Enantiospecific synthesis of estrone

JOHN H. HUTCHINSON AND THOMAS MONEY
Department of Chemistry, The University of British Columbia, 2036 Main Mall, Vancouver, B.C., Canada V6T 1Y6

Received January 2, 1986

This paper is dedicated to Dr. O. E. (Ted) Edwards

JOHN H. HUTCHINSON and THOMAS MONEY. Can. J. Chem. **65**, 1 (1987).

Efficient cleavage of the C(1)—C(2) bond in 9,10-dibromocamphor (**3**) provides a chiral intermediate (**5**) that can be used in a new enantiospecific synthesis of estrone.

JOHN H. HUTCHINSON et THOMAS MONEY. Can. J. Chem. **65**, 1 (1987).

Le clivage efficace de la liaison C(1)—C(2) du dibromo-9,10 camphre (**3**) fournit un intermédiaire chiral (**5**) qui peut être utilisé dans une nouvelle synthèse énantiospécifique de l'estrone.

[Traduit par la revue]

Can. J. Chem. Downloaded from www.nrcresearchpress.com by 80.58.250.72 on 09/07/12
For personal use only.

Recent research in our laboratory has shown that (+)-camphor (**1**)[1] can be converted to (+)-9,10-dibromocamphor (**3**) (2*a*,*b*) and that the latter compound undergoes facile, efficient ring cleavage (1*b*, 2*c*,*d*, 5*g*) with base to provide monocyclic bromoacid (**4**) or hydroxyacid (**5**) in >90% yield. The development of an enantiospecific synthesis[2] of estrone[3] from the monocyclic hydroxyacid **5** or its enantiomer is described below and outlined in Scheme 1.

In our initial studies we recognized that bromoacid **4** (2*c*,*d*) could represent ring D and part of ring C of (−)-estrone **20** and that the exocyclic double bond in **4** could be regarded as the eventual precursor of the 17-keto group. Our investigations also made us aware of the tendency of the exocyclic double bond in **4** to undergo acid-catalyzed isomerization to the thermodynamically more stable endocyclic position (6). This isomerization would, of course, greatly diminish the synthetic usefulness of bromoacid **4** or hydroxyacid **5** and thus it was necessary to avoid prolonged acidic conditions during the synthetic sequence until oxidative cleavage of the exocyclic double bond had been accomplished. Initially we considered the possibility of constructing the *trans*-C,D hydrindane ring system in estrone by intramolecular alkylation of the bromoketone **6** derived from bromoacid **4**. However, this proved to be only partially successful since reaction of **6** with LDA/HMPA at −78°C provided a mixture of the desired bicyclic ketone **9** and a monocyclic hydroxyketone **7**, which was presumably formed by hydrolysis of the intermediate bicyclic enol ether **10**. A molecular model of the kinetic enolate derived from bromoketone **6** indicates that there is some strain involved in achieving the proper trajectory for the desired 6-(enolendo)-*exo*-tet cyclization (7) and therefore the 6-*exo*-tet cyclization (*O*-alkylation) leading to enol ether **10** becomes a viable alternative (7–9).

The disappointing results described above prompted us to consider an alternative route to the C,D ring system of estrone, which involved the intermediacy of hydroxyacid **5** (2*c*) derived directly from (+)-9,10-dibromocamphor (**3**). As shown in Scheme 1, conversion of hydroxyacid **5** to hydroxyketone **7** followed by oxidation to ketoaldehyde **8** and subsequent intramolecular aldol condensation provided the *trans*-bicyclic dienone **11** in ~40% overall yield. The remaining task in the synthesis was construction of the A, B ring system of estrone, and our initial attempts to accomplish this by alkylation of dienone **11** with *m*-methoxyphenethyl iodide were unsuccessful in spite of reasonable analogy (10). A similar difficulty has been reported by other research groups (11, 12) when they tried to use *m*-methoxyphenethyl iodide as alkylating agent and is presumably due to the tendency of this compound to undergo elimination rather than substitution. We decided, therefore, to construct rings A and B by adaptation of a previous approach described by Cohen and co-workers (13), i.e., conjugate addition of *m*-methoxybenzylmagnesium chloride to an exocyclic bicyclic enone system. The intermediate trienone **13** required for this purpose was synthesized by heating dienone **11** with Brederick's reagent ($Bu^tOCH(NMe_2)_2$) (14–18) followed by DIBAL reduction of the intermediate vinylogous amide **12**. However, all attempts to achieve regiospecific conjugate addition of *m*-methoxybenzylmagnesium chloride to trienone **13** in the presence or absence of CuI or CuII salts (13*b*, 19) gave mixtures of 1,2 and 1,4 addition products.

The failure of this approach prompted us to consider conjugate addition of *m*-methoxybenzylmagnesium chloride to the vinylogous amide **12**. This type of reaction was first reported by Benary (20), who found that conjugate addition of Grignard reagent to vinylogous amides followed by acid hydrolysis provides α,β-unsaturated ketones. Since then similar reactions have been described by other research groups (21, 22). In the event, treatment of vinylogous amide **12** with *m*-methoxybenzylmagnesium chloride provided trienones **14***a*,*b* in ~70% yield. The major product (**14***a*) (~90%) and minor product (**14***b*) (~10%) were identified as *trans*- and *cis*-trienones respectively by nOe (nuclear Overhauser effect) difference spectra. For example, irradiation at the chemical shift (δ 6.94) of the C(7) vinyl proton in *trans*-trienone **14***a* produced positive enhancement for protons at C(6) (steroid numbering), while irradiation of the corresponding proton (δ 5.85) in the *cis*-trienone **14***b* resulted in enhancement of the C(6), C(14), and C(15) proton signals.

The stereoselectivity of conjugate addition of Grignard reagent to the *trans*-vinylogous amide (stereochemistry assumed by analogy with similar systems (16, 21*a*)) can be explained (Scheme 2) by the smaller steric interactions in the rotamer

[1]The development of elegant synthetic routes from camphor to various steroid systems has been described by the late Professor R. V. Stevens and co-workers (1).

[2]We define enantiospecific synthesis as one in which readily available enantiomeric starting materials provide enantiomeric products. The term "stereospecific synthesis" is defined (3) as one in which stereoisomeric starting materials (which, of course, include geometric isomers) provide stereoisomeric products and therefore would also include all enantiospecific syntheses.

[3]Syntheses of estrone published up to the end of 1981 have been reviewed in ref. 4; syntheses of estrone since 1982 include those in ref. 5.

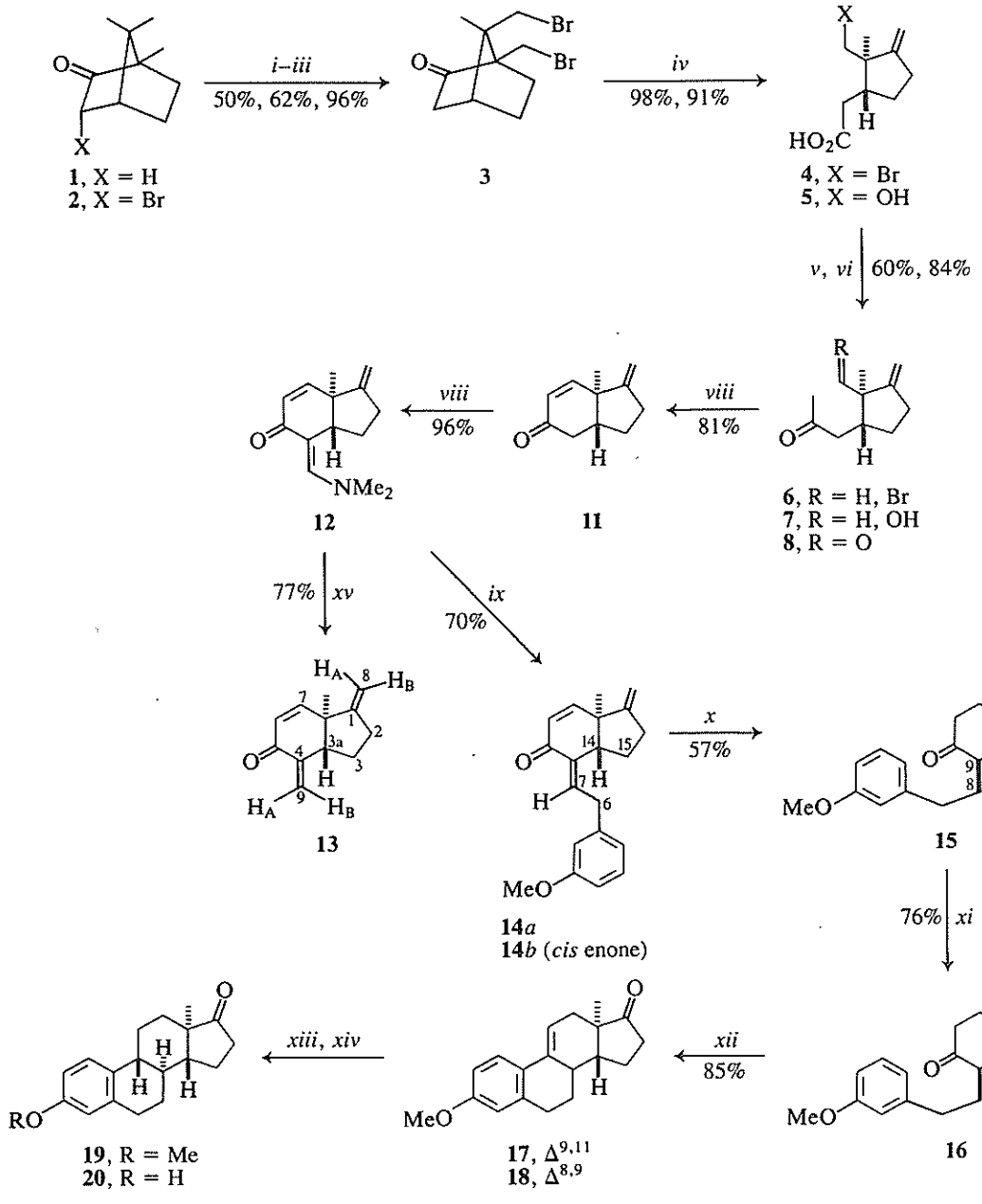

i $Br_2/ClSO_3H/1$ h; *ii* $Br_2/ClSO_3H/5$ days; *iii* Zn/HOAc/Et_2O/0°C; *iv* KOH/DMSO/H_2O/24 h; *v* MeLi/THF; Me_3SiCl; 1 *N* HCl; *vi* PDC/CH_2Cl_2/20°C/24 h; *vii* 2 *N* NaOH/MeOH/0°C/5 min; MsCl/Et_3N/DMAP; DBU; *viii* Bu^{t}OCH$(NMe_2)_2$/heat; *ix* *m*-$CH_3OC_6H_4CH_2MgCl/Et_2O$; *x* $Li/NH_3/Et_2O$; *xi* O_3/CH_2Cl_2; Me_2S; *xii* HCl/HOAc; *xiii* H_2/Pd; *xiv* BBr_3/CH_2Cl_2; *xv* DIBAL/THF

SCHEME 1

(**22***a*) of the intermediate enolate adduct (**21**) that leads to the major product (**14***a*).

The final stages of the synthetic route involved stereoselective reduction of trienone **14***a* with Li/NH_3 in ether, followed by ozonolysis to provide the known diketone **16** (23) in ~50% overall yield. Subsequent cyclodehydration of diketone **16** with concentrated HCl/HOAc (24) at 0°C led to a mixture (97:3) of (−)-9,11-dehydroestrone methyl ether **17** (5*b*, 23, 25, 26) and the $\Delta^{8,9}$ isomer **18** (5*b*, 25*b*, 26, 27) in ~85% yield. Finally, catalytic hydrogenation (Pd/C) of **17** (5*b*, 23, 25*b*) gave (−)-estrone methyl ether **19**, which was demethylated with boron tribromide (28) to provide (−)-estrone **20** having ir, nmr (400 MHz), and mass spectra identical to those of authentic (+)-estrone.[4]

To obtain natural (+)-estrone would of course require the use of (−)-3-bromocamphor in the reaction sequence. This can be obtained inexpensively by oxidizing (−)-borneol to (−)-camphor (29) followed by bromination in acetic acid (30). The commercial availability of (+)-3-bromocamphor (**2**), however, prompted us to conduct our investigations in the *ent*-series.

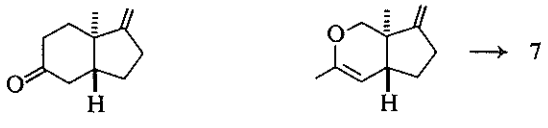

9 **10**

[4]The synthesis of estrone shown in Scheme 1 was presented at the International Symposium on the Chemistry of Natural Products in Edmonton, Alberta, June 23–26, 1985.

Can. J. Chem. Downloaded from www.nrcresearchpress.com by 80.58.250.72 on 09/07/12
For personal use only.

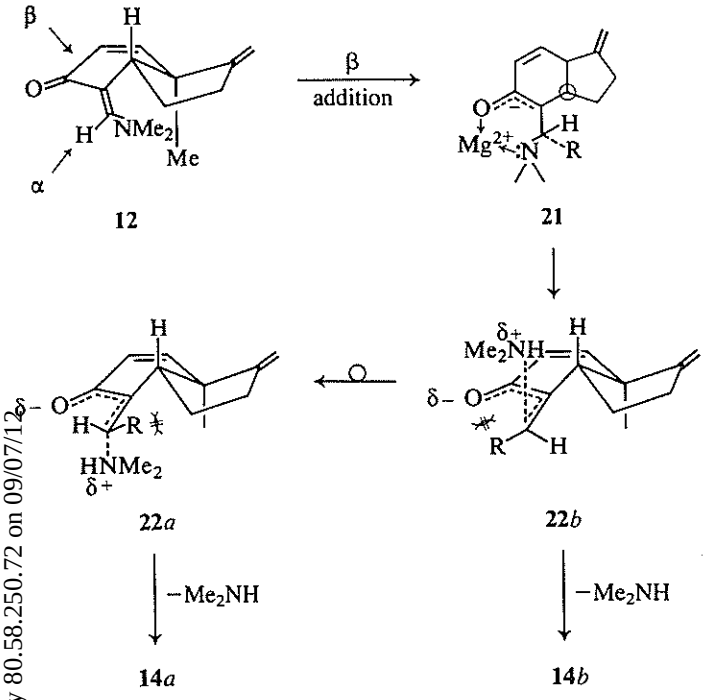

SCHEME 2

Experimental

Melting points (mp) were determined on a Kofler micro heating stage and are uncorrected. Infrared spectra were recorded on a Perkin–Elmer 137 spectrophotometer and optical rotations were made on a Perkin–Elmer 141 polarimeter. The ^{1}H nmr spectra were recorded on Bruker WH-400, Bruker WP-80, or Nicolet–Oxford H-270 instruments. Signal positions are given in delta (δ) with tetramethylsilane (TMS) as internal reference (except for compounds containing trialkylsilyl groups where TMS was used as an external reference). The integrated areas and signal multiplicities are indicated in parentheses. Low resolution mass spectra were determined on a MAT CH-4 spectrometer and high resolution spectra were recorded on a Kratos MS-50 spectrometer. Gas–liquid chromatography was performed on a Hewlett–Packard model 5830A gas chromatograph with a 6 ft × 1/8 in. column (3% OV-17) or a Hewlett–Packard model 5880A gas chromatograph using 50 or 12 m × 0.2 mm columns (Carbowax 10M). Column chromatography was done using Merck silica gel 60 (230–400 MHz) and thin-layer chromatography (tlc) utilizing silica gel HLF5 UV254 (Analtech) or silica gel 1B2-F (Baker-flex) sheets. Microanalyses were performed by Mr. P. Borda, Microanalytical Laboratory, University of British Columbia.

Bromoketone (6)

Methyllithium (2.43 mL, 3.0 mmol; 1.25 *M* solution in ether) was added to a solution of the bromoacid (**4**) (2*c*) (250 mg, 1.0 mmol) in tetrahydrofuran (10 mL, 0°C). After 2 h, freshly distilled trimethylsilyl chloride (2.54 mL, 20 mmol) was added and the solution warmed to room temperature over 45 min (31). Hydrochloric acid (1 *N*) was added and the solution extracted 3 times with ether. The organic phase was washed twice with water, dried over $MgSO_4$, and the solvent removed to give a pale yellow oil (241 mg).

Column chromatography on silica gel using distilled toluene as eluant gave the bromoketone **6** as a colorless oil (173 mg, 70%); $[\alpha]_D$ −48.3° (*c* 0.4, MeOH); ν_{max} ($CHCl_3$): 1715, 1650, 890 cm^{-1}; δ ($CDCl_3$, 400 MHz): 1.05 (3H, s), 1.24 (1H, m), 1.95 (1H, m), 2.18 (3H, s), 2.26 (1H, dd, *J* = 16 Hz, 10 Hz), 2.31–2.45 (2H, m), 2.54 (1H, m), 2.68 (1H, dd, *J* = 16 Hz, 4 Hz), 3.39 (d) and 3.47 (d) (2H, AB quartet, *J* = 10 Hz), 4.84 (1H, br s), 4.99 (1H, br s); *m/e* (relative intensity): 246/244 (M^+, 0.1/0.1), 231/229 (0.6/0.6), 188/186 (26/27), 165 (10), 109 (23), 107 (100), 93 (26), 91 (23). *Mol. Wt.* calcd. for $C_{11}H_{17}O$ ($M-Br$)$^+$: 165.1279; found (high resolution mass spectrometry): 165.1280.

Hydroxyketone (7)

The hydroxyacid **5** (2*c*) (5.0 g, 27.2 mmol) in dry tetrahydrofuran (250 mL) at 0°C under argon was treated with methyllithium (200 mL, 200 mmol; 1 *M* solution in ether) over 30 min. After 1 h at 0°, the reaction was warmed to room temperature and left to stir overnight. Trimethylsilyl chloride (52 mL, 408 mmol; freshly distilled) was added slowly (**care**!) and after 10 min the solution was treated with hydrochloric acid (1 *N*; 100 mL) for 30 min. The solution was then made basic with potassium hydroxide (2 *N*) and extracted twice with ether. The ether layers were washed with 2 *N* potassium hydroxide (twice), then water, dried ($MgSO_4$), and the ether removed to yield the crude hydroxyketone **7** (3.60 g). It was found that the best overall yield of the ketoaldehyde (**8**) was obtained by oxidizing this crude material without purification. Isolation of a portion of the crude product was achieved by flash chromatography on silica gel (petroleum ether/ether 2:1) to yield pure hydroxyketone **7**; ν_{max} (film): 3420, 1705, 1650, 885 cm^{-1}; δ ($CDCl_3$, 400 MHz): 0.84 (3H, s), 1.28 (1H, m), 1.90 (1H, m), 2.09 (1H, br s, exchangeable with D_2O), 2.17 (3H, s), 2.32 (1H, m), 2.32 (1H, dd, *J* = 16 Hz, 8.5 Hz), 2.45 (2H, m), 2.60 (1H, dd, *J* = 16 Hz, 5 Hz), 3.36 (d) and 3.52 (d) (2H, AB quartet, *J* = 11 Hz), 4.82 (1H, t, *J* = 2.5 Hz), 5.00 (1H, t, *J* = 2 Hz); *m/e* (relative intensity): 182 (M^+, 0.4), 151 (11), 109 (35), 95 (15), 94 (100), 93 (30), 89 (34). *Mol. Wt.* calcd. for $C_{11}H_{18}O_2$: 182.1307; found (high resolution mass spectrometry): 182. 1297.

Acidification of the combined aqueous phases with 6 *N* hydrochloric acid and extraction with ether (×3), then washing the ether layers with water, gave (after drying and evaporation) a white solid (1.16 g). Chromatography on Florisil (elution with ether) afforded starting material **5** (754 mg).

Oxidation of the crude hydroxyketone[5] **7** (3.4 g, ~18.7 mmol) was carried out with pyridinium dichromate (14 g, 37.4 mmol) in dichloromethane (200 mL) at room temperature under argon for 24 h. The usual work-up provided a crude oil (3.16 g). Column chromatography (silica gel; petroleum ether/ether 5:1) gave the keto aldehyde **8** (2.21 g, 48% yield over 2 steps); $[\alpha]_D$ −22.2° (*c* 0.315, CH_2Cl_2); ν_{max} ($CHCl_3$): 2725, 1720, 1650, 900 cm^{-1}; δ ($CDCl_3$, 400 MHz): 1.03 (3H, s), 1.42 (1H, m), 2.0 (1H, m), 2.13 (3H, s), 2.34–2.57 (4H, m), 2.73 (1H, 6-line multiplet), 4.75 (1H, t, *J* = 2.5 Hz), 5.09 (1H, t, *J* = 2 Hz), 9.31 (1H, s); *m/e* (relative intensity): 151 (12), 109 (32), 95 (15), 94 (100), 93 (30), 79 (37). *Mol. Wt.* calcd. for $C_{11}H_{16}O_2$ − CHO: 151.1123; found (high resolution mass spectrometry): 151.1131. *Anal.* calcd. for $C_{11}H_{16}O_2$: C 73.30, H 8.95; found: C 73.05, H 9.00.

Hydrindienone (11)

Sodium hydroxide (2 *N*, 50 mL) was added to a cooled (0°C) solution of ketoaldehyde **8** (1.6 g, 8.9 mmol) in methanol (50 mL). after 1 min, tlc indicated the reaction was complete and the mixture was poured into brine and carefully treated with 6 *N* hydrochloric acid until neutral. After extracting with ether (×5), the combined ether layers were washed with brine, dried, and concentrated *in vacuo* to give crude aldol product as a pale yellow solid (1.75 g); ν_{max} (film): 3450 (br), 1705, 1650, 890 cm^{-1}; δ ($CDCl_3$, 80 MHz): 1.08 (3H, s), 4.00 (1H, dd, *J* = 20 Hz, 12 Hz), 4.82 (1H, m), 5.38 (1H, m); *m/e* (relative intensity): 180 (M^+, 0.9), 120 (3), 91 (99), 79 (100).

The crude aldol product (1.75 g) was converted to the corresponding mesylate (methanesulphonyl chloride, 1.8 mL; triethylamine, 4.4 mL; 4-dimethylaminopyridine, 0.4 g; dichloromethane, 60 mL; argon; 24 h), which was then treated with 1,5-diazabicyclo[5.4.0]undec-5-ene (DBU) (1.3 g, 8.9 mmol) in dry dichloromethane (50 mL) for 45 min. The solution was diluted with dichloromethane, washed successively with 1 *N* hydrochloric acid and water (twice), dried, and evaporated to provide the dienone **11** (1.21 g, 84%) as a white crystalline solid that was sufficiently pure for further reactions. Low temperature recrystallization of this material from pentane provided pure dienone **11**, mp 60.5–61.5°C (sealed tube); $[\alpha]_D$ −13.5° (*c* 0.17, CH_2Cl_2); ν_{max} ($CHCl_3$): 1670, 1665, 890 cm^{-1}; δ ($CDCl_3$, 400 MHz): 1.03 (3H, s), 1.57 (1H, m), 1.81 (1H, m), 2.17 (1H, m), 2.41 (1H, dd, *J* = 17 Hz, 14 Hz), 2.41 (1H, m), 2.58 (1H, dd, *J* = 17 Hz, 4.5 Hz),

[5]Oxidation of the pure hydroxyketone **7** provided ketoaldehyde **8** in 81% yield.

Can. J. Chem. Downloaded from www.nrcresearchpress.com by 80.58.250.72 on 09/07/12
For personal use only.

Can. J. Chem. Downloaded from www.nrcresearchpress.com by 80.58.250.72 on 09/07/12
For personal use only.

2.58 (1H, m), 4.87 (1H, t, J = 2 Hz), 4.92 (1H, t, J = 2.5 Hz), 5.90 (1H, d, J = 10 Hz), 7.30 (1H, d, J = 10 Hz); m/e (relative intensity): 162 (M^+, 14), 147 (22), 120 (100), 105 (37), 91 (47), 77 (33). *Mol. Wt.* calcd. for $C_{11}H_{14}O$: 162.1045; found (high resolution mass spectrometry): 162.1042. *Anal.* calcd. for $C_{11}H_{14}O$: C 81.44, H 8.70; found: C 81.22, H 8.78.

*Vinylogous amide (**12**)*

Dienone **11** (280 mg, 1.73 mmol) and *tert*-butoxybis(dimethylamino)methane (14) (870 mg) were stirred at 70°C for 6 h. Water was added and the solution extracted with dichloromethane. The combined organic extracts were washed with water, dried, and concentrated to provide the vinylogous amide **12** as a brown oil (386 mg). This material was used without any further purification; ν_{max} (film): 1640, 1610, 1560, 890, 820 cm^{-1}; δ ($CDCl_3$, 270 MHz): 0.90 (3H, s), 1.60 (1H, m), 1.81 (1H, m), 2.45 (1H, m) and 2.55 (1H, m), 3.05 (6H, s), 4.89 (1H, t, J = 2 Hz), 4.93 (1H, t, J = 2.5 Hz), 5.90 (1H, d, J = 9.5 Hz), 6.21 (1H, s), 6.98 (1H, d, J = 9.5 Hz); m/e (relative intensity): 217 (M^+, 100), 202 (99), 200 (13), 85 (51), 84 (44), 83 (75), 73 (68), 72 (43). *Mol. Wt.* calcd. for $C_{14}H_{19}ON$: 217.1467; found (high resolution mass spectrometry): 217.1467.

*Trienone (**13**)*

To a cold (−78°C) solution of the vinylogous amide **12** (377 mg, 1.69 mmol) in tetrahydrofuran (10 mL) under an argon atmosphere was added diisobutylaluminum hydride (DIBAL) (1.75 mL, 1.75 mmol; 1 *M* solution in hexane). The reaction was stirred for 3 h (−78°C to room temperature), then ammonium chloride solution (10 mL) was added and stirring continued for a further 10 h. The mixture was partitioned between ether and 1 *N* hydrochloric acid. The aqueous layer was extracted twice more with ether and the combined ether extracts washed with water (×3), dried, and the solvent removed. A pale yellow oil resulted, which was subjected to chromatography on silica gel (petroleum ether/ether 24:1) to provide the trienone (225 mg, 1.29 mmol, 76%); $[\alpha]_D$ +123.2° (c 0.41, CH_2Cl_2); ν_{max} (film): 1675, 1660, 1630, 885, 840 cm^{-1}; δ ($CDCl_3$, 400 MHz): 0.94 (3H, s), 1.80 (1H, 9-line multiplet; C(3)-H), 1.94 (1H, m; C(3)-H); 2.52 (1H, m; C(2)-H), 2.64 (1H, m; C(2)-H), 2.82 (1H, dddd, J = 12 Hz, 6 Hz, 2.5 Hz, 2.5 Hz; C(3a)-H), 4.89 (1H, dd, J = 2 Hz, 2 Hz; C(8)-H_B), 4.94 (1H, dd, J = 2.5 Hz, 2.5 Hz; C(8)-H_A), 5.21 (1H, ddd, J = 2.5 Hz, 1.5 Hz, 0.75 Hz; C(9)-H_B), 6.03 (1H, dd, J = 10 Hz, 0.75 Hz; C(6)-H), 6.13 (1H, dd, J = 2.5 Hz, 1.5 Hz; C(9)-H_A), 7.35 (1H, d, J = 10 Hz; C(7)-H). Irradiation at δ 5.2 (C(9)-H_B) causes the following signals to collapse: δ 6.13 (C(9)-H_A) to a doublet (J = 2.5 Hz); 6.03 (C(6)-H) to a doublet (J = 10 Hz); and δ 2.82 (C(3a)-H) to a ddd (J = 12 Hz, 6 Hz, 2.5 Hz). Irradiation at δ 2.52 (C(2)-H) causes both δ 4.89 (C(8)-H_B) and 4.94 (C(8)-H_A) to collapse to doublets (J = 2 Hz and 2.5 Hz respectively). Similarly, irradiation at δ 2.64 (C(2)-H) gives doublets at δ 4.89 and δ 4.94 (J = 2 Hz and 2.5 Hz respectively). Irradiating δ 1.94 (C(3)-H) causes 2.82 to become a ddd (J = 12 Hz, 2.5 Hz, 2.5 Hz), and irradiation at δ 1.80 (C(3)-H) causes 2.82 to collapse to a broad singlet. The nOe difference experiments provided the following results: (i) irradiation at δ 1.80 (C(3)-H), enhancement at δ 2.64 (C(2)-H) and 5.21 C(9)-H_B; (ii) irradiation at δ 2.82 (C(3a)-H), enhancement at δ 1.94 (C(3)-H) and 2.52 (C(2)-H); (iii) irradiation at δ 7.35 (C(7)-H), enhancement at δ 4.94 C(8)-H_A). m/e (relative intensity): 174 (M^+, 100), 159 (50), 146 (19), 145 (21), 131 (42), 105 (18), 91 (36). *Mol. Wt.* calcd. for $C_{12}H_{14}O$: 174.1045; found (high resolution mass spectrometry). 174.1049.

*Benzyltrienone (**14**a,b)*

m-Methoxybenzyl chloride (32) (1.74 g, 11.1 mmol) in ether (20 mL) was added to magnesium turnings (534 mg, 22.2 mmol) at a rate that maintained a vigorous reflux. A further 20 mL of ether was added and the solution refluxed for 30 min and then cooled to room temperature. A 1-mL aliquot was removed, added to water, and titration with 0.05 *N* hydrochloric acid using phenolphthalein as indicator indicated that the Grignard solution was 0.425 *M*.

To vinylogous amide **12** (680 mg, 3.08 mmol) in dry ether (40 mL) at −78°C under argon was added a solution of *m*-methoxybenzylmagnesium chloride (9 mL, 3.8 mmol). After 40 min the cold bath was removed and the reaction warmed at room temperature over 30 min. The solution was then transferred via cannula to a rapidly stirred solution of ammonium chloride. Extraction with ether (×3) and work-up in the usual way provided a pale yellow oil (973 mg) that, on column chromatography (silica gel: petroleum ether/ether 12:1), gave a mixture of *meta*-methylanisole and 1,2-di-(3-methoxyphenyl)ethane (144 mg) followed by the *cis* enone (**14***b*) (61 mg, 7%) as a colourless oil; $[\alpha]_D$ −34.6 (c 0.24, MeOH); ν_{max} (film): 1670, 1630, 1605, 1590, 1495, 890 cm^{-1}; δ ($CDCl_3$, 400 MHz): 0.95 (3H, s), 1.67–1.86 (2H, m), 2.48 (1H, m), 2.60 (1H, m), 2.82 (1H, m; C(14)-H), 3.80 (3H, s), 3.93–4.08 (2H, m; C(6)-H), 4.89 (1H, t, J = 2 Hz), 4.94 (1H, t, J = 2.5 Hz), 5.85 (1H, ddd, J = 7.5 Hz. 7.5 Hz, 2.5 Hz; C(7)-H), 6.00 (1H, d, J = 10 Hz), 6.73–6.85 (3H, m), 7.21 (1H, t, J = 8 Hz), 7.24 (1H, d, J = 10 Hz). In an nOe difference experiment irradiation at δ 5.85 gives a positive enhancement at δ 1.67–1.86, δ 2.82, and δ 3.93–4.08; m/e (relative intensity): 294 (M^+, 100), 279 (36), 173 (32), 135 (24), 121 (41), 91 (28). *Mol. Wt.* calcd. for $C_{20}H_{22}O_2$: 294.1620; found (high resolution mass spectrometry): 294.1625.

Elution with petroleum ether/ether (2:1) provided the *trans*-enone **14***a* (595 mg, 66%) as a colourless oil; $[\alpha]_D$ +24.5° (c 0.2, MeOH); ν_{max} (film): 1680, 1660, 1620, 1600, 1590, 1495, 890 cm^{-1}; δ ($CDCl_3$, 400 MHz): 1.04 (3H, s), 2.18 (1H, 9-line multiplet), 2.29 (1H, m), 2.48 (1H, m), 2.66 (1H, m), 2.90 (1H, m; C(14)-H), 3.60 (1H, ddd, J = 16 Hz, 8 Hz, 2 Hz; C(6)-H), 3.70 (1H, ddd, J = 16 Hz, 8 Hz, 1 Hz; C(6)-H), 3.78 (3H, s), 4.94 (1H, t, J = 2 Hz), 4.98 (1H, t, J = 2.5 Hz), 6.04 (1H, d, J = 10 Hz), 6.72–6.81 (3H, m), 6.94 (1H, ddd, J = 8 Hz, 8 Hz, 2.5 Hz; C(7)-H), 7.22 (1H, t, J = 7.5 Hz), 7.30 (1H, d, J = 10 Hz). Decoupling the proton at δ 6.94 (C(7)-H) simplifies signals at δ 3.70, 3.60, and 2.90. The nOe difference experiment: irradiation at δ 6.94 gave enhanced signals at δ 6.72–6.81 and δ 3.60–3.70; m/e (relative intensity): 294 (M^+, 100), 279 (53), 173 (99), 171 (34), 160 (38), 145 (40), 135 (38), 134 (31), 121 (69), 115 (35), 91 (70), 77 (43). *Mol. Wt.* calcd. for $C_{20}H_{22}O_2$: 294.1620; found (high resolution mass spectrometry): 294.1625.

*Enone (**15**)*

To a solution of lithium (45 mg, 9.1 mmol) in ammonia (30 mL) under argon was added the trienone **14***a* (102 mg, 0.34 mmol) in ether (7 mL). After 2 h, the ammonia was removed and saturated ammonium chloride solution was added. The mixture was extracted with ether (×3) and the ether layers washed twice with water, dried, and the solvent removed to provide a pale yellow oil (100 mg). Subsequent chromatography on silica gel (petroleum ether/ether 10:1) afforded enone **15** (40.6 mg), followed by a mixture of starting material **14***a* and an unknown dihydro derivative (32.2 mg). This mixture was subjected to the same reduction conditions described above (lithium, 20 mg; ammonia, 20 mL; ether, 5 mL; 30 min) and the product, after chromatography, provided a further quantity of the desired enone **15** (18.1 mg) (58.7 mg total, 57% combined yield); $[\alpha]_D$ −28.6° (c 0.405, MeOH); ν_{max} (film): 1705, 1660, 1600, 1590, 1490, 880 cm^{-1}; δ ($CDCl_3$, 400 MHz): 1.09 (3H, s), 1.51 (1H, m), 1.61–1.76 (3H, m), 1.82 (1H, m), 1.93 (1H, m), 2.00 (1H, ddd, J = 13 Hz, 7 Hz, 2 Hz), 2.30–2.67 (6H, m), 2.73 (1H, 8-line multiplet), 3.80 (3H, s), 4.68 (1H, t, J = 2.5 Hz), 4.73 (1H, t, J = 2 Hz), 6.70–6.81 (3H, m), 7.19 (1H, t, J = 8 Hz); m/e (relative intensity): 298 (M^+, 27), 164 (35), 134 (100), 122 (29), 121 (37), 94 (82), 91 (29). *Mol. Wt.* calcd. for $C_{20}H_{26}O_2$: 298.1933; found (high resolution mass spectrometry): 298.1928.

*Diketone (**16**)*

Ozone was bubbled through a cold (−78°C) solution of the enone **15** (143.9 mg, 0.48 mmol) in dry methanol (25 mL). At the first sign of a pale blue colour, the flow of ozone was stopped and the system purged with oxygen until colourless. Dimethylsulphide (1 mL) was added and the reaction allowed to warm to room temperature. After 3 h the solvent was removed *in vacuo* and the crude product (202.5 mg) purified by flash chromatography (petroleum ether/ether 2:1) to provide pure diketone (**16**) (110.6 mg, 76%) as a viscous oil; $[\alpha]_D$ −77.2° (c 0.47, MeOH); ν_{max} (film): 1740, 1710, 1605, 780, 695 cm^{-1} (lit. (23) ν_{max} (film): 1740, 1710, 1600, 780, 690 cm^{-1}; lit (25*a*) ν_{max} (film): 1740, 1715, 1600, 1585 cm^{-1}); δ ($CDCl_3$, 400 MHz): 1.13 (3H, s),

Can. J. Chem. Downloaded from www.nrcresearchpress.com by 80.58.250.72 on 09/07/12
For personal use only.

1.62–1.80 (3H, m), 1.86 (1H, ddd, J = 13 Hz, 12.5 Hz, 5.5 Hz), 1.94–2.09 (3H, m), 2.21 (1H, 6-line multiplet), 2.41–2.62 (5H, m), 2.76 (1H, m), 3.80 (3H, s), 6.71–6.83 (3H, m), 7.19 (1H, t, J = 8 Hz); m/e (relative intensity): 300 (M^+, 9), 135 (14), 134 (100), 122 (12). *Mol. Wt.* calcd. for $C_{19}H_{24}O_3$: 300.1726; found (high resolution mass spectrometry): 300.1730.

(−)-9,11-Dehydroestrone methyl ether (17) and (−)-8,9-dehydroestrone methyl ether (18)

Ketone **16** (57.4 mg, 0.19 mmol) was dissolved in ether (1 mL) and a mixture of glacial acetic acid/concentrated hydrochloric acid (10:1) (2 mL) at 0°C. After 2 h, the reaction was poured into brine and extracted with ether. The ether layers were washed with sodium bicarbonate solution, brine (twice), dried ($MgSO_4$), and evaporated to yield a white crystalline solid (53.5 mg) that, on column chromatography (silica gel; petroleum ether/ether 4:1), provided the tetracyclic products **17** and **18** (45.8 mg, 85%) in the ratio 97:3 (capillary glc, OV-101, 200°C).[6] Recrystallization from methanol provided pure (−)-9,11-dehydroestrone methyl ether **17**, mp 143–145.5°C (lit. (5*b*) mp 143–144°C, lit. (25*a*) mp 142.5–144°C); $[\alpha]_D$ −284° (*c* 0.208, $CHCl_3$) (lit. (5*b*) $[\alpha]_D$ −288.20 (*c* 0.5, dioxane) and, for the enantiomer, lit. (5*b*) $[\alpha]_D$ +288.7° (*c* 0.479, dioxane), lit. (25*a*) $[\alpha]_D$ +290.0° (*c* 0.5, $CHCl_3$)); ν_{max} ($CHCl_3$) 1735, 1610, 1500 cm^{-1}; δ ($CDCl_3$, 400 MHz): 0.95 (3H, s), 1.47 (1H, m), 1.68 (2H, m), 2.10–2.40 (6H, m), 2.54 (1H, m), 2.83–3.00 (2H, m), 3.80 (3H, s), 6.14 (1H, m; C(11)-H), 6.63 (1H, d, J = 3 Hz; C(4)-H), 6.73 (1H, dd, J = 8 Hz, 3 Hz; C(2)-H), 7.54 (1H, d, J = 8 Hz; C(1)-H); m/e (relative intensity): 282 (M^+, 100), 267 (49), 249 (19), 225 (30), 224 (36), 211 (22). *Mol. Wt.* calcd. for $C_{19}H_{22}O_2$: 282.1620; found (high resolution mass spectrometry): 282.1618. *Anal.* calcd. for $C_{19}H_{22}O_2$: C 80.82, H 7.85; found: C 80.71, H 7.88.

(−)-Estrone methyl ether (19)

Dehydroestrone methyl ether (38.4 mg; **17**:**18** 93:7), palladium-on-charcoal (10% catalyst, 13.1 mg), and methanol (8 mL) were stirred under an atmosphere of hydrogen for 2 h (23). The solution was diluted with ether, filtered through a pad of Celite, and the solvent removed to yield a white crystalline solid (35.0 mg). Capillary glc analysis (OV-101, 220°C) showed this to be two compounds, estrone methyl ether **19** and an unidentified by-product[7] in the ratio 65:35. Recrystallization from methanol provided pure (−)-estrone methyl ether **19** (18.2 mg, 47%), mp 167.5–170°C (lit. (13*b*) mp 164–167°C); $[\alpha]_D$ −149.2° (*c* 0.126, dioxane) (lit. (13*b*) $[\alpha]_D$ +153.98° (*c* 1.0, dioxane) for enantiomer); ν_{max} ($CHCl_3$): 1735, 1620, 1500 cm^{-1}; δ ($CDCl_3$, 400 MHz): 0.91 (3H, s; C(18)-methyl), 1.35–1.70 (6H, m), 1.93–2.20 (4H, m), 2.26 (1H, m), 2.40 (1H, m), 2.50 (1H, dd, J = 20 Hz, 8 Hz), 2.90 (2H, m), 3.78 (3H, s), 6.66 (1H, d, J = 3 Hz), 6.73 (1H, dd, J = 8 Hz, 3 Hz), 7.21 (1H, d, J = 8 Hz); m/e (relative intensity): 284 (M^+, 100), 199 (56), 186 (24), 160 (32). *Mol. Wt.* calcd. for $C_{19}H_{24}O_2$: 284.1775; found (high resolution mass spectrometry): 284.1775. The synthetic material was found to be identical (tlc, ir, ^1H nmr, and ms) to an authentic sample of (+)-estrone methyl ether prepared from (+)-estrone.

(−)-Estrone (20)

Boron tribromide (11.5 L, 0.12 mmol) was added to a solution of (−)-estrone methyl ether **19** (31.3 mg, 0.11 mmol) in dichloromethane (2 mL) at −78°C under argon (28). The cold bath was removed and after 30 min the reaction mixture was added to ice and brine. Dilution with dichloromethane followed by extraction with 2*N* potassium hydroxide solution, acidification of the aqueous layer, extraction with chloroform, and removal of solvent provided a crude product that, on titration with petroleum ether/ether, afforded (−)-estrone **20** (16 mg, 54%); ν_{max} ($CHCl_3$): 3600 (sharp), 3350 (br), 1735, 1610 cm^{-1}; δ ($CDCl_3$, 400 MHz): 0.90 (3H, s), 1.38–1.70 (6H, m), 1.93–2.28 (5H, m), 2.38 (1H, m), 2.50 (1H, dd, J = 19 Hz, 9 Hz), 2.86 (2H, m), 4.69 (1H, br s), 6.59 (1H, d, J = 3 Hz), 6.64 (1H, dd, J = 8 Hz, 3 Hz), 7.15 (1H, d, J = 8 Hz); m/e (relative intensity): 270 (M^+, 100), 185 (47), 172 (38), 146 (40). The synthetic (−)-estrone was found to be identical (tlc, ir, ^1H nmr, and ms) with authentic (+)-estrone (Sigma Chemical Co.).

(+)-Estrone methyl ether (ent-*19*)

(+)-Estrone (*ent*-**20**) (108 mg, 0.4 mmol; Sigma Chemical Co.), potassium hydroxide (100 mg, 1.79 mmol), methanol (6 mL), water (2 mL), and dimethyl sulphate (0.6 mL, 6.3 mmol) were stirred for 24 h. The mixture was added to ammonium hydroxide solution, extracted with ether, and the ether layers washed with potassium hydroxide solution (2 *N*) followed by washing with water. The dried solution was evaporated to provide a white crystalline solid (113 mg), which was crystallized from acetonitrile to give pure (+)-estrone methyl ether (*ent*-**19**), mp 170–173°C (lit. (13*b*) mp 164–167°C); $[\alpha]_D$ +154.0° (*c* 1.02, dioxane) (lit. (13*b*) $[\alpha]_D$ +153.98° (*c* 1.0, dioxane)).

[6]When the reaction was carried out at room temperature the ratio of **17** to **18** was found to be 3.7:1 by integration of the C(18)-methyl resonances in the 400-MHz ^1H nmr spectrum. (−)-9,11-Dehydroestrone methyl ether **17** has the C(18)-methyl at δ 0.94 (25*b*, 26) while the (−)-8,9-dehydroestrone methyl ether **18** has the C(18)-methyl resonance at δ 0.90 (26, 27).

[7]Analysis of the crude product by glc–ms (DB-17 column, 220°C) showed the by-product to be isomeric with (−)-estrone methyl ether; m/e (relative intensity): 284 (M^+, 100), 199 (38), 186 (15), 160 (24). It seems reasonable to assume that this compound is the 9α-isomer (23, 33) of **19**.

Acknowledgement

We thank the Natural Sciences and Engineering Research Council of Canada

1. (*a*) R. V. STEVENS, F. C. A. GAETA, and D. S. LAWRENCE. J. Am. Chem. Soc. **105**, 7713 (1983); (*b*) R. V. STEVENS and D. S. LAWRENCE. Tetrahedron, **41**, 93 (1985).
2. (*a*) W. M. DADSON, M. LAM, T. MONEY, and S. E. PIPER. Can. J. Chem. **61**, 343 (1983); (*b*) T. MONEY. Nat. Prod. Rep. **2**, 253 (1985); (*c*) J. H. HUTCHINSON, T. MONEY, and S. E. PIPER. Can. J. Chem. **64**, 1404 (1986); (*d*) J. H. HUTCHINSON and T. MONEY. Can. J. Chem. **63**, 3182 (1985); (*e*) R. V. STEVENS, N. BEAULIEU, W. H. CHAN, A. R. DANIEWSKI, T. TAKEDA, A. WALDNER, P. G. WILLIARD, and U. ZUTTER. J. Am. Chem. Soc. **108**, 1039 (1986).
3. E. L. ELIEL. Stereochemistry of carbon compounds. J. Wiley and Sons, New York. 1962. p. 436.
4. D. TAUB. *In* The total synthesis of natural products. Vol. 2. *Edited by* J. W. ApSimon. John Wiley and Sons, New York. 1973; Vol. 6. 1984, and references cited therein.
5. (*a*) F. E. ZIEGLER and H. LIM. J. Org. Chem. **47**, 5229 (1982); (*b*) G. QUINKERT, U. SCHWARTZ, H. STARK, W.-D. WEBER, F. ADAM, H. BAIER, G. FRANK, and G. DURNER. Justus Liebigs Ann. Chem. 1999 (1982); (*c*) G. QUINKERT and H. STARK. Angew. Chem. Int. Ed. Engl. **22**, 637 (1983), and references cited therein; (*d*) P. MAGRIOTIS and F. JOHNSON. J. Org. Chem. **49**, 1460 (1984); (*e*) E. D. STERNBERG and K. P. C. VOLHARDT. J. Org. Chem. **49**, 1574 (1984); (*f*) M. E. JUNG and K. M. HALWEG. Tetrahedron Lett. **25**, 2121 (1984); (*g*) J. H. HUTCHINSON and T. MONEY. Tetrahedron Lett. **26**, 1819 (1985); (*h*) D. A. BLEASDALE and D. W. JONES. J. Chem. Soc. Chem. Commun. 1027 (1985); (*i*) A. R. DANIEWSKI and T. KOWALCZYK-PRZEWLOKA. J. Org. Chem. **50**, 2976 (1985); (*j*) G. H. POSNER and C. SWITZER. J. Am. Chem. Soc. **108**, 1239 (1986).
6. (*a*) R. B. TURNER and R. H. GARNER. J. Am. Chem. Soc. **79**, 253 (1957); (*b*) R. FLECK. J. Org. Chem. **22**, 439 (1957).
7. J. E. BALDWIN and M. J. LUSCH. Tetrahedron, **38**, 2939 (1982), and references cited.
8. H. O. HOUSE, W. V. PHILLIPS, T. S. B. SAYER, and C.-C. YAU. J. Org. Chem. **43**, 700 (1978).
9. S. J. ETHERIDGE. J. Org. Chem. **31**, 1990 (1966).

10. G. MIKHAIL and M. DEMUTH. Helv. Chim. Acta, **66**, 2362 (1983).
11. D. J. CRISPIN, A. E. VANSTONE, and J. S. WHITEHURST. J. Chem. Soc. (C), 10 (1970).
12. U. EDER, H. GIBIAN, G. HAFFER, G. NEEF, G. SAUER, and R. WIECHERT. Chem. Ber. **109**, 2948 (1976).
13. (*a*) R. A. MICHELI, Z. G. HAJOS, N. COHEN, D. R. PARRISH, L. A. PORTLAND, W. SCIAMANNA, M. A. SCOTT, and P. S. WEHRLI. J. Org. Chem. **40**, 675 (1975); (*b*) N. COHEN, B. L. BANNER, W. F. EICHEL, D. R. PARRISH, and G. SAUCY. J. Org. Chem. **40**, 681 (1975).
14. H. BREDERICK, G. SIMCHEN, S. REBSDAT, W. KANTLEHNER, P. HORN, R. WAHL, H. HOFFMANN, and P. GRIESHABER. Chem. Ber. **101**, 41 (1968).
15. F. E. ZIEGLER, J.-M. FANG, and C. C. TAM. J. Am. Chem. Soc. **104**, 7174 (1982).
16. B. M. TROST, M. PRECKEL, and L. M. LEICHTER. J. Am. Chem. Soc. **97**, 2224 (1975).
17. R. H. SCHLESSINGER, J. L. WOOD, A. J. POSS, R. A. NUGENT, and W. H. PARSONS. J. Org. Chem. **48**, 1147 (1983).
18. S. DANISHEFSKY, M. HIRAMA, K. GOMBATZ, T. HARAYAMA, E. BERMAN, and P. F. SCHUDA. J. Am. Chem. Soc. **101**, 7020 (1979), and references cited.
19. (*a*) R. E. IRELAND, S. W. BALDWIN, and S. W. WELCH. J. Am. Chem. Soc. **94**, 2056 (1972); (*b*) K. BISCHOFBERGER and J. R. BULL. J. Chem. Soc. Chem. Commun. 1051 (1982).
20. E. BENARY. Chem. Ber. **64**, 2543 (1931).
21. (*a*) R. F. ABDULLA and K. H. FUHR. J. Org. Chem. **43**, 4248 (1978); (*b*) R. F. ABDULLA and R. S. BRINKMEYER. Tetrahedron, **35**, 1675 (1979).
22. F. E. ZIEGLER, T. GUENTHER, and R. V. NELSON. Synth. Commun. **10**, 661 (1980).
23. G. H. DOUGLAS, J. M. G. GRAVES, D. HARTLEY, G. A. HUGHES, B. J. MCLOUGHLIN, J. SIDDALL, and H. SMITH. J. Chem. Soc. 5072 (1963).
24. D. J. FRANCE, J. J. HAND, and M. LOS. J. Org. Chem. **35**, 468 (1970).
25. (*a*) N. COHEN, B. L. BANNER, J. F. BLOUNT, M. TSAI, and G. SAUCY. J. Org. Chem. **38**, 3229 (1973); (*b*) G. QUINKERT, W.-D. WEBER, U. SCHWARTZ, and G. DURNER. Angew. Chem. Int. Ed. Engl. **19**, 1027 (1980).
26. G. H. POSNER, J. P. MALLAMO, and A. Y. BLACK. Tetrahedron, **37**, 3921 (1981).
27. C. RUFER, E. SCHRODER, and H. GIBIAN. Justus Liebigs Ann. Chem. **705**, 211 (1967).
28. E. H. VICKERY, L. F. PAHLER, and E. J. EISENBRAUN. J. Org. Chem. **44**, 4444 (1979).
29. (*a*) R. V. STEVENS, K. T. CHAPMAN, and H. N. WELLER. J. Org. Chem. **45**, 2030 (1980); (*b*) S. O. NWAUKWA and P. M. KEEHN. Tetrahedron Lett. **23**, 35 (1982); (*c*) R. V. STEVENS, K. T. CHAPMAN, C. A. STRUBBS, W. W. TAM, and K. F. ALBIZATI. Tetrahedron Lett. **23**, 4647 (1982).
30. W. L. MEYER, A. P. LOBO, and R. N. MCCARTY. J. Org. Chem. **32**, 1754 (1967).
31. G. M. RUBOTTOM and C.-W. KIM. J. Org. Chem. **48**, 1551 (1983).
32. R. GRICE and L. N. OWEN. J. Chem. Soc. 1947 (1963).
33. K. BISCHOFBERGER and J. R. BULL. Tetrahedron, **41**, 365 (1985).

Can. J. Chem. Downloaded from www.nrcresearchpress.com by 80.58.250.72 on 09/07/12
For personal use only.

Metabolites of the honey mushroom, *Armillaria mellea*

WILLIAM A. AYER and JOHN B. MACAULAY
Department of Chemistry, University of Alberta, Edmonton, Alta., Canada T6G 2G2

Received March 26, 1986

This paper is dedicated to Dr. O. E. (Ted) Edwards

WILLIAM A. AYER and JOHN B. MACAULAY. Can. J. Chem. **65**, 7 (1987).

The fungus *Armillaria mellea* (Vahl ex. Fr.) Kummer is responsible for severe losses in timber and fruit production.The metabolites isolated when certain strains of this fungus are grown in liquid culture have been identified as diterpenoid acids possessing the abietane (**1**) and pimarane (**2**) skeletons. These compounds, known collectively as resin acids, have not been reported previously from a fungal source. In addition to the resin acids dehydroabietic acid (**3**), pimaric acid (**4**), isopimaric acid (**5**), and sandaracopimaric acid (**6**), three additional acids, levopimaric acid *endo*-peroxide (**7**), 7-oxodehydroabietic acid (**9**), and 7-oxo-15-hydroxydehydroabietic acid (**10**) were obtained. On one occasion three orange pigments, austocystin F (**11**), averufin (**12**), and averufanin (**13**), all previously known fungal metabolites, were isolated.

WILLIAM A. AYER et JOHN B. MACAULAY. Can. J. Chem. **65**, 7 (1987).

Le champignon *Armillaria mellea* (Vahl ex. Fr.) Kummer est responsable de pertes importantes dans l'industrie du bois et dans la production des fruits. On a identifié les métabolites qui ont été isolés lorsqu'on fait croître certaines souches de ce champignon dans des milieux de cultures liquides; il s'agit de diterpénoïdes possédant des squelettes de l'abiétane (**1**) et du pimarane (**2**). Ces composés sont connus collectivement comme des acides résiniques; leur production à partir de champignons n'avait pas été rapportée jusqu'à maintenant. En plus des acides résiniques, déhydroabiétique (**3**), pimarique (**4**), isopimarique (**5**) et sandaracopimarique (**6**), on a aussi obtenu trois acides additionnels, soit le peroxide-*endo* de l'acide lévopimarique (**7**), l'acide oxo-7 déhydroabiétique (**9**) et l'acide oxo-7 hydroxy-15 déhydroabiétique (**10**). À une occasion, on a aussi isolé trois pigments oranges, l'austocystine F (**11**), l'avérufine (**12**) et l'avérufanine (**13**), qui sont tous des métabolites de champignons qui étaient connus antérieurement.

[Traduit par la revue]

Introduction

The fungus commonly regarded as *Armillaria mellea* (Vahl ex. Fr.) Kummer, also known as shoe string root rot (the fruiting body is the "honey mushroom"), is a vigorous pathogen of many commercially important types of trees (1). Larch, cedar, willow, walnut, and apple trees are all very susceptible to attack by this fungus. Fir, oak, and birch, although frequently attacked, show fewer adverse effects. The fungus invades the healthy tree via the roots. Sheets of white mycelium develop just beneath the outer bark as the fungus spreads. The mycelium may completely girdle small trees and shrubs. This girdling, combined with extensive damage to the root system, deprives the leaves of water, and the tree wilts and dies (1, 2). *A. mellea* has been reported to produce antibacterial and antifungal metabolites (3, 4). Previous examinations of the metabolites produced by the fungus have yielded the sesquiterpenoid orsellinates of armillol (4*a*), a neoilludol derivative (4*a*), and melleolide (4*b*). Ergosterol (5), unsaturated analogues of ergosterol (5), and polysaccharides (6) also have been reported. In this paper we report the isolation of metabolites afforded by three strains (NFRC-621, 624, and 631) of this fungus, indigenous to western Canada, when they are grown in liquid culture.

Among the metabolites, several are diterpenoid carboxylic acids possessing the abietane (**1**) and pimarane (**2**) skeletons. These compounds have not been reported previously from a fungal source (7). They are known collectively as resin acids and are the major constituents of resin exuded by coniferous trees. Some resin acids are known to display antibiotic, antifungal, and antilarval activity (8). In addition, three orange pigments, all previously known fungal metabolites, have been isolated and identified.

Liquid still cultures of *A. mellea* were grown on either 10% (v/v) clarified V-8 juice solution containing 1% (w/v) glucose or on potato dextrose broth. After a growth period of between 34 and 92 days, the mycelial mat was removed by filtration, and the culture broth was extracted with chloroform. The mycelium was separately subjected to Soxhlet extraction with chloroform or methanol. The crude broth metabolites were separated by chromatography over silica gel to give four major components, dehydroabietic acid (**3**) and three isomeric compounds, pimaric acid (**4**), isopimaric acid (**5**), and sandaracopimaric acid (**6**). The more polar fractions of the crude extract afforded three additional metabolites, levopimaric acid *endo*-peroxide (**7**), 7-oxodehydroabietic acid (**9**), and 7-oxo-15-hydroxydehydroabietic acid (**10**). On one occasion[1] one of the strains (NFRC-631) produced orange pigments in both the broth and mycelial extracts. Chromatography over silica gel afforded three compounds, austocystin F (**11**), averufin (**12**), and averufanin (**13**) (also known as avermutin).

Discussion

Metabolites **3–6** initially were obtained as a mixture after preliminary separation of the crude broth extract. Mass spectroscopy (ms) indicated that the mixture was composed of compounds of molecular weight 302 ($C_{20}H_{30}O_2$) and 300 ($C_{20}H_{28}O_2$). The infrared (ir) spectrum of the mixture shows broad OH absorption (3300–2400 cm^{-1}) and strong carbonyl absorption (1692 cm^{-1}) indicative of carboxylic acids. Esterification with diazomethane converted all four components to the corresponding methyl esters (the ir spectrum reveals no OH absorption, while the carbonyl peak is shifted to 1720 cm^{-1}). The ^1H nuclear magnetic resonance (nmr) spectrum of the mixture of esters is virtually identical with that of the acids except for the appearance of methyl singlets at δ 3.63, 3.66, and 3.67. Hydrogenation (H_2, 10% Pd/C) of the mixture of acids resulted in the uptake of four atoms of hydrogen by the $C_{20}H_{30}O_2$ components but left the $C_{20}H_{28}O_2$ compound

[1]This result was not reproducible, thus the production of the orange pigments due to a contamination by another fungus cannot be ruled out.

Can. J. Chem. Downloaded from www.nrcresearchpress.com by 80.58.250.72 on 09/07/12
For personal use only.

Can. J. Chem. Downloaded from www.nrcresearchpress.com by 80.58.250.72 on 09/07/12
For personal use only.

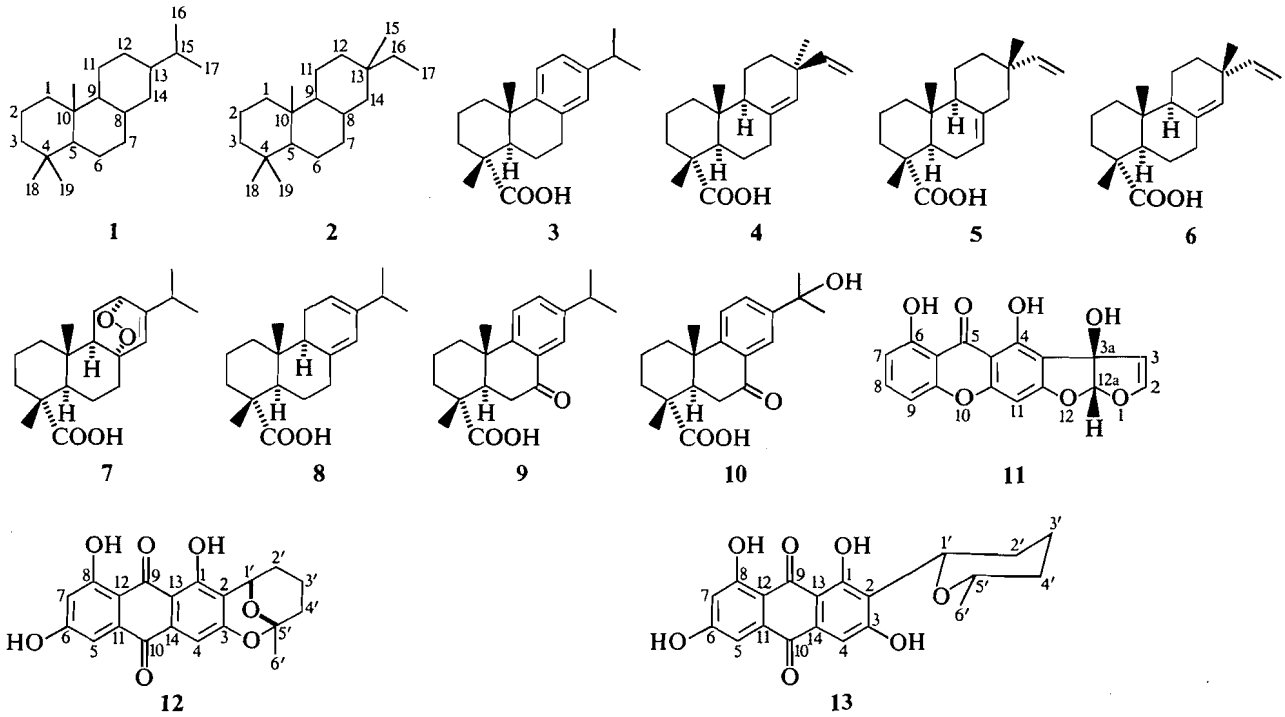

unchanged. The acids **3–6** were further separated by careful chromatography over silica gel impregnated with silver nitrate.

Inspection of the ^{1}H nmr spectrum reveals that the $C_{20}H_{28}O_2$ component contains a 1,2,4-trisubstituted benzenoid nucleus and that one of the substituents is an isopropyl group. Thus the three aromatic protons (δ 6.87, 6.98, 7.14) possess *ortho* (J = 8 Hz), *ortho* and *meta* (J = 8, 1.75 Hz), and *meta* (J = 1.75 Hz) couplings respectively. Three benzylic protons are evident, two as a multiplet centred at δ 2.90 and an isopropyl methine appearing at δ 2.82 (septet, J = 7 Hz). The ir spectrum shows absorptions for a carboxylic acid at 3200–2400 cm^{-1} (OH) and 1692 cm^{-1} (C=O). The fragmentation pattern of the mass spectrum is indicative of an abietane (**1**) skeleton (as judged by comparison with mass spectra of other compounds that possess the abietane framework). Comparison (thin-layer chromatography (tlc), ^{1}H nmr, and ir) with an authentic sample showed that this component is dehydroabietic acid (**3**). The optical rotation ([α]$_D$ +54°) confirmed the absolute configuration (9).

The isomeric $C_{20}H_{30}O_2$ compounds could not be completely separated. One component, **4**, was obtained in pure form, while **5** and **6** were isolated as an inseparable mixture. The ^{1}H nmr spectra of all three components show an AMN splitting pattern in the region δ 4.8–5.9 characteristic of a vinyl group. This suggested that compounds **4–6** possess the pimarane skeleton **2**, which is closely related biogenetically to the abietane skeleton **1**. The presence of an additional olefinic proton (see Table 1) indicated that each of the three components possesses a trisubstituted (nuclear) carbon–carbon double bond. The equatorial disposition of the carboxyl group in the three compounds is confirmed (10) by the C—O stretch (1244 cm^{-1}) in the ir spectra of the corresponding methyl esters (formed by treatment of the acids with diazomethane). It has been observed (11) that the ir frequency of the out-of-plane C—H bend of the vinyl group in pimarane-type structures is particularly diagnostic with respect to the relative stereochemistry of the vinyl and methyl groups attached to C-13. Thus a 914 cm^{-1} absorption in the ir spectrum of the methyl ester of **4** indicates a β-vinyl substituent

TABLE 1. ^{1}H nuclear magnetic resonance data of olefinic protons in **4–6**

Compound	Proton	δ (ppm)	Multiplicity	J (Hz)
4	H_A	5.72	dd	17.5, 10.5
	H_B	4.96	dd	10.5, 2
	H_C	4.91	dd	17.5, 2
	Nuclear H	5.15	bs	—
5	H_A	5.81	dd	17.5, 10.5
	H_B	4.87	dd	10.5, 1.5
	H_C	4.93	dd	17.5, 1.5
	Nuclear H	5.33	bd	5
6	H_A	5.78	dd	17.5, 10.5
	H_B	4.89	dd	10.5, 1.5
	H_C	4.91	dd	17.5, 1.5
	Nuclear H	5.22	bs	—

group while the mixture of the methyl esters of **5** and **6** shows absorption at 909 cm^{-1}, suggesting an α-vinyl substituent. These data led to the assignment of the three isomers as pimaric (**4**), isopimaric (**5**), and sandaracopimaric (**6**) acids respectively. Identification was confirmed by comparison (tlc, ^{1}H nmr) with authentic samples.

Compound **7** contains a carboxyl function that can be methylated (diazomethane), resulting in a shift of the carbonyl frequency in the ir spectrum from 1692 cm^{-1} to 1720 cm^{-1}. In the ^{1}H nmr spectrum, a septet at δ 2.50 (J = 7 Hz) again suggests an isopropyl group and thus the abietane skeleton. It is noteworthy that the methyl groups of the isopropyl unit in **7** give rise to two well-separated doublets, δ 1.08 and 1.12 (J = 7 Hz), indicating that the environments of the two methyls differ more than in **3**, where the isopropyl methyl doublets overlap (δ 1.22, J = 7 Hz). Compound **7** has one olefinic proton appearing as a singlet at δ 5.87. Since the isopropyl methine is allylic (δ 2.50), the singlet nature of the olefinic proton indicates a $\Delta^{13,14}$ double bond with C-8 fully substituted. The appearance of signals at

Can. J. Chem. Downloaded from www.nrcresearchpress.com by 80.58.250.72 on 09/07/12
For personal use only.

δ 76.9 (s) and δ 74.6 (d) in the ^{13}C nmr spectrum indicates the presence of two oxygenated sp^3 carbons. This, coupled with the fact that the base peak in the mass spectrum (m/z 302) corresponds to the loss of a molecule of oxygen, suggested that **7** might be the *endo*-peroxide of levopimaric acid (**8**). Comparison of the methyl ester of **7** with an authentic sample confirmed the identity. Although the *endo*-peroxide is not an auto-oxidation product (12) of levopimaric acid (**8**), the presence of light and a photosensitizing substance in the crude extract (13) may bring about the incorporation of molecular oxygen in the homoannular diene component of **8**.

7-Oxodehydroabietic acid (**9**) was obtained in the flash chromatography fractions eluting after the acids **3–6**. The ^1H nmr spectrum reveals three aromatic protons with a coupling pattern similar to that of **3**, although at somewhat lower field. A benzylic isopropyl methine proton appears at δ 2.92 (septet, J = 7 Hz), but the C-7 benzylic protons of **3** are absent. A ketonic carbon is evident in the ^{13}C nmr spectrum at δ 198.4. In addition to the carboxyl carbonyl at 1695 cm^{-1} in the ir spectrum, an unsaturated ketone appears at 1685 cm^{-1}. The two carbonyl bands become better resolved (1727 and 1684 cm^{-1}) when the acid is esterified (diazomethane). The ultraviolet spectrum indicates the presence of an aromatic ketone (217 (ε 10 500), 255 (ε 7700), 304 (ε 1830) nm). Comparison of the spectroscopic data with literature values (23) for methyl 7-oxodehydroabietate confirmed the identity. This uv-active compound may be an artifact since upon standing dehydroabietic acid gives a number of auto-oxidation products, including **9** (14).

The identity of 7-oxo-15-hydroxydehydroabietic acid (**10**) was established from the ^1H nmr, ir, and mass spectra, and by comparison with the spectral data of **3** and **9**. Thus, the three aromatic protons with the coupling pattern found in the C-ring of **3** appear again in **10**. As in **9**, these three protons are deshielded relative to **3**. Both the C-7 methylene and the benzylic isopropyl proton of **3** are absent in **10**, while two methyl singlets appear at δ 1.60 and 1.61. Thus the ketone and hydroxyl groups are assigned to C-7 and C-15, respectively. Although 15-hydroxy compounds are not among the reported (14) auto-oxidation products of **3**, the fact that benzylic auto-oxidation may give rise to **9** suggests that **10** also may be an artifact.

The pigment austocystin F (**11**) was obtained as orange crystals, mp 232–234°C. The molecular formula $C_{17}H_{10}O_7$ was established by high resolution mass spectroscopy. The ir spectrum shows an OH band at 3480 cm^{-1}, and absorption at 1663 and 1645 cm^{-1} characteristic of the γ-pyrone unit. The ^1H nmr spectrum shows three protons exchangeable with D_2O, two hydrogen-bonded phenolic protons that appear as singlets at δ 11.80 and 12.38, and an alcoholic proton at δ 2.88. A 1,2,3-trisubstituted aromatic system is apparent from the coupling of the aromatic protons at δ 6.80, 6.89, and 7.59. The low-field position of the latter proton, which shows two *ortho* couplings, indicates its location *para* to an electron-withdrawing substituent. Protons at δ 5.73 and 6.58 are coupled (J = 2.75 Hz). The small coupling constant and the large difference in their chemical shifts indicate they are located on a highly polarized *Z*-olefin. This suggested the presence of the *bis*-dihydrofuran moiety, typical of the aflatoxins (15). Such a structure also accounts for two low-field singlets at δ 6.44 and 6.46. One is a methine deshielded by two ethereal oxygens while the other is assigned to the isolated aromatic proton at C-4. Thus the alcoholic OH must be the other ring junction substituent. The linear nature of the fused pentacyclic system follows from the chemical shift (δ 6.44 or 6.46) of the proton at C-11 (16). Comparison (tlc, ir) with an authentic sample of austocystin F confirmed the identity of the metabolite as well as the *cis* fusion of the dihydrofuran rings. Austocystin F has been isolated previously as a member of a series of austocystins produced by *Aspergillus ustus* (16).

Averufin (**12**) and averufanin (**13**) were found to cocrystallize from chloroform. The mixture appeared homogeneous by tlc and could not be separated.[2] The mixture was shown to be composed of two components by chemical ionization mass spectroscopy, which gives M + 1 peaks at m/z 369 (100%) and 371 (78%). In conjunction with the high resolution mass spectrum, the molecular formulae were established as $C_{20}H_{16}O_7$ (368) and $C_{20}H_{18}O_7$ (370). The ir spectrum reveals OH (3380 cm^{-1}) as well as unsaturated carbonyls (1669 and 1622 cm^{-1}). That the latter of these is a quinone carbonyl hydrogen-bonded to two *peri*-phenolic groups is indicated by the appearance of singlets in the ^1H nmr spectrum ($CDCl_3$) at δ 12.34 (1H) and 12.51 (1H). In acetone-d_6 + D_2O the spectrum shows two aromatic protons, displaying mutual *meta* coupling (2 Hz) at δ 6.58 and 7.13, and an isolated aromatic proton at δ 7.03. These data give rise to the anthraquinone partial structure **14**.

Acetylation (acetic anhydride – pyridine) of the mixture afforded products that were separated by preparative tlc. Mass spectral analysis shows these to be a tetraacetate ($C_{28}H_{26}O_{11}$) arising from the component of molecular weight 370, and a triacetate ($C_{26}H_{22}O_{10}$) formed from the compound of molecular weight 368. The ^1H nmr spectrum of the triacetate possesses a multiplet at δ 5.29 (1H) and a singlet at δ 1.56 (3H). These features helped establish the structure of averufin (**12**) as the parent compound of the triacetate. The identity was confirmed by comparison (tlc, ir, ms) with an authentic sample.

The location of an hydroxyl at C-3 in **13** follows from the magnitude (Δ ppm = 0.79) of the downfield shift of H-4 upon acetylation (18). Such a large change can be attributed to the acetylation of both *ortho* and *para* phenolic hydroxyls. In **12** H-4 experiences a downfield shift of only 0.41 ppm, due to acetylation of the *para* OH substituent. The ^1H nmr spectrum of **13** contains signals at δ 1.31 (3H, d, J = 6 Hz), 3.8 (1H, m), and 5.13 (1H, dd, J = 11.5, 2.25 Hz), suggesting a methyl substituted tetrahydropyran ring, which accounts for the single remaining degree of unsaturation. Acetylation (acetic anhydride – pyridine) of an authentic sample of averufanin afforded a product identical (tlc, ir) with the tetraacetate of the compound in hand.

A thorough examination of the mycelial extracts afforded several steroidal compounds, ergosterol peroxide (**15**), sitostanol (**16**), and β-sitosterol (**17**). The presence of the saturated compound (**16**) in the sample of **17** was indicated by the mass spectrum, which shows a peak of 19% intensity at m/z 416 (M^+ of **16**), whereas an intensity of only 5% would be anticipated for the M + 2 peak of m/e 414 (M^+ of **17**).

Saturated fatty acids possessing 18, 20, 22, and 24 carbon atoms were present in the mycelial extract. Triglycerides were also isolated, which upon basic hydrolysis (10% KOH (w/v)) yielded a mixture of saturated fatty acids (having 16 and 18 carbons) and the unsaturated fatty acid linoleic acid (**18**).

Fifteen distinct species (five in Europe and ten in North

[2]In our hands, averufin and averufanin could not be separated by tlc using the method of Berger and Jadot (17). Observed R_f values were significantly lower than those reported and no separation was obtained.

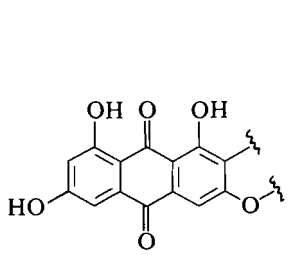

14

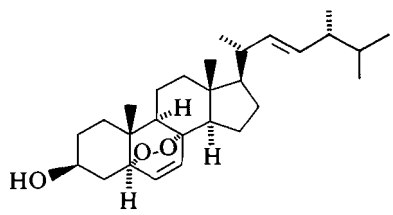

15

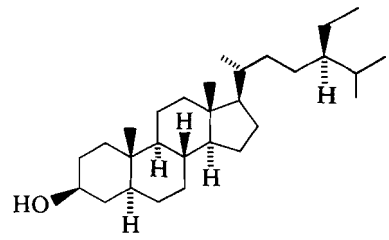

16

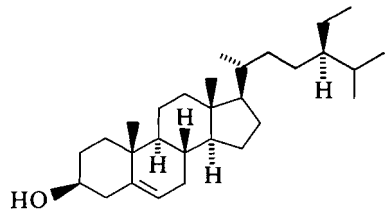

17

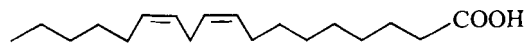

18

America) of the *A. mellea* complex have been identified (19). The three strains employed in this study are "biological species I" of Anderson and Ullrich (19) or the closely related "foothills type" of Mallett (20). They correspond to a taxonomic species *Armillaria ostoyae* (Romagn.) Herink (= *A. obscura* (Persoon) Herink), one of the species recognized within the *Armillaria mellea* complex in recent years (21). Thus it is possible that the species used in this study has not been examined previously for its metabolites, while reported metabolites of *A. mellea* (broad sense), including those of Oduro *et al.* (3*a*) may have been isolated from one or more of the other species. The strains studied in this investigation are parasitic on pine and spruce, themselves producers of resin acids, but the media used in this study (V-8 juice, potato dextrose) do not contain resin acids. The biological significance of this observation is not clear to us. However, it is interesting to note that in conifers large amounts of resin are exuded through the bark at the point of infection and the area of resinosis increases as the fungus spreads in the bark (2*a*). As noted previously, resin acids hitherto have not been identified as fungal metabolites.

Experimental

General

High resolution electron impact mass spectra (hreims) were recorded on an AEI MS-50 mass spectrometer. Unless diagnostically significant, only those peaks with intensity of >30% of the base peak are recorded. Chemical ionization mass spectra (cims) were obtained using an AEI MS-12 mass spectrometer with ammonia as the reagent gas. The data were processed in DS-55 and Nova-4 computers. Fourier transform infrared (Ftir) spectra were recorded as $CHCl_3$, CH_2Cl_2, or CH_3OH casts on a Nicolet 7199 FTIR interferometer. Single scan infrared (ir) spectra were recorded on a Perkin Elmer 297 spectrometer. Nuclear magnetic resonance (nmr) spectra (^1H and ^{13}C) were obtained on Bruker WH-200 or WH-400 spectrometers with an Aspect 2000 computer system. Tetramethylsilane was used as the internal standard. Ultraviolet (uv) spectra were obtained on a Unicam SP 1700 spectrophotometer and optical rotations on a Perkin Elmer 141 polarimeter. Melting points are uncorrected and were determined on Zeitz–Wetzlar and Thomas Model 40 melting point apparatus. Macherey Nagel silica gel 60 (less than 200 mesh) was used for column chromatography. Fractions were collected with a Buchler Fracto Mette 200 fraction collector. E. Merck silica gel 60 (230–400 mesh) was used for flash chromatography. Preparative thin-layer chromatography (ptlc) was carried out on Terochem silica gel G containing a trace of electronic phosphor (General Electric), 20 × 20 cm, 10 × 20 cm, or 5 × 20 cm plates, 0.35 mm thickness. Analytical thin-layer chromatography (tlc) was carried out on glass plates (75 × 25 or 75 × 50 mm) coated with the same adsorbent as ptlc, or on E. Merck precoated plates of silica gel 60 F-254. Analytical tlc plates with adsorbed silver nitrate ($AgNO_3$) were prepared by dipping the precoated plates into a solution of 20% (w/v) $AgNO_3$ in H_2O–CH_3OH, 1:1 (stored in the dark) for several seconds, then drying with a heat gun. The plates were used immediately. Unless otherwise indicated, R_f values are for single elutions. Ultraviolet active materials were detected by visualization under a uv lamp (254 or 350 nm). The plate (only a thin vertical band in the case of ptlc) was then sprayed with a solution of 10% or 30% sulphuric acid and charred on a hot plate. Unless specified, all solvents, with the exception of ether, hexane, and tetrahydrofuran, were distilled prior to use. Skellysolve B refers to Skelly Oil Company light petroleum, bp 62–70°C.

Fungal strains

The strains of *Armillaria mellea* used in this study were obtained from Dr. Y. Hiratsuka, Northern Forest Research Centre (NFRC), Edmonton. They were collected from the following host trees in British Columbia. Slant tube cultures of these strains were transferred to potato dextrose agar (PDA) slant tubes, which were kept as stock cultures at 4°C.

Strain	Host	Rhizomorph type*
NFRC-621	Lodgepole pine	Modified *A. bulbosa*
NFRC-624	Ponderosa pine	*A. mellea*
NFRC-631	White spruce	No rhizomorphs

*As determined by K. Mallett.

Still cultures of the fungus were initiated by inoculation into 1-L Fernbach flasks charged with sterile culture medium (either a 10% (v/v) solution of clarified V-8 juice containing 1% (w/v) glucose or potato dextrose broth (PDB)). The flasks were stoppered with foam rubber plugs covered loosely with aluminum foil. Growth periods were from 34 to 92 days.

Bioassays

The resin acids **3–7** and **9** show mild (0.5–2 mm zones of inhibition) antibiotic activity against *Staphylococcus aureus*, *Streptococcus pyogenes*, and *Klebsiella pneumoniae* at a concentration of 1% (w/v) (3.4% (w/v) for **7**). Antibiotic activity of resin acids against *S. aureus* has been reported previously (8*a*–*c*).

In vitro bioassays of the resin acid mixture **3–6** (1–5% (w/v) concentration) showed inhibition of *Fomes annosus*, *F. roseus*, and *F. pini*. A plug of *A. mellea* NFRC-621 also inhibited the growth

Can. J. Chem. Downloaded from www.nrcresearchpress.com by 80.58.250.72 on 09/07/12
For personal use only.

Can. J. Chem. Downloaded from www.nrcresearchpress.com by 80.58.250.72 on 09/07/12
For personal use only.

of *F. roseus* in vitro. Resin acids have been reported to inhibit the mycelial growth of *F. annosus* (8*d*).

The resin acid mixture **3–6** was also found to inhibit the growth of lodgepole pine seedlings at a concentration of 0.1% (w/v).

Extraction of the metabolites

The culture mixture was separated into broth and mycelium by filtration through cheesecloth. The culture broth was extracted with chloroform (ca. equal volume). The chloroform extracts contained emulsions, and vacuum filtration through Celite facilitated the separation of organic and aqueous phases. The chloroform was dried over sodium sulphate and evaporated *in vacuo* to afford the crude metabolites. Although yields of crude metabolites varied with different growth periods, the resin acids (*vide infra*) were produced consistently by all three strains. The mycelium was extracted with chloroform or methanol in a Soxhlet extractor. The organic extract was dried over sodium sulphate and concentrated to dryness.

*Isolation of dehydroabietic acid (**3**), pimaric acid (**4**), isopimaric acid (**5**), and sandaracopimaric acid (**6**)*

The crude broth metabolites of strain NFRC-621 (1.8 g) were subjected to flash chromatography (chloroform – ethyl acetate – acetic acid, 94:5:1) to afford 0.547 g of a mixture of compounds **3–6**. A 40-mg sample of the mixture was applied to a 20 × 20 cm ptlc plate and developed 12 times with Skellysolve B – ethyl acetate – acetic acid, 98:2:1. Careful scraping of the lower edge of the band corresponding to the mixture and elution from the silica gel yielded 3.2 mg of impure **3**. This sample was further purified by ptlc on a 5 × 20 cm plate using the same solvent system as above and eluting five times, followed by scraping and elution to give **3**, pure as judged by multiple-elution tlc on silver nitrate-impregnated silica gel, using both protic and aprotic solvent systems.

A 90-mg sample of the mixture **3–6** was chromatographed on 10 g of silica gel that had been thoroughly mixed with 2 g powdered silver nitrate. The column (1.5 cm diameter) was wrapped in aluminum foil. Fractions (5 mL) were collected from elution with chloroform – Skellysolve B, 50:50, then 75:25 (each for approximately one column volume), then 100% chloroform to fraction 175, and finally chloroform – ethyl acetate, 98:2, to fraction 260.

Fractions 30–69 gave 31 mg of impure **3**. Further purification by flash chromatography (chloroform – ethyl acetate, 98:2) afforded 19 mg of **3**, mp 162–168°C (CH_3OH–H_2O) (lit. (9) mp 171–172°C); $[\alpha]_D$ +54° (*c* 1.9, 95% EtOH) (lit. $[\alpha]_D^{25}$ +61° (95% EtOH); tlc: R_f 0.6 (Skellysolve B – ethyl acetate – acetic acid, 75:25:1), R_f 0.72 (chloroform – ethyl acetate – acetic acid, 97:2:1, 3×, silver nitrate-impregnated silica gel); Ftir (CH_2Cl_2 cast): 3200–2400 (b), 2950, 2925, 2865, 1692 cm^{-1}; uv (CH_3OH): 220 (ε 2180), 268 (ε 630), 276 (ε 600) nm; ^1H nmr ($CDCl_3$) δ: 1.0–1.9 (7H, m), 1.23 (6H, d, J = 7 Hz, C-15 2 × CH_3), 1.25 (3H, s, C-10 CH_3), 1.29 (3H, s, C-4 CH_3), 2.24 (1H, dd, J = 12.5, 2 Hz), 2.30 (1H, bd, J = 12.5 Hz), 2.82 (1H, septet, J = 7 Hz, C-15 H), 2.90 (2H, m, C-7 CH_2), 6.87 (1H, d, J = 1.75 Hz, C-14 H), 6.98 (1H, dd, J = 8, 1.75 Hz, C-12 H), 7.14 (1H, d, J = 8 Hz, C-11 H); ^{13}C nmr ($CDCl_3$) δ: 16.3, 24.0 (2 C's), 25.2 (CH_3); 18.6, 21.9, 30.1, 36.9, 38.1 (CH_2); 33.5, 44.7, 124.0, 124.2, 127.0 (CH); 37.0, 47.5, 134.8, 145.8, 146.9 (C); 185.0 (C=O); hreims, m/z calcd. for $C_{20}H_{28}O_2$ (M^+): 300.2089; found: 300.2093 (30), 285 (100), 239 (74).

Fractions 95–169 from the above chromatography of 90 mg of the mixture **3–6** afforded 3.3 mg of **4**, mp 200–208°C (95% EtOH) (lit. (22) mp 212°C); tlc R_f 0.65 (chloroform – ethyl acetate – acetic acid, 97:2:1, 3×, silver nitrate-impregnated silica gel); Ftir ($CHCl_3$ cast): 3600–2400(b), 2925, 2870, 2850, 1695 cm^{-1}; ^1H nmr ($CDCl_3$): see Table 1; δ: 0.80 (3H, s, C-10 CH_3), 0.8–1.8 (13H, m), 1.02 (3H, s, C-13 CH_3), 1.23 (3H, s, C-4 CH_3), 1.95 (1H, dd, J = 12.5, 2.5 Hz), 2.13 (1H, m), 2.29 (1H, m); ^{13}C nmr ($CDCl_3$) δ: 15.0, 16.7, 29.4 (CH_3); 18.0, 18.9, 25.1, 35.3, 35.6, 37.0, 38.1, 116.4 (CH_2); 48.7, 51.4, 128.4, 147.2 (CH); 37.8, 38.6, 47.3, 137.9 (C); 185.8 (C=O); hreims, m/z calcd. for $C_{20}H_{30}O_2$ (M^+): 302.2246; found: 302.2243 (49), 287 (69), 167 (37), 121 (100), 91 (31).

The later fractions from the above chromatography of 90 mg of the mixture **3–6** gave 40 mg of impure **5** and **6**. After this sample was subjected twice more to flash chromatography (Skellysolve B – ethyl acetate – acetic acid, 95:5:1, and chloroform – ethyl acetate, 9:1, respectively) a trace of **4** was still present by tlc (silver nitrate). The remainder (17 mg) was subjected to flash chromatography (chloroform – ethyl acetate – acetic acid, 97:2:1) on silica gel (2.4 g) thoroughly mixed with powdered silver nitrate (0.6 g) to give 5 mg of **5** and **6**, appearing as a single spot by tlc: R_f 0.52 (chloroform – ethyl acetate – acetic acid, 97:2:1, 3×, silver nitrate-impregnated silica gel); ^1H nmr ($CDCl_3$): see Table 1; δ: 0.85 (s, C-10 CH_3 of **6**), 0.87 (s, C-10 CH_3 of **5**), 0.91 (s, C-13 CH_3 of **5**), 1.05 (s, C-13 CH_3 of **6**), 1.1–2.0 (m), 1.22 (s, C-4 CH_3 of **6**), 1.28 (s, C-4 CH_3 of **5**); hreims, m/z calcd. for $C_{20}H_{30}O_2$ (M^+): 302.2246; found: 302.2250 (100), 287 (47), 273 (29), 257 (27), 241 (34), 187 (30), 105 (31), 91 (33).

*Esterification of **3–6***

An excess of diazomethane in ether was added to a magnetically stirred solution of **3–6** (28 mg; tlc: R_f 0.67 (Skellysolve B – ethyl acetate – acetic acid, 75:25:1); ir ($CHCl_3$): 3400–2400(b), 1690 cm^{-1}) dissolved in ether (1 mL). Evaporation to dryness gave a colourless oil (28 mg), tlc: R_f 0.82 (Skellysolve B – ethyl acetate – acetic acid, 75:25:1); ir ($CHCl_3$): 1720 cm^{-1}; cims, m/z: 334 (M + 18 for esters of **4–6**), 332 (M + 18 for ester of **3**), 317 (M + 1 for esters of **4–6**), 315 (M + 1 for ester of **3**).

Similarly 2.5 mg of purified **4** was esterified to give methyl pimarate; tlc: R_f 0.67 (chloroform – ethyl acetate – acetic acid, 97:2:1, 2×, silver nitrate-impregnated silica gel); Ftir ($CHCl_3$ cast): 2918, 2849, 1728, 1244, 914 cm^{-1}.

*Chromatography of the methyl esters of **3–6***

The mixture of esters (47 mg) was subjected to column chromatography over neutral alumina (36.4 g; Woelm, ICN Pharmaceuticals), mixed thoroughly with powdered silver nitrate (7.3 g). The column (1.5 cm diameter) was wrapped in aluminum foil and eluted with hexane (7 fractions, 8 mL), hexane–ether, 98:2 (to fraction 38), and finally hexane–ether, 95:5. Methyl dehydroabietate (methyl ester of **3**) and methyl pimarate (methyl ester of **4**) eluted together; however, methyl isopimarate and methyl sandaracopimarate (6 mg; methyl esters of **5** and **6** respectively) eluted in fractions 67–88; tlc: R_f 0.44 (Skellysolve B – ethyl acetate, 90:10, silver nitrate-impregnated silica gel); Ftir ($CHCl_3$ cast): 3080 (w), 2950, 2920, 2865, 2845, 1728 (s), 1637 (w), 1244, 909 cm^{-1}; ^1H nmr ($CDCl_3$) δ: 0.83 (s), 0.86 (s), 0.90 (s), 1.04 (s), 1.1–2.0 (m), 1.20 (s), 1.26 (s), 3.65 (s), 3.67 (s), 4.86 (dd, J = 10.5, 1.5 Hz), 4.88 (dd, J = 10.5, 1.5 Hz), 4.90 (dd, J = 17.25, 1.5 Hz), 4.92 (dd, J = 17.25, 1.5 Hz), 5.21 (bs), 5.31 (dd, J = 7.5, 1.5 Hz), 5.77 (dd, J = 17.25, 10.5 H), 5.80 (dd, J = 17.25, 10.5 Hz); cims, m/z: 334 (M + 18).

*Hydrogenation of **3–6***

The mixture **3–6** (10 mg) was dissolved in dry ethyl acetate (9 mL) and activated 10% palladium on charcoal (102 mg) was added. The mixture was pressurized with hydrogen (15 psi; 1 psi = 6.9 kPa) and shaken in a Parr hydrogenator for 24 h at room temperature. The catalyst was removed by filtration through Celite. Evaporation of the filtrate *in vacuo* afforded 10 mg of a colourless solid; tlc: R_f 0.56 (Skellysolve B – ethyl acetate – acetic acid, 75:25:1) ir ($CHCl_3$ cast): 3400–2400(b), 1695 (s) cm^{-1}; cims, m/z: 324 (M + 18 for hydrogenation products of **4–6**), 318 (M + 18 for unchanged **3**).

Isolation of levopimaric acid endo-*peroxide (**7**)*

The crude broth metabolites of strain NFRC-631 (0.74 g) were subjected to flash chromatography (chloroform – ethyl acetate, 9:1, to fraction 16, then chloroform – ethyl acetate – acid, 97:2:1, to fraction 21, and 94:5:1 to fraction 25). Elution was continued with Skellysolve B – ethyl acetate, 3:1 (100 mL), 1:1 (100 mL), and ethyl acetate (100 mL). A 389-mg fraction (eluting with chloroform – ethyl acetate – acetic acid (97:2:1) after **3–6**) contained **7** and was further purified by flash chromatography (chloroform – ethyl acetate – acetic acid, 97:2:1) to give **7** (269 mg); tlc: R_f 0.43 (chloroform–acetone – acetic acid, 89:10:1, 5×); Ftir ($CHCl_3$ cast): 3600–2400 (b), 2955, 2935, 2870, 1692 cm^{-1}; ^1H nmr ($CDCl_3$) δ: 0.56 (3H, s, C-10 CH_3), 0.9–2.4 (14H, m), 1.08 and 1.12 (2 × 3H, d, J = 7 Hz, C-15 CH_3), 1.15 (3H, s, C-4 CH_3), 2.50 (1H, septet, J = 7 Hz, C-15 H), 4.61 (1H, m, C-12

Can. J. Chem. Downloaded from www.nrcresearchpress.com by 80.58.250.72 on 09/07/12
For personal use only.

H), 5.87 (1H, s, C-14 H), 9.0 (1H, bs, COOH); ^{13}C nmr ($CDCl_3$) δ: 15.1, 16.2, 20.1, 20.3 (CH_3); 16.9, 21.6, 24.9, 32.0, 36.1, 36.6 (CH_2); 31.0, 48.8, 50.0, 74.6, 124.6 (CH); 36.8, 46.8, 76.9, 149.0 (C); 184.9 (C=O); hreims, m/z calcd. for $C_{20}H_{30}O_4$ (M^+): 334.2144; found: 334.2149 (18), 319 (14), 316 (18), 302 (100), 291 (18), 285 (21), 275 (25), 245 (51), 146 (37), 121 (56), 113 (32), 107 (32), 105 (38), 93 (38), 91 (58).

Esterification of levopimaric acid endo*-peroxide (7)*

Treatment of **7** (12 mg) with excess diazomethane in ether overnight at room temperature yielded 12 mg of the methyl ester upon evaporation to dryness; tlc: R_f 0.56 (chloroform–acetone – acetic acid, 89:10:1, 5×); ir ($CHCl_3$): 2950, 2875, 1720, 1300–1190 (b) cm^{-1}; ^{1}H nmr ($CDCl_3$) δ: 0.58 (3H, s), 0.9–2.4 (14H, m), 1.10 (3H, d, J = 7 Hz), 1.14 (3H, d, J = 7 Hz), 1.17 (3H, s), 2.5 (1H, septet), 3.70 (3H, s), 4.62 (H, m), 5.89 (1H, s); hreims, m/z calcd. for $C_{21}H_{32}O_4$ (M^+): 348.2300; found: 348.2302 (9), 333 (5), 316 (100), 146 (48), 121 (70), 91 (36).

Isolation of 7-oxodehydroabietic acid (9)

Flash chromatography of the crude broth metabolites of strain NFRC-621 (*vide supra*) afforded impure **9** in fractions eluting with chloroform – ethyl acetate – acetic acid, (94:5:1) after the fractions containing the mixture **3–6**. This material (153 mg) was further subjected to flash chromatography (chloroform – ethyl acetate 94:6, containing 3 drops acetic acid per 10 mL) to give impure **9** (37 mg). Preparative tlc (chloroform – ethyl acetate, 90:10, 5×) yielded, after careful scraping and elution, 12 mg of **9**, $[\alpha]_D$ −3° (*c* 1.56, 95% EtOH); tlc: R_f 0.23 (Skellysolve B – ethyl acetate – acetic acid, 85:15:1); Ftir ($CHCl_3$ cast): 3500–2400 (b), 2955, 2930, 2870, 1695, 1685 cm^{-1}; uv (CH_3OH): 217 (ε 10 500), 255 (ε 7700), 304 (ε 1830) nm; ^{1}H nmr ($CDCl_3$) δ: 0.8–1.9 (4H, m), 1.234 and 1.237 (2 × 3H, d, J = 7 Hz, C-15 2 × CH_3), 1.26 (3H, s, C-4 CH_3), 1.34 (3H, 3H, s, C-10 CH_3), 2.36 (2H, bd, J = 13 Hz), 2.49 and 2.70 (2 × 1H, d, J = 14 Hz, C-6 H_{eq} and C-5 H), 2.76 (1H, dd, J = 14 Hz, C-6 H_{ax}), 2.92 (1H, septet, J = 7 Hz, C-15 H), 7.29 (1H, d, J = 8 Hz, C-11 H), 7.41 (1H, dd, J = 8, 2 Hz, C-12 H), 7.87 (1H, d, J = 2 Hz, C-11 H); ^{13}C nmr ($CDCl_3$) δ: 16.2, 23.65, 23.69, 23.76 (CH_3); 18.2, 36.7, 37.2, 37.8 (CH_2), 33.6, 43.8, 123.4, 125.3, 132.5 (CH); 29.7, 46.4, 130.9, 147.0, 153.0 (C); 182.1, 198.4 (C=O); hreims, m/z calcd. for $C_{20}H_{26}O_3$ (M^+): 314.1882; found: 314.1883 (58), 299 (35), 253 (100), 211 (26).

Esterification of 7-oxodehydroabietic acid (9)

An excess of diazomethane in ether was added to a magnetically stirred solution of **9** (4.5 mg) in $CHCl_3$ (2 mL) and the reaction mixture was stirred for 15 min at room temperature. Evaporation to dryness afforded 4.5 mg of the methyl ester; $[\alpha]_D$ +2° (*c* 4.5, 95% EtOH) (lit. (23) $[\alpha]_D$ +7.9° (EtOH)); tlc: R_f 0.41 (Skellysolve B – ethyl acetate – acetic acid, 85:15:1); Ftir ($CHCl_3$ cast): 2955, 2936, 2868, 1727 (s), 1684 (s), 1608 (w), 1250 cm^{-1}; ^{1}H nmr ($CDCl_3$) δ: 0.8–1.9 (5H, m), 1.255 (6H, d, J = 7 Hz, C-15 2× CH_3), 1.27 (3H, s, C-4 CH_3), 1.35 (3H, s, C-10 CH_3), 2.36 (2H, m), 2.73 (2H, m), 2.93 (1H, septet, J = 7 Hz, C-15 H), 3.66 (3H, s, OCH_3), 7.29 (1H, d, J = 8 Hz, C-11 H), 7.40 (1H, dd, J = 8, 2 Hz, C-12 H), 7.87 (1H, d, J = 2 Hz, C-14 H); hreims, m/z calcd. for $C_{21}H_{28}O_3$ (M^+): 328.2038; found: 328.2037 (66), 313 (6), 253 (100).

Isolation of 7-oxo-15-hydroxydehydroabietic acid (10)

The polarity of the eluent in the flash chromatography of the crude broth metabolites of strain NFRC-621 (*vide supra*) was increased to chloroform – ethyl acetate – acetic acid, 84:15:1 after 31 fractions. A polar fraction (210 mg) containing **10** was further subjected to flash chromatography (Skellysolve B – ethyl acetate – acetic acid, 70:30:1, to fraction 18, then 65:35:1; sample dissolved in chloroform). Fractions 29–34 gave 12 mg of material, which was further purified by flash chromatography (chloroform–acetone – acetic acid, 90:10:1) to afford pure **10** (3 mg); tlc: R_f 0.4 (chloroform–acetone – acetic acid, 89:10:1, 3×); Ftir ($CHCl_3$ cast): 3600–2400 (b), 2970, 2930, 2867, 1696 (b), 1237, 756 cm^{-1}; ^{1}H nmr ($CDCl_3$) δ: 0.8–1.9 (5H, m), 1.29 (3H, s, C-10 CH_3), 1.37 (3H, s, C-4 CH_3), 1.60 and 1.61 (2 × 3H, s, C-15 2 × CH_3), 2.38 (2H, bd, J = 11 Hz), 2.49 and 2.58 (2 × 1H, d, J = 12.5 and 12.25 Hz respectively, C-6 H_{eq} and C-5 H), 2.74 (1H, dd, J = 12.5, 12.25 Hz, C-6 H_{ax}), 7.39 (1H, d, J = 8.5 Hz, C-11 H), 7.77 (1H, dd, J = 8.5, 2.25 Hz, C-12 H), 8.09 (1H, d, J = 2.25 Hz, C-14 H); hreims, m/z calcd. for $C_{20}H_{26}O_4$ (M^+): 330.1831; found: 330.1826 (3), 315 (100), 312 (3), 269 (8).

Isolation of austocystin F (11)

Flash chromatography of the crude broth metabolites of strain NFRC-631 (*vide supra*) gave 109 mg of material containing **3–6** as well as **11–13** in fractions eluting with chloroform – ethyl acetate – acetic acid. This sample was further purified by flash chromatography (Skellysolve B – ethyl acetate – acetic acid, 92:7:1; sample dissolved in chloroform) to afford **3–6**, then Skellysolve B – ethyl acetate – acetic acid (87:12:1) coeluted **12** and **13**, and Skellysolve B – ethyl acetate – acetic acid (79:20:1) gave **11**. Recrystallization from toluene provided **11** (2 mg, mp 232–234°C (lit. (16) mp 230–233°C); $[\alpha]_D$ −180° (*c* 1.1, pyridine) (lit. (16) $[\alpha]_D^{22}$ −244° (*c* 0.91, pyridine)); tlc: R_f 0.35 (Skellysolve B – ethyl acetate – acetic acid, 85:15:1, 3×); Ftir (CH_2Cl_2 cast): 3480 (b), 1663, 1645, 1606, 1491 cm^{-1}; ^{1}H nmr ($CDCl_3$) δ: 2.88 (1H, bs, C-3a OH), 5.73 (1H, d, J = 2.75 Hz, C-3 H), 6.44 and 6.46 (2 × 1H, s, C-11 H and C-12a H), 6.58 (1H, d, J = 2.75 Hz, C-2 H), 6.80 (1H, d, J = 8.25 Hz, C-7 H), 6.89 (1H, d, J = 8.25 Hz, C-9 H), 7.59 (1H, t, J = 8.25 Hz, C-8 H), 11.80 (1H, s, C-4 OH), 12.38 (1H, s, C-6 OH); hreims, m/z calcd. for $C_{17}H_{10}O_7$ (M^+): 326.0426; found: 326.0423 (58), 297 (100), 271 (15).

Isolation of averufin (12) and averufanin (13)

The amounts of **12** and **13** from the broth extract of strain NFRC-631 (*vide supra*) were too small for identification purposes. Soxhlet extraction (chloroform) of the mycelium of the same growth of NFRC-631 mentioned above provided 7.2 g of crude metabolites. A portion (3.3 g) was subjected to flash chromatography (sample dissolved in chloroform), eluent Skellysolve B – ethyl acetate, 93:7 (750 mL), then Skellysolve B – ethyl acetate, 85:15 (750 mL), then chloroform—methanol, 99:1 (500 mL), then chloroform–methanol, 98:2 (750 mL), and finally chloroform–methanol, 95:5 (500 mL). Fraction 24 (eluting with Skellysolve B – ethyl acetate, 85:15) afforded orange crystals upon concentration and cooling to ca. 5°C. The crystalline material (23 mg) was a mixture of **12** and **13**; tlc: R_f 0.50 (Skellysolve B – ethyl acetate – acetic acid, 85:15:1, 3×); R_f 0.20 (chloroform – ethyl acetate, 98:2, 3×); Ftir ($CHCl_3$ cast): 3380 (b), 1669 (w), 1622, 1399, 1268, 1258, 1156, 751 cm^{-1}; ^{1}H nmr (acetone-d_6 + D_2O) δ: 1.1–2.1 (m), 1.24 (<3H, d, J = 6.5 Hz, C-5′ CH_3 of **12**), 3.73 (<1H, m, C-5′ H of **13**), 5.04 (<1H, dd, J = 11.5, 2.25 Hz, C-1′ H of **13**), 5.22 (<H, d, J = 2.75 Hz, C-1′ H of **12**), 6.58 (1H, d, J = 2 Hz, C-7 H), 7.03 (1H, s, C-4 H), 7.13 (1H, d, J = 2 Hz, C-5 H); hreims, m/z calcd. for $C_{20}H_{18}O_7$ (M^+ for **13**): 370.1052; found: 370.1040 (17); m/z calcd. for $C_{20}H_{16}O_7$ (M^+ for **12**): 368.0896; found: 368.0891 (57), 350 (22), 325 (89), 310 (100), 297 (71), 286 (58); cims, m/z: 386 (M + 18 for **12**), 371 (M + 1 for **13**), 369 (M + 1 for **12**).

Acetylation of averufin (12) and averufanin (13)

Acetic anhydride (1.0 mL) and pyridine (1.0 mL) were added to the mixture of **12** and **13** (3.5 mg) and the reaction mixture was stirred for 18 h at room temperature. The solvents were evaporated *in vacuo* and the crude products were separated by preparative tlc (chloroform–methanol, 99:1) to give averufin triacetate (1.3 mg), mp 205–210°C (Skellysolve B – benzene) (lit. (24) mp 210–214°C): $[\alpha]_D$ −25° (*c* 2.2, $CHCl_3$) (lit. (24) $[\alpha]_D$ −15° ($CHCl_3$)); tlc: R_f 0.45 (chloroform–methanol, 99:1, 2×); Ftir (CH_2Cl_2 cast): 1770, 1677, 1662, 1600, 1346, 1325, 1197 cm^{-1}; ^{1}H nmr (acetone-d_6) δ: 1.6–2.2 (6H, m), 1.56 (3H, s, C-5′ CH_3), 2.37, 2.40, and 2.44 (3 × 3H, s, 3 × $COCH_3$), 5.29 (1H, m, C-1′ H), 7.39 (1H, d, J = 3 Hz, C-7 H), 7.51 (1H, s, C-4 H), 7.93 (1H, d, J = 3 Hz, C-5 H); hreims, m/z calcd. for $C_{26}H_{22}O_{10}$ (M^+): 494.1213; found: 494.1211 (10), 452 (61), 410 (100), 368 (49), 352 (84), 340 (32), 325 (77), 310 (99), 309 (56), 297 (69), 286 (34), 285 (41), 281 (37).

The above mentioned ptlc also gave 0.5 mg of averufanin tetra-

Can. J. Chem. Downloaded from www.nrcresearchpress.com by 80.58.250.72 on 09/07/12
For personal use only.

acetate; tlc: R_f 0.29 (chloroform–methanol, 99:1, 2×); Ftir ($CHCl_3$ cast): 2920, 2850, 1776, 1677, 1595, 1367, 1324, 1183 cm^{-1}; ^1H nmr (acetone-d_6) δ: 1.15 (3H, d, J = 6 Hz, C-5′ CH_3), 1.6–2.3 (6H, m), 2.37, 2.40, 2.41, and 2.44 (4 × 3H, s, 4 × $COCH_3$), 3.8 (1H, m, C-5′ H), 4.93 (1H, m, C-1′ H), 7.41 (1H, d, J = 2.25 Hz, C-7 H), 7.89 (1H, s, C-4 H), 7.94 (1H, d, J = 2.25 Hz, C-5 H); hreims, m/z calcd. for $C_{28}H_{26}O_{11}$ (M^+): 538.1475; found: 538.1475 (8), 496 (42), 478 (24), 454 (73), 436 (11), 412 (76), 394 (28), 352 (42), 300 (27), 299 (38), 297 (31), 172 (50), 57 (100).

Averufanin tetraacetate was also prepared from authentic averufanin for comparative purposes, using the same procedure described above for the mixture of **12** and **13**.

*Isolation of ergosterol peroxide (**15**)*

The crude mycelial extract (0.94 g) from strain NFRC-621 was subjected to flash chromatography. Elution with chloroform gave a fraction (86 mg) that was further chromatographed (Skellysolve B – ethyl acetate, 85:15; changed to 75:25 after 11 fractions) to provide impure **15** (16 mg). Preparative tlc (chloroform–methanol, 97:3, 3×) afforded **15** (5 mg), which was recrystallized from ether–hexane, mp 178–181°C (lit. (25) mp 181.5–183°C). The compound was identical (tlc, ftir, ^1H nmr) with an authentic sample.

Analysis of other mycelial extracts by tlc showed **15** to be produced by strains NFRC-624 and 631 as well. Although not isolated in pure form, ergosterol was also shown to be present in the mycelial extracts of NFRC-624 by comparative tlc with an authentic sample.

*Isolation of sitostanol (**16**) and β-sitosterol (**17**)*

Flash chromatography of the crude mycelial extract of strain NFRC-624 (0.82 g) afforded 30 mg from fractions eluting with Skellysolve B – ethyl acetate (75:25). Preparative tlc of this material (Skellysolve B – ethyl acetate, 85:15, 4×) yielded a mixture of **16** and **17** (6 mg), which was recrystallized from methanol–ether (mp 136–138°C) (lit. (26) mp 136–137°C); tlc: R_f 0.37 (Skellysolve B – ethyl acetate, 85:15, 3×); Ftir ($CHCl_3$ cast): 3600–3100 (b), 2955, 2930, 2865, 1465, 1375, 1057 cm^{-1}; ^1H nmr ($CDCl_3$) δ: 0.66 and 0.69 (2s, C-10 CH_3 of **16** and **17**), 0.7–2.4 (m), 0.81–0.87 (m, C-13 CH_3 of **16**, C-25 2 × CH_3 and C-28 CH_3 of **16** and **17**), 0.90–0.95 (2d, J = 7 Hz, C-20 CH_3 of **16** and **17**), 1.03 (s, C-13 CH_3 of **17**), 3.52 (bs, C-3 H of **16** and **17**), 5.38 (m, C-6 H of **16**); hreims, m/z calcd. for $C_{29}H_{52}O$ (M^+ for **16**): 416.4018; found: 416.4005 (19); m/z calcd. for $C_{29}H_{50}O$ (M^+ for **17**): 414.3861; found: 414.3871 (73), 401 (6), 399 (19), 396 (30), 303 (32), 159 (30), 145 (40), 133 (32), 121 (33), 119 (33), 109 (33), 107 (62), 105 (41), 95 (67), 93 (46), 91 (36), 81 (74), 69 (62), 57 (82), 55 (100).

Isolation of fatty acids and triglycerides

Flash chromatography of the crude mycelial extracts of strain NFRC-631 (see isolation of **12** and **13**) afforded crude triglycerides (531 mg) in fractions 4–5. These were further purified by flash chromatography (Skellysolve B – ethyl acetate, 95:5) to give mixed triglycerides (370 mg) as a colourless liquid; tlc: R_f 0.68 (Skellysolve B – ethyl acetate – acetic acid, 85:15:1, 2×); Ftir ($CHCl_3$ cast): 3005 (w), 2925, 2850, 1745, 1465, 1163 cm^{-1}.

From several fractions of the above flash chromatography of the NFRC-631 mycelial extract, a mixture of fatty acids crystallized upon concentration, mp 59–61°C; Ftir ($CHCl_3$ cast): 3300–2400 (b), 2915, 2850, 1697 cm^{-1}; ^1H nmr ($CDCl_3$) δ: 0.88 (3H, t, J = 7 Hz, CH_3—$(CH_2)_n$—), 1.26 (s, CH_3—$(CH_2)_n$—CH_2CH_2CO—), 1.63 (2H, quintet, J = 7.5 Hz, —CH_2—CH_2—CO—), 2.35 (2H, t, J = 7.5 Hz, —CH_2—CO); cims, m/z: 386 (M + 18 for lignoceric acid (C24)), 358 (M + 18 for behenic acid (C22)), 330 (M + 18 for arachic acid (C20)), 302 (M + 18 for stearic acid (C18)).

Hydrolysis of triglycerides

A solution of triglycerides (158 mg) in tetrahydrofuran (4 mL) and 10% (w/v) potassium hydroxide (2 mL) was stirred overnight at room temperature. After evaporation of the tetrahydrofuran *in vacuo*, the solution was acidified (5 *N* hydrochloric acid) and extracted with chloroform (5 × 20 mL). The combined chloroform extracts were washed with water (3 × 25 mL) and brine (3 × 25 mL) and dried over sodium sulphate. Filtration and evaporation afforded crude hydrolysis products (96 mg). Crystallization from ethyl acetate gave mixed fatty acids (11 mg), mp 55–57°C; cims, m/z: 302 (M + 18 for stearic acid (C18)), 198 (M + 18 for linoleic acid (18)), 274 (M + 18 for palmitic acid (C16)).

The remainder of the hydrolysis products was subjected to flash chromatography (Skellysolve B – ethyl acetate – acetic acid (gradient), 94:5:1 to 89:10:1 to 84:15:1) to afford additional fatty acids (62 mg); ir ($CHCl_3$): 3500–2400 (b), 1930, 2860, 1706 cm^{-1}; ^1H nmr ($CDCl_3$): δ: 0.88 (m, CH_3—$(CH_2)_n$—), 1.26 (m, CH_3—$(CH_2)_n$—CH_2CH_2CO—), 1.64 (m, —CH_2—CH_2—CO), 2.05 (m, —CH_2—CH=CH— of **18**), 2.36 (t, J = 7.5 Hz, —CH—CO), 2.79 (t, J = 6 Hz, —CH=CH—CH_2—CH=CH— of **18**), 5.35 (m, —CH=CH— of **18**), 9.7 (bs, —COOH); hreims, m/z calcd. for $C_{18}H_{36}O_2$ (stearic acid) (M^+): 284.1715; found: 284.1714 (8); m/z calcd. for $C_{18}H_{32}O_2$ (linoleic acid) (**18**) (M^+): 280.2402; found: 280.2400 (10); m/z calcd. for $C_{16}H_{32}O_2$ (palmitic acid) (M^+): 256.2402; found: 256.2403 (20).

Acknowledgements

We gratefully acknowledge the financial support of the Natural Sciences and Engineering Research Council of Canada in the form of operating grants (W.A.A.) and scholarships (J.B.M.). We thank Dr. Y. Hiratsuka, Northern Forest Research Centre, Edmonton, for bringing this problem to our attention and for providing cultures of *A. mellea*, Dr. K. Mallett for mycological information on the strains used in this study, and A. Szenthe for carrying out the later culture growths. For kindly providing authentic samples we wish to thank Dr. O. E. Edwards and Dr. E. Wenkert for pimaric, isopimaric, and sandaracopimaric acids; Dr. R. Vleggaar for austocystin F; Dr. J. C. Vederas for averufin; and Dr. A. Castonguay for averufanin.

1. E. L. PALMER. Fieldbook of natural history. McGraw–Hill Book Company Inc., New York. 1949. p. 63.
2. (*a*) D. J. MORRISON. Armillaria root disease. A guide to disease diagnosis, development and management in British Columbia. Canadian Forestry Service, Pacific Forest Research Centre, Victoria, B.C. BC-X-203. July, 1981; (*b*) C. DICKINSON and J. LUCAS (*Editors*). The encyclopedia of mushrooms. G. P. Putnam's Sons, New York. 1979. p. 46.
3. (*a*) K. ODURO, D. MUNNECKE, J. SIMS, and N. KEEN. Trans. Br. Mycol. Soc. **66**, 195 (1976); (*b*) H. OHR and D. MUNNECKE. Trans. Br. Mycol. Soc. **62**, 65 (1974); (*c*) A. OPPERMANN. Arch. Mikrobiol. **16**, 364 (1951); (*d*) C. RICHARD. Can. J. Microbiol. **17**, 395 (1971).
4. (*a*) D. DONNELLY, S. SANADA, J. O'REILLY, J. POLONSKY, T. PRANGE, and C. PASCARD. J. Chem. Soc. Chem. Commun. 135 (1982); (*b*) S. MIDLAND, R. IZAC, R. WING, A. ZAKI, D. MUNNECKE, and J. SIMS. Tetrahedron Lett. **23**, 2515 (1982), and references therein.
5. F. DESIMONE, F. SENATORE, D. SICA, and F. ZOLLO. Phytochemistry, **18**, 1572 (1979).
6. H. BOVENG, R. FRASER, and B. LINDBERG. Carbohydr. Res. **4**, 12 (1967); **4**, 20 (1967).
7. (*a*) W. B. TURNER. Fungal metabolites. Academic Press, London. 1971; (*b*) W. B. TURNER and D. B. ALDRIDGE. Fungal metabolites II. Academic Press, London. 1983.
8. (*a*) E. HARTMANN, B. RENZ, and J. JUNG. Phytopathol. Z, **101**, 31 (1981); (*b*) N. MAKARENKO, E. SCHMIDT, V. RALDUGIN, and Z. DUBOVENKO. Mikrobiol. Zh. **42**, 98 (1980); (*c*) W. OLECHNOWICZ-STEPIEN and E. LAMER-ZARAWSKA. Herba Pol. **27**, 145 (1981); (*d*) M. HENRIKS, R. EKMAN, and K. VON WEISSENBERG. Acta Acad. Abo. Ser. B, 39 (1979); (*e*) To. SATO and Ts. SATO. Gyomu Hokoku-Akita-Ken Ringyo Senta, 185 (1979); (*f*) C. ELLIGER, D. ZINKEL, B. CHAN, and A. WAISS. Experientia, **32**, 1364 (1976).

9. L. F. FIESER and W. CAMPBELL. J. Am. Chem. Soc. **60**, 159 (1938).
10. S. BORY and M. FETIZON. Bull. Soc. Chem. Fr. 570 (1964).
11. R. E. IRELAND and P. SCHIESS. J. Org. Chem. **28**, 6 (1963).
12. E. AKIO and K. KITAO. Mokuzai Gakkaishi, **20**, 600 (1974).
13. H. ADAM, I. CAMPBELL, and N. MCCORKINDALE. Nature, **216**, 397 (1967).
14. N. AVDYUKOVA, E. SHMIDT, and V. PENTEGOVA. Izv. Sib. Otd. Akad. Nauk SSSR Ser. Khim. Nauk, 85 (1975).
15. T. ASAO, G. BUCHI, M. ABDEL-KADER, S. CHANG, E. WICK, and G. WEGAN. J. Am. Chem. Soc. **87**, 882 (1965).
16. P. STEYN and R. VLEGGAAR. J. Chem. Soc. Perkin Trans. 1, 2250 (1974).
17. Y. BERGER and J. JADOT. Bull. Soc. R. Sci. Liege, 633 (1975).
18. J. MASSICOT, J. MARTHE, and S. HEITZ. Bull. Soc. Chim. Fr. 2712 (1963).
19. J. ANDERSON and R. ULLRICH, Mycologia, **71**, 402 (1979).
20. K. MALLETT. Ph.D. thesis, University of Alberta, Edmonton, Alberta. 1985.
21. R. WATLING, G. KILE, and N. GREGORY. Trans. Br. Mycol. Soc. **78**, 271 (1982).
22. T. K. DEVON and A. I. SCOTT. Handbook of naturally occurring compounds. Vol. II. Academic Press, New York. 1975. p. 215.
23. E. WENKERT and B. JACKSON. J. Am. Chem. Soc. **80**, 211 (1958).
24. R. THOMSON. Naturally occurring quinones. 2nd ed. Academic Press, London. 1971. p. 485.
25. T. RAKAHASHI, O. TANAKA, and S. SHIBATA. Phytochemistry, **11**, 1850 (1972).
26. DICTIONARY OF ORGANIC COMPOUNDS. 5th ed. Chapman and Hall, New York. 1982. pp. 5009–5010.

Can. J. Chem. Downloaded from www.nrcresearchpress.com by 80.58.250.72 on 09/07/12
For personal use only.

Bullerone, a novel sesquiterpenoid from *Cyathus bulleri* Brodie[1]

WILLIAM A. AYER AND ROBERT H. MCCASKILL
Department of Chemistry, University of Alberta, Edmonton, Alta., Canada T6G 2G2

Received May 21, 1986

This paper is dedicated to Dr. O. E. (Ted) Edwards

WILLIAM A. AYER and ROBERT H. MCCASKILL. Can. J. Chem. **65**, 15 (1987).

The structure of bullerone (**3**), a minor metabolite of the bird's nest fungus *Cyathus bulleri* Brodie, has been determined by a combination of chemical and spectroscopic methods. The possible biogenesis of bullerone, a new skeletal class of sesquiterpenoid, is discussed.

WILLIAM A. AYER et ROBERT H. MCCASKILL. Can. J. Chem. **65**, 15 (1987).

Faisant appel à des méthodes tant chimiques que spectroscopiques, on a déterminé la structure de la bullérone (**3**), un métabolite mineur du champignon *Cyathus bulleri* Brodie des nids d'oiseaux. On discute des diverses possibilités de biogénèse de la bullérone qui, du point de vue du squelette, appartient à une nouvelle classe de sesquiterpénoïdes.

[Traduit par la revue]

Can. J. Chem. Downloaded from www.nrcresearchpress.com by 80.58.250.72 on 09/07/12
For personal use only.

Recently we reported (2) that the bird's nest fungus *Cyathus bulleri* Brodie, when grown in liquid culture, elaborates a series of humulene derived metabolites of which cybrodol (**1**) is representative. Subsequently, we described (3) the isolation and structural elucidation of the biogenetically unique sesquiterpenoid nidulol (**2**) from the same source. We report herein the structure of bullerone (**3**),[2,3] a minor metabolite of this fungus. Bullerone represents a new skeletal type of sesquiterpenoid.

Bullerone ($C_{15}H_{18}O_3$)[4] was obtained as a light yellow oil that resisted all attempts to induce crystallization. The functionality of bullerone was determined in the following manner. Bullerone shows infrared (ir) absorption in the carbonyl region at 1752 cm^{-1} and does not show hydroxyl absorption. The ^{13}C nmr spectrum of bullerone shows only one carbonyl signal at δ 214.4. Bullerone is thus a keto diether and the ketone is most likely located in a five-membered ring. Reduction of bullerone with sodium borohydride in methanol gave a complex reaction mixture from which bullerol (**4**, $C_{15}H_{20}O_3$, ir 3420 cm^{-1}) was isolated in 20% yield. Recourse to the method of Luche (4) (sodium borohydride, methanol, ceric chloride) gave bullerol in 88% yield. The carbinol proton and carbon of bullerol are evident in the ^1H nmr (δ 3.26) and ^{13}C nmr (δ 84.7) spectra, respectively. Acetylation (acetic anyhydride, pyridine) of bullerol afforded the acetyl derivative **5** ($C_{17}H_{22}O_4$, ir 1742 cm^{-1}) in which the characteristic secondary alcohol acetylation shift of 1.50 ppm is observed for the carbinol proton (δ 4.76) in the ^1H nmr spectrum.

In the olefinic carbon region of the ^{13}C nmr spectrum of **3** four signals are evident, two of which (δ 121.9, 132.9) correspond to carbons bearing hydrogen while the remaining pair (δ 134.1, 144.9) represent fully substituted carbons. Thus bullerone possesses two double bonds and is therefore tetracyclic. In the ^1H nmr spectrum of **3**, two vinylic protons ($CDCl_3$, δ 5.58, 5.62; C_6D_6, δ 5.14, 5.35) mutually coupled by 1.5 Hz are observed. This coupling constant is too small to arise from a vicinal arrangement (5) but may be rationalized in terms of a conjugated diene in which the hydrogens are in a 1,4 *anti* relationship, as in **3** (ref. 5, pp. 341–342). The presence of a conjugated diene is substantiated by the ultraviolet (uv) spectrum (CH_3OH) of **3**, which shows bands at 215 (ε 2800), 250 (ε 3300), and 342 nm (ε 600) assigned respectively to the ketone n–π* end absorption, the conjugated diene chromophore, and (likely) an uv-active impurity, since bullerone was isolated as a light yellow oil. The uv spectrum of **4** (CH_3OH) shows only one absorption band at 246 nm (ε 3500), in good agreement with the calculated value (6) of 244 nm.

The singly oxygenated carbon region of the ^{13}C nmr spectrum of **3** has two signals (δ 77.6, 77.7) assigned[5] to fully substituted and methylene carbons respectively. Consistent with this, the ^1H nmr spectrum of **3** shows the presence of a geminate pair of

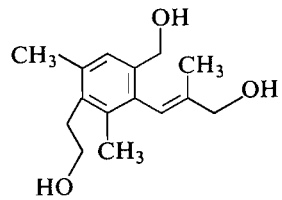

1

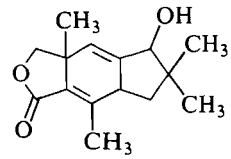

2

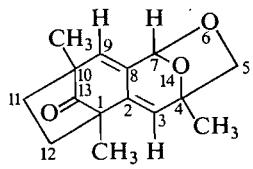

3

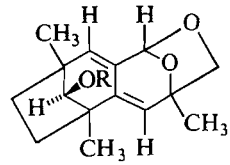

4 R = H
5 R = CH_3CO

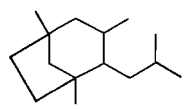

6

[1]Part 20 in the series: Metabolites of bird's nest fungi. For Part 19, see ref. 1.

[2]The numbering reflects the systematic name for bullerone: 1,4,10-trimethyl-6,14-dioxa-13-oxotetracyclo[8.2.1.$1^{4,7}$.$0^{2,8}$]-tetradeca-2,8-diene.

[3]To facilitate a concise presentation, the evidence will be presented in terms of the adduced structure. No stereochemistry is implied for **3**.

[4]Because of the small amounts available, all molecular formulas were established by high resolution mass spectrometry. Chemical ionization mass spectrometry was used to confirm the molecular weights.

[5]The multiplicities of all ^{13}C nmr signals were determined by single frequency off-resonance decoupling.

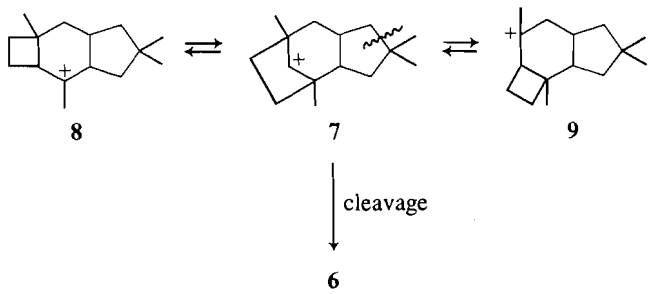

SCHEME 1

protons (δ 3.43, 3.84) mutually coupled by 6 Hz. The acetal function of **3** is revealed by a ^{13}C nmr signal at δ 101.3 arising from a carbon bearing a hydrogen and bonded to two oxygens. This hydrogen appears as a singlet at δ 5.62 in the ^1H nmr spectrum of **3**. No coupling is observed between H-7 and H-9 in accord with an allylic angle of nearly 0° (ref. 5, p. 316). The nmr parameters of the hydrogens and carbons associated with the acetal function are in accord with model compounds (7). Efforts to chemically characterize the acetal system of **3** were unsuccessful. Thus exposure to boron trifluoride etherate in methanol (2 days, 25°C) gave only recovered starting material, as did treatment with methanol saturated with hydrogen chloride (2 days, 25°C). When the latter reaction mixture was heated under reflux overnight an intractable mixture resulted.

Bullerone has three methyl groups (^1H nmr: δ 1.16, 1.19, 1.50; ^{13}C nmr: δ 15.2, 17.2, 20.2) all bonded to fully substituted carbons. The remaining four protons of bullerone appear in the ^1H nmr spectrum as an isolated spin system of four single-proton triple doublets (δ 1.70, 1.82, 1.90, 2.11) whose complexity and chemical shifts are consistent with contiguous methylene groups flanked by fully substituted carbons as per C-11 and C-12 of **3**.

The carbinol proton of **4** is coupled only to vinyl proton H-9 (δ 5.45) by 1.5 Hz. Since bullerone is clearly not an α,β-unsaturated ketone, these two protons cannot be vicinal and thus the carbonyl carbon of bullerone must be flanked by fully substituted carbons. Inspection of models of **3** and **4** indicates that hydride reduction of **3** from the less hindered face of the carbonyl would place the carbinol hydrogen of **4** in a four-bond "w" relationship to H-9, thus explaining the coupling between these protons. With the connectivity between the cyclopentanone fragment and the diene component thus indicated, insertion of the remaining structural elements (methyls, acetal, contiguous methylenes) into the partial structure thus derived leads to **3** as the only structure that is not subject to very severe bond angle strain.

We make no stereochemical assignment for bullerone, although of the two possible relative stereoisomers, that in which the C-5, O-6 bridge is *syn* rather than *anti* with respect to the carbonyl is somewhat more likely since we do observe pyridine-induced chemical shifts of 0.04 and 0.10 ppm for the C-5 hydrogens of **4**. This could indicate that the environment of one of these hydrogens is influenced somewhat by the C-13 hydroxyl. Lack of material precluded further studies to confirm the assignment.

The mass spectral fragmentation pattern of **3** shows loss of formaldehyde (presumably C-5 and O-6) and carbon monoxide (carbonyl carbon) leading to a base peak at *m/e* 188. Bullerol (**4**) loses formaldehyde (*m/e* 218), then ethylene (*m/e* 190), followed by CH_3 (*m/e* 175, 100%) or OH (*m/e* 173, 89%).

The carbon skeleton (**6**)[6] of bullerone, to the best of our knowledge, is unprecedented. It appears to be derived from a cation (**7**) that was proposed as an intermediate connecting the sterpurane system **8** (8) with the *proto*-illudane system **9** (Scheme 1).[7] It is significant that *C. bulleri* appears to be producing metabolites derived from cations **7**, **8**, and **9**. Thus nidulol (**2**) is likely derived from **8**, cybrodol (**1**) from **9**, and bullerone (**3**) from **7**. Interestingly, derivation of skeleton **6** from **7** requires the same bond cleavage as that which gives rise to cybrodol (**1**) from **9**.

Experimental

Cyathus bulleri was cultured and worked up as previously described (2). All solvents were distilled prior to use. Skellysolve B refers to Skelly Oil Company light petroleum, bp 62–70°C. Macherey Nagel silica gel (<80 μm) was used for column chromatography. Analytical thin-layer chromatography (tlc) was carried out on glass plates (75 × 25 or 75 × 50 mm) coated (0.3 mm) with silica gel G (E. Merck, Darmstadt) containing 1% electronic phosphor (General Electric, Cleveland). Materials were detected by visualization under an ultraviolet lamp. The plate was then sprayed with a solution of vanillin (1%) in concentrated sulfuric acid and carefully charred with a heat gun.

Mass spectra (ms) were recorded on a A.E.I. MS-50 mass spectrometer coupled to a DS 50 computer or a A.E.I. MS-9 mass spectrometer (chemical ionization). Data is reported as *m/e* (relative intensity) and, unless diagnostically significant, peaks with intensities less than 20% of the base peak are omitted. Infrared (ir) spectra were recorded on a Nicolet 7199 FT interferometer and ultraviolet (uv) spectra on a Unicam SP 1700 uv spectrophotometer. The ^1H nmr spectra were measured on a Varian HA-100 spectrometer interfaced to a Digilab FTS/NMR-3 data system or a Bruker WH-400 spectrometer. The ^{13}C nmr spectra were measured on a Bruker HFX-90 spectrometer interfaced to a Nicolet 1085 computer. All nuclear magnetic resonance measurements employed tetramethylsilane (TMS) as an internal standard.

Isolation of bullerone (3)

The crude neutral fungal extract (1.6 g) described previously (2) showed a prominent red spot (vanillin, H_2SO_4 visualization) on tlc at R_f 0.75 (eluent benzene–ether, 1:1). The extract was chromatographed over Sephadex LH-20 (100 g, 7-mL fractions) with fractions 42 and 43 (195 mg) containing the material responsible for the red spot. Silica gel chromatography (Skellysolve B – chloroform, 1:1; 10 g of silica gel) of this crude material afforded bullerone (18 mg) as a yellow oil; uv (CH_3OH) λ_{max}: 215 (ε 2800), 250 (ε 3300), 342 nm (ε 600); ir ($CHCl_3$ cast): 1752, 1645, 1605, 1450, 1375, 1340, 1315, 1295, 1235, 1195, 1090, 1080, 1020, 1000, 990, 940, 910, 840 cm^{-1}; ^1H nmr ($CDCl_3$) δ: 1.16 (3H, s), 1.19 (3H, s), 150 (3H, s), 1.70 (1H, ddd (6.8, 10.8, 12.0 Hz)), 1.82 (1H, ddd (3.6, 12.0, 12.0 Hz)), 1.90 (1H, ddd (6.8, 12.0, 12.8 Hz)), 2.11 (1H, ddd, (3.6, 10.8, 12.8 Hz)), 3.43 (1H, d (6 Hz)), 3.84 (1H, d (6 Hz)), 5.58 (1H, d (1.5 Hz)), 5.62 (1H, d (1.5 Hz)), 5.62 (1H, s); (C_6D_6) δ: 0.99 (3H, s), 1.16 (6H, s), 1.3–1.7 (4H, m), 3.29 (1H, d (6 Hz)), 3.60 (1H, d (6 Hz)), 5.14 (1H, d (1.5 Hz)), 5.35 (1H, d (1.5 Hz)), 5.69 (1H, s); ^{13}C nmr ($CDCl_3$) δ: 15.2, 17.2, 20.0 (CH_3); 33.5, 35.1, 77.7 (CH_2); 101.3, 121.9, 132.9 (CH); 47.2, 49.6, 77.6, 134.1, 144.9, 214.4 (C); ms *m/e* calcd. for $C_{15}H_{18}O_3$ (M^+): 246.1255; found: 246.1245 (49), 231 (16), 218 (20), 216 (34), 203 (24), 201 (20), 188 (100), 173 (25), 160 (28), 145 (22), 128 (21). Chemical ionization (NH_3) ms shows peaks at *m/e* 247 (*M* + 1) and 264 (*M* + 18).

Sodium borohydride – ceric chloride reduction of bullerone (3)

Sodium borohydride (5 mg) was added to a stirred solution of bullerone (**3**, 25 mg) and ceric chloride hexahydrate (353 mg) in

[6]We propose the trivial name bullerane for skeleton **6**.

[7]For a discussion of fungal terpene chemistry, including biogenesis, see ref. 9.

Can. J. Chem. Downloaded from www.nrcresearchpress.com by 80.58.250.72 on 09/07/12
For personal use only.

methanol (10 mL) at room temperature. After stirring for 5 min, the mixture was diluted with water (25 mL) and extracted with methylene chloride (5 × 10 mL). The extracts were washed with brine (10 mL) and dried ($MgSO_4$). Work-up in the usual way was followed by silica gel chromatography (chloroform, 8 g of silica gel) giving pure bullerol (**4**) as a clear oil (22 mg, 88%); uv (CH_3OH) λ_{max}: 246 nm (ϵ 3500); ir ($CHCl_3$ cast): 3420, 1650, 1610 cm^{-1}; ^1H nmr ($CDCl_3$) δ: 1.17 (3H, s), 1.21 (3H, s), 1.52 (3H, s), 1.5–1.8 (4H, m), 3.26 (1H, d (1.5 Hz)), 3.46 (1H, d (6 Hz)), 3.86 (1H, d (6 Hz)), 5.45 (1H, dd (1.5, 1.5 Hz)), 5.68 (1H, s), 5.73 (1H, d (1.5 Hz)); (C_5D_5N) δ: 1.22 (3H, s), 1.37 (3H, s), 1.50 (3H, s), 3.48 (1H, d (1.5 Hz)), 3.50 (1H, d (6 Hz)), 3.96 (1H, d (6 Hz)), 5.50 (1H, dd (1.5, 1.5 Hz)), 5.85 (1H, d (1.5 Hz)), 6.02 (1H, s); ^{13}C nmr ($CDCl_3$) δ: 19.8, 20.6, 21.9 (CH_3); 34.2, 36.2, 77.3 (CH_2); 84.7, 102.0, 125.1, 130.3 (CH); 44.4, 45.3, 78.1, 135.5, 140.3 (C); ms *m/e* calcd. for $C_{15}H_{20}O_3$ (M^+): 248.1413; found: 248.1416 (2), 218 (85), 190 (20), 175 (100), 173 (89).

Acetylation of bullerol (4)

A mixture of bullerol (**4**, 2.7 mg) and acetic anhydride – pyridine (10:1, 1 mL) was stirred at ambient temperature for 3 days. Evaporation to dryness left the acetyl derivative **5** (2.8 mg) as a yellow oil; ir ($CHCl_3$ cast): 1742 cm^{-1}; ^1H nmr ($CDCl_3$) δ: 1.09 (3H, s), 1.14 (3H, s), 1.50 (3H, s), 1.5–1.8 (4H, m), 2.00 (3H, s), 3.47 (1H, d (6 Hz)), 3.83 (1H, d (6 Hz)), 4.76 (1H, d (1.5 Hz)), 5.44 (1H, dd (1.5, 1.5 Hz)), 5.61 (1H, d (1.5 Hz)), 5.68 (1H, s); ms *m/e* calcd. for $C_{17}H_{22}O_4$ (M^+): 290. 1518; found: 290.1531 (4), 260 (35), 173 (100).

Acknowledgements

We wish to thank Dr. T. T. Nakashima and his associates for assistance in obtaining nmr measurements, Dr. A. Hogg and associates for the mass spectral measurements, and Drs. D. J. Burnell and D. E. Ward for useful discussions. We acknowledge the financial support of the Natural Sciences and Engineering Research Council of Canada in the form of operating grants (W.A.A.) and scholarships (R.H.M).

1. W. A. AYER, R. J. FLANAGAN, and T. REFFSTRUP. Tetrahedron, **40**, 2069 (1984).
2. W. A. AYER and R. H. McCASKILL. Can. J. Chem. **59**, 2150 (1981).
3. W. A. AYER, R. H. McCASKILL, and T. REFFSTRUP. Rev. Latinoam. Quim. **13**, 118 (1982).
4. J. L. LUCHE. J. Am. Chem. Soc. **100**, 2226 (1978).
5. L. M. JACKMAN and S. STERNHELL. Applications of nuclear magnetic resonance spectroscopy in organic chemistry. 2nd ed. Pergamon Press, Oxford. 1969. pp. 301–304.
6. A. I. SCOTT. Interpretation of the ultraviolet spectra of natural products. Pergamon Press, Oxford. 1964. p. 50.
7. R. R. FRASER, R. U. LEMIEUX, and J. D. STEVENS. J. Am. Chem. Soc. **83**, 3901 (1961); L. F. FIESER, T. GOTO, and B. K. BHATTACHARYVA. J. Am. Chem. Soc. **82**, 1700 (1962); W. E. WILLY, G. BINSCH, and E. ELIEL. J. Am. Chem. Soc. **92**, 5394 (1970).
8. W. A. AYER, M. H. SAEEDI-GHOMI, D. VAN ENGEN, B. TAGLE, and J. CLARDY. Tetrahedron, **37**, Suppl. No. 1, 379 (1981); W. A. AYER and M. H. SAEEDI-GHOMI. Can. J. Chem. **59**, 2536 (1981); W. A. AYER, T. T. NAKASHIMA, and M. H. SAEEDI-GHOMI. Can. J. Chem. **69**, 531 (1984).
9. W. A. AYER and L. M. BROWNE. Tetrahedron, **37**, 2199 (1981).

Can. J. Chem. Downloaded from www.nrcresearchpress.com by 80.58.250.72 on 09/07/12
For personal use only.

Sulfur extrusion from 1,4-benzothiazepines: formation of 3-aryl-4-carbomethoxyisoquinolines

LAJOS FODOR[1] AND DAVID B. MACLEAN[2]

Department of Chemistry, McMaster University, Hamilton, Ont., Canada L8S 4M1

Received May 16, 1986

This paper is dedicated to Dr. O. E. (Ted) Edwards

LAJOS FODOR and DAVID B. MACLEAN. Can. J. Chem. **65**, 18 (1987).

Treatment of 3-aryl-2-carbomethoxy-4,5-dihydro-1,4-benzothiazepines with *N*-chlorosuccinimide in ether gave 3-aryl-4-carbomethoxyisoquinolines in a reaction in which the sulfur atom was extruded from the seven-membered thiazepin ring.

LAJOS FODOR et DAVID B. MACLEAN. Can. J. Chem. **65**, 18 (1987).

La réaction des aryl-3 carbométhoxy-2 dihydro-4,5 benzothiazépines-1,4 avec la *N*-chlorosuccinimide dans l'éther conduit aux aryl-3 carbométhoxy-4 isoquinoléines; dans ces réactions, l'atome de soufre est expulsé du cycle à sept chaînons de la thiazépine.

[Traduit par la revue]

Can. J. Chem. Downloaded from www.nrcresearchpress.com by 80.58.250.72 on 09/07/12
For personal use only.

The extrusion of sulfur from thiepins and benzothiepins, a reaction leading to the formation of benzenes and naphthalenes, respectively, is well documented (1, 2). The extrusion of sulfur from a heterocyclic system containing both nitrogen and sulfur in the same ring has also been reported. It was shown that indoles were formed from 4*H*-3,1-benzothiazines on prolonged heating (3) but reactions of this type are rare. Here we report the novel formation of isoquinolines when 3-aryl-2-carbomethoxy-4,5-dihydro-1,4-benzothiazepines were oxidized with *N*-chlorosuccinimide (NCS).

The benzothiazepines used in this investigation were prepared by established methods (see Scheme 1). Szabo *et al.* (4) have reported the reaction of thiophenol (**1**) with the hydroxymethylamides (**2***a* and **2***b*) yielding the amides (**3***a* and **3***b*). Treatment of the amides with $POCl_3$ led to the formation of the 2-aryl-4*H*-1,3-benzothiazines (**4***a* and **4***b*). It was shown (5, 6) that the latter reacted with chloroacetyl chloride in the presence of triethylamine yielding the β-lactams (**5***a* and **5***b*) and that the β-lactams rearranged to 4,5-dihydro-1,4-benzothiazepines (**6***a* and **6***b*) in the presence of sodium methoxide in methanol. We prepared **6***a*, **6***b*, and the analogue **6***c* by the methods described (4–6). The spectroscopic properties of **6***c* and of the intermediates leading to it closely resemble those of the previously reported **6***a* and **6***b* and their precursors and do not merit discussion.

The treatment of **6***a*, **6***b*, and **6***c* with *N*-chlorosuccinimide in diethyl ether gave the corresponding 6,7-dimethoxy-3-aryl-4-carbomethoxyisoquinolines (**9***a*, **9***b*, and **9***c*). The three isoquinolines were identified by their spectroscopic properties of which the ^1H nmr spectra were most revealing. The three compounds have in common two aromatic methoxy signals appearing in the region of δ 4.0 and one ester methoxy signal near δ 3.70. Each compound shows three signals in the aromatic region associated with the protons at C-1, C-5, and C-8 of the isoquinoline ring system. The signal for C-1 appears in all three compounds near δ 9.2. The aromatic protons and other signals associated with the aryl group at C-3 of the isoquinoline ring are in accord with the nature and number of substituents on the aromatic ring. Other spectroscopic data also support the assigned structures.

We conclude that the reaction with NCS proceeds by halogenation at nitrogen followed by elimination of HCl to yield the transient benzothiazepines **7** and that subsequent elimination of sulfur through intermediates **8** provides the isoquinolines **9**.[3] 1,4-Benzothiazepines, to our knowledge, have not been reported in the literature so that there is no precedent for the sulfur extrusion reaction reported in this system. However, 1-benzothiepins (ref. 1 and references therein) have been extensively studied and are known to eliminate sulfur with ease, leading to formation of naphthalenes. It is generally considered that episulfides such as **8** are intermediates in the extrusion pathway of benzothiepins and thiepins (1, 2). The ease of sulfur elimination is a function of structure, but half-lives of less than 1 h (1, 2) have been reported. The fact that we did not observe intermediates **7** suggests that benzothiazepines decompose during work-up of the reaction mixture.

The substituted isoquinolines prepared in this study have not been previously reported. They are potentially useful intermediates for the synthesis of several classes of isoquinoline alkaloids of which the protoberberines, the benzophenanthridines, and the 3-arylisoquinolines are specific examples (7).

Experimental

The ^1H nmr spectra were recorded on a Bruker AM500 at 500 MHz and the ^{13}C nmr spectra on the same instrument at 125.8 MHz. The samples were dissolved in $CDCl_3$ using tetramethylsilane (TMS) as internal standard; chemical shifts are reported in ppm (δ) downfield from TMS. The symbols, s (singlet), d (doublet), t (triplet), q (quartet), m (multiplet), and br (broadened), are used to report the multiplicity and shape of the signals. EI mass spectra were recorded either on a VG Micro Mass 7070F or a VG ZAB E mass spectrometer at an ionizing voltage of 70 eV. Infrared spectra were recorded on a Perkin–Elmer 283 infrared spectrometer. Melting points were determined using a Gallenkamp apparatus and are uncorrected. *N*-hydroxymethylpiperonylamide **2***c* was prepared by a modification of a literature procedure (8). Compounds **6***a* and **6***b* were prepared as described (4, 6, 8). Thin-layer chromatography was performed using Polygram Sil G/UV_{254} or Polygram Aloxn/UV_{254} plates. The homogeneity of

[1]Present address: Central Laboratory, County Hospital, H-5701 Gyula, POB. 46, Hungary.

[2]Author to whom correspondence may be addressed.

[3]An alternative route to intermediate **7** has been suggested by a referee, namely, that chlorination may occur initially at sulfur, and that HCl and H^+ may be eliminated subsequently.

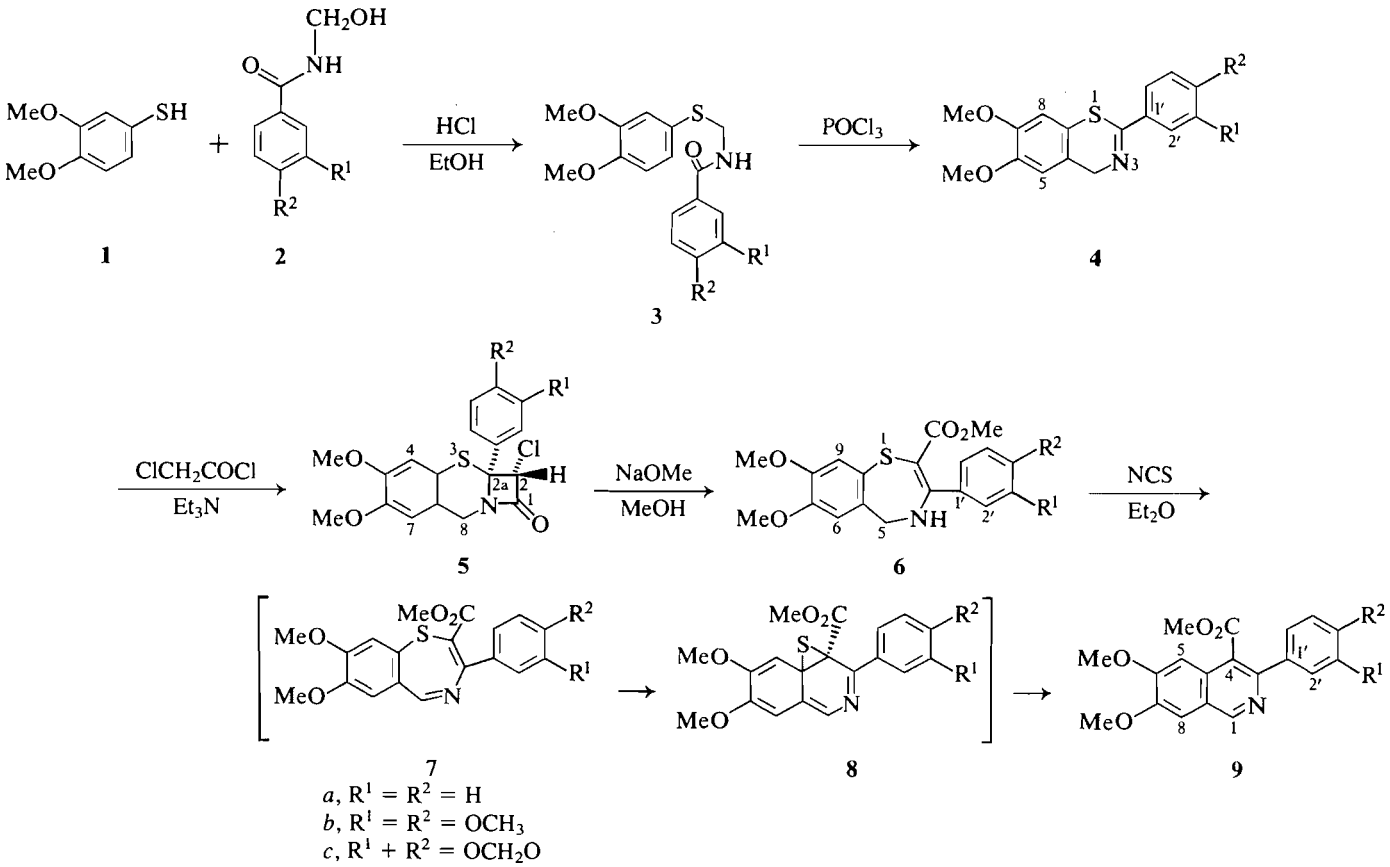

SCHEME 1

the products was established on the basis of chromatographic and spectroscopic (^{1}H nmr, ^{13}C nmr, and mass spectral) examination.

*6,7-Dimethoxy-2-(3',4'-methylenedioxyphenyl)-4*H*-1,3-benzothiazine (4c)*

Preparation of N*-(3,4-dimethoxyphenylthiomethyl)-piperonylamide (3c)*

A solution of 3,4-dimethoxythiophenol (**1**) (8.5 g, 0.05 mol) and *N*-(hydroxymethyl)-piperonylamide (**2***c*) (9.75 g, 0.05 mol) in EtOH was treated with 5 mL of a saturated solution of HCl in EtOH. The solution was maintained at room temperature for 3 h after which the crystalline product (14.8 g, 88.2%) was separated by filtration and recrystallized from EtOH, mp 108–109°C; ^{1}H nmr (500 MHz) $CDCl_3$ δ: 3.82 (3H, s, OMe), 3.86 (3H, s, OMe), 4.77 (2H, apparent d, J = 6.2 Hz, CH_2), 6.01 (2H, s, OCH_2O), 6.42 (1H, br s, NH), 6.80 (2H, m, Ar H's), 7.04 (2H, m, Ar H's), 7.20 (2H, m, Ar H's); ms (EI), m/z (%): 347(2) $M^{+\bullet}$, 177 (2), 170 (53), 169 (20), 155 (13), 149 (100), 121 (34).

Conversion of **3**c *to* **4**c

A mixture of **3***c* (6.94 g, 0.02 mol) and $POCl_3$ (10 mL) was heated on a boiling water bath for 1 h. The mixture was cooled to room temperature and ice was added to decompose the excess $POCl_3$. The solution was then neutralized with sodium carbonate, extracted with benzene, and the extract dried over anhydrous Na_2SO_4. The benzene solution was filtered, evaporated, and the residue taken up in 20 mL of hot EtOH. The crystals (3.12 g, 47.2%) that separated melted at 169–170°C after recrystallization from methanol; ^{1}H nmr (500 MHz, $CDCl_3$) δ: 3.89 (3H, s, OCH_3), 3.90 (3H, s, OCH_3), 4.72 (2H, s, C-4 H's), 6.03 (2H, s, OCH_2O), 6.85 (1H, s, C-5 or C-8 H), 6.87 (1H, s, C-8 or C-5 H), 6.86 (1H, d, J = 8.2 Hz, C-5' H), 7.55 (1H, d, J = 1.7 Hz, C-2' H), 7.63 (1H, q, J = 8.2 and 1.7 Hz, C-6' H); ^{13}C nmr (125.8 MHz), $CDCl_3$ δ: 55.4 (C-4), 56.4 (2 × OCH_3), 102.0 (OCH_2O), 108.3, 109.7, 110.4, 121.1, 123.6, 123.8, 148.4, 149.1, 149.4, 151.2 (aromatic and imine C-atoms);[4] ms (EI), m/z (%): 329 (15) $M^{+\bullet}$, 182 (100), 167 (56), 147 (3), 146 (5), 139 (4). *Mol. Wt.* calcd. for $C_{17}H_{15}NO_4S$: 329.0721; found (hrms): 329.0720.

cis*-2-Chloro-2,2a-dihydro-5,6-dimethoxy-2a-(3',4'-methylenedioxy)-1*H*,8*H*-azeto[2,1-b][1,3]benzothiazin-1-one (5*c*)*

A solution of compound **4***c* (1.645 g, 0.005 mol) in benzene (30 mL) was treated with chloroacetyl chloride (0.60 g). The mixture was heated to boiling under reflux and a solution of triethylamine (0.60 g) in benzene (30 mL) was added dropwise, with stirring, over a period of 1 h. The crystalline $Et_3\overset{+}{N}H\ Cl^-$ that separated was removed by filtration. The benzene filtrate was evaporated to dryness and the residue taken up in ethanol. The colorless crystals (1.88 g, 94%) were collected by filtration and melted at 141–142°C. ir (ν_{max} cm^{-1}), 1790; ^{1}H nmr (500 MHz, $CDCl_3$) δ: 3.83 (3H, s, OMe), 3.84 (3H, s, OMe), 4.26 and 4.90 (2H, ABq, J = 16.3 Hz, C-8 H's), 5.07 (1H, s, C-2 H), 5.98 (2H, s, OCH_2O), 6.66 (1H, s, C-4 or C-7 H), 6.67 (1H, s, C-4 or C-7 H), 6.78 (1H, d, J = 8.3 Hz, C-5' H), 6.93 (1H, q, J = 8.3 and 1.8 Hz, C-6' H), 6.94 (1H, apparent s, C-2' H); ms (EI), m/e (%): 405 (14) $M^{+\bullet}$, 369 (18), 329 (5), 182 (100), 167 (73), 147 (28), 146 (42). *Mol. Wt.* calcd. for $C_{19}H_{16}NO_5S^{35}Cl$: 405.0438; found (hrms): 405.0443.

2-Carbomethoxy-4,5-dihydro-7,8-dimethoxy-3-[3',4'-methylenedioxyphenyl]-1,4-benzothiazepine (6c)

A solution of compound **5***c* (0.405 g, 0.001 mol) in MeOH (10 mL) was treated with sodium methoxide (0.054 g, 0.001 mol) and the mixture heated under reflux for 3 h. Water was added to the cooled solution and the mixture extracted with $CHCl_3$. The extract was dried, evaporated, and the residue dissolved in MeOH. The crystals (0.334 g, 84%), which separated on standing, melted at 170–171°C.

[4]There are 10 signals for the 13 sp^2 hydridized C atoms of **4***c*, indicating that three pairs of C atoms have similar resonances.

Can. J. Chem. Downloaded from www.nrcresearchpress.com by 80.58.250.72 on 09/07/12
For personal use only.

ir (ν_{max}, cm^{-1}): 1710; ^1H nmr (500 MHz, DMSO-d_6 with D_2O added) δ: 3.31 (3H, s, CO_2Me), 3.81, 3.82 (6H, 2s, 2 × OMe), 4.80 (2H, d, J = 5.0 Hz, C-5 H's), 6.05 (2H, s, OCH_2O), 6.62 (1H, q, J = 8.0 and 1.6 Hz, C-6′ H), 6.69 (1H, d, J = 1.6 Hz, C-2′ H), 6.87 (1H, d, J = 8.0 Hz, C-5′ H), 6.97 (1H, s, C-6 H or C-9 H), 7.08 (1H, s, C-6 H or C-9 H); ^{13}C nmr (125.8 MHz, DMSO-d_6) δ: 47.7 (C-5), 51.1 (CO_2Me), 56.1 (2 × OMe), 101.5 (OCH_2O), 108.1, 108.5, 112.8, 115.4, 121.8 (ArCH), 101.5, 129.2, 134.6, 135.8, 147.0, 147.8, 148.6, 149.0, 158.1 (Ar and vinylic C's devoid of H), 167.8 (CO_2Me). ms (EI), m/z (%): 401 (68) $M^{+\cdot}$, 368 (100), 342 (67), 254 (28), 195 (49). *Mol. Wt.* calcd. for $C_{20}H_{19}NO_6S$: 401.0933; found (hrms): 401.0945. *Anal.* calcd. for $C_{20}H_{19}NO_6S$: C 59.8, H 4.7, N 3.5; found: C 60.0, H 4.9, N 4.0%.

*4-Carbomethoxy-6,7-dimethoxy-3-phenylisoquinoline (**9**a)*

A solution of **6***a* (0.5 mmol) and 0.10 g *N*-chlorosuccinimide was stirred in Et_2O at room temperature for 48 h. The crystals that separated were recovered by filtration, dissolved in $CHCl_3$, and the solution washed with 5% Na_2CO_3 solution. The $CHCl_3$ layer was separated, dried over anhydrous Na_2SO_4, evaporated, and the residue dissolved in a mixture of Et_2O–MeOH. The product (0.111 g, 68.7%) that separated melted at 185–186°C; ir ($\nu_{max,\ cm}{}^{-1}$), $CHCl_3$: 1700; ^1H nmr (500 MHz, $CDCl_3$) δ: 3.70 (3H, s, CO_2Me), 4.04 (6H, s, 2 × OMe), 7.26 (1H, s, C-5 or C-8 H), 7.33 (1H, s, C-5 or C-8 H), 7.41 (1H, m, Ar), 7.47 (2H, m, Ar), 7.69 (2H, m, Ar), 9.16 (1H, s, C-1 H); ^{13}C nmr[5] (125.8 MHz, $CDCl_3$) δ: 52.5 (CO_2Me), 56.2, 56.3, (2 × OMe), 102.6, 105.7, 121.8, 123.3, 128.5, 128.7, 130.6, 140.5, 150.3, 150.76, 150.80, 154.4 (Ar C's), 169.7; ms (EI), m/z (%): 323 (87), 308 (100), 292 (39), 265 (11), 264 (9), 248 (10). *Mol. Wt.* calcd. for $C_{19}H_{17}NO_4$: 323.1158; found (hrms): 323.1164.

*4-Carbomethoxy-6,7-dimethoxy-3(3′,4′-dimethoxyphenyl)-isoquinoline (**9**b)*

This compound was prepared from **7***b* in the manner described for the preparation of **7***a*. Yield: 0.108 g, 56.4%; mp 127–129°C (ether–MeOH); ir ν_{max} (cm^{-1}): 1710; ^1H nmr (500 MHz, $CDCl_3$) δ: 3.76 (3H, s, CO_2Me), 3.95 (3H, s, OMe), 3.99 (3H, s, OMe), 4.07 (6H, s, 2 × OMe), 6.97 (1H, d, J = 8.3 Hz, C-5′ H), 7.23 (1H, d, J = 8.3 Hz, C-6′ H), 7.31, (2H, apparent s, two of C-2′, C-5, C-8 H), 7.36 (1H, s, one of C-2′, C-5, C-4 H), 9.22 (1H, s, C-1 H); EI (ms), m/z (%): 383 (100) $M^{+\cdot}$, 368 (46), 352 (29), 337 (8), 324 (5). *Mol. Wt.* calcd. for $C_{21}H_{21}NO_6$: 383.1369; found (hrms): 383.1376.

*4-Carbomethoxy-6,7-dimethoxy-3(3′,4′-methylenedioxyphenyl)-isoquinoline (**9**c)*

This compound was prepared from **7***c* in the manner described for the preparation of **9***a*. Yield: 0.112 g, 61%; mp 148–149°C (ether–MeOH); ir, ν_{max} (cm^{-1}) $CHCl_3$: 1710; ^1H nmr (500 MHz, $CDCl_3$) δ: 3.78 (3H, s, CO_2Me), 4.05 (6H, s, 2 × OMe), 6.03 (2H, s, OCH_2O), 6.89 (2H, d, J = 8.0 Hz, C-5′ H), 7.19 (2H, d, J = 8.0 Hz, C-6′ H), 7.23, 7.27, 7.29 (1H each, singlets, C-2′, C-5, and C-8 H), 9.15 (1H, s, C-1 H); ^{13}C nmr (125.8 MHz, $CDCl_3$) δ: 52.8 (CO_2CH_3), 56.4, 56.4 (2 × OMe), 101.5 (OCH_2O), 102.6, 105.8, 108.5, 109.3, 122.9, 150.2 (Ar CH), 121.8, 123.2, 131.0, 133.9, 148.2, 148.3, 149.1, 150.9, 154.8 (Ar quaternary), 169.6 (CO_2Me). ms (EI), m/z (%): 367 (100), 352 (84), 336 (33), 308 (11), 306 (12), 278 (18). *Mol. Wt.* calcd. for $C_{20}H_{17}NO_6$: 367.1056; found (hrms): 367.1053. *Anal.* calcd. for $C_{20}H_{17}NO_6$: C 65.4, H 4.7, N 3.8; found: C 65.4, H 4.8, N 3.7%.

[5]There are several overlapping signals associated with the C_6H_5 group.

Acknowledgements

We gratefully acknowledge financial support from the Natural Sciences and Engineering Research Council of Canada through an International Scientific Exchange Award and an Operating Grant.

1. D. N. Reinhoudt. Recl.: J.R. Neth. Chem. Soc. **101**, 277 (1982).
2. R. Gleiter, G. Krennrich, D. Cremer, K. Yamamoto, and I. Murata. J. Am. Chem. Soc. **107**, 6874 (1985).
3. D. Lednicer and D. E. Emmert. J. Heterocycl. Chem. **8**, 903 (1971).
4. J. Szabo, L. Fodor, I. Varga, E. Vinkler, and P. Sohar. Acta Chim. Acad. Sci. Hung. **93**, 403 (1977).
5. L. Fodor, J. Szabo, G. Bernath, L. Parkanyi, and P. Sohar. Tetrahedron Lett. **22** 5077 (1981).
6. L. Fodor, J. Szabo, E. Szucs, G. Bernath, P. Sohar, and J. Tamas. Tetrahedron, **40**, 4089 (1984).
7. M. Shamma. The isoquinoline alkaloids, chemistry and physiology. Academic Press, New York. 1972; M. Shamma and J. L. Moniot. Isoquinoline alkaloid research 1972–1977. Plenum Press, New York. 1978.
8. J. Szabo, L. Fodor, I. Varga, E. Vinkler, and P. Sohar. Acta Chim. Acad. Sci. Hung. **92**, 317 (1977).

Can. J. Chem. Downloaded from www.nrcresearchpress.com by 80.58.250.72 on 09/07/12
For personal use only.

The conversion of podocarpic acid to hexahydrophenalene derivatives: an approach to the synthesis of edulone A[1]

ROBERT H. BURNELL[2] AND JEAN-MARC DUFOUR
Chemistry Department, Université Laval, Québec (Qué.), Canada G1K 7P4

Received April 21, 1986

This paper is dedicated to Dr. O. E. (Ted) Edwards

ROBERT H. BURNELL and JEAN-MARC DUFOUR. Can. J. Chem. **65**, 21 (1987).

To test the feasibility of a biogenetically inspired synthesis of edulone A **1**, podocarpic acid **3***a* has been transformed into a substituted hexahydrophenalene **16***b*. The critical steps involve introduction of a double bond into the A ring, cleavage by ozone, and, after suitable manipulation, an epoxy-arene cyclization. A second product from this cyclization is an octahydrophenaleno[1,9-*bc*]furan **17**.

ROBERT H. BURNELL et JEAN-MARC DUFOUR. Can. J. Chem. **65**, 21 (1987).

Afin de vérifier que notre plan de synthèse de l'édulone A **1** inspiré d'une biosynthèse est réalisable, nous avons transformé l'acide podocarpique **3***a* en un hexahydrophénalène substitué **16***b*. Les étapes critiques de la synthèse impliquent l'introduction d'une insaturation dans le cycle A, l'ouverture de ce cycle par l'ozone et la cyclisation de la chaîne ainsi obtenue sur le cycle aromatique via l'époxyde **15**. De plus, nous avons isolé un second produit de cette cyclisation, soit l'octahydrophénalèno[1,9-*bc*]furanne **17**.

Edulone A **1** was isolated from *Plectranthus edulis* (1) and is unusual in that this 2[*H*]-1-oxapyrene skeletal type of diterpene is unknown elsewhere. When the accepted structure was proposed by Eugster and co-workers (1), they also suggested a logical biogenesis involving cleavage of the C4—C5 bond of a normal tricyclic diterpene intermediate, appropriate oxidations, and cyclization of the resulting long sidechain to the relevant positions on the C ring (C11 and the oxygen at C12). For some time our interests (2) have been the elaboration of complex structures starting from commercially affordable chiral materials, for instance podocarpic acid **3***a*. We felt that a biogenetically inspired approach to the laboratory synthesis of edulone A merited investigation and in a preliminary study we wished to test the feasibility of transforming methyl *O*-methyl podocarpate **3***b* into the model hexahydrophenalene system **2** (in which X and Y could be virtually any functional group). Since the absolute stereochemistry at the quaternary carbon C10 of podocarpic acid will be preserved throughout the transformations, this could be used to induce a stereoselective edulone sythesis later.

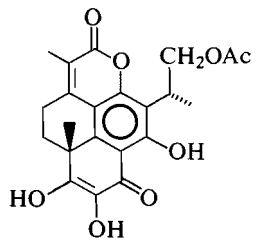

1

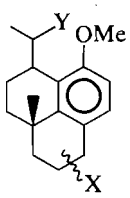

2

The rupture of the C4—C5 bond in methyl *O*-methyl podocarpate **3***b* under laboratory conditions, which is critical to the project, would be considerably easier if one of the substituents at C4 were sacrificed. To this end a conjugated enone function was introduced by the known DDQ[2] oxidation of the B ring (3) to give **4***a* and the ester moiety was then replaced by hydrogen using organic bases such as *quinuclidinol*-3, DBU, or DBN[3] (4), affording the demethoxycarbonylated enone **4***b*. The yield in the DDQ oxidation was only moderate since the crude product was very discolored and required repeated chromatography, so we actually used a longer but more manageable route when larger quantities of **4***b* were needed. The steps involved were: benzylic oxidation to the aromatic ketone **5***a* (5) and then bromination using copper bromide (6) to afford the 6-bromo derivative **5***b*, which was both dehydrobrominated and demethoxycarbonylated by treatment with DBU.

To open the A ring it was necessary to shift the double bond and, after unsuccessfully trying to do this by formation of the ketal or by reducing the enol acetate, we found the best method was the deconjugation of the enone **4***b* by potassium *tert*-amylate (7), which gave the β,γ-enone **6** in high yield. This reaction must be performed in a rigorously inert atmosphere. Sodium borohydride reduction of **6** leads to the homoallylic alcohol **7** and the A ring was then opened by cleavage of the double bond with ozone. Cautious work-up gave a product that was partly the β-hydroxy ketone **8** but, as anticipated, the latter dehydrated almost spontaneously; we therefore found it expedient to isolate only the conjugated enone **9**, by stirring the material in dichloromethane containing acetic acid until tlc showed the presence of but one product. The ring B double bond was easily hydrogenated to the diketone **10** in which the two carbonyls should show markedly different reactivity due to the sterically imposing quaternary carbon adjacent to the ring ketone. The reduction of the enone **9** afforded a second product that turned out to be the hydroxy ketone **13***a* (see later).

Since we needed to retain a function in the B ring while transforming the sidechain, it was necessary to provide adequate protection, which was achieved in the following manner. Mild conditions (ethylene glycol, BF_3-etherate at −9°C) (8) afforded the monoketal **11** with barely a trace of the diketal. The remaining hindered carbonyl was then reduced with lithium aluminium hydride, giving exclusively the hydroxy compound **12***a*. After acetylation to **12***b*, the ketal residue was hydrolysed to give the acetoxy ketone **13***b*, which proved to be identical

[1]The structure of edulone A has been revised very recently, see ref. 12.

[2]Author to whom correspondence may be addressed.

[3]DDQ: 2,3-dichloro-5,6-dicyano-*p*-benzoquinone; DBU: 1,8-diazabicyclo[5.4.0]undec-7-ene; DBN: 1,5-diazabicyclo[4.3.0]non-5-ene.

Can. J. Chem. Downloaded from www.nrcresearchpress.com by 80.58.250.72 on 09/07/12
For personal use only.

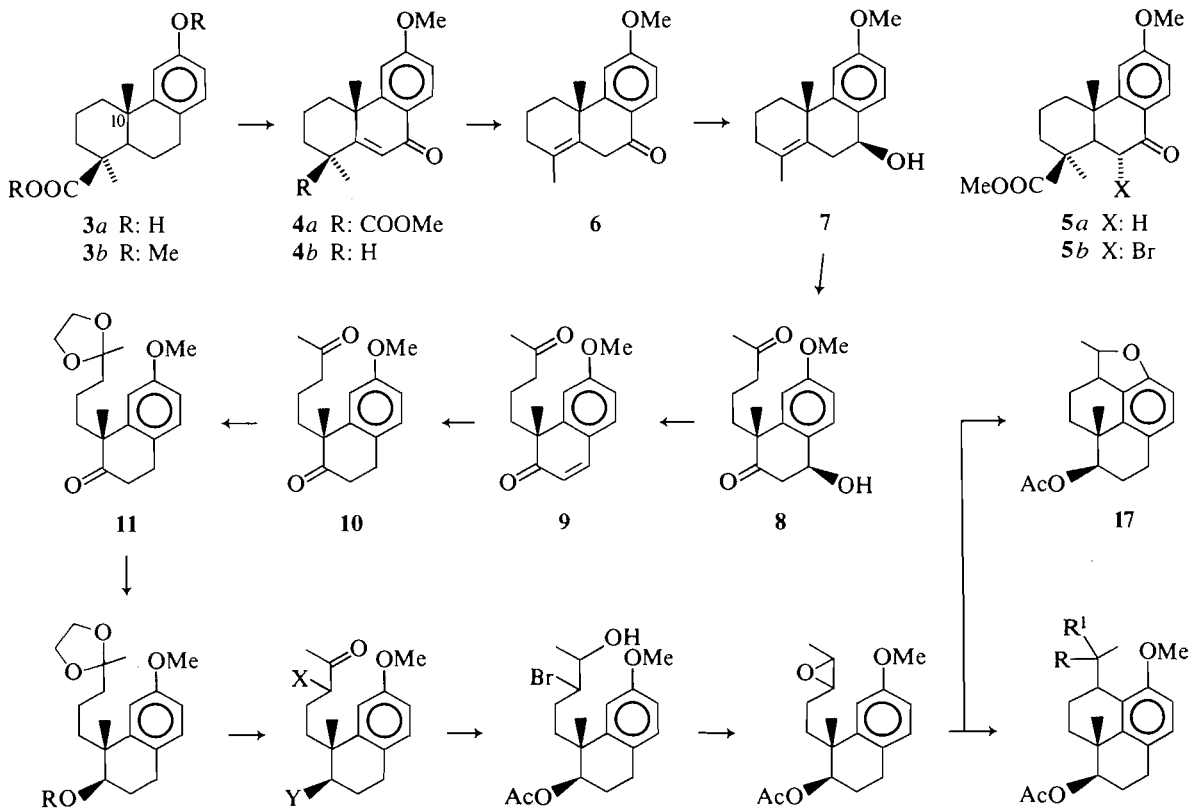

with the product obtained by acetylating the hydroxy ketone **13***a* referred to above.

Using the copper bromide technique (6), the ketone **13***b* was brominated selectively at the methylene group to afford **13***c*, which, when reduced with sodium borohydride, afforded only a 15% yield of the bromohydrin **14** since the major part of the product had precociously formed the mixture of stereoisomeric epoxides **15**. Cyclization of the latter was promoted by stannic chloride (9) and gave rise to the tricyclic hexahydrophenalene alcohol **16***a* (58%), which, for easier characterization, was oxidized (10) to the methyl ketone **16***b* (thus eliminating some of the diastereomeric possibilities). A second product, also obtained from the cyclization, was shown to be the tetracyclic dihydrobenzofuran **17** (38%). The distribution of products was not altered by lowering the temperature of the cyclization reaction, which suggests that the stereochemistry of the epoxide dictates the outcome of the process. Examination of molecular models does not immediately reveal which of the four epoxides should suffer subsequent cyclization but it seems likely that the terminal methyl, arising from the electrophilic opening of the epoxide, forces the still complexed potential hydroxyl residue close to the aromatic methoxyl residue to provoke the ready cyclization.

These model results assured us that an approach to the synthesis of edulone A based on Eugster's suggested biosynthetic pathway has a good chance of success. Our efforts are now directed towards preparing, from podocarpic acid, the suitably functionalized aromatic starting material for the total synthesis.

Experimental

Unless otherwise stated, the conditions and instruments used to characterize the products were the following: melting points, Electrothermal, uncorrected; ultraviolet spectra, ethanol solutions (log ε in parentheses), Hewlett Packard 8450A; infrared spectra, solids as KBr pellets, others as carbon tetrachloride solutions, Beckman 4250 and Perkin Elmer 457; proton magnetic resonance spectra, deuteriochloroform solutions, TMS internal standard, (multiplicity, integrated peak areas, and, where important, coupling constants and assignments in parentheses: D_2O infers that resonances were no longer detectable after shaking the solution for a few minutes with deuterium oxide), Bruker HX 90 and Varian XL-200; carbon-13 magnetic resonance spectra, deuteriochloroform solutions, TMS internal standard, Bruker WP 80; the peaks were assigned after recording the ^{1}H-decoupled and the off-resonance spectra, by comparison with the spectra of the many similar compounds previously described (2*a*–*d*) and by calculation using standard empirical parameters (11); mass spectra, Hewlett Packard 5992; high resolution mass spectra were recorded on an AEI MS30. Elemental analyses were by Galbraith Laboratories, Knoxville, Tenn.

Dry column chromatography (abbreviated dry col chrom) implies the use of Merck Kieselgel 60F (70–230 mesh) in Nylon foil tubing and development with either hexane – ethyl acetate or carbon tetrachloride – ethyl acetate (proportions determined by prior thin-layer chromatography using Machery–Nagel precoated plastic sheets).

9-Oxo-6-methoxy-1,4a(S)-dimethyl-2,3,4,4a,9,10-hexahydrophenanthrene (6)

Potassium (15.1 g) was added to *tert*-amyl alcohol (500 mL) in small amounts and the resulting solution was refluxed for 12 h under argon. The conjugated enone **4***b*, prepared as described in the literature (3, 4) (6.59 g), was added to the cooled amylate solution and the mixture was stirred at room temperature for 48 h. The solution changed color to become red and finally almost black. Under cooling, the reaction was neutralized with 10% acetic acid (300 mL, added rapidly) and the whole was then poured into saturated sodium bicarbonate solution, extracted with ether, dried over magnesium sulfate, evaporated, and chromatographed (silica gel, CCl_4 with 10% EtOAc). This afforded the deconjugated enone **6** (4.73 g; 72%) as a pale yellow solid, mp

Can. J. Chem. Downloaded from www.nrcresearchpress.com by 80.58.250.72 on 09/07/12
For personal use only.

Can. J. Chem. Downloaded from www.nrcresearchpress.com by 80.58.250.72 on 09/07/12
For personal use only.

114–118°C; uv: 226 (10 700), 278 (11 400), and 287 (10 300) nm; ir: 1680, 1600, and 790 cm^{-1}; ^1H nmr δ: 1.45 (s, Me-C10), 1.68 (s br, Me-C4), 3.29 and 3.63 (ABq, J = 18 Hz, H_2-C6), 3.86 (s, Me-O), 6.82 (dd, J = 2.5 and 9 Hz, H-C13), 6.89 (d, J = 2.5 Hz, H-C11), and 7.97 (d, J = 9 Hz, H-C14); ms m/z: 256 (20, M^+), 242 (14), 241 (100), 223 (8), 213 (9), 211 (7), and 198 (6). *Exact Mass* calcd. for $C_{17}H_{20}O_2$: 256.1464; found (hrms): 256.1462 (base peak calcd. for $C_{16}H_{17}O_2$: 241.1229; found: 241.1246, $M^+ - CH_3$); ^{13}Cmr, see Table 1.

6-Methoxy-9(S)-hydroxy-1,4a(S)-dimethyl-2,3,4,4a,9,10-hexahydrophenanthrene (7)

To the ketone **6** (4.66 g) in methanol (100 mL) was added sodium borohydride (0.73 g) in small portions. After stirring the solution for 3 h, it was poured into water and extracted with ether. The yellow solid obtained by evaporation was chromatographed (silica gel, CCl_4 with 10% EtOAc) to give the homoallylic alcohol **7** (4.35 g; 93%); ir: 3450, 1600, and 1570 cm^{-1}; ^1H nmr δ: 1.47 (s, Me-C10), 1.77 (s br, $w_{1/2}$ = 3 Hz, Me-C4), 3.18 (dd, J = 12 and 6 Hz, H_{eq}-C6), 3.93 (s, Me-O), 4.75 (dd, J = 11 and 6 Hz, H-C7), 6.73 (dd, J = 7.5 and 2.5 Hz, H-C13), 6.79 (d, J = 2.5 Hz, H-C11), and 7.50 (dd, J = 7.5 and 1 Hz, H-C14); ms m/z: 258 (18, M^+), 243 (34), 240 (17), and 225 (100); ^{13}Cmr, see Table 1.

Ozonolysis of the homoallylic alcohol 7

A solution of the alcohol **7** (1.72 g) in dichloromethane (500 mL) was cooled to −78°C and a current of oxygen containing about 3% ozone was bubbled through for 20 min. Dimethyl sulfide was added (5 mL) and the solution was allowed to warm to room temperature when a saturated solution of potassium iodide (30 mL, aqueous) and acetic acid (5 mL glacial) was added. The mixture was stirred for 45 min and then washed with saturated sodium thiosulfate solution. The organic phase was dried ($MgSO_4$), evaporated, and the residue purified by dry col chrom (silica gel, CCl_4 with 15% EtOAc) to give enone **9** (762 mg; 42%) and the β-hydroxy ketone **8** (575 mg; 30%). The latter was quantitatively converted to the enone by taking it up in dichloromethane containing a trace of glacial acetic acid and stirring at room temperature. The enone **9** was a colorless oil; uv: 221 (16 000), 245 (13 700), and 342 (12 300) nm; ir: 3005, 1710, 1650, 1620, and 1605 cm^{-1}; ^1H nmr δ: 1.38 (s, Me-C10), 2.02 (s, Me-C=O), 2.28 (t, J = 7 Hz, CH_2—C=O), 3.89 (s, Me-O), 6.07 (d, J = 9.5 Hz, H-C6), 6.82 (dd, J = 8 and 2.5 Hz, H-C13), 6.99 (d, J = 2.5 Hz, H-C11), 7.29 (d, J = 8 Hz, H-C14), and 7.42 (d, J = 9.5 Hz, H-C7); ms m/z: 272 (4, M^+), 214 (2), and 188 (100). *Exact Mass* calcd. for $C_{17}H_{20}O_3$: 272.1412; found (hrms): 272.1411 (base peak calcd. for $C_{12}H_{12}O_2$: 188.0837; found: 188.0821); ^{13}Cmr, see Table 1.

Catalytic hydrogenation of the enone 9

The enone **9** (762 mg) in ethyl acetate (30 mL) was shaken with 10% palladium on charcoal (100 mg) under hydrogen at 40 psi (1 psi = 6.9 kPa) during 1 h. After filtering the catalyst and evaporating the solvent, the residue was purified by dry col chrom (silica gel, CCl_4 with 25% EtOAc) affording, as the less polar product, *1-(4'-oxopentyl)-2-oxo-7-methoxy-1(R)-methyl-1,2-dihydronaphthalene* ***10*** (479 mg; 63%) as a viscous oil; uv: 220 (20 000), 280 (6 000), and 287 (5 400) nm; ir: 1705, 1605, and 1570 cm^{-1}; ^1H nmr δ: 1.38 (s, Me-C10), 2.06 (s, Me-C=O), 2.33 (t, J = 7 Hz, CH_2—C=O), 2.62 (dd, J = 7.5 and 6 Hz, H-C7), 2.66 (dd, J = 7.5 and 5.5 Hz, H-C7), 2.99 (2H, dd, J = 11.5 and 5.5 Hz, H_2-C6), 3.84 (s, Me-O), 6.77 (dd, J = 8 and 3 Hz, H-C13), 6.88 (d, J = 3 Hz, H-C11), and 7.13 (d, J = 8 Hz, H-C14); ms m/z: 274 (25, M^+), 256 (60), 216 (2), 189 (100), and 175 (11). *Exact Mass* calcd. for $C_{17}H_{22}O_3$: 274.1569; found (hrms): 274.1578 (base peak calcd. for $C_{12}H_{13}O_2$: 189.0916; found: 189.0889); ^{13}Cmr, see Table 1.

The chromatogram afforded a more polar compound, *1-(4'-oxopentyl)-2-hydroxy-7-methoxy-1(R)-methyl-1,2-dihydronaphthalene* ***13***a, as a slightly yellow oil (229 mg; 30%); ir (film): 3460, 1700, and 1605 cm^{-1}; ^1H nmr δ: 1.24 (s, Me-C10), 2.11 (s, Me—C=O), 3.13 (br s, OH, D_2O), 3.81 (s, Me-O), 3.94 (m, H-C5), 6.63 (dd, J = 8 and 3 Hz, H-C13), 6.80 (d, J = 3 Hz, H-C11), and 6.97 (d, J = 8 Hz, H-C14); ms m/z: 276 (8, M^+), 258 (4, $M - H_2O$), 243 (3), 200 (4), 186 (4), and 173 (64). *Exact Mass* calcd. for $C_{17}H_{24}O_3$: 276.1726; found (hrms): 276.1729 (base peak calcd. for $C_{12}H_{13}O$: 173.0966; found: 173.0968). Acetylation of this alcohol ***13****a* using acetic anhydride – pyridine gave an acetate, which is described later; ^{13}Cmr, see Table 1.

Monoketalization of the diketone 10

The diketone **10** (203 mg) was dissolved in dichloromethane (20 mL) containing ethylene glycol (5 mL) and the solution cooled to −9°C (ice; isopropanol). Boron trifluoride etherate (0.4 mL) was added and stirring was continued for 5 h, after which the reaction mixture was poured into water and extracted with dichloromethane. After washing, drying, and evaporating, the residue was chromatographed over silica gel (hexane:EtOAc 6:4) to give the ketal **11** (198 mg; 84%: *1-(4',4'-ethylenedioxypentyl)-7-methoxy-1(R)-methyl-2-tetralone)*, as a colorless oil; uv: 220 (8 600), 279 (2 800), and 286 (2 500) nm; ^1H nmr δ: 1.22 and 1.41 (2s, Me-C), 3.89 (s, Me-O), 3.92 (m, 4H, —OCH_2CH_2O—), 6.74 (dd, J = 8 and 3 Hz, H-C13), 6.87 (d, J = 3 Hz, H-C11), and 7.08 (d, J = 8 Hz, H-C14); ms m/z: 318 (1.2), 303 (1.4), 190 (60), 161 (16), and 87 (100). *Exact Mass* calcd. for $C_{19}H_{26}O_4$: 318.1831; found (hrms): 318.1815; ^{13}Cmr, see Table 1.

Reduction of ketone 11

Lithium aluminium hydride (14 mg) was added slowly to a solution of ketone **11** (72 mg) in dry ether (20 mL). After 12 h of stirring, the excess hydride was decomposed by adding water and the product was obtained by extraction into ether. Chromatography of the crude material (silica gel, CCl_4 with 25% EtOAc) afforded the alcohol ***12****a* (64 mg; 88%: *1-(4',4'-ethylenedioxypentyl)-7-methoxy-2-hydroxy-1(R)-methyl-1,2,3,4-tetrahydronaphthalene)*, colorless oil; ir: 3380, 1605, and 1565 cm^{-1}; ^1H nmr δ: 1.25 and 1.28 (2s, Me-C), 2.30 (br s, OH, D_2O), 3.79 (s, Me-O), 3.92 (br s, —OCH_2CH_2O—), arom. protons at 6.72 (dd, J = 8 and 2.5 Hz), 6.91 (d, J = 2.5 Hz), and 7.04 (d, J = 8 Hz); ms m/z: 320 (1.1), 258 (10), 200 (5), 188 (10), 174 (15), 173 (23), and 158 (15). *Exact Mass* calcd. for $C_{19}H_{28}O_4$: 320.1988; found (hrms): 320.1983 (also calcd. for $C_{12}H_{14}O$: 174.1045; found: 174.1034); ^{13}Cmr, see Table 1.

The alcohol ***12****a* (290 mg) was acetylated by stirring at room temperature for 18 h in pyridine (25 mL) containing acetic anhydride (11 mL). The reaction was stopped by pouring the mixture into ice/water and the product was extracted into ether, which was then well washed. The residue was chromatographed over silica gel (hexane:EtOAc 8:2) to give the acetate ***12****b* (293 mg; 89%: *1-(4',4'-ethylenedioxypentyl)-2(R)-acetoxy-7-methoxy-1(R)-methyl-1,2,3,4-tetrahydronaphthalene)*, as a colorless oil; ir: 1730, 1605, 1565, and 1240 cm^{-1}; ^1H nmr δ: 1.28 and 1.29 (2s, Me-C), 2.08 (s, Me—C=O), 3.83 (s, Me-O), 3.96 (br s, —OCH_2CH_2O—), 5.12 (dd, J = 6 and 3.5 Hz, H-C5), arom. protons at 6.67 (dd, J = 8 and 3 Hz), 6.83 (d, J = 3 Hz), and 6.99 (d, J = 8 Hz); ms m/z: 362 (5, M^+), 347 (2), 302 (2), 240 (6), 225 (9), 200 (10), 173 (26), and 87 (100). *Exact Mass* calcd. for $C_{21}H_{30}O_5$: 362.2093; found (hrms): 362.2092; ^{13}Cmr, see Table 1.

*Hydrolysis of the ketal 12*b

Aqueous hydrochloric acid (15 mL of 2%) was added to a solution of the ketal ***12****b* (290 mg) in THF (40 mL). After stirring at room temperature for 15 h, the reaction mixture was poured into water and extracted with ether. After washing, drying, and evaporating, the residue was chromatographed over silica gel (hexane:EtOAc 8:2) to give the ketone ***13****b* (231 mg; 91%: *1-(4'-oxopentyl)-2(R)-acetoxy-7-methoxy-1(R)-methyl-1,2,3,4-tetrahydronaphthalene)*, as a colorless oil; ir: 1730, 1715, 1610, 1570, and 1240 cm^{-1}; ^1H nmr δ: 1.26 (s, Me-C10), 2.08 and 2.09 (2s, acetate and methyl ketone), 2.38 (t, J = 6.4 Hz, CH_2—C=O), 2.79 (2H, m, H_2-C7), 3.77 (s, Me-O), 5.00 (dd, J = 8.3 and 3.2 Hz, C*H*—OAc), 6.66 (dd, J = 8.3 and 2.5 Hz, H-C13), 6.77 (d, J = 2.2 Hz, H-C11), and 6.96 (d, J = 8.3 Hz, H-C14); ms m/z: 318 (2.1, M^+), 258 (5.3), 200 (7.2), 191 (11.4), 185 (14.2), 173 (100), and 158 (19.7). *Exact Mass* calcd. for $C_{19}H_{26}O_4$: 318.1831; found (hrms): 318.1827 (also calcd. for $C_{17}H_{22}O_2$ (M^+ −

Can. J. Chem. Downloaded from www.nrcresearchpress.com by 80.58.250.72 on 09/07/12
For personal use only.

TABLE 1. ^{13}C nuclear magnetic resonance data[a]

	Compound[b]																			
Carbon	**4***a*	**4***b*	**5***a*	**5***b*	**6**	**7**	**9**	**10**	**11**	**12***a*	**12***b*	**13***a*	**13***b*	**13***c*[c]		**14**[c]		**15**[c]	
1	40.2	41.4	38.6	37.0	29.5	29.9	41.3	38.6	38.7	26.6	38.5	27.1	26.9	27.3	27.4	27.7	27.5	27.1	26.7
2	19.3	22.2	19.8	19.4	19.5	19.2	19.5	19.7	19.9	23.9	21.1	25.0	23.7	26.3	26.1	23.7	23.9	23.2	23.0
3	37.4	37.2	37.7	38.4	32.6	32.0	43.7	43.8	40.8	40.0	40.2	44.0	44.3	55.4	55.7	67.1		52.7	
4	48.1	34.3	44.2	45.6	129.4	131.0	208.4	208.2	110.1	110.3	110.1	209.7	208.3	201.7	201.4	70.5	70.0	57.4	
5	164.4	170.2	50.6	49.0	128.8	132.4	204.3	214.3	214.5	73.5	76.1	73.1	76.1	76.1		76.1	76.0	76.2	
6	126.7	121.4	37.5	57.7	40.4	35.3	122.9	39.5	39.4	25.1	27.0	26.5	25.3	25.3		25.1		25.3	
7	184.2	184.3	197.1	193.2	195.9	70.0	145.3	27.4	27.0	37.5	38.5	29.9	29.9	29.4	29.2	30.9	30.6	29.7	
8	124.0	124.2	124.8	125.4	125.6	127.4	123.4	128.4	128.5	127.2	127.2	127.7	127.2	127.2		127.3		127.2	
9	154.9	154.9	157.1	154.0	155.9	149.0	148.5	143.4	143.9	144.9	144.6	144.7	144.2	143.5		143.9		143.9	
10	42.1	41.6	38.9	39.2	39.4	39.1	51.9	52.0	52.1	41.7	40.7	41.6	40.6	40.5		40.4		40.4	
11	111.9	111.0	110.1	109.1	110.6	111.3	112.0	112.1	111.8	111.6	111.7	111.4	111.7	112.0		112.0	111.8	111.8	
12	163.7	163.4	164.5	164.5	164.5	159.2	161.9	159.2	159.1	158.1	158.2	158.1	158.2	158.3		158.3		158.3	
13	113.1	113.0	112.2	112.0	111.7	112.0	113.3	112.7	112.8	113.0	112.6	113.0	112.2	112.5		112.6		112.7	
14	128.8	128.8	130.0	130.7	129.6	127.0	131.3	129.3	129.1	129.9	129.8	129.9	129.9	130.1		130.0		130.0	
18	28.0	18.4	28.0	29.4	37.0	38.2	29.6	29.6	23.8	26.5	25.2	37.0	37.8	35.9	36.1	36.5		13.2	
19	175.7	—	177.0	177.1	—	—	—	—	—	—	—	—	—	—		—		—	
20	27.4	27.1	21.5	24.7	19.5	19.2	29.3	27.8	27.8	19.0	23.6	18.6	21.2	23.9		21.2		23.7	
O-Me	55.5	55.5	55.4	55.5	55.5	55.2	55.5	55.5	55.5	55.4	55.3	55.4	55.4	55.4		55.4		55.4	
Others	52.0	—	51.4	52.0	—	—	—	—	64.7	64.7	64.7								
											170.7		170.8	170.6		170.8		170.8	
											19.0		19.0	21.3		21.0		21.2	

[a]In ppm from TMS.
[b]The carbon atoms are always numbered as a function of their "origin" in the abieta-8,11,13-triene skeleton.
[c]Some of the signals are "doubled" due to the presence of diastereomers.

CH_3COOH): 258.1620; found: 258.1616 and, for base peak, calcd. for $C_{12}H_{13}O$: 173.0966; found: 173.0949); ^{13}Cmr, see Table 1.

Bromination of the methyl ketone ***13****b*

The methyl ketone **13***b* (229 mg) was dissolved in a mixture of chloroform and ethyl acetate (12.5 mL of each), and cupric bromide (209 mg) was added. The mixture was refluxed for 18 h with efficient stirring, cooled, filtered, and evaporated. Chromatography (silica gel, CCl_4 with 10% EtOAc) allowed the isolation of some starting material (36 mg) and then the bromo-ketone **13***c* (222 mg; 78%, which rises to 92% if the recovery of the starting material is considered); ir: 1725; 1605, and 1570 cm^{-1}; ^{1}H nmr δ: 1.30 (s, Me-C10), 2.12 (s, O—CO—CH_3), 2.36 (s, methyl ketone), 3.87 (s, Me-O), 4.24 (m, —C*H*—Br), 5.11 (dd, J = 5.5 and 4.5 Hz, —C*H*—OAc), aromatic protons at 6.71 (dd, J = 8 and 2.5 Hz, 6.78 (d, J = 2.5 Hz), and 7.03 (d, J = 8 Hz); ms m/z: 398 and 396 (0.4, M^+), 257 (9.5), 213 (7.8), 191 (13.1), 187 (13.5), 174 (20.1), 173 (100), and 158 (32.4). *Exact Mass* calcd. for $C_{19}H_{25}O_4Br$: 398.0916 and 396.0936; found (hrms): 398.0914 and 396.0914; ^{13}Cmr, see Table 1.

Borohydride reduction of the α-bromo-ketone ***13****c*

To the bromo-ketone **13***c* (84 mg) in methanol (20 mL) was added sodium borohydride (13 mg) and the mixture was stirred at room temperature for 3 h. After diluting with water, the crude product was extracted into ether and the residue purified by dry col chrom (CCl_4 with 10% EtOAc) affording two products:

Epoxide ***15***, colorless oil (50 mg; 75%); ir: 1735, 1610, and 1575 cm^{-1}; ^{1}H nmr δ: 1.23 (d, J = 7 Hz, Me-CH), 1.28 (s, Me-C10), 2.08 (s, acetate), 3.82 (s, Me-O), 5.03 (dd, J = 5.5 and 4 Hz, C*H*—OAc), 6.70 (dd, J = 8 and 3 Hz, H-C13), 6.83 (d, J = 3 Hz, H-C11), and 7.05 (d, J = 8 Hz, H-C14); ^{13}Cmr, see Table 1.

Bromohydrin ***14***, colorless oil (13 mg; 15%); ir: 1725, 1610, and 1575 cm^{-1}; ^{1}H nmr δ: 1.27 (d, J = 7 Hz, Me—C*H*(OH)-), 1.30 (s, Me-C10), 2.10 (s, acetate), 3.82 (s, Me-O), 5.03 (dd, J = 5 and 4 Hz, C*H*—OAc), aromatic protons at 6.72 (dd, J = 8 and 2.5 Hz), 6.87 (d, J = 2.5 Hz), and 7.05 (d, J = 8 Hz); ms m/z: 400 and 398 (0.1, M^+), 241 (3.6), 225 (2.8), 213 (3.9), 191 (16.1), 185 (16.6), 173 (100), 171 (16.7), 158 (27.6), and 145 (8.6); ^{13}Cmr, see Table 1.

Cyclization of epoxide ***15***

To the epoxide **15** (50 mg) in dichloromethane (40 mL, anhydrous) was added stannic chloride dissolved in dichloromethane (0.3 mL of 1 *M*) and the mixture was then refluxed for 90 min. The cooled solution was poured into ice/water and extracted with more dichloromethane. Evaporation gave a mixture of two products (tlc), which were separated by dry col chrom (CCl_4 with 10% EtOAc):

Alcohol ***16****a*, colorless oil (29 mg; 58%: *4-(1'-hydroxyethyl)-7(*R*)-acetoxy-3-methoxy-6a(*R*)-methyl-4,5,6,6a,7,8-hexahydro[1*H*]phenalene)*; ir: 3450, 1730, 1610, and 1595 cm^{-1}; ^{1}H nmr δ: 1.15 (s, Me-C), 1.28 (br s, $w_{1/2}$ = 6 Hz, Me—CH(OH)—), 1.95 (s, acetate), 3.83 (s, Me-O), 5.03 (m, C*H*—OAc), 6.73 (d, J = 8 Hz, H-C13) and 7.03 (d, J = 8 Hz, H-C14).

Benzodihydrofuran ***17***, colorless oil (18 mg; 38%: *5(*R*)-acetoxy-2,4a(*R*)-dimethyl-2,2a,3,4,4a,5,6,7-octahydrophenaleno[1,9-*bc*]furan)*; ir: 1730, 1630, and 1600 cm^{-1}; ^{1}H nmr δ: 1.16 (s, Me-C), 1.61 (d, J = 6 Hz, Me-CH), 1.97 (s, acetate), 4.52 (m, Me—C*H*-O-), 5.19 (dd, J = 3.5 and 3 Hz, C*H*—OAc), 6.46 (d, J = 8 Hz, H-C13), and 6.78 (d, J = 8 Hz, H-C14); ms m/z: 286 (11.6, M^+), 243 (1.1), 227 (12.7), 226 (66.2), 212 (16.7), 211 (88.7), 193 (23), 183 (36), and 171 (30.3). *Exact Mass* calcd. for $C_{18}H_{22}O_3$: 286.1569; found (hrms): 286.1555.

Oxidation of alcohol ***16****a*

Pyridinium dichromate (37 mg) was added to a solution of the alcohol **16***a* (29 mg) in dichloromethane (10 mL). After vigorous stirring for 22 h the reaction mixture was diluted with ether and the precipitated solids removed by filtration. The brownish oil obtained by evaporation was purified by dry col chrom (CCl_4 with 25% EtOAc), which afforded the methyl ketone **16***b* (24 mg; 84%: pale yellow oil); ir: 1722 (br) cm^{-1}; ^{1}H nmr δ: 1.18 and 1.25 (2s, Me-C), 1.96 (s, CH_3—C=O), 2.14 and 2.20 (2s, $OCOCH_3$), 2.88 (m, 2H, H_2-C7), 3.73 and 3.74 (2s, Me-O), 3.94 (m, 1H, H-C3), 5.02 (t, J = 2.9 Hz, *H*—C—OAc), 6.68 (dd, J = 8.3 and 2.5 Hz, H-C14), and 7.00 (dd, J = 8.3 and 0.95 Hz, H-C13); ms m/z: 316 (9.6, M^+), 273 (9.5, M − 43), 256 (7.6), 213 (87.5), 198 (10.0), 187 (10.8), 185 (12.8), 171 (100), and 165 (12.8). *Exact Mass* calcd. for $C_{19}H_{24}O_4$: 316.1675; found (hrms): 316.1669.

Acknowledgments

We thank the Natural Sciences and Engineering Research Council of Canada and the Ministère de l'éducation du Québec for operating and equipment grants. A graduate bursary (F.C.A.R., Québec) is also gratefully acknowledged.

1. G. Buchbauer, P. Ruedi, and C. H. Eugster. Helv. Chim. Acta, **61**, 1969 (1978).
2. (*a*) R. H. Burnell, A. Andersen, M. Neron, and S. Savard. Can. J. Chem. **63**, 2769 (1985); (*b*) R. H. Burnell, M. Jean, D. Poirier, and S. Savard. Can. J. Chem. **62**, 2822 (1984); (*c*) R. H. Burnell, M. Jean, and S. Savard. Can. J. Chem. **61**, 2461 (1983); (*d*) R. H. Burnell, A. Andersen, M. Neron-Desbiens, and S. Savard. Can. J. Chem. **59**, 2820 (1981).
3. J. W. A. Findlay and A. B. Turner. J. Chem. Soc. (C), 547 (1971).
4. E. J. Parrish, B. S. Huang, and D. H. Miles. Synth. Commun. **5**, 341 (1975).
5. R. C. Cambie, L. N. Mander, A. K. Bose, and N. S. Mankas. Tetrahedron, **20**, 409 (1964).
6. L. C. King and G. Ostrum. J. Org. Chem. **29**, 3459 (1964).
7. (*a*) S. K. Malhotra and H. J. Ringold. J. Am. Chem. Soc. **87**, 3228 (1965); (*b*) J. Am. Chem. Soc. **86**, 1997 (1964); (*c*) J. Am. Chem. Soc. **85**, 1538 (1963); (*d*) Tetrahedron Lett. 669 (1962); (*e*) J. Am. Chem. Soc. **84**, 3402 (1962).
8. J. S. Swenton, R. M. Blankenship, and R. Sanitra. J. Am. Chem. Soc. **97**, 4941 (1975).
9. S. K. Taylor, G. H. Hockerman, G. L. Karrick, S. B. Lyle, and S. B. Schramm. J. Org. Chem. **48**, 2449 (1983).
10. E. J. Corey and G. Schmidt. Tetrahedron Lett. 399 (1979).
11. F. W. Wehrli and T. Wirthlin. Interpretation of carbon-13 NMR spectra. Heydon, New York. 1976.
12. J. M. Künzle, P. Rüedi, R. Prewo, and C. H. Eugster. Helv. Chim. Acta, **69**, 1513 (1986).

Can. J. Chem. Downloaded from www.nrcresearchpress.com by 80.58.250.72 on 09/07/12
For personal use only.

The formylacetate synthon. Studies related to the synthesis of the penam and oxapenam ring systems

SAUL WOLFE AND ROMAN Z. STERZYCKI
Department of Chemistry, Queen's University, Kingston, Ont., Canada K7L 3N6

Received May 29, 1986

This paper is dedicated to Dr. O. E. (Ted) Edwards

SAUL WOLFE and ROMAN Z. STERZYCKI. Can. J. Chem. **65**, 26 (1987).

Methyl penicillanate has been synthesized by condensation of D-penicillamine with three different variations of the synthon RO_2CCH_2CHO, followed by esterification of the resulting 4-carboxythiazolidine-2-acetic acid ester, removal of R, and Mukaiyama ring closure. The conditions for the synthesis of an analogous 4-carboxyoxazolidine-2-acetic acid ester, containing an *N*-benzoyl protecting group, have been worked out. The condensation of threonine with diethinylketone does not lead directly to a vinylogous oxapenam.

SAUL WOLFE et ROMAN Z. STERZYCKI. Can. J. Chem. **65**, 26 (1987).

On a réalisé la synthèse du pénicillanate de méthyle en procédant à une condensation de la D-pénicillamine avec trois variations différentes du synthon RO_2CCH_2CHO, suivie d'une estérification de l'ester de l'acide carboxy-4 thiazolidine acétique-2 qui en resulte, d'une élimination du groupement R et d'une cyclisation selon la méthode de Mukaiyama. On a aussi mis au point les conditions permettant de réaliser la synthèse d'un ester analogue de l'acide carboxy-4 oxazolidine acétique-2 contenant un groupement protecteur *N*-benzoyle. La condensation de la thréonine avec la diéthinylcétone ne conduit pas directement à la formation de l'oxapénam vinylogue.

[Traduit par la revue]

The biosynthesis of clavulanic acid (**1**) proceeds via a 5-carbon precursor (most probably L-ornithine (1)) and a 3-carbon precursor (most probably 3-hydroxypropionate (2, 3)). Since the bridgehead carbon atom (C5) of clavulanic acid is a masked aldehyde, and the 3-carbon moiety formylacetate (**2**, X = Y = H) has the required oxidation level, the condensations depicted in **3** and **4** could have biomimetic relevance. However,

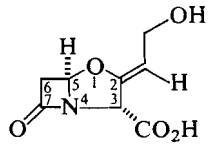

1

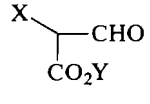

2

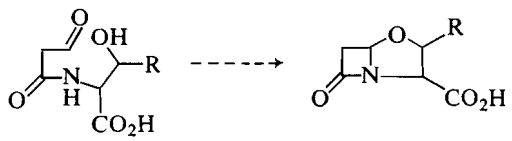

3

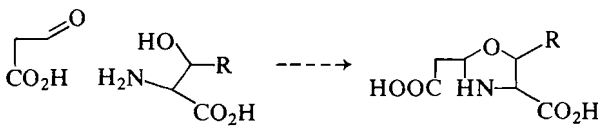

4

monocyclic oxazolidine-4-carboxylic acids are not stable in aqueous solution below pH 7, and can be characterized only following N-acylation (**5**) (4). In addition, although formylacetic acid (malonaldehydic acid) is a known biochemical substrate (5), it must be prepared *in situ*, in dilute aqueous solution, and used rapidly. Accordingly, a realization of **3** or **4** will require attention to two problems: the development of an effective equivalent to formylacetate, and the development of conditions or protecting groups to stabilize an appropriately substituted monocyclic oxazolidinecarboxylic acid at an intermediate stage of a synthetic sequence. This manuscript is

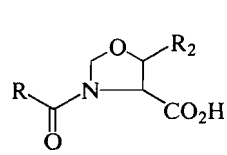

5

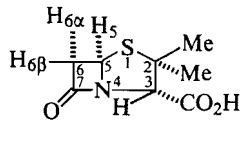

6

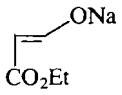

7

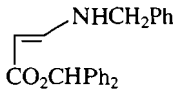

8

concerned with **4**, and reports a solution to the first problem, exemplified by a successful synthesis of methyl penicillanate, and a partial solution to the second.

Like clavulanic acid, penicillanic acid (**6**) contains a formylacetate skeleton at C5—C7 but, in this case, the condensation of a mercaptoamino acid with an aldehyde leads to a chemically stable *thia*zolidine-4-carboxylic acid (6). Indeed, Sheehan's celebrated total synthesis of penicillin (7) begins with the condensation of the aldehyde **2** (X = phthalimido, Y = *tert*-butyl) with D-penicillamine. However, despite this precedent, a synthesis of **6** from the parent aldehyde **2** (X = Y = H) or its equivalent has not yet been completed (8).

Following Vanderhaeghe and co-workers (8*a*), we first examined the reaction of D-penicillamine with the synthons **7** (9) and **8**. Since the enamine **8** is obtained easily by addition of benzylamine to benzhydryl propiolate (**9**), it was then realized (correctly (8*b*)) that **9** may condense with penicillamine without prior activation.

Table 1 summarizes reactions of penicillamine with **7**, **8**, and **9** to form the thiazolidines **10**, as approximately 1:1 mixtures of C5 epimers.[1] Vanderhaeghe and co-workers had found that the epimers of the ethyl ester **10***a* could not be separated by chromatography on a Lobar RP8 column. In the present work, complete separation of C5 epimers was possible on a Lobar

[1]Penicillin numbering is employed. See **6**.

Can. J. Chem. Downloaded from www.nrcresearchpress.com by 80.58.250.72 on 09/07/12
For personal use only.

TABLE 1. Condensation of D-penicillamine with various formylacetate equivalents

Reactant	Solvent	Time (h)	Additional reagents (equiv.)	Product (% yield)
7	EtOH–H_2O (1:1)	16	None	**10***a* (10)
	H_2O (pH 6)	40	*p*-TsOH (1)	**10***a* (18)
8	THF–H_2O (1:1)	16	Na_2CO_3 (1)	(0)
	EtOH–H_2O (1:1)	16	None	**10***b* (47)
	DMF–H_2O (1:1)	16	HCl (1.5)	**10***b* (51)
	DMF–H_2O (2:1)	16	*p*-TsOH (1)	**10***b* (80)
	DMF–H_2O (3:2)	16	*p*-TsOH (1)	**10***b* (85)
9	DMF	16	None	**10***b* (56)

LiChroprep Si60 column, following esterification of **10***b* to **11** (**11***a,b*: CH_2N_2, 2:1 methylene chloride – methanol (10); **11***c,d*: *p*-nitrobenzyl bromide – triethylamine – acetonitrile). The esters **11** could be deprotected selectively at C7,[1] using 98% formic acid (11), to give C3-protected[1] thiazolidineacetic acids **12**.

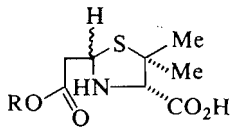

10*a*: R = Et
b: R = $CHPh_2$

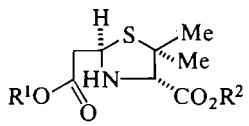

11*a*: $R^1 = CHPh_2$; $R^2 = CH_3$
c: $R^1 = CHPh_2$; R^2 = *p*-nitrobenzyl

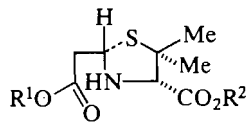

11*b*: $R^1 = CHPh_2$; $R^2 = CH_3$
d: $R^1 = CHPh_2$; R^2 = *p*-nitrobenzyl

12*a*: R^1 = H; $R^2 = CH_3$
c: R^1 = H; R^2 = *p*-nitrobenzyl

12*b*: R^1 = H; $R^2 = CH_3$
d: R^1 = H; R^2 = *p*-nitrobenzyl

Cyclization to the penam ring system was pursued with the methyl esters **11***a,b* and **12***a,b*, under four sets of conditions: (*A*) PhMgBr (on **11***a,b*) (12); (*B*) benzotriazolyl *N*-oxytrisdimethylaminophosphonium hexafluorophosphate (BOP) (on **12***a,b*) (13); (*C*) methanesulfonyl chloride – potassium bicarbonate – tetrabutylammonium bisulfate under phase transfer conditions (on **12***a,b*) (14); (*D*) triphenylphosphine – 2-mercaptopyridine disulfide – acetonitrile (on **12***a,b*) (15).

The Mukaiyama phase transfer procedure (*C*) led to 20% isolated yields of the 5*R*-penicillanate **13**, and the 5*S*-penicillanate **14**. The Ohno method (*D*) afforded only 2% isolated

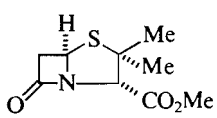

13

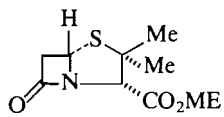

14

yields of penicillanates; this compares to the 8–9% yields obtained with this procedure in the parent system lacking a carboxyl group (8*b*). Grignard cyclization (*A*) produced less than 1% of penicillanates; and the BOP reagent (*B*) gave no β-lactam containing products.

The ^{1}Hmr spectrum of **14**, but not **13**, shows long-range coupling (1.4 Hz) between H3 and H6β. This confirms the configurational assignment for this compound and, therefore, that of its thiazolidineacetic acid precursor. In each of **11–14**, H3 is at higher field when it is *cis* to H5 (16).

Sulbactam (penicillanic acid sulfone) is a potent β-lactamase inhibitor (17). Although the β-lactam forming step of the present synthesis proceeds in low yield, it is reproducible, and the sequence is easily accomplished and applicable to syntheses of ^{14}C-labelled analogs of Sulbactam and its C5 epimer.

Following these exploratory studies, condensation reactions of **7–9** were reexamined, with L-threonine or its methyl ester as the substrate in place of D-penicillamine. With the conditions of the earlier oxazolidine synthesis as a precedent (4), the salt **7** was allowed to react with threonine in water, and the reaction mixture was then benzoylated (PhCOCl, $NaHCO_3$, acetone). Exhaustive chromatography was necessary to obtain the oxazolidine **15***a*, in only 8% yield.

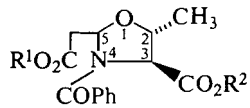

15*a*: R^1 = Et; R^2 = H
b: $R^1 = Ph_2CH$; $R^2 = CH_3$

The enamine **8** is a crystalline compound, but its ^{1}Hmr spectrum in chloroform solvent changes with time, from that of the *E*-isomer (7.61 ppm, 1H, q, 8.0, 14.0 Hz, =CHN; 4.92 ppm, 1H, d, 14.0 Hz, =CHC) to that of a 1:3 *E*:*Z* mixture (*Z*-isomer: 6.70 ppm, 1H, q, 8.0, 14.0 Hz, =CHN; 4.72 ppm, 1H, d, 8.0 Hz, =CHC). This spectral information facilitated the structural determination of the complex mixture of products formed initially in the reactions of **8** and **9** with threonine.

Treatment of threonine with **8** (DMF–H_2O, 3:2), at room temperature, followed by benzoylation (PhCOCl, $NaHCO_3$, acetone) and esterification (CH_2N_2) of the acidic fraction, led to a 2:1 adduct (A_1) (38%), *which did not contain a benzoyl group*. Under slightly different conditions (DMF–H_2O, 3:2, 1 equiv. *p*-TsOH, then benzoylation and esterification as above), a different 2:1 adduct (A_2) (48%) could be isolated, and *this also lacked a benzoyl group*. The same adducts were obtained, but in lower yields, when the condensations were carried out with the synthon **9**.

The adduct A_1 was found to have the formula $C_{37}H_{35}NO_7$, and its mass spectrum contained a series of peaks corresponding to successive loss of Ph_2CH, CO_2, CH_2, and CO. The ^{1}Hmr spectrum featured an *E*-enamine vinyl moiety. Structure **16** is assigned to A_1; its configuration at C5[1] is uncertain, because only one epimer was isolated.

The adduct A_2 has two sets of vinyl protons (7.88, 4.62 ppm, J = 13.5 Hz; and 4.95 ppm, 4.54 ppm, J = 17.0 Hz), and it is assigned the acyclic structure **17**.

Can. J. Chem. Downloaded from www.nrcresearchpress.com by 80.58.250.72 on 09/07/12
For personal use only.

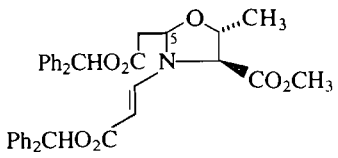

16

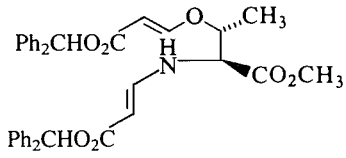

17

Treatment of the oxazolidine **16** with benzoyl chloride (CH_2Cl_2–*pyridine*) led to loss of the enamine moiety, and formation of the *N*-benzoyloxazolidine **15***b* as a single epimer, mp 123–124°C. The ^{1}Hmr spectrum of this compound was consistent with the structure assigned and, in addition, showed the expected evidence for restricted rotation about the amide bond (4).

Reaction of the methyl ester of threonine with **9** (CH_3CN, 20°C, 48 h) led to **16** (42%). However, this compound was not formed when *pyridine* was present in the reaction mixture (18). Instead, a mixture of three compounds (tlc) was produced, whose ^{1}Hmr spectrum was interpretable in terms of **17**–**19**.

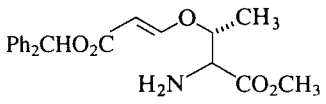

18

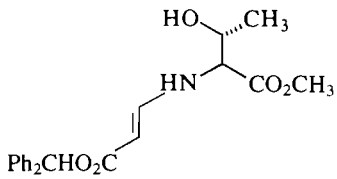

19

Addition of benzoyl chloride transformed this complex mixture to a single crystalline substance, the *N*-benzoyloxazolidine **15***b*.

The nitrogen atom of a 4-carboxyoxazolidine-2-acetic acid derivative thus seems to be an effective nucleophile for Michael addition reactions. It was therefore considered that the incorporation of two ethinyl acceptor groups into the same molecule, as in diethinylketone (**20**), might lead, via **21**, to a vinylogous oxapenam **22** (19).

The ketone **20** was synthesized by oxidation (MnO_2) of diethinylcarbinol (20). Condensation of **20** with the methyl ester of threonine in ether or ether–acetonitrile led to the same major product, isolable in 38–48% yield. This product did not contain an RCH_2CO moiety. Its infrared spectrum featured acetylene (2095 cm^{-1}), ester (1730 cm^{-1}), and enamine (1620 cm^{-1}) absorptions. The ^{1}Hmr spectrum confirmed the presence of a *Z*-enamine and an ethinyl group, with the ethinyl signal indicating the presence of a 2:1 mixture of isomers. The product is assigned structure **23**, a mixture of epimers at C5. The formation of **23** can be understood in terms of oxazolidine formation onto the carbonyl group of **24**, in preference to the cyclization **24** → **21**. Attempts to obtain a 1:1 adduct, by use of an excess of **20** in this reaction, have not been successful.

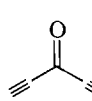

20

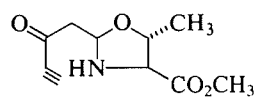

21

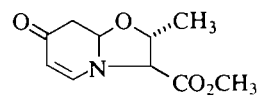

22

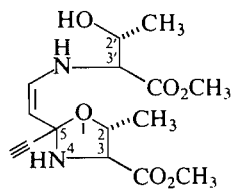

23

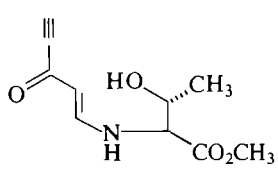

24

In summary, a strategy for bicyclic azetidinone synthesis, based on the formylacetate synthon, has been applied successfully to obtain a penam, and to reach the first (condensation) intermediate of a projected extension to an oxapenam. Whether such intermediates can be carried further will require the development of an appropriate alternative to benzoyl at the acylation stage.

Experimental

Solvents were routinely distilled before use, dried as required by standard methods (21), and stored over molecular sieves. Analytical thin-layer chromatography (tlc) was performed on precoated Merck silica gel 60 F-254 plates, with aluminium backing. Merck 60 mesh silica gel was used for column chromatography. High performance liquid chromatography used Merck prepacked Lobar columns, and a Fluid Metering Inc. model RP-SY pump and model PD-60-LF pulse dampener. The ^{1}Hmr spectra were recorded at 200 MHz or 400 MHz. Mass spectra were obtained on an AEI-MS 3074/DS 50 instrument. Analyses are by Galbraith Laboratories, Knoxville, TN.

Ethyl formylacetate sodium salt (7) (9)

Sodium hydride (50% in mineral oil, 24 g, 0.5 mol) was washed with ether under dry nitrogen, dried, and suspended in ether (100 mL), to which ethanol (23 g, 0.5 mol) was added dropwise, with stirring. After the addition was complete, more ether (50 mL) was added, and the mixture was cooled to −15°C. Then a mixture of ethyl acetate (44 g, 0.5 mol) and ethyl formate (37 g, 0.5 mol) was added with stirring, at such a rate as to maintain the temperature below −10°C. When this addition was complete, the mixture was allowed to warm to room temperature, cooled to −5°C, and filtered under nitrogen. The salt was washed with dry ether, dried, and stored under nitrogen.

Benzhydryl propiolate (9)

A solution of diphenyldiazomethane (5.92 g, 30 mmol) in methylene chloride (75 mL) was added dropwise, with stirring, to a solution of propiolic acid (2.1 g, 30 mmol) in methylene chloride (25 mL). When the reaction was complete, the solvent was removed, and the residue was purified by chromatography on silica gel (6% ethyl acetate in hexane).

Benzhydryl 2-N-benzylacrylate (8)

A solution of benzhydryl propiolate (6.7 g, 28.4 mmol), in ether (50 mL), was cooled to 0°C, and benzylamine (3.04 g, 28.4 mmol) was added dropwise. The product crystallized slowly, and was collected after 18 h, washed with ether, and dried (6.3 g, 65%), mp 122–123°C; ^{1}Hmr ($CDCl_3$) δ: 8.14 (1H, bm, NH), 7.46–7.16 (15H, m), 7.61 (1H, q, 8.0, 14.0, =CHN), 6.94 (1H, s), 4.92 (1H, d, 14.0, =CHC), 4.16 (2H, d, 5.5). *Anal.* $C_{23}H_{21}NO_2$: C, H, N.

Reaction of penicillamine with 7

The salt **7** (276 mg, 2 mmol), D-penicillamine (149 mg, 1 mmol), and *p*-toluenesulfonic acid (380 mg, 2 mmol) were dissolved in water (3 mL), the pH was adjusted to 6.0 with KH_2PO_4, and the solution was stirred at room temperature for 50 h. The mixture, containing some precipitated material, was then diluted with water, acidified to pH 2, and extracted with ether. This extract was dried and evaporated. The residue was crystallized from ether–hexane to give 53 mg (18%) of **10***a*, mp 132–133°C; ^{1}Hmr ($CDCl_3$) δ: 5.18 (0.5H, t, H5), 4.99 (0.5H, t, H5), 4.17 (2H, q), 4.01 (0.5H, s, H3), 3.83 (0.5H, t, H3), 3.20–2.71 (2H, m), 1.64 (3H, br s), 1.32 (3H, br s), 1.23 (3H, t). Mass spectrum, M^+.

Reaction of penicillamine with 8

p-Toluenesulfonic acid hydrate (2.32 g, 12.2 mmol) and D-penicillamine (1.79 g, 12.0 mmol) were dissolved in water (7 mL) and DMF (3 mL). To this solution, with stirring, was added a solution of the enamine (4.2 g, 12.2 mmol) in DMF (12 mL). The clear solution was stirred for 18 h, and some insoluble material was then removed by filtration. The filtrate was diluted with ether and extracted with 5% sodium carbonate. The aqueous extract was washed thoroughly with

Can. J. Chem. Downloaded from www.nrcresearchpress.com by 80.58.250.72 on 09/07/12
For personal use only.

Can. J. Chem. Downloaded from www.nrcresearchpress.com by 80.58.250.72 on 09/07/12
For personal use only.

ether, and then layered with ether and acidified with 6 *N* HCl. The ether extract was dried and evaporated to give 3.7 g (80%) of the product **10***b*. 5*S*-epimer, ^{1}Hmr (acetone-d_6) δ: 7.48–7.17 (10H, m), 6.89 (1H, s), 4.97 (1H, t, H5), 3.67 (1H, s, H3), 3.28–2.77 (2H, m), 1.61 (3H, s,) 1.23 (3H, s); 5*R*-epimer, ^{1}Hmr (acetone-d_6) δ: 7.48–7.17 (10H, m), 6.88 (1H, s), 5.20 (1H, t, H5), 3.88 (1H, s, H3), 1.61 (3H, s), 1.28 (3H, s).

Reaction of penicillamine with ***9***

D-Penicillamine (449 mg, 3 mmol) was suspended in DMF (15 mL), and a solution of benzhydryl propiolate (850 mg, 3.6 mmol) in DMF (15 mL) was added. The mixture was stirred at room temperature for 5 days, and then diluted with 5% sodium carbonate and extracted exhaustively with ethyl acetate. The aqueous phase was then layered with ethyl acetate and acidified to pH 2.5. Evaporation of the dried organic phase gave 643 mg (56%) of **10***b*, which crystallized upon trituration with methylene choride, mp 134–136°C. *Anal.* $C_{21}H_{23}NO_4S$: C, H, N.

Conversion of ***10***b *to the methyl esters* ***11***a *and* ***11***b

The acid **10***b* (a 1:1 mixture of epimers at C5) (870 mg, 2.3 mmol) was added to 2:1 methylene chloride – methanol (20 mL), and treated with excess ethereal diazomethane. After 30 min, the residual diazomethane was destroyed by addition of silica gel. The product was extracted from the silica gel with methanol. After removal of the solvent, the ester was chromatographed (Lobar, 10% acetone–hexane) to yield **11***b* (312 mg), followed by **11***a* (300 mg); **11***a*, ^{1}Hmr ($CDCl_3$) δ: 7.34 (10H, s, Ph), 6.92 (1H, s, $CHPh_2$), 5.16 (1H, t, 6.0 Hz, H5), 3.78 (4H, s, CH_3 + H_3), 3.34 (1H, br s, NH), 2.97 (1H, q, 6.0, 12.0 Hz, H6), 2.75 (1H, q, 6.0, 12.0 Hz, H6), 1.63 (3H, s), 1.22 (3H, s); **11***b*, ^{1}Hmr ($CDCl_3$) δ: 7.32 (10H, br s, Ph), 6.90 (1H, s, $CHPh_2$), 4.93 (1H, br t, 5.0 Hz, H5), 3.75 (3H, s, CH_3), 3.60 (1H, s, H3), 3.27 (1H, br, NH), 2.97 (1H, d, 5.0 Hz, H6), 1.63 (3H, s, CH_3), 1.14 (3H, s, CH_3).

Conversion of ***10***b *to the* p*-nitrobenzyl esters* ***11***c,d

The acid **10***b* (1.75 g, 4.7 mmol) and *p*-nitrobenzyl bromide (1.02 g, 4.7 mmol) were dissolved in acetonitrile (10 mL), triethylamine (0.735 mL, 5.3 mmol) was added, and the mixture was refluxed under nitrogen for 2 h. The mixture was then cooled, diluted with methylene chloride (50 mL), and extracted exhaustively with brine. After drying and evaporation, a portion of the product (total 2.3 g, 93%) was purified by chromatography (Lobar, 10% ethyl acetate – hexane) to separate the esters; **11***c*, ^{1}Hmr ($CDCl_3$) δ: 8.24 (2H, d, 8.5 Hz), 7.53 (2H, d, 8.5 Hz), 7.32 (10H, s, Ph), 6.88 (1H, s, $CHPh_2$), 5.26 (2H, s, CH_2Ar), 5.13 (1H, t, 6 Hz, H5), 3.78 (1H, br s, H3), 3.46 (1H, br s, NH), 2.90 (1H, dd, 6.0, 15.0 Hz, H6), 2.72 (1H, dd, 6.0, 15.0 Hz, H6), 1.56 (3H, s, CH_3), 1.13 (3H, s, CH_3); **11***d*, ^{1}Hmr ($CDCl_3$) δ: 8.24 (2H, d, 9.0 Hz), 7.54 (2H, d, 5.0 Hz), 7.34 (10H, s, Ph), 6.91 (1H, s, $CHPh_2$), 5.29 (2H, s, CH_2Ar), 4.92 (1H, dt, 5.5, 11.5 Hz, H5), 3.62 (1H, t, 11.5 Hz, NH), 3.53 (1H, d, 11.5 Hz, H3), 3.02 (1H, q, 5.5, 16.0 Hz, H6), 2.91 (1H, q, 5.5, 16.0 Hz, H6), 1.59 (3H, s, CH_3), 1.06 (3H, s, CH_3).

Conversion of ***11***a *into* ***12***a

The diester **11***a* (65 mg, 0.16 mmol) was dissolved in 98% formic acid (1 mL), and the solution was left at room temperature for 3 h, and then freeze-dried. The residue was dissolved in water, extracted with ethyl acetate (5 × 1 mL), and freeze-dried again; ^{1}Hmr ($CDCl_3$) δ: 4.90 (1H, t, 6.0 Hz, H6), 3.76 (3H, s, CH_3), 3.75 (1H, s, H3), 2.87 (2H, d, 6.0 Hz), 1.64 (3H, s, CH_3), 1.23 (3H, s, CH_3).

Conversion of ***12***a *into methyl* 5R*-penicillanate (****13****)*

The substrate (130 mg, 0.56 mmol), potassium bicarbonate (240 mg, 2.4 mmol), and tetra-*n*-butylammonium bisulfate (30 mg) were dissolved in water (5 mL). Then chloroform (10 mL) was added, followed, all at once, by a solution of methanesulfonyl chloride (137 mg, 1.2 mmol), in chloroform (15 mL). The mixture was stirred at room temperature for 18 h and then partitioned between ether and water. The organic layer was dried and evaporated, and the residue was purified by column chromatography (20–30% ethyl acetate – hexane) to yield the penam (24 mg, 20%); ^{1}Hmr ($CDCl_3$) δ: 5.31 (1H, q, 2.0, 3.8 Hz, H5), 4.48 (1H, s, H3), 3.78 (3H, s, CH_3), 3.58 (1H, q, 3.8, 16.8 Hz, H6α), 3.08 (1H, q, 2.0, 16.8 Hz, H6β), 1.68 (3H, s, CH_3), 1.48 (3H, s, CH_3).

Conversion of ***12***b *into methyl* 5S*-penicillanate (****14****)*

The reaction was carried out as described for **13**; ^{1}Hmr ($CDCl_3$) δ: 5.09 (1H, q, 2.1, 4.2 Hz, H5), 3.83 (3H, s, CH_3), 3.78 (1H, d, 1.4 Hz, H3), 3.44 (1H, dq, 1.4, 4.2, 16.1 Hz, H6β), 3.21 (1H, q, 2.1, 16.1 Hz, H6α), 1.65 (3H, s, CH_3), 1.52 (3H, s, CH_3).

Reaction of threonine with ***7***

L-Threonine (119 mg, 1 mmol) and the salt **7** (138 mg, 1 mmol) were dissolved in water (2 mL); the solution was stored for 3 days at 4°C and then treated with a solution of benzoyl chloride (141 mg, 1 mmol) in acetone (1 mL), with addition of $NaHCO_3$ (1 g) to maintain the pH above 7. After 2 h, the mixture was diluted with water and extracted with ether. This extract was discarded. The aqueous phase was acidified to pH 1, and extracted successively with ether and ethyl acetate. The combined organic extracts were dried and evaporated to yield 135 mg of material, which (tlc, 80:1:4 butanone – acetic acid – water) was a mixture of at least six products. This mixture was chromatographed (Lobar, 1:1 ethyl acetate – hexane, followed by 3:1 ethyl acetate – hexane, followed by ethyl acetate). The fifth substance eluted was identified as the oxazolidine **15***a*, 24 mg (8%); ^{1}Hmr ($CDCl_3$) δ: 7.44 (2H, m, Ar), 7.31 (3H, br s, Ar), 5.07 (1H, br s, H5), 4.19 (2H, q, 6 Hz, CH_2), 4.02 (1H, d, 6.0 Hz, H3), 3.72 (1H, dq, 6.0, 6.0 Hz, H2), 2.60 (1H, m, H6), 2.27 (1H, m, H6), 1.15 (3H, d, 6.0 Hz, CH_3), 0.89 (3H, t, 6.0 Hz, CH_3).

Reaction of threonine with ***8****. Preparation of* ***16***

A solution of L-threonine (119 mg, 1 mmol) in water (2 mL) was treated dropwise with a solution of the enamine **8** (343 mg, 1 mmol) in DMF (3 mL). The mixture was stirred in an ice bath for 3 h, and was then left overnight at 4°C. Then sodium bicarbonate (1 g) was added, followed by a solution of benzoyl chloride (140 mg, 1 mmol) in acetone (3 mL). The next day, the mixture was diluted with water (50 mL), extracted exhaustively with ether, and then acidified to pH 2. Extraction with ether, followed by drying and evaporation, afforded an acidic fraction, which was converted to the methyl ester with ethereal diazomethane. The product was isolated by chromatography (Lobar, 10% ethyl acetate – hexane), 230 mg (38%); ^{1}Hmr ($CDCl_3$) δ: 7.59 (1H, d, 13.5 Hz, =CHN), 7.34 (20H, Ph), 6.93 (2H, s, $CHPh_2$, $CHPh_2$), 5.57 (1H, dd, 4.5, 7.5 Hz, H5), 4.73 (1H, d, 13.5 Hz, =CHC), 4.50 (1H, dq, 6.0, 6.0 Hz, H2), 3.80 (1H, d, 6.0 Hz, H3), 3.78 (3H, s, CH_3), 2.97 (1H, dd, 4.5, 15.3 Hz, H6), 2.87 (1H, dd, 7.5, 15.3 Hz, H6), 1.39 (3H, d, 6.0 Hz, CH_3); ms, *m/z*: 605 (M^+), 448 (M − Ph_2CH), 404, 390, 362. *Anal.* $C_{37}H_{35}NO_7$: C, H, N.

Reaction of threonine with ***8****. Preparation of* ***17***

The reaction was carried out as described above, except that the initial mixture also contained *p*-toluenesulfonic acid hydrate (190 mg, 1 mmol). The product was eluted with 20% ethyl acetate – hexane; ^{1}Hmr ($CDCl_3$) δ: 8.7 (1H, br), 7.88 (1H, d, 13.5 Hz), 7.32 (10H, br), 7.29 (10H, d), 6.88 (2H, s), 4.95 (1H, d, 17.0 Hz), 4.62 (1H, d, 13.5 Hz), 4.54 (1H, d, 13.5 Hz), 3.76 (1H, dq, 6.0, 8.1 Hz), 3.65 (1H, d, 6.0 Hz), 3.63 (3H, s), 1.40 (3H, d, 8.1 Hz).

Conversion of ***16*** *into the* N*-benzoyloxazolidine* ***15***b

The enamine **16** (350 mg, 0.58 mmol) was dissolved in CH_2Cl_2 (7 mL), and pyridine (49 mg, 0.62 mmol) was added. After 1 h, benzoyl chloride (241 mg, 1.72 mmol) was added. The reaction mixture was stirred at room temperature for 4 h, and the solvent was then removed. The residue was chromatographed (Lobar, 30% ethyl acetate – hexane) to yield **15***b* (219 mg, 80%), mp 123–124°C (ethyl acetate – hexane); ^{1}Hmr ($CDCl_3$) δ: 7.43 (5H, Ph), 7.32 (10H, Ph), 6.90 (1H, $CHPh_2$), 6.05 (1H, br d, 9.0 Hz, H5), 4.50 (1H, dq, 5.4, 5.4 Hz, collapses to a doublet J = 5.4 Hz upon irradiation at 1.35 ppm, H2), 4.20 (1H, br, H3), 3.71 (3H, s, CH_3), 3.19 (1H, br, H6), 2.97 (1H, dd, 9.0, 15.0 Hz, collapses to a doublet J = 15.0 Hz upon irradiation at 6.05 ppm, H6), 1.35 (3H, d, 5.4 Hz, CH_3); ms, *m/z*:

473 (M^+). *Anal.* $C_{28}H_{27}NO_6$, C, H, N. The H3 and H5 protons and one of the H6 protons show temperature-dependent broadening, characteristic of restricted rotation about the amide bond (4).

*Formation of **16** in the reaction of **9** with threonine methyl ester*

The methyl ester of L-threonine (386 mg, 2.90 mmol) was suspended in acetonitrile (10 mL), and treated with a solution of **9** (700 mg, 2.97 mmol) in acetonitrile (5 mL). The mixture was stirred at room temperature for 48 h, filtered to remove 250 mg of insoluble material, and evaporated to give 832 mg of crude product. This was purified by chromatography (20% → 50% ethyl acetate – benzene) to yield **16** (370 mg, 42% based on threonine), identified by comparison with the aforementioned material.

*Reaction of **9** with the methyl ester of threonine in the presence of pyridine*

A solution of **9** (344 mg, 1.46 mmol) in acetonitrile (2 mL), was added during 1 h to a suspension of the methyl ester of L-threonine (194 mg, 1.46 mmol) in acetonitrile (3 mL), containing pyridine (115 mg, 1.46 mmol). During the addition the reaction mixture turned yellow and then orange, and a white semicrystalline precipitate then formed slowly. This was collected after 10 h (55 mg), and the filtrate was evaporated to dryness. The tlc of the precipitate and the residue were similar (3 spots). The ^{1}Hmr spectra in $CDCl_3$, acetone-d_6, and DMSO-d_6 showed varying proportions of **17** and two other enamines. Treatment of the residue with benzoyl chloride (204 mg) in 1:1 methylene chloride – pyridine (4 mL) effected quantitative conversion to a single product, **15***b*.

Reaction of diethinylketone with the methyl ester of threonine

Diethinylcarbinol (450 mg, 5.6 mmol) was dissolved in 1,1,2,2-tetrachloroethane (4 mL), and added dropwise under nitrogen to a suspension of activated manganese dioxide (5 g) in the same solvent (6 mL). The mixture was stirred, gradually warmed to 50°C, and evacuated (1 Torr; 1 Torr = 133.3 Pa). The distillate was collected in two traps, ice–water and Dry Ice – ethanol. The contents of the Dry Ice – ethanol trap were used in the following experiment. The methyl ester of L-threonine (140 mg, 1.05 mmol) was suspended in ether (10 mL), diethinylketone (80 mg, 1.02 mmol) was added, and the reaction mixture was stirred at room temperature for 1 week. The solvent was then removed, and the residual oil was chromatographed (Lobar, 35:10:55 ethyl acetate – methanol–hexane) to yield the main product; ^{1}Hmr ($CDCl_3$) δ: 8.37 (1H, br, NH), 6.85 (1H, q, 7.1, 12.5 Hz, collapses to a doublet, J = 12.5 Hz upon irradiation at 5.38 ppm, =CHN), 6.50 (1H, br, NH), 5.38 (1H, d, 7.1 Hz, =CHC), 4.73 (1H, dd, 2.2, 8.5 Hz, H3), 4.44 (1H, dq, 2.2, 8.4 Hz, collapses to a doublet, J = 2.2 Hz upon irradiation at 1.29 ppm, H2), 4.32 (1H, dq, 3.6, 8.7 Hz, collapses to a doublet J = 3.6 Hz upon irradiation at 1.29 ppm, H2′), 3.85 (3H, s, CH_3), 3.84 (3H, s, CH_3), 3.77 (1H, dd, 3.6, 8.5 Hz, H3′), 3.11 + 3.06 (1H, s + s, ≡CH), 1.84 (1H, br, OH), 1.29 (6H, d, 8.5 Hz, CH_3).

Acknowledgements

The authors thank the Natural Sciences and Engineering Research Council of Canada for financial support.

1. C. A. TOWNSEND and M. HO. J. Am. Chem. Soc. **107**, 1065 (1985).
2. C. A. TOWNSEND and M. HO. J. Am. Chem. Soc. **107**, 1066 (1985).
3. A. L. GUTMAN, V. RIBON, and A. BOLTANSKI. J. Chem. Soc. Chem. Commun. 1627 (1985).
4. S. WOLFE, G. MILITELLO, C. FERRARI, and S. L. LEE. Tetrahedron Lett. 3913 (1979).
5. A. PINNER and C. BISCHOFF. Ann. Chem. **179**, 74 (1875); H. DEN, W. G. ROBINSON, and M. J. COON. J. Biol. Chem. **234**, 1666 (1959); E. W. YAMADA and W. B. JAKOBY. J. Biol. Chem. **235**, 589 (1960); O. HAYAISHI, Y. NISHIZUKA, M. TITIBANA, M. TAKESHITA, and S. KUNO. J. Biol. Chem. **236**, 781 (1961).
6. A. H. COOK and I. M. HEILBRON. *In* The chemistry of penicillin. *Edited by* H. T. Clarke, J. R. Johnson, and R. Robinson. Princeton University Press, Princeton, NJ. 1949. Chapt. XXV.
7. J. C. SHEEHAN and K. R. HENERY-LOGAN. J. Am. Chem. Soc. **81**, 3089 (1959).
8. (*a*) P. J. CLAES, P. HERDEWIJN, and H. VANDERHAEGHE. Nouv. J. Chim. **6**, 273 (1982); (*b*) J. SAKAKI, T. TAKAHASHI, and C. KANEKO. Chem. Lett. 659 (1985).
9. W. DEUTSCHEL. Helv. Chim. Acta, **35**, 1587 (1952).
10. S. E. JENSEN, D. W. S. WESTLAKE, R. J. BOWERS, and S. WOLFE. J. Antibiot. **35**, 1351 (1982).
11. S. WOLFE, R. J. BOWERS, S. K. HASAN, and P. M. KAZMAIER. Can. J. Chem. **59**, 406 (1981); S. E. JENSEN, D. W. S. WESTLAKE, R. J. BOWERS, C. F. INGOLD, M. JOUANY, L. LYUBECHANSKY, and S. WOLFE. Can. J. Chem. **62**, 2712 (1985).
12. T. N. SALZMANN, R. W. RATCLIFFE, B. G. CHRISTENSEN, and F. A. BOUFFARD. J. Am. Chem. Soc. **102**, 6161 (1980).
13. B. CASTRO, J. R. DORMOY, G. EVIN, and C. SELVE. Tetrahedron Lett. 1219 (1975); J. R. DORMOY and B. CASTRO. Tetrahedron Lett. 3321 (1979); J. C. ROZÉ, J. P. PRADÈRE, G. DUGUAY, A. GUÉVEL, and H. QUINIOU. Tetrahedron Lett. **23**, 2315 (1982).
14. Y. WATANABE and T. MUKAIYAMA. Chem. Lett. 443 (1981).
15. S. KOBAYASHI, T. IIMORI, T. IZAWA, and M. OHNO. J. Am. Chem. Soc. **103**, 2406 (1981).
16. I. MCMILLAN and R. J. STOODLEY. Chem. Commun. 11 (1968).
17. A. R. ENGLISH, J. A. RETSEMA, A. E. GIRARD, J. E. LYNCH, and W. E. BARTH. Antimicrob. Agents Chemother. **14**, 414 (1978); D. G. BRENNER and J. R. KNOWLES. Biochemistry, **23**, 5833 (1984).
18. A. W. MCCULLOCH and A. G. MCINNES. Can. J. Chem. **52**, 3569 (1974).
19. R. C. FUSON. Chem. Rev. **16**, 1 (1935).
20. E. R. H. JONES, H. H. LEE, and M. C. WHITING. J. Chem. Soc. 3483 (1960).
21. D. D. PERRIN, W. L. F. ARMAGO, and D. R. PERRIN. Purification of laboratory chemicals. Pergamon Press, Toronto. 1966.

Can. J. Chem. Downloaded from www.nrcresearchpress.com by 80.58.250.72 on 09/07/12
For personal use only.

Studies in anthracyclinone synthesis. The oxidative decyanation route to aklavinone and 4,11-dideoxy-α-rhodomycinone

J. APPA RAO, K. RAVICHANDRAN, G. J. O'MALLEY, AND M. P. CAVA[1]

Department of Chemistry, University of Alabama, Box H, University, AL 35486, U.S.A.

Received April 9, 1986

This paper is dedicated to Dr. O. E. (Ted) Edwards

J. APPA RAO, K. RAVICHANDRAN, G. J. O'MALLEY, and M. P. CAVA. Can. J. Chem. **65**, 31 (1987).

The formal synthesis of aklavinone and the first synthesis of 4,11-dideoxy-α-rhodomycinone are described. Oxidative decyanation of the tetracyclic nitrile to the corresponding ketone using a strong base (LDA) constitutes an important strategy in the synthesis of both these compounds.

J. APPA RAO, K. RAVICHANDRAN, G. J. O'MALLEY et M. P. CAVA. Can. J. Chem. **65**, 31 (1987).

On décrit la synthèse formelle de l'aklavinone ainsi que la première synthèse de la didéoxy-4,11 α–rhodomycinone. La décyanation oxydante du nitrile tétracyclique, sous l'influence d'une base forte (LDA), constitue une stratégie importante dans la synthèse de chacun de ces deux composés.

[Traduit par la revue]

Can. J. Chem. Downloaded from www.nrcresearchpress.com by 190.90.36.8 on 09/07/12
For personal use only.

Recently we reported (1) the conversion of some simple hydroxyanthraquinone dye intermediates into the tetracyclic ketonitriles **8** and **14**; a tandem Michael vicarious aromatic substitution reaction on the enones **7** and **13** formed the key step of the synthetic sequence.

We now report the use of **8** to complete a new formal synthesis of aklavinone (**1**), as well as the elaboration of **14** to afford the first synthesis of 4,11-dideoxy-α-rhodomycinone (**6**).

Synthesis of aklavinone

As part of the continuing search for new anthracyclines that may show decreased side effects and (or) increased antitumor activity relative to daunomycin and adriamycin, much interest has focused on aclacinomycin A (2). Since microbiological methods permit the transformation of the aglycon, aklavinone (**1**), to aclacinomycin A, significant efforts have been expended on the synthesis of **1** (3).

The research described in this section emanated from our search for a method to convert nitrile **8** into the versatile intermediate 4,6-dihydroxy-9-ethyl-7,8,9,10-tetrahydronaphthacenetrione **12**, which has already found use as a late stage precursor to aklavinone, as well as a potential starting material for the synthesis of other 11-deoxyanthracyclinones such as decarbomethoxyaklavinone **2** (4) and β_1-citromycinone **3** (5).

We envisaged that the ketone functionality of **8** would be troublesome to maintain since it would contribute a driving force for the aromatization of the "A" ring. Hence the removal of this functionality seemed advantageous. The carbonyl group could be reduced directly using triethylsilane/TFA (6) to afford **10** (46%), although a better yield (~80%) was obtained by conversion of **8** to the dithioketal **9** and subsequent reduction using tri-*n*-butyltin hydride (7).

We first expected that the anionic oxygenation of **10** to ketone **11** would succeed using a mild base such as K_2CO_3 in DMSO (8). However, varying the temperature from room temperature to 100°C and prolonging the oxidation time for 72 h failed to afford the required product. Changing the base to NaH and (or) *t*-BuOK, together with varying the oxygenation temperature, also proved futile.

The only success in obtaining **11** required the use of the strong base LDA (lithium diisopropylamide) (1.5 equiv.) and dry oxygen (9). Compound **11** was easily demethylated in the conventional way ($AlCl_3/CH_2Cl_2$) to obtain **12**; both **11** and **12** were identical in all respects (tlc, ^{1}Hmr, mp, ms) with authentic samples.[2]

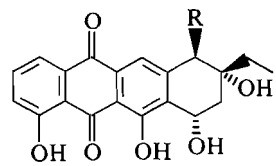

1 Aklavinone, R = CO_2CH_3
2 Decarbomethoxyaklavinone, R = H
3 β_1-Citromycinone, R = OH

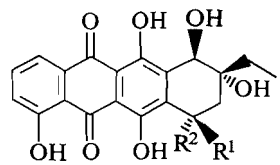

4
Rhodomycinone
R^1 = H; R^2 = OH (β)
R^1 = OH; R^2 = H (α)

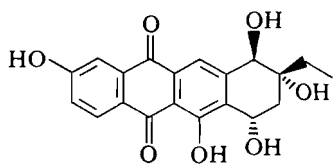

5
2-Hydroxy-4,11-dideoxy-β-rhodomycinone

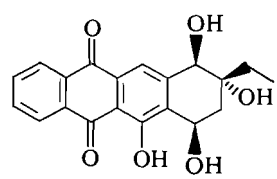

6
4,11-Dideoxy-α-rhodomycinone

[1]Author to whom correspondence may be addressed.

[2]We are grateful to Drs. Confalone and G. Pizzolato for providing us authentic samples.

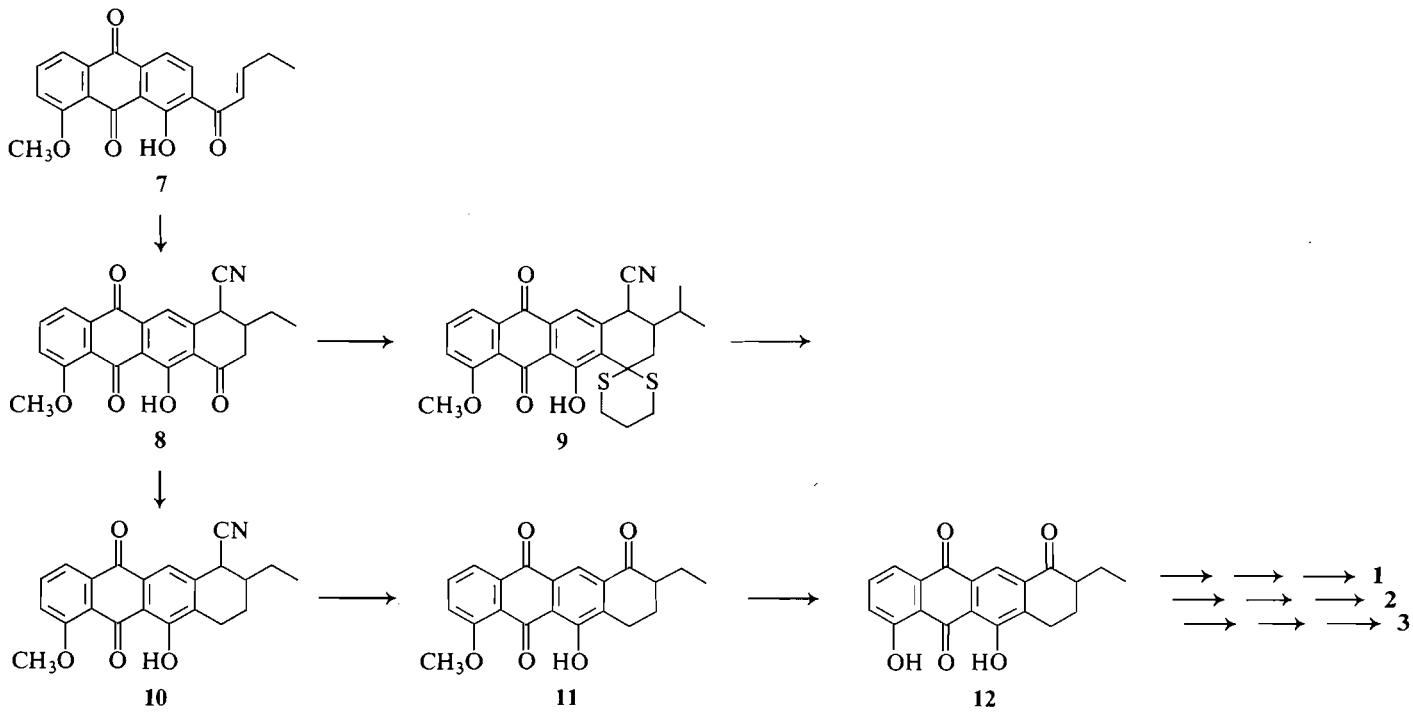

SCHEME 1

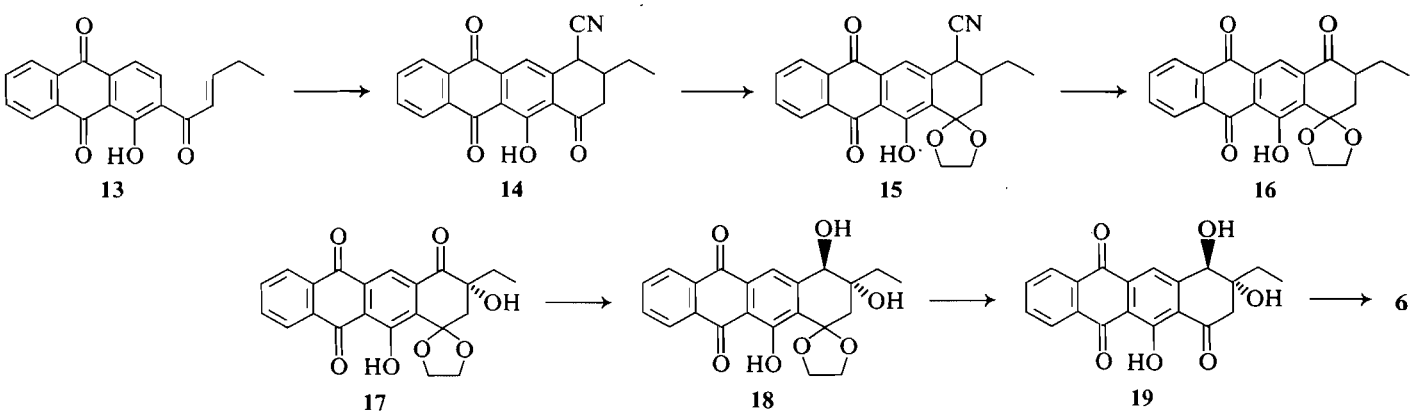

SCHEME 2

Since **12** has been previously converted to aklavinone (3*a*,*b*), decarbomethoxyaklavinone (4), and β_1-citromycinone (5), our route to this versatile intermediate by a conceptually different approach constitutes new formal syntheses of these anthracyclinones.

Synthesis of 4,11-dideoxy-α-rhodomycinone

The rhodomycinones (**4**) are the principal aglycones of the aminoglycoside antibiotics of the rhodomycin group produced by various strains of streptomyces (10). Several elegant studies have been described, aimed at the synthesis of these molecules (11). Recently 4,11-dideoxy-2-hydroxy-β-rhodomycinone (**5**) (12), has been synthesized: this compound comprises of a hybrid analog of 2-hydroxyaklavinone and β-rhodomycinone. We now report the first synthesis of 4,11-dideoxy-α-rhodomycinone (**6**), a structure that constitutes a hybrid analog of 4-deoxyaklavinone and α-rhodomycinone.

Earlier we synthesized (1) the ketonitrile **14** by a two-step sequence in 56% overall yield from the enone **13**. However, treatment of the enone **13** with $PhSCH_2CN$ improved the yield of **14** to 72% in a single-step operation.

Unlike in the aklavinone synthesis, we decided to keep the carbonyl function intact at the 7 position in the ketonitrile **14**; hence, this was protected as the ethylene ketal **15** in 76% yield. Oxidative decyanation of **15** using LDA as described in the previous section conveniently provided the requisite ketone **16**. Enolate hydroxylation of the ketone **16** with oxodiperoxymolybdenum(pyridine)hexamethylphosphoramide (MoOPH) (13) gave the α-hydroxyketone **17** in 60% yield. Reduction of the carbonyl group in **17** was accomplished with sodium cyanoborohydride at pH 5 to afford the desired 9,10-*trans* diol **18** in 80% yield; the remainder was the *cis* isomer, which could be eliminated by chromatography followed by crystallization.

Cleavage of the ketal function by 5% HCl proceeded smoothly to afford **19** in 68% yield. Reduction of the C-7 carbonyl of **19** with an excess (10 equivalents) of $NaCNBH_3$ at pH 5 provided **6** together with its isomer, albeit in modest yield due to extensive aromatization of the "A" ring. The separation of these isomers was easily achieved using benzeneboronic acid/PTS (14) to provide the desired *trans* isomer as a yellow solid, mp 238–240°C (dec.).

In conclusion, we have completed a new formal synthesis

Can. J. Chem. Downloaded from www.nrcresearchpress.com by 190.90.36.8 on 09/07/12
For personal use only.

Can. J. Chem. Downloaded from www.nrcresearchpress.com by 190.90.36.8 on 09/07/12
For personal use only.

of aklavinone, as well as the first synthesis of 4,11-dideoxy-α-rhodomycinone, using the oxidative decyanation of fully constructed tetracyclic molecules derived from simple hydroxyanthraquinone precursors.

Experimental

Melting points were determined on a Thomas–Hoover apparatus and are uncorrected. The ^{1}H nmr spectra were obtained on a Bruker 250 FT instrument using $CDCl_3$ as solvent and Me_4Si as an internal standard; shifts are expressed in δ units. Infrared (ir) spectra were obtained on a Perkin–Elmer 781 grating spectrophotometer using polystyrene film as a standard; absorbances are expressed in units of cm^{-1}. Mass spectra were determined on a V-G 70-70 Micromass. Thin-layer chromatographic plates were obtained from JT Baker Chemical Co. (Si 250 F). Products were detected by viewing under an uv source and (or) exposing to I_2 vapours. All organic extracts were washed and dried over anhydrous Na_2SO_4 prior to filtration and evaporation.

4-Methoxy-6-hydroxy-9-ethyl-10-cyano-7,8,9,10-tetrahydronaphthacene-dione ***10***

Method A

To a stirred solution of the keto nitrile **8** (100 mg, 0.26 mmol) and triethylsilane (150 mg, 1.3 mmol) in CH_2Cl_2 (15 mL) at 0°C, was added trifluoroacetic acid (0.2 mL, 2.34 mmol). After stirring at 0°C for 1 h, the reaction mixture was gradually warmed to room temperature and left overnight. The contents were poured over crushed ice, extracted with methylene chloride, and washed thoroughly with $NaHCO_3$. Column chromatography followed by crystallization (95% EtOH) afforded **10** (45 mg, 0.124 mmol, 46%), mp 192–194°C (dec.); nmr: 1.03 (t, 3H, J = 7.4 Hz), 1.62 (m, 1H), 1.82–2.04 (m, 2H), 2.20–2.38 (m, 1H), 2.42–2.60 (m, 1H), 2.86–2.94 (m, 1H), 3.10–3.24 (m, 1H), 3.78 (d, 1H, J = 9.1 Hz), 4.10 (s, 3H), 7.40 (d, 1H, J = 7.5 Hz), 7.70 (t, 1H, J = 7.5 Hz), 13.50 (s, 1H); ms: 362 (32), 351 (92), 250 (18), 69 (100). *Mol. Wt.* (high resolution ms) calcd. for $C_{22}H_{19}O_4N$: (M^+ + 1), 362.1350; found: 362.0242.

Method B

To a stirred solution of the ketonitrile **8** (100 mg, 0.26 mmol), 1,3-propanedithiol (66.6 mg, 0.53 mmol), and trimethylsilyl chloride (50 mg, 0.53 mmol) in a flame-dried, nitrogen flushed flask containing CH_2Cl_2 (15.0 mL) was added 1 drop of trimethylsilyl triflate. After stirring at room temperature for 20 min, the dark green solution was diluted with H_2O (100 mL). This was extracted with methylene chloride, dried over anhydrous Na_2SO_4, and evaporated to dryness. Chromatography (silica gel, hexane – ethyl acetate 2:1) provided **9** (106 mg, 0.23 mmol, 85%) as an *unstable* light orange solid, ((mp 138–140°C); nmr: 1.09–1.15 (m, 3H), 2.14–2.19 (m, 2H), 2.66–2.90 (m, 2H), 3.04–3.30 (m, 6H), 3.85 (d, 1H, J =9.1 Hz), 4.18 (s, 3H), 7.40 (d, 1H, J = 7.5 Hz), 7.70 (t, 1H, J = 7.5 Hz), 7.64 (s, 1H), 14.6 (s, 1H); ms: 465 (0.5), 423 (4.6), 361 (100), 343 (15.8), 332 (69.9)), which was immediately refluxed in *dry* benzene (15.0 mL) containing tri-*n*-butyltin hydride (296 mg, 1.02 mmol) and AIBN (catalyst, 20 mg). After 3 h the solvent was removed under reduced pressure, extracted with methylene chloride, washed several times with water, dried over anhydrous Na_2SO_4, and finally evaporated to dryness. Chromatography (silica gel, hexane–EtOAc 3:1) followed by crystallization (95% EtOH) afforded **10** (77 mg, 0.21 mmol, 94%), which was identical in all respects with the sample obtained by Method A.

*7,8-Dihydro-4-methoxy-6-hydroxy-9-ethyl-5,10,12(9*H*)-naphthacenetrione* ***11***

To a solution of 0.152 mmol of lithium diisopropylamide in 3.0 mL of anhydrous THF at −78°C under a nitrogen atmosphere was added a solution of **10** (50 mg, 0.138 mmol) in 2 mL THF and 0.5 mL HMPA. Dry O_2 was bubbled (250 mL/min) into the lithionitrile solution for 1 h at −78°C. The reaction was quenched with 6.0 mL of 1 *M* aqueous $NaHSO_3$ solution and stirred at 0°C for 1. After further stirring at room temperature for 30 min, the reaction mixture was diluted with ether, washed successively with water, 1 *M* NaOH solution, water, and brine, and dried over anhydrous Na_2SO_4. Chromatography of the crude product followed by crystallization (95% EtOH) afforded **11** (27 mg, 0.77 mmol, 55%), mp 224–225°C (lit. (*3a*) mp 224–225°C); nmr: 1.03 (t, 3H, J = 7.4 Hz), 1.60 (quintet, 1H, J = 7.4 Hz), 1.82–2.04 (m, 2H), 2.30–2.40 (m, 1H), 2.42–2.51 (m, 1H), 2.85–2.94 (m, 1H), 3.17–3.24 (m, 1H), 7.30 (d, 1H, J = 7.5 Hz), 7.70 (t, 1H, J = 7.5 Hz), 7.84 (d, 1H, J = 7.5 Hz), 8.37 (s, 1H), 13.42 (s, 1H); ms: 350 (3.1), 256 (14.1), 149 (50.5), 57 (100). This substance was identical in all respects with an authentic sample.[2]

4,6-Dihydroxy-9-ethyl-7,8,9,10-tetrahydronaphthacenetrione ***12***

To a suspension of anhydrous $AlCl_3$ (100 mg, excess) in 15 mL of dry CH_2Cl_2 was added a solution of ketone **11** (25 mg, 0.07 mmol) in CH_2Cl_2 (2.0 mL) at room temperature under N_2. After 24 h, all solvent was removed under reduced pressure; 5% HCl (2.0 mL) and saturated brine (15 mL) were added and stirred further for 1 h. This was extracted with ether (2 × 15 mL) dried over anhydrous Na_2SO_4, evaporated, and crystallized (CH_2Cl_2/ether/hexane) to afford **12** (18 mg, 0.05 mmol, 75%); mp 203–204°C (lit. (*3a,b*) mp 203–204°C, 204–205°C); nmr: 1.03 (t, 3H, J = 7.4 Hz), 1.60 (quintet, 1H, J = 7.4 Hz), 1.88–2.03 (m, 2H), 2.29–2.38 (m, 1H), 2.44–2.51 (m, 1H), 2.85–2.94 (m, 1H), 3.17–3.24 (m, 1H), 7.29 (d, 1H, J = 7.5 Hz), 7.70 (t, 1H, J = 7.5 Hz), 7.84 (d, 1H, J = 7.5 Hz), 8.37 (s, 1H), 12.0 (s, 1H), 12.46 (s, 1H); ms: 336 (5.9), 252 (2.5), 123 (8.3), 81 (48.4), 69 (100). This substance was identical in all respects with an authentic sample.[2]

*10-Cyano-9,10-dihydro-9-ethyl-6-hydroxy-5,7,12(8*H*)-naphthacenetrione* ***14***

To a suspension of 200 mg (4.36 mmol) of NaH (60% dispersion in oil) in 20 mL of DMF, 0.375 mL (2.18 mmol) of $PhSCH_2CN$ was added under nitrogen with stirring. After 15 min, 500 mg (1.64 mmol) of the enone **13** was added in one lot. The reaction mixture was stirred at room temperature for 3 h and was poured onto ice (50 g) containing 2 mL of acetic acid. The mixture was extracted with CH_2Cl_2 (100 mL), washed with water (2 × 50 mL), dried (Na_2SO_4), and the solvent evaporated. The residue was chromatographed over silica gel (3:1 hexane:ethyl acetate) to give, after crystallization from benzene, the cyanoketone **14** (400 mg, 1.16 mmol, 72%) as yellow crystalline solid, mp 205–206°C (lit. (1) mp 205–206°C); nmr: 1.07–1.14 (t, 3H, J = 7.4 Hz), 1.59–1.83 (m, 2H), 2.37–2.42 (m, 1H), 2.75–2.96 (m, 2H), 4.29–4.30 (d, 1H, J = 3.6 Hz), 7.84–7.86 (m, 3H), 8.26–8.35 (m, 2H), 13.97 (s, 1H); ms: 346 (M^++1, 100), 345 (33), 289 (37), 205 (4), 177 (5), 150 (4), 113 (8), 84 (11). *Mol. Wt.* (high resolution ms) calcd. for $C_{21}H_{15}NO_4$; 345.0966; found: 345.1187.

10-Cyano-9-ethyl-7,7-ethylenedioxy-6-hydroxy-7,8,9,10-tetrahydro-5,12-naphthacenedione ***15***

A mixture of 500 mg (1.45 mmol) of the cyanoketone **14,** 0.1 mL (1.8 mmol) of ethyleneglycol, and 25 mg of *p*-toluenesulfonic acid in 50 mL of benzene was refluxed for 2 h under nitrogen with azeotropic removal of water. The reaction mixture was cooled, washed successively with 10% $NaHCO_3$ solution (25 mL), water (2 × 25 mL), dried (Na_2SO_4), and solvent removed. The residue was chromatographed over silica gel (4:1 hexane:ethyl acetate) to afford, after crystallization from CH_2Cl_2–MeOH, the cyanoketal **15** (420 mg, 1.08 mmol, 76%) as bright yellow crystals, mp 224–226°C; nmr: 1.05–1.11 (t, 3H, J = 7.3 Hz), 1.56–1.71 (m, 2H), 2.04–2.17 (m, 3H), 4.07–4.49 (m, 5H), 7.74 (s, 1H), 7.81–7.86 (m, 2H), 8.27–8.34 (m, 2H), 13.64 (s, 1H); ms: 390 (M^+ + 1, 57), 389 (M^+, 11), 347 (21), 346 (88), 334 (24), 333 (100). *Mol. Wt.* (high resolution ms) calcd. for $C_{23}H_{19}NO_5$: 389.1257; found: 389.1250.

*9-Ethyl-6-hydroxy-7,8-dihydro-7,7-ethylenedioxy-5,10,12 (9*H*)-naphthacenetrione* ***16***

LDA was prepared from 0.25 mL (1.87 mmol) of diisopropylamine and 0.75 mL of 2.5 *M n*-BuLi in 10 mL of THF at −78°C. Cyanoketal **15** (250 mg, 0.625 mmol) dissolved in 10 mL of THF was added at −78°C. After stirring for 30 min, dry oxygen was bubbled through the solution for 2 h at −78°C. The reaction mixture was brought to 0°C and 2.5 mL of 1 *M* stannous chloride in 2 *M* HCl was added. After 30 min, the reaction mixture was extracted with CH_2Cl_2 (100 mL), and washed with 1 *N* NaOH (50 mL). The aqueous solution was acidified with acetic acid and extracted with CH_2Cl_2 (100 mL). The organic

Can. J. Chem. Downloaded from www.nrcresearchpress.com by 190.90.36.8 on 09/07/12
For personal use only.

phase was washed with water (2 × 50 mL), dried, and solvent removed. The residue was chromatographed over silica gel (4:1 hexane:ethyl acetate) to afford, after crystallization from CH_2Cl_2–MeOH, the ketone **16** (165 mg, 0.43 mmol, 68%) as reddish brown crystals, mp 212–214°C; ir: 1710 (C=O), 1685 and 1640 (quinone C=O); nmr: 1.01–1.08 (t, 3H, J = 7.4 Hz), 1.54–1.77 (m, 1H), 1.95–2.05 (m, 1H), 2.11–2.23 (m, 1H), 2.33–2.40 (dd, 1H, J = 13.9 and 4.3 Hz), 2.81–1.91 (m, 1H), 4.13–4.58 (m, 4H), 7.80–7.89 (m, 2H), 8.29–8.37 (m, 2H), 8.38 (s, 1H), 13.58 (s, 1H); ms: 379 (M^+ + 1, 100), 378 (M^+, 36), 335 (41), 307 (66), 294 (88), 138 (20). *Mol. Wt.* (high resolution ms) calcd. for $C_{22}H_{18}O_6$: 378.1110; found: 378.1135.

6,9-Dihydroxy-7,8-dihydro-9-ethyl-7,7-ethylenedioxy-5,10,12(9H)-naphthacenetrione **17**

LDA was prepared from 0.17 mL (1.2 mmol) of diisopropylamine and 0.51 mL of 2.5 *M n*-BuLi in 10 mL of THF at −78°C. A solution of 150 mg (0.4 mmol) of the ketone **16** in 10 mL of THF was added at −78°C. After 30 min, 210 mg (0.48 mmol) of MoOPH was added with vigorous stirring. After stirring the reaction mixture at −78°C for 1 h, it was slowly brought to room temperature over a period of 1 h and stirred for another 2 h. The contents were poured onto ice (50 g) containing 2 mL of acetic acid, extracted with CH_2Cl_2 (75 mL), washed with water (2 × 25 mL), dried (Na_2SO_4), solvent evaporated, and the residue was chromatographed over silica gel (3:1 hexane:ethyl acetate) to furnish, after crystallization from CH_2Cl_2–MeOH, the α-hydroxyketone **17** (94 mg, 0.24 mmol, 60%) as reddish brown needles, mp 226–227°C; ir: 1710 (C=O), 1680 and 1640 (quinone C=O); nmr: 0.86–0.92 (t, 3H, J = 7.2 Hz), 1.82–1.86 (m, 2H), 2.33–2.66 (ABq, 2H, J =14.4 Hz), 3.74 (s, 1H), 4.21–4.51 (m, 4H), 7.84–7.87 (m, 2H), 8.30–8.34 (m, 2H), 8.36 (s, 1H), 13.57 (s, 1H); ms: 395 (M^+ + 1, 100), 394 (M^+, 34), 377 (28), 338 (16), 294 (27), 293 (22), 85 (41), 83 (57). *Mol. Wt.* (high resolution ms) calcd. for $C_{22}H_{18}O_7$: 394.1050; found: 394.1008.

9-Ethyl-7,7-ethylenedioxy-7,8,9,10-tetrahydro-6,9,10-trihydroxy-5,12-naphthacenedione **18**

To a solution of 100 mg (0.25 mmol) of the α-hydroxyketone **17**, in CH_2Cl_2 (10 mL) and MeOH (10 mL), was added acetic acid (~1 mL) to give a solution of pH 5. $NaBH_3CN$ (0.32 g, 0.5 mmol) was added and the solution stirred at room temperature for 36 h. Solvent was removed under reduced pressure, the residue was dissolved in CH_2Cl_2 (25 mL), washed with water (3 × 25 mL), dried, and the residue, after removal of the solvent, was chromatographed over silica gel (2:1 hexane: ethyl acetate) to afford, after crystallization from benzene, **18** (80 mg, 0.20 mmol, 80%) as yellow needles, mp 228–230°C (dec.); nmr: 1.02–1.08 (t, 3H, J = 7.4 Hz), 1.56–1.60 (m, 2H), 2.00–2.06 and 2.43–2.49 (ABq, 2H, J = 14.5 Hz), 2.25–2.27 (d, 1H, J = 5.0 Hz), 2.93 (s, 1H), 4.19–4.48 (m, 4H), 4.62–4.64 (d, 1H, J = 5.0 Hz), 7.81–7.84 (m, 2H), 7.93 (s, 1H), 8.28–8.33 (m, 2H), 13.63 (s, 1H); ms: 397 (M^+ + 1, 40), 396 (2), 379 (28), 334 (43), 278 (25), 116 (18), 91 (100), 79 (25), 72 (32), 70 (44). *Mol. Wt.* (high resolution ms) calcd. for $C_{22}H_{20}O_7$: 396.1210; found: 396.1179.

9,10-Dihydro-9-ethyl-6,9,10-trihydroxy-5,7,12(8H)-naphthacenetrione **19**

To a solution of the ketal **18** (60 mg, 0.15 mmol) in 5 mL of THF, 2 mL of 5% HCl was added while cooling in ice and the mixture stirred for 90 min. Solvent was removed under reduced pressure, the residue was taken up in CH_2Cl_2 (25 mL), washed with water (2 × 25 mL), and dried (Na_2SO_4). Removal of the solvent gave yellowish brown solid, which on chromatographic purification over silica gel (1:1 hexane:ethyl acetate) furnished, after crystallization from benzene, **19** (40 mg, 0.11 mmol, 66%) as yellow solid, mp 205–210°C (dec.); nmr: 1.00–1.06 (t, 3H, J = 7.4 Hz), 1.54–1.63 (m, 2H), 1.81–1.93 (m, 1H), 2.69 (s, 1H), 2.73–2.79 and 3.14–3.21 (ABq, J = 17.1 Hz), 4.89 (s, 1H), 7.81–7.85 (m, 2H), 8.05 (s, 1H), 8.25–8.35 (m, 2H), 13.89 (s, 1H); ms: 353 (M^+ + 1, 32), 352 (4), 335 (66), 334 (100). *Mol. Wt.* (high resolution ms) calcd. for $C_{20}H_{16}O_6$: 352.0950; found: 352.0932.

4,11-Dideoxy-α-rhodomycinone **6**

To a solution of **19** (50 mg, 0.142 mmol) in CH_2Cl_2 (10 mL) and MeOH (10 mL) was added acetic acid (~1 mL) to give a solution of pH 5. $NaBH_3CN$ (90 mg, 1.42 mmol) was added and the solution stirred at room temperature for 3 h. Solvent was removed under reduced pressure, the residue was dissolved in CH_2Cl_2 (25 mL), washed with water (3 × 25 mL), dried (Na_2SO_4), and the residue after evaporation of the solvent was chromatographed over silica gel (1:1 hexane:ethyl acetate) to give a mixture of triols (10 mg, 0.028 mmol, 20%) as yellow solid. The solid was dissolved in a mixture of benzene (10 mL) and CH_2Cl_2 (10 mL), and benzeneboronic acid (6 mg) and PTS (2 mg) were added. The solution was stirred at room temperature for 24 h, and was then washed with 5% aqueous $NaHCO_3$ solution (10 mL), dried (Na_2SO_4), solvent evaporated, and the residue chromatographed over silica gel (1:1 hexane:ethyl acetate) to afford, after crystallization from hexane CH_2Cl_2, **6** (6 mg, 0.017 mmol, 12%) was yellowish powder, mp 238–240°C (dec.); nmr: 1.03–1.10 (t, 3H, J = 7.4 Hz), 1.80–1.88 (m, 2H), 2.22–2.31 (m, 1H), 2.45–2.49 (m, 1H), 4.55 (bs, 1H), 5.29–5.32 (m, 1H), 7.66–7.95 (m, 2H), 8.16 (s, 1H), 8.18–8.45 (m, 2H), 13.39 (s, 1H); ms: 355 (M^+ + 1, 10), 354 (14), 349 (42), 336 (24), 319 (45), 318 (19), 303 (20), 302 (18), 278 (17), 264 (24), 224 (14), 207 (17), 199 (27), 181 (14), 175 (26), 151 (21), 133 (24), 113 (100). *Mol. Wt.* (high resolution ms) calcd. for $C_{20}H_{18}O_6$: 354.1100; found: 354.1065.

Acknowledgements

Technical assistance from Mr. John Dykins and Mr. Roger Powers (University of Pennsylvania) in the determination of mass spectra is gratefully acknowledged. This work was supported by NIH-CA 30377.

1. M. P. Cava, Z. Ahmed, N. Benfaremo, R. A. Murphy, Jr., and G. J. O'Malley. Tetrahedron, **40**, 4767 (1984).
2. T. Oki, Y. Matsuzawa, A. Yoshimoto, K. Numata, I. Kitamura, S. Hori, A. Takamatsu, H. Umezawa, M. Ishizuka, H. Naganawa, H. Suda, M. Hamada, and T. Takeuchi. J. Antibiot. **28**, 830 (1975).
3. (*a*) P. N. Confalone and G. Pizzolato. J. Am. Chem. Soc. **103**, 4251 (1981); (*b*) R. K. Boeckman, Jr., and F. W. Sum. J. Am. Chem. Soc. **104**, 4604 (1982); (*c*) T. Li and Y. L. Wu. J. Am. Chem. Soc. **103**, 7007 (1981); (*d*) A. S. Kende and J. P. Rizzi. J. Am. Chem. Soc. **103**, 4247 (1981); (*e*) B. A. Pearlman, J. M. McNamara, I. Haran, S. Hatakeyama, H. Sekizaki, and Y. Kishi. J. Am. Chem. Soc. **103**, 4251 (1981).
4. A. S. Kende and J. P. Rizzi. Tetrahedron Lett. **22**, 1779 (1981).
5. K. Krohn. Liebigs Ann. Chem. 2285 (1981).
6. C. T. West, S. J. Donnelly, D. A. Kooistra, and M. P. Doyle. J. Org. Chem. **38**, 2675 (1978).
7. C. G. Gutierrez, R. R. Stringham, T. Nitasaka, and K. G. Glasscock. J. Org. Chem. **45**, 3393 (1980).
8. S. S. Kulp and M. J. McGee. J. Org. Chem. **48**, 4097 (1983).
9. R. W. Freerksen, S. J. Selikson, R. R. Wrobble, K. S. Kyler, and D. S. Watt. J. Org. Chem. **48**, 4087 (1983).
10. H. Brockmann. Fortschr. Chem. Org. Naturst. **21**, 121 (1963); H. Brockmann and J. Niemeyer. Chem. Ber. **100**, 3578 (1967).
11. (*a*) A. S. Kende. J. Chem. Soc. Chem. Commun. 140 (1977); (*b*) K. Krohn and W. Priyono. Tetrahedron, **40**, 4609 (1984), and references therein.
12. H. Tanaka, T. Yoshioka, Y. Shimauchi, A. Yoshimoto, T. Ishikura, H. Naganawa, T. Takeuchi, and H. Umezawa. Tetrahedron Lett. **25**, 3355 (1984)
13. E. Vedejs, D. A. Engles, and J. E. Telschow. J. Org. Chem. **43**, 188 (1978).
14. (*a*) M. J. Broadhurst, C. H. Hassal, and G. J. Thomas. J. Chem. Soc. Perkin Trans. 1, 2229 (1982); (*b*) K. Ravichandran, F. A. J. Kerdesky, and M. P. Cava. J. Org. Chem. **51**, 2044 (1986).

Trijugins *A* and *B*, tetranortriterpenoids with a novel rearranged carbon skeleton from *Heynea trijuga* (Meliaceae)

KOZHIPARAMBIL K. PURUSHOTHAMAN, MATHURAM VENKATANARASIMHAN, AND AYYAPPATH SARADA
Captain Srinivasa Murti Drug Research Institute for Ayurveda, Arumbakkam, Madras 600106, India

AND

JOSEPH D. CONNOLLY[1] AND DAVID S. RYCROFT
Department of Chemistry, University of Glasgow, Glasgow, G12 8QQ, Scotland

Received June 4, 1986

This paper is dedicated to Dr. O. E. (Ted) Edwards

KOZHIPARAMBIL K. PURUSHOTHAMAN, MATHURAM VENKATANARASIMHAN, AYYAPPATH SARADA, JOSEPH D. CONNOLLY, and DAVID S. RYCROFT. Can. J. Chem. **65**, 35 (1987).

Two new tetranortriterpenoids, trijugins *A* (**1**) and *B* (**3**), isolated from the leaves of *Heynea trijuga* (Meliaceae), have been shown to be derivatives of methyl angolensate but with a novel carbon skeleton having a contracted ring C. The structures were assigned on the basis of detailed ^1H and ^{13}C nuclear magnetic resonance spectroscopic examination including 2D long-range δ_C/δ_H correlation and homonuclear ^1H nuclear Overhauser effect difference experiments.

KOZHIPARAMBIL K. PURUSHOTHAMAN, MATHURAM VENKATANARASIMHAN, AYYAPPATH SARADA, JOSEPH D. CONNOLLY et DAVID S. RYCROFT. Can. J. Chem. **65**, 35 (1987).

On a démontré que deux nouveaux tétranortriterpénoïdes, les trijugines *A* (**1**) et *B* (**3**), isolés des feuilles du *Heynea trijuga* (Meliaceae) sont des dérivés de l'angolensate de méthyle qui possèdent toutefois un nouveau squelette carboné comportant un cycle C ayant subi une contraction. On a attribué les structures en se basant sur un examen détaillé des spectres rmn du ^1H et du ^{13}C comportant des corrélations δ_C/δ_H 2-D et à longue distance ainsi que des expériences de différences d'eOn ^1H homonucléaire.

[Traduit par la revue]

Introduction

Previous work (1) on the leaves of *Heynea trijuga* Roxb., which are bitter and known to possess tonic properties, resulted in the isolation of 24-methylenecycloartane-3β,21-diol and heynic acid. We have now examined the more polar fractions of the extract and have obtained two new tetranortriterpenoids, trijugins *A* and *B*, which have been shown to have the novel structures **1** and **3** respectively and which represent a new skeletal type of compound.

Results and discussion

Trijugin *A* (**1**), $C_{29}H_{34}O_{11}$ (*m/z* 498.1893 (M^+ − HOAc)), mp 265–266°C, $[\alpha]_D^{30}$ −32.5° (*c* 2.0 in $CHCl_3$), ir (KBr) ν_{max}: 3450, 1742, 1702 cm^{-1}, has ^1H and ^{13}C resonances (see Tables 1 and 2) for four tertiary methyl groups, a secondary acetate with abnormally highly shielded methyl protons (δ_H 1.75), a carbomethoxyl, an exomethylene, a ketonic carbonyl, a ring D lactone, a β-substituted furan, and four further oxygen-bearing carbons, two secondary, one quaternary (δ_C 88.4), and one a ketal or hemiketal (δ_C 108.4). These signals together with two methylenes, two methine, and three quaternary carbon atoms account for all the carbon and all but one of the hydrogen atoms. Hence there is one hydroxyl group, but this is not acetylated under normal conditions. Trijugin *A* is therefore bicarbocyclic with two oxygen bridges and the above features suggest it is a derivative of methyl angolensate (**2**) (2). The signal at δ_C 108.4 is then assigned to the hemiketal carbon of a cyclic hemiketal involving a secondary oxygen function.

Further insight was obtained from ^1H nOe (nuclear Overhauser effect) difference and 2D COSY experiments. Support for a methyl angolensate type of structure comes from the observation of ^1H resonances for an ABX system associated with 2H-2 and H-1, and an isolated AB quartet arising from 2H-15. The large geminal coupling constants of the C-2 and C-15 methylene protons are consistent with their situation α to carbonyl groups. The ring D lactone terminus H-17, identified by its coupling to H-21 of the furan, shows a large nOe (8%) from the secondary acetate methine proton (δ_H 5.84); this implies that the acetate is attached α to C-12, consistent with the high shielding of its methyl protons. H-12 is coupled (4.2 Hz) to a proton at δ_H 3.06. This coupling must be vicinal and the proton must be H-11 since the alternative, a ^4J W-interaction

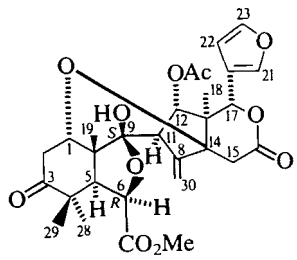

1

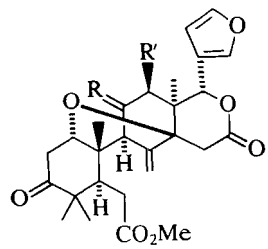

	R	R′
2	H_2	H
5	O	OAc

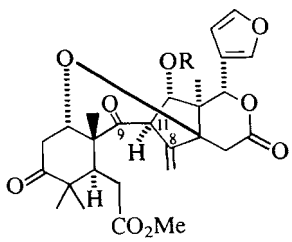

	R
3	H
4	Ac

[1]Author to whom correspondence may be addressed.

Can. J. Chem. Downloaded from www.nrcresearchpress.com by 190.90.36.8 on 09/07/12
For personal use only.

TABLE 1. ^{1}H nuclear magnetic resonance shifts[a] of trijugins *A* (**1**) and *B* (**3**), and acetate **4**

Proton	1	3	4
1	3.93 (dd, 2.9, 6.7)	4.40 (t, 3.7)	4.39 (dd, 4.5, 3.1)
2α	2.52 (dd, 2.9, 17.2)	2.44 (dd, 3.6, 15.4)	2.50 (dd, 3.1, 16.3)
2β	2.94 (dd, 6.7, 17.2)	2.97 (dd, 3.8, 15.4)	2.96 (dd, 4.5, 16.3)
5	3.24 (d, 8.4)	2.97 (dd, 7.6, 2.1)	3.29 (dd, 8.5, 2.5)
6	4.81 (d, 8.3)	2.34 (dd, 2.1, 17.8)	2.40 (dd, 8.5, 18.0) *pro R*
		2.84 (dd, 7.6, 17.8)	2.76 (dd, 2.5, 18.0) *pro S*
11	3.06 (dt, 4.2, 1.4)	3.38 (dt, 3.3, 1.2)	3.36 (dt, 2.9, 1.1)
12	5.82 (d, 4.2)	5.39 (d, 3.3)	5.58 (d, 2.9)
15β 15α	2.72 2.82 (AB_q, 17.9)	2.74 2.90 (AB_q, 17.9)	2.81 2.95 (AB_q, 17.9)
17	5.92 (s)	5.95 (d, 0.9)	6.10 (bd, 0.9)
18	0.90	0.84	0.89
19	1.16	1.22	1.14
21	7.33 (m)	7.51 (dt, 1.6, 0.9)	7.52 (dt, 1.6, 0.9)
22	6.31 (m)	6.45 (dd, 0.9, 1.9)	6.36 (dd, 0.9, 1.9)
23	7.33 (m)	7.39 (t, 1.7)	7.38 (dd, 1.6, 1.9)
28	1.35	1.08	1.08
29	1.06	1.06	1.11
30 *Z*	5.13 (d, 1.5)	5.19 (bd, 0.9)	5.23 (bt)
30 *E*	5.50 (d, 1.4)	5.34 (dd, 0.5, 1.2)	5.40 (dd, 0.8, 1.1)
OMe	3.75	3.65	3.65
Ac	1.75		1.81
OH	4.2 (bs)		

[a]In ppm relative to internal $CHCl_3$ at δ 7.25 for solutions in $CDCl_3$ run at 200.13 MHz. Multiplicities and splittings (Hz) are given in brackets.

between H-12 and H-9, would require an α-H at C-12 and is inconsistent with the nOes observed between H-11 and H-12 (both 3%), and H-12 and H-17 (8 and 5%). H-11 couples allylically to the exomethylene protons. This fact is significant and indicates that we are not dealing with a normal ring B-cleaved tetranortriterpenoid but with one containing a cyclopentanoid ring C. This conclusion is supported by several nOes. Thus the resonance for H-11 is enhanced (6%) by irradiation of 3H-18 but not of 3H-19. The spatial relationships are therefore different from the normal methyl angolensate type of structure, where H-9 is equatorial in ring C and remote from C-18 but *gauche* to C-19, and where H-9 and 2H-30 are coplanar. Complementary results for methyl angolensate (to be published) confirm these conclusions. The remaining coupled ^{1}H spin system consists of the secondary terminus of the cyclic hemiketal H-6 coupled to H-5, both with large nOes (6%) from {3H-28}. Hence the hemiketal carbon is C-9. The large nOe (7%) of the hemiketal hydroxyl proton from {3H-19} agrees with this assignment and shows that the configuration of C-9 is *S*. The large nOe (13%) of H-6 from {H-5} means that the coupling involved (8.3 Hz) arises from a *syn* rather than an *anti* relationship and that the configuration of C-6 is *R* as in related compounds (3). These data lead to structure **1** for trijugin *A*.

Definitive assignments of all the ^{13}C resonances and confirmation of the structure were achieved using 2D δ_C/δ_H correlation experiments. 2D One-bond δ_C/δ_H correlation permitted the assignments of all the protonated carbons including the tertiary methyl groups. Prior identification of the ^{1}H resonances of the tertiary methyl groups was effected using small *J* 2D COSY, which revealed the ^4J couplings between 3H-28 and 3H-29 and between H-17 and 3H-18. The quaternary carbons were assigned on the basis of the 2D long-range δ_C/δ_H correlations listed in Table 3. The hemiacetal carbon has long-range correlations with H-6 (^3J via oxygen), H-11 (^2J), H-12 (^3J), and 3H-19 (^3J), which support its assignment as C-9. In contrast C-12 exhibits long-range correlations with H-11 (^2J) and 3H-18 (^3J). C-11 correlates with 2H-30 (^3J) but not with 3H-19.

It is clear from the spectroscopic properties of trijugin *B* (**3**), $C_{27}H_{32}O_9$ (*m/z* 500.2066 (M^+)), mp 230–231°C, $[\alpha]_D^{30}$ −15° (*c* 2.0 in $CHCl_3$), ir (KBr) ν_{max}: 3 450, 1 730, 1 685 cm^{-1}, that it is closely related to trijugin *A* (**1**). The ^{1}H and ^{13}C nmr data (Tables 1 and 2) show all the same features except for a secondary hydroxyl group instead of an acetate at C-12, a ketone instead of a cyclic hemiketal at C-9, and a second proton at C-6 (J_{gem} 17.8 Hz). Acetylation of trijugin *B* (**3**) afforded the acetate **4**, mp 222°C, ir (CCl_4) ν_{max}: 1 750, 1 710, 1 694 cm^{-1}, *m/z* 542.2156. The acetate protons are again shielded (δ_H 1.81), consistent with their position at C-12, and the five-membered ring C was established for compound **4** by evidence similar to that for compound **1**. Irradiation of 3H-18 gave a 4% nOe at H-11, and the H-12, {H-17} nOe was 6%. The C-9 ketone was confirmed by 2D long-range δ_C/δ_H correlations (Table 3) to H-11, H-12, and 3H-19. Thus trijugin *B* has structure **3**.

Trijugins *A* (**1**) and *B* (**3**) represent a new skeletal type of tetranortriterpenoid. The contraction of ring C may occur by a pinacol–pinacolone rearrangement of a 9,11-dihydroxy precursor. The structural elucidation of trijugins *A* and *B* provides another illustration of the use of 2D long-range δ_C/δ_H correlation in the solution of structural problems and for definitive assignment of nonprotonated carbons, although in this case nOe difference experiments provided the vital clues to the new tetranortriterpenoid skeleton. Spectroscopically the distinction between the new cyclopentanoid and the normal six-membered ring C is rather subtle and with acetate **4**, for example, the data obtained initially pointed towards structure **5**. Several tetranortriterpenoids with multiple oxygenation of ring C are known (3) and it is clear that in future more

Can. J. Chem. Downloaded from www.nrcresearchpress.com by 190.90.36.8 on 09/07/12
For personal use only.

Can. J. Chem. Downloaded from www.nrcresearchpress.com by 190.90.36.8 on 09/07/12
For personal use only.

TABLE 2. ^{13}C nuclear magnetic resonance shifts[a] of trijugins *A* (**1**) and *B* (**3**), and acetate **4**

Carbon	1	3	4
1	74.5	74.9	74.3
2	43.4	41.6	41.9
3	211.3	210.0	210.6
4	46.9	48.9	49.1
5	54.1	42.4	41.2
6	75.8	30.5	30.1
7	175.5	174.7	173.5
8	143.2	142.7	142.5
9	108.4	207.3	204.9
10	53.0	54.7	56.3
11	60.1	70.8	69.1
12	74.8	75.7	75.8
13	48.8	49.6	49.9
14	88.4	89.5	88.5
15	33.7	34.4	34.9
16	168.3	168.2	167.8
17	77.9	78.4	77.4
18	11.4	10.2	11.7
19	18.4	18.6	18.7
20	120.6	121.4	120.9
21	141.3	140.3	140.7
22	109.5	109.2	108.8
23	142.9	143.2	143.3
28	27.4	25.2	26.5
29	20.3	22.3	22.4
30	113.4	110.2	114.9
MeO	52.6	52.2	52.0
Me*C*O	169.4		169.0
*Me*CO	20.9		20.4

[a]In ppm relative to internal TMS for solutions in $CDCl_3$ at 25 MHz. Multiplicities were determined from 2D one-bond δ_C/δ_H correlation spectra run at 50 MHz.

TABLE 3. 2D Long-range δ_C/δ_H correlations[a] of trijugin *A* (**1**) and acetate **4**

	Protons showing correlations	
Carbon	1	4
1	2α, 5, 19	2α, 19
3	2α and β, 28, 29	1, 2α and β, 28, 29
4	5, 28, 29	5, 6 *pro R* and *pro S*, 28, 29
6	5	
7	5, OMe	5, 6 *pro R* and *pro S*, OMe
8	11, 30*E*	11, 12, 30*E*
9	6, 11, 12, 19	11, 12, 19
10	2α, 5, 6, 19	2α, 5, 6 *pro S*, 19
11	30*E* and *Z*	30*E* and *Z*
12	11, 18	11, 18
13	12, 15,[b] 17, 18	12, 15β, 17, 18
14	11, 15,[b] 18, 30*E* and *Z*	1, 11, 12, 15β, 18, 30*E* and *Z*
16	15α and β	15α and β
17	12, 18	12, 18
Me*C*O	12, OAc	12, OAc

[a]Standard 2D δ_C/δ_H correlation experiments giving heteronuclear decoupling in both dimensions and performed (4), with phase-cycling to achieve quadrature detection in both dimensions (5); the fixed delay for coherence transfer was 40 ms and the fixed delay for refocussing of transverse ^{13}C magnetisation was 20 ms.

[b]It was not possible to distinguish between the α and β positions because of the 2nd-order character of 2H-15: the correlation observed corresponded to the inner lines of the AB quartet, which are not resolved in the 2D experiment.

detailed examination of such compounds will be necessary than has been the norm in the past. Subsequent to this work we ourselves have found that the ekebergolactones (3) also possess the cyclopentanoid ring C (to be published).

Experimental

All mps are uncorrected. Acme's silica gel (100–200 mesh) was used for column chromatography. Separations were monitored by tlc (silica gel G).

Isolation

The leaves of *H. trijuga* Roxb. (syn. *Trichilia connaroides* (W. & A.) Bentilezen) were collected at Pune, India, in May and identified by Mr. S. Usman Ali, Assistant Director, Jawaharlal Nehru Ayurvedic Medicinal Plants Garden and Herbarium, Pune. A specimen (Reg. No. 275) has been deposited at the Herbarium of the Captain Srinivasa Murti Drug Research Institute.

Dried, powdered leaves (2 kg) were defatted with *n*-hexane and then extracted with $CHCl_3$ in the cold for 48 h. The residue (30 g), after removal of the solvent, was chromatographed over a column of silica gel (600 g). The column was eluted with *n*-hexane, benzene, and $CHCl_3$ followed by mixtures of $CHCl_3$–EtOAc. $CHCl_3$–EtOAc (19:1) yielded 24-methylenecycloartane-3β,21-diol (300 mg) (1) while $CHCl_3$–EtOAc (9:1) gave heynic acid (600 mg) (1). Elution with 15% EtOAc–$CHCl_3$ (200 mL) and removal of solvent afforded a green mass, which on further chromatography over silica gel and crystallization from acetone–*n*-hexane gave *trijugin A* (**1**) (300 mg), mp 265–266°C. *Anal.* calcd. for $C_{29}H_{34}O_{11}$: C 62.4, H 6.1%; found: C 62.8, H 6.3. The product obtained on elution with 20% EtOAc–$CHCl_3$ (300 mL) was rechromatographed over silica gel and crystallized from acetone–*n*-hexane to give *trijugin B* (**3**) (350 mg), mp 230–231°C. *Exact Mass* calcd. for $C_{27}H_{32}O_9$: 500.2046; found (*m/z*): 500.2066.

Acetate 4

Trijugin *B* (**3**) (100 mg) in dry pyridine (1 mL) was treated with acetic anhydride (2 mL) at room temperature for 12 h. The usual work-up, followed by filtration through a short column of silica gel and crystallization from acetone–*n*-hexane, afforded the *acetate* **4** (80 mg) mp 222°C. *Exact Mass* calcd. for $C_{29}H_{34}O_{10}$: 542.2152; found (*m/z*): 542.2156.

Acknowledgements

We thank the Central Council for Research in Ayurveda and Siddha, New Delhi, for financial assistance to K.K.P., M.V., and A.S., Mr. S. Usman Ali for supplying and identifying the plant material, and the Science and Engineering Research Council for financial assistance towards purchase of the nmr spectrometer.

1. K. K. PURUSHOTHAMAN, A. SARADA, and V. MATHURAM. Indian J. Chem. **22B**, 820 (1983).
2. C. W. L. BEVAN, J. W. POWELL, D. A. H. TAYLOR, T. G. HALSALL, P. TOFT, and M. WELFORD. J. Chem. Soc. (C), 163 (1967); W. R. CHAN, K. E. MAGNUS, and B. S. MOOTOO. J. Chem. Soc. (C), 171 (1967).
3. D. A. H. TAYLOR. Prog. Chem. Org. Nat. Prod. **45**, 1 (1984).
4. R. FREEMAN and G. A. MORRIS. J. Chem. Soc. Chem. Commun. 684 (1978).
5. A. BAX and G. A. MORRIS. J. Magn. Reson. **42**, 501 (1981).

Reactions of sulfonhydrazides with benzeneseleninic acid, selenium halides, and sulfur halides. A convenient preparation of selenosulfonates and thiosulfonates

THOMAS G. BACK,[1] SCOTT COLLINS,[2,3] AND M. VIJAYA KRISHNA
Department of Chemistry, University of Calgary, Calgary, Alta., Canada T2N 1N4

Received May 28, 1986

This paper is dedicated to Dr. O. E. (Ted) Edwards

THOMAS G. BACK, SCOTT COLLINS, and M. VIJAYA KRISHNA. Can. J. Chem. **65**, 38 (1987).

The oxidation of sulfonhydrazides with benzeneseleninic acid provides an efficient and convenient preparation of selenosulfonates. Se-Phenyl *p*-tolueneselenosulfonate was also produced in good to excellent yield from the reaction of *p*-toluenesulfonhydrazide with PhSeCl, $PhSeBr_3$, or $PhSeCl_3$. Sulfonhydrazides react with sulfenyl halides or with $PhSBr_3$ to produce thiosulfonates in generally high yield. The treatment of *p*-toluenesulfonhydrazide with benzenetellurinic acid, $PhTeCl_3$, or $PhTeBr_3$ afforded only diphenyl ditelluride and not the corresponding tellurosulfonate.

THOMAS G. BACK, SCOTT COLLINS et M. VIJAYA KRISHNA. Can. J. Chem. **65**, 38 (1987).

L'oxydation des sulfonhydrazides par l'acide benzènesélénique s'avère une méthode efficace et intéressante de préparer des sélénosulfonates. On a aussi préparé le *p*-toluènesélénosulfonate de Se-phényle avec un rendement de bon à excellent en faisant réagir la *p*-toluènesulfonhydrazide avec le PhSeCl, le $PhSeBr_3$ ou le $PhSeCl_3$. Les sulfonhydrazides réagissent avec les halogènures de sulfényles ou avec le $PhSBr_3$ pour conduire aux thiosulfonates, généralement avec des rendements élevés. La réaction de la *p*-toluènesulfonhydrazide avec l'acide benzènetellurinique, le $PhTeCl_3$ ou le $PhTeBr_3$ ne conduit qu'au ditellurure de diphényle et non pas au tellurosulfonate correspondant.

[Traduit par la revue]

Can. J. Chem. Downloaded from www.nrcresearchpress.com by 190.90.36.8 on 09/07/12
For personal use only.

Introduction

Selenosulfonates (RSO_2SeR') are stable, crystalline, odourless compounds, which were first reported by Foss (1) in 1947. They were then almost completely ignored until quite recently, when we and others began an investigation of their electrophilic (2) and free-radical (2–8) additions to olefins (2–4), allenes (5), acetylenes (6, 7), and diazomethane (8). The synthetic utility of these processes, collectively named "selenosulfonations", has now been firmly established and the need for a convenient source of the required selenosulfonates is evident.

Previously, a few selenosulfonates had been obtained by the reactions of areneselenenyl bromides with sulfinates (eq. [1]) (1, 9). However, the scope of this method and its limitations were never clearly established. We now report several new procedures for preparing diverse selenosulfonates from readily available sulfonhydrazides via their oxidations with benzeneseleninic acid ($PhSeO_2H$) or from their reactions with selenenyl halides or trihalides. The similar syntheses of the well-known corresponding sulfur analogues, the thiosulfonates (RSO_2SR') (for lead references, see ref. 11), using sulfenyl halides or sulfur trihalides are also described. While this work was in progress (preliminary communication, ref. 10), Gancarz and Kice (3*b*, 12) reported a related preparation of selenosulfonates from the oxidation and sulfinic acids with benzeneseleninic acid (eq. [2]).

[1] $ArSeBr + Ar'SO_2^- \rightarrow Ar'SO_2SeAr + Br^-$

[2] $2ArSO_2H + PhSeO_2H \rightarrow ArSO_2SePh + ArSO_3H + H_2O$

Results and discussion

The oxidations of several types of hydrazo compounds with seleninic acids and anhydrides have been investigated previously (13, 14). In particular, *N*-acylhydrazines are known to afford selenoesters (eq. [3]), as well as other products, depending on the conditions (15). It appeared reasonable that, by analogy, the oxidation of sulfonhydrazides with benzeneseleninic acid ($PhSeO_2H$) should produce the desired selenosulfonates via eq. [4].

[3] $RC(=O)NHNH_2 + PhSeO_2H \longrightarrow RC(=O)SePh + N_2 + 2H_2O$

[4] $RS(=O)_2NHNH_2 + PhSeO_2H \longrightarrow RS(=O)_2SePh + N_2 + 2H_2O$

1

Our results are summarized in Table 1, which indicates that generally high yields of Se-phenyl areneselenosulfonates (**1**, R = aryl) are available via the process shown in eq. [4]. Both electron-donating and electron-withdrawing substituents are tolerated on the arylsulfonyl group. The method is also applicable to alkaneselenosulfonates, as illustrated by the methane derivative (**1**, R = Me), obtained in 65% yield (entry 9, Table 1).

Typically, the sulfonhydrazide in dichloromethane is added dropwise to benzeneseleninic acid in the same solvent at 0°C. Vigorous evolution of nitrogen occurs and the product is isolated by evaporation of the solvent, followed by crystallization of the yellow or red residue, generally from methanol. In some instances (entries 1 and 4) it was more expedient to employ methanol as the reaction solvent instead of dichloromethane, as the product then crystallized directly from the reaction medium in a high state of purity. This procedure therefore constitutes an exceptionally rapid, convenient, and efficient preparation of selenosulfonates.

A plausible mechanism for the oxidation is shown in Scheme 1. Seleninylation of the sulfonhydrazide is followed by selenoxide elimination to produce the corresponding azene **2** and benzeneselenenic acid (PhSeOH). Further reaction of these two

[1]Author to whom correspondence may be addressed.

[2]Holder of an NSERC Postgraduate Scholarship and an Honorary Killam Scholarship.

[3]Present address: Department of Chemistry, University of Waterloo, Waterloo, Ont., Canada N2L 3G1.

TABLE 1. Preparation of selenosulfonates

$$RSO_2NHNH_2 \xrightarrow{PhSeO_2H} RSO_2SePh$$

Entry	R of sulfonhydrazide	(mmol)	$PhSeO_2H$ (mmol)	Solvent	Isolated yield of RSO_2SePh (%)
1	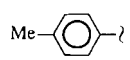	(100)	100	MeOH	96
2	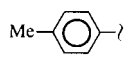	(20)	20	CH_2Cl_2	92
3	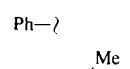	(20)	20	CH_2Cl_2	88
4	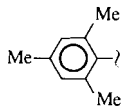	(3)	3	MeOH	91
5	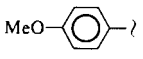	(10)	10	CH_2Cl_2	83
6	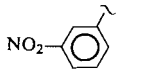	(0.5)	0.55	CH_2Cl_2	82
7	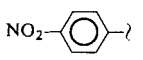	(4)	4	CH_2Cl_2	83
8	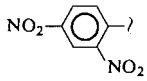	(0.5)	0.5	CH_2Cl_2	68
9	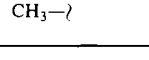	(9.5)	11.5	CH_2Cl_2	65

Can. J. Chem. Downloaded from www.nrcresearchpress.com by 190.90.36.8 on 09/07/12
For personal use only.

$$RSO_2NHNH_2 + PhSeO_2H \longrightarrow [RSO_2NHNHSePh] + H_2O$$

$$[RSO_2NHNHSePh] \longrightarrow [RSO_2N{=}NH] + [PhSeOH]$$
2

$$[RSO_2N{=}NH] + [PhSeOH] \longrightarrow [RSO_2N{=}NSePh] + H_2O$$
2 **3**

$$[RSO_2N{=}NSePh] \longrightarrow RSO_2SePh + N_2$$
3 **1**

SCHEME 1

intermediates is expected to furnish the selenadiazene **3**, from which nitrogen extrusion affords the desired selenosulfonate.[4]

We also investigated the reactions of *p*-toluenesulfonhydrazide with benzeneselenenyl chloride (PhSeCl), phenylselenium tribromide ($PhSeBr_3$), and phenylselenium trichloride ($PhSeCl_3$), in each case affording Se-phenyl *p*-tolueneselenosulfonate (**1**, R = *p*-tolyl) in high yield. The reactions were carried out in dichloromethane at 0°C in the presence of pyridine to remove HCl or HBr. When PhSeCl was employed, 3 molar equivalents of the reagent were required and, unfortunately, the simultaneous formation of one mole of diphenyl diselenide (PhSeSePh) necessitated the chromatographic isolation of the selenosulfonate (eq. [5]).

A plausible mechanism for the above process is given in Scheme 2, which invokes the same intermediates **2** and **3** as in

[5] 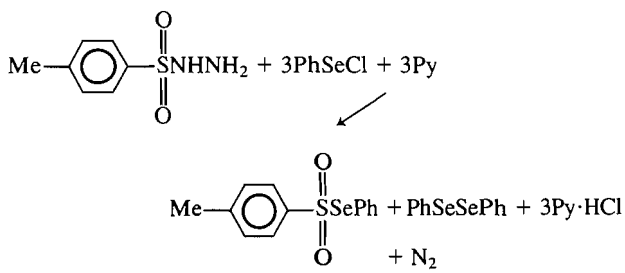

the oxidation of sulfonhydrazides with $PhSeO_2H$ as shown in Scheme 1.

The undesired formation of PhSeSePh in the preceding reaction prompted us to examine the use of selenium trihalides instead of PhSeCl, with the expectation that the higher oxidation state of the selenium atom (Se(IV) vs. Se(II)) would result in the stoichiometry shown in eq. [6], thus avoiding the unwanted diselenide by-product.

Phenylselenium tribromide (16) was prepared *in situ* by adding 3 molar equivalents of bromine to PhSeSePh in dichloromethane. The subsequent addition of the sulfonhydrazide and

$$ArSO_2NHNH_2 + PhSeCl + Py \longrightarrow [ArSO_2NHNHSePh] + Py{\cdot}HCl$$

$$[ArSO_2NHNHSePh] + Py \longrightarrow [ArSO_2N{=}NH] + PhSe^- {}^+PyH$$
2

$$[ArSO_2N{=}NH] + PhSeCl + Py \longrightarrow [ArSO_2N{=}NSePh] + Py{\cdot}HCl$$
2 **3**

$$[ArSO_2N{=}NSePh] \longrightarrow ArSO_2SePh + N_2$$
3

$$PhSe^- {}^+PyH + PhSeCl \longrightarrow PhSeSePh + Py{\cdot}HCl$$

(Ar = *p*-tolyl)

SCHEME 2

[4] A referee has pointed out that nitrogen extrusion from **2** would produce a sulfinic acid (RSO_2H), which could react with PhSeOH (or PhSeCl in Scheme 2) to produce the selenosulfonate **1** without the intermediacy of **3**. Indeed, this variation cannot be ruled out on the basis of the available evidence, as indicated previously (29).

TABLE 2. Preparation of thiosulfonates

$$RSO_2NHNH_2 \xrightarrow[R'SBr_3]{R'SCl \text{ or } R'SBr \text{ or}} RSO_2SR'$$

Entry	R of sulfonhydrazide[a]	Sulfur halide reagent (mmol)[b]		Isolated yield of RSO_2SR' (%)
1	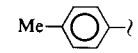	PhSBr	(3)	65[c]
2	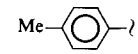	PhSCl	(3)	79[c]
3	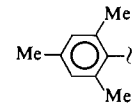	$CH_3(CH_2)_4SCl$	(3)	88[c]
4	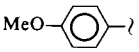	$PhCH_2SCl$	(3)	89[c]
5	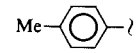	$PhSBr_3$	(1)	42[d]

[a]All reactions were performed in CH_2Cl_2 at 0°C, using 1 mmol of sulfonhydrazide.
[b]The reagents were prepared *in situ* by adding Br_2 or SO_2Cl_2 to the corresponding disulfides in the presence of a catalytic amount of Et_3N.
[c]An approximately equimolar amount of R'SSR' was also produced.
[d]*p*-Toluenesulfonyl bromide was also isolated in 20% yield.

[6] 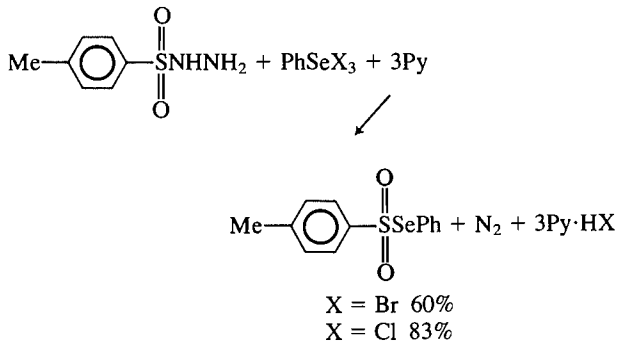

pyridine afforded the expected selenosulfonate in 60% yield. Closer scrutiny of the reaction mixture revealed the accompanying formation of *p*-toluenesulfonyl bromide, which was isolated in 21% yield. It therefore appears that the selenium tribromide functions as a brominating agent[5] as well as a selenenylating agent in this reaction. Similar results were obtained with $PhSeCl_3$, which was also generated *in situ* from the diselenide and sulfuryl chloride (17). In this case an improved yield of the selenosulfonate (83%) was realized and only a small quantity of *p*-toluenesulfonyl chloride (11%) was produced. The use of selenium halide reagents therefore comprises an alternative approach to the synthesis of selenosulfonates, although the need for the removal of by-products renders the method less convenient than the oxidation of sulfonhydrazides with $PhSeO_2H$.

We also wished to determine whether similar procedures would permit the preparation of the synthetically useful thiosulfonates (RSO_2SR', **4**) (11), and the, as yet unreported, tellurosulfonates (RSO_2TePh, **5**). We first attempted to react *p*-toluenesulfonhydrazide with *p*-toluenesulfinic acid (by analogy to eq. [4]); however, no reaction was observed, indicating that the sulfinic acid is a considerably less powerful oxidant than $PhSeO_2H$ in this process. On the other hand, the treatment of several sulfonhydrazides with 3 molar equivalents of sulfenyl chlorides or bromides in the presence of pyridine afforded high yields of the desired thiosulfonates, as indicated in Table 2. As in the case of the selenium series (ca. eq. [5]), the products were accompanied by the formation of an equimolar amount of the corresponding disulfides. The use of phenylsulfur tribromide ($PhSBr_3$) proved less satisfactory (entry 5, Table 2), affording only 42% of the thiosulfonate (cf. eq. [6]) as well as 20% of *p*-toluenesulfonyl bromide.

Attempts to react *p*-toluenesulfonhydrazide with benzenetellurinic acid ($PhTeO_2H$) (19), phenyltellurium trichloride ($PhTeCl_3$) (20), or phenyltellurium tribromide ($PhTeBr_3$) (20) all failed to afford significant quantities of the corresponding tellurosulfonate RSO_2TePh (**5**, R = *p*-tolyl). In each case diphenyl ditelluride (PhTeTePh) was the only major tellurium-containing product that could be isolated.

These experiments demonstrate that sulfonhydrazides can be used as convenient precursors of both selenosulfonates and thiosulfonates, but not of tellurosulfonates.

Experimental

Melting points were obtained on an A. H. Thomas hot-stage apparatus and are uncorrected. Spectroscopic data were recorded on the following instruments, ir: Perkin–Elmer 467 or Nicolet 5DX FTIR; ^1H nmr: Hitachi Perkin–Elmer R24B or Varian XL200; ms: Varian MAT CH5 or Kratos MS80. All nmr spectra were obtained in $CDCl_3$ solution with internal TMS as the standard unless otherwise indicated. Elemental analyses were performed by Dr. W. S. Lin (University of Calgary) or by Guelph Chemical Laboratories.

Benzeneseleninic acid, diphenyl diselenide, and benzeneselenenyl chloride were purchased from the Aldrich Co. and used without further purification. Sulfonhydrazides were obtained from commercial sources except for the following compounds, which were prepared by literature methods: 4-methoxybenzenesulfonhydrazide (21), 3-, 4-, and 2,4-dinitrobenzenesulfonhydrazides (22), and methanesulfonhydrazide (23). Diphenyl ditelluride (24) and phenyltellurium trihalides (20) were obtained by published procedures. Benzenetellurinic acid (19) was prepared by the hydrolysis of $PhSeBr_3$, according to a known general method (25). Diphenyl, di-*n*-amyl, and dibenzyl disulfides, as well as all other required reagents, were purchased commercially and purified by standard methods as necessary.

[5]It has been reported that selenium trihalides are in equilibrium with the corresponding selenenyl halides and free halogen (18), as in the following example: $PhSeBr_3 \rightleftharpoons PhSeBr + Br_2$.

Can. J. Chem. Downloaded from www.nrcresearchpress.com by 190.90.36.8 on 09/07/12
For personal use only.

Can. J. Chem. Downloaded from www.nrcresearchpress.com by 190.90.36.8 on 09/07/12
For personal use only.

Preparation of selenosulfonates via the oxidation of sulfonhydrazides with $PhSeO_2H$ (see Table 1)

Se-Phenyl p-*tolueneselenosulfonate (entries 1 and 2)*

p-Toluenesulfonhydrazide (18.6 g, 100 mmol) in 75 mL of methanol was added dropwise over ca. 15 min to a suspension of benzeneseleninic acid (18.9 g, 100 mmol) in 75 mL of methanol at 0°C. Vigorous evolution of nitrogen was observed. The solution gradually turned clear yellow and towards the end of the addition a yellow precipitate formed. After cooling at −5°C overnight, the product was filtered to afford 27.65 g of the title compound, mp 77–78°C (lit. (26) mp 77–79°C.). The concentrated mother liquor provided a second crop of 2.25 g, mp 70–73°C. Total yield: 96%.

When the reaction was repeated with 20 mmol of each reactant in dichloromethane, the yield of the selenosulfonate was 92% after evaporation *in vacuo* and recrystallization from methanol, mp 79.5–80°C.

Se-Phenyl benzeneselenosulfonate (entry 3)

The procedure of entry 2 was followed to afford 88% of the title compound, mp 56–58°C (lit. (9) mp 51°C).

Se-Phenyl 2,4,6-trimethylbenzeneselenosulfonate (entry 4)

The procedure of entry 1 was followed to afford 91% of the title compound, mp 75–76°C (from methanol); ir ($CHCl_3$): 1315, 1133 cm^{-1}; ^1H nmr (60 MHz) δ: 7.55–7.25 (m, 5H), 6.82 (s, 2H), 2.31 (s, 6H), 2.29 (s, 3H); mass spectrum, *m/e*: 340 (M^+, ^{80}Se), 338 (M^+, ^{78}Se). *Anal.* calcd. for $C_{15}H_{16}O_2SSe$: C 53.07, H 4.76, S 9.46; found: C 53.40, H 4.87, S 9.58.

Se-Phenyl 4-methoxybenzeneselenosulfonate (entry 5)

The procedure of entry 2 was followed to afford 83% of the title compound, mp 79–80°C (from methanol); ir (Nujol): 1316, 1139 cm^{-1}; ^1H nmr (60 MHz) δ: 7.60–7.25 (m, 7H), 6.82 (d, J = 9 Hz, 2H), 3.88 (s, 3H); mass spectrum, *m/e*: 328 (M^+, ^{80}Se), 326 (M^+, ^{78}Se). *Anal.* calcd. for $C_{13}H_{12}O_3SSe$: C 47.69, H 3.70, S 9.80; found: C 47.85, H 3.85, S 10.19.

Se-Phenyl 3-nitrobenzeneselenosulfonate (entry 6)

3-Nitrobenzenesulfonhydrazide (108 mg, 0.50 mmol) was added in portions over 15 min to $PhSeO_2H$ (104 mg, 0.55 mmol) in 10 mL of dichloromethane. The solvent was removed *in vacuo* and the residue was separated by preparative tlc on silica gel with 20% chloroform–benzene to furnish 139 mg (82%) of the title compound, mp 125–127°C (from methanol); ir (KBr): 1545, 1350, 1320, 1145 cm^{-1}; ^1H nmr (60 MHz) δ: 8.42 (dt, J = 8, 2 Hz, 1H), 8.21 (t, J = 2 Hz, 1H), 7.85 (dt, J = 8, 2 Hz, 1H), 7.65–7.20 (m, 6H); mass spectrum, *m/e*: 343 (M^+, ^{80}Se), 341 (M^+, ^{78}Se). *Anal.* calcd. for $C_{12}H_9NO_4SSe$: C 42.12, H 2.65, N 4.09, S 9.37; found: C 41.76, H 2.64, N 4.00, S 9.24.

Se-Phenyl 4-nitrobenzeneselenosulfonate (entry 7)

4-Nitrobenzenesulfonhydrazide (0.87 g, 4.0 mmol) was added in portions over 15 min to $PhSeO_2H$ (0.76 g, 4.0 mmol) in 75 mL of dichloromethane. After stirring for several additional minutes, a small amount of insoluble material was filtered, the filtrate was concentrated, and the product crystallized upon addition of hexane to give 1.14 g (83%), mp 143–145°C; ir (KBr): 1528, 1351, 1308, 1134 cm^{-1}; ^1H nmr (60 MHz) δ: 8.28 (d, J = 8 Hz, 2H), 7.65 (d, J = 8 Hz, 2H), 7.41 (br s, 5H); mass spectrum, *m/e*: 343 (M^+, ^{80}Se), 341 (M^+, ^{78}Se). *Anal.* calcd. for $C_{12}H_9NO_4SSe$: C 42.12, H 2.65, N 4.09, S 9.37; found: C 42.30, H 2.59, N 4.11, S 9.61.

Se-Phenyl 2,4-dinitrobenzeneselenosulfonate (entry 8)

The preceding procedure was followed to afford 68% of the title compound, mp 147–150°C (from dichloromethane–hexane); ir (Nujol): 1566, 1540, 1362, 1344, 1319, 1135 cm^{-1}; ^1H nmr (60 MHz, DMSO-d_6) δ: 8.91 (d, J = 3 Hz, 1H), 8.55 (dd, J = 8, 3 Hz, 1H), 7.61 (d, J = 8 Hz, 1H), 7.55 (m, 5H); mass spectrum, *m/e*: 388 (M^+, ^{80}Se), 386 (M^+, ^{78}Se). *Anal.* calcd. for $C_{12}H_8N_2O_6SSe$: C 37.20, H 2.08, N 7.24, S 8.18; found: C 38.12, H 2.30, N 7.35, S 8.37. Attempts at further purification by crystallization resulted in decomposition.

Se-Phenyl methaneselenosulfonate (entry 9)

The procedure of entry 2 was followed to afford 65% of the title compound, mp 88–90°C (from methanol); ir ($CHCl_3$): 1330, 1131 cm^{-1}; ^1H nmr (60 MHz, CCl_4) δ: 7.80 (m, 2H), 7.46 (m, 3H), 3.18 (s, 3H); mass spectrum, *m/e*: 236 (M^+, ^{80}Se), 234 (M^+, ^{78}Se). *Anal.* calcd. for $C_7H_8O_2SSe$: C 35.73, H 3.43, S 13.64; found: C 35.87, H 3.59, S 13.48.

Reaction of p-*toluenesulfonhydrazide with PhSeCl*

The sulfonhydrazide (186 mg, 1.00 mmol) in 2 mL of dichloromethane was added dropwise to a solution of PhSeCl (574 mg, 3.00 mmol) and pyridine (0.24 mL, 3 mmol) in 4 mL of dichloromethane at 0°C. After 15 min, the mixture was concentrated *in vacuo* and separated by flash chromatography on silica gel. Diphenyl diselenide was eluted with hexane and elution with 60% dichloromethane–hexane afforded 300 mg (96%) of Se-phenyl *p*-tolueneselenosulfonate (**1**, R = *p*-tolyl), mp 76–78°C.

Reaction of p-*toluenesulfonhydrazide with $PhSeBr_3$*

Bromine (77 μL, 1.5 mmol) in 2 mL of dichloromethane was added dropwise to a solution of PhSeSePh (157 mg, 0.50 mmol) in 2 mL of dichloromethane at 0°C and stirring was continued for 1.5 h. A solution of the sulfonhydrazide (186 mg, 1.00 mmol) and pyridine (0.24 mL, 3 mmol) in 3 mL of dichloromethane was then added to the $PhSeBr_3$ solution at 0°C. The mixture was concentrated and flash chromatographed over silica gel. A small amount of PhSeSePh was removed with hexane, followed by elution of *p*-toluenesulfonyl bromide (50 mg, 21%) with 30% dichloromethane–hexane, mp 90–93°C (lit. (27) mp 93–94°C), identified by its ir and mass spectra. Further elution with 40% dichloromethane–hexane afforded 188 mg (60%) of the selenosulfonate **1** (R = *p*-tolyl), mp 74–76°C.

Reaction of p-*toluenesulfonhydrazide with $PhSeCl_3$*

Sulfuryl chloride (0.12 mL, 1.5 mmol) was added to PhSeSePh (157 mg, 0.50 mmol) in 1 mL of dichloromethane at 0°C and stirring was continued for 0.5 h. The $PhSeCl_3$ thus produced was then treated with the sulfonhydrazide and pyridine as in the preceding procedure to afford 21 mg (11%) of *p*-toluenesulfonyl chloride, identical to an authentic sample, and 257 mg (83%) of the selenosulfonate **1** (R = *p*-tolyl), mp 77–78°C.

Preparation of thiosulfonates from sulfonhydrazides and sulfur halides (see Table 2)

S-*Phenyl* p-*toluenethiosulfonate (entries 1, 2, and 5)*

Bromine (77 μL, 1.5 mmol) in 2 mL of dichloromethane was added to PhSSPh (327 mg, 1.50 mmol) in 2 mL of dichloromethane at 0°C. After several minutes, *p*-toluenesulfonhydrazide (186 mg, 1.00 mmol) and pyridine (0.24 mL, 3.0 mmol) in 3 mL of dichloromethane was added to the sulfenyl bromide solution. The mixture was concentrated and separated by flash chromatography to furnish 257 mg (118% based on the expected formation of 1.0 mmol) of PhSSPh (eluant: hexane), 48 mg (20%) of *p*-toluenesulfonyl bromide (eluant: 20% dichloromethane–hexane), mp 92–93°C, identical to the sample prepared from the sulfonhydrazide and $PhSeBr_3$, and 172 mg (65%) of the title compound, mp 75–76°C (lit. (28) mp 75–76°C), with an ir spectrum as reported in the literature (28).

In a second experiment, sulfuryl chloride (0.12 mL, 1.5 mmol) was added to PhSSPh (327 mg, 1.5 mmol) in 1 mL of dichloromethane containing a trace of triethylamine at 0°C. After several minutes, the sulfonhydrazide and pyridine were added to the resulting sulfenyl chloride as in the above procedure. Flash chromatography in the same manner provided 230 mg (105% based on the expected formation of 1.0 mmol) of PhSSPh and 209 mg (79%) of the title compound, mp 73–75°C.

In a third experiment, bromine (77 μL, 1.5 mmol) in 2 mL of dichloromethane was added to PhSSPh (109 mg, 0.50 mmol) in 2 mL of dichloromethane at 0°C. The addition of the sulfonhydrazide and pyridine to the resulting $PhSBr_3$ solution, and subsequent flash chromatography, were performed as in the preceding two procedures. The products thus obtained were 48 mg (20%) of *p*-toluenesulfonyl bromide, mp 92°C, and 111 mg (42%) of the title compound, mp 73–75°C.

S-n-*Amyl 2,4,6-trimethylbenzenethiosulfonate (entry 3)*

The procedure of entry 2 was followed to afford 88% of the title compound as a colourless oil, bp 132–134°C (0.2 Torr; 1 Torr =

133.3 Pa) by short-path distillation; ir (film): 1602, 1325, 1141, 1047, 1033, 853, 714, 645 cm^{-1}; ^1H nmr (200 MHz) δ: 6.97 (s, 2H), 3.03 (t, $J = 7$ Hz, 2H), 2.70 (s, 6H), 2.31 (s, 3H), 1.6 (m, 2H), 1.3 (m, 4H), 0.83 (t, $J = 7$ Hz, 3H); mass spectrum, m/e: 286 (M^+). *Anal.* calcd. for $C_{14}H_{22}O_2S_2$: C 58.74, H 7.69, S 22.37; found: C 58.54, H 7.83, S 22.23.

S-Benzyl 4-methoxybenzenethiosulfonate (entry 4)

The procedure of entry 2 was followed to afford 89% of the title compound as a colourless oil, bp 185–188°C (0.25 Torr) by short-path distillation; ir (film): 1593, 1496, 1326, 1263, 1137, 1080, 1024, 834, 802, 701, 660 cm^{-1}; ^1H nmr (200 MHz) δ: 7.78 (d, $J = 9$ Hz, 2H), 7.23 (m, 5H), 6.92 (d, $J = 9$ Hz, 2H), 4.25 (s, 2H), 3.88 (s, 3H); mass spectrum, m/e: 294 (M^+). *Anal.* calcd. for $C_{14}H_{14}O_3S_2$: C 57.14, H 4.76, S 21.76; found: C 57.14, H 4.85, S 21.83.

Attempted preparation of tellurosulfonates

The reaction of *p*-toluenesulfonhydrazide with $PhTeO_2H$, $PhTeBr_3$, and $PhTeCl_3$ was performed in both methanol and dichloromethane, with and without the presence of pyridine. In each case flash chromatography on silica gel afforded 55–60% of diphenyl ditelluride, identical to an authentic sample. The only other tellurium-containing products were either insoluble or highly polar, and were not isolated.

Acknowledgement

We thank the Natural Sciences and Engineering Research Council of Canada and the Research Corporation for financial support.

1. O. Foss. J. Am. Chem. Soc. **69**, 2236 (1947).
2. (*a*) T. G. Back and S. Collins. Tetrahedron Lett. **21**, 2215 (1980); (*b*) J. Org. Chem. **46**, 3249 (1981).
3. (*a*) R. A. Gancarz and J. L. Kice. Tetrahedron Lett. **21**, 4155 (1980); (*b*) J. Org. Chem. **46**, 4899 (1981); (*c*) Y.-H. Kang and J. L. Kice. J. Org. Chem. **49**, 1507 (1984).
4. (*a*) L. A. Paquette and W. A. Kinney. Tetrahedron Lett. **23**, 5127 (1982); (*b*) L. A. Paquette and G. D. Crouse. J. Org. Chem. **48**, 141 (1983); (*c*) W. A. Kinney, G. D. Crouse, and L. A. Paquette. J. Org. Chem. **48**, 4986 (1983).
5. (*a*) Y.-H. Kang and J. L. Kice. Tetrahedron Lett. **23**, 5373 (1982); (*b*) J. L. Kice and Y.-H. Kang. Tetrahedron, **41**, 4739 (1985).
6. (*a*) T. G. Back and S. Collins. Tetrahedron Lett. **22**, 5111 (1981); (*b*) T. G. Back, S. Collins, and R. G. Kerr. J. Org. Chem. **48**, 3077 (1983); (*c*) T. G. Back, S. Collins, U. Gokhale, and K.-W. Law. J. Org. Chem. **48**, 4776 (1983); (*d*) T. G. Back, S. Collins, and K.-W. Law. Tetrahedron Lett. **25**, 1689 (1984); (*e*) Can. J. Chem. **63**, 2313 (1985); (*f*) T. G. Back, J. R. Proudfoot, and C. Djerassi. Tetrahedron Lett. **27**, 2187 (1986).
7. T. Miura and M. Kobayashi. J. Chem. Soc. Chem. Commun. 438 (1982).
8. T. G. Back. J. Org. Chem. **46**, 5443 (1981).
9. T. Austad. Acta Chem. Scand. Ser. A, **30**, 479 (1976).
10. T. G. Back and S. Collins. Tetrahedron Lett. **21**, 2213 (1980).
11. (*a*) L. Field. Synthesis, 101 (1972); 713 (1978); (*b*) *In* Organic chemistry of sulfur. *Edited by* S. Oae. Plenum Press, New York. 1977. Chapt. 7. pp. 323–325 and 348–350.
12. R. A. Gancarz and J. L. Kice. Tetrahedron Lett. **21**, 1697 (1980).
13. (*a*) D. H. R. Barton, D. J. Lester, and S. V. Ley. J. Chem. Soc. Chem. Commun. 445 (1977); 276 (1978); (*b*) J. Chem. Soc. Perkin Trans. 1, 1212 (1980).
14. (*a*) T. G. Back. J. Chem. Soc. Chem. Commun. 278 (1978); 530 (1981); (*b*) T. G. Back and R. G. Kerr. Can. J. Chem. **60**, 2711 (1982).
15. (*a*) T. G. Back and S. Collins. Tetrahedron Lett. 2661 (1979); (*b*) T. G. Back, S. Collins, and R. G. Kerr. J. Org. Chem. **46**, 1564 (1981).
16. (*a*) O. Behaghel and K. Hofmann. Chem. Ber. **72**, 582 (1939); (*b*) O. Behaghel and W. Muller. Chem. Ber. **68**, 1540 (1935).
17. L. Engman. Tetrahedron Lett. **26**, 6385 (1985).
18. D. L. Klayman. *In* Organic selenium compounds: their chemistry and biology. *Edited by* D. L. Klayman and W. H. H. Gunther. Wiley, New York. 1973. p. 140.
19. K. Lederer. Chem. Ber. **48**, 1345 (1915).
20. W. R. McWhinnie and P. Thavornyutikarn. J. Chem. Soc. Dalton Trans. 551 (1972).
21. H. Zinner, H. Brenken, W. Braun, I. Falk, E. Fechtner, and E. Hähner. Annalen, **622**, 133 (1959).
22. W. Davies, F. R. Storrie, and S. H. Tucker. J. Chem. Soc. 624 (1931).
23. J. W. Powell and M. C. Whiting. Tetrahedron, **7**, 305 (1959).
24. D. Seebach and A. K. Beck. Chem. Ber. **108**, 314 (1975).
25. P. Thavornyutikarn and W. R. McWhinnie. J. Organomet. Chem. **50**, 135 (1973).
26. D. H. R. Barton, M. R. Britten-Kelly, and D. Ferreira. J. Chem. Soc. Perkin Trans. 1, 1090 (1978).
27. T. Zincke and W. Frohneberg. Ber. Dtsch. Chem. Ges. **43**, 837 (1910).
28. S. Oae, Y. H. Kim, D. Fukushima, and K. Shinhama. J. Chem. Soc. Perkin Trans. 1, 913 (1978).
29. S. Collins. Ph.D. Thesis, University of Calgary, 1983. p. 80.

Can. J. Chem. Downloaded from www.nrcresearchpress.com by 190.90.36.8 on 09/07/12
For personal use only.

Synthesis of 11- and 12-membered rings by a direct cyclization method

DENIS BRILLON AND PIERRE DESLONGCHAMPS[1]

Laboratoire de synthèse organique, Département de chimie, Faculté des sciences, Université de Sherbrooke, Sherbrooke (Qué.), Canada J1K 2R1

Received May 1, 1986

This paper is dedicated to Dr. O. E. (Ted) Edwards

DENIS BRILLON and PIERRE DESLONGCHAMPS. Can. J. Chem. **65**, 43 (1987).

The malonate anion intramolecular displacement of propargylic or allylic chlorides, and of primary bromide, in eleven- and twelve-carbon chains containing either two, one, or no unsaturation centers leads to the corresponding 11- and 12-membered ring compounds in good yield under conditions of medium dilution.

DENIS BRILLON et PIERRE DESLONGCHAMPS. Can. J. Chem. **65**, 43 (1987).

Le déplacement intramoléculaire de bromure primaire et de chlorures allyliques ou propargyliques par l'anion malonate de chaînes de onze et douze carbones contenant soit deux, une ou aucune insaturation conduit aux composés cycliques à 11 et 12 membres correspondants, avec d'excellents rendements dans des conditions de dilution moyenne.

Can. J. Chem. Downloaded from www.nrcresearchpress.com by 80.58.250.72 on 09/07/12
For personal use only.

The study of the conformation and the chemical reactivity of medium and large carbocyclic and heterocyclic rings containing various functional groups and substituents is an interesting area of research that has so far been essentially unexplored.[2,3] The discovery of reliable direct methods of cyclization for the preparation of these macrocyclic compounds is an important step in starting such a study.

We have recently reported (1) that 10-membered rings can be obtained in good yield by a direct method of cyclization at 10^{-2} and 10^{-3} molar solutions (not high dilution) provided that the aliphatic chains contain two unsaturation centers (double or triple bond). The success of this method was due to the presence of the unsaturation centres, which diminish the number of degrees of freedom of the chain and which eliminate, at the same time, most of the transannular steric interactions (the two main factors that render macrocyclization difficult).

Since previous studies on cyclization of aliphatic saturated chains have shown generally the difficulty of preparing C-9 to C-12 membered rings (with a drop in yield for C-10) (4), we have undertaken a study of 11- and 12-membered ring formation via the above strategy and we wish to report this work.[4]

Cyclization reactions were carried out for the C-11 and C-12 acyclic precursors **1***a* and **1***b* (Scheme 1), which have two unsaturation centers (either a triple bond or a double bond (*cis* or *trans*)), and which can yield either the corresponding cyclic monomers (**2***a* and **2***b*) or dimers (**3***a* and **3***b*) in competition with the polymerization process. The cyclization of the C-11 and C-12 acyclic precursors **4***a* and **4***b* containing only one unsaturation center (a triple bond) was also studied. Similarly, the cyclization of the C-11 and C-12 saturated precursors **5***a* and **5***b* was also carried out to confirm the validity of our approach. In competition with the polymerization process, compounds **4***a,b* and **5***a,b* can yield either their corresponding cyclic monomers (**6***a,b* and **7***a,b* respectively) or dimers (structures not shown).

An interesting synthetic route for the preparation of all the C-11 and C-12 precursors, starting with simple acetylene derivatives, was found, and is summarized in Schemes 2–4. The C-6 and C-7 acetylenic key intermediates **8***a* and **8***b* were prepared as described in Scheme 2. Using these two intermediates, the corresponding C-6 and C-7 intermediates having a *cis* olefin (**9***a* and **9***b*), a *trans* olefin (**10***a* and **10***b*), or no unsaturation (**11***a* and **11***b*) were prepared as shown in Scheme 3. The same scheme summarizes also the conversion of the C-6 and C-7 key intermediates **8***a*, **8***b*, **9***a*, **9***b*, **10***a*, and **10***b* respectively into the C-11 and C-12 doubly unsaturated aliphatic precursors **1***a* and **1***b* [A–A, A–T, A–C, T–T, T–C, and C–C] (A = acetylene, T = *trans* olefin, and C = *cis* olefin). It also describes the preparation of the mono-unsaturated C-11 and C-12 aliphatic chains **4***a* and **4***b* (containing one triple bond) from the saturated C-6 and C-7 intermediates **11***a* and **11***b*, as well as the formation of the fully saturated C-11 and C-12 aliphatic chains **5***a* and **5***b* obtained respectively from the catalytic hydrogenation of **4***a* and **4***b*.

The general strategy for the preparation of the unsaturated C-11 and C-12 aliphatic chains **1***a*, **1***b*, **4***a*, and **4***b* from the C-6 and C-7 aliphatic chains is further detailed in Scheme 4: alkylation of intermediates **8**–**11** (*a* or *b*) with an appropriate alkylating agent (*cis* or *trans* 1,4-dichloro-2-butene or 1,4-dichloro-2-butyne) gave the corresponding chlorides **14***a* and **14***b*. SN_2 displacement of these chlorides with dimethyl malonate gave the THP-malonates **15***a* and **15***b*. Acid hydrolysis then provided the primary alcohol malonates **16***a* and **16***b*, which were then respectively converted into the C-11 and C-12 allylic or propargylic chlorides **1***a* and **1***b* [A–A, A–T, A–C, T–T, T–C, and C–C] as well as the primary bromides **4***a* and **4***b*.

The reactions of cyclization were performed at 2×10^{-2} and 2×10^{-3} molar dilution and not high dilution. The results are summarized in Tables 1 and 2 for the 11- and 12-membered rings respectively. The monomers and dimers are readily separated by column chromatography. All the cyclic monomers (except for **2***a* [T–T]) and dimers are crystalline compounds. For all new substances, the spectra (ir, 250-MHz and 80-MHz ^{1}H nmr, ^{13}C nmr, and high resolution mass spectra) were in complete agreement with the assigned structures. The corresponding ^{1}H nmr, ^{13}C nmr, and mass spectral characteristics and melting points for the cyclic compounds are listed in Table 3.

As previously observed with C-10 aliphatic chains (1), dimerization always competes effectively with the polymerization process, even at 10^{-2} *M*. At 10^{-3} *M*, the monomers are generally produced in a yield greater than 60% except for **2***a* [C–C] (54%), **2***a* [T–T] (32%), **2***a* [A–T] (44%), and **2***b* [C–T] (38%). Better yields of monomers are obtained in the C-12 series except for **2***b* [C–T] and **2***b* [A–A]. The increase in yield of monomer on passing from the saturated chain to the monoacetylene and to the bisacetylene is clearly seen in the

[1]Author to whom correspondence may be addressed.

[2]For a general discussion, see ref. 2.

[3]For previous work in this area, see references cited in refs. 1–3.

[4]For a preliminary account, see ref. 5.

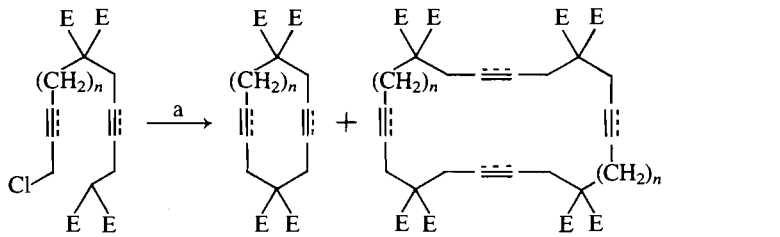

1a (n = 2) **2a** (n = 2) **3a** (n = 2)
1b (n = 3) **2b** (n = 3) **3b** (n = 3)

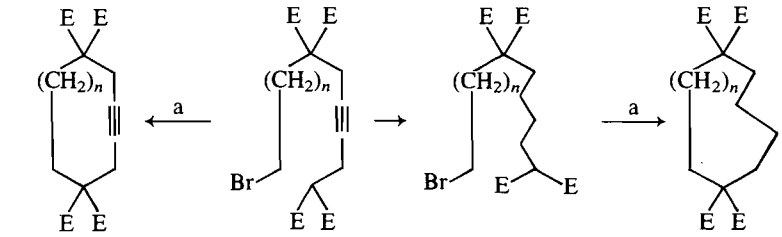

6a (n = 4) **4a** (n = 4) **5a** (n = 4) **7a** (n = 4)
6b (n = 5) **4b** (n = 5) **5b** (n = 5) **7b** (n = 5)

(E = $COOCH_3$)

(a) K_2CO_3, THF–DMF, 90°C, ref. 1

SCHEME 1

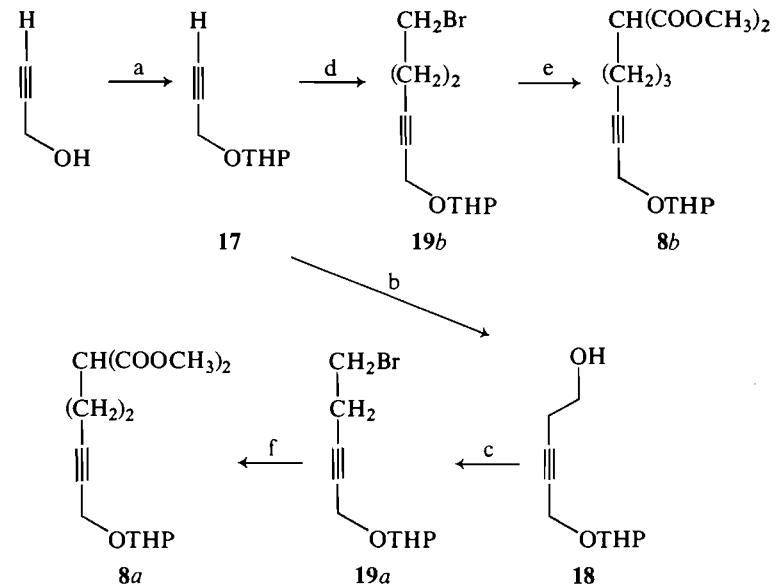

17 **19b** **8b**

8a **19a** **18**

(a) DHP, CF_3CO_2H, CH_2Cl_2, r.t., 93%
(b) n-BuLi, Et_2O–THF–HMPA, −40°C → r.t., $(CH_2)_2O$, r.t.
(c) CBr_4, Ph_3P, pyridine, CH_2Cl_2, 0°C → r.t., 66%
(yield for b and c), ref. 6
(d) n-BuLi, THF–HMPA, −40°C, $CH_2(CH_2Br)_2$, reflux, 83%, ref. 7
(e) K_2CO_3, $CH_2(COOCH_3)_2$, DMF–THF, 80°C, 97%, ref. 1
(f) NaH, $CH_2(COOCH_3)_2$, THF–DMF, reflux, 90%, ref. 8

SCHEME 2

C-12 series (29, 39, and 79%), but is much more dramatic in the C-11 series (2, 40, and 87%). This must be a consequence of the transannular steric interactions, which must be more important in the C-11 than in the C-12 series. Further analysis of these results requires detailed molecular modeling studies.

In conclusion, the above results fully illustrate the use of unsaturation in the chain to obtain good yield in macrocyclization processes. We have also studied the cyclization of 13- and 14-membered rings and these results are reported in the following publication (13).

Can. J. Chem. Downloaded from www.nrcresearchpress.com by 80.58.250.72 on 09/07/12
For personal use only.

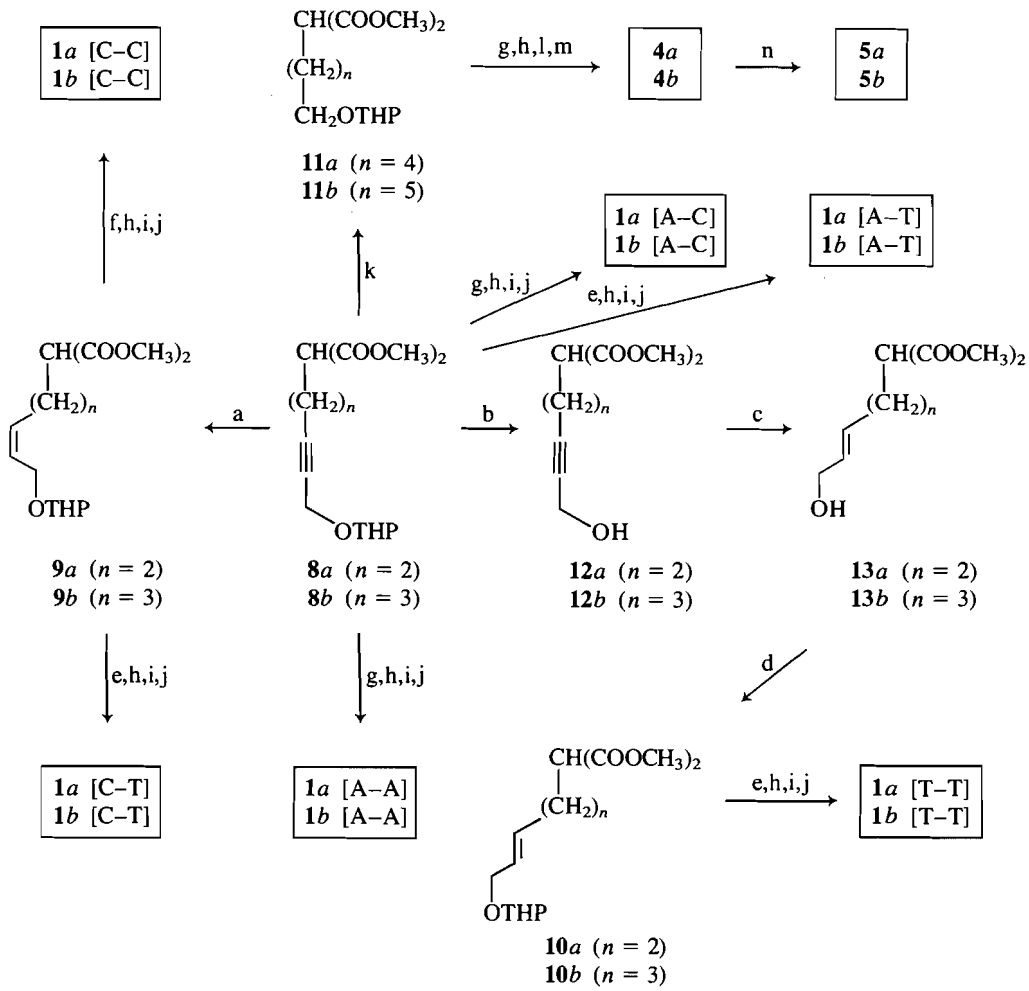

(a) H_2, $Pd/CaCO_3$–PbO, cyclohexane – ethyl acetate, r.t., 96–100%, ref. 9
(b) PPTS, CH_3OH, 50°C, 95–99%
(c) $CrCl_2$, Na_2SO_4, CH_3COONa, H_2O–DMF, r.t., 75–84%, ref. 10
(d) DHP, CF_3CO_2H, CH_2Cl_2, r.t., 90–92%
(e) NaH, $ClCH_2$—CH=CH—CH_2Cl (*trans*), THF, reflux, 80–90%
(f) NaH, $ClCH_2$—CH=CH—CH_2Cl (*cis*), THF, reflux, 81–89%
(g) NaH, $ClCH_2$—C≡C—CH_2Cl, THF, reflux, 54–75%
(h) NaH, $CH_2(COOCH_3)_2$, DMF–THF, reflux, 90–100%, ref. 8
(i) PPTS, CH_3OH, r.t., 96–100%, ref. 11
(j) MsCl, LiCl, collidine, DMF, 0°C → r.t., 75–90%, ref. 12
(k) H_2, 5% Pd/C, cyclohexane – ethyl acetate, r.t., 99%
(l) PPTS, CH_3OH, reflux, 95–98%
(m) CBr_4, Ph_3P, pyridine, CH_2Cl_2, 0°C → r.t., 77–83%, ref. 6
(n) H_2, PtO_2, Na_2SO_4, ethyl acetate, r.t., 98%

SCHEME 3

Experimental

Proton nmr spectra ($CDCl_3$) were recorded on Bruker WP-80 and WM-250 instruments. The ^{13}C nmr spectra were recorded on a Bruker WM-250 instrument. Infrared (ir) spectra were recorded on a Perkin–Elmer 681 spectrophotometer ($CHCl_3$). Mass spectra (ms) and peak matching assays were obtained using a VG Micromass ZAB-1F mass spectrometer. Vapor phase chromatographic (vpc) analysis was performed on a Hewlett–Packard 5710A gas chromatograph with flame ionization detection (capillary column OV-101, 25 m). Melting points were determined on a Reichert apparatus. For flash chromatography, silica gel Kiesel gel 60 (230–400 mesh ASTM) from Merck was used.

All reactions were carried out under an argon atmosphere. Ground anhydrous potassium carbonate was used for cyclization reactions. Tetrahydrofuran was dried by distilling over sodium/benzophenone, whereas *N,N*-dimethylformamide was dried over calcium hydride, followed by decantation and distillation under reduced pressure. All reagents were distilled prior to use: 1,4-dichloro-2-butyne (Aldrich) was thus obtained in 99% purity (vpc analysis), *cis*-1,4-dichloro-2-butene in 95% purity, and *trans*-1,4-dichloro-2-butene in 85% purity (contaminated with *cis* isomer) from distillation.

Purification of trans-*1,4-dichloro-2-butene*

Freshly distilled *trans*-1,4-dichloro-2-butene (150 mL) was kept in a closed addition funnel for 16 h at −15°C (freezer). The remaining liquid (found to be a 1:2 mixture of *cis* and *trans* isomers from vpc

Can. J. Chem. Downloaded from www.nrcresearchpress.com by 80.58.250.72 on 09/07/12
For personal use only.

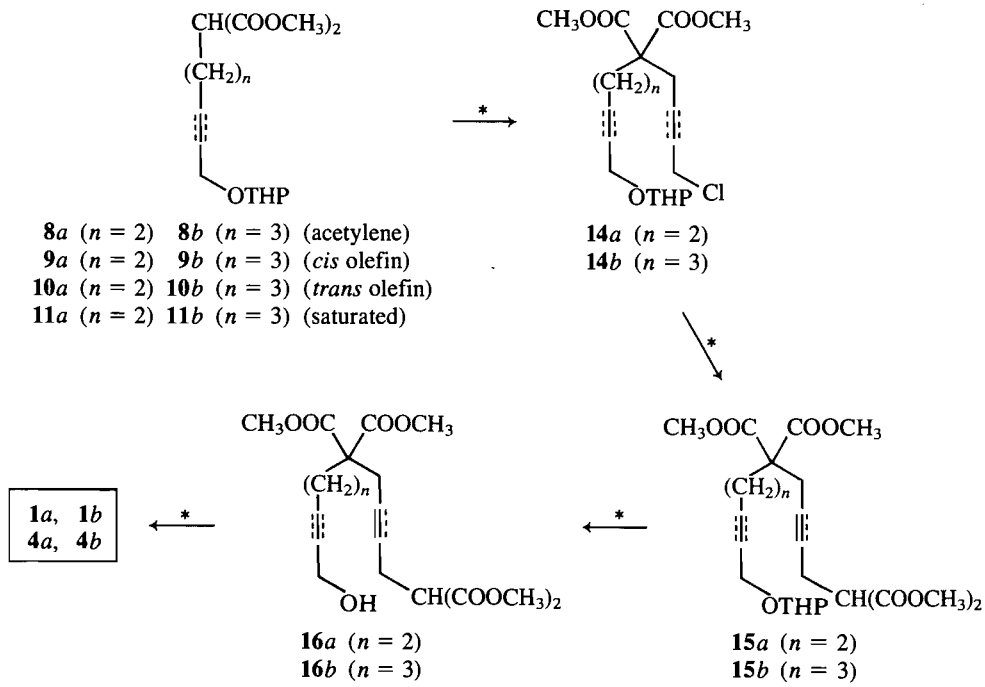

*See Scheme 3.

SCHEME 4

TABLE 1. Cyclization of C-11 aliphatic chains in K_2CO_3/DMF–THF[a]

Compound	Time (h)	T (°C)	$10^3 M$	% Monomer[b]	% Dimer[b]
1*a* [C–C]	45	90	20	16	29
			2	54	12
1*a* [C–T]	20	90	20	22	46
			2	66	15
1*a* [T–T]	42	95	20	8[c]	63
			2	32[c]	37
1*a* [A–C]	15	90	20	47	29
			2	85	8
1*a* [A–T]	18	90	20	16	20
			2	44	7
1*a* [A–A]	14	90	20	54	25
			2	87	8
4*a*	44	90	2	40	17
5*a*	48	90	2	2	2[d]

[a]Each experiment was carried out twice.
[b]Yield of isolated material after chromatography.
[c]Value obtained from capillary gc analysis.
[d]Value obtained from 250-MHz ^{1}H nmr spectral analysis.

TABLE 2. Cyclization of C-12 aliphatic chains in K_2CO_3/DMF–THF[a]

Compound	Time (h)	T (°C)	$10^3 M$	% Monomer[b]	% Dimer[b]
1*b* [C–C]	24	90	20	28	42
			2	61	15
1*b* [C–T]	21	90	20	11	58
			2	38	33
1*b* [T–T]	43	90	20	28	46
			2	63	14
1*b* [A–C]	18	90	20	80	3
			2	90	—
1*b* [A–T]	22	90	20	59	22
			2	86	5
1*b* [A–A]	15	90	20	51	19
			2	79	4
4*b*	48	90	20	39	16
5*b*	40	90	2	29	6[c]

[a]Each experiment was carried out twice.
[b]Yield of isolated material after chromatography.
[c]Value obtained from 250-MHz ^{1}H nmr spectral analysis.

analysis) was removed and the remaining crystals were washed twice with 10 mL of diethyl ether precooled to −30°C. After warming to 25°C and removal of solvent under vacuum, 62 g of 98.5% pure *trans* isomer was obtained (contaminated with 1.4% of *cis* isomer).

General Procedure 1:

Propargyl alcohol tetrahydropyranyl ether ***17***

To a stirred solution of dihydropyran (45.5 g, 0.542 mol) and trifluoroacetic acid (0.15 g, 1.3 mmol) in dichloromethane (200 mL), was added over a 30-min period a solution of propargyl alcohol (26.8 g, 0.514 mol) dissolved in dichloromethane (50 mL). After 18 h of stirring, the mixture was distilled under vacuum to afford compound **17** as a liquid (66.9 g, 93%); bp 54–56°C (3 Torr; 1 Torr = 133.3 Pa); ir: 3280, 2115, and 1025 cm^{-1}; ^{1}H nmr δ: 1.30–1.80 (6H, m, C—$(CH_2)_3$—C), 2.38 (1H, t, J = 2.4 Hz, —C≡C—H), 3.45–4.00 (2H, m, —OCH_2—, cyclic), 4.22 (2H, d, J = 2.3 Hz, —OCH_2—C≡C—), 4.80 (1H, m, —O_2CH—).

*5-[(Tetrahydro-2*H*-pyran-2-yl)oxy]-3-pentyn-1-ol (****18****)*

To a stirred solution of **17** (3.00 g, 21.4 mmol), hexamethylphosphoramide (1.14 mL, 6.40 mmol), and triphenylmethane (1 mg) dissolved in diethyl ether (30 mL) and tetrahydrofuran (12 mL), was added *n*-butyllithium (1.6 *M* in hexanes) until the coloration change from yellow to orange at −40°C. Neat ethylene oxide (2.2 mL, 43 mmol) was added at 25°C through the septum and the reaction mixture was stirred for 30 h. Diethyl ether (200 mL) was added and the organic phase was washed twice with brine/water (4:1) (50 mL), dried on sodium sulfate, and evaporated to give crude alcohol **18** as an oil (4.08 g, 103%); ir: 3620, 3200–3600, 1025 cm^{-1}; ^{1}H nmr δ: 1.60 (6H, m, —$C(CH_2)_3$C—), 2.07 (1H, m, —OH), 2.47 (2H, m, —CCH_2C≡C—), 3.40–4.00 (4H, m, —CH_2O—), 4.22 (2H, m, THPOCH_2—), 4.77 (1H, m, —O_2CH—).

General Procedure 2:

Bromide ***19****a from alcohol* ***18***

To a solution of alcohol **18** (4.08 g crude), carbon tetrabromide

Can. J. Chem. Downloaded from www.nrcresearchpress.com by 80.58.250.72 on 09/07/12
For personal use only.

Can. J. Chem. Downloaded from www.nrcresearchpress.com by 80.58.250.72 on 09/07/12
For personal use only.

(9.50 g, 28.6 mmol, 1.15 equiv.), and pyridine (0.4 mL) in dichloromethane (70 mL) at 0°C, was added rapidly a solution of triphenylphosphine (8.13 g, 30.9 mmol, 1.3 equiv.) in dichloromethane (10 mL). The solution was stirred 1 h at 0°C, then left overnight at 25°C. The solvent was evaporated, followed by the addition of dichloromethane (10 mL) and hexanes (150 mL), filtration, and evaporation. Bromide **19***a* was obtained as an oil (3.48 g, 66% from **17**) by flash chromatography (hexanes/ethyl acetate 15:1); ir: 2240, 1018 cm^{-1}; ^1H nmr δ: 1.30–1.80 (6H, m, —$C(CH_2)_3C$—), 2.65–2.90 (2H, m, —$CCH_2C{\equiv}C$—), 3.43 (2H, t, J = 6 Hz, —CH_2Br), 3.40–4.00 (2H, m, —OCH_2—, cyclic), 4.24 (2H, m, —$OCH_2C{\equiv}C$—), 4.80 (1H, m, —O_2CH—); ms m/e: 247 (MH^+).

*1-Bromo-6-[(tetrahydro-2H-pyran-2-yl)oxy]-4-hexyne (**19**b)*

To a solution of acetylene **17** (10.0 g, 71.4 mmol), hexamethylphosphoramide (1.25 mL, 7.0 mmol), and triphenylmethane (3 mg) in tetrahydrofuran (200 mL) was added *n*-butyllithium (1.6 *M* in hexane) at −40°C until the color of the solution passed from yellow to orange. To this solution was added distilled 1,3-dibromopropane (36 mL, 356 mmol) and the mixture was refluxed for 28 h. To the cooled solution was added diethyl ether (200 mL) and the organic phase was washed with water (3 × 50 mL) and dried over sodium sulfate. Volatile materials were evaporated and pure bromide **19***b* was obtained from a Kugelrohr distillation (65–75°C at 0.015 Torr) (15.0 g, 83%); ir: 2200, 1020 cm^{-1}; ^1H nmr δ: 1.30–1.80 (6H, m, —$C(CH_2)_3C$—), 2.03 (2H, m, —CH_2CH_2Br), 2.42 (2H, m, —CH_2—$CH_2C{\equiv}C$—), 3.50 (2H, t, J = 6 Hz, —CH_2Br), 3.40–4.00 (2H, m, —OCH_2—, cyclic), 4.23 (2H, m, —$C{\equiv}C$—CH_2O—), 4.78 (1H, m, —O_2CH—); ms m/e: 261 (MH^+).

General Procedure 3:

*Malonate **8**a from **19**a*

To a solution of bromide **19***a* (3.43 g, 13.9 mmol) and dimethyl malonate (7.9 mL, 69.2 mmol) in tetrahydrofuran (55 mL) and *N,N*-dimethylformamide (18 mL) at room temperature (r.t.), was added sodium hydride (1.01 g, 25.2 mmol, 60% in mineral oil). The solution was refluxed for 1.5 h. Hexane (20 mL) and water (100 mL) were then added at r.t. The aqueous phase was washed with a 1:1 mixture of diethyl ether and hexane (2 × 30 mL). Combined organic phases were dried on sodium sulfate. The solvents were evaporated and volatile materials distilled at 90°C (oil bath temperature) at 1 Torr. Compound **8***a* was obtained pure by flash chromatography (ethyl acetate/dichloromethane/hexanes 1:2:7) (3.78 g, 91%); ir: 1732 cm^{-1}; ^1H nmr δ: 1.61 (6H, m, —$C(CH_2)_3C$—), 1.95–2.40 (4H, m, —$C{\equiv}C$—$(CH_2)_2$—), 3.35–4.00 (3H, m, —$CH(CO_2Me)_2$ and —OCH_2—, cyclic), 3.74 (6H, s, CH_3), 4.24 (2H, m, —$C{\equiv}CCH_2O$—), 4.78 (1H, m, —O_2CH—); ms m/e: 299 (MH^+).

*Methyl 2-carbomethoxy-8-[(tetrahydro-2H-pyran-2-yl)oxy]-6-octynoate (**8**b)*

To a solution of bromide **19***b* (15.0 g, 57.4 mmol) and dimethyl malonate (33.6 mL, 294 mmol) in a 1:1 mixture of tetrahydrofuran and *N,N*-dimethylformamide (220 mL) was added potassium carbonate (40.6 g, 294 mmol). The mixture was heated at 90°C for 15 h. Hexane (100 mL) was then added at r.t. The mixture was filtered on Celite, the solvents were evaporated, and the volatile materials removed by Kugelrohr distillation (30°C, 0.02 Torr). The crude residue was dissolved in diethyl ether (250 mL) and washed with a 5% aqueous solution of sodium bicarbonate (3 × 50 mL). The organic phase was dried on magnesium sulfate and evaporation of solvents afforded pure malonate **8***b* as an oil (17.5 g, 98%); ir: 1740 cm^{-1}; ^1H nmr δ: 1.30–1.80 (8H, m, —$C(CH_2)_3$—C and —$CH_2CH_2CH_2C{\equiv}C$—), 1.80–2.30 (4H, m, —$CH_2CH_2CH_2C{\equiv}C$—), 3.38 (1H, t, J = 6 Hz, —$CH(CO_2Me)_2$), 3.40–4.00 (2H, m, —OCH_2—, cyclic), 3.73 (6H, s, CH_3), 4.22 (2H, m, —$C{\equiv}CCH_2O$—), 4.78 (1H, m, —O_2CH—); ms m/e: 313 (MH^+).

General Procedure 4:

cis-*Alkene **9**a from **8**a*

Malonate **8***a* (2.8 g, 9.4 mmol) was dissolved in cyclohexane (10 mL) and ethyl acetate (2 mL) under argon. Lyndlar catalyst ($Pd/CaCO_3/PbO$ from Aldrich) (0.5 g) was added and this mixture was stirred for 44 h under hydrogen (1.03 atm; 1 atm = 101.3 kPa). The solution was filtered, then evaporated to give pure *cis*-alkene **9***a* (2.8 g, 99.5%); ir: 1736 cm^{-1}; ^1H nmr δ: 1.40–1.80 (6H, m, —$C(CH_2)_3C$—), 1.90–2.20 (4H, m, —$CH_2CH_2C{=}C$—), 3.30–4.30 (5H, m, —$CH(CO_2Me)_2$ and —OCH_2—), 3.73 (6H, s, CH_3), 4.60 (1H, m, —O_2CH—), 5.30–5.80 (2H, m, —HC=CH—); ms m/e: 301 (MH^+).

*Methyl (Z)-2-carbomethoxy-8-[(tetrahydro-2H-pyran-2-yl)oxy]-6-octenoate (**9**b)*

Following procedure 4: Malonate **8***b* (3.00 g, 9.61 mmol) gave, under an hydrogenation pressure of 1.00 atm, alkene **9***b* (2.90 g, 96%); ir: 1740 cm^{-1}; ^1H nmr δ: 1.20–2.25 (12H, m, C—CH_2—C), 3.20–4.30 (5H, m, —$CH(CO_2Me)_2$ and —OCH_2—), 3.72 (6H, s, CH_3), 4.60 (1H, m, —O_2CH—), 5.25–5.80 (2H, m, H—C=C—H); ms m/e: 315 (MH^+).

General Procedure 5:

*Alcohol **12**a from **8**a*

Malonate **8***a* (2.35 g, 7.88 mmol) was dissolved in methanol (18 mL) containing pyridinium *p*-toluenesulfonate (170 mg, 0.67 mmol). This solution was refluxed for 1.5 h, and methanol was evaporated under vacuum. The residue was dissolved in methylene dichloride (5 mL) and filtered on silica gel (hexanes/dichloromethane/ethyl acetate 2:2:1) until complete recovery of alcohol **12***a*, which was obtained as a colorless oil (1.68 g, 99.5%); ir: 3600 and 1732 cm^{-1}; ^1H nmr δ: 1.90 (1H, m, —OH), 2.00–2.40 (4H, m, —CH_2CH_2—), 3.57 (1H, t, J = 6 Hz, —$CH(CO_2Me)_2$), 3.74 (6H, s, CH_3), 4.23 (2H, m, —CH_2OH); ms m/e: 215 (MH^+).

General Procedure 6:

trans-*Allylic alcohol **13**a*

A solution of chromous chloride was prepared by the slow addition, under an argon stream, of chrome powder (3.34 g, 64.2 mmol, 325 mesh from Aldrich) to a 8:9 mixture of degassed water and concentrated hydrochloric acid (15 mL) at 10°C. After 45 min of stirring, deoxygenated water (80 mL) was added, followed by sodium acetate (2.50 g, 30.5 mmol) and sodium sulfate (4.40 g, 30.9 mmol). Alcohol **12***a* (1.68 g, 7.84 mmol), dissolved in deoxygenated *N,N*-dimethylformamide (30 mL), was added to the chromous solution and stirred for 45 h at 25°C. The reaction mixture was extracted with diethyl ether (7 × 50 mL), dried on sodium sulfate, and evaporated. The alcohol **13***a* was purified by flash chromatography (ethyl acetate/dichloromethane/hexanes 1:2:2) (1.30 g, 77%); ir: 1732 cm^{-1}; ^1H nmr δ: 1.26 (1H, m, —OH), 2.07 (4H, m, —CH_2CH_2—), 3.39 (1H, t, —$CH(CO_2Me)_2$), 3.74 (6H, s, CH_3), 4.10 (2H, m, —CH_2O—), 5.67 (2H, m, —HC=CH—); ms m/e: 217 (MH^+).

*Methyl (E)-2-carbomethoxy-7-[(tetrahydro-2H-pyran-2-yl)oxy]-5-heptenoate (**10**a)*

Following procedure 1: Alcohol **13***a* (370 mg, 1.72 mmol) was transformed into **10***a*, which was purified by flash chromatography (ethyl acetate/dichloromethane/hexanes 1:2:7) (466 mg, 91%); ir: 1732 cm^{-1}; ^1H nmr δ: 1.40–1.80 (6H, m, C—$(CH_2)_3$—C), 2.06 (4H, m, —$C{=}CCH_2CH_2$—), 3.30–4.30 (5H, m, —$CH(CO_2Me)_2$ and —CH_2O—), 3.73 (6H, s, CH_3), 4.62 (1H, m, —O_2CH—), 5.64 (2H, m, —HC=CH—); ms m/e: 301 (MH^+).

*Methyl (E)-2-carbomethoxy-8-hydroxy-6-octenoate (**13**b)*

The malonate **8***b* was converted directly into alcohol **13***b* via a modification of procedure 6: the malonate **8***b* (2.00 g, 6.37 mmol) was heated for 4 h at 60°C under the conditions of procedure 6 without using sodium acetate. Then sodium acetate (1.80 g, 21.9 mmol) was added at 25°C and, after 36 h, the alcohol **13***b* was isolated (1.23 g, 84%); ir: 1733 cm^{-1}; ^1H nmr δ: 1.30–2.20 (6H, m, —$(CH_2)_3$—), 3.36 (1H, t, —$CH(CO_2Me)_2$), 3.73 (6H, s, CH_3), 4.10 (2H, m, —CH_2O—), 5.66 (2H, m, —HC=CH—); ms m/e: 231 (MH^+).

*Methyl (E)-2-carbomethoxy-8-[(tetrahydro-2H-pyran-2-yl)oxy]-6-octenoate (**10**b)*

Following procedure 1: Malonate **10***b* (1.55 g, 92%) was obtained from alcohol **13***b* (1.23 g, 5.35 mmol); ir: 1740 cm^{-1}; ^1H nmr δ: 1.30–2.20 (12H, m, C—CH_2—C), 3.36 (1H, t, J = 6 Hz, —$CH(CO_2Me)_2$),

TABLE 3. Spectral characteristics of monomers and dimers

Compound[a]	^{1}H nmr 250-MHz δ(ppm)[b]	^{13}C nmr 62.9-MHz δ(ppm)[b]	*Exact mass*[c]	Melting point (°C)[d]
2*a* [C–C]	1.90–2.05 (10H, m, CH_2), 3.73, 3.74 (12H, s, CH_3), 5.0–5.70 (4H, m, H—C=C—H)	22.4, 30.1 (2), 32.0, 32.2 (CH_2), 52.4, 52.5 (CH_3), 57.0, 57.8 (CH_2), 124.3, 127.0, 129.5, 133.2 (C=C), 171.2, 171.9 (C=O)	382.1645 (382.1628)	135–136
3*a* [C–C]	1.89 (8H, m, CH_2—CH_2), 2.58 12H, m, $E_2CCH_2C\equiv$), 3.71 (24H, s, CH_3), 5.14–5.50 (8H, m, HC=CH)	22.3, 30.6, 31.1 (2), 32.4 (CH_2), 52.3 (CH_3), 57.2 (CE_2), 124.2, 126.8, 126.9, 132.0 (C=C), 171.2, 171.4 (C=O)	764 (764)	149–153
2*a* [C–T]	2.00–2.10 (4H, m, CH_2—CH_2), 2.55–2.65 (6H, m, E_2CCH_2=C), 3.73, 3.74 (12H, s, CH_3), 5.00, 5.35, 5.45–5.75 (4H, m, HC=CH)	22.4, 30.4, 33.1, 37.0, 38.4 (CH_2), 52.3 (CH_3), 56.3, 57.8 (CE_2), 121.8, 128.2, 129.3, 133.2 (C=C), 171.7, 172.0 (C=O)	382.1645 (382.1628)	134–135.5
3*a* [C–T]	1.90 (8H, m, CH_2—CH_2), 2.55–2.70 (12H, m, $E_2CCH_2C\equiv$), 3.70, 3.71 (24H, s, CH_3), 5.10–5.60 (8H, m, HC=CH)	22.2, 29.7, 31.8, 35.3, 36.0 (CH_2), 52.3 (CH_3), 57.2, 57.6 (CE_2), 123.7, 128.4, 128.8, 132.1 (C=C), 171.1, 171.4 (C=O)	764 (764)	194–297
2*a* [T–T]	2.03, 2.17 (4H, m, CH_2—CH_2), 2.50–2.83 (6H, m, E_2CCH_2C=), 3.72, 3.75 (12H, s, CH_3), 4.90–5.60 (4H, m, HC=CH)	27.4, 33.4, 38.6 (2), 39.1 (CH_2), 52.5 (CH_3), 59.2 (CE_2), 126.9, 130.9, 131.6, 137.2 (C=C), 171.8, 172.4 (C=O)	382.1628 (382.1628)	—
3*a* [T–T]	1.90 (8H, m, CH_2—CH_2), 2.49–2.64 (12H, m, E_2C—CH_2C=), 3.71, 3.74 (24H, s, CH_3), 5.00–5.62 (8H, m, HC=CH)	27.8, 31.8, 34.6, 35.0, 35.7 (CH_2), 52.5 (CH_3), 56.7, 57.7 (CE_2), 124.4, 128.4, 128.8, 134.5 (C=C), 171.3, 171.4 (C=O)	764	214–222
2*a* [A–C]	1.85, 2.24 (4H, m, CH_2—CH_2), 2.60, 3.07, 3.40 (4H, m, E_2CCH_2C=), 2.75 (2H, m, $E_2CCH_2C\equiv$), 3.73, 3.75 (12H, s, CH_3), 5.26, 5.49 (2H, m, HC=CH)	13.9, 23.6, 29.8, 30.9, 31.2 (CH_2), 52.6, 52.8 (CH_3), 55.6, 58.1 (CE_2), 77.3, 83.4 (C≡C), 126.2, 127.7 (C=C), 171.0, 171.5 (C=O)	349.1293 (349.1288) (M^+ − OMe)	104–106
3*a* [A–C]	2.05, 2.25 (8H, m, CH_2—CH_2), 2.67–2.85 (12H, m, $E_2CCH_2C\equiv$), 3.72, 3.73, 3.73, 3.74 (24H, s, CH_3), 5.20, 5.45 (4H, m, HC=CH)	14.4, 22.8, 29.8, 31.7, 33.3 (CH_2), 52.3, 52.7 (CH_3), 56.9 (CE_2), 75.3, 82.3 (C≡C), 126.0, 128.5 (C=C), 170.3, 171.1 (C=O)	729 (729) (M^+ − OMe)	195–198
2*a* [A–T]	2.08, 2.21 (4H, m, CH_2—CH_2), 2.75 (6H, m, $E_2CCH_2C\equiv$), 3.72, 3.75 (12H, s, CH_3), 5.55–5.80 (2H, m, HC=CH)	13.6, 24.4, 31.8, 36.7, 36.8 (CH_2), 52.6, 52.7 (CH_3), 56.3, 58.8 (CE_2), 78.9, 87.2 (C≡C), 128.1, 130.5 (C=C), 170.8, 171.7 (C=O)	380.1472 (380.1472)	82–84
3*a* [A–T]	2.10 (8H, m, CH_2—CH_2), 2.60–2.80 (12H, m, $E_2CCH_2C\equiv$), 3.71 (24H, s, CH_3), 5.15–5.60 (4H, m, HC=CH)	14.4, 22.5, 31.3, 35.1, 35.8 (CH_2), 52.4, 52.6 (CH_3), 56.0, 56.9 (CE_2), 74.8, 82.2 (C≡C), 128.3, 128.7 (C=C), 170.3, 171.0 (C=O)	761 (761) (MH^+)	208–213
2*a* [A–A]	2.16, 2.42 (4H, m, CH_2—CH_2), 2.79, 2.91 (6H, m, ≡C—CH_2CE_2), 3.72, 3.76 (12H, s, CH_3)	13.7, 23.1, 25.0, 25.8, 31.8 (CH_2), 52.7 (CH_3), 56.0, 57.1 (CE_2), 77.8, 80.0, 81.1, 84.8 (C≡C), 169.7, 170.6 (C=O)	347.1139 (347.1131) (M^+ − OMe)	112–113
3*a* [A–A]	2.06, 2.25 (8H, m, CH_2—CH_2), 2.78, 2.93 (12H, m, $E_2CCH_2C\equiv$), 3.72, 3.74 (24H, s, CH_3)	14.3, 22.8 (2), 23.2, 31.5 (CH_2), 52.8 (CH_3), 56.6 (CE_2), 74.5, 77.6, 78.0, 82.1 (C≡C), 169.4, 170.2 (C=O)	756 (756)	189–192
6*a*	1.41 (6H, m, $E_2CCH_2(CH_2)_3$), 2.05 (4H, m, $E_2CCH_2CH_2$), 2.94 (4H, m, $E_2CCH_2C\equiv$), 3.724, 3.726 (12H, s, CH_3)	18.1 (2), 22.8 (2), 25.6, 29.7 (2) (CH_2), 52.7 (CH_3), 55.9 (CE_2), 79.9 (C≡C), 171.5 (C=O)	382.1622 (382.1628)	115–119

Can. J. Chem. Downloaded from www.nrcresearchpress.com by 80.58.250.72 on 09/07/12
For personal use only.

TABLE 3. (*continued*)

Compound[a]	^{1}H nmr 250-MHz δ(ppm)[b]	^{13}C nmr 62.9-MHz δ(ppm)[b]	*Exact mass*[c]	Melting point (°C)[d]
Dimer (from **4***a*)	1.12–1.38 (12H, m, $E_2CCH_2(CH_2)_3$), 2.03 (8H, m, $E_2CCH_2CH_2$), 2.78 (8H, m, $E_2CCH_2C{\equiv}$), 3.70, 3.72 (24H, s, CH_3)	23.2 (2), 24.4 (2), 30.8, 32.3 (2) (CH_2), 52.5 (CH_3), 57.1 (CE_2), 77.8 (C≡C), 170.7 (C=O)	764 (764)	225–228
2*a*	1.25–1.45 (10H, m, $E_2CCH_2CH_2$), 1.96, 2.05 (8H, m, E_2CCH_2), 3.68, 3.69 (12H, s, CH_3)	20.8 (2), 23.1 (2), 26.1, 28.9 (2), 30.1 (2) (CH_2), 52.2 (CH_3), 57.6 (CE_2), 172.1 (C=O)	387.2011 (387.2019) (MH^+)	114–126
Dimer (from **5***a*)	1.05–1.35 (20H, m, $E_2CCH_2CH_2$), 1.86 (16H, m, E_2CCH_2), 3.69, 3.70 (24H, s, CH_3)	—	772 (772)	185–211[e]
2*b* [C–C]	1.23 (2H, m, $CH_2CH_2CH_2$), 1.86–2.03 (4H, m, CH_2—CH_2), 2.60–2.75 (6H, m, $E_2CCH_2C{\equiv}$), 3.71, 3.75 (12H, s, CH_3), 5.05–5.70 (4H, m, HC=CH)	24.3, 27.7, 30.1, 30.4 (2), 32.0 (CH_2), 52.5 (CH_3), 57.5 (CE_2), 123.6, 126.9, 127.2, 134.2 (C=C), 171.4, 171.8 (C=O)	396.1790 (396.1784)	157–158
3*b* [C–C]	1.17 (4H, m, CH_2—CH_2—CH_2), 1.82, 2.01 (8H, m, CH_2—CH_2—CH_2), 2.60 (12H, m, $E_2CCH_2C{=}$), 3.72 (24H, s, CH_3), 5.05–5.50 (8H, m, HC=CH)	24.0, 27.5, 30.0 (2), 30.5, 32.1 (CH_2), 52.3 (CH_3), 57.0, 57.3 (CE_2), 123.4, 126.9 (2), 133.0 (C=C), 171.4, 171.6 (C=O)	792 (792)	128–131
2*b* [C–T]	1.45 (2H, m, CH_2—CH_2—CH_2), 1.87, 2.04 (4H, m, CH_2—CH_2—CH_2), 2.68 (6H, m, $E_2CCH_2C{=}$), 3.71, 3.74 12H, s, CH_3), 5.08–5.60 (4H, m, HC=CH)	21.1, 25.2, 29.8 (2), 34.6, 35.5 (CH_2), 52.3, 52.5 (CH_3), 56.0 (CE_2), 124.6, 127.7, 128.5, 130.6 (C=C), 171.6, 172.0 (C=O)	396.1794 (396.1784)	108–109
3*b* [C–T]	1.17 (4H, m, $CH_2CH_2CH_2$), 1.82, 2.07 (8H, m, $CH_2CH_2CH_2$), 2.60 (12H, m, $E_2CCH_2C{=}$), 3.710, 3.713 (24H, s, CH_3), 5.15–5.60 (8H, m, HC=CH)	23.9, 27.4, 29.4, 31.2, 35.3, 35.4 (CH_2), 52.3 (CH_3), 57.1, 57.6 (CE_2), 123.1, 128.6, 128.7, 133.2 (C=C), 171.2, 171.6 (C=O)	792 (792)	130–133
2*b* [T–T]	1.22 (2H, m, CH_2—CH_2CH_2), 1.76, 1.88 (4H, m, $CH_2CH_2CH_2$), 2.61, 2.72 (6H, d, $E_2CCH_2C{=}$), 3.70, 3.75 (12H, s, CH_3), 5.00–5.70 (4H, m, HC=CH)	23.8, 28.6, 28.7, 35.0, 37.4, 38.5 (CH_2), 52.4, 52.6 (CH_3), 55.7, 57.6 (CE_2), 124.7, 128.2, 131.2, 133.4 C=C), 171.8, 172 (C=O)	396.1795 (396.1784)	104.5–106
3*b* [T–T]	1.19 (4H, m, $CH_2CH_2CH_2$), 1.75, 2.03 (8H, m, $CH_2CH_2CH_2$), 2.57 (12H, m, $E_2CCH_2C{=}$), 3.70 (24H, s, CH_3), 5.15–5.60 (8H, m, HC=CH)	23.6, 30.7, 32.6, 35.4 (3) (CH_2), 52.3 (CH_3), 57.2, 57.9 (CE_2), 124.5, 128.4, 128.8, 134.5 (C=C), 171.2, 171.7 (C=O)	792 (792)	159–160
2*b* [A–C]	1.33 (2H, m, $CH_2CH_2CH_2$), 2.05 (4H, m, $CH_2CH_2CH_2$), 2.45–3.15 (6H, m, $E_2CCH_2C{=}$), 3.717, 3.735 (12H, s, CH_3), 5.10, 5.30 (2H, m, HC=CH)	18.4, 22.6, 23.9, 28.5, 29.5, 30.3 (CH_2), 52.4, 52.8 (CH_3), 55.7, 56.6 (CE_2), 76.3, 84.1 (C≡C), 126.80, 126.86 (C=C), 170.9, 171.5 (C=O)	394.1628 (394.1628)	166–167
3*b* [A–C]	1.37 (4H, m, $CH_2CH_2CH_2$), 1.90 2.15 (8H, m, $CH_2CH_2CH_2$), 2.70–2.85 (12H, m, $E_2CCH_2C{\equiv}$), 3.718, 3.735 (24H, s, CH_3), 5.35 (4H, m, HC=CH)	—	788 (788)	—

Can. J. Chem. Downloaded from www.nrcresearchpress.com by 80.58.250.72 on 09/07/12
For personal use only.

TABLE 3. (*concluded*)

Compound[a]	^{1}H nmr 250-MHz δ(ppm)[b]	^{13}C nmr 62.9-MHz δ(ppm)[b]	*Exact mass*[c]	Melting point (°C)[d]
2*b* [A–T]	1.30 (2H, m, $CH_2CH_2CH_2$), 2.05 (4H, m, $CH_2CH_2CH_2$), 2.69 (4H, m, $E_2CCH_2C{=}$), 2.81 (2H, t, $E_2CCH_2C{\equiv}$), 3.72, 3.75 (12H, s, CH_3), 5.21, 5.86 (2H, m, HC=CH)	18.5, 22.0, 24.2, 29.2, 34.7, 38.4 (CH_2), 52.3, 52.6 (CH_3), 55.6, 57.5 (CE_2), 77.4, 83.7 (C≡C), 125.7, 130.7 (C=C), 170.6, 171.7 (C=C)	394.1631 (394.1627)	123.5–126
3*b* [A–T]	1.33 (4H, m, $CH_2CH_2CH_2$), 1.95, 2.16 (8H, m, $CH_2CH_2CH_2$), 2.60–2.75 (12H, m, $E_2CCHC{=}$), 3.71, 3.72 (24H, s, CH_3), 5.40 (4H, m, HC=CH)	18.9, 23.0, 23.3, 31.1, 35.4, 35.7 (CH_2), 52.3, 52.5 (CH_3), 57.1, 57.3 (CE_2), 75.0, 82.7 (C≡C), 128.1, 129.0 (C=C), 170.4, 171.5 (C=O)	788 (788)	157–159
2*b* [A–A]	1.33 (2H, m, $CH_2CH_2CH_2$), 2.17, 2.28 (4H, m, $CH_2CH_2CH_2$), 2.80–2.90 (6H, m, $E_2CCH_2C{\equiv}$), 3.72, 3.76 (12H, s, CH_3)	18.7, 22.0, 22.6, 25.1, 25.5, 30.0 (CH_2), 52.5, 52.8 (CH_3), 55.5, 56.3 (CE_2), 76.1, 76.8, 77.5, 79.3 (C≡C), 169.7, 170.8 (C=O)	361.1290 (361.1288) (M^+ − OMe)	118–119
3*b* [A–A]	1.38 (4H, m, $CH_2CH_2CH_2$), 2.10–2.25 (8H, m, $CH_2CH_2CH_2$), 2.81–2.95 (12H, m, $E_2CCH_2C{\equiv}$), 3.73, 3.74 (24H, s, CH_3)	18.9, 23.0 (2), 23.3, 23.4, 31.5 (CH_2), 52.6, 52.8 (CH_3), 56.89 (CE_2), 74.7, 77.7, 77.9, 82.8 (C≡C), 169.5, 170.7 (C=O)	785 (785) (MH^+)	159–160
6*b*	1.46 (8H, m, $E_2CCH_2(CH_2)_4$), 2.05 (4H, m, $E_2CCH_2CH_2$), 2.87 (4H, s, $E_2CCH_2C{\equiv}$), 3.72 (12H, s, CH_3)	19.9 (2), 23.8 (2), 26.0 (2), 32.1 (2) (CH_2), 52.6 (CH_3), 56.2 (CE_2), 78.7 (C≡C), 171.2 (C=O)	396.1790 (396.1784)	88–88.5
Dimer (from **4***b*)	1.15 (8H, m, $E_2CCH_2CH_2CH_2$), 1.36 (8H, m, $E_2CCH_2CH_2$), 2.03 (8H, m, $E_2CCH_2CH_2$), 2.76 (8H, m, $E_2CCH_2C{\equiv}$), 3.71 (24H, s, CH_3)	22.7 (4), 24.4 (4), 29.8 (4), 31.6 (4) (CH_2), 52.6 (CH_3), 57.0 (CE_2), 77.6 (C≡C), 170.8 (C=O)	792 (792)	158–164
7*b*	1.16 (4H, m, $E_2CCH_2CH_2CH_2$), 1.27 (4H, m, $E_2CCH_2CH_2CH_2$), 1.43 (4H, m, $(E_2CCH_2CH_2)_2$), 1.88 (4H, m, $(E_2CCH_2)_2)_2$), 2.06 (4H, m, $(E_2CCH_2CH_2)_2$), 3.69 (12H, s, CH_3)	18.0 (2), 22.3 (2), 24.8 (2), 27.0 (2), 29.1 (2) (CH_2), 52.3 (CH_3), 57.8 (CE_2), 172.2 (C=O)	401.2162 (401.2175) (MH^+)	155–155.5
Dimer (from **5***b*)	1.11–1.29 (24H, m, $E_2CCH_2CH_2$), 1.85 (16H, m, E_2CCH_2), 3.69 (24H, s, CH_3)	23.7, 24.4, 29.6, 31.8, 32.0 (CH_2), 52.2 (CH_3), 57.4 (CE_2), 172.2 (C=O)	800 (800)	167–168

[a]For notation: C (*cis*), T (*trans*), A (Acetylene).
[b]"E" refers to the ester group (CO_2Me).
[c]Only for monomers; mass spectra for dimers; calculated values in parentheses.
[d]Recrystallized sample ($CHCl_3$/hexanes).
[e]Unrecrystallized sample.

3.40–4.30 (4H, m, —OCH_2—), 3.73 (6H, s, CH_3), 4.62 (1H, m, —O_2CH—), 5.64 (2H, m, H—C=C—H); ms *m/e*: 315 (MH^+).

General Procedure 7:

Saturated malonate ***11****a from* ***8****a*

Malonate **8***a* (1.80 g, 6.04 mmol) was dissolved under an argon atmosphere in a 5:1 mixture of cyclohexane and ethyl acetate (12 mL). To this solution was added 5% palladium on charcoal (100 mg) and the solution was stirred under hydrogen (1.0 atm) until gas uptake ceased. The solution was filtered on Celite and the solvents removed to give crude malonate **11***a* (1.81 g, 99%); ir: 1731 cm^{-1}; ^{1}H nmr δ: 1.20–2.05 (14H, m, C—CH_2—C), 3.20–4.10 (5H, m, —$CH(CO_2Me)_2$ and —OCH_2—), 3.73 (6H, s, CH_3), 4.56 (1H, m, —O_2CH—); ms *m/e*: 303 (MH^+).

*Methyl 2-carbomethoxy-8-[(tetrahydro-2*H*-pyran-2-yl)oxy]-octanoate (****11****b)*

Following procedure 7: Crude malonate **11***b* (3.15 g, 100%) was obtained from acetylene **8***b* (3.11 g, 9.97 mmol); ir: 1740 cm^{-1}; ^{1}H nmr δ: 1.10–2.00 (16H, m, C—CH_2—C), 3.10–4.10 (5H, m, —$CH(CO_2Me)_2$ and —OCH_2—), 3.74 (6H, s, CH_3), 4.55 (1H, m, —O_2CH—); ms *m/e*: 317 (MH^+).

General Procedure 8:

*Methyl (*Z*)-2-carbomethoxy-2-[(*Z*)-4-chloro-2-butenyl]-7-[(tetrahydro-2*H*-pyran-2-yl)oxy]-5-heptenoate (****14****a [C–C])*

A mixture of malonate **9***a* (1.30 g, 4.33 mmol) and sodium hydride (207 mg, 5.20 mmol, 60% in mineral oil) in tetrahydrofuran (18 mL) was refluxed for 30 min. (Z)-1,4-Dichloro-2-butene (2.3 mL, 21.6 mmol)

Can. J. Chem. Downloaded from www.nrcresearchpress.com by 80.58.250.72 on 09/07/12
For personal use only.

Can. J. Chem. Downloaded from www.nrcresearchpress.com by 80.58.250.72 on 09/07/12
For personal use only.

was added at 25°C and the mixture refluxed for 30 min. The solution was cooled to 0°C, followed by the addition of 10% aqueous ammonium chloride (20 mL) and extraction with diethyl ether (3 × 50 mL). The organic phases were dried on sodium sulfate, evaporated, and purified by flash chromatography (ethyl acetate/dichloromethane/hexanes 1:2:8) to afford compound **14***a* [C–C] (1.49 g, 89%) as an oil; ir: 1730 cm^{-1}; ^1H nmr δ: 1.63 (6H, m, C—$(CH_2)_3$—C), 1.97 (4H, m, —CH_2—CH_2—$C(CO_2Me)_2$—), 2.68 (2H, m, —C=$CCH_2C(CO_2Me)_2$—), 3.40–4.20 (4H, m, —OCH_2—), 3.78 (6H, s, CH_3), 4.15 (2H, m, —CH_2Cl), 4.59 (1H, m, —O_2CH—), 5.30–5.80 (4H, m, H—C=C—H); ms *m/e*: 389 (MH^+).

Methyl (Z),(Z)-*2,7,7-tricarbomethoxy-12-[(tetrahydro-2*H*-pyran-2-yl)oxy]-4,10-dodecadienoate (**15**a [C–C])*

Following procedure 3, compound **14***a* [C–C] (1.48 g, 3.8 mmol) was transformed into the malonate **15***a* [C–C] (1.71 g, 92%); ir: 1732 cm^{-1}; ^1H nmr δ: 1.30–1.70 (6H, m, C—$(CH_2)_3$—C), 1.95 (4H, m, —CH_2—CH_2—), 2.65 (4H, m, —C=$CCH_2C(CO_2Me)_2$—), 3.25–4.20 (5H, m, —$CH(CO_2Me)_2$ and —OCH_2—), 3.71, 3.73 (12H, s, CH_3), 4.59 (1H, m, —O_2CH—), 5.20–5.65 (4H, m, H—C=C—H); ms *m/e*: 485 (MH^+).

General Procedure 9:

Methyl (Z),(Z)-*2,7,7-tricarbomethoxy-12-hydroxy-4,10-dodecadienoate (**16**a [C–C])*

Malonate **15***a* [C–C] (1.70 g, 3.51 mmol) was dissolved in methanol (5 mL) containing pyridinium *p*-toluenesulfonate (77 mg, 0.31 mmol) and this solution was stirred at r.t. for 2 days, followed by removal of volatile materials under vacuum. Methanol (10 mL) was added and this solution was stirred for 1 day, followed by evaporation of solvent. The crude oil was filtered on silica gel using ethyl acetate/dichloromethane/hexanes 1:2:2 as eluent and this method afforded alcohol **16***a* [C–C] (1.37 g, 98%) as a pure oil; ir: 3400 (weak), 1732 cm^{-1}; ^1H nmr δ: 1.60 (1H, m, —OH), 1.97 (4H, m, —CH_2CH_2—), 2.66 (4H, m, —C=C—$CH_2C(CO_2Me)_2$), 3.40 (1H, t, —$CH(CO_2Me)_2$), 3.75, 3.76 (12H, s, CH_3), 4.14 (2H, m, —CH_2O—), 5.20–5.70 (4H, m, H—C=C—H); ms *m/e*: 401 (MH^+).

General Procedure 10:

Methyl (Z),(Z)-*2,7,7-tricarbomethoxy-12-chloro-4,10-dodecadienoate (**1**a [C–C])*

To a solution of **15***a* [C–C] (1.36 g, 3.40 mmol), lithium chloride (287 mg, 6.90 mmol), and 2,4,6-collidine (671 μL, 5.45 mmol) in *N,N*-dimethylformamide (35 mL) at 0°C, was added methanesulfonyl chloride (396 μL, 5.45 mmol). This solution was stirred for 2 h at 0°C, 1 h at 25°C, poured onto ice-water (400 mL), and extracted with a mixture of diethyl ether/hexanes 1:1 (4 × 80 mL). The organic phase was dried on sodium sulfate and evaporated. Purification of the resulting oil by flash chromatography, using ethyl acetate/dichloromethane/hexanes 1:2:4 as eluent, afforded compound **1***a* [C–C] as an oil (1.18 g, 83%); ir: 1735 cm^{-1}; ^1H nmr δ: 1.98 (4H, m, —CH_2CH_2—), 2.70 (4H, m, C=$CCH_2C(CO_2Me)_2$—), 3.41 (1H, t, —$CH(CO_2Me)_2$), 3.73, 3.75 (12H, s, CH_3), 4.10 (2H, m, —CH_2Cl), 5.30–5.70 (4H, m, H—C=C—H); ms *m/e*: 419 (MH^+).

General Procedure 11:

(Z),(Z)-*1,1,6,6-Tetracarbomethoxy-3,8-cycloundecadiene* (**2**a *[C–C])* and (Z),(Z),(Z),(Z)-*1,1,6,6,12,12,17,17-octacarbomethoxy-3,9,14,20-cyclodocosatetraene* (**3**a *[C–C])*

To a solution of **1***a* [C–C] (204 mg, 0.489 mmol) in tetrahydrofuran and *N,N*-dimethylformamide (1:1) (24 mL) was added potassium carbonate (330 mg, 2.40 mmol). This mixture was refluxed (oil bath at 90°C) for 45 h, then cooled, and hexane (10 mL) was added followed by filtration on Celite. The solvents were removed under reduced pressure and the residue purified by flash chromatography (ethyl acetate/dichloromethane/hexanes in successive ratios of 1:2:6, 1:2:4, and 1:2:3) to give monomer **2***a* [C–C] (29.4 mg, 15.7%) and dimer **3***a* [C–C] (53.1 mg, 28.4%). Both compounds were recrystallized in a minimum amount of chloroform, followed by addition at 25°C of excess hexanes and cooling to −15°C for a few hours (see Table 3 for melting point); ir of **2***a*: 1730, 1290, 1210 cm^{-1}; ir of **3***a*: 1735, 1230 cm^{-1}.

Methyl (Z)-*2-carbomethoxy-2-[(*E*)-4-chloro-2-butenyl]-7-[(tetrahydro-2*H*-pyran-2-yl)oxy]-5-heptenoate (**14**a [C–T])*

Following procedure 8: Compound **9***a* (1.203 g, 4.01 mmol) was reacted with (*E*)-1,4-dichloro-2-butene (2.1 mL, 20 mmol) to afford **14***a* [C–T] as an oil (1.24 g, 80%); ir: 1730 cm^{-1}; ^1H nmr δ: 1.62 (6H, m, C—$(CH_2)_3$—C), 1.94 (4H, m, —CH_2CH_2—), 2.71 (2H, m, C=$CCH_2C(CO_2Me)_2$—), 3.30–4.00 (2H, m, —CH_2O—, cyclic), 3.73 (6H, s, CH_3), 4.00–4.15 (4H, m, —CH_2Cl and —OCH_2C=C—), 4.61 (1H, m, —O_2CH—), 5.45–5.75 (4H, m, H—C=C—H); ms *m/e*: 389 (MH^+).

Methyl (E),(Z)-*2,7,7-tricarbomethoxy-12-[(tetrahydro-2*H*-pyran-2-yl)oxy]-4,10-dodecadienoate (**15**a [C–T])*

Following procedure 3: Chloride **14***a* [C–T] (1.23 g, 3.17 mmol) gave **15***a* [C–T] (1.51 g, 99%); ir: 1732 cm^{-1}; ^1H nmr δ: 1.61 (6H, m, C—$(CH_2)_3$—C), 1.90 (4H, m, —CH_2CH_2—), 2.54 (4H, m, —C=$CCH_2C(CO_2Me)_2$), 3.40 (1H, t, —$CH(CO_2Me)_2$—), 3.40–4.00 (2H, m, —CH_2O—, cyclic), 3.71, 3.74 (12H, s, CH_3), 4.13 (2H, m, —O—CH_2—C=C—), 4.61 (1H, m, —O_2CH—), 5.53 (4H, m, H—C=C—H); ms *m/e*: 485 (MH^+).

Methyl (E),(Z)-*2,7,7-tricarbomethoxy-12-hydroxy-4,10-dodecadienoate (**16**a [C–T])*

Following procedure 9: Compound **15***a* [C–T] (1.5 g, 3.1 mmol) gave alcohol **16***a* [C–T] (1.24 g, 100%); ir: 3300–3700, 1730 cm^{-1}; ^1H nmr δ: 1.80–1.90 (5H, m, —OH and —CH_2CH_2—), 2.58 (4H, m, —C=$CCH_2C(CO_2Me)_2$—), 3.41 (1H, t, —$CH(CO_2Me)_2$), 3.71 (12H, s, CH_3), 4.15 (2H, m, —CH_2O—), 5.50 (4H, m, H—C=C—H); ms *m/e*: 401 (MH^+).

Methyl (E),(Z)-*2,7,7-tricarbomethoxy-12-chloro-4,10-dodecadienoate (**1**a [C–T])*

Following procedure 10: Chloride **1***a* [C–T] (1.11 g, 86%) was obtained from the alcohol **16***a* [C–T] (1.23 g, 3.07 mmol); ir: 1730 cm^{-1}; ^1H nmr δ: 1.94 (4H, m, —CH_2CH_2—), 2.60 (4H, m, —C=$CCH_2C(CO_2Me)_2$), 3.40 (1H, t, —$CH(CO_2Me)_2$), 3.72 (12H, s, CH_3), 4.05 (2H, m, —CH_2Cl), 5.3–5.7 (4H, m, —HC=CH—); ms *m/e*: 419 (MH^+).

(E),(Z)-*1,1,6,6-Tetracarbomethoxy-3,8-cycloundecadiene* (**2**a *[C–T])* and (E),(Z),(E),(Z)-*1,1,6,6,12,12,17,17-octacarbomethoxy-3,9,14,20-cyclodocosatetraene* (**3**a *[C–T])*

Following procedure 11: After 20 h of treatment chloride **1***a* [C–T] (198 mg, 0.474 mmol) afforded **2***a* [C–T] (38.1 mg, 21%) and **3***a* [C–T] (83.1 mg, 45.8%); ir of **2***a*: 1730, 1280, 1180 cm^{-1}; ir of **3***a*: 1730, 1250 cm^{-1}.

Methyl (E)-*2-carbomethoxy-2-[*(E)*-4-chloro-2-butenyl]-7-[(tetrahydro-2*H*-pyran-2-yl)oxy]-5-heptenoate (**14**a [T–T])*

Following procedure 8: Using (*E*)-1,4-dichloro-2-butene: compound **10***a* (1.58 g, 5.27 mmol) gave chloride **14***a* [T–T] (1.71 g, 84%); ir: 1731 cm^{-1}; ^1H nmr δ: 1.59 (6H, m, C—$(CH_2)_3$—C), 1.97 (4H, m, —CH_2CH_2—), 2.63 (2H, m, C=$CCH_2C(CO_2Me)_2$), 3.40–4.20 (6H, m, —CH_2Cl and —OCH_2—), 3.72 (6H, s, CH_3), 4.61 (1H, m, —O_2CH—), 5.64 (4H, m, —HC=CH—); ms *m/e*: 389 (MH^+).

Methyl (E),(E)-*2,7,7-tricarbomethoxy-12-[(tetrahydro-2*H*-pyran-2-yl)oxy]-4,10-dodecadienoate (**15**a [T–T])*

Following procedure 3: Chloride **14***a* [T–T] (1.71 g, 4.41 mmol) gave **15***a* [T–T] (2.06 g, 97%); ^1H nmr δ: 1.62 (6H, m, C—$(CH_2)_3$—C), 1.94 (4H, m, —CH_2CH_2—), 2.54 (4H, m, C=$CCH_2C(CO_2Me)_2$), 3.40 (1H, t, —$CH(CO_2Me)_2$), 3.30–4.20 (4H, m, —OCH_2—), 3.70, 3.74 (12H, s, CH_3), 4.63 (1H, m, —O_2CH—), 5.2–5.7 (4H, m, —HC=CH—); ms *m/e*: 485 (MH^+).

Methyl (E),(E)-*2,7,7-tricarbomethoxy-12-hydroxy-4,10-dodecadienoate (**16**a [T–T])*

Following procedure 9: Compound **15***a* [T–T] (1.45 g, 3.00 mmol)

gave **16***a* [T–T] (1.17 g, 98%); ir: 3600–3200, 1740, 1733 cm^{-1}; ^1H nmr δ: 1.66 (1H, m, —OH), 1.92 (4H, m, $—CH_2CH_2—$), 2.57 (4H, m, $—C{=}CCH_2C(CO_2Me)_2—$), 3.40 (1H, t, $—CH(CO_2Me)_2$), 3.71, 3.75 (12H, s, CH_3), 4.11 (2H, m, $—CH_2O—$), 5.40–5.80 (4H, m, —HC=CH—).

Methyl (E),(E)-*2,7,7-tricarbomethoxy-12-chloro-4,10-dodecadienoate (1*a *[T–T])*

Following procedure 10: Alcohol **16***a* [T–T] (1.16 g, 2.91 mmol) gave chloride **1***a* [T–T] (0.826 g, 68%); ir: 1739, 1730 cm^{-1}; ^1H nmr δ: 1.92 (4H, m, $—CH_2CH_2—$), 2.55 (4H, m, $—C{=}C—CH_2C(CO_2Me)_2$), 3.38 (1H, t, $—CH(CO_2Me)_2$), 3.70, 3.73 (12H, s, CH_3), 4.03 (2H, m, $—CH_2Cl$), 5.30–5.75 (4H, m, H=C=CH—); ^{13}C nmr δ: 26.6, 31.5, 31.7, 35.9 (CH_2), 44.9 (CH_2Cl), 51.6 ($—CH(CO_2Me)_2$), 52.3, 52.4 (CH_3), 57.3 ($—(CH_2)_2C(CO_2Me)_2$), 126.7, 127, 130.2, 134.2 (C=C), 169.0, 171.2 (C=O); ms *m/e*: 419 (MH^+).

(E),(E)-*1,1,6,6-Tetracarbomethoxy-3,8-cycloundecadiene (2*a *[T–T]) and* (E),(E),(E),(E)-*1,1,6,6,12,12,17,17-octacarbomethoxy-3,9,14,20-cyclodocosatetraene (3*a *[T–T])*

Following procedure 11: At 2×10^{-3} *M*, chloride **1***a* [T–T] (187 mg, 0.447 mmol) gave the monomer **2***a* [T–T] (60% pure from vpc analysis) (88.5 mg, 52%) and dimer **3***a* [T–T] (64.6 mg, 38%); ir of **2***a*: 1728, 1241 cm^{-1}; ir of **3***a*: 1730, 1273, 1200, 1138 cm^{-1}.

*Methyl 2-carbomethoxy-2-[(Z)-4-chloro-2-butenyl]-7-[(tetrahydro-2H-pyran-2-yl)oxy]-5-heptynoate (14*a *[A–C])*

Following procedure 8: Malonate **8***a* (1.13 g, 3.79 mmol) gave chloride **14***a* [A–C] (1.294 g, 88%); ir: 1731 cm^{-1}; ^1H nmr δ: 1.40–1.80 (6H, m, $—C(CH_2)_3C—$), 2.20 (4H, m, $—CH_2CH_2—$), 2.72 (2H, bd, $C{=}CCH_2C(CO_2Me)_2—$), 3.40–3.90 (2H, m, $—OCH_2—$, cyclic), 3.72 (6H, s, CH_3), 4.07 (2H, bd, $—CH_2Cl$), 4.21 (2H, m, $THPOCH_2—$), 4.76 (1, m, $—O_2CH—$), 5.35–5.95 (2H, m, —HC=CH—); ms *m/e*: 387 (MH^+).

Methyl (Z)-*2,7,7-tricarbomethoxy-12-[(tetrahydro-2*H*-pyran-2-yl)oxy]-4-dodecen-10-ynoate (15*a *[A–C])*

Following procedure 3: In tetrahydrofuran as solvent, compound **14***a* [A–C] (1.28 g, 3.32 mmol) gave malonate **15***a* [A–C] (1.30 g, 80%); ir: 1732 cm^{-1}; ^1H nmr δ: 1.64 (6H, m, $C—(CH_2)_3—C$), 2.17 (4H, m, $—CH_2CH_2—$), 2.68 (4H, m, $C{=}CCH_2C(CO_2Me)_2$), 3.30–3.90 (3H, m, $—CH_2O—$, cyclic and $—CH(CO_2Me)_2$), 3.72, 3.74 (12H, s, CH_3), 4.20 (2H, m, $THPOCH_2—$), 4.77 (1H, m, $—O_2CH—$), 5.40 (2H, m, —HC=CH—); ms *m/e*: 481 (MH^+).

(Methyl (Z)-*2,7,7-tricarbomethoxy-12-hydroxy-4-dodecen-10-ynoate (16*a *[A–C])*

Following procedure 9: Compound **15***a* [A–C] (1.29 g, 2.69 mmol) gave **16***a* [A–C] (1.06 g, 99%); ir: 3610 (weak), 1731 cm^{-1}; ^1H nmr δ: 1.63 (1H, m, —OH), 2.17 (4H, m, $—CH_2CH_2—$), 2.70 (4H, m, $—C{=}CH_2C(CO_2Me)_2—$), 3.40 (1H, t, $—CH(CO_2Me)_2$), 3.73, 3.74 (12H, s, CH_3), 4.22 (2H, m, $—CH_2O—$), 5.40 (2H, m, —HC=CH—); ms *m/e*: 399 (MH^+).

Methyl (Z)-*2,7,7-tricarbomethoxy-12-chloro-4-dodecen-10-ynoate (1*a *[A–C])*

Following procedure 10: Compound **16***a* [A–C] (1.05 g, 2.64 mmol) gave chloride **1***a* [A–C] (0.910 g, 83%); ir: 1732 cm^{-1}; ^1H nmr δ: 2.16 (4H, m, $—CH_2CH_2—$), 2.65 (4H, m, $—C{=}CCH_2C(CO_2Me)_2$), 3.39 (1H, t, $—CH(CO_2Me)_2$), 3.72, 3.74 (12H, s, CH_3), 4.11 (2H, m, $—CH_2Cl$), 5.38 (2H, m, —HC=CH—); ms *m/e*: 417 (MH^+).

(Z)-*1,1,6,6-Tetracarbomethoxy-3-cycloundecen-8-yne (2*a *[A–C])* and (Z),(Z)-*1,1,6,6,12,12,17,17-octacarbomethoxy-3,14-cyclodocosadien-9,20-diyne (3*a *[A–C])*

Following procedure 11: Chloride **1***a* [A–C] (250 mg, 0.6 mmol) gave, after 15 h, **2***a* [A–C] (107 mg, 46.8%) and dimer **3***a* [A–C] (67.0 mg, 29.3%); ir of **2***a*: 1730, 1285, 1230 cm^{-1}; ir of **3***a*: 1732, 1290 cm^{-1}.

*Methyl 2-carbomethoxy-2-[(E)-4-chloro-2-butenyl]-7-[(tetrahydro-2H-pyran-2-yl)oxy]-5-heptynoate (14*a *[A–T])*

Following procedure 8: Using *trans*-1,4-dichloro-2-butene, compound **8***a* (1.15 g, 3.86 mmol) gave **14***a* [A–T] (1.34 g, 90%); ir: 1732 cm^{-1}; ^1H nmr δ: 1.62 (6H, m, $—C(CH_2)_3C—$), 2.17 (4H, m, $—CH_2CH_2—$), 2.65 (2H, m, $—C{=}CCH_2C(CO_2Me)_2—$), 3.40–3.90 (2H, m, $—CH_2O—$, cyclic), 3.73 (6H, s, CH_3), 4.02 (2H, m, $—CH_2Cl$), 4.20 (2H, m, $THPOCH_2—$), 4.77 (1H, m, $—O_2CH—$), 5.66 (2H, m, —HC=CH—); ms *m/e*: 387 (MH^+).

Methyl (E)-*2,7,7-tricarbomethoxy-12-[(tetrahydro-2*H*-pyran-2-yl)oxy]-4-dodecen-10-ynoate (15*a *[A–T])*

Following procedure 3: Using tetrahydrofuran as solvent, chloride **14***a* [A–T] (1.33 g, 3.44 mmol) gave malonate **15***a* [A–T] (1.38 g, 83%); ir: 1730 cm^{-1}; ^1H nmr δ: 1.62 (6H, m, $—C(CH_2)_3C—$), 2.12 (4H, m, $—CH_2CH_2—$), 2.55 (4H, m, $—C{=}CCH_2C(CO_2Me)_2$), 3.40 (1H, t, $—CH(CO_2Me)_2$), 3.40–4.00 (2H, m, $—OCH_2—$, cyclic), 3.71, 3.74 (12H, s, CH_3), 4.2 (2H, m, $—CH_2OTHP$), 4.77 (1H, m, $—O_2CH—$), 5.43 (2H, m, —HC=CH—); ms *m/e*: 399 ($M^+ - THP$).

Methyl (E)-*2,7,7-tricarbomethoxy-12-hydroxy-4-dodecen-10-ynoate (16*a *[A–T])*

Following procedure 9: Compound **15***a* [A–T] (1.36 g, 2.82 mmol) gave alcohol **16***a* [A–T] (1.12 g, 100%); ir: 1732 cm^{-1}; ^1H nmr δ: 1.67 (1H, m, —OH), 2.12 (4H, m, $—CH_2CH_2—$), 2.57 (4H, m, $—C{=}CCH_2C(CO_2Me)_2$), 3.40 (1H, m, $—CH(CO_2Me)_2$), 3.72, 3.74 (12H, s, CH_3), 4.20 (2H, m, $—CH_2OH$), 5.45 (2H, m, —HC=CH—); ms *m/e*: 399 (MH^+).

Methyl (E)-*2,7,7-tricarbomethoxy-12-chloro-4-dodecen-10-ynoate (1*a *[A–T])*

Following procedure 10: Alcohol **16***a* [A–T] (1.11 g, 2.79 mmol) gave **1***a* [A–T] (0.94 g, 81%); ir: 1732 cm^{-1}; ^1H nmr δ: 2.13 (4H, m, $—CH_2CH_2—$), 2.55 (4H, m, $—C{=}CCH_2C(CO_2Me)_2$), 3.39 (1H, t, $—CH(CO_2Me)_2$), 3.72, 3.74 (12H, s, CH_3), 4.12 (2H, m, $—CH_2Cl$), 5.40 (2H, m, —HC=CH—); ms *m/e*: 417 (MH^+).

(E)-*1,1,6,6-Tetracarbomethoxy-3-cycloundecen-8-yne (2*a *[A–T])* and *(E),(E)-1,1,6,6,12,12,17,17-octacarbomethoxy-3,14-cyclodocosadien-9,20-diyne (3*a *[A–T])*

Following procedure 11: After 18 h and at 2×10^{-3} *M*, the chloride **1***a* [A–T] (166 mg, 0.4 mmol) gave the monomer **2***a* [A–T] (68.0 mg, 45%) and **3***a* [A–T] (10.3 mg, 7%, 85% pure estimated from ^{13}C nmr); ir of **2***a*: 1730, 1229 cm^{-1}; ir of **3***a*: 3040, 1730, 1235 cm^{-1}.

*Methyl 2-carbomethoxy-2-(4-chloro-2-butynyl)-7-[(tetrahydro-2*H*-pyran-2-yl)oxy]-5-heptynoate (14*a *[A–A])*

Following procedure 8: Using 1,4-dichloro-2-butyne, malonate **8***a* (1.4 g, 4.7 mmol) gave **14***a* [A–A] (1.36 g, 75%); ir: 1733 cm^{-1}; ^1H nmr δ: 1.62 (6H, m, $—C(CH_2)_3C—$), 2.27 (4H, m, $—CH_2CH_2—$), 2.89 (2H, t, J = 2.5 Hz, $—C{\equiv}CCH_2C(CO_2Me)_2—$), 3.40–4.00 (2H, m, $—CH_2O—$, cyclic), 3.75 (6H, s, CH_3), 4.08 (2H, t, J = 2.5 Hz, $—CH_2Cl$), 4.21 (2H, m, $—C{\equiv}CCH_2O—$), 4.78 (1H, m, $—O_2CH—$); ms *m/e*: 385 (MH^+).

*Methyl 2,7,7-tricarbomethoxy-12-[(tetrahydro-2*H*-pyran-2-yl)oxy]-4,10-dodecadiynoate (15*a *[A–A])*

Following procedure 3: Using tetrahydrofuran as solvent, chloride **14***a* [A–A] (1.29 g, 3.36 mmol) gave compound **15***a* [A–A] (1.23 g, 76%); ir: 1740, 1732 cm^{-1}; ^1H nmr δ: 1.40–1.70 (6H, m, $—C(CH_2)_3C—$), 2.22 (4H, m, $—CH_2CH_2—$), 2.76 (4H, m, $—C{\equiv}CCH_2C(CO_2Me)_2$), 3.35–4.00 (3H, m, $—CH(CO_2Me)_2$ and $—OCH_2—$, cyclic), 3.72, 3.75 (12H, s, CH_3), 4.19 (2H, m, $—C{\equiv}CCH_2O—$), 4.76 (1H, m, $—O_2CH—$); ms *m/e*: 481 (MH^+).

*Methyl 2,7,7-tricarbomethoxy-12-hydroxy-4,10-dodecadiynoate (16*a *[A–A])*

Following procedure 5: Malonate **15***a* [A–A] (1.22 g, 2.54 mmol) at 50°C gave alcohol **16***a* [A–A] (0.947 g, 94%) as an oil containing some impurities; ir: 1735 cm^{-1}; ^1H nmr δ: 1.57 (1H, m, —OH), 2.24 (4H, m, $—CH_2CH_2—$), 2.79 (4H, m, $—C{\equiv}CCH_2C(CO_2Me)_2$), 3.52 (1H, t, $—CH(CO_2Me)_2$), 3.73, 3.77 (12H, s, CH_3), 4.21 (2H, m, $—CH_2O—$); ms *m/e*: 397 (MH^+).

Can. J. Chem. Downloaded from www.nrcresearchpress.com by 80.58.250.72 on 09/07/12
For personal use only.

Can. J. Chem. Downloaded from www.nrcresearchpress.com by 80.58.250.72 on 09/07/12
For personal use only.

*Methyl 2,7,7-tricarbomethoxy-12-chloro-4,10-dodecadiynoate (**1**a [A–A])*

Following procedure 10: Alcohol **16***a* [A–A] (0.937 g, 2.37 mmol) gave chloride **1***a* [A–A] (0.73 g, 75%) as an oil; ir: 2240, 1740 cm^{-1}; ^1H nmr δ: 2.24 (4H, m, $—CH_2CH_2—$), 2.77 (4H, m, $—C{\equiv}CCH_2C(CO_2Me)_2—$), 3.51 (1H, t, $—CH(CO_2Me)_2$), 3.73, 3.77 (12H, s, CH_3), 4.11 (2H, m, $—CH_2Cl$); ms *m/e*: 415 (MH^+).

*1,1,6,6-Tetracarbomethoxy-3,8-cycloundecadiyne (**2**a [A–A]) and 1,1,6,6,12,12,17,17-octacarbomethoxy-3,9,14,20-cyclodocosatetrayne (**3**a [A–A])*

Following procedure 11: After 14 h, chloride **1***a* [A–A] (169 mg, 0.408 mmol) gave monomer **2***a* [A–A] (81.1 mg, 53%) and dimer **3***a* [A–A] (36.0 mg, 24%); ir of **2***a*: 1730, 1232 cm^{-1}; ir of **3***a*: 1730, 1295 cm^{-1}.

*Methyl 2-carbomethoxy-2-[4-chloro-2-butynyl)-7-[(tetrahydro-2H-pyran-2-yl)oxy]-5-heptanoate (**14**a [A])*

Following procedure 8: Crude malonate **11***a* (1.40 g, 4.65 mmol) gave chloride **14***a* [A] as an impure oil (0.975 g, 54%); ir: 1732 cm^{-1}; ^1H nmr δ: 1.30–2.20 (14H, m, $—C(CH_2)_3C—$ and $C—(CH_2)_4—C$), 2.87 (2H, t, J = 2.5 Hz, $—C{\equiv}CCH_2C(CO_2Me)_2—$), 3.20–4.00 (4H, m, $—OCH_2—$), 3.74 (6H, s, CH_3), 4.08 (2H, t, J = 2.5 Hz, $—CH_2Cl$), 4.55 (1H, m, $—O_2CH—$); ms *m/e*: 389 (MH^+).

*Methyl2,7,7-tricarbomethoxy-12-[(tetrahydro-2H-pyran-2-yl)oxy]-4-dodecynoate (**15**a [A])*

Following procedure 3: Compound **14***a* [A] (0.955 g, 2.46 mmol) gave **15***a* [A] (0.983 g, 83%) as an oil; ir: 1735 cm^{-1}; ^1H nmr δ: 1.30–2.10 (14H, m, $—C(CH_2)_3C—$ and $—C(CH_2)_4C—$), 2.77 (4H, m, $—C{\equiv}CCH_2C(CO_2Me)_2$), 3.20–4.10 (5H, m, $—CH(CO_2Me)_2$ and $—OCH_2—$), 3.72, 3.76 (12H, s, CH_3), 4.56 (1H, m, $—O_2CH—$); ms *m/e*: 485 (MH^+).

*Methyl 2,7,7-tricarbomethoxy-12-hydroxy-4-dodecynoate (**16**a [A])*

Following procedure 5: Compound **15***a* [A] (0.983 g, 2.03 mmol) gave, after 2.5 h, alcohol **16***a* [A] (0.786 g, 98%); ir: 1732 cm^{-1}; ^1H nmr δ: 1.10–2.20 (9H, m, —OH and $—C(CH_2)_4C—$), 2.76 (4H, m, $—C{\equiv}CCH_2C(CO_2Me)_2$), 3.30–3.70 (3H, m, $—CH(CO_2Me)_2$ and $—OCH_2—$), 3.72, 3.76 (12H, s, CH_3); ms *m/e*: 401 (MH^+).

*Methyl 12-bromo-2,7,7-tricarbomethoxy-4-dodecynoate (**4**a)*

Following procedure 2: Alcohol **16***a* [A] (0.786 g, 1.76 mmol) gave, after flash chromatography (ethyl acetate/dichloromethane/hexanes 1:2:4), bromide **4***a* (0.704 g, 77%); ir: 2350, 1732 cm^{-1}; ^1H nmr δ: 1.00–2.10 (8H, m, $—C(CH_2)_4C—$), 2.76 (4H, m, $—C{\equiv}CCH_2C(CO_2Me)_2$), 3.40 (2H, t, J = 6 Hz, $—CH_2Br$), 3.50 (1H, m, $—CH(CO_2Me)_2$), 3.72, 3.76 (12H, s, CH_3); ms *m/e*: 463 (MH^+).

*1,1,6,6-Tetracarbomethoxy-3-cycloundecyne (**6**a) and 1,1,6,6,12,12,17,17-octacarbomethoxy-3,14-cyclodocosadiyne* (dimer)

Following procedure 11: After 44 h bromide **4***a* (166.4 mg, 0.359 mmol) gave **6***a* (58.6 mg, 42%) and dimer (25.2 mg, 18%) at 2×10^{-3} *M*; ir of **6***a* 1732, 1460, 1270 cm^{-1}; ir of dimer: 1733, 1285, 1120 cm^{-1}.

General procedure 12:

*Methyl 12-bromo-2,7,7-tricarbomethoxy-dodecanoate (**5**a)*

Bromide **4***a* (454 mg, 0.983 mmol) was dissolved in cyclohexane (10 mL) and ethyl acetate (2 mL) under argon. Platinum(IV) oxide (25 mg) and sodium sulfate (100 mg) were added at 25°C and the mixture was stirred under a hydrogen atmosphere for 3 h. The solution was filtered on Celite and the solvents were evaporated under vacuum to give **5***a* (448 mg, 98%); ir: 1730 cm^{-1}; ^1H nmr δ: 1.00–2.10 (16H, m, $—CCH_2C—$), 3.33 (1H, t, $—CH(CO_2Me)_2$), 3.38 (2H, t, J = 6 Hz, $—CH_2Br$), 3.70, 3.73 (12H, s, CH_3); ms *m/e*: 467 (MH^+).

*1,1,6,6-Tetracarbomethoxy-cycloundecane (**7**a) and 1,1,6,6,12,12,17,17-octacarbomethoxy-cyclodocosane* (dimer)

Following procedure 11: After 48 h, bromide **5***a* (172 mg, 0.369 mmol) gave monomer **7***a* (4.8 mg, 3%) and dimer (3.5 mg, 2%) at 2×10^{-3} *M*; ir of **7***a*: 1728, 1250, 1192 cm^{-1}; ir of dimer: 1730, 1230 cm^{-1}.

*Methyl (Z)-2-carbomethoxy-2-[(Z)-4-chloro-2-butenyl]-8-[(tetrahydro-2H-pyran-2-yl)oxy]-6-octenoate (**14**b [C–C])*

Following procedure 8: Compound **9***b* (1.37 g, 3.4 mmol) gave chloride **14***b* [C–C] (1.49 g, 85%); ir: 1732 cm^{-1}; ^1H nmr δ: 1.25–2.30 (12H, m, $—C(CH_2)_3C—$), 2.70 (2H, m, $—C{=}CCH_2C(CO_2Me)_2$), 3.30–4.00 (6H, m, $—CH_2Cl$ and $—OCH_2—$), 3.72 (6H, s, CH_3), 4.60 (1H, m, $—O_2CH—$), 5.30–5.90 (4H, m, $—HC{=}CH—$); ms *m/e*: 403 (MH^+).

*Methyl (Z),(Z)-2,7,7-tricarbomethoxy-13-[(tetrahydro-2H-pyran-2-yl)oxy]-4,11-tridecadienoate (**15**b [C–C])*

Following procedure 3: Compound **14***b* [C–C] (1.48 g, 3.67 mmol) gave the malonate **15***b* [C–C] (1.77 g, 97%); ir: 1730–1740 cm^{-1}; ^1H nmr δ: 1.30–2.10 (12H, m, $—C(CH_2)_3C—$), 2.61 (4H, m, $—C{=}CCH_2C(CO_2Me)_2$), 3.37 (1H, t, $—CH(CO_2Me)_2$), 3.30–4.00 (2H, m, $—OCH_2—$, cyclic), 3.71, 3.74 (12H, s, CH_3), 4.14 (2H, m, $THPOCH_2—$), 4.63 (1H, m, $—O_2CH—$), 5.30–5.70 (4H, m, $—HC{=}CH—$); ms *m/e*: 499 (MH^+).

*Methyl (Z),(Z)-2,7,7-tricarbomethoxy-13-hydroxy-4,11-tridecadienoate (**16**b [C–C])*

Following procedure 9: Compound **15***b* [C–C] (1.76 g, 3.53 mmol) gave alcohol **16***b* [C–C] (1.43 g, 98%); ir: 3200–3600, 1730 cm^{-1}; ^1H nmr δ: 1.2–2.1 (7H, m, —OH and $—(CH_2)_3—$), 2.63 (4H, m, $—C{=}CCH_2C(CO_2Me)_2$), 3.38 (1H, t, $—CH(CO_2Me)_2$), 3.71, 3.74 (12H, s, CH_3), 4.17 (2H, m, $—CH_2O—$), 5.20–5.70 (4H, m, $—HC{=}CH—$); ms *m/e*: 415 (MH^+).

*Methyl(Z),(Z)-2,7,7-tricarbomethoxy-13-chloro-4,11-tridecadienoate (**1**b [C–C])*

Following procedure 10: Alcohol **16***b* [C–C] (1.42 g, 3.43 mmol) gave chloride **1***b* [C–C] (1.27 g, 86%); ir: 1730–1745 cm^{-1}; ^1H nmr δ: 1.30–2.20 (6H, m, $—(CH_2)_3—$), 2.72 (4H, m, $—C{\equiv}CCH_2C(CO_2Me)_2—$), 3.37 (1H, t, $—CH(CO_2Me)_2$), 3.70, 3.73 (12H, s, CH_3), 4.12 (2H, m, $—CH_2Cl$), 5.25–5.70 (4H, m, $—HC{=}CH—$); ms *m/e*: 433 (MH^+).

*(Z),(Z)-1,1,6,6-Tetracarbomethoxy-3,8-cyclododecadiene (**2**b [C–C] and (Z),(Z),(Z),(Z)-1,1,6,6,13,13,18,18-octacarbomethoxy-3,10,15,22-cyclotetracosatetraene (**3**b [C–C])*

Following procedure 11: After 24 h, the chloride **1***b* [C–C] (184 mg, 0.427 mmol) gave the monomer **2***b* [C–C] (50.1 mg, 29.1%) and **3***b* [C–C] (70.4 mg, 40.9%); ir of **2***b*: 1731, 1271, 1060 cm^{-1}; ir of **3***b*: 1730, 1136, 1103 cm^{-1}.

*Methyl (Z)-2-carbomethoxy-2-[(E)-4-chloro-2-butenyl]-8-[(tetrahydro-2H-pyran-2-yl)oxy]-6-octenoate (**14**b [C–T])*

Following procedure 8: Using *trans*-1,4-dichloro-2-butene, compound **9***b* (1.33 g, 4.26 mmol) gave chloride **14***b* [C–T] (1.38 g, 81%); ir: 1733 cm^{-1}; ^1H nmr δ: 1.10–2.10 (12H, m, $—C(CH_2)_3C—$), 2.67 (2H, m, $—C{=}CCH_2C(CO_2Me)_2$), 3.40–4.00 (2H, m, $—OCH_2—$, cyclic), 3.72 (6H, s, CH_3), 4.00–4.15 (4H, m, $—CH_2Cl$ and $THPOCH_2—$), 4.62 (1H, m, $—O_2CH—$), 5.30–5.70 (4H, m, $—HC{=}CH—$); ms *m/e*: 403 (MH^+).

*Methyl (E),(Z)-2,7,7-tricarbomethoxy-13-[(tetrahydro-2H-pyran-2-yl)oxy]-4,11-tridecadienoate (**15**b [C–T])*

Following procedure 3: Compound **14***b* [C–T] (1.37 g, 3.40 mmol) gave **15***b* [C–T] (1.54 g, 91%); ir: 1730 cm^{-1}; ^1H nmr δ: 1.20–2.10 (12H, m, $—(CH_2)_3—$), 2.59 (4H, m, $—C{=}CCH_2C(CO_2Me)_2$), 3.38 (1H, t, $—CH(CO_2Me)_2$), 3.40–4.00 (2H, m, $—OCH_2—$, cyclic), 3.70, 3.74 (12H, s, CH_3), 4.10 (2H, m, $THPOCH_2—$), 4.61 (1H, m, $—O_2CH—$), 5.30–5.70 (4H, m, $—HC{=}CH—$); ms *m/e*: 499 (MH^+).

*Methyl (E),(Z)-2,7,7-tricarbomethoxy-13-hydroxy-4,11-tridecadienoate (**16**b [C–T])*

Following procedure 9: Compound **15***b* [C–T] (1.52 g, 3.06 mmol) gave alcohol **16***b* [C–T] (1.29 g, 100%); ir: 3620, 1730 cm^{-1}; ^1H nmr δ: 1.10–2.20 (7H, m, —OH and $—(CH_2)_3—$), 2.52 (4H, m, $—C{=}CCH_2C(CO_2Me)_2$), 3.37 (1H, t, $—CH(CO_2Me)_2$), 3.69, 3.73 (12H, s, CH_3), 4.17 (2H, m, $—CH_2O—$), 5.10–5.80 (4H, m, $—HC{=}CH—$); ms *m/e*: 415 (MH^+).

Can. J. Chem. Downloaded from www.nrcresearchpress.com by 80.58.250.72 on 09/07/12
For personal use only.

Methyl (E),(Z)-*2,7,7-tricarbomethoxy-13-chloro-4,11-tridecadienoate* (**1**b *[C–T]*)

Following procedure 10: Compound **16***b* [C–T] (1.27 g, 3.07 mmol) gave **1***b* [C–T] (1.11 g, 84%); ir: 1730 cm^{-1}; ^1H nmr δ: 1.10–2.25 (6H, m, $—(CH_2)_3—$), 2.60 (4H, m, $—C{=}CCH_2C(CO_2Me)_2$), 3.38 (1H, t, $—CH(CO_2Me)_2$), 3.70–3.73 (12H, s, CH_3), 4.08 (2H, m, $—CH_2Cl$), 5.20–5.75 (4H, m, —HC=CH—); ms *m/e*: 433 (MH^+).

(E),(Z)-*1,1,6,6-Tetracarbomethoxy-3,8-cyclododecadiene* (**2**b *[C–T]*) *and* (E),(Z),(E),(Z)-*1,1,6,6,13,13,18,18-octacarbomethoxy-3,10,15,22-cyclotetracosatetraene* (**3**b *[C–T]*)

Following procedure 11: After 20 h, chloride **1***b* [C–T] (187.6 mg, 0.434 mmol) gave **2***b* [C–T] (20.6 mg, 12%) and dimer **3***b* [C–T] (102.4 mg, 60%); ir of **2***b*: 1730, 1265, 1063 cm^{-1}; ir of **3***b*: 1730, 1175, 1131 cm^{-1}.

Methyl (E)-*2-carbomethoxy-2-[*(E)-*4-chloro-2-butenyl]-8-[(tetrahydro-2*H*-pyran-2-yl)oxy]-6-octenoate* (**14**b *[T–T]*)

Following procedure 8: Using *trans*-1,4-dichloro-2-butene, malonate **10***b* (1.33 g, 3.29 mmol) gave chloride **14***b* [T–T] (1.39 g, 75%); ir: 1730 cm^{-1}; ^1H nmr δ: 1.20–2.10 (12H, m, $—C(CH_2)_3—C—$), 2.60 (2H, m, $—C{=}C—CH_2C(CO_2Me)_2—$), 3.40–4.00 (2H, m, $—OCH_2—$, cyclic), 3.70 (6H, s, CH_3), 4.10 (4H, m, $—CH_2Cl$ and $THPOCH_2—$), 4.61 (1H, m, $—O_2CH—$), 5.63 (4H, m, —HC=CH—); ms *m/e*: 403 (MH^+).

Methyl (E),(E)-*2,7,7-tricarbomethoxy-13-[(tetrahydro-2*H*-pyran-2-yl)oxy]-4,11-tridecadienoate* (**15**b *[T–T]*)

Following procedure 3: Chloride **14***b* [T–T] (1.63 g, 3.26 mmol) gave **15***b* [T–T] (1.306 g, 100%); ir: 1732 cm^{-1}; ^1H nmr δ: 1.20–2.10 (12H, m, $C(CH_2)_3C$), 2.55 (4H, m, $—C{=}CCH_2C(CO_2Me)_2—$), 3.30–4.10 (5H, m, $—CH(CO_2Me)_2$ and $—OCH_2—$), 3.69, 3.74 (12H, s, CH_3), 4.59 (1H, m, $—O_2CH—$), 5.30–5.70 (4H, m, —HC=CH—); ms *m/e*: 499 (MH^+).

Methyl (E),(E)-*2,7,7-tricarbomethoxy-13-hydroxy-4,11-tridecadienoate* (**16**b *[T–T]*)

Following procedure 9: Compound **15***b* [T–T] (1.29 g, 3.13 mmol) gave **16***b* [T–T] (1.61 g, 96%); ir: 3200–3600, 1740, 1730 cm^{-1}; ^1H nmr δ: 1.20–2.10 (7H, m, —OH and $—(CH_2)_3—$), 2.61 (4H, m, $—C{=}CCH_2C(CO_2Me)_2$), 3.38 (1H, t, $—CH(CO_2Me)_2$), 3.70, 3.74 (12H, s, CH_3), 4.10 (2H, m, $—CH_2O—$), 5.20–5.70 (4H, m, —HC=CH—); ms *m/e*: 415 (MH^+).

Methyl (E),(E)-*2,7,7-tricarbomethoxy-13-chloro-4,11-tridecadienoate* (**1**b *[T–T]*)

Following procedure 10: Compound **16***b* [T–T] (1.27 g, 3.08 mmol) gave chloride **1***b* [T–T] (1.20 g, 90%); ir: 1730–1740 cm^{-1}; ^1H nmr δ: 1.20–2.10 (6H, m, $—(CH_2)_3—$), 2.61 (4H, m, $—C{=}CCH_2C(CO_2Me)_2$), 3.38 (1H, t, $—CH(CO_2Me)_2$), 3.70, 3.74 (12H, s, CH_3), 4.08 (2H, m, $—CH_2Cl$), 5.30–5.70 (4H, m, —HC=CH—); ms *m/e*: 433 (MH^+).

(E),(E)-*1,1,6,6-Tetracarbomethoxy-3,8-cyclododecadiene* (**2**b *[T–T]*) *and* (E),(E),(E),(E)-*1,1,6,6,13,13,18,18-octacarbomethoxy-3,10,15,22-cyclotetracosatetraene* (**3**b *[T–T]*)

Following procedure 11: After 43 h, chloride **1***b* [T–T] (186 mg, 0.432 mmol) gave monomer **2***b* [T–T] (118 mg, 65%) and dimer **3***b* [T–T] (25.2 mg, 15%) at 2×10^{-3} *M*; ir of **2***b*: 1740, 1730, 1250, 1135 cm^{-1}; ir of **3***b*: 1730, 1270, 1175 cm^{-1}.

Methyl 2-carbomethoxy-2-[(Z)-*4-chloro-2-butenyl]-8-[(tetrahydro-2*H*-pyran-2-yl)oxy]-6-octynoate* (**14**b *[A–C]*)

Following procedure 8: Malonate **8***b* (1.25 g, 4.02 mmol) gave **14***b* [A–C] (1.31 g, 81%); ir: 1730 cm^{-1}; ^1H nmr δ: 1.20–2.40 (12H, m, $C—(CH_2)_3—C$), 2.72 (2H, m, $—C{=}CCH_2C(CO_2Me)_2$), 3.40–3.90 (2H, m, $—OCH_2—$, cyclic), 3.73 (6H, s, CH_3), 4.07 (2H, m, $—CH_2Cl$), 4.23 (2H, m, $THPOCH_2—$), 4.79 (1H, m, $—O_2CH—$), 5.60 (2H, m, —HC=CH—); ms *m/e*: 401 (MH^+).

Methyl (Z)-*2,7,7-tricarbomethoxy-13-[(tetrahydro-2*H*-pyran-2-yl)oxy]-4-tridecen-11-ynoate* (**15**b *[A–C]*)

Following procedure 3: Compound **14***b* [A–C] (1.24 g, 3.10 mmol) gave the malonate **15***b* [A–C] (1.54 g, 100%); ir: 1731 cm^{-1}; ^1H nmr δ: 1.20–2.20 (12H, m, $—(CH_2)_3—$), 2.67 (4H, m, $—C{=}CCH_2C(CO_2Me)_2$), 3.30–3.90 (3H, m, $—CH(CO_2Me)_2$ and $—OCH_2$, cyclic), 3.71, 3.74 (12H, s, CH_3), 4.23 (2H, m, $THPOCH_2—$), 4.78 (1H, m, $—O_2CH—$), 5.38 (2H, m, —HC=CH—); ms *m/e*: 497 (MH^+).

Methyl (Z)-*2,7,7-tricarbomethoxy-13-hydroxy-4-tridecen-11-ynoate* (**16**b *[A–C]*)

Following procedure 9: Compound **15***b* [A–C] (1.53 g, 3.08 mmol) gave alcohol **16***b* [A–C] (1.19 g, 94%); ir: 3200–3600, 1732 cm^{-1}; ^1H nmr δ: 1.25–2.20 (7H, —OH and $—(CH_2)_3—$), 2.69 (4H, m, $—C{=}CCH_2C(CO_2Me)_2$), 3.39 (1H, t, $—CH(CO_2Me)_2$), 3.72, 3.74 (12H, s, CH_3), 4.23 (2H, m, $—CH_2O—$), 5.37 (2H, m, —HC=CH—); ms *m/e*: 413 (MH^+).

Methyl (Z)-*2,7,7-tricarbomethoxy-13-chloro-4-tridecen-11-ynoate* (**1**b *[A–C]*)

Following procedure 10: Alcohol **16***b* [A–C] (1.18 g, 2.87 mmol) gave chloride **1***b* [A–C] (0.85 g, 70%); ir: 1740, 1790 cm^{-1}; ^1H nmr δ: 1.20–2.30 (6H, m, $—(CH_2)_3—$), 2.69 (4H, m, $—C{=}CCH_2C(CO_2Me)_2$), 3.38 (1H, t, $—CH(CO_2Me)_2$), 3.735, 3.739 (12H, s, CH_3), 4.13 (2H, m, $—CH_2Cl$), 5.44 (2H, m, —HC=CH—); ms *m/e*: 431 (MH^+).

(Z)-*1,1,6,6-Tetracarbomethoxy-3-cyclododecen-8-yne* (**2**b *[A–C]*) *and* (Z),(Z)-*1,1,6,6,13,13,18,18-octacarbomethoxy-3,15-cyclotetracosadien-10,22-diyne* (**3**b *[A–C]*)

Following procedure 11: Chloride **1***b* [A–C] (180 mg, 0.418 mmol) gave monomer **2***b* [A–C] (132.6 mg, 80%) and dimer **3***b* [A–C] (5.8 mg, 3.5%) after 18 h; ir of **2***b*: 1730, 1272, 1178 cm^{-1}; ir of **3***b*: 1732, 1200 cm^{-1}.

Methyl-2-carbomethoxy-2-[(E)-*4-chloro-2-butenyl]-8-[(tetrahydro-2*H*-pyran-2-yl)oxy]-6-octynoate* (**14**b *[A–T]*)

Following procedure 8: Using *trans*-1,4-dichloro-2-butene, malonate **8***b* (1.43 g, 4.57 mmol) gave chloride **14***b* [A–T] (1.40 g, 77%); ir: 1731 cm^{-1}; ^1H nmr δ: 1.20–2.20 (12H, m, $—C(CH_2)_3C—$), 2.59 (2H, m, $—C{=}CCH_2C(CO_2Me)_2$), 3.40–3.90 (2H, m, $—OCH_2—$, cyclic), 3.72 (6H, s, CH_3), 4.00 (2H, m, $—CH_2Cl$), 4.24 (2H, m, $THPOCH_2—$), 4.79 (1H, m, $—O_2CH—$), 5.66 (2H, m, —HC=CH—); ms *m/e*: 401 (MH^+).

Methyl (E)-*2,7,7-tricarbomethoxy-13-[(tetrahydro-2*H*-pyran-2-yl)oxy]-4-tridecen-11-ynoate* (**15**b *[A–T]*)

Following procedure 3: Chloride **14***b* [A–T] (1.39 g, 3.47 mmol) gave **15***b* [A–T] (1.71 g, 99%); ir: 1735 cm^{-1}; ^1H nmr δ: 1.20–2.20 (12H, m, $C—(CH_2)_3—C$), 2.59 (4H, m, $—C{=}CCH_2C(CO_2Me)_2$), 3.30–3.80 (3H, m, $—CH(CO_2Me)_2$ and $—OCH_2—$, cyclic), 3.70, 3.73 (12H, s, CH_3), 4.23 (2H, m, $THPOCH_2—$), 4.78 (1H, m, $—O_2CH—$), 5.42 (2H, m, —HC=CH—); ms *m/e*: 497 (MH^+).

Methyl (E)-*2,7,7-tricarbomethoxy-13-hydroxy-4-tridecen-11-ynoate* (**16**b *[A–T]*)

Following procedure 9: Compound **15***b* [A–T] (1.68 g, 3.40 mmol) gave alcohol **16***b* [A–T] (1.42 g, 100%); ir: 3610, 1730 cm^{-1}; ^1H nmr δ: 1.20–2.20 (7H, —OH and $—(CH_2)_3—$), 2.61 (4H, m, $—C{=}CCH_2C(CO_2Me)_2$), 3.40 (1H, t, $—CH(CO_2Me)_2$), 3.71, 3.75 (12H, s, CH_3), 4.23 (2H, m, $—CH_2O—$), 5.42 (2H, m, —HC=CH—); ms *m/e*: 413 (MH^+).

Methyl (E)-*2,7,7-tricarbomethoxy-13-chloro-4-tridecen-11-ynoate* (**1**b *[A–T]*)

Following procedure 10: Alcohol **16***b* [A–T] (1.41 g, 3.42 mmol) gave **1***b* [A–T] (1.24 g, 85%); ir: 1735 cm^{-1}; ^1H nmr δ: 1.20–2.24 (6H, m, $—(CH_2)_3—$), 2.61 (4H, m, $—C{=}CCH_2C(CO_2Me)_2$), 3.38 (1H, t, $—CH(CO_2Me)_2$), 3.71, 3.73 (12H, s, CH_3), 4.14 (2H, t, J = 4.5 Hz, $—CH_2Cl$), 5.42 (2H, m, —HC=CH—); ms *m/e*: 431 (MH^+).

(E)-*1,1,6,6-Tetracarbomethoxy-3-cyclododecen-8-yne* (**2**b *[A–T]*) *and* (E),(E)-*1,1,6,6,13,13,18,18-octacarbomethoxy-3,15-cyclotetracosadien-10,22-diyne* (**3**b *[A–T]*)

Following procedure 11: After 22 h chloride **1***b* [A–T] (185.9 mg,

Can. J. Chem. Downloaded from www.nrcresearchpress.com by 80.58.250.72 on 09/07/12
For personal use only.

0.432 mmol) gave monomer **2***b* [A–T] (100 mg, 59%) and dimer **3***b* [A–T] (39.5 mg, 23%); ir of **2***b*: 1730, 1251, 1135 cm^{-1}; ir of **3***b*: 1740, 1730, 1180–1260 cm^{-1}.

*Methyl 2-carbomethoxy-2-[4-chloro-2-butynyl)-8-[(tetrahydro-2*H*-pyran-2-yl)oxy]-6-octynoate (**14**b [A–A])*

Following procedure 8: Using 1,4-dichloro-2-butyne, malonate **8***b* (1.14 g, 3.66 mmol) gave **14***b* [A–A] (1.09 g, 75%); ir: 1731 cm^{-1}; ^{1}H nmr δ: 1.30–2.40 (12H, m, C—$(CH_2)_3$—C), 2.87 (2H, t, J = 3 Hz, —C≡C$CH_2C(CO_2Me)_2$), 3.40–4.00 (2H, m, —OCH_2—, cyclic), 3.74 (6H, s, CH_3), 4.10 (2H, t, J = 3 Hz, —CH_2Cl), 4.22 (2H, m, THPOCH_2—), 4.78 (1H, m, —O_2CH—); ms m/e: 399 (MH^+).

*Methyl2,7,7-tricarbomethoxy-13-[(tetrahydro-2*H*-pyran-2-yl)oxy]-4,11-tridecadiynoate (**15**b [A–A])*

Following procedure 3: Chloride **14***b* [A–A] (1.08 g, 2.70 mmol) gave malonate **15***b* [A–A] (0.99 g, 74%) by performing the reaction in tetrahydrofuran; ir: 1735 cm^{-1}; ^{1}H nmr δ: 1.25–2.40 (12H, m, C—$(CH_2)_3$—C), 2.76 (4H, m, —C≡C$CH_2C(CO_2Me)_2$), 3.35–3.90 (3H, m, —$CH(CO_2Me)_2$ and —OCH_2—, cyclic), 3.72, 3.76 (12H, s, CH_3), 4.23 (2H, m, THPOCH_2—), 4.79 (1H, m, —O_2CH—); ms m/e: 411 (M^+ − THP).

*Methyl 2,7,7-tricarbomethoxy-13-hydroxy-4,11-tridecadiynoate (**16**b [A–A])*

Following procedure 9: Malonate **15***b* [A–A] (0.98 g, 1.98 mmol) gave alcohol **16***b* [A–A] (0.81 g, 100%); ir: 1734 cm^{+1}; ^{1}H nmr δ: 1.20–1.60 (3H, m, —OH and $(CH_2)_2CH_2$—), 1.80–2.40 (4H, m, $(CH_2)_2CH_2$—), 2.76 (4H, m, —C≡C$CH_2C(CO_2Me)_2$), 3.52 (1H, m, —$CH(CO_2Me)_2$), 3.73, 3.78 (12H, s, CH_3), 4.25 (2H, dt, J = 8 Hz and 3 Hz, —CH_2—O); ms m/e: 411 (MH^+).

*Methyl 2,7,7-tricarbomethoxy-13-chloro-4,11-tridecadiynoate (**1**b [A–A])*

Following procedure 10: Alcohol **16***b* [A–A] (800 mg, 1.95 mmol) gave chloride **1***b* [A–A] (0.76 g, 91%); ir: 1738 cm^{-1}; ^{1}H nmr δ: 1.20–1.60 (2H, m, —$(CH_2)_2CH_2$—), 1.90–2.40 (4H, m, $(CH_2)_2CH_2$), 2.77 (4H, m, —C≡C$CH_2C(CO_2Me)_2$—), 3.51 (1H, m, —$CH(CO_2Me)_2$), 3.73, 3.77 (12H, s, CH_3), 4.14 (2H, t, J = 3 Hz, —CH_2Cl); ms m/e: 429 (MH^+).

*1,1,6,6-Tetracarbomethoxy-3,8-cyclododecadiyne (**2**b [A–A]) and 1,1,6,6,13,13,18,18-octacarbomethoxy-3,10,15,22-cyclotetracosatetrayne (**3**b [A–A])*

Following procedure 11: Chloride **1***b* [A–A] (162 mg, 0.380 mmol) after 15 h gave the monomer **2***b* [A–A] (71.5 mg, 48%) and dimer **3***b* [A–A] (17.3 mg, 12%); ir of **2***b*: 1736, 1250, 1080 cm^{-1}; ir of **3***b*: 1736, 1292, 910 cm^{-1}.

*Methyl 2-carbomethoxy-2-(4-chloro-2-butynyl)-8-[(tetrahydro-2*H*-pyran-2-yl)oxy]-octanoate (**14**b [A])*

Following procedure 8: Using 1,4-dichloro-2-butyne, compound **11***b* (2.09 g, 6.61 mmol) gave **14***b* [A] as an impure oil (2.06 g, 77.5%); ir: 1732 cm^{-1}; ^{1}H nmr δ: 1.20–2.20 (16H, m, C—CH_2—C), 2.86 (2H, t, J = 3 Hz, C≡C$CH_2C(CO_2Me)_2$), 3.20–3.90 (4H, m, —OCH_2C—), 3.73 (6H, s, CH_3), 4.08 (2H, t, J = 3 Hz, —CH_2Cl), 4.55 (1H, m, —O_2CH—); ms m/e: 403 (MH^+).

*Methyl2,7,7-tricarbomethoxy-13-[(tetrahydro-2*H*-pyran-2-yl)oxy]-4-tridecynoate (**15**b [A])*

Following procedure 3: Chloride **14***b* [A] (2.05 g, 5.1 mmol) gave malonate **15***b* [A] (1.93 g, 76%) as an oil; ir: 1733 cm^{-1}; ^{1}H nmr δ: 1.20–2.20 (16H, m, C—CH_2—C), 2.75 (4H, m, C≡C$CH_2C(CO_2Me)_2$), 3.20–4.00 (5H, m, —$CH(CO_2Me)_2$ and —OCH_2—), 3.71, 3.75 (12H, s, CH_3), 4.55 (1H, m, —O_2CH—); ms m/e: 499 (MH^+).

*Methyl 2,7,7-tricarbomethoxy-13-hydroxy-4-tridecynoate (**16**b [A])*

Following procedure 9: Compound **15***b* [A] (1.92 g, 3.85 mmol) gave alcohol **16***b* [A] (1.52 g, 95%); ir: 3300–3600, 1732 cm^{-1}; ^{1}H nmr δ: 1.20–2.10 (11H, m, —OH and —$(CH_2)_5$—), 2.76 (4H, m, C≡C$CH_2C(CO_2Me)_2$), 3.30–3.80 (3H, m, —CH_2O— and —$CH(CO_2Me)_2$), 3.71, 3.76 (12H, s, CH_3); ms m/e: 415 (MH^+).

*Methyl 13-bromo-2,7,7-tricarbomethoxy-4-tridecynoate (**4**b)*

Following procedure 2: Alcohol **16***b* [A] (1.51 g, 3.65 mmol) gave bromide **4***b* (1.45 g, 83%); ir: 1731 cm^{-1}; ^{1}H nmr δ: 1.20–2.10 (10H, m, —$(CH_2)_5$—), 2.77 (4H, m, C≡C$CH_2C(CO_2Me)_2$), 3.40 (2H, t, J = 6 Hz, —CH_2Br), 3.51 (1H, m, —$CH(CO_2Me)_2$), 3.72, 3.76 (12H, s, CH_3); ms m/e: 477 (MH^+).

*1,1,6,6-Tetracarbomethoxy-3-cyclododecyne (**6**b) and 1,1,6,6,13,13,18,18-octacarbomethoxy-3,15-cyclotetracosadiyne* (dimer)

Following procedure 11: After 48 h, bromide **4***b* (205.6 mg, 0.432 mmol) gave monomer **6***b* (63.4 mg, 37%) and dimer (33.5 mg, 19%); ir of **6***b*: 1732, 1247, 1108 cm^{-1}; ir of dimer: 1730, 1282, 1200 cm^{-1}.

*Methyl 13-bromo-2,7,7-tricarbomethoxy-tridecanoate (**5**b)*

Following procedure 12: The compound **4***b* (597 mg, 1.25 mmol) gave **5***b* (598 mg, 99%); ir: 1729 cm^{-1}; ^{1}H nmr δ: 1.20 and 1.83 (18H, m, C—CH_2—C), 3.31 (1H, t, —$CH(CO_2Me)_2$), 3.36 (2H, t, J = 6.5 Hz, —CH_2Br), 3.68, 3.71 (12H, s, CH_3); ms m/e: 481 (MH^+).

*1,1,6,6-Tetracarbomethoxy-cyclododecane (**7**b) and 1,1,6,6,13,13,18,18-octacarbomethoxy-cyclotetracosane* (dimer)

Following procedure 11: After 40 h, compound **5***b* (199.6 mg, 0.415 mmol) gave monomer **7***b* (46.6 mg, 28%) and dimer (estimated to be 50% pure by ^{1}H nmr) (18.1 mg, 11%); ir of **7***b*: 1730, 1472, 1276 cm^{-1}; ir of dimer: 1728, 1460, 1172 cm^{-1}.

Acknowledgements

Support for this work by the Natural Sciences and Engineering Research Council of Canada (NSERCC) and by the "Ministère de l'Éducation (FCAR)", Québec, is gratefully acknowledged.

1. P. Deslongchamps, S. Lamothe, and H.-S. Lin. Can. J. Chem. **62**, 2395 (1984).
2. (*a*) P. Deslongchamps. Aldrichimica Acta, **17**, 59 (1984); (*b*) Bull Soc. Chim. Fr. II, **9–10**, 349 (1984).
3. (*a*) W. C. Still and D. Mobilio. J. Org. Chem. **48**, 4786 (1983); (*b*) W. C. Still, L. L. MacPherson, T. Harada, J. F. Callahan, and A. L. Rheingold. Tetrahedron, **40**, 2275 (1984).
4. (*a*) G. Illuminati and L. Mandolini. Acc. Chem. Res. **14**, 95 (1981); (*b*) M. A. Casadei, C. Galli, and L. Mandolini. J. Org. Chem. **46**, 3127 (1981); (*c*) M. A. Casadei, C. Galli, and L. Mandolini. J. Am. Chem. Soc. **106**, 1051 (1984).
5. D. Brillon and P. Deslongchamps. Tetrahedron Lett. **27**, 1131 (1986).
6. A. B. Smith, III and A. S. Thompson. J. Org. Chem. **49**, 1469 (1984).
7. M. Schwartz and X. M. Waters. Synthesis, 567 (1972).
8. D. Brillon. Synth. Commun. **16**, 291 (1986).
9. H. Lindlar and R. Dubuis. Org. Synth. **46**, 89 (1966).
10. (*a*) D. G. Holah and J. P. Fackler, Jr. Inorganic synthesis. Vol. 10. McGraw–Hill, New York, NY. 1967. p. 26; (*b*) C. E. Castro and R. P. Stephens. J. Am. Chem. Soc. **86**, 4358 (1964).
11. M. Miyashita, A. Yoshikoshi, and P. A. Grieco. J. Org. Chem. **42**, 3772 (1977).
12. E. W. Collington and A. I. Meyers. J. Org. Chem. **36**, 3044 (1971).
13. D. Brillon and P. Deslongchamps. Can. J. Chem. **65**, 56 (1987).

Synthesis of 13- and 14-membered rings by a direct cyclization method

DENIS BRILLON AND PIERRE DESLONGCHAMPS[1]

Laboratoire de synthèse organique, Département de chimie, Faculté des sciences, Université de Sherbrooke, Sherbrooke (Qué.), Canada J1K 2R1

Received May 1, 1986

This paper is dedicated to Dr. O. E. (Ted) Edwards

DENIS BRILLON and PIERRE DESLONGCHAMPS. Can. J. Chem. **65**, 56 (1987).

The malonate anion intramolecular displacement of propargylic or allylic chlorides, and primary bromide, in thirteen- and fourteen-carbon chains containing either two, one, or no unsaturation sites, yields the corresponding 13- and 14-membered ring compounds under conditions of medium dilution.

DENIS BRILLON et PIERRE DESLONGCHAMPS. Can. J. Chem. **65**, 56 (1987).

Le déplacement intramoléculaire de bromure primaire et de chlorures allyliques ou propargyliques par l'anion malonate de chaînes de treize et quatorze carbones contenant soit deux, une ou aucune insaturation conduit aux composés cycliques à 13 et 14 membres correspondants, dans des conditions de dilution moyenne.

Can. J. Chem. Downloaded from www.nrcresearchpress.com by 80.58.250.72 on 09/07/12
For personal use only.

We have recently published (1) a simple and good method for the preparation of 10-membered rings by direct cyclization, under conditions of medium dilution, of C-10 aliphatic chains containing two sites of unsaturation (double or triple bonds). In the preceding publication (2) we reported a similar study on the cyclization of C-11 and C-12 aliphatic chains. In this report, we wish to disclose an analogous study on the cyclization of C-13 and C-14 aliphatic chains.[2]

We have studied the cyclization of the C-13 and C-14 aliphatic chains **1***a* and **1***b*, which can yield, beside polymerization, either the corresponding cyclic monomers (**2***a* and **2***b*) or dimers (**3***a* and **3***b*) (Scheme 1). The two unsaturations in the chain can be (two of) a *cis* (C), a *trans* (T) olefin, and (or) an acetylene (A). The following combinations were studied: **1***a* or **1***b* -[C–C], -[C–T], -[T–T], -[A–C], -[A–T], and -[A–A]. The cyclization of C-13 and C-14 aliphatic precursors containing only one unsaturation center, an acetylene, i.e. compounds **4***a* and **4***b*, was also studied. Similarly, the cyclization of the fully saturated C-13 and C-14 chains **5***a* and **5***b* was also carried out. These compounds (**4***a*, *b* and **5***a*, *b*) can yield the corresponding cyclic monomers (**6***a*, *b* or **7***a*, *b* respectively) and dimers (structures not shown), or undergo polymerization.

The various C-13 and C-14 aliphatic precursors were obtained by a route (Schemes 2–4) similar to that used for the preparation of the C-11 and C-12 aliphatic chains (2). Scheme 2 describes the preparation of the C-8 and C-9 acetylenic key intermediates **8***a* and **8***b*. The C-8 and C-9 key intermediates having a *cis* olefin (**9***a* and **9***b*), a *trans* olefin (**10***a* and **10***b*), or no unsaturation (**11***a* and **11***b*) were prepared from the acetylenic intermediates **8***a* and **8***b* (Scheme 3). The same scheme summarizes also the conversion of the C-8 and C-9 key intermediates **8***a*, **8***b*, **9***a*, **9***b*, **10***a*, **10***b*, **11***a*, and **11***b* respectively into the C-13 and C-14 doubly unsaturated aliphatic precursors **1***a* and **1***b* [A–A, A–T, A–C, T–T, T–C, and C–C]. It also describes the preparation of the C-13 and C-14 monoacetylenic chains **4***a* and **4***b* (via **11***a* and **11***b*) as well as that of the saturated chains **5***a* and **5***b* obtained from the hydrogenation of **4***a* and **4***b* respectively.

The preparation of the various C-13 and C-14 aliphatic chains from the C-8 and C-9 key intermediates (**8***a*, *b*, **9***a*, *b* **10***a*, *b*, and **11***a*, *b*) is further detailed in Scheme 4: Alkylation of intermediates **8**–**11** (*a* or *b*) with an appropriate alkylating agent (*cis* or *trans* 1,4-dichloro-2-butene or 1,4-dichloro-2-butyne) gave the corresponding chlorides **14***a* and **14***b*. SN_2 displacement of these unsaturated chlorides with dimethyl malonate gave the THP-malonates **15***a* and **15***b*. Acid hydrolysis then gave the primary alcohol malonates **16***a* and **16***b*, which were then respectively transformed into the C-13 and C-14 allylic and propargylic chlorides **1***a* and **1***b* [A–A, A–T, A–C, T–T, T–C, and C–C] as well as the monoacetylenic primary bromides **4***a* and **4***b*.

The cyclization reactions (K_2CO_3/DMF–THF, 90°C) were carried out at 2×10^{-2} and 2×10^{-3} molar dilution, not high dilution, and are presented in Tables 1 and 2 for the C-13 and C-14 aliphatic chains respectively. The cyclic monomers and dimers are readily separated by column chromatography and are all crystalline, except for the monomer **2***b* [C–C]. For all new substances, the spectra (ir, 250-MHz and 80-MHz ^{1}H nmr, ^{13}C nmr, and high resolution mass spectra; low resolution mass spectra were obtained for the dimers) were in complete agreement with the assigned structure. The corresponding ^{1}H nmr, ^{13}C nmr, and mass spectral characteristics and melting points for the cyclic compounds are listed in Table 4.

In most cases, at 10^{-2} *M*, the formation of monomer plus dimer competes effectively with polymerization and, at 10^{-3} *M*, formation of monomer is the main process. During the cyclization of the bromides (**4***a*, *b* and **5***a*, *b*), better yields of monomers were obtained if cesium carbonate was used in addition to potassium carbonate. Under those conditions, cyclization is faster and the formation of a secondary product (a formate resulting from DMF displacement of bromides) was negligible.

The increase in yield on passing from the saturated chain, the monoacetylene, and the bisacetylene is important (44, 53, and 89%) in the C-13 series, but much less in the C-14 series (66, 55, and 76%). Low yields of monomers observed in the cyclization of **1***a* [C–T] (20%), **1***a* [T–T] (45%), **1***b* [T–T] (20%), and **1***b* [A–T] (41%) show that in the C-13 and C-14 series the presence of unsaturation (especially *trans* olefin) can even decrease the yield, by comparison with the cyclization of the monoacetylenes and the fully saturated chains. Somewhat surprisingly, the C-14 series gave lower yields than the C-13 series except for the cyclization of saturated chains **5***b* and **1***b* [C–T].

A comparison of yields obtained at 10^{-3} *M* for monomers and

[1]Author to whom correspondence may be addressed.

[2]For a preliminary account, see ref. 3.

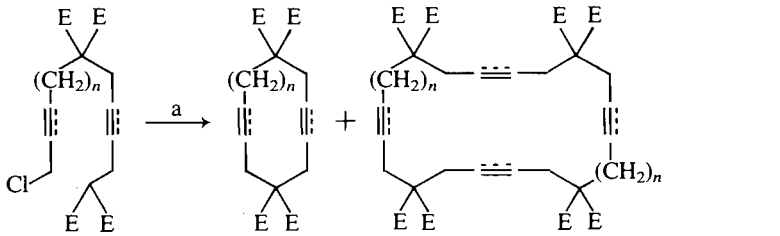

1a (n = 4) **2a** (n = 4) **3a** (n = 4)
1b (n = 5) **2b** (n = 5) **3b** (n = 5)

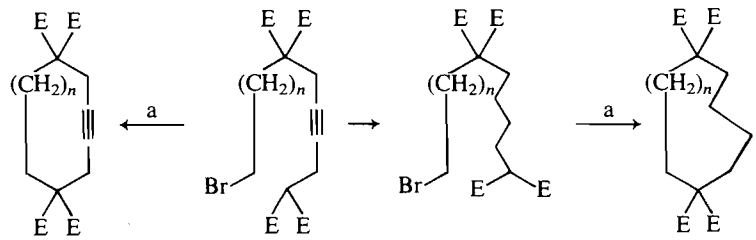

6a (n = 6) **4a** (n = 6) **5a** (n = 6) **7a** (n = 6)
6b (n = 7) **4b** (n = 7) **5b** (n = 7) **7b** (n = 7)

(E = $COOCH_3$)

(a) K_2CO_3, THF–DMF, 90°C, refs. 1, 2

SCHEME 1

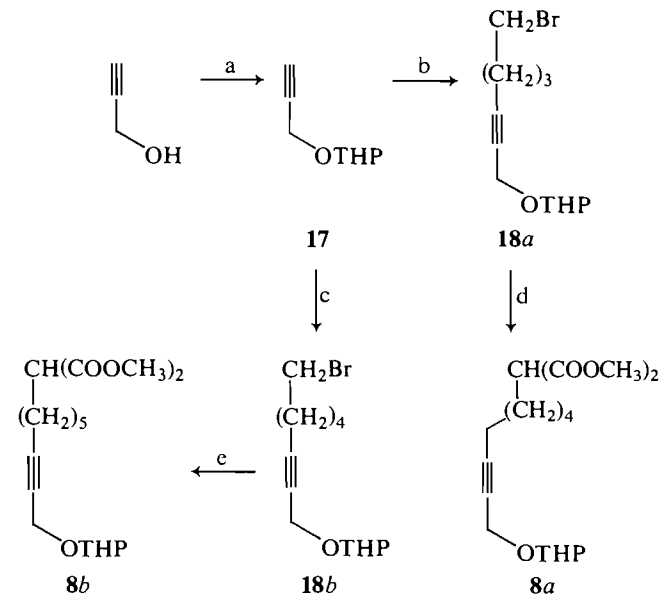

(a) DHP, CF_3COOH, CH_2Cl_2, r.t., 93%, ref. 2
(b) n-BuLi, THF–HMPA, −40°C; $BrCH_2$—$(CH_2)_2$—CH_2Br, reflux, 86%, ref. 2
(c) n-BuLi, THF–HMPA, −40°C; $BrCH_2$—$(CH_2)_3$—CH_2Br, reflux, 82%, ref. 2
(d) K_2CO_3, $CH_2(COOCH_3)_2$, DMF–THF, 80°C, 96%, ref. 1
(e) K_2CO_3, $CH_2(COOCH_3)_2$, DMF–THF, 80°C, 99%, ref. 1

SCHEME 2

dimers with aliphatic chain length from C-10 to C-14 is made in Table 3. The results are in agreement with previous studies on saturated systems, which indicate easier formation of monomers from C-13 and C-14 chains, in comparison with C-10, C-11, and C-12 chains (10). This table also shows clearly that, generally, the introduction of unsaturation in the chain is much more important for a good yield in the C-10, C-11, and C-12 than in the C-13 and C-14 series. In addition, much better yields

Can. J. Chem. Downloaded from www.nrcresearchpress.com by 80.58.250.72 on 09/07/12
For personal use only.

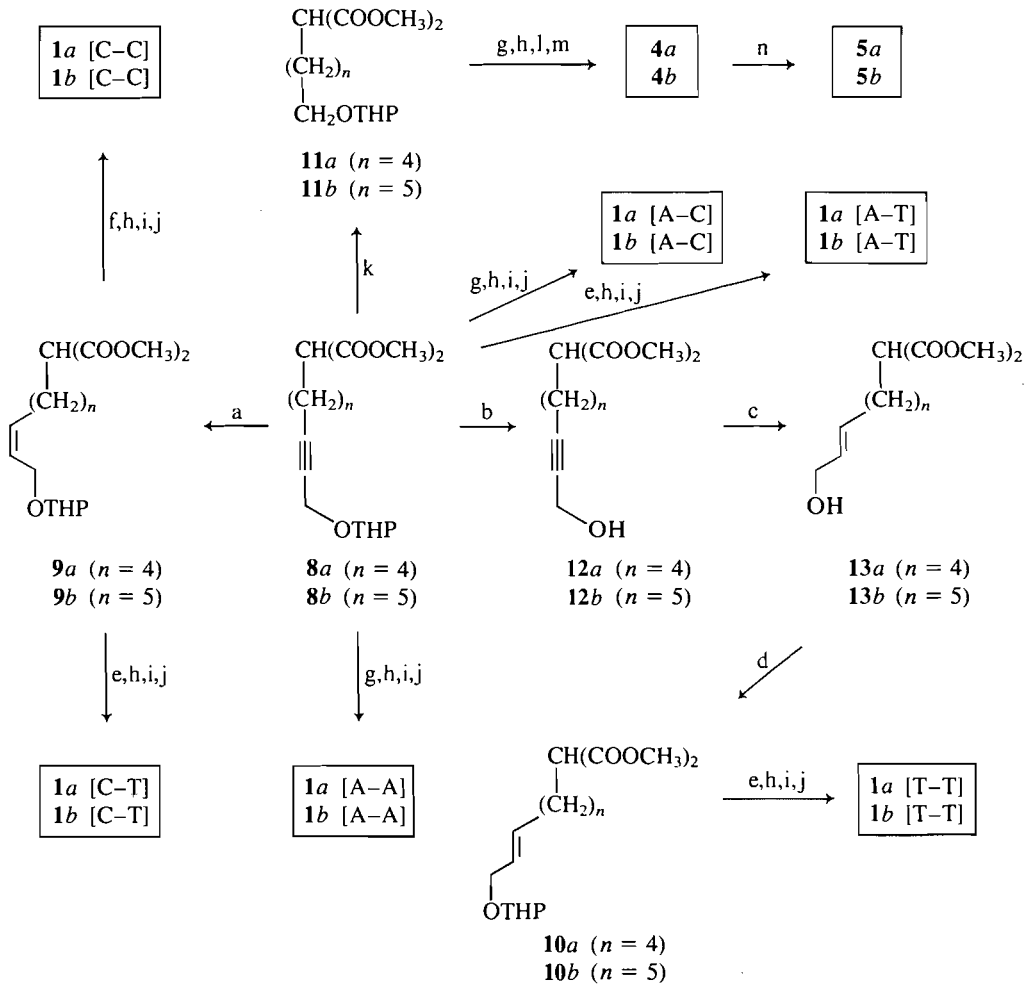

(a) H_2, $Pd/CaCO_3$–PbO, cyclohexane – ethyl acetate, r.t., 96–100%, ref. 4
(b) PPTS, CH_3OH, 50°C, 100%
(c) $CrCl_2$, Na_2SO_4, CH_3COONa, H_2O–DMF, r.t., 92–94%, ref. 5
(d) DHP, CF_3CO_2H, CH_2Cl_2, r.t., 95–96%, ref. 2
(e) NaH, $ClCH_2$—CH=CH—CH_2Cl (*trans*), THF, reflux, 75–84%, ref. 2
(f) NaH, $ClCH_2$—CH=CH—CH_2Cl (*cis*), THF, reflux, 82–87%, ref. 2
(g) NaH, $ClCH_2$—C≡C—CH_2Cl, THF, reflux, 70–91%, ref. 2
(h) NaH, $CH_2(COOCH_3)_2$, DMF–THF, reflux, 90–100%, refs. 2, 9
(i) PPTS, CH_3OH, r.t., 93–100%, ref. 6
(j) MsCl, LiCl, collidine, DMF, 0°C → r.t., 72–92%, ref. 7
(k) H_2, 5% Pd/C, cyclohexane – ethyl acetate, r.t., 100%
(l) PPTS, CH_3OH, reflux, 97–99%
(m) CBr_4, Ph_3P, CH_2Cl_2, 0°C → r.t., 89–91%, ref. 8
(n) H_2, PtO_2, Na_2SO_4, ethyl acetate, r.t., 98–99%

SCHEME 3

are obtained when an acetylenic grouping is present in the chains, and *cis* olefins appear to increase the yield better than *trans* olefins.

In conclusion, these results show clearly that C-10 to C-14 membered rings can be obtained in good yield by a direct cyclization method under conditions of medium dilution. A detailed molecular modeling study of the above result is necessary to understand further the factors that influence these macrocyclization reactions.

Experimental

Proton nmr spectra were recorded in $CDCl_3$ on Bruker WP-80 and WM-250 instruments. The ^{13}C nmr spectra were recorded on a Bruker WM-20 instrument. The infrared (ir) spectra were taken on a Perkin–Elmer 681 spectrophotometer ($CHCl_3$). The mass spectra (ms) and peak matching assays were obtained using a VG Micromass ZAB-1F mass spectrometer. Vapor phase chromatographic (vpc) analyses were carried out on a Hewlett–Packard 5710A gas chromatograph with a flame ionization detector (capillary column OV-101, 25 m). Melting points were determined on a Reichert apparatus. For flash chromatography, the silica gel Kieselgel-60 (from Merck) was used.

All reactions were carried out under an argon atmosphere. Tetrahydrofuran was dried by distilling over sodium/benzophenone whereas *N,N*-dimethylformamide was dried over calcium hydride followed by decantation and distillation under reduced pressure. Ground anhydrous potassium carbonate was used for cyclization reactions.

Can. J. Chem. Downloaded from www.nrcresearchpress.com by 80.58.250.72 on 09/07/12
For personal use only.

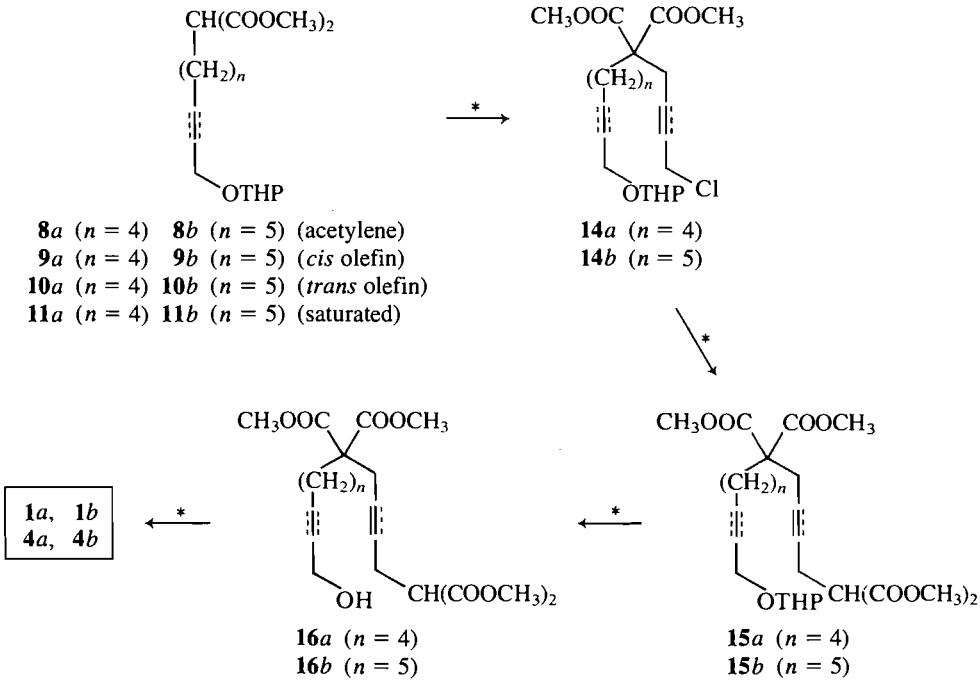

8*a* (n = 4) **8***b* (n = 5) (acetylene)
9*a* (n = 4) **9***b* (n = 5) (*cis* olefin)
10*a* (n = 4) **10***b* (n = 5) (*trans* olefin)
11*a* (n = 4) **11***b* (n = 5) (saturated)

14*a* (n = 4)
14*b* (n = 5)

16*a* (n = 4)
16*b* (n = 5)

15*a* (n = 4)
15*b* (n = 5)

*See Scheme 3.

SCHEME 4

TABLE 1. Cyclization of C-13 aliphatic chains in K_2CO_3/DMF–THF at 90°C[a]

Compound	Time (h)	$10^3 M$	% Monomer[b]	% Dimer[b]
1*a* [C–C]	42	20	67[c]	11
	42	2	77[c]	3
1*a* [C–T]	62	20	8[d]	48
	62	2	20[d]	23
1*a* [T–T]	46	20	13	40
	46	2	45	21
1*a* [A–C]	36	20	91	4
	36	2	95	—
1*a* [A–T]	42	20	59	23
	42	2	83	4
1*a* [A–A]	15	20	68	18
	21	2	89	3
4*a*	40	2	53	14
5*a*	44	2	44	—
	16[e]	2	56	—

[a]Each experiment was carried out twice.
[b]Yield of isolated material after chromatography.
[c]Value obtained from capillary gc analysis.
[d]Value obtained from 250-MHz ^{1}H nmr spectral analysis.
[e]Carried with a mixture of K_2CO_3 and Cs_2CO_3.

TABLE 2. Cyclization of C-14 aliphatic chains in K_2CO_3/DMF–THF at 90°C[a]

Compound	Time (h)	$10^3 M$	% Monomer[b]	% Dimer[b]
1*b* [C–C]	58	20	69[c]	4
	58	2	76[c]	—
1*b* [C–T]	60	20	21	40
	60	2	52	19
1*b* [T–T]	60	20	7[c]	33
	60	2	20[c]	17
1*b* [A–C]	36	20	81	3
	36	2	85	—
1*b* [A–T]	38	20	10[c]	27
	46	2	41[c]	19
1*b* [A–A]	15	20	41	26
	20	2	76	7
4*b*	30[e]	2	55	16
5*b*	48	2	52	4[d]
	16[e]	2	66	4[d]

[a]Each experiment was carried out twice.
[b]Yield of isolated material after chromatography.
[c]Value obtained from capillary gc analysis.
[d]Value obtained from 250-MHz ^{1}H nmr spectral analysis.
[e]Carried with a mixture of K_2CO_3 and Cs_2CO_3.

(E) and (Z)-1,4-Dichloro-2-butene and acetylene **17**

The same samples that were prepared in the preceding work (2) were used.

General procedure 1:

Bromide **18***a from* **17**

To a stirred solution of **17** (10.0 g, 71.3 mmol), triphenylmethane (3 mg), and hexamethylphosphoramide (1.25 mL, 7.0 mmol) in tetrahydrofuran (200 mL), at −40°C, was added *n*-butyllithium (1.6 *M* in hexanes) until the coloration of the solution changed from yellow to dark yellow. Then 1,4-dibromobutane (77.0 g, 356 mmol) was added and the solution was refluxed for 30 h. Diethyl ether (250 mL) was added after cooling and the organic phase was washed with 10% aqueous sodium chloride (3 × 50 mL), dried on sodium sulfate, and evaporated. The remaining volatile materials were removed by Kugelrohr distillation (35°C at 0.02–0.08 Torr) and similarly pure bromide **18***a* was obtained by heating at 85–90°C (0.005–0.01 Torr) (16.5 g, 86%); ^{1}H nmr δ: 1.25–2.40 (12H, m, —C(CH$_2$)$_3$C—), 3.43 (2H, t, J = 7 Hz, —CH$_2$Br), 3.40–3.95 (2H, m, —OCH$_2$—, cyclic), 4.24 (2H, m, THPOCH$_2$—), 4.79 (1H, bs, —O$_2$CH—); ms m/e: 275 (MH$^+$).

*1-Bromo-8-[(tetrahydro-2*H*-pyran-2-yl)oxy]-6-octyne (***18***b)*

Following procedure 1: Using 1,5-dibromopentane (82.0 g, 356 mmol), acetylene **17** (10.0 g, 71.3 mmol) gave bromide **18***b* (16.9 g, 82%), which was obtained as a pure oil by a Kugelrohr distillation (100–110°C at 0.005 Torr); ir: 3008, 2230, 1020 cm^{-1}; ^{1}H nmr δ:

Can. J. Chem. Downloaded from www.nrcresearchpress.com by 80.58.250.72 on 09/07/12
For personal use only.

TABLE 3. Yields of cyclic monomer and dimer from C-10 to C-14 aliphatic precursors containing two, one, and zero sites of unsaturation in the chain[a]

Length of chain	C–C	C–T	T–T	A–C	A–T	A–A	Mono A	Saturated
	%M–%D[b]	%M–%D	%M–%D	%M–%D	%M–%D	%M–%D	%M–%D	%M–%D
C-10[e]	84---[c]	44–25[c]	43–13	73–9	57–15	39–12	—[d]	—[d]
C-11[f]	54–12	66–15	32–37	85–8	44–7	87–8	40–17	2–2
C-12[f]	61–15	38–33	63–14	90---	86–5	79–4	39–16	29–6
C-13	77–3	20–23	45–21	95---	83–4	89–3	53–14	44---
C-14	76---	52–19	20–17	85---	41–19	76–7	55–16	52–4

[a]Cyclization at 2×10^{-3} *M*.
[b]M = monomer, D = dimer.
[c]Cyclization at 2×10^{-2} *M*.
[d]Not carried out.
[e]Reference 1.
[f]Reference 2.

Can. J. Chem. Downloaded from www.nrcresearchpress.com by 80.58.250.72 on 09/07/12
For personal use only.

1.20–2.00 (12H, m, C—$(CH_2)_3$—C, cyclic and $BrCH_2$—$(CH_2)_3$—), 2.24 (2H, m, —C≡CCH_2—C), 3.41 (2H, t, *J* = 7 Hz, —CH_2Br), 3.40–4.00 (2H, m, —OCH_2—, cyclic), 4.24 (2H, m, THPOCH_2—), 4.80 (1H, bs, —O_2CH—); ms *m/e*: 289 (MH^+).

General procedure 2:

*Malonate 8*a *from 18*a

A stirred mixture of bromide **18***a* (16.5 g, 61.3 mmol), dimethyl malonate (40.0 mL, 306 mmol), and potassium carbonate (42.0 g, 306 mmol) in tetrahydrofuran (110 mL) and *N,N*-dimethylformamide (110 mL) was heated at 80°C for 15 h. The mixture was cooled and hexane (150 mL) was added, followed by filtration through a Celite pad and removal of solvents under reduced pressure. The residue was dissolved in a (1:1) mixture of diethyl ether/hexane (350 mL), washed with 10% aqueous sodium bicarbonate (60 mL), dried on sodium sulfate, and the solvents were evaporated. The volatile materials were removed by Kugelrohr distillation at 40°C (0.02 Torr) to afford pure malonate **8***a* as an oil (18.7 g, 96%); ir: 1760–1740 cm^{-1}; ^{1}H nmr δ: 1.20–2.30 (14H, m, C—$(CH_2)_3$—C and C—$(CH_2)_4$—C), 3.33 (1H, t, *J* = 6 Hz, —$CH(CO_2Me)_2$), 3.40–4.00 (2H, m, —OCH_2—, cyclic), 3.70 (6H, s, CH_3), 4.20 (2H, m, THPOCH_2—), 4.76 (1H, bs, —O_2CH—); ms *m/e*: 340 (M^+).

*Methyl 2-carbomethoxy-10-[(tetrahydro-2*H*-pyran-2-yl)oxy]-8-decynoate (8*b*)*

Following procedure 2: Bromide **18***b* (16.9 g, 58.5 mmol) gave malonate **8***b* (19.8 g, 99%); ir: 2251, 1730 cm^{-1}; ^{1}H nmr δ: 1.20–2.30 (16H, m, C—$(CH_2)_5$—C and C—$(CH_2)_3$—C), 3.25–4.00 (3H, m, —$CH(CO_2Me)_2$ and —OCH_2—, cyclic), 3.70 (6H, s, CH_3), 4.20 (2H, m, THPOCH_2—), 4.76 (1H, bs, —O_2CH—); ms *m/e*: 341 (MH^+).

General procedure 3:

*(Z)-Alkene 9*a *from 8*a

Lindlar's catalyst (Pd/$CaCO_3$/PbO from Aldrich (300 mg) was added under an argon atmosphere to a solution of **8***a* (2.8 g, 8.1 mmol) in ethyl acetate (3 mL) and cyclohexane (13 mL). This mixture was then carefully stirred under hydrogen (1.00 atm (1 atm = 101.3 kPa) at the end) until the hydrogen uptake ceased. The mixture was filtered through a Celite pad and the filtrate evaporated to afford **9***a* as an oil (2.81 g, 100%); ir: 1730 cm^{-1}; ^{1}H nmr δ: 1.20–2.20 (14H, m, C—$(CH_2)_4$—C and C—$(CH_2)_3$—C), 3.35 (1H, t, *J* = 6 Hz, —$CH(CO_2Me)_2$), 3.35–4.00 (2H, m, —OCH_2—, cyclic), 3.73 (6H, s, CH_3), 4.14 (2H, m, THPOCH_2—), 4.61 (1H, bs, —O_2CH—), 5.55 (2H, m, —HC=CH—); ms *m/e*: 329 (MH^+).

*Methyl (Z)-2-carbomethoxy-10-[(tetrahydro-2*H*-pyran-2-yl)oxy]-8-decenoate (9*b*)*

Following procedure 3: Malonate **8***b* (3.0 g, 9.4 mmol) gave **9***b* (3.0 g, 99%); ir: 1731 cm^{-1}; ^{1}H nmr δ: 1.10–2.20 (16H, m, C—$(CH_2)_5$—C and C—$(CH_2)_3$C), 3.35 (1H, t, *J* = 6.5 Hz, —$CH(CO_2Me)_2$), 3.40–4.00 (2H, m, —OCH_2—, cyclic), 3.74 (6H, s, CH_3), 4.15 (2H, m, THPOCH_2—), 4.62 (1H, bs, —O_2CH—), 5.56 (2H, m, —HC=CH—); ms *m/e*: 343 (MH^+).

General procedure 4:

*Alcohol 12*a *from 8*a

Malonate **8***a* (2.04 g, 6.20 mmol) and pyridinium *p*-toluenesulfonate (170 mg, 0.680 mmol) were dissolved in methanol (15 mL). This solution was heated at 50°C for 1.5 h. After evaporation of methanol under reduced pressure, the residual oil was purified on a silica gel column with ethyl acetate/dichloromethane/hexanes (1:2:2) as eluent. The evaporation of solvents afforded crude alcohol **12***a* as an oil (1.53 g, 99.5%); ^{1}H nmr δ: 1.25–2.35 (9H, m, C—$(CH_2)_4$—C and —OH), 3.38 (1H, t, *J* = 6 Hz, —$CH(CO_2Me)_2$), 3.75 (6H, s, CH_3), 4.2 (2H, dt, *J* = 6 and 2.5 Hz, —OCH_2—); ms *m/e*: 243 (MH^+).

General procedure 5:

*Alcohol 13*a *from 12*a

To a solution of chromous chloride (80 mL) (see ref. 2) was added sodium sulfate (3.30 g, 23.2 mmol), sodium acetate (1.90 g, 23.1 mmol), and alcohol **12***a* (1.53 g, 62.2 mmol) dissolved in deoxygenated *N,N*-dimethylformamide (27 mL). This mixture was stirred at room temperature for 36 h, followed by extraction with diethyl ether (5 × 60 mL). The organic phase was dried over sodium sulfate and evaporated. The residual oil was purified by flash chromatography (ethyl acetate/dichloromethane/hexanes (1:2:2)) to afford the pure alcohol **13***a* as an oil (1.38 g, 92%); ir: 3600, 1732 cm^{-1}; ^{1}H nmr δ: 1.20–1.60 (5H, m, —OH and —$CH_2(CH_2)_2CH_2$—), 1.70–2.20 (4H, m, —$CH_2(CH_2)_2CH_2$—), 3.25 (1H, t, *J* = 6.5 Hz, —$CH(CO_2Me)_2$), 3.74 (6H, s, CH_3), 4.08 (2H, m, —OCH_2—), 5.68 (2H, m, —HC=CH—); ms *m/e*: 245 (MH^+).

General procedure 6:

*(E)-Alkene 10*a *from 13*a

Trifluoroacetic acid (0.05 mL) was added at room temperature to a solution of alcohol **13***a* (1.37 g, 5.52 mmol) and dihydropyran (0.66 mL, 7.2 mmol) in dichloromethane (20 mL). The reaction mixture was stirred at 25°C for 18 h. Dichloromethane was evaporated under reduced pressure and the residual oil was purified by flash chromatography (ethyl acetate/hexanes 1:5) to afford the compound **10***a* (1.77 g, 96%); ir: 1732 cm^{-1}; ^{1}H nmr δ: 1.20–2.20 (14H, m, C—$(CH_2)_3$—C and C—$(CH_2)_4$—C), 3.20–4.30 (5H, m, —$CH(CO_2Me)_2$, —OCH_2—), 3.73 (6H, s, CH_3), 4.61 (1H, bs, —O_2CH—), 5.63 (2H, m, —HC=CH—); ms *m/e*: 329 (MH^+).

*Methyl 2-carbomethoxy-10-hydroxy-8-decynoate (12*b*)*

Following procedure 4: Malonate **8***b* (2.00 g, 5.78 mmol) gave alcohol **12***b* as a crude oil; ir: 3610, 1732 cm^{-1}; ^{1}H nmr δ: 1.25–2.35 (11H, m, C—$(CH_2)_5$—C, —OH), 3.37 (1H, t, —$CH(CH_2Me)_2$),

Can. J. Chem. Downloaded from www.nrcresearchpress.com by 80.58.250.72 on 09/07/12
For personal use only.

3.74 (6H, s, CH_3), 4.20 (2H, dt, J = 3 and 7 Hz, —CH_2O—); ms m/e: 257 (MH^+).

*Methyl (*E*)-2-carbomethoxy-10-hydroxy-8-decenoate (**13**b)*

Following procedure 5: Crude alcohol **12***b* afforded purified alcohol **13***b* (1.36 g, 91% from **8***b*); ir: 1730 cm^{-1}; ^1H nmr δ: 1.20–2.20 (11H, m, C—$(CH_2)_5$—C and —OH), 3.35 (1H, t, —$CH(CO_2Me)_2$), 3.73 (6H, s, CH_3), 4.24 (2H, m, —CH_2O—), 5.65 (2H, m, —HC=CH—); ms m/e: 259 (MH^+).

*Methyl (*E*)-2-carbomethoxy-10-[(tetrahydro-2*H*-pyran-2-yl)oxy]-8-decenoate (**10**b)*

Following procedure 6: Alcohol **13***b* (1.43 g, 5.42 mmol) gave malonate **10***b* (1.79 g, 95%); ir: 1732 cm^{-1}; ^1H nmr δ: 1.10–2.20 (16H, m, C—$(CH_2)_3$—C and C—$(CH_2)_5$—C), 3.20–4.30 (5H, —$CH(CO_2Me)_2$ and —OCH_2—), 3.73 (6H, s, CH_3), 4.63 (1H, bs, —O_2CH—), 5.60 (2H, m, —HC=CH—); ms m/e: 343 (MH^+).

General procedure 7:

*Malonate **11**a from **8**a*

The catalyst 5% palladium on activated carbon (90 mg) was added under argon to a solution of malonate **8***a* (3.10 g, 8.95 mmol) in cyclohexane (10 mL) and ethyl acetate (2 mL). This mixture was then stirred under hydrogen (1.00 atm) until no more hydrogen uptake was observed. The solution was filtered through a Celite pad and the evaporation of solvents afforded crude malonate **11***a* (3.13 g, 100%) (impure from tlc analysis); ir: 1733 cm^{-1}; ^1H nmr δ: 1.10–2.00 (18H, m, C—$(CH_2)_6$—C and C—$(CH_2)_3$—C), 3.20–4.00 (5H, m, —$CH(CO_2Me)_2$, —OCH_2—), 3.71 (6H, s, CH_3), 4.50 (1H, bs, —O_2CH—); ms m/e: 331 (MH^+).

*Methyl 2-carbomethoxy-10-[(tetrahydro-2*H*-pyran-2-yl)oxy]-decanoate (**11**b)*

Following procedure 7: Alkyne **8***b* (2.10 g, 5.83 mmol) gave crude malonate **11***b* (2.13 g, 100%); ir: 1732 cm^{-1}; ^1H nmr δ: 1.15–2.00 (20H, m, C—$(CH_2)_7$—C and C—$(CH_2)_3$—C), 3.15–4.00 (5H, m, —$CH(CO_2Me)_2$ and —OCH_2—), 3.66 (6H, s, CH_3), 4.49 (1H, bs, —O_2CH—); ms m/e: 345 (MH^+).

General procedure 8:

*Methyl (Z)-2-carbomethoxy-2-[(Z)-4-chloro-2-butenyl]-9-[(tetrahydro-2*H*-pyran-2-yl)oxy]-7-nonenoate (**14**a [C–C])*

To a stirred solution of **9***a* (1.36 g, 4.15 mmol) in tetrahydrofuran (18 mL) was added sodium hydride (190 mg, 60% in mineral oil, 4.77 mmol) and this mixture was refluxed for 20 min. After cooling, (*Z*)-1,4-dichloro-2-butene (2.0 mL, 20 mmol) was added and the solution was heated under reflux for 20 min, cooled to 0°C, followed by addition of diethyl ether/hexanes (1:1) (100 mL). The organic phase was washed with 10% aqueous ammonium chloride (10 mL) and dried over sodium sulfate. After filtration and evaporation of solvents under reduced pressure, the residual oil was purified by flash chromotography (ethyl acetate/dichloromethane/hexanes 1:2:7) to afford chloride **14***a* (1.42 g, 82%) as an oil; ir: 1730 cm^{-1}; ^1H nmr δ: 1.10–2.20 (14H, m, C—$(CH_2)_3$—C and C—$(CH_2)_4$—C), 2.66, 2.75 (2H, d, J = 7 Hz, —C=$CCH_2C(CO_2Me)_2$—), 3.30–4.25 (6H, m, —OCH_2— and —CH_2Cl), 3.73 (6H, s, CH_3), 4.61 (1H, bs, —O_2CH—), 5.60 (4H, bm, —HC=CH—); ms m/e: 417 (MH^+).

General procedure 9:

*Methyl (Z),(Z)-2,7,7-tricarbomethoxy-14-[(tetrahydro-2*H*-pyran-2-yl)oxy]-4,12-tetradecadienoate (**15**a [C–C])*

To a stirred solution of **14***a* [C–C] (1.41 g, 3.38 mmol) and dimethyl malonate (2.2 mL, 16.9 mmol) in tetrahydrofuran (14 mL) and *N*,*N*-dimethylformamide (4 mL), was added sodium hydride (354 mg, 60% in mineral oil, 8.8 mmol). This solution was heated under reflux for 1.5 h, then cooled to room temperature. Water (50 mL) was added and the aqueous phase was extracted with a 1:1 mixture of diethyl ether/hexanes (3 × 80 mL). The combined organic phases were dried over sodium sulfate, filtered, and concentrated under reduced pressure (1 Torr (133.3 Pa), 90°C). The crude oil was then purified by flash chromatography (ethyl acetate/dichloromethane/hexanes 1:2:4) to afford **15***a* [C–C] (1.70 g, 98%) as an oil; ir: 1731 cm^{-1}; ^1H nmr δ: 1.10–2.20 (14H, m, C—$(CH_2)_4$—C and C—$(CH_2)_3$—C), 2.70 (4H, m, C=$CCH_2C(CO_2Me)_2$—), 3.30–4.00 (3H, m, —$CH(CO_2Me)_2$ and —OCH_2—, cyclic), 3.70, 3.73 (12H, s, CH_3), 4.14 (2H, m, THPOCH_2—), 4.61 (1H, bs, —O_2CH—), 5.20–5.70 (4H, m, —HC=CH—); ms m/e: 513 (MH^+).

General procedure 10:

*Methyl (Z),(Z)-2,7,7-tricarbomethoxy-14-hydroxy-4,12-tetradecadienoate (**16**a [C–C])*

The malonate **15***a* [C–C] (1.69 g, 3.3 mmol) and pyrdinium *p*-toluenesulfonate (100 mg, 0.4 mmol) were stirred in methanol (10 mL) for 24 h at room temperature. The solvent was evaporated, the volatile materials removed under vacuum, and methanol (5 mL) was added. The solvent was evaporated after 24 h, and the crude oil was filtered on silica gel (ethyl acetate/dichloromethane/hexanes (1:2:2)) to afford alcohol **16***a* [C–C] (1.38 g, 97%) as an oil; ir: 3620, 1730 cm^{-1}; ^1H nmr δ: 1.10–1.60 (5H, m, —OH, —$CH_2(CH_2)_2CH_2$—), 2.70–3.30 (4H, m, —$CH_2(CH_2)_2CH_2$—), 2.63 (4H, m, —C=$CCH_2C(CO_2Me)_2$), 3.37 (1H, t, J = 6 Hz, —$CH(CO_2Me)_2$), 3.71, 3.74 (12H, s, CH_3), 4.18 (2H, t, J = 6 Hz, —CH_2O—), 5.10–5.80 (4H, m, —HC=CH—); ms m/e: 429 (MH^+).

General procedure 11:

*Methyl (Z),(Z)-2,7,7-tricarbomethoxy-14-chloro-4,12-tetradecadienoate (**1**a [C–C])*

To a solution of the alcohol **16***a* [C–C] (1.36 g, 3.18 mmol), *s*-collidine (0.78 mL, 5.1 mmol), and lithium chloride (340 mg, 8.1 mmol) in *N*,*N*-dimethylformamide (25 mL) at 0°C, was added methanesulfonyl chloride (0.46 mL, 8.1 mmol). This solution was stirred 1 h at 0°C, then 2 h at room temperature, and finally poured into water (at 0°C) and extracted with diethyl ether/hexanes (1:1) (5 × 60 mL). The combined organic phases were dried over sodium sulfate and the solvents were evaporated. The residual oil was purified by flash chromatography (ethyl acetate/dichloromethane/hexanes, 1:2:4) to afford chloride **1***a* [C–C] (1.08 g, 77%) as an oil; ir: 1730 cm^{-1}; ^1H nmr δ: 1.00–1.60 (4H, m, —$CH_2(CH_2)_2CH_2$—), 1.70–2.30 (4H, m, —$CH_2(CH_2)_2$—(CH_2—), 2.63 (4H, m, C=$CCH_2(CO_2Me)_2$), 3.37 (1H, t, J = 7 Hz, —$CH(CO_2Me)_2$), 3.71, 3.73 (12H, s, CH_3), 4.03, 4.11 (2H, d, J = 6 Hz, —CH_2Cl), 5.20–5.70 (4H, m, —HC=CH—); ms m/e: 447 (MH^+).

General procedure 12:

*(Z),(Z)-1,1,6,6-Tetracarbomethoxy-3,8-cyclotridecadiene (**2**a [C–C]) and (Z),(Z),(Z),(Z)-1,1,6,6,14,14,19,19-octacarbomethoxy-3,8,16,21-cyclohexacosatetraene (**3**a [C–C])*

Chloride **1***a* [C–C] (185 mg, 0.450 mmol) was dissolved in tetrahydrofuran (11 mL) and *N*,*N*-dimethylformamide (11 mL) containing potassium carbonate (330 mg, 2.40 mmol) and the reaction mixture was heated at 90°C for 42 h. The solution was cooled and hexane (20 mL) was added. After filtration through a Celite pad, the solvents were removed by distillation under reduced pressure and the residual solid was purified by flash chromatography (ethyl acetate/dichloromethane/hexanes in successive ratios of 1:2:7, 1:2:4, 1:2:3) to afford monomer **2***a* [C–C] (118 mg, 70%, 95% pure from vpc analysis) and dimer **3***a* [C–C] (18.6 mg, 11%). Dimer **3***a* was recrystallized from chloroform/hexanes at −15°C. Monomer **2***a* was recrystallized from a (5:1) hot mixture of methanol/chloroform; ir of **2***a*: 3012, 1735, 1220 cm^{-1}; ir of **3***a*: 2955, 1733, 1200 cm^{-1}.

*Chloride **14**a [C–T] from **9**a*

Following procedure 8: Using (*E*)-1,4-dichloro-2-butene, malonate **9***a* (1.28 g, 3.9 mmol) gave **14***a* [C–T] (1.24 g, 76%); ir: 1731 cm^{-1}; ^1H nmr δ: 1.10–2.20 (14H, m, C—$(CH_2)_3$—C and C—$(CH_2)_4$—C), 2.63 (2H, m, C=CCH_2—$C(CO_2Me)_2$), 3.30–4.30 (6H, m, —OCH_2— and —CH_2Cl), 3.71 (6H, s, CH_3), 4.62 (1H, m, —O_2CH—), 5.60 (4H, m, —HC=CH—).

*Malonate **15**a [C–T] from **14**a [C–T]*

Following procedure 9: Chloride **14***a* [C–T] (1.23 g, 2.95 mmol) gave **15***a* [C–T] (1.40 g, 93%); ir: 1730, 1740 cm^{-1}; ^1H nmr δ:

TABLE 4. Spectral characteristics of monomers and dimers

Compound	^{1}H nmr 250-MHz δ(ppm)	^{13}C nmr 62.9-MHz δ(ppm)	*Exact mass*[a]	Melting point (°C)[b]
2*a* [C–C]	1.00, 1.45 (4H, 2m, —$CH_2(CH_2)_2CH_2$—), 1.75, 2.02 (4H. 2m, —$CH_2(CH_2)_2CH_2$—), 2.65 (6H, m, —C=$CCH_2C(CO_2Me)_2$—), 3.71, 3.74 (12H, 2s, CH_3), 4.98, 5.11, 5.25 (4H, 3m, —HC=CH—)	19.9, 24.5, 27.0, 29.5 (2), 29.6, 29.9 (CH_2), 52.4, 52.5 (CH_3), 56.6, 57.2 ($C(CO_2Me)_2$), 124.0, 127.0, 127.3, 135.2 (C=C), 171.4, 171.7 (C=O)	410.1941 (410.1941)	210–212
3*a* [C–C]	1.15, 1.32 (8H, 2m, —$CH_2(CH_2)_2CH_2$—), 1.85, 2.02 (8H, 2m, —$CH_2(CH_2)_2CH_2$—), 2.61 (12H, m, C=$CCH_2C(CO_2Me)_2$), 3.71 (24H, s, CH_3), 5.15, 5.35, 5.50 (8H, 3m, —HC=CH—)	23.8, 27.1, 29.6, 30.1, 30.6, 30.7, 32.0 (CH_2), 52.4 (CH_3), 57.3, 57.3 ($C(CO_2Me_2)$), 123.1, 126.9, 126.9, 133.6 (C=C), 171.4, 171.7 (C=O)	821 (821) (MH^+)	191–194
2*a* [C–T]	1.05, 1.47 (4H, 2m, CH_2—$(CH_2)_2CH_2$), 1.84, 2.10 (4H, 2m, —$CH_2(CH_2)_2CH_2$—), 2.58, 2.69 (6H, 2m, C=C—$CH_2C(CO_2Me)_2$), 3.71 and 3.74 (12H, s, CH_3), 5.00–5.45 (4H, m, —HC=CH—)	21.4, 26.0, 27.2, 30.1, 31.0, 35.5, 35.8 (CH_2), 52.4, 52.8 (CH_3), 56.0, 56.5 ($C(CO_2Me)_2$), 123.8, 127.7, 128.1, 132.2 (C=C), 171.9, 172.0 (C=O)	410.1933 (410.1941)	112–121
3*a* [C–T]	1.12, 1.36 (8H, 2m, —$CH_2(CH_2)_2CH_2$—), 1.81, 2.04 (8H, 2m, —$CH_2(CH_2)_2CH_2$—), 2.59 (12H, m, C=$CCH_2C(CO_2Me)_2$), 3.70, 3.70 (24H, s, CH_3), 5.05–5.60 (8H, m, —HC=CH—)	23.5, 27.3, 29.2, 29.5, 31.3, 34.9, 35.2 (CH_2), 52.2 (CH_3), 56.9, 57.3 ($C(CO_2Me)_2$), 122.5, 128.1, 128.5, 133.4 (C=C), 171.0, 171.4 (C=O)	820 (820)	164–169
2*a* [T–T]	1.09 and 1.44 (4H, 2m, —$CH_2(CH_2)_2CH_2$—), 1.74 and 2.02 (4H, 2m, —$CH_2(CH_2)_2CH_2$—), 2.58 and 2.70 (2H and 4H, d, J = 7.1 Hz, C=$CCH_2C(CO_2Me)_2$), 3.71, 3.74 (12H, s, CH_3), 5.10–5.55 (4H, m, —HC=CH—)	20.6, 26.3, 30.8, 31.3, 35.2, 36.7 (2) (CH_2), 52.4, 52.5 (CH_3), 56.9, 57.4 ($C(CO_2Me)_2$), 126.1, 126.2, 130.1, 132.4 (C=C), 171.9 (2) (C=O)	410.1937 (410.1941)	85–87
3*a* [T–T]	1.13, 1.37 (8H, 2m, —$CH_2(CH_2)_2CH_2$—), 1.83 (8H, 2m, —$CH_2(CH_2)_2CH_2$), 2.53 (12H, m, C=$CCH_2C(CO_2Me)_2$), 3.70, 3.71 (24H, s, CH_3), 4.97–5.40, 5.57 (8H, 2m, —HC=CH—)	23.9, 30.1, 31.5, 32.9, 34.6, 34.9, 35.2 (CH_2), 52.4 (CH_3), 56.8, 57.6 ($C(CO_2Me)_2$), 123.5, 128.4, 128.5, 135.5 (C=C), 171.3, 171.6 (C=O)	820 (820)	193–196
2*a* [A–C]	1.35, 1.44, 1.86, 2.15 (8H, 4m, C—$(CH_2)_4$—C), 2.75, 2.83, 2.94 (6H, 3m, C=$CCH_2C(CO_2Me)_2$), 3.72, 3.73 (12H, s, CH_3), 5.10–5.40 (2H, m, —HC=CH—)	17.7, 22.0, 22.6, 26.3, 29.8, 30.1, 31 (CH_2), 52.3, 52.7 (CH_3), 55.7, 57.0 ($C(CO_2Me)_2$), 75.2, 82.7 (C≡C), 126.1, 126.4 (C=C), 170.5, 171.5 (C=O)	408.1789 (408.1784)	147–148
3*a* [A–C]	1.31, 1.49, 1.87, 2.19 (16H, 4m, C—$(CH_2)_4$—C), 2.55–2.95 (12H, bm, —C=$CCH_2C(CO_2Me)_2$—), 3.72 (24H, s, CH_3), 5.10–5.50 (4H, m, —HC=CH—)	18.4, 22.8, 23.3, 29.0, 29.9, 30.7, 32.4 (CH_2), 52.1, 52.4 (CH_3), 57.0, 57.4 ($C(CO_2Me)_2$), 74.7, 83.4 (C≡C), 126.1, 128.3 (C=C), 170.2, 171.5 (C=O)	816 (816)	
2*a* [A–T]	1.26, 1.42 (4H, 2m, —$CH_2(CH_2)_2CH_2$—), 1.93, 2.14 (4H, 2m, —$CH_2(CH_2)_2CH_2$—), 2.61 (4H, t, J = 7.8 Hz, —C=CCH_2—), 2.76 (2H, m, —C≡$CCH_2C(CO_2Me)_2$), 3.69, 3.73 (12H, s, CH_3), 5.25 and 5.82 (2H, 2m, —HC=CH—)	17.8, 21.2, 23.5, 25.7, 30.4, 34.6, 38.4 (CH_2), 52.2, 52.4 (CH_3), 56.7, 57.1 ($C(CO_2Me)_2$), 76.5, 82.6 (C≡C), 127.2, 129.2 (C=C), 170.7, 171.6 (C=O)	408.1789 (408.1784)	93.5–96
3*a* [A–T]	1.23, 1.50, 1.84, 2.16 (16H, 4m, —$(CH_2)_4$—), 2.63 and 2.76 (4H and 8H, 2m, C=$CCH_2C(CO_2Me)_2$), 3.70, 3.72 (24H, s, CH_3), 5.35 (4H, bm, —HC=CH—)	18.2, 22.5, 22.7, 28.8, 30.6, 34.7, 35.1 (CH_2), 52.3, 52.6 (CH_3), 56.9, 57.3 ($C(CO_2Me)_2$), 74.6, 83.3 (C≡C), 127.8, 129.0 (C=C), 170.4, 171.5 (C=O)	816 (816)	174–177

Can. J. Chem. Downloaded from www.nrcresearchpress.com by 80.58.250.72 on 09/07/12
For personal use only.

TABLE 4. (*continued*)

Compound	^{1}H nmr 250-MHz δ(ppm)	^{13}C nmr 62.9-MHz δ(ppm)	*Exact mass*[a]	Melting point (°C)[b]
2*a* [A–A]	1.38–1.62 (4H, m, —$CH_2(CH_2)_2CH_2$—), 2.10 and 2.28 (4H, 2m, —$CH_2(CH_2)_2CH_2$—), 2.86 and 2.97 (2H and 4H, 2t, J = 2.3 Hz, —C≡$CCH_2C(CO_2Me)_2$), 3.72, 3.74 (12H, s, CH_3)	16.8, 20.7, 22.7, 24.1 (2), 25.9, 30.2 (CH_2), 52.6, 52.9 (CH_3), 55.5, 57.0 ($C(CO_2Me)_2$), 77.0, 78.2, 78.9, 82.5 (C≡C), 170.1, 171.1 (C=O)	407.1706 (407.1706) (MH^+)	74–75
3*a* [A–A]	1.25 and 1.51 (8H, 2m, —$CH_2(CH_2)_2CH_2$—), 2.00, 2.18 (8H, 2m, —$CH_2(CH_2)_2CH_2$—), 2.85, 2.93, 2.99 (12H, 3 bs, —C≡$CCH_2C(CO_2Me)_2$), 3.72, 3.74 (24H, s, CH_3)	18.1, 22.6 (2), 23.0 (2), 28.8, 31.2 (CH_2), 52.6, 52.8 (CH_3), 56.9, 56.9 ($C(CO_2Me)_2$), 74.6, 77.8, 78.0, 82.3 (C≡C), 169.5, 170.8 (C=O)	812 (812)	159–162
6*a*	1.30 and 1.44 (10H, 2m, —$CH_2(CH_2)_5CH_2$—), 2.09 (4H, m, —$CH_2(CH_2)_5CH_2$—), 2.86 (4H, s, —C≡C—CH_2—), 3.72 (12H, s, CH_3)	21.2 (2), 22.8 (2), 24.6, 26.7 (2), 31.2 (2) (CH_2), 52.7 (CH_3), 56.7 ($C(CO_2Me)_2$), 78.7 (C≡C), 171.1 (C=O)	410.1933 (410.1941)	—
Dimer of **6***a*	1.15 and 1.34 (20H, 2m, —$CH_2(CH_2)_5CH_2$—), 2.04 (8H, m, —$CH_2(CH_2)_5CH_2$—), 2.78 (8H, s, —C≡C—CH_2—), 3.72 (24H, s, CH_3)	22.9 (2), 24.1 (2), 29.5, 30.2 (2), 31.93 (2) (CH_2), 52.5 (CH_3), 56.9 ($C(CO_2Me)_2$), 77.6 (C≡C), 170.8 (C=O)	820 (820)	158–160
7*a*	1.29 and 1.41 (14H, 2m, —$(CH_2)_xCH_2C(CO_2Me)_2$—), 1.95 (8H, m, —$CH_2C(CO_2Me)_2$—), 3.69 (12H, s, CH_3)	22.0 (2), 23.7 (2), 23.9, 28.2 (2), 29.4 (2), 30.5 (2) (CH_2), 52.2 (CH_3), 57.9 ($C(CO_2Me)_2$), 172.2 (C=C)	415.2339 (415.2332)	142.5–144
2*b* [C–C]	1.10, 1.31, 1.48, 1.75, 2.12 (10H, 5m, C—$(CH_2)_5$—C), 2.63 (6H, m, —C=$CCH_2C(CO_2Me)_2$—), 3.70, 3.72 (12H, s, CH_3), 5.17 and 5.47 (4H, 2m, —HC=CH—)	21.5, 24.5, 26, 26.5, 28.8, 30.6, 31.6, 32.1 (CH_2), 52.1 (CH_3), 56.7, 56.8 ($C(CO_2Me)_2$), 123.1, 126.3, 128.3, 134.6 (C=C), 171.1, 171.3 (C=O)	424.2097 (424.2097)	—
3*b* [C–C]	1.12, 1.30, 1.82, 1.98 (4, 8, 4, and 4H, 4m, C—$(CH_2)_5$—C), 2.60 (12H, m, —C=$CCH_2C(CO_2Me)_2$), 3.71 (24H, s, CH_3), 5.00–5.60 (8H, 3m, —HC=CH—)	—	848 (848)	—
2*b*	1.15, 1.36 (2H and 4H, 2m, —$CH_2(CH_2)_3CH_2$—), 1.79, 2.00 (4H, 2m, —$CH_2(CH_2)_3CH_2$—), 2.62 and 2.69 (2H and 4H, 2m, C=$CCH_2C(CO_2Me)_2$), 3.71 (12H, s, CH_3), 5.07, 5.27, and 5.48 (1, 1, and 2H, 3m, —HC=CH—)	19.6, 25.5, 26.1, 27.1, 29.9, 30.6, 34, 34.7 (CH_2), 52.4 (CH_3), 56.4 ($C(CO_2Me)_2$), 122.7, 127.3, 128.2, 134.2 (C=C), 171.4, 171.9 (C=O)	424.2110 (424.2097)	117–122
3*b* [C–T]	1.10, 1.31 (4H and 8H, 2m, —$CH_2(CH_2)_3CH_2$—), 1.78, 2.03 (8H, 2m, —$CH_2(CH_2)_3CH_2$—), 2.56 (12H, m, C=CCH_2—$C(CO_2Me)_2$), 3.69 (24H, s, CH_3), 5.12, 5.24, 5.50 (1, 2, and 1H, 3m, —HC=HC—)	23.8, 27.4, 29.3, 29.4, 29.5, 31.6, 35.2, 35.4 (CH_2), 52.3 (CH_3), 57.2, 57.4 ($C(CO_2Me)_2$), 122.6, 128.4, 128.7, 133.7 (C=C), 171.2, 171.6 (C=O)	848 (848)	106–107
2*b* [T–T]	0.96, 1.23, 1.43, 1.72, and 2.09 (10H, 5m, C—$(CH_2)_5$—C), 2.68 (6H, m, C=$CCH_2C(CO_2Me)_2$), 3.711, 3.719 (12H, s, CH_3), 5.30, 5.44, 5.61 (1, 2, and 1H, 3m, —HC=CH—)	20.4, 25.7, 27.1, 30.8, 31.9, 35.2, 36.2, 37.2 (CH_2), 52.4 (CH_3), 56.4, 57.9 ($C(CO_2Me)_2$), 125.9, 127.3, 129.7, 134.3 (C=C), 171.6, 172.0 (C=O)	424.2097 (424.2097)	—
3*b* [T–T]	1.10, 1.31, 1.81, 1.96 (4, 8, 4, and 4H, 4m, C—$(CH_2)_5$—C), 2.55 (12H, m, C=$CCH_2C(CO_2Me)_2$), 3.70, 3.71 (24H, s, CH_3), 5.13, 5.28, 5.54 (2, 4, and 2H, 3m, —HC=CH—)	23.6, 29.1 (2), 31.3, 32.6, 35, 35.1, 35.2 (CH_2), 52.3 (CH_3), 57.3 ($C(CO_2Me)_2$), 123.5, 128.4, 128.5, 135.3 (C=C), 171.2, 171.7 (C=O)	848 (848)	155–158

Can. J. Chem. Downloaded from www.nrcresearchpress.com by 80.58.250.72 on 09/07/12
For personal use only.

TABLE 4. (*concluded*)

Compound	^{1}H nmr 250-MHz δ(ppm)	^{13}C nmr 62.9-MHz δ(ppm)	*Exact mass*[a]	Melting point (°C)[b]
2*b* [A–C]	1.09, 1.44, 1.82, 2.20 (10H, 4m, C—$(CH_2)_5$—C), 2.77 and 2.87 (4H, and 2H, 2m, C≡CCH_2C$(CO_2Me)_2$), 3.72, 3.73 (12H, s, CH_3), 5.20 (2H, m, —HC=CH—)	16.4, 21.4, 23.1, 24.6, 27.0, 29.5, 29.9, 31.5 (CH_2), 52.2, 52.5 (CH_3), 56.3, 56.8 (*C*$(CO_2Me)_2$), 75.4, 82.1 (C≡C), 126.1, 126.6 (C=C), 170.3, 171.6 (C=O)	423.2019 (423.2019) (MH^+)	124–125
3*b* [A–C]	1.16, 1.36, 1.48, 1.85, 2.15 (20H, 5m, C—$(CH_2)_5$—C), 2.70 and 2.80 (8H and 4H, 2m, C=CCH_2C$(CO_2Me)_2$), 3.70, 3.72 (24H, s, CH_3), 5.15–5.50 (4H, m, —HC=CH—)	—	844 (844)	
2*b* [A–T]	1.04, 1.44 (2), 1.84, 2.22 (10H, 4m, C—$(CH_2)_5$—C), 2.68 (4H, bd, —C=CCH_2—), 2.83 (2H, t, J = 2.4 Hz), C≡CCH_2C$(CO_2Me)_2$—), 3.72, 3.74 (12H, s, CH_3), 5.30 and 5.97 (2H, 2m, —HC=CH—)	16.4, 19.9, 24.2, 24.7, 26.4, 31.5, 35.0, 38.7 (CH_2), 52.3, 52.6 (CH_3), 56.5, 57.1 (*C*$(CO_2Me)_2$), 77.3, 81.6 (C≡C), 127.6, 128.8 (C=C), 170.6, 171.9 (C=O)	423.2022 (423.2019)	116.5–118
3*b* [A–T]	1.16, 1.46 (2), 1.88, 2.13 (20H, 5m, C—$(CH_2)_5$—C), 2.70 (12H, m, C=CCH_2C$(CO_2Me)_2$), 3.70, 3.72 (24H, s, CH_3), 5.30, 5.42 (4H, 2m, —HC=CH—)	18.4, 22.6, 23.3, 28.3, 28.7, 31.3, 35.1 (2) (CH_2), 52.2, 52.5 (CH_3), 56.7, 57.4 (C(*C*$O_2Me)_2$), 74.3, 83.2 (C≡C), 127.7, 129.0 (C=C), 170.3, 171.5 (C=O)	844 (844)	134–140
2*b* [A–A]	1.52 (6H, m, —CH_2(*C*$H_2)_3CH_2$—), 2.09 and 2.19 (4H, 2m, —*C*H_2($CH_2)_3$*C*H_2—), 2.83, 3.01 (2H and 4H, t, J = 2.5 Hz, —C≡CCH_2C$(CO_2Me)_2$), 3.72, 3.74 (12H, s, CH_3)	19.1, 23.0, 23.2, 23.5, 23.6, 25.9, 29.45, 32.6 (CH_2), 52.6, 52.9 (CH_3), 55.4, 56.8 (*C*—$(CO_2Me)_2$), 75.0, 78.3, 79.0, 84.1 (C≡C), 169.9, 171.2 (C=O)	421.1862 (421.1862) (MH^+)	99–97
3*b* [A–A]	1.16, 1.48 (2), 2.05, 2.14 (20H, 4m, C—$(CH_2)_5$—C), 2.80, 2.91, 2.94 (12H, 3 bt, J = 2.3 Hz, —C≡C—CH_2C$(CO_2Me)_2$), 3.73, 3.74 (24H, s, CH_3)	18.5, 22.9 (3), 23.4, 28.3, 28.7, 31.7 (CH_2), 52.6, 52.8 (CH_3), 56.8, 56.9 (*C*$(CO_2Me)_2$), 74.1, 77.6, 77.9, 83.5 (C≡C), 169.5, 170.8 (C=O)	840 (840)	111–113
6*b*	1.17, 1.35, 1.41 (12H, 3m, —CH_2(*C*$H_2)_6$—CH_2—), 2.05 (4H, m, —*C*H_2—($CH_2)_6$—*C*H_2—), 2.82 (4H, s, —C≡CCH_2—), 3.72 (12H, s, CH_3)	20.2, 22.6, 24.4, 27.1, 30.1 (CH_2), 52.5 (CH_3), 56.6 (*C*$(CO_2Me)_2$), 77.9 (C≡C), 170.8 (C=O)	424.2110 (424.2097)	129–130
Dimer of **6***b*	1.13, 1.31 (24H, 2m, —CH_2—(*C*$H_2)_6$—CH_2—), 2.02 (8H, m, —*C*H_2—($CH_2)_6$—*C*H_2—), 2.78 (8H, m, —C≡CH_2—), 3.72 (24H, s, CH_3)	22.8, 24.3, 29.9, 30.0, 31.8 (CH_2), 52.6 (CH_3), 56.9 (*C*$(CO_2Me)_2$), 77.5 (C≡C), 170.9 (C=O)	848 (848)	110–120
7*b*	1.16, 1.31, 1.38 (16H, 3m, —CH_2(*C*$H_2)_6$—CH_2— and (*C*H_2CH_2C$(CO_2Me)_2$—)$_2$), 1.92 (8H, m, —CH_2C$(CO_2Me)_2$—), 3.69 (12H, s, CH_3)	20.25, 24.3, 25, 27.4, 29.7, 30.2 (CH_2), 52.1 (CH_3), 57.1 (*C*$(CO_2Me)_2$), 172.0 (C=O)	429.2488 (429.2488)	129–130
Dimer of **7***b*	1.13, 1.27 (32H, 2m, —CH_2(*C*$H_2)_6CH_2$— and (*C*H_2CH_2C$(CO_2Me)_2)_2$—), 1.86 (16H, m, —CH_2C$(CO_2Me)_2$), 3.70 (24H, s, CH_3)	—	856 (856)	202–206

[a]Only for monomers; mass value for dimers; calculated values in parentheses.
[b]From recrystallized samples.

1.10–2.20 (14H, m, C—$(CH_2)_3$—C and C—$(CH_2)_4$—C), 2.57 (4H, m, C=CCH_2C$(CO_2Me)_2$), 3.20–4.25 (5H, m, —CH$(CO_2Me)_2$ and —OCH_2—), 3.72, 3.79 (12H, s, CH_3), 4.60 (1H, m, —O_2CH—), 5.3–5.7 (4H, m, —HC=CH—).

Alcohol ***16****a* *[C–T] from* ***15****a* *[C–T]*

Following procedure 10: Compound ***15****a* [C–T] (1.40 g, 2.73 mmol) gave ***16****a* [C–T] (1.20 g, 100%); ir: 3610, 1730 cm^{-1}; ^{1}H nmr δ: 1.10–2.20 (9H, m, —OH, C—$(CH_2)_4$—C), 2.60 (4H, m, C=CCH_2C$(CO_2Me)_2$), 3.38 (1H, t, —CH$(CO_2Me)_2$), 3.70, 3.73 (12H, s, CH_3), 4.21 (2H, m, —CH_2O—), 5.30–5.70 (4H, m, —HC=CH—).

Chloride ***1****a* *[C–T] from* ***16****a* *[C–T]*

Following procedure 11: Alcohol ***16****a* [C–T] (1.20 g, 2.75 mmol) gave chloride ***1****a* [C–T] (0.90 g, 72%); ir: 1732 cm^{-1}; ^{1}H nmr δ: 1.16 and 1.38 (4H, 2 m, —CH_2(*C*$H_2)_2CH_2$—), 1.82 and 2.10 (4H, 2 m,

Can. J. Chem. Downloaded from www.nrcresearchpress.com by 80.58.250.72 on 09/07/12
For personal use only.

Can. J. Chem. Downloaded from www.nrcresearchpress.com by 80.58.250.72 on 09/07/12
For personal use only.

—$CH_2(CH_2)_2CH_2$—), 2.57 (4H, m, C=$CCH_2C(CO_2Me)_2$), 3.38 (1H, t, J = 7.5 Hz, —$CH(CO_2Me)_2$), 3.70, 3.73 (12H, s, CH_3), 4.10 (2H, d, J = 7 Hz, —CH_2Cl), 5.28–5.72 (4H, m, —HC=CH—); ms m/e: 447 (MH^+).

(E),(Z)-1,1,6,6-Tetracarbomethoxy-3,8-cyclotridecadiene (2a [C–T]) and (E),(Z),(E),(Z)-1,1,6,6,14,14,19,19-octacarbomethoxy-3,8,16,21-cyclohexacosatetraene (3a [C–T]) from 1a [C–T]

Following procedure 12: Chloride **1***a* [C–T] (158 mg, 0.354 mmol) gave, after 62 h, monomer **2***a* [C–T] (15.3 mg, 10.5%, estimated to be 75% pure from ^{13}C nmr analysis; no vpc analysis was possible due to decomposition during analysis) and dimer **3***a* [C–T] (68.3 mg, 46.9%); ir of **2***a*: 1729, 1212 cm^{-1}; ir of **3***a*: 1732, 1202 cm^{-1}.

Chloride 14a [T–T] from 10a

Following procedure 8: Using (*E*)-1,4-dichloro-2-butene, malonate **10***a* (1.59 g, 4.86 mmol) gave **14***a* [T–T] (1.59 g, 79%); ir: 1731 cm^{-1}; ^1H nmr δ: 1.00–2.20 (14H, m, C—$(CH_2)_4$—C and C—$(CH_2)_3$—C), 2.67 (2H, m, C=$CCH_2C(CO_2Me)_2$), 3.30–4.40 (6H, m, —OCH_2— and —CH_2Cl), 3.71 (6H, s, CH_3), 4.61 (1H, m, —O_2CH—), 5.65 (4H, bm, —HC=CH—); ms m/e: 417 (MH^+).

Malonate 15a [T–T] from 14a [T–T]

Following procedure 9: Compound **14***a* [T–T] (1.58 g, 3.8 mmol) gave **15***a* [T–T] as an oil; ir: 1733 cm^{-1}; ^1H nmr δ: 1.10–2.20 (14H, m, C—$(CH_2)_4$—C and C—$(CH_2)_3$—C), 2.60 (4H, m, C=$CCH_2C(CO_2Me)_2$), 3.38 (1H, t, —$CH(CO_2Me)_2$), 3.70 and 3.74 (12H, s, CH_3), 3.40–4.20 (4H, m, —OCH_2—), 4.61 (1H, bs, —O_2CH—), 5.41 and 5.66 (4H, 2 m, —HC=CH—); ms m/e: 429 (MH^+ − THP).

Alcohol 16a [T–T] from 15a [T–T]

Following procedure 10: Malonate **15***a* [T–T] gave **16***a* [T–T] (1.43 g, 88% from **14***a* [T–T]); ir: 3610, 1728 cm^{-1}; ^1H nmr δ: 1.00–2.20 (9H, m, —OH and C—$(CH_2)_4$—C), 2.58 (4H, m, C=$CCH_2C(CO_2Me)_2$), 3.38 (1H, t, —$CH(CO_2Me)_2$), 3.69, 3.73 (12H, s, CH_3), 4.09 (2H, m, —CH_2O—), 5.40 and 5.64 (4H, 2 m, —HC=CH—); ms m/e: 429 (MH^+).

Chloride 1a [T–T] from 16a [T–T]

Following procedure 11: Alcohol **16***a* [T–T] (1.42 g, 3.32 mmol) gave chloride **1***a* [T–T] (1.26 g, 85%); ir: 1730 cm^{-1}; ^1H nmr δ: 1.00–2.20 (8H, m, C—$(CH_2)_4$—C), 2.60 (4H, m, C=CCH_2—$C(CO_2Me)_2$), 3.38 (1H, t, —$CH(CO_2Me)_2$), 3.70 and 3.73 (12H, s, CH_3), 3.99 (2H, d, J = 5 Hz, —CH_2Cl), 5.40 and 5.62 (4H, 2 m, —HC=CH—); ms m/e: 447 (MH^+).

(E),(E)-1,1,6,6-Tetracarbomethoxy-3,8-cyclotridecadiene (2a [T–T]) and (E),(E),(E),(E)-1,1,6,6,14,14,19,19-octacarbomethoxy-3,8,16,21-cyclohexacosatetraene (3a [T–T]) from 1a [T–T]

Following procedure 12: Chloride **1***a* [T–T] (188 mg, 0.420 mmol) gave, after 60 h, monomer **2***a* (24.1 mg, 14%) and dimer **3***a* (70.3 mg, 40.8%); ir of **2***a*: 1731, 1205–1225 cm^{-1}; ir of **3***a*: 1730, 1279, 1200 cm^{-1}.

Chloride 14a [A–C] from 8a

Following procedure 8: Malonate **8***a* (1.43 g, 4.39 mmol) gave compound **14***a* [A–C] 0.97 g, 54%); ir: 1736 cm^{-1}; ^1H nmr δ: 1.10–2.20 (14H, m, C—$(CH_2)_4$—C and C—$(CH_2)_3$—C), 2.80 (2H, d, J = 6 Hz, —C=$CCH_2C(CO_2Me)_2$—), 3.30–4.00 (2H, m, —OCH_2—, cyclic), 3.72 (6H, s, CH_3), 4.10 (2H, d, J = 5 Hz, —CH_2Cl), 4.22 (2H, m, THPOCH_2—), 4.78 (1H, bs, —O_2CH—), 5.61 (2H, bm, —HC=CH—).

Malonate 15a [A–C] from 14a [A–C]

Following procedure 9: Chloride **14***a* [A–C] (0.96 g, 2.31 mmol) gave malonate **15***a* [A–C] (0.98 g, 77%); ir: 1733 cm^{-1}; ^1H nmr δ: 1.10–2.40 (14H, m, C—CH_2)$_4$—C and C—$(CH_2)_3$—C), 2.65 (4H, m, C=$CCH_2C(CO_2Me)_2$), 3.37 (1H, t, —$CH(CO_2Me)_2$), 3.40–4.00 (2H, m, —OCH_2—, cyclic), 3.71, 3.74 (12H, s, CH_3), 4.22 (2H, m, THPOCH_2—), 4.77 (1H, bs, —O_2CH—), 5.40 (2H, m, —HC=CH—).

Alcohol 16a [A–C] from 15a [A–C]

Following procedure 10: Compound **15***a* [A–C] (0.97 g, 1.9 mmol) gave alcohol **16***a* [A–C] (0.81 g, 100%); ir: 3300–3620, 1730 cm^{-1}; ^1H nmr δ: 1.40, 1.87, 2.22 (9H, 3 m, —OH and C—$(CH_2)_4$—C), 2.65 (4H, m, C=$CCH_2C(CO_2Me)_2$), 3.38 (1H, t, —$CH(CO_2Me)_2$), 3.71, 3.74 (12H, s, CH_3), 4.26 (2H, dt, J = 1.5 and 4.5 Hz, $HOCH_2$—), 5.40 (2H, bm, —HC=CH—).

Chloride 1a [A–C] from 16a [A–C]

Following procedure 11: Alcohol **16***a* [A–C] (0.800 g, 1.88 mmol) gave the precursor **1***a* [A–C] (0.64 g, 77%); ir: 1730 cm^{-1}; ^1H nmr δ: 1.26, 1.51, 1.85 (6H, m, —$(CH_2)_3C(CO_2Me)_2$—), 2.24 (2H, tt, J = 2.3 and 7 Hz, —C≡CCH_2—$(CH_2)_3$—), 2.66 (4H, m, —C=CCH_2—), 3.37 (1H, t, J = 7.5 Hz, —$CH(CO_2Me)_2$), 3.71, 3.74 (12H, s, CH_3), 4.13 (2H, t, J = 2.3 Hz, —CH_2Cl), 5.38 (2H, bm, —HC=CH—); ms m/e: 445 (MH^+).

(Z)-1,1,6,6-Tetracarbomethoxy-3-cyclotridecen-8-yne (2a [A–C]) and (Z),(Z)-1,1,6,6,14,14,19,19-octacarbomethoxy-3,16-cyclohexacosadiene-8,21-diyne (3a [A–C])

Following procedure 12: After 36 h, chloride **1***a* [A–C] (125.1 mg, 0.28 mmol) gave monomer **2***a* [A–C] (105 mg, 91.4%) and dimer **3***a* [A–C] (5.7 mg, 5%); ir of **2***a*: 1730, 1075 cm^{-1}; ir of **3***a*: 1732 cm^{-1}.

Chloride 14a [A–T] from 8a

Following procedure 8: Compound **8***a* (1.35 g, 4.13 mmol) and (*E*)-1,4-dichloro-2-butene gave **14***a* [A–T] (1.28 g, 75%); ir: 1732 cm^{-1}; ^1H nmr δ: 1.10–2.40 (14H, m, C—$(CH_2)_3$—C and C—$(CH_2)_4$—C), 2.65 (2H, m, C=$CCH_2C(CO_2Me)_2$), 3.30–4.00 (2H, m, —OCH_2—, cyclic), 3.72 (6H, s, CH_3), 3.97 (2H, d, —CH_2Cl), 4.22 (2H, m, THPOCH_2—), 4.77 (1H, bs, —O_2CH—), 5.65 (2H, m, —HC=CH—).

Malonate 15a [A–T] from 14a [A–T]

Following procedure 9: Chloride **14***a* [A–T] (1.27 g, 3.07 mmol) gave compound **15***a* [A–T] (1.51 g, 97%); ir: 1735 cm^{-1}; ^1H nmr δ: 1.10–2.40 (14H, m, C—$(CH_2)_4$—C and C—$(CH_2)_3$—C), 2.60 (4H, m, —C=CCH_2—), 3.38 (1H, t, —$CH(CO_2Me)_2$), 3.30–4.00 (2H, m, —OCH_2—, cyclic), 3.70, 3.73 (12H, s, CH_3), 4.22 (2H, m, THPOCH_2—), 4.78 (1H, bs, —O_2CH—), 5.40 (2H, m, —HC=CH—).

Alcohol 16a [A–T] from 15a [A–T]

Following procedure 10: Malonate **15***a* [A–T] (1.50 g, 2.94 mmol) gave **16***a* [A–T] (1.23 g, 99%); ir: 3620, 1735 cm^{-1}; ^1H nmr δ: 1.10–2.35 (9H, m, —OH and C—$(CH_2)_4$—C), 2.58 (4H, m, —C=CCH_2—), 3.39 (1H, t, —$CH(CO_2Me)_2$), 3.70, 3.74 (12H, s, CH_3), 4.23 (2H, dt, —CH_2O—), 5.40 (2H, m, —HC=CH—).

Chloride 1a [A–T] from 16a [A–T]

Following procedure 11: Alcohol **16***a* [A–T] (1.22 g, 2.87 mmol) gave chloride **1***a* [A–T] (0.945 g, 74%); ir: 1730 cm^{-1}; ^1H nmr δ: 1.26, 1.50, 1.81 (6H, 3 m, —$(CH_2)_3C(CO_2Me)_2$), 2.23 (2H, tt, J = 2.3 and 7 Hz, —C≡CCH_2—$(CH_2)_3$—), 2.58 (4H, m, —C=C—CH_2—), 3.38 (1H, t, J = 7.6 Hz, —$CH(CO_2Me)_2$), 3.70, 3.73 (12H, s, CH_3), 4.13 (2H, t, J = 2.4 Hz, —CH_2Cl), 5.25–5.60 (2H, m, —HC=CH—); ms m/e: 445 (MH^+).

(E)-1,1,6,6-Tetracarbomethoxy-3-cyclotridecen-8-yne (2a [A–T]) and (E),(E)-1,1,6,6,14,14,19,19-octacarbomethoxy-3,16-cyclohexacosadiene-8,21-diyne (3a [A–T])

Following procedure 12: Chloride **1***a* [A–T] (156 mg, 0.35 mmol) gave, after 42 h, monomer **2***a* [A–T] (86.8 mg, 61%) and **3***a* [A–T] (33.7 mg, 23.5%); ir of **2***a*: 1730, 1095 cm^{-1}; ir of **3***a*: 1732, 1282 cm^{-1}.

Chloride 14a [A–A] from 8a

Following procedure 8: 1,4-Dichloro-2-butyne and malonate **8***a* (1.39 g, 4.26 mmol) gave **14***a* [A–A] (1.57 g, 90%); ir: 1736 cm^{-1}; ^1H nmr δ: 1.10–2.35 (14H, m, C—$(CH_2)_3$—C and C—$(CH_2)_4$—C), 2.90 (2H, t, J = 2.5 Hz, C≡$CCH_2C(CO_2Me)_2$—), 3.30–4.00 (2H, m, —OCH_2—, cyclic), 3.74 (6H, s, CH_3), 4.09 (2H, t, J = 2.5 Hz, —CH_2Cl), 4.22 (2H, m, THPOCH_2—), 4.79 (1H, bs, —O_2CH—); ms m/e: 413 (MH^+).

Can. J. Chem. Downloaded from www.nrcresearchpress.com by 80.58.250.72 on 09/07/12
For personal use only.

Malonate ***15***a *[A–A] from* ***14***a *[A–A]*

Following procedure 9: Compound ***14a*** [A–A] (1.56 g, 3.79 mmol) gave ***15a*** [A–A] (1.82 g, 95%); ir: 1736 cm^{-1}; ^1H nmr δ: 1.10–2.40 (14H, m, C—$(CH_2)_4$—C and C—$(CH_2)_3$—C), 2.60–2.80 (4H, m, —C≡C—CH_2—$C(CO_2Me)_2$), 3.3–4 (3H, m, —$CH(CO_2Me)_2$ and —OCH_2—, cyclic), 3.72, 3.77 (12H, s, CH_3), 4.24 (2H, m, $THPOCH_2$—), 4.78 (1H, bs, —O_2CH—); ms *m/e*: 508 (M^+).

Alcohol ***16***a *[A–A] from* ***15***a *[A–A]*

Following procedure 10: Compound ***15a*** [A–A] (1.81 g, 3.56 mmol) gave ***16a*** [A–A] (1.49 g, 99%); ir: 1730 cm^{-1}; ^1H nmr δ: 1.10–2.40 (9H, m, —OH and C—$(CH_2)_4$—C—), 2.77 (4H, m, C≡$CCH_2C(CO_2Me)_2$), 3.53 (1H, t, —$CH(CO_2Me)_2$), 3.73, 3.77 (12H, s, CH_3), 4.21 (2H, dt, *J* = 2 and 7 Hz, —CH_2O—); ms *m/e*: 425 (MH^+).

Chloride ***1***a *[A–A] from* ***16***a *[A–A]*

Following procedure 11: Alcohol ***16a*** [A–A] (1.48 g, 3.49 mmol) gave ***1a*** [A–A] (1.27 g, 82%); ir: 1735 cm^{-1}; ^1H nmr δ: 1.10–2.40 (8H, m, C—$(CH_2)_4$—C), 2.78 (4H, m, —C≡$CCH_2C(CO_2Me)_2$—C), 3.50 (1H, m, —$CH(CO_2Me)_2$), 3.73–3.77 (12H, s, CH_3), 4.13 (2H, t, *J* = 2 Hz, —CH_2Cl); ms *m/e*: 443 (MH^+).

*1,1,6,6-Tetracarbomethoxy-3,8-cyclotridecadiyne (***2***a [A–A]) and 1,1,6,6,14,14,19,19-octacarbomethoxy-3,8,16,21-cyclohexacosatetrayne (***3***a [A–A])*

Following procedure 12: Chloride ***1a*** [A–A] (233 mg, 0.527 mmol) gave ***2a*** [A–A] (144 mg, 67%) and ***3a*** [A–A] (38 mg, 18%); ir of ***2a***: 1735, 1280 cm^{-1}; ir of ***3a***: 1738, 1200 cm^{-1}.

Chloride ***14***a *[A] from* ***11***a

Following procedure 8: 1,4-Dichloro-2-butyne and malonate ***11a*** (1.60 g, 4.85 mmol) gave ***14a*** [A] (1.42 g, 70%); ir: 2250, 1732 cm^{-1}; ^1H nmr δ: 1.10–2.20 (18H, m, C—$(CH_2)_3$—C and C—$(CH_2)_6$—C), 2.85 (2H, m, C≡$CCH_2C(CO_2Me)_2$), 3.30–4.10 (4H, m, —OCH_2—), 3.72 (6H, s, CH_3), 4.08 (2H, m, —CH_2Cl), 4.56 (1H, bs, —O_2CH—).

Malonate ***15***a *[A] from* ***14***a *[A]*

Following procedure 9: Compound ***14a*** [A] (1.41 g, 3.39 mmol) gave ***15a*** [A] (1.40 g, 85%); ir: 1735 cm^{-1}; ^1H nmr δ: 1.00–2.15 (18H, m, C—$(CH_2)_3$—C and C—$(CH_2)_6$—C), 2.75 (4H, bs, —C≡$CCH_2C(CO_2Me)_2$), 3.20–4.10 (5H, m, —$CH(CO_2Me)_2$, —OCH_2—), 3.70, 3.75 (12H, s, CH_3), 4.56 (1H, bs, —O_2CH—).

Alcohol ***16***a *[A] from* ***15***a *[A]*

Following procedure 10: Compound ***15a*** [A] (1.39 g, 2.71 mmol) gave ***16a*** [A] (1.12 g, 97%); ^1H nmr δ: 1.10–1.70 (11H, m, —OH and —$(CH_2)_5$—$C(CO_2Me)_2$—), 1.95 (2H, m, —CH_2CH_2O—), 2.76 (4H, bs, —C≡CCH_2—), 3.30–3.90 (3H, m, —OCH_2— and —$CH(CO_2Me)_2$), 3.71, 3.76 (12H, s, CH_3).

General procedure 13:

Bromide ***4*** *from* ***16*** *[A]*

*Methyl 14-bromo-2,7,7-tricarbomethoxy-4-tetradecynoate (***4***a)*

The alcohol ***16a*** [A] (1.115 g, 2.60 mmol) and carbon tetrabromide (1.0 g, 3.0 mmol) were dissolved in dichloromethane (15 mL) at 0°C. To this solution was rapidly added a solution of triphenylphosphine (0.900 g, 3.39 mmol) in dichloromethane (5 mL). The solution was stirred for 2 h at 0°C, and for 10 h at room temperature. The solvents were evaporated under vacuum and the solid residue was dissolved in a minimum amount of dichloromethane and purified by flash chromatography (ethyl acetate/dichloromethane/hexanes, 1:2:4) to afford ***4a*** (1.14 g, 89%) as an oil; ir: 1730 cm^{-1}; ^1H nmr δ: 1.31 (8H, m, —$(CH_2)_4$—$CH_2C(CO_2Me)_2$), 1.86 (4H, m, —$CH_2(CH_2)_4CH_2C(CO_2Me)_2$—), 2.74 (4H, bs, —C≡$CCH_2$—), 3.39 (3H, bt, —$CH_2Br$ and —$CH(CO_2Me)_2$), 3.70, 3.74 (12H, s, CH_3); ms *m/e*: 491 (MH^+).

1,1,6,6-Tetracarbomethoxy-3-cyclotridecyne ***6***a *and 1,1,6,6,14,14,19,19-octacarbomethoxy-3,16-cyclohexacosadiyne* (dimer)

Following procedure 12: After 40 h, bromide ***4a*** (172 mg, 0.349 mmol) gave at 2×10^{-3} *M* the monomer ***6a*** (78.6 mg, 54.8%) and dimer (18.7 mg, 13%); ir of ***6a***: 1736, 1060 cm^{-1}; ir of dimer: 2935, 1736, 1203 cm^{-1}.

General procedure 14:

Bromide ***5*** *from* ***4***

*Methyl 14-bromo-2,7,7-tricarbomethoxytetradecanoate (***5***a)*

To a solution of ***4a*** (551 mg, 1.11 mmol) dissolved in ethyl acetate (10 mL) was added sodium sulfate (100 mg) and platinum(IV) oxide (25 mg) under an argon atmosphere. This mixture was stirred for 2 h under a hydrogen atmosphere, then filtered through a Celite pad. Evaporation of solvents afforded bromide ***5a*** (549 mg, 99%) as an oil; ir: 1731 cm^{-1}; ^1H nmr δ: 0.90–1.50 and 1.50–2.10 (20H, m, —$(CH_2)_6$—$C(CO_2Me)_2$—$(CH_2)_4$—), 3.31 (1H, t, *J* = 7 Hz, —$CH(CO_2Me)_2$), 3.38 (2H, t, *J* = 7 Hz, —CH_2Br), 3.68, 3.70 (12H, s, CH_3); ms *m/e*: 495 (MH^+).

*1,1,6,6-Tetracarbomethoxycyclotridecane (***7***a) and 1,1,6,6,14,14,19,19-octacarbomethoxycyclohexacosane* (dimer)

Following procedure 12: At 2×10^{-3} *M*, bromide ***5a*** (171 mg, 0.345 mmol) gave, after 44 h, monomer ***7a*** (60.6 mg, 42.5%) as an impure solid. Another run in the presence of a 4:1 mixture of potassium carbonate and cesium carbonate (250 mg) gave, after 16 h, monomer ***7a*** (57.8% and 54.1%); ir of ***7a***: 2932, 1730, 1179 cm^{-1}. No dimer was detected from mass spectral (ms) analysis.

Chloride ***14***b *[C–C] from* ***9***b

Following procedure 8: Malonate ***9b*** (1.41 g, 4.12 mmol) gave ***14b*** [C–C] (1.19 g, 67%); (no spectral data available).

Malonate ***15***b *[C–C] from* ***14***b *[C–C]*

Following procedure 9: Compound ***14b*** [C–C] (1.19 g, 2.77 mmol) gave ***15b*** [C–C] (1.08 g, 75%); ir: 1730–1740 cm^{-1}; ^1H nmr δ: 1.00–2.15 (16H, m, C—$(CH_2)_5$—C and C—$(CH_2)_3$—C), 2.63 (4H, m, —C=$CCH_2C(CO_2Me)_2$), 3.25–4.25 (5H, m, —$CH(CO_2Me)_2$ and —OCH_2—), 3.70, 3.73 (12H, s, CH_3), 4.61 (1H, m, —O_2CH—), 5.20–5.70 (4H, m, —HC=CH—).

Alcohol ***16***b *[C–C] from* ***15***b *[C–C]*

Following procedure 10: Compound ***15b*** [C–C] (1.07 g, 2.04 mmol) gave ***16b*** [C–C] (0.901 g, 100%); ir: 1736 cm^{-1}; ^1H nmr δ: 1.28 (7H, m, —OH, —$CH_2(CH_2)_3CH_2$—), 1.95 (4H, m, —CH_2—$(CH_2)_3CH_2$—), 2.63 (4H, m, C=$CCH_2C(CO_2Me)_2$), 3.37 (1H, t, —$CH(CO_2Me)_2$), 3.71, 3.74 (12H, s, CH_3), 4.25 (2H, t, *J* = 5 Hz, —CH_2O—), 5.20–5.70 (4H, m, —HC=CH—).

Chloride ***1***b *[C–C] from* ***16***b *[C–C]*

Following procedure 11: Alcohol ***16b*** [C–C] (890 mg, 2.01 mmol) gave chloride ***1b*** [C–C] (785 mg, 85%); ir: 1731 cm^{-1}; ^1H nmr δ: 1.18, 1.35, 1.85, 2.10 (10H, 4 m, —$C(CH_2)_5C$—), 2.66 (4H, m, C=$CCH_2C(CO_2Me)_2$), 3.36 (1H, t, *J* = 7.6 Hz, —$CH(CO_2Me)_2$), 3.70, 3.73 (12H, s, CH_3), 4.08 (2H, m, —CH_2Cl), 5.38, 5.61 (4H, 2 m, —HC=CH—); ms *m/e*: 461 (MH^+).

*(Z),(Z)-1,1,6,6-Tetracarbomethoxy-3,8-cyclotetradecadiene (***2***b [C–C]) and (Z),(Z),(Z),(Z)-1,1,6,6,15,15,20,20-octacarbomethoxy-3,8,17,22-cyclooctacosatetraene (***3***b [C–C])*

Following procedure 12: After 58 h, chloride ***1b*** [C–C] (142.7 mg, 0.31 mmol) gave monomer ***2b*** [C–C] (101 mg, 77.1%, 90% pure from vpc analysis) and ***3b*** [C–C] (4.9 mg, 3.7%); ir of ***2b***: 1730, 1100 cm^{-1}; ir of ***3b***: 1732, 975 cm^{-1}. The monomer could not be recrystallized or purified.

Chloride ***14***b *[C–T] from* ***9***b

Following procedure 8: Malonate ***9b*** (1.41 g, 4.14 mmol) and (*E*)-1,4-dichloro-2-butene gave compound ***14b*** [C–T] (1.41 g, 79%); ^1H nmr δ: 1.00–2.20 (16H, m, C—$(CH_2)_3$—C and C—$(CH_2)_5$—C), 2.63 (2H, m, —C=$CCH_2C(CO_2Me)_2$), 3.20–4.00 (2H, m, —OCH_2—, cyclic), 3.71 (6H, s, CH_3), 3.99 (2H, m, —CH_2Cl), 4.17 (2H, m, $THPOCH_2$—), 4.61 (1H, bs, —O_2CH—), 5.63 (4H, m, —HC=CH—).

Malonate ***15***b *[C–T] from* ***14***b *[C–T]*

Following procedure 9: Chloride ***14b*** [C–T] (1.41 g, 3.28 mmol) gave compound ***15b*** [C–T] (1.55 g, 90%); ir: 1735 cm^{-1}; ^1H nmr δ:

Can. J. Chem. Downloaded from www.nrcresearchpress.com by 80.58.250.72 on 09/07/12
For personal use only.

1.10–2.20 (16H, m, C—$(CH_2)_3$—C and C—$(CH_2)_5$—C), 2.59 (4H, m, C=$CCH_2C(CO_2Me)_2$), 3.25–4.00 (3H, m, —$CH(CO_2Me)_2$ and —OCH_2—, cyclic), 3.70, 3.73 (12H, s, CH_3), 4.15 (2H, m, THPOCH_2—), 4.62 (1H, bs, —O_2CH—), 5.50 (4H, m, —HC=CH—).

Alcohol ***16***b *[C–T] from* ***15***b *[C–T]*

Following procedure 10: Compound ***15****b* [C–T] (1.54 g, 2.93 mmol) gave alcohol ***16****b* [C–T] (1.28 g, 99%); ir: 3620, 1731 cm^{-1}; ^1H nmr δ: 1.28, 1.90 (11H, 2 m, —OH and C—$(CH_2)_5$—C), 2.59 (4H, m, C=$CCH_2C(CO_2Me)_2$—), 3.39 (1H, t, —$CH(CO_2Me)_2$), 3.70, 3.73 (12H, s, CH_3), 4.18 (2H, t, —CH_2O—), 5.50 (4H, m, —HC=CH—).

Chloride ***1***b *[C–T] from* ***16***b *[C–T]*

Following procedure 11: Alcohol ***16****b* [C–T] (1.27 g, 2.88 mmol) gave chloride ***1****b* [C–T] (1.10 g, 87%); ir: 1735 cm^{-1}; ^1H nmr δ: 1.13–1.34 (2H and 4H, 2 m, —$CH_2(CH_2)_3$—CH_2—), 1.80, 2.08 (4H, 2 m, —$CH_2(CH_2)_3CH_2$—), 2.58 (4H, m, C=$CCH_2C(CO_2Me)_2$), 3.37 (1H, t, J = 7.7 Hz, —$CH(CO_2Me)_2$), 3.70, 3.73 (12H, 2 s, CH_3), 4.08 (2H, m, —CH_2Cl), 5.40, 5.61 (4H, 2 m, —HC=CH—); ms m/e: 461 (MH^+).

*(E),(Z)-1,1,6,6-Tetracarbomethoxy-3,8-cyclotetradecadiene (****2****b [C–T]) and (E),(Z),(E),(Z)-1,1,6,6,15,15,20,20-octacarbomethoxy-3,8,17,22-cyclooctacosatetraene (****3****b [C–T])*

Following procedure 12: After 60 h, chloride ***1****b* [C–T] (123 mg, 0.376 mmol) gave ***2****b* [C–T] (32 mg, 20%) and dimer ***3****b* [C–T] (60.6 mg, 38%); ir of ***2****b*: 1732, 1278 cm^{-1}; ir of ***3****b*: 1730, 1239 cm^{-1}. The monomer was recrystallized in hot methanol, followed by addition of hexanes and cooling at 0°C.

Chloride ***14***b *[T–T] from* ***10***b

Following procedure 8: (*E*)-1,4-Dichloro-2-butene and malonate ***10****b* (1.39 g, 4.06 mmol) gave chloride ***14****b* [T–T] (1.29 g, 74%); ir: 1731 cm^{-1}; ^1H nmr δ: 1.10–2.15 (16H, m, C—$(CH_2)_3$—C and C—$(CH_2)_5$—C), 2.63 (2H, m, —C=$CCH_2C(CO_2Me)_2$—), 3.30–4.30 (6H, m, —CH_2O—, CH_2Cl), 3.72 (6H, s, CH_3), 4.61 (1H, bs, —O_2CH—), 5.65 (4H, m, —HC=CH—); ms m/e: 431 (MH^+).

Malonate ***15***b *[T–T] from* ***14***b *[T–T]*

Following procedure 9: Chloride ***14****b* [T–T] (1.27 g, 2.95 mmol) gave ***15****b* [T–T] (1.52 g, 98%); ir: 1730 cm^{-1}; ^1H nmr δ: 1.25, 1.64, 2.03 (16H, 3 m, C—$(CH_2)_3$—C and C—$(CH_2)_5$—C), 2.60 (4H, m, C=$CCH_2C(CO_2Me)_2$), 3.38 (1H, t, —$CH(CO_2Me)_2$), 3.70, 3.74 (12H, s, CH_3), 3.40–4.20 (4H, m, —OCH_2—), 4.63 (1H, bs, —O_2CH—), 5.41 and 5.64 (4H, 2 m, —HC=CH—); ms m/e: 527 (MH^+).

Alcohol ***16***b *[T–T] from* ***15***b *[T–T]*

Following procedure 10: Compound ***15****b* [T–T] (1.51 g, 2.87 mmol) gave ***16****b* [T–T] (1.265 g, 100%); ir: 1731 cm^{-1}; ^1H nmr δ: 1.10–1.60, 1.60–2.20 (11H, 2 m, —OH and C—$(CH_2)_5$—C), 2.59 (4H, m, C=$CCH_2C(CO_2Me)_2$), 3.38 (1H, t, —$CH(CO_2Me)_2$), 3.69, 3.79 (12H, s, CH_3), 4.07 (2H, m, —CH_2O—), 5.39, 5.65 (4H, 2 m, —HC=CH—); ms m/e: 443 (MH^+).

Chloride ***1***b *[T–T] from* ***16***b *[T–T]*

Following procedure 11: Alcohol ***16****b* [T–T] (1.26 g, 285 mmol) gave ***1****b* [T–T] (1.08 g, 83%); ir: 1735 cm^{-1}; ^1H nmr δ: 1.27 and 1.85 (6H and 4H, 2 m, C—$(CH_2)_5$—C), 2.59 (4H, m, C=$CCH_2C(CO_2Me)_2$), 3.38 (1H, t, —$CH(CO_2Me)_2$), 3.69, 3.73 (12H, 2 s, CH_3), 4.02 (2H, d, J = 5 Hz, —CH_2Cl), 5.40, 5.64 (4H, 2 m, —HC=CH—); ms m/e: 461 (MH^+).

*(E),(E)-1,1,6,6-Tetracarbomethoxy-3,8-cyclotetradecadiene (****2****b [T–T]) and (E),(E),(E),(E)-1,1,6,6,15,15,20,20-octacarbomethoxy-3,8,17,22-cyclooctacosatetraene (****3****b [T–T])*

Following procedure 12: Chloride ***1****b* [T–T] (173 mg, 0.377 mmol) gave, after 60 h, the monomer ***2****b* [T–T] (12.5 mg, 7.9%, 85% pure from vpc analysis) and ***3****b* [T–T] (47.2 mg, 31%). The monomer was purified by recrystallization in a 4:1 mixture of acetone/water followed by cooling at 0°C; ir of ***2****b*: 1730, 1230, 970 cm^{-1}; ir of ***3****b*: 1730, 1197, 971 cm^{-1}.

Chloride ***14***b *[A–C] from* ***8***b

Following procedure 8: Malonate ***8****b* (1.52 g, 4.47 mmol) gave ***14****b* [A–T] (1.66 g, 87%); ir: 1730, 1021 cm^{-1}; ^1H nmr δ: 1.00–2.30 (16H, m, C—$(CH_2)_3$—C and C—$(CH_2)_5$—C), 2.70 (2H, bd, J = 6 Hz, —C=$CH_2C(CO_2Me)_2$), 3.30–4.00 (2H, bm, —OCH_2—, cyclic), 3.72 (6H, s, CH_3), 4.08 (2H, d, J = 6 Hz, —CH_2Cl), 4.23 (2H, q, THPOCH_2—), 4.79 (1H, bs, —O_2CH—), 5.60 (2H, bm, —HC=CH—).

Malonate ***15***b *[A–C] from* ***14***b *[A–C]*

Following procedure 9: Compound ***14****b* [A–C] (1.65 g, 3.85 mmol) gave ***15****b* [A–C] (2.00 g, 100%); ir: 1735 cm^{-1}; ^1H nmr δ: 1.00–2.40 (16H, m, C—$(CH_2)_3$—C and C—$(CH_2)_5$—C), 2.63 (4H, m, C=$CCH_2C(CO_2Me)_2$), 3.25–4.00 (3H, m, —OCH_2—, cyclic and —$CH(CO_2Me)_2$), 3.71, 3.74 (12H, s, CH_3), 4.23 (2H, q, THPOCH_2—), 4.79 (1H, bs, —O_2CH—), 5.40 (2H, bm, —HC=CH—).

Alcohol ***16***b *[A–C] from* ***15***b *[A–C]*

Following procedure 10: Compound ***15****b* [A–C] (1.995 g, 3.81 mmol) gave alcohol ***16****b* [A–C] (1.66 g, 99%); ir: 3300–3620, 1720–1750 cm^{-1}; ^1H nmr δ: 1.40–1.76, 2.20 (11H, 3 m, —OH and C—$(CH_2)_5$—C), 2.63 (4H, m, —C=$CCH_2C(CO_2Me)_2$), 3.39 (1H, t, J = 7.5 Hz, —$CH(CO_2Me)_2$), 3.71, 3.74 (12H, s, CH_3), 4.22 (2H, dt, J = 2 and 6 Hz, —CH_2O—), 5.40 (2H, bm, —HC=CH).

Chloride ***1***b *[A–C] from* ***16***b *[A–C]*

Following procedure 11: Alcohol ***16****b* [A–C] (1.65 g, 3.75 mmol) gave ***1****b* [A–C] (1.59 g, 92%); ir: 1731 cm^{-1}; ^1H nmr δ: 1.15, 1.26, 1.38, 1.84, 2.21 (10H, 5 m, C—$(CH_2)_5$—C), 2.63 (4H, m, —C=$CCH_2C(CO_2Me)_2$), 3.36 (1H, t, J = 7.5 Hz, —$CH(CO_2Me)_2$), 3.69, 3.73 (12H, s, CH_3), 4.12 (2H, t, J = 2.3 Hz, —CH_2Cl), 5.35 (2H, m, —HC=CH—); ms m/e: 459 (MH^+).

*(Z)-1,1,6,6-Tetracarbomethoxy-3-cyclotetradecen-8-yne (****2****b [A–C]) and (Z),(Z)-1,1,6,6,15,15,20,20-octacarbomethoxy-3,17-cyclooctacosadiene-8,20-diyne (****3****b [A–C])*

Following procedure 12: Chloride ***1****b* [A–C] (184.9 mg, 0.404 mmol) after 38 h gave ***2****b* [A–C] (135.5 mg, 79.6%) and dimer ***3****b* [A–C] (3.3 mg, 1.9%); ir of ***2****b*: 1730, 1047 cm^{-1}; ir of ***3****b*: 1730, 1100 cm^{-1}.

Chloride ***14***b *[A–T] from* ***8***b

Following procedure 8: (*E*)-1,4-Dichloro-2-butene and malonate ***8****b* (1.50 g, 4.49 mmol) gave ***14****b* [A–T] (1.59 g, 84%) as an impure oil; ir: 1732 cm^{-1}; ^1H nmr δ: 1.16, 1.40, 1.53, 1.85 (8H, 4 m, —$(CH_2)_4$—$C(CO_2Me)_2$), 2.21 (2H, tt, J = 7 and 2.1 Hz, —C≡CCH_2C—), 2.64 (2H, d, J = 6.3 Hz, C=$CCH_2C(CO_2Me)_2$), 3.52 and 3.84 (2H, 2 m, —OCH_2—, cyclic), 3.72 (6H, s, CH_3), 3.99 (2H, d, J = 5.9 Hz, —CH_2Cl), 4.24 (2H, q of t, J = 12.3 and 2.1 Hz, THPOCH_2—), 4.81 (1H, bt, —O_2CH—), 5.64 (2H, bm, —HC=CH—); ms m/e: 429 (MH^+).

Malonate ***15***b *[A–T] from* ***14***b *[A–T]*

Following procedure 9: Compound ***14****b* [A–C] (1.58 g, 3.73 mmol) gave ***15****b* [A–T] (1.73 g, 88%); ir: 1736 cm^{-1}; ^1H nmr δ: 1.15, 1.28, 1.52, 1.80, 2.20 (10H, 5 m, C—$(CH_2)_5$—C), 2.57 (4H, m, C=$CCH_2C(CO_2Me)_2$), 3.37 (1H, t, J = 7.5 Hz, —$CH(CO_2Me)_2$), 3.50 and 3.84 (2H, 2 m, —OCH_2—, cyclic), 3.69, 3.73 (12H, s, CH_3), 4.23 (2H, q of t, J = 11.9 and 2.2 Hz, THPOCH_2—), 4.79 (1H, bt, —O_2CH—), 5.40 (2H, bm, —HC=CH—); ms m/e: 525 (MH^+).

Alcohol ***16***b *[A–T] from* ***15***b *[A–T]*

Following procedure 10: Compound ***15****b* [A–T] (1.73 g, 3.30 mmol) gave alcohol ***16****b* [A–T] (1.41 g, 98%); ir: 1732 cm^{-1}; ^1H nmr δ: 1.18, 1.40, 1.48, 1.82 (9H, 4 m, —OH and —$(CH_2)_4$—$C(CO_2Me)_2$), 2.20 (2H, t of t, J = 6.1 and 2.1 Hz, —C≡CCH_2C—), 2.58 (4H, m, C=$CCH_2C(CO_2Me)_2$), 3.39 (1H, t, J = 7.4 Hz, —$CH(CO_2Me)_2$), 3.70, 3.74 (12H, s, CH_3), 4.25 (2H, d of t, J = 6 and 2.2 Hz, —CH_2O—), 5.40 (2H, bm, —HC=CH—); ms m/e: 441 (MH^+).

Chloride ***1***b *[A–T] from* ***16***b *[A–T]*

Following procedure 11: Alcohol ***16****b* [A–T] (1.4 g, 3.21 mmol)

gave chloride **1***b* [A–T] as an oil (1.29 g, 88%); ir: 1736 cm^{-1}; ^1H nmr δ: 1.15, 1.37, 1.48, 1.81 (8H, 4 m, —$(CH_2)_4C(CO_2Me)_2$—), 2.21 (2H, t of t, J = 5.7 and 2.2 Hz, —C≡CCH_2C—), 2.58 (4H, m, C=$CCH_2C(CO_2Me)_2$), 3.38 (1H, t, J = 7.5 Hz, —$CH(CO_2Me)_2$), 3.70, 3.73 (12H, s, CH_3), 4.14 (2H, t, J = 2.3 Hz, —CH_2Cl), 5.4 (2H, bm, —HC=CH—); ms m/e: 459 (MH^+).

*(*E*)-1,1,6,6-Tetracarbomethoxy-3-cyclotetradecen-8-yne (***2**b *[A–T]) and (*E*),(*E*)-1,1,6,6,15,15,20,20-octacarbomethoxy-3,17-cyclooctacosadien-8,22-diyne (***3**b *[A–T])*

Following procedure 12: Chloride **1***b* [A–T] (152 mg, 0.332 mmol) gave, after 38 h, monomer **2***b* [A–T] (15.2 mg, 10.8%, 85% pure from vpc analysis) and dimer **3***b* [A–T] (34.2 mg, 28.4%). The monomer was purified from recrystallization in hot methanol; ir of **2***b*: 1735, 1035 cm^{-1}; ir of **3***b*: 1733, 1198 cm^{-1}.

*Chloride **14**b [A–A] from **8**b*

Following procedure 8: 1,4-Dichloro-2-butyne and malonate **8***b* (1.37 g, 4.03 mmol) gave **14***b* [A–A] (1.57 g, 91%); ir: 1733 cm^{-1}; ^1H nmr δ: 1.10–2.30 (16H, m, C—$(CH_2)_3$—C and C—$(CH_2)_5$—C), 2.90 (2H, m, —C≡$CCH_2C(CO_2Me)_2$), 3.77 (6H, s, CH_3), 3.30–4.00 (2H, m, —OCH_2—, cyclic), 4.12 (2H, t, J = 3 Hz, —CH_2Cl), 4.27 (2H, m, THPOCH_2—), 4.84 (1H, bs, —O_2CH—); ms m/e: 426 (M^+).

*Malonate **15**b [A–A] from **14**b [A–A]*

Following procedure 9: Compound **14***b* [A–A] (1.56 g, 3.66 mmol) gave **15***b* [A–A] (1.76 g, 92%); ir: 1734 cm^{-1}; ^1H nmr δ: 1.10–2.30 (16H, m, C—$(CH_2)_3$—C and C—$(CH_2)_5$—C), 2.78 (4H, m, —C≡$CCH_2C(CO_2Me)_2$—), 3.41 (1H, —$CH(CO_2Me)_2$), 3.30–4.00 (2H, m, —OCH_2—, cyclic), 3.73, 3.75 (12H, s, CH_3), 4.25 (2H, m, THPOCH_2—), 4.82 (1H, bs, —O_2CH—); ms m/e: 522 (M^+).

*Alcohol **16**b [A–A] from **15**b [A–A]*

Following procedure 10: Compound **15***b* [A–A] (1.75 g, 3.75 mmol) gave **16***b* [A–A] (1.4 g, 95%); ir: 1733 cm^{-1}; ^1H nmr δ: 1.00–2.40 (11H, m, —OH and C—$(CH_2)_5$—C), 2.78 (4H, m, C≡$CCH_2C(CO_2Me)_2$), 3.40 (1H, t, —$CH(CO_2Me)_2$), 3.73, 3.78 (12H, s, CH_3), 4.25 (2H, d of t, J = 6 and 2 Hz, —CH_2O—); ms m/e: 439 (MH^+).

*Chloride **1**b [A–A] from **16**b [A–A]*

Following procedure 11: Compound **16***b* [A–A] (1.39 g, 3.17 mmol) gave **1***b* [A–A] (1.13 g, 78%); ir: 1734 cm^{-1}; ^1H nmr δ: 1.00–2.40 (10H, 2 m, C—$(CH_2)_5$—C), 2.78 (4H, m, C≡$CCH_2C(CO_2Me)_2$), 3.52 (1H, —$CH(CO_2Me)_2$), 3.72, 3.78 (12H, s, CH_3), 4.20 (2H, t, J = 5 Hz, —CH_2Cl); ms m/e: 457 (MH^+).

*1,1,6,6-Tetracarbomethoxy-3,8-cyclotetradecadiyne (***2**b *[A–A]) and 1,1,6,6,15,15,20,20-octacarbomethoxy-3,8,17,22-cyclooctacosatetrayne (***3**b *[A–A])*

Following procedure 12: Chloride **1***b* [A–A] (204 mg, 0.448 mmol) after 15 h gave **2***b* [A–A] (75.4 mg, 40%) and **3***b* [A–A] (47 mg, 24.9%); ir of **2***b*: 1732, 1230, 1132 cm^{-1}; ir of **3***b*: 1735, 1201 cm^{-1}.

*Chloride **14**b [A] from **11**b*

Following procedure 8: Malonate **11***b* (1.67 g, 4.85 mmol) and 1,4-dichloro-2-butyne gave chloride **14***b* [A] (1.65 g, 79%); ir: 1736 cm^{-1}; 250-MHz ^1H nmr δ: 1.31 (6H, m, $C(CH_2)_3$—C, cyclic), 1.16, 1.45–1.95, 2.02 (14H, 3 m, C—$(CH_2)_7$—C), 2.87 (2H, t, J = 2.3 Hz, C≡$CCH_2C(CO_2Me)_2$), 3.38 and 3.72 (2H, 2 d of t, J = 9.6 and 6.6 Hz, —OCH_2—, acyclic), 3.50 and 3.88 (2H, 2 m, —OCH_2—, cyclic), 3.74 (6H, s, CH_3), 4.09 (2H, t, J = 2.3 Hz, —CH_2Cl), 4.57 (1H, bt, —O_2CH—); ms m/e: 431 (MH^+).

*Malonate **15**b [A] from **14**b [A]*

Following procedure 9: Compound **14***b* [A] (1.65 g, 3.84 mmol) gave malonate **15***b* [A] (1.71 g, 85%) as an oil; ir: 1738 cm^{-1}; ^1H nmr δ: 1.30 (6H, m, C—$(CH_2)_3$—C), 1.11, 1.55–1.89, 1.96 (14H, 3 m, C—$(CH_2)_7$—C), 2.74 (4H, m, —C≡CCH_2—), 3.38 and 3.72 (1H and 1H, 2 d of t, J = 9.6 and 6.7 Hz, —OCH_2— acyclic), 3.50, 3.88 (2H, 2 m, —OCH_2—, cyclic), 3.52 (1H, m, —$CH(CO_2Me)_2$), 3.72, 3.76 (12H, s, CH_3), 4.57 (1H, bt, —O_2CH—); ms m/e: 527 (MH^+).

*Alcohol **16**b [A] from **15**b [A]*

Following procedure 10: Compound **15***b* [A] (1.71 g, 3.25 mmol) gave alcohol **16***b* [A] (1.43 g, 99%); ir: 3630, 1735 cm^{-1}; ^1H nmr δ: 1.11, 1.30, 1.56, 1.96 (2, 9, 2, and 2H, 4 m, —OH and C—$(CH_2)_7$—C), 2.75 (4H, m, —C≡CCH_2—), 3.51 (1H, t, J = 7.5 Hz, —CH—$(CO_2Me)_2$), 3.63 (2H, t, J = 6.5 Hz, —CH_2O—), 3.71, 3.76 (12H, s, CH_3); ms m/e: 443 (MH^+).

*Bromide **4**b from **16**b [A]*

Following procedure 13: Alcohol **16***b* [A] (1.42 g, 3.20 mmol) gave bromide **4***b* (1.46 g, 91%); ir: 1733 cm^{-1}; ^1H nmr δ: 1.12, 1.31, 1.42, 1.85, 1.97 (2, 6, 2, 2, and 2H, 5 m, C—$(CH_2)_7$—C), 2.74 (4H, m, —C≡CCH_2—), 3.40 (2H, t, J = 5.8 Hz, —CH_2Br), 3.51 (1H, t, J = 7.5 Hz, —$CH(CO_2Me)_2$), 3.72, 3.76 (12H, s, CH_3); ms m/e: 505 (MH^+).

*1,1,6,6-Tetracarbomethoxy-3-cyclotetradecyne (**6**b) and 1,1,6,6,15,15,20,20-octacarbomethoxy-3,17-cyclooctacosadiyne* (dimer)

Following procedure 12: Bromide **4***b* (85.9 mg, 0.170 mmol) in the presence of a 7:1 mixture of potassium carbonate and cesium carbonate (230 mg) gave, after 30 h, **6***b* (39.1 mg, 53.9%) and dimer (10.5 mg, 14.5%); ir of **6***b*: 1738, 1279, 1118 cm^{-1}; ir of dimer: 1737, 1466, 1200–1230 cm^{-1}.

*Bromide **5**b from **4**b*

Following procedure 14: Bromide **4***b* (0.925 g, 1.82 mmol) dissolved in ethyl acetate (12 mL) and cyclohexane (12 mL) gave **5***b* after 5 h (0.915 g, 98%); ir: 1733 cm^{-1}; ^1H nmr δ: 1.05–1.5 (14H, m, —CH_2—$(CH_2)_5$—CH_2—CH_2Br and —$(CH_2)_2CH_2CH(CO_2Me)_2$—), 1.86 (8H, m, —CH_2CH_2Br and —$CH_2C(CO_2Me)_2$—), 3.34 (1H, t, J = 7.6 Hz, —$CH(CO_2Me)_2$), 3.40 (2H, t, J = 6.8 Hz, —CH_2Br), 3.70, 3.73 (12H, s, CH_3); ms m/e: 509 (MH^+).

*1,1,6,6-Tetracarbomethoxycyclotetradecane (**7**b) and 1,1,6,6,15,15,20,20-octacarbomethoxycyclooctacosane* (dimer)

Following procedure 12: Bromide **5***b* (165.9 mg, 0.326 mmol) in the presence of a 4:1 mixture of potassium carbonate and cesium carbonate (500 mg) gave, after 16 h, monomer **7***b* (91.9 mg, 65.7%), dimer (6.5 mg, 4.6%), and a saturated formate ester (3.4%; 13.5% in absence of cesium carbonate); ir of **7***b*: 1730, 1260, 1120 cm^{-1}; ir of dimer: 1736, 1200–1230 cm^{-1}.

Acknowledgements

Support for this work by the Natural Sciences and Engineering Research Council of Canada (NSERCC) and by the "Ministère de l'Éducation (FCAR)", Québec, is gratefully acknowledged.

1. P. Deslongchamps, S. Lamothe, and H.-S. Lin. Can. J. Chem. **62**, 2395 (1984).
2. D. Brillon and P. Deslongchamps. Can. J. Chem. **65**, 43 (1987).
3. D. Brillon and P. Deslongchamps. Tetrahedron Lett. **27**, 1131 (1986).
4. H. Lindlar and R. Dubuis. Org. Synth. **46**, 89 (1966).
5. (*a*) D. G. Holah and J. P. Fackler, Jr. Inorganic Synthesis. Vol. 10. McGraw–Hill, New York, NY. 1967. p. 26; (*b*) C. E. Castro and R. P. Stephens. J. Am. Chem. Soc. **86**, 4358 (1964).
6. M. Miyashita, A. Yoshikoshi, and P. A. Grieco. J. Org. Chem. **42**, 3772 (1977).
7. E. W. Collington and A. I. Meyers. J. Org. Chem. **36**, 3044 (1971).
8. A. B. Smith III and A. S. Thompson. J. Org. Chem. **49**, 1469 (1984).
9. D. Brillon. Synth. Commun. **16**, 291 (1986).
10. (*a*) G. Illuminati and L. Mandolini. Acc. Chem. Res. **14**, 95 (1981); (*b*) M. A. Casadei, C. Galli, and L. Mandolini. J. Org. Chem. **46**, 3127 (1981); (*c*) M. A. Casadei, C. Galli, and L. Mandolini. J. Am. Chem. Soc. **106**, 1051 (1984).

Can. J. Chem. Downloaded from www.nrcresearchpress.com by 80.58.250.72 on 09/07/12
For personal use only.

Synthesis of cedranoid sesquiterpenes. III. Functionalization at carbon 4[1]

PETER YATES, D. JEAN BURNELL,[2] VERNON J. FREER,[3] AND JEFFERY F. SAWYER
Lash Miller Chemical Laboratories, University of Toronto, Toronto, Ont., Canada M5S 1A1

Received June 16, 1986

This paper is dedicated to Dr. O. E. (Ted) Edwards

PETER YATES, D. JEAN BURNELL, VERNON J. FREER, and JEFFERY F. SAWYER. Can. J. Chem. **65**, 69 (1987).

Dimethyl 6,6-dimethyl-5,7-dioxobicyclo[2.2.2]oct-2-ene-2,3-dicarboxylate (**8**) on irradiation in acetophenone gives dimethyl 6,6-dimethyl-4,7-dioxotricyclo[3.2.1.$0^{2,8}$]octane-1,8-dicarboxylate (**13**), which on treatment with lithium dimethylcuprate followed by monodecarbomethoxylation gives methyl 4,4-*endo*-8-trimethyl-3,6-dioxo-*cis*-bicyclo[3.3.0]octane-1-carboxylate (**17**). Similar irradiation of dimethyl 4,6,6-trimethyl-5,7-dioxobicyclo[2.2.2]oct-2-ene-2,3-dicarboxylate (**24**) and its 7,7-ethylenedioxy derivative (**25**) followed by treatment with DBU and concentrated H_2SO_4, respectively, gives dimethyl 3-hydroxy-4,4,8-trimethyl-6-oxo-*cis*-bicyclo[3.3.0]-octa-2,7-diene-1,2-dicarboxylate (**30**). This, on acetylation, reduction with $NaBH_4/CeCl_3$, methanolysis, monodecarbomethoxylation, and hydrogenation, gives methyl *endo*-6-hydroxy-4,4-*endo*-8-trimethyl-3-oxo-*cis*-bicyclo[3.3.0]octane-1-carboxylate (**38**), while on reduction with Li/NH_3 followed by monodecarbomethoxylation it gives a methyl 6-hydroxy-4,4-*exo*-8-trimethyl-3-oxo-*cis*-bicyclo[3.3.0]octane-1-carboxylate (**33**).

PETER YATES, D. JEAN BURNELL, VERNON J. FREER et JEFFERY F. SAWYER. Can. J. Chem. **65**, 69 (1987).

L'irradiation du diméthyl-6,6 dioxo-5,7 bicyclo[2.2.2]octène-2 dicarboxylate-2,3 de diméthyle (**8**) dans l'acétophénone conduit au diméthyl-6,6 dioxo-4,7 tricyclo[3.2.1.$0^{2,8}$]octane dicarboxylate-1,8 de diméthyle (**13**) qui, par une réaction avec du diméthylcuprate de lithium suivie d'une monodécarbométhoxylation, conduit au triméthyl-4,4,8-*endo* dioxo-3,6 bicyclo[3.3.0]octane-*cis* carboxylate-1 de méthyle (**17**). Des irradiations semblables du triméthyl-4,6,6 dioxo-5,7 bicyclo[2.2.2]octène-2 dicarboxylate-2,3 de diméthyle (**24**) et de son dérivé éthylènedioxy-7,7 (**25**), suivies par des traitements respectifs avec de la DBU et du H_2SO_4 concentré, conduisent à l'hydroxy-3 triméthyl-4,4,8 oxo-6 bicyclo[3.3.0]octadiène-2,7-*cis* dicarboxylate-1,2 de diméthyle (**30**). Ce composé, soumis à une acétylation, une réduction par le $NaBH_4/CeCl_3$, une méthanolyse, une monodécarbométhoxylation et une hydrogènation, conduit à l'hydroxy-6-*endo* triméthyl-4,4,8-*endo* oxo-3 bicyclo[3.3.0]octane-*cis* carboxylate-1 de méthyle (**38**) alors que sa réduction par Li/NH_3, suivie d'une monodécarbométhoylation, conduit à un hydroxy-6 triméthyl-4,4,8-*exo* oxo-3 bicyclo[3.3.0]octane-*cis* carboxylate-1 de méthyle (**33**).

[Traduit par la revue]

The cedranoid sesquiterpenes have the tricyclo[5.3.1.$0^{1,5}$]undecane ring system. The simplest members of the series are α-cedrene (**1**), β-cedrene (**2**), and cedrol (**3**).[4] Two members, α-biotol (**4**) and β-biotol (**5**), have been shown to have a hydroxyl substituent at C-4 (4).

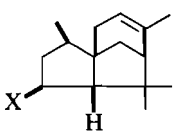

1 X = H
4 X = OH

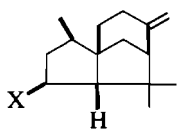

2 X = H
5 X = OH

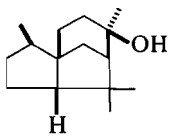

3

In continuation of our synthetic studies in this series (1, 2) we report now on work directed towards the incorporation of an oxygen function at C-4. Our general approaches have included the photosensitized oxa-di-π-methane rearrangement of bicyclo[2.2.2]octenone **6** to the tricyclo[3.2.1.$0^{2,8}$]octenone **7**. We have used an analogous route in the present work with the introduction of an oxygen substituent at C-7 in **6**, which places the corresponding substituent at C-4 in **7**. Accordingly the diketone **8** was synthesized by the route shown in Scheme 1.

Oxidation of 5,5-dimethyl-2-cyclohexen-1-one (**9**) (5) under the somewhat arcane conditions described in the patent literature (6) for the corresponding oxidation of isophorone (3,5,5-trimethyl-2-cyclohexen-1-one) gave enedione **10** (7). This was

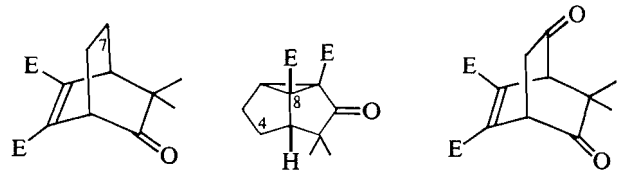

6 **7** (E = CO_2Me) **8**

treated with an excess of isopropenyl acetate and dimethyl acetylenedicarboxylate (DMAD) and a catalytic amount of *p*-toluenesulfonic acid to give the Diels–Alder adduct (**12**) of DMAD and the acetoxy diene **11** without isolation of the latter (cf. ref. 8). Attempted purification of **12** by chromatography on silica led to partial hydrolysis to **8**, but the ^1H nmr spectrum of **12** could be shown to be in accord with expectation by

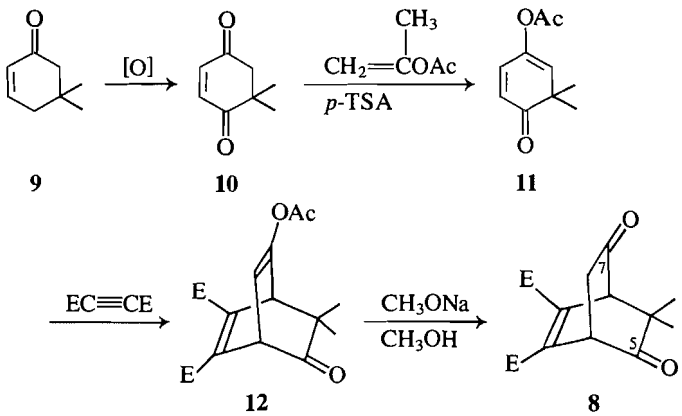

9 **10** **11**

12 **8**

(E = CO_2Me)

SCHEME 1

[1]For earlier papers in this series see refs. 1 and 2.

[2]Present address: Department of Chemistry, Memorial University of Newfoundland, St. John's, Nfld., Canada A1B 3X7.

[3]Present address: Schenectady Chemicals Ltd., Scarborough, Ont., Canada M1L 2H3.

[4]For an account of the chemistry of the cedrenes and cedrol see ref. 3.

Can. J. Chem. Downloaded from www.nrcresearchpress.com by 190.90.36.8 on 09/07/12
For personal use only.

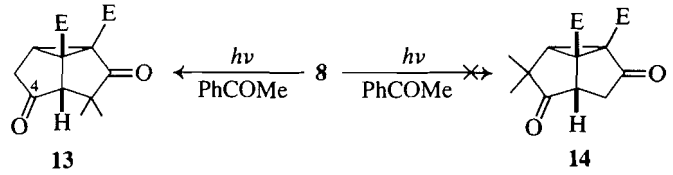

(E = CO_2Me)

SCHEME 2

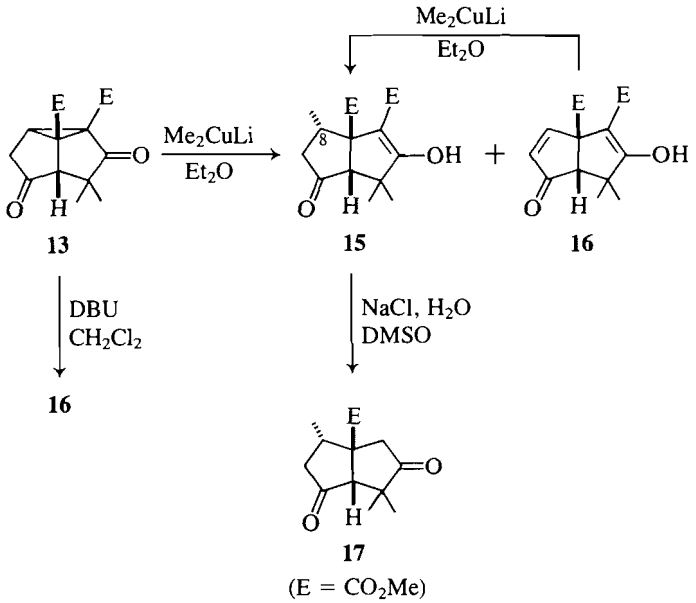

(E = CO_2Me)

SCHEME 3

comparison of the spectrum of the mixture of **8** and **12** with that of **8**. Deliberate conversion of **12** to **8** was effected by methanolysis with methanolic sodium methoxide.

Because of the likelihood that the dione **8** would give a mixture of oxa-di-π-methane products on photosensitized reaction, attempts were made initially to convert it selectively to a monoacetal by treatment with ethylene glycol and *p*-toluenesulfonic acid. However, ^{1}H nmr spectroscopy and tlc showed that the product was a mixture of both monoacetals, the diacetal, and starting material. The photosensitized reaction of the dione **8** itself was therefore examined. This gave a single product in 95% yield that was shown (*vide infra*) to be the desired tricyclic diketone **13**, derived by an oxa-di-π-methane rearrangement involving the C-5 carbonyl group, rather than **14**, involving the C-7 carbonyl group (Scheme 2).[5]

Reaction of **13** with lithium dimethylcuprate in ether gave two products. (Scheme 3). The ir spectrum (λ_{max} 5.78, 6.01, 6.16 μm) and ^{1}H nmr spectrum (δ 0.92 (d, J = 7 Hz, 3H), 10.78 (br s, 1H)) of the major product (67%) led to the assignment to it of a gross structure corresponding to **15**. Its relative configuration at C-8 was established by its decarbomethoxylation by the method of Krapcho and Lovey (9) to give **17**, whose relative configuration was independently determined (*vide infra*). The minor product (20%) is assigned structure **16**. Its α,β-unsaturated, five-membered cyclic ketone and enolized β-keto ester moieties are apparent from its ir and ^{1}H nmr spectra (λ_{max} 5.88, 5.98, 6.13, 6.29 μm; δ 6.13 (d, J = 6 Hz, 1H), 7.92 (d, J = 6 Hz, 1H), 10.46 (br s, 1H)). It is considered to

[5]The origin of the remarkable selectivity in this reaction is uncertain and is under investigation; ADDED IN PROOF: cf. ref. 20.

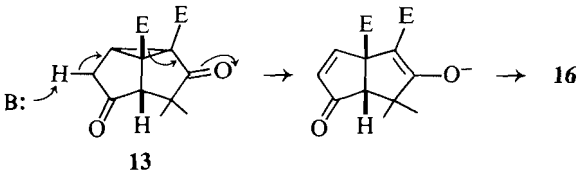

(E = CO_2Me)

SCHEME 4

arise from **13** via removal of a proton from C-7 by a species in the cuprate reagent (10) and opening of the cyclopropane ring to give the anion of the β-keto ester system (Scheme 4) (or by a Lewis-acid-catalyzed variant of this reaction). This type of pathway was confirmed by the demonstration that treatment of **13** with DBU in dichloromethane for 10 min at room temperature gives **16** in 98% yield. The formation of **16** from the photoproduct from **8** establishes that the latter has structure **13**, since an analogous product could not be formed from **14**.

It had been hoped that reaction of lithium dimethylcuprate with **13** would give the *exo* C-8 methyl product **18** rather than the *endo* epimer **15**, in analogy with the reaction of this reagent with **19** to give **20** in our earlier work on the synthesis of cedrene (1). The difference may be directly due to the presence of the carbonyl group at C-4 in **13** or to the formation of **15** by conjugate addition to **16** rather than homoconjugate addition to **13**. Indeed, reaction of **16** with lithium dimethylcuprate was observed to give **15**. It has been postulated that these two types of addition can proceed by different mechanisms (11), and they thus may follow different stereochemical courses. In any event compound **15** has the wrong relative configuration at C-8 for eventual elaboration to the biotols **4** and **5** and, since there appeared to be no simple method for epimerization at C-8, it was necessary to pursue a different approach.

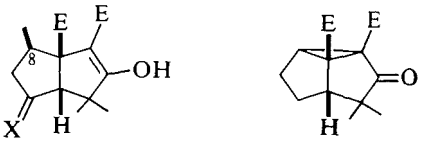

(E = CO_2Me)

This involved the incorporation of what was to become the C-8 methyl group of **18** earlier in the synthesis. Oxidation of isophorone to the enedione **21** was effected under the conditions used for the oxidation of **9** to **10** (6, 7). In a run where the crude product was worked up with aqueous sodium hydroxide, a by-product was isolated whose elemental composition and spectra are in accord with the assignment to it of structure **22** (7). This is considered to arise by base-catalyzed condensation of **21** with **23**, formed by over-oxidation of isophorone,[6] followed by aromatization of the resulting cyclohexadiene ring by air oxidation.

Compound **21** was converted to the dione **24** by a reaction sequence analogous to that of Scheme 1. Unlike its analogue **8**, **24** could be converted selectively to a monoacetal by treatment

[6]S. Ito and M. Matsumoto (quoted in ref. 12) have oxidized the 3-methyl group of isophorone to a formyl group with O_2/$FeCl_3$. D. J. Burnell, R. Grewal, and P. Yates (unpublished results) have observed the formation of both this product and 3,3,5-trimethyl-5-cyclohexene-1,2,4-trione on oxidation of isophorone with selenium dioxide in dioxane.

Can. J. Chem, Downloaded from www.nrcresearchpress.com by 190.90.36.8 on 09/07/12
For personal use only.

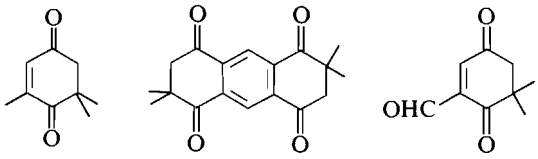

21 22 23

with ethylene glycol and *p*-toluenesulfonic acid. This is assigned structure **25** rather than **26** for the following reasons: (*i*) Its ^{1}H nmr spectrum has the bridge methylene and bridgehead methine proton signals at δ 2.06 and 3.29, respectively, showing that these protons are not on carbon atoms adjacent to the remaining carbonyl group (cf. the chemical shifts for the protons in the spectrum of **24**, δ 2.34 and 3.85), and (*ii*) the presence in the mass spectrum of the monoacetal of a strong peak with *m/z* 86 that can be assigned to the fragment ion **27**, which is readily derivable from **25**, but not from **26**. The selectivity in the monoacetalization of **24** relative to **8** can be attributed to increased steric hindrance to acetalization of the C-5 carbonyl group because of the presence of the C-4 methyl group.

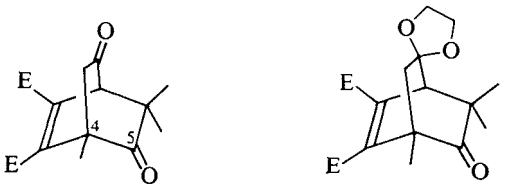

24 25

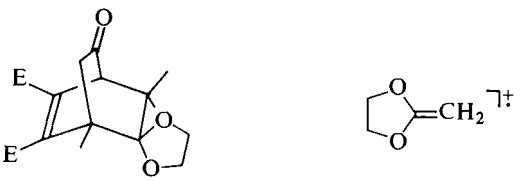

26 27

Photosensitized rearrangement of **25** gave the tricyclo-octane derivative **28** (Scheme 5). It was planned to convert **28** to the dione **29** and then treat this with base to give **30**. Attempts to convert the acetal function of **28** to a ketone by hydrolysis in the presence of *p*-toluenesulfonic acid or pyridinium *p*-toluenesulfonate (13) or by treatment with triphenylcarbenium tetrafluoroborate (14) were unsuccessful, and so we had to resort to dissolution of **28** in concentrated sulfuric acid followed by quenching in ice-water. This led to the direct conversion of **28** to **30**, presumably via **29**. Longer reaction times with sulfuric acid led to yet another desired transformation, that of **30** by decarbomethoxylation to **31**, which could also be prepared from **30** by the method of Krapcho and Lovey (9). It was subsequently found that the unprotected dione **24**, like the dione **8**, gave a single product (94%) on photosensitized rearrangement that was shown to be **29**[5] by its conversion to **30** on treatment with 1,8-diazabicyclo[5.4.0]undec-7-ene (DBU).

It was now necessary to reduce the ethylenic double bond of **31** stereoselectively to give a product with an *exo* methyl group at C-8. Since dissolving metal reductions of α,β-unsaturated ketones often lead to the more stable product (15), the reduction of **31** with lithium in liquid ammonia was investigated. This led to the production of compounds **32** and **33** (Scheme 6), in low yields. The gross structures of these products followed from their spectra (each showed a three-proton doublet in its ^{1}H nmr spectrum). In contrast, hydrogenation of **31** over platinum yielded only **17** (89%). This suggested the *endo* configuration at C-8 shown in **17**, but it was still not possible to assign unambiguously the relative stereochemistry at this center.

Since eventually it would be necessary to build the third ring of the biotols by selective reaction at C-3, we next investigated the selective reduction of the C-6 ketone group of the 3,6-diones **32** and **17**, but this could not be achieved with either sodium borohydride or aluminum isopropoxide, and was also unsuccessful in the case of their enolized precursor **30**. However, protection of the hydroxyl group of **30** by conversion with acetic anhydride, triethylamine, and 4-(dimethylamino)pyridine (DMAP) (16) to the enol acetate **34**, followed by reduction with sodium borohydride and cerous chloride heptahydrate in methanol,[7] gave the C-6 hydroxy compound **35** (Scheme 7). Removal of the acetyl group by methanolysis yielded the β-keto ester **36**. Interestingly, this was the only methyl 4,4-dimethyl-3-oxobicyclo[3.3.0]octane-2-carboxylate of the many encountered in our present and earlier (1, 2) work that was isolated as the unenolized form.[8] Decarbomethoxylation of **36** in the usual manner (9) gave **37**. This on treatment with hydrogen over platinum gave **38**, whose relative stereochemistry was established by X-ray crystallographic analysis to be that shown.[9]

Establishment of the relative configuration at C-6 in **38** leads immediately to the assignment of the corresponding relative configuration shown for compounds **35**, **36**, and **37**. More importantly, the now-established relative configuration at C-8 in **38** together with the observation that **38** is oxidized by pyridinium dichromate (18) to **17** leads to the unambiguous assignment of the *endo* configuration to the secondary methyl group in **17** (Scheme 8). This in turn leads to the assignment of the *exo* configuration for the C-8 methyl group in **32**, which can only differ from **17** by its configuration at C-8. Furthermore, since oxidation of **33** with pyridinium dichromate gives **32**, the former also can be assigned a structure with an *exo* C-8 methyl group (Scheme 8).

Thus in the hydrogenation of the ethylenic double bonds of **31** and **37** over platinum, addition of hydrogen occurs exclusively from the *exo* face of the bicyclo[3.3.0]oct-7-ene system and reduction of the ketone group of **34** with sodium borohydride/cerous chloride occurs in the same stereochemical sense. Preference for reaction on the convex, *exo* face rather than the concave, *endo* face of bicyclo[3.3.0]octane derivatives has been observed previously for similar reactions. However, it was previously uncertain in the present cases whether this stereoselectivity would be operative in the presence of the carbomethoxy substituent C-1.

When reduction of **31** was effected with lithium/ammonia, products (**32** and **33**) with *exo* C-8 methyl groups were obtained (Scheme 6). Since the corresponding methyl group of the biotols has the *exo* configuration, it was clear that we would have to resort to dissolving metal reduction of the C-7—C-8 double bond of a bicyclo[3.3.0]oct-7-ene derivative to obtain the correct relative configuration at C-8. However, as the yields of **32** and **33** from **31** were very low, it was necessary

[7]Gemal and Luche (17) have shown that conditions of this type favor 1,2 rather than 1,4 reduction of enones.

[8]This may be the result of hydrogen bonding between the *endo* C-6 hydroxyl group and the C-2 carbomethoxyl group, if the latter has the *endo* configuration.

[9]The details of this analysis will be published elsewhere.

Can. J. Chem. Downloaded from www.nrcresearchpress.com by 190.90.36.8 on 09/07/12
For personal use only.

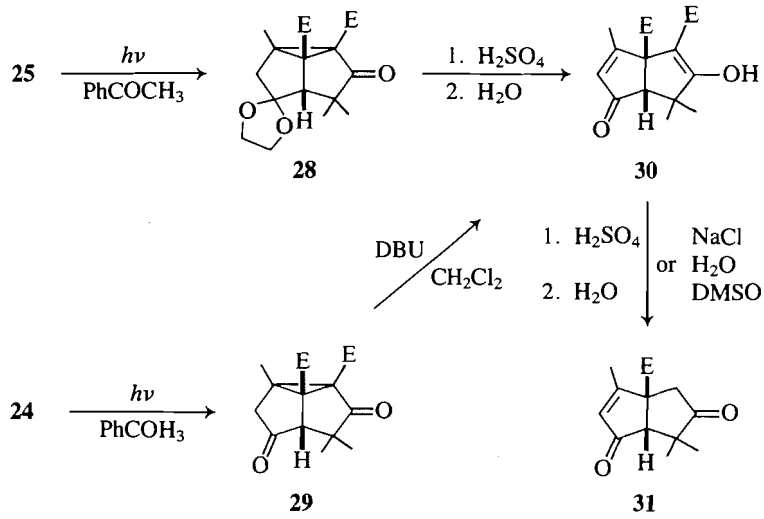

SCHEME 5

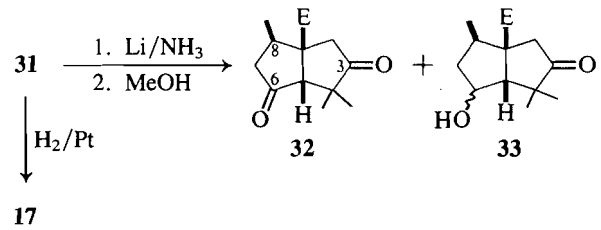

SCHEME 6

to modify this route, which was done by carrying out the lithium/ammonia reduction on **30**, the precursor of **31**. The major product (40%) was an alcohol, which was shown to be **39** by decarbomethoxylation in the usual manner to give **33**. Compound **18** was also formed in the reduction of **30** (Scheme 9).

Thus the *exo* C-8 methyl series can be entered more efficiently in this way, although additional work is needed to further improve the yields, which should be possible since the second product, **18**, from the reduction of **30** also has an *exo* C-8 methyl group. The relative configuration of the C-6 hydroxyl group cannot be assigned unambiguously on the basis of available data. However, this is not critical because, if it is found that the hydroxyl group in **33** has the undesired *endo* configuration, routes are available for inversion at C-6 (cf. ref. 19 and references cited therein).

Experimental

Melting points were determined on a Fisher-Johns apparatus and are uncorrected. The uv spectra were taken in CH_3OH solution and the ir spectra in CCl_4 solution, unless otherwise stated; ir bands are strong unless specified as medium (m) or weak (w) and are sharp unless specified as broad (br). The ^1H nmr spectra were taken in $CDCl_3$ solution at 60 MHz, unless specified to have been taken at 200 MHz. The ^{13}C nmr spectra were taken in $CDCl_3$ solution; chemical shifts were determined by recording the spectra in the proton noise-decoupled mode; the recorded multiplicities were determined from spectra obtained in the single frequency off-resonance decoupled mode.

Diethyl ether and tetrahydrofuran were freshly distilled from benzophenone sodium ketyl and were introduced to the reaction vessel (flame-dried under a flow of nitrogen) through a rubber septum via syringe. Other solvents used for work-ups or chromatography were either distilled or were of ACS Reagent Grade quality. Solutions were concentrated on a rotary evaporator under water aspirator pressure and subsequently under high vacuum provided by a two-stage vacuum pump. Liquid ammonia was dried and distilled from sodium.

Ultraviolet irradiations were conducted in a Rayonet Srinivasan–Griffin photochemical reactor equipped with 11 low-pressure RPR lamps. Solutions were degassed with a stream of nitrogen or argon for 0.3–1 h prior to irradiation.

*5,5-Dimethyl-2-cyclohexen-1-one (**9**)*

A solution of 5,5-dimethylcyclohexane-1,3-dione (dimedone; 2.80 g, 0.0206 mol) and tosylhydrazine (3.83 g, 0.0206 mol) in anhydrous methanol (50 mL) containing concentrated sulfuric acid (3 drops) was stirred at room temperature for 18 h under nitrogen. The methanol was

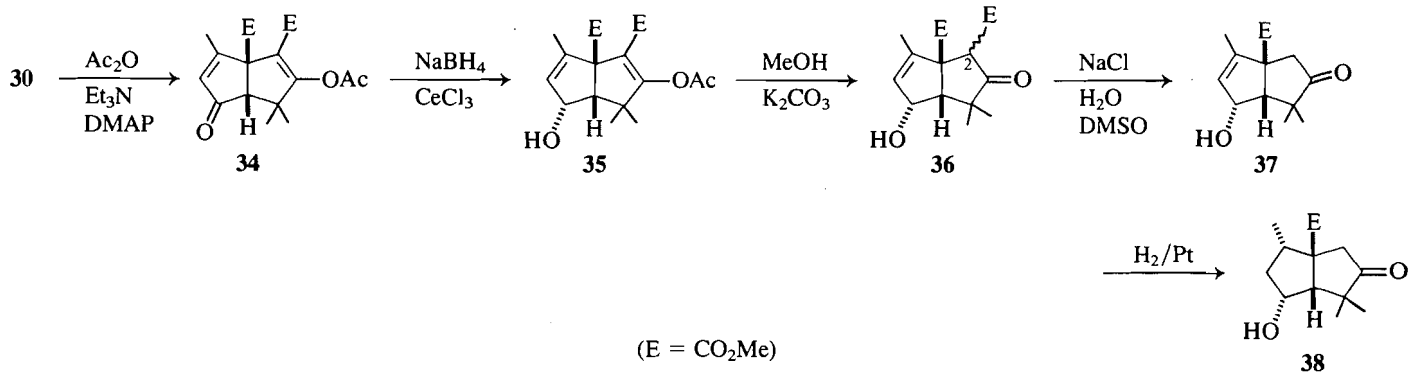

SCHEME 7

Can. J. Chem. Downloaded from www.nrcresearchpress.com by 190.90.36.8 on 09/07/12
For personal use only.

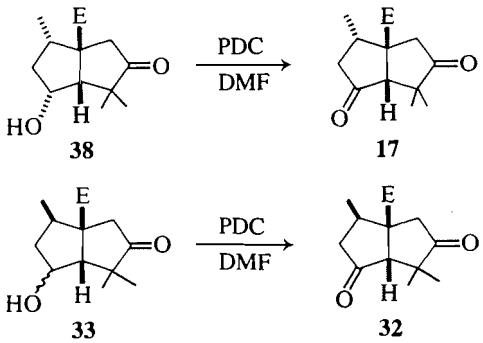

SCHEME 8

removed, potassium carbonate (22.1 g, 0.160 mol) and distilled water (250 mL) were added, and the solution was heated to steam distil the product. The distillate was saturated with sodium chloride and extracted with ether (3 × 30 mL). The organic extracts were washed with saturated brine (2 × 20 mL) and dried over Na_2SO_4. The ethereal solution was concentrated to give **9** as a yellow oil. Purification was accomplished by column chromatography on silica with hexanes/ethyl acetate (4:1 v/v) as the eluent to give **9** (1.28 g, 0.0103 mol, 50%) as a colorless oil; ir λ_{max}: 5.93 μm; ^{1}H nmr δ: 1.07 (s, 6H), 2.20 (m, 2H), 2.27 (s, 2H), 6.00 (dt, J = 10, 2 Hz, 1H), 6.83 (dt, J = 10, 4 Hz, 1H).

*5,5-Dimethyl-2-cyclohexene-1,4-dione (**10**)*

Compound **9** (4.0 g, 0.032 mol) was added to phosphomolybdic acid (0.0148 g, 0.0089 mmol), potassium dichromate (0.0018 g, 0.006 mmol), and cupric sulfate pentahydrate (0.0071 g, 0.045 mmol). The reaction mixture was stirred and maintained at 100°C while air was blown into it through a gas delivery frit at a flow rate of 300 mL/min. Consumption of starting material was complete after 84 h. The viscous black mixture was extracted with ether (100 mL) and the extract was washed with distilled water (4 × 50 mL) and saturated brine (2 × 50 mL). The ethereal solution was dried over $MgSO_4$ and concentrated. The residual oil was distilled (0.5 Torr (1 Torr = 133.3 Pa), 90°C) to give **10** (2.66 g, 0.019 mol, 60%) as a clear, yellow, mobile oil. Crystallization of this oil from hexanes and cooling with ice gave **10** as yellow plates, mp 39.0–39.5°C; ir λ_{max}: 5.89 μm; ^{1}H nmr δ: 1.38 (s, 6H), 2.83 (s, 2H), 6.75 (s, 2H); ^{13}C nmr δ: 25.6 (q), 45.0 (s), 51.3 (t), 139.0 (d), 139.8 (d), 197.5 (s), 202.6 (s); ms *m/z*: 138 (30%). *Exact Mass* calcd. for $C_8H_{10}O_2$: 138.0681; found: 138.0687. *Anal.* calcd. for $C_8H_{10}O_2$: C 69.54, H 7.30; found: C 69.41, H 7.31.

Compound **10** has been prepared previously in 32% yield by oxidation of **9** with *tert*-butyl hydroperoxide and palladium(II) catalysts (12).

*Dimethyl 7-acetoxy-6,6-dimethyl-5-oxobicyclo[2.2.2]octa-2,7-diene-2,3-dicarboxylate (**12**)*

A solution of compound **10** (0.211 g, 1.53 mmol), freshly distilled dimethyl acetylenedicarboxylate (1.42 g, 10.0 mmol), and hydroquinone (3 mg) in isopropenyl acetate (5 mL) was stirred at 25°C for 0.5 h under nitrogen, after which *p*-toluenesulfonic acid (20 mg) was added and the solution was boiled at reflux for 96 h. The isopropenyl acetate and excess dimethyl acetylenedicarboxylate were distilled under water aspirator pressure to leave crude **12**. Chromatography on silica with dichloromethane/ethyl acetate (17:3 v/v) as the eluent gave **12** as a clear yellow oil contaminated with **8** (total combined weight of both materials was 0.466 g), indicating some of **12** underwent hydrolysis on the silica column; ir λ_{max}: 5.72 (br) μm; ^{1}H nmr δ: 1.12 (s, 3H), 1.30 (s, 3H), 2.67 (s, 3H), 3.87 (s, 3H), 3.90 (s, 3H), 3.97 (d, J = 2 Hz, 1H), 4.37 (d, J = 6 Hz, 1H), 6.20 (dd, J = 6, 2 Hz, 1H).

*Dimethyl 6,6-dimethyl-5,7-dioxobicyclo[2.2.2]oct-2-ene-2,3-dicarboxylate (**8**)*

A solution of compound **12** (0.466 g, 1.45 mmol) in methanol (50 mL) containing sodium methoxide (50 mg, 0.926 mmol) was stirred at room temperature for 1 h. The reaction mixture was treated with glacial acetic acid (2 drops) and concentrated. The crude product was redissolved in dichloromethane and the solution was passed through a small plug of neutral alumina and concentrated to give **8** (0.304 g, 1.09 mmol, 75%) as a yellow oil. Purification was accomplished by flash chromatography with hexanes/ethyl acetate (85:15 v/v) as eluent to give **8** as colorless crystals, mp 101.5–102°C; uv λ_{max} (ε) 219 (2 750), 252 (2 800), 307 (850) nm; ir λ_{max}: 5.75 (br) μm; ^{1}H nmr δ: 1.35 (s, 3H), 1.40 (s, 3H), 2.45 (d, J = 3 Hz, 2H), 3.56 (s, 1H), 3.83 (s, 6H), 3.87 (t, J = 3Hz, 1H); ^{13}C nmr δ: 24.7 (q), 25.2 (q), 33.9 (t), 41.7 (s), 50.5 (d), 52.8 (q), 63.5 (d), 136.0 (s), 138.1 (s), 163.8 (s), 164.5 (s), 203.8 (s), 209.2 (s); ms m/*z*: 280 (1%). *Exact Mass* calcd. for $C_{14}H_{16}O_6$: 280.0947; found: 280.0964. *Anal.* calcd. for $C_{14}H_{16}O_6$: C 59.99 H 5.75; found: C 60.06, H 5.81.

*Dimethyl 6,6-dimethyl-4,7-dioxotricyclo[3.2.1.0^{2,8}]octane-1,8-dicarboxylate (**13**)*

A solution of compound **8** (2.14 g, 7.64 mmol) in freshly distilled acetophenone (25 mL) was degassed with nitrogen for 30 min and then irradiated at 350 nm for 32 h in a Pyrex tube. The acetophenone was removed by distillation at 0.5 Torr. The residual solid was recrystallized from hexanes/ethyl acetate (3:1 v/v) to give **13** (2.04 g, 7.28 mmol, 95%) as colorless prisms, mp 112.5–113.5°C; ir λ_{max}: 5.70 (br) μm; ^{1}H nmr (200 MHz) δ: 0.95 (s, 3H), 1.36 (s, 3H), 2.24 (d, J = 20 Hz, 1H), 2.65 (ddd, J = 20, 7, 3 Hz, 1H), 3.17 (d, J = 3 Hz,

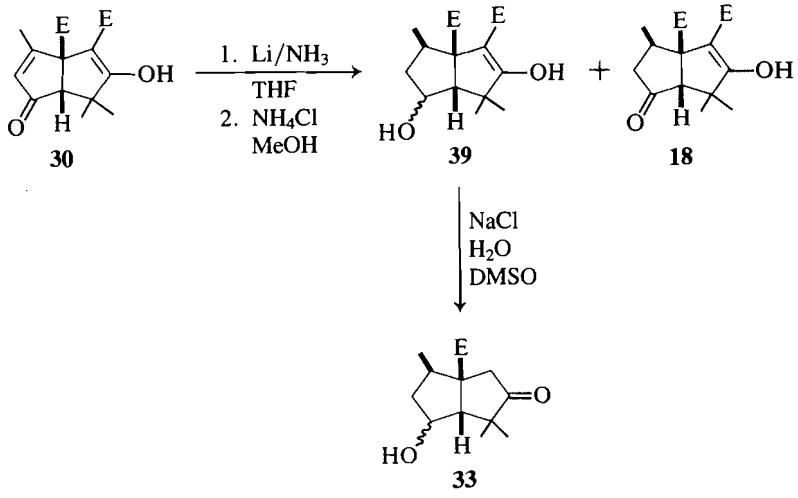

SCHEME 9

Can. J. Chem. Downloaded from www.nrcresearchpress.com by 190.90.36.8 on 09/07/12
For personal use only.

Can. J. Chem. Downloaded from www.nrcresearchpress.com by 190.90.36.8 on 09/07/12
For personal use only.

1H), 3.33 (d, J = 7 Hz, 1H), 3.77 (s, 3H), 3.80 (s, 3H); ^{13}C nmr δ: 17.4 (q), 25.9 (q), 33.8 (t), 36.4 (d), 46.8 (s), 52.9 (q), 53.3 (q), 54.1 (s), 55.9 (s), 58.8 (d), 164.9 (s), 168.4 (s), 207.0 (s), 210.8 (s); ms m/z: 280 (5%). *Exact Mass* calcd. for $C_{14}H_{16}O_6$: 280.0947; found: 280.0956. *Anal.* calcd. for $C_{14}H_{16}O_6$: C 59.99, H 5.75; found: C 60.18, H 5.86.

*Dimethyl 3-hydroxy-4,4-*endo*-8-trimethyl-6-oxo-*cis*-bicyclo[3.3.0]oct-2-ene-1,2-dicarboxylate (**15**)*

A solution of methyllithium – lithium bromide complex in ether (1.53 *M*; 0.96 mL, 1.47 mmol) was added over 20 min to a cold (0°C) slurry of cuprous iodide (0.142 g, 0.747 mmol) in ether (8 mL) under nitrogen. After 1 h a solution of compound **13** (0.100 g, 0.355 mmol) in ether (4 mL) was added over 30 min. The reaction mixture was stirred at 0°C for 5 h and was then siphoned into cold 10% hydrochloric acid (20 mL). The mixture was filtered through Celite. The filtrate was separated and the aqueous phase was extracted with ether (2 × 10 mL). The organic phases were combined and washed with saturated aqueous sodium bicarbonate (5 mL), 1 *M* aqueous sodium thiosulfate (5 mL), and saturated brine (2 × 5 mL). The organic extract was dried over $MgSO_4$ and concentrated to give a yellow oil (0.096 g) containing **15** and **16.**

The ^{1}H nmr spectrum of the oil showed that the ratio of **15** and **16** was 3:1. Chromatography of the mixture with hexanes/ethyl acetate (3:1 v/v) as the eluent gave **15** (0.064 g, 0.219 mmol, 67%) as a colorless solid, mp 102–103.5°C; ir λ_{max}: 5.78, 6.01 (m), 6.16 (m) μm; ^{1}H nmr (200 MHz) δ: 0.92 (d, J = 7 Hz, 3H), 1.18 (s, 3H), 1.35 (s, 3H), 2.02 (dd, J = 17, 8 Hz, 1H), 2.51 (d, J = 2 Hz, 1H), 2.60 (ddd, J = 17, 7.5, 2 Hz, 1H), 3.10 (m, $W_{1/2}$ = 10 Hz, 1H), 3.71 (s, 3H), 3.77 (s, 3H), 10.78 (br s, 1H); ^{13}C nmr δ: 17.6 (q), 21.6 (q), 29.1 (q), 34.2 (d), 46.0 (s), 47.3 (t), 51.4 (q), 52.6 (q), 60.5 (s), 62.6 (d), 98.1 (s), 170.1 (s), 175.4 (s), 181.6 (s), 214.3 (s); ms m/z: 296 (21%). *Exact Mass* calcd. for $C_{15}H_{20}O_6$: 296.1254; found: 296.1243.

Compound **16** (*vide infra*) (20%) was also isolated during chromatography.

*Dimethyl 3-hydroxy-6-oxo-4,4-dimethyl-*cis*-bicyclo[3.3.0]octa-2,7-diene-1,2-dicarboxylate (**16**)*

A solution of compound **13** (0.099 g, 0.354 mmol) in dichloromethane (4 mL) containing 1,8-diazabicyclo[5.4.0]undec-7-ene (DBU; 0.4 mL) was stirred at 25°C under nitrogen. After 10 min the reaction mixture was treated with 10% hydrochloric acid (5 mL). The mixture was extracted with ethyl acetate (2 × 25 mL). The extract was washed with 10% hydrochloric acid (2 × 5 mL), distilled water (2 × 5 mL), and saturated brine (2 × 5 mL), dried over $MgSO_4$, and concentrated to give a yellow oil. Crystallization of the oil from hexanes/ethyl acetate (3:1 v/v) gave **16** (0.097 g, 0.343 mmol, 98%) as colorless plates, mp 119.5–120.5°C; ir λ_{max}: 3.33 (br, w), 5.88, 5.98, 6.13, 6.29 μm; ^{1}H nmr δ: 1.23 (s, 3H), 1.50 (s, 3H), 2.70 (s, 1H), 3.80 (s, 3H), 3.90 (s, 3H), 6.13 (d, J = 6 Hz, 1H), 7.92 (d, J = 6 Hz, 1H), 10.46 (br s, 1H); ^{13}C nmr δ: 22.0 (q), 28.9 (q), 45.6 (s), 51.7 (q), 52.8 (q), 59.6 (d), 61.7 (s), 99.5 (s), 133.1 (d), 163.4 (d), 168.6 (s), 173.0 (s), 180.9 (s), 206.2 (s); ms m/z: 280 (16%). *Exact Mass* calcd. for $C_{14}H_{16}O_6$: 280.0947; found: 280.0950. *Anal.* calcd. for $C_{14}H_{16}O_6$: C 59.99, H 5.75; found: C 60.13, H 5.84.

Treatment of compound **16** with lithium dimethylcuprate under similar conditions gave **15** in 62% yield.

*Methyl 4,4-*endo*-8-trimethyl-3,6-dioxo-*cis*-bicyclo[3.3.0]octane-1-carboxylate (**17**)*

A mixture of compound **15** (0.0451 g, 0.190 mmol) and sodium chloride (0.96 mg, 0.016 mmol) was stirred and heated (112°C) in reagent grade dimethyl sulfoxide (4 mL) containing added water (30 μL) for 18 h under nitrogen. The mixture was diluted with distilled water (5 mL) and extracted with ether (2 × 10 mL). The combined organic extracts were washed with distilled water (2 × 5 mL) and saturated brine (2 × 5 mL), dried over $MgSO_4$, and concentrated to give a yellow oil. Purification of the oil was accomplished by column chromatography on silica with hexanes/ethyl acetate (4:1 v/v) as the eluent, giving **17** (0.0255 g, 0.107 mmol, 56%) as a colorless oil. Crystallization of the oil from pentane/dichloromethane provided **17** as colorless plates, mp 70.5–71°C; ir λ_{max}: 5.65, 5.71 μm; ^{1}H nmr (200 MHz) δ: 1.08 (s, 3H), 1.09 (s, 3H), 1.10 (d, J = 5 Hz, 3H), 2.04 (dd, J = 13.5, 17.5 Hz, 1H), 2.41 (d, J = 19 Hz, 1H), 2.51 (ddd, J = 17.5, 7, 1.5 Hz, 1H), 2.79 (m, 1H), 2.93 (m, $W_{1/2}$ = 4 Hz, 1H), 3.10 (dd, J = 19, 2 Hz, 1H), 3.78 (s, 3H); ^{13}C nmr δ: 14.9 (q), 21.3 (q), 27.1 (q), 35.6 (d), 38.3 (t), 45.2 (t), 49.2 (s), 52.8 (q), 54.9 (s), 64.9 (d), 175.4 (s), 213.3 (s), 217.8 (s); ms m/z: 238 (35%). *Exact Mass* calcd. for $C_{13}H_{18}O_4$: 238.1200; found: 238.1199. *Anal.* calcd. for $C_{13}H_{18}O_4$: C 65.53, H 7.61; found: C 65.54, H 7.69.

*2,6,6-Trimethyl-2-cyclohexene-1,4-dione (**21**)*

3,5,5-Trimethyl-2-cyclohexen-1-one (isophorone; 250 g, 1.81 mol) was added to phosphomolybdic acid (4.0 g, 2.2 mmol), potassium dichromate (0.081 g, 0.28 mmol), and cupric sulfate pentahydrate (0.346 g, 1.39 mmol). The reaction mixture was stirred and maintained at 90–95°C while air was blown into it through a gas delivery frit at a flow rate of 300 mL/min. Consumption of starting material was complete after 100 h. The black mixture was extracted with ether (300 mL) and the extract was washed with distilled water (3 × 50 mL) and saturated brine, dried over $MgSO_4$, and concentrated. The residual liquid was distilled (20 Torr, 99–101°C) to give **21** (152.7 g, 1.01 mol, 56%) as a pale yellow liquid; ir λ_{max}: 5.96 μm; ^{1}H nmr δ: 1.25 (s, 6H), 2.02 (br s, 3H), 2.74 (s, 2H), 6.54 (m, $W_{1/2}$ = 3.5 Hz, 1H); ms m/z: 152 (3%).

In an experiment in which the crude product was treated with aqueous base, a by-product, **22** (2,2,6,6-tetramethylanthracene-1,4,5,8(2*H*,3*H*,6*H*,7*H*)-tetraone), was obtained as yellow flakes, mp 224.5–225°C; uv λ_{max} (ε): 238 (58 000), 262 (40 000), 324 (3 000) nm; ir λ_{max}: 5.87 μm; ^{1}H nmr δ: 1.33 (s, 12H), 3.00 (s, 4H), 8.73 (s, 2H); ^{13}C nmr δ: 25.5 (q), 45.8 (s), 51.8 (t), 126.8 (d), 137.1 (s), 138.6 (s), 194.4 (s), 199.5 (s); ms m/z: 298 (72%). *Exact Mass* calcd. for $C_{18}H_{18}O_4$: 298.1205; found: 298.1219. *Anal.* calcd. for $C_{18}H_{18}O_4$: C 72.45, H 6.09; found: C 72.42, H 6.17.

*Dimethyl 4,6,6-trimethyl-5,7-dioxobicyclo[2.2.2]oct-2-ene-2,3-dicarboxylate (**24**)*

A solution of compound **21** (26.67 g, 0.178 mol), freshly distilled dimethyl acetylenedicarboxylate (25.32 g, 0.178 mol), and hydroquinone (0.167 g, 1.52 mmol) in isopropenyl acetate (20.20 g, 0.202 mol) was stirred at 25°C for 0.5 h under nitrogen. After 30 min *p*-toluenesulfonic acid was added and the solution was heated to 91°C for 48 h. The excess isopropenyl acetate was removed by distillation under water aspirator pressure to leave a solid. This was repeatedly recrystallized from a mixture of hexanes and ethyl acetate to give dimethyl 7-acetoxy-4,6,6-trimethyl-5-oxobicyclo[2.2.2]octa-2,7-diene-2,3-dicarboxylate (49.49 g, 0.148 mol, 83%) as colorless crystals; ir λ_{max} ($CHCl_3$): 5.75 (br) μm; ^{1}H nmr δ: 1.07 (s, 3H), 1.20 (s, 3H), 1.43 (s, 3H), 2.18 (s, 3H), 3.80 (s, 6H), 3.88 (d, J = 3 Hz, 1H), 5.79 (d, J = 3 Hz, 1H); ^{13}C nmr δ: 13.2 (q), 21.1 (q), 26.3 (q), 26.5 (q), 39.7 (s), 52.0 (q), 52.4 (s), 52.6 (q), 57.3 (d), 113.0 (d), 136.2 (s), 147.6 (s), 157.0 (s), 163.3 (s), 166.0 (s), 167.5 (s), 206.6 (s).

A solution of the above product (0.250 g, 0.744 mmol) and sodium methoxide (0.010 g, 0.185 mmol) in methanol (10 mL) was stirred at room temperature for 1 h under nitrogen. Concentrated glacial acetic acid (2 drops) was added and the solution was concentrated to give a yellow oil. The oil was dissolved in dichloromethane, and the solution was passed through a short plug of neutral alumina and concentrated. Repeated crystallization of the residue from hexanes/ethyl acetate (4:1 v/v) gave **24** (0.182 g, 0.618 mmol, 83%) as large colorless plates, mp 82–83°C; uv λ_{max} (ε): 216 (3 270), 251 (3 040), 307 (817) nm; ir λ_{max}: 5.78 (br), 6.12 (m) μm; ^{1}H nmr δ: 1.16 (s, 6H), 1.31 (s, 3H), 2.26 (d, J = 19 Hz, 1H), 2.42 (d, J = 19 Hz, 1H), 3.78 (s, 1H), 3.81 (s, 3H), 3.85 (s, 3H); ^{13}C nmr δ: 13.9 (q), 24.9 (q), 25.0 (q), 41.1 (t), 41.6 (s), 52.5 (s), 52.5 (q), 52.8 (q), 61.0 (d), 130.8 (s), 146.6 (s), 162.7 (s), 165.3 (s), 204.7 (s), 210.0 (s); ms m/z: 294 (6%). *Anal.* calcd. for $C_{15}H_{18}O_6$: C 61.22, H 6.16; found: C 61.22, H 6.15.

Can. J. Chem. Downloaded from www.nrcresearchpress.com by 190.90.36.8 on 09/07/12
For personal use only.

*Dimethyl 7,7-ethylenedioxy-4,6,6-trimethyl-5-oxobicyclo[2.2.2]oct-2-ene-2,3-dicarboxylate (**25**)*

Ethylene glycol (10 mL) and *p*-toluenesulfonic acid (50 mg) were added to a solution of compound **24** (6.02 g, 0.021 mol) in dry benzene (100 mL) under nitrogen. The mixture was boiled at reflux for 40 h in a Dean–Stark apparatus. After cooling, the mixture was concentrated, the residual oil was dissolved in ether (60 mL), and the solution was washed with 5% aqueous sodium hydroxide (2 × 10 mL), distilled water (2 × 10 mL), and saturated brine (2 × 10 mL). The ethereal layer was dried over $MgSO_4$ and concentrated. Repeated crystallization of the residual oil from a mixture of hexanes and ethyl acetate gave **25** (6.40 g, 0.019 mol, 92%) as colorless plates, mp 88–89°C; ir λ_{max}: 5.71 (br), 6.08 (w) μm; ^{1}H nmr (200 MHz) δ: 1.07 (s, 3H), 1.21 (s, 3H), 1.32 (s, 3H), 2.06 (s, 2H), 3.29 (s, 1H), 3.79 (s, 3H), 3.81 (s, 3H), 3.85–4.00 (m, 4H), ^{13}C nmr δ: 14.0 (q), 25.0 (q), 27.6 (q), 41.3 (s), 43.5 (t), 50.8 (d), 51.2 (s), 51.9 (q), 52.2 (q), 63.4 (t), 64.4 (t), 111.4 (s), 135.3 (s), 142.7 (s), 163.5 (s), 165.9 (s), 212.1 (s); ms *m/z*: 338 (4%). *Anal.* calcd. for $C_{17}H_{22}O_7$: C 60.35, H 6.55; found: C 60.47, H 6.54.

*Dimethyl 4,4-ethylenedioxy-2,6,6-trimethyl-7-oxotricyclo[3.2.1.0^{2,8}]octane-1,8-dicarboxylate (**28**)*

A solution of compound **25** (6.40 g, 0.019 mol) in freshly distilled acetophenone (20 mL) was degassed with nitrogen for 15 min and then irradiated at 350 nm for 96 h in a Pyrex tube. The acetophenone was removed by distillation at 0.5 Torr. The residual solid was recrystallized from hexanes/ethyl acetate (3:1 v/v) to give **28** (6.03 g, 0.018 mol, 94%) as colorless prisms, mp 112–113°C; uv λ_{max} (ε): 216 (3 125), 248 (3 660), 304 (570) nm; ir λ_{max} ($CHCl_3$): 5.75, 5.80 μm; ^{1}H nmr (200 MHz) δ: 1.14 (s, 3H), 1.23 (s, 3H), 1.59 (s, 3H), 1.83 (d, *J* = 14 Hz, 1H), 1.95 (dd, *J* = 14, 3 Hz, 1H), 2.81 (d, *J* = 3 Hz, 1H), 3.74 (s, 3H), 3.78 (s, 3H), 3.81–4.00 (m, 4H); ^{13}C nmr δ: 17.1 (q), 18.0 (q), 27.7 (q), 41.9 (t), 42.4 (s), 50.8 (s), 52.2 (q), 52.4 (q), 53.6 (s), 55.5 (d), 57.6 (s), 62.2 (t), 66.1 (t), 118.4 (s), 164.8 (s), 168.9 (s), 210.0 (s); ms *m/z*: 338 (5%). *Anal.* calcd. for $C_{17}H_{22}O_7$: C 60.35, H 6.55; found: C 60.42, H 6.57.

*Dimethyl 3-hydroxy-4,4,8-trimethyl-6-oxo-*cis*-bicyclo[3.3.0]octa-2,7-diene-1,2-dicarboxylate (**30**)*

A solution of compound **28** (6.03 g, 0.018 mol) in concentrated sulfuric acid (20 mL) was stirred for 10 min. The reaction mixture was poured into an ice–water mixture and extracted with ether (4 × 50 mL). The combined organic layers were washed with distilled water (3 × 25 mL), saturated aqueous sodium bicarbonate (3 × 50 mL), and saturated brine (3 × 25 mL). The ethereal layer was dried over $MgSO_4$ and concentrated to give a yellow oil. Repeated crystallization of this oil from hexanes/ethyl acetate (3:1 v/v) gave **30** (5.11 g, 0.017 mol, 98%) as colorless plates, mp 122–123°C; ir λ_{max}: 3.40 (br, w), 5.73, 5.87, 6.02, 6.19 μm; ^{1}H nmr (200 MHz) δ: 1.14 (s, 3H), 1.39 (s, 3H), 2.19 (d, *J* = 1.5 Hz, 3H), 2.73 (s, 1H), 3.73 (s, 3H), 3.82 (s, 3H), 5.92 (q, *J* = 1.5 Hz, 1H), 10.9 (br s, 1H); ^{13}C nmr δ: 17.8 (q), 22.0 (q), 28.9 (q), 45.2 (s), 51.5 (q), 52.7 (q), 62.7 (d), 63.9 (s), 98.6 (s), 132.2 (d), 169.4 (s), 172.8 (s), 178.1 (s), 183.0 (s), 204.8 (s); ms *m/z*: 294 (6%). *Anal.* calcd. for $C_{15}H_{18}O_6$: C 61.22, H 6.16; found: C 61.11, H 6.19.

Treatment of compound **30** with concentrated sulfuric acid for 18 h under otherwise similar conditions gave **31** in 95% yield.

*Dimethyl 2,6,6-trimethyl-4,7-dioxotricyclo[3.2.1.0^{2,8}]octane-1,8-dicarboxylate (**29**)*

A solution of compound **24** (0.489 g, 1.66 mmol) in freshly distilled acetophenone (5 mL) was degassed with nitrogen for 20 min and then irradiated at 350 nm for 144 h in a Pyrex tube. The acetophenone was removed by distillation at 0.5 Torr. The residual oil was crystallized from a mixture of pentane and dichloromethane to give **29** (0.440 g, 1.49 mmol, 90%) as a colorless crystalline solid, mp 111.5–112.5°C; ir λ_{max}: 5.70, 5.75 μm; ^{1}H nmr δ: 0.97 (s, 3H), 1.37 (s, 3H), 1.68 (s, 3H), 2.47 (br s, 2H), 3.20 (br s, 1H), 3.93 (s, 6H); ^{13}C nmr δ: 16.4 (q), 17.1 (q), 25.5 (q), 40.5 (s), 43.4 (t), 47.2 (s), 52.3 (q), 52.5 (q), 55.3 (s), 56.3 (s), 60.0 (d), 164.0 (s), 167.5 (s), 207.4 (s), 209.9 (s); ms *m/z*: 294 (1%). *Exact Mass* calcd. for $C_{15}H_{18}O_6$: 294.1098; found: 294.1125.

Treatment of compound **29** with DBU under conditions similar to those used for the conversion of **13** to **16** gave **30** in 89% yield.

*Methyl 4,4,8-trimethyl-3,6-dioxo-*cis*-bicyclo[3.3.0]oct-7-ene-1-carboxylate (**31**)*

A mixture of compound **30** (0.095 g, 0.323 mmol) and sodium chloride (0.029 g, 0.501 mmol) was stirred in reagent grade dimethyl sulfoxide (4 mL) containing added water (50 μL) and heated to 80°C for 11 h under nitrogen. After cooling, the mixture was diluted with distilled water and extracted with ether (3 × 25 mL). The combined ethereal extracts were washed with distilled water (2 × 10 mL) and saturated brine. The organic layer was dried over $MgSO_4$ and concentrated to give a brown oil. The oil was passed through a silica plug with hexanes/ethyl acetate (4:1 v/v) as the eluent to give **31** (0.064 g, 0.269 mmol, 83%) as a colorless oil; ir λ_{max}: 5.72, 5.83, 6.12 (m) μm; ^{1}H nmr (200 MHz) δ: 1.07 (s, 3H), 1.25 (s, 3H), 2.09 (d, *J* = 1 Hz, 3H), 2.54 (d, *J* = 19 Hz, 1H), 2.93 (s, 1H), 3.42 (d, *J* = 19 Hz, 1H), 3.78 (s, 3H), 6.03 (q, *J* = 1 Hz, 1H); ^{13}C nmr δ: 15.4 (q), 20.1 (q), 27.0 (q), 40.7 (t), 48.0 (s), 52.7 (q), 57.0 (s), 61.9 (d), 131.8 (d), 172.4 (s), 174.9 (s), 204.6 (s), 215.7 (s); ms *m/z*: 236 (1%). *Exact Mass* calcd. for $C_{13}H_{16}O_4$: 236.1044; found: 236.1049.

*Reduction of compound **31** with lithium and ammonia. Formation of compounds **32** and **33***

Lithium (90.4 mg) was added to liquid ammonia (100 mL) and the mixture was stirred for 45 min to ensure complete dissolution. A solution of compound **31** (0.84 g) in dry tetrahydrofuran (10 mL) was added by syringe. After 10 min solid ammonium chloride (3 g) was added and the ammonia was allowed to evaporate. Water (200 mL) was added to the residue and the mixture was extracted with ether (4 × 75 mL) to give a brown oil (0.63 g). Flash chromatography with 3:1 hexanes – ethyl acetate gave a very low yield of compound **32** in the early fractions, which was identified by comparison with the product obtained by oxidation of compound **33** (*vide infra*).

In another run compound **31** (60 mg) in dry tetrahydrofuran was added to liquid ammonia (10 mL), followed by lithium (12 mg). Within 1 min the solution became dark blue and methanol (2.5 mL) was added rapidly, followed by ammonium chloride (1 g). Work-up as before gave a brown oil, which on flash chromatography with 2:1 hexanes – ethyl acetate gave a low yield of compound **33**, identified by comparison with product obtained by decarbomethoxylation of compound **39** (*vide infra*).

*Conversion of compound **31** to compound **17***

Compound **31** (0.523 g, 2.22 mmol) was hydrogenated at 3 atm (1 atm = 101.3 kPa) in ethyl acetate (30 mL) over platinum (formed from platinum oxide *in situ*; 0.040 g) for 16.5 h. The catalyst was filtered and the filtrate was concentrated to give a yellow oil. Purification was accomplished by chromatography on silica with hexanes/ethyl acetate (3:1 v/v) as the eluent and subsequent crystallization from hexanes/ethyl acetate (3:1 v/v) with cooling to give **17** (0.474 g, 1.99 mmol, 89%) as colorless plates, mp 70.5–71°C. The spectroscopic data for the product were identical with those reported for compound **17** prepared by decarbomethoxylation of **15** (*vide supra*).

*Dimethyl 3-acetoxy-4,4,8-trimethyl-6-oxo-*cis*-bicyclo[3.3.0]octa-2,7-diene-1,2-dicarboxylate (**34**)*

A solution of compound **30** (1.62 g, 5.51 mmol) in acetic anhydride (16 mL) and triethylamine (2 mL) containing 4-(dimethylamino)pyridine (0.005 g, 0.04 mmol) was stirred at room temperature under nitrogen for 16 h. The reaction mixture was treated with distilled water (15 mL) and extracted with ethyl acetate (3 × 20 mL). The combined organic extracts were washed with water (3 × 25 mL), saturated aqueous sodium bicarbonate (2 × 25 mL), and saturated brine (2 × 20 mL). The solution was dried over $MgSO_4$ and concentrated to give a brown solid. Crystallization from hexanes/ethyl acetate

Can. J. Chem. Downloaded from www.nrcresearchpress.com by 190.90.36.8 on 09/07/12
For personal use only.

(3:1 v/v) gave **34** (1.46 g, 4.35 mmol, 79%) as a colorless crystalline solid, mp 124.5–125°C; ir λ_{max}: 5.57 (m), 5.73, 5.83, 6.04 (w), 6.16 (w) μm; ^{1}H nmr δ: 1.07 (s, 3H), 1.37 (s, 3H), 2.22 (m, 3H), 2.28 (s, 3H), 2.78 (s, 1H), 3.77 (s, 6H), 6.02 (m, 1H); ^{13}C nmr δ: 17.7 (q), 20.4 (q), 21.4 (q), 28.6 (q), 46.0 (s), 51.3 (q), 52.4 (q), 61.0 (d), 64.7 (s), 115.5 (s), 132.7 (d), 162.5 (s), 166.0 (s), 166.5 (s), 171.7 (s), 177.3 (s), 204.1 (s); ms *m/z*: 336 (2%). *Anal.* calcd. for $C_{17}H_{20}O_7$: C 60.71, H 5.99; found: C 60.86, H 6.02.

Dimethyl 3-acetoxy-endo-*6-hydroxy-4,4,8-trimethyl*-cis-*bicyclo[3.3.0]-octa-2,7-diene-1,2-dicarboxylate (35)*

Compound **34** (0.193 g, 0.575 mmol) and cerous chloride hexahydrate (0.217 g, 0.613 mmol) were added to methanol (10 mL) and the mixture was stirred for 10 min at room temperature. Sodium borohydride (0.0271 g, 0.715 mmol) was added in one portion to the resulting solution and stirring was continued for 3 h. The pH was adjusted to neutrality with 10% hydrochloric acid before the mixture was concentrated on the rotary evaporator to yield a yellow oil. The crude material was extracted with ether (2 × 30 mL). The extracts were combined and washed with distilled water (2 × 10 mL) and saturated brine (2 × 20 mL). The solution was dried over $MgSO_4$ and concentrated to give **35** as an oil (0.145 g, 0.429 mmol, 75%); ir λ_{max}: 2.95 (w), 5.59, 5.75, 5.78, 6.00 (w), 6.13 (w) μm; ^{1}H nmr δ: 1.20 (s, 3H), 1.33 (s, 3H), 1.78 (m, $W_{1/2}$ = 5 Hz, 3H), 2.12 (br, 1H), 2.27 (s, 3H), 2.71 (d, J = 7 Hz, 1H), 3.65 (s, 6H), 4.67–4.98 (m, $W_{1/2}$ = 13 Hz, 1H), 5.73 (m, $W_{1/2}$ = 6 Hz, 1H); ^{13}C nmr δ: 14.8 (q), 20.4 (q), 20.7 (q), 27.5 (q), 46.1 (s), 51.0 (q), 52.1 (q), 60.9 (s), 66.8 (d), 75.3 (d), 117.2 (s), 134.0 (d), 142.3 (s), 163.1 (s), 167.3 (s), 167.9 (s), 174.1 (s); ms *m/z*: 338 (1%). *Exact Mass* calcd. for $C_{17}H_{22}O_7$: 338.1365; found: 338.1366.

Dimethyl endo-*6-hydroxy-4,4,8-trimethyl-3-oxo*-cis-*bicyclo[3.3.0]oct-7-ene-1,2-dicarboxylate (36)*

A mixture of compound **35** (0.118 g, 0.349 mmol) and potassium carbonate (0.025 g, 0.181 mmol) in methanol (6 mL) was stirred for 2.5 h under nitrogen. The reaction was quenched with 10% aqueous hydrochloric acid (3 mL) and the mixture was concentrated. The residual oil was extracted with ether (2 × 20 mL) and the combined extracts were dried over $MgSO_4$. The ethereal solution was concentrated to give a colorless oil. Purification of the oil was accomplished by flash chromatography on silica with dichloromethane/ethyl acetate (9:1 v/v) as the eluent to give **36** (0.088 g, 0.297 mmol, 85%) as a colorless solid, mp 102.5–104°C; ir λ_{max}: 3.03 (w), 5.68, 5.79 (br), 6.03 (w), 6.13 (w) μm; ^{1}H nmr δ: 1.00 (s, 3H), 1.40 (s, 3H), 1.57 (m, 3H), 1.77 (br s, 1H), 2.88 (d, J = 6 Hz, 1H), 3.75 (s, 3H), 3.80 (s, 3H), 4.41–4.77 (m, 1H), 4.63 (s, 1H), 5.97 (m, 1H); ms *m/z*: 296 (5%).

Methyl endo-*6-hydroxy-4,4,8-trimethyl-3-oxo*-cis-*bicyclo[3.3.0]oct-7-ene-1-carboxylate (37)*

A mixture of compound **36** (0.340 g, 1.15 mmol) and sodium chloride (0.117 g, 2.00 mmol) was stirred in reagent grade dimethyl sulfoxide (4 mL) containing added water (40 μL) and heated to 80°C for 14 h under nitrogen. After cooling, the mixture was diluted with distilled water and extracted with ethyl acetate (2 × 25 mL). The combined organic extracts were washed with distilled water (2 × 25 mL) and saturated brine (2 × 25 mL) before being dried over $MgSO_4$. The solution was concentrated to yield a clear yellow oil. Flash chromatography of the oil on silica with chloroform/ethyl acetate (4:1 v/v) as the eluent gave **37** (0.271 g, 1.14 mmol, 99%) as a colorless crystalline solid, mp 123.5–124.5°C; ir λ_{max}: 2.99 (br, w), 5.75 μm; ^{1}H nmr δ: 0.98 (s, 3H), 1.30 (s, 3H), 1.44 (d, J = 5 Hz, 1H), 1.70 (m, $W_{1/2}$ = 3 Hz, 3H), 2.18 (d, J = 19 Hz, 1H), 2.87 (d, J = 6 Hz, 1H), 3.36 (d, J = 19 Hz, 1H), 3.73 (s, 3H), 4.58–4.98 (m, $W_{1/2}$ = 10 Hz, 1H), 5.62–5.80 (m, $W_{1/2}$ = 6 Hz, 1H); ^{13}C nmr δ: 14.0 (q), 18.7 (q), 26.1 (q), 42.7 (t), 48.6 (s), 52.6 (q), 60.5 (s), 61.3 (d), 75.7 (d), 130.8 (d), 148.3 (s), 175.7 (s), 217.8 (s); ms *m/z*: 238 (6%). *Exact Mass* calcd. for $C_{13}H_{18}O_4$: 238.1200; found: 238.1203.

Methyl endo-*6-hydroxy-4,4*-endo-*8-trimethyl-3-oxo*-cis-*bicyclo[3.3.0]-octane-1-carboxylate (38)*

Compound **37** (0.0677 g, 0.284 mmol) was hydrogenated at atmospheric pressure in ethyl acetate (12 mL) over platinum (formed from platinum oxide *in situ;* 0.010 g) for 50 min. The catalyst was filtered and the filtrate was concentrated to give a colorless oil. Purification was accomplished by flash chromatography on silica with chloroform/ethyl acetate (4:1 v/v) as the eluent and crystallization from pentane containing 5–10% dichloromethane to yield **38** (0.0622 g, 0.259 mmol, 91%) as colorless crystals, mp 122.5–123°C; ir λ_{max}: 3.00 (br, w), 5.72, 5.78 μm; ^{1}H nmr (200 MHz) δ: 0.89 (s, 3H), 1.14 (d, J = 7.5 Hz, 3H), 1.25 (s, 3H), 1.53 (ddd, J = 14.0, 2.5, 1.0 Hz, 1H), 1.55 (br, 1H), 2.32 (ddd, J = 14.0, 10.5, 3.5 Hz, 1H), 2.57 (qdd, J = 10.5, 7.5, 2.5 Hz, 1H), 2.72 (d, J = 19.5 Hz, 1H), 2.85 (d, J = 3.5 Hz, 1H), 3.03 (d, J = 19.5 Hz, 1H), 3.74 (s, 3H), 4.38 (m, $W_{1/2}$ = 6.5 Hz, 1H); ^{13}C nmr δ: 19.5 (q), 25.7 (q), 39.2 (t), 41.7 (d), 44.1 (t), 48.0 (s), 52.5 (q), 56.3 (s), 63.5 (d), 75.1 (d), 179.1 (s), 220.1 (s); ms *m/z*: 240 (6%). *Exact Mass* calcd. for $C_{13}H_{20}O_4$: 240.1361; found: 240.1361. *Anal.* calcd. for $C_{13}H_{20}O_4$: C 64.98, H 8.39; found: C 64.54, H 8.27.

Oxidation of compounds 33 and 38 to compounds 32 and 17

A solution of compound **33** (0.050 g, 0.208 mmol) and pyridinium dichromate (0.118 g, 0.313 mmol) in anhydrous *N,N*-dimethylformamide (5 mL) was stirred for 18 h under nitrogen at room temperature. The reaction mixture was extracted with ethyl acetate (2 × 10 mL) and the extract was washed with distilled water (3 × 5 mL) and saturated brine (3 × 5 mL), dried over $MgSO_4$, and concentrated. The residual oil was chromatographed on silica with hexanes/ethyl acetate (3:1 v/v) as the eluent to yield **32** (0.030 g, 0.126 mmol, 61%) as a colorless oil; ^{1}H nmr (200 MHz) δ: 1.03 (s, 3H), 1.08 (d, J = 6.5 Hz, 3H), 1.21 (s, 3H), 2.23 (m, 1H), 2.39–2.47 (m, 2H), 2.61 (d, J = 19 Hz, 1H), 2.91 (s, 1H), 3.12 (d, J = 19 Hz, 1H), 3.76 (s, 3H). *Anal.* calcd. for $C_{13}H_{18}O_4$: C 65.53, H 7.61; found: C 65.34; H 7.69.

Oxidation of compound **38** under similar conditions gave **17**.

Dimethyl 3,6-dihydroxy-4,4-exo-*8-trimethyl*-cis-*bicyclo[3.3.0]oct-2-ene-1,2-dicarboxylate (39)*

Lithium wire (36 mg, 5.2 mg-atom) was added to a stirred solution of **30** (0.514 g, 1.75 mmol) in anhydrous tetrahydrofuran (15 mL) and ammonia (50 mL) under nitrogen. After 20 min the reaction was quenched with methanol (3 mL), solid ammonium chloride was added, and the ammonia was allowed to evaporate. Saturated aqueous ammonium chloride (15 mL) was added and the layers were separated. The aqueous phase was extracted with ethyl acetate (2 × 10 mL). The combined organic layers were washed with distilled water (3 × 10 mL), saturated brine (3 × 10 mL), dried over $MgSO_4$, and concentrated. The residual oil was chromatographed on silica with dichloromethane/ethyl acetate (20:3 v/v) as the eluent to give **39** (40%); ir λ_{max}: 2.75 (w), 5.77 (br), 6.04 (br), 6.21 μm; ^{1}H nmr δ: 1.12 (s, 3H), 1.12 (d, J = 6 Hz, 3H), 1.30 (s, 3H), 1.53–2.27 (m, 4H), 2.50 (d, J = 9 Hz, 1H), 3.70 (s, 3H), 3.80 (s, 3H), 4.12 (m, $W_{1/2}$ = 26 Hz, 1H), 10.90 (br s, 1H); ^{13}C nmr δ: 16.0 (q), 18.9 (q), 28.3 (q), 40.7 (t), 43.8 (d), 44.2 (s), 51.1 (q), 51.6 (q), 61.0 (s), 64.8 (d), 73.9 (d), 102.5 (s), 170.8 (s), 175.7 (s), 180.5 (s); ms *m/z*: 298 (3%). *Exact Mass* calcd. for $C_{15}H_{22}O_6$: 298.1410; found: 298.1434.

The presence of both compounds **39** and **18** in the crude product was demonstrated by its decarbomethoxylation to both **33** and **32** (*vide infra*).

Decarbomethoxylation of compound 39 to compound 33

A mixture of compound **39** (0.090 g, 0.302 mmol) and sodium chloride (0.010 g, 0.171 mmol) in reagent grade dimethyl sulfoxide (4 mL) containing added distilled water (30 μL) was stirred and heated (80°C) for 24 h under nitrogen. The mixture was diluted with distilled water (10 mL) and extracted with ethyl acetate (2 × 10 mL). The combined organic extracts were washed with distilled water (4 × 5 mL) and saturated brine (2 × 5 mL), and dried over $MgSO_4$. The solution was concentrated to give **33** as an oil (0.049 g, 0.204 mmol, 68%); ^{1}H nmr (200 MHz) δ: 0.98 (d, J = 6.5 Hz, 3H), 1.07 (s, 3H), 1.14

(s, 3H), 1.75 (m, 2H), 2.18 (m, 1H), 2.20 (d, J = 19 Hz, 1H), 2.5 (br, exchangeable with D_2O, 1H), 2.67 (d, J = 6.5 Hz, 1H), 3.25 (d, J = 19 Hz, 1H), 3.78 (s, 3H), 4.04 (m, $W_{1/2}$ = 10 Hz, 1H); ^{13}C nmr δ: 14.9 (q), 19.1 (q), 28.2 (q), 43.2 (t), 44.2 (d), 45.0 (t), 48.1 (s), 52.1 (q), 55.3 (s), 63.8 (d), 74.2 (d), 176.3 (s), 219.8 (s); ms m/z: 240 (6%). Exact Mass calcd. for $C_{13}H_{20}O_4$: 240.1356; found: 240.1354.

When a sample of the crude product mixture from the lithium/ammonia reduction of **30** was similarly decarbomethoxylated, the ^1H nmr spectrum of the product showed the presence of both **33** and **32**.

Acknowledgments

We thank Mr. N. Plavac for obtaining the 200-MHz ^1H nmr spectra and the Natural Sciences and Engineering Research Council of Canada for financial support.

1. P. YATES and K. E. STEVENS. Tetrahedron, **37,** 4401 (1981).
2. P. YATES and K. E. STEVENS. Can. J. Chem. **60**, 825 (1982).
3. P. YATES. Structure determination. W. A. Benjamin, Inc., New York. 1967.
4. B. TOMITA, Y. HIROSE, and T. NAKATSUKA. Tetrahedron Lett. 843 (1968); P. BRUN. Tetrahedron Lett. 2269 (1977).
5. G. A. HIEGEL and P. BURK. J. Org. Chem. **38**, 3637 (1973).
6. M. SUERET and E. WIDMER. Belg. Patent 830 273 (1975) (Chem. Abstr. **84**, 164296e (1976)); cf. H. G. W. LEUENBERGER, W. BOGUTH, E. WIDMER, and R. ZELL. Helv. Chim. Acta, **59**, 1832 (1976).
7. V. J. FREER and P. YATES. Chem. Lett. 2031 (1984).
8. S. GERIBALDI, G. TORRI, and M. AZZARO. Bull. Soc. Chim. Fr. 2521 (1973).
9. A. P. KRAPCHO and A. J. LOVEY. Tetrahedron Lett. 957 (1973).
10. G. H. POSNER. Org. React. **22**, 253 (1975).
11. H. O. HOUSE. Acc. Chem. Res. **9**, 59 (1976).
12. T. HOSOKAWA, S. INUI, and S.-I. MURAHASHI. Chem. Lett. 1081 (1983).
13. R. STERZYCKI. Synthesis, 724 (1979).
14. D. H. R. BARTON, P. D. MAGNUS, G. SMITH, G. STRECKERT, and D. ZURR. J. Chem. Soc. Perkin Trans. 1, 542 (1972).
15. D. CAINE. Org. React. **23**, 1 (1976).
16. G. HOFLE, W. STEGLICH, and H. VORBRUGGEN. Angew. Chem. Int. Ed. Engl. **17**, 569 (1978).
17. A. L. GEMAL and J.-L. LUCHE. J. Am. Chem. Soc. **103**, 5454 (1981).
18. E. J. COREY and G. SCHMIDT. Tetrahedron Lett. 399 (1979).
19. G. CAINELLI, F. MANESCALCHI, G. MARTELLI, M. PANUNZIO, and L. PLESSI. Tetrahedron Lett. **26**, 3369 (1985).
20. M. DEMUTH, P. RITTERSKAMP, E. WEIGT, and K. SCHAFFNER. J. Am. Chem. Soc. **108**, 4149 (1986).

Can. J. Chem. Downloaded from www.nrcresearchpress.com by 190.90.36.8 on 09/07/12
For personal use only.

(Trialkylstannyl)copper(I) reagents: preparation and reaction with α,β-unsaturated carbonyl systems. Preparation of β-trialkylstannyl α,β-unsaturated ketones

EDWARD PIERS, HOWARD E. MORTON, AND J. MICHAEL CHONG
Department of Chemistry, University of British Columbia, 2036 Main Mall, University Campus, Vancouver, B.C., Canada V6T 1Y6

Received May 16, 1986

This paper is dedicated to Dr. O. E. (Ted) Edwards

EDWARD PIERS, HOWARD E. MORTON, and J. MICHAEL CHONG. Can. J. Chem. **65**, 78 (1987).

Reaction of Me_3SnLi with 1 equivalent of $CuBr \cdot Me_2S$, PhSCu, $Me_2(MeO)C—C\equiv C—Cu$, or CuCN in tetrahydrofuran (THF) affords the (trimethylstannyl)copper(I) reagents $Me_3SnCu \cdot Me_2S$ (**1**) and $[Me_3SnCuY]Li$ (Y = PhS (**2**), $Me_2(MeO)C—C\equiv C$ (**4**), CN (**5**)), respectively. Similarly, treatment of a THF solution of Me_3SnLi with 0.5 equivalent of $CuBr \cdot Me_2S$ provides $(Me_3Sn)_2CuLi$ (**3**), while reaction of *n*-Bu_3SnLi with PhSCu (1 equivalent) gives [*n*-$Bu_3SnCuSPh]Li$ (**6**). Reagents **2** and **6** readily transfer (in a conjugate sense) the R_3Sn group to conjugated enones (e.g. **7–9**) and structurally simple enoates (e.g. **10**), but do not react with β,β-disubstituted α,β-unsaturated esters (e.g. **11–13**). Reaction of reagent **2** with the enone **26** under "normal" conditions produces, in addition to the expected ketone **28**, a significant amount of the double conjugate addition product **30**. A similar result is obtained with ethyl propenoate (**27**). However, reaction of **26** and **27** with reagent **2** in the presence of acetic acid provides cleanly and efficiently the "simple" conjugate addition products **28** and **29**, respectively. Reagent **1** does not react, or reacts very sluggishly, with α,β-unsaturated carbonyl compounds. β-Trialkylstannyl α,β-unsaturated ketones (e.g. **37–46**) can be produced smoothly and efficiently by reaction of the corresponding β-iodo enones (e.g. **32–36**) with reagents **2** (or **1**) and **6**.

EDWARD PIERS, HOWARD E. MORTON et J. MICHAEL CHONG. Can. J. Chem. **65**, 78 (1987).

Les réactions du Me_3SnLi avec un équivalent de $CuBr \cdot Me_2S$, de PhSCu, de $Me_2(MeO)C—C\equiv C—Cu$ ou de CuCN, dans le tétrahydrofuranne (THF), conduisent respectivement aux réactifs de (triméthylstannyl)cuivre(I) suivants : $Me_2SnCu \cdot Me_2S$ (**1**), $[Me_3SnCuY]Li$ (Y = Phs (**2**), $Me_2(MeO)C—C\equiv C$ (**4**) ou CN (**5**). De la même manière, la réaction d'une solution de THF de Me_3SnLi avec 0,5 équivalent de $CuBr \cdot Me_2S$ conduit au $(Me_3Sn)_2CuLi$ (**3**) alors que la réaction du *n*-Bu_3SnLi avec le PhSCu (1 équivalent) conduit au [*n*-$Bu_3SnCuSPh]Li$ (**6**). Les réactifs **2** et **6** transfèrent facilement (d'une façon conjuguée) le groupement R_3Sn aux énones conjuguées (comme **7–9**) et aux énoates simples d'un point de vue des structures (comme **10**); toutefois, ils ne réagissent pas avec les esters α,β-non-saturées portant deux substituants en position-β,β (comme les composés **11–13**). La réaction de **2** avec l'énone **26**, utilisant des conditions "normales", conduit à une quantité importante du produit **30** provenant d'une double addition conjuguée, en plus de la cétone **28** attendue. Des résultats semblables ont été obtenus avec le propènoate d'éthyle (**27**). Toutefois, la réaction des composés **26** et **27** avec le réactif **2**, en présence d'acide acétique, conduit d'une façon propre et efficace aux produits **28** et **29** provenant d'une addition conjuguée «simple». Le réactif **1** ne réagit pas, ou ne réagit que très lentement, avec les composés carbonylés portant une insaturation en α,β. On peut obtenir les cétones α,β-non-saturées portant un groupement trialkylstannyle en position β (comme **37–46**) d'une façon douce et efficace en faisant réagir les β-iodo énones correspondantes (comme **32–36**) avec les réactifs **2** (ou **1**) et **6**.

[Traduit par la revue]

Can. J. Chem. Downloaded from www.nrcresearchpress.com by 190.90.36.8 on 09/07/12
For personal use only.

Introduction

Over the past two decades, organocopper reagents derived from the interaction of alkyl-lithium, alkenyl-lithium, and (or) related Grignard reagents with copper(I) salts have become well established in organic synthesis (1). Indeed, carbocuprates of various types and constitutions have been found to react efficiently with a wide range of electrophilic substrates and it is difficult to overestimate the importance of these reactions, particularly as methods for forming carbon–carbon bonds.

Recently, cuprate reagents derived from anions other than carbanions have been prepared and have found increasing use in organometallic synthesis. In this connection, the elegant work of Fleming and co-workers (2; see also ref. 3) on the preparation and use of silyl-cuprate reagents deserves explicit mention. The formation of germyl-cuprates from triethyl- and triphenylgermyl-lithium has also been reported (4).

Recently, we initiated investigations into the preparation and chemical reactivity of (trialkylstannyl)copper species, a new class of organometallic reagents first prepared in our laboratory. Our work thus far has focussed mainly on the reactions of these reagents with a variety of electrophilic substrates, and some of the results of these studies have been published in preliminary form (5; see also ref. 6). We report herein (*a*) the preparation of (trimethylstannyl)copper(I)-dimethyl sulfide (**1**), the (trimethylstannyl)cuprate reagents **2–5**, and lithium (phenylthio)(tri-*n*-butylstannyl)cuprate (**6**); (*b*) a study of the reaction of reagents **1**, **2**, and **6** with α,β-unsaturated ketones and esters; and (*c*) the use of reagents **1**, **2**, and **6** for the conversion of β-iodo α,β-unsaturated ketones into the corresponding β-trialkylstannyl enones, a hitherto unknown class of organostannane compounds.

Results and discussion

(a) Preparation of the (trialkylstannyl)copper(I) reagents 1–6

Reaction of trimethylstannyl-lithium[1] with 1.0 or 0.5 equivalents of cuprous bromide – dimethyl sulfide complex (8) in

$Me_3SnCu \cdot Me_2S$	$[Me_3SnCuY]Li$
1	**2** Y = SPh
	3 Y = $SnMe_3$
[*n*-$Bu_3SnCuSPh]Li$	**4** Y = $C\equiv C—C(OMe)Me_2$
6	**5** Y = CN

[1]Trimethylstannyl-lithium and tri-*n*-butylstannyl-lithium were prepared by reaction of hexamethylditin and hexa-*n*-butylditin with 1.0 equivalent of methyl-lithium and *n*-butyl-lithium, respectively. See ref. 7.

Can. J. Chem. Downloaded from www.nrcresearchpress.com by 190.90.36.8 on 09/07/12
For personal use only.

cold (−48°C), dry tetrahydrofuran (THF) provided solutions of reagents **1** and **3**, respectively. Similarly, the cuprate reagents **2**, **4**, and **5** were prepared by addition of 1.0 equivalent of solid phenylthiocopper(I) (9), 3-methoxy-3-methyl-1-butynylcopper(I) (10), or cuprous cyanide, respectively, to cold solutions of trimethylstannyl-lithium[1] in dry THF. Lithium (phenylthio)(tri-*n*-butylstannyl)cuprate (**6**) was obtained in analogous fashion by reaction of tri-*n*-butylstannyl-lithium[1] with phenylthiocopper(I) (9) in THF at −20°C.

The formulations shown in **1**–**6** are not meant to imply actual structures, but are used for convenience and to show stoichiometry. These formulas are, of course, analogous to those commonly used to represent alkylcuprate reagents.[2] It is interesting to note that THF solutions of reagents **1**–**4** and **6** are dark red in color, while solutions of the cyanocuprate **5** are bright orange.

Although the preparation of reagents **1**–**6** is relatively straightforward, it is important to discuss a number of details. In analogy with alkylcuprates, the (trialkylstannyl)copper(I) reagents are thermally unstable and are sensitive to oxygen. Therefore, it is imperative to maintain relatively low reaction temperatures (certainly ≤ room temperature) and to carefully exclude oxygen from the reaction mixtures. An explicit study regarding the relative stabilities of **1**–**6** was not carried out, but on the basis of observations made during the course of our work with these species, it appears that the phenylthiocuprates **2** and **6** and the cyanocuprate **5** are somewhat more stable than reagents **1**, **3**, and **4**.

For the preparation of reagents **1** and **3**, it is best to use white, recently prepared (8) cuprous bromide – dimethyl sulfide complex. Furthermore, we have found that, although phenylthiocopper(I) (9) remains a uniform yellow color even after storage (ambient temperatures, argon atmosphere) for periods of time greater than one year, the phenylthiocuprates **2** and **6** did not form consistently when the phenylthiocopper(I) used was more than about six months old. In a similar vein, the cuprate reagent **4** should be prepared within a few days of preparing 3-methoxy-3-methyl-1-butynylcopper(I) (10). For the formation of the cyanocuprate **5**, purification of commercially available cuprous cyanide is not necessary.

(b) Reaction of reagents 1, 2, and 6 with α,β-unsaturated carbonyl compounds

It is well known that the reactivity patterns of alkyl-lithium reagents are notably different from those of alkylcuprates (1). For example, reaction of alkyl-lithiums with α,β-unsaturated carbonyl compounds normally results in direct attack of the alkyl group on the carbonyl carbon (1,2-addition). In contrast, alkylcuprate reagents of various types and constitutions usually transfer the alkyl group to the β carbon of conjugated enones and enoates (1,4-addition) (1).

Still has shown (7) that reaction of trimethylstannyl-lithium with 2-cyclohexen-1-ones *in diethyl ether* results largely in 1,2-addition products. However, treatment of α,β-unsaturated ketones and esters with Me_3SnLi *in THF or THF–hexamethylphosphoramide (HMPA)* provides conjugate addition products in high yields. (7). Interestingly, these reactions take place rapidly even at −78°C. Thus, although both alkyl-lithiums and trialkylstannyl-lithiums are highly reactive reagents, their reactivity patterns with respect to enones and enoates are not entirely analogous.

TABLE 1. Reaction of trialkylstannyl reagents with α,β-unsaturated ketones and esters

Entry	Substrate	Reagent (equiv.)	Reaction conditions[a]	Product (yield, %)[b]
1	**7**	Me_3SnLi		**14** (93)[c]
2	**7**	**1** (1.3)	A	**14** (trace)[d]
3	**7**	**2** (1.3)	B	**14** (76)
4	**7**	**6** (1.5)	C	**15** (69)
5	**8**	Me_3SnLi		**16** (96)[c]
6	**8**	**1** (1.3)	A	**16** (32)[e]
7	**8**	**2** (2.0)	B	**16** (91)
8	**8**	**6** (1.5)	C	**17** (78)
9	**9**	Me_3SnLi		**18** (77)[c]
10	**9**	**1** (1.3)	A	**18** (—)[d]
11	**9**	**2** (2.0)	B	**18** (69)
12	**9**	**6** (1.5)	C	**19** (64)
13	**10**	Me_3SnLi (1.1)	D	**20** (71)
14	**10**	**1** (1.3)	A	**20** (trace)[d]
15	**10**	**2** (1.1)	B	**20** (67)
16	**10**	**6** (1.5)	C	**21** (74)
17	**11**	Me_3SnLi (1.1)	D	**22** (74)
18	**11**	**2** (1.3)	B	**22** (—)[d]
19	**12**	Me_3SnLi		**23** (80)[c]
20	**12**	**2** (1.3)	B	**23** (—)[d]
21	**13**	Me_3SnLi (1.1)	D	**24** (75)
22	**13**	**2** (1.3)	B	**24** (—)[d]

[a]A: THF, −48°C, 2 h; −20°C, 1 h; room temperature, 1 h. B: THF, −20°C, 15 min; room temperature, 1 h. C: THF, −78°C, 1 h; −20°C, 1 h; room temperature, 1 h. D: THF, −78°C, 15 min.

[b]Yields from the experiments described herein refer to isolated, purified material.

[c]Taken from ref. 7.

[d]Starting material was recovered in high yield.

[e]The diketone **25** was also produced (24% yield) in this reaction (see text).

It might be expected that (trialkylstannyl)copper(I) reagents would also transfer, in a conjugate sense, the R_3Sn group to α,β-unsaturated carbonyl compounds.[3] Furthermore, it was of interest to compare the reactivity of these reagents with that of the "parent" trialkylstannyl-lithium species. Therefore, we investigated initially the reactions of reagents **1**, **2**, and **6** with a number of representative α,β-unsaturated ketones (**7**–**9**) and esters (**10**–**13**), and compared the results obtained with those derived from reaction of these substrates with trimethylstannyl-lithium. The results of this study are summarized in Table 1.

A number of points should be made with respect to the data given in Table 1. In terms of its ability to transfer conjugatively the trimethylstannyl group to α,β-unsaturated carbonyl systems, lithium (phenylthio)(trimethylstannyl)cuprate (**2**) was found to be less reactive than Me_3SnLi. Thus, reagent **2** readily transformed the enones **7**–**9** and methyl (*E*)-2-butenoate (**10**) into the corresponding 1,4-addition products **14**, **16**, **18**, and **20**, respectively (Table 1, Entries 3, 7, 11, 15). However, the cuprate **2** failed to react with ethyl 3-methyl-2-butenoate (**11**) or with the β,β-disubstituted enoates **12** and **13** (Entries 18, 20,

[2]For very interesting recent work regarding the constitutions of various cuprate reagents derived by interaction of methylcopper(I) and varying amounts of methyl-lithium, see ref. 11. See also ref. 12.

[3]Hudec (13) reported that treatment of two 2-cyclohexen-1-one derivatives with a "black" THF solution of trimethylstannyl-lithium in the presence of a *catalytic amount* of cuprous iodide provided the corresponding conjugate addition products. However, in view of Still's work (7), it is not clear that the CuI catalyst played a significant role in these transformations.

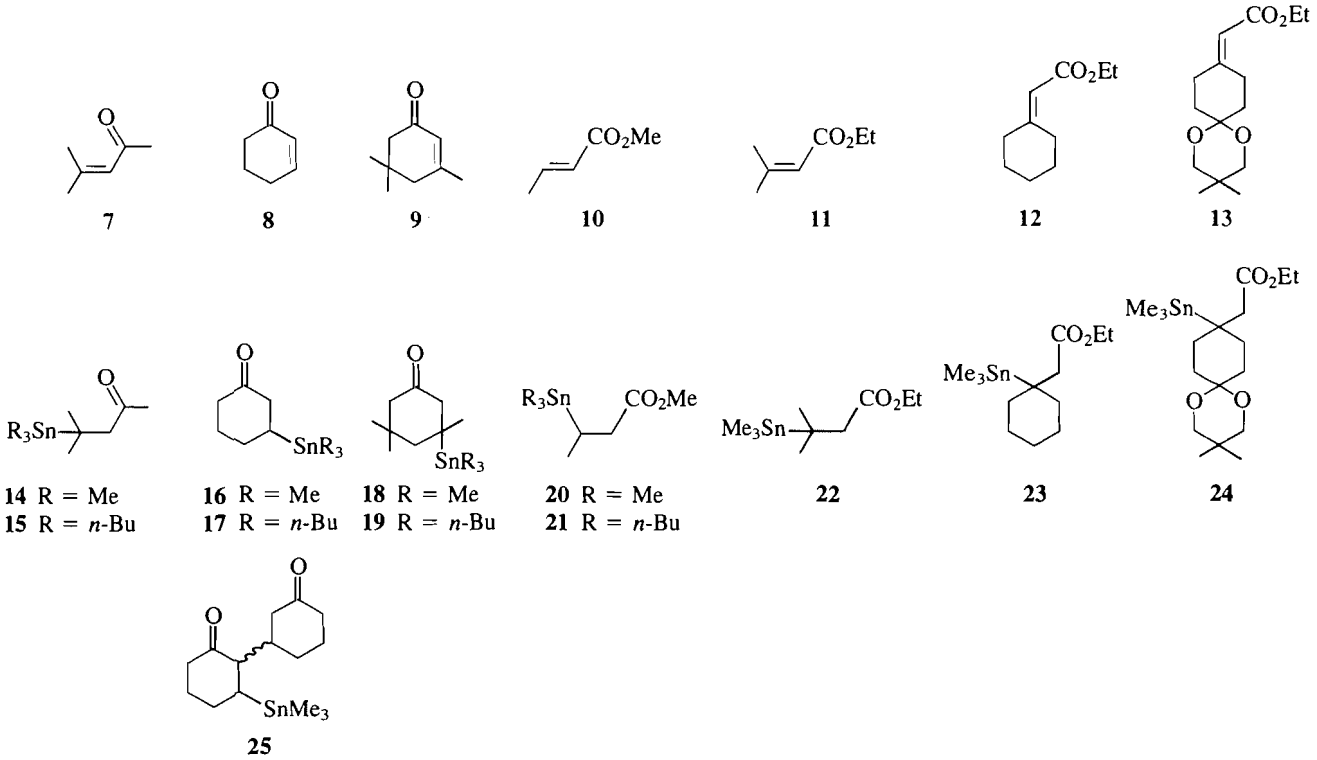

CHART 1

22). In each case, a high proportion of the starting material was recovered. In contrast, trimethylstannyl-lithium smoothly and efficiently converted all of the substrates **7**–**13** into the corresponding conjugate addition products (Entries 1, 5, 9, 13, 17, 19, 21).

Lithium (phenylthio)(tri-*n*-butylstannyl)cuprate (**6**) evidently has reactivity similar to that of the trimethylstannyl analog **2**. Thus, reaction of the substrates **7**–**10** with **6** provides the tri-*n*-butylstannyl derivatives **15**, **17**, **19**, and **21**, respectively, in good yields (Entries 4, 8, 12, 16).

The results summarized in Table 1 also show that (trimethylstannyl)copper(I)-dimethyl sulfide (**1**) is relatively unreactive towards α,β-unsaturated carbonyl compounds. In fact, treatment of the substrates **7**, **9**, and **11** with reagent **1** did not produce any products; in each case, starting material was recovered in high yield (Entries 2, 10, 14). On the other hand, reaction of 2-cyclohexen-1-one (**8**) with **1** (Entry 6) provided a low yield (32%) of 3-trimethylstannylcyclohexanone (**16**). Also produced in this reaction, in 48% yield, was the diketone **25**. Thus, although reagent **1** does transfer the Me_3Sn group to the β carbon of enone **8**, conjugate addition of the enolate anion thus formed to a second molecule of **8** is competitive with the initial addition.

The problem of "double" conjugate addition is also observed in the reactions of trimethylstannyl-lithium and the cuprate reagent **2** with the structurally simple substrates 3-buten-2-one (**26**) and ethyl propenoate (**27**) (see Chart 2 and Table 2). Thus, treatment of **26** and **27** with 1 equivalent of Me_3SnLi (−78°C, THF) provided, in each case, a mixture of mono-addition (**28**, **29**, respectively) and di-addition (**30**, **31**, respectively) products (Table 2, Entries 1 and 3). Similarly, reaction of the enone **26** with reagent **2** afforded products **28** (27%) and **30** (37%) (Entry 2), while an analogous transformation involving the enoate **27** gave a low yield (18%) of the diester **31** as essentially the only volatile product.

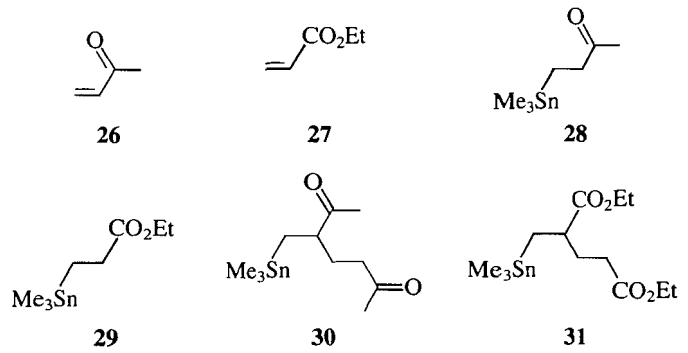

CHART 2

Interestingly, however, it was found that the reactions of **26** and **27** with the cuprate reagent **2** can be controlled experimentally so as to produce good yields of the conjugate addition products **28** and **29**. Thus, treatment of **26** with reagent **2** (1.3 equivalents) *in the presence of 1.3 equivalents of acetic acid* provided the ketone **28** in 77% yield (Entry 5).[4] Under these conditions, only trace amounts of the diketone **30** was formed. Evidently, conjugate addition of cuprate reagent **2** to the enone **26** is considerably faster than protonation (destruction) of **2** by acetic acid. Furthermore, protonation (HOAc) of the initially formed enolate anion (from **26** + **2**) is relatively fast compared with a second conjugate addition reaction (to produce **30**). In similar fashion, treatment of a cold THF solution of reagent **2** (4 equivalents) with a mixture of ethyl propenoate (**27**) and acetic acid (2 equivalents) afforded the mono-ester **29** in 70% yield (Entry 6).

The results just described revealed an interesting and import-

[4]Reaction of the enone **26** with trimethylstannyl-lithium in the presence of acetic acid gave only trace amounts of the conjugate addition product **28**.

Can. J. Chem. Downloaded from www.nrcresearchpress.com by 190.90.36.8 on 09/07/12
For personal use only.

Can. J. Chem. Downloaded from www.nrcresearchpress.com by 190.90.36.8 on 09/07/12
For personal use only.

TABLE 2. Reaction of Me_3SnLi and $[Me_3SnCuSPh]Li$ (**2**) with 3-buten-2-one (**26**) and ethyl propenoate (**27**)

Entry	Substrate	Reagent (equiv.)	Reaction conditions[a]	Products (yield, %)[b]
1	**26**	Me_3SnLi (1.0)	A	**28** (43), **30** (31)
2	**26**	**2** (1.3)	B	**28** (27), **30** (37)
3	**27**	Me_3SnLi (1.0)	A	**29** (20), **31** (29)
4	**27**	**2** (1.3)	B	**29** (trace), **31** (18)
5	**26**	**2** (1.3)	B[c]	**28** (77), **30** (trace)
6	**27**	**2** (4.0)	B[d]	**29** (70), **31** (trace)

[a]A: THF, −78°C, 1 h. B: THF, −78°C, 30 min; −20°C, 1 h; room temperature, 30 min.

[b]Yields refer to isolated, purified products.

[c]HOAc (1.3 equiv.) was added along with the substrate **26** to a solution of reagent **2**.

[d]HOAc (2.0 equiv.) was added along with the substrate **27** to a solution of reagent **2**.

ant characteristic of (trialkylstannyl)cuprate reagents. Unlike the "parent" trialkylstannyl-lithiums, the corresponding copper(I) species are relatively weak bases in THF.[5] This property not only allows one to perform successfully transformations such as **26** → **28** and **27** → **29**, but proved to be important in subsequent investigations concerning the use of these reagents in synthesis (5).

(c) Reaction of reagents 1, 2, and 6 with β-iodo α,β-unsaturated ketones

Recent work in our laboratory (14) has shown that β-iodo α,β-unsaturated ketones (15) (general formulas **A**, **B**) serve as excellent synthetic equivalents of unsaturated a^3 synthons of general structures **C** and **D**, respectively. In connection with an investigation (16) aimed at employing β-iodo enones as synthetic equivalents of the unsaturated d^3 synthons **E** and **F** we

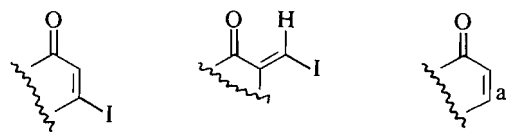

wished to convert substances of general structures **A** and **B** into the corresponding β-trialkylstannyl α,β-unsaturated ketones.

Treatment of 3-iodo-2-cyclohexen-1-one (**32**) (see Chart 3) with 1 equivalent of trimethylstannyl-lithium in THF at −78°C for 1 h afforded a mixture (gas–liquid chromatographic analysis) of starting material **32** (42%), the desired enone **37** (32%), the di-addition product **47** (15%), and a number of minor constituents. Pure samples of **37** and **47** were obtained by preparative gas–liquid chromatography and these substances were fully characterized. In general, this reaction was not very reproducible and attempts to increase the yield of **37** by varying reaction conditions proved to be unfruitful.

In contrast, reaction of the iodo enone **32** with 1.1 equivalents of lithium (phenylthio)(trimethylstannyl)cuprate (**2**) in THF (−20°C to room temperature) gave 3-trimethylstannyl-2-cyclohexen-1-one (**37**) in 86% yield (see Table 3, Entry 1). In similar fashion, the cuprate reagent **6** smoothly converted substrate **32** into the tri-*n*-butylstannyl derivative **38** (81%, Table 3, Entry 2). Both reactions were clean and none of the corresponding di-addition products (e.g. **47**) could be detected in the materials initially isolated.

Similar transformations involving the β-iodo enones **33–36** and the cuprate reagents **2** and **6** were carried out and the results are summarized in Table 3 (Entries 3–10). Although the conversions of **32–35** into the β-trialkylstannyl enones **37–44** were generally clean and efficient, the corresponding transformations of (*E*)-2-(iodomethylene)cyclohexanone (**36**) into **45** and **46** were not entirely reproducible. The yields of isolated, purified products obtained from several reactions varied considerably (~35–80% for **45** and 45–70% for **46**). In general, best results were obtained when the crude reaction products were subjected to chromatography on silica gel prior to bulb-to-bulb distillation.

The stereochemistry of products **45** and **46** was assigned on the basis of the following comparisons. In the ^1H nmr spectra of compounds **48** and **49** (see Chart 4), the olefinic protons resonate at δ 5.6 and 6.62, respectively (17). On the other hand, the olefinic protons adjacent to the methyl group in (*E*)-2-heptene (**50**) and to the Me_3Sn function in (*E*)-1-trimethylstannyl-1-hexene (**51**) give rise to signals at δ 5.40 and 5.92 (18), respectively. Thus, replacing the methyl substituent on the double bond of **50** by a trimethylstannyl group (cf. **51**) causes a downfield shift of about 0.5 ppm for the adjacent olefinic proton. Analysis of the data given above would lead one to predict that the alkene protons of **45** and **46** should resonate at approximately δ 7.1 (~6.6 + ~0.5). In fact, the olefinic protons in question exhibit triplets (J = 2 Hz) at δ 7.03 (**45**) and δ 7.04 (**46**). These values provide excellent evidence for the stereochemical assignments.

The reactions of β-iodo enones with other (trimethylstannyl)copper(I) reagents were also examined. For example, reaction of **32** with $Me_3SnCu \cdot Me_2S$ (**1**) in THF (−48°C to room temperature) provided **37** in excellent yield (Table 3, Entry 11).[6] In similar fashion, the β-iodo enones **34–36** were converted efficiently into the corresponding products **41**, **43**, and **45**, respectively (Table 3, Entries 12–14). The yields of these reactions were comparable to those obtained from reaction of **32** and **34–36** with the cuprate reagent **2**. Furthermore, reaction of **36** with **1** (to produce **45**) was found to be much more reproducible than the corresponding transformation involving **36** and the cuprate reagent **2**.

It was also found that reaction of 3-iodo-2-methyl-2-cyclopenten-1-one (**35**) with reagent **1** under conditions identical with those used for the iodo enones **32** and **34** gave, in addition to the desired product **43**, a significant amount of starting material. However, addition of HMPA to the reaction mixture improved the efficiency of this conversion (Table 3, Entry 13).

[5]Similar observations were made independently by Cox and Wudl (see the last citation in ref. 6).

[6]The β-iodo enone **32** could also be converted efficiently into **37** by reaction with the bis(trimethylstannyl)cuprate **3** or the cyanocuprate **5**. However, since two equivalents of Me_3SnLi are required to prepare one equivalent of **3**, it seems clear that the mixed cuprates **2** and **5** or the (trimethylstannyl)copper(I) reagent **1** are the preferred reagents. Thus far, most of our work has employed reagents **1** and **2**.

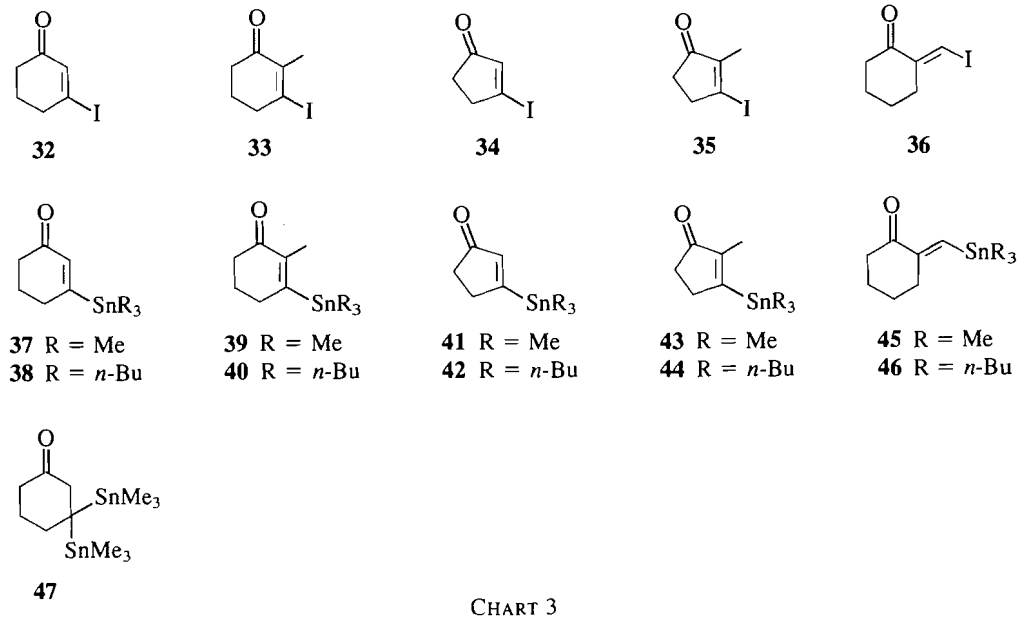

CHART 3

TABLE 3. Preparation of β-trialkylstannyl α,β-unsaturated ketones

Entry	Substrate	Reagent (equiv.)	Reaction conditions[a]	Product (yield, %)[b]
1	**32**	**2** (1.1)	A	**37** (86)
2	**32**	**6** (1.1)	A	**38** (81)
3	**33**	**2** (1.1)	A	**39** (84)
4	**33**	**6** (1.3)	A	**40** (79)
5	**34**	**2** (1.1)	A	**41** (83)
6	**34**	**6** (1.1)	A	**42** (76)
7	**35**	**2** (1.1)	A	**43** (82)
8	**35**	**6** (1.3)	A	**44** (79)
9	**36**	**2** (1.3)	A	**45** (77)
10	**36**	**6** (1.1)	A	**46** (69)
11	**32**	**1** (1.3)	B	**37** (84)
12	**34**	**1** (1.3)	B	**41** (80)
13	**35**	**1** (1.3)	B[c]	**43** (82)
14	**36**	**1** (1.3)	C	**45** (75)

[a]A: THF, −20°C, 15 min; room temperature, 30 min. B: THF, −48°C, 2 h; −20°C, 1 h; room temperature, 1 h. C: THF, −48°C, 2 h.

[b]Yields refer to isolated, purified products.

[c]In this reaction, HMPA was added to the reaction mixture prior to addition of the β-iodo enone **35**.

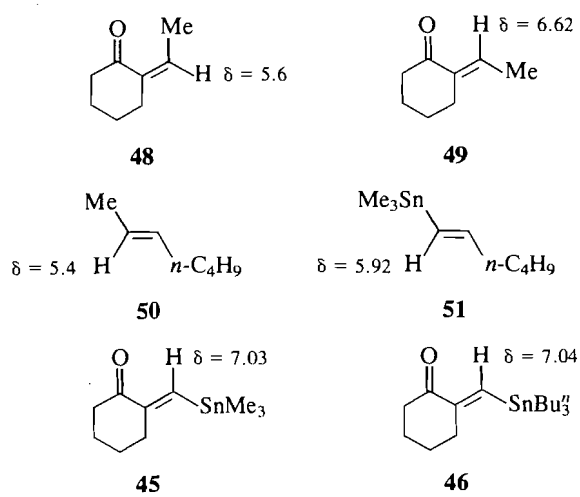

CHART 4

TABLE 4. Longest wavelength π→π* ultraviolet absorption bands of β-trialkylstannyl α,β-unsaturated ketones (methanol solution)

Entry	Compound	λ_{max}, nm (ε)
β-Trimethylstannyl α,β-unsaturated ketones		
1	**37**	236 (12 000)
2	**39**	250 (14 300)
3	**41**	233 (15 200)
4	**43**	242 (15 800)
5	**45**	246 (8 300)
β-Tri-*n*-butylstannyl α,β-unsaturated ketones		
6	**38**	242 (10 900)
7	**40**	256 (12 000)
8	**42**	235 (12 100)
9	**44**	246 (13 200)
10	**46**	250 (7 400)

(d) Ultraviolet spectra of β-trialkylstannyl α,β-unsaturated ketones

Prior to the work described herein, cyclic β-trialkylstannyl α,β-unsaturated ketones were unknown. Therefore, it was of interest to record the ultraviolet spectra of compounds **37**–**46** to determine the effect of β R_3Sn groups on the position of the longest wavelength π→π* absorption band of the enone system. The data are recorded in Table 4.

The π→π absorption maxima of the "parent" enones 2-cyclohexen-1-one, 2-cyclopenten-1-one, and 2-(methylene)cyclohexanone appear at 226, 218, and 231 nm, respectively. The data given in Table 4 show that a β Me_3Sn group causes a significant bathochromic shift (10–15 nm) in the position of the absorption maxima (Entries 1, 3, 5). As expected (19), introduction of an α methyl group results in a further shift to longer wavelengths (Entries 2,4). Similar trends are seen with β-tri-*n*-butylstannyl enones, although the bathochromic shifts (16–19 nm, Entries 6,8,10) associated with the *n*-Bu_3Sn group are consistently larger than those related to the Me_3Sn group. Finally, it is interesting to note that the molar absorptivities of the β-trimethylstannyl enones are consistently greater than those of the tri-*n*-butylstannyl analogs.

Can. J. Chem. Downloaded from www.nrcresearchpress.com by 190.90.36.8 on 09/07/12
For personal use only.

Can. J. Chem. Downloaded from www.nrcresearchpress.com by 190.90.36.8 on 09/07/12
For personal use only.

Experimental

General information

Melting points and distillation temperatures, which refer to short path (Kugelrohr) distillations, are uncorrected. Ultraviolet (uv) spectra were measured with a Cary 15 spectrophotometer. Infrared (ir) spectra were recorded on Perkin Elmer models 710 or 710B spectrophotometers and were calibrated using the 1601 cm^{-1} band of polystyrene film. Proton nuclear magnetic resonance (^1H nmr) spectra were recorded at 80 MHz (Bruker WP-80 spectrometer) or at 100 MHz (Varian Associates HA-100 or XL-100 spectrometers). Signal positions are given in δ units and were measured relative to the chloroform signal (δ 7.25). The tin–proton coupling constants (J_{Sn-H}) are given as an average of the ^{117}Sn and ^{119}Sn values. High resolution mass spectra were recorded with Kratos/AEI MS50 or MS 902 mass spectrometers. For compounds containing trialkylstannyl groups, molecular mass measurements were based on ^{120}Sn. Microanalyses were performed in the Microanalytical Laboratory of the University of British Columbia.

Note: All reactions described below were carried out under an atmosphere of dry argon in carefully dried glassware.

Trimethylstannyl-lithium

To a cold (−20°C), stirred solution of hexamethylditin in dry THF (~10 mL per mmol of $Me_3Sn–SnMe_3$) was added a solution of methyl-lithium (1.0 equiv.) in ether. The mixture was stirred at −20°C for 15 min to afford a pale yellow solution of trimethylstannyl-lithium.

Tri-n-butylstannyl-lithium

To a cold (0°C), stirred solution of hexa-*n*-butylditin in dry THF (~10 mL per mmol of the ditin) was added a solution of *n*-butyl-lithium (1.0 equiv.) in hexane. The mixture was stirred at 0°C for 15 min to afford a yellow solution of tri-*n*-butylstannyl-lithium.

Lithium (phenylthio)(trimethylstannyl)cuprate (2)

To a cold (−20°C), stirred solution of trimethylstannyl-lithium (0.75 mmol) in 10 mL of dry THF was added in one portion solid phenylthiocopper(I) (132 mg, 0.75 mmol). The slurry was stirred at −20°C for 15 min to afford a dark red solution of the cuprate reagent **2**.

Lithium (phenylthio)(tri-n-butylstannyl)cuprate (6)

To a cold (−20°C), stirred solution of tri-*n*-butylstannyl-lithium (0.55 mmol) in 7 mL of dry THF was added in one portion solid phenylthiocopper(I) (97 mg, 0.55 mmol). The mixture was stirred at −20°C for 15 min to produce a dark red solution of the cuprate reagent **6**.

Lithium bis(trimethylstannyl)cuprate (3)

To a cold (−48°C), stirred solution of trimethylstannyl-lithium (1.1 mmol) in 10 mL of dry THF was added in one portion solid cuprous bromide – dimethyl sulfide complex (117 mg, 0.55 mmol). The mixture was stirred at −48°C for 20 min to afford a dark red solution of the cuprate reagent **3**.

Lithium (3-methoxy-3-methyl-1-butynyl)(trimethylstannyl)cuprate (4)

To a cold (−48°C), stirred solution of trimethylstannyl-lithium (0.39 mmol) in 5 mL of dry THF was added, in one portion, solid (3-methoxy-3-methyl-1-butynyl)copper(I) (63 mg, 0.39 mmol). The mixture was stirred at −48°C for 15 min to afford a dark red solution of the cuprate reagent **4**.

Lithium (cyano)(trimethylstannyl)cuprate (5)

To a cold (−78°C), stirred solution of trimethylstannyl-lithium (0.39 mmol) in 5 mL of dry THF was added, in one portion, solid cuprous cyanide (35 mg, 0.39 mmol). The mixture was stirred at −78°C for 5 min and at −48°C for 15 min to afford a bright orange solution of the cuprate reagent **5**.

(Trimethylstannyl)copper(I)-dimethyl sulfide (1)

To a cold (−48°C), stirred solution of trimethylstannyl-lithium (0.65 mmol) in 5 mL of dry THF was added, in one portion, solid cuprous bromide – dimethyl sulfide complex (113 mg, 0.65 mmol). The mixture was stirred at −48°C for 10 min to give a dark red solution of the cuprate reagent **1**.

Preparation of β-trialkylstannyl ketones and esters

(a) General procedure A

To a cold (−20°C), stirred solution of lithium (phenylthio)(trimethylstannyl)cuprate (**2**) (1.1–2.0 equiv.) in dry THF (10 mL) was added a solution (THF, ~1 mL) of the appropriate α,β-unsaturated ketone or ester (0.58–1.5 mmol). The reaction mixture was stirred at −20°C for 15 min and at room temperature for 1 h. Methanol (~0.2 mL) and diethyl ether (~30 mL) were added and the mixture was stirred at room temperature for several minutes. The resulting yellow slurry was filtered through a short column of Florisil (10 g, 100–200 mesh). The column was eluted with 50 mL of diethyl ether. Removal of the solvent from the combined eluate, followed by bulb-to-bulb distillation of the residual oil, gave the product(s).

(b) General procedure B

To a cold (−78°C), stirred solution of lithium (phenylthio)(tri-*n*-butylstannyl)cuprate (**6**) (1.3–1.5 equiv.) in dry THF (10 mL) was added a solution (THF, ~1 mL) of the α,β-unsaturated ketone or ester (0.67–1.0 mmol). The reaction mixture was stirred at −78°C for 1 h, at −20°C for 1 h, and at room temperature for 1 h. Methanol (~0.2 mL) and diethyl ether (~30 mL) were added and work-up was carried out as described in procedure A, above. The crude, undistilled product was subjected to column chromatography on 20 g of silica gel. Elution of the column with 1:9 diethyl ether – petroleum ether gave initially a mixture of tetra-*n*-butylstannane and hexa-*n*-butylditin. Further elution, followed by concentration of the appropriate fractions and bulb-to-bulb distillation of the residue, afforded the product(s).

(c) General procedure C

To a cold (−78°C), stirred solution of trimethylstannyl-lithium (1.0–1.1 equiv.) in dry THF (10 mL) was added a solution (THF, ~1 mL) of the α,β-unsaturated ketone or ester (0.5–1.5 mmol). After the reaction mixture had been stirred at −78°C for the appropriate length of time, methanol (~0.5 mL) and diethyl ether (~30 mL) were added. The mixture was allowed to warm to room temperature and then was filtered through a column of Florisil (10 g, 100–200 mesh). The column was eluted with 50 mL of diethyl ether. Removal of the solvent from the combined eluate and bulb-to-bulb distillation of the residual oil gave the product(s).

4-Methyl-4-trimethylstannyl-2-pentanone (14)

Following general procedure A, 4-methyl-3-penten-2-one (**7**) (57 mg, 0.58 mmol) was allowed to react with 0.75 mmol of the cuprate reagent **2** in 11 mL of dry THF. Work-up and distillation (air-bath temperature 40–47°C/0.3 Torr (1 Torr = 133.3 Pa), receiver cooled to −78°C) afforded 116 mg (76%) of the ketone **14**. An analytical sample, prepared by preparative tlc on silica gel (developing solvent 2:98 diethyl ether – petroleum ether), exhibited ir (film): 1713, 765 cm^{-1}; ^1H nmr δ: −0.02 (s, 9H, J_{Sn-H} = 50 Hz), 1.06 (s, 6H, J_{Sn-H} = 62 Hz), 2.10 (s, 3H), 2.49 (s, 2H, J_{Sn-H} = 66 Hz). *Anal.* calcd. for $C_9H_{20}OSn$: C 41.11, H 7.67; found: C 41.10, H 7.70. *Exact Mass* calcd. (M^+ −15): 249.0301; found: 249.0288.

4-Methyl-4-tri-n-butylstannyl-2-pentanone (15)

Following general procedure B, 4-methyl-3-penten-2-one (**7**) (66 mg, 0.67 mmol) was allowed to react with 1.0 mmol of the cuprate reagent **6** in 11 mL of dry THF. Work-up, followed by column chromatography of the crude product and distillation (air-bath temperature 120–128°C/0.2 Torr) of the oil obtained from the appropriate fractions, gave 181 mg (69%) of the ketone **15**. An analytical sample, obtained by preparative tlc on silica gel (developing solvent 2:98 diethyl ether – petroleum ether), exhibited ir (film): 1718 cm^{-1}; ^1H nmr δ: 0.62–1.64 (m, 27H), 1.04 (s, 6H), 2.03 (s, 3H), 2.44 (s, 2H, J_{Sn-H} = 64 Hz). *Anal.* calcd. for $C_{18}H_{38}OSn$: C 55.55, H 9.84; found: C 55.66, H 9.74.

3-Trimethylstannylcyclohexanone (16)

(a) Via general procedure A

2-Cyclohexen-1-one (**8**) (66 mg, 0.68 mmol) was allowed to react with 1.36 mmol of the cuprate reagent **2** in 11 mL of dry THF. Work-up, followed by distillation (air-bath temperature 75–90°C/0.2 Torr) of the crude product, gave 162 mg (92%) of the ketone **16** (one spot by tlc and one peak by glc). This material exhibited ir (film):

1712, 770 cm^{-1}; ^1H nmr δ: −0.02 (s, 9H, J_{Sn-H} = 51 Hz), 1.40–2.15 (m, 5H), 2.15–2.54 (m, 4H). *Exact Mass* calcd. for $C_9H_{18}OSn$: 262.0380; found: 262.0394.

(b) Via reaction of 2-cyclohexen-1-one (8) with (trimethylstannyl)copper(I)-dimethyl sulfide (1)

To a cold (−48°C), stirred solution of the copper reagent **1** (0.65 mmol) in 5 mL of dry THF was added a solution of the enone **8** (48 mg, 0.50 mmol) in dry THF (0.5 mL). The reaction mixture was stirred at −48°C for 2 h, at −20°C for 1 h, and at room temperature for 1 h. Saturated aqueous ammonium chloride (pH 8, 5 mL) and diethyl ether were added and the mixture was stirred for several minutes. The layers were separated and the organic phase was washed with saturated aqueous ammonium chloride (pH 8) and dried ($MgSO_4$). Removal of the solvent gave a yellow oil that, on the basis of glc analysis, consisted of a mixture (~1:1) of 3-trimethylstannylcyclohexanone (**16**) and 2-(3-ketocyclohexyl)-3-trimethylstannylcyclohexanone (**25**). These substances were separated by distillation. Ketone **16** (42 mg, 32%) exhibited spectral data identical with those given above.

The diketone **25** (43 mg, 48%; distillation temperature 148–159°C/0.09 Torr) exhibited ir (film): 1705, 775 cm^{-1}; ^1H nmr δ: 0.02 (s, 9H, J_{Sn-H} = 51 Hz), 1.30–2.66 (br diffuse m, 17H). *Exact Mass* calcd. for $C_{15}H_{26}O_2Sn$: 358.0955; found: 358.0964.

3-Tri-n-butylstannylcyclohexanone (17)

Reaction of 2-cyclohexen-1-one (**8**) (64 mg, 0.67 mmol) with the cuprate reagent **6** (1.0 mmol) in 11 mL of dry THF was carried out via general procedure B. Work-up, followed by column chromatography of the crude product and distillation (air-bath temperature 165–169°C/0.2 Torr) of the desired material, gave 202 mg (78%) of the ketone **17**; ir (film): 1710 cm^{-1}; ^1H nmr δ: 0.76–1.02 (m, 15H), 1.08–2.08 (m, 17H), 2.08–2.48 (m, 4H). *Exact Mass* calcd. for $C_{18}H_{36}OSn$: 388.1786; found: 388.1791.

3,5,5-Trimethyl-3-trimethylstannylcyclohexanone (18)

Following general procedure A, 3,5,5-trimethyl-2-cyclohexen-1-one (**9**) (94 mg, 0.68 mmol) was allowed to react with the cuprate reagent **2** (1.36 mmol) in 11 mL of dry THF. Work-up afforded a yellow oil, which consisted (glc analysis) of the starting material **9** and the β-trimethylstannyl ketone **18** in a ratio of 7:93, respectively. Distillation (air-bath temperature 80–93°C/0.06 Torr) afforded 52 mg (69%) of the ketone **18** (homogeneous by tlc and glc analyses); ir (film): 1712, 750 cm^{-1}; ^1H nmr δ: 0.07 (s, 9H, J_{Sn-H} = 49 Hz), 1.00, 1.07 (s, s, 3H each), 1.28 (s, 3H, J_{Sn-H} = 64 Hz), 1.59 (d, 1H, J = 15 Hz), 1.91 (d, 1H, J = 15 Hz), 2.11–2.18 (unresolved m, 3H), 2.54 (d, 1H, J = 14 Hz). *Exact Mass* calcd. for $C_{12}H_{24}OSn$: 304.0849; found: 304.0870.

3,5,5-Trimethyl-3-tri-n-butylstannylcyclohexanone (19)

This compound was prepared, via general procedure B, by reaction of the enone **9** (92 mg, 0.67 mmol) with 1.0 mmol of the cuprate reagent **6** in 11 mL of dry THF. Work-up, column chromatography of the crude product, and distillation (air-bath temperature 169–177°C/0.2 Torr) of the desired material yielded 185 mg (64%) of the ketone **19**. The later substance was homogeneous by tlc and glc analyses and exhibited ir (film): 1711 cm^{-1}; ^1H nmr δ: 0.81–0.97 (m, 15H) 1.01, 1.06, 1.34 (s, s, s, 3H each), 1.20–1.56 (m, 12H), 1.64 (d, 1H, J = 13 Hz), 1.98 (d, 1H, J = 13 Hz), 2.10–2.38 (m, 3H), 2.61 (d, 1H, J = 13 Hz). *Exact Mass* calcd. for $C_{21}H_{42}OSn$: 430.2258; found: 430.2264.

4-Trimethylstannyl-2-butanone (28)

(a) Via general procedure C

Following general procedure C, 3-buten-2-one (**26**) (70 mg, 1 mmol) was allowed to react with 1.0 mmol of trimethylstannyl-lithium in 11 mL of THF at −78°C for 1 h. Work-up afforded a yellow oil, which was subjected to column chromatography on 2.7 g of silica gel. Elution of the column with petroleum ether (~10 mL) gave hexamethylditin. Further elution with diethyl ether (~12 mL) provided a colorless oil, which, on the basis of a glc analysis, consisted of a mixture of the ketone **28** and the diketone **30** in a ratio of about 3:1, respectively.

Distillation (air-bath temperature 98–110°C/35 Torr) of the oil afforded 102 mg (43%) of the ketone **28**; ir (film): 1710, 767 cm^{-1}; ^1H nmr δ: −0.02 (s, 9H, J_{Sn-H} = 52 Hz), 0.83 (t, 2H, J = 7.5 Hz, J_{Sn-H} = 54 Hz), 2.08 (s, 3H), 2.60 (t, 2H, J = 7.5 Hz, J_{Sn-H} = 58 Hz). *Anal.* calcd. for $C_7H_{16}OSn$: C 35.79, H 6.87; found: C 35.78, H 6.95.

Distillation (air-bath temperature 110–120°C/0.35 Torr) of the remaining oil gave 47 mg (31%) of the diketone **30**; ir (film): 1708, 770 cm^{-1}; ^1H nmr δ: 0.06 (s, 9H, J_{Sn-H} = 52 Hz), 0.81 (dd, 1H, J = 13, 8 Hz), 0.98 (dd, 1H, J = 13, 7 Hz), 1.54–1.96 (m, 2H), 2.09, 2.11 (s, s, 3H each), 2.34–2.37 (m, 2H), 2.49–2.64 (m, 1H). *Anal.* calcd. for $C_{11}H_{22}O_2Sn$: C 43.32, H 7.27; found: C 43.36, H 7.30.

(b) Via reaction of 3-buten-2-one with the cuprate reagent 2

To a cold (−78°C), stirred solution of the cuprate reagent **2** (2.0 mmol) in 10 mL of dry THF was added a solution of 3-buten-2-one (**26**) (105 mg, 1.5 mmol) in dry THF (1 mL). The red solution was stirred at −78°C for 30 min, at −20°C for 1 h, and at room temperature for 30 min. Saturated aqueous ammonium chloride (0.2 mL) and diethyl ether (30 mL) were added. Further work-up as described in general procedure A, followed by column chromatography of the residual oil as described in (*a*), above, gave a colorless oil. Analysis (glc) of this material showed that it consisted of a mixture of the ketone **28** and the diketone **30**, in a ratio of about 2:1, respectively. Separation of these substances by distillation gave 96 mg (27%) of **28** and 85 mg (37%) of **30**. The spectral properties of these compounds were identical with those reported above.

(c) Via reaction of 3-buten-2-one with the cuprate reagent 2 in the presence of acetic acid

To a cold (−78°C), stirred solution of the cuprate reagent **2** (2.0 mmol) in 10 mL of dry THF was added, dropwise, a solution of 3-buten-2-one (**26**) (105 mg, 1.5 mmol) and glacial acetic acid (120 mg, 2.0 mmol) in dry THF (1 mL). The red solution was stirred at −78°C for 30 min and at −20°C for 1 h. The cooling bath was removed and, after 20 min, saturated aqueous ammonium chloride (0.2 mL) and diethyl ether (30 mL) were added. Further work-up (see general procedure A) and column chromatography of the crude material on silica gel as described in (*a*), above, afforded a colorless oil. This material consisted of a mixture of the ketone **28** and the diketone **30** in a ratio of 97:3, respectively. Distillation (air-bath temperature 90–100°C/30 Torr) provided 271 mg (77%) of 4-trimethylstannyl-2-butanone (**28**). The spectral properties of this material were identical with those reported above.

Methyl 3-trimethylstannylbutanoate (20)

(a) Via general procedure A

Following general procedure A, methyl (*E*)-2-butenoate (**10**) (68 mg, 0.68 mmol) was allowed to react with the cuprate reagent **2** (0.75 mmol) in 11 mL of dry THF. Work-up and distillation (air-bath temperature 41–50°C/0.2 Torr; receiver cooled to −78°C) of the crude product gave 122 mg (67%) of the ester **20**, which exhibited ir (film): 1738, 1202, 770 cm^{-1}; ^1H nmr δ: 0.02 (s, 9H, J_{Sn-H} = 51 Hz), 1.17 (d, 3H, J = 7 Hz, J_{Sn-H} = 68 Hz), 1.30–1.62 (m, 1H), 2.50 (d, 2H, J = 7 Hz), 3.66 (s, 3H). *Anal.* calcd. for $C_8H_{18}O_2Sn$: C 36.27, H 6.85; found: C 36.64, H 6.94.

(b) Via general procedure C

Reaction of methyl (*E*)-2-butenoate (**10**) (68 mg, 0.68 mmol) with 0.75 mmol of trimethylstannyl-lithium in 11 mL of dry THF for 5 min (general procedure C), followed by work-up and bulb-to-bulb distillation of the crude product, gave 108 mg (71%) of the ester **20**. The spectral properties of this material were identical with those given above.

Methyl 3-tri-n-butylstannylbutanoate (21)

Following general procedure B, methyl (*E*)-2-butenoate (**10**) (100 mg, 1 mmol) was allowed to react with 1.3 mmol of the cuprate reagent **6** in 11 mL of dry THF. Work-up, followed by column chromatography of the crude product and distillation (air-bath temperature 110–115°C/0.25 Torr) of the desired material, afforded 287 mg (74%) of the ester **21**. An analytical sample, obtained by preparative tlc on silica gel (developing solvent 2:98 diethyl ether – petroleum ether),

Can. J. Chem. Downloaded from www.nrcresearchpress.com by 190.90.36.8 on 09/07/12
For personal use only.

Can. J. Chem. Downloaded from www.nrcresearchpress.com by 190.90.36.8 on 09/07/12
For personal use only.

exhibited ir (film): 1738, 1200 cm^{-1}; ^1H nmr δ: 0.81–0.95 (m, 15H), 1.21 (d, 3H, J = 7 Hz, J_{Sn-H} = 60 Hz), 1.26–1.37 and 1.41–1.53 (m, m, 12H), 1.57–1.68 (m, 1H), 2.45 (dd, 1H, J = 15, 9 Hz), 2.55 (dd, 1H, J = 15, 7 Hz), 3.69 (s, 3H). *Anal.* calcd. for $C_{17}H_{36}O_2Sn$: C 52.20, H 9.28; found: C 52.46, H 9.21.

Ethyl 3-methyl-3-trimethylstannyl-2-butenoate (22)

Following general procedure C, ethyl 3-methyl-2-butenoate (**11**) (87 mg, 0.68 mmol) was allowed to react with trimethylstannyl-lithium (0.75 mmol) in 11 mL of dry THF at −78°C for 15 min. Work-up and distillation (air-bath temperature 115–123°C/25 Torr) of the crude product gave 147 mg (74%) of the ester **22**, which exhibited ir (film): 1733, 760 cm^{-1}; ^1H nmr δ: 0.01 (s, 9H, J_{Sn-H} = 50 Hz), 1.12 (s, 6H, J_{Sn-H} = 61 Hz), 1.24 (t, 3H, J = 7 Hz), 2.32 (s, 2H, J_{Sn-H} = 67 Hz), 4.11 (q, 2H, J = 7 Hz). *Exact Mass* calcd. for $C_{10}H_{22}O_2Sn$: 282.9781; found: 282.9792.

Ketal ester 24

Following general procedure C, the α,β-unsaturated ester **13** (134 mg, 0.5 mmol) was allowed to react with 0.53 mmol of trimethylstannyl-lithium in 11 mL of dry THF at −78°C for 15 min. Work-up and distillation (air-bath temperature 130–150°C/0.07 Torr) of the crude product gave 162 mg (75%) of the ketal ester **24**, which exhibited ir (film): 1730, 1097, 758 cm^{-1}; ^1H nmr δ: 0.03 (s, 9H, J_{Sn-H} = 60 Hz), 0.94 (s, 6H), 1.21 (t, 3H, J = 7 Hz), 1.42–2.04 (diffuse m, 8H), 2.49 (s, 2H, J_{Sn-H} = 74 Hz), 4.08 (q, 2H, J = 7 Hz). *Exact Mass* calcd. for $C_{18}H_{34}O_4Sn$: 434.1479; found: 434.1495.

Ethyl 3-trimethylstannylpropanoate (29)

(a) Via general procedure C

Ethyl propenoate (**27**) (150 mg, 1.5 mmol) was allowed to react with 1.5 mmol of trimethylstannyl-lithium in 11 mL of dry THF at −78°C for 1 h. Work-up gave a yellow oil, which was subjected to column chromatography on 2.7 g of silica gel. Elution with petroleum ether (10 mL) gave hexamethylditin. Further elution with diethyl ether (12 mL) produced a colorless oil, which was shown (glc analysis) to consist of a mixture of the ester **29** and the diester **31** in a ratio of about 3:2, respectively.

Distillation (air-bath temperature 100–118°C/30 Torr) of the oil afforded 80 mg (20%) of the ester **29**, which exhibited ir (film): 1732, 775 cm^{-1}; ^1H nmr δ: 0.01 (s, 9H, J_{Sn-H} = 52 Hz), 0.95 (t, 2H, J = 8 Hz), 1.21 (t, 3H, J = 7 Hz), 2.47 (t, 2H, J = 8 Hz, J_{Sn-H} = 59 Hz), 4.12 (q, 2H, J = 7 Hz). *Anal.* calcd. for $C_8H_{18}O_2Sn$: C 36.27, H 6.85; found: C 36.56, H 6.81.

Distillation (air-bath temperature 100–118°C/0.3 Torr) of the remaining oil produced 81 mg (29%) of the diester **31**, which exhibited ir (film): 1727, 772 cm^{-1}; ^1H nmr δ: 0.03 (s, 9H, J_{Sn-H} = 53 Hz), 0.93–1.06 (m, 2H), 1.21 (t, 6H, J = 7 Hz), 1.63–2.03 (m, 2H), 2.08–2.43 (m, 2H), 2.43–2.73 (m, 1H), 4.09 (q, 4H, J = 7 Hz). *Anal.* calcd. for $C_{13}H_{26}O_4Sn$: C 42.77, H 7.18; found: C 42.41, H 7.03.

(b) Via reaction of ethyl propenoate (27) with the cuprate reagent 2 in the presence of acetic acid

To a cold (−78°C), stirred solution of the cuprate reagent **2** (2 mmol) in 10 mL of dry THF was added, dropwise, a solution of ethyl propenoate (**27**) (50 mg, 0.5 mmol) and glacial acetic acid (60 mg, 1.0 mmol) in dry THF (1 mL). The red mixture was stirred at −78°C for 30 min and at −20°C for 1 h. After removal of the cooling bath, the mixture was stirred for 30 min and then was treated with saturated aqueous ammonium chloride (0.2 mL) and diethyl ether (30 mL). Work-up as described in general procedure A, followed by column chromatography of the crude product as described in (*a*), above, gave a colorless oil. Analysis (glc) of this material showed that it was composed of a mixture of the ester **29** and the diester **31** in a ratio of 93:7, respectively. Distillation (air-bath temperature 105–110°C/38 Torr) of the oil provided 92 mg (70%) of the ester **29**, which exhibited spectral data identical with those reported above.

Preparation of β-trialkylstannyl α,β-unsaturated ketones

(a) General procedure D

To a cold (−20°C), stirred solution of the cuprate reagent **2** (0.75 mmol) in 10 mL of dry THF was added a solution of the appropriate β-iodo α,β-unsaturated ketone (0.57–0.68 mmol) in 1 mL of dry THF. The dark red mixture was stirred at −20°C for 15 min and at room temperature for 30 min. Methanol (0.2 mL) and diethyl ether (30 mL) were added and the mixture was stirred for several minutes. The resulting yellow slurry was filtered through a short column of Florisil (10 g, 100–120 mesh). The column was eluted with 50 mL of diethyl ether. Removal of the solvent from the combined eluate, followed by bulb-to-bulb distillation of the residual oil, gave the desired β-trimethylstannyl enone.

(b) General procedure E

To a cold (−48°C), stirred solution of (trimethylstannylcopper(I)-dimethylsulfide (**1**) (0.65 mmol) in 5 mL of dry THF was added a solution of the appropriate β-iodo α,β-unsaturated ketone (0.5 mmol) in 0.5 mL of dry THF. The dark red solution was stirred at −48°C for 2 h, at −20°C for 1 h, and at room temperature for 1 h. Saturated aqueous ammonium chloride (pH 8, 5 mL) and diethyl ether (30 mL) were added and the mixture was stirred for several minutes. The organic layer was separated, washed with saturated aqueous ammonium chloride, and dried ($MgSO_4$). Removal of the solvent, followed by bulb-to-bulb distillation of the crude product, gave the desired β-trimethylstannyl enone.

(c) General procedure F

To a cold (−20°C), stirred solution of the cuprate reagent **6** (0.55–0.65 mmol) in 10 mL of dry THF was added a solution of the appropriate β-iodo α,β-unsaturated ketone (0.5 mmol) in 0.5 mL of dry THF. The mixture was stirred at −20°C for 15 min and at room temperature for 30 min. Methanol (0.2 mL) and diethyl ether (30 mL) were added and the mixture was stirred at room temperature for several minutes. The yellow slurry was filtered through a short column of Florisil (10 g, 100–200 mesh) and the column was eluted with a further 50 mL of diethyl ether. Removal of the solvent from the combined eluate gave a yellow oil, which was subjected to column chromatography on 20 g of silica gel. Elution of the column with a 1:9 mixture of diethyl ether – petroleum ether gave initially a mixture of tetra-*n*-butyltin and hexa-*n*-butylditin and then the desired β-tri-*n*-butylstannyl enone. Distillation (air-bath) of this material provided the pure product.

3-Trimethylstannyl-2-cyclohexen-1-one (37)

(a) Via reaction of the β-iodo enone 32 with trimethylstannyl-lithium

To a cold (−78°C), stirred solution of trimethylstannyl-lithium (0.5 mmol) in 10 mL of dry THF was added a solution of 3-iodo-2-cyclohexen-1-one (**32**) (111 mg, 0.5 mmol) in 0.25 mL of dry THF. The orange solution was stirred at −78°C for 1 h. Saturated aqueous ammonium chloride (5 mL) and diethyl ether (30 mL) were added and the mixture was allowed to warm to room temperature. The organic layer was separated, washed with brine, and dried ($MgSO_4$). Removal of the solvent, followed by distillation (air-bath temperature 65–69°C/0.15 Torr) of the residual oil, afforded a mixture (100 mg) that, on the basis of a glc analysis, was composed of the starting material **32** (~42%), 3-trimethylstannyl-2-cyclohexen-1-one (**37**) (~32%), and 3,3-bis(trimethylstannyl)cyclohexanone (**47**) (~15%), along with minor unidentified substances. A pure sample of each of the major components was obtained by preparative glc.

The enone **37** exhibited ir (film): 1670, 1582, 766 cm^{-1}; ^1H nmr δ: 0.17 (s, 9H, J_{Sn-H} = 54 Hz), 1.82–2.14 (m, 2H), 2.28–2.66 (m, 4H), 6.22 (t, 1H, J = 2 Hz, J_{Sn-H} = 64 Hz). *Anal.* calcd. for $C_9H_{16}OSn$: C 41.75, H 6.23; found: C 41.75, H 6.22. *Exact Mass* calcd.: 260.0223; found: 260.0216.

The ketone **47** exhibited mp 50–51°C; ir ($CHCl_3$): 1701 cm^{-1}; ^1H nmr δ: 0.04 (s, 18H, J_{Sn-H} = 49 Hz), 1.76–2.18 (m, 4H), 2.18–2.46 (m, 2H), 2.67 (br s, 2H). *Anal.* calcd. for $C_{12}H_{26}OSn_2$: C 34.02, H 6.19; found: C 34.08, H 6.26.

(b) Via general procedure D

Following general procedure D, the cuprate reagent **2** (0.75 mmol) was allowed to react with the β-iodo enone **32** (151 mg, 0.68 mmol) in 11 mL of dry THF. Work-up and distillation (air-bath temperature 65–80°C/0.09 Torr) of the crude product provided 153 mg (86%) of

Can. J. Chem. Downloaded from www.nrcresearchpress.com by 190.90.36.8 on 09/07/12
For personal use only.

the β-trimethylstannyl enone **37**, which showed spectral data identical with those given above.

(c) Via general procedure E

Following general procedure E, 0.65 mmol of the (trimethylstannyl-copper(I) reagent **1** was allowed to react with the β-iodo enone **32** (111 mg, 0.5 mmol) in 5.5 mL of dry THF. Work-up and distillation (air-bath temperature 71–79°C/0.1 Torr) of the crude product gave 129 mg (84%) of the enone **37**.

*3-Tri-*n*-butylstannyl-2-cyclohexen-1-one (38)*

Following general procedure F, the cuprate reagent **6** (0.55 mmol) was allowed to react with the β-iodo enone **32** (111 mg, 0.5 mmol) in 10.5 mL of dry THF. Work-up, followed by column chromatography of the crude product on silica gel and distillation (air-bath temperature 150–158°C/0.2 Torr) of the desired crude product, afforded 157 mg (81%) of the enone **38**. This material exhibited ir (film): 1672, 1575 cm^{-1}; ^1H nmr δ: 0.78–1.05 (m, 15H), 1.08–1.70 (m, 12H), 1.82–2.14 (m, 2H), 2.30–2.60 (m, 4H), 6.22 (t, 1H, J = 2 Hz, J_{Sn-H} = 57 Hz). *Anal.* calcd. for $C_{18}H_{34}OSn$: C 56.13, H 8.90; found: C 56.22, H 9.00. *Exact Mass* calcd.: 386.1632; found: 386.1632.

2-Methyl-3-trimethylstannyl-2-cyclohexen-1-one (39)

Following general procedure D, 0.75 mmol of the cuprate reagent **2** was allowed to react with the β-iodo enone **33** (160 mg, 0.68 mmol) in 11 mL of dry THF. Work-up and distillation (air-bath temperature 58–69°C/0.07 Torr) of the resultant crude product yielded 158 mg (84%) of the β-trimethylstannyl enone **39**, which exhibited ir (film): 1665, 1595, 760 cm^{-1}; ^1H nmr δ: 0.22 (s, 9H, J_{Sn-H} = 54 Hz), 1.78–2.08 (m, 2H), 1.86 (t, 3H, J = 1.8 Hz), 2.32–2.56 (m, 4H). *Exact Mass* calcd. for $C_{10}H_{18}OSn$: 274.0378; found: 274.0374.

*2-Methyl-3-tri-*n*-butylstannyl-2-cyclohexen-1-one (40)*

Following general procedure F, the cuprate reagent **6** (0.65 mmol) was allowed to react with the β-iodo enone **33** (118 mg, 0.5 mmol) in 10.5 mL of dry THF. Work-up, column chromatography of the crude product on silica gel, and distillation (air-bath temperature 160–163°C/0.2 Torr) of the oil thus obtained gave 157 mg (79%) of the β-tri-*n*-butylstannyl enone **40**. This material exhibited ir (film): 1677, 1590 cm^{-1}; ^1H nmr δ: 0.75–1.09 (m, 15H), 1.11–1.63 (m, 12H), 1.88 (t, 3H, J = 2 Hz), 1.72–2.14 (m, 2H), 2.28–2.62 (m, 4H). *Exact Mass* calcd. for $C_{19}H_{36}OSn$: 400.1788; found: 400.1801.

3-Trimethylstannyl-2-cyclopenten-1-one (41)

(a) Via general procedure D

The cuprate reagent **2** (0.75 mmol) was allowed to react with the β-iodo enone **34** (141 mg, 0.68 mmol) in 11 mL of dry THF. Work-up and distillation (air-bath temperature 60–72°C/0.17 Torr) of the crude product gave 138 mg (83%) of the β-trimethylstannyl enone **41**, which exhibited ir (film): 1685, 1558, 762 cm^{-1}; ^1H nmr δ: 0.25 (s, 9H, J_{Sn-H} = 56 Hz), 2.23–2.35 (m, 2H), 2.73–2.90 (m, 2H), 6.37 (t, 1H, J = 2.3 Hz, J_{Sn-H} = 33 Hz). *Exact Mass* calcd. for $C_8H_{14}OSn$: 247.0145; found: 247.0143.

(b) Via general procedure E

Reaction of the (trimethylstannyl)copper(I) reagent **1** (0.65 mmol) with the β-iodo enone **34** (104 mg, 0.50 mmol) in 5.5 mL of dry THF, followed by work-up and distillation (air-bath temperature 65–71°C/0.15 Torr) of the crude product, provided 98 mg (80%) of the enone **41**. The spectral properties of this material were identical with those given above.

*3-Tri-*n*-butylstannyl-2-cyclopenten-1-one (42)*

Following general procedure F, the cuprate reagent **6** (0.55 mmol) was allowed to react with the β-iodo enone **34** (104 mg, 0.5 mmol) in 10.5 mL of dry THF. Work-up, column chromatography of the crude product on silica gel, and distillation (air-bath temperature 150–154°C/0.2 Torr) of the desired material gave 141 mg (76%) of the enone **42**. This material exhibited ir (film): 1705, 1555 cm^{-1}; ^1H nmr δ: 0.76–1.18 (m, 15H), 1.18–1.72 (m, 12H), 2.24–2.39 (m, 2H), 2.76–2.96 (m, 2H), 6.40 (t, 1H, J = 2 Hz), J_{Sn-H} = 29 Hz). *Anal.* calcd. for $C_{17}H_{32}OSn$: C 55.02, H 8.69; found: C 54.79, H 8.70. *Exact Mass* calcd.: 372.1475; found: 372.1488.

2-Methyl-3-trimethylstannyl-2-cyclopenten-1-one (43)

(a) Via general procedure D

The cuprate reagent **2** (0.75 mmol) was allowed to react with the β-iodo enone **35** (151 mg, 0.68 mmol) in 11 mL of dry THF. Work-up and distillation (air-bath temperature 65–73°C/0.2 Torr) of the crude oil produced 144 mg (82%) of the β-trimethylstannyl enone **43**, which exhibited ir (film): 1690, 1601, 765 cm^{-1}; ^1H nmr δ: 0.26 (s, 9H, J_{Sn-H} = 56 Hz), 1.83 (t, 3H, J = 2 Hz), 2.28–2.40 (m, 2H), 2.56–2.76 (m, 2H). *Exact Mass* calcd. for $C_9H_{16}OSn$: 260.0224; found: 260.0234.

(b) Via reaction of the β-iodo enone 35 with (trimethylstannyl)copper(I)-dimethyl sulfide (1)

To a cold (−48°C), stirred solution of the (trimethylstannyl)copper(I) reagent **1** (0.65 mmol) in 5 mL of dry THF was added, sequentially, hexamethylphosphoramide (2 mL) and a solution of the β-iodo enone (111 mg, 0.50 mmol). The red solution was stirred at −48°C for 2 h, at −20°C for 1 h, and at room temperature for 1 h. Work-up as described in general procedure E, followed by distillation (air-bath temperature 63–75°C/0.2 Torr) of the crude product, provided 105 mg (82%) of the β-trimethylstannyl enone **43**. The spectra of this material were identical with those summarized above.

*2-Methyl-3-tri-*n*-butylstannyl-2-cyclopenten-1-one (44)*

Following general procedure F, 0.65 mmol of the cuprate reagent **6** was allowed to react with the β-iodo enone **35** (110 mg, 0.5 mmol) in 10.5 mL of dry THF. Work-up, followed by column chromatography of the crude product on silica gel and distillation (air-bath temperature 158–164°C/0.2 Torr) of the oil thus obtained, yielded 152 mg (79%) of the enone **44**. This material exhibited ir (film): 1702 cm^{-1}; ^1H nmr δ: 0.70–1.18 (m, 15H), 1.18–1.67 (m, 12H), 1.84 (t, 3H, J = 2 Hz), 2.28–2.42 (m, 2H), 2.58–2.80 (m, 2H). *Anal.* calcd. for $C_{18}H_{34}OSn$: C 56.13, H 8.90; found: C 56.37, H 9.00. *Exact Mass* calcd.: 386.1632; found: 386.1609.

(E)-*2-(Trimethylstannylmethylene)cyclohexanone (45)*

(a) Via general procedure D

The cuprate reagent **2** (0.75 mmol) was allowed to react with the β-iodo enone **36** (134 mg, 0.57 mmol) in 11 mL of dry THF. Work-up produced a red oil, which was purified by preparative tlc on silica gel (developing solvent 1:9 diethyl ether – petroleum ether). Distillation (air-bath temperature 80–90°C/0.17 Torr) of the oil thus obtained gave 120 mg (77%) of the β-trimethylstannyl enone **45**, which exhibited ir (film): 1687, 1577, 775 cm^{-1}; ^1H nmr δ: 0.17 (s, 9H, J_{Sn-H} = 56 Hz), 1.63–2.05 (m, 4H), 2.27–2.64 (m, 4H), 7.03 (t, 1H, J = 2 Hz, J_{Sn-H} = 68 Hz.) *Exact Mass* calcd. for $C_9H_{15}OSn$ (M^+-15): 259.0145; found: 259.0142.

(b) Via general procedure E

Reaction of the β-iodo enone **36** (118 mg, 0.5 mmol) with the trimethylstannylcopper(I) reagent **1** (0.65 mmol) in 5.5 mL of dry THF at −48°C for 2 h afforded, after work-up, purification of the crude product by preparative tlc, and distillation of the desired material, 102 mg (75%) of the β-trimethylstannyl enone **45**. The spectra of this material were identical with those summarized above.

(E)-*2-(Tri-*n*-butylstannylmethylene)cyclohexanone (46)*

Following general procedure F, the cuprate reagent **6** (0.55 mmol) was allowed to react with the β-iodo enone **36** (118 mg, 0.5 mmol) in 10.5 mL of dry THF. Work-up, column chromatography of the crude product on silica gel, and distillation (air-bath temperature 160–171°C/0.2 Torr) of the oil thus obtained produced 136 mg (69%) of the enone **46**. This material exhibited ir (film): 1690, 1581 cm^{-1}; ^1H nmr δ: 0.77–1.13 (m, 15H), 1.17–1.66 (m, 12H), 1.66–2.00 (m, 4H), 2.38–2.68 (m, 4H), 7.04 (t, 1H, J = 2 Hz, J_{Sn-H} = 62 Hz). *Exact Mass* calcd. for $C_{19}H_{36}OSn$: 400.1788; found: 400.1763.

Acknowledgements

Financial support from the Natural Sciences and Engineering Research Council of Canada (NSERCC) and NSERCC post-graduate scholarships (to H.E.M. and J.M.C.) are gratefully acknowledged.

1. G. H. POSNER. Org. React. **19**, 1 (1972); J. F. NORMANT. Synthesis, 63 (1972); A. E. JUKES. Adv. Organomet. Chem. **12**, 215 (1974); G. H. POSNER. Org. React. **22**, 253 (1975); J. F. NORMANT. J. Organomet. Chem. Libr. **1**, 219 (1976); H. O. HOUSE. Acc. Chem. Res. **9**, 59 (1976); J. F. NORMANT. Pure Appl. Chem. **50**, 709 (1978); G. H. POSNER. An introduction to synthesis using organocopper reagents. John Wiley & Sons, New York, NY. 1980; J. F. NORMANT and A. ALEXAKIS. Synthesis, 841 (1981); E. ERDIK. Tetrahedron, **40**, 641 (1984); B. H. LIPSHUTZ, R. S. WILHELM, and J. A. KOZLOWSKI. Tetrahedron, **40**, 5005 (1984); R. J. K. TAYLOR. Synthesis, 364 (1985).
2. D. J. AGER and I. FLEMING. J. Chem. Soc. Chem. Commun. 177 (1978); I. FLEMING and F. ROESSLER. J. Chem. Soc. Chem. Commun. 276 (1980); I. FLEMING and D. MARCHI. Synthesis, 560 (1981); D. G. AGER, I. FLEMING, and S. K. PATEL. J. Chem. Soc. Perkin Trans. 1, 2520 (1981); I. FLEMING, T. W. NEWTON, and F. ROESSLER. J. Chem. Soc. Perkin Trans. 1, 2527 (1981); I. FLEMING and T. W. NEWTON. J. Chem. Soc. Perkin Trans. 1, 119, 1805 (1984); I. FLEMING and D. WATERSON. J. Chem. Soc. Perkin Trans. 1, 1809 (1984); I. FLEMING and N. K. TERRETT. Tetrahedron Lett. **25**, 5103 (1984); I. FLEMING and A. P. THOMAS. J. Chem. Soc. Chem. Commun. 411 (1985).
3. B. M. TROST and D. M. T. CHAN. J. Am. Chem. Soc. **104**, 3733 (1982); J. G. SMITH, N. R. QUINN, and M. VISWANATHAN. Synth. Commun. **13**, 1 (1983); B. LAYCOCK, W. KITCHING, and G. WICKHAM. Tetrahedron Lett. **24**, 5785 (1983).
4. H. ODA, Y. MORIZAWA, K. OSHIMA, and H. NOZAKI. Tetrahedron Lett. **25**, 3217 (1984).
5. E. PIERS and H. E. MORTON. J. Chem. Soc. Chem. Commun. 1033 (1978); E. PIERS and H. E. MORTON. J. Org. Chem. **45**, 4263 (1980); E. PIERS, J. M. CHONG, and H. E. MORTON. Tetrahedron Lett. **22**, 4905 (1981); E. PIERS and J. M. CHONG. J. Org. Chem. **47**, 1602 (1982); E. PIERS and J. M. CHONG. J. Chem. Soc. Chem. Commun. 934 (1983); E. PIERS and H. L. A. TSE. Tetrahedron Lett. **25**, 3155 (1984); E. PIERS, J. M. CHONG, and B. A. KEAY. Tetrahedron Lett. **26**, 6265 (1985).
6. M. GILL, H. P. BAINTON, and R. W. RICKARDS. Tetrahedron Lett. **22**, 1437 (1981); D. E. SEITZ and S.-H. LEE. Tetrahedron Lett. **22**, 4909 (1981); H. WESTMIJZE, K. RUITENBERG, J. MEIJER, and P. VERMEER. Tetrahedron Lett. **23**, 2797 (1982); K. RUITENBERG, H. WESTMIJZE, J. MEIJER, C. J. ELSEVIER, and P. VERMEER. J. Organomet. Chem. **241**, 417 (1983); S. D. COX and F. WUDL. Organometallics, **2**, 184 (1983).
7. W. C. STILL. J. Am. Chem. Soc. **99**, 4836 (1977).
8. H. O. HOUSE, C. Y. CHU, J. M. WILKENS, and M. J. UMEN. J. Org. Chem. **40**, 1460 (1975); P. G. M. WUTS. Synth. Commun. **11**, 139 (1981).
9. G. H. POSNER, D. J. BRUNELLE, and L. SINOWAY. Synthesis, 662 (1974).
10. E. J. COREY, D. FLOYD, and B. H. LIPSHUTZ. J. Org. Chem. **43**, 3418 (1978); R. E. ATKINSON, R. F. CURTIS, and J. A. TAYLOR. J. Chem. Soc. (C), 578 (1967).
11. B. H. LIPSHUTZ, J. A. KOZLOWSKI, and C. M. BRENEMAN. J. Am. Chem. Soc. **107**, 3197 (1985).
12. B. H. LIPSHUTZ, J. A. KOZLOWSKI, and C. M. BRENEMAN. Tetrahedron Lett. **26**, 5911 (1985).
13. J. HUDEC. J. Chem. Soc. Perkin Trans. 1, 1020 (1975).
14. E. PIERS, K. F. CHENG, and I. NAGAKURA. Can. J. Chem. **60**, 1256 (1982); E. PIERS, J. BANVILLE, C. K. LAU, and I. NAGAKURA. Can. J. Chem. **60**, 2965 (1982); E. PIERS, C. K. LAU, and I. NAGAKURA. Can. J. Chem. **61**, 288 (1983); E. PIERS, H. E. MORTON, I. NAGAKURA, and R. W. THIES. Can. J. Chem. **61**, 1226 (1983); E. PIERS and E. H. RUEDIGER. Can. J. Chem. **61**, 1239 (1983).
15. E. PIERS, J. R. GRIERSON, C. K. LAU, and I. NAGAKURA. Can. J. Chem. **60**, 210 (1982).
16. E. PIERS and H. E. MORTON. J. Org. Chem. **44**, 3437 (1979).
17. J. E. DUBOIS and M. DUBOIS. C. R. Acad. Sci. **256**, 715 (1963).
18. A. J. LEUSINK, H. A. BUDDING, and J. W. MARSMAN. J. Organomet. Chem. **9**, 285 (1967).
19. R. M. SILVERSTEIN, G. C. BASSLER, and T. C. MORRILL. Spectrometric identification of organic compounds. 4th ed. John Wiley and Sons, Inc., New York, NY. 1981. pp. 316–319.

Can. J. Chem. Downloaded from www.nrcresearchpress.com by 190.90.36.8 on 09/07/12
For personal use only.

β-Lactams. XII.
A study of the synthesis of N-unsubstituted β-lactams, and of 4-styryl monobactams

DENISE DUGAT, GEORGE JUST, AND SOUMYA SAHOO
Department of Chemistry, McGill University, Montreal, P.Q., Canada H3A 2K6

Received April 29, 1986

This paper is dedicated to Dr. O. E. (Ted) Edwards

DENISE DUGAT, GEORGE JUST, and SOUMYA SAHOO. Can. J. Chem. **65**, 88 (1987).

A few types of amines XNH_2 were investigated for the formation of β-lactams via the cycloaddition of the corresponding Schiff bases with azidoacetyl chloride. Among the β-lactams formed, only the *N-p,p'*-dimethoxybenzhydryl compounds could be transformed to N-unsubstituted azetidinones by removal of the N-substituent with ceric ammonium nitrate. Conversion of those N-unsubstituted intermediates to 3-acylated monobactams was studied in the 4-styryl series.

DENISE DUGAT, GEORGE JUST et SOUMYA SAHOO. Can. J. Chem. **65**, 88 (1987).

Dans le but de déterminer leur abilité à former des β-lactames, on a étudié la cycloaddition d'un certain nombre de bases de Schiff, dérivées de quelques types d'amines XNH_2, avec le chlorure d'azidoacétyle. Parmi les β-lactames qui se sont formées, seuls les composés *N-p,p'*-diméthoxybenzhydryles ont pu être transformés, sous l'influence du nitrate d'ammonium cérique, en azétidones ne portant pas de substituants sur le N. Dans la série des dérivés styrylés en position 4, on a étudié la conversion de ces intermédiaires ne portant pas de substituants sur le N en monobactames acylés en position 3.

[Traduit par la revue]

Can. J. Chem. Downloaded from www.nrcresearchpress.com by 80.58.250.72 on 09/07/12
For personal use only.

Introduction

We have been interested for some time in the synthesis of monocyclic β-lactams in which ring strain imparted by a second ring in classical β-lactams such as penicillins and cephalosporins was replaced by strain induced by electron withdrawal (1).

Recently, a new class of antibiotics was discovered (2, 3): the monobactam **A** in which this electronic strain is created by *N*-sulfonation of a monocyclic β-lactam.

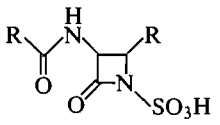

A

Subsequently, powerful antibiotics were developed by chemical modification of **A** (4, 5). The required β-lactam nucleus has been synthesized by conversion of 6-amino penicillanic acid (5), by cyclization of the appropriate threonine derivative (6) or α,β-diaminocarboxylic acids (7), or by cycloaddition of azidoacetyl chloride with a Schiff base of type **2** and **3** where X is a group that can be subsequently removed without the destruction of the β-lactam ring. Examples of this last approach were mentioned in recently published papers. Thus 2-(phenylselenenyl)ethylamine (8), *p*-anisidine (9), and threonine (10) have been used as the amine from which Schiff bases were derived. The removal of the N-substituents was effected respectively by elimination and oxidative hydrolysis (8), by ceric ammonium nitrate (CAN) oxidation (9), and by oxidation with an excess of Jones reagent (10).

We would like to report our results in this field, which indicate that only certain types of amines may be used for the formation of β-lactams via the cycloaddition reaction pioneered by Bose *et al.* (11) and developed by Doyle *et al.* (12).

In a second part, we describe our studies of the synthesis of 4-styryl monobactams, since some 4-styryl monocyclic β-lactams[1] had shown weak antibacterial properties.

[1]G. Just, W. Y. Liu, and A. Ugolini. Unpublished results.

Results and discussion

Formation of unsubstituted β-lactams

The prototype aldehydes used for this investigation were acetaldehyde and cinnamaldehyde; the amines covered the range described (**1***a*–**1***i*).

The first two amines investigated, hydroxylamine **1***a* and its *O*-benzyl derivative **1***b*, where the X group can be removed by known methods (14), formed oximes **2***a,b* and **3***a,b*; neither of these underwent cycloaddition with azidoacetyl chloride.

Next, we investigated trityl amine **1***c* and *tert*-butyldimethylsilylamine **1***d* where the X group might be removed by hydrogenolysis or tetra-*n*-butylammonium fluoride; neither amine formed a Schiff base, even under forcing conditions.

The next two amines investigated, trimethylsilylethylamine **1***e* (prepared from vinyltrimethylsilane according to Kabalka *et al.* (15)) and allylamine **1***f*, were found to be too reactive for Schiff base formation with acetaldehyde; they reacted smoothly with cinnamaldehyde to generate the corresponding Schiff bases **3***e,f*, which upon reaction with azidoacetyl chloride gave the *cis* β-lactams **5***e,f* in good yield. However, the removal of the trimethylsilylethyl group in **5***e*, using a variety of conditions recently described by Lipshutz *et al.* (16), failed. Similarly, the removal of the allyl group in **5***f*, using $(Ph_3P)_3RhCl$, according to Laguzza and Ganem (17), was also unsuccessful.

We finally investigated *l*-methylphenylcarbinyl amine **1***g*, benzhydrylamine **1***h*, and *p,p'*-dimethoxybenzhydrylamine **1***i*. All three gave Schiff bases **2***g,h,i* and **3***g,h,i* in excellent yield. Cycloaddition of these with azidoacetyl chloride led in good yields to *cis*-styryl β-lactams **5***g,h,i* and *trans*-methyl β-lactams **4***g,h* (12), except in the case of Schiff base **2***i*, which gave in moderate yield the *cis* β-lactam **4***i*.

Hydrogenolysis using a variety of catalysts did not effect the removal of the X group in **4***g,h,i* and **5***g,h,i*. The *p,p'*-dimethoxybenzhydryl group of **4***i* and **5***i* could be removed in 75% yield by means of ceric ammonium nitrate using a modification of the described conditions (9) (overall from **1**, **6**: 13.5%, **7**: 44%).

We have no explanation for the formation of **4***i* in the *cis* configuration rather than the expected *trans* arrangement.

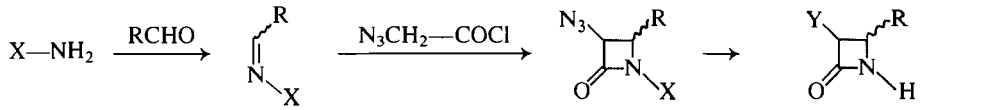

X—NH_2	Imines		β-Lactams	
	R = CH_3	R = styryl	R = CH_3	R = styryl
a X = OH	**2***a*	**3***a*	—	—
b X = OCH_2Ph	**2***b*	**3***b*	—	—
c X = CPh_3	—	—	—	—
d X = $SiMe_2t$-Bu	—	—	—	—
e X = $CH_2CH_2SiMe_3$	—	**3***e*	—	**5***e cis*
f X = $CH_2CH{=}CH_2$	—	**3***f*	—	**5***f cis*
g X = CHMePh	**2***g*	**3***g*	**4***g trans*	**5***g cis*
h X = $CHPh_2$	**2***h*	**3***h*	**4***h trans*	**5***h cis*
i X = $CH(p\text{-}C_6H_4OMe)_2$	**2***i*	**3***i*	**4***i cis*	**5***i cis*

Due to the low yield of **6**, further work was carried out only on 4-styryl β-lactam **7**.

Selective reduction of the azide function in the presence of the styryl group was effected either by catalytic hydrogenation, using nickel boride (18) as catalyst, or by treatment with triphenyl phosphine, followed by aqueous hydrolysis of the resulting iminophosphorane (19), giving amine **8**.

4-Styryl-monobactams

Acylation of **8** with phenylacetyl chloride provided **11** (yield 51%), which was transformed to the *N*-potassium sulfonate **12***b* by sulfonation of **11** with the pyridine – sulfur trioxide complex in pyridine (20), followed by extraction of the sulfonic acid as its tetra-*n*-butylammonium salt **12***a*; passage through an ion-exchange resin gave the potassium salt **12***b* in 48% yield from **11**.

A synthesis of **18***c*, in which the styryl β-lactam **10** was acylated with the aminothiazolylcarboxylic acid **14**, a side chain similar to that used of the highly active aztreonam, has been described in a patent of the Squibb Institute (21), but no information was given concerning its antibacterial activity. We report here two other routes leading to **18***c*.

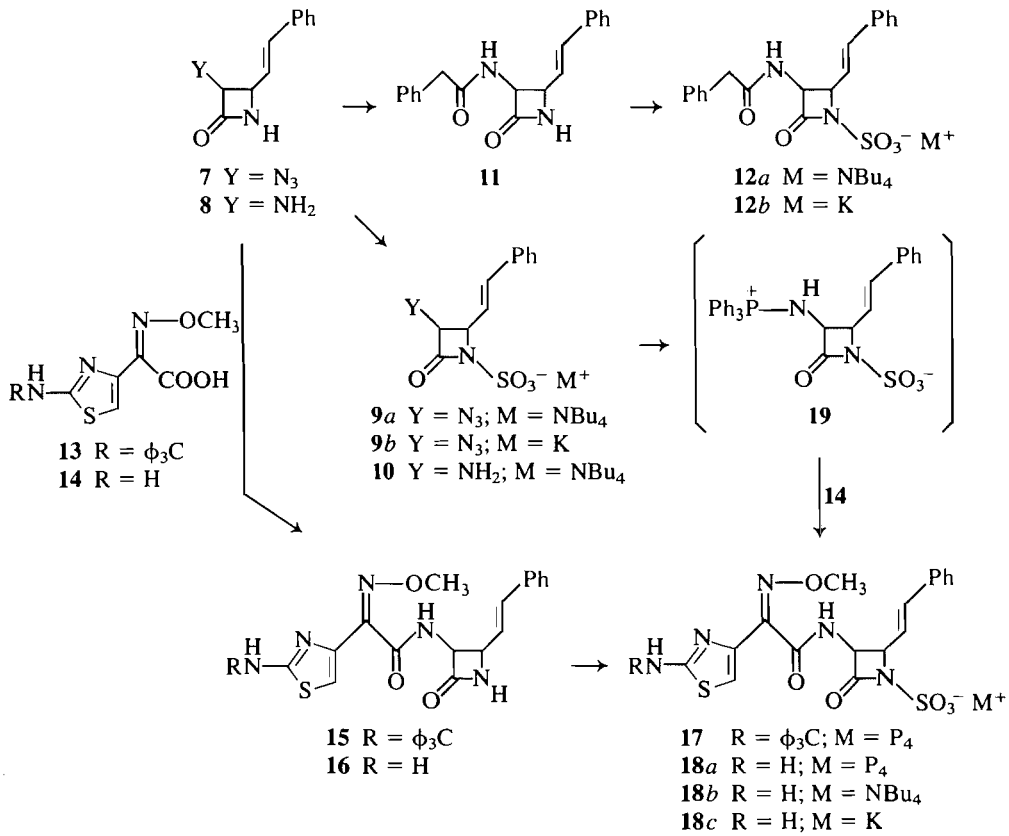

Can. J. Chem. Downloaded from www.nrcresearchpress.com by 80.58.250.72 on 09/07/12
For personal use only.

Can. J. Chem. Downloaded from www.nrcresearchpress.com by 80.58.250.72 on 09/07/12
For personal use only.

The first approach reproduces the sequence condensation–sulfonation as developed above for **12***b*. Thus, reaction of **8** with the trityl-amino acid **13** was carried out in CH_2Cl_2/DMF using *N*-ethoxycarbonyl-2-ethoxy-1,2-dihydroquinoline (EEDQ) (22) as coupling agent (yield of **15**: 62%), and gave better yields than dicyclohexylcarbodiimide (DCC) and *N*-hydroxybenzotriazole. The sulfonation reaction, which required more forcing conditions than before, due to solubility problems, was carried out in DMF/pyridine directly on the trityl-amino β-lactam **15** or on its deprotected amino analogue **16**. Deblocking of the trityl group of **15** and **17** was performed by refluxing for 7 h in a methanolic solution of formic acid. The pyridinium sulfonate **18***a* obtained in both cases could not be isolated and purified as before as its *N*-butylammonium salt **18***b*, because of the low solubility of **18***b* in organic solvents; it was directly converted to potassium salt **18***c* by means of potassium 2-ethyl hexanoate (23), and was obtained with greater purity and better yield in the first sequence (path A) (**15** → **17** → **18**: yield 75%) than in the second one (path B) (**15** → **16** → **18**: yield 50%).

β-Lactam sulfonic salt **18***c* could also be obtained, albeit in lower yield and purity, by another approach involving a modification of the peptide synthesis from an azide and a carboxylic acid, a reaction pioneered by Vilarrasa and co-workers (24) and recently developed by Roberts and co-workers (25). Thus, the tetrabutylammonium salt of 3-azido β-lactam **9***a*, generated from **7** in the conditions previously used, was treated with triphenylphosphine in THF–DMF to form the zwitterion intermediate **19**, which partially precipitated during the reaction (24). Heating of the crude mixture in the presence of carboxylic acid **14** afforded **18***b* contaminated with side products that were difficult to remove. Passage through an ion-exchange resin gave **18***c*.

All compounds reported gave good interpretable nmr and mass spectra. Positive-ion fast atom bombardment mass spectra of **18***c* and aztreonam (26) were compared; both are characterized by the following fragments: MK^+, MH^+, $MH^+ - SO_3$, $MH^+ - HSO_3NCHR$ (**18***c*: R = styryl; aztreonam: R = Me), and 126 ($C_4H_4N_3S$).

None of the monobactamates **9***b*, **12***b*, and **18***c* showed notable antibacterial activity when tested against a panel of Gram positive and negative bacteria. The presence of a 4-styryl group seemed to decrease the intrinsic activity of those compounds, especially of aminothiazolyl methoxyimino monobactam **18***c* as compared to its 4-methyl analogue (4, 5).

This result may be explained by either a steric effect, where the antibacterial activity decreases for side chains larger than ethyl (5, 13), or, as suggested by Cimarusti,[2] by the increased lipophilicity of the aromatic ring at an inappropriate binding site.

Experimental

Thin-layer chromatography was performed on Merck Silica Gel 60 F_{254} aluminum-backed plates. Flash chromatography was done with Woelm silica (32–63 μm) using predistilled solvents. Melting points were determined on a Gallenkamp block and are uncorrected. Infrared spectra were run on a Perkin–Elmer 297 spectrophotometer. Nuclear magnetic resonance spectra were recorded on Varian T-60, T-60A, XL-200, and XL-300 spectrometers. Mass spectra were taken on an LKB-9000 and FAB mass spectra on a VG-analytical mass spectrometer.

[2]Personal discussions during the XIth European Heterocyclic Colloquium, Ferrara, Italy, October 1985.

Amines

Trityl amine ***1***c *and* tert-*butyldimethylsilylamine* ***1***d

To a solution of trityl chloride (1.114 g, 4 mmol) or *tert*-butyldimethylsilylchloride (602 mg, 4 mmol) in ether at −50°C was added ether (80 mL) previously saturated by ammonia (at −78°C). After stirring overnight until elimination of excess ammonia, the solvent was removed *in vacuo* to afford the corresponding amines in 90% yield.

Trimethylsilylethylamine ***1***e (ref. 15)

To a solution of vinyltrimethylsilane (900 mg, 9 mmol) in THF (3 mL) was added under nitrogen, at −5°C, BH_3–THF (3 mmol, 3 mL of a 1 *M* solution). The solution was stirred for 2 h and allowed to warm to 10°C. Then, to the organoborane (3 mmol), cooled again to 0°C, was added dropwise under nitrogen aqueous solutions of ammonium hydroxide (3 mmol) and sodium hypochlorite (3.3 mmol). The mixture was stirred for 15 min and allowed to warm to 10°C. The reaction mixture was extracted with ether (3 × 10 mL). The organic layers were combined, washed with brine, and dried on $MgSO_4$. Removal of the solvent gave the expected amine (yield: 65%); ^{1}H nmr (60 MHz, $CDCl_3$) δ: 0.1 (s, 9H, $SiMe_3$), 0.80–1.3 (m, 2H, $SiCH_2$), 1.9 (br s, 2H, NH_2), 3.0 (m, 2H, CH_2—N).

p,p′-*Dimethoxybenzhydrylamine* ***1***i

To a solution of *p,p′*-dimethoxybenzhydrol (1.22 g, 5 mmol) in dry CH_2Cl_2 (100 mL) at −50°C, under nitrogen, was added dropwise mesylchloride (0.87 mL, 1.145 g, 10 mmol) and triethylamine (2.78 mL, 2.20 g, 20 mmol). The mixture was stirred for ½ h and allowed to warm up to −20°C maximum. As shown by tlc, the alcohol was rapidly converted into its mesylate. The reaction mixture was then cooled again to −50°C and THF (100 mL), previously saturated by ammonia (at −78°C), was added. After stirring overnight, the solvents were removed *in vacuo* and replaced with ether (200 mL). The solution was washed with 1 *N* HCl solution (3 × 20 mL); the aqueous layer was then made slightly basic with aqueous sodium hydroxide and extracted several times with ether. The organic extract was dried on $MgSO_4$ and stripped of solvent under reduced pressure to afford the desired amine, which was essentially pure by tlc analysis; yield: 70%; ^{1}H nmr (60 MHz, $CDCl_3$) δ: 2.3 (br s, 2H, NH_2), 3.8 (s, 6H, $2OCH_3$), 5.1 (s, 1H, CH), 7.0 (AB spectra, 8H, 2φ, J = 8.0 Hz, $\Delta\nu$ = 25 Hz).

Schiff bases ***2***a,b,g,h,i, ***3***a,b,e,f,g,h,i

All the Schiff bases were prepared in a similar manner and used without purification. The following is a representative procedure.

A solution of the amine **1***i* (1.21 g, 5 mmol) in dry CH_2Cl_2 (50 mL) was treated with magnesium sulfate (2.4 g, 20 mmol) and cooled to −20°C under a nitrogen atmosphere. Freshly distilled acetaldehyde (660 mg, 15 mmol) or cinnamaldehyde (660 mg, 5 mmol) was added dropwise. The mixture was stirred for 2 h, filtered, and evaporated to give a crude material that was directly used for the next reaction.

2*i*: yield: 90%; ^{1}H nmr (60 MHz, $CDCl_3$) δ: 1.95 (d, 3H, CH_3, J = 5.0 Hz), 3.7 (s, 6H, $2OCH_3$), 5.35 (br s, 1H, CH), 7.0 (AB spectra, 8H, 2φ, J = 9.0 Hz, $\Delta\nu$ = 21 Hz), 7.85 (q, 1H, CH=, J = 5.0 Hz).

3*i*: yield: 78%; ^{1}H nmr (60 MHz, $CDCl_3$) δ: 3.9 (s, 6H, $2OCH_3$), 5.45 (br s, 1H, CH), 6.8–7.5 (m, 15H, 3φ + C*H*=C*H*), 8.1 (br s, 1H, *H*C=N).

Azido β-lactams ***4***g–i, ***5***e–i

All β-lactams were prepared in an identical manner. To a solution of Schiff base (2 mmol) and triethylamine (292 μL, 212 mg, 2.1 mmol) in dry CH_2Cl_2 (10 mL) at −30°C, under nitrogen, was added dropwise a solution of azidoacetyl chloride (263 mg, 2.2 mmol) in CH_2Cl_2 (10 mL). The reaction mixture, after stirring for 1 h, was allowed to warm up to 0°C, washed with brine, dried on $MgSO_4$, and evaporated. The crude material was purified by flash chromatography and obtained in approximately 75% yield except for compound **4***i* (yield: 20%); ir ($CHCl_3$) ν_{max}: 2100 (N_3), 1750–1760 (CO β-lactam) cm^{-1}.

Compound *trans* **4***g*: ^{1}H nmr (60 MHz, $CDCl_3$) δ: 1.2 and 1.3 (2d, 3H, CH—*CH*$_3$, J = 6.5 Hz), 1.65 and 1.8 (2d, 3H, CHPh—*CH*$_3$, J = 8.0 Hz), 3.4 (dg, 1H, C*H*Me, J = 6.5, 2.0 Hz), 4.1 (d, 1H, C*H*N_3, J = 2.0 Hz), 4.4—5.1 (m, 1H, C*H*MePh), 7.3 (s, 5H, φ).

Can. J. Chem. Downloaded from www.nrcresearchpress.com by 80.58.250.72 on 09/07/12
For personal use only.

Compound *trans* **4***h*: ^{1}H nmr (60 MHz, $CDCl_3$) δ: 1.2 (d, 3H, $CHCH_3$, J = 6.5 Hz), 3.5 (dg, 1H, CHMe, J = 6.5, 2.0 Hz), 4.2 (d, 1H, CHN_3, J = 2.0 Hz), 6.0 (s, 1H, $CHPh_2$), 7.3 (s, 10H, 2φ).

Compound *cis* **4***i*: ^{1}H nmr (60 MHz, $CDCl_3$) δ: 1.6 (d, 3H, $CHCH_3$, J = 6.0 Hz), 3.8 (s, 6H, $2OCH_3$), 4.1 (dg, 1H, CHMe, J = 6.0, 5.0 Hz), 4.7 (d, 1H, CHN_3, J = 5.0 Hz), 5.7 (s, 1H, $CH(\phi OMe)_2$), 6.7–7.2 (m, 8H, 2φ).

Compound *cis* **5***e*: ^{1}H nmr (60 MHz, $CDCl_3$) δ: 0.2 (s, 9H, $SiMe_3$), 0.8–1.6 (m, 2H, CH_2—Si), 3.2–3.8 (m, 2H, N—CH_2), 4.6 (dd, 1H, CH—CH=, J = 9.0, 5.5 Hz), 5.0 (d, 1H, CHN_3, J = 5.5 Hz), 6.1–7.1 (m, 2H, CH=CH), 7.6 (s, 5H, φ).

Compound *cis* **5***f*: ^{1}H nmr (60 MHz, $CDCl_3$) δ: 3.4–4.3 (m, 2H, N—CH_2), 4.45 (dd, 1H, CH—CH=, J = 9.0, 5.5 Hz), 4.85 (d, 1H, CHN_3, J = 5.5 Hz), 5.1–6.9 (m, 5H, 3CH= and CH_2=), 7.4 (s, 5H, φ).

Compound *cis* **5***g*: ^{1}H nmr (60 MHz, $CDCl_3$) δ: 1.8 and 1.95 (2d, 3H, CHφ—CH_3, J = 8.0 Hz), 4.1 (dd, 1H, CH—CH=, J = 9.5, 5.0 Hz), 4.5–5.1 (m, 2H, CHMePh + CHN_3), 6.2–7.2 (m, 12H, 2φ + CH=CH).

Compound *cis* **5***h*: ^{1}H nmr (60 MHz, $CDCl_3$) δ: 4.3 (dd, 1H, CH—CH=, J = 9.0, 5.5 Hz), 4.7 (d, 1H, CHN_3, J = 5.5 Hz), 6.0 (s, 1H, $CHPh_2$), 6.1–6.7 (m, 2H, CH=CH), 6.9–7.3 (m, 15H, 3φ).

Compound *cis* **5***i*: ^{1}H nmr (60 MHz, $CDCl_3$) δ: 3.7 and 3.8 (2s, 6H, $2OCH_3$), 4.4 (dd, 1H, CH—CH=, J = 9.0, 5.0 Hz), 4.8 (d, 1H, CHN_3, J = 5.0 Hz), 5.8–6.5 (m, 3H, $CH(\phi\text{-}OMe)_2$ + CH=CH—), 6.7–7.3 (m, 13H, 3φ).

3-Azido N-unsubstituted β-lactams ***6*** *and* ***7*** (ref. 9)

Both β-lactams **6** and **7** were prepared in an identical manner from the corresponding *N*-dimethoxybenzhydryl compounds **4***i* and **5***i*, using the following procedure. A solution of *N*-dimethoxybenzhydryl azetidinone (1 mmol) in acetonitrile (10 mL) was cooled at 0°C and treated with a solution of ceric ammonium nitrate (CAN) (1.64 g, 3 mmol) in water (5 mL) over 5 min. The reaction was stirred at −5° to 0°C for 45 min and diluted with 40 mL of water. The mixture was extracted with ethyl acetate (3 × 15 mL). The organic extracts were washed with 5% sodium bicarbonate (30 mL) and the aqueous extracts back-washed with ethyl acetate (10 mL). The combined organic solutions were washed with 10% sodium sulfite (until the aqueous layer remained colorless), 5% sodium bicarbonate (5 mL), and brine. The resulting solution was swirled over charcoal for 30 min; sodium sulfate was added and the mixture was filtered through Celite. Removal of the solvent yielded a crude material, which was purified by flash chromatography (ethyl acetate – hexane: 30:70) to afford the N-unsubstituted β-lactams in approximately 75% yield.

Compound **6**: ir ($CHCl_3$) ν_{max}: 3400 (NH), 2930 (CH), 2840 (CH_3), 2100 (N_3), 1760 (CO β-lactam) cm^{-1}; ^{1}H nmr (60 MHz, $CDCl_3$) δ: 1.5 (d, 3H, CH_3, J = 6.0 Hz), 4.2 (dq, 1H, CHMe, J = 6.0, 5.0 Hz), 4.8 (dd, 1H, CHN_3, J = 5.0, 1.0 Hz), 6.7 (br d, 1H, NH, J = 1.0 Hz).

Compound **7**: mp 100–102°C (lit. (9) mp 103–105°C); ir ($CHCl_3$) ν_{max}: 3410 (NH), 2920 (CH), 2100 (N_3), 1775 (CO β-lactam), 1650 (w, C=C) cm^{-1}; ^{1}H nmr (60 MHz, $CDCl_3$) δ: 4.5 (dd, 1H, CH—C=, J = 7.5, 5.5 Hz), 4.8 (dd, 1H, CHN_3, J = 5.5, 1.5 Hz), 6.2 (dd, 1H, —CH=CHφ, J = 16.0, 7.5 Hz), 6.5 (d, 1H, CH=CHφ, J = 16.0 Hz), 6.95 (br d, 1H, NH, J = 1.5 Hz), 7.4 (m, 5H, φ).

3-Amino β-lactam ***8***

(a) Method 1

To nickel acetate (249 mg, 1 mmol), in a 2-necked flask equipped with a septum, was added 2 mL of 95% ethanol. The flask was connected to the hydrogenation apparatus and was flushed with hydrogen. The catalyst was produced by injecting 2 mL of a 0.5 *M* solution of sodium borohydride in 95% ethanol to the rapidly stirred solution of nickel acetate. The reaction vessel was reflushed with hydrogen. Hydrogenation was then initiated by introducing 214 mg (1 mmol) of azido β-lactam **7** in 2 mL ethanol via the septum. The reaction was stopped after 2 h, just before that the absorbed quantity of hydrogen was larger than the liberated quantity of nitrogen. The reaction mixture was then filtered through Celite, the ethanol removed under reduced pressure, and the residue diluted in acetone. The solution was filtered again and evaporated. The crude compound was purified on aluminium oxide (eluant: $CHCl_3$–MeOH, 98:2) to give 56 mg of pure β-lactam **8** (yield 30%); ir ($CHCl_3$) ν_{max}: 3420 (NH, NH_2), 2930 (CH), 1760 (CO β-lactam), 1600 (w, C=C) cm^{-1}; ^{1}H nmr (200 MHz, $CDCl_3$) δ: 1.8 (br s, 2H, NH_2), 4.4–4.5 (m, 2H, CH—CH), 6.22 (dd, 1H, CH=CHφ, J = 16.0, 6.5 Hz), 6.4 (s, 1H, NH), 6.65 (d, 1H, =CHφ, J = 16.0 Hz), 7.25–7.41 (m, 5H, φ); ms (70 eV) *m/e*: 188 (85, M^+), 187 (64), 145 (103, H_2N—CH—CH—CH=$CH\phi^+$), 144 (163), 143 (35), 133 (110), 132 (1000, $M^+ - H_2NCHCO + 1$), 117 (96), 116 (64), 115 (374), 91 (75), 72 (131), 57 (124, H_2N—CH—CO), 51 (150), 43 (60, CONH).

(b) Method 2

To a solution of azido β-lactam **7** (214 mg, 1 mmol) in dry THF (10 mL) was added, under nitrogen and at room temperature, triphenylphosphine (288 mg, 1.1 mmol). After 2 h stirring, 2 or 3 equivalents of water were added and the reaction mixture was stirred overnight. The solvent was then evaporated and the residue dissolved in acetone (5 mL). *para*-Toluenesulfonic acid (209 mg, 1.1 mmol) was added and the solution stirred again for 3 h. The precipitate was filtered and washed with 1 mL of acetone to give 188 mg of the *para*-toluenesulfonate salt of β-lactam **8** (yield: 52%); mp 198–200°C; ir (KBr) ν_{max}: 3400 (NH_3), 2930 (CH), 1750 (CO β-lactam), 1610 (C=C), 1030 (SO_3), 1000, 955 cm^{-1}; ^{1}H nmr (200 MHz, DMSO-d_6) δ: 2.04 (s, 3H, CH_3), 4.48 (dd, 1H, CH—C=, J = 7.5, 5.0 Hz), 4.62 (d, 1H, H_3N—CH, J = 5.0 Hz), 6.34 (dd, 1H, CH=CHφ, J = 16.0, 7.5 Hz), 6.78 (d, 1H, =CHφ, J = 16.0 Hz), 7.04–7.46 (m, 9H, 2φ), 8.42 (br s, 3H, NH_3), 8.85 (s, 1H, NH β-lactam).

4-Styryl 3-azido 2-oxo 1-azetidine sulfonic acid ***9*** (ref. 20)

(a) Tetrabutylammonium salt ***9***a

A solution of 3-azido β-lactam **7** (214 mg, 1 mmol) in 3 mL of pyridine was heated under nitrogen to 80°C, and 477 mg (3 mmol) of pyridine – sulfur trioxide complex added. The mixture, which quickly became homogeneous, was stirred for 2 h and then poured into 35 mL of 0.5 *N* KH_2PO_4. The resulting solution was extracted with CH_2Cl_2 (2 × 10 mL) and EtOAc (1 × 10 mL); the organic extracts were back-washed with phosphate solution (4 × 10 mL). The combined aqueous layers were then treated with 355 mg (1.05 mmol) of tetrabutylammonium hydrogen sulfate (TBAHS) and extracted with methylene chloride (1 × 20 mL and 2 × 10 mL). The organic extract was dried on $MgSO_4$ and concentrated to yield the desired tetra-*n*-butylammonium salt, which was essentially pure by tlc analysis ($CHCl_3$–MeOH, 9:1); yield: 80%; ir (film) ν_{max}: 2960, 2930 and 2875 (CH_3, CH_2), 2100 (N_3), 1770 (CO β-lactam), 1485, 1465, 1380, 1265, 1050 (SO_3), 790, 760 cm^{-1}; ^{1}H nmr (200 MHz, $CDCl_3$) δ: 0.95 (t, 12H, $4CH_3$, J = 7.3 Hz), 1.40 (m, 8H, 4 × CH_2—Me), 1.57 (m, 8H, $4CH_2$), 3.19 (m, 8H, $4NCH_2$), 4.65 (d, 1H, N_3—CH—, J = 5.7 Hz), 4.80 (dd, 1H, CH—C=, J = 5.7, 7.9 Hz), 6.28 (dd, 1H, CH=CHφ, J = 15.9, 7.9 Hz), 6.85 (d, 1H, CH=CHφ, J = 15.9 Hz), 7.25 (m, 5H, φ); ms (70 eV) *m/e*: 242 (1000, NBu_4), 243 (200).

(b) Potassium salt ***9***b

A solution of tetra-*n*-butylammonium salt (148 mg, 0.28 mmol) in distilled water – methanol (3:1) was applied to a column of ion exchange resin (12 mL) (Dowex: 50 × 8-200) previously charged in K^+ ions with a 1 *N* KCl solution. Elution was made with distilled water. The eluate was freeze-dried to give 44 mg of the desired potassium salt as a yellow powder (yield: 50%); ir (KBr) ν_{max}: 3460 (br, OH), 2100 (N_3), 1765 (CO β-lactam), 1615 (C=C), 1245 and 1050 (SO_3), 970, 755, 695, 650 cm^{-1}; ^{1}H nmr (200 MHz, DMSO-d_6) δ: 4.65 (dd, 1H, CH—C=, J = 7.8, 5.6 Hz), 5.12 (d, 1H, N_3—CH—, J = 5.6 Hz), 6.22 (dd, 1H, —CH=CHφ, J = 16.1, 7.8 Hz), 6.8 (d, 1H, CH=CHφ, J = 16.1 Hz), 7.33 (m, 5H, φ); ms *m/e* (negative FAB): 293 (814, M − K), 265 (161, M − K − N_2), 252 (137), 210 (710, $O_3SNC_9H_8$), 185 (225), 161 (170), 153 (433), 145 (185), 122 (1000,

Can. J. Chem. Downloaded from www.nrcresearchpress.com by 80.58.250.72 on 09/07/12
For personal use only.

O_3SNCO); *m/e* (positive FAB): 371 (244, M + K), 332 (71, M), 261 (118), 247 (102), 242 (1000), 168 (457), 158 (496), 142 (275).

4-Styryl 3-phenylacetamido 2-azetidinone ***11***

To a solution of amino β-lactam **8** (34 mg, 0.18 mmol) and pyridine (43 mg, 0.54 mmol) in dry methylene chloride (4 mL) was added dropwise at 0°C, under nitrogen, a solution of phenylacetyl chloride (40 mg, 0.25 mmol) in dry methylene chloride (1 mL). After the addition was complete, the solution was stirred for 3 h, washed with pH 4.5 buffer solution, 5% $NaHCO_3$ solution, and brine. The organic layer was dried on $MgSO_4$ and evaporated. The solid that precipitated was washed with chloroform to give 28 mg (51%) of pure compound, mp 210°C; ir (KBr) ν_{max}: 3280 (NH), 1770 (CO β-lactam), 1660 (CO amide), 1600 (w, C=C), 1540, 1190, 970, 750, 690 cm^{-1}; ^1H nmr (200 MHz, CD_3COCD_3) δ: 3.5 (AB spectra, 2H, CH_2, J = 12.7 Hz, $\Delta\nu$ = 15.5 Hz), 4.47 (ddd, 1H, C*H*—C=, J = 7.0, 5.5, 0.8 Hz), 5.31 (ddd, 1H, NH—C*H*, J = 9.5, 5.5, 1.0 Hz), 6.17 (dd, 1H, —C*H*=CHφ, J = 16.0, 7.0 Hz), 6.71 (dd, 1H, —CH=C*H*φ, J = 16.0, 0.8 Hz), 7.0 (m, 5H, φ), 7.2 (m, 5H, φ), 7.50 (d, 1H, NH β-lactam, J = 1.0 Hz), 7.76 (d, 1H, NH amide, J = 9.5 Hz); ms (70 eV) *m/e*: 306 (1.5, M^+), 289 (5), 263 (15, M^+ − CONH), 188 (19), 187 (20), 175 (23, M^+ − PhCH= − CH—CH—NH), 171 (855), 132 (1000, M^+ − $PhCH_2CONHCHCO$ + 1), 119 (15, $PhCH_2CO$), 115 (309).

4-Styryl 3-phenylacetamido 2-oxo 1-azetidine sulfonic acid ***12*** (ref. 20)

(*a*) *Tetrabutylammonium salt* ***12a***

Tetrabutylammonium salt ***12a*** was prepared from **11** (15 mg, 0.05 mmol) following the procedure described for ***9a***. Yield: 57%; ir ($CHCl_3$) ν_{max}: 3420 (NH), 2960, 2940, 2880 (CH_3, CH_2), 1760 (CO β-lactam), 1670 (CO amide), 1600 (C=C), 1460, 1265 and 1050 (SO_3) cm^{-1}; ^1H nmr (200 MHz, $CDCl_3$) δ: 0.92 (t, 12H, $4CH_3$, J = 7.3 Hz), 1.40 (m, 8H, 4 × CH_2—Me), 1.60 (m, 8H, $4CH_2$), 3.22 (m, 8H, $4NCH_2$), 3.50 (s, 2H, CH_2φ), 4.85 (dd, 1H, C*H*—C=, J = 6.7, 5.9 Hz), 5.33 (dd, 1H, NH—C*H*—, J = 9.7, 5.9 Hz), 5.98 (d, 1H, NH, J = 9.7 Hz), 6.20 (dd, 1H, C*H*=CHφ, J = 16.0, 6.7 Hz), 6.75 (d, 1H, CH=C*H*φ, J = 16.0 Hz), 7.0 (m, 5H, φ), 7.3 (m, 5H, φ); ms *m/e* (positive FAB): 629 (13, MH_2^+), 332 (138), 307 (35, MH_2^+ − NBu_4 − SO_3), 302 (103), 272 (161), 258 (172), 242 (1000, NBu_4), 240 (1000), 212 (63, $HSO_3NC_9H_8$ + H^+), 142 (CH_2NBu_2), 123 (115, HSO_3NCO).

(*b*) *Potassium salt* ***12b***

Potassium salt ***12b*** was prepared from ***12a*** (11 mg, 0.017 mmol) as described for ***9b***. However, in the present case the tetrabutylammonium salt was dissolved in distilled water – methanol (1:1). Elution of the ion-exchange resin was made first with a MeOH–H_2O (1:1) solution, then distilled water. The eluate was partially evaporated *in vacuo* and freeze-dried to afford 6 mg of potassium salt. Yield: 83%; ir (KBr) ν_{max}: 3485, 3310 (NH), 1760 (CO β-lactam), 1660 (CO amide), 1600 (C=C), 1540, 1295, 1240, 1050 and 1040 (SO_3) cm^{-1}; ^1H nmr (200 MHz, DMSO-d_6) δ: 3.38 (AB spectra, 2H, CH_2, J = 12 Hz, $\Delta\nu$ = 16 Hz), 4.53 (dd, 1H, C*H*—C=, J = 8.4, 5.7 Hz), 5.13 (dd, 1H, NH—C*H*, J = 9.4, 5.7 Hz), 6.31 (dd, 1H, C*H*=CHφ, J = 16.0, 8.4 Hz), 6.60 (d, 1H, CH=C*H*φ, J = 16.0 Hz), 6.95–7.40 (m, 10H, 2φ), 8.92 (d, 1H, NH, J = 9.4 Hz).

4-Styryl 3[[(2-trityl-amino 4-thiazolyl)(methoxyimino)acetyl]amino] 2-azetidinone ***15***

To a solution of (2-trityl-amino 4-thiazolyl)(methoxyimino) acetic acid **13** (443 mg, 1 mmol) in dry CH_2Cl_2 (5 mL) was added dropwise, at 0°C under nitrogen, a solution of EEDQ (296 mg, 1.2 mmol) in CH_2Cl_2 (5 mL). The mixture was stirred for 1 h. Simultaneously, to a solution of *para*-toluenesulfonate salt of β-lactam **8** (360 mg, 1 mmol) in 6 mL CH_2Cl_2–DMF (4:1) was added dropwise, at 0°C under nitrogen, triethylamine (167 μL, 121 mg, 1.2 mmol). The mixture was allowed to warm up to 25°C over 1 h and was then added dropwise to the first solution at 0°C. After stirring overnight, the precipitate was filtered and washed with 1 mL CH_2Cl_2 to give 380 mg of trityl β-lactam **15** (yield: 62%); mp 235°C; ir (KBr) ν_{max}: 3410 (w, NH β-lactam), 3280 (br, NH), 1780 (CO β-lactam), 1670 (CO amide), 1590 (C=C) cm^{-1}; ^1H nmr (200 MHz, DMSO-d_6) δ: 3.6 (s, 3H, OCH_3), 4.4 (dd, 1H, C*H*—C=, J = 8.0, 5.0 Hz), 5.22 (dd, 1H, NH—C*H*—, J = 9.0, 5.0 Hz), 6.1 (dd, 1H, C*H*=CHPh, J = 16.0, 8.0 Hz), 6.34 (s, 1H, S—C*H*=), 6.6 (d, 1H, =C*H*Ph, J = 16.0 Hz), 7.26 (m, 20H, $4C_6H_5$), 8.48 (s, 1H, NH β-lactam), 8.78 (s, 1H, ϕ_3C—N*H*), 9.24 (d, 1H, NH amide, J = 9.0 Hz); ms (70 eV) *m/e*: 614 (9, M^+ + 1), 483 (9, M^+ − φCH=CH—NH + 1), 244 (1000, ϕ_3CH), 243 (195, ϕ_3C), 223 (110), 207 (235), 205 (101), 183 (128), 165 (167), 153 (104), 131 (147, C_6H_5—CH=CH—CH—NH), 115 (387).

4-Styryl 3[[(2-amino 4-thiazolyl)(methoxyimino)acetyl]amino] 2-azetidinone ***16***

Trityl β-lactam **15** (306 mg, 0.5 mmol) in 40 mL methanol – formic acid (2:1) was refluxed for 7 h. After evaporation of the solvent, the crude material was washed with chloroform (3 × 2 mL) and MeOH (1 × 1 mL) to give 173 mg (93%) of amino β-lactam **16**; mp 226–229°C; ir (KBr) ν_{max}: 3400 (NH β-lactam), 3300, 3200 (NH_2), 1770 (CO β-lactam), 1660 (CO amide), 1590 (C=C) cm^{-1}; ^1H nmr (200 MHz, DMSO-d_6) δ: 3.6 (s, 3H, OCH_3), 4.46 (dd, 1H, C*H*—C=, J = 8.0, 5.0 Hz), 5.26 (dd, 1H, NH—C*H*—, J = 9.0, 5.0 Hz), 6.26 (dd, 1H, C*H*=CHφ, J = 16.0, 8.0 Hz), 6.4 (s, 1H, S—C*H*=), 6.64 (d, 1H, C*H*φ, J = 16.0 Hz), 7.13 (s, 2H, NH_2), 7.24–7.44 (m, 5H, φ), 8.5 (s, 1N, NH β-lactam), 9.26 (d, 1H, NH amide, J = 9.0 Hz); ms (70 eV) *m/e*: 371 (3, M^+), 328 (3, M^+ − CONH), 240 (M^+ − PhCH=CH—CHNH), 210 (169), 181 (182), 156 (209, $C_5H_6N_3OS$), 131 (346, C_6H_5—CH=CH—CH—NH), 130 (1000), 126 (218, $C_4H_4N_3S$), 125 (349), 115 (224), 103 (230), 84 (307), 43 (353, CHNO).

4-Styryl 3-[[(2-amino 4-thiazolyl)(methoxyimino)acetyl]amino] 2-oxo 1-azetidine sulfonic acid, potassium salt ***18c***

(a) Method 1 (path A)

A solution of trityl-amino azetidinone **15** (184 mg, 0.3 mmol) in 2 mL pyridine–DMF (1:1) was heated under nitrogen to 80°C, and 215 mg (1.35 mmol) of pyridine – sulfur trioxide complex was added. The mixture was stirred at 80°C for 15 h until tlc showed no more starting material. Evaporation of the solvents *in vacuo* afforded **17** as a crude material; ir ($CHCl_3$) ν_{max}: 3500–2500 (br), 1770 (CO β-lactam), 1385, 1255 (SO_3), 1100, 1050 (SO_3), 920, 760, 730 cm^{-1}; ^1H nmr (60 MHz, $CDCl_3$) δ: 3.7 (s, 3H, OCH_3), 4.5–5.2 (m, 2H, N—C*H*—C*H*—), 6.1–7.0 (m, 3H, 3CH=), 7.2 and 8.0 (m, φ).

Crude **17** was dissolved in 16 mL methanol – formic acid (3:1); the solution was refluxed for 7 h and evaporated to dryness. The residue was washed with chloroform (5 × 2 mL), dissolved in methanol (0.5 mL), and 2 mL of potassium 2-ethyl hexanoate (0.5 *M* in ethyl acetate) was added. The slurry was cooled to 0°C, filtered, washed with ethyl acetate, and dried to give 105 mg of potassium salt ***18c***; yield ~ 75–80%; mp 200°C (dec.); pH = 4.5; ir (KBr) ν_{max}: 3650–2800 (br), 1770 (CO β-lactam), 1670 (CO amide), 1635, 1535, 1250 (SO_3), 1130 (strong), 1050 (SO_3), 980, 620 cm^{-1}; ^1H nmr (300 MHz, DMSO-d_6) δ: 3.9 (s, 3H, OCH_3), 4.64 (dd, 1H, C*H*—CH=, J = 8.0, 5.0 Hz), 5.3 (dd, 1H, NH—C*H*—, J = 10.0, 5.0 Hz), 6.37 (dd, 1H, C*H*=CHφ, J = 16.0, 8.0 Hz), 6.45 (s, 1H, S—C*H*=), 6.68 (d, 1H, C*H*φ, J = 16.0 Hz), 7.25 (br s, 2H, NH_2), 7.29–7.5 (m, 5H, φ), 9.2 (d, 1H, NH, J = 10.0 Hz); ms *m/e* (positive FAB): 529 (55, MH^+ + K), 528 (151, MK^+), 490 (151, MH^+), 452 (82), 451 (94, MH^+ − K), 410 (166, MH^+ − SO_3), 390 (121), 359 (272), 353 (121), 343 (91), 329 (70, MH^+ − KSO_3NCO), 321 (145), 279 (151, MH^+ − $HSO_3NC_9H_8$), 242 (1000), 240 (91, 279 − K), 165 (424, $C_4H_4N_3S$ + K), 126 (575, $C_4H_4N_3S$), 91 (363, $C_6H_5CH_2$).

(b) Method 1 (path B)

A solution of amino β-lactam **16** (93 mg, 0.25 mmol) in 1.5 mL pyridine–DMF (1:2) was heated under nitrogen to 80°C and 159 mg (1 mmol) of pyridine – sulfur trioxide complex was added. The mixture was stirred at 80°C for 10 h. Evaporation of the solvents *in vacuo* gave a crude material, which was washed with chloroform (5 × 1.5 mL) and dissolved in methanol (0.5 mL). A solution of potassium 2-ethyl hexanoate in ethyl acetate (1.5 mL, 0.5 *M*) was added. The slurry was cooled to 0°C, filtered, and dissolved in distilled water (1 mL). The

aqueous solution was washed with ethyl acetate (2 × 0.5 mL), partially evaporated *in vacuo*, and freeze-dried to afford 62 mg of potassium salt **18***c* as a white powder (yield: 51%).

(c) Method 2 (refs. 24, 25)

To a solution of triphenylphosphine (208 mg, 0.8 mmol) in 1.5 mL THF–DMF (2:1) was added a solution of 3-azido *N*-sulfonyl β-lactam **9***a* (390 mg, 0.73 mmol) in 1 mL THF. The mixture was stirred for 1 h at room temperature. A light precipitate of zwitterion **19** appeared during the reaction; ir (KBr) ν_{max}: 3480 (br), 3080, 2895, 2790, 1780 (CO β-lactam), 1590 (C=C), 1480, 1440, 1290, 1230 (SO_3), 1180, 1120, 1050 (SO_3), 990 cm^{-1}; ^1H nmr (300 MHz, DMSO-d_6) δ: 4.44 (m, 1H, C*H*—CH=), 4.88 (br s, 1H, N—C*H*), 6.48 (m, 2H, C*H*=), 7.4–8.1 (m, 22H); ms *m/e* (positive FAB): 551 (6, MNa^+), 529 (14, MH^+), 450 (12), 449 (27, $MH^+ - SO_3$), 406 (10, $MH^+ - HSO_3NCO$), 332 (20), 318 (10, $MH^+ - HSO_3C_9H_8$), 262 (47, $P\phi_3$), 242 (1000), 142 (322), 91 (57), 90 (161).

Thereupon, a solution of amino-thiazolyl acid **14** (147 mg, 0.73 mmol) in 2 mL THF–DMF (1:1) was added to the above solution and the mixture was heated to 50°C for 8 h. The solution was then cooled, filtered, and evaporated *in vacuo* to afford 500 mg of crude *N*-butylammonium salt **18***b*; ir (film) ν_{max}: 3380 (br), 2940, 2880 (CH_3, CH_2), 1750 (CO β-lactam), 1640 (CO amide), 1460, 1240 and 1040 (SO_3), 880, 750 cm^{-1}; ^1H nmr (300 MHz, $CDCl_3$) δ: 1.05 (t, 12H, $4CH_3$, J = 7.3 Hz), 1.5 (m, 8H, $4CH_2Me$), 1.7 (m, 8H, $4CH_2$), 3.34 (m, 8H, $4CH_2N$), 3.40 (s, 3H, OCH_3), 4.8–5.5 (m, 2H, C*H*—C*H*), 6.35–7.8 (m, 11H, φ, 3CH=, NH_2, NH); ms *m/e* (positive FAB): 332 (14, 240 + G), 242 (1000, NBu_4), 240 (72, $MH^+ - NBu_4$—$HSO_3NC_9H_8$), 165 (9, $C_4H_4N_3S$ + K), 142 (287, CH_2NBu_2), 126 (8, $C_4H_4N_3S$), 100 (46), 98 (40), 91 (9).

The *N*-butylammonium salt **18***b* was dissolved in distilled water – methanol (2:1) and the solution was applied to a column of ion-exchange resin (12 mL) (Dowex 50 × 8-200) previously charged in K^+ ions with a 1 *N* KCl solution. Elution was made first with a MeOH–H_2O solution (1:1) and then distilled water. The eluate was washed with chloroform (2 × 0.5 mL) to remove the small amount of unexchanged *N*-butylammonium salt (18 mg). The aqueous layer was partially evaporated *in vacuo* and freeze-dried to afford 36 mg of potassium salt **18***c* in 11% overall yield from **9***a*.

Acknowledgements

We wish to thank the Natural Sciences and Engineering Research Council of Canada and Lederle Laboratories for financial support, Ms. Nida Kuck for biological tests, Dr. S. Lang for providing a sample of acid **13**, Dr. Françoise Sauriol and Guerino Sacripante for taking the 300-MHz and 200-MHz ^1H nmr spectra, Dr. O. Mamer, Ms. J. Montgomery, and Dr. C. Kozikoff for the mass spectral data, Alexis Carpenter and Norman Hebert for preparation of some starting material, and Dr. Christopher M. Cimarusti, Squibb Institute, for valuable discussions during the XIth European Heterocyclic Colloquium in Ferrara, Italy, October 1985.

1. G. Just and R. Zamboni. Can. J. Chem. **56**, 2720 (1978); **56**, 2725 (1978).
2. A. Imada, K. Kitano, K. Kintaka, M. Muroi, and M. Asai. Nature, **289**, 590 (1981).
3. R. B. Sykes, C. M. Cimarusti, D. P. Bonner, K. Bush, D. M. Floyd, N. H. Georgopapadakou, W. H. Koster, W. C. Liu, W. L. Parker, P. A. Principe, M. L. Rathnum, W. A. Slusarchyk, W. H. Trejo, and J. S. Wells. Nature, **291**, 489 (1981).
4. H. Breuer, C. M. Cimarusti, T. Denzel, W. H. Koster, W. A. Slusarchyk, and U. D. Treuner. J. Antimicrob. Chemother. **8**, Suppl. E 21 (1981).
5. C. M. Cimarusti, D. P. Bonner, H. Breuer, H. W. Chang, A. W. Fritz, D. M. Floyd, T. P. Kissick, W. H. Koster, D. Kronenthal, F. Massa, R. H. Mueller, J. Pluscec, W. A. Slusarchyk, R. B. Sykes, M. Taylor, and E. R. Weaver. Tetrahedron, **39**, 2577 (1983).
6. D. M. Floyd, A. W. Fritz, and C. M. Cimarusti. J. Org. Chem. **47**, 176 (1982).
7. S. Kobayashi, T. Iimori, T. Izawa, and M. Ohno. J. Am. Chem. Soc. **103**, 2406 (1981).
8. J. V. Heck and B. G. Christensen. Tetrahedron Lett. 5027 (1981).
9. D. R. Kronenthal, C. Y. Han, and M. K. Taylor. J. Org. Chem. **47**, 2765 (1982).
10. A. K. Bose, M. S. Manhas, J. E. Vincent, K. Gala, and I. F. Fernandez. J. Org. Chem. **47**, 4075 (1982).
11. A. K. Bose, G. Spiegelman, and M. S. Manhas. J. Am. Chem. Soc. **90**, 4506 (1968).
12. T. W. Doyle, B. Belleau, B. Y. Luh, C. F. Ferrari, and M. P. Cunningham. Can. J. Chem. **55**, 468 (1977).
13. C. M. Cimarusti and R. B. Sykes. Med. Res. Rev. **4**, 1 (1984).
14. P. G. Mattingly and M. J. Miller. J. Org. Chem. **45**, 410 (1980).
15. G. W. Kabalka, K. A. R. Sastry, G. W. McCollum, and H. Yoshioka. J. Org. Chem. **46**, 4296 (1981).
16. B. H. Lipshutz, J. J. Pegram, and M. C. Morey. Tetrahedron Lett. 4603 (1981).
17. B. C. Laguzza and B. Ganem. Tetrahedron Lett. 1483 (1981).
18. C. A. Brown and V. K. Ahuja. J. Chem. Soc. Chem. Commun. 553 (1973); H. C. Brown and C. A. Brown. J. Am. Chem. Soc. **85**, 1005 (1963).
19. M. Vaultier, N. Knouzi, and R. Carrié. Tetrahedron Lett. 763 (1983).
20. D. M. Floyd, A. W. Fritz, J. Pluscec, E. R. Weaver, and C. M. Cimarusti. J. Org. Chem. **47**, 5160 (1982).
21. R. B. Sykes, W. L. Parker, C. M. Cimarusti, W. H. Koster, W. A. Slusarchyk, A. W. Fritz, and D. M. Floyd. Eur. Pat. Appl. EP 48,953, 07 Apr 1982; Chem. Abstr. **97**, 92116w (1982); Neth. Appl. NL 81 00,571, 01 Sept 1981; Chem. Abstr. **96**, 181062x (1982).
22. B. Belleau and G. Malek. J. Am. Chem. Soc. **90**, 1651 (1968); G. Just, D. Dugat, and W. Y. Liu. Can. J. Chem. **61**, 1730 (1983).
23. P. D. Jeffrey and S. W. McCombie. J. Org. Chem. **47**, 587 (1982); M. Kamber and G. Just. Can. J. Chem. **63**, 823 (1985).
24. J. Garcia, F. Urpi, and J. Vilarrasa. Tetrahedron Lett. 4841 (1984).
25. J. Zaloom, M. Calandra, and D. C. Roberts. J. Org. Chem. **50**, 2601 (1985).
26. A. I. Cohen, P. T. Funke, and B. N. Green. J. Pharm. Sci. **71**, 1065 (1982).

Can. J. Chem. Downloaded from www.nrcresearchpress.com by 80.58.250.72 on 09/07/12
For personal use only.

Synthesis of erythrina and related alkaloids. 17.[1] Total synthesis of *dl*-coccuvinine and *dl*-coccolinine

TAKEHIRO SANO,[2] JUN TODA, AND NOBUTERU MAEHARA
Showa College of Pharmaceutical Sciences, Tsurumaki, Setagaya-ku, Tokyo 154, Japan

AND

YOSHISUKE TSUDA
Faculty of Pharmaceutical Sciences, Kanazawa University, Takara-machi, Kanazawa 920, Japan

Received June 2, 1986

This paper is dedicated to Dr. O. E. (Ted) Edwards

TAKEHIRO SANO, JUN TODA, NOBUTERU MAEHARA, and YOSHISUKE TSUDA. Can. J. Chem. **65**, 94 (1987).

Total synthesis of *dl*-coccuvinine **1***a* and *dl*-coccolinine **2***a*, "abnormal-type" erythrinan alkaloids lacking the C(16) O-function at the aromatic ring, was effectively achieved by using the Diels–Alder reaction of dioxopyrroline. Isoquinolinopyrrolinedione **6***a*, a key dienophile, was synthesized via the tetrahydroisoquinoline **5***a*, which was prepared by Bischler–Napieralski cyclization of the amide **4***a* at the unactivated position. The Diels–Alder adduct **7***a* of 1,3-bis(trimethylsilyloxy)-butadiene with **6***a* with converted stereoselectively into these alkaloids in short steps.

TAKEHIRO SANO, JUN TODA, NOBUTERU MAEHARA et YOSHISUKE TSUDA. Can. J. Chem. **65**, 94 (1987).

Faisant appel à une réaction de Diels–Alder de la dioxopyrroline, on a effectivement réalisé la synthèse totale de la (*dl*)-coccuvinine (**1***a*) et de la (*dl*)-coccolinine (**2***a*), des alcaloïdes de l'érythrinane d'un «type anormal» et qui ne portent pas de fonction oxygénée en position C(16) du cycle aromatique. On a synthétisé l'isoquinolinopyrrolinedione (**6***a*), un diénophile clé, par le biais de la tétrahydroisoquinoléine **6***a* qui a été préparée par une cyclisation de Bischler–Napieralski de l'amide **4***a* vers la position qui n'est pas activée. L'adduit de Diels–Alder **7***a* du bis(triméthylsilyloxy)-1,3 butadiène avec le composé **6***a* peut être transformé stéréosélectivement dans les deux alcaloïdes par des étapes courtes.

[Traduit par la revue]

Introduction

Coccuvinine **1***a*, the alkaloid isolated from *Cocculus laurifolius* DC. (Menispermaceae), is an "abnormal-type" erythrinan alkaloid in the sense that it contains no oxygen function at the C(16) position (1). Coccolinine **2***a* is the 8-oxo derivative of **1***a*. This non-basic lactam alkaloid was also isolated from the same plant (2). The synthesis of "abnormal-type" erythrinan alkaloids is of interest because of their biological activity, such as hypotensive and neuromuscular blocking action (3). We wish to report in detail the total synthesis of *dl*-coccuvinine **1***a* and *dl*-coccolinine **2***a*.

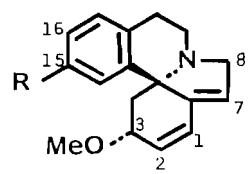

1

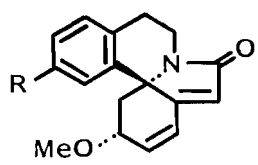

2

a: R=OMe, b: R=H

We have recently developed a new effective synthetic route to the erythrinan alkaloids using Diels–Alder reaction of isoquinolinopyrrolinedione with 1,3-*O*-disubstituted butadiene as a key step (4–6). This method provides a short synthesis of these alkaloids, if the isoquinoline ring closure occurs at the *meta* position with respect to the methoxy group on the aromatic ring. Ju-ichi *et al.* (7), who accomplished the first total synthesis of the abnormal-type erythrinan alkaloids by the method developed by Mondon *et al.* (8, 9), solved this problem by the introduction of an ethoxycarbamide group at the C(16) position as a regioselective *para*-directing group. Eventually this function was replaced with hydrogen after ring closure. However, this conversion itself requires several additional steps, thus lowering the total yield. Therefore, to further prove the efficiency of our method of erythrinan alkaloid synthesis, we have chosen these alkaloids as target molecules.

Total synthesis of dl-*coccuvinine and* dl-*coccolinine*

Condensation of 2-(4-methoxyphenyl)-ethylamine **3***a* with methyl chloroformylacetate afforded the amide **4***a* in good yield. As anticipated, the isoquinoline ring closure of **4***a* was very difficult. Treatment of **4***a* with phosphorus oxychloride under reflux afforded the tetrahydroisoquinoline **5***a* in only 3% yield. No starting material was recovered. Heating of **4***a* with polyphosphate ester (PPE) (10) in chloroform under reflux for 18 h afforded **5***a* in 15% yield together with an appreciable amount of the starting material (22%). Increase of the reaction time (48 h) resulted in greater decomposition of **5***a*, thus lowering the yield of **5***a* (9%). A fairly good result, although not optimized, was obtained by heating **4***a* in PPE without solvent for 18 h. Under these conditions **5***a* was formed in 34% yield and the starting material recovered in 33% yield. Since the starting material can be recycled, the net yield of **5***a* was calculated to be 51%. Condensation of **5***a* with oxalyl chloride provided the isoquinolinopyrrolinedione **6***a* in 78% yield. The structure of the dioxopyrroline moiety was readily characterized by the visible absorption band at 430 nm (11). Thus the key intermediate **6***a* was obtained from the commercially available amine **3***a* in 38% overall yield.

The Diels–Alder reaction of **6***a* with 1,3-trimethylsilyloxy-butadiene proceeded in a regio- and stereoselective manner. Thus, heating of **6***a* with the diene in toluene at 130°C for 20 min afforded the adduct **7***a* in 71% yield. The stereochemical assignment of the C(1) OTMS group as having the *endo* configuration results from comparison of the nmr spectrum of **7***a* with those of the adducts reported in the previous papers

[1]For part 16 see ref. 6. This paper also constitutes Part XXXIX of Dioxopyrrolines.

[2]Author to whom correspondence may be addressed.

Can. J. Chem. Downloaded from www.nrcresearchpress.com by 80.58.250.72 on 09/07/12
For personal use only.

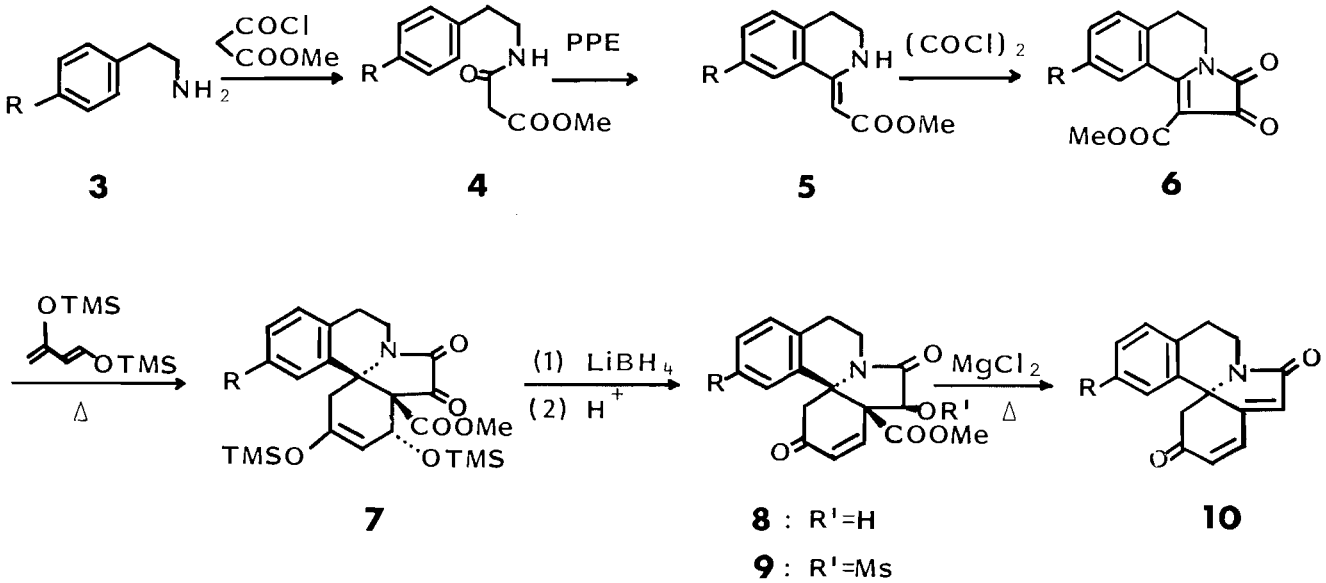

(6, 12). Reduction of **7***a* with lithium borohydride at −63°C occurred selectively at the C(7) keto group and treatment of the resulting alcohol with hydrochloric acid afforded the enone **8***a* in 56% yield. Removal of the methoxycarbonyl group at the C(6) position was effected by heating **8***a* with magnesium chloride in DMSO (13), giving rise to the dienone **10***a* with concomitant dehydration of the C(7) OH group in 32% yield. Substitution of the C(7) OH by a good leaving group markedly improved this step. Thus mesylation of **8***a* and demethoxycarbonylation of the resulting mesylate **9***a* under similar conditions produced **10***a* in 72% yield.

Meerwein–Ponndorf reduction of **10***a* occurred stereoselectively at the C(3) ketone to give the α-alcohol **11***a* and the β-alcohol **12***a* in 76 and 18% yields, respectively. Methylation of **11***a* with methyl iodide in the presence of a phase transfer catalyst afforded *dl*-coccolinine **2***a* in 93% yield. Reduction of **2***a* with aluminum hydride generated by lithium aluminum hydride, and aluminum chloride in THF occurred site-selectively at the C(8) lactam carbonyl group to furnish *dl*-coccuvinine **1***a* in 93% yield. The identity of **1***a* and **2***a* with authentic samples was confirmed by their spectral comparison. Thus, the total synthesis of *dl*-coccuvinine was effectively accomplished in 10 steps, proceeding in 6–7% overall yield from the commercially available amine **3***a*.

Synthesis of 15-demethoxycoccuvinine

Because of physiological interest, we have synthesized 15-demethoxycoccuvinine **1***b*, an unnatural erythrinan compound that lacks an O-function at the aromatic ring. The synthesis was achieved via the same route starting from phenylethylamine. Bischler–Napieralski cyclization of the amide **4***b*, using PPE as a condensing reagent as described above, afforded the tetra-

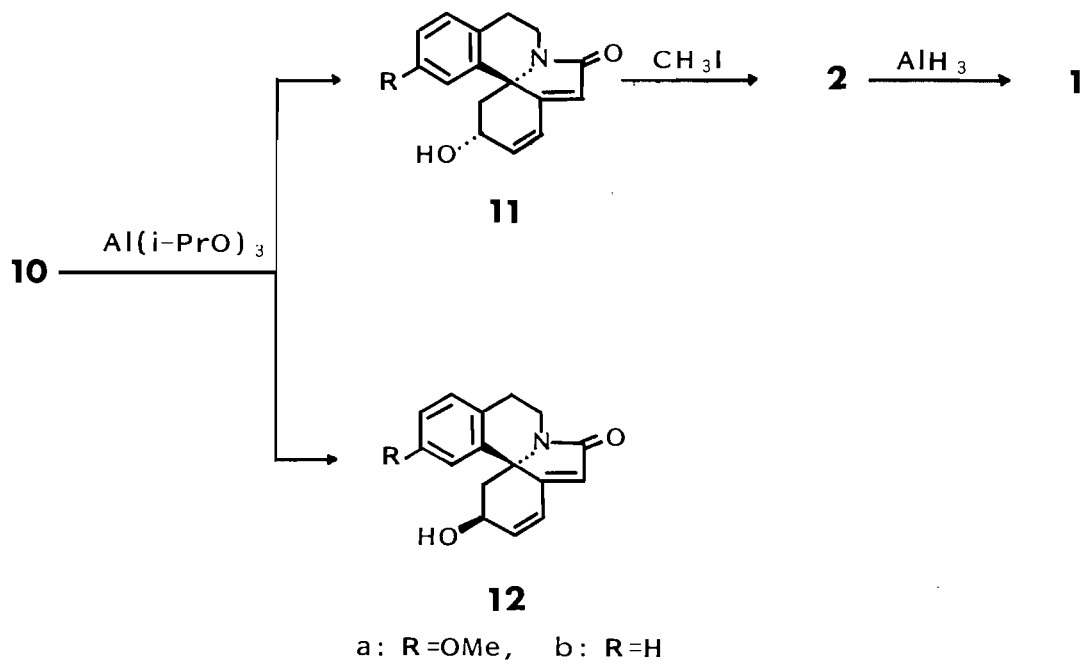

Can. J. Chem. Downloaded from www.nrcresearchpress.com by 80.58.250.72 on 09/07/12
For personal use only.

hydroisoquinoline **5***b* in 47% yield. The subsequent reactions proceeded in similar manner and afforded *dl*-15-demethoxycoccuvinine **1***b* in a comparable yield.

Experimental

Unless otherwise stated, the following procedures were adopted. Melting points were taken on a Yanagimoto hot-stage apparatus and are uncorrected. Organic extracts were dried over anhydrous Na_2SO_4 and concentrated *in vacuo*. Column chromatography was performed on silica gel (Wakogel C-200). Thin-layer chromatographic (tlc) analyses were carried out by using silica gel plates (Merck precoated plates, silica gel 60F-254). Infrared spectra were taken in Nujol mulls with a Hitachi 260-10 spectrometer, and are given in cm^{-1}. Ultraviolet spectra were recorded in dioxane solution with a Hitachi 200-10 spectrophotometer. Proton nuclear magnetic resonance spectra were taken in $CDCl_3$ solution with tetramethylsilane (TMS) as an internal standard on a JEOL JNM-FX100 (FT-NMR; 100 MHz) spectrometer.

*General procedure for condensation reaction of arylethylamine **3** with methyl chloroformylacetate*

A solution of methyl chloroformylacetate (1.2 equiv. of **3**) in CH_2Cl_2 (50 mL) was added dropwise to a mixed solution of arylethylamine **3** in CH_2Cl_2 (100 mL) and 10% K_2CO_3 (1.2 equiv.) at 0°C, and stirring was continued for 1 h. The reaction mixture was neutralized with 5% HCl and the organic layer was washed with water, dried, and evaporated. Crystallization of the residue gave the amide **4**.

*Methoxycarbonylaceto-2-(4-methoxyphenyl)ethylamide (**4**a)*

Compound **4***a* (7.96 g, 96%) was prepared from **3***a* (5.00 g), mp 88–89°C, as colorless needles from AcOEt; ir ν_{max}: 3260, 1740, 1630 cm^{-1}; ^{1}Hmr δ: 2.77 (t, J = 7 Hz, 2H, $ArCH_2$—), 3.28 (s, 2H, —$COCH_2CO$—), 3.47 (t, J = 7 Hz, $>NCH_2$—), 3.72 (s, 3H, $COOCH_3$), 3.79 (s, 3H, OCH_3), 6.85 (d, J = 9 Hz, 1H, ArH), 7.14 (d, J = 9 Hz, 1H, ArH). *Mol. Wt.* calcd. for $C_{13}H_{17}NO_4$: 251.1156; found (ms): 251.1143.

*Methoxycarbonylaceto-2-phenylethylamide (**4**b)*

Compound **4***b* (16.1 g, 88%) was prepared from **3***b* (10 g), mp 65–67°C, as colorless needles from AcOEt; ir ν_{max}: 3230, 1740, 1640 cm^{-1}; ^{1}Hmr δ: 2.83 (t, J = 7 Hz, 2H, $ArCH_2$—), 3.48 and 3.61 (d, J = 7 Hz, each 1H, $>NCH_2$—), 3.71 (s, 3H, $COOCH_3$), 7.24 (m, 5H, ArH). *Mol. Wt.* calcd. for $C_{12}H_{15}NO_3$: 221.1050; found (ms): 221.1033.

*General procedure for Bischler–Napieralski reaction of nonactivated amide **4***

A mixture of **4** and polyphosphate ester (PPE) (20 times the amount of **4**) was heated at 80°C for the appropriate time (18 h for **4***a* and 40 h for **4***b*). After the excess of PPE was decomposed with ice water, the solution was basified with 10% K_2CO_3 and extracted with $CHCl_3$. The extract was washed with water, dried, and evaporated. The residue was chromatographed on silica gel using $CHCl_3$ as eluent to give the isoquinoline **5**.

*(Z)-7-Methoxy-1-methoxycarbonylmethylidene-1,2,3,4-tetrahydroisoquinoline (**5**a)*

Compound **5***a* (1.60 g, 34%) was obtained from **4***a* (5.00 g) as a pale yellow oil; ir ν_{max}: 3300, 1650 cm^{-1}; ^{1}Hmr δ: 2.77 (t, J = 7 Hz, 2H, $ArCH_2$—), 3.39 (t, J = 7 Hz, 2H, $>NCH_2$—), 3.69 (s, 3H, $COOCH_3$), 3.78 (s, 3H, OCH_3), 5.12 (s, 1H, $>C$=$CHCO$—), 6.9–7.1 (m, 3H, ArH). *Mol. Wt.* calcd. for $C_{13}H_{15}NO_3$: 233.1052; found (ms): 233.1059.

The starting amide **4***a* (1.70 g, 33%) was recovered from the column chromatography.

*(Z)-1-Methoxycarbonylmethylidene-1,2,3,4-tetrahydroisoquinoline (**5**b)*

Compound **5***b* (2.20 g, 47%) was obtained from **4***b* (5.08 g) as a pale yellow oil; ir($CHCl_3$) ν_{max}: 3300, 1650 cm^{-1}; ^{1}Hmr δ: 2.81 (t, J = 6 Hz, 2H, $ArCH_2$—), 3.42 (m, 2H, $>NCH_2$—), 3.68 (s, 3H, $COOCH_3$), 5.15 (s, 1H, $>C$=$CHCO$—), 7.39 (m, 4H, ArH).

The starting amide **4***b* (709 mg, 14%) was recovered from the column chromatography.

*General procedure for condensation reaction of **5** with oxalylchloride*

Oxalylchloride (1.1 equiv. of **5**) was added dropwise to a solution of **5** in anhydrous ether (50 mL) at 0°C under stirring, and the stirring was continued for one additional hour. The precipitate was collected by filtration and chromatographed on silica gel, using $CHCl_3$ as eluent, to give the dioxopyrroline **6**.

*8-Methoxy-1-methoxycarbonyl-2,3-dioxo-2,3,5,6-tetrahydropyrrolo[2,1-a]isoquinoline (**6**a)*

Compound **6***a* (892 mg, 78%) was obtained from **5***a* (930 mg), mp 181–185°C, as red prisms from AcOEt; ir ν_{max}: 1760, 1730, 1680 cm^{-1}; uv (dioxane, 25°C) λ_{max} (ε): 220 (15 800), 300 (12 600), 383 (4 900), 425 (4 100; sh); ^{1}Hmr δ: 3.03 (t, J = 6 Hz, 2H, $ArCH_2$—), 3.81 (t, J = 6 Hz, 2H, $>NCH_2$—), 3.87 (s, 6H, $COOCH_3$ and OCH_3), 7.17 (dd, J = 3 and 9 Hz, 1H, ArH), 7.29 (d, J = 9 Hz, 1H, ArH), 8.08 (d, J = 3 Hz, 1H, ArH). *Mol. Wt.* calcd. for $C_{15}H_{13}NO_4$: 287.0794; found (ms): 287.0797.

*1-Methoxycarbonyl-2,3-dioxo-2,3,5,6-tetrahydropyrrolo[2,1-a]isoquinoline (**6**b)*

Compound **6***b* (1.15 g, 61%) was obtained from **5***b* (1.5 g), mp 203–206°C, as red prisms from AcOEt; ir ν_{max}: 1760, 1720, 1700 cm^{-1}; ^{1}Hmr δ: 3.10 (t, J = 4 Hz, 2H, $ArCH_2$—), 3.84 (t, J = 4 Hz, 2H, $>NCH_2$—), 3.88 (s, 3H, $COOCH_3$), 7.53 (m, 4H, ArH). *Mol. Wt.* calcd. for $C_{14}H_{11}NO_4$: 257.0687; found (ms): 257.0687.

*General procedure for Diels–Alder reaction of **6** with 1,3-bis(trimethylsilyloxy)-1,3-butadiene*

A solution of **6** and the diene (5 equiv. of **6**) in toluene (10 mL) was heated at 130°C for 20 min in a sealed tube. The solution was concentrated to dryness to give a residue, which was triturated with *n*-hexane to give the adduct **7**.

(4R, 4aR*, 13bR*)-12-Methoxy-4a-methoxycarbonyl-5,6-dioxo-2,4-bis(trimethylsilyloxy)-4,4a,5,6,8,9-hexahydro-1H-indolo[7a,1-a]isoquinoline (**7**a)*

Compound **7***a* (256 mg, 71%) was prepared from **6***a* (200 mg), mp 144–146°C, as colorless prisms from EtOAc–*n*-hexane; ir ν_{max}: 1780, 1740, 1720, 1660 cm^{-1}; ^{1}Hmr δ: 0.05 and 0.12 (each s, 9H, $Si(CH_3)_3$), 2.90 (s, 3H, $COOCH_3$), 3.59 (s, 3H, OCH_3), 5.12 (d, J = 6 Hz, 1H, $>CHOTMS$), 5.25 (d, J = 6 Hz, 1H, C=CH—), 6.60–7.20 (m, 3H, ArH). *Mol. Wt.* calcd. for $C_{25}H_{35}NO_7Si_2$: 517.1952; found (ms): 517.1958.

(4R, 4aR*, 13bR*)-4a-Methoxycarbonyl-5,6-dioxo-2,4-bis(trimethylsilyloxy)-4,4a,5,6,8,9-hexahydro-1H-indolo[7a,1-a]isoquinoline (**7**b)*

Compound **7***b* (780 mg, 67%) was prepared from **6***b* (617 mg), mp 155–158°C, as colorless prisms from EtOAc; ir ν_{max}: 1760, 1710, 1650 cm^{-1}; ^{1}Hmr δ: 0.11 (s, 18H, 2 × $Si(CH_3)_3$), 2.83 (s, 3H, $COOCH_3$), 5.12 (d, J = 5 Hz, 1H, $>CHOTMS$), 5.22 (d, J = 5 Hz, 1H, C=CH—), 7.02 (m, 4H, ArH). *Mol. Wt.* calcd. for $C_{24}H_{35}NO_6Si_2$: 487.1844; found (ms): 487.1824.

*General procedure for reduction of **7** with $LiBH_4$*

A mixture of **7** and $LiBH_4$ in anhydrous THF was stirred for 20 min at −60°C under an argon atmosphere. The mixture was diluted with Et_2O, washed with saturated NaCl solution and water, dried, and evaporated. The residue in 5% HCl–THF (1:1) (10 mL) was heated on a water bath for 1 h. The mixture was extracted with $CHCl_3$, washed with water, dried, and evaporated. Recrystallization of the residue gave the enone **8**.

Can. J. Chem. Downloaded from www.nrcresearchpress.com by 80.58.250.72 on 09/07/12
For personal use only.

Can. J. Chem. Downloaded from www.nrcresearchpress.com by 80.58.250.72 on 09/07/12
For personal use only.

(4aS,5S*,13bR*)-5-hydroxy-12-methoxy-4a-methoxycarbonyl-2,6-dioxo-2,4a,5,6,8,9-hexahydro-1*H*-indolo[7a,1-a]isoquinoline (**8**a)*

Compound **8***a* (77 mg, 56%) was obtained by reduction of **7***a* (202 mg) with $LiBH_4$ (5 mg) in THF (6 mL), mp 189–192°C, as colorless prisms from Et_2O–acetone; ir ν_{max}: 3250, 1740, 1690 cm^{-1}; ^{1}Hmr δ: 3.27 (s, 3H, $COOCH_3$), 3.64 (s, 3H, OCH_3), 4.77 (s, 1H, >CHOH), 6.43 and 7.53 (each d, J = 11 Hz, 1H, —COCH=CH—), 6.5–7.0 (m, 3H, ArH). *Mol. Wt.* calcd. for $C_{19}H_{19}NO_6$: 357.1211; found (ms): 357.1206.

(4aS,5S*,13bR*)-5-Hydroxy-4a-methoxycarbonyl-2,6-dioxo-2,4a,5,6,8,9-hexahydro-1*H*-indolo[7a,1-a]isoquinoline (**8**b)*

Compound **8***b* (300 mg, 89%) was obtained by reduction of **7***b* (500 mg) with $LiBH_4$ (26 mg) in THF (9 mL), mp 191–194°C, as colorless prisms from Et_2O–MeOH; ir ν_{max}: 3250, 1740, 1690 cm^{-1}; ^{1}Hmr δ: 2.80 and 3.20 (d, J = 16 Hz, each 1H, —$COCH_2$—), 3.22 (s, 3H, $COOCH_3$), 4.79 (s, 1H, —COCH=CH—), 7.04 (m, 4H, ArH), 7.55 (d, J = 11 Hz, 1H, —COCH=CH—). *Mol. Wt.* calcd. for $C_{18}H_{17}NO_5$: 327.1105; found (ms): 327.1100.

*General procedure for mesylation reaction of **8** with methanesulfonylchloride*

A mixture of **8** and methanesulfonylchloride (4 equiv. of **8**) in pyridine (5 mL) was stirred at room temperature for 2 h. The reaction mixture was basified with 10% K_2CO_3 and extracted with $CHCl_3$. The extract was washed with water, dried, and evaporated. Recrystallization of the residue gave the mesylate **9**.

(4aS,5S*,13bR*)-5-Methanesulfonyloxy-12-methoxy-4a-methoxycarbonyl-2,6-dioxo-2,4a,5,6,8,9-hexahydro-1*H*-indolo[7a,1-a]isoquinoline (**9**a)*

Compound **9***a* (145 mg, 80%) was obtained by reaction of **8***a* (156 mg) and CH_3SO_2Cl (200 mg) in pyridine (2 mL), mp 211–212°C, as colorless prisms from Et_2O–MeOH; ir ν_{max}: 1750, 1725, 1695, 1620 cm^{-1}; ^{1}Hmr δ: 3.31 (s, 3H, $COOCH_3$), 3.37 (s, 3H, OSO_2CH_3), 3.65 (s, 3H, OCH_3), 5.50 (s, 1H, >CHOMs), 6.50 (d, J = 11 Hz, 1H, —COCH=CH—), 6.5–7.0 (m, 3H, ArH), 7.47 (d, J = 11 Hz, —COCH=CH—). *Mol. Wt.* calcd. for $C_{20}H_{21}NO_8S$: 435.0985; found (ms): 435.0985.

(4aS,5S*,13bR*)-5-Methanesulfonyloxy-4a-methoxycarbonyl-2,6-dioxo-2,4a,5,6,8,9-hexahydro-1*H*-indolo[7a,1-a]isoquinoline (**9**b)*

Compound **9***b* (329 mg, 81%) was prepared from **8***b* (328 mg), mp 181–183°C, as colorless prisms from Et_2O–MeOH; ir ν_{max}: 1740, 1720, 1690 cm^{-1}; ^{1}Hmr δ: 3.25 (s, 3H, $COOCH_3$), 3.37 (s, 3H, —OSO_2CH_3), 5.57 (s, 1H, >CH—OMs), 7.16 (m, 4H, ArH), 7.17 (d, J = 11 Hz, —COCH=CH—), 7.44 (d, J = 11 Hz, —COCH=CH—). *Mol. Wt.* calcd. for $C_{19}H_{19}NO_7S$: 405.0811; found (ms): 405.0896.

*General procedure for demethoxycarbonylation of the mesylate **9***

A mixture of **9** and $MgCl_2$ (5 equiv. of **9**) in DMSO (5 mL) was heated at 160°C for 2 h in a sealed tube. The mixture was extracted with $CHCl_3$. After an addition of water the extract was washed with water, dried, and evaporated. The residue was chromatographed on silica gel using $CHCl_3$ as eluent to give the dienone **10**.

*12-Methoxy-2,6-dioxo-2,6,8,9-tetrahydro-1*H*-indolo[7a,1-a]isoquinoline (**10**a)*

Compound **10***a* (30 mg, 89%) was prepared from **9***a* (52 mg), mp 180–183°C, as pale yellow prisms from AcOEt; ir ν_{max}: 1690, 1665 cm^{-1}; ^{1}Hmr δ: 2.78 and 3.27 (d, J = 15 Hz, each 1H, —$COCH_2$—), 3.70 (s, 3H, OCH_3), 6.38 (d, J = 10 Hz, —COCH=CH—), 6.76–7.13 (m, 3H, ArH), 7.75 (d, J = 10 Hz, —COCH=CH—). *Mol. Wt.* calcd. for $C_{17}H_{15}NO_3$: 281.1052; found (ms): 281.1065.

*2,6-Dioxo-2,6,8,9-tetrahydro-1*H*-indolo[7a,1-a]isoquinoline (**10**b)*

Compound **10***b* (22 mg, 68%) was prepared from **9***b* (52 mg), mp 147–149°C, as pale yellow prisms from AcOEt; ir ν_{max}: 1720, 1670 cm^{-1}; ^{1}Hmr δ: 2.79 and 3.27 (d, J = 15 Hz, each 1H, —$COCH_2$—), 6.37 (d, J = 10 Hz, 1H, —COCH=CH—), 6.38 (s, 1H, —C=CH—CO—), 7.18 (m, 4H, ArH), 7.76 (d, J = 10 Hz, 1H, —COCH=CH—). *Mol. Wt.* calcd. for $C_{16}H_{13}NO_2$: 251.0947; found (ms): 251.0965.

*General procedure for Meerwein–Ponndorf reduction of **10** with aluminium isopropoxide*

A mixture of **10** and Al(i-PrO)$_3$ (20 equiv. of **10**) in anhydrous i-PrOH was heated under reflux for 24 h under an argon atmosphere. The mixture was acidified with 5% HCl and extracted with $CHCl_3$. The extract was washed with water, dried, and evaporated. The residue was purified by preparative tlc (developed by $CHCl_3$–MeOH (30:1)) to give two fractions. The more polar fraction gave the α-alcohol (**11**) and the less polar fraction gave the β-alcohol (**12**).

(2S,13bR*)-2-Hydroxy-12-methoxy-6-oxo-2,6,8,9-tetrahydro-1*H*-indolo[7a,1-a]isoquinoline (**11**a)*

Compound **11***a* (38 mg, 76%) was prepared from **10***a* (50 mg), mp 102–103°C, as colorless prisms from MeOH; ir ν_{max}: 3350, 1640 cm^{-1}; ^{1}Hmr δ: 1.69 (dd, J = 5 Hz, 1H, H-1′), 2.79 (dd, J = 5 and 11 Hz, H-1′), 3.72 (s, 3H, C_{12}-OCH_3), 4.1–4.3 (m, 1H, —CH—OH), 5.97 (s, 1H, —COCH=C—), 6.25 (br d, J = 10 Hz, 1H, —COCH=CH—), 6.7–6.9 (m, 2H, ArH), 6.80 (dd, J = 2 and 10 Hz, 1H, —CH=CH—CH(OH)—), 7.13 (d, J = 9 Hz, ArH). *Mol. Wt.* calcd. for $C_{17}H_{17}NO_3$: 283.1208; found (ms): 283.1208. *Anal.* calcd. for $C_{17}H_{17}NO_3$: C 72.07, H 6.05, N 4.94; found: C 72.22, H 6.13, N 4.96.

(2R,13bR*)-2-Hydroxy-12-methoxy-6-oxo-2,6,8,9-tetrahydro-1*H*-indolo[7a,1-a]isoquinoline (**12**a)*

Compound **12***a* (9 mg, 18%) was prepared from **10***a* (50 mg), mp 83–85°C, as colorless prisms from Et_2O; ir ν_{max}: 3300, 1640 cm^{-1}; ^{1}Hmr δ: 2.11 (dd, J = 5 and 14 Hz, 1H, H-1′), 2.73 (br d, J = 14 Hz, 1H, H-1′), 3.75 (s, 3H, C_{12}-OCH_3), 4.47 (br t, J = 5 Hz, 1H, —CH—OH), 6.01 (s, 1H, —COCH=C—), 6.29 (dd, J = 5 and 10 Hz, 1H, —CH=CH—CH(OH)—), 6.78 (dd, J = 3 and 8 Hz, ArH), 6.91 (d, J = 10 Hz, 1H, —CH=CH—CH(OH)—), 6.93 (d, J = 3 Hz, 1H, ArH), 7.20 (d, J = 8 Hz, 1H, ArH).

(2S,13bR*)-2-Hydroxy-6-oxo-2,6,8,9-tetrahydro-1*H*-indolo[7a,1-a]isoquinoline (**11**b)*

Compound **11***b* (81 mg, 83%) was prepared from **10***b* (97 mg), mp 196–198°C, as colorless prisms from MeOH; ir ν_{max}: 3350, 1650 cm^{-1}; ^{1}Hmr δ: 4.12 (m, 1H, —CHOH), 5.96 (s, 1H, —COCH=C—), 6.25 (d, J = 10 Hz, 1H, H-4′), 6.80 (dd, J = 3 and 10 Hz, 1H, H-3′), 7.12 (m, 4H, ArH). *Mol. Wt.* calcd. for $C_{16}H_{15}NO_2$: 253.1101; found (ms): 253.1088.

(2R,13bR*)-2-Hydroxy-6-oxo-2,6,8,9-tetrahydro-1*H*-indolo[7a,1-a]isoquinoline (**12**b)*

Compound **12***b* (13 mg, 13%) was prepared from **10***b* (97 mg), mp 75–77°C, as colorless prisms from Et_2O; ir ν_{max}: 3200, 1670, 1650 cm^{-1}; ^{1}Hmr δ: 4.46 (t, J = 5 Hz, 1H, —CHOH), 6.02 (s, 1H, H-5′), 6.28 (dd, J = 5 and 10 Hz, 1H, H-3′), 6.93 (d, J = 10 Hz, 1H, H-4′), 7.27 (m, 4H, ArH). *Mol. Wt.* calcd. for $C_{16}H_{15}NO_6$: 253.1101; found (ms): 253.1076.

Synthesis of dl*-coccolinine (**2**a) and* dl*-15-demethoxycoccolinine (**2**b)*

A mixture of **11***a* (50 mg), CH_3I (280 mg), Et_4NBr (210 mg), and KOH (99 mg) in anhydrous THF (10 mL) was stirred for 18 h at room temperature. The mixture was diluted with water and extracted with $CHCl_3$. The extract was washed with water, dried, and evaporated. Recrystallization of the residue from MeOH gave *dl*-coccolinine **2***a* (49 mg, 93%) as colorless prisms, mp 152–154°C; ir ν_{max}: 1670, 1610 cm^{-1}; ^{1}Hmr δ: 2.82 (dd, J = 4 and 12 Hz, 1H, H-4′), 3.34 (s, 3H, OCH_3), 3.74 (s, 3H, OCH_3), 3.90 (m, 1H, —CHOMe), 6.03 (s, 1H, —COCH=C—), 6.30 (d, J = 9 Hz, 1H, H-1′), 6.70–7.30 (m, 3H, ArH), 6.79 (d, J = 9 Hz, 1H, H-2′). *Mol. Wt.* calcd. for $C_{18}H_{19}NO_3$: 297.1365; found (ms): 297.1365.

The ir and ^{1}Hmr spectra were identical with those of natural coccolinine. The difference in melting point of *dl*-coccolinine from

that reported (lit. (7) mp 179–180°C) might be attributable to the presence of dimorphic forms.

Similarly, a solution of **11***b* (67 mg) in anhydrous THF (10 mL) was treated with CH_3I (600 mg) in the presence of Et_4NBr (210 mg) and KOH (80 mg). Working up as described above, *dl*-demethoxycoccolinine **2***b* (65 mg, 95%) was obtained as colorless needles from AcOEt, mp 165–168°C; ir ν_{max}: 1675 cm^{-1}; ^{1}Hmr δ: 1.74 (d, J = 12 Hz, 1H, H-4′), 2.82 (dd, J = 5 and 12 Hz, 1H, H-4′), 3.33 (s, 3H, OCH_3), 3.99 (m, 1H, H-3′), 6.02 (s, 1H, H-8′), 6.30 (d, J = 10 Hz, 1H, H-1′), 6.88 (dd, J = 2 and 10 Hz, 1H, H-2′). *Mol. Wt.* calcd. for $C_{17}H_{17}NO_2$: 267.1257; found (ms): 267.1255.

Synthesis of dl-*coccuvinine (**1**a) and* dl-*15-demethoxycoccuvinine (**1**b)*

An ethereal solution of excess AlH_3 (prepared from $LiAlH_4$:$AlCl_3$ = 3:1) was added to a solution of **2***a* (60 mg) in anhydrous THF (15 mL) at room temperature under an argon atmosphere. The reaction mixture was stirred for a further 2 h. The mixture was basified with 10% NH_4OH and extracted with $CHCl_3$. The extract was washed with water, dried, and evaporated to give *dl*-coccuvinine **1***a* (52 mg, 91%) as a colorless oil (picrate, yellow prisms from EtOH, mp 166–167°C); ^{1}Hmr δ: 1.90 (t, J = 11 Hz, 1H, H-4′), 2.52 (dd, J = 5.5 and 11 Hz, 1H, H-4′), 3.31 (s, 3H, OCH_3), 3.73 (s, 3H, OCH_3), 3.96 (m, 1H, H-3′), 5.72 (s, 1H, H-7′), 5.99 (d, J = 10 Hz, H-1′), 6.56 (dd, J = 2 and 10 Hz, 1H, H-2′), 6.70 (d, J = 2.7 Hz, 1H, ArH), 6.81 (dd, J = 2.7 and 8.0 Hz, 1H, ArH), 7.08 (d, J = 8.0 Hz, 1H, ArH).

The ir and ^{1}Hmr spectra were identical with those of natural coccuvinine.

Similarly, **2***b* (50 mg) in anhydrous THF (13 mL) was reduced with excess AlH_3 as described above to give 15-demethoxycoccuvinine **1***b* (44 mg, 93%) as a colorless oil (picrate, yellow prisms from EtOH, mp 191–193°C); ^{1}Hmr δ: 1.84 (t, J = 11 Hz, 1H, H-4′), 2.54 (dd, J = 6 and 11 Hz, 1H, H-4′), 3.29 (s, 3H, OCH_3), 3.85 (m, 1H, H-3′), 5.71 (s, 1H, H-7′), 5.97 (d, J = 10 Hz, 1H, H-1′), 6.55 (dd, J = 2 and 10 Hz, 1H, H-2′), 7.14 (m, 5H, ArH).

Acknowledgement

We are grateful to Professor M. Ju-ichi, Mukogawa Women's University, for providing the spectral data of coccolinine and coccuvinine.

1. A. N. Singh and D. S. Bhakuni. J. Indian Chem. Soc. **15**B, 388 (1977).
2. H. Pande, N. K. Saxena, and D. S. Bhakuni. J. Indian Chem. Soc. **14**B, 366 (1976).
3. V. B. Zakirov, Kh. V. Aliev, and N. V. Abdumalikova. Farmakol. Alkaloidov Serdechnykh Glikozidov (USSR), 197 (1971); Chem. Abstr. **77**, 135092 (1972).
4. T. Sano, J. Toda, N. Kashiwaba, Y. Tsuda, and Y. Iitaka. Heterocycles, **16**, 1151 (1981).
5. T. Sano. J. Toda, and Y. Tsuda. Heterocycles, **18**, 229 (1982).
6. T. Sano, J. Toda, N. Kashiwaba, T. Ohshima, and Y. Tsuda. Chem. Pharm. Bull. In press.
7. M. Ju-ichi, Y. Fujitani, and Y. Ando. Chem. Pharm. Bull. **29**, 396 (1981).
8. A. Mondon, K. F. Hansen, K. Boeme, H. P. Faro, H. J. Nestler, H. G. Vihuber, and K. Bottcher. Chem. Ber. **103**, 615 (1970).
9. A. Mondon and H. J. Nestler. Chem. Ber. **112**, 1329 (1979).
10. Y. Kanaoka, E. Sato, O. Yonemitsu, and Y. Ban. Chem. Pharm. Bull. **12**, 793 (1964).
11. T. Sano, Y. Horiguchi, J. Toda, K. Imafuku, and Y. Tsuda. Chem. Pharm. Bull. **32**, 497 (1984).
12. Y. Tsuda, T. Ohshima, T. Sano, and J. Toda. Heterocycles, **19**, 2027 (1982).
13. Y. Tsuda and Y. Sakai. Synthesis, 119 (1981).

Can. J. Chem. Downloaded from www.nrcresearchpress.com by 80.58.250.72 on 09/07/12
For personal use only.

^{13}C Nuclear magnetic resonance spectroscopy in the elucidation of structures of diterpenoid alkaloids[1]

BALAWANT S. JOSHI, JOHN K. WUNDERLICH, AND S. WILLIAM PELLETIER[2]

Institute for Natural Products Research and the School of Chemical Sciences, The University of Georgia, Athens, GA 30602, U.S.A.

Received May 28, 1986

This paper is dedicated to Dr. O. E. (Ted) Edwards

BALAWANT S. JOSHI, JOHN K. WUNDERLICH, and S. WILLIAM PELLETIER. Can. J. Chem. **65**, 99 (1987).

^{13}C Nuclear magnetic resonance spectroscopy is an exceptionally useful tool for the structure determination of diterpenoid alkaloids. A detailed study of the ^{1}H and ^{13}C nmr spectra of aconitine and 3-deoxyaconitine has permitted definite assignments to all the carbon atoms of the molecule. Chemical shift revisions have been suggested for certain carbon atoms of the C_{19}-diterpenoid alkaloids. Chemical examination of *Aconitum columbianum* Nutt. ssp. *columbianum*, *A. forrestii* Stapf, *Delphinium tatsienense* Franch., and *D. vestitum* Wall. resulted in the isolation of several new C_{19}-diterpenoid alkaloids. The structure derivation of those alkaloids was based mainly on ^{13}C nmr spectroscopic evidence.

BALAWANT S. JOSHI, JOHN K. WUNDERLICH et S. WILLIAM PELLETIER. Can. J. Chem. **65**, 99 (1987).

La spectroscopie rmn du ^{13}C est un outil d'une utilité exceptionnelle pour déterminer la structure des alcaloïdes diterpéniques en C_{13}. Une étude détaillée des spectres rmn du ^{1}H et ^{13}C de l'aconitine et de la déoxy-3 aconitine a permis d'attribuer d'une façon définitive tous les déplacements de tous les atomes de carbone de la molécule. Des revisions des déplacements chimiques ont été suggérées pour certains atomes de carbone d'alcaloïdes diterpéniques en C_{19}. Un examen des produits chimiques contenus dans les sources naturelles suivantes *Aconitum columbianum* Nutt. ssp. *columbianum*, *A. forrestii* Stapf, *Delphinium tatsienense* Franch. et *D. vestitum* Wall. a permis d'isoler plusieurs nouveaux alcaloïdes diterpéniques en C_{19}. Les structures de ces alcaloïdes ont été déterminées en se basant principalement sur des données de la rmn du ^{13}C.

[Traduit par la revue]

To date, the structures of about 175 naturally occurring C_{19}-diterpenoid alkaloids have been reported and a large majority of these structures have been elucidated during the last ten years (1). The structure determination of these complex alkaloids has largely been possible because of the developments in isolation methods (2) and advances in spectroscopic techniques, e.g. proton nmr, carbon-13 nmr, high resolution mass spectra, and X-ray analysis. However, by far the most useful technique for the structure elucidation of these alkaloids has been the application of ^{13}C nmr spectroscopy. By a systematic study of more than 100 naturally occurring C_{19}-diterpenoid alkaloids and their derivatives, we have accumulated a data base that has proved very useful in the derivation of structures of newly isolated alkaloids.

Jones and Benn made the initial contribution to ^{13}C nmr spectroscopy of diterpenoid alkaloids (3). In 1976, Pelletier and Djarmati studied the ^{13}C nmr spectra of various closely related aconitine-type alkaloids and suggested assignments of all the carbon atoms making use of substituent effects (4). Undoubtedly, these data on the ^{13}C chemical shifts of various functional groups in C_{19}-diterpenoid alkaloids have been useful in structure determination of newly isolated alkaloids. Although errors in assignment may be averaged out over a large number of compounds having similar structural features, and the correct structure may be derived in the case of new alkaloids, the assigned chemical shifts may not be absolutely correct. We therefore undertook a detailed study of the ^{13}C nmr chemical shift assignments for the well-known alkaloid aconitine (**1***A*). A variety of methods were used to obtain the ^{1}H and ^{13}C nmr assignments, with the major emphasis on the use of the 2-D nmr technique (5). The assignments of the acetyl and benzoyl groups have been well studied and there is no doubt about these values.

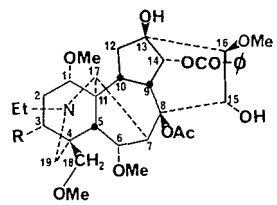

1*A* R=OH Aconitine

1*B* R=H 3-Deoxyaconitine

First, homonuclear proton decoupling experiments were carried out and then $^{1}H-^{1}H$ correlated (COSY) 2-D experiments, without and with the addition of pyridine, to note the dispersion of some signals. A summary of the results of the COSY experiment is given in Table 1. A slice through the data-matrix at δ 4.88 showed two off-diagonal elements: a doublet of doublets at δ 2.90 and a doublet at δ 3.33. The correlation with the doublet at δ 3.33 can best be attributed to "*w*" coupling between H-14 and H-16. A slice taken at δ 2.90 showed as an off-diagonal element, a doublet at δ 4.88 (H-14) and a doublet of doublets of doublets at δ 2.33. Assuming that H-9 appears at δ 2.9, the signal at δ 2.33 should be assigned to H-10. A slice taken at δ 4.48 showed, as off-diagonal elements, a doublet at δ 4.39 and a doublet at δ 3.33. Based on earlier evidence, since H-16 appears at δ 3.33, the signal at δ 4.48 must be assigned to H-15 and the doublet at δ 4.39 should be due to C(15)—OH. By this process most of the proton assignments were made as shown in Table 1. These ^{1}H nmr assignments are essentially in agreement with the reported values of Katz and Rudin for aconitine (6).

A C/H correlation experiment was performed on aconitine without the addition of pyridine. The quaternary carbon resonances will not appear since the experiment relies on a polarization transfer step to observe the C/H correlation. A slice taken at the downfield carbon resonance at 90.1 ppm showed a correlation with the H-16 resonance at δ 3.33, indicating that the signal at 90.1 should be assigned to C(16). Similarly, the signal

[1]Presented at the R.H.F. Manske Symposium held during the 10th International Congress of Heterocyclic Chemistry in Waterloo, Canada, August 15, 1985.

[2]Author to whom correspondence may be addressed.

Can. J. Chem. Downloaded from www.nrcresearchpress.com by 190.90.36.8 on 09/07/12
For personal use only.

TABLE 1. COSY experiment on aconitine **1A**[a]

Slice (δ)	Proton assignment	Off-diagonal elements	Proton assignment
4.88 d	14	3.33 d	16
		2.90 dd	9
4.48 dd	15	4.39 d	C(15)—OH
		3.33 d	16
4.39 d	C(15)—OH	4.48 dd	15
4.04 brd	6	2.84 brs	7
		2.10 brd	5
3.63 d	18	3.49 d	18
3.33 d	16	4.88 d	14
		4.48 dd	15
2.90 dd	9	4.88 d	14
		2.33 ddd	10
2.73 dq	N—CH_2CH$_3$	2.39 dq	N—CH_2CH$_3$
		1.10 t	N—CH$_2$CH_3
2.34 ddd[b]	2 (α)	3.77 dd	3
		3.16 dd	1
		2.02 ddd	2 (β)
2.10 brd	5	4.04 brd	6
		3.11 brs	17

[a]NOTE: For Tables 1, 2, and 3 the 2D-nmr spectra were taken on a JEOL FX-270 MHz instrument using JEOL FAFT-84 2D software. Aconitine (90 mg) and 3-deoxyaconitine (79.8 mg) were dissolved in 0.5 mL or 1 mL of $CDCl_3$ for 5-mm or 10-mm (od) nmr tubes, respectively. All chemical shifts are reported in ppm (δ) relative to internal tetramethylsilane; s: singlet, d: doublet, t: triplet, q: quartet, br: broad, m: multiplet.

[b]COSY experiment after addition of pyridine.

TABLE 2. C/H Correlation of aconitine **1A**[a]

Carbon (ppm)	Assignment	Proton correlation (ppm)
92.1 s	C(8)	—
90.1 d	C(16)	3.33 d
83.4 d	C(6)	4.04 brd
82.4 d	C(1)	3.16 dd
78.9 d	C(14)	4.88 d
78.8 d	C(15)	4.48 d
76.2 t	C(18)	3.63 d, 3.49 d
74.0 s	C(13)	—
71.0 d	C(3)	3.77 dd
61.1 q	OCH_3(16′)	3.76 s
60.9 d	C(17)	3.11 brs
59.1 q	OCH_3(18′)	3.30 s
58.0 q	OCH_3(6′)	3.17 s
55.9 q	OCH_3(1′)	3.27 s
50.0 s	C(11)	—
48.9 t	N—CH_2	2.73 dq, 2.39 dq
47.0 t	C(19)	2.80 m, 2.37 m
46.9 d	C(5)	2.10 brd
44.8 d	C(7)	2.84 brs
44.2 d	C(9)	2.90 dd
43.2 s	C(4)	—
40.9 d	C(10)	2.33 ddd
35.9 d	C(12)	2.74 m, 2.12 m
33.9 t	C(2)	2.34 ddd, 2.02
13.4 q	N—CH$_2$—CH_3	—

[a]See NOTE, Table 1.

TABLE 3. DIFNOE experiment on aconitine **1A**[a]

OMe	^{1}H signal	Nuclear Overhauser enhancement (δ)	Assignment ^{1}H	Assignment ^{13}C
16′	3.76	4.48 dd	H-15	61.1
		4.39 d	OH-15	—
		3.97 s	OH-13	—
		3.33 d	H-16	—
18′	3.30	—	—	59.1
1′	3.27	3.16 dd	H-1	55.9
6′	3.17	4.04 d	H-6	58.0
		1.39 s	C(8)-OAc	

[a]See NOTE, Table 1.

83.4 ppm was assigned to C(6) as it was correlated with H-6, appearing at δ 4.04. Using the same approach, assignments were made for C(1), C(3), C(14), C(15), C(17), and C(18) (Table 2). The signals at 48.9 and 47.0 ppm showed correlation with the methylene proton resonances of an *N*-ethyl group and C(19), respectively. The methine carbons appearing at 46.9, 44.8, and 44.2 ppm were correlated with H-5, H-7, and H-9 resonating at 2.1, 2.84, and 2.9, respectively. The doublet at 40.9 ppm was assigned to C(10) as it showed an overlap with the H-10 resonance at δ 2.33. The remaining chemical shifts for C(2) and C(12) were assigned to the signals appearing at 33.9 and 35.9 ppm, respectively.

The DIFNOE (difference nuclear Overhauser enhancement) technique was used for assigning the methoxyl protons. Irradiation at δ 3.76 gave four enhanced signals, due to H-15, 15-OH, 13-OH, and H-16, suggesting that the δ 3.76 signal belongs to the 16′-methoxyl group. The C/H correlation shows that the signal at 61.1 ppm can be assigned to the 16′-methoxyl. The remaining three methoxyls were similarly assigned (Table 3).

These investigations provided accurate ^{13}C chemical shift assignments for all the carbon atoms of aconitine. Table 4 shows a comparison of the previously assigned values (4) and the revised chemical shift assignments. By a similar set of experiments, the ^{1}H and ^{13}C chemical shifts of 3-deoxyaconitine (**1B**) were derived (Table 4).

On the basis of published data of the ^{13}C nmr spectra of more than 160 C_{19}-diterpenoid alkaloids and their derivatives, we have prepared a table indicating the general chemical shift ranges of all the carbon atoms (1). These data are only approximations but are useful in studying the structures of newly isolated alkaloids.

Even when correct structures may be derived on the basis of these chemical shift values, the individual carbon atoms could have been assigned incorrectly. One such error has been noticed in the chemical shift assignments for C(10) and C(13). For most of the alkaloids, the higher field resonance appearing in the range 37–43 ppm has been ascribed to C(10) and the lower field signal around 43–46 ppm to C(13), when neither of these carbons bears an oxygen function. It is well established that within a group of closely related compounds, a given substituent produces remarkably similar effects on the shielding of the carbons at or near the site of substitution. Thus, when a hydrogen is replaced by a hydroxyl group, a downfield shift of about 7–8 ppm is observed on the β carbon (β-effect) and an upfield shift of 2–4 ppm on the γ carbon (γ-effect).

These generalized β- and γ-effects are not observed in the published chemical shifts of C(10) and C(13) in closely related C_{19}-diterpenoid alkaloids; e.g. placement of a hydroxyl at C(9) in monticoline (**2**) leads to a related alkaloid ranaconine (**3**). The chemical shifts for C(10) and C(13) in monticoline (**2**) have

Can. J. Chem. Downloaded from www.nrcresearchpress.com by 190.90.36.8 on 09/07/12
For personal use only.

Can. J. Chem. Downloaded from www.nrcresearchpress.com by 190.90.36.8 on 09/07/12
For personal use only.

TABLE 4. ^{13}C Chemical shift assignments of aconitine (**1A**) and 3-deoxyaconitine (**1B**)

Carbon	Aconitine New	Aconitine Original (4)	Deoxyaconitine New	Deoxyaconitine Original (4)
1	82.4 d	83.4	85.2 d	85.0
2	33.9 t	36.0	26.3 t	26.3
3	71.0 d	70.4	35.1 t	35.2
4	43.2 s	43.2	39.0 s	39.0
5	46.9 d	46.6	49.1 d	49.1
6	83.4 d	82.3	83.3 d	83.3
7	44.8 d	44.8[a]	45.1 d	45.1[a]
8	92.1 s	92.0	92.1 s	92.0
9	44.2 d	44.2[a]	44.5 d	44.6[a]
10	40.9 d	40.8	41.0 d	41.0
11	50.0 s	49.8	49.9 s	49.9
12	35.9 t	34.0	36.6 t	36.7
13	74.0 s	74.0	74.1 s	74.0
14	78.9 d	78.9	79.0 d	78.8[b]
15	78.8 d	78.9	78.8 d	79.0[b]
16	90.1 d	90.1	90.2 d	90.2
17	60.9 d	61.0	61.2 d	61.2
18	76.2 t	75.6	80.3 t	80.2
19	47.0 t	48.8	53.2 t	53.3
N—CH_2	48.9 t	46.9	49.1 t	49.1
CH_3	13.4 q	13.3	13.4 q	13.4
1′	55.9 q	55.7	56.0 q	56.0
6′	58.0 q	57.9	57.9 q	57.9
16′	61.1 q	60.7	60.9 q	60.9
18′	59.1 q	58.9	59.0 q	59.0
C=O	172.3 s	172.2	172.2 s	172.2
CH_3	21.4 q	21.3	21.3 q	21.3
C=O	166.0 s	165.9	166.0 s	165.9
C_6H_5	129.8 s	129.8	130.0 s	129.9
	129.6 d	129.6	129.5 d	129.5
	128.6 d	128.6	128.6 d	128.5
	133.3 d	133.2	133.1 d	133.1

[a,b]Values may be interchanged.

been assigned the values 37.1 and 42.0 ppm, respectively (7). In ranaconine (**3**), C(10) and C(13) have been assigned 37.5 and 51.1 ppm (8), which point to a downfield shift of 0.4 ppm on C(10) (β-effect) and a downfield shift of 9.1 ppm on C(13) (γ-effect). Similarly, the published values for sachaconitine (**4**) (9) and lappaconine (**5**) (10) indicate an upfield shift of 1.1 ppm on C(10) and a downfield shift of 4.9 ppm on C(13) when C(9) is substituted with a hydroxyl group contrary to the expected β- and γ-effects. If the presently assigned values of C(10) and

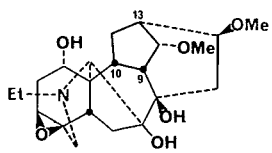

2 Monticoline

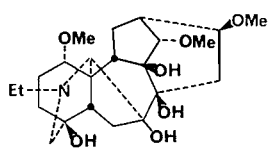

3 Ranaconine

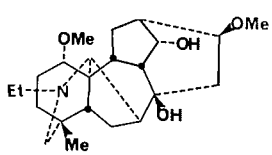

4 Sachaconitine

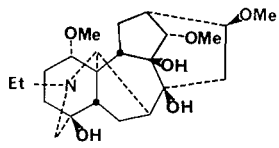

5 Lappaconine

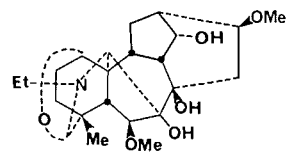

6 Gadesine

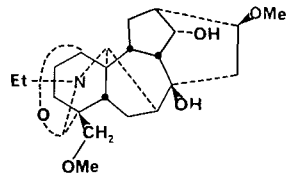

7 Nevadenine

C(13) are reversed, then the expected β- and γ-effects are observed. We have therefore suggested that the earlier assigned chemical shifts for C(10) and C(13) of many of the C_{19}-diterpenoid alkaloids should be reversed, assigning the downfield signal occurring around 43–46 ppm to C(10) and the upfield signal around 37–43 ppm to C(13) (11).

Another assignment that needs to be corrected in the literature is that of C(1) and C(19) in gadesine (**6**) (1, 12), nevadenine (**7**) (13), and other alkaloids containing a 1,19-oxygen bridge. The low field signals at 89.0 and 87.6 ppm respectively in **6** and **7** should be assigned to C(19) and the upfield signals at 68.3 and 69.4 ppm should be assigned to C(1) for these compounds instead of the reversed assignments reported. The C(19) signal generally appears in the range 52.0–52.5 ppm when it does not bear an oxygen function. When it does, a downfield shift of around 40 ppm would be expected and C(19) should show a signal around 90 ppm (14).

Recent examples of our application of ^{13}C nmr spectroscopy in the field of diterpenoid alkaloid structure elucidation include the following:

Alkaloids of Delphinium tatsienense *Franch.*

From the roots of *Delphinium tatsienense* Franch., a Chinese medicinal plant, more than ten alkaloids were isolated and their structures determined mainly on the basis of ^{13}C nmr spectroscopy. Tatsiensine, $C_{27}H_{39}NO_7$, an amorphous alkaloid, was formulated as **8** on the basis of ^1H nmr and ^{13}C nmr evidence (15). The structure of tatsinine (**9**), $C_{22}H_{35}NO_6$, mp 132–

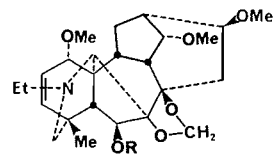

8 R=Ac Tatsiensine

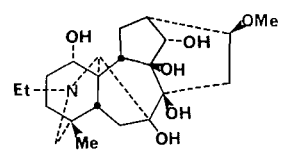

9 Tatsinine

133°C, was proposed solely on the basis of ^{13}C nmr spectral data (16). This structure has recently been confirmed by an X-ray crystal structure determination (17). The isolation and structure determination of another amorphous alkaloid, $C_{25}H_{41}NO_7$ (**10**), designated as deltatsine, was based on ^1H nmr and ^{13}C nmr spectroscopic data and a chemical correlation with delcosine (**11**) (18). The other C_{19}-diterpenoid alkaloids from *D. tatsienense,* whose structures were determined by ^{13}C nmr spectra, were browniine, delcosine, lycoctonine, and the C_{20}-diterpenoid alkaloids ajaconine, hetisine, and hetisinone (15). A C_{20}-diterpenoid alkaloid, $C_{21}H_{33}NO_3$, mp 181–182°C, isolated from

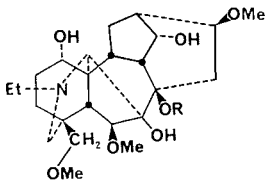

10 R=Me Deltatsine

11 R=H Delcosine

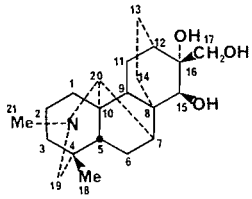

12 Dictyzine

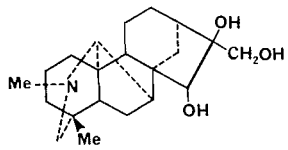

13

this plant, was shown to be identical with dictyzine (**12**), first obtained from *D. dictyocarpum* DC. The structure **13** proposed for this alkaloid based on chemical studies (19) was revised to **12** from an X-ray crystal structure determination (20). We derived the structure of this alkaloid from its ^{13}C nmr spectrum, which showed the following signals ($CDCl_3$; TMS): C(1) 40.2t, C(2) 20.8t, C(3) 27.7[a]t, C(4) 34.4s, C(5) 44.2d, C(6) 26.6[a]t, C(7) 36.2d, C(8) 42.0s, C(9) 52.8d, C(10) 45.6s, C(11) 21.9t, C(12) 42.8d, C(13) 23.1t, C(14) 26.6[a]t, C(15) 86.7d, C(16) 79.8s, C(17) 59.8t, C(18) 23.6q, C(19) 67.8t, C(20) 73.5d ppm ([a] these values may be interchanged).

From the roots of another Chinese medicinal plant, *Aconitum forrestii* Stapf, we had isolated two new C_{19}-diterpenoid alkaloids forestine (**14**) and foresticine (**15**) together with three known alkaloids chasmanine, talatizamine, and yunaconitine (21). These alkaloids were isolated from the crude alkaloid fraction obtained at pH 8 and the structures were derived mainly on ^{13}C nmr spectroscopic evidence. From the alkaloidal fraction taken at pH 5–6, we have isolated four new alkaloids acoforine (**16**), acoforesticine (**17**), acoforestine (**18**), and acoforestinine (**19**), besides crassicauline A (**20**) and yunaconitine (**21**).

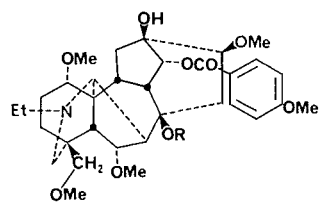

14 R=H Forestine

18 R=Et Acoforestine

20 R=Ac Crassicauline A

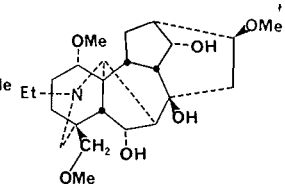

15 Foresticine

Except for acoforestine, mp 203–204°C, the three alkaloids **16**, **17**, and **19** are amorphous. The structures of all these alkaloids were derived from their ^{13}C nmr spectral data and correlation studies. Acoforine (**16**) was shown to be identical with 14-acetylcolumbidine, prepared from columbidine (*vide infra*). When acoforesticine (**17**) was acetylated with acetic anhydride and *p*-toluenesulfonic acid it gave the known alkaloid foresaconitine (vilmorrianine C) (**22**). Heating crassicauline A (**20**) with ethanol in a sealed tube at 130°C afforded acoforestine (**18**). As the structure of **20** was based only on spectral and chemical evidence, an X-ray crystal structure determination of acoforestine was carried out, confirming the structure proposals **18** and **20** for these alkaloids (22).

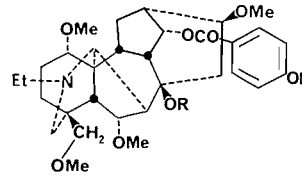

17 R=H Acoforesticine

22 R=Ac Foresaconitine

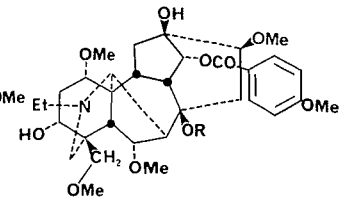

19 R=Et Acoforestinine

21 R=Ac Yunaconitine

C_{19}-Diterpenoid alkaloids containing a methoxyl or an ethoxyl group at C(8) have been reported in the literature, e.g. alkaloid A, ambiguine, puberaconitidine, septentrionine, columbidine. The question as to whether these alkaloids containing an alkoxyl group at C(8) are artefacts or are present in the plants cannot be answered with certainty until the extraction procedures are repeated, avoiding the use of methanol and ethanol during the isolation.

The conversion of the 8-acetoxy group in C_{19}-diterpenoid alkaloids to afford the 8-alkoxy compounds can be considered as a Grob type fragmentation, when the free electron pair on the nitrogen atom is oriented periplanar with respect to the Cβ,Cγ bond that undergoes cleavage (23).

Aconitum columbianum Nutt. ssp *columbianum*, growing in the Western parts of the USA, afforded the known alkaloids cammaconine, deltaline, dictyocarpine, talatizamine (**23**), 8-*O*-methyl talatizamine, and a new alkaloid columbidine (**24**) (11). The structures of all the alkaloids were derived mainly on the basis of ^{13}C nmr spectral data.

Delphinium vestitum Wall., growing in the Western Himalayas, was found to contain two closely related alkaloids delvestine (**25**) and delvestidine (**26**), the structures of which

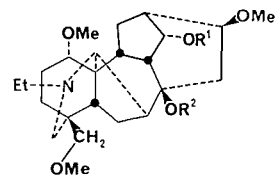

16 R^1=Ac; R^2=Et Acoforine

23 R^1=R^2=H Talatizamine

24 R^1=H; R^2=Et Columbidine

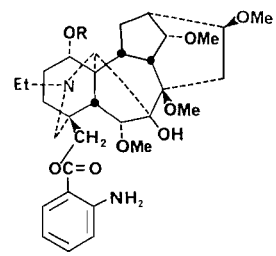

25 R=H Delvestine

26 R=Me Delvestidine

were based on ^{13}C nmr spectroscopic data and correlation with gigactonine and lycoctonine, respectively (24).

In summary, our work indicates that a data bank of ^{13}C nmr spectra of C_{19}-diterpenoid alkaloids is valuable in deriving structures of newly isolated compounds of this class. Also, in the case of amorphous alkaloids, where an X-ray crystal structure determination is not possible, ^{13}C nmr spectroscopy is a very useful tool for derivation of structure.

1. S. W. Pelletier, N. V. Mody, B. S. Joshi, and L. C. Schramm. *In* Alkaloids: chemical and biological perspectives. Vol. 2. *Edited by* S.W. Pelletier. John Wiley, New York. 1984. Chapt. 5. p. 205.
2. S. W. Pelletier, B. S. Joshi, and H. K. Desai. *In* Advances in medicinal plant research. Wissenschaftliche Verlagsgesellsehaft mbH, Stuttgart. 1985. pp. 153–195; H. K. Desai, B. S. Joshi, A. M. Panu, and S. W. Pelletier. J. Chromatogr. **322**, 223 (1985).
3. A. J. Jones and M. H. Benn. Can. J. Chem. **51**, 486 (1973).
4. S. W. Pelletier and Z. Djarmati. J. Am. Chem. Soc. **98**, 2626 (1976).

Can. J. Chem. Downloaded from www.nrcresearchpress.com by 190.90.36.8 on 09/07/12
For personal use only.

5. J. WUNDERLICH. Ph.D. thesis, University of Georgia, Athens, Georgia. 1985.
6. A. KATZ and H. RUDIN. Helv. Chim. Acta, **67**, 2017 (1984).
7. E. F. AMETOVA, M. S. YUNUSOV, V. E. BANNIKOVA, N. D. ABDULLAEV, and V. A. TEL'NOV. Khim. Prir. Soedin. 466 (1981).
8. S. W. PELLETIER, N. V. MODY, A. P. VENKOV, and N. M. MOLLOV. Tetrahedron Lett. 5045 (1978).
9. S. W. PELLETIER, N. V. MODY, and N. KATSUI. Tetrahedron Lett. 4027 (1977); C. R. YANG, D. Z. WANG, D. G. WU, X. J. HAO, and H. ZHOU. Acta Chim. Sin. **39**, 445 (1981).
10. S. W. PELLETIER, N. V. MODY, and R. S. SAWHNEY. Can. J. Chem. **57**, 1652 (1979).
11. S. W. PELLETIER, S. K. SRIVASTAVA, B. S. JOSHI, and J. D. OLSEN. Heterocycles, **23**, 331 (1985).
12. A. G. GONSALEZ, G. DE LA FUENTE, R. DIAZ, J. FAYOS, and M. MARTINEZ-RIPOLL. Tetrahedron Lett. 79 (1979).
13. A. G. GONSALEZ, G. DE LA FUENTE, T. ORRIBO, and R. D. ACOSTA. Heterocycles, **23**, 2979 (1985).
14. E. BREITMAIER and W. VOELTER. ^{13}C-NMR spectroscopy. Verlag Chemie, Weinheim, New York. 1978. p. 153.
15. S. W. PELLETIER, J. A. GLINSKI, B. S. JOSHI, and S. Y. CHEN. Heterocycles, **20**, 1347 (1983).
16. J. A. GLINSKI, B. S. JOSHI, S. Y. CHEN, and S. W. PELLETIER. Tetrahedron Lett. **25**, 1211 (1984).
17. J. A. MADDRY. Ph.D. Thesis, University of Georgia, Athens, Georgia. 1985.
18. B. S. JOSHI, J. A. GLINSKI, H. P. CHOKSHI, S. Y. CHEN, S. K. SRIVASTAVA, and S. W. PELLETIER. Heterocycles, **22**, 2037 (1984).
19. B. J. SALIMOV, M. S. YUNUSOV, Y. V. RASHKES, and S. Y. YUNUSOV. Khim. Prir. Soedin. 812 (1979).
20. B. TASHKHADZHAEV. Khim. Prir. Soedin. 812 (1979); B. J. SALIMOV, B. TASHKHODZHAEV, and M. S. YUNUSOV. Khim. Prir. Soedin. 86 (1981).
21. S. W. PELLETIER, S. Y. CHEN, B. S. JOSHI, and H. K. DESAI. J. Nat. Prod. **47**, 474 (1984).
22. S. W. PELLETIER, B. S. JOSHI, J. A. GLINSKI, H. P. CHOKSHI, S.-Y. CHEN, K. BHANDARY, and K. GO. Heterocycles. In press.
23. C. A. GROB, H. R. KIEFER, H. LUTZ, and H. WILKENS. Tetrahedron Lett. 2901 (1964).
24. H. K. DESAI, B. S. JOSHI, and S. W. PELLETIER. Heterocycles, **23**, 2483 (1985).

Can. J. Chem. Downloaded from www.nrcresearchpress.com by 190.90.36.8 on 09/07/12
For personal use only.

Synthesis of tricyclic azetidinones by intramolecular free radical cyclization

GEORGE JUST[1] AND GUERINO SACRIPANTE
Department of Chemistry, McGill University, Montreal, P.Q., Canada H3A 2K6

Received June 6, 1986

This paper is dedicated to Dr. O. E. (Ted) Edwards

GEORGE JUST and GUERINO SACRIPANTE. Can. J. Chem. **65**, 104 (1987).

The synthesis of strained tricyclic azetidinones was achieved by free radical cyclization of N-substituted azetidinones involving a tributyltin hydride/AIBN mediated chain reaction. The 5-*exo* cyclization led to benzo carbapenems **10**, **12**, and **13**, which were relatively unstable in solution. The 6-*exo* mode, however, afforded stable benzo carbacephems **20**, **22**, **24**, and **25**.

GEORGE JUST et GUERINO SACRIPANTE. Can. J. Chem. **65**, 104 (1987).

On a réalisé la synthèse d'azétidinones tricycliques tendues en faisant appel à une cyclisation radicalaire d'azétidinones N-substituées qui implique une réaction en chaîne provoquée par le couple hydrure de tributylétain/AIBN. La cyclisation *exo*-5 conduit aux benzo carbapénèmes **10**, **12** et **13** qui sont relativement instables en solution. Toutefois, dans le mode *exo*-6, les cyclisations conduisent aux benzo carbacéphèmes **20**, **22**, **24** et **25** stables.

[Traduit par la revue]

Introduction

Since the discovery of the antibacterial drug thienamycin, **1**, numerous modifications of its carbapenem structure have been carried out to determine the effect of the ring size on biological activity (1). Our interests in preparing nonclassical tricyclic azetidinones (2) prompted us to investigate the stabilities of the more strained tricyclic benzo carbapenem ($n = 0$) or carbacephem ($n = 1$) of type **2**. The syntheses of carbapenems or carbacephems were previously achieved by ionic methods. In view of the known instability of tricyclic carbacephems towards acids and nucleophilic reagents, we sought a free radical method for their synthesis (3).

As suitable precursors for the intramolecular free radical annelation yielding **2**, the radicals were generated either β ($n = 0$) or γ ($n = 1$) to the nitrogen atom of the azetidinone **3**, and a phenyl substituent (R^1) was chosen so that the *exo* mode of addition should be favoured over the *endo* process. Similar free radical cyclizations yielding bicyclic azetidinones have been described elsewhere (4, 5).

Results and discussion

The *cis*-azido azetidinones were prepared by known methods (2) involving the condensation of an appropriate Schiff base with azidoacetyl chloride in the presence of equimolar amounts of triethylamine. Reduction of the azide substituent using hydrogen sulfide and triethylamine followed by acylation of the amine intermediate with phenylacetyl chloride and triethylamine gave fair to good yields of the expected amido azetidinones **4**–**8**.

Free radical cyclization of **4** (0.02 *M* in refluxing benzene), with slow addition of tributyltin hydride and catalytic AIBN over a 20-h period under an inert atmosphere, gave the reduction product **9** (15%), tricyclic azetidinone **10** (5%), and the azepinone **11** (35%), together with some starting material, after separation using a neutral silica hplc column. The configuration of **10** was assigned, based on its coupling constant of 8 Hz (J_{H4-H5}), by analogy with diastereomers **20** and **26** discussed below. When this tricyclic benzo carbapenam **10** was placed in an nmr tube ($CDCl_3$), it decomposed within a week, and **11** was isolated as the major product. Due to the instability of **10** in solution, the free radical annelation of **4** was repeated using 1.5 equiv. of tributyltin hydride over a shorter period of time (3 h). After evaporation of the solvent, the crude residue was redissolved in carbon tetrachloride, and **10** precipitated as colorless crystals (24%). The infrared spectrum of **10** displayed the azetidinone carbonyl frequency at 1805 cm^{-1}, which is considerably higher than for less strained bicyclic azetidinones such as cephalosporanic acid (1765 cm^{-1}). The decomposition of **10** to **11** most likely resulted via proton abstraction at C5 with a double bond formation at C4—C5 and ring opening at the C4—N position to give **11**, which is closely related to diazepam (see arrows, **10**). To avoid this decomposition, we decided to carry out the next experiment on a propargyl azetidinone **5**, where the resulting product **12**/**13** lacks the C5 proton.

Thus, the free radical cyclization of **5** gave two tricyclic azetidinones **12** and **13** in a 4:3 ratio as a crystalline mixture (31%), mp 140–145°C. Also, the reduction product **14** (27%), some starting material, and several decomposition products were obtained. The mixture of **12** and **13** did not survive chromatography using various types of silica and only **13** was recovered partially when neutral silica gel was used. Attempts to recrystallize this mixture also failed, giving decomposition in solution within a few days. From this decomposed mixture was isolated the azepinone **15**, which most likely resulted via proton abstraction at C3 forming a double bond at C3—C4 and ring opening at N—C4 of the azetidinone rings **12** and **13**. The infrared spectra of **12** and **13** showed the azetidinone carbonyl frequency vibration at 1824 cm^{-1}.

Since the benzo carbapenems obtained were found to be unstable in solution, we next investigated the formation of the somewhat less strained benzo carbacephems **2** ($n = 1$). Desilylation of **6**–**8** using tetrabutylammonium fluoride, followed by bromination of the corresponding alcohol with triphenylphosphine/carbon tetrabromide, gave good yields of the bromo azetidinones **16**, **17**, and **18** respectively.

Free radical cyclization of **16** gave some reduction product **19** and 65% tricyclic benzo carbacephem, mp 256°C, exclusively, as the less crowded diastereomer **20**. The infrared spectrum showed the azetidinone carbonyl absorption at 1755 cm^{-1}. This tricyclic product resulting from a 6-*exo* addition was found to be highly stable in solution. Similarly, free radical cyclization of **17** gave the reduction product **21** and a good yield of the analogous tricyclic azetidinone **22** (70%), mp 273°C, which displayed the infrared carbonyl vibration at 1770 cm^{-1}.

[1]Author to whom correspondence may be addressed.

Can. J. Chem. Downloaded from www.nrcresearchpress.com by 80.58.250.72 on 09/07/12
For personal use only.

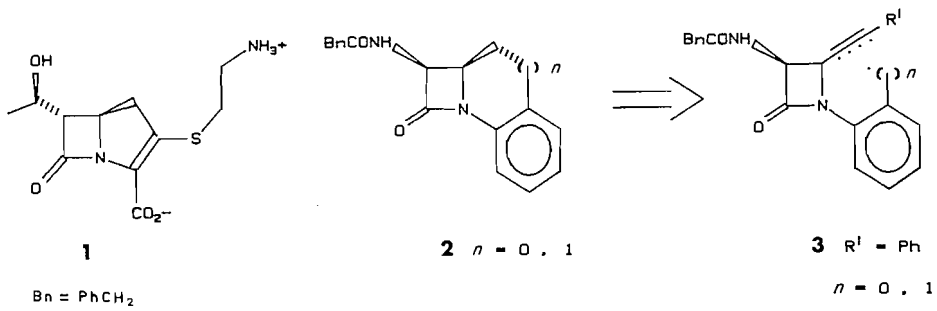

1 Bn = $PhCH_2$

2 n = 0, 1

3 R^1 = Ph, n = 0, 1

FIG. 1

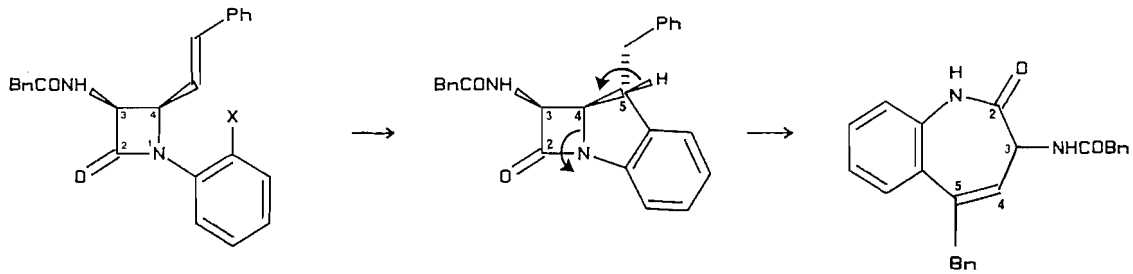

4 X = Br
9 X = H

10

11

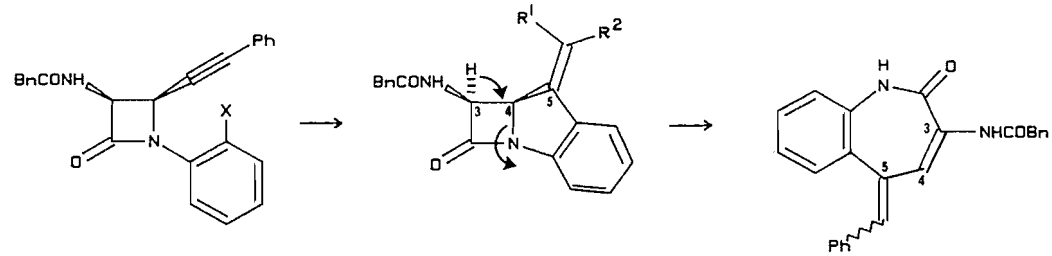

5 X = Br
14 X = H

12 R^1 = H, R^2 = Ph
13 R^1 = Ph, R^2 = H

15

FIG. 2

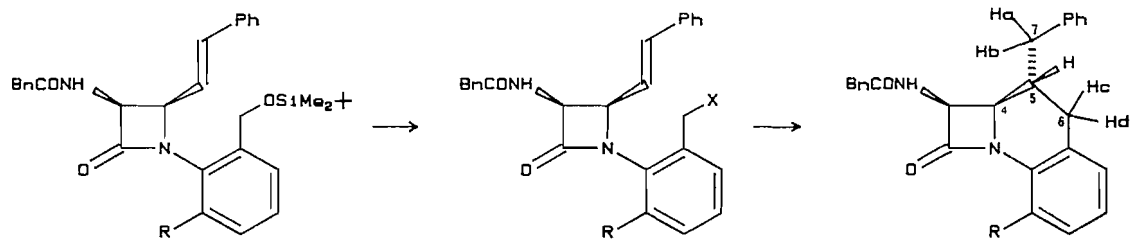

6 R = H
7 R = OBn

16 X = Br, R = H
17 X = Br, R = OBn
19 X = H, R = H
21 X = H, R = OBn

20 R = H
22 R = OBn
23 R = OH

FIG. 3

Hydrogenolysis of **22** using palladium on charcoal in DMF afforded an almost quantitative yield of the tricyclic phenol **23**, which displayed the carbonyl frequency at lower wave numbers, 1715 cm^{-1}, due to H-bonding of the phenol proton with the azetidinone carbonyl. The presence of the azetidinone was proven by silylation with Me_3SiCl/Et_3N, which gave a product for which the azetidinone frequency reverted to its expected position at 1773 cm^{-1}. In both of the above cyclizations, no diastereomer of **20**/**22** or 7-*endo* cyclization product was detected.

The free radical cyclization of **18** gave the 6-*exo* intramolecular cyclization products as a 1:1 mixture of geometic isomers

Can. J. Chem. Downloaded from www.nrcresearchpress.com by 80.58.250.72 on 09/07/12
For personal use only.

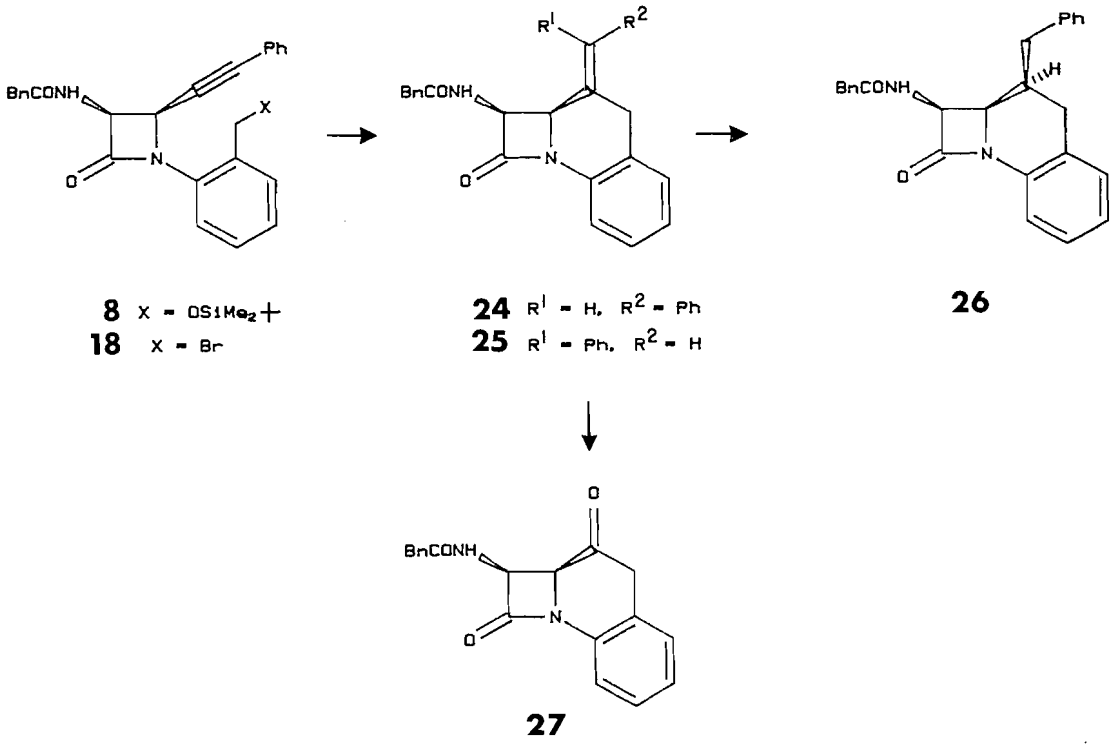

FIG. 4

in over 75% combined yield. These tricyclic azetidinones **24** and **25** were easily separated by flash chromatography and their structures assigned unambiguously by nOe (nuclear Overhauser effect) nmr experiments. The tricyclic azetidinones **24** and **25**, mp 189 and 196°C respectively, were found to be soluble in most organic solvents and stable in solution. Interestingly, the more sterically crowded *Z* isomer **25** displayed a slightly higher azetidinone carbonyl frequency at 1753 cm^{-1}, as compared to 1748 cm^{-1} for **24**. Hydrogenation of either **24** or **25**, using platinum black as catalyst, reduced the exocyclic double bond from the less hindered side to give the more crowded tricyclic benzo carbacephem **26** as the only product, mp 236–237°C. The coupling constant between H-4 and H-5 was found to be 3 Hz, distinctly smaller than for its diastereomer **20** (10 Hz). The infrared spectrum showed the carbonyl frequency at 1768 cm^{-1}, which was, not surprisingly, 13 wave numbers higher than its less constrained diastereomer **20**. Finally, a mixture of **24** and **25** was ozonolyzed to give the corresponding ketone **27** in good yield. Its infrared spectrum showed the azetidinone frequency at 1793 cm^{-1} and the ketone absorption at 1722 cm^{-1}. This ketone was considerably less stable than its olefinic precursor, and slowly decomposed on silica gel.

Overall, the infrared data indicate a trend of higher instability as the azetidinone carbonyl frequency increases from 1755 to 1824 cm^{-1}. The reactions carried out establish the usefulness of a radical process for the carbon–carbon bond formation in strained azetidinone. These free radical reactions also give good stereochemical control in the intramolecular cyclization onto an olefinic bond.

Experimental

The nmr spectra were recorded on a Varian XL-200 or XL-300 spectrometer using TMS as internal standard, and the assignments were determined unambiguously by decoupling, nOe, or 2D experiments when necessary. The infrared spectra were recorded on Perkin Elmer 297 or Nicolet FT 7000 ir spectrometers. Mass spectra (ms) were obtained on MP 5984A or LKB 9000 mass spectrometers, ion source 250°C and 70 eV electron impact, direct inlet (unless otherwise stated); *m/z* (assignment, relative intensity). Melting points were determined on a Gallenkamp block and are uncorrected. Column chromatography was performed using Woelm Silica, 32–63 μm size, and the hplc separations were performed using an Altex Ultrasphere-Si column.

The *cis*-azetidinones **4**, **5**, and **8** were prepared by a procedure as described for **6** (2*a*) and **7** (2*b*).

Bromo azetidinone 4

Prepared in 78% yield from its corresponding azide; mp 138–139°C; ir (KBr) ν_{max}: 3300 (NH), 1771 (azetidinone), 1654 (amide); ^1H nmr ($CDCl_3$) δ: 3.51 (s, 2H, CH_2), 5.31 (dd, 1H, C3-H, J = 5.3, 8), 5.45 (dd, 1H, C4-H, J = 5.4, 8), 5.9 (dd, 1H, C5-H, J = 8, 16), 6.15 (d, 1H, N-H, J = 8), 6.52 (d, 1H, C6-H, J = 16), 7.03–7.51 (m, 14H, Ar-H); ^{13}C nmr ($CDCl_3$) δ: 43.4 (CH_2), 59.9 (C3), 63.4 (C4), 117–136 (20 C, C5, C6 and Ar-C), 165.7 (C2), 171.4 (amide carbonyl); ms (150°C): 460/462 (M^+, 0.6), 284 ($M^+ - C_{10}H_9NO_2$, 32), 263 ($M^+ - C_{18}H_{17}NO$, 38.8), 197 (40.7), 171 (72.6), 145 (67.6), 91 (100). *Mol. Wt.* (high resolution ms) calcd. for $C_{25}H_{21}O_2N_2Br$: 460.0783; found: 460.0799.

Free radical cyclization of 4

Tributyltin hydride (170 mg, 0.55 mmol), AIBN (catalytic amount), and dry benzene (3 mL) were added to azetidinone **4** (213 mg, 0.46 mmol) and dry benzene (20 mL) at reflux temperature during 20 h (syringe pump) under an inert atmosphere. The mixture was cooled to room temperature and the solvent removed. The residual yellow oil was dissolved in acetonitrile (30 mL), washed with hexane (3 × 30 mL), and the solvent removed. High performance liquid chromatography (hplc) using isopropanol/hexane (1:5) as eluent gave starting material (same spectroscopic data as **4**) and the following products:

Reduction product **9** (15%); ir (KBr) ν_{max}: 1765 (azetidinone), 1657 (amide); ^1H nmr ($CDCl_3$) δ: 3.56 (s, 2H, CH_2), 4.95 (dd, 1H, C4-H, J = 5, 8), 5.53 (dd, 1H, C3-H, J = 5, 8), 5.98 (dd, 1H, C5-H, J = 8, 16), 6.61 (d, 1H, C6-H, J = 16), 7.01–7.44 (m, 16H, N-H and Ar-H).

Tricyclic benzo carbapenem **10** (5%); mp 121°C: ir (KBr) ν_{max}: 3305 (NH), 1805 (azetidinone), 1664 (amide); ^1H nmr ($CDCl_3$) δ: 2.95 (dd, 1H, C6-Hb, J = 13.8, 18), 3.18 (dd, 1H, C6-Ha, J = 6.2, 13.8), 3.34–3.45 (m, 1H, C5-H), 3.45 (dd, 2H, CH_2, J = 4, 16), 4.32 (dd,

Can. J. Chem. Downloaded from www.nrcresearchpress.com by 80.58.250.72 on 09/07/12
For personal use only.

Can. J. Chem. Downloaded from www.nrcresearchpress.com by 80.58.250.72 on 09/07/12
For personal use only.

1H, C4-H, J = 5, 8), 5.39 (dd, 1H, C3-H, J = 5, 8), 5.73 (d, 1H, N-H, J = 8), 7.05–7.32 (m, 14H, Ar-H); ms (260°C): 382 (M^+, 100), 337 ($M^+ - 45$, 56), 247 ($M^+ - BnCONH_2$, 96), 207 ($M^+ - C_{10}H_9NO_2$, 53.1). *Mol. Wt.* (high resolution ms) calcd. for $C_{25}H_{22}N_2O_2$: 382.1681; found: 382.1734.

Azepinone **11** (35%); ir (KBr) ν_{max}: 3290 (NH), 1680 (lactam), 1657 (amide); ^{1}H nmr ($CDCl_3$) δ: 3.63 (s, 2H, CH_2CO), 4.31 (dd, 2H, CH_2Ar, J = 3, 5), 4.56 (d, 1H, C4-H, J = 5.2), 5.68 (dd, 1H, C3-H, J = 5, 6), 6.78 (d, 1H, N-H, J = 6), 6.93–8.0 (m, 15H, Ar-H); ms (111°C): 382 (M^+, 0.23), 291 ($M^+ - Bn$, 0.3), 207 ($M^+ - C_{10}H_9NO_2$, 31.3), 206 (24.4), 130 (100).

Repeating the above cyclization, except adding 1.5 equiv. of tributyltin hydride over a 3-h period, gave a precipitate, after evaporation of the solvent and trituration of the corresponding residue with carbon tetrachloride. The crystals were filtered off and washed with hexane to give **10** (24%) as colorless crystals, with identical spectroscopic data as before.

Bromo azetidinone 5

Prepared in 71% yield from its corresponding azide; mp 151–152°C as colorless crystals; ir (KBr) ν_{max}: 2280 (C≡C), 1741 (azetidinone), 1647 (amide); ^{1}H nmr ($CDCl_3$) δ: 3.65 (s, 2H, CH_2), 5.48 (d, 1H, C4-H, J = 5.4), 5.75 (dd, 1H, C3-H, J = 5.4, 9), 6.78 (d, 1H, N-H, J = 9), 7.11–7.6 (m, 14H, Ar-H); ^{13}C nmr ($CDCl_3$) δ: 43.46 (CH_2), 53.62 (C4), 59.22 (C3), 81.34 (C5); 90.07 (C6), 118–133 (18C, Ar-C), 165.5 (C2), 171.22 (amide carbonyl); ms (195°C): 458/460 (M^+, 5.7), 283/285 ($M^+ - C_{10}H_9NO_2$, 20.8), 175 ($M^+ - 283$, 5.7).

Free radical cyclization of 5

Tributyltin hydride (150 mg, 0.5 mmol), AIBN (cat.), and dry benzene (1 mL) were added to azetidinone **5** (193 mg, 0.42 mmol) and dry benzene (20 mL) at reflux temperature during 5 h (syringe pump) under an inert atmosphere. The mixture was cooled to room temperature and the solvent removed. The residue was dissolved in acetonitrile (30 mL), washed with hexanes (3 × 30 mL), and the solvent removed. Trituration of the residue with carbon tetrachloride/acetonitrile gave the tricyclic azetidinones **12** and **13** as a yellow precipitate (4:3 ratio respectively, 31%), mp 140–145°C. From the filtrate was isolated starting material (5%), reduction product **14** (11%), and the azepinone **15** (27%), after separation by column chromatography using ethyl acetate/hexane as eluent (1:1).

Tricyclic azetidinone **12**; ^{1}H nmr ($CDCl_3$) δ: 3.60 (dd, 1H, CH_2, J = 2.5, 17), 5.79 (dd, 1H, C3-H, J = 5.9, 9.2), 6.00 (d, 1H, N-H, J = 9.2), 6.32 (d, 1H, C6-H, J = 2.5), 7.07–7.54 (m, 14H, Ar-H); ^{13}C nmr ($CDCl_3$) δ: 43.42 (CH_2), 58.34 (C4), 62.13 (C3), 126.01 (C6), 122–144 (Ar-C and C5), 171.00 (C1), 175.87 (amide carbonyl).

Tricyclic azetidinone **13**; ^{1}H nmr ($CDCl_3$) δ: 3.06 (dd, 2H, CH_2, J = 17, 34), 5.51 (dd, 1H, C4-H, J = 3.3, 6), 5.66 (d, 1H, N-H, J = 10), 6.10 (dd, 1H, C3-H, J = 6, 10), 6.99 (d, 1H, C6-H, J = 3.3), 7.07–7.54 (m, 14H, Ar-H); ^{13}C nmr ($CDCl_3$) δ: 42.79 (CH_2), 58.02 (C4), 61.86 (C3), 123.42 (C6), 122–144 (Ar-C and C5), 170.32 (C2), 175.77 (amide carbonyl); ir of **14** and **15** (KBr) ν_{max}: 3290–3310 (NH), 1824 (azetidinone), 1640–1647 (amide).

Reduction product **14**; ir (KBr) ν_{max}: 3300 (NH), 1745 (azetidinone), 1649 (amide); ^{1}H nmr ($CDCl_3$) δ: 3.65 (s, 2H, CH_2), 5.03 (d, 1H, C4-H, J = 5), 5.72 (dd, 1H, C3-H, J = 5, 8), 6.26 (d, 1H, N-H, J = 8), 7.05–7.59 (m, 15H, Ar-H); ms (111°C) chemical ionization, isobutane: 381 ($M^+ + 1$, 22.1), 363 ($M^+ - BnCO$, 15.8), 353 (381 − CO, 10.1), 206 ($M^+ - C_{10}H_9NO_2$, 100), 176 ($M^+ - 206$, 65.7).

Azepinone **15**; ^{1}H nmr ($CDCl_3$) δ: 4.19 (s, 2H, CH_2CO), 6.86–7.50 (m, 11H, Ar-H and C=CH), 8.85 (bs, 1H, NH).

Bromo azetidinone 8

Prepared in 49% yield from its corresponding azide; mp 123–124°C (colorless crystals); ir (KBr) ν_{max}: 3210 (NH), 1768 (azetidinone), 1645 (amide); ^{1}H nmr ($CDCl_3$) δ: 0.048 and 0.056 (s, 6H, $SiMe_2$), 0.907 (s, 9H, *tert*-butyl), 3.67 (s, 2H, CH_2CO), 5.18 (2, 1H, C4-H, J = 8), 5.7 (s, 2H, CH_2O), 5.71 (dd, 1H, C3-H, J = 5, 10), 6.3 (d, 1H, N-H, J = 10), 7.1–7.5 (m, 14H, Ar-H); ms (175°C): 524 (M^+, 0.1) 467 (M^+ − *tert*-butyl, 1.9), 349 ($M^+ - C_{10}H_9NO_2$, 1.7), 292 (M^+ − C2C3 − *tert*-butyl, 26.1).

Silyl azetidinone 16

Tetrabutylammonium fluoride (4.69 g, 17 mmol) and THF (5 mL) were added to azetidinone **6** (5.0 g, 9.5 mmol) and 150 mL of dry THF at 0°C under a nitrogen atmosphere. After 30 min, water (2 mL) was added and the solvent removed. The residue was then purified by flash chromatography using ethyl acetate/hexane (1:1) as eluent to give the alcohol as colorless crystals (72%); mp 174–175°C; ir (KBr) ν_{max}: 1756 (azetidinone), 1660 (amide); ^{1}H nmr (DMSO-d_6) δ: 3.34 (s, 2H, CH_2CO), 4.52–4.56 (bs, 1H, O-H), 4.53 (s, 2H, CH_2—O), 4.82 (dd, 1H, C4-H, J = 5, 86), 5.25 (dd, 1H, CH_3-H, J = 5, 8), 6.05 (dd, 1H, C5-H, J = 8, 16), 6.40 (d, 1H, C6-H, J = 16), 6.8–7.28 (m, 19H, Ar-H), 8.26 (d, 1H, N-H, J = 8); ms (230°C): 410 ($M^+ - 2H^+$, 2.6), 333 (410 − Ph, 3.3), 320 ($M^+ - Bn - H^+$, 50.1).

To the above alcohol (700 mg, 1.7 mmol) and dry methylene chloride (100 mL) at 0°C under a nitrogen atmosphere were added carbon tetrabromide (560 mg) followed by slow addition of triphenylphosphine (430 mg, 1.97 mmol). After 3 h of stirring, the solution was allowed to warm up to room temperature, and purified by column chromatography using ethyl acetate/hexane (1:3) to give the azetidinone **16** as colorless crystals (62.5%) after recrystallization from ethyl acetate/hexane; mp 123–124°C; ir (KBr) ν_{max}: 3310 (NH), 1744 (azetidinone), 1644 (amide); ^{1}H nmr ($CDCl_3$) δ: 3.60 (s, 2H, CH_2—O), 4.72 (dd, 2H, CH_2Br, J = 10.4, 22), 5.02 (dd, 1H, C4-H, J = 5, 8.2), 5.55 (dd, 1H, C3-H, J = 5, 8), 6.08 (dd, 1H, C5-H, J = 8.2, 16), 6.38 (d, 1H, N-H, J = 8), 6.64 (d, 1H, C6-H, J = 16), 7.1–7.34 (m, 14H, Ar-H); ms (305°C): 474/476 (M^+, 4/3.9), 395 ($M^{+\bullet} - Br^\bullet$, 33), 394 ($M^+ - HBr$, 100), 317 ($M^+ - Ph - HBr$, 70.5), 275 ($M^+ - HBr - BnCO$, 43.7), 220 ($M^{+\bullet} - C_{10}H_9NO_2 - Br^\bullet$, 45), 263 ($M^+ - C_{18}H_{17}NO$, 17).

Silyl azetidinone 17

Prepared as described for **16**. The alcohol was obtained in 65% yield from **9** as colorless crystals, mp 163°C; ^{1}H nmr ($CDCl_3$) δ: 3.50 (s, 2H, CH_2CO), 4.12 (dd, 1H, O-H, J = 4, 8), 4.64 and 4.82 (dd, 2H, CH_2—O, J = 8, 12 and 4, 12), 5.08 (s, 1H, $PhCH_2Ar$), 5.13 (dd, 1H, C4-H, J = 5, 8), 5.24 (dd, 1H, C3-H, J = 5, 8), 6.07 (dd, 1H, C5-H, J = 8, 16), 6.40 (d, 1H, C6-H, J = 16), 6.80 (d, 1H, N-H, J = 8), 6.9–7.39 (m, 13H, Ar-H); ms (200°C): 518 (M^+, 0.1), 343 ($M^+ - C_{10}H_9NO_2$, 0.9), 263 ($M^+ - C_{15}H_{13}NO_3$, 42.7), 175 ($M^+ - NC_4$, 3.0).

Azetidinone **17** was obtained as colorless crystals in 81% yield from the above alcohol; mp 145–146°C; ir (KBr) ν_{max}: 3270 (NH), 1758 (azetidinone), 1656 (amide); ^{1}H nmr ($CDCl_3$) δ: 3.56 (s, 2H, CH_2CO), 4.66 (dd, 2H, CH_2Br, J = 10, 10.1), 5.05 (s, 2H, $PhCH_2Ar$), 5.12 (dd, 1H, C4-H, J = 5, 8), 5.41 (dd, 1H, C3-H, J = 5.8), 5.96 (bd, 1H, N-H, J = 8), 6.09 (dd, 1H, C5-H, J = 8, 16), 6.42 (d, 1H, C6-H, J = 16), 6.88–7.39 (m, 18H, Ar-H); ms (285°C): 580/582 (M^+, 0.8/0.7), 501 ($M^{+\bullet} - Br$, 38.4), 500 ($M^+ - HBr$, 100), 423 ($M^+ - HBr - Ph$, 30), 381 ($M^+ - HBr - BnCON$, 19.9).

Silyl azetidinone 18

Prepared as described for **17**. The alcohol was obtained in 51% yield from **8** as colorless crystals; mp 184–185°C; ir (KBr) ν_{max}: 3305 (NH), 1768 (azetidinone), 1650 (amide); ^{1}H nmr (DMSO-d_6) δ: 3.29 (s, 1H, O-H), 3.61 (s, 2H, CH_2CO), 4.69 (s, 2H, CH_2—O), 5.23 (d, 1H, C4-H, J = 5), 5.50 (dd, 1H, C3-H, J = 5, 8), 7.08–7.46 (m, 15H, Ar-H and N-H); ms (208°C) chemical ionization, isobutane: 411 ($M^+ + 1$, 19.4), 319 ($M^+ + 1 - C_{10}H_9NO_2$, 9.1). *Mol. Wt.* (high resolution ms (208°C)) calcd. for $C_{26}H_{22}N_2O_3$: 410.1629; found: 410.1685.

Azetidinone **18** was obtained in 63% yield from the above alcohol as colorless crystals; mp 135–136°C; ir (KBr) ν_{max}: 3290 (NH), 1755 (azetidinone), 1666 (amide); ^{1}H nmr ($CDCl_3$) δ: 3.69 (s, 2H, CH_2CO), 4.64 (dd, 2H, CH_2Br, J = 10, 18), 5.21 (d, 1H, C4-H, J = 5), 5.75 (dd, 1H, C3-H, J = 5, 8), 6.30 (d, 1H, N-H, J = 8), 7.05–7.51 (m, 14H, Ar-H); ms (195°C): 472/474 (M^+, 0.3), 343 ($M^{+\bullet} - Br^\bullet$, 1.8), 392 ($M^+ - Bn$, 1.8), 392 ($M^+ - HBr$, 5.8), 218 ($M^{+\bullet} - Br^\bullet - C_{10}H_9NO_2$, 56.8), 217 (41.2), 175 (28.2).

Can. J. Chem. Downloaded from www.nrcresearchpress.com by 80.58.250.72 on 09/07/12
For personal use only.

Radical cyclization of ***16***

Tributyltin hydride (442 mg, 1.52 mmol), AIBN (cat.), and benzene (5 mL) were added to azetidinone **16** (600 mg, 1.27 mmol) and dry benzene (55 mL) at reflux temperature during 10 h under an inert atmosphere. The mixture was cooled to room temperature and the precipitate filtered off and washed with hexane to give the azetidinone **20** (340 mg, 68%) as colorless crystals. From the filtrate, after the usual work-up and column chromatography, was recovered the reduction product **19** (12%) using ethyl acetate/hexane as eluent.

Benzo carbacephem **20**; mp 256°C; ir (KBr) ν_{max}: 3290 (NH), 1755 (azetidinone), 1642 (amide); ^{1}H nmr (pyridine-d_5, 60°C) δ: 1.95 (m, 1H, C5), 2.19 (dd, 1H, C6-Hc, J = 10, 13), 2.32 (dd, 1H, C7-Ha, J = 15, 13), 2.59 (dd, 1H, C7-Hb, J = 4, 15), 2.97 (dd, 1H, C6-Hd, J = 4, 13), 3.74 (dd, 1H, C4-H, J = 5, 10), 3.82 (s, 2H, CH_2CO), 5.96 (dd, 1H, C3-H, J = 5, 9), 6.99—7.63 (m, 14H, Ar-H), 9.91 (d, 1H, N-H, J = 9); ^{13}C nmr (DMSO-d_6) δ: 30.45 (C7), 32.32 (C5), 36.85 (C6), 42.11 (CH_2Ph), 56.77 (C4), 58.56 (C3), 117–138.3 (Ar-C), 165.68 (C2), 170.57 (amide carbonyl); ms (225°C): 396 (M^+, 2.2), 305 (M^+ − Bn, 2.1), 277 (M^+ − BnCO, 6.6), 222 (M^+ + 1 − $C_{10}H_9NO_2$, 35.7), 175 (1.9), 77 (100). *Mol. Wt.* (high resolution ms) calcd. for $C_{26}H_{24}O_2N_2$: 396.1837; found: 396.1830.

Reduction product **19**; ir (KBr) ν_{max}: 3305 (NH), 1740 (azetidinone), 1675 (amide); ^{1}H nmr ($CDCl_3$) δ: 2.32 (s, 3H, CH_3), 3.50 (s, 2H, CH_2CO), 4.92 (dd, 1H, C4-H, J = 5, 8), 5.56 (dd, 1H, C3-H, J = 5, 8), 6.15 (dd, 1H, C5-H, J = 8, 16), 6.56 (d, 1H, C5-H, J = 16), 6.92–7.57 (m, 15H, Ar-H and N-H); ms (100°C): 396 (M^+, 3.2), 395 (5.7), 305 (M^+ − Bn, 1.8), 277 (M^+ − BnCO, 6.0), 221 (M^+ − $C_{10}H_9NO_2$, 33), 222 (100).

Radical cyclization of ***17***

Tributyltin hydride (72 mg, 0.25 mmol), AIBN (cat.), and benzene (1.5 mL) were added to azetidinone **17** and dry benzene (10 mL) at reflux temperature during 5 h (syringe pump) under an inert atmosphere. After a further 3 h at the same temperature, the reaction mixture was cooled to room temperature, whereby a white precipitate formed. The precipitate was filtered off and washed with hexane to give azetidinone **22** (39 mg, 70%) as colorless crystals. The solvent was removed to give an oily residue, which after the usual work-up and purification by column chromatography (ethyl acetate/hexane 1:1) gave the reduction product **21** (12%).

Tricyclic benzo carbacephem **22**; mp 273–274°C; ir (KBr) ν_{max}: 3282 (NH), 1770 (azetidinone), 1655 (amide); ^{1}H nmr (pyridine-d_5) δ: 2.25–2.4 (m, 3H, C5-H, C7-Ha, and C6-Hc), 2.63 (dd, 1H, C7-H6, J = 1.2, 14), 2.98 (dd, 1H, C6-Hd, J = 1.2, 10), 3.69 (dd, 2H, C4-H, J = 5, 10.2), 3.81 (s, 2H, CH_2CO), 5.17 (dd, 2H, CH_2—O, J = 12, 22), 5.97 (dd, 1H, C3-H, J = 5, 9), 6.84–7.7 (m, 14H, Ar-H), 9.97 (d, 1H, N-H, J = 9); ms (273°C): 502 (M^+, 0.96), 411 (M^+ − Bn, 4.5), 383 (M^+ − BnCO, 1.6), 328 (M^+ + 1 − $C_{10}H_9NO_2$, 100), 148 (M^+ − 328, 0.5). *Mol. Wt.* (high resolution ms (270°C)) calcd. for M^+ − Bn, $C_{26}H_{23}O_3N_2$: 411.171; found: 411.171.

Reduction product **21**; ir (KBr) ν_{max}: 3278 (NH), 1748 (azetidinone), 1650 (amide); ^{1}H nmr ($CDCl_3$) δ: 2.33 (s, 3H, CH_3), 3.50 (s, 2H, CH_2CO), 4.95 (dd, 1H, CH4-H, J = 5, 8), 5.06 (dd, 2H, $PhCH_2$—O, J = 12, 16), 5.38 (dd, 1H, C3-H, J = 5, 8), 5.95 (dd, 1H, C5-H, J = 8, 16), 6.17 (d, 1H, N-H, J = 8), 6.44 (d, 1H, C6-H, J = 16), 6.75–7.39 (m, 18H, Ar-H); ms (282°C): 502 (M^+, 2.7), 411 (M^+ − Bn, 4.5), 327 (M^+ − $C_{10}H_9NO_2$, 21.3), 328 (41.9), 237 (17.1).

Phenol carbacephem ***23***

Azetidinone **22** (25 mg), ethanol (5 mL), and dimethylformamide (2.5 mL) were hydrogenated with palladium on charcoal (2.5 mg, 10%) until 2.5 mL of hydrogen had been absorbed. The mixture was filtered and the solvent removed. Recrystallization from hot ethyl acetate and precipitation with hexane gave quantitative yield of azetidinone **23** as colorless crystals; mp 282–283°C; ir (KBr) ν_{max}: 3420 (b, OH), 3280 (NH), 1715 (azetidinone), 1658 (amide); ^{1}H nmr (pyridine-d_5) δ: 2.35–2.47 (m, 3H, C5-H, C6-Hc, and C7-Ha), 2.71 (d, 1H, C7-Hb, J = 12), 3.01 (d, 1H, C6-Hd, J = 10), 3.78 (dd, 1H, C4-H, J = 5, 9.2), 3.85 (s, 2H, CH_2CO), 5.02 (bs, 1H, OH), 5.95 (dd, 1H, C3-H, J = 5, 9), 6.87–7.49 (m, 14H, Ar-H), 9.98 (d, 1H, N-H, J = 9); ms (220°C): 412 (M^+, 2.9), 293 (M^+ − BnCO, 5.5), 237 (M^+ − $C_{10}H_9NO_2$, 15.5), 238 (100). *Mol. Wt.* (high resolution ms (260°C)) calcd. for $C_{26}H_{24}O_3N_2$: 412.1786; found: 412.1835.

Free radical cyclization of ***18***

Tributyltin hydride (125 mg, 0.42 mmol), AIBN (cat.), and benzene (2 mL) were added to azetidinone **18** (170 mg, 0.36 mmol) and dry benzene (18 mL) at reflux temperature during 12 h (syringe pump) under an inert atmosphere. The mixture was cooled to room temperature and the solvent removed. The residue was dissolved in acetonitrile (30 mL), washed with hexane (3 × 30 mL), and the solvent removed. Column chromatography using ethyl acetate/hexane as eluent gave the following products:

Tricyclic azetidinone **24** (37%); *E* isomer; mp 189°C (colorless crystals); ir (KBr) ν_{max}: 3305 (NH), 1748 (azetidinone), 1690 (amide); ^{1}H nmr ($CDCl_3$) δ: 3.30 (dd, 2H, C7-H, J = 16, 30), 3.47 (s, 2H, CH_2CO), 4.78 (d, 1H, C4-H, J = 5), 5.77 (d, 1H, N-H, J = 8), 5.78 (dd, 1H, C3-H, J = 5, 8), 6.60 (s, 1H, C6-H), 6.96–7.41 (m, 14H, Ar-H); ms (270°C): 394 (M^+, 0.7), 275 (M^+ − BnCO, 0.6), 260 (M^+ − BnCONH, 0.93), 221 (M^+ − $C_{10}H_9NO_2$, 18.2), 220 (100). *Mol. Wt.* (high resolution ms (270°C)) calcd. for $C_{26}H_{26}O_2N_2$: 394.1681; found: 394.1695.

Tricyclic azetidinone **25** (38%): *Z* isomer: mp 196°C: ir (KBr) ν_{max}: 3260 (NH), 1753 (azetidinone), 1655 (amide); ^{1}H nmr ($CDCl_3$) δ: 3.60 (s, 2H, CH_2CO), 3.63 (dd, 2H, C7-H, J = 19, 28), 4.62 (d, 1H, C4-H, J = 5), 5.64 (dd, 1H, C3-H, J = 5, 8), 6.04 (d, 1H, N-H, J = 8), 6.29 (s, 1H, C6-H), 7.06–7.44 (m, 14H, Ar-H); ms (269°C): 394 (1.6), 260 (11), 275 (0.9), 221 (21.7), 220 (100), 219 (19.6). *Mol. Wt.* (high resolution ms) calcd. 394.1681; found: 394.1710.

Tricyclic benzo carbacephem ***26***

To a mixture of azetidinones **24** (10 mg) and **25** (10 mg), ethyl acetate (5 mL), and ethanol (3 mL) was added platinum black (3 mg). The mixture was stirred overnight at room temperature under a hydrogen atmosphere, was then filtered off, and the solvent removed. The residue was purified by flash chromatography using ethyl acetate/hexane as eluent to give, after recrystallization from chloroform/carbon tetrachloride, the tricyclic azetidinone **26** as colorless crystals (25%); mp 237°C; ir (KBr) ν_{max}: 3305 (NH), 1768 (azetidinone), 1641 (amide); ^{1}H nmr ($CDCl_3$) δ: 1.91–2.04 and 2.36–2.65 (m, 5H, C5-H, C6-H, and C7-H), 3.65 (dd, 2H, CH_2CO, J = 2.5, 6), 4.25 (dd, 1H, C4-H, J = 3, 5), 5.41 (dd, 1H, C3-H, J = 5, 6), 6.01 (d, 1H, N-H, J = 6), 6.7–7.5 (m, 14H, Ar-H); ms (220°C): 396 (M^+, 2.1), 305 (M^+ − Bn, 1.7), 277 (M^+ − BnCO, 23.1), 262 (M^+ − $BnCONH_2$, 20), 222 (M^+ + H − $C_{10}H_9NO_2$, 14.2), 175 (14.4). *Mol. Wt.* (high resolution ms) calcd. for $C_{26}H_{24}O_2N_2$: 396.1837; found: 396.1758.

Tricyclic ketoazetidinone **27**

A mixture of azetidinones **24** (10 mg) and **25** (10 mg), methanol (2 mL), and dichloromethane (2 mL) at −78°C was ozonized for 5 min. The light blue solution was stirred for 15 min, and a stream of nitrogen was passed through the solution for 15 min. Dimethylsulfide (excess) was added and the mixture left overnight at room temperature. The solvents were removed and the residue purified by column chromatography using ethyl acetate/hexane (1:1) to give the ketone **27** as a yellow **oil (75% yield)**; ir (neat) ν_{max}: 3160 (NH), 1793 (azetidinone), 1722 (ketone), 1647 (amide); ^{1}H nmr ($CDCl_3$) δ: 3.55 (dd, 1H, C6-Ha, J = 1.8, 22), 3.56 (s, 2H, CH_2CO), 4.06 (d, 1H, C6-Hb, J = 22), 4.06 (dd, 1H, C4-H, J = 1.8, 5.7), 4.74 (dd, 1H, C3-H, J = 5.7, 7.2), 6.05 (d, 1H, N-H, J = 7.2), 7.17–7.39 (m, 9H, Ar-H); ms (148°C) chemical ionization, isobutane: 321 (M^+ + 1, 48.4), 320 (M^+, 2.7), 319 (14.7), 304 (321 − 17, 38.8), 303 (321 − 18, 48.3), 176 (14.6), 146 (M^+ + 1 − $C_{10}H_9NO_2$, 100).

Acknowledgements

We wish to thank Drs. John Finkenbine and Orval Mamer of the Biomedical Mass Spectrometry Unit, McGill University, for mass spectra, Dr. Werner Hinz for helpful discussions, and

the Natural Sciences and Engineering Research Council of Canada, Lederle Laboratories, and Fonds FCAR, Province de Québec, for generous financial support.

1. (*a*) J. H. BATESON, P. M. ROBERTS, T. C. SMALE, and R. SOUTHGATE. J. Chem. Soc. Chem. Commun. 185 (1980); (*b*) N. T. SALZMANN, R. W. RATCLIFFE, and B. G. CHRISTENSEN. Tetrahedron Lett. **21**, 1193 (1980).
2. (*a*) G. JUST and R. ZAMBONI. Can. J. Chem. **56**, 2720 (1978); (*b*) **56**, 2725 (1978); (*c*) G. JUST, Y. S. TSANTRIZOS, and A. UGOLINI. Can. J. Chem. **59**, 2781 (1981).
3. J. FINKELSTEIN, K. G. HOLDEN, and C. C. PERCHONOCK. Tetrahedron Lett. **19**, 1629 (1978).
4. (*a*) M. D. BACHI and C. HOORNAERT. Tetrahedron Lett. **22**, 2689 (1981); (*b*) **22**, 2693 (1981); (*c*) **22**, 2505 (1981); (*d*) M. D. BACHI, F. FROWLOW, and C. HOORNAERT. J. Org. Chem. **48**, 1841 (1983).
5. (*a*) J. KNIGHT, P. J. PARSONS, and R. SOUTHGATE. J. Chem. Soc. Chem. Commun. 788 (1986); (*b*) A. L. J. BECKWITH and R. D. BOATHE. Tetrahedron Lett. **26**, 1761 (1985).

Can. J. Chem. Downloaded from www.nrcresearchpress.com by 80.58.250.72 on 09/07/12
For personal use only.

Stereochemistry of 3-carboxylated 2,5-dihydrothiophene formation[1,2]

JOHN M. MCINTOSH AND IVY E. E. HAYES[3]
Department of Chemistry, University of Windsor, Windsor, Ont., Canada N9B 3P4

Received May 20, 1986

This paper is dedicated to Dr. O. E. (Ted) Edwards

JOHN M. MCINTOSH and IVY E. E. HAYES. Can. J. Chem. **65**, 110 (1987).

The preparation of 2-carboxylated-1,3-dienes from carbomethoxy vinylphosphonates and 2-mercaptocarbonyl compounds has been shown to give stereoisomeric mixtures. This may be due to the formation of stereoisomers of the intermediate 2,5-dihydrothiophenes and (or) to the occurrence of both modes of disrotatory sulfur dioxide elimination.

JOHN M. MCINTOSH et IVY E. E. HAYES. Can. J. Chem. **65**, 110 (1987).

On démontre que la préparation de diènes-1,3 portant un groupement carboxyle en position-2, effectuée à partir de carbométhoxy vinylphosphonates et de composés mercapto-2 carbonyles, conduit à des mélanges de stéréoisomères. Ce résultat peut être dû à formation de stéréoisomères des dihydro-2,5 thiophènes intermédiaires et (ou) à la présence de chacun des deux modes d'éliminations disrotatoires du dioxyde de soufre.

[Traduit par la revue]

Can. J. Chem. Downloaded from www.nrcresearchpress.com by 190.90.36.8 on 09/07/12
For personal use only.

Some time ago we described the reaction of 2-mercaptoaldehydes and ketones (**1**) with vinylphosphonium salts as a preparative route to substituted 2,5-dihydrothiophenes (DHT's) (**3**) (2). This Michael–Wittig sequence was shown to afford products that were predominantly the *cis* 2,5-disubstituted stereoisomers when the 3-substituent was small (R′ = H), but increasing amounts of the *trans*-isomer were formed as the steric bulk of the ring substituents increased (3). These results were rationalized on the basis of a model (**2**) in which the substitutents were preferentially on the side opposite the bulky triphenylphosphine moiety. Oxidation of the DHT to the sulfone, followed by thermolysis, led to the disrotatory (4) elimination of sulfur dioxide and the formation of a 1,3-diene in a regiospecific and stereoselective manner by the formal joining of two vinyl moieties (Scheme 1).

In subsequent work it was shown that vinylphosphonates (**4**) bearing an α-carbomethoxy group afforded excellent yields of 3-carboxylated DHT's (**6**) and, after oxidation and thermolysis, 2-carbomethoxy-1,3-dienes **8** (Scheme 2) (5). In view of the potential applications of compounds of type **8** to natural product syntheses (6), an examination of the stereochemistry of the DHT formation and decomposition was deemed to be worthwhile and this brief report deals with that aspect of the reaction.

It is known that the attack of the anion of a phosphonate, like that of a phosphorane, on a carbonyl group is a reversible process (7). Thus the isomeric distribution of DHT's should reflect the thermodynamic stabilities of the intermediate **5** that is undergoing irreversible decomposition. Comparison of the intermediate **2** (Scheme 1), in which a hydrogen is attached to the phosphorus-bearing carbon atom (α-substituted vinylphosphonium salts do not give DHT products (8)), with **5** (Scheme 2), in which a carbomethoxy group is in this position, suggests that the tendency toward the formation of the *cis* 2,5-disubstituted isomers should be lowered in the latter case.

Two vinylphosphonates (**4***a* and **4***b*) were utilized with one 2-mercaptoaldehyde (**1***a*) and two 2-mercaptoketones (**1***b*, *c*) giving five DHT's (**6***a–e*) with varying substitution patterns, two of which can exist in only one stereoisomeric form. The products and their yields are shown in Table 1, and Table 2 summarizes the spectroscopic data for the new compounds. As was found with the noncarboxylated DHT's (2), it was not possible to separate the stereoisomers by either thin-layer chromatography (tlc) or gas chromatography (gc). In addition, the spectra, although confirming the presence of stereoisomeric mixtures in many cases, could not be used to unambiguously determine isomer ratios. In an attempt to circumvent this problem, the DHT's were oxidized to the corresponding sulfones **7** (2), and thermolysis to the dienes **8** under two conditions was studied. Direct injection into a gas chromatograph (inlet temperature 270°C) led to the elution of the component dienes. Integration of the peaks led to the isomer ratios. Alternatively, decomposition of the sulfones in refluxing toluene for varying lengths of time gave the same dienes, but in ratios that were, in some cases, time dependent. Because separation of the components on a preparative basis was not achieved, the stereochemistry of each component is uncertain. However, the number of components and the time dependence of their abundance gives information regarding the stereochemistry of the DHT's and also of the cheletropic sulfur dioxide elimination reaction.

The results of the diene decompositions are presented in Table 3. From these data, the following conclusions can be drawn. The two sulfones (**7***a* and **7***b*) that can exist in only one stereoisomeric form both give two dienes. Collection of the mixture and reinjection into the gas chromatograph gave the same peaks in the same ratios, establishing that, at least in these cases, no diene isomerization was occurring under these "direct decomposition" conditions. If it is assumed that the presence of the 3-carbomethoxy group does not affect the stereochemical nature of the sulfur dioxide elimination, it can be stated that both modes of disrotatory ring opening are occurring. The initial product favors the *Z*-isomer but prolonged heating causes equilibration toward the more stable *E* form. In the case of **7***c*, two sulfone stereoisomers are possible but only two dienes are expected since the cyclohexene double bond must be *cis*. In this case, a 1:1 mixture of two dienes is obtained under direct decomposition conditions and this ratio does not change on prolonged heating, a result which can be rationalized either on the basis of equal amounts of the two sulfone stereoisomers or on very rapid equilibration of the two isomers. In the final two instances (**7***d* and **7***e*), two sulfone isomers and four diene components are possible, but only three of the latter are formed.

[1]Dihydrothiophenes, part 11. For part 10 see ref. 1.

[2]Taken in part from the M.Sc. thesis of I. E. E. Smith, University of Windsor, 1985.

[3]Present address: Department of Chemistry, York University, North York, Ontario.

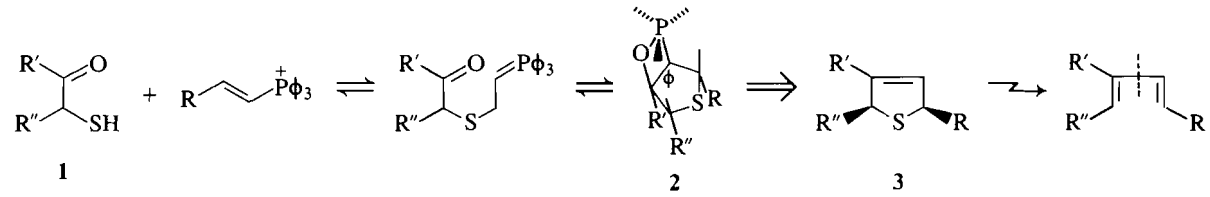

SCHEME 1

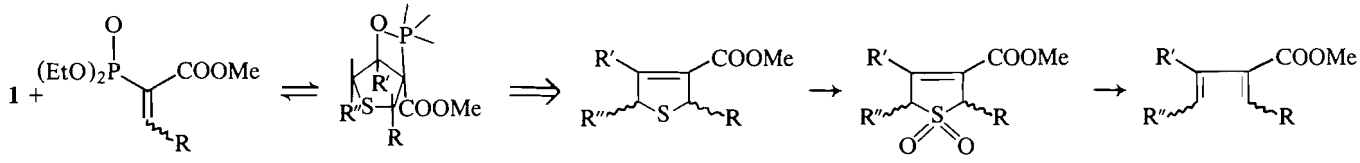

SCHEME 2

TABLE 1. Products and yields of compounds **6** and **7**

Phosphonate		Mercaptan			2,5-DHT		Sulfone	
No.	R	No.	R′	R″	No.	Yield (%)	No.	Yield (%)
4*a*	Ph	**1***a*	H	H	**6***a*[a]	47	**7***a*	83
4*b*	iPr	**1***a*	H	H	**6***b*	100	**7***b*	63
4*a*	Ph	**1***b*	—$(CH_2)_4$—		**6***c*	100	**7***c*	70
4*a*	Ph	**1***c*	Me	Me	**6***d*	71	**7***d*	23
4*b*	iPr	**1***c*	Me	Me	**6***e*	31	**7***e*	69

[a]Reference 5*a*.

Prolonged heating of these does not significantly alter the component ratios. In the absence of definitive identification of the diene component stereochemistry, it is not possible to unambiguously determine the stereochemical composition of the sulfone mixtures. However, at best, **7***d* is a 9:1 mixture and, at worst (the more likely scenario), a 3:1 mixture. Similar considerations apply to **7***e*.

In conclusion, the following can be stated. The presence of a 3-carbomethoxy group significantly and negatively affects the stereochemical outcome of the use of DHT's for 1,3-diene synthesis. This may be due to steric influences in the transition state for DHT formation, which gives larger *trans*/*cis* ratios than when vinylphosphonium salts are used, and (or) to significant interactions in the transition state for sulfur dioxide elimination, which allows both modes of disrotatory ring opening to occur. The overall result is that, although assembly of the carbon skeleton of the 2-carbomethoxy-1,3-diene system remains facile, stereochemical control of the process is not feasible.

Experimental

Infrared spectra were obtained on a Perkin Elmer Model 180 instrument or a Nicolet 5:DX (FT) instrument in $CHCl_3$ solution (unless otherwise noted) and are reported in cm^{-1}. The ^1H nmr spectra were obtained on a Varian EM360 or Bruker WP-80 instrument in $CDCl_3$ solution and the chemical shift values are relative to internal TMS as standard. Gas chromatographic analyses were performed on a Varian Model 3700 instrument using a helium flow rate of 1 cm^3/s. The injector port temperature was 270°C and the columns used were 10 ft × 0.25 in. 20% SE-30 on Chromosorb W or 50 cm × 0.125 in. 5% OV-101 on Chromosorb W.

Starting materials

Mercaptoaldehyde **1***a* was purchased in the form of its dimer (1,4-dithiane-2,5-diol); compounds **1***b* (9), **1***c* (10), and **4***a* (5*a*) were prepared according to literature procedures.

*Methyl 2-diethylphosphono-4-methyl-2-pentenoate (4*b*)*

To a stirred solution of isobutyraldehyde (11.97 g, 0.166 mol) and diethyl phosphonoacetate (6.99 g, 0.033 mol) in 250 mL of dry benzene was added a mixture of 1.5 mL acetic acid and 0.5 g of piperidine. The solution was heated at reflux under a Dean–Stark water separator for 55 h, at which time gc analysis indicated the reaction was complete. The solvent was evaporated and the residue distilled to give 7.39 g (90%) of **4***b* as a mixture of diastereomers; bp 97–105°C (0.5 Torr; 1 Torr = 133.3 Pa). *Anal.* calcd. ($C_{11}H_{21}O_5P$): C 49.99, H 8.01; found: C 50.23, H 7.84.

General procedure for dihydrothiophene preparation and oxidation

To a refluxing, nitrogen-blanketed suspension or solution of **1** (0.033 mol) in 250 mL of CH_2Cl_2 containing 5.3 g of Et_3N was added dropwise a solution of 0.02 mol of vinyl phosphonate **4** in 50 mL of CH_2Cl_2. After 14–24 h the reaction was complete, as shown by gc analysis. The solution was cooled, washed with water (2 × 200 mL), 5% HCl (2 × 150 mL), dried, and evaporated to give the crude dihydrothiophene as a yellow oil. Chromatography (neutral alumina, activity grade I) using 1:1 petroleum ether:ether as eluant eluted the pure DHT in the first 300 mL. Yields of products are given in Table 1 and physical and spectroscopic data in Table 2. Analytical data for new compounds are given in Table 4.

Oxidation to the sulfones 7 was accomplished according to the literature procedure (5*a*). In the case of **6***e*, oxidation was incomplete even with several equivalents of peracid and the sulfone was contaminated with small amounts of sulfoxide (ir and mass spectra). DHT sulfoxides are known to decompose nonstereospecifically but at much

Can. J. Chem. Downloaded from www.nrcresearchpress.com by 190.90.36.8 on 09/07/12
For personal use only.

TABLE 2. Physical and spectroscopic data for **6** and **7**

Compound	Melting point (°C)	Infrared (cm^{-1})[a]	^1H nmr[b]
6*a*	70	3020, 1725, 1650, 1275	7.19 (s, 5), 6.97 (m, 1), 5.45 (m, 1), 4.00 (m, 2), 3.57 (s, 3)
6*b*		2925, 1722, 1436, 1380, 1260, 1195	6.83 (m, 1), 4.57–4.30 (m, 1), 3.70 (s, 3), 3.65 (m, 2), 1.30 (m, 1), 0.97, 0.80 (2d, 6, J = 7 Hz)
6*c*		2950, 1715, 1285, 1265	7.27, 7.30 (2s, 5), 5.45 (m, 1), 4.63–4.00 (m, 1), 3.40, 3.47 (2s, 3), 2.50–1.30 (m, 8)
6*d*	60	2925, 1717, 1436, 1281, 1232	7.20 (s, 5), 5.50 (m, 1), 4.40 (m, 1), 3.50 (s, 3), 2.17 (s, 3), 1.43 (d, 3, J = 7 Hz)
6*e*		2961, 1717, 1434, 1380, 1214, 1067	4.38 (m, 1), 4.20–3.93 (m, 1), 3.65 (s, 3), 2.55–2.01 (bs, 4), 1.36 (d, 3, J = 7 Hz), 0.90, 0.76 (2d, 6, J = 7 Hz)
7*a*	170 (dec.)	[c]1735, 1460, 1335, 1200	[d]7.41 (m, 6), 5.46 (bs, 1), 4.33 (d, 2, J = 4 Hz), 3.90 (s, 3)
7*b*	78 (dec.)	2977, 1723, 1436, 1325, 1257, 1199	7.12 (m, 1), 4.00–3.77 (m, 3), 3.77 (s, 3), 2.60–1.94 (m, 1), 1.14 (d, 6, J = 7 Hz)
7*c*	118 (dec.)	3056, 2880, 1719, 1317, 1245, 1166	7.05 (m, 5), 5.20–4.97 (m, 1), 3.75–3.45 (m, 1), 3.52, 3.45 (2s, 3), 2.28–1.05 (m, 8)
7*d*	111 (dec.)	[c]2937, 1713, 1313, 1237, 1136	7.32 (m, 5), 5.20 (m, 1), 3.95 (m, 1), 3.58 (s, 3), 2.37 (s, 3), 1.63 (d, 3, J = 7 Hz)
7*e*	—	[e]2964, 1721, 1436, 1310, 1234, 1139	

[a]Most intense peaks; in $CHCl_3$ solution.
[b]In $CDCl_3$. Coding: chemical shift (multiplicity, number of hydrogens, coupling constant).
[c]KBr pellet.
[d]In CF_3COOD solution.
[e]Mixture of sulfone and sulfide.

TABLE 3. Results of sulfone thermolysis

Sulfone No.	Peak ratios[a,b] Gas chromatographic injection	Thermolysis (h)[c]
7*a*	72:28	49:51 (4) 23:77 (19)
7*b*	80:20	45:55 (20)
7*c*	45:55	50:50 (10)
7*d*	13:77:10	14:76:10 (2.5) 12:82:6 (5.2)
7*e*	15:70:15	10:85:5 (6)

[a]Isomers in order of elution from gc.
[b]Injection port temperature 270°C.
[c]Toluene at reflux.

TABLE 4. Analytical data for new compounds

Compound	Calculated Carbon	Calculated Hydrogen	Found Carbon	Found Hydrogen
6*b*	58.03	7.57	58.21	7.49
6*d*	67.70	6.49	67.85	6.55
6*e*	61.64	8.46	61.13	8.42
7*a*	57.12	4.79	56.98	4.81
7*b*	49.52	6.46	49.44	6.40
7*c*	62.72	5.92	62.32	5.92
7*d*	59.98	5.75	59.68	5.75

higher temperatures than sulfones (11), and this mixture was used directly in the thermolysis experiments.

Sulfone thermolyses

Injection of sulfones into the injection port of a gas chromatograph (neat or in solution) effected elimination of SO_2, and the dienes were eluted. Flask thermolyses were performed by suspending the sulfone in dry toluene and heating at reflux under nitrogen until tlc indicated the absence of starting material. The solvent was removed by distillation and the residue chromatographed on silica gel using 20% petroleum ether in ether. The collected fractions of dienes were combined and analyzed by gc. Results of all thermolyses are given in Table 3. The mass spectra (field desorption) and ir and nmr spectra of the diene mixtures indicated that only the expected dienes were present, but were not interpretable in terms of the stereochemistry of the components.

Acknowledgements

The financial assistance of the Natural Sciences and Engineering Research Council of Canada made this work possible and is gratefully acknowledged.

1. J. M. McIntosh and L. Z. Pillon. Can. J. Chem. **62**, 2089 (1984).
2. (*a*) J. M. McIntosh, H. B. Goodbrand, and G. M. Masse. J. Org. Chem. **39**, 202 (1974); (*b*) J. M. McIntosh and R. S. Steevensz. Can. J. Chem. **52**, 1934 (1974).

Can. J. Chem. Downloaded from www.nrcresearchpress.com by 190.90.36.8 on 09/07/12
For personal use only.

3. J. M. McINTOSH and G. M. MASSE. J. Org. Chem. **40**, 1294 (1975).
4. W. L. MOCK, J. Am. Chem. Soc. **88**, 2857 (1966); S. D. McGREGOR and D. M. LEMAL. J. Am. Chem. Soc. **88**, 2859 (1966).
5. (*a*) J. M. McINTOSH and R. A. SIELER. Can. J. Chem. **56**, 226 (1978); (*b*) J. M. McINTOSH and R. A. SIELER. J. Org. Chem. **43**, 4431 (1978).
6. A. S. KENDE and B. H. TODER. J. Org. Chem. **47**, 163 (1982).
7. W. S. WADSWORTH. Organic reactions. Vol. 25. Wiley, New York, NY. 1977. p. 204.
8. J. M. McINTOSH and R. S. STEEVENSZ. Can. J. Chem. **55**, 2445 (1977).
9. F. ASINGER, M. THIEL, and H. KALTWASSER. Justus Liebigs Ann. Chem. **606**, 67 (1957).
10. P. HROMATKA and R. HABERL. Monatsh. Chem. **85**, 830 (1954).
11. D. M. LEMAL and P. CHAO. J. Amer. Chem. Soc. **95**, 920, 922 (1973).

Can. J. Chem. Downloaded from www.nrcresearchpress.com by 190.90.36.8 on 09/07/12
For personal use only.

A general intramolecular Diels–Alder approach to tricyclic sesquiterpenes: stereoselective total syntheses of (±)-sinularene and (±)-5-epi-sinularene

KAZIMIERZ ANTCZAK,[1] JOHN F. KINGSTON,[2] AND ALEX G. FALLIS[3]
Department of Chemistry, Memorial University of Newfoundland, St. John's, Nfld., Canada A1B 3X7

AND

ALFRED W. HANSON
National Research Council of Canada, Atlantic Research Laboratory, Halifax, N.S., Canada B3H 3Z1

Received Received June 4, 1986

This paper is dedicated to Dr. O. E. (Ted) Edwards

KAZIMIERZ ANTCZAK, JOHN F. KINGSTON, ALEX G. FALLIS, and ALFRED W. HANSON. Can. J. Chem. **65**, 114 (1987).

Stereoselective total syntheses of (±)-sinularene and (±)-5-epi-sinularene are described. The sequence employs a "blocked" cyclopentadiene in which the cyclopropane unit also serves as a latent methyl group. Thus intramolecular [4 + 2] cycloaddition of the substituted methyl spiro[2.4]hepta-4,6-dien-1-yl-2-pentenoate **13***c* affords 5-benzyloxy-6-isopropyl-8-carbomethoxytetracyclo[5.4.$0^{1,7}$.$0^{2,4}$.$0^{2,9}$]undec-10-ene (**14***c*), which after selective hydrogenolysis generates the tricyclo[4.4.$0^{1,6}$.$0^{2,8}$]decane (sinularene) ring system. Removal of the secondary hydroxyl function by elimination and hydrogenation ($Ph_3P/CCl_4/CH_3CN$; H_2/Pd/C), reduction of the methyl ester ($LiAlH_4$), and introduction of the exocyclic double bond (acetate pyrolysis, 550°C) completes the synthesis of (±)-sinularene in 12 steps from aldehyde **7**. A parallel series of reactions employing the isopropyl triene epimer **13***a* affords (±)-5-epi-sinularene. X-ray analyses of the triene **13***a* and the adduct **14***a* are also reported.

KAZIMIERZ ANTCZAK, JOHN F. KINGSTON, ALEX G. FALLIS et ALFRED W. HANSON. Can. J. Chem. **65**, 114 (1987).

On décrit les synthèses stéréosélectives du (±)-sinularène et du (±)-épi-5 sinularène. Ces synthèses impliquent l'utilisation d'un cyclopentadiène «bloqué» dans lequel l'unité cyclopropane sert aussi de groupement méthyle latent. Ainsi, la cycloaddition intramoléculaire [4 + 2] du spiro[2.4]heptadiène-4,6 yl-1 pentène-2 oate de méthyle substitué (**13***c*) conduit au benzyloxy-5 isopropyl-6 carbométhoxy-8 tétracyclo[5.4.$0^{1,7}0^{2,4}0^{2,9}$]undécène-10 (**14***c*) qui, après hydrogénolyse sélective, conduit au système cyclique tricyclo[4.4.$0^{1,6}0^{2,8}$]décane du sinularène. L'enlèvement de la fonction hydroxyle secondaire, par le biais d'une élimination suivie d'une hydrogénation ($Ph_3P/CCl_4/CH_3CN$; H_2/Pd/C), suivie d'une réduction de l'ester méthylique ($LiAlH_4$) et de l'introduction de la double liaison exocyclique (pyrolyse de l'acétane, 550°C) complètent la synthèse du (±)-sinularène, en 12 étapes à partir de l'aldéhyde **7**. Une série de réactions parallèles, appliquée au triène portant un groupement isopropyle de stéréochimie épimère **13***a*, conduit au (±)-épi-5 sinularène. On rapporte aussi des études par diffraction des rayons-X qui ont été effectuées sur le triène **13***a* ainsi que sur l'adduit **14***a*.

[Traduit par la revue]

Introduction

Marine invertebrates are a rich source of secondary metabolites and in recent years have afforded a broad cross section of interesting terpenoid skeletons (1). The coelenterates, particularly, have provided an array of new sesquiterpenes including the structurally unusual hydrocarbon (−)-sinularene (**1**). Sinularene was isolated from the alcyonacean soft coral *Sinularia mayi* and its structure established in 1977 by X-ray analysis (2, 3). More recently, the related esters 12-acetoxysinularene (**2**) and 12-acetoxycyclosinularene (**4**) were obtained from a

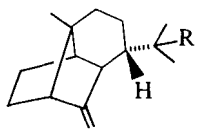

1 R = H
2 R = OAc

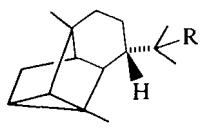

3 R = H
4 R = OAc

closely related stoloniferan soft coral *Claularia inflata* (4). To the best of our knowledge the corresponding parent hydrocarbon cyclosinularene (**3**) still awaits discovery.

The synthesis of natural products continues to play a significant role in the development of modern organic chemistry and thus, not surprisingly, these structures have attracted considerable attention as synthetic targets. Three total syntheses of (±)-sinularene have been reported. The first by Collins and Wege utilized a Wagner–Meerwein rearrangement, followed by intramolecular alkylative ring closure (5). Subsequently Oppolzer *et al.* employed an intramolecular "magnesium-ene" reaction as the key step (6) and, more recently, have also prepared 12-acetoxysinularene by this procedure (7). Coincident with the completion of our own work (8), Piers and Jung described an efficient Cope rearrangement sequence to the bicyclo[3.2.1]octane nucleus, followed by intramolecular alkylation to generate sinularene (9).

Results

(a) Synthetic plan (see Scheme 1)

Our own approach is based on an intramolecular Diels–Alder reaction sequence, a reaction in which there is considerable current interest and which has recently been applied to a number of natural product syntheses with notable success (10–13). The route selected, outlined briefly in retrosynthetic fashion in Scheme 1, utilizes the cyclopropane ring present in the spiro[2.4]heptatriene system **6** to block the normally dominant 1,5 sigmatropic rearrangement of cyclopentadienes. This cyclopropyl unit subsequently serves as a source of latent functionality to generate the requisite tertiary methyl group from the tetracyclic Diels–Alder adduct of type **5** by selective cyclo-

[1]Present address: Torcan Chemical Ltd., P.O. Box 308, 110 Industrial Pkwy. N., Aurora, Ont., Canada L4G 1X9.

[2]Present address: Explosives Research Laboratory, C.I.L. Inc., McMasterville, Que., Canada J3G 1T9.

[3]Author to whom enquiries may be addressed.

Can. J. Chem. Downloaded from www.nrcresearchpress.com by 80.58.250.72 on 09/07/12
For personal use only.

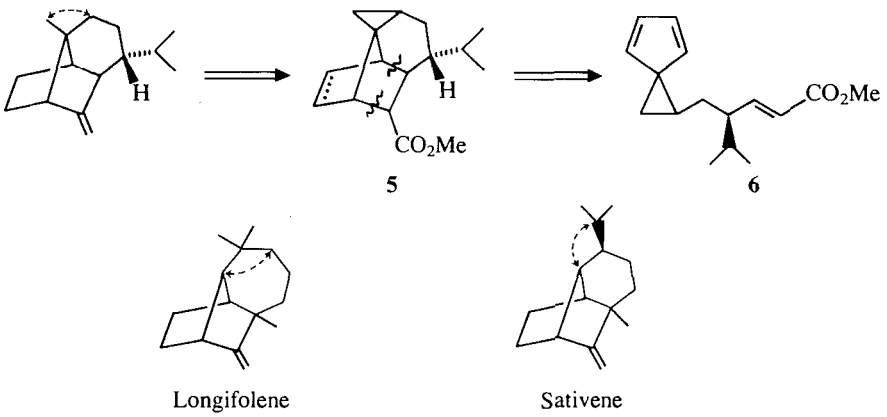

SCHEME 1

propane bond cleavage to provide a direct entry into the tricyclo[4.4.$0^{1,6}$.$0^{2,8}$]decane ring system possessed by sinularene. This strategy thus requires, in a retrosynthetic sense, the construction of a bond between the tertiary methyl group and the neighbouring methylene position (arrows) prior to double disconnection of the "bicyclo[2.2.1]heptane" nucleus. In the forward, synthetic direction the cyclopropane step corresponds to the reverse of an intramolecular alkylation. We have described earlier the general potential of this strategy for the eventual total synthesis of longifolene (14, 15) and sativene (16, 17) by controlled cleavage of the other cyclopropane bonds with suitably substituted precursors (arrows) (18).

(b) Preparation of hydroxy-ester 8 (see Figure 1)

Our initial intention to utilize triene **6** directly was thwarted by the discovery that it would not cyclize and that a C5 oxygen substituent was essential to ensure that the desired intramolecular cycloaddition proceeded as required (19). In addition, carrying the isopropyl function in the sidechain seemed advantageous so the correct stereochemistry could be established at an early stage. These considerations indicated that the substituted triene **13** (Scheme 2) was a desirable intermediate target, as it possessed these features as well as containing all 15 carbon atoms required for the natural product.[4]

The substituted triene **13** was elaborated from a series of condensations commencing with the aldehyde **7**, which was prepared by oxidation of the corresponding primary alcohol (20, 21) with active manganese dioxide (19). The initial aldol condensation of **7** with the anion derived from methyl 3-methylbutyrate and lithium diisopropylamide (LDA) was conducted at −78°C in tetrahydrofuran (THF). This led to a 47:30:14:2 mixture (based on isolated yields, total yield 93%) of the hydroxy-ester stereoisomers **8** (Fig. 1). The major isomer **8***c* (47%) arose from preferential attack of the *E*(O) enolate, as illustrated in **9**, on the aldehyde carbonyl from the less hindered direction and was assigned the (2*S**,3*S**,1′*S**)-configuration based on its conversion to (±)-sinularene.[4] The (2*R**,3*S**,1′*S**)-stereochemistry of the isomer **8***a* (30%) followed from the X-ray-difraction analysis described below and its conversion to (±)-5-epi-sinularene. Experimentally the chromatographic behaviour of the 14% component **8***b* and that of the **8***c* hydroxy-ester were very similar and thus it was more efficient to separate these compounds at the ether-alcohol stage (i.e., **11**, Scheme 2). In principle, the 2,3-*anti* selectivity of this coupling could be further enhanced if the conditions were altered to afford the *E*(O) enolate preferentially using modified aldol conditions (22). This has not been examined in the present instance due to our desire to have access to the various isomeric trienes **13***a–c*, in order to learn more about their cycloaddition behaviour and the unusual stereoelectronic effects of oxygen substituents in this series.

(c) Preparation of Diels–Alder adducts 14 (see Scheme 2)

The following set of parallel reactions converted the individual diastereomers **8** into the (4*R**,5*R**,1′*S**)-triene **13***c*, the (4*S**,5*R**,1′*S**)-triene **13***a*, and the (4*R**,5*S**,1′*S**)-triene **13***b*. The secondary alcohol **8** was protected as its benzyl ether in 80% yield upon generation of the alkoxide with sodium hydride in dimethoxyethane (DME) and alkylation with benzyl bromide. The resulting ether-ester **10** was reduced with lithium aluminum hydride in 95% yield to the primary alcohol **11**. Oxidation of **11** with pyridinium dichromate gave the aldehyde **12**, which was subjected to Wittig condensation with methyl (triphenylphosphoranylidene)acetate in refluxing tetrahydrofuran. In contrast to our earlier experience with **6**, these conditions resulted in simultaneous cyclization of triene **13***c* to the tetracyclic ester **14***c* in 72% overall yield. This implied a cycloaddition yield of approximately 95% and dramatically illustrated the beneficial influence of the C5 oxygen substituent.

In similar fashion the (4*S**,5*R**,1′*S**)-triene **13***a* also cyclized at 67°C (THF), although recycling was required since at this temperature the initial Diels–Alder reaction stopped at 50% completion. This implied that an equilibrium was established. However, this does not appear to be the exact explanation, since there was no evidence (^{1}H nmr) for any triene formation when a sample of the adduct **14***a* was heated in refluxing THF for 8 h, and cyclization at a higher temperature (110°C, toluene) failed to improve the cycloaddition yield beyond 50%. In contrast to the behaviour of **13***c* and **13***a*, the related isomeric (4*R**,5*S**,1′*S**)-triene **13***b* failed to cyclize to a detectable extent even in refluxing *o*-dichlorobenzene (180°C).

(d) Conversion of 14 into (±)-sinularene and (±)-5-epi-sinularene (see Scheme 2)

The direct preparation of the desired tetracyclic adducts **14***c* and **14***a* now permitted the introduction of the latent methyl functionality by hydrogenolysis. As expected from our pre-

[4]All the compounds described are racemic but only the enantiomers leading to the natural configuration of sinularene and 5-epi-sinularene are illustrated. The relative stereochemistries are indicated commencing with the *S** isomer of aldehyde **7** from which the (4*R**,5*R**,1′*S**)-triene **13***c* and sinularene were prepared. Thus rotation of the (4*S**,5*R**,1′*S**)-triene **13***a* affords the X-ray conformation in Fig. 3 and ring closure leads to **14***a* (Fig. 2).

Can. J. Chem. Downloaded from www.nrcresearchpress.com by 80.58.250.72 on 09/07/12
For personal use only.

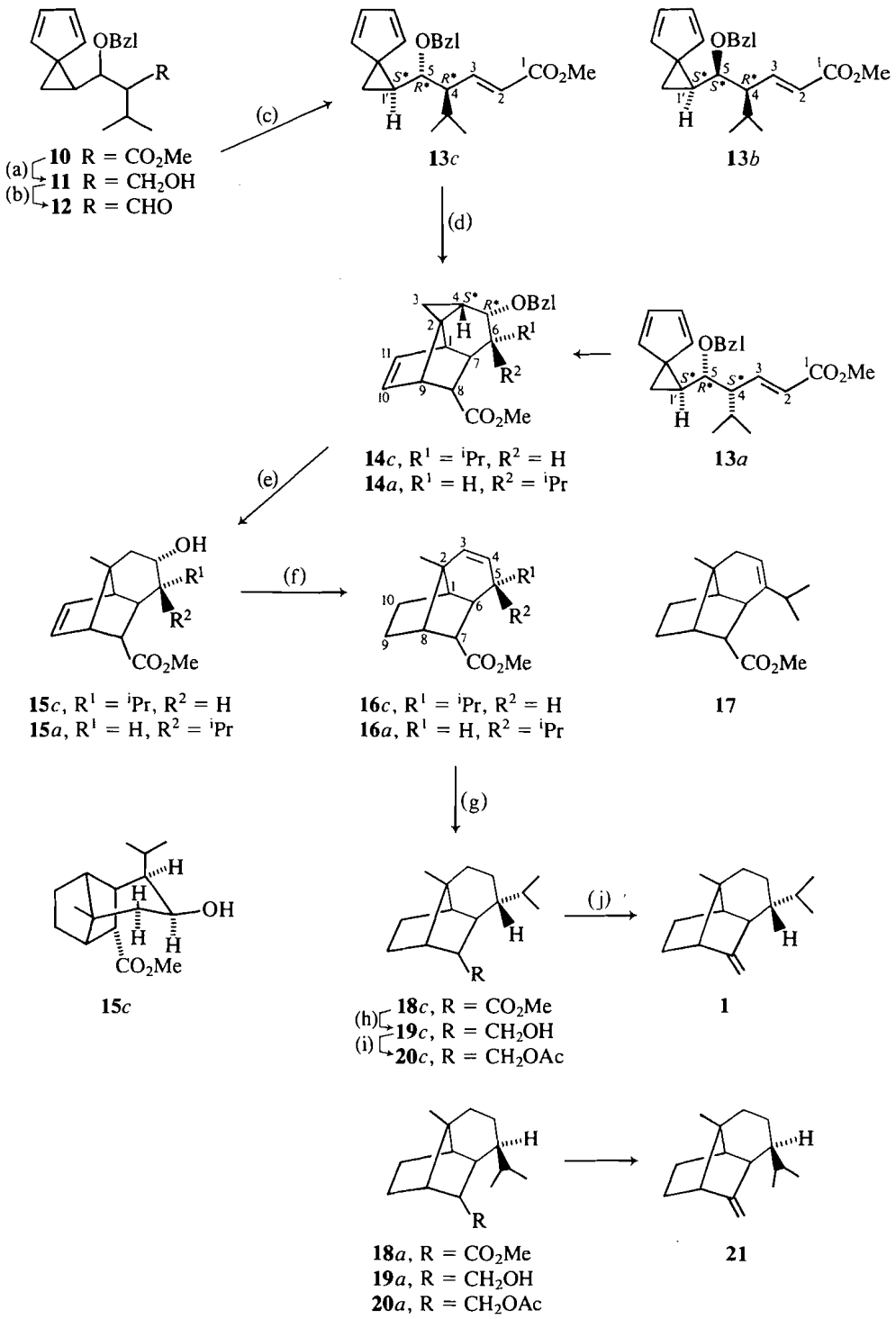

For natural series: (a) $LiAlH_4$, ether, 0°C, 1 h, 95%; (b) PDC, CH_2Cl_2, 21°C, 24 h, 64%; (c) $Ph_3P{=}CHCO_2Me$, THF, 67°C, 12 h, 76%; (d) THF, 67°C, 12 h, 95%; (e) H_2, 10% Pd/C, 50 psi, MeOH, 21°C, 24 h, 85%; (f) Ph_3P/CCl_4, CH_3CN, 21°C, 24 h, 97%; (g) H_2, 10% Pd/C, 1 atm, MeOH, 21°C, 48 h, 99%; (h) $LiAlH_4$, ether, 0°C, 0.5 h, 99%; (i) Ac_2O/pyridine, 4°C, 15 h, 99%; (j) 550°C, flow, 77%.

SCHEME 2

liminary studies of related cyclopropyl ketones (18), hydrogenolysis of **14** in the presence of 10% Pd/C at 50 psi (1 psi = 6.9 kPa) cleaved the least substituted cyclopropane bond exclusively, with concomitant removal of the benzyl function and hydrogenation of the double bond to give the hydroxy-ester **15***c* in 85% yield. Originally we intended to convert the secondary alcohol function into a halide substituent for subsequent hydride displacement and ester reduction in the next step. However, attempted conversion of **15***c* into a secondary bromide with triphenylphosphine dibromide afforded a significant amount of the olefin **16***c*, accompanied by unreacted alcohol and only a trace of the desired bromide. Elimination is

Can. J. Chem. Downloaded from www.nrcresearchpress.com by 80.58.250.72 on 09/07/12
For personal use only.

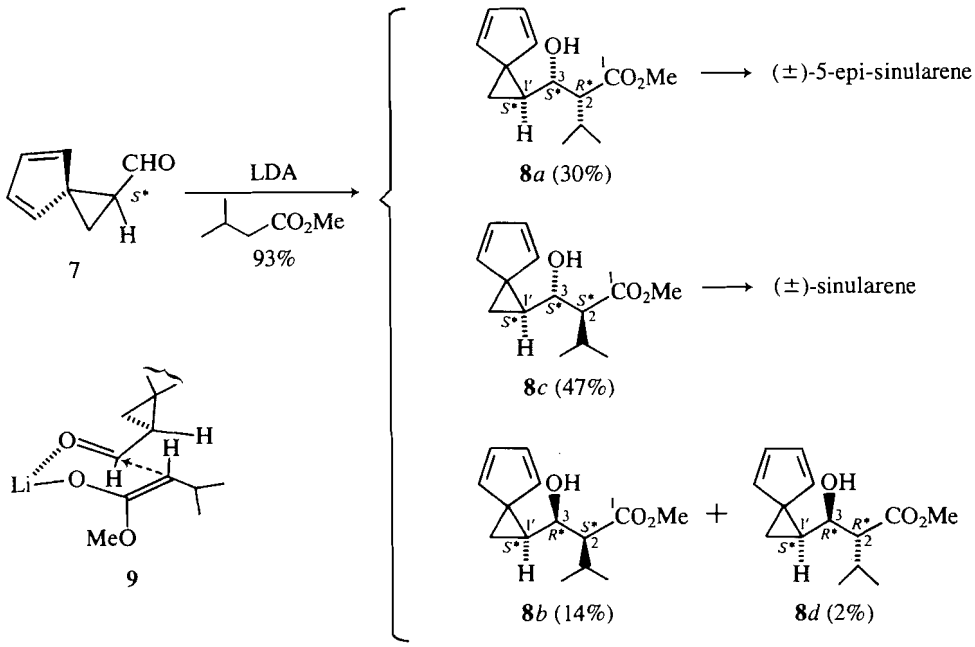

FIG. 1.

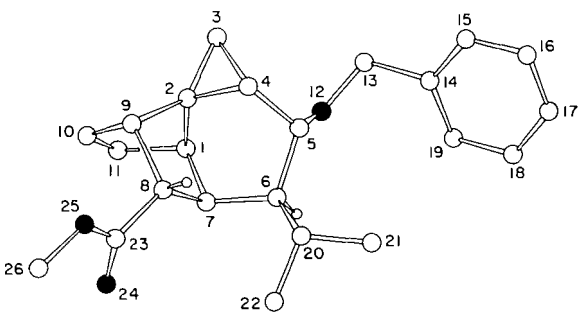

FIG. 2. A view of the adduct **14***a* ((4*S**,5*R**,6*S**)-5-benzyloxy-6-isopropyl-8-carbomethoxytetracyclo[5.4.$0^{1,7}$.$0^{2,4}$.$0^{2,9}$]undec-10-ene); H-atoms are shown only where they help in visualizing the stereochemistry. Here and in Fig. 3, C and O atoms are represented by open and solid circles, and H atoms by smaller open circles.

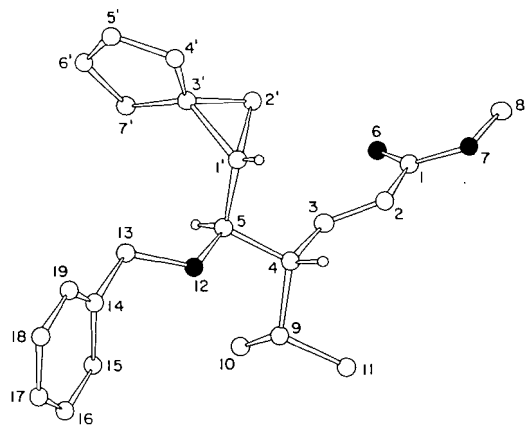

FIG. 3. A view of the triene **13***a* (4*S**,5*R**,1′*S**)-4-isopropyl-5-benzyloxy-5-(spiro[2.4]hepta-4,6-dien-1-yl)-2-pentenoate); H-atoms (assumed positions) are shown only where they help in visualizing the stereochemistry.

known to accompany substitution in these cases (23) and, by conducting the reaction at 21°C in acetonitrile with triphenylphosphine/carbon tetrachloride, the single ester-olefin **16***c* was obtained in 97% yield. The ^{13}C nmr spectrum contained only two olefinic carbon signals at δ 135.3 and 128.9, confirming that there was none of the more highly substituted double bond isomer **17** present. This result is consistent with a facile *trans* diaxial elimination from **15***c* in which inversion of the secondary alcohol has occurred to give the axial chloride prior to the elimination with loss of the axial methylene proton. In the epi series two antiperiplanar axial hydrogens are available in the halide intermediate, and consequently both olefins **16***a* and **17** are produced (~1:1).

Hydrogenation of **16***c* (H_2, 10% Pd/C, CH_3OH, 1 atm (101.3 kPa), 99%) provided the saturated ester **18***c* directly. It is important that pressure be avoided during this hydrogenation to avoid partial double bond isomerization and subsequent epimerization of the isopropyl substituent due to hydrogenation from the less hindered, back side of the molecule. In the epi series, similar hydrogenation of **16***a* and **17** afforded the ester **18***a* as the predominant product. Unfortunately, the selectivity in the hydrogenation of **17** was not quite complete and the product was accompanied by a small amount of the natural isomer, which was separated by chromatography.

Completion of the synthesis now required the conversion of the ester functionality into a double bond. The esters **18** were reduced quantitatively with lithium aluminum hydride to the primary alcohols **19** but, unfortunately, direct introduction of the exocyclic methylene using either selenoxide elimination or dehydrobromination proved impractical. Therefore, the acetate **20***c* was prepared (Ac_2O, pyridine, 99%) and (±)-sinularene was obtained in 77% yield via pyrolysis of this acetate in a flow apparatus at 550°C (5, 6). The sesquiterpene possessed spectral features (^{1}H nmr, ir, ms) identical to those published for the natural product (3) and completed a direct stereoselective synthesis of (±)-sinularene in 22% overall yield from the major aldol diastereomer **8** (9% from **7**). It required 14 steps from cyclopentadiene (12 from **7**), the same ultimate starting material as employed in the syntheses of both refs. 5 and 6. In parallel

Can. J. Chem. Downloaded from www.nrcresearchpress.com by 80.58.250.72 on 09/07/12
For personal use only.

fashion, pyrolysis of the **20***a* acetate afforded (±)-5-epi-sinularene in 85% yield.

Discussion

In spite of considerable recent attention, the subtle substituent effects governing intramolecular Diels–Alder reactions are still imperfectly understood (10, 11, 19, 24–30). The key cycloaddition steps in the syntheses above were diastereospecific and were clearly dominated by the presence of the benzyl ether substituent and its orientation. Molecular models suggested that the steric bulk of this substituent in the (4*R**,5*S**,1′*S**)-triene **13***b* was sufficient to impede the close approach of the diene and dienophilic components as required for cyclization. As illustrated in **22**, a particularly favourable conformation results from the π stacking of the cyclopentadiene, phenyl, and dienophilic units in a series of parallel planes, which precludes cycloaddition and indicates that the barrier to cyclization will be large. Transition state interactions of a related type were encountered during the total synthesis of patchouli alcohol (31). In that instance only the diastereomer **23** underwent Diels–Alder cycloaddition due to the nonbonded interaction in the methyl epimer. More recently, the steric interaction between a vinyl bromide (29) or vinyl silane (30) substituent and an allylic ether group (benzyl or methoxymethyl) has been employed, to encourage enhanced levels of diastereoselection due to cyclization from a conformation resembling **24** in which this interaction is minimized, rather than other possible diastereomeric arrangements.

It is of fundamental interest that this sort of steric limitation was not present in triene **6**, which lacks a benzyloxy substituent and yet also failed to cyclize (19)! The exact role of the C5 oxygen substituent awaits further clarification but it is likely that this group alters the conformation of the triene to one in which the diene is positioned near the cyclopentadiene ring in an alignment that facilitates the cycloaddition. Fortunately, in the present study the **13***a* triene and its adduct **14***a* were crystalline and thus permitted the determination of the interatomic distances in the crystalline state. The crystal structure analyses confirm the proposed formulations and establish unambiguously the stereochemistries of these compounds.

The critical C_1—C_7 and C_9—C_8 distances (adduct numbering) between the reacting olefinic centres in the triene are 4.78 and 6.01 Å respectively. In the adduct **14***a* these new bonds (1.560 and 1.586 Å) are longer than average, a characteristic that appears to be common in spiro adducts of a similar type (32). Recent theoretical calculations (33–35) for the cycloaddition of butadiene to ethylene support a synchronous C_s Diels–Alder transition structure in which bond formation is concerted, although it seems likely that highly substituted intramolecular cases are represented more accurately by a twist-asynchronous model (27). The separation of the diene and the dienophile in these cases is approximately 2.2 Å. It is apparent from Fig. 3 and molecular models that rotation of the sidechain about the C1′—C5 bond relieves any interaction between the phenyl and cyclopentadiene rings and places the dienophile in close promimity to the diene.

To ascertain if the observed rate enhancement due to the presence of the oxygen substituent adjacent to the diene is a general phenomenon we have conducted a competitive experiment between the spiro-dienes **25** and **26** and *N*-phenylmaleimide. However, it was found that they react at comparable rates at 21°C, indicating that in this instance the hydroxyl function

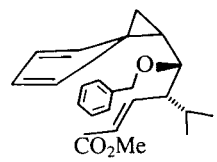

22

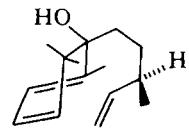

23

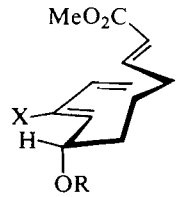

24
X = Br, $SiMe_3$
R = Bzl, MOM

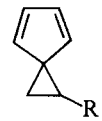

25 R = H
26 R = CH_2OH

does not exert a significant beneficial influence.[5] In related studies, we are conducting *ab initio* calculations on less substituted spirotrienes to ascertain the effect that varying the C5 substituent has on the energy minima.[6] At present we have insufficient data, both theoretical and experimental, to draw an unambiguous conclusion on the origin of this steric and (or) stereoelectronic effect. As a referee has indicated, the fact that Diels–Alder additions to **25** and **26** proceed at similar rates implies that the steric bulk of the benzyloxy group, rather than an electronic influence, is the dominant factor. Nevertheless this effect played a crucial role in the success of these syntheses and has set the stage for the extension of these concepts and procedures to related targets, such as 12-acetoxysinularene (4, 7) and (+)-longifolene, utilizing this intramolecular Diels–Alder – cyclopropane ring-opening strategy.

Experimental

Melting points were determined in capillary tubes with a Thomas–Hoover Uni-Melt apparatus or on a Fisher–Johns melting point apparatus, and are uncorrected. Infrared spectra were recorded on a Perkin–Elmer 237B or 451 grating spectrophotometer, and were calibrated with the 2850 and 1601 cm^{-1} bands of polystyrene film. Ultraviolet spectra were recorded on a Perkin–Elmer 202 uv–visible spectrophotometer and were calibrated with the 279.4-nm band of a Holmium oxide filter. Proton magnetic resonance spectra were measured at 80 MHz with a Bruker WP80 spectrometer employing a chloroform lock, at 60 MHz with a Varian EM 360 spectrometer, or at 400 MHz (at the University of Alberta) with a Bruker WH 400 spectrometer. Signal positions are reported in ppm downfield from tetramethylsilane (δ scale) as an internal standard; multiplicity, the number of protons, coupling constants, and proton assignments are indicated in parentheses. Mass spectra were determined on a V.G. Micromass 7070 HS instrument using an ionization energy of 70 eV. A Picker four-circle diffractometer was used for crystallographic measurements.

Thin-layer chromatographic analyses were carried out on commercial precoated silica gel plates with fluorescent indicator (Eastman Kodak silica gel 13181). Preparative thin-layer chromatography was conducted on 20 × 20 cm glass plates coated with silica gel $PF^{254+366}$ type 60 (E. Merck). Flash chromatography using BDH silica gel Kieselgel 60, 230–400 mesh, was employed for all column chromatography.

Petroleum ether refers to a fraction with boiling range 30–60°C.

[5]Lei Bo and A. G. Fallis, unpublished results; we are grateful to K. U. Ingold for a fruitful discussion.

[6]R. Porier and A. G. Fallis, unpublished work.

Can. J. Chem. Downloaded from www.nrcresearchpress.com by 80.58.250.72 on 09/07/12
For personal use only.

Can. J. Chem. Downloaded from www.nrcresearchpress.com by 80.58.250.72 on 09/07/12
For personal use only.

Anhydrous diethyl ether (ether), tetrahydrofuran (THF), dimethoxyethane (DME), and dioxane were obtained by distillation from lithium aluminium hydride or potassium/benzophenone. Absolute ethanol and methanol were dried by distillation from magnesium. Dry hexamethylphosphoramide (HMPA), dimethylformamide (DMF), dimethyl sulfoxide (DMSO), and diisopropylamine were prepared by distillation from calcium hydride. Solutions in organic solvents were dried over anhydrous magnesium sulphate and stripped of solvent with a Buchi rotary evaporator connected to a water aspirator. Unless otherwise indicated all reactions were conducted under an atmosphere of dry nitrogen.

Parallel reactions were conducted on the same scale in both the sinularene and epi-sinularene series and are grouped under the single compound name.

Methyl 3-hydroxy-2-isopropyl-3-(spiro[2.4]hepta-4,6-dien-1-yl)propanoate (8)

Methyl isovalerate (13 g, 0.115 mol) in THF (20 mL) was added dropwise to a THF solution maintained at −78°C with an external, solid carbon dioxide/acetone bath, containing lithium diisopropylamide (LDA, prepared from 2.6 *M* *n*-butyllithium solution (Aldrich, 65.4 mL, 0.17 mol) and diisopropylamine (16.8 mL, 0.12 mol) in THF (250 mL) at −78°C). The reaction mixture was stirred for 0.5 h and the aldehyde **7** (19) (12 g, 0.1 mol) in THF (20 mL) added dropwise. After stirring for a further 10 min at −78°C, the cooling bath was removed and replaced by an ice bath. Once the reaction mixture had reached 0°C it was quenched with saturated aqueous ammonium chloride solution and extracted with diethyl ether (3×). The combined ether extracts were dried, filtered, concentrated, and the residue purified by chromatography (petroleum ether/diethyl ether; 3:1) to afford the hydroxy-ester **8** as three separate fractions; **8***a*, 7.32 g (30%), recrystallized from dichloromethane/hexane, mp 59–60°C; ir (film): 3570 (OH), 3430 (sh, OH), 1725 (C=O), 1635 (w, C=C) cm^{-1}; ^1H nmr (CCl_4) δ: 0.99 (d, 3H, *J* = 6.5 Hz, CH_3CH), 1.01 (d, 3H, *J* = 6.5 Hz, CH_3CH), 1.52 (d, 1H, *J* = 2 Hz, OH), 1.80 (m, 2H, $HCMe_2$, cyclopropyl H), 2.09 (m, 1H, *J* = 6 Hz, HC—C=O), 2.45 (m, 2H, cyclopropyl H), 3.58 (m, 1H, H-C—OH), 3.62 (s, 3H, OCH_3), 6.00 (m, 1H, cyclopentadienyl H), 6.21 (m, 1H, cyclopentadienyl H), 6.46 (m, 1H, cyclopentadienyl H), 6.58 (m, 1H, cyclopentadienyl H). *Exact Mass* calcd. for $C_{14}H_{20}O_3$: 236.1412; found: 236.1399.

Hydroxy-esters **8***b* and **8***c*, 15.1 g (64%); ir (film): 3400 (br, OH), 1725 (C=O) cm^{-1}; ^1H nmr (CCl_4) δ: 0.89 (d, 6H, *J* = 7 Hz, $(CH_3)_2CH$), 1.6–2.5 (m, 5H), 3.25 (d, 1H, *J* ~5 Hz, OH), 3.54 (s, 3H, OCH_3), 3.75 (m, 1H, H-C—OH), 5.9–6.5 (m, 4H, cyclopentadienyl H). *Exact Mass* calcd. for $C_{14}H_{20}O_3$: 236.1412; found: 236.1420.

Hydroxy-ester **8***d*, 0.47 g (2%); ir (film): 3510 (OH), 1730 (C=O), 1625 (w, C=C) cm^{-1}; ^1H nmr (CCl_4) δ: 1.00 (dd, 6H, *J* = 6.5, $(CH_3)_2CH$), 1.5–2.5 (m, 6H), 3.65 (m, 1H, H-C—OH), 3.70 (s, 3H, OCH_3), 5.99 (m, 1H, cyclopentadienyl H), 6.26 (m, 1H, cyclopentadienyl H), 6.46 (m, 2H, cyclopentadienyl H). *Exact Mass* calcd. for $C_{14}H_{20}O_3$: 236.1412; found: 236.1372.

Methyl 3-benzyloxy-2-isopropyl-3-(spiro[2.4]hepta-4,6-dien-1-yl)propanoate (10)

The hydroxyester **8** (4.72 g, 0.02 mol) in dimethoxyethane (DME, 5 mL) was added dropwise to a suspension of sodium hydride (0.8 g, 0.02 mol, 60% oil dispersion, Aldrich) in DME (15 mL) maintained at 0°C with an external ice bath. Tetrabutylammonium iodide (150 mg) was added after hydrogen evolution had ceased (approximately 0.5 h), followed by benzyl bromide (3.9 g, 0.023 mol, Aldrich). The resulting mixture was stirred at 0°C for approximately 4 h (monitored by tlc) until no hydroxy-ester remained. The reaction was quenched by careful dropwise addition of saturated aqueous ammonium chloride, the mixture was extracted with ether (3×), the combined ether extracts dried and concentrated, and the products purified by chromatography (5% ethyl ether/petroleum ether) to give the ester **10***a* 5.02 g (77%) recrystallized from ether/hexane, mp 81.5–82.5°C; ir (CCl_4): 1735 (C=O) cm^{-1}; ^1H nmr (CCl_4) δ: 0.94 (d, 6H, *J* = 6.5 Hz, $(CH_3)_2CH$), 1.57 (m, 2H, cyclopropyl H), 1.8–2.7 (m, 3H), 3.46 (m, 1H, HCOBzl), 3.58 (s, 3H, OCH_3), 4.05 (s, 2H, H_2COBzl), 5.97 (m, 1H, cyclopentadienyl H), 6.39 (m, 3H, cyclopentadienyl H), 7.11 (s, 5H, phenyl H).

Ether-esters **10***b* and **10***c*, 5.35 g (82%); ir (film): 1735 (C=O) cm^{-1}; ^1H nmr (CCl_4) δ: 0.92 (overlapping d's, 2 × 6H, $(CH_3)_2CH$'s), 3.48 and 3.53 (s, 2 × 3H, OCH_3), 4.58 (m, 2 × 2H, H_2COBzl's), 5.98 (m, 2 × 1H, cyclopentadienyl H's), 6.35 (m, 2 × 3H, cyclopentadienyl H's), 7.19 (s, 2 × 5H, phenyl H's).

3-Benzyloxy-2-propyl-3-(spiro[2.4]hepta-4,6-dien-1-yl)propanol (11)

The benzyloxy-ester **10** (5.28 g, 0.015 mol) dissolved in diethyl ether (25 mL) was added dropwise to an ether solution (100 mL) of lithium aluminium hydride (0.6 g) maintained at 0°C with an external ice bath. The reaction mixture was stirred for a further hour after addition was complete and the excess lithium aluminium hydride destroyed by dropwise addition of ethyl acetate. This was followed by the addition of aqueous 20% sodium tartrate solution (150 mL) and extraction with ether (4×). The combined ether extracts were dried, filtered, and concentrated. The product was purified by chromatography (petroleum ether/diethyl ether; 3:1) to give the alcohol **11***a*, 4.20 g (94%); ir (film): 3380 (br, OH) cm^{-1}; ^1H nmr (CCl_4) δ: 0.96 (d, 6H, *J* = 6.5 Hz, $(CH_3)_2CH$), 3.00 (br s, 1H, OH), 3.56 (m, 3H, CH_2OH, HCOBzl), 4.06 (s, 2H, CH_2Ph), 5.91 (m, 1H, cyclopentadienyl H), 6.31 (m, 3H, cyclopentadienyl H), 7.05 (s, 5H, phenyl H).

Alcohol **11***b*, 0.94 g (21%); ir (film): 3490 (OH) cm^{-1}; ^1H nmr (CCl_4) δ: 0.90 (d, 6H, *J* = 6.5 Hz, $(CH_3)_2CH$), 3.54 (m, 3H, CH_2OH, HCOBzl), 4.54 (AB system, 2H, *J* = 12 Hz, OCH_2Ph), 5.95 (m, 2H, cyclopentadienyl H), 6.35 (m, 2H, cyclopentadienyl H), 7.20 (s, 5H, phenyl H).

Alcohol **11***c*, 3.40 g (76%); ir (film): 3400 (br, OH) cm^{-1}; ^1H nmr (CCl_4) δ: 0.85 (d, 6H, *J* = 6.5 Hz, $(CH_3)_2CH$), 2.62 (br s, 1H, OH), 3.51 (m, 3H, CH_2OH, HCOBzl), 4.55 (AB system, 2H, *J* = 12 Hz, OCH_2Ph), 5.95 (m, 2H, cyclopentadienyl H), 6.33 (m, 2H, cyclopentadienyl H).

3-Benzyloxy-2-isopropyl-3-(spiro[2.4]hepta-4,6-dien-1-yl)propanal (12)

The primary alcohol **11** (4.47 g, 0.015 mol) was dissolved in dichloromethane (50 mL) and added to pyridinium dichromate (PDC, 9.4 g, 0.08 mol) contained in dichloromethane (100 mL). The reaction mixture was stirred for 24 h at 21°C, diluted with diethyl ether, and filtered through magnesium sulfate. The residue obtained after concentration was purified by chromatography (petroleum ether/diethyl ether; 10:1) to give the aldehyde **12***a*, 2.66 g (60%); ir (film): 3070 (HC=C), 3035 (HC=C), 2630 (HC=O), 1722 (C=O) cm^{-1}; ^1H nmr (CCl_4) δ: 1.02 (d, 3H, *J* = 6.5 Hz, CH_3CH), 1.08 (d, 3H, *J* = 6.5 Hz, CH_3CH), 1.5–2.5 (m, 5H), 3.94 (dd, 1H, *J* = 6, 8 Hz, HCOBzl), 4.24 (s, 2H, OCH_2Ph), 6.11 (m, 1H, cyclopentadienyl H), 6.40 (m, 1H, cyclopentadienyl H), 6.54 (m, 2H, cyclopentadienyl H), 7.27 (s, 3H, phenyl H), 7.36 (m, 1H, *o*-phenyl H), 7.62 (m, 1H, *o*-phenyl H), 9.78 (d, 1H, *J* = 3 Hz, HC=O).

Aldehyde **12***b*, 2.84 g (64%); ir (film): 3070 (HC=C), 3035 (HC=C), 2735 (HC=O), 1720 (C=O) cm^{-1}; ^1H nmr (CCl_4) δ: 0.84 (d, 3H, *J* = 6.5 Hz, CH_3CH), 0.92 (d, 3H, *J* = 6.5 Hz, CH_3CH), 1.7–2.5 (m, 5H), 3.57 (dm, 1H, *J* = 8 Hz, HCOBzl), 4.67 (AB system, 2H, *J* = 12 Hz, OCH_2Ph), 5.95 (m, 2H, cyclopentadienyl H), 6.39 (m, 2H, cyclopentadienyl H), 7.26 (s, 5H, phenyl H), 9.60 (d, 1H, *J* = 3 Hz, HC=O).

Aldehyde **12***c*, 2.84 g (64%); ir (film): 3075 (HC=C), 3035 (HC=C), 2725 (HC=O), 1722 (C=O) cm^{-1}; ^1H nmr (CCl_4) δ: 0.93 (d, 3H, *J* = 6.5 Hz, CH_3CH), 1.03 (d, 3H, *J* = 6.5 Hz, CH_3CH), 1.7–2.4 (m, 5H), 3.82 (dd, 1H, *J* = 5.5, 8 Hz, HCOBzl), 4.68 (AB system, 2H, *J* = 12 Hz, OCH_2Ph), 6.10 (m, 2H, cyclopentadienyl H), 6.45 (m, 2H, cyclopentadienyl H), 7.30 (s, 3H, phenyl H), 7.46 (m, 1H, *o*-phenyl H), 7.78 (m, 1H, *o*-phenyl H), 9.42 (d, 1H, *J* = 3 Hz, HC=O).

Can. J. Chem. Downloaded from www.nrcresearchpress.com by 80.58.250.72 on 09/07/12
For personal use only.

*Methyl 5-benzyloxy-4-isopropyl-5-(spiro[2.4]hepta-4,6-dien-1-yl)-2-pentenoate (**13**) and 5-benzyloxy-6-isopropyl-8-carbomethoxy-tetracyclo[5.4.0^{1,7}.0^{2,4}.0^{2,9}]undec-10-ene (**14**)*

The aldehyde **12** (2.96 g, 10 mmol) was dissolved in THF (10 mL), mixed with methyl (triphenylphosphoranylidene)acetate (4 g, 12 mol, Aldrich) in THF (50 mL), and stirred under reflux for 12 h. The solution was concentrated and the product purified by chromatography (5% diethyl ether/petroleum ether) to give the triene **13***a*, 1.41 g, (40%), recrystallized from hexane, mp 76–77°C; ir ($CHCl_3$): 3050 (HC=C), 3035 (HC=C), 1715 (C=O), 1655 (C=C) cm^{-1}; ^{1}H nmr ($CDCl_3$) 400 MHz, δ: 0.87 (d, 3H, J = 6.5 Hz, CH_3CH), 0.88 (d, 3H, J = 6.5 Hz, CH_3CH), 1.64 (dd, 1H, J = 4.5, 7 Hz, cyclopropyl H), 1.75 (dd, 1H, J = 4.5, 8.5 Hz, cyclopropyl H), 2.10 (dd, 1H, J = 8.5 Hz, cyclopropyl H), 2.26 (m, 1H, J ~ 7 Hz, $HC(CH_3)_2$), 2.37 (m, 1H, HCC=C), 3.58 (dd, 1H, J = 7, 8.5 Hz, HCOBzl), 3.75 (s, 3H, CH_3O), 4.25 (AB system, 2H, J = 11.5 Hz, OCH_2Ph), 5.78 (d, 1H, 15.5 Hz, C=CHC=O), 6.09 (dt, 1H, J = 2, 5 Hz, cyclopentadienyl H), 6.37 (dt, 1H, J = 2, 5 Hz, cyclopentadienyl H), 6.54 (ddt, 2H, J = 1.5, 5 Hz, cyclopentadienyl H), 6.88 (dd, 1H, J = 11, 15.5 Hz, HC=CC=O), 7.28 (m, 5H, phenyl H); and the Diels–Alder adduct **14***a* 1.76 g (50%), recrystallized from diethyl ether, mp 115–116°C; ir ($CHCl_3$): 3065 (HC=C), 1730 (C=O) cm^{-1}; ^{1}H nmr ($CDCl_3$) 400 MHz δ: 0.47 (dt, 1H, J = 5.5, 8.5 Hz, cyclopropyl H-CC—OBzl), 0.90 (d, 3H, J = 6.5 Hz, CH_3CH), 0.92 (d, 3H, J = 6.5 Hz, CH_3CH), 1.09 (t, 1H, J = 5.5 Hz, cyclopropyl H), 1.21 (dd, 1H, J = 5.5, 8.5 Hz, cyclopropyl H), 1.46 (br septet, 1H, J ~ 6.5 Hz, $HC(CH_3)_2$), 1.88 (dd, 1H, J = 5.5, 11 Hz, *endo*-H-C), 2.33 (dd, 1H, J = 2.5, 5.5 Hz, *exo*-H-CCOOCH$_3$), 2.39 (br s, 1H, $W_{1/2}$ = 7 Hz, H-C*i*Pr), 2.51 (m, 1H, $W_{1/2}$ = 9 Hz, bridgehead H), 2.58 (dd, 1H, J = 2.5, 4.5 Hz, bridgehead H), 3.62 (s, 3H, CH_3O), 3.74 (d, 1H, J = 5.5 Hz, HCOBzl), 4.43 (AB system, 2H, J = 12 Hz, OCH_2Ph), 6.05 (dm, 1H, J ~ 0.5, 2.5, 5.5 Hz, HC=C), 6.26 (dm, 1H, J ~ 1, 3, 5.5 Hz, HC=C), 7.29 (m, 5H, phenyl H).

Alternatively, a solution of the triene **13***a* (1.41 g) in THF (50 mL) was refluxed for 12 h. Concentration followed by chromatography (5% diethyl ether/petroleum ether) afforded the tetracyclic ester **14***a* in 45% yield, accompanied by uncyclized triene (50%), which was recycled; the combined total yield from aldehyde **12***a* was 72%.

Triene **13***b*, 3.41 g (97%), recrystallized from dichloromethane/hexane, mp 101–103°C; ir (CCl_4): 3070 (HC=C), 3030 (HC=C), 1725 (C=O), 1655 (C=C) cm^{-1}; ^{1}H nmr ($CDCl_3$) 400 MHz δ: 0.77 (d, 3H, J = 6.5 Hz, CH_3CH), 0.88 (d, 3H, J = 6.5 Hz, CH_3CH), 1.4–2.2 (m, 5H), 3.47 (dd, 1H, J = 2, 8 Hz, HCOBzl), 3.66 (s, 3H, OCH_3), 4.68 (AB system, 2H, J = 12 Hz, OCH_2Ph), 5.10 (d, 1H, J = 16 Hz, C=CHC=O), 6.05 (m, 2H, cyclopentadienyl H), 6.50 (m, 2H, cyclopentadienyl H), 6.92 (dd, 1H, J = 10, 16 Hz, HC=CC=O), 7.31 (s, 5H, phenyl H). Cyclization did not occur in separate experiments for 24 h in refluxing THF, toluene, xylene, and *o*-dichlorobenzene.

Triene **13***c* cyclized spontaneously under the Wittig reaction conditions to the adduct **14***c*; 2.52 g (72%, from aldehyde); ir (film): 3070 (HC=C), 3035 (HC=C), 1735 (C=O) cm^{-1}; ^{1}H nmr ($CDCl_3$) 400 MHz δ: 0.46 (m, 1H, J ~ 5 Hz, cyclopropyl H), 0.84 (d, 3H, J = 6.5 Hz, CH_3CH), 1.00 (d, 3H, J = 6.5 Hz, CH_3CH), 1.25 (m, 2H, cyclopropyl H), 2.06 (m, 2H, $HCCOOCH_3$, HC*i*Pr), 2.85 (m, 2H, bridgehead H), 3.61 (m, 1H, HCOBzl), 3.62 (s, 3H, OCH_3), 4.61 (AB system, 2H, J = 12 Hz, OCH_2Ph), 6.09 (t, 2H, J = 1 Hz, HC=CH), 7.33 (s, 5H, phenyl H).

*7-Carbomethoxy-5-isopropyl-2-methyltricyclo[4.4.0^{1,6}.0^{2,8}]decan-4-ol (**15**)*

The tetracyclic ester **14** (1.76 g, 5 mol) dissolved in methanol (25 mL) was mixed with 10% Pd/C (200 mg) and hydrogenated in a Parr apparatus at 50 psi for 24 h at 21°C. The catalyst was removed by filtration, washed with diethyl ether, and the product purified by chromatography (petroleum ether/diethyl ether; 3:1) to give the hydroxy-ester **15***a*, 1.08 g (81%), recrystallized from hexane, mp 87–88°C; ir (CCl_4): 3400 (br, OH), 1725 (C=O) cm^{-1}; ^{1}H nmr (CCl_4) δ: 0.78 (d, 3H, J = 6.5 Hz, CH_3CH), 1.00 (s, 3H, CH_3C), 1.00 (d, 3H, J = 6.5 Hz, CH_3CH), 2.34 (m, 1H, bridgehead H), 2.65 (m, 1H, *exo*-H-CCOOCH$_3$), 2.96 (br s, 1H, OH), 3.63 (s, 3H, OCH_3), 3.83 (m, 1H, HCOH). *Exact Mass* calcd. for $C_{16}H_{26}O_3$: 266.1882; found: 266.1884.

Hydroxy-ester **15***c*, 1.13 g (85%); ir (film): 3375 (br OH), 1730 (C=O) cm^{-1}; ^{1}H nmr ($CDCl_3$) δ: 0.82 (d, 3H, J = 6.5 Hz, CH_3CH), 0.91 (d, 3H, J = 6.5 Hz, CH_3CH), 0.96 (s, 3H, CH_3), 2.05 (d, 1H, J = 3 Hz, bridgehead H), 2.25 (s, 1H, OH), 2.63 (m, 1H, *exo*-H-CCOOCH$_3$), 3.52 (m, 1H, HCOH), 3.55 (s, 3H, OCH_3); ^{13}C nmr ($CDCl_3$) δ: 18.60, 20.91, 21.25, 22.79, 24.67, 29.37, 40.82, 41.16, 42.01, 46.88, 48.59, 51.24, 55.26, 58.33, 67.73, 175.39. *Exact Mass* calcd. for $C_{16}H_{26}O_3 - H_2O$: 248.1786; found: 248.1776.

*7-Carbomethoxy-5-isopropyl-2-methyltricyclo[4.4.0^{1,6}.0^{2,8}]dec-3-ene (**16**)*

The hydroxy ester **15** (120 mg, 0.45 mmol) was dissolved in anhydrous acetonitrile (1 mL) and triphenyl phosphine (157 mg, 0.6 mmol), carbon tetrachloride (92 mg, 0.6 mmol), and pyridine (80 mg) added. The reaction mixture was stirred for 24 h at 21°C, concentrated, and the product purified by chromatography (5% diethyl ether/petroleum ether) to give the alkene **16***a* and its positional isomer **17**, ~1:1, 96 mg (93%); ir (film): 3035 (HC=C), 1740 (C=O) cm^{-1}; ^{1}H nmr ($CDCl_3$) δ: 3.60 (s, 6H, OCH_3), 5.08 (m, 1H, HC=C), 5.50 (m, 2H, HC=CH), ^{13}C nmr ($CDCl_3$) δ: 117.6, 128.5, 134.7, 156.2, 174.7, 175.8. *Exact Mass* calcd. for $C_{16}H_{24}O_2$: 248.1776; found: 248.1777.

Olefin **16***c*, 100 mg (97%); ir (film): 3030 (HC=C), 1735 (C=O) cm^{-1}; ^{1}H nmr ($CDCl_3$) δ: 0.90 (d, 3H, J = 6.5 Hz, CH_3CH), 0.93 (d, 3H, J = 6.5 Hz, CH_3CH), 0.99 (s, 3H, CH_3C), 2.15 (m, 2H), 2.30 (m, 1H), 2.56 (m, 1H), 3.60 (s, 3H, OCH_3), 5.50 (br s, 2H, HC=CH). ^{13}C nmr ($CDCl_3$) δ: 18.0, 21.3, 21.5, 23.5, 24.6, 41.8, 43.0, 50.5, 51.4, 52.4, 53.4, 128.9, 135.3, 175.9. *Exact Mass* calcd. for $C_{15}H_{24}O_2$: 248.1776; found: 248.1816.

*7-Carbomethoxy-5-isopropyl-2-methyltricyclo[4.4.0^{1,6}.0^{2,8}]decane (**18**)*

A methanol solution of olefin ester **16** (1.24 g, 5 mmol) was hydrogenated in the presence of 10% Pd/C (100 mg) in a Parr apparatus at 21°C at atmospheric pressure. (Under pressure (30–50 psi) the reaction requires ~8 h, but the double bond undergoes partial isomerization, resulting in epimerization of the isopropyl group, which is avoided at atmospheric pressure although the reaction is much slower, 24–48 h.) The catalyst was removed by filtration, washed thoroughly with ether, the combined washings and filtrate dried, and the solvent removed to give the saturated ester **18***a*, 1.23 g (98%); ir (film): 1735 (C=O) cm^{-1}; ^{1}H nmr ($CDCl_3$) δ: 0.92 (triplet-like, 9H, overlapping CH_3's), 2.60 (m, 1H, bridgehead H), 2.72 (m, 1H, $HCOOCH_3$), 3.57 (s, 3H, OCH_3). ^{13}C nmr ($CDCl_3$) δ: 20.00, 20.77, 25.13, 25.73, 30.77, 33.59, 43.42, 44.70, 46.33, 47.78, 49.92, 50.94, 175.22.

Ester **18***c*, 1.24 g (99%); ir (film): 1735 (C=O) cm^{-1}; ^{1}H nmr (CCl_4) δ: 0.84 (s shoulder, 3H, CH_3C), 0.93 (overlapping d's, 6H, J = 6.5 Hz, CH_3CH), 2.72 (m, 1H, $HCOOCH_3$), 3.57 (s, 3H, OCH_3). *Exact Mass* calcd. for $C_{16}H_{26}O_2$: 250.1933; found: 250.1936.

*7-Hydroxymethyl-5-isopropyl-2-methyltricyclo[4.4.0^{1,6}.0^{2,8}]decane (**19**)*

The ester **18** (0.5 g, 2 mmol) in diethyl ether (5 mL) was added dropwise to an ether suspension (20 mL) of lithium aluminium hydride (76 mg, 2 mmol) maintained at 0°C with an external ice bath. The reaction was stirred at this temperature for 0.5 h, ethyl acetate added dropwise followed by aqueous 20% sodium potassium tartrate (10 mL), and the aqueous layer extracted with ether (3 × 10 mL). The combined ether extracts were dried, concentrated, and the product purified by chromatography (diethyl ether/petroleum ether) to give the alcohol **19***a*, 435 mg, (98%); ir (film): 3350 (br, OH) cm^{-1}; ^{1}H nmr (CCl_4) δ: 0.90 (9H, overlapping CH_3's), 2.18 (m, 1H, *exo*-H), 3.40 (d, 2H, J = 16 Hz, CH_2O), 3.93 (s, 1H, OH).

Alcohol **19***c*, 440 mg (99%); ir (film): 3350 (br, OH) cm^{-1}; ^{1}H nmr (CCl_4) δ: 0.98 (9H, overlapping CH_3's), 2.80 (s, 1H, OH), 3.47

Can. J. Chem. Downloaded from www.nrcresearchpress.com by 80.58.250.72 on 09/07/12
For personal use only.

(d, 2H, J = 16 Hz, CH_2O). *Exact Mass* calcd. for $C_{15}H_{26}O$: 222.1984; found: 222.1999.

*7-Acetoxymethyl-5-isopropyl-2-methyltricyclo[4.4.0^{1,6}.0^{2,8}]decane (**20**)*

The alcohol **19** (444 mg, 2 mmol) was dissolved in pyridine (3 mL) and acetic anhydride (0.76 mL, 8 mmol) was added. The reaction mixture was maintained at 4°C for 15 h, diluted with diethyl ether, and poured into ice acidified with a few drops of concentrated hydrochloric acid. The resulting mixture was extracted with diethyl ether (3×), the combined ether extracts washed with aqueous 10% sodium bicarbonate solution and then with brine, dried, and concentrated. The product was purified by chromatography (petroleum ether/diethyl ether; 5:1) to give the acetate **20***a*, 523 mg (99%); ir (film): 1745 (C=O) cm^{-1}; ^{1}H nmr (CCl_4) δ: 0.90 (9H, overlapping CH_3's), 1.94 (s, 3H, CH_3C=O), 3.90 (d, 2H, J = 15 Hz, CH_2O); ^{13}C nmr ($CDCl_3$) δ: 19.97, 21.08, 22.45, 23.98, 25.61, 26.72, 29.96, 33.72, 39.96, 46.20, 46.37, 46.88, 48.34, 50.47, 66.79, 171.6.

Acetate **20***c*, 525 mg (99%); ir (film): 1740 (C=O) cm^{-1}; ^{1}H nmr (CCl_4) δ: 0.94 (9H, overlapping CH_3's), 1.92 (s, 3H, CH_3C=O), 3.91 (d, 2H, J = 16 Hz, CH_2OAc); ^{13}C nmr ($CDCl_3$) δ: 20.40, 20.91, 25.52, 30.90, 32.10, 39.96, 46.20, 46.54, 46.80, 47.82, 49.79, 66.53, 170.4.

*(±)-5-Epi-sinularene (**21**) and (±)-sinularene (**1**)*

The acetate **20** (200 mg, 0.76 mmol) was dissolved in benzene (2 mL) and injected, under a stream of nitrogen, into a Pyrex tube (14 × 60 cm, packed with glass helices) preheated to 550°C and attached to a receiver that was cooled to −78°C with an external solid carbon dioxide/acetone bath. Once injection of the sample was complete it was followed by two further aliquots of benzene (2 mL) and the collected material was concentrated and purified by chromatography (petroleum ether) to give (±)-5-epi-sinularene, 130 mg (85%); ir (film): 3070 (H-C=C), 1658 (C=C), 877 (C=C) cm^{-1}; ^{1}H nmr ($CDCl_3$) δ: 0.82 (d, 3H, J = 6.5 Hz, CH_3CH), 0.89 (s, 3H, CH_3C), 0.96 (d, 3H, J = 6.5 Hz, CH_3CH), 2.08 (br s, 1H, allylic *endo*-H), 2.38 (br s, 1H, allylic bridgehead H), 4.52 (br s, 1H, H-C=C), 4.80 (br s, 1H, H-C=C); ^{13}C nmr ($CDCl_3$) δ: 20.65, 21.34, 24.92, 26.55, 29.02, 31.93, 34.84, 47.31, 48.08, 49.62, 51.24, 52.86, 102.2, 159.2. *Exact Mass* calcd. for $C_{15}H_{24}$: 204.1878; found: 204.1898.

(±)-Sinularene (**1**), 119 mg (77%); ir (film): 3070 (H-C=C), 1665 (C=C), 875 (C=C) cm^{-1}; ^{1}H nmr ($CDCl_3$) δ: 0.90 (d, 3H, J = 6 Hz, CH_3CH), 0.92 (d, 3H, J = 6 Hz, CH_3CH), 0.92 (s, 3H, CH_3C), 4.59 (br s, 1H, H-C=C), 4.79 (br s, 1H, H-C=C); ^{13}C nmr ($CDCl_3$) δ: 20.74, 21.51, 22.36, 26.03, 29.02, 30.22, 31.67, 42.95, 48.42, 49.19, 50.22, 53.29, 101.2, 162.9. *Exact Mass* calcd. for $C_{15}H_{24}$: 204.1878; found: 204.1875.

Sinularene and epi-sinularene can be separated by plc using isooctane as the eluent on Beckman silica gel$_{PF\,254}$ treated with 20% silver nitrate.

Crystallography

(4S,5R*,6S*)-5-Benzyloxy-6-isopropyl-8-carbomethoxytetracyclo[5.4.0^{1,7}.0^{2,4}.0^{2,9}]undec-10-ene (**14**a)*

All procedures at nominal 22°C, using Ni-filtered CuKα radiation. Unit-cell constants from least-squares analysis of diffractometer angles of a number of well-centered reflections (α_1 component) of large Bragg angle. The intensities of the accessible independent reflections were measured using θ–2θ scans, with analysis of individual reflection profiles (36). The standard deviations of the intensities were evaluated from counting statistics. Absorption corrections were deemed to be unnecessary, and were not applied. The structure solution was by direct methods (MULTAN 78) (37). Refinement was by block-diagonal least squares, minimizing $\Sigma w\Delta F^2$, where $1/w = \sigma^2(F_o) + kF_o^2$. Hydrogen atoms were initially located in physically reasonable positions (C—H = 1.08 Å) or located in a ΔF synthesis. The parameters refined were scale factor, secondary extinction coefficient g (38), atomic coordinates, and temperature factors (anisotropic for C and O). Refinement was terminated when all parameter shifts were acceptably small. The final ΔF synthesis revealed no detail inconsistent with the proposed structure.

TABLE 1. Atomic coordinates (e.s.d.'s) and equivalent isotropic B value (B_{eq}, Å^2) for (4*S**,5*R**,6*S**)-5-benzyloxy-6-isopropyl-8-carbomethoxytetracyclo[5.4.0^{1,7}.0^{2,4}.0^{2,9}]undec-10-ene (**14***a*) (H-atoms omitted)

Atom	x	y	z	B_{eq}
C(1)	0.35419(6)	−0.1045(3)	0.25652(15)	3.2
C(2)	0.38121(7)	0.0920(3)	0.27259(15)	3.3
C(3)	0.35446(8)	0.2821(3)	0.26138(17)	4.2
C(4)	0.38558(6)	0.2066(3)	0.15613(16)	3.3
C(5)	0.36474(6)	0.1054(3)	0.03826(15)	3.1
C(6)	0.38287(6)	−0.1107(3)	0.03780(14)	2.9
C(7)	0.39431(6)	−0.1934(2)	0.17128(14)	2.9
C(8)	0.44618(6)	−0.1280(3)	0.24107(15)	3.1
C(9)	0.42872(7)	0.0134(3)	0.34674(16)	3.7
C(10)	0.40458(8)	−0.1140(3)	0.44078(16)	4.4
C(11)	0.36165(8)	−0.1859(3)	0.38655(17)	4.1
O(12)	0.30911(4)	0.1055(2)	0.02587(11)	3.6
C(13)	0.28854(7)	0.2854(3)	−0.02099(17)	4.2
C(14)	0.29126(6)	0.3062(3)	−0.16056(17)	3.6
C(15)	0.29583(8)	0.4879(3)	−0.21205(19)	4.6
C(16)	0.29689(9)	0.5119(4)	−0.33989(21)	6.0
C(17)	0.29424(9)	0.3528(4)	−0.41642(20)	6.0
C(18)	0.29005(9)	0.1709(4)	−0.36680(21)	5.9
C(19)	0.28792(9)	0.1477(3)	−0.23912(20)	5.1
C(20)	0.42668(7)	−0.1425(3)	−0.04983(16)	3.9
C(21)	0.40944(8)	−0.1015(4)	−0.18625(17)	4.8
C(22)	0.44777(11)	−0.3466(4)	−0.04188(20)	6.9
C(23)	0.47934(7)	−0.2927(3)	0.29358(15)	3.6
O(24)	0.46942(6)	−0.4616(2)	0.29036(14)	5.4
O(25)	0.52350(5)	−0.2239(2)	0.34711(13)	5.0
C(26)	0.56049(8)	−0.3655(4)	0.39688(22)	5.8

[a]In this and the following table, B_{eq} is the arithmetic mean of the principal axes of the thermal ellipsoid.

Methyl (4S,5R*,1'S*)-4-isopropyl-5-benzyloxy-5-(spiro[2,4]hepta-4,6-dien-1-yl)-2-pentenoate (**13**a)*

Except where noted, same procedures as for **14***a*. The specimen was extremely small, and poorly diffracting. It was not possible to observe reflections for which 2θ ≥ 100°C. Therefore, in measuring the cell constants, α_1–α_2 overlap problems were avoided by using the K_β components of lower-angle reflections. Refinement was hindered by the low yield of observable reflections and by severe thermal motion (or disorder) of the benzene ring. (The carbon atoms of this ring must be regarded as poorly resolved.) The methyl H atoms of the carbomethoxy group could not be located; H atom parameters were not refined, nor was the secondary extinction coefficient g.

The atomic coordinates for both structures are given in Tables 1 and 2, and selected bond lengths in Tables 3 and 4. The computer programs and the source of the atomic scattering factors are identified in the references (36–39). Supplementary data[7] include H-atom coordinates, temperature factors, all bond lengths, and structure factors.

Crystal and other numerical data

(4S,5R*,6S*)-5-Benzyloxy-6-isopropyl-8-carbomethoxytetracyclo[5.4.0^{1,7}.0^{2,4}.0^{2,9}]undec-10-ene (**14**a)*

$C_{23}H_{28}O_3$ fw = 352.5

Monoclinic, $P2_1/a$, a = 26.002(2), b = 6.8817(3), c = 10.7454(5) Å, β = 94.00(1)° (CuKα_1, λ = 1.54056 Å, 43 reflections, 114° < 2θ < 128°), V = 1918.1 Å^3, Z = 4, ρ = 1.220 g cm^{-3}. Nominal specimen

[7]Tables of supplementary data may be purchased from the Depository of Unpublished Data, CISTI, National Research Council of Canada, Ottawa, Ont., Canada K1A 0S2.

Can. J. Chem. Downloaded from www.nrcresearchpress.com by 80.58.250.72 on 09/07/12
For personal use only.

TABLE 2. Atomic coordinates (e.s.d.'s) and equivalent isotropic B values (B_{eq}, Å^2) for methyl (4*S**,5*R**,1′*S**)-4-isopropyl-5-benzyloxy-5-(spiro[2.4]hepta-4,6-dien-1-yl)-2-pentenoate (**13***a*) (H atoms omitted)

Atom	x	y	z	B_{eq}
C(1)	0.3939(12)	0.8589(14)	0.5613(14)	7.1
C(2)	0.5308(12)	0.7822(12)	0.4800(15)	5.6
C(3)	0.5861(13)	0.6480(12)	0.4332(13)	5.1
C(4)	0.7216(14)	0.5577(14)	0.3477(15)	8.1
C(5)	0.7945(12)	0.4461(12)	0.4294(14)	5.7
O(6)	0.3269(9)	0.8060(9)	0.5922(11)	8.6
O(7)	0.3584(10)	0.9882(9)	0.5942(12)	9.9
C(8)	0.2223(16)	1.0739(14)	0.6759(19)	12.2
C(9)	0.7150(12)	0.4934(12)	0.1883(12)	5.1
C(10)	0.6345(15)	0.4155(16)	0.1653(17)	9.6
C(11)	0.6609(15)	0.6020(15)	0.1114(15)	8.9
O(12)	0.9201(8)	0.3572(7)	0.3421(9)	5.7
C(13)	0.9844(13)	0.2337(12)	0.3740(15)	6.8
C(14)	1.1016(13)	0.1399(13)	0.2663(16)	7.1
C(15)	1.0822(23)	0.0974(24)	0.1270(21)	21.6
C(16)	1.1957(27)	0.0129(27)	0.0241(21)	26.3
C(17)	1.3183(21)	−0.0411(19)	0.0605(21)	16.2
C(18)	1.3267(16)	0.0013(21)	0.1857(23)	16.6
C(19)	1.2228(17)	0.0884(18)	0.2909(19)	13.3
C(1′)	0.8227(13)	0.5102(13)	0.5759(14)	6.2
C(2′)	0.7189(12)	0.5812(14)	0.7057(13)	6.3
C(3′)	0.8367(11)	0.4478(13)	0.7099(15)	6.2
C(4′)	0.9372(12)	0.4452(14)	0.8031(14)	7.6
C(5′)	0.9708(12)	0.3368(14)	0.8553(14)	7.5
C(6′)	0.8869(14)	0.2718(17)	0.7980(17)	9.8
C(7′)	0.8113(14)	0.3339(15)	0.7022(15)	7.7

TABLE 3. Selected bond lengths (e.s.d.'s) in Å for (4*S**,5*R**,6*S**)-5-benzyloxy-6-isopropyl-8-carbomethoxytetracyclo[5.4.0^{1,7}.0^{2,4}.0^{2,9}]-undec-10-ene (**14***a*)

Bond	Length (Å)	Bond	Length (Å)
C(1)—C(2)	1.528(3)	C(5)—C(12)	1.443(2)
C(1)—C(7)	1.560(2)	C(6)—C(7)	1.553(2)
C(1)—C(11)	1.505(2)	C(7)—C(8)	1.563(2)
C(2)—C(3)	1.482(3)	C(8)—C(9)	1.586(3)
C(2)—C(4)	1.490(2)	C(8)—C(23)	1.509(3)
C(2)—C(9)	1.522(2)	C(9)—C(10)	1.508(3)
C(3)—C(4)	1.527(3)	C(10)—C(11)	1.319(3)
C(4)—C(5)	1.512(2)	C(12)—C(13)	1.426(2)
C(5)—C(6)	1.560(3)		

TABLE 4. Selected interatomic distances (e.s.d.'s) in Å, for methyl (4*S**,5*R*,1′*S**)-4-isopropyl-5-benzyloxy-5-(spiro[2.4]hepta-4,6-dien-1-yl)-2-pentenoate (**13***a*)

Atoms	Distance (Å)	Atoms	Distance (Å)
C(1)—C(2)	1.50(2)	C(1′)—C(2′)	1.50(2)
C(2)—C(3)	1.33(2)	C(1′)—C(3′)	1.60(2)
C(3)—C(4)	1.51(2)	C(2′)—C(3′)	1.55(2)
C(4)—C(5)	1.59(2)	C(3′)—C(4′)	1.42(2)
C(4)—C(9)	1.53(2)	C(3′)—C(7′)	1.41(2)
C(5)—C(12)	1.44(1)	C(4′)—C(5′)	1.36(2)
C(12)—C(13)	1.40(2)	C(5′)—C(6′)	1.43(2)
C(5)—C(1′)	1.50(2)	C(6′)—C(7′)	1.37(2)
C(2)...C(4′)	6.01(2)	C(3)...C(7′)	4.78(2)

dimensions 0.40 × 0.27 × 0.20 mm, μ = 5.9 cm^{-1}; 3257 reflections scanned ($2\theta \leq 130°$, $\pm h$, $+k$, $+l$) giving 2345 "observed" ($I \geq 3\sigma(I)$). Final R = 0.038 (0.06 including unobserved), wR = 0.051, k in weighting scheme, 0.0005. Maximum shift in final cycle 0.15σ; final ΔF map, −0.14 to 0.17 e Å^{-3}.

Methyl (4S,5R*,1′S*)-4-isopropyl-5-benzyloxy-5-(spiro[2.4]hepta-4,6-dien-1-yl)-2-pentenoate (**13**a)*

$C_{23}H_{28}O_3$ fw = 352.5

Triclinic, $P\bar{1}$, a = 11.033(3), b = 11.316(4), c = 9.610(2) Å, α = 104.90(2), β = 90.41(2), γ = 65.72(2)° (CuK$_\beta$, λ = 1.39217 Å, 34 reflections, 29° < 2θ < 46°), V = 1050.3 Å^3, Z = 2, ρ = 1.114 g cm^{-3}. Nominal specimen dimensions 0.20 × 0.10 × 0.07 mm, μ = 5.4 cm^{-1}; 2153 reflections scanned (CuKα, $2\theta \leq 100°$, $\pm h$, $\pm k$, $+l$) giving 579 "observed" ($I \geq 3\sigma(I)$). Final R = 0.071 (0.27 including unobserved), wR = 0.091, k in weighting scheme, 0.002. Maximum shift in final cycle, 0.3σ; final ΔF map, −0.2 to 0.2 e Å^{-3}.

Acknowledgements

We are grateful to Memorial University of Newfoundland and the Natural Sciences and Engineering Research Council of Canada for financial support of this research, to G. Gallacher and S. K. Attah-Poku for preliminary experiments, to B. Gregory for high resolution mass spectra, to H. J. Liu (University of Alberta) for 400-MHz ^{1}H nmr spectra, to D. J. Burnell, S. Tuladhar, and G. Bérubé for stimulating discussions, and to the referees for their constructive comments.

1. D. J. FAULKNER. Nat. Prod. Rep. **1**, 551 (1984).
2. C. M. BEECHAN, C. DJERASSI, J. S. FINER, and J. CLARDY. Tetrahedron Lett. 2395 (1977).
3. C. M. BEECHAM, C. DJERASSI, and H. EGGERT. Tetrahedron, **34**, 2503 (1978).
4. J. C. BRAEKMAN, D. DALOZE, A. DUPONT, B. TURSCH, J. P. D. CLERCQ, G. GERMAIN, and M. MEERSSCHE. Tetrahedron, **37**, 179 (1981).
5. P. A. COLLINS and D. WEGE. Aust. J. Chem. **32**, 1819 (1979).
6. W. OPPOLZER, H. F. STRAUSS, and D. P. SIMMONS. Tetrahedron Lett. **23**, 4673 (1982).
7. W. OPPOLZER, T. BEGLEY, and A. ASHCROFT. Tetrahedron Lett. **25**, 825 (1984).
8. K. ANTCZAK, J. F. KINGSTON, and A. G. FALLIS. Can. J. Chem. **63**, 993 (1985).
9. E. PIERS and G. L. JUNG. Can. J. Chem. **63**, 996 (1985).
10. A. G. FALLIS. Can. J. Chem. **62**, 183 (1984).
11. E. CIGANEK. Org. React. **32**, 1 (1984).
12. D. F. TABER. Intramolecular Diels–Alder reactions and alder ene reactions. Springer Verlag, Berlin. 1984.
13. G. BRIEGER and J. N. BENNETT. Chem. Rev. **80**, 63 (1980).
14. G. OURISSON. Bull. Soc. Chim. Fr. 895 (1955).
15. J. THIERRY and R. WEISS. Tetrahedron Lett. 2663 (1969).
16. P. DEMAYO and R. E. WILLIAMS. J. Am. Chem. Soc. **87**, 3275 (1965).
17. L. A. SMEDMAN, E. ZAVARIN, and R. TERANISHI. Phytochemistry, 1457 (1969).
18. S. K. ATTAH-POKU, K. ANTCZAK, S. J. ALWARD, and A. G. FALLIS. Can. J. Chem. **62**, 1717 (1984).
19. G. GALLACHER, A. S. NG, S. K. ATTAH-POKU, K. ANTCZAK, S. J. ALWARD, J. F. KINGSTON, and A. G. FALLIS. Can. J. Chem. **62**, 1709 (1984).
20. K. BANGERT and V. BOEKELHEIDE. Tetrahedron Lett. 1119 (1963).
21. M. NEUENSCHWANDER, D. MEUCHE, and H. SCHALTEGGER. Helv. Chim. Acta, **46**, 1760 (1963).
22. S. MASAMUNE, W. CHOY, J. S. PETERSEN, and L. R. SITA. Angew. Chem. Int. Ed. Engl. **24**, 1 (1985).
23. R. APPEL and H. WIHLER. Chem. Ber. **109**, 3446 (1976).

24. S. J. ALWARD and A. G. FALLIS. Can. J. Chem. **62**, 121 (1984).
25. S. J. HECKER and C. H. HEATHCOCK. J. Org. Chem. **50**, 5159 (1985).
26. T. WU and K. N. HOUK. Tetrahedron Lett. **26**, 2293 (1985).
27. F. K. BROWN and K. N. HOUK. Tetrahedron Lett. **26**, 2297 (1985).
28. L. L. KLEIN. J. Org. Chem. **50**, 1770 (1985).
29. W. R. ROUSH and M. KAGEYAMA. Tetrahedron Lett. **26**, 4327 (1985).
30. R. K. BOECKMAN, JR. and T. E. BARTA. J. Org. Chem. **50**, 3421 (1985).
31. F. NAF, R. DECORZANT, W. GIERSCH, and G. OHLOFF. Helv. Chim. Acta, **64**, 1387 (1981).
32. R. E. R. CRAIG, A. C. CRAIG, R. D. LARSEN, and C. N. CAUGHLAN. J. Org. Chem. **42**, 3188 (1977).
33. F. K. BROWN and K. N. HOUK. Tetrahedron Lett. **25**, 4609 (1984).
34. F. BERNARDI, A. BOTTONI, M. A. ROBB, M. J. FIELD, I. H. HILLIER, and M. F. GUEST. J. Chem. Soc. Chem. Commun. 1051 (1985).
35. K. N. HOUK, Y. LIN, and F. K. BROWN. J. Am. Chem. Soc. **108**, 554 (1986).
36. D. F. GRANT and E. J. GABE. J. Appl. Crystallogr. **11**, 114 (1978).
37. P. MAIN, S. E. HULL, L. LESSINGER, G. GERMAIN, J. DECLERCQ, and M. M. WOOLFSON. A system of computer programs for the automatic solution of crystal structures from X-ray diffraction data. University of York, University of Louvain. York, England; Louvain, Belgium. 1978.
38. A. C. LARSON. *In* Crystallographic computing. *Edited by* F. R. Ahmed, S. R. Hall, and C. P. Huber. Munksgaard, Copenhagen. 1970. pp. 291–294.
39. A. C. LARSON and E. J. GABE. *In* Computing in crystallography. *Edited by* H. Schenk, R. Olthof-Hazekamp, H. van Koningsveld, and G. C. Bassi. Delft University Press, Delft. 1978. pp. 81–89; International tables for X-ray crystallography. Vol. 4. Kynoch Press (distributor D. Reidel, Dordrecht), Birmingham, England.

Can. J. Chem. Downloaded from www.nrcresearchpress.com by 80.58.250.72 on 09/07/12
For personal use only.

Directed *ortho* metalation reactions. Convergent synthesis of "angular" anthracyclinones ochromycinone and X-14881 C[1]

K. KATSUURA AND V. SNIECKUS[2]

Guelph–Waterloo Centre for Graduate Work in Chemistry, University of Waterloo, Waterloo, Ont., Canada N2L 3G1

Received June 16, 1986

This paper is dedicated to Dr. O. E. (Ted) Edwards

K. KATSUURA and V. SNIECKUS. Can. J. Chem. **65**, 124 (1987).

Convergent syntheses of the benz[*a*]anthraquinone natural products X-14881 C (**2***c*) and ochromycinone (**2***d*) have been achieved using aromatic directed metalation strategies. Key steps involve (a) the condensations of dilithiated *cis*-tetralol (**13***a*) with the aldehydo *o*-anisamide **14** and of methoxymethyl protected aldehyde **17***b* with lithiated *o*-anisamide (**18**) to give, after acid-catalyzed cyclization, the phthalide **16**, and (b) the regiospecific hydroxyselenylation of anthraquinone **22** to provide the hydroxyselenide **23**.

K. KATSUURA et V. SNIECKUS. Can. J. Chem. **65**, 124 (1987).

Faisant appel à des stratégies de métalations orientées par les groupements aromatiques, on a réalisé des synthèses convergentes des produits naturels X-14881 C (**2***c*) et ochromycinone (**2***d*) de la série des benz[*a*]anthraquinones. Les étapes clés impliquent: (a) les condensations du tétralol-*cis* dilithié (**13***a*) avec l'aldéhydo *o*-anisamide (**14**) ainsi que de l'aldéhyde **17***b*, protégé par un groupement méthoxyméthyle, avec la *o*-anisamide lithiée (**18**) qui conduisent toutes les deux au phtalide **16** après une cyclisation acido-catalysée; et (b) l'hydroxysélénylation régiospécifique de l'anthraquinone **22** qui conduit à l'hydroxysélénide **23**.

[Traduit par la revue]

Can. J. Chem. Downloaded from www.nrcresearchpress.com by 80.58.250.72 on 09/07/12
For personal use only.

The benz[*a*]anthraquinones (**1**) constitute a distinct class of antibiotic substances isolated from cultures of several strains of *Streptomyces* (2). Represented by several ring A oxidation states, levels of oxygenation, and functional group complexity (e.g. tetrangulol (**1**) (2*a*), rabelomycin (**2***a*) (2*b*), X-14881 A (**3**) (2*e*)), this group of structural "angular" analogues of the anthracyclinones (3) has been shown to exhibit weak antibacterial (2*b*, 2*d*), enzyme inhibitory (2*c*), and antitumor (2*d*) activity. Synthesis of the benz[*a*]anthraquinone antibiotics is limited to a classical route to tetrangulol (**1**) (4) and an interesting convergent construction of the non-naturally occurring 3-deoxyrabelomycin (**2***b*) (5) based on regioselectively generated anionic 1-tetralol chromium tricarbonyl complex intermediates (6). We detail herein the first total syntheses of X-14881 C (**2***c*) and ochromycinone (**2***d*) by a strategy which originated with our general anthraquinone synthesis (7) and which focusses on the application of *ortho* metalated benzamide (8) and **uncomplexed** 1-tetralol (6) intermediates.

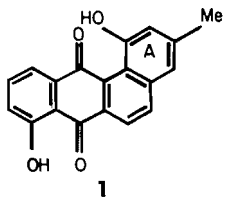

1

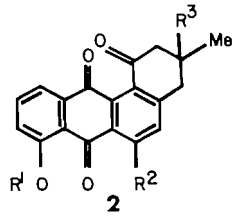

2

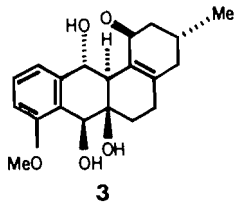

3

	R^1	R^2	R^3
a	H	OH	OH
b	H	OH	H
c	Me	H	H
d	H	H	H
e	Ac	H	H

Maximum synthetic convergence to the benz[*a*]anthraquinone skeleton **4** is gained by dissections a and b (Scheme 1) leading to fragments **5**, **6** and **7**, **8** respectively. These retro-

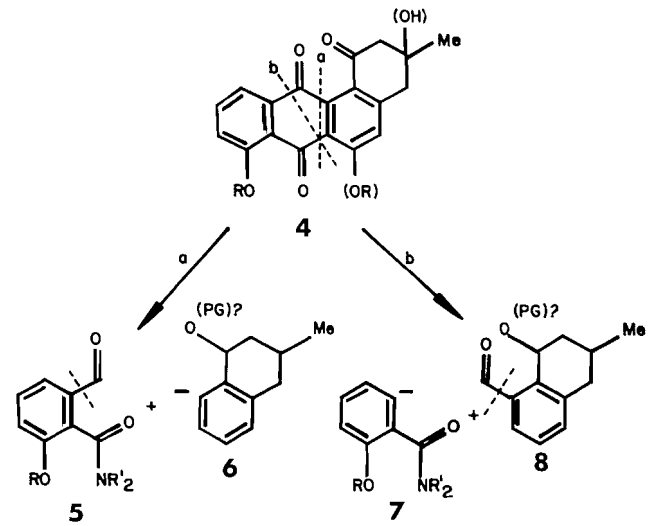

SCHEME 1

synthetic paths are mutually interactive in that aldehydes **5** and **8** are obtainable from **7** and **6** respectively by reaction with DMF. The question of necessity to protect the 1-tetralol function was considered to be best answered by experimentation. Of the two approaches, route a proved to be the more efficient.

The tetralone derivative **12** (Scheme 2), obtained by unexceptional chemistry (see experimental section), was reduced to a *cis–trans* mixture of tetralols **13***a*, *b* (**13***a* major) according to a reported procedure (9). Since the isomers had been separated and fully characterized (9), the opportunity to test stereochemical effects involving a benzyl alcohol directed *ortho* metalation group was presented for the first time (6, 10). Dilithiation of the *cis* isomer (**13***a*) using *n*-BuLi/TMEDA complex in refluxing Et_2O followed by D_2O quench at 0°C resulted in 86% d_1 incorporation, while metalation and deuteration of the *trans* isomer (**13***b*) under essentially identical conditions gave only 24% d_1 incorporation (nmr analysis). This distinct stereochemical consequence, perhaps the result of better coordinative stabilization in the planar dilithiated species

[1]For preliminary communication of this work, see ref. 1.

[2]Author to whom correspondence may be addressed.

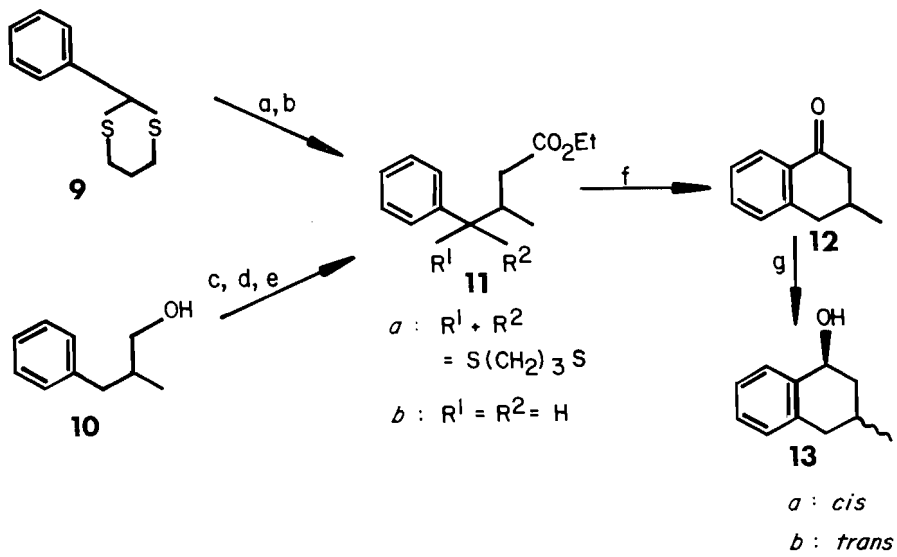

a: *n*-BuLi/THF/−78°C; ethyl crotonate; b: Raney Ni/EtOH/reflux (75% overall); c: TsCl/py; d: NaCN/methyl cellosolve/reflux; e: conc. H_2SO_4/EtOH/reflux (68% overall); f: 75% aq. H_2SO_4/100°C (79%); g: $NaBH_4$/*i*-PrOH–H_2O/room temp. (quant.).

SCHEME 2

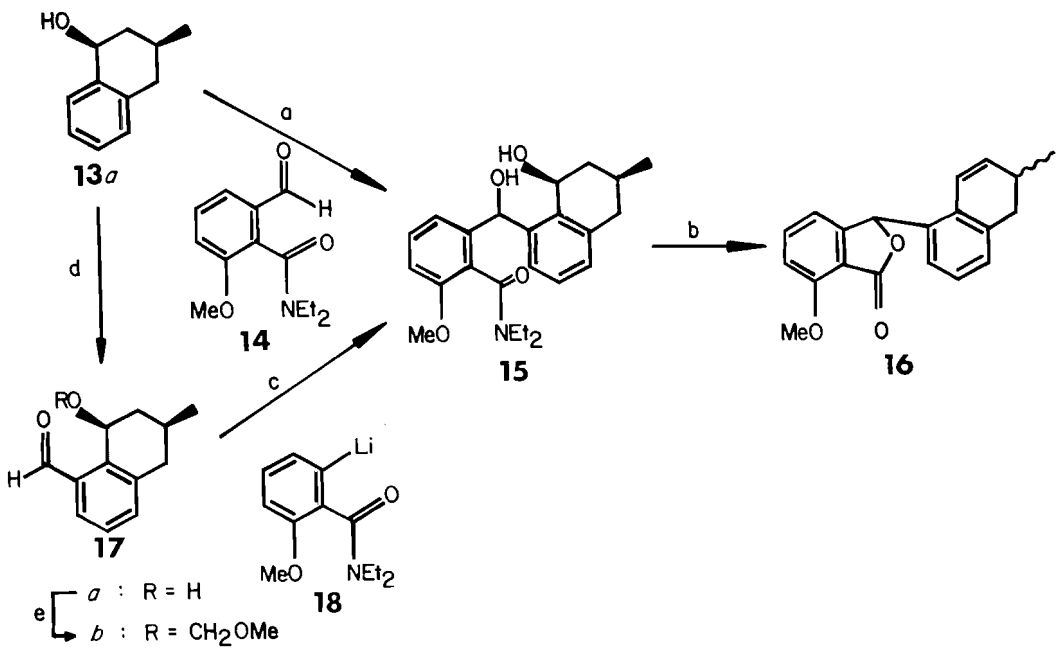

a: 2 equiv. *n*-BuLi/TMEDA/Et_2O/reflux; **14**/Et_2O/−45°C; b: TsOH/Tol/reflux (77% overall); c: **18** (*s*-BuLi/TMEDA/Et_2O/−78°C; **17**/Et_2O/room temp.; d: *n*-BuLi/TMEDA/Et_2O/reflux; DMF/0°C (quant.); e: $ClCH_2OMe$/*i*-Pr_2NEt/THF/room temp. (89%)

SCHEME 3

derived from the *cis* isomer, provided persuasive evidence that further metalation reactions be effected on pure **13***a*.

The *cis*-isomer (**13***a*) (Scheme 3) was thus dilithiated as before and the resulting species was coupled at −45°C with the amide aldehyde **14**, derived in high yield from lithiated *N*,*N*-diethyl *o*-anisamide by reaction with DMF (11). The conditions for this coupling to give optimum yields of product were achieved after considerable experimentation.

As previously encountered for related systems (7), manipulation and purification of the intermediate amide alcohol **15** proved to be problematical. Therefore, **15** was treated directly with TsOH in refluxing benzene to give the phthalide alcohol **19***a* (42%) and the corresponding dehydrated product **16** (4%) as a stereoisomeric nonhomogeneous material. Chromium trioxide – pyridine oxidation of **19***a* to the keto phthalide **19***b* followed by zinc hydrogenolysis in basic solution produced the keto benzoic acid **20**. Friedel–Crafts cyclization directly to the anthrone corresponding to X-14881 C (**2***c*) was unsuccessful using TFAA (7) or concentrated sulfuric acid, undoubtedly due in part to the deactivated nature of the aromatic ring. These failures and the possibility of the Hayashi rearrangement under more vigorous Lewis acid catalyzed conditions (12) forced a reexamination of the conditions for the TsOH-catalyzed lactonization of the intermediate **15**. When the solvent was

Can. J. Chem. Downloaded from www.nrcresearchpress.com by 80.58.250.72 on 09/07/12
For personal use only.

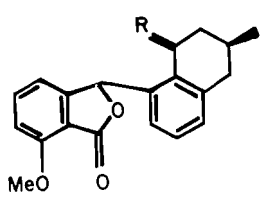

19

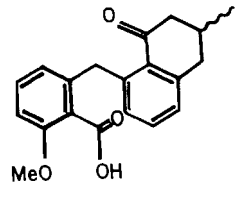

20

a: R = H, OH
b: R = O

changed to toluene, the olefin phthalide **16** was obtained in high yield, a result also observed by Uemura *et al.* in a similar system (6). This finding and the expected minor effect of the double bond in the projected Friedel–Crafts reaction changed the strategy to one incorporating a functional group conversion step at the terminal stage of the synthesis.

The alternate convergent strategy to **16** (route b, Scheme 1) was initiated by dimetalation and formylation of **13***a* to give, in quantitative yield, the formyl tetralol **17***a*. Protection of the secondary alcohol with the popular methoxymethyl group, followed by coupling with **18** at −78°C and acid-catalyzed cyclization, furnished the same phthalide **16** in substantially lower overall yield (58%) than that obtained by condensation of **13***a* with **14**.

Zinc-mediated hydrogenolysis (7) of **16** (Scheme 4) led to the benzoid acid **21** (93%), which upon sequential TFAA-catalyzed Friedel–Crafts reaction and aerial oxidation in the presence of Triton B (13) afforded the dihydrobenz[*a*]anthraquinone **22**. Regiospecific C-1 hydroxylation of **22** using the well-documented hydroxymercuration method (14) failed. However, the Nicolaou procedure of selenohydroxylation with phenylselenylphthalimide (15*a*) afforded the required product **23**. Compound **23** was also prepared by Clive's phenylselenyl chloride procedure (15*b*) in comparable yield. Although the assigned regiochemistry was in agreement with the ^{1}H nmr data (δ 3.87, 1H, br t, C-2 H; 4.84, 1H, d, J = 4 Hz, D_2O-exchangeable; 5.34, 1H, dd, J = 4, 2.5 Hz, C-1 H), it was deduced only after correlation of synthetic X-14881 C (**2***c*) with the natural product. The *trans* stereochemistry was tentatively assigned on the basis of the generally accepted *trans* mode addition of selenium electrophiles to simple olefin systems (16). The small coupling constant, J = 2.5 Hz, for C-1 H suggests *cis* (17) or *trans*-diaxial relationship between the hydroxyl and phenylselenyl groups. We prefer the latter assignment on the basis of the accepted mechanism of addition (16) and the recent evidence that the PhSe group prefers axial orientation in both *cis* and *trans* cyclohexanone derivatives (18). A mechanistic rationalization (Scheme 5) for the formation of **23** involves assistance in the delivery of acetate to the benzylic carbon by initial coordination with the quinone oxygen. The stereochemistry of **23** is, of course, inconsequential to the synthetic end result (**2***c*, **2***d*).

Adoption of the standard excess Ph_3SnH conditions (19) on **23** to reductively cleave the C—Se bond resulted in the formation of the olefin **22**, presumably by thermal dehydration of the deselenylated intermediate. However, when hydroxy selenide **23** was first subjected to CrO_3 oxidation and the intermediate selenyl ketone was treated with Ph_3SnH, X-14881 C (**2***c*) was obtained cleanly and in good yield. Synthetic **2***c* was shown to be identical with the natural product by comparison of physical and spectral data with those reported in the literature (2*e*). Demethylation using $AlCl_3$ afforded ochromycinone (**2***d*) whose identity with the natural product (20) was similarly established. Direct comparison of ochromycinone acetate (**2***e*) with an authentic sample further established identity of the two materials.

To conclude, syntheses of X-14881 C (**2***c*) and ochromycinone (**2***d*) have been completed in 21% overall yield and 8–9 steps based on compound **9** and consideration of the higher yield sequences. This work demonstrates the viability of coupling aromatic directed *ortho* metalation reactions (8) for regiospecific and convergent construction of these substituted benz[*a*]anthraquinone antibiotics and invites further application of this strategy in organic synthesis (21).

Experimental

Melting points were measured on a Büchi SMP-20 apparatus and are uncorrected. The ^{1}H nmr spectra were recorded on a Bruker WP-80 spectrometer in deuteriochloroform using tetramethylsilane as an internal standard unless otherwise stated. The ir spectra were determined on a Perkin–Elmer 983 spectrometer. Mass spectra were recorded on a high resolution CH-7 spectrometer. Column chromatog-

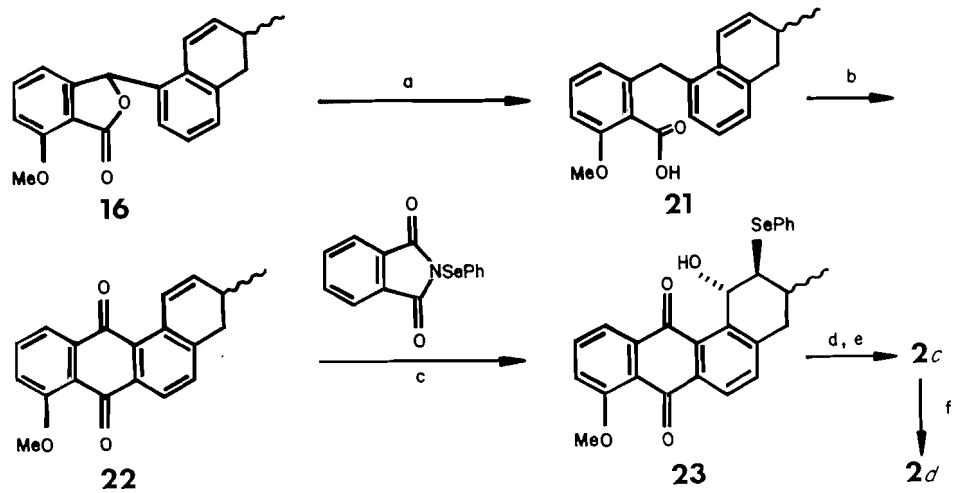

a: Zn/10% aqueous NaOH/reflux (90%); b: TFAA/CH_2Cl_2/reflux; O_2/Triton B/MeOH/room temp.; c: TsOH/CH_2Cl_2–H_2O/room temp. (85% overall); d: CrO_3/py/H_2O/room temp. (72%); e: Ph_3SnH/ AIBN/PhH/reflux (67%); f: $AlCl_3$/CH_2Cl_2/room temp. (99%)

SCHEME 4

Can. J. Chem. Downloaded from www.nrcresearchpress.com by 80.58.250.72 on 09/07/12
For personal use only.

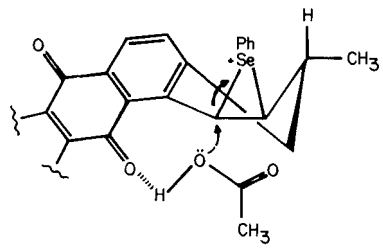

SCHEME 5

raphy was performed with Silica Gel 60 (Merck, 230–400 mesh) or aluminum oxide (Aldrich, neutral). The phrase "standard work-up" refers to washing of the organic phase with water, drying over $MgSO_4$, filtration, and evaporation under reduced pressure.

*Ethyl 3-methyl-4-(1,3-dithiopropano)-4-phenylbutyrate (**11**a) from **9***

To a stirred solution of **9** (23.04 g, 118 mmol) in dry THF (350 mL) was added dropwise a solution of *n*-BuLi (78 mL, 118 mmol, 1.5 *M* solution) at −78°C under nitrogen. After stirring 1 h at −78°C, the solution was treated with ethyl crotonate (14.8 mL, 119 mmol). The resulting mixture was stirred for 1 h at −78°C and treated with aqueous NH_4Cl solution. The mixture was concentrated to ca. 200 mL and extracted with ether. Standard work-up gave an oil, which upon distillation afforded 28.58 g (78%) of ethyl 3-methyl-4-(1,3-dithiopropano)-4-phenylbutyrate (**11***a*) as a pale yellow oil, bp 160–180°C/0.03 Torr (1 Torr = 133.3 Pa); ir (neat) ν_{max}: 1730 cm^{-1}; ^1H nmr δ: 0.98 (3H, d, *J* = 6.5 Hz), 1.20 (3H, t, *J* = 7 Hz), 1.60–3.20 (9H, m), 4.07 (2H, q, *J* = 7 Hz), 7.10–8.00 (5H, m); ms *m/e* (rel. intensity): 310 (4, M^+), 195 (49), 84 (61).

Hydrolysis of **11***a* (20% aqueous NaOH–EtOH, reflux) furnished in 90% yield *3-methyl-4-(1,3-dithiopropano)-4-phenylbutyric acid*, mp 137–138°C (EtOAc); ir (Nujol) ν_{max}: 1711 cm^{-1}; ^1H nmr δ: 1.00 (3 H, d, *J* = 6 Hz), 1.80–3.10 (9H, m), 7.20–7.50 (3H, m), 7.85–8.00 (2H, m); ms *m/e* (rel. intensity): 282 (11, M^+), 195 (100). *Anal.* calcd. for $C_{14}H_{18}O_2S_2$: C 59.53, H 6.43, S 22.70; found: C 59.58, H 6.56, S 22.98.

*Ethyl 3-methyl-4-phenylbutyrate (**11**b) from **10***

To an ice-cooled solution of *p*-toluenesulfonyl chloride (53.0 g, 0.28 mol) in dry pyridine (230 mL) was added **10***a* (38.2 g, 0.25 mol) (22), and the reaction mixture was stirred overnight at room temperature. Concentration to remove pyridine was followed by acidification (dilute HCl) and extraction with Et_2O. Standard work-up furnished a colorless syrup of the tosylate; ^1H nmr δ: 0.88 (3H, d, *J* = 7 Hz), 1.90–2.90 (3H, m), 2.44 (3H, s), 3.86 (2H, d, *J* = 5.5 Hz), 7.00–7.85 (9H, m).

A stirred suspension of the above tosylate and powdered NaCN (11.6 g, 0.24 mol) in methyl cellosolve (270 mL) was refluxed for 2.5 h under nitrogen. After removal of the solvent, the reaction mixture was diluted with Et_2O and the heterogeneous mixture was filtered. Standard work-up followed by distillation gave 33.4 g (82%) of the nitrile as a colorless oil, bp 80–92°C/0.14 Torr (lit. (23) bp 100–105°C/1.5 Torr); ir (neat) ν_{max}: 2246 cm^{-1}; ^1H nmr δ: 1.11 (3H, d, *J* = 6.5 Hz), 1.90–2.30 (3H, m), 2.66 (2H, d, *J* = 6.5 Hz), 7.10–7.40 (5H, m); ms *m/e* (rel. intensity): 159 (100, M^+).

A stirred mixture of the above nitrile (1.00 g, 6.3 mmol) and concentrated H_2SO_4 (2 mL) in 95% EtOH (5 mL) was refluxed for 18 h. The reaction mixture was poured into ice-water and extracted with ether. The extract was washed with aqueous $NaHCO_3$ solution and subjected to the standard work-up to give 1.08 g (83%) of a pale yellow oil, which was shown to be identical with **11***b* obtained as described below by comparison of ^1H nmr and ir spectra.

*3-Methyl-1-tetralone (**12**)*

A stirred suspension of **11***a* (14.19 g, 45.8 mmol) and Raney-Ni (W-7, 50 g) in absolute EtOH (200 mL) was refluxed for 2 h. After removal of the catalyst and the solvent, the residue was dissolved in $CHCl_3$. Standard work-up gave 10.10 g of *ethyl 3-methyl-4-phenylbutyrate* (**11***b*) as a colorless oil; ir (neat) ν_{max}: 1730 cm^{-1}; ^1H nmr δ: 0.90–1.32 (6H, m), 2.15–2.65 (5H, m), 4.10 (2H, q, *J* = 7 Hz), 7.10–7.30 (5H, m).

A stirred mixture of the crude ester (**11***b*) and 75% H_2SO_4 (50 mL) was heated at 100°C for 8 h. The reaction mixture was poured into ice-water and extracted with $CHCl_3$. Standard work-up gave material that was distilled to afford 5.79 g (79%) of **12** as a pale yellow oil bp 80–90°C/0.14 Torr (lit. (24) bp 94–96°C/0.3 Torr); ^1H nmr δ: 1.13 (3H, d, *J* = 6 Hz), 2.10–3.10 (5H, m), 7.15–7.60 (4H, m), 8.02 (1H, dd, *J* = 1.5 and 7.5 Hz).

Cis- *and* trans-*3-methyl-1-tetralol (**13**a, **13**b)*

The method of Mitsui *et al.* (9) was adopted. To an ice-cooled stirred solution of the tetralone **12** (6.75 g, 42.0 mmol) in a mixture of *i*-PrOH (60 mL) – water (6 mL) was added $NaBH_4$ (1.50 g, 39.0 mmol) in one portion. The reaction mixture was stirred at room temperature for 44 h and evaporated to a slurry, which was diluted with water and extracted with $CHCl_3$. The extract was washed with H_2O, dried ($MgSO_4$), and evaporated to dryness to give a colorless solid (16.82 g, quantitative). Recrystallization from Et_2O–hexane gave 5.21 g (76%) of colorless needles of the *cis*-tetralol **13***a*, mp 95–96°C (lit. (9) mp 96.5–98°C); nmr (acetone-d_6) δ: 4.80 (dd, *J* = 6.3, 10.6 Hz) (9).

By fractional crystallization of the mother liquor of several reduction experiments from Et_2O–hexane, the *trans*-tetralol **13***b* was obtained, mp 110.5–112°C (lit. (9) mp 113–115°C); nmr (acetone-d_6)δ: 4.81 (t, 1H, *J* = 3.1 Hz) (9).

Lithiation of the cis-*tetralol **13**a*

To a stirred solution of **13***a* (110 mg, 0.68 mmol) and TMEDA (0.21 mL, 1.39 mmol) in dry ether (10 mL) was added *n*-BuLi solution (1.2 mL, 1.68 mmol, 1.40 *M* solution) and the mixture was refluxed for 5 h under nitrogen. The resulting red solution was quenched with MeOD (0.5 mL) at 0°C. The reaction mixture was stirred for 1 h at room temperature, treated with aqueous NH_4Cl solution, and concentrated. The resulting aqueous solution was extracted with Et_2O and the extract was washed with dilute HCl. Standard work-up gave 110 mg (quantitative) of **13***a* as a colorless solid whose ^1H nmr spectrum (acetone-d_6) showed 86% d_1 incorporation by comparison of aromatic and C-Me and C1-H integrations.

Lithiation of the trans-*tetralol **13**b*

Lithiation and deuteration of **13***b* was carried out under conditions identical to those described for **13***a*. From **13***a* (144 mg, 0.89 mmol), TMEDA (0.3 mL, 1.99 mmol), and *n*-BuLi (1.8 mL, 2.63 mmol, 1.46 *M* solution) in anhydrous Et_2O (25 mL), there was obtained after the identical work-up but with chromatography (silica gel, 30% EtOAc–hexane eluent), 130 mg (90%) of **13***b* whose ^1H nmr spectrum (acetone-d_6) showed, by appropriate integration, 24% d_1 incorporation.

*Phthalide **16** from* cis-*tetralol **13**a*

To a stirred solution of **13***a* (7.80 g, 48.1 mmol) and TMEDA (14.6 mL, 96.9 mmol) in dry ether (700 mL) was added a solution of *n*-BuLi (75 mL, 109.5 mmol, 1.46 *M* solution) under argon and the mixture was refluxed for 6 h. To the resulting red solution was added dropwise a solution of **14** (11) (11.00 g, 46.8 mmol) in dry ether (10 mL) at −45°C with stirring. The reaction mixture was stirred overnight at ambient temperature, treated with aqueous NH_4Cl solution, and washed with dilute HCl. Standard work-up gave crude amide alcohol **15** as a solid.

A solution of crude **15** and TsOH (6.80 g, 35.8 mmol) in toluene (800 mL) was refluxed for 18 h with azeotropic removal of water. The reaction mixture was washed with aqueous $NaHCO_3$ solution and subjected to standard work-up. The residue was chromatographed (silica gel, 40% EtOAc–hexane eluent) to give 11.04 g (77%) of **16**; ir (Nujol) ν_{max}: 1764 cm^{-1}; ^1H nmr δ: 1.14 (3H, d, *J* = 6 Hz), 2.50–3.00 (3H, m), 4.00 (3H, s), 6.42 (1H, br d, *J* = 10 Hz), 6.70–7.70 (8H, m); ms *m/e* (rel. intensity): 306 (34, M^+), 273 (35), 83 (100).

*Phthalide **16** from methylenemethoxy* cis-*tetralol aldehyde **17**b*

To a stirred solution of TMEDA (0.18 mL, 1.2 mmol) and *s*-BuLi (1.0 mL, 1.3 mmol, 1.27 *M* solution) in dry ether (15 mL) was added a

Can. J. Chem. Downloaded from www.nrcresearchpress.com by 80.58.250.72 on 09/07/12
For personal use only.

Can. J. Chem. Downloaded from www.nrcresearchpress.com by 80.58.250.72 on 09/07/12
For personal use only.

solution of *N,N*-diethyl *o*-anisamide (207 mg, 1.0 mmol) (11) in anhydrous Et_2O (2 mL) at −78°C under argon and the mixture was stirred for 1 h. The resulting milky suspension was quenched with a solution of **17***b* (227 mg, 1.0 mmol) in dry ether (3 mL) and the mixture was stirred overnight at ambient temperature. The solution was treated with aqueous NH_4Cl solution and concentrated. The residue was acidified with dilute HCl and extracted with Et_2O. Standard work-up gave 443 mg of a pale yellow syrup.

A mixture of the crude product and TsOH (240 mg) in toluene (60 mL) was refluxed for 6 h. The reaction mixture was washed with aqueous $NaHCO_3$ solution and subjected to standard work-up to give material that was chromatographed (ptlc, silica gel) to give 193 mg (65%) of a colorless solid. This solid was shown to be identical with compound **16** prepared above, by comparison of ^1H nmr and ir spectra.

*3-Methyl-8-formyl-*cis*-1-tetralol (17*a*)*

A mixture of **13***a* (1.01 g, 6.2 mmol), TMEDA (1.9 mL, 12.6 mmol), and a solution of *n*-BuLi (12.7 mL, 17.8 mmol, 1.40 *M*) in dry Et_2O (70 mL) was refluxed for 6 h under argon. The resulting red solution was quenched with DMF (2.4 mL, 31.1 mmol) at 0°C. The reaction mixture was stirred overnight at ambient temperature and treated with aqueous NH_4Cl solution. The Et_2O layer was washed with dilute HCl and subjected to standard work-up to give a colorless syrup. Chromatography (silica gel, 25% EtOAc–hexane) gave 1.18 g (quantitative) of **17***a* as a colorless syrup; ir (neat) ν_{max}: 3396, 1679 cm^{-1}; ^1H nmr δ: 1.12 (3H, d, J = 6 Hz), 1.30–2.80 (5H, m), 4.76 (1H, br s, exchangeable with D_2O), 5.20 (1H, t, J = 8 Hz), 7.20–7.80 (3H, m), 10.05 (1H, s); ms (20 eV) m/e: 190.0984 (M^+) (calcd. for $C_{12}H_{14}O_2$: 190.0990).

Methylenemethoxy cis*-1-tetralol aldehyde **17**b*

A mixture of **17***a* (0.75 g, 4.0 mmol), diisopropylethylamine (2.6 mL, 15.0 mmol), and chloromethyl methyl ether (2.3 mL, 30.3 mmol) in dry THF (40 mL) was stirred for 7 days at room temperature. The reaction mixture was evaporated to dryness and the residue was dissolved in water. The solution was acidified (dilute HCl) and extracted with Et_2O. The extract was washed with brine and worked up in the standard manner to give a residue that was chromatographed (silica gel, 15% EtOAc–hexane) to give 0.82 g (89%) of **17***b* as a colorless syrup; ir (neat) ν_{max}: 1690 cm^{-1}; ^1H nmr δ: 1.14 (3H, d, J = 6 Hz), 1.30–2.80 (5H, m), 3.40 (3H, s), 4.81 (2H, s), 5.39 (1H, t, J = 7 Hz), 7.20–7.80 (3H, m), 10.31 (1H, s); ms (20 eV) m/e (rel. intensity): 189 (100, $M^+ - CH_2OMe$), 172 (71).

*Phthalide alcohol **19**a*

A mixture of **13***a* (4.35 g, 26.9 mmol), TMEDA (8.3 mL, 55.1 mmol), and *n*-BuLi solution (41.0 mL, 62.3 mmol, 1.52 *M*) in dry Et_2O (400 mL) was refluxed for 6 h under argon. The resulting red solution was treated with a solution of **14** (6.34 g, 27.0 mmol) (11) in dry Et_2O (20 mL) at −40°C with stirring. The reaction mixture was stirred overnight at ambient temperature and treated with aqueous NH_4Cl solution. The Et_2O layer was washed with dilute HCl and worked up in standard manner to give crude material used directly in the following reaction.

A solution of the crude product and TsOH (1.28 g, 6.7 mmol) in benzene (350 mL) was refluxed for 8 h. The reaction mixture was washed successively with aqueous $NaHCO_3$ solution and worked up in the standard manner to give a residue that was chromatographed (silica gel, 20% EtOAc–hexane eluent) to give 0.84 g (19%) of the tetralol **13***a*. Elution with 30% EtOAc–hexane gave 0.36 g (4%) of a colorless solid, which was identified as **16** by comparison of ^1H nmr and ir spectra. Elution with 60% EtOAc–hexane gave a yellow syrup, which was crystallized from MeOH to give 3.65 g (42%) of **19***a* as colorless prisms, mp 195–197°C; ir (Nujol) ν_{max}: 3466, 1736 cm^{-1}; ^1H nmr δ: 1.14 (3H, d, J = 6 Hz), 1.20–3.00 (5H, m), 2.67 (1H, d, J = 5.5 Hz, exchangeable with D_2O), 3.99 (3H, s), 5.28 (1H, m, convertible into t, J = 7 Hz by D_2O exchange), 6.60–7.70 (7H, m); ms m/e (rel. intensity): 306 (100, $M^+ - H_2O$). *Anal.* calcd. for $C_{20}H_{20}O_4$: C 74.06, H 6.21; found: C 73.82, H 6.47.

*Phthalide ketone **19**b*

Cornforth's reagent (25) (5 mL, prepared from CrO_3 (1.0 g), H_2O (1 mL), and pyridine (10 mL)) was added to a stirred solution of **19***a* (681 mg, 2.1 mmol) in pyridine (15 mL) and the mixture was stirred at room temperature for 16 h. *i*-PrOH (1 mL) was added, the reaction mixture was diluted with EtOAc, and the whole was filtered. The filtrate was concentrated and the residue was dissolved in EtOAc. The solution was washed with dilute HCl and subjected to standard work-up to give a colorless foam. Crystallization from Et_2O gave 618 mg (91%) of **19***b* as colorless prisms, mp 140–154°C; ir (Nujol) ν_{max}: 1758, 1672 cm^{-1}; ^1H nmr δ: 1.18 (3H, d, J = 5 Hz), 2.10–3.20 (5H, m), 4.00 (3H, s), 6.80–7.70 (7H, m); ms m/e (rel. intensity): 322 (100, M^+). *Anal.* calcd. for $C_{20}H_{18}O_4$: C 74.52, H 5.63; found: C 74.30, H 5.74.

*Keto benzoic acid **20***

A suspension of **19***b* (244 mg, 0.76 mmol) and zinc powder (3.0 g) in 10% NaOH solution (30 mL) was refluxed for 24 h with stirring. After filtration, the reaction mixture was washed with Et_2O, acidified with dilute HCl, and extracted with Et_2O. The extract was washed with brine, dried, and concentrated. The residue was chromatographed (silica gel, 70% EtOAc–hexane eluent) to give 133 mg (54%) of **20**. Crystallization (toluene) gave colorless needles, mp 139.5–140°C; ir (Nujol) ν_{max}: 1696 cm^{-1}; ^1H nmr δ: 1.08 (3H, d, J = 5.5 Hz), 2.00–3.20 (5H, m), 3.85 (3H, s), 4.52 (2H, s), 6.40–7.50 (6H, m), 9.61 (1H, br s, exchangeable with D_2O); ms m/e (rel. intensity): 280 (10, $M^+ - CO_2$), 143 (100%). *Anal.* calcd. for $C_{20}H_{20}O_4$: C 74.06, H 6.21; found: C 73.82, H 6.43.

*Ene benzoic acid **21***

A stirred suspension of **16** (327 mg, 1.1 mmol) and zinc powder (4.0 g) in 10% NaOH solution (40 mL) was refluxed for 24 h. The reaction mixture was subjected to filtration. The filtrate was washed with Et_2O, acidified with dilute HCl, and extracted with $CHCl_3$. Crystallization (EtOAc–hexane) gave colorless prisms, mp 169.5–171°C; ir (Nujol) ν_{max}: 1706 cm^{-1}; ^1H nmr δ: 1.04 (3H, d, J = 6 Hz), 2.30–3.00 (3H, m), 3.92 (3H, s), 4.20 (2H, s), 5.87 (1H, dd, J = 10 and 2.5 Hz), 6.50–7.40 (7H, m); ms m/e (rel. intensity): 308 (18, M^+), 143 (100). *Anal.* calcd. for $C_{20}H_{20}O_3$: C 77.90, H 6.54; found: C 77.70, H 6.60.

*Anthraquinone **22***

A mixture of **21** (2.79 g, 9.1 mmol) and trifluoroacetic anhydride (20 mL) in dry CH_2Cl_2 (75 mL) was refluxed for 4 h under argon. The reaction mixture was concentrated to dryness and the residue was used immediately for the next step.

A stream of oxygen was bubbled through a stirred solution of the above residue and 30% Triton B (15 mL) in MeOH (180 mL) for 2 h at room temperature. After removal of the solvent, the reaction mixture was dissolved in $CHCl_3$ and subjected to standard work-up to give material that was chromatographed (silica gel, 20% EtOAc–hexane eluent) to give 2.31 g (84%) of **22**. This was crystallized (MeOH–$CHCl_3$) to furnish red needles, mp 172–172.5°C; ir (Nujol) ν_{max}: 1664 cm^{-1}; ^1H nmr δ: 1.14 (3H, d, J = 6 Hz), 2.50–3.00 (3H, m), 4.04 (3H, s), 6.25 (1H, dd, J = 10 and 2.5 Hz), 7.20–8.20 (6H, m); ms m/e (rel. intensity): 304 (100, M^+), 289 (88). *Anal.* calcd. for $C_{20}H_{16}O_3$: C 78.93, H 5.30; found: C 79.19, H 5.54.

*Hydroxyselenide **23***

*Method a (15*a)*

The *N*-phenylselenophthalimide (N-PSP) reagent was prepared as follows: To a stirred suspension of potassium phthalimide (500 mg, 2.7 mmol) in dry CH_2Cl_2 (10 mL) was added phenylselenenyl chloride (500 mg, 2.6 mmol) and the mixture was filtered to give N-PSP reagent (0.26 *M*) as a colorless solution.

To a stirred solution of **22** (39 mg, 0.13 mmol) and TsOH (10 mg, 0.05 mmol) in CH_2Cl_2 saturated with water (20 mL) was added the N-PSP reagent (0.6 mL, 0.17 mmol) at room temperature. After 15 h, the reaction mixture was treated with additional N-PSP reagent (1.0 mL, 0.26 mmol) and the mixture was stirred for a total of 84 h at

Can. J. Chem. Downloaded from www.nrcresearchpress.com by 80.58.250.72 on 09/07/12
For personal use only.

room temperature. The resulting solution was diluted with Et_2O and washed with aqueous NaOH solution. Standard work-up followed by chromatography (silica gel, 30% EtOAc–hexane eluent) gave 52 mg (85%) of **23** as a yellow-brown solid; ir ($CHCl_3$) ν_{max}: 3504, 1664 cm^{-1}; ^1H nmr δ: 1.31 (3H, d, J = 6 Hz), 2.60–3.10 (3H, m), 3.87 (1H, br t), 4.05 (3H, s), 4.84 (1H, d, J = 4 Hz, exchangeable with D_2O), 5.34 (1H, dd, J = 4 and 2.5 Hz, convertible into d, J = 2.5 Hz by D_2O exchange), 7.10–7.90 (9H, m), 8.21 (1H, d, J = 8 Hz).

Method b (15 b)

To a stirred solution of **22** (2.50 g, 8.22 mmol) and anhydrous sodium acetate (2.40 g, 29.3 mmol) in HOAc (50 mL) and dry CH_2Cl_2 (25 mL) was added phenylselenenyl chloride (5.26 g, 27.4 mmol) and the mixture was stirred for 4 days at room temperature. After removal of solvent, the reaction mixture was dissolved in $CHCl_3$ and the resulting solution was washed with aqueous $NaHCO_3$ solution. Standard work-up gave a reddish-yellow syrup. The crude product was treated with 10% K_2CO_3 solution (70 mL) in THF (70 mL) and MeOH (70 mL) and the whole was refluxed for 4 h. The reaction mixture was concentrated and the resulting aqueous mixture was extracted with $CHCl_3$. Standard work-up followed by chromatography (alumina; 35% EtOAc–hexane eluent) gave 3.50 g (89%) of a yellow solid, which was identified as **23** by comparison of ir and ^1H nmr spectra and tlc with the product obtained by Method a).

X-14881 C (2c)

A mixture of **23** (945 mg, 1.98 mmol) and Cornforth's reagent (25) (5 mL), prepared as described in the synthesis of **19***b*, in pyridine (15 mL) was stirred for 18 h at room temperature. *i*-PrOH (1 mL) was added and the mixture was concentrated. The residue was treated with $CHCl_3$ and the resulting mixture was subjected to filtration. The filtrate was washed with dilute HCl. Standard work-up and chromatography (alumina, $CHCl_3$ eluent) gave 682 mg (72%) of the ketoselenide as a yellow solid; ir ($CHCl_3$) ν_{max}: 1697, 1667 cm^{-1}.

A solution of the ketoselenide (640 mg, 1.35 mmol), triphenyltin hydride (1.46 g, 4.15 mmol), and azobisisobutyronitrile (8 mg) in dry benzene (50 mL) was refluxed for 1 day under argon. The reaction mixture was concentrated to half of the initial volume and chromatographed (alumina, 20% EtOAc–hexane eluent) to give 27 mg (7%) of **22**, identical by ir and ^1H nmr comparison with material obtained above.

Elution (35% EtOAc–hexane) gave 288 mg (67%) of X-14881 (**2***c*). Crystallization ($CHCl_3$–MeOH) gave orange needles, mp 236–237°C (lit. (2*e*) mp 235°C (dec.)), which was shown to be identical with an authentic sample by comparison of ir, ^1H nmr, uv, and mass spectra provided by Dr. H. Maehr.

Further elution (30% $CHCl_3$–EtOAc) gave 147 mg (23%) of the starting ketoselenide as a yellow solid.

Ochromycinone (2 d)

A mixture of **2***c* (74 mg, 0.23 mmol) and anhydrous $AlCl_3$ (307 mg, 2.30 mmol) in dry CH_2Cl_2 (35 mL) was stirred for 4 h at room temperature. Ice-water was added and the mixture was extracted with $CHCl_3$. Standard work-up followed by chromatography (silica gel, $CHCl_3$ eluent) gave 70 mg (99%) of *ochromycinone* (**2***d*). Crystallization (MeOH) gave yellow prisms, mp 168–169°C (lit. (20) mp 152–153°C),[3] shown to be identical with natural ochromycinone by comparison of its ir, ^1H nmr, and uv spectra with those provided by Prof. J. H. Bowie.

Ochromycinone acetate (2e)

To an ice-cooled solution of **2***d* (73 mg, 0.24 mmol) in dry pyridine (10 mL) was added Ac_2O (3 mL) and the mixture was stirred overnight at room temperature. The reaction mixture was concentrated and the residue was dissolved in $CHCl_3$. Standard work-up gave 82 mg (99%) of **2***e*. Crystallization (EtOAc) afforded yellow prisms, mp 175–176°C (J. H. Bowie, personal communication, mp 170.5–171.5°C); ir (KBr) ν_{max}: 1768, 1708, 1672 cm^{-1}; ^1H nmr δ: 1.20 (3H, d, J = 5.5 Hz), 2.48 (3H, s), 2.50–3.10 (5H, m), 7.37 (1H, dd, J = 1.5 and 8 Hz), 7.51 (1H, d, J = 8 Hz), 7.78 (1H, t, J = 8 Hz), 8.11 (1H, dd, J = 1.5 and 8 Hz), 8.21 (1H, d, J = 8 Hz); ms m/e (rel. intensity): 348 (4, M^+), 306 (77), 263 (100).

Compound **2***e* was shown to be identical by ir and uv comparison, and by mixture mp determination with an authentic sample of ochramycinone acetate provided by Prof. J. H. Bowie.

[3]The mp discrepancies are probably due to impurities present in the originally isolated ochromycinone: J. H. Bowie, personal communication, March 13, 1984.

Acknowledgements

We gratefully acknowledge the financial support of NSERC Canada and Merck Frosst Canada. We thank E. G. Doadt for experimental work, which pointed the way towards the successful synthesis; Dr. M. Uemura, Osaka City University for a preprint of ref. 5 and beneficial discussion; and Dr. H. Maehr for spectral data of X-14881 C. Prof. J. H. Bowie kindly provided spectral data of ochromycinone, a sample of ochromycinone acetate, and much encouragement.

1. K. Katsuura and V. Snieckus. Tetrahedron Lett. 9, (1985).
2. (*a*) R. H. Thomson. Naturally occurring quinones. 2nd ed. Academic Press, New York, 1971. p. 648 ff; (*b*) W.-C. Liu, W. L. Parker, D. S. Slusarchyk, G. L. Greenwood, S. F. Graham, and E. Meyers. J. Antibiot. **23**, 437 (1970); (*c*) M. Sezaki, S. Kondo, K. Maeda, H. Umezawa, and M. Ohno. Tetrahedron, **26**, 5171 (1970); (*d*) N. Imamura, K. Kakinuma, N. Ikekawa, H. Tanaka, and S. Omura. J. Antibiot. **35**, 602 (1982); (*e*) H. Maehr, C.-M. Liu, A. Perrotta, J. M. Smallheer, T. H. Williams, and J. F. Blout. J. Antibiot. **35**, 1627 (1982); (*f*) J. F. Blout, D. N. Greenley, H. Maehr, A. Perrotta, R. G. Pitcher, L. Todaro, and T. H. Williams. J. Antibiot. **38**, 1270 (1985); (*g*) R. W. Richards and J.-P. Wu. J. Antibiot. **38**, 513 (1985); (*h*) Y. Hayakawa, T. Iwakiri, K. Imamura, H. Seto, and N. Otake. J. Antibiot. **38**, 957 (1985); **38**, 960 (1985); (*i*) T. Uchida, M. Imoto, Y. Watanabe, K. Miura, T. Dobashi, N. Matsuda, T. Sawa, H. Naganawa, M. Hamada, T. Takeuchi, and H. Umezawa. J. Antibiot. **38**, 1171 (1985).
3. F. Arcamone. Doxorubicin. Academic Press, New York. 1981; S. T. Crooke and S. D. Reich. Anthracyclines: current status and new developments. Academic Press, New York. 1980.
4. P. M. Brown and R. H. Thomson. J. Chem. Soc. Perkin Trans. 1, 2149 (1976).
5. M. Uemura, K. Take, and Y. Hayashi. J. Chem. Soc. Chem. Commun. 858 (1983); M. Uemura, K. Take, K. Isobe, T. Minami, and Y. Hayashi. Tetrahedron, **41**, 5571 (1985).
6. M. Uemura, N. Nishikawa, K. Take, M. Ohnishi, K. Hirotsu, T. Higuchi, and Y. Hayashi. J. Org. Chem. **48**, 2349 (1983), and references cited therein.
7. S. O. de Silva, M. Watanabe, and V. Snieckus. J. Org. Chem. **44**, 4802 (1979).
8. V. Snieckus. J. Heterocycl. Chem. Suppl. 95 (1984).
9. S. Mitsui, A. Kasahara, and K. Hanaya. Bull. Chem. Soc. Jpn. **41**, 2526 (1968), and references cited therein.
10. N. Meyer and D. Seebach. Chem. Ber. **113**, 1304 (1980).
11. S. O. de Silva, J. N. Reed, and V. Snieckus. Tetrahedron Lett. 5099 (1978).
12. R. H. Thomson. *In* The chemistry of the quinonoid compounds. Part 1. *Edited by* S. Patai. Wiley, New York, 1974. p. 136; M. S. Newman. Acc. Chem. Res. **5**, 354 (1972).
13. Y. Sprinzak. J. Am. Chem. Soc. **80**, 5449 (1958).
14. H. C. Brown and P. Geoghegan, Jr. J. Org. Chem. **35**, 1844 (1970).
15. (*a*) K. C. Nicolaou, D. A. Claremon, W. E. Barnette, and S. P. Seitz. J. Am. Chem. Soc. **101**, 3704 (1979); (*b*) D. L. J. Clive, G. Chittattu, and C. K. Wong. J. Chem. Soc. Chem.

Commun. 441 (1978); (*c*) K. C. NICOLAU, N. A. PETASIS, and D. A. CLAREMON. Tetrahedron, **41**, 4835 (1985).
16. D. LIOTTA. Acc. Chem. Res. **17**, 28 (1984).
17. D. LIOTTA, G. ZIMA, and M. SAINDANE. J. Org. Chem. **47**, 1258 (1982).
18. M. ZERROS, L. WARTSKI, N. GOASDOUE, and N. PLATZER. J. Org. Chem. **51**, 1293 (1986).
19. D. L. J. CLIVE, G. J. CHITTATTU, V. FARINA, W. A. KIEL, S. M. MENCHEN, C. G. RUSSELL, A. SINGH, C. K. WONG, and N. J. CURTIS. J. Am. Chem. Soc. **102**, 4438 (1980).
20. J. H. BOWIE and A. W. JOHNSON. Tetrahedron Lett. 1449 (1967).
21. J. N. REED and V. SNIECKUS. Tetrahedron Lett. 5505 (1984); M. P. SIBI, S. CHATTOPADHYAY, J. W. DANKWARDT, and V. SNIECKUS. J. Am. Chem. Soc. **107**, 6312 (1985).
22. S. ABE and T. YASUKAWA. Yuki Gosei Kagaku Kyokai Shi, **22**, 209 (1964).
23. J. VEBREL and R. CARRIÉ. Bull. Soc. Chim. Fr. II, 116 (1982).
24. W. E. BACHMANN and W. S. STRUVE. J. Am. Chem. Soc. **62**, 1618 (1940).
25. R. H. CORNFORTH, J. W. CORNFORTH, and G. POPJAK. Tetrahedron, **18**, 1351 (1962).

Can. J. Chem. Downloaded from www.nrcresearchpress.com by 80.58.250.72 on 09/07/12
For personal use only.

The Michael adduct of L-ascorbic acid to methyl vinyl ketone: its remarkable self-condensation and other reactions

REGINA ARNOLD AND GABOR FODOR[1]
Department of Chemistry, West Virginia University, Morgantown, WV 26506, U.S.A.

AND

CLIFFORD GEORGE AND ISABELLA KARLE
Laboratory for the Structure of Matter, Naval Research Laboratory, Washington, DC 20375, U.S.A.

Received May 28, 1986

This paper is dedicated to Dr. O. E. (Ted) Edwards

REGINA ARNOLD, GABOR FODOR, CLIFFORD GEORGE, and ISABELLA KARLE. Can. J. Chem. **65**, 131 (1987).

The structure of the Michael adduct of L-ascorbic acid (**1**) to methyl vinyl ketone was established as 2-(3-oxobutyl)-3-oxo-L-gulonolactone⟨3,6⟩hemiketal (**3**). In aqueous solution **3** is prone to undergo base- or acid-promoted degradations. 1-(2-Furyl)-1,4-pentanedione was isolated from the acidic product mixture. Under strictly anhydrous acid-catalyzed conditions, if a suitable nucleophile like ethanol is present, the tricyclic ethyl ketal **6***b* forms. In the absence of a nucleophile, the unexpected self-condensation of **3** occurs leading to cyclo-trimer **7**, the structure of which was established by X-ray crystallography. Trimer **7**, held together via ketal bridges, is converted quantitatively into the tricyclic methyl ketal **6***a* in methanolic hydrogen chloride. Mechanisms are proposed for the formation of **6***a* and *b* or **7**.

REGINA ARNOLD, GABOR FODOR, CLIFFORD GEORGE et ISABELLA KARLE. Can. J. Chem. **65**, 131 (1987).

On a établi que le produit d'addition de Michael de l'acide L-ascorbique (**1**) sur la méthyl vinyl cétone est le (oxo-3 butyl)-2 oxo-3 L-gulonolactone⟨3,6⟩hémicétal (**3**). En solution aqueuse, le composé **3** est sujet à subir des dégradations sous l'influence tant des acides que des bases. On a isolé la (furyl-2)-1 pentanedione-2,4 du mélange des produits obtenus en milieu acide. En milieu acide strictement anhydre et en présence d'un nucléophile approprié, comme l'éthanol, il se forme l'éthyl cétal tricyclique **6***b*. En l'absence d'un nucléophile, il se produit une auto-condensation surprenante du composé **3** qui conduit au cyclo-trimère **7** dont la structure a été établie par diffraction des rayons-X. Sous l'influence du chlorure d'hydrogène en milieu méthanolique, le trimère **7**, qui est retenu ensemble par des ponts cétals, se transforme quantitativement en méthyl cétal tricyclique **6***a*. On propose des mécanismes pour la formation des composés **6***a* et *b* ou du composé **7**.

[Traduit par la revue]

Introduction

L-Ascorbic acid (**1**) has been found recently to act as a Michael carbanion donor towards α,β-unsaturated aldehydes and ketones (1). The reaction with acrolein leads to the tricyclic hemiacetal lactone **2**. The homologous aldehydes methacrolein

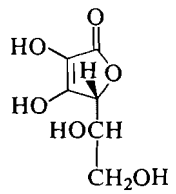

1

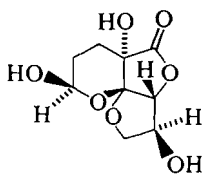

2

and crotonaldehyde likewise give tricyclic adducts (2). In contrast, addition of **1** to methyl vinyl ketone yields the bicyclic lactone **3**. More recently the list of Michael acceptors has been extended to include cyclic enones and also benzoquinone monoepoxide (3).

The L-ascorbic acid – methyl vinyl ketone adduct 2-(3-oxobutyl)-3-oxo-L-gulonolactone⟨3,6⟩hemiketal (**3**) attracted our attention early because of its potential synthetic utility as a chiral intermediate. The tautomer of **3**, namely the monocyclic diketo lactone **4**, appeared to be set up for an intramolecular aldol condensation in a Robinson annulation sequence.

Although there was no spectral evidence that **4** is present in neutral solution, its transient existence under base- or acid-catalyzed conditions was envisaged. This working hypothesis prompted us to expose adduct **3** to various reaction conditions.

[1]Author to whom correspondence may be addressed.

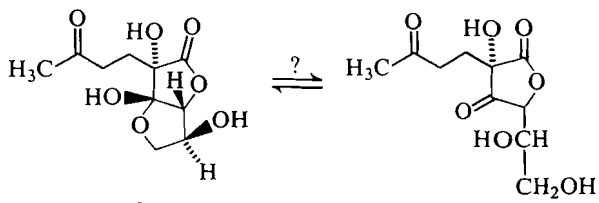

3 **4**

It soon became clear that the idea of using **3** in a Robinson annulation had to be abandoned. In return, however, we learned what conditions promote the degradation of **3**, and we discovered that **3** can undergo a remarkable self-condensation (preliminary paper, ref. 4). These and other aspects of the chemistry of **3** will be the subject of this paper.

Results and discussion

Adduct **3** is a hydrophilic molecule and therefore readily soluble in protic solvents. One of our first findings was that in such an environment bases as well as acids promote the degradation of **3**. In 1% ethanolic potassium hydroxide the lactone opens up to the carboxylic acid, which is subsequently decarboxylated. This degradation was proven by the spectral evidence that the products had lost the lactone functionality. Degradation of the structurally related 2-*C*-benzyl ascorbic acid was reported earlier (5).

The acid-promoted degradation was studied in more detail. Thus it was shown that **3** decarboxylates in dilute hydrochloric acid; the reaction proceeds rapidly on heating to 80°C. One neutral component, 1-(2-furyl)-1,4-pentanedione (**5**) was isolated. Its ir and nmr characteristics were in accord with literature values for **5** reported by Severin and König (6). The pathway

Can. J. Chem. Downloaded from www.nrcresearchpress.com by 190.90.36.8 on 09/07/12
For personal use only.

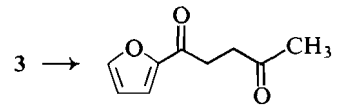

5

from **3** to **5** can be rationalized by a straightforward mechanism (2). Our results are in line with the known degradation of piptosidin (*7a*), a natural product that is structurally similar to **3**. Also, the slow spontaneous degradation of **3** in aqueous solution should be mentioned. Compound **5** was shown (by tlc) to be present in an "aged" solution of **3**.

No ascorbic acid (**1**) was detected in these experiments, proving that the Michael addition of **1** to methyl vinyl ketone is not reversible, unlike the formation of ascorbigen by C-2 alkylation of **1** with 3-(hydroxymethyl)-indole (8).

The impact of catalytic amounts of acids in an anhydrous medium was studied next. We found that the lactone ring of **3** remains intact, but two unexpected condensation reactions occur. None of the transformations that are to be described involve tautomer **4**. Therefore the existence of **4** as a reactive intermediate was ruled out.

When compound **3** and a trace of *p*-toluenesulfonic acid were refluxed in a benzene–ethanol mixture under strictly anhydrous conditions (azeotropic removal of water), a crystalline product was isolated from the reaction mixture, namely the tricyclic ethyl ketal **6***b*. The methyl ketal **6***a* had been prepared earlier (1) when **3** was exposed to glycosidation conditions, i.e., 2% methanolic hydrogen chloride. One should rationalize why methyl or ethyl ketal formation at C-3 of adduct **3** is not observed. This ketalization would require a puckered bridgehead carbonium ion at the transition state. In contrast, the carbonyl group in the 3-oxobutyl side chain is less restricted to participate in mixed ketalization. However, methyl glycoside formation at C-3 has been reported for R = benzyl (5) and R = skatyl (3-methylindolyl) (8), where intramolecular ketalization with the substituent at C-2 is excluded.

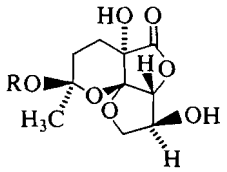

6*a*, R = CH_3
6*b*, R = C_2H_5

The mechanism for the formation of the tricyclic ethyl ketal **6***b* involves continuous removal of water, which shifts the overall reaction irreversibly towards the C-3′ carbonium ion, which is then captured by an intramolecular stereospecific attack of the C-3 hemiketal hydroxyl upon one face of the planar ion at C-3′. We did not observe the formation of diastereoisomers of either **6***a* or **6***b*.

The intramolecular ketalization depends upon the presence of a reactive nucleophile. Therefore it was deemed of interest to study the behavior of **3** with no external nucleophile present. Upon refluxing a suspension of **3** in benzene under anhydrous conditions in the presence of an acid catalyst, a crystalline product formed. It was practically insoluble in all common solvents except methylene chloride. In further experiments methylene chloride was used as the solvent of choice.

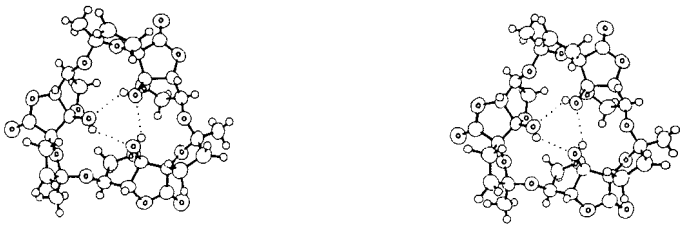

FIG. 1. Stereodiagram of **7** from experimental coordinates determined by X-ray diffraction. Thermal ellipsoids enclose 50% probability.

The spectral and chemical properties of the new compound were controversial. The ir spectrum showed only one carbonyl band at a position (1800 cm^{-1}) that is unusually high for a lactone absorption. The keto carbonyl, present in **3**, disappeared. Several osmometric molecular weight determinations gave high (≥500) but inconsistent values. Therefore the possibility of an intermolecular reaction had to be considered. However, the mass spectrum showed no M^+ peak in that order of magnitude (highest peak: *m/e* 228). Furthermore, the ^{13}C nmr spectrum showed ten resonances; hence the number of carbons of **3** was preserved. The chemical shifts also indicated that the skeleton of **3** did not undergo a drastic structural change. The ^1H nmr spectrum (60 MHz) confirmed a methyl singlet at δ 1.65, a singlet at δ 4.50, comparable to the C-4 proton in **3**, and only one hydroxyl proton resonance. Unlike results for compound **3**, resonances of uncertain multiplicities were found up- and downfield of the C-4 proton singlet. The data suggested, however, that the unknown compound was a symmetrical oligomer.

X-ray analysis revealed a highly symmetrical crown-like structure (Fig. 1). This remarkable macrocycle **7**, itself com-

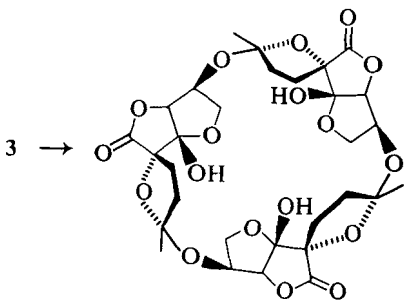

7

posed of nine rings, is the product of a self-condensation of **3**. Now the ten peaks in the proton decoupled ^{13}C nmr spectrum were readily assigned (Fig. 2). The highest peak in the mass spectrum corresponds to the M^+ peak of the monomeric unit of **7**. We were able to obtain a high resolution (600 MHz) ^1H nmr spectrum of **7**, the downfield portion of which clearly shows the coupling pattern of the C-4, C-5, and C-6 protons (Fig. 3). The geminal protons H-6 and H-6′ are separated by 1.0 ppm, because H-6′ is deshielded by the tetrahydrofuryl oxygen of the adjacent monomeric unit. This "through space" effect reflects the spatial arrangement of the nine rings and the overall conformational rigidity of **7**. The integrated intensity of the C-4 proton was consistently less than expected. A small increase in the height of the singlet was observed when one of the C-2′ protons was selectively irradiated. These observations suggest a nuclear Overhauser effect (nOe). However, the percentage of intensity increase was not determined. Scale models show that

Can. J. Chem. Downloaded from www.nrcresearchpress.com by 190.90.36.8 on 09/07/12
For personal use only.

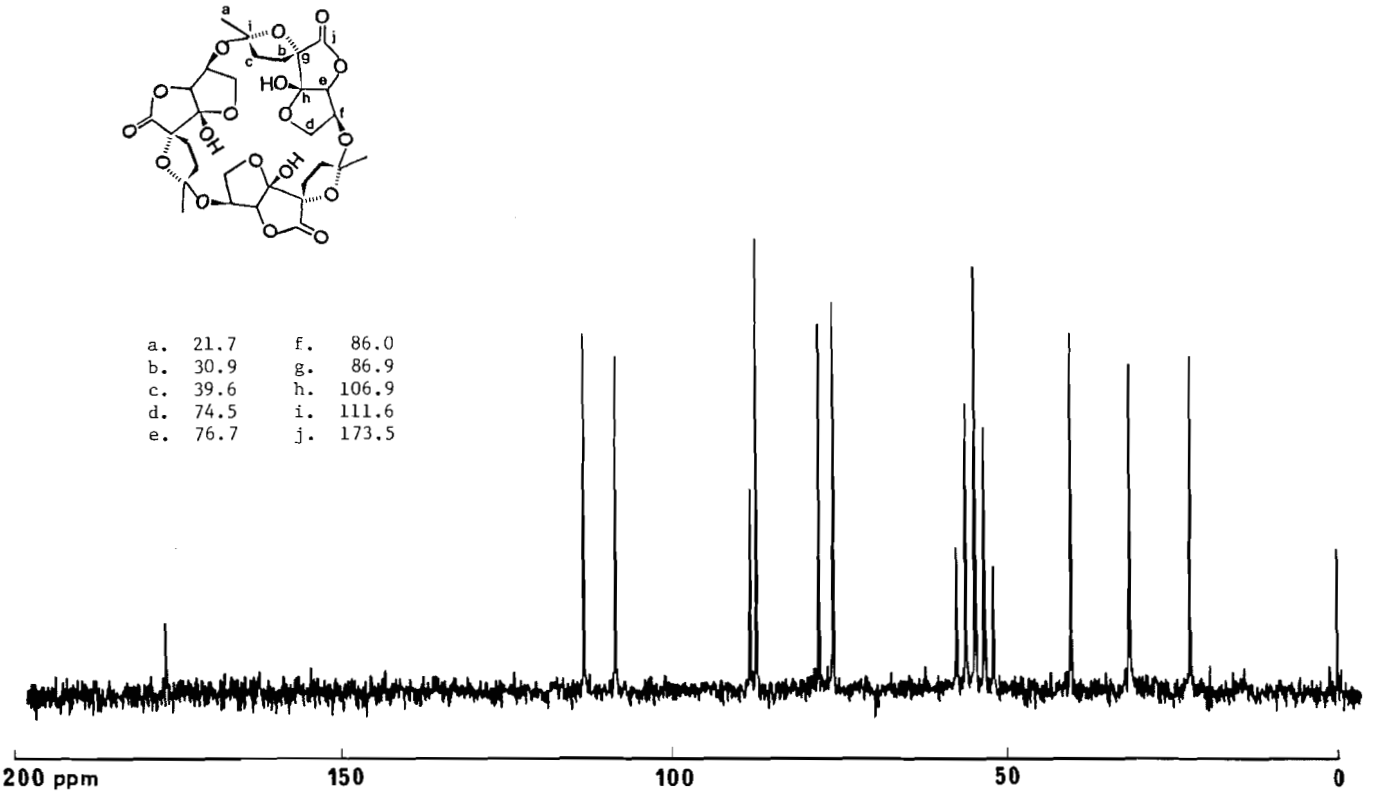

FIG. 2. Proton decoupled ^{13}C nmr spectrum of trimer **7** in CD_2Cl_2.

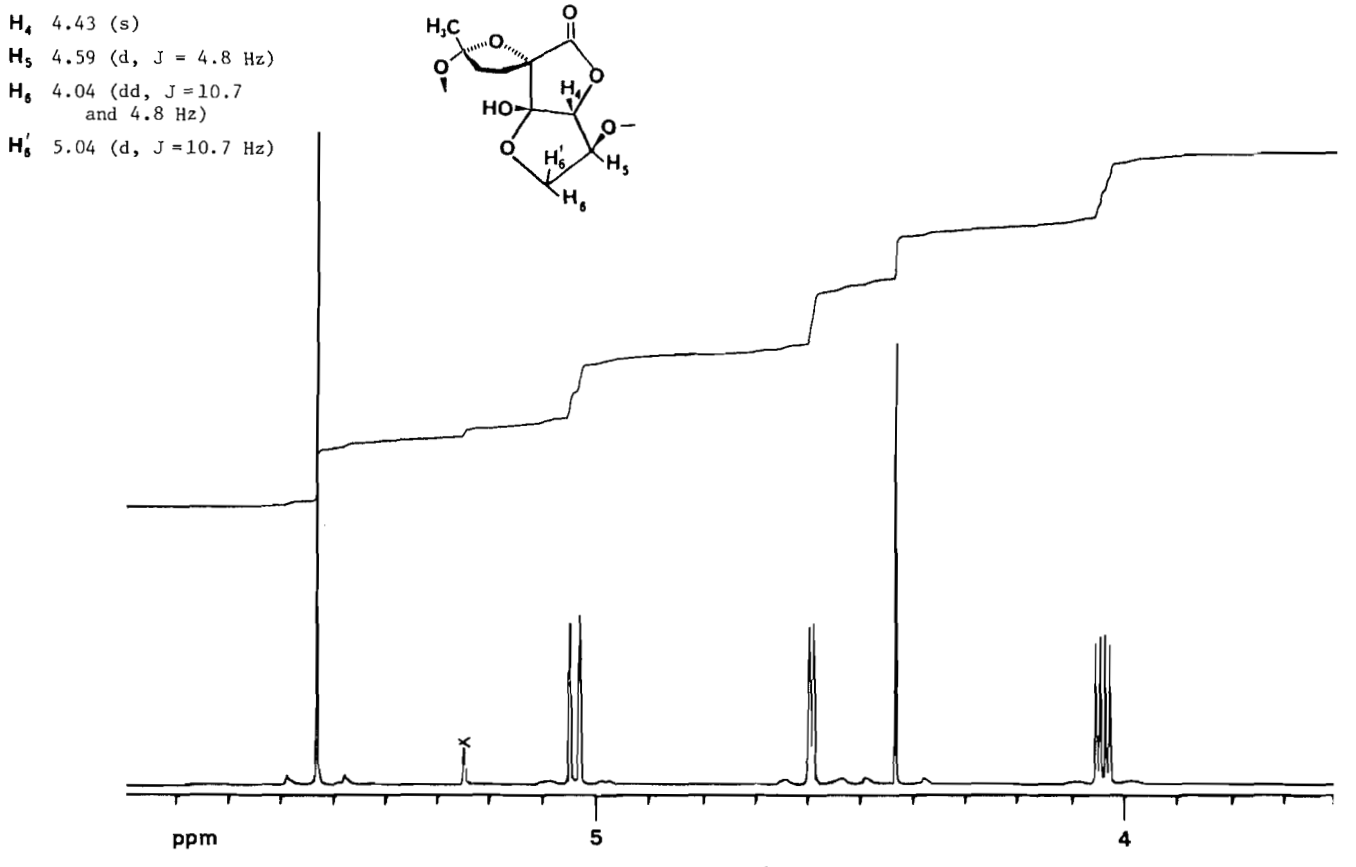

FIG. 3. Downfield portion of the 600-MHz ^1H nmr spectrum of trimer **7**.

Can. J. Chem. Downloaded from www.nrcresearchpress.com by 190.90.36.8 on 09/07/12
For personal use only.

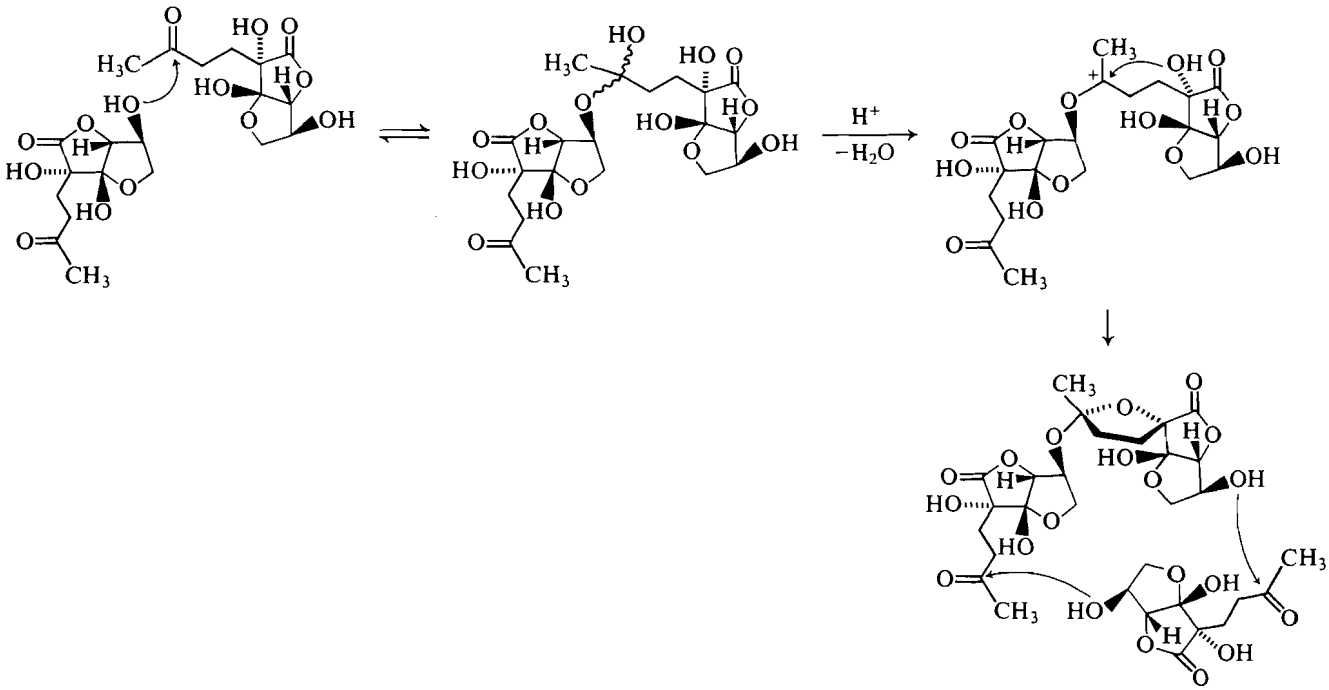

SCHEME 1

the protons in question are very closely situated, a prerequisite for the nOe.

The self-condensation (cyclo-trimerization) of **3** occurs almost quantitatively. Yields of 90% were reproducible with no polymeric by-products. The solvent dependency was demonstrated when ketolactone **3** failed to trimerize in anhydrous tetrahydrofuran under comparable conditions (acid catalysis, reflux, presence of molecular sieves 4Å to remove water if formed). Thus only anhydrous aprotic solvents that are unable to participate in hydrogen bonding to the hydroxyls of **3** promote this self-condensation.

Any reaction mechanism for **7** should be viewed under the premise that the solvent prompts the hydrophilic monomer as well as oligomeric intermediates to "curl up" during the reaction sequence. Thereby the spatial prerequisite for the successful cyclo-trimerization of **3** can be achieved. As a first step, reversible hemiketal formation may occur intramolecularly with either the C-2 or the C-3 hydroxyl, or intermolecularly with the C-5 hydroxyl of another molecule of **3**. We propose in Scheme 1 that the latter hemiketal is preferentially and irreversibly dehydrated, thus linking two molecules of **3**. An intramolecular reaction involving the C-3 hydroxyl appears to be prevented on steric grounds. This view was supported by examining a Dreiding model of the assumed dimeric carbonium ion intermediate. The C-2 hydroxyl, however, can approach the carbonium ion without steric restrictions. The intramolecular ketalization has to be stereospecific, for only the "right" configuration at the ketal carbon allows the self-condensation to proceed and ultimately leads to the cyclo-trimer **7**. In keeping with the carbohydrate derived name for the parent molecule **3**, we chose the following name for trimer **7**: tris⟨3′,5⟩ketal of 2-(3′-oxobutyl)-3-oxo-L-gulonolactone⟨2,3′⟩hemiketal⟨3,6⟩hemiketal.

A drawback of this nomenclature is that the spiro junction of **7** is not mentioned explicitly. The atom numbering scheme used in the discussion of the X-ray analysis is somewhat different to avoid ambiguities. As for the spiro junction, piptosidin, a spirodilactone (*7a,b*), attracted our attention, since its skeleton is strikingly similar to the monomeric unit of **7**.

The trimer **7** is held together via ketal bridges. For that reason, the otherwise very stable substance was expected to be sensitive to acid. Furthermore, if our mechanistic ideas are correct, the acid-catalyzed breakdown of **7** should lead, in the presence of a nucleophile, to the respective tricyclic ketal (**6**). We found that transketalization in methanolic hydrogen chloride yields the methyl ketal **6***a* quantitatively.

The cyclo-trimer **7** is a lipophilic molecule but the three inwardly oriented hydroxyls should render the cavity hydrophilic. Crown ethers exhibit comparable features, although on a simpler structural level. It was an intriguing thought to use **7** as a macrocyclic ligand for metal ions. Initial experiments designed to probe the idea gave only negative results.

The Dreiding model of **7** is somewhat misleading with respect to the size of the cavity in the macrocycle, because the model is conformationally flexible. The X-ray structure analysis revealed after the final refinement that the hydroxyl hydrogens participate in hydrogen bonding within the trimer. As a result, the molecule is locked into one conformation in which the oxygens of the three hydroxyls occupy fixed position at the corners of an equilateral triangle (2.76(1) Å). In this conformation there is no cavity that could accommodate a guest cation.

Experimental

Melting points were determined on a Electrothermal melting point apparatus and are uncorrected.

Infrared spectra were recorded on a Beckman IR 10 or IR 8 spectrometer. For measurements in solution a pair of matched cells (NaCl) with a pathlength of 0.11 mm was used.

The ^{1}H nmr spectra were recorded on a Varian EM-360 (60 MHz) spectrometer or on a Varian CFT-20 spectrometer equipped with a proton probe at 80 MHz. The 600-MHz nmr data were obtained at the Carnegie–Mellon NMR Center for Biomedical Studies in Pittsburgh. Tetramethylsilane was used as internal standard. The ^{13}C nmr spectra were taken on a Varian CFT-20 spectrometer at 20 MHz. For deuterium oxide as a solvent, *p*-dioxane was the internal standard.

Can. J. Chem. Downloaded from www.nrcresearchpress.com by 190.90.36.8 on 09/07/12
For personal use only.

Can. J. Chem. Downloaded from www.nrcresearchpress.com by 190.90.36.8 on 09/07/12
For personal use only.

A Perkin–Elmer Model 141 M polarimeter was used for the optical rotation measurements.

Mass spectra were obtained on a Finnigan 4021 mass spectrometer with an INCOS data system. The ionizing voltage was 70 eV unless otherwise indicated.

Elemental analyses and osmometric molecular weight determinations were performed by Galbraith Laboratories, Inc., Knoxville, Tennessee.

2-(3-Oxobutyl)-3-oxo-L-gulonolactone⟨3,6⟩hemiketal (**3**) was prepared following the published procedure (1). Benzene was dried by distillation from sodium metal. The 2% w/v methanolic hydrogen chloride solution was prepared by passing dry hydrogen chloride gas through methanol that had been dried by treatment with magnesium metal, and subsequent distillation. The acid content was determined by titration with a standard 0.10 *M* sodium hydroxide solution.

Degradation of compound **3** *in acidic medium. Isolation of 1-(2-furyl)-1,4-pentanedione (***5***)*

A solution of 1.1 g (4.5 mmol) of adduct **3** in 100 mL 1 *M* hydrochloric acid was prepared in a flask fitted with a thermometer and an adapter for gas outlet. The solution was stirred and slowly heated to 80°C, while the evolving carbon dioxide was collected in a graduated cylinder. After 40 min the desired temperature was reached and the expected gas volume (110 mL) had been collected. The distinctly yellow solution was allowed to cool to room temperature and extracted with chloroform (2 × 40 mL). Thin-layer chromatography (tlc) (silica, ethyl acetate) revealed at least three unresolved components of R_f's <0.31 and one component of R_f 0.59. The combined extracts were shaken with 5 mL of 0.5 *M* sodium hydroxide solution and subsequently washed with 20 mL water. The basic aqueous layer turned bright yellow at first, then became brown, and was discarded. The almost colorless chloroform solution was dried ($MgSO_4$) and checked by tlc. Only the component of R_f 0.59 (silica, ethyl acetate) was present. After removal of chloroform the residue, a yellow mobile oil, was kept *in vacuo* for several hours. The oily product (208 mg, 28%) was identified as 1-(2-furyl)-1,4-pentanedione (**5**); ir (in $CHCl_3$): 1720 (s, C=O), 1680 (vs, furoyl C=O) cm^{-1}; ^1H nmr ($CDCl_3$, 80 MHz) δ: 2.21 (s, 3H), 2.98 (m, A_2B_2 system, 4H), 6.53 (dd, 1H), 7.21 (d, $J \simeq$ 4 Hz, 1H), 7.58 (unresolved d, 1H); ^{13}C nmr ($CDCl_3$): 29.9, 32.1, 36.7, 112.2, 117.0, 146.4, 152.5, 187.7, and 206.9 ppm.

These spectral characteristics are in agreement with data reported in the literature (6).

Preparation of the tricyclic ethyl ketal lactone **6**b

To 4 g (16.3 mmol) of adduct **3** a mixture of dry benzene (90 mL) and absolute ethanol (30 mL) was added, together with a catalytic amount of *p*-toluenesulfonic acid. The flask was equipped with a Dean and Stark moisture test receiver allowing the continuous removal of water. The suspension was stirred and heated to reflux, whereupon the solid dissolved. After 12 h at reflux the pale yellow reaction mixture was cooled to room temperature before the solvents were evaporated. The residue, a yellow viscous liquid, was stirred vigorously, while the flask was immersed in an ice bath until a crystalline solid precipitated. After being kept in the cold for several hours the crystalline mass was diluted with dry benzene, the crystals were filtered off, washed with a small amount of cold absolute ethanol, and dried *in vacuo* at 78°C. First crop: 1.1 g of pure **6***b*. The mother liquor was concentrated and subjected to the same work-up sequence three more times. The combined crops afforded 3 g (67%) of ethyl ketal **6***b*. Recrystallization from ethyl acetate gave large transparent prisms and plates; mp 145–147°C; $[\alpha]_D^{25}$ +53.9 ± 0.3° (*c* 1, methanol); ir (KBr): 3500 (s, sh, O—H), 3330 (s, O—H), 3000–2950 (m, C—H), 1730 (vs, lactone C=O) cm^{-1}; ir (1.5% w/w in $CHCl_3$): ~3500 (m, br, O—H), 3000–2900 (m, C—H), 1730 (vs, sh, lactone C=O) cm^{-1}; ^1H nmr (DMSO-d_6, 60 MHz) δ: 1.24 (t, 3H), 1.40 (s, 3H), 1.5–2.3 (m, 4H), 3.7–4.4 (q and m, 5H), 4.43 (s, ~1H); D_2O exchangeable resonances: δ 5.35 (b, d, 1H) and 5.75 (s, 1H); ^{13}C nmr (D_2O): 14.2, 23.4, 31.2, 35.2, 63.6, 73.1, 75.5, 77.6, 86.6, 112.8, 114.9, and 173.3 ppm; ^{13}C nmr (DMSO-d_6): 13.9, 23.7, 31.1, 34.9, 60.4, 71.9, 74.8, 76.3, 85.8, 110.0, 114.1, and 171.2 ppm; ms (20 eV) *m/e*: 274 (M^+ peak), 246, 213, 186, 173, 158, 141, 113, 99, 85, and 59 (base peak). *Anal.* calcd. for $C_{12}H_{18}O_7$: C 52.55, H 6.57, O 40.88; found: C 52.63, H 6.70, O 40.61.

*Self-condensation of 2-(3-oxobutyl)-3-oxo-L-gulonolactone⟨3,6⟩hemiketal (***3***)*

Adduct **3** (2 g, 8.1 mmol) was suspended in 100 mL methylene chloride in a flask equipped with a moisture test receiver (recycle type). To prevent reentry of water traces during recycling of the solvent the receiver was charged with molecular sieves 4Å. A catalytic amount (15–25 mg) of *p*-toluenesulfonic acid was added; the suspension was stirred and heated to reflux. After about 7 h the reaction mixture had become homogeneous. The pale yellow solution was allowed to cool to room temperature and evaporated to dryness. The residue, a crystalline yellowish solid, was suspended in 30 mL cold 95% ethanol and stirred vigorously (~30 min). The white crystals were filtered and dried *in vacuo* at 78°C. Cyclo-trimer **7** (1.67 g, 90%) was obtained. Recrystallization from methylene chloride gave small white needles. Recrystallization from methylene chloride with a trace of absolute ethanol afforded long transparent needles, among which were single crystals suitable for X-ray analysis, mp 240–242°C dec. (sealed capillary tube); $[\alpha]_D^{25}$ +57.1 ± 0.3° (*c* 0.5, methylene chloride); ir (KBr): 3400 (s, O—H), 2980–2860 (w, C—H), 1800 (vs, lactone C=O) cm^{-1}; ^1H nmr (CD_2Cl_2, 600 MHz) δ: 1.58 (s, 9H), 1.98 (m, 6H), 2.15 (m, 3H), 2.68 (m, 3H), 4.04 (dd, J = 10.7 and 4.8 Hz, 3H), 4.43 (s, <3H), 4.59 (d, J = 4.8 Hz, 3H), 5.04 (d, J = 10.7 Hz, 3H), 5.53 (s, 3H, hydroxyl protons); ^{13}C nmr (CD_2Cl_2): 21.7, 30.9, 39.6, 74.5, 76.7, 86.0, 86.9, 106.9, 111.6, and 173.5 ppm; ms *m/e*: 228 (M^+, monomeric unit), 127, 110, 82, 71, 55, and 43 (base peak, CH_3—C≡O). Molecular weight (osmometry): 495–570. *Anal.* calcd. for $C_{30}H_{36}O_{18}$: C 52.63, H 5.26, O 42.11; found: C 52.55, H 5.50, O 41.85. *Note*: The decomposition point of **7** is not a reliable physical constant. Depending on the rate of heating and whether an open or sealed capillary was used, the decomposition was found to start as low as 228°C, or as high at 250°C.

X-Ray crystallographic analysis of compound **7** *(tris⟨3′,5⟩ketal of 2-(3′-oxobutyl)-3-oxo-L-gulonolactone⟨2,3′⟩hemiketal⟨3,6⟩hemiketal)*

A clear 0.70 × 0.12 × 0.10 mm crystal was mounted in a general orientation. Unit cell parameters were refined from 24 centered reflections ($16° < 2\theta < 54°$) on an automated diffractometer with a graphite incident beam monochromater. Crystal data are

$C_{10}H_{12}O_6$ fw 228.20

Hexagonal, space group $P6_3$ (C_6^6, No. 173), $a = b = 18.997(3)$, $c = 5.691(1)$ Å, $\gamma = 120.0°$, $V = 1778.7(6)$ Å^3, $Z = 6$, $\rho c = 1.278$ gm cm^{-3}, $\mu = 8.80$ cm^{-1}, $F(000) = 720$ (22°C; CuKα, $\lambda = 1.54178$ Å). Reflection condition $000l = 2n$.

Intensities were measured on a Nicolet R3M diffractometer in the $\theta/2\theta$ mode with scan width of $(2.0 + \Delta_{\alpha 1\alpha 2})°$. The scan rate was a function of the count rate (4°/min minimum, 30°/min maximum). The range of hkl was: $-17 \leq h \leq 20$, $-20 \leq k \leq 17$, $0 \leq l \leq 7$ with $(\sin\theta/\lambda)_{max} = 0.54$. The intensities of the 3 check reflections 210, 631, and 203 were monitored every 60 reflections and showed a maximum random variation of 3.2% over the data collection. In total, 4242 reflections were measured, 1464 unique, with 1434 observed with $|F_o| > 3\sigma|F_o|$. The value of $R_{int} = \Sigma|F - \langle F\rangle|/\Sigma F = 0.02$ from merging equivalent data. The data were corrected for Lorentz and polarization, but not for absorption, effects.

The structure was solved by direct methods (9), and refined using the program SHELXTL (10). In the "block cascade" least squares the function minimized was $\Sigma w(|F_o| - |F_c|)^2$ where $w = 1/[\sigma^2(|F_o|) + g(F_o)^2]$, and $g = 0.0003$ for this work. The 149 parameters refined include the C and O coordinates, anisotropic thermal parameters, and atom positions for the hydroxyl hydrogen. All other hydrogens were fixed in idealized positions with isotropic thermal parameters fixed at 1.1 times the value of the atom to which they are bonded. The final R values were $R = 0.042$ and $wR = 0.054$ for the 1434 independent reflections, with maximum and mean shift-to-error ratio $\Delta/\sigma = 0.32$ and 0.09, respectively. The mean error in the observation of unit

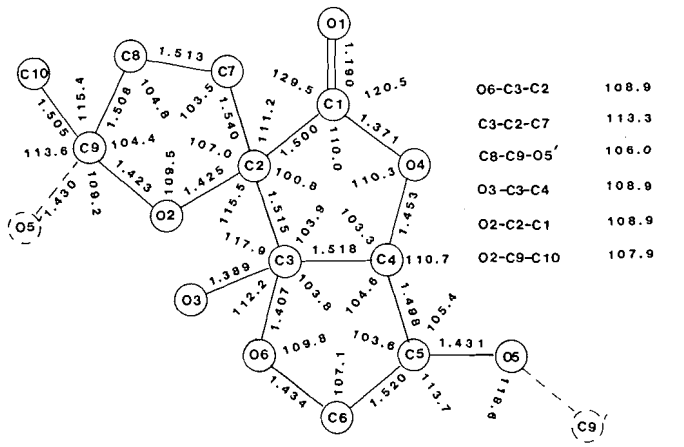

FIG. 4. Bond distances (esd's ≈ 0.004 Å) and bond angles (esd's ≈ 0.3°) for **7**.

weight was 2.02 and the final difference Fourier excursions were +0.27 and −0.34 e/Å^3.

Table 1 lists fractional coordinates for the C and O atoms as well as the equivalent isotropic thermal parameters.[2] The bond distances and angles are given in Fig. 4. The molecular geometry of the trimer is shown in the stereodiagram, Fig. 1. The asymmetric unit is linked by ketal bridges about the 3-fold axis to form a trimer with the three portions of the molecule related by symmetry operations (x, y, z), ($1.0 - y$, $1.0 + x - y$, z), and ($-x + y$, $1.0 - x$, z).

The absolute configuration of **7** is based on the chirality of L-ascorbic acid as referenced to the chiral centers of **7**. The fused lactone-furanose rings are twisted about their common bond with torsion angles C2—C3—C4—C5 = −147.5(2)° and O6—C3—C4—O4 = 82.2(2)°. This portion of the molecule has nearly the same molecular geometry as the L-ascorbic acid derivatives previously reported (1, 11): the cyclic hemiacetal of 2-(3-oxopropyl)-3-oxo-L-gulonolactone⟨3,6⟩hemiketal (**2**) and 2-(5-methyl-2-furyl)-3-oxo-L-gulonolactone⟨3,6⟩hemiketal. The respective torsion angles are −139.3(4)° and 89.8(4)° for **2**, and −140.3(4)° and 87.0(5)° for the latter. Orientation of the methyltetradydrofuryl ring at the spiro junction is described by torsion angles C(4)—C(3)—C(2)—C(7) = 85.9(3)° and C(4)—C(3)—C(2)—O(2) = 150.1(2)°.

Intermolecular contacts (trimer–trimer) in this compound are at normal van der Waals separations. The nearest approaches are H(4)--H(6B)′ = 2.26(1) Å, H(8B)--H(10B)′ = 2.39(1) Å, and O(4)--H(4)′ = 2.63(1) Å.

Within the trimer, intramolecular hydrogen bonding occurs between the hydroxyls. O(3) acts as a donor to one of its symmetry equivalents and as an acceptor from the other symmetrically equivalent hydroxyl oxygen within the trimer, as do each of the equivalent hydroxyl oxygens. The H--O and O--O distances and O--H—O angles are 2.17(4) Å, 2.76(1) Å, and 138.2(4.5)°. Near approaches within the trimer occur at H(6A)--O(2)′ = 2.56(1) Å and H(6A)--O(6)′ = 2.57(1) Å.

Atomic scattering factors are from the International Tables for X-ray Crystallography, 1974.

Preparation of the tricyclic methyl ketal ***6a*** *from the cyclo-trimer* ***7***

Trimer **7** (1.5 g, 2.2 mmol) was suspended in 120 mL anhydrous methanol that contained 2% hydrogen chloride. The suspension was stirred at room temperature in a flask fitted with a drying tube ($CaSO_4$). After 5 h a clear, colorless solution was obtained. The hydrochloric acid was neutralized with the stoichiometric amount of solid silver carbonate (8.8 g). Silver chloride was removed by suction filtration, and the filtrate was dried (Na_2SO_4). After an additional filtration with Celite the methanol was evaporated to near dryness. The residue was a clear, colorless syrup. Scratching with a glass rod induced crystallization immediately. The flask was kept in the cold for some time before the crystals were washed with a small portion of cold anhydrous ether and dried *in vacuo*. The crystalline product (mp 153–154°C) was shown to be pure methyl ketal ***6a***; yield 1.72 g (100%); ms (20 eV) m/e: 260 (M^+ peak), 232, 199, 172, 159, 141, 99, 85, and 59 (base peak).

Other spectral and chemical data of ***6a*** have been reported previously (1).

Acknowledgements

This work has been accomplished with the help of the National Foundation for Cancer Research, which supported one of us (RA) with a stipend and the West Virginia University research group with chemicals.

1. G. FODOR, R. ARNOLD, T. MOHACSI, I. KARLE, and J. FLIPPEN-ANDERSON. Tetrahedron, **39**, 2137 (1983).
2. R. ARNOLD. Dissertation, West Virginia University, Morgantown. 1984.
3. K. SUSSANGKARN and G. FODOR. Abstract ORGN 266, 191st ACS National Meeting, New York City, NY. 1986.
4. R. ARNOLD, G. FODOR, I. KARLE, and C. GEORGE. Abstract ORGN 36, 187th ACS National Meeting, St. Louis, MO. 1984.
5. K. G. A. JACKSON and J. K. N. JONES. Can. J. Chem. **43**, 450 (1965).
6. TH. SEVERIN and D. KÖNIG. Chem. Ber. **107**, 1499 (1974).
7. (*a*) N. V. RIGGS and J. D. STEVENS. Aust. J. Chem. **19**, 683 (1966); (*b*) J. B. LOWRY, J. B. MCALPINE, and N. V. RIGGS. Aust. J. Chem. **28**, 109 (1975).
8. G. KISS and H. NEUKOM. Helv. Chim. Acta, **49**, 989 (1966).
9. J. KARLE and I. L. KARLE. Acta Crystallogr. **21**, 849 (1966).
10. G. M. SHELDRICK. SHELXTL. Minicomputer programs for structure determination. University of Göttingen, West Germany. 1980.
11. G. FODOR, K. SUSSANGKARN, H. MATHELIER, R. ARNOLD, I. KARLE, and C. GEORGE. J. Org. Chem. **49**, 5064 (1984).

[2]Lists of structure factors, anisotropic thermal parameters, and hydrogen coordinates may be purchased from the Depository of Unpublished Data, CISTI, National Research Council of Canada, Ottawa, Ont., Canada K1A 0S2.

Can. J. Chem. Downloaded from www.nrcresearchpress.com by 190.90.36.8 on 09/07/12
For personal use only.

Schmidt reaction on camphor. Part I. Structure of the products[1]

NORMAN R. HUNTER,[2] M. ZAFAR KHAN,[3] AND KIRK MARAT
Department of Chemistry, University of Manitoba, Winnipeg, Man., Canada R3T 2N2
AND
OSSAMA A. L. EL-KABBANI AND LOUIS T. J. DELBAERE[4]
Department of Biochemistry, University of Saskatchewan, Saskatoon, Sask., Canada S7N 0W0

Received March 5, 1986

This paper is dedicated to Dr. O. E. (Ted) Edwards

NORMAN R. HUNTER, M. ZAFAR KHAN, KIRK MARAT, OSSAMA A. L. EL-KABBANI, and LOUIS T. J. DELBAERE. Can. J. Chem. **65**, 137 (1987).

A reinvestigation of the major product from the Schmidt reaction on camphor has led to the assignment of the structure as 1,9,9-trimethyl-3-oxo-2,8-diazabicyclo[3.3.1]nonane (**5**). The structure has been established by high-field proton and carbon-13 nuclear magnetic resonance, as well as degradation to the imine ester **4**. Confirmation of the structure of **5** was achieved by X-ray crystallography. Compound **5**, $C_{10}H_{18}N_2O$, crystallized in space group $P2_1/a$ with a = 14.934(1) Å, b = 10.973(1) Å, c = 12.341(1) Å, β = 92.0°, and Z = 8. The relatively rare *cis* amide linkage is present in the molecule. In addition to the amino amide **5**, the Schmidt reaction on camphor leads to small amounts of the tetrazole **8** and the imine nitrile **9**.

NORMAN R. HUNTER, M. ZAFAR KHAN, KIRK MARAT, OSSAMA A. L. EL-KABBANI et LOUIS T. J. DELBAERE. Can. J. Chem. **65**, 137 (1987).

Un réexamen du produit principal de la réaction de Schmidt effectuée sur le camphre a permis d'établir que sa structure est le triméthyl-1,9,9 oxo-3 diaza-2,8 bicyclo[3.3.1]nonane (**5**). On a établi cette structure en se basant sur ses spectres de rmn du ^1H et du ^{13}C ainsi que sur le fait que sa dégradation conduit à l'imine ester **4**. On a confirmé la structure **5** par diffraction des rayons-X. Le composé **5**, $C_{10}H_{18}N_2O$, cristallise dans le groupe d'espace $P2_1/a$ avec a = 14,934(1), b = 10,973(1) et c = 12,341(1) Å, β = 92,0° et Z = 8. Dans cette molécule, on retrouve une liaison amide-*cis* qui est relativement rare. En plus de l'amide aminé **5**, la réaction de Schmidt effectuée sur le camphre conduit aussi à de faibles quantités du tétrazole **8** et du nitrile aminé **9**.
[Traduit par la revue]

Introduction

Since the first report by Karl F. Schmidt (1) on the reaction of hydrazoic acid on carbonyl compounds in the presence of a mineral acid, this reaction has been carried out on a variety of organic compounds including alkenes and carbonyl compounds (2). Bridged bicyclic ketones have been studied in the Schmidt reaction. This reaction, which involves the insertion of nitrogen into the bicyclic system, yields bicyclic lactams as the major product (3). Occasionally some cleavage products are also obtained. In some cases, where excess hydrazoic acid is used, tetrazoles are also isolated. Schmidt has claimed the isolation of the tetrazole **1** in 20% yield from the reaction of hydrazoic acid on camphor (4). It has also been reported that in an attempt to prepare α-camphidone **2** by the reaction of camphor with sodium azide in the presence of concentrated sulfuric acid, less than 1% yield of **2** was obtained (5). The major product from this reaction (approximately 30%) had a mp of 178–180°C and was assigned the structure of the urea **3**.

Recently we reexamined this product using carbon-13 nuclear magnetic resonance spectroscopy. The spectrum showed a downfield absorption at 173.8 ppm, which is characteristic of an amidic carbonyl and not the carbonyl of a urea. This observation led us to reinvestigate the reaction of camphor under Schmidt reaction conditions and to reconsider the structure previously assigned to the major product.

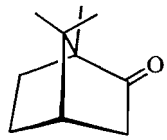

Camphor

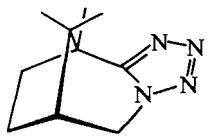

1

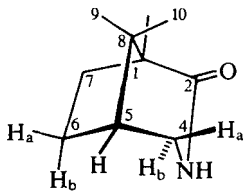

2

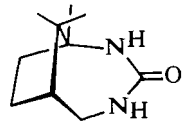

3

Results and discussion

Structure of the major product

The Schmidt reaction on camphor was carried out using two different orders of addition of reagents. Either sodium azide (2.1 equiv.) was added slowly to the rapidly stirred mixture of *dl*-camphor, chloroform, and concentrated sulfuric acid or, alternatively, concentrated sulfuric acid was added slowly to the rapidly stirred mixture of *dl*-camphor, chloroform, and sodium azide (2.1 equiv.). Identical work-up (see Experimental) gave almost the same yield of the major product regardless of the order of addition of reagents. The yield of the major product obtained over a number of trials varied from 30 to 42%. (The best conditions for this reaction are given in the experimental section.) The yields for this exothermic reaction were lowest

[1]Portions of the results presented herein have been given as preliminary communications at the 28th IUPAC Congress, Vancouver, August 1981 (Paper 0R77) and the 65th CIC Conference, Toronto, June 1982 (Paper 0R163). Taken in part from the Ph.D. Thesis of M. Zafar Khan, 1984.

[2]Author to whom correspondence regarding chemistry should be addressed.

[3]University of Manitoba Fellowship holder from September 1981 to December 1983.

[4]Author to whom correspondence regarding X-ray crystallography should be addressed.

Can. J. Chem. Downloaded from www.nrcresearchpress.com by 80.58.250.72 on 09/07/12
For personal use only.

TABLE 1. The 400-MHz ^{1}H nmr spectrum of imine ester **4** (chemical shifts in ppm relative to TMS; solvent CD_2Cl_2)

Chemical shifts	Assignments	Couplings (Hz)
0.979	C11 Me	—
1.147	C12 Me	—
1.404	H5a	^3J(5a,4) = 11.00, ^2J(5a,5e) = −13.70, ^3J(5a,6e) = 5.50, ^3J(5a,6a) = 10.00
1.642	H5e	^3J(5e,4) = 3.80, ^2J(5e,5a) = −13.70, ^3J(5e,6e) = 3.20, ^3J(5e,6a) = 5.50
1.922	C10 Me	^5J(Me,6e) = 1.60, ^5J(Me,6a) = 2.00
1.942	H4	^3J(4,5a) = 11.00, ^3J(4,5e) = 3.80, ^3J(4,7) = 3.80, ^3J(4,7*) = 11.00
2.043	H7*	^2J(7*,7) = −15.00, ^3J(7*,4) = 11.00
2.462	H7	^2J(7,7*) = −15.00, ^3J(7,4) = 3.80
3.372	H6a	^2J(6a,6e) = −18.00, ^3J(6a,5e) = 5.50, ^3J(6a,5a) = 10.00, ^5J(6a,Me) = 2.00
3.582	H6e	^2J(6e,6a) = −18.00, ^3J(6e,5e) = 3.20, ^3J(6e,5a) = 5.50, ^5J(6e,Me) = 1.60
3.619	-OMe	

when the temperature was controlled at room temperature or lower, and in such cases a large amount of unreacted camphor was recovered. Other products that were isolated in low yields will be discussed later. The mass spectrum of the major product showed a molecular ion peak at m/z 182, indicating an even number of nitrogen atoms. The proton magnetic resonance (90 MHz) spectrum showed two different deuterium exchangeable protons, one at 5.90 ppm and the other at 1.60 ppm. The infrared spectrum showed NH stretching of secondary amines at 3310 cm^{-1} and 3285 cm^{-1}, N—H stretching for amides at 3180 cm^{-1}, carbonyl stretching (amide band I) at 1662 cm^{-1} and (amide band II) at 1640–1655 cm^{-1}. The carbon-13 nuclear magnetic resonance (22.63 MHz) spectrum (broad band proton decoupled) showed 10 peaks. The Fourier transform polarization transfer (proton decoupled INEPT) technique (6) was used to assign the carbon-13 chemical shifts (in ppm) to methine, methylene, methyl, and quaternary carbons as 71.8 (quaternary), 37.9 (methine), 37.4 (methylene), 35.9 (methylene), 35.8 (quaternary), 28.5 (methylene), 24.0 (methyl), 23.1 (methyl), and 22.9 (methyl). The peak at 173.8 ppm was assigned to an amidic carbon atom.

To assign a new structure to this major product (hereafter called the amino amide), it was mixed with 3% HCl in methanol (prepared by the addition of acetyl chloride to methanol) and heated at reflux for 3 days. The product obtained after work-up was a clear liquid, bp 85–90°C at 0.4 Torr (1 Torr = 133.3 Pa) (74% yield). The infrared spectrum showed absorption for ester and imine functional groups. The proton magnetic resonance (90 MHz) spectrum showed a singlet at 3.65 ppm (3 H's) (—CO—O—Me), a double doublet at 1.91 ppm (3 H's), and two singlets at 1.15 ppm (3 H's) and 0.97 ppm (3 H's). The mass spectrum showed a parent ion at m/z 197.

The high resolution proton magnetic resonance (400 MHz) spectrum (Fig. 1*a*) of this hydrolysis product (cf. Table 1 for chemical shifts, assignments, and couplings) established the structure of the imine ester as **4**. The methyl group attached to the C2 carbon of **4** absorbs at 1.922 ppm and is coupled to two protons on C6 through long range coupling showing a double doublet (three-bond couplings of 1.6 and 2.0 Hz).

The values for the chemical shifts and coupling constants given in Table 1 were obtained from the spectrum simulated on an Amdal 470 computer (LAME–LAOCOON program). The experimental and simulated spectra are shown in Fig. 1*b*. The carbon-13 magnetic resonance spectral data (broad band proton decoupled, and proton decoupled INEPT) and assignments are shown in Table 2.

Since only amino amide **5** would give rise to the imine ester **4**, the structure of the amino amide from the Schmidt reaction on camphor is therefore assigned as **5**. This assignment of structure **5** was confirmed by the high resolution proton magnetic resonance (400 MHz) spectrum studies (Fig. 2*a*). The chemical shifts, assignments, and coupling constants are given in Table 3. Again the values for the chemical shifts and coupling constants were taken from the simulated spectrum obtained on an Amdal 470 computer (LAME–LAOCOON program). The experimental and simulated spectra of **5** are shown in Fig. 2*b*. The carbon-13 spectral assignments for **5** are given in Table 2.

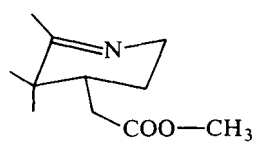

4

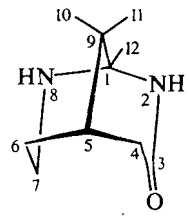

5

Proton decoupled INEPT was used to assign all carbons except the two methylenes C4 and C7. Carbon–proton shift mapping (Fig. 3) was used to distinguish between these two methylenes. The downfield absorption at 37.4 ppm was assigned to C7 and the upfield absorption at 35.9 ppm was assigned to C4.

To confirm that one nitrogen atom is amidic and the other a secondary amine, the N8 phenylcarbamoylamino derivative **6** and the N8 methyl derivative **7** were prepared by standard procedures (see Experimental).

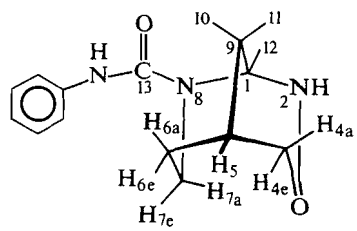

6

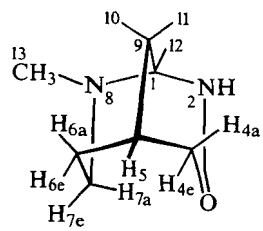

7

Based on the proton and carbon-13 magnetic resonance studies of the amino amide as well as its derivatives and degradation product, it is clear that the structure of the amino amide obtained from the Schmidt reaction on camphor is that of compound **5**. An X-ray analysis further confirmed this assignment.

X-Ray crystallographic confirmation of amino amide 5

X-Ray results and discussion

Table 4 illustrates the bond lengths and angles determined for the two molecules in the crystallographic asymmetric unit. These two molecules are related by an appropriate noncrystallographic center of symmetry present at approximately (0.19, 0.25, 0.61). A perspective drawing of the two molecules is given in stereo in Fig. 4 (11).

The average values for the bond angles around the *cis* amide bond, C4—C3—O3, N2—C3—O3, N2—C3—C4, C1—N2—C3 are 120.3(2), 121.8(2), 118.0(2), 126.2(2)°, respectively. The average bond distances N2—C3, C1—N2

Can. J. Chem. Downloaded from www.nrcresearchpress.com by 80.58.250.72 on 09/07/12
For personal use only.

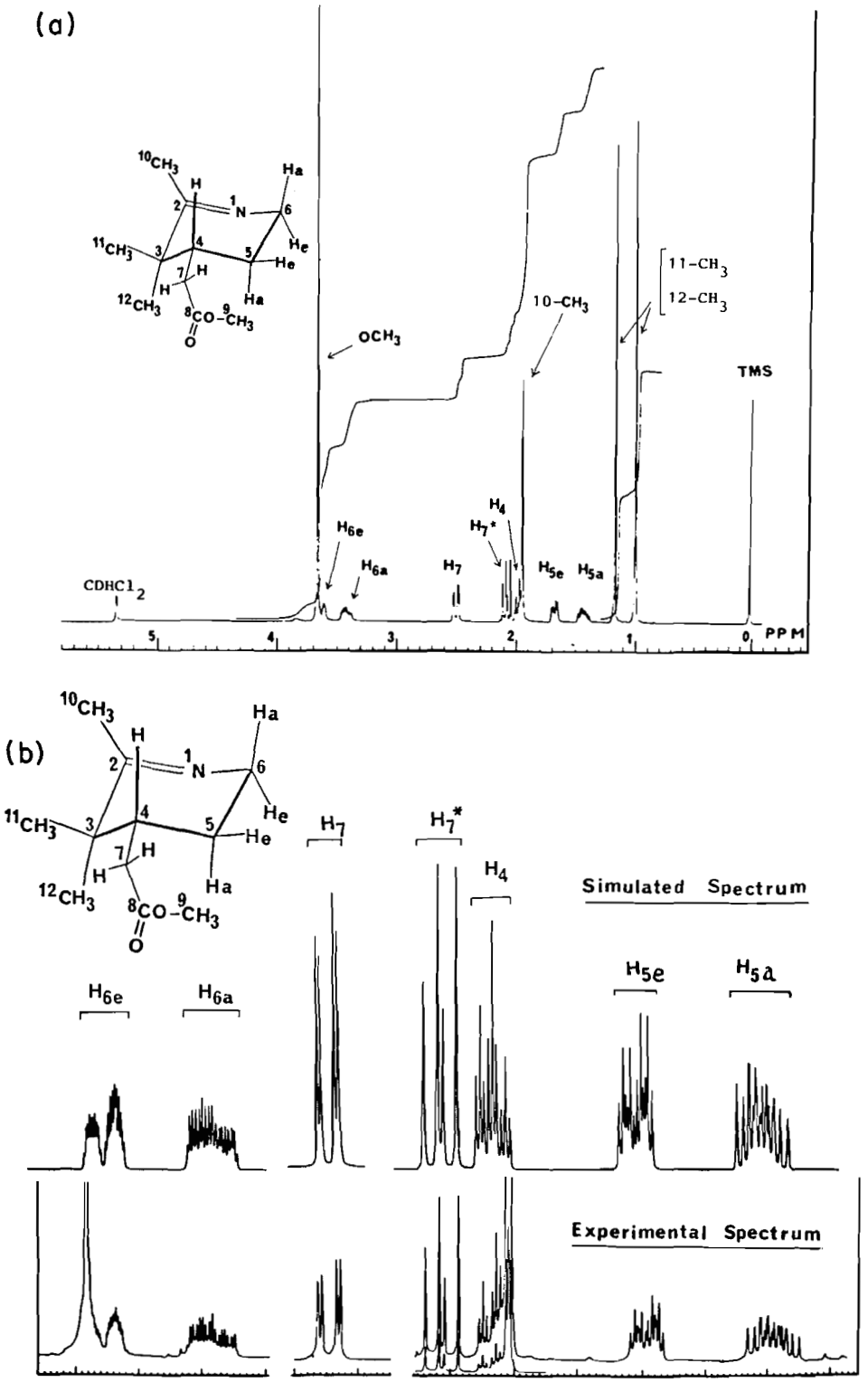

FIG. 1. (*a*) The ^{1}H nmr spectrum (400 MHz) of imine ester **4**. (*b*) The ^{1}H nmr spectrum of imine ester **4**; top: simulated spectrum; bottom: experimental spectrum (400 MHz).

for the two molecules have values of 1.335(3) and 1.489(3) Å respectively. On the other hand the bond angles around a *trans* amide bond have values of 121, 122, 117, and 120° with corresponding bond distances of 1.32 and 1.45 Å, respectively (12). The N2—C3 average distance of 1.335(3) Å is similar to the bond distance of 1.32 Å in *trans* peptide bonds, which shows that there is also double bond character for this bond in compound **5**. The average C1—N2 distance of 1.489(3) Å represents a single bond and may be compared with the other single C—N bonds of compound **5**, C1—N8 and C7—N8, which have average bond distances of 1.465(3) and 1.454(4) Å, respectively, for molecules A and B. Furthermore the bond angles C1—N8—C7 and N8—C7—C6 for the two molecules have average values of 114.4(2) and 109.3(2)°, respectively.

Can. J. Chem. Downloaded from www.nrcresearchpress.com by 80.58.250.72 on 09/07/12
For personal use only.

TABLE 2. The ^{1}H-decoupled, and ^{1}H-decoupled INEPT, data and carbon assignments for compounds **2**, **4**, **5**, **6**, **7**, **8**, and **9**

Compound	Chemical shift (ppm)	Carbon type (INEPT)	Assignment
α-Camphidone **2**	178.98	—	2
	52.27	Quaternary	1
	47.20	Methylene	4
	43.71	Methine	5
	42.32	Quaternary	8
	37.96	Methylene	7
	27.76	Methylene	6
	23.05	Methyl	9,10
	19.32	Methyl	
	13.39	Methyl	11
Amino amide **5**	173.84	—	3
	71.80	Quaternary	1
	37.87	Methine	5
	37.39	Methylene	7
	35.92	Methylene	4
	35.80	Quaternary	9
	28.46	Methylene	6
	23.89	Methyl	10,11
	23.11	Methyl	
	22.87	Methyl	12
Imine ester **4**	173.57	—	8,2
	172.83	—	
	51.58	Methyl	9
	48.63	Methylene	6
	38.66	Quaternary	3
	38.66	Methine	4
	35.40	Methylene	7
	25.33	Methyl	10
	24.44	Methylene	5
	22.56	Methyl	11,12
	21.01	Methyl	
N-Phenylcarbamoyl amino amide **6**	171.11	—	3
	155.20	—	13
	140.56	—	Aromatic C_1
	128.54	—	Aromatic C_3
	120.89	—	Aromatic C_4
	117.62	—	Aromatic C_2
	88.55	—	1
	39.29	Quaternary	9
	37.17	Methylene	7
	34.47	Methylene	4
	32.63	Methine	5
	30.12	Methylene	6
	20.92	Methyl	10, 11, 12
	17.14	Methyl	
	17.06	Methyl	
N-Methyl amino amide **7**	174.09	—	3
	75.09	—	1
	47.22	—	13
	37.90	—	5
	37.85	—	7
	36.76	—	4,9
	35.86	—	
	28.39	—	6
	24.90	—	10,11,12
	23.14	—	
	20.56	—	
Tetrazole **8**	150.37	—	3
	72.35	Quaternary	1
	45.44	Quaternary	8
	42.55	Methine	5

Can. J. Chem. Downloaded from www.nrcresearchpress.com by 80.58.250.72 on 09/07/12
For personal use only.

TABLE 2. (*concluded*)

Compound	Chemical shift (ppm)	Carbon type (INEPT)	Assignment
	39.76	Methylene	4
	27.74	Methylene	7
	23.47	Methyl	9,10,11
	19.57	Methyl	
	14.53	Methyl	
Imine nitrile **9**	172.1	—	2
	119.4	—	8
	48.3	Methylene	6
	39.3	Methine	4
	38.6	Quaternary	3
	25.5	Methyl	9
	23.8	Methylene	5
	22.4	Methyl	10,11
	20.7	Methyl	
	18.6	Methylene	7

Table 5 shows the torsion angles involving non-hydrogen atoms in the two molecules. The six-membered ring C9—C1—N2—C3—C4—C5 has a distorted chair conformation due to the *cis*-amide bond at N2—C3 in molecules A and B. This amide bond is not strictly planar (planar within 0.04 and 0.11 Å in molecules A and B, respectively) with the C1—N2—C3—C4 torsion angles being −6.7 and 15.4° for molecules A and B, respectively. The six-membered ring C1—C9—C5—C6—C7—N8 has a chair conformation in the two molecules. The torsion angles calculated for this ring in the two molecules are listed in Table 5.

There are two intermolecular hydrogen bonds between these molecules, O3(b)...N2(A) = 3.103(6), O3(B)...H(N2A) = 2.26(3) Å, angle N2(A)—H...O3(B) = 168(3)° and O3(A)...N2(B) = 2.864(6), O3(A)...H(N2B) = 1.97(3) Å, angle N2(B)—H...O3(A) = 172(3)°. The thermal parameters for the non-hydrogen atoms, the hydrogen atom parameters, and the structure amplitude table for **5** are available from the Depository of Unpublished Data.[5]

Other products from the Schmidt reaction on camphor

Other minor products that were obtained and identified from the Schmidt reaction on camphor are α-camphidone **2**, the tetrazole **8**, and the imine nitrile **9**.

(a) α-Camphidone 2

This compound was isolated from the acidic reaction mixture (along with the tetrazole **8**) in 5.3% yield and had a melting point range of 242–244°C. The infrared spectrum showed absorptions for N—H stretch and imidic carbonyl stretch. The mass spectrum showed the parent ion peak at m/z 167. The proton magnetic resonance (90 MHz) spectrum showed the amidic N—H proton resonance at 5.90 ppm (1H, m). The protons at the 4a and 4e positions were coupled to the amidic proton (^3J = 1–2 Hz). This coupling was confirmed by examination of an N—H decoupled proton magnetic resonance (90 MHz) spectrum where the coupling of H4a and H4e to the amidic N—H was removed. The carbon-13 magnetic resonance (broad band decoupled, and proton decoupled INEPT) data and assignments are given in Table 2. The lactam **2** has previously been reported as a product from the Schmidt reaction on camphor in only 1% yield (5).

(b) Tetrazole 8 (see Scheme 1)

This tetrazole, obtained in 1% yield, is N-bridge substituted and is different from the tetrazole **1** claimed by Schmidt as the major product from camphor (4). The structure of tetrazole **1**, assigned by Schmidt, was supported only by its elemental analysis and melting point (242–243°C). The tetrazole isolated by us, and assigned structure **8**, melts over the range 245–247°C in a sealed tube. The mass spectrum of **8** shows a parent ion at m/z 192. In addition, nitrogen is readily lost from the parent ion to give a fragment ion at m/z 164. The assignment of structure **8**, rather than structure **1**, to this tetrazole is based largely on its proton magnetic resonance spectrum. At 90 MHz the spectrum showed a double-double-doublet centered at 3.15 ppm for proton H4a (^2J(4a,4b) = −17 Hz, ^3J(4a,5) = 3.1 Hz, and ^4J(4a,6a) = 1.5 Hz) and a double-doublet centered at 2.95 ppm for proton H4b (^2J(4b,4a) = −17 Hz, ^3J(4b,5) = 2 Hz). A singlet at 1.78 ppm (3 H) is assigned to the hydrogens of the C11 methyl group, which are deshielded by the ring current of the tetrazole ring. A singlet at 0.81 ppm (3 H) is assigned to the hydrogens on the shielded methyl group C10. The chemical shifts of H4a and H4b, at 3.15 and 2.95 ppm respectively, are more upfield than one would predict from the corresponding hydrogens adjacent to N3 in tetrazole **1** (13). The carbon-13 magnetic resonance (broad band decoupled, and proton decoupled INEPT) data and assignments for **8** are shown in Table 2.

(c) Imine nitrile 9 (see Scheme 1)

This compound (bp 65°C at 0.1 Torr) was isolated in 1% yield from the mother liquors of the recrystallization of amino amide **5**. The infrared spectrum of **9** showed absorptions for nitrile and imine functional groups. The proton magnetic resonance (90 MHz) spectrum showed a double-doublet at 1.88 ppm (3 H) due to the protons on the C9 methyl group. This methyl group is coupled to H6a and H6b as in the imine ester **4** obtained from amino amide **5**. (All the proton couplings of imine nitrile **9** were very similar to those of imine ester **4**. The major difference in the proton magnetic resonance spectrum of these compounds was in the chemical shifts for the protons at C4 in the side chain.) The carbon-13 nmr (broad band decoupled, and proton decoupled INEPT) data and assignments are shown in Table 2.

[5]Copies may be purchased from the Depository of Unpublished Data, CISTI, National Research Council of Canada, Ottawa, Ont., Canada K1A 0S2.

Can. J. Chem. Downloaded from www.nrcresearchpress.com by 80.58.250.72 on 09/07/12
For personal use only.

Can. J. Chem. Downloaded from www.nrcresearchpress.com by 80.58.250.72 on 09/07/12
For personal use only.

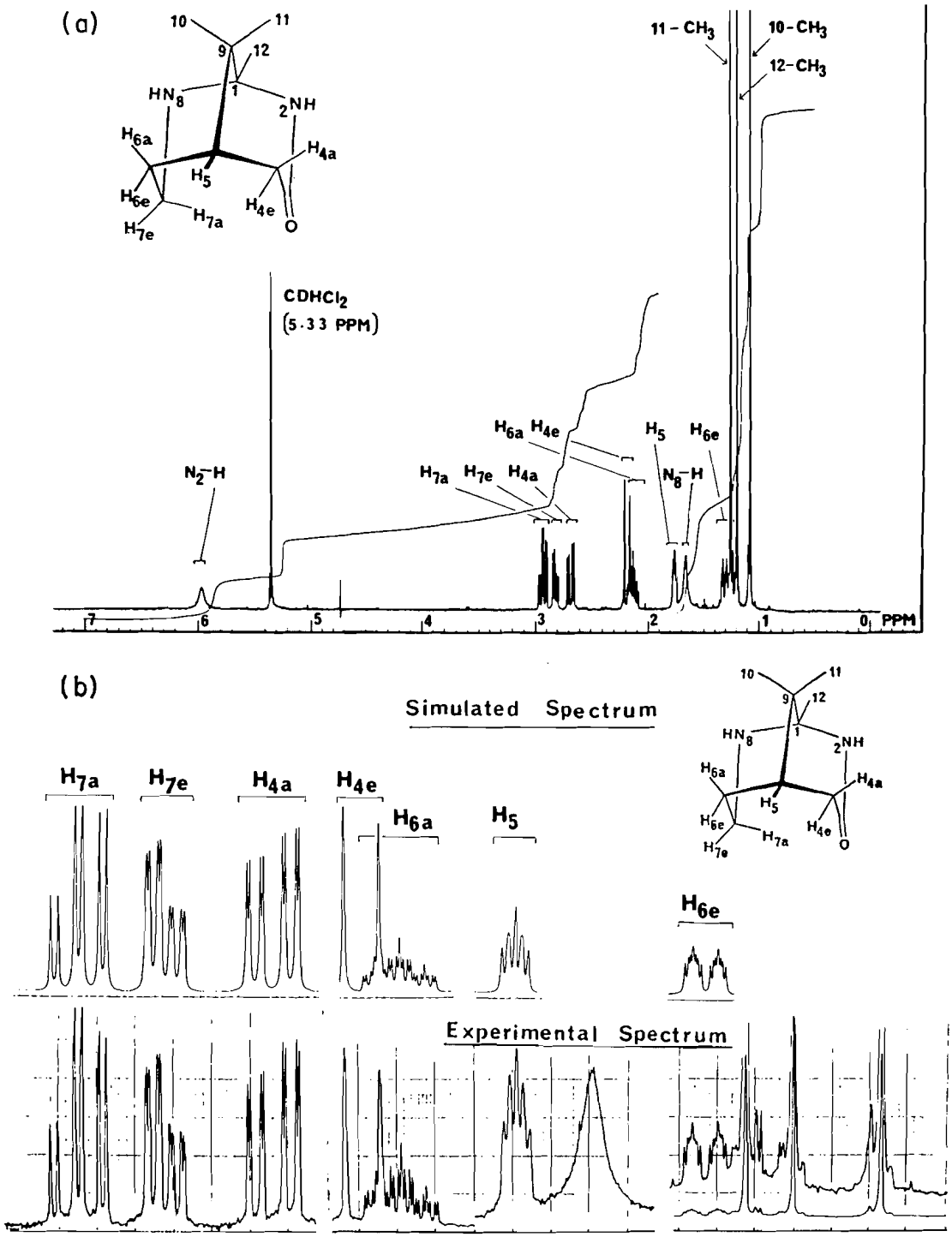

FIG. 2. (*a*) The ^{1}H nmr spectrum (400 MHz) of amino amide **5**. (*b*) The ^{1}H nmr spectrum of amino amide **5**; top: simulated spectrum; bottom: experimental spectrum (400 MHz).

Here also, with the exception of the C4 carbon, the chemical shifts are similar for both compounds **4** and **9**.

Mechanistic discussion

The mechanism established for the formation of the major product **5** will be discussed in a separate paper. However, the formation of the product **9** and the regioisomeric nitrogen insertion products **2** and **8**, though low in yield, is worthy of mechanistic comment at this stage. We suggest the simultaneous action of five different mechanisms to explain the formation of products **2**, **5**, **8**, and **9**.

We believe that, initially, camphor adds one mole of hydrazoic acid to generate the intermediate protonated azidohydrin **11** (Scheme 1). Molecular models show that the attack of hydrazoic acid on the carbonyl carbon of camphor should occur from the *endo* face due to hindrance of the *exo* face by the *syn*-7 methyl group. Nucleophilic attack at a ketonic carbonyl group requires the attainment of a 110° angle of Nu-C=O at the time of attack (14). This angle is only favourable in the case of camphor when attack is from the *endo* face. Attack of hydrazoic acid on the ketonic carbon of norcamphor (15) and of peracid during the Baeyer–Villiger oxidation of norcamphor (16) and fenchone

TABLE 3. The 400-MHz ^1H nmr spectrum of amino amide **5** (chemical shifts in ppm relative to TMS; solvent CD_2Cl_2)

Chemical shifts	Assignments	Couplings
1.058	C10 Me	—
1.176	C12 Me	—
1.236	C11 Me	—
1.290	H6e	^2J(6e,6a) = −13.43, ^3J(6e,5) = 2.80, ^3J(6e,7a) = 4.00, ^3J(6e,7e) = 1.68
1.642	N8-H	—
1.744	H5	^3J(5,4a) = 7.00, ^3J(5,6a) = 4.02, ^3J(5,6e) = 2.80, ^4J(5,7e) = 0.62, ^3J(5,4e) = 0.50 (assigned)
2.116	H6a	^2J(6a,6e) = −13.43, ^3J(6a,5) = 4.02, ^4J(6a,4a) = 1.51, ^3J(6a,7e) = 5.82, ^3J(6a,7a) = 13.39
2.169	H4e	^2J(4e,4a) = −18.63, ^3J(4e,5) = 0.5 (assigned)
2.655	H4a	^2J(4a,4e) = −18.63, ^3J(4a,5) = 7.00, ^4J(4a,6a) = 1.51
2.799	H7e	^2J(7e,7a) = −12.49, ^3J(7e,6a) = 5.82, ^3J(7e,6e) = 1.68, ^4J(7e,5) = 0.62
2.911	H7a	^2J(7a,7e) = −12.49, ^3J(7a,6a) = 13.39, ^3J(7a,6e) = 4.00, + long range
5.950	N2-H	—

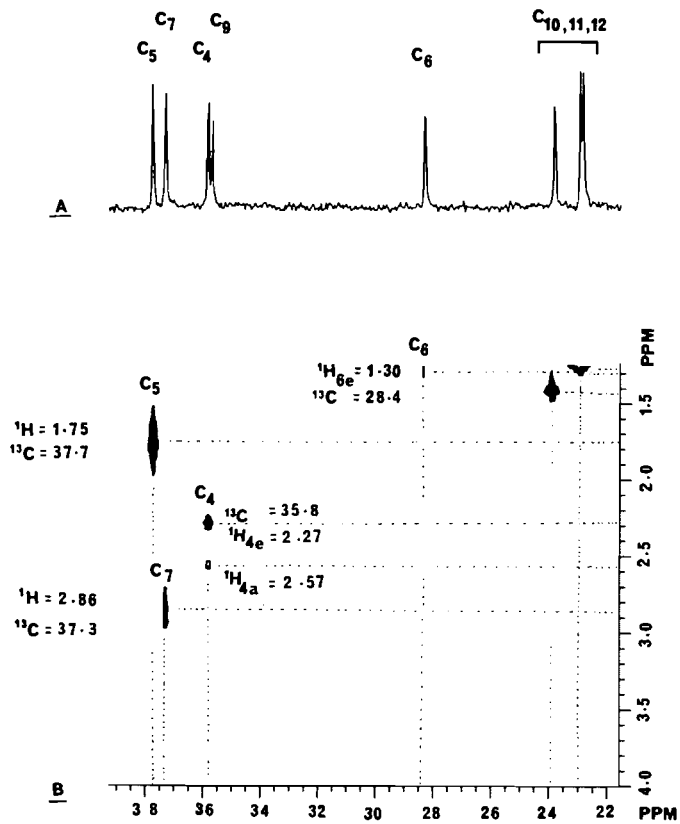

FIG. 3. *A*: The ^{13}C nmr spectrum of amino amide **5** (C1 at 71.8 ppm and C3 at 173.8 ppm not shown). *B*: Carbon–proton shift map.

(17) is believed to take place from the *exo* face because of the absence of the *syn*-7 methyl group. Based on the relative percentage yield of the amino amide **5**, we infer that most of the protonated azidohydrin **11** undergoes cleavage (Scheme 2) to generate the intermediate α-campholenoamide **16**. One mole of hydrazoic acid then adds to **16** to ultimately produce the amino amide **5**. Experimental support for this conclusion will be presented in a separate paper. In addition, some of the protonated azidohydrin **11** rearranges with methylene migration to nitrogen to produce α-camphidone **2** (*vide infra*). The isolation of compounds **8** and **9** indicates that some of the intermediate **11** dehydrates to generate the iminodiazonium ion **12***a*, which is analogous to camphor oxime **12***b*. The iminodiazonium ion **12***a* then rearranges in two ways to produce **8** and **9**: (*i*) Bridgehead carbon migration to nitrogen leading to the intermediate iminium ion **13**, which then adds one mole of hydrazoic acid to yield the tetrazole **8** (13*b*). (Iminium ion **13** may also lead to **10**. This type of cleavage between the bridgehead carbon and the imine carbon of the iminium ion has been suggested for the iminium ion formed during the Schmidt reaction of *cis*-8-methylhydrindan-1-one (13*b*) (*vide infra*).) (*ii*) Cleavage between the bridgehead carbon and imine carbon leads to α-campholenonitrile **10**. This type of cleavage has been observed for camphor oxime **12***b* (18) and fenchone oxime (19). α-Campholenonitrile **10** then reacts with one mole of hydrazoic acid to produce the iminonitrile **9**. (α-Campholenonitrile **10** was not isolated during any of the trials.)

Roberts and co-workers (20*a*) have established the configuration of camphor oxime as having the OH group *anti* to the bridgehead carbon. This assignment has been confirmed by an X-ray crystallographic study (20*b*).[6] For the present argument it is assumed that the iminodiazonium ion **12***a* and the camphor oxime **12***b* are isosteric since the iminodiazonium ion is larger than OH. It is known (21) that iminodiazonium ion intermediates rearrange according to the rule of *anti*-migration which also operates in the Beckmann rearrangement. *anti*-Migration of the bridgehead carbon to nitrogen for **12***a* would result in the iminium ion **13**, which in principle should lead to the 2-azalactam **15** and, in the case of reaction with a second mole of hydrazoic acid, the tetrazole **8**. The isolation of **8** and the absence of **15** can be explained by the fact that the excess hydrazoic acid present would react very rapidly with iminium ion **13** to produce the tetrazole **8**. The small amount of water present would not compete effectively for the iminium ion **12**. (It is known that tetrazoles cannot be produced under Schmidt reaction conditions (13*b*) from the corresponding lactams.) The same arguments can be applied to the iminium ion **14**, which

[6]We thank one of the referees for bringing this reference to our attention.

Can. J. Chem. Downloaded from www.nrcresearchpress.com by 80.58.250.72 on 09/07/12
For personal use only.

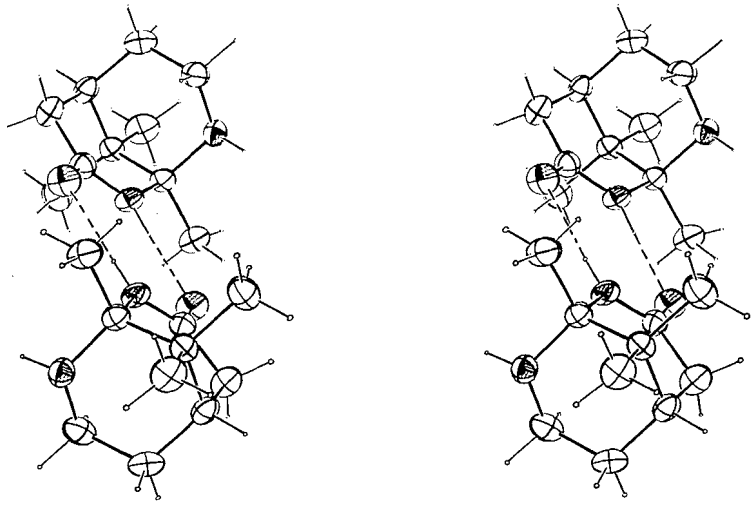

FIG. 4. Stereo drawing of the two crystallographically independent molecules of amino amide **5**. The nitrogen and oxygen atoms have one octant shaded. Hydrogen bonds are indicated by dashed lines.

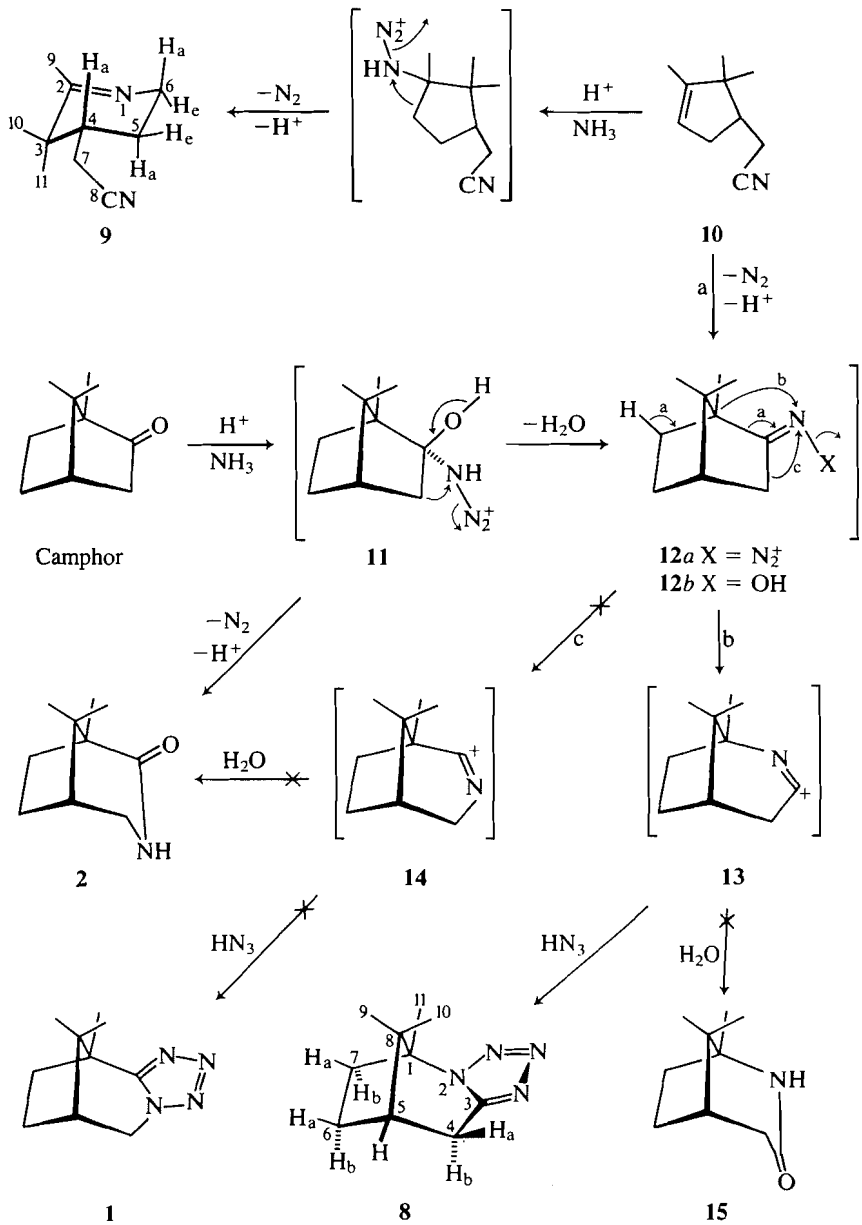

SCHEME I

Can. J. Chem. Downloaded from www.nrcresearchpress.com by 80.58.250.72 on 09/07/12
For personal use only.

TABLE 4. Bond distances and angles for amino amide **5**

Bond	Bond distance (Å)*		
	Molecule A	Molecule B	Mean
C1—N2	1.494(4)	1.483(4)	1.489(3)
C1—N8	1.464(4)	1.466(4)	1.465(3)
C1—C9	1.548(4)	1.543(5)	1.546(3)
C1—C12	1.509(5)	1.519(5)	1.514(4)
N2—C3	1.338(4)	1.332(4)	1.335(3)
C3—O3	1.240(4)	1.239(4)	1.240(3)
C3—C4	1.505(5)	1.514(6)	1.510(4)
C4—C5	1.520(5)	1.535(5)	1.528(4)
C5—C6	1.526(5)	1.522(5)	1.524(4)
C5—C9	1.557(5)	1.555(5)	1.556(4)
C6—C7	1.518(5)	1.516(6)	1.517(4)
C7—N8	1.453(5)	1.455(5)	1.454(4)
C9—C10	1.534(5)	1.530(5)	1.532(4)
C9—C11	1.531(5)	1.530(5)	1.531(4)
	Bond angle (deg)*		
Bonds	Molecule A	Molecule B	Mean
N2—C1—N8	111.5(2)	111.1(2)	111.3(1)
N2—C1—C9	107.5(2)	108.1(2)	107.8(1)
N2—C1—C12	107.2(3)	107.5(3)	107.4(2)
N8—C1—C9	108.4(2)	108.9(2)	108.7(1)
N8—C1—C12	107.3(3)	106.8(3)	107.1(2)
C9—C1—C12	115.0(3)	114.4(2)	114.7(2)
C1—N2—C3	126.0(3)	126.4(3)	126.2(2)
N2—C3—O3	121.9(3)	121.6(3)	121.8(2)
N2—C3—C4	118.7(3)	117.2(3)	118.0(2)
O3—C3—C4	119.4(3)	121.1(3)	120.3(2)
C3—C4—C5	115.5(3)	115.7(3)	115.6(2)
C4—C5—C6	110.9(3)	111.0(3)	111.0(2)
C4—C5—C9	109.4(3)	110.1(3)	109.8(2)
C6—C5—C9	112.0(3)	111.0(3)	111.5(2)
C5—C6—C7	111.7(3)	111.1(3)	111.4(2)
C6—C7—N8	108.7(3)	109.9(3)	109.3(2)
C1—N8—C7	114.2(3)	114.5(3)	114.4(2)
C1—C9—C5	105.4(2)	105.3(2)	105.4(1)
C1—C9—C10	111.1(3)	111.2(3)	111.2(2)
C1—C9—C11	112.4(3)	112.0(3)	112.2(2)
C5—C9—C10	110.5(3)	110.9(3)	110.7(2)
C5—C9—C11	110.7(3)	110.1(3)	110.4(2)
C10—C9—C11	106.9(3)	107.4(3)	107.2(2)

*Estimated standard deviation of the last digit is given in parentheses.

TABLE 5. Torsion angles in amino amide **5** involving non-hydrogen atoms (esd's are ~0.4°)

Bonds	Torsion angle (deg)	
	Molecule A	Molecule B
C9—C1—N2—C3	32.9	−39.0
C1—N2—C3—C4	−6.7	15.4
N2—C3—C4—C5	10.6	−16.0
C3—C4—C5—C9	−41.2	41.7
C4—C5—C9—C1	66.3	−63.6
C5—C9—C1—N2	−59.9	59.8
N8—C1—C9—C5	60.7	−61.1
C1—C9—C5—C6	−57.0	59.7
C9—C5—C6—C7	54.3	−56.5
C5—C6—C7—N8	−52.2	52.2
C6—C7—N8—C1	59.9	−56.9
C7—N8—C1—C9	−66.1	63.0

would be produced if camphor iminodiazonium ion has the configuration with the iminodiazonium ion *syn* to the bridgehead carbon. Since tetrazole **1** was not isolated, as would be expected if the iminium ion **14** had formed, the formation of **2** probably proceeds directly from rearrangement of the protonated azidohydrin **12**. This rearrangement is analogous to that proposed by Krow and Szezepanski (22) for the formation of α-camphidone from reaction of camphor with hydroxylamine-*O*-sulfonic acid.

Similar to the rearrangement of **11** to **2**, the methylene migration during the rearrangement of other intermediate protonated azidohydrins and the intermediates formed by the attack, from the *endo* face, of peracids on camphor have been explained by considering different factors. Murray *et al.* (23), while determining the structure of steroidal D-ring lactones, have tried to identify the electronic factors involved in the Baeyer–Villiger oxidation of camphor. They suggested that the migration of the tertiary bridgehead carbon involves a high-energy transition state of the boat form (Scheme 3), while migration of the methylene carbon involves a lower energy transition state of the chair form.

Di Maio and Permutti (13*b*) have suggested the simultaneous action of two mechanisms to explain the formation of regioisomeric nitrogen insertion products obtained during the Schmidt reaction on *cis*-8-methyl hydrindan-1-one (Scheme 4).

The first mechanism proposed by Di Maio and Permutti involves the stereospecific migration of bridgehead carbon *anti* to the leaving group in the intermediate (Scheme 4) to form the iminium ion **B**, which then undergoes either ring opening to yield the corresponding nitrile or attack by excess hydrazoic acid to give the corresponding tetrazoles. The second mechanism was based upon the relative boat–chair conformational strain energies, as proposed by Murray *et al.* (23), to explain the formation of the isoquinoline-type lactam **D**. The formation of lactam **D** would be favoured by the chair transition state obtained during migration of the methylene group as indicated in structure **C**. If the relative boat–chair conformational strain energies are a factor during the rearrangement of intermediates produced in the Baeyer–Villiger reaction and the Schmidt reaction of bridged bicyclic ketones, then the formation of α-camphidone **2** from **11** can be explained on precisely the same basis. As indicated by the arrows in **11** (Scheme 1), the migration of the methylene group would result in the formation of **2** via a transition state with an energetically favoured chair conformation. The bridgehead migration of **11** to produce **15** (which we have not detected) would occur via the less favourable boat transition state.

Sauers and Beisler (17) have observed mainly methylene migrated products from the Baeyer–Villiger oxidation of *syn* 7-chloronorcamphor and *syn* 7-bromonorcamphor because the predominently *endo* attack of the peracid leads to chair conformations in the transition state. To rationalize their observations, as well as those of others (24), they considered forces that might work in opposition to both electronic and boat–chair conformational interactions in the transition state. The conformation of the leaving group would not be an important factor provided it is able to attain *trans*-coplanarity with either of the possible migrating groups (25). These authors proposed that an extra factor, associated with the torsional strain caused by the eclipsed nonbonded interactions between substituents on C2 and the hydrogens on C3, is involved in these

Can. J. Chem. Downloaded from www.nrcresearchpress.com by 80.58.250.72 on 09/07/12
For personal use only.

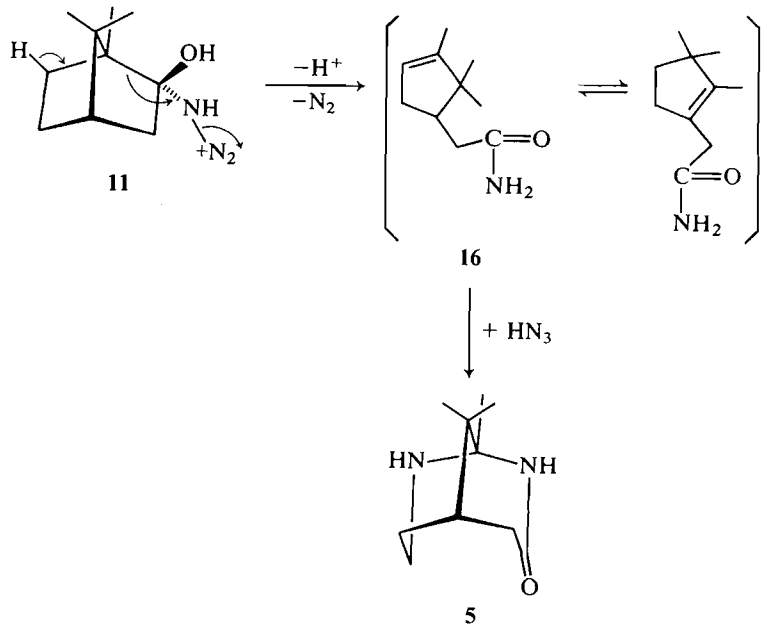

SCHEME 2

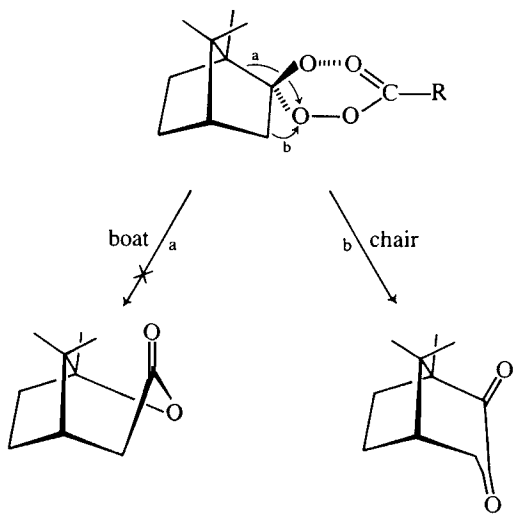

SCHEME 3

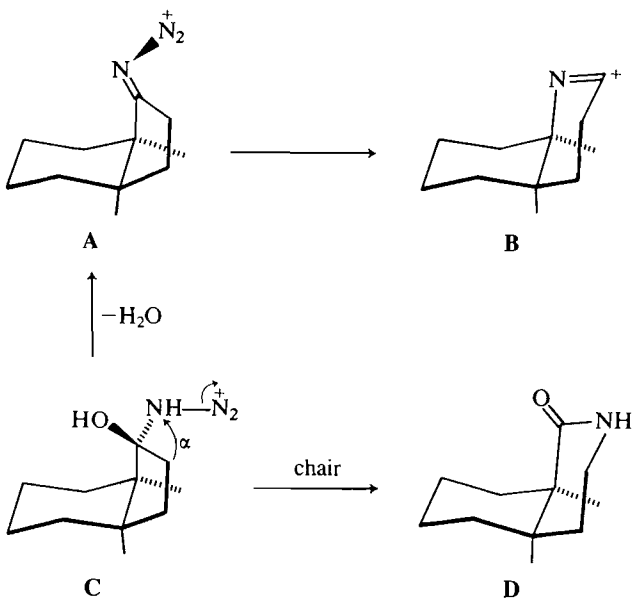

SCHEME 4

migrations. The similar nonbonded interaction between substituents on C2 and the bridgehead carbon are much less severe since the dihedral angles involved are approximately 44° (H1 with the C2 *exo* substituent) and 79° (H1 with the C2 *endo* substituent). Thus migration of the C2—C3 bond would proceed with considerable relief of eclipsing strain. Sauers and Beisler concluded that migration of the C2—C3 bond during the Baeyer–Villiger reaction of bicyclic ketones will always be favoured by torsional factors regardless of the substitution or orientation of the hydroxy-perester function. Such a rationalization was used to predict the migration of the C2—C3 bond in fenchone under peracid oxidation conditions (17). In the case of fenchone, the electronic effects are essentially equal and the competition is between formation of the boat form and relief of torsional strain. The major product (approximately 60%) was the one predicted on the latter basis.

We could apply the same arguments to the case of protonated azidohydrin **11** where there would be torsional strain caused by the eclipsed nonbonded interactions between the substituents on C2 and the hydrogens on C3. Migration of the C2—C3 bond, yielding **2**, would proceed with greater relief of eclipsing strain. It appears that the two effects of (*i*) forces due to the energetically favoured chair conformation and (*ii*) the greater relief of torsional strain caused by the eclipsed nonbonded interactions between substituents on C2 and C3 operate concurrently to cause migration in the same direction during the C2—C3 bond migration of protonated azidohydrin **11** to produce **2**. However, considering the 3-way rearrangement of **11** and the 2-way rearrangement of iminodiazonium ion **12***a*, and also the C1—C2 bond or C2—C3 bond migration or ring opening observed by other workers during the Schmidt or Beckmann reactions on bridged bicyclic ketones, it will be very difficult to predict the products of a ring enlargement owing to the different factors involved.

We could not detect or isolate compounds **15** or **1**, which would be produced from the intermediates **13** and **14**, respectively. The total yield of the identified products **2**, **5**, **8**, and **9** from the Schmidt reaction on camphor is approximately 50%. Since no unreacted camphor was recovered from the reaction under *optimum conditions* (see Experimental), it is apparent that the other product(s) obtained must be water soluble. Attempts

Can. J. Chem. Downloaded from www.nrcresearchpress.com by 80.58.250.72 on 09/07/12
For personal use only.

to obtain identifiable products from the aqueous layer have so far been unsuccessful. It is probable that some of the lactam produced (**2** or **15**) undergoes hydrolysis to water soluble amino acids prior to work-up of the Schmidt reaction. Because of the relatively low material balance it is not possible to draw definitive conclusions about the migratory ratios involved in the total reaction of hydrazoic acid with camphor.

Experimental

Melting points were determined using a precalibrated Thermopan (Kofler hot stage) melting point apparatus or, in the case of a sealed tube melting point, a Canlab–Gallenkamp apparatus. Infrared spectra were recorded on a Unicam SP 1000 spectrophotometer. Mass spectra were recorded using a Finnigan 1015 mass spectrometer under electron-impact at 70 eV ionization voltage, and on a high resolution A.E.I. model MS 50 mass spectrometer (hrms). Proton magnetic resonance spectra were recorded on a Varian EM-360 (60 MHz), a Bruker WH 90 (90 MHz), or a Bruker WH 400 (400 MHz) spectrometer. Carbon-13 nuclear magnetic resonance spectra were obtained on a Bruker WH 90 (at 22.63 MHz) spectrometer equipped with a NIC 1180 computer, 293 A′ pulse programmer, homebuilt phase shifter, and NTL FT software. Analytical thin-layer chromatography (tlc) was performed on sheets precoated with silica gel 60 F(254) (EM reagents) of 0.2 mm thickness. Spots were detected under uv light or visualized in an iodine chamber. Silica gel Kieselgel 60 (230–400 mesh ASTM) was used in columns for flash chromatography. All solvent evaporations were carried out on rotary evaporators.

X-Ray experimental

Colorless crystals of compound **5** were obtained as rods elongated along the *b* axis exhibiting the forms [100], [010], and [001]. The crystal data are given in Table 6. The systematically absent reflections that occurred for the crystal were $h0l$; $h = 2n + 1$ and $0k0 = 2n + 1$. This is consistent with the monoclinic space group $P2_1/a$.

Quantitative data collection was carried out on an Enraf–Nonius CAD4F diffractometer with an $\omega/2\theta$ scan. Observational weights (7) for the reflections were derived from the formula $W = (2I)^2/F_o^2(T + (0.02I)^2 + r^2B)$, where I is the net intensity, F_o is the observed structure amplitude, T is the total peak count, B is the sum of the background counts, and r is the ratio of the peak-scan time to the total background counting time ($r = 2$ for this data). Lorentz and polarization corrections were applied.

X-Ray diffraction data collected on the crystal were processed by using the XRAY76 system (8). The observed structure amplitudes were then converted into normalized structure factors, E values, by using a Wilson plot (9). The overall B was 3.4 Å^2. The structure was solved by employing the MULTAN80 package of computer programs (10). Both figures of merit, ABSFOM and RESID, were used to choose the best set of phases used in the structure determination; ABSFOM was 1.0700 and RESID had a value of 13.08.

The positions of the non-hydrogen atoms of the molecule were determined from a calculated E map. Least-squares isotropic refinement gave an R value of 0.148. Anisotropic refinement was then carried out and gave an R value of 0.109. The positions of the hydrogen atoms were located by using a difference Fourier map. Finally, full-matrix least-squares refinement of anisotropic temperature factors for the non-hydrogen atoms and isotropic refinement for the hydrogen atoms converged to an R index of 0.042. The largest shift/error value for the coordinates of the non-hydrogen atoms was 0.38 and the average shift/error for all of the parameters was 0.12 for the final cycle of refinement. The final atomic parameters are given in Table 7. The DEC 2060 computer at the University of Saskatchewan was used to carry out all crystallographic computations.

Schmidt reaction on camphor

(a) Amino amide ***5***

d,l-Camphor (30.4 g, 0.2 mol) was dissolved in chloroform (400 mL). Concentrated H_2SO_4 (100 mL) was then added. To this rapidly stirred two-phase system, sodium azide (27.0 g, 0.41 mol) was added in small portions over a period of 3.25 h. During this addition

TABLE 6. Crystal data

Parameter	Value
Formula	$C_{10}H_{18}N_2O$
Formula weight (fw)	182.27
Space group	$P2_1/a$
Equivalent positions	$x, y, z; \bar{x}, \bar{y}, \bar{z}; \frac{1}{2} - x, \frac{1}{2} + y, \bar{z}; \frac{1}{2} + x, \frac{1}{2} - y, z$
Crystal size	0.20 × 0.30 × 0.12 mm
a (Å)	14.934(1)
b (Å)	10.973(1)
c (Å)	12.341(1)
β	92.0°
V (Å^3)	2019.9
Z	8
ρ_o (g cm^{-3}, determined by floatation in a mixture of pentane and carbon tetrachloride	1.21
ρ_c (g cm^{-3})	1.20
Radiation	Cu K_α (λ = 1.5418 Å)
$2\theta_{max}$	120
Total reflections measured	3002
No. of unique reflections with net $I > 3\sigma(I)$	1867
Merging $R_I = (\sum_i \|I - I_i\| / \sum_i I_i) \times 100$ (%)	1.4 for 135 reflections
$R = (\Sigma \|\|F_o\| - \|F_c\|\| / \Sigma \|F_o\|)$	0.042
$R_w = (\Sigma w\Delta^2 / \Sigma w F_o^2)^{1/2}$	0.054
Maximum decay correction	1.04

TABLE 7. Atomic coordinates of compound **5***

Atom	x/a	y/b	z/c	U_{eq}†(Å^2)
Molecule B				
O(3A)	0.2814(1)	0.1725(2)	0.6286(2)	0.046
N(2A)	0.2421(2)	0.2709(2)	0.4738(2)	0.037
N(8A)	0.3135(2)	0.4214(3)	0.3590(2)	0.038
C(1A)	0.2569(2)	0.3125(3)	0.3606(2)	0.034
C(3A)	0.2963(2)	0.1976(3)	0.5330(2)	0.037
C(4A)	0.3749(3)	0.1400(3)	0.4796(3)	0.044
C(5A)	0.3951(2)	0.1887(3)	0.3678(2)	0.039
C(6A)	0.4505(2)	0.3053(3)	0.3764(3)	0.046
C(7A)	0.3971(2)	0.4101(3)	0.4218(3)	0.046
C(9A)	0.3056(2)	0.2084(3)	0.3017(2)	0.036
C(10A)	0.3241(3)	0.2438(4)	0.1843(3)	0.049
C(11A)	0.2502(3)	0.0908(4)	0.2968(3)	0.052
C(12A)	0.1666(3)	0.3470(4)	0.3112(3)	0.049
Molecule A				
O(3B)	0.0848(1)	0.3604(2)	0.6112(2)	0.051
N(2B)	0.1331(2)	0.2481(3)	0.7536(2)	0.038
N(8B)	0.0679(2)	0.0677(3)	0.8340(2)	0.042
C(1B)	0.1200(2)	0.1789(3)	0.8551(2)	0.034
C(3B)	0.0741(2)	0.3225(3)	0.7044(2)	0.039
C(4B)	−0.0044(3)	0.3644(3)	0.7694(3)	0.048
C(5B)	−0.0217(2)	0.2909(3)	0.8724(3)	0.042
C(6B)	−0.0740(2)	0.1751(4)	0.8456(3)	0.051
C(7B)	−0.0189(2)	0.0879(3)	0.7798(3)	0.048
C(9B)	0.0686(2)	0.2610(3)	0.9332(2)	0.037
C(10B)	0.0525(3)	0.1954(4)	1.0402(3)	0.054
C(11B)	0.1195(3)	0.3786(4)	0.9603(3)	0.056
C(12B)	0.2118(2)	0.1387(4)	0.8982(3)	0.047

†$U_{eq} = (U_{11} + U_{22} + U_{33})/3$.
*Estimated standard deviation of last digit in parentheses.

Can. J. Chem. Downloaded from www.nrcresearchpress.com by 80.58.250.72 on 09/07/12
For personal use only.

Can. J. Chem. Downloaded from www.nrcresearchpress.com by 80.58.250.72 on 09/07/12
For personal use only.

the temperature of the reaction mixture remained above 35°C and occasionally reached 50°C. The reaction mixture was stirred for an additional 3.5 h and then placed in the freezer overnight. The upper $CHCl_3$ layer was decanted from the thick yellow gum at the bottom of the flask. This yellow gum was diluted with ice-water (600 g) and stirred for 5 min before extraction with $CHCl_3$ (1 × 200 mL). This $CHCl_3$ extract was reserved for later work-up (see below). The acidic aqueous layer was adjusted to pH 10 with 60% NaOH solution and then extracted with $CHCl_3$ (3 × 150 mL). These combined $CHCl_3$ extracts were dried with anhydrous Na_2SO_4 and then evaporated to dryness on the rotary evaporator. The semisolid obtained was crystallized from ethyl acetate to give 14.3 g (39.4%) of pure compound, mp 181–183°C (sealed tube); ir (Nujol) cm^{-1}: 3310 (m) and 3285 (m) (NH stretch of amine), 3180 (m) (NH stretch of amide), 1662 (s) (C═O, amide band I), 1655–1640 (s) (amide band II). The carbon-13 nmr and proton nmr (400 MHz) data and assignments are given in Tables 2 and 3 respectively. Mass spectra *m/z*: 182 (38) (M^+), 167 (10) (M − (CH_3)), 139 (23) (M − (NH═C═O)), 114 (46), 101 (98), 98 (77) (139 − (CH_2CH═CH_2)) 82 (100) (98 − (NH_2)). *Exact Mass* calcd. for $C_{10}H_{18}N_2O$: 182.1419; found (hrms, 100%): 182.1420. This compound was assigned the structure of the amino amide **5**.

The mother liquor saved from the crystallization of the amino acid **5** was concentrated on the rotary evaporator and the product obtained was chromatographed on a silica gel column (10 in. × 1.5 in.). Sixty-four fractions (10 mL) were collected using $CHCl_3$–EtOH (20:1) as the eluting system. A white solid (mp 181–182°C in sealed tube), 0.995 g, 2.7%, was obtained from fractions 30–62. This material was identified as the amino amide **5** by ir, nmr, and mass spectra.

(b) Imine nitrile 9

Fractions 15–21 from above were combined and concentrated. A brown liquid (0.548 g) was obtained. This product was purified by treatment with activated charcoal and rechromatography on silica gel with $CHCl_3$. The tlc pure fraction (R_f 0.38 in $CHCl_3$–EtOH (10:1, v:v)) collected was distilled at 65°C oil bath temperature (0.1 Torr) to give 0.315 g of colourless liquid, ir (thin film) cm^{-1}: 2240 (m) (CN), 1651 (s) (C═N); ^{1}H nmr (90 MHz) in $CDCl_3$, δ: m centred at 3.54 (2H, H6a, H6e), dd at 2.44 (1H, H) [^2J(7, 7*) = 16.5 Hz, ^3J(7, 4a) = 4.0 Hz], dd at 2.08 (1H, H7*) [^2J(7*, 7) = −16.6 Hz, ^3J(7*, 4a) = 9.5 Hz], dd at 1.88 (3H, C9 methyl) [^5J(Me, 6a) = 1.9 Hz, ^5J(Me, 6e) = 1.6 Hz], m at 1.97–1.41 (3H, H4a, H5a, H5e), s at 1.13 (3H) and s at 0.97 (3H) due to C10 and C11 methyls. The carbon-13 nmr (proton decoupled and proton decoupled INEPT) data and assignments are given in Table 2. Mass spectra *m/z*: 164 (18) (M^+), 149 (2) (M − (CH_3)), 124 (16) (M − (CH_3—C═N—CH_2—CH_2)), 83 (100) (124 − (CH_3—CN)), 68 (47) (83 − (CH_3)), 55 (76) (83 − (CH_2═CH_2)). This mass fragmentation pattern is analogous to that of the imine ester **4** (see below).

(c) Tetrazole 8 and α-camphidone 2

The chloroform extract of the acidic aqueous layer (see Sect. (*a*) above) was washed with water, dried, and concentrated. A white solid (4.44 g) was obtained. Thin-layer chromatography with CH_2Cl_2–CH_3OH (100:2, v:v) showed two spots (R_f 0.75 and 0.44). This white solid was chromatographed on a silica gel column using CH_2Cl_2–CH_3OH (100:2, v:v) as eluant.

(i) Tetrazole 8

Fractions 18 and 19 from the above chromatography were combined and concentrated to give a white crystalline solid (0.349 g) that was pure by tlc. After recrystallization from ethyl acetate the product had mp 245–247°C (sealed tube); ir (thin film) cm^{-1}: 1520 (m) (C═N of tetrazole ring), 1417 (s) (C—N stretch); ^{1}H nmr (90 MHz) in $CDCl_3$, δ: ddd at 3.15 (1H, H4a) [^2J(4a, 4b) = 17 Hz, ^3J(4a, 5) = 3.1 Hz, ^4J(4a, 6a) = 1.5 Hz], dd at 2.95 (1H, H4b) [^2J(4b, 4a) = −17 Hz, ^3J(4b, 5) = 2 Hz], set of multiplets from 2.42 to 1.92 (4H, H5, H6a, H7a, H7b), s at 1.78 (3H, C11 methyl), m at 1.60 to 1.33 (1H, H6b), s at 1.16 (3H, C9 methyl), and s at 0.81 (3H, C10 methyl). The carbon-13 nmr (proton decoupled and proton decoupled INEPT) data and assignments are given in Table 2. Mass spectra *m/z*: 192 (8) (M^+), 164 (5) (M − (N_2)), 163 (10) (164 − (H)), 149 (20) (164 − (CH_3)), 124 (15), 109 (9) (149 − (CH_2—CN)), 108 (25) (109 − (H)), 107 (33) (108 − (H)), 97 (79), 82 (100) (M − (N_2)). *Anal.* calcd. for $C_{10}H_{16}N_4$: C 62.47, H 8.39, N 29.14; found: C 62.35, H 8.39, N 29.12.

(ii) α-Camphidone 2

Fractions 23–36 from the above chromatography were combined and evaporated to dryness to yield a white solid, which was recrystallized from ethyl acetate (1.76 g, 5.3%) (mp 242–244°C in a sealed tube). Thin-layer chromatography showed that this product was pure; ir (Nujol) cm^{-1}: 3310 (w), 3220 (m) and 3090 (w) (all N—H stretchings), 1667 (s) (C═O); ^{1}H nmr (90 MHz) in $CDCl_3$, δ: broad m centred at 5.90 (1H, N3 H), dddd at 3.44 (1H, H4a) [^2J (4a, 4e) = −11.1 Hz, ^3J(4a, 5) = 3.5 Hz, ^3J(4a, NH) = 1–2 Hz, ^4J(4a, 6a) = 1.6 Hz], ddd at 2.99 (1H, H4e) [^2J(4e, 4a) = −11.1 Hz, ^3J(4e, 5) = 2 Hz), ^3J(4e, NH) = 2.0 Hz], set of m at 2.22 to 1.42 (5H, H5, H6a, H6b, H7a, H7b), 3 s at 1.10 (3H), 1.04 (3H), and 0.96 (3H) (C9, C10, and C11 methyls); NH-decoupled ^{1}H nmr (90 MHz) in $CDCl_3$, δ: ddd at 3.46 (1H, H4a) [^2J(4a, 4e) = 11.1 Hz, ^3J(4a, 5) = 3.5 Hz, ^4J(4a, 6a) = 1.6 Hz], dd at 3.01 (1H, H4e) [^2J(4a, 4e) = 11.1 Hz, ^3J(4e, 5) = 2.0 Hz], no N—H absorption, and the rest of the spectrum similar to the NH coupled spectrum. The carbon-13 magnetic resonance (proton decoupled and proton decoupled INEPT) data and assignments are given in Table 2. Mass spectra *m/z*: 167 (61) (M^+), 152 (97) (M − (CH_3)), 139 (6) (M − (CO)), 138 (15) (139 − (H)), 124 (27) (M − (HN═C═O)), 98 (94) (M − (Me_2C═CH—CH_2)), 69 (100) (Me_2C═CH—CH_2), 55 (73) (69 − (CH_2)).

Imine ester 4

Acetyl chloride (12 g) was slowly added to methanol (240 mL) over a period of 0.5 h (26). Amino amide **5** (2.0 g, 0.11 mol) was added and this solution was heated under reflux for 3 days while the reaction was monitored by tlc. The reaction mixture was concentrated to dryness and the solid obtained was dissolved in water (30 mL). This aqueous solution was made basic (pH 9–10) with dilute sodium bicarbonate solution and extracted with $CHCl_3$ (3 × 30 mL). The combined $CHCl_3$ extracts were dried with sodium sulfate and evaporated to dryness. A clear liquid (2.08 g) was obtained. After distillation (bp 85–90°C at 0.4 Torr), 1.60 g (74%) of a colourless liquid was obtained; tlc: R_f 0.55 in $CHCl_3$–EtOH (10:1, v:v); ir (thin film) cm^{-1}: 1745 (s) (O═C—OCH_3), 1655 (s) (C═N); ^{1}H nmr data (400 MHz) are given in Table 1. Carbon-13 nmr (proton decoupled and proton decoupled INEPT) data and assignments are given in Table 2. Mass spectra *m/z*: 197 (15) (M^+), 182 (11) (M − (CH_3)), 166 (12) (M − (OCH_3)), 138 (8) (M − (CO—OCH_3)), 128 (47) (Me_2C═CH—CH_2COOCH_3), 124 (47) (M − (CH_2—$COOCH_3$)), 96 (77), 69 (100). *Exact Mass* calcd. for $C_{11}H_{19}NO_2$: 197.1416; found (hrms, 64.8%): 197.1419.

N8-Phenylcarbamoylamino amide 6

A benzene solution (50 mL) of phenyl isocyanate (0.81 g, 0.006 mol) was added to a benzene solution (50 mL) of the amino amide **5** (1.09 g, 0.006 mol). Within 2 min a white solid started to appear. The mixture was stirred for an additional 16 h. The white solid suspended in the solution was filtered off, washed with fresh benzene (15 mL), and dried under suction (yield 1.78 g). This highly polar compound was recrystallized from EtOAc–MeOH (3:1, v:v) to give 1.07 g (60%) of **6**; mp 163–165°C; ir (Nujol) cm^{-1}: 3330 (m), 3200 (m) and 3080 (m) (all N—H stretch), 1675 (s) (C═O, urea), 1645 (s) (C═O, amide), 1595 (s) (C═C, aromatic); ^{1}H nmr (90 MHz) in DMSO-d_6, δ: br s at 8.18 (^{1}H, N14 proton), set of m at 7.46–6.80 (5H, aromatic), br m at 6.10 (H, N2 proton), m at 3.22–2.73 (3H, H7a, H7e, H4a), sets of m at 2.40–1.50 (3H, H4e, H6a, H5), m at 1.32–1.04 (1H, H6e), three s at 1.23 (3H), 0.92 (3H), and 0.80 (3H) (C10, C11, and C12 methyls). The spectrum also shows a br s at 8.38 (OH of methanol), s at 3.31 (H_2O from recrystallization and DMSO-d_6 solvent), s at 3.12 (CH_3 of methanol). The CH_3 and OH of methanol integrate for 0.85 mol of methanol of crystallization. Mass spectra *m/z*: 301 (3) (M^+), 286 (3) (M − (CH_3)), 209 (5) (M − (Ph—NH)), 182 (33) (M − (Ph—N═C═O)), 167 (11) (182 − (CH_3)), 139 (22) (182 − (NH═C═O)), 119 (100) (Ph—N═C═O), 101 (76), 98 (54) (139 − (CH_2—CH═CH_2)), 93 (74) (Ph—NH_2), 82 (72) (98 − NH_2). *Anal.* calcd. for $C_{17}H_{23}N_3O_2 \cdot 0.85\,CH_3OH \cdot 0.5\,H_2O$: C 63.50, H 8.18, N 12.45; found: C 63.84, H 8.05, N 12.31. The carbon-13 nmr

(proton decoupled and proton decoupled INEPT) data and assignments are given in Table 2. (The INEPT experiments also demonstrated the presence of methanol by the observance of a peak at 48.26 ppm.)

N8-Methylamino amide **7**

(*a*) Amino amide **5** (3.62 g, 0.02 mol) was dissolved in methylene chloride (50 mL). Magic Methyl® (97% methyl fluorosulphonate) (1.90 mL, 0.022 mol) was added to this solution over a period of 10 min (27). A white precipitate began forming immediately after the addition of the methyl fluorosulphonate. After stirring at room temperature for an additional 1.5 h, the methylene chloride was decanted from the white solid that had formed. This product was washed with cold methylene chloride (5 mL) and then suspended in 35 mL of methylene chloride. A 1 *N* solution of sodium hydroxide (30 mL) was added to the organic solution and the mixture was stirred for 5 min while the white solid dissolved. After separation of the two layers, the aqueous layer was extracted with chloroform (3 × 20 mL). The combined organic extracts were dried with sodium sulphate and evaporated to dryness. The white solid that remained was recrystallized from ethyl acetate to give 2.73 g (70%) of compound **7**; tlc: R_f 0.5 in $CHCl_3$–EtOH (10:1, v:v); mp 150–150°C; ir (Nujol) cm^{-1}: 3188 (m) (NH stretch), 1672–1664 (s) (C=O, amide band I overlapped by amide band II); ^1H nmr (90 MHz), δ: dd at 2.67 (^1H, H4a) [^2J(4a, 4e) = −18 Hz, ^3J(4a, 5) = 7 Hz], sets of m at 2.65–2.36 (2H, H7a, H7e), d at 2.22 (1H, H4e) [^2J(4e, 4a) = −18 Hz] overlapped by a br m at 2.32–1.94 (1H, H6a), s at 2.16 (3H, N8 methyl), m at 1.72 (1H, H5), m at 1.45–1.25 (1H, H6e), s at 1.24 (6H), and s at 1.08 (3H) (C10, C11, and C12 methyls). Carbon-13 nmr (proton decoupled, and proton decoupled INEPT) data and assignments are given in Table 2. Mass spectra *m/z*: 196 (100) (M^+), 181 (22) (M − (CH_3)), 153 (44) (M − (HN=C=O)), 138 (56) (181 − (HN=C=O) or 153 − (CH_3)), 127 (58), 124 (50) (138 − (CH_2)), 112 (96), 110 (89). *Exact Mass* calcd. for $C_{11}H_{20}N_2O$: 196.1576; found (hrms, 100%): 196.1578. *Anal.* calcd. for $C_{11}H_{20}N_2O$: C 67.31, H 10.27, N 14.27; found: C 66.78, H 10.38, N 14.13.

(*b*) A methanol solution of amino amide **5** (3.0 g, 0.0165 mol) and MeI (7.5 g, 0.0532 mol) was heated for 3 days at oil-bath temperature of 55–62°C in a pressure bottle. The hot solution was then filtered under gravity and the methanol removed to leave a pale yellow solid. Recrystallization from methanol/pentane (1:1, v:v) gave a white hydroiodide salt (3.55 g). The filtrate from this salt was diluted with water and made basic (pH 12) with dilute NaOH. Extraction with $CHCl_3$ (2 × 30 mL) gave, after drying and evaporation, a yellowish solid (0.65 g, 20% crude). The hydroiodide salt from above was converted to the free base by dissolving it in water, adjusting to pH 10 with dilute NaOH, and extraction with $CHCl_3$ (3 × 60 mL). After drying and evaporation to dryness, the combined $CHCl_3$ extracts yielded a white solid (1.86 g, 58% crude). The two solids were identified as the *N*-methyl amino amide **7** by ir, ms, and ^1H nmr. *N*-Methylamino amide **7** could also be prepared by reacting the amino amide **5** and MeI in isopropyl alcohol at room temperature but the yield of recrystallized product was only 37%.

Acknowledgements

N.R.H. is grateful for financial support through operating grants from the Natural Sciences and Engineering Research Council of Canada and the University of Manitoba Research Board. L.T.J.D. thanks the Medical Research Council of Canada for financial support. The 400-MHz proton magnetic resonance spectra were obtained at the University of Alberta through the kind cooperation of Thomas Nakashima. The high resolution mass spectra were obtained at the University of Alberta through the courtesy of Hsing-Jang Liu. Mr. Wayne Blonski is thanked for his help with the spectral simulations.

1. K. F. SCHMIDT. Angew. Chem. **36**, 511 (1923).
2. L. G. DONARUMA and W. Z. HELDT. Org. React. **11**, 1 (1960).
3. G. R. KROW. Tetrahedron Report Number R106, Tetrahedron, **37**, 1283 (1981).
4. K. F. SCHMIDT. U.S. Patent No. 2,029,799 (1936); Chem. Abstr. **30**, 1950 (1936).
5. J. W. APSIMON and N. R. HUNTER. Tetrahedron Lett. 187 (1972).
6. (*a*) G. A. MORRIS and R. FREEMAN. J. Am. Chem. Soc. **101**, 760 (1979); (*b*) D. M. DODDRELL and D. T. PEGG. J. Am. Chem. Soc. **102**, 6388 (1980); (*c*) D. P. BURUM and R. R. ERNST. J. Magn. Reson. **39**, 163 (1980).
7. F. R. AHMED, S. R. HALL, M. E. PIPPY, and C. P. HUBER. N.R.C. Crystallographic Programs for the IBM/360 System. Accession Nos. 133–147. *In* J. Appl. Crystallogr. **6**, 309 (1973).
8. J. M. STEWART. The X-ray system of crystallographic computer programs. Computer Science Center, University of Maryland, College Park, MD. 1976.
9. A. J. C. WILSON. Nature, **150**, 152 (1942).
10. P. MAIN, S. J. FISKE, S. E. HULL, L. LESSINGER, G. GERMAIN, J.-P. DECLERCQ, and M. M. WOOLFSON. MULTAN80. A system of computer programs for the automatic solution of crystal structures from X-ray diffraction data. University of York, England. 1980.
11. C. K. JOHNSON. ORTEP-II. Report ORNL-5138. Oak Ridge National Laboratory, Oak Ridge, TN. 1976.
12. A. L. LEHNINGER. Biochemistry. 2nd ed. Worth Publishers Inc., New York. 1977. p. 127.
13. (*a*) T. SASAKI, S. EGUCHI, and T. TORU. J. Org. Chem. **36**, 2454 (1971); (*b*) G. DI MAIO and V. PERMUTTI. Tetrahedron, **22**, 2059 (1966).
14. (*a*) J. E. BALDWIN. J. Chem. Soc. Chem. Commun. 734 (1976); (*b*) J. E. BALDWIN, J. CUTTING, W. DUPONT, L. KRUSE, L. SILBERMAN, and R. C. THOMAS. J. Chem. Soc. Chem. Commun. 736 (1976); (*c*) J. E. BALDWIN. J. Chem. Soc. Chem. Commun. 738 (1976).
15. R. C. ELDERFIELD and E. T. LOSIN. J. Org. Chem. **26**, 1072 (1961).
16. J. MEINWALD and E. FRAUENGLASS. J. Am. Chem. Soc. **82**, 5235 (1960).
17. R. R. SAUERS and J. A. BEISLER. J. Org. Chem. **29**, 210 (1964).
18. (*a*) T. SATO and H. OBASE. Tetrahedron Lett. 1633 (1967); (*b*) T. SATO, T. INOUE, and K. YAMAMOTO. Bull. Chem. Soc. Jpn. **45**, 1176 (1972).
19. R. W. COTTINGHAM. J. Org. Chem. **25**, 1473 (1960).
20. (*a*) G. E. HAWKES, K. HERWIG, and J. D. ROBERTS. J. Org. Chem. **39**, 1017 (1974); (*b*) F. BAERT and R. FOURET. Acta Crystallogr. Sect. B, **34**, 2546 (1978).
21. P. A. S. SMITH and J. P. HORWITZ. J. Am. Chem. Soc. **72**, 3718 (1950).
22. G. R. KROW and S. SZEZEPANSKI. Tetrahedron Lett. 4593 (1980).
23. M. F. MURRAY, B. A. JOHNSON, R. L. PEDERSON, and A. C. OTT. J. Am. Chem. Soc. **78**, 981 (1956).
24. (*a*) R. R. SAUERS and R. J. TUCKER. J. Org. Chem. **28**, 876 (1963); (*b*) J. BERSON and D. WILLNER. J. Am. Chem. Soc. **84**, 675 (1962); (*c*) C. L. ARCUS, R. E. MARKS, and R. VITTERLAIN. Chem. Ind. (London), 1193 (1960).
25. M. F. HAWTHORNE, W. D. EMMONS, and K. S. MCCALLUM. J. Am. Chem. Soc. **80**, 6393 (1958).
26. L. F. FIESER and M. FIESER. Reagents for organic synthesis. Vol. 1. John Wiley and Sons, Inc., New York. 1967. p. 668.
27. M. G. AHMED, R. W. ALDER, G. H. JAMES, M. L. SINNOTT, and M. C. WHITING. J. Chem. Soc. Chem. Commun. 1533 (1968).

Can. J. Chem. Downloaded from www.nrcresearchpress.com by 80.58.250.72 on 09/07/12
For personal use only.

Chemical constituents of *Lansium anamallayanum* Bedd.

K. K. PURUSHOTHAMAN, A. SARADA, AND A. SARASWATHY
Captain Srinivasa Murti Drug Research Institute for Ayurveda, Arumbakkam, Madras-600106, India

Received May 12, 1986

This paper is dedicated to Dr. O. E. (Ted) Edwards

K. K. PURUSHOTHAMAN, A. SARADA, and A. SARASWATHY. Can. J. Chem. **65**, 150 (1987).

Several triterpenoids and steroids have been isolated from *Lansium anamallayanum* Bedd. The leaves yielded an unknown triterpene lansitriol and four new steroids, lansisterone *E* **1**, lansisterone *Z* **2**, lansisterol B, and lansisterol A **3**. From the bark, a new triterpene lactone designated as lansilactone **4** was isolated. Structures for compounds **1**, **2**, **3**, and **4** have been proposed as 3β,4β-dihydroxy-17(20)-*cis* 5α-pregna-16-one; 3β,4β-dihydroxy-17(20)-*trans* 5α-pregna-16-one; 24-methylene 3β,4β,7β, 20-tetrahydroxy cholest-5-ene, and 25,26,27-lanostane trisnorlactone.

K. K. PURUSHOTHAMAN, A. SARADA et A. SARASWATHY. Can. J. Chem. **65**, 150 (1987).

On a isolé plusieurs triterpènoïdes et stéroïdes du *Lansium anamallayanum* Bedd. Les feuilles ont fourni un triterpène inconnu, le lansitriol, ainsi que quatre nouveaux stéroïdes, la lansistérone-(E) (**1**), la lansistérone-(Z) (**2**), le lansistérol B et le lansitérol A (**3**). À partir de l'écorce, on a isolé une nouvelle lactone triterpénique que l'on a appelé lansilactone (**4**). On propose que les structures des composés **1**, **2**, **3** et **4** sont respectivement celles de la dihydroxy-3β,4β 17(20)-*cis* 5α-pregnanone-16; de la dihydroxy-3β,4β 17(20)-*trans* 5α-pregnanone-16; du méthylène-24 tétrahydroxy-3β,4β,7β,20 cholestène-5 et de la lanostane trisnor-25,26,27 lactone.

[Traduit par la revue]

Can. J. Chem. Downloaded from www.nrcresearchpress.com by 190.90.36.8 on 09/07/12
For personal use only.

From the leaves of *Lansium anamallayanum* Bedd. (Meliaceae), syn: *Reinwardtiodendron anamallayanum* (Bedd) Saldanha (1), we have isolated five new compounds: lansitriol, lansisterone *E* (**1**), lansisterone *Z* (**2**), lansisterol B, and lansisterol A (**3**). The bark yielded a new triterpene lactone, lansilactone (**4**). Both the bark and the leaves yielded, as well, α-amyrin acetate, *n*-octacosanol, α-amyrin, and β-sitosterol.

Lansisterone E *(1)*

Lansisterone *E* (**1**), mp 205°C, $[\alpha]_D^{30}$ −130°C (*c* 1, in chloroform), $C_{21}H_{32}O_3$ (M^+ 332), ir ν_{max}: 3425 (hydroxyls), 1725, 1660 cm^{-1} (α,β-unsaturated five-membered ketone), answered the Libermann Burchard test characteristic of steroids. The formation of a diacetate showed the presence of two hydroxyls. All three oxygens of the molecule were accounted for by these functionalities. The ^1H nmr spectrum more precisely settled the position of the α,β-unsaturated moiety. There were signals for three methyls, two of them were tertiary and the other a vinylic methyl at δ 1.85 (d, 3H, C=C(H)CH_3). There was one olefinic proton as a quartet at δ 6.5, showing that the vinylic methyl and the vinylic proton are attached to the same carbon.

The two hydroxyls present in the compound are vicinal, as **1** readily underwent cleavage by periodate to yield the corresponding dialdehyde. Of the two aldehyde protons, one appeared as a triplet (δ 9.74) and the other as a doublet (δ 9.86) in the ^1H nmr.

In the ^1H nmr of **1**, there was a proton at δ 3.75 as a multiplet, having one diaxial and two axial–equatorial interactions. Both the multiplicity and the chemical shift were in agreement for the 3β-hydroxyl. The H4 appeared as dd at δ 3.98 (J_{3-4} = 3.5 Hz and J_{4-5} = 3.5 Hz), which could be ascribed to the equatorial H4 proton. Therefore the 4-hydroxyl is axial. The coupling constant of H4–H5 was further deduced by irradiation at δ 3.75, which reduced the H4 double doublet into a doublet (3.5 Hz), which agrees with H4 equatorial and H5 axial coupling. The compound, therefore, belongs to the 5α-pregnane series, which is found to occur abundantly in nature. Lansisterone *E* is assigned structure 3β,4β-dihydroxy-17(20)-*cis* 5α-pregna-16-one (**1**). The ^{13}C nmr measurements were in agreement with the structure.

Lansisterone Z *(2)*

During the course of acetylation of **1**, two acetates were formed. One isomer of the acetate $C_{25}H_{36}O_5$, mp 176°C, was assigned from its ^1H nmr spectrum as the acetate corresponding to **1**. The other isomer, mp 193°C, had, as a distinguishing feature, the olefinic hydrogen appearing as a quartet at δ 5.75 instead of at δ 6.50 as observed in the diacetate of **1**. In **1**, the vinylic hydrogen is deshielded due to the proximity of the carbonyl. In **2**, this hydrogen is disposed away from the carbonyl and therefore appeared at higher field. So the acetate having mp 193°C corresponds to the *Z* isomer (**2**). The lansisterone *Z* (**2**) itself was not separated from the crude extract but its presence could be detected spectroscopically.

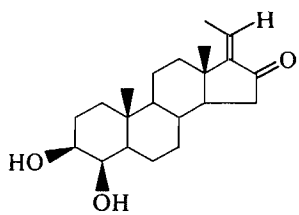

1

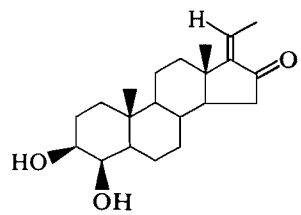

2

Lansisterol A (3)

Lansisterol A, mp 130°C, $[\alpha]_D^{30}$ −107°C (*c* 2, in chloroform), $C_{28}H_{46}O_4$ (M^+ 446), had three secondary and one tertiary hydroxyl groups, δ 64.82 (d), 71.84 (d), 78.49 (d), and 74.92 (s) and δ H 3.58 (H3), 3.93 (H7), and 4.15 (H4) shifted to, in the triacetate, δ H 4.85, 5.05, and 5.52 (three hydroxy methines), δ C 156.2 (s) and 106.22 (t) and δ H 4.72 (2H), an exomethylene, and δ C 146.55 (s) and 129.48 (d) and δ H 5.83 (H6), trisubstituted double bond, and gave a positive colour test for steroids. The compound is tetracarbocyclic. The tertiary nature of one hydroxyl was further proved by the ir spectrum of the triacetate, which still retained the hydroxyl absorption at 3480 cm^{-1}. There were five methyls at δ H 0.88 (s, 3H, —CH_3), 1.0 (s, 3H, —CH_3), 1.1 and 1.2 (s, 3H, each, isopropyl *methyls*), and 1.3 (s, 3H, —CH_3). The absorption at 1.3 should correspond to a methyl group attached to an oxygen-bearing carbon (C20). The presence of a CH_2—$C(CH_2)$—$CH(CH_3)_2$ moiety in the side chain was concluded from the

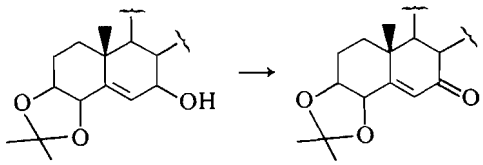

infrared and mass spectra, 1660, 890 (exomethylene), 1389, 1385 cm^{-1} (isopropyl group) and the mass fragment of 83 amu. Lansisterol A underwent periodate oxidation to give a dialdehyde without loss of a carbon atom. Of the two aldehyde protons, one was a triplet (δ 9.60) and the other a singlet (δ 9.35) and the corresponding hydroxy methines, which disappeared, were δ 3.58 (H3) and 4.15 (H4). The chemical shifts of the two hydroxy methines suggested that H4, H7 were allylic. Lansisterol A formed an acetonide that was smoothly oxidized to an α,β-unsaturated ketone (ν_{max} 1672 cm^{-1} and λ_{max} 235 nm).

An examination of the chemical shifts and the multiplicities of ^1H nmr of lansisterol A, the acetonide, and the corresponding ketone indicated that in **3** the signal at 3.93 corresponds to H7.

Double irradiation studies on the triacetate of **3** confirmed the various proton assignments and their configurations. Irradiation of the H7 proton at δ 5.05 (dd, J_{6-7} = 4.5 Hz, J_{7-8} = 7.5 Hz) collapsed the H6 signal at 5.95 (d, J_{6-7} = 4.5 Hz) to a singlet. Irradiation of the H3 proton at δ 4.85 (m) similarly collapsed the H4 proton at 5.52 (d, J_{3-4} = 4.5 Hz) to a singlet and irradiation of the H6 proton at 5.95 (d, J_{6-7} = 4.5 Hz) collapsed the H7 (dd) at 5.05 to a doublet of 7.5 Hz. From the foregoing experiments and the observed multiplicities (2), the structure for lansisterol A is proposed as 24-methylene 3β,4β,7β,20-tetrahydroxy cholest-5-ene (**3**).

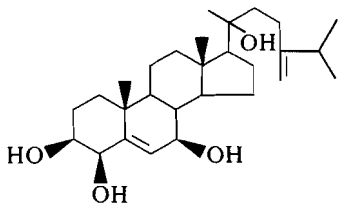

3

Lansilactone (4)

Lansilactone, $C_{27}H_{44}O_3$, ir ν_{max}: 3450 (hydroxyl), 1750 (γ-lactone) cm^{-1}, gave a colour reaction for triterpene with tin and thionyl chloride. The ^1H nmr showed six C-methyls at δ 0.82, 0.84, 0.89, 0.92, 0.95, and 1.35; the last signal indicated that the methyl is attached to a carbon carrying the lactonic oxygen. Formation of such a lactone by the elimination of three carbon atoms from the side chain had been earlier reported by Beillmann and Ourisson (3) while suggesting a structure for diterocarpol trisnorlactone. Lansilactone formed a monoacetate; the shift of hydroxy methine was in agreement with 3β-hydroxyl. Further confirmation of the 3β-hydroxyl was obtained by observing the chemical shift of 4α,α-dimethyls in the ^1H nmr of the ketone taken in $CDCl_3$, and the shift (0.36 ppm) by the addition of 30% benzene was in agreement with the reported value (0.33 ppm (4)). Diterocarpol trisnorlactone, which belongs to the dammarane series, and lansilactone, though having identical molecular formulae and functional groups, were not found to be identical by direct comparison. On biogenetic grounds and in conformity with the lanostane series, lansilactone is assigned structure **4**.

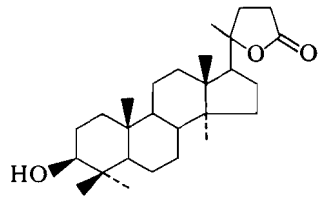

4

Experimental

Melting points are uncorrected and were determined in open-ended capillaries and expressed in degrees centigrade. Thin-layer chromatographic analyses were performed on silica gel-G (Mira chem), plates developed by ceric sulphate. Known compounds have been identified by their mp, mmp, ir, and specific rotation. Infrared spectra were obtained on a Perkin–Elmer 337 instrument using KBr pellets, and the uv spectra were recorded in methanol solution on a Pye–Unicam 1800 uv spectrophotometer. The ^1H nmr spectra were recorded on a Varian-XL 100 at 100 MHz or on an EM 390 90-MHz spectrometer with TMS as internal standard. The ^{13}C nmr spectra were recorded at 25.2 MHz. The chemical shifts are expressed as δ ppm.

Leaves and bark of *Lansium anamallayanum* Bedd. were collected at Bhimashankar, State of Maharashtra, India during the month of July 1981, shade dried, and coarsely powdered. Specimens of these samples were kept in the herbarium of this Institute under the registry number 277.

The coarsely powdered leaves (1.5 kg) were extracted successively with *n*-hexane, chloroform, and alcohol. Each extraction was carried out in an aspirator bottle by the cold percolation method for a period of 72 h. The solvents were removed (up to 80%) by distillation of a water bath at room temperature and then *in vacuo*. The hexane and chloroform extracts showed similar spots on tlc, so they were combined. The combined extract (26.5 g) was chromatographed over silica gel (Acme 100–200 mesh, 1:22) which was eluted with solvents of increasing polarity in the order hexane, hexane–benzene, benzene, chloroform, and ethyl acetate. The hexane eluate after removal of the waxy material afforded *n*-octacosanol and a gum, which on crystallization using methanol gave α-amyrin (250 mg).

Benzene-eluted fractions on concentration resulted in the isolation of β-sitosterol (0.85 g).

Isolation of lansitriol

The column was then eluted with chloroform and the eluted material was further chromatographed through a column of neutral alumina (Acme) using hexane, benzene, chloroform, and ethyl acetate and their mixtures. The residue obtained from the chloroform–ethyl acetate (20:1) eluates crystallized from benzene to give lansitriol (200 mg), mp 178°C; $[\alpha]_D^{30}$ +35° (*c* 1, in chloroform); ν_{max}: 3400, 1030 cm^{-1}; ^1H nmr ($CDCl_3$) δ: 0.33 and 0.55 (d, 1H each, *J* = 5 Hz, cyclopropane protons), 0.78 (s, 3H, CH_3), 0.88 (s, 3H, CH_3), 0.94 (s, 6H, 2 × CH_3), 1.13 (s, 3H, CH_3), 1.19 (s, 6H, 2 × CH_3), and 3.3 (m, 2H, C*H*—OH); ^{13}C nmr ($CDCl_3$) δ: 79.64 (s), 78.84 (s), 73.23 (d); *m/z*: 460, 447, 427, 409, 399, 320, 315, 255, 241, 229, 227, 215, 203, 202, 191, 189, 177, 175, 173, 171, 163, 162, 161, 159, 157, 149, 145, 135, 134, 133, 131, 127, 121, 119, 95, 71, 69, 67, 59 (100%), 55, 43, 41. *Anal.* calcd. for $C_{30}H_{52}O_3$: C 78.25, H 11.31; found: C 78.50, H 11.15.

Isolation of lansisterol B

Fractions eluted with chloroform – ethyl acetate (10:1) were combined and crystallized from alcohol to give lansisterol B (130 mg), mp 238°C; ν_{max}: 3400, 1075, 965, 895 cm^{-1}; ^1H nmr ($CDCl_3$) δ: 0.98 (s, 6H, 2 × CH_3), 1.06 (s, 3H, CH_3), 1.13 (d, 6H, 2 × CH_3), 2.56 (d, 1H, $W_{1/2}$ = 4.5 Hz), 3.36 (m, 1H, C*H*—OH), 4.0 (dd, *J* = 8.5 Hz and 4.5 Hz, 1H), 4.25 (m, 1H, C*H*—OH), 4.85 (d, 2H, *J* = 6.5 Hz, exomethylene), 5.3 (bd, 1H, olefinic proton). *Anal.* calcd. for $C_{28}H_{44}O_3$: C 78.50, H 10.28; found: C 78.56, H 10.21.

Isolation of lansisterone E *(1) and lansisterone* Z *(2)*

Eluates of a mixture of chloroform and ethyl acetate (1:1) were

Can. J. Chem. Downloaded from www.nrcresearchpress.com by 190.90.36.8 on 09/07/12
For personal use only.

Can. J. Chem. Downloaded from www.nrcresearchpress.com by 190.90.36.8 on 09/07/12
For personal use only.

combined and rechromatographed over a short column of neutral alumina. Crystallization of the solid from chloroform–benzene gave **1** (240 mg), mp 205°C; $[\alpha]_D^{30}$ −130° (*c* 1, in chloroform); ν_{max}: 3425, 1725, 1660 cm^{-1}; ^1H nmr ($CDCl_3$) δ: 0.82 (s, 3H, C*H*$_3$), 1.0 (s, 3H, C*H*$_3$), 1.85 (d, 3H, C=C(H)C*H*$_3$), 3.75 (m, 1H, C*H*—OH, H3), 3.98 (dd, J_{3-4} = 3.5 Hz and J_{4-5} = 3.5 Hz, 1H, C*H*—OH, H4), 6.5 (q, 1H, C=C(*H*)CH$_3$, olefinic proton); ^{13}C nmr ($CDCl_3$) δ: 37.9 (t), 33.5 (t), 69.0 (d), 69.2 (d), 40.5 (d), 12.4 (t), 36.2 (t), 34.2 (d), 50 (d), 37.0 (s), 20.7 (t), 31.8 (t), 43.4 (s), 53.9 (d), 38.1 (t), 206.7 (s), 147.9 (s), 13.2 (q), 17.6 (q), 129.3 (d), 27.40 (q); *m/z*: 332, 317, 314, 299, 281, 234, 216, 201, 191, 190, 175, 161, 149, 147, 143, 135, 133, 123, 121, 119, 109, 107, 106, 105, 95, 94, 93, 90, 83 (100%), 81, 80, 79 (81.22%), 78, 77, 69, 67, 65, 57, 55 (73.21%), 34. *Anal.* calcd. for $C_{21}H_{32}O_3$: C 75.91, H 9.64; found: C 75.85, H 9.64.

The presence of lansisterone *Z* (**2**) was indirectly concluded during acetylation of **1** (see later).

Isolation of lanisterol A (3)

Ethyl acetate fractions from the main column yielded a gum, which on crystallization from dilute acetone afforded **3** (600 mg), mp 138°C; $[\alpha]_D^{30}$ −107° (*c* 2, in chloroform); ν_{max} (CCl_4): 3450, 1660, 1389, 1385, 890 cm^{-1}; ^1H nmr ($CDCl_3$) δ: 0.88 (s, 3H, 18-C*H*$_3$), 1.0 (s, 3H, 19-C*H*$_3$), 1.1 (s, 3H, —CH(C*H*$_3$)CH$_3$), 1.2 (s, 3H, —CH(CH$_3$)C*H*$_3$), 1.3 (s, 3H, 21-C*H*$_3$), 3.58 (m, 1H, —C*H*—OH, H3), 3.98 (m, 1H, —C*H*—OH, H7), 4.15 (m, 1H, C*H*, —OH, H4), 4.72 (d, 2H, *J* = 6 Hz, exomethylene), 5.83 (d, 1H, *J* = 5 Hz, olefinic proton, H6). The ^{13}C nmr spectrum taken in $CDCl_3$ and CD_3COCD_3 showed a singlet at 156.2 (C24), a triplet at 106.22 (C28), a singlet at 146.55 (C5), a doublet at 129.48 (C6), a singlet at 74.92 (C21), and three doublets at 78.49, 71.84, and 64.82 (C4, C7, and C3) respectively. Mass spectra *m/z*: 446, 428, 390, 349, 313, 295, 270, 173, 159, 157, 147, 145, 135, 133, 131, 129, 123, 121, 119, 109, 107, 105, 97, 95, 93, 91, 83, 81, 79, 77, 69, 67, 55, 43, 28 (base). *Anal.* calcd. for $C_{28}H_{46}O_4$: C 75.34, H 10.55; found: C 75.28, H 10.60.

Later fractions of ethyl acetate yielded a gummy material containing a few crystals. The crystals were washed with methanol and recrystallized from absolute alcohol to get sitosterol-3β-glucopyranoside (200 mg), mp 288°C. It was hydrolysed to get β-sitosterol, mp 131°C.

Isolation of lansilactone (4)

The coarsely powdered bark (1.5 kg) of *Lansium anamallayanum* Bedd. was extracted by the cold percolation method. The hexane and chloroform extracts were combined and chromatographed over silica gel (1:22). The column was eluted with solvents in the order hexane, benzene, chloroform, and ethyl acetate and their mixtures.

Hexane eluates yielded α-amyrin acetate. Material obtained from hexane–benzene mixtures was identified as *n*-octacosanol and α-amyrin. Fractions eluted with benzene gave β-sitosterol. Benzene–chloroform (1:1) and chloroform fractions were combined and rechromatographed and the chloroform eluate on crystallization with benzene–hexane afforded lansilactone (4) (200 mg), mp 239°C; $[\alpha]_D^{30}$ +20° (*c* 1, in chloroform); ν_{max}: 3450, 2920, 1750, 1450, 1380, 1270, 1255, 1080, 945 cm^{-1}; ^1H nmr ($CDCl_3$) δ: 0.82, 0.84, 0.89, 0.92, 0.95, and 1.35, each (s, 3H, C*H*$_3$), and 3.4 (t, 1H, —C*H*—OH, H3); ^{13}C nmr ($CDCl_3$) δ: 176.8 (s), 90.13 (s), 75.8 (d). *Anal.* calcd. for $C_{27}H_{44}O_3$: C 77.90, H 10.58; found: C 78.40, H 10.20.

Acetylation of 1

Lansisterone *E* (70 mg) in pyridine (2 mL) was treated with freshly distilled acetic anhydride (3 mL) and the mixture was heated for 3 h on a water bath. The product was worked up in the usual way and then purified on silica gel. The material (40 mg) eluted with hexane crystallized from hexane (minimum) giving the diacetate (35 mg), mp 176°C; ^1H nmr δ: 0.88 (s, 3H, C*H*$_3$), 0.98 (s, 3H, C*H*$_3$), 1.93 (d, *J* = 7 Hz, 3H, C=C(H)C*H*$_3$), 2.06 (s, 3H, —O—CO—C*H*$_3$), 2.12 (s, 3H, —O—CO—C*H*$_3$), 4.97 (bm, 1H, —C*H*—OAc, H3), 5.28 (dd, *J* = 3 and 4 Hz, 1H, —C*H*—OAc, H4), 6.5 (q, 1H, C=C(*H*)CH$_3$, olefinic proton); ^{13}C nmr ($CDCl_3$) δ: 206.23 (s), 170.38 (s), 170.30 (s), 147.78 (s), 130.10 (d), 69.90 (d), 69.2 (d), 53.85 (d), 49.93 (d), 43.32 (s), 39.42 (d), 39.42 (t), 37.83 (t), 37.16 (s), 36.15 (t), 33.48 (d), 32.27 (t), 31.61 (t), 27.14 (q), 21.21 (q), 21.09 (q), 20.64 (t), 17.63 (q), 13.15 (q), 12.5 (t); *m/z*: 416, 402, 401 (100%), 356, 314, 299, 296, 281, 177, 175, 163, 161, 159, 149, 145, 136, 135, 133, 131, 123, 121, 119, 117, 109, 107, 105, 95, 93, 91, 83, 81, 79, 76, 67, 55, 53. *Anal.* calcd. for $C_{25}H_{36}O_5$: C 72.11, H 8.65; found: C 72.04, H 8.53.

Isolation of lansisterone Z (2) acetate

The column on further elution yielded yet another 20 mg of a compound that showed a different spot. The product was further rechromatographed and gave **2** acetate. Subsequently further runs of acetylation were carried to separate the acetate in a pure form, which was crystallized from alcohol, mp 193°C; ν_{max} (CCl_4): 1744, 1722 (enone), 1650 cm^{-1}; ^1H nmr ($CDCl_3$) δ: 0.9 (s, 6H, 2 × CH$_3$), 1.88 (s, 6H, 2 × —O—CO—C*H*$_3$), 2.08 (s, 3H, 21-C*H*$_3$), 4.98 (m, 1H, —C*H*—OAc, H3), 5.30 (dd, *J* = 3 and 4 Hz, 1H, C*H*—OAc, H4), 5.75 (q, 1H, C=C(*H*)CH$_3$); ^{13}C nmr ($CDCl_3$) δ: 208.46 (s), 170.38 (s), 170.30 (s), 148.21 (s), 130.10 (d), 69.90 (d), 69.20 (d), 54.07 (d), 49.43 (d), 43.24 (s), 39.42 (d), 39.42 (t), 37.83 (t), 37.2 (s), 35.62 (t), 33.82 (d), 32.27 (t), 31.61 (t), 27.14 (q), 27.21 (q), 21.09 (q), 20.64 (t), 19.65 (q), 14.04 (q), 12.50 (t). *Anal.* calcd. for $C_{25}H_{30}O_5$: C 72.11, H 8.65; found: C 72.04, H 8.7.

Periodate oxidation of 1

Lansisterone *E* (40 mg) in methanol (2 mL) was treated with potassium metaperiodate solution (100 mg in 2 mL of water) and kept aside for 24 h. Methanol was removed *in vacuo*. Water was added and the product extracted into chloroform. Removal of the solvent by distillation gave the dialdehyde gum (25 mg), ^1H nmr ($CDCl_3$) δ: 9.74 (t, 1H, —CH$_2$—C*H*O), 9.86 (d, 1H, —CH—C*H*O). *Anal.* calcd. for $C_{21}H_{30}O_3$: C 76.37, H 9.14; found: C 76.20, H 9.04.

Acetonide of 1

A suspension of **1** (40 mg) and anhydrous copper sulphate (200 mg) in anhydrous acetone (10 mL) was refluxed on a water bath for 24 h. This suspension was filtered and evaporation of the filtrate gave the acetonide gum (25 mg). *Anal.* calcd. for $C_{24}H_{36}O_5$: C 71.29, H 8.91; found: C 71.35, H 8.85.

Jones oxidation of 1

Lansisterone *E* (85 mg) in dry acetone (3 mL) was oxidized with Jones reagent with constant shaking for 5 min at room temperature. The excess reagent was destroyed by adding methanol, diluted with water, and extracted with chloroform. The product was absorbed on silica gel. Elution with benzene yielded ketone (60 mg), which was crystallized from benzene–hexane (55 mg), mp 251°C; ^1H nmr (CD_3OD) δ: 0.85 (s, 3H, C*H*$_3$), 1.02 (s, 3H, —C*H*$_3$), 1.84 (d, *J* = 7 Hz, 3H, C=C(H)C*H*$_3$), and 6.46 (q, 1H, C=C(*H*)CH$_3$); ^{13}C nmr (CD_3OD) δ: 208.43 (s), 174.94 (s), 177.31 (s) for carbonyl carbons; *m/z*: 328, 303, 287, 243, 241, 219, 218, 201, 135, 131, 129, 128, 123, 122, 121, 119, 109, 108, 107, 105, 95, 93, 92, 91 (100%), 83, 81, 79, 77, 69, 67, 65, 55, 53. *Anal.* calcd. for $C_{21}H_{28}O_3$: C 76.83, H 8.54; found: C 76.75, H 8.34.

Acetylation of 3

Compound **3** (100 mg) was acetylated in pyridine (3 mL) and acetic anhydride (2 mL) by heating on a water bath. After 2.5 h, reaction was completed. The product (60 mg) obtained after the usual work-up was crystallized from dichloromethane and alcohol; ν_{max}: 3480, 2930, 1740, 1720, 1460, 1370, 1240, 1038, 890 cm^{-1}; ^1H nmr ($CDCl_3$) δ: 0.85 (s, 3H, 18-C*H*$_3$), 1.0 (s, 3H, 19-C*H*$_3$), 1.08 (s, 3H, —CH(C*H*$_3$)CH$_3$), 1.15 (s, 3H, —CH(CH$_3$)C*H*$_3$), 1.30 (s, 3H, C(OH)—C*H*$_3$), 1.98 (s, 3H, —O—COC*H*$_3$), 2.04 (s, 6H, 2 × O—COC*H*$_3$), 4.72 (d, *J* = 6 Hz, 2H, exomethylene), 4.85 (m, 1H, —C*H*—OAc, H3), 5.05 (dd, J_{6-7} = 4.5 Hz and J_{7-8} = 7.5 Hz, 1H, C*H*—OAc, H7), 5.52 (d, J_{4-3} = 4.5 Hz, 1H, C*H*—OAc, H4), and 5.95 (d, J_{6-7} = 4.5 Hz, H6, olefinic proton); ^{13}C nmr ($CDCl_3$) δ: 170.32 (s), 170.19 (s), 169.65 (s), 156.20 (s), 143.82 (s), 128.28 (d), 106.29 (t), 74.98 (s), 74.92 (d), 72.12 (d), 67.41 (d), 57.84 (d), 49.14 (d), 43.29 (d), 42.50 (s), 42.24 (t), 39.17 (t), 36.90 (s), 36.26 (t), 35.09 (d), 33.91 (d), 28.79 (t), 26.11 (q), 23.53 (t), 22.37 (t), 22.27 (t), 21.90 (q), 21.88 (q), 21.25 (q), 21.18 (q), 21.01 (q), 19.97 (t), 13.72 (q), 13.06 (q). *Anal.* calcd. for $C_{34}H_{52}O_7$: C 71.34, H 9.09; found: C 71.41, H 9.13.

Can. J. Chem. Downloaded from www.nrcresearchpress.com by 190.90.36.8 on 09/07/12
For personal use only.

Acetonide of 3

A mixture of **3** (120 mg) and anhydrous copper sulphate (3 g) in permanganate-distilled acetone (4 mL) was refluxed on a water bath for 3 days. It was diluted with acetone and filtered, then purified by chromatography (100 mg), mp 202°C; ^{1}H nmr ($CDCl_3$) δ: 0.85 (s, 3H, 18-CH_3), 0.97 (s, 3H, 19-CH_3), 1.04 (s, 6H, —CH(CH_3)CH_3), 1.16 (s, 3H, —C(OH)—CH_3), 1.29 (s, 6H, C(CH_3)CH_3), 3.6 (m, 1H, —C*H*—O—(O)C(Me)Me, H3), 3.95 (m, 1H, C*H*—OH, H7), 4.15 (d, J_{4-3} = 4.5 Hz, 1H, C*H*—O—(O)C(Me)Me, H4), 4.72 (d, J = 6 Hz, 2H, exomethylene), and 5.85 (d, J_{6-7} = 4.5 Hz, 1H, olefinic proton). *Anal.* calcd. for $C_{31}H_{50}O_4$: C 76.54, H 10.29; found: C 76.46, H 10.35.

Acetylation of 3 acetonide

Lansisterol A acetonide (50 mg) was acetylated in pyridine – acetic anhydride (1:1) by heating on a water bath for 2 h. Crystals (40 mg) from benzene–hexane, mp 169°C; ν_{max}: 3500, 2950, 1750, 1380, 1250, 1065, 1055, 1020, 930, 890 cm^{-1}; ^{1}H nmr ($CDCl_3$) δ: 0.8 (s, 3H, 18-CH_3), 0.9 (s, 3H, 19-CH_3), 1.03 (s, 3H, —CH(CH$_3$)CH_3), 1.1 (s, 3H, —CH(CH_3)CH$_3$), 1.2 (s, 3H, —C(OH)—CH_3), 1.3 (s, 3H, —O—(O)C(CH_3)CH$_3$), 1.53 (s, 3H, —O—(O)C(CH$_3$)CH_3), 2.07 (s, 3H, —O—CO—CH_3), 4.17 (m, 1H, —C*H*—O—C(Me)Me), 4.43 (dd, J_{6-7} = 4.5 Hz and J_{7-8} = 7.8 Hz, —C*H*—OAc, H7), 4.72 (d, J = 6 Hz, 2H, exomethylene), 5.06 (d, J_{4-3} = 4.5 Hz, 1H, —C*H*—O—C(Me)Me, H4), 5.9 (d, J_{6-7} = 4.5 Hz, olefinic proton, H6). *Anal.* calcd. for $C_{33}H_{52}O_5$: C 74.96, H 9.85; found: C 74.85, H 9.60.

Jones oxidation of 3 acetonide

Compound **3** acetonide (50 mg) was oxidized with Jones reagent as before to get the product (35 mg), mp 163°C; ν_{max}: 3450, 2925, 1672, 1380, 1105, 890 cm^{-1}; ^{1}H nmr ($CDCl_3$) δ: 0.9 (s, 3H, 18-CH_3), 1.0 (s, 3H, 19-CH_3), 1.08 (s, 6H, —CH(CH_3)CH_3), 1.33 (s, 3H, C(CH$_3$)CH$_3$), 1.55 (s, 3H, —O—(O)C(Me)Me), 4.3 (m, 1H, C*H*—O—(O)C(Me)Me, H3), 4.54 (d, J_{4-3} = 5 Hz, 1H, C*H*—O—(O)C(Me)Me, H4), 4.72 (d, J = 6 Hz, 2H, exomethylene), and 5.9 (s, 1H, olefinic proton, H6). *Anal.* calcd. for $C_{31}H_{48}O_4$: C 76.85, H 9.92; found: C 76.79, H 9.83.

Periodate oxidation of 3

Lansisterol A (240 mg) in alcohol (5 mL) was treated with sodium metaperiodate solution (120 mg in 3 mL of water) and set aside for 24 h. Alcohol was removed at room temperature and the product extracted into ether as gum (120 mg); ν_{max} ($CHCl_3$): 1720, 1090, 860 cm^{-1}; λ_{max} (EtOH): 232 nm; λ_{max} (NaOH): 215 nm; ^{1}H nmr ($CDCl_3$) δ: 0.8 (s, 3H, 18-CH_3), 0.9 (s, 3H, 19-CH_3), 1.0 (s, 3H, —CH(CH_3)CH$_3$), 1.06 (s, 3H, —CH(CH$_3$)CH_3), 1.25 (s, 3H, —C(OH)—CH_3), 3.2 (m, 2H, —CH_2 protons), 4.15 (m, 1H, C*H*—OH, H7), 4.70 (d, J = 6 Hz, exomethylene), 6.82 (t, 1H, olefinic proton, H6), 9.35 (s, 1H, CC*H*O), and 9.60 (t, 1H, —CH$_2$C*H*O). *Anal.* calcd. for $C_{28}H_{42}O_4$: C 76.04, H 9.50; found: C 76.15, H 9.39.

Acetylation of 4

Lansilactone (80 mg) was acetylated in pyridine (3 mL) and acetic anhydride (2 mL) by heating on a water bath for 2 h, and then worked up in usual way affording **4** acetate as crystals from hexane (60 mg), mp 179°C; ^{1}H nmr ($CDCl_3$) δ: 0.84 (s, 3H, CH_3), 0.86 (s, 6H, 2 × CH_3), 0.92 (s, 3H, CH_3), 0.97 (s, 3H, CH_3), 1.35 (s, 3H, 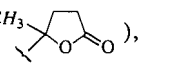), 1.96 (s, 3H, —OCO—CH_3), and 4.65 (t, 1H, —C*H*—OAc, H3). *Anal.* calcd. for $C_{29}H_{46}O_4$: C 75.98, H 10.04; found: C 75.86, H 10.13.

Jones oxidation of 4

Lansilactone (60 mg) dissolved in acetone was shaken with 6 drops of Jones reagent for 15 min, worked up, and crystallized from alcohol (38 mg), mp 182°C; ν_{max}: 2900, 1750, 1695 cm^{-1}; ^{1}H nmr ($CDCl_3$) δ: 0.9 (s, 3H, CH_3), 0.95 (s, 3H, CH_3), 1.0 (s, 3H, CH_3), 1.05 (s, 6H, 2 × CH_3), and 1.35 (s, 3H, 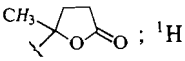 ; ^{1}H nmr ($CDCl_3$ and benzene) δ: 0.84 (s, 3H, 4β-CH_3), 0.9 (s, 3H, CH_3), 0.95 (s, 3H, CH_3), 1.0 (s, 3H, CH$_3$), 1.20 (s, 3H, 4α-CH_3), and 1.35 (s, 3H, 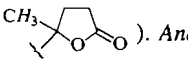). *Anal.* calcd. for $C_{27}H_{42}O_3$: C 78.25, H 10.14; found: C 78.15, H 10.21.

Acknowledgements

The authors wish to thank Dr. J. D. Connolly, Department of Chemistry, University of Glasgow, U.K. for most of the spectroscopic data and helpful discussions; Dr. Guy Ourisson, Institute de Chimie, Strasbourg, France for an authentic sample of diterocarpol trisnorlactone; Mr. S. Usman Ali, Assistant Director, Jawaharlal Nehru Medicinal Plants Garden & Herbarium, Pune for supply for the plant material; and Central Council for Research in Ayurveda and Siddha for financial support.

1. T. D. Pennington and B. T. Styles. Blumea, **22**, 483 (1975).
2. T. Matsura, M. Kawai, R. Nakashima, and Y. Butsugan. J. Chem. Soc. (C), 664 (1970).
3. J. F. Beillmann and G. Ourisson. Bull. Soc. Chim. Fr. 348 (1960).
4. N. S. Bhacca and D. H. Williams. Application of NMR spectroscopy in organic chemistry. Holden–Day Inc. London. 1964. pp. 84, 167.

Facial (*syn–anti*) stereoselectivity in the Diels–Alder reactions of spiro(bicyclo[2.2.2]octane-2,1′-[2,4]cyclopentadiene)

D. Jean Burnell,[1] H. Bruce Goodbrand, Stephanie M. Kaiser, and Zdenek Valenta[2]

Department of Chemistry, University of New Brunswick, Bag Service #45222, Fredericton, N.B., Canada E3B 6E2

Received May 28, 1986

This paper is dedicated to Professor O. E. (Ted) Edwards

D. Jean Burnell, H. Bruce Goodbrand, Stephanie M. Kaiser, and Zdenek Valenta. Can. J. Chem. **65**, 154 (1987).

Spiro(bicyclo[2.2.2]octane-2,1′-[2,4]cyclopentadiene) (**3**) has been synthesized in ten steps, and its Diels–Alder cycloadditions, both thermal and catalysed, have been studied with a variety of *Z*-ethylenic dienophiles. No significant differences in facial stereoselectivity were observed. This suggests that, in the *exo* region, the distance between the addends at the transition state is approximately the same in all the cases studied.

D. Jean Burnell, H. Bruce Goodbrand, Stephanie M. Kaiser et Zdenek Valenta. Can. J. Chem. **65**, 154 (1987).

On a synthétisé le spiro(bicyclo[2.2.2]octane[2,4]cyclopentandiène-2,1′) (**3**) en dix étapes et on a étudié la nature de ses cycloadditions de Diels–Alder, tant thermiques que catalysées, avec divers diénophiles portant un groupement éthyléniques *Z*. On n'a pas observé de différences remarquables dans les stéréosélectivités faciales. Ceci suggère que, dans la région *exo* de l'état de transition, les distances entre les réactifs sont approximativement les mêmes dans tous les cas étudiés.

[Traduit par la revue]

Introduction

Facial (*syn–anti*) stereoselectivity in a Diels–Alder reaction involving a plane-nonsymmetric diene is dependent on the different steric interactions which an incoming dienophile encounters as it approaches either face of the diene. In most instances, the major product is the one resulting from addition to the less hindered face (1). However, in some cases facial stereoselectivity is governed by what might loosely be called "electronic" effects. Dramatic examples are the well-documented contrasteric additions of 5-heterosubstituted cyclopentadienes (2). Furthermore, dienes fused to some bridged systems give major addition products that have been rationalized in terms of electronic effects (3).

In the course of total syntheses of steroids we found that significant changes in facial selectivity could be accomplished by seemingly modest alterations in the structure of the diene-bearing molecule. Thus, whereas addition of a dienophile to **1** was predominantly *syn* to the methyl group (4), addition to **2**

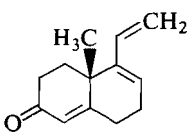

1

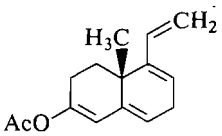

2

was predominantly *anti* to the methyl group (5). We believed that this difference could be explained largely in terms of steric effects; however, a perusal of the literature revealed that there has been little systematic study of steric control of facial selectivity in the Diels–Alder reaction.

Purely synthetic considerations were not the only reason for the initiation of a study of facial selectivity. Frontier orbital theory has been used by Sustmann (6*a*) and by Houk (6*b*) to explain orientation in Diels–Alder additions. To rationalize the increase in *endo* stereoselectivity in catalysed reactions and the heightening of asymmetric induction with chiral dienophiles in the presence of Lewis acid catalysts, Houk and Strozier (6*c*), in an extension of the frontier orbital theory to catalyzed additions,

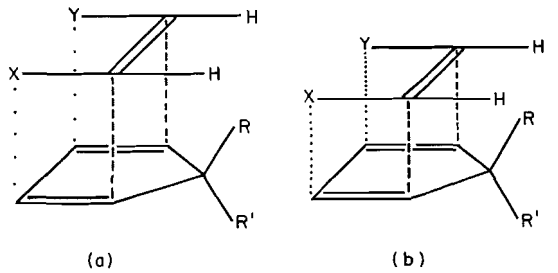

FIG. 1. The transition state structures of the additions of less reactive dienophiles (a) and of more reactive or catalysed dienophiles (b), with the same plane-nonsymmetric diene, are illustrated. According to the tight-transition-state hypothesis, in (b) secondary orbital interactions (dotted lines) are stronger, resulting in a shorter distance between the addends, which implies that the distance between the dienophile and the point of plane-nonsymmetry is also shorter in (b).

invoked the idea of a "tighter" transition state as a consequence of much stronger (attractive) secondary orbital interactions. In other words, they postulated that at the transition state the addends may be significantly closer together in a catalysed reaction than in the corresponding thermal reaction. The idea of a "tighter" transition state has been extended to explain why relatively reactive dienophiles, such as maleic anhydride and *N*-phenylmaleimide, tend to react thermally with greater *endo* stereoselectivity than less reactive dienophiles, such as methyl acrylate and 3-buten-2-one (7).

We expected that reactions of plane-nonsymmetric dienes might provide valuable clues to the geometry of the Diels–Alder transition state. This was based on the following reasoning: The two faces of a plane-nonsymmetric diene present different amounts of steric hindrance toward an incoming dienophile, while the magnitude of these steric interactions at the transition state should be a function of the distance between interacting centres. If the tight-transition-state hypothesis is correct, then with a given plane-nonsymmetric diene the catalysed reactions (with the tightest transition states) should be the most sensitive to the different amounts of steric repulsion presented by the two faces of the diene (Fig. 1). Therefore, catalysed reactions should give the greatest facial (*syn–anti*) stereoselectivity, followed by relatively thermally-reactive dienophiles, followed by less thermally-reactive dienophiles.

[1]Present address: Department of Chemistry, Memorial University of Newfoundland, St. John's, Newfoundland, Canada A1B 3X7.

[2]Author to whom correspondence may be addressed.

Can. J. Chem. Downloaded from www.nrcresearchpress.com by 190.90.36.8 on 09/07/12
For personal use only.

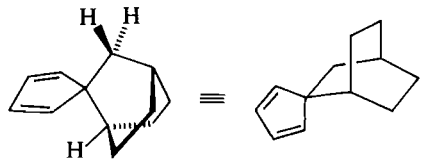

3

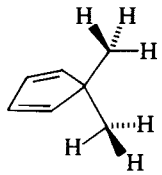

4

We chose the cyclopentadiene derivative **3** as our test diene for the following reasons:

(*i*) It avoids the potential problem of significant electronic effects which heteroatoms or additional π-orbitals might present.[3]

(*ii*) Although **3** is plane-nonsymmetrical, it does have a plane of symmetry perpendicular to the diene moiety; regioisomeric mixtures can, therefore, not be produced.

(*iii*) Steric interactions should preclude the formation of *exo* addition products; therefore only *syn-anti* stereoisomerism should be observed in the adducts.

(*iv*) It is fairly rigid, which avoids conformational ambiguities. In fact, the steric difference between the two faces is analogous to the difference in steric hindrance between the methyl groups of 5,5-dimethylcyclopentadiene **4** with its methyl groups "frozen" in two different conformations.

The synthesis of, and the details of our Diels–Alder study with, the diene **3** are presented here. The cycloaddition results have been published in preliminary form (9).

Synthesis of the diene

Our strategy for the construction of **3** was to form the bicyclo[2.2.2]octanyl moiety by a Diels–Alder reaction, then to build the five-membered ring by paralleling methodology developed by Martin and co-workers (10). The synthesis is shown in Scheme 1.

The cycloaddition of 1,3-cyclohexadiene to acrolein could be effected in yields of up to 77% by heating the reactants in a Carius tube as described by Krantz and Lin (11) followed by vacuum distillation to remove some troublesome polymeric material. A better thermal procedure involved heating the reactants for several days in a high-pressure hydrogenation apparatus under an argon atmosphere. Yields of up to 94% were achieved, with very little, or no, polymer. These thermal procedures provided the *endo* and the *exo* adducts, **5***a* and **5***b* respectively, in a ratio of about 9:1. Alternately, catalysis of the Diels–Alder reaction by the introduction of tin(IV) chloride (in dichloromethane at −78°C) gave exclusively the *endo* adduct **5***a*, but polymerization of the acrolein resulted in a yield of only 71%.

Hydrogenation of the adduct(s) yielded the aldehyde **6** in excellent yield. However, overhydrogenation was surprisingly facile, yielding not the corresponding alcohol, but the symmetrical ether **7**. Indeed, prolonged hydrogenation of **6** provided a respectable yield of **7**. This ether must arise by hydrogenolysis

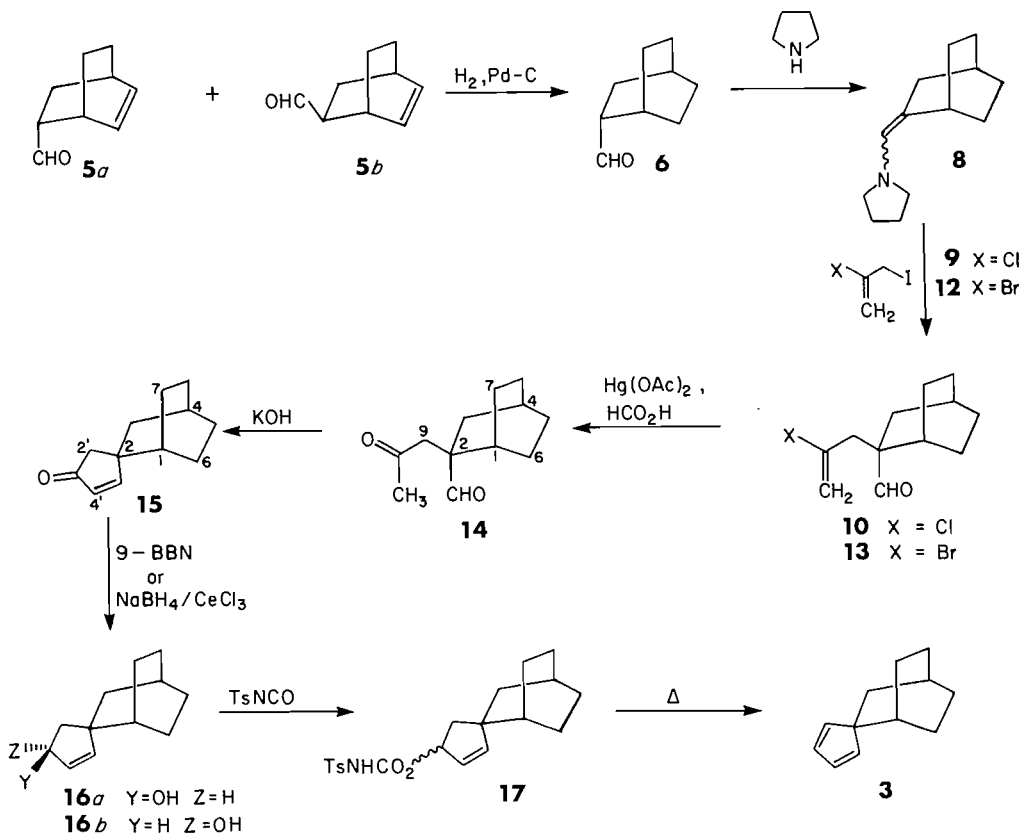

SCHEME 1

[3]Calculations have suggested that 5-methylcyclopentadiene is a system in which there is very little π-orbital perturbation by the methyl group (8).

Can. J. Chem. Downloaded from www.nrcresearchpress.com by 190.90.36.8 on 09/07/12
For personal use only.

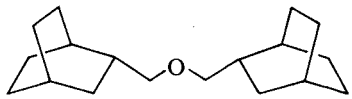

7

of an intermediate hemiacetal formed by attack of the alcohol onto unreduced aldehyde **6**.

Slow addition of the aldehyde **6** to a solution of pyrrolidine in benzene gave the enamine **8** in high yield,[4] but prolonged heating of a solution of **8** with 2,3-dibromo-1-propene in acetonitrile provided no alkylated material. Fortunately, the enamine **8** would slowly attack 2-chloro-3-iodo-1-propene (**9**) to give, following hydrolysis of the intermediate immonium salt and vacuum distillation, the chloro-aldehyde **10** in 60% yield.

A significant amount of **6** was always recovered, even if the alkylation was allowed to proceed for five days with a large excess of **9**. Continued heating of the pot residue after vacuum distillation of **10** resulted in the sublimation of a white powder. The ^{13}C nmr spectrum of this material (which was evidently relatively pure) showed that the compound had a high degree of symmetry. It was interesting to note that the proton noise-decoupled spectrum contained a perfect triplet (1:2:1) centred at δ 104.5. The spectral evidence pointed towards a cyclic trimer **11**. Because the aldehyde **6** was racemic, trimer **11** must have

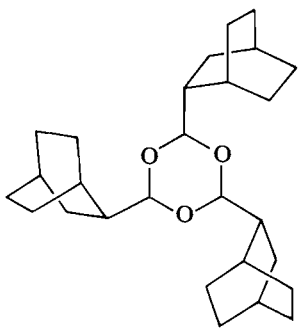

11

been a mixture of two pairs of enantiomers *RRR/SSS* and *RRS/RSS* in ratio of 1:3, respectively, by random attachment. The *RRS/RSS* forms might give rise to two signals for the *s*-trioxane carbons (ratio 2:1), whereas the *RRR/SSS* form should give just one. Thus the "triplet" signal in the ^{13}C nmr spectrum could be explained (assuming that all three substituents on the *s*-trioxane ring were equatorial). Not unexpectedly, thin-layer chromatography (tlc) of **11** on silica gel gave only one spot that corresponded to the carboxylic acid to which **6** readily oxidizes in air.

Alkylation of the enamine **8** with the bromo-iodide **12** gave a marginally better yield (67%) of product **13** in a four-day reaction.

Whereas mercury(II) acetate with boron trifluoride etherate (10) or trifluoroacetic acid proved completely ineffective in the transformation of **10** to the keto-aldehyde **14**, with formic acid (12) the yield of **14** was very good. Cyclization of **14** to the enone **15** proceeded cleanly with potassium hydroxide in ethanol. This two-step conversion was much better (89%) than direct conversion of **10** to **15** with cold sulphuric acid, which was a very capricious reaction. Much of the product of the latter process was isomeric with **15**; column chromatography was required to isolate the desired enone, which, even in one of the better runs, was obtained in only 21% yield. Welch *et al.* (13) have reported similar results with this direct conversion reaction.

The ketone of **15** could be reduced in high yield by 9-borabicyclo[3.3.1]nonane (9-BBN) in dry tetrahydrofuran (14) to a mixture of epimeric alcohols **16***a* and **16***b*. However, this procedure was relatively long (involving column chromatography) compared to the extremely simple procedure consisting of sodium borohydride reduction of **15** in the presence of hydrated cerium(III) chloride (15). Again, a mixture of epimers **16***a* and **16***b* was obtained, in a ratio of about 55:45, respectively.[5]

Attempted dehydration of this mixture of alcohols using tosyl chloride, mesyl chloride, and thionyl chloride gave mainly rearranged materials. Hoping to avoid cationic intermediates, we formed the carbamates **17** with *para*-toluenesulphonylisocyanate (17). Subsequent pyrolysis in a Kugelrohr apparatus yielded crude diene **3** along with sulphonamide and a few minor contaminants. A more convenient procedure was merely to add the isocyanate to a benzene solution of the alcohols, then to heat this mixture under reflux for a few days. To have very pure materials for the Diels–Alder study, the product was chromatographed very carefully. We obtained an 81% yield of **3** containing no impurities detectable by tlc, ^1H nmr, or ^{13}C nmr spectroscopy. The latter spectrum demonstrated that no rearrangement had taken place: only two olefinic signals were evident and, of the remaining six resonances, two were doubled in size as expected for a symmetric molecule.

The overall yield of diene **3** from 1,3-cyclohexadiene was 37% via the chloro-aldehyde **10** and 40% via the bromo-aldehyde **13**.

Diels–Alder reactions

To avoid possible complications arising from solvent effects (18) we chose dichloromethane as the solvent for all the Diels–Alder reactions. Thermal reactions with maleic anhydride, *N*-phenylmaleimide, and *para*-benzoquinone were heated under reflux for 12 h. The less reactive dienophiles (dimethyl maleate, acrolein, methyl acrylate, and 3-buten-2-one) required much longer reaction times with a large excess of dienophile. The crude products of these slower reactions were freed of excess dienophile and secondary products by preparative tlc. (To confirm that no significant amount of adduct had been overlooked, the silica gel remaining on each plate was extracted; the ^1H nmr spectra of the extracts displayed no signals attributable to the desired adducts.)

Catalysed reactions were carried out with three dienophiles using one equivalent of boron trifluoride etherate as the Lewis acid catalyst. Rate enhancement was obvious; the reactions were complete within a few hours at −78°C.

The adduct mixtures were analysed by high-field ^1H nmr, and signals for a major and a minor adduct were seen in every case. The signals arising from the bicyclo[2.2.1]heptene moieties were found downfield of the signals due to the unfunctionalized bicyclo[2.2.2]octane moieties. The latter resonances were generally poorly resolved, even at 360 MHz, and in the upfield region the signals due to the minor adducts could not be

[4]Addition of pyrrolidine to the aldehyde **6** gave inconsistent results.

[5]This was estimated by integration of the ^{13}C nmr spectrum of the mixture with suppression of the nuclear Overhauser enhancements, obtained by a gated decoupling experiment. The δ-*syn* effect (16) of the hydroxyl group was used to show that the major isomer was **16***a* and the minor one was **16***b*.

Can. J. Chem. Downloaded from www.nrcresearchpress.com by 190.90.36.8 on 09/07/12
For personal use only.

TABLE 1. Diels–Alder adducts obtained by reaction with **3**

Dienophile	Adducts		Thermal reaction[a]		Catalysed reaction[b]	
	Type I	Type II	Yield (%)	Type I/Type II	Yield (%)	Type I/Type II
Maleic anhydride	**18***a*	**18***b*	95	86:14	71	90:10
N-Phenylmaleimide	**19***a*	**19***b*	100	86:14	98	93: 7
para-Benzoquinone	**20***a*	**20***b*	100	86:14	95	89:11
Dimethyl maleate	**21***a*	**21***b*	80	89:11	—	—
Acrolein	**22***a*	**22***b*	85	86:14	—	—
Methyl acrylate	**23***a*	**23***b*	83	88:12	—	—
3-Buten-2-one	**24***a*	**24***b*	61	89:11	—	—

[a]In boiling dichloromethane (40°C). Thus, for the thermal reaction with *N*-phenylmaleimide the $\Delta\Delta G^{\ddagger}$ is 1.1 kcal/mol.
[b]With one equivalent of BF_3 etherate in dichloromethane at −78°C. The $\Delta\Delta G^{\ddagger}$ of the catalysed reaction with *N*-phenylmaleimide is 1.0 kcal/mol.

discerned. The major to minor adduct ratios were determined by integration of all the well-separated pairs of downfield signals. (We estimated the precision to be ±5%.)

Although the signals due to the bicyclo[2.2.1]heptene moieties could be assigned with reasonable confidence based on chemical shifts and couplings, we verified our assignments with spin-decoupling experiments (19). Coupling constants in the minor adducts were very similar to those in the major adducts. In both cases there was appreciable coupling between the proton on the carbon α to the carbonyl group(s) and the vicinal bridgehead proton(s); therefore in both cases the α-protons must have been *exo* with respect to the bicyclo[2.2.1]heptene moiety (20). Hence, in every case the adducts differed from each other only in the configuration of the spiro junction (Fig. 2), i.e. one adduct (Type I) must have resulted by *endo* addition to the face of the diene moiety of **3** *syn* to the C-3 methylene, and the other adduct (Type II) was the result of *endo* addition to the face of the diene moiety of **3** *syn* to the C-1 methine.

As expected, the protons nearest the carbonyl group(s) showed the largest chemical shift changes when deuterochloroform was replaced with perdeuterobenzene as the nmr solvent. Dramatically moving upfield were signals that decoupling experiments showed were due to the two C-3 protons of the bicyclo[2.2.2]octane moieties of the major adducts (only). This, along with a careful comparison of the relative chemical shifts (major versus minor) (19), implied that *every* major adduct was the Type I adduct, with the bicyclo[2.2.2]octane C-3 methylene *syn* to the carbonyl(s). This was demonstrated unequivocally by careful irradiation of the α-proton resonance of the major adduct with maleic anhydride (**18***a*). This resulted in an 11% nuclear Overhauser enhancement of the C-3 methylene signal as measured from a difference spectrum.[6]

The adduct yields and the Type I to Type II ratios for all additions are given in Table 1. All the dienophiles should provide the same steric interaction with **3**. That is, during cycloaddition, each dienophile projects two hydrogens towards the bicyclo[2.2.2]octane moiety of **3**. We found very little difference in the facial stereoselectivity between dienophiles. Furthermore, the effect of Lewis acid catalysis on the facial selectivity was not significant.

Before attempting to rationalize these results it seemed prudent to resolve the question of kinetic versus thermodynamic control. Regardless of the substantial precedent for kinetically

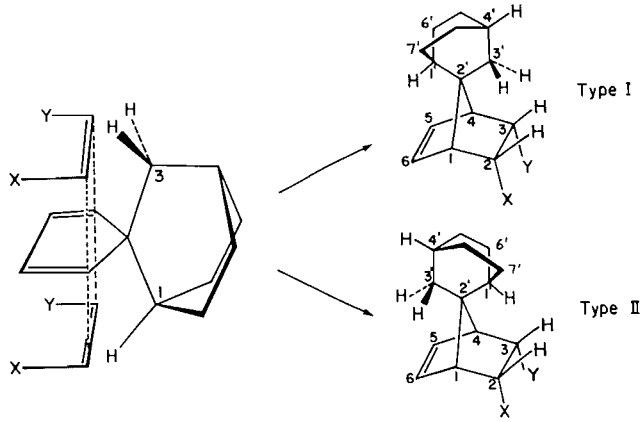

X	Y	Type I	Type II
—C(=O)—O—C(=O)—		**18***a*	**18***b*
—C(=O)—N(Ph)—C(=O)—		**19***a*	**19***b*
—C(=O)—CH=CH—C(=O)—		**20***a*	**20***b*
CO_2CH_3	CO_2CH_3	**21***a*	**21***b*
CHO	H	**22***a*	**22***b*
CO_2CH_3	H	**23***a*	**23***b*
$COCH_3$	H	**24***a*	**24***b*

FIG. 2. Two modes of *endo*-addition in diene **3**. The Type I adduct results from addition to the face of the cyclopentadienyl ring *syn* to the C-3 methylene of the bicyclo[2.2.2]octane moiety. The Type II adduct results from addition to the opposite diene face, i.e., *syn* to the C-1 methine of the bicyclo[2.2.2]octane moiety.

controlled reactions in Diels–Alder cycloadditions involving nonheterocyclic dienes, the fact that our product ratios were so similar suggested that these ratios might have been the result of equilibrating conditions. The major adduct (**18***a*) from the cycloaddition with maleic anhydride was isolated by multiple recrystallization. A solution of this very pure Type I adduct was heated under reflux for two days, after which we could find no evidence of isomerization to **18***b*. Furthermore, heating a

[6]We thank Dr. Thomas T. Nakashima, Department of Chemistry, University of Alberta, for kindly running this experiment on a Bruker WH-400 instrument.

Can. J. Chem. Downloaded from www.nrcresearchpress.com by 190.90.36.8 on 09/07/12
For personal use only.

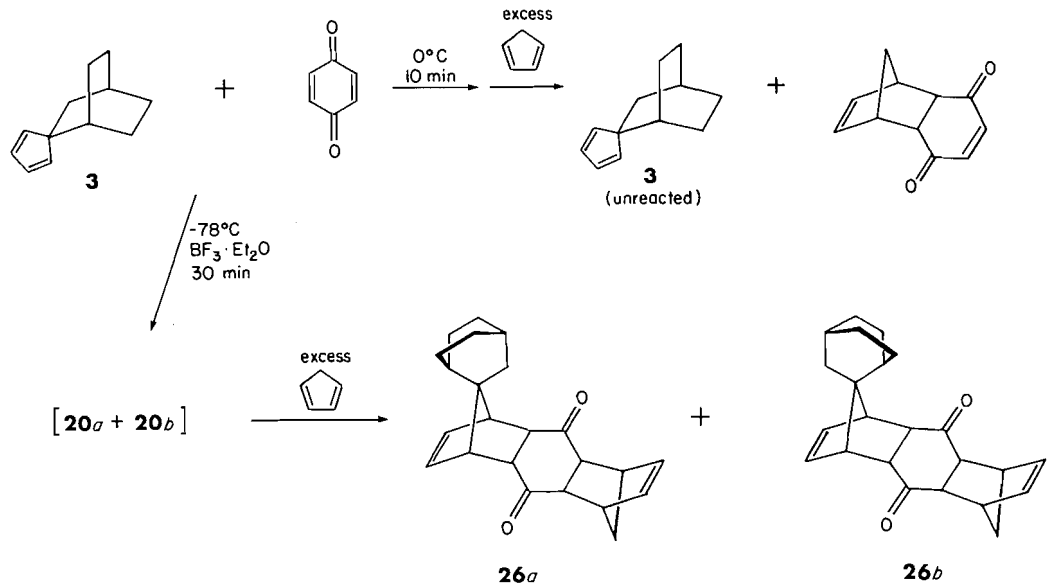

SCHEME 2

solution of **19***a* and **19***b* with a large excess of cyclopentadiene failed to produce any cyclopentadiene adduct **25**.

We knew from competitive experiments that diene **3**, like 5,5-dimethylcyclopentadiene **4** (21), is much less reactive than cyclopentadiene. We used this fact to prove that our so-called catalysed reactions were indeed taking place efficiently at

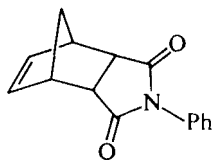

25

−78°C (Scheme 2). Thus, without the catalyst, **3** did not react appreciably with *para*-benzoquinone even at 0°C. However, at −78°C in the presence of boron trifluoride etherate, cycloaddition of **3** to *para*-benzoquinone was efficient and, after quenching the reaction with excess cyclopentadiene, the double-adducts **26***a* and **26***b* were obtained. (Had **3** not reacted readily at −78°C the cyclopentadiene double adduct **27** (22) would have been the result.)

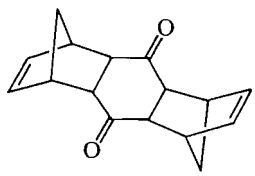

27

Discussion

All the dienophiles used in this study were mono- or *cis*-disubstituted ethylenes. The nmr data showed that both the major (Type I) and the minor (Type II) adducts resulted by *endo* addition. Therefore, with every dienophile studied we expected that the important steric interactions would be between a pair of (*cis*) hydrogens on the incoming dienophile and plane-nonsymmetric substituents in the *exo* region of diene **3** as shown in Fig. 2. The hydrogens of the C-1 methine and the C-3 methylene of **3** are situated between 2 and 2.2 Å from the plane of the diene moiety. This is the distance between addends at the Diels–Alder transition state, as determined by *ab initio* calculations (23, 24). As **3** was much less reactive than cyclopentadiene, steric interactions were indeed very important and therefore it seemed resonable to assume that these interactions must have governed the observed facial stereoselectivity. Nevertheless, the data in Table 1 show that there was very little, if any, correlation between the inherent reactivity of the system and the stereoselectivity; i.e., the Type I to Type II ratios were roughly constant. This is clearly *not* what would be expected considering the tight-transition-state hypothesis.

During cycloaddition with diene **3**, the dienophiles experienced steric interactions in the *exo* region of the transition-state structure. In contrast, the experimental data that led to the formulation of the tight-transition-state hypothesis involved *endo*-controlled phenomena. Furthermore, our previous studies (4, 5), in which different *syn–anti* ratios were observed for thermal and catalysed reactions, employed dienes (**1** and **2**) that were plane-nonsymmetrical in the *endo* region.

All these data are consistent with the following hypothesis, which emphasizes the degree of rehybridization at the reacting centres rather than the actual distance between the addends. Isotope effects have suggested that the Diels–Alder transition state is very early on the reaction coordinate (25), but obviously some rehybridization of the reacting centres from sp^2 to sp^3 must be evident at the transition state. This is borne out by *ab initio* calculations of the butadiene plus ethylene reaction (23, 24). The simplest rationalization for the data in Table 1 is that the distance between the sterically interacting atoms must be roughly constant for all the reactions studied. This implies that the angles ϕ_3 and ϕ_4, in the *exo* region of the generic Diels–Alder transition-state structure shown in Fig. 3, are roughly constant (regardless of the reactivity of the dienophile). On the other hand, we might expect the angles ϕ_1 and ϕ_2, in the *endo* region of Fig. 3, to be significantly smaller with more reactive dienophiles because they generally have stronger attractive interactions between the secondary, ultimately non-reacting, centres (6*c*, 7, 26).

As originally postulated (6*c*), the tight-transition-state hypothesis seems somewhat at variance with Hammond's postulate (27). Intuitively, one would expect that, if anything, the more reactive systems should be *further* apart at the transition state! Figure 3 serves to illustrate that, in fact, the more reactive

Can. J. Chem. Downloaded from www.nrcresearchpress.com by 190.90.36.8 on 09/07/12
For personal use only.

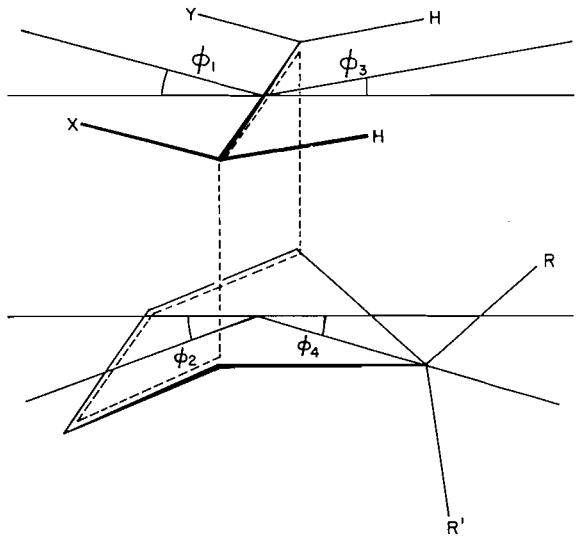

FIG. 3. Diels–Alder transition-state geometry.

systems are more reactant-like in that at the transition state of a reaction involving a more reactive dienophile the addends are flatter, i.e. more sp^2, than at the transition state of a reaction involving a less reactive dienophile.

The hypothesis outlined above is, of course, predicated on the assumption that the observed facial stereoselectivity was governed by steric factors. In our communication (9) we mentioned that signals corresponding to C-1 and C-3 in the ^{13}C nmr spectrum of **3** were found significantly upfield of their expected positions. We conjectured that this might be symptomatic of appreciable hyperconjugation of various σ-orbitals of the bicyclo[2.2.2]octane moiety with the diene π-orbital(s). This, in turn, suggested that electronic factors might be important in controlling the facial stereoselectivity of **3**, just as Gleiter, Paquette, Vogel, and others (3) have proposed for isodicyclopentadiene and related systems.[7] We should therefore mention here the result of recent calculations. Evaluation of the steric interactions in an MM2 model for the addition of ethylene to **3** gave reasonable agreement with the ratios in Table 1. This is consistent with steric factors being dominant in determining facial stereoselectivity with **3**.[8]

In the course of steroid syntheses we encountered instances in which substituted benzoquinones reacted with significantly better regioselectivity than other dienophiles (28). Hence, we were particularly interested to see whether *para*-benzoquinone would react in a different manner when compared to nonquinonoid dienophiles of similar reactivity. Table 1 shows that *para*-benzoquinone reactions, be they thermal or catalysed, gave the same *syn–anti* ratios as reactions with maleic anhydride and *N*-phenylmaleimide.[9] Thus, it appears that the "anomalous" quinone behavior is not related to significant differences in the geometry of the *exo* region of its Diels–Alder transition-state structures.

In conclusion, we have demonstrated that facial stereoselectivity, when governed by steric interactions in the *exo* region, is insensitive to dienophile reactivity. The implication is that the transition-state geometry is fairly constant in the *exo* region.

Experimental

Melting points (mp) were determined on a Kofler hot stage and are uncorrected. Ultraviolet (uv) spectra were obtained with a Beckman Model 25 spectrophotometer. Infrared (ir) spectra were recorded on a Perkin–Elmer 727B spectrophotometer in $CHCl_3$ solution. Routine ^1H nuclear magnetic resonance (nmr) spectra were obtained at 60 MHz (Varian T-60) in $CDCl_3$ solution, unless otherwise noted. Some spectra were also recorded at 200 MHz (Varian XL-200), 220 MHz, and 360 MHz (via Mr. Alan Lee, Department of Medical Genetics, University of Toronto). Routine ^{13}C nmr spectra were obtained on a Varian CFT-20 or a Bruker WP-80 instrument in $CDCl_3$ solution. Chemical shifts are given in ppm downfield of the tetramethylsilane internal reference. Standard abbreviations apply, but *apparent* multiplicities are usually reported. (In many instances the actual coupling is very complicated.) Signal multiplicities for ^{13}C nmr data refer to single-frequency off-resonance decoupled (SFORD) spectra. Considerable signal overlap was encountered in the ^{13}C nmr SFORD spectra of some compounds; this was overcome by simple spin-echo experiments. Low resolution electron impact mass spectra (ms) were provided by a Hitachi Perkin–Elmer RMU-6D instrument (70 eV). High resolution spectra were run by Dr. A. M. Hogg, Department of Chemistry, University of Alberta, on an AEI MS-50 spectrometer. Microanalyses were by Dr. F. Pascher, Mikroanalytisches Laboratorium, Bonn, and Mr. H. Seguin, National Research Council, Ottawa. Unless otherwise specified, reactions were performed under an atmosphere of dry nitrogen or argon. Solvents were distilled or were of A.C.S. Reagent Grade quality. Aqueous solutions are implied by saturated NaCl, $NaHCO_3$, etc.

*(1RS,2RS,4RS)- and (1RS,2SR,4RS)-5-bicyclo[2.2.2]octene-2-carboxaldehyde (**5**a and **5**b)*

(a) Thermal reaction

1,3-Cyclohexadiene[10] (39.1 g, 0.488 mol), freshly distilled acrolein (60.0 mL, 0.898 mol), and hydroquinone (approximately 100 mg) were placed in a Parr Series 4000 high pressure hydrogenation apparatus attached to an argon cylinder. Over a period of 5 h the pressure and temperature were increased to 194 atm and 85°C. After 60 h the reaction mixture was allowed to cool to room temperature (11 h), and the pressure was released. The product was removed from the reaction vessel with CH_2Cl_2. Rotary evaporation followed by vacuum distillation (bp 42–50°C/0.5 Torr; 1 Torr = 133.3 Pa) afforded 62.6 g (94%) of a 9:1 mixture (by ^1H nmr spectroscopy) of the *endo*- and *exo*-addition products, ***5a*** and ***5b*** respectively.

(b) Catalysed reaction

A stirred solution of 1,3-cyclohexadiene[10] (23.0 g, 0.287 mol) in CH_2Cl_2 (625 mL), containing a very small amount of hydroquinone, was cooled in a Dry Ice – acetone bath. Tin(IV) chloride (144 mL of a 1 *M* solution in CH_2Cl_2) was introduced, and freshly distilled acrolein (43.7 g, 0.780 mol) was added over a period of 2 h, then stirred for an additional 4 h. (Initially the reaction mixture was bright yellow, but it gradually became paler and more turbid.) The mixture was allowed to warm to room temperature, and water (230 mL) was added slowly. The CH_2Cl_2 layer was washed with saturated $NaHCO_3$, water, and saturated NaCl, then dried (Na_2SO_4) and concentrated by rotary evaporation. The viscous residue was distilled under vacuum (bp 54–58°C/0.4 Torr) to provide pure ***5a*** (27.8 g, 71%). For ***5a***: ir ν_{max}:

[7]For an alternative explanation of the facial stereoselectively of isodicyclopentadiene see ref. 24.

[8]F. K. Brown, K. N. Houk, D. J. Burnell, and Z. Valenta. Manuscript in preparation.

[9]Competitive experiments with cyclopentadiene as the diene in dichloromethane solution at room temperature gave the following relative reaction rates: maleic anhydride, 8.6; *N*-phenylmaleimide, 6.1; and *para*-benzoquinone, 1.0. Our results were similar to, but not identical with, the following relative rates reported by Sauer (18) for the same reactions in dioxane (20°C): maleic anhydride, 6.1; *N*-phenylmaleimide, 7.7; and *para*-benzoquinone, 1.0.

[10]The 1,3-cyclohexadiene was prepared by free-radical bromination of cyclohexene (*N*-bromosuccinimide, *hν*, 2.5 h; 69%) followed by dehydrobromination (quinoline, heating to 150°C while fractionally distilling the product; 79%) (29). We found this to be somewhat superior to the Organic Syntheses procedure (30).

Can. J. Chem. Downloaded from www.nrcresearchpress.com by 190.90.36.8 on 09/07/12
For personal use only.

Can. J. Chem. Downloaded from www.nrcresearchpress.com by 190.90.36.8 on 09/07/12
For personal use only.

2945, 2880, 2835 and 2740 (both m, aldehyde C—H), 1720, 1380, and 910 cm^{-1}; ^1H nmr δ: 9.44 (d, J = 1.5 Hz, 1H), 6.32 (ddd, J = 1.7, 6.4, 8.6 Hz, 1H) and 6.09 (ddd, J = 1.8, 6.3, 8.6 Hz, 1H) in an AB relationship, 2.45–3.1 (m, 3H), and 1.1–1.9 (m, 6H). For **5***b*: ^1H nmr δ: 9.77 (br s, 1H).

*Bicyclo[2.2.2]octane-2-carboxaldehyde (**6**)*

A solution of **5***a* and **5***b* (11.3 g, 83.2 mmol) in ethyl acetate (50 mL) was hydrogenated in the presence of 10% Pd on charcoal (1.0 g) for 1 h at 3.4 atm (1 atm = 101.3 kPa) on a Parr apparatus. After filtration through Celite, evaporation of the solution *in vacuo* provided **6** (11.5 g, 100%); bp 90°C/14 Torr: ir ν_{max}: 2945, 2875, 2830 and 2735 (both m, aldehyde C—H), and 1720 cm^{-1}; ^1H nmr δ: 9.73 (s, 1H), 2.3–2.7 (br m, 1H), and 1.3–2.3 (m, 12H) including two large pseudosinglets at δ 1.50 and 1.65.

*Di(bicyclo[2.2.2]octane-2-methylyl)ether (**7**)*

A solution of **5***a* and **5***b* (26.8 g, 0.197 mol) in ethyl acetate (60 mL) was hydrogenated in the presence of 10% Pd on charcoal (3.5 g) for 74.5 h at 5 atm. Filtration and evaporation yielded 23.8 g of a 3:4 mixture of **6** and **7**. A relatively pure sample of **7** was obtained by precipitation from cold ethyl acetate followed by preparative tlc; ir ν_{max}: 2920, 2870, and 1090 cm^{-1}; ^1H nmr δ: 3.32 (d, J = 7 Hz, 4H) and 1.35–2.1 (m) including a large pseudosinglet at δ 1.58; ^{13}C nmr δ: 74.7 (t, C-9), 35.9 (d, C-2), 30.6 (t, C-3), 27.2 (t, C-7), 26.2 (t, C-5), 25.6 (t, C-8), 25.3 (d, C-1), 24.5 (d, C-4), and 20.9 (t, C-6).

*2-(Pyrrolidinomethylene)-bicyclo[2.2.2]octane (**8**)*

A solution of pyrrolidine (100 mL) in dry benzene (1000 mL) was heated under reflux as a solution of **6** (35.0 g, 0.253 mol) in benzene (200 mL) was added over 5 h; evolved water was removed by means of a Barrett water separator. Reflux was maintained for a further 14 h. Rotary evaporation of the benzene and excess pyrrolidine left a red-brown residue, which was distilled under vacuum to provide **8** (46.0 g, 95%), bp 100°C/0.55 Torr; ir ν_{max}: 3200 (br), 1710, 1660, 1455, and 1360 cm^{-1}; ^1H nmr δ: 5.68 (t, 1H), 3.03 (br t, 4H), 2.39 (br t, 2H), and 1.4–2.0 (m, 14H); ms m/z (%): 191 (100, M^+), 190 (15), 162 (79), 148 (29), 123 (21), 122 (68), 120 (23), 109 (36), 94 (21), 93 (29), 91 (32), 84 (33), 81 (63), 80 (67), 79 (44), 77 (25), 70 (36), 69 (21), 67 (63), 57 (36), 55 (40), 44 (82), 43 (38), and 41 (69).

*2-Chloro-3-iodo-1-propene (**9**)*

Sodium iodide (425 g, 2.84 mol) was added to a solution of 2,3-dichloro-1-propene (174 g, 1.57 mol) in spectral-grade acetone (1.5 L). After heating under reflux for 3.5 h,[11] the mixture was cooled and water and ether were introduced. The organic layer was washed with $NaHSO_3$, water, and saturated NaCl, then dried ($MgSO_4$) and evaporated to yield essentially pure **9** (290 g, 91%), bp 101–102°C; ^1H nmr δ: 5.60 (br d, 1H), 5.32 (d, J = 1.6 Hz, 1H), and 4.11 (s, 2H).

*2-(2-Chloro-2-propenyl)-bicyclo[2.2.2]octane-2-carboxaldehyde (**10**)*

The chloro-iodide **9** (290 g, 1.43 mol) was added dropwise to a stirred solution of **8** (71.4 g, 0.373 mol) in dry acetonitrile (approx. 1.8 L). The reaction mixture was heated under reflux for 5 days. Following rotary evaporation of most of the acetonitrile, the residue was stirred for several hours with 560 mL of a water–THF mixture (1:1). The volume was reduced by about one third by rotary evaporation, and this was extracted with ether. The organic solution was washed with 5% HCl, 10% $Na_2S_2O_3$, 10% $NaHCO_3$ and saturated NaCl, then dried ($MgSO_4$), and the solvent was evaporated. The residue was distilled under vacuum; the initial fractions were unreacted **9** and aldehyde **6**, followed by the desired chloro-aldehyde **10** (47.6 g, 60%), bp 99–104°C/0.3 Torr, which, when stored in a freezer, slowly crystallized to provide pale yellow crystals, mp 30–33°C; ir ν_{max}: 2950, 2875, 1720, 1640, and 890 cm^{-1}; ^1H nmr δ: 9.63 (s, 1H), 5.24 (d, J = 1.5 Hz, 1H), 5.10 (br d, 1H), 2.73 (br s, 2H), 2.4 (m, 1H), 2.2 (m, 1H), and 1.2–2.0 (10H); ^{13}C nmr, see Table 2. Remaining in the distillation flask, and subliming slowly as a white powder, was *2,4,6-tri(bicyclo[2.2.2]octan-2-yl)-1,3,5-trioxane* (**11**): ir ν_{max}: 2930, 2855, 1720 (w), 1350, and 1085 cm^{-1}; ^1H nmr δ: 4.77 (br d, J = 7 Hz, 3H), and 1.2–2.1 (39 H), mostly in the form of one large pseudosinglet centred at δ 1.53; ^{13}C nmr δ: 104.7, 104.5 and 104.3 (1:2:1, doublets, —O—CH—O—), 40.0 (d, C-2), 28.3 (t, C-3), 26.8 (t, C-7), 26.1 (t, C-5), 25.4 (t, C-8), 24.0 (d, C-4), 23.8 (d, C-1), and 21.5 (t, C-6). *Anal.* calcd. for $C_{27}H_{42}O_3$: C 78.21, H 10.21; found: C 77.65, H 9.99.[12]

TABLE 2. ^{13}C nuclear magnetic resonance spectra of synthetic intermediates and **3** in $CDCl_3$

	Chemical shift (δ)					
Carbon[a]	**10**	**14**	**15**	**16***a*	**16***b*	**3**
1	29.7	31.2	34.4	36.0	34.5	31.4
2(1′)	50.4	47.8	46.0	48.7	49.1	57.5
3	30.6	35.0	39.8	40.6	42.6	28.9
4	24.8	24.4	24.9	25.6	25.7	24.1
5	25.4	25.1[b]	24.9[c]	25.2[d]	25.2[d]	25.1
6	23.2	23.0	23.9	23.7	23.6	26.0
7	22.0	22.6	22.6	23.2	23.0	26.0
8	24.1	24.7[b]	24.5[c]	25.0[d]	25.0[d]	25.1
9 or 2′	46.0	53.4	51.2	49.7	50.3	146.3
10 or 3′	138.4	206.5	210.2	76.8	76.8	127.4
11 or 4′	115.9	29.9	130.7	130.7	130.7	127.4
CHO or 5′	205.9	208.7	172.3	144.1	144.7	146.3

[a]C-7 and C-8 are *syn* to C-9 or C-2′.
[b–d]Assignments may be interchanged.

*2-Bromo-3-iodo-1-propene (**12**)*

Sodium iodide (8.78 g, 58.5 mmol) was added to a solution of 2,3-dibromo-1-propene (6.50 g, 32.5 mmol) in spectral-grade acetone (19 mL). After heating under reflux for 4 h, the mixture was cooled and water and ether were introduced. The dark purple organic layer was washed with dilute $NaHSO_3$, then saturated NaCl, dried ($CaCl_2$), and evaporated to yield **12** as a colourless liquid (6.09 g, 76%); ^1H nmr δ: 6.03 (br d, 1H), 5.88 (d, J = 2 Hz, 1H), and 4.23 (s, 2H).

*2-(2-Bromo-2-propenyl)-bicyclo[2.2.2]octane-2-carboxaldehyde (**13**)*

The enamine **8** (0.50 g, 2.6 mmol) was added to a solution of **12** (6.1 g, 25 mmol) in dry acetonitrile (50 mL). After heating under reflux for 4 days, the solvent was removed by rotary evaporation, and the residue was worked up as for **10**. Unreacted **12** was removed by vacuum distillation in a Kugelrohr apparatus leaving crude **13** as the residue (0.45 g, 67%), bp 104°C/0.18 Torr; ^1H nmr δ: 9.67 (s, 1H), 5.53 (br s, 2H), 2.91 (br s, =CBr-CH_2-, 2H), 2.4 (m, 1H), 2.2 (m, 1H), and 1.2–2.0 (10 H).

*2-(2-Oxopropyl)-bicyclo[2.2.2]octane-2-carboxaldehyde (**14**)*

*(a) From the chloro-aldehyde **10***

Mercury(II) acetate (13.1 g, 41.2 mmol) was added to a solution of **10** (8.77 g, 41.2 mmol) in 98% formic acid (175 mL). After stirring for 19.5 h at 23°C, the reaction mixture was poured into saturated NaCl (1000 mL), which was extracted with ether. The organic solution was washed with water and saturated NaCl, then dried ($MgSO_4$) and evaporated to provide essentially pure **14** (7.42 g, 93%). Recrystallization of a portion of this from CH_2Cl_2–CH_3OH gave colourless plates, mp 40.5–42°C; ir ν_{max}: 2945, 2875, 2730 (w), 1720 (very strong), 1365, and 1165 cm^{-1}; ^1H nmr δ: 9.80 (s, 1H), 2.98 (slightly broadened

[11]Prolonged heating of the reaction mixture, as advocated by Letsinger and Traynham (31), produces an appreciable amount of a second product, tentatively identified as 2,5-dichloro-1,5-hexadiene; ^1H nmr δ: 5.18 (br s) and 2.60 (br s).

[12]Purification of this cyclic trimer is problematic. Our attempts resulted in the production of *more* of the major contaminant, *bicyclo[2.2.2]octane-2-carboxylic acid*. (The monomer **6** is very susceptible to aerial oxidation.)

Can. J. Chem. Downloaded from www.nrcresearchpress.com by 190.90.36.8 on 09/07/12
For personal use only.

s, 2H), 2.5 (m, 1H), 2.3 (m, 1H), 2.13 (s, 3H), and 1.2–2.0 (10H) mainly in the form of a large, broad pseudodoublet, $J \simeq 4$ Hz, centred at δ 1.47; ^{13}C nmr, see Table 2; ms m/z (%): 194 (6, M^+), 166 (25), 136 (44), 108 (24), 81 (21), 80 (26), 79 (33), 43 (100), and 41 (21).

(b) From the bromo-aldehyde ***13***

The procedure was very similar to the above. The bromo-aldehyde **13** (0.454 g, 1.77 mmol) and mercury(II) acetate (0.564 g, 1.77 mmol) in 98% formic acid (9.0 mL), stirred for 22 h at 23°C, ultimately provided **14** in a 92% yield (0.420 g).

*Spiro(bicyclo[2.2.2]octane-2,1'-[4]cyclopenten-3-one) (**15**)*

(a) From the keto-aldehyde ***14***

A solution of **14** (4.46 g, 22.9 mmol) in 6% ethanolic KOH (200 mL) was heated under reflux for 1.5 h, after which the reaction mixture was poured into water, and the product was extracted into ether. The organic solution was washed with 5% HCl, water, and saturated NaCl, then dried ($MgSO_4$) and evaporated to provide the cyclic enone **15** (3.85 g, 95%), mp 30–31.5°C; bp 89°C/0.4 Torr; ir ν_{max}: 2945, 2870, 1710, 1680, and 1590 cm^{-1}; uv λ_{max} (hexane): 220.7 nm (ε 8600); ^{1}H nmr δ: 7.67 (d, J = 6 Hz, 1H), 5.98 (d, J = 6 Hz, 1H), 2.55 (d, J = 18 Hz, 1H) and 2.22 (d, J = 18 Hz, 1H) as an AB quartet, and 1.2–2.0 (12H) mostly in the form of one large broad peak at δ 1.67; ^{13}C nmr, see Table 2; ms m/z (%): 176.1201 (76, M^+), 148.1252 (34, $C_{11}H_{16}^+$), 95.0497 (100, $C_6H_7O^+$), 94.0418 (21, $C_6H_6O^+$), 80.0626 (28, $C_6H_8^+$), and 67.0555 (35, $C_5H_7^+$). *Anal.* calcd. for $C_{12}H_{16}O$: C 81.77, H 9.15; found: C 81.64, H 9.11.

(b) Directly from the chloro-aldehyde ***10***

A solution of **10** (1.92 g, 9.03 mmol) in CH_2Cl_2 (5 mL) was added slowly to 20 mL of ice-bath cooled, concentrated H_2SO_4. Within a few minutes the reaction mixture became deep red. Stirring was continued for 8 h with gradual warming to room temperature. The reaction mixture was poured onto crushed ice and repeatedly extracted with CH_2Cl_2. The combined organic solutions were washed with 10% $NaHCO_3$ and saturated NaCl, dried ($MgSO_4$), and evaporated. The residue was chromatographed on a silica gel HF (65 g) column eluted with hexane containing an increasing proportion of ethyl acetate to provide pure **15** (0.332 g, 21%).

*(2RS,3'RS)- and (2RS,3'SR)-spiro(bicyclo[2.2.2]octane-2,1'-[4]cyclopenten-3-ol) (**16**a and **16**b)*

(a) By reduction with 9-BBN

A solution of 9-BBN (Aldrich; 8.00 mmol) in dry THF (35 mL) was added over a period of 30 min to an ice-bath cooled solution of **15** (1.39 g, 7.87 mmol) in dry THF (approximately 200 mL). The reaction mixture was stirred at this temperature for an additional 3.5 h, then at room temperature for 11.5 h. Approximately 0.5 mL of CH_3OH was added, then all the solvent was removed by rotary evaporation, and pentane (200 mL) was added. 2-Aminoethanol (0.5 mL) was added, producing a greenish gum; the pentane was decanted, and the gum was reextracted with fresh pentane (2 × 50 mL). After evaporation of the pentane, the combined extracts were chromatographed on a silica gel HF (40 g) column eluted with hexane, containing an increasing proportion of ethyl acetate, to provide a nearly 1:1 mixture of the epimeric alcohols **16***a* and **16***b* (1.31 g, 93%).

(b) By reduction with $NaBH_4$–$CeCl_3$

To an ice-bath cooled solution of **15** (6.54 g, 37.1 mmol) in CH_3OH (300 mL) was added solid $CeCl_3 \cdot 7H_2O$ (B.D.H; 13.8 g, 37.1 mmol). After stirring for 5 min, $NaBH_4$ (2.00 g, 52.8 mmol) was added in small portions over a period of 5 min. Water (100 mL) was added, and the mixture was reduced in volume to approximately one third by rotary evaporation. This was extracted with ether. The organic extract was washed with water and saturated NaCl, dried ($MgSO_4$), and evaporated to yield 6.32 g (96%) of a mixture of **16***a* (56% of product) and **16***b* (44% of product); ir ν_{max}: 3615, 3470 (br), 2940, 2865, and 1620 (w) cm^{-1}; ^{1}H nmr δ: 6.05 (d, J = 5 Hz, 1H), 5.75 (br d, J = 5 Hz, $W_{1/2}$ of each line ≃ 3.5 Hz, 1H), 4.8 (br m, 1H), 3.1 (concentration dependent, 1H), 1.8–2.6 (m, 2H, C-5'H_2), and 1.1–2.0 (12H) mainly as a broad pseudosinglet at δ 1.61; ^{13}C nmr of both isomers, see Table 2; ms m/z (%): 178.1358 (77, M^+, $C_{12}H_{18}O^+$ requires 178.1358), 160.1251 (20, $C_{12}H_{16}^+$), 135.1175 (25, $C_{10}H_{15}^+$), 96.0572 (73, $C_6H_8O^+$), 95.0498 (100, $C_6H_7O^+$), 93.0702 (20, $C_7H_9^+$), 91.0550 (26, $C_7H_7^+$), 83.0500 (22, $C_5H_7O^+$), 82.0423 (27, $C_5H_6O^+$), 81.0704 (32, $C_6H_9^+$), 80.0627 (39, $C_6H_8^+$), 79.0552 (47, $C_6H_7^+$), 77.0397 (20, $C_6H_5^+$), and 67.0555 (33, $C_5H_7^+$).

N-para-*Toluenesulphonylspiro(bicyclo[2.2.2]octane-2,1'-[4]cyclopenten-3-yl)carbamate (**17**)*

A mixture of **16***a* and **16***b* (2.06 g, 11.6 mmol) and *para*-toluenesulphonylisocyanate (2.28 g, 11.6 mmol) in dry benzene (50 mL) was stirred at room temperature overnight. The benzene was evaporated to yield **17** as a white powder (4.34 g, 100%); ^{1}H nmr δ: 7.6–8.4 (very br, 1H, NH), 7.92 (d, J = 8 Hz, 2H), 7.30 (br d, J = 8 Hz, 2H), 6.12 (br d, J = 6 Hz, 1H), 5.62 (br d, J = 6 Hz, 1H), 5.6 (br m, 1H), 2.45 (br s, 3H), and 0.9–2.3 (14H) including a large broad pseudosinglet at δ 1.53.

*Spiro(bicyclo[2.2.2]octane-2,1'-[2,4]cyclopentadiene) (**3**)*

(a) By pyrolysis of ***17***

The carbamate **17** (4.30 g, 11.4 mmol) was heated to 130°C under vacuum (approximately 0.2 Torr) in a Kugelrohr apparatus. Initially, a yellow liquid was evolved, followed by a white solid. Column chromatography of the distillate on silica gel HF (30 g), eluted with hexane – ethyl acetate (15:1) provided the diene **3** as a colourless liquid (1.46 g, 80%).

(b) Without isolation of ***17***

para-Toluenesulphonylisocyanate (6.75 g, 34.2 mmol) was added to a solution of **16***a* and **16***b* (6.09 g, 34.2 mmol) in dry benzene at 23°C. The mixture was warmed to reflux. After 20 h an additional 1.5 g of *para*-toluenesulphonylisocyanate was added; then after a further 14 h under reflux the solvent was evaporated. The resulting gum was dissolved in a 1:1 mixture of dry CH_3OH and hexane. Addition of a few drops of water separated the layers, and the methanolic layer was reextracted with hexane. The combined hexane extracts were evaporated, and the residue was chromatographed on a silica gel HF (40 g) column, eluted with hexane – ethyl acetate (20:1) to yield pure diene **3** as a colourless liquid (4.45 g, 81%), bp 65°C/0.1 Torr; uv λ_{max} (hexane): 205.0 nm (ε 1200) and 258.2 nm (ε 1100); ^{1}H nmr 360 MHz in $CDCl_3$ [60 MHz in C_6D_6] δ: 6.505 [6.48] (m, $W_{1/2}$ = 8.5 Hz, 2H, C-2'H and C-5'H) and 6.160 [6.17] (m, $W_{1/2}$ = 8.5 Hz, 2H, C-3'H and C-4'H) as an AA'XX' [AA'BB'] spin system, and 0.8–2.1 [1.0–2.2] (complex signals, 12H) appearing mainly as a very large pseudosinglet at δ 1.72 [1.53] at 60 MHz; ^{13}C nmr, see Table 2; ms m/z (%): 160.1252 (100, M^+, $C_{12}H_{16}^+$ requires 160.1252), 132.0933 (29, $C_{10}H_{12}^+$), 131.0860 (43, $C_{10}H_{11}^+$), 117.0704 (46, $C_9H_9^+$), 91.0549 (45, $C_7H_7^+$), 81.0707 (23, $C_6H_9^+$), 80.0632 (37, $C_6H_8^+$), 79.0554 (31, $C_6H_7^+$), and 67.0557 (24, $C_5H_7^+$).

Diels–Alder additions to ***3***

The Diels–Alder study used pure diene **3** and commercially available dienophiles, which in all cases were further purified. In order that the ratio of adducts be undisturbed, in most instances 360-MHz ^{1}H nmr spectra were run on the crude reaction mixtures, which usually contained a small amount of unreacted dienophile. Other spectra were taken on adduct mixtures from which impurities had been removed. Adduct ratios, which were determined by integration of the 360-MHz nmr, and percentage yields are reported in Table 1.

Addition of maleic anhydride ***3***

(a) Thermal reaction

Maleic anhydride (122.2 mg, 1.246 mmol) was added to solution of **3** (195.8 mg, 1.222 mmol) in CH_2Cl_2 (10 mL). The mixture was heated under reflux for 12 h. Rotary evaporation provided an off-white powder (300.4 mg) composed of **18***a* (major) and **18***b* (minor) (respectively, *(2s,3'aR,4'S,7'R,7'aS)-* and *(2r,3'aR,4'S,7'R,7'aS)-3'a,4',7',7'a-tetrahydro-1',3'-dioxospiro(bicyclo[2.2.2]octane-2,8'-[4,7]methanoisobenzofuran))*.

(b) Catalysed reaction

The diene **3** (288.9 mg, 1.803 mmol) was added to a stirred solution of maleic anhydride (187.9 mg, 1.907 mmol) in CH_2Cl_2 (8 mL) cooled

TABLE 3. ^{13}C nuclear magnetic resonance data of some adducts in $CDCl_3$[a]

Adduct	Carbon[b]:	Chemical shift (δ) 1	2	3	4	5	6	1′	2′	3′	4′	5′	6′	7′	8′	Others
18*a*		52.7	46.1	46.1	52.7	135.2	135.2	25.9	70.4	35.1	25.8	24.8	23.7	23.7	24.8	172.2
18*b*		52.7	46.6	46.6	52.7	135.1	135.1	27.8	68.0	34.4	25.5	24.7	22.0	22.0	24.7	172.0
19*a*		52.1	44.8	44.8	52.1	134.2	134.2	25.9	69.4	34.8	25.8	24.9	23.7	23.7	24.9	177.4
19*b*		52.4	45.3	45.3	52.4	134.2	134.2	27.4	67.2	34.9	25.6	24.8	22.2	22.2	24.8	177.2
21*a*		53.1	46.9	46.9	53.1	134.6	134.6	26.2	63.4	34.9	25.3	25.1	23.7	23.7	25.1	173.2 51.5
21*b*		53.4	47.2	47.2	53.4	134.5	134.5	27.5	61.0	35.0	25.9	25.0	22.2	22.2	25.0	173.2 51.5
22*a*		51.7	49.5	26.2	51.5	137.7	131.7	26.3	64.3	35.0	25.2	25.1	24.1	23.9	25.1	205.4
23*a*		52.6	42.0	27.6	49.1	137.5	132.2	26.3	63.9	35.0	25.5	25.3	24.1	23.8	25.2	175.7 51.4
24*a*		52.8	49.3	25.9	51.4	137.6	131.1	26.3	64.3	35.2	25.5	25.3	24.1	23.8	25.2	209.5 29.1
26*a*		55.1	48.9	48.9	55.1	136.4	136.4	26.2	63.8	35.1	24.3	25.0	23.8	23.8	25.0	213.5 136.4 53.3 52.0 49.9

[a]Assignments are in accordance with SFORD and (or) spin echo data. However, signals of similar chemical shift with the same multiplicity should be considered interchangeable.

[b]Adducts are numbered as in Fig. 2. Although this is not always in accordance with strict IUPAC rules, it does allow convenient comparison of signals.

in a Dry Ice – acetone bath, followed quickly by addition of 220 μL (1.80 mmol) of freshly distilled BF_3 etherate. After 10 h the reaction mixture was allowed to warm to room temperature, and water (10 mL) was introduced. The organic solution was washed with water, saturated $NaHCO_3$, and saturated NaCl, then evaporated to yield a mixture of **18***a* (major) and **18***b* (minor) as a yellow powder (332.4 mg). Repeated (×6) recrystallization of the product from CH_2Cl_2 – ethyl acetate afforded a small amount of pure **18***a*, mp 172–175°C (sub.); ir ν_{max}: 1810 (m), 1775 (s), 1075, and 905 cm^{-1}; ^1H nmr 360 MHz in $CDCl_3$ [200 MHz in C_6D_6] δ: 6.235 [5.76] (t, J = 2.0 Hz, 2H), 3.676 [2.78] (dd, J = 1.5, 2.9 Hz, 2H, H α to C=O), 3.169 [2.54] (quintet, $W_{1/2}$ = 6 Hz, 2H, [2.2.1] bridgehead H), 1.855 [1.44] (br t, $W_{1/2}$ = 7 Hz, 1H, [2.2.2] C-1H), 1.685 [1.33] (distorted br q, $W_{1/2}$ = 10 Hz, 1H, [2.2.2] C-4H), 1.377 [0.65] (br d, J = 3.2 Hz, 2H, [2.2.2] C-$3H_2$), and remaining signals unresolved 1.35–1.55 [0.95–1.33]; ^{13}C nmr in $CDCl_3$, see Table 3 (100 MHz in C_6D_6 δ: 171.8 (2C), 135.2 (2C), 69.9, 52.6 (2C), 46.0 (2C), 34.7, 26.2, 25.9, 25.0 (2C), and 23.7 (2C)); ms m/z (%): (M^+ not apparent), 230.1305 (8, $C_{15}H_{18}O_2^+$), 185.1331 (100, $C_{14}H_{17}^+$), 117.0704 (12, $C_9H_9^+$), 104.0627 (12, $C_8H_8^+$), 91.0549 (17, $C_7H_7^+$), and 81.0706 (11, $C_6H_9^+$). *Anal.* calcd. for $C_{16}H_{18}O_3$: C 74.40, H 7.02; found: C 74.26, H 6.94. For **18***b* (determined from mixture): ^1H nmr 360 MHz in $CDCl_3$ δ: 6.272 (t, J = 2 Hz, 2H), 3.555 (dd, J = 1.5, 2.9 Hz, 2H, H α to C=O), and 3.225 (quintet, $W_{1/2}$ = 6 Hz, 2H, [2.2.2] bridgehead H); ^{13}C nmr, see Table 3.

Addition of N-*phenylmaleimide to* **3**

(a) Thermal reaction

N-Phenylmaleimide (54.0 mg, 0.312 mmol) was added to a solution of **3** (50.0 mg, 0.312 mmol) in CH_2Cl_2 (3 mL). The mixture was heated under reflux for 12 h. Rotary evaporation yielded a pale yellow powder (103.6 mg) composed of **19***a* (major) and **19***b* (minor) (respectively, *(2s,3′aR,4′S,7′R,7′aS)-* and *(2r,3′aR,4′S,7′R,7′aS)-3′a,4′,7′,7′a-tetrahydro-1′,3′-dioxo-2′-phenylspiro(bicyclo[2.2.2]octane-2,8′-[4,7]methanoisoindole))*.

(b) Catalysed reaction

A solution of **3** (40.5 mg, 0.253 mmol) in CH_2Cl_2 (4 mL) was cooled in a Dry Ice – acetone bath; *N*-phenylmaleimide (43.9 mg, 0.253 mmol) was added, followed immediately by 31 μL (≡ 0.25 mmol) of BF_3 etherate. After stirring for 2 h, the solution was allowed to attain room temperature slowly. The red-brown reaction mixture was added to ether (25 mL), which was washed with saturated NaCl, then dried ($MgSO_4$) and evaporated to afford an off-white solid (82.7 mg) composed of **19***a* (major) and **19***b* (minor); ir ν_{max}: 2930 (m), 2860 (w), 1710, 1600, 1380, 1050, and 1010 cm^{-1}; ^1H nmr of **19***a* 360 MHz in $CDCl_3$ [60 MHz in C_6D_6] δ: 7.12–7.46 [7.0–7.5] (5H), 6.178 [5.93] (t, J = 2.0 Hz, 2H), 3.542 [2.93] (dd, J = 1.5, 2.8 Hz, 2H, H α to C=O), 3.195 [2.85] (m, $W_{1/2}$ = 6 Hz, 2H, [2.2.1] bridgehead H), 1.88 [1.67] (m, 1H, [2.2.2] C-1H), 1.68 (m, 1H, [2.2.2] C-4H), [0.95] (br, $W_{1/2}$ = 6 Hz, 2H, [2.2.2] C-$3H_2$), and remaining signals 1.3–1.6 [1.0–1.5] mainly in the form of a large pseudosinglet at δ 1.45 [1.25]; ^1H nmr of **19***b* 360 MHz in $CDCl_3$ δ: 6.214 (t, J = 2.0 Hz, 2H), 3.429 (dd, J = 1.6, 2.7 Hz, 2H, H α to C=O), and 3.243 (m, $W_{1/2}$ = 6 Hz, 2H, [2.2.1] bridgehead H); ^{13}C nmr of **19***a* and **19***b*, see Table 3; ms (of the mixture of **19***a* and **19***b*) m/z (%): 333.1730 (100, M^+), 186.1407 (12, $C_{14}H_{18}^+$), 119.0370 (10, $C_7H_5NO^+$), 104.0628 (38, $C_8H_8^+$), 95.0858 (10, $C_7H_{11}^+$), 92.0622 (12, $C_7H_8^+$), 91.0548 (17, $C_7H_7^+$), 79.0549 (11, $C_6H_7^+$), and 78.0472 (10, $C_6H_6^+$). Multiple recrystallization of the product from CH_3OH provided colourless crystals, which sublimed above 200°C, recondensing as beautiful plates, mp 227°C. *Anal.* calcd. for $C_{22}H_{23}NO_2$: C 79.25, H 6.95, N 4.20; found: C 79.34, H 6.99, N 4.31.

Addition of para-*benzoquinone to* **3**

(a) Thermal reaction

The procedure was the same as for the *N*-phenylmaleimide addition; 33.7 mg (0.312 mmol) of *para*-benzoquinone and 50.0 mg (0.312 mmol) of **3** provided 83.7 mg of an off-white solid[13] composed of **20***a* (major) and **20***b* (minor) respectively, *(2s,1′R,4′S,4′aR,8′aS)-* and *(2r,1′R,4′S,4′aR,8′aS)-1′,4′,4′a,8′a-tetrahydrospiro(bicyclo[2.2.2]octane-2,9′-[1,4]methanonaphthalene)-5′,8′-dione)*.

(b) Catalysed reaction

BF_3 etherate (145 μL, 1.17 mmol) was added to a stirred solution of *para*-benzoquinone (126.5 mg, 1.170 mmol) in CH_2Cl_2 (25 mL) cooled in a Dry Ice – acetone bath. This was followed by addition of

[13]Attempts to recrystallize this adduct mixture from a number of common solvents resulted in the production of a significant amount of very sparingly soluble material, which did not appear to be either photocyclized or aromatized.

Can. J. Chem. Downloaded from www.nrcresearchpress.com by 190.90.36.8 on 09/07/12
For personal use only.

Can. J. Chem. Downloaded from www.nrcresearchpress.com by 190.90.36.8 on 09/07/12
For personal use only.

a solution of **3** (187.2 mg, 1.168 mmol) in CH_2Cl_2 (approximately 2 mL). After stirring for 6 h, the reaction mixture was allowed to attain room temperature slowly. The mixture was poured into approximately 75 mL of ether, and this solution was washed with saturated $NaHCO_3$ and saturated NaCl, then dried (Na_2SO_4) and evaporated to provide a pale brown solid[13] (297.1 mg) composed predominantly of the adducts **20***a* (major) and **20***b* (minor); ir ν_{max}: 2930, 2870, and 1670 cm^{-1}; ^1H nmr of **20***a* 220 MHz in $CDCl_3$ [360 MHz in C_6D_6] δ: 6.64 [6.099] (s, 2H, olefinic H of enedione), 6.04 [5.715] (t, J = 2.0 Hz, 2H, [2.2.1] olefinic H), 3.40 [2.812] (dd, J = 1.4, 2.3 Hz, 2H, H α to C=O), 3.25 [3.035] (m, 2H, [2.2.1] bridgehead H), 1.82 [1.612] (m, $W_{1/2}$ = 8 Hz, 1H, [2.2.2] C-1H), 1.69 [1.400] (m, $W_{1/2}$ = 9.5 Hz, 1H, [2.2.2] C-4H), [0.91] (br d, J = 2 Hz, 2H, [2.2.2] C-3H_2), and remaining signals 1.3–1.75 (1.1–1.35), in $CDCl_3$ mainly in the form of one large pseudosinglet at δ 1.43; ^1H nmr of **20***b* 220 MHz in $CDCl_3$ [360 MHz in C_6D_6] δ: 6.63 [6.093] (s, 2H, olefinic H of enedione), 6.07 [5.781] (t, J = 2.0 Hz, 2H, [2.2.1] olefinic H), [3.068] (m, 2H, [2.2.1] bridgehead H), and [2.633] (m, 2H, H α to C=O); ms (of the mixture of **20***a* and **20***b*) m/z (%): 268.1465 (50, M^+, $C_{18}H_{20}O_2^+$ requires 268.1463), 240.1514 (100, $C_{17}H_{20}O^+$), 160.1252 (18, $C_{12}H_{16}^+$), 131.0496 (23, $C_9H_7O^+$), 117.0704 (20, $C_9H_9^+$), 104.0628 (19, $C_8H_8^+$), and 91.0548 (31, $C_7H_7^+$).

Thermal addition of dimethyl maleate to 3

A large excess of dimethyl maleate (0.5 mL) was added to a solution of **3** (30.9 mg, 0.193 mmol) in CH_2Cl_2 (4 mL), and the mixture was heated under reflux for 72 h. The solvent was evaporated, and the residue was purified by preparative tlc to yield 47.2 mg (80%) of a semisolid composed of **21***a* (major) and **21***b* (minor) (respectively, *dimethyl (1*R,*2*S,*3*R,*4*S,*7*s)- and *dimethyl (1*R,*2*S,*3*R,*4*S,*7*r)-*spiro(bicyclo[2.2.1]hept-5-ene-7,2'-bicyclo[2.2.2]octane)-2,3-dicarboxylate;* ir ν_{max}: 2935, 2865, 1740, 1605, 1165, and 1020 cm^{-1}; ^1H nmr of **21***a* 360 MHz in $CDCl_3$ [360 MHz in C_6D_6] δ: 6.175 [6.215] (t, J = 1.9 Hz, 2H), 3.613 [3.429] (s, 6H), 3.427 [3.233] (m, $W_{1/2}$ = 4 Hz, H α to C=O), 2.836 [2.646] (m, $W_{1/2}$ = 5 Hz, [2.2.1] bridgehead H), 1.905 [1.850] (m, $W_{1/2}$ = 7.5 Hz, 1H, [2.2.2] C-1H), 1.644 [1.380] (m, $W_{1/2}$ = 9 Hz, 1H, [2.2.2] C-4H), [0.961] (br d, J = 3 Hz, 2H, [2.2.2] C-3H_2), and remaining signals 1.34–1.5 [1.1–1.35], in $CDCl_3$ mainly in the form of a large pseudosinglet at δ 1.41; ^1H nmr of **21***b* 360 MHz in $CDCl_3$ [360 MHz in C_6D_6] δ: 6.211 [6.285] (t, J = 1.9 Hz, 2H), 3.601 [3.415] (s, 6H), 3.323 [3.120] (m, $W_{1/2}$ = 4 Hz, 2H, H α to C=O), 2.921 [2.733] (m, $W_{1/2}$ = 5.5 Hz, 2H [2.2.1] bridgehead H), and [0.907] (m, 1H, [2.2.2] C-1H ?); ^{13}C nmr of **21***a* and **21***b*, see Table 3; ms (of the mixture of **21***a* and **21***b*) m/z (%): 304.1674 (8, M^+), 273.1486 (17, $C_{17}H_{21}O_3^+$), 244.1465 (100, $C_{16}H_{20}O_2^+$), 185.1333 (95, $C_{14}H_{17}^+$), 146.0580 (17, $C_6H_{10}O_4^+$), 117.0704 (18, $C_9H_9^+$), 113.0240 (23, $C_5H_5O_3^+$), and 91.0549 (24, $C_7H_7^+$). A small amount was recrystallized from CH_3OH. *Anal.* calcd. for $C_{18}H_{24}O_4$: C 71.03, H 7.95; found: C 70.85, H 7.93.

Thermal addition of acrolein to 3

A large excess of acrolein (approximately 1 mL) was added to a solution of **3** (42.0 mg, 0.262 mmol) in CH_2Cl_2 (4 mL), and the mixture was heated under reflux for 48 h. The solvent was evaporated, and the oily product was purified by preparative tlc to yield a white solid (48.0 mg, 85%) composed of **22***a* (major) and **22***b* (minor) (respectively, *(1*RS,*2*RS,*4*RS,*7*SR)- and *(1*RS,*2*RS,*4*RS,*7*RS)-*spiro(bicyclo[2.2.1]hept-2-ene-7,2'-bicyclo[2.2.2]octane)-2-carboxaldehyde);* ir ν_{max}: 2930, 2870, 2710 (w), and 1710 cm^{-1}; ^1H nmr of **22***a* 360 MHz in $CDCl_3$ [360 MHz in C_6D_6] δ: 9.509 [9.335] (d, J = 2.1 [1.6] Hz, 1H, CHO), 6.124 [5.810] (dd, J = 3.2, 5.9 Hz, 1H, C-5H), 5.902 [5.636] (dd, J = 2.9, 5.9 Hz, 1H, C-6H), 2.996 [2.575] (dddd, J = 2.1 [1.6], 3.7, 3.9, 8.6 Hz, 1H, C-2H), 2.910 [2.473] (m, $W_{1/2}$ = 7.5 Hz, 1H, C-1H), 2.597 [2.192] (br t, $W_{1/2}$ = 8 Hz, 1H, C-4H), 2.064 [1.703] (ddd, J = 3.7, 8.6, 12.4 Hz, 1H, C-3$_{exo}$H), 1.827 [1.753] (m, $W_{1/2}$ = 7.5 Hz, 1H, [2.2.2] C-1H) 1.636 [1.460] (m, $W_{1/2}$ = 8.5 Hz, 1H, [2.2.2] C-4H), 1.455[14] [1.374[14]] (dd, J = 3.9, 12.4 Hz, 1H, C-3$_{endo}$H), [1.054 and 0.993] (second-order doublets with much additional coupling, J_{gem} = 13.8 Hz, 2H, [2.2.2] C-3H_2), and remaining signals 1.25–1.6 [1.2–1.45]; ^1H nmr of **22***b* 360 MHz in $CDCl_3$ [360 MHz in C_6D_6] δ: 9.501[14] [9.312] (d, J = 2.0 [1.7] Hz, 1H, CHO), 6.159 [5.869] (dd, J = 3.2, 5.9 Hz, 1H, C-5H), 5.944 [5.699] (dd, J = 2.8, 5.9 Hz, 1H, C-6H), 2.91[14] [2.56[14]] (m, 1H, C-1H), 2.90[14] [2.440[14]] (dddd, J = 2.0 [1.7], 3.7, 3.9, 8.6 Hz, 1H, C-2H), 2.690 [2.289] (br t, $W_{1/2}$ = 8 Hz, 1H, C-4H), and 1.952 [1.566] (ddd, J = 3.7, 8.6, 12.3 Hz, 1H, C-3$_{exo}$H); ^{13}C nmr of **22***a*, see Table 3; ms (of the mixture of **22***a* and **22***b*) m/z (%): 216.1513 (13, M^+, $C_{15}H_{20}O^+$ requires 216.1513), 187.1488 (16, $C_{14}H_{19}^+$), 160.1248 (10, $C_{12}H_{16}^+$), 131.0860 (8, $C_{10}H_{11}^+$), 117.0704 (9, $C_9H_9^+$), 109.1019 (100, $C_8H_{13}^+$), 91.0549 (18, $C_7H_7^+$), 79.0552 (18, $C_6H_7^+$), and 67.0554 (46, $C_5H_7^+$).

Thermal addition of methyl acrylate to 3

A large excess of methyl acrylate (approximately 1 mL) was added to a solution of **3** (25.3 mg, 0.158 mmol) in CH_2Cl_2 (2.5 mL). The mixture was heated under reflux for 5 days. The solvent and excess dienophile were evaporated, and the residue was subjected to preparative tlc to yield 32.3 mg (83%) of white needles composed of **23***a* (major) and **23***b* (minor) (respectively, *methyl (1*RS,*2*RS,*4*RS,*7*SR)- and *methyl (1*RS,*2*RS,*4*RS,*7*RS)-*spiro(bicyclo[2.2.1]hept-5-ene-7,2'-bicyclo[2.2.2]octane)-2-carboxylate);* ir ν_{max}: 2935, 2865, 1715, and 1165 cm^{-1}; ^1H nmr of **23***a* 360 MHz in $CDCl_3$ [360 MHz in C_6D_6] δ: 6.118 [5.987] (dd, J = <0.5,[15] 3.2, 5.8 Hz, 1H, C-5H), 5.832 [5.891] (dd, J = <0.5,[15] 2.9, 5.8 Hz, 1H, C-6H), 3.621 [3.375] (s, 3H, OCH_3), 3.055 [2.911] (dt, J = 3.8, 3.9, 8.8 Hz, 1H, C-2H), 2.848 [2.836] (m, $W_{1/2}$ = 8 Hz, J = <0.5, 1, 2.9, 3.8 Hz,[15] 1H, C-1H), 2.511 [2.230] (m, $W_{1/2}$ = 8 Hz, J = <0.5, 1, 3.2, 3.7 Hz,[15] 1H, C-4H), 2.059 [1.907] (ddd, J = 3.7, 8.8, 12.2 Hz, 1H, C-3$_{exo}$H), 1.812 [1.846] (m, $W_{1/2}$ = 7 Hz, 1H, [2.2.2] C-1H), 1.619 [1.459] (m, $W_{1/2}$ = 8 Hz, 1H, [2.2.2] C-4H), 1.43[14] [1.645] (dd, J = 3.9, 12.2 Hz, 1H, C-3$_{endo}$H), [1.089] (multiplets with J_{gem} = 14 Hz, 2H, [2.2.2] C-3H_2), and remaining signals 1.3–1.6 [1.2–1.45]; ^1H nmr of **23***b* 360 MHz in $CDCl_3$ [360 MHz in C_6D_6] δ: 6.144[14] [6.039] (dd, J = 3.2, 5.6 Hz, 1H, C-5H), 5.872 [5.953] (dd, J = 2.6, 5.6 Hz, 1H, C-6H), 3.614 [3.366] (s, 3H, OCH_3), 2.953[14] [2.763] (dt, J = 3.9, 3.9, 8.7 Hz, 1H, C-2H), 2.934[14] [2.90[14]] (m, 1H, C-1H), 2.602 [2.333] (m, $W_{1/2}$ = 8 Hz, C-4H), 1.947 [1.777] (ddd, J = 3.9, 8.7, 12.2 Hz, 1H, C-3$_{exo}$H), and [1.64[14]] (dd, 1H, C-3$_{endo}$H); ^{13}C nmr of **23***a*, see Table 3; ms (of the mixture of **23***a* and **23***b*) m/z (%): 246.1616 (100, M^+, $C_{16}H_{22}O_2^+$ requires 246.1620), 187.1473 (39, $C_{14}H_{19}^+$), 186.1409 (71, $C_{14}H_{18}^+$), 109.1018 (53, $C_8H_{13}^+$), 105.0706 (25, $C_8H_9^+$), 104.0630 (29, $C_8H_8^+$), 91.0544 (31, $C_7H_7^+$), 79.0544 (33, $C_6H_7^+$), 77.0391 (20, $C_6H_5^+$), and 67.0556 (27, $C_5H_7^+$).

Thermal addition of 3-buten-2-one to 3

A large excess of 3-buten-2-one (approximately 1 mL) was added to a solution of **3** (44.1 mg, 0.275 mmol) in CH_2Cl_2 (4 mL). The mixture was heated under reflux for 7 days. The solvent and excess dienophile were evaporated, and the residue was subjected to preparative tlc to yield 38.8 mg (61%) of a white semisolid composed of **24***a* (major) and **24***b* (minor) (respectively, *(1*RS,*2*RS,*4*RS,*7*SR)- and *(1*RS,*2*RS,*4*RS,*7*RS)-*2-acetylspiro(bicyclo[2.2.1]hept-5-ene-7,2'-bicyclo[2.2.2]octane));* ir ν_{max}: 2930, 2865, 1700, 1600 (w), 1350, 1055, and 1015 cm^{-1}; ^1H nmr of **24***a* 360 MHz in $CDCl_3$ [360 MHz in C_6D_6] δ: 6.084 [5.910] (dd, J = 3.2, 5.9 Hz, 1H, C-5H), 5.767 [5.644] (dd, J = 2.9 [2.6], 5.9 Hz, 1H, C-6H), 3.050 [2.636] (ddd, J = 3.8 [3.7], 4.0 [5.2], 8.5 [7.0] Hz, 1H, C-2H), 2.869 [2.583] (m, $W_{1/2}$ = 8 [7] Hz, 1H, C-1H), 2.515 [2.228] (m, $W_{1/2}$ = 8.5 [8] Hz, 1H, C-4H), 2.119 [1.744] (s, 3H, $COCH_3$), 1.895 [1.69[16]] (ddd, J = 3.8, 8.5, 12.3 Hz, 1H, C-3$_{exo}$H), 1.818 [1.831] (m, $W_{1/2}$ = 7 Hz, 1H, [2.2.2] C-1H), 1.641 [1.510] (m, $W_{1/2}$ = 8 Hz, 1H, [2.2.2] C-4H), 1.508[14] [1.69[16]] (dd, J = 4.0, 12.3 Hz, 1H, C-3$_{endo}$H), [1.15 and 1.09] (second-order doublets with much additional coupling, J_{gem} =

[14]Partially or completely overlapped signal.

[15]Couplings determined with the aid of spin decoupling experiments.

[16]In C_6D_6 these protons have essentially the same shift, resulting in a very complicated 2H signal.

Can. J. Chem. Downloaded from www.nrcresearchpress.com by 190.90.36.8 on 09/07/12
For personal use only.

13.6 Hz, 2H, [2.2.2] C-3H_2), and remaining signals 1.35–1.55 [1.24–1.47]; ^{1}H nmr of **24***b* 360 MHz in $CDCl_3$ [360 MHz in C_6D_6] δ: 6.110[14] [5.956] (dd, J = 3.2, 5.9 Hz, 1H, C-5H), 5.807 [5.696] (dd, J = 2.9, 5.9 Hz, 1H, C-6H), 2.965[14] [2.62[14]] (m, $W_{1/2}$ = 8 Hz, 1H, C-1H), 2.956[14] [2.479] (dt, J = 3.8, 3.9, 8.5 Hz, 1H, C-2H), 2.606 [2.317] (m, $W_{1/2}$ = 8 Hz, 1H, C-4H), and 2.108 [1.732] (s, 3H, $COCH_3$); ^{13}C nmr of **24***a*, see Table 3; ms (of the mixture of **24***a* and **24***b*) *m/z* (%): 230.1668 (11, M^+), 187.1486 (27, $C_{14}H_{19}^+$), 186.1408 (8, $C_{14}H_{18}^+$), 109.1018 (100, $C_8H_{13}^+$), 91.0549 (12, $C_7H_7^+$), 79.0551 (11, $C_6H_7^+$), and 67.0555 (35, $C_5H_7^+$). An analytical sample was recrystallized from ethyl acetate. *Anal.* calcd. for $C_{16}H_{22}O$: C 83.43, H 9.63; found: C 83.29, H 9.75.

Reactivity of **3** *versus cyclopentadiene*

A solution of **3** (19.2 mg, 0.120 mmol) and freshly cracked cyclopentadiene (7.7 μL ≡ 0.093 mmol) in C_6D_6 (approximately 0.5 mL) was rapidly mixed in an nmr tube with a solution of *para*-benzoquinone (12.9 mg, 0.119 mmol) in C_6D_6 (0.5 mL). The ^{1}H nmr spectra taken at intervals showed reaction of all the cyclopentadiene with the dienophile within a few minutes, but at the same time there was no detectable production of **20***a*. However, after 2.5 h much of the remaining *para*-benzoquinone had reacted with **3** to provide mainly **20***a*. After 24 h the amount of diene **3** in solution had not decreased significantly.

Reactivity of **3** *at 0°C*

A solution of **3** (11.3 mg, 0.070 mmol) in CH_2Cl_2 (5 mL) was cooled in an ice bath as *para*-benzoquinone (7.6 mg, 0.070 mmol) was added. After 10 min approximately 30 mg of cyclopentadiene was added, and the solution was allowed to attain room temperature. The solvent and excess cyclopentadiene were evaporated. The ^{1}H nmr spectrum of the product showed that it consisted solely of unreacted **3** and of cyclopentadiene adduct.

This mixture was redissolved in CH_2Cl_2 (3 mL) and cooled again in an ice bath. One drop of BF_3 etherate was added followed quickly by *para*-benzoquinone (7.2 mg). The mixture was stirred for 4 min before a large excess of cyclopentadiene was added. The mixture was added to water. The organic layer was dried (Na_2SO_4) and evaporated. The ^{1}H nmr spectrum of the product showed signals attributable to the double adducts **26***a* and **26***b* (*vide infra*), but no trace of **3** or of **20***a*.

Reactivity of **3** *at −78°C in the presence of a Lewis acid*

A solution of **3** (50.0 mg, 0.312 mmol) in CH_2Cl_2 (4 mL) was cooled in a Dry Ice – acetone bath; BF_3 etherate (38.5 μL, 0.313 mmol) was added, followed quickly by a solution of *para*-benzoquinone (33.7 mg, 0.312 mmol) in CH_2Cl_2 (approximately 1 mL). The mixture was stirred at −78°C for 30 min, and the cyclopentadiene (0.35 μL, 4.2 mmol) was added at once. The solution was allowed to warm above 0°C, then it was diluted with ether, and this solution was washed (×2) with saturated NaCl. Evaporation of the solvent provided a yellow solid the ^{1}H nmr spectrum of which was consistent with a mixture of **26***a* and **26***b*, but there were no signals corresponding to **3**, **20***a*, the cyclopentadiene adduct, or the double cyclopentadiene adduct **27**.

Attempts at thermal equilibration

(a) Of pure **18***a*

A solution of pure (by 400-MHz ^{1}H and 100-MHz ^{13}C nmr) adduct **18***a* in CH_2Cl_2 was heated under reflux for 48 h, then the solvent was evaporated. In the 400-MHz ^{1}H nmr spectrum of the product, only signals due to **18***a* were apparent, i.e. not even a trace of **18***b* could be detected.

(b) Of **19***a and* **19***b with cyclopentadiene*

A solution of adducts **19***a* and **19***b* and a large excess of freshly-cracked cyclopentadiene in CH_2Cl_2 was heated under reflux for 15.5 h, then the solvent was evaporated. The ^{1}H nmr spectrum of the product revealed that no cyclopentadiene adduct **25** had formed. (What remained was unchanged **19***a* and **19***b*.)

Double addition of para*-benzoquinone to* **3** *and cyclopentadiene*

A stirred solution of **3** (50.0 mg, 0.312 mmol) in CH_2Cl_2 (3 mL) was cooled in a Dry Ice – acetone bath. BF_3 etherate (38.4 μL, 0.312 mmol) and *para*-benzoquinone (33.7 mg, 0.312 mmol) were added, and the mixture was stirred for 6 h. Freshly cracked cyclopentadiene (27.5 μL, 0.312 mmol) was added, and the mixture was stirred for a further 20 min, after which the mixture was allowed to attain room temperature. Ether was added, and the organic solution was washed with saturated NaCl, dried ($MgSO_4$), and evaporated to yield 101.0 mg of a pale yellow solid composed of **26***a* (major) and **26***b* (minor) (respectively, *(2s,1'R,4'S,4'aR,5'S,8'R,8'aS,9'aS,10'a*R- and *(2r,1'R,4'S,4'aR,5'S,8'R,8'aS,9'aS,10'aR)-1',4',4'a,5',8',-8'a,9'a,10'a-octahydrospiro(bicyclo[2.2.2]octane-2,11'-[1,4][5,8]dimethanoanthracene)-9',10'-dione)* and small amounts of **20***a* and **20***b*. Crystallization from ethyl acetate – CH_2Cl_2 provided colourless crystals; ir ν_{max}: 2930, 2870, and 1685 cm^{-1}; ^{1}H nmr of **26***a* 60 MHz in $CDCl_3$ [360 MHz in C_6D_6] δ: 6.20 [5.998] (t, J = 1.8 Hz, 2H, C-6'H + C-7'H), 6.07 [5.895] (t, J = 1.9 Hz, 2H, C-2'H + C-3'H), 3.39 [3.181] (m, $W_{1/2}$ = 4.5 Hz, 2H, C-5'H + C-8'H), 3.0[14] [2.943] (m, $W_{1/2}$ = 5 Hz, 2H, C-1'H + C-4'H), 3.0[14] [2.793] (m, $W_{1/2}$ = 5 Hz, 2H, C-4'aH + C-9'aH), 2.9[14] [2.592] (m, $W_{1/2}$ = 5 Hz, 2H, C-8'aH + C-10'aH), [1.729] (m, $W_{1/2}$ = 8 Hz, 1H, [2.2.2] C-1H), [1.392] (m, $W_{1/2}$ = 9.5 Hz, 1H, [2.2.2] C-4H), [1.159] (d of very small t, J_{gem} = 9 Hz, 1H, C-12'*s*H), [0.938] (br d, J = 2 Hz, 2H, [2.2.2] C-3H_2), [0.783] (br d, J_{gem} = 9 Hz, 1H, C-12'*r*H), and remaining signals unresolved 1.1–2 [1.1–1.35]; ^{1}H nmr of **26***b* [360 MHz in C_6D_6] δ: [5.982] (t, J = 2.0 Hz, 2H, C-2'H + C-3'H), and [3.02] (m, 2H, C-1'H + C-4'H), with the majority of signals being partially or completely overlapped with signals due to **26***a*; ^{13}C nmr of **26***a*, see Table 3; ms (of mixture of **26***a* and **26***b*) *m/z* (%): 334.1929 (1.5, M^+), 268.1463 (53, $C_{18}H_{20}O_2^+$), 240.1514 (100, $C_{17}H_{20}O^+$), 160.1251 (42, $C_{12}H_{16}^+$), 160.0524 (17, $C_{10}H_8O_2^+$), 131.0860 (20, $C_{10}H_{11}^+$), 131.0497 (24, $C_9H_7O^+$), 117.0704 (28, $C_9H_9^+$), 109.1020 (22, $C_8H_{13}^+$), 104.0628 (23, $C_8H_8^+$), 91.0549 (46, $C_7H_7^+$), 82.0062 (67, $C_4H_2O_2^+$), 79.0550 (25, $C_6H_7^+$), 67.0554 (26, $C_5H_7^+$), and 66.0479 (31, $C_5H_6^+$). *Anal.* calcd. for $C_{23}H_{26}O_2$: C 82.60, H 7.84; found: C 82.43, H 7.83.

*(1*R*,4*S*,4a*R*,5*S*,8*R*,8a*S*,9a*S*,10a*R*)-1,4,4a,5,8,8a,9a,10a-octahydro[1,4],[5,8]dimethanoanthracene (27)*[17]

Cyclopentadiene (2.5 mL) was added to a solution of *para*-benzoquinone (1.02 g, 9.44 mmol) in CH_2Cl_2 (approximately 50 mL). The mixture was heated under reflux for 60 h. After evaporation of the solvent, the residue was crystallized from CH_2Cl_2–ether–pentane yielding colourless crystals (1.77 g, 78%), mp 165–166.5°C (lit. (22, 32) mp 157°C; ir ν_{max}: 2980, 2930, 2860, and 1685 cm^{-1}; ^{1}H nmr 60 MHz in $CDCl_3$ [360 MHz in C_6D_6] δ: 6.22 [5.928] (t, J = 1.8 Hz, 4H), 3.37 [3.119] (m, $W_{1/2}$ = 4.5 Hz, 4H), 2.88 [2.503] (br t, $W_{1/2}$ = 4 Hz, 4H), 1.45 [1.117] (dt, J = 2, 9.6 Hz, 2H, C-11H + C-12H *syn* to double bonds), and 1.31 [0.743] (br d, J = 9.6 Hz, 2H, C-11H + C-12H *anti* to double bonds (20)); ms *m/z* (%): 240 (12, M^+), 212 (12), 174 (48), 146 (11), 91 (10), and 66 (100).

Acknowledgements

We thank Dr. Žarko Stojanac of this Department for many stimulating discussions and helpful suggestions. We are pleased to acknowledge Professor K. N. Houk of the University of California in Los Angeles for an interesting exchange of opinions. We are grateful to the Natural Sciences and Engineering Research Council for financial support in the form of operating grants and a postgraduate scholarship to D.J.B.

1. V. A. Mironov, T. M. Fadeeva, and A. A. Akhrem. Dokl. Akad. Nauk SSSR, **174**, 852 (1967); E. J. Corey, N. M. Weinshenker, T. K. Schaaf, and W. Huber. J. Am. Chem. Soc. **91**, 5675 (1969); D. Bellus, G. Helferich, and C. D. Weis. Helv. Chim. Acta, **54**, 463 (1971); N. Stojanac, A. Sood, Ž. Stojanac, and Z. Valenta. Can. J. Chem. **53**, 619

[17]Included here for comparison of its spectroscopic data with those of **26***a* and **26***b*.

(1975); H. AUKSI and P. YATES. Can. J. Chem. **59**, 2510 (1981), and references therein; D. J. BURNELL and Z. VALENTA. J. Chem. Soc. Chem. Commun. 1247 (1985).
2. S. WINSTEIN, M. SHATAVSKY, C. NORTON, and R. B. WOODWARD. J. Am. Chem. Soc. **77**, 4183 (1955); K. L. WILLIAMSON, Y.-F. L. HSU, R. LACKO, and C. H. YOUN. J. Am. Chem. Soc. **91**, 6129 (1969); V. A. MIRONOV, M. E. DOLGAYA, V. T. LUK'YANOV, and S. A. YANKOVSKII. Zh. Org. Khim. **12**, 1436 (1976); D. W. JONES. J. Chem. Soc. Chem. Commun. 739 (1980).
3. M. HARDY, P.-A. CARRUPT, and P. VOGEL. Helv. Chim. Acta, **59**, 1685 (1976); M. AVENATI, J.-P. HAGENBUCH, C. MAHAIM, and P. VOGEL. Tetrahedron Lett. **21**, 3167 (1980); J.-P. HAGENBUCH, P. VOGEL, A. A. PINKERTON, and D. SCHWARZENBACH. Helv. Chim. Acta, **64**, 1818 (1981); M. AVENATI, O. PILET, P.-A. CARRUPT, and P. VOGEL. Helv. Chim. Acta, **65**, 178 (1982); M. AVENATI, P.-A. CARRUPT, D. QUARROZ, and P. VOGEL. Helv. Chim. Acta, **65**, 188 (1982); M. AVENATI and P. VOGEL. Helv. Chim. Acta, **65**, 204 (1982); C. MAHAIM and P. VOGEL. Helv. Chim. Acta, **65**, 866 (1982); C. MAHAIM, L. SCHWAGER, P.-A. CARRUPT, and P. VOGEL. Tetrahedron Lett. **34**, 3603 (1983); R. GLEITER and L. A. PAQUETTE. Acc. Chem. Res. **16**, 328 (1983); J. C. GALLUCCI, T. M. KRAVETZ, K. E. GREEN, and L. A. PAQUETTE. J. Am. Chem. Soc. **107**, 6592 (1985); L. A. PAQUETTE, T. M. KRAVETZ, and L.-Y. HSU. J. Am. Chem. Soc. **107**, 6598 (1985), and references therein.
4. M. KAKUSHIMA, L. ALLAIN, R. A. DICKINSON, P. S. WHITE, and Z. VALENTA. Can. J. Chem. **57**, 3354 (1979).
5. M. KAKUSHIMA, J. DAS, G. R. REID, P. S. WHITE, and Z. VALENTA. Can. J. Chem. **57**, 3356 (1979); J. DAS, R. A. DICKINSON, M. KAKUSHIMA, G. M. KINGSTON, G. R. REID, Y. SATO, and Z. VALENTA. Can. J. Chem. **62**, 1103 (1984).
6. (*a*) R. SUSTMANN. Tetrahedron Lett. 2721 (1971); (*b*) K. N. HOUK. J. Am. Chem. Soc. **95**, 4092 (1973); (*c*) K. N. HOUK and R. W. STROZIER. J. Am. Chem. Soc. **95**, 4094 (1973).
7. K. SEGUCHI, A. SERA, Y. OTSUKI, and K. MARUYAMA. Bull. Chem. Soc. Jpn. **48**, 3641 (1975).
8. S. INAGAKI, H. FUJIMOTO, and K. FUKUI. J. Am. Chem. Soc. **98**, 4054 (1976).
9. D. J. BURNELL, H. B. GOODBRAND, S. M. KAISER, and Z. VALENTA. Can. J. Chem. **62**, 2398 (1984).
10. S. F. MARTIN, T.-S. CHOU, and C. W. PAYNE. J. Org. Chem. **42**, 2520 (1977); S. F. MARTIN and T.-S. CHOU. J. Org. Chem. **43**, 1027 (1978).
11. A. KRANTZ and C. Y. LIN. J. Am. Chem. Soc. **95**, 5662 (1973).
12. M. JULIA and C. BLASIOLI. Bull. Soc. Chim. Fr. 1941 (1976).
13. S. C. WELCH, S. CHAYABUNJONGLERD, and A. S. C. P. RAO. J. Org. Chem. **45**, 4086 (1980).
14. S. KRISHNAMURTHY and H. C. BROWN. J. Org. Chem. **40**, 1864 (1975).
15. J.-L. LUCHE. J. Am. Chem. Soc. **100**, 2226 (1978); J.-L. LUCHE, L. RODRIGUEZ-HAHN, and P. CRABBÉ. J. Chem. Soc. Chem. Commun. 601 (1978).
16. S. H. GROVER, J. P. GUTHRIE, J. B. STOTHERS, and C. T. TAN. J. Magn. Reson. **10**, 227 (1973); S. H. GROVER and J. B. STOTHERS. Can. J. Chem. **52**, 870 (1974); J. B. STOTHERS, C. T. TAN, and K. C. TEO. Can. J. Chem. **54**, 1211 (1976); H. BEIERBECK and J. K. SAUNDERS. Can. J. Chem. **54**, 2985 (1976).
17. L. C. ROACH and W. H. DALY. J. Chem. Soc. Chem. Commun. 606 (1970).
18. J. SAUER. Angew. Chem. Int. Ed. Engl. **6**, 16 (1967); J. SAUER and R. SUSTMANN. Angew. Chem. Int. Ed. Engl. **19**, 779 (1980).
19. D. J. BURNELL. Ph.D. thesis. University of New Brunswick. 1983.
20. P. LASZLO and P. VON R. SCHLEYER. J. Am. Chem. Soc. **86**, 1171 (1964); I. FLEMING and D. H. WILLIAMS. Tetrahedron, **23**, 2747 (1967).
21. R. S. ROUSE and W. E. TYLER III. J. Org. Chem. **26**, 3525 (1961).
22. R. C. COOKSON, R. R. HILL, and J. HUDEC. J. Chem. Soc. 3043 (1964).
23. L. A. BURKE, G. LEROY, and M. SANA. Theor. Chim. Acta, **40**, 313 (1975); R. F. TOWNSHEND, G. RAMUNNI, G. SEGAL, W. J. HEHRE, and L. SALEM. J. Am. Chem. Soc. **98**, 2190 (1976); L. A. BURKE and G. LEROY. Theor. Chim. Acta, **44**, 219 (1977).
24. F. K. BROWN and K. N. HOUK. Tetrahedron Lett. **25**, 4609 (1984).
25. VAN SICKLE and J. O. RODIN. J. Am. Chem. Soc. **86**, 3091 (1964); P. BROWN and R. C. COOKSON. Tetrahedron, **21**, 1977 (1965); **21**, 1993 (1965).
26. K. N. HOUK. J. Am. Chem. Soc. **95**, 4092 (1973).
27. G. S. HAMMOND. J. Am. Chem. Soc. **77**, 334 (1955).
28. J. DAS. Ph.D. thesis. University of New Brunswick. 1978; J. DAS, R. KUBELA, G. A. MACALPINE, Ž. STOJANAC, and Z. VALENTA. Can. J. Chem. **57**, 3308 (1979).
29. N. S. ISAACS. Experiments in physical organic chemistry. Macmillan, London. 1969. pp. 276–277; N. A. DOMNIN and M. A. LARIONOVA. Zh. Obshch. Khim. **26**, 1398 (1956).
30. J. P. SCHAEFER and L. ENDRES. Org. Synth. Collect. Vol. V, 285 (1973).
31. R. L. LETSINGER and J. G. TRAYNHAM. J. Am. Chem. Soc. **70**, 2818 (1948).
32. W. ALBRECHT. Justus Liebigs Ann. Chem. **348**, 31 (1906).

Can. J. Chem. Downloaded from www.nrcresearchpress.com by 190.90.36.8 on 09/07/12
For personal use only.

Thermolysis of geminal diazides: a novel route to 1,3,4-oxadiazoles

WILLIAM OGILVIE[1] AND WERNER RANK[2]

Department of Chemistry, Laurentian University, Ramsey Lake Road, Sudbury, Ont., Canada P3E 2C6

Received July 8, 1986

This paper is dedicated to Dr. O. E. (Ted) Edwards

WILLIAM OGILVIE and WERNER RANK. Can. J. Chem. **65**, 166 (1987).

The geminal diazides ethyl α,α-diazidoacetoacetate and α,α-diazidobenzoylacetate were prepared from the corresponding dibromo precursors by nucleophilic azide displacement. Thermolysis of the diazido compounds led to the formation of 2,5-disubstituted 1,3,4-oxadiazoles in high yield.

WILLIAM OGILVIE et WERNER RANK. Can. J. Chem. **65**, 166 (1987).

Utilisant les dérivés dibromés correspondants comme précurseurs et faisant appel à des réactions de déplacements nucléophiles par des azotures, on a préparé les dérivés diazidés géminés, α,α-diazidoacétoacétate et α,α-diazidobenzoylacétate d'éthyle. La thermolyse des composés diazidés conduit à la formation, avec de très bons rendements, d'oxadiazoles-1,3,4 disubstitués dans les positions 2 et 5.

[Traduit par la revue]

Can. J. Chem. Downloaded from www.nrcresearchpress.com by 190.90.36.8 on 09/07/12
For personal use only.

Interest in azido compounds stems partially from their potential for thermal and photolytic decomposition to highly reactive nitrenes. Depending on the structure and on conditions, the nitrenes rearrange to more stable products where a major stabilization process may lead to the formation of azomethines (1). Thus nitrenes may undergo 1,2-hydrogen shifts leading to the formation of imines, or alkyl and aryl shifts leading to the formation of N-substituted azomethines. Less commonly observed is the migration of an acyl group from carbon onto nitrogen, leading to the formation of *N*-acyl imines (2–4). In some cases the evidence for the intermediacy of *N*-acyl imines is indirect. An intermediate *N*-acyl imine has been postulated in the thermolytic conversion of the geminal diazide 2,2-diazido-1,3-indandione to a tetrazole derivative (3) (eq. [1]).

[1] 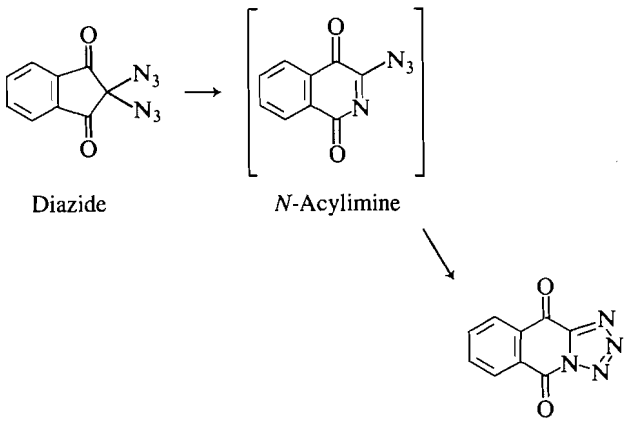

Diazide *N*-Acylimine Tetrazole

The photolytic decomposition of dimethyl diazidomalonate provides another example of this nature (5). To further explore the structural requirements for acyl migration onto nitrogen we chose to study the thermolysis of ethyl α,α-diazido-acetoacetate and -benzoylacetate.

To undertake this study we first had to synthesize these two hitherto unknown geminal diazides. For this purpose ethyl acetoacetate and ethyl benzoylacetate were first brominated to the known dibromo derivatives **1***a* (6) and **1***b* (7). Nucleophilic displacement of halogen by the azide ion was achieved when the dibromo derivatives were treated with sodium azide in dimethyl formamide. Fractional distillation[3] gave pure ethyl α,α-diazidoacetoacetate (**2***a*) and pure ethyl α,α-diazidobenzoylacetate (**2***b*) in yields of 76% and 63%, respectively. The structural identity of the diazido derivatives was established from their spectral and microanalytical data. An ir absorption characteristic for the azido group was observed at 2135 cm^{-1} for **2***a* and at 2130 cm^{-1} for **2***b*.

Thermolysis of the two diazido compounds gave in each case one major product, which proved to be a 2,5-disubstituted 1,3,4-oxadiazole (Scheme 1). This complex rearrangement is not only of synthetic utility as a good route to 1,3,4-oxadiazoles, but also has mechanistic significance in that it presents an example of acyl migration to nitrogen.

When ethyl α,α-diazidoacetoacetate was heated in refluxing dry xylene under a N_2 atmosphere the ir azide absorption at 2135 cm^{-1} disappeared completely after 2 h. Flash chromatography through silica gel gave a crude material (94%) that proved to be almost pure 2-carboxyethyl-5-methyl-1,3,4-oxadiazole (**3***a*) according to its ^{1}Hmr spectrum. Further purification by Kugelrohr distillation and recrystallization gave 76% of pure 1,3,4-oxadiazole **3***a*. The ir absorption at 1745 cm^{-1}, the ^{1}Hmr signals at 4.60 (2H, q) and 1.50 (3H, t), as well as the ^{13}Cmr signals at 166.18, 63.45, and 14.08 supported the presence of an ethyl carboxylate function. Medium ir absorption bands at 1565 and 1540 cm^{-1} were attributed to the presence of two C=N bonds. These spectral data supported the structure of the 2,5-disubstituted 1,3,4-oxadiazole **3***a*. However, the possibility of an isomeric 1,2,4-oxadiazole structure (Scheme 2) could not be excluded unequivocally, either mechanistically or on the basis of the spectral data. It was therefore decided to prove the structure of the thermolytic product by an independent synthesis (Scheme 1). For this purpose 5-methyltetrazole (**4**) was prepared from acetonitrile and covalent aluminum azide, in analogy to a procedure reported by Behringer and Kohl (8). The tetrazole so obtained was acylated with oxalyl chloride mono-

[1]Undergraduate participant in research.

[2]Author to whom correspondence may be addressed.

[3]Attention should be drawn to the potentially hazardous nature of azides (5). In our laboratory no difficulties were encountered when they were handled in solution or when small amounts were distilled under reduced pressure. However, proper caution should be exercised at all times.

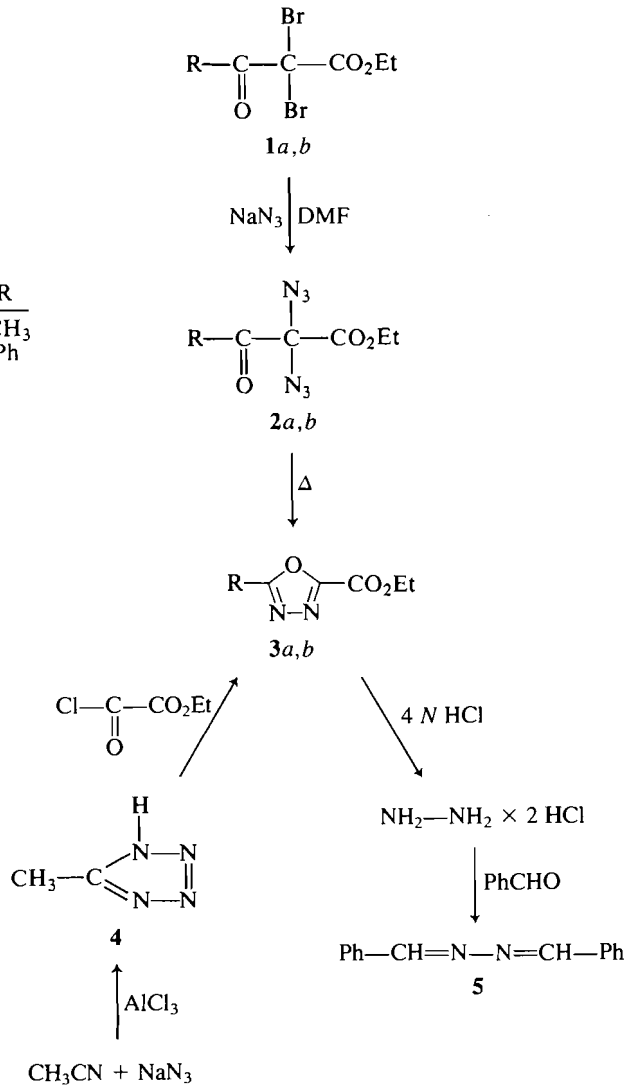

SCHEME 1

ethyl ester in refluxing xylene, in analogy to a method described by Huisgen *et al.* (9). The 2-carboxyethyl-5-methyl-1,3,4-oxadiazole obtained by this route melted at 45°C and had ir and ^{1}Hmr spectral data identical to those of the thermolytic oxadiazole.

In a further experiment the thermolytic oxadiazole **3***a* was hydrolyzed with refluxing 4 *N* hydrochloric acid. The residue obtained upon evaporation was reacted with benzaldehyde to give crystalline benzalazine (**5**), which was identified by a mixture melting point with authentic benzalazine (10). Since in benzalazine the nitrogen atoms are linked to each other, the thermolytic oxadiazole **3***a* must have the 1,3,4-oxadiazole rather than the 1,2,4-oxadiazole structure.

Thermolysis of ethyl α,α-diazidobenzoylacetate **2***b* in refluxing xylene under a N_2 atmosphere showed complete conversion of the starting material after 2 h by the absence of an ir absorption band at 2130 cm^{-1}. Evaporative work-up followed by medium pressure column chromatography gave recrystallized 2-carboxyethyl-5-phenyl-1,3,4-oxadiazole **3***b* (83%) with a melting point of 72–73°C. This melting point as well as the uv spectral data were in agreement with the data reported in the literature (9). The ir absorption at 1740 cm^{-1}, the ^{1}Hmr signals at 4.53 (2H, q) and 1.43 (3H, t), as well as the ^{13}Cmr signals at 166.42, 63.50, and 14.12 confirmed the presence of an ethyl carboxylate function. The remaining ^{13}Cmr data of 1,3,4-oxadiazole **3***b* at 156.57 and 154.41 were comparable to the data of the 1,3,4-oxadiazole **3***a* at 157.11 and 154.41.

Mechanistic considerations

Upon thermolysis, both diazido compounds **2***a* and **2***b* followed the same reactivity pattern, leading to the formation of 1,3,4-oxadiazoles **3***a* and **3***b* in excellent yields (Scheme 2). Although no intermediates could be isolated, we would like to propose that initially the diazido compound probably loses one molar equivalent of nitrogen to form a nitrene. Subsequent migration of the acyl group onto nitrogen leads then to the formation of an azidoazomethine intermediate.[4]

Alternatively, the negatively charged azido nitrogen may attack the electrophilic carbonyl carbon. A subsequent rearrangement with concomitant loss of one molar equivalent of nitrogen may then lead to the formation of the same azidoazomethine intermediate.

Azidoazomethines usually isomerize readily to tetrazoles in a reversible reaction (11). Loss of a second molar equivalent of nitrogen from either the azidoazomethine directly or from the tetrazole might lead to the diazir-2-ene, which finally rearranges to the 2,5-substituted 1,3,4-oxadiazole. Huisgen and Blaschke (12) considered such a diazirene intermediate as a possibility in the formation of 1,3,4-oxadiazoles in both the photolytic and thermolytic reaction of ethyl azidoformate with nitriles. Since in our case no intermediates have been isolated or spectrally detected, these mechanistic considerations are speculative. However, the correctness of an initial acyl migration onto nitrogen can be assumed.

Experimental

Infrared (ir) spectra were obtained with a Perkin–Elmer spectrometer, model 735B, using chloroform as solvent. Ultraviolet (uv) spectra of ethanolic solutions were measured on a Hitachi Perkin–Elmer double beam spectrometer, model 124-0031. Proton magnetic resonance (^{1}Hmr) spectra were recorded with a Varian T-60 spectrometer and ^{13}C magnetic resonance (^{13}Cmr) spectra were recorded with a Bruker WP-80 FT spectrometer. The chemical shift data are quoted in δ units and refer to solutions in deuterochloroform using tetramethylsilane as internal reference. Thin-layer chromatography (tlc) was performed on precoated silica gel GF Redi Plates (Fisher Scientific Co.). Preparative layer chromatography (plc) was carried out on 20 × 20 cm glass plates precoated with silica gel Sil G-100 UV_{254} (Brinkmann Instruments, Inc.). Column chromatography was done under medium pressure with silica gel G-type 60 (E. Merck) as adsorbent, or by gravity flow using silica gel (60–200 mesh) "Baker Analyzed Reagent" (J. T. Baker Chemical Co.). Unless otherwise stated, anhydrous sodium sulfate was used for drying organic solutions. Solvents were usually removed on a rotary evaporator at reduced pressure using bath temperatures of 30–40°C. Melting points and boiling points are uncorrected.

*Ethyl α,α-dibromoacetoacetate (**1**a)*

To a vigorously stirred mixture of ethyl acetoacetate (13.0 g, 0.10 mol) and water (25 mL) was added dropwise (2 h) bromine (33.6 g, 0.2 mol) at room temperature. After additional stirring for 1 h methylene chloride (50 mL) was added. The organic phase was then separated, washed with water (3×), and dried. Evaporation of the solvent gave a yellow oil, which was purified by fractional distillation to give ethyl α,α-dibromoacetoacetate (20.7 g, 72%), $bp_{1.6}$ 83–84°C; $n_D^{20} = 1.4988$.

[4]It should be noted that there was no evidence of migration of the carboxyethyl group onto nitrogen.

Can. J. Chem. Downloaded from www.nrcresearchpress.com by 190.90.36.8 on 09/07/12
For personal use only.

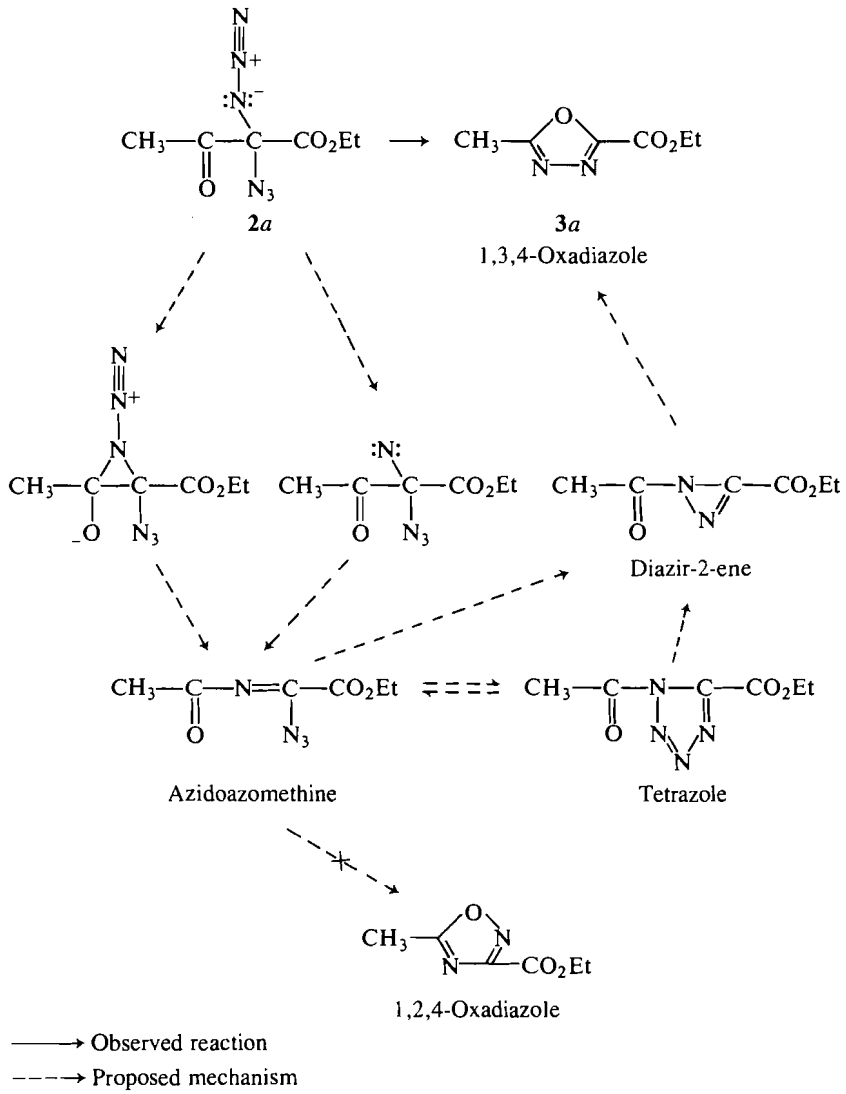

SCHEME 2

Ethyl α,α-dibromobenzoylacetate (1b)

To a refluxing solution of ethyl benzoylacetate (19.2 g, 0.1 mol) in carbon tetrachloride (100 mL), bromine (33.6 g, 0.21 mol) was added gradually (1.5 h). After additional reflux for 1 h the solvent was removed and the residue was distilled to give ethyl α,α-dibromobenzoylacetate (23.5 g, 67%), $bp_{0.3}$ 121–124°C; $n = 1.5705$ (lit. (7) bp_1 153–154°C; $n_D^{20} = 1.5703$).

Ethyl α,α-diazidoacetoacetate (2a)

To an ice cold solution of ethyl α,α-dibromoacetoacetate (14.4 g, 0.05 mol) in dimethylformamide (50 mL), sodium azide (7.15 g, 0.11 mol) was added portionwise during 30 min. After the reaction mixture reached room temperature, stirring was continued for another hour. Then water (100 mL) was added and the ester extracted with ether (2 × 50 mL). The combined ether extracts were washed with water (50 mL) and with brine (50 mL). After drying and evaporation of the solvent a yellowish liquid (9.6 g) was obtained. Fractional distillation (footnote 3) gave pure ethyl α,α-diazidoacetoacetate (8.1 g, 76%) with $bp_{0.8}$ 69–72°C and $n_D^{20} = 1.4627$. Spectral data corroborated the structural assignment; ir ν_{max}: 2135, 1740, 1715 cm^{-1}; ^{1}Hmr: 4.41 (2H, q, J = 7 Hz), 2.31 (3H, s), 1.38 (3H, t, J = 7 Hz). *Anal.* calcd. for $C_6H_8N_6O_3$: C 33.96, H 3.80, N 39.61; found: C 34.21, H 3.98, N 39.30.

Ethyl α,α-diazidobenzoylacetate (2b)

Ethyl α,α-dibromobenzoylacetate (14.0 g, 0.04 mol) was reacted as above with sodium azide. Extractive work-up followed by fractional distillation (footnote 3) gave pure ethyl α,α-diazidobenzoylacetate (6.9 g, 63%) with $bp_{0.1}$ 105–115°C and $n_D^{20} = 1.5395$. Spectral data supported the structural assignment; ir ν_{max}: 2130, 1745, 1700 cm^{-1}; ^{1}Hmr: 7.2–8.0 (5H, m), 4.18 (2H, q, J = 7 Hz), 1.13 (3H, t, J = 7 Hz). *Anal.* calcd. for $C_{11}H_{10}N_6O_3$: C 48.18, H 3.68, N 30.64; found: C 48.32, H 3.85, N 30.29.

2-Carboxyethyl-5-methyl-1,3,4-oxadiazole (3a)

(a) Thermolysis of ethyl α,α-diazidoacetoacetate (2a)[5,6]

A solution of diazide **2a** (1 g, 47 mmol) in sodium-dried xylene (3 mL) was heated to reflux under a N_2 atmosphere. An ir spectrum after 2 h indicated the complete disappearance of the azide signal at 2135 cm^{-1}. A crude purification of the products was achieved by putting the reaction mixture on a short column of silica gel (5 g, 60–200 mesh). Elution with cyclohexane removed the xylene. Subsequent elution with ethyl acetate gave a brownish viscous material (690 mg), which proved to be almost pure 2-carboxyethyl-5-methyl-1,3,4-oxadiazole according to the ^{1}Hmr spectrum. Kugelrohr distillation by heating this material up to 130°C at a pressure of 0.1 Torr (1 Torr =

[5]The above experiment was scaled up to 5 g of diazide **2a** without any difficulties.

[6]When the thermolysis was carried out in refluxing toluene instead of xylene the reaction was much slower. After a reaction time of 13 h the reaction mixture consisted of about 40% diazide **2a** and 60% oxadiazole **3a**.

Can. J. Chem. Downloaded from www.nrcresearchpress.com by 190.90.36.8 on 09/07/12
For personal use only.

133.3 Pa) furnished white crystalline oxadiazole **3***a* (556 mg, 75%). Recrystallization from ether/cyclohexane gave pure oxadiazole **3***a* with a melting point of 45°C. Spectral data were in agreement with the structural assignment; ir ν_{max}: 1745, 1565, 1540 cm^{-1}; uv λ_{max} (EtOH): 218 nm (ε 8000); ^{1}Hmr: 4.60 (2H, q, J = 7 Hz), 2.73 (3H, s), 1.50 (3H, t, J = 7 Hz); ^{13}Cmr: 166.18, 157.11, 154.41, 63.45, 14.08, 11.21. *Anal.* calcd. for $C_6H_8N_2O_3$: C 46.15, H 5.16, N 17.94; found: C 46.07, H 5.09, N 17.81.

*(b) Independent synthesis of 2-carboxyethyl-5-methyl-1,3,4-oxadiazole (3*a*)*

Oxadiazole **3***a* was prepared through acylation of 5-methyl tetrazole **4** in analogy to a reaction described by Huisgen *et al.* (9).

5-Methyltetrazole (4)

In analogy to a method developed for the synthesis of other tetrazoles (8), sodium azide (48.75 g, 0.75 mol) was added to a solution of acetonitrile (10.25 g, 0.25 mol) in dry tetrahydrofuran (50 mL). To this suspension was added a solution of aluminum trichloride (35 g, 0.26 mol) in dry tetrahydrofuran (250 mL). This reaction mixture was heated to reflux for 25 h, then cooled to room temperature and stirred for 1 h with 10% hydrochloric acid (50 mL). The mixture was then evaporated to dryness. Extraction of the residue with hot acetone gave an oil that crystallized upon standing. Recrystallization from chloroform gave pure 5-methyl tetrazole (7.2 g, 34.3%) with a melting point of 143°C (lit. (9) mp 143°C).

*Oxadiazole 3*a

To a solution of 5-methyl tetrazole (168 mg, 2 mmol) in dry xylene (10 mL) was added oxalylchloride monoethyl ester (316 mg, 2.5 mmol). After reflux for 1 h, tlc indicated the absence of starting tetrazole **4***a* and the formation of a new major product with a polarity equaling that of the thermolytic oxadiazole **3***a*. Evaporative work-up gave a viscous residue (247 mg) that was purified by plc to give pure 2-carboxyethyl-5-methyl-1,3,4-oxadiazole (194 mg, 62%), which after recrystallization from cyclohexane melted at 45°C. Identical ir and nmr spectra for the oxadiazoles generated by the two different routes proved the identity of the products.

Hydrolysis of 2-carboxyethyl-5-methyl-1,3,4-oxadiazole

The oxadiazole **3***a* (156 mg, 1 mmol) was hydrolyzed with refluxing 4 *N* hydrochloric acid (5 mL) during 3 h. The reaction mixture was then evaporated, followed by several coevaporations with ethanol to furnish a white, solid residue (91 mg). An ir spectrum in Nujol indicated the absence of any carbonyl absorption. An aqueous solution of this residue formed a voluminous precipitate with a solution of silver nitrate. These properties suggested that this material was hydrazine hydrochloride, which was confirmed by its conversion to benzalazine **5**. For this purpose a solution of the above residue (65 mg) and of sodium acetate (200 mg) in water (5 mL) was reacted with benzaldehyde (5 drops) in methanol (2 mL). Upon gentle warming of this mixture (heat gun, 10 min) a yellow precipitate formed. After cooling, the precipitate was filtered off, washed thoroughly with water, and dried to yield benzalazine **5** (108 mg, 84%). The melting point of 92°C and mixture melting point of 92°C established the identity of this material with authentic benzalazine (lit. (10) mp 93°C).

*2-Carboxyethyl-5-phenyl-1,3,4-oxadiazole (3*b)

A solution of diazide **2***b* (5.0 g, 18 mmol) in sodium-dried xylene (15 mL) was heated to reflux under a N_2 atmosphere. The progress of the reaction was monitored by ir and after 2 h there was no longer a detectable azide absorption at 2130 cm^{-1}. Evaporation of the solvent, followed by oil pump evacuation, left a liquid residue that was purified by medium pressure column chromatography to give a major product. Recrystallization from ethanol/cyclohexane afforded pure 2-carboxyethyl-5-phenyl-1,3,4-oxadiazole (3.3 g, 83%) with a melting point of 72–73°C. Spectral data supported the structural assignment; ir ν_{max}: 1740, 1605, 1540 cm^{-1}; uv λ_{max} (EtOH): 265 nm (ε 20 540); ^{1}Hmr: 7.33–8.23 (5H, m), 4.53 (2H, q, J = 7 Hz), 1.43 (3H, t, J = 7 Hz); ^{13}Cmr: 166.42, 156.57, 154.41, 63.50, 14.12. *Anal.* calcd. for $C_{11}H_{10}N_2O_3$: C 60.55, H 4.62, N 12.84; found: C 60.28, H 4.60, N 12.98. Literature (9) mp 71°C and λ_{max} (EtOH): 266 nm (ε 19 540).

Acknowledgements

The authors thank the Natural Sciences and Engineering Research Council of Canada for financial support and Mr. H. Seguin for the microanalyses.

1. T. Sheradsky. *In* The chemistry of the azido group. *Edited by* S. Patai. Interscience, London. 1971. pp. 331–395.
2. J. S. Millership and H. Suschitzky. Chem. Commun. 1496 (1971).
3. H. W. Moore and D. S. Pearce. Tetrahedron Lett. 1621 (1971).
4. W. A. Court, O. E. Edwards, C. Grieco, W. Rank, and T. Sano. Can. J. Chem. **53**, 463 (1975).
5. R. M. Moriarty, J. M. Kliegman, and C. Shovlin. J. Am. Chem. Soc. **89**, 5958 (1967).
6. K. J. Pedersen. Acta Chem. Scand. **2**, 252 (1948).
7. B. W. Howk and S. M. McElvain. J. Am. Chem. Soc. **54**, 282 (1932).
8. H. Behringer and K. Kohl. Chem. Ber. **89**, 2648 (1956).
9. R. Huisgen, J. Sauer, H. J. Sturm, and J. H. Markgraf. Chem. Ber. **93**, 2106 (1960).
10. R. C. Weast (*Editor*). CRC handbook of chemistry and physics. CRC Press, Boca Raton, Florida. 1980. p. C-140.
11. M. Tisler. Synthesis, 123 (1973).
12. R. Huisgen and H. Blaschke. Liebigs Ann. Chem. **686**, 145 (1965).

Can. J. Chem. Downloaded from www.nrcresearchpress.com by 190.90.36.8 on 09/07/12
For personal use only.

Biosynthesis of lupanine: incorporation of [3,3-$^2H_2$]cadaverine

THOMAS HEMSCHEIDT AND IAN D. SPENSER[1]
Department of Chemistry, McMaster University, Hamilton, Ont., Canada L8S 4M1

Received June 19, 1986

This paper is dedicated to Dr. O. E. (Ted) Edwards

THOMAS HEMSCHEIDT and IAN D. SPENSER. Can. J. Chem. **65**, 170 (1987).

The mode of incorporation of ^2H from [3,3-$^2H_2$]cadaverine into lupanine (**2**) and 13α-hydroxylupanine (**3**) in *Lupinus angustifolius* was determined by ^2H nmr spectroscopy. Lupanine carried deuterium at positions 4α, 4β, 8α, 8β, 13α, and 13β. These six sites were approximately equally enriched. Similarly, 13α-hydroxylupanine carried label approximately equally at five sites, 4α, 4β, 8α, 8β, and 13β. [3,3-$^2H_2$]Cadaverine was prepared by borodeuteride reduction in D_2O of the *p*-toluenesulfonylhydrazone of *N*-benzoylpiperid-4-one, followed by degradation of the resulting *N*-benzoyl[4,4-$^2H_2$]piperidine into 1,5-dibromo[3,3-$^2H_2$]pentane, conversion into 1,5-diphthalimido[3,3-$^2H_2$]pentane, and acid hydrolysis.

THOMAS HEMSCHEIDT et IAN D. SPENSER. Can. J. Chem. **65**, 170 (1987).

Faisant appel à la rmn du ^2H, on a déterminé le mode d'incorporation du ^2H de la [3,3-$^2H_2$]cadavérine dans la lupanine (**2**) et dans l'hydroxy-3α lupanine (**3**) dans le *Lupinus angustifolius*. La lupanine porte des atomes de deutérium dans les positions 4α, 4β, 8α, 8β, 13α et 13β. Les taux d'enrichissement de chacun de ces sites sont approximativement égaux. De la même manière, l'hydroxy-13α lupanine porte des quantités a peu près égales de marqueurs dans les positions 4α, 4β, 8α, 8β et 13β. On a préparé la [3,3-$^2H_2$]cadavérine en procédant à une réduction de la *p*-toluènesulfonylhydrazone de la *N*-benzoylpipéridone-4 par le borodeutêrure dans le D_2O, suivie d'une dégradation de la *N*-benzoyl [4,4-$^2H_2$]pipéridine qui en résulte en dibromo-1,5[3,3-$^2H_2$]pentane, d'une conversion en diphtalimido-1,5[3,3-$^2H_2$]pentane et finalement d'une hydrolyse acide.

[Traduit par la revue]

Introduction

Cadaverine, derived by decarboxylation from L-lysine (1), is a key intermediate in the biosynthesis of the lupine alkaloids. Label from [1-^{14}C]cadaverine is incorporated into specific sites of the tetracyclic $C_{15}N_2$ lupine alkaloids, sparteine (**1**) (2, 3), lupanine (**2**) (4–6), and 13α-hydroxylupanine (**3**) (4, 7). Each

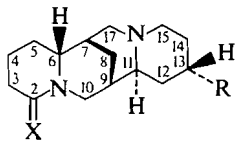

1 R = H, X = H_2
2 R = H, X = O
3 R = OH, X = O

of these sites contained approximately one-sixth of the total activity of the intact alkaloid. Experiments with stable isotopes revealed the entire regiochemistry of the incorporation of label from [1-^{13}C]cadaverine. In (−)sparteine (**1**) (8, 9), in (+)lupanine (**2**) (10, 11), and in 13α-hydroxylupanine (**3**) (10), each of the six C-atoms adjacent to nitrogen (C-2, -6, -10, -11, -15, -17) are equally enriched with ^{13}C. Thus, three cadaverine-derived C_5 units supply the carbon skeleton of the $C_{15}N_2$ alkaloids.

Furthermore, the mode of incorporation of intramolecularly doubly labelled [1-^{13}C,1-^{15}N]cadaverine (8–11) shows that each of the two nitrogen atoms enters the alkaloids as part of an intact cadaverine-derived C—N fragment, (N-1,C-2 and N-16,C-15, respectively).

Thus, two cadaverine-derived C_5N units supply the outer C_5N units (N-1,C-2 to C-6 and N-16,C-15 to C-11, respectively), whereas a cadaverine-derived C_5 unit supplies the central C_5 chain, C-17,C-7 to C-10, of the alkaloids. That this central chain cannot originate from a cadaverine-derived C_5 unit with C_{2v} symmetry is shown by the mode of incorporation of label from [2-^{14}C]- and [6-^{14}C]-Δ^1-piperideine (12).

These two compounds are equivalent to 5-amino[1-^{14}C]pentanal and 5-amino[5-^{14}C]pentanal, respectively, i.e., they represent labelled C_5N units that are derivable from cadaverine but lack C_{2v} symmetry. [2-^{14}C]-Δ^1-Piperideine delivers radioactivity into C-6, C-17, and C-11, but not into C-2, C-10, or C-15 of lupanine, whereas [6-^{14}C]-Δ^1-piperideine delivers label into C-2, C-10, and C-15 of lupanine, but not into C-6, C-17, or C-11. These findings suggest that the same cadaverine-derived C_5N precursor that supplies the outer rings, N-1,C-2 to C-6 and N-16,C-15 to C-11, also supplies the inner C_5 chain, and that nitrogen is lost from this segment at a late stage of biosynthesis.

Whereas experiments with [1-^{13}C,1-^{15}N]cadaverine have clarified the regiochemistry of incorporation, tracer work with chirally deuteriated samples of [1-$^2H_1$]cadaverine have shed light on stereochemical aspects of the biosynthetic events that occur in the vicinity of the nitrogen atoms of sparteine and lupanine (11, 13, 14).

Despite the wealth of tracer evidence that has been accumulated, intermediates between cadaverine and the alkaloids have not been unequivocally identified or generally accepted and the biosynthetic steps leading from cadaverine into the alkaloids are currently the subject of controversy. Several biogenetic hypotheses are under consideration (12, 15–17) and have been scrutinized in recent texts (18) and reviews (17, 19, 20).

In an attempt to add to the evidence that might lead to a clearer understanding of the steps on the biosynthetic route from cadaverine into the alkaloids, we have studied the incorporation of label from [3,3-$^2H_2$]cadaverine into lupanine and 13α-hydroxylupanine in *Lupinus angustifolius*.

Results and discussion

[3,3-$^2H_2$]Cadaverine carries deuterium at the only site within the molecule that is not affected, directly or indirectly, by the reactivity of the nitrogen atom and at the only site that is proprochiral (Caabb) rather than prochiral (Caabc).

Loss of deuterium or protium, as the case may be, on the route from [1,1-$^2H_2$]- or (*S*)- and (*R*)-[1-$^2H_1$]cadaverine into sparteine or lupanine (11, 13, 14) is the inevitable consequence of the process that converts cadaverine into the biosynthetic C_5N

[1]Author to whom correspondence may be addressed.

Can. J. Chem. Downloaded from www.nrcresearchpress.com by 190.90.36.8 on 09/07/12
For personal use only.

Can. J. Chem. Downloaded from www.nrcresearchpress.com by 190.90.36.8 on 09/07/12
For personal use only.

intermediate, presumably free or bound $NH_2—\overset{5}{C}H_2—\overset{4}{C}H_2—\overset{3}{C}H_2—\overset{2}{C}H_2—\overset{1}{C}HO$, and loss of deuterium or protium, as the case may be, on the route from [2,2-$^2H_2$]- or (*S*)- and (*R*)-[2-$^2H_1$]cadaverine is the necessary consequence of keto–enol or imine–enamine equilibration of this intermediate (e.g., $NH_2—\overset{5}{C}H_2—\overset{4}{C}H_2—\overset{3}{C}H_2—\overset{2}{C}H_2—\overset{1}{C}H{=}NH \rightleftarrows NH_2—\overset{5}{C}H_2—\overset{4}{C}H_2—\overset{3}{C}H_2—\overset{2}{C}H{=}\overset{1}{C}H—NH_2$), and the distribution of label within the alkaloids from [1-^{2}H]- and [2-^{2}H]cadaverines thus throws light mainly on the early, pre-alkaloid stages of the pathway. Distribution within the alkaloids of deuterium from [3,3-$^2H_2$]cadaverine, on the other hand, may expose stereochemical events that take place at a later stage of biosynthesis, after ring formation has taken place and the proprochiral site of the precursor, containing homotopic protons, has been transformed into prochiral sites, containing diastereotopic protons.

Label from [3,3-$^2H_2$]cadaverine can be predicted to enter C-4, C-8, and C-13 of the $C_{15}N_2$ alkaloids. If, at any one of these sites, there is nonequivalent deuterium enrichment at the α and β position, then a chiral event must have taken place at this site in the course of biosynthesis. If, at any one of these sites, deuterium enrichment at the α and the β positions is identical, then an intact CH_2 (or CD_2) unit from C-3 of the substrate has survived at that site.[2]

[3,3-$^2H_2$]Cadaverine was prepared in five steps from commercially available *N*-benzoylpiperid-4-one. The *p*-toluenesulfonylhydrazone of the piperidone was reduced to *N*-benzoyl[4,4-$^2H_2$]piperidine with sodium borodeuteride in a solution of tetrahydrofuran containing 20% (v/v) D_2O. Reaction with a mixture of bromine and phosphorus tribromide (21) cleaved the piperidine derivative to yield 1,5-dibromo[3,3-$^2H_2$]pentane, which was then converted into 1,5-diphthalimido[3,3-$^2H_2$]pentane, i.e., *N*,*N*′-diphthaloyl[3,3-$^2H_2$]cadaverine. Acid hydrolysis gave the dihydrochloride of [3,3-$^2H_2$]cadaverine. The overall yield of deuterocadaverine with respect to sodium borodeuteride was 9.5%.

The ^{2}H nmr spectrum of the deuteriated sample of *N*,*N*′-diphthaloylcadaverine shows a major and a minor signal. The major signal, at δ 1.31 ppm (relative signal area 4) is due to deuterium at C-3. Since the ^{1}H nmr spectrum of the sample does not exhibit a signal at this chemical shift, the sample is fully deuteriated at this position. The minor signal appears at δ 1.65 (relative signal area 1). This signal is due to deuterium at the C-2 and C-4 atoms. Each of four spin-equivalent hydrogen atoms at these two positions carried 5% deuterium. The ^{1}H nmr spectra of the labelled samples of diphthaloylcadaverine and cadaverine dihydrochloride confirm the presence of deuterium at C-2, -4, in that in each case the relative signal area of the upfield triplet (δ 1.64, 1.80, respectively), due to the four hydrogen atoms of the two β-carbons, is 10% smaller than that of the downfield triplet (δ 3.60, 3.15, respectively), due to the four hydrogen atoms on the α-carbons.

The deuterium at C-2, -4 was introduced into the positions adjacent to the hydrazone carbon atom of *N*-benzoylpiperid-4-one *p*-toluenesulfonylhydrazone by proton–deuteron exchange, in the course of the reduction. The presence of this small but

[2]The possibility that biochemical events might have taken place, which, in entirely nonstereospecific manner, remove and then replace each of the diastereotopic protons to an equal extent, is regarded as too remote to be considered within the context of the biosynthetic route to a product with four or five chiral and 11 or 10 or 9 prochiral centres.

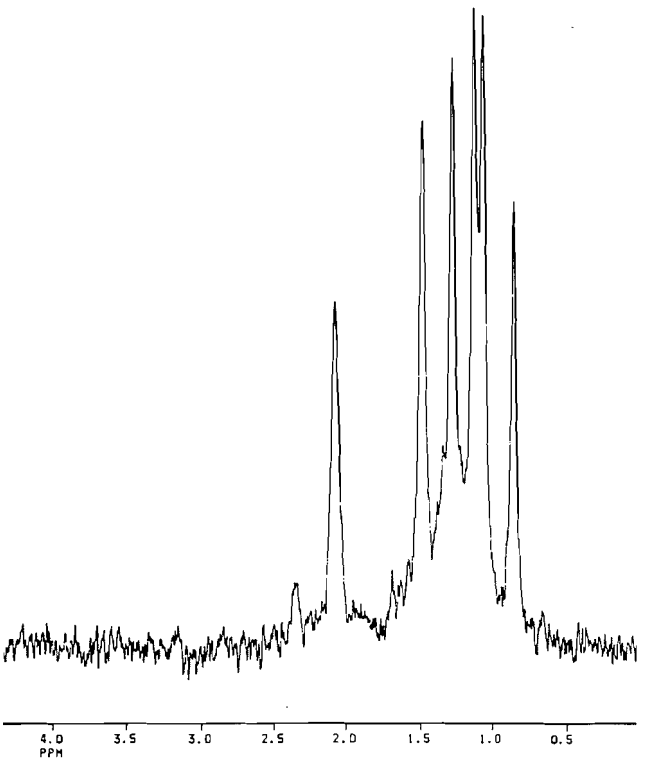

FIG. 1. The ^{2}H nmr spectrum (76.8 MHz) of a deuterium enriched sample of lupanine isolated from *L. angustifolius* after administration of [3,3-$^2H_2$]cadaverine. Lupanine (53 mg) in benzene (0.66 mL); 3000 scans. The spectrum was recorded in the Fourier mode on a Bruker AM 500 spectrometer, in a 5-mm tube, with the natural abundance signal of the solvent as internal reference, 45° pulses, 16 K data points, 4.8 s acquisition time.

significant amount of deuterium at C-2, -4 (5% at each of four hydrogen atoms) in the [3,3-$^2H_2$]cadaverine, nevertheless does not substantially interfere with the interpretation of the results of the tracer experiment.

An aqueous solution of the labelled cadaverine dihydrochloride (100 mg in 100 mL) was administered to 100 six-weeks-old plants of *Lupinus angustifolius* by infusion through cotton wicks over a period of a week. Lupanine (53 mg) and 13α-hydroxylupanine (71 mg) was then isolated by standard procedures (22).

The ^{2}H nmr spectra of the two alkaloids are shown in Figs. 1 and 2.

Direct entry of label from [3,3-$^2H_2$]cadaverine into the alkaloids would be expected to lead to deuteriation at C-4, C-8, and C-13. As expected, six deuterium signals appear in the spectrum of lupanine (Fig. 1) and five in that of 13α-hydroxylupanine (Fig. 2). The specific incorporation (100 × (deuterium enrichment per C_5 unit of alkaloid)/(deuterium enrichment of precursor)) of [3,3-$^2H_2$]cadaverine into lupanine (1.3%) and 13-hydroxylupanine (0.11%) was determined by comparing the signal area due to natural abundance deuterium in the solvent with the signal areas of the two signals due to deuterium at carbon-8 of each alkaloid. The signals were assigned on the basis of heteronuclear 2D COSY spectra of nonenriched samples of the two alkaloids, and on the basis of chemical deuteriation studies.[3]

Complete (24) and partial (25, 26) assignments of the signals due to the protons at C-4 (24, 25), C-8 (24–26), and C-13 (24)

[3]T. Hemscheidt. Unpublished results.

Can. J. Chem. Downloaded from www.nrcresearchpress.com by 190.90.36.8 on 09/07/12
For personal use only.

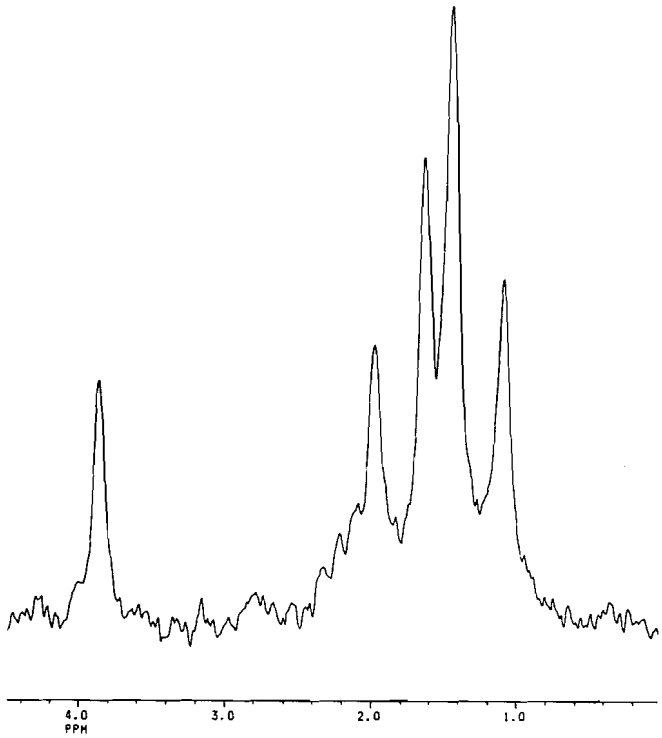

FIG. 2. The ^2H nmr spectrum (76.8 MHz) of a deuterium enriched sample of 13α-hydroxylupanine isolated from *L. angustifolius* after administration of [3,3-$^2H_2$]cadaverine. 13α-Hydroxylupanine (71 mg) in dichloromethane (0.65 mL); 15 520 scans. The spectrum was recorded in the Fourier mode on a Bruker AM 500 spectrometer, in a 5-mm tube, with the natural abundance signal of the solvent as internal reference, 45° pulses, 16 K data points, 4.8 s acquisition time.

of lupanine and due to the protons at C-8 (25) and the proton at C-13 (25) of 13α-hydroxylupanine, based on homonuclear 2D COSY and 2D *J*-resolved nmr spectra (24), and by application of an Europium shift reagent (25), and of homonuclear INDOR spectroscopy (26), have been published.

The six signals in the ^2H nmr spectrum of lupanine derived from [3,3-$^2H_2$]cadaverine are due to the three pairs of diastereotopic deuterons, at C-4 (δ 1.12, 1.28), at C-8 (δ 0.84, 2.08), and at C-13 (δ 1.06, 1.49) (Fig. 1). The weak signal at δ 2.44 ppm is at a chemical shift assigned to one of the hydrogens at C-3, i.e., the C atom adjacent to the lactam carbonyl group. Deuterium enrichment at this position is to be expected due to the presence of 5% ^2H within each of the four hydrogen atoms at C-2 and C-4 of the labelled substrate (see above). The strong background noise of deuterium in the region δ 1.0–1.6 is, similarly, due to this additional labelling, which would be expected to reside at C-5, -7, -9, -12, and -14. All ten hydrogen atoms at these centers resonate in this region of the spectrum. The deuterium signals due to the three pairs of deuterium atoms, at C-4, C-8, and C-13, clearly emerge from the background. Within the limits of error, the deuterium enrichment is the same at each of the two members of each of the three pairs. It follows that in the course of biosynthesis the CH_2 group at C-3 of cadaverine has maintained its integrity on the route to C-4, C-8, and C-13 of the alkaloids. Thus, no hidden biochemical event has occurred at any of these sites. This finding disposes of a biogenetic scheme (16) that includes, as essential steps, loss of a hydrogen from C-8 (either by deprotonation or by dehydrogenation) and reintroduction of a hydrogen, at the same site, in a subsequent step.

The ^2H nmr spectrum of 13α-hydroxylupanine (Fig. 2) shows a distribution of ^2H analogous to that in lupanine. Since deuterium enrichment in 13α-hydroxylupanine was lower[4] than enrichment in lupanine from the same experiment, the signal-to-noise ratio in the spectrum, Fig. 2, is less favourable than in the spectrum of Fig. 1. Nonetheless, five deuterium-enriched sites are evident, two pairs at C-4 (δ 1.43, 1.63) and C-8 (δ 1.08, 1.97) and the β-hydrogen at C-13 (δ 3.86).

As in Fig. 1, and for the same reason, there is again a significant background of deuterium in the region, δ 1.0–2.2, of the spectrum. Nevertheless, the conclusion is confirmed that the integrity of the CH_2 group at C-3 of the precursor is preserved on the route into C-4 and C-8 of 13α-hydroxylupanine. The fact that deuterium is maintained at the 13β site of 13α-hydroxylupanine (δ 3.86) shows that introduction of oxygen at C-13 does not proceed by way of a carbonyl intermediate.

Experimental

Synthesis of [3,3-$^2H_2$]cadaverine

N-*Benzoylpiperid-4-one*-p-*toluenesulfonylhydrazone*

N-Benzoylpiperid-4-one (5.8 g, 28.6 mmol) was dissolved in ethanol (30 mL), *p*-toluenesulfonylhydrazide (6.3 g, 35 mmol) was added, and the solution was boiled 1 h under reflux. The product crystallized on cooling and was recrystallized from ethanol, mp 186°C (dec.); yield 9.53 g (90%); ir (KBr) cm^{-1}: 3250 (NH), 1635 (CO), 1420, 1330, 1160, 1030; ^1H nmr ($CDCl_3$, 90 MHz) δ: 2.45 (s(br), 7H, CH_3 and H-4, -5), 3.65 (s(br), 4H, H-2, -6), 7.25–7.90 (AB q, *J* 8 Hz, 4H, tosyl), 7.50 (s, 5H, phenyl); ^{13}C nmr ($CDCl_3$, 127 MHz) δ: 170.8 (CO), 156.6 (CN), 143.8, 135.4, 135.2, 129.9, 129.4, 128.5, 127.9, 126.7 (aromatic C atoms), 47.3, 44.9, 42.2, 40.8, 34.3, 33.0, 27.8, 26.9 (piperidine ring C atoms), 21.5 (CH_3); ($^2H_6$-DMSO, 127 MHz, 50°C) δ: aromatic C atoms unchanged, 40–46 (br), 33.2, 27.6, 20.8 (CH_3) ppm;[5] ms (DCI, NH_3): 389 (14%, M + 1 + NH_3), 372 (46%, M + 1), 216 (50%, M^+ minus CH_3—C_6H_4—SO_2), 188 (100%, M^+ minus CH_3—C_6H_4—SO_2NN), 105 (22%, C_6H_5CO). *Anal.* calcd. for $C_{19}H_{21}N_3O_3S$: C 61.4, H 5.7, N 11.3%; found: C 61.1, H 5.9, N 11.2%.

[4]There are several possible explanations for the observation that the level of deuterium enrichment within 13α-hydroxylupanine is lower than that within lupanine. Among these are the following: (*a*) The plant may contain a larger store of preformed 13α-hydroxylupanine than of preformed lupanine. Newly biosynthesized 13α-hydroxylupanine would then be more highly diluted with preformed natural abundance material than newly biosynthesized lupanine. (*b*) 13α-Hydroxylupanine may be formed from lupanine. Further experimentation is required to distinguish among these possibilities.

[5]The ^{13}C nmr spectrum of *N*-benzoylpiperid-4-one *p*-toluenesulfonylhydrazone in $CDCl_3$ at room temperature exhibits eight broad lines between δ 27 and 47 ppm. At elevated temperature (50°C) these eight signals collapse into two sharp lines together with a broad signal between δ 40 and 46 ppm. It is suggested that eight, instead of the expected two, lines for the α- and β-carbon atoms of the piperidine nucleus appear as a consequence of the existence, at room temperature, of two stereoisomers of the *p*-toluenesulfonylhydrazone, in which the benzoyl and the *p*-toluenesulfonyl groups are, respectively, *syn* and *anti*. In either of these isomers the two α-carbon atoms and the two β-carbon atoms of the piperidine nucleus are nonequivalent, so that the piperidine nucleus of each isomer gives rise to four carbon signals. At elevated temperature, fast equilibration of the isomers occurs by restored rotation of the benzoyl group, as a result of which the eight signals collapse to yield a broad signal due to the α-carbons and two lines due to the two nonequivalent β-carbon atoms.

Can. J. Chem. Downloaded from www.nrcresearchpress.com by 190.90.36.8 on 09/07/12
For personal use only.

N-Benzoyl[4,4-$^2H_2$]piperidine

The above *p*-toluenesulfonylhydrazone (3.7 g, 10 mmol) was dissolved in a mixture of dry tetrahydrofuran (40 mL) and ^2H_2O (99.8% at.% ^2H, 10 mL). The solution was refluxed 30 min under dry nitrogen, cooled, and concentrated *in vacuo*. The residual suspension was extracted with dichloromethane (3 × 35 mL) and the combined organic extracts were washed with ^2H_2O (10 mL), dried (Na_2SO_4), and evaporated *in vacuo*. The residual foam was dissolved in dry tetrahydrofuran (40 mL), ^2H_2O (10 mL) was added, the mixture was refluxed 30 min, and then cooled to 0°C. Sodium borodeuteride (820 mg) was added in small portions with vigorous stirring over 15 min. The mixture was refluxed gently for 18 h and was then cooled and concentrated *in vacuo*. The residue was extracted with chloroform (3 × 25 mL), the combined organic extracts were washed with water (2 × 25 mL) and saturated sodium chloride (25 mL), dried (Na_2SO_4), and evaporated.

Bulb-to-bulb distillation of the residue (80°C air-bath temperature, 0.005 Torr (1 Torr = 133.3 Pa)), gave *N*-benzoyl[4,4-$^2H_2$]piperidine as a yellowish oil. Yield: 1.29 g (68%); ^1H nmr ($CDCl_3$, 90 MHz) δ: 1.65 (s(br), 4H, H-3, -5), 3.50 (s(br), 4H, H-2, -6), 7.40 (s, 5H, phenyl); ^{13}C nmr ($CDCl_3$, 22.63 MHz) δ: 170.3 (CO), 136.6, 128.9, 128.4, 126.8 (phenyl), 47.0 (br, α-C), 43.0 (br, α-C), 25.9 (β-C).

1,5-Dibromo[3,3-$^2H_2$]pentane (cf., ref. 21)

N-Benzoyl[4,4-$^2H_2$]piperidine (1.29 g, 6.8 mmol) was mixed at 0°C with phosphorus tribromide (1.7 g, 6.4 mmol). After 10 min, bromine (1.0 g, 6.1 mmol) was added dropwise at 0°C with vigorous stirring. The flask was connected to a bulb-to-bulb distillation apparatus, which was flushed with nitrogen gas and connected to a pump. The mixture was distilled by raising the temperature of the air bath slowly to 160°C at 20 Torr. The distillate was collected over 2 h in a trap cooled with Dry Ice/acetone. The distillate was mixed with crushed ice (2 g), ice-cold hydrobromic acid (48%, w/v, 8 mL) was added, and the mixture was then refluxed under nitrogen 4 h at 110°C with vigorous stirring. After cooling, the reaction mixture was extracted with dichloromethane (2 × 25 mL). The combined organic extracts were washed with water (3 × 50 mL), with saturated sodium bicarbonate solution (3 × 50 mL), and with saturated sodium chloride (50 mL), dried (Na_2SO_4), and evaporated. The residue was used in the subsequent reaction without further purification.

1,5-Diphthalimido[3,3-$^2H_2$]pentane

The dark-brown product of the previous reaction was dissolved in dry dimethylformamide (15 mL), potassium phthalimide (5.5 g, 30 mmol) was added, and the mixture was heated 36 h at 90°C under nitrogen with vigorous stirring. The reaction mixture was cooled, filtered, and the solids were extracted repeatedly with hot chloroform (3 × 75 mL). The filtrate and the chloroform extracts were combined and washed in turn with water (100 mL), dilute sodium hydroxide (0.3 *M*, 3 × 100 mL), water (100 mL), and saturated sodium chloride solution (50 mL), dried (Na_2SO_4), and concentrated. 1,5-Diphthalimido[3,3-$^2H_2$]pentane, i.e., *N,N'*-diphthaloyl[3,3-$^2H_2$]cadaverine, crystallized on addition of methanol; mp 181–183°C (lit. (23) mp 186°C); yield 0.7 g (29% with reference to *N*-benzoylpiperidine); ^1H nmr ($CDCl_3$, 90 MHz) δ: 7.74–7.62 (m, 8H, phthaloyl), 3.60 (t, 4H, *J* 7.1 Hz), 1.64 (t, 3.6H, *J* 7.0 Hz); ^2H nmr ($CHCl_3$, 76.8 MHz) δ: 1.31 (s, rel. area 4), 1.65 (s, rel. area 1).

[3,3-$^2H_2$]Cadaverine dihydrochloride

1,5-Diphthalimido[3,3-$^2H_2$]pentane (0.36 g, 1 mmol) and concentrated hydrochloric acid (3 mL) were heated in a sealed tube 8 h at 180°C. On cooling, the reaction mixture was diluted with water, solids were filtered off and washed with water, and the aqueous filtrate repeatedly evaporated from water. The solid residue was recrystallized from ethanol yielding [3,3-$^2H_2$]cadaverine dihydrochloride as hygroscopic needles. Yield 130 mg (90%); ^1H nmr (D_2O, 90 MHz) δ: 3.15 (t, *J* 7 Hz, 4H), 1.80 (t, *J* 7 Hz, 3.6H).

Administration of [3,3-$^2H_2$]cadaverine to Lupinus angustifolius *plants and isolation of alkaloids*

Plants of *Lupinus angustifolius* were grown from seed in the greenhouse and were used for the feeding experiment with [3,3-$^2H_2$]cadaverine 6 weeks after germination.

Tracer solution (100 mg [3,3-$^2H_2$]cadaverine dihydrochloride in 100 mL glass-distilled water) was administered by wick to 100 plants over 5 days (20 mL/day). The plants were allowed to grow for a further 3 days before being harvested.

Lupanine and 13α-hydroxylupanine were isolated and purified by conventional methods (22). The plant material (1050 g) was dried 12 h at 50°C and was then ground and extracted 16 h in a Soxhlet extractor with methanol. The extract was evaporated and the residue partitioned between chloroform (100 mL) and hydrochloric acid (3% v/v, 25 mL). The aqueous phase was washed with chloroform (2 × 100 mL), filtered through Celite, and concentrated *in vacuo*. The solution was then neutralized by addition of solid potassium carbonate, made strongly alkaline with concentrated potassium hydroxide (50% w/v), and the alkaloids extracted into dichloromethane. The extract was dried (K_2CO_3) and evaporated *in vacuo*. The residue was dissolved in dilute hydrochloric acid (3% v/v, 3 mL), the solution was extracted with ether, neutralized by addition of solid potassium carbonate, basified with potassium hydroxide solution (50% w/v), and extracted with ether–dichloromethane (1:1, 3 × 5 mL). The organic extract was dried (Na_2SO_4) and evaporated and the residue taken through one more acid–base cycle. The alkaline solution so obtained was mixed with kieselguhr (7 g); the mixture was kept 30 min at room temperature and was then added to a column containing kieselguhr (7 g) moistened with potassium hydroxide solution (50% w/v, 5 mL). The column was eluted first with petroleum ether (30–60°C, 125 mL) to yield lupanine (53 mg), and then with dichloromethane to yield 13α-hydroxylupanine (71 mg).

Acknowledgments

This investigation was supported by a grant from the Natural Sciences and Engineering Research Council of Canada. We thank Thelma Leech, Greenhouse Supervisor, McMaster University, for providing facilities for this work.

1. E. Leistner and I. D. Spenser. Pol. J. Chem. **53**, 49 (1979).
2. H. R. Schütte, F. Bohlmann, and W. Reusche. Arch. Pharm. **294**, 610 (1961).
3. H. R. Schütte, H. Hindorf, K. Mothes, and G. Hübner. Liebigs Ann. Chem. **680**, 93 (1964).
4. H. R. Schütte, E. Nowacki, and Ch. Schäfer. Arch. Pharm. **295**, 20 (1962).
5. H. R. Schütte and Ch. Schäfer. Naturwissenschaften, **48**, 669 (1961).
6. E. Nowacki and R. U. Byerrum. Bull. Acad. Pol. Sci. Cl. 5, **12**, 489 (1964).
7. H. R. Schütte and D. Knöfel. Z. Pflanzenphysiol. **57**, 188 (1967).
8. J. Rana and D. J. Robins. J. Chem. Soc. Chem. Commun. 1335 (1983).
9. W. M. Golebiewski and I. D. Spenser. J. Chem. Soc. Chem. Commun. 1509 (1983).
10. J. Rana and D. J. Robins. J. Chem. Research (S), 196 (1985).
11. W. M. Golebiewski and I. D. Spenser. J. Am. Chem. Soc. **106**, 7925 (1984).
12. W. M. Golebiewski and I. D. Spenser. J. Am. Chem. Soc. **98**, 6726 (1976).
13. A. M. Fraser and D. J. Robins. J. Chem. Soc. Chem. Commun. 1477 (1984).
14. A. M. Fraser and D. J. Robins. J. Chem. Soc. Chem. Commun. 545 (1986).
15. E. Leete. *In* Biogenesis of natural compounds. 2nd ed. *Edited by* P. Bernfeld. Pergamon Press, Oxford. 1967. p. 973.
16. M. Wink, T. Hartmann, and H.-M. Schiebel. Z. Naturforsch. C: Biosci. **34**, 704 (1979).
17. E. Leete. Biosynthesis (Specialist Periodical Reports), **7**, 110 (1983).

18. D. R. DALTON. The alkaloids, a biogenetic approach. Marcel Dekker Inc., New York. 1979. p. 105.
19. A. D. KINGHORN and M. F. BALANDRIN. *In* Alkaloids: chemical and biological perspectives. Vol 2. *Edited by* S. W. Pelletier. Wiley, New York. 1984. p. 118.
20. I. D. SPENSER. Pure Appl. Chem. **57**, 453 (1985).
21. J. VON BRAUN. Org. Synth. Coll. Vol. **1**, 428 (1941).
22. M. D. BRATEK-WIEWIOROWSKA, M. WIEWIOROWSKI, I. REIFER, K. GOLANKIEWICZ, E. NOWACKI, W. BOCZON, and M. DEZOR. Acta Biochim. Polon. **12**, 395 (1965).
23. J. VON BRAUN. Chem. Ber. **37**, 3583 (1904).
24. W. M. GOLEBIEWSKI. Magn. Reson. Chem. **24**, 105 (1986).
25. J. BARCISZEWSKI, A. J. RAFALSKI, and M. WIEWIOROWSKI. Bull. Acad. Polon. Sci. Ser. Sci. Chim. **19**, 545 (1971).
26. A. S. SADYKOV, F. G. KAMAYEV, V. A. KORENEVSKY, V. B. LEONT'EV, and YU. A. USTYNYUK. Org. Magn. Reson. **4**, 837 (1972).

Can. J. Chem. Downloaded from www.nrcresearchpress.com by 190.90.36.8 on 09/07/12
For personal use only.

Synthesis and spectroscopic investigations of 1,4-benzothiazepine derivatives[1]

JÁNOS SZABÓ, GÁBOR BERNÁTH, ÁGNES KATÓCS, AND LAJOS FODOR
Institute of Pharmaceutical Chemistry, University Medical School, POB 121, H-6701 Szeged, Hungary

AND

PÁL SOHÁR[2]
Spectroscopic Department, EGIS Pharmaceuticals, POB 100, H-1475 Budapest, Hungary

Received July 16, 1986

This paper is dedicated to Dr. O. E. (Ted) Edwards

JÁNOS SZABÓ, GÁBOR BERNÁTH, ÁGNES KATÓCS, LAJOS FODOR, and PÁL SOHÁR. Can. J. Chem. **65**, 175 (1987).

The reaction of sodium 3,4-dimethoxythiophenolate (**1**) with 2-bromoethylamine (**2**) gave 2′-aminoethyl-3,4-dimethoxyphenyl sulfide hydrochloride (**3**). Ring closure of the acyl derivatives **4***a–c* with phosphoryl chloride furnished the 2,3-dihydro-1,4-benzothiazepines **5***a–c*. In a reaction competing with the cyclization, the acid amides **4** decomposed to 2′-chloroethyl-3,4-dimethoxyphenyl sulfide (**7**) and the corresponding nitrile. A few derivatives (**8–10**) of **5***c* were prepared. Sodium borohydride reduction of **5***b*, *c* yielded the 2,3,4,5-tetrahydro-1,3-benzothiazepines **11***a*, *b*. With substituted acetyl chlorides, compounds **5***c* and **10** were converted to the β-lactam derivatives **12***a–f* and **13**, the configurations and conformations of which were determined by nmr spectroscopy; under similar reaction conditions the analogous compounds **5***a*, *b* gave the enamides **14**, **15**, and **16**.

JÁNOS SZABÓ, GÁBOR BERNÁTH, ÁGNES KATÓCS, LAJOS FODOR et PÁL SOHÁR. Can. J. Chem. **65**, 175 (1987).

La réaction du diméthoxy-3,4 thiphénolate de sodium (**1**) avec la bromo-2 éthylamine (**2**) conduit au chlorhydrate du sulfure d'amino-2 éthyle et de diméthoxy-3,4 phényle (**3**). La cyclisation des dérivés acyles **4***a–c* avec le chlorure de phosphoryle conduit aux dihydro-2,3 benzothiazépines-1,4 **5***a–c*. Les amides acides **4** subissent en même temps une réaction de décomposition qui conduit au sulfure de chloro-2 éthyle et de diméthoxy-3,4 phényle (**7**) et au nitrile correspondant. On a préparé quelques dérivés (**8–10**) de **5***c*. La réduction des composés **5***b*, *c* par le borohydrure de sodium conduit aux tétrahydro-2,3,4,5 benzothiazépines-1,3 **11***a*, *b*. À l'aide de chlorures d'acétyles substitués, on a pu transformer les composés **5***c* et **10** en dérivés β-lactames **12***a–f* et **13** dont on a déterminé les configurations et les conformations en faisant appel à la rmn; dans des conditions semblables, les composés analogues **5***a*, *b* conduisent aux énamides **14**, **15** et **16**.

[Traduit par la revue]

Introduction

Many researchers have dealt with the syntheses of 3-oxo, 5-oxo, and 3,5-dioxo derivatives of 1,4-benzothiazepines, but there are only a few publications (2–9) relating to the preparation of 2,3- and 3,4-dihydro- or 2,3,4,5-tetrahydro-1,4-benzothiazepines containing no carbonyl group. Only a single procedure, following a different pathway, was found in the literature for the synthesis of a β-lactam derivative of 1,4-benzothiazepine (10).

We earlier reported the syntheses of 4,5-dihydro-1,4-benzothiazepine and 4,5-dihydro-1,4-benzothiazepin-3(2*H*)-one derivatives (8, 9, 11). In the present work, convenient preparations of suitably substituted 2,3-dihydro- and 2,3,4,5-tetrahydro-1,4-benzothiazepines and the syntheses of their β-lactam and other derivatives are described.

Syntheses

The reaction of sodium 3,4-dimethoxythiophenolate (**1**) with 2-bromoethylamine (**2**) gave 2′-aminoethyl-3,4-dimethoxyphenyl sulfide, which was isolated as the hydrochloride **3**. With acid anhydrides or acid chlorides, compound **3** was converted to the acid amides **4***a–c*. Heating of the latter with $POCl_3$ furnished the benzothiazepine derivatives **5***a–c* (Scheme 1) in poor yields, since a competitive reaction, probably via disintegration of the intermediary imide chloride **6**, gave rise mainly to the decomposition products 2′-chloroethyl-3,4-dimethoxyphenyl sulfide (**7**) and the corresponding nitrile. Compound **7** and benzonitrile, formed simultaneously with the cyclization of the acid amide **4***c*, were isolated from the reaction mixture. A definitive synthesis of compound **7** was its preparation from sodium 3,4-dimethoxythiophenolate and 1,2-dichloroethane (Scheme 1).

A few characteristic derivatives were prepared from **5***c*, such as the methiodide **8** with methyl iodide, the sulfoxide **9** with $NaIO_4$, and the sulfone **10** with $KMnO_4$. Reduction of **5***b* and **5***c* with $NaBH_4$ furnished the corresponding tetrahydro-1,4-benzothiazepines **11***a*, *b* (Scheme 2).

Analogously to the cycloaddition reactions of imines with acid chlorides, **5***c* gave the β-lactams **12***a–f*. It was found that, except for one case, only one of the diastereomers was formed; thus, the reactions were regio- and stereospecific. However, when **5***c* and 2-chloro-2-phenylacetyl chloride were reacted in the presence of TEA (triethylamine), both stereoisomers **12***e* and **12***f* were isolable (Scheme 3).

The β-lactam **13** obtained from the benzothiazepine dioxide **10** by treatment with phenylacetyl chloride was identical with the compound formed from the β-lactam **12***a* by oxidation with peracetic acid (Scheme 4).

Compound **5***a* with benzoyl chloride and, analogously, **5***b* with dichloroacetyl chloride or benzoyl chloride in the presence of TEA gave the enamides **14**, **15**, and **16**, respectively (Scheme 5), similar to the reactions of 1-alkyl-3,4-dihydroisoquinolines and 4-alkyl-2*H*-1,3-benzothiazines (12, 13). Further investigations relating to these compounds are in progress.

Spectroscopic evidence of structures

The ir and ^1H and ^{13}C nmr data supporting the structures of

[1]Presented in part at the 7th Symposium on the Chemistry of Heterocyclic Compounds, Bratislava, August 31 – September 3, 1981. Abstracts p. 146. This paper is regarded as Part 116 of the series "Saturated Heterocycles." Part 115: see ref. 1.

[2]Author to whom correspondence should be addressed.

Can. J. Chem. Downloaded from www.nrcresearchpress.com by 80.58.250.72 on 09/07/12
For personal use only.

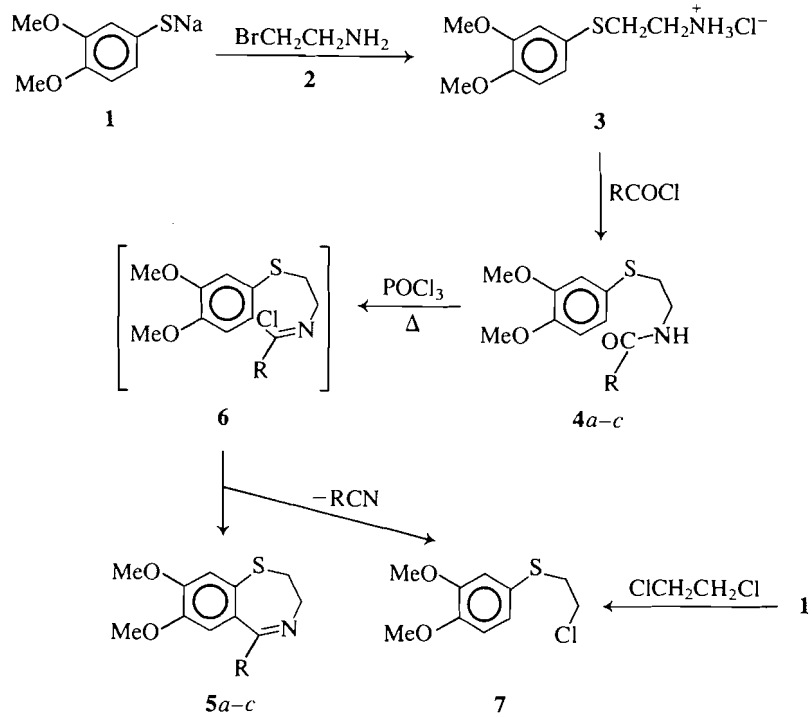

a: R = Me *b*: R = CH_2Ph *c*: R = Ph

SCHEME 1

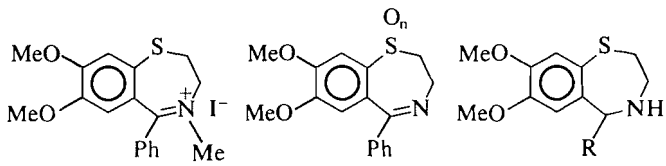

SCHEME 2

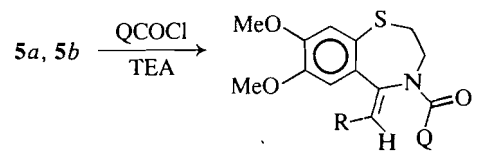

SCHEME 5

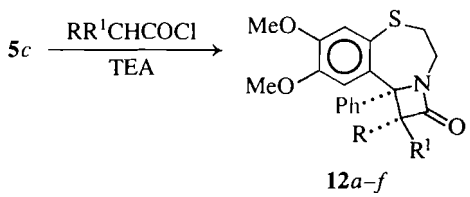

a: R = Ph; R^1 = H *d*: R = R^1 = Cl
b: R = OPh; R^1 = H *e*: R = Ph; R^1 = Cl
c: R = Cl; R^1 = H *f*: R = Cl; R^1 = Ph

SCHEME 3

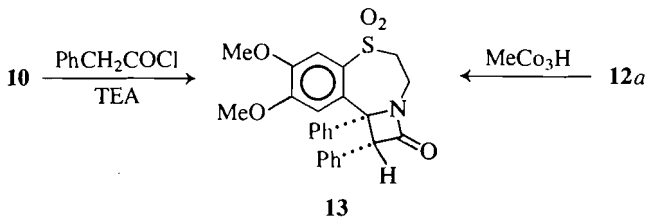

SCHEME 4

the new compounds are given in the Experimental; those of the β-lactams are listed in Tables 1–3.

In the ^1H nmr spectrum of the sulfone analog **10**, the two methylene groups give a singlet of 4H intensity. Thus, the two methylene groups appear to be isochronous in $CDCl_3$ solution, owing to the practically identical substituent effects of the sp^2 nitrogen and the sulfone group. The chemical equivalence of both pairs of methylene protons indicates a rapid interconversion of the thiazepine ring.

The ArH-9 signal of **11***b* shows a very marked upfield shift (−0.5 ppm) as compared with the value for the starting compound **5***c*. This shift is a consequence of the anisotropic shielding of the phenyl substituent (14*a*) attached to the saturated hetero ring, confirming the preference for a conformation in which the ArH-9 atom is situated "above" the plane of the phenyl ring and near to it. This conformation is also indicated by the upfield shift of the C-8 methoxy signal.

The configurations of the C-1 and C-10 atoms in the β-lactams **12***a–f* and **13** remain to be elucidated; this is hampered by the fact that the thiazepine ring may assume several conformations, differing according to the substitution.

In determining the steric structures of the diastereomeric pair **12***e–f*, it is helpful to start with the ^1H nmr data, since there are

Can. J. Chem. Downloaded from www.nrcresearchpress.com by 80.58.250.72 on 09/07/12
For personal use only.

TABLE 1. Infrared data (KBr, cm^{-1}) and ^1H nmr chemical shifts[a] ($CDCl_3$, δ_{TMS} = 0 ppm) for compounds **12***a–f* and **13**

Compound	ν C=O band	CH_2 (3, 4) 4dd (4 × 1H)[b]	OCH_3 (7, 8) 2s (2 × 3H)	H-10 s(1H)	ArH-6 s(1H)	ArH-9 s(1H)	ArH (1Ph, 10Ph) 2m/4m (5H/10H)
12*a*	1745	2.77, 2.88 3.46, 4.58	3.92, 4.00	5.35	7.05	7.12	6.73,[c] 7.0–7.3
12*b*	1760	2.76, 2.84 3.41, 4.45	3.48, 3.88	5.76	7.03[e]	6.43	6.68,[c] ≈7.02,[d,e] 7.19,[c] ≈7.38
12*c*	1771	2.74, 2.85 3.43, 4.46	3.92, 3.95	5.53	6.82	7.10	≈6.95,[c] ≈7.35[d]
12*d*	1784	2.67, 2.89 3.38, 4.19	3.92[e]	—	6.86	6.94	≈7.25,[c] ≈7.40[d]
12*e*	1774	2.70, 2.96 3.30, 4.36	3.94, 4.00	—	7.04	7.33	6.87,[c] 7.10,[f] 7.15,[g] 7.45[c]
12*f*	1778	2.70, 2.91 3.53, 4.36	3.43, 3.77	—	6.73	6.03	7.15,[d] 7.3–7.5[h]
13	1770 1753	3.32, 3.46 3.71, 4.50	4.01, 4.07	5.30	7.74	7.32	6.80,[c] 7.05–7.2

[a]For coupling constants, see Table 2.
[b]Assignments, in order of increasing downfield shifts, are: δ H-4*e*, δ 4′*a*, δ H-3′*a*, δ H-3*e* (**12***a–c*), δ H-4′*a*, δ H-4*e*, δ H-3*e*, δ H-3′*a* (**12***d–f*), δ H-4*e*, δ H-3′*a*, δ H-4′*a*, δ H-3*e* (**13**).
[c]H-2′,6′ (2H).
[d]H-3′,4′,5′ (3H).
[e]Two coalesced signals.
[f]H-3′,5′ (2H).
[g]4H.
[h]7H.

TABLE 2. Geminal and vicinal proton–proton coupling constants for compounds **12***a–b* and **13** (Hz)

Compound	$^2J(4,4')$	$^2J(3,3')$	$^3J(3',4')$	$^3J(3',4)$	$^3J(3,4')$	$^3J(3,4)$
12*a*	14.2	10.9	11.6	2.9	2.9	2.9
12*b*	14.4	13.8	7.8	3.6	3.4	3.6
12*c*	14.5	13.7	11.0	3.2	3.1	3.3
12*d*	15.0	13.3	9.0	4.2	4.0	5.4
12*e*	14.6	13.4	8.0	4.0	3.5	6.9
12*f*	15.0	13.4	9.5	4.5	4.0	4.9
13	14.5	14.5	11.8	3.2	2.9	3.2

no significant differences either in the ir frequencies or in the chemical shifts of the carbon resonance signals. On the other hand, in the ^1H nmr spectrum of **12***f* both methoxy signals and also the H-6 and H-9 singlets, mainly one of each, reveal very considerable upfield shifts. The two larger shifts amount to about −0.5 and −1.0 ppm. This is indicative of a configuration and conformation in which the C-10 phenyl ring, occupying different positions in the diastereomers, has come near to the methoxy groups. This steric structure is possible only when the C-1 and C-10 phenyl rings are in the *trans* position, i.e. if the relative configuration is 1*R*,10*S* (1*S*,10*R*). Further evidence for this is given in the spectrum of **12***e* by the higher shielding of some of the aromatic hydrogens, indicating that the two rings in this compound are nearer to each other, i.e. in the *cis* position relative to the β-lactam ring. In view of the data listed in Table 1, **12***b* and **12***f* have analogous structures (the C-1 phenyl and C-10 phenoxy groups are in the *trans* position), whereas the structures of the β-lactams **12***a*,*c*,*d* and **13** are identical with that of isomer **12***e*.

Information about the conformations is obtained primarily from the vicinal proton–proton coupling constants of the methylene groups (Table 2). As shown by molecular models,

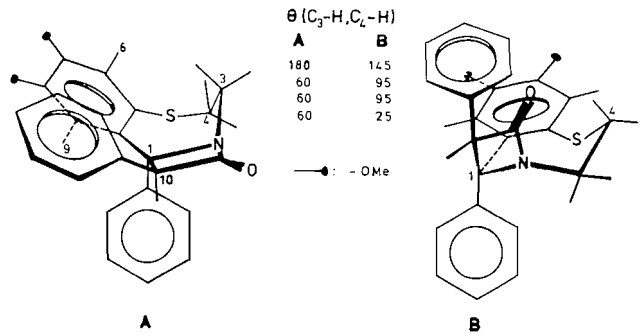

FIG. 1. The possible conformations of compounds **12***a–c* (A) and **12***d–f* (B), respectively.

two sterically favored, relatively stable conformations are possible (Fig. 1). In one of these (**A**), the thiazepine ring is in a boat-like form; the β-lactam ring is attached *quasi-equatorially*, and the dihedral angles of the methylene hydrogens are about 180, 60, 60, and 60°. In the other conformation (**B**), there is a chair-like seven-membered heterocycle (in which C-1 and C-4 are situated out of the plane of the other five atoms constituting the ring), and a *quasi-axially* annelated β-lactam ring is coupled

Can. J. Chem. Downloaded from www.nrcresearchpress.com by 80.58.250.72 on 09/07/12
For personal use only.

Can. J. Chem. Downloaded from www.nrcresearchpress.com by 80.58.250.72 on 09/07/12
For personal use only.

TABLE 3. The ^{13}C nmr chemical shifts ($\delta_{TMS} = 0$ ppm) for compounds **12***a–f* and **13** in $CDCl_3$ solution at 20.14 MHz

Compound	C-1	C-3	C-4	C-5a	C-6,9	C-7	C-8	C-9a	C-10	OCH_3(7,8)	C-1′	C-2′,3′,5′,6′	C-4′	C=O
12*a*	74.4	42.3	33.0	126.8	115.3 118.6	148.3[a]	148.6[a]	138.3[b]	66.8	56.2 56.6	137.6[b]	127.8[c] 128.0 128.5[d]	127.3 128.5[d]	167.3
12*b*[e]	76.5[f]	42.2	32.4	126.8	114.1 117.4	148.0[a]	148.3[a]	136.4[b]	91.6	55.8 56.0	135.6[b] 157.6[g]	118.8[g] 128.7 128.1[c] 129.5	123.5[g] 128.1[c]	165.7
12*c*[e]	74.8	43.2	32.7	127.1	114.0 118.2	148.8[c]	136.2[d]		67.6	56.3 56.7	136.2[d]	128.3 128.5	128.6	163.4
12*d*	81.4	43.7	31.6	126.9	115.1 116.4	146.9	148.7	136.7	91.4	55.9 56.3	129.3[b]	128.4[c]	129.2[b]	162.1
12*e*[e]	80.0	43.0	32.4	127.8	116.1 118.4	147.0[a]	148.5[a]	137.8[b]	84.1	56.1 56.7	130.6[g] 136.3[b]	128.2 128.4[h] 128.9[c]	128.4[h] 128.9[c]	165.8
12*f*[e]	86.1	43.8	32.0	127.5	114.8 117.3	146.5	148.0	138.2	84.3	56.0[c]	129.0[g] 135.7	128.0[d] 128.1 129.7	128.7 128.9	166.2
13[e]	75.1	34.1[i]	55.1[i]	133.2[a]	112.4 115.2	148.7	152.2	133.1[a]	70.1	56.6 56.8	128.5[c,g] 136.7	127.3[b] 127.4[b] 128.0[b] 128.4[b]	127.9[b] 128.5[c,b]	166.7

[a,b]Assignments may be reversed.
[c,d]Two overlapping lines.
[e]Assignments were proved by DEPT measurements.
[f]Measured in DMSO-d_6 solution (in $CDCl_3$ this line is hidden by the triplet of the solvent).
[g]Phenyl in position 10.
[h]Three overlapping lines.
[i]These assignments are due to α and β effects of the SO_2 substituent.

to it. (The C-H,C-H dihedral angles of the C-3 and C-4 methylene groups are approximately 145, 95, 95, and 25°.) In this more strained skeletal structure, the substituent in the position *trans* to the C-1 phenyl group is sterically favored. The distance between H-9 and the C-1 phenyl group is increased. It is therefore obvious that compounds **12***d–f* have the **B** conformation, whereas for the analogs **12***a*,*c* and **13**, which have no C-10 substituent in the position *trans* to the C-1 phenyl group, the preferred conformation is the boat-like form **A**. In **12***b*, with *trans* C-1 and C-10 substituents in the postulated configuration, the phenoxy group can avoid steric hindrance through rotation about the C_{10}—O—C_{aryl} chain. Consequently, the predominant conformer is **A**. This is indicated by the higher value of the ^3J(H-3′,H-4′) coupling constant and the lower value of its ^3J(H-3,H-4) counterpart in compounds **12***a–c* and **13**.

Evidence of the conformational difference is furnished by the switchover of the relative chemical shifts of the methylene proton pairs. In **12***a–c* and **13** the usual relations δ H-3*e* > δ H-3′*a* and δ H-4*e* < δ H-4′*a* were observed (it is characteristic of sulfur-containing saturated heterocycles (14*b*) that the sequence of shifts of the C-4 methylene hydrogens is opposite in direction to that for the cyclohexane derivatives, i.e. the *equatorial* proton is more shielded than its *axial* counterpart); in the C-10 disubstituted analogs, just the opposite sequence is found. This is probably due to the anisotropic effect of the β-lactam ring, which increases the shielding around H-4′*a* and decreases it around H-3*e*, the chair-like conformation of the thiazepine ring. The assignments given in Table 1 are based partly on a consideration of the expected substituent effects, and partly on the magnitudes of the coupling constants.

The preferred conformations of compounds **14–16** are supported by the broadening and downfield shifts of some of the ^1H nmr signals. In the spectrum of **14**, the C-8 methoxy signal is found at 3.63 ppm, upfield by about 0.25 ppm in comparison with the average shifts in the other compounds. The ArH-9 singlet is at 6.22 ppm, i.e. in the same direction, but with a very markedly larger shift and broadened. This strongly suggests a predominant conformation in which the benzoyl group is near to the C-8 methoxy group and the ArH-9 atom. In one of the rotamers, the aromatic ring exerts an anisotropic shielding effect on this group and atom; this is the reason why the upfield shifts appear, while the broadening of the signal is caused by the slow interconversion of the rotational isomers. In this conformation, the ethylidene group is *quasi-axial* relative to the hetero ring; in the *N*-benzoyl substituent, the phenyl ring and the amide group are not coplanar. This is evidenced by the observation that the signals of the phenyl *ortho* hydrogens are not separated in the downfield direction from the signals of the *meta* and *para* protons, as generally occurs in benzoyl compounds, due to the anisotropic effect of a coplanar carbonyl group (14*c*).

The conformation of **15** is analogous to that of **14**; the relative positions of the benzylidene ring to the C-8 methoxy group and to the ArH-9 atom are also quite similar; accordingly, similar upfield shifts of these signals are found, and there is a broadening of the latter, due to the hindered amide rotation.

The combined anisotropic effect of the two phenyl groups in compound **16** results in anomalous upfield shifts of the corresponding signals; that of the 8-methoxy group is found at 3.13 ppm, i.e. shifted by about −0.8 ppm as compared with the usual value for these compounds; the very broad ArH-9 signal is at 5.50 ppm, the chemical shift being about 1.5 ppm smaller

Can. J. Chem. Downloaded from www.nrcresearchpress.com by 80.58.250.72 on 09/07/12
For personal use only.

than the average. This is evidence of the analogous conformation; at the same time the *E*-configuration about the olefin bond in compounds **15** and **16** is shown, in which the phenyl ring of the benzylidene group is situated in the direction of the fused veratryl ring, and the olefin hydrogen toward the benzoyl group.

Experimental

The ir spectra were run in KBr discs on a Perkin–Elmer 125 (**3**, **4***a–c*, **5***c*, **8–10**, **11***b*, and **15**) or an Aspect 2000 computer-controlled Bruker IFS-113v-FT spectrometer (all other compounds).

The nmr spectra were recorded in 5- or 10-mm tubes at room temperature on a Varian EM-60 (**3**, **4***a–c*, **5***a–c*, **8**, **11***b*, and **15**) or a Bruker WM-250 (all others) instrument (^{1}H) at 60 and 250 MHz, respectively, and on a WP-80-SY FT spectrometer controlled by an Aspect 2000 computer at 20.14 MHz (^{13}C) in $CDCl_3$ or DMSO-d_6 solution, using the deuterium signal to the solvent as the lock and TMS as internal reference. The most important measuring parameters for the FT mode were as follows: sweep width: 5 kHz; pulse width: 1 (^{1}H) or 3.5 (^{13}C) μs (ca. 20° or 30° flip angle); acquisition time 1.64 s; number of scans: 16 or 2^{10}–2^{16}; computer memory: 16K; Lorentzian exponential multiplication for signal-to-noise enhancement (LB 0.7 or 1.0 Hz) and complete proton noise decoupling (ca. 1.5 W) for ^{13}C measurements were applied.

DEPT experiments (16) were performed (for compounds **12***b*, *c*, *e*, *f* and **13**) in a standard way (17), using only the θ = 135° pulse to separate the CH/CH_3 and CH_2 lines phase "up" and "down", respectively. Typical acquisition data were number of scans: 128–2048 K; relaxation delay for proton 3 s; 90° pulse width: 10.8 and 22.8 μs for ^{13}C and ^{1}H, respectively. The estimated value for J(C,H) resulted in a 3.7 ms delay for polarization.

Spectral data on the β-lactams **12***a–f* and **13** are given in Tables 1–3; parameters on the other structures are listed separately below.

Melting points are uncorrected.

2'-Aminoethyl-3,4-dimethoxyphenyl sulfide hydrochloride **3**

Sodium 3,4-dimethoxythiophenolate (19.22 g; 100 mmol) was added to a solution of 2-bromoethylamine (12.4 g; 100 mmol) in dry benzene (100 mL). The mixture was stirred and refluxed for 1 h, then extracted with 5% NaOH solution (50 mL), and the benzene phase was dried (Na_2SO_4) and evaporated to dryness. The residue was dissolved in ethanol (15 mL) and ethanol (20 mL) saturated with HCl was added. Compound **3** precipitated as colorless crystals (18.48 g; 74%), mp 175–176°C (EtOH); ir: ν N^+H: 3200–2300, ≈1990 cm^{-1}; ^{1}H nmr (D_2O): CH_2: 3.30 s (4H); OCH_3: 3.90 s (6H); ArH-5: 6.90 d (8 Hz, 1H); ArH-2,6: ≈7.1 m (2H). *Anal.* calcd. for $C_{10}H_{16}NO_2S$: C 48.09, H 6.46, N 5.61; found: C 48.11, H 6.85, N 5.22%.

2'-Acetaminoethyl-3,4-dimethoxyphenyl sulfide **4**a

Compound **3** (2.5 g; 10 mmol) was refluxed in acetic anhydride for 2 h. The mixture was poured into water and extracted with benzene. The extract was washed with dilute Na_2CO_3 solution and then with dilute H_2SO_4 and water, dried (Na_2SO_4), and evaporated. The residue was crystallized from CCl_4 to give colorless needles (1.66 g; 65%), mp 82–83°C. *Anal.* calcd. for $C_{12}H_{17}NO_3S$: C 56.44, H 5.53, N 5.49; found: C 56.59, H 5.72, N 5.60%.

3,4-Dimethoxyphenyl-2'-phenylacetaminoethyl sulfide **4**b

Compound **3** (2.5 g; 10 mmol) was dissolved in ice-water (20 g) and, with continuous stirring, phenylacetyl chloride (2 mL) and then a solution of NaOH (1.1 g NaOH in 5 mL of water) were added dropwise. The mixture was extracted with benzene, and the extract was dried (Na_2SO_4) and evaporated. The residue crystallized. Recrystallization from methanol gave colorless needles (2.92 g; 88%), mp 99–100°C. *Anal.* calcd. for $C_{18}H_{21}NO_3S$: C 65.23, H 6.39, N 4.23; found: C 65.62, H 6.73, N 4.29%.

2'-Benzoylaminoethyl-3,4-dimethoxyphenyl sulfide **4**c

Compound **3** (2.5 g; 10 mmol) was dissolved in pyridine (10 mL). Benzoyl chloride (1.7 mL) was added with stirring, and the mixture was allowed to stand for 30 min. It was then poured into ice-cold dilute H_2SO_4 and the crystals that separated were collected by filtration (2.85 g; 90%); colorless prisms, mp 108–109°C (MeOH); ir: ν NH: 3310 (**4***a*), 3270 (**4***b*), 3380 (**4***c*); amide-I: 1635, 1640, 1650 cm^{-1}; ^{1}H nmr: $COCH_3$ (**4***a*): 1.93 s (3H); SCH_2: 2.95 t (2H, **4***a*), 2.90 t (2H, **4***b*), 3.03 t (2H, **4***c*); NCH_2: 3.45, 3.35, 3.60 q (2H); $PhCH_2$ (**4***b*): 3.50 s (2H); OCH_3: 3.83, 3.86 2s (2 × 3H, **4***a*), 3.80 s (6H, **4***b*), 3.78 s (6H, **4***c*); NH: ≈6.2 br s (1H, **4***a*), ≈6.1 br s (1H, **4***b*), ≈7.0 m (overlapped with the ArH, **4***c*); ArH-5: 6.78, 6.75, 6.75 d (8 Hz, 1H); ArH-2: 6.90, 6.85, 6.93 d (2 Hz, 1H); ArH-6: 6.95, 6.90, 6.98 dd (1H); Ar (Ph): 7.20 ≈s (5H, **4***b*); ArH-3',5' (Ph): ≈7.4 m (3H); ArH-2',6' (Ph): ≈7.7 m (2H, **4***c*). *Anal.* calcd. for $C_{17}H_{19}NO_3S$: C 64.33, H 6.03, N 4.41; found: C 64.01, H 6.17, N 4.70%.

2,3-Dihydro-7,8-dimethoxy-5-methyl-1,4-benzothiazepine **5**a

A mixture of compound **4***a* (10.2 g; 40 mmol) and $POCl_3$ (15 mL) was heated on a steam bath for 1 h. The reaction mixture was decomposed in ice-water, made alkaline with Na_2CO_3, and extracted with benzene. The extract was reextracted with 10% HCl (100 mL). The acid phase was neutralized with Na_2CO_3 and extracted with benzene. After drying (Na_2SO_4), the benzene solution was evaporated. The pale-yellow oily residue was dissolved in ethanol, and **5***a* was precipitated from the solution as yellow crystals of the picrate (1.55 g; 8.3%), mp 195–197°C (dec.). The base liberated from the picrate was a pale-yellow, slowly crystallizing oil. Recrystallization from petroleum ether yielded a product melting at 100–102°C, in all respects identical with the compound synthesized in a different way (2).

5-Benzyl-2,3-dihydro-7,8-dimethoxy-1,4-benzothiazepine **5**b

A mixture of **4***b* (2.31 g; 10 mmol) and $POCl_3$ (3 mL) was heated on a steam bath for 1 h. The mixture was treated with ice-water, made alkaline with Na_2CO_3, and extracted with benzene. The organic phase was dried (Na_2SO_4) and concentrated. The residue was dissolved in ethanol (2 mL) and **5***b*·HCl was precipitated, by the addition of ethanol saturated with HCl, as pale-yellow crystals (0.32 g; 14.7%), mp 195–196°C. *Anal.* calcd. for $C_{18}H_{20}ClNO_2S$: C 61.79, H 5.76, Cl 10.14; found: C 62.18, H 6.09, Cl 10.66%.

The *picrate* was prepared as yellow crystals (EtOH), mp 197–199°C (dec.).

The base liberated from **5***b*·HCl was a viscous oil. *Anal.* calcd. for $C_{18}H_{19}NO_2S$: C 68.98, H 6.11, N 4.47; found: C 69.10, H 6.35, N 4.60%.

2,3-Dihydro-7,8-dimethoxy-1,4-benzothiazepine **5**c *and 2'-chloroethyl-3,4-dimethoxyphenyl sulfide* **7**

Compound **4***c* (9.51 g; 30 mmol) and $POCl_3$ (11 mL) were heated in a steam bath for 3 h. The mixture was poured into ice-water (150 mL) and extracted with benzene. The extract was dried (Na_2SO_4) and the solvent was evaporated. Fractional distillation of the oily residue in a water-pump vacuum gave benzonitrile (1.55 g), and 2'-chloroethyl-3,4-dimethoxyphenyl sulfide (3 g); $n_\alpha^{20°}$ 1.5816. *Anal.* calcd. for $C_{10}H_{13}ClO_2S$: C 51.60, H 5.63, Cl 15.24; found: C 51.76, H 5.53, Cl 15.45%.

The acidic aqueous solution was made alkaline and extracted with benzene. After drying (Na_2SO_4), the solvent was evaporated and the residue was crystallized from ethanol to give colorless prisms of **5***c* (3.3 g; 36.7%), mp 167–168°C. *Anal.* calcd. for $C_{17}H_{17}NO_2S$: C 68.20, H 5.73, N 4.68; found: C 69.09, H 6.03, N 4.89%.

The *picrate* crystallized from ethanol as a yellow product, mp 238–240°C (dec.); ^{1}H nmr: $COCH_3$ (**5***a*): 2.36 s (3H); CH_2: 3.50 s (4H, **5***a*), 3.47, and 3.56 2m (2 × 2H, **5***b*), ≈3.65 AA'BB'-type m (4H) with close A and B parts (**5***c*); OCH_3: 3.90 s (6H, **5***a*), 3.73 and 3.84 2s (2 × 3H, **5***b*), 3.73 and 3.82 2s (2 × 3H, **5***c*); $PhCH_2$ (**5***b*): 4.01 s (2H); ArH-6: 6.80, 6.95, 7.08 s (1H); ArH-9: 7.00, 6.63, 6.60 s (1H); ArH(Ph): 7.1–7.3 m (5H, **6***b*), 7.2–7.7 m (5H, **5***c*). *Anal.* calcd. for $C_{23}H_{20}N_4O_9S$: C 52.27, H 3.82, N 10.60; found: C 52.02, H 3.88, N 10.66%.

2'-Chloroethyl-3,4-dimethoxyphenyl sulfide **7**

3,4-Dimethoxythiophenol (1.7 g; 10 mmol) was dissolved in 1,2-dichloroethane (10 mL). The solution was refluxed under a nitrogen protecting atmosphere while a solution of $NaOCH_3$ (10 mmol)

in methanol (10 mL) was added dropwise. The mixture was refluxed for 3 h. It was then diluted with water and extracted with $CHCl_3$. The extract was washed with $NaHCO_3$ solution, dried (Na_2SO_4), and evaporated. The oily residue was distilled, in the vacuum of a water pump, on an air bath at 125°C. The product was a colorless oil (1.6 g; 70%), $n_\alpha^{20°}$ 1.5808, in all properties identical with compound **7** isolated from the reaction mixture in the preparation of **5***c*; ^{1}H nmr: CH_2: 3.11, 3.58 AA'BB'-type m (4H); OCH_3: 3.87, 3.88 2s (2 × 3H); ArH-5: 6.81 d (8.5 Hz, 1H); ArH-2: 6.97 d (2.0 Hz, 1H); ArH-6: 7.03 dd (1H); ^{13}C nmr: SCH_2: 38.0; $ClCH_2$: 42.4; OCH_3: 56.01, 56.05; C(Ar)-2: 112.3; C(Ar)-5: 116.4; C(Ar)-1: 125.1; C(Ar)-6: 125.4; C(Ar)-3,4: 149.5, 149.6.

2,3-Dihydro-7,8-dimethoxy-4-methyl-5-phenyl-1,4-benzothiazepinium iodide ***8***

Compound **5***c* (0.75 g; 2.5 mmol) was dissolved in CH_3CN (5 mL). CH_3I (0.4 mL) was added and the mixture was refluxed for 1 h. On cooling, crystals of **8** separated (0.72 g; 65.5%). Recrystallization from CH_3CN gave a product with mp 204–205°C (dec.); ^{1}H nmr: N^+CH_3: 3.67 s (3H); OCH_3: 4.00, 4.05 2s (2 × 3H); CH_2: ≈4.05 (overlapped by the OCH_3 singlets), 4.45, AA'BB'-type m (4H); ArH-9: 6.60 s (1H); ArH-6: 7.20 s (1H); ArH(Ph): ≈7.65 m (5H). *Anal.* calcd. for $C_{18}H_{20}INO_2S$: C 48.99, H 4.57, N 3.17; found: C 48.80, H 4.82, N 3.16%.

2,3-Dihydro-7,8-dimethoxy-5-phenyl-1,4-benzothiazepine 1-oxide ***9***

A solution of **5***c* (1 g; 3.3 mmol) in methanol (40 mL) was stirred at room temperature for 3 days with a solution of $NaIO_4$ (0.7 g) in water (10 mL). After dilution with water, the precipitate was filtered off. Recrystallization from methanol (3 mL) gave colorless prisms (0.67 g; 63.8%), mp 157–158°C; ir: ν SO: 1065 cm^{-1} (the strongest band of the ir spectrum); ^{1}H nmr: CH_2: 3.10 dd (1H), 3.44 dt (1H), ≈4.1 (1H, overlapped by one of the OCH_3 singlets), 4.63 dt (1H); OCH_3: 3.83, 4.07 2s (2 × 3H); ArH-9: 6.75 s (1H); ArH-3′,5′ (Ph): 7.4 m (3H); ArH-6: 7.53 s (1H); ArH-2′,6′ (Ph): 7.60 ≈d (2H). *Anal.* calcd. for $C_{17}H_{17}NO_3S$: C 64.74, H 5.44, N 4.44; found: C 64.56, H 5.67, N 4.19%.

The *picrate*, yellow crystals from ethanol, had mp 210–211°C (dec.). *Anal.* calcd. for $C_{23}H_{20}N_4O_{10}S$: C 50.73, H 3.70, N 10.29; found: C 50.89, H 3.98, N 10.58%.

2,3-Dihydro-7,8-dimethoxy-5-phenyl-1,4-benzothiazepine 1,1-dioxide ***10***

Compound **5***c* (1 g; 3.3 mmol) was dissolved in a mixture of dioxan (5 mL) and acetic acid (5 mL). A solution $KMnO_4$ (3 g) in water (20 mL) was added, in portions, to the stirred mixture and stirring was continued for 1 h. H_2O_2 was added dropwise until dissolution of the MnO_2 was complete. The solution was diluted with water (100 mL), made alkaline with Na_2CO_3, and stirred for 1 h more. It was then extracted with benzene, and the extract was dried (Na_2SO_4) and evaporated to dryness. The residue was crystallized from a small amount of ethanol as colorless prisms (0.6 g, 54.5%), mp 162–164°C; ir: ν_{as} SO_2: 1315; ν_s SO_2: 1125 cm^{-1}; ^{1}H nmr: OCH_3: 3.79, 4.01 2s (2 × 3H); CH_2: 3.88 s (4H); ArH-9: 6.68 s (1H); ArH-3′,5′ (Ph): 7.40 m (3H); ArH-6: 7.58 s (1H); ArH-2′,6′ (Ph): 7.62 d (2H). *Anal.* calcd. for $C_{17}H_{17}NO_4S$: C 61.61, H 5.17, N 4.23; found: C 61.20, H 5.24, N 4.48%.

Picrate: yellow crystals from ethanol, mp 245–246°C (dec.). *Anal.* calcd. for $C_{23}H_{20}N_4O_{11}S$: C 49.28, H 3.60, N 10.00; found: C 49.08, H 3.85, N 9.91%.

5-Benzyl-7,8-dimethoxy-2,3,4,5-tetrahydro-1,4-benzothiazepine ***11****a*

Compound **5***b*·HCl (0.35 g; 1 mmol) was dissolved in methanol (25 mL). $NaBH_4$ (0.5 g) was added in portions, and the mixture was allowed to stand overnight. After the addition of water (0.5 mL), the mixture was evaporated to dryness and extracted with ether. The ethereal extract was concentrated and a solution of HCl in ether was added to precipitate **11***a*·HCl as colorless crystals (0.29 g; 82.6%), mp 110–112°C. *Anal.* calcd. for $C_{18}H_{22}ClNO_2S$: C 61.44, H 6.30, Cl 10.08, N 3.98; found: C 61.11, H 6.60, Cl 10.38, N 3.68%.

The base **11***a* liberated from the hydrochloride was a viscous oil; ^{1}H nmr: NH: 1.80 s (1H); SCH_2: 2.68 m (2H); CH_2(Ph): 3.0–3.2 m (2H); NCH_2: 3.3–3.4 m (2H); NCH: 4.59 dd (9.6 and 5.6 Hz, 1H); ArH-9: 6.77 s (1H); ArH-6: 7.08 s (1H); ArH(Ph): ≈7.25 ≈s (5H); ^{13}C nmr: C-4: 35.4; C-3: 40.0; CH_2Ph: 49.9; OCH_3: 55.9 (two overlapping lines); C-1: 61.4; C-6: 111.2; C-9: 117.0; C-4′: 126.0; C-5a: 126.9; C-3′,5′: 128.2; C-2′,6′: 128.9; C-9a: 139.2; C-1′: 140.3; C-7: 147.1; C-8: 148.5. *Anal.* calcd. for $C_{18}H_{21}NO_2S$: C 68.54, H 6.71, N 4.44; found: C 68.70, H 6.95, N 4.20%.

7,8-Dimethoxy-5-phenyl-2,3,4,5-tetrahydro-1,4-benzothiazepine ***11****b*

Compound **5***c* (1.5 g; 5 mmol) was dissolved in methanol (50 mL). $NaBH_4$ (1 g) was added in small portions, and the mixture was left to stand overnight. Water (1 mL) was then added, and the mixture was evaporated to dryness and extracted with benzene. The extract was concentrated, whereupon the residue crystallized to give colorless prisms (1.45 g; 96%), mp 145–146°C (from methanol); ir: ν NH: 3340 cm^{-1} (weak); ^{1}H nmr: NH: 1.70 s (1H); CH_2: ≈2.7 m (2H), ≈3.4 m (2H, overlapped by one of the OCH_3 singlets); OCH_3: 3.50, 3.82 2s (2 × 3H); NCH: 5.60 s (1H); ArH-9: 6.10 s (1H); ArH-6: 7.05 s (1H); ArH(Ph): 7.30 ≈s (5H). *Anal.* calcd. for $C_{17}H_{19}NO_2S$: C 67.74, H 6.35, N 4.65; found: C 67.41, H 6.57, N 4.79%.

The **11***b*·HCl was precipitated from benzene with ether containing HCl; mp 102–105°C. *Anal.* calcd. for $C_{17}H_{20}ClNO_2S$: C 60.43, H 5.97, Cl 10.49, N 4.15; found: C 60.27, H 6.27, Cl 10.52, N 4.16%.

General procedure for preparation of β-lactams **12***a–f and* **13**

The appropriate acid chloride (5 mmol) was added to a solution of **5***c* (1.5 g; 5 mmol) in benzene (30 mL). The mixture was refluxed and, with continuous stirring, TEA (0.5 g; 5 mmol) in benzene (30 mL) was added dropwise during 1 h. The crystalline TEA·HCl was removed by filtration, the filtrate was evaporated, and the residue was crystallized from ethanol to yield colorless crystals (cf. Table 4).

Separation of diastereomers **12***e and* **12***f*

The reaction was effected according to the general procedure. The residue was dissolved in ethanol and, after the mixture had stood for 3 h, the precipitated crystals of **12***e* were collected by filtration. The mother liquor was stored in a refrigerator at 5°C overnight, whereupon compound **12***f* crystallized.

Synthesis of compounds **13** *by oxidation of* **12***a*

Compound **12***a* (1.40 g; 3.3 mmol) was dissolved in acetic acid (20 mL); peracetic acid (15 mL) was added, and the solution was left to stand overnight. The crystals (1.07 g; 71.3%) that separated on dilution with water were filtered off and recrystallized from ethanol; the colorless product had mp 239–240°C and was in all respects identical with compound **13** prepared from **10**.

4-Benzoyl-2,3-dihydro-7,8-dimethoxy-5-methylene-1,4-benzothiazepine ***14***

A solution of TEA (1.01 g; 10 mmol) in benzene (20 mL) was added to **5***a*·HCl (1.75 g; 5 mmol) and, with constant stirring, a solution of benzoyl chloride (0.70 g; 5 mmol) in benzene (20 mL) was added. Stirring was continued for 1 h more. After removal of the TEA·HCl by filtration, the filtrate was evaporated to dryness. The residue crystallized slowly. It was suspended in petroleum ether and filtered off to yield the product (0.35 g; 20.6%), which was recrystallized from benzene; mp 140–142°C; ir: amide-I: 1647, ν C=C(H_2): 1622, ν (=CH_2): 864, 792 cm^{-1}; ^{1}H nmr: SCH_2: 3.23 ≈t (5.8 Hz, 2H); OCH_3: 3.63, 3.84 2s (2 × 3H); NCH_2: 4.21 ≈t (2H); =CH_2: 5.24, 5.38 2 × ≈s (2 × 1H); ArH-9: 6.22 s (1H, broadened due to hindered rotation of the *N*-benzoyl group); ArH-6: 6.76 s (1H); ArH(Ph) ≈7.3 m (5H); ^{13}C nmr: C-4: 31.8; C-3: 50.4; OCH_3: 55.8 (two overlapping lines); C-6: 112.9; =CH_2: 113.3; C-9: 116.0; C-5a: 125.2; C-2′,6′ and C-3′,5′: 127.3, 127.4; C-4′: 129.0; C-1′: 130.5; C-9a: 136.7; C-1 and C-8: 147.3 (two overlapping lines); C-7: 148.9; C=O: 170.8. *Anal.* calcd. for $C_{19}H_{19}NO_3S$: C 66.84, H 5.61, N 4.10; found: C 66.56, H 5.90, N 4.32%.

5-Benzylidene-7,8-dimethoxy-4-dichloroacetyl-2,3-dihydro-1,4-benzothiazepine ***15***

TEA (1.01 g; 10 mmol) in benzene (20 mL) was added to **5***b*·HCl (1.75 g; 5 mmol). With constant stirring, a solution of dichloroacetyl

Can. J. Chem. Downloaded from www.nrcresearchpress.com by 80.58.250.72 on 09/07/12
For personal use only.

TABLE 4. Physical and analytical data for compounds **12***a–f* and **13**

Compound	Yield (%)	Melting point (°C)	Molecular formula Mol. Wt.	Analysis Calculated C	H	N	S	Found C	H	N	S
12*a*	57.6	205–206	$C_{25}H_{23}NO_3S$ 417.50	71.92	5.55	3.36	7.68	72.20	5.81	3.25	7.93
12*b*	89.1	176–177	$C_{25}H_{23}NO_4S$ 433.50	69.26	5.35	3.23	—	69.08	5.32	3.19	—
12*c*	92	220–221	$C_{19}H_{18}ClNO_3S$ 375.86	60.71	4.83	3.73	—	60.79	4.81	3.85	—
12*d*	95	192–193	$C_{19}H_{17}Cl_2NO_3S$ 410.31	55.61	4.18	3.41	—	55.42	44.6	3.54	—
12*e*	87	217–218	$C_{25}H_{22}ClNO_3S$ 451.96	66.43	4.91	3.10	—	66.73	5.04	3.23	—
12*f*	8	209–210	$C_{25}H_{22}ClNO_3S$ 451.96	66.43	4.91	3.10	—	66.56	5.02	3.01	—
13	40.4	239–240	$C_{25}H_{23}NO_5S$ 449.50	66.80	5.16	3.12	7.13	67.08	5.07	3.27	7.49

chloride (0.74 g; 5 mmol) in benzene (20 mL) was added and stirring was continued for 1 h. After removal of the TEA·HCl by filtration, the benzene solution was evaporated to dryness in vacuum. Recrystallization of the residue from ethanol gave pale-yellow crystals (1.2 g; 56.6%), mp 160–161°C (dec.); ir: amide-I: 1685 cm^{-1}; ^1H nmr: SCH_3: 3.25 t (6 Hz, 2H); OCH_3: 3.53, 3.90 2s (2 × 3H); NCH_2: ≈4.3 ≈t (2H, broad due to hindered rotation of the amide group); $CHCl_2$: 6.33 s (1H); ArH-9: 6.60 s (1H, br); =CH(Ph): 6.85 s (1H); ArH-6: 6.90 s (1H); ArH(Ph): 7.27 ≈s (5H). *Anal.* calcd. for $C_{20}H_{19}Cl_2NO_3S$: C 56.61, H 4.51, Cl 16.71, N 3.30; found: C 56.23, H 4.80, Cl 17.00, N 3.57%.

4-Benzoyl-5-benzylidene-2,3-dihydro-7,8-dimethoxy-1,4-benzothiazepine ***16***

Compound **5***b* (0.70 g; 2 mmol) was dissolved in benzene (15 mL). TEA (0.20 g) and then, with constant stirring, a solution of benzoyl chloride (0.28 g; 2 mmol) in benzene (10 mL) were added, and the mixture was stirred for 1 h more. The precipitated TEA·HCl was removed by filtration, the filtrate was evaporated in vacuum, and the residue was crystallized from a mixture of benzene and petroleum ether to give colorless crystals, mp 165–166°C; ir: amide-I: 1655 cm^{-1}; ^1H nmr: SCH_2: 3.19 ≈t (2H); OCH_3: 3.13, 3.84 2s (2 × 3H); NCH_2: br t (2H); ArH-9: 5.50 br s (1H); =CHPh: 6.82 s (1H); ArH-6: 6.89 s (1H); ArH^o(=CHPh): ≈7.02 dd (2H); $ArH^{m,p}$(=CHPh): ≈7.13 m (3H); $ArH^{m,p}$(COPh): ≈7.27 m (3H); ArH^o(COPh): 7.36 m (2H). *Note*: broadening of the NCH_2 and ArH-9 signals due to hindered rotation of the amide group; ^{13}C nmr: C-4: 31.8; C-3: 53.1; OCH_3: 55.3, 55.8; C-6: 113.7; C-9: 114.5; C-5a: 126.1; C-1′(COPh): 127.6 (two overlapping lines), C-2′,3′,4′,5′(=CHPh and COPh): 127.6, 127.9, 128.1, and 128.7; C-4′(=CHPh): 129.3; C-1′(=CHPh): 131.4; C-4′(COPh): 132.0; =CH: 134.9; C-9a: 137.2; C-1: 140.3; C-8: 147.0; C-7: 148.4; C=O: 171.0. *Anal.* calcd. for $C_{25}H_{23}NO_3S$: C 71.92, H 5.55, N 3.36; found: C 72.30, H 5.72, N 3.64%.

1. G. STÁJER, A. E. SZABÓ, G. BERNÁTH, and P. SOHÁR. Tetrahedron. In press.
2. L. H. STERNBACH, H. LEHR, E. REEDER, T. HAYER, and N. STEIGER. J. Org. Chem. **30**, 2812 (1965).
3. T. HIRODASHI, T. IZUMI, and M. YAKAMOTO. Japan Pat. No. 7227107, 1972; Chem. Abstr. **77**, 140187 (1972).
4. R. BOUDET and D. BOURGOIN-LEGAY. C. R. Acad. Sci. Ser. C, **282**, 249 (1976); Chem. Abstr. **84**, 150605 (1976).
5. R. M. ACHESON and N. F. ELMORE. Adv. Heterocycl. Chem. **23**, 263 (1978).
6. M. SINDLER-KULYK and D. C. NECKERS. Tetrahedron Lett. **22**, 529 (1981).
7. M. SINDLER-KULYK, D. C. NECKERS, and I. R. BLOUNT. Tetrahedron, **37**, 3377 (1981).
8. L. FODOR, J. SZABÓ, G. BERNÁTH, L. PÁRKÁNYI, and P. SOHÁR. Tetrahedron Lett. **22**, 5077 (1981).
9. L. FODOR, J. SZABÓ, E. SZÜCS, G. BERNÁTH, P. SOHÁR, and J. TAMÁS. Tetrahedron, **40**, 4089 (1984).
10. A. K. BOSE, W. A. HOFFMANN, and M. S. MANHAS. J. Chem. Soc. Perkin Trans. 1, 2343 (1976).
11. J. SZABÓ, L. FODOR, Á. KATÓCS, G. BERNÁTH, and P. SOHÁR. Chem. Ber. **119**, 2904 (1986).
12. I. NINOMIYA. Heterocycles, **1**, 105 (1974).
13. P. SOHÁR, L. FODOR, J. SZABÓ, and G. BERNÁTH. Tetrahedron, **40**, 4387 (1984).
14. P. SOHÁR. *In* Nuclear magnetic resonance spectroscopy. CRC Press, Boca Raton, Florida. 1983; (*a*) Vol. 1, pp. 35–38; (*b*) Vol. 2, p. 44; (*c*) Vol. 2, p. 69 and Vol. 3, p. 69.
15. S. HOLLY and P. SOHÁR. Theoretical and Technical Introduction to the series Absorption Spectra in the Infrared Region. *Edited by* L. Láng and W. H. Prichard. Akadémiai Kiadó, Budapest. 1975; (*a*) pp. 113–114; (*b*) pp. 128–129.
16. D. T. PEGG, D. M. DODDRELL, and M. R. BENDALL. J. Chem. Phys. **77**, 2745 (1982).
17. M. R. BENDALL, D. M. DODDRELL, D. T. PEGG, and W. E. HULL. High resolution multipulse NMR spectrum editing and DEPT. Bruker, Karlsruhe. 1982.

Can. J. Chem. Downloaded from www.nrcresearchpress.com by 80.58.250.72 on 09/07/12
For personal use only.

Total synthesis of a proposed structure of isohimachalone[1]

HSING-JANG LIU AND ERIC N. C. BROWNE[2]
Department of Chemistry, The University of Alberta, Edmonton, Alta., Canada T6G 2G2

Received May 21, 1986

This paper is dedicated to Dr. O. E. (Ted) Edwards

HSING-JANG LIU and ERIC N. C. BROWNE. Can. J. Chem. **65**, 182 (1987).

A proposed structure **5** of the naturally occurring sesquiterpene ketone isohimachalone has been synthesized by a route using the unique Diels–Alder chemistry developed in our laboratory. The product has been shown to be non-identical with the natural material by comparison of spectral data, a result which has been implied by the work of an independent group using direct methods. Spectroscopic differences between our synthetic material and the natural and closely related products are discussed.

HSING-JANG LIU et ERIC N. C. BROWNE. Can. J. Chem. **65**, 182 (1987).

Utilisant la chimie unique de Diels–Alder qui a été développé dans notre laboratoire, on a synthétisé le composé **5** dont la structure avait été proposée pour la cétone sesquiterpénique naturelle isohimachalone. Une comparaison des données spectrales a permis de démontrer que le produit obtenu n'est pas identique avec le produit naturel; ce résulte a déjà été suggéré par le travail d'un groupe indépendant qui a utilisé des méthodes directes. On discute des différences observées dans les spectres du produit de synthèse, du produit naturel et d'autres produits qui leur sont fortement apparentés.

[Traduit par la revue]

Can. J. Chem. Downloaded from www.nrcresearchpress.com by 190.90.36.8 on 09/07/12
For personal use only.

Introduction

As described by us in a previous paper (1), the himachalane class of naturally occurring sesquiterpenes represented by skeleton **1** has grown significantly since the first examples were reported (2, 3). In the 1970's two other very closely related skeletal types were disclosed. The allohimachalane skeleton **2** is characteristic of two compounds isolated by Dev and co-workers (4–6) while the related isohimachalane skeleton **3** is characteristic of two reported compounds. Teisseire first reported the isolation (7) from *Cedrus atlantica* of a ketone to which he has assigned the *trans*-fused structure **4** (8). Dev later reported (4) the isolation from *Cedrus deodara* Loud. of a ketone to which he originally assigned *cis*-fused structure **5** and which he named isohimachalone.

It has been suggested (8) that *trans*-ketone **4** arises by a rearrangement of the epoxide **6**. One or both of the epimeric epoxides **6** and **7** are reportedly (9) auto-oxidation products of β-himachalene **8**, and so conceivably the *cis*-fused structure could arise by a similar rearrangement of the naturally occurring epoxide **7**. Both epimeric epoxides **6** (7, 10, 11) and **7** (10) have been shown to occur naturally. The allohimachalane skeleton **2** would arise in a similar fashion by migration of a different carbon–carbon bond in these same epoxide intermediates **6** and **7**.[3]

Recently, a collaborative effort of Dev and Clardy and co-workers (14, 15) using X-ray analysis has resulted in revision of the stereochemistry of himachalol from **9** (16) to **10**. Consequently, the structures of a number of related natural products whose stereochemistries were logically derived from that of himachalol must also be revised, in particular that of the non-naturally derived (17) β-himachalene oxide originally assigned in 1977 (9) as **7**, which now stands corrected to **6**. By implication (ref. 14, footnote 6), although not specifically stated in that paper, this general revision includes the structure of

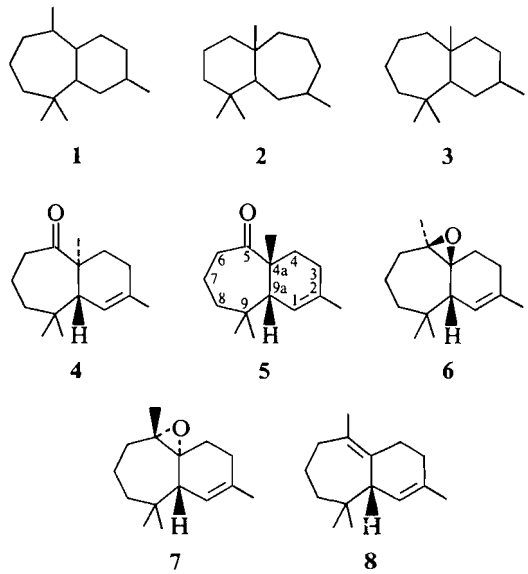

isohimachalone,[4] the stereochemistry of which was assigned after partial synthesis from β-himachalene via the 6,7-epoxide. This implied revision of the structure of isohimachalone to *trans*-fused structure **4** confirms an earlier independently reached conclusion of this group (18) that the *cis*-compound **5** could not be identical with that of the reported naturally occurring material by either group.

A number of different synthetic approaches to the himachalane skeleton **1** have been reported (19–24). Our own group has achieved the synthesis of α-(**11**) and β-himachalene (**8**) by a unique Diels–Alder approach (1). We wish at this time to report our synthesis of the *cis*-fused compound **5** using the unique Diels–Alder chemistry previously developed by this group. Spectroscopic differences between **5** and the natural product will be demonstrated, which support the implication of the Dev/Clardy group's results.

A modern synthetic scheme should be designed to achieve the rapid assembly of the target carbon skeleton in an intermediate containing functional groups that require only simple modifica-

[1]The content of this paper represents a part of the Ph.D. thesis of E. N. C. Browne, the University of Alberta, 1980.

[2]Present address: DeVoe-Holbein Canada Inc., 175 Bouchard Blvd., Dorval, Québec, Canada H9S 1A9.

[3]The stereochemistry of allohimachalol and related compounds has recently been revised following X-ray analysis (12, 13).

[4]Confirmed by S. Dev in private communication, January, 1986.

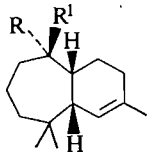

9 R = OH, R′ = CH_3
10 R = CH_3, R′ = OH

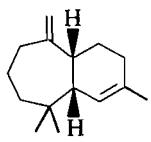

11

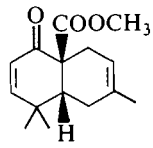

12

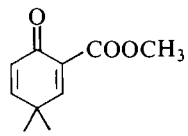

13

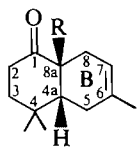

14 R = $COOCH_3$
15 R = CH_3

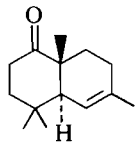

16

tions to give the synthetic target. On this basis, keto ester **12** prepared by Diels–Alder addition of isoprene to dienone ester **13** (1) offers a suitable key intermediate for synthesis of the isohimachalane skeleton **3**. Reduction to saturated ketone **14** followed by conversion of the carbomethoxyl substituent to an angular methyl group would give ketone **15**, which requires only homologation of the A ring and isomerization of the double bond to give *cis*-ketone **5**.

A similar approach could be applied to the synthesis of *trans*-ketone **4** (isohimachalone). Starting with the *cis*-fused ketone **15**, isomerization of the double bond and epimerization of the ring junction could give *trans*-fused ketone **16**, which, after homologation of the A ring, would give the ketone **4** (isohimachalone). The synthesis of *cis*-ketone **5** has been achieved and found to be not identical with naturally occurring isohimachalone. The synthesis of *trans*-ketone **4** is under study and the progress in this study will be reported in a future publication.

Results and discussion

For the proposed synthesis of *cis*-ketone **5** the previously reported saturated keto-ester **14** (1), obtained by hydrosilylation/hydrolysis of keto ester **12** was used as the key intermediate. Conversion of the carbomethoxyl group of **14** to an angular methyl group required protection of the ketone prior to the reduction step. Thus ketone **14** was treated with ethylene glycol and *p*-toluenesulfonic acid in refluxing benzene for 47 h and a ketal was obtained in 93% yield to which structure **17** was tentatively assigned.

To ascertain that the acidic ketalization conditions had not also caused migration of the double bond to give ketal **18**, the ketal group was removed by treatment with *p*-toluenesulfonic acid in acetone for 14 days. A single product was obtained in quantitative yield (based on recovery of 46% of the starting ketal), which was identical by ^1H nmr, ir, and tlc analysis with the original keto ester **14**. The production of un-isomerized keto ester **14** from the very mild transketalization conditions indicated that the ketalization of **14** had occurred without migration of the double bond and that **17** was the structure of the product obtained.

Conversion of the carbomethoxy group of **17** to a methyl group required reduction of the ester to the alcohol **19**, followed by attachment of a leaving group and further reduction to give the methyl derivative **20**. The ester **17** was easily reduced with lithium aluminum hydride in ether to give alcohol **19** in 92% yield.

The further reduction of the hydroxymethylene group of **19** to an angular methyl required the use of a derivative that could be reduced without steric interference from the adjacent neopentyl center. It has been shown (25) that tetramethyl phosphorodiamidate (TMPDA) derivatives of alcohols can be reduced to hydrocarbons with lithium in ethylamine/tetrahydrofuran/*tert*-butyl alcohol. Such TMPDA derivatives of sterically hindered alcohols are, however, difficult to prepare directly from reaction of the alcohol with tetramethylphosphorodiamidic chloride. This difficulty can be overcome (26) by conversion of the alcohol, first to the dimethyl chlorophosphoramidate derivative using dimethylphosphoramidic dichloride followed by treatment of the resulting intermediate with dimethylamine to give the TMPDA derivative. Accordingly, alcohol **19** was converted to the corresponding alkoxy anion by treatment with *n*-butyllithium in 1,2-dimethoxyethane/tetramethylethylenediamine (80:20) at 0°C for 15 min. The anion was treated *in situ* with dimethylphosphoramidic dichloride (27) at room temperature for 23 h to give complete conversion to the intermediate **21**. This compound was not isolated but was rapidly converted, by the addition of excess liquid dimethylamine to the solution at 0°C, into the TMPDA derivative **22** in 84% overall yield from alcohol **19**.

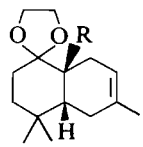

17 R = $COOCH_3$
19 R = CH_2OH
20 R = CH_3
21 R = $CH_2OPO(Cl)N(CH_3)_2$
22 R = $CH_2OPO[N(CH_3)_2]_2$

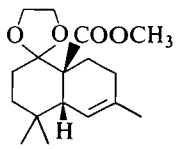

18

Reduction of the TMPDA derivative **22** with lithium in ethylamine/tetrahydrofuran/*tert*-butyl alcohol gave three principal products. One product, obtained in 14% yield, was found to be identical with the alcohol **19** and clearly resulted from cleavage of the P—O bond rather than C—O cleavage. The minor product, obtained in 5% yield, was found to be identical with the *trans*-ketone **23** obtained previously (1). Possibly, this ketone could have been formed via a 1,3-glycol type cleavage in the radical, which would result from P—O bond fission in the TMPDA derivative **22**. The major product, obtained in 69% yield, was identified as the desired ketal **20**.

Transketalization of ketal **20** with acetone in the presence of *p*-toluenesulfonic acid rapidly (2.5 h) gave a product identifiable as *cis*-ketone **15** in 97% yield.

The synthesis of **5** could proceed from ketone **15** by two different routes: isomerization of the double bond (**15** → **24**) followed by homologation of the ketone ring, or homologation first (**15** → **25**) and then isomerization of the double bond. The isomerization of **25** to **5** has precedent in the acid catalyzed isomerization of **26** → **27** in which the equilibrium ratio of the two compounds was approximately 33:67 (1, 18, 28). On the other hand, examination of Dreiding models of **15** and **24** showed that in **15** the B ring could not achieve a stable quasi-chair conformation without exerting considerable torsional strain on the C-4a/C-8a bond. In ketone **24**, however, the quasi-chair conformation of the B ring could be attained without undue torsional strain. Ketone **24** therefore might be expected to predominate in an equilibrium mixture of **15** and **24**.

Treatment of **15** with *p*-toluenesulfonic acid in refluxing benzene for 2 h gave an 85:15 equilibrium mixture of two

Can. J. Chem. Downloaded from www.nrcresearchpress.com by 190.90.36.8 on 09/07/12
For personal use only.

TABLE 1. ^{13}C magnetic resonance spectra (δ) of ketones **15** and **24**

Ketone	C-1	C-2	C-3	C-4	C-4a	C-5	C-6	C-7	C-8	C-8a	CH_3	CH_3	CH_3	CH_3
15	216.2	34.9	40.7	33.9	48.9	28.0	132.1	117.7	33.7	46.4	32.2	23.6	23.2	21.0
24	217.3	35.1	38.5	34.0	52.3	120.5	133.7	26.2	29.3	46.0	31.5	23.8	23.1	22.8

inseparable compounds in 89% yield. The minor component was identified as ketone **15** by its gc retention time and by comparison of the minor signals in the ^{1}Hmr spectrum of the mixture with the spectrum of pure **15**. The major component showed ^{1}Hmr signals at δ 5.40 (multiplet) due to a vinyl proton and at δ 1.71, 1.04, 0.97, and 0.94 (singlets) due to methyl groups. The structure **24** was tentatively assigned and this was confirmed by comparison of the ^{13}Cmr spectra (Table 1) of **15** and **24**. In both cases the signal due to C-4a appeared as the only high-field doublet in the off-resonance decoupled spectrum. In **15** the signal appeared at δ 48.9 whereas in **24** the signal appeared at δ 52.3 because of deshielding by the closer proximity of the double bond. As well, the olefinic carbon C-5 in **24** was deshielded (δ 120.5) relative to C-7 of **15** (δ 117.7) by the β-effect (29) caused by C-4.

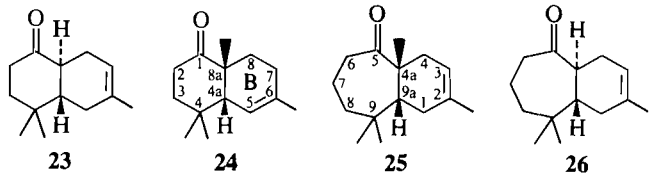

23 **24** **25** **26**

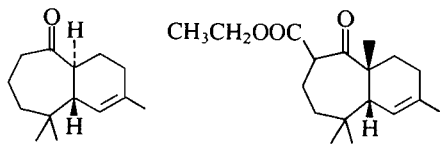

27 **28**

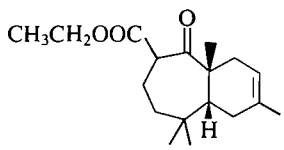

29

As was stated for the synthesis of himachalenes (1), the ring expansion of ketones such as **24** with ethyl diazoacetate (30) was expected (31, 32) to proceed with predominant migration of the less substituted α-carbon to give β-keto esters such as **28**. Treatment of **24**[5] with ethyl diazoacetate and boron trifluoride etherate in ether for seven days gave two products (~1:1) in a combined yield of 41%, which were separated by column chromatography. The ^{1}Hmr spectrum of the faster-moving product showed a doublet at δ 5.32 due to a vinylic proton and a signal at δ 3.92 that was assigned to a proton on the α-carbon of a β-keto ester. This latter signal was a doublet of doublets with coupling constants of 12 and 4 Hz, indicating that two protons were adjacent. The spectroscopic data, especially the coupling patterns of the vinyl and keto ester protons, indicated that the structure of this product was **28**.

The other product of the ring expansion reaction was conclusively identified as **29** by comparison with an authentic sample obtained directly by ring expansion of pure ketone **15** (*vide infra*). The presence of **29** among the reaction products probably stemmed from the ring expansion of **15**, which was present as an impurity (~15%) in the starting material.

The decarboxylation of keto ester **28** with lithium iodide dihydrate (33) proceeded to give a ketone in 10% yield. The product showed a molecular ion at *m/e* 220.1823 in the mass spectrum and showed a band at 1699 cm^{-1} in the ir spectrum, indicating a ketone in a seven-membered ring. The ^{1}Hmr spectrum showed a vinyl proton as a doublet at δ 5.34 with a coupling constant of 4 Hz. Methyl groups appeared as singlets at δ 1.69, 1.01, 0.97, and 0.69. The appearance of the vinyl proton as a doublet strongly suggested that this product had structure **5**. The relatively poor yield obtained for conversion of **24** to **5** prompted investigation of the alternate route to **5** via ring expansion of ketone **15**.

Treatment of **15** with ethyl diazoacetate and boron trifluoride etherate in ether for 48 h gave a single product (18 lines in the ^{13}Cmr spectrum) in 82% yield. In the ^{1}Hmr spectrum, a signal at δ 3.86 was assigned to a proton at the α-carbon of a β-keto ester and appeared as a doublet of doublets with two coupling constants of 10 Hz each, indicating that there were two protons adjacent to it. The spectral data indicated that the structure of the ring expansion product was **29**.

Decarboxylation of **29** with lithium iodide dihydrate (33) gave a product identified as the corresponding ketone **25** in 86% yield.

The attempted acid catalyzed isomerization of **25** to **5** with oxalic acid in aqueous dioxane at reflux for 12 h gave only recovered starting material (89%). However, treatment of **25** with *p*-toluenesulfonic acid hydrate in refluxing benzene for 2 h produced two isomeric ketones, in addition to a 5% recovery of starting material. The major product, obtained in 53% yield, was identical in all respects with the ketone **5** produced by decarboxylation of keto ester **28**. The second product, obtained in 15% yield, gave a molecular ion at *m/e* 220.1831 in the mass spectrum. The ir spectrum showed a band at 1699 cm^{-1} due to a seven-membered ring ketone. The ^{1}Hmr spectrum showed a vinyl proton as a multiplet at δ 5.17 and methyl groups as singlets at δ 1.60, 1.26, 0.94, and 0.75. Although the spectral data indicated that this compound was very closely related to ketones **5** and **25**, the structure could not be assigned with certainty; however, mechanistic (Scheme 1), structural, and spectroscopic considerations give weight to our tentative assignment of structure **30**, the epimer of allohimachalone (5, 6, 12), to this product.[6]

Conclusive evidence in support of the assignment of the double bond position in ketones **5** and **25** was obtained from their ^{13}Cmr spectra (Table 2). In **5**, C-9a appeared as the only high-field doublet at δ 50.2, deshielded relative to C-9a of **25** (δ 45.0) by the adjacent double bond. Also the olefinic carbon C-1 of **5** (δ 121.8) was deshielded relative to C-3 of **25** (δ 119.7) due to a β-effect from the adjacent C-9.

With the placement of the double bond in **5** and **25** clearly

[5]The sample was contaminated with ~15 ± 5% of the isomeric ketone **15**.

[6]Continued heating of the acidic reaction mixture for 22 h gave this ketone as the major product.

Can. J. Chem. Downloaded from www.nrcresearchpress.com by 190.90.36.8 on 09/07/12
For personal use only.

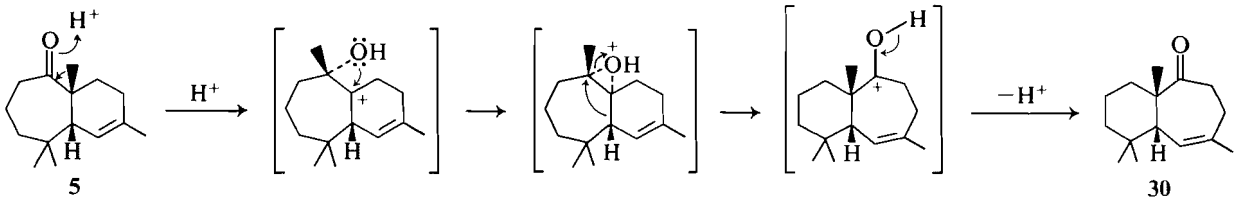

SCHEME 1

TABLE 2. ^{13}C magnetic resonance spectra (δ) of ketones **5** and **25**

Ketone	C-1	C-2	C-3	C-4	C-4a	C-5	C-6	C-7	C-8	C-9	C-9a	CH_3	CH_3	CH_3	CH_3
5	121.8	134.1	27.1[a]	23.4	49.7	218.0	40.5	[b,a]	46.2	39.6	50.2	33.4	26.0	24.5	23.4
25	18.1	132.1	119.7	29.5[a]	49.1	217.8	35.4	30.1[a]	38.2	37.5	45.0	29.6	26.6	26.1	23.1

[a]This signal cannot be assigned with certainty.
[b]This signal is probably obscured by the signal of the cyclohexane standard (δ 27.7).

TABLE 3. ^{1}H magnetic resonance spectra (δ) of several isohimachalane derivatives

Synthetic **5**	Isohimachalone (4)	*trans*-Ketone **4** (8)	Ketone **25**	Ketone **30**
5.44	5.50	5.53	5.30	5.17
2.56	2.60	2.55	2.84	
		2.00		
1.69	1.80	1.81	1.63	1.60
1.01	1.13	1.12	0.97	1.26
0.97	0.98	0.90 (0.94)[a]	0.95	0.94
0.69	0.75	0.74	0.69	0.75

[a]Although the text of the paper refers to the chemical shift of this signal as δ 0.90, the spectrum, which is illustrated in the paper, shows a shift at ~δ 0.94.

defined by the spectroscopic evidence, and with the *cis* stereochemistry of the ring junction fixed by the structure of the key intermediate, Diels–Alder adduct **14**, the assignment of structures **5** and **25** to their respective compounds was assured.

It is essential to note at this point that the spectral data (Table 3) of neither ketone **5** nor **25**, nor indeed of the tentatively identified ketone **30** were identical with those reproted by Dev (4) for naturally occurring isohimachalone. Examination of the data in Table 3 further indicated that a very close similarity existed between the ^{1}Hmr spectra of Dev's (4) isohimachalone and Teisseire's (8) *trans*-ketone **4**. This, together with the non-identity of our synthetic **5** with the naturally occurring compound, strongly suggested that the naturally occurring isohimachalone isolated by Dev (4) might be identical with the *trans*-ketone **4** isolated by Teisseire (8). Unfortunately, authentic samples of both naturally occurring ketones were no longer available[7,8] and so direct comparison of the compounds with each other and with **5** was not possible.

Experimental

General

Melting points were determined on a Kofler hot stage apparatus and are uncorrected. Elemental analyses were performed by the microanalytical laboratory of this department. The ir spectra were recorded on a Perkin–Elmer model 457 or Nicolet 7-199 FT-IR spectrophotometer and, except where otherwise stated, were obtained on solutions in chloroform. The ^{1}Hmr spectra were recorded on a Varian HA-100, HA-100/Digilab, or Bruker WH-200 spectrometer and, except where otherwise stated, were obtained on solutions in carbon tetrachloride with tetramethylsilane as internal reference. The ^{13}Cmr spectra were recorded on a Bruker WP-60/Nicolet BNC-12 system or a Bruker HFX-90/Nicolet 1085 system and were obtained on solutions in deuteriochloroform using tetramethylsilane as internal reference. Mass spectra (ms) were recorded using A.E.I. model MS9, MS12, or MS50 mass spectrometers. All gas chromatography (gc) was performed on a Hewlett–Packard 5750 research chromatograph using stainless steel columns (8 ft × ⅛ in.) packed with 10% diethylene glycol succinate on 80–100 mesh Chromosorb-W, acid washed, and treated with dimethylchlorosilane. Unless stated otherwise, anhydrous magnesium sulfate was used for drying organic solutions.

Materials

Benzene was distilled over lithium aluminum hydride. Pyridine was distilled over barium oxide and stored over potassium hydroxide pellets. Boron trifluoride etherate was distilled over calcium hydride according to the procedure of Zweifel and Brown (34, 35). Nitrogen was passed through a purification train of Fieser's solution (35), saturated aqueous lead acetate, concentrated sulfuric acid, and potassium hydroxide pellets. Starting ketone **14** was prepared according to the procedure previously reported by this group (1). All products and raw materials used are racemic where applicable.

8aβ-Carbomethoxy-1,1-ethylenedioxo-4,4,6-trimethyl-1,2,3,4,4aβ,-5,8,8a-octahydronaphthalene (17)

Ketone **14** (1.01 g, 4.02 mmol) was dissolved in dry benzene (50 mL), and ethylene glycol (2.78 g, 45 mmol) and *p*-toluenesulfonic acid monohydrate (10 mg, 0.053 mmol) were added. The reaction flask was fitted with a Dean–Stark water separator with type 3 Å molecular sieve in the take-off arm. The reaction mixture was heated at reflux for 47 h, then cooled to room temperature. Saturated aqueous sodium bicarbonate (2 mL) was added and the resulting mixture was extracted with methylene chloride. The extracts were washed with water, dried,

[7]P. Teisseire, personal communication.
[8]S. Dev, personal communication.

Can. J. Chem. Downloaded from www.nrcresearchpress.com by 190.90.36.8 on 09/07/12
For personal use only.

filtered, and concentrated. Column chromatography of the residue on silica gel, eluting with 7–30% ether in petroleum ether, gave ketal **17** (1.09 g, 93% yield); ir: 1728 (C=O), 1386, 1368 (CH_3), and 794 (C=CH) cm^{-1}; ^{1}Hmr δ: 5.20 (dm, 1H, J = 5 Hz, =CH—), 3.73 (m, 4H, —O—CH_2—CH_2—O—), 3.54 (s, 3H, —O—CH_3), 2.81 (dd, 1H, J = 17, J' = 5 Hz, C-8 H_β), 1.56 (s, 3H, =C—CH_3), 0.96 (s, 3H, —CH_3), and 0.80 (s, 3H, —CH_3); ^{13}Cmr δ: 174.1, 133.3, 118.7, 111.5, 64.7, 64.5, 53.6, 52.0, 41.2, 37.6, 33.2, 32.9, 29.3, 28.9, 28.6, 23.5, and 21.3; ms M^+: 294.1833 (calcd. for $C_{17}H_{26}O_4$: 294.1830). *Anal.* calcd. for $C_{17}H_{26}O_4$: C 69.36, H 8.90; found: C 69.13, H 9.01.

Deketalization of ketal 17

Ketal **17** (28 mg, 0.095 mmol) was dissolved in acetone (2 mL) and *p*-toluenesulfonic acid hydrate (2.0 mg, 0.011 mol) was added. After stirring for 14 days the mixture was diluted with water and extracted with methylene chloride. The extracts were washed with water, dried, filtered, and concentrated. Column chromatography of the residue on silica gel, eluting with 1% ether in petroleum ether, gave keto ester **14** (14 mg, 59% yield, 100% based on consumption of 54% of starting ketal **17**). Further elution with 1–5% ether in petroleum ether gave recovered ketal **17** (13 mg, 46% recovery).

*1,1-Ethylenedioxo-8aβ-hydroxymethyl-4,4,6-trimethyl-1,2,3,4,4aβ,-5,8,8a-octahydronaphthalene (**19**)*

Ketal **17** (954 mg, 3.24 mmol) was dissolved in anhydrous ether (50 mL) and lithium aluminum hydride (369 mg, 9.71 mmol) was added. After 4.5 h the mixture was cooled to 0°C and water (5 mL) was added dropwise. The resulting mixture was extracted with methylene chloride and the extracts were washed with water, dried, filtered, and concentrated. Column chromatography of the residue on silica gel, eluting with 10–15% ether in petroleum ether, gave recovered ketal **17** (75 mg, 9% recovery). Further elution with 15–50% ether in petroleum ether gave alcohol **19** (721 mg, 84% yield, 92% based on consumption of 91% of the starting material), which crystallized on standing. Three recrystallizations from petroleum ether gave white crystals of pure alcohol **19**, the melting point of which did not change on further recrystallization; mp 109–112°C; ir 3546 (—OH), 1390, 1380, 1366 (CH_3), and 790 (C=CH) cm^{-1}; ^{1}Hmr δ: 5.14 (br s, 1H, —CH=), 3.95 (s, 4H, —O—CH_2—CH_2—O—), 3.51 (dd, 1H, J = 11, J' = 2 Hz, HO—C*H*), 3.10 (dd, 1H, J = J' = 11 Hz, HO—C*H*), 2.42 (dd, 1H, J = 11, J' = 2 Hz, —OH), 1.62 (br s, 3H, =C—CH_3), 0.97 (s, 3H, —CH_3), and 0.83 (s, 3H, —CH_3); ^{13}Cmr δ: 133.0, 118.2, 115.2, 64.9, 64.3, 63.8, 43.0, 39.1, 38.1, 33.5, 32.9, 29.1, 27.9, 26.7, 32.5, and 22.1; ms M^+: 266.1886 (calcd. for $C_{16}H_{26}O_3$: 266.1882). *Anal.* calcd. for $C_{16}H_{26}O_3$: C 72.14, H 9.84; found: C 71.85, H 9.85. After exchanging the ^{1}Hmr sample with D_2O, the following changes were observed in the ^{1}Hmr spectrum: δ 3.51 (d, 1H, J = 11 Hz, DO—C*H*), 3.10 (d, 1H, J = 11 Hz, DO—C*H*), and the disappearance of the signal at δ 2.42.

*1,1-Ethylenedioxo-8aβ-(N,N,N′,N′-tetramethylphosphorodiamidyl-oxymethyl)-4,4,6-trimethyl-1,2,3,4,4aβ,5,8,8a-octahydronaphthalene (**22**)*

Alcohol **19** (515 mg, 1.94 mmol) was dissolved in a 20% solution of *N,N,N′,N′*-tetramethylethylenediamine (distilled over sodium) in 1,2-dimethoxyethane (freshly distilled over lithium aluminum hydride) (19.4 mL of solution) under an atmosphere of nitrogen. The resulting solution was cooled to 0°C and a 1.99 *N* solution of *n*-butyllithium in hexane (1.47 mL, 2.92 mmol) was added dropwise with stirring over 5 min. The mixture was allowed to warm to room temperature over 10 min, then *N,N*-dimethylphosphoramidic dichloride (26) was added. After 23 h the mixture was cooled to 0°C and dimethylamine gas was passed through a potassium hydroxide drying tube and condensed (60 drops, ~3 mL) into the reaction mixture. After 30 min the resulting mixture was poured into ice-cold water and extracted with ether. The extracts were washed with water until the washings were neutral to pH paper, dried, filtered, and concentrated. Column chromatography of the residue on silica gel, eluting with 5–20% methanol in ether, gave TMPDA derivative **22** (652 mg, 84% yield), which crystallized on standing. One recrystallization from ether gave colourless rhombic crystals of pure TMPDA derivative **22** (330 mg); mp 100–102°C; ir 1383, 1372, 1359 (CH_3), 1296 (P=O) cm^{-1}; ^{1}Hmr δ: 5.20 (br s, 1H, =CH—), 4.18–3.73 (complex, total 5H, —O—CH_2—CH_2—O— and *H*—CH—O—), 3.39 (dd, 1H, J = 11, J' = 4 Hz, *H*—CH—O—), 2.57, 2.55 (both d, total 12H, each J = 10 Hz, 2× —$N(CH_3)_2$), 1.64 (br s, 3H, =C—CH_3), 0.93 (s, 3H, —CH_3), and 0.81 (s, 3H, —CH_3); ms M^+: 400.2487 (calcd. for $C_{20}H_{37}N_2O_4P$: 400.2491). *Anal.* calcd. for $C_{20}H_{37}N_2O_4P$: C 59.98, H 9.31, N 6.99; found: C 59.89, H 9.48, N 6.77.

*1,1-Ethylenedioxo-4,4,6-8aβ-tetramethyl-1,2,3,4,4aβ,5,8,8a-octahydronaphthalene (**20**)*

Ethylamine (400 mL) was distilled from lithium into a reaction vessel under an atmosphere of argon. Small pieces of lithium ribbon (2.74 g, 392 g-atom) were added and the mixture was stirred for 1 h to effect solution. Then a solution of TMPDA derivative **22** (15.7 g, 39.2 mmol) and *tert*-butyl alcohol (5.80 g, 78.4 mmol, dried over type 3 Å molecular sieves) in tetrahydrofuran (270 mL, freshly distilled over lithium aluminum hydride) was added dropwise over 1 h with stirring. After an additional 40 min water was added slowly to discharge the blue colour and the reaction mixture was poured into ice-cold water. The resulting mixture was extracted with ether and the extracts were washed with ice-cold water until the washings were neutral. The extracts were then dried, filtered, and concentrated. Column chromatography of the residue on silica gel, eluting with 2% ether in petroleum ether, gave ketal **20** (6.75 g, 69% yield), which crystallized on standing. One recrystallization from petroleum ether gave colourless rhombs of pure ketal **20**; mp 28–30°C; ir: 1388, 1371, 1363 (CH_3) and 780 (C=CH) cm^{-1}; ^{1}Hmr δ: 5.22 (br s, 1H, =CH—), 3.86 (s, 4H, —O—CH_2—CH_2—O—), 1.62 (br s, 3H, =C—CH_3), 0.88 (s, 3H, —CH_3), 0.83 (s, 3H, —CH_3), and 0.76 (s, 3H, —CH_3); ms M^+: 250.1930 (calcd. for $C_{16}H_{26}O_2$: 250.1933). *Anal.* calcd. for $C_{16}H_{26}O_2$: C 76.75, H 10.47; found: C 76.82, H 10.56. Further elution with 2–5% ether in petroleum ether gave *trans*-ketone **23** (354 mg, 5% yield) and further elution with 5–100% ether in petroleum ether gave alcohol **19** (1.42 g, 14% yield).

*4,4,6,8aβ-Tetramethyl-3,4,4aβ,5,8,8a-hexahydro-1(2H)-naphthalenone (**15**)*

Ketal **20** (265 mg, 1.06 mmol) was dissolved in acetone (20 mL) and *p*-toluenesulfonic acid monohydrate (110 mg, 0.58 mmol) was added. The resulting mixture was stirred for 2.5 h and then diluted with methylene chloride. The resulting solution was washed with saturated aqueous sodium bicarbonate and water, dried, filtered, and concentrated. Column chromatography on silica gel, eluting with 2–8% ether in petroleum ether, gave pure ketone **15** (211 mg, 97% yield); ir: 1706 (C=O), 1390, 1375 (CH_3), 820 and 790 (C=CH) cm^{-1}; ^{1}Hmr δ: 5.27 (m, 1H, =CH—), 2.68 (ddd, 1H, J = 15, J' = 12, J'' = 8 Hz, —CO—CH_α), 2.08 (ddd, 1H, J = 15, J' = J'' = 4 Hz, —CO—CH_β), 1.65 (s, 3H, =C—CH_3), 1.02 (s, 3H, —CH_3), and 0.95 (s, 6H, 2× —CH_3); ^{13}Cmr δ: 216.2, 132.1, 117.7, 48.9, 46.4, 40.7, 34.9, 33.7, 32.2, 28.0, 23.6, 23.2, and 21.0; ms M^+: 206.1671 (calcd. for $C_{14}H_{22}O$: 206.1671). *Anal.* calcd. for $C_{14}H_{22}O$: C 81.50, H 10.75; found: C 81.77, H 10.74.

*4,4,6,8aβ-Tetramethyl-3,4,4aβ,7,8,8a-hexahydro-1(2H)-naphthalenone (**24**)*

Ketone **15** (758 mg, 3.68 mmol) was dissolved in benzene (50 mL) under an atmosphere of nitrogen, and *p*-toluenesulfonic acid hydrate (350 mg, 1.84 mmol) was added. The mixture was heated to reflux with

Can. J. Chem. Downloaded from www.nrcresearchpress.com by 190.90.36.8 on 09/07/12
For personal use only.

stirring for 2 h and then cooled to room temperature, diluted with water, and extracted with methylene chloride. The extracts were washed with saturated aqueous sodium bicarbonate and water, dried, filtered, and concentrated. Column chromatography of the residue on silica gel, eluting with 2–4% ether in petroleum ether, gave a mixture of ketones **24** and **15** (85:15 by gc analysis, 67.5 mg, 89% yield). The ^{1}Hmr and ^{13}Cmr spectra of this mixture showed the following signals, which were attributed to ketone **24**: ^{1}Hmr δ: 5.40 (m, 1H, =CH—), 1.71 (s, 3H, =C(CH$_3$)—), 1.04 (s, 3H, —CH$_3$), 0.97 (s, 3H, —CH$_3$), and 0.94 (s, 3H, —CH$_3$); ^{13}Cmr δ: 217.3, 133.7, 120.5, 52.3, 46.0, 38.5, 35.1, 34.0, 29.3, 26.2, 23.8, 23.1, and 22.8. The following spectra were also recorded: ir: 1703 (C=O), 1384, 1374, 1362 (CH$_3$) cm^{-1}; ms M$^+$: 206.1672 (calcd. for $C_{14}H_{22}O$: 206.1670). *Anal.* calcd. for $C_{14}H_{22}O$: C 81.50, H 10.75; found: C 81.48, H 10.95.

*6-Carboethoxy-2,4aβ,9,9-tetramethyl-3,4,4a,6,7,8,9,9aβ-octahydro(5*H*)-benzocyclohepten-5-one (28)*

Ketone **24**[9] (42 mg, 0.20 mmol) was dissolved in ether (4 mL) in a flask wrapped in aluminum foil to exclude light. Boron trifluoride etherate (145 mg, 1.02 mmol) was added, followed by ethyl diazoacetate (107 μL, 116 mg, 1.02 mmol). After stirring for 4 days, additional boron trifluoride etherate (145 mg, 1.02 mmol) and ethyl diazoacetate (116 mg, 1.02 mmol) were added. After further 3 days, saturated aqueous sodium bicarbonate (1 mL) was added and the resulting mixture was extracted with methylene chloride. The extracts were washed with water, dried, filtered, and concentrated. Column chromatography of the residue on silica gel, eluting with 2% ether in petroleum ether, gave ketone **24** (3 mg, 7% recovery). Continued elution gave keto ester **28** (12 mg, 20% yield, 21% based on recovered ketone **24**); ir: 1748 (ester C=O), 1706 (ketone C=O), 1389 and 1367 (CH$_3$) cm^{-1}; ^{1}H nmr δ: 5.32 (d, 1H, J = 5 Hz, =CH—), 4.09, 4.07 (both q, total 2H, both J = 7 Hz, —O—C*H*$_2$—CH$_3$), 3.92 (dd, 1H, J = 12, J' = 4 Hz, —CO—CH(—CO$_2$—)), 1.71 (br s, 3H, =C(CH$_3$)—), 1.21 (dd, 3H, $J = J'$ = 7 Hz, —O—CH$_2$—C*H*$_3$), 1.09 (s, 3H, —CH$_3$), 0.97 (s, 3H, —CH$_3$), and 0.67 (s, 3H, —CH$_3$); ms M$^+$: 292.2031 (calcd. for $C_{18}H_{28}O_3$: 292.2039). Continued elution gave keto ester **29** (11 mg, 19% yield, 20% based on recovered ketone **24**).

Lithium iodide dihydrate – collidine reagent

Finely divided anhydrous lithium iodide (514 mg, 3.84 mmol) was suspended in 2,4,6-collidine (3.05 mL) with vigorous stirring. Water (138 μL, 138 mg, 7.68 mmol) was added and the suspension rapidly dissolved. The resulting pale yellow solution had a calculated concentration of 1.28 *N* in lithium iodide dihydrate. The reagent was prepared fresh for each use.

*2,4aβ,9,9-Tetramethyl-3,4,4a,6,7,8,9,9aβ-octahydro-(5*H*)-benzocyclohepten-5-one (5) via keto ester 28*

Keto ester **28** (23 mg, 0.078 mmol) was dissolved in lithium iodide dihydrate – collidine reagent (244 μL, 0.312 mmol) and heated to reflux. After 45 min, the mixture was cooled to room temperature, poured into cold aqueous 5% hydrochloric acid, and extracted with ether. The extracts were washed with 5% hydrochloric acid and water, dried, filtered, and concentrated. Column chromatography of the residue on silica gel, eluting with 1% ether in petroleum ether, gave ketone **5** (1.4 mg, 10% yield based on recovered **28**). Further elution with 2–5% ether in petroleum ether gave keto ester **28** (5.4 mg, 23% recovery).

*6-Carboethoxy-2,4aβ,9,9-tetramethyl-1,4,4a,6,7,8,9,9aβ-octahydro-(5*H*)-benzocyclohepten-5-one (29)*

Ketone **15** (178 mg, 0.86 mmol) was dissolved in anhydrous ether (5 mL) in a flask wrapped in aluminum foil to exclude light. Boron trifluoride etherate (491 mg, 3.46 mmol) was added, followed by ethyl diazoacetate (394 mg, 3.46 mmol). After stirring for 48 h, the reaction mixture was cooled to 0°C and saturated aqueous sodium bicarbonate (2 mL) was added. The resulting mixture was extracted with methylene chloride and the extracts were washed with water, dried, filtered, and concentrated. Column chromatography of the residue on silica gel, eluting with 3–5% ether in petroleum ether, gave keto ester **29**[10] (205 mg, 82% yield), which crystallized on standing. One recrystallization from ether gave white crystals of pure keto ester **29**; mp 76–78°C; ir 1750 (ester C=O), 1700 (ketone C=O), 1392, 1364 (CH$_3$), 791 (C=CH) cm^{-1}; ^{1}Hmr δ: 5.34 (br s, 1H, =CH—), 4.11, 4.08 (both q, total 2H, both J = 7 Hz, —O—CH$_2$—), 3.86 (dd, 1H, $J = J'$ = 10 Hz, —CO—CH(—CO$_2$), 2.10 (br s, 4H, 2× =C—CH$_2$—), 1.66 (s, 3H, =C(CH$_3$)—), 1.22 (dd, 3H, $J = J'$ = 7 Hz, —O—CH$_2$—C*H*$_3$), 1.09 (s, 3H, —CH$_3$), 0.98 (s, 3H, —CH$_3$), and 0.71 (s, 3H, —CH$_3$); ^{1}Hmr ($CDCl_3$) δ: 5.35 (br s, 1H, =CH—), 4.20, 4.19 (both q, total 2H, both J = 7 Hz, —O—CH$_2$—), 4.14 (dd, 1H, $J = J'$ = 10 Hz, —CO—CH(—CO$_2$—)), 2.20 (br s, 4H, 2× =C—CH$_2$—), 1.68 (s, 3H, =C(CH$_3$)—), 1.24 (dd, 3H, J = 7 Hz, —O—CH$_2$—C*H*$_3$), 1.15 (s, 3H, —CH$_3$), 0.99 (s, 3H, —CH$_3$), and 0.72 (s, 3H, —CH$_3$); ^{13}Cmr δ: 212.1, 170.8, 132.0, 119.2, 61.0, 50.3, 49.5, 44.7, 37.3, 37.1, 29.6, 29.3 (two carbons), 26.0, 25.9, 23.1, 20.8, and 14.1; ms M$^+$: 292.2037 (calcd. for $C_{18}H_{28}O_3$: 292.2038). *Anal.* calcd. for $C_{18}H_{28}O_3$: C 73.93, H 9.65; found: C 73.75, H 9.61.

*2,4aβ,9,9-Tetramethyl-1,4,4a,6,7,8,9,9aβ-octahydro-(5*H*)-benzocyclohepten-5-one (25)*

Keto ester **29** (166 mg, 0.57 mmol) was dissolved in 2,4,6-collidine (1.8 mL) under an atmosphere of nitrogen. Lithium iodide (304 mg, 2.27 mmol) and water (82 μL, 4.54 mmol) were added and the mixture was heated to reflux with stirring for 2 h. The reaction mixture was then cooled to room temperature, poured into cold aqueous 5% hydrochloric acid, and extracted with ether. The extracts were washed with aqueous 5% hydrochloric acid and water, dried, filtered, and concentrated. Column chromatography of the residue on silica gel, eluting with 2–3% ether in petroleum ether, gave ketone **25** (108 mg, 86% yield), which crystallized on standing. One recrystallization from petroleum ether gave white clusters of pure ketone **25** (63 mg); mp 53–56°C; ir: 1701 (C=O), 1387, 1372, 1362 (CH$_3$), and 838 (C=CH) cm^{-1}; ^{1}Hmr δ: 5.30 (br s, 1H, =CH—), 2.84 (ddd, 1H, J = 11, J' = J'' = 9 Hz, —CO—CH*H*), 1.63 (br s, 3H, =C(CH$_3$)—), 0.97 (s, 3H, —CH$_3$), 0.95 (s, 3H, —CH$_3$), and 0.69 (s, 3H, —CH$_3$); ^{13}Cmr δ: 217.8, 132.1, 119.7, 49.1, 45.0, 38.2, 37.5, 35.04, 30.1, 29.6, 29.5, 26.6, 26.1, 23.1, and 18.1; ms M$^+$: 220.1829 (calcd. for $C_{15}H_{20}O$: 220.1827). *Anal.* calcd. for $C_{15}H_{20}O$: C 81.76, H 10.98; found: C 81.63, H 10.87.

*2,4aβ,9,9-Tetramethyl-3,4,4a,6,7,8,9,9aβ-octahydro-(5*H*)-benzocyclohepten-5-one (5) via ketone 25*

Ketone **25** (20 mg, 0.09 mmol) was dissolved in dry benzene (5 mL) under an atmosphere of nitrogen. *p*-Toluenesulfonic acid hydrate was added and the mixture was heated to reflux for 2 h. The reaction mixture was then cooled to room temperature, poured into water, and extracted with ether. The extracts were washed with water, dried, filtered, and concentrated. Column chromatography of the residue on silica gel, eluting with 0.5% ether in petroleum ether, gave a ketone (3 mg, 15% yield) to which structure **30** was tentatively assigned. The compound showed the following spectroscopic data: ir 1699 (C=O), 1384, 1377 and 1364 (CH$_3$) cm^{-1}; ^{1}Hmr δ: 5.17 (m, 1H, =CH—), 1.60 (s, 3H, =C(CH$_3$)—), 1.26 (s, 3H, —CH$_3$), 0.94 (s, 3H, —CH$_3$), and 0.75

[9]This material was contaminated with ~15% of the isomeric ketone **15**.

[10]This material required 24 h under vacuum (0.5 Torr) to remove an impurity which is thought to be ethyl glycolate on the basis of the ^{1}Hmr spectrum of the mixture.

Can. J. Chem. Downloaded from www.nrcresearchpress.com by 190.90.36.8 on 09/07/12
For personal use only.

(s, 3H, —CH_3); ms M^+: 220.1831 (calcd. for $C_{15}H_{24}O$: 220.1827). Continued elution gave ketone **5** (10.6 mg, 53% yield), which crystallized on standing; mp 48–54°C; ir 1699 (C=O), 1388, 1365 (CH_3), and 870 (C=CH) cm^{-1}; ^{1}Hmr δ: 5.34 (d, 1H, J = 4 Hz, =CH—), 2.66 (ddd, 1H, $J = J' = 10$, $J'' = 4$ Hz, —C*H*H), 1.69 (br s, 3H, =C—CH_3), 1.01 (s, 3H, —CH_3), 0.97 (s, 3H, —CH_3), and 0.69 (s, 3H, —CH_3); ^{13}Cmr δ: 218.0, 134.1, 121.8, 50.2, 49.7, 46.2, 40.5, 39.6, 33.4, 27.1, 25.7, 24.5, 23.4 (two carbons);[11] ms M^+: 220.1823 (calcd. for $C_{15}H_{24}O$: 220.1827). Further elution with 1% ether in petroleum ether gave recovered ketone **25** (1 mg, 5% recovery).

Acknowledgements

We are grateful to the Natural Sciences and Engineering Research Council of Canada and the University of Alberta for financial support and to Dr. S. Dev for informing us the revised structure of himachalol.

1. H. J. Liu and E. N. C. Browne. Can. J. Chem. **59**, 601 (1981).
2. T. C. Joseph and S. Dev. Tetrahedron Lett. 216 (1961).
3. J. B. Bredenberg and H. Erdtman. Acta Chem. Scand. **15**, 685 (1961).
4. R. Shankaranarayan, S. Krishnappa, and S. Dev. Tetrahedron, **33**, 885 (1977).
5. S. C. Bisarya and S. Dev. Tetrahedron Lett. 3761 (1964).
6. S. C. Bisarya and S. Dev. Tetrahedron, **24**, 3869 (1968).
7. M. Plattier and P. Teisseire. Recherches, **19**, 131 (1974).
8. P. Teisseire and M. Plattier. Recherches, **19**, 167 (1974).
9. A. P. S. Narula and S. Dev. Tetrahedron, **33**, 813 (1977).
10. D. R. Adams, S. P. Bhatnagar, and R. C. Cookson. J. Chem. Soc. Perkin Trans. 1, 1502 (1975).

[11]The fifteenth signal, which was expected to appear at ~δ 27 to δ 28, was probably obscured by the signal at δ 27.7 due to cyclohexane, which was used as an internal reference in this case.

11. M. Plattier and P. Teisseire. An. Acad. Bras. Cienc. **44**, 392 (1972).
12. A. G. Bajaj, S. Dev, B. Tagle, J. Tesler, and J. Clardy. Tetrahedron Lett. 325 (1980).
13. S. Dev. Pure Appl. Chem. **51**, 837 (1979).
14. P. Bhan, S. Dev, L. S. Bass, B. Tagle, and J. Clardy. J. Chem. Res. (S), 344 (1982).
15. P. Bhan, S. Dev, L. S. Bass, B. Tagle, and J. Clardy. J. Chem. Res. (M), 3473 (1982).
16. S. C. Bisarya and S. Dev. Tetrahedron, **24**, 3861 (1968).
17. V. S. Joshi, N. P. Damodaran, and S. Dev. Tetrahedron, **27**, 459 (1971).
18. E. N. Browne. Ph.D. Thesis, The University of Alberta, Edmonton, Alberta. 1980.
19. R. C. Pandey and S. Dev. Tetrahedron, **24**, 3829 (1968).
20. B. D. Challand, G. Kornis, G. L. Lange, and P. de Mayo. J. Chem. Soc. Chem. Commun. 704 (1967).
21. B. D. Challand, H. Hikino, G. Kornis, G. Lange, and P. de Mayo. J. Org. Chem. **34**, 794 (1969).
22. E. Wenkert and K. Naemura. Synth. Commun. **3**, 45 (1973).
23. W. Oppoltzer and R. L. Snowden. Helv. Chim. Acta, **64**, 2592 (1981).
24. E. Piers and E. H. Ruediger. J. Chem. Soc. Chem. Commun. 166 (1979).
25. R. E. Ireland, D. C. Muchmore, and U. Hengartner. J. Am. Chem. Soc. **94**, 5098 (1972).
26. H. J. Liu, S. P. Lee, and W. H. Chan. Can. J. Chem. **55**, 3797 (1977).
27. E. N. Walsh and A. D. F. Toy. Inorg. Synth. **7**, 69 (1963).
28. T. C. Joseph and S. Dev. Tetrahedron, **24**, 3853 (1968).
29. J. B. Stothers. Carbon-13 NMR spectroscopy. Academic Press, New York. 1972.
30. W. T. Tai and E. W. Warnhoff. Can. J. Chem. **42**, 1333 (1964).
31. H. J. Liu and T. Ogino. Tetrahedron Lett. 4937 (1973).
32. H. J. Liu and S. P. Majumdar. Synth. Commun. **5**, 125 (1975).
33. F. Elzinger. Org. Synth. **45**, 7 (1965).
34. G. Zweifel and H. C. Brown. Org. React. **13**, 28 (1963).
35. L. F. Fieser and M. Fieser. Reagents for organic synthesis. Vol. 1. Wiley, New York. 1967.

Can. J. Chem. Downloaded from www.nrcresearchpress.com by 190.90.36.8 on 09/07/12
For personal use only.

A simple and efficient synthesis of 5′-($^2H_3$)olivetol

MICHEL GIRARD,[1a,2] DAVID B. MOIR,[1b] AND JOHN W. APSIMON[2]

Ottawa–Carleton Chemistry Institute, Department of Chemistry, Carleton University, Ottawa, Ont., Canada K1S 5B6

Received May 28, 1986

This paper is dedicated to Dr. O. E. (Ted) Edwards

MICHEL GIRARD, DAVID B. MOIR, and JOHN W. APSIMON. Can. J. Chem. **65**, 189 (1987).

The title compound **1** was prepared in 13% overall yield starting from the commercially available and inexpensive 3,5-dimethoxybenzoic acid (**4**). The *n*-pentyl side chain was elaborated from cross-coupling reactions between halides.

MICHEL GIRARD, DAVID B. MOIR et JOHN W. APSIMON. Can. J. Chem. **65**, 189 (1987).

On rapporte la synthèse du composé **1** à partir de l'acide diméthoxy-3,5-benzoïque (**4**) commercial. L'élaboration de la chaîne *n*-pentyle se fait par deux réactions de couplages croisés d'halogénures.

Can. J. Chem. Downloaded from www.nrcresearchpress.com by 190.90.36.8 on 09/07/12
For personal use only.

In the course of studies directed towards the synthesis of isotopically substituted cannabinoid standards (for a recent review on cannabinoid synthesis, see ref. 1) we required the preparation of 5′-($^2H_3$)olivetol (**1**). The unlabelled parent compound olivetol (**2**) is generally best prepared by the method of Focella *et al.* (2) (Scheme 1). We reasoned, however, that the applicability of this method for the preparation of **1** suffers from two serious disadvantages: first, the lack of an easy access to the suitably labelled starting material (i.e., hexanal), and secondly, the high cost associated with the introduction of the label in the early stages of the synthetic scheme. Similarly, the only previous synthesis of **1**, reported by Pitt *et al.* (3), uses the relatively expensive 3,5-dimethoxybenzaldehyde (**3**) as starting

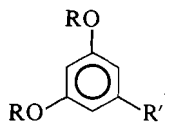

1 R = H, R′ = $(CH_2)_4C^2H_3$
2 R = H, R′ = $(CH_2)_4CH_3$
3 R = CH_3, R′ = CHO

compound. We have therefore devised an efficient synthesis of **1** that makes use of relatively inexpensive starting material and labelling agent and that allows for the introduction of the label in the penultimate step of the synthetic scheme.

We wish to report here the preparation of **1** by a stepwise elaboration of the labelled *n*-pentyl side chain starting from the commercially available 3,5-dimethoxybenzoic acid (**4**) (Scheme 2). Our approach relies on the use of two cross-coupling reactions between alkyl halides and Grignard reagents (for an overview, see ref. 4) to provide the side chain.

The starting acid **4** was first converted to bromide **5** by successive hydride reduction and nucleophilic displacement using phosphorus tribromide. A first cross-coupling reaction was then used to achieve a three-carbon unit chain extension by reacting bromide **5** with allyl magnesium bromide. The best yields of olefin **6** were obtained by using a 1:2 molar ratio of **4** to Grignard reagent. Hydroboration–oxidation at the terminal carbon of olefin **6**, followed by nucleophilic displacement according to the recently reported method of Olah *et al.* (5),

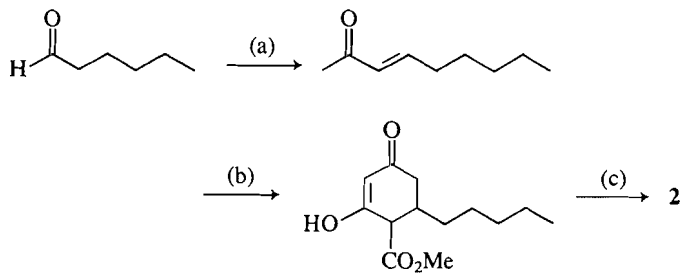

(a) NaOH, acetone; (b) NaOMe, $CH_2(CO_2Me)_2$; (c) Br_2, DMF

SCHEME 1

afforded bromide **7** in good yield. The label was then introduced by means of a second cross-coupling reaction between bromide **7** and deuterated methyl magnesium iodide in the presence of dilithium tetrachlorocuprate as catalyst (6). The labelled dimethoxyolivetol **8** thus obtained was demethylated using trimethylsilyliodide (7) to afford the title compound **1** in 13% overall yield.

Experimental

The ^1H and ^{13}C nmr spectra were recorded on a Varian XL-200 spectrometer. Deuterated chloroform ($CDCl_3$) was used as the standard solvent and tetramethylsilane (TMS) as an internal reference. All chemical shifts are expressed in ppm downfield from TMS. Infrared spectra were measured on a Perkin–Elmer 237-B grating infrared spectrophotometer. Mass spectra were obtained on a VG-7070E instrument.

All reactions were routinely monitored by analytical thin-layer chromatography (tlc) on precoated silica gel plates (Merck-60 PF-254). Silica gel (Davison Chemical Co., grade 923, 100–200 mesh) was used for column chromatography. High-performance liquid chromatography (hplc) was performed using a Waters Prep-500 high performance liquid chromatograph.

Dry solvents were obtained by distillation over lithium aluminum hydride (DME and THF) or sodium (ether and benzene).

3,5-Dimethoxybenzyl bromide (5)

To a suspension of lithium aluminum hydride (3.8 g, 0.10 mol) in 100 mL of anhydrous ether was added acid **3** (18.2 g, 0.10 mol) dissolved in 60 mL of ether at such a rate that a gentle reflux was maintained. The reaction was stirred for 16 h at room temperature, then worked up by the slow addition of 5 mL of water, 5 mL of 15% aqueous NaOH, and a further 15 mL of water. The suspension was filtered through a pad of Celite, which was washed with ether. The combined ether washings were concentrated under reduced pressure and the residual oil was immediately dissolved in 50 mL of anhydrous dichloromethane. After cooling the mixture to 0°C, phosphorus tribromide (27.1 g, 0.10 mol) was added dropwise and the reaction was allowed to warm to room temperature, then stirred for 1 h. The mixture

[1]Current address: (*a*) Drug Identification Division, Bureau of Drug Research, Health Protection Branch, Health and Welfare Canada, Tunney's Pasture, Ottawa, Ont., Canada K1A 0L2. (*b*) Division of Biological Sciencies, National Research Council of Canada, Ottawa, Ont., Canada K1A 0R6.

[2]Authors to whom correspondence may be addressed.

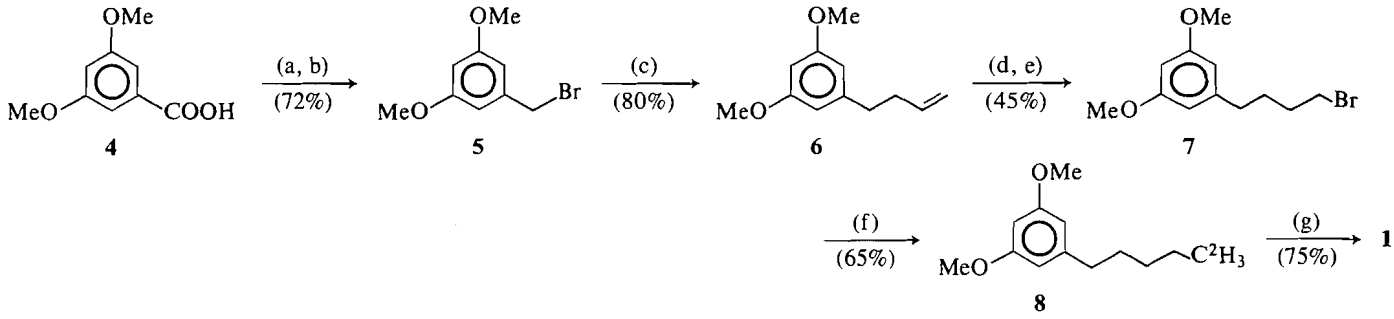

(a) LAH, ether; (b) PBr_3, CH_2Cl_2; (c) $H_2C{=}CHCH_2MgBr$, ether; (d) $BH_3{\cdot}Me_2S$, then $H_2O_2/NaOH$; (e) TMSCl, LiBr, MeCN; (f) $^2H_3CMgI$, Li_2CuCl_4, THF; (g) TMSI, $CHCl_3$

SCHEME 2

was poured into ice-water and the organic layer was collected. The aqueous phase was extracted with dichloromethane (75 mL) and the combined organic phases were washed with water (100 mL), saturated $NaHCO_3$ (100 mL), and saturated NaCl (100 mL), then dried over magnesium sulfate. Concentration gave 22 g (78%) of bromide **5** as a colorless solid; ^1H nmr: 3.8 (6H, s, OMe), 4.3 (2H, s, benzylic), 6.2–6.6 (3H, m, aromatic).

4-(3,5-Dimethoxyphenyl)-1-butene (6)

To a cooled solution of allyl magnesium bromide (286 mL of 1 *M* ether solution, 0.286 mol) was added dropwise bromide **5** (33.0 g, 0.14 mol) in ether (200 mL). The reaction was allowed to warm to room temperature and then stirred for 30 h. The reaction mixture was quenched by addition of a saturated ammonium chloride solution, followed by water (250 mL). The organic layer was separated and the aqueous layer was extracted with ether (200 mL). The resulting emulsion was passed through glass wool and the organic layers were combined and dried over magnesium sulfate. Solvent evaporation and purification by hplc (10% ethyl acetate in hexane) afforded olefin **6** (22.0 g, 80%); ir (neat): 1640 (C=C); 920 (C=CH_2) cm^{-1}; ^1H nmr: 2.2–2.8 (4H, m, CH_2's), 3.75 (6H, s, OMe), 4.8–5.3 and 5.5–6.1 (3H, m, CH=CH_2), 6.35 (3H, s, aromatics); ms *m/e* (relative intensity): 192 (M^+, 62), 177 (15), 151 (100). High resolution ms: M^+ calcd. for $C_{12}H_{16}O_2$: 192.1150; found: 192.1157.

4-(3,5-Dimethoxyphenyl)-1-bromobutane (7)

Olefin **6** (20.0 g, 0.104 mol) was dissolved in dichloromethane (35 mL) and cooled to 0°C. Borane–dimethyl sulfide complex (3.8 mL of 10.2 *M* BH_3, 38 mmol) was then added dropwise. The temperature was maintained at 0°C for 25 min, then allowed to rise to room temperature. The reaction was stirred for 3 h, then concentrated under reduced pressure. Dichloromethane (35 mL) and ethanol (35 mL) were added, followed by 12.8 mL of 3 *N* NaOH (38.5 mmol). The mixture was cooled to 0°C and an equivalent volume of 30% aqueous hydrogen peroxide was added. The reaction was refluxed for 1 h, cooled, and poured into 500 mL of ice-water. The mixture was extracted with ether (3 × 100 mL) and the combined organics were washed with water (200 mL) and brine (200 mL) and dried over magnesium sulfate. Concentration and purification by hplc afforded 14.2 g (65%) of 4-(3,5-dimethoxyphenyl)-1-butanol as an oil; ^1H nmr: 1.3–2.0 (4H, br m, CH_2's), 2.55 (2H, t, benzylic), 3.75 (6H, s, OMe), 3.5–3.7 (2H, m, CH_2OH), 6.3 (3H, br s, aromatics).

Lithium bromide (8.30 g, 0.095 mol) was suspended in 250 mL of acetonitrile. Trimethylsilyl chloride (12.93 g, 0.119 mol) was added, followed by the addition of a solution of the previously prepared alcohol (10.00 g, 0.048 mol) in acetonitrile (120 mL). The reaction was refluxed for 12 h. The solution was then poured into ice-water and extracted with ether (3 × 200 mL). The combined organic phases were washed with saturated sodium bicarbonate solution, then with brine, and dried over anhydrous magnesium sulfate. Purification by flash chromatography afforded 8.5 g of pure title compound (70% yield); ^1H nmr: 1.7–2.0 (4H, br m, CH_2's), 2.6 (2H, t, benzylics), 3.55 (2H, t, CH_2Br), 3.80 (6H, s, OMe), 6.4 (3H, br s, aromatics).

5'-($^2H_3$)-Olivetol dimethyl ether (8)

Bromide **7** (11.00 g, 0.040 mol) was dissolved in dry THF (30 mL) and cooled to 0°C. The Grignard reagent, prepared by the addition of ($^2H_3$)-iodomethane (7.60 g, 0.052 mol, MSD Isotopes >99.5%) in dry ether (15 mL) to magnesium (1.37 g, 0.056 mol) in ether (10 mL), was then added dropwise to the bromide **7** solution via stainless steel cannula. Li_2CuCl_4 (2.02 mL of a 0.1 *M* solution in THF, 0.2 mmol) (6) was added with a syringe. The reaction was allowed to warm to room temperature and stirred for 16 h. Sulfuric acid (1.8 *M*) was added slowly until all the precipitate had dissolved. The mixture was extracted with ether (3 × 150 mL). The combined organic layers were washed with saturated sodium bicarbonate solution, then with brine, and dried over $MgSO_4$. Concentration and purification by hplc (5% ethyl acetate in hexane) provided 6.55 g (60%) of the title compound as a viscous oil; bp 79–82°C (0.05 Torr; 1 Torr = 133.3 Pa); ^1H nmr: 2.3–2.6 (2H, t, benzylics), 3.8 (6H, s, OMe), 6.3 (3H, s, arom.); ^{13}C nmr: 14–15 ppm (septuplet, C^2H_3), 22.3, 31.05, 31.5, 36.3, 55.2 (OMe), 97.5, 106.5, 145.4, 160.7; ms *m/e* (relative intensity): 211 (M^+, 30), 192 (2.5), 169 (12), 165 (10), 152 (100). High resolution ms: M^+ calcd. for $C_{13}H_{17}{}^2H_3O_2$: 211.1665; found: 211.1671. The percentage of incorporation was determined by mass spectrometry and was found to be: $^2H_3$ = 98.7%; $^2H_2$ = 0.1%; $^2H_1$ = 0.1%; $^2H_0$ = 1.1%.

5'-($^2H_3$)-Olivetol (1)

The labelled dimethyl ether **8** (6.55 g, 0.031 mol) was dissolved in chloroform (30 mL) and treated with trimethylsilyl iodide (18.60 g, 0.093 mol). The mixture was heated to 40°C until no more starting material was detected by tlc (48 h). The reaction was cooled, poured into 150 mL of methanol, and evaporated *in vacuo*. Ether (100 mL) was added and the solution was washed with aqueous sodium bisulfite (100 mL), sodium bicarbonate, brine, and dried over magnesium sulfate. Concentration under reduced pressure and purification afforded the title compound (4.25 g, 75%); mp 38–39°C; ir ($CDCl_3$): 3400 (OH) cm^{-1}; ^1H nmr: 2.55 (2H, t, benzylics), 6.4 (3H, br s, arom.).

Acknowledgements

This work was supported in part by operating grants from the Natural Sciences and Engineering Research Council of Canada. We thank Carleton University for scholarships to M.G. and D.B.M.

1. R. K. RAZDAN. *In* The total synthesis of natural products. Vol. 4. *Edited by* J. W. ApSimon. John Wiley, New York. 1981. pp. 185–262.
2. A. FOCELLA, S. TEITEL, and A. BROSSI. J. Org. Chem. **42**, 3456 (1977).
3. C. G. PITT, D. T. HOBBS, H. SCHRAN, C. E. TWINE, JR., and D. L. WILLIAMS. J. Labelled Compd. **9**, 551 (1975).
4. M. S. KHARASCH and O. REINMUTH. Grignard reactions of non-metallic substances. Prentice–Hall, New York. 1954.
5. G. A. OLAH, B. G. BALARAM GUPTA, R. MALHOTRA, and S. R. NARANG. J. Org. Chem. **45**, 1638 (1980).
6. M. TAMURA and J. KOCHI. Synthesis, 303 (1971).
7. M. JUNG and M. A. LYSTER. J. Org. Chem. **42**, 3761 (1977).

Can. J. Chem. Downloaded from www.nrcresearchpress.com by 190.90.36.8 on 09/07/12
For personal use only.

γ-Lactam formation by a novel intramolecular rearrangement involving β-cyanoketones. Crystal structure of 1,7-dioxo-10a-methyl-perhydrophenanthrene-4a,8a-carbolactam[1,2]

MICHEL GIRARD[3] AND JOHN W. APSIMON

Ottawa–Carleton Chemistry Institute, Department of Chemistry, Carleton University, Ottawa, Ont., Canada K1S 5B6

AND

CAROL P. HUBER

Division of Biological Sciences, National Research Council of Canada, Ottawa, Ont., Canada K1A 0R6

Received June 10, 1986

This paper is dedicated to Dr. O. E. (Ted) Edwards

MICHEL GIRARD, JOHN W. APSIMON, and CAROL P. HUBER. Can. J. Chem. **65**, 191 (1987).

Treatment of cyano-triketone **1** with bases such as ethoxide or methoxide ions affords the tetracyclic lactam **4** in high yield. Its formation can be rationalized by invoking a novel intramolecular rearrangement. Crystals of **4** are orthorhombic, $a = 10.351(3)$, $b = 11.503(2)$, $c = 11.935$ (2) Å, $Z = 4$, space group $P2_12_12_1$, $R = 0.043$ for 2037 observations. The structure analysis establishes the formation of a γ-lactam, with the lactam ring bridging a six-membered ring. The three six-membered rings are in chair conformations with some distortions, and the lactam ring is envelope shaped.

MICHEL GIRARD, JOHN W. APSIMON et CAROL P. HUBER. Can. J. Chem. **65**, 191 (1987).

La cyano-tricétone **1** conduit à la lactame tétracyclique **4** en présence d'un excès de bases comme l'éthylate ou le méthylate de sodium. On peut expliquer cette transformation par une transposition intramoléculaire inédite. Le composé **4** cristallise dans le système orthorhombique avec des dimensions de maille $a = 10{,}351(3)$, $b = 11{,}503(2)$, $c = 11{,}935(2)$ Å, $Z = 4$, et le groupe spatial $P2_12_12_1$. La valeur de R est 0,043 pour 2037 réflexions. L'analyse par diffraction de rayons-X confirme la présence d'une γ-lactame pontée. Chacun des trois cycles à six membres existe dans la conformation «chaise» avec une distortion variable et le cycle γ-lactame possède la forme d'une enveloppe.

Can. J. Chem. Downloaded from www.nrcresearchpress.com by 190.90.36.8 on 09/07/12
For personal use only.

Since the pioneering work of Ireland *et al.* (1), the use of nitrile groups as precursors of angular methyl substituents has become common practice in the field of pentacyclic triterpene synthesis (for a recent review, see ref. 2). Our interest in that field led us to prepare the bicyclic cyano-triketone **1** as a key intermediate in a new approach to the naturally occurring friedelin **2**.[4] After several unsuccessful attempts at modifying (i.e., reducing, hydrolysing, ...) the nitrile functionality in suitably protected derivatives of **1**, we attempted a base-catalyzed aldol condensation on **1** to obtain the tricyclic enone **3**

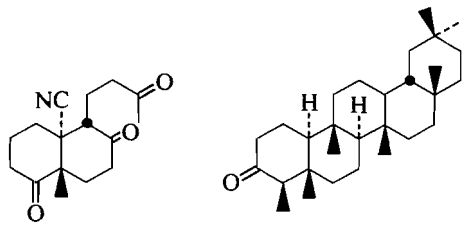

1

2

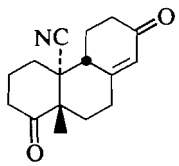

3

with the hope that the latter would prove a better substrate for reduction of the nitrile. Treatment of triketone **1** with an excess of sodium ethoxide in anhydrous ethanol afforded a single crystalline compound, which was tentatively identified as lactam **4** on the basis of spectroscopic properties, the most significant being the absence of the characteristic nitrile absorption band around 2200 cm^{-1} in the ir spectrum of the product. The presence of the lactam was revealed in the ^{13}C nmr spectrum by a resonance at 177.9 ppm. The structure was established by a single-crystal X-ray diffraction experiment.

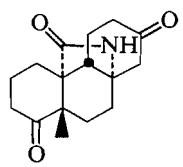

4

X-ray structural studies

Figure 1 shows a view of the molecule with the numbering scheme. Final atomic coordinates are listed in Table 1, and bond lengths and angles are given in Fig. 2.

Compounds having a γ-lactam ring bridging a six-membered ring[5] have seldom been subjected to X-ray structure analysis. A search of the Cambridge Structural Database (3) (January 1986 release with 50 499 entries) found only three other compounds with such a feature (4–6), one of which (6) is *N*-substituted and therefore excluded from further discussion. The bond lengths and angles for the lactam moiety of the title compound agree well with the corresponding values in the two unsubstituted structures.

Nørskov-Lauritsen *et al.* (7) have compiled average bond lengths and angles for various lactams and lactones. Agreement of the pertinent values in the present structure with corresponding average values that they give for 41 γ-lactams is within 2.5 σ, but the e.s.d.'s associated with the averages are relatively large. The largest difference, perhaps due to the bridging

[1]Taken in part from the Ph.D. dissertation of M. Girard, Carleton University, 1985.

[2]NRCC No. 26490.

[3]Present address: Drug Identification Division, Bureau of Drug Research, Health Protection Branch, Sir Frederick G. Banting Research Centre, Health and Welfare Canada, Tunney's Pasture, Ottawa, Ont., Canada K1A 0L2.

[4]This approach will be the subject of a future paper.

[5]The lactam ring in this compound, as can be seen, also shares the B/C ring junction.

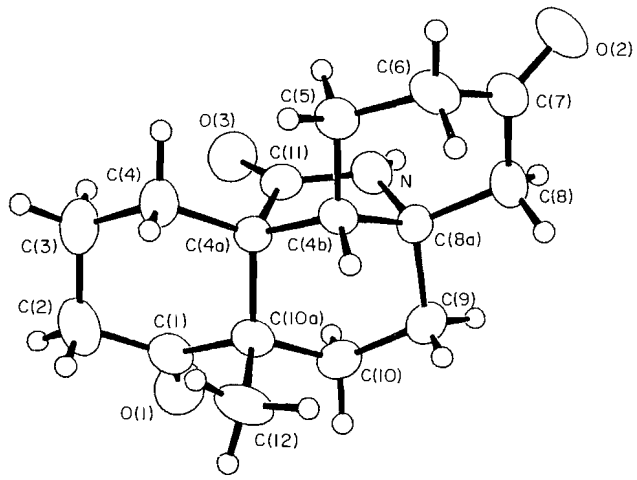

FIG. 1. A perspective view of the molecule prepared with ORTEP-II (14) showing the numbering scheme. Anisotropic ellipsoids enclose 50% probability and H atoms are shown as spheres of 0.1 Å radius.

TABLE 1. Final fractional coordinates ($\times 10^4$) and equivalent isotropic temperature factors, B_{eq} (Å^2), for the non-H atoms; $B_{eq} = \frac{8}{3}\pi^2\Sigma_i\Sigma_j U_{ij} a_i^* a_j^* \mathbf{a}_i \cdot \mathbf{a}_j$

Atom	x	y	z	B_{eq}
O(1)	4742(2)	−3018(2)	1216(2)	4.8
O(2)	10797(2)	1717(2)	665(2)	4.9
O(3)	6208(2)	−1018(2)	−753(1)	4.3
N	8048(2)	−685(2)	251(1)	3.1
C(1)	4689(2)	−1990(2)	1413(2)	3.4
C(2)	3496(2)	−1288(3)	1220(3)	4.6
C(3)	3785(2)	−221(3)	503(2)	4.6
C(4)	4919(2)	479(2)	966(2)	3.5
C(4a)	6133(2)	−242(2)	1177(1)	2.4
C(4b)	7277(2)	419(2)	1699(1)	2.5
C(5)	7479(2)	1627(2)	1191(2)	3.1
C(6)	8784(2)	2136(2)	1535(2)	3.7
C(7)	9867(2)	1368(2)	1167(2)	3.4
C(8)	9740(2)	119(2)	1519(2)	3.8
C(8a)	8389(2)	−408(2)	1414(2)	2.8
C(9)	8297(2)	−1511(2)	2131(2)	3.8
C(10)	7030(2)	−2158(2)	1931(2)	3.6
C(10a)	5847(2)	−1355(2)	1912(2)	2.8
C(11)	6761(2)	−692(2)	90(2)	2.8
C(12)	5470(3)	−1021(2)	3119(2)	4.3

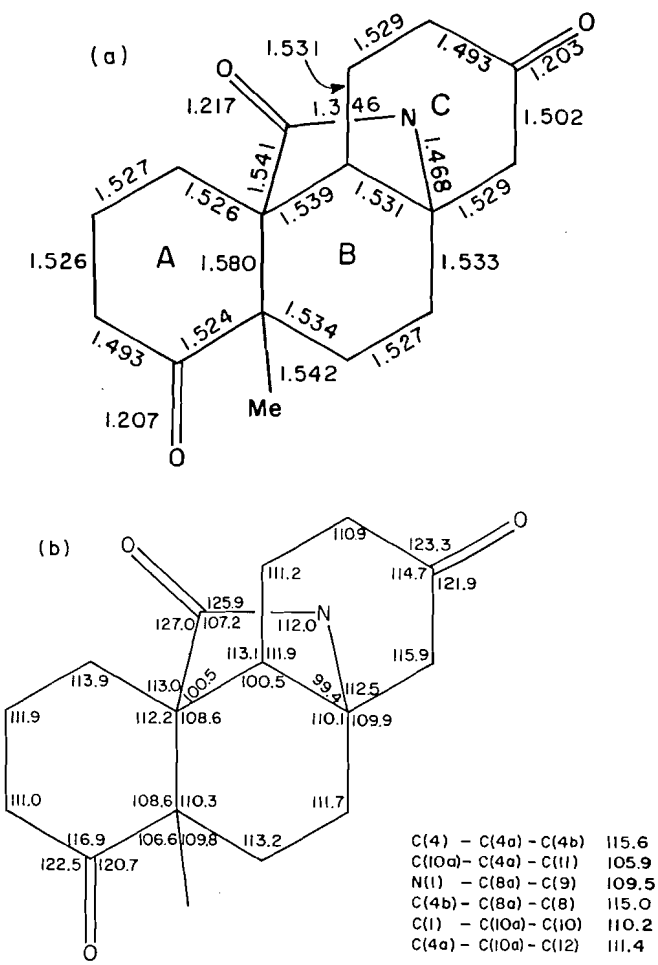

FIG. 2. (*a*) Bond lengths (Å) and (*b*) bond angles (°). Estimated standard deviations are 0.003–0.004 Å and 0.14–0.23°.

geometry, is in the C—N—C angles; the average value is 114.9(13)°, while the present value is 112.0(2)°. Corresponding values from refs. 4 and 5 are 111.8° and 112.4°, respectively.

In the present structure there is a small but significant (~3.9σ) difference between the C(4a)—C(11)—O(3) (127.0(2)°) and N—C(11)—O(3) (125.9(2)°) angles, whereas the average C—C=O and N—C=O angles are essentially equal (within the e.s.d.'s) for the 41 γ-lactams (7). It is not clear to us whether the slight enlargement of the C(4a)—C(11)—O(3) angle here, relative to N—C(11)—O(3), serves primarily to relieve intramolecular repulsion between O(3) and H(31), which are separated by only 2.44(3) Å, or whether a small anomeric effect is involved, or both. The latter effect should be smaller for lactams than for lactones (7).

Conformation

Ring A is in a relatively undistorted, although slightly flattened, chair conformation. Displacements of the ring carbon atoms from the mean plane vary in magnitude between 0.209(3) and 0.222(2) Å. The conformation of ring B is essentially a chair, with some distortion toward envelope form; C(4b) deviates most (0.377(2) Å) from the mean plane. This distortion is very probably due to the bridging lactam ring. Ring C is also in a distorted chair conformation, the distortion in this case being toward a half-chair form. The smallest torsional angle, C(4b)—C(8a)—C(8)—C(7), is −37.1(3)°, and the two largest displacements, for C(5) and C(6), are −0.274(2) and 0.259(3) Å. The lactam ring is close to envelope conformation with apex at C(4b); puckering parameters (8) for all four rings are given in Table 2. The amide group is significantly nonplanar; the C(8a)—N—C(11)—C(4a) torsional angle is 7.3(2)° and displacements from the mean plane through these four atoms plus O(3) vary from 0.018(2) (C(11)) up to 0.069(2) Å (N).

The molecules are linked into chains parallel to the *a* axis by intermolecular hydrogen bonds between the N—H and C=O(1) groups; the N···O distance is 2.892(3) Å, the N—H···O and H···O=C angles are 177(3) and 127.0(7)° respectively, and the H(1)···O(1) distance is 2.12(3) Å. The packing arrangement is shown in Fig. 3.

Formation of lactam **4** can be rationalized as shown in Scheme 1. Presumably the cyclic six-membered transition state of the intramolecular aldol condensation adopts the more stable chair conformation **5**, which leads to β-face attack by the side-chain enolate onto the ring ketone. The alkoxide thus generated can attack the nitrile group to give an intermediate cyclic imino-ether **6**. Such an intramolecular base-catalyzed

Can. J. Chem. Downloaded from www.nrcresearchpress.com by 190.90.36.8 on 09/07/12
For personal use only.

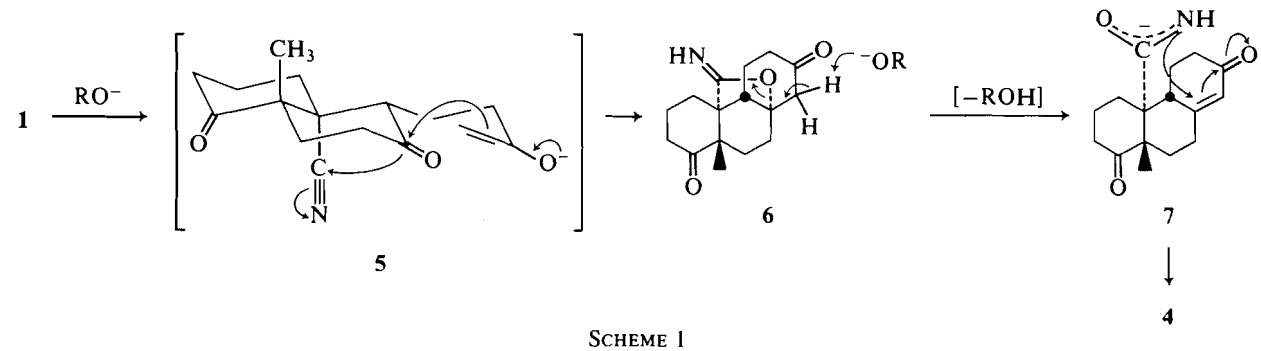

SCHEME 1

TABLE 2. Ring puckering parameters

Ring	q_2 (Å)	ϕ_2 (°)	q_3 (Å)
A	0.002	189.9	0.525
B	0.212	244.7	0.619
C	0.143	−40.4	−0.480
Lactam	0.445	173.0	—

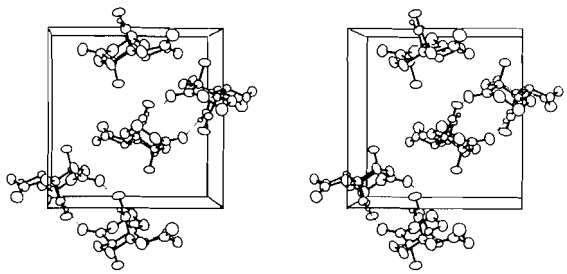

FIG. 3. Stereoscopic view of the packing arrangement, drawn with ORTEP-II (14). The axial directions are $b\rightarrow$, $c\uparrow$, a up out of the plane of the paper. Hydrogen bonds are indicated by single lines.

Pinner synthesis has recently been described (9). Finally, deprotonation at C(8) in **6** followed by ring opening of the imino-ether leads to enone-amide anion **7**, which then closes back via an intramolecular Michael-type addition to afford lactam **4**.

Lactam **4** is also obtained, although in slightly lower yield, when sodium methoxide is used as a base. We are now investigating the generality of the reaction as a tool for the formation of lactams.

Experimental

1,7-Dioxo-10a-methyl-perhydrophenanthrene-4a,8a-carbolactam (4)

To a solution of triketone **1** (0.23 mmol, 63 mg) in anhydrous ethanol (10 mL) was added a sodium ethoxide solution (7 mL of 0.44 *M*, 3 mmol) in anhydrous ethanol. The reaction mixture was stirred at room temperature for 20 h after which time no starting material could be detected by thin-layer chromatography. After evaporation of ethanol under reduced pressure, water was added and the mixture was extracted several times with chloroform. The combined organic phases were washed with dilute HCl solution, saturated $NaHCO_3$ solution, brine, and dried over anhydrous magnesium sulfate. Evaporation under reduced pressure afforded 57 mg (91%) of the title compound **4**, which crystallized in $CHCl_3$–MeOH mixtures; mp ($CHCl_3$–MeOH) 245–250°C (dec.); ir ($CDCl_3$) ν_{max}: 3210 (NH), 1700 and 1680 (C=O) cm^{-1}; ^1H nmr ($CDCl_3$) in ppm, δ: 1.3 (s, 3H, CH_3), 1.6–2.8 (br m, 17H), 7.65 (br s, 1H, NH); ^{13}C nmr ($CDCl_3$) in ppm, δ: 210.1 and 212.7 (q, C1 and C7), 177.9 (q, HN—C=O), 61.3 (C8a), 56.4 (C4a); ms (*m/e*, %): 275 (M^+, 100), 247 (44), 220 (78), 190 (25), 163 (31), 91 (28), 55 (36), 41 (49).

Compound **4** crystallized from a chloroform/methanol mixture as colourless transparent plates. A specimen 0.23 × 0.45 × 0.50 mm was cut for X-ray measurements, which were made with a CAD-4 diffractometer using Zr-filtered MoKα radiation.

Crystal data

$C_{16}H_{21}NO_3$ M. Wt. 275.33

Orthorhombic, space group $P2_12_12_1$, a = 10.351(3), b = 11.503(2), c = 11.935(2) Å, V = 1421.1 Å^3, Z = 4, ρ_c = 1.287 Mg m^{-3} (293 K, MoKα, λ = 0.7107 Å), μ(MoKα) = 0.095 mm^{-1}.

Cell dimensions were obtained by least-squares refinement on the θ angles of 24 reflections with $7 < \theta < 21°$. Relative intensities were measured with $\omega/2\theta$ scans of scan width $\Delta\omega(°) = 1.5(0.75 + 0.35 \tan\theta)$, and scan speed 0.59–1.68° min^{-1}. Three standards, monitored every hour of exposure time, showed only random fluctuations in intensity. A total of 2357 independent reflections with $\theta \leqq 30°$ were measured, of which 2037 with $I \geqq \sigma(I)$ were considered observed. Net intensities, after scaling, were corrected for Lorentz and polarization factors, but not for absorption. A correction for secondary extinction ($g/\mu = 0.285 \times 10^{-6}$) was made during refinement. The structure was solved by direct methods, using the MULTAN78 (10) program. Refinement was by block-diagonal least squares, minimizing $\Sigma w(\Delta F)^2$. Hydrogen atoms were located on difference maps and refined isotropically while non-hydrogen atoms were refined anisotropically. The weighting scheme used during the later cycles of refinement was $w = w_1 w_2$ where $w_1 = 20.0/|F_o|$ if $|F_o| > 20.0$, $w = 1.0$ otherwise; $w_2 = \sin^2\theta/0.05$ if $\sin^2\theta < 0.05$, $w_2 = 1.0$ otherwise. This scheme made $\langle w\Delta F^2\rangle$ essentially independent of $|F_o|$ and of $\sin^2\theta$. The final R value is 0.043 on all 2037 observed reflections, R_w = 0.046. At convergence the mean (shift/e.s.d.) was 0.045 and $(\Delta/\sigma)_{max}$ was 0.21, for a H parameter. Scattering factor values for O, N, C were taken from ref. 11 without any corrections for anomalous dispersion; those for H were from ref. 12. Calculations were made with the NRC set of crystallographic programs (13) unless otherwise specified. A difference map calculated from the final structure factors[6] shows density between 0.24 and −0.16 e/Å^3; the eight peaks over 0.19 e/Å^3 ($4\sigma(\rho)$) are essentially at the midpoints of C—C bonds, and presumably correspond to bonding electron density.

Acknowledgements

This work was supported by a grant from the Natural Sciences and Engineering Research Council of Canada. We are grateful to Carleton University for a scholarship to M.G.

1. R. E. IRELAND, M. I. DAWSON, S. C. WELCH, A. HAGENBACH, J. BORDNER, and B. TRUS. J. Am. Chem. Soc. **95**, 7829 (1973).
2. J. W. APSIMON, K. E. FYFE, and A. M. GREAVES. *In* The total synthesis of natural products. Vol. 6. *Edited by* J. W. ApSimon. Wiley–Interscience, New York. 1984. pp. 85–139.
3. F. H. ALLEN, S. BELLARD, M. D. BRICE, B. A. CARTWRIGHT, A. DOUBLEDAY, H. HIGGS, T. HUMMELINK, B. G. HUMMELINK-

[6]Tables of observed and calculated structure amplitudes, of hydrogen atom parameters, and of anisotropic thermal parameters may be purchased from the Depository of Unpublished Data, CISTI, National Research Council of Canada, Ottawa, Ont., Canada K1A 0S2.

Can. J. Chem. Downloaded from www.nrcresearchpress.com by 190.90.36.8 on 09/07/12
For personal use only.

PETERS, O. KENNARD, W. D. S. MOTHERWELL, J. R. RODGERS, and D. G. WATSON. Acta Crystallogr. Sect. B, **35**, 2331 (1979).
4. D. J. CHADWICK and J. D. DUNITZ. Acta Crystallogr. Sect. B, **34**, 968 (1978).
5. K. BLAHA, P. MALON, M. TICHY, I. FRIC, R. USHA, S. RAMAKUMAR, and K. VENKATESAN. Collect. Czech. Chem. Commun. **43**, 3241 (1978).
6. G. T. FURST, M. A. WACHSMAN, J. PIERONI, J. G. WHITE, and E. J. MORICONI. Tetrahedron, **29**, 1675 (1973).
7. L. NØRSKOV-LAURITSEN, H.-B. BÜRGI, P. HOFMANN, and H. R. SCHMIDT. Helv. Chim. Acta, **68**, 76 (1985).
8. D. CREMER and J. A. POPLE. J. Am. Chem. Soc. **97**, 1354 (1975).
9. J. F. LE BORGNE, T. CUVIGNY, M. LARCHEVÊQUE, and H. NORMANT. Synthesis, 238 (1976).
10. P. MAIN, S. E. HULL, L. LESSINGER, G. GERMAIN, J.-P. DECLERCQ, and M. M. WOOLFSON. MULTAN78. A system of computer programs for the automatic solution of crystal structures from X-ray diffraction data. Universities of York, England, and Louvain, Belgium. 1978.
11. International Tables for X-ray Crystallography. Vol. IV, Kynoch Press, Birmingham. 1974.
12. R. F. STEWART, E. R. DAVIDSON, and W. T. SIMPSON. J. Chem. Phys. **42**, 3175 (1965).
13. F. R. AHMED, S. R. HALL, M. E. PIPPY, and C. P. HUBER. J. Appl. Crystallogr. **6**, 309, accession nos. 133–147 (1973).
14. C. K. JOHNSON. ORTEP-II. Report 5138, Oak Ridge National Laboratory, Tennessee. 1976.

Can. J. Chem. Downloaded from www.nrcresearchpress.com by 190.90.36.8 on 09/07/12
For personal use only.

A synthetic strategy for tricholomic acid and acivicin

STEPHEN HANESSIAN AND BENOIT VANASSE
Department of Chemistry, Université de Montréal, Montréal (Qué.), Canada H3C 3J7

Received June 10, 1986

This paper is dedicated to Dr. O. E. (Ted) Edwards

STEPHEN HANESSIAN and BENOIT VANASSE. Can. J. Chem. **65**, 195 (1987).

A synthetic strategy towards tricholomic acid and acivicin has been established using the aldol condensation of *N*-pyruvilideneglycinatoaquocopper(II) and an optically active aldehyde derived from *S*-malic acid as the key bond-forming reaction. Although a viable strategy was developed, no asymmetric induction was observed.

STEPHEN HANESSIAN et BENOIT VANASSE. Can. J. Chem. **65**, 195 (1987).

La condensation aldolique entre le *N*-pyruvilidineglycinatoaquo cuivre(II) et un aldéhyde optiquement actif provenant de l'acide *S*-malique est utilisée comme réaction-clé dans une stratégie de synthèse de l'acide tricholomique et de l'acivicine. Bien que notre stratégie soit opérationnelle, nous n'avons pas observé d'induction asymétrique.

Can. J. Chem. Downloaded from www.nrcresearchpress.com by 190.90.36.8 on 09/07/12
For personal use only.

Tricholomic acid **1** isolated from *tricholoma muscarium* by Takemodo (1) in 1964 is an unusual amino acid (2) having flycidal properties (3). It bears stereochemical and structural resemblance to acivicin (AT-125) **2**, an antitumor antibiotic (4) isolated by Martin and co-workers (5), to its 4-hydroxy analog (6), and to ibotenic acid **3** (7).

The close relationship between tricholomic acid and acivicin makes the former an ideal target for the synthesis of this particular class of dihydroisoxazoleacetic acids. Indeed, several total syntheses of acivicin have been reported that utilize tricholomic acid as a precursor (8*a*).[1] Syntheses of tricholomic acid are also known (9).

We envisaged a synthetic route to tricholomic acid based on a precursor related to a protected β-hydroxy glutamic acid,[2] since there was precedent (11) for displacing a leaving group in the β position of such a derivative with inversion of configuration.

Our strategy was to disconnect between C-2 and C-3, giving a malonaldehyde equivalent and a suitably activated glycine[3] unit as shown in Scheme 2.

It was reasoned that an aldol condensation of a glycine copper complex **4** and a suitable aldehyde derivative **8** would give the desired acyclic framework with the required functionality. *N*-Pyruvylideneglycinatoaquocopper(II) was used as a glycine anion equivalent (13), and the malonic amide hemialdehyde equivalent was derived from *S*-malic acid via a well-established route (14) (Scheme 3). Thus *S*-malic acid was expected to provide a chiral precursor to aldehyde **8**, which can be considered to be a latent malonic acid derivative.

Furthermore, it was hoped that some diastereofacial selectivity might be encountered in the aldol reaction[4] by virtue of the presence of an asymmetric center bearing an oxygen substituent in the aldehyde (16). Reaction of *N*-pyruvylideneglycinatoaquocopper(II) **4** with aldehyde **8** proceeded smoothly at room temperature at pH 9.8 (NaOH) to give a diastereomeric mixture of β-hydroxy α-amino acids **9** (Scheme 4). Although possible, isolation of **9** was not deemed necessary and the products were carried through without purification.

Protection of the α-amino group as its *N*-benzyloxycarbonyl (Z) derivative and esterification with benzyl bromide in the presence of triethylamine gave a good yield of a 3:2 mixture of diastereoisomers, which could be separated by chromatography. The major isomer **10***a* was then protected as the acetate derivative **11***a*, and the acetal function was hydrolyzed in excellent overall yield (90%). The resulting diol was subjected to oxidative cleavage with $KMnO_4/NaIO_4$ to give the monoacid **13***a* as an oil, in 81% yield. The identity of the diastereomeric monoacids **13***a* and **13***b* (*erythro* series not shown) was established by comparison with products obtained by a different route (11).

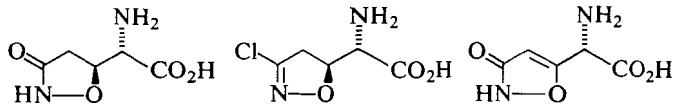

1 **2** **3**

SCHEME 1

The *threo* five-carbon monoacid **13***a* encompasses all the required functionality and oxidation state present in the target, except for an inversion of configuration at C-3. On the other hand, the *erythro* diastereomer **13***b* does have the correct relative stereochemistry of tricholomic acid and acivicin. However, access to the heterocycle from **13***b* would require cyclization mediated by the C-3 hydroxyl group in the formation of the dihydroisoxazole ring.

We opted to converge with the known synthetic route (11) in which intramolecular heterocycle formation utilizes the nucleophilic character of an *N*-substituted hydroxamate (17). Tricholomic acid thus obtained has been resolved (18) to give the optically pure natural product.

The *threo* isomer **13***a* was converted into the corresponding *O*-benzylhydroxamate derivative **14***a*, in the presence of 1-ethyl-3-(3-diethylaminopropyl) carbodiimide hydrochloride. Deacetylation of **14***a* gave a crystalline compound **15***a* whose physical constants were identical with the expected *threo* product (11). The *erythro* isomer **11***b* was subjected to the same protocol to give the *erythro* hydroxamate derivative **15***b*. Comparison of its physical constants with values reported in the literature (11) confirmed the *erythro* relative stereochemistry.

The carbon framework and functionality present in tricholomic acid (hence acivicin) was easily accessible by the methodology described in this work. There was a modest preference for the *threo* isomer, but the products were racemic in each diastereomeric series, which could be due to the unfavorable disposition of the oxygen-bearing asymmetric

[1]For other approaches to acivicin, see ref. 8*b*.

[2]For a recent synthesis of *threo* β-hydroxy L-glutamic acid, see ref. 10.

[3]For a recent review on the synthesis of α-amino acids including the use of activated glycine units, see ref. 12.

[4]For a detailed discussion of the aldol reaction, see ref. 15.

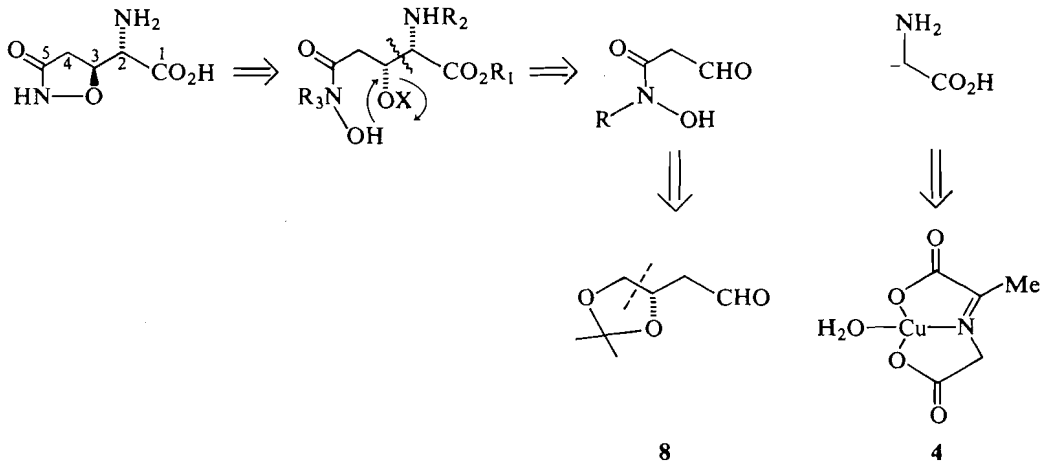

SCHEME 2

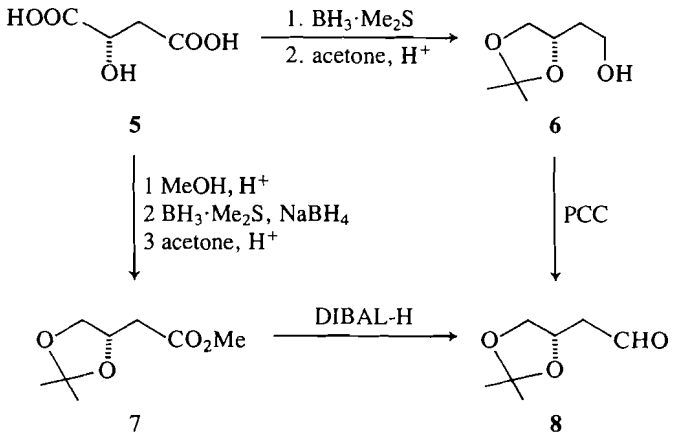

SCHEME 3

center in the aldehyde **8** (19).[5] Normally, a heteroatom assisted diastereoselection proceeds better in five-membered chelates (15) compared to the six-membered counterparts. In fact, Ishido and co-workers (13) had shown that reaction of 1,2-*O*-isopropylidene-D-glyceraldehyde with **4** gives 2-amino-2-deoxy-D-xylonic acid (31%) as the preponderant isomer. It is of interest, however, that there was a modest 3:2 preference in favor of the *syn* (*threo*) isomer in the condensation. Also noteworthy is the fact that the aldol condensation was carried out in *water*, hence the guidelines established for diastereofacial bias and stereoselection in nonaqueous systems (e.g. THF, etc.) may not be applicable here.

We are continuing to explore the synthetic utility of aldol and related C—C bond-forming reactions based on copper chelates of amino acids in aqueous and nonaqueous polar media.

Experimental

Melting points are uncorrected. Optical rotations were measured on a Perkin–Elmer automatic spectropolarimeter model 141. The ^{1}H nmr spectra were recorded on Varian 60 and Bruker 400 MHz instruments with tetramethylsilane as internal standard in deuteriochloroform as solvent. Mass spectra were recorded on a VG 1212 low resolution mass spectrometer by the direct chemical ionization technique (DCI). Column chromatography was done by the flash technique.

(S)-2,2-Dimethyl-1,3-dioxolane-4-ethanal

Method A

To a stirred suspension of pyridinium chlorochromate (20 g; 93 mmol) and molecular sieves (3Å, freshly activated; 20 g) in dichloromethane (125 mL) was added alcohol **6**[6] (3.8 g; 26 mmol) in dichloromethane (10 mL). After being stirred for an hour, the mixture was diluted with ether, then filtered on silica gel and evaporated to give aldehyde **8** (3.4 g; 23 mmol; 88%); ν_{max} (film): 1725 cm^{-1}; ^{1}H nmr (60 MHz) ppm: 1.37 (s, 3H), 1.42 (s, 3H), 2.70 (ddd, 2H, J = 2, 6, 17 Hz), 3.60 (dd, 1H, J = 6, 7.5 Hz), 4.20 (dd, 1H, J = 6, 7.5 Hz), 4.55 (9.1H, J = 6 Hz), 9.8 (t, 1H, J = 2 Hz).

Method B

To a stirred solution of ester **7** (14) (5.11 g; 29 mmol) in toluene (100 mL) at −78°C was added, dropwise over an hour, DIBAL-H (38.2 mL; 38.2 mmol) in toluene. The cold solution was then transferred through a cannula into a rapidly stirring solution of 50% aqueous acetic acid (130 mL). After being stirred for 30 min the mixture was extracted with toluene (3 × 100 mL), and the organic phases were combined, dried, and evaporated to dryness to give aldehyde **8** (3.4 g; 23 mmol; 80%).

(2R,3R,5S), (2R,3S,5S), (2S,3R,5S), and (2S,3S,5S)-2-amino-5,6-O-isopropylidine-3,5,6-trihydroxyhexanoic acids (9)

To a suspension of *N*-pyruvylideneglycinatoaquocopper(II) **4** (13) (5.2 g; 20 mmol) in water (200 mL) was added 2 *M* NaOH to pH 9.8, then a solution of **8** (3.4 g; 23 mmol) in ethanol (10 mL) was added dropwise. The resulting mixture was stirred for 4 h at room temperature while maintaining a constant pH. The solution was saturated with H_2S gas, then concentrated to approximately 30 mL, and ethanol (70 mL) was added. Filtration and washing gave **9** (2.19 g; 10 mmol; 50%), mp 215°C (dec.); ν_{max} (film): 1700 (br, COOH) cm^{-1}; ^{1}H nmr (D_2O) (60 MHz) ppm: 1.38 (s, 3H), 1.40 (s, 3H), 2.2–2.5 (m, 2H), 4.0–4.8 (m, 5H), 5.1 (HOD); ms: 220 (M + 1).

*Benzyl (2S,3R,5S) and (2R,3S,5S)-2-benzyloxycarbonylamino-5,6-O-isopropylidene-3,5,6-trihydroxyhexanoates **10**a, and benzyl (2R,3R,5S) and (2S,3S,5S)-2-benzyloxycarbonylamino-5,6-O-isopropylidene-3,5,6-trihydroxyhexanoates **10**b*

To a solution of **9** in water (100 mL) and DMF (200 mL) was added *N*-(benzyloxycarbonyloxy) succinimide (5.5 g; 22 mmol) in DMF (50 mL). After being stirred at room temperature overnight, the mixture was treated with 5% $NaHCO_3$ (200 mL), washed twice with ether (250 mL), acidified to pH ~2.0 with 10% HCl (slowly), and subsequently extracted with ether (4 × 100 mL) to give a syrup. To the crude syrup dissolved in dry DMF (50 mL), triethylamine (3.4 mL;

[5]See ref. 19*a* for usage of **8** in aldol condensation. For a related case in a Grignard reaction, see ref. 19*b*.

[6]This material is contaminated with 10% of the corresponding six-membered acetonide, see ref. 20.

Can. J. Chem. Downloaded from www.nrcresearchpress.com by 190.90.36.8 on 09/07/12
For personal use only.

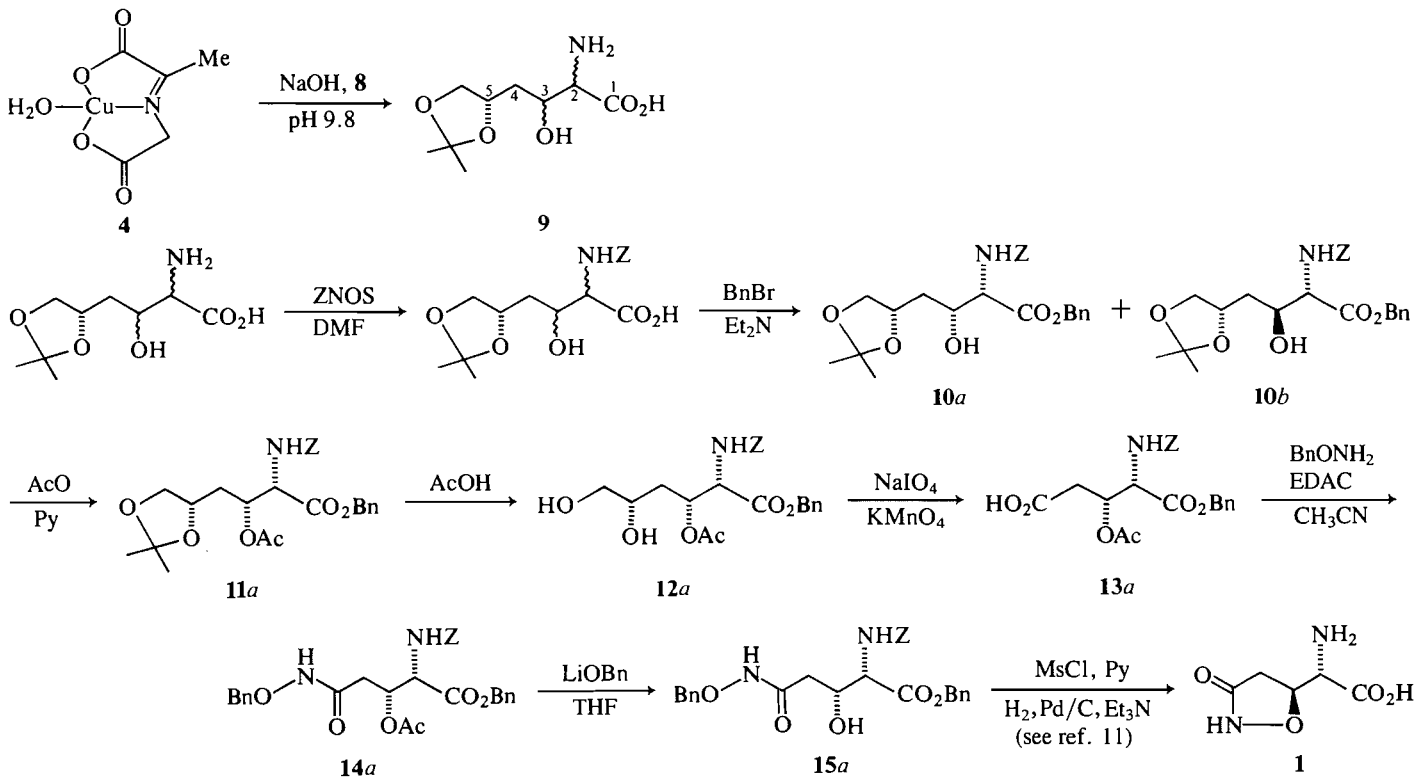

SCHEME 4

24 mmol) and benzylbromide (2.6 mL; 21.8 mmol) were added at room temperature. After stirring overnight, water (100 mL) was added and the mixture was extracted with ether (3 × 100 mL). The organic phase was washed with saturated $NaHCO_3$; then with brine, dried ($MgSO_4$), filtered, and evaporated to a syrup, which upon chromatography (ethyl acetate – chloroform–*n*-hexane 25:10:65) gave **10***a* (2.07 g; 4.68 mmol; 23% (3 steps)), **10***b* (1.38 g; 3.12 mmol; 16% (3 steps)), and benzyl *N*-benzyloxycarbonylamino glycinate (1.0 g; 3.34 mmol).

Compound **10***a*: mp 61.5–62.5°C; $[\alpha]_D$ +6.0° (*c* 1, $CHCl_3$); ν_{max} (film): 1740–1750 (ester, carbamate) cm^{-1}; ^1H nmr (400 MHz) ppm: 1.34–1.39 (2s, 6H, 2 × CH_3), 1.65–1.85 (m, 2H, H-4A, H-4B), 2.75 (d, 1H, OH, *J* = 4.9 Hz), 3.54 (dd, 1H, H-6A, *J* = 7.8, 7.9 Hz), 4.01 (dd, 1H, H-6B, *J* = 6.2, 7.9 Hz), 4.25–4.35 (m, 1H, H-5), 4.40–4.48 (m, 2H, H-3 + H-2), 5.19 (bs, 2H, CH_2Ph), 5.22 (bs, 2H, CH_2Ph), 5.89 (d, 1H, NH, *J* = 9.2 Hz), 7.35–7.40 (bs, 10H, arom); ms: 444 (*M* + 1).

Compound **10***b*: mp 72.5–73.5°C; $[\alpha]_D$ −2.8 (*c* 1, $CHCl_3$); ν_{max} (film): 1740 (ester, carbamate) cm^{-1}; ^1H nmr (400 MHz) ppm: 1.35, 1.41 (2s, 6H, 2 × CH_3), 1.73–1.76 (m, 2H, H-4A, H-4B), 3.52 (bs, 1H, OH), 3.54 (dd, 1H, H-6A, *J* = 7.1, 8.1 Hz), 4.07 (dd, 1H, H-6B, *J* = 6.1, 8.1 Hz), 4.25–4.32 (m, 1H, H-5), 4.40 (bd, 1H, H-2, *J* = 9.5 Hz), 4.45–4.50 (m, 1H, H-3), 5.13 (s, 2H, CH_2Ph), 5.22 (d, 2H, CH_2Ph, *J* = 3.4 Hz), 5.80 (d, 1H, NH, *J* = 9.5 Hz), 7.30–7.40 (bs, 10H, arom); ms: 444 (*M* + 1).

*Benzyl (2*R*,3*R*,5*S*) and (2*R*,3*S*,5*S*)-3-*O*-acetyl-2-benzyloxycarbonylamino-5,6-*O*-isopropylidene trihydroxyhexanoates **11***a*

To a solution of **10***a* (450 mg; 1.01 mmol) in pyridine (5 mL) was added acetic anhydride (2.5 mL) and 4-dimethylaminopyridine (catalytic). The mixture was stirred at room temperature for 3 h. Ethyl acetate was then added and the mixture was washed three times with $CuSO_4$ (saturated solution). The organic phase was then washed with water, dried ($MgSO_4$), filtered, and evaporated to an oil, which was chromatographed (ethyl acetate – *n*-hexane 15:85) to give **11***a* as an oil (460 mg; 94%); $[\alpha]_D$ +17.7° (*c* 1, $CHCl_3$); ν_{max} (film): 1740–1750 (carbamate, esters) cm^{-1}; ^1H nmr (400 MHz) ppm: 1.31, 1.41 (2s, 6H, 2 × CH_3), 1.80 (ddd, 1H, H-4A, *J* = 4.8, 6.0, 15.2 Hz), 1.86 (s, 3H, OAc), 1.96 (ddd, 1H, H-4B, *J* = 7.6, 9.2, 15.2 Hz), 3.55 (dd, 1H, H-6A, *J* = 6.7, 7.9 Hz), 4.03 (dd, 1H, H-6B, *J* = 6.0, 7.9 Hz), 4.15 (m, 1H, H-5), 4.67 (dd, 1H, H-2, *J* = 2.1, 9.8 Hz), 5.13, 5.14 (2s, 4H, 2 × CH_2Ph), 5.49 (d, 1H, NH, *J* = 9.8 Hz), 5.54 (m, 1H, H-3), 7.30–7.40 (s, 10H, arom, *J* = 9.8 Hz); ms: 486 (*M* + 1).

*Benzyl (2*R*,3*R*,5*S*) and (2*S*,3*S*,5*S*)-3-*O*-acetyl-2-benzyloxycarbonylamino-5,6-isopropylidene trihydroxyhexanoate **11** b*

Using the same procedure as for **11***a*, compound **11***b* was obtained as a solid (308 mg, 94%); mp 80–81°C; $[\alpha]_D$ −27.8° (*c* 1.2, $CHCl_3$); ν_{max} (film): 1740–1750 (br, esters, carbamate) cm^{-1}; ^1H nmr (400 MHz) ppm: 1.32, 1.37 (2s, 6H, 2 × CH_3), 1.84–1.90 (m, 2H, H-4A, H-4B), 1.92 (s, 3H, OAc), 350 (dd, 1H, H-6A, *J* = 7.4, 7.8 Hz), 4.00 (dd, 1H, H-6B, *J* = 6.1, 7.8 Hz), 4.05–4.15 (m, 1H, H-5), 4.65 (dd, 1H, H-2, *J* = 2.2, 9.7 Hz), 5.09–5.18 (m, 4H, 2 × CH_2Ph), 5.45 (d, 1H, NH, *J* = 9.7 Hz), 5.52 (m, 1H, H3), 7.30–7.40 (bs, 10H, arom); ms: 486 (*M* + 1).

*Benzyl (2*R*,3*S*,5*S*) and (2*S*,3*R*,5*S*)-3-*O*-acetyl-2-benzyloxycarbonylamino-5,6-dihydroxy trihydroxyhexanoates, **12***a*

A solution of **11***a* (460 mg; 0.95 mmol) in acetic acid – water (4:1, 10 mL) was stirred overnight at room temperature. Toluene was then added and the solution was evaporated twice under reduced pressure. The resulting oil was purified by chromatography (ethyl acetate – *n*-hexanes 7:3) to give **12***a* (400 mg; 95%) as a solid; mp 73–74°C, $[\alpha]_D$ +13.8° (*c* 1.0, HCl_3); ν_{max} (film): 1700–1760 (esters, carbamate) cm^{-1}; ^1H nmr (400 MHz) ppm: 1.74–1.78 (m, 2H, H-4A, H-4B), 1.81 (s, 3H, OAc), 2.9–3.2 (bs, 2H, 2 × OH), 3.31 (dd, 1H, H-6A, *J* = 6.7, 11.2 Hz), 3.46 (dd, 1H, H-6B, *J* = 2.8, 11.2 Hz), 3.65–3.75 (m, 1H, H-5), 4.63 (dd, 1H, H-2, *J* = 1.9, 9.8 Hz), 5.03 (bs, 4H, 2 × CH_2Ph), 5.41–5.50 (m, 1H, H-3), 5.54 (d, 1H, NH, *J* = 9.8 Hz), 7.30–7.40 (m, *J* = 10 Hz, arom); ms: 446 (*M* + 1).

*Benzyl (2*R*,3*R*,5*S*) and (2*S*,3*S*,5*S*)-3-*O*-acetyl-2-benzyloxycarbonylamino-5,6-dihydroxy trihydroxyhexanoates **12** b*

Using the same procedure as for **12***a*, compound **12***b* was obtained as an oil (267 mg, 95%); $[\alpha]_D$ −18.7° (*c* 1, $CHCl_3$); ν_{max} (film): 1700–1760 (esters, carbamate) cm^{-1}; ^1H nmr (400 MHz) ppm: 1.66–

Can. J. Chem. Downloaded from www.nrcresearchpress.com by 190.90.36.8 on 09/07/12
For personal use only.

1.69 (m, 2H, H-4A, H-4B), 1.84 (s, 3H, OAc), 2.2–2.8 (bs, 2H, 2 × OH), 3.47 (dd, 1H, H-6A, J = 7.1, 12.9 Hz), 3.53 (dd, 1H, H6-B, J = 2.8, 12.9 Hz), 4.68 (dd, 1H, H-2, J = 1.9, 9.6 Hz), 5.10–5.12 (m, 4H, 2 × CH_2Ph), 5.56–5.62 (m, 2H, H-3 + NH), 7.30–7.40 (m, 10H, arom); ms: 446 (M + 1).

(d,l)-threo-3-O-Acetyl-2-benzyloxycarbonylamino-3-hydroxyglutaric acid α-benzyl esters, ***13****a*

To a suspension of $NaIO_4$ (481 mg, 2.25 mmol), and potassium permanganate (18 mg, 0.11 mmol) in acetone–water (10:1, 11 mL) was added **12***a* (400 mg, 0.9 mmol) in acetone (1 mL) followed by $NaHCO_3$ (227 mg, 2.7 mmol). The resulting dark purple suspension was stirred overnight. The dark brown precipitate was filtered through Celite and the solids washed with ether. The organic phase was extracted with 5% $NaHCO_3$, the aqueous phase was washed twice with ether, acidified to pH ~2.0 with HCl 10%, then extracted twice with ether. The ether phase was dried ($MgSO_4$), filtered, and evaporated to give **13***a* as a yellow oil (350 mg, 81%); ν_{max} (film): 1735 (ester, carbamate, acid) cm^{-1}; ^1H nmr (400 MHz) ppm: 1.80 (s, 3H, OAc), 2.75 (bs, 1H, H-4A), 2.80 (bs, 1H, H-4B), 4.70–4.80 (m, 1H, H-2), 5.10 (bs, 4H, 2 × CH_2Ph), 5.50–5.65 (m, 2H, H-3, N-H), 7.35 (bs, 10H, arom), 9.50–9.70 (bs, 1H, COOH); ms: 430 (M + 1).

(d,l)-erythro-3-O-Acetyl-2-benzyloxycarbonylamino-3-hydroxyglutaric acid α-benzyl ester, ***13****b*

Using the same procedure as for **13***a*, compound **13***b* was obtained as an oil (200 mg, 80%); ν_{max} (film): 1735 (ester, carbamate, acid) cm^{-1}; ^1H nmr (400 MHz) ppm: 1.84 (s, 3H, OAc), 2.75 (bs, 1H, H-4A), 2.82 (bs, 1H, H-4B), 4.70–4.80 (m, 1H, H-2), 5.15 (bs, 4H, 2 × CH_2Ph), 5.50–5.65 (m, 2H, H-3, NH), 7.30–7.40 (bs, 10H, arom), 9.50–9.70 (bs, 1H, COOH); ms: 430 (M + 1).

(d,l)-threo-3-O-Acetyl-2-benzyloxycarbonylamino-3-hydroxyglutaric acid α-benzyl ester (δ-N-benzyloxyamide), ***14****a*

To a solution containing **13***a* (70 mg, 0.16 mmol) and *O*-benzylhydroxylamine (40 mg, 0.33 mmol) in acetonitrile (10 mL), was added successively 1-ethyl-3-(3-dimethylaminopropyl) carbodiimide hydrochloride (67.1 mg; 0.35 mmol) and 4-dimethylaminopyridine (catalytic quantity). The resulting solution was stirred for 15 h; the mixture was then poured into water (20 mL), extracted with CH_2Cl_2, dried ($MgSO_4$), and evaporated to an oil, which upon chromatography (ethyl acetate – *n*-hexanes 15:85) gave **14***a* (35 mg; 80%) as a solid, mp 104–105°C; ν_{max} (film): 1750 (br, ester, carbamate, hydroxamate) cm^{-1}; ^1H nmr (400 MHz) ppm: 1.80 (s, 3H, OAc), 2.70–2.81 (m, 2H, H-4A, H-4B), 4.70–4.80 (m, 1H, H-2), 4.90 (s, 2H, $PhCH_2ON$), 5.10 (bs, 4H, CH_2Ph), 5.5–5.65 (m, 3H, 2 × NH), 7.3–7.4 (bs, 15H, arom); ms: 535 (M + 1).

(d,l)-erythro-3-O-Acetyl-2-benzyloxycarbonylamino-3-hydroxyglutaric acid α-benzyl ester (δ-N-benzyloxyamide), ***14****b*

Using the same procedure as for **13***a*, compound **14***b* was obtained as an oil (80%); ν_{max} (film): 1740–1760 (ester, carbamate, hydroxamate) cm^{-1}; ^1H nmr (400 MHz) ppm: 1.81 (s, 3H, OAc), 2.71–2.83 (m, 2H, H-4A, H-4B), 4.72–4.80 (m, 1H, H-2), 4.90 (s, 2H, $PhCH_2ON$), 5.10 (bs, 4H, 2 × CH_2Ph), 5.5–5.65 (m, 3H, H-3, 2 × NH), 7.3–7.4 (bs, 15H, arom); ms: 535 (M + 1).

(d,l)-threo-2-Amino-3-hydroxyglutaric acid α-benzyl ester (δ-N-benzyloxyamide), ***15****a*

To a cooled solution of **14***a* (35 mg; 0.065 mmol) in THF (4 mL) was added dropwise a solution of lithium benzyloxide (LiOBn) in THF (0.65 mL of 0.1 M solution) at 0°C. After stirring at that temperature for an hour, Dowex H^+ resin was added, the suspension was filtered, and the filtrate was processed in the usual way to give a yellow oil, which was chromatographed (ethyl acetate – *n*-hexane 1:1) to give **15***a* (25 mg, 80%) as an oil that solidified on standing; recrystallization from ethyl acetate – *n*-hexane showed mp 131–132°C (lit. (11) mp 132–133.5°C); ν_{max} (film): 1750 (ester, carbamate, hydroxamate) cm^{-1}; ^1H nmr (400 MHz) ppm: 2.7–2.8 (m, 2H, H-4A, H-4B), 4.72–4.80 (m, 1H, H-2), 4.90 (s, 2H, $PhCH_2ON$), 5.10 (bs, 4H, 2 × CH_2Ph), 5.5–5.65 (m, 3H, H-3, NH (2×)), 7.3–7.4 (bs, 15H, arom); ms: 493 (M + 1).

(d,l)-erythro-2-Amino-3-hydroxyglutaric acid benzyl ester (δ-N-benzyloxyamide, ***15****b*

Using the same procedure as for **15***a*, compound **15***b* was obtained as a solid (81%); recrystallization in ethyl acetate – *n*-hexanes) gave crystals, mp 161–162°C (lit. (11) mp 166–167°C); ν_{max} (film): 1750 (ester, carbamate, hydroxamate) cm^{-1}; ^1H nmr (400 MHz) ppm: 2.7–2.8 (m, 2H, H-4A, H-4B), 4.70–4.82 (m, 1H, H-2), 4.92 (s, 2H, $PhCH_2ON$), 5.10 (bs, 4H, 2 × CH_2Ph), 5.52–5.65 (m, 3H, H-3, 2 × NH), 7.30–7.40 (bs, 15H, arom); ms: 493 (M + 1).

Acknowledgements

We thank the Natural Sciences and Engineering Research Council of Canada and FCAR (Fonds pour la formation de chercheurs et l'aide à la recherche) for financial support, Dr. Phan Viet Tan for nmr data, and Michael Evans for mass spectra.

1. T. Takemodo. J. Pharm. Soc. Jpn. **84**, 1183 (1964).
2. H. Musso. Angew. Chem. Int. Ed. Engl. **22**, 816 (1983).
3. M. Terasaki. Eiyo To Shokuryo, **18**, 178 (1965).
4. L. J. Hanka, D. G. Martin, and G. L. Neil. Cancer Chemother. Rep. **57**, 141 (1973); D. A. Cooney, H. N. Jarayam, J. A. Ryan, and V. H. Bono. Cancer Chemother. Rep. **58**, 793 (1974); H. N. Jarayam, D. A. Cooney, J. A. Ryan, G. Neil, R. L. Dion, and V. H. Bono. Cancer Chemother. Rep. **59**, 481 (1975); D. Houchens, A. Ovejera, R. Johnson, A. Bogden, and G. Neil. Proc. Am. Assoc. Cancer Res. **19**, 40 (1978); G. L. Neil, A. E. Berger, R. P. McPartland, G. B. Grindley, and A. Bloch. Cancer Res. **39**, 852 (1979); G. L. Neil, A. E. Berger, B. K. Bhuyan, C. L. Blowers, and S. L. Kuentzel. Adv. Enzyme Regul. **17**, 375 (1979); J. Y. Tso, S. G. Bower, and H. Zalkin. J. Biol. Chem. **255**, 6734 (1980); H. N. Jarayam, D. A. Cooney, J. K. Swiniarski, and R. K. Johnson. Proc. Am. Assoc. Cancer Res. **21**, 22 (1980); H. Rosenfeld and J. Roberts. Cancer Res. **41**, 1324 (1981); J. P. McGovern, G. L. Neil, P. C. C. Sem, and J. C. Stewart. J. Pharmacol. Exp. Ther. **216**, 433 (1981).
5. D. G. Martin, D. J. Duchamp, and C. G. Chidester. Tetrahedron Lett. 2549 (1973); L. J. Hanka and A. Dietz. Antimicrob. Agents Chemother. **3**, 425 (1973); D. G. Martin, L. J. Hanka, and G. L. Neil. Cancer Chemother. Rep. **58**, 935 (1974).
6. D. G. Martin, C. G. Chidester, S. A. Mizsak, D. J. Duchamp, L. Baczynskyj, W. C. Krueger, R. J. Wnuk, and P. A. Meulman. J. Antibiot. **28**, 91 (1975); L. J. Hanka, S. A. Gerpheide, P. R. Spieles, D. G. Martin, P. A. Belter, T. A. Coleman, and H. F. Meyer. Antimicrob. Agents Chemother. **7**, 807 (1975).
7. C. H. Euster. Fortschr. Chem. Org. Naturst. **27**, 261 (1969), and refs. cited therein: see also ref. 2.
8. (*a*) R. C. Kelly, I. Schletter, S. J. Stein, and W. Wierenga. J. Am. Chem. Soc. **101**, 1054 (1979); J. E. Baldwin, L. I. Kruse, and J. K. Cha. J. Am. Chem. Soc. **103**, 942 (1981); R. B. Silverman and M. N. Holladay. J. Am. Chem. Soc. **103**, 7357 (1981); (*b*) J. E. Baldwin, C. Hoskins, and L. I. Kruse. J. Chem. Soc. Chem. Commun. 795 (1976); A. A. Hagedorn III, B. J. Miller, and J. O. Nagy. Tetrahedron Lett. **21**, 229 (1980); P. A. Wade, M. K. Pillay, and S. M. Singh. Tetrahedron Lett. **23**, 4563 (1982); R. V. Stevens and R. P. Polniaszek. Tetrahedron, **39**, 743 (1983); P. A. Wade, S. M. Singh, and M. K. Pillay. Tetrahedron, **40**, 601 (1984); D. M. Vyas, Y. Chiang, and T. W. Doyle. Tetrahedron Lett. **25**, 487 (1984).
9. T. Kamiya. Chem. Pharm. Bull. **17**, 895 (1969), and refs. therein; R. M. Khomutove, E. S. Severin, and G. V. Kovaleva. Dokl. Akad. Nauk SSSR, **161**, 1227 (1965); Chem. Abstr. **63**, 5734e (1965).

Can. J. Chem. Downloaded from www.nrcresearchpress.com by 190.90.36.8 on 09/07/12
For personal use only.

10. P. GARNER. Tetrahedron Lett. 3855 (1984), and refs. therein.
11. T. KAMIYA. Chem. Pharm. Bull. **17**, 886 (1969) and refs. therein.
12. G. C. BARRETT. *In* Chemistry and biochemistry of the amino acids. *Edited by* G. C. Barrett. Chapman–Hall, New York. 1985. Chapt. 8.
13. T. ICHIKAWA, S. MAEDA, T. OKAMOTO, Y. ARAKI, and Y. ISHIDO. Bull. Chem. Soc. Jpn. **44**, 2779 (1971); S. M. HECHT, K. M. RUPPRECHT, and P. M. JACOBS. J. Am. Chem. Soc. **101**, 3982 (1979).
14. S. HANESSIAN, A. UGOLINI, D. DUBÉ, and A. GLAMYAN. Can. J. Chem. **62**, 2146 (1984); S. SAITO, T. HASEGAWA, M. INABA, R. NISHIDA, T. FUJII, S. NOMIZU, and T. MORIWAKE. Chem. Lett. 1389 (1984).
15. C. H. HEATHCOCK. *In* Asymmetric synthesis. Vol. III. *Edited by* J. D. Morrisson. Academic Press, New York. 1984. Chapt. 2.
16. M. T. REETZ and A. JUNG. J. Am. Chem. Soc. **105**, 4833 (1983).
17. J. E. BALDWIN, J. K. CHA, and L. I. KRUSE. Tetrahedron, **41**, 5241 (1985).
18. H. IWASAKI, T. KAMIYA, O. OKA, and J. UEYANAGI. Chem. Pharm. Bull. **17**, 866 (1969).
19. (*a*) T. NAKATA, S. NAGAO, N. MORI, and T. OISHI. Tetrahedron Lett. 6461 (1985); T. ROSEN, M. J. TASCHNER, and C. H. HEATHCOCK. J. Org. Chem. **49**, 3994 (1984); (*b*) S. HANESSIAN, A. UGOLINI, and M. THERIEN. J. Org. Chem. **48**, 4427 (1983).
20. A. I. MEYERS and J. P. LAWSON. Tetrahedron Lett. 4883 (1982).

Can. J. Chem. Downloaded from www.nrcresearchpress.com by 190.90.36.8 on 09/07/12
For personal use only.

Assignment of the ^1H and ^{13}C spectra of aspidocarpine and assignment of the structure and stereochemistry of the von Braun reaction product of aspidocarpine by 2D nmr spectroscopy

STEWART MCLEAN, WILLIAM F. REYNOLDS, AND XINGPEI ZHU[1]

Department of Chemistry, University of Toronto, Toronto, Ont., Canada M5S 1A1

Received June 17, 1986

This paper is dedicated to Dr. O. E. (Ted) Edwards

STEWART MCLEAN, WILLIAM F. REYNOLDS, and XINGPEI ZHU. Can. J. Chem. **65**, 200 (1987).

The ^{13}C and ^1H spectra of aspidocarpine and the spectra, structure, and stereochemistry of the product of its von Braun reaction with cyanogen bromide have been totally assigned by a combination of homonuclear (COSY-45) and direct and indirect heteronuclear shift-correlated 2D nmr spectra.

STEWART MCLEAN, WILLIAM F. REYNOLDS et XINGPEI ZHU. Can. J. Chem. **65**, 200 (1987).

En se basant sur une combinaison de techniques impliquant des spectres rmn en 2D homonucléaires (COSY-45) et hétéronucléaires comportant une corrélation directe et indirecte avec les déplacements, on a pu faire des attributions pour toutes les bandes des spectres rmn ^1H et ^{13}C de l'aspidocarpine et de son produit de réaction avec le bromure de cyanogène (von Braun); de plus, ces techniques ont permis d'établir la structure et la stéréochimie de ce dernier composé.

[Traduit par la revue]

Can. J. Chem. Downloaded from www.nrcresearchpress.com by 80.58.250.72 on 09/07/12
For personal use only.

As part of our investigation (1) that led us to the elucidation of the structure of aspidocarpine (**1**), we subjected the alkaloid to a von Braun degradation by treatment with cyanogen bromide. The bromocyanamide formed without difficulty, but the normal solvolytic completion of the degradation failed and it was observed that merely heating the bromocyanamide in ethanol caused it to revert to aspidocarpine. Aspidospermine had been found to behave in a very similar manner (2) and Conroy *et al.* presented evidence that the bromocyanamide included a $-CH_2Br$ unit as part of a carbon chain with "few degrees of freedom" (2). Although the unprecedented reversal of the von Braun reaction was of considerable interest, the degradation provided little significant structural information and the question of the structure of the bromocyanamide has lain dormant since then. Once the structure of **1** was established, it was possible to conjecture that the bromocyanamide had structure **2** but alternative structures could also be suggested.

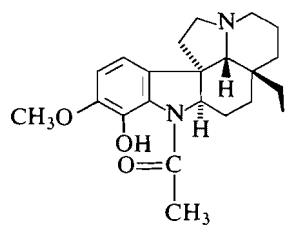

1

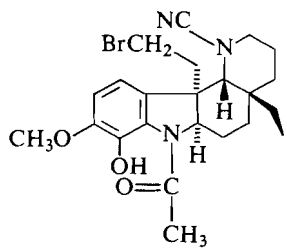

2

Aspidocarpine and aspidospermine were among the first alkaloids to which ^1H nmr spectroscopy was applied for purposes of structure elucidation (1, 2). However, the techniques available then were of limited power and the ^1H spectra were poorly resolved, providing limited and sometimes confusing information (2) regarding molecular structure. The importance of the aspidosperimidine alkaloids subsequently became apparent and a considerable range of nmr data for them is now available (3). However, only limited ^1H data (1) and no ^{13}C data are available for **1**. Consequently, we decided to apply modern nmr spectroscopic techniques to assign unambiguously the ^1H and ^{13}C spectra of **1** as well as to determine whether the structure of the von Braun reaction product was indeed **2**. We have succeeded not only in confirming **2** and totally assigning the spectra of **1** and **2**, but also have succeeded in deducing the conformations of rings C and D of **1** and **2**. These results are reported below.

[1]On leave of absence from the Department of Chemistry, Beijing Normal University, People's Republic of China.

Results and discussion

(a) Assignment of ^1H and ^{13}C spectra of 1

As a first step in assignment, normal and DEPT-edited (4) ^{13}C spectra of **1** were obtained. Then a two-dimensional (2D) heteronuclear (^1H–^{13}C) chemical shift correlation experiment (5) was carried out to determine the chemical shift(s) of the hydrogen(s) directly bonded to each protonated carbon. Next, a ^1H COSY-45 spectrum (6) (Fig. 1) was used to establish connectivities between coupled protons. There are four distinct sequences in the saturated carbon region that could be assigned from this experiment: C(2)H—C(3)H_2—C(4)H_2, C(6)H_2—C(7)H_2—C(8)H_2, C(10)H_2—C(11)H_2, and C(α)H_2—C(β)H_3. The COSY experiment did not allow distinction between C(6)H_2 and C(8)H_2 in the second sequence and C(10)H_2 and C(11)H_2 in the third sequence (due to the symmetry of each sequence). However, C(8)H_2 and C(10)H_2 were readily assigned due to their deshielding by the adjacent nitrogen. Assignments are summarized in Table 1.

Nonprotonated carbons were assigned by carrying out a heteronuclear shift-correlated experiment with delay times optimized for coupling between indirectly bonded carbons and hydrogens (e.g., $^2J_{CH}$ or $^3J_{CH}$). This experiment was performed using the recently proposed 2D pulse sequence XCORFE (7). This sequence detects cross peaks corresponding to ^{13}C–X–^1H and ^{13}C–X–C–^1H pairs (where X = C, N, O, etc.). Two-bond connectivities involving a pair of protonated carbons are distinguished from three-bond connectivities because the former are split by vicinal ^1H–^1H coupling, while the latter appear as singlets (7). Observed connectivities are summarized in Table 2. The remaining carbons are easily assigned using these connectivities (see Table 1). For example, it is trivial to distinguish C(5) from C(12) on the basis of their numerous cross peaks to adjacent protons. The aromatic carbons are assigned on the basis of cross peaks to OH, OCH_3, and to aromatic and saturated protons. Note that the aromatic protons show much stronger three-bond than two-bond peaks due to the relatively

Can. J. Chem. Downloaded from www.nrcresearchpress.com by 80.58.250.72 on 09/07/12
For personal use only.

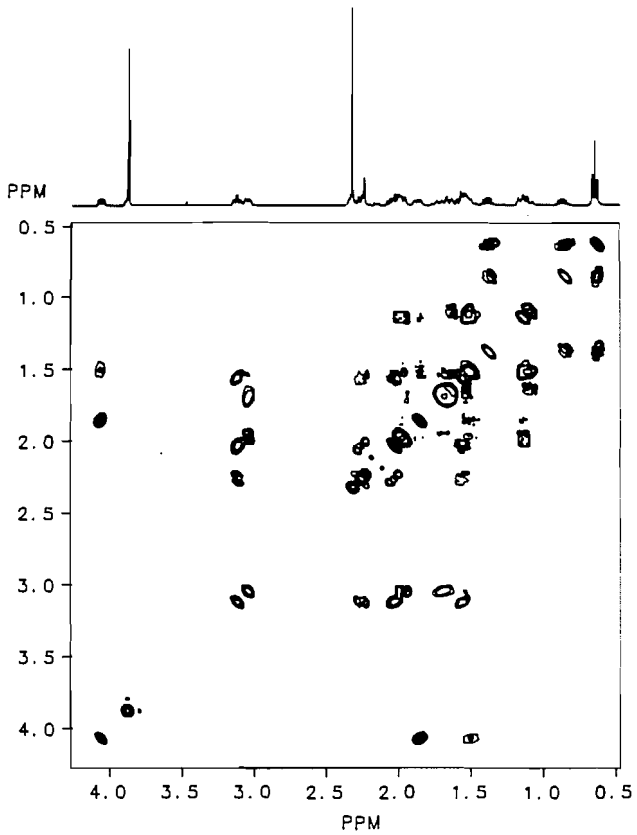

FIG. 1. COSY-45 spectrum for **1**. The normal spectrum lies along the diagonal with off-diagonal peaks indicating connectivities between coupled protons.

small magnitudes of $^2J_{CH}$ (12). The fact that the OH proton shows a three-bond cross peak with C(16) but not with C(18) may reflect stereospecific coupling arising from hydrogen bonding to the *N*-acetyl group (1).

The data in Table 2 also support the earlier assignments of C(8)H_2 and C(10)H_2 (made on chemical shift grounds), which are confirmed by the observation of three-bond connectivities between H(19) and C(8) and between H(8) and C(10). These connectivities, the cross peaks involving OH and OCH_3 protons, as well as several other connectivities in Table 2 illustrate the ability of this experiment to establish connectivities through heteroatoms.

(b) Assignment of the structure and ^1H and ^{13}C spectra of 2

Exactly the same combination of experiments as outlined in (*a*) was used to investigate **2** (e.g., see the COSY spectrum in Fig. 2) and spectral assignments were made in a similar manner. Results are summarized in Tables 3 and 4.

Several observations clearly indicate that **2** is the correct structure for the reaction product. First, the carbon assigned as C(10) is shifted from δ 52.4 in **1** to δ 27.0 in **2**, consistent with replacement of a bond to nitrogen by one to bromine (8). Second, the large nonequivalence of the methylene protons of C(10) in **1** has almost been eliminated in **2**, consistent with the fact that a bond has been broken between C(10) and the chiral nitrogen. Finally, the XCORFE experiment revealed two connectivities to the cyano group, one to H(19) and the other to the H(8) proton at δ 3.02, consistent with attachment of the cyano group to the nitrogen, as shown in **2**. The fact that no significant cross peak was observed involving the second H(8) proton at δ 3.63 provides useful conformational information. This is discussed below.

TABLE 1. Assigned ^{13}C and ^1H chemical shifts and ^1H–^1H coupling constants for **1** in $CDCl_3$

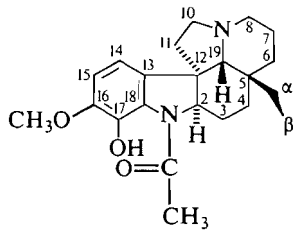

Carbon[a]	δ_C	δ_H (J_{HH})[b,c]
2	70.25	4.07 (dd, 11, 6)
3	25.10	1.86 (m), 1.52 (m)
4	22.92	2.00 (td, 12, 14), 1.15 (dm, 12)
5	35.46	
6	34.02	1.11 (td, 12, 4), 1.65 (dt, 12, 4)
7	21.50	1.72 (tm, 12), 1.53 (dm, 12)
8	53.67	1.98 (td, 12, 4), 3.04 (dm, 12)
10	52.43	2.27 (m), 3.12 (m)
11	39.37	1.57 (m), 2.04 (m)
12	52.20	
13	133.13	
14	112.36	6.61 (d, 8)
15	110.04	6.69 (d, 8)
16	149.35	
17	137.47	
18	127.51	
19	70.62	2.25 (s)
α	30.03	0.93 (m), 1.44 (m)
β	6.76	0.63 (t, 7.5)
OCH_3	56.43	3.88 (s)
$COCH_3$	22.68	2.33 (s)
$COCH_3$	169.31	
—	—	OH 10.98

[a]Numbering shown below.

[b]Splitting pattern in parentheses (multiplicity, coupling constant (in Hz) where resolved).

[c]In cases of protons in rings C and D, the first listed proton of a methylene pair is the axial proton, while the second is equatorial. For C(10), C(11), and C(α), the protons are listed in chemical shift order.

(c) Deduction of the conformations of 1 and 2 from three-bond ^1H–^{13}C connectivities

The solution conformation of **1** is unknown. The *N*-methiodide of the closely related alkaloid aspidospermine has been shown by X-ray crystallography to have a chair conformation for ring C but a boat conformation for ring D (see **3**) (9). However, on the basis of infrared spectroscopy, it was concluded that ring D most probably is in a chair conformation in the free base (see **4**) (10). The nmr data strongly suggest that the conformation of **1** is very close to that shown in **4**. For example, the ^1H spectrum of **1** shows multiplets for the methylene protons of C(4), C(6), and C(8), all of which show the expected couplings for *axial* and *equatorial* proton pairs

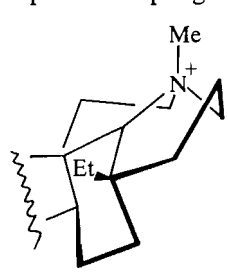

3

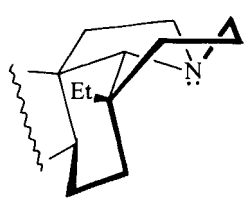

4

Can. J. Chem. Downloaded from www.nrcresearchpress.com by 80.58.250.72 on 09/07/12
For personal use only.

TABLE 2. Observed two-bond and three-bond $^{13}C-^{1}H$ connectivities from XCORFE experiments on **1**

Carbon	^{1}H connectivities[a]
2	3_a(d), 3_e, 4_e, 11_l, 19
3	2, 4_a(d), 4e
4	3_a(d), 6_a, 19
5	3_e, 4_a, 4_e, 6_a, 6_e, 19, α_l, α_h, β
6	7_a(d), 7_e, 8_e
7	6_a(d), 8_a(d)
8	6^e, 7_a(d), 10_l
10	(8_e), 11_l(b), 11_h(d), 19
11	2, 10_l(b), 10_h(d)
12	2, 3_e, 10_l, 10_h, 11_l, 11_h, 19
13	(2), 11_h, 15, 19
14	15(d)
15	14(d)
16	14, OCH_3, OH
17	15, OH
18	(2), 14
19	4_e, 6_e, 8_e, (10_h)
α	4_e, (10), β(b)
β	α_l(b), α_h(b)
OCH_3	
$COCH_3$	
$COCH_3$	$COCH_3$

[a]The number indicates the proton while the subscript indicates whether it is axial (a) or equatorial (e) in ring C or D, or high field (h) or low field (l) for other methylene pairs. Weak connectivities are indicated in parentheses. d = a doublet splitting, while b = a broadened line with unresolved splitting. Observation of coupling indicates a two-bond connectivity between a proton and an adjacent protonated carbon (see ref. 7). Couplings of less than 7 Hz are not detected due to limited data point resolution.

TABLE 3. Assigned ^{13}C and ^{1}H chemical shifts and $^{1}H-^{1}H$ coupling constants for **2** in $CDCl_3$

Carbon[a]	δ_C	δ_H (J_{HH})
2	65.67	4.56 (dd, 11, 6)
3	24.71	2.15 (m), 1.56 (m)
4	21.93	2.24 (td, 12, 4), 1.33 (dm, 12)
5	38.47	
6	34.38	1.11 (td, 12, 4), 1.41 (dt, 12, 4)
7	20.12	2.02 (tm, 12), 1.65 (dm, 12)
8	53.51	3.02 (td, 12, 4), 3.63 (dm, 12)
10	26.97	{3.27} (m)[b]
11	41.03	1.93 (m), 2.82 (m)
12	50.07	
13	129.38	
14	114.01	6.56 (d, 8)
15	108.92	6.77 (d, 8)
16	150.42	
17	138.44	
18	126.13	
19	64.68	3.29 (s)
α	31.16	0.72 (m), 1.17 (m)
β	6.93	0.58 (t, 7.5)
OCH_3	56.45	3.91 (s)
$COCH_3$	22.80	2.38 (s)
$COCH_3$	169.74	
CN	119.94	
—	—	OH 10.90

[a]Numbering is identical to that in Table 1.
[b]The C(10) protons appear as a complex multiplet centered at δ 3.27. The nonequivalence of these protons is approximately 0.03 ppm.

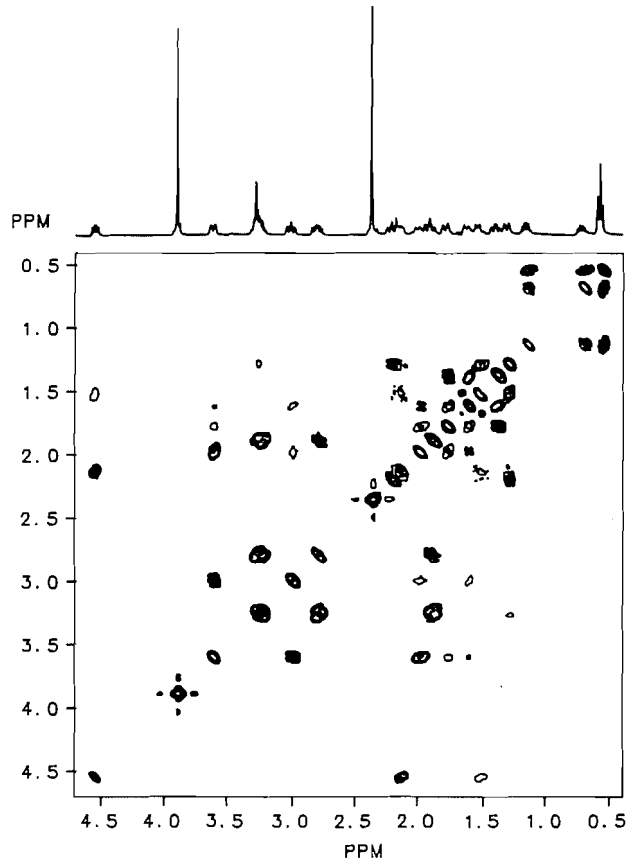

FIG. 2. COSY-45 spectrum for **2**.

in a chair form (11). i.e., the axial protons show two large (ca. 12 Hz) splittings corresponding to $^{2}J_{H(a)H(e)}$ and $^{3}J_{H(a)H(a)}$ plus a smaller splitting (ca. 4 Hz) corresponding to $^{3}J_{H(a)H(e)}$, while the equatorial protons show one large $^{2}J_{H(a)H(e)}$ splitting and two smaller splittings assignable as $^{3}J_{H(e)H(a)}$ and $^{3}J_{H(e)H(e)}$ (see Table 1). Similar splitting patterns are observed for the corresponding protons in **2** (see Table 2), suggesting that rings C and D in both **1** and **2** are in chair conformations.

Further evidence concerning the specific chair conformations in each case is provided by the indirect shift-correlated experiments. $^{3}J_{CH}$ couplings are conformationally dependent with typical values for *anti*, *syn*, and *gauche* couplings being, respectively, ca. 8, 5, and 2 Hz (12). Polarization transfer between ^{1}H and ^{13}C is maximum when the fixed delay, T, equals $(2J_{CH})^{-1}$ (7). Most spectra were run using $T = 0.06$ s (see Experimental), corresponding to an optimum $J_{CH} \cong 8$ Hz. Consequently, *gauche* $^{3}J_{CH}$ coupling vectors are still far removed from the antiphase orientation that leads to maximum polarization transfer (5). After polarization transfer, a second delay allows the $^{13}C-^{1}H$ coupling vectors to return to an in-phase orientation prior to ^{1}H decoupling and ^{13}C detection (5). Once again the delay is too short for *gauche* $^{3}J_{CH}$ coupling vectors to reach this optimum orientation. Consequently three-bond *gauche* C—H connectivities are effectively suppressed, while those corresponding to *anti* pathways are optimized.[2]

This allows one to probe conformations of rings C and D in terms of observed or missing three-bond peaks. Specifically, equatorial hydrogen should show three-bond $^{1}H-^{13}C$ cross peaks, while axial hydrogens do not. For example, the isolated

[2]A somewhat similar approach has recently been used to deduce conformational information for ryanodine (13).

TABLE 4. Observed two-bond and three-bond $^{13}C-^{1}H$ connectivities from XCORFE experiments on **2**

Carbon	^{1}H connectivities[a]
2	3_a(d), 3_e, 4_e, 19
3	2, 4_a(d), 4_e
4	3_a(d), 6_a, 19
5	3_e, 4_a, 4_e, 6_a, 6_e, 7_e, 19, α_l, α_h, β
6	7_e, 8_e
7	6_a(d), 6_e, 8_a(d), 8_e
8	6_e, 7_a(d), (19)
10	11_l(d), 11_h(b)
11	2, 10(d)
12	2, 3_e, (11_l), 11_h, 14, 19
13	2, (11_h), 15, 19
14	15(d)
15	14(d)
16	14, (15), (OH), OCH_3
17	(14), 15, (OH)
18	(2), 14, (OH)
19	4_e, 6_e, 8_e (11_l)
α	4_a, (6_a), (19), β(b)
β	α_l(b), α_h(b)
OCH_3	
$COCH_3$	
$COCH_3$	$COCH_3$
CN	8_a, 19

[a]See footnote *a* of Table 2.

proton, H(19), is in an axial orientation with respect to ring D and an equatorial orientation with respect to ring C. As expected, it shows strong three-bond cross peaks with C(2) and C(4) of ring C but no significant cross peaks with C(6) or C(8) in ring D. By contrast, in both **1** and **2** C(19) shows strong cross peaks with hydrogens $H(4)_e$ (δ 1.33), $H(6)_e$ (δ 1.82), and $H(8)_e$ but not from H(2), which is in a pseudo-axial orientation with respect to ring C. Similarly, there is a cross peak between C(2) and $H(4)_e$ but not between C(4) and H(2), while strong cross peaks are also observed between C(6) and $H(8)_e$ and C(8) and $H(6)_e$. All of these observations are entirely consistent with chair forms for rings C and D of **1** and **2**, similar to **4**.

The connectivity data also strongly imply an axial orientation for the cyano group bonded to nitrogen in **2** (see **5**). Three-bond connectivities are observed between the cyano group and both $H(8)_a$ and H(19) but not with $H(8)_e$. Since this indicates an *anti* orientation of the cyano group with respect to the two axial hydrogens, it follows that the former group is axial. This was further supported by selectively ^{1}H decoupled ^{13}C spectra for the cyano group, which indicated couplings of 9, 2, and 9 Hz to $H(8)_a$, $H(8)_e$, and H(19), respectively.

While the mechanism of the von Braun cyanogen bromide reaction received little earlier attention, it is now established that the reaction proceeds through the *N*-cyanoammonium salt (14). The reversal of the reaction, eliminating CNBr from the bromocyanamide, is rarely observed. The conformation deduced for the bromocyanamide (**5**) in the present case suggests an explanation for the reversal of the reaction: the equatorially disposed lone-pair electrons on nitrogen are well placed to effect an intramolecular displacement of the bromide. It is reasonable to suppose that this process corresponds to the microscopic reversal of the bond cleavage in the forward direction and leads to the conclusion that the configuration at the nitrogen of the cyanoammonium intermediate is opposite to that in the methiodide (see **3**). It follows then that the cyanogen bromide in the von Braun reaction undergoes a facile reaction with the free base in its dominant conformation (**4**), while methyl iodide fails to react with the nitrogen in this conformation and selectively quaternizes the nitrogen of the minor conformational isomer.

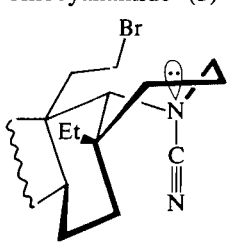

5

Experimental

The isolation of aspidocarpine has been described elsewhere (1). The von Braun reaction was carried out using previously described conditions (1).

All nmr data were obtained on a Varian XL-400 nmr spectrometer (^{13}C 90° pulse width = 13.5 μs, ^{1}H 90° pulse width **4** 13.6 μs, ^{1}H 90° pulse width through decoupler coil of multinuclear probe = 27.0 μs, probe temperature = 18°C). In each case, 70 mg of **1** or **2** was dissolved in ca. 0.5 mL of $CDCl_3$ in a 5-mm tube. Typical parameters for the COSY spectrum were $f_1 = f_2 = 2200$ Hz with 512 time increments (zero filled to 1024), 1024 data points, 16 transients per time interval, and 0.5 s relaxation delay. Pseudo-echo processing was used in both domains, followed by symmetrization by triangular folding. Typical parameters for direct heteronuclear shift-correlated spectra were $f_1 = 2200$ Hz, $f_2 = 7500$ Hz, 256 time increments (zero filled to 1024), 2048 data points, 64 transients per time interval, and 0.5 s relaxation delay. Separate spectra were obtained for the aromatic region.

Two sets of XCORFE spectra were obtained in each case with fixed times $T = 0.062$ s (272 time increments for 2200 Hz, f_1 spectral width) and $T = 0.08$ s (352 time increments for 2200 Hz, f_1 spectral width) and 256 transients per time interval. These are, respectively, optimized for $J_{CH} \cong 8$ Hz and $J_{CH} \cong 6$ Hz. Note that in XCORFE (7) and other similar 2D experiments (15, 16) one not only must choose $T \sim (^{2}J_{CH})^{-1}$ but also avoid the condition $T \sim (2J_{HH})^{-1}$ since polarization transfer is eliminated if $^{1}H-^{1}H$ coupling vectors are antiphase at the end of T (16). $T = 0.062$ is a good choice in most cases since J_{HH} is generally less than 5 Hz or greater than 10 Hz. However, in some cases (H(2), H(α), H(β), and the aromatic protons) $J_{HH} \sim 8$ Hz. The alternative time generally gave better cross peaks for these protons.

Acknowledgements

Financial support from the Natural Sciences and Engineering Research Council of Canada (to S.McL. and W.F.R.) and the Government of the People's Republic of China (to X.Z.) is gratefully acknowledged.

1. S. McLEAN, K. PALMER, and L. MARION. Can. J. Chem. **38**, 1547 (1960).
2. H. CONROY, P. R. BROOK, M. K. ROUT, and N. SILVERMAN. J. Am. Chem. Soc. **80**, 5178 (1958).
3. G. A. CORDELL. *In* The alkaloids. Vol. 17. *Edited by* R. H. F. Manske and R. Rodrigo. Academic Press, New York. 1979.
4. D. M. DODDRELL, D. T. PEGG, and M. R. BENDALL. J. Magn. Reson. **48**, 323 (1982).
5. A. BAX and G. A. MORRIS. J. Magn. Reson. **42**, 501 (1981).
6. A. BAX and R. FREEMAN. J. Magn. Reson. **44**, 542 (1981).
7. W. F. REYNOLDS, D. W. HUGHES, M. PERPICK-DUMONT, and R. G. ENRIQUEZ. J. Magn. Reson. **63**, 413 (1985).
8. G. E. MACIEL. *In* Topics in carbon-13 nmr spectroscopy. Vol. 1. *Edited by* G. C. Levy. Wiley–Interscience, New York. 1974.
9. J. F. D. MILLS and S. C. NYBURG. J. Chem. Soc. 1458 (1960).
10. G. F. SMITH and J. T. WROBEL. J. Chem. Soc. 1463 (1960).
11. L. JACKMAN and S. STERNHELL. Applications of nuclear mag-

Can. J. Chem. Downloaded from www.nrcresearchpress.com by 80.58.250.72 on 09/07/12
For personal use only.

netic resonance spectroscopy in organic chemistry. Pergamon Press, Oxford. 1969.
12. P. E. HANSEN. Prog. Nucl. Magn. Reson. Spectrosc. **14**, 175 (1981).
13. A. L. WATERHOUSE, I. HOLDEN, and J. E. CASIDA. J. Chem. Soc. Perkin Trans. 2, 1011 (1985).
14. G. FODOR, S. ABIDI, and T. C. CARPENTER. J. Org. Chem. **39**, 1507 (1974).
15. H. KESSLER, C. GRIESENGER, J. ZARBOCK, and H. R. LOOSI. J. Magn. Reson. **57**, 331 (1984).
16. C. BAUER, R. FREEMAN, and S. WIMPERIS. J. Magn. Reson. **58**, 526 (1984).

Can. J. Chem. Downloaded from www.nrcresearchpress.com by 80.58.250.72 on 09/07/12
For personal use only.

A comparative study on the dynamics of epimeric 1-hydroxymethylquinolizidines: I. Conformational analysis of monomers and spectroscopic data for solid state, liquid state, and dilute solutions

K. KULIŃSKA AND M. WIEWIÓROWSKI

Institute of Bioorganic Chemistry, Polish Academy of Sciences, Noskowskiego 12, 61-704 Poznań, Poland

Received June 11, 1986

This paper is dedicated to Dr. O. E. (Ted) Edwards

K. KULIŃSKA and M. WIEWIÓROWSKI. Can. J. Chem. **65**, 205 (1987).

A systematic comparative study of the conformational dynamics of lupinine and epilupinine, two 1-hydroxymethyl quinolizidine epimers, as a function of phase transition and of their protonation is presented. Lupinine and epilupinine have a *trans*-quinolizidine configuration and they differ only in the position of the CH_2OH group. The axial position of this group allows the formation of an intramolecular hydrogen bond OH...N in lupinine, in contrast to epilupinine in which this group is in the equatorial position. Intrinsic conformational equilibria for both epimers have been defined. Despite the significant difference in the population of the preferred rotamers of lupinine and epilupinine, both epimers adopt very similar crystal structures, but in all other states and forms, e.g., pure liquids, solutions in inert and polar solvents, and protonated salts, they behave in drastically different ways.

K. KULIŃSKA et M. WIEWIÓROWSKI. Can. J. Chem. **65**, 205 (1987).

On présente une étude comparative systématique des dynamiques conformationnelles de la lupinine et de l'épilupinine (deux épimères de l'hydroxyméthyl-1 quinolizidine) en fonction de la transition de phase ainsi que de leur protonation. La lupinine et l'épilupinine possèdent une configuration *trans* au niveau de la quinolizidine et leur seule différence réside dans la position du groupement CH_2OH. Le fait que ce groupement soit en position axiale dans la lupinine lui fournit l'occasion de former des liaisons hydrogènes intramoléculaires OH...N qui ne se forment pas dans le cas de l'épilupinine dans laquelle le groupement se trouve en position équatoriale. On a défini les équilibres conformationnels intrinsèques des deux épimères. Malgré l'existence de différences importantes dans les populations des rotamères préférés dans la lupinine et dans l'épilupinine, chacun des épimères existe dans des structures cristallines assez semblables; toutefois, dans tous les autres états et formes (liquides purs, solutions dans des solvants inertes et polaires et sous formes de sels protonés), il se comportent très différemment.

[Traduit par la revue]

Introduction

Two 1-hydroxymethyl quinolizidine epimers, lupinine and epilupinine (Fig. 1), have a *trans*-quinolizidine configuration (*trans* Q) (1). Rotation of the exocyclic hydroxymethylene group makes three staggered conformers of lupinine and epilupinine (Fig. 2) possible. The axial position of the CH_2OH group creates good stereochemical conditions for the formation of an intramolecular hydrogen bond OH...N in the *syn*/−60° rotamer of lupinine. In contrast, the equatorial position of the CH_2OH group in epilupinine makes a similar intramolecular interaction impossible, because of the long nitrogen–oxygen atomic distance (in the most favourable rotamer it is >3 Å).

In previously published papers (2–4) it has been shown that the lupinine rotamer with an intramolecular hydrogen bond predominates in solution, in contrast to the solid state, where only a crystal structure with an *anti*/180° lupinine conformation was found (5).

This paper presents a systematic comparative study of the conformational dynamics of lupinine and epilupinine as a function of phase transition and of their protonation. Various self-association properties of both epimers, possessing analogous proton-donor and -acceptor centers, will be discussed in the light of different configuration and conformational dynamics in the next paper of this series.

Experimental

Infrared spectra were measured on a Perkin–Elmer ir spectrometer, type 180. The ir spectra of solids were obtained by the powder method of suspension in Fluorolub (4000–1400 cm^{-1}). The ir spectra of liquids were obtained using cells of various thickness with NaCl or CaF_2 windows, depending on the solvent and concentration of the solution.

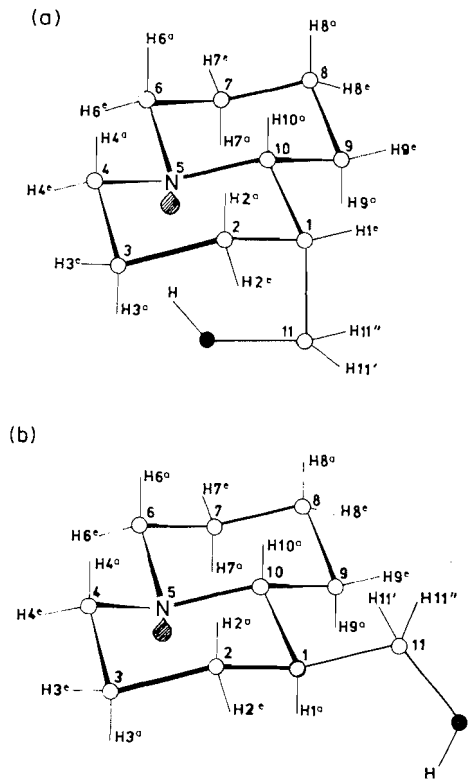

FIG. 1. Molecular structure of quinolizidine epimers: (*a*) lupinine and (*b*) epilupinine. Open circles denote carbon atoms; filled circles, oxygen atoms; "a" denotes axial, "e" equatorial, orientation of the hydrogen atoms.

Can. J. Chem. Downloaded from www.nrcresearchpress.com by 190.90.36.8 on 09/07/12
For personal use only.

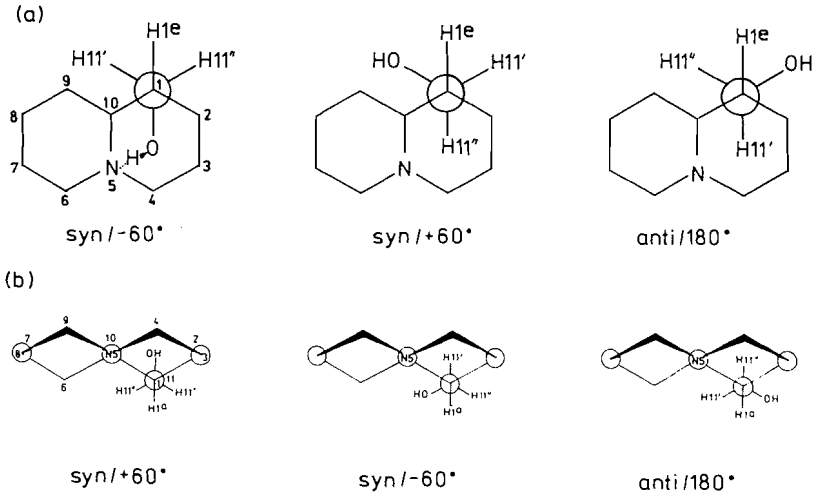

FIG. 2. Staggered (*a*) lupinine and (*b*) epilupinine conformers induced by rotations of the exocyclic CH_2OH group around the C1—C11 bond. The plane of projection of both epimers is perpendicular to C1—C11. Open rings indicate carbon atoms overlapped in projection. The terms "*syn*" and "*anti*" pertain to the relative position of the oxygen and C10 carbon atoms; the angular value describes the C10—C1—C11—O torsion angle.

Can. J. Chem. Downloaded from www.nrcresearchpress.com by 190.90.36.8 on 09/07/12
For personal use only.

All solvents were spectrally pure (Merck) and were dried prior to the experiment by passing through an aluminum oxide filled column and storing above 3 or 4 Å sieves.

The concentration of solutions was achieved by a precise weighing of each compound, which was then dissolved in an amount of solvent accurately measured with a micro pipette, or by the extinction of the C—H band at 2670 cm^{-1} (particularly in the series of concentration spectra). To avoid hydration of the solution, contact of the solvent with the environment was minimized, and the operation carried out partly in a dry box. Infrared spectra at higher temperatures were measured with the aid of a Specac temperature attachment, which enables stabilization of the temperature of the sample with a precision of ± 1°C.

The ^1H nmr and ^{13}C nmr spectra were recorded on JEOL FX-90Q Fourier transfer impulse equipment by the standard method and by double resonance, which facilitated the assignment of signals in the spectra. The ^{13}C nmr spectra were done by the noise band decoupling (NBD) and the single frequency of resonance decoupling (SFORD) techniques.

Results and discussion

Intrinsic conformational equilibrium

Conformational equilibrium can be defined by the free energy difference between conformations A and B

$$-RT \ln \frac{A}{B} = \Delta G^0(A) - \Delta G^0(B)$$

where ΔG^0 of each conformer is assumed to be equal to the algebraic sum of its 1,3 synaxial conformational interactions (6). The ΔG^0 values of 1,3 synaxial interactions were taken from the literature (4, 6).

Lupinine:

$$\Delta G^0(syn/-60°) = \Delta G^0(CH_2/OH) + \Delta G^0(CH_2/H) - \Delta G^0(OH\ldots N)$$
$$= 2.85 - \Delta G^0(OH\ldots N) \text{ kcal mol}^{-1}$$
$$\Delta G^0(anti/180°) = 2\Delta G^0(CH_2/H) + \Delta G^0(CH_2/N) + \Delta G^0(OH/H)$$
$$= 2.50 \text{ kcal mol}^{-1}$$
$$\Delta G^0(syn/+60°) = \Delta G^0(CH_2/OH) + \Delta G^0(CH_2/N) + \Delta G^0(CH_2/H)$$
$$= 3.30 \text{ kcal mol}^{-1}$$

TABLE 1. Lupinine and epilupinine free energy values and the population distribution of three staggered rotamers

	Rotamers	Free energies ΔG^0 (kcal mol^{-1})	Relative population of rotamers (%) 1[a]	2[b]
Lupinine	*syn*/−60°	2.85[c]	31	89
	anti/180°	2.50	55 }	11
	syn/+60°	3.30	14 }	
Epilupinine	*syn*/+60°	1.55	31	
	anti/180°	1.20	55	
	syn/−60°	2.00	14	

[a]Relative population of rotamers calculated according to the semi-empirical formula from refs. 4*a* and 6.

[b]Relative population of rotamers calculated from ir spectra of dilute lupinine and epilupinine solutions in inert solvent.

[c]Calculated without the contribution of the free energy, ΔG^0(OH...N), of the intramolecular OH...N hydrogen bond.

Epilupinine:

$$\Delta G^0(syn/+60°) = 2\Delta G^0(OH/H) + \Delta G^0(CH_2/H) = 1.55 \text{ kcal mol}^{-1}$$
$$\Delta G^0(anti/180°) = \Delta G^0(OH/H) + \Delta G^0(CH_2/H) = 1.20 \text{ kcal mol}^{-1}$$
$$\Delta G^0(syn/-60°) = \Delta G^0(OH/CH_2) = 2.00 \text{ kcal mol}^{-1}$$

The conformational equilibrium defined in this way is called an intrinsic conformational equilibrium, because it is determined exclusively by intramolecular steric tension. The free energy values obtained and the population of particular lupinine and epilupinine rotamers calculated on this basis are listed in Table 1.

Molecular structure in dilute solutions of inert solvent

The ir spectra of dilute lupinine and epilupinine solutions in CCl_4 in the region of stretching vibrations of the OH group are presented in Fig. 3. At low concentration, about 10^{-3} *M*, nearly all molecules of lupinine and epilupinine occur as monomers (4*a*). In the ir spectra of dilute epilupinine – carbon tetrachloride (CCl_4) solutions, where homoassociation processes take place

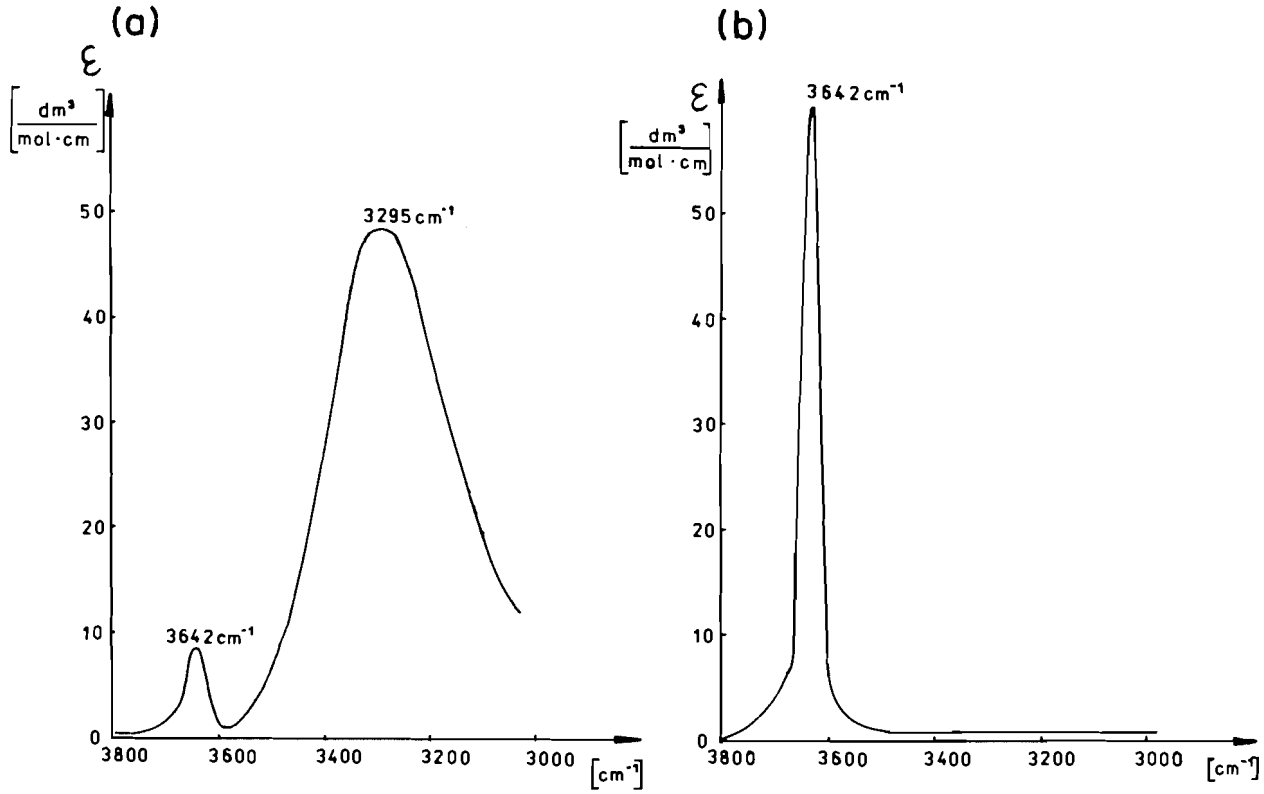

FIG. 3. The ir spectra of dilute (*a*) lupinine and (*b*) epilupinine solutions in CCl_4 in the region of stretching vibrations of the OH group (c = 0.003 M, 30°C).

only to a very small extent, only one ν(OH) band at 3642 cm^{-1} is present, indicating that "free" OH groups vibrate in the same manner in all rotamers of epilupinine. The ir spectrum of a dilute lupinine solution is in accordance with theoretical expectations and previous literature reports (4*b*), and exhibits two bands within this spectral range: (*i*) a low intensity band in the same position as in an epilupinine ir spectrum ν(OH) = 3642 cm^{-1}, corresponding to rotamers with a "free" OH group (*syn*/+60° and *anti*/180°); and (*ii*) a band ν(OH...N) = 3295 cm^{-1} corresponding to the *syn*/−60° rotamers in which the OH group is engaged in an intramolecular hydrogen bond. Integrative absorptions of the ν(OH) = 3642 cm^{-1} bands in the ir spectra of lupinine and epilupinine solutions in CCl_4 were compared, on the assumption that the molar extinction coefficient of free stretching vibrations of the OH group is identical for the epimeric compounds (4*b*). Approximately 11% of lupinine molecules occur in the *syn*/+60° and *anti*/180° conformations, from which it follows that 89% of the molecules take on the *syn*/−60° conformation.

Comparing the spectroscopically determined conformational equilibrium of lupinine with its intrinsic conformational equilibrium, one can calculate the unknown free energy value of the intramolecular hydrogen bond formation (4*a*), which equals ΔG^0 (OH...N) = −1.8 kcal mol^{-1}.

An increasing concentration of lupinine and epilupinine in such solutions as *n*-heptane, *n*-hexane, CCl_4, 1,2-dichloroethane, and benzene causes bands of homoassociated molecules to appear in the ir spectra beside those of solvated monomers.[1] Concentration does not influence the conformational equilibrium between intramolecular hydrogen bonded (*syn*/−60°) and other forms (*syn*/+60° and *anti*/180°) of lupinine monomers, as long as no crystallization takes place in the solution, since the ratio of integrative absorptions ν(OH) and ν(OH...N) is independent of concentration.

The ^{1}H nmr spectra of lupinine solutions in CCl_4 and deuterated chloroform ($CDCl_3$) add new information about the rotation of the exocyclic CH_2OH group. The ^{1}H nmr spectrum of a lupinine solution in $CDCl_3$, presented in Fig. 4*a*, shows four groups of signals originating from (*1*) the hydroxyl proton, δ 5.38 ppm, (*2*) protons H11′ and H11″ of the exocyclic CH_2OH group, δ 4.3–3.6 ppm, (*3*) equatorial protons from α carbons, δ 2.9–2.7 ppm, (*4*) the remaining protons of the quinolizidine ring, which give a broad band in the range δ 2.3–1.0 ppm. (The chemical shift assignments in the ^{1}H nmr and ^{13}C nmr spectra were made by comparison with previously reported values (7) and off-resonance decoupling. An extensive analysis of ^{1}H nmr spectra of lupinine and epilupinine solutions is presented in ref. 8.)

In solutions of lupinine in dilute CCl_4 and in 0.01–2.0 M $CDCl_3$ the signals of the H11′ and H11″ methylene protons of the CH_2OH group appear as doublets and quartets (Fig. 4*a*). The vicinal coupling constants of H11′ and H11″ protons with the H1^e proton, observed in the ^{1}H nmr spectrum, are the weighted average of vicinal coupling constants for all three lupinine rotamers. The fact that the value of the vicinal coupling constant for one of the methylene protons is reduced to 0 Hz can be attributed to the deformation of the ideal *syn*/−60° conformer, by an intramolecular hydrogen bond, into a *syn*/−30° form in which a dihedral angle of H1—C1—C11—H11″ equals nearly 90° (Fig. 5). Then, in accordance with the Karplus dependence, its vicinal coupling constant is a small negative number equilibrating the impact of the few (about 10%)

[1]A detailed discussion of homoassociation processes of lupinine and epilupinine will be presented in the following paper of this series (K. Kulińska and M. Wiewiórowski, in preparation).

Can. J. Chem. Downloaded from www.nrcresearchpress.com by 190.90.36.8 on 09/07/12
For personal use only.

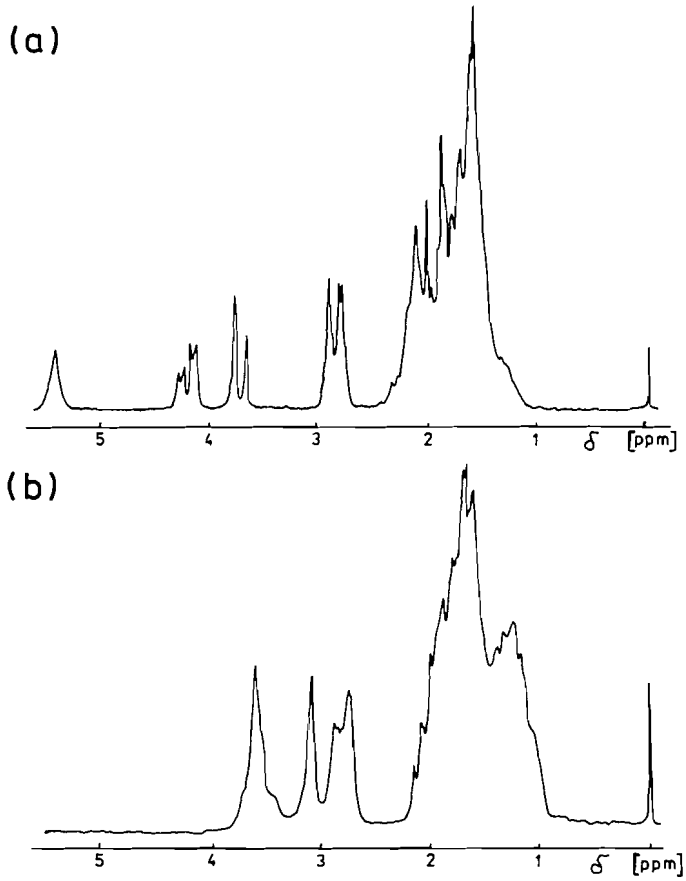

FIG. 4. The ^1H nmr spectra of (*a*) lupinine and (*b*) epilupinine solutions in $CDCl_3$ ($c = 0.4\,M$, 30°C).

anti/180° and *syn*/+60° rotamers. From model observations it follows that the *syn*/−30° conformation creates the most favourable geometrical conditions for the intramolecular hydrogen bond because the distance between the nitrogen and oxygen atoms becomes the shortest and the hydrogen bond is almost linear. The mean vicinal coupling constant of the H11′ methylene proton with $H1^e$ equals 6 Hz, as determined from the ^1H nmr spectrum (Fig. 4), which according to the Karplus correlation (9) should correspond to the values for dihedral angles of about 30° or 150°. The first value fits very well to the assumed 90° torsion angle for H1—C1—C11—H11″ bonds shown in Fig. 5*b*. In the ^1H nmr spectra of CCl_4–lupinine solutions of higher concentration, the methylene proton signals appear as two quartets, since as well as monomers among which the conformers with intramolecular hydrogen bonds dominate by 90%, there appear in increasing amounts associated molecules without intramolecular hydrogen bonds, i.e., without the deformed *syn*/−30° conformation in which the value of the vicinal coupling constant $J(H1^eH11'')$ is a small negative number.

Conformational dynamics of the hydrated and protonated quinolizidine ring system in aqueous solutions

A comparison of ^1H nmr spectra of aqueous solutions of lupinine and epilupinine measured under identical concentration and temperature conditions shows a lower resolution of the former (Fig. 6). This cannot be due to the high viscosity of lupinine solution in D_2O (9) because the spectra of epilupinine, which possesses a similar viscosity, show a much better resolution. Moreover, a decrease in the concentration of

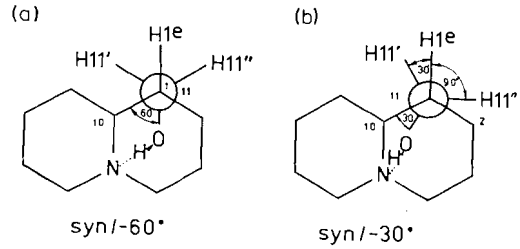

FIG. 5. Schematic presentation of lupinine rotamer with intramolecular hydrogen bond in its ideal *syn*/−60° and deformed *syn*/−30° form.

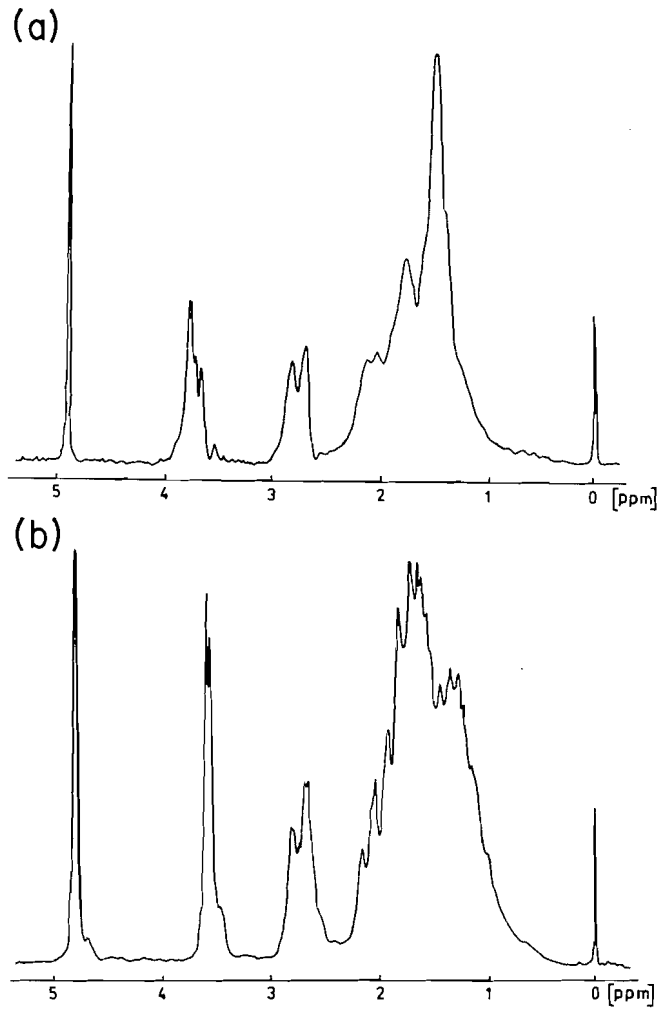

FIG. 6. The ^1H nmr spectra of (*a*) lupinine and (*b*) epilupinine aqueous solutions ($c = 0.4\,M$, 30°C).

lupinine solution decreases its viscosity but does not increase the resolution of the spectrum. On the other hand, an increase in temperature is accompanied by greater resolution of the ^1H nmr spectra of lupinine solution in D_2O, and by a shift of signals originating from the protons of the quinolizine rings within the range 1.0–2.3 ppm (Fig. 7).

In the second paper of this series[1] we will show that in aqueous solution intramolecular hydrogen bonds are not present within lupinine. Relatively small water molecules can interact specifically both with tertiary nitrogen and with the hydroxyl group. It is known from earlier papers that N-methylation and N-oxidation of lupinine cause inversion at the nitrogen atom

Can. J. Chem. Downloaded from www.nrcresearchpress.com by 190.90.36.8 on 09/07/12
For personal use only.

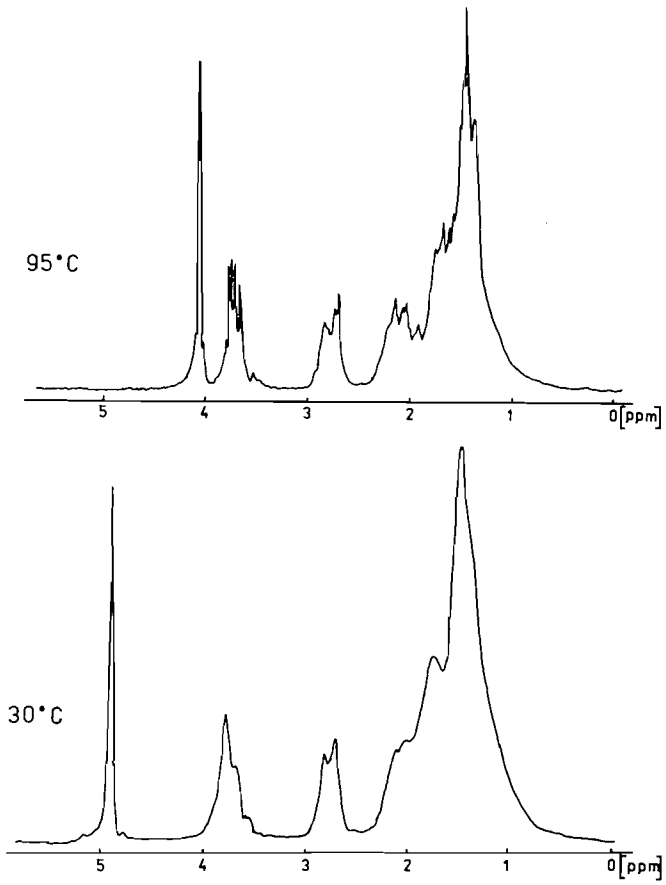

FIG. 7. The ^{1}H nmr spectra of aqueous solutions of lupinine at different temperatures (c = 0.8 M).

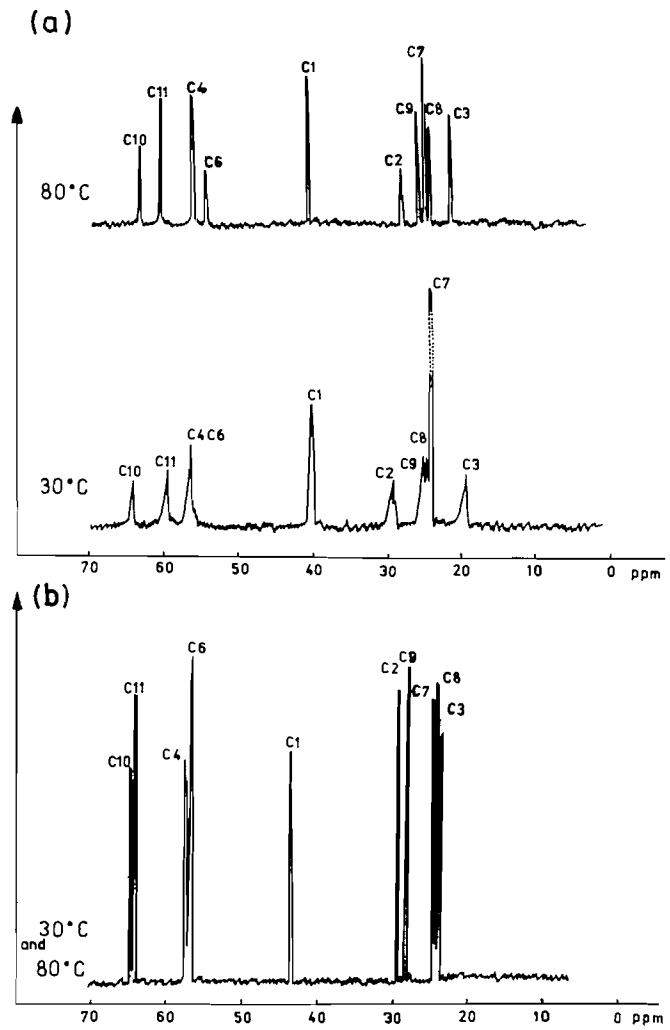

FIG. 8. The ^{13}C nmr spectra of aqueous solutions of (a) lupinine and (b) epilupinine (c = 0.4 M).

(10). We assume that the hydration of a lupinine molecule can also bring about a similar inversion and, in consequence, the occurrence of lupinine molecules in aqueous solution also in the "*cis*" configuration.

The above spectroscopic observations confirm the existence of this type of conformational and configurational dynamism in the quinolizidine system of lupinine.

At room temperature the *cis* ⇄ *trans* transformation is so slow that it only causes a broadening of the signals in the spectrum, but an increase in temperature accelerates the rate of configurational changes. In the ^{1}H nmr spectrum of an aqueous solution of epilupinine, increase in temperature does not bring about any changes, and the spectrum has a relatively good resolution over the whole temperature range. The presence of configurational *cis–trans* dynamism in a lupinine molecule, and the absence of this dynamism in a molecule of epilupinine in aqueous environment, is further confirmed by ^{13}C nmr spectra of aqueous solutions of these molecules.

The signals in a ^{13}C nmr spectrum of lupinine in D_2O vary in intensity and are broadened (Fig. 8*a*), contrary to the ^{13}C nmr spectra of aqueous solutions of epilupinine (Fig. 8*b*). By increasing the temperature the signals in a ^{13}C nmr lupinine spectrum become sharp, their intensities unified, and considerable shifts are also observed. In the ^{13}C nmr spectrum of the aqueous solution of lupinine the signal of carbon C7 exhibits an exceptionally high intensity. If one compares the Dreiding models of *trans* and *cis* lupinine conformers one notices that only the environment of carbon C7 does not undergo any changes as a consequence of a transition from the *trans* into the *cis* Q form. The high intensity of this signal in the ^{13}C nmr spectrum indicates long relaxation times T_1 and T_2. A broadening of the signals and their shift resulting from temperature changes indicate the presence of, and dynamic transition between, the *trans* and *cis* forms of lupinine.

Configurational changes within the quinolizidine system that were observed in aqueous solution of lupinine made us expect that the *cis* ⇄ *trans* equilibrium would also appear in solutions of protonated lupinine derivatives such as lupinine hydrochloride and perchlorate.

Crystalline lupinine hydrochloride preserves the *trans*-quinolizidine configuration (5) whereas the N-methylated derivative of lupinine occurs exclusively in the "*cis*" form (5). This indicates that, in the process of N-alkylation, inversion takes place at the nitrogen atom.

The ^{13}C nmr spectra of the aqueous lupinine hydrochloride solution contain a double number of signals (Fig. 9). This is evidence of the coexistence of comparable populations of the *trans* and *cis* forms of protonated lupinine molecules in aqueous solution. Either both these forms are stable and do not undergo mutual transformation, or the mutual transformation of both forms is very slow.

In the ^{13}C nmr spectra of aqueous epilupinine solutions no changes indicating the presence of a dynamic *cis* ⇄ *trans* equilibrium are observed, just as in the ^{1}H nmr spectra. As

Can. J. Chem. Downloaded from www.nrcresearchpress.com by 190.90.36.8 on 09/07/12
For personal use only.

Can. J. Chem. Downloaded from www.nrcresearchpress.com by 190.90.36.8 on 09/07/12
For personal use only.

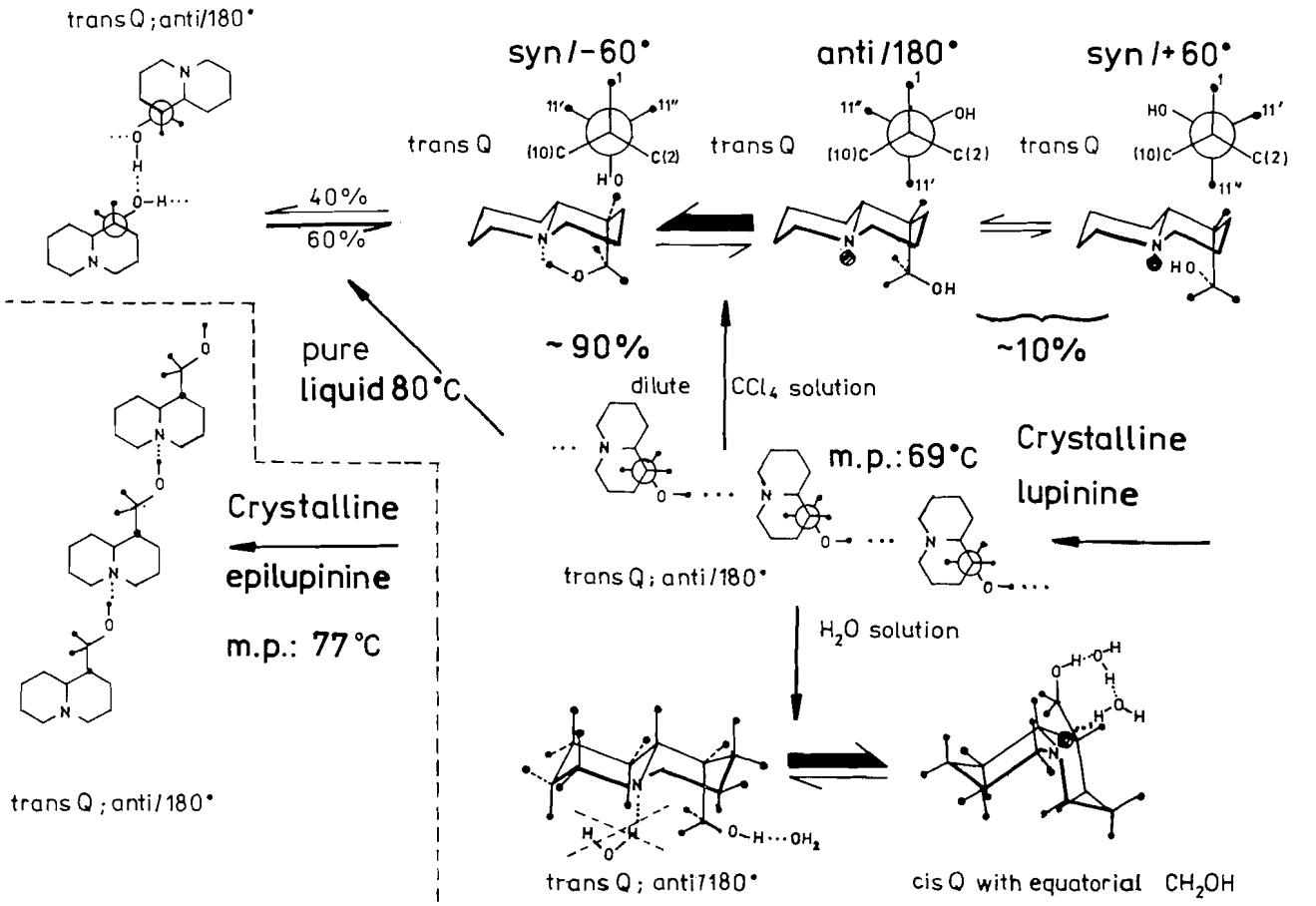

SCHEME 1. Schematic presentation of structural changes of lupinine molecule occurring on solid ⇄ liquid and solid ⇄ solute phase transitions.

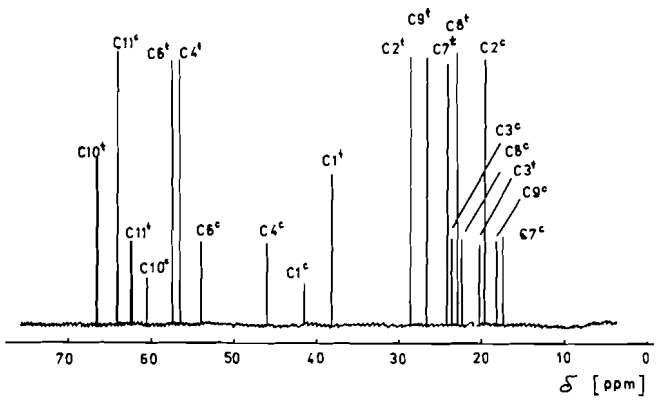

FIG. 9. The ^{13}C nmr spectra of aqueous solutions of lupinine hydrochloride (c = 0.4 M, 30°C).

expected, epilupinine exhibits no conformational dynamism other than the rotation of the exocyclic CH_2OH group around the C1—C11 bond.

Molecular structure in the solid and liquid states

In the crystalline structure, lupinine and epilupinine occur in the *anti*/180° conformation and form infinitely long linear polyassociates linked by intermolecular hydrogen bonds OH...N′ (Scheme 1). To compare the strengths of the OH...N′ intermolecular hydrogen bonds present in the monocrystals of lupinine and epilupinine, the ΔHB and $-\Delta H^0$ parameters were calculated (11*a*,*b*). The values of the ΔHB parameters, approximate values of enthalpy $-\Delta H^0$ corresponding to them,

TABLE 2. Selected parameters characterizing the geometry and strength of the intermolecular hydrogen bonds OH...N′ in the crystalline structure of lupinine and epilupinine

	ΔHB[a]	$-\Delta H^0$ (kcal mol^{-1})	d (Å)[b]	∢β[c]
Lupinine	132	2	2.868	10.2°
Epilupinine	98	1.5	2.902	15.1°

[a]The ΔHB parameter indicates the value by which the distance between the hydrogen bonded proton donor and acceptor groups is shorter than the sum of corresponding van der Waals radii. The following values of the van der Waals radii have been used: r_O = 1.45 Å; r_N = 1.55 Å; ΔHB = $(r_O + r_N - d) \times 10^3$ (Å).
[b]d = the distance between the oxygen atom and the nitrogen atom, from X-ray data.
[c]∢β = 180° − ∢(OH, ON′).

as well as some X-ray data describing the geometry of the O...N′ intermolecular hydrogen bonds are given in Table 2.

The values of the ΔHB parameters show that the OH...N′ intermolecular hydrogen bonds, which occur in the crystalline structure of both epimers, are of comparable strength and belong to the group of weak hydrogen bonds. The above observation is confirmed by the ir spectra of the solid state of lupinine and epilupinine (Fig. 10). The bands of the stretching vibrations of the OH group are shifted towards lower frequencies in respect to the band of the stretching vibrations of "free" OH, by 470 cm^{-1} in lupinine and by 480 cm^{-1} in epilupinine. The bigger shift in epilupinine suggests a stronger intermolecular hydrogen bonding OH...N′ in this compound, while X-ray data (namely, the distances between the hydrogen

TABLE 3. The stretching vibrations of the OH group (cm^{-1}) (free and involved in different types of hydrogen bonds)

Phase	Lupinine				Epilupinine		
	ν(OH)	ν(OH...O′)	ν(OH...N)	ν(OH...N′)	ν(OH)	ν(OH...O′)	ν(OH...N)
Solid				3170 s			3160 s
Liquid		3420 m	3310 m			3410 m	3200 m
Amorphic		3420 sh	3310 m	3170 s			
CCl_4 $c = 0.003\ M$	3640 w		3295 s		3640 s		
CCl_4 $c = 0.7\ M$	3640 w	3400 m	3295 m	3170 sh	3640 w	3380 m	3200 m

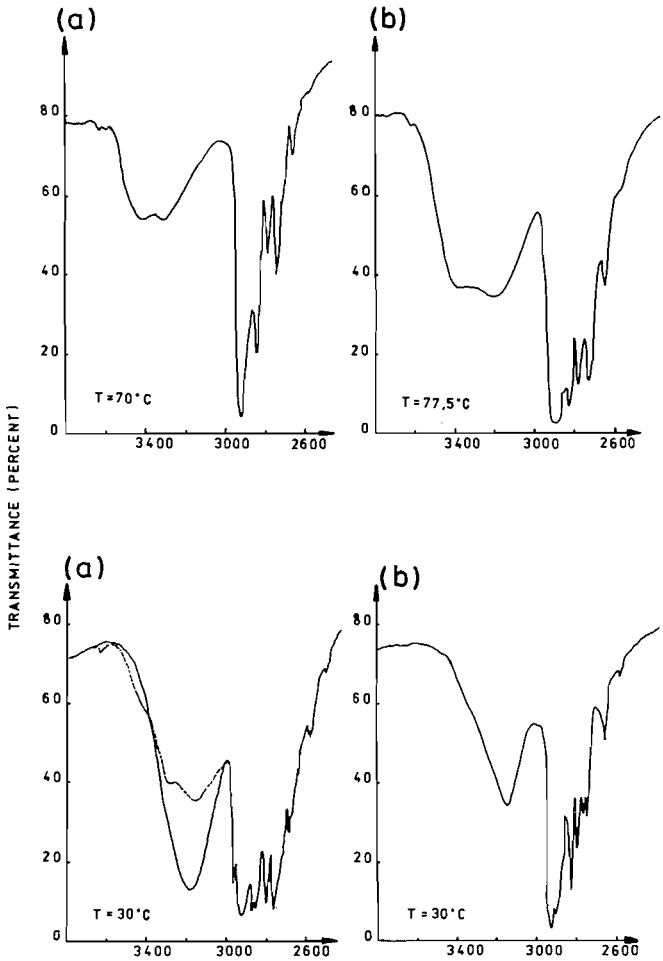

FIG. 10. The ir spectra of (*a*) lupinine and (*b*) epilupinine in the solid state at 30°C and at temperatures above the melting point. Dotted line denotes ir spectrum of lupinine in the amorphic phase ((*a*), 30°C).

bonded proton donor and acceptor groups and the ΔHB related parameters) suggest the opposite.

In spite of numerous attempts at the crystallization of lupinine under various conditions, we failed to obtain a different polymorphic crystalline form, in which lupinine would preserve the intramolecular hydrogen bond that is present in solution (see above). However, it has been observed that lupinine has a tendency to form an amorphic solid state. When the crystallization process of lupinine is fast, because of rapid cooling or the insertion of a crystalline germ into the supersaturated solution, the obtained ir spetrum of the solid state differs considerably from the ir spectrum of lupinine crystals obtained by way of slow crystallization (Fig. 10*a*, broken line).

The increase in temperature from 20°C to the melting point (69–70°C for lupinine, 77–78°C for epilupinine) does not cause any significant changes in the ir spectrum of the crystalline phase of either compound.

In the liquid state (temperature >70°C) nearly 50% of lupinine molecules adopt the form of a monomer with an intramolecular hydrogen bond (ν(OH...N) = 3310 cm^{-1}). A comparable number of molecules associate through the OH...O′ intermolecular hydrogen bond (ν(OH...O′) = 3420 cm^{-1}), and a small fraction of molecules (less than 10%) through the OH...N′ intermolecular hydrogen bond (the shoulder at 3170 cm^{-1}).

In liquid epilupinine, comparable fractions of the molecules associate through the OH...O′ (ν(OH...O′) = 3410 cm^{-1}) and OH...N′ (ν(OH...N′) = 3200 cm^{-1}) intermolecular hydrogen bonds.

The ir spectrum of the condensed amorphic phase of lupinine seems to be a superposition of the ir spectra of the crystalline and liquid phases (Fig. 10*a*, Table 3).

Summary and final remarks

Lupinine and epilupinine, two epimeric amino alcohols, differ in the position of the exocyclic hydroxymethyl group. This relatively small structural change has a drastic influence on the molecular and intermolecular dynamism of both epimers. The conformational and configurational dynamism of lupinine is much greater due to a sterically unfavourable axial location of the *exo* hydroxymethyl group. The exocyclic CH_2OH groups can rotate around the C1—C11 bonds and are the most dynamic fragments of both molecules.

Intrinsic conformational equilibria for lupinine and epilupinine have been defined in a semi-empirical way by calculation of conformational free energies assumed to depend only on intramolecular steric hindrances (6). Populations of the three staggered rotamers for lupinine and epilupinine are summarized in Table 1.

The *syn*/−60° rotamer in lupinine is additionally stabilized by an intramolecular OH...N hydrogen bond whose contribution to the conformational energy is ~1.8 kcal mol^{-1}. In consequence, the population of the *syn*/−60° rotamer of lupinine in dilute solution in inert solvents rises to ~90%, whereas that of the two remaining rotamers (*anti*/180° and *syn*/+60°) decreases to ~7 and ~3%, respectively.

Despite the significant difference in the populations of the preferred rotamers of lupinine (*syn*/−60°, 90%) and epilupinine (*anti*/180°, 55%), both epimeric amino alcohols adopt very similar crystal structures (5) containing infinite chains of hydrogen bonded *anti*/180° rotamers (Scheme 1). Close values of ν(OH) (3170 and 3160 cm^{-1}, Table 3) in the ir spectra of both crystalline samples indicate that also the strengths of the intermolecular hydrogen bonds in the above chains are almost identical.

Can. J. Chem. Downloaded from www.nrcresearchpress.com by 190.90.36.8 on 09/07/12
For personal use only.

Can. J. Chem. Downloaded from www.nrcresearchpress.com by 190.90.36.8 on 09/07/12
For personal use only.

In all other states and forms, e.g. pure liquids, dilute solutions (in inert and polar solvents), and protonated salts, the two epimers behave in drastically different ways.

In the case of epilupinine, the melting and dissolution processes do not show any unusual features. In pure liquid at 80°C, in addition to the OH...N polyassociated chain present in the crystalline solid (ν(OH...N) at 3200 cm^{-1}), there appears another type of homoassociation with —O—H...O— hydrogen bonds (ν(OH) at 3410 cm^{-1}, Table 3). In dilute epilupinine solution in inert solvents there exist, mostly or exclusively, solvated monomeric epilupinine molecules characterized in ir spectra by a ν(OH) band at 3640 cm^{-1}. When the concentration of epilupinine increases, the two homoassociates begin to appear (Table 3).

In the case of lupinine, phase transitions (i.e., melting and dissolution) are accompanied by disappearance of the polyassociated OH...N chains, present as exclusive forms in the single crystal of lupinine. Two forms dominate in pure liquid (temperature 70°C): monomeric *syn*/−60° rotamers with intramolecular hydrogen bonds, and OH...OH homoassociated *anti*/180° rotamers.

Scheme 1 presents in a very simplified manner the structural changes occurring in the solid ⇄ liquid and solid ⇄ solute phase transitions of lupinine.

In liquid lupinine, besides the association through intermolecular hydrogen bonds —OH...OH presented in Scheme 1, there certainly exist significant amounts of symmetric

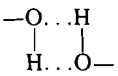

and especially asymmetric dimers where *syn*/−60° rotamers with an intramolecular hydrogen bond are associated by intermolecular hydrogen bond with the *anti*/180° rotamers:

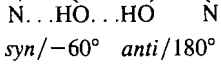

syn/−60° *anti*/180°

Lupinine molecules in dilute inert solvent solutions (e.g. CCl_4 or $C_2H_4Cl_2$) exist exclusively in two monomeric forms: homosolvated (rotamers, *syn*/−30° with intramolecular hydrogen bonds) and heterosolvated (rotamers, *anti*/180° and *syn*/+60°, solvated by solvent molecules).

The drastic change of conformational equilibrium in lupinine upon conversion to the crystalline phase seems to be brought about by competition between intermolecular OH...N′ and intramolecular OH...N hydrogen bonds. In solution and in the liquid state the formation of polymeric structures is hardly probable because of unfavourable entropy and limitations of the kinetics of the molecules. That is why the OH...N intramolecular hydrogen bond dominates, and the stronger OH...N′ intermolecular hydrogen bond is unstable. Only in the crystalline structure, when the molecular kinetics is blocked, is the *anti*/180° conformation of lupinine energetically more favourable. This facilitates the formation of the stronger OH...N′ intermolecular hydrogen bond. This is confirmed by recrystallization of the amorphic phase of condensed lupinine, in which process frozen structures containing intramolecular hydrogen bonds OH...N are gradually transformed into crystalline structures with OH...N′ intermolecular hydrogen bonds.

Both epimeric amino alcohols are very soluble in polar solvents, e.g. H_2O and DMSO. There is no doubt that these solvents are active enough to break the intermolecular hydrogen bonds existing in crystalline samples of lupinine and epilupinine. Water molecules, having both proton-donor and proton-acceptor centers, tend to interact with donor as well as acceptor centers of the epimeric amino alcohols. In epilupinine both the N and O atoms can be easily hydrated, especially in the *anti*/180° rotamer. However, in the case of lupinine, the axial CH_2OH group, even in the *anti*/180° form, creates significant steric hindrance around the nitrogen atoms and in consequence only the OH group can be easily hydrated when lupinine exists in the *trans* Q configuration. The ^{13}C nmr data of lupinine in D_2O suggest that, due to hydration, it is transformed in aqueous solution from the *trans* Q into the *cis* Q configuration by inversion at the nitrogen atoms. Thus the CH_2OH groups become equatorial and hence easily accessible by water molecules (Scheme 1). We assume that in an aqueous solution of lupinine the equilibrium between *trans* Q and *cis* Q is shifted almost completely to the *cis* side, but further evidence is needed. This statement is strongly supported by the previous chemical finding that the reactions of aqueous lupinine solution with H_2O_2 and CH_3I lead to the N-oxide and N-methyl derivatives of lupinine with the *cis* Q ring system (10).

1. R. H. F. Manske and H. L. Holmes. The alkaloids, chemistry and physiology. Academic Press, New York. Vol. III. 1953; Vol. VII. 1960; Vol. IX. 1967.
2. A. F. Thomas, R. J. Vipond, and L. Marion. Can. J. Chem. **35**, 1290 (1955).
3. M. Wiewiórowski and L. Lompa-Krzymień. Rocz. Chem. **44**, 1231 (1970).
4. (*a*) H. S. Aaron and C. P. Ferguson. Tetrahedron, **30**, 803 (1974); (*b*) J. Am. Chem. Soc. **98**, 7013 (1976).
5. A. Kozioł, Z. Kosturkiewicz, and N. Podkowińska. Acta Crystallogr. Sect. B, **34**, 3491 (1978); (*b*) A. Kozioł, N. Gdaniec, and Z. Kosturkiewicz. Acta Crystallogr. Sect. B, **36**, 982 (1980).
6. F. L. Eliel, N. L. Allinger, S. J. Angyal, and G. A. Morrison. Conformational analysis. John Wiley & Sons Inc., New York. 1965. p. 74.
7. (*a*) F. Bohlmann and R. Zeisberg. Chem. Ber. **108**, 1043 (1975); (*b*) E. Wenkert, B. Chauncy, K. G. Dave, A. R. Jeffcoat, F. M. Schell, and H. P. Schenk. J. Am. Chem. Soc. **95**, 8427 (1973); (*c*) H. Podkowińska and J. Skolik. Org. Magn. Reson. **22**, 6 (1984).
8. K. Kulińska. Ph.D. Thesis. UAM. Poznań.
9. P. S. Knowles, D. Marsh, and H. V. F. Rattle. Magnetic resonance of biomolecules. John Wiley & Sons Inc., New York. 1976. pp. 56, 64.
10. T. K. Janusow, W. B. Leontiew, F. G. Kamajew, A. H. Aslanow, and A. S. Sadykow. Chem. Prir. Soedin. **4**, 477 (1972).
11. (*a*) W. Krzyżosiak, M. Jaskólski, H. Sierzputowska-Gracz, and M. Wiewiórowski. Nucleic Acids Res. **10**, 2741 (1982); (*b*) A. Perkowska, M. Wiewiórowski, E. Skrzypczak-Jankun, and Z. Kałuski. J. Mol. Struct. **101**, 147 (1983).

Influence of solvent on the magnitude of the anomeric effect

J.-P. PRALY[1] AND R. U. LEMIEUX[2]
University of Alberta, Edmonton, Alta., Canada T6G 2G2

Received July 3, 1986

This paper is dedicated to Dr. O. E. (Ted) Edwards

J.-P. PRALY and R. U. LEMIEUX. Can. J. Chem. **65**, 213 (1987).

A novel application of ^{13}C nuclear magnetic resonance provided the effects of solvent polarity and hydrogen-bond formation on the conformational equilibria for a range of 2-substituted tetrahydropyrans and the results are interpreted in terms of how solvent affects the competition between the *endo*- and *exo*-anomeric effects in determining the magnitude of the anomeric effect. In accord with the generally accepted origin of the *endo*- and *exo*-anomeric effects (*anti*-periplanar n–σ^* interaction of the oxygen lone-pair orbital with the antibonding orbital of the adjacent C—O bond), the *exo*-anomeric effect for the α anomer is expected to be weaker because charge delocalization from the glycosidic oxygen to anomeric center is in competition with delocalization from the ring-oxygen atom. The effects of solvent on the relative magnitudes of the *endo*- and *exo*-anomeric effects are then considered to arise from the formation of specific complexes with the solvent, and the *exo*-anomeric effect of a β-glycoside is more strongly influenced. It is contended that hydrogen bonding of solvent to the ring oxygen increases the *exo*-anomeric effects. For this reason water is particularly effective for the strengthening of the *exo*-anomeric effect and, thereby, the conformational rigidity of glycosides. Experimental evidence is presented that indicates that the anomeric hydroxyl groups of free sugars dissolved in water tend to prefer the equatorial orientation because these provide stronger hydrogen bonds as proton donors to water.

J.-P. PRALY et R. U. LEMIEUX. Can. J. Chem. **65**, 213 (1987).

Une nouvelle application de la rmn du ^{13}C permet de déterminer les effets de la polarité du solvant et de la formation de liaisons hydrogènes sur l'équilibre conformationnel d'une série de tétrahydropyrannes portant un substituant en position 2; on interprète les résultats en fonction de comment les solvants affectent la compétition entre les effets anomères *endo* et *exo* dans la détermination de l'amplitude de l'effet anomère. En accord avec l'origine généralement acceptée des effets anomères *endo* et *exo* (interaction n–σ^* *anti*-périplanaire de l'orbitale de la paire libre de l'oxygène avec l'orbitale antiliante de la liaison C—O adjacente), il est prévu que l'effet anomère-*exo* de l'anomère-α sera plus faible parce que la délocalisation de la charge de l'oxygène glycosidique vers le centre anomère est en compétition avec la délocalisation de l'atome d'oxygène du cycle. On considère alors que les effets de solvant sur les amplitudes relatives des effets anomères *endo* et *exo* proviennent de la formation de complexes spécifiques avec le solvant et que l'effet anomère-*exo* d'un β-glycoside est plus fortement influencé. On prétend que la liaison hydrogène du solvant avec l'oxygène du cycle augmente les effets anomères-*exo*. Pour cette raison, l'eau est particulièrement efficace pour rehausser l'effet anomère-*exo* et, finalement, la rigidité conformationnelle des glycosides. On présente des données expérimentales qui indiquent que les groupements hydroxyles anomères de sucres libres dissous dans l'eau tendent à préférer l'orientation équatoriale parce que celle-ci donne lieu à des liaisons hydrogènes plus fortes comme donneurs de protons à l'eau.

[Traduit par la revue]

Can. J. Chem. Downloaded from www.nrcresearchpress.com by 190.90.36.8 on 09/07/12
For personal use only.

Introduction

The term "anomeric effect" was introduced in 1959 (1) to indicate the existence of a stereoelectronic influence on chemical bonding that had been detected (2) in a study of the anomerization equilibria for acetylated glycopyranoses of known ring conformation (3). Since then, the subject has received major attention (4, 5). It was initially proposed (6) that the anomeric effect was the result of bond dipole – bond dipole interactions. Mainly on the basis of X-ray crystallographic data, Altona (7) suggested that the anomeric effect was a manifestation of charge delocalization (no-bond resonance) from the oxygen atom of the acetal group toward the anomeric carbon. Thus, the stabilization gained was greater for the anomer with the aglycon in axial orientation since this placed the polar glycosidic bond *anti*-periplanar to an unshared pair of electrons of the ring oxygen. The subject then drew very substantial attention from theoretical chemists. Wolfe *et al.* (8) have presented a fine review of these developments. The nature of the orbitals and how these are considered to interact for the stabilization of an acetal bond has been qualitatively presented in detail by Kirby (4).

The differences in conformational energy for the various conformers for dimethoxymethane as estimated by the *ab initio* molecular orbital calculations of Jeffrey, Pople, and co-workers (9) were used in this laboratory (10) to assign a value to what had been termed the *exo*-anomeric effect (11). Subsequently (12), this contribution to the energy of a glycosidic bond was expressed in terms of two torsion expressions, namely

$$[1]\quad exo\text{-}A_\beta = 2.61(1 - \cos\theta^\circ) - 1.21(1 - \cos 2\theta^\circ) - 1.18(1 - \cos 3\theta^\circ) + 2.86 \text{ kcal/mol}$$

$$[2]\quad exo\text{-}A_\alpha = 1.58(1 - \cos\theta^\circ) - 0.74(1 - \cos 2\theta^\circ) - 0.70(1 - \cos 3\theta^\circ) + 1.72 \text{ kcal/mol}$$

That the *exo*-anomeric effect appears some 1.66 times stronger for the anomers (**1**) that have the aglycon in equatorial orientation (normally the β anomers) is not surprising, even in the absence of theoretical calculation. As seen in formula **1**, both the unshared pairs of electrons of the ring oxygen are *syn*-clinal to the glycosidic bond and, therefore, unfavorably disposed for delocalization toward the anomeric carbon. Thus, there exists no important competition for delocalization of charge (back bonding) (13) from the glycosidic oxygen that, in the sterically most favorable orientation, has an unshared pair

[1]University of Alberta Postdoctoral Fellow, 1983–1985. Present address: Universite Claude-Bernard Lyon 1, Ecole Superieure de Chimie Industrielle de Lyon, Laboratoire de Chimie Organique 2, ESCIL, 43 Boulevard du 11-Novembre-1918, 69622 Villeurbanne CEDEX, France.

[2]Author to whom correspondence may be addressed.

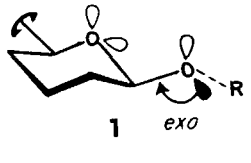

1

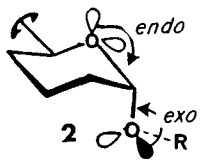

2

of electrons *anti*-periplanar to the C1—ring oxygen bond. In contrast to the β anomers, the α-glycosides have the aglycon in axial orientation and therefore, as displayed in **2**, are importantly stabilized by an *endo*-anomeric effect. However, for these α-anomers (**2**), competition exists between the *endo* and *exo*-anomeric effects for the electron deficiency at the anomeric carbon. Consequently, in accord with calculation (9, 14), the *exo*-anomeric effect for **2** should be weaker than that for the β anomer (**1**).

Fuchs *et al.* (15) examined the X-ray crystallographic data for 111 carbohydrate structures and found only orientations for the aglycon that are compatible with stabilization by way of an *exo*-anomeric effect.

The values for the *exo*-anomeric effects provided by expressions [1] and [2] are of course only a hopefully useful approximation. Certainly, the values for these stereoelectronic contributions to molecular stability will depend on the electronegativities of the substituents, both on the pyranose ring and on the aglycon (16). As will be discussed below, the solvent also appears to influence the values of *exo*-anomeric effects. Nevertheless, it was considered possible that the values for the α and β *exo*-anomeric effects, in conformers for dimethoxymethane as derived by *ab initio* molecular orbital calculation (9), would serve usefully for the molecular modelling of oligosaccharides. To date, this has proven to be the case. It was found, for example, that the conformational preference required by ^{1}H nmr data for the B human blood group trisaccharide determined in aqueous solution was not provided by hard-sphere calculation (12). However, addition of a contribution by the *exo*-anomeric effect to the hard-sphere calculations (12) provided a structure that was not only in accord with the nmr data but also present in the crystal structure (17).

Despite much such definitive evidence for the importance of the *exo*-anomeric effect (12, 13), this stereoelectronic feature continues to be disregarded in efforts to assess the conformational preferences of oligosaccharides. For example, Lipkind, Verovsky, and Kochetkov (18) recently published on the conformational states of cellulose, lactose, and maltose, and state, in the absence of acceptable experimental support, that the *exo*-anomeric effect does "not play a significant role under the conditions of an aqueous medium." In fact, as will be demonstrated below, the *exo*-anomeric effect appears to be not only of major importance but even of special importance in aqueous solution. The main purpose of this communication is to provide experimental support for this contention. Indeed, the neglect of a consideration of the *exo*-anomeric effect renders obsolete a large literature on the theoretical calculation of the conformational preferences of glycosidic structures. The fact that the *exo*-anomeric effect adds rigidity about the glycosidic bonds of oligosaccharides is a matter of major importance to an understanding of their interactions with the receptor sites of proteins to form specific carbohydrate–protein complexes. In this regard, it has become apparent that oligosaccharides present well-defined and substantially rigid surfaces about which the protein becomes organized (19).

The conformational analyses of compounds that contain polar bonds and atoms with unshared pairs of electrons require a consideration of specific solvent effects. For example, the conformational equilibrium for methyl 3-deoxy-β-L-*erythro*-pentopyranoside was more sensitive to the chemical nature of the solvent than to its polarity (20). Similarly, specific solvation effects were found to influence the conformational equilibrium for 2-methoxytetrahydropyran (2-MeO-THP) (**3**) (11).

The equilibrium data presented in Table 1 confirm the observation made in 1969 (11) that the polar solvent CD_3CN favors the more polar equatorial conformer **3e** to a greater extent

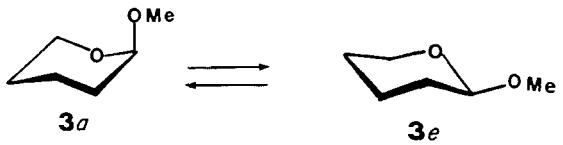

3a **3e**

than does the nonpolar CCl_4. In D_2O the two conformers have a near equal population (11). Thus, the anomeric effect for **3** is weak in water. Also, the mutarotation of many aldopyranoses in water favors the anomer with the anomeric hydroxyl in equatorial orientation (4). It is these kinds of observations that have led to the widespread notion that the anomeric effect is unimportant when the solvent is water. However, the stereoelectronic factors that are responsible for the anomeric effect cannot be expected to simply disappear in certain solvents. Instead, it must be considered that stereoelectronic effects on the strengths of the two C—O bonds of acetals remain but are exhibited differently in different environments because of changes in the interactions involving the unshared pairs of electrons. That this is the case clearly evident from the fact that, as seen in Table 1, weakly polar $CDCl_3$ is as effective as CD_3CN in favoring the more polar (11) conformer **3e**. In contrast, Tvaroska and Kozar (21) have presented a theoretical study of the hydration of the acetal segment in glycosides and concluded that hydration does not operate against the anomeric and *exo*-anomeric effects. Also, as already mentioned, Lipkind *et al.* (18) concluded, on the basis of a theoretical conformational analysis of disaccharide derivatives in aqueous solution, that the *exo*-anomeric effect and intramolecular hydrogen bonding are of no significance. We disagree. It is to be kept in mind, however, now that the origin of the anomeric effect has become established (8, 9), that an anomeric effect (ΔA) must be considered as the *difference* between the sum (A_{3e}) of the *endo*- and *exo*-anomeric effects in the equatorial conformer and the sum (A_{3a}) of these for the other conformer (22, 23). It is on this basis that the anomeric effect for **3** is defined as shown in expression [3]. As was mentioned above, the *endo*-A_e contributions are considered negligible and, therefore, A_{3e} is assumed to be equal to *exo*-A_{3e}.

$$[3]\quad \Delta A_3 = (exo\text{-}A_{3e} + endo\text{-}A_{3e}) - (exo\text{-}A_{3a} + endo\text{-}A_{3a}) = A_{3e} - A_{3a}$$

On the basis of eq. [3], anomeric effects will have a wide range of values, including negative and positive values, depending on the relative magnitudes of the various *exo*- and *endo*-anomeric effects. Indeed, for the equilibrium **3a** ⇄ **3e**, the axial conformer **3a** is strongly favored in CCl_4 and, therefore, A_{3e} must be less negative (less stabilizing) than A_{3a} in order that ΔA_3 be positive. In contrast, 2-methylaminotetrahydropyran (**4**) because of the basic nitrogen is expected to possess strong *exo*-anomeric effects. The *exo*-A_{4e} effect should be greater than the *exo*-A_{4a} contribution to the stability and, perhaps, sufficiently greater for the equilibrium to favor **4e** even though **4a** should be additionally stabilized by an *endo*-

Can. J. Chem. Downloaded from www.nrcresearchpress.com by 190.90.36.8 on 09/07/12
For personal use only.

Can. J. Chem. Downloaded from www.nrcresearchpress.com by 190.90.36.8 on 09/07/12
For personal use only.

TABLE 1. The conformational equilibria for 2-methoxytetrahydropyran in a variety of solvents at 308 K as estimated from studies of its 4,4,5,5-tetradeuterio derivative (**6**)

Solvent	Dielectric constant	Mole fraction (n_e) of the equatorial conformer			
			Present study		
		Lit. (11)	$J_{H,H}$[a]	nOe[b]	J_{HD}[c]
CCl_4	2.2	0.17	—	—	
C_6D_6	2.3	0.18	—	—	
CCl_4–C_6D_6 (10%)	~2.2	—	0.20	0.18	0.21
CCl_4–C_6F_6 (10%)	~2.3	—	0.20	—	0.26
$CDCl_3$	4.8	0.29	0.33	0.34	0.36
$(CD_3)_2CO$	21	0.28	—	—	
$(CD_3)_2SO$	36	0.26	—	—	
CD_3CN	38	0.32	0.37	0.37	0.37
D_2O	78	0.48	0.48	—	0.47

[a]From the time-averaged coupling of H-2 with H-3*c* and H-3*t*.

[b]From the relative enhancements (R) of the signals for H-6*c* and the methyl group on saturation of H-2 of **6**. Setting R = nOe (H-6*c*)/nOe (CH_3), R = 0.18 (CCl_4–C_6D_6), R = 0.34 ($CDCl_3$), R = 0.37 (CD_3CN).

[c]From the coupling between H-6*c* and H-6*t* and deuterium atoms at C-5.

anomeric effect. In fact, Booth *et al.* (24) have recently shown that the process **4a** ⇄ **4e** favors the equatorial conformer. De Hoog (25) had earlier demonstrated a similar situation for 2-dimethylaminotetrahydropyran (**5**). On the other hand, the

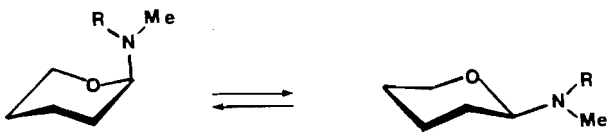

4*a*, R=H
5*a*, R=Me

4*e*, R=H
5*e*, R=Me

substitution of the ring oxygen of a glycosidic structure by the stronger electron-donating NH group should increase the *endo*-anomeric effect of an α anomer but decrease the strengths of the *exo*-anomeric effects. Indeed, Pinto and Wolfe (26) have shown that the antibiotic Nojirimycin (5-amino-5-deoxy-D-glucopyranose) mutarotates in water to an equilibrium α/β = 1.7, in contrast to D-glucopyranose for which α/β = 0.56.

The conformational analysis of the equilibrium **3a** ⇄ **3e** can be expressed as

$$\Delta G^0 \simeq (\Delta A^0 + \Delta R^0) - T\Delta S^0$$

where ΔA^0 = anomeric effect, ΔR^0 = change in nonbonded interactions, and ΔS^0 = change in entropy. ΔG^0 is positive since **3a** is favored. For compound **3**, in nonpolar solvents, ΔS^0 should be negligible. The highest value to date for the anomeric effect (ΔA^0) is the 2.1 kcal/mol proposed by Franck (27) using CCl_4 as solvent. The change in nonbonded destabilizing interactions (ΔR^0) is not known but, because of the short C—O bond in the tetrahydropyranyl ring, should be greater than the *A* value (0.6 kcal/mol) (28) for a methoxy group. Assuming that **3a** is destabilized by 1.1 kcal/mol and that the change in entropy is negligible (27), the change in enthalpy ($\Delta H^0 = \Delta A^0 + \Delta R^0$) would appear to be about 1 kcal/mol in favor of **3a**. That this result has some validity is indicated by the fact that, with CCl_4 as solvent, ΔG^0 is near 1 kcal/mol (11) (see Table 5). However, Booth *et al.* (24) found ΔH for **3a** ⇄ **3e** with $CFCl_3$–$CDCl_3$ as solvent to be near zero. It was suggested that **3a** may be favored (K_e = 0.256) because of an unusually high difference in conformational entropy. On the other hand, Lemieux *et al.* (11) had provided evidence that **3** forms specific complexes with polar solvents and especially with solvents such as $CDCl_3$ and D_2O, which can provide a proton to hydrogen bond formation. Thus, it seemed possible that the near temperature independence of the change in free energy noted by Booth *et al.* (24) was due to stronger bonding of the solvent ($CFCl_3/CDCl_3$) with **3e** to form solvated species of nearly equal enthalpy contents. Since $CDCl_3$ solvent molecules are less prone to self-association than to bonding with the acetal (**3**), the decrease in entropy for the solvation of **3e** should be greater than that for **3a**. Thus, the net change in entropy should favor **3a**, as was observed. An examination of this possibility was a main purpose for this investigation. Deslongchamps (5*a*) has discussed the importance of stereoelectronic factors to the reactivity of acetals and, in this regard, pointed out (5*b*) that stereoelectronic effects should "influence the basicity of the oxygen atoms of the acetal function, thence their relative ease of protonation." The results to be presented below are in strong support of this contention.

Discussion of results

As already mentioned, this investigation was undertaken mainly because the conformational equilibrium for **3** in $CFCl_3$–$CDCl_3$ (85:15 v/v) was found to be essentially independent of temperature (23). The extension of temperature studies to other solvents appeared possible by the procedure used in 1969 (11), which involved measurement of the time-averaged values of $J_{2,3cis}$ and $J_{2,3trans}$ for 4,4,5,5-tetradeuterio-**3**; namely, the equilibrium **6a** ⇄ **6e**.

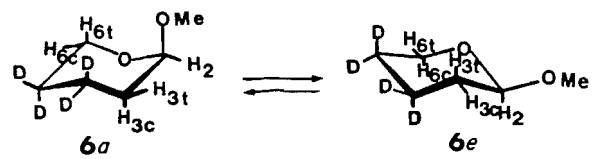

6*a* **6*e***

The conformational equilibria for the tetradeuterio compound **6** were estimated using the same procedure as previously described (11) except that the spacings in the ^1H nmr spectra were more precisely determined by operating at 400 MHz with deuterium decoupling. The results obtained using five different solvents and two different temperatures are presented in Table 2. As was previously done (11), the $J_{1,2a}$ and $J_{1,2e}$ coupling constants for the methyl 2-deoxy-α- and 2-deoxy-β-D-*arabino*-hexopyranosides were used to calculate the conformational equilibria from the observed values for $J_{2,3c}$ and $J_{2,3t}$. These equilibria are presented in Table 1, where it is seen that the results at 308 K agree well with those previously obtained (11) using a spectrometer operating at 100 MHz in the CW mode. The use of the coupling constants found for the 2-deoxyglucosides to calculate conformational equilibria for 2-MeO-THP (**3**) is, of course, arbitrary. That the procedure provides results useful for the present purposes was previously (11) supported by the optical rotations of an optically active sample of 2-MeO-THP in the various solvents. This conclusion is now supported, as described in the Experimental and involving structures **7**–**10**, by two other procedures: (*a*) the coupling of the H-6 atoms with deuterium atoms at C-5, and (*b*) the nuclear Overhauser enhancements (nOe) observed on saturation on H-2.

The above-described procedure for the determination of conformational equilibria of **6** by ^1H nmr was prohibitively

TABLE 2. ^{1}H nuclear magnetic resonance data for the estimation of changes in the conformational equilibrium of 2-methoxytetrahydropyran (**3**) with changes in solvent and temperature

Solvent	Chemical shifts (ppm)						Coupling constants (Hz)				
	H-2	H-3*c*	H-3*t*	H-6*c*	H-6*t*	OCH_3	H-2,H-3*c*	H-2,H-3*t*	H-3*c*,H-3*t*	H-6*c*,H-6*t*	n_{6e}
1. 2-Methoxy-4,4,5,5-tetradeuteriotetrahydropyran (**6**)											
At 308 K											
$CCl_4 + C_6D_6$ (10%)	4.41	1.57	1.53	3.40	3.70	3.27	3.15	3.20	−13.17	−11.11	0.20
$CCl_4 + C_6F_6$ (10%)	4.39	1.57	1.51	3.39	3.70	3.27	3.16	3.22	−13.19	−11.11	0.20
$CDCl_3$	4.50	1.69	1.57	3.50	3.84	3.40	3.04	4.24	−13.33	−11.28	0.33
CD_3CN	4.44	1.63	1.46	3.44	3.76	3.31	2.98	4.54	−13.24	−11.29	0.37
D_2O	4.61	1.75	1.50	3.58	3.86	3.42	2.96	5.30	−13.53	−11.52	0.48
At 268 K											
$CCl_4 + C_6D_6$ (10%)	4.42	1.57	1.54	3.40	3.68	3.27	3.16	2.87	−13.22	−11.15	0.15
$CCl_4 + C_6F_6$ (10%)	4.40	1.57	1.51	3.39	3.68	3.26	3.16	3.00	−13.20	−11.15	0.17
$CDCl_3$	4.54	1.72	1.58	3.52	3.85	3.41	3.03	4.23	−13.35	−11.30	0.33
CD_3CN	4.46	1.62	1.46	3.44	3.75	3.30	2.99	4.41	−13.21	−11.30	0.35
At 278 K											
D_2O	4.63	1.75	1.50	3.59	3.86	3.42	2.96	5.25	−13.59	−11.47	0.47

2. Methyl 2-deoxy-D-*arabino*-hexopyranosides in D_2O at 308 K

	H-1	H-2a	H-2e	H-3	H-4	OCH_3	H-1,H-2a	H-1,H-2e	H-2a,H-2e	H-2a,H-3	H-2e,H-3
α Anomer	4.90	1.70	2.13	3.85	3.35	3.35	3.71	1.32	−13.51	11.87	5.27
β Anomer	4.61	1.46	2.24	3.70	3.24	3.51	9.79	2.00	−12.38	11.76	5.09

expensive, both in time and facilities, for broader application. However, it proved possible using the mole-fraction data presented in Table 2 to establish an efficient procedure based in ^{13}C nmr for the study of the conformational equilibria, not only under a variety of solvent conditions but also for a range of different 2-substituted tetrahydropyrans. The procedure, which is described in the Experimental, involves the assignment of "absolute" chemical shifts for C-4 in the conformations **3a** and **3e**. On this basis, time-averaged chemical shifts for C-4 could be interpreted to yield the mole fractions of **3a** and **3e** under the prevailing conditions. This procedure is made possible by the great stability of the magnetic fields produced by the superconducting solenoids of the modern high-frequency nmr spectrometers.

The equilibrium data at 308 K presented in Table 3, using CCl_4–C_6D_6 (10%) as solvent, are in accord with expectations based on the nature of the anomeric effect as it exists in the literature (4) and as discussed in the Introduction. The electronegativities of the aglycons CH_2FCH_2, CH_2OAcCH_2, and CH_3 are similar and, indeed, the conformational equilibria are all in the range 0.22 ± 0.02. As expected, the monofluoro compound (**12**) most favors the conformer with the aglycon in axial

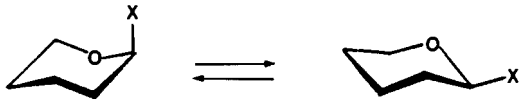

11, X = CF_3CH_2O
12, X = CH_2FCH_2O
13, X = CH_2OAcCH_2O

orientation. Replacement of the CH_2F group of **12** by the much more electronegative CF_3 group to form **11** is seen to greatly enrich the population of the axial conformer. This consequence has long been appreciated (29), but is now considered to occur in part because the CF_3CH_2O group of **11** strengthens the *endo*-anomeric effect for conformer **11a** to a greater extent than does the less electronegative CH_2FCH_2O group of **12**. Also, however, the more electronegative CF_3CH_2 group of **11** weakens both the *exo*-anomeric effects to a greater extent than does the CH_2FCH_2 group.

As already discussed with reference to the amino compounds **4** and **5**, the equatorial orientation for the aglycon of a 2-substituted THP compound will be favored the stronger the *exo*-anomeric effect—an effect that increases with increasing ease for charge delocalization from the aglycon to the anomeric carbon. On this basis, the trimethylsilyl ether **14** was expected (30) to favor conformer **14e**, as compared to **3** favoring **3e**. In fact, the equilibrium for **14** in CCl_4–C_6D_6 is much more in favor of the equatorial conformer than is that for **3** and, for that matter, also those for **12** and **13**.

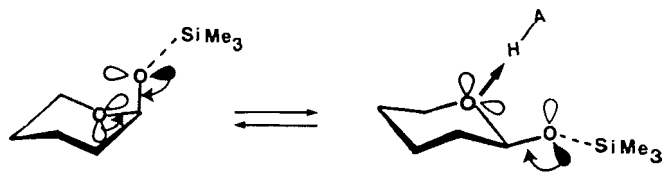

14a **14e**

As indicated in the conformational equilibrium for **14**, the ring oxygen of the **14e** conformer should serve best as proton acceptor for hydrogen bond formation with a protic solvent. Therefore, the population of **14e** at equilibrium should increase when the solvent is changed from carbon tetrachloride to chloroform (A = CCl_3). As seen in Table 3, the mole fraction of **14e** does increase from 0.28 to 0.47 on changing the solvent from CCl_4–C_6D_6 (10%) to $CDCl_3$. In D_2O, the mole fraction of **14e** was even greater at 0.70. This high abundance of **14e** can be

Can. J. Chem. Downloaded from www.nrcresearchpress.com by 190.90.36.8 on 09/07/12
For personal use only.

TABLE 3. Conformational equilibria for various 2-substituted tetrahydropyrans in different solvents at 308 K

2-Substituent	Chemical shifts, ppm: Observed C-4	Chemical shifts, ppm: "Absolute" [C-4]	n_e	K_e	ΔG^0 (kcal mol^{-1})
1. In CCl_4–C_6D_6 (10%)					
CF_3CH_2O-(**11**)	18.119	18.12	0.05	0.05	1.81
CH_2FCH_2O-(**12**)	18.713	18.71	0.17	0.20	0.98
CH_2OAcCH_2O-(**13**)	18.797	18.80	0.19	0.23	0.89
CH_3O-(**3**)	18.818	18.82	0.19	0.23	0.89
$(CH_3)_3SiO$-(**14**)	19.330	19.33	0.28	0.39	0.58
CH_2ODCH_2O-(**15**)	19.414	19.41	0.31	0.45	0.49
DO-(**16**)	19.463	19.46	0.32	0.47	0.47
2. In $CDCl_3$					
CF_3CH_2O-(**11**)	18.387	18.60	0.15	0.18	1.06
CH_2FCH_2O-(**12**)	19.168	19.38	0.30	0.43	0.52
CH_2OAcCH_2O-(**13**)	19.267	19.48	0.32	0.47	0.46
CH_3O-(**3**)	19.280	19.49	0.32	0.47	0.46
$(CH_3)_3SiO$-(**14**)	20.057	20.27	0.47	0.89	0.07
CH_2ODCH_2O-(**15**)	19.887	20.10	0.44	0.79	0.15
DO-(**16**)	20.138	20.35	0.49	0.96	0.02
2. In CD_3CN					
CF_3CH_2O-(**11**)	23.858	19.01	0.23	0.30	0.74
CH_2FCH_2O-(**12**)	24.533	19.68	0.36	0.56	0.35
CH_2OAcCH_2O-(**13**)	24.573	19.72	0.37	0.59	0.33
CH_3O-(**3**)	24.588	19.74	0.37	0.59	0.33
$(CH_3)_3SiO$-(**14**)	25.103	20.25	0.47	0.89	0.07
CH_2ODCH_2O-(**15**)	24.801	19.95	0.41	0.69	0.22
DO-(**16**)	25.648	20.80	0.58	1.38	−0.20
4. In D_2O					
CF_3CH_2O-(**11**)	21.112	19.71	0.36	0.56	0.35
CH_2FCH_2O-(**12**)	21.703	20.30	0.48	0.92	0.05
CH_2OAcCH_2O-(**13**)	21.682	20.28	0.48	0.92	0.05
CH_3O-(**3**)	21.628	20.23	0.47	0.89	0.07
$(CH_3)_3SiO$-(**14**)	22.833	21.43	0.70	2.33	−0.52
CH_2ODCH_2O-(**15**)	21.833	20.43	0.50	1.00	−0.00
DO-(**16**)	22.835	21.43	0.70	2.33	−0.52

attributed to both the high polarity of D_2O as well as to its ability to behave as a "proton" donor for hydrogen bond formation. The polar CD_3CN provided an equilibrium with nearly the same population of **14e** as does the much less polar solvent $CDCl_3$ (11).

In CCl_4–C_6D_6, the abundance of conformer **15e** of the hydroxyethyl compound **15** is significantly greater (n_{15e} = 0.31) than that (0.19) of conformer **3e** for compound **3** although the CH_2ODCH_2 group of **15** is certainly more electronegative than the CH_3 group of **3**. This apparent anomaly can be attributed to involvement of the ring oxygen of **15** in hydrogen bonding with the hydroxyl of the aglycon as is displayed in the formulas for **15a** and **15e**. This driving force in favor of **15e** would be eliminated in solvents such as CD_3CN and D_2O, which can act as good proton acceptors. In fact, the mole fractions of **15e** in these solvents are greater and nearly the same as those for **12e**, **13e**, and **3e**. On the other hand, $CDCl_3$ is a very poor proton acceptor, and therefore **15e** should be favored to a greater extent in this solvent than would be either **12e**, **13e**, or **3e**. As seen in Table 3, this is the case and provides convincing evidence that engagement of the ring oxygen in hydrogen bond formation favors the equatorial orientation for the aglycon.

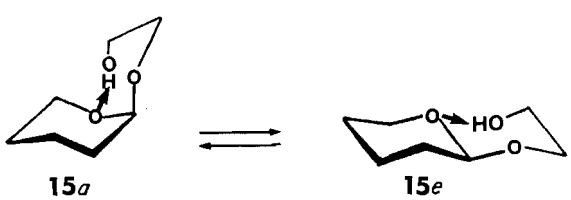

15a **15e**

Since the proposals made in the Introduction to rationalize the influences of solvent on the anomeric effect appear well supported, it was of interest to interpret the solvent effects on 2-hydroxy-THP (**16**) on the same basis. In fact, to do so not only provides an attractive rationalization of the effect of solvent on the conformational equilibrium of **16** but also on the anomerization equilibria for a number of sugars, such as glucose, which favor the equatorial orientation for the anomeric hydroxyl group.

As seen in Table 3, the conformational equilibria for **16** in both the solvents CCl_4–C_6D_6 (10%) and $CDCl_3$ are nearly the

Can. J. Chem. Downloaded from www.nrcresearchpress.com by 190.90.36.8 on 09/07/12
For personal use only.

Can. J. Chem. Downloaded from www.nrcresearchpress.com by 190.90.36.8 on 09/07/12
For personal use only.

same as those for the hydroxyethyl compound (**15**). However, major differences in equilibria (0.58 versus 0.41 and 0.70 versus 0.50) occur when the solvent is CD_3CN or D_2O, respectively. These differences are attributed to the fact that when dissolved in these latter solvents, both **15** and **16** become extensively hydrogen bonded as hydrogen donors to solvent molecules. The changes in bond polarity that arise from the formation of these hydrogen bonds should not much influence the electronegativity of the CH_2OHCH_2 group of **15**. In fact, **15e** has nearly the same population (0.41) in CD_3CN as in $CDCl_3$ (0.44). On the other hand, the population of **16e** is significantly greater in CD_3CN than in $CDCl_3$ (0.58 versus 0.49). This is as expected, since hydrogen bonding of the hydroxyl group of **16** with a solvent molecule must enrich the electron density on the oxygen atom (20) and thereby increase the *exo*-anomeric effects, but more so that for the equatorial conformer (**16e**). Thus, the proton-accepting solvent should, as was observed, enrich the population of the equatorial conformer (**16e**). The situation is similar with water as solvent. As seen in Table 3, the 0.50 mole fraction for **15e** in D_2O is nearly the same as those for **12e**, **13e**, and **3e**, namely, 0.48, 0.48, and 0.47. On the other hand, the mole fraction for **16e** is 0.70 in D_2O. This result is attributed to a greater strengthening of the *exo*-anomeric effects, but more so for **16e** as the result of the

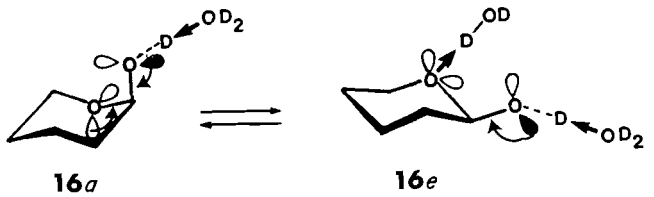

16a **16e**

hydrogen bonding with water as is indicated in the formula for **16e**. Experimental evidence exists for increased electron density on an oxygen atom of an hydroxyl group as the result of hydrogen bond formation (20), and Jeffrey and Mitra (31) have provided evidence, based in crystal structures, that anomeric hydroxyls are in fact strong proton donors but poor proton acceptors for hydrogen bond formation.

To better establish the influence of hydrogen bonding on the conformational equilibrium for **16**, a study was made of the effect of the addition of dimethylsulfoxide to solutions in CCl_4–C_6D_6 (10%). The results, presented in Fig. 1, show that the population of **16e** increases in a manner consistent with increasing hydrogen bonding of **16** with the DMSO, as displayed by the chemical shifts for both H-2 and OH-2. In contrast, the same addition of DMSO to solutions of 2-CH_3O-THP (**3**) had no effect on the chemical shift for H-2 and very little effect on the conformational equilibrium. We therefore abandon the earlier postulate that the influence of water on the conformational equilibria for 2-methoxytetrahydropyran (**3**) (11) and 2-hydroxytetrahydropyran (**16**) (32) is related to a more favorable water bridge between the two oxygen atoms when the conformer has the aglycon in equatorial orientation.

In view of the above observations on the effects of solvents on the conformational equilibria for **16**, we propose that certain sugars such as glucose, galactose, and xylose favor the β anomer when dissolved in water because of a strong β *exo*-anomeric effect. To further support this proposal, a brief study was made of the mutarotation of 2,3,4,6-tetra-*O*-methyl-D-glucopyranose (**17**) (33). The mole fraction of the β anomer, which has the anomeric hydroxyl in equatorial orientation, at

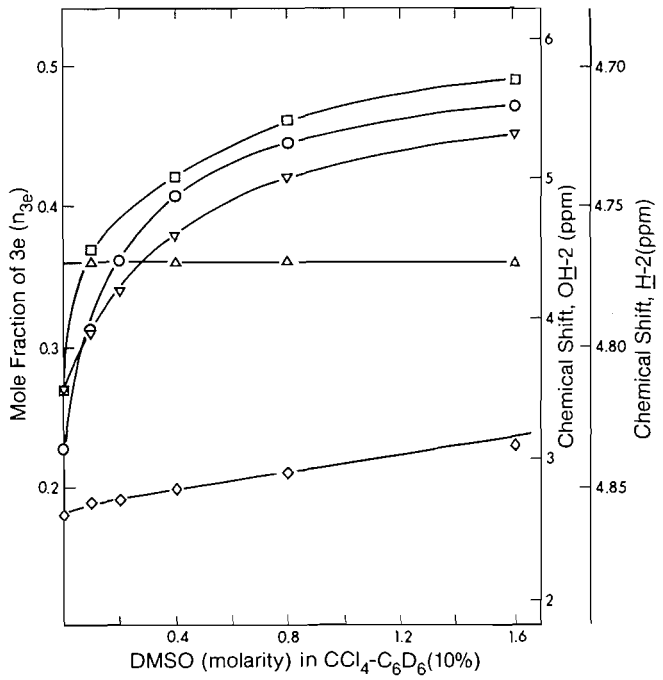

FIG. 1. The effects of additions of DMSO to 0.1 *M* solutions of 2-MeO-THP (△, $\delta_{H\text{-}2}$; ◇, n_e) and 2-HO-THP (○, $\delta_{OH\text{-}2}$; ▽, $\delta_{H\text{-}2}$; □, n_e) in CCl_4–C_6D_6 (10%), at 308 K, on chemical shifts and the conformational equilibria.

equilibrium in water and at 298 K was found to be 0.39. This result contrasts with that for the parent D-glucose for which the mole fraction at equilibrium is 0.64. Evidently the situation is not as straightforward for these complex structures as it is for **16**. Nevertheless, the mutarotation of the methylated glucose (**17**) (0.1 *M*) was examined in CCl_4–C_6D_6 (10%) and found to be well catalyzed at 298 K by the addition of 2-hydroxypyridone (34) (0.001 *M*). Under these conditions, at equilibrium, the mole fraction of the β anomer was 0.41. On rendering the solution 0.8 *M* in DMSO, the mole fraction of this anomer increased to 0.51, in accordance with the expectation that the hydrogen bonding with the DMSO more strongly strengthens the β *exo*-anomeric effect.

It was earlier suggested, with reference to the conformational equilibrium for 2-hydroxyethyloxy-THP (**15**), that the *exo*-anomeric effect is enhanced by hydrogen bonding involving the ring oxygen (O-5). It was further proposed that this enhancement is greater for the equatorial conformer since, for this conformer, O-5 is not importantly involved in an *endo*-anomeric effect. Intramolecular hydrogen bonding is supported by the presence of a bond between the hydroxyl and the ring oxygen of 2(*R*)-hydroxy-1(*R*)-cyclohexyl β-D-glucopyranoside tetraacetate in the crystalline form (35). To further test the hypothesis, the data reported in Table 4 were obtained. It is well known that phenol is a good proton donor to hydrogen bond formation. Therefore the addition of this substance to a solution of **3** in a nonpolar aprotic solvent such as CCl_4–C_6D_6 (10%) is expected to lead to hydrogen bonding between the phenol and the acetal group. As mentioned above, the ring oxygen of the equatorial conformer of **3** is expected to form the strongest hydrogen bond and, thereby, cause a shift of the conformational equilibrium toward a higher population of the equatorial conformer. As seen in Table 4, the addition of phenol at 308 K to a solution of **3** in CCl_4–C_6D_6 in fact led to an increase of n_{3e} from 0.18 to 0.29. In contrast, a similar addition of

TABLE 4. The effect of intermolecular hydrogen bonding on the conformational equilibrium of 0.1 *M* 2-MeO-THP (**3**) in CCl_4–C_6D_6

	Chemical shifts (ppm)			Mole fraction
	$\delta^{3}_{C\text{-}4}$	$\delta^{THP}_{C\text{-}4}$	$[\delta_{C\text{-}4}]$	n_{3e}
Additive[a] at 308 K				
None	18.790	0	18.79	0.18
DMSO	18.878	0.027	18.91	0.21
DTBPC	18.818	0.027	18.85	0.20
DTBPC–DMSO (1:1)	18.928	0.055	18.98	0.22
PhOH	18.762	0.578	19.34	0.29
PhOH–DMSO (1:1)	18.95	0.163	19.12	0.25
At 268 K				
None	18.693	−0.029	18.71	0.17
DMSO	19.796	0.039	18.84	0.19
DTBPC	18.683	0.049	18.73	0.17
DTBPC–DMSO (1:1)	18.844	0.054	18.90	0.20
PhOH	18.639	0.701	19.34	0.29
PhOH–DMSO (1:1)	18.87	0.138	19.01	0.23

[a]DMSO = dimethylsulfoxide; DTBPC = 2,6-di-*tert*-butyl-4-methylphenol; PhOH = phenol. All additions rendered the solution 0.8 *M* in the additive.

DMSO increased n_{3e} to only 0.21. The addition of both these compounds should increase n_{3e} to a lesser extent since the DMSO would compete with **3** for bonding with the phenol. This was the case (Table 4). Similar experiments were conducted using the highly hindered 2,6-di-*tert*-butyl-4-methylphenol, to strengthen the evidence that hydrogen bonding is responsible for the increase in the population of the equatorial conformer that occurred on adding phenol. As seen in Table 4, addition of this hindered phenol (DTBPC) had little influence on the conformational equilibrium whether or not DMSO was present. This is as expected, since the OH group of DTBPC is too hindered to form intermolecular hydrogen bonds.

As was discussed in the Introduction, the change in enthalpy for the conformational equilibrium **3a** ⇄ **3e** should be positive and about 1 kcal/mol. Table 5 reports the effects of changes in temperature and solvent on the equilibrium **3a** ⇄ **3e** as assessed by ^{13}C nmr. The effects of temperature change were then used to estimate the changes in enthalpy and entropy. As seen in Table 5, with the nonpolar and weakly associating solvent CCl_4–C_6D_6 (10%), the change in enthalpy (0.8 kcal/mol) is in fact nearly 1 kcal/mol and the conformational change involves a very small decrease in entropy. For reasons to be discussed below with reference to more polar solvents, it is apparent that C_6F_6 associates more strongly with **3** than does C_6D_6, and this is reasonable because of the presence of much more polar bonds in C_6F_6. The change in enthalpy with $CDCl_3$ as solvent was −0.2 kcal/mol, a value that is near the zero value observed by Booth *et al.* (24) using a mixture of $CDCl_3$ and $CFCl_3$ as solvent. Thus, in $CDCl_3$, the change in free energy (0.48 kcal/mol) is mainly determined by the decrease in entropy. This is not surprising, since $CDCl_3$ must form (through hydrogen bonding) much better defined (ordered) complexes with **3** by associating with the acetal oxygens than it can through self-association by way of extremely weak intermolecular hydrogen bonds. Furthermore, as was to be expected from the foregoing discussions, the interaction of $CDCl_3$ with **3e** should be stronger than with **3a**. Therefore $CDCl_3$ should decrease the enthalpy for **3e** to a greater extent than for **3a** and thereby, as was observed, lead to a smaller change in enthalpy in this solvent than in the non-hydrogen-binding solvent CCl_4–C_6D_6 (10%).

The results obtained with CD_3CN and D_2O as solvents are also in accord with the postulate that **3e** forms more stable and more ordered complexes with polar solvents than does **3a**. In other words, we contend that the changes in free energy with changes in solvent presented in Table 5 have their origins in the differences between the polar interactions of the solvent molecules with the two conformers. To reiterate, the polar interactions are considered to be stronger for an equatorial conformer because the absence of an *endo*-anomeric effect renders further charge delocalization energetically more facile. By affecting the charge delocalizations within the conformers, polar and hydrogen-bonding solvents must influence the magnitudes of the *endo*- and *exo*-anomeric effects, but these intramolecular effects cannot be separated from the forces of association.

These studies have shown that stereoelectronic influences on molecular structure are affected by interactions with polar molecules. Effects on the *exo*-anomeric effect present in β-glycopyranosides wherein the aglycon is in equatorial orientation can be expected to be especially large. In the case of the α anomers, the solvation influences the strengths of both the *endo*- and *exo*-anomeric effects. However, there can be no doubt that *hydration* of the ring oxygen will strengthen the *exo*-anomeric effect for both the anomers and thereby increase its contribution to the conformational rigidity of all glycosides. In this regard, the contributions used in HSEA calculations (12) that refer to an isolated molecule of dimethoxymethane are likely minimum values. It is of interest to note that simple rotation about a glycosidic bond must weaken the *exo*-anomeric effect and thereby activate the anomeric carbon toward nucleophilic attact. Likely, such rotations occur in the course of the formation of activated complexes with enzymes that catalyze transformations involving the replacement of the aglycons of glycosides.

Experimental

General procedures

Except for D_2O, all solvents were purified and stored over 3Å molecular sieves (BDH, Toronto).

The 2-alkoxytetrahydropyrans (**3**, **11**, **12**, **13**) were prepared, in the usual manner, by hydrogen chloride catalyzed addition of the alcohol to 2,3-dihydro-4*H*-pyran; **12**: bp 69°C, 17 Torr (1 Torr = 133.3 Pa); **13**: bp 126–127°C, 20 Torr. Deacetylation of **13** provided the 2-(2-hydroxyethoxy)tetrahydropyran (**15**) (bp 73–77°C, 3 Torr). Trimethylsilylation of the 2-hydroxytetrahydropyran (**16**) (36) readily afforded **14**.

The addition of either hexadeuteriobenzene or hexafluorobenzene (10%) to carbon tetrachloride was made for field frequency lock purposes.

Unless otherwise stated, the various solutions of the 2-substituted tetrahydropyrans were 0.1 *M*. These solutions were 0.05 *M* in tetrahydropyran, which served as the internal standard.

All the ^{13}C spectra recorded at 90.56 MHz in the FT mode used a Bruker WM 360 spectrometer interfaced with an Aspect-2000 computer for data accumulation and processing. The temperature was regulated with a VT-1000 temperature controller. Except for the studies involving **4**, the same spectrometer was used to measure the ^1H nmr spectra (360.13 MHz).

2-Methoxy-4,4,5,5-tetradeuterio-tetrahydropyran (6)

The compound was prepared as previously reported (11) except that pent-3-yne-5-ol-1-al dimethyl acetal was acetylated prior to the deuteration. The product was deacetylated (sodium methoxide – methanol) prior to treatment with a solution of methanol saturated with hydrogen chloride in dichloromethane for 15 min at 0°C. The product

Can. J. Chem. Downloaded from www.nrcresearchpress.com by 190.90.36.8 on 09/07/12
For personal use only.

TABLE 5. Approximate thermodynamic parameters for the conformational equilibria of 2-MeO-THP (**3**) in different solvents

Solvent	Temperature (K)	Chemical shifts (ppm) Observed $\delta_{C\text{-}4}$	Chemical shifts (ppm) "Absolute" $[\delta_{C\text{-}4}]$	n_e	K_e	ΔG^0 (kcal mol^{-1})	ΔH^0 (kcal mol^{-1})	ΔS^0 (cal K^{-1} mol^{-1})
$CCl_4 + C_6D_6$ (10%)	348	18.883	18.92	0.21	0.27	0.92	0.8	−0.3
	308	18.818	18.82	0.19	0.23	0.89		
	288	18.737	18.71	0.17	0.20	0.91		
	268	18.679	18.66	0.16	0.19	0.89		
$CCl_4 + C_6F_6$ (10%)	308	19.042	18.82	0.19	0.23	0.89	0.6	−1
	268	18.774	18.71	0.17	0.20	0.85		
$CDCl_3$	328	19.275	19.49	0.32	0.47	0.49	−0.2	−2
	308	19.280	19.49	0.32	0.47	0.46		
	288	19.304	19.52	0.33	0.49	0.41		
	268	19.288	19.53	0.33	0.49	0.38		
CD_3CN	348	24.608	19.75	0.37	0.59	0.37	0.1	−0.7
	308	24.588	19.74	0.37	0.59	0.33		
	288	24.561	19.71	0.36	0.56	0.33		
	268	24.525	19.69	0.36	0.56	0.31		
D_2O	348	22.138	20.20	0.46	0.85	0.11	−0.1	−0.6
	308	21.628	20.23	0.47	0.89	0.07		
	288	21.298	20.25	0.47	0.89	0.07		
	278	21.162	20.25	0.47	0.89	0.07		

TABLE 6. Determination of the conformational equilibria at 308 K of **6** in a variety of solvents from the coupling of H-6*c* and H-6*t* with deuterium atoms at C-5

Solvent[a]	Chemical shifts (ppm) H-6*c*	Chemical shifts (ppm) H-6*t*	Half-height widths $J_{H,D} + J_{H,H}$[b] H-6*c*	$J_{H,D} + J_{H,H}$[b] H-6*t*	$J_{H,H}$[c] H-6*c*	$J_{H,H}$[c] H-6*t*	$J_{H,D}$[d] H-6*c*	$J_{H,D}$[d] H-6*t*	n_{6e}[a]
CCl_4–C_6D_6 (10%)	3.40	3.70	2.30	5.55	1.08	1.06	1.22	4.49	0.21
CCl_4–C_6F_6 (10%)	3.39	3.70	2.45	5.55	0.92	1.3	1.53	4.25	0.26
$CDCl_3$	3.50	3.84	2.95	4.85	0.96	1.28	1.99	3.57	0.36
CD_3CN	3.44	3.76	3.00	4.75	0.84	1.10	2.16	3.65	0.37
D_2O	3.65	3.92	3.20	3.85	0.72	1.08	2.48	2.77	0.47

[a]Mole fraction **6***e* = half height width H-6*c* divided by the sum of the half heights of H-6*c* and H-6*t* (see Table 1).
[b]Without decoupling.
[c]With deuterium decoupling.
[d]By subtracting the values for *J* with and without deuterium coupling.

(73% yield) was isolated by distillation and contained about 10% dichloromethane. The proton and deuterium decoupled ^{13}C spectrum was recorded at 100.61 MHz. The 5020 scans were accumulated at 308 K using a 0.5-mL sample containing 10 μL of 2-methoxytetrahydropyran (**3**) and 40 μL of the 4,4,5,5-tetradeuterated derivative (**6**) with 10% hexafluorobenzene in carbon tetrachloride as solvent. To assign the chemical shifts, a spectrum was recorded under the same conditions but in the absence of **3**.

The gc–ms using a 30-m capillary silicon-coated (DB-1) column (temperature increase: 8°C/min from 60 to 200°C) produced the following relative intensities for the various tetrahydropyranyl ions in the range $86 \leq m/e \leq 91$: 9, 25, 70, 100, 43, 9. Thus the product was a mixture of several deuterated derivatives of **3** with the main components being tri (27%), tetra (37%), and penta (18%) species. Nevertheless, the material proved useful for the planned application. In this regard, the ^1H nmr spectra in the various solvents (Table 2) all showed a major component that provided, on deuterium decoupling, a well-defined ABX pattern for H-3*c*, H-3*t*, and H-2 and an AB pattern for H-6*c*, H-6*t*. An examination of the ^{13}C nmr spectrum of the mixture under conditions of both hydrogen and deuterium decoupling showed that these signals arose from the 4,4,5-tri- and 4,4,5,5-tetradeuterio compounds (about 50% abundance). The ^{13}C nmr spectrum confirmed the presence of the 4,5,5- and 4,4,5-trideuterio and the 4,4,5,5-tetradeuterio compounds for the following reason. It is known (37) that the effect of deuteration on a ^{13}C atom in cyclohexane is an upfield shift of 0.418 ppm when the separation is by one bond, 0.104 ppm by two bonds, and 0.025 ppm by three bonds. Since the chemical shift for C-3 of MeO-THP (**3**) under the conditions used was 30.519 ppm, it could be expected that the mixture would produce signals for C-3 at 30.365, 30.286, and 30.261 ppm for the 4,5,5-, 4,4,5-, and 4,4,5,5-deuterated compounds, respectively. In fact, signals occurred at 30.366, 30.285, and 30.260 ppm. Low intensity signals at 30.013 and 29.900 ppm suggest that some exchange of H-3 atoms by deuterium had occurred. Since the deuteration was conducted prior to ring formation, the

Can. J. Chem. Downloaded from www.nrcresearchpress.com by 190.90.36.8 on 09/07/12
For personal use only.

TABLE 7. Effects of solvent and temperature on the ^{13}C chemical shifts of TMS and C-4 of THP

Solvent	Temperature (K)	Observed chemical shifts (ppm) TMS	C-4 THP	$\Delta C\text{-}4^{THP}$[a] (ppm)
CCl_4–C_6D_6 (10%)	348	−0.195	23.585	−0.033
	308	0.0	23.618	0
	288	0.119	23.642	0.024
	268	0.209	23.639	0.021
CCl_4–C_6F_6 (10%)	308	0.002	23.840	0.222
	268	0.003	23.684	0.066
$CDCl_3$	328	−0.243	23.402	−0.216
	308	−0.134	23.403	−0.215
	288	−0.033	23.401	−0.217
	268	0.041	23.374	−0.244
CD_3CN	348	4.134	28.479	4.861
	308	4.181	23.470	4.852
	288	4.208	28.469	4.851
	268	4.230	28.451	4.833
D_2O	348	—	25.553	1.935
	308	—	25.020	1.402
	288	—	24.669	1.051
	278	—	24.534	0.916

[a]Observed $\delta_{C\text{-}4}^{THP}$ minus 23.618 ppm.

trideuterated compounds must be present in the mixture as equal amounts of their diastereoisomeric forms; namely, **7** and **8** for the 4,4,5- and **9** and **10** for the 4,5,5-deuterated compounds.

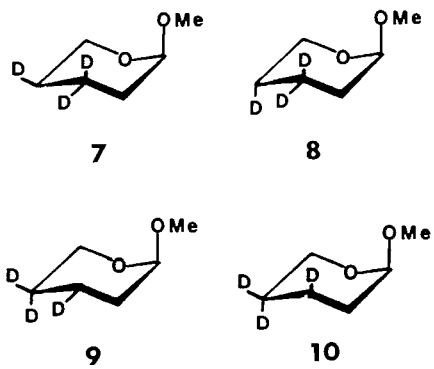

Conformational equilibria by ^1H nuclear magnetic resonance

The proton spectra of 2-methoxy-4,4,5,5-tetradeuteriotetrahydropyran, under deuterium decoupling (61.42 MHz, 30 db), were recorded at 400.13 MHz using a 2400-Hz spectral window and 32K data points (digital resolution after transformation: 0.15 Hz/pt). Since the deuterium signal was useless for lock purposes and in the absence of fluorine in the samples, one single scan was recorded after a 90° pulse. Prior to Fourier transformation, resolution enhancement was achieved through a Lorentz–Gauss transformation ($0.25 \leq$ Gaussian broadening ≤ 0.4, $-0.7 \leq$ line broadening ≤ -0.55), then the spin parameters were optimized through iterative calculations using the LAOCOON-III-like (38) PANIC program (39) for the above mentioned Aspect computer, resulting in a ± 0.02 Hz probable error for the coupling constants assigned to H-2, H-3*c*, H-3*t*, H-6*c*, and H-6*t*.

As was mentioned above, the ^1H nmr spectra of the mixture comprising mainly (37%) **6** but about equal amounts of **7**–**10** (each about 7% of the mixture) produced, on deuterium decoupling, readily distinguishable ABX patterns assignable to compounds **6**, **7**, and **8** and an A′B′ pattern assignable to H-6*c* and H-6*t* of compounds **6**, **9**, and **10**. The spectra of course displayed much weaker signals in close proximity to these main patterns, which are attributable to the other deuterated derivatives of **3** present in the mixture. Integration of the spectra and assuming that the methoxy group contained only natural abundance deuterium required very little, if any, deuteration of C-2 or C-6. As mentioned above, some deuteration of C-3 had occurred.

For an nOe study of **6** at 360.13 MHz, specially treated (40) 5-mm glass tubes were used. Argon was bubbled throughout the solutions for 5 min, then the tubes were immediately sealed. For these experiments, 99.96% enriched deuterium oxide with low paramagnetic impurity content was used. The data were obtained at 308 K in the difference mode from at least 950 accumulated scans.

The signals for the hydrogens at C-6 of **6** were readily assigned since saturation of H-2, while observing the signals for the hydrogens at C-6, showed that only one of these, the higher field signal, was enhanced and, therefore, the signal for the hydrogen (H-6*c*), which is in *cis*-relationship to H-2. The signal for the methyl group was also enhanced. For the two conformers, the distances between the average positions of the methyl group hydrogens and H-2 are very nearly the same. Therefore, the nOe's observed for the methyl group signals should be nearly equilibrium independent. Consequently, the ratio *R* for the nOe's observed for H-6*c* and the methyl group under a given set of experimental conditions should be proportional to the point of equilibrium and should increase as the population of **3e** increases. The *R* values in three different solvents are reported in the footnote to Table 1. That these values correspond to the mole fractions of **3e** is surely coincidental. This finding reinforces the contention that **6** exists essentially only in conformers **6a** and **6e**.

Further support for the equilibria reported in Table 1 was provided by the coupling of H-6*c* and H-6*t* with deuterium atoms at C-5 in the deuterated 2-MeO-THP preparation discussed above with reference to Table 1. As seen in Table 6, the decoupling of the deuterium atoms reduced the half-band widths observed for H-6*c* and H-6*t* and thereby provided a measure of the relative strengths of the deuterium couplings. It is expected that the coupling of the axial H-6*t* of the **6a** conformer with the deuteriums at C-5 will be the same as that for the axial H-6*c* of conformer **6e**, since their orientations relative to the deuteriums must be very similar, if not the same. Similarly, H-6*c* of **6a** is in an environment also present for H-6*t* of **6e**. Therefore the ratio of the change in the coupling with deuterium of one of the H-6's to the sum of the changes involving both H-6*t* and H-6*c* should provide a measure of the mole fraction of one of the two conformers. In fact, as seen in Table 6, the deuterium coupling with H-6*c* increased on increasing the polarity of the solvent in accord with an increasing abundance of **6e**. This follows, since in conformer **6e**, H-6*c* is *anti*-periplanar and *syn*-clinal to deuteriums at C-5 but is *syn*-clinal to both the deuteriums at C-5 in the case of **6a**. As seen in Table 1, the conformational equilibria estimated in this manner proved to be in fine agreement with those found by the other procedures.

Conformational equilibria by ^{13}C nuclear magnetic resonance

The frequency corresponding to tetramethylsilane (TMS) in CCl_4–C_6D_6 (10%) at 308 K was taken as the ultimate external reference chemical shift. To be sure that no appreciable drift in magnetic field had occurred, the position of this reference signal at the prevailing temperature was checked by repeating selected experiments at some later date. The chemical shift for C-4 of tetrahydropyran (THP) was then used as internal standard to adjust the observed chemical shifts for solvent and temperature effects. This was expected to be useful since the environments for C-4 in conformers **3a** and **3e** are very similar. The choice of the signal for C-4 in tetrahydropyran as a reference signal was also attractive because Booth *et al.* (24) had shown that there exists an important (4.59 ppm) chemical shift difference at 143 K for C-4 in these conformers. For these reasons, the chemical shifts for C-4 of THP, relative to the external TMS signal, are reported in Table 7. These shift differences ($\Delta C\text{-}4^{THP}$) are then used in Table 8 to adjust the observed values for C-4 of 2-MeO-THP (**3**) to the so-called "absolute" chemical shifts, i.e., chemical shifts that are expected to be indepen-

Can. J. Chem. Downloaded from www.nrcresearchpress.com by 190.90.36.8 on 09/07/12
For personal use only.

TABLE 8. Data for the calculation of "absolute" chemical shifts for C-4 of **3***a* and **3***e*

Solvent	Expt. No.	Temperature (K)	Mole fraction[a] n_{3e}	Chemical shifts (ppm) Observed $\delta_{C\text{-}4}$	Chemical shifts (ppm) "Absolute"[b] $[\delta_{C\text{-}4}]$
CCl_4–C_6D_6 (10%)	1	308	0.20	18.818	18.82
	2	278	(0.16)	—	(18.70)
	3	268	0.15	18.679	18.66
CCl_4–C_6F_6 (10%)	4	308	0.20	19.042	18.82
	5	278	(0.18)	—	(18.74)
	6	268	0.17	18.774	18.71
$CDCl_3$	7	308	0.33	19.280	19.50
	8	278	(0.33)	—	(19.52)
	9	268	0.33	19.288	19.53
CD_3CN	10	308	0.37	24.588	19.74
	11	278	(0.36)	—	(19.70)
	12	268	0.35	24.525	19.69
D_2O	13	308	0.48	21.628	20.23
	14	278	0.47	21.162	20.25

[a]From Table 3 with the values at 278 K in parentheses obtained by interpolation.
[b]By substitution of the $\Delta^{THP}_{C\text{-}4}$ values in Table 4 from the observed chemical shift for C-4 of **3**. The values in parentheses were obtained by interpolation.

TABLE 9. Calculation of "absolute" chemical shifts for C-4 of **3** in the axial (**3***a*) and equatorial (**3***e*) conformers

Combinations[a]	"Absolute" chemical shifts (ppm) $[\delta_{C\text{-}4}]_{3e}$	"Absolute" chemical shifts (ppm) $[\delta_{C\text{-}4}]_{3a}$	$[\delta_{C\text{-}4}]_{3e} - [\delta_{C\text{-}4}]_{3e}$ (ppm)
At 308 K 1– 7	23.01	17.77	
1–10	23.15	17.74	
1–13	22.85	17.81	
4– 7	23.01	17.77	
4–10	23.15	17.74	
4–13	22.85	17.81	
7–13	22.76	17.89	
10–13	22.55	18.09	
Average:	22.92	17.83	5.09
At 278 K 2– 8	22.75	17.93	
2–11	22.90	17.90	
2–14	22.90	17.90	
5– 8	23.00	17.80	
5–11	23.11	17.78	
5–14	23.01	17.80	
8–14	23.01	17.80	
11–14	22.90	17.90	
Average:	22.95	17.85	5.10
At 268 K 3– 9	22.77	17.93	
3–12	23.04	17.89	
6– 9	22.96	17.84	
6–12	23.23	17.78	
Average:	23.00	17.86	5.14
Overall average	22.96 ± 0.16	17.85 ± 0.09	5.11 ± 0.25

[a]Using the data in Table 5 and the expression, $[\delta_{C\text{-}4}] = n_{3e}[\delta_{C\text{-}4}]_{3e} + n_{3a}[\delta_{C\text{-}4}]_{3a}$.

dent of solvent and temperature. On this basis, these chemical shifts were used in conjunction with the conformational equilibria reported in Table 3 to estimate "absolute" chemical shifts [δ] for C-4 in the conformers **3a** and **3e**. This was accomplished by solving the sets of simultaneous equations presented in Table 9. The data in Table 9 indicate that effects of changes in temperature on chemical shifts were not detected. Consequently, the simple expression

$$n_e = ([\delta]_{obs} - [\delta_a])/([\delta_e] - [\delta_a]) = ([\delta]_{obs} - 17.85)/5.11$$

was used to estimate the conformational equilibria, not only for compound **3**, but also for other 2-substituted tetrahydropyrans, since it was expected that changes at C-2 would not significantly affect the chemical shift of C-4. Following this procedure, the only requirement is that the observed chemical shift for C-4 be corrected for the general solvent and temperature effects using the Δ values for C-4 of tetrahydropyran as provided in Table 7. Application of the procedure is justified since it well reproduces the conformational equilibria measured by way of ^{1}H nmr. Although its accuracy cannot be predicted, the procedure is certainly not misleading.

Acknowledgement

The authors are particularly indebted to Dr. Ole Hindsgaul for his supervision of the work done on the 360-MHz ^{1}H nmr spectrometer, but also deeply thankful for the guidance by Dr. T. Nakashima and G. Bigam of the nmr-spectral service laboratory of the department. The research was supported by the Natural Sciences and Engineering Research Council of Canada (Grant A-172 to R.U.L.) and by the Alberta Heritage Foundation for Medical Research (grant to R.U.L.).

1. R. U. LEMIEUX. Abstr. Pap. Am. Chem. Soc. **135**, 5E (1959).
2. R. U. LEMIEUX and P. CHÜ. Abstr. Pap. Am. Chem. Soc. **133**, 31N (1958).
3. R. U. LEMIEUX, R. K. KULLNIG, H. J. BERNSTEIN, and W. G. SCHNEIDER. J. Am. Chem. Soc. **80**, 6098 (1958).
4. A. J. KIRBY. The anomeric effect and related stereoelectronic effects at oxygen. *In* Reactivity and structure concepts in organic chemistry. Vol. 15. Springer Verlag, New York. 1983.

Can. J. Chem. Downloaded from www.nrcresearchpress.com by 190.90.36.8 on 09/07/12
For personal use only.

5. P. DESLONGCHAMPS. Stereoelectronic effects in organic chemistry. Pergamon Press, New York. 1983; (*a*) pp. 4–53; (*b*) p. 31.
6. R. U. LEMIEUX. Molecular rearrangements. Part Two. *Edited by* P. de Mayo. Interscience, New York. 1964. p. 709.
7. C. ALTONA. Ph.D. Thesis, University of Leiden, 1964.
8. S. WOLFE, M.-H. WHANGBO, and D. J. MITCHELL. Carbohydr. Res. **69**, 1 (1979).
9. G. A. JEFFREY, J. A. POPLE, J. S. BINKLEY, and S. VISHVESHWARA. J. Am. Chem. Soc. **100**, 373 (1978).
10. R. U. LEMIEUX, K. BOCK, L. T. J. DELBAERE, S. KOTO, and V. S. RAO. Can. J. Chem. **58**, 631 (1980).
11. R. U. LEMIEUX, A. A. PAVIA, J. C. MARTIN, and K. A. WATANABE. Can. J. Chem. **47**, 4427 (1969).
12. H. THØGERSEN, R. U. LEMIEUX, K. BOCK, and B. MEYER. Can. J. Chem. **60**, 44 (1982).
13. R. U. LEMIEUX, S. KOTO, and D. VOISIN. ACS Symp. Ser. No. 87. 1979. Chapt. 2. p. 17.
14. I. TVAROSKA and T. KOZAR. J. Am. Chem. Soc. **104**, 6929 (1980).
15. B. FUCHS, L. SCHLIEFER, and E. TARTAKOVSKY. Nouv. J. Chim. **8**, 275 (1984).
16. A. J. BRIGGS, R. GLENN, P. G. JONES, A. J. KIRBY, and P. RAMASWAMY. J. Am. Chem. Soc. **106**, 6200 (1984).
17. R. BALL, A. P. VENOT, O. HINDSGAUL, and R. U. LEMIEUX. Manuscript in preparation.
18. G. M. LIPKIND, V. E. VEROVSKY, and N. K. KOCHETKOV. Bioorgan. Khim. **9**, 1269 (1983); Carbohydr. Res. **133**, 1 (1984).
19. R. U. LEMIEUX, A. P. VENOT, U. SPOHR, P. BIRD, G. MANDAL, N. MORISHIMA, O. HINDSGAUL, and D. R. BUNDLE. Can. J. Chem. **63**, 2664 (1985), and references therein.
20. R. U. LEMIEUX and A. A. PAVIA. Can. J. Chem. **47**, 4441 (1969).
21. I. TVAROSKA and T. KOZAR. Int. J. Quantum Chem. **23**, 765 (1983).
22. R. U. LEMIEUX. Proceedings VIIth International Symposium on Medicinal Chemistry. Vol. 1. Swedish Pharmaceutical Press, Stockholm. 1985. p. 329.
23. H. BOOTH and K. A. KHEDHAIR. J. Chem. Soc. Chem. Commun. 467 (1985).
24. H. BOOTH, T. B. GRINDLEY, and A. K. KHEDHAIR. J. Chem. Soc. Chem. Commun. 1047 (1982).
25. A. J. DE HOOG. Org. Magn. Reson. **6**, 233 (1974).
26. B. M. PINTO and S. WOLFE. Tetrahedron Lett. **23**, 3687 (1982).
27. R. W. FRANCK. Tetrahedron, **39**, 3251 (1983).
28. E. L. ELIEL and M. H. GIANNI. Tetrahedron Lett. 97 (1962).
29. G. A. PIERSON and O. A. RUNQUIST. J. Org. Chem. **33**, 2572 (1968).
30. B. FUCHS, A. ELLENCWEIG, E. TARTAKOVSKY, and P. APED. Angew. Chem. **98**, 289 (1986).
31. G. A. JEFFREY and J. MITRA. Acta Crystallogr. Sect. B, **34***a*, 469 (1983).
32. A. EL-KAFRAWY and R. PERRAUD. C.R. Acad. Sci. Paris, **280**, 1219 (1975).
33. B. JOHNSEN and P. E. SØRENSEN. Acta Chem. Scand. Ser. A, **33**, 241 (1979).
34. S. J. ANGYAL, V. A. PICKLES, and R. AHLUWALIA. Carbohydr. Res. **3**, 300 (1967).
35. J. P. PRALY, G. DESCOTES, R. FAURE, and H. LOISELEUR. Cryst. Struct. Commun. **11**, 1323 (1982).
36. L. E. SCHNIEPP and H. H. GELLER. J. Am. Chem. Soc. **68**, 1646 (1946).
37. R. AYDIN and H. GUNTHER. J. Am. Chem. Soc. **103**, 1301 (1981).
38. S. COSTELLANO and A. A. BOTHNER-BY. J. Chem. Phys. **41**, 3863 (1964).
39. PANIC Program: Copyright, Bruker Spectrospin AG, Switzerland.
40. Y. THERIAULT, Y. MORIO, and G. KOTOVYCH. Can. J. Biochem. **57**, 165 (1979).

Can. J. Chem. Downloaded from www.nrcresearchpress.com by 190.90.36.8 on 09/07/12
For personal use only.

Attempted novel preparation of dihydrocoumarin and coumarin; obtention of aryl acrylates and 3-chloropropionates

JASWANT R. MAHAJAN AND HUGO C. ARAÚJO
Departamento de Química, Universidade de Brasília, 70910-Brasília, DF, Brasil

Received May 27, 1986

This paper is dedicated to Dr. O. E. (Ted) Edwards

JASWANT R. MAHAJAN and HUGO C. ARAÚJO. Can. J. Chem. **65**, 224 (1987).

It has been found that, contrary to the published report, there is no noticeable reaction between phenol and methyl acrylate in the presence of aluminum chloride to produce phenyl acrylate (**1**) and dihydrocoumarin (**2**). Although products having the reported spectral data can be obtained by the reaction of phenol with acrylyl chloride, these products are actually phenyl acrylate and phenyl 3-chloropropionate (**4**), there being detected no dihydrocoumarin. This reaction has now been extended to several substituted phenols and some naphthols. Attempts at cyclization of phenyl acrylate, phenyl 3-chloropropionate, or their mixtures have been unsuccessful.

JASWANT R. MAHAJAN et HUGO C. ARAÚJO. Can. J. Chem. **65**, 224 (1987).

Contrairement à ce qui a déjà été publié, on a trouvé que le phénol et l'acrylate de méthyle, en présence de chlorure d'aluminium, ne réagissent pratiquement pas pour donner de l'acrylate de phényle (**1**) et de la dihydrocoumarine (**2**). Même si la réaction du phénol avec le chlorure d'acrylyle conduit à des produits possédant les caractéristiques spectrales rapportées, on n'obtient que de l'acrylate de phényle et du chloro-3 propionate de phényle (**4**) et on ne détecte pas de formation de dihydrocoumarine. On a maintenant étendu cette réaction à plusieurs phénols substitués et à quelques naphtols. Des essais effectués en vue de cycliser l'acrylate de phényle, le chloro-3 propionate de phényle ou leurs mélanges se sont avérés inutiles.
[Traduit par la revue]

Can. J. Chem. Downloaded from www.nrcresearchpress.com by 80.58.250.72 on 09/07/12
For personal use only.

Dihydrocoumarin (**2**) and coumarin (**3**) are important flavor and fragrance substances and are accessible by several routes (1–8). Our interest in these compounds led us to repeat a simple preparation, by the reaction of phenol with methyl acrylate, as reported by Reddy (9) and illustrated by eq. [1].

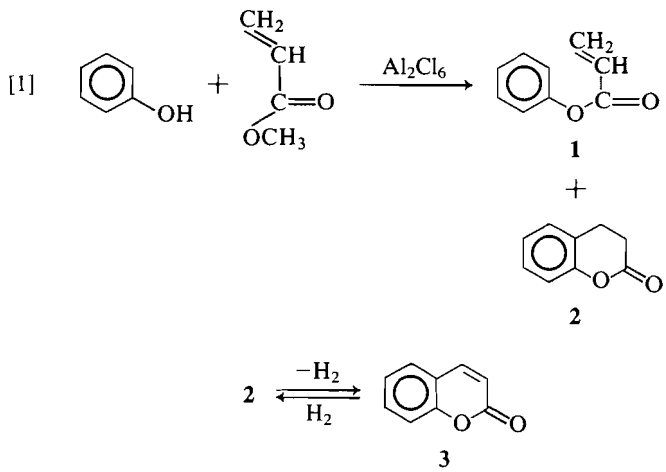

However, we were unable to duplicate the reported results under a variety of experimental conditions. Eventually, we treated phenol with acrylyl chloride in the presence of aluminum chloride and obtained two products having spectral properties almost identical with the reported data. Subsequently, we found that the reaction could also be brought about by the reaction of phenol with acrylic acid, in the presence of $SOCl_2$, PCl_3, $POCl_3$, or PCl_5. However, due to the formation of some side products, prior conversion of the acid to its chloride was found to be advantageous. In view of the earlier reports on the preparation of acrylyl chloride (10) and based on our own experiments, we concluded that phosphorus pentachloride was best; 40–50 mol% of this reagent, with respect to acrylic acid, gave optimum results. The subsequent acylation of phenol could then be carried out either *in situ* or by using the distilled acid chloride. The optimized reaction conditions were applied to several substituted phenols and some naphthols, which also gave similar pairs of products (see Experimental).

However, when we undertook the dehydrogenation of the supposed dihydro compound, we again met with repeated failures, even when all such hypotheses as bad catalyst, impure sample or solvent, catalyst poison, etc., were discounted; the only doubt now resided in the identity of the alleged dihydrocoumarin. As an authentic sample of this compound was not at hand, we compared our spectra with those in the Aldrich spectra catalogs (11, 12) and proved beyond doubt that the compound under investigation was not dihydrocoumarin! Subsequent reasoning, and circumstantial as well as analytical evidence then revealed that we were dealing instead with phenyl 3-chloropropionate (**4**), the addition product of phenyl acrylate with hydrogen chloride, which are the initial products of the acylation reaction. The same was true for the rest of the supposed dihydrocoumarins obtained from other phenols and naphthols. The mistake was caused by the spectral data reported by Reddy being in an acceptable range for the alleged dihydrocoumarin; chemical shifts (δ ppm) from Reddy (9*a*), Aldrich (11, 12); values in parentheses), and those found for compound **4** are shown below.

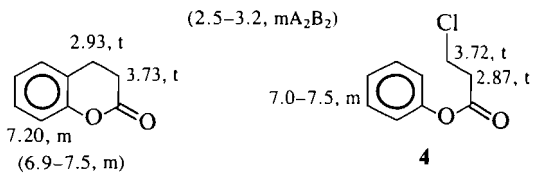

ν_{max}(neat; C=O) cm^{-1}: 1760(1761); 1767

Finally, attempts at cyclization of phenyl acrylate, phenyl 3-chloropropionate, or their mixtures, using aluminum chloride, concentrated sulphuric acid, phosphorus pentoxide, boron trifluoride etherate *N,N*-dimethylaniline, etc., were unsuccessful, confirming earlier reports (13).

Experimental

Reagent grade chemicals were used as received from suppliers.

Can. J. Chem. Downloaded from www.nrcresearchpress.com by 80.58.250.72 on 09/07/12
For personal use only.

Infrared spectra were taken on a Perkin–Elmer 137 Infracord spectrophotometer. The ^{1}Hmr spectra were recorded on a Varian EM-390 (90 MHz) spectrometer. Mass spectra were obtained on a Hewlett–Packard spectrometer model 5987A, using direct inlet probe, 70 eV, and temperature program (40–250°C). Progress of reaction was followed by thin-layer chromatography (tlc; silica gel, toluene/EtOAc 95:5, I_2 vapours). An authentic sample of phenyl acrylate was prepared by exposing an aqueous solution of sodium phenolate to acrylyl chloride; ir ν_{max} (neat): 1750 cm^{-1}; ^{1}Hmr (CCl_4) δ: 5.8–6.7 (m, 3H, H_2C=CH—) and 7.0–7.4 (m, 5H, arom.).

Reaction of phenol with acrylyl chloride

Acrylyl chloride (Aldrich; 5 mL, 5.57 g, 61.5 mmol) was added dropwise to a mixture of phenol (4.8 g, 51 mmol) and anhydrous aluminum chloride (230 mg) contained in a flask cooled by tap water. The whole was stirred for 16 h, when the reaction mixture was put on a hot water bath (~80°C) for 4 h. The reaction mixture was decomposed with cold water (20 mL) and extracted with petroleum ether (bp 40–60°C), the organic phase being washed with water and brine. Drying over anhydrous Na_2SO_4 and evaporation of solvent gave a colorless liquid (6.31 g); ir ν_{max} (neat): 1770, 1748 cm^{-1}; ^{1}Hmr (CCl_4) δ: 2.90 (t, CH_2), 3.76 (t, CH_2), 5.8–6.7 (m, vinyl group), and 7.0–7.5 (m, aromatic H). Quantitative integral evaluation of the vinyl and methylene region indicated a 68:32 ratio for phenyl acrylate to phenyl 3-chloropropionate.

Fractional distillation afforded phenyl 3-chloroproprionate, virtually free from phenyl acrylate; bp 125–127°C/4 Torr (1 Torr = 133.3 Pa); ir and ^{1}Hmr as reported in the discussion section for structure **4**; ms *m/e*: 186 (*M* + 2, 1), 184 (M^+, 3), 94 (100).

General acylation procedure using acrylic acid and PCl_5

(*a*) Acrylic acid (13.7 mL, 14.4 g, 0.2 mol) containing hydroquinone (110 mg) was added dropwise, with care, onto phosphorus pentachloride powder (20.8 g, 0.1 mol) contained in a 3-necked flask, under magnetic stirring and anhydrous conditions. There was an immediate exothermic reaction with the evolution of HCl gas, which was led to a water trap. The reaction mixture soon turned fluid and the vigour of reaction was controlled by the slow addition of the acid. After complete addition, the reaction mixture was heated slowly to distill the crude acyl chloride (bp 70–88°C) directly onto phenol (18.8 g, 0.2 mol) containing hydroquinone (110 mg), and under magnetic stirring. Finally, anhydrous aluminum chloride (267 mg) was added and the whole heated with stirring in an air bath (80–90°C) for 3 h, followed by heating at 100°C for 1 h. After removing any low-boiling material on a rotary evaporator, the reaction mixture was distilled to afford a colorless liquid (28.8 g), bp 100–110°C/1.5 Torr. Redistillation furnished almost pure (^{1}Hmr, tlc) chloro ester **4** (19.4 g), bp 132–134°C/5 Torr, preceded by its mixture with phenyl acrylate (8.9 g).

(*b*) Acrylic acid (1.58 g, 22 mmol) was added slowly to PCl_5 (1.88 g, 9 mmol) and the whole gently refluxed in an air bath (110–120°C) for 1 h. After cooling, phenol (1.88 g, 20 mmol) was added and stirring continued at room temperature for 2.5 h, when the air bath was heated slowly to bring its temperature to 90°C during ~1 h, and maintained there for another 3 h. The cooled reaction mixture was taken up in ether (50 mL) and washed successively with water, 1 *N* NaOH, and brine. Drying (Na_2SO_4) and evaporation gave the crude product (3.5 g), which on short-path distillation furnished a colorless liquid (2.7 g) whose ^{1}Hmr analysis indicated a 7.5:92.5 ratio between phenyl acrylate and phenyl 3-chloropropionate.

2-Chlorophenol, *o*-, *m*-, and *p*-cresol, as well as 1- and 2-naphthol could be acylated similarly either by procedure (*a*) or (*b*), affording a 60–80% yield of the acylated mixture as indicated by their ^{1}Hmr spectra, which had a very close resemblance to those of phenyl acrylate and compound **4** in the vinyl and methylene region, respectively. In the case of 1-naphthol, the acylated product was predominantly (>90%) the corresponding acrylic ester, while in the case of 2-naphthol, the 3-chloropropionate ester was obtained as a colorless solid from ethanol (43% yield); mp 53–55°C; ir ν_{max} (KBr): 1761 cm^{-1}; ^{1}Hmr (CCl_4) δ: 2.85 (t, 2H, H_2CCO_2—), 3.70 (t, 2H, H_2C-Cl), and 7.0–7.8 (m, 7H arom.). *Anal.* calcd. for $C_{13}H_{11}O_2Cl$: C 66.52, H 4.69; found: C 66.76, H 4.66.

Acknowledgement

We thank Prof. J. N. Cardoso (UFRJ – Instituto de Química) for the mass spectra.

1. K. Bauer and D. Garbe. Common fragrance and flavor materials—preparation, properties, and uses. VCH Verlagsgesellschaft mbH, Weinheim. 1985.
2. O. DeGarmo. *In* Kirk–Othmer: Encyclopedia of chemical technology. 1st ed. Vol. 4. John Wiley, New York. 1949. pp. 588–593.
3. T. E. Furia and N. Bellanca (*Editors and translators*). Fenaroli's handbook of flavor ingredients. The Chemical Rubber Co., Cleveland. 1971.
4. V. G. Cherkaev, G. F. Yakovleva, L. A. Shutikova, and G. D. Kayukova. U.S.S.R. SU 1,030,363. 1983; Chem. Abstr. **99**, 194811c (1983).
5. S. Schaafsma and J. Deumens. Ger. Offen. 2,309,536. 1973; Chem. Abstr. **79**, 136983m (1973).
6. J. A. Thoma, J. M. Deumens, and E. J. Verheijen. N.L. Patent 72,02,539. 1972; Chem. Abstr. **80**, 37000c (1974).
7. T. Symon and A. K. Sparks. U.S. Patent 3,859,311. 1972; Chem. Abstr. **82**, 97941m (1975).
8. N. J. Christensen. U.S. Patent 3,888,883. 1973; Chem. Abstr. **83**, 163995f (1975).
9. (*a*) V. B. Reddy. Chem. Ind. 414 (1976); (*b*) W. Theilheimer (*Editor*). Synthetic methods of organic chemistry. Vol. 32. Karger, Basel. 1978. Item 745.
10. C. E. Rehberg, M. B. Dixon, and C. H. Fisher. J. Am. Chem. Soc. **67**, 209 (1945); G. H. Stempel, Jr., R. P. Cross, and R. P. Mariella. J. Am. Chem. Soc. **72**, 2299 (1950).
11. C. J. Pouchert. The Aldrich library of infrared spectra. The Aldrich Chemical Company, Milwaukee. 1970. Spectrum 769-C.
12. C. J. Pourchet and J. R. Campbell. The Aldrich library of NMR spectra. Vol. 7. The Aldrich Chemical Company, Milwaukee. 1974. Spectrum 45B; W. W. Simons and M. Zanger. The Sadtler guide to NMR spectra. Sadtler Research Laboratories, Philadelphia. 1972. Spectrum 397.
13. T. Amakasu and K. Sato. J. Org. Chem. **31**, 1433 (1966).

Stereochemistry of the 1,2-migration of the carboxyl group that occurs during the biosynthesis of tropic acid from phenylalanine[1,2]

EDWARD LEETE
Natural Products Laboratory, School of Chemistry, University of Minnesota, Minneapolis, MN 55455 U.S.A.

Received June 3, 1986

This paper is dedicated to Dr. O. E. (Ted) Edwards

EDWARD LEETE. Can. J. Chem. **65**, 226 (1987).

(2*S*,3*R*)- and (2*S*,3*S*)-[1-^{14}C,3-^{3}H]phenylalanine were fed in separate experiments to *Datura innoxia* plants. The distribution of isotopes in the resultant labeled hyoscyamine and scopolamine indicates that the biosynthesis of the acid moiety of these ester alkaloids, namely (*S*)-tropic acid, involves the migration of the carboxyl group of phenylalanine to its prochiral C-3 position with retention of configuration.

EDWARD LEETE. Can. J. Chem. **65**, 226 (1987).

Au cours d'expériences séparées, on a fait croître des plants de *Datura innoxia* en présence de [^{14}C-1,^{3}H-3]-phénylalanines soit (2*S*,3*R*) soit (2*S*,3*S*). En se basant sur la distribution des isotopes dans les hyoscyamine et scopolamine marquées qui en résultent, on peut en conclure que la biosynthèse de la portion acide de ces esters d'alcaloïdes, soit l'acide tropique-(*S*), implique la migration du groupement carboxyle de la phénylalanine vers sa position prochirale-3 et que cette migration se fait avec rétention de configuration.

[Traduit par la revue]

Can. J. Chem. Downloaded from www.nrcresearchpress.com by 190.90.36.8 on 09/07/12
For personal use only.

Introduction

It has been established that the biosynthesis of (*S*)-tropic acid (**1**), the acid moiety of the tropane alkaloids hyoscyamine (**2**) and scopolamine (**3**), involves the intramolecular 1,2-migration of the carboxyl group of phenylalanine, from C-2 to C-3 (2). Recently, it has been shown that the biosynthesis of tropic acid also involves a 1,2-migration of hydrogen from C-3 of phenylalanine to C-2, which ultimately becomes the hydroxymethyl group of tropic acid (3). This preliminary result was obtained by feeding a mixture of all four possible stereoisomers of [1-^{14}C,3-^{3}H]phenylalanine (2*R*,3*R*; 2*R*,3*S*; 2*S*,3*R*; and 2*S*,3*S*) to *Datura innoxia* plants. The stereochemistry of the migration of the carboxyl group has now been probed by carrying out feeding experiments with (2*S*)-phenylalanine stereospecifically labeled with one tritium at its prochiral C-3 position. These substrates were obtained as previously described (4). The stereochemical purity at the C-3 position was determined by conversion to *trans*-cinnamic acid with the enzyme phenylalanine ammonia-lyase (PAL). This enzyme catalyses the *trans* elimination of ammonia. From the retention of tritium relative to carbon-14 (located at C-1), it was calculated that both the (3*R*)- and (3*S*)-[1-^{14}C,3-^{3}H]phenylalanine were 89% enantiomerically pure at their prochiral C-3 positions. The doubly labeled phenylalanines were fed to *Datura innoxia* plants by the wick method. The alkaloids were isolated and separated as previously described (5) from plants that were harvested 10 days after the initial feeding.

Results and discussion

Scheme 1 illustrates the fate of hydrogen at C-3 of phenylalanine when tropic acid is formed. If the migration of the carboxyl group occurs with retention of configuration, (2*S*,3*R*)-[1-^{14}C,3-^{3}H]phenylalanine (**5**) will afford (*S*)-tropic acid (**4**), retaining tritium at its chiral center. If the migration occurs with inversion, the tritium will be displaced and will be found on the hydroxymethyl group of (*S*)-tropic acid (**6**).

The results recorded in Table 1 are consistent with the first mechanism, that is, migration with retention of configuration. The interpretation of the results is complicated by the fact that the tropic acid moiety of hyoscyamine and scopolamine is readily racemized. Such racemization will result in loss of tritium from the chiral center of tropic acid. Thus the hyoscyamine isolated from the feeding of (2*S*,3*R*)-[1-^{14}C,3-^{3}H]phenylalanine (Expt. 1) had 50% enantiomeric excess of the (−)-isomer. However, it retained 65% of tritium relative to carbon-14. When this hyoscyamine was racemized (by addition of a trace of sodium hydroxide to a solution of the alkaloid in ethanol), the reisolated racemic hyoscyamine (atropine) retained only 10% of its tritium, indicating that most of the tritium was located at the chiral center of the tropic acid. Hydrolysis of the racemized hyoscyamine with aqueous barium hydroxide yielded racemic tropic acid with the same relative amount of tritium. The scopolamine, which is optically more stable than hyoscyamine, retained 83% of tritium relative to carbon-14. However, hydrolysis of this alkaloid with aqueous barium hydroxide yielded tropic acid that was almost racemic (18% enantiomeric excess), and retained only 13% of tritium relative to carbon-14. The residual tritium found in the racemic tropic acid presumably arises from the (2*S*,3*S*)-[1-^{14}C,3-^{3}H]phenylalanine (11%) present in the administered precursor.

Complementary results were obtained with (2*S*,3*S*)-[1-^{14}C,3-^{3}H]phenylalanine (Expt. 2). The alkaloids isolated from this feeding experiment retained most of the tritium relative to carbon-14. Racemization of the alkaloids caused little change in their ^{3}H/^{14}C ratios, indicating that the tritium was not located at the chiral center of tropic acid. Basic hydrolysis of the alkaloids yielded racemic tropic acid that retained 85% of the tritium, which was shown to be present on the hydroxymethyl group using the degradation previously described (3).

Independently, Haslam and co-workers (6) fed (2*S*,3*R*)- and (2*S*,3*S*)-[2-^{14}C,3-^{3}H]phenylalanine to *Datura stramonium* plants. They considered that their results were consistent with a stereospecific loss of the pro-*R* hydrogen at C-3 of phenylalanine, the carboxyl group migrating with inversion of configuration at this position. This conclusion is the direct opposite of the one reported in the present article. However, the authors apparently failed to realize that tritium located at the chiral center of tropic acid is very labile. The ^{3}H/^{14}C ratio of the isolated alkaloids was not reported. The mixture of alkaloids

[1]This article is Part 35 in the series "Chemistry of the Tropane Alkaloids." For Part 1, see ref. 1.

[2]Communication No. 202 from this laboratory.

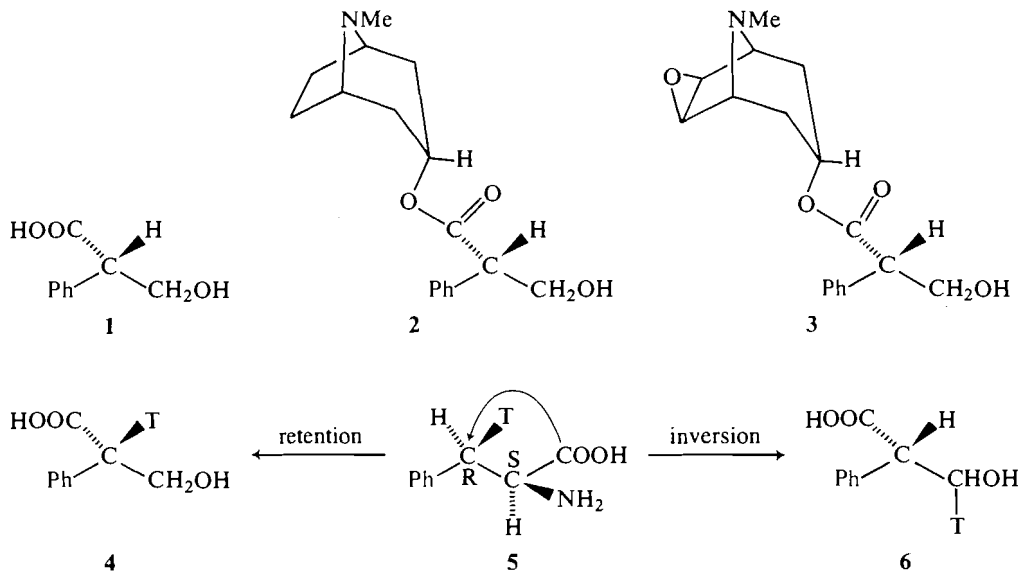

SCHEME 1

TABLE 1. Feeding of labeled phenylalanines to *Datura innoxia*

Exp. No.	Experiment No. 1			Experiment No. 2		
Precursor fed:	(2*S*,3*R*)-[1-^{14}C,3-^{3}H]phenylalanine			(2*S*,3*S*)-[1-^{14}C,3-^{3}H]phenylalanine		
Time of feeding	April			June		
Fresh weight of plants (g)	220			350		
		^{14}C (dpm/mmol)	^{3}H/^{14}C		^{14}C (dpm/mmol)	^{3}H/^{14}C
Activity		1.83×10^7	10.6		4.89×10^6	3.60
Amount fed	0.5 mmol			0.5 mmol		
Alkaloids isolated						
Hyoscyamine·HCl						
Weight (mg)	119			142		
Enantiomeric excess[a]	50%			51%		
Activity		7.40×10^4	6.9		6.32×10^4	3.25
Absolute inc.[b] (^{14}C)	0.30%			1.13%		
Tropic acid		7.23×10^4	1.1		6.19×10^4	3.05
Scopolamine·HCl						
Weight (mg)	202			297		
Enantiomeric excess[a]	82%			95%		
Activity		5.21×10^4	8.8		5.74×10^4	3.48
Absolute inc.[b] (^{14}C)	0.34%			2.05%		
Tropic acid		5.06×10^4	1.35		5.70×10^4	3.10

[a]The optical purity was obtained by determination of the specific rotations of the alkaloid hydrochlorides. Optically pure hyoscyamine·HCl has $[\alpha]_D^{25}$ −24.2° (*c* 3.5, EtOH) and scopolamine·HCl has $[\alpha]_D^{25}$ −17.7° (*c* 4.5, EtOH).
[b]Absolute inc. = total activity (dpm) found in the isolated alkaloid divided by the total activity (dpm) fed to the plants.

was hydrolyzed by refluxing with aqueous 10% sodium hydroxide for 30 min, conditions which would cause racemization of tropic acid. The tropic acid was assayed for radioactivity after conversion to methyl-3-*O*-acetyltropate. It was reported that this tropic acid derived from (2*S*,3*R*)-[2-^{14}C,3-^{3}H]phenylalanine (88% enantiomeric excess at C-3) had lost 88–93% of its tritium relative to carbon-14. The tropic acid derived from (2*S*,3*S*)-[2-^{14}C,3-^{3}H]phenylalanine (83% enantiomeric excess at C-3) lost 30–35% of the tritium. These experimental results are thus entirely consistent with ours, the retention of tritium in the tropic acid derived from the [3*S*-^{3}H]phenylalanine being due to its migration to the hydroxymethyl group, and not because it remained at the chiral center of tropic acid.

The 1,2-migration of the carboxyl group of phenylalanine to ultimately yield (*S*)-tropic acid is analogous to the biochemical conversion of (2*R*)-methylmalonyl coenzyme A (**7**) to succinyl coenzyme A (**8**) (7), which is illustrated in Scheme 2. In this reaction, it is the thioester group that undergoes an intramole-

Can. J. Chem. Downloaded from www.nrcresearchpress.com by 190.90.36.8 on 09/07/12
For personal use only.

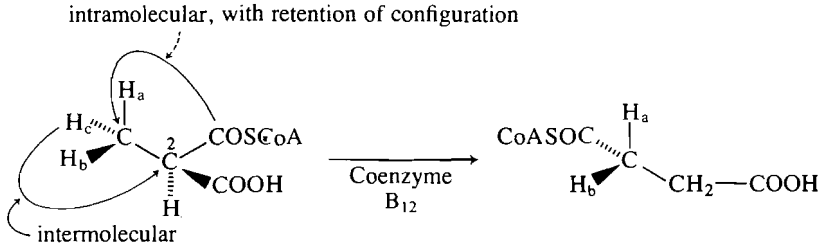

7 8

SCHEME 2

cular migration with retention of configuration. The displaced hydrogen also migrates in the opposite direction; however, this migration is intermolecular. It has not yet been determined whether the 1,2-migration of the 3-pro-*S* hydrogen of phenylalanine that occurs during tropic acid biosynthesis is inter- or intra-molecular. Another point of interest is the fact that the conversion of **7** to **8** is catalyzed by coenzyme B_{12}. However, the presence of vitamin B_{12} or its derivatives in higher plants is tenuous and controversial (8–10). Twenty years ago I sent an extract of *Datura* plants to Professor R. H. Abeles (then at the University of Michigan), but he was unable to detect any vitamin B_{12} in this material.

Experimental

Radioactivity assay

Radioactivity measurements were carried out in a Tracor Analytic Mark III liquid scintillation counter. Samples (assayed in duplicate) were dissolved in water or EtOH (1 mL), which was then diluted with liquid scintillation solution (10 mL). The liquid scintillation solution was made by dissolving naphthalene (50 g), 2,5-diphenyloxazole (3.5 g), and 1,4-(5-phenyloxazol-2-yl)-benzene (0.25 g) in spectroscopic grade dioxane (500 mL). The backgrounds in the ^{14}C and ^{3}H channels were 8 and 14 dpm, respectively. In unquenched samples the efficiency of counting in the ^{14}C and ^{3}H channels was 60 and 45%, respectively, and spillover of ^{14}C into the ^{3}H channel was 10%.

(2S,3R)- and (2S,3S)-[1-^{14}C,3-^{3}H]phenylalanine

The (2*S*,3*R*)- and (2*S*,3*S*)-[1-^{14}C,3-^{3}H]phenylalanine were obtained from [*formyl*-^{3}H]benzaldehyde and [1-^{14}C]glycine as previously described (4). The enantiomeric excess at C-3 was determined by incubation with phenylalanine ammonia-lyase (EC 4.3.1.5) from *Rhodotorula glutinis* (Sigma Chem. Co.), as previously described (4).

Administration of the labeled phenylalanine to Datura innoxia *plants and isolation of the alkaloids*

The plants were 3 months old, growing in soil in a greenhouse at the time of feeding, which was done by means of cotton wicks inserted into the stems of the plants near to ground level. After 10 days the plants (both the roots and aerial parts) were harvested and the alkaloids, hyoscyamine and scopolamine, isolated and separated by thin-layer chromatography (tlc) as previously described (5).

Racemization of hyoscyamine and scopolamine

The following is a typical procedure, the optical rotations being determined in a Perkin–Elmer 242 polarimeter. The hyoscyamine hydrochloride (113.7 mg) from Expt. 1 was dissolved in absolute EtOH (10 mL) at 25°C. Aqueous 10% NaOH (0.05 mL) was added. Under these conditions the rotation was reduced by half in 12.5 min. After 2 h the solution was acidified with a drop of acetic acid and then evaporated to dryness. The residue was subjected to tlc on silica gel PF 254 (Merck), developing with a mixture of $CHCl_3$, EtOH, concentrated NH_3 (80:20:1). The zone (R_f 0.3) corresponding to atropine (detected by uv) was extracted with MeOH. This extract was neutralized with HCl, evaporated to dryness, and the residue crystallized from a mixture of EtOH and ethyl acetate to afford atropine hydrochloride. This salt had essentially the same ^{14}C specific activity as the initial hyoscyamine hydrochloride, but its $^{3}H/^{14}C$ ratio changed from 6.9 to 1.1. Scopolamine hydrochloride was similarly racemized; however, its half-life under the same conditions was longer (22 min).

Hydrolysis of the alkaloids

The alkaloid hydrochloride (200 mg) was dissolved in aqueous saturated $Ba(OH)_2$ solution (10 mL) and the mixture refluxed for 30 min. The cooled solution was acidified with HCl and extracted with Et_2O (3 × 30 mL). The residue obtained on evaporation of the dried (Na_2SO_4) Et_2O extract was crystallized from a mixture of benzene and hexane, affording tropic acid (50–60 mg), mp 118°C. Optically pure tropic acid has mp 129°C (11).

Acknowledgements

This research was supported by a research grant GM-13246 from the National Institutes of Health, U.S. Public Health Service. Seeds of *Datura innoxia* were obtained from the Zentral Institut für Genetik und Kulturpflanzenforschung, Gatersleben, D.D.R.

1. E. LEETE, L. MARION, and I. D. SPENSER. Nature, **174**, 650 (1954).
2. E. LEETE, N. KOWANKO, and R. A. NEWMARK. J. Am. Chem. Soc. **97**, 6826 (1975).
3. E. LEETE. J. Am. Chem. Soc. **106**, 7271 (1984).
4. R. H. WIGHTMAN, J. STAUNTON, A. R. BATTERSBY, and K. R. HANSON. J. Chem. Soc. Perkin Trans. 1, 2355 (1972).
5. E. LEETE. Phytochemistry, **11**, 1713 (1973).
6. R. V. PLATT, C. T. OPIE, and E. HASLAM. Phytochemistry, **23**, 2211 (1984).
7. J. RÉTEY. *In* New comprehensive biochemistry, stereochemistry. Vol. 3. *Edited by* Ch. Tamm. Elsevier Biochem. Press, New York. 1982. pp. 261–265.
8. L. FRIES. Physiol. Plantarum, **15**, 566 (1962).
9. J. M. POSTON. Phytochemistry, **17**, 401 (1978).
10. W. S. BECK. *In* B_{12}. Vol. 2. *Edited by* D. Dolphin. John Wiley and Sons, New York. 1982. pp. 9–10.
11. M. B. WATSON and G. W. YOUNGSON. J. Chem. Soc. Perkin Trans. 1, 1597 (1972).

Can. J. Chem. Downloaded from www.nrcresearchpress.com by 190.90.36.8 on 09/07/12
For personal use only.

Spiro steroids via the Barbier–Grignard reaction of steroidal ketones with allyl bromide and magnesium

ZDZISŁAW PARYZEK AND KRZYSZTOF BŁASZCZYK
Faculty of Chemistry, Adam Mickiewicz University, 60-780 Poznań, Poland

Received June 3, 1986

This paper is dedicated to Dr. O. E. (Ted) Edwards

ZDZISŁAW PARYZEK and KRZYSZTOF BŁASZCZYK. Can. J. Chem. **65**, 229 (1987).

Barbier–Grignard reaction of 3- and 17-steroidal ketones gave excellent yields of the allyl steroids **1** + **2** and **15**. These were transformed into a mixture of 1,3- and 1,4-diols by hydroboration–oxidation. The diols **3**, **5**, and **18** were used for the preparation of spirolactones and spiroethers. Thus, the Barbier–Grignard allylation–hydroboration–cyclization sequence proved to be an effective method for the spiroannelation of steroidal ketones. It was also shown that an earlier assignment of the stereochemistry of the diols **3** and **5** was erroneous.

ZDZISŁAW PARYZEK et KRZYSZTOF BŁASZCZYK. Can. J. Chem. **65**, 229 (1987).

Par réaction de Barbier–Grignard sur des stéroïdes portant des groupements cétoniques en positions 3 ou 17, on peut obtenir les stéroïdes allyliques **1** + **2** et **15**. En soumettant ces composés à des réactions d'hydroboration/oxydation, on a pu les transformer en des mélanges de diols-1,3 ét-1,4. On a utilisé les diols **3**, **5** et **18** pour préparer des spirolactones et des spiroéthers. Ainsi, la séquence de réactions d'allylation selon Barbier–Grignard—d'hydroboration/oxydation et de cyclisation s'avère une méthode efficace pour effectuer la spiroannelation de cétones stéroïdales. On a aussi démontré qu'une attribution antérieure de stéréochimie des diols **3** et **5** était erronée.

[Traduit par la revue]

Can. J. Chem. Downloaded from www.nrcresearchpress.com by 190.90.36.8 on 09/07/12
For personal use only.

The γ-butyrolactone and α-methylene-γ-butyrolactone structural units have been suggested to be responsible for the biological activity of many natural compounds and their synthetic analogues (1). In the steroidal series, some spirolactones were found to possess tumor-inhibiting activity (2). Other important steroids possess a spirolactone moiety in position 17 of the steroidal skeleton and exhibit aldosterone blocking activity (3). Since the first reports on the synthesis and antialdosterone activity of several steroid 17-spirolactones (e.g. 7α-acetylthio-3-oxo-17α-pregn-4-ene-21,17 carbolactone) (3*a*, 4), several synthetic methods leading to spirolactone steroids have been developed (5).

A simple and attractive possibility for synthesizing spirolactones is the introduction of the three-carbon unit in a Barbier–Grignard reaction of an alicyclic ketone with an allyl magnesium halide, followed by a two-step transformation leading to a spirolactone (eq. [1]). Since α-methylenation of lactones is a well-known process (6), the sequence shown in eq. [1] might be

[1] 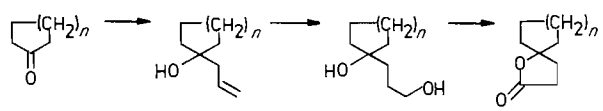

extended to the synthesis of steroidal spiro-α-methylene-γ-butyrolactones. The Barbier–Grignard reaction of aldehydes and ketones with allyl halides and magnesium has been extensively studied (7). However, reports on further chemical transformation of the allyl carbinols to spiro compounds are scarce (8). Surprisingly, this approach to spirolactones has not been attempted with steroidal ketones.

In our investigation 5α-cholestan-3-one and 3β-hydroxy-5α-androstan-17-one were chosen as model steroids. Barbier–Grignard (9) reaction of 5α-cholestan-3-one with allyl bromide and magnesium afforded two isomeric allyl derivatives **1** and **2** in 51 and 48% yield, respectively. The stereochemistry of the epimers was assigned on the basis of ^{1}H nmr and ir spectra and the expected polarity difference, since greater polarity of the isomer with an equatorial hydroxy group was reported for compounds bearing alkyl (10) and alkynyl (11) substituents in position 3 of the cholestane skeleton. According with the

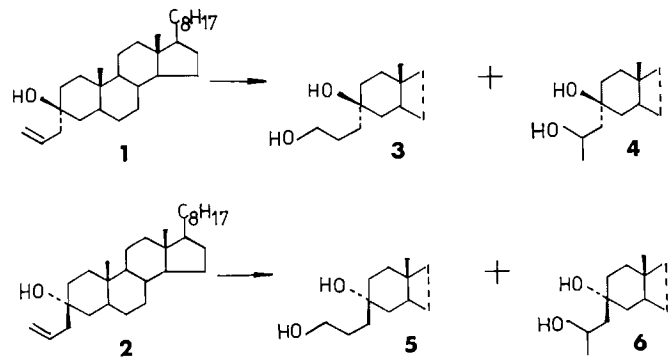

suggestion (12) that steric compression due to typical 1,3 interactions with protons on the cyclohexyl ring would cause proton signals for axially situated methylene groups to be shifted to lower field, ^{1}H nmr analysis of both isomers showed distinctly that the allylic methylene group in **1** resonates at lower field (δ 2.31) than the analogous protons in **2** (δ 2.16). Compounds **1** and **2** were previously obtained in the reaction of allylzinc with 5α-cholestan-3-one (13).

Hydroborations of allyl steroids, irrespective of the source of diborane, were less regioselective than was anticipated on the basis of the published data (8). Hydroboration–oxidation of the allyl compound **1** gave 1,4-diol **3** in 75% yield along with 1,3-diol **4** (21%). Similar regioselectivity was observed in hydroboration of the epimeric allyl compound **2**, the diols **5** and **6** being isolated in 74 and 23% yield, respectively. Fortunately, the regioisomers could be readily separated by chromatography on silica gel. The diols **3** and **5** were quantitatively oxidized with Jones reagent to the respective lactones **7** and **8**. The same diols on intramolecular etherification with *p*-toluenesulfonyl chloride in pyridine (15) gave spiroethers **9** and **10**.

Because the assigned configuration of the diols **3** and **5**, and consequently of the other C-3 stereoisomers, was opposite to that reported by Bladon and Rae (14), the 900–1150 cm^{-1} region in the infrared spectra of compounds belonging to the two epimeric series was carefully examined. The higher carbon–oxygen stretching frequencies were found in compounds with

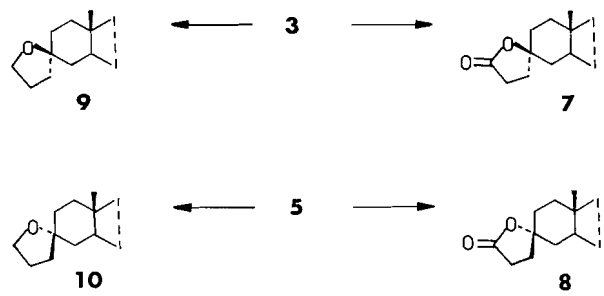

equatorial C(3)—O bonds when compared with the axial analogues (8, 11, 16) (see Table 1).

Spirolactones **7** and **8** have been synthesized previously from 5α-cholestan-3-one in two steps. Thus the ketone reacted with diazocyclopropane to give two isomeric spirocyclobutanone steroids, which could be oxidized to the appropriate lactones. In view of our stereochemical assignments, the stereochemistry of the nucleophilic addition of diazocyclopropane to 5α-cholestan-3-one (14) has to be revised. It is proposed that formation of the lactone **8** occurs by the route shown in eq. [2], assuming the predominantly equatorial approach (17) of diazocyclopropane to the carbonyl group.

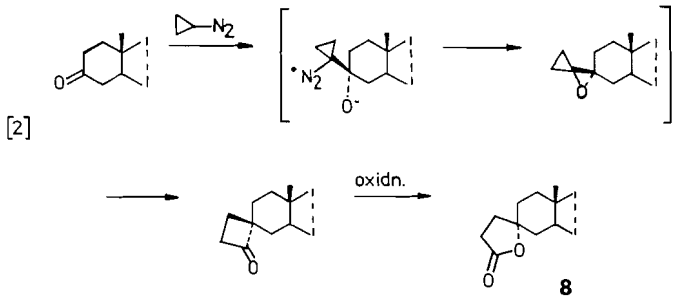

Jones oxidation of 1,3-diols **4** and **6** afforded two β-hydroxyketones **11** and **12**, which were dehydrated with *p*-toluenesulfonic acid in benzene to the mixture of conjugated and unconjugated ketones **13** and **14**. The ratio of these isomers, estimated by the integration of vinylic protons in the ^{1}H nmr spectra of the crude reaction products, was 9:1 when the substrate was compound **11** and 7:3 in the case of compound **12**. After prolonged treatment with methanolic potassium hydroxide the conjugated ketone **13** was entirely transformed to the unconjugated ketone **14**. The position of the olefinic double bond in **14** was assigned on the basis of the broad multiplet at δ 5.47 present in the ^{1}H nmr spectrum.

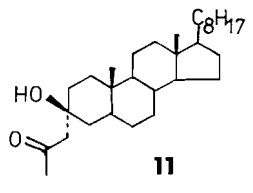

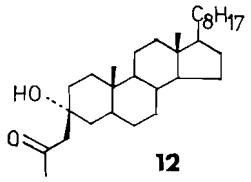

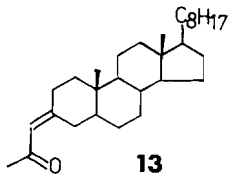

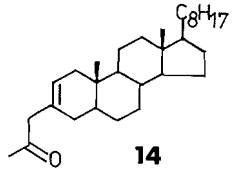

Next, the spiroannelation sequence was repeated on a 17-steroidal ketone. Accordingly, 17-oxo-5α-androstan-3β-yl-2-tetrahydropyranyl ether was treated with allyl bromide and magnesium in a Barbier–Grignard reaction to give a quantitative yield of the allyl carbinol **15**. The 17β orientation of the OH group in this compound was assigned on the basis of the known stereochemistry of addition of Grignard reagents to 17-oxosteroids (18). Acid hydrolysis of **15**, followed by acetylation, gave compound **17** (19). Hydroboration–oxidation of **17** gave a mixture from which the 1,4-diol **18** was isolated in 74% yield. The ^{1}H nmr spectrum of the second product (homogenous on tlc) suggested a mixture of C-2′ epimers of the 1,3-diol **19**. Thus the 10-methyl group of this compound resonates at δ 0.91 while the 13-methyl group gives two low intensity singlets at δ 0.84 and 0.82. Oxidation–lactonization of the diol **18** to compound **21** proceeded smoothly, as did the cyclization to the spiroether **20**. Each step leading from the 17-steroidal ketone to **20** and **21**, except the hydroboration step (74% of **18**), proceeded in over 95% isolated yield. Thus, the overall yield of compound **20** and **21** was considerably better than that reported earlier (3*a*, 19) and in more recent work (3*c*, 5).

TABLE 1. C—O Stretching frequencies in the infrared spectra of the cholestane derivatives ($CHCl_3$ solutions)

Compound	C(3)—O_{eq}	C(3)—O_{ax}
1	1020 m	—
2	—	995 m
3	995 m	—
5	—	985 m
7	1010 m	—
8	—	990 m
9	1045 s	—
10	—	1035 s
11	1050 m	—
12	—	1035 m
3-OH, 3-CH_3	1095 s	1065 w

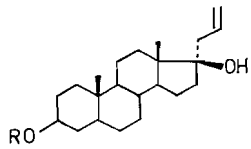

15 R = THP
16 R = H
17 R = Ac

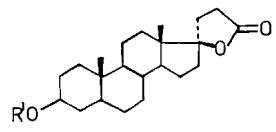

21 R = Ac
22 R = H

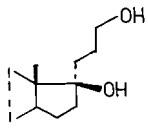

18 (3β-OAc)

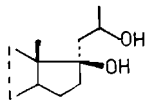

19 (3β-OAc)

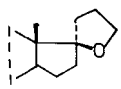

20 (3β-OAc)

The results obtained with the unhindered 3-steroidal ketone and the sterically hindered 17-ketone showed that the reaction sequence: Barbier–Grignard allylation–hydroboration–cyclization is a simple and effective method for the spiroannelation of steroidal ketones. Since Grignard-type reactions are known to proceed smoothly even with hindered steroidal ketones, it is assumed that the described spiroannelation can be extended to other positions in the steroidal skeleton.

Experimental

Melting points were determined on a Kofler hot-stage apparatus and are uncorrected. The ir spectra were determined with a Perkin–Elmer 580 spectrophotometer for solutions in chloroform. The ^{1}H nmr spectra

Can. J. Chem. Downloaded from www.nrcresearchpress.com by 190.90.36.8 on 09/07/12
For personal use only.

Can. J. Chem. Downloaded from www.nrcresearchpress.com by 190.90.36.8 on 09/07/12
For personal use only.

were recorded with a Varian EM-360 or JEOL FX 90 spectrometer for solutions in deuteriochloroform. The chemical shifts (δ) are expressed in ppm relative to tetramethylsilane. Mass spectra were recorded with a JEOL JMS-D spectrometer using electron impact.

Barbier–Grignard reaction of 5α-cholestan-3-one with allyl bromide

To a mixture of magnesium (0.72 g), allyl bromide (0.05 g), and a few crystals of iodine in benzene (5 mL) stirred under argon, a solution of 5α-cholestan-3-one (2.3 g) and allyl bromide (1.43 g) in diethyl ether (30 mL) was added dropwise in 30 min. The reaction mixture was stirred at room temperature for 2 h, diluted with benzene, and washed with water. The dried ($MgSO_4$) organic layer was evaporated and the crude reaction product was chromatographed on silica gel with benzene as eluent. The two products obtained are listed in the order of their emergence: 3β-allyl-5α-cholestan-3α-ol (**2**) (1.30 g, 51%), which had mp 89–91°C (methanol) (lit. (13) mp 90–92°C), and 3α-allyl-5α-cholestan-3β-ol (**1**) (1.22 g, 48%), which had mp 114–116°C (methanol) (lit. (13) mp 112–114°C); ^{1}H nmr and ir spectra of compounds **1** and **2** were in accordance with the reported data (13).

Hydroboration of compound 1

To a stirred solution of **1** (100 mg) and sodium borohydride (18 mg) in diglyme (7.5 mL) kept at room temperature under argon was added dropwise boron trifluoride diethyl ether complex (80 μL) over 5 min. After 40 min a mixture of potassium hydroxide (10%, 1.2 mL) and hydrogen peroxide (30%, 0.8 mL) was added dropwise over 5 min, and stirring was continued for 30 min. The reaction mixture was then poured into water and extracted with a 1:1 mixture of diethyl ether – benzene. The product was chromatographed on a silica gel column with benzene – ethyl acetate mixtures as eluent. Two compounds were obtained. 3α-(2′-Hydroxypropyl)-5α-cholestan-3β-ol (**4**) (22 mg, 21%) was a colorless oil; ir ν_{max}: 3610 and 3480 cm^{-1}; ^{1}H nmr δ: 4.10 (1H, m), 2.88 (2H, br s, $W_{1/2}$ = 18 Hz), 0.88, 0.79, 0.77, and 0.62; mass spectrum *m/z*: 446 (M^+), 387, 331, 330, 141, 128, 116, 109, 95, and 81. *Anal.* calcd. for $C_{30}H_{54}O_2$: C 80.65, H 12.18; found: C 80.51, H 12.44. 3α-(3′-Hydroxypropyl)-5α-cholestan-3β-ol (**3**) (78 mg, 75%) was recrystallized from methanol; mp 168–170°C; $[\alpha]_D$ +24.0° (*c* 1.7 pyridine) (lit. (14) mp 164–170°C; $[\alpha]_D$ +24.4° (*c* 0.41, pyridine)); ir ν_{max}: 3.600 and 3410 cm^{-1}; ^{1}H nmr δ: 3.64 (2H, m), 2.91 (2H, s), 0.88, 0.83, 0.77, and 0.62; mass spectrum *m/z*: 446 (M^+), 387, 141, 128, 115. *Anal.* calcd. for $C_{30}H_{54}O_2$: C 80.65, H 12.18; found: C 80.43, H 12.33.

Hydroboration of compound 2

The reaction of **2** (103 mg) was carried out in a similar manner to that described above. After chromatography on silica gel two compounds were obtained. 3β-(2′-Hydroxypropyl)-5α-cholestan-3α-ol (**6**) (25 mg, 23%) had mp 140–147°C (methanol); ir ν_{max}: 3610 and 3480 cm^{-1}; ^{1}H nmr δ: 4.27 (1H, m, $W_{1/2}$ = 22 Hz), 3.10 (2H, br s, $W_{1/2}$ = 16 Hz), 0.88, 0.79, 0.72, and 0.62; mass spectrum *m/z*: 446 (M^+), 387, 232, 128, 95. *Anal.* calcd. for $C_{30}H_{54}O_2$: C 80.65, H 12.18; found: C 80.44, H 12.30. 3β-(3′-Hydroxypropyl)-5α-cholestan-3α-ol (**5**) (80 mg, 74%) had mp 141–142°C (methanol); $[\alpha]_D$ +27.2° (*c* 0.6 pyridine) (lit. (14) mp 141–142°C; $[\alpha]_D$ +45.0° (*c* 0.6 pyridine)); ir ν_{max}: 3610 and 3410 cm^{-1}; ^{1}H nmr δ: 3.65 (2H, m), 2.17 (2H, s), 0.93, 0.89, 0.82, 0.74, and 0.65; mass spectrum *m/z*: 446 (M^+), 387, 95. *Anal.* calcd. for $C_{30}H_{54}O_2$: C 80.65, H 12.18; found: C 80.64, H 12.51.

(R)-Spiro[(5α-cholestane-3,5′-(2′-oxotetrahydrofuran)] (7)

Jones reagent was added dropwise to a stirred solution of compound **3** (75 mg) in acetone (20 mL) kept at 0°C until all the substrate had reacted (tlc control). Then a few drops of ethanol were added and the reaction mixture was poured into water. After extraction with a 1:1 mixture of benzene – diethyl ether, the crude product was purified on a column of silica gel to give lactone **7** (74 mg, 99%), which had mp 218–221°C (chloroform–methanol) and $[\alpha]_D$ +21.7° (*c* 0.91 chloroform) (lit. (14) mp 217–222°C; $[\alpha]_D$ +21.7° (chloroform); ir ν_{max}: 1760 cm^{-1}; ^{1}H nmr δ: 2.75–2.41 (2H, m), 0.87, 0.81, 0.78, and 0.63; mass spectrum *m/z*: 442 (M^+), 427, 287, and 180. *Anal.* calcd. for $C_{30}H_{50}O_2$: C 81.38, H 11.38; found: C 81.33, H 11.43.

(S)-Spiro[(5α-cholestane)-3,5′-(2′-oxotetrahydrofuran)] (8)

Oxidation of compound **5** (244 mg), carried out as described above, gave lactone **8** (229 mg, 94%), which had mp 199–201°C (methanol) and $[\alpha]_D$ +20.4° (*c* 6.13, chloroform) (lit. (14) mp 202–206°C; $[\alpha]_D$ +6.6° (*c* 0.91, chloroform)); ir ν_{max}: 1755 cm^{-1}; ^{1}H nmr δ: 2.60–2.33 (2H, m), 0.90, 0.87, 0.76, and 0.62; mass spectrum *m/z*: 442 (M^+), 427, 287, and 95. *Anal.* calcd. for $C_{30}H_{50}O_2$: C 81.38, H 11.38; found: C 81.45, H 11.46.

(R)-Spiro[(5α-cholestane)-3,2′-(tetrahydrofuran)] (9)

To a stirred solution of compound **3** (40 mg) in pyridine (0.5 mL) kept at 0°C under argon was added a solution of *p*-toluenesulfonyl chloride (34 mg) in pyridine (0.5 mL). After 1.5 h an additional portion of *p*-toluenesulfonyl chloride (34 mg) was added and stirring was continued for 18 h. The reaction mixture was poured into water. The usual work-up gave 38 mg (99%) of chromatographically pure **9**, which had mp 117–118°C (acetone); ir ν_{max}: 1045 cm^{-1}; ^{1}H nmr δ: 3.80 (2H, m), 0.88, 0.78, 0.70, and 0.62; mass spectrum *m/z*: 428 (M^+), 331, 123, 110, and 98. *Anal.* calcd. for $C_{30}H_{52}O$: C 84.04, H 12.23; found: C 83.77, H 12.12.

(S)-Spiro[(5α-cholestane)-3,2′-(tetrahydrofuran)] (10)

The reaction was carried out as above. Compound **5** (50 mg) and *p*-toluenesulfonyl chloride (42 mg) gave compound **10** (44 mg, 92%), which had mp 103–104°C (acetone); ir ν_{max}: 1035 cm^{-1}; ^{1}H nmr δ: 3.79 (2H, m), 0.87, 0.81, 0.77, 0.75, and 0.62; mass spectrum *m/z*: 428 (M^+), 123, 110, 98. *Anal.* calcd. for $C_{30}H_{52}O$: C 84.04, H 12.23; found: C 84.14, H 12.30.

3α-Acetonyl-5α-cholestan-3β-ol (11)

Compound **4** (40 mg) dissolved in acetone (10 mL) was oxidized with Jones reagent at 0°C. The usual work-up gave 38 mg (96%) of slightly impure (tlc) product. This was filtered through a column of silica gel to give **11** (28 mg, 71%), which had mp 109–111°C (pentane); ir ν_{max}: 3510 and 1700 cm^{-1}; ^{1}H nmr δ: 3.79 (1H, m, $W_{1/2}$ = 24 Hz, O*H*), 2.74 (2H, s, CH_2 α to CO), 2.17 (3H, s, CH_3CO), 0.91, 0.80, and 0.65; mass spectrum *m/z*: 444 (M^+), 426, 386, 368, 44. *Anal.* calcd. for $C_{30}H_{52}O_2$: C 81.02, H 11.79; found: C 80.63, H 11.70.

3β-Acetonyl-5α-cholestan-3α-ol (12)

Compound **6** (24 mg) was dissolved in acetone (5 mL) and oxidized with Jones reagent at 0°C. The usual work-up gave a crude product (20.5 mg, 86%), which was crystallized from pentane to give **12** (15 mg). It had mp 125–128°C; ir ν_{max}: 3520 and 1700 cm^{-1}; ^{1}H nmr δ: 3.45 (1H, br s, $W_{1/2}$ = 14 Hz, O*H*), 2.55 (2H, s, CH_2CO), 2.16 (3H, s, CH_3CO), 0.93, 0.89, 0.82, 0.74, and 0.64; mass spectrum *m/z*: 444 (M^+), 426, 368. *Anal.* calcd. for $C_{30}H_{52}O_2$: C 81.02, H 11.79; found: C 80.85, H 11.75.

Dehydration of 12

A solution of compound **12** (20 mg) and *p*-toluenesulfonic acid (2 mg) in benzene (0.6 mL) was stirred at room temperature for 22 h. The usual work-up and chromatography on a silica gel column gave a product (16 mg, 83%) consisting of **13** and **14** in the ratio 9:1 (estimated from ^{1}H nmr spectrum by the integration of olefinic proton signals at δ 5.98 and 5.47). This material, mostly 3-(2′-oxopropylidene)-5α-cholestane (**13**), was an oil; ir ν_{max}: 1680 and 1620 cm^{-1}; uv $\lambda_{max}(\varepsilon)$: 248 (12 800) (ethanol); ^{1}H nmr δ: 5.98 (1H, br s), 2.16 (3H, s), 0.93, 0.90, 0.82, and 0.65; mass spectrum *m/z*: 426 (M^+) and 368. *Accurate Mass* calcd. for $C_{30}H_{50}O$: 426.3862; found: 426.3845.

Dehydration of 11

A solution of compound **11** (14.5 mg) and *p*-toluenesulfonic acid (1.5 mg) in benzene (0.2 mL) was stirred at room temperature for 25 h. The usual work-up and filtration through a silica gel column gave a product (11 mg, 79%) consisting of **13** and **14** in the ratio 7:3, estimated from the ^{1}H nmr spectrum as in the preceding experiment.

3-Acetonyl-5α-cholest-2-ene (14)

To a solution of compound **13** (10.5 mg) in methanol (2 mL) stirred under argon was added a solution of potassium hydroxide in methanol (10%, 0.1 mL). The reaction mixture was stirred at room temperature

for 16 h. The usual work-up gave compound **14** (9 mg), which had mp 104–106°C (methanol); ir ν_{max}: 1705 cm^{-1}; ^1H nmr δ: 5.47 (1H, m), 3.00 (2H, s), 2.12 (3H, s), 0.96, 0.90, 0.83, 0.73, and 0.66; mass spectrum *m/z*: 426 (M^+), 368, 43. *Accurate Mass* calcd. for $C_{30}H_{50}O$: 426.3861; found: 426.3857.

17α-Allyl-3β-(tetrahydropyran-2-yloxy)-5α-androstan-17β-ol (15)

To a mixture of magnesium (60 mg), allyl bromide (0.014 g), and a few crystals of iodine in diethyl ether (1 mL) stirred under argon was added a solution of 3β-(tetrahydropyran-2-yloxy)-5α-androstan-17-one (300 mg) and allyl bromide (86 mg) in diethyl ether (9 mL). After completion of the addition (45 min) the reaction mixture was refluxed with stirring for 1.5 h, then poured into water and extracted with a 1:1 mixture of diethyl ether – benzene. The dried ($MgSO_4$) organic layer was evaporated to give chromatographically pure compound **15** (328 mg, 98%), which had mp 117–126°C (methanol); ir ν_{max}: 3620, 1630, and 1020 cm^{-1}; ^1H nmr δ: 5.94 (1H, m, $W_{1/2}$ = 34 Hz), 5.26–4.85 (2H, m), 4.67 (1H, m), 3.79 (1H, m), 3.51 (2H, m), 2.22 (2H, d, J = 6 Hz), 1.81 (1H, s), 0.86, and 0.82; mass spectrum *m/z*: 416 (M^+), 315, 297, 273, 255, 85. *Anal.* calcd. for $C_{27}H_{44}O_3$: C 77.83, H 10.64; found: C 77.42, H 10.69.

17α-Allyl-5α-androstan-3β,17β-diol (16)

A solution of **15** (252 mg) and concentrated hydrochloric acid (0.04 mL) in absolute ethanol was stirred at room temperature for 6 h. The usual work-up gave chromatographically pure compound **16** (190 mg, 95%), which had mp 173–174°C (methanol) (lit. (19*a*) mp 176–177°C); ir ν_{max}: 3605, 3450, 1635, and 1030 cm^{-1}; ^1H nmr δ: 5.97 (1H, m, $W_{1/2}$ = 32 Hz), 5.38–4.92 (2H, m), 3.53 (1H, m), 2.24 (2H, d, J = 7 Hz), 1.52 (2H, s), 0.87, and 0.82; mass spectrum *m/z*: 332 (M^+), 291, 273, 255, 161, 147, 107, 42. *Anal.* calcd. for $C_{22}H_{36}O_2$: C 75.38, H 10.92; found: C 75.57, H 10.95.

3β-Acetoxy-17α-allyl-5α-androstan-17β-ol (17)

Crude compound **16**, obtained from the Barbier–Grignard reaction of 3β-(tetrahydropyran-2-yloxy)-5α-androstan-17-one (300 mg) and subsequent hydrolysis of THP–ether, was acetylated in a mixture of pyridine (2 mL) and acetic anhydride (2 mL) at room temperature for 26 h. The usual work-up gave a crude product (284 mg, 95%). This was crystallized from hexane to give compound **17** (251 mg, total yield of the three-step sequence 84%), which had mp 124–128°C (lit. (19*a*) mp 132–133°C); ir ν_{max}: 3620, 3560, 1720, 1630, and 1250 cm^{-1}; ^1H nmr δ: 5.95 (1H, m, $W_{1/2}$ = 34 Hz), 5.33–4.90 (2H, m), 4.65 (1H, m), 2.22 (2H, d, J = 7 Hz), 1.97 (3H, s), 1.65 (1H, s), 0.83, and 0.80; mass spectrum *m/z*: 374 (M^+), 333, 273, 255, and 43. *Anal.* calcd. for $C_{24}H_{38}O_2$: C 76.95, H 10.22; found: C 76.30, H 10.56.

Hydroboration of compound 17

To a solution of compound **17** (1.072 g) in tetrahydrofuran (10 mL), stirred under argon at room temperature, three portions (1 mL each) of $BH_3 \cdot (CH_3)_2S$ complex (1 *M*) in methylene chloride were added at 0.5 h intervals. After the substrate had reacted (tlc control), a solution of sodium hydroxide (10%, 6 mL) was added, followed by dropwise addition of hydrogen peroxide (30%, 14 mL) during 4 h. The product was extracted with a 1:1 mixture of benzene – diethyl ether and purified chromatographically (silica gel, benzene – ethyl acetate 5:1). The major product was 3β-acetoxy-17α-(3′-hydroxypropyl)-5α-androstan-17β-ol (**18**) (830 mg, 74%), which had mp 219–221°C (methanol); ir ν_{max}: 3620, 3415, 1720, and 1255 cm^{-1}; ^1H nmr δ: 4.60 (1H, m, $W_{1/2}$ = 18 Hz), 3.62 (2H, m), 2.64 (2H, s), 1.97 (3H, s), 0.80; mass spectrum *m/z*: 374, 333, 115, 102, 97, and 43. *Anal.* calcd. for $C_{24}H_{40}O_4$: C 73.42, H 10.27; found: C 73.50, H 10.69. The minor product was a compound whose spectra were in agreement with structure **19**. It had mp 175–177°C (methanol); ir ν_{max}: 3620, 3480, 1720, and 1265 cm^{-1}; ^1H nmr δ: 4.66 (1H, m, $W_{1/2}$ = 16 Hz), 4.16 (1H, m, $W_{1/2}$ = 16 Hz), 2.56 (2H, s), 1.99 (3H, s), 0.91 (3H, s), 0.84, and 0.82 (two s integrating to 3H); mass spectrum *m/z*: 392 (M^+), 333, 115. This material did not give satisfactory analytical data.

(S)-Spiro[(3β-acetoxy-5α-androstane)-17,2′-tetrahydrofuran] (20)

A solution of **18** (50 mg) and *p*-toluenesulfonyl chloride (97 mg) in pyridine (1 mL) was stirred under argon at room temperature for 3.5 h. The usual work-up gave compound **20** (46 mg, 97%, homogenous on tlc), which had mp 113–114°C (methanol) (lit. (19*b*) mp 116–120°C and 124–125°C); ir ν_{max}: 1720 and 1255 cm^{-1}; ^1H nmr δ: 4.65 (1H, m, $W_{1/2}$ = 26 Hz), 3.74 (2H, m), 2.00 (3H, s), 0.85, and 0.82; mass spectrum *m/z*: 374 (M^+), 97, 84.

(R)-Spiro[(3β-acetoxy-5α-androstane)-17,5′-(2′-oxotetrahydrofuran)] (21)

Oxidation of compound **18** (650 mg) with Jones reagent gave a crude product (637 mg) that was crystallized from heptane to give lactone **21** (605 mg, 94%), which had mp 162–163°C (lit. (19*b*) mp 162–163°C); ir ν_{max}: 1760, 1720, and 1250 cm^{-1}; ^1H nmr δ: 4.65 (1H, m, $W_{1/2}$ = 20 Hz), 2.44 (2H, m), 1.97 (3H, s), 0.86, and 0.78; mass spectrum *m/z*: 388 (M^+), 328, 217, 147, 107, and 43.

(R)-Spiro[(3β-hydroxy-5α-androstane)-17,5′-(2′-oxotetrahydrofuran)] (22)

To a solution of lactone **21** (400 mg) in methanol (20 mL) was added potassium carbonate in methanol (1%, 20 mL), and the mixture was kept at room temperature for 17 h. The usual work-up gave a crude product, which was filtered through a column of silica gel. Compound **22** (343 mg, 96%) had mp 200–202°C (methanol) (lit. (3*a*) mp 199–201°C); ir ν_{max}: 3605, 3480, and 1760 cm^{-1}; ^1H nmr δ: 3.52 (1H, m), 2.45 (2H, m), 2.07 (1H, s), 0.88, and 0.79; mass spectrum *m/z*: 346 (M^+), 246, 217, 107, and 41.

Acknowledgement

Financial support of this work from the Polish Academy of Sciences MR I.12.1.5 and from the Ministry of Sciences and Higher Education RP II.13.2 is gratefully acknowledged.

1. H. M. R. Hoffmann and J. Rabe. Angew. Chem. Int. Ed. Engl. **24**, 94 (1985).
2. K. H. Lee, T. Ibuka, S. H. Kim, B. R. Vestal, I. H. Hall, and E. S. Huang. J. Med. Chem. **18**, 812 (1975); G. Schlewer, J. L. Stampf, and C. Benezra. J. Med. Chem. **23**, 1031 (1980); C. Lindig. J. Prakt. Chem. **325**, 587 (1983).
3. (*a*) J. A. Cella, E. A. Brown, and R. R. Burtner. J. Org. Chem. **24**, 743 (1959); (*b*) J. A. Cella and R. C. Tweit. J. Org. Chem. **24**, 1109 (1959); (*c*) D. Bittler, H. Hofmeister, H. Laurent, K. Nickisch, R. Nickolson, K. Petzoldt, and R. Wiechert. Angew. Chem. Int. Ed. Engl. **21**, 696 (1982).
4. J. A. Cella and C. M. Kagawa. J. Am. Chem. Soc. **79**, 4808 (1957); C. M. Kagawa, J. A. Cella, and C. G. Van Armau. Science, **126**, 1015 (1957).
5. P. L. Creger. J. Am. Chem. Soc. **89**, 2500 (1967); D. Caine and A. S. Frobese. Tetrahedron Lett. 883 (1978); E. Ehlinger and P. Magnus. Tetrahedron Lett. **21**, 11 (1980); G. Sturtz and J.-J. Yaouanc. Synthesis, 289 (1980); K. Kano, K. Hayashi, and H. Mitsuhashi. Chem. Pharm. Bull. **30**, 1198 (1982).
6. P. A. Grieco. Synthesis, 67 (1975); P. Brownbridge, E. Egert, P. G. Hunt, O. Kennard, and S. Warren. J. Chem. Soc. Perkin Trans. 1, 2751 (1981); T. Oida, S. Tanimoto, H. Ikehira, and M. Okano. Bull. Chem. Soc. Jpn. **56**, 645 (1983).
7. C. Blomberg and F. A. Hartog. Synthesis, 18 (1977).
8. P. Picard and J. Moulines. Bull. Soc. Chim. Fr. 3377 (1973); B. M. Trost and M. J. Bogdanowicz. J. Am. Chem. Soc. **95**, 5321 (1973); O. S. Bhanot, T. K. Das, I. Gupta, H. S. Suri, and P. C. Dutta. J. Org. Chem. **42**, 1623 (1977).
9. M. P. Dreyfuss. J. Org. Chem. **28**, 3269 (1963).
10. D. H. R. Barton, A. S. Campos-Neves, and R. C. Cookson. J. Chem. Soc. 3500 (1956).
11. H. Berbalk, K. Eichinger, and R. Schuster. Helv. Chim. Acta, **60**, 2499 (1977).
12. R. A. Y. Jones, A. R. Katritzky, and P. G. Lehman. J. Chem. Soc. (B), 1316 (1971).
13. P. D. Woodgate, B. R. Davies, and M. H. Lee. Aust. J. Chem. **28**, 1785 (1975).

Can. J. Chem. Downloaded from www.nrcresearchpress.com by 190.90.36.8 on 09/07/12
For personal use only.

14. P. BLADON and D. R. RAE. J. Chem. Soc. Perkin Trans. 1, 2240 (1974).
15. D. D. REYNOLDS and W. O. KENYON. J. Am. Chem. Soc. **72**, 1593 (1950).
16. A. R. H. COLE, R. N. JONES, and K. DOBRINER. J. Am. Chem. Soc. **74**, 5571 (1952); H. ROSENKRANTZ and L. ZABLOW. J. Am. Chem. Soc. **75**, 903 (1953).
17. J. B. JONES and P. PRICE. J. Chem. Soc. Chem. Commun. 1478 (1969).
18. D. N. KIRK and M. P. HARTSHORN. *In* Steroid reaction mechanism. Elsevier, Amsterdam. 1968. Chapt. 4.
19. (*a*) J. EUW and T. REICHSTEIN. Helv. Chim. Acta, **24**, 401 (1941); (*b*) V. WENNER and T. REICHSTEIN. Helv. Chim. Acta, **27**, 24 (1944).

Can. J. Chem. Downloaded from www.nrcresearchpress.com by 190.90.36.8 on 09/07/12
For personal use only.

Medium effects on activation parameters on alkaline hydrolysis of 2-carbomethoxypropionate ion in aqueous mixtures of ethylene glycol

PRASANTA KUMAR BISWAS, BIKAS CHANDRA BAG, AND MIHIR NATH DAS[1]

Department of Chemistry, Jadavpur University, Calcutta 700 032, India

Received May 27, 1986

PRASANTA KUMAR BISWAS, BIKAS CHANDRA BAG, and MIHIR NATH DAS. Can. J. Chem. **65**, 235 (1987).

The standard free energies of transfer (ΔG_{tr}^0) of the 2-carbomethoxypropionate ion (R^-) have been determined from the solubilities of the silver salt (AgR) in water and six aqueous mixtures of ethylene glycol (1–60%) at 25°C, using the literature values of ΔG_{tr}^0 of Ag^+. Utilizing these values of the R^- ion as well as the literature values of $\Delta G_{tr}^{\ddagger}$ of the OH^- ion, combined with the experimental values of $\Delta G^{\ddagger}$ for the alkaline hydrolysis of R^- ion, the corresponding transfer parameters of the transition states ($\Delta G_{tr}^{\ddagger}$) for the hydrolysis reaction in aquo-glycolic media at 25°C have been calculated. Attempts have been made to correlate the rates and activation parameters with the transfer quantities and solvent properties.

PRASANTA KUMAR BISWAS, BIKAS CHANDRA BAG et MIHIR NATH DAS. Can. J. Chem. **65**, 235 (1987).

En se basant sur les solubilités, mesurées à 25°C, du sel d'argent (AgR) dans l'eau et dans six mélanges aqueux d'éthylène glycol (10–60%) et utilisant les valeurs de la littérature pour le ΔG_{tr}^0 de l'ion Ag^+, on a déterminé les énergies libres standards de transfert (ΔG_{tr}^0) de l'ion carbométhoxy-2 propionate (R^-). Utilisant ces valeurs pour l'ion R^- et les valeurs de la littérature de ΔG_{tr}^0 pour l'ion OH^- en combinaison avec les valeurs expérimentales de $\Delta G^{\ddagger}$ pour l'hydrolyse alcaline de l'ion R^-, on a calculé les paramètres correspondants de transfert des états de transition ($\Delta G_{tr}^{\ddagger}$ pour la réaction d'hydrolyse, à 25°C, dans des milieux glycoliques aqueux. On a essayé d'établir une corrélation entre les vitesses de réaction et les paramètres d'activation d'une part avec les quantités de transfert et les propriétés de solvant d'autre part.

[Traduit par la revue]

Introduction

Rates and activation parameters for alkaline hydrolysis of the 2-carbomethoxypropionate ion (R^-), a negatively charged ester, in aqueous mixtures of ethylene glycol (EG) were reported earlier (1, 2). The reaction is

$$^-OCOCH_2CH_2COOCH_3 + OH^- \rightleftharpoons {}^-OCOCH_2CH_2COO^- + CH_3OH$$

Attempts were made to correlate the results by dissecting the parameters into electrostatic and non-electrostatic components. A meaningful analysis of the results, however, requires a knowledge of the relevant thermodynamic transfer parameters, and the present paper essentially deals with medium effects in the light of the transfer free energies of the reacting ions and the transition state in aquo-glycolic mixtures at 25°C.

Experimental

2-Carbomethoxypyropionic acid (the half ester of succinic acid) was prepared by a standard method (3). Ethylene glycol (E. Merck, India) was purified by the usual procedure (4). Aqueous mixtures of six different compositions (10–60% EG) were prepared by weight. The silver salt of the half ester (AgR) was prepared and its solubilities (S) in water and the aquo-glycolic mixtures at 25°C were measured by the same procedures as described earlier (5).

Results

From the rate constants at zero ionic strengths (k_0) at 20, 30, and 40°C, reported earlier (2), the k_0 values corresponding to 25°C were evaluated by interpolation for all the media, and are shown in Table 1, together with the ratios k_s/k_w, where k_w denotes the value of k_0 in water and k_s that in any mixed medium. The activation parameters on the molar scale were also evaluated for 25°C (Table 1).

The standard free energies of transfer of the silver salt, ΔG_{tr}^0(AgR), from water to the respective media were evaluated by eq. [1], assuming complete dissociation of AgR in all the media.

TABLE 1. Rate constants (L mol^{-1} min^{-1}) and activation parameters (in KJ mol^{-1}) at zero ionic strength at 25°C (molar scale)

Wt. % of EG	k_0	k_s/k_w	$\Delta H^{\ddagger}$	$T\Delta S^{\ddagger}$	$\Delta G^{\ddagger}$	$m\delta\Delta G^{\ddagger}$
0	3.58	—	48.9	−31.1	80.0	—
10	2.57	0.72	52.1	−28.7	80.8	0.80
20	2.09	0.58	53.9	−27.5	81.4	1.40
30	1.66	0.46	57.5	−24.5	82.0	2.00
40	1.26	0.35	63.8	−18.8	82.6	2.60
50	1.07	0.30	65.9	−17.2	83.1	3.10
60	1.00	0.28	68.0	−15.2	83.2	3.20

$$[1] \quad \Delta G_{tr}^0(\text{AgR}) = RT \ln \frac{K_{sp}(w)}{K_{sp}(s)}$$

where K_{sp} denotes the solubility product of AgR and w and s representing water and any other medium, respectively.

The standard free energies of transfer of the substrate ion, $\Delta G_{tr}^0(R^-)$, from water to the mixed media were calculated by subtracting from ΔG_{tr}^0(AgR) the corresponding values of transfer of Ag^+ ion, $\Delta G_{tr}^0(Ag^+)$, as obtained from literature (6). These latter values are based on the well-known extrathermodynamic TATB assumption that ΔG_{tr}^0 for the tetraphenyl arsonium (TA^+) ion is equal to that for the tetraphenyl boride (TB^-) ion for any particular medium at a given temperature.

The ΔG_{tr}^0 values for the other reactant, OH^- ion, were obtained from literature (7), these being based on the self-ionization constants of water and the mixed media (8), combined with the TATB assumption (9, 10). Wells (11) has used a different assumption for calculating $\Delta G_{tr}^0(OH^-)$, and his values are slightly different. The TATB assumption is, however, generally considered to be more sound (9, 12).

The medium effect on the free energy of activation, $m\delta\Delta G^{\ddagger}$,

[1]To whom all correspondence should be addressed.

Can. J. Chem. Downloaded from www.nrcresearchpress.com by 80.58.250.72 on 09/07/12
For personal use only.

TABLE 2. Solubilities (S) of AgR and standard free energies of transfer (in KJ mol^{-1}) of AgR, Ag^+, R^-, OH^-, and the transition states at 25°C (molar scale)

Wt. % of EG	$S(M \times 10^3)$	ΔG^0_{tr}(AgR)	$\Delta G^0_{tr}(Ag^+)^a$	$\Delta G^0_{tr}(R^-)$	$\Delta G^0_{tr}(OH^-)^b$	$\Delta G^{\ddagger}_{tr}$
0	4.19	—	—	—	—	—
10	2.47	2.60	−0.20	2.80	0.40	4.00
20	2.42	2.70	−0.40	3.10	−0.30	4.20
30	2.36	2.90	−0.70	3.60	−0.45	5.15
40	2.18	3.30	−1.00	4.30	−0.95	5.95
50	1.86	4.00	−1.40	5.40	−1.10	7.40
60	1.79	4.20	−2.00	6.20	−0.90	8.50

[a]Reference 6.
[b]Reference 7 (reported as $\Delta G^0_{tr}(S^-)$).

is given by eq. [2].

$$[2] \quad m\delta\Delta G^{\ddagger} = \Delta G^{\ddagger}(s) - \Delta G/(w)$$

where s and w denote any mixed medium and water, respectively (Table 1). The standard free energy of transfer of the transition state, $\Delta G^{\ddagger}_{tr}$, for any medium is given by eq. [3].

$$[3] \quad \Delta G^{\ddagger}_{tr} = m\delta\Delta G^{\ddagger} + \Delta G^0_{tr}(OH^-) + \Delta G_{tr}{}^0(R^-)$$

The values of the standard free energies of transfer of the different species from water to the aquo-glycolic media of varying compositions are shown in Table 2.

Discussion

The rate constant monotonically decreases with increase in the proportion of glycol in the medium (Table 1). Only a small part of this decrease can, however, be ascribed to a decrease in the dielectric constant. In a series of isodielectric media (D = 50.38) comprising water and an organic solvent like acetone, dioxane, ethanol, and ethylene glycol, the rate constant for the same reaction at 30°C is the lowest in the aqueous mixture of glycol (1). A similar result was also found for the alkaline hydrolysis of another negatively charged ester, acetyl mandelate ion (13). It is true that amongst all these isodielectric media, the glycolic medium has the lowest mole fraction of water, and this may or may not be just a case of coincidence. But then, the rate of the title reaction in aqueous DMSO mixtures monotonically increases with decreasing mole fraction of water (5). Increase in rate with decrease in water content has also been found for the same reaction in some other aquo-organic mixtures (14).

In aquo-glycolic media, a disturbing factor to be considered (7, 15) is the possibility of formation of the glycoxide ion (OG^-) by reaction between the OH^- ion and the glycol molecule (GOH)

$$OH^- + GOH \rightleftharpoons OG^- + H_2O$$

If the glycoxide ion be present in an appreciable concentration, a parallel reaction between this ion and the ester ion is likely to occur. Hence, the rate constants and the activation parameters as well as the transfer free energies, $\Delta G^0_{tr}(OH^-)$ and $\Delta G^{\ddagger}_{tr}$, reported in the present work ought to be considered as composite quantities involving both OH^- and OG^- ions. This aspect of the problem, which has been discussed by Kundu and co-workers (7) in connection with the alkaline fading of crystal violet ion in aqueous mixtures of ethylene glycol, is an involved one and will remain so till the above equilibrium is studied quantitatively, and separate values for the two rate constants (for reactions with OH^- and OG^- ions) as well as the transfer free energies of the OH^- and OG^- ions for the different aquo-glycolic media are available. Certain plausible conclusions may, however, be profitably drawn from the observed overall values of the rate constants and the thermodynamic parameters, as presented below.

The observed decrease in rate, on changing the medium from water to aqueous glycol, may occur as a result of stabilization of the reacting ions and/or destabilization of the transition state. The observed $\Delta G^0_{tr}(OH^-)$ values (Table 2) are negative and rather small in magnitude, implying that the OH^- ion is slightly stabilized on adding glycol to water, but this becomes appreciable only beyond 40% glycol. The OH^- ion should thus be somewhat less reactive on adding glycol to water. The $\Delta G^0_{tr}(R^-)$ values (Table 2), however, are positive and of a higher magnitude, indicating that the substrate ion is appreciably destabilized and should become more reactive on adding glycol. It is significant that the ΔG^0_{tr} values for the anions, Cl^-, Br^-, and I^- are also reported to be positive on the basis of the TATB assumption (9, 10) as well as the other assumption used by Wells (11, 15). For the transition state, which is a doubly charged anion, the free energies of transfer ($\Delta G^{\ddagger}_{tr}$) are also positive and appreciably larger, indicating a relatively larger degree of destabilization. In fact, it is the destabilization of the transition state which essentially dictates the overall effect leading to decreased rates in aquo-glycolic media. In aqueous DMSO mixtures, on the other hand, it is the combined destabilization of the reacting ions, which predominates over even the very large destabilization effect on the transition state, leading to enhanced rates (5).

The greater destabilization of the transition state and also of the substrate ion to a smaller extent, on gradual replacement of water by glycol molecules, possibly arises from the reduced solvating capacity of glycol because of intramolecular hydrogen bond formation between the twin OH groups in the molecule (11). The $T\Delta S^{\ddagger}$ values (Table 1) become less negative with increasing proportion of glycol, thereby implying progressively less solvation of the transition state. The electrostatic effect arising from reduced dielectric constant also contributes to a smaller extent towards destabilization of the doubly charged transition state. For this reaction, the $\Delta H^{\ddagger}$ values (Table 1) in aquo-glycolic media are much higher than in any other medium studied so far (1, 2, 5, 14). The excess free energy function (G^E) for aqueous mixtures of ethylene glycol is negative (16, 17), but the observed results cannot be rationalized by the model of Caldin and Bennetto (18) according to which negative G^E for the solvent mixture should reduce the enthalpy of

Can. J. Chem. Downloaded from www.nrcresearchpress.com by 80.58.250.72 on 09/07/12
For personal use only.

activation (19). Other unfavourable contributory factors, particularly desolvation, obviously preponderate over the effect of negative G^E.

On the basis of the classification of solvents into typically aqueous (TA) and typically nonaqueous with negative G^E (TNAN) (17, 20), the behaviour of ethylene glycol in aqueous mixtures is considered to form a borderline between TA and TNAN, but lying more towards TA (17). The present kinetic results also point towards a similar conclusion.

Acknowledgements

We thank the University Grants Commission, New Delhi, for the award of teacher fellowships to P.K.B. and B.C.B. and the authorities of R. B. C. College, Naihati, and B. N. Mahavidyalaya, Itachuna, West Bengal, for granting them leave of absence.

1. B. C. Bag and M. N. Das. Indian J. Chem. **21**A, 1035 (1982).
2. B. C. Bag and M. N. Das. J. Indian Chem. Soc. **60**, 1118 (1983).
3. J. Cason (*Editor*). Organic synthesis. Vol. 25. John Wiley, New York. 1945. p. 19.
4. A. Weissberger (*Editor*). Technique of organic chemistry. Vol. VII. 2nd ed. Interscience, New York. 1955. p. 363.
5. P. K. Biswas and M. N. Das. J. Chem. Soc. Faraday Trans. 1, 82, 1973 (1986).
6. K. K. Kundu and A. J. Parker. J. Soln. Chem. **12**, 847 (1981).
7. U. Mandal, S. Sen, K. Das, and K. K. Kundu. Can. J. Chem. **64**, 700 (1986).
8. S. K. Banerjee, K. K. Kundu, and M. N. Das. J. Chem. Soc. A, 1166 (1967).
9. A. K. Das and K. K. Kundu. Indian J. Chem. **16**A, 467 (1978).
10. A. Bhattacharyya, A. K. Das, and K. K. Kundu. Can. J. Chem. **59**, 1153 (1981).
11. C. F. Wells. J. Chem. Soc. Faraday Trans: 1, **71**, 1868 (1975).
12. J. I. Kim. J. Phys. Chem. **82**, 1191 (1978).
13. A. K. Ray and M. N. Das. J. Chem. Soc. A, 1576 (1970).
14. V. Holba and J. Benko. Collect. Czech. Chem. Commun. **45**, 2873 (1980).
15. C. F. Wells. J. Chem. Soc. Faraday 1, **77**, 1515 (1981).
16. H. M. Trimble and W. Potts. Ind. Eng. Chem. **27**, 66 (1935).
17. M. J. Blandamer. *In* Advances in physical organic chemistry. Vol. 14. *Edited by* V. Gold and D. Bethel. Academic Press, New York. 1977. p. 327.
18. E. F. Caldin and H. P. Bennetto. *In* The physical chemistry of aqueous systems. *Edited by* R. L. Kay. Plenum, New York. 1973. pp. 129–131.
19. P. P. Tejeda, J. R. Velasco, and F. S. Burgos. J. Chem. Soc. Dalton Trans. 2679 (1983).
20. M. J. Blandamer and J. Burges. Chem. Soc. Rev. **4**, 55 (1975).

Can. J. Chem. Downloaded from www.nrcresearchpress.com by 80.58.250.72 on 09/07/12
For personal use only.

Fluorescence properties of polyene antibiotics in phospholipid bilayer membranes

N. O. PETERSEN, R. GRATTON, AND E. M. PISTERS
Department of Chemistry, The University of Western Ontario, London, Ont., Canada N6A 5B7

Received May 27, 1986

N. O. PETERSEN, R. GRATTON, and E. M. PISTERS. Can. J. Chem. **65**, 238 (1987).

The fluorescence characteristics of the polyene antibiotic Nystatin have been studied by measurements of quantum yields, lifetimes, and anisotropies in a model bilayer membrane. These measurements have been performed as a function of temperature and fluorophore-to-phospholipid molar ratio. Comparisons with data available for the parinaric acids demonstrate that the photophysics of the two polyene chromophores is similar. The quantum yield decreases at increasing Nystatin densities while the lifetimes are constant. These observations combined with quantitative comparisons with calculations of the density dependence of dynamic quenching in two-dimensional systems show that Nystatin fluorescence is quenched in bilayer membranes by a static process. This is likely due to the formation of complexes within the bilayer. The quenching is equally efficient in both the gel and liquid crystalline phases of the bilayer which suggests that the formation of the complexes occurs at all temperatures. At high Nystatin densities, there is also a quenching of the polarization, but the mechanism whereby this occurs is not clear. The limiting anisotropy at low concentrations is between 0.33 and 0.35 at all temperatures, suggesting that the Nystatin monomer is highly restricted in its reorientational motion in both gel and liquid crystalline phases.

N. O. PETERSEN, R. GRATTON et E. M. PISTERS. Can. J. Chem. **65**, 238 (1987).

En effectuant des mesures de rendements quantiques, de temps de vie et d'anisotropies dans une membrane modèle à double couche, on a étudié les caractéristiques de fluorescence de l'antibiotique polyénique Nystatine. On a effectué ces mesures en fonction de la température et du rapport molaire fluorophore/phospholipide. Des comparaisons avec les données disponibles pour les acides parinariques démontre que les photophysiques des deux chromophores polyéniques sont semblables. Le rendement quantique diminue avec une augmentation des densités des Nystatines; toutefois, les temps de vie sont constants. Ces observations, combinées avec des comparaisons quantitatives et avec des calculs de corrélation entre la densité et le piégeage dynamique dans des systèmes bidimensionnels, démontrent que la fluorescence de la Nystatine est piégée dans les membranes à doubles couches par un processus statique. Ceci est probablement dû à la formation de complexes à l'intérieur de la double couche. Le piégeage est également efficace tant des les phases en gel que dans les cristaux liquides de la double couche; ceci suggère que la formation des complexes se produit à toutes les températures. A des densités élevées de Nystatine, il se produit aussi un piégeage de la polarisation, mais le mécanisme par lequel ce piégeage se produit n'est pas clair. A des concentrations faibles et à toutes les températures, l'anisotropie limite se situe entre 0,33 et 0,35 et ceci suggère que le monomère de Nystatine est fortement restreint dans son mouvement de réorientation, tant dans la phase de gel que dans la phase cristalline liquide.
[Traduit par la revue]

Can. J. Chem. Downloaded from www.nrcresearchpress.com by 80.58.250.72 on 09/07/12
For personal use only.

Introduction

Fluorescence properties of polyene antibiotics (1–4) have been used to characterize their interactions with sterols in solution and in some membrane preparations (5–7). Detailed interpretations have been hampered by a poor understanding of the photophysics of the polyene antibiotics, and in some cases by the presence of highly fluorescent impurities (8).

Recent lifetime and quantum yield measurements (9) suggest that in solution the fluorescence properties of Nystatin (a tetraene antibiotic) are virtually identical to those of the parinaric acids and similar to those of diphenyl hexatriene. These observations now make it possible to utilize the fluorescence of several polyene antibiotics in both solution and membrane preparations to investigate their intermolecular interactions, their incorporation into bilayers and their effect on bilayer structure (10). In this report we characterize the fluorescence properties of Nystatin in a simple bilayer membrane by measurements of quantum yields, lifetimes, and anisotropies as functions of temperature and Nystatin to phospholipid molar ratios. These experiments are compared to available data (11–14) for other polyenes, notably parinaric acid, and to calculations (15–17) of the concentration-dependent quenching of emission and polarization in two dimensions.

Experimental

Materials

Polyene antibiotic derivatives were prepared as described previously (8, 9). Nystatin and the lipids used were obtained from Sigma (St. Louis, MO). Solvents were spectroscopic grade and were obtained from Fisher.

Lipid dispersions of small vesicles were prepared by injection of concentrated ethanol solutions of the lipids and polyene antibiotics in the desired proportions into warm buffer solutions (Phosphate Buffered Saline at pH 7.4 (PBS)) which were stirred vigorously (15).

Fluorescence spectroscopy

(*A*) Quantum yield measurements: Fluorescence spectra were recorded on an MPF-4 (Perkin Elmer) fluorescence spectrophotometer. The quantum yields were calculated relative to micromolar concentrations of quinine sulphate (recrystallized from water) in 0.1 *N* H_2SO_4 using the quantum yield of 0.52 (18). The calculations were not corrected for refractive index differences between lipid suspensions and the sulfuric acid solutions, but were corrected for measurements in organic solvents (19). The quantum yields were calculated from the areas by cutting and weighing. The absorbance spectra were measured on a Cary 219 uv–visible spectrophotometer, in most cases on more concentrated solutions. We have not detected any concentration dependence of the absorbance spectra in these samples beyond that expected from the Beer–Lambert Law.

(*B*) Lifetime measurements: Fluorescence lifetimes were made using single photon counting equipment in Professor W. R. Ware's laboratory (Chemistry, University of Western Ontario). The Photochemical Research Associates Model 3000 ns lifetime system has been described elsewhere (20). The lifetimes were estimated from fitting by standard procedures to, in most cases, double exponential decays. In all cases the χ^2 values were close to unity.

(*C*) Anisotropy measurements: The fluorescence anisotropy was measured on a Photochemical Research Associates prototype fluorescence polarization spectrophotometer employing appropriate excitation and emission filters along with an excitation monochromator. The fluorescence intensity was always measured in all combinations of polarization: I_{vv}, I_{vh}, I_{hv}, and I_{hh} for both the solution of interest and for a membrane suspension at the same lipid concentration but without

the chromophore. The anisotropy, r, is corrected for the background light scattering by the calculation (21):

$$r = (I_{vv(corr)} - I_{vh(corr)} \times G)/(I_{vv(corr)} + 2 \times I_{vh(corr)} \times G)$$

where G corrects for the different detection efficiency for vertical and horizontal emission polarization ($G = I_{hv(corr)}/I_{hh(corr)}$; in all cases where the data were meaningful, the value for G was in the range 0.95–0.97). In these expressions $I_{(corr)}$ is calculated as the difference between the emission intensity of the sample and the blank membrane suspension (e.g. $I_{vv(corr)} = I_{vv(sample)} - I_{vv(blank)}$).

Results

The absorption, fluorescence emission, and fluorescence excitation spectra of the polyene antibiotic Nystatin and its nitrobenzoxadiazole derivative (NBD-Nys) have been reported for solutions in several solvents (9). These spectra are fairly insensitive to the solvent except that the quantum yield of fluorescence decreases as the polarity of the solvent increases. There are small changes in both the position and the relative amplitude of the four characteristic peaks. The absorption spectra of Nystatin in phospholipid membrane preparations is obscured by the substantial background scattering relative to the absorbance at the low concentrations employed in most of the experiments described in this report, but was measured for a few samples with larger amounts of Nystatin. The fluorescence spectra, in contrast, could be measured with good precision at concentrations as low as 10^{-7} M and in some cases lower than that. Examples of these spectra are shown in Fig. 1 at several temperatures along with the structure of Nystatin. The quantum yields and the peak positions are summarized in Table 1 for a particular Nystatin-to-lipid ratio, and are compared to the corresponding values in a few solvents. Clearly, the quantum yield is highly temperature dependent in the lipid system, ranging from 0.049 at low temperatures (comparable to that in THF) to 0.003 at high temperatures (comparable to that in water). This change is a result of a decrease in the lifetime of the emission (*vide infra*) rather than a transfer of the Nystatin from the membrane to the aqueous solution.

Figure 2 illustrates the temperature dependence of the fluorescence emission intensity at several concentrations of Nystatin in the lipid. The data are normalized to the intensities at 15°C for each composition and are compared to the temperature dependence in ethanol.

The fluorescence intensity is affected by the change in lipid matrix from the gel state to the more fluid liquid crystalline state. This is particularly evident at low Nystatin concentrations where the intensity drop occurs at the usual phase transition temperature of 23°C for dimyristoyl phosphatidyl choline. At higher concentrations of Nystatin the presence of the polyene antibiotic affects the phase transition temperature range, causing a broadening. At high (about 1%) Nystatin concentrations the relative intensity is almost insensitive to the phase transition. Thus small molar amounts of Nystatin cause perturbations in the bilayer structure, at least in the immediate vicinity of the emitting polyene chromophore.

The temperature variations in fluorescence intensity are reversible. On cooling the fluorescence intensity increase as rapidly as the temperature equilibration permits. This indicates that the polyene antibiotic remains in the membrane throughout the heating–cooling cycle. The vesicles with the Nystatin are also generated at high temperature, and cooled prior to any of the experiments. We, therefore, believe that the fluorescence changes reflect changes in equilibrium properties within the membrane rather than transient, nonequilibrium effects.

Fluorescence decay measurements of Nystatin emission in

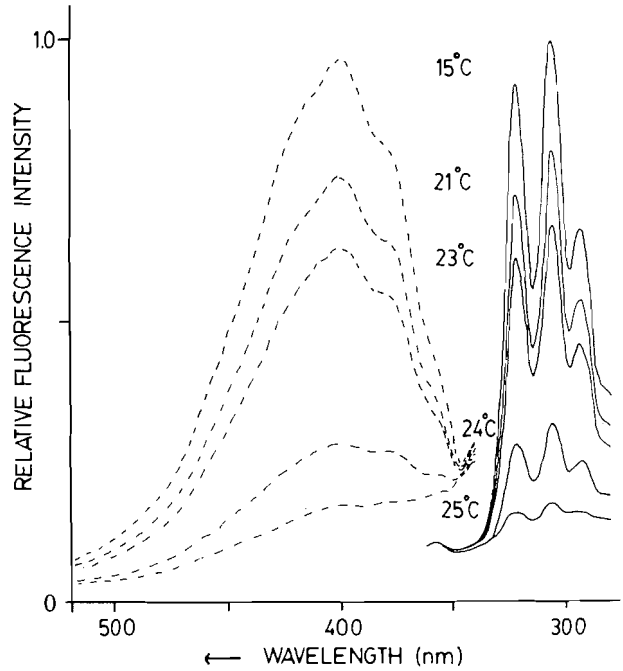

FIG. 1. Fluorescence emission and excitation spectra of Nystatin in dimyristoyl phosphatidylcholine at selected temperatures for a Nystatin-to-lipid molar ratio of 1:2500. The molecular structure of the polyene antibiotic Nystatin is

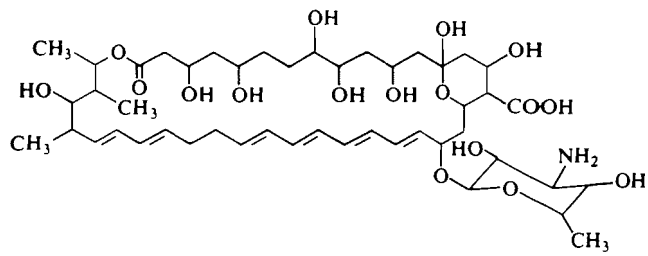

THF are fit well by a single lifetime (9). In contrast, decays of Nystatin emission in bilayer membranes require at least two lifetimes for the fits to converge with χ^2 values close to unity (Table 2 (*A*)). In some preparations, light scattering provides a small, rapidly decaying component (<0.8 ns) in addition to the two major lifetimes shown in the tables.

At low temperatures (when the bilayer is in the gel phase) the lifetimes are long (33 and 17 ns) and approach the estimated radiative lifetime of 57 ns (9) as expected for a chromophore imbedded in a rigid medium. At higher temperatures (when the bilayer is in the less rigid liquid crystalline phase) the lifetimes are reduced about five-fold. This behaviour parallels that observed for the parinaric acids in membrane preparations (13). For comparison, the lifetimes measured for *trans*-parinaric acid (*t*PnA) in gel and liquid crystalline phases are listed in Table 2 (*B*). Although the numbers differ in details, there is a close correspondence: in solution the emission decays with a single, short lifetime while in bilayers it decays with two lifetimes which are long in the rigid gel phase and short (but not as short as in solution) in the liquid crystalline phase.

These data contrast with those for diphenylhexatriene (DPH) (Table 2 (*C*); 11, 14). This probe exhibits single exponential decays (or nearly so) in all systems with little variation in lifetime between solution, gel, and liquid crystalline phases.

The quantum yield of Nystatin fluorescence in the gel phase of the bilayer is comparable to that in THF even though the

Can. J. Chem. Downloaded from www.nrcresearchpress.com by 80.58.250.72 on 09/07/12
For personal use only.

TABLE 1. Comparison of absorption and fluorescence parameters for Nystatin in solutions and membranes

Medium	Temperature/°C	λ^a_{max}/nm	$\epsilon/10^4\,M^{-1}\,cm^{-1}$	ϕ_F
EtOH	23	305	7.6	0.032
THF	23	306	6.8	0.046
DMPC[b]	15	306	~6.8	0.049
	18			0.037
	21			0.030
	22	306	~6.8	0.029
	23			0.024
	24	306	~6.8	0.016
	25			0.004
	27	306	~6.8	0.003
	30			0.003
H_2O	23	307	6.0	0.0019

[a]The wavelength at the maximum of the tallest of the four-line spectrum.
[b]8×10^{-7} *M* Nystatin plus 8×10^{-4} *M* lipid for 1:1000 molar ratio.

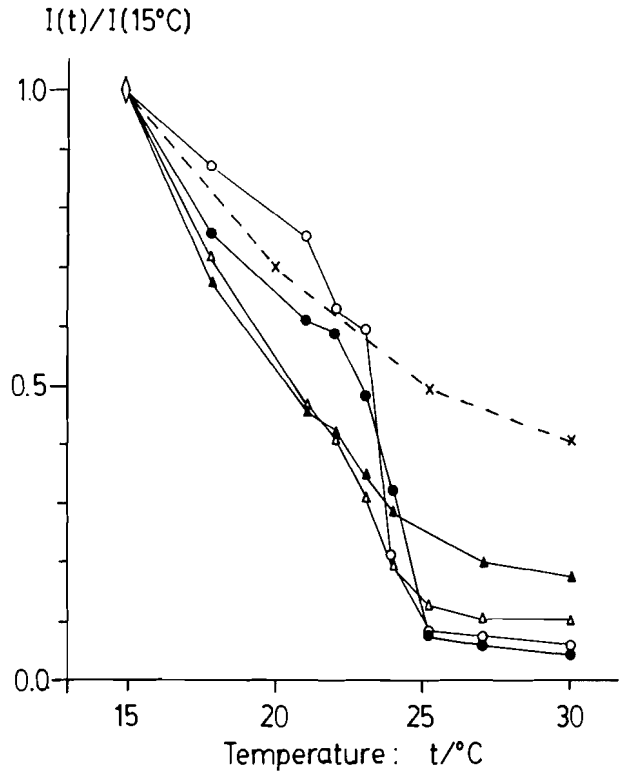

FIG. 2. Relative fluorescence intensity as a function of temperature for Nystatin in dimyristoyl phosphatidylcholine at selected mole ratios of Nystatin-to-lipid. In each case, the fluorescence is normalized to that at 14.8°C. For comparison the relative intensity is plotted for the same temperature range for Nystatin in an ethanol solution at a total concentration of 10^{-6} *M*. The Nystatin concentration in solution is 8×10^{-7} in all cases whereas the lipid concentrations were 2×10^{-3} (○); 8×10^{-4} (●); 2×10^{-4} (△), and 8×10^{-5} (▲).

lifetime is about ten-fold longer. Correspondingly, the lifetime in the liquid crystalline phase approaches that in THF while the quantum yield is at least ten-fold smaller (Table 2 (*A*)). These observations suggest strongly that the quantum yield of Nystatin fluorescence is reduced by a static quenching process in the bilayer environment. The quantum yields of the *t*PnA emission in bilayers were not reported (13) so it is unclear whether similar quenching occurs for the parinaric acids in bilayers.

The quantum yield of Nystatin fluorescence is sensitive to the Nystatin-to-lipid mole ratio (N/L), whereas the lifetimes are not. This appears to be true at both low and high temperatures, but it is difficult to get accurate or meaningful lifetime measurements at high temperatures and high N/L values since the quantum yield becomes less than 0.001. Table 3 lists the variation in quantum yields and lifetimes for samples in which the total concentration of Nystatin was kept constant and the phospholipid concentration was varied to achieve a 25-fold change in the mole fraction. While the quantum yield measured at 15°C changes from 0.055 to 0.006, the average lifetime (calculated as indicated in Table 3) remains unchanged. This indicates that the quenching process is a static quenching of Nystatin by itself.

Dynamic quenching in bilayer membrane systems have been calculated for several models and have been observed in a few systems (15–17). The results are typically presented as the relative intensity (I/I_0) as a function of the mole ratio of the acceptor to the lipid. Figure 3 shows the variation in relative intensity of Nystatin fluorescence as a function of the Nystatin-to-lipid ratio (N/L) at both 20 and 32°C. The graph also illustrates the expected variation for a dynamically quenched system for which the quenching cross-section radius (R_0) is either 4.5, 6.0, or 10.0 nm. It is evident that the quenching observed for Nystatin occurs with equal efficiency at both temperatures. It is also evident that the quenching occurs at a greater efficiency at lower N/L values than would be expected for a dynamic quenching process, unless the quenching cross-section radius is about 10.0 nm. For Nystatin this is an unreasonably large value, particularly because of the large Stoke shift (9) which reduces the spectral overlap of the absorption and emission bands. The data in Table 3 and Fig. 3 therefore both strongly suggest that the Nystatin is quenching itself in a static, density-dependent process. This may be understood if Nystatin forms complexes within the bilayer (3, 4, 10), in which the Nystatin chromophores interact to facilitate non-radiative decay processes, rather than internal conversion and emission.

The data in Fig. 3 also provide support for the assertion that

Can. J. Chem. Downloaded from www.nrcresearchpress.com by 80.58.250.72 on 09/07/12
For personal use only.

TABLE 2. Comparison of measured lifetimes of Nystatin, *trans*-parinaric acid (*t*PnA), and diphenylhexatriene fluorescence in solutions and phospholipid membranes

Chromophore	Solvent	Temperature/°C	ϕ_F	τ_1/ns	τ_2/ns	$\langle\tau\rangle^a$/ns
A: Nystatin	THF[c]	23	0.046	2.6	—	2.6
	DMPC(1:1250)[d]	20	0.030	33(0.5)[b]	17(0.5)	25
	DMPC(1:1250)[d]	32	0.003	7.4(0.6)	1.6(0.4)	5.1
B: *t*PnA	Dioxane[e]	Amb	0.025	2.5	—	2.5
	DPPC(1:400)[f]	23	—	50(0.7)	15(0.3)	40
	DPPC(1:100)[f]	23	—	50(0.7)	14(0.3)	40
	DPPC(1:160)[f]	53	—	4.5(0.1)	2.3(0.9)	2.5
	DEPC(1:150)[f]	23	—	6.8(0.5)	3.1(0.5)	4.9
C: DPH	Benzene[g]	Amb	0.68	5.5	—	5.5
	DMPC[h]	7	—	10.2	—	10.2
	DMPC[h]	39	—	7.8	—	7.8

[a]Average lifetime calculated as $\langle\tau\rangle = \Sigma a_i\tau_2^2/\Sigma a_i\tau_i$.
[b]The fractional quantum efficiency = $a_i\tau_i/\Sigma a_i\tau_i$.
[c]Petersen (1985), ref. 9.
[d]This work.
[e]Sklar *et al.* (1977), ref. 12.
[f]Wolber and Hudson (1981), ref. 13.
[g]Hudson and Kohler (1973), ref. 11.
[h]Lakowicz *et al.* (1985) ref. 14.

TABLE 3. Concentration dependence of Nystatin fluorescence quantum yield and lifetime[a]

N:L	X_{NYS}	ϕ^b	τ_1/ns	τ_2/ns	$\langle\tau\rangle$/ns[c]
1:2500	0.0004	0.055	30.4(0.76)[d]	13.2(0.24)	26.2
1:1000	0.0010	0.049	32.2(0.72)	15.4(0.28)	27.4
1:250	0.0040	0.018	30.4(0.75)	12.2(0.25)	25.8
1:100	0.0100	0.006	30.3(0.66)	8.9(0.33)	23.2

[a]Both measurements were performed on the same sample within hours.
[b]Quantum yield relative to that of quinine sulphate (ϕ = 0.52) measured at 15°C. Lifetimes were measured at 20°C.
[c]Average lifetime defined as $\langle\tau\rangle = \Sigma_i a_i\tau_i^2/\Sigma_i a_i\tau_i$.
[d]Values in parentheses represent the relative quantum efficiency of that process and is $a_i\tau_i/\Sigma_i a_i\tau_i$.

the Nystatin remains within the bilayer at all temperatures. Indeed, the close correspondence between the relative intensity drop at the two temperatures suggest that the complexes responsible for the static quenching exist to the same extent in both phases of the lipid bilayer.

In two-dimensional systems, processes which result in intensity quenching can also give rise to quenching of fluorescence polarization (17). Figure 4 illustrates this for the Nystatin–phospholipid system studied here. The anisotropy, measured in samples in which the concentration of lipid is constant and the Nystatin concentration is changed to provide a range of N/L values, drops systematically as the N/L value increases (Fig. 4*A*).

Snyder and Friere (17) have calculated, by numerical methods, the decrease in the anisotropy as a function of acceptor density for systems with either random or non-random distributions of fluorophores in a two-dimensional membrane. They fit their calculated changes in the relative polarization function ($g(p)/g(p_0)$) to a fourth-order polynomial function of the logarithm of a normalized fluorophore density (log γ) and express their results in terms of the five coefficients in the polynomial. The polarization function is $g(p) = 1/(1/p - 1/3) = 3r/2$, where p is the polarization and r is the anisotropy. Thus $g(p)/g(p_0) = r/r_0$. The normalized fluorophore density is $\gamma = NR_0^2/LA_L$, where R_0 is the quenching cross-section radius, A_L is the area per phospholipid (0.7 nm^2), and N/L is defined above. Thus $\log\gamma = \log(N/L) + \log(R_0^2/A_L)$.

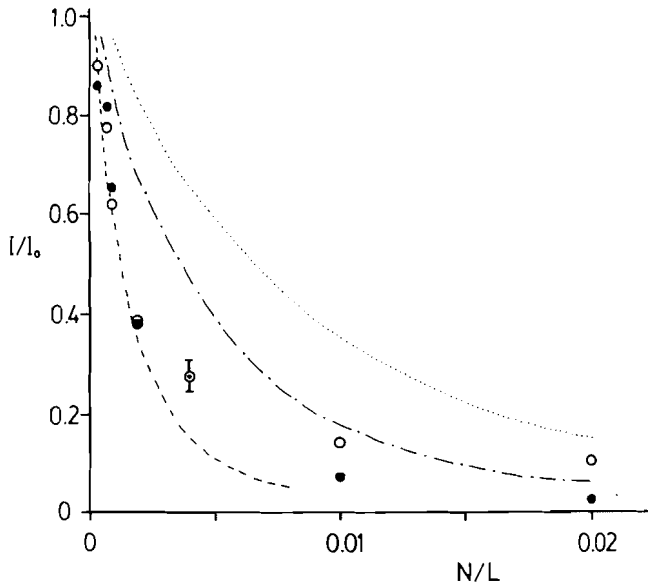

FIG. 3. Relative fluorescence intensity of Nystatin in dimyristoyl phosphatidylcholine as a function of the molar ratio of Nystatin-to-lipid at 20 (○) and 32°C (●). The smooth curve indicates the expected quenching if the fluorescence is dynamically quenched with a quenching cross section radius of 4.5 nm (···); 6.0 nm (-···-), and 10.0 nm (---). The intensity is normalized to that of infinite dilution, which is estimated from extrapolation of the actual fluorescence to zero Nystatin concentration. The uncertainty in the measurements are indicated by the error bar on one data point.

Figures 4 *A* and *B* compare the anisotropies measured for Nystatin to the anisotropies calculated by adjusting the anisotropy at infinite dilution (r_0) to a value of 0.33 and the

Can. J. Chem. Downloaded from www.nrcresearchpress.com by 80.58.250.72 on 09/07/12
For personal use only.

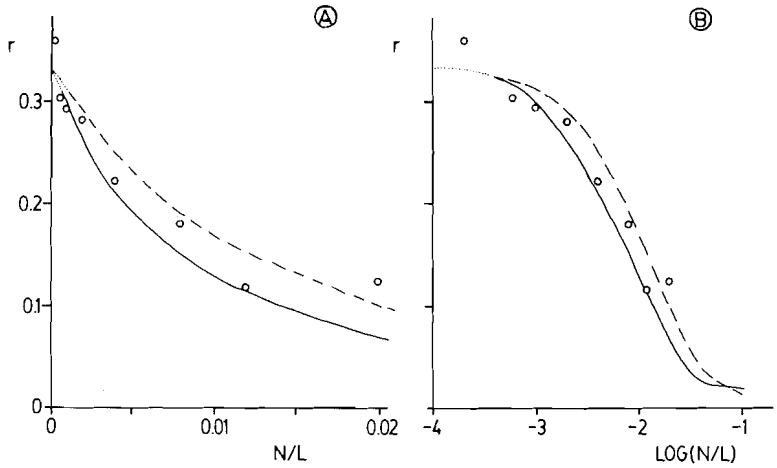

FIG. 4. The anisotropy of emission of Nystatin monomers in dimyristoyl phosphatidylcholine as a function the molar ratio (*A*) or the logarithm of the molar ratio (*B*) of Nystatin-to-lipid at 20°C. The smooth curves correspond to the expected curves using the numerical calculations in ref. 17 for a random (- - -) or a non-random (—) distribution of quenchers assuming a quenching cross section radius of 4.5 nm in both cases. Figures 4*A* and *B* contain the same data but in two representations to facilitate the comparison of the data with Fig. 3 and with ref. 17.

quenching radius (R_0) to a value of 4.5 nm for both a random (dashed lines) and the most non-random distribution (solid lines). These are not necessary the only or the best fit values. Qualitatively, the data correspond with the calculated values, but it is impossible to distinguish between random and non-random distributions without additional information. In either case, the infinite dilution value of the anisotropy is about 0.33 at 20°C. This compares with 0.36 measured for the limiting anisotropy of parinaric acids in the gel phase. It is possible that the difference corresponds to a slightly larger difference in the orientation of the absorption and emission transition moments for Nystatin than for parinaric acid. At the very least, the Nystatin monomer (whose emission is being measured) is reorienting only a little during the 20–30 ns lifetime. This is not surprising for a large polyene antibiotic molecule imbedded in a rigid phospholipid matrix. The corresponding quenching of polarization at 32°C is much harder to measure because the fluorescence intensities decrease rapidly. However, at low concentrations, the anisotropy is as large or larger than that at the corresponding concentration at lower temperature. This means that the Nystatin monomer undergoes less reorientation during the 5 ns lifetime at high temperatures than during its 23 ns lifetime at low temperatures. In either environment, the rotational motion of the Nystatin monomer is slow and as a consequence the anisotropy measurement is not likely to be a good measure of the membrane environment of polyene antibiotics.

Discussion

Characteristics of the fluorescence of tetraenes

In non-polar solvents (THF, dioxane) the fluorescence quantum yield of both Nystatin and parinaric acid is small and the emission decay is rapid (Table 2). These data yield intrinsic lifetimes of about 57 ns for Nystatin and 100 ns for parinaric acid. In isotropic solution non-radiative decay processes are therefore about 20-fold faster than the radiative process.

In aqueous suspensions of Nystatin better than 90% of the initial intensity decays within 100 ps (Turnbull and Petersen, unpublished results) and the quantum yield approaches the detection limit (Table 1). This rapid decay may arise from solvent relaxation and quenching.

In phospholipid membranes in their gel phase ($T < 23$°C) the lifetime for Nystatin and parinaric acid increases at least ten-fold and there is evidence for multiple radiative processes. Although the present data are fit to, and reported as, two exponential decays, more recent evidence with more precise data (200 000 counts in the peak channel) suggests that the decay is best described by a distribution of lifetimes whose mean and variance is sensitive to temperature (Turnbull, James, Petersen, and Ware, unpublished results). Accordingly, interpretation of τ_1 and τ_2, and changes in these, in terms of molecular processes is tenuous. Nevertheless, the lack of change in the lifetimes reported in Table 3 and discussed below is unambiguous.

The overall increase is decay time in the rigid membrane is compatible with a decrease in the rate of non-radiative decay. This is expected if the non-radiative relaxation requires conformational changes, i.e. twisting, in the conjugated polyene segment. These are hindered in the gel phase of the membrane but freely accessible in the isotropic liquid. The liquid crystalline membrane then provides an intermediate environment with intermediate lifetimes.

In our hands, the lifetimes of the parinaric acids in DMPC membranes are slightly shorter than those reported (Table 2) (e.g. 33 ns vs. 55 ns for the longer component in *trans*-parinaric acid). For these suspensions, the quantum yield is about 0.3–0.4. Hence the about ten-fold increase in lifetime is accompanied by a ten-fold increase in quantum yield as expected in systems where the rates of non-radiative processes are slowed down. In contrast, the quantum yield of Nystatin emission in DMPC is less than or about equal to that in solution even though the lifetimes increase about ten-fold. As discussed below, this provides strong evidence for static quenching of Nystatin even at the lowest concentrations measured.

Evidence for Nystatin incorporation into the bilayer

Several sets of data provide evidence that Nystatin is incorporated into the bilayer membrane at temperatures both above and below the phase transition temperature (23°C). The quantum yield drops dramatically at the phase transition temperature for low Nystatin density showing that it can monitor the change in phase. The decrease in quantum yield could be a result of Nystatin being transferred to the aqueous phase at higher temperatures. However, the lifetime of the

Can. J. Chem. Downloaded from www.nrcresearchpress.com by 80.58.250.72 on 09/07/12
For personal use only.

Can. J. Chem. Downloaded from www.nrcresearchpress.com by 80.58.250.72 on 09/07/12
For personal use only.

emission decreases in direct proportion to the decrease in quantum yield while it remains much higher than that expected in solution (~0.1 ns). The fluorescence decay is bi-exponential at both high and low temperatures, suggesting that the chromophore remains in an anisotropic environment. The lifetime changes are similar to those observed for the parinaric acids (13) in various membrane systems. The close correspondence between the photophysics of these chromophores was previously shown for solutions (9) and the extension seen here for the bilayers suggest that these polyenes are sensitive to the same environmental changes. Presuming that parinaric acid remains in the membrane at all temperatures, these lifetimes suggest that the polyene segment of Nystatin does as well.

The partition constant for partitioning of the polyene antibiotic Amphotericin B, which differs from Nystatin only by having an additional site of unsaturation (9), between water and the liquid crystalline phase of lecithin at room temperature has been estimated to be 5×10^5 (22). Assuming this number is applicable to Nystatin, the fraction of Nystatin in the bilayer at high temperatures ranges from 0.999 to 0.923 in the experiments presented here.

The anisotropy is between 0.33 and 0.35 for Nystatin in the bilayer at all temperatures. This compares with anisotropies measured in THF of 0.13 and in ethanol of 0.01. The environment of the Nystatin therefore permits much less, or much slower, reorientation of the chromophore during its much longer lifetime while in the membrane. This further suggests that the Nystatin remains within the bilayer.

The perhaps most convincing evidence for full incorporation at all temperatures comes from the virtually identical density dependence of the static quenching. This suggests that the complexes which are responsible for the static quenching form with equal ease at both 20 and 32°C (see next section).

Taken together, all these observations provide convincing evidence that Nystatin is predominantly within the bilayer structure at all temperatures and at all concentrations. The fluorescence lifetimes, quantum yields, and anisotropies are therefore characteristic of the emission from the monomeric species in a phospholipid matrix.

Evidence for static quenching in bilayer membranes

The lifetime of emission from the Nystatin fluorophore is longer in the more rigid, but still non-polar, environment of the phospholipid bilayer than in the non-polar solvent, THF. Yet, the quantum yield of emission is less. The quantum yield of emission can in general be expressed as

$$\phi_F = X_i \times \phi_i = X_i \times (k_F/(k_F + k_{NR} + k_Q \times [Q]))_i$$
$$= X_i \times (k_F \times t_F)_i$$

where the subscript denotes the ith species and the summation is over all species in the system each present at a mole fraction X_i. The measured lifetime of emission (t_F) equals the inverse of the sum of the rate constants in the denominator.

Dynamic quenching of a single species results in a decrease in the measured lifetime and a proportional decrease in the quantum yield as the quencher concentration is increased. This is not observed for Nystatin in the lipid bilayer (Table 3).

Dynamic quenching of only one of a pair of emitting species would result in a decrease in the lifetime of the quenched species along with an overall decrease in the quantum yield. The lifetime of the non-quenched species would remain unaltered. The small decrease in the shorter of the lifetimes observed for Nystatin (Table 3) is not enough to account for the ten-fold change in the total quantum yield, especially since this is the smaller component in the decay.

Static quenching is usually thought of as a highly efficient quenching process for those chromophores within a critical radius of the quencher, while ineffective for the remainder of the emitters. The static quenching will therefore divide the chromophores into two populations: "dark complexes" which are totally quenched and whose emission is not observed, and "normal" chromophores which are not affected in either quantum yield or lifetime. The total quantum yield is then solely a reflection of the mole fraction of the chromophores which are not complexed and hence not quenched. However, since only the normal chromophores are emitting, the measured fluorescence lifetime is unchanged. This general pattern fits the quantum yield and lifetime measurements listed in Table 3.

The static quenching observed for Nystatin in bilayers is sensitive to the Nystatin concentration relative to the lipid concentration. Since these measurements are for samples with a constant Nystatin concentration, and since the extent of quenching decreases as the amount of lipid in the sample increases it is highly unlikely that the quenching arises from addition of or changing concentrations of impurities. It follows that the Nystatin emission is quenched by the increasing density of Nystatin in the bilayer. This is compatible with the formation of Nystatin complexes within the lipid bilayer (3, 4, 10). The implication is that Nystatin aggregates cannot emit fluorescence, while the monomeric species in the bilayer can. The formation of Nystatin complexes is favoured at higher densities so the mole fraction of monomers decreases and the result is a lower quantum yield.

The density dependence of the fluorescence quenching is the same in both the gel and the liquid crystalline phases of the bilayer. Hence Nystatin complexes form with about equal ease in both rigid and fluid membranes. The thermodynamics controlling the monomer–complex equilibrium and stabilizing the complex must then be more important than any differences in solubility of the Nystatin between the two phases. The low density at which the complexes form (molar ratios < 0.001) also attest to their stability.

The fluorescence comes exclusively from the monomer. The lifetime and anisotropy measurements therefore reflect the properties of the monomer only. Correspondingly, the quantum yield is a direct measure of the mole fraction of Nystatin which exist as monomers. These points will be important for the interpretation of any fluorescence studies in the future. It should now be possible to measure whether sterols interact with Nystatin monomers and affect their emission lifetime, or whether they shift the equilibrium between monomers and complexes. In fact, careful quantum yield and lifetime measurements can in principle be used to measure the binding constant between various sterols and either the Nystatin complexes or the monomers within the bilayer. Analogous experiments have been used to measure lipid:protein binding affinities employing spin-labeled lipids as quenchers (23).

Concentration quenching of anisotropy

The anisotropy is quenched at high Nystatin densities (Fig. 4). Although the density dependence can be fitted to numerical predictions, the data cannot distinguish between random and non-random distributions of the emitting species. In this case, the anisotropy is always that of the monomer, so there should not be any correlation between the intensity quenching (which is static) and the anisotropy quenching

(which must be dynamic). It is important to recognize that the quenching of anisotropy cannot be through energy transfer to the Nystatin complexes, unless these can emit or transfer back. The concentration quenching of the monomer polarization must be a result of energy transfer among monomers. The fits of the data in Fig. 4 indicate that the Nystatin–Nystatin energy transfer can occur with a characteristic radius R_0 of about 4.5 mm.

The limiting anisotropy at low densities appears to approach 0.33. This value is close to the limiting anisotropy of the parinaric acids in rigid media. Consequently the Nystatin monomer does not reorient rapidly in the bilayer at low temperatures. This is not surprising because of the large cylindrical shape of the molecule. The slightly larger anisotropy measured at higher temperatures (0.33–0.35) shows that the Nystatin monomer is too bulky to reorient about its long axis even in the more fluid bilayer phase.

The anisotropy data have no bearing on the complexes, so their orientation (and location) is uncertain. It is nevertheless tempting to speculate that the traditional pore model (3, 4) is substantially correct.

Acknowledgements

We greatly appreciate the use of the lifetime equipment in Professor W. R. Ware's laboratory. The interpretation of these data was facilitated by discussions with Dr. D. R. James. The work was supported by NSERC grant U0109 and National Institute of Health (NIAID) grant AI16228. R. Gratton and E. M. Pisters were NSERC Summer Undergraduate Research Fellows.

1. G. Medoff, J. Bolard, J. Brajtburg, and G. S. Kobayashi. Ann. Rev. Pharmacology and Toxicology. Vol. 23. *Edited by* R. George, R. Okun, and A. K. Cho. Palo Alto, CA. 1983. p. 303.
2. A. W. Norman, A. M. Spielvogel, and R. G. Wong. Adv. Lipid Res. **14**, 127 (1976).
3. B. Dekruijff, W. J. Gerritsen, A. Oerlemans, R. A. Demel, and L. L. M. Van Deenen. Biochim. Biophys. Acta, **339**, 30 (1974).
4. P. Van Hoogevest and B. Dekruijff. Biochim. Biophys. Acta, **511**, 397 (1978).
5. R. Bitmann and S. A. Fischkoff. Proc. Natl. Acad. Sci. US **69**, 3795 (1972).
6. J. M. Patterson, J. Holland, and L. L. Bieber. J. Antibiot. **32**, 646 (1979).
7. J. M. Patterson, M. R. Olinger, J. F. Holland, and L. L. Beiber. J. Antibiot. **32**, 1193 (1979).
8. N. O. Petersen. Spectrosc. Intl. J. **2**, 408 (1983).
9. N. O. Petersen. Can. J. Chem. **63**, 77 (1985).
10. L. J. O'Neill, J. G. Miller, and N. O. Petersen. Biochemistry, **25**, 177 (1986).
11. B. S. Hudson and B. E. Kohler. J. Chem. Phys. **59**, 4984 (1973).
12. L. A. Sklar, B. S. Hudson, M. Petersen, and J. Diamond. Biochem. **16**, 813 (1977).
13. P. K. Wolber and B. S. Hudson. Biochemistry, **20**, 2800 (1981).
14. J. R. Lakowicz, H. Cheryk, B. P. Maliwal, and E. Gratton. Biochemistry, **24**, 376 (1985).
15. B. K.-K. Fung and L. Stryer. Biochemistry, **17**, 5341 (1978).
16. P. K. Wolber and B. S. Hudson. Biophys. J. **28**, 197 (1979).
17. B. Snyder and E. Freire. Biophys. J. **40**, 137 (1982).
18. S. R. Meech and D. Phillips. J. Photochem. **23**, 193 (1983).
19. C. A. Parker. Photoluminescence of solutions. Elsevier Publ. Co., Amsterdam. 1968. p. 263.
20. W. R. Ware, M. Pratinidhi, and R. K. Bauer. Rev. Sci. Instrum. **54**, 1148 (1983).
21. E. A. Haigh, K. R. Thulborn, and W. H. Sawyer. Biochemistry, **18**, 3525 (1979).
22. G. Strauss. Can. J. Spectrosc. **26**, 95 (1981).
23. E. London and G. W. Feigenson. Biochemistry, **20**, 1939 (1981).

Can. J. Chem. Downloaded from www.nrcresearchpress.com by 80.58.250.72 on 09/07/12
For personal use only.

Charge transfer fluorescence of some *N*-benzoylindoles[1]

BIMSARA W. DISANAYAKA AND ALAN C. WEEDON[2]

The Photochemistry Unit, Department of Chemistry, The University of Western Ontario, London, Ont., Canada N6A 5B7

Received July 28, 1986

BIMSARA W. DISANAYAKA and ALAN C. WEEDON. Can. J. Chem. **65**, 245 (1987).

The fluorescence properties of various *N*-carbonyl-substituted indoles (compounds **1**–**7**) are examined. The *N*-benzoyl-indole derivatives **1** and **3**–**5** are shown to fluoresce weakly and the effect of solvent polarity upon the energy of the emitting state and upon the quantum yield of fluorescence is described. It is concluded that the initially formed singlet excited state is non-emissive and can relax to an intramolecular charge transfer state which is weakly fluorescent. The solvent effects are consistent with a general type of solvent interaction, and the solvent-induced shifts in the wavelength of the fluorescence emission correlate well with the Lippert equation relating the stabilisation of the excited state to a function of solvent dielectric and refractive index. A poor correlation with the empirical $E_T(30)$ solvent polarity parameter is observed.

BIMSARA W. DISANAYAKA et ALAN C. WEEDON. Can. J. Chem. **65**, 245 (1987).

On a étudié les propriétés de fluorescence de divers indoles substitués portant un groupement *N*-carbonyle (composés **1** à **7**). On démontre que les dérivés *N*-benzoyle indoles **1** et **3**–**5** possèdent une légère fluorescence et on décrit aussi l'effet de la polarité du solvant sur l'énergie de l'état donnant naissance à l'émission ainsi que sur le rendement quantique de la fluorescence. On en conclut que l'état singulet qui se forme initialement ne donne pas lieu à de l'émission et qu'il peut subir une relaxation conduisant à un état de transfert de charge intramoléculaire qui est faiblement fluorescent. Les effets de solvant sont en accord avec un type général d'interaction de solvant; de plus, les déplacements de longueurs d'onde d'émission de fluorescence induits par le solvant sont en bon accord avec l'équation de Lippert qui établit une relation entre la stabilisation de l'état excité et une fonction de la constante diélectrique du solvant et l'indice de réfraction. On a observé une mauvaise corrélation avec le paramètre empirique $E_T(30)$ de la polarité du solvant.

[Traduit par la revue]

Introduction

Indole is relatively unreactive photochemically and the major route for decay of the excited state produced by ultraviolet light irradiation is fluorescence (1). However, if a carbonyl substituent is present upon the indole nitrogen then the excited state will readily undergo a reaction with alkenes to yield cyclobutane derivatives in which the alkene has become attached to the 2- and 3-positions of the indole nucleus. Thus *N*-benzoyl and *N*-acetyl indoles will form cyclobutane adducts when irradiated with simple alkenes (2), as will *N*-carboethoxy-substituted indoles.[3] As part of a study of the mechanism of this reaction we attempted to determine the multiplicity of the excited state involved. Sensitisation and quenching experiments indicated that the reaction proceeds via the triplet excited state of the indole derivative.[4] In order to demonstrate that the reaction did not also proceed through the singlet excited state we attempted to record the fluorescence spectra of some *N*-carbonyl-substituted indoles in the presence and absence of alkenes. No fluorescence quenching, which would have been indicative of a singlet excited state reaction, was observed. However, the fluorescence, which was much weaker than that of indole itself, occurred at anomalously long wavelength, and the position and intensity of this emission was exceedingly solvent dependent.

Given the common occurrence of indole rings in tryptophan-containing living tissue, and the potential utility of the solvent-dependent fluorescence of the *N*-carbonyl-substituted derivatives for studies of their environment in proteins, we digressed from our mechanistic examination in order to study the emission properties of some *N*-carbonyl-substituted indole derivatives. The results are described here.

Results

The absorption and emission spectra of compounds **1**–**7** were recorded at room temperature in various solvents. The absorption spectra were substantially different from that of indole itself and exhibited a strong band at ca. 250 nm (ϵ = ca. 5×10^5) along with a weaker band at ca. 300 nm (ϵ = ca. 1×10^5) which showed evidence of vibrational structure (see Fig. 1). The position of the absorption bands for each compound were not solvent dependent. At room temperature *N*-acetyl indole, **2**, and the cyclic analogue **6** did not emit detectably while compounds **1** and **3**–**5** fluoresced weakly and with very large Stokes' shifts. Compound **7** fluoresced strongly

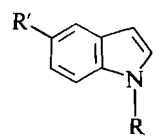

	R′	R
1	H	C_6H_5CO
2	H	MeCO
3	H	*p*-MeO—C_6H_5CO
4	H	*p*-NO_2—C_6H_5CO
5	MeO	C_6H_5CO

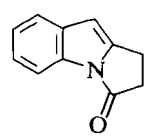

6

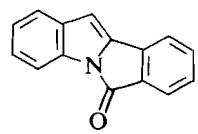

7

[1]Contribution number 368 from the Photochemistry Unit, the University of Western Ontario.

[2]To whom all correspondence should be addressed.

[3]V. Dave and A. C. Weedon. Unpublished work.

[4]B. W. Disanayaka and A. C. Weedon. Unpublished work.

Can. J. Chem. Downloaded from www.nrcresearchpress.com by 80.58.250.72 on 09/07/12
For personal use only.

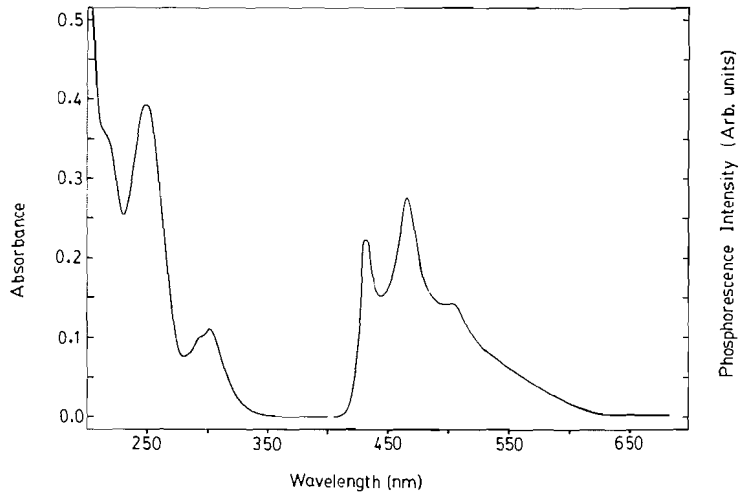

FIG. 1. Absorption spectrum at room temperature (23°C) in hexane (left hand curve) and phosphorescent emission spectrum in acetonitrile at 77 K (right hand curve) for compound **1** (10^{-5} *M*). The spectra were identical in all solvents.

but with a smaller Stokes' shift than compounds **1** and **3–5**. The wavelength and intensity of the emission was highly solvent dependent for those compounds which did emit, and this was most pronounced for compounds **1** and **3–5**. Generally, the more polar the solvent, the broader and weaker was the emission and the longer the wavelength of maximum intensity. The position of the emission maxima and some quantum yields of emission are given in Tables 1 and 2, and the appearance of the emission in some of the solvents examined is shown in Fig. 2 for compound **1**. The positions of the fluorescence maxima were not concentration dependent and the excitation spectra in all cases were in agreement with the emission being derived from the compound under study, and not from any strongly emitting impurity, of which indole was the most likely. The phosphorescence spectra were also measured at 77 K for compound **1** in three solvents (see Fig. 1); the position of the emission band was different from that of the fluorescence and did not shift with changing solvent. Its intensity was much greater than that of the room temperature fluorescence and completely masked it.

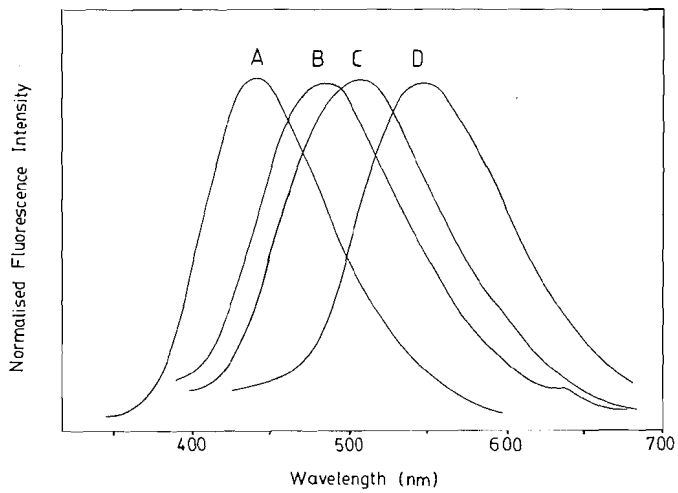

FIG. 2. Normalised fluorescence spectra of compound **1** (10^{-5} *M*). Curve *A*: hexane; curve *B*: diethyl ether; curve *C*: THF; curve *D*: MeCN.

Discussion

The appearance of the spectra in Fig. 1 indicates that the absorption and low temperature (phosphorescent) emission properties of compound **1** are unexceptional. However, the room temperature fluorescent emission (shown in Fig. 2) is at unexpectedly long wavelength, and the wavelength of the emission increases greatly with solvent polarity. The excitation spectra indicated that the emission at room temperature was indeed due to *N*-benzoyl indole and not some impurity. The possibility that the emission is due to an excimer species can be excluded since at the concentrations of the *N*-benzoyl indole used (10^{-5} *M*) the singlet excited state would have insufficient time to form an exciplex with a ground state molecule.

The fact that for compound **1** the positions of the absorption maxima do not change with solvent polarity suggests that the initially formed excited state possesses a similar degree of charge separation to the ground state molecule. In contrast, the large Stokes' shift of the fluorescent emission, along with the marked solvent dependence of the emission wavelength suggests that the emitting species is a singlet state possessing a large degree of charge transfer character, which is formed rapidly from the initially formed, non-emissive excited state. Thus as the solvent polarity increases the charge transfer state becomes more stabilised and therefore emits to longer wavelength. This type of long wavelength fluorescence has been observed previously in systems where potential electron donating systems are conjugated with chromophores capable of accepting charge. Examples of such systems are *p*-*N*,*N*-dimethylaminobenzonitrile and various aminononaphthalene sulphonates (3, 4).

The effect of structural changes in the fluorescing molecules suggests that the charge transfer is most probably from the indole ring to the benzoyl chromophore. Thus in hexane the energies of the charge transfer states for compounds **1**, **3**, **4**, and **5**, as determined from the positions of the emission maxima, is in the order **4** < **5** < **1** < **3**. This order is that which would be expected for charge transfer from the indole ring to the benzoyl group since an electron donor is present in the indole ring of **5** and an electron acceptor is present in the benzoyl ring of **4**, and these substituents would stabilise the charge transfer state. Similarly, the presence of an electron donor in the benzoyl group in **3** would be expected to destabilise the charge transfer state and result in a shorter wavelength emission, as is observed. This rationalisation is also consistent with the failure of *N*-acetyl

Can. J. Chem. Downloaded from www.nrcresearchpress.com by 80.58.250.72 on 09/07/12
For personal use only.

TABLE 1. Wavelengths of absorption and fluorescence emission for compounds **1–7** in various solvents[a]

Compound	Solvent	λ_{abs} (nm)	λ_{em} (nm)	$\bar{\nu}_{abs} - \bar{\nu}_{em}$ (cm^{-1})	$E_T(30)$ (kcal/mol)	Δf_n
1	*n*-Pentane	302	440	10390	32.4	0.0101
	n-Hexane	302	440	10390	33.1	0.0000
	Et_2O	302	480	12280	34.6	0.1671
	1,4-Dioxane	303	504	13270	36.0	0.0203
	THF	302	506	13350	37.4	0.2097
	CH_3CO_2Et	301	504	13270	38.1	0.1997
	HCO_2Et	302	503	13230	40.9	0.2205
	$(i\text{-}Pr)_2O$	302	476	12100	34.4	0.1450
	$(MeOCH_2)_2$	302	504	13270	38.6	0.2141
	$(n\text{-}Bu)_2O$	302	468	11750	34.0	0.0959
	n-PrCN	302	521	13920	43.1	0.2751
	MeCN	302	540	14590	46.0	0.3055
	$CHCl_3$	303	519	13850	39.1	0.1492
	CCl_4	304	466	11650	33.6	0.0119
	CH_2Cl_2	303	518	13800	41.1	0.2171
	$ClCH_2CH_2Cl$	303	520	13880	41.9	0.2208
	$MeCCl_3$	303	490	12700	36.2	0.1987
2	*n*-Hexane	299	—			
5	*n*-Hexane	314	452	9723	33.1	0.0000
	Et_2O	314	496	11690	34.6	0.1671
	THF	314	518	12540	37.4	0.2097
	MeCN	314	560	13990	46.0	0.3055
	CH_2Cl_2	315	540	13230	41.1	0.2171
4	*n*-Hexane	288	518	15420	33.1	0.0000
	Et_2O	288	—			
	MeCN	289	—			
	CH_2Cl_2	289	—			
3	*n*-Hexane	302	418	9189	33.1	0.0000
	Et_2O	301	456	11290	34.6	0.1671
	THF	302	474	12020	37.4	0.2097
	MeCN	301	514	13770	46.0	0.3055
	CH_2Cl_2	302	496	12950	41.1	0.2171
6	*n*-Hexane	290	—			
7	*n*-Hexane	359	460	6116	33.1	0.0000
	MeCN	357	494	7768	46.0	0.3055
	CH_2Cl_2	360	492	7453	41.1	0.2171

[a]Absorption and emission spectra were recorded on solutions of ca. 10^{-5} *M* concentration. λ_{abs} is the wavelength of the lowest absorption maximum. λ_{em} is the wavelength of maximum emission. $\bar{\nu}_{abs} - \bar{\nu}_{em}$ is $(1/\lambda_{abs} - 1/\lambda_{em}$ expressed in cm^{-1}. $E_T(30)$ is the Kosower solvent polarity parameter (see text). Δf_n is:

$$\frac{\epsilon - 1}{2\epsilon + 1} - \frac{n^2 - 1}{2n^2 + 1}$$

where ϵ is the solvent dielectric constant and n is the solvent refractive index.

indole **2** and its cyclic analogue **6** to fluoresce as no charge transfer would be expected if the delocalised π-system of the benzoyl group is necessary to accept the charge.

The cyclic analogue of *N*-benzoyl indole, compound **7**, was found to be highly fluorescent and the Stokes' shift was much smaller and less solvent sensitive than for *N*-benzoyl indole, and more reminiscent of indole (5). Whether this is due to the rigidity of the molecule which prevents rotation of the benzoyl group and enforces interaction with the indole ring through overlap with the nitrogen "non-bonding" pair, or whether it is due to the conjugation of the benzene ring with the indole ring is unclear.

The quantum yields of fluorescent emission for compounds **1** and **3–5** (Table 2) indicate that the efficiency of emission drops with increasing solvent polarity. This effect can be ascribed to a lowering of the energy gap between the polar, solvent-stabilised charge transfer excited state and the relatively non-polar ground state. The energy gap law which dominates transitions between electronic states predicts that this should accelerate the rate of internal conversion to the ground state so that emission from the

Can. J. Chem. Downloaded from www.nrcresearchpress.com by 80.58.250.72 on 09/07/12
For personal use only.

Can. J. Chem. Downloaded from www.nrcresearchpress.com by 80.58.250.72 on 09/07/12
For personal use only.

TABLE 2. Quantum yields of fluorescence (Φ_{em}) for compounds **1–7** in various solvents

Compound	Solvent	Φ_{em}
1	*n*-Hexane	0.041
	MeCN	0.018
	CH_2Cl_2	0.028
2	*n*-Hexane	0.0[a]
3	*n*-Hexane	0.03
	CH_2Cl_2	0.15
4	*n*-Hexane	0.06
5	*n*-Hexane	0.07
	MeCN	$<10^{-2}$ [b]
	CH_2Cl_2	0.03
6	*n*-Hexane	0.0[a]
7	*n*-Hexane	0.9
	MeCN	0.44
	CH_2Cl_2	0.62

[a]No emission was observed.
[b]The emission was too weak to be quantified.

charge transfer state competes less effectively. An alternative explanation is that as the charge transfer state is stabilised by increasingly polar solvents the energy gap between it and the initially formed S_1 state will be increased. This will slow down the rate of formation of the charge transfer state and the charge transfer process will become less competitive with intersystem crossing to the triplet state. Thus less of the charge transfer state will be formed and the quantum yield of fluorescence from it will be reduced. It should be noted that the triplet state appears to be non-polar (since the position of the phosphorescent emission is not solvent dependent) and that it cannot be populated from the charge transfer state because in all the solvents examined the latter is lower in energy than the former (for *N*-benzoyl indole the triplet energy is 68 kcal/mol from phosphorescence measurements at 77 K; the energy of the charge transfer state is 65 kcal/mol at room temperature in hexane and lower in more polar solvents).

For the fluorescent charge transfer states which have been observed previously for molecules capable of intramolecular electron transfer between conjugated groups, the effect of solvent interactions upon the energy, and hence the wavelength of emission have been classified into specific solvent interactions (e.g. hydrogen bonding etc.) and general solvent effects (i.e. the way in which the solvent reorganises to stabilise the charge separated state electrostatically) (6). For non-hydrogen bonding solvents, the stabilisation of the charge transfer state arising from the general type of solvent interaction can be related to the polarisability of the solvent expressed in terms of a function of the solvent dielectric and refractive index. The relationship, derived by Lippert *et al.* (6, 7), takes the form:

$$\bar{\nu}_{abs} - \bar{\nu}_{em} \simeq \frac{2}{hc}\left\{\frac{\epsilon - 1}{2\epsilon + 1} - \frac{n^2 - 1}{2n^2 + 1}\right\}\frac{(\mu^* - \mu)^2}{r^3} + \text{constant}$$

or

$$\bar{\nu}_{abs} - \bar{\nu}_{em} \simeq \frac{2}{hc}\Delta f_n \frac{(\mu^* - \mu)^2}{r^3} + \text{constant}$$

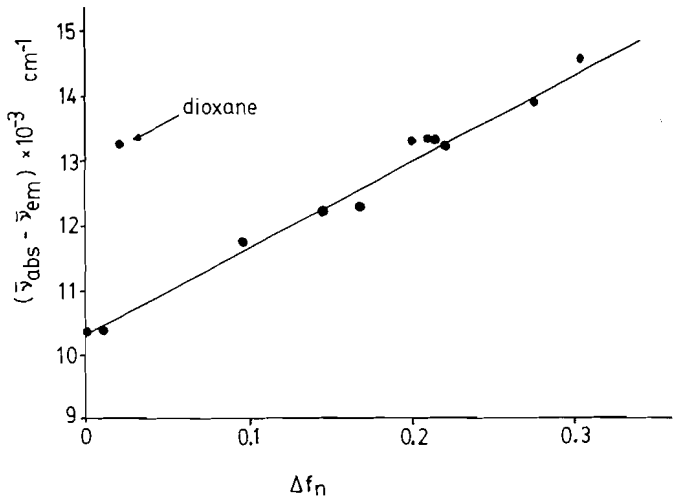

FIG. 3. Lippert plot for compound **1**.

where $\bar{\nu}_{abs}$ and $\bar{\nu}_{em}$ represent the absorption and emission energies in cm^{-1}, respectively, h is Plank's constant, c is the speed of light, ϵ is the solvent dielectric constant, n is the solvent refractive index, r is the Onsager radius (i.e. the radius of the sphere occupied by the molecule in the solvent), and μ and μ^* are the dipole moments of the ground state and emitting excited state, respectively.

By plotting the degree of solvent stabilisation of the excited state (i.e. $\bar{\nu}_{abs} - \bar{\nu}_{em}$) against the solvent polarisability function Δf_n it is possible to obtain a value of the change in dipole moment in going from the initially formed excited state to the charge transfer state if a value of the Onsager radius, r, can be estimated. Such a plot is shown for *N*-benzoyl indole in Fig. 3, and similar plots were obtained for the substituted derivatives **3** and **5**. The data point corresponding to dioxane is off the line; this has been observed (8) in other systems and it may arise because the conformation of the dioxane molecule may be altered when it is solvating the charge transfer excited state. From other solvent polarisability–fluorescence wavelength correlations it has been found (8) that the effective dielectric constant of dioxane is 6 or 7. Using a value of this order brings the dioxane point onto the line in Fig. 3. In addition, the chlorinated solvents examined did not fall on the line and are not included in Fig. 3. Presumably these solvents stabilise the charge transfer state by a specific solvent interaction. With the exception of dioxane, the data obtained in the 12 non-chlorinated, non-hydrogen bonding solvents examined give a good fit to the Lippert equation. This supports the assignment of a charge transfer state to the fluorescent emission of compounds **1** and **3–5**, and allows an estimate of the dipole moment change in going from the initially formed singlet excited state to the charge transfer state. The results are shown in Table 3; for reasonable values of r (i.e. 5.5 Å for **1** and 6.5 Å for **3** and **5**) the change in dipole moment is thus of the order of 15 D for **1** and 20 D for **3** and **5**. Since 4.8 D corresponds to the separation of a unit charge by one Å, these values of the change in dipole moment correspond to a movement of a unit charge across the molecules of 3 Å in **1** and 4 Å in **3** and **5**. These distances are of the order of the separation of the major chromophores in the *N*-benzoyl indoles and are consistent with the conclusion that the charge transfer occurs between the indole nucleus and the benzoyl ring.

For some systems exhibiting charge transfer fluorescence a correlation between the energy of the emitting state (as determined from the position of the fluorescence maximum)

TABLE 3. Dipole moment changes derived from the Lippert plots for compounds **1**, **3**, and **5**

Compound	$(\mu^* - \mu)/r^3$	$(\mu^* - \mu)^b$
1	13700±500[a]	15 D[b]
3	14800±800[a]	20 D[b]
5	13900±700[a]	20 D[b]

[a]From the gradient of the Lippert plot, omitting dioxane and chlorinated solvents (see text).
[b]Assuming values of the Onsager radius, r, of 5.5 Å for **1** and 6.5 Å for **3** and **5**.

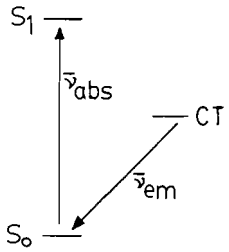

FIG. 4. Energy diagram showing relationship between the ground state (S_0), initially formed singlet excited state (S_1), and charge transfer state (CT) for *N*-benzoyl indoles **1**, **3**, **4**, and **5**. $\bar{\nu}_{abs}$ is the energy of the $S_0 \rightarrow S_1$ transition in cm^{-1}, and $\bar{\nu}_{em}$ is the energy of the CT $\rightarrow S_0$ transition in cm^{-1}.

and the empirical solvent polarity parameter $E_T(30)$ has been claimed (4). The $E_T(30)$ parameter for a solvent is obtained by measuring the position of the absorption maximum of the charge transfer transition of a pyridinium betaine dissolved in the solvent. In some cases the correlation is linear and in others the correlation takes the form of two intersecting lines, indicative of two emitting states, one charge transfer in nature and the other relatively non-polar (4). In principle, this situation could also apply to the *N*-benzoyl indole system described here. An energy-state diagram for compound **1** is shown in Fig. 4; in non-polar solvents the charge transfer state will be highly destabilised and it is possible that its energy could lie above that of the singlet state. As the solvent polarity is increased the charge transfer state will be lowered in energy and eventually will become much lower than that of the initially formed state. In this situation, the emission observed at low solvent polarity would be derived from the initially formed, non-polar singlet excited state and the wavelength of the emission maximum will be relatively insensitive to solvent polarity. At high polarity the emission will be derived from the charge transfer state and the wavelength of maximum intensity will change rapidly with solvent polarity. Thus a plot of the emission energy against solvent polarity should show two lines of different gradient. At low polarities the line would be near horizontal, while at high polarities a line of greater slope would be expected, corresponding to solvation of the charge transfer state. This has been observed for systems such as the *N*-phenylamino-naphthalene sulphonates (4).

A plot of the energy of the emitting state (derived from the wavelength of emission) for *N*-benzoyl indole against the solvent $E_T(30)$ value is shown in Fig. 5. It would appear that at low solvent polarities the position of the fluorescence is highly sensitive to the changing solvent polarity and that at higher polarity the position of the emission band is less dependent. This is the reverse of the trend which would be expected and would correspond to an unidentified non-polar low-lying electronic

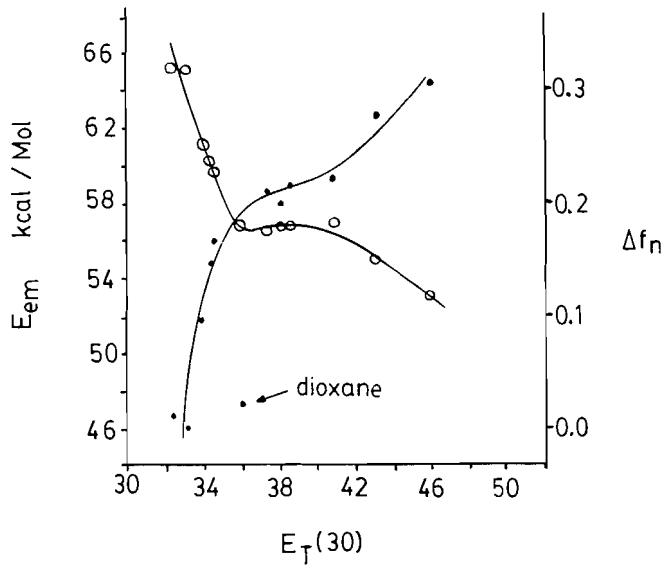

FIG. 5. Plots of energy of the $S_0 \rightarrow S_1$ transition in kcal/mol against the solvent $E_T(30)$ value (full circles), and solvent $E_T(30)$ value against the Lippert function Δf_n (open circles).

state of the *N*-benzoyl indole molecule. However, if the $E_T(30)$ parameter is plotted against the polarisability function Δf_n the curve obtained mirrors that for the $E_T(30)$ vs. emission energy plot for compound **1** (see Fig. 5). This would suggest that the curvature seen in the $E_T(30)$ vs. emission energy plot is an artifact of the $E_T(30)$ parameter and does not relate to a change in emitting state. These observations suggest that care should be exercised in correlating the $E_T(30)$ parameter with emission energy when large solvent polarity ranges and solvents of widely varying chemical structure are used.

Conclusions

The observations described are consistent with the existence of a fluorescent charge transfer state in *N*-benzoyl-substituted indoles. The pronounced solvent-induced shifts in the position of the fluorescence maximum suggest that *N*-benzoyl indole derivatives could be useful probes of environment.

Experimental

The *N*-benzoyl indoles **1**, **3–5** were prepared by treatment of indole or 5-methoxy indole with benzoyl chloride, or its *para*-methoxy or *para*-nitro derivatives using the two phase procedure described by Illi (9). *N*-Acetyl indole, **2**, was prepared similarly from indole and acetyl chloride. The cyclic analogues of *N*-acetyl indole and *N*-benzoyl indole, compounds **6** and **7**, were prepared by the literature procedure (10) which involves intramolecular Wittig cyclisation of the phosphonium salts of *ortho*-succinimidylbenzyl bromide and *ortho*-phthalimidobenzyl bromide, respectively.

Absorption spectra were recorded on a Hewlett Packard 8450 A diode array spectrophotometer. Fluorescence spectra were recorded on a Perkin-Elmer 650-40 fluorescence spectrometer and quantum yields of fluorescence were measured on this instrument relative to indole. Phosphorescence spectra were recorded on a Perkin-Elmer MPF-4 emission spectrometer.

Acknowledgements

The authors thank Dr. A. Siemiarczuk for many valuable discussions, and the Natural Sciences and Engineering Research Council of Canada for financial support.

1. K. YAMASAKI, T. MATSUURA, and I. SAITO. J. Chem. Soc. Chem. Commun. 944 (1974); R. LUMRY and M. HERSCHBERGER. Photochem. Photobiol. **27**, 819 (1978); D. C. NECKERS and A. H.

Can. J. Chem. Downloaded from www.nrcresearchpress.com by 80.58.250.72 on 09/07/12
For personal use only.

A. TINNEMANS. *In* Synthetic organic photochemistry. *Edited by* W. H. Horspool. Plenum, New York. 1984.
2. D. R. JULIAN and R. FOSTER. J. Chem. Soc. Chem. Commun. 311 (1973); M. IKEDA, K. OHNO, S. MOHRI, M. TAKAHASHI, and Y. TAMURA. J. Chem. Soc. Perkin Trans. I, 405 (1984).
3. C. J. SELISKAR and L. BRAND. J. Am. Chem. Soc. **93**, 5414 (1971); G. WEBER and F. J. FARRIS. Biochemistry, **18**, 3075 (1979); Z. R. GRABOWSKI, K. ROTKIEWICZ, A. SIEMIARCZUK, D. J. COWLEY, and W. BAUMAN. Nouv. J. Chim. **3**, 443 (1979); W. RETTIG and M. SANDER. Chem. Phys. Lett. **87**, 229 (1982); A. SIEMIARCZUK. Chem. Phys. Lett. **110**, 437 (1984).
4. E. M. KOSOWER and H. KANETY. J. Am. Chem. Soc. **105**, 6236 (1983); E. M. KOSOWER. Acc. Chem. Res. **15**, 259 (1982).
5. M. SUN and P.-S. SONG. Photochem. Photobiol. **25**, 3 (1977).
6. J. R. LAKOWICZ. Principles of fluorescence spectroscopy. Plenum, New York. 1983. Chapt. 7.
7. E. VON LIPPERT. Z. Electrochem. **61**, 962 (1957).
8. W. BAUMAN, F. PETZKE, and K.-D. LOOSEN. Z. Naturforsch. **34**a, 1070 (1979); W. LIPTAY. Z. Naturforsch. **20**a, 1441 (1965); **21**a, 1606 (1966).
9. V. O. ILLI. Synthesis, 387 (1979).
10. M. D. CRENSHAW and H. ZIMMER. J. Het. Chem. **21**, 623 (1984).

Can. J. Chem. Downloaded from www.nrcresearchpress.com by 80.58.250.72 on 09/07/12
For personal use only.

Kinetics of the reaction of *p*-dinitrobenzene with basic hydrogen peroxide

RAYMOND A. HELLER AND RICHARD WEILER[1]
Department of Chemistry, Wilfrid Laurier University, Waterloo, Ont., Canada N2L 3C5

Received April 28, 1986

RAYMOND A. HELLER and RICHARD WEILER. Can. J. Chem. **65**, 251 (1987).

Kinetic studies of the reaction of *p*-dinitrobenzene with H_2O_2 and NaOH in 10%, 30%, and 50% aqueous dioxane have been carried out at 30.0°C. The reaction involves the formation of a reasonably stable intermediate which absorbs strongly in the visible region, with the rate of formation being about 18 times faster than the rate of conversion to final product which is *p*-nitrophenol. Proton and ^{13}C nmr spectra of the kinetic solution provide strong evidence that the intermediate is *p*-nitrophenyl hydroperoxide, apparently the first time that a true aryl peroxide species has been identified.

RAYMOND A. HELLER et RICHARD WEILER. Can. J. Chem. **65**, 251 (1987).

Opérant à 30,0°C et dans des solutions aqueuses de dioxanne à 10, 30 et 50%, on a mesuré la cinétique de la réaction du *p*-dinitrobenzène avec le H_2O_2 et le NaOH. La réaction implique la formation d'un intermédiaire relativement stable qui absorbe fortement dans la région du visible, avec une vitesse de formation qui est environ 18 fois plus rapide que sa vitesse de transformation en *p*-nitrophénol qui est le produit final. Les spectres rmn du ^1H et du ^{13}C des solutions fournissent de fortes indications que l'intermédiaire est l'hydroperoxyde de *p*-nitrophényle; apparemment, il s'agit de la première fois qu'une véritable espèce peroxyde d'aryle a pu être identifiée.

[Traduit par la revue]

Can. J. Chem. Downloaded from www.nrcresearchpress.com by 80.58.250.72 on 09/07/12
For personal use only.

In comparison with other aromatic processes, nucleophilic displacements of aromatic nitro groups have not been investigated extensively, but the last few years have seen the publication of theoretical treatments of the reaction mechanism (1), a discussion of the synthetic utility of such reactions (2), and various related studies (3).

We recently published a paper (4) describing the results of our work on the reaction of *o*-dinitrobenzene (*o*DNB) with NaOH and H_2O_2 in 50% aqueous dioxane. In brief, we found that the presence of hydrogen peroxide results in accelerated, clean production of *o*-nitrophenol (*o*NP) and that absorbance changes corresponding to two distinct reaction steps can be discerned in the visible spectrum. Our kinetic analysis led to the conclusion that the rate constants for the two steps were of similar magnitude and that both were dependent on the concentration of hydrogen peroxide. We also suggested that the intermediate was the radical anion formed by the transfer of an electron from hydrogen peroxide anion to *o*DNB.

In this paper we report the results of our parallel investigations on the related compound, *p*-dinitrobenzene (*p*DNB), as well as our new conclusions concerning the nature of the intermediate in reactions of this kind.

Experimental

With minor modifications, the experimental methods used in this work were the same as those previously described (4). Commercial *p*DNB, mp 172–174°C uncorrected; lit. (5) mp 174°C) was used as supplied. The purity of the *p*DNB could be satisfactorily confirmed by diluting an accurately measured portion of *p*DNB stock solution to a specific volume with aqueous NaOH, heating the mixture overnight in a sealed tube, and then measuring the absorbance due to phenolate product (λ_{max} = 405 nm; ϵ = 20500 M^{-1} cm^{-1}).

For a typical kinetic run (50% v/v dioxane in water) 20 mL of redistilled 1,4-dioxane, 5 mL of aqueous H_2O_2 stock solution, and about 19 mL of NaOH stock solution were placed in a 50 mL volumetric flask. Both this flask and a separate container of *p*DNB–dioxane stock solution were brought to temperature equilibrium in a 30.0°C bath. To initiate the reaction, 5 mL of *p*DNB solution were added to the 50 mL volumetric flask which was quickly made up to volume by the dropwise addition of more NaOH solution. This sequence of addition minimizes the temperature increase (heat of mixing) which affected our *o*DNB experiments. Absorbance measurements and scans were done on a Beckman DU-7 spectrophotometer with the cell compartment thermostatted at 30.0°C.

The esr and nmr experiments were carried out at ambient temperature in the same (or appropriately deuterated) solvent system, but with reactant concentrations much higher than those used in the kinetic mixtures. The esr spectra were run on a Bruker ER100D epr spectrometer operating in the X/band mode. Proton and ^{13}C nmr spectra were recorded on Bruker WP-80, AM-250, and AM-500 spectrometers.

Results

In the absence of H_2O_2, both *o*DNB and *p*DNB slowly react with NaOH to form the corresponding phenol, the reaction likely occurring by straightforward nucleophilic displacement of nitrite ion. The kinetics of the *para* reaction in aqueous dioxane were examined some years ago by Tommila and Murto (6) who found that their experimental data did not conform to either first- or second-order rate behaviour.

In our kinetic study, we have determined that H_2O_2 triggers an accelerated *p*DNB-to-*p*NP reaction involving a reasonably stable intermediate which is spectrophotometrically detectable in the visible region. Thus, the *para* isomer behaves much like the *ortho* in the presence of hydrogen peroxide (reaction [1])

$$[1]\quad \mathrm{DNB} + \mathrm{HO_2^-} \xrightarrow{k_1} \text{intermediate} \xrightarrow{k_2} \mathrm{NP}$$

but noteworthy differences are apparent when a detailed comparison is made.

Figure 1 shows a set of spectra taken at various times during the reaction of *p*DNB with NaOH–H_2O_2 in 50% dioxane. The scans illustrate the key spectral characteristics common to the *ortho* and *para* reactions; (*a*) gradual shift of the λ_{max} from lower wavelength to the position of maximum nitrophenolate absorption; (*b*) early increase of absorbance in the 340 nm region followed by a decrease. These observations argue for the involvement of a long-lived intermediate in the reaction. The major difference between the *ortho* and *para* processes is the clear development of an isosbestic point (374 nm) in the *para* case. This feature, indicating that only two species are present during the latter stage of the reaction (7), allows the k_2 step to be analyzed independently. Although the isosbestic point could

[1]WLU Undergraduate Summer Research Assistant, 1983.

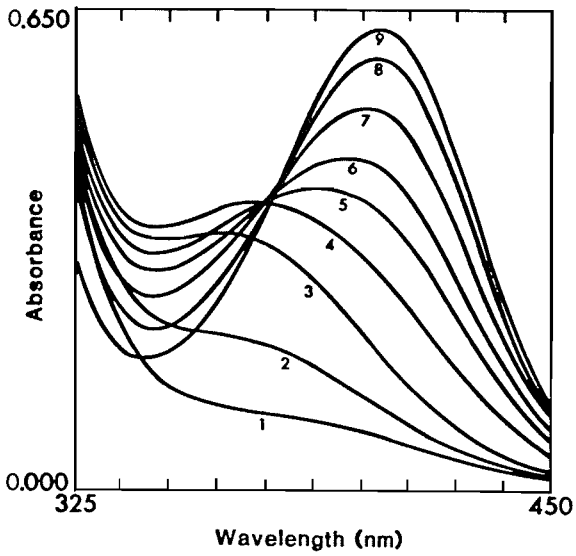

FIG. 1. Conversion of *p*-dinitrobenzene to *p*-nitrophenolate anion. Spectral changes during the course of the reaction (30.0°C; 50% v/v dioxane in water; $[p\text{DNB}]_0 = 3.0 \times 10^{-5}$ *M*; $[\text{NaOH}]_0 = 0.378$ *M*; $[H_2O_2]_0 = 0.230$ *M*). Scans started at: *1*, 2 min; *2*, 7 min; *3*, 22 min; *4*, 80 min; *5*, 123 min; *6*, 170 min; *7*, 260 min; *8*, 400 min; *9*, 1200 min.

reflect a reaction scheme as shown in [2] with the equilibrium shifted overwhelmingly toward the dead-end intermediate, we believe it is more reasonably interpreted in the context of sequence [1] which conforms to traditional models of aromatic

[2] $\text{DNB} + HO_2^- \longrightarrow \text{NP}$

$\downarrow \uparrow$

Intermediate

substitution. Working from this assumption, we anticipated that the kinetic elucidation of the *para* reaction would be more straightforward than the time-consuming computer matching which we were forced to adopt for the rationalization of our *ortho* data.

Instead, we discovered that the k_2 values (Table 1) were not cleanly reproducible and neither were they dependent on $[H_2O_2]$ contrary to the conclusion we reached in our *o*DNB studies. The supposed relationship between k_2 and $[H_2O_2]$ established in that earlier work can only be ascribed to unsuspected shortcomings of the computer-model methodology.

The rather high degree of uncertainty in the k_2 values prompted a brief examination of the secondary factors which might affect the reaction pathway. We found that although the reaction proceeded to >95% formation of *p*NP in quartz uv cells, the yield in Pyrex vessels was as much as 25% lower as measured by the infinity absorbance. Not only the yield, but also the apparent reaction rate was detectably different in Pyrex containers. We did not investigate this phenomenon in detail, but we have reason to suspect that both the composition and the relative wall area of the reaction vessel is important in this regard. For example, in Pyrex nmr tubes appreciable amounts of secondary product(s) are formed, giving rise to permanent peaks which are well upfield from the aromatic region. Some of them are partly obscured by the water signal.[2] It therefore

[2]Speculating that some fraction of the intermediate was undergoing additional nucleophilic displacement and ring opening as a result of surface catalysis, we subjected 1,4-benzoquinone and 1,4-hydroquinone to our reaction conditions, but these experiments did not reproduce the extraneous peaks obtained in the kinetic runs.

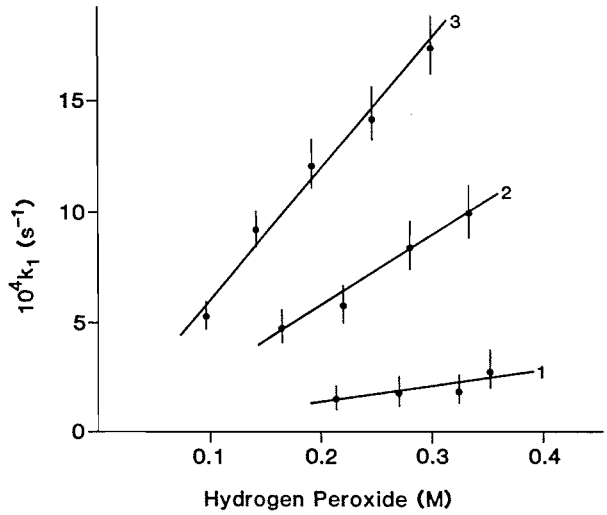

FIG. 2. Variation of k_1 with H_2O_2 concentration (30.0°C; [NaOH] = 0.35 *M*): *1*, 10% dioxane, $r = 0.857$; *2*, 30% dioxane, $r = 0.989$; *3*, 50% dioxane, $r = 0.993$.

TABLE 1. Values of k_2 ([NaOH] = 0.35 *M*, 30.0°C)

% Dioxane	$10^5 \times k_2$ (s^{-1})
10	11.75 ± 4.48
30	9.87 ± 2.47
50	6.78 ± 1.40

appears that our reaction is subject to surface effects for which peroxide decomposition reactions are well-known (8) and we ascribe our inconsistent results to such effects. It is likely that the *o*DNB reaction which we studied previously (4) behaves similarly although we were not aware of it at the time.

The absorbance changes in the 340 nm region allow us to determine t_{max}, the time at which the concentration of the intermediate reaches a maximum. In a well-behaved two-step kinetic system, t_{max} is directly related to the numerical values of k_1 and k_2 (9). Because of the uncertainty in our k_2 values, the evaluation of k_1 via t_{max} is subject to some error, but nevertheless the relationship between $[H_2O_2]$ and k_1 is apparently linear in aqueous solutions containing 10%, 30%, and 50% dioxane, as shown in Fig. 2. The larger k_1 values for the reactions in dioxane-rich media agree with the common observation that nucleophilic processes involving charge dispersal in the transition state are faster in solvents of lower polarity, presumably because of the greater, but relatively unsatisfied solvation requirements of the original ion in comparison with those of the transition state (10).

Our kinetic results therefore show that, within the framework of reaction [1], k_1 is considerably greater than k_2 for the *para* isomer whereas our earlier work (4) established that for the *ortho* compound, k_1 and k_2 are of comparable magnitude. Experimental values for the pseudo first-order rate constants under equivalent conditions are shown in Table 2.

Discussion

Kinetic results

A comparison of our k_1 values with those for similar aromatic substitutions is of some interest. Unfortunately, although there is an abundance of such data available for nucleophilic attack on 2,4-dinitro- and 2,4,6-trinitroaromatics, very little work has

Can. J. Chem. Downloaded from www.nrcresearchpress.com by 80.58.250.72 on 09/07/12
For personal use only.

TABLE 2. Rate constants for *o*- and *p*-dinitrobenzene (50% v/v dioxane in water, 30.0°C, $[H_2O_2]$ = 0.2 *M*, [NaOH] = 0.35–0.45 *M*)

Dinitrobenzene	$10^5 \times$ Rate constant (s^{-1}) k_1	k_2
Ortho	(45)[a]	(30)[a]
Para	121	6.8

[a]Approximate; from ref. 4.

been done on simpler systems such as ours. In particular, the vast majority of previous studies involve displacement (or Meisenheimer addition) at a position adjacent to a nitro group without a comparative examination of attack at a position free of *ortho* interference.

One directly analogous study is that of Tommila and Murto (6) who found that $k_{para}/k_{ortho} \sim 10$ for reaction [3]

[3] $DNB + RO^- \rightarrow (NO_2)C_6H_4OR + NO_2^-$

[4] $DNB + HO^- \rightarrow (NO_2)C_6H_4OH + NO_2^-$

(R = Me, Et) in aqueous alcohol while the ratios for [4] under the same solvent conditions were in the range 1.6–2.7. They also found that reaction [4] in pure water gave $k_{para}/k_{ortho} \sim 0.5$. Our k_1 ratio for attack by HO_2^- is 2.7, similar to their findings for HO^- attack in less polar solvent mixtures. This agreement is not surprising in light of the view that both HO^- and HO_2^- are "sterically unhindered" nucleophiles (11).

It is also interesting to compare our results with roughly equivalent electrophilic processes. Keeping in mind the "unhindered" nature of the HOO— moiety, one can argue that the σ complexes formed in our reactions have a reasonable *steric* resemblance to the *ortho* and *para* intermediates generated in the nitration of nitrobenzene and therefore their relative rates of formation might be similar. From the partial rate factors for nitrobenzene nitration (68–84% H_2SO_4; temperature 0–40°C) it is possible to calculate $k_{para}/k_{ortho} = 0.11$ (12*a*). A similar treatment of toluene nitration data (various solvents; temperature 0–40°C) gives $k_{para}/k_{ortho} = 1.4$ (12*b*) which is close to our result.

The "α-effect" phenomenon continues to arouse the curiosity of chemists even though its underlying origins remain obscure (13*a*) and its evaluation remains controversial (13*b*). Our data allow the α-effect, $(k_{HO_2^-}/k_{HO^-})$, to be estimated for attack on *p*DNB. Given the pK_a of H_2O_2 (14) and the pH of our reaction solutions, it is not unreasonable to assign $[HO_2^-]$ as being equal to the titrated H_2O_2 concentration. Then the slope (5.78×10^{-3}) of the 50% dioxane plot in Fig. 2 may be taken as $k_{HO_2^-}$, the second order rate constant for the reaction of HO_2^- with *p*DNB. From ref. 6, interpolation yields a value, $k_{HO^-} = 4.0 \times 10^{-5}\ M^{-1}\ s^{-1}$ for the same conditions, leading to an α-effect ratio of 145. In comparison, Behrman *et al.* report a ratio of 200 for displacement of chloride from 2,4-dinitrochlorobenzene (15) although $k_{HO_2^-}/k_{HO^-}$ ratios as large as 10 000 have been observed for attack on carbocation and carbonyl centers (13*a*) which are, like the benzene substrates, sp^2 hybridized.

Structure of the intermediate

Our previous work (4) in this field led us to suggest that the intermediate in the *o*DNB–H_2O_2 reaction was a radical anion formed by electron transfer from HO_2^- to the aromatic electrophile. There is ample precedent for the formation of nitroaromatic radical anions in strong base (16), but an examination of our kinetic solutions by esr spectroscopy yields no evidence for the presence of long-lived organic radicals. In light of this, a radical anion must be ruled out as the intermediate which absorbs so noticeably in the 340–450 nm region during the first few hours of a kinetic run.

There is little published information dealing with the intermediates arising from reaction between peroxidic anions and nitroaromatic compounds. Some reports (11, 15, 17) touch on the empirically observed visible spectra of the intermediates formed when peroxide anions are reacted with 2,4-dinitrohalobenzenes; in one case (17) the intermediate is referred to as "2,4-dinitrophenyl peroxide anion" but no definitive structural evidence is put forward. Also on the basis of visible spectroscopy, Meisenheimer complexes are reported to result from the reaction of substituted 2,4,6-trinitroaromatics with alkyl peroxide anions (18). Parallel reasoning suggests that the Meisenheimer structure **1** and the aryl hydroperoxide **2** are sequentially involved in our reaction system, but which of these two is the long-lived intermediate?

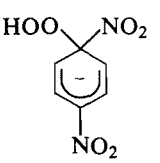

1

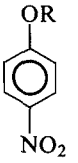

2*a* R = OH
2*b* R = O$^-$

Over the years, many different Meisenheimer complexes (mostly di- and trinitro-) have been characterized in detail (19) and there can be no doubt as to their existence as a class. In contrast, aryl hydroperoxides are so notoriously unstable that no example of the class has ever been identified. Although there are many literature references to "aryl hydroperoxides" and "aryl peroxides", these invariably prove to be erroneously classified aralkyl compounds, usually derivatives of cumene, in which the peroxidic oxygens are bonded to an alkyl rather than an aryl carbon atom.

Mononitro–Meisenheimer complexes are not common but the proton nmr characteristics of a few such structures have been studied by Ohsawa (20). For *para*-nitro systems, Ohsawa reports that there is little shift of the ring proton signals when a mononitro–Meisenheimer complex is formed; for example, if methoxide is reacted with *p*-nitroaniline, the ring hydrogens appear at δ 6.56 and 7.97, a shift of less than 0.15 ppm, and the reaction of NH_2^- with the same substrate moves the signals only about 0.5 ppm to δ 6.02, 7.50. Such findings are in contrast to those observed for dinitro–Meisenheimer complexes which typically show a large upfield shift of about 2 or 3 ppm to δ 4–5 for protons *ortho* or *para* to the point of anion attack (19*a*, 21).

Our concentrated kinetic solutions yielded the proton nmr spectra shown as **2***a*–**2***d* in Fig. 3. The spectra taken early in the time sequence show considerable line broadening which may be associated with precipitation which occurs when the necessarily concentrated solutions are mixed to begin the runs for nmr studies. However, we have independently determined that a mixture of NaOD and *p*DNB displays some broadening of the *p*DNB peak even when no precipitate is present, suggesting chemical exchange involving a charge transfer complex. Another reasonable explanation[3] is the presence of very small quantities of dinitrobenzene radical anions and therefore, despite the

[3]We thank one of the referees for alerting us to this point.

Can. J. Chem. Downloaded from www.nrcresearchpress.com by 80.58.250.72 on 09/07/12
For personal use only.

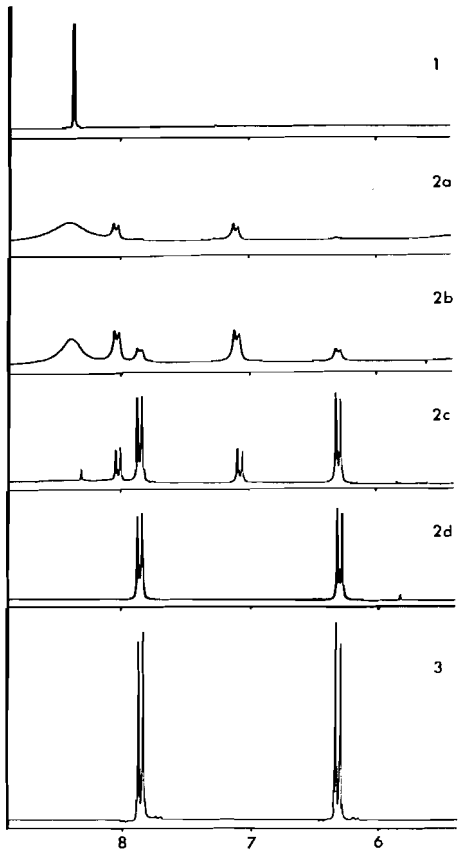

FIG. 3. 250 MHz proton nmr spectra. (*1*) *p*DNB (≈0.05 *M* in 50% aq. dioxane); (*2*) kinetic solution (50% aq. dioxane; [*p*DNB] ~ 0.05 *M*; [NaOD] ~ 0.4 *M*; [H_2O_2] ~ 0.2 *M*; 25°C): (*a*) 7 min; (*b*) 40 min; (*c*) 132 min; (*d*) 18 h; (*3*) *p*NP (~0.1 *M* in 50% aq. dioxane; [NaOD] ~ 0.7 *M*).

TABLE 3. Proton chemical shifts of *para*-nitro systems

Compound	Ring protons (δ)	Reference
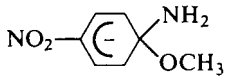	6.56, 7.97	20
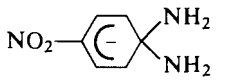	6.02, 7.50	20
p-Nitrophenolate	6.3, 7.8	This work
p-Nitrophenol	6.9, 8.1	22*a*
p-Nitroanisole	6.9, 8.1	22*b*
p-Nitrophenylhydrazine	6.9, 8.0	22*c*
Intermediate	7.06, 8.01	This work

negative esr results, we cannot totally eliminate the possibility that the radical anion is involved as an extremely short-lived intermediate in the first step of the reaction (16*b*). The line broadening develops as soon as the reactants are mixed together but, at the concentrations used in our regular kinetic runs, we detect no corresponding absorbance changes in the uv/visible regions. Therefore this phenomenon is not a direct factor in the analysis of our results.

Aside from the broadening, our spectra clearly show temporary peaks (AA′BB′ quartet; δ 7.06, 8.01) during the time period corresponding to uv/visible absorption by the intermediate in our kinetic runs. These temporary peaks are distinctly different

TABLE 4. Carbon-13 nmr data

Compound	Chemical shift (ppm) C-1	C-2	C-3	C-4
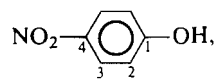	161.2	116.7	125.1	141.2
p-Nitroanisole, calcd (23)	165.7	115.0	124.7	140.8
Intermediate, obsd (this work)	172.8	113.5	127.3	141.0
p-Nitrophenolate, obsd (this work)	180.0	120.6	129.2	134.7

from the *p*-nitrophenolate product signals at δ 6.30 and 7.84. They are moved upfield by 1.30 and 0.35 ppm from the parent *p*DNB signal at δ 8.36, a difference which seems rather large compared to the small shifts observed by Ohsawa. In fact, as shown in Table 3, the positions of the intermediate's peaks agree rather better with those for simple aromatic systems having an oxygen or nitrogen substituent *para* to the nitro group. This observation seems to favour the aryl hydroperoxide **2**, as the structure of the intermediate, but the Meisenheimer complex **1** cannot be rigorously excluded on this basis.

The question is cleanly resolved by ^{13}C nmr spectroscopy. Structure **1** has an sp^3 carbon but as shown in Table 4, our intermediate displays only aromatic carbons, similar to, but not identical with the signals given by *p*-nitrophenolate anion. Furthermore, the peak positions observed for the intermediate correspond closely to those calculated (23) for *p*-nitroanisole and for unionized *p*-nitrophenol (which is totally converted to *p*-nitrophenolate under our reaction conditions). It is therefore logical to conclude that the intermediate has the aromatic structure *p*-NO_2—C_6H_4—OR, specifically, *p*-nitrophenyl hydroperoxide **2**. The high pH of the reaction medium coupled with the probable pK_a (14) of an aryl hydroperoxide suggest that the intermediate is actually in the form of the anion **2***b*.

In summary, the results presented here constitute the first firm evidence for the existence of an aryl hydroperoxide species and the overall reaction is best described by sequence [3]:

$$[3]\quad \mathrm{DNB} + \mathrm{HO_2^-} \xrightarrow{k_1} \mathbf{1} \xrightarrow[\text{fast}]{\text{very}} \mathbf{2a/2b} \xrightarrow{k_2} \mathrm{NP}$$

We are pursuing similar work on related aromatic systems.

Acknowledgements

Financial support from the Wilfrid Laurier University Research Office and from the Natural Sciences and Engineering Research Council of Canada is gratefully acknowledged. The continued laboratory assistance of Mrs. A. Kinastowski is very much appreciated. We are also grateful to Dr. R. Rodrigo for helpful discussions and arranging nmr services at the University of Waterloo. Special thanks to Dr. R. A. Bell and his co-workers at McMaster University's 500 MHz Nuclear Magnetic Resonance Facility. We thank Dr. Politzer for providing a preprint of ref. 1*b*.

1. (*a*) P. POLITZER, L. ABRAHMSEN, and P. SJOBERG. J. Am. Chem. Soc. **106**, 855 (1984); (*b*) P. POLITZER, P. R. LAURENCE, L. ABRAHMSEN, B. A. ZILLES, and P. SJOBERG. Chem. Phys. Lett. **111**, 75 (1984).
2. J. R. BECK. Tetrahedron, **34**, 2057 (1978).
3. (*a*) A. ANNULLI, P. MENCARELLI, and F. [illegible] J. Org. Chem. **49**, 4065 (1984); (*b*) G. P. STAHLY. J. [illegible] (1985); (*c*) R. G. SUTHERLAND, R. L. [illegible] the intack on anion fork has

Can. J. Chem. Downloaded from www.nrcresearchpress.com by 80.58.250.72 on 09/07/12
For personal use only.

and C. C. LEE. Abstracts of the 68th Annual Conference of the Chemical Institute of Canada. 1985. p. 125.
4. R. A. HELLER, M. FEWSTER, and T. LAMBERT. Can. J. Chem. **61**, 2455 (1983).
5. R. C. WEAST (*Editor*). Handbook of chemistry and physics. 60th ed. CRC Press, Cleveland. 1976. p. C-164.
6. E. TOMMILA and J. MURTO. Acta Chem. Scand. **16**, 53 (1962).
7. T. N. HALL and C. F. PARANSKI, JR. Chemistry of the nitro and nitroso groups. Part II. *Edited by* H. Fener. Interscience, New York. 1970. p. 341.
8. (*a*) I. R. WILSON. *In* Comprehensive chemical kinetics. Vol. 6. *Edited by* C. H. Bamford and C. F. H. Tipper. Elsevier Publishing Co., Amsterdam. 1972. p. 335; (*b*) R. C. P. CUBBON. *In* Progress in reaction kinetics. Vol. 5. *Edited by* G. Porter. Pergamon Press, London. 1970. pp. 32, 39, 48; (*c*) J. T. BARBES and J. E. LEFFLER. J. Org. Chem. **50**, 705 (1985).
9. A. A. FROST and R. G. PEARSON. Kinetics and mechanism. John Wiley and Sons, Inc., New York. 1953. p. 155.
10. (*a*) C. K. INGOLD. Structure and mechanism in organic chemistry. G. Bell and Sons Ltd., London. 1963. p. 347; (*b*) J. HINE. Physical organic chemistry. 2nd ed. McGraw-Hill Book Co. Ltd., New York. 1962. pp. 73, 74.
11. C. D. RITCHIE and M. SAWADA. J. Am. Chem. Soc. **99**, 3754 (1977).
12. P. B. D. DE LAMARE and J. H. RIDD. Aromatic substitution. Butterworth Scientific Publications, London. 1959. (*a*) p. 83; (*b*) p. 88.
13. C. H. DEPUY, E. W. DELLA, J. FILLEY, J. J. GRABOWSKI, and V. M. BIERBAUM. J. Am. Chem. Soc. **105**, 2481 (1983); (*b*) S. HOZ and E. BUNCEL. Tetrahedron Lett. **25**, 3411 (1984).
14. T. MOELLER. Inorganic chemistry. John Wiley and Sons, Inc., New York. 1952. p. 505.
15. J. E. MCISAAC JR., L. R. SUBBARAMAN, J. SUBBARAMAN, H. A. MULHAUSEN, and E. J. BEHRMAN. J. Org. Chem. **37**, 1037 (1972).
16. (*a*) M. R. CRAMPTON. Adv. Phys. Org. Chem. **7**, 211 (1969); (*b*) T. ABE and Y. IKEGAMI. Bull. Chem. Soc. Jpn. **51**, 196 (1978); (*c*) I. BIL'KIS and S. SHEIN. Izv. Akad. Nauk. SSR Ser. Khim. 961 (1973); Chem. Abstr. **79**, 52546k (1973).
17. J. E. DIXON and T. C. BRUICE. J. Am. Chem. Soc. **93**, 6592 (1971).
18. H. KROPF, M. BALL, K. H. SIEGFRIEDT, and S. WAGNER. J. Chem. Res. (S), 339 (1981).
19. (*a*) M. J. STRAUSS. Chem. Rev. **70**, 667 (1970); (*b*) E. BUNCEL, A. R. NORRIS, and K. E. RUSSELL. Q. Rev. **22**, 123 (1967).
20. S. OHSAWA. Nippon Kagaku Kaishi, 1491 (1973); 460 (1976).
21. W. E. BYRNE, E. J. FENDLER, J. H. FENDLER, and C. E. GRIFFIN. J. Org. Chem. **32**, 2506 (1967).
22. C. J. POUCHERT and J. R. CAMPBELL. The Aldrich Library of nmr spectra. Aldrich Chemical Co. Inc., Milwaukee, Wisconsin. 1974. (*a*) V, 154D; (*b*) V, 155A; (*c*) V, 155C.
23. G. C. LEVY and G. L. NELSON. Carbon-13 nuclear magnetic resonance for organic chemists. Wiley-Interscience, New York. 1972. p. 80.

Can. J. Chem. Downloaded from www.nrcresearchpress.com by 80.58.250.72 on 09/07/12
For personal use only.

Stereochemistry of dopaminergic ergoline derivatives: structures of pergolide and pergolide mesylate

LILIAN Y. Y. MA AND NORMAN CAMERMAN[1]
Department of Biochemistry, University of Toronto, Toronto, Ont., Canada M5S 1A8

JOHN K. SWARTZENDRUBER AND NOEL D. JONES
Lilly Research Laboratories, Eli Lilly and Company, Indianapolis, IN 46285, U.S.A.

AND

ARTHUR CAMERMAN
Departments of Medicine (Neurology) and Pharmacology, University of Washington, Seattle, WA 98195, U.S.A.

Received February 25, 1986[2]

LILIAN Y. Y. MA, NORMAN CAMERMAN, JOHN K. SWARTZENDRUBER, NOEL D. JONES, and ARTHUR CAMERMAN. Can. J. Chem. **65**, 256 (1987).

The crystal and molecular structures of the dopaminergic ergoline derivative pergolide have been determined both as the free base and as the mesylate salt. Despite differences in protonation at the nitrogen atom, the two structures are extremely similar in all aspects. Stereochemical comparisons are made with bromocriptine, and possible dopaminergic pharmacophores in ergolines are discussed.

LILIAN Y. Y. MA, NORMAN CAMERMAN, JOHN K. SWARTZENDRUBER, NOEL D. JONES et ARTHUR CAMERMAN. Can. J. Chem. **65**, 256 (1987).

On a déterminé les structures cristallines et moléculaires, tant à l'état de base libre que sous la forme d'un sel mésylate, de la pergolide, un dérivé dopaminergique de l'ergoline. En dépit de différences dans la protonation de l'atome d'azote, les deux structures sont extrêmement semblables. Des comparaisons stéréochimiques ont été faites avec la bromocriptine et on discute des diverses possibilités de pharmacophores dopaminergiques dans les ergolines.

[Traduit par la revue]

Introduction

Physiological properties of ergots have been recognized since the Middle Ages when the fungus *Claviceps purpurea*, found on rye grain, was identified as the causative agent of St. Anthony's fire. More recently ergot alkaloids have been shown to exhibit dopaminergic, serotonergic, and α-adrenergic properties. As part of a program to separate these activities, the semisynthetic ergot, pergolide, (8β)-8-[(methylthio)methyl]-6-propylergoline (**1**), was prepared. Pergolide shows profound dopamine

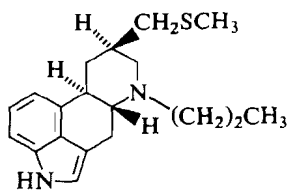

1

agonist activity (1) and is currently being evaluated clinically for the treatment of Parkinson's Syndrome (2–4), as well as for a number of hyperprolactinemia characterized diseases (5–7). Its antiparkinson efficacy, like that of the other ergolines, can be attributed to the postsynaptic stimulation of central dopaminergic receptors (8, 9).

Attempts to delineate the dopaminergic pharmacophore of the ergot derivatives by stereochemical comparisons with dopamine and other dopamine receptor agonists, notably apomorphine, have resulted in postulations of imino-phenylethylamine (10, 11), pyrrolethylamine (12), and indolethylamine (13) as the dopaminomimetic entity. Among the criteria considered in some of the modelling attempts has been the direction of the amino nitrogen lone-pair electrons. Crystal structure determinations of protonated (10) and unprotonated[3] bromocriptine revealed opposite nitrogen lone-pair directions in the two cases, showing that inter- (and intra-) molecular attractions, rather than inherent stability, are determinants of this feature. Here we report the results of crystal structure determinations of pergolide as the free base and as the mesylate salt to further investigate the effects of molecular contacts on nitrogen lone-pair orientation and to provide more data for delineation of the stereochemical features of the ergoline type of dopamine agonists.

TABLE 1. Crystal data

Parameter	Pergolide	Pergolide mesylate
Formula	$C_{19}H_{26}N_2S$	$C_{19}H_{27}N_2S \cdot CH_3O_3S$
Molar mass, g	314.5	410.6
Crystal form	Orthorhombic	Triclinic
Space group	$P2_12_12_1$	$P1$
a, Å	7.038(5)	6.841(2)
b, Å	12.109(8)	9.319(2)
c, Å	20.430(10)	9.678(2)
α, deg	90	64.42(2)
β, deg	90	69.67(2)
γ, deg	90	76.74(2)
V, Å^3	1741.1	519.6
d_x g/cm^3	1.20	1.31
Z	4	1
μ, cm^{-1}	15.73	22.47

Experimental

A. Pergolide

Colorless crystals were obtained by shaking the mesylate salt (from Lilly; LY127809) with a mixture of aqueous ammonia and ethyl

[1]Author to whom correspondence may be addressed.
[2]Revision received August 27, 1986.
[3]H. P. Weber, private communication.

Can. J. Chem. Downloaded from www.nrcresearchpress.com by 80.58.250.72 on 09/07/12
For personal use only.

TABLE 2. Fractional atomic coordinates ($\times 10^4$) and equivalent isotropic temperature factors (in Å^2)

	Pergolide				Pergolide mesylate			
Atom	x	y	z	B_{eq}	x	y	z	B_{eq}
N1	−12084(13)	−3024(7)	−7333(5)	3.48	5222(8)	2120(6)	9790(7)	3.55
C2	−10883(15)	−2522(8)	−7760(5)	3.24	7092(5)	2164(4)	8597(5)	3.32
C3	−9730(15)	−1803(9)	−7457(5)	3.07	8094(5)	3462(4)	8232(4)	2.84
C4	−8131(17)	−1076(9)	−7688(5)	3.39	10090(9)	4133(7)	7098(8)	2.84
C5	−6842(18)	−766(8)	−7085(5)	3.04	10679(6)	5251(4)	7663(5)	2.45
N6	−5482(12)	110(7)	−7262(4)	3.21	12486(4)	6159(3)	6385(3)	2.37
C7	−4114(17)	327(10)	−6724(6)	4.09	13248(5)	7151(4)	6932(4)	2.76
C8	−5125(17)	720(10)	−6123(6)	4.34	11502(8)	8369(7)	7339(7)	2.61
C9	−6563(16)	−142(10)	−5900(5)	4.14	9620(8)	7547(7)	8596(8)	2.84
C10	−7943(17)	−414(8)	−6460(5)	3.48	8878(4)	6498(4)	8069(4)	2.53
C11	−9441(16)	−1275(8)	−6263(6)	3.40	6977(8)	5657(7)	9287(7)	2.61
C12	−10176(18)	−1469(9)	−5652(6)	4.53	5419(6)	6198(5)	10379(5)	3.16
C13	−11631(17)	−2254(10)	−5565(6)	4.40	3646(6)	5535(5)	11330(5)	3.79
C14	−12425(17)	−2824(8)	−6074(6)	4.30	3398(7)	3948(6)	11277(6)	3.63
C15	−11720(17)	−2646(9)	−6711(6)	3.76	4951(7)	3399(5)	10187(6)	3.08
C16	−10259(16)	−1830(8)	−6788(5)	2.86	6712(5)	4258(4)	9255(4)	2.84
C17	−4399(16)	−181(9)	−7868(5)	3.42	14298(5)	5057(5)	5801(5)	3.08
C18	−3031(19)	657(9)	−8107(6)	4.19	16106(7)	5966(6)	4505(6)	3.95
C19	−2250(19)	413(13)	−8795(7)	7.60	17652(7)	4806(7)	3796(7)	4.74
C20	−3691(18)	901(12)	−5547(6)	5.71	12286(6)	9371(5)	7928(5)	2.92
S21	−1972(7)	1975(5)	−5719(2)	8.95	14718(2)	10257(2)	6698(3)	4.58
C22	−3344(30)	3163(16)	−5583(8)	11.03	14094(11)	11450(6)	4861(6)	6.00
S23					1077(2)	9295(1)	2710(1)	3.47
O24					912(5)	7636(4)	3826(4)	4.89
O25					12790(5)	9460(4)	1262(4)	5.61
O26					11048(11)	10352(7)	3423(6)	8.37
C27					−1239(10)	9824(9)	2117(9)	7.11

acetate, isolating the ethyl acetate layer, and allowing the solvent to evaporate slowly in a refrigerator. Crystal data are given in Table 1. A thin plate, 0.33 × 0.20 × 0.03 mm, was mounted along a and intensities of 1647 independent X-ray diffraction maxima were measured on an automated four circle diffractometer by using Ni-filtered CuKα (λ = 1.54178 Å) radiation with the θ–2θ scan technique ($2\theta_{max}$ = 125°, scan rate = 1°/min). Empirical absorption corrections were applied by measuring variation of intensities of 2 reflections (200 and 400 at 2θ = 25.33° and 52.02° respectively) with φ at χ = 90°. After data reduction 887 reflections were considered as observed ($I > 3\sigma(I)$) and were used in the structure refinement.

The structure was solved using the direct phasing methods program MULTAN80 (14), and was refined by full matrix least-squares techniques on F with weights = $1/(\sigma(F))^2$. Hydrogen atoms (located on difference Fourier plots) were assigned fixed positional and thermal parameters (B_{iso} = 6.0 Å^2) and were not refined. Non-hydrogen atoms were refined anisotropically. The absolute configuration was determined by Hamilton's test (15) using anomalous scattering from the S, N, and C atoms (16). Final values for R, Rw, and S for the presently determined enantiomer were 0.0737, 0.0778, and 1.8133 as compared to corresponding values of 0.0740, 0.0783, and 1.8251 for the other enantiomer.

B. Pergolide mesylate

Prismatic crystals were obtained from absolute methanol. Crystal data are given in Table 1. Intensities of 1547 unique reflections, to 2θ = 116°, were measured on an automated four-circle diffractometer by using monochromatic copper radiation (θ/2θ scan). After the usual Lorentz and polarization corrections, the data were put on an absolute scale with a calculated overall temperature factor, B = 3.71 Å^2. A total of 973 reflections had $I > 2.5\sigma(I)$ and were included in the refinement procedure. The structure was determined using the SOLV routine of the SHELXTL program (17) and was refined by least squares to an R value of 0.0497 (Rw = 0.0504). The final refinement included anisotropic temperature factors for all atoms except hydrogen, the latter being included with isotropic temperature factors at calculated positions. The weighting scheme was $w = 1/[\sigma^2(F) + G|F|^2]$ where G refined to 0.047. The absolute configuration of the molecule was determined by the anomalous dispersion technique, using the procedure of Rogers (18); the measure of fit parameter was 0.95 (σ = 0.06). The largest residual in the final difference electron density map was 0.4 ē/Å^3.

Table 2 lists the atomic fractional coordinates and equivalent isotropic thermal parameters for the heavy atoms for the two crystal structures. The anisotropic thermal parameters, hydrogen atomic positional parameters, and the observed and calculated structure factors have been deposited and are available.[4]

Results and discussion

Figure 1 shows the atomic numbering scheme and the bond lengths and angles; because the overall conformations and molecular parameters of pergolide and the mesylate salt are so similar (see below), the values shown are the averages of the two structures. Tables of bond lengths and angles for each compound have been deposited.[4] As expected, the bond lengths involving N6 are longer (by 0.02–0.04 Å) in the protonated form of pergolide but, because N6 is involved in intermolecular interactions in both structures, bond angles around N6 have (similar) tetrahedral values. The other bond lengths and angles exhibit normal values.

Figure 2 is a stereoscopic superposition of the two pergolide structures. The two structure determinations have each independently confirmed the absolute configurations at the three asymmetric centers, C5, C8, and C10. As can be seen from the figure, unprotonated pergolide and the pergolide cation of the

[4]A complete set of data may be purchased from the Depository of Unpublished data, CISTI, National Research Council of Canada, Ottawa, Ont., Canada K1A 0S2.

Can. J. Chem. Downloaded from www.nrcresearchpress.com by 80.58.250.72 on 09/07/12
For personal use only.

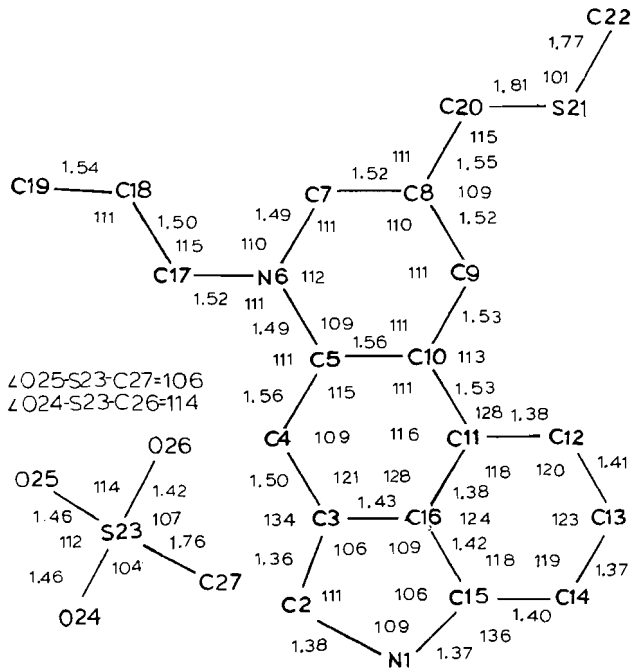

FIG. 1. Averaged bond lengths and angles in pergolide and pergolide mesylate. Standard deviations are less than 0.01 Å and 1°.

mesylate salt have virtually identical conformations, including the configuration at N6. This arises as a consequence of the molecular packing schemes: although N6 of the pergolide cation is an H-bond donor (to an oxygen of the mesylate ion) and N6 of unprotonated pergolide is an H-bond acceptor (from N1 of another molecule), both interactions occur on the same side of the pergolide moiety in the two crystal structures, thus giving rise to identical conformations. This is in contrast to the situation in the crystal structures of bromocriptine mesylate (10) and unprotonated bromocriptine: the hydrogen-bonding scheme in the former is similar to pergolide mesylate, resulting in a similar configuration at N6, but in the latter N6 is an H-bond acceptor in an intramolecular interaction from the opposite direction. This results in the opposite nitrogen lone-pair orientation at N6 (Fig. 3) in the unprotonated bromocriptine structure. Taken together, these results strongly suggest that the direction of the nitrogen atom lone pair of electrons in ergoline derivatives is variable and can be influenced by the side of approach of an interacting species, e.g. a hydrogen-bonding or charged side chain of a receptor.

As in the bromocriptine structures, the indole nucleus in pergolide is planar, and the adjoining ring adopts a half-chair conformation with C5 lying out of the plane of the other atoms. In contrast to bromocriptine, in which the C9—C10 double bond causes the heterocyclic six-membered ring to be skewed, the saturated character of the ring in pergolide results in a chair conformation.

Details of the molecular packing are shown in Fig. 4. The hydrogen bonding in unprotonated pergolide has dimensions N1...N6 = 2.95 Å, H1...N6 = 2.03 Å, and the angle N1—H1...N6 = 163°. There are two intermolecular interactions with the mesylate ion in the pergolide salt structure, involving two different molecules; the parameters are N6...O24 = 2.72 Å, H6...O24 = 1.79 Å, and the N6—H6...O24 angle is 164°, and N1...O25 = 2.85 Å, H1...O25 = 1.90 Å, and the N1—H1...O25 angle is 170°.

The delineation of the dopamine pharmacophore in ergolines has been a subject of considerable interest. Syntheses of dopaminergic ergoline analogues (**2**) that lack the phenyl A-ring of the ergot compounds have resulted in the proposal (19, 20) that the pyrrolethylamine moiety (rather than the dopamine-like phenylethylamine) is the ergoline dopaminomimetic entity. However, as noted by Camerman and Camerman (21), if the hydrogen-bonding NH of the pyrrole (analogous to the *meta* OH of dopamine) rather than the phenyl or pyrrole ring per se is important for dopaminergic activity, then these syntheses do not differentiate between models. The primary function of the phenyl or pyrrole ring may be to position the NH properly, and neither ring may be necessary per se. If so, it would be

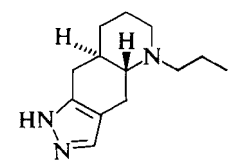

2

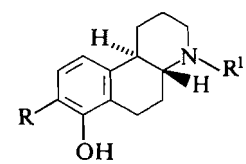

3

inaccurate to label either the phenylethylamine or the pyrrolethylamine as the ergoline dopamine pharmacophore. The structure determination of a dopaminergic ergoline analogue that lacks a pyrrole ring (22) (**3**) and subsequent stereochemical

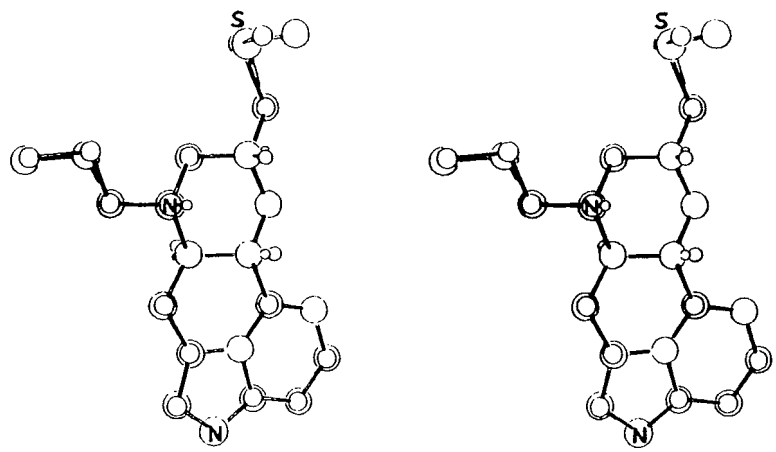

FIG. 2. Stereoscopic superposition of the structures of pergolide (large circles) and the pergolide ion of the mesylate (small circles).

Can. J. Chem. Downloaded from www.nrcresearchpress.com by 80.58.250.72 on 09/07/12
For personal use only.

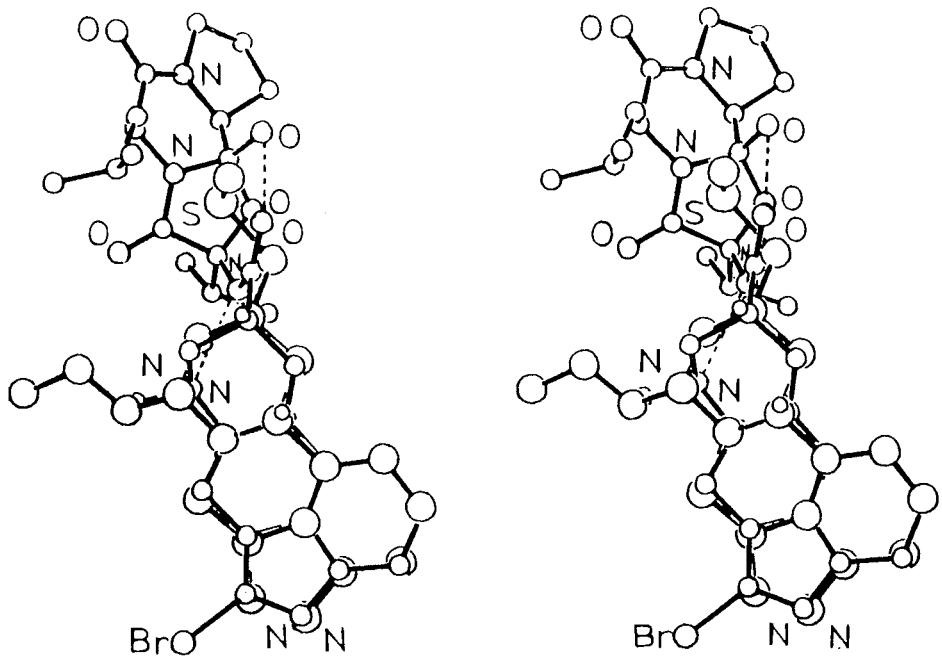

FIG. 3. Stereoscopic superposition of pergolide (large circles) and bromocriptine (small circles).

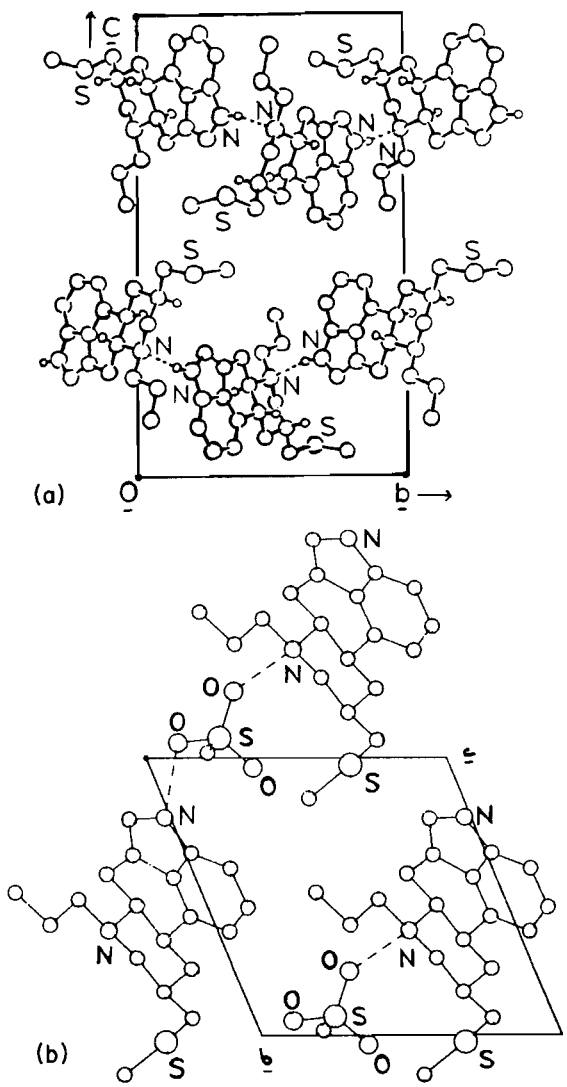

FIG. 4. Molecular packing and hydrogen bonding in the crystal structures of (*a*) pergolide, (*b*) pergolide mesylate.

comparisons would be of interest in addressing the pharmacophore question. Two such structures have recently been reported (23, 24); in the latter case, pharmacological structure–activity relationships of resolved enantiomers have indicated comparable activity at post-synaptic DA receptors for both enantiomers (but activity of unexplainably higher magnitude at DA autoreceptors for the absolute configuration opposite to that pictured in **3**).

Acknowledgements

Supported by National Institutes of Health grant NS09839 from the NINCDS (National Institute of Neurological and Communicative Disorders and Stroke). A.C. is a Klingenstein Senior Fellow in the Neurosciences.

1. R. W. FULLER, J. A. CLEMENS, E. C. KORNFIELD, H. D. SNODDY, E. B. SMALSTIG, and N. J. BACH. Life Sci. **24**, 375 (1979).
2. A. N. LIEBERMAN, M. LEIBOWITZ, A. NEOPHYTIDES, M. KUPERSMITH, S. MEHL, D. KLEINBERG, M. SERBY, and M. GOLDSTEIN. Lancet, **2**, 1129 (1979).
3. A. N. LIEBERMAN, M. LEIBOWITZ, M. KUPERSMITH, A. NEOPHYTIDES, V. PACT, S. MEHL, D. KLEINBERG, and M. GOLDSTEIN. Clin. Pharmacol. Ther. **27**, 266 (1980).
4. A. LIEBERMAN, M. GOLDSTEIN, M. LIEBOWITZ, A. NEOPHYTIDES, M. KUPERSMITH, V. PACT, and D. KLEINBERG. Neurology, **31**, 675 (1981).
5. D. L. KLEINBERG, A. LIEBERMAN, J. TODD, J. GRIESING, A. NEOPHYTIDES, and M. KUPERSMITH. J. Clin. Endocrinol. Metab. **51**, 152 (1980).
6. S. FRANKS, P. M. HORROCKS, S. S. LYNCH, W. R. BUTT, and D. R. LONDON. Lancet, **2**, 659 (1981).
7. J. T. CALLAGAN, R. E. CLEARLY, R. CRABTREE, and L. LEMBERGER. Life Sci. **28**, 951 (1981).
8. W. C. KOLLER, W. J. WEINER, B. I. DIAMOND, P. A. NAUSIEDA, and H. L. KLAWANS. Neuropharmacology, **19**, 831 (1980).
9. M. GOLDSTEIN, A. LIEBERMAN, L. Y. LEW, T. ASANO, M. R. ROSENFELD, and M. H. HAKMAN. Proc. Natl. Acad. Sci. **77**, 3725 (1980).
10. N. CAMERMAN, L. Y. CHAN, and A. CAMERMAN. Mol. Pharmacol. **16**, 729 (1979).

Can. J. Chem. Downloaded from www.nrcresearchpress.com by 80.58.250.72 on 09/07/12
For personal use only.

11. J. G. CANNON. Adv. Biosci. **20**, 87 (1979).
12. D. E. NICHOLS. J. Theor. Biol. **59**, 167 (1976).
13. J. G. CANNON, B. J. DEMOPOULOS, J. T. LONG, J. R. FLYNN, and F. M. SHARABI. J. Med. Chem. **24**, 238 (1981).
14. P. MAIN, S. J. FISKE, S. E. HULL, L. LESSINGER, G. GERMAIN, J. P. DECLERCQ, and W. W. WOOFSON. MULTAN80. A system of computer programs for the automatic solution of crystal structures from X-ray diffraction data. University of York, England. 1980.
15. W. C. HAMILTON. Statistics in physical sciences. Ronald Press, New York. 1964. pp. 157–162.
16. International tables for X-ray crystallography. Vol. IV. Kynoch Press, Birmingham. 1974. p. 149.
17. G. M. SHELDRICK. SHELXTL. A computer program for crystal structure determination. University of Cambridge, Cambridge, England. 1981.
18. D. ROGERS. Acta Crystallogr. Sect. A, **37**, 734 (1981).
19. N. J. BACH, E. C. KORNFELD, N. D. JONES, M. O. CHANEY, D. E. DORMAN, J. W. PASCHAL, J. A. CLEMENS, and E. B. SMALSTIG. J. Med. Chem. **23**, 481 (1980).
20. R. NORDMANN and T. J. PETCHER. J. Med. Chem. **28**, 367 (1985).
21. N. CAMERMAN and A. CAMERMAN. Mol. Pharmacol. **19**, 517 (1981).
22. J. G. CANNON, C. SUAREZ-GUTIERREZ, T. LEE, J. P. LONG, B. COSTALL, D. H. FORTUNE, and R. J. NAYLOR. J. Med. Chem. **22**, 341 (1979).
23. L. Y. Y. MA, N. CAMERMAN, and A. CAMERMAN. Annual Meeting of the American Crystallographic Association, Stanford, California, Aug. 18–19, 1985. Abstract PC-29.
24. H. B. WIKSTROM, B. ANDERSSON, D. SANCHEZ, P. LINDBERG, L.-E. ARVIDSON, A. M. JOHANSSON, J. L. G. NILSSON, K. SUENSSON, S. HJORTH, and A. CARLSSON. J. Med. Chem. **28**, 215 (1985).

Can. J. Chem. Downloaded from www.nrcresearchpress.com by 80.58.250.72 on 09/07/12
For personal use only.

Structural and vibrational studies of 1,1,3,3-tetracyanopropane and 2,2,4,4,6-pentacyanocyclohexenamine

R. A. BELL, B. E. BROWN, M. DUARTE, H. E. HOWARD-LOCK, AND C. J. L. LOCK[1]

Department of Chemistry and the Institute for Materials Research, McMaster University, Hamilton, Ont., Canada L8S 4M1

Received May 5, 1986

R. A. BELL, B. E. BROWN, M. DUARTE, H. E. HOWARD-LOCK, and C. J. L. LOCK. Can. J. Chem. **65**, 261 (1987).

1,1,3,3-Tetracyanopropane, **1**, was prepared in low yields by a literature method with 2,2,4,4,6-pentacyanocyclohexenamine, **2**, as a major by-product. The products were examined by X-ray crystallography. **1** has an orthorhombic space group, *Pbcn* (No. 60) with cell dimensions, $a = 7.158(2)$, $b = 10.510(3)$, $c = 9.733(2)$ Å and has four formula units in the unit cell. **2** has a monoclinic cell, $P2_1/c$ (No. 14) with cell dimensions $a = 14.368(3)$, $b = 6.626(1)$, $c = 12.300(2)$ Å, $\beta = 115.60(1)°$ and has 4 formula units in the unit cell. Data were collected with use of MoKα radiation and a Nicolet P3 diffractometer. The crystal structures were determined by standard methods and refined to $R_w = 0.037$ (**1**) and $R_w = 0.040$ (**2**) on the basis of 782 and 2108 unique reflections. Bond lengths and angles in the two compounds are normal. **2** has what has been considered to be the less likely tautomeric structure. Both compounds were examined by ^1H, ^{13}C nmr, vibrational spectroscopy, and mass spectroscopy. For **2** there was no evidence of the alternative tautomeric structure. New methods were developed for the preparation of both compounds and the mechanism of the original reaction rationalized.

R. A. BELL, B. E. BROWN, M. DUARTE, H. E. HOWARD-LOCK et C. J. L. LOCK. Can. J. Chem. **65**, 261 (1987).

Faisant appel à une méthode décrite dans la littérature, on a préparé le tétracyano-1,1,3,3 propane, **1**, avec un faible rendement; on a obtenu la pentacyano-2,2,4,4,6 cyclohexylamine, **2**, comme sous-produit principal. On a étudié les produits par diffraction des rayons-X. Le composé **1** cristallise dans le groupe d'espace orthorhombique *Pbcn* (No. 60) avec $a = 7,158(2)$, $b = 10,510(3)$ et $c = 9,733(2)$ Å et il compte quatre unités par cellule de base. Le composé **2** possède une cellule monoclinique $P2_1/c$ (No. 14) avec $a = 14,368(3)$, $b = 6,626(1)$ et $c = 12,300(2)$ Å et $\beta = 115,60(1)°$ et il comporte quatre unités dans la cellule de base. On a obtenu les données à l'aide d'une radiation MoKα et un diffractomètre Nicolet P3. On a déterminé les structures par des méthodes standards et on les a affiné jusqu'à des valeurs respectives de R_w de 0,037 (**1**) et 0,040 (**2**) sur la base de 782 et 2108 réflexions uniques. Les longueurs de liaisons observées dans les deux composés sont normales. Le composé **2** possède ce qui est considéré comme la structure tautomère la moins probable. On a étudié les deux composés par rmn du ^1H et du ^{13}C ainsi que par spectroscopies vibrationnelles et de masse. Dans le cas du composé **2**, il n'y a aucune indication qu'une autre structure tautomère puisse exister. On a développé de nouvelles méthodes pour préparer les deux composés et on a proposé un mécanisme qui rationalise la réaction originale.

[Traduit par la revue]

Can. J. Chem. Downloaded from www.nrcresearchpress.com by 80.58.250.72 on 09/07/12
For personal use only.

Introduction

Alkyl cyanides are good solvents for many transition metal complexes (1), often because they act as ligands (2). Recently, we have examined the complex $Pt(CH_3CN)_2Cl_2$ (3). Alkyl groups substituted by more than one cyanide group have the potential of binding more than one metal ion. To this end we have been interested in the preparation of 1,1,3,3-tetracyanopropane. The synthesis of 1,1,3,3-tetracyanopropane, **1**, was reported by Diels *et al.* in 1922 (4) who prepared it by the condensation of malononitrile with formaldehyde at 0°C. These authors noted the strong influence of reaction temperature and stoichiometry on the product yield and suggested a structure for a minor product formed in the reaction as 1,1,3,3,5,5-hexacyanopentane (5). The identity of this compound was subsequently questioned (6) and it was suggested a more likely formulation was either **3** or less likely **2**.

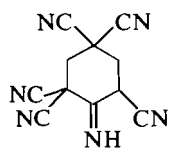

3

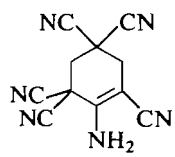

2

We have repeated the literature preparations and obtained **1** and established that the minor product is **2**. We could not, however, obtain the compounds from these reactions in a pure state. In addition, after long reaction times an orange insoluble material was obtained. The true natures of **1** and **2** were established by X-ray crystal structure determinations of selected single crystals. Subsequently, better methods of obtaining pure samples of **1** and **2** were developed and a study of the reactions of these compounds allowed an explanation of the course of the original preparation. We describe this work here.

[1]To whom all correspondence should be addressed.

Experimental methods

Reagents used in preparations

Malonitrile was purchased from Canlab and used without further purification. Formaldehyde (37% aqueous solution) was certified A.C.S. and purchased from Fisher Scientific Company. β-Alanine was purchased from Sigma Chemical Company and used without further purification.

Preparation of 1,1,3,3-tetracyanopropane, 1

A modified version of the preparation reported by Rybkina *et al.* (7) was followed. Malononitrile 1.500 g (0.0227 mol) was dissolved in 7.5 mL of absolute ethanol that contained 0.01% HCl. To this was added 0.860 mL (0.0144 mol) of a 37% aqueous solution of formaldehyde and 0.040 g of β-alanine. This mixture was stirred at room temperature for 4 to 5 h, and the resulting precipitate filtered off and washed with distilled water (5 × 20 mL) and ethanol (5 × 20 mL). The product was dried under vacuum for 1 h at room temperature. Recrystallizations were made from tetrahydrofuran or acetone. The product was obtained as 0.586 g of white microcrystals in 73% yield, mp 132–135°C. *Anal.* calcd. for $C_7H_4N_4$: C 58.3, H 2.8, N 38.9; found: C 58.3, H 3.0, N 38.8.

Preparation of 2,2,4,4,6-pentacyanocyclohexenamine, 2

1,1,3,3-Tetracyanopropane (0.3626 g, 0.00163 mol) prepared as above was dissolved in 50 mL distilled water by heating to 75–80°C. The reaction mixture was filtered hot and the filtrate allowed to cool and refrigerated for 3 h. White crystalline needles precipitated from the

TABLE 1. Crystal data

Compound	$(NC)_2CHCH_2CH(CN)_2$, $C_7H_4N_4$	$NH_2.\overline{C(CN).CH_2.C(CN)_2CH_2.C(CN)_2}$, $C_{11}H_6N_6$
f.w.	144.14	222.21
Crystal size (mm)	0.23 × 0.33 × 0.43	0.23 × 0.27 × 0.43
Systematic absences	$h0l, h = 2n + 1, 0kl, l = 2n + 1$ $hk0, h + k = 2n + 1$	$h0l, l = 2n + 1, 0k0$ $k = 2n + 1$
Space group	$Pbcn$(No. 60)	$P2_1/c$(No. 14)
Unit cell parameters (Å and deg)	a = 7.158(2) b = 10.510(3) c = 9.733(2)	a = 14.368(3) b = 6.626(1), β = 115.60(1) c = 12.300(2)
Volume (Å^3)	732.2(2)	1056.0(4)
Z	4	4
μ linear absorption coefficient (cm^{-1})	0.957	1.020
ρ_{calcd}, ρ_{obsd} (g cm^{-3})	1.308, 1.30(1)	1.385, 1.37(1)
max 2θ, reflections, measured	55°, $h, k, \pm l$	55°, $h, k, \pm l$
Standard reflections (e.s.d.%)	−1 1 3 (1.22) 0 0 4 (1.55)	0 1 2 (1.13) 3 1 4 (1.45)
Temperature (°C)	22	22
No. of reflections, measured	1633	2541
R_{int}	0.0249	0.0174
No. of independent reflections	852	2447
No. with $I > 0$ (used)	782	2108
Final R, R_w[a]	0.115, 0.037	0.094, 0.040
Final shift error max(ave)	0.001 (<0.001)	0.009 (0.001)
Final difference map		
Highest peak, lowest valley (e Å^{-3})	0.44, −0.42	0.45, −0.51
Weighting	$w = (\sigma_F^2)^{-1}$	$w = (\sigma_F^2)^{-1}$
F(000)	296	456
Number of variables	61	178
Error in obs. of unit weight	1.77	1.70

[a] $R = \Sigma||F_o| - |F_c||/\Sigma|F_o|$; $R_w = (\Sigma w(|F_o| - |F_c|)^2/\Sigma wF_o^2)^{1/2}$.

solution and were filtered and washed with absolute ethanol. The product was then vacuum dried for 1 h at room temperature. The melting point of the product was 225°C and the yield 0.125 g (68%). *Anal.* calcd. for $C_{11}H_6N_6$: C 59.5, H 2.7, N 37.8; found: C 59.9, H 2.7, N 37.4.

Apparatus

Infrared spectra were recorded on a Perkin–Elmer 283 grating spectrometer in the range 4000–200 cm^{-1}. The samples were prepared as KBr pellets. The spectra were calibrated against polystyrene and indene. Spectra were also collected in the 500–100 cm^{-1} region on a Nicolet 7199 FT-IR Spectrometer with samples between polyethylene plates.

Raman spectra were obtained from powder samples at room temperature in the range 3000–50 cm^{-1} on a Spex spectrometer Model 14018 with a Coherent Radiation Argon Laser Model 52. The spectra were calibrated against $HgCl_2$.

The ^1H and ^{13}C nmr were recorded at room temperature on a Bruker WP80 instrument using tetramethylsilane as a reference. Samples were dissolved in dimethylsulphoxide-d_6. Carbon-13 data were acquired in 8K and over 6000 Hz with a pulse angle of approximately 15°.

Ultraviolet spectra were recorded on a Hewlett Packard 8451A Diode Array Spectrophotometer with samples in quartz cells. Samples were dissolved in tetrahydrofuran.

The mass spectra were recorded on a Micromass 70-70 mass spectrometer. The source temperature was varied from 100 to 250°C, and the ionization voltage was 70 eV.

Collection of diffraction data and solution of the structures

The plate-like crystals of compound **1** and the needle-like crystals of compound **2** were cut to acicular crystals of suitable size and each sealed in a Lindemann capillary. Systematic absences from the precession photographs were consistent with the space group $Pbcn$ for **1** and $P2_1/c$ for **2**. The cell parameters of both crystals were determined by a least-squares refinement based on 15 automatically centered independent reflections in the range 18° < 2θ < 27°, **1** and 20° < 2θ < 29°, **2**. Intensities were measured at 22°C on a Nicolet P3 diffractometer with the use of graphite monochromatized MoKα radiation (λ = 0.71069 Å). Crystal data and other numbers related to data collection are summarized in Table 1. Corrections were made for Lorentz-polarization effects but not for absorption. This will introduce a maximum error in F_o of 0.8% for **1** and 0.5% for **2**.[2]

For **1** and **2** the phases were determined by direct methods using 124 reflections with $|E| > 1.6$, and 50 reflections with $|E| > 1.6$ for **1** and **2**, respectively, and 12 sets of starting phases for each. All non-hydrogen atoms were found in the subsequent E map. Hydrogen atoms were found from subsequent difference maps and the coordinates of all atoms (C and N with anisotropic temperature factors) were then refined by minimizing the function $\Sigma w(|F_o| - |F_c|)^2$ until the final maximum shift/error was <0.001 for **1** and 0.009 for **2**. The large difference in R and R_w in both structures is because we have used an $I > 0$ cut-off. Refinement based on reflections with $I > 3\delta(I)$ cut-off gave R = 0.048 and R_w = 0.028 for **1** and R = 0.046, R_w = 0.033 for **2**. Nevertheless, the inclusion of the greater number of reflections gives a more accurate structure (13). No corrections for secondary extinction were necessary for either crystal. Scattering curves were taken from Cromer and Waber (12). The atom parameters are listed in Tables 2 and 3.

Discussion[3]

We were able to prepare 1,1,3,3-tetracyanopropane, **1**, in rather poor yields from the methods in the literature (4, 7),

[2]All calculations were carried out on a CYBER 170/730 computer. The programs DATCO5, ABSORB, and DATDRN from the XRAY 76 program (8) were used for preliminary data treatment. The structure was solved with SHELX (9). Plane and dihedral angles were made with NRC 22 (10). Diagrams were prepared with the program ORTEP II (11).

[3]Complete set of data may be purchased from the Depository of Unpublished Data, CISTI, National Research Council of Canada, Ottawa, Ont., Canada K1A 0S2.

Can. J. Chem. Downloaded from www.nrcresearchpress.com by 80.58.250.72 on 09/07/12
For personal use only.

Can. J. Chem. Downloaded from www.nrcresearchpress.com by 80.58.250.72 on 09/07/12
For personal use only.

TABLE 2. Atomic position parameters and temperature factors ($Å^2$) for 1,1,3,3-tetracyanopropane (x, y, $z \times 10^4$ for C and N, $\times 10^3$ for H, U_{eq} or $U \times 10^3$ for all atoms)*

Atom	x	y	z	U_{eq}† or U
C(1)	5000	2802(3)	2500	31(2)
C(2)	3409(3)	3619(2)	1889(2)	32(1)
C(3)	2560(3)	4459(2)	2935(2)	38(1)
C(4)	1972(3)	2760(2)	1293(2)	39(2)
N(3)	1996(3)	5105(2)	3767(2)	61(2)
N(4)	912(3)	2076(2)	847(2)	60(2)
H(1)	446(3)	223(2)	326(2)	38(7)
H(2)	390(3)	418(2)	109(2)	45(7)

*C(1) lies on the a two-fold axis and thus x and z were not refined.
†$U_{eq} = (1/3)(U_{11} + U_{22} + U_{33})$.

TABLE 3. Atomic position parameters and temperature factors ($Å^2$) for 2,2,4,4,6-pentacyanocyclohexenamine (x, y, $z \times 10^4$ for C and N, $\times 10^3$ for H, and U_{eq} or $U \times 10^3$ for all atoms)

Atom	x	y	z	U_{eq} or U ($\times 10^3$)
C(1)	7451(2)	−140(4)	289(2)	23(1)
C(2)	8451(2)	251(4)	573(2)	22(1)
C(3)	8854(2)	2098(4)	206(2)	26(2)
C(4)	8027(2)	2980(4)	−991(2)	22(1)
C(5)	7001(2)	3260(4)	−877(2)	24(2)
C(6)	6595(2)	1257(4)	−582(2)	22(2)
C(7)	9203(2)	−1235(4)	1271(2)	29(2)
C(8)	8356(2)	5010(4)	−1198(2)	27(2)
C(9)	7882(2)	1684(4)	−2036(2)	25(2)
C(10)	5989(2)	47(4)	−1691(2)	28(2)
C(11)	5886(2)	1835(4)	−35(2)	27(2)
N(1)	7099(2)	−1774(4)	655(2)	40(2)
N(7)	9796(2)	−2453(4)	1770(2)	43(2)
N(8)	8596(2)	6600(4)	−1322(2)	41(2)
N(9)	7749(2)	735(4)	−2854(2)	38(2)
N(10)	5546(2)	−931(4)	−2504(2)	49(2)
N(11)	5355(2)	2295(4)	386(2)	44(2)
H(11)	754(2)	−261(4)	129(2)	60(10)
H(12)	648(2)	−208(4)	45(2)	60(10)
H(31)	905(2)	323(4)	85(2)	42(8)
H(32)	952(2)	168(4)	8(2)	43(7)
H(51)	645(2)	389(3)	−165(2)	34(7)
H(52)	712(2)	424(3)	−20(2)	35(7)

*$U_{eq} = (1/3)(U_{11} + U_{22} + U_{33} + 2\cos\beta U_{13})$.

and also cyclic 2,4,4,6,6-pentacyanocyclohexenamine, **2**, in considerable yield. In addition, we also obtained, as the major product at long reaction times, an unidentified orange material which is probably polymeric. The natures of **1** and **2** were demonstrated by a number of physical methods, and subsequently much better methods of preparation were devised. The reactions of these pure materials allowed us to formulate mechanisms of reactions and explain the low yields obtained by the literature methods.

The structures of the compounds **1** and **2** were established by X-ray crystallography. The X-ray structure of **1** is shown in Fig. 1 and the bond lengths and angles are given in Table 4. The molecule has a two-fold axis through the CH_2 (C(1)) group and the C_2 arrangement of the cyanide groups minimizes intramolecular steric repulsion. Bond lengths and angles agree well with those found in similar compounds (14–19). The structure of **2** is shown in Fig. 2 and bond lengths and angles are

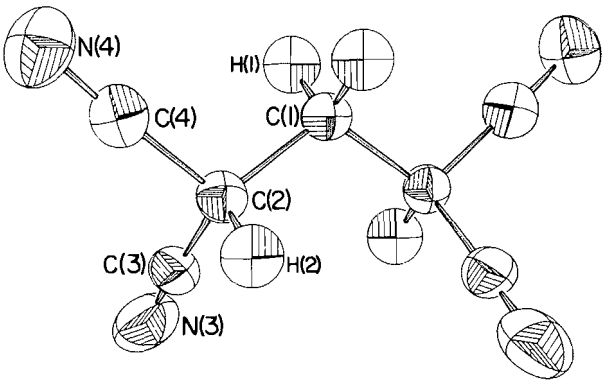

FIG. 1. 1,1,3,3-Tetracyanopropane showing the atom numbering.

TABLE 4. Selected interatomic distances (Å) and angles (deg) for 1,1,3,3-tetracyanopropane

Bond	Length	Bonds	Angle
C(1)—C(2)	1.546(3)	H(1)—C(1)—H(1a)	109(2)
C(3)—N(3)	1.132(3)	H(1a)—C(1)—C(2)	109(1)
C(2)—H(2)	1.04(2)	C(1)—C(2)—C(4)	108.8(2)
C(2)—C(3)	1.478(3)	C(3)—C(2)—C(4)	110.3(2)
C(4)—N(4)	1.132(3)	C(2)—C(1)—C(2a)	112.5(2)
C(2)—C(4)	1.486(3)	C(1)—C(2)—H(2)	111(1)
C(1)—H(1)	1.03(2)	H(2)—C(2)—C(3)	108(1)
		C(2)—C(3)—N(3)	176.6(3)
		H(1)—C(1)—C(2)	109(1)
		C(1)—C(2)—C(3)	111.7(2)
		H(2)—C(2)—C(4)	107(1)
		C(2)—C(4)—N(4)	117.9(3)

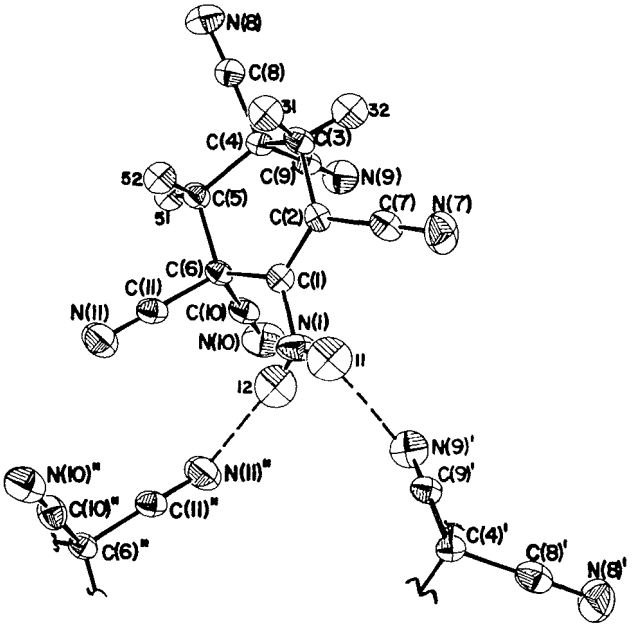

FIG. 2. 2,2,4,4,6-Pentacyanocyclohexenamine showing the atom numbering. The weak hydrogen bonds are shown by dotted lines. Primed atoms are related to those in Table 1 by the transformation $x, -\frac{1}{2} - y, \frac{1}{2} + z$ and double primed atoms by the transformation $1 - x, -y, -z$.

TABLE 5. Selected interatomic distances (Å) and angles (deg) for 2,2,4,4,6-pentacyanocyclohexanamine

Bond	Length	Bond	Length	Bond	Length
C(1)—C(2)	1.349(3)	C(2)—C(3)	1.504(3)	C(3)—C(4)	1.552(3)
C(4)—C(5)	1.550(3)	C(5)—C(6)	1.554(3)	C(1)—C(6)	1.542(3)
C(2)—C(7)	1.440(3)	C(4)—C(8)	1.484(3)	C(4)—C(9)	1.484(3)
C(6)—C(10)	1.495(3)	C(6)—C(11)	1.494(3)	C(1)—N(1)	1.354(3)
C(7)—N(7)	1.141(3)	C(8)—N(8)	1.139(3)	C(9)—N(9)	1.131(3)
C(10)—N(10)	1.128(3)	C(11)—N(11)	1.133(3)	N(1)—H(11)	0.94(3)
N(1)—H(12)	0.85(3)	C(3)—H(32)	1.07(2)	C(3)—H(31)	1.03(2)
C(5)—H(51)	1.03(2)	C(5)—H(52)	1.01(2)		

Bonds	Angle	Bonds	Angle
C(2)—C(1)—C(6)	120.3(2)	C(1)—C(6)—C(5)	114.1(2)
C(1)—C(2)—C(3)	125.7(2)	C(2)—C(3)—C(4)	110.8(2)
C(3)—C(4)—C(5)	109.1(2)	C(2)—C(1)—N(1)	125.3(2)
C(4)—C(5)—C(6)	112.7(2)	C(6)—C(1)—N(1)	114.3(2)
C(1)—C(2)—C(7)	117.6(2)	C(7)—C(2)—C(3)	116.7(2)
C(3)—C(4)—C(8)	109.5(2)	C(8)—C(4)—C(9)	108.2(2)
C(5)—C(4)—C(8)	107.0(2)	C(3)—C(4)—C(9)	111.5(2)
C(5)—C(6)—C(10)	112.0(2)	C(5)—C(4)—C(9)	111.3(2)
C(5)—C(6)—C(11)	106.5(2)	C(1)—C(6)—C(11)	109.6(2)
C(10)—C(6)—C(11)	107.9(2)	C(1)—C(6)—C(10)	106.7(2)
C(4)—C(8)—N(8)	177.1(3)	C(2)—C(7)—N(7)	176.4(3)
C(6)—C(10)—N(10)	117.4(3)	C(4)—C(9)—N(9)	117.9(3)
C(1)—N(1)—H(11)	122(2)	C(6)—C(11)—N(11)	179.1(3)
H(11)—N(1)—H(12)	110(2)	C(1)—N(1)—H(12)	127(2)
C(2)—C(3)—H(32)	107(1)	H(32)—C(3)—H(31)	109(2)
C(4)—C(3)—H(32)	112(1)	C(2)—C(3)—H(31)	109(1)
C(4)—C(5)—H(51)	111(1)	C(4)—C(3)—H(31)	108(1)
C(6)—C(5)—H(51)	110(1)	C(4)—C(5)—H(52)	108(1)
H(51)—C(5)—H(52)	107(2)	C(6)—C(5)—H(52)	108(1)

given in Table 5. It can be seen that the structure is that of the tautomer considered by Westfahl and Gresham to be least likely (6). Despite the unusual temperature factor on N(1) which might suggest a disorder between the two tautomers, there is no evidence in our work for the presence of the other tautomer. The olefinic bond causes the molecule to adopt a half-chair conformation with C(4) being the atom furthest out of the best plane. Bond lengths and angles are normal. There is considerable conjugation involving the amine and the olefin, but it is not as great as has been observed in similar structures (20–22). Thus, C(1)—N(1) (1.354(3) Å) is considerably shorter than 1.475 Å, which is typical for aliphatic C—N distances (23) but it is at the upper end of the range (1.30(1)–1.33(1) Å) observed in amine–olefin compounds (20–22). Conversely, C(1)—C(2), 1349(3) Å is marginally longer than a normal olefin distance, 1.337 Å (22) but not as long as similar distances (range 1.372(5)–1.390(5) Å) in other amine–olefin compounds (20–22). In addition, C(2)—C(3), 1.504(3) Å, and C(2)—C(7), 1.440(3) Å, are shorter than the other C—C ring (range 1.542(3)–1.554(3) Å) and C—C(cyanide) (range 1.484(3)–1.495(3) Å) distances. Surprisingly, considering this conjugation, the NH_2 group is twisted with respect to the N(1)C(1)C(2) framework (dihedral angle N(1)H(11)H(12)—N(1)—C(1)—C(2) 13(2)°). This is probably caused by intramolecular hydrogen bonding (see below).

The packing of **1** within the cell is unnoteworthy and all intermolecular distances are equal to or greater than van der Waals distances. Similarly, packing of **2** within the unit cell is primarily determined by van der Waals interactions, although there are two very weak intermolecular hydrogen bonds involving the amine group, (N(1)—H(11)...N(9), N(1)...N(9) 3.104(3) Å, H(11)...N(9) 2.28(3) Å, N(1)—H(11)...N(9) 145(1)°, N(1)—H(12)...N(11), N(1)...N(11) 3.207(3) Å, N(1)...H(12) 0.85 (3), H(12)...N(11) 2.37(3) Å, N(1)—H(12)...N(11) 168(1)°) (see Fig. 2).

The mass spectral data for **1** and **2** are given in Table 6. Since the mass spectra of **1** always showed a peak at $m/z = 222$, corresponding to the parent ion of **2**, the question arose as to whether this was caused by contamination of **1** with **2** or whether small amounts of **2** were formed by thermal decomposition on the inlet probe.

In early preparations of **1**, we knew from other experiments that there was contamination by **2**, but with improved preparative methods and examination of the samples by chromatography we are sure that in later samples there was no contamination. The $m/z = 222$ peak persisted, however, and thus we conclude that it is caused by thermal decomposition of **1** on the probe. We obtained evidence for this decomposition by obtaining spectra at different times after the sample was injected and the sample heated. At short times relatively reproducible spectra were obtained (see **1***a* and **1***b* in Table 6) but at longer times there are marked changes in the spectra. The decomposition is complex, since the extra peaks in addition to $m/z = 222$ clearly do not come from the decomposition of **2**; **2** had a reproducible mass spectrum.

Our principal evidence for the thermal decomposition formation of peak $m/z = 222$ in the mass spectrum of **1** is the low intensity of the peak $m/z = 62$ and the absence of peaks 58–61 in the spectrum of **1**. Peak $m/z = 62$ is a major peak in the decomposition of **2** and the other peaks also have considerable

Can. J. Chem. Downloaded from www.nrcresearchpress.com by 80.58.250.72 on 09/07/12
For personal use only.

TABLE 6. Mass spectra of 1,1,3,3-tetracyanopropane, **1**, and 2,2,4,4,6-pentacyanocyclohexenamine, **2**

	Intensity					Intensity			
m/z	**1***A*	**1***B*	**1***C*	**2**	*m/z*	**1***A*	**1***B*	**1***C*	**2**
224	—	—	—	1.0	106	—	—	—	0.3
223	2.0	1.8	11.4	11.1	105	1.6	1.4	15.9	5.1
222	13.7	10.0	20.3	59.3	104	1.3	1.4	12.4	4.4
221	—	—	—	0.4	103	1.1	1.8	18.7	5.8
197	1.0	1.4	—	1.3	102	—	—	10.7	2.4
196	—	—	—	1.6	101	0.6	—	16.2	2.9
195	—	—	—	0.6	100	—	—	16.5	1.3
194	—	—	—	1.6	95	—	—	—	0.4
177	1.3	—	—	—	94	—	—	—	0.4
170	—	—	—	1.4	93	1.0	—	—	2.2
169	—	1.1	13.3	3.8	92	4.8	5.4	28.9	15.2
168	1.0	0.7	12.7	3.5	91	2.9	2.8	22.2	8.6
167	—	—	—	1.4	90	1.6	2.3	21.9	5.8
157	—	—	—	0.7	89	3.2	3.2	29.2	10.2
156	—	—	—	0.6	88	1.4	2.1	23.5	6.3
155	—	—	—	1.0	87	—	—	14.0	1.9
154	—	—	—	0.3	86	—	—	8.3	0.9
149	3.5	—	—	—	80	1.1	1.1	13.3	—
146	—	—	—	2.0	79	15.2	18.9	57.1	3.2
145	8.9	10.4	29.8	44.4	78	15.2	5.7	22.2	58.4
144	100	100	100	100	77	8.3	6.4	33.0	48.9
143	1.3	1.3	12.1	—	76	2.4	2.8	29.8	33.0
142	1.0	1.4	16.5	5.4	75	1.3	2.1	23.5	8.6
141	0.6	1.1	17.1	3.2	74	—	—	9.2	4.3
140	—	—	12.4	1.6	73	—	—	—	1.0
133	—	—	—	0.3	68	—	—	8.9	—
132	1.0	1.1	13.3	4.4	67	3.5	6.4	29.2	—
131	2.5	2.1	14.6	7.0	66	39.4	48.5	79.3	—
130	0.6	1.1	12.1	2.9	65	4.4	5.4	36.8	0.4
129	—	—	—	0.6	64	5.7	6.4	33.7	1.0
128	—	—	8.9	1.3	63	2.9	3.9	32.3	15.2
127	—	—	—	1.1	62	0.8	2.1	21.6	100
126	—	—	8.6	0.4	61	—	—	8.9	17.1
125	—	—	—	0.3	60	—	—	—	18.4
120	—	1.1	—	0.6	59	—	—	—	9.8
119	2.9	10.0	17.1	7.0	58	—	—	—	5.8
118	1.0	1.4	11.4	5.1	57	—	—	—	1.0
117	2.9	3.6	20.3	14.6	55	—	—	7.6	—
116	1.7	1.4	14.6	5.1	54	2.2	3.2	26.6	—
115	1.7	2.1	20.3	7.0	53	7.0	10.7	45.1	—
114	—	—	11.1	2.0	52	13.3	21.4	73.0	—
113	—	—	10.8	1.6	51	13.3	8.2	38.1	—
112	—	—	—	0.2	50	1.6	—	—	—

intensity. If **1** were contaminated with **2** then peaks at the following values of *m/z* and intensity, in parentheses, should occur: 62 (22); 61 (3.7); 60 (4.0); 59 (2.1); 58 (1.3). None of these were observed, however.

The most important mass peaks are quite similar for the two compounds, differences being extra peaks at *m/z* = 119, 79, 66, and 52 for **1** and *m/z* = 168, 117, 104, 88, 62, and 60 for **2**. Masses 222 and 144 are the parent ions for **2** and **1** and the 168 peak is most likely formed by 4,6 cleavage of the hexenamine ring. Peaks at *m/z* = 131, 119, 117, and 92 are derived from **1** by the loss of CH, CN, with H transfer, HCN and 2CN, respectively. Peak *m/z* = 104 is derived from 131 by loss of HCN and 77 is similarly derived from 104. The fragment *m/z* = 66, $HC(CN)_2^+$ is derived from simple 1,2 cleavage of **1** giving the alternate fragment *m/z* = 79. Peaks *m/z* = 62, 60 corresponding to the fragments C_4N^+ and C_5^+ must be derived from the ring skeleton and *m/z* = 52 is either $(CN)_2^+$ or $(H_2C{=}CH{-}CN)^+$.

The infrared and Raman bands of malononitrile, 1,1,3,3-tetracyanopropane, and 2,4,4,6,6-pentacyanocyclohexenamine, are listed in Table 7. The assignments for the first two compounds are straightforward. The assignments for the last

Can. J. Chem. Downloaded from www.nrcresearchpress.com by 80.58.250.72 on 09/07/12
For personal use only.

TABLE 7. Vibrational spectra of cyano ligands, bands in cm^{-1}

Malononitrile	1,1,3,3-Tetracyanopropane		2,2,4,4,6-Pentacyanocyclohexenamine			
Infrared*	Infrared*	Raman†	Infrared*	Raman†	Infrared‡	Assignment§
			3440, 85	3435, w, br	[2575]	ν_a NH_2, ND_2, ρ = 1.34
					3392	ν NH
			3360, 93	3354, 8	[2460]	ν_s NH_2, ND_2, ρ = 1.37
			3290, w			2 × 1652
			3241, 59	3240, w, br	[2430]	ρ = 1.34, 2 × 1627
	3026, 61	3020, w				ν CH
			3010, 15	3002, w		
	2986, 57	2984, 20	2990, vw	2986, 12		ν_a CH_2
2960, vs			2970, 12	2966, 12		
2930, vs	2911, 78	2914, 58	2940, 7	2930, 15		ν_s CH_2
	2845, vw		2865, vw			
					2500, shp	ν ND
2285, w				2270, 34		
2265, vs	2260, 53	2263, 100	2262, 8	2257, 27	2260	ν C≡N
			2218, 48	2215, 55	2220	
			1652, 100	1653, 53	[1245]	δ NH_2, δ ND_2, ρ = 1.33
			1627, 67	1627, 40	1630, s	ν C=C
					1527	δ NH
					1465	δ CH_2
	1445, 82	1443, 12	1452, 46	1452, 5		
			1438, 21	1435, 10		
1390, vs			1382, 36		1382, s	δ NH
1378, vs	1369, 41, br		1369, 41			δ CH, ω CH_2
		1330, 12	1328, 21	1328, w	1328	
			1303, 25	1303, 8	1303	ring C—N
	1290, 51	1284, 12				δ CH
	1280, 65					
1230, vw	1242, 84		1242, 27		1242, s	ω NH_2
1210, vw			1218, 23			
	1180, 49	1180, 15				
			1155, vw	1155, ms	[862]	ρ = 1.34
			1135, 40	1120, w		τ CH_2
					1100	δ ND, ρ = 1.38, 1527
	1070, sh				1070	ρ = 1.34, 1465
	1056, 90	1058, 13				ν C_2—C_3
			1040, 12, br	1040, w	1030	ν C—C
			1016, 100			ν C_1—C_3
					1010	δ ND, ρ = 1.37, 1382
975, s				990, vw		
930, m, br	945, 61					ω CH_2
	920, 34, br					
					938	ν ND_2, ρ = 1.32, 1242
			906, 13	906, w		
885, s			880, 6	880, vw		
	840, 39	849, 29				
			830, w	831, w, br		r NH_2
	790, sh					r CH_2
	780, 44					
			740, 9, br			ω NH_2
725, vw	720, 25		718, 12	720, 12	700	r CH_2
700, vw				680, 9		
	658, w, br		658			358 + 310
	595, 15					
	568	575, 13	575, w	575, 11		δ CCC
578, m	58, db					scissor
	560	560, w				
			548, 32			
			520, 16	500, 8		
			500, 8			
	479, 50					
		461, 15				δ C—C≡N
	463, 47					in plane
			449, 26	450, 11		

Can. J. Chem. Downloaded from www.nrcresearchpress.com by 80.58.250.72 on 09/07/12
For personal use only.

TABLE 7. (*concluded*)

Malononitrile	1,1,3,3-Tetracyanopropane		2,2,4,4,6-Pentacyanocyclohexenamine			
Infrared*	Infrared*	Raman†	Infrared*	Raman†	Infrared‡	Assignment§
440, w			431, 45	431, 13	425	
			415, 45	420, w		
			375, 25			
360, s	363, 49	365, 32				δ C—C≡N out-of-plane
328, m			336, 38		315	
	316, 36	315, 17			305	
				266, w	278	
	214, 100	218, 10	214, vw			
		200, 17		205, 14		
			193, vw	190, 25		
			164, 81	156, 36		C—(CN_2) scissor
	143, 92	144, 58		142, 49		
		120, 63	123, 100	128, 88		C—(CN_2) scissor
				96, 100		
		75, 37		73, 60		
		60, 17				

*Infrared data, ν, I: 4000–450 cm^{-1}, intensity relative to strongest band = 100; 450 cm^{-1} and below, FTIR; intensity relative to 214 or 123 cm^{-1} band = 100. Abbreviations: s = strong, v = very, m = medium, w = weak, br = broad, shp = sharp, sh = shoulder, db = doublet, ρ is frequency ratio of normal to deuterated form.

†Raman data $\Delta\nu$, I: intensity relative to strongest band = 100.

‡Data from deuterated form (D_2O exchange).

§Assignments: ν = stretching frequency, a = antisymmetric, s = symmetric, δ = deformation, τ = twist, r = rock, ω = wag.

compound and its deuterated derivatives are discussed here. The NH_2 region was typical of most liquid aromatic amines, with two absorptions >3300 cm^{-1} and with a weaker band at 3250–3170 cm^{-1}. The relationship $\nu_s = 345.5 + 0.876\nu_a$ (24) holds exactly for the two observed NH_2 stretching bands, $\nu_a = 3440\,cm^{-1}$, $\nu_s = 3360\,cm^{-1}$. The slightly weaker band at 3240 cm^{-1} can be assigned as the overtone of the deformation which is intensified by Fermi resonance.

Primary amines with tertiary carbon atoms (C—NH_2) absorb weakly at 1038–1022 and more strongly at 1240–1170 cm^{-1} (24) (observed 1040 and 1242, 1218 cm^{-1}).

Nitriles are characterized by νC≡N at 2260–2240 cm^{-1} (24), which is lowered by conjugation to the ring system to 2235–2215 cm^{-1} (24). This vibration was observed at 2218 cm^{-1} for **2**. A nitrile group is reported to lower δCH_2 to 1425 cm^{-1} (24). The lowering is not so great in **2** where two bands are observed at 1452 and 1438 cm^{-1} and no lowering is observed in the deuterated compound. The CH_2 wag (a similar motion to $\delta_s CH_3$) occurs at 1328 cm^{-1}.

The calculated shifts on deuteration are 1.333 for ND_2/NH_2, 1.369 for ND/NH, and 1.372 for NHD/NH_2. It is apparent that the pentacyano compound subjected to D_2O exchange gave a mixture of —NHD and —ND_2, the former yielding new single bands νNH at 3392 cm^{-1}, νND at 2500 cm^{-1}, δNH at 1527 cm^{-1}, and δND at 1100 cm^{-1}.

The δNH_2 was observed at 1652 cm^{-1} (δND_2, 1245 cm^{-1}) and the νC=C observed at 1630 cm^{-1} was unshifted on deuteration. Our assignments are in the reverse order from those of Baldwin (δNH_2, 1631, 1650 cm^{-1}) (25). Our choices for these assignments, however, are in agreement with those for cyclohexenamine (26) and acrylonitrile (27) and are confirmed by the changes on deuteration. The lower frequency NH_2 bands (w, γ and τ) were less well-defined but followed the same general pattern of ND_2 shifts. In conclusion, the vibrational spectral results agree with the findings of the X-ray study, that compound **2** exists as the cyclohexenamine.

The results of the proton and carbon-13 nmr are given in Table 8. The ^1H nmr spectrum of a solution of 1,1,3,3-tetracyanopropane in DMSO-d_6 showed two triplets of equal intensities and a weak singlet. The minor peak at 4.44 ppm was ascribed to a small amount of the starting material, malononitrile, $CH_2(CN)_2$. The triplet centered at 2.96 ppm was assigned to the two H(1) hydrogens of the CH_2 group which were coupled to the two chemically equivalent H(2) hydrogen atoms. The triplet centered at 5.10 ppm was attributed to the two H(2) hydrogens.

The proton decoupled carbon 13-nmr of 1,1,3,3-tetracyanopropane exhibit singlets at 112.6 ppm, 28.2 ppm, and 20.5 ppm with relative intensities of 16:9:18 respectively. The peak at 112.6 ppm was assigned to the four CN carbons. The assignment of the remaining two peaks was confirmed with use of results of a "spin-sort" experiment (28).

The ^1H nmr spectrum of 2,2,4,4,6-pentacyanocyclohexenamine consisted of three singlets at 3.23 ppm, 3.66 ppm, and 7.68 ppm all of equal intensity. The peak at 7.68 ppm was assigned to the amine group, the peak at 3.66 ppm to the two hydrogen atoms on carbon 3, and that at 3.23 ppm to the two hydrogen atoms on carbon 5 (see Table 8).

The assignment of carbon-13 nmr spectrum is ambiguous with regard to some peaks. The singlet at 143.88 ppm was assigned to carbon C1 being adjacent to the electron-withdrawing nitrogen. The signal at 69.9 ppm was assigned to carbon C2. The high field position of this signal arises from the back donation of electron density from the nitrogen atom into the π-system of the alkene. From the intensities of the peaks at 117.3, 113.52, and 112.07 ppm these are assigned to the CN groups, with the first being assigned to the C-2 CN. It was not possible to distinguish between the remaining C-4 and C-6 groups. The assignments of C(3) and C(5) were confirmed by selective proton irradiation experiments.

The overall reaction and mechanism for the formation of the tetracyanopropane **1** are shown in Scheme 1. The initial process

Can. J. Chem. Downloaded from www.nrcresearchpress.com by 80.58.250.72 on 09/07/12
For personal use only.

TABLE 8. Nuclear magnetic resonance results

^{1}H spectra[a]				^{13}C spectra[a]			
Chemical shift (ppm)	Multiplicity	Relative intensity	Assignment	Chemical shift (ppm)	Multiplicity	Relative intensity[b]	Assignment
Compound **1**							
2.96	Triplet[e]	1	H(1)	20.5	Doublet	18	C(2)
*4.44	Singlet	—	Malononitrile	28.2	Triplet	9	C(1)
5.10	Triplet[e]	1	H(2)	112.6		16	C(3), C(4)
Compound **2**							
3.23	Singlet	1	H(51), H(52)	28.1	Triplet	1.5	C(4)[c]
3.66	Singlet	1	H(31), H(32)	31.1		1.5	C(5)
7.68	Singlet	1	H(11), H(12)	32.0		1.5	C(6)[c]
				34.5	Triplet	1.7	C(3)
				69.9		1.3	C(2)
				112.1		1.7	C(8),[d] C(9)[d]
				113.5		1.9	C(10),[d] C(11)
				117.3		0.9	C(7)
				143.9		1.3	C(1)

[a]Samples ran in DMSO with TMS reference.
[b]Pulse angles of approximately 15° were used to enable relative intensities to be used.
[c]Assignments may be interchanged.
[d]Assignments may be interchanged.
[e]$J_{1,2}$ = 7.4 Hz.

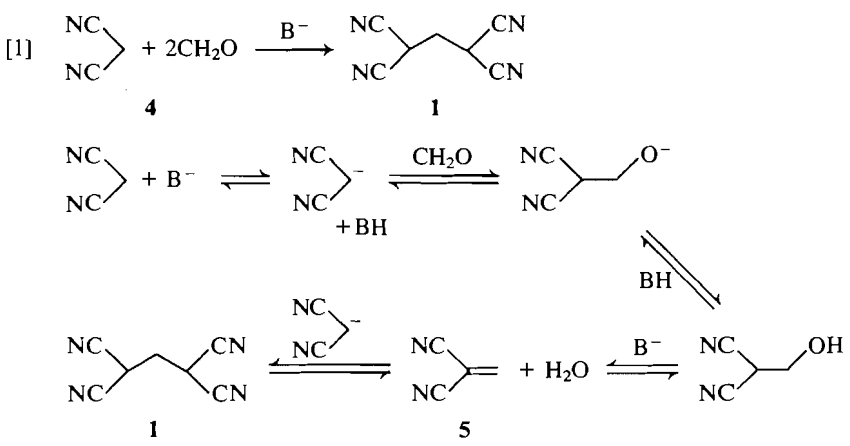

SCHEME 1

is a normal aldol condensation between the malononitrile anion and formaldehyde leading to the 1,1-dicyanoethylene, **5**. This intermediate then undergoes conjugate addition and protonation with another malononitrile anion. It should be noted that compound **1** is a kinetic product, its formation in good yield being governed by its rapid crystallization from the reaction medium. The continued exposure of **1** to base results in its transformation into either polymer or the mono-cyclic product **2** as the thermodynamic products (*vide infra*).

The overall reaction and suggested mechanism for the transformation of compound **1** into the pentacyanocyclohexenamine **2** are shown in Scheme 2. Traces of base in water (or other alcohol solvents) are sufficient to generate the anion of **1** and set up the reverse conjugate addition equilibrium between **1** and **5** and malononitrile anion as shown in Scheme 1. The anion of **1** can now add to 1,1-dicyanoethylene, **5**, to give an intermediate anion **6** which can either undergo further conjugate additions (giving polymer) or carry out an intramolecular aldol condensation which upon protonation and tautomerization leads to the vinylogous amino-nitrile **2**. The driving force which displaces the equilibria to **2** is the ease of formation of the six-membered ring and the stability of the vinylogous amino-nitrile system.

As noted above, the original preparation (7) will only give the desired product in good yields if the product crystallizes from solution and stops further reaction. If this does not occur then either the cyclic product or the polymer is formed.

The results of our ultraviolet–visible spectroscopic studies are assembled in Table 9. The malononitrile solution instability illustrated by the variations in peak intensities and peak positions was first documented by Mendelson *et al.* (29). We have also observed a similar dynamic nature in the uv spectra of the tetracyanopropane solutions. The instability was suspected given the ease of formation of the cyclic compound, **2** from the tetracyanide. As can be seen, the low ϵ values of the transitions for both malononitrile and tetracyanopropane represent $n \rightarrow \pi^*$ spin forbidden transitions. The spectra of the 2,4,4,6,6-pentacyanocyclohexenamine exhibited two intense transitions at 260 nm and 288 nm. The peak at 260 nm agrees well with a π–π^* transition reported for 2-cyanocyclohexenamine (26). Williams had previously reported a peak at 271 nm for this

Can. J. Chem. Downloaded from www.nrcresearchpress.com by 80.58.250.72 on 09/07/12
For personal use only.

TABLE 9. Ultraviolet and visible spectroscopy results[a]

Compound	λ (cm^{-1})[b]	A	ε (M^{-1} cm^{-1})
Malononitrile	238	0.86	3
	264(sh)	0.38	1
	288(br)	0.27	1
	356(w)	0.27	1
	440(br)	0.20	1
1,1,3,3-Tetracyanopropane	242	0.15	30
	254	0.14	50
(24 h later)	246	0.40	60
	276	0.04	6
	292	0.07	10
	348	0.07	10
2,4,4,6,6-Pentacyanocyclohexenamine	260	0.23	10 000
	288	0.08	4 000
(ref. 30)[c]	271		12 500
Cyanocyclohexenamine (ref. 26)[c]	262		11 000

[a]Unless otherwise stated the solvent was THF.
[b]Cell path length = 1 cm, sh shoulder, br broad, w weak.
[c]Solvent was ethanol, reference.

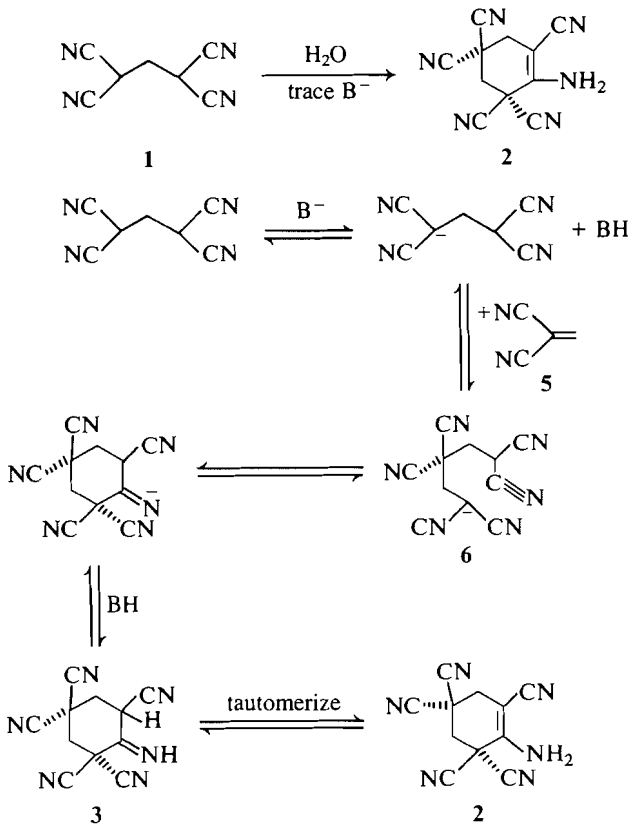

SCHEME 2

compound (30). This deviation from our value can be explained by a bathochromic shift to 271 nm caused by the more polar solvent ethanol.

Acknowledgements

We thank Romolo Faggiani for assistance in acquiring the X-ray data, Brian Sayer for assistance in acquiring the nmr data, and F. A. Ramelan for obtaining the mass spectra. Financial support for this work was given by Natural Sciences and Engineering Research Council of Canada, the National Cancer Institute of Canada, and the McMaster University Science and Engineering Research Board.

1. B. N. STORHOFF and H. C. LEWIS. Coord. Chem. Rev. **23**, 1 (1977).
2. F. A. COTTON and G. WILKINSON. Advanced inorganic chemistry. Interscience Publishers, Toronto. 1972. pp. 721–723.
3. F. D. ROCHON, R. MELANSON, H. E. HOWARD-LOCK, C. J. L. LOCK, and G. TURNER. Can. J. Chem. **62**, 860 (1984).
4. O. DIELS, H. GARTNER, and R. KAACK. Berichte, **55B**, 3949 (1922).
5. O. DIELS and B. CONN. Berichte, **56B**, 2076 (1923).
6. J. C. WESTFAHL and T. L. GRESHAM. J. Org. Chem. **21**, 319 (1956).
7. N. M. RYBKINA, A. A. BYLINKINA, and G. I. MIKHAILOV. Metody Poluch. Khim. Reaktivov Prep. (1969), No. 18, 180 (Russ.).
8. J. M. STEWART. The Xray 76 System Tech. Rept. TR-446, Computer Science Center, University of Maryland, College Park, Maryland (1976).
9. G. M. SHELDRICK. Shelx, Program for crystal structure determination. University of Cambridge, England. 1976.
10. M. E. PIPPY and F. A. AHMED. NRC-22. Mean plane and torsional angles. National Research Council of Canada, Ottawa, Canada. 1978.
11. C. K. JOHNSON. ORTEP-II. Report ORNL-5138, Oak Ridge National Laboratory, TN. 1976.
12. D. T. CROMER and J. T. WABER. International tables for X-ray crystallography. Vol. IV. *Edited by* J. A. Ibers and W. C. Hamilton. Kynoch Press, Birmingham, England. 1974. Table 2.2B. pp. 99–101.
13. P. SEILER, W. B. SCHWEIZER, and J. D. DUNITZ. Acta Crystallogr. B**40**, 319 (1984).
14. M. T. DOVE and A. I. M. RAE. Faraday Discuss. Chem. Soc. **69**, 98 (1980).
15. L. E. ALEXANDER, R. ENGMANN, and H. G. CLARK. J. Phys. Chem. **70**, 252 (1966).
16. M. J. KORNBLAU and R. E. HUGHES. Acta Crystallogr. **17**, 1033 (1964).
17. C. PICCINI-LEOPARDI, B. TINART, J. P. DECLERCQ, and G. GERMAIN. Bull. Soc. Chim. Belg. **92**, 311 (1983).

Can. J. Chem. Downloaded from www.nrcresearchpress.com by 80.58.250.72 on 09/07/12
For personal use only.

18. N. C. BAENZIGER, S. WAWZONEK, and D. C. SWENSON. Acta Crystallogr. B**35**, 2793 (1979).
19. H. C. GARDNER and J. K. KOCHI. J. Am. Chem. Soc. **98**, 558 (1976).
20. V. G. ANDRIANOV, Y. T. STRUCHKOV, and K. K. BABIEVSKY. Cryst. Struct. Commun. **11**, 35 (1982).
21. P. B. SARKAR and S. P. SEN GUPTA. Cryst. Struct. Commun. **10**, 1133 (1981).
22. G. D. FALLON, B. M. GATEHOUSE, A. PRING, I. D. RAE, and J. A. WEIGOLD. Can. J. Chem. **58**, 1821 (1980).
23. D. T. CROMER and J. T. WABER. International tables for X-ray crystallography. Vol. III. *Edited by* J. A. Ibers and W. C. Hamilton. Kynoch Press, Birmingham, England. 1974. (*a*) Table 4.2.4, (*b*) Table 4.2.2.
24. N. B. COLTHUP, L. H. DALY, and S. E. WIBERLEY. Introduction to infrared and Raman spectroscopy. Academic Press, New York. 1961. pp. 278–290.
25. S. BALDWIN. J. Org. Chem. **26**, 3288 (1961).
26. S. S. KULP. Can. J. Chem. **45**, 1981 (1967).
27. F. HALVERSON, R. F. STAMM, and J. J. WHALEN. J. Chem. Phys. **16**, 808 (1948).
28. M. R. BENDALL, D. M. DODDRELL, and D. T. PEGG. J. Am. Chem. Soc. **103**, 4603 (1981).
29. J. MENDELSON, J. H. MENDELSON, B. J. BAX, and R. G. GRENELL. Science, **120**, 266 (1954).
30. J. K. WILLIAMS. J. Org. Chem. **28**, 1054 (1963).

Can. J. Chem. Downloaded from www.nrcresearchpress.com by 80.58.250.72 on 09/07/12
For personal use only.

Structure and conformation of 2′,5′-anhydroarabinosylcytosine: X-ray, ^{1}H nmr and ^{13}C nmr analyses[1]

GEORGE I. BIRNBAUM
Division of Biological Sciences, National Research Council of Canada, Ottawa, Ont., Canada K1A 0R6

AND

MILOŠ BUDĚŠÍNSKÝ AND JIŘÍ BERÁNEK
Institute of Organic Chemistry and Biochemistry, Czechoslovak Academy of Sciences, Fleming Sq. 2, 16610 Prague 6, Czechoslovakia

Received June 18, 1986

GEORGE I. BIRNBAUM, MILOŠ BUDĚŠÍNSKÝ, and JIŘÍ BERÁNEK. Can. J. Chem. **65**, 271 (1987).

Crystals of 2′,5′-anhydroarabinosylcytosine hemihydrate belong to the monoclinic space group $P2_1$. The cell dimensions are a = 9.643(2), b = 10.328(1), c = 10.544(2) Å, β = 94.55(1)°. X-ray intensity data were measured on a diffractometer and the structure was determined by direct methods. Least-squares refinement, which included all nucleoside hydrogen atoms, converged at R = 0.041 for 2298 observed reflections. The asymmetric unit contains two molecules of the nucleoside and one molecule of water. In both nucleoside molecules, the conformation about the glycosyl bond is *anti*, with χ_{CN} values of 15.5(3) and 26.3(3)°, respectively. In the bicyclic sugar moiety, the arabinofuranose rings adopt a C(3′)*exo*/C(2′)*endo* conformation and are highly puckered (τ_m = 57°). The solution conformation was studied by ^{1}H and ^{13}C nmr spectroscopy. A difference nOe proton nmr spectrum and ^3J(C,H) coupling constants reveal an *anti* conformation in solution, with torsion angles very similar to those obtained from X-ray analysis. A comparison of observed ^3J(H,H) coupling constants with those calculated on the basis of a modified Karplus equation shows significant differences, probably due to the presence of the bicyclic system.

GEORGE I. BIRNBAUM, MILOŠ BUDĚŠÍNSKÝ et JIŘÍ BERÁNEK. Can. J. Chem. **65**, 271 (1987).

Les cristaux de l'hémihydrate de l'anhydro-2′,5′ arabinosylcytosine cristallisent dans le groupe d'espace monoclinique $P2_1$, avec a = 9,643(2), b = 10,328(1) et c = 10,544(2) Å et β = 94,55(1)°. On a mesuré les intensités de rayons-X à l'aide d'un diffractomètre et on a déterminé la structure par des méthodes directes. L'affinement par la méthode des moindres carrés, qui comporte tous les atomes d'hydrogène du nucléoside, converge à R = 0,041 pour 2298 réflexions observées. L'unité asymétrique contient deux molécules de nucleoside et une molécule d'eau. Dans chacune des molécules de nucléoside, la conformation autour de la liaison glycosyle est *anti* avec des valeurs de χ_{CN} qui sont respectivement de 15,5(3) et 26,3(3)°. Dans la portion du sucre, les cycles arabinofurannose adoptent une conformation C(3′)*exo*/C(2′)*endo* et ils sont fortement repliés (τ_m = 57°). On a étudié la conformation en solution à l'aide de la rmn du ^{1}H et du ^{13}C. En se basant sur un spectre rmn du proton en différentiel d'effet Overhauser nucléaire et sur les constantes de couplage ^3J(C,H), on peut en déduire que, en solution, la conformation est *anti* et que les angles de torsion sont très semblables à ceux observés par diffraction des rayons-X. Une comparaison des constantes de couplage ^3J(H,H) observées avec celles calculées en se basant sur une équation de Karplus modifiée présente des différences notables qui sont probablement dues à la présence du système bicyclique.

[Traduit par la revue]

Introduction

In order to study structure–activity relationships (1–5), various derivatives of deoxynucleosides were recently synthesized, in particular those incorporating the cancerostatic agents 5-fluorouracil (1, 6) and arabinosylcytosine (2, 7). Attention was focussed on 5′-deoxy derivatives which are unable to form 5′-phosphate esters, the proposed active forms of both agents (8–10). In the 5-fluorouracil series, 5′-chloro-5-fluorouridine (6) and 5′-deoxy-5-fluorouridine (6) were later found to possess promising biological activities (11–13).

In the arabinosylcytosine series, 5′-chloroarabinosylcytosine (7) is a selective, very strong inhibitor of nucleic acid synthesis in L1210 cells (3). Both in alkaline medium and in a biological system, in a study with cytidine deaminase (14), the 5′-halogeno (chloro or bromo) derivatives of arabinosylcytosine as well as 5′-chloro-2,2′-cyclocytidine are converted to 2′,5′-anhydroarabinosylcytosine (15). The latter has an inhibitory effect against growth of L1210 cells which is comparable to that of 5′-bromoarabinosylcytosine, but lower than that of 5′-chloroarabinosylcytosine (2); however, it has a higher resistance to deaminase (14). One of the possible mechanisms of action of 5′-chloroarabinosylcytosine we envisage involves its conversion to 2′,5′-anhydroarabinosylcytosine. Consequently, it appeared worthwhile to determine the detailed conformation of the latter compound in the solid state and in solution.

[1]NRC No. 26555.

Experimental

Colorless prismatic crystals of 2′,5′-anhydroarabinosylcytosine hemihydrate were grown from water. X-ray precession photographs indicated space group $P2_1$. A crystal fragment measuring 0.45 × 0.55 × 0.65 mm was mounted on an Enraf-Nonius CAD-4 diffractometer; it provided the following data:

$C_9H_{11}N_3O_4.\frac{1}{2}H_2O$ fw = 234.21

Monoclinic, a = 9.643(2), b = 10.328(1), c = 10.544(2) Å, β = 94.55(1)°, V = 1046.80 Å^3, ρ_c = 1.49 g cm^{-3}, Z = 4 (20°C; CuKα$_1$, λ = 1.54056 Å); F(000) = 492, μ(CuKα) = 9.87 cm^{-1}.

The cell dimensions were determined from angular settings of 23 high-order (2θ > 107°) reflections. Intensities were measured with Ni-filtered CuKα radiation, using ω/2θ scans with variable scan ranges and speeds. Three standard reflections were monitored at frequent intervals; their intensities fluctuated by ± 1%. There were 2316 unique reflections accessible to the diffractometer (2θ ≤ 152°), of which two with $I \leq 3\sigma(I)$ were considered unobserved. The intensities were corrected for Lorentz and polarization factors; absorption corrections were considered unnecessary.

The structure was determined by direct methods with the aid of the computer program MULTAN78 (16). Of the 16 starting sets subjected to tangent refinement, the solution with the highest combined figure of merit yielded an E map on which all atoms of the two independent

Can. J. Chem. Downloaded from www.nrcresearchpress.com by 80.58.250.72 on 09/07/12
For personal use only.

Can. J. Chem. Downloaded from www.nrcresearchpress.com by 80.58.250.72 on 09/07/12
For personal use only.

TABLE 1. Final atomic coordinates and temperature parameters[a]

Atom	x/a	y/b	z/c	U_{eq}
N(1A)	4067(2)	6819	3681(2)	273
C(2A)	3435(2)	5680(2)	4001(2)	286
O(2A)	3081(2)	4897(2)	3129(2)	422
N(3A)	3201(2)	5431(2)	5215(2)	305
C(4A)	3518(2)	6328(2)	6102(2)	291
N(4A)	3169(2)	6079(2)	7276(2)	390
C(5A)	4198(2)	7507(2)	5821(2)	340
C(6A)	4454(2)	7714(2)	4596(2)	307
C(1'A)	4301(2)	7038(2)	2321(2)	308
C(2'A)	2998(2)	7522(3)	1537(2)	410
O(2'A)	2469(2)	8621(3)	2167(2)	537
C(3'A)	3666(3)	8127(3)	413(2)	417
O(3'A)	4371(3)	7232(2)	−306(2)	521
C(4'A)	4573(3)	8987(2)	1313(2)	357
O(4'A)	5259(2)	8064(2)	2192(1)	318
C(5'A)	3460(4)	9654(3)	2019(3)	520
N(1B)	9394(2)	7075(2)	2517(1)	259
C(2B)	9102(2)	8054(2)	1626(2)	258
O(2B)	8779(2)	9143(2)	2006(1)	348
N(3B)	9185(2)	7793(2)	375(2)	290
C(4B)	9586(2)	6617(2)	15(2)	276
N(4B)	9760(3)	6434(2)	−1216(2)	408
C(5B)	9827(2)	5586(2)	897(2)	321
C(6B)	9724(2)	5861(2)	2134(2)	305
C(1'B)	9324(2)	7398(2)	3865(2)	252
C(2'B)	7891(2)	7170(2)	4347(2)	292
O(2'B)	7464(2)	5874(2)	4020(2)	405
C(3'B)	8302(2)	7063(2)	5782(2)	301
O(3'B)	8939(2)	8148(2)	6378(1)	337
C(4'B)	9334(3)	5983(2)	5540(2)	330
O(4'B)	10200(2)	6558(2)	4636(1)	314
C(5'B)	8368(3)	5030(2)	4842(2)	420
O(W)	3397(2)	3407(4)	1034(3)	856

[a]All values were multiplied by 10^4.

nucleoside molecules were located. The oxygen atom of the water molecule was found on a subsequent difference Fourier map. Other such maps, calculated at later stages, revealed the positions of all hydrogen atoms except one belonging to the water molecule. All atomic parameters were refined by block-diagonal least squares with anisotropic and isotropic temperature parameters for nonhydrogen and hydrogen atoms, respectively. The scattering factors were taken from the "International tables for X-ray crystallography" (17) and the oxygen curve was corrected for anomalous dispersion (17). Throughout the refinement the function $\Sigma w(|F_o| - |F_c|)^2$ was minimized and a factor of 0.8 applied to all shifts. The following weighting scheme was used during the final stages: $w = w_1 \cdot w_2$, where $w_1 = 1$ for $|F_o| \leq 4$, $w_1 = 4/|F_o|$ for $|F_o| > 4$; and $w_2 = \sin^2\theta/0.9$ for $\sin^2\theta < 0.9$, $w_2 = 1$ for $\sin^2\theta \geq 0.9$. This scheme made the average value of $w(\Delta F^2)$ independent of $|F_o|$ and $\sin^2\theta$. The refinement converged to a conventional residual index $R = 0.041$ and a weighted index $R' = 0.051$ for 2298 observed reflections (sixteen strong low-order reflections suffered from secondary extinction and were given zero weights). A final difference Fourier map showed no significant features. The coordinates of nonhydrogen atoms are listed in Table 1. Anisotropic temperature parameters, hydrogen atom parameters, and a list of observed and calculated structure factors are available.[2] A stereoscopic view of one of the molecules is shown in Fig. 1.

^{1}H and ^{13}C nmr spectra were measured at 30°C on a Varian XL-200 FT-NMR spectrometer at frequencies of 200 MHz and 50.3 MHz, respectively. For the ^{1}H nmr measurements, solutions were made up by dissolving ca. 5 mg in 0.4 mL of DMSO-d_6, CD_3OD, CD_3OD + pyridine-d_5 (2:1), and D_2O. Selective decoupling of H(1') was used for the determination of its coupling constants with other protons. The difference nOe spectrum in CD_3OD was obtained as difference of two spectra, with the irradiation frequency placed on the signal of H(5') and H(5") and the decoupler "on" or "off" during 5.3 s before data acquisition. The nOe enhancement values were determined by a comparison with the intensity of the signal for H(5') and H(5") (200%) in the difference spectrum. ^{13}C chemical shifts and the number of directly bonded protons were obtained from the "attached proton test" ^{13}C nmr spectrum (18) in DMSO-d_6. Signals were referenced to DMSO-d_6 and recalculated to the δ-scale using $\delta_{DMSO} = 39.7$. Coupling constants J(C,H) were extracted from the proton-coupled ^{13}C nmr spectrum with nOe enhancement.

[2]These tables may be purchased from the Depository of Unpublished Data, CISTI, National Research Council of Canada, Ottawa, Ont., Canada K1A 0S2.

Results and discussion

Pyrimidine moiety

Most bond lengths and bond angles in the cytosine residues (Tables 2 and 3) agree with previously observed values (19); only the N(1)—C(2)—N(3) angle in molecule A is slightly larger than normal. The difference between this angle and the corresponding one in molecule B is significant and so are the differences between the N(1)—C(2) and N(1)—C(1') bond lengths in the two molecules. These differences may reflect variations in electron delocalization. We note that the sums of the N(1)—C(2) and N(1)—C(1') bond lengths are equal in the two molecules, but the deviations of the six ring atoms from the mean plane are larger in molecule B than in molecule A.

Glycosyl linkage

In pyrimidine arabinonucleosides the glycosyl torsion angles have been found to have values of 30 ± 7° (20). In the present structure this torsion angle is restricted by intramolecular steric interactions to a narrow range of smaller values. On the one hand, it is desirable to avoid the total eclipsing of N(1)—C(6) and C(1')—O(4') bonds; on the other hand, the distance between H(6) and one of the hydrogen atoms attached to C(5') becomes unacceptably short with increasing χ_{CN}. In molecule A, with $\chi_{CN} = 15.5(3)°$, this nonbonded H···H distance is 2.22 Å (after normalizing the C—H distances to 1.09 Å), while in molecule B, with $\chi_{CN} = 26.3(3)°$, the H(6)···H(5') distance (2.00 Å) is extremely short.

Arabinosyl moiety

To the best of our knowledge, this is the first X-ray analysis of a 2',5'-anhydroarabinonucleoside. It is therefore of interest to compare the geometry of this moiety to that of normal nucleosides. The bridging of O(2') and C(5') imposes a C(3') *exo* pucker on the furanose ring. The phase angles of pseudorotation (P) are 193.9 and 195.0° for molecules A and B, respectively. These values are just outside the usual range. The [2,2,1]-bicyclic system makes the arabinofuranose ring much more puckered than normal: the maximum amplitudes of puckering (τ_m) are 57.5 and 57.1° in the two molecules rather than the usual value of ~39°. The similarities of P and τ_m in molecules A and B, as well as of the torsion angles shown in Figs. 2 and 3, reflect the rigidity of the bicyclic system.

The strain present in this portion of the molecule is made evident by the distortion of some bond angles. In particular, the C(2')—C(3')—C(4') and C(3')—C(4')—C(5') angles are at least 10° smaller than normal. The O(2')—C(5') bond is significantly longer (weaker) than O(2')—C(2'), particularly in molecule B. The apparent difference between the two molecules is very likely attributable to the significantly larger vibrational parameters of C(2'), O(2'), and C(5') in molecule A. An

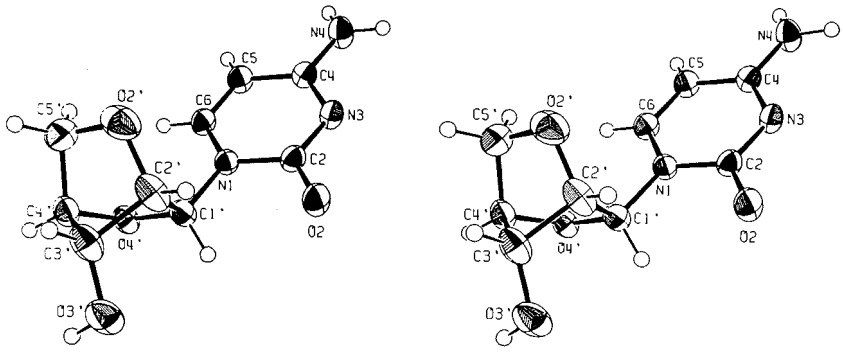

FIG. 1. Stereoscopic view of molecule A of 2′,5′-anhydroarabinosylcytosine. The ellipsoids correspond to 50% probability.

TABLE 2. Bond lengths (in Å)[a]

Bond	Length	
	Molecule A	Molecule B
N(1)—C(2)	1.379	1.394
N(1)—C(6)	1.367	1.362
N(1)—C(1′)	1.486	1.467
C(2)—O(2)	1.251	1.242
C(2)—N(3)	1.342	1.355
N(3)—C(4)	1.334	1.338
C(4)—N(4)	1.334	1.336
C(4)—C(5)	1.425	1.420
C(5)—C(6)	1.351	1.346
C(1′)—C(2′)	1.532	1.528
C(1′)—O(4′)	1.419	1.420
C(2′)—O(2′)	1.430	1.435
C(2′)—C(3′)	1.527	1.538
O(2′)—C(5′)	1.449	1.466
C(3′)—O(3′)	1.405	1.403
C(3′)—C(4′)	1.524	1.529
C(4′)—O(4′)	1.453	1.445
C(4′)—C(5′)	1.519	1.506

[a]The esd's are 0.002–0.004 Å.

TABLE 3. Bond angles (in deg)[a]

Angle	Molecule A	Molecule B
C(2)—N(1)—C(6)	120.4	120.5
C(2)—N(1)—C(1′)	118.0	117.7
C(6)—N(1)—C(1′)	121.6	121.8
N(1)—C(2)—O(2)	118.1	118.9
N(1)—C(2)—N(3)	120.5	119.2
O(2)—C(2)—N(3)	121.4	122.0
C(2)—N(3)—C(4)	119.3	119.8
N(3)—C(4)—N(4)	117.1	117.7
N(3)—C(4)—C(5)	122.1	122.0
N(4)—C(4)—C(5)	120.8	120.2
C(4)—C(5)—C(6)	117.1	117.1
N(1)—C(6)—C(5)	120.5	121.2
N(1)—C(1′)—C(2′)	112.9	113.5
N(1)—C(1′)—O(4′)	110.8	110.1
O(4′)—C(1′)—C(2′)	102.6	103.2
C(1′)—C(2′)—O(2′)	108.4	108.3
C(1′)—C(2′)—C(3′)	100.0	99.7
O(2′)—C(2′)—C(3′)	102.9	102.5
C(2′)—O(2′)—C(5′)	105.8	105.4
C(2′)—C(3′)—O(3′)	113.7	116.9
C(2′)—C(3′)—C(4′)	90.7	90.5
O(3′)—C(3′)—C(4′)	116.2	113.0
C(3′)—C(4′)—O(4′)	103.0	103.2
C(3′)—C(4′)—C(5′)	100.2	99.9
O(4′)—C(4′)—C(5′)	106.8	108.3
C(1′)—O(4′)—C(4′)	106.5	106.3
O(2′)—C(5′)—C(4′)	102.5	102.5

[a]The esd's are 0.2°.

additional indication of the strain is the C(2′)···C(4′) nonbonded distance (2.174(3) Å), shortened by ~0.2 Å from normal (20).

Hydrogen bonding and packing

Three protons in each nucleoside molecule and two in the water molecule are capable of participating in hydrogen bonding and all of them are involved in intermolecular hydrogen bonds. The network can be represented schematically as follows:

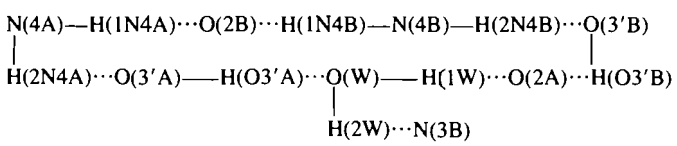

The geometrical details of these hydrogen bonds are given in Table 4. As commonly observed in X-ray analyses, the N—H and O—H bonds appear shorter than their real length. By extending these covalent bond lengths to their nominal values of 1.04 and 0.97 Å, respectively, one obtains corrected H···*A* distances which reflect more accurately the strengths of these hydrogen bonds. The strongest bonds are seen to be those in which the proton donor also acts as an acceptor, a phenomenon

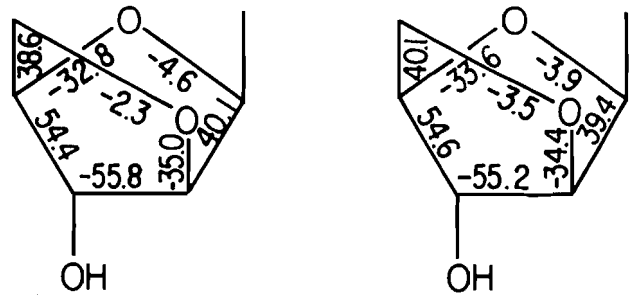

FIG. 2. Endocyclic torsion angles in the sugar moieties of molecules A (left) and B (right).

Can. J. Chem. Downloaded from www.nrcresearchpress.com by 80.58.250.72 on 09/07/12
For personal use only.

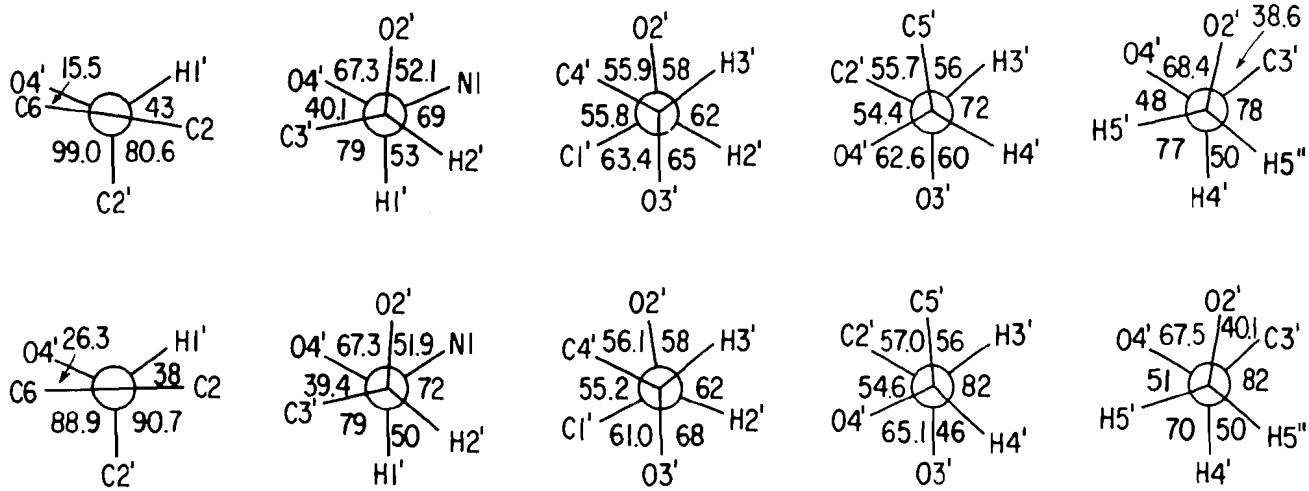

FIG. 3. Newman projections along (left to right) N(1)—C(1'), C(1')—C(2'), C(2')—C(3'), C(3')—C(4'), and C(4')—C(5') in molecules A (top) and B (bottom).

TABLE 4. Distances and angles for hydrogen bonds[a]

			Distances, Å			Angles, deg
D	*A*	*A* at	*D*···*A*	H···*A*	H···A_{corr}	*D*—H···*A*
N(4A)—H(1N4A)···O(2B)	$-1-x, -\frac{1}{2}+y, 1-z$	2.886	2.00	1.88	162
N(4A)—H(2N4A)···O(3'A)	$x, y, 1+z$	2.965	2.09	1.95	167
O(3'A)—H(O3'A)···O(W)	$-1-x, \frac{1}{2}+y, \bar{z}$	2.637	1.70	1.67	177
N(4B)—H(1N4B)···O(2B)	$\bar{x}, -\frac{1}{2}+y, \bar{z}$	2.909	2.04	1.89	168
N(4B)—H(2N4B)···O(3'B)	$x, y, -1+z$	3.143	2.28	2.14	163
O(3'B)—H(O3'B)···O(2A)	$-1-x, \frac{1}{2}+y, 1-z$	2.736	1.86	1.77	179
O(W)—H(1W)···O(2A)	x, y, z	2.729	1.82	1.76	174
O(W)—H(2W)···N(3B)	$-1-x, -\frac{1}{2}+y, \bar{z}$	2.868			

[a]The esd's are 0.003–0.005 Å, 0.04–0.05 Å, and 3–5° for *D*···*A*, H···*A*, and *D*—H···*A*, respectively.

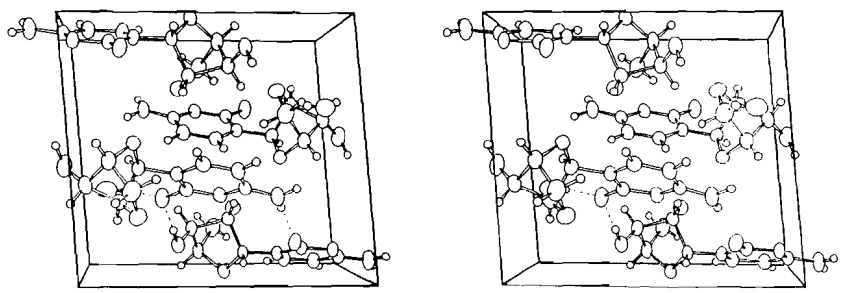

FIG. 4. Stereoscopic view, along the *y* axis, of molecular packing in the crystal.

known as the cooperativity effect (21). The ether oxygens do not participate in hydrogen bonding and only one N(3) atom acts as an acceptor. On the other hand, each carbonyl oxygen accepts two protons. One may therefore speculate that the carbonyl group, as well as the amino group, could play a significant role in binding to a receptor.

The packing of the molecules in the crystal is shown in Fig. 4. The A and B molecules form hydrogen-bonded dimers, involving both base and sugar moieties. There is neither base pairing nor base stacking.

Solution conformation

^1H and ^{13}C nmr spectra were studied in order to compare the conformation in solution with that determined by the X-ray analysis. In view of the rigidity of the bicyclic system in the sugar moiety, one would expect the differences, if any, to be due, primarily, to a different orientation about the glycosyl bond. On the other hand, the rigid system provides us with an opportunity to compare the experimentally obtained coupling constants with those calculated by the method of Haasnoot *et al.* (22).

The ^1H nmr spectra were recorded in four different solvents in order to find an optimal distribution of signals for H(2')—H(5"). As shown in Table 5, the best resolution was achieved in a mixture of CD_3OD and pyridine-d_5. While the proton chemical shifts are rather solvent dependent, the coupling constants remain unaffected. This fact, together with the long-range couplings of H(1'), indicates the rigidity of the

Can. J. Chem. Downloaded from www.nrcresearchpress.com by 80.58.250.72 on 09/07/12
For personal use only.

TABLE 5. Proton and ^{13}C nmr data

Proton	Chemical shifts (in ppm) DMSO-d_6	CD_3OD	CD_3OD + Py-d_5	D_2O	Coupling constants (in Hz)[a] H,H	J(H,H)
H(5)	5.75	5.91	5.95	6.22	5,6	7.5
H(6)	7.78	7.95	7.98	8.12	1′,2′	1.1
H(N4)	7.07				1′,3′	0.7
H(1′)	6.08	6.17	6.37	6.22	1′,5′	0.5
H(2′)	4.14	4.37	4.49	4.66	1′,5″	0.25
H(3′)	4.43	4.55	4.52	4.80	2′,3′	2.6
H(4′)	4.41	4.46	4.63	4.77	3′,4′	0.8
H(5′)	3.96	3.99	4.05	4.18	3′,OH	3.2
H(5″)	3.90		4.01		4′,5′	0.65
H(O3′)	5.91				4′,5″	1.0
					5′,5″	8.9

Carbon	Chemical shifts (in ppm)	Coupling constants (in Hz)[b] C,H	J(C,H)	C,H	J(C,H)
C(2)	155.52	2,6	5.5	2,1′	0
C(4)	166.00	4,5	1.5	4,6	9.2
C(5)	93.00	5,5	172.8		
C(6)	141.64	6,6	181.0	6,1′	4.8
		6,5	2.4		
C(1′)	90.27	1′,1′	171.6		
C(2′)	75.99	2′,2′	168.5		
C(3′)	75.11	3′,3′	155.0		
C(4′)	80.62	4′,4′	167.2		
C(5′)	72.19	5′,5′	143.4[c]	5′,5″	147.6[c]

[a]The same J values were found in all solvents.
[b]Long-range J(C,H) values were determined only for cytosine carbons.
[c]These values may be interchanged.

sugar moiety of the molecule. The small values of all vicinal coupling constants (<3 Hz) are in agreement with the *gauche* orientations of interacting protons shown in Fig. 3. Using the generalized Karplus relations derived by Haasnoot *et al.* (22), we calculated the vicinal coupling constants corresponding to the torsion angles obtained from the X-ray analysis. As seen in Table 6, some values differ significantly from those obtained experimentally. We have shown recently that good agreement can be obtained for a pyranose (23) and for a diazepine ring (24). It is likely, therefore, that the differences can be attributed to the distortions and interactions occurring in bicyclic systems. In fact, Haasnoot *et al.* (22) specifically excluded derivatives of norbornane and norbornene from their dataset. The unusual conformation is also evidenced by the differences between the J values in Table 6 and those published by de Leeuw and Altona (25) for arabinonucleosides with a $_3T^2$ ring pucker. However, de Leeuw and Altona did not calculate J's for a highly puckered ring with $\tau_m = 57°$. Thus, the values presented in Table 6 should be useful in future studies of 2′,5′-anhydronucleosides.

The difference nOe proton nmr spectrum provided information about the orientation of the cytosine base with respect to the sugar moiety. Upon irradiation of H(5′) and H(5″) (it is not possible to irradiate selectively only one of them), we observed a 14% nOe enhancement of the H(6) signal. The proximity of H(6) to the C(5′) methylene group indicates the *anti* conformation about the glycosyl bond. We also observed smaller nOe enhancements on the H(3′) (6%) and H(4′) (10%) signals.

In DMSO-d_6 the hydroxyl proton H(O3′) gives a doublet at

TABLE 6. Proton torsion angles (in deg) and interproton coupling constants (in Hz)

Protons	Torsion angles[a] Mol. A	Mol. B	^3J(H,H) Mol. A[b]	Mol. B[b]	Exp.[c]
H(1′),H(2′)	53	50	1.3	1.5	1.1
H(2′),H(3′)	62	62	3.6	3.6	2.6
H(3′),H(4′)	72	82	1.4	1.0	0.8
H(4′),H(5′)	77	70	1.6	2.1	0.7
H(4′),H(5″)	50	50	1.8	1.8	1.0

[a]From the X-ray analysis.
[b]Calculated (22) from the torsion angles listed on the left.
[c]From the nmr analysis.

δ 5.91 with J(3′,O3′) = 3.2 Hz, indicating a *gauche* orientation of these interacting hydrogens. In the crystal structure, where H(O3′) participates in hydrogen bonds, the H—C(3′)—O(3′)—H torsion angles are 92° and −49° in molecules A and B, respectively.

The proton decoupled "attached proton test" ^{13}C nmr spectrum (18) afforded nine signals. Structural assignment (Table 5) was done on the basis of numbers of directly bonded protons, chemical shift arguments, and a comparison with ^{13}C nmr data of cytosine nucleosides and arabinofuranoses. Very near signals of C(2′) and C(3′) at δ 75.99 and 75.11 were structurally distinguished by using ^1J(C,H) obtained from the

Can. J. Chem. Downloaded from www.nrcresearchpress.com by 80.58.250.72 on 09/07/12
For personal use only.

proton-coupled ^{13}C nmr spectrum. Of the two values 168.5 and 155.0 Hz, only the former is very similar to the value 167.2 Hz for C(4′). Therefore, we assigned the signal at 75.99 to C(2′) which has the same substitution as C(4′) (ether oxygens) and the signal at 75.11 to C(3′) whose lower value of ^1J(C,H) is due to the hydroxyl substituent. All one-bond couplings J(C,H) and long-range couplings of cytosine carbons were determined from the proton-coupled ^{13}C nmr spectrum. Poorly resolved multiplets with many splittings make it very difficult to determine long-range couplings of the sugar carbons. The proof of individual interactions by heteronuclear selective decouplings is complicated by the close spacing of the signals for H(2′)—H(5″).

Two coupling constants are relevant to the orientation about the glycosyl bond, viz. ^3J(C(6),H(1′)) and ^3J(C(2),H(1′)). The significantly higher value of the former (4.8 Hz) provides additional evidence for a *trans* orientation of the fragment C(6)—N(1)—C(1′)—H(1′). Using a relation between J(C,H) and the torsion angle in the fragment C—N—C—H (26), we obtain values of 130° and 50° for the torsion angles C(6)—N(1)—C(1′)—H(1′) and C(2)—N(1)—C(1′)—H(1′), respectively. These values are in good agreement with the results of the X-ray analysis, viz. 137(3)° and 43(3)° in molecule A and 142(2)° and 38(2)° in molecule B. Thus, the results of the nmr analysis confirm the conclusion we mentioned above, i.e. the torsion angle about the glycosyl bond is restricted to a relatively narrow range.

Acknowledgements

Apart from MULTAN78 (16), all crystallographic computations were carried out with programs written by Ahmed *et al.* (27). Figures 1 and 4 were drawn with the ORTEP program of Johnson (28).

1. H. HŘEBABECKÝ and J. BERÁNEK. Collect. Czech. Chem. Commun. **43**, 3268 (1978).
2. H. HŘEBABECKÝ and J. BERÁNEK. Nucleic Acids Res. Symp. Ser. No. 9, 99 (1981).
3. J. BERÁNEK and E. M. ACTON. Collect. Czech. Chem. Commun. **49**, 2551 (1984).
4. M. BÁRTOVÁ, M. RYBA, Z. JEDLIČKOVÁ, L. NOVOTNÝ, H. HŘEBABECKÝ, and H. BERÁNEK. Collect. Czech. Chem. Commun. **48**, 2088 (1983).
5. L. NOVOTNÝ, H. FARGHALI, M. RYBA, I. JANKŮ, and J. BERÁNEK. Cancer Chemother. Pharmacol. **13**, 195 (1984).
6. H. HŘEBABECKÝ and J. BERÁNEK. Nucleic Acids Res. **5**, 1029 (1978).
7. H. HŘEBABECKÝ and J. BERÁNEK. Collect. Czech. Chem. Commun. **45**, 599 (1980).
8. S. S. COHEN, J. G. FLAKS, H. D. BARNER, M. R. LOEB, and J. LICHTENSTEIN. Proc. Natl. Acad. Sci. U.S.A. **44**, 1004 (1958).
9. M. Y. CHU and G. A. FISCHER. Biochem. Pharmacol. **14**, 333 (1965).
10. J. J. FURTH and S. S. COHEN. Cancer Res. **28**, 2061 (1968).
11. S. AJMERA and P. V. DANENBERG. J. Med. Chem. **25**, 999 (1982).
12. A. F. COOK, M. J. HOLMAN, M. J. KRAMER, and P. W. TROWN. J. Med. Chem. **22**, 1330 (1979).
13. A. ROSOWSKY, S.-H. KIM, D. TRITES, and M. WICK. J. Med. Chem. **25**, 1034 (1982).
14. J. KÁRA, M. BÁRTOVÁ, M. RYBA, H. HŘEBABECKÝ, J. BROKEŠ, L. NOVOTNÝ, and J. BERÁNEK. Collect. Czech. Chem. Commun. **47**, 2824 (1982).
15. H. HŘEBABECKÝ, J. BROKEŠ, and J. BERÁNEK. Collect. Czech. Chem. Commun. **47**, 2961 (1982).
16. P. MAIN, S. E. HULL, L. LESSINGER, G. GERMAIN, J.-P. DECLERCQ, and M. M. WOOLFSON. MULTAN78, University of York, England, and University of Louvain, Belgium. 1978.
17. J. A. IBERS and W. C. HAMILTON (*Editors*). International tables for X-ray crystallography. Vol. IV. Kynoch Press, Birmingham, England. 1974.
18. C. LECOCQ and J.-Y. LALLEMAND. J. Chem. Soc. Chem. Commun. 150 (1981).
19. R. TAYLOR and O. KENNARD. J. Am. Chem. Soc. **104**, 3209 (1982).
20. G. I. BIRNBAUM and G. A. GENTRY. J. Am. Chem. Soc. **105**, 5398 (1983).
21. G. A. JEFFREY and J. MITRA. Acta Crystallogr. Sect. B, **39**, 469 (1983).
22. C. A. G. HAASNOOT, F. A. A. M. DE LEEUW, and C. ALTONA. Tetrahedron, **36**, 2783 (1980).
23. G. I. BIRNBAUM and D. R. BUNDLE. Can. J. Chem. **63**, 739 (1985).
24. G. I. BIRNBAUM, J. R. BRISSON, S. H. KRAWCZYK, and L. B. TOWNSEND. J. Am. Chem. Soc. **107**, 7635 (1985).
25. F. A. A. M. DE LEEUW and C. ALTONA. J. Chem. Soc. Perkin Trans. **2**, 375 (1982).
26. V. F. BYSTROV, YU. D. GAVRILOV, and V. N. SOLKAN. J. Magn. Reson. **19**, 123 (1975).
27. F. R. AHMED, S. R. HALL, M. E. PIPPY, and C. P. HUBER. J. Appl. Crystallogr. **6**, 309 (1973).
28. C. K. JOHNSON. "ORTEP-II", Report ORNL-5138. Oak Ridge National Laboratory, Oak Ridge, TN. 1976.

Can. J. Chem. Downloaded from www.nrcresearchpress.com by 80.58.250.72 on 09/07/12
For personal use only.

Kinetics and mechanisms of oxidations by metal ions. Part VIII.[1] Oxidation of *n*-propanol by aquomanganese(III) ions

MAHENDRA MEHTA, RATAN R. NAGORI, AND RAJ N. MEHROTRA[2]
Department of Chemistry, University of Jodhpur, Jodhpur 342 001, India

Received January 24, 1986[3]

MAHENDRA MEHTA, RATAN R. NAGORI, and RAJ N. MEHROTRA. Can. J. Chem. **65**, 277 (1987).

The oxidation of *n*-propanol by aquomanganese(III) ions in perchlorate medium of constant ionic strength (4 mol dm^{-3}, $NaClO_4$) is described by the rate law [i] which is based on the consideration of the reactions [ii]–[ix].

$$[i] \quad \frac{-d[Mn^{III}]}{dt} = \frac{2(kK_a\beta[Mn^{II}]^{-1} + k_1\beta_1K_h[H^+]^{-1})[Mn^{III}][C_3H_7OH]}{(1 + K_c[H^+])(1 + K_h[H^+]^{-1}) + (\beta + \beta_1K_h[H^+]^{-1})[C_3H_7OH]}$$

[ii] $Mn^{3+}(aq) \overset{K_h}{\rightleftharpoons} MnOH^{2+}(aq) + H^+(aq)$

[iii] $C_3H_7OH + H^+(aq) \overset{K_c}{\rightleftharpoons} C_3H_7OH_2^+$

[iv] $C_3H_7OH + Mn^{3+}(aq) \overset{\beta}{\rightleftharpoons} C_3H_7OHMn^{3+}(aq)$

[v] $C_3H_7OH + MnOH^{2+}(aq) \overset{\beta_1}{\rightleftharpoons} C_3H_7OMn^{2+}(aq) + H_2O$

[vi] $C_3H_7OHMn^{3+}(aq) \overset{K_a}{\rightleftharpoons} C_2H_5CH_2\overset{+}{O}H + Mn^{2+}$

[vii] $C_2H_5CH_2\overset{+}{O}H \overset{k}{\rightarrow} C_2H_5\dot{C}HOH + H^+$

[viii] $C_2H_5CH_2OMn^{2+}(aq) \overset{k_1}{\longrightarrow} C_2H_5\dot{C}HOH + Mn^{2+}$

[ix] $C_2H_5\dot{C}HOH + Mn^{III} \rightarrow C_2H_5CHO + Mn^{II} + H^+$ (fast)

A further analysis of the rate law in terms of the results indicated that $MnOH^{2+}(aq)$ is the major oxidant. The values of the equilibrium constant (β_1) and rate determining constant (k_1) are reported together with the associated thermodynamic parameters. The values of the other constants, k, K_a, and β, could not be determined though an assumption was made that $\beta \approx \beta_1$.

MAHENDRA MEHTA, RATAN R. NAGORI et RAJ N. MEHROTRA. Can. J. Chem. **65**, 277 (1987).

La vitesse de la réaction du *n*-propanol avec les ions manganeux(III) aqueux, dans une solution perchlorique de force ionique constante (4 mol dm^{-3}, $NaClO_4$), est décrite par l'équation [i] qui est basée sur la considération des réactions [ii]–[ix] :

$$[i] \quad \frac{-d[Mn^{III}]}{dt} = \frac{2(kK_a\beta[Mn^{II}]^{-1} + k_1\beta_1K_h[H^+]^{-1})[Mn^{III}][C_3H_7OH]}{(1 + K_c[H^+])(1 + K_h[H^+]^{-1}) + (\beta + \beta_1K_h[H^+]^{-1})[C_3H_7OH]}$$

[ii] $Mn^{3+}(aq) \overset{K_h}{\rightleftharpoons} MnOH^{2+}(aq) + H^+(aq)$

[iii] $C_3H_7OH + H^+(aq) \overset{K_c}{\rightleftharpoons} C_3H_7OH_2^+$

[iv] $C_3H_7OH + Mn^{3+}(aq) \overset{\beta}{\rightleftharpoons} C_3H_7OHMn^{3+}(aq)$

[v] $C_3H_7OH + MnOH^{2+}(aq) \overset{\beta_1}{\rightleftharpoons} C_3H_7OMn^{2+}(aq) + H_2O$

[vi] $C_3H_7OHMn^{3+}(aq) \overset{K_a}{\rightleftharpoons} C_2H_5CH_2\overset{+}{O}H + Mn^{2+}$

[vii] $C_2H_5CH_2\overset{+}{O}H \overset{k}{\rightarrow} C_2H_5\dot{C}HOH + H^+$

[viii] $C_2H_5CH_2OMn^{2+}(aq) \overset{k_1}{\longrightarrow} C_2H_5\dot{C}HOH + Mn^{2+}$

[ix] $C_2H_5\dot{C}HOH + Mn^{III} \rightarrow C_2H_5CHO + Mn^{II} + H^+$ (vite)

Une analyse plus poussée de la loi de vitesse, en fonction des résultats, a indiqué que le $MnOH^{2+}(aq)$ est l'oxydant principal. On rapporte les valeurs de la constante d'équilibre (β_1) et de la constante de la réaction déterminant la vitesse (k_1) ainsi que les paramètres thermodynamiques qui leurs sont associés. On n'a pas pu déterminer les valeurs des autres constantes k, K_a et β bien qu'on suppose que $\beta \approx \beta_1$.

[Traduit par la revue]

[1]For Part VII, see ref. 1.

[2]To whom all correspondence should be addressed.

[3]Revision received September 13, 1986.

Can. J. Chem. Downloaded from www.nrcresearchpress.com by 80.58.250.72 on 09/07/12
For personal use only.

Can. J. Chem. Downloaded from www.nrcresearchpress.com by 80.58.250.72 on 09/07/12
For personal use only.

Introduction

Although the oxidation of secondary alcohols, isopropanol (2) and *s*-butanol and cyclohexanol (3), by aquomanganese(III) ions has been discussed in detail, the oxidation of primary alcohols has received scant attention. The only study reported so far is that of methanol (4). That the oxidation of methanol is different from those of *s*-alcohols is exemplified by the effect of Mn^{2+} ions on the rates of oxidation. The rate of oxidation of *s*-alcohols is independent of $[Mn^{2+}]$ whereas that of methanol is retarded by it. The retarding effect of Mn^{2+} ions was explained by the suggestion that the Mn^{2+} ion, the $\dot{C}H_2OH$ radical, and H^+ ion are formed in a solvent cage in the initial stage and that the backward reaction increased by additional Mn^{2+} ions present in the wall of the solvent cage. However, this explanation became untenable when it was found that Mn^{2+} ions did not retard the rate of oxidation of glycolic acid (5) which generates the $\dot{C}H_2OH$ radical during its oxidation.

It was therefore considered necessary to examine the oxidation of another primary alcohol with a view to understand its mechanism of oxidation with respect to the role of Mn^{2+} ions. The choice of *n*-propanol was influenced by the fact that there is spectrophotometric evidence (6) for its complexation by aquomanganese(III) ions.

Experimental

Solutions of aquomanganese(III) ions were freshly prepared by the electrolytic oxidation of stock manganese(II) perchlorate solution under nitrogen. The stock manganese(II) perchlorate (G. F. Smith) solution was standardized against a standard solution of sodium ethylenediaminetetraacetate (BDH) in the presence of ammonium hydroxide using 4-(2-pyridylazo)resorcinol as indicator.

The solution of aquomanganese(III) ions was standardized by allowing it to react with a known volume of standard iron(II) solution. The unreacted iron(II) solution was estimated titrimetrically using a standard vanadium(V) solution (barium diphenylamine sulphonate indicator used in presence of phosphoric acid). Other details are described elsewhere (7). Perchloric acid (E. Merck, GR) was standardized against standard sodium hydroxide using phenolphthalein as indicator. Anhydrous sodium perchlorate (G. F. Smith) was standardized gravimetrically and used with Mn(II) perchlorate to maintain the ionic strength at 4 mol dm^{-3}. *n*-Propanal (E. Merck) was refluxed with 2,4-dinitrophenylhydrazine to remove carbonyl impurities and distilled. The middle fraction, bp 97.8°C, was collected for use. Reductant solutions were made by direct weighing.

Stoichiometry

Reaction mixtures, aerobic or under nitrogen, with [alcohol] $\gg$ $[Mn^{III}]$ were prepared and left at 25°C until the reaction was complete. The reaction mixture was then treated with 2,4-dinitrophenylhydrazine and the precipitated phenylhydrazone was separated and purified. Its mp (156°C) did not change on mixing with the hydrazone prepared from an authentic sample of *n*-propanol (lit. (8), 155°C). The yield, 90–96% of the calculated amount, of the hydrazone was independent of acidity and atmospheric conditions. The $[Mn^{III}]/[\text{hydrazone}] = 2.15 \pm 0.1$ indicated that the oxidation of excess *n*-propanol is given by reaction [1]

$$[1] \quad 2Mn^{III} + C_2H_5CH_2OH \rightarrow C_2H_5CHO + 2Mn^{II} + 2H^+$$

Rate measurements

The kinetics were followed under pseudo-first order conditions, i.e. *n*-propanol was always present in large excess. Other details are described elsewhere (7). Temperature was maintained to ±0.1°C. In adopting the titrimetric method it was ensured that the presence of *n*-propanol in concentrations present in the reaction mixtures did not affect the titre value of Fe^{II} solution against vanadium(V) solution. The rates under nitrogen were similar to those in air. The rates reported are the mean of the values obtained from replicate runs which agreed to within ±2–3%.

The values of the pseudo first-order rate constant k_{obs} were calculated from the slopes of linear plots of log (titre change) vs. time. The slopes were obtained with a statistical calculator. The plots were linear for at least two half-lives and the correlation coefficients were always >0.99.

Test for free radicals

The formation of the free radical during the progress of the reaction was indicated by the observed polymerisation of acrylonitrile added to partially oxidised reaction mixtures which were previously saturated with nitrogen. The blank tests in which acrylonitrile was added separately to solutions of Mn^{III} and *n*-propanol did not show any polymerisation of acrylonitrile.

TABLE 1. The retarding effect of $[Mn^{II}]$ on the observed rate*

$[Mn^{II}]$ (mol dm^{-3})	$10^5 k_{obs}$ (s^{-1})	$[Mn^{II}]$ (mol dm^{-3})	$10^5 k_{obs}$ (s^{-1})
0.059	8.6	0.099	6.5
0.066	7.8	0.199	6.0
0.079	7.0	0.140	5.6

*$10^3[Mn^{III}]$ = 2.0 mol dm^{-3}, $[C_3H_7OH]$ = 0.2 mol dm^{-3}, T = 35°C, $[HClO_4]$ = 3.0 mol dm^{-3}, I = 4 mol dm^{-3}.

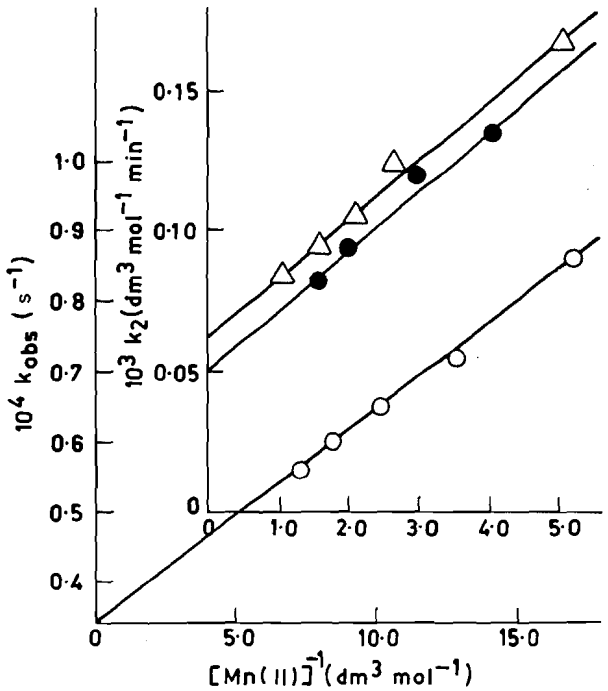

FIG. 1. Plots of k_{obs} against $[Mn^{II}]^{-1}$. The innermost plot between k_2 (dm^3 mol^{-1} min^{-1}) and $[Mn^{II}]^{-1}$ in the oxidation of methanol, at different acidities, is based on the rate data of ref. 4. The plots are (○) for *n*-propanol, and for methanol at $[HClO_4]$ = 1.0 (△) and (●) 2.0 mol dm^{-3} at 35°C.

Results

Dependence on $[Mn^{II}]$

The results in Table 1 at constant $[H^+]$ = 3 mol dm^{-3} and 35°C indicate that k_{obs} decreases with increasing $[Mn^{II}]$ at constant ionic strength (4 mol dm^{-3}). An analysis of the results indicated that the plot, Fig. 1, between k_{obs} and $[Mn^{II}]^{-1}$ was linear with an intercept on the rate axis. It is interesting to note

TABLE 2. Dependence of the observed rate constant k_{obs} on the initial [substrate]*

[Pr^{n}OH] (mol dm^{-3})	$10^5 k_{obs}$(s^{-1}) 30°C	35°C	40°C	45°C
0.16	—	—	15.6	25.6
0.24	4.8	9.2	21.2	35.2
0.32	6.2	11.8	25.1	43.3
0.40	7.0	13.5	29.2	51.0
0.48	7.2	14.5	31.6	58.1
0.64	8.1	16.5	35.7	67.6
0.80	8.6	17.9	39.7	75.8

*10^3[Mn^{III}] = 2.0 mol dm^{-3}, [Mn^{II}] = 0.066 mol dm^{-3}, [$HClO_4$] = 3.0 mol dm^{-3}, I = 4 mol dm^{-3}.

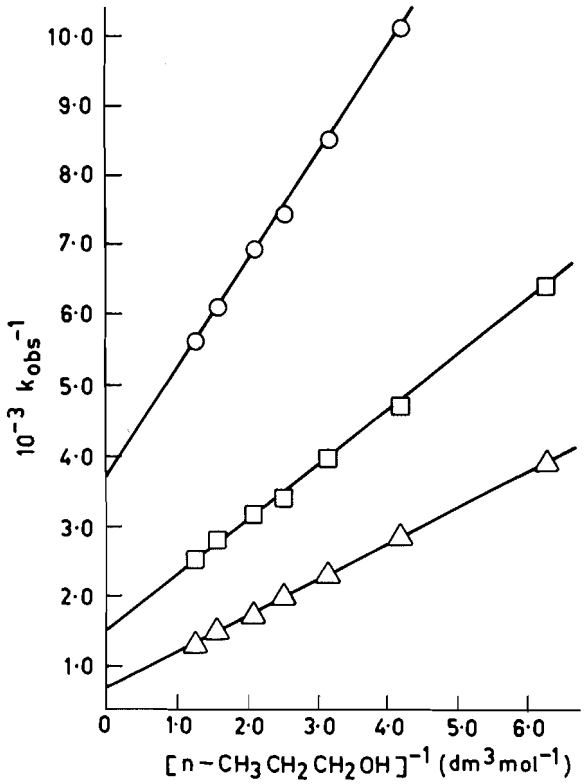

FIG. 2. Plots of k_{obs}^{-1} against [n-propanol]$^{-1}$ at (○) 35, (□) 40, and (△) 45°C. 10^3[Mn^{III}] = 2.0 mol dm^{-3}, [$HClO_4$] = 3.0 mol dm^{-3}, [Mn^{II}] = 0.066 mol dm^{-3}, and I = 4 mol dm^{-3}.

that the intercept/slope ratio is greater than 12. The significance of this ratio is discussed in a later section.

Dependence on [n-propanol]

The effect of the initial [n-propanol] on k_{obs} was investigated at different temperatures. The results in Table 2 indicated that the plot, Fig. 2, between k_{obs}^{-1} and [n-propanol]$^{-1}$ was linear with an intercept on the ordinate axis. These plots are consistent with complex formation between aquomanganese(III) ions and n-propanol (6).

Dependence on [H^+]

The results in Table 3 indicated that k_{obs} decreased with the increasing [H^+] at constant ionic strength. The actual relationship between k_{obs} and [H^+] is discussed later.

Discussion

Michaelis–Menten plots, Fig. 2, are consistent with the spectrophotometric evidence (6, 9) for the existence of Mn^{III}–Pr^{n}OH complexes. The retarding effect of [Mn^{2+}] on the observed rate could be explained by one of several possible alternatives discussed below:

(*a*) There is a possibility of the existence of equilibrium [2]. The equilibrium constant K for equilibrium [2] has an upper limit of 10^{-2} in 6 mol dm^{-3} perchloric acid (10) which is consistent with the value found in sulphuric acid (11) and the conclusions of Wells and Davies (12). The equilibrium [2] is attractive in the sense that alcohols are reported (13) to be oxidised by Mn^{IV}. However, consideration of this equilibrium implies that the reaction, at least partially, has a second order dependence in [Mn^{III}] which is contrary to the observed first-order dependence in [Mn^{III}].

[2] $Mn^{III} + Mn^{III} \rightleftarrows Mn^{IV} + Mn^{II}$

(*b*) The retardation in k_{obs} was also expected if Mn^{II} complexes the reductant which would cause a decrease in the reactive [n-propanol]. This possibility was not favoured because no spectral change in the uv–visible region was observed in the spectra of Mn^{II} in the presence of n-propanol. A similar conclusion is based on the absence of any effect of Mn^{II} on the spectra of Mn^{III} in aqueous methanol. Further a rate law deduced with this assumption predicted a linear correlation between k_{obs}^{-1} and [Mn^{II}]. However, a curved plot is obtained when k_{obs}^{-1} is plotted against [Mn^{II}], which eliminates this possibility.

(*c*) There could be a reversible rate determining reaction [3] where Ṡ is the free radical corresponding to the substrate SH. A variation of this idea in which an interaction between Mn^{II} and the free radical $\dot{C}H_2OH$ was assumed inside the solvent cage whose walls contained additional Mn^{II} ions at high [Mn^{II}] was considered in the oxidation of methanol (4).

[3] Mn^{III}–SH $\rightleftarrows Mn^{II} + \dot{S} + H^+$

This proposal is not favoured because Mn^{II} did not retard the rate of oxidation of glycolic acid (5) which gives the same free radical $\dot{C}H_2OH$ produced in the oxidation of methanol (4). There seems to be no reason to believe that, unlike the Mn^{III}–methanol complex, the Mn^{III}–glycolic acid complex cannot undergo intramolecular electron transfer inside the solvent cage. Moreover, the rate law deduced with this assumption is not consistent with the correlation between k_{obs} and [Mn^{II}]$^{-1}$ in Fig. 1.

Mechanism

The following mechanism, consisting of reactions [4]–[11], is suggested for the oxidation of n-propanol. It is consistent with the observed linearity of the plot between k_{obs} and [Mn^{II}]$^{-1}$ illustrated in Fig. 1. Reaction [4] is well established hydrolytic equilibrium between Mn^{3+}(aq) and $MnOH^{2+}$(aq) ions. The value of K_h at different temperatures was obtained from the known ΔH_h value (12). Reaction [5] is consistent with the known protonation of alcohols in aqueous solutions of strong mineral acids (14). The formation of $C_3H_7OHMn^{3+}$(aq) and $C_3H_7OMn^{2+}$(aq) complexes is consistent with the spectrophotometric studies reported earlier (6, 9).

[4] $Mn^{3+}(aq) \overset{K_h}{\rightleftharpoons} MnOH^{2+}(aq) + H^+$

[5] $C_3H_7OH + H^+(aq) \overset{K_c}{\rightleftharpoons} C_3H_7OH_2^+$

Can. J. Chem. Downloaded from www.nrcresearchpress.com by 80.58.250.72 on 09/07/12
For personal use only.

TABLE 3. Dependence of the observed rate constant k_{obs} on $[H^+]$*

	$10^5 k_{obs}(s^{-1})$					$10^5 k_{obs}(s^{-1})$			
$[HClO_4]$	30°C	35°C	40°C	45°C	$[HClO_4]$	30°	35°C	40°C	45°C
1.0	8.34	21.8	56.0	—	2.75	4.00	7.80	20.8	33.2
1.5	7.20	14.4	36.0	61.6	3.00	3.70	7.30	18.6	30.5
1.75	6.10	12.2	31.0	51.4	3.25	3.47	6.80	17.0	28.0
2.00	5.52	10.8	28.0	45.0	3.50	3.20	6.30	15.8	26.0
2.25	4.76	9.4	25.0	40.2	3.80	2.80	5.60	14.6	24.2
2.50	4.46	8.8	22.0	36.5					

*$10^3[Mn^{III}]$ = 2.0 mol dm^{-3}, $[Mn^{II}]$ = 0.066 mol dm^{-3}, $[Pr^nOH]$ = 0.2 mol dm^{-3}, I = 4 mol dm^{-3}.

[6] $C_3H_7OH + Mn^{3+}(aq) \overset{\beta}{\rightleftharpoons} C_3H_7OHMn^{3+}(aq)$

[7] $C_3H_7OH + MnOH^{2+}(aq) \overset{\beta_1}{\rightleftharpoons} C_3H_7OMn^{2+}(aq) + H_2O$

[8] $C_3H_7OHMn^{3+}(aq) \overset{K_a}{\rightleftharpoons} C_2H_5CH_2\overset{+}{O}H + Mn^{2+}$

[9] $C_2H_5CH_2\overset{+}{O}H \overset{k}{\rightarrow} C_2H_5\dot{C}HOH + H^+$

[10] $C_2H_5CH_2OMn^{2+}(aq) \xrightarrow{k_1} C_2H_5\dot{C}HOH + Mn^{2+}$

[11] $C_2H_5\dot{C}HOH + Mn^{III} \xrightarrow{fast} C_2H_5CHO + Mn^{II} + H^+$

Based on the above sequence of reactions, the rate of disappearance of $[Mn^{III}]$ is given by eq. [12].

$$[12]\quad \frac{-d[Mn^{III}]}{dt} = \frac{2(kK_a\beta[Mn^{II}]^{-1} + k_1\beta_1K_h[H^+]^{-1})[Mn^{III}][C_3H_7OH]}{(1 + K_c[H^+])(1 + K_h[H^+]^{-1}) + (\beta + \beta_1K_h[H^+]^{-1})[C_3H_7OH]}$$

where reaction [9] is considered as disproportionation of $C_2H_5CH_2\overset{+}{O}H$ ion and not as a deprotonation reaction. Further if reaction [9] is considered reversible, then there is a need to consider a rate-limiting reaction which is obviously the reaction of $C_2H_5\dot{C}HOH$ radical with Mn^{III} ion. The resultant rate law under this condition will thus have a second order term in Mn^{III} which is contrary to the first order dependence in $[Mn^{III}]$.

It might be noted that reactions [8] and [10] differ by protonation, yet reaction [8] is written as an equilibrium reaction because of the demand to explain the retardation of Mn(II) in such a way that the plot of k_{obs} and $[Mn^{II}]^{-1}$ has an intercept on the rate ordinate. If reaction [10] is also considered to be reversible, the retardation by Mn(II) could still be explained but the resultant rate law will no longer explain the intercept on the rate ordinate. The plot will be expected to pass through the origin.

Equation [12] is consistent with the observed linearity of the plot between k_{obs} and $[Mn^{II}]^{-1}$ in Fig. 1. Also illustrated are two other linear plots based on the rate data taken from the study of Wells and Barnes (4) for the oxidation of methanol at different acidities. The linearity of these two latter plots indicates that the mechanism proposed here is equally applicable to the oxidation of methanol (4) and there is no need for the assumption made (4) to explain the retarding effect of Mn^{2+} ions.

Now if we assume that $\beta \approx \beta_1$, eq. [12] is simplified to eq. [13] which can be rearranged to eq. [14]. The latter equation is consistent with the linearity of the plots between k_{obs}^{-1} and $[C_3H_7OH]^{-1}$ illustrated in Fig. 2. The slopes and intercepts of these plots are given by eqs. [15] and [16], respectively. The intercept/slope ratio, eq. [17], can be used to calculate the value of β_1. The value of β_1 obtained at different temperatures, Table 4, are essentially constant within the experimental limits. Hence the assumption of rapid equilibria [6] and [7] is justified.

$$[13]\quad k_{obs} = \frac{2\beta_1(kK_a[Mn^{II}]^{-1} + k_1K_h[H^+]^{-1})[C_2H_5CH_2OH]}{(1 + K_cH^+])(1 + K_h[H^+]^{-1}) + \beta_1(1 + K_h[H^+]^{-1})[C_2H_5CH_2OH]}$$

$$[14]\quad k_{obs}^{-1} = \frac{(1 + K_c[H^+])(1 + K_h[H^+]^{-1})}{2\beta_1(kK_a[Mn^{II}]^{-1} + k_1K_h[H^+]^{-1})[C_3H_7OH]} + \frac{(1 + K_h[H^+]^{-1})}{2(kK_a[Mn^{II}]^{-1} + k_1K_h[H^+]^{-1})}$$

$$[15]\quad \text{Slope} = \frac{(1 + K_c[H^+])(1 + K_h[H^+]^{-1})}{2\beta_1(kK_a[Mn^{II}]^{-1} + k_1K_h[H^+]^{-1})}$$

$$[16]\quad \text{Intercept} = \frac{(1 + K_h[H^+]^{-1})}{2(kK_a[Mn^{II}]^{-1} + k_1K_h[H^+]^{-1})}$$

$$[17]\quad \frac{\text{Intercept}}{\text{Slope}} = \frac{\beta_1}{1 + K_c[H^+]}$$

It should be noted that the value of K_c for *n*-propanol is available (14) only at 25°C. The temperature dependence of K_c for methanol (15) exhibits a slight maximum. Assuming similar behaviour for *n*-propanol, it is considered that the use of K_c(25°C) at other temperatures does not lead to serious error in the determination of β_1 from eq. [17].

Equation [18], obtained from [13], indicated that a plot of the left hand term against $[H^+]^{-1}$ should be linear with an intercept

Can. J. Chem. Downloaded from www.nrcresearchpress.com by 80.58.250.72 on 09/07/12
For personal use only.

TABLE 4. Values of β_1 at different temperatures

T (°C)	β_1
30	5.0
35	3.0
40	4.0
45	2.0
	Ave. 4±1

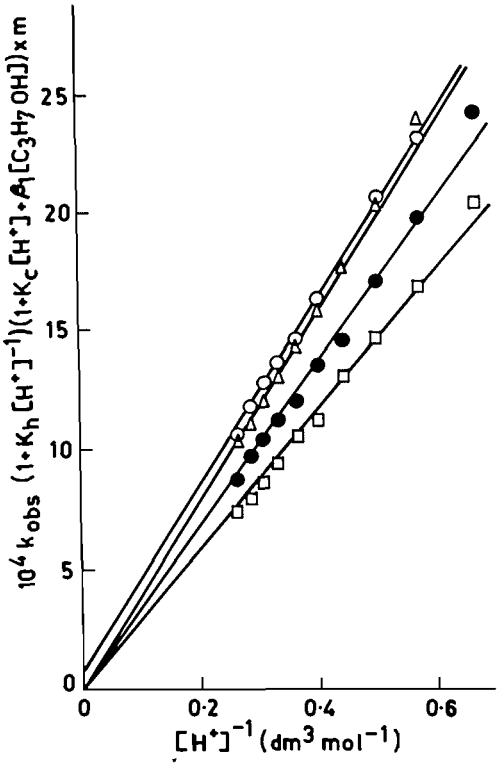

FIG. 3. Plots between k_{obs} $(1 + K_h[H^+]^{-1})(1 + K_c[H^+] + \beta_1[C_3H_7OH]) \times m$ and $[H^+]^{-1}$ at 30°C with $m = 0.1$ (○), 35°C with $m = 0.25$ (●), 40°C with $m = 0.8$ (□), and 45°C with $m = 1$ (△). $10^3[Mn^{III}] = 2.0$ mol dm^{-3}, $[Mn^{II}] = 0.066$ mol dm^{-3}, $[C_3H_7OH] = 0.2$ mol dm^{-3}, and $I = 4$ mol dm^{-3}.

on the rate ordinate. The plots at 35, 40, and 45°C, Fig. 3, have zero intercept indicating that $kK_a[Mn^{II}]^{-1} \ll k_1K_h$.

$$[18]\quad k_{obs}(1 + K_h[H^+]^{-1})(1 + K_c[H^+] + \beta_1[C_3H_7OH]) = 2\beta_1(kK_a[Mn^{II}]^{-1} + k_1K_h[H^+]^{-1})[C_3H_7OH]$$

However, the plot at 30°C does have an intercept on the rate ordinate confirming the validity of the eq. [18] at least at lower temperatures. The intercept $kK_a[Mn^{II}]^{-1}$, is 1×10^{-5} s^{-1}, and since $[Mn^{II}] = 0.066$ mol dm^{-3} the value of kK_a is 6.6×10^{-7} mol dm^{-3} s^{-1}. The corresponding slope value $K_1K_h = 2.28 \times 10^{-4}$ mol dm^{-3} s^{-1}, which explains the small retarding effect of Mn^{II}. The k_1 values at different temperatures, obtained from the slopes of Fig. 3 are given in Table 5 together with calculated activation parameters.

TABLE 5. Rate constant k_1 at different temperatures*

T (°C)	$10^4 k_1$ (s^{-1})
30	2.0
35	5.3
40	13
45	17

*Activation parameters are $\Delta H^{\ddagger} = 116 \pm 10$ kJ mol^{-1} and $\Delta S^{\ddagger} = 140 \pm 16$ kJ mol^{-1}.

The oxidation of *n*-propanol is faster than that of isopropanol (2) and the two oxidations appear to have different mechanisms. The formation of Pr^nOH–Mn^{III} complexes lowers the energy of activation. The $\Delta H^{\ddagger}$ value for *n*-propanol is about 12 kJ mol^{-1} less than that for isopropanol. Similarly the $\Delta S^{\ddagger}$ value for *n*-propanol is more positive because the formation of Pr^nOH–Mn^{III} complexes causes much more restructuring of the solvent molecules than caused by the approach of isopropanol and Mn^{III} molecules to a minimum distance before the electron is transferred. The formation of Pr^nOH–Mn^{III} in reaction [8] may explain the retarding effect of Mn^{II} ion: Mn^{II} retards the rate of oxidation of primary alcohols whereas it has no effect in the oxidation of *s*-alcohols.

Acknowledgement

The authors thank Professor R. C. Kapoor for encouragement. R.R.N. and M.M. thank CSIR and UGC respectively for the award of Junior Research Fellowships during the tenure of this work. Thanks are also due to the reviewers for helpful suggestions.

1. P. CHAUDHARY, R. R. NAGORI, and R. N. MEHROTRA. Indian J. Chem. In press.
2. C. F. WELLS and G. DAVIES. Trans. Faraday Soc. **63**, 2737 (1967).
3. C. F. WELLS, C. BARNES, and G. DAVIES. Trans. Faraday Soc. **64**, 3067 (1968).
4. C. F. WELLS and C. BARNES. J. Chem. Soc. (A), 430 (1971).
5. M. MEHTA, R. R. NAGORI, A. KUMAR, and R. N. MEHROTRA. Indian J. Chem. **21**A, 777 (1982).
6. C. F. WELLS and C. BARNES. J. Chem. Soc. (A), 1626 (1968).
7. M. MEHTA, R. R. NAGORI, and R. N. MEHROTRA. J. Chem. Soc. Dalton Trans., 211 (1979).
8. H. T. CLARK. A handbook of organic analysis. Arnold and Co., London. 1952. p. 12.
9. C. F. WELLS, D. MAYS, and C. BARNES. J. Inorg. Nucl. Chem. **30**, 1341 (1968).
10. H. DIEBLER and N. SUTIN. J. Phys. Chem. **68**, 174 (1964).
11. R. J. SELIM and J. J. LINGANE. Anal. Chim. Acta, **21**, 536 (1959).
12. C. F. WELLS and G. DAVIES. J. Chem. Soc. (A), 1858 (1967).
13. E. F. PRATT and J. F. VAN DE CASTLE. J. Org. Chem. **26**, 2973 (1961).
14. C. F. WELLS. Trans. Faraday Soc. **62**, 2815 (1966).
15. C. F. WELLS. Trans. Faraday Soc. **61**, 2194 (1965).

Can. J. Chem. Downloaded from www.nrcresearchpress.com by 80.58.250.72 on 09/07/12
For personal use only.

Preparation of α-aminothioamides from aldehydes

MARTINO PAVENTI AND JOHN T. EDWARD
Department of Chemistry, McGill University, 801 Sherbrooke Street West, Montreal (Que.), Canada H3A 2K6

Received January 24, 1986[1]

MARTINO PAVENTI and JOHN T. EDWARD. Can. J. Chem. **65**, 282 (1987).

The conversion of aldehydes into α-aminonitriles and thence into imidazolidin-4-thiones has been studied. Hydrolysis of the appropriate imidazolidin-4-thiones gave thioamides of nine naturally occurring α-amino acids. The possible pre-biotic significance of these compounds is discussed.

MARTINO PAVENTI et JOHN T. EDWARD. Can. J. Chem. **65**, 282 (1987).

On a étudié la transformation des aldéhydes en α-amino-nitriles et éventuellement en imidazolidinethiones-4. L'hydrolyse des imidazolidinethiones-4 appropriées conduit aux thioamides de neuf acides α-aminés naturels. On discute de l'implication pré-biotique possible de ces composés.

[Traduit par la revue]

Can. J. Chem. Downloaded from www.nrcresearchpress.com by 80.58.250.72 on 09/07/12
For personal use only.

In 1953, Miller (1) showed that sparking a mixture of methane, ammonia, hydrogen, and water vapour furnished traces of glycine, alanine, and other common α-amino acids. This historic experiment awakened the interest of many organic chemists in possible pre-biotic routes to proteins, nucleic acids, and polysaccharides on the primitive earth.

It seems likely that under the conditions of Miller's experiment aldehydes and hydrogen cyanide are formed (2). These can react with ammonia to give α-aminonitriles **1**, which are hydrolysed to α-amino acids (2). However, the polymerization of α-amino acids to polypeptides and proteins requires an activation process. Various possible modes of activation that might operate under pre-biotic conditions (heat, cyanamide, adsorption on clays, etc.) have been suggested (2, 3) but are not very plausible.

This activation step might have been avoided on the primitive earth if α-aminonitriles had been converted into reactive α-amino acid derivatives rather than into unreactive α-amino acid zwitterions. One such derivative might have been the thioamide. The reactivity of these compounds was demonstrated more than 70 years ago by Johnson and Burnham (4), in the course of their attempts to obtain the thioamide **2** ($R^1 = R^2 = H$) by treatment of the nitrile **1** ($R^1 = R^2 = H$) with hydrogen sulfide (a constituent of the earth's primitive atmosphere (3)) in ethanol saturated with ammonia. They obtained instead a small amount of the thiodipeptide derivative **3** ($R^1 = R^2 = H$), and possibly of the thiotripeptide and larger amounts of the cyclic product **4** ($R^1 = R^2 = H$), all presumably arising from further reaction of the sought-for thioamide **2** ($R^1 = R^2 = H$) (Scheme 1). Later attempts by Gatewood and Johnson (5, 6) to obtain other α-aminothioamides by this route gave either no product (6), or products from further reaction of initially formed α-aminothioamides (5, 6). However, Cook *et al.* (7) obtained **2** (R^1 = Ph, $R^2 = H$) in 12% yield by treating **1** (R^1 = Ph, $R^2 = H$) with H_2S for 24 h in ether containing a little pyridine.

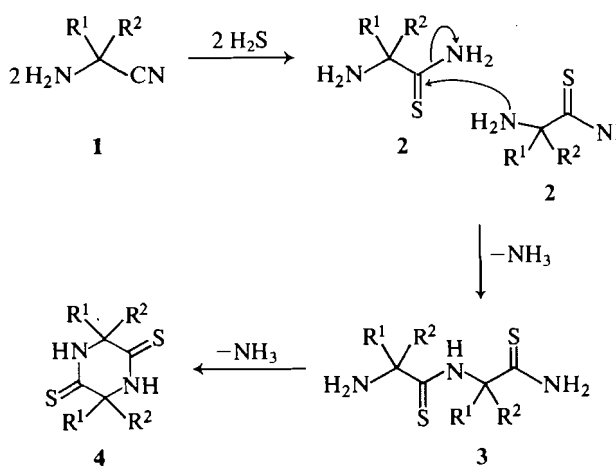

SCHEME 1

This work indicates a possibility of producing thiopolypeptides and thence polypeptides by the general route of Scheme 1. Consequently, we have prepared α-aminothioamides **2** corresponding to several common α-amino acids as a preliminary to searching for conditions to convert them into linear thiopolypeptides.

We first required a convenient and general preparation of α-aminonitriles **1**. These compounds have long been obtained by the Strecker reaction:

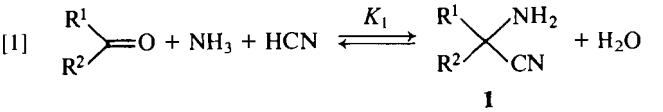

[1]

1

but yields are often low and the products often decompose on standing. Commeyras *et al.*, in a masterly series of papers (reviewed in ref. 8), have explained the thermodynamic and kinetic factors underlying the formation of **1**. Because of the reversibility of the reaction, α-aminonitriles decompose completely in solutions sufficiently acidic to convert NH_3 to NH_4^+, and in solutions sufficiently alkaline to convert HCN into CN^-. Consequently the pH most favourable for the formation of **1** is ca. 9.2, given by the equation

$$[2] \quad pH = \frac{1}{2}(pK_{HCN} + pK_{NH_4^+})$$

However, while α-aminonitriles are thermodynamically unstable in weakly acid solution, complete protonation of $-NH_2$ to $-NH_3^+$ by strong acid renders them kinetically stable. Based on these considerations, we devised a simple two-phase (2P) procedure for the synthesis of these compounds. For safety and convenience, NH_4Cl and NaCN (≡ NaCl + NH_4CN ≡ NaCl + NH_3 + HCN) were used instead of liquid or gaseous NH_3 and HCN; enough aqueous ammonia was added to buffer the system to pH ≈ 9. The reaction was started in the two-phase system THF–H_2O (salts), but water was removed during the course of

[1]Revision received September 22, 1986.

TABLE 1. Yields of α-aminonitriles **1** obtained by two-phase (2P) procedure (as salts) and by literature procedures

Structure				Yield (%)		Melting point (°C)		Hydantoin melting point (°C)	
R^1	R^2	X^-	Solvent[a]	2P	Lit. (ref.)	2P	Lit. (ref.)	2P	Lit. (ref.)
Me	H	Cl	A	30	14(9), 34(10)	130–132	125–128(9)	142–143[b]	147–150(11)
n-Pr	H	Cl	A	67	13(9)	145–150	148–150(9)	134–136	136.5(12)
i-Pr	H	Cl	A	82	44(13), 64(14)	205–210	204–210(14)	145–147[b]	145(12)
n-Bu	H	Cl	A	69	18(9)	143–145	—	137–139[b]	139.5(15)
sec-Bu	H	Cl	A	57	—	182–184	—	123–125[b]	—
i-Bu	H	Cl	A	78	—	170–172	175–180(16)	208–210[b]	212(17)
Ph	H	Cl	E/DE 1:10	61	30[c]	169–172	169–172[c]	174–176	178(12, 18)
$PhCH_2$	H	NO_3	A	25	—	149–151	—	187–188[b]	190(18)
$-(CH_2)_5-$		Cl	E/EA 1:7	79	77(19)	183–185	187–189(20)	—	—
Me	Me	Cl	A	77	72(21)	144–146	—	—	—

[a]Recrystallization solvents: A, acetonitrile; E, ethanol; DE, diethyl ether; EA, ethyl acetate.
[b]The identities of these compounds were also established by comparison of ^1H nmr spectra with those reported in the literature (22).
[c]Results of F. L. Chubb using published procedure (23).

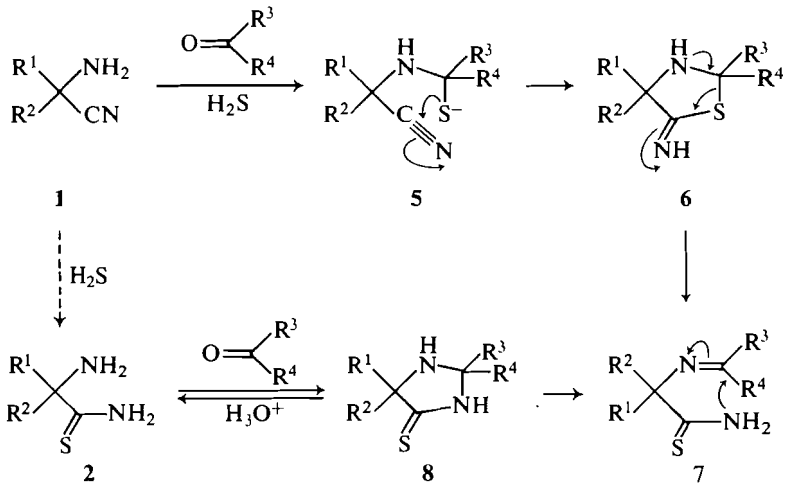

SCHEME 2

the reaction by addition of anhydrous sodium sulfate, to push reaction [1] to the right. The product was isolated as the stable and relatively insoluble hydrochloride or nitrate by treating the oily product in diethyl ether with HCl gas or 70% HNO_3. No systematic studies were made to optimize the yields shown in Table 1, but it is evident that the two-phase procedure usually gave better yields of α-aminonitriles from aldehydes (R^1 = H), if not from ketones, than the procedures described in the literature. This may be due in part to the isolation of the α-aminonitriles as salts rather than as the unstable free bases.

The identity of the α-aminonitrile salts was confirmed by their ir and nmr spectra, and by their conversion into the stable hydantoins when heated with ammonium carbonate (24). The ir spectra of the α-aminonitrile salts did not show a C≡N stretching band at 2200 cm^{-1}, but were otherwise unexceptional.

The formation of α-aminothioamides from the treatment of α-aminonitriles with hydrogen sulfide was mentioned above. This is a capricious reaction. Thus treatment of α-aminobenzyl cyanide (**1**; R^1 = Ph, R^2 = H) with hydrogen sulfide in 95% ethanol for 24 h gave the polymer $-(CH_2Ph\text{-}S)-_n$ (25), presumably because of the reversibility of [1] under these conditions. We have found the most convenient preparation of α-aminothioamides to be that of Cook, Heilbron, and Mahadevan (7), in which α-aminonitriles are treated with hydrogen sulfide and a ketone (a plausible pre-biotic reagent (26)) in basic solution to afford imidazolidin-4-thiones **8** in good yield[2] (Scheme 2). These in turn may be hydrolysed in dilute acids to yield α-aminothioamides **2** (7, 28).

Cook *et al.* (7) proposed that the imidazolidin-4-thiones **8** were formed by the route **1** → **2** → **8**. However, the rate of formation of **8** is much too great for this mechanism, when account is taken of the slowness of the proposed step **1** → **2**. Thus α-aminobenzyl cyanide (**1**; R^1 = pH, R^2 = H) reacted with hydrogen sulfide and cyclohexanone within ten minutes to give a 30% yield of the imidazolidin-4-thione **8** (R^1 = Ph, R^2 = H, R^3R^4 = $-(CH_2)_5-$); within an hour the reaction was essentially complete. In this time no detectable amount of the α-aminothioamide **2** (R^1 = Ph, R^2 = H) is formed by reaction of the α-aminonitrile with hydrogen sulfide.

A more plausible mechanism is the "assisted" thiohydrolysis of the nitrile group shown in Scheme 2. This mechanism parallels the assisted hydrolysis of the nitrile group of α-aminonitriles in the presence of aldehydes or ketones in basic

[2]The procedure described in the experimental section is a considerable improvement over those described in the literature (7, 27). In particular, some of the procedures of Asinger *et al.* (27) are unnecessarily complicated because of mistaken ideas of the mechanism of the reaction.

Can. J. Chem. Downloaded from www.nrcresearchpress.com by 80.58.250.72 on 09/07/12
For personal use only.

TABLE 2. 5-Phenyl-2,2-disubstituted imidazolidin-4-thiones (**8**; R^1 = Ph, R^2 = H) from the reaction of α-aminobenzyl cyanide with H_2S and various ketones

Substituents				
R^3	R^4	Ketone	Yield (%)	Melting point (°C)
Me	Me	Acetone	86[a]	159–162[b]
Et	Me	2-Butanone	89	132–134[c]
-$(CH_2)_4$-		Cyclopentanone	75	164–166
-$(CH_2)_5$-		Cyclohexanone	95[d]	168–170[e]
-$CH_2CHMe(CH_2)_3$-		3-Methylcyclohexanone	97	143–146
-$(CH_2)_2CHMe(CH_2)_2$-		4-Methylcyclohexanone	86	151–153
-$(CH_2)_2CHBu^t(CH_2)_2$-		4-*tert*-Butylcyclohexanone	94	183–188

[a]Reported (7) yield 76%, (27) 74%.
[b]Reported (7) mp 163°C, (27) 163–164°C.
[c]Reported (7) mp 135°C.
[d]Reported (27) yield 91%.
[e]Reported (27) mp 170–171°C.

TABLE 3. Substituted imidazolidin-4-thiones **8** from the reaction of α-aminonitriles with H_2S and either acetone or cyclohexanone

Substituent					
R^1	R^2	R^3	R^4	Yield (%)	Melting point (°C)
Me	H	Me	Me	42	158–160
n-Pr	H	Me	Me	58	113–114
i-Pr	H	Me	Me	51	101–103
n-Bu	H	Me	Me	~80	174–176[a]
sec-Bu	H	Me	Me	91	104–106
i-Bu	H	Me	Me	81	157–159
$PhCH_2$	H	Me	Me	91	133–134
H	H	-$(CH_2)_5$-		100[b]	193–195[b]
Me	H	-$(CH_2)_5$-		87[c]	150–153[c]
n-Pr	H	-$(CH_2)_5$-		94	138–140
i-Pr	H	-$(CH_2)_5$-		96	144–146
n-Bu	H	-$(CH_2)_5$-		86	115–117
sec-Bu	H	-$(CH_2)_5$-		46	147–150
i-Bu	H	-$(CH_2)_5$-		71	151–153
Me	Me	Me	Me	Low, 96[d,e]	152–156[e]
-$(CH_2)_5$-		Me	Me	Low[f]	213–216[f]
-$(CH_2)_5$-		-$(CH_2)_5$-		59, 91[d,g]	227–229[g]

[a]Melting point of hydrochloride; free base mp ~30°C.
[b]Reported (27) yield 93%, mp 217–219°C.
[c]Reported (27) yield 81%, mp 152–153°C.
[d]Using modified procedure (see Experimental).
[e]Reported (6) yield 20%, mp 153–155°C.
[f]Reported (27) yield 77%, mp 215–217°C.
[g]Reported (27) yield 98%, mp 228.5°C.

solution to give the Schiff bases **7** (O in place of S), very thoroughly studied by Commeyras and others (29–32). The two reactions differ in that further cyclization of the Schiff bases **7** (O in place of S) requires strongly basic conditions or heating (32, 33), while cyclization of the corresponding thio compounds **7** → **8** takes place very easily, so that imidazolidin-4-thiones **8** are the ultimate products of this procedure.

The imidazolidin-4-thiones **8** from the reaction of α-aminobenzyl cyanide with H_2S and various ketones are listed in Table 2. None of the ketones gave significantly higher yields than cyclohexanone, as would be expected from the fact that cyclohexanone is one of the most reactive of the common ketones (34).[3] Consequently, the other α-aminonitriles were treated only with acetone and (or) cyclohexanone in the presence of hydrogen sulfide to give the imdazolidin-4-thiones listed in Table 3. Yields were good to excellent with all the α-aminonitriles (**1**; R^2 = H) derived from aldehydes, but poorer with the α-aminonitriles (**1**; R^1 and R^2 alkyl) derived from ketones, perhaps because of steric hindrance to the step **1** → **2** of the overall reaction sequence. Furthermore, in 95% ethanol the reaction with H_2S and ketones of α-aminonitriles having both R^1 and R^2 alkyl sometimes gave mixtures of products, because the slowness of the reaction sequence **1** → **5** → **8** gave time for appreciable decomposition of the α-aminonitrile to ketone, HCN, and NH_3 (8). Thus, the reaction of the α-aminonitrile **10** with acetone and H_2S would be expected to give only the imidazolidin-4-thione **9**. In fact, a mixture of the imidazolidin-4-thiones **9**, **11**, and **12** was obtained in the yields shown in Scheme 3.[4] These latter products require the decomposition of **10** to cyclohexanone, which can then react with more **10** and H_2S to form **11**, and to ammonia and hydrocyanic acid, which can then react with acetone to form the α-aminonitrile **13** and thence **12**.

The ease of acid hydrolysis of imidazolidin-4-thiones to α-aminothioamides and ketones depends upon their substitution pattern. When R^2 = H (i.e., the original α-aminonitrile was derived from an aldehyde) and $R^3 = R^4$ = Me (i.e., acetone was used in the assisted thiohydrolysis), the imidazolidin-4-thione was readily hydrolysed by one equivalent of hydrochloric acid in aqueous alcoholic solution to give the hydrochlorides of the α-aminothioamides. In this way the thioamides of the nine α-amino acids, glycine, phenylglycine, alanine, norvaline, valine, norleucine, isoleucine, leucine, and phenylalanine, were obtained as their hydrochlorides; these are listed in Table 4. However, when both R^1 and R^2 were alkyl, hydrolysis became very difficult, as already observed by Asinger *et al.*

[3]While aldehydes are more reactive than ketones in catalyzing the intramolecular assisted hydrolysis of α-aminonitriles (31), they were ineffective in promoting the conversion **1** → **8**, apparently because of their preferential reaction with H_2S to form linear or cyclic polythianes.

[4]Similar schemes can explain the formation of imidazolidin-4-thiones from the treatment of α-aminonitriles with hydrogen sulfide (6, 27) and of cyanohydrins with ammonium sulfide (27, 35).

Can. J. Chem. Downloaded from www.nrcresearchpress.com by 80.58.250.72 on 09/07/12
For personal use only.

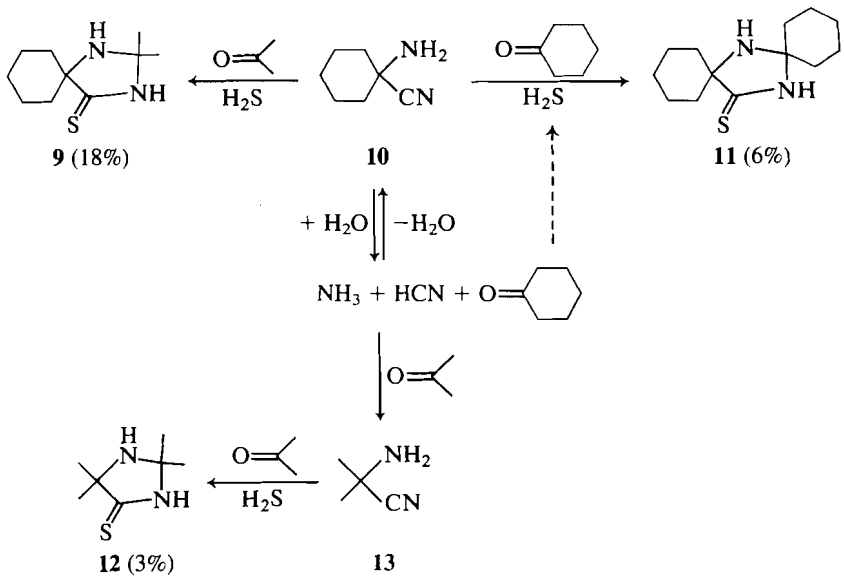

SCHEME 3

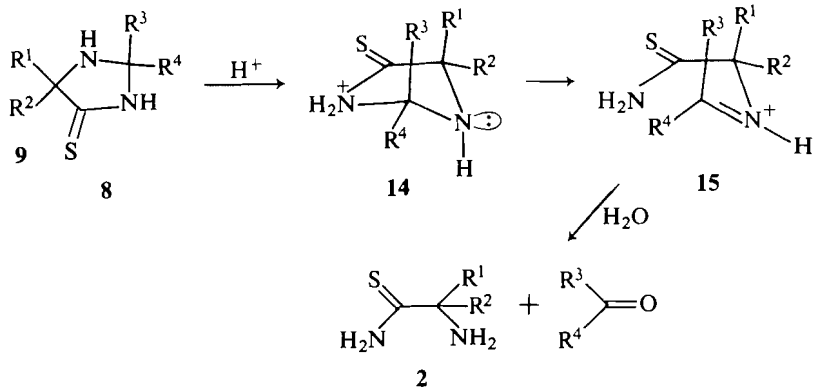

SCHEME 4

TABLE 4. Hydrochlorides of α-aminothioamides **2** obtained by hydrolysis of imidazolidin-4-thiones **8**

Parent amino acid	R^1	R^2	Yield (%)	Melting point (°C)
Glycine	H	H	64	160–161[a]
Alanine[b]	Me	H	61	110[b]
Norvaline	*n*-Pr	H	85[c]	146–148
Valine	i-Pr	H	80	178–180
Norleucine	*n*-Bu	H	88	153–155
Isoleucine	*sec*-Bu	H	91	166–168
Leucine	i-Bu	H	88	141–144
Phenylglycine	Ph	H	80[d]	208–209
Phenylalanine	$PhCH_2$	H	91	209–210

[a]Reported (7) mp 173°C.
[b]Free base; hydrochloride could not be crystallized.
[c]Reported (27) yield of free base 87%.
[d]Reported (27) yield of free base 93%.

TABLE 5. Infrared spectra (KBr) of α-aminonitrile **1** hydrochlorides

Structure		
R^1	R^2	Infrared peaks (cm^{-1})
Me	H	2960, 2850, 2690, 2480, 2000 (w, br), 1570, 1480, 1440
n-Pr	H	2960, 2860, 2680, 2600, 2540, 1950 (w, br), 1575, 1480
i-Pr	H	2980, 2880, 2700, 2630, 2570, 2480, 1900 (w, br), 1580, 1525, 1460
n-Bu	H	2940, 2850, 2700, 2610, 2530, 1970 (w, br), 1580, 1480, 1460, 1450
sec-Bu	H	2980, 2950, 2890, 2670, 2630, 2580, 1910 (w, br), 1586, 1504, 1460
i-Bu	H	2940, 2850, 2640, 2540, 1980 (w, br), 1580, 1560, 1480
Ph	H	2950, 2860, 2600, 2590, 2350, 1965, 1890, 1830, 1770, 1578, 1480, 1448
$PhCH_2$	H	3040, 2950, 2870, 2670, 2480, 1945, 1880, 1775, 1745, 1602, 1520, 1413

(28). This may be explained by the mechanism[5] of Scheme 4, in which the rate-determining step is the breaking of the C—N bond of **14** to give **15** (the protonated form of **7**). Stereoelectronic theory would require the facility of this rupture to depend on the C—N bond being as closely as possible antiperiplanar to the free electron pair of nitrogen shown in **14** (36). Such an antiperiplanar arrangement requires the five-membered ring of **14** to be strongly puckered. The puckering will become difficult when R^1, R^2, R^3, and R^4 are all alkyl

[5]We are grateful to a referee for suggesting this mechanism.

Can. J. Chem. Downloaded from www.nrcresearchpress.com by 80.58.250.72 on 09/07/12
For personal use only.

TABLE 6. Chemical shifts of ^{1}H nmr peaks of α-aminonitrile **1** hydrochlorides

Structure		^{1}H nmr peaks (δ)[a]		
R^1	R^2	NH_3^{+}[b]	$CH(NH_3^{+})CN$	R^1 peaks
Me	H	9.30	4.57 q (7.0)	1.62 d (7.0) (Me)
n-Pr	H	9.42	4.58 t (7.0)	0.97 t (7.0) (Me), 1.17–2.10 m (CH_2CH_2)
i-Pr	H	9.38	4.59 d (5.6)	1.07 d (6.4) (Me), 1.10 d (6.4) (Me), 2.33 m (CH)
n-Bu	H	9.30	4.60 t (7.0)	0.92 t (5.4) (Me), 1.40 m (CH_2CH_2), 1.94 m (CH_2)
sec-Bu	H	9.47	4.59 d (5.0), 4.55 d (6.0)	1.00 t (7.4) (Me), 1.08 d (6.0) (Me), 1.42 m (CH_2), 2.07 m (CH)
i-Bu	H	9.40	4.57 t (7.4)	0.95 d (6.2) (Me), 0.98 d (6.2) (Me), 1.47–2.06 m (CH_2CH)
Ph	H	9.86	6.03 s	7.65 m (Ph)
$PhCH_2$	H	9.60	4.97 d of d (10.0, 6.0)	3.28 m (CH_2), 7.37 s (Ph)

[a]Peak splitting and *J* (in Hz) indicated after δ values.
[b]All broad singlets.

TABLE 7. Combustion analyses of imidazolidine-4-thiones **8**

Structure				Empirical formula	Calcd.			Found		
R^1	R^2	R^3	R^4		C	H	N	C	H	N
Ph	H	-$(CH_2)_4$-		$C_{13}H_{16}N_2S$	67.20	6.94	12.06	67.17	7.03	12.02
Ph	H	-$(CH_2)_5$-		$C_{14}H_{18}N_2S$	68.25	7.36	11.37	68.47	7.81	11.21
Ph	H	-$(CH_2)_2CHBu^t(CH_2)_2$-		$C_{18}H_{26}N_2S$	71.48	8.66	9.26	71.49	8.50	9.02
H	H	-$(CH_2)_5$-		$C_8H_{14}N_2S$	56.43	8.29	16.45	56.14	8.27	16.26
Me	H	-$(CH_2)_5$-		$C_9H_{16}N_2S$	58.65	8.75	15.20	58.46	8.81	15.00
n-Pr	H	-$(CH_2)_5$-		$C_{11}H_{20}N_2S$	62.22	9.49		62.49	9.83	
i-Pr	H	-$(CH_2)_5$-		$C_{11}H_{20}N_2S$	62.22	9.49	13.19	62.50	9.61	13.14
n-Bu	H	-$(CH_2)_5$-		$C_{12}H_{22}H_2S$	63.67	9.79		63.97	10.10	
sec-Bu	H	-$(CH_2)_5$-		$C_{12}H_{22}N_2S$	63.67	9.79	12.37	63.76	9.45	12.31
i-Bu	H	-$(CH_2)_5$-		$C_{12}H_{22}N_2S$	63.67	9.79	12.37	63.84	9.56	12.10
-$(CH_2)_5$-		-$(CH_2)_5$-		$C_{13}H_{22}N_2S$	65.50	9.30	11.75	65.17	8.79	11.52

TABLE 8. Principle infrared peaks of imidazolidin-4-thiones **8**

R^1	R^2	R^3	R^4	Infrared peaks (KBr) (cm^{-1})
Ph	H	Me	Me	3280, 3080, 2953, 2825, 2680, 2610, 1510, 1450, 1420
Ph	H	Et	Me	3300, 3275, 3095, 2968, 2830, 2610, 1495, 1420
Ph	H	-$(CH_2)_4$-		3295, 3110, 2960, 2870, 2690, 2590, 1500, 1420
Ph	H	-$(CH_2)_5$-		3270, 3125, 2920, 2840, 2680, 2580, 1592, 1575, 1495, 1432
Ph	H	-$CH_2CHMe(CH_2)_3$-		3270, 3120, 2960, 2930, 2880, 2850, 2710, 1505, 1448
Ph	H	-$(CH_2)_2CHMe(CH_2)_2$-		3292, 3140, 2925, 2860, 2695, 1600, 1490, 1440
Ph	H	-$(CH_2)_2CHBu^t(CH_2)_2$-		3260, 3130, 3080, 3040, 2950, 2937, 2910, 2860, 1510, 1500, 1450
Me	H	Me	Me	3220, 3160, 2982, 2940, 2880, 2820, 2650, 1510, 1445
n-Pr	H	Me	Me	3230, 3120, 2980, 2960, 2870, 2820, 2730, 2670, 2610, 2500, 1510, 1450
i-Pr	H	Me	Me	3310, 3180, 3030, 2980, 2965, 2935, 2870, 2695, 1535, 1462, 1430
n-Bu	H	Me	Me	3235, 3140, 2955, 2930, 2855, 1510, 1458, 1448
sec-Bu	H	Me	Me	3340, 3290, 3110, 2970, 2940, 2860, 2740, 2640, 1515, 1460, 1430
i-Bu	H	Me	Me	3310, 3260, 3150, 2960, 2938, 2870, 2700, 2620, 1525, 1450
$PhCH_2$	H	Me	Me	3280, 3130, 2990, 2935, 2880, 2700, 1620, 1527, 1450
H	H	-$(CH_2)_5$-		3227, 3080, 2930, 2850, 2730, 2580, 1505, 1448
Me	H	-$(CH_2)_5$-		3235, 3158, 2980, 2940, 2875, 2860, 1493, 1458, 1448
n-Pr	H	-$(CH_2)_5$-		3260, 3145, 2935, 2855, 2700, 1510, 1460
i-Pr	H	-$(CH_2)_5$-		3310, 3145, 2960, 2925, 2860, 2830, 2700, 1510, 1460, 1442
n-Bu	H	-$(CH_2)_5$-		3258, 3222, 3140, 2940, 2860, 2705, 1505, 1460
sec-Bu	H	-$(CH_2)_5$-		3320, 3150, 2960, 2930, 2860, 2700, 1500, 1445
i-Bu	H	-$(CH_2)_5$-		3258, 3148, 2940, 2870, 2700, 1503, 1459, 1432
Me	Me	Me	Me	3330, 3150, 3015, 2980, 2930, 2890, 2860, 2710, 1530, 1460, 1450
-$(CH_2)_5$-		Me	Me	3315, 3125, 2990, 2940, 2860, 2710, 1528, 1452, 1444, 1425
-$(CH_2)_5$-		-$(CH_2)_5$-		3332, 3300, 3140, 2995, 2930, 2865, 2720, 2670, 1510, 1450

Can. J. Chem. Downloaded from www.nrcresearchpress.com by 80.58.250.72 on 09/07/12
For personal use only.

TABLE 9. Chemical shifts of ^{1}H nmr peaks of 2,2-disubstituted 5-phenylimidazolidin-4-thiones **8** of Table 2

Structure		^{1}H nmr peaks (δ)[a]				
R^3	R^4	N(1)-H	N(3)-H[b]	C(5)-H	C(5)-Ph[c]	2-Substituents (R^3 and R^4)
Me	Me	3.37s	10.93	4.97s	7.37	1.43s (2 Me)
Et	Me	3.33s	10.89	4.97s	7.37	0.96t (8.4) (Me),[d] 0.92t (8.4) (Me),[d] 1.38s (Me),[e] 1.43s (Me),[e] 1.67q (8.4) (CH_2)
$-(CH_2)_4-$		3.56d (8.8)	11.02	4.88d (8.8)	7.37	1.75m ($-(CH_2)_4-$)
$-(CH_2)_5-$		3.42d (9.0)	11.00	4.95d (9.0)	7.40	1.67m ($-(CH_2)_5-$)
$-CH_2CHMe(CH_2)_3-$		3.73d, 3.75d	10.88	4.95d (9.0), 4.97d (9.0)	7.37	0.92d (6.0) (Me), 1.20–2.33m ($-CH_2CH(CH_2)_3-$)
$-(CH_2)_2CHMe(CH_2)_2-$		3.40d (8.0)	11.20	4.97d (8.0)	7.40	0.93s br (Me), 1.60m ($-(CH_2)_2CH(CH_2)_2-$)
$-(CH_2)_2CHBu^t(CH_2)_2-$		3.40d (8.0)	11.43	4.97d (8.0)	7.35	0.90s (3 Me), 1.67 br m ($-(CH_2)_2CH(CH_2)_2-$)

[a]Peak multiplicities (singlet, triplet, quartet, etc.) and J values (in Hz) shown after δ values.
[b]Broad singlets.
[c]Multiplets.
[d,e]Adding up to 3H, indicating two diastereomers.

TABLE 10. Chemical shifts of ^{1}H nmr peaks of 2,2-disubstituted imidazolin-4-thiones **8** of Table 3

Structure				^{1}H nmr peaks (δ)[a]				
R^1	R^2	R^3	R^4	N(1)-H[b]	N(3)-H[b]	C(5)-H	C(5)-R	C(2)-R^3 and R^4
Me	H	Me	Me	2.91	10.63	3.78q (6.8)	1.35d (6.8)	1.29s (Me), 1.40s (Me)
n-Pr	H	Me	Me	3.36	10.80	3.63m	0.93t (5.6) (Me), 1.68br m (CH_2CH_2)	1.29s (Me), 1.38s (Me)
i-Pr	H	Me	Me	3.23	10.70	3.81d (2.8)	0.79d (7.0) (Me), 0.97d (7.0) (Me), 2.31m (CH)	1.36s (2 Me)
sec-Bu	H	Me	Me	3.32	10.65	3.90d (~2)	0.81t (6.4) (Me), 0.97d (6.4) (Me), 2.09m (CH_2), 2.67m (CH)	1.33s (2 Me)
i-Bu	H	Me	Me	3.29	10.67	3.72m	0.92d (7.6) (Me), 0.96d (7.6) (Me), 1.12–2.16 ($CHCH_2$)	1.29s (Me), 1.37s (Me)
$PhCH_2$	H	Me	Me	2.83	10.92	3.98m	2.59–3.59m (CH_2), 7.30s (Ph)	1.28s (Me), 1.32s (Me)
H	H	$-(CH_2)_5-$		3.20	10.75	3.69s	3.69s (H)	1.57br s
Me	H	$-(CH_2)_5-$		2.94	10.77	3.73q (6.9)	1.33d (6.0) (Me)	1.57br s
n-Pr	H	$-(CH_2)_5-$		2.70	10.87	3.63br s	0.93t (6.4) (Me), 1.13–2.23m (CH_2CH_2)	1.57br s
i-Pr	H	$-(CH_2)_5-$		2.56	10.73	3.78br s	0.77d (6.6) (Me), 0.96d (7.0) (Me), 2.40m (CH)	1.55br s
n-Bu	H	$-(CH_2)_5-$		3.00	9.97	3.27s	0.83br t (5.6) (Me), 1.00–3.60m ($CH_2CH_2CH_2$)	1.41br s
sec-Bu	H	$-(CH_2)_5-$		3.33	10.77	3.80br m	0.80t (5.6) (Me), 1.00d (6.8) (Me), 1.1–2.27m (CH_2CH)	1.57br s
i-Bu	H	$-(CH_2)_5-$		2.53	9.95	3.27br s	0.82d (5.8) (Me), 0.85d (5.8) (Me), 1.0–2.0br m ($CHCH_2$)	1.43br s
Me	Me	Me	Me	2.85	10.73	—	1.37s (2 Me)	1.33s (2 Me)
$-(CH_2)_5-$		Me	Me	2.63	10.60	—	1.57s ($-(CH_2)_5-$)	1.33s (2 Me)
$-(CH_2)_5-$		$-(CH_2)_5-$		2.40	10.67	—	1.58s ($-(CH_2)_5-$)	1.58s ($-(CH_2)_5-$)

[a]Multiplicity (doublet, triplet, quartet, etc.) and J values (in Hz) shown after δ.
[b]Broad singlets.

groups, because then two alkyl groups are brought close together in an interaction similar to the 1,3-diaxial interaction of alkyl groups in cyclohexanes (see Scheme 4). The interconversion of **14** and **15** is a 5-*endo-trig* process (37), but is evidently not impossible here and elsewhere (29–32; see also ref. 38 and references therein).

α-Aminothioamides may be stored indefinitely as the stable hydrochlorides or other salts but, as the free bases, they decompose at differing rates into other products on standing. The nature of these products is being investigated.

Experimental

General

Melting points are uncorrected. Infrared spectra (KBr) were recorded with a Perkin–Elmer 297 spectrophotometer. Mass spectra were recorded on a Du Pont 21–492 B spectrometer. Proton magnetic resonance (^{1}H nmr) spectra in DMSO-d_6 were recorded with a Varian T-60 spectrometer using the hydrate of sodium 3-(trimethylsilyl)-1-propanesulfonate (TSPSA) as internal standard. Ultraviolet spectra were recorded using a Unicam SP800 spectrophotometer.

Two-phase procedure for preparing α-aminonitriles

The aldehyde (0.10 mol) was added to a stirred mixture of ammonium hydroxide (7.0 mL, 0.11 mol) and tetrahydrofuran (30 mL). After 10 min solid ammonium chloride or nitrate (0.10 mol) and potassium cyanide (6.51 g, 0.10 mol) were added, and the mixture was stirred for 1.5 h in a lightly stoppered flask. Then sodium sulfate (30 g) and diethyl ether (80 mL) were added, and the mixture was swirled frequently for 30 min. The solution was decanted from the solids, which were washed with ether. The combined solution and washings were concentrated under reduced pressure to a syrup, which was dissolved in ethyl ether

Can. J. Chem. Downloaded from www.nrcresearchpress.com by 80.58.250.72 on 09/07/12
For personal use only.

TABLE 11. Combustion analyses of α-aminothioamides **2** as salts or free bases

Structure				Calcd.			Found		
R^1	R^2	Salt	Empirical formula	C	H	N	C	H	N
H	H	HCl	$C_2H_7N_2SCl$	18.97	5.57	—	19.20	5.44	—
Me	H	PA[a]	$C_9H_{11}N_5O_7S$	38.40	4.56	18.66	38.68	4.83	18.65
n-Pr	H	HCl	$C_5H_{13}N_2SCl$	35.60	7.77	—	35.67	7.46	—
i-Pr	H	PA[a]	$C_{11}H_{15}N_5O_7S$	36.56	4.18	19.38	36.52	4.34	19.39
n-Bu	H	HCl	$C_6H_{15}N_2SCl$	39.44	8.27	15.33	39.10	7.95	15.04
sec-Bu	H	HCl	$C_6H_{15}N_2SCl$	39.44	8.27	—	39.11	7.99	—
i-Bu	H	—	$C_6H_{14}N_2S$	49.28	9.65	19.15	49.59	9.99	19.12
i-Bu	H	PA[a]	$C_{12}H_{17}N_5O_7S$	38.40	4.56	18.66	38.68	4.83	18.85
Ph	H	HCl	$C_8H_{11}N_2SCl$	47.40	5.47	—	47.44	5.52	—
$PhCH_2$	H	HCl	$C_9H_{13}N_2SCl$	49.88	6.05	—	49.74	6.25	—
$-(CH_2)_5-$		HNO_3	$C_7H_{15}N_3O_3S$	38.00	6.83	—	38.32	6.91	—
$-(CH_2)_5-$		PA[a]	$C_{13}H_{17}N_5O_7S$	40.31	4.42	18.08	40.19	4.64	17.78

[a]Picric acid.

TABLE 12. Infrared peaks of hydrochlorides of α-aminothioamides **1**

R^1	R^2	Infrared peaks (KBr) (cm^{-1})
H	H	3300, 3140, 2995, 2940, 2930, 2880, 2865, 2690, 2590, 2455, 2360, 2075, 1935, 1687, 1643, 1590, 1465
Me	H	3290, 3140, 3060, 2900, 2780, 2690, 2570, 2330, 1630, 1585, 1435
n-Pr	H	3260, 3100, 2960, 2870, 2820, 2560, 2450, 2360, 1950 (br), 1630, 1570, 1465
i-Pr	H	3300, 3170, 2980, 2940, 2740, 2670, 2620, 1935, 1640, 1592, 1570, 1440
n-Bu	H	3260, 3120, 3090, 2950, 2930, 2920, 2850, 2570, 1950, 1625, 1590, 1560, 1460
sec-Bu	H	3300, 3140, 3040, 2960, 2920, 2610, 1960, 1640, 1600, 1575, 1500, 1465
i-Bu	H	3280, 3080, 2960, 2870, 2750, 2690, 2630, 2570, 2520, 2460, 1985, 1648, 1588, 1457
Ph	H	3275, 3125, 3035, 2990, 2945, 2885 (br), 2825, 2785, 2695, 2645, 2600, 2560, 1985, 1965, 1915 (w, br), 1895, 1638, 1583, 1575, 1475, 1440
$PhCH_2$	H	3300, 3280, 3155, 3090, 3070, 3030, 3010, 2990, 2940, 2900, 1960 (w, br), 1630, 1597, 1580, 1470, 1455, 1430

(300 mL). Hydrogen chloride gas was bubbled through the solution until precipitation was complete. (Alternatively, concentrated nitric acid (6 mL, ~0.10 mol) was added to the stirred ethereal solution). The solid precipitate was suction filtered, air-dried, and weighed. Yields are given in Table 1 and spectral data in Tables 5 and 6.

The two-phase mixture derived from ketones and from benzaldehyde was stirred for 7 h and dried over sodium sulfate overnight, but the procedure was otherwise identical to the one above. Recrystallization of **1** (R^1 = Ph, R^2 = H) was from ethanol/ether 1:10.

General procedure for preparing imidazolidin-4-thiones **8**

Hydrogen sulfide was bubbled for 1 h into an ethanolic solution (sometimes containing some water) (30 mL total) at 0°C containing the α-aminonitrile salt (0.020 mol), triethylamine (2.05 g, 0.020 mol), and the ketone (0.20 mol). The product started to separate after 10–45 min, depending on the ketone. After standing overnight in the stoppered reaction vessel, hydrogen sulfide was purged by a stream of N_2 that was passed into sodium hydroxide traps, the reaction vessel being kept in a water bath at 50–60°C. The suspension was then concentrated on a rotatory evaporator. The solid residue was treated with water (50 mL), removed by filtration, and washed with water (2 × 50 mL). Yields are shown in Tables 2 and 3, combustion analyses in Table 7, ir data in Table 8, and nmr data in Tables 9 and 10.

A modified procedure, in which the reaction was carried out in 30 mL of concentrated ammonium hydroxide with a little ethanol to obtain a homogenous solution, and with potassium hydroxide (1.12 g, 0.020 mol) instead of triethylamine, gave 96% and 91% yields of **8** ($R^1 = R^2 = R^3 = R^4$ = Me) and **8** ($R^1R^2 = R^3R^4 = -(CH_2)_5-$) respectively (cf. end of Table 3).

Hydrochlorides of the imidazolidin-4-thiones, prepared by bubbling hydrogen chloride into acetone solutions of the compounds, crystallized out as sharply melting, pure compounds.

*Reaction of 1-aminocyclohexane carbonitrile (**1**; $R^1R^2 = -(CH_2)_5-$) with acetone and hydrogen sulfide*

The hydrochloride (3.2 g) of the α-aminonitrile was neutralized with 2 *N* sodium hydroxide (10 mL), taken up in ether (3 × 30 mL), and dried (Na_2SO_4). The residue left by evaporation of the ether was dissolved in ethanol (10 mL) and acetone (4.5 mL), two drops of triethylamine were added, and then hydrogen sulfide was bubbled through the solution for 1.5 h. The solution was left for 24 h at room temperature, purged of H_2S by a stream of N_2, and concentrated to yield 1.2 g of white solid. Chromatography on Florisil with ethyl acetate – light petroleum yielded three compounds: cyclohexanespiro-2′-(imidazolidin-4′-thione)-5′-spirocyclohexane **11** (0.19 g), mp 227–228°C, identical (mp, ir, nmr) with authentic material (35); cyclohexanespiro-5′-(2′,2′-dimethylimidazolidin-4′-thione) **9** (0.50 g), mp 213–216°C (lit. (27) mp 215–216°C), identified by ir (Table 9) and nmr (Table 10) spectra; and 2,2,5,5-tetramethylimidazolidin-4-thione **12** (0.06 g), mp 152–156°C (lit. (6) mp 153–155°C), identified by ir (Table 9) and nmr (Table 10) spectra.

General procedure for preparing α-aminothioamide hydrochlorides

The hydrochloride of the requisite imidazolidin-4-thione **8** (R^2 = H) (0.010 mol) in 95% ethanol (15 mL) containing 3 drops of ethanolic hydrogen chloride (4.0 *M*) was refluxed for 2 h. The solution was evaporated under reduced pressure and the residual solids were recrystallized from acetonitrile. Yields are shown in Table 4. The hydrochloride of the thioamide of alanine turned out to be an oil, and so was treated in ethanol with excess bicarbonate and, isolated as

Can. J. Chem. Downloaded from www.nrcresearchpress.com by 80.58.250.72 on 09/07/12
For personal use only.

TABLE 13. Chemical shifts of ^{1}H nmr peaks of salts[a] of α-aminothioamides **2**

Structure		^{1}H nmr peaks (δ)[b]			
R^1	R^2	$-NH_3^+$[c]	$-CSNH_2$[c]	-H (R^2)	R^1
H	H	8.47	10.03	3.78s	3.78s (H)
Me[d]	H	8.08	9.60, 9.90	4.13q (6.4)	1.42d (6.4) (Me)
n-Pr	H	8.40	10.00	4.10t (6.6)	0.88t (5.6) (Me), 1.33m (CH_2), 1.72m (CH_2)
i-Pr	H	8.46	10.08	3.93d (7.6)	0.99d (7.0) (Me), 1.06d (7.0) (Me), 2.15m (CH)
n-Bu	H	8.57	10.20	4.10m	0.90t (4.8) (Me), 1.30m (CH_2CH_2), 1.77m (CH_2)
sec-Bu	H	8.42	10.05	3.95m	0.89t (6.4) (Me), 1.01d (6.4) (Me), 1.38m (CH_2), 1.85m (CH)
i-Bu	H	9.43	10.37	4.13t (6.6)	0.96d (6.0) (Me), 0.99d (6.0) (Me), 1.71m ($CHCH_2$)
Ph	H	8.93	10.05, 10.43	5.40s	7.4–7.9m (Ph)
$PhCH_2$	H	8.63	9.93	4.43m	3.20m (CH_2), 7.30s (Ph)

[a]Hydrochlorides, except when noted otherwise.
[b]Multiplicity (singlet, doublet, etc.) and *J* value (in Hz) shown after δ values.
[c]Broad singlet.
[d]Picrate, not hydrochloride.

the base, crystallized from benzene/light petroleum. Several of the hydrochlorides gave poor combustion analyses, perhaps because of hygroscopicity, and were converted into picrates for analysis: see Table 11. The ir spectra are given in Table 12, and ^{1}H nmr spectra in Table 13.

When the above procedure was applied to the hydrochloride of 2,2,5,5-tetramethylimidazolidin-4-thione, no hydrolysis was observed after refluxing for 10 h.

Acknowledgement

We are grateful for financial support from the Natural Sciences and Engineering Research Council of Canada.

1. S. L. MILLER. Science, **117**, 528 (1953).
2. S. L. MILLER. *In* Mineral deposits and the evolution of the biosphere. *Edited by* H. D. Holland and M. Schidlowski. Springer Verlag, Berlin. 1982. p. 164.
3. J. P. FERRIS. Chem. Eng. News, **61**, 22 (1984).
4. T. B. JOHNSON and G. BURNHAM. J. Biol. Chem. **9**, 449 (1961).
5. E. GATEWOOD and T. B. JOHNSON. J. Am. Chem. Soc. **48**, 2800 (1926).
6. E. GATEWOOD and T. B. JOHNSON. J. Am. Chem. Soc. **50**, 1422 (1928).
7. A. H. COOK, I. M. HELLBRON, and A. P. MAHADEVAN. J. Chem. Soc. 1064 (1949).
8. A. COMMEYRAS, J. TAILLADES, L. MION, and M. LASPERAS. Inf. Chim. 194 (1976).
9. J. JENNI, H. KUHNE, and B. PRIJS. Helv. Chim. Acta, **45**, 1163 (1962).
10. J. V. DUBSKY. Ber. **49**, 1045 (1916).
11. S. KOMATSU. Mem. Coll. Sci. Eng. Kyoto, **3**, 1 (1911); Chem. Abstr. **5**, 2819 (1911); H. D. DAKIN. J. Chem. Soc. **107**, 434 (1915).
12. H. BERGS. Chem. Abstr. **27**, P. 1001[7] (1933).
13. D. J. ABERHART and L. J. LIN. J. Chem. Soc. Perkin Trans. 1, 2320 (1974).
14. H. IINUMA, N. YAGISAWA, S. SHIBAHARA, Y. SUHARA, S. KONDO, K. MAEDA, T. TAKEUCHI, M. OHNO, and H. UMEZAWA. Agric. Biol. Chem. **38**, 2099 (1974).
15. H. R. HENZE and R. J. SPEER. J. Am. Chem. Soc. **64**, 522 (1942).
16. G. T. NEWBOLD, W. SHARP, and F. S. SPRING. J. Chem. Soc. 2679 (1951).
17. F. LIPPICH. Ber. **41**, 2953 (1908); Chem. Abstr. **3**, 59[9] (1908).
18. H. T. BUCHERER and V. A. LIEB. J. Prakt. Chem. **89**, 361 (1914).
19. R. M. HERBST and T. B. JOHNSON. J. Am. Chem. Soc. **54**, 2463 (1932).
20. A. SNAESSAREW. J. Prakt. Chem. **89**, 361 (1914).
21. J. TAILLADES and A. COMMEYRAS. Tetrahedron, **30**, 3407 (1974).
22. T. SUZUKI, T. TOMIOKA, and K. TUZIMURA. Can. J. Biochem. **55**, 521 (1977).
23. L. NEELAKATAN and W. H. HARTUNG. J. Org. Chem. **24**, 1943 (1959).
24. J. T. EDWARD and C. JITRANGSRI. Can. J. Chem. **53**, 3339 (1975).
25. H. KLINGER. Ber. **9**, 1895 (1876).
26. J. P. FERRIS and C. T. CHEN. J. Am. Chem. Soc. **97**, 2962 (1975).
27. P. ASINGER, W. SCHAFER, H. HEISEL, H. KERSTEIN, and A. SAUS. Monatsh. Chem. **98**, 338 (1967).
28. F. ASINGER, W. SCHAFER, H. KERSTEIN, and A. SAUS. Monatsh. Chem. **98**, 1843 (1967).
29. R. PASCAL, J. TAILLADES, and A. COMMEYRAS. Bull. Soc. Chim. Fr. II, 177 (1978).
30. R. PASCAL, J. TAILLADES, and A. COMMEYRAS. Tetrahedron, **34**, 2275 (1978).
31. R. PASCAL, J. TAILLADES, and A. COMMEYRAS. Tetrahedron, **36**, 2999 (1980).
32. J. T. EDWARD and F. L. CHUBB. Proc. R. Ir. Acad. Sect. B, **83**, 57 (1983).
33. A. C. DAVIS and A. L. LEVY. J. Chem. Soc. 3479 (1951).
34. J. HINE. Structural effects in organic chemistry. John Wiley, New York. 1975. Chapt. 8.
35. H. T. BUCHERER and W. BRANDT. J. Prakt. Chem. **140**, 129 (1934).
36. P. DESLONGCHAMPS. Stereoelectronic effects in organic chemistry. Pergamon Press, Oxford. 1983.
37. J. E. BALDWIN. J. Chem. Soc. Chem. Commun. 734 (1976).
38. B. A. KEAY, D. RAJAPAKSA, and R. RODRIGO. Can. J. Chem. **62**, 1093 (1984).

Can. J. Chem. Downloaded from www.nrcresearchpress.com by 80.58.250.72 on 09/07/12
For personal use only.

Flash vacuum pyrolysis of anthracenic Diels–Alder adducts, a convenient source of methanethial and methanethial *S*-oxide[1]

YANNICK VALLEE AND JEAN-LOUIS RIPOLL[2]
Laboratoire de Chimie des Composés Thioorganiques (UA CNRS N° 480), Université de Caen, 14032 Caen, France

AND

CHRISTOPHE LAFON AND GENEVIÈVE PFISTER-GUILLOUZO
Laboratoire de Physico-Chimie Moléculaire (UA CNRS N° 474), Université de Pau, 64000 Pau, France

Received June 17, 1986

YANNICK VALLEE, JEAN-LOUIS RIPOLL, CHRISTOPHE LAFON, and GENEVIÈVE PFISTER-GUILLOUZO. Can. J. Chem. **65**, 290 (1987).

The flash vacuum pyrolysis of Diels–Alder adducts of anthracene constitutes a rapid and selective route to methanethial **1** and methanethial *S*-oxide **2**, as analyzed in the gas phase by photoelectron spectroscopy. Low temperature infrared and nuclear magnetic resonance (^1H, ^{13}C) spectra are also reported for sulfine **2**.

YANNICK VALLEE, JEAN-LOUIS RIPOLL, CHRISTOPHE LAFON et GENEVIÈVE PFISTER-GUILLOUZO. Can. J. Chem. **65**, 290 (1987).

La thermolyse éclair d'adduits de Diels–Alder dérivés de l'anthracène constitue une voie d'accès rapide et sélective au méthanethial **1** et au *S*-oxyde de méthanethial **2**, analysés en phase gazeuse par spectrométrie photoélectronique. Les spectres infrarouge et de résonance magnétique nucléaire (^1H et ^{13}C) à basse température sont également rapportés pour la sulfine **2**.

Can. J. Chem. Downloaded from www.nrcresearchpress.com by 80.58.250.72 on 09/07/12
For personal use only.

Introduction

The title compounds, methanethial **1** (thioformaldehyde) and methanethial *S*-oxide **2**, first members in the classes of thioaldehydes and sulfines, respectively, present a particular interest related to their simplicity (four and five atoms) and high reactivity. Methanethial **1** is also an interstellar molecule (1).

The Diels–Alder cyclo-addition and reversion has been employed several times as a protection–regeneration sequence for the purification of substituted thioaldehydes (2). Methanethial **1** and its *S*-oxide **2**, when generated by other thermal decompositions or eliminations, are easily contaminated with volatile co-formed reaction products and/or starting materials; these methods thus require careful optimization of the experimental conditions (3, 4).

The retro-Diels–Alder reaction under flash vacuum pyrolysis (fvp), hitherto not applied to the synthesis of **1** or **2**, was expected by us to constitute a simple, rapid alternative synthetic route. The anthracene adducts **3** and **4**, smoothly prepared from thiophosgene and anthracene (5), should lead more readily to clean thio-compounds **1** and **2**, owing to the low-volatility of both the precursors **3** or **4** and the formed anthracene (Fig. 1) (the formal Diels–Alder adduct between sulfene $H_2C{=}SO_2$ and anthracene, closely related to **3** and **4**, gives upon pyrolysis SO_2 elimination in place of the $(4\pi + 2\pi)$ cycloreversion (6)).

Experimental

Adducts **3** and **4** were sublimed under 10^{-6} Torr through a short path fvp oven (quartz tube 6 cm length × 1.6 cm i.d.). Anthracene, and eventually the unreacted starting material, crystallized immediately at the exit of the oven. Volatile products were condensed at 77 K, on frozen $CFCl_3$ for nmr analysis and attempts at chemical trapping, or on a NaCl pellet for ir spectroscopy (see ref. 7 for more experimental details). Gas phase analysis was performed, as previously described (8), by direct coupling of the fvp oven with a Helectros 0078 photoelectron spectrometer. The present impurities (CS_2, H_2S, SO_2) were identified by comparing their photoelectron spectra with those of authentic samples (9).

[1]Part 21 of the series "Retrodienic reactions"; for part 20, see ref. 16.

[2]To whom all correspondence should be addressed.

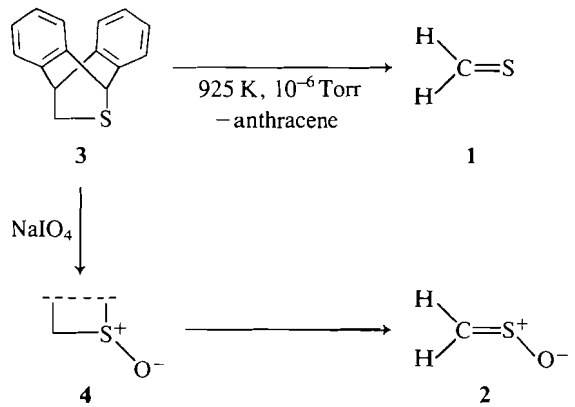

FIG. 1. Flash vacuum pyrolysis to synthesize **1** and **2**.

Results and discussion

A complete cycloreversion of sulfide **3** takes place at an oven temperature of 925 K, leading to anthracene in ~100% yield. Whereas only polymeric methanethial **1** was observed both in condensed phase and in solution (^1H nmr (CCl_4) 4.03 and 4.10 ppm; ir (film) 1368, 1173, 735, and 708 cm^{-1}, in agreement with ref. 10), the gas phase photoelectron analysis indicates the presence of monomeric **1** in a practically pure state (ionisations at 9.36, 11.87, 14.02, and 15.23 eV, in good agreement with ref. 11), the only impurities being traces of CS_2 and H_2S (Fig. 2).

On the other hand, the fvp of sulfoxide **4** at 925 K gives, besides anthracene (quantitatively obtained) and polymeric material, methanethial *S*-oxide **2** as evidenced by its nmr spectra recorded at 173 K (δ ^1H ($CFCl_3$): 7.73 and 7.84 ppm (2H AB, J 5.5 Hz); δ ^{13}C ($CFCl_3$ + CD_2Cl_2): 158.8 ppm; spectra in accordance with those of substituted sulfines (3, 12), no nmr data were hitherto reported for sulfine **2** itself). A rapid loss of the signals attributed to **2** takes place upon warming, and the concomitant formation of an insoluble white polymer is observed (attempts at trapping **2** by methyllithium, cyclopentadiene, or 1,3-diphenylisobenzofuran were unsuccessful).

The ir spectrum of the pyrolysis product of **4**, recorded

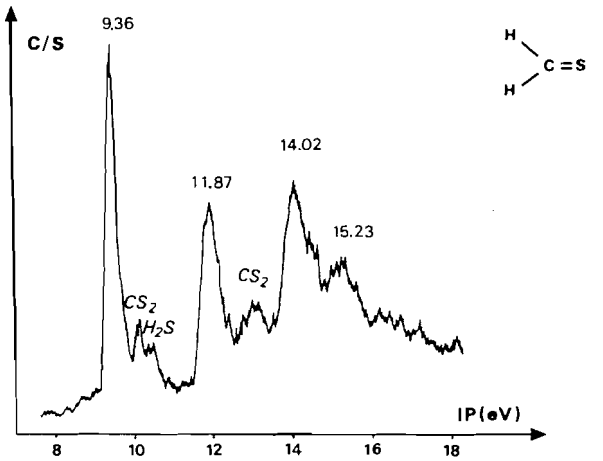

FIG. 2. Photoelectron spectrum of methanethial, **1**.

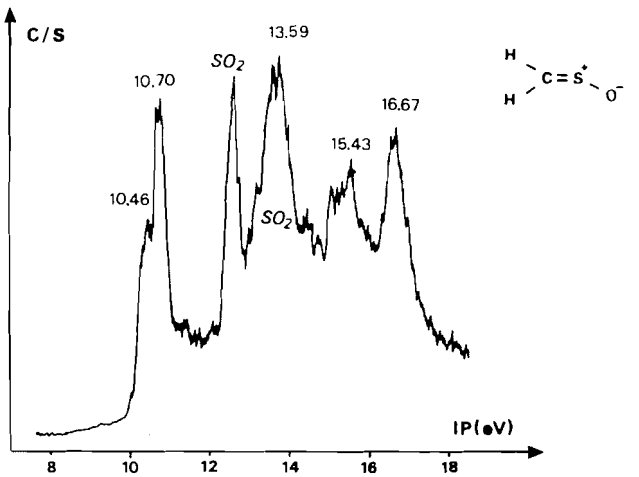

FIG. 3. Photoelectron spectrum of methanethial *S*-oxide, **2**.

under vacuum at 77 K, shows main transient absorptions at 1375, 1125, and 820 cm^{-1} and weaker bands at 3100 and 990 cm^{-1}. They are replaced at about 173 K by an intense band at 1048 cm^{-1}, assigned to polymers. Owing to the different conditions, these bands may be compatible with those reported in an argon matrix for sulfine **2** (13) (1357, 1165, 767 cm^{-1}). Also, fvp of the reported precursor of **2**, 1,3-dithietane-1-oxide (14), gave in our experimental conditions, in a less pure state, the above described ^1H nmr and ir spectra attributed to sulfine **2** in the pyrolysis of sulfoxide **4**.

The photoelectron spectrum of the pyrolysis product of **4** also agrees with that described for sulfine **2** (15) (Fig. 3); the characteristic ionisation pattern of SO_2, a known evolution product of **2** in the gas phase (14), is the only observed impurity.

Acknowledgements

We wish to thank Professor E. Block, State University of New York at Albany, for helpful comments and gift of a sample of 1,3-dithietane-1-oxide.

1. A. P. C. MANN and D. A. WILLIAMS. Nature, **283**, 721 (1980).
2. M. C. LASNE and J. L. RIPOLL. Synthesis, 121 (1985).
3. H. BOCK, T. HIRABAYASHI, and S. MOHMAND. Chem. Ber. **115**, 492 (1982) and references therein.
4. E. BLOCK. *In* Organic sulfur chemistry. *Edited by* R. Zh. Freidlina and A. E. Skorova. Pergamon Press, Oxford. 1981. p. 15; E. BLOCK and A. WALL. Tetrahedron Lett. **26**, 1425 (1985) and references therein.
5. H. ALLGEIER and T. WINKLER. Tetrahedron Lett. 215 (1976).
6. N. J. HALES, D. J. H. SMITH, and M. E. SWINDLES. J. Chem. Soc. Chem. Commun. 981 (1976).
7. Y. M. MALECOT, J. L. RIPOLL, and A. THUILLIER. J. Chem. Res. S-86, M-0959 (1983).
8. C. LAFON, D. GOMBEAU, G. PFISTER-GUILLOUZO, M. C. LASNE, J. L. RIPOLL, and J. M. DENIS. Nouv. J. Chim. **10**, 69 (1986).
9. K. KIMURA, S. KATSUMATA, Y. ACHIBA, T. YAMAZAKI, and S. IWATA. *In* Handbook of He I photoelectron spectra of fundamental organic molecules. *Edited by* Japan Scientific Society Press, Tokyo. 1981.
10. M. OHSAKU. Bull. Chem. Soc. Jpn. **47**, 965 (1974).
11. H. W. KROTO and R. J. SUFFOLK. Chem. Phys. Lett. **15**, 545 (1972); B. SOLOUKI, P. ROSMUS, and H. BOCK. J. Am. Chem. Soc. **98**, 6054 (1976); H. BOCK, B. SOLOUKI, S. MOHMAND, E. BLOCK, and L. K. REVELLE. J. Chem. Soc. Chem. Commun. 287 (1977).
12. E. BLOCK and S. AHMAD. J. Am. Chem. Soc. **107**, 6731 (1985).
13. D. E. POWERS, C. A. ARRINGTON, W. C. HARRIS, E. BLOCK, and V. F. KALASINSKY. J. Phys. Chem. **83**, 1890 (1979).
14. E. BLOCK, R. E. PENN, R. J. OLSEN, and P. F. SHERWIN. J. Am. Chem. Soc. **98**, 1264 (1976).
15. E. BLOCK, H. BOCK, S. MOHMAND, P. ROSMUS, and B. SOLOUKI. Angew. Chem. Int. Ed. Engl. **15**, 383 (1976); E. BLOCK, E. R. COREY, R. E. PENN, T. L. RENKEN, P. F. SHERWIN, H. BOCK, T. HIRABAYASHI, S. MOHMAND, and B. SOLOUKI. J. Am. Chem. Soc. **104**, 3119 (1982).
16. M. C. LASNE and J. L. RIPOLL. Bull. Soc. Chim. Fr. 766 (1986).

Can. J. Chem. Downloaded from www.nrcresearchpress.com by 80.58.250.72 on 09/07/12
For personal use only.

Open-chain nitrogen compounds. Part XII.[1] Methanolysis of 3-alkyl-3,4-dihydro-1,2,3-benzotriazin-4-ols: evidence for ring-chain tautomerism with the cytotoxic monoalkyltriazenes

RONALD J. LAFRANCE, HARTFORD W. MANNING, AND KEITH VAUGHAN[2]
Department of Chemistry, Saint Mary's University, Halifax, N.S., Canada B3H 3C3

Received September 27, 1985[3]

RONALD J. LAFRANCE, HARTFORD W. MANNING, and KEITH VAUGHAN. Can. J. Chem. **65**, 292 (1987).

A series of 4-hydroxy-3,4-dihydro-1,2,3-benzotriazines ("triazinols"), potential pro-drugs for the cytotoxic monoalkyltriazenes, have been investigated for anti-tumor activity and have been found to have marginal activity against the TLX5 tumor. The in vivo anti-tumor activity correlates with previously observed in vitro cytotoxicity of the compounds. The chemical behaviour of the triazinols is consistent with carbinolamine ⇌ triazene ring-chain tautomerism in solution. The triazinols undergo methanolysis to give a series of new 4-methoxytriazines; the rate of methanolysis is primarily dependent on the substituent at C-4 of the triazinol. Those triazinols that undergo methanolysis rapidly are also more active biologically, suggesting that cytotoxicity and anti-tumor activity derive from the *in situ* generation of the open chain triazene.

RONALD J. LAFRANCE, HARTFORD W. MANNING et KEITH VAUGHAN. Can. J. Chem. **65**, 292 (1987).

On a évalué l'activité contre les tumeurs d'une série d'hydroxy-4 dihydro-3,4 benzotriazines-1,2,3 («triazinols»), des pro-drogues potentielles pour les monoalkyltriazènes cytotoxiques; on a trouvé que ces composés n'ont qu'un effet marginal sur les tumeurs TLX5. Il existe une corrélation entre l'activité in vivo contre les tumeurs et la cytotoxicité in vitro observée antérieurement pour ces composés. Le comportement chimique des triazinols en solution est en accord avec une tautomérisation cycle/chaîne carbinolamine ⇌ triazène. Les triazinols subissent une méthanolyse qui conduit à une série de nouvelles méthoxy-4 triazines; les vitesses de méthanolyse dépendent principalement de la nature du substituant en position C-4 du triazinol. Les triazinols qui subissent la méthanolyse le plus rapidement sont aussi les composés qui sont les plus actifs d'un point de vue biologique; ces résultats suggèrent que la cytotoxicité ainsi que l'activité contre les tumeurs provient de la génération *in situ* du triazène en chaîne ouverte.

[Traduit par la revue]

Introduction

Imidazotetrazinones (**1**) have been shown to possess pronounced anti-tumor activity against mouse L1210 and P388 leukemias (1), and one of these agents, the N-chloroethyl derivative ("mitozolomide," CCRG 81010, M&B 39565, NSC 353451) has entered Phase II clinical trial (2). A mechanism of action study of this novel and potent anti-tumor agent has shown (3) that cytotoxicity is exerted by a metabonate of the drug and that the most likely species responsible for cytotoxicity is the monochloroethyltriazenoimidazole ("MCTIC") (**2**). Thus

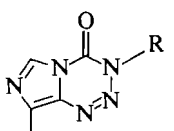

1

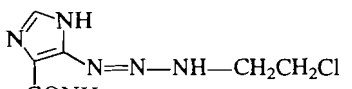

2

mitozolomide acts as a "pro-drug," without the need for metabolic activation, for the cytotoxic monoalkyltriazene, in contrast to the anti-tumor dimethyltriazenes, which require metabolic N-demethylation to generate the cytotoxic monomethyltriazene (4).

The observation that mitozolomide is indeed a pro-drug for an acyclic triazene suggests that other nitrogen-containing heterocycles with NNN linkages might act as slow release forms of cytotoxic triazenes. In a previous report (5), it was shown that *o*-acylphenyltriazenes (**3**) undergo facile cyclization to the novel 4-hydroxy-3,4-dihydrobenzo-1,2,3-triazines ("triazinols", e.g. **4**). Nuclear magnetic resonance spectra of these novel cyclic carbinolamines suggest that they exist in equilibrium with the open-chain triazene tautomers in solution, and these triazinols have been shown to be cytotoxic towards M21 tumor cells in vitro *without* metabolic activation (6). These preliminary observations prompted us to investigate the anti-tumor activity of the triazinols and to determine the extent to which biological activity correlates with the tendency of the molecules towards ring-chain tautomerism with the open-chain triazenes.

The triazinols are important to us not only for their potential as anti-tumor agents. It has not escaped our attention that these 4-hydroxy-1,2,3-benzotriazines represent rare examples of stable α-carbinolamines (i.e., —N—C—OH). Although such species are widely reported in the literature as transient metabolites of N-alkyl xenobiotic molecules (7), very few examples of stable carbinolamines are available chemically for direct study. Thus molecules of type **4** represent excellent model compounds to test some widely accepted metabolic hypotheses. In this paper, we report (a) some chemistry of the cyclic triazinol – acyclic triazene system, (b) the anti-tumor evaluation of representative molecules of this series, and (c) some observations relevant to the metabolism of N-alkyl xenobiotic molecules.

Experimental

Synthesis

The 4-hydroxy-3,4-dihydro-1,2,3-benzotriazines (**4**, **5**, **7**, **8**, **10**, **13**) were prepared by the reported method (5).

*3-(2-Chloroethyl)-4-hydroxy-3,4-dihydro-1,2,3-benzotriazine (**6**)*

2-Aminobenzaldehyde (15 mmol) dissolved in chloroform (50 mL) was added to a solution of sodium nitrite (1.25 g) in water (50 mL) and the two-phase mixture cooled to 0°C. The cold mixture was stirred vigorously while 2 *N* hydrochloric acid (25 mL) was added dropwise. The chloroform layer was separated and washed once with water

[1]For part XI, see ref. 15.
[2]Author to whom all correspondence should be addressed.
[3]Revision received September 17, 1986.

Can. J. Chem. Downloaded from www.nrcresearchpress.com by 80.58.250.72 on 09/07/12
For personal use only.

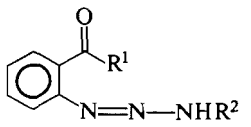

3 *a*, R^1 = H, R^2 = CH_2CH_2Cl
b, R^1 = Et, R^2 = CH_2CH_2Cl
c, R^1 = Ph, R^2 = CH_2CH_2Cl

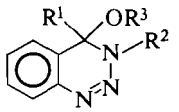

4 R^1 = R^3 = H, R^2 = Me
5 R^1 = R^3 = H, R^2 = Et
6 R^1 = R^3 = H, R^2 = CH_2CH_2Cl
7 R^1 = R^2 = Me, R^3 = H
8 R^1 = Et, R^2 = Me, R^3 = H
9 R^1 = Et, R^2 = CH_2CH_2Cl, R^3 = H
10 R^1 = Ph, R^2 = Me, R^3 = H
11 R^1 = Ph, R^2 = Et, R^3 = H
12 R^1 = Ph, R^2 = CH_2CH_2Cl, R^3 = H
13 R^1 = 2-fluorophenyl, R^2 = Me, R^3 = H
14 R^1 = H, R^2 = R^3 = Me
15 R^1 = R^2 = R^3 = Me
16 R^1 = Et, R^2 = R^3 = Me
17 R^1 = Ph, R^2 = R^3 = Me
18 R^1 = H, R^2 = CH_2CH_2Cl, R^3 = Me
19 R^1 = Ph, R^2 = CH_2CH_2Cl, R^3 = Me
20 R^1 = Et, R^2 = CH_2CH_2Cl, R^3 = Me

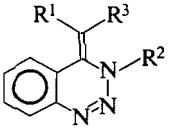

21 R^1 = R^3 = H, R^2 = Me
22 R^1 = H, R^2 = R^3 = Me
23 R^3 = H, R^1 = R^2 = Me
24 R^1 = H, R^2 = CH_2CH_2Cl, R^3 = Me

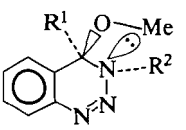

25

(20 mL); the aqueous washing was combined with the aqueous diazonium salt layer. A solution of 2-chloroethylamine hydrochloride (16 mmol) in water (10 mL) was added slowly to the cold diazonium salt solution; the resulting solution was cooled below 0°C and rendered basic by the slow addition of saturated potassium carbonate solution (5 mL). The product was extracted into chloroform and evaporation of the dried chloroform extract gave the chloroethyltriazine (**6**) (10.3 mmol, 69%), mp 72–78°C; ir (Nujol): 3150 (br, OH) cm^{-1}; δ ($CDCl_3$): 3.85–4.00 and 4.21–4.38 (4H, m, $-CH_2CH_2-$), 5.87 (1H, s, CH at C-4), 7.16 (d, *J* 8.0 Hz), 7.34 (t, *J* 8.0 Hz), 7.35 (d, *J* 8.1 Hz), and 7.43 (t, *J* 7.3 Hz, aromatic) ppm; δ ($CDCl_3$): 42.8 (CH_2), 54.3 (CH_2), 73.3 (C4 of triazine), 119.4, 122.9, 126.8, 129.5, 130.0, 135.3 (arom), and 194.3 (*C*=O) ppm.

3-Alkyl-4-hydroxy-3,4-dihydro-1,2,3-benzotriazines

General procedure

The appropriate 2′-aminophenylketone (15 mmol) was dissolved in 1 *N* hydrochloric acid (50 mL), cooled to 0°C, and diazotized with sodium nitrite (15 mmol) in water (10 mL). A solution of the alkylamine hydrochloride (16 mmol) in water (10 mL) was added slowly to the diazonium salt solution; the resulting solution was cooled below 0°C and rendered basic with saturated potassium carbonate solution (5 mL). After stirring for 1 h, the precipitate was filtered, washed with water, and dried to afford the following 4-hydroxy-1,2,3-benzotriazines:

9, from 2′-aminopropiophenone and 2-chloroethylamine, 11 mmol (73%), mp 77–80°C; ir (Nujol): 3110 (br, OH) cm^{-1}; δ ($CDCl_3$): 1.20 (3H, t, *J* 8 Hz, $-CH_3$), 3.00 (2H, q, *J* 8 Hz, $-CH_2-$), 3.7–4.2 (4H, m, $-CH_2CH_2-$), and 6.9–8.0 (4H, m, arom) ppm; δ ($CDCl_3$): 8.4 (q, *J* 131 Hz, CH_3), 32.7 (t, *J* 126 Hz, N-CH_2), 42.0 (t, *J* 154 Hz, CH_2), 62.2 (t, *J* 140 Hz, CH_2), 114.3 (d, *J* 168 Hz, arom), 117.9 (s, arom), 120.2 (d, *J* 168 Hz, arom), 130.6 (d, *J* 157 Hz, arom), 134.3 (d, *J* 163 Hz, arom), 143.7 (s, arom), and 203.6 (s, C=O) ppm.

12, from 2′-aminobenzophenone and 2-chloroethylamine, 10.4 mmol (70%), mp 102–105°C; ir (Nujol): 2500–3300 (OH) cm^{-1}; δ ($CDCl_3$): 3.7–4.1 (4H, m, $-CH_2CH_2-$) and 7.2–7.9 (10H, m, arom + OH) ppm; δ ($CDCl_3$): 42.2 (CH_2), 44.3 (CH_2), 77.1 (C4 of triazine), 104.3, 111.0, 114.5, 116.8, 117.7, 127.9, 128.9, 130.8, 134.1, 134.4, 134.9, 135.5, 150.8 (arom), 199.2 (C=O) ppm.

11, from 2′-aminobenzophenone and ethylamine, 13 mmol (87%), mp 118–124°C; ir (Nujol): 3440 (br, OH) cm^{-1}; δ ($CDCl_3$): 1.3 (3H, t, *J* 8 Hz, CH_3), 3.7 (2H, br q, CH_2), 7.0–7.9 (10H, m, arom + OH) ppm.

*3-Alkyl-4-methoxy-3,4-dihydro-1,2,3-benzotriazines (**14–19**)*

General procedure

(a) The 4-hydroxy-1,2,3-benzotriazine (0.2 mmol) was dissolved in methanol (5.0 mL) and the solution stirred at room temperature until reaction was complete. Evaporation of the methanol under reduced pressure afforded the pure product as an oil.

(b) In those cases in which the 4-hydroxy-1,2,3-benzotriazine did not react readily at room temperature, the triazine was refluxed in methanol for 2 h and the product isolated as before.

Details of reaction times, reaction temperatures, and yields are given in Table 1. The 4-methoxytriazines were identified by analysis of infrared spectra and complete interpretation of ^1H nmr data (Table 1). Since the compounds were all prepared by the same sequence of reactions, and since the ^1H nmr spectra are consistent for the series, only representative compounds were analyzed (Table 2). The ^{13}C nmr data for representative compounds are as follows:

14: δ ($CDCl_3$): 40.3 (q, *J* 139 Hz, N-Me), 49.4 (dq, *J* 6, 143 Hz, O-Me), 78.9 (d, *J* 168 Hz, C4 of triazine ring), 115.3 (s, arom), 125.2 (dd, *J* 5, 163 Hz, arom), 126.9 (d, *J* 152 Hz, arom), 129.9 (dd, *J* 7, 163 Hz, arom), 130.2 (dd, *J* 8, 162 Hz), and 138.3 (t, *J* 8.3 Hz) ppm.

16: δ ($CDCl_3$): 8.5 (C-Me), 31.4 (CH_2), 35.8 (N-Me), 50.4 (O-Me), 87.2 (C4), 117.3, 124.3, 125.1, 129.6, and 139.5 (arom) ppm.

18: δ ($CDCl_3$): 42.3 (Cl-*C*H_2), 49.6 (O-*C*H_3), 54.3 (N-*C*H_2), 78.9 (*C*4), 115.6, 125.7, 126.7, 127.1, 130.4 and 136.3 (arom) ppm.

19: δ ($CDCl_3$): 41.6 (Cl-*C*H_2), 50.5 (O-*C*H_3), 50.9 (N-*C*H_2), 85.9 (*C*4), 119.8, 125.3, 127.4, 127.6, 128.2, 128.5, 129.8, 130.1, 137.9, and 143.1 (arom) ppm.

*Z-4-Ethylidene-3-methyl-3,4-dihydro-1,2,3-benzotriazine (**22**)*

(a) 4-Ethyl-4-hydroxy-3-methyl-3,4-dihydro-1,2,3-benzotriazine (**8**) (0.2 mmol) was refluxed in benzene (5 mL) containing a trace of *p*-toluenesulfonic acid for 2 h. Evaporation of the benzene under reduced pressure afforded the ethylidenebenzotriazine (**22**) (quantitative) as an oil; ^1H nmr, δ ($CDCl_3$): 1.98 (3H, d, *J* 8 Hz, *C*H_3—C=), 3.53 (3H, s, N-Me), 4.78 (1H, q, *J* 8 Hz, *H*—C=), and 7.17–7.88 (4H, m, arom) ppm; (Minor component: δ 1.94 (d), 3.52 (s), 3.60 (q), and 7.2–7.8 (m) ppm.) ^{13}C nmr δ ($CDCl_3$): 13.84 (ethylidene Me), 40.6 (N-Me), 94.6 (exocyclic sp^2 carbon of ethylidene group), 125.3, 126.0, 129.3, 129.6, 130.7/131.0, 134.0/134.4, 139.3 (arom) ppm.

(b) The 4-ethyl-4-hydroxytriazine (**8**) was dissolved in methanol and the solution stirred at room temperature for 1 h. Evaporation of the methanol afforded an oil; the nmr spectrum of the oil showed two components, the major product being the methyl ether (**16**) with a small

Can. J. Chem. Downloaded from www.nrcresearchpress.com by 80.58.250.72 on 09/07/12
For personal use only.

TABLE 1. Physical and spectroscopic data of the 3-alkyl-4-methoxy-3,4-dihydro-1,2,3-benzotriazines

Compound no.	R^1	R^2	Reaction temperature (°C)	Time	Yield (%)	^{1}H nuclear magnetic resonance (δ)			
						R^1	R^2	O-Me	Ar
14	H	Me	20	1 h	100	5.95(1H)	3.63(3H)	2.74(3H)	7.15–7.63(4H)
15	Me	Me	Reflux[a] / 20	2 h / 1 h	22[b] / 23[b]	1.90(3H)	3.50(3H)	2.78(3H)	7.3–7.7(4H)
16	Et	Me	Reflux[a] / 20	2 h / 120 h	100 / 25	0.16(t)[c](3H) / 2.19(q) (2H)	3.51(3H)	2.81(3H)	7.39–7.54(4H)
17	Ph	Me	20	9 days	82.5	(arom)	3.21(3H)	2.90(3H)	7.2–7.7(9H)
18	H	CH_2CH_2Cl	20	1.5 h	100	6.03(1H)	4.0(t) / 4.23(t) (4H)	2.80(3H)	7.3–7.7(4H)
19	Ph	CH_2CH_2Cl	20	1 h	100	(arom)	3.6–3.9(m, 4H)	2.90(3H)	7.3–7.8(9H)

[a]65°C.
[b]Minor product of dehydration of **7** (see discussion).
[c]*J* 7.5 Hz.

TABLE 2. Elemental analysis and molecular ion mass measurement

Compound no.	Analysis								Molecular formula	Mass measurement	
	Calculated (%)				Found (%)					Found	Calculated
	C	H	N	Cl	C	H	N	Cl			
18	53.2	5.4	18.6	15.7	53.2	5.3	18.0	15.1	$C_{10}H_{12}N_3OCl$	227.0645/ 225.0069	227.0636/ 225.0666
19	63.7	5.3	13.9	11.8	64.2	5.3	13.5	11.8	$C_{16}H_{16}N_3OCl$	303.0965/ 301.0991	303.0978/ 303.0948
14	—	—	—		—	—	—		$C_9H_{11}N_3O$	177.0905	177.0899

amount of the dehydration product (**22**). The mixture was redissolved in methanol and stirred at room temperature for 5 days. The methanol was evaporated under vacuum and the residue examined by nmr, showing the same two components as before but with the ethylidene-triazine (**22**) now the major component.

(c) 4-Ethyl-4-methoxy-3-methyl-3,4-dihydro-1,2,3-benzotriazine (**16**) was dissolved in 10% aqueous methanol and the solution left at room temperature for 24 h. Evaporation of the solution gave an oil residue; the nmr spectrum of the oil showed that the major component (77%) was the ethylidene triazine (**22**). The minor component was unchanged methyl ether (**16**).

Anti-tumor activity

In vivo anti-tumor activity against the P388 (6) and TLX5 (8) tumors was determined as described previously.

Discussion

Diazotization of the 2-acylaniline and coupling with the appropriate alkylamine affords the triazenes (**3**), which cyclize spontaneously to give the 4-hydroxytriazine, as described previously (5). A modified method for the diazotization of 2-aminobenzaldehyde is reported here, which gives improved yields of the triazinols **4** and **5**. This method was also extended to the 3-chloroethyl derivative (**6**); other chloroethyl derivatives **9** and **12** were prepared by the conventional diazotization method. The products were characterized by nmr spectroscopy, which showed some variation in the behaviour of the chloro-ethyl derivatives in deuteriochloroform solution. The 4-phenyl-(**12**) and 4-hydro-(**6**) 3-chloroethyltriazines exist in $CDCl_3$ in equilibrium with the openchain forms (**3***c* and **3***a* respectively); the ^{13}C nmr spectra of these compounds show signals from C-4 of the cyclic triazine (77.1 and 73.3 ppm respectively) and from the carbonyl carbon of the acyclic triazene (199.2 and 193.4 ppm). This behaviour is predictable, based on previous experience (5) with the N-methyl analogues. However, the 4-ethyl-3-chloroethyltriazine (**9**) is unusual in that it exists exclusively as the triazene form (**3***b*) in $CDCl_3$ solution. There is no doubt that these compounds exist in the cyclic form in the solid; the ir spectra in Nujol show an absorption band for the hydroxyl group but not for the carbonyl group.

Recrystallization of some of the triazinols from solvent mixtures containing methanol frequently resulted in failure to recover the 4-hydroxytriazine and it became apparent that the carbinolamines were undergoing methanolysis to give new products, the 4-methoxytriazines (**14–20**). When this methanolysis was studied in pure methanol, it was found that the reaction can give virtually quantitative yields of the methyl ethers and also that the rate of reaction is strongly dependent on the nature of the substituents R^1 and R^2. Table 1 summarizes the results of this study and also shows the ^{1}H nmr data of the 4-methoxytriazines.

Reaction of the 3-methyl-4-hydroxy-1,2,3-benzotriazine (**4**) with methanol takes place rapidly at room temperature and results in 100% conversion to the methoxytriazine (**14**). The analogous 3-chloroethyltriazine (**6**) also reacts rapidly at room temperature to give the analogous ether (**18**). In contrast, the 4-phenyl-4-hydroxy-3-methyltriazine (**10**) reacts much less readily in methanol and required 9 days at room temperature to achieve 82.5% conversion to the methoxymethyltriazine (**17**). When the N-Me group of **10** is replaced by N-chloroethyl, i.e., in **12**, the reactivity is restored and the rate of conversion

Can. J. Chem. Downloaded from www.nrcresearchpress.com by 80.58.250.72 on 09/07/12
For personal use only.

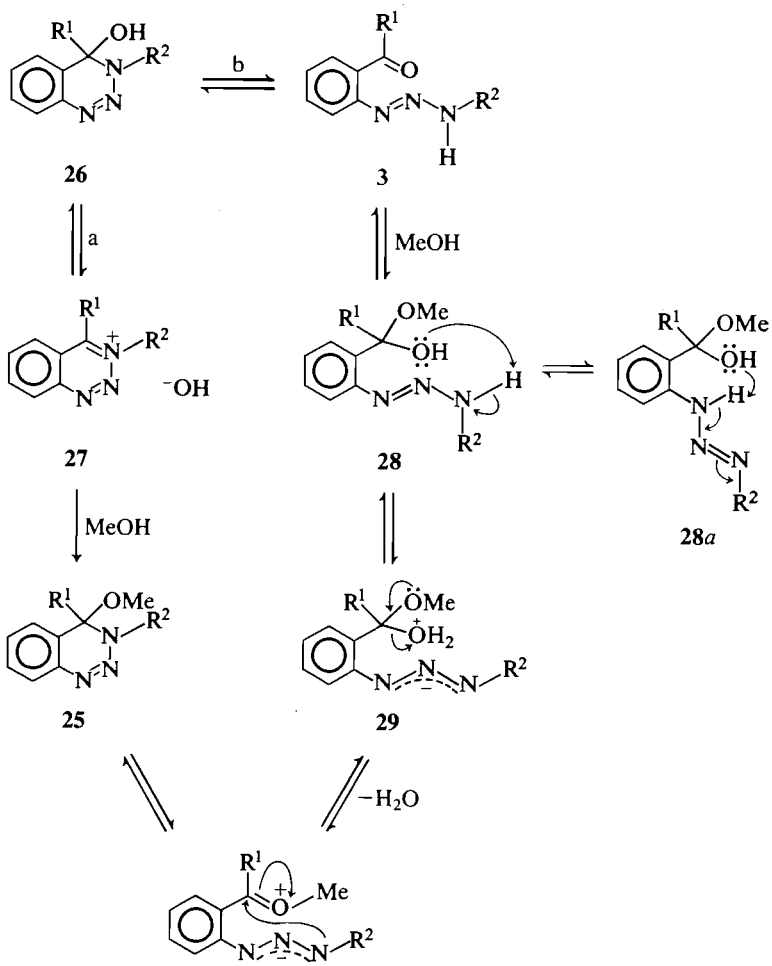

SCHEME 1

of **12** to the ether (**19**) at room temperature is comparable to the conversion **4** → **14**.

The reactivity of the 4-methyl-(**7**) and 4-ethyl-(**8**) 4-hydroxytriazines is complicated by a competing reaction by dehydration to give 4-methylenetriazines (9), e.g., **21**. The 4-methyl-4-hydroxytriazine (**7**) does react rapidly in methanol at room temperature, giving 80% conversion to products after one hour. However, the major component of the product mixture is the 3-methyl-4-methylenetriazine (**21**) (58%), which was evident from the characteristic vinylic proton doublets in the nmr spectrum (9). The yield of the methyl ether (**15**) from this reaction was 23%. Refluxing the hydroxytriazine (**7**) in methanol did not appreciably change the course of the reaction; after 2 h, the product mixture contained unreacted **7** (13%), **15** (22%), and **21** (65%). An attempt to alkylate the hydroxytriazine (**7**) with diazomethane in methylene chloride surprisingly resulted in complete dehydration to the methylenetriazine (**21**) within 0.5 h. The methylenetriazine (**21**) was recovered unchanged after refluxing in ethanol for 1.5 h; thus it is unlikely that the dehydration product (**21**) is an intermediate in the conversion of **7** → **15**.

Refluxing the 3-methyl-4-ethyl-4-hydroxytriazine (**8**) in methanol was more successful and resulted in 100% conversion to the methyl ether (**16**) after 2 h, whereas reaction of **8** in methanol at room temperature was slow (120 h) and gave a mixture of the ether (**16**) (25%) and the analogous dehydration product, the 4-ethylidene triazine (**22**) (75%). Quantitative conversion of the hydroxytriazine (**8**) to the ethylidenetriazine (**22**), together with a trace of its geometric isomer **23**, was achieved by reaction in benzene with a trace of *p*-toluenesulfonic acid as catalyst. An interesting phenomenon was observed when the methyl ether (**16**) was left in aqueous methanol at room temperature for 24 h, which resulted in a 77% conversion to the ethylidenetriazine (**22**). This observation suggests that the methanolysis is reversible in the presence of water; the regenerated 4-hydroxytriazine (**8**) then undergoes irreversible dehydration to the observed product (**22**). The reversibility of the methanolysis is also evident in the reaction of the 3-chloroethyl-4-methoxytriazine (**18**), which reverts to the alcohol (**6**) when left in an aqueous medium for 12 h. Dehydration was also the major pathway of reaction of the 3-chloroethyl-4-ethyltriazin-4-ol (**9**) in methanol for 4 h at room temperature, which affords a 9:1 mixture of the *Z*-ethylidenetriazine (**24**) and the ether (**20**) respectively; refluxing **9** in methanol for 1 h gave a 4:1 mixture of the same products, with **24** in excess.

The ^{1}H nmr spectrum of the 4-ethylidenetriazine (**22**) confirms the assigned structure; the stereochemistry around the exocyclic C=C group is assigned as *Z* on the basis of comparisons of the chemical shift of the vinylic proton in **22** with the spectrum of the methylenetriazine (**21**). In **22**, the vinylic proton is in the R^1 position and is thus strongly deshielded, resulting in a chemical shift of 4.78 ppm for this proton; the analogous proton in **21** has a chemical shift of 4.4 ppm. The nmr spectrum of **22** shows a small but detectable amount of the *E* isomer (**23**), in which the vinylic proton (quartet), now situated at the more shielded position R^3, is

Can. J. Chem. Downloaded from www.nrcresearchpress.com by 80.58.250.72 on 09/07/12
For personal use only.

found at 3.60 ppm; the analogous proton in **21** is found at 3.8 ppm.[4] The estimated composition, from nmr, of the mixture is 94% *Z*-(**22**) and 6% *E* isomer (**23**). The structure of **22** is corroborated by the ^{13}C nmr spectrum.

The structural assignment for the 4-methoxytriazines (**14**–**19**) is based on ^{1}H and ^{13}C nmr and ir data. The chemical shift of the OMe protons is in the range 2.7–2.9 ppm, which is an unusually high field for an O-Me group. The ^{13}C signal of the O-Me carbon, observed at ca. 50 ppm in **14** and **16**, is also an unusually high field for a methyl ether carbon (11). A possible explanation for this observation is that the O-Me carbon is shielded by the effect of the electron lone-pair at N-3, which could be held in close proximity to the O-Me group if the triazine ring is nonplanar (see structure **25**). Indeed, there is evidence that compounds of this type do have some deviation from planarity in the triazine ring, as shown by a crystal structure determination of a related compound 3-ethyl-4-hydroxy-3,4-dihydro-1,2,3-benzotriazine (**14**, Et for Me at R^2) (12).

The results of this study clearly show that the rate of methanolysis of the benzotriazinol is strongly dependent on the nature of the substituent R^1 at C-4 of the triazine. Thus, for triazinols in which R^2 is fixed as a methyl group, the reactivity order for various R^1 groups is: H ~ Me > Et > Ph. Scheme 1 shows two possible pathways for the mechanism of the methanolysis. Path (a), an addition/elimination mechanism, involves heterocyclic pseudo-base dissociation of **26** to give the benzotriazinium cation (**27**), which would be expected to undergo facile reaction with the solvent to give the methyl ether (**25**). However, the observed reactivity sequence does not accord with this hypothesis, since electron-donating groups at R^1 should stabilize the intermediate triazinium ion (**27**) and facilitate formation of the methyl ether. On the other hand, if the rate-determining step in path (a) is the addition of methanol to the triazinium ion, then the observed reactivity sequence would be consistent with the steric effect of R^1 rather than with its electron-releasing character.

The alternative mechanism for the methanolysis, path (b), involves the triazinol ⇆ triazene ring-chain tautomerism (**26** ⇆ **3**). The open-chain triazene (**3**) could react with methanol reversibly to afford the hemi-acetal or -ketal (**28**) and the reactivity sequence for variation of R^1 is consistent with the predicted reactivity of the carbonyl group towards nucleophilic addition by methanol in the steps **3** → **28**. Cyclization of **28**, or more likely from the tautomer **28***a*, then proceeds by an intramolecular proton transfer to give the zwitterionic-triazenido compound **29**, which is then set up for elimination of water and ring closure of the triazenido-methyloxonium zwitterion to give the observed product (**25**).

Although the evidence reported here does not clearly establish path (a) or (b) as the correct mechanism for the methanolysis, the authors favour path (b) since the triazinol ⇆ triazene tautomerism (**26** ⇆ **3**) has been clearly demonstrated (5) whereas the pseudo-base character of **26** has not.

It is worthwhile to compare the facility of methanolysis of these benzotriazinols with the apparent inactivity of their acyclic analogues, the hydroxymethyltriazenes (**30***a*). Analogous reaction of **30***a* with methanol would be expected to afford the methoxymethyltriazene (**30***b*); however, the only reaction we have observed with compounds of type **30***a* in methanol is loss of formaldehyde to afford the monomethyltriazene (Ar·N=N·NHMe). Furthermore, the hydroxymethyl group in **30***a* can be activated by derivatization to the acetoxymethyltriazene (**30***c*), which does react with methanol to give the methyl ether (**30***b*). This latter reaction has been shown by kinetic analysis to involve intermediate iminium ion (**31**) formation (13).

TABLE 3. In vivo antitumor activity of the 4-hydroxy-3,4-dihydro-1,2,3-benzotriazines

Compound no.	R^1	R^2	Tumor	Optimum dose (mg/kg)	%T/C[a]
4	H	Me	TLX5	160	138
			P388	200	Toxic[c]
5	H	Et	TLX5	160	128
			P388	100	Toxic
6	H	CH_2CH_2Cl	TLX5	160	131
8	Et	Me	TLX5	160	Toxic
			P388	Inactive[b]	
9	Et	CH_2CH_2Cl	TLX5	Inactive	
10	Ph	Me	TLX5	Inactive	
			P388	Inactive	
11	Ph	Et	TLX5	Inactive	
12	Ph	CH_2CH_2Cl	TLX5	Inactive	
13	2-Fluoro phenyl	CH_3	TLX5	Inactive	

[a]Control = 100%.

[b]"Inactive" implies no increase or decrease in the life-span of treated animals as compared with a control group, i.e. %T/C < 125(TLX5); < 120(P388).

[c]"Toxic" means that the life-span of the treated animals was less than that of the control group, i.e. %T/C < 100.

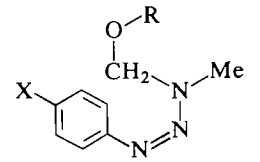

30 *a*, R = H
b, R = Me
c, R = Ac

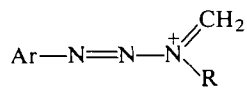

31

The formation of α-carbinolamines by enzymatic oxidation is an ubiquitous pathway in the metabolism of N-alkyl xenobiotic molecules (7). A typical xenobiotic is the tobacco alkaloid nicotine, which undergoes enzymatic oxidation to a transient α-carbinolamine; it has been suggested (14) that the carbinolamine, and analogous metabolites from other xenobiotics (e.g., phencyclidine), might undergo ionization to give an electrophilic iminium ion analogous to **31**. The iminium ion could be an active metabolite capable of covalent interaction with biological nucleophiles, e.g. protein, DNA.

α-Carbinolamines of the type suggested as metabolites of nicotine and phencyclidine are not chemically isolable and consequently it has been difficult to provide a chemical model to test the iminium ion hypothesis. Clearly the 4-hydroxytriazines (e.g. **4**) and hydroxymethyltriazenes (**30***a*) are suitable model compounds to test these hypotheses. The mechanisms by which these compounds interact with nucleophiles have direct relevance to the biochemistry and pharmacology of many important xenobiotic molecules, and further studies of these

[4]A similar pair of geometric isomers in an ethylidene heterocyclic system has been observed in some isoquinoline enamides and characterized by the variation of nmr chemical shift (10).

Can. J. Chem. Downloaded from www.nrcresearchpress.com by 80.58.250.72 on 09/07/12
For personal use only.

mechanisms are being undertaken to assess the importance of the iminium ion hypothesis in their metabolism.

Anti-tumor activity

Table 3 shows the results of in vivo anti-tumor evaluation of the 4-hydroxytriazines. Only the triazines (**4**–**6**) without an alkyl or aryl substituent at C-4 are active against the TLX5 tumor, and the level of activity is only a little above marginal. None of the compounds tested had any activity against the P388 tumor; two of the compounds with TLX5 activity were found to be severely toxic during the P388 assay and one of the P388 inactive compounds (**8**) was similarly toxic during the TLX5 test. Substitution of the N-methyl group of the 4-hydroxytriazine by the chloroethyl group causes little change in the biological activity.

Although the degree of activity observed for these compounds is low and does not encourage consideration of further testing of analogues, there is an interesting correlation of these in vivo results with previous results of in vitro cytotoxicity (6). Compounds **4** and **5** are active on the TLX5 tumor *and* show significant in vitro cytotoxicity *without* metabolic activation, whereas two of the TLX5-inactive compounds, **10** and **13**, have a much lower degree of in vitro cytotoxicity. There appears to be a structure–activity correlation in this series: the biologically active compounds are those without an alkyl, or aryl, substituent at C-4 of the triazine. This activity correlates with the chemical reactivity of the triazinol in the methanolysis reaction.

Thus, there does appear to be a correlation between the biological activity of the triazinol and the facility of the triazinol to undergo chemical ring opening. For example, the 3-methyl-4-hydroxy-4-hydrotriazine (**4**) is cytotoxic to M21 tumor cells in culture (6), has measurable in vivo anti-tumor activity against the TLX5 tumor, and also undergoes facile methanolysis to give the methyl ether (**14**). In contrast, the 3-methyl-4-hydroxy-4-phenyltriazine (**10**) has only marginal cytotoxicity in vitro, is inactive against the TLX5 tumor, and undergoes methanolysis extremely slowly.

Acknowledgements

Financial support for this project was provided by the Natural Sciences and Engineering Research Council of Canada. High resolution nmr spectra were provided by the Atlantic Regional Nuclear Magnetic Resonance Centre at Dalhousie University, Halifax. Anti-tumor activity was determined at the Cancer Research Campaign Laboratories of the Department of Pharmaceutical Sciences, University of Aston in Birmingham (U.K.) and at the National Cancer Institute, Bethesda, MD (U.S.A.). High resolution mass spectra were recorded at the Mass Spectrometry Laboratory at the University of Alberta, Edmonton.

1. J. A. HICKMAN, M. F. G. STEVENS, N. W. GIBSON, S. P. LANGDON, C. FIZAMES, F. LAVELLE, G. ATASSI, E. LUNT, and R. M. TILSON. Cancer Res. **45**, 3008 (1985).
2. E. S. NEWLANDS, G. BLACKLEDGE, J. A. SLACK, C. GODDARD, C. J. BRINDLEY, L. HOLDEN, and M. F. G. STEVENS. Cancer Treat. Rep. **69**, 801 (1985).
3. C. M. T. HORGAN and M. J. TISDALE. Biochem. Pharmacol. **33**, 2185 (1984).
4. K. VAUGHAN and M. F. G. STEVENS. Chem. Soc. Rev. **7**, 377 (1978).
5. P. L. FAYE, K. VAUGHAN, and D. L. HOOPER. Can. J. Chem. **61**, 179 (1983); K. VAUGHAN, R. J. LAFRANCE, Y. TANG, and D. L. HOOPER. Can. J. Chem. **63**, 2455 (1985).
6. D. J. KOHLSMITH, K. VAUGHAN, and S. J. LUNER. Can. J. Physiol. Pharmacol. **62**, 396 (1984).
7. M. OVERTON, J. A. HICKMAN, M. D. THREADGILL, K. VAUGHAN, and A. GESCHER. Biochem. Pharmacol. **34**, 2055 (1985).
8. A. GESCHER, J. A. HICKMAN, R. J. SIMMONS, M. F. G. STEVENS, and K. VAUGHAN. Biochem. Pharmacol. **30**, 89 (1981).
9. H. FONG and K. VAUGHAN. Can. J. Chem. **53**, 3714 (1975).
10. I. NINOMIYA, T. NAITO, and H. TAKASUGI. J. Chem. Soc. Perkin Trans. 1, 1791 (1975).
11. J. B. STOTHERS. Carbon-13 NMR spectroscopy. Academic Press, New York. 1972. p. 144.
12. K. K. LAI, C. H. SCHWALBE, K. VAUGHAN, R. J. LAFRANCE, and C. D. WHISTON. Can. J. Chem. **63**, 581 (1985).
13. C. M. HEMENS and K. VAUGHAN. J. Chem. Soc. Perkin Trans. 2, 11 (1986); C. M. HEMENS, H. W. MANNING, K. VAUGHAN, R. J. LAFRANCE, and Y. TANG. Can. J. Chem. **62**, 741 (1984).
14. D. P. WARD, A. J. TREVOR, A. KALIR, J. D. ADAMS, T. A. BAILLIE, and N. CASTAGNOLI, JR. Drug. Metab. Dispos. **10**, 690 (1982), and references therein.
15. R. D. SINGER, K. VAUGHAN, and D. L. HOOPER. Can. J. Chem. **64**, 1567 (1986).

Can. J. Chem. Downloaded from www.nrcresearchpress.com by 80.58.250.72 on 09/07/12
For personal use only.

1,2,6-Thiadiazin-3,5(2*H*,6*H*)-dione 1,1-dioxide derivatives: crystal structure, physico-chemical and biological properties

PILAR GOYA, ROSA NIEVES, AND CARMEN OCHOA[1]
Instituto de Química Médica-CSIC, Juan de la Cierva 3, 28006 Madrid, Spain

AND

CARMEN RODELLAS, MARTÍN MARTINEZ-RIPOLL, AND SEVERINO GARCÍA-BLANCO
Instituto Rocasolano-CSIC, Serrano 119, 28006 Madrid, Spain

Received April 10, 1986

PILAR GOYA, ROSA NIEVES, CARMEN OCHOA, CARMEN RODELLAS, MARTÍN MARTINEZ-RIPOLL, and SEVERINO GARCÍA-BLANCO. Can. J. Chem. **65**, 298 (1987).

Crystal structure, ^{1}H and ^{13}C nmr spectroscopy and pK_a measurements of 1,2,6-thiadiazin-3,5(2*H*,6*H*)-dione derivatives related with phenylbutazone are reported. An anomalous variation in the pK_a values of compounds **1**, **2**, and **3** has been observed. Antiinflammatory, analgesic, and antipyretic activities of these compounds have been evaluated.

PILAR GOYA, ROSA NIEVES, CARMEN OCHOA, CARMEN RODELLAS, MARTÍN MARTINEZ-RIPOLL et SEVERINO GARCÍA-BLANCO. Can. J. Chem. **65**, 298 (1987).

On a déterminé la structure cristalline, les spectres rmn du ^{1}H et du ^{13}C et les valeurs des pK_a de dérivés de la thiadiazine-1,2,6 dione-3,5(2*H*,6*H*) qui sont apparentés avec la phénylbutazone. On a observé une variation anormale dans les valeurs des pK_a des composés **1**, **2** et **3**. On a évalué les propriétés antiinflammatoire, analgésique et antipyrétique de ces composés.

[Traduit par la revue]

Can. J. Chem. Downloaded from www.nrcresearchpress.com by 80.58.250.72 on 09/07/12
For personal use only.

Introduction

In a previous paper (1) we carried out a comparative study between the physicochemical properties of 1,2,6-thiadiazine 1,1-dioxide derivatives and related pyrazoles. We have now extended the comparison to compounds of this series with antiinflammatory activity. Thus, we now wish to report the physico-chemical properties and preliminary biological screening of 1,2,6-thiadiazin-3,5(2*H*,6*H*)-dione 1,1-dioxides **1** (2), **2** and **3** (3), structurally related to phenylbutazone **4**. Compound **3** can be considered as pyrazolidindione **4** in which an SO_2 group has been introduced between the two nitrogen atoms. Thiadiazine derivatives **1** and **2** have been chosen because the cyclohexyl moiety seems to be useful for inducing antiinflammatory activity (4–6). Thus, whilst 1,2-dicyclohexyl pyrazole derivatives have shown some activity (7), the corresponding cyclopentyl compounds turned out to be inactive (8).

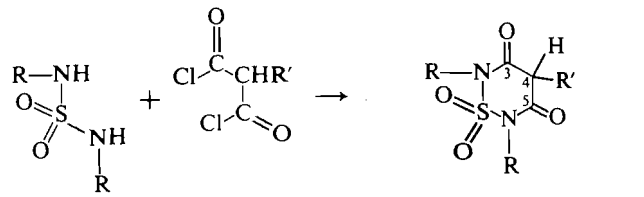

1 R = C_6H_{11}, R′ = H
2 R = C_6H_{11}, R′ = *n*-C_4H_9
3 R = C_6H_5, R′ = *n*-C_4H_9

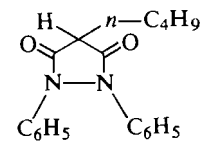

SCHEME 1

Results and discussion

Synthesis, nmr data and pK_a values

Compound **2** was prepared from *N*,*N*′-dicyclohexylsulfamide and *n*-butylmalonyl chloride using the procedure used to prepare **1** (2).

The ^{1}H nmr data of compounds **1**, **2**, and **3** can be found in the experimental part. The assignments have been made by chemical correlation and signal multiplicity. The spectrum of compound **1** at 300 MHz shows the signals belonging to the protons of the cyclohexyl moieties separated in six multiplets. It was therefore possible to assign most of these signals on the basis of their multiplicity and coupling constants. The multiplet, a triplet of triplets, appearing at lower field ($J_{1'a,2'a}$ = 12.36 Hz, $J_{1'a,2'e}$ = 3.85 Hz) corresponds to H1′a indicating that the heterocyclic rest is, as expected, in the equatorial position. The following signal that corresponds to H2′a, appears as a double quartet indicating that J_{gem}, $J_{H2'a,H1'a}$, and $J_{H2'a,H3'a}$ have very close values ($J \sim |12|$ Hz). In this way, the signals corresponding to the other axial protons appear like a triplet of quartets and the signals corresponding to the equatorial protons as distorted doublets ($J_{gem} = \sim -12$ Hz, and $2.5 < J_{e,e}, J_{a,e} < 4$ Hz).

The ^{13}C nmr data of compounds **1**, **2**, **3**, and phenylbutazone (**4**) (9) are gathered in Table 1.

The effect of an SO_2 group on ^{13}C nmr chemical shift can be evaluated by comparing the data of thiadiazine derivatives **1**, **2**, **3**, and those of phenylbutazone (**4**). Thus, the signal belonging to the equivalent C3 and C5 is shifted to lower field (~5 ppm) in phenylbutazone, whilst the C4 signal is shifted to higher field (~6 ppm) as can be seen from the data of **3** and **4**. The signals corresponding to the *ortho*, *meta*, and *para* carbons of phenylbutazone are separated from each other about 3 ppm, whilst in compound **3** they appear with a difference of 0.3 ppm, the one corresponding to the *p*-carbon atom being that appearing at lower field.

The pK_a values (water) were measured using the spectrophotometric method and the data are shown in Table 2.

The substitution of a C—H (**1**) by a C-*n*-butyl group (**2**) slightly affects the acidity (+0.16 pK_a units), taking into account the statistical effect (10). On the other hand, the pK_a variation between compounds **3** and **4** can be explained by

[1]To whom all correspondence should be addressed.

TABLE 1. ^{13}C nmr chemical shifts[a] (δ ppm) of **1**, **2**, **3**, and phenylbutazone (**4**) (9)

	δ									
Compd.[b]	C3,C5	C4	C1′	C2′	C3′	C4′	C7	C8	C9	C10
1	163.1	45.1	57.8	29.9	25.8	24.6	—	—	—	—
2	165.1	51.8	58.4	29.9	25.8	24.7	28.6	25.1	22.2	13.6
3	164.8	51.5	132.0	129.6[c]	128.9[c]	130.1	28.8	24.7	22.2	13.6
4	169.9	45.6	135.8	122.3	128.1	125.3	27.0	26.2	21.4	12.9

[a]DMSO-d_6 as solvent.
[b]C3, C4, C5 correspond to the heterocyclic rest, C1′, C2′, C3′, and C4′ to the cyclohexyl or phenyl rings and C7, C8, C9, and C10 to the *n*-butyl moiety.
[c]The assignments may be reversed.

TABLE 2. pK_a values of **1**, **2**, **3**, and phenylbutazone (**4**)

Compound	pK_{a_1}
1	6.04±0.11
2	6.18±0.06
3	3.92±0.04
4	4.42±0.10

the electron-withdrawing effect of the SO_2 group. The strong variation of the pK_a values between the two dicyclohexyl derivatives and the diphenyl derivative **3** is not easily explained. In related barbiturates, the presence of monooxo or dioxo tautomer forms in the salt formation accounts for changes in the pK_a values (11). However, in thiadiazine derivatives **1**, **2**, and **3** the variation in pK_a values cannot be due to the existence of different tautomers since their uv spectra are very similar and the ^1H nmr spectra of the three compounds show only the signal corresponding to the CH tautomers (dioxo form). Despite the fact that electronic and steric effects of substituents cause changes in pK_a values in barbituric acid derivatives (12), these effects do not seem to be enough to account for such strong variations in the pK_a values of the thiadiazines.

X-ray discussion

The crystal structures of **2** and **3** have been determined by single crystal X-ray diffraction techniques. Figures 1 and 2 are perspective drawings of their final X-ray models (13). A list of bond lengths and bond angles is given in Tables 3 and 4, which compare well with other thiadiazine compounds (1, 14–20), taking into account the different location of the double bonds within these molecules.

The thiadiazine rings of both compounds present boat conformations (21), $\phi 2$ = 179.8(3) and $\theta 2$ = 93.2(3) for **2**, $\phi 2$ = 0.0(2) and $\theta 2$ = 89.2(2) for **3**, with the C4 and S atoms at the flaps (see also Table 5). These structures, together with another one reported previously (22), are examples of thiadiazine rings showing boat conformations. The best planes of the cyclohexyl rings in **2** (C22, C23, C25, C26 and C62, C63, C65, C66) form similar angles, 88(1)°, with the best plane of the thiadiazine ring. The phenyl rings in **3** are also symmetrically oriented with respect to the best plane of the thiadiazine ring and make an angle of 95(1)° with it. This symmetrical orientation of the substituted rings does not occur in the analogue compound phenylbutazone (23), where the two phenyl rings make angles of ~60° and ~40°, respectively, with the main ring, this situation occurring in the two crystallographically independent molecules. The other structural difference of phenylbutazone is

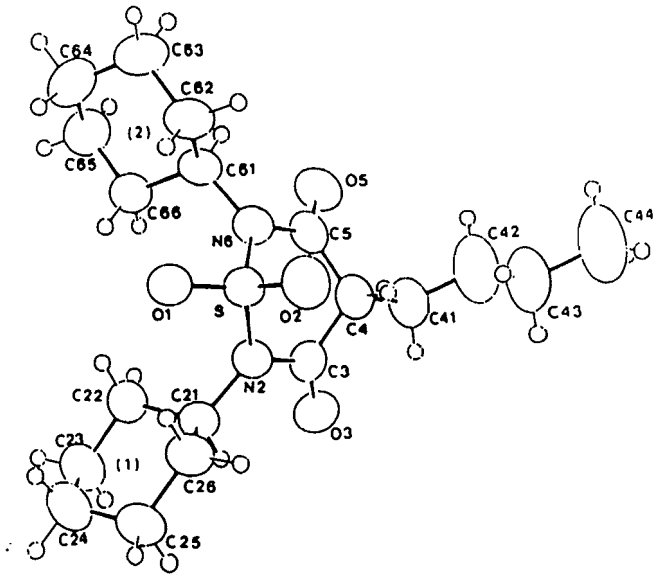

FIG. 1. A perspective view of molecule **2**.

the lack of planarity around its nitrogen atoms, which is not observed in **2** and **3**. Thus, the incorporation of the SO_2 group to phenylbutazone to produce the present thiadiazine derivatives plays an important role in determining the final molecular geometry.

The conformation of the thiadiazine rings in **2** and **3** described above causes the H-atom bonded to C4 to get near to one of the oxygen atoms of the SO_2 group (Fig. 3). In compound **2** (pK_a = 6.18) the distance H4...O2 = 2.48 Å is less than in compound **3** (2.70 Å, pK_a = 3.92). The contact H4...O2 cannot be considered as a typical hydrogen bond, but it indicates (24) a certain attractive interaction, that produces a major structural fixation of the H4 atom in **2**.

Biological results

The antipyretic, analgesic, and antiinflammatory activity of thiadiazines **1**, **2**, and **3** has been evaluated. The preliminary results are shown in Table 6.

Compound **3**, closely related with phenylbutazone, shows an antiinflammatory activity similar to this compound, whilst **1** and **2** present much lower activity. Compound **2** presents a remarkable analgesic activity and this result is the only one that is statistically significant.

There seems to be a correlation between the pK_a values and the antiinflammatory activity since the two more active compounds are also the more acidic.

In previous reports (25, 26) a relationship between the carbon

Can. J. Chem. Downloaded from www.nrcresearchpress.com by 80.58.250.72 on 09/07/12
For personal use only.

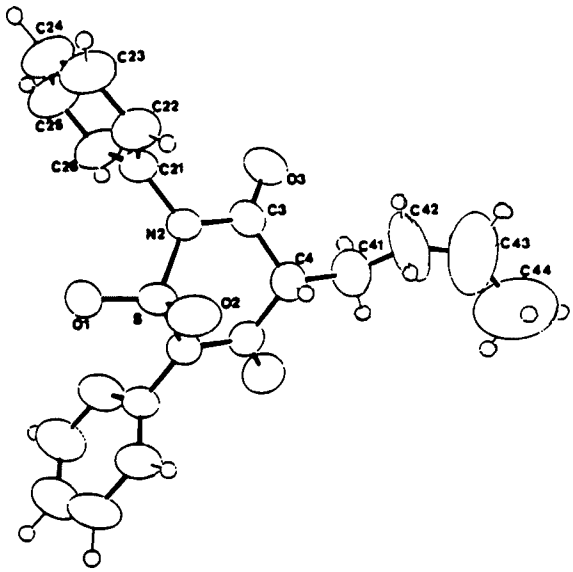

FIG. 2. A perspective view of molecule **3**. A crystallographic mirror plane passes through O1, O2, S, C4, and C41. Atoms C42, C43, and C44 are disordered.

TABLE 3. Bond lengths (Å) and bond angles (deg) for **2** with standard deviations in parentheses

Bond	Length	Bond	Length
S—O1	1.411(3)	C21—C26	1.521(6)
S—O2	1.422(3)	C22—C23	1.527(7)
S—N2	1.649(3)	C23—C24	1.527(8)
S—N6	1.653(4)	C24—C25	1.504(7)
O3—C3	1.207(5)	C25—C26	1.529(7)
O5—C5	1.209(6)	C41—C42	1.444(8)
N2—C3	1.399(6)	C42—C43	1.43 (1)
N2—C21	1.505(5)	C43—C44	1.44 (1)
N6—C5	1.395(6)	C61—C62	1.515(6)
N6—C61	1.492(5)	C61—C66	1.515(6)
C3—C4	1.519(6)	C62—C63	1.525(6)
C4—C5	1.516(6)	C63—C64	1.518(8)
C4—C41	1.530(7)	C64—C65	1.517(8)
C21—C22	1.519(5)	C65—C66	1.519(7)

Bonds	Angle	Bonds	Angle
N2—S—N6	101.0(2)	O5—C5—N6	121.0(4)
O2—S—N6	108.9(2)	N2—C21—C26	113.1(3)
O2—S—N2	109.2(2)	N2—C21—C22	112.4(3)
O1—S—N6	109.0(2)	C22—C21—C26	111.9(4)
O1—S—N2	108.4(2)	C21—C22—C23	109.1(4)
O1—S—O2	118.9(2)	C22—C23—C24	111.3(4)
S—N2—C21	122.8(3)	C23—C24—C25	111.2(4)
S—N2—C3	118.2(3)	C24—C25—C26	111.8(4)
C3—N2—C21	119.1(3)	C21—C26—C25	108.6(3)
S—N6—C61	122.3(3)	C4—C41—C42	116.1(5)
S—N6—C5	118.0(3)	C41—C42—C43	125.1(6)
C5—N6—C61	119.7(3)	C42—C43—C44	119.7(7)
O3—C3—N2	120.7(4)	N6—C61—C66	112.3(3)
N2—C3—C4	115.6(3)	N6—C61—C62	113.2(3)
O3—C3—C4	123.7(4)	C62—C61—C66	112.3(3)
C3—C4—C41	111.8(4)	C61—C62—C63	109.0(4)
C3—C4—C5	110.7(3)	C62—C63—C64	110.8(4)
C5—C4—C41	112.6(4)	C63—C64—C65	111.4(5)
N6—C5—C4	115.9(4)	C64—C65—C66	110.9(4)
O5—C5—C4	123.1(4)	C61—C66—C65	109.3(4)

TABLE 4. Bond lengths (Å) and bond angles (deg) for **3** with standard deviations in parentheses

Bond	Length	Bond	Length
S—O1	1.414(3)	C21—C26	1.369(4)
S—O2	1.420(3)	C22—C23	1.398(6)
S—N2	1.658(2)	C23—C24	1.363(7)
O3—C3	1.197(4)	C24—C25	1.365(6)
N2—C3	1.396(4)	C25—C26	1.375(6)
N2—C21	1.454(3)	C41—C42	1.47 (1)
C3—C4	1.517(4)	C42—C43	1.36 (3)
C4—C41	1.499(7)	C43—C44	1.40 (4)
C21—C22	1.367(4)		

Bonds	Angle	Bonds	Angle
N2—S—N2′	101.1(7)	N2—C21—C26	118.9(2)
O2—S—N2	109.3(1)	N2—C21—C22	120.1(3)
O1—S—N2	108.2(1)	C22—C21—C26	121.0(3)
O1—S—O2	119.2(2)	C21—C22—C23	118.2(3)
S—N2—C21	117.1(2)	C22—C23—C24	120.9(4)
S—N2—C3	121.1(2)	C23—C24—C25	119.8(4)
C3—N2—C21	121.6(2)	C24—C25—C26	120.2(4)
O3—C3—N2	120.4(3)	C21—C26—C25	120.0(3)
N2—C3—C4	115.1(2)	C4—C41—C42	115.6(5)
O3—C3—C4	124.5(2)	C41—C42—C43	120 (2)
O3—C4—C41	114.1(1)	C42—C43—C44	127 (2)

TABLE 5. Intracyclic torsional angles for **2** and **3** with standard deviations in parentheses

2		**3**	
Bonds	Angle	Angle	Bonds
S—N2—C3—C4	−2.6(5)	0.3(4)	S—N2—C3—C4
N2—C3—C4—C5	−48.4(5)	47.4(4)	N2—C3—C4—C3′
C3—C4—C5—N6	48.4(5)	−47.4(4)	C3—C4—C3′—N2′
C4—C5—N6—S	2.8(5)	−0.3(4)	C4—C3′—N2′—S
C5—N6—S—N2	−47.3(3)	40.5(1)	C3′—N2′—S—N2
N6—S—N2—C3	47.2(3)	−40.5(1)	N2′—S—N2—C3

chemical shifts of the biological active center and hypnotic activity in barbituric acid derivatives and analgesic activity in antipyrine derivatives has been described. No relationship seems to exist between the chemical shifts of C4 and the biological activities of compounds **1**, **2**, **3**, and **4**, since the pairs of compounds with similar C4 chemical shifts (**1** and **4**, **2** and **3**) do not have similar activities. No more correlations have been made due to the few data available.

Although the antiinflammatory activity found in compound **3** seems to indicate that the parallelism between pyrazole and thiadiazine derivatives (1) exists also in what biological activities are concerned, the high toxicity of **3** and the not very significant activities of **1** and **2** do not encourage further development.

Experimental

Melting points were determined in a Kofler apparatus and are uncorrected. ^{1}H nmr spectra were recorded at 90 MHz on a Varian EM-390 or at 300 MHz on a Varian XL-300 spectrometers. ^{13}C nmr spectra were recorded at 20.15 MHz on a Bruker WP-80 spectrometer. Infrared spectra were recorded on a Perkin-Elmer 257 spectrophoto-

Can. J. Chem. Downloaded from www.nrcresearchpress.com by 80.58.250.72 on 09/07/12
For personal use only.

Can. J. Chem. Downloaded from www.nrcresearchpress.com by 80.58.250.72 on 09/07/12
For personal use only.

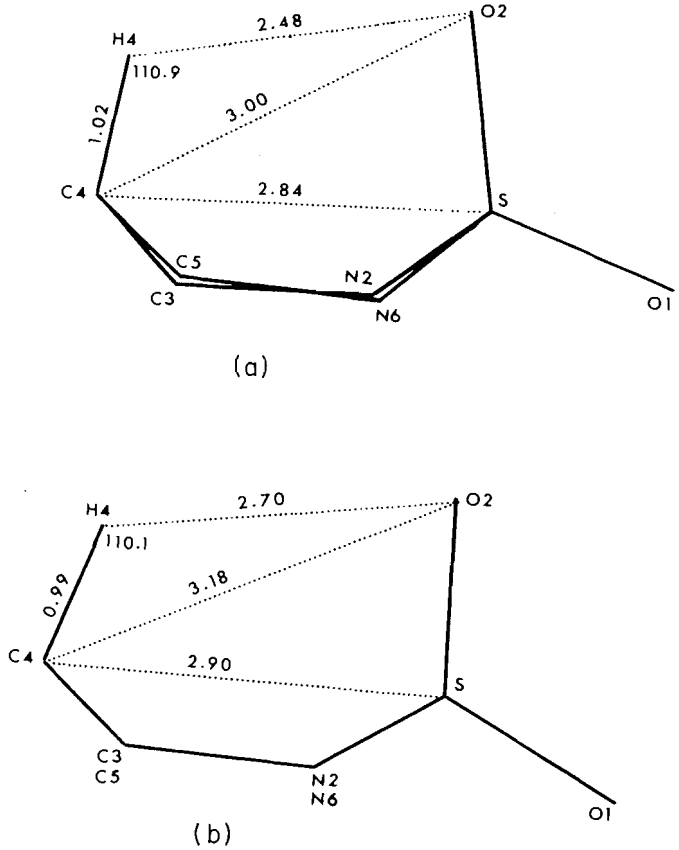

FIG. 3. Projection of a fragment of the molecule onto a plane normal to the best ring plane: (*a*) for **2**, (*b*) for **3**.

TABLE 6. Antipyretic (AP), analgesic (AN), antiinflammatory (AI) activities (in %) and LD_{50} of thiadiazines

Compound[a]	AP[b]	AN[c]	AI[d]	LD_{50} (mg/kg)
1	55	41	30	300–1000
2	28	67[e]	10	300–1000
3	—	—	100	100
4	—	—	100	500

[a]All compounds have been tested at the same dose as the standard.
[b]Aminopyrine as standard (100% activity, dose 50 mg/kg).
[c]Acetylsalicylic acid as standard (100% activity, dose 100 mg/kg).
[d]Phenylbutazone (**4**) as standard (100% activity, dose 50 mg/kg).
[e]Significant difference: $0.02 < p < 0.05$.

meter. Ultraviolet spectra were registered on a Perkin-Elmer 402 spectrophotometer.

Crystal data for **2** are as follows:

$C_{19}H_{32}N_2O_4S$ m.w. = 384.53
Triclinic, $P1$, a = 11.45(1), b = 15.678(2), c = 5.7669(2) Å, α = 90.22(1), β = 99.35(2), γ = 93.62(1), Z = 2, V = 1019.4(2) Å^3, D_x = 1.25 Mg m^{-3}, μ(CuKα) = 1.58 mm^{-1}, F(000) = 416.

Crystal data for **3** are as follows:

$C_{19}H_{20}N_2O_4S$ m.w. = 372.23
Orthorhombic, *Pnma*, a = 9.9891(3), b = 13.3077(4), c = 13.9982(2) Å, Z = 4, V = 1860.8(1) Å^3, D_x = 1.32 Mg m^{-3}, μ(CuKα) = 1.56 mm^{-1}, F(000) = 784.

Needle shaped colourless crystals, mounted on a PW1100 four circle diffractometer. Intensities were recorded in the $\omega/2\theta$ scan mode with θ between 2° and 65°. Graphite monochromatized CuKα radiation (λ = 1.54178 Å) was used. A total of 3710, for **2**, and 1659, for **3**, independent reflexions were measured, of which 2933 (for **2**) and 1200 (for **3**) were flagged as observed with $I > 2\sigma(I)$. Intensity data were corrected by Lorentz and polarization effects. No absorption correction was applied. Lattice parameters were determined by least-squares fit of the θ values for 45 and 32 reflexions respectively ($15° < \theta < 30°$) measured at 295 K for both positive and negative Bragg angles (gravity centres of the peaks), using only the most accurate circle (ω) of the diffractometer. Scattering factors for neutral atoms and anomalous dispersion corrections for S and O atoms were taken from International tables for X-ray crystallography (27). The structures were solved using MULTAN (28). Atoms C42, C43, and C44 of compound **3** are disordered as they do not lie on the mirror plane passing through O1, O2, S, C4, and C41, and so they have been assigned to a population parameter of 0.5. The structures were refined by full-matrix least-squares analysis using anisotropic temperature coefficients (H atoms as isotropic fixed contributors). All H atoms were located in a difference map, except those attached to C42, C43, and C44 in compound **3** which were calculated geometrically. A convenient weighting scheme of type $w = w_1 w_2$, with $w_1 = k/(a + b|F_o|)^2$ and $w_2 = 1/(c + d \sin\theta/\lambda)$, was used to obtain flat dependence in $\langle w\Delta^2 F\rangle$ vs. $\langle F_o\rangle$ and vs. $\langle \sin\theta/\lambda\rangle$ (29); the coefficients used for **2** are a = 0.9, b = −0.2 for $F_o < 11$, a = 0.3, b = 0 for $F_o > 11$, c = 1.85 and k = 0.6, d = −1.9 for all reflexions; the coefficients used for **3** are a = 1.4, b = −0.2 for $F_o < 12$, a = 0.5, b = 0 for $F_o > 12$, k = 0.4, c = 2.5, d = −5.0 for all reflexions. The unweighted and weighted final R values were 0.066 and 0.080 for **2** and 0.047 and 0.051 for **3**. Most calculations were performed with the XRAY76 System (30). Tables 7 and 8 show the final atomic parameters.[2]

The analgesic activity was tested following the Siegmund, Cadmus, and Lu method (31), using acetylsalicilic acid as standard. The antiinflammatory activity was measured by the Winter method (32)

TABLE 7. Atomic parameters for **2**

Atom	x/a	y/b	z/c	U_{eq}[a]
S	0.0728(1)	0.2489(1)	0.5502(2)	54
O1	0.1948(2)	0.2560(2)	0.5357(5)	60
O2	−0.0110(3)	0.2430(2)	0.3389(5)	78
O3	−0.0826(3)	0.1007(2)	0.9251(6)	74
O5	−0.0930(3)	0.3785(2)	0.9191(6)	79
N2	0.0477(3)	0.1667(2)	0.7167(6)	55
N6	0.0418(3)	0.3288(2)	0.7128(6)	56
C3	−0.0573(4)	0.1617(3)	0.8119(7)	58
C4	−0.1354(4)	0.2363(3)	0.7585(8)	63
C5	−0.0631(4)	0.3207(3)	0.8071(7)	60
C21	0.1334(4)	0.0978(2)	0.7718(7)	54
C22	0.2432(4)	0.1282(3)	0.9437(7)	64
C23	0.3174(5)	0.0521(4)	1.0152(9)	80
C24	0.3486(5)	0.0068(4)	0.8006(10)	84
C25	0.2390(5)	−0.0196(3)	0.6283(8)	72
C26	0.1649(4)	0.0564(3)	0.5532(7)	63
C41	−0.2423(4)	0.2293(4)	0.8873(9)	80
C42	−0.3501(5)	0.2624(6)	0.7659(13)	121
C43	−0.4063(5)	0.2382(5)	0.5326(13)	115
C44	−0.5159(7)	0.2737(8)	0.4341(19)	169
C61	0.1251(4)	0.4056(2)	0.7730(7)	56
C62	0.1581(4)	0.4509(3)	0.5589(7)	65
C63	0.2305(5)	0.5339(3)	0.6378(9)	78
C64	0.3391(5)	0.5166(3)	0.8158(10)	86
C65	0.3052(5)	0.4691(3)	1.0262(9)	79
C66	0.2330(4)	0.3863(3)	0.9494(7)	65

[a]$U_{eq} = (1/3)\Sigma[U_{ij}a_i^* a_j^* a_i a_j \cos(a_i, a_j) \times 10^3]$.

[2]Lists of observed and calculated structure factors, atomic parameters for H-atoms and anisotropic thermal coefficients are included as supplementary material. Complete set of data may be purchased from the Depository of Unpublished Data, CISTI, National Research Council of Canada, Ottawa, Ont., Canada K1A 0S2.

TABLE 8. Atomic parameters for **3**

Atom	x/a	y/b	z/c	U_{eq}[a]
S	0.0349(1)	0.2500(—)	0.1810(1)	52
O1	−0.0153(4)	0.2500(—)	0.0865(2)	68
O2	0.1755(3)	0.2500(—)	0.1958(3)	72
O3	−0.0937(3)	0.0842(2)	0.3788(2)	75
N2	−0.0327(2)	0.1538(1)	0.2388(2)	50
C3	−0.0475(3)	0.1552(2)	0.3379(2)	54
C4	0.0015(5)	0.2500(0)	0.3868(3)	63
C21	−0.0701(3)	0.0665(2)	0.1822(2)	51
C22	0.0252(3)	−0.0012(3)	0.1546(3)	73
C23	−0.0146(5)	−0.0826(3)	0.0981(3)	93
C24	−0.1447(5)	−0.0934(3)	0.0704(3)	89
C25	−0.2379(4)	−0.0247(3)	0.0990(3)	93
C26	−0.2008(3)	0.0556(3)	0.1548(3)	74
C41	−0.0166(8)	0.2500(—)	0.4930(4)	102
C42	0.0865(13)	0.1954(9)	0.5477(6)	145
C43	0.1012(28)	0.2117(25)	0.6431(17)	269
C44	0.1704(26)	0.2906(14)	0.6864(13)	214

[a] $U_{eq} = (1/3)\Sigma[U_{ij}a_i^*a_j^*a_ia_j \cos(a_i, a_j) \times 10^3]$.

with phenylbutazone as standard and the antipyretic activity by the Bianchi method (33) using aminopyrine as standard.

General synthetic method

To a stirred solution of the corresponding *N,N'*-disubstituted sulfamide (0.01 mol) in dry toluene (50 mL) a solution of malonyl or *n*-butylmalonyl chloride (0.01 mol) in dry toluene (10 mL) was added dropwise. The mixture was heated at 50°C for 30 min and then at 70°C for 4 h. On cooling, the resulting solution was evaporated to dryness *in vacuo* and the residue crystallized from ethanol. With this procedure, the following compounds were obtained.

*2,6-Dicyclohexyl-4*H*-1,2,6-thiadiazin-3,5(2*H*,6*H*)-dione 1,1-dioxide (1)*

Yield 70%, mp 152°C (lit. (2) 152°C); uv λ_{max} (MeOH): 213 (ε, 1400), 277 nm (ε, 850); ^{1}H nmr ($CDCl_3$) δ: 1.18 (m, 2H, H4′a, $J_{gem} \sim J_{a,a} = |12|$ Hz), 1.33 (m, 4H, H3′a, $J_{gem} \sim J_{a,a} = |12|$ Hz), 1.66 (m, 2H, H4′e, $J_{gem} = -12.4$ Hz), 1.80[3] (m, 4H, H3′e), 1.85[3] (m, 4H, H2′e), 2.16 (d.q, 4H, H2′a, $J_{gem} \sim J_{1'a,2'a} \sim J_{2'a,3'a} = |12|$ Hz, $J_{2'a,3'e} = 3.36$ Hz), 3.91 (s, 2H, H4), 4.48 (tt, 2H, H1′a, $J_{1'a,2'a} = 12.36$ Hz, $J_{1'a,2'e} = 3.85$ Hz), ir (Nujol) ν: 1760 cm^{-1} (C=O).

*4-*n*-Butyl-2,6-dicyclohexyl-1,2,6-thiadiazin-3,5-(2*H*,6*H*)-dione 1,1-dioxide (2)*

Yield 66%, mp 96°C; uv λ_{max} (MeOH): 225 (ε, 6650), 291 nm (ε, 3650); ^{1}H nmr ($CDCl_3$) δ: 0.9 (t, 3H, CH_3), 1.0–2.2 (m, 26H, H2′, H3′, H4′, $3CH_2$ butyl moiety), 3.9 (t, 1H, H4, $J = 4.5$ Hz), 4.3 (tt, 2H, H1′a, $J_{1'a,2'a} = 12$ Hz, $J_{1'a,2'e} = 4$ Hz); ir (Nujol) ν: 1700, 1740 cm^{-1} (C=O). *Anal.* calcd. for $C_{19}H_{32}N_2O_4S$: C 59.35, H 8.38, N 7.28; found: C 59.44, H 8.49, N 6.97.

*4-*n*-Butyl-2,6-diphenyl-1,2,6-thiadiazin-3,5-(2*H*,6*H*)-dione 1,1-dioxide (3)*

Yield 65%, mp 177–178°C (lit. (3) 177–178.5°C); uv λ_{max} (MeOH): 215 (ε, 1050), 289 nm (ε, 450); ^{1}H nmr ($CDCl_3$) δ: 1.0 (t, 3H, CH_3), 1.2–1.8 (m, 4H, CH_2-8, CH_2-9), 2.2 (m, 2H, CH_2-7), 4.5 (t, 1H, H4, $J = 6$ Hz), 7.4–7.7 (m, 10H, arom.); ir (Nujol) ν: 1720, 1760 cm^{-1} (C=O).

Acknowledgments

The financial support of the Comisión Asesora de Investigación Científica y Técnica (CAICYT) of Spain is gratefully acknowledged. The authors wish to thank Prof. Dr. W. Pfleiderer for the determination of the pK_a values.

[3] Assignments may be reversed.

1. J. ELGUERO, C. OCHOA, M. STUD, C. ESTEBAN-CALDERON, M. MARTINEZ-RIPOLL, J. P. FAYET, and M. C. VERTOUT. J. Org. Chem. **47**, 536 (1982).
2. A. M. PAQUIN. Angew. Chem. **60**, 316 (1948).
3. H. TEUFEL. U.S. Patent 2, 956, 997 (1960).
4. J. GIELDANOWSKI, B. BOBRANSKI, J. DECKERT, and B. SZAGA. Il Farmaco, Ed. Sc. **29**, 81 (1974).
5. H. SLADOWSKA. Il Farmaco, Ed. Sc. **32**, 866 (1977).
6. J. GIELDANOWSKI, B. BOBRANSKI, J. DECKERT, B. SZAGA, and B. TEODOCZYK. Arch. Immun. Ther. Exp. **21**, 517 (1972).
7. E. WAGNER, B. BOBRANSKI, J. KUPRINSKA, B. CEBO, and T. LIBROWSKI. Il Farmaco, Ed. Sc. **35**, 1039 (1980).
8. A. BURGER and R. T. STANDRIDGE. J. Med. Chem. **6**, 221 (1963).
9. S. P. SINGH, S. S. PARMAR, V. I. STENBERG, and S. A. FARNUM. J. Heterocycl. Chem. **15**, 13 (1978).
10. R. P. BELL. The proton in chemistry. Cornell University Press, New York. 1959.
11. M. WOLFF (*Editor*). Burger's medicinal chemistry. John Wiley and Sons, New York. 1981. p. 795.
12. R. H. MC. KEOWN. J. Chem. Soc. Perkin II, 515 (1980).
13. C. K. JOHNSON. ORTEP. Report ORNL-3794. Oak Ridge National Laboratory, TN. 1965.
14. M. D. CABEZUELO, F. H. CANO, C. FOCES-FOCES, and S. GARCIA-BLANCO. Acta Crystallogr. B**33**, 3598 (1977).
15. C. ESTEBAN-CALDERON, M. MARTINEZ-RIPOLL, and S. GARCIA-BLANCO. Acta Crystallogr. B**35**, 2795 (1979).
16. C. ESTEBAN-CALDERON, M. MARTINEZ-RIPOLL, and S. GARCIA-BLANCO. Acta Crystallogr. B**38**, 1128 (1982).
17. C. ESTEBAN-CALDERON, M. MARTINEZ-RIPOLL, and S. GARCIA-BLANCO. Acta Crystallogr. B**38**, 1340 (1982).
18. C. ESTEBAN-CALDERON, M. MARTINEZ-RIPOLL, and S. GARCIA-BLANCO. Acta Crystallogr. B**38**, 2296 (1982).
19. C. ESTEBAN-CALDERON, M. MARTINEZ-RIPOLL, and S. GARCIA-BLANCO. Acta Crystallogr. B**39**, 440 (1983).
20. C. ESTEBAN-CALDERON, M. MARTINEZ-RIPOLL, and S. GARCIA-BLANCO. Acta Crystallogr. B**40**, 80 (1984).
21. D. CREMER and J. A. POPLE. J. Am. Chem. Soc. **97**(6), 1354 (1975).
22. P. BROUANT, M. PIERROT, A. BALDY, C. OCHOA, P. GOYA, J. C. SOYFER, and J. BARBE. Acta Crystallogr. In press.
23. T. P. SINGH and M. VIJAYAN. J. Chem. Soc. Perkin II, 693 (1977).
24. R. TAYLOR and O. KENNARD. J. Am. Chem. Soc. **104**(19), 5063 (1982).
25. J. OKADA and T. ESAKI. Chem. Pharm. Bull. **22**, 1580 (1974).
26. J. OKADA, T. ESAKI, and K. FUJIEDA. Chem. Pharm. Bull. **24**, 61 (1976).
27. International tables for X-ray crystallography. Vol. IV, Birmingham, Kynoch Press. 1974.
28. P. MAIN, S. J. FISKE, S. E. HULL, L. LESSINGER, G. GERMAIN, J. P. DECLERCQ, and M. M. WOOLFSON. MULTAN. A system of computer programs for the automatic solution of crystal structures from X-ray diffraction data. University of York, England and Louvain, Belgium. 1980.
29. M. MARTINEZ-RIPOLL and F. H. CANO. PESOS. A computer program for the automatic treatment of weighting schemes. Instituto Rocasolano, CSIC, Serrano 119, 28006 Madrid, Spain. 1975.
30. J. M. STEWART, F. A. KUNDELL, and J. C. BALDWIN. The XRAY 76 System. Tech. Rep. TR-446. Computer Science Center, University of Maryland, College Park, Maryland. 1976.
31. E. SIEGMUND, R. CADMUS, and G. LU. Proc. Soc. Exp. Biol. Med. **95**, 729 (1957).
32. C. A. WINTER, E. A. RISLEY, and C. W. NUSS. Proc. Soc. Exp. Biol. Med. **111**, 544 (1962).
33. C. BIANCHI, B. LUMACHI, and L. PEGRASSI. Arztneim.-Forsch. **17**, 246 (1967).

Can. J. Chem. Downloaded from www.nrcresearchpress.com by 80.58.250.72 on 09/07/12
For personal use only.

Ultrasonic and thermodynamic studies of tetracyclines in solutions

J. D. PANDEY, K. MISHRA, A. SHUKLA, AND R. D. RAI

Department of Chemistry, University of Allahabad, Allahabad 211 002, U.P., India

Received June 11, 1986

J. D. PANDEY, K. MISHRA, A. SHUKLA, and R. D. RAI. Can. J. Chem. **65**, 303 (1987).

The ultrasonic velocity, U, density, and viscosity of aqueous and non-aqueous (water + dioxan) solutions of tetracycline hydrochloride and chlorotetracycline have been measured at two different temperatures. Partial molal volumes, ϕ_v, partial molal compressibility, ϕ_k, Vand's interaction coefficients, Q and C, and thermodynamic activation parameters ΔG^*, ΔS^*, and ΔH^* of these solutions have been computed from the ultrasonic velocity, density, and viscosity data. The results are interpreted in terms of solute–solvent interaction.

J. D. PANDEY, K. MISHRA, A. SHUKLA et R. D. RAI. Can. J. Chem. **65**, 303 (1987).

Opérant à deux températures différentes, on a déterminé la vitesses ultrasoniques, U, et d'autres propriétés, comme la densité et la viscosité, de solutions aqueuses (eau + dioxanne) et non-aqueuses du chlorhydrate de tétracycline et de la chlorotétracycline. Utilisant les données de vitesse ultrasonique, de densité et de viscosité, on a calculé les volumes molals partiels, ϕ_v, la compressibilité molale partielle, ϕ_k, les coefficients d'interaction Q et C de Vand et les paramètres thermodynamiques d'activation ΔG^*, ΔS^* et ΔH^* de ces solutions. On interprète les résultats en fonction d'interactions soluté/solvant.

[Traduit par la revue]

Introduction

Tetracyclines are a group of broad spectrum antibiotics. These compounds are well known for their prophylatic and therapeutic values. Their contribution to the medical profession has been substantial since they act as antibiotics against a wide range of human and animal pathogens (1, 2). They are a group of structurally related complex compounds, the parent compound being tetracycline. Their mode of action (3), biogenesis (4–8), and chemical properties have been worked out extensively.

The different tetracyclines used as antibiotics have comparable activity (9). The exact mechanism of their drug action, so far, has not been proposed. However, they do form coordination complexes with metal ions *in vitro* (10–12).

The results of ultrasonic, volumetric, and viscometric studies of tetracycline hydrochloride and chlorotetracycline in water and water–dioxan system are presented in this work. They may throw some light on the intricate drug interaction mechanism.

Experimental

Analytical grade tetracycline (TC) and chlorotetracycline (CTC) were obtained from Cynamide India Limited (Ledereley Division) as hydrochlorides and used as such. These antibiotics were kept in a vacuum desiccator for 48 h before use. Melting points were checked.

Preparation of aqueous solutions

Stock solutions (10^{-3} M) of (TC) and (CTC) were prepared in double distilled water. Nine solutions of different concentrations ranging from 0.0001 to 0.0009 M were prepared.

Preparation of non-aqueous solutions

Stock solutions (10^{-3} M) of (TC) and (CTC) were prepared in double distilled water and in 1,4-dioxane. Nine different solutions were prepared having varying compositions (10–90% of water–dioxan mixture).

Density measurements

The density measurements were performed for different solutions at 25 and 35±0.01°C with the help of precalibrated bicapillary pyknometer. The estimated error in the density measurements were found to be ±0.005%, as reported in an earlier paper (13).

Ultrasonic measurements

Ultrasonic velocity (U) measurement has been performed by variable path ultrasonic interferometer having frequency of 2 MHz, as described earlier (13). The estimated error has been found to be ±0.02% which is an improvement over the previous estimated accuracy (±0.05%).

Viscosity measurements

Viscosity was measured with a calibrated modified Ostwald type viscometer 03 at 25 and 35 ± 0.01°C. Uncertainties in the measured viscosities were within ±0.03%. Viscosity data were analysed using Jones–Dole (14) and Vand's (15) equations.

Thermodynamic parameters have been evaluated from the experimental viscosity values.

Results and discussion

The apparent molal volumes, ϕ_v, and apparent molal compressibilities, ϕ_k, of tetracycline solutions were determined from density and adiabatic compressibility, using the following equations:

$$[1] \quad \phi_v = \frac{10^3(d_s - d_0)}{m d_s d_0} + \frac{M}{d_0}$$

$$[2] \quad \phi_k = \frac{10^3(\beta_s - \beta_0)}{m d_0} + \beta_s \phi_v$$

where d_0, d_s, β_0, and β_s are densities and compressibilities of solvent and solution, respectively, m is the molality, and M is the molecular weight of the true solute (Table 1).

The adiabatic compressibility, β_s, of the aqueous solutions were determined from the sound velocity using the relation,

$$\beta_s = \frac{1}{U^2 d}$$

Values of S_v and S_k at infinite dilution were obtained from the Masson's (16) equations [3] and [4] respectively.

$$[3] \quad \phi_v = \phi_v^0 + S_v\sqrt{C}$$

$$[4] \quad \phi_k = \phi_k^0 + S_k\sqrt{C}$$

where S_v and S_k are the experimental slope of ϕ_v vs. $\sqrt{C}$ and ϕ_k vs. $\sqrt{C}$ plots. ϕ_v^0 and ϕ_k^0 are the standard partial molal volume and partial molal compressibility, respectively. The

Can. J. Chem. Downloaded from www.nrcresearchpress.com by 80.58.250.72 on 09/07/12
For personal use only.

TABLE 1. Compressibility lowering, apparent molal volume, apparent molal compressibility and Jones–Dole parameter for the system tetracycline hydrochloride + water and chlorotetracycline + water at different temperatures

System	C (dm^{-3} mol × 10^{-4})	$\Delta\beta_s$ (TPa^{-1})* 25°C	$\Delta\beta_s$ (TPa^{-1})* 35°C	ϕ_v (dm^3 mol^{-1}) 25°C	ϕ_v (dm^3 mol^{-1}) 35°C	ϕ_k (MPa^{-1} mol^{-1} m)† 25°C	ϕ_k (MPa^{-1} mol^{-1} m)† 35°C	Jones–Dole parameter $\eta/\eta_0 - 1/\sqrt{C}$ 25°C	Jones–Dole parameter $\eta/\eta_0 - 1/\sqrt{C}$ 35°C
1. Tetracycline hydrochloride + water	1	0.17	0.13	1.488	0.483	−0.164	−0.129	1.93	0.35
	2	0.36	0.31	1.990	0.989	−0.172	−0.152	2.59	1.75
	3	0.79	0.66	2.827	1.495	−0.252	−0.215	3.49	3.14
	4	1.16	1.00	3.496	1.747	−0.260	−0.244	4.15	4.12
	5	1.41	1.29	3.896	2.101	−0.266	−0.251	4.61	4.79
	6	1.78	1.63	4.162	2.168	−0.280	−0.264	5.05	5.42
	7	2.13	1.97	4.351	2.360	−0.286	−0.273	5.58	6.13
	8	2.49	2.36	4.492	2.504	−0.293	−0.286	5.83	6.49
	9	2.84	2.69	4.402	2.615	−0.297	−0.290	5.83	6.54
2. Chlorotetracycline + water	1	0.12	0.08	2.491	1.493	−0.109	−0.074	3.27	3.84
	2	0.37	0.20	2.993	1.999	−0.172	−0.092	3.54	4.23
	3	0.79	0.38	3.160	2.167	−0.250	−0.118	4.26	5.16
	4	1.16	0.57	3.243	2.503	−0.277	−0.132	4.82	5.87
	5	1.52	0.81	3.493	2.705	−0.290	−0.151	5.20	6.34
	6	1.88	1.04	3.659	2.839	−0.298	−0.162	5.60	7.05
	7	2.23	1.33	2.920	2.935	−0.303	−0.179	5.86	7.34
	8	2.58	1.57	3.990	3.132	−0.306	−0.184	6.05	7.38
	9	2.93	1.85	4.045	3.173	−0.309	−0.193	6.06	7.42

*TPa^{-1} (teraPascal^{-1}) = 10^{12} Pa^{-1}.
†MPa^{-1} (megaPascal^{-1}) = 10^6 Pa^{-1}.

TABLE 2. Apparent molal volume, apparent molal compressibility, viscosity interaction coefficient of Jones–chlorotetracycline + water

System	ϕ_v^0 (dm^3 mol^{-1}) 25°C	ϕ_v^0 (dm^3 mol^{-1}) 35°C	S_v Slope of ϕ_v^0 vs. $\sqrt{C}$ 25°C	S_v Slope of ϕ_v^0 vs. $\sqrt{C}$ 35°C	ϕ_k^0 (MPa^{-1} mol^{-1} m) 25°C	ϕ_k^0 (MPa^{-1} mol^{-1} m) 35°C	S_k Slope of ϕ_k^0 vs. $\sqrt{C}$ 25°C	S_k Slope of ϕ_k^0 vs. $\sqrt{C}$ 35°C
1. Tetracycline hydrochloride + water	1.38	0.82	0.18	0.10	0.22	0.19	0.346	0.375
2. Chlorotetracycline + water	2.46	1.46	0.09	0.08	0.24	0.07	0.500	0.570

TABLE 3. Apparent molal volume, apparent molal compressibility, viscosity interaction coefficient of chlorotetracycline + (dioxan–water)

System†	ϕ_v^0 (dm^3 mol^{-1}) 25°C	ϕ_v^0 (dm^3 mol^{-1}) 35°C	S_v Slope of ϕ_v^0 vs. $\sqrt{C}$ 25°C	S_v Slope of ϕ_v^0 vs. $\sqrt{C}$ 35°C	ϕ_k^0 (MPa^{-1} mol^{-1} m) 25°C	ϕ_k^0 (MPa^{-1} mol^{-1} m) 35°C	S_k Slope of ϕ_k^0 vs. $\sqrt{C}$ 25°C	S_k Slope of ϕ_k^0 vs. $\sqrt{C}$ 35°C
1. TC hydrochloride + (dioxan–water)	6.80	6.00	0.46	0.45	0.40	0.13	1.190	0.2142
2. CTC + (dioxan–water)	9.20	8.70	0.33	0.31	0.22	0.12	0.628	0.2121

†TC = tetracycline, CTC = chlorotetracycline.

Can. J. Chem. Downloaded from www.nrcresearchpress.com by 80.58.250.72 on 09/07/12
For personal use only.

values of ϕ_v, ϕ_k, and S_v, S_k are listed in Table 2 and Table 3. The values of coefficients B and Q of viscosity data were obtained from Jones–Dole (14) and Vand's (15) equations

$$[5] \quad \eta/\eta_0 = 1 + A\sqrt{C} + BC$$

$$[6] \quad \frac{C}{\log \eta_r} = \frac{2.303}{2.5\,\bar{V}} - \frac{2.303\,QC}{2.5}$$

where η/η_0 is relative viscosity, A and B are empirical coefficients obtained from $(\eta/\eta_0 - 1/\sqrt{C}$ vs. $\sqrt{C}$ plots. Values of A and B are listed in Table 2. In eq. [6], C is the molar concentration and $\bar{V}$ is the molar volume of the solute which is the effective flowing volume. Q is a generalised particle interaction coefficient dealing with mutual interference between the spheres and with their Brownian motion. The values of Q and $\bar{V}$ were obtained from C (log $\eta_\gamma)^{-1}$ vs. C plots, and are presented in Table 3.

Calculated values of apparent molal volume, ϕ_v, have been found to be in good agreement with Masson's equation, as the plot of ϕ_v vs. $\sqrt{C}$ is linear. Calculated values of partial molal volumes, ϕ_v^0, are summarized in Tables 2 and 3. The values of ϕ_v^0 in the water–dioxan system are comparatively higher than those of pure water. This is attributed to the fact that dioxan does not penetrate the three dimensional structure of water. Positive values of ϕ_v^0 indicate that this does not restrict molecular motion within the solution.

Values of S_v obtained from the slope of ϕ_v vs. $\sqrt{C}$ are incorporated in Tables 2 and 3. Results of the experimental slope S_v reveal that solute–solute interaction decreases with the rise in the temperature. Values are comparatively low in water system compared to water–dioxan system, which indicates that solute–solute interaction is maximum at 25°C in the solute dioxan – water system (13, 17–26). Standard partial molal compressibilities, ϕ_k^0, obtained from the linear plot of ϕ_k vs. $\sqrt{C}$ are listed in Tables 2 and 3. Results show that the values are comparatively higher in tetracycline + dioxan – water system than chlorotetracycline + dioxan – water system in comparison to water alone. Negative values of ϕ_k are attributed to the loss of structural compressibility of the solvent molecules due to the increased population of four bonded water molecules in the water–dioxan mixtures (13, 17–26).

Viscosity data are analysed in the terms of Jones–Dole and Vand's equations. Values of B and Q interaction coefficients are displayed in Tables 2 and 3. Positive B and Q values indicate a strong alignment of solvent molecules with those of the solute (22–26). B and Q values increase with rise in temperature, showing that solute–solvent interaction are influenced by the temperature. The behaviour of tetracyclines in water–dioxan mixture can be analysed by observing the Q values. Tables 2 and 3 reveal that the tetracycline hydrochloride and chlorotetracycline have low positive B and Q values and are slightly influenced by variation in the temperature. Therefore, it can be stated that positive B and Q values for tetracycline hydrochloride and chlorotetracycline are exclusively due to solute–solvent interaction (22–26). Thus the tetracycline molecules can be labelled as "structure makers" in aqueous solution.

The analysis of solute activation parameters are presented in Tables 2 and 3. This has been done in light of Nightingale (27) and Feakins (28) formulations. It has been mentioned already that these tetracyclines have been used as therapeutic and prophylatic agents against bacterial activity. The data have been reported at 25 and 35°C, because at higher temperature these compounds may decompose. Besides, the main object of this work is to investigate the solute–solvent interaction

Dole equation and average value of thermodynamic parameters for the system tetracycline hydrochloride and at infinite dilution

ΔG^* (kcal)		ΔS^* (eu)		ΔH^* (cal)		A coefficient		B coefficient	
25°C	35°C	25°C	35°C	25°C	35°C	25°C	35°C	25°C	35°C
15.77	16.17	15.78	16.19	4719.02	5001.50	−1.65	−0.40	2.20	3.18
15.77	16.19	15.78	16.20	4719.85	5006.30	−3.10	−3.05	1.82	2.50

Vand's equation and average value of thermodynamic parameters for the system tetracycline hydrochloride mixture at infinite dilution

ΔG^* (kcal)		ΔS^* (eu)		ΔH^* (cal)		Q coefficient		$\bar{V}$ coefficient	
25°C	35°C	25°C	35°C	25°C	35°C	25°C	35°C	25°C	35°C
16.29	16.63	16.31	16.65	4876.38	5145.79	0.017	0.050	0.010	0.009
16.25	16.61	16.27	16.63	4864.91	5137.70	0.019	0.062	0.011	0.010

Can. J. Chem. Downloaded from www.nrcresearchpress.com by 80.58.250.72 on 09/07/12
For personal use only.

TABLE 4. Compressibility lowering, apparent molal volume, apparent molal compressibility, and Vand's parameter for the system tetracycline hydrochloride + (dioxan–water) and chlorotetracycline + (dioxan–water) mixture at different temperatures

System	Mole fraction of dioxan $\times 10^{-4}$		$\Delta\beta_s$ (TPa^{-1})		ϕ_v ($dm^3\ mol^{-1}$)		ϕ_k ($MPa^{-1}\ mol^{-1}\ m$)		Vand's parameter $C/\log \eta r$ $\times 10^{-4}$	
	25°C	35°C	25°C	35°C	25°C	35°C	25°C	35°C	25°C	35°C
1. Tetracycline hydrochloride + (dioxan–water) mixture	288	227	4.68	1.89	8.672	7.824	−0.358	−0.126	116	161
	816	813	4.81	2.78	12.384	11.952	−0.222	−0.108	135	185
	1687	1682	5.40	4.02	17.549	16.848	−0.144	−0.091	141	222
	3111	3103	4.25	4.81	20.063	19.040	−0.063	−0.087	154	236
	5861	5853	0.45	3.61	22.072	21.362	−0.084	−0.019	161	267
2. Chlorotetracycline + (dioxan–water) mixture	228	227	2.97	1.97	10.156	9.971	−0.206	−0.124	133	184
	816	813	4.22	2.89	14.395	12.947	−0.180	−0.110	152	214
	1687	1681	4.95	3.97	17.215	16.056	−0.127	−0.092	162	249
	367	3103	5.58	3.45	18.894	17.523	−0.109	−0.044	171	279
	5859	5849	0.65	3.21	20.507	19.131	−0.070	−0.015	180	309

(tetracyclines in water and water–dioxan mixture) near body temperature. The observed appreciable changes in the viscosities enabled us to evaluate the thermodynamic activation parameters. The Gibbs–Helmholtz equation was used. The values of ΔH^* was deduced from the estimates of ΔS^* and ΔG^* (28). The values of ΔS^* were obtained from the slope of the plot of $\ln \eta_v/hN$ vs. T. The evaluation of ΔS^* values from such plots at only two temperature can not yield reliable results. The average values of the thermodynamic activation parameters are given in Tables 2 and 3.

The careful scrutiny of the thermodynamic parameters indicates that these values increase with increase in temperature. However, it is found that the ΔG^*, ΔS^*, and ΔH^* values are higher in the water–dioxan system than those in water alone. The positive value of the free energy of activation, ΔG^*, suggests that water has more affinity for tetracycline hydrochloride and chlorotetracycline than have water–dioxan mixtures (13, 17–25). Similarly, other activation parameters, such as ΔH^* and ΔS^*, have positive values at all solvent compositions of water–dioxan, thereby showing that entropies and enthalpies in water–dioxan mixtures are both enhanced relative to pure water and hence the net order created by the solutes in water–dioxan mixture is less than that in pure water. The hydrophilicities (lipophobicities) of tetracycline hydrochloride and chlorotetracycline are thus in accordance with their drug activity (Table 4). The conclusion drawn from the thermodynamic behaviour of these antibiotics in solution, viz., the lower entropies and enthalpies in pure water as compared to water–dioxan mixture are very much in keeping with their minimal requirement for drug action *in vivo*.

Acknowledgements

We are very grateful to Dr. V. P. Tewari for his valuable cooperation in this work. We also thank the C.S.I.R., New Delhi, for financial assistance.

1. R. E. KIRK and D. F. OTHMER (*Editors*). Encyclopedia of chemical technology. Vol. 13. Interscience, New York. 1954. (*a*) p. 185; (*b*) pp. 800, 808.
2. H. K. SPITZY. Antibiotics. Chemother. **10**, 193 (1962).
3. G. C. BARRETT. J. Pharm. Sci. **52**, 309 (1963).
4. J. R. D. MCCORMICK. Biogenesis of antibiotics substances. *Edited by* Z. Vanek and Z. Hostaick. Academic Press, New York. 1965. p. 73.
5. J. H. MARTIN, L. A. MITSCHER, P. A. MILLER, P. SHUAR, and J. N. BOBONOS. Antimicrobial agents and chemotherapy. Am. Soc. Microbial. Ann. Arost. Michigan. 1966. p. 563.
6. P. A. MILLER, A. SATURNELL, J. H. MARTIA, L. A. MITSCHER, and N. BOHONOS. Biochem. Biophys. **16**, 285 (1964).
7. J. R. D. MCCORMICK, U. H. JOSCHIM, and JOHODAC. J. Am. Chem. Soc. **87**, 1793 (1965).
8. P. A. MILLER, J. H. HESCH, M. LINCIS, and N. BOHNOS. Biochem. Biophys. Res. Commun. **18**, 325 (1965).
9. J. R. BROWN and D. S. IRELAND. Adv. Pharmacol. Chemother. **15**, 161 (1978).
10. N. P. SACHAN and C. M. GUPTA. Talanta, **27**, 457 (1980).
11. N. P. SACHAN. Ph.D. Thesis, University of Rajasthan, Jaipur. 1981.
12. T. R. TRILTON. Biochemistry, **16**, 4133 (1977).
13. J. D. PANDEY, A. K. PURI, and K. MISRA. Thermochim. Acta, **74**, 313 (1984).
14. D. JONES and M. DOLE. J. Am. Chem. Soc. **51**, 2050 (1929).
15. V. VAND. J. Phys. Colloid. Chem. **52**, 277 (1948).
16. D. O. MASSON. Phil. Mag. **8**, 218 (1929).
17. A. SHUKLA. Ph.D. Thesis, Allahabad University, Allahabad. 1985.
18. H. P. BENNETO, D. FEABINS, and K. G. LAWRENCE. J. Chem. Soc. A, 1493 (1968).
19. A. FMATIELLO and D. C. DOUGLASS. J. Mol. Spectrosc. II, 465 (1963).
20. A. BANNAIM and D. MONAN. Trans. Faraday Soc. **61**, 821 (1965).
21. R. K. MOHANTY, T. S. SAVIMA, S. SUBRAMANIAM, and J. C. AHLUWALIA. Trans. Faraday Soc. **65**, 2333 (1969).
22. P. B. DAS, N. C. DAS, and P. P. MISRA. Thermochim. Acta, **44**, 113 (1981).
23. S. P. MOULIK and A. K. MITRA. Carbohydr. Res. **23**, 65 (1972).
24. P. B. DAS. Thermochim. Acta, **44**, 379 (1981).
25. P. B. DAS and N. C. DAS. Thermochim. Acta, **41**, 247 (1980).
26. P. B. DAS, S. MOHANTY, and B. K. DAS. Thermochim. Acta, **43**, 385 (1981).
27. E. R. NIGHTINGALE and R. F. BENCH. J. Phys. Chem. **63**, 1777 (1959).
28. D. FEAKINS, D. F. MANTLE, and K. C. LAWRENCE. J. Chem. Soc. Faraday Trans. I, **70**, 795 (1974).

Can. J. Chem. Downloaded from www.nrcresearchpress.com by 80.58.250.72 on 09/07/12
For personal use only.

Chloration de l'acétanilide et de la benzanilide en présence des cyclodextrines et de l'amylose

ROBERT CHÊNEVERT [1] ET GUY AMPLEMAN

Département de chimie, Faculté des sciences et de génie, Université Laval, Québec (Qué.), Canada G1K 7P4

Reçu le 28 avril 1986

ROBERT CHÊNEVERT et GUY AMPLEMAN. Can. J. Chem. **65**, 307 (1987).

La présence des cyclodextrines ou de l'amylose lors de la chloration de l'acétanilide ou de la benzanilide favorise la formation de l'isomère *para* au détriment de l'isomère *ortho*. La constante de dissociation du complexe acétanilide–α-cyclodextrine ainsi que la disposition moléculaire de l'acétanilide dans la cavité de l'α-cyclodextrine ont été déterminées par spectroscopie de résonance magnétique nucléaire du proton et du carbone-13.

ROBERT CHÊNEVERT and GUY AMPLEMAN. Can. J. Chem. **65**, 307 (1987).

The ratio of *ortho* to *para* isomers in chlorination of acetanilide and benzanilide is changed in favour of the *para* isomer when the reactants are entrapped in cyclodextrins or amylose. The dissociation constant and the time-averaged position of acetanilide in the α-cyclodextrin cavity have been determined by proton and carbon-13 nuclear magnetic resonance spectroscopy.

Can. J. Chem. Downloaded from www.nrcresearchpress.com by 80.58.250.72 on 09/07/12
For personal use only.

Introduction

Les cyclodextrines forment des composés d'inclusion en solution aqueuse avec une grande variété de substrats et elles sont des catalyseurs de certaines réactions organiques (1). Ces systèmes sont des modèles de la réaction enzymatique et leur cinétique a été fortement étudiée (2–4). Plus récemment, l'intérêt s'est porté vers l'étude de la sélectivité des réactions en présence de cyclodextrines. Les premiers travaux sont ceux de Breslow *et al.* sur la chloration de l'anisole par l'acide hypochloreux en présence de l'α-cyclodextrine (5, 6). Les cyclodextrines ont aussi une influence sur la réaction de Reimer–Tiemann (7), le réarrangement photochimique de Fries (8, 9), le réarrangement du tétrafluoroborate de benzylméthylsulfonium (10) et sur la réduction des énones par le borohydrure de sodium (11). D'autre part, l'amylose ou poly-(1→4)-α-D-glucose peut dans des conditions adéquates adopter la conformation d'une hélice α et inclure des substrats à l'intérieur de cette hélice. Malgré ce fait, l'amylose a rarement été employée comme catalyseur dans les réactions organiques. Hui *et al.* ont rapporté une cinétique de saturation de type enzymatique lors de l'étude de l'hydrolyse d'esters en présence de l'amylose ou de ses dérivés (12). Plus récemment nous avons décrit l'effet de l'amylose sur la réduction d'énones par le borohydrure de sodium (13) et sur un réarrangement photochimique de Fries (14). Nous décrivons dans cet article les effets des cyclodextrines et de l'amylose sur la chloration de l'acétanilide et de la benzanilide.

Résultats et discussion

La chloration de l'acétanilide et de la benzanilide par le chlore a d'abord été réalisée dans l'eau pure, puis les résultats ont été comparés à ceux obtenus en présence de l'α-cyclodextrine (α-CD), de la β-cyclodextrine (β-CD) ou de l'amylose. Un équivalent molaire de cyclodextrine (α-CD et β-CD) a été employé alors que la concentration relative d'amylose était de 1 g/mmol de substrat. Les résultats sont décrits par l'équation [1] et le tableau 1. Dans tous les cas, la cyclodextrine favorise l'introduction du chlore en position *para* et l'effet est plus prononcé avec l'α-CD. Nous avons donc étudié plus particulièrement le complexe α-CD–acétanilide. La constante de dissociation K_d du complexe a été mesurée par spectroscopie de résonance magnétique nucléaire du proton. Les déplacements

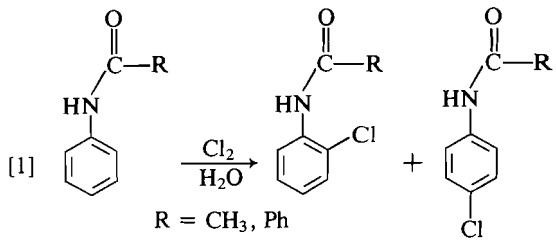

[1] R = CH_3, Ph

chimiques des protons aromatiques du substrat ont été mesurés en fonction de la concentration de l'α-CD (tableau 2). Les valeurs obtenues ont été traitées suivant la méthode décrite par Bergeron *et al.* (15, 16) (diagramme de Benesi–Hildebrand). La constante de dissociation trouvée est $5{,}0 \pm 0{,}3 \times 10^{-2}\ M$. Cette constante est comparable à celle de l'acétate de phényle ($2{,}2 \times 10^{-2}\ M$) (17) ou du *p*-nitrotrifluoroacétanilide ($6{,}1 \times 10^{-2}\ M$) (18) avec l'α-cyclodextrine.

La spectroscopie rmn à haute résolution (400 MHz) permet aussi de déterminer la position moyenne de l'acétanilide à l'intérieur de la cavité de la cyclodextrine. En effet, les protons méthine en position 3 et 5 de chaque unité de glucose pointent vers l'intérieur de la cavité de la cyclodextrine. L'observation de ces protons en rmn montre qu'ils sont blindés lorsqu'ils se trouvent dans le champ magnétique du nuage d'électrons π d'un noyau aromatique (15, 16, 19–23). Les déplacements chimiques des protons de l'α-cyclodextrine en fonction de la concentration de l'acétanilide sont rassemblés dans le tableau 3. Les constantes de couplage entre les différents protons de l'α-CD ($J_{1,2} = 3{,}3$ Hz, $J_{2,3} = 9{,}8$ Hz, $J_{3,4} = 8{,}8$ Hz, $J_{4,5} = 9{,}6$ Hz) varient très peu lors de l'addition d'acétanilide, ce qui signifie qu'il n'y a pas distorsion des cycles de glucose. À l'échelle des temps de la rmn ^{1}H, les six unités de glucose sont dans des conformations identiques. Les valeurs des constantes de couplage vicinaux sont en accord avec la conformation chaise *C*1. Il y a un déplacement vers les champs forts des protons H3 et H5, alors que les autres protons situés à l'extérieur de la cavité ne montrent pas de déplacements significatifs. Le déplacement de H3 est nettement plus prononcé que celui de H5. D'autre part, le déblindage des protons en position *ortho* du substrat est similaire à celui des protons *meta* et *para*. Ces résultats montrent que le noyau aromatique se trouve vis-à-vis le proton H3 de l'α-CD, c'est-à-dire du coté des hydroxyles secondaires (coté le plus large du tore). Le schéma 1 montre la position du noyau aromatique dans la cavité de la cyclodextrine. A priori, la molécule d'acétanilide peut prendre deux orienta-

1. Auteur à qui adresser la correspondance.

TABLEAU 1. Chloration de l'acétanilide et de la benzanilide

Substrat	Conditions	Rendements relatifs, %[a] (±3%) *ortho*	*para*	Rapport *ortho/para*
R = CH_3	Sans CD	49	51	0,96
	α-CD	10	90	0,11
	β-CD	39	61	0,64
	Amylose	48	52	0,92
R = phenyl	Sans CD	45	55	0,82
	α-CD	28	72	0,39
	β-CD	32	68	0,47
	Amylose	31	69	0,45

[a]Moyennes de trois essais. Taux de conversion : acétanilide (100%); benzanilide (90%). Le taux de récupération des produits est supérieur à 90% dans tous les cas.

TABLEAU 2. Déplacements chimiques des protons aromatiques de l'acétanilide[a] dans le D_2O en fonction de la concentration de l'α-cyclodextrine (200 MHz)

[α-CD] (*M*)	δ_{obs} H *ortho* (Hz)	δ_{obs} H *para*, *meta* (Hz)	Δδ *ortho* (Hz)	Δδ *meta*, *para* (Hz)
0,000	1485,1	1481,0	—	—
0,001	1486,2	1481,9	1,1	0,9
0,005	1486,7	1482,6	1,6	1,6
0,010	1488,3	1484,1	3,2	3,1
0,020	1490,8	1486,4	5,7	5,4
0,030	1492,7	1488,3	7,6	7,3
0,040	1494,0	1489,5	8,9	8,6
0,050	1495,3	1490,8	10,2	9,8

[a]Concentration de l'acétanilide fixe à 0,006 *M*.

tions différentes dans la cavité de α-CD : le groupement amide peut être orienté vers l'intérieur de la cavité ou encore émerger du coté des fonctions hydroxyles secondaires. L'orientation réelle pourrait être établie par une étude des déplacements chimiques (rmn ^1H) des protons sur le noyau aromatique du substrat : plus de déblindage est fort plus le proton est inclu profondement dans la cavité de la cyclodextrine (21). Toutefois, dans le cas de l'acétanilide, les déplacements des protons *ortho* sont presqu'identiques à ceux des protons *méta* et *para* et il est impossible d'établir l'orientation du substrat selon ce critère. L'orientation peut aussi être déterminée par une étude des déplacements chimiques en rmn ^{13}C des carbones du noyau aromatique. Les carbones 1 et 4 situés dans l'axe de l'α-CD seront blindés (déplacement vers les champs forts) s'ils sont profondement inclus dans la cavité et déblindés (déplacement vers les champs faibles s'ils sont dans la position inverse (24–26)). Il s'agit d'un effet de solvant, la cavité de la cyclodextrine fournissant un milieu moins polaire que son environnement. Les déplacements ont été prédits par des calculs de mécanique quantique et les orientations prédites sont conformes à celles déterminées en solution par la rmn ^1H et à l'état solide par des études de rayons-X (24). Ainsi, il a été démontré que l'acide benzoïque, l'acide *p*-hydroxybenzoïque et le *p*-nitrophénol ont respectivement leurs groupements acide et nitro orientés vers l'intérieur de la cavité de l'α-CD (24). Dans le cas de l'acétanilide le carbon 1 est déblindé de 0,29 ppm et le

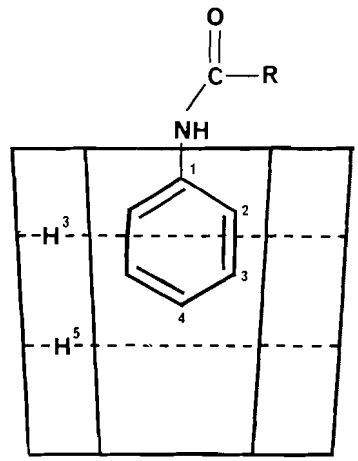

SCHÉMA 1

carbone 4 est blindé de 0,35 ppm (tableau 4). La fonction amide émerge donc de la cavité de la cyclodextrine par le coté des hydroxyles secondaires (schéma 1). Cette disposition du substrat permet d'expliquer la sélectivité de la réaction de chloration. Les positions *ortho* de l'acétanilide sont masquées par la cyclodextrine alors que la position *para* qui occupe l'axe de la cavité est relativement dégagée. Le chlore pénétre donc dans la cavité du coté des hydroxyles primaires pour réagir avec la position *para* de l'acétanilide. Un mécanisme similaire a été rapporté par Komiyama et Hirai (27, 28) lors d'une étude de la réaction de Reimer–Tiemann en présence de cyclodextrines. Ils ont démontré que l'addition de l'α-CD rend la réaction sélective en *para* et que le chloroforme pénétre dans la cavité de l'α-CD pour attaquer la position *para* du noyau aromatique. Lors de l'étude de la chloration de l'anisole par l'acide hypochloreux en présence de α-CD, Breslow a noté une augmentation de vitesse et une grande sélectivité en *para*. Cet effet avait deux origines : les positions en *ortho* sont masquées par la formation du complexe et la chloration en *para* est favorisée par la formation d'un ester hypochloreux avec un hydroxyle de la cyclodextrine permettant une réaction intra-complexe (5, 6, 29). Plus récemment, Tee et Bennett ont étudié la cinétique de la bromation de l'anisole par le brome en présence de α-CD et ont noté une réduction du taux de bromation en présence de α-CD; ils ont aussi démontré que la réaction n'implique pas l'acide hypobromeux ou son ester (30). Dans notre cas, la formation d'acide hypochloreux est possible par réaction entre le chlore et l'eau mais la constante d'équilibre est défavorable ($K = 4{,}2 \times 10^{-4}$) (31). Nos résultats doivent être expliqués principalement par un encombrement de position *ortho* car la formation d'un ester hypochloreux et une réaction intra-complexe devrait conduire à une plus grande sélectivité comparable à celle rapportée par Breslow.

Nous n'avons pas effectué d'études similaires de spectroscopie rmn pour le complexe α-CD–benzanilide car la solubilité de la benzanilide est infime dans l'eau et la présence de deux noyaux aromatiques sur le substrat rend l'interprétation des données complexes. La sélectivité plus faible de la benzanilide est due au moins en partie à la présence de deux noyaux aromatiques, le noyau benzoyle occupant la cavité de la cyclodextrine environ la moitié du temps. Il est à noter que la chloration d'un noyau aromatique par le chlore sans catalyseur n'est possible que sur un noyau activé; la chloration est impossible sur le noyau benzoyle car il est désactivé et nous

Can. J. Chem. Downloaded from www.nrcresearchpress.com by 80.58.250.72 on 09/07/12
For personal use only.

TABLEAU 3. Déplacements chimiques (400 MHz) des protons de l'α-CD en fonction du rapport substrat/α-CD (S/CD)

		δ (Hz)					Δδ (Hz)			
Protons	S/CD :	0[a]	0,25	0,50	1,00	2,00	0,25	0,50	1,00	2,00
H1		1941,2	1942,1	1941,1	1940,9	1942,6	0,9	−0,1	−0,3	1,4
H2		1372,6	1373,9	1372,4	1372,7	1375,4	1,3	−0,2	0,1	2,8
H3		1512,8	1503,4	1501,5	1494,5	1489,5	−9,4	−11,3	−18,3	−23,3
H4		1353,6	1355,3	1353,9	1353,8	1357,2	1,7	0,3	0,2	3,6
H5		1454,1	1452,2	1452,0	1451,9	1494,4	−1,9	−2,1	−2,2	−4,7
H6a		1476,9	1472,0	1479,1	1480,2	1480,1	2,1	2,2	3,3	3,2
H6b		1464,7	1466,9	1465,4	1467,9	1464,9	2,2	0,7	3,2	0,2

[a][CD] = 0,04 *M*; *T* = 23°C. Les conditions d'obtention sont décrites dans la partie expérimentale.

TABLEAU 4. Déplacements chimiques en ^{13}C de l'acétanilide

Carbone	Amide libre (ppm)	Complexe[a] (ppm)	Δδ (ppm)[b]
$C_{C=O}$	173,79	173,75	−0,04
C1	137,57	137,86	+0,29
C2	122,96	122,81	−0,15
C3	129,98	129,99	+0,01
C4	126,43	126,08	−0,35

[a]Concentration : α-CD = 0,10 *M*; acétanilide = 0,04 *M*.
[b]Une valeur négative indique un déplacement vers les champs forts.

n'avons pas détecté d'autres produits que ceux décrits au tableau 1.

L'amylose est sans effet notable sur la chloration de l'acétanilide mais, tous comme les cyclodextrines, favorise l'introduction du chlore en *para* de la benzanilide. Nous avons déjà décrit des résultats similaires lors du réarrangement photochimique de Fries des acétate et benzoate de phényle (14). Le réarrangement du benzoate était modifié par la présence de l'amylose alors que celui de l'acétate ne l'était pas. Il semble que l'amylose requiert des substrats volumineux afin d'exercer son effet. Hui a rapporté lors de l'étude de l'hydrolyse d'esters de *p*-nitrophénol en présence d'amylose que l'effet catalytique est nul sur l'acétate et que l'effet augmente avec la longueur de la chaîne de l'ester (12). De même, Whitten et coll. ont étudié la photochimie de stilbènes porteurs de chaînes de diverses longueurs en présence d'amylose et ont aussi noté que l'effet de l'amylose augmente avec la longueur de chaîne (32). Nos résultats peuvent donc s'expliquer ainsi : l'amylose est sans effet sur la chloration de l'acétanilide car le complexe d'inclusion est instable; par contre, la benzanilide, plus volumineuse, est inclu dans l'hélice α de l'amylose, et la position *para* qui occupe l'axe de l'hélice est dégagée alors que les positions *ortho* sont masquées par les unités glucose formant cette hélice. L'amylose existe sous forme d'hélice α à un pH inférieur à 12 et une température inférieure à 60°C (32–34). Les hydrates de carbone de petite taille tel que le glucoside de méthyle sont sans effet sur la réaction.

L'amylose est un produit naturel abondant et moins dispendieux que les cyclodextrines. Il présente un site de complexation similaire à celui des cyclodextrines mais ce site est plus flexible et de dimensions variables dans le sens de l'axe de l'hélice. Enfin Hui (12) a souligné que le processus de complexation peut s'accomplir par de simples changements de conformation de la macromolécule mimant ainsi le processus enzymatique d'adaptation induite («Induced fit»).

Partie expérimentale

Réactifs

L'acétanilide et la benzanilide (Aldrich Chem. Co.) ont été recristallisés jusqu'à point de fusion constant et séchés sous vide. Des échantillons authentiques des chloro-2 et chloro-4 acétanilides ont été préparés par acétylation des chloroanilines correspondantes avec l'anhydride acétique. Les chloro-2 et chloro-4 benzanilides ont été préparés par benzoylation des chloroanilines correspondantes avec le chlorure de benzoyle. La masse moléculaire moyenne de l'amylose (Type III, Sigma Chem. Co.), mesurée par viscosimétrie, est de $4{,}38 \times 10^5$ g/mol (35).

Appareils

Les produits de chloration ont été analysés avec un chromatographe en phase gazeuse Varian 3740 couplé avec un intégrateur Varian 4270. Les spectres de rmn ont été enregistrés sur des spectromètres multinoyaux Varian XL-200 et Bruker WH-400. Le dioxane a été utilisé comme référence externe en rmn du carbone-13 et l'acétate de sodium 0,05 *M* comme référence externe en rmn du proton. Le solvant est l'eau deutériée.

Chloration des amides. Méthode générale

La cyclodextrine (1 mmol) et le substrat (1 mmol) sont dissous dans l'eau distillée (450 mL) et la solution est agitée durant 3 h. Dans le cas de l'amylose on utilise 1,0 g d'amylose/mmol de substrat. La solution est ensuite traversée par un filet de chlore (en excès) durant une heure. L'excès de chlore est chassé par de l'azote et la solution aqueuse est extraite à l'éther (3 × 100 mL). La phase organique est séchée sur du sulfate de magnésium puis évaporée sous vide. Le mélange brut est analysé par chromatographie en phase gazeuse à l'aide d'une colonne SE-30, 6 pi × 1/8 po. Le programme de température est le suivant : isotherme à 100°C durant 2 min, augmentation de 7°C/min jusqu'à 240°C, isotherme à 240°C.

Remerciements

Les auteurs remercient le Conseil de recherches en sciences naturelles et en génie du Canada et le Ministère de l'éducation du Québec qui ont financé ce travail. Les spectres de rmn 400 MHz proviennent du Centre régional de RMN à haut champ (Université de Montréal).

1. W. SAENGER. Angew. Chem. Int. Ed. Engl. **19**, 344 (1980).
2. C. SIRLIN. Bull. Soc. Chim. Fr. II-5 (1984).
3. I. TABUSHI. Acc. Chem. Res. **15**, 66 (1982).
4. I. TABUSHI et Y. KURODA. Adv. Catal. **32**, 417 (1983).
5. R. BRESLOW et P. CAMPBELL. J. Am. Chem. Soc. **91**, 3085 (1969).
6. R. BRESLOW, H. KOHN et B. SIEGEL. Tetrahedron Lett. 1645 (1976).
7. M. KOMIYAMA et H. HIRAI. J. Am. Chem. Soc. **105**, 2018 (1983).
8. M. OHARA et K. WATANABE. Angew. Chem. Int. Ed. Engl. **14**, 820 (1975).

Can. J. Chem. Downloaded from www.nrcresearchpress.com by 80.58.250.72 on 09/07/12
For personal use only.

9. R. CHÊNEVERT et R. PLANTE. Can. J. Chem. **61**, 1092 (1983).
10. M. MITANI, T. TSUCHIDA et K. KOYAMA. J. Chem. Soc. Chem. Commun. 869 (1974).
11. R. CHÊNEVERT et D. CHAMBERLAND. Chem. Lett. 1117 (1985).
12. Y. HUI, S. WANG et X. JIANG. J. Am. Chem. Soc. **104**, 347 (1982).
13. R. CHÊNEVERT et G. AMPLEMAN. Chem. Lett. 1489 (1985).
14. R. CHÊNEVERT et N. VOYER. Tetrahedron Lett. **25**, 5007 (1984).
15. R. BERGERON, M. A. CHANNING, G. J. GIBEILY et D. M. PILLOV. J. Am. Chem. Soc. **99**, 5146 (1977).
16. R. BERGERON, M. A. CHANNING, K. A. MCGOVERN et W. P. ROBERTS. Bioorg. Chem. **8**, 263 (1979).
17. R. L. VAN ETTEN, J. F. SEBASTIAN, G. A. CLOWES et M. L. BENDER. J. Am. Chem. Soc. **89**, 3242 (1967).
18. M. KOMIYAMA et M. L. BENDER. J. Am. Chem. Soc. **99**, 8021 (1977).
19. D. J. WOOD, F. E. HRUSKA et W. SAENGER. J. Am. Chem. Soc. **99**, 1735 (1977).
20. P. V. DEMARCO et A. L. THAKKAV. J. Chem. Soc. Chem. Commun. 2 (1970).
21. R. J. BERGERON, M. A. CHANNING et K. A. MCGOVERN. J. Am. Chem. Soc. **100**, 2878 (1978).
22. R. BERGERON et R. ROWAN III. Bioorg. Chem. **5**, 425 (1976).
23. M. KOMIYAMA et H. HIRAI. Polym. J. **13**, 171 (1981).
24. Y. INOUE, H. HOSHI, M. SAKURAI et R. CHÛJÔ. J. Am. Chem. Soc. **107**, 2319 (1985).
25. R. I. GELB, L. M. SCHWARTZ, B. CARDELINO, H. S. FUHRMAN, R. F. JOHNSON et D. A. LAUFER. J. Am. Chem. Soc. **103**, 1750 (1981).
26. M. KOMIYAMA et H. HIRAI. Bull. Chem. Soc. Jpn. **54**, 828 (1981).
27. M. KOMIYAMA et H. HIRAI. J. Am. Chem. Soc. **106**, 174 (1984).
28. M. KOMIYAMA et H. HIRAI. J. Am. Chem. Soc. **105**, 2018 (1983).
29. R. BRESLOW et P. CAMPBELL. Bioorg. Chem. **1**, 140 (1971).
30. O. S. TEE et J. M. BENNETT. Can. J. Chem. **62**, 1585 (1984).
31. F. A. COTTON et G. WILKINSON. Advanced inorganic chemistry. 4e éd. Interscience, New York. 1980. Chap. 17. p. 556.
32. Y. HUI, J. C. RUSSELL et D. G. WHITTEN. J. Am. Chem. Soc. **105**, 1374 (1983).
33. A. HAYASHI, K. KINOSHITA et Y. MIYABE. Polym. J. **13**, 537 (1981).
34. H. NAKATANI, K. I. SHIBATA, H. KONDO et K. HIROMI. Biopolymers, **16**, 2363 (1977).
35. D. P. SHOEMAKER, C. W. GARLAND et J. I. STEINFELD. Experiments in physical chemistry. 3e éd. McGraw–Hill, New York. 1974. p. 392.

Can. J. Chem. Downloaded from www.nrcresearchpress.com by 80.58.250.72 on 09/07/12
For personal use only.

Rate constant for chlorine abstraction from CCl_4 by the 5-hexenyl radical

DEBORAH RAE JEWELL, LUKOSE MATHEW, AND JOHN WARKENTIN[1]
Department of Chemistry, McMaster University, Hamilton, Ont., Canada L8S 4M1

Received September 15, 1986

This paper is dedicated to Dr. O. E. (Ted) Edwards

DEBORAH RAE JEWELL, LUKOSE MATHEW, and JOHN WARKENTIN. Can. J. Chem. **65**, 311 (1987).

Cyclization of the 5-hexenyl free radical to the cyclopentylmethyl free radical was used to clock chlorine atom abstraction by 5-hexenyl from carbon tetrachloride in solution. The source of 5-hexenyl radicals was 5-hexenyl[1-hydroxy-1-methylethyl]diazene ($(CH_3)_2C(OH)N{=}N(CH_2)_4CH{=}CH_2$), which decomposes thermally in CCl_4 by a radical chain mechanism to afford chloroform, acetone, nitrogen, 6-chloro-1-hexene, cyclopentylchloromethane, 1-hexene, and methylcyclopentane as primary products. 6-Chloro-1-hexene is converted, in part, to a secondary product, 1,1,1,3,7-pentachloroheptane, by radical chain addition of CCl_4 to the double bond. The rate constant for chlorine atom abstraction, k_{Cl}, was calculated from the product composition and the known rate constant for cyclization of the 5-hexenyl radical. For the temperature range 274–353 K, k_{Cl} is given by $\log (k_{Cl}/M^{-1}\,s^{-1}) = (8.4 \pm 0.3) - (6.2 \pm 0.4)/\theta$ where $\theta = 2.3\,RT$ kcal mol^{-1}, which leads to $k_{Cl}^{25°C} = 7.2 \times 10^3\,M^{-1}\,s^{-1}$. This value is significantly smaller than recently reported estimates for other primary alkyl radicals.

DEBORAH RAE JEWELL, LUKOSE MATHEW et JOHN WARKENTIN. Can. J. Chem. **65**, 311 (1987).

On utilisé la cyclisation du radical libre hexène-5 yle en cyclopentylméthyle pour mesurer le temps qu'il faut au radical hexène-5 yle pour enlever un atome de chlore du tétrachlorure de carbone en solution. On a utilisé l'hexène-5 yl[hydroxy-1 méthyl-1 éthyl]diazène ($(CH_3)_2C(OH)N{=}N(CH_2)_4CH{=}CH_2$) comme source de radicaux hexène-5 yles qui se décomposent thermiquement en solution dans le CCl_4 par un mécanisme radicalaire en chaîne pour donner du chloroforme, de l'acétone, de l'azote, du chloro-6 hexène-1, du cyclopentylchlorométhane, de l'hexène-1 et du méthylcyclopentane comme produits primaires. Le chloro-6 hexène-1 se transforme, en partie, en un produit secondaire, le pentachloro-1,1,1,3,7 heptane, par une addition radicalaire en chaîne du CCl_4 à la double liaison. On a calculé la constante de vitesse pour la réaction d'abstraction de l'atome de chlore, k_{Cl}, en se basant sur la composition des produits et sur la constante de vitesse connue pour la cyclisation du radical hexène-5 yle. À des températures allant de 274 à 353 K, la valeur de k_{Cl} est exprimée par l'équation $\log (k_{Cl}/M^{-1}\,s^{-1}) = (8{,}4 \pm 0{,}3) - (6{,}2 \pm 0{,}4)/\theta$ dans laquelle $\theta = 2{,}3RT$ kcal mol^{-1}; ceci conduit à une valeur de $k_{Cl}^{25°C} = 7{,}2 \times 10^3\,M^{-1}\,s^{-1}$. Cette valeur est beaucoup plus faible que les évaluations qui ont été rapportées récemment pour d'autres radicaux alkyles primaires.
[Traduit par la revue]

Introduction

Rate constants for abstraction of a chlorine atom from CCl_4 by carbon centered free radicals are of considerable current interest. The reaction is a potential kinetic standard for determination of a variety of other free radical reaction rate constants by the competition method. Two groups (1, 2) have recently pointed to the need for reliable values of k_{Cl} for solution work with alkyl radicals. There are two problems with literature values for k_{Cl}. First, the numbers from solution work with similar or identical alkyl radicals in different laboratories are widely scattered and, second, the numbers from gas phase studies are considerably smaller than most of the lowest values of k_{Cl} for condensed systems.[2] Under the circumstances, it was necessary to redetermine values of k_{Cl}.

Ingold and co-workers (1) estimated k_{Cl} for the neophyl radical (N) by using values of $k_i^N/k_{HSnBu_3}^N$ (where i stands for isomerization) from the literature (3) and substituting for $k_{HSnBu_3}^N$ the average value $k_{HSnBu_3}^{Et\cdot,n\text{-}Bu\cdot}$ from laser flash photolysis work (4). That procedure gave $\log (k_{Cl}^N/M^{-1}\,s^{-1}) = (8.14 \pm 0.42) - (5.52 \pm 0.63)/\theta$ or $k_{Cl}^{N,25°C} = 1.2 \times 10^4\,M^{-1}\,s^{-1}$. Ethyl and *n*-butyl radicals were the best models then available. More recently, $k_{HSnBu_3}^{neopentyl}$ has been determined (5) by laser flash photolysis over a range of temperatures, and use of those values, which presumably represent $k_{HSnBu_3}^N$ more closely, leads to $\log (k_{Cl}^N/M^{-1}\,s^{-1}) = (7.6 \pm 0.4) - (4.5 \pm 0.5)/\theta$ and to $k_{Cl}^{N,25°C} = 2 \times 10^4\,M^{-1}\,s^{-1}$. Although the value of k_{Cl} is quite well defined, a question just as important regarding its magnitude is whether or not N is a good model for estimating the reactivities of unbranched 1°-alkyl radicals. Moreover, a recent estimate (2) of $k_{Cl}^{n\text{-}butyl}$ ($5.8 \times 10^4\,M^{-1}\,s^{-1}$ at 27°C) based on a kinetic epr (electron paramagnetic resonance) method (2), raised the possibility that k_{Cl}^N might indeed be 3- to 5-fold (or more, given the errors) smaller than k_{Cl}^N for a straight chain 1°-alkyl radical.

We now report the Arrhenius equation for attack of the 5-hexenyl radical (5-h) on CCl_4. The results represent an independent check of $k_{Cl}^{n\text{-}Bu}$ (epr) (2), because *n*-butyl and 5-hexenyl radicals are structurally similar. They also answer the question of whether or not the neophyl clock can be used with confidence to estimate reactivities of unbranched primary alkyl radicals toward CCl_4. Finally, a new source of 5-hexenyl radicals for clocking experiments is introduced.

Method, results, and discussion

Choice of radical source

An ideal source of free radicals for a competition study involving CCl_4 is one that undergoes facile induced decomposition, by trichloromethyl radicals, to generate the desired radical. Long kinetic chains are possible with such a source and the product mixture is potentially simple, being largely devoid of products from radical–radical reactions. Since the competition method requires the determination of product ratios, it is advantageous to have a relatively clean system, so that the chances of counting one or more coproducts accidentally with the products of interest are reduced.

Hydroxydiazene **1** was chosen for this study because of evidence that compounds with the combination of functional groups, $\rangle C(OH)N{=}N-$, decompose readily in CCl_4 at temperatures near room temperature to afford chloroform and

[1]Author to whom correspondence may be addressed.

[2]Up to date citations to the primary literature, and some of the data, can be found in refs. 1 and 2.

Can. J. Chem. Downloaded from www.nrcresearchpress.com by 80.58.250.72 on 09/07/12
For personal use only.

Can. J. Chem. Downloaded from www.nrcresearchpress.com by 80.58.250.72 on 09/07/12
For personal use only.

$(CH_3)_2C(OH)N{=}N(CH_2)_4CH{=}CH_2 \xrightarrow{\text{initiation}}$

1

$(CH_3)_2\dot{C}OH + N_2 + \cdot CH_2(CH_2)_3CH{=}CH_2$

(R·)

$R\cdot + CCl_4 \xrightarrow{k_{Cl}} ClCH_2(CH_2)_3CH{=}CH_2 + \cdot CCl_3$

(RCl)

$R\cdot \xrightarrow{k_i^{5\text{-h}}} c\text{-}C_5H_9CH_2\cdot$

(R′·)

R′· + CCl_4 → 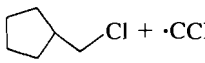 + ·CCl_3

1 + ·CCl_3 $\xrightarrow[\text{decomposition}]{\text{induced}}$ $HCCl_3 + (CH_3)_2CO + N_2 + R\cdot$

1 + R·(R′·) $\xrightarrow[\text{decomposition}]{\text{induced}}$ $RH(R'H) + (CH_3)_2CO + N_2 + R\cdot$

$2Cl_3C\cdot \rightarrow C_2Cl_6$

$(CH_3)_2\dot{C}OH + \cdot CCl_3 \rightarrow HCCl_3 + (CH_3)_2CO$

SCHEME 1

(*a*) **1** + ·CCl_3 → $(CH_3)_2C(OH)N{=}N(CH_2)_4\dot{C}HCH_2CCl_3$

4

$\xrightarrow{CCl_4}$ $(CH_3)_2C(OH)N{=}N(CH_2)_4CH(Cl)CH_2CCl_3 + \cdot CCl_3$

5

5 + ·CCl_3 $\xrightarrow[\text{decomposition}]{\text{induced}}$

$HCCl_3 + (CH_3)_2CO + N_2 + \cdot CH_2(CH_2)_3CH(Cl)CH_2CCl_3$

(R″·)

$R''\cdot + CCl_4 \rightarrow ClCH_2(CH_2)_3CH(Cl)CH_2CCl_3$

(R″Cl)

(*b*) RCl (Scheme 1) + ·CCl_3 → $ClCH_2(CH_2)_3\dot{C}HCH_2CCl_3$

(R‴·)

$R'''\cdot + CCl_4 \rightarrow R''Cl + \cdot CCl_3$

SCHEME 2

other products (6). We therefore expected **1** to decompose in CCl_4 according to Scheme 1. The facile decomposition of **1** at temperatures between 30 and 80°C, and the product composition, are in keeping with the postulate that those reactions are the major primary processes.[3] Secondary processes, including radical chain addition of CCl_4 to RCl, are discussed below.

Addition of CCl_4 to double bonds

A potential flaw in the use of a ring closure reaction of an unsaturated radical to clock Cl abstraction from CCl_4 is that radical chain addition of CCl_4 can occur prior to release of the radical from the source (Scheme 2(*a*)) or after the radical has abstracted from CCl_4, Scheme 2(*b*).

Any contribution from the steps under Scheme 2(*a*) would interfere with the competition method for determining k_{Cl} because there is no way to partition the R″Cl obtained overall between that from the pathway involving competition, Scheme 1, and that formed without competition from ring closure, Scheme 2(*a*). However, since k_{Cl} is obtained from eq. [1], it is clear that any R″Cl measured, over and above that which should

$$[1]\quad k_{Cl} = \frac{k_i^{5\text{-h}}([RCl] + [R''Cl])}{([R'Cl] + [R'H])[CCl_4]}$$

go into the equation, serves to increase the value of k_{Cl}. Thus, even if there are two pathways to R″Cl, the method will still serve to set an upper limit on the value of k_{Cl}.

There are several reasons for believing that the undesired pathway to R″Cl was not an important contributor. The fact that both RH and R′H (Scheme 1) were formed in competition with products from Cl abstraction (Table 1) indicates that H abstraction from **1**, and (or) from $HN{=}NR^2$, is a fast process. A preliminary estimate of $k_H^{R\cdot}$ ($k_H^{R\cdot}$ is the rate constant for H abstraction from **1** by the 5-hexenyl radical), obtained by thermolysis of **1** in C_6F_6 to ca. 10% conversion followed by analysis for RH and R′H, indicates a value near $1 \times 10^5\ M^{-1}\ s^{-1}$ at 25°C.[4] If a similar value is assumed for $k_H^{Cl_3C\cdot}$, and if the rate constant for addition of $Cl_3C\cdot$ to the C=C bond of **1** is taken to be $\leq 2 \times 10^3$ at 25°C,[5] then it follows that one out of 50 $Cl_3C\cdot$ would add to **1** rather than abstract from it. In spite of potential errors in the assumptions, the above analysis suggests that most of the R″Cl can be expected to come from the route of Scheme 2(*b*) and that R″Cl should therefore be included (as was done) in eq. [1]. Values of k_{Cl} in Table 1 would be reduced by small factors only, between 0.79 and 0.87 for the three highest temperatures, if none of the R″Cl were counted. For the 274 K experiments, the analogous factor would be 0.49, as those photo-initiated runs gave the highest relative yields of R″Cl. However, a control experiment, in which a solution of RCl in CCl_4 was photolyzed, indicated ca. 34% conversion to R″Cl in 2 h, suggesting that the photochemical conditions were simply more conducive than were the thermal conditions to the consumption of initially-formed RCl by radical chain addition of CCl_4. Finally, any radicals **4** that are formed from **1** cannot be expected to form **5** efficiently in any case, because **4** is set up for closure in the 6-*exo* sense.[6] That process, followed by H transfer and dehydration, could yield hydrazone **6**, eq. [2].

[2] **4** → 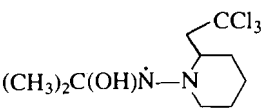 $\xrightarrow{\mathbf{1}}$ 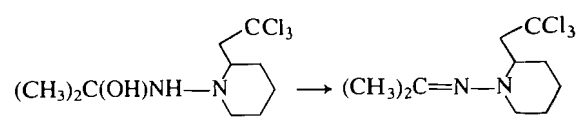

5 **6**

[3]A referee has pointed out that the equilibrium **1** ⇄ Me_2CO + $HN{=}N(CH_2)_4CH{=}CH_2$ could be involved. Such a contribution would not invalidate the conclusions from this study because it does not matter whether the 5-hexenyl radicals come directly or indirectly from **5**.

[4]L. Mathew and J. Warkentin. Unpublished observations.

[5]The rate constant for addition of $Cl_3C\cdot$ to vinyl acetate at 50°C is $2.16 \times 10^3\ M^{-1}\ s^{-1}$ (7).

[6]The rate constant for 6-*exo* cyclization of a primary alkyl radical onto a C=C bond is about $1.1 \times 10^4\ s^{-1}$ at 65°C (8). Corresponding cyclization involving the N=N bond is considerably faster (A. L. J. Beckwith, S. F. Wang, and J. Warkentin, unpublished observations).

TABLE 1. Product ratios from thermolysis of **1** in CCl_4[a]

T(k)	$[CCl_4]$[e]	Relative yields[b–d] (RCl)	(R″Cl)	(R′H)	(R′Cl)	Ratio[f]	Mean[g]	$k_i^{5\text{-h}}$ $s^{-1} \times 10^{-5}$ [h]	k_{Cl} (M^{-1} s^{-1})
274[i]	10.17	0.188	0.237	0.112	1.00	0.382	0.392	0.791	3.05×10^3
		0.268	0.183	0.160	1.00	0.389	± 0.011		
		0.197	0.251	0.110	1.00	0.404			
303	9.81	0.390	0.067	0.128	1.00	0.405	0.401	2.66	1.11×10^4
		0.332	0.127	0.120	1.00	0.410	± 0.005		
		0.418	0.108	0.272	1.00	0.414			
323	9.66	0.355	0.078	0.220	1.00	0.355	0.337	5.40	1.87×10^4
		0.351	0.056	0.210	1.00	0.336	± 0.017		
		0.392	0.054	0.387	1.00	0.322			
353	9.39	0.315	0.055	0.331	1.00	0.278	0.268	13.5	3.85×10^4
		0.305	0.036	0.293	1.00	0.264	± 0.009		
		0.303	0.037	0.298	1.00	0.262			

[a]Initial concentations of **1** were between 0.26 and 0.32 *M* for all runs.
[b]Each set of numbers represents a separate run and the average results of at least three gc analyses of the products of that run. Actual average intergrator counts have been reduced to relative counts, to facilitate visualization of the ratio of products (unrearranged/rearranged or the inverse).
[c]Absolute yields estimated by gc: 274 K, RCl + R′Cl + R″Cl + R′H = 70%, azine ≤ 0.3%, $CHCl_3$ = 85%, 1-hexene = 2%; 323 K, RCl + R′Cl + R″Cl + R′H = 89%, azine ≤ 2%, $CHCl_3$ = 62%, 1-hexene = 7%.
[d]The ratios $CHCl_3/C_2Cl_6$ for the two runs in footnote *c* were 56 and 43, respectively.
[e]Neat CCl_4; concentrations corrected for **1** present and for thermal expansion of CCl_4.
[f](RCl + R″Cl)/(R′Cl + R′H); RCl = 6-chloro-1-hexene, R″Cl = 1,1,1,3,7-pentachloroheptane, R′Cl = cyclopentylmethyl chloride, R′H = methylcyclopentane.
[g]The error is expressed as the standard deviation.
[h]Calculated from the equation $\log (k_i^{5\text{-h}}/s^{-1}) = 10.4 - 6.9/\theta$, where $\theta = 2.3\,RT$ kcal mol^{-1}.
[i]Photolysis.

Examination of crude product mixtures by ^1H nmr spectroscopy showed, for all but the runs at 274 K, two singlets (δ 1.74 and 1.98, CCl_4, 250 MHz) suggestive of a hydrazone or an azine of acetone. The maximum yield of that product, estimated by gc analysis, was about 15% from one thermal run. Other thermal runs gave lower yields (ca. 2–8%). Analysis of products from the photo-induced (274 K) reactions by gc revealed a material with the same retention time (≤0.3%). Attempts to isolate the hydrazone or azine by-product were unsuccessful, but the possibility that it was acetone azine could be excluded by coinjection of authentic acetone azine.

Although the identity of the hydrazone or azine by-product is of interest, formation of **6** (eq. [2]) would not interfere with the operation of the 5-hexenyl clock. The fact that yields of the by-product varied, and that they were lowest from the low temperature, photo-initiated runs (complete in ≤3 h) suggests that the by-product actually came from a competing polar reaction, eq. [3], catalyzed by trace impurities or by wall surfaces.

[3] $\mathbf{1} \rightarrow H_2O + Me_2C{=}NN{=}CH(CH_2)_3CH{=}CH_2$

In summary, the inclusion of the total yield of R″Cl in eq. [1] is unlikely to have caused errors larger than the experimental errors involved in determining the product ratios (Table 1), and the formation of an unidentified by-product (azine or hydrazone), in significant quantity in some cases, is unlikely to invalidate the kinetic results. Numerous minor compounds formed in trace amounts (≤1% each) are probably the products expected from the many radical–radical reactions (coupling and disproportionation) that are not included in Scheme 1. Although some of those products should also be counted in eq. [1], the fact that they are very minor components and that their inclusion in eq. [1] would increase both the numerator and the denominator very slightly, and would therefore alter the ratio insignificantly, means that they can be ignored. Incidentally, the low yields of products expected from radical–radical reactions and the high ratio of chain transfer product ($CHCl_3$) to a chain termination product (C_2Cl_6), Table 1 (footnote *d*), point to the dominance of radical-chain decomposition of **1** in CCl_4.

Magnitude of k_{Cl}

The most reliable published (4) Arrhenius relationship for isomerization of 5-h is eq. [4]. That equation can now be modified slightly to eq. [5] by using the most recent data (5) for

[4] $\log (k_i^{5\text{-h}}/s^{-1}) = (10.37 \pm 0.32) - (6.85 \pm 0.42)/\theta$

[5] $\log (k_i^{5\text{-h}}/s^{-1}) = (10.4 \pm 0.3) - (6.9 \pm 0.4)/\theta$

H abstraction from $HSnBu_3$ by ethyl and *n*-butyl radicals. Equation [5] was used to calculate $k_i^{5\text{-h}}$ values for use in eq. [1].

The Arrhenius relationship for chlorine atom abstraction by 5-h, from the data in Table 1, is eq. [6], in which the errors are

[6] $\log (k_{Cl}^{5\text{-h}}/M^{-1}\,s^{-1}) = (8.4 \pm 0.3) - (6.2 \pm 0.4)/\theta$

estimated and in which $\theta = 2.3\,RT$ kcal mol^{-1}. Equation [6] gives $k_{Cl}^{5\text{-h},25°C} = 7.2 \times 10^3\ M^{-1}\ s^{-1}$, which is a factor of eight smaller than $k_{Cl}^{n\text{-butyl}}$ (esr) determined by Griller and co-workers (2) and a factor of 2.8 smaller than the best estimate of k_{Cl}^{N}, based on the $HSnBu_3$ method (1) and recalculated as outlined in the Introduction. The disagreement with the results from esr work (2) is not outside the considerable errors associated with that approach and the good agreement with k_{Cl}^{N} removes any serious qualms about the use of the neophyl radical as a model for unbranched 1°-alkyls in this case.

In summary, the present Arrhenius equation for $k_{Cl}^{5\text{-h}}$ should

Can. J. Chem. Downloaded from www.nrcresearchpress.com by 80.58.250.72 on 09/07/12
For personal use only.

be used for studies of unhindered 1°-alkyl radicals in which abstraction from CCl_4 is the competitive clocking reaction. Reagent **1** is a promising source of 5-hexenyl radicals for studies such as this one because its radical chain decomposition eliminates the cage coupling that can complicate product analyses when non-chain sources are used.

Experimental

5-Hexenyl[1-hydroxy-1-methylethyl]diazene, 1

This compound was prepared by treatment of the corresponding hydroperoxide (**2**), described below, in ice-cooled petroleum ether with triphenylphosphine in petroleum ether, bp 30–60°C. When addition of the phosphine solution was complete, the reaction mixture was kept for several hours in a freezer to complete precipitation of triphenylphosphine oxide. Filtration, removal of most of the solvent with a rotary evaporator, and bulb-to-bulb distillation at room temperature (10^{-2} Torr) afforded **1**; uv (hexane, λ_{max}, log ε): 232 (1.97), 328 (1.33); ir (neat): 3412 (OH) cm^{-1}; ^1H nmr (CCl_4, 250 MHz) δ: 1.25 (s, 6H), 1.37 (quintet, 2H), 1.72 (quintet, 2H), 2.00 (m, 2H), 3.77 (m, 2H), 4.28 (s, br, 1H), 4.87 (m, 2H), 5.64 (m, 1H); ^{13}C nmr ($CDCl_3$, 250 MHz) δ: (5-hexenyl group) 26.50 (C-2 or C-3), 27.04 (C-3 or C-2), 33.36 (C-4), 66.57 (C-1), 114.80 (C-6), 138.30 (C-5); (1-hydroxy-1-methylethyl group) 26.94 (C-2), 93.61 (C-1); ms (high resolution) *m/z*: calcd. for $C_9H_{17}N_2$ ($M^+ - OH$): 153.1393; found: 153.1387.

5-Hexenyl[1-hydroperoxy-1-methylethyl]diazene, 2

Autoxidation of the 5-hexenyl hydrazone of acetone (**3**, described below, 1.02 g, 6.6 mmol), in light petroleum until the uptake of oxygen ceased, afforded **2** in solution for direct reduction to **1**. A small aliquot was freed from solvent by blowing N_2 onto the surface of the solution; uv (hexane, λ_{max}, log ε): 222 (1.98), 362 (1.35); ir (neat): 3317 (OH) cm^{-1}; iodometric titration: 97%, 98%; ^1H nmr (CCl_4, 90 MHz) δ: 1.32 (s, 6H), 1.32–2.25 (m, 6H), 3.81 (t, 2H), 4.97 (m, 2H), 5.73 (m, 1H), 9.33 (s, 1H); ^{13}C nmr ($CDCl_3$, 250 MHz) δ: (5-hexenyl group) 26.53 (C-3 or C-2), 26.96 (C-2 or C-3), 33.35 (C-4), 68.69 (C-1), 128.34 (C-6), 138.24 (C-5); 1-hydroperoxy-1-methylethyl group 21.63 (C-2), 102.73 (C-1).

5-Hexenylhydrazone of acetone, 3

To a cold solution of acetone (ca. 15 mL) in ether (50 mL) containing acetic acid was added, drop by drop, a solution of 5-hexenyl hydrazine (13.23 g, 0.116 mol) in 50 mL of ether. After it had been stirred for an hour the solution was washed with water (2 × 50 mL) and with brine (50 mL). The ether layer was dried over $MgSO_4$, the ether was then evaporated, and the residual liquid was distilled at 2.8 Torr. The fraction boiling at 71–72°C (15.6 g, 87% yield) was used in small scale autoxidations described above; uv (hexane, λ_{max}, log ε): 224 (1.93), 246 (1.96), 364 (0.88); ^1H nmr ($CDCl_3$, 250 MHz, ref. $CHCl_3$ at δ 7.21) δ: 1.32–1.42 (m, 4H), 1.57 (s, 3H), 1.77 (s, 3H), 1.47 (q, 2H), 2.94 (t, 2H), 4.05 (s, br, 1H), 4.84 (m, 2H), 5.65 (m, 1H); ^{13}C nmr ($CDCl_3$, 250 MHz) δ: (5-hexenyl group) 26.27 (C-3 or C-2), 28.97 (C-2 or C-3), 33.48 (C-4), 50.85 (C-1), 114.30 (C-6), 138.56 (C-5); remainder, 15.34 (*Z*-Me), 25.00 (*E*-Me), 145.15 (Me_2C); ms (high resolution) *m/z*: calcd. for $C_9H_{18}N_2$: 154.1471; found: 154.1478.

5-Hexenylhydrazine

5-Hexenyl tosylate (42.97 g, 0.169 mol) was added during 20 min, with stirring, to an ice-cooled solution of hydrazine hydrate (90 g, 1.8 mol) in absolute ethanol (100 mL). Stirring was continued for 2 h after addition was complete before most of the ethanol was removed with a rotary evaporator. Continuous extraction of the residue with ether (250 mL) for two days, drying of the ether layer with Na_2SO_4, and evaporation of the ether left a residue, which was distilled under N_2 at 3 Torr. The fraction boiling at 56–58°C was a clear, colourless liquid (13.23 g, 68% yield); ^1H nmr (CCl_4, 90 MHz) δ: 1.15 (m, 4H), 1.80 (m, 2H), 2.45 (m, 2H), 2.83 (s, 3H), 4.70 (m, 2H), 5.27–5.77 (m, 1H).

6-Chloro-1-hexene

A solution of 5-hexen-1-ol (1.8 g, 0.018 mol) in benzene (30 mL) containing *N,N*-dimethylaniline (2.18 g, 0.018 mol) was cooled to −5°C and thionyl chloride (2.22 g, 0.019 mol) in benzene (20 mL) was dropped in during 10 min, with stirring. The resulting yellow-brown mixture was stirred at ice-bath temperature for 1 h before it was heated to the reflux temperature for 1 h. The solution, now green, was washed twice with water, three times with 3 *M* HCl (25 mL), three times with saturated $NaHCO_3$ solution, and, finally, with water until the wash was neutral to litmus. Drying over $MgSO_4$ followed by evaporation of the solvent left a yellow liquid from which colourless 5-chloro-1-hexene was obtained by distillation, bp 130–132°C (760 Torr); ^1H nmr (CCl_4, 250 MHz) δ: 1.48–1.54 (m, 2H), 1.72 (m, 2H), 2.04 (m, 2H), 3.44 (t, 2H), 4.93 (m, 2H), 5.70 (m, 1H); ms (low resolution) *m/z*: 120, 118 (M^+), 55 ($C_4H_7^+$, 100%).

Cyclopentylmethyl chloride

A procedure similar to that described above afforded the title compound (9) from cyclopentyl methanol; ^1H nmr (CCl_4, 250 MHz, ref. $CHCl_3$ at δ 7.21) δ: 1.16–1.33 (m, 2H), 1.54–1.82 (2m, partly resolved, 6H), 2.21 (quint, 1H), 3.37 (d, 2H); ms (low resolution) *m/z*: 120, 118 (M^+), 55 ($C_4H_7^+$, 100%).

1,1,1,3,7-Pentachloroheptane

A solution of 6-chloro-1-hexene (0.10 g, 0.84 mmol) and benzoyl peroxide (0.010 g, 4.1×10^{-5} mol) in 2 mL of carbon tetrachloride was degassed and sealed at 10^{-2} Torr. It was then heated at 80°C for 48 h. The desired pentachloroheptane was obtained by preparative gc separation of the reaction mixture on OV-17 (10%); ^1H nmr (CCl_4, 250 MHz) δ: 1.7 (m, 6H), 2.9–3.3 (AB quartet, J_{AB} = 15.5 Hz, each line a doublet, J = 4.79 Hz for A, 5.21 Hz for B, 2H), 3.5 (m, 2H), 4.2 (m, 1H).

Purification of CCl_4

Reagent grade CCl_4 was washed thoroughly with dilute sodium bicarbonate solution. The CCl_4 layer was separated and dried over anhydrous K_2CO_3. A center cut from distillation in a grease-free glass system was stored in a brown bottle.

Thermolysis of 1

A small quantity of **1** (20–30 mg) was weighed in a small vial. Carbon tetrachloride (ca. 0.5 mL) was added to make a solution, near 0.3 *M* in **1**, which was transferred to an nmr tube fitted with a ground glass joint. The sample was degassed by means of freeze–pump–thaw cycles and the tube was sealed at 10^{-2}–10^{-3} Torr. A constant temperature oil bath was used for thermolysis of **1** in the sample and progress was monitored by nmr spectroscopy. When the *gem*-dimethyl signal of **1** had disappeared, the tube was opened and the contents were analyzed by gas chromatography, using authentic compounds to establish retention times and detector response factors. Identification of products was based also on the results of analysis by gc/ms and on comparison of ^1H nmr spectra of samples obtained by preparative gc with spectra of authentic materials.

Photolysis of 1

Diazene **1** (0.0430 g) was weighed in a calibrated, 1-mL volumetric flask and CCl_4 was added up to the calibration mark. The flask was shaken to mix the contents and 300 μL of the solution was transferred into each of three nmr tubes. The tubes were sealed after three freeze–pump–thaw cycles and they were transferred to a quartz Dewar flask, equipped with a stirrer and filled with ice and water, after acquisition of the ^1H nmr spectrum, which showed no evidence of either acetone or chloroform. After photolysis for 3 h with 300 nm light in a Rayonet apparatus, the ^1H nmr spectrum was free from the *gem*-dimethyl signal of **1** and the tubes were cut for analysis. During the photolysis, the temperature was monitored (1 ± 0.5°C) with a thermometer placed near to the sample tubes and portions of ice were added from time to time to maintain the temperature.

Chromatographic analysis

A Varian Vista 6000 gas chromatograph with a flame ionization detector at 300°C and an off-column flash injector at 220°C were used for analytical work. Two columns were used to check for signal overlap and (or) thermal decomposition during analysis. One was a 5 ft × 1/8 in. glass column packed with Carbowax 20 M (5%) on

Can. J. Chem. Downloaded from www.nrcresearchpress.com by 80.58.250.72 on 09/07/12
For personal use only.

Chromosorb P (AW, 100–120 mesh). The other was a 10 ft × 1/8 in. stainless steel column packed with Carbowax 20 M (10%) on the same support. Nitrogen, at 12 mL min^{-1}, was used as carrier gas and the column temperature was normally held at 40°C for 3 min before it was increased at 5°C min^{-1} to a maximum temperature of 220°C.

Acknowledgements

This work was financed from grants provided by Imperial Oil Limited and by the Natural Sciences and Engineering Research Council of Canada.

1. D. A. LINDSAY, K. LUSZTYK, and K. U. INGOLD. J. Am. Chem. Soc. **106**, 7087 (1984).
2. J. A. HAWARI, S. DAVIS, P. S. ENGEL, B. C. GILBERT, and D. GRILLER. J. Am. Chem. Soc. **107**, 4721 (1985).
3. J. A. FRANZ, R. D. BARROWS, and D. M. CAMAIONI. J. Am. Chem. Soc. **106**, 3964 (1984).
4. C. CHATGILIALOGLU, K. U. INGOLD, and J. C. SCAIANO. J. Am. Chem. Soc. **103**, 7739 (1981).
5. L. J. JOHNSTON, J. LUSZTYK, D. D. M. WAYNER, A. N. ABEYWICKREYMA, A. L. J. BECKWITH, J. C. SCAIANO, and K. U. INGOLD. J. Am. Chem. Soc. **107**, 4594 (1985).
6. D. W. K. YEUNG and J. WARKENTIN. Can. J. Chem. **54**, 1349 (1976).
7. J. P. LORAND. *In* Landolt Bornstein (New Series), Radical reactions in liquids. Vol. 13. subvolume a. *Edited by* H. Fischer. Springer Verlag, Berlin. 1984. p. 135.
8. (*a*) A. L. J. BECKWITH and K. U. INGOLD. *In* Rearrangements in ground and excited states. *Edited by* P. de Mayo. Academic Press, New York. 1980. p. 201; (*b*) A. L. J. BECKWITH. Tetrahedron, **37**, 3073 (1981).
9. W. E. DUPUY, H. R. HUDSON, and P. A. KARAM. J. Chromatogr. **71**, 347 (1972).

Can. J. Chem. Downloaded from www.nrcresearchpress.com by 80.58.250.72 on 09/07/12
For personal use only.

Haloselenate(IV) formation and selenous acid dissociation equilibria in hydrochloric and hydrofluoric acids

JOHN MILNE

Ottawa–Carleton Institute for Research and Graduate Studies in Chemistry, University of Ottawa Campus, Ottawa, Ont., Canada KIN 9B4

Received June 4, 1986

JOHN MILNE. Can. J. Chem. **65**, 316 (1987).

Raman spectroscopy has shown that the initial stages of haloselenate(IV) formation equilibria are the same in HF and HCl solutions.

$$H_2SeO_3 + H^+ + X^- \overset{K_4}{=} HSeO_2X + H_2O \qquad (X = F, Cl)$$

$$HSeO_2X + H^+ + X^- \overset{K_5}{=} SeOX_2 + H_2O$$

The constants K_4 and K_5, evaluated by quantitative Raman measurements, for HCl solutions are 0.015 ($\pm$0.001) L^2 mol^{-2} and 0.9 ($\pm$0.1) $\times$ 10^{-5} L^2 mol^{-2}, respectively. These constants yield the minimum average deviation in normalized molar scattering intensity for the species formed in three regions of the spectra, 690 and 890 cm^{-1} (SeO stretching) and 100–450 cm^{-1} (deformation and SeCl stretching). Before the onset of haloselenate(IV) formation, changes in the SeO stretching band intensities with HX concentration occur due to repression of ionic dissociation of selenious acid

$$H_2SeO_3 \overset{K_1}{=} H^+ + HSeO_3^-$$

Quantitative Raman measurements yield K_1 = 9.8 ($\pm$0.3) $\times$ 10^{-3} mol L^{-1}. Reasons for the high value of this constant, compared to reported values, are discussed.

JOHN MILNE. Can. J. Chem. **65**, 316 (1987).

Il a été montré par la spectroscopie Raman que les équilibres initiaux de la formation des halosélénate(IV)s sont les mèmes dans les solutions de HF et HCl.

$$H_2SeO_3 + H^+ + X^- \overset{K_4}{=} HSeO_2X + H_2O \qquad (X = F, Cl)$$

$$HSeO_2X + H^+ + X^- \overset{K_5}{=} SeOX_2 + H_2O$$

Les constantes K_4 et K_5, evaluées à l'aide de mésures quantitatives Raman, pour les solutions d'HCl, sont respectivement 0.015 ($\pm$0.001) L^2 mol^{-2} et 0.9 ($\pm$0.1) $\times$ 10^{-5} L^2 mol^{-2}. Ces constantes donnent les écarts moyens minimums dans l'intensité molaire normalisée de la lumière diffusée à trois regions des spectres, 690 et 890 cm^{-1} (SeO allongements) et 100–450 cm^{-1} (déformations et SeCl allongements). Avant la formation de haloselenate(IV)s, les changements d'intensité des bandes de SeO allongement avec des changements de la concentration d'HCl ont lieu à cause de la repression de la dissociation ionique de l'acide sélénieux,

$$H_2SeO_3 \overset{K_1}{=} H^+ + HSeO_3^-$$

Les mésures quantitatives Raman donnent K_1 = 9.8 ($\pm$0.3) $\times$ 10^{-3} mol L^{-1}. Des causes de la haute valeur de cette constante en comparaison aux valeurs dans la literatures, sont discutées.

Introduction

While there is a considerable body of quantitative information concerning complexation equilibria involving metal ions in aqueous solution, little work has been done on semimetal complexation. The present work deals with Se(IV) complexation in hydrofluoric and hydrochloric acid and represents an extension of earlier studies on SeO_2 on HF (1), HCl (2), and HBr (3). The reasons for the extension of previous work are threefold. Firstly, it was reported without complete explanation in earlier work (2) that the relative intensities of the SeO double and single bond stretching bands in the Raman spectra of SeO_2 solutions changed with increasing HCl concentration (0.0 to 5.0 *M*), a range where only H_2SeO_3 was considered to be present, and it was felt that some rationalization of this change was necessary. Secondly, the activities of hydrochloric acid were applied erroneously in earlier work (2) and, while the equilibria occuring at high HCl concentrations (8.0–12.0 *M* HCl) were correctly identified, the formation constants calculated were incorrect. A reinterpretation of the quantitative Raman intensities with more detailed measurements over the entire HCl concentration range was called for. Finally, while the monohaloselenate(IV) anions, SeO_2X^- (X = F, Cl, Br) (4, 5) are familiar, only in the case of the SeO_2–HBr system (3) has one of the parent acids, $HSeO_2Br$, been observed. It seems likely that the analogous acids would be present in SeO_2–HF and SeO_2–HCl systems also.

Experimental section

Solutions were made up from SeO_2 (Alfa), which was found by permanganometric analysis (6) to be partially converted to H_2SeO_3. The SeO_2 used was found to be 95% pure. Hydrofluoric and hydrochloric acids (Baker) were analyzed by titration before use.

The methods for obtaining quantitative Raman spectra have been described elsewhere (2). The spectra of the hydrofluoric acid solutions were recorded at 488 nm using a sapphire cell and those of the hydrochloric acid solutions were recorded at 514.5 nm. The normalization assumption for calibration of band intensities was that the 925 cm^{-1} band in the spectrum of 1 *M* perchloric acid solution, used as an external standard, had an area intensity of 6.45 cm^2 (1 $in.^2$). This

Can. J. Chem. Downloaded from www.nrcresearchpress.com by 80.58.250.72 on 09/07/12
For personal use only.

Can. J. Chem. Downloaded from www.nrcresearchpress.com by 80.58.250.72 on 09/07/12
For personal use only.

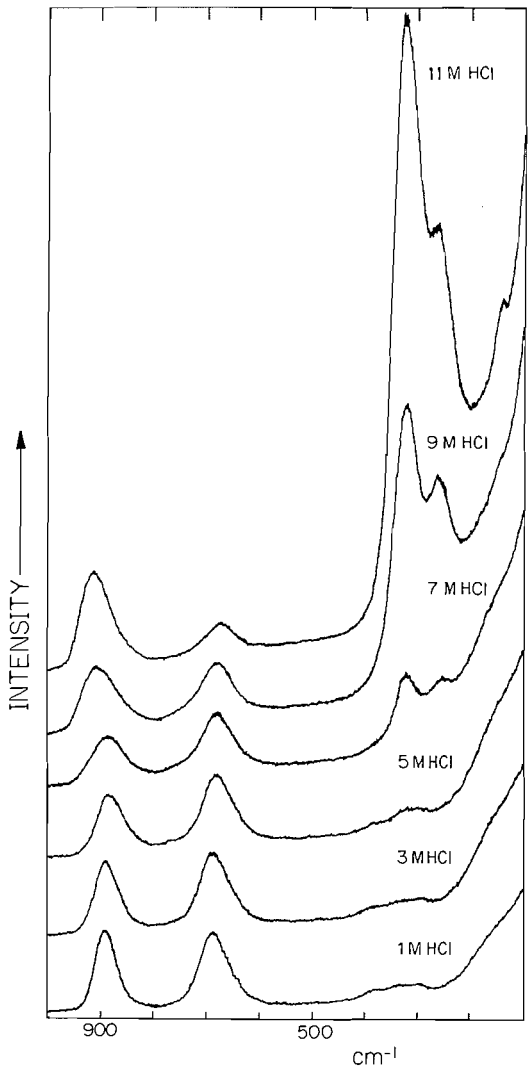

FIG. 1. Raman spectra of solutions of SeO_2 (0.95 *M*) in HCl (0.0–12.0 *M*).

standard was run before and after each SeO_2 solution spectrum with all spectrometer and laser conditions held constant.

Results and discussion

From consideration of the Raman spectra of 0.95 *M* SeO_2 in solutions with HCl concentration in the range 0.0 to 4.0 *M*, shown in Fig. 1, it is apparent that the SeO single bond stretching mode at 690 cm^{-1} increases in intensity relative to the SeO double bond mode at 890 cm^{-1}. Normalized intensities given in Table 1 for these bands show that there is an absolute increase in intensity of the 690 cm^{-1} band and a decrease in intensity of the 890 cm^{-1} band. These changes are not accompanied by the appearance of an Se—Cl stretching band near 300 cm^{-1} and must involve changes in selenous acid dissociation equilibria connected with changes in proton activity accompanying the increase in HCl concentration. An understanding of these changes requires first of all a consideration of the equilibria governing selenious acid and the various other non-chloro-coordinated Se(IV) species in solution. It should be noted that the changes in peak intensity and frequency for a single species due to changes in ionic strength as a result of differing solvation effects are normally small relative the effects discussed here. For instance, the position of the 925 cm^{-1} band of the perchlorate ion in solutions of perchloric acid over the

TABLE 1. Interpolated intensities for 0.95 *M* SeO_2 in 0.0–12.0 *M* HCl solutions

c_{HCl} (mol L^{-1})	$i_{100-450}$ (cm^2)	i_{690} (cm^2)	i_{890}[a] (cm^2)
0.0	2.26	6.05	5.33
1.0	3.09	6.20	5.01
2.0	4.17	6.46	4.94
3.0	4.95	6.66	4.88
4.0	5.23	6.80	4.81
5.0	5.37	6.98	4.75
6.0	5.53	7.01	4.70
7.0	6.56	6.93	4.77
8.0	12.80	6.52	5.13
9.0	28.60	6.38	6.03
10.0	42.70	4.08	7.18
11.0	65.40	2.74	8.55
12.0	77.00	1.42	10.00

[a]Intensity of total band envelope (850 and 890 cm^{-1}).

concentration range 0.3 to 9 *M* increases by 5 cm^{-1} and the intensity varies directly as the concentration.

Cesium hydrogen selenate(IV) solutions

Plots of normalized intensity of peaks at 850 and 610 cm^{-1}, the double and single bond stretches for $HSeO_3^-$, for solutions of $CsHSeO_3$ (0.38, 0.57, 0.78, and 0.95 *M*) yield straight lines with molar intensities $I_{850}(HSeO_3^-) = 8.10\ (\pm 0.25)\ cm^2$ and $I_{610}(HSeO_3^-) = 2.40\ (\pm 0.30)\ cm^2$. These solutions apparently contain $HSeO_3^-$ ion as the only Se(IV) species. This is expected in view of the magnitude of the dissociation and hydrolysis constants for $HSeO_3^-$, $K_2 = 7.9 \times 10^{-9}$ mol L^{-1} and $K_h = 3.1 \times 10^{-12}$ mol L^{-1}, respectively (7). A single measurement of the bands in the deformation region (100–450 cm^{-1}) at $c(CsSeO_3) = 0.76\ M$ gave a molar intensity $I_{100-450}(HSeO_3^-) = 3.0\ cm^2$.

Selenous acid solutions

At low selenous acid concentrations and ambient temperatures the equlibria,

[1] $H_2SeO_3 = H^+ + HSeO_3^-$

[2] $HSeO_3^- \overset{K_2}{=} H^+ + SeO_3^{2-}$

governed by dissociation constants, $K_1 = 3.2 \times 10^{-3}$ mol L^{-1} and $K_2 = 7.9 \times 10^{-9}$ mol L^{-1}, occur (7). However, at higher concentrations more complex species such as $(H_2SeO_3)_2$, $H(HSeO_3)_2^-$, and $(HSeO_3)_2^{2-}$ may be formed (7–9). For concentrations in the range studied here the SeO double bond envelope at 890 cm^{-1} consists of two peaks, a main peak at 890 cm^{-1} due to H_2SeO_3 and a shoulder at 850 cm^{-1} due to $HSeO_3^-$ (8). This is shown in Fig. 2 where the relative intensity of the 850 cm^{-1} peak to the 890 cm^{-1} peak decreases with increasing concentration in accordance with equilibrium (1). It should also be noted at this time that the intensity of the 850 cm^{-1} peak in the 0.95 *M* SeO_2 in 1 *M* HCl solution spectrum is virtually eliminated compared to those in 0.95 *M* SeO_2 in water, confirming the origin of this peak. It is clear from the magnitude of K_2 that, in these solutions, the small concentration of SeO_3^{2-} ion would not be detected by Raman spectroscopy. However, an estimate of K_1 was made by resolving the SeO double bond envelope into contributions from H_2SeO_3 and $HSeO_3^-$ and determining $[HSeO_3^-]$ from the molar intensity at 850 cm^{-1}, $I_{850}(HSeO_3^-)$. $[H_2SeO_3]$ was

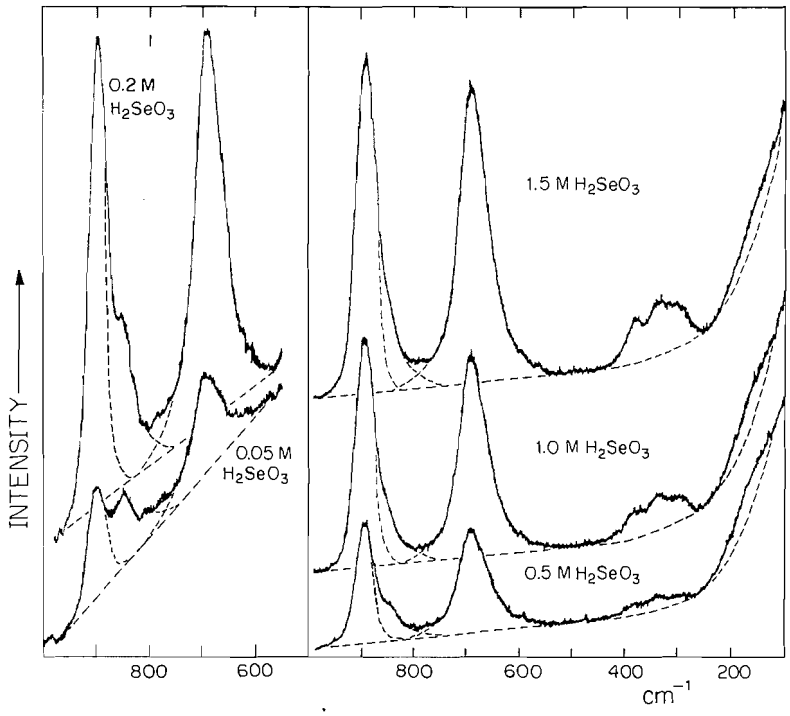

FIG. 2. Raman spectra of solutions of SeO_2 in water.

then calculated from stoichiometry. In the absence of measured ionic activity coefficients, those calculated from Debye–Hückel theory were used (10). In the range of ionic strength for these solutions (ca. 0.1 *M*), DH coefficients for strong acids with oxoanions are usually within 10% (lower) of measured values (ref. 10, p. 491) and this should apply for H^+ and $HSeO_3^-$ ions. The first dissociation constant,

$$[3] \quad K_1 = \frac{[H^+][HSeO_3^-]y_\pm^2}{[H_2SeO_3]}$$

where $y_\pm$ is the molar activity coefficient, was determined to be $9.3\,(\pm 0.7) \times 10^{-3}$ mol L^{-1}. The agreement between the values of K_1, as well as the reasonably constant value of the molar intensities calculated for H_2SeO_3 from the concentrations and molar intensities for the $HSeO_3^-$ ion given above, for the five solutions studied supports the interpretation and calculations. The data and calculated values are shown in Table 2. The value calculated for K_1 is higher than that reported in the literature (7). The large apparent concentration of hydrogen selenate(IV) ion may be due to the equilibrium,

$$[4] \quad H_2SeO_3 + HSeO_3^- \overset{K_3}{=} H(HSeO_3)_2^-$$

for which there is evidence from pH studies (7). However, calculations which include eq. [4] and which use as criteria of acceptability, the constancy of K_1 and K_3, lead to little change in K_1 (10% lower). Another possible reason for the relatively high value of K_1 is ion-pair formation. There exist instances of moderately strong acids where the dissociation constant, measured by infinite dilution methods or by methods which can be used in the millimolar range where $y_\pm = 1$ is a good approximation, is lower than that measured by high concentration methods such as nmr or Raman spectroscopy (11, 12). It has been proposed that the high dissociation constants at high concentration are due to the formation of the "hydronium ion – acid anion" ion pair, which would contribute to the high apparent anion concentration (12) and dissociation constant. Finally another possible reason for the difference may be the simplicity of the equilbria model chosen. Barcza and Sillen (7) have found evidence for the dimerization of H_2SeO_3 and $HSeO_3^-$ in solutions of moderately low selenous acid concentration (0.02–3.00 *M*). However, Raman studies show evidence for the formation of $(H_2SeO_3)_2$ only at much higher concentrations (8.07 *M*) (8) than those studied here and it is claimed in other potentiometric and spectrophotometric work (13) that anion dimerization does not occur under the acid conditions which exist in this work. At present the discrepancy between low and high concentration dissociation constants, K_1, is best accounted for in terms of ion-pair formation. The trend towards higher values of K_1 with increasing concentration shown in Table 2 might also be accounted for by ion-pair formation although $H(HSeO_3)_2^-$ formation would also cause the same change in the apparent K_1.

Solutions of selenium dioxide in hydrochloric acid

The changes in intensity of the 690 and 890 cm^{-1} bands in the spectra of 0.95 *M* SeO_2 in 0.0 to 4.0 *M* HCl solutions, which are in the opposite direction (Fig. 1), can be readily accounted for in terms of the repression of equilibrium (1). The 690 cm^{-1} band increases with increasing c_{HCl} because this band is more intense for H_2SeO_3 ($I_{690}(H_2SeO_3) = 7.4\ cm^2$) than for $HSeO_3^-$ ($I_{690}(HSeO_3^-) = 2.4\ cm^2$) while the 890 cm^{-1} band decreases since $I_{890}(H_2SeO_3)$ (5.45 cm^2) is lower than $I_{890}(HSeO_3^-)$ (8.1 cm^2). Quantitative treatment of this region of HCl concentration is difficult, since there is no clear way to deal with the ionic activities. Debye–Hückel activities are unrealistic in this range of ionic strength especially for acid electrolytes (except at $c_{HCl} = 0.0$). The measured molar ionic activities for HCl (H^+, Cl^-) probably represent a closer description of these activities for H^+ and $HSeO_3^-$ in these solutions than do Debye–Hückel activities. In view of these uncertainties as well as the relatively small changes in intensity of the 690 and

Can. J. Chem. Downloaded from www.nrcresearchpress.com by 80.58.250.72 on 09/07/12
For personal use only.

TABLE 2. Band intensities and apparent $[HSeO_3^-]$ for solutions of SeO_2 in water and K_1 for simple dissociation

c_{SeO_2} (M)	i_{850} (cm^2)	$[HSeO_3^-]^a$ (M)	$[H_2SeO_3]$ (M)	$y_\pm{}^b$	$10^3 K_1$ (M)	$i_{890}{}^c$ (cm^2)	$i_{690}{}^d$ (cm^2)	$i_{100-450}{}^e$ (cm^2)
0.048	0.143	0.0176	0.0299	0.855	7.59	0.19	0.29	—
0.190	0.386	0.0477	0.1423	0.773	9.56	0.82	1.24	—
0.475	0.706	0.0872	0.3878	0.706	9.78	1.87	2.95	1.34
0.950	1.104	0.1363	0.8137	0.6474	9.57	4.27	6.02	2.21
1.425	1.513	0.1868	1.2380	0.6011	10.18	6.49	9.17	3.17

[a]Apparent concentration, see text.
[b]Debye–Hückel molar activity coefficient.
[c]Average $I_{890}(H_2SeO_3) = 5.45 (\pm 0.45)$ cm^2 L mol^{-1}.
[d]Average $I_{690}(H_2SeO_3) = 7.43 (\pm 0.49)$ cm^2 L mol^{-1}.
[e]Average $I_{100-450}(H_2SeO_3) = 2.18 (\pm 0.23)$ cm^2 L mol^{-1}.

TABLE 3. Calculated molar intensities for $HSeO_2Cl$ and $SeOCl_2$ and concentrations of Se(IV) species for solutions of SeO_2 in 5.0–12.0 M HCl solutions for $K_4 = 0.015$ L^2 mol^2 and $K_5 = 9 \times 10^{-6}$ L^2 mol^2

c_{HCl} (M)	$I_{690}{}^a$ ($HSeO_2Cl$) (cm^2 M^{-1})	$[H_2SeO_3]$ (M)	$[HSeO_2Cl]$ (M)	$[SeOCl_2]$ (M)	$[Cl^-]^b$ (M)	a_w	$a_{\pm HCl}$ (M)	$I_{890}{}^c$ ($SeOCl_2$) (cm^2 M^{-1})	$I_{100-450}{}^d$ ($SeOCl_2$) (cm^2 M^{-1})
5.0	7.3	0.276	0.673	—	4.33	0.743	11.2	—	—
6.0	7.4	0.112	0.835	—	5.16	0.677	18.4	—	—
7.0	7.4	0.035	0.901	—	6.07	0.596	32.4	12.8	—
8.0	7.2	—	0.892	—	7.01	0.509	56.0	14.9	—
9.0	6.7	—	0.801	0.146	7.91	0.430	93.1	14.4	97
10.0	6.6	—	0.616	0.334	8.72	0.363	148	12.4	95
11.0	7.2	—	0.380	0.573	9.47	0.310	228	11.7	107
12.0	8.3	—	0.172	0.768	10.29	0.254	355	11.9	96

[a]Calculated.
[b]$[Cl^-] = [H^+]$.
[c]Values calculated by choosing $I_{890}(HSeO_2Cl) = 4.92$ cm^2 M^{-1}, which gave the lowest average deviation from the mean of $I_{890}(SeOCl_2)$ $(= 13.0 \pm 1.1$ cm^2 $M^{-1})$.
[d]Values calculated by choosing $I_{100-450}(HSeO_2Cl) = 18$ cm^2 M^{-1}, which gave the lowest average deviation from the mean of $I_{100-450}(SeOCl_2)$ $(= 98 \pm 2$ cm^2 $M^{-1})$.

890 cm^{-1} bands (Table 1), it was not considered worthwhile to fit these data to K_1.

As HCl concentration is increased above 4.0 M, a band is seen to grow in intensity at 330 cm^{-1} in the SeCl stretching region of the spectrum. This peak is 50 cm^{-1} higher than that of the SeO_2Cl^- anion (5) in acetonitrile and is, therefore, unlikely to be due to this species. Moreover, the growth of this peak is accompanied by a growth in the intensity of the Se—OH stretching peak (690 cm^{-1}) over the range 4.0 to 6.0 M HCl where $[H_2SeO_3]$ is virtually constant if not decreasing. For these reasons it appears likely that $HSeO_2Cl$ is formed in these solutions. At even higher concentrations, $SeOCl_2$ is formed (2) and its spectrum is apparent in Fig. 1. In the range 4.0–12.0 M HCl the Se(IV) equilibria which occur are,

$$[5] \quad H_2SeO_3 + H^+ + Cl^- \overset{K_4}{=} HSeO_2Cl + H_2O$$

$$[6] \quad HSeO_2Cl + H^+ + Cl^- \overset{K_5}{=} SeOCl_2 + H_2O$$

Interpretation in terms of K_4 and K_5 is consistent with the observed peak intensities. If it is assumed that only $SeOCl_2$ is formed (2), the formation constants calculated vary by several orders of magnitude over the HCl concentration range 5.0–12.0 M.

The formation constants K_4 and K_5 may be evaluated from any one of the three peak intensity regions of the spectra, 100–450, 690, or 890 cm^{-1}. However, the 690 cm^{-1} region is simpler to deal with since only H_2SeO_3 and $HSeO_2Cl$ contribute to the peak intensity of this region. In addition, in the case of the deformation/SeCl stretching region, while greater peak intensity at high HCl concentrations yields greater accuracy, uncertainty in the background correction and of the H_2SeO_3 molar intensity remove this advantage except for the most concentrated solutions. The unknowns, K_4, K_5, and $I_{690}(HSeO_2Cl)$ may be evaluated by means of the following equations,

$$[7] \quad c_{IV} = [H_2SeO_3] + [HSeO_2Cl]$$

$$[8] \quad i_{690} = I_{690}(H_2SeO_3)[H_2SeO_3] + I_{690}(HSeO_2Cl)[HSeO_2Cl]$$

$$[9] \quad K_4 = \frac{[HSeO_2Cl]\,a_w}{[H_2SeO_3]\,a_{\pm HCl}{}^2}$$

$$[10] \quad K_5 = \frac{[SeOCl_2]\,a_w}{[HSeO_2Cl]\,a_{\pm HCl}{}^2}$$

$$[11] \quad [H^+] = [Cl^-] = c_{HCl} - [HSeO_2Cl] - 2[SeOCl_2]$$

where a_w is the activity of water, $a_{\pm HCl}$ is the molar activity of HCl (ref. 10, Appendix 8.10; refs. 14, 15) and c_{IV} and c_{HCl} are the stoichiometric concentrations of Se(IV) and HCl, respectively. Various values of K_4 and K_5 were chosen in increments of 10^{-3} and 10^{-6}, respectively, to yield a minimum in the average deviation in $I_{690}(HSeO_2Cl)$ for the eight highest

Can. J. Chem. Downloaded from www.nrcresearchpress.com by 80.58.250.72 on 09/07/12
For personal use only.

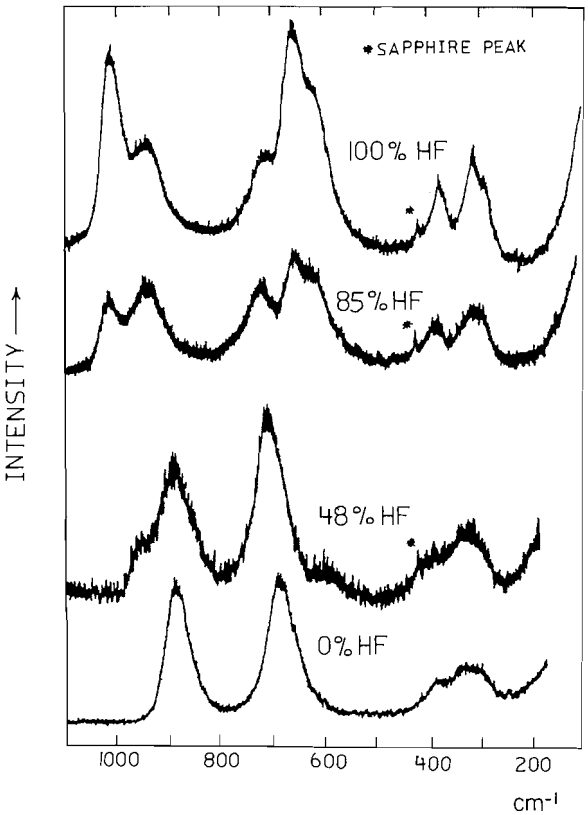

FIG. 3. Raman spectra of solutions of SeO_2 (3 M) in HF (0.0–100%).

HCl concentrations measured (5.0–12.0 M HCl). Smaller incremental changes in K_4 and K_5 were not felt to be useful since the minimum in the deviation on $I_{690}(HSeO_2Cl)$ then became very shallow. The best results were given by $K_4 = 1.5 \times 10^{-2}$ L^2 mol^{-2} and $K_5 = 9 \times 10^{-6}$ L^2 mol^{-2} which gave an average $I_{690}(HSeO_2Cl) = 7.25$ cm^2. The individual values of $I_{690}(HSeO_2Cl)$ at each c_{HCl} and mean value with average deviation as well as the concentrations of all species are given in Table 3. It is possible to calculate the molar intensities of $SeOCl_2$, $I_{890}(SeOCl_2)$ and $I_{100-450}(SeOCl_2)$, by choosing the analogous values for $HSeO_2Cl$, $I_{890}(HSeO_2Cl)$ and $I_{100-450}(HSeO_2Cl)$, which yield the minimum variation in the $I(SeOCl_2)$ values via the equations,

$$[12] \quad i_{890} = I_{890}(HSeO_2Cl)[HSeO_2Cl] + I_{890}(SeOCl_2)[SeOCl_2] + 5.45[H_2SeO_3]$$

$$[13] \quad i_{100-450} = I_{100-450}(HSeO_2Cl)[HSeO_2Cl] + I_{100-450}(SeOCl_2)[SeOCl_2] + 2.18[H_2SeO_3]$$

because of the low $[SeOCl_2]$, and thus the small influence on the intensity of the bands, at low c_{HCl}, these calculations were only carried out for solutions with $c_{HCl} > 7$ M. The molar intensities for H_2SeO_3 are taken from Table 2 and the concentrations from Table 3. The least variation, as judged by average deviation, in $SeOCl_2$ molar intensities was given by choosing $I_{890}(HSeO_2Cl) = 4.9$ cm^2 and $I_{100-450}(HSeO_2Cl) = 18$ cm^2. The individual $I(SeOCl_2)$ for each c_{HCl} and mean value with average deviation are given in Table 3. Because of the uncertainty in the background contribution to the 100–450 cm^{-1} envelope at low peak intensities and the uncertainty in $I_{100-450}(H_2SeO_3)$, the $I_{100-450}(SeOCl_2)$ calculated at $c_{HCl} < 9.0$ M are unreliable. The excellent agreement between $I_{100-450}(SeOCl_2)$ calculated for the range $c_{HCl} = 9.0$ to 12.0 M, when $i_{100-450}$ changes three-fold in intensity, is strong support for the interpretation in terms of equilibria [5] and [6] as well as the calculated values of K_4 and K_5.

Solutions of SeO_2 in hydrofluoric acid

The Raman spectra of solutions of SeO_2 in hydrofluoric acid shown in Fig. 3 exhibit the same changes at low HF concentrations as those of the corresponding solutions in hydrochloric acid. The changing intensities of the 690 and 890 cm^{-1} peaks reflect the repression of the dissociation equilibria of H_2SeO_3. When the HF concentration of the solvent used reaches 28.0 M the spectrum of a 3 M SeO_2 solution exhibits new peaks in addition to those of H_2SeO_3. A new peak appears at 930 cm^{-1} corresponding to an SeO double bond stretch, another peak appears at 600 cm^{-1} in the SeF stretching region and the SeO single bond peak at 690 cm^{-1} increases in intensity relative to that at 890 cm^{-1} indicating that the new species being formed has an SeO single bond. The spectral changes are consistent with the equilibrium

$$[14] \quad H_2SeO_3 + HF = HSeO_2F + H_2O$$

With 52.0 M HF as solvent the spectrum due to H_2SeO_3 has completely disappeared, the three principal peaks of $HSeO_2F$ are clearly evident but, in addition, peaks corresponding to those of $SeOF_2$ at 1008 and 650 cm^{-1} are apparent. The formation of $SeOF_2$ from SeO_2 and 100% HF has been demonstrated earlier (1). With 100% HF as solvent the spectrum of $SeOF_2$ is even more pronounced relative to that of $HSeO_2F$. In the absence of activity data for HF at the concentrations at which $HSeO_2F$ and $SeOF_2$ are formed, it is not possible to calculate formation constants.

Conclusions

In solutions of SeO_2 in HX (X = F, Cl, Br), as the concentration of HX is increased, there is first of all a repression of the ionic dissociation of H_2SeO_3 which then undergoes a stepwise substitution of OH groups by halogen X yielding first the monohaloselenous acid which is undissociated in HX solutions. Subsequently, the second OH group is substituted, giving seleninyl halide, which in HBr acts as a Br^- acceptor, forming the $SeOBr_3^-$ anion. Seleninyl fluoride is the most highly fluoride coordinated species in HF but in HCl and HBr, SeX_5^- and SeX_6^{2-} species are formed (2, 3).

Acknowledgements

The Natural Sciences and Engineering Research Council of Canada is thanked for research support. W. D. Moffett is thanked for the measurement of the SeO_2/HF spectra.

1. H. SELIG and U. EL-GAD. J. Inorg. Nucl. Chem. Suppl. 233 (1976).
2. J. MILNE and P. LAHAIE. Inorg. Chem. **18**, 3180 (1979).
3. J. MILNE and P. LAHAIE. Inorg. Chem. **24**, 840 (1985).
4. R. PAETZOLD and K. AURICH. Z. anorg. allg. Chem. **335**, 281 (1965).
5. J. MILNE and P. LAHAIE. Spectrochim. Acta, Pt. A, **39A**, 555 (1983).
6. A. I. VOGEL. Quantitative inorganic analysis. 3rd ed. Longman, London. 1972. p. 302.

Can. J. Chem. Downloaded from www.nrcresearchpress.com by 80.58.250.72 on 09/07/12
For personal use only.

7. L. BARCZA and L. G. SILLEN. Acta Chem. Scand. **25**, 1250 (1971).
8. G. E. WALRAFEN. J. Chem. Phys. **36**, 90 (1962).
9. G. E. WALRAFEN. J. Chem. Phys. **37**, 1468 (1962).
10. R. A. ROBINSON and R. H. STOKES. Electrolyte solutions. Butterworths, London. 1965.
11. J. MILNE and T. PARKER. J. Solution Chem. **10**, 479 (1981).
12. A. K. COVINGTON, J. G. FREEMAN, and T. H. LILLEY. J. Phys. Chem. **74**, 3773 (1970).
13. E. SH. GANELINA, V. P. KUZ'MICHEVA, and M. B. KRASNOPO'SKAYA. Zh. neorg. Khim. **18**, 1321 (1973).
14. R. C. WEAST. Handbook of chemistry and physics. Chemical Rubber Publishing Co., Cleveland. 1970. D184.
15. M. RANDALL and L. E. YOUNG. J. Am. Chem. Soc. **50**, 989 (1928).

Can. J. Chem. Downloaded from www.nrcresearchpress.com by 80.58.250.72 on 09/07/12
For personal use only.

Ultrasonic speeds and isentropic compressibilities of binary mixtures of *n*-octane with each of the hexane isomers at 298.15 K[1]

GEORGE C. BENSON[2] AND CARL J. HALPIN
Division of Chemistry, National Research Council of Canada, Ottawa, Ont., Canada K1A 0R6

Received June 9, 1986

GEORGE C. BENSON and CARL J. HALPIN. Can. J. Chem. **65**, 322 (1987).

Measurements of ultrasonic speed were carried out for *n*-octane + each of the five hexanes at 298.15 K. The results were combined with excess molar volumes reported previously to obtain excess isentropic compressibilities and isentropic pressure derivatives of the excess molar volumes. These are in good agreement with estimates from the Flory theory of mixtures.

GEORGE C. BENSON et CARL J. HALPIN. Can. J. Chem. **65**, 322 (1987).

Opérant à 298,15 K, on a effectué des mesures de vitesses ultrasoniques pour les mélanges de *n*-octane avec chacun des cinq hexanes. On a combiné les résultats obtenus avec les valeurs des volumes molaires en excès qui ont été déterminés antérieurement pour évaluer les compressibilités isentropiques en excès et les pressions isentropiques dérivées des volumes molaires en excès. Celles-ci sont en bon accord avec les évaluations faites à l'aide de la théorie de Flory pour les mélanges.

[Traduit par la revue]

Can. J. Chem. Downloaded from www.nrcresearchpress.com by 80.58.250.72 on 09/07/12
For personal use only.

Previous papers from our laboratory have reported excess enthalpies (1), excess volumes (2), and excess isobaric heat capacities (3) of (*n*-octane + a hexane isomer) for the five hexanes: *n*-hexane (*n*-C_6), 2-methylpentane (2-MP), 3-methylpentane (3-MP), 2,2-dimethylbutane (2,2-DMB), and 2,3-dimethylbutane (2,3-DMB). As an extension of those studies, we have determined the speed of ultrasound in the same set of mixtures.

Experimental

Component liquids

The *n*-octane was Aldrich Chemical Co. Gold Label reagent with a specified purity of 99+ mol%. The isomeric hexanes were Phillips Research Grade reagents with purities of 99.88 mol% or greater. The component liquids were stored over molecular sieve pellets (BDH Type 4A) and partially degassed prior to their use. At 298.15 K, the densities (in kg m^{-3}) of the samples used for the ultrasonic studies were as follows: *n*-octane, 698.64; *n*-C_6, 654.92; 2-MP, 648.50; 3-MP, 659.81; 2,2-DMB, 644.44; 2,3-DMB, 657.02.

Ultrasonic measurements

A pulse-echo-overlap technique was used to determine the ultrasonic speed of 2 MHz waves in mixtures formed in a successive dilution cell. The apparatus and experimental procedure have been described in previous publications (4, 5). The speed of sound in pure water (1496.739 m s^{-1} at 298.15 K), reported by Kroebel and Mahrt (6), was used to determine the distance between the transducer and the reflector. The error of the ultrasonic speeds is estimated to be less than 0.2 m s^{-1}, and their reproducibility was about 0.02 m s^{-1}. The mole fractions of the mixtures are known with an accuracy better than $\pm 1 \times 10^{-4}$.

Results and discussion

The experimental results for the speed u of ultrasound in $\{xC_8H_{18} + (1 - x)C_6H_{14}\}$ mixtures at 298.15 K and ambient standard atmospheric pressure are summarized in Table 1 for the five hexanes. Also listed there are isentropic compressibilities κ_S, excess isentropic compressibilities κ_S^E, and values of the differential coefficient $(\partial V_m^E/\partial p)_S$ calculated from the relations:

$$[1] \quad \kappa_S = (\rho u^2)^{-1}$$

$$[2] \quad \kappa_S^E = \kappa_S - \kappa_S^{id}$$

and

$$[3] \quad (\partial V_m^E/\partial p)_S = [xV_1^0 + (1 - x)V_2^0]\kappa_S^{id} - V_m\kappa_S$$

where ρ is the density of the mixture and κ_S^{id} is the isentropic compressibility of the corresponding ideal mixture, V_1^0 and V_2^0 are the molar volumes of pure *n*-octane and hexane isomer, respectively, and V_m is the molar volume of the mixture. Values of ρ and V_m were estimated from the densities of the pure components and our previous results for the excess molar volumes V_m^E of the mixtures (2). The formula for evaluating κ_S^{id} has already been described (7). Values of the isobaric expansivities and molar isobaric heat capacities used in the present application were taken from our previous publications (2, 3).

For each system, an equation of the form

$$[4] \quad \Phi(x) = x(1 - x)\sum_{j=1}^{n} c_j(1 - 2x)^{j-1}$$

was fitted to the deviations Δu defined by the equation

$$[5] \quad \Delta u = u - xu_1^0 - (1 - x)u_2^0$$

where u_1^0 and u_2^0 are the ultrasonic speeds in pure *n*-octane and the hexane isomer, respectively. Values of the coefficients were determined by least-squares analyses in which all points were weighted equally. Equation [4] was also fitted to the results for κ_S^E and $(\partial V_m^E/\partial p)_S$. The coefficients c_j and standard deviations s for these representations are listed in Table 2.

The experimental results for Δu and their representations by eq. [4] are plotted in Fig. 1. The values of Δu at corresponding x decrease in the order:

$$2,2\text{-DMB} > 2,3\text{-DMB} > 2\text{-MP} > 3\text{-MP} > n\text{-}C_6$$

Similar plots for κ_S^E and $(\partial V_m^E/\partial p)_S$ are shown in Figs. 2 and 3, respectively. For both these functions, the order of the absolute values at corresponding x differs from the order for Δu by the interchange of the curves for 2,3-DMB and 2-MP. These features are qualitatively similar to our previous findings for (*n*-heptane + hexane isomer) mixtures (8) and (*n*-dodecane + hexane isomer) mixtures (9). Comparison of results for different *n*-alkanes with the same hexane isomer shows that the magnitudes of Δu, κ_S^E, and $(\partial V_m^E/\partial p)_S$ increase with increasing size of the *n*-alkane component, and that the curves for the longer *n*-alkanes tend to be more skewed toward $x = 0$.

[1]NRCC No. 26589.

[2]Present address: Department of Chemical Engineering, University of Ottawa, 770 King Edward Avenue, Ottawa, Ont., Canada K1N 9B4.

TABLE 1. Ultrasonic speeds u, isentropic compressibilities κ_S, excess isentropic compressibilities κ_S^E, and differential coefficients $(\partial V_m^E/\partial p)_S$ for $\{xC_8H_{18} + (1-x)C_6H_{14}\}$ mixtures at 298.15 K

x	u / m s^{-1}	κ_S / TPa^{-1}	κ_S^E / TPa^{-1}	$(\partial V_m^E/\partial p)_S$ / cm^3 mol^{-1} GPa^{-1}	x	u / m s^{-1}	κ_S / TPa^{-1}	κ_S^E / TPa^{-1}	$(\partial V_m^E/\partial p)_S$ / cm^3 mol^{-1} GPa^{-1}
				n-Octane + *n*-C_6					
0.00000	1076.55	1317.48	0.00	0.000	0.49917	1129.20	1154.83	−14.24	2.101
0.03667	1080.82	1303.16	−2.57	0.341	0.54939	1133.69	1142.08	−13.36	1.993
0.07244	1084.93	1289.59	−4.81	0.644	0.61816	1139.98	1124.79	−12.34	1.868
0.11155	1089.38	1275.14	−7.02	0.949	0.69553	1146.86	1106.28	−10.74	1.652
0.16856	1095.69	1255.01	−9.61	1.316	0.76829	1153.07	1089.87	−8.68	1.355
0.23827	1103.20	1231.58	−12.02	1.673	0.83809	1158.88	1074.84	−6.39	1.012
0.31655	1111.28	1206.98	−13.59	1.925	0.89654	1163.60	1062.80	−4.21	0.674
0.39342	1119.02	1184.10	−14.42	2.079	0.94684	1167.61	1052.76	−2.23	0.360
0.45606	1125.07	1166.55	−14.40	2.104	1.00000	1171.76	1042.48	0.00	0.000
				n-Octane + 2-MP					
0.00000	1040.90	1423.22	0.00	0.000	0.49702	1113.53	1193.00	−27.07	4.009
0.09755	1056.43	1369.25	−11.76	1.597	0.52925	1117.53	1181.69	−26.20	3.906
0.16176	1066.42	1336.10	−17.75	2.447	0.60314	1126.75	1156.35	−24.04	3.639
0.21434	1074.35	1310.50	−21.49	2.997	0.69157	1137.59	1127.58	−20.68	3.186
0.27556	1083.32	1282.35	−24.62	3.479	0.75923	1145.48	1107.16	−17.08	2.667
0.33927	1092.36	1254.72	−26.66	3.820	0.82547	1152.97	1088.20	−12.98	2.052
0.40900	1101.83	1226.55	−27.38	3.981	0.89052	1160.10	1070.52	−8.43	1.350
0.41530	1102.78	1223.85	−27.62	4.022	0.94547	1166.03	1056.14	−4.36	0.705
0.45943	1108.64	1206.91	−27.52	4.044	1.00000	1171.76	1042.48	0.00	0.000
0.46109	1108.75	1206.51	−27.27	4.009					
				n-Octane + 3-MP					
0.00000	1071.16	1320.91	0.00	0.000	0.43275	1121.02	1172.32	−17.33	2.509
0.03879	1076.14	1305.01	−3.41	0.449	0.44352	1121.98	1169.59	−17.02	2.471
0.07920	1081.22	1289.07	−6.48	0.863	0.50913	1128.51	1151.78	−16.50	2.431
0.12495	1086.80	1271.81	−9.37	1.263	0.59164	1136.46	1130.58	−15.18	2.277
0.17136	1092.33	1255.01	−11.80	1.608	0.68962	1145.49	1107.11	−12.64	1.938
0.23208	1099.36	1234.09	−14.24	1.968	0.77729	1153.24	1087.49	−9.68	1.511
0.30257	1107.23	1211.17	−16.12	2.265	0.84372	1158.86	1073.51	−6.94	1.100
0.36740	1114.23	1191.25	−17.11	2.441	0.89569	1163.14	1063.02	−4.61	0.738
0.39091	1116.54	1184.66	−16.92	2.427	1.00000	1171.76	1042.48	0.00	0.000
				n-Octane + 2,2-DMB					
0.00000	998.87	1555.25	0.00	0.000	0.48840	1095.13	1237.79	−50.32	7.462
0.05015	1010.09	1513.16	−13.16	1.780	0.55952	1107.11	1204.38	−47.54	7.150
0.08439	1017.55	1486.01	−20.76	2.828	0.61279	1115.96	1180.55	−44.71	6.794
0.11619	1024.32	1461.89	−26.85	3.683	0.63321	1119.06	1172.21	−42.93	6.550
0.15595	1032.64	1432.98	−33.42	4.624	0.65899	1123.25	1161.27	−41.18	6.314
0.19961	1041.55	1402.82	−39.30	5.490	0.70513	1130.34	1142.89	−37.05	5.732
0.20428	1042.50	1399.67	−39.87	5.574	0.75972	1138.47	1122.23	−31.43	4.914
0.25389	1052.35	1367.39	−44.91	6.345	0.80584	1145.17	1105.58	−26.18	4.129
0.25433	1052.36	1367.32	−44.75	6.322	0.84372	1150.56	1092.41	−21.57	3.426
0.30803	1062.62	1334.67	−48.29	6.901	0.88444	1156.24	1078.74	−16.31	2.611
0.31035	1063.19	1332.97	−48.74	6.969	0.95825	1166.25	1055.17	−6.12	0.992
0.37322	1074.87	1297.14	−51.03	7.391	1.00000	1171.76	1042.48	0.00	0.000
				n-Octane + 2,3-DMB					
0.00000	1046.44	1389.91	0.00	0.000	0.45870	1112.60	1190.78	−25.86	3.776
0.03269	1051.83	1372.19	−4.51	0.596	0.52031	1120.25	1170.19	−25.06	3.709
0.06595	1057.15	1354.95	−8.45	1.127	0.58910	1128.42	1148.65	−23.23	3.489
0.10779	1063.74	1334.01	−12.86	1.732	0.66490	1137.16	1126.21	−20.50	3.130
0.16011	1071.70	1309.24	−17.27	2.355	0.74842	1146.34	1103.19	−16.49	2.563
0.22964	1081.93	1278.29	−21.68	3.005	0.83424	1155.39	1081.09	−11.56	1.828
0.30194	1092.08	1248.46	−24.54	3.458	0.89799	1161.87	1065.60	−7.45	1.193
0.38158	1102.79	1217.97	−26.04	3.737	0.94625	1166.61	1054.45	−4.02	0.650
0.41222	1106.63	1207.17	−25.88	3.741	1.00000	1171.76	1042.48	0.00	0.000
0.42102	1107.93	1203.67	−26.25	3.801					

Can. J. Chem. Downloaded from www.nrcresearchpress.com by 80.58.250.72 on 09/07/12
For personal use only.

TABLE 2. Coefficients c_j and standard deviations s for least-squares representations of Δu, κ_S^E, and $(\partial V_m^E/\partial p)_S$ for $\{xC_8H_{18} + (1 - x)C_6H_{14}\}$ mixtures at 298.15 K by eq. [4]

Mixture	c_1	c_2	c_3	c_4	s
n-Octane					
		$\Phi = \Delta u/(\text{m s}^{-1})$			
+ *n*-C_6	20.265	2.684			0.04
+ 2-MP	30.145	3.342			0.07
+ 3-MP	24.762	4.657			0.05
+ 2,2-DMB	47.567	4.555	1.007	1.947	0.05
+ 2,3-DMB	34.650	5.133	1.381		0.04
		$\Phi = \kappa_S^E/\text{TPa}^{-1}$			
+ *n*-C_6	−56.443	−16.405	−3.085		0.09
+ 2-MP	−107.740	−31.219	−5.352		0.14
+ 3-MP	−66.787	−22.674	−3.466		0.11
+ 2,2-DMB	−200.702	−61.710	−17.511	−8.280	0.12
+ 2,3-DMB	−101.630	−33.185	−9.658		0.08
		$\Phi = (\partial V_m^E/\partial p)_S/(\text{cm}^3\ \text{mol}^{-1}\ \text{GPa}^{-1})$			
+ *n*-C_6	8.3548	1.5050			0.015
+ 2-MP	16.0029	2.9424			0.023
+ 3-MP	9.8403	2.2179			0.016
+ 2,2-DMB	29.8322	6.1826	1.6144	0.9723	0.018
+ 2,3-DMB	14.9785	3.1906	0.8742		0.012

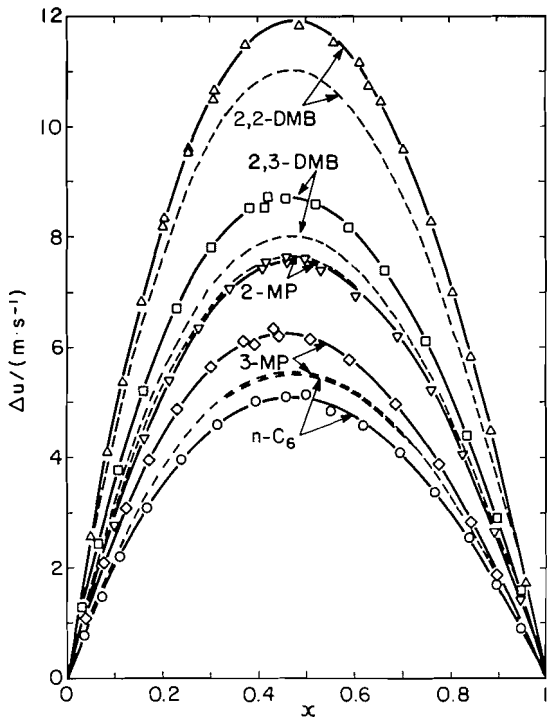

FIG. 1. Deviations Δu of the speed of ultrasound from mole fraction linearity, for $\{xC_8H_{18} + (1 - x)C_6H_{14}\}$ at 298.15 K. Experimental results: ○, *n*-C_6; ▽, 2-MP; ◇, 3-MP; △, 2,2-DMB; □, 2,3-DMB. Curves: —, calculated from eq. [4] with coefficients from Table 2; ---, calculated from Flory theory.

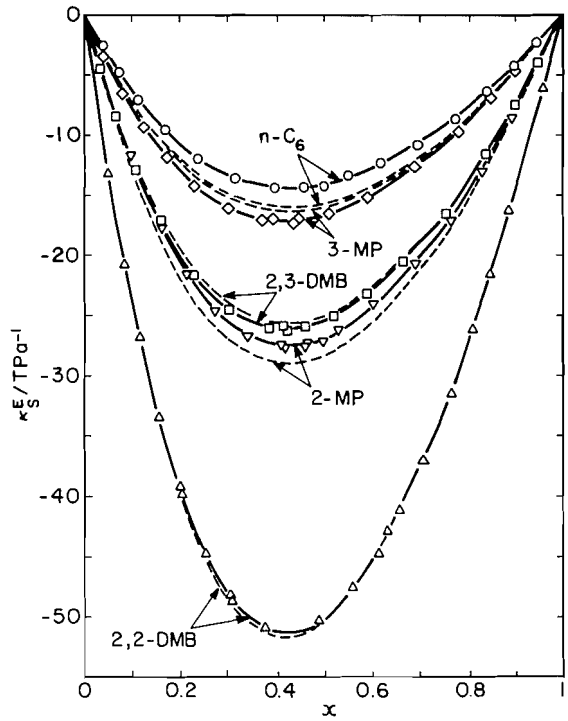

FIG. 2. Excess isentropic compressibilities κ_S^E for $\{xC_8H_{18} + (1 - x)C_6H_{14}\}$ at 298.15 K. Experimental results: ○, *n*-C_6; ▽, 2-MP; ◇, 3-MP; △, 2,2-DMB; □, 2,3-DMB. Curves: —, calculated from eq. [4] with coefficients from Table 2; ---, calculated from Flory theory.

Previously (2) we found that the Flory theory (10, 11) provided useful estimates of the excess molar volumes of (*n*-octane + hexane isomer) mixtures when the interchange energy parameter X_{12} was selected to give a least-squares fit between the experimental and theoretical excess molar enthalpy curves (1). A further investigation (3) showed that the excess molar isobaric heat capacities of these mixtures could also be reproduced fairly well by the theory when X_{12} was assumed to be a linear function of the temperature, and a suitable value was assigned to $(\partial X_{12}/\partial T)_p$. Table 3 summarizes the Flory characteristic pressures p^*, molar volumes V, and temperatures T^* for the component liquids; also listed there are values of X_{12} and $(\partial X_{12}/\partial T)_p$ for their mixtures. Details of the derivation of these values can be found in our earlier works (2, 3).

Can. J. Chem. Downloaded from www.nrcresearchpress.com by 80.58.250.72 on 09/07/12
For personal use only.

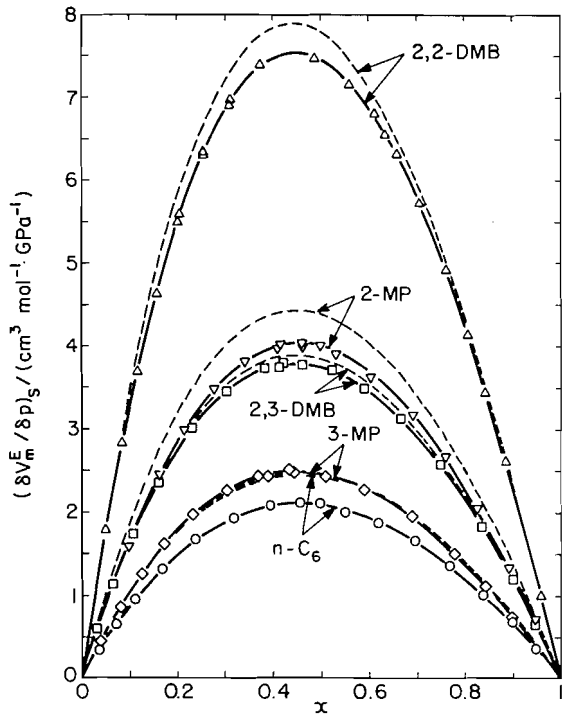

FIG. 3. Differential coefficients $(\partial V_m^E/\partial p)_S$ for $\{xC_8H_{18} + (1 - x)C_6H_{14}\}$ at 298.15 K. Experimental results: ○, n-C_6; ▽, 2-MP; ◇, 3-MP; △, 2,2-DMB; □, 2,3-DMB. Curves: —, calculated from eq. [4] with coefficients from Table 2; ---, calculated from Flory theory.

TABLE 3. Parameters p^*, V^*, T^*, X_{12}, and $(\partial X_{12}/\partial T)_p$ used in calculations for $\{xC_8H_{18} + (1 - x)C_6H_{14}\}$ mixtures at 298.15 K by the Flory theory[a]

Component	p^* / J cm^{-3}	V^* / cm^3 mol^{-1}	T^* / K	X_{12} / J cm^{-3}	$(\partial X_{12}/\partial T)_p$ / J cm^{-3} K^{-1}
n-C_8H_{18}	436.9	127.70	4827.0		
n-C_6	424.2	99.52	4436.1	0.3382	−0.00444
2-MP	408.3	99.99	4380.8	0.9996	−0.01354
3-MP	424.2	98.68	4423.0	0.8284	−0.01949
2,2-DMB	389.0	100.07	4324.8	1.6123	−0.04062
2,3-DMB	405.3	99.16	4430.2	0.8391	−0.02508

[a]Values of p^*, V^*, T^*, and X_{12} taken from ref. 2; $(\partial X_{12}/\partial T)_p$ from ref. 3.

Estimates of Δu, κ_S^E and $(\partial V_m^E/\partial p)_S$ were calculated from the Flory theory in the following way. According to the theory, the isothermal compressibility κ_T at zero pressure is given by the formula

$$[6] \quad \kappa_T = (3\tilde{v}^2/p^*)(\tilde{v}^{1/3} - 1)/(4 - 3\tilde{v}^{1/3})$$

where $\tilde{v}$ is the reduced volume of the mixture, obtained by solving the Flory equation of state. The isentropic compressibility is calculated from the thermodynamic relation

$$[7] \quad \kappa_S = \kappa_T - TV_m\alpha_p^2/C_{p,m}$$

using the theoretical expressions for the molar volume

$$[8] \quad V_m = \tilde{v}[xV_1^* + (1 - x)V_2^*] = \tilde{v}V_m^*$$

the isobaric expansivity

$$[9] \quad \alpha_p = (3\tilde{v}^{4/3}/T^*)/(4 - 3\tilde{v}^{1/3})$$

and the molar isobaric heat capacity

$$[10] \quad C_{p,m} = -xp_1^*V_1^*\alpha_{p,1}^0/\tilde{v}_1 - (1 - x)p_2^*V_2^*\alpha_{p,2}^0/\tilde{v}_2 + [xp_1^*V_1^* + (1 - x)p_2^*V_2^* - xV_1^*\theta_2X_{12}](\alpha_p/\tilde{v}) + (xV_1^*\theta_2/\tilde{v})(\partial X_{12}/\partial T)_p + xC_{p,1}^0 + (1 - x)C_{p,2}^0$$

where $\alpha_{p,1}^0$ and $\alpha_{p,2}^0$ are respectively the isobaric expansivities of the pure n-octane and hexane isomer, and $C_{p,1}^0$ and $C_{p,2}^0$ are their molar isobaric heat capacities. As in our previous work, it is assumed that the site fraction for the hexane isomer can be approximated by the expression

$$[11] \quad \theta_2 = (1 - x)/[1 + x\{(V_1^*/V_2^*)^{2/3} - 1\}]$$

Values of κ_S^{id} for the corresponding ideal mixture are obtained from eq. [7] where κ_T^{id} and α_p^{id} are volume fraction averages of the pure component values, and $C_{p,m}^{id}$ is a mole fraction average.

Values of u can be calculated from eq. [1] using the Flory estimates of ρ and κ_S. The corresponding Δu are shown as broken curves in Fig. 1. Theoretical estimates of κ_S^E and $(\partial V_m^E/\partial p)_S$, obtained from eqs. [3] and [4], are plotted in Figs. 2 and 3. It can be seen that the Flory model provides a fairly satisfactory representation of Δu, κ_S^E, and $(\partial V_m^E/\partial p)_S$ for the present mixtures. The order of the curves is reproduced correctly, however the differences between the curves for n-C_6 and 3-MP are underestimated.

1. S. E. M. HAMAM, M. K. KUMARAN, and G. C. BENSON. Fluid Phase Equilib. **18**, 147 (1984).
2. M. K. KUMARAN and G. C. BENSON. Can. J. Chem. **62**, 2369 (1984).
3. G. C. BENSON and P. J. D'ARCY. Can. J. Chem. **64**, 2139 (1986).
4. O. KIYOHARA, J.-P. E. GROLIER, and G. C. BENSON. Can. J. Chem. **52**, 2287 (1974).
5. O. KIYOHARA, C. J. HALPIN, and G. C. BENSON. Can. J. Chem. **55**, 3544 (1977).
6. W. KROEBEL and K.-H. MAHRT. Acustica, **35**, 154 (1976).
7. O. KIYOHARA and G. C. BENSON. J. Chem. Thermodyn. **11**, 861 (1979).
8. E. AICART, M. K. KUMARAN, C. J. HALPIN, and G. C. BENSON. J. Chem. Thermodyn. **15**, 919 (1983).
9. G. C. BENSON, C. J. HALPIN, and M. K. KUMARAN. J. Chem. Thermodyn. In press.
10. P. J. FLORY. J. Am. Chem. Soc. **87**, 1833 (1965).
11. A. ABE and P. J. FLORY. J. Am. Chem. Soc. **87**, 1838 (1965).

Can. J. Chem. Downloaded from www.nrcresearchpress.com by 80.58.250.72 on 09/07/12
For personal use only.

Molecular conformation of 2′-deoxy-3′,5′-di-*O*-acetyl adenosine. Crystal structure and high resolution proton nuclear magnetic resonance investigations

LEO H. KOOLE[1] AND HENK M. BUCK

Department of Organic Chemistry, Eindhoven University of Technology, P.O. Box 513, 5600 MB Eindhoven, The Netherlands

AND

JAN A. KANTERS AND ARIE SCHOUTEN

Laboratory of Crystal and Structural Chemistry, State University of Utrecht, Utrecht, The Netherlands

Received July 3, 1986

LEO H. KOOLE, HENK M. BUCK, JAN A. KANTERS, and ARIE SCHOUTEN. Can. J. Chem. **65**, 326 (1987).

2′-Deoxy-3′,5′-di-*O*-acetyl adenosine crystallizes in the orthorhombic space group $P2_12_12_1$, and the cell dimensions are a = 7.768(1) Å, b = 12.890(1) Å, c = 15.495(1) Å; Z = 4 molecules per cell. Least-squares refinement converged at R = 0.054 for 1752 observed reflections. The adenine bases are linked via N_6—H...N_1 and N_6—H...N_7 hydrogen bonds, in such a way that infinite one-dimensional chains are formed. Comments are made on the fact that this structure is entirely different from the parallel dimer that was found for 3′,5′-di-*O*-acetyl thymidine. Furthermore, the conformational preferences of the title compound in aqueous solution have been determined with 300- and 500-MHz ^{1}H nmr. It is found that the X-ray structure and the solution conformation are essentially similar, except for the $C_{4'}$—$C_{5'}$ conformation, that is γ^- in the solid state, and predominantly γ^+ in solution.

LEO H. KOOLE, HENK M. BUCK, JAN A. KANTERS et ARIE SCHOUTEN. Can. J. Chem. **65**, 326 (1987).

La désoxy-2′ di-*O*-acétyl-3′,5′ adénosine cristallise dans le groupe d'espace orthorhombique $P2_12_12_1$, avec a = 7,768(1), b = 12,890(1) et c = 15,495(1) Å et Z = 4 molécules par maille. On a affiné la structure par la méthode des moindres carrés jusqu'à une valeur de R = 0,054 pour 1752 réflexions observées. Les bases adénines sont liées par le biais de liaisons hydrogènes N_6—H...N_1 et N_6—H...N_7 et elles forment ainsi des chaînes unidimentionnelles infinies. On fait des commentaires sur le fait que cette structure est entièrement différente de celle du dimère parallèle qui a été trouvé pour la di-*O*-acétyl-3′,5′ thymidine. De plus, faisant appel à la rmn du ^{1}H à 300 et à 500 MHz, on a déterminé les préférences conformationnelles du composé mentionné dans le titre, en solution aqueuse. On a trouvé que les structures observées par diffraction des rayons-X ainsi qu'en solution sont essentiellement semblables, excepté pour la conformation autour de la liaison $C_{4'}$—$C_{5'}$ qui est γ^- à l'état solide et en prédominance γ^+ en solution.

[Traduit par la revue]

Introduction[2]

The crystal structures of several acetylated nucleosides have been determined during the previous years (1–4). The interest in these compounds stems partly from their possible function as antitumor, antibacterial, and antiviral agents. For instance, the 1:1 complex of 2′,3′,5′-tri-*O*-acetyl uridine and *cis*-$Pt(H_2O)_2(NH_3)_2$ was shown to be particularly active (5). Moreover, this complex has the advantages of a high water solubility and a low renal toxicity. In addition, it is of interest that acetylated nucleosides generally show peculiar stacking interactions and hydrogen-bonded self-association of the nucleobases in the solid state. For example, the crystal structure of 3′,5′-di-*O*-acetyl thymidine shows a thymine–thymine dimer in which the bases are parallel and linked via two N_3—H...O_4 hydrogen bonds (2, 3). Using the hexanucleoside pentaphosphate $d(T_pT_pT_pT_pT_pT)$, it was shown that this type of base pairing results in the formation of a non-Watson and Crick parallel DNA duplex structure, provided that the phosphate groups are methylated (3). In the present work, we report the crystal structure of 2′-deoxy-3′,5′-di-*O*-acetyl adenosine (Fig. 1). The adenine bases are linked via two different hydrogen bonds (i.e. N_6—H...N_1 and N_6—H...N_7) to form infinite one-dimensional chains. The X-ray data of 2′-deoxy-3′,5′-di-*O*-acetyl adenosine are compared with the aqueous solution conformation, as determined with 300- and 500-MHz ^{1}H nmr spectroscopy.

[1]To whom all correspondence should be addressed.

[2]Nomenclature in this work follows the recent IUPAC-IUB recommendations on nucleotide conformational nomenclature. See ref. 27.

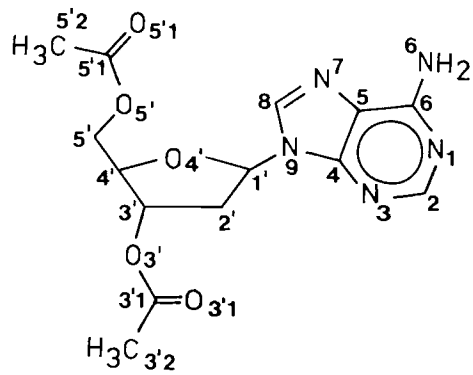

FIG. 1. Structural formula and atomic labelling of the 2′-deoxy-3′,5′-di-*O*-acetyl adenosine molecule.

Experimental section

Preparation

Acetic anhydride (1.06 g, 10.38 mmol) was added to a cooled (0°C) and stirred solution of 2′-deoxyadenosine (2.00 g, 8.00 mmol) in 30 mL of anhydrous pyridine. (2′-Deoxyadenosine was previously dissolved with heating and vigorous stirring.) The reaction mixture was stirred overnight at room temperature. After evaporation of the pyridine, thin layer chromatography using chloroform–ethanol (6:1 v/v) as eluent indicated the presence of four substances: 2′-deoxy-3′,5′-di-*O*-acetyladenosine (R_f = 0.41), 2′-deoxy-3′-*O*-acetyladenosine (R_f = 0.32), 2′-deoxy-5′-*O*-acetyladenosine (R_f = 0.16), and unreacted 2′-deoxyadenosine (R_f = 0). The isolation of 2′-deoxy-3′,5′-di-*O*-acetyladenosine was accomplished via chromatography on a Woelm silica gel column. The product was initially obtained as a white solid, yield 0.75 g, 28%. Recrystallization from

Printed in Canada / Imprimé au Canada

Can. J. Chem. Downloaded from www.nrcresearchpress.com by 80.58.250.72 on 09/07/12
For personal use only.

H_2O yielded rod-shaped colorless crystals, mp 148–150°C (6). *Anal.* calcd. for $C_{14}H_{17}N_5O_5$: C 50.15, H 5.11, N 20.89; found: C 50.08, H 5.11, N 20.38. ^{1}H nmr (solvent D_2O): δ 1.98 (3H, s, CH_3), 2.16 (3H, s, CH_3), 2.76 (1H, m, $H_{2''}$), 3.00 (1H, m, $H_{2'}$), 4.32 (2H, m, $H_{5'}/H_{5''}$), 4.50 (1H, m, $H_{4'}$), 5.50 (1H, m, $H_{3'}$), 6.44 (1H, dd, $H_{1'}$), 8.21 (1H, s, H_2), 8.30 (1H, s, H_8).

Crystallographic measurements and structure resolution

$C_{14}H_{17}N_5O_5$ fw = 335.32

Orthorhombic, a = 7.768(1) Å, b = 12.890(1) Å, c = 15.495(1) Å, V = 1551.5(3) Å^3, Z = 4, D_c = 1.435 g cm^{-3}, λ(CuKα) = 1.54184 Å, t = 20°C, μ(CuKα) = 9.53 cm^{-1}, F(000) = 704. Absent reflections: $h00$, h odd; $0k0$, k odd; and $00l$, l odd; space group $P2_12_12_1$ (D_2^4, No. 19).

A crystal of dimensions (mm) 0.75 × 0.25 × 0.25 was mounted on a Nonius CAD4 diffractometer. Unit cell dimensions were determined by least-squares refinement of the setting angles of 24 reflections in the θ range 11.4–45.8°. Intensities of 1842 reflections were measured within the sphere of reflection limited by 2θ = 150° and $0 \leqq h \leqq 9$, $0 \leqq k \leqq 16$, and $0 \leqq l \leqq 19$, using Ni-filtered Cu Kα radiation. The ω/2θ scan technique was applied with ω = (0.70 + 0.15 tan θ)°. The intensities of two reference reflections (024 and 210), measured every 60 reflections showed an average deviation less than 1% during the duration of the data collection. The intensities were corrected for Lorenz-polarization effects, but not for absorption. A total of 1752 reflections that satisfied the criterion $I \geqq 2.5\sigma(I)$ were retained for the structure determination and refinement. $\sigma(I)$ was derived from counting statistics. The structure was solved with the direct methods program of SHELXS84 (7), the coordinates of all non-hydrogen atoms being determined from an E-map. The hydrogen atoms, with the exception of one hydrogen atom of each methyl group, were located on subsequent difference maps. The hydrogen atoms of the methyl groups were placed at idealized positions (C—H 1.00 Å, H—C—H 109.5°) such that two hydrogen atoms of each methyl group were close to the maxima observed in the difference map. In the refinement the methyl groups were treated as rigid groups. The remaining hydrogen atoms were included in the refinement with constant isotropic thermal parameters, equal to those of their carrier atoms. Anisotropic blocked full-matrix refinement (5 blocks) on F of 260 parameters converged at R = 0.054 and R_w = 0.056 with $w = [\sigma^2(F_o) + 0.01697F_o^2]^{-1}$. The quantity minimized was $\Sigma w\Delta F^2$, the goodness of fit, $s = [\Sigma w\Delta F^2/(m - n)]^{-1/2}$, was 0.61 and the average shift to error ratio 0.048. A final ΔF map showed maximal fluctuations of +0.25 and −0.40 e Å^{-3}. Scattering factors were those of Cromer and Mann (8) and for hydrogen of Stewart, Davidson, and Simpson (9). Programs used include SHELX76 (10) (refinement) and EUCLID (11) (geometry and illustrations).

Nuclear magnetic resonance spectroscopy

One-dimensional spectra were recorded at different sample temperatures on a Bruker CXP-300 spectrometer[3] (^{1}H frequency: 300.13 MHz), operating in the Fourier transform mode. An internal D_2O field-frequency lock, and a spectral window of 3000 Hz (16 K data points) were used. Before Fourier transformation, the spectra were zero-filled to 32 K, and resolution enhanced by an appropriate Gaussian multiplication (12). A standard computer simulation–iteration procedure was employed to obtain accurate values for spin–spin coupling constants and chemical shifts. All nuclear Overhauser enhancement experiments reported in this work were performed at 300 MHz. In addition, a two-dimensional J-resolved spectrum (13, 14) was recorded at 500 MHz on a Bruker WM-500 spectrometer[4] (sample temperature 20°C). In this experiment, we used a spectral window of 4000 Hz on the chemical shift axis (16 K data points), and 15.6 Hz on the J axis (256 data points).

[3]NMR facility at the Eindhoven University of Technology.

[4]Dutch National 500/200 hf nmr facility at Nijmegen, The Netherlands.

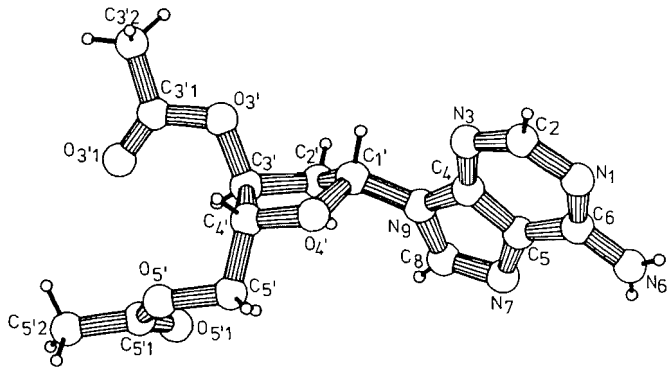

FIG. 2. Perspective drawing and atomic labelling of the 2'-deoxy-3',5'-di-*O*-acetyl adenosine molecule.

Results and discussion

Crystal structure[5]

The atomic labelling and a perspective drawing of the 2'-deoxy-3',5'-di-*O*-acetyl adenosine molecule are given in Fig. 2. The fractional coordinates are listed in Table 1. Table 2 summarizes bond angles between non-hydrogen atoms. Table 3 lists a selected set of torsion angles describing the geometry of the furanose ring, the acetylated backbone and the base, as well as the conformation around the glycosidic bond.

Furanose and backbone conformation

The 2'-deoxyribofuranose ring is found in the $C_{2'}$—endo envelope (^2E) conformation; the phase angle and amplitude of pseudorotation (15) are 156.0(6)° and 31.1(4)°, respectively. The furanose pucker deviates slightly from the standard South pucker. The bond lengths $O_{4'}$—$C_{1'}$ (1.419(2) Å) and $O_{4'}$—$C_{4'}$ (1.440(2) Å) exhibit the expected difference of approximately 0.02 Å, which is due to the anomeric effect (16). The conformation around the $C_{4'}$—$C_{5'}$ bond is γ^-, with $\gamma(O_{5'}—C_{5'}—C_{4'}—C_{3'})$ = −74.7(2)°. The acetyl geometries are as previously noted (1–4), showing short C=O bonds ($C_{3'1}$—$O_{3'1}$ = 1.186(3) Å, and $C_{5'1}$—$O_{5'1}$ = 1.204(3) Å). The glycosyl bond length N_9—$C_{1'}$ and bond angle N_9—$C_{1'}$—$O_{4'}$ are 1.451(2) Å and 108.5(1)°, respectively. The conformation around the glycosyl bond is *anti* with a value of 84.0(2)° for $\chi(O_{4'}—C_{1'}—N_9—C_8)$.

Base geometry

The values of the bond lengths and angles for the adenine base are similar to those reported for the "standard" adenine ring (17). Largest deviations were found for C_6—N_1 and C_8—N_7 (bond lengths smaller than the standard values by 0.036 and 0.051 Å, respectively), as well as for C_5—C_6 and C_5—N_7 (bond lengths greater than the standard values by 0.058 and 0.069 Å, respectively). The adenine ring is planar, the mean deviation of the nine atoms from the least-squares plane is 0.012(4) Å.

Hydrogen bonding and molecular stacking

In the structure each molecule is bonded to two molecules by intermolecular hydrogen bonds of the donor NH_2 group (Fig. 3). One hydrogen bond is between N_6 and N_7 at $(-\frac{1}{2} + x,$

[5]Bond distances, tables of structure factor amplitudes, anisotropic temperature factors of non-hydrogen atoms, hydrogen atom coordinates, as well as analyses of short intra- and intermolecular contacts and the hydrogen bond network, may be purchased from the Depository of Unpublished Data, CISTI, National Research Council of Canada, Ottawa, Ont., Canada K1A 0S2.

Can. J. Chem. Downloaded from www.nrcresearchpress.com by 80.58.250.72 on 09/07/12
For personal use only.

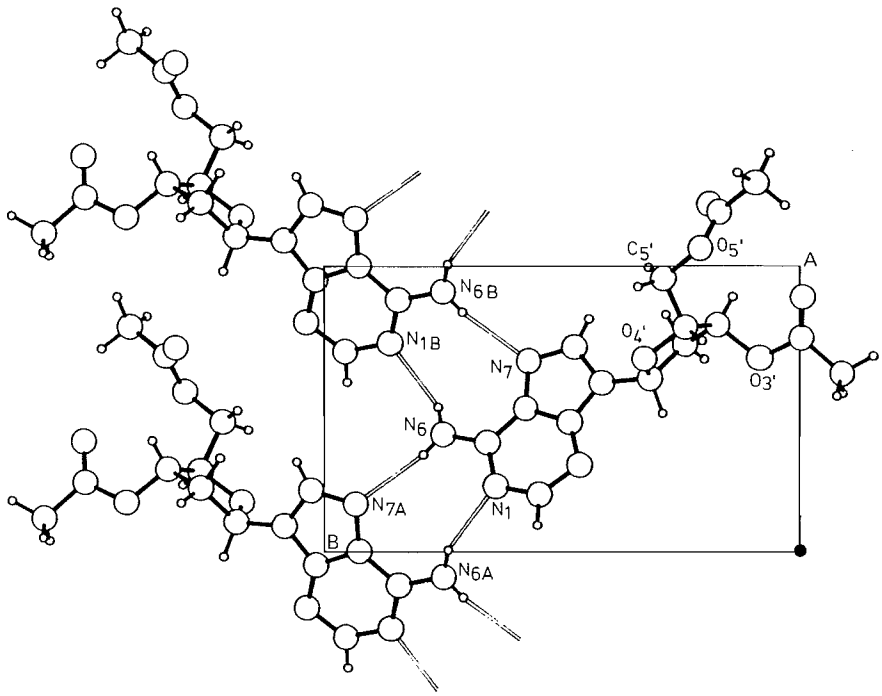

FIG. 3. Projection of a part of the structure down the *c* axis, showing the hydrogen-bonded chain in the *ab* plane. The cell origin is shown as a black dot. Some furanose and backbone atoms are labelled in the parent molecule. The others can be identified by comparison with Figs. 1 and 2. Molecule A is at $-\frac{1}{2} + x$, $1\frac{1}{2} - y$, $-z$; molecule B is at $\frac{1}{2} + x$, $1\frac{1}{2} - y$, $-z$.

TABLE 1. Refined fractional coordinates of non-hydrogen atoms, and equivalent isotropic temperature factors U_{eq} (Å^2)[a]

Atom	*x*	*y*	*z*	U_{eq}
$C_{1'}$	0.6061(3)	0.3141(1)	0.0939(1)	0.0302(5)
$C_{2'}$	0.7255(3)	0.2402(2)	0.0474(1)	0.0378(5)
$C_{3'}$	0.7923(2)	0.1706(1)	0.1184(1)	0.0305(5)
$C_{4'}$	0.7854(3)	0.2397(1)	0.1990(1)	0.0347(5)
$C_{5'}$	0.9567(4)	0.2858(2)	0.2256(2)	0.0503(6)
$C_{3'1}$	0.7466(3)	−0.0034(2)	0.1604(1)	0.0394(5)
$C_{3'2}$	0.6205(5)	−0.0907(2)	0.1631(2)	0.0610(8)
$C_{5'1}$	1.1886(3)	0.1665(2)	0.2183(2)	0.0439(6)
$C_{5'2}$	1.2914(4)	0.0909(3)	0.2689(2)	0.0730(10)
C_2	0.2013(3)	0.5453(2)	0.1027(2)	0.0397(5)
C_4	0.4543(2)	0.4821(1)	0.0646(1)	0.0266(4)
C_5	0.5027(2)	0.5745(1)	0.0257(1)	0.0294(4)
C_6	0.3828(2)	0.6562(1)	0.0285(1)	0.0300(5)
C_8	0.7163(3)	0.4721(1)	0.0121(2)	0.0375(5)
$O_{3'}$	0.6760(2)	0.0832(1)	0.1259(1)	0.0380(4)
$O_{4'}$	0.6752(2)	0.3259(1)	0.1781(1)	0.0453(4)
$O_{5'}$	1.0624(2)	0.2075(1)	0.2650(1)	0.0471(5)
$O_{3'1}$	0.8904(3)	−0.0064(2)	0.1858(2)	0.0673(6)
$O_{5'1}$	1.2166(3)	0.1880(2)	0.1440(1)	0.0607(6)
N_1	0.2308(2)	0.6392(1)	0.0681(1)	0.0367(5)
N_3	0.3042(2)	0.4623(1)	0.1041(1)	0.0363(5)
N_6	0.4120(3)	0.7500(1)	−0.0064(2)	0.0432(5)
N_7	0.6677(2)	0.5672(1)	−0.0070(1)	0.0369(5)
N_9	0.5914(2)	0.4160(1)	0.0548(1)	0.0303(4)

[a] U_{eq} = (1/3)(trace of diagonalized *U*).

TABLE 2. Bond angles (deg)

Bonds	Angle	Bonds	Angle
$C_{3'}$—$O_{3'}$—$C_{3'1}$	114.9(2)	N_7—C_8—N_9	113.2(2)
$C_{1'}$—$O_{4'}$—$C_{4'}$	110.4(1)	$C_{2'}$—$C_{1'}$—$O_{4'}$	105.9(2)
$C_{5'}$—$O_{5'}$—$C_{5'1}$	118.0(2)	$C_{2'}$—$C_{1'}$—N_9	114.8(2)
C_2—N_1—C_6	118.5(2)	$O_{4'}$—$C_{1'}$—N_9	108.5(1)
C_4—N_3—C_2	111.1(2)	$C_{3'}$—$C_{2'}$—$C_{1'}$	103.7(1)
C_5—N_7—C_8	104.3(2)	$O_{3'}$—$C_{3'}$—$C_{2'}$	107.8(1)
$C_{1'}$—N_9—C_4	125.2(2)	$O_{3'}$—$C_{3'}$—$C_{4'}$	111.4(1)
$C_{1'}$—N_9—C_8	128.3(2)	$C_{2'}$—$C_{3'}$—$C_{4'}$	103.6(1)
C_4—N_9—C_8	105.9(1)	$O_{4'}$—$C_{4'}$—$C_{3'}$	106.6(1)
N_3—C_2—N_1	128.8(2)	$O_{4'}$—$C_{4'}$—$C_{5'}$	106.3(1)
N_9—C_4—N_3	127.4(1)	$C_{3'}$—$C_{4'}$—$C_{5'}$	114.7(2)
N_9—C_4—C_5	105.9(1)	$C_{4'}$—$C_{5'}$—$O_{5'}$	110.0(2)
N_3—C_4—C_5	126.7(1)	$O_{3'}$—$C_{3'1}$—$O_{3'1}$	122.7(2)
C_4—C_5—C_6	116.7(1)	$O_{3'}$—$C_{3'1}$—$C_{3'2}$	111.5(2)
C_4—C_5—N_7	110.6(1)	$O_{3'1}$—$C_{3'1}$—$C_{3'2}$	125.8(3)
C_6—C_5—N_7	132.6(1)	$O_{5'}$—$C_{5'1}$—$O_{5'1}$	124.2(2)
N_1—C_6—C_5	118.2(1)	$O_{5'}$—$C_{5'1}$—$C_{5'2}$	111.8(2)
N_1—C_6—N_6	118.5(2)	$O_{5'1}$—$C_{5'1}$—$C_{5'2}$	124.0(3)
C_5—C_6—N_6	123.3(2)		

$1\frac{1}{2} - y$, $-z$) with N...N 3.033(2), H...N 2.26(3) Å, and N—H...N 170(3)°, the other one involves N_6 and N_1 at ($\frac{1}{2} + x$, $1\frac{1}{2} - y$, $-z$) with N...N 3.014(3), H...N 2.23(3) Å, and N—H...N 149(2)°. The hydrogen-bond accepting molecules are one translation apart along the *a* axis and this results in a one-dimensional chain of hydrogen-bonded molecules, approximately parallel the *ab* plane, propagating along the *a* direction (Fig. 3). In addition there are three weak C—H...O contacts involving the polar carbonyl O atoms of the acetyl side chains. One contact is intramolecular, $C_{3'}$—H...$O_{3'1}$ with C...O 2.622(3), H...O 2.16(3) Å, and C—H...O 112(2)°. The other two are intermolecular, $C_{5'}$—H...$O_{3'1}$ at ($2 - x$, $\frac{1}{2} + y$, $\frac{1}{2} - z$) and $C_{1'}$—H...$O_{5'1}$ at ($1 - x$, y, z) with C...O, H...O, and C—H...O 3.236(4), 2.57(3) Å, 131(2)° and 3.521(3) Å, 2.57(2) Å, 157(1)°, respectively.

It has been reported (1, 2, 4) that acetyl groups play an important role in the stacking of acetyl-substituted nucleosides in that the polar carbonyl group takes up important stacking

Can. J. Chem. Downloaded from www.nrcresearchpress.com by 80.58.250.72 on 09/07/12
For personal use only.

TABLE 3. Selected torsion angles (deg)

Bonds	Angle	Bonds	Angle
($C_{4'}$—$O_{4'}$—$C_{1'}$—$C_{2'}$)	−21.4(2)	(C_8—N_9—$C_{1'}$—$O_{4'}$)	84.0(2)
($O_{4'}$—$C_{1'}$—$C_{2'}$—$C_{3'}$)	31.0(2)	($C_{1'}$—N_9—C_8—N_7)	−172.5(2)
($C_{1'}$—$C_{2'}$—$C_{3'}$—$C_{4'}$)	−28.4(2)	(C_5—N_7—C_8—N_9)	0.7(3)
($C_{2'}$—$C_{3'}$—$C_{4'}$—$O_{4'}$)	16.4(2)	(C_8—N_7—C_5—C_4)	0.1(2)
($C_{1'}$—$O_{4'}$—$C_{4'}$—$C_{3'}$)	3.0(2)	(N_9—C_4—C_5—N_7)	−0.7(2)
($C_{3'1}$—$O_{3'}$—$C_{3'}$—$C_{2'}$)	155.7(2)	(C_8—N_9—C_4—C_5)	1.1(2)
($C_{3'}$—$O_{3'}$—$C_{3'1}$—$C_{3'2}$)	−178.0(2)	(C_2—N_3—C_4—C_5)	−0.6(3)
($C_{3'}$—$O_{3'}$—$C_{3'1}$—$O_{3'1}$)	2.9(3)	(C_4—N_3—C_2—N_1)	0.2(4)
($C_{3'}$—$C_{4'}$—$C_{5'}$—$O_{5'}$)	−74.7(2)	(C_6—N_1—C_2—N_3)	0.1(4)
($C_{5'1}$—$O_{5'}$—$C_{5'}$—$C_{4'}$)	102.8(2)	(C_2—N_1—C_6—C_5)	−0.1(3)
($C_{5'}$—$O_{5'}$—$C_{5'1}$—$C_{5'2}$)	177.2(2)	(C_4—C_5—C_6—N_1)	−0.2(2)
($C_{5'}$—$O_{5'}$—$C_{5'1}$—$O_{5'1}$)	−2.7(4)	(C_2—N_1—C_6—N_6)	179.7(2)

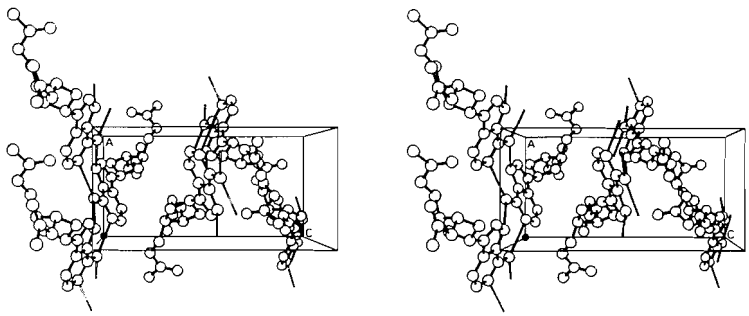

FIG. 4. Stereo view of the unit cell down the *b* axis. The cell origin is indicated by a black dot. The left of the cell also shows the hydrogen-bonded chain along *a*. Hydrogen atoms have been omitted for clarity.

positions in relation to neighbouring base rings. The stacking force involved in such an approach could be due to the polarization of the ring system by the polar carbonyl group (18). In the present structure there is a very close contact of 3.180(3) Å between the carbonyl $O_{5'1}$ and C_8 of a neighbouring base at $(\frac{1}{2} + x, \frac{1}{2} - y, -z)$, substantially to one side of the ring system. Though the $O_{3'1}$ acetyl group is one atom shorter and should therefore show less flexibility in bending toward a neighbouring ring (2) there are contacts of 3.419(3) and 3.612(3) Å with C_2 and N_3, respectively, of a base ring at $(1 - x, -\frac{1}{2} + y, \frac{1}{2} - z)$ and of 3.503(3) and 3.596(3) Å with C_5 and N_7 respectively of a base ring at $(\frac{1}{2} + x, \frac{1}{2} - y, -z)$. So, both $O_{3'1}$ and $O_{5'1}$ are bent toward the same base ring and $O_{3'1}$ is stacked between two different base rings. A stereo view of the contents of the unit cell is given in Fig. 4. Note that Fig. 4 also provides a stereoscopic view of the hydrogen-bonded chain that propagates in the *a* direction.

Conformation in solution

$C_{4'}$—$C_{5'}$ conformation

In solution, rapid interconversion between the three staggered rotamers γ^+, γ^t, and γ^- (Fig. 5) yields weighted time-averaged coupling constants $J_{4'5'}$ and $J_{4'5''}$ which are related to the individual rotamers and their populations $x(\gamma^+)$, $x(\gamma^t)$, and $x(\gamma^-)$:

$$^3J_{4'5'(5'')} = x(\gamma^+)J^{\gamma^+}_{4'5'(5'')} + x(\gamma^t)J^{\gamma^t}_{4'5'(5'')} + x(\gamma^-)J^{\gamma^-}_{4'5'(5'')}$$

with $x(\gamma^+) + x(\gamma^t) + x(\gamma^-) = 1$. The rotamer populations were obtained with the help of the empirically generalized Karplus equation developed by Altona *et al.* (19), from which $J_{4'5'}$ and $J_{4'5''}$ in the various rotamers can be calculated. Table 4 lists the proton–proton torsion angles in γ^+, γ^t, and γ^-,

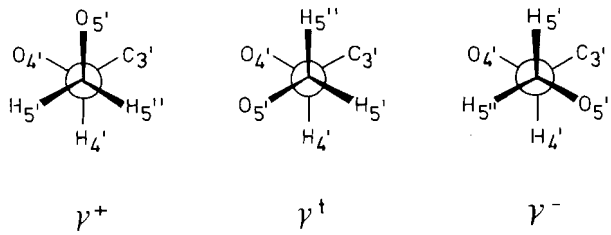

FIG. 5. Newman projection of the three staggered rotamers around the $C_{4'}$—$C_{5'}$ bond.

and the corresponding calculated coupling constants (20). The assignment of $H_{5'}$ and $H_{5''}$ was accomplished with variable temperature ^{1}H nmr at 300 MHz (21), and is found to agree with the Remin and Shugar rule (22). From the experimental data (Table 5), $J_{4'5'} = 3.8$ Hz and $J_{4'5''} = 4.3$ Hz, one calculates in this way: $x(\gamma^+) = 0.56$, $x(\gamma^t) = 0.28$, and $x(\gamma^-) = 0.16$. Thus, the γ^+ rotamer is clearly dominant in aqueous solution.

$C_{1'}$—N_9 conformation

The conformation around the $C_{1'}$—N_9 bond can be described in terms of a *syn* ⇄ *anti* equilibrium of the adenine base, on the basis of the relative Overhauser enhancements of the H_8 resonance, obtained by selective irradiation of $H_{1'}$, $H_{2'}$, and $H_{3'}$. Using the method of Guéron *et al.* (23, 24), it can be concluded from the experimental data $f_8\{1'\} = 0.10$, $f_8\{2'\} = 0.12$, and $f_8\{3'\} = 0.05$, that the contributions of the *syn* and *anti* conformations are roughly equal. This result is not surprising, since it is known that purine bases correspond with a marked rotational flexibility around the glycosidic bond. Pyrimidine bases, on the other hand, usually show a strong preference for the *anti* orientation of the base, since unfavorable

Can. J. Chem. Downloaded from www.nrcresearchpress.com by 80.58.250.72 on 09/07/12
For personal use only.

TABLE 4. Proton–proton torsion angles and calculated coupling constants[a]

$C_{4'}$—$C_{5'}$ conformation	$\phi[H_{4'}—C_{4'}—C_{5'}—H_{5'}]$ (deg)	$J_{4'5'}$ (Hz)	$\phi[H_{4'}—C_{4'}—C_{5'}—H_{5''}]$ (deg)	$J_{4'5''}$ (Hz)
γ^+	−64	2.4	55	1.3
γ^t	64	2.6	−178	10.5
γ^-	174	10.6	−68	3.8

[a]Calculated according to refs. 19 and 20.

TABLE 5. Vicinal coupling constants (in Hz) between the protons of the backbone and the 2′-deoxyribofuranose ring, measured in aqueous solution at 20°C

Atoms	^3J	Atoms	^3J
1′2′	6.8	3′4′	2.9
1′2″	6.3	4′5′	3.8
2′2″	−14.1	4′5″	4.3
2′3′	6.8	5′5″	−12.6
2″3′	3.5		

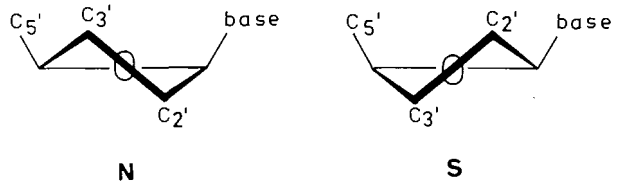

FIG. 6. Standard N (phase angle of pseudorotation 0°) and S (phase angle of pseudorotation 180°) conformations of the 2′-deoxyribofuranose ring in nucleosides and nucleotides.

steric interactions between the C=O group at the 2-position of the base, and the furanose ring exist in the *syn* conformation (25).

Furanose conformation

The conformation of the furanose ring was determined with the PSEUROT method (26), which yields a quantitative picture of the solution conformation of the sugar ring in nucleosides and nucleotides. The procedure is based on the fact that the furanose ring is involved in a rapid conformational equilibrium between two states, which are denoted North (N) and South (S), see Fig. 6. The PSEUROT algorithm calculates the best fit of P_N, P_S (the phase angles of pseudorotation in the N and S forms), $\nu_{max,N}$, $\nu_{max,S}$ (the pucker amplitudes in the N and S forms), and the mole fraction of one of the participating conformers, to the experimental vicinal spin–spin couplings between the ring protons. The procedure was run in two ways, on the basis of the experimental data, listed in Table 5. First, $\nu_{max,N}$ and $\nu_{max,S}$ were assumed to be equal to 31°, i.e. the pucker amplitude for 2′-deoxy-3′,5′-di-*O*-acetyl adenosine in the crystalline state, yielding $P_N = 10°$, $P_S = 160°$, and 0.68 for the mole fraction of the S conformer. The rms error is 0.22. Secondly, the program was run under the assumption that one of the participating sugar conformations equals the crystal structure, i.e. $P_S = 156°$, and $\nu_{max,S} = 31°$. This results in $P_N = -40°$, $\nu_{max,N} = 40°$, and again a mole fraction of 0.68 for the S conformer. In this case, an rms error of 0.15 is achieved. Based on these results, it can be concluded that the furanose ring conformation in solution represents an equilibrium between an N conformer with $P \approx -40°$, and an S conformer as is found in the crystal structure. Presumably, the N conformer is slightly more puckered than its S counterpart.

Conclusion

The crystal structure of 2′-deoxy-3′,5′-di-*O*-acetyl adenosine consists of peculiar one-dimensional chains by virtue of intermolecular N_6—H...N_1 and N_6—H...N_7 hydrogen bonds. Obviously, the participation of the imidazole nitrogen N_7 in the hydrogen bonding scheme is essential in realizing this compact and complex structure, which differs markedly from the parallel base–base dimer that was encountered in the crystal structure of 3′,5′-di-*O*-acetyl thymidine. Comparison of the solution conformation of 2′-deoxy-3′,5′-di-*O*-acetyl adenosine with the X-ray structure reveals a close correspondence with respect to the structure of the 2′-deoxyribofuranose ring, and the glycosidic conformation. In the solid state, the sugar ring resides in an S-type conformation, which is also dominant in solution. The glycosidic conformation is *anti* in the solid state, which agrees well with experimental NOE data, obtained in solution. However, a remarkable anomaly is found for the $C_{4'}$—$C_{5'}$ conformation, which is in the very rare γ^- conformation in the solid state (20), and predominantly γ^+ in solution. The γ^+ conformation is commonly encountered for nucleosides and nucleotides, since a favorable *gauche* effect interaction exists between $O_{5'}$ and $O_{1'}$, as well as a stabilizing electrostatic attraction between $O_{5'}$ and the base proton H_8. Detailed examination of the crystal structure of 2′-deoxy-3′,5′-di-*O*-acetyl adenosine reveals that the γ^- conformation allows a favorable intermolecular stacking of $O_{5'1}$ and an adenine ring. Therefore, the present structural study adds another example to the growing number of compounds showing different conformations in the solid state and in solution.

1. J. N. LOW and C. C. WILSON. Acta Crystallogr. C**40**, 1030 (1984).
2. C. C. WILSON, J. N. LOW, P. TOLLIN, and H. R. WILSON. Acta Crystallogr. C**40**, 1712 (1984).
3. L. H. KOOLE, M. H. P. VAN GENDEREN, H. FRANKENA, H. J. M. KOCKEN, J. A. KANTERS, and H. M. BUCK. Proc. Kon. Ned. Akad. van Wetensch. **89**, 51 (1986).
4. C. C. WILSON, J. N. LOW, and P. TOLLIN. Acta Crystallogr. C**41**, 1123 (1985).
5. Patent Research Corp. Brit. 1,473,148 (Cl. C07D239/52) Appl. 74/40,175 (1977).
6. W. ANDERSEN, D. H. HAYES, A. M. MICHELSON, and A. R. TODD. J. Am. Chem. Soc. **21**, 1882 (1954).
7. G. M. SHELDRICK. SHELXS84. Program for crystal structure solution. University of Göttingen, Federal Republic of Germany.
8. D. T. CROMER and J. B. MANN. Acta Crystallogr. A**24**, 321 (1968).
9. R. F. STEWART, E. R. DAVIDSON, and W. T. SIMPSON. J. Chem. Phys. **42**, 3175 (1965).
10. G. M. SHELDRICK. SHELX76. Program for crystal structure determination. University of Cambridge, England.

Can. J. Chem. Downloaded from www.nrcresearchpress.com by 80.58.250.72 on 09/07/12
For personal use only.

11. A. L. SPEK. EUCLID. Computational crystallography. *Edited by* D. Sayre. Oxford, Clarendon Press. 1982. p. 528.
12. R. R. ERNST. Advances in magnetic resonance. Vol. 2. *Edited by* J. S. Waugh. Academic Press, New York. 1966, pp. 1–125.
13. W. P. AUE, J. KARHAN, and R. R. ERNST. J. Chem. Phys. **64**, 4226 (1976).
14. K. NAGAYAMA, K. WÜTHRICH, P. BACKMANN, and R. R. ERNST. Biochem. Biophys. Res. Commun. **78**, 99 (1977).
15. C. ALTONA and M. SUNDARALINGAM. J. Am. Chem. Soc. **94**, 8205 (1972).
16. A. J. KIRBY. The anomeric effect and related stereoelectronic effects at oxygen. Springer Verlag, Berlin. 1983.
17. R. TAYLOR and O. KENNARD. J. Am. Chem. Soc. **104**, 3209 (1982).
18. C. C. WILSON, J. N. LOW, and D. W. YOUNG. Acta Crystallogr. C**39**, 1103 (1983).
19. C. A. G. HAASNOOT, F. A. A. M. DE LEEUW, H. P. M. DE LEEUW, and C. ALTONA. Recl. Trav. Chim. Pays-Bas, **98**, 576 (1979).
20. H. P. M. DE LEEUW, C. A. G. HAASNOOT, and C. ALTONA. Isr. J. Chem. **20**, 108 (1980).
21. C. ALTONA. Recl. Trav. Chim. Pays-Bas, **101**, 413 (1982).
22. M. REMIN and D. SHUGAR. Biochem. Biophys. Res. Commun. **48**, 636 (1972).
23. S. TRAN-DINH, W. GUSCHLBAUER, and M. GUÉRON. J. Am. Chem. Soc. **94**, 7903 (1972).
24. L. H. KOOLE, R. J. L. VAN KOOYK, and H. M. BUCK. J. Am. Chem. Soc. **107**, 4032 (1985).
25. J. J. C. VAN LIER, L. H. KOOLE, and H. M. BUCK. Recl. Trav. Chim. Pays-Bas, **102**, 148 (1983).
26. F. A. A. M. DE LEEUW and C. ALTONA. J. Chem. Soc. Perkin Trans. II. 375 (1982), and Quantum Chemistry Program Exchange Program 463.
27. D. B. DAVIES and H. B. E. DIXON. IUPAC-IUB discussion draft on abbreviations and symbols for the description of polynucleotide chains. Document J.C.B.N. 14.2 (1980).

Can. J. Chem. Downloaded from www.nrcresearchpress.com by 80.58.250.72 on 09/07/12
For personal use only.

FOR ERRATA SEE
v. 65 #9 1987 P. 2316

Preparation[1] of (4*R*,5*S*)-(5-methyl-2,2-dimethyl-1,3-dioxolane-4-ylmethyl)-phosphonium iodide. A synthetic approach to olguine: further model studies

SERAFIN VALVERDE, BERNARDO HERRADON, ROSA M. RABANAL,[2] AND MANUEL MARTIN-LOMAS
Instituto de Química Orgánica, C.S.I.C., Juan de la Cierva 3, Madrid 28006, Spain

Received May 13, 1986

SERAFIN VALVERDE, BERNARDO HERRADON, ROSA M. RABANAL, and MANUEL MARTIN-LOMAS. Can. J. Chem. **65**, 332. (1987).

The enantiomerically pure title compound ((4*R*,5*S*)-(5-methyl-2,2-dimethyl-1,3-dioxolane-4-ylmethyl)-phosphonium iodide) has been synthesized starting from (*R*,*R*)-(+)-tartaric acid. The synthesis of an olguine analog has been carried out. Attempts have been made to improve the stereoselectivity and yield of key steps.

SERAFIN VALVERDE, BERNARDO HERRADON, ROSA M. RABANAL et MANUEL MARTIN-LOMAS. Can. J. Chem. **65**, 332 (1987).

Utilisant l'acide (+)-tartrique-(*R*,*R*) comme produit de départ, on a réalisé la synthèse du composé mentionné dans le titre (l'iodure du (méthyl-5 diméthyl-2,2 dioxolane-1,3 yl-4 méthyl)-(4*R*,5*S*) phosphonium) sous une forme énantiomèrement pure. On a réalisé une synthèse d'un analogue olguine. On a fait des essais dans le but d'améliorer la stéréosélectivité et le rendement des étapes clés.

[Traduit par la revue]

Introduction

The synthesis of enantiomerically pure compounds has become one of the main concerns of organic chemists. In connection with our planned synthesis of olguine we were confronted with the need of preparing an enantiomerically pure phosphonium salt. Tartaric acid is one of the few compounds both enantiomers of which occur abundantly in nature in a readily isolable form. It has found wide application in this type of synthesis (1, 2). In the following, we describe our efforts to use (*R*,*R*)-(+)-tartaric acid for the synthesis of the required phosphonium salt.

There are numerous natural products containing an α,β-unsaturated lactone structure (3). Examples are the α,β-unsaturated δ-lactones olguine **1** and anamarine **2**, which have been isolated from an unclassified Hyptis species (4, 5), or asperlin **3**, an antibiotic isolated from *Aspergillus nidulans* (6).

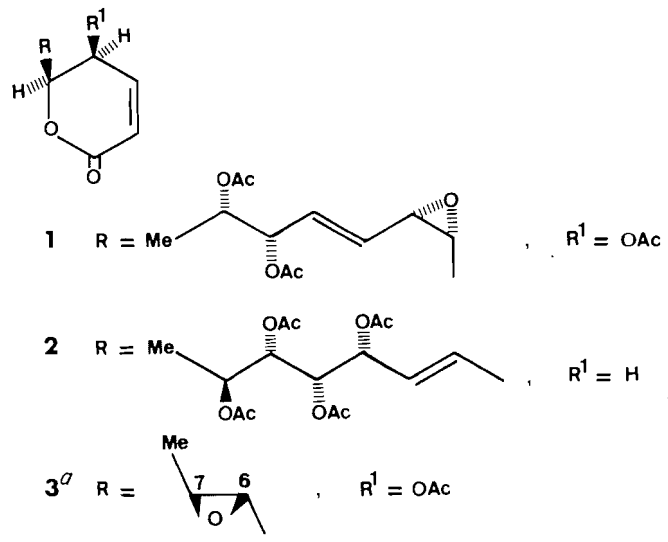

[a]The stereochemistry indicated (6*S*,7*R*) for the oxirane ring has been assigned by synthesis (ref. 27)

[1]For part 1 of this series, see ref. 2.

[2]Present address: Departamento de Farmacología y Farmacognosia, Facultad de Farmacia, La Laguna, Tenerife, Spain.

Printed in Canada / Imprimé au Canada

The synthesis of these substances from carbohydrate precursors could be envisaged (7). We had previously made some synthetic efforts, directed towards the preparation of the side chain of these compounds (8), which have now been completed with the construction of the side chain of olguine **1**, using the same model compound.

Results and discussion

Compound **4** (see Scheme 1) was prepared from D-galactose using standard literature procedures (9). The oxidation step was carried out with PCC (pyridinium chlorochromate) in the presence of molecular sieves (10), and 82% of isolated product **4** was obtained. To achieve a two carbon atom chain extension, a Wittig olefination reaction appeared as most appropriate. In the case of compound **1** a *cis* stereoselectivity was desirable.

We have partly achieved this goal using the phosphorane derived from (1,3-dioxolan-2-ylmethyl)triphenylphosphonium bromide (8), which yielded a *Z*/*E* olefin mixture in a 7:3 ratio. Better results were obtained when compound **4** was reacted with methoxycarbonyltriphenylphosphorane (11) in methanol to give compound **5** in a 20:1 *Z*/*E* ratio. Both isomers were separated by flash chromatography. Compound **5** (*Z* isomer) was subjected to reduction with DIBAH (diisobutylaluminum hydride) at 0°C, affording alcohol **6** (8) in 87% yield. Almost the same yield (84%) was obtained when the reduction was carried out with $LiAlH_4$ in THF at −20°C.

The next step consisted in an epoxidation of compound **6**. It was important to achieve a good degree of stereoselectivity. With this aim in mind we essayed a variety of conditions, which have been collected in Table 1. The stereoselectivity obtained was only moderate, except in the case of asymmetric epoxidation (entry 7), which yielded a single isomer. It is also obvious that opposite results were obtained using *m*-CPBA (*m*-chloroperbenzoic acid) and TBHP (*tert*-butylhydroperoxide).

The oxidation of these epoxy-alcohols, **7** and **8**, was carried out separately using PCC/molecular sieves, with excellent yields, 92% in the case of **7** and 96% in the case of **8**.

At this point it was important to prepare a four carbon fragment and to establish adequate conditions to carry out the second extension of the side chain present in olguine **1**. The reaction of the dimethyl ester of L-(+)-tartaric acid **11** with benzaldehyde afforded (12) the corresponding benzylidene

Can. J. Chem. Downloaded from www.nrcresearchpress.com by 80.58.250.72 on 09/07/12
For personal use only.

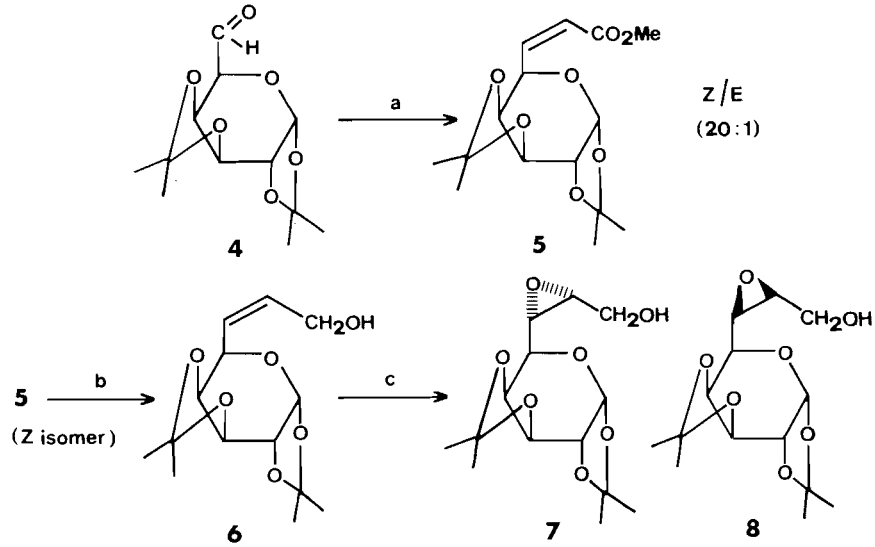

(a) $Ph_3P{=}CHCO_2Me$, MeOH
(b) DIBAH, Et_2O or $LiAlH_4$, THF, −20°C
(c) conditions collected in Table 1

SCHEME 1

TABLE 1. Reaction conditions for the epoxidation of compound **6**

Reagents (equiv.)	Solvents	T (°C)	Time	Catalyst (mequiv.)	Yield:7 (%)	Yield:8 (%)
1 *m*CPBA (1.7)	CH_2Cl_2	0	52 h	—	21	50
2 *m*CPBA (1.5)	CH_2Cl_2	Room temp.	5 h	—	20	60[a]
3 *m*CPBA (1.7)	$CHCl_3$	20	40 h	—	38	34
4 TBHP (7.3)	CH_2Cl_2	0	82 h	$VO(acac)_2$ (7.0)	66	16
5 TBHP (8.0)	CH_2Cl_2	0	148 h	$Mo(CO)_6$ (5.0)	—	—
6 TBHP (2.0)	CH_2Cl_2	15	40 h	$VO(acac)_2$ (5.0)	59	39
7 TBHP	CH_2Cl_2	−20	31 d	L-(+)-DET $Ti(i\text{-}Pro)_4$	—	60[b]

[a]Data taken from ref. 8.
[b]Sharpless asymmetric epoxidation conditions (24).

acetal **12** with good yield (see Scheme 2). Next we carried out the $LiAlH_4$ reduction to the corresponding diol **13**, obtaining a disappointing low yield. Attempted monotosylation of **13**, under phase transfer conditions (13), was even more discouraging since, although the corresponding monotosylate could be detected in the reaction medium (^1H nmr and tlc), it reacted further during the chromatographic separation, leading to a complex mixture of compounds, none of which could be identified. It was decided then to modify our synthetic scheme to that represented in Scheme 3. In this new approach the unstability of the benzylidene group of **12** under reductive conditions was avoided, by preparing the acetonide derivative **14** instead. Compound **14** was prepared as previously described (14) (see Scheme 3) in good yield (90%). The $LiAlH_4$ reduction of **14** occurred as predicted (15, 16), with good yield (77%), leading to diol **15**. Tosylation of **15**, under phase transfer conditions, afforded the monotosylate derivative **17** (17) (89%) and a small amount of the corresponding ditosylate **16** (3.6%). Reductive displacement of the tosyl group was achieved using $NaBH_4$ in acetonitrile as solvent under reflux conditions. The alcohol **18** was obtained in good yield (69%).[3]

Using other solvents (HMPTA; HMPTA/DMF) led to zero or low yield of **18**. There was no formation of **18** when the reduction was attempted with $NaBH_4$ in toluene–water under phase transfer conditions (18).

The steps leading from **18** to the final product **21** are depicted in Scheme 4.

The monotosyl derivative was prepared from **18** using standard procedures but the substitution of this group by halogen appeared rather sluggish under a variety of conditions. To overcome this difficulty we decided to prepare the mesyl derivative instead. The reaction of **18** with mesyl chloride in THF and a slight excess of triethylamine gave compound **19** in excellent yield (96%). Refluxing an anhydrous acetone solution of **19** in the presence of NaI gave, after three days, compound

[3]The same reaction in DMF led to the formation of **18** in moderate yield only (40%).

Can. J. Chem. Downloaded from www.nrcresearchpress.com by 80.58.250.72 on 09/07/12
For personal use only.

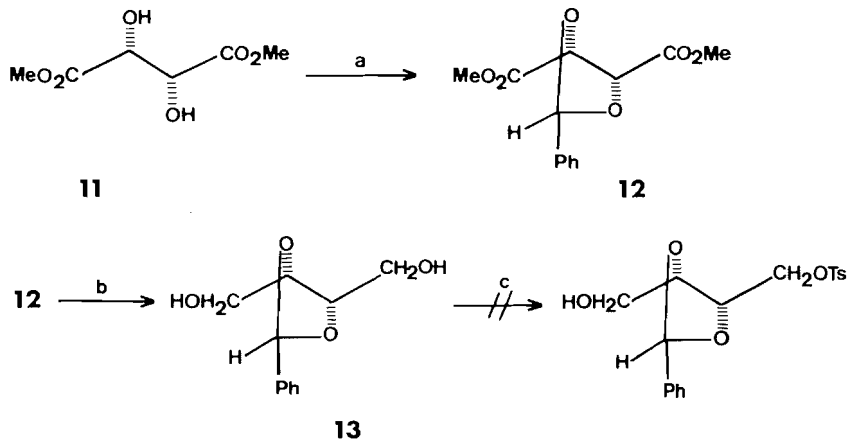

(a) PhCHO, TsOH, C_6H_6; (b) $LiAlH_4$, THF; (c) TsCl, $(n\text{-}Bu)_4NHSO_4$, NaOH, H_2O

SCHEME 2

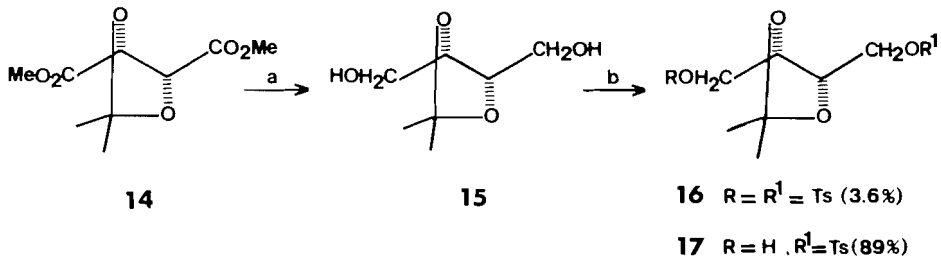

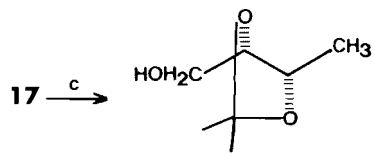

(a) $LiAlH_4$, THF; (b) TsCl, $(n\text{-}Bu)_4NHSO_4$, NaOH, H_2O; (c) $NaBH_4$, CH_3CN

SCHEME 3

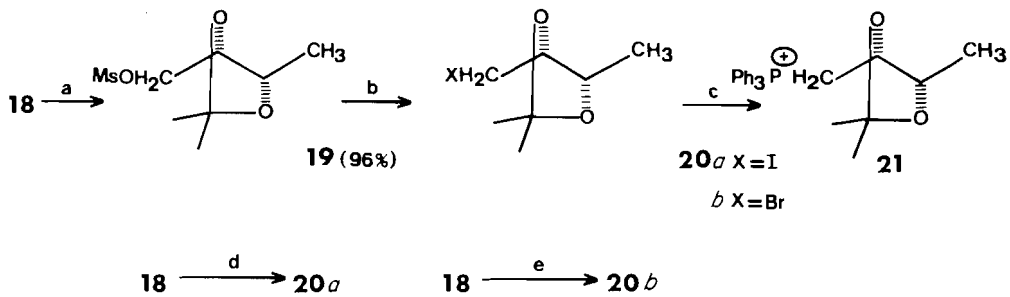

(a) MsCl, C_6H_5N; (b) NaI, CH_3COCH_3; (c) Ph_3P, CH_3CN or Ph_3P (neat); (d) I_2, Ph_3P, $C_3H_4N_2$, C_6H_6, or Ph_3P, $C_3HI_3N_2$(TII); (e) $ZnBr_2$, Ph_3P, DEAD, THF

SCHEME 4

20*a* in 45% yield. Compound **20***a* was relatively volatile and this fact may account, in part, for the moderate yield obtained since some of the product may be lost during the isolation procedure.

Compound **20***a* could be prepared directly from **18** by treatment with triiodoimidazol and triphenylphosphine in toluene solution (19). In this method the amount of toluene used was critical since an excess of solvent increases the coevaporation of **20***a* and causes fluctuation of the isolated **20***a*, 77% being the best yield we managed to obtain. Another more reproducible method of preparing **20***a* was by the reaction of **18** with triphenylphosphine, imidazole, and iodine in benzene solution, according to the method described by Ley and co-workers (20).

The corresponding bromide derivative **20***b* was also prepared

Can. J. Chem. Downloaded from www.nrcresearchpress.com by 80.58.250.72 on 09/07/12
For personal use only.

TABLE 2. Reaction conditions for the Wittig condensation of the aldehyde **9** and the phosphonium salt **21**

	21:**9** (Molar ratio)	Base (equiv.)	Solvent	*T* (°C)	Total yield (%)	*E*/*Z* (ratio)
1.	1.0	LDA (1.1)	THF	−70–0	15	1:1
2.	1.7	LHMDS (1.7)	THF/HMPTA (6:1)	−70–0	90	1:5
3.	1.5	LHMDS (1.6)	THF/HMPTA (28:1)	−70–0	40	1:1
4.	1.1	K*t*-BuO	THF	0–room temp.	—	—

TABLE 3. Reaction conditions for the Wittig condensation of aldehyde **10** and the phosphonium salt **21**

	21:**10** (Molar ratio)	Base (equiv.)	Solvent	*T* (°C)	Total yield (%)	*E*/*Z* (ratio)
1.	1.3	*n*-Bu Li (3.0)	THF	−70–room temp.	—	—
2.	1.1	LDA (1.1)	THF	−70–room temp.	40	2:3
3.	1.3	LDA (1.3)	THF	−70(3 h)–0	40	2:3
4.	1.0	Ethylene oxide (catalytic)	CH_2Cl_2	Room temp.	50	[a]
5.	1.0	Ethylene oxide (1.0)	CH_2Cl_2	Room temp.	—	—
6.	1.5	LiHMDS	THF/HMPTA	−70–0	79	1:3

[a] The isolated yield of *Z*-olefin was 10%. The yield of *E*-olefin (40%) was estimated from a mixture with compounds **10** and **27**.

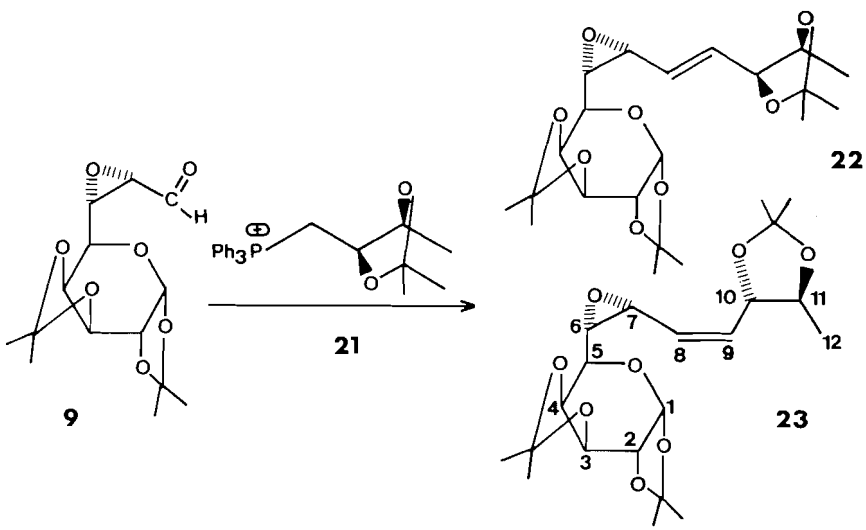

SCHEME 5

from **18** by treatment with zinc bromide and triphenylphosphine in THF solution and in the presence of DEAD (diethyl azodicarboxylate) (21).

Finally, reaction of **20***a* with triphenylphosphine in acetonitrile solution led to the formation of **21** in moderate yield (58%) with recovery of the remaining starting material (42%). When the same reaction was carried out in the absence of any solvent at 80°C (bath temperature) the yield of phosphonium salt **21** was 90%. Compound **21** is an amorphous solid, mp 71–73°C, rather hygroscopic, which was characterized by its ^{1}H nmr spectrum; $[\alpha]_D$ −35° (*c* 0.97).

Compound **21** could be used as one of the fragments required in a Wittig condensation leading to olguine (4). The reaction of the epoxy-aldehydes **9** and **10** with the phosphonium salt **21** gave a *Z* and *E* mixture of the olefins **22–25** in good yield (90% and 79% respectively) (see Tables 2 and 3, Schemes 5 and 6), when the reaction was carried out in THF/HMPTA (6:1). Unfortunately the use of these conditions (entries 2 and 6) led to mixtures of compounds of opposite stereoselectivity to the desired one.

In the case of aldehyde **9**, better *E*/*Z* ratios were achieved using the conditions specified in entries 1 and 3 (Table 2), but

Can. J. Chem. Downloaded from www.nrcresearchpress.com by 80.58.250.72 on 09/07/12
For personal use only.

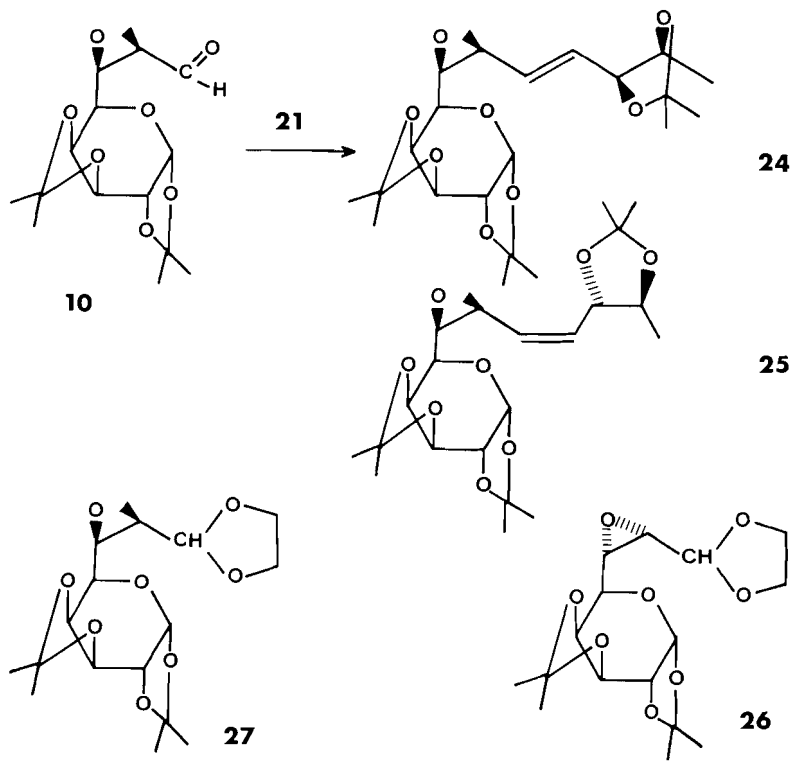

SCHEME 6

with low yield. For aldehyde **10**, the best *E*-stereoselectivity was achieved working in dichloromethane solution and with catalytic amounts of ethylene oxide (Table 3, entry 4).

Using large amounts of ethylene oxide (22) (1 equivalent or more) led to the formation of the acetals **26** and **27** as the main reaction products.

Experimental

Flash column chromatography (25) was done on silica gel 40–63 μm (Merck); tlc was carried out on plates on silica gel 60 F_{254} (Merck). The ^1H nmr spectra were measured either with a Varian 390 (90 MHz) or a Varian XL-300 (300 MHz) spectrometer and the ^{13}C nmr spectra were measured with a Bruker WP-80 (20.1 MHz) spectrometer in $CDCl_3$ solution with tetramethylsilane as internal reference. Assignments of ^{13}C nmr shifts were made with the aid of off-resonance and noise decoupled ^{13}C nmr spectra. Melting points were determined in a Kofler hot-stage apparatus. Optical rotations were measured in chloroform solution, unless otherwise stated, with a Perkin–Elmer 141 polarimeter. All the reactions with sensitive substrates were carried out under argon or nitrogen atmosphere.

Preparation of compounds 5

A solution of methoxycarbonyltriphenylphosphorane (3 mmol) in methanol (2 mL/mmol)[4] was added to aldehyde **4** (1 mmol) dissolved in the same solvent (2 mL/mmol). The mixture was stirred for 8 h at room temperature. The solvent was evaporated in the water pump and the residue subjected to flash chromatography with hexane – ethyl acetate (85:15) to yield **5** (*Z* isomer 77%; *E* isomer 3.6%), identified by its spectroscopic data (23).

Reduction of compound 5 (Z isomer)

Method A

To a cold solution (0°C) of **5** (*Z* isomer) (5.05 g, 16 mmol) in ether (90 mL) was added 56 mL of a 1.2 *M* solution of DIBAH in hexane (4.2 equiv.). The solution was stirred during 12 h and excess DIBAH was destroyed by the addition of MeOH (1 mL). The solvents were removed under vacuum and the residue purified by flash chromatography. Compound **6** (4.0 g, 87%) was isolated and identified (tlc, ^{13}C nmr, $[\alpha]_D$) with authentic material (8).

Method B

A solution of $LiAlH_4$ (505 mg, 2.2 equiv.) in THF (100 mL) was cooled at −20°C. To this solution, while stirring, was added **5** (*Z* isomer) (1.388 g, 5.93 mmol) in THF. The mixture was allowed to reach room temperature, cooled at −20°C, and then aqueous saturated Na_2SO_4 was added. The white precipitate was filtered and the solvents evaporated. Chromatography separation of the residue afforded **6** (1.42 g, 84%) and its dihydro derivative (102 mg, 6%).

Epoxidation of compound 6

A typical procedure for this transformation was the following.

With m*CPBA (see Table 1 for details)*

To a solution of the alcohol **6** in CH_2Cl_2, *m*CPBA was added. The solution was diluted and successively washed with aqueous $NaHSO_3$ and $NaHCO_3$ and, finally, with water. The residue obtained by evaporation of the solvents was purified by flash chromatography, affording compounds **7** and **8** in the yields stated in Table 1.

With TBHP

To a solution of **6** in CH_2Cl_2 the catalyst indicated in Table 1 was added, followed by a solution of TBHP in toluene (24). Excess of TBHP was destroyed by the addition of dimethyl sulphide. Evaporation of the solvents gave a residue, which was chromatographically separated to yield **7** and **8** (yields indicated in Table 1).

Preparation of compounds 8 and 10

The following procedure was applied to compounds **7** and **18** separately.

To a solution of PCC (3 equiv.) in CH_2Cl_2 (10 mL), 4 Å molecular sieves and anhydrous sodium acetate were added. After stirring for 1 h, a solution of the epoxy-alcohol (**7** or **8**) (1 equiv.) was added. Stirring was continued for 90 min, and finally the solution was diluted with ethyl ether and filtered through a short column of silica gel G. Epoxy-aldehydes **9** and **10**, identical (^1H nmr and ^{13}C nmr, $[\alpha]_D$) to

[4]Larger amounts of solvent or longer reaction times caused a lowering of the overall yield of isolated **5**, due to the formation of by-products through Michael type addition of methanol to the α,β-unsaturated ester.

Can. J. Chem. Downloaded from www.nrcresearchpress.com by 80.58.250.72 on 09/07/12
For personal use only.

Can. J. Chem. Downloaded from www.nrcresearchpress.com by 80.58.250.72 on 09/07/12
For personal use only.

those previously described (8), were obtained in 92% and 96% yield respectively.

Reduction of compound ***12***

To a suspension of $LiAlH_4$ (408 mg, 11 mmol), in dry ethyl ether, was added compound **12** (12) (2.215 g, 8 mmol). The mixture was stirred for 2 h under reflux, excess $LiAlH_4$ destroyed by the cautious addition of water and 15% aqueous NaOH, and the solids separated by filtration. Evaporation of the solvent left a complex residue, which was purified by flash chromatography affording **13** (505 mg, 30%) (26).

Attempted preparation of the monotosyl derivative of compound ***13***

A CH_2Cl_2 solution of *p*-toluenesulphonyl chloride (718 mg, 2.9 mmol) was added to a flask containing diol **13** (647 mg, 3.1 mmol), tetrabutylammonium bisulfate (84 mg, 0.25 mmol), CH_2Cl_2 (10 mL), and 15% solution of aqueous NaOH (120 mg, 3 mmol). The mixture was strongly stirred during 90 min at room temperature. The two layers were separated and the organic layer was sequentially washed with water, aqueous saturated $NaHCO_3$, water, aqueous 5% HCl, and brine. Solvents were finally dried and evaporated, yielding a residue that showed spots on tlc attributable to a tosyl derivative. Flash chromatography of this residue failed to provide any of the possible monotosylate of **13**.

Reduction of the diester ***14***

A solution of $LiAlH_4$ (29 g, 0.76 mol) in anhydrous THF was mixed with compound **14** (14) (128.5 g, 0.59 mol) under nitrogen. The mixture was refluxed during 4 h, cooled at −20°C, and a saturated aqueous Na_2SO_4 solution was added to the THF solution. The white precipitate was filtered through a Celite layer and the solids washed with abundant CH_2Cl_2–MeOH mixture (3:1). Flash chromatography of the residue obtained by evaporation of the solvents provided diol **15** (73 g) (77%), identified by its physical and spectroscopic data (15).

Monotosylation of ***15***

A CH_2Cl_2 solution of tosyl chloride (25.7 g, 135 mmol) was added to a mixture of **15** (19.8 g, 122 mmol), tetrabutylammonium bisulfate (4.3 g), 15% aqueous NaOH (35 mL, 135 mmol), and CH_2Cl_2 (500 mL). This mixture was stirred at room temperature for 45 min and worked up as described previously (see above). The ditosylate **16** (3.6%) and the monotosylate **17** (89%) were isolated and identified by comparison with previously described products (17); ^{13}C nmr δ: 145.1 (s), 132.9 (s), 130.0 (d), 128.0 (d), 110.1 (s), 78.2 (d), 74.8 (d), 69.1 (t), 61.9 (t), 27.0 (q), 26.8 (q), 21.6 (q).

$NaBH_4$ reduction of ***17***

To a solution of **17** (7.8 g, 24.7 mmol) in acetonitrile (120 mL), $NaBH_4$ (4.7 g, 124.2 mmol) was added and the mixture heated under reflux for 20 h. Once cooled in an ice bath, the solution was diluted with ethyl ether and water, and enough 5% aqueous HCl added to reach pH 6.0. The two phases were separated and the aqueous layer washed with ethyl ether. All the organic solvents were washed with brine, dried, and evaporated. The residue was formed by pure compound **18**. An analytical sample could be obtained by bulb-to-bulb distillation (bp 35–40°C/0.1 Torr (1 Torr = 133.3 Pa)); $[\alpha]_D$ +1° (*c* 2.193); ^1H nmr δ: 4.10–3.40 (m, 4H), 2.0 (br s, exchangeable with D_2O), 1.33 (s, 3H), 1.30 (s, 3H), 1.20 (d, *J* = 6 Hz, 3H); ^{13}C nmr δ: 108.5 (d), 82.9 (d), 72.9 (d), 61.5 (t), 27.4 (q), 26.9 (q), 17.6 (q); ms *m/e*: 131 (M^+ − 15). *Anal.* calcd. for $C_7H_{14}O_3$: C 57.51, H 9.65; found: C 57.38, H 9.58.

Mesylation of compound ***18***

To a cold solution (10°C) of **18** (1.95 g, 13.4 mmol) in CH_2Cl_2 (20 mL) containing anhydrous triethylamine (4.4 mL, 31.6 mmol) was added, dropwise, mesyl chloride (1.2 mL, 16 mmol) dissolved in CH_2Cl_2 (25 mL). The mixture was allowed to reach room temperature and stirred during 2 h. It was then poured over saturated aqueous $NaHCO_3$, while cooling in an ice bath. The organic layer was separated and washed with saturated aqueous ammonium chloride. After drying and evaporating the organic solvents, a residue of **19** was obtained (2.35 g, 96%) that required no further purification; thick oil, $[\alpha]_D$ −3.6° (*c* 0.283); ^1H nmr δ: 4.25 (d, *J* = 4 Hz, 2H), 4.15–3.65 (m, 2H), 3.05 (s, 3H), 1.38 (s, 3H), 1.35 (s, 3H), 1.30 (d, *J* = 6 Hz, 3H); ^{13}C nmr δ: 109.3 (s), 79.9 (d), 73.5 (d), 68.5 (t), 37.7 (q), 27.3 (q), 26.8 (q), 17.7 (q); ms *m/e*: 209 (M^+ − 15).

Preparation of ***20***a

Method A

An anhydrous acetone solution (30 mL), containing **19** (1.211 g, 5.0 mmol) and NaI (3.5 g, 25.3 mmol), was heated under reflux during three days. After cooling, water and CH_2Cl_2 were added to the medium and the two phases separated. The organic layer was washed with 10% aqueous sodium thiosulfate and brine. The solvents were dried and evaporated, yielding a residue that was purified by flash chromatography (hexane – ethyl acetate, 95:5), affording **20***a* (600 mg, 45%).

Method B

A toluene solution (180 mL) of **18** (2.316 g, 15.9 mmol), triphenylphosphine (6.3 g, 24 mmol), and triiodomidazol (5.3 g, 11.9 mmol) was stirred under reflux at a bath temperature of 120°C for 3 h, following the procedure indicatd in ref. 19. Working up and chromatography of the crude product gave **20***a* (3.13 g, 77%).[5]

Method C

To a solution of **18** (369 mg, 2.53 mmol) in 70 mL of anhydrous benzene were successively added triphenylphosphine (1.5 g, 5.7 mmol, 2.2 equiv.), imidazole (500 mg, 11.6 mmol, 4.6 equiv.), and iodine (1.4 g, 5.5 mmol, 2.1 equiv.). The mixture was refluxed for 90 min. After this time the reaction was worked up as in ref. 20. Purification by flash chromatography yielded 648 mg (80%) of **20***a*, bp 30°C/1 Torr; $[\alpha]_D$ +6.2° (*c* 0.113); ^1H nmr δ: 3.85 (m, 1H), 3.60 (m, 1H), 3.30 (d, *J* = 6 Hz, 2H), 1.50 (s, 6H), 1.40 (d, *J* = 6 Hz, 3H); ^{13}C nmr δ: 108.1 (s), 81.2 (d), 77.3 (d), 27.2 (q), 22.5 (q), 18.6 (q), 4.9 (t). *Anal.* calcd. for $C_7H_{13}O_2I$: C 33.17, H 5.25; found: C 32.83, H 5.12.

Preparation of ***21***

Method A

Compound **20***a* (2.48 g, 9.7 mmol) and triphenylphosphine (2.75 g, 10.5 mmol) in acetonitrile (60 mL) were heated at a bath temperature of 80°C under argon. After nine days, elimination of the solvent left a residue, which was chromatographed. Compound **21** (2.88 g, 58%) and starting material **20***a* (1.04 g, 42%) were thus obtained.

Method B

Compound **20***a* (1.04 g, 4.1 mmol) and triphenylphosphine (1.18 g, 4.5 mmol) were mixed and heated in an oil bath at 80°C during 50 h. Flash chromatography of the residue gave **21** (1.9 g, 90%). Compound **21** is a rather hygroscopic solid, mp 71–73°C; $[\alpha]_D$ −35° (*c* 0.097); ^1H nmr δ: 7.95–7.65 (m, 15H), 4.45–4.25 (m, 2H), 4.05–3.95 (m, 1H), 1.25 (s, 3H), 1.15 (s, 3H). *Anal.* calcd. for $C_{25}H_{28}O_2P$: C 57.92, H 5.44; found: C 55.84, H 5.25.

Preparation of ***20***b

The alcohol **18** (552 mg, 3.8 mmol) and triphenylphosphine (3.0 g, 11.4 mmol) were dissolved in anhydrous THF (25 mL) under argon. Anhydrous zinc bromide (860 mg, 3.8 mmol) in THF (40 mL) and diethyl azidodicarboxylate (DEAD) (1.8 mL, 11.4 mmol) in THF (12 mL) were added consecutively. The mixture was stirred for 44 h, the solvents were removed, and the residue was chromatographed to yield 430 mg (55%) of **15***b*;[6] ^1H nmr δ: 4.1–3.6 (m, 2H), 3.45 (d, *J* = 5 Hz, 2H), 1.35 (s, 6H), 1.30 (d, *J* = 6 Hz, 3H).

Wittig condensation of the epoxyaldehyde ***9*** *and the phosphonium salt* ***21***

The following general procedure was used.

To a solution of the appropriate base in THF or THF/HMPTA (see Tables 2 and 3) was added compound **21** dissolved in the same solvent. After 2 min, a solution of compounds **9** or **10** in THF was added. The mixture was allowed to warm to 0°C and the reaction quenched by the addition of wet ethyl ether. Any solids formed were separated by filtration, and the residue dissolved in ethyl ether. This solution was washed with water, aqueous saturated $NaHSO_3$, and again with water. The organic layer was dried and evaporated, yielding a residue that was

[5]This compound appears to be relatively volatile and losses were detected at the water and oil pumps.

[6]Compound **20***b* was partially lost during the isolation process due to its appreciable volatility.

purified by flash chromatography, affording compounds **22**, **23**, **24**, and **25** (conditions and amounts collected shown in Tables 2 and 3).

22, ^{1}H nmr (300 MHz) δ: 5.58 (dd, J = 17.0 and 4.6 Hz, olefinic H), 5.50 (dd, J = 17.0 and 4.6 Hz, olefinic H), 4.92 (d, J = 5.8 Hz, anomeric H), 4.65 (m, 1H), 4.38 (m, 1H), 4.32 (m, 1H), 4.0 (m, 3H), 3.35 (m, epoxidic 2H), 1.50 (s, 6H), 1.49 (s, 3H), 1.43 (s, 3H), 1.37 (s, 3H), 1.36 (s, 3H), 1.32 (d, J = 3.8 Hz, 3H).

23, melting point 90–92°C, $[\alpha]_D$ −154° (c 0.16); ^{1}H nmr (300 MHz) δ: 5.75 (dd, J = 12.9 and 8.4 Hz, H-9), 5.54 (dd, J = 12.9 and 8.4 Hz, H-8), 5.48 (d, J = 4.8 Hz, H-1), 4.63 (dd, J = 8.1 and 2.7 Hz, H-3), 4.44 (dd, J = 9.0 and 9.0 Hz, H-11), 4.36 (dd, 8.1 and 1.8 Hz, H-4), 4.30 (dd, J = 5.1 and 2.4 Hz, H-2), 3.80 (m, H-7 and H-10), 3.54 (dd, J = 8.0 and 1.0 Hz, H-5), 3.40 (dd, J = 8.0 and 4.0 Hz, H-6), 1.49, 1.47, 1.38, 1.31 (s, 3H); 1.32 (d, J = 3.8 Hz, 3H); ^{13}C nmr δ: 128.5 (d), 118.1 (d), 109.5 (s), 108.7 (s), 108.6 (s), 96.0 (d), 78.5 (d), 76.8 (d), 71.3 (d), 70.5 (d), 70.4 (d), 65.2 (d), 55.7 (d), 53.0 (d), 27.3 (q), 27.0 (q), 26.1 (q), 26.0 (q), 24.9 (q), 24.2 (q), 16.3 (q); ms m/e: 397 (M^+ − 15), 229. *Anal.* calcd. for $C_{21}H_{32}O_8$: C 61.15, H 7.82; found: C 61.08, H 8.13.

24, ^{1}H nmr (300 MHz) δ: 5.77 (dd, J = 15.0 and 7.5 Hz, olefinic H), 5.72 (dd, J = 15.0 and 7.5 Hz, olefinic H), 5.03 (d, J = 5.6 Hz, anomeric H), 3.33 (m, epoxidic H), 3.13 (m, epoxidic H).

25, syrup, $[\alpha]_D$ +8° (c 0.16); ^{1}H nmr δ: 5.55 (m, olefinic 2H), 5.4 (d, J = 3 Hz, anomeric H), 4.45 (dd, J = 7 and 2 Hz, 1H), 4.3–4.0 (m, 3H), 3.75–3.55 (m, 2H), 3.45–3.2 (m, epoxidic 2H), 1.60 (s, 3H), 1.35 (s, 6H), 1.25 (s, 6H), 1.2 (s, 3H), 1.2 (d, J = 6 Hz, 3H). *Anal.* calcd. for $C_{21}H_{32}O_8$: C 61.15, H 7.82; found: C 60.79, H 8.30.

1. D. Seebach and E. Hungerbuhler. Modern synthetic methods. *Edited by* R. Scheffold. Salle and Sauerlander, Berlin. 1980; (*a*) p. 115; (*b*) p. 91.
2. S. Valverde, B. Herradon, and M. Martin-Lomas. Tetrahedron Lett. **26**, 3731 (1985).
3. T. K. Devon and A. I. Scott. Handbook of naturally occurring compounds. Vol. 1. Academic Press, New York. 1975.
4. A. Alemany, C. Marquez, C. Pascual, S. Valverde, A. Perales, J. Fayos, and M. Martinez-Ripoll. Tetrahedron Lett. 3579 (1979).
5. A. Alemany, C. Marquez, C. Pascual, S. Valverde, A. Perales, J. Fayos, and M. Martinez-Ripoll. Tetrahedron Lett. 3583 (1979).
6. A. D. Argoudelis and J. F. Zieserl. Tetrahedron Lett. 1969 (1966).
7. S. Hanessian. Total synthesis of natural compounds: the chiron approach. Pergamon Press, Oxford. 1983; F. Gillard and J.-J. Riehl. Tetrahedron Lett. **24**, 587 (1983).
8. R. M. Rabanal, L. Escudero, M. Martin-Lomas, S. Valverde, A. Perales, and J. Fayos. Carbohydr. Res. **141**, 49 (1985).
9. D. Horton, N. Nakadate, and J. M. Tronchet. Carbohydr. Res. **7**, 56 (1968).
10. J. Herscovici and K. Antonakis. J. Chem. Soc. Chem. Commun. 561 (1980).
11. O. Tisler, H. Gutmann, M. Montavon, R. Ruegg, G. Rysen, and P. Zeller. Helv. Chim. Acta, **40**, 1242 (1957).
12. H. O. L. Fischer and H. Appel. Helv. Chim. Acta, **17**, 1574 (1934).
13. P. J. Garegg, T. Iversen, and S. Oscarson. Carbohydr. Res. **53**, C5-C7 (1977).
14. J. A. Musich and H. Rapoport. J. Am. Chem. Soc. **100**, 4865 (1978).
15. P. W. Feit. J. Med. Chem. **7**, 14 (1964).
16. M. Carmack and C. J. Kelley. J. Org. Chem. **23**, 2171 (1968).
17. H. Meyer and D. Seebach. Liebigs Ann. Chem. 2261 (1975).
18. F. Rolla. J. Org. Chem. **46**, 3909 (1981).
19. P. J. Garegg and B. Samuelson. J. Chem. Soc. Perkin Trans. 1, 2866 (1980).
20. M. P. Edwards, S. V. Ley, S. G. Lester, B. D. Palmer, and D. H. Williams. J. Org. Chem. **49**, 3503 (1984).
21. P.-T. Ho and N. Davies. J. Org. Chem. **49**, 3027 (1984).
22. J. Buddrus. Angew. Chem. Int. Ed. Engl. **7**, 536 (1968).
23. J. M. J. Tronchet and M. A. M. Massard. Helv. Chim. Acta, **62**, 1632 (1979).
24. T. Katsuki and K. B. Sharpless. J. Am. Chem. Soc. **102**, 5974 (1980).
25. W. C. Still, M. Kahn, and A. Mitra. J. Org. Chem. **43**, 2923 (1978).
26. W. D. Curtis, D. A. Laidler, J. F. Stoddart, and G. H. Jones. J. Chem. Soc. Perkin Trans. 1, 1756 (1977).
27. S. Valverde, B. Herradon, R. M. Rabanal, and M. Martin-Lomas. Can. J. Chem. **65**, 339 (1987).

Can. J. Chem. Downloaded from www.nrcresearchpress.com by 80.58.250.72 on 09/07/12
For personal use only.

The synthesis of D-asperlin

SERAFIN VALVERDE, BERNARDO HERRADON, ROSA M. RABANAL,[1] AND MANUEL MARTIN-LOMAS
Instituto de Química Orgánica, C.S.I.C., Juan de la Cierva 3, Madrid 28006, Spain

Received May 13, 1986

SERAFIN VALVERDE, BERNARDO HERRADON, ROSA M. RABANAL, and MANUEL MARTIN-LOMAS. Can. J. Chem. **65**, 339 (1987).

The synthesis of the D-enantiomer of asperlin has been carried out. The stereochemistry of the epoxide ring has been assigned as 6*R*,7*S* for this D-enantiomer.

SERAFIN VALVERDE, BERNARDO HERRADON, ROSA M. RABANAL et MANUEL MARTIN-LOMAS. Can. J. Chem. **65**, 339 (1987).

On a réalisé la synthèse de l'énantiomère D de l'asperline. On a attribué la stéréochimie 6*R*,7*S* au cycle époxyde de cet énantiomère D.

[Traduit par la revue]

Introduction

Asperlin is an antibiotic (U-13393) isolated from *Aspergillus nidulans* (1). It was assigned (1) the structure indicated in formula **1** (see Scheme 2). The D-enantiomer of asperlin was later synthesized (2), confirming the gross structural features of **1** and assigning a *trans* stereochemistry to the epoxide ring. A synthesis of racemic asperlin has recently appeared (3). Despite these synthetic efforts, the absolute stereochemistry of the epoxide ring remained to be established. Spin-lattice relaxation and nuclear Overhauser enhancement (nOe) measurements were used to tentatively propose the configuration of natural asperlin (4) as 6*R*,7*S*.

We have carried out an enantioespecific synthesis of the D-enantiomer of asperlin, which permits an unequivocal assignment of the stereochemistry of the oxirane ring, which turned out to be 6*R*,7*S*, **1***a*.

Results and discussion

The synthesis was initiated with tri-*O*-acetyl-D-glucal **2**, which was transformed into **3** by standard methods. Inversion of the configuration at C-4 (5) and manipulation of the C-4 and C-6 functions allowed for the preparation of aldehyde **4** (see Scheme 1). Reaction of **4** with the phosphorane derived from chloroacetaldehyde gave the *trans*-olefin **5** almost exclusively. $NaBH_4$ reduction of **5** at −20°C in methanol afforded **6** (95%) and the corresponding dihydro derivative (5%).

Epoxidation of **6** with *m*CPBA (*m*-chloroperbenzoic acid) in dichloromethane yielded a 5:4 ratio of the two possible epoxides (86% overall yield of isolated products). The major component (higher R_f) corresponds to the only product obtained by epoxidation of **6** using Sharpless conditions (6) (titanium isopropoxide, L-(+)-diethyl tartrate, and *tert*-butylhydroperoxide (TBHP)).

The mixture of epoxides **7***a* and **7***b* was separated by flash chromatography and the next sequence of reactions (see Scheme 2) was carried out separately with each isomer.

Epoxide **7***a* (6*R*,7*S*) was mesylated under standard conditions and this derivative treated (7) with $NaBH_4$ in acetonitrile under reflux. The 8-desoxy derivative **8***a* was obtained with good yield (90%). The same result was obtained (8) using "Red-Al", but the yield was significantly lower (50%).

Treatment of **8***a* (6*R*,7*S*) with Jones reagent (9) at 0–5°C during 30 min led to the formation of the lactone **9***a* (30%) and the recovery of starting material (60%). Accounting for this possible turnover, the overall yield of this oxidation approaches the 60%. Attempts to improve the lactone yield by carrying out a controlled hydrolysis of **8***a*, followed by oxidation of the corresponding hemiacetal, were not successful.

The attempted removal of the *tert*-butyldimethylsilyl (*t*-BDMSi) group of **9***a*, using conditions (10) (tetra-*n*-butylammonium fluoride in THF) ordinarily successful with this protecting group, also failed. Apparently, the basicity of the fluoride salt was sufficient to open the lactone ring, leading to a complex mixture of products. Hydrolysis (AcOH–H_2O, 7:3) (10) was rather sluggish at room temperature and led to undesirable side products when forcing these conditions.

The removal of the *t*-BDMSi group took place smoothly when compound **8***a* was treated with tetra-*n*-butylammonium fluoride in THF solution. Compound **10***a* (6*R*,7*S*), obtained in this way, was easily acetylated using standard conditions (Ac_2O/pyridine), and afforded the corresponding acetyl derivative **11***a* (100%).

Jones oxidation of **11***a* at 0–5°C, during 2 h, led to the isolation of the D-enantiomer of asperlin **1***a* (30%) and the recovery of starting material (60%). The identity with asperlin was established by comparison of the ^1H nmr spectra of **1***a* in $CDCl_3$ and C_6D_6 with published data (1, 4) (see Experimental).

The reaction sequence depicted in Scheme 2 was also applied to **7***b* (6*S*,7*R*). Compounds **8***b*, **9***b*, **10***b*, **11***b*, and **1***b* were thus obtained, and their data can be found in the Experimental.

We can then conclude that if the Sharpless rule for the asymmetric epoxidation of allylic alcohols is applicable to compound **6**, this synthesis establishes the absolute stereochemistry of natural asperlin as 6*S*,7*R*.

Experimental

For general experimental details see the preceding paper (16).

Preparation of compound ***3***

Compound **3** was prepared following literature procedures (12, 13).

Partial hydrolysis of ***3***

To a cold solution (−20°C) of **3** (120 mg, 0.32 mmol) in methanol (1.5 mL), a small amount (3 mg) of solid KOH was added and the solution stirred at −20°C for 12 h. Aqueous 5% HCl was added to reach pH 7.0. The solvent was removed and the residue separated by flash chromatography to yield 60 mg (67.5%) of ethyl 6-*O*-benzoyl-2,3-dideoxy-α-D-*threo*-hex-2-enopyranoside (14) and 6.0 mg each of starting material (4.9%) and ethyl 4-*O*-benzoyl-2,3-dideoxy-α-D-*threo*-hex-2-enopyranoside (6.7%).

[1]Present address: Departamento de Farmacología y Farmacognosia, Facultad de Farmacia, La Laguna, Tenerife, Spain.

Printed in Canada / Imprimé au Canada

Can. J. Chem. Downloaded from www.nrcresearchpress.com by 80.58.250.72 on 09/07/12
For personal use only.

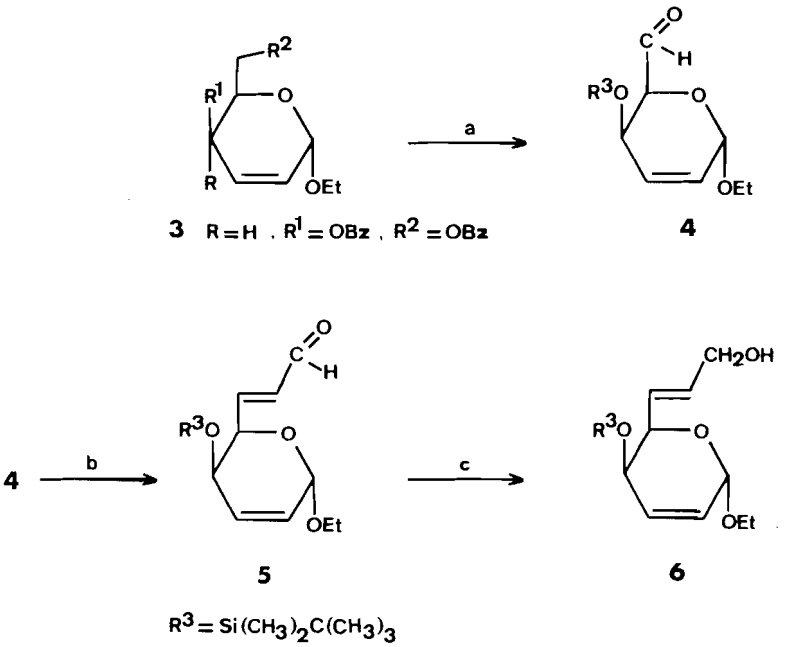

(a) MeOH, KOH, −20°C; DMAP, Et_3N, $(CH_3)_3CSi(CH_3)_2Cl$, CH_2Cl_2; MeOH, KOH, r.t.; PCC, molecular sieves, CH_2Cl_2; (b) $Ph_3P{=}CHCHO$, C_6H_6; (c) $NaBH_4$, MeOH, −5°C

SCHEME 1

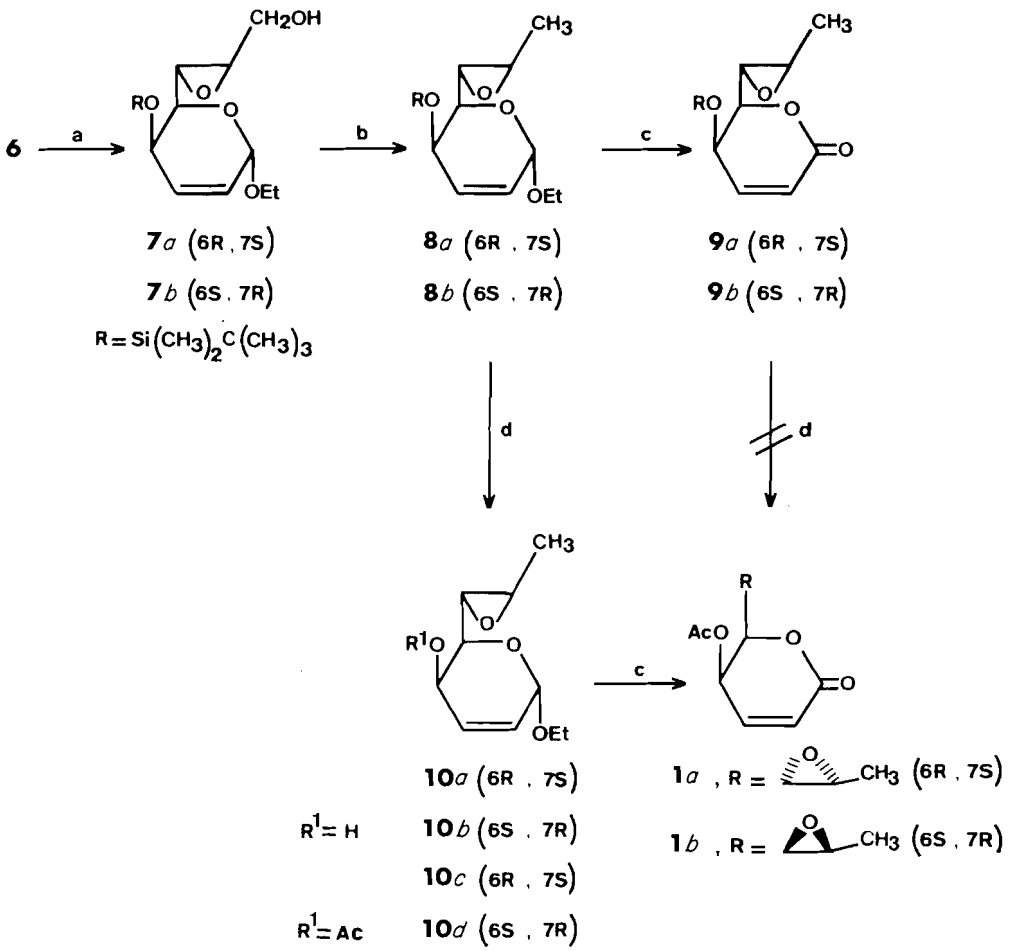

(a) *m*-CPBA, CH_2Cl_2 or Ti(O—i-Pr)$_4$, L-(+)-diethyl tartrate, TBHP, CH_2Cl_2, −20°C; (b) MsCl, C_6H_5N, 0°C; $NaBH_4$, CH_3CN, molecular sieves; (c) CrO_3, H_2SO_4, CH_3COCH_3; (d) (*n*-Bu)$_4$NF, THF

SCHEME 2

Can. J. Chem. Downloaded from www.nrcresearchpress.com by 80.58.250.72 on 09/07/12
For personal use only.

Can. J. Chem. Downloaded from www.nrcresearchpress.com by 80.58.250.72 on 09/07/12
For personal use only.

Preparation of the tert-*butyldimethylsilyl derivative* ***4***

To a solution of **3***a*, ethyl 6-*O*-benzoyl-2,3-dideoxy-α-D-*threo*-hex-2-enopyranoside (4.0 g, 14.3 mmol), in CH_2Cl_2 (20 mL), under argon, were sequentially added DMAP (4-dimethylamino pyridine) (610 mg, 4.7 mmol), Et_3N (1.53 g, 18 mmol), and *t*-BDMSiCl (2.416 g, 16 mmol). The mixture was stirred at room temperature overnight. The organic layer was washed with water, brine, and again with water.

The residue obtained was dissolved in methanol (20 mL) and a catalytic amount of KOH was added to this solution. After 3 h the solution was diluted with water and extracted with CH_2Cl_2. Column chromatography of the crude product gave pure ethyl 4-*O*-*tert*-butyldimethylsilyl-2,3-dideoxy-α-D-*threo*-hex-2-enopyranoside (2.7 g, 81%).

PCC (pyridinium chlorochromate) (6.45 g, 3 equiv.) was dissolved in anhydrous CH_2Cl_2 (50 mL) and molecular sieves (3Å, 10 g) were added to this solution. After stirring for 2 h, a CH_2Cl_2 solution of the alcohol prepared above (2.5 g, 1 equiv.) was added to the reaction mixture. The oxidation was complete after 2 h. The solids were eliminated by filtering through a Celite layer. Evaporation afforded crude aldehyde **4**, which was purified by column chromatography yielding 1.8 g of pure **4** (67%, aldehyde proton at δ 9.70).

Preparation of the aldehyde ***5***

A solution of formylmethylenetriphenylphosphorane (11) (5.0 g, 16.4 mmol) in dry benzene (125 mL) was mixed with the aldehyde **4** (2.87 g, 10 mmol) dissolved in benzene (10 mL). The mixture was heated in an oil bath at 110°C for 2 h. Evaporation of the solvent and chromatographic separation yielded **5** (2.7 g, 86%), mp 69–71°C; $[\alpha]_D$ −170° (*c* 0.642); ^{1}H nmr δ: 7.0 (dd, *J* = 3 and 15 Hz, H-6), 6.68 (ddd, *J* = 1.5, 7.0, and 15.0 Hz, H-7), 9.65 (d, *J* = 7 Hz, H-8).

$NaBH_4$ reduction of ***5***

A solution of **5** (1.4 g, 4.8 mmol) in methanol (50 mL) was reduced with excess $NaBH_4$ at −20°C. The methanol was poured over water and the aqueous solution extracted with CH_2Cl_2. The residue obtained by evaporation of the CH_2Cl_2 solution was purified by flash chromatography, yielding **6** (1.3 g, 95%) and its dihydro derivative (63 mg, 5%); **6**, mp 70°C, $[\alpha]_D$ −124° (*c* 1.07); ^{1}H nmr δ: 6.07 (m, 4H, olefinic protons), 4.32 (d, *J* = 5 Hz, H-8).

Epoxidation of ***6***

(a) With m*CPBA*

To a solution of **6** (800 mg, 2.5 mmol) in anhydrous CH_2Cl_2 (40 mL) was added *m*CPBA (600 mg, 3.3 mmol). The epoxidation was complete after 2 h. The organic solvent was washed with aqueous $NaHSO_3$, aqueous $NaHCO_3$, and water. Evaporation of the solvent yielded a mixture of **7***a* and **7***b*. Careful flash chromatography of the crude product (hexane – ethyl acetate 9:1) afforded **7***a* (400 mg, 48%) and **7***b* (320 mg, 38%); **7***a*, thick oil, $[\alpha]_D$ −123° (*c* 0.75); ^{1}H nmr (300 MHz) δ: 5.04 (dd, *J* = 1.0 and 2.9 Hz, H-1), 5.88 (dd, *J* = 2.9 and 10.2 Hz, H-2), 6.01 (ddd, *J* = 1.0, 5.3, and 10.2 Hz, H-3), 3.98 (dd, *J* = 2.5 and 5.3 Hz, H-4), 3.78 (dd, *J* = 2.5 and 5.7 Hz, H-5), 3.28 (dd, *J* = 2.3 and 5.7 Hz, H-6), 3.23 (m, H-7), 3.60 (m, H-8), 4.00 (m, H-8′); ^{13}C nmr (δ): 93.7 (C-1), 127.8 (C-2),[2] 129.1 (C-3),[2] 62.3 (C-4), 70.6 (C-5), 54.1 (C-6), 57.2 (C-7), 61.7 (C-8). *Anal.* calcd. for $C_{16}H_{30}O_5Si$: C 58.19, H 9.08; found: C 58.41, H 9.27.

7*b* mp 51°C, $[\alpha]_D$ −69° (0.68); ^{1}H nmr (300 MHz) δ: 5.09 (dd, *J* = 1.0 and 2.9 Hz, H-1), 5.90 (dd, *J* = 2.9 and 10.2 Hz, H-2), 5.98 (ddd, *J* = 1.0, 5.1, and 10.2 Hz, H-3), 3.93 (dd, *J* = 2.6 and 5.1 Hz, H-4), 3.63 (dd, *J* = 2.6 and 6.8 Hz, H-5), 3.35 (dd, *J* = 2.3 and 6.8 Hz, H-6), 3.10 (m, H-7), 3.60 (m, H-8), 4.00 (m, H-8′); ^{13}C nmr (δ): 93.7 (C-1), 127.8 (C-2),[2] 129.1 (C-3),[2] 62.3 (C-4), 70.6 (C-5), 54.1 (C-6), 57.2 (C-7), 61.7 (C-8). *Anal.* calcd. for $C_{16}H_{30}O_5Si$: C 58.19, H 9.08; found: C 58.20, H 9.15.

(b) With TBHP

To a cold (−20°C), serum-capped flask, containing anhydrous CH_2Cl_2 (15 mL), under argon, the following compounds were sequentially added: titanium isopropoxide (42 mg, 1.4 mmol), L-(+)-diethyl tartrate (0.25 mL), **6** (400 mg, 1.25 mmol), and a solution (15) of TBHP in toluene (0.84 mL, 2.8 mmol). The mixture was kept at −20°C overnight. Aqueous 10% tartaric acid (5 mL) was added with stirring, and the organic layer was washed with water and aqueous $NaHCO_3$. Chromatography of the residue afforded **7***a* (300 mg, 72%) (see above).

Preparation of compound ***8***

The following procedure was applied separately to **7***a* and **7***b*.

To a cold solution (0°C) of the alcohol (**7***a* or **7***b*) (330 mg, 1 mmol) in pyridine (5 mL) was added, dropwise, 0.18 mL of mesyl chloride. After 2 h, the solution was poured over cold, aqueous saturated $NaHCO_3$ (30 mL). The aqueous solution was extracted with CH_2Cl_2 (3 × 20 mL) and the organic solvent dried and evaporated, yielding the mesyl derivative, which was used in the next step without further purification.

The whole crude product, obtained as above (~1 mmol), was dissolved in acetonitrile (15 mL) and powdered molecular sieves (3Å) were added to this solution, which was heated under reflux for 1 h. $NaBH_4$ (150 mg) was added and the heating continued for 24 h. A single product was formed, which was chromatographically purified to give **8***a* or **8***b* in 90 and 70% yields, respectively.

8*a*, thick oil, $[\alpha]_D^{20}$ −124° (*c* 0.98); ^{1}H nmr (300 MHz) δ: 5.02 (d, *J* = 3.3 Hz, H-1), 5.84 (dd, *J* = 3.3 and 11.3 Hz, H-2), 6.00 (ddd, *J* = 1.3, 6.0, and 11.3 Hz, H-3), 3.95 (dd, *J* = 3.0 and 6.0 Hz, H-4), 3.63 (dd, *J* = 3.0 and 7.0 Hz, H-5), 2.96 (dd, *J* = 2.3 and 7.0 Hz, H-6), 3.03 (m, H-7), 1.35 (d, *J* = 6.0 Hz, H-8). *Anal.* calcd. for $C_{16}H_{30}O_4Si$: C 61.15, H 9.55; found: C 61.43, H 9.44.

8*b*, mp 68–70°C; $[\alpha]_D^{20}$ −87.5° (*c* 0.665); ^{1}H nmr (300 MHz) δ: 3.03 (dd, *J* = 2.3 and 8.0 Hz, H-6), 2.89 (m, H-7). *Anal.* calcd. for $C_{16}H_{30}O_4Si$: C 61.15, H 9.55; found: C 60.92, H 9.85.

Preparation of the lactone ***9***

The following procedure (9) was applied separately to epoxides **8***a* and **8***b*.

To a cold (0–5°C) solution of **8***a* (157 mg, 0.5 mmol) in acetone (10 mL), a large excess (1.5 mL, 0.07 mL required) of Jones reagent was added, followed by solid $MgSO_4$. The mixture was stirred for 30 min. A few drops of isopropyl alcohol were added, the pH of the solution made neutral by the addition of solid $NaHCO_3$, and the solids filtered off. The solution was diluted with water and most of the acetone eliminated under vacuum. Finally, it was extracted with CH_2Cl_2 and this solvent dried and evaporated to give a mixture that was purified by tlc yielding **9***a* (42 mg, 30%) and **8***a* (86 mg, 60%).

9*a*, thick oil, $[\alpha]_D^{20}$ −167° (*c* 0.862); ^{1}H nmr (300 MHz) δ: 6.08 (d, *J* = 10.6 Hz, H-2), 6.86 (dd, *J* = 6.0 and 10.6 Hz, H-3), 4.29 (d, *J* = 3.0 and 6.0 Hz, H-4), 3.83 (dd, *J* = 3.0 and 7.6 Hz, H-5), 3.05 (m, H-6 and H-7), 1.35 (d, *J* = 5.3 Hz, H-8); ^{13}C nmr (δ): 162.2 (C-1), 122.5 (C-2), 144.2 (C-3), 61.3 (C-4), 81.3 (C-5), 55.4 (C-6),[2] 54.6 (C-7),[2] 17.2 (C-8).

9*b*, mp 93–95°C; $[\alpha]_D^{20}$ −78° (*c* 0.329); ^{1}H nmr (300 MHz) δ: 5.99 (d, *J* = 10.6 Hz, H-2), 6.69 (dd, *J* = 4.3 and 10.6 Hz, H-3), 4.5 (dd, *J* = 4.3 and 5.3 Hz, H-4), 4.09 (dd, *J* = 5.3 and 5.6 Hz, H-5), 3.14 (dd, *J* = 2.6 and 5.6 Hz, H-6), 2.93 (m, H-7), 1.31 (d, *J* = 6.0 Hz, H-8); ^{13}C nmr (δ): 165.8 (C-1), 122.1 (C-2), 144.5 (C-3), 63.4 (C-4), 80.2 (C-5), 56.5 (C-6), 50.4 (C-7), 17.0 (C-8).

Preparation of compound ***10***

The following procedure was applied separately to epoxides **8***a* and **8***b*.

To a solution of **8***a* (157 mg, 0.5 mmol) in freshly distilled THF (7 mL) was added tetra-*n*-butylammonium fluoride (260 mg, 1 mmol). The mixture was stirred for 30 min at room temperature. The solvent, once washed with water, was evaporated under vacuum and the residue, **10***a*, was acetylated with Ac_2O/pyridine at room temperature during 4 h. The usual work-up yielded compound **11***a* (120 mg, 100%) as a thick oil; ^{1}H nmr (300 MHz) δ: 5.06 (d, partially overlapping with H-4, H-1), 6.02 (dd, *J* = 2.6 and 11.0 Hz, H-2), 6.15 (ddd, *J* = 1.3, 6.0, and 11.0 Hz, H-3), 5.08 (ddd, *J* = 0.6, 3.0, and 6.0 Hz, H-4), 3.96 (dd, *J* = 3.0 and 6.0 Hz, H-5), 2.90 (dd, *J* = 6.0 and 2.3 Hz, H-6), 3.09 (m, H-7), 1.36 (d, *J* = 5.2 Hz, H-8).

[2]These assignments can be reversed.

Preparation of compound ***1***

The same procedure was applied to compounds **11***a* and **11***b* (this last one was not further characterized).

To a cold solution (0–5°C) of **11***a* (120 mg, 0.5 mmol) in acetone (10 mL), a large excess (1.5 mL, 0.07 mL required) of Jones reagent was added, followed by the addition of anhydrous $MgSO_4$ (140 mg). The mixture was stirred for 2 h. A few drops of isopropyl alcohol were then added and the solids filtered off. The solution was adjusted to pH 7.0 by the addition of solid $NaHCO_3$, diluted with water, and most of the acetone eliminated under vacuum. The solution was extracted with CH_2Cl_2 and this solvent dried and evaporated, affording a mixture of compounds that was separated by tlc. Compounds **1***a* (22 mg, 20%) and **11***a* (70 mg, 60%) were isolated; **1***a*, mp 69–71°C (lit. (1) mp 71–73°C), $[\alpha]_D^{30}$ −320° (*c* 0.951, $CHCl_3$); uv, λ_{max} (EtOH): 220 nm; ^{1}H nmr (300 MHz) ($CDCl_3$) δ: 6.22 (d, *J* = 9.6 Hz, H-2), 7.08 (dd, *J* = 5.7 and 9.6 Hz, H-3), 5.32 (dd, *J* = 3.0 and 5.7 Hz, H-4), 4.12 (dd, *J* = 3.0 and 7.2 Hz, H-5), 3.08 (m, H-6 and H-7), 1.39 (d, *J* = 5.1 Hz, H-8) (identical to published data, see ref. 1); (C_6D_6, 0.1 *M*) δ: 5.61 (d, *J* = 10.6 Hz, H-2), 6.19 (dd, *J* = 6.3 and 10.6 Hz, H-3), 4.76 (dd, *J* = 3.0 and 6.3 Hz, H-4), 3.23 (dd, *J* = 3.0 and 7.0 Hz, H-5), 2.69 (dd, *J* = 2.0 and 7.0 Hz, H-6), 2.48 (m, H-7), 0.82 (d, *J* = 5.6 Hz, H-8) (see ref. 4).

1*b* (prepared as above) (13 mg, 11%), mp 63–65°C; $[\alpha]_D^{30}$ −170° (*c* 0.355, $CHCl_3$); uv λ_{max} (EtOH): 220 nm; ^{1}H nmr (300 MHz) ($CDCl_3$) δ: 6.22 (d, *J* = 9.9 Hz, H-2), 6.87 (dd, *J* = 5.1 and 9.9 Hz, H-3), 5.51 (dd, *J* = 3.6 and 5.1 Hz, H-4), 4.36 (dd, *J* = 3.6 and 4.8 Hz, H-5), 3.02 (m, H-6 and H-7), 1.35 (d, *J* = 5.1 Hz, H-8); (C_6D_6) δ: 5.61 (d, *J* = 10.6 Hz, H-2), 5.81 (dd, *J* = 5.6 and 10.6 Hz, H-3), 4.73 (dd, *J* = 3.0 and 5.6 Hz, H-4), 3.41 (dd, *J* = 3.0 and 6.0 Hz, H-5), 2.53 (m, H-6), 2.46 (m, H-7), 0.80 (d, *J* = 5.6 Hz, H-8).

Acknowledgments

Financial support from CSIC and the Comision Asesora de Investigacion Cientifica y Tecnica is gratefully acknowledged.

1. A. D. Argoudelis and J. F. Zieserl. Tetrahedron Lett. 1969 (1966).
2. S. Lesage and A. S. Perlin. Can. J. Chem. **56**, 2889 (1978).
3. H. Hiraoka, K. Furuta, N. Ikeda, and H. Yamamoto. Bull. Chem. Soc. Jpn. **57**, 2777 (1984).
4. Ph. Dais and A. S. Perlin. Can. J. Chem. **63**, 1009 (1985).
5. O. Mitsunobu. Synthesis, 1 (1981).
6. T. Katsuki and K. B. Sharpless. J. Am. Chem. Soc. **102**, 5974 (1980).
7. D. Pica, G. Carret, and D. Anker. Tetrahedron Lett. **26**, 1863 (1985).
8. V. Bazant, M. Capka, M. Cerny, V. Chvalovsky, K. Kochloefl, M. Kraus, and J. Malek. Tetrahedron Lett. 3303 (1968).
9. R. Rangarajan and E. J. Eisenbraun. J. Org. Chem. **50**, 2435 (1985).
10. E. J. Corey and A. Venkateswarlu. J. Am. Chem. Soc. **94**, 6190 (1972).
11. S. Tripett and D. M. Walker. J. Chem. Soc. 1266 (1961).
12. R. J. Ferrier and N. Prasad. J. Chem. Soc. C, 570 (1969).
13. H. W. Pauls and B. Fraser-Reid. Can. J. Chem. **62**, 1532 (1984).
14. B. Fraser-Reid, S. Y.-K. Tam, and B. Radatus. Can. J. Chem. **53**, 2005 (1975).
15. J. G. Hill, B. E. Rossiter, and K. B. Sharpless. J. Org. Chem. **48**, 3607 (1983).
16. S. Valverde, B. Herradon, R. M. Rabanal, and M. Martin-Lomas. Can. J. Chem. **65**, 332 (1987).

Can. J. Chem. Downloaded from www.nrcresearchpress.com by 80.58.250.72 on 09/07/12
For personal use only.

Alcaloïdes bisbenzylisoquinoléiques de *Albertisia* cf. *A. papuana*

MARIE LAVAULT ET JEAN BRUNETON[1]
Centre d'études des plantes médicinales, Unité de formation et de recherche de médecine et de pharmacie, 16, Boulevard Daviers, 49000 Angers, France

ADRIEN CAVÉ
C.C.I.P.E., BP 5055, 34033 Montpellier Cedex, France

KAI CHEONG CHAN
Department of Chemistry, University of Malaysia, Kuala Lumpur, Malaysia

JEAN ROBERT DEVERRE ET THIERRY SEVENET
I.C.S.N., Centre national de la recherche scientifique, 91190 Gif sur Yvette, France

ET

HÉLÈNE GUINAUDEAU
Unité de formation et de recherche de pharmacie, 87025 Limoges, France

Reçu le 27 mai 1986

MARIE LAVAULT, JEAN BRUNETON, ADRIEN CAVÉ, KAI CHEONG CHAN, JEAN ROBERT DEVERRE, THIERRY SEVENET et HÉLÈNE GUINAUDEAU. Can. J. Chem. **65**, 343 (1987).

Quatre nouveaux alcaloïdes de structure bisbenzylisoquinoléique ont été isolés de *Albertisia* cf. *A. papuana* Becc. (Ménispermacées). Ce sont la (−)-bisnor-2,2′ phaeanthine (**5**), la (+)-pangkoramine (**7**), la (+)-pangkorimine (**9**) et la (+)-nor-2′ cocsuline (**14**). Ils sont accompagnés de la (+)-daphnoline (**2**), majoritaire, et de sept autres dimères déjà connus, mono-, di- ou tripontés.

MARIE LAVAULT, JEAN BRUNETON, ADRIEN CAVÉ, KAI CHEONG CHAN, JEAN ROBERT DEVERRE, THIERRY SEVENET, and HÉLÈNE GUINAUDEAU. Can. J. Chem. **65**, 343 (1987).

Four new bisbenzylisoquinoline alkaloids were obtained from *Albertisia* cf. *A. papuana* Becc. (Menispermaceae). These are (−)-2,2′-bisnorphaeanthine (**5**), (+)-pangkoramine (**7**), (+)-pangkorimine (**9**), and (+)-2′-norcocsuline (**14**). They are accompanied by the known (+)-daphnoline (**2**), which is the main alkaloid, and by seven known dimers with one, two, or three ether bridges.

Le genre *Albertisia* Becc. (1), longtemps demeuré monospécifique, comprend, depuis les travaux de Forman (2), 17 espèces dont la majorité, d'origine africaine, fût initialement classée dans le genre *Epinetrum* Hiern. Des cinq espèces spontanées dans le sud-est asiatique une seule, *A. papuana* Becc., a fait l'objet d'une étude chimique (3); l'échantillon étudié provenait du sud de Padang dans la partie occidentale de Sumatra (Indonésie). Ayant eu à notre disposition un lot de cette liane en provenance de l'Ile de Pangkor (Malaisie), il nous a semblé intéressant d'en étudier la composition alcaloïdique compte tenu de la très large dispersion de cette espèce (Sarawak, Moluques, Papouasie–Nouvelle-Guinée...(4)) et de l'hypothèse, un temps retenue, d'une subdivision de l'espèce en deux variétés (var. *bancana* et var. *buruensis*) (5).

La présente étude a permis l'isolement et l'identification de 12 alcaloïdes bisbenzylisoquinoléines. Huit sont connues : un dérivé monoponté 11–12′, la (+)-lindoldhamine **1**; trois dérivés dipontés 7–8′, 11–12′ de configuration 1*R*,1′*S*, la (+)-daphnoline **2**, la (+)-daphnandrine **3** et la (+)-bisnoraromoline **4**; quatre dérivés à enchaînement dibenzo-dioxine (6–7′, 7–8′, 11–12′) de configuration 1*S*,1′*S* : (+)-cocsuline **10**, (+)-cocsoline **11** et (+)-*O*-méthyl cocsoline **12**, ou de configuration 1*R*,1′*S* : c'est le cas de la (+)-apateline **13**. Tous ces alcaloïdes ont déjà été isolés à plusieurs reprises, en particulier à partir de diverses Ménispermacées (6–8), et ont été identifiés par comparaison de leurs constantes physiques et de leurs données spectrales avec celles publiées ainsi que par une comparaison directe avec des échantillons authentiques.

Les quatre autres alcaloïdes sont des bisbenzylisoquinoléines originales. La (−)-bisnor-2,2′ phaeanthine **5**, $C_{36}H_{38}N_2O_6$, présente, sur son spectre de masse, un pic moléculaire à *m/z* 594. Le pic de base à *m/z* 367 est caractéristique du fragment monovalent bisisoquinoléique formé par la rupture des liaisons benzyliques chez les dimères dipontés «tête à tête – queue à queue» (9). Le spectre de rmn du proton montre l'absence de singulets dûs à des N-CH_3 vers 2,5 ppm, ce qui indique le caractère bis-amine secondaire de **5**; cette absence de substituant sur les atomes d'azote est par ailleurs soulignée par le fort déblindage subi par les protons en 1 (4,06 ppm) et 1′ (4,35 ppm). La méthylation ($HCHO/NaBH_4$) conduit au composé **6** dont les groupements N-CH_3 apparaissent, sur le spectre de rmn protonique, sous la forme de deux singulets nettement séparés ($\Delta\delta$ = 0,29 ppm) comme cela est habituel chez les dérivés dipontés 8–7′, 11–12′ (10). La configuration de **5** et de **6** ne peut être que 1*R*,1*R*′ ou 1*S*,1*S*′ comme le montrent les positions du doublet dédoublé du proton en 10 (6,42 et 6,54 ppm) et du singulet du méthoxyle en 6′ (3,41 et 3,37 ppm) (cf. tableau 1); ces positions sont tout à fait comparables à celles observées dans le cas de la (−)-limacine ou de la (−)-gyroaméricine (11) : respectivement 6,56 et 6,53, 3,35 et 3,37 ppm pour ces deux signaux alors qu'ils apparaissent vers 6,25–6,40 et 3,60–3,90 pour la série 1*R*,1*S*′ (6, 7). Le pouvoir rotatoire négatif de **6** permet de l'identifier à la (−)-phaeanthine. Une comparaison directe avec un échantillon authentique confirme cette conclusion et démontre ainsi sans équivoque la structure de l'alcaloïde **5**.

L'alcaloïde **7** est également un dérivé «bis-nor» (absence de N-méthyle en rmn). Son spectre de masse est compatible avec une formule brute en $C_{34}N_{34}N_2O_6$ (M^+ 566) et, comme pour le composé **5** indique sa nature bipontée «tête à tête –

1. Auteur à qui adresser toute correspondance.

Can. J. Chem. Downloaded from www.nrcresearchpress.com by 80.58.250.72 on 09/07/12
For personal use only.

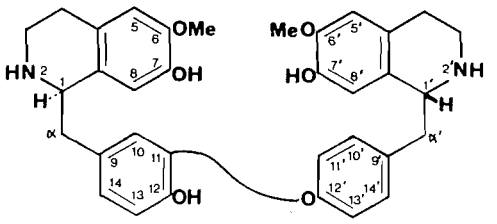

1

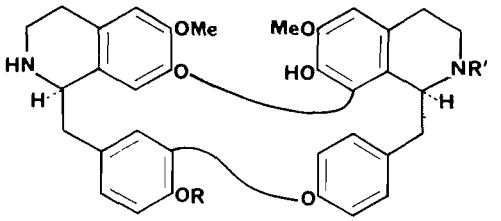

2 R=H , R'=Me
3 R=Me , R'=Me
4 R=H , R'=H

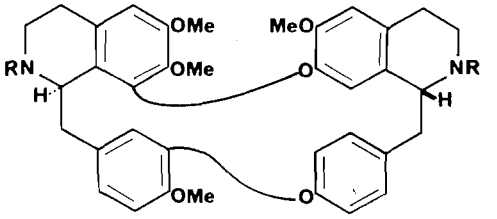

5 R=H
6 R=Me

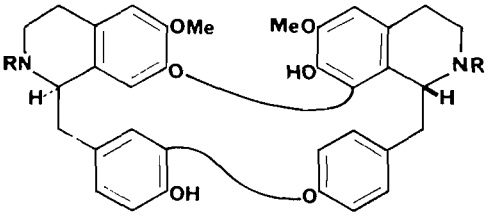

7 R=H
8 R=Me

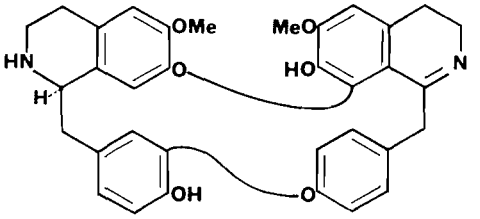

9

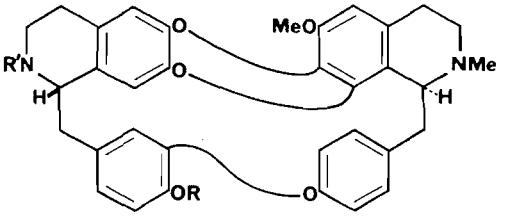

10 R=H , R'=Me
11 R=R'=H
12 R=Me , R'=H

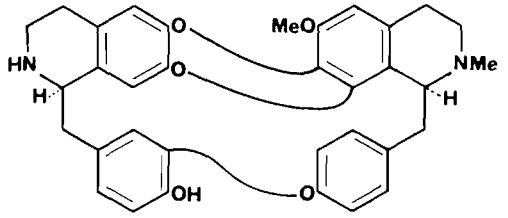

13

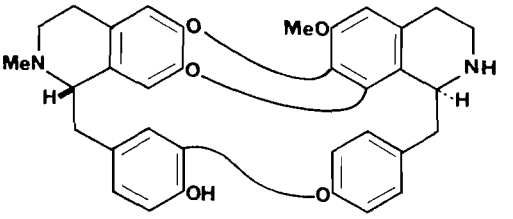

14

queue à queue» : pic de base à m/z 353 (cette valeur de 353 indique de plus que l'une des unités tétrahydroisoquinoléique est phénolique). La méthylation ($HCHO/NaBH_4$) conduit à un dérivé **8** qui est un dimère à deux ponts diphényl éther 7–8′, 11–12′ ($\Delta\delta$ des signaux des N-CH_3 = 0,1 ppm), de configuration 1*S*,1*S*′ ou 1*R*,1*R*′ (le signal du proton en 10 est à 6,56 ppm au lieu de 5,40–5,60 dans le cas des énantiomères 1*R*,1*S*′ : ((+)-daphnoline **2**, 5,59, (+)-daphnandrine **3**, 5,60) ou 1*S*,1*R*′ : ((−)-gyrolidine, 5,47, (−)-gyrocarpine, 5,48 (11)). La mesure du pouvoir rotatoire ainsi que l'enregistrement des courbes de dichroïsme circulaire permettent d'identifier le dérivé diméthylé **8** à la 1*R*,1*R*′(+)-candicusine isolée et décrite récemment chez une Ménispermacée sud-américaine : *Curarea candicans* Barneby et Krukoff (12). Cette corrélation prouve la structure proposée pour la (+)-pangkoramine **7** (ou (+)-bisnor-2,2′ candicusine) (tableau 2).

Le troisième alcaloïde nouveau, la (+)-pangkorimine **9** présente un spectre de masse décalé de deux unités et simplifié par rapport à celui du précédent. Le pic de masse à m/z 564 est le pic de base; il est accompagné d'un pic très intense à m/z 563 ce qui traduit une conjugaison supplémentaire de la molécule. Le spectre uv confirme cette observation : il montre en particulier un effet bathochrome en milieu acide caractéristique de la présence d'une fonction imine (13). Le spectre de rmn ne présente pas de singulet vers 2,5 ppm attribuable à un N-CH_3 et ne comporte qu'un seul signal (à 4,13 ppm) dû à un proton en 1 ou 1′. On remarque en outre un système AB (4,04 et 4,63 ppm, J = 13,6 Hz) attribuable aux protons du CH_2 benzylique situé du côté de l'imine. Le reste du spectre de rmn présente de fortes analogies avec ceux de **7** et de **8** comme le montre le tableau 1. La réduction de l'imine ($NaBH_4$–MeOH) conduit à une bis-amine secondaire identique en tous points à la (+)-pangkoramine **7**. La position exacte de la fonction imine est déduite des observations suivantes : le doublet du proton

Can. J. Chem. Downloaded from www.nrcresearchpress.com by 80.58.250.72 on 09/07/12
For personal use only.

Can. J. Chem. Downloaded from www.nrcresearchpress.com by 80.58.250.72 on 09/07/12
For personal use only.

TABLEAU 1. Spectre rmn (360 MHz) des alcaloïdes **5** et **6**

	2-NMe	2′-NMe	H-1	H-1′	H-5	H-5′	H-8′	H-10	H-13	H-14	H-10	H-11′	H-13′	H-14′	MeO-6	MeO-6′	MeO-7	MeO-12
Phaeanthine	2,33	2,62	3,75	3,88	6,30	6,51	5,99	6,54	6,85	6,88	6,29	6,81	7,13	7,33	3,74	3,37	3,19	3,94
Bisnor-2,2′ phaeanthine	NH	NH	4,06	4,35	6,33	6,53	6,03	6,42	6,89	6,79	6,40	6,87	7,16	7,44	3,78	3,41	3,25	3,95

TABLEAU 2. Spectre rmn (360 MHz) des alcaloïdes **7**, **8** et **9**

	2-NMe	2′-NMe	H-1	H-1′	H-5	H-5′	H-8	H-10	H-13	H-14	H-10′	H-11′	H-13′	H-14′	MeO-6	MeO-6′	MeO-7	MeO-12
Candicusine	2,55	2,54	3,47	4,29	6,38	6,39	6,45	6,56	7,00	6,88	6,83	6,83	7,13	7,37	3,41	3,78	OH	OH
Pangkoramine	NH	NH	4,07	4,99	6,41	6,41	6,25	6,71	6,84	6,76	6,82	6,89	6,82	7,40	3,57	3,81	OH	OH
Pangkorimine[a]	NH	—	4,13	—	6,53	6,57	6,22	5,02	6,79	6,67	7,25	6,41	6,78	7,41	3,97	3,92	OH	OH

[a]H-α_1' 4,63 d, H-α_2' 4,04 d, J = 13,6 Hz.

TABLEAU 3. Spectre rmn (360 MHz) des alcaloïdes **10**, **11** et **14**

	2-NMe	2′-NMe	H-1	H-1′	H-5	H-5′	H-8	H-10	H-13	H-14	H-10′	H-11′	H-13′	H-14′	MeO-6′	MeO-12
(+)Cocsuline	2,40	2,58	3,35	4,02	6,62	6,33	6,14	6,52	6,88	6,82	7,15	6,93	7,14	7,58	3,86	OH
(+)Cocsoline	NH	2,60	3,65	3,97	6,63	6,33	6,19	6,54	6,90	6,85	7,10	6,80	7,18	7,51	3,86	OH
Nor-2′ cocsuline	2,44	NH	3,32	4,35	6,60	6,31	6,12	6,50	6,90	6,79	7,13	6,96	7,17	7,63	3,86	OH

aromatique en 10 apparaît, dans le cas de **9**, à 5,02 ppm comme cela se produit dans le cas d'une autre imine en 1′,2′, la (−)-épistéphanine (14), qui appartient à la même série (liaisons 7–8′, 11–12′; configuration *R* du carbone 1) et dont le proton 10 apparaît à 4,98 ppm. Si la fonction imine était en 1,2 ce proton serait beaucoup moins affecté : ainsi, toujours dans la même série et avec une configuration 1′*R*, la (−)-déhydro-1,2 limacusine voit son proton en 10 résonner à 6,36 ppm (15). Ces indications, qui ne constituent que des présomptions, sont confirmées par mesure des nOe (effet Overhauser nucléaire) qui montre en particulier une augmentation de 8% et de 3% du signal des protons en α′ après irradiation du proton en 10′ ou en 14′ (réciproque : 14 et 4%); (les résultats des principales mesures figurent dans la partie expérimentale).

Le dernier alcaloïde nouveau est une bisbenzylisoquinoléine à trois ponts éther, monophénolique : la (+)-nor-2′cocsuline **14** : $C_{34}H_{32}N_2O_5$. La présence de l'enchaînement dibenzodioxine est reconnue par la classique réaction de ce type de composé en milieu nitro-sulfurique (16, 17) et par le spectre de masse qui montre des fragmentations superposables à celles observées dans le cas de la (+)-cocsoline **11** (9). Comme ce dernier composé, l'alcaloïde **14** conduit, par méthylation, à la (+)-cocsuline **10**; il s'agit donc bien d'un dérivé déméthylé à l'azote de la (+)-cocsuline. Le seul groupe *N*-methyle présent est en 2 comme le montre la valeur de son déplacement chimique à 2,44 ppm (cf. tableau 1 et la réf. 17; tableau 3).

Bien que tous les alcaloïdes minoritaires de cette espèce ne soient pas identifiés (des dimères ayant un cycle B ou B′ aromatique sont en cours d'étude), quelques remarques peuvent être formulées sur la composition alcaloïdique de cet échantillon qui montre des différences importantes par rapport à celle rapportée pour le matériel indonésien (3). Certes, comme dans le cas de l'étude citée, nous n'avons isolé que des alcaloïdes dimères mais les constituants majoritaires sont très différents : (+)-daphnoline (47%) et (+)-pangkoramine (16%) pour le lot malais, (+)-cocsoline (44%) et (+)-cocsuline (15%) pour le lot indonésien. Pour les autres alcaloïdes un seul, la (+)-lindoldhamine, est présent en quantité notable dans les deux cas : 12% dans notre échantillon, 5% dans celui étudié par Cavé et coll. (3). Enfin notons que six dimères décrits dans le spécimen indonésien n'ont pas été détectés dans celui récolté en Malaisie et que ce dernier fournit sept bisisoquinoléines absentes dans le premier.

Ces différences quantitatives et qualitatives semblent indiquer, si l'on exclut une division de l'espèce,[2] l'existence de chimiotypes : la saison de récolte étant la même dans les deux cas, de simples variations saisonnières sont à priori exclues. Comme dans le cas de l'échantillon récolté dans la partie occidentale de Sumatra, nous n'avons isolé que des dimères dipontés «queue à queue», ce qui démarque bien les *Albertisia* du sud-est asiatique des *Albertisia* africains initialement étudiés sous le nom générique d'*Epinetrum* et caractérisés par des dimères dipontés «tête à queue» (18, 19); cette observation est sans doute à mettre en relation avec un développement parallèle des Ménispermacées (originaires de l'Ouest du Pacifique) sur les deux continents.

Partie expérimentale

Appareillage

Les points de fusion sont mesurés en tube capillaire et ne sont pas corrigés. Les pouvoirs rotatoires sont mesurés à la température ambiante sur polarimètre Schmidt–Haensch, dans le chloroforme ou le méthanol. Les spectres sont enregistrés sur les appareils suivants : uv, Beckman 530, éthanol (λ_{max}, (log ε)); ir, Perkin–Elmer 580, KBr (ν cm^{-1}); rmn, Varian EM 360 (60 MHz) et Bruker WB 360 (360 MHz), $CDCl_3$, δ ppm, TMS = 0; spectres de masse, Varian MAT 311 (*m/z* (%)). Les chromatographies sur colonne sont réalisées sur Kieselgel 60 (Merck 7734) ou 60 H (Merck 7736) et les ccm analytiques sur DC Alufolien 60 F 254 (Merck 5554).

Matériel végétal

Les tiges de *A. papuana* ont été récoltées dans l'Ile de Pangkor le 7-12-1983. Un échantillon de référence est conservé sous le n° SD 42.

Extraction et isolement des alcaloïdes

La drogue pulvérisée (4,6 kg) et dégraissée par l'hexane est extraite par le chloroforme en milieu alcalin selon un procédé déjà décrit (15). Un premier fractionnement des alcaloïdes totaux (207 g) est obtenu par chromatographie sur colonne d'alumine désactivée par addition de 6% d'eau. La purification des différents constituants est obtenue par une suite de chromatographies sur colonnes de silice pour ccm avec pour éluant des mélanges $CHCl_3$–MeOH 95:5–90:10 + 0,3% NH_4OH; les chromatographies préparatives sur ccm sont développées avec des mélanges $CHCl_3$–MeOH 92:8, NH_4OH 0,2% ou $CHCl_3$–Me_2CO–MeOH 40:40:3 avec 5–10% de diéthylamine.

Description des produits isolés

Les constantes physiques et données spectrales des composés antérieurement décrits ne seront pas redonnées ici. Les composés **1**, **2**, **3** et **10** ont été formellement identifiés par comparaison avec des échantillons authentiques. Les constantes et données spectrales mesurées pour les autres alcaloïdes sont en bon accord avec celles de la bibliographie. L'identification des composés **5**, **7**, **9**, **11** et **14** est vérifiée par corrélation chimique.

Description des alcaloïdes nouveaux isolés

(−)-Bisnor-2,2′ phaeanthine **5**, amorphe, $[\alpha]_D$ −272° ($CHCl_3$, *c* 0,1); uv : 213 (4,29), 232 (4,58), 283 (3,86); rmn : cf. tableau 1; sm : 594 (6), 593 (8), 367 (100), 184 (28), 161 (10).

(+)-Pangkoramine **7**, amorphe, $[\alpha]_D$ +126° (MeOH, *c* 0,05); uv : 214 (4,72), 230 (4,39), 280 (4,58); OH^+ : 212, 290; sm *m/z* : 564, M^+ (24), 563 (36), 353 (100), 339 (9), 192 (22), 177 (35).

(+)-Pangkorimine **9**, $[\alpha]_D$ +65° (MeOH, *c* 0,05); uv : 213 (4,64), 228 (4,48), 283 (4,26), 314 (3,80); H^+ : 213 (4,63), 279 (4,13), 333 (4,09); sm *m/z* : 564, M^+ (100), 563 (94), 562 (46), 549 (8), 534 (20), 533 (53), 283 (16).

Principaux effets nOe observés : H-α'_1 sur H-10′ (14%), réciproque : 8%; H-α'_2 sur H-14′ (4%), réciproque : 3%; H-8 sur H-1 (7%), réciproque : 5%; H-5 sur OMe-6 (13%), réciproque : 18%; H-5′ sur OMe-6′ (14%), réciproque : 20%.

(+)-Nor-2′cocsuline **15**, $[\alpha]_D$ +238° ($CHCl_3$, *c* 0,15); uv : 212 (4,53), 225 (4,43), 287 (3,60); sm *m/z* : 548 (27), 547 (27), 335 (100), 321 (27), 319 (24), 168 (32), 167 (7)).

N-méthylation de **7**, **9** : 30 mg de l'alcaloïde sont dissous dans 20 mL de MeOH; on ajoute 2 mL de HCHO puis, sous agitation, du borohydrure de sodium en excès. Le produit réactionnel est purifié par ccm préparative.

Réduction de **9** en **7** : 20 mg de **11** sont dissous dans 10 mL de MeOH; on ajoute 50 mg de $NaBH_4$ et laisse sous agitation 2 h.

Remerciements

Ce travail a été effectué dans le cadre du programme de Recherche en Coopération CNRS Université de Malaisie. Les auteurs remercient MM. A. Cavé et M. Leboeuf (Université de Paris XI, centre de Châtenay–Malabry) pour la fourniture d'échantillons de référence, et M. A. J. Freyer (Pennsylvania State University) pour l'enregistrement de spectres de rmn à 360 MHz.

1. O. Beccari. Malesia, I, 1877.
2. L. L. Forman. Kew Bull. **30**, 77 (1977).

2. Le matériel étudié présente quelques différences morphologiques mineures avec celui étudié par Cavé et coll. Toutefois l'absence d'inflorescences ne permet pas de détermination univoque (L. L. Forman, communication personelle).

Can. J. Chem. Downloaded from www.nrcresearchpress.com by 80.58.250.72 on 09/07/12
For personal use only.

3. M. LEBOEUF, M.-L. ABOUCHACRA, T. SÉVENET et A. CAVÉ. Plant. Med. Phytother. **16**, 280 (1982).
4. G. BUCCHEIM. Menispermaceae. *Dans* A. Engler's Syllabus der Pflanzenfamilien, Berlin. 1964.
5. J. G. BOERLAGE. Cat. Pl. Phan. Hort. Bogor. **1**, 44 (1899).
6. K. P. GUHA, B. MUKHERJEE et R. MUKHERJEE. J. Nat. Prod. **42**, 1 (1979).
7. P. L. SCHIFF, JR. J. Nat. Prod. **46**, 1 (1983).
8. K. W. BENTLEY. Nat. Prod. Rep. **1**, 355 (1984); **2**, 81 (1985).
9. J. BALDAS, I. R. C. BICK, T. IBUKA, R. S. KAPIL et Q. N. PORTER. J. Chem. Soc. 592 (1972).
10. M. SHAMMA. The isoquinoline alkaloids, chemistry and pharmacology. Academic Press, New York. 1972.
11. M.-C. CHALANDRE, P. CABALION, H. GUINAUDEAU et J. BRUNETON. Can. J. Chem. **64**, 123 (1986).
12. M. LAVAULT, A. FOURNET, H. GUINAUDEAU et J. BRUNETON. J. Chem. Res. S, 248 (1985).
13. I. R. C. BICK et S. SOTHEESWARAN. Aust. J. Chem. **31**, 2077 (1978).
14. H. GUINAUDEAU, A. J. FREYER et M. SHAMMA. Natural Products Reports. À paraître.
15. M. LAVAULT, A. FOURNET, H. GUINAUDEAU et J. BRUNETON. Chem. Pharm. Bull. **34**, 1148 (1986).
16. I. R. C. BICK et A. R. TODD. J. Chem. Soc. 1606 (1950).
17. D. S. BHAKUNI et J. P. JOSHI. Tetrahedron, **31**, 2575 (1975).
18. M.-M. DEBRAY, M. PLAT et J. LE MEN. Ann. Pharm. Fr. **24**, 551 (1967).
19. A. BOUQUET et A. CAVÉ. Plant. Med. Phytother. **5**, 131 (1971).

Can. J. Chem. Downloaded from www.nrcresearchpress.com by 80.58.250.72 on 09/07/12
For personal use only.

Solution and solid state studies of some ternary complexes of Cu(II) involving heteroaromatic *N*-bases and *o*-hydroxy aromatic carbonyls

NEELIMA D. KULKARNI AND P. K. BHATTACHARYA[1]

Department of Chemistry, Faculty of Science, M.S. University of Baroda, Baroda-390 002, India

Received May 26, 1986

NEELIMA D. KULKARNI and P. K. BHATTACHARYA. Can. J. Chem. **65**, 348 (1987).

Stability constants of some ternary complexes of *o*-hydroxy aldehydes (HL) with Cu(II) as central metal ion and bis(2-pyridyl)amine (dpa) and 5-nitro-1,10-phenanthroline (5-N-phen) as primary ligands (A) have been determined potentiometrically in 50% aqueous dioxane medium using a computer technique. The values of $\Delta \log K$ ($\log K^{MA}_{MAL} - \log K^{M}_{MA}$) have been compared within the series as well as with the corresponding bipyridyl complexes. The stability order has been explained on the basis of the electron repulsion concept. The complexes have been isolated in the solid state and characterized by elemental analysis, conductance and magnetic measurements, and ir and electronic spectral studies. Shifts in ligand field absorption wave numbers of the mixed ligand complex from the average value of the ligand field absorption wave numbers of $[MA_2]^{2+}$ and $[ML_2]$ have been correlated with the potentiometrically determined $\Delta \log K$ values.

NEELIMA D. KULKARNI et P. K. BHATTACHARYA. Can. J. Chem. **65**, 348 (1987).

Opérant dans un milieu formé de dioxanne/eau à 50%, faisant appel à la potentiométrie et à une technique d'ordinateur, on a déterminé les constantes de stabilité de quelques complexes ternaires des *o*-hydroxy aldéhydes (HL) avec le Cu(II) comme ion métallique central et avec la bis(pyridyl-2)amine (dpa) et la nitro-5 phénanthroline-1,10 (N-5-phen) comme ligands primaires (A). On procède à une comparaison des valeurs de $\Delta \log K$ ($\log K^{MA}_{MAL} - \log K^{M}_{MA}$) tant dans la série des composés examinés que dans celle des complexes bipyridyles correspondants. On explique l'ordre de stabilité en fonction du concept de repulsion électronique. On a isolé les complexes à l'état solide et on les a caractérisé par leurs analyses élémentaires, par des mesures magnétiques et de conductivité ainsi que par des études spectrales électroniques et infrarouges. On a établi une corrélation entre les valeurs de $\Delta \log K$ déterminées d'une façon potentiométrique et les déplacements des nombres d'onde d'absorbtion dans le champ de ligand du complexe avec un ligand mixte par rapport à la valeur moyenne des nombres d'onde d'absorbtion dans le champ de ligand de $[MA_2]^{2+}$ et $[ML_2]$.

[Traduit par la revue]

During the last two decades exhaustive studies have been made on ternary metal complexes with a variety of ligands to understand the factors governing the stability and behaviour of these complexes. Most of the work has been done on complexes containing bidentate heteroaromatic N bases (A) (1–3). A discriminating behaviour of $[MA]^{2+}$ has been shown towards the ligands containing N—N, O^-—N, and O^-—O^- coordinating sites (1, 4–6). Complexes $[MAL]^{n+}$ where L = O^-—O^- coordinating ligands were shown to be the most stable (ref. 1, Chapt. 2, p. 67; refs. 8–10).

Sigel *et al.* have studied pyrocatechol complexes (11) with dipyridyl analogues and explained the stability order of the complexes in terms of the electron-withdrawing or -releasing nature of the substituent on the primary ligand. To see the "cooperative effects" (6, 12, 13) which may occur between the π-systems of the amine and O^-—O^- containing ligand bound to the same Cu^{2+}, they made a comparative study of the complexes of $[Cudipy]^{2+}$ and $[Cu\text{-}o\text{-}phen]^{2+}$ with pyrocatechol and its derivatives (14). Their observation is similar to that made later by Bhattacharya and co-workers (15), who explained the stability order on the basis of an electron repulsion concept. The effect of dipyridyl analogues on the stability of the ternary complexes involving copper(II) and substituted *o*-hydroxy aldehyde has also been studied (16). Both groups conclude that the electron density over the ligand (L) with O^- as donor site has significant influence on the stability of the ternary $[CuAL]^+$ complexes. Electron-withdrawing substituents on L lower the stability of the complex and electron-donating substituents increase it (14, 16).

However, very few attempts have been made to isolate the ternary complexes in the solid state and to correlate their properties with solution characteristics. This would enable the study of various spectral and magnetic properties for the structural assignment of the complexes.

The present study involves the potentiometric determination of the stability constants of the ternary complexes $[CuAL]^+$ where A = bis(2pyridyl) amine (dpa = A^1) or 5-nitro-1,10-phenanthroline (5-N-phen, A^2) and HL = salicylaldehyde (SAL, HL^1), 5-bromosalicylaldehyde (5-B-SAL, HL^2), 5-nitrosalicylaldehyde (5-N-SAL, HL^3), 2-hydroxynaphthaldehyde (2-OH-naph, HL^4), and 2-hydroxyacetophenone (2-OH-acph, HL^5). These complexes have been isolated and characterised.

Experimental

Chemicals

The ligands dpa, 2-OH-acph, and 2-OH-naph were obtained from Fluka AG, 5-nitro-1,10-phenanthroline was from Sigma. Salycylaldehyde was reagent grade and was purified by distillation. 5-Nitrosalicylaldehyde was prepared by the known method (17), mp 127°C (126–127°C reported). 5-Bromosalicylaldehyde was prepared by low temperature (<5°C) bromination of salicylaldehyde by liquid bromine in acetic acid. The product, separated after addition of the reaction mixture to cold water, was recrystallised twice from ethanol; mp 107°C (lit. 18, 105–107°C).

Potentiometric determination of stability constants

An extended Irving–Rossotti titration technique (19) was used to determine preliminary values of formation constants of the complexes in aqueous dioxane (50% v/v) medium at $I = 0.2$ *M* ($NaClO_4$) and at temperature 30°C, using 0.2 *M* NaOH. pH values were corrected on the basis of experimental results,[2] to give the concentration of hydrogen

[1]To whom all correspondence should be addressed.

[2]pH values of standard perchloric acid solutions under the experimental conditions have been determined and compared with theoretical values. This difference takes into account liquid junction potential across the membrane and effect of the ionic strength of the medium (21). The constant difference has been considered as correction for other titration data.

Can. J. Chem. Downloaded from www.nrcresearchpress.com by 80.58.250.72 on 09/07/12
For personal use only.

TABLE 1. Stability constants of ternary complexes [CuAL] in aqueous dioxan (1:1, v/v) medium at 30°C, $I = 0.2\ M\ NaClO_4$[a]

			A^1 = dpa		A^2 = 5-N-phan		Δ log K	
L	log K_1^H	log K_{ML}^M	log K_{MAL}^{MA}	Δ log K	log K_{MAL}^{MA}	Δ log K	A^3	A^4
SAL	8.55 (±0.06)	5.92 (±0.08)	6.03 (±0.07)	+0.11	6.43 (±0.04)	+0.51	+0.75	+0.94
5-B-SAL	7.68 (±0.07)	5.29 (±0.03)	4.66 (±0.24)	−0.63	5.38 (±0.09)	+0.09	+0.35	+0.60
5-N-SAL	5.67 (±0.02)	3.79 (±0.06)	3.87 (±0.08)	+0.08	3.95 (±0.05)	+0.16	+0.24	+0.42
2-OH-naph	7.66 (±0.06)	6.23 (±0.02)	6.22 (±0.04)	−0.01	6.47 (±0.05)	+0.24	+0.62	+0.73
2-OH-acph	10.09 (±0.04)	6.61 (±0.03)	6.74 (±0.11)	+0.13	7.09 (±0.07)	+0.48	+0.96	+1.14

[a]A^3 = 1,10-phenanthroline and A^4 = 2,2′-bipyridyl. Δ log K values are taken from ref. 16. Values in parentheses indicate standard deviation.

ion in the solution. Formation constant values were further refined by using the computer program SCOGS (22) wherein activity coefficient has been considered to be equal to 1 (23) and ionic product of water in 50% aqueous dioxane (1.419×10^{-16}) (23, 24) has been used. Both stepwise formation of the ternary complex, as well as simultaneous existence of all the species LH, L^-, AH^+, A, Cu^{2+}, $[CuA]^{2+}$, $[CuA_2]^{2+}$, $[CuL]^{1+}$, $[CuL_2]$, and $[CuAL]^+$ were considered.

General method for the preparation of complexes

To 2.5 mmol $Cu(Ac)_2.H_2O$ in 50% alcohol – water mixture was added a mixture of equimolar amounts of ligands A and L in alcohol–water mixture. The resulting solution was refluxed for 15–20 min[3] followed by the addition of concentrated $NaClO_4$ solution. The resulting crystalline solid was separated by filtration, washed with alcohol, and analyzed for Cu (by acid decomposition and iodometric titration with standard $Na_2S_2O_3$ solution) for C, H (on a Coleman analyzer model No. 33), and for N by Duma's method.

Room temperature magnetic susceptibility measurements were done using Gouy method. Electronic spectra of the complexes in 50% aqueous dioxane solutions and diffuse reflectance spectra (d.r.s.) of the powdered samples were recorded on a Shimadzu UV 240 spectrophotometer with $BaSO_4$ as reference. Infrared spectra were recorded in KBr phase (as discs) on a Perkin Elmer IR spectrophotometer model No. 567.

Results and discussion

The formation of the complex $[CuAL]^+$ can take place either in steps (reactions [1] and [2] or reactions [3] and [4]) or the two ligands may combine simultaneously with the metal ion leading to reaction [5]:

$$[1]\quad M + A \overset{K_{MA}^M}{\rightleftharpoons} MA$$

$$[2]\quad MA + L \overset{\beta_{MAL}^M}{\rightleftharpoons} MAL$$

$$[3]\quad M + L \overset{K_{ML}^M}{\rightleftharpoons} ML$$

$$[4]\quad ML + A \overset{K_{MLA}^{ML}}{\rightleftharpoons} MAL$$

$$[5]\quad M + A + L \overset{\beta_{MLA}^M}{\rightleftharpoons} MAL$$

[3]Cu(II) complexes are known to be formed at room temperature instantaneously. However, the solutions were refluxed just to ensure completion of the reaction and to avoid any possibility of $[CuA_2]$ or $[CuL_2]$ being left out.

The overall formation constant β_{MAL}^M can then be given by either of the following combinations:

$$[6]\quad \log \beta_{MAL}^M = \log K_{MA}^M + \log K_{MAL}^{MA} = \log K_{ML}^M + \log K_{MAL}^{ML}$$

and the relative stability of the ternary complex with respect to the binary complex can be given as

$$[7]\quad \Delta \log K = \log K_{MAL}^{MA} - \log K_{ML}^M = \log K_{MLA}^{ML} - \log K_{MA}^M$$

Close agreement between the values, log K_{MAL}^{MA}, determined by considering stepwise formation of the complex (reactions [1] and [2]) and the values $\log \beta_{MAL}^M - \log K_{MA}^M$ determined by considering simultaneous formation of all the species indicate that the complex formation takes place in steps.

Table 1 reveals that Δ log K values of the ternary complexes of dpa are less positive compared to their 5-N-phen analogues. However, both of them are less positive than their bipyridyl and 1,10-phenanthroline analogues (16). Δ log K values for the latter two have been incorporated in Table 1. Δ log$K$ values for 5-N-phen complexes clearly indicate that the electron-withdrawing —NO_2 group has a destabilizing effect. This is in keeping with the observation made earlier that 2-(2′-pyridyl) benzimidazol, 2-hydroxyaldehydatocopper(II) complexes are less stable than 2,2′-bipyridyl, 2-hydroxyaldehydato-copper(II) complexes. This has been explained to be due to the lowering of M → 2-OH-aldehyde π-interaction in the ternary complex, involving another stranger π-acid ligand.

The electron-withdrawing —NO_2 group makes 5-N-phen a stronger π-acceptor. Hence, the Cu-2-hydroxyaldehyde π-bond is weakened and a less stable [Cu-5-N-phen-L] complex is formed compared to [Cu-*o*-phen-L] (16). However, the electron-releasing >NH group in dpa does not exert a stabilizing effect. This may be because in [Cu-dpa-L] complexes, where L = aromatic *o*-hydroxy aldehydes, both the ligands form six-membered chelate rings which are observed to be less stable than a combination of 5–6 membered chelate rings (26) as formed in [Cu-dipy-L].

It is also interesting to observe the effect of the nature of substitution over salicylaldehyde on the formation constant of

Can. J. Chem. Downloaded from www.nrcresearchpress.com by 80.58.250.72 on 09/07/12
For personal use only.

TABLE 2. Elemental analyses, magnetic moment, and molar conductivity data of the complexes $[CuAL]ClO_4$

Complex	Analyses % Cu	% C	% H	% N	μ (BM)	Λ^a (10^{-3} M)
$[CuA^1L^1].ClO_4$	14.15 (13.96)	43.74 (44.83)	2.86 (3.07)	9.12 (9.23)	1.75	105
$[CuA^1L^2].ClO_4$	11.84 (11.90)	38.70 (38.21)	2.63 (2.44)	8.09 (7.87)	1.71	110
$[CuA^1L^3].ClO_4$	12.53 (12.70)	40.33 (40.79)	2.74 (2.56)	10.84 (11.20)	1.78	94
$[CuA^1L^4].ClO_4$	12.66 (12.58)	50.02 (49.88)	3.02 (3.16)	8.16 (8.31)	1.79	100
$[CuA^1L^5].ClO_4$	33.07 (13.57)	45.77 (46.15)	3.88 (3.42)	8.77 (8.97)	1.70	110
$[CuA^2L^1].ClO_4$	12.59 (12.48)	44.71 (44.77)	2.35 (2.36)	8.93 (8.32)	1.65	96
$[CuA^2L^2].ClO_4$	10.82 (10.81)	38.33 (38.78)	2.04 (2.04)	6.67 (7.14)	1.82	91
$[CuA^2L^3].ClO_4$	11.41 (11.46)	40.73 (41.15)	2.41 (1.98)	9.99 (10.11)	1.77	110
$[CuA^2L^4].ClO_4$	11.50 (11.36)	48.92 (49.35)	2.55 (2.50)	7.37 (7.51)	1.72	92
$[CuA^2L^5].ClO_4$	12.12 (12.15)	45.81 (45.88)	2.41 (2.87)	7.57 (8.03)	1.84	97

[a]Equivalent conductances measured for 10^{-3} M methanolic solutions are reported in Ω^{-1} cm^2 mol^{-1}. The values in parentheses are those calculated for the formula $[CuAL].ClO_4$.

the ternary complex. From Table 1 it can be seen that Δ log K is less positive for $[CuAL]^+$ complexes where HL = 5-bromo, or 5-nitro-salicylaldehyde than the respective [CuA salicylaldehydate]$^+$ complexes. This is also true for [CuA 2-hydroxynaphthaldehydate]$^+$ complexes where the phenyl ring is fused in the 5–6 position. This is because of the electron-withdrawing effect of the nitro, and bromo groups or the fused phenyl ring. Complexes of $[CuA]^{2+}$ with 2-hydroxy acetophenone, having an electron-releasing methyl group as a substituent at carbonyl carbon, are expected to be slightly more stable than their salicylaldehyde analogues due to the electron-releasing effect of the $—CH_3$ group. However, in the present study we found Δ log K for [CuA salicylaldehydate]$^+$ and [CuA-2-hydroxyacetophenonate]$^+$ to be very close, probably because of the small electron-releasing tendency of the $—CH_3$ group. These observations are in agreement with the earlier results (16). This can be explained on the basis of the electron repulsion concept. When a ligand coordinates with the metal ion through O^-, there is coulombic repulsion between the metal d_π electron and the extra lone pair of electrons on O^-. Coordination with a π-bonding ligand like tertiary diamine (A) decreases the π-electron density over the metal ion through metal-to-ligand π-bonding. When a secondary ligand with O^-—O coordinating sites binds with $[MA]^{n+}$, it realizes less repulsion from the metal d_π electrons than when it binds with the free metal ion. This results in greater stability of the ternary complex compared to the corresponding binary complex. Substitution over the secondary ligand will affect the electron density over the coordinating atom and hence stability of the complex. Observations made in the present study are in accordance with the expectation that the electron-withdrawing group lowers the negative charge density over O^-—O whereas an electron-releasing $—CH_3$ group increases the electron density, resulting in stabilization or destabilization, respectively, of ternary complexes.

Isolation of complexes

The elemental analyses of the complexes (Table 2) correspond to the empirical formula $[CuAL].ClO_4$. Molar conductivity values of methanolic solutions indicated that these are 1:1 electrolytes. On the basis of these results the general structure of dpa complexes can be given as follows:

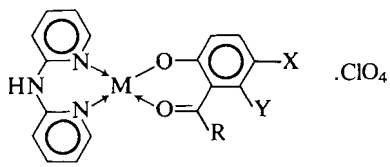

1, 6 X = H, Y = H, R = H
2, 7 X = Br, Y = H, R = H
3, 8 X = NO_2, Y = H, R = H
4, 9 XY = $—(CH)_4—$, R = H
5, 10 X = H, Y = H, R = CH_3
6 to **10** dpa is replaced by 5-N-phen

Room temperature magnetic susceptibility measurements correspond to one unpaired electron except in some cases where a slight lowering in magnetic moment indicates a possibility of weak intermolecular spin–spin interaction between the Cu(II) centres in the dimers, possibly formed by the linking of Cu(II) of one molecule with O^- of the aldehyde of the adjacent molecule in the solid state. According to a very recent report (7) crystal

Can. J. Chem. Downloaded from www.nrcresearchpress.com by 80.58.250.72 on 09/07/12
For personal use only.

TABLE 3. Ligand field bands of [CuAL] complexes ($\bar{\nu}$ in 10^3 cm^{-1})

		A = A^1			A = A^2		
			In 50% aq. dioxane			In 50% aq. dioxane	
L	CuL_2	$\bar{\nu}_c$ in d.r.s.	$\bar{\nu}_c$	$\Delta\bar{\nu}_c$	$\bar{\nu}_c$ in d.r.s.	$\bar{\nu}_c$	$\Delta\bar{\nu}_c$
A_1	15.20	—	—	—	—	—	—
A^2	14.28	—	—	—	—	—	—
L^1	12.63	15.87	15.87 (87)[a]	1.95	16.08	15.82 (84)	2.37
L^2	12.53	16.45	15.77 (88)	1.90	16.18	15.75 (103)	2.34
L^3	12.66	16.75	15.67 (86)	1.74	16.89	15.70 (89)	2.23
L^4	13.11	16.39	16.45 (114)	2.29	16.67	16.29 (96)	2.59
L^5	12.45	16.45 14.08	16.08 (96)	2.26	18.03 15.62(sh)	18.11, 15.87[b] (179) (169)	—

[a]Molar absorbance values in parentheses.
[b]Two bands observed in solution spectrum, hence estimation of the energy of the $d_{xy} \rightarrow d_{x^2-y^2}$ transition is not possible.

structure of (di-2-pyridylamine)salicylaldehydatocopper(II) perchlorate consists of a dimeric unit with two large apical Cu—O distances, one towards the O of the ClO_4 anion and the other one, linking two monomeric units, towards the O of the nearest salycylaldehyde molecule.

Electronic spectra

The complexes exhibit a broad band characteristic of paramagnetic Cu(II) centers in the region ~15 500 – 17 000 cm^{-1}. Diffuse reflectance spectra of these complexes in the solid state exhibit an unsymmetrical band which, in some cases, is split, giving two band maxima. This suggests a five coordinate structure due to dimerization. However, in solution there is only one band observed in all cases except in $[CuA^2L^5].ClO_4$. This indicates that the complex is four coordinated in solution. However, distortion from square planar geometry can not be ruled out.

Presuming D_{4h} geometry, the broad band in Cu(II) complexes (20) is due to the merger of three possible transitions, $A_{1g} \leftarrow B_{1g}$, $B_{2g} \leftarrow B_{1g}$, and $E_g \leftarrow B_{1g}$, which are close in energy. The central part of the broad band can be considered to correspond roughly to D_{qxy}. If we consider the $\bar{\nu}(d\text{–}d)$ in binary complexes $[CuA_2]$ and $[CuL_2]$ of primary and secondary ligands to be $\bar{\nu}_1$ and $\bar{\nu}_2$, respectively, and $\bar{\nu}_c$ for the ternary complex then the difference between observed $\bar{\nu}_c$ and the mean of $\bar{\nu}_1$ and $\bar{\nu}_2$ (eq. [8]) will be a measure of extra stabilization or destabilization of the ternary complex.

$$[8] \quad \Delta\bar{\nu} = \bar{\nu}_c - (\bar{\nu}_1 + \bar{\nu}_2)/2$$

It is observed that $\Delta\bar{\nu}$ has a positive value, indicating that the ternary complex is more stabilized than expected from average field created by the two ligands. The order of $\Delta\bar{\nu}$ can be correlated with $\Delta \log K$ value (eq. [7]) determined by potentiometric method. However, a linear relation between $\Delta\bar{\nu}$ and $\Delta \log K$ is not observed. This can not be expected because the stereochemistry of the binary and mixed complexes may not be perfect square planar and similar to each other.

Infrared spectra

All ten ternary complexes reported here exhibit carbonyl stretching frequencies between 1615–1640 cm^{-1}. They are shifted by about 50 cm^{-1} to the lower energy region in the complex compared to the corresponding bands in the free ligands, occurring at 1680–1700 cm^{-1} for aromatic $\diagdown$C=O and at 1695–1715 cm^{-1} for —CHO. The lowering in $\nu_{C=O}$ is due to its coordination with the metal ion. The complexes exhibit a strong absorption band at 1100 cm^{-1} corresponding to $\nu_{as\,Cl-O}$, supporting the presence of ionic perchlorate (25).

Acknowledgement

We are grateful to Council of Scientific and Industrial Research (CSIR), New Delhi, for financial assistance.

1. H. SIGEL (*Editor*). Metal ions in biological systems. Vol. 2. Marcel Dekker, Inc., New York. 1973.
2. H. SIGEL. Inorg. Chem. **19**, 1411 (1980).
3. P. K. BHATTACHARYA. J. Sci. Ind. Res. **40**, 382 (1981).
4. H. SIGEL. Chimia, **21**, 489 (1967).
5. H. SIGEL and B. PRIJS. Chimia, **29**, 138 (1975).
6. R. GRIESSER and H. SIGEL. Inorg. Chem. **9**, 1238 (1970).
7. M. T. GARLAND, J. Y. LE MAROUILLE, and E. SPONDINE. Acta Crystallogr., Sect. C: Cryst. Struct. Commun. C**41**(6), 855 (1985); Chem. Abstr. **103**(6), 46247*j* (1985).
8. P. J. PATEL, V. K. PATEL, and P. K. BHATTACHARYA. Indian J. Chem. **21**A, 590 (1982).
9. P. J. PATEL, V. K. PATEL, and P. K. BHATTACHARYA. Inorg. Chem. **21**, 3163 (1982).
10. R. GRIESSER, B. PRIJS, and H. SIGEL. Inorg. Nucl. Chem. Lett. **4**, 443 (1968).
11. B. E. FISCHER and H. SIGEL. Inorg. Chem. **18**, 425 (1979).
12. P. R. HUBER, R. GRIESSER, and H. SIGEL. Inorg. Chem. **10**, 945 (1971).
13. F. A. WALKER, H. SIGEL, and D. B. MCCORMICK. Inorg. Chem. **11**, 2756 (1972).

Can. J. Chem. Downloaded from www.nrcresearchpress.com by 80.58.250.72 on 09/07/12
For personal use only.

14. H. SIGEL, P. R. HUBER, R. GRIESSER, and B. PRIJS. Inorg. Chem. **12**, 1198 (1973).
15. P. J. PATEL and P. K. BHATTACHARYA. J. Ind. Chem. Soc. **59**, 310 (1982).
16. P. J. PATEL and P. K. BHATTACHARYA. J. Coord. Chem. **13**, 113 (1984).
17. S. DANDEGAONKAR and S. G. SHET. J. Ind. Chem. Soc. **42**, 323 (1965).
18. K. AUWERS and O. BURGER. Ber. **37**, 3934 (1904).
19. (*a*) H. M. IRVING and H. S. ROSSOTTI. J. Chem. Soc. 3397 (1953); (*b*) H. M. IRVING and H. S. ROSSOTTI. J. Chem. Soc. 2907 (1954).
20. A. B. P. LEVER. *In* Inorganic electronic spectroscopy. Elsevier Publishing Co., Amsterdam. 1968.
21. H. M. IRVING, M. G. MILES, and L. D. PETIT. Anal. Chim. Acta, **38**, 475 (1967).
22. (*a*) I. G. SAYCE. Talanta, **15**, 1397 (1968); (*b*) I. G. SAYCE. Talanta, **18**, 653 (1971); (*c*) I. G. SAYCE and V. S. SHARMA. Talanta, **19**, 831 (1972).
23. H. S. HARNED and B. B. OWEN. Physical chemistry of electrolytic solutions. Am. Chem. Soc. monograph 2nd ed. Reinhold Publ. Corp, New York. 1950.
24. H. S. HARNED and L. D. FALLON. J. Am. Chem. Soc. **61**, 2377 (1939).
25. K. NAKAMOTO. *In* Infrared and Raman spectra of inorganic and coordinate compounds. 3rd ed. John Wiley and Sons Inc. 1978.
26. H. SIGEL, P. R. HUBER, and R. F. PASTERNACK. Inorg. Chem. **10**, 2226 (1971).

Can. J. Chem. Downloaded from www.nrcresearchpress.com by 80.58.250.72 on 09/07/12
For personal use only.

Pronounced solvent effect on the absorption spectra of the photochemically produced 2,4-dinitrobenzyl carbanion

ROBERT A. MCCLELLAND
Department of Chemistry, University of Toronto, Toronto, Ont., Canada M5S 1A1

AND

STEEN STEENKEN
Max-Planck-Institut fur Strahlenchemie, D-4330 Mülheim, West Germany

Received August 6, 1986

ROBERT A. MCCLELLAND and STEEN STEENKEN. Can. J. Chem. **65**, 353 (1987).

The photochromism of 2,4-dinitrotoluene in aqueous solution has been attributed to formation of the 2,4-dinitrobenzyl carbanion (J. Chem. Phys. **39**, 1218 (1963)). The spectrum of the colored transient is, however, significantly different from that of ground state carbanion when formed in aprotic solvents through thermal decarboxylation of potassium 2,4-dinitrophenylacetate (J. Org. Chem. **49**, 413 (1984)). In this paper absorption spectra obtained upon 248 nm laser photolysis are reported, for solutions in water, acetonitrile, and their mixtures. The spectrum in acetonitrile does closely resemble that of the carbanion formed by decarboxylation. It is suggested that the same ion is formed in water, and a solvent effect is responsible for the significantly different spectrum. Spectra in the mixed solvents suggest that there is an equilibrium between differently solvated forms of the anion, the extremes being an unspecifically solvated form with λ_{max} 400 and 640 nm as in acetonitrile and a form in water that is hydrogen bonded through the nitro group with λ_{max} 350 and 500 nm. Experiments with conductivity detection provide corroborative evidence for carbanion formation. In acetonitrile a non-conducting transient is produced as a precursor to the anion. This is suggested to be the conjugate acid of the aci-nitro anion, formed by intramolecular hydrogen abstraction in the excited nitrotoluene.

ROBERT A. MCCLELLAND et STEEN STEENKEN. Can. J. Chem. **65**, 353 (1987).

Le photochromisme du dinitro-2,4 toluène dans des solutions aqueuses a été attribué à la formation du carbanion dinitro-2,4 benzyle (J. Chem. Phys. **39**, 1218 (1963)). Toutefois, le spectre de l'espèce de transition colorée est très différent de celui du carbanion dans son état fondamental, formé dans des solvants atropiques par le biais d'une décarboxylation thermique du dinitro-2,4 phénylacétate de potassium (J. Org. Chem. **49**, 413 (1984)). Dans la présente publication, on rapporte le spectre d'absorption obtenu par photolyse laser à 248 nm pour des solutions dans l'eau, dans l'acétonitrile et dans leurs mélanges. Le spectre dans l'acétonitrile ressemble beaucoup à celui du carbanion qui se forme par décarboxylation. On suggère que le même ion se forme dans l'eau et qu'un effet de solvant est responsable pour le spectre qui est passablement différent. Les spectres dans des solvants mixtes suggèrent qu'il existe un équilibre entre les diverses formes solvatées de l'anion; les extrêmes sont, d'une part, une forme qui n'est pas solvatée d'une façon spécifique, avec λ_{max} 400 et 640 nm et que l'on retrouve dans l'acétonitrile, et, d'autre part, une forme observée dans l'eau qui est liée par une liaison hydrogène par le biais du groupement nitro et qui présente des λ_{max} à 350 et 500 nm. Des expériences impliquant une détection de conductivité fournissent une corraboration de la formation du carbanion. Dans l'acétonitrile, il se forme une entité transitoire non-conductrice comme précurseur de l'anion. On suggère que cette entité est l'acide conjugué de l'anion aci-nitro qui se forme par un enlèvement intramoléculaire d'hydrogène dans le nitrotoluène excité.

[Traduit par la revue]

The photochromism of aqueous solutions of derivatives of 2-nitrotoluene is a well studied phenomenon (1–4). Flash photolysis experiments have provided spectra of the colored species produced upon irradiation, and life-times of these relatively long-lived species have been measured (5–10). The structure of the intermediate has been assumed to be that of an aci-nitro anion or, in its other resonance contributor, a 2-nitrobenzyl carbanion. There is evidence (ref. 11, see also later) that this is not the initial photoproduct. Yip and co-workers (12) have shown recently that both singlet and triplet excited states can be involved as precursors of the carbanion. Intermediates with the same spectra as the carbanion have also been found in the photodecarboxylation of 2-nitrophenylacetate ions in aqueous solutions (13, 14).

Recently Buncel and co-workers working in aprotic media have generated relatively stable solutions of nitrobenzyl carbanions, through toluene deprotonation (15) and by the thermal decarboxylation of the potassium salt of the corresponding nitrophenylacetate (16). The absorption spectra recorded for these solutions, however, proved to be significantly different from those (13, 14) generated in the flash experiments. Two alternative explanations were offered to account for the difference (16) — (*a*) that there are significant solvent effects on the spectra and (*b*) that the photochemical intermediates are radical or radical anion in nature.

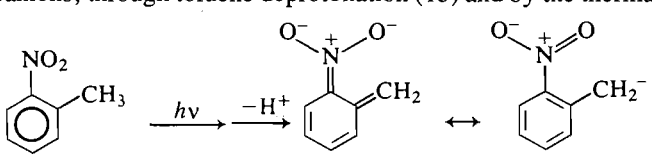

To resolve this question we have reinvestigated the photochemistry of the 2,4-dinitrotoluene system, employing laser flash photolysis with both optical and conductivity detection. Our results clearly establish that it is the 2,4-dinitrobenzyl carbanion which is formed upon irradiation, and that there are significant and interesting medium effects upon its absorption spectrum.

Results and discussion

Argon-bubbled solutions containing 1.6×10^{-4} molar 2,4-dinitrotoluene were irradiated with the 248.5 nm light of a Lambda Physik EMG 103 MSC excimer laser. As observed in previous flash experiments (9) transients of relatively long life-times are formed. Figure 1 shows spectra recorded in water and acetonitrile. In water, an intermediate is formed within the

Can. J. Chem. Downloaded from www.nrcresearchpress.com by 80.58.250.72 on 09/07/12
For personal use only.

Can. J. Chem. Downloaded from www.nrcresearchpress.com by 80.58.250.72 on 09/07/12
For personal use only.

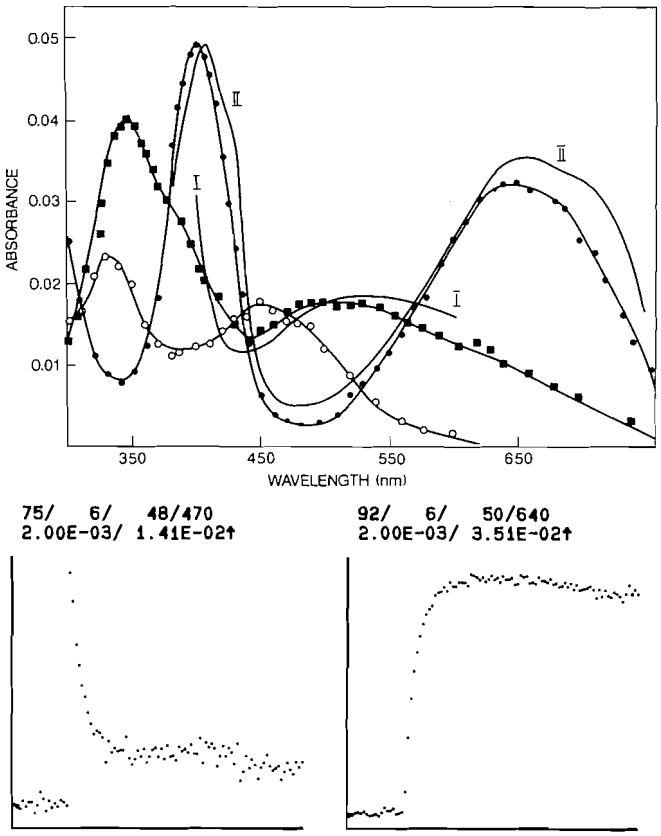

FIG. 1. Absorption spectra following 248.5 nm photolysis of 1.6×10^{-4} molar solutions of 2,4-dinitrotoluene in water (■) and in acetonitrile (○ and ●). (○) – intermediate **A**, spectrum recorded 3–5 $\times 10^{-6}$ s after flash and (●) – intermediate **B**, 3–5 $\times 10^{-4}$ s after flash. Spectrum I is the literature spectrum obtained upon flash photolysis in water (ref. 9). Spectrum II is the literature spectrum of the 2,4-dinitrobenzyl carbanion ion in dimethyl sulfoxide, obtained after ground state decarboxylation of potassium 2,4-dinitrophenylacetate (ref. 16). (Spectra I and II have been scaled such as to illustrate their correspondence to the laser spectra.) The bottom figures show time-resolved (2 ms entire trace) OD changes at 470 nm (left) and 640 nm (right) in acetonitrile.

25 ns pulse of the laser, undergoing pH dependent first-order decay in the seconds time range. The spectrum in this solvent agrees with that obtained previously using flash photolysis by Wettermark and Ricci (9), although these workers covered a narrower wavelength range and did not see the absorption maximum at 349 nm.

In acetonitrile a transient (**A**) also forms within the laser flash, but, in contrast to water, this intermediate undergoes a first-order change (see Fig. 1, bottom section) over a period of about 100 μs resulting in a second transient (**B**). The spectrum of the latter closely resembles that of the thermally generated 2,4-dinitrobenzyl carbanion in dimethyl sulfoxide (16). We conclude therefore that it is this ion which is being produced photochemically, not radical products.[1] An extinction coefficient of 1.4×10^4 M^{-1} cm^{-1} at the λ_{max} of 408 nm was determined for this carbanion (16). The 0.05 absorbance

[1]This conclusion is supported by in-situ photolysis esr experiments which show that radicals are barely detectable, unless a good hydrogen donor such as propan-2-ol is present, in which case the radical anion of 2,4-dinitrotoluene is observed.

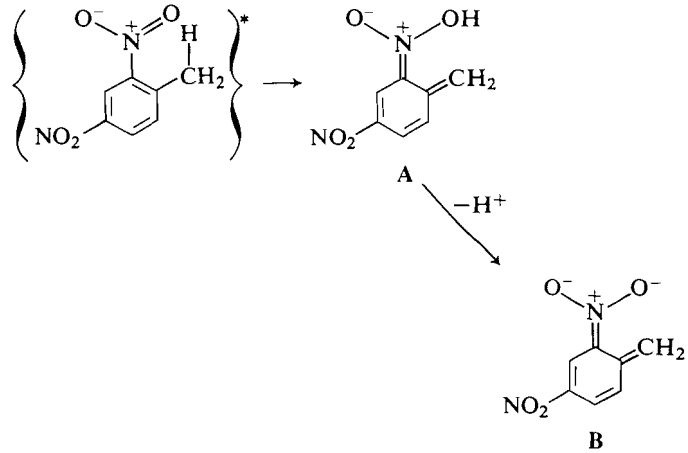

observed in the flash experiments therefore corresponds to 3.5×10^{-6} molar carbanion being produced (with the assumption that extinction coefficients are the same in the two solvents).

The presence in acetonitrile of a precursor to the anion suggests a mechanism with the excited state reaction involving hydrogen abstraction forming initially a neutral aci-nitro compound. Atherton and Craig (11) have recently reported similar observations with the same interpretation after laser photolysis of 2,6-dinitrotoluene in methanol and methanol:water mixtures. They have also carried out a detailed kinetic study of the deprotonation. We qualitatively observed that the transformation **A** → **B** is strongly accelerated by small amounts of water and amine bases. The possibility exists that even in the pure solvent, trace amounts of water are responsible for the ionization, not the weakly basic solvent. Wettermark and Ricci were able to observe a species assigned the structure of the acid form **A** in aqueous solutions by using strong acids (1 *M* $HClO_4$) to shift the **A** ⇄ **B** equilibrium (9). They observed also that the spectrum of the acid form is considerably shifted to lower wavelengths. A pK_a of 1 was determined by these workers from the spectroscopic change as a function of pH, and also from an analysis of the decay kinetics (9). We find that in water and in all water:acetonitrile mixtures investigated (Fig. 3) the neutral form is not observed as a precursor to the anion except in strongly acidic solutions (pH < 1). This is not unexpected. If **A** is a normal O—H acid, a pK_a of 1 means that deprotonation by the water solvent will occur with a rate constant of 10^8–10^9 s^{-1}, so that ionization will occur within the 25 ns flash.

Corroborating evidence comes from experiments carried out with conductivity detection. In dilute aqueous base irradiation results in a rapid conductivity decrease (Fig. 2*A*). This can be explained by the neutralization of hydroxide ion, that is, the replacement of hydroxide in the solution by the less mobile organic anion. In acid solution (Fig. 2*B*) a conductivity burst is observed. Here the photolysis is producing the anion and an equivalent amount of hydronium ion. In both acid and base solutions the conductivity returns to its original level in an exponential fashion. Rate constants for this change agree with those measured for the decay of the anion using optical detection. These also correspond with rate constants reported by Wettermark and Ricci (9). (Note the faster decay in acid as observed by these workers).

In aqueous solution the initial conductivity changes occur within the one μs resolution of the AC conductivity method, but as illustrated in Fig. 2*C* in acetonitrile irradiation results initially in a non-conducting solution. A conductivity increase then

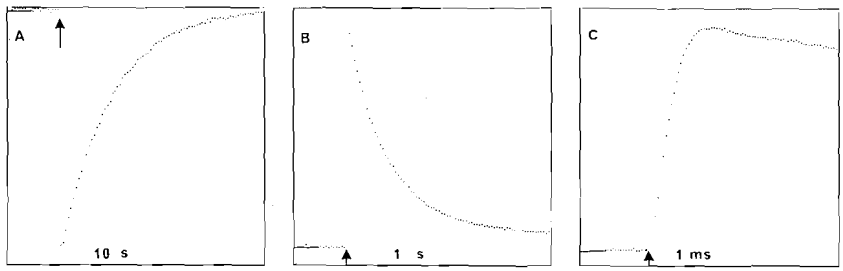

FIG. 2. Conductivity changes following 248.5 nm excitation of 1.6×10^{-4} *M* solutions of 2,4-dinitrotoluene. *A*, 10^{-4} *M* NaOH in water; *B*, 10^{-4} *M* HCl in water; *C*, acetonitrile. The arrow indicates the position of the laser flash. The time indicated is for the entire trace including the pre-flash.

occurs, on the same time scale as the spectral transformation **A** → **B**. This observation is consistent with the formation in acetonitrile of the neutral aci-nitro form as the initial intermediate, followed by its slower deprotonation to produce charged species, the aci-nitro anion and H^+. A slower conductivity decrease follows, part of which can be seen in Fig. 2*C*.

As seen in Fig. 1 there is a very large solvent effect on the spectra of the carbanion. In order to probe this in more detail spectra were obtained in a series of water:acetonitrile mixtures (Fig. 3). These suggest that there are two quite different forms of the anion, and acetonitrile or aprotic solvent form absorbing at 400 nm and 640 nm, and a water form absorbing at 350 nm and 500 nm. In the mixed solvents both forms are present, although the water content must be relatively high to observe a large amount of water form. It is possible that even in pure water some of the 400 nm/640 nm form is present, since there appear shoulders at these wavelengths on the 350 nm/500 nm bands.

The phenomenon of two differently absorbing forms of a nitro anion has been encountered previously, for the anion derived from 4-nitrophenylacetonitrile (17, 18). The explanation which has been offered is that the anion exists in two differently solvated forms, one where a water molecule or molecules are tightly hydrogen bonded to the nitro group and a second unspecifically solvated form lacking this hydrogen bonding. This is indicated by the structures below, although

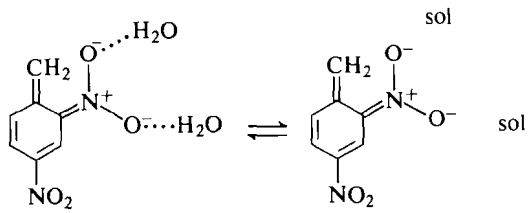

the actual number of water molecules involved in hydrogen bonding is unknown. The negative charge is obviously also delocalized to the 4-nitro group, and the relative contribution of this is also unknown. The exact nature of these solvations is unclear. As seen in Fig. 3 there are four reasonably isosbestic regions, indicating that there is an equilibrium between these two forms, with the concentration ratio depending upon the solvent composition.

Experimental section

2,4-Dinitrotoluene was a commercial sample and was used as received. Solvents were prepared with spectroscopic grade acetonitrile and water from a Millipore Milli-Q system. Solutions were prepared with 1.6×10^{-4} *M* nitro compound and had OD/cm = 0.6 at 248 nm. These were argon saturated and photolyzed with ≈20 ns pulses

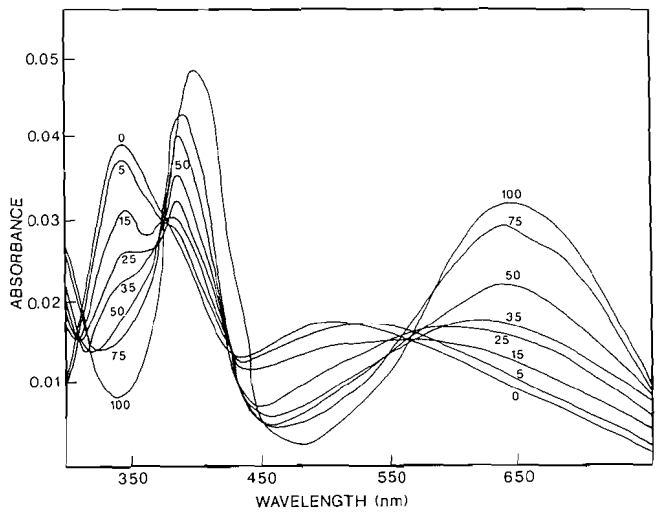

FIG. 3. Absorption spectra of the 2,4-dinitrobenzyl carbanion in water:acetonitrile mixtures (percent by volume acetonitrile shown). Curves have been drawn to provide the best fit to the experimental points.

(≈100 mJ) of 248 nm light (KrF) from a Lambda Physik EMG 103 MSC excimer laser. The optical and conductance signals were digitized by a Tektronix 7612 transient recorder interfaced with a DEC 11/73 computer which also ran the experiment and was used for the analysis and documentation of the data.

Acknowledgements

This work was conducted at the Max-Planck-Institut, whom R.A.M. thanks for their gracious hospitality. The technical assistance of Ms. Claudia Thom is acknowledged. R.A.M. also thanks the Natural Sciences and Engineering Research Council of Canada for its continued financial support. We also thank Dr. E. Buncel for useful discussions.

1. R. HARDWICK, H. S. MOSHER, and P. PASSAILAIGUE. Trans. Faraday Soc. **56**, 44 (1960).
2. H. S. MOSHER, C. SOUERS, and R. HARDWICK. J. Chem. Phys. **32**, 1888 (1960).
3. J. A. SOUSA and J. WEINSTEIN. J. Org. Chem. **27**, 3155 (1962).
4. J. D. MARGERUM, L. J. MILLER, E. SAITO, M. S. BROWN, H. S. MOSHER, and R. HARDWICK. J. Phys. Chem. **66**, 2434 (1962).
5. G. WETTERMARK. Nature, **194**, 677 (1962).
6. G. WETTERMARK. J. Phys. Chem. **66**, 2560 (1962).
7. H. S. MOSHER, E. R. HARDWICK, and D. BEN HUR. J. Chem. Phys. **37**, 904 (1962).
8. G. WETTERMARK. J. Am. Chem. Soc. **84**, 3658 (1962).
9. G. WETTERMARK and R. RICCI. J. Chem. Phys. **39**, 1218 (1963).

Can. J. Chem. Downloaded from www.nrcresearchpress.com by 80.58.250.72 on 09/07/12
For personal use only.

10. G. WETTERMARK, E. BLACK, and L. DOGLIOTTI. Photochem. Photobiol. **4**, 229 (1965).
11. S. J. ATHERTON and B. B. CRAIG. Chem. Phys. Lett. **127**, 7 (1986).
12. R. W. YIP, D. K. SHARMA, R. GIASSON, and D. GRAVEL. J. Phys. Chem. **89**, 5328 (1985).
13. J. D. MARGERUM. J. Am. Chem. Soc. **87**, 3772 (1965).
14. J. D. MARGERUM and C. T. PETRUSIS. J. Am. Chem. Soc. **91**, 2467 (1969).
15. E. BUNCEL and B. C. MENON. J. Am. Chem. Soc. **102**, 3499 (1980).
16. E. BUNCEL, T. K. VENKATACHALAM, and B. C. MENON. J. Org. Chem. **49**, 413 (1984).
17. M. J. MINCH, M. GIACCIO, and R. WOLFF. J. Am. Chem. Soc. **97**, 3766 (1975).
18. E. A. WALTERS. J. Phys. Chem. **81**, 1955 (1977).

Can. J. Chem. Downloaded from www.nrcresearchpress.com by 80.58.250.72 on 09/07/12
For personal use only.

A carbon-13 nuclear magnetic resonance study of solid tetracyclines

SANDRA MOOIBROEK[1] AND RODERICK E. WASYLISHEN[2]
Department of Chemistry, Dalhousie University, Halifax, N.S., Canada B3H 4J3

Received June 2, 1986

SANDRA MOOIBROEK and RODERICK E. WASYLISHEN. Can. J. Chem. **65**, 357 (1987).

Magic angle sample spinning and proton/carbon-13 cross-polarization techniques have been used to obtain high resolution solid state ^{13}C nuclear magnetic resonance spectra of several tetracycline antibiotics. Carbon-13 resonances in the solid state are assigned by measuring the extent of dipolar broadening due to neighbouring quadrupolar nuclei and by using a pulse sequence that suppresses non-quaternary carbon resonances. The observed ^{13}C chemical shifts are discussed in light of the known solid state structures derived from X-ray diffraction, and are compared with those in solution. It is shown that the solid state nuclear magnetic reosnance technique is capable of clearly distinguishing between the neutral and zwitterionic forms of the tetracycline free bases.

SANDRA MOOIBROEK et RODERICK E. WASYLISHEN. Can. J. Chem. **65**, 357 (1987).

On a utilisé les techniques de l'angle magique de couplage de l'échantillon et de polarisation croisée proton/carbone-13 pour obtenir des spectres rmn ^{13}C à l'état solide de plusieurs antibiotiques de la famille des tétracyclines. On a attribué les résonances en ^{13}C du spectre à l'état solide en mesurant l'amplitude de l'élargissement dipôlaire provenant du noyau quadrupôlaire voisin et en utilisant une séquence pulsée qui supprime les résonances de carbones qui ne sont pas quaternaires. On discute des déplacements chimiques observés pour les ^{13}C en fonction des structures à l'état solide qui ont été obtenues par diffraction des rayons-X et on les compare avec ceux observés en solutions. On démontre que la technique rmn à l'état solide peut distinguer sans ambiguïtés entre les formes neutre et zwitterioniques des tétracyclines existant sous la forme de bases neutres.
[Traduit par la revue]

Can. J. Chem. Downloaded from www.nrcresearchpress.com by 80.58.250.72 on 09/07/12
For personal use only.

Introduction

Since the solid state nmr techniques of cross-polarization (CP) (1) and magic-angle spinning (MAS) (2) were first used in combination (3), high resolution ^{13}C nmr of many important biological and chemical compounds has become possible (4). The advantages of using CPMAS to obtain solid state ^{13}C nmr spectra are many. The solid state spectrum may contain unique structural features, which in solution are averaged and hence not observed in the corresponding solution spectrum. Problems with finding a solvent to dissolve the material, overlapping solvent peaks in the spectrum, or solvent effects on chemical shifts are obviously avoided. In addition, the chemical shifts of a ^{13}C spectrum obtained from a powdered sample are sensitive to the conformational and electronic properties of exactly the same structures reported by X-ray diffraction studies. The technique can thus provide a "bridge" between crystal structure information and ^{13}C nmr solution data. For this reason, we have obtained solid state ^{13}C CPMAS nmr spectra of tetracycline and some of its derivatives (**1**), to clarify subtle differences in the various forms.

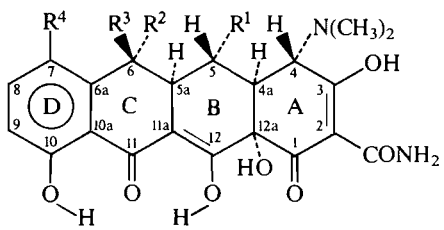

Generic Name	R^1	R^2	R^3	R^4	Abbreviation
Tetracycline	H	CH_3	OH	H	TC
Oxytetracycline	OH	CH_3	OH	H	OTC
Chlortetracycline	H	CH_3	OH	Cl	CTC
Demeclocycline	H	H	OH	Cl	
Doxycycline	OH	CH_3	H	H	
Minocycline	H	H	H	$N(CH_3)_2$	

[1]Holder of an NSERC 1967 Science and Engineering Scholarship.
[2]Author to whom correspondence may be addressed.

The chemical properties of this broad class of antibiotics have been of considerable interest (5), particularly the conformation of the free (6–23) and the complexed (24–32) molecules, since the mechanism by which the drug enters the cell and blocks ribosomal protein production, and what role metal ions or other complexes play in the action, are still not clear (33).

Crystal structures have been reported for the chlortetracycline (CTC) (6), oxytetracycline (OTC) (7), tetracycline (TC) (10), doxycycline (6-deoxy-OTC) (18), and demeclocycline (6-demethyl-7-CTC) (23) hydrochloride salts, and for the TC and OTC free bases (15–17). The conformations of the hydrochloride salts are very similar, differing mainly in the tautomeric form of the amide substituent (**2**, **3**), and in localization of the hydroxy proton, depicted on the C3 hydroxy in **1** as is commonly found in the literature, but, more realistically, is associated with the amide carbonyl in **2** and **3** as is reported by X-ray crystallographers (6, 18, 23).

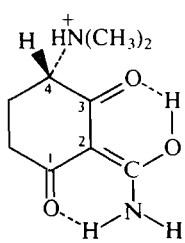

2

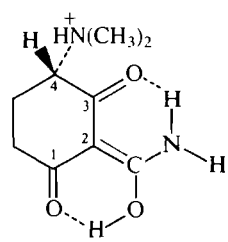

3

By contrast, oxytetracycline free base has been shown (15, 16) to crystallize in either a non-ionized anhydrous form (OTC^0, **4**), or as the zwitterionic dihydrate (OTC ±, **5**). The two differ markedly in intra- and intermolecular hydrogen bonding, and in the conformation of the A ring with respect to the plane of the BCD rings; OTC ± being very similar to the fully protonated salt, and OTC^0 displaying a conformation similar to that of an inactive derivative, 5,12a-diacetyloxytetracycline (8, 34). While Palenik *et al.* (23) argue that due to the relatively extreme methods used to obtain the anhydrous crystal (15), the OTC^0 modification is probably not biologically significant, Stezowski and co-workers (19) report that both forms of the free base

TABLE 1. Solid state ^{13}C nmr chemical shifts

Compound	CH_3	5	4a	5a	$N(Me)_2$	6	4	12a	2
TC HCl	23.3	30.5	35.8	43.1	37.5, 44.6	68.8	69.8	74.5	97.4
TC ±	22.4	29.9	32.5	40.6	35.4, 40.6	69.5	71.7	75.8	99.5
TC (non-ionized)[b]	20.8	24.5	38.4	43.5	44.1, 44.1	69.1	69.4	75.2	96.7
epi-TC HCl	19.8	22.7	37.7	44.1	37.3, 39.0	69.6	65.9	77.6	101.9
TC HCl in D_2O	22.3	26.9	35.4	42.3	43.3	70.7	70.4	74.4	97.5
TC base in DMSO	22.8	22.5	37.4	40.8	42.4	68.1	69.8	74.3	98.5
epi-TC in DMSO	22.4	19.8	43.3	42	42	68.0	66.0	73.7	95.5
OTC HCl	26.8	66.7	43.2	51.8	38.9, 44.9	69.7	63.5	73.4	97.7
OTC ±	24.1	67.7	40.8	48.6	38.5, 42.8	71.0	69.0	74.6	98.7
OTC (non-ionized)	25.8	67.7	47.3	49.5	34.5, 45.1	68.9	61.3	74.1	101.7
OTC HCl in D_2O	24.5	65.9	43.3	51.2	43.6	71.2	67.4	74.0	97.7
CTC HCl	26.4	31.4	35.5	43.1	38.2, 44.1	72.6	70.1	74.4	97.1
Demeclocycline HCl	—	31.8	34.6	37.6	37.5, 44.3	64.0	69.0	74.8	94.1
Doxycycline HCl	17.5	67.0	36.6	44.8	40.9, 43.8	40.1	71.6	73.6	99.2
	15.7	67.0	36.6	43.8	43.8, 46.4	39.5	69.3	73.6	95.2
Minocycline HCl	—	27.4	35.6	31.9	39.5, 43.8	35.6	68.9	76.4	100.2

[a]Solution shifts are from ref. 14. Errors in peak positions are approximately ±0.2 ppm. Where appropriate, corrections have
[b]Errors in peak positions for TC (non-ionized) estimated to be ±1.0 ppm.

coexist in $EtOH/H_2O$ solutions, and that when the composition of the solvent is less than 20% H_2O, the non-ionized form (OTC^0) predominates. They propose that biological activity of the antibiotic involves both conformations, and that interconversion occurs in vivo in aqueous or lipid-rich phases.

Solvent induced changes in conformation have not been discussed in ^{13}C nmr solution studies (11, 13, 14), although differences in the ^{13}C chemical shifts of tetracycline derivatives in DMSO-d_6 and in H_2O are noted (14). These differences, though subtle for most of the resonance peaks, are nonetheless critical for the understanding of chemical shifts due to structural changes (e.g., **4** vs. **5**).

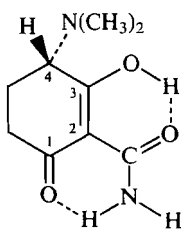

4

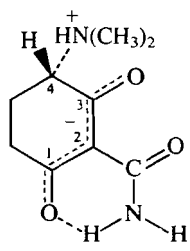

5

In this respect, we present the solid state ^{13}C nmr chemical shifts of the fully protonated, zwitterionic, and non-ionized forms of tetracycline and oxytetracycline, as well as the solid state ^{13}C shifts of several other tetracycline-derived salts. The results are discussed in terms of both corresponding solution values (14) and X-ray crystal data (6, 7, 10, 15–23), and should serve as the basis for further ^{13}C nmr studies of tetracycline derivatives and their metal complexes (26, 27).

Experimental

The hydrochloride salts of TC, OTC, CTC, demeclocycline, doxycycline, and minocycline and the free base hydrates of TC and OTC were purchased from the Sigma Chemical Company. All gave well-resolved, good signal-to-noise solid state nmr spectra except for tetracycline hexahydrate, which was purified by recrystallization from aqueous acetone solution. Anhydrous TC and OTC free base were prepared by the method of Stezowski (15); 4-epi-TC was prepared by the method of Doerschuk *et al.* (35). The purity of the samples was checked by the appearance of the solid state nmr spectrum, and, in the case of the salt, base, and epimer of TC, by ultraviolet absorbance ratio assay (36).

Powdered samples of the tetracyclines (≈0.5 g) were packed into cylindrical rotors made from alumina. Carbon-13 nmr spectra were obtained at 50.3 MHz on a Bruker MSL-200 while magic angle spinning at a rate of 4.5–5 kHz. Cross-polarization was acomplished using the Hartmann–Hahn match with 90° pulses of about 4 μs and contact times of 2–3 ms. Data tables of 8 K points were collected over a sweep width of 13.5 kHz. To improve signal-to-noise, spectra were signal averaged for at least 100 transients using recycle times of 2–3 s. Also, a sensitivity enhancement corresponding to 15 Hz of line broadening was applied before Fourier transformation. During non-quaternary suppression experiments (37), the high power decoupler was switched off for 40–50 μs.

All carbon-13 chemical shifts were referenced with respect to external adamantane, which has shifts of 29.50 ppm (*C*H) and 38.56 ppm (CH_2) with respect to TMS (38).

Results and discussion

Representative spectra are shown in Fig. 1 and chemical shifts are listed in Table 1. Assignment of the spectra was primarily based upon non-quaternary suppression experiments, comparison to solution state results (14), and the solid state ^{13}C shifts of other tetracycline derivatives.

The non-quaternary suppression sequence (37) suppresses resonance signals from strongly dipolar coupled nuclei, and thus only quaternary and methyl resonances are observed. In the case of the tetracycline family, use of the experiment can immediately distinguish signals C6a from C8, C10a from C7 and C9, C6 from C4, and the methyl resonances of C6-CH_3 and the C4-$N(CH_3)_2$ group. Important to note here is the inequivalence of the amino-methyls: the two resonance signals typically diverge by 3–7 ppm (see Table 1), except in TC^0 and OTC^0 where the amino group is not protonated (15, 16), and in the inactive 4-epimer of TC in which the configuration of the C4-H and C4-$N(CH_3)_2$ is opposite to that in TC and the other derivatives (39). The separation of the $N(CH_3)_2$ peaks in these cases is unresolved, ≤2 ppm, 10.6 ppm, and 1.7 ppm, for TC^0,

Can. J. Chem. Downloaded from www.nrcresearchpress.com by 80.58.250.72 on 09/07/12
For personal use only.

of tetracycline derivatives, given in ppm from TMS[a]

Carbon											
11a	9	10a	7	8	6a	10	$CONH_2$	12	3	1	11
108.9	114.3	115.0	119.5	140.1	150.3	163.5	173.1	172.8	187.4	192.0	195.7
107.3	115.7	115.7	118.6	135.4	146.0	161.1	170.5	176.1	185.9	187.4	193.2
106.3	114.2	114.4	116.5	137.0	147.3	162.1	174.0	177.6	190.2	192.5	193.7
103.5	114.1	118.2	118.2	134.1	145.1	162.2	171.1	180.8	187.0	194.0	196.0
107.1	116.8	114.9	118.7	138.5	146.9	162.0	173.5	174.1	187.2	193.8	193.8
105.9	114.5	114.4	116.9	136.4	148.0	161.4	172.4	176.8	191.8	192.3	192.9
106.6	115.9	114.5	117.5	136.5	148.0	161.4	172.9	175.1	187.8	191.3	193.0
106.1	114.5	114.5	119.6	140.2	150.1	164.0	174.8	172.3	188.0	191.4	195.9
105.3	115.9	116.4	118.6	140.1	147.4	161.7	170.6	177.5	183.2	191.9	194.1
103.9	118.5	112.2	118.5	140.5	146.1	163.7	171.2	170.5	191.5	192.4	193.7
105.6	116.7	115.2	118.7	138.4	147.7	162.6	172.5	173.5	187.2	193.6	194.6
108.2	121.5	117.6	128.2	143.0	146.9	164.1	172.3	174.1	187.3	191.9	194.3
106.0	122.8	115.2	130.7	138.2	140.3	163.6	173.0	173.0	187.8	192.7	192.7
107.8	115.9	115.8	118.9	138.0	149.2	161.5	171.8	174.0	186.0	193.1	197.1
106.6	115.9	115.2	118.9	137.8	146.1	160.6	171.8	175.2	189.4	192.4	193.8
108.7	120.7	115.3	133.9	130.4	133.9	158.8	171.2	177.2	187.0	189.5	194.4

been made for C—N dipolar splitting.

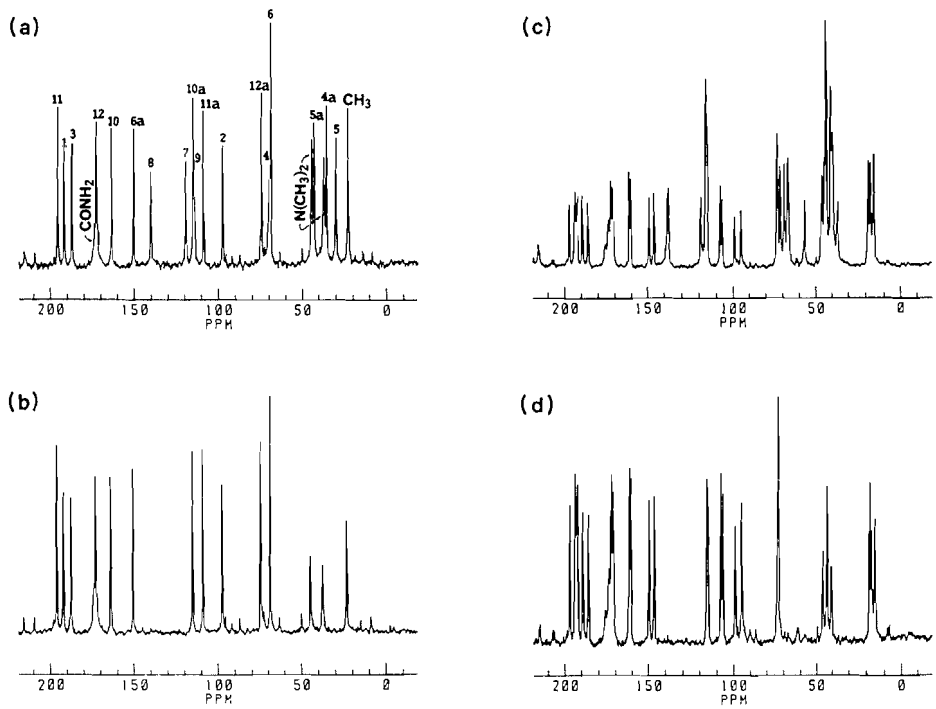

FIG. 1. ^{13}C CPMAS solid state nmr spectra of (*a*),(*b*) tetracycline·HCl and (*c*),(*d*) doxycycline·HCl. Spectra (*b*) and (*d*) were obtained using the non-quaternary suppression pulse sequence (37).

OTC^0, and epi-TC, respectively. In solution, the dimethylamino signals are averaged to a single peak, which in DMSO-d_6 is buried underneath the solvent septet centred at 39.5 ppm, along with the C5a signal (14a). At low pH the proton resonances of the two methyl groups are inequivalent (14*b*).

Also unique to the solid state spectra is the observation of broadening and (or) splitting of the resonance signals of carbons attached to quadrupolar nuclei having nonzero electric field gradients (EFG) (40, 41). The most obvious example is the C7 resonance of chlortetracycline and demeclocycline hydrochlorides (see Fig. 2). The chlorine substituent has such a large quadrupole coupling constant that the spin 3/2 nucleus (^{35}Cl, natural abundance 75.53%, or ^{37}Cl, natural abundance 24.47%) is not quantized along the magnetic field (B_0) direction. As a result, ^{13}C–chlorine dipolar coupling cannot be averaged by rapid spinning at the magic angle (54.7°) with respect to B_0 (40, 41).

The actual ^{13}C nmr lineshape for an aromatic carbon dipolar coupled to directly bonded ^{35}Cl can be estimated using the analysis of Zumbulyadis *et al.* (41). Assuming a quadrupolar coupling constant A of 71.09 MHz (42), the ratio of the chlorine Zeeman interaction, Z, to A is 0.276 at $B_0 = 4.7$ T. Carbon-13

Can. J. Chem. Downloaded from www.nrcresearchpress.com by 80.58.250.72 on 09/07/12
For personal use only.

Can. J. Chem. Downloaded from www.nrcresearchpress.com by 80.58.250.72 on 09/07/12
For personal use only.

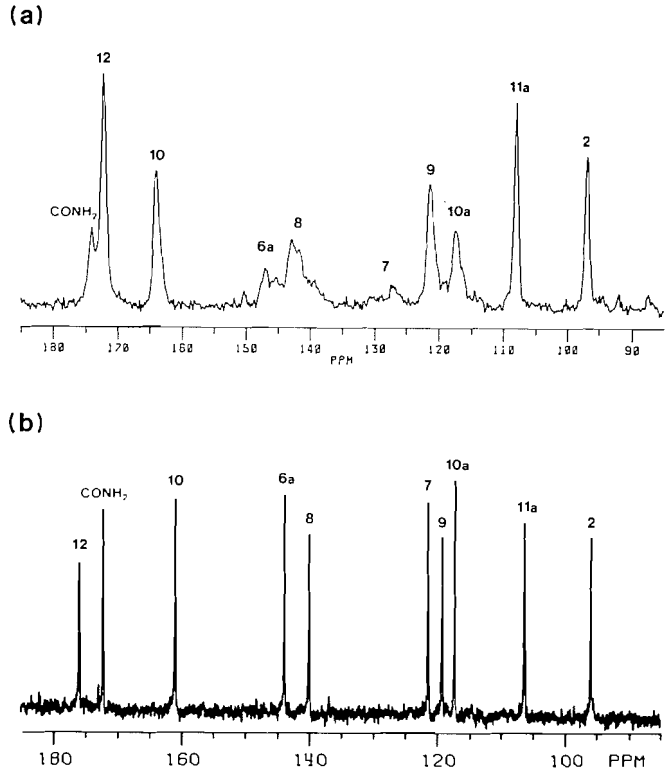

FIG. 2. Expanded region of (*a*) of the solid and (*b*) solution state ^{13}C nmr spectra of chlortetracycline·HCl, showing $^{13}C-^{35}Cl$ dipolar broadening of the substituted carbon 7 and neighbouring carbons 6a and 8. The solution spectrum was obtained with a 0.2 *M* DMSO-d_6 solution, using the central DMSO-d_6 transition (39.56 ppm (51)) as reference.

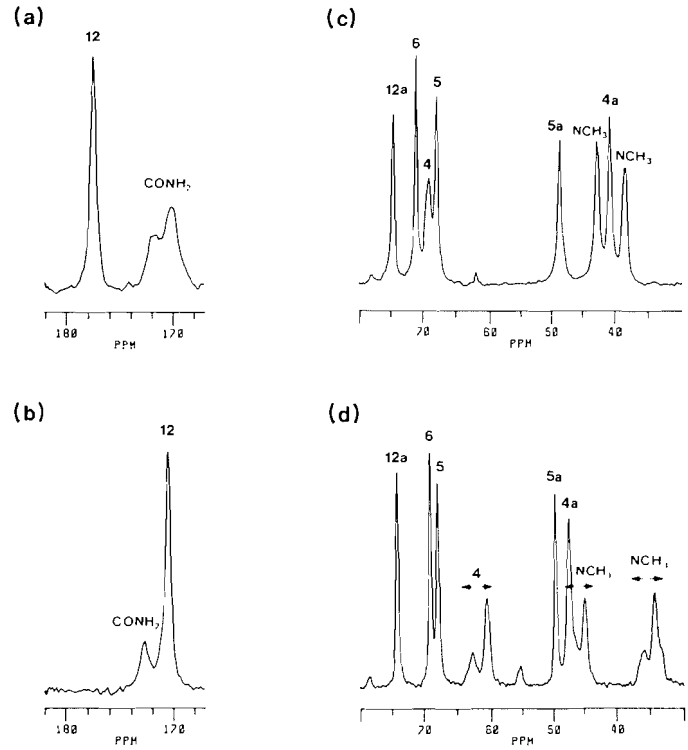

FIG. 3. Segments of the ^{13}C solid state nmr spectrum of (*a*),(*c*) OTC·$2H_2O$ and (*b*),(*d*) OTC^0 showing $^{13}C-^{14}N$ dipolar splitting in the C_{amide} carbonyl peak (*a*) and deprotonated $N(CH_3)_2$ methyl peaks (*d*).

nmr spectra calculated using Z/A ratios of 0.25 and 0.33 are illustrated in Fig. 2 of ref. 41. If the ^{35}Cl relaxation times are long enough to neglect $^{13}C-^{35}Cl$ self-decoupling (43), the calculated spectrum is expected to span a range of at least 2.0 D, where $D = (\gamma_C\gamma_{Cl}\hbar)/2\pi r^3 = 590$ Hz. In Fig. 2*a*, the expanded region of the ^{13}C solid state spectrum of CTC·HCl shows a broadening and splitting of at least 200 Hz of the C7 resonance signal, and neighbouring carbons C6a and C8 are also substantially broadened by the chlorine substituent. The signal-to-noise and overlap with other resonances make it difficult to rule out the possibility of partial self-decoupling. Similar effects were observed in demeclocycline hydrochloride.

Another example of dipolar broadening due to directly bonded quadrupolar nuclei is the amide carbonyl signal, which is affected by the amino ^{14}N. The breadth and low intensity of this signal serve to distinguish it from the nearby C12 peak. In solution, the amide shift is always reported to be upfield of the C12 signal (14), but in the solid this order is occasionally reversed. Typically, the amide resonance appeared as an asymmetric doublet (41, 44–46) with an apparent splitting of approximately 100 Hz (Fig. 3*a*). In some cases part of the doublet was obscured by the C12 resonance (e.g., Fig. 3*b*). The magnitude of the observed splitting is in good agreement with that calculated (47) using the method of Hexem *et al.* (45). Assuming a ^{14}N quadrupolar coupling constant of 2.274 MHz ($\eta = 0.378$) for the amide moiety (48) and a nitrogen–carbon bond length of 1.35 Å, calculations predict an apparent splitting of approximately 125 Hz, in good agreement with experiment.

The effect of ^{14}N on the C4 resonance signal is of particular interest. The peak is very sharp when the dimethylamino group is fully protonated (Fig. 3*c*) and the symmetry about the ^{14}N is approximately tetrahedral (i.e., the field gradient is small (49), and the ^{14}N nuclear spins are quantized along B_0). In the non-ionized form of OTC base, however, the $N(CH_3)_2$ group is not protonated (15) and the large EFG of the nitrogen (50) broadens and splits the C4 and $N(CH_3)_2$ resonance signals as shown in Fig. 3*d*. This feature of the C4 signal is useful not only for its sensitivity to the degree of $N(CH_3)_2$ protonation, but also as a means of differentiating the C4 and C5 signals in OTC and doxycycline (**1**). The two peaks are close together in the spectra of these compounds due to the 35–40 ppm downfield shift of the C5 signal by the hydroxy substituent.

Assignment of most of the other resonance peaks is straightforward since the chemical shifts differ little from solution values. Exceptions include: (*i*) C7 and C9 signals that are very close and may be interchanged (except in CTC, demeclocycline, and minocycline where C7 is shifted to higher frequency by substituents); (*ii*) C11a and C2, which are assigned by similarity to solution shifts (14), but are too close in epi-TC and non-ionized OTC^0 for the assignment to be reliable; and (*iii*) the group of low field carbonyls C11, C1, and C3. These last three have been tentatively assigned by consideration of the available X-ray data (6, 7, 15, 23), and by comparison to pH induced shifts obtained in solution (12).

Asleson and Frank (12) report that tetracycline carbon-13 signals that have an appreciable change in chemical shift (≥ 1.0 ppm) in the pH 1–6 range are the C1, C2, amide, C3, C4, $N(CH_3)_2$, C4a, C5, C12 and C12a carbons, and associate the observed pK_a (≈ 3.3) to the deprotonation of the A ring

tricarbonyl system. Their results indicate low frequency (high field) shifts in the positions of the C1, C3, and Cam peaks of −2.3, −2.7, and −1.9 ppm, respectively, upon increasing the pH from 1 to 6 for TC·HCl in 50% DMSO, 50% H_2O solution. The assigned solid shifts in TC·HCl as compared to TC·hexahydrate are −4.6, −1.5, and −2.6 ppm for the C1, C3 and Cam, while the corresponding shifts in OTC·HCl as compared to OTC/$2H_2O$ are +0.5, −4.8, and −4.2 ppm, respectively. The different behavior of C1, C3, and Cam in TC·HCl and OTC·HCl upon deprotonation of the A ring tricarbonyl system is consistent with the different known solid state structures of TC± (15, 17) and OTC± (15). X-ray diffraction studies indicate that the amide group of OTC± exists in a conformation depicted by **2** (15) while in TC± the conformation of the amide group is that shown in **3** (15, 17); the hydrochloride salts of both TC and OTC exist in form **2** (7, 10). The high frequency shifts of C12, C2, C4, and C12a, and the concurrent low frequency shifts of C4a, C11, and C11a confirm that the crystalline TC±·$6H_2O$ and OTC±·$2H_2O$ correspond to the solution zwitterionic free bases of TC and OTC respectively (10, 14).

The ^{13}C shifts of the anhydrous free base derivatives are consistent with the non-ionized (enol) conformation (**4**) reported by Stezowski and co-workers for both the anhydrous OTC^0 crystal (15) and for the free base in nonaqueous solution (19). The deprotonation of the C4-$N(CH_3)_2$ group and enolization of the A ring is particularly noticeable in (*i*) TC, by the high frequency shifts of C4a (+5.9 ppm) and C1 (+5.1 ppm), and the low frequency shift of C5 (−5.4 ppm); (*ii*) also in OTC, by the high frequency shifts of C4a (+6.5 ppm) and C3 (+8.3 ppm), and the low frequency shifts of C4 (−7.7 ppm) and C12 (−7.0 ppm). The magnitude and direction of these shifts is comparable to the results of Asleson and Frank upon deprotonation of the dimethylamino group in solution (12). Again, the observed shifts depend on the tautomeric form of the amide and conformation of the A ring, with TC shifts being more influenced in the adjacent B ring carbons (C5, C5a) than the OTC chemical shifts, which show a more pronounced effect on A ring carbon positions.

Shifts due to tautomeric form and slight changes in conformation are also clearly seen in the ^{13}C solid state spectrum of doxycycline hydrochloride, Fig. 1*c*,*d*. Unlike the salts of other TC derivatives, which have only one type of molecule per unit cell (6, 7, 10, 23), doxycycline·HCl crystallizes with one ethanol, one water, and two unique doxycycline molecules per unit cell (18). The two molecules differ mainly in the amide conformation, with DOXY(1) having the form indicated in **2** and DOXY(2) having the form shown in **3**. Each molecule has its own set of resonance peaks and hence many of the ^{13}C signals are split, some by as much as 4 ppm (e.g., C2). Signals due to ethanol in the crystal are also observed at 56.9 ppm and 18.6 ppm (see Fig. 1*d*).

In most cases, the assignment of a pair of signals to a particular carbon is quite obvious, but the high frequency carbonyl resonance peaks overlap and the choice of which two belong to C1, C3, or C11 is not clear. On the basis of the development of peak intensity with increasing contact time, these resonance signals were paired and tentatively assigned as shown in Table 1. The change in amide conformation appears to affect the C3 position much more than C1. Surprisingly, the shift difference between the C11 peaks is also quite large, as is the range of C11 shifts in the different forms of TC and OTC. Since the conformation of the BCD rings and the C11—O11 and $O_{11}\cdots H$ bond lengths show little variation among the crystal structures determined so far (15, 23), the range of C11 shifts is likely due to intermolecular effects such as packing or hydrogen bonding with water.

Conclusions

^{13}C CPMAS nmr has proven to be particularly useful in clarifying the chemical shift differences between various forms of tetracycline and oxytetracycline. These differences must be understood to interpret ^{13}C nmr data of the complexed antibiotics. In addition, the solid state spectra have displayed interesting phenomena that are not observed in the corresponding ^{13}C solution state spectra, namely, inequivalence of the amino methyl groups and quadrupole effects of adjacent ^{35}Cl and ^{14}N nuclei. The latter are particularly important in distinguishing the zwitterionic and neutral forms of the tetracycline.

Acknowledgements

We wish to thank Mr. Ross Dickson for several lineshape calculations and NSERC for financial support in the form of an equipment grant, an operating grant, and a 1967 Scholarship.

1. A. Pines, M. G. Gibby, and J. S. Waugh. J. Chem. Phys. **59**, 569 (1973).
2. (*a*) E. R. Andrew, A. Bradbury, and R. G. Eades. Nature, **182**, 1659 (1958); **183**, 1802 (1959); (*b*) I. J. Lowe. Phys. Rev. Lett. **2**, 285 (1959).
3. J. Schaefer and E. O. Stejskal. J. Am. Chem. Soc. **98**, 1031 (1976).
4. C. A. Fyfe. Solid state NMR for chemists. CFC Press, Guelph. 1985.
5. (*a*) W. Duerckheimer. Angew. Chem. Int. Ed. Engl. **14**, 721 (1975); (*b*) J. J. Hlavka and J. H. Boothe (*Editors*). The tetracyclines. Springer Verlag, Berlin, Heidelberg. 1985.
6. J. Donohue, J. D. Dunitz, K. N. Trueblood, and M. S. Webster. J. Am. Chem. Soc. **85**, 851 (1963).
7. H. Cid-Dresdner. Z. Kristallogr. Kristallgeom. Kristallphys. Kristallchem. **121**, 170 (1965).
8. M. Schach von Wittenau and R. K. Blackwood. J. Org. Chem. **31**, 613 (1966).
9. L. A. Mitscher, A. C. Bonacci, and T. D. Sokolski. Tetrahedron Lett. 5361 (1968).
10. K. Kamiya, M. Asai, Y. Wada, and M. Nishikawa. Experientia, **27**, 363 (1971).
11. G. L. Asleson and C. W. Frank. J. Am. Chem. Soc. **97**, 6246 (1975).
12. G. L. Asleson and C. W. Frank. J. Am. Chem. Soc. **98**, 4745 (1976).
13. E. P. Mazzola, J. A. Melin, and L. G. Wayland. J. Pharm. Sci. **69**, 229 (1980).
14. (*a*) A. F. Casy and A. Yasin. J. Pharm. Biomed. Anal. **2**, 19 (1984); (*b*) Magn. Reson. Chem. **23**, 767 (1985).
15. J. J. Stezowski. J. Am. Chem. Soc. **98**, 6012 (1976).
16. R. Prewo and J. J. Stezowski. J. Am. Chem. Soc. **99**, 1117 (1977).
17. M. R. Caira, L. R. Nassimbeni, and J. C. Russell. Acta Crystallogr. Sect. B, **33**, 1171 (1977).
18. J. J. Stezowski. J. Am. Chem. Soc. **99**, 1122 (1977).
19. L. J. Hughes, J. J. Stezowski, and R. E. Hughes. J. Am. Chem. Soc. **101**, 7655 (1979).
20. R. Prewo and J. J. Stezowski. J. Am. Chem. Soc. **101**, 7657 (1979).
21. R. Prewo and J. J. Stezowski. J. Am. Chem. Soc. **102**, 7015 (1980).
22. R. Prewo, J. J. Stezowski, and R. Kirschlechner. J. Am. Chem. Soc. **102**, 7021 (1980).

Can. J. Chem. Downloaded from www.nrcresearchpress.com by 80.58.250.72 on 09/07/12
For personal use only.

23. G. J. PALENIK, M. MATTHEW, and R. RESTIVO. J. Am. Chem. Soc. **100**, 4458 (1978).
24. J. T. DOLUISIO and A. N. MARTIN. J. Med. Chem. **6**, 16 (1963).
25. D. E. WILLIAMSON and G. W. EVERETT, JR. J. Am. Chem. Soc. **97**, 2397 (1975).
26. (*a*) J. GULBIS and G. W. EVERETT, JR. J. Am. Chem. Soc. **97**, 6248 (1975); (*b*) Tetrahedron, **32**, 913 (1976); (*c*) J. Y. LEE and G. W. EVERETT, JR. J. Am. Chem. Soc. **103**, 5221 (1981).
27. R. B. MARTIN. *In* Metal ions in biological systems. Vol. 19. *Edited by* H. Sigel. Marcel Dekker, Inc., New York. 1985. p. 19.
28. M. CELOTTI and G. V. FAZAKERLY. J. Chem. Soc. Perkin Trans. 2, **6**, 1319 (1977).
29. K. H. JOGUN and J. J. STEZOWSKI. J. Am. Chem. Soc. **98**, 6018 (1976).
30. G. J. PALENIK and M. MATTHEW. J. Am. Chem. Soc. **100**, 4464 (1978).
31. C. COIBION and P. LASZLO. Biochem. Pharmacol. **28**, 1367 (1979).
32. G. BERTHON, M. BRION, and L. LAMBS. J. Inorg. Biochem. **19**, 1 (1983).
33. E. F. GALE *et al.* (*Editors*). Molecular basis of antibiotic action. 2nd ed. John Wiley & Sons, New York. 1981. pp. 447–453.
34. R. B. VON DREELE and R. E. HUGHES. J. Am. Chem. Soc. **93**, 7290 (1971).
35. A. P. DOERSCHUK, B. A. BITLER, and J. R. D. MCCORMICK. J. Am. Chem. Soc. **77**, 4687 (1955).
36. J. R. D. MCCORMICK, S. M. FOX, L. L. SMITH, B. A. BITLER, J. REICHENTHAL, V. E. ORIGONI, W. H. MULLER, R. WINTERBOTTOM, and A. P. DOERSCHUK. J. Am. Chem. Soc. **79**, 2849 (1957).
37. S. J. OPELLA and M. H. FREY. J. Am. Chem. Soc. **101**, 5854 (1979).
38. W. L. EARL and D. L. VANDERHART. J. Magn. Reson. **48**, 35 (1982).
39. C. H. STEPHENS, L. H. CONOVER, P. N. GORDON, F. C. PENNINGTON, R. L. WAGNER, K. J. BRUNINGS, and F. J. PILGRIM. J. Am. Chem. Soc. **78**, 1515 (1956).
40. P. C. TAYLOR, J. F. BAUGHER, and H. M. KRIZ. Chem. Rev. **75**, 203 (1975).
41. N. ZUMBULYADIS, P. M. HENRICHS, and R. H. YOUNG. J. Chem. Phys. **75**, 1603 (1981).
42. (*a*) Y. SAITO. Can. J. Chem. **43**, 2530 (1965); (*b*) W. CAMINATI and A. M. MIRRI. Chem. Phys. Lett. **12**, 127 (1971).
43. H. W. SPIESS, U. HAEBERLEN, and H. ZIMMERMANN. J. Magn. Reson. **25**, 55 (1977).
44. A. NAITO, S. GANAPATHY, and C. A. MCDOWELL. J. Chem. Phys. **74**, 5393 (1981).
45. J. G. HEXEM, M. H. FREY, and S. OPELLA. J. Chem. Phys. **77**, 3847 (1982).
46. R. K. HARRIS, P. JONSEN, and K. J. PACKER. Magn. Reson. Chem. **23**, 565 (1985).
47. R. M. DICKSON. Honours chemistry thesis, Dalhousie University. 1986.
48. L. GUIBE and E. A. C. LUCKEN. C. R. Seances Acad. Sci. Ser. B, **263**, 815 (1966).
49. M. J. HUNT. J. Magn. Reson. **15**, 113 (1974).
50. J. M. LEHN and J. P. KINTZINGER. *In* Nitrogen NMR. *Edited by* M. Witanowski and G. A. Webb. Plenum Press, London. 1973. p. 79.
51. G. C. LEVY, R. L. LICHTER, and G. L. NELSON. Carbon-13 nuclear magnetic resonance spectroscopy. John Wiley and Sons, New York. 1980. p. 30.

Can. J. Chem. Downloaded from www.nrcresearchpress.com by 80.58.250.72 on 09/07/12
For personal use only.

The ion-pair mechanism and bimolecular displacement at saturated carbon. VI.[1] Racemization and *radio*-bromide exchange for substituted 1-phenylbromoethanes; solvent effects

ALLAN R. STEIN
Department of Chemistry, Memorial University of Newfoundland, St. John's, Nfld., Canada A1B 3X7

Received May 14, 1986

ALLAN R. STEIN. Can. J. Chem. **65**, 363 (1987).

Racemization and *radio*-bromide exchange kinetics for 1-phenylbromoethanes in acetonitrile and in nitromethane using tetrabutylammonium bromide are reported. The results, together with those previously reported for acetone solutions, provide direct empirical support for the ion-pair mechanism for nucleophilic substitution at saturated carbon. Changing the substituents on the phenyl from the 4-nitro through to the 3,4-dimethyl substrate and the solvent from acetone to the more polar acetonitrile and nitromethane shifts the transition state for bromide substitution from an early to a late stage of the equilibria series substrate ⇄ intimate ion pair ⇄ various solvated ion pairs ⇄ free or dissociated ions. For all the substrates in acetone and, for the species giving the less stable carbocations, in acetonitrile and nitromethane, both racemizations and exchanges are bimolecular. In the latter solvents, the substrates giving the more stable carbocations show mixed kinetics.

ALLAN R. STEIN. Can. J. Chem. **65**, 363 (1987).

On rapporte les cinétiques de la racémisation et de l'échange du *radio*-bromure de phényl-1 bromoéthanes, dans l'acétonitrile et dans le nitrométhane, sous l'influence du bromure de tétrabutylammonium. Les résultats obtenus, considérés avec ceux rapportés antérieurement pour des solutions dans l'acétone, fournissent un support empirique direct pour le mécanisme par paires d'ions pour les substitutions nucléophiles au niveau de carbones saturés. Lorsqu'on change les substituants portés par le groupement phényle de nitro-4 à diméthyl-3,4 et le solvant de l'acétone aux solvants plus polaires comme l'acétonitrile et le nitrométhane, l'état de transition se déplace, pour les substitutions de bromures, d'une étape du début vers une étape plus tardive de la série d'équilibres substrat ⇄ pair d'ions intimes ⇄ paires d'ions diversement solvatés ⇄ ions dissociés ou libres. Pour tous les substrats observés dans l'acétone et, pour les espèces donnant les carbocations les moins stables, dans l'acétonitrile et dans le nitrométhane, tant les racémisations que les échanges sont bimoléculaires. Dans ces derniers solvants, les substrats donnant lieu aux carbocations les plus stables présentent des cinétiques qui ne sont pas claires.

[Traduit par la revue]

Can. J. Chem. Downloaded from www.nrcresearchpress.com by 80.58.250.72 on 09/07/12
For personal use only.

Over fifty years ago, Hughes and Ingold first published what must surely be the most broadly known and accepted reaction mechanisms in organic chemistry, the S_N1 (1) and the S_N2 (2) mechanisms for the uni- and bimolecular nucleophilic substitutions at saturated carbon. Their proposals brought order to, and, hence for organic chemists, understanding of, large amounts of empirical data that had already been and have continued to be accumulated. Despite their apparent generality and success, the two mechanistic schemes are not universally successful. An alternate mechanistic proposal, an elaboration of an earlier ion pair scheme due to Winstein (3), was made by Sneen and Larsen in 1969 (4). Their ion-pair mechanistic scheme, as summarized in Scheme 1, facilitates explanation and understanding of the "mixed" or "intermediate" behavior shown by many reactions. Such reactions, which most commonly show mixed stereochemistry — that is, bimolecular reactions which show considerable racemization or unimolecular ones which show considerable net inversion of stereochemistry (see, for example, ref. 5) — or, rarely, intermediate or mixed kinetics which are not cleanly uni- or bimolecular (see, for example, ref. 6), have long troubled organic chemists (see, for example, ref. 7).

The ion-pair mechanism for nucleophilic substitution at saturated carbon was presented in some detail in the previous paper in this series (8). It was pointed out that while there was much direct empirical evidence for the involvement of ion pairs, especially for solvolysis in reactions at or near the unimolecular extreme (3, 9), perhaps the best direct empirical evidence for their involvement in bimolecular substitutions was provided in that paper.

Chiral 1-phenylbromoethanes were prepared (10) with the following substituents on the phenyl group: 4′-nitro, 4′-bromo, unsubstituted, 3′-methyl, 4′-methyl, and 3′,4′-dimethyl. The rates of racemization of chiral substrate and of *radio*-bromide–bromide exchange on racemic substrate were determined in acetone containing lithium bromide. If the Hughes–Ingold mechanisms apply, the rate constants of racemization and exchange should be equal for a unimolecular process whereas for a bimolecular one the ratio should be 2.00:1.00 since the inversion of one half of the substrate results in a racemic mixture. In fact Hughes and Ingold reported that, for the parent compound, 1-phenylbromoethane itself, the rate of racemization was, within experimental error, indeed twice the rate of bromide exchange (2), an observation we previously confirmed (11). With the 4-methyl compound, by contrast, the racemization to exchange rate constant ratio (k_{rac}/k_{exch}) was found to average 2.36:1.00. Both racemization and exchange were bimolecular, first order in each of alkyl bromide concentration and bromide activity.[2] These results are very difficult to accommodate with the Hughes–Ingold mechanisms but present no problem with the ion pair cheme (Scheme 1). Apparently a portion of the initially formed contact ion pair is being sufficiently solvent separated for some of the carbocations to turn over with respect to the bromide ion before collapsing to starting material with partial racemization. The observed rate ratio means that racemization via the internal pathway is more than one third as fast as substitution.

Substrates which would give a less stable carbocation, and hence less stable and shorter-lived ion-pair species, would be

[1]For Part V, see ref. 8.

[2]Lithium bromide associates to form ion pairs in acetone. Bromide ion activities were calculated using the data in ref. 25.

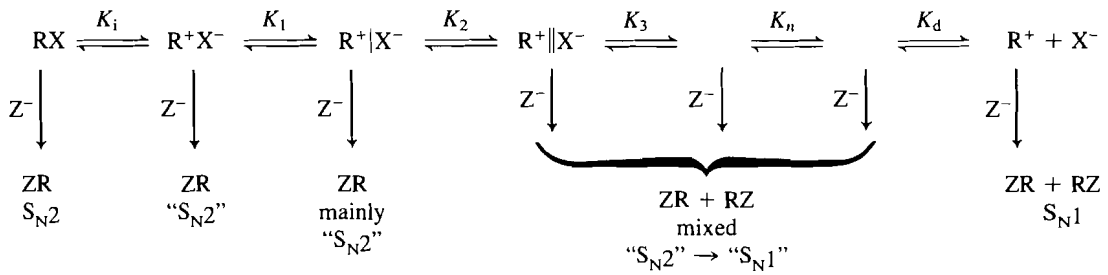

SCHEME 1

less likely to show such racemization with internal return. Indeed, in acetone, the nitro-, bromo-, and unsubstituted substrate had racemization to exchange rate constant ratios that deviated little from 2:1. The 1-(3′,4′-dimethylphenyl)bromoethane substrate, on the other hand, gave stereochemical behavior intermediate between S_N1 and S_N2 with an average racemization to exchange ratio of 1.52:1.00; the kinetics remained bimolecular, however. These results in acetone suggested that extending the study to both less polar and to more polar solvents was warranted. We report results for the more polar solvents acetonitrile and nitromethane in this paper.

Results

Racemization kinetics were done in acetonitrile and nitromethane containing the indicated concentrations of tetrabutylammonium bromide, Bu_4NBr, by starting with the corresponding chiral 1-phenylbromoethane (10) and following the loss of optical activity as previously described for the parent compound in acetone (11). Exchange kinetics were followed by the electrodeposition method of Beronius (12), again as previously described for acetone (11), except that Bu_4NBr rather than LiBr was used to make up the electrolyte solution. Irradiation of Bu_4NBr at the high neutron flux required to make ^{82}Br resulted in charring and decomposition so that LiBr was used. The solid, radioactive LiBr was dissolved in the appropriate solvent, acetonitrile or nitromethane, and a small aliquot added to the Bu_4NBr solution in the exchange cell. In all cases, the lithium ion concentration was less than 0.75%, generally less than 0.4%, of that of the tetrabutylammonium ion and was consequently ignored.

The results reported in this paper were obtained in three different laboratories; all racemization kinetics were done in one, exchanges in a second, and eliminations in a third. Each reaction type was followed by a different method with different equipment, solvents from different suppliers and with different thermometers calibrated only at 0°C where that temperature was within the thermometer's range. (The previously reported results for acetone (8), some of which are summarized in Table 1, with the exception of the exchanges with 1-(3′,4′-dimethylphenyl)bromoethane, were all done using the same thermometer and hence are more internally consistent.) Consequently, small systematic errors due to slight solvent property and temperature differences are to be expected; care must be exercised when considering small differences in rates, etc.

The ratio of the racemization to exchange rate constants (k_{rac}/k_{exch}) for acetonitrile and nitromethane, together with those for acetone, are reported in Table 1. Elimination, a competing process, would lead to isotopic dilution of *radio*-labelled ionic bromide and hence contribute to the rate assigned to bromide exchange. The elimination product, the appropriate styrene (or its readdition product) would be achiral (or racemic)

TABLE 1. Racemization to exchange rate ratios for 1-phenylbromoethanes in several solvents[a]

Substrate	Acetone[b]	Acetonitrile[c]	Nitromethane[c]
4′-Nitro	2.14	2.12	2.18
4′-Bromo	2.09	2.22	2.25
Unsubstituted	1.94	2.17	2.01
4′-Methyl	2.36	3.65	5.50
3′,4′-DiMe	1.52	4.26	2.82

[a]Rate ratios reported are average values for $[M^+Br^-] = 0.0002\ M$ at various temperatures.
[b]LiBr was used (ref. 8).
[c]Bu_4NBr was used.

so that elimination would also contribute to the observed racemization rate. Elimination rate determinations were done with added lutidine to prevent readdition of liberated HBr. Some results, along with the corresponding racemization rates, are reported in Table 2 for acetone, acetonitrile, and nitromethane. The relative and absolute rates of elimination increase progressively through those three solvents. Additional elimination results appear in Table 6.

Rate constants for racemization and bromide exchange are tabulated in Table 3 for acetonitrile and in Table 4 for nitromethane. The reported values are the average of two-to-four runs.

Discussion

In the previous paper of this series where the acetone results were reported (8), the racemization:exchange rate constant ratios were discussed in some detail. As perusal of the data in Table 1 shows, deviations in the ratio from the theoretical 2.00 are relatively small for the unsubstituted substrate and for those substrates with elecron-withdrawing *p*-Br and *p*-NO_2 substituents. Deviations are far greater for the substrates substituted with electron-donating substituents. The 4′-methyl-substituted material shows a rate ratio much greater than 2.00 for all three solvents while that for the 3′,4′-dimethyl substrate is much more erratic, falling below 2.00 in acetone, above in the other two solvents but lower than that for 4′-methyl in nitromethane; in acetonitrile it is perhaps lower than would have been anticipated considering the value for the 4′-methyl substrate. Before these rate constant ratios are further discussed, the more detailed kinetic results must be considered.

Average racemization rate constants are reported in Table 3 for acetonitrile. If the observed rate of racemization, that is $k_{rac}[Bu_4NBr]$ is plotted vs. $[Bu_4NBr]$, as has been done in Fig. 1, the first four substrates, 4′-NO_2, 4′-Br, unsubstituted, and 3′-Me behave as expected — the rate increases linearly with $[Bu_4NBr]$ and shows essentially a zero intercept, that is,

Can. J. Chem. Downloaded from www.nrcresearchpress.com by 80.58.250.72 on 09/07/12
For personal use only.

TABLE 2. *Pseudo*-first order racemization and elimination,[a] [MBr] = 0.002 *M*, all *k*'s × 10^{-5} s^{-1}, [lutidine] = 0.0343 *M* (for elimination)

	Acetone		Acetonitrile		Nitromethane	
T (°C)	k_{rac}	Rac/elim	k_{rac}	Rac/elim	k_{rac}	Rac/elim
3′,4′-Dimethyl						
30	2.51	37.3	15.06	8.99		
45	7.74	22.5	60.32±1.1	9.91	91.54	2.94
55			142.0	7.33		
4′-Methyl						
30	3.218±0.006	131.0	7.64±0.64	13.7		
45	10.02±0.01	76.8	33.25	10.61	59.4±1.4	5.84
55			83.28	10.36		
Unsubstituted						
45	5.082±0.014	77.7	5.193±0.077	80.0		
55			12.16	62.3		
4′-Nitro						
55			13.18	1919.		

[a] k_{rac} with error limits are empirical values, others are recalculated from activation parameters.

there is no racemization without added Bu_4NBr. The last two substrates, 4′-methyl and 3′,4′-dimethylphenylbromoethane, behave quite differently. They have a large positive intercept while still showing a linear rate increase with concentration of ionic bromide. Such behavior is that expected for mixed kinetics with a uni- and a bimolecular component, that is:

$$\text{Rate} = k_1[RX] + k_2[RX][X^-]$$

Similar behavior was found in nitromethane but, as reported earlier, not in the less dipolar acetone where all compounds gave a near zero intercept (8).

Separated uni- and bimolecular components for racemizations in acetonitrile and nitromethane are reported in Table 5. The reported bimolecular component would include any salt effect due to the increasing ionic strength of the medium as the concentration of the Bu_4NBr was increased. The racemization and exchange rates were to be compared and earlier studies in acetone (11) had shown that all "inert electrolytes" added, lithium chlorate, perchlorate, nitrate, picrate, ..., either interfered with the electrodeposition of AgBr or were not sufficiently soluble. The tetrabutylammonium salts of most of the above anions should be sufficiently soluble in acetonitrile and nitromethane to permit racemization kinetics at constant ionic strength to access the salt effects. Such studies have not yet been done. Racemization studies with 1-phenylbromomethane in acetone using LiBr at constant lithium ion concentration ($LiNO_3$) have, however, been reported (13). The rate of racemization decreased progressively as the ionic strength increased, falling by 46% as the lithium ion concentration was increased ten fold, from 0.01 to 0.1 *M*, with [LiBr] = 0.01 *M* at 40.38°C. Of course there are a number of components in this "salt effect". While the ionic strength increased so did the degree of association of the lithium bromide, decreasing the activity of the bromide ion. Also, of course, there was no or at most a very small unimolecular contribution in that racemization. These results cannot be extrapolated to the present situation because, at the concentrations used, Bu_4NBr does not show significant association and the reactions of the

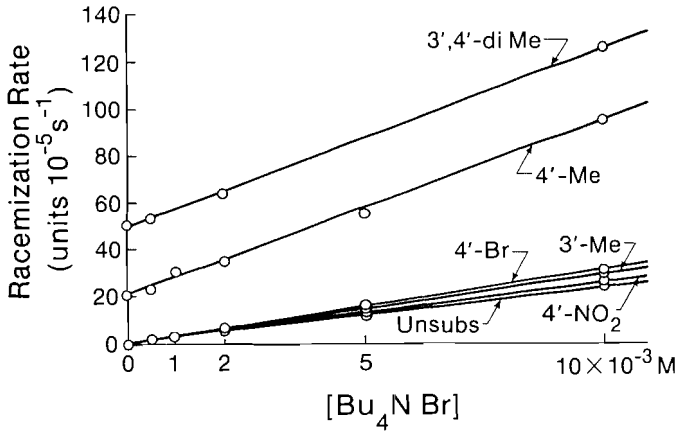

FIG. 1. Observed racemization rate versus the concentration of added Bu_4NBr in acetonitrile at 45°C.

4′-methyl and 3′,4′-dimethyl substrates do have large unimolecular components. While hundreds of papers report salt or ionic strength effects in solvolysis, such studies for "identity" or symmetrical substitution reactions are rare indeed. Fava *et al.* (6) have examined thiocyanate exchanges for various benzhydryl thiocyanates in acetone and in acetonitrile at constant ionic strength and separated uni- and bimolecular components. Unfortunately they did not undertake ionic strength effect studies, in part because of problems with association of NaSCN. We found LiBr association problems in acetone (8, 11, 13). Beronius and Gupta report such problems for various halides, including Et_4NI in the iodide exchange at methyl iodide (14).

There is an ionic strength effect contribution to all of our rate constants, including both the uni- and bimolecular components of those reactions showing mixed kinetics. How large that contribution is and indeed that it is an accelerating one, can not be stated with certainty at this time. For the cleanly bimolecular reactions, the salt effects must be small since the second order rate constant is apparently very nearly independent of the concentration of Bu_4NBr — a small rate retardation may in

Can. J. Chem. Downloaded from www.nrcresearchpress.com by 80.58.250.72 on 09/07/12
For personal use only.

TABLE 3. Racemization and exchange rate constants: acetonitrile

1-Phenylbromoethane	T (°C)	Reaction	k_{rac} and k_{exch} at given [Bu_4NBr], units $\times 10^{-3}$ L/m s 0.01000 M	0.00500 M	0.00200 M	0.00100 M	0.00050 M
4′-Nitro	30	Rac	6.15±0.05	—	6.106±0.020	—	—
		Exch			2.89±0.03		
	40	Rac	16.12±0.07	—	16.54±0.11	—	—
		Exch			7.37±0.05		
	45	Rac	25.54±0.20	26.28±0.08	26.60±0.51	27.39±0.14	27.20±0.10
		Exch	11.62±0.06		12.96±0.47		
4′-Bromo[a]	30	Rac	—	—	7.72±0.04	—	—
		Exch			3.59±0.05		
	40	Rac	18.83±0.14	19.81±0.21	20.41±0.78	20.32±0.76	20.63±0.14[b]
		Exch			8.514±0.012		
	45	Rac	30.06±0.07	30.57±0.62	31.55±0.35	29.52±0.04	33.75±0.34[b]
		Exch	14.037±0.013		14.96±0.61		
Unsubstituted[c]	30	Rac	5.90±0.03	—	6.312±0.012	—	—
		Exch			2.995±0.021		
	40	Rac	14.79±0.02	—	15.85±0.05	—	—
		Exch			7.426±0.014		
	45	Rac	23.31±0.11	24.16±0.04	25.96±0.38	28.05±0.12[b]	33.27±0.76[b]
		Exch	11.24±0.11	—	11.52±0.40	12.26±0.18	12.09±0.36
3′-Methyl	30	Rac	7.32±0.12	—	6.84±0.08	—	—
	40	Rac	17.91±0.14	—	18.70±0.09	—	—
	45	Rac	28.41±0.23	29.04±0.57	31.00±0.63	34.89±0.13[b]	36.9±2.2[b]
4′-Methyl[d]	30	Rac	20.65±1.10	28.25±0.33	38.2±3.2	55.4±3.1[b]	147.1±10.0[b]
		Exch			12.050±0.003		
	40	Rac	69.10±1.06	71.27±0.87	97.1±1.8	146.46±0.33[b]	257.0±1.6[b]
		Exch			25.23±0.13		
	45	Rac	90.5±4.3	108.74±1.05	172.8±3.5	303.2±3.4[b]	454.2±2.0[b]
		Exch	38.05±0.70		43.7±1.1		
3′,4′-diMe[e]	30	Rac	—	—	—	—	—
		Exch			18.61±1.07		
	40	Rac	—	—	192.7±7.2	—	—
		Exch			42.2±1.9		
	45	Rac	124.8±2.0	—	301.6±5.6	—	1063.9±7.2[b]
		Exch	52.4±1.1		75.9±1.2		

[a]With no added Bu_4NBr, at 40 and 45°C, there was no change in rotation in the racemization studies for the first 90 min — racemization commenced over longer times.

[b]Initial slopes were used to calculate k_{rac} — racemization accelerated in later stages.

[c]With no added Bu_4NBr, at 45°C, the initial rate of racemization was $(0.344 \pm 0.012) \times 10^{-5}$ s^{-1}.

[d]With no added Bu_4NBr, at 30, 40, and 45°C, respectively, the initial rates of racemization were (4.392 ± 0.033), (10.77 ± 0.38), and $(20.78 \pm 0.26) \times 10^{-5}$ s^{-1}.

[e]With no added Bu_4NBr, at 40 and 45°C, respectively, the initial rates of racemization were (33.02 ± 0.44) and $(50.49 \pm 0.30) \times 10^{-5}$ s^{-1}.

fact be present. Certainly the bimolecular rate constants, k_2, reported in Table 5 are not unrealistic for the 4′-methyl and 3′,4′-dimethyl substrates even though there is most likely a positive salt effect on the unimolecular component which would increase the apparent k_2. In acetone at 30°C, for example, where any unimolecular component was very small, the second order rate constant for the 4′-methyl compound was slightly more than double that of the unsubstituted compound, in acetonitrile at 45°C it is triple. Still, as Bunton *et al.* have shown, there is most likely a positive salt effect on the unimolecular component, a contribution which probably increases linearly with Bu_4NBr concentration (15). Just how large a fraction of the k_2 value should be assigned to that salt effect remains to be established.

Table 5 also includes the elimination rate constants measured with added excess lutidine to prevent readdition. As pointed out previously (8), the elimination rate given should be considered an upper limit since there is evidence that in buffered solutions, even such weak bases as the trifluoroacetate ion in trifluoroacetic acid (16) or various chloro- and trifluoroacetate ions in 50:50 2,2,2-trifluoroethanol:water (17) promote elimination side reactions, for the solvolysis of butyl tosylate and 1-(4′-methylphenyl)chloroethane, respectively. Without added lutidine, eliminations were slower and the bromide ion concentration tended to reach a plateau value a bit above the initial concentration, a plateau value that varied considerably even in duplicate runs. With lutidine added, the elimination rate was quite insensitive to the concentration of Bu_4NBr, decreasing

Can. J. Chem. Downloaded from www.nrcresearchpress.com by 80.58.250.72 on 09/07/12
For personal use only.

TABLE 4. Racemization and exchange rate constants: nitromethane

1-Phenylbromoethane	T (°C)	Reaction	k_{rac} and k_{exch} at given [Bu_4NBr], units × 10^{-3} L/m s 0.01000 M	0.00500 M	0.00200 M	0.00100 M	0.00050 M
4′-Nitro	30	Rac	2.965±0.018	—	2.78±01.04	—	—
		Exch	1.049±0.022		1.368±0.003		
	40	Rac	8.19±0.11	—	7.64±0.49	—	—
		Exch			3.17±0.05		
	45	Rac	13.54±0.07	13.59±0.02	12.97±0.13	12.24±0.10	11.36±0.42
		Exch					
	50	Rac	—	—	21.23±0.27	—	—
		Exch			10.20±0.09		
4′-Bromo	30	Rac	—	—	4.59±0.04	—	—
		Exch	1.701±0.038		1.79±0.09		
	40	Rac	11.68±0.41	11.23±0.07	11.83±0.17	11.15±0.05	14.10±0.37[a]
		Exch			4.36±0.12		
	50	Rac	28.24±0.08	—	29.35±0.34	—	—
		Exch			12.95±0.16		
Unsubstituted	30	Rac	—	—	4.79±0.03	—	—
		Exch	1.648±0.057		1.94±0.06		
	40	Rac	10.04±0.19	10.75±0.16	11.77±0.33	13.75±0.27	15.89±0.13[a]
		Exch			6.63±0.58		
	50	Rac	—	—	28.19±0.45	—	—
		Exch			15.99±0.26		
3′-Methyl	30	Rac	5.602±0.011		5.798±0.026		
	40	Rac	13.42±0.17		15.291±0.018		
	45	Rac	21.12±0.39	20.79±0.24	23.65±0.60	30.76±0.34[a]	45.84±0.79[a]
	50	Rac	31.44±0.24		37.09±0.52		
4′-Methyl	30	Rac	29.24±0.66	—	83.1±3.6	—	—
		Exch			12.74±0.31		
	40	Rac	72.2±4.8	120.1±9.0	230.0±14.2	465.6±10.4[a]	853.8±5.9[a]
		Exch			38.08±1.06		
	45	Rac	103.6±5.7	—	297.0±6.8	—	1030.0±9.4[a]
		Exch					
	50	Rac	—	—	500.1±11.2	—	—
		Exch			120.0±14.0		
3′,4′-diMe	20	Exch		—	10.3±0.11	—	—
	30	Rac	39.99±1.13	—	110.8±5.9[a]	—	—
		Exch	15.31±0.29		24.27±0.64		
	40	Rac	90.36±1.90	152.0±3.1	282.4±14.4[a]	528.2±9.2[a]	1046.0±22.0[a]
		Exch			101.5±8.3		
	50	Rac	210.7±1.1	—	722.7±22.0[a]	—	—
		Exch			253.5±0.3		

[a] Initial slopes were used to calculate k_{rac} — racemization accelerated in later stages.

TABLE 5. Separation of uni- and bimolecular components at 45°C (k_1, × 10^{-5} s^{-1}; k_2, × 10^{-3} L/m s; k_{elim}, × 10^{-5} s^{-1})

Substrate	Acetonitrile k_1	Acetonitrile k_2	Acetonitrile k_{elim}	Nitromethane k_1	Nitromethane k_2	Nitromethane k_{elim}
4′-Nitro	0.238±0.062	25.40±0.13	<0.005	−0.123±0.021	13.97±0.04	
4′-Bromo	0.37±0.27	29.31±0.29		0.010±0.09[a]	11.58±0.17[a]	
Unsubstituted	0.57±0.05	22.81±0.10	0.0649±0.0005	0.42±0.06[a]	9.66±0.10[a]	
3′-Methyl	0.57±0.06	27.86±0.13		1.01±0.10	19.90±0.19	
4′-Methyl	20.62±0.70	69.5±1.4	3.19±0.06	51.4±1.7	51.4±2.6	13.493±0.007
3′,4′-diMe	46.7±1.9	76.7±2.9	7.73±0.01	47.9±0.7[a]	53.4±1.6[a]	~20[a,b]

[a] At 40°C.
[b] k_{elim} = (31.42±0.009) × 10^{-5} s^{-1} at 45°C.

Can. J. Chem. Downloaded from www.nrcresearchpress.com by 80.58.250.72 on 09/07/12
For personal use only.

TABLE 6. Elimination rate vs. [Bu_4NBr]: acetonitrile, 4′-methyl, 55°C [lutidine] = 34.3×10^{-3} *M*

$[Br_4NBr] \times 10^{-3}$ *M*	$k_{elim} \times 10^{-5}$ s^{-1}
5.000	8.012±0.0066
2.000	8.375±0.059
1.000	8.936±0.010
(rate vs. $\sqrt{\mu}$, slope = −0.4)	

only very slightly with increasing concentration (Table 6). This elimination contributes to the unimolecular component of the racemizations.

Thus the observed racemization rate is made up of the components:

$$\text{Rate observed} = [RBr](k_{1\,rac} + k_{1\,elim} + k_{2\,rac}[Bu_4NBr])$$

For the 4′-methyl substrate in acetonitrile at 40°C the values of the three rate constants are:

$$k_{1\,rac} = (17.43 \pm 0.70) \times 10^{-5}\ s^{-1}$$

$$k_{1\,elim} = (3.19 \pm 0.06) \times 10^{-5}\ s^{-2}$$

$$k_{2\,rac} = (69.5 \pm 1.4) \times 10^{-3}\ L/m\ s$$

or at $[Bu_4NBr] = 0.01$ *M*,

$$k_{2\,rac}[Bu_4NBr] = (69.5 \pm 1.4) \times 10^{-5}\ s^{-1}$$

Thus at the highest concentration of salt used, the elimination would account for only 3.5% of the observed rate, at the lowest concentration (0.0005 *M* Bu_4NBr) it would be 13.2%, whereas in nitromethane the corresponding percentages would be 13.1% and 25.0%. In all cases, elimination, even with added lutidine, accounts for only a fraction of the unimolecular component.

The simplest approach is to assume there are uni- and bimolecular processes with the carbocation formed in the former partitioning between elimination and nucleophile addition and the latter being simple bimolecular nucleophilic substitution as represented in Scheme 2. This is not, however, a complete picture.

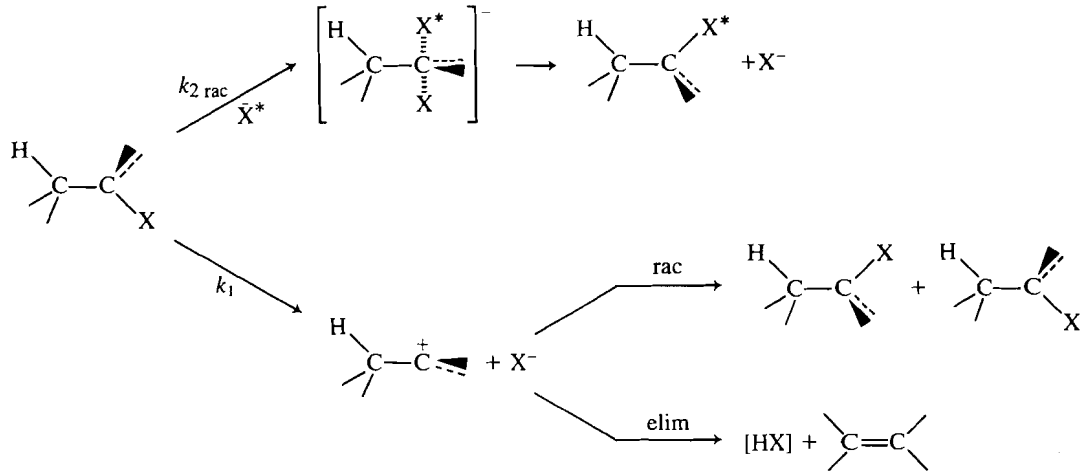

SCHEME 2

For such a scheme the rate ratio for racemization:exchange should fall between the value of 2.00 for S_N2 and 1.00 for S_N1 mechanisms. Instead, in acetonitrile, it is 3.65, in nitromethane, 5.50 for the 4′-methyl substrate. This discrepancy is more easily accommodated in the ion-pair mechanistic scheme (Scheme 1). A considerable amount of internal return with racemization is occurring in a reaction where the average stage for nucleophilic attack is quite far over towards dissociation. This explanation is supported by the fact that the rac:exch rate ratios increase as the concentration of bromide ion decreases. Thus, for example, at 45°C, for the unsubstituted compound the ratios are 2.07, 2.25, 2.29 and 2.75 at 0.01, 0.002, 0.001 and 0.0005 *M* respectively, for 4′-methyl the ratios are 2.37 and 3.93 and for 3′,4′-dimethyl 2.38 and 3.98 at 0.01 and 0.002 *M*, respectively. This behavior is exactly what would be predicted since at the higher concentrations of nucleophile, the average stage of nucleophilic attack should be earlier in the ion pair solvation–dissociation sequence and the amount of internal return with racemization would be reduced both by faster, earlier nucleophilic attack and by reducing the total amount of internal return.

The drop in $k_{rac}:k_{exch}$ ratio for 1-(3′,4′-dimethylphenyl)bromoethane is consistent with an even more stable carbocation than that from the 4′-methyl substrate. Consequently, the average stage of nucleophilic attack is farther delayed, the reaction has a larger S_N1 component (i.e. dissociation of more of the ion pair before reaction) and shows a reduced amount of internal return.

The picture presented above is incomplete. As pointed out by Bentley *et al.* (18) chemists tend to treat the ion pair scheme of Winstein or as applied by Sneen and represented in Scheme 1 as though it was "exact" and "complete". Even unimolecular processes in relatively non-ionizing solvents are greatly accelerated by added "inert" electrolyte giving rise to the "special salt effects" first noted by Winstein *et al.* (for a summary, see ref. 3). That this is through some sort of one-on-one process is confirmed by the fact that, at higher electrolyte concentration, the rate acceleration reverts to a "normal salt effect". Clearly other ionic species present directly affect the ionization–dissociation process.

In recent years, nucleophilic substitutions in the gas phase have received extensive study (19–21). Studies of methyl

Can. J. Chem. Downloaded from www.nrcresearchpress.com by 80.58.250.72 on 09/07/12
For personal use only.

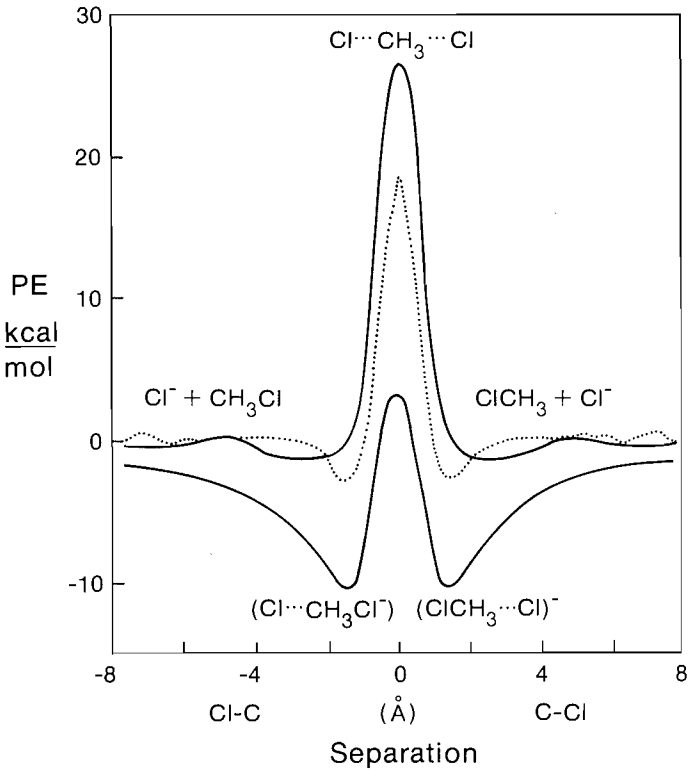

FIG. 2. Calculated energies as a function of reaction coordinate separation in Å for the reaction of Cl^- with CH_3Cl in aqueous solution (upper), in DMF (middle), and in the gas phase (lower curve) (from ref. 19*a*).

halide – halide ion exchange in the gas phase by Olmstead and Brauman (20) show an energy well with the transition state for substitution being a maximum within that well, a potential energy profile which is supported by the calculations of Jorgensen *et al.* (19*a*), Fig. 2, lowest curve. The minima preceding and following the transition state correspond to the exothermic "solvation" or ion–dipole interaction of $X^-\cdots H_3\overset{\delta+}{C}—\overset{\delta-}{X}$ and $\overset{\delta-}{X}—\overset{\delta+}{C}H_3\cdots X^-$, respectively. While the effect of progressive solvation of the nucleophile apparently has not been reported for such degenerate processes, empirical (19*b*, 21) and theoretical (22) results have been reported for gas phase substitutions on methyl halides by hydrated hydroxide ions. Thus for $OH^-(H_2O)_n$ as the nucleophile with methyl bromide, Bohme and MacKay (21) found that, as the degree of hydration, n, is progressively increased, n = 0, 1, 2, 3, ..., that is, as the nucleophile is stabilized by solvation, the depth of the pre-transition state energy well decreases and the net energy barrier to reaction increases from near zero towards the aqueous solution value of E_a = 23 kcal/mol. The observed reaction rate also decreases progressively, being 1×10^{-9}, 6×10^{-10}, 2×10^{-12}, $\lesssim 2 \times 10^{-13}$, and 2.3×10^{-25} cm^3/molecule s for the reactions with n = 0, 1, 2, 3, and in aqueous solution, respectively.

Solvent effects on the potential energy profile of a degenerate process have been considered by Chandrasekhar and Jorgensen (19*a*) and are summarized in Fig. 2. Notice that small energy minima corresponding to the ion–dipole association of Cl^- and CH_3Cl are still predicted for even such polar solvents as DMF (d.c. = 36.7). Presumably, solvents of similar polarity, such as acetonitrile (d.c. = 37.5) and nitromethane (d.c. = 35.9), would have similar minima to that calculated for DMF while a much less polar solvent like acetone (d.c. = 20.7) would show much more pronounced minima, falling somewhere between the gas phase and DMF pictures of Fig. 2. As Chandrasekhar and Jorgensen point out, such results "lead one to question the likelihood of concerted S_N2 reactions in nonaqueous media, i.e. (reactions) preceding without ... intermediates" (19*a*).

Our results, which show a large uni-molecular component for the species which would give the most stable carbocation in the relatively polar aprotic solvents, acetonitrile and nitromethane, prove that at least in such favourable cases nucleophilic assistance is not necessary to promote ion-pair formation–dissociation. The unassisted unimolecular process is in competition with the nucleophile-assisted, bimolecular one. Yamabe and Hirao (23) have done SCF computations which show the chloride ion in acetonitrile to be tetrahedrally solvated, through the carbon of the methyl group, by four acetonitrile molecules. Kebarle and co-workers (19*c*), on the other hand, find that in DMSO, the chloride ion is solvated through the sulfur of the S—O group and is located between and below the methyls, directly along the S—O bond. It is unlikely the bromide ion would differ greatly in those two solvents; as for the chloride, solvation would be considerably better in DMSO with the concomitant reduction in nucleophilicity. Apparently analogous calculations have not been done for nitromethane but our results suggest the bromide ion is less reactive, better solvated in that solvent since the uni-molecular components are proportionally much larger. Presumably, solvational exchange, that is, displacement of nitromethane from a solvation site by alkyl bromide ($—\overset{\delta\oplus}{C}—\overset{\delta\ominus}{Br}$), is less exothermic and the pre- and post-transition state energy wells are shallower than for acetonitrile. For acetone apparently those wells are considerably deeper. Unfortunately, preliminary exchange experiments in dimethylformamide and in dimethylsulfoxide indicated problems in the electrodeposition — unstable AgBr films formed and current efficiencies were less than 100% and irreproducible.

A parallel solvational effect would be acting on the leaving group — the better the solvation, the less the assistance of the nucleophile would be required for, first, ionization to ion pair and, then, dissociation to solvated carbocation and bromide ion.

We now have a fairly complete picture for the range of transition states. For the less dipolar, "poorer" solvents like acetone, ionization–dissociation does not proceed without involvement of the nucleophile. For the more dipolar, "better" solvents like acetonitrile and nitromethane, the same applies for those substrates giving the less stable carbocations and, hence, ion pairs. For these cases, nucleophilic assistance is required. Except for the most readily ionized substrates, once formed the ion pair either collapses to starting material or undergoes nucleophilic attack fairly early in the ionization–dissociation process since there is little or no internal return with racemization. The k_{rac}:k_{exch} ratio is 2:1, the value predicted for the S_N2 mechanism and racemization and exchange show "clean" second order kinetics.

Even in acetone, a more readily ionized substrate, one giving a more stable carbocation such as 1-(4′-methylphenyl)bromoethane, has the transition state for nucleophilic substitution shifted sufficiently towards dissociation to show considerable internal return with racemization. k_{rac}:k_{exch} becomes greater than 2:1. For the even more readily ionized substrate, 1-(3′,4′-dimethylphenyl)bromoethane, the rate ratio falls to less than 2:1 but both racemization and exchange remain bimolecular; the bromide ion is still necessary to promote ionization–

Can. J. Chem. Downloaded from www.nrcresearchpress.com by 80.58.250.72 on 09/07/12
For personal use only.

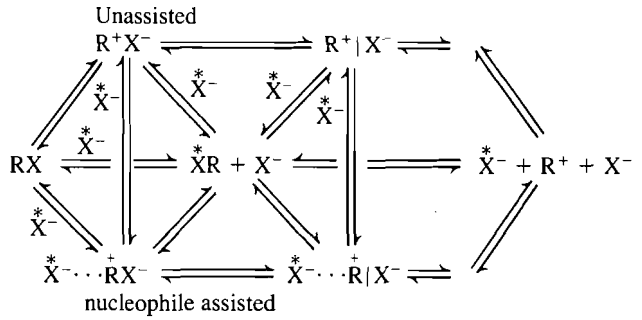

SCHEME 3

dissociation. Here though either a significant fraction of the ion pairs "dissociate" before reaction with the nucleophile or the separation is sufficient for considerable leaving group — nucleophile exchange before collapse.

In more ionizing media, nucleophilic involvement is still essential for those substrates giving the less stable carbocations–ion pairs. Substrates giving somewhat more stable species, the 4′-methyl substrate in our case, show large amounts of internal return with racemization but here, and more markedly with the 3′,4′-dimethyl substrate, nucleophilic assistance is no longer crucial. A unimolecular component has appeared. These reactions show mixed kinetics as well as mixed stereochemistry.

The evolving picture is difficult to represent in two dimensions. Lowry and Richardson (24) have given one of the better representations which is presented, somewhat modified, in Scheme 3.

If such a scheme is operating here, the bulk of the reactions follow the nucleophile assisted pathway. Only the unimolecular component of those reactions showing mixed kinetics, that is those substrates giving the most stable carbocations/ion pairs in the more polar solvents acetonitrile and nitromethane, represent reaction via the unassisted pathway. (3′,4′-Dimethylphenyl)bromoethane in acetone, which reacts with bimolecular kinetics but gives a k_{rac}/k_{exch} ratio halfway between that expected for uni- and bimolecular processes, presumably undergoes "intersystem crossing"; it starts along the nucleophile assisted pathway but, because the carbocation/ion pair is sufficiently stable, nucleophile involvement is not essential for completion of ion pair separation. The reaction proceeds, at least in part, by crossing to the unassisted pathway.

Obviously even Scheme 3 is far from complete since it includes reactions of only one solvated ion pair and does not consider stereochemistry, the possibility of return with racemization, and elimination. As such, it is a much better representation of the bromide exchange than of the racemization process. The scheme does, however, contain most other components.

Experimental

All solvents were reagent or Analar grade and were stored over a generous quantity of Type 4A molecular sieves before being freshly distilled under dry tank nitrogen which had been further dried by bubbling through concentrated H_2SO_4 followed by a column of Type 3A molecular sieves. Analytical grade tetrabutylammonium bromide (Eastman) was pumped at 0.1 mm Hg and 60°C overnight and kept under vacuum or, for brief periods, tightly stoppered in a glove box. Stock solutions 0.0200 or 0.0500 *M* in Bu_4NBr were prepared, sealed in Hypo-vials and stored in a dry nitrogen flushed glove box (racemizations) or bag (exchanges and eliminations). Solutions of the appropriate concentration for kinetics were prepared using freshly distilled solvent as required. Normally the stock solutions were used within 1–2 weeks, the diluted solutions within 1–2 days. Racemization rates obtained using stock solutions that had been stored for several months were within a few percent of those obtained using freshly prepared stock solutions for acetonitrile and for nitromethane; the rate decreased somewhat more, about 8% for three month storage, for acetone. The dilute solutions which were kept in stoppered volumetric flasks went "off" much more quickly.

Except as indicated below, all experimental details and data handling were analogous or identical to those previously described (8, 11, 13).

Kinetics of exchange were followed as outlined for LiBr in acetone (8) except that Bu_4NBr was used. Since that salt was destroyed when irradiated at the high neutron fluxes required to prepare ^{82}Br, $Li^{82}Br$ was used instead. LiBr, 0.87 mg was sealed *in vacuo* in a thin-walled quartz vial — the appropriate volume of aqueous LiBr was added to the vial, the water evaporated and the vial heated at 225–250°C before sealing. After irradiation, the vial was broken below the surface of 5 mL of the solvent being used in a small erlenmeyer flask. Aliquots of this 0.002 *M* solution were then added to the kinetics cell containing 50 mL of the Bu_4NBr solution. The aliquot volume was 0.05–0.5 mL, chosen to give a reasonable count rate after electrodeposition of AgBr on the silver electrodes. The volume added was smallest for the lowest concentrations with the freshest radioactive material.

Acknowledgements

The author wishes to thank Memorial University of Newfoundland and the Natural Sciences and Engineering Research Council of Canada for financial assistance; Atomic Energy of Canada Ltd., Chalk River, Ont., Canada, for use of their research facilities and equipment for the exchange studies; and the University of Auckland, Auckland, New Zealand, for use of their laboratories and equipment for the elimination studies.

1. E. D. HUGHES and C. K. INGOLD. J. Chem. Soc. 244 (1935).
2. J. L .GLEAVE, E. D. HUGHES, and C. K. INGOLD. J. Chem. Soc. 236 (1935).
3. S. WINSTEIN, B. APPEL, R. BAKER, and S. DIAZ. *In* Organic reaction mechanisms. Chem. Soc. Spectrosc. Publ. No. 19, 1965. pp. 109–130.
4. (*a*) R. A. SNEEN and J. W. LARSEN. J. Am. Chem. Soc. **91**, 363 (1969); **91**, 6031 (1969); (*b*) R. A. SNEEN. Acc. Chem. Res. **6**, 46 (1973).
5. C. K. INGOLD. Structure and mechanism in organic chemistry. 2nd ed. Cornell University Press, Ithaca, NY. 1969. pp. 515–544.
6. A. FAVA, A. ILICETO, and A. CECCON. Tetrahedron Lett. 685 (1963); A. CECCON, I. PAPA, and A. FAVA. J. Am. Chem. Soc. **88**, 4643 (1966).
7. (*a*) A. STREITWIESER, JR. Solvolytic displacement reactions. McGraw Hill, New York, NY. 1962. p. 59ff; (*b*) V. GOLD. J. Chem. Soc. 4633 (1956).
8. A. R. STEIN and E. A. MOFFATT. Can. J. Chem. **63**, 3433 (1985).
9. (*a*) H. L. GOERING and H. HUNSKI. J. Org. Chem. **40**, 920 (1975) and references therein; (*b*) H. L. PEETENS and M. ANTEUNIS. J. Org. Chem. **40**, 307 (1975); **40**, 312 (1975); (*c*) F. G. BORDWELL, P. F. WILEY, and T. G. MECCA. J. Am. Chem. Soc. **97**, 132 (1975) and references therein; (*d*) J. M. W. SCOTT and R. E. ROBERTSON. Can. J. Chem. **50**, 167 (1972); (*e*) C. PARADISI and J. F. BUNNETT. J. Am. Chem. Soc. **107**, 8225 (1985).
10. A. R. STEIN, R. D. DAWE, and J. R. SWEET. Can. J. Chem. **63**, 3442 (1985).
11. A. R. STEIN. J. Org. Chem. **41**, 519 (1976).
12. P. BERONIUS. Trans. R. Inst. Technol. Stockholm No. 213 (1963).
13. A. R. STEIN. J. Org. Chem. **38**, 4022 (1973).
14. P. BERONIUS and R. P. GUPTA. Acta Chem. Scand. Ser. A, **A30**, 477 (1976) and references therein.
15. C. A. BUNTON, T. W. DEL PESCO, A. M. DUNLOP, and K.-U. YANG. J. Org. Chem. **36**, 887 (1971).

Can. J. Chem. Downloaded from www.nrcresearchpress.com by 80.58.250.72 on 09/07/12
For personal use only.

16. J. J. DANNEBERG. J. Am. Chem. Soc. **103**, 7764 (1981).
17. J. P. RICHARD and W. P. JENCKS. J. Am. Chem. Soc. **106**, 1373 (1984); **106**, 1383 (1984).
18. T. W. BENTLEY, C. T. BOWEN, D. H. MORTEN, and P. v. R. SCHLEYER. J. Am. Chem. Soc. **103**, 5466 (1981).
19. (*a*) J. CHANDRASEKHAR and W. L. JORGENSEN. J. Am. Chem. Soc. **107**, 2974 (1985); J. CHANDRASEKHAR, S. F. SMITH, and W. L. JORGENSEN. J. Am. Chem. Soc. **107**, 154 (1985); **106**, 3049 (1984); (*b*) D. K. BOHME and A. B. RAKSIT. Can. J. Chem. **63**, 3007 (1985); J. Am. Chem. Soc. **106**, 3447 (1984) and references therein; (*c*) T. F. MAGNERA, G. CALDWELL, J. SUNNER, S. IKUTA, and P. KEBARLE. J. Am. Chem. Soc. **106**, 6140 (1984); J. SUNNER and P. KEBARLE. J. Am. Chem. Soc. **106**, 6135 (1984); G. CALDWELL, T. F. MAGNERA, and P. KEBARLE. J. Am. Chem. Soc. **106**, 959 (1984); (*d*) M. J. PELLERITE and J. I. BRAUMAN. J. Am. Chem. Soc. **105**, 2672 (1983) and references therein; (*e*) M. HENCHMAN, J. F. PAULSON, and P. M. HIERL. J. Am. Chem. Soc. **105**, 5509 (1983); (*f*) S. WOLFE and D. J. MITCHELL. J. Am. Chem. Soc. **103**, 7692 (1981); **103**, 7694 (1981); (*g*) T. H. MORTON. Tetrahedron Report Number 137, Tetrahedron **38**, 3195 (1982); J. H. BOWIE. Acc. Chem. Res. **13**, 76 (1980).
20. W. N. OLMSTEAD and J. I. BRAUMAN. J. Am. Chem. Soc. **99**, 4219 (1977).
21. D. K. BOHME and G. I. MACKAY. J. Am. Chem. Soc. **103**, 978 (1981).
22. K. OHTA and K. MOROKUMA. J. Phys. Chem. **89**, 5845 (1985).
23. S. YAMABE and K. HIRAO. Chem. Phys. Lett. **84**, 598 (1981); K. HIRAO, S. YAMABE, and M. SANO. J. Phys. Chem. **86**, 2626 (1982).
24. T. H. LOWRY and K. S. RICHARDSON. Mechanism and theory in organic chemistry. 2nd ed. Harper and Row Publishers, New York, NY. 1981. p. 303.
25. P. BERONIUS, U. ISACSSON, and A.-M. NILSSON. Acta Chem. Scand. **24**, 189 (1970).

Can. J. Chem. Downloaded from www.nrcresearchpress.com by 80.58.250.72 on 09/07/12
For personal use only.

Substitution reactions of some pseudo-halides in *trans*-$[Ru(NH_3)P(OEt)_3(H_2O)]^{2+}$

SONIA MARIA NEIVA, LUCÍDIO SOUZA SANTOS, SEBASTIÃO BARROS ARAÚJO,
JOSÉ CARDOSO DO NASCIMENTO FILHO, AND DOUGLAS WAGNER FRANCO
Instituto de Física e Química de São Carlos, USP São Carlos, 13.560 – SP, CP. 369 – Brasil

Received October 1, 1984[1]

SONIA MARIA NEIVA, LUCÍDIO SOUZA SANTOS, SEBASTIÃO BARROS ARAÚJO, JOSÉ CARDOSO DO NASCIMENTO FILHO, and DOUGLAS WAGNER FRANCO. Can. J. Chem. **65**, 372 (1987).

The kinetics and mechanism of the formation of *trans*-$[Ru(NH_3)_4P(OEt)_3X]^{1+}$ (X = SCN^-, CN^-, and N_3^-) have been investigated. The second order specific rate constants k_1 for the substitution of the water molecule in *trans*-$[Ru(NH_3)_4P(OEt)_3(H_2O)]^{2+}$ for CN^-, N_3^-, and SCN^- are $(3.1 \pm 0.3) \times 10^2$, $(1.7 \pm 0.1) \times 10^2$, and $(1.4 \pm 0.1) \times 10^2\ M^{-1}\,s^{-1}$, respectively, at 25°C, μ = 1.0 ($NaCF_3COO$). Under the same experimental conditions the aquation of the pseudohalide derivatives, *trans*-$[Ru(NH_3)_4P(OEt)_3X]^+$, proceeds at specific rates of $(1.8 \pm 0.1) \times 10$ and $(2.8 \pm 0.1) \times 10\,s^{-1}$ for X = N_3^- and SCN^-, respectively, and the upper limit for the rate of CN^- loss from *trans*-$[Ru(NH_3)_4P(OEt)_3CN]^+$ was estimated as $1.2 \times 10^{-1}\,s^{-1}$. The order of affinities for the monophosphite complex in the series of ligands studied is:

$$SO^{2-} \sim P(OEt)_3 > CN^- > imN > isn > pyr > Mepyr^+ > N_3^- > SCN^-$$

where imN = imidazol, pyr = pyrazine, and $Mepyr^+$ = methylpyrazinium. From enthalpies of activation it is possible to estimate that net replacement of H_2O in *trans*-$[Ru(NH_3)_4P(OEt)_3(H_2O)]^{2+}$ by azide ions is exothermic by 2.8 ± 2 kcal/mol.

SONIA MARIA NEIVA, LUCÍDIO SOUZA SANTOS, SEBASTIÃO BARROS ARAÚJO, JOSÉ CARDOSO DO NASCIMENTO FILHO et DOUGLAS WAGNER FRANCO. Can. J. Chem. **65**, 372 (1987).

On a étudié la cinétique et le mécanisme de formation du complexe $[Ru(NH_3)_4P(OEt)_3X]^{1+}$-*trans* (X = SCN^-, CN^- et N_3^-). On a déterminé que, à 25°C et à une valeur de μ = 1,0 ($NaCF_3COO$), les constantes de vitesses spécifiques du deuxième ordre, k_1, pour la substitution de CN^-, N_3^- et SCN^- par la molécule d'eau dans le $[Ru(NH_3)_4P(OEt)_3(H_2O)]^{2+}$-*trans* sont respectivement de $(3{,}1 \pm 0{,}3) \times 10^2$, $(1{,}7 \pm 0{,}1) \times 10^2$ et $(1{,}4 \pm 0{,}1) \times 10^2\ M^{-1}\,s^{-1}$. Dans des conditions expérimentales semblables, les réactions d'aquation des dérivés pseudo halogénés, $[Ru(NH_3)_4P(OEt)_3X^-]^{1+}$-*trans* dans lesquels X = N_3^- et SCN^-, se produisent respectivement à des vitesses spécifiques de $(1{,}8 \pm 0{,}1) \times 10$ et $(2{,}8 \pm 0{,}1) \times 10\,s^{-1}$ et on a évalué que la limite supérieure pour la vitesse de la perte du CN^- du $[Ru(NH_3)_4P(OEt)_3CN]^{1+}$-*trans* est égale à $1{,}2 \times 10^{-1}\,s^{-1}$. L'ordre des affinités pour le complexe monophosphite dans la série des ligands étudiés est

$$SO^{2-} \sim P(OEt)_3 > CN^- > imN > isn > pyr > Mepyr^+ > N_3^- > SCN^-$$

dans lesquels imn = imidazole, pyr = pyrazine et $Mepyr^+$ = méthylpyrazinium. A partir des enthalpies d'activation, il est possible d'évaluer que le remplacement net de l'eau dans $[Ru(NH_3)_4P(OEt)_3(H_2O)]^{2+}$-*trans* par les ions azotures et exothermique par 2,8 ± 2 kcal/mol.

[Traduit par la revue]

Introduction

The substitution of one of the ammonia molecules in $[Ru(NH_3)_6]^{2+}$ by the $P(OEt)_3$ ligand provides a good model for the study of the substitutional reactivity of the ligand *trans* to the phosphite molecule.

The substitution of the water molecule in the monophosphite complex *trans*-$[Ru(NH_3)_4P(OEt)_3(H_2O)]^{2+}$ by some nucleophilic and electrophilic reagents was reported earlier (1).

In contrast to other ruthenium(II) ammines (2–4), it was observed for the monophosphite complex that the mechanism of the substitution reactions is sensitive to the properties of the substituent ligand. Proceeding with our investigations on this subject we report further studies on the substitution reactions of monophosphite complex by azide, thiocyanate, and cyanide ions.

Experimental section

Doubly distilled water was used throughout, and all chemicals of analytical grade were used as supplied. Sodium azide (Sigma), sodium thiocyanate (Merck), sodium cyanide (Merck), and triethyl phosphite (Aldrich) were purified as described previously (1).

The $[Ru(NH_3)_5Cl]Cl_2$ and *trans*-$[Ru(NH_3)_4SO_2(H_2O)](CF_3SO_3)_2$ were prepared from $[Ru(NH_3)_6]Cl_3$ (Matthey-Bishop) and $[Ru(NH_3)_5Cl]Cl_2$ according to the literature (5, 6). The *trans*-$[Ru(NH_3)_4(P(OEt)_3)_2](CF_3SO_3)_2$ was prepared by reaction of *trans*-$[Ru(NH_3)_4SO_2(H_2O)](CF_3SO_3)_2$ with $P(OEt)_3$ in acetone (1). The monophosphite complex *trans*-$[Ru(NH_3)_4P(OEt)_3(H_2O)]^{2+}$ was generated in solution by aquation (1, 7) of the biphosphite complex *trans*-$[Ru(NH_3)_4(P(OEt)_3)_2](CF_3SO_3)_2$. Due to air sensitivity of ruthenium(II) complexes all the manipulations were carried out in an inert atmosphere of argon or nitrogen. Electronic spectra of solutions were recorded on a Varian Techtron model 635 spectrophotometer. Reactions were run under pseudo-first-order conditions (excess of ligand), and kinetic determinations made by following changes in absorbance at a selected wavelength in an Aminco-Morrow stopped-flow spectrophotometer. The observed pseudo-first-order rate constant for the approach to equilibrium in reaction [2] is expressed by:

$$[1] \quad k_{obsd} = k_1[X^-] + k_{-1}$$

Values of k_1 and k_{-1} were calculated from the slope and intercept of plots of k_{obsd} versus $[X^-]$ and by employing an H.P. 97 calculator with a standard least squares program. The K_{eq} were calculated from the quotient k_1/k_{-1}. The thermodynamic parameters were evaluated from data at three different temperatures using the Eyring equations (8). The temperature of cell compartment of the spectrophotometer was kept within ±0.1°C by circulating water from a thermostat.

Zwickel flask (9), Teflon tubing, or syringe techniques were used to transfer air-sensitive materials.

Results

The pseudo-halides react with the monophosphite complex according to:

[1]Revision received September 8, 1986.

Can. J. Chem. Downloaded from www.nrcresearchpress.com by 80.58.250.72 on 09/07/12
For personal use only.

TABLE 1. Band maxima and molar absorptivities for the monophosphite complexes

Complex	λ, nm[a]	ε, M^{-1} cm^{-1}	Conditions
trans-$[Ru(NH_3)_4P(OEt)_3N_3]^+$	323	$(7.0 \pm 0.4) \times 10^2$	0.20 *M* NaN_3, 0.80 *M* $NaCF_3CO_2$
trans-$[Ru(NH_3)_4P(OEt)_3CN]^+$	312	$(2.8 \pm 0.2) \times 10^2$	0.20 *M* NaCN, 0.005 *M* NaOH, 0.79 *M* $NaCF_3CO_2$
trans-$[Ru(NH_3)_4P(OEt)_3SCN]^+$	310	$(4.7 \pm 0.4) \times 10^2$	0.20 *M* NaSCN, 0.80 *M* $NaCF_3CO_2$

[a]With an uncertainty of ±1 nm, 25 ± 0.2°C.

TABLE 2. Substitution in *trans*-$[Ru(NH_3)_4P(OEt)_3(H_2O)]^{2+}$ by azide ion[a]

T (°C)	$C_{N_3^-}$ (*M*)	k_{obsd}[b] (s^{-1})
25.0 ± 0.2	0.07	29.5
25.0 ± 0.2	0.10	36.0
25.0 ± 0.2	0.14	41.7
25.0 ± 0.2	0.18	49.0
25.0 ± 0.2	0.22	55.0
15.0 ± 0.2	0.07	20.0
15.0 ± 0.2	0.10	24.0
15.0 ± 0.2	0.14	29.0
15.0 ± 0.2	0.18	33.5
15.0 ± 0.2	0.22	39.0
5.0 ± 0.2	0.07	14.7
5.0 ± 0.2	0.10	19.2
5.0 ± 0.2	0.14	22.6
5.0 ± 0.2	0.18	26.0
5.0 ± 0.2	0.22	31.0

[a]μ = 1.0 ($NaCF_3CO_2$); $C_{Ru(II)} = 3.5 \times 10^{-3}$; 0.010 *M* $NaHCO_3$.
[b]Each value is a mean of at least three independent determinations whose agreement is better than 95%.

[2] *trans*-$[Ru(NH_3)_4P(OEt)_3(H_2O)]^{2+} + X^-$ $\underset{k_{-1}}{\overset{k_1}{\rightleftharpoons}}$ *trans*-$[Ru(NH_3)_4P(OEt)_3X]^+ + H_2O$

where X indicates N_3^-, SCN^-, and CN^-, respectively.

The characteristics of the electronic spectra of the products of reaction [2] are listed in Table 1.

The kinetic data obtained for the above reaction are summarized in Tables 2–4.

There is no evidence in the plots of k_{obsd} versus $[X^-]$ for rate saturation even with pseudo-halide concentrations as high as 0.22 *M*.

The second order specific rates k_1 for the substitution of the water molecule in *trans*-$[Ru(NH_3)_4P(OEt)_3(H_2O)]^{2+}$ for CN^-, N_3^-, and SCN^- are $(3.1 \pm 0.3) \times 10^2$, $(1.7 \pm 0.1) \times 10^2$, and $(1.4 \pm 0.1) \times 10^2$ M^{-1} s^{-1}, respectively, at 25°C, μ = 1.0 ($NaCF_3COO$ 0.90 *M*/$NaHCO_3$ 0.10 *M*). Under the same experimental conditions the aquation of the pseudo-halide derivatives, *trans*-$[Ru(NH_3)_4P(OEt)_3X]^+$, proceeds at specific rates k_{-1} of $(1.2 \pm 0.1) \times 10^{-1}$, $(1.8 \pm 0.1) \times 10$, and $(2.8 \pm 0.1) \times 10$ s^{-1} for $X^- = CN^-$, N_3^-, and SCN^-, respectively.

Since the intercept of the plot k_{obsd} versus $[X^-]$ for the cyanide system is very close to the origin the rate for CN^- loss from *trans*-$[Ru(NH_3)_4P(OEt)_3CN]^+$ was estimated from a least-squares treatment of the experimental data; therefore, the values of 1.2×10^{-1} s^{-1} and 2.6×10^3 M^{-1} must be considered as the upper and lower limits for k_{-1} and K_{eq}, respectively.

TABLE 3. Substitution in *trans*-$[Ru(NH_3)_4P(OEt)_3(H_2O)]^{2+}$ by thiocyanate ion[a]

C_{SCN^-}	k_{obsd}[b] (s^{-1})
0.0250	29.8
0.0500	35.5
0.100	43.3
0.200	57.7
0.300	70.0
0.400	86.0

[a]μ = 1.0 ($NaCF_3CO_2$), $C_{Ru(II)} = 3.0 \times 10^{-3}$ *M*, 0.01 *M* $NaHCO_3$, 25 ± 0.2°C.
[b]Each value is a mean of at least three independent determinations whose agreement is better than 95%.

TABLE 4. Substitution in *trans*-$[Ru(NH_3)_4P(OEt)_3(H_2O)]^{2+}$ by cyanide ion[a]

C_{CN^-}	k_{obsd}[b] (s^{-1})
0.0200	5.9
0.0400	12.5
0.0600	18.0
0.0800	25.0
0.100	32.2
0.140	42.0
0.180	55.4

[a]μ = 1.0 $NaCF_3CO_2$, $C_{Ru(II)} = 1.0 \times 10^{-3}$ *M*, 0.005 *M* NaOH, 25 ± 0.2°C.
[b]Each value is a mean of at least three independent determinations whose agreement is better than 92%.

Discussion

The reactions between Ru(II) centers and CN^-, SCN^-, and N_3^- are not simple substitution processes (10–15). The decomposition observed even in the solid state of the $[Ru(NH_3)_5N_3]^{2+}$ ion or of the $[Ru(trien)(N_3)_2]^+$ ion to the corresponding $[Ru(NH_3)_5N_2]^{2+}$ and the $[Ru(trien)N_3N_2]^+$ ions illustrates such reactivity (16).

For the azide ion, a strong oxidizing agent in acidic media the specific second order rates for these reactions show dependence

Can. J. Chem. Downloaded from www.nrcresearchpress.com by 80.58.250.72 on 09/07/12
For personal use only.

Can. J. Chem. Downloaded from www.nrcresearchpress.com by 80.58.250.72 on 09/07/12
For personal use only.

on the driving force of the Ru(III)/Ru(II) couple in these complexes (17).

Since triethyl phosphite stabilizes Ru(II) with respect to Ru(III) in *trans*-$[Ru(NH_3)_4P(OEt)_3(H_2O)]^{2+}$ ($E^0 = +0.46$ V versus s.c.e.) and the monophosphite complex (1) is weaker acid than aquopentaammine-ruthenium(II), it was expected that the reaction between the monophosphite complex with N_3^- and the other pseudo-halides could be studied without further complications.

The activation parameters for the N_3^- system, calculated from values in Table 2 are $\Delta H_1^{\ddagger} = 3.4 \pm 1.8$ kcal mol^{-1}, $\Delta H_{-1}^{\ddagger} = 6.0 \pm 2.0$ kcal mol^{-1}, $\Delta S_1^{\ddagger} = -37 \pm 6$ cal mol^{-1} deg^{-1}, $\Delta S_{-1}^{\ddagger} = -32 \pm 6$ cal mol^{-1} deg^{-1}. The net replacement of the water in the *trans*-$[Ru(NH_3)_4P(OEt)_3(H_2O)]^{2+}$ by N_3^- is exothermic by 2.8 ± 2.0 kcal mol^{-1} and the entropy change is $\Delta S_{eq}^{\ddagger} = -5 \pm 6$ cal mol^{-1} deg^{-1}.

The stability constants for the *trans*-$[Ru(NH_3)_4P(OEt)_3X]^+$ complexes, calculated from the quotient k_1/k_{-1} are $2.6 \times 10^3\ M^{-1}$, $10 \pm 1\ M^{-1}$, and $5.0 \pm 0.5\ M^{-1}$ for CN^-, N_3^-, and SCN^-, respectively. The position of CN^-, N_3^-, and SCN^- arranged in order of decreasing affinity for the monophosphite complex in the series of the ligands studied (1) is

$$SO^{2-} \sim P(OEt)_3 > CN^- > imN > isn > pyr > Mepyr^+ > N_3^- > SCN^-$$

where imN, isn, pyr, and $Mepyr^+$ are imidazol, isonicotinamide, pyrazine, and methylpyrazinium respectively.

CN^- and SCN^- are both ambidentate ligands and no structural work has been carried out on these systems. However, based on the literature data (10, 18) for similar Ru(II) complexes, it seems reasonable to expect the carbon and sulphur atoms to be the coordination sites for CN^- and SCN^-, respectively, in the monophosphite complexes.

The position of CN^- in the series above, close to $P(OEt)_3$ and SO_3^{2-} can be understood on the basis of its biphilic character. A synergistic effect between the π and σ components of the $(OEt)_3P$—Ru—CN^- bonds must be operative, strengthening the Ru—CN^- linkage. For the azide ion, a weak π acid and moderate σ base, and for the thiocyanate, a weak π acid and weak σ base, the synergism between the π and σ components of the $(OEt)_3P$—Ru—SCN^- and $(EtO)_3P$—Ru—N_3^- bonds should be very weak if not absent.

The formation constants for monoazide and monothiocyanate complexes for divalent metal ions where back-bonding is not significant and those for the *trans*-$[Ru(NH_3)_4P(OEt)_3N_3]^+$ and *trans*-$[Ru(NH_3)_4P(OEt)_3(SCN)]^+$ are of the same order of magnitude. The increase in stability (19–21) of these complexes follow the order

$$Mn^{2+} < Fe^{2+} < Co^{2+} < Ni^{2+} < Zn^{2+} < Ru(II) < Cd^{2+}$$

For electrophilic substituents such as isonicotinamide, pyrazine, and methylpyrazinium, a tendency to rate saturation has been observed on the plots of k_{obsd} versus ligand concentration (1). This behavior is explained by a mechanism of the type:

[3] $[Ru(NH_3)_4P(OEt)_3(H_2O)]^{2+} + X^- \xrightarrow{K_{os}} [[Ru(NH_3)_4P(OEt)_3(H_2O)]^{2+}.X^-]$

[4] $[Ru(NH_3)_4P(OEt)_3(H_2O)]^{2+}.X^- \underset{k'_{-1}}{\overset{k_{1'}}{\rightleftharpoons}} [Ru(NH_3)_4P(OEt)_3X]^{1+} + H_2O$

where X^- represents the entering ligand regardless of its formal charge.

The plots of k_{obsd} versus $[X^-]$ for N_3^-, SCN^-, and CN^- exhibit the same patterns as those observed for good nucleophilic substituents such as imidazole and sulphite ion. The dependence of k_{obsd} upon $[X^-]$ is first order in all the range of ligand concentration and no tendency for rate saturation has been observed.

The overwhelming evidence for the substitution reactions of ruthenium(II) complexes favours a dissociative process (1, 2, 4, 6, 10, 11, 22). Although this mechanism is governed principally by dissociative activation, it is unlikely from the above data that the behavior of N_3^-, SCN^-, and CN^- could be interpreted assuming the formation of the outer-sphere type complexes $[[Ru(NH_3)_4P(OEt)_3(H_2O)^{2+}].X^-]$. It should also be noted that the stability of the outer-sphere complexes is directly related to the extent of charge transfer from Ru(II) to the π acid ligand. Therefore the outer-sphere association of the monophosphite complex with N_3^-, SCN^-, CN^-, imN, and SO^{2-} — weak π acids — should be very weak if it exists (1).

A linear relationship could be found between $\log k_1$ versus $\log K_{eq}$, and $\log k_{-1}$ versus $\log 1/K_{eq}$ for reaction [2] (X = SO^{2-}, CN^-, N_3^-, imN, and SCN^-). For anation reaction the slope is about 0 (indeed 0.05), which implies a transition state resembling the reactants. In the aquation reaction the observed slope for the free energy relationship is 0.89, suggesting that the departing group X^- is only weakly bound in the transition state that resembles the products (23, 24). These results suggest a dissociative activation and are in agreement with our previous observation (1) that the activated complex contains one metal complex and one ligand with some degree of bond making.

It is well known that the extension of bond making relative to bond breaking in the activated complexes changes continuously from one extreme to the other as a function of the experimental conditions, ligands and of the metal center. Small changes could sometimes modify the reaction mechanism (23–25).

In spite of the chemical similarity between phosphite (1) and sulphite systems, no experimental evidence for rate saturations has been reported for substitution reactions on *trans*-$[Ru(NH_3)_4SO_3(H_2O)]$ and related complexes (3, 4). The monophosphite complex seems to be the first reported example on Ru(II) chemistry where the same metal center is able to discriminate through a different mechanism between electrophilic and nucleophilic entering ligands.

Acknowledgements

Support of the research by Conselho Nacional de Pesquisa (CNPq) and Fundação de Amparo à Pesquisa do Estado de São Paulo (FAPESP) in the form of grants is gratefully acknowledged.

1. D. W. Franco and H. Taube. Inorg. Chem. **17**, 571 (1978).
2. H. Taube. Surv. Prog. Chem. **6**, 1 (1973).
3. S. S. Isied and H. Taube. Inorg. Chem. **15**, 3070 (1976).
4. H. Taube. Comm. Inorg. Chem. **1**, 17 (1981).
5. L. H. Vogt, J. L. Katz, and S. E. Wiberley. Inorg. Chem. **4**, 1157 (1963).
6. S. S. Isied and H. Taube. Inorg. Chem. **13**, 1545 (1974).
7. D. W. Franco. Inorg. Chim. Acta, **48**, 1 (1981).
8. J. H. Espenson. Chemical kinetics and reaction mechanism. McGraw-Hill Book Company, NY. 1981.
9. C. G. Kuehn and H. Taube. J. Am. Chem. Soc. **98**, 689 (1976).
10. S. S. Isied and H. Taube. Inorg. Chem. **14**, 2561 (1975).
11. R. E. Shepherd and H. Taube. Inorg. Chem. **12**, 1392 (1973).
12. B. Bosnich and F. P. Dwyer. Aust. J. Chem. **19**, 2235 (1966).
13. N. R. Davies and T. L. Mullins. Aust. J. Chem. **21**, 915 (1968).
14. A. D. Allen, F. Bottomley, R. O. Harris, V. P. Reinsalu, and C. V. Senoff. J. Am. Chem. Soc. **89**, 5595 (1967).

15. L. A. P. KANE-MAGUIRE, P. S. SHERIDAN, F. BASOLO, and R. G. PEARSON. J. Am. Chem. Soc. **92**, 5865 (1970).
16. T. ELIADES, R. O. HARRIS, and P. REINSALU. Can. J. Chem. **47**, 3823 (1969).
17. J. F. ENDICOTT and H. TAUBE. Inorg. Chem. **4**, 437 (1965) and references therein.
18. R. A. LEE and J. E. EARLEY. Inorg. Chem. **20**, 1739 (1981) and references therein.
19. L. G. SILLEN and A. E. MARTELL. Stability constant of metal ion complexes. The Chemical Society, London. 1964 (Special Publication n° 17).
20. E. A. NEVES and L. SANT'AGOSTINHO. Anal. Chim. Acta, **49**, 591 (1970).
21. O. E. GODINHO and L. M. ALEIXO. J. Coord. Chem. **6**, 245 (1977).
22. J. E. BYRD and W. K. WILMARTH. Inorg. Chim. Acta Rev. **5**, 7 (1971).
23. R. G. WILKINS. The study of kinetics and mechanism of transition metal complexes. Allyn and Bacon Inc., Boston. 1974.
24. J. R. CHIPPERFIELD. *In* Advances in linear free energy relationships. *Edited by* N. B. Chapman and J. Shorter. Plenum Press, London. 1972. p. 321 and references therein.
25. C. K. POON and T. C. LAU. Inorg. Chem. **22**, 1664 (1983).

Can. J. Chem. Downloaded from www.nrcresearchpress.com by 80.58.250.72 on 09/07/12
For personal use only.

Minor metabolites of the marine hydroid *Garveia annulata*

EOIN FAHY AND RAYMOND J. ANDERSEN[1]

Departments of Chemistry and Oceanography, University of British Columbia, Vancouver, B.C., Canada V6T 1W5

Received June 5, 1986

EOIN FAHY and RAYMOND J. ANDERSEN. Can. J. Chem. **65**, 376 (1987).

Garvalones A (**8**) and B (**18**), garvins A (**11**) and B (**13**), garveatin D (**20**), garveatin A quinone (**29**), 2-hydroxygarveatins A (**21**) and B (**26**), and 2-hydroxygarvin B (**16**) have been isolated from methanol extracts of the marine hydroid *Garveia annulata*. The structures of all nine metabolites were inferred from their spectral data and chemical derivatization reactions. 2-(3-Oxobutyl)garveatin A (**10**) was synthesized as a model compound for the garvalones and the same methodology was applied to the synthesis of garvalone B (**18**). Dimeric compounds **30** and **32**, formed from 2,2′ coupling of two molecules of garveatin B (**2**) or one molecule of garveatin B (**2**) and one molecule of garvin B (**13**) respectively, were also isolated and shown to be artifacts.

EOIN FAHY et RAYMOND J. ANDERSEN. Can. J. Chem. **65**, 376 (1987).

Les garvalones A (**8**) et B (**18**), les garvines A (**11**) et B (**13**), la garvéatine D (**20**), la garvéatine A quinone (**29**), les hydroxy-2 garvéatines A (**21**) et B (**26**) et l'hydroxy-2 garvine B (**16**) ont été isolées des extraits méthanoliques de l'hydroïde marin *Garveia annulate*. On a déduit les structures des neuf métabolites à partir de leurs données spectrales et de réactions de dérivatisations chimiques. On a synthétisé la (oxo-3 butyl)-2 garvéatine A (**10**) comme composé modèle pour les garvalones et on a appliqué la même méthodologie à la synthèse de la garvalone B (**18**). On a aussi isolé les composés dimères **30** et **32**, qui se forment respectivement par le couplage 2,2′ de deux molécules de garvéatine B (**2**) ou d'une molécule de garvéatine B (**2**) et d'une molécule de garvine B (**13**), et on a démontré qu'il s'agit là de produits qui ne sont pas d'origine.

[Traduit par la revue]

Garveia annulata is a small orange hydroid[2] that is reasonably abundant in the rocky subtidal habitats of Barkley Sound, British Columbia, during the late winter months. Methanol extracts of *G. annulata* are very rich in metabolites that display potent in vitro antimicrobial activity. We have recently reported the isolation of garveatin A (**1**) (2), garveatin B (**2**), garveatin C (**3**), 2-hydroxygarvin A (**4**), garvin A quinone (**5**) (3), annulin A

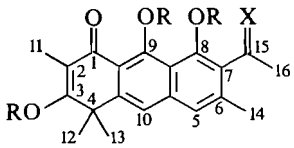

1 R = H X = O
2 R = H X = H_2
23 R = Ac X = O

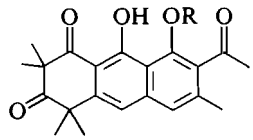

3 R = Me
20 R = H

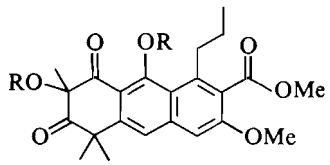

4 R = H
24 R = Ac

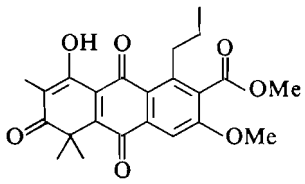

5

(**6**), and annulin B (**7**) (4) from these extracts. Our continuing investigations of *G. annulata* have resulted in the isolation of a number of minor metabolites whose structures we report herein.

Garvalone A (**8**) was obtained as an optically inactive pale yellow oil that gave a parent ion in the hrms (high resolution mass spectrum) appropriate for a molecular formula of $C_{27}H_{32}O_7$. A close relationship between the aromatic portion of the previously reported 2-hydroxygarvin A (**4**) and a fragment of **8** was immediately apparent from a comparison of their spectral data. The uv spectrum (λ_{max} 228, 279, 317, 330, and 382 nm) of **8** was virtually identical to that of **4** (λ_{max} 226, 278, 318, 332,

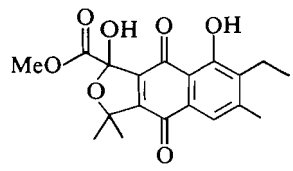

6

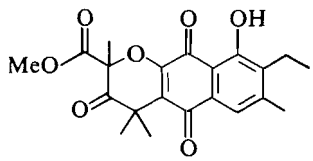

7

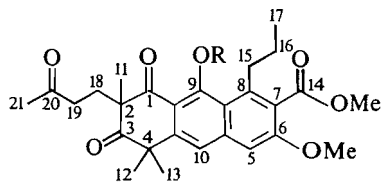

8 R = H
9 R = Me

and 385 nm) and its ^1H (Table 1) and ^{13}C (Table 2) nmr spectra contained resonances that could be assigned to the naphthalenic substructure **i**.

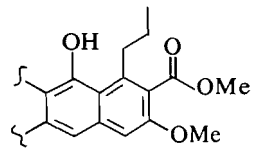

i

Functionality, which accounted for the remaining atoms ($C_{11}H_{16}O_3$) of garvalone A (**8**), could be readily identified upon further consideration of its ^1H and ^{13}C nmr spectra. Four methyl singlets at 1.47, 1.55, 1.59, and 2.04 and a complex multiplet at 2.23 (4H) ppm located the remaining hydrogen atoms. Carbon

[1]Author to whom correspondence may be addressed.

[2]For chemical studies of hydroids other than *G. annulata* see ref. 1.

Can. J. Chem. Downloaded from www.nrcresearchpress.com by 80.58.250.72 on 09/07/12
For personal use only.

Can. J. Chem. Downloaded from www.nrcresearchpress.com by 80.58.250.72 on 09/07/12
For personal use only.

TABLE 1. ^{1}H nuclear magnetic resonance data. Chemical shifts are in ppm from TMS

Proton on carbon no.	Carbon									
	Garvalone A (**8**)	2-(3-Oxobutyl) garveatin A (**10**)	Garvin A (**11**)	Garvin B[a] (**13**)	2-OH garvin B (**16**)	Garvalone B (**18**)	Garveatin D (**20**)	Triacetate (**22**)	Triacetate (**27**)	Garveatin A quinone (**29**)
1OR	—	—	—	—	—	—	—	—	—	11.45*
2OR	—	—	—	—	4.02, br s	—	—	2.20	2.22	—
5	6.93	6.65	6.91	7.16	7.11	7.06	7.05	7.61	7.55	7.55
6OR	3.96&	—	3.95*	11.14#	11.44 (11.45)#	11.50#	—	—	—	—
8OR	—	10.13*	—	—	—	—	10.2	2.34*	2.45	11.66*
9OR	15.10	16.29*	15.14	17.85#	14.61 (14.62)#	15.44#	—	2.41*	2.45	—
10	7.13	7.12	7.17	7.35	7.11	7.10	7.12	7.79	7.70	—
11	1.47	1.48	1.99	1.85	1.65 (1.66)	1.46	1.50	1.45	1.44	1.98
11a	—	—	—	—	—	—	1.50	—	—	—
12	1.55#	1.54#	1.64	1.54*	1.65 (1.66)*	1.55*	1.58	1.57#	1.55#	1.63
13	1.59#	1.58#	1.64	1.58*	1.80 (1.82)*	1.57*	1.58	1.79#	1.78#	1.63
14	—	2.34	—	—	—	—	2.41	2.41	2.50	2.41
14OR	3.93&	—	3.97*	—	—	—	—	—	—	—
15	3.15	—	3.18, m	3.23, dd 4.35, dd	3.41 (3.44), dd 4.38, dd	3.42, dd 4.39, dd	—	—	2.70, q	—
16	1.75, m	2.55	1.73, m	4.77, m	4.74, m	4.72, m	2.63	2.50	1.13, t	2.60
17	1.11, t	—	1.03, t	1.50, d	1.64 (1.65), d	1.62, d	—	—	—	—
18	2.23, m	2.24, m	—	—	—	2.24, m	—	—	—	—
19	2.23, m	2.24, m	—	—	—	2.24, m	—	—	—	—
21	2.04	2.04	—	—	—	2.06	—	—	—	—

[a]Spectrum of **13** was run in DMSO-d_6. All other spectra were run in $CDCl_3$. All signals are singlets unless indicated otherwise. *, &, # indicate assignment may be reversed.

TABLE 2. ^{13}C nuclear magnetic resonance data. Chemical shifts are in ppm from TMS. All spectra were run in $CDCl_3$

Carbon no.	Compound			
	2-Hydroxy garvin A (**4**)	Garvalone A (**8**)	2-(3-Oxobutyl) garveatin A (**10**)	2-Hydroxy garvin B (**16**)
1	—	203.9	204.1	199.71 (199.55)
2	—	58.3	58.0	81.64 (81.57)
3	—	211.9	211.3	209.83
4	—	47.9	47.9	47.14 (47.05)
4a	142.9	143.0	—	145.40 (145.26)*
5	105.0	105.0	—	111.81
6	157.7	157.4	—	161.27 (161.16)
7	126.9	126.5	—	115.94
8	142.1	142.5	—	144.58 (144.54)*
8a	116.7	116.8	—	110.81 (110.77)
9	166.0	166.6	—	167.39 (167.17)
10	116.5	116.8	—	116.03
9a	107.3	108.7	—	107.00 (106.88)
10a	142.0	142.8	—	143.84
11	—	24.2	24.1	28.43 (27.99)#
12	—	29.9	29.9	29.15 (29.04)#
13	—	27.0	27.1	30.70 (30.44)#
14	168.3	168.6	—	169.85 (169.80)
15	36.0	36.1	—	34.60 (34.36)
16	25.3	25.4	—	75.43 (75.35)
17	14.7	14.8	—	20.83
18	—	31.4	31.3	—
19	—	39.1	38.9	—
20	—	207.0	206.9	—
21	—	30.5	30.7	—
6OR	55.9&	55.9&	—	—
14OR	52.3&	52.5&	—	—

*, #, and & indicate that the assignments may be interchanged.

resonances at 39.1 (t) and 31.4 (t) required that the protons resonating at 2.23 ppm be attached to two methylene carbons. Carbonyl resonances at 211.9, 207.0, and 203.9 showed that the three oxygens were present as ketone functionalities and resonances at 58.3 (s) and 47.9 (s) ppm identified quaternary carbons.

The carbon resonances at 203.9, 58.3, 211.9, and 47.9 ppm in the spectrum of **8** were very similar to the resonances exhibited by carbons 1 to 4 in garveatin C (**3**) (C1, 204.9; C2, 55.3; C3, 211.6; C4, 48.1) (3), suggesting that both metabolites had the 1-oxo, 2-dialkyl, 3-oxo, 4-dialkyl functionalities in common. Demonstration of an nOe (nuclear Overhauser enhancement) between the aromatic proton resonance at 7.13 (H10) and two methyl resonances at 1.55 and 1.59 ppm in the ^1H nmr of **8** provided evidence for a *gem*-dimethyl group at C4. The ^1H nmr resonance at 1.47 (s, 3H) was assigned to a methyl substituent at C2 by analogy with the other *Garveia* metabolites, and a methyl ketone residue was indicated by the ^1H nmr resonance at 2.04 (s, 3H) and the ^{13}C nmr resonances at 207.0 (s) and 30.5 (q) ppm. Insertion of the two methylene carbons between the carbonyl carbon of the methyl ketone residue and the remaining unsatisfied valence at C2 of the anthracenone skeleton gave the proposed structure **8** for garvalone A. In the mass spectrum, **8** shows intense fragment ions at 398 ($M^+ + H - (CH_3COCH_2CH_2$-): 100%) and 397 ($M^+ - (CH_3COCH_2CH_2$-): 89%) as would be expected.

2-(3-Oxobutyl)garveatin A (**10**), a model for **8**, was obtained from a Michael reaction (5) between garveatin A (**1**) and methyl vinyl ketone (benzene, room temperature, K_2CO_3, 18-crown-6). The ^1H nmr, ^{13}C nmr, and mass spectra of **10** were in complete accord with the structure assigned to garvalone A (**8**) (see Tables 1 and 2).

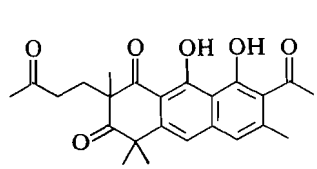

10

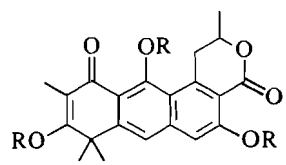

13 R = H
15 R = Ac

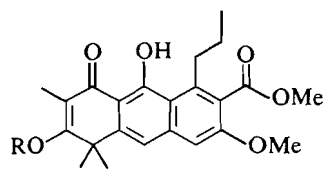

11 R = H
12 R = Me

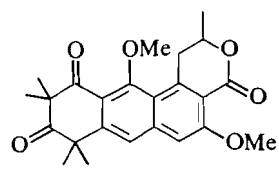

14

Three of the new minor metabolites from the *Garveia* extracts belong to the garvin family. Garvin A (**11**) was obtained as a bright yellow solid that gave a parent ion in the mass spectrum at m/z 398 appropriate for a molecular formula of $C_{23}H_{26}O_6$. Its ^1H nmr spectrum showed resonances (Table 1) assignable to the *n*-propyl, methyl ester, and methyl ether functionalities found in the substructure **i** of 2-hydroxygarvin A (**4**) (3). Additional resonances at 1.64 (s, 6H), 1.99 (s, 1.5H), 1.50 (d, J = 7 Hz,

Can. J. Chem. Downloaded from www.nrcresearchpress.com by 80.58.250.72 on 09/07/12
For personal use only.

Can. J. Chem. Downloaded from www.nrcresearchpress.com by 80.58.250.72 on 09/07/12
For personal use only.

1.5H), and 4.01 (q, $J = 7$ Hz, 0.5H) ppm corresponded closely to the signals assigned to the two tautomeric forms of the alicyclic ring in garveatin B (**2**) (3). A simple combination of the two fragments led to the assignment of structure **11** to garvin A. Treatment of garvin A (**11**) with diazomethane gave monomethyl garvin A (**12**) as the major product.

Garvin B (**13**) was obtained as an optically active yellow solid that was shown by hrms to have a molecular formula of $C_{21}H_{20}O_6$. Methyl resonances at 1.54, 1.58, and 1.85 ppm in the ^{1}H nmr (DMSO-d_6; Table 1) of garvin B showed a strong resemblance to the resonances for the methyl groups in the alicyclic ring of garveatin A (**1**) (2) (DMSO-d_6; 1.59, 6H; 1.90, 3H), indicating that the two molecules had this substructure in common. Aromatic resonances at 7.16 (s, 1H) and 7.35 (s, 1H) could be assigned to protons on C5 and C10 of an anthracenone skeleton by analogy with other *Garveia* metabolites. A six-proton spin system (1.50 (d, $J = 7$ Hz, 3H), 4.77 (m, 1H), 3.23 (dd, $J = 19$, 13 Hz, 1H), 4.35 (dd, $J = 19$, 3 Hz, 1H)) could be assigned to a propyl residue that contained an oxygen substituent at the central carbon and an aryl substituent at one of the terminal carbons. Carbon resonances at 20.4, 75.4, and 34.0 ppm were assigned to the substituted propyl residue. The remaining substituents on the aromatic nucleus were shown to be two phenols by methylation and acetylation reactions that gave **14** and **15** respectively, and an ester carbonyl by the observation of a ^{13}C nmr resonance at 170.6 ppm. Modification of the structure of garvin A (**11**) by replacing the methoxy substituent at C6 with a phenol, and formation of a delta (δ) lactone between an alcohol at C16 and the carboxyl at C14, leads to a new structure **13**, which effectively accounts for all the properties of garvin B.

2-Hydroxygarvin B (**16**) was obtained as a yellow solid, which showed a parent ion in its mass spectrum at m/z 384 appropriate for a molecular formula of $C_{21}H_{20}O_7$. A preliminary examination of the ^{1}H nmr spectrum of **16** (Table 1) revealed that a number of the resonances were doubled (ratio approximately 1:1), indicating that a mixture of two diastereomers was present. It was readily apparent from both the ^{1}H and ^{13}C nmr spectra of **16** (Tables 1 and 2) that each of the diastereomers contained an alicyclic ring identical to that found in 2-hydroxygarvin A (**4**), and a naphthalenic fragment identical to that found in garvin B (**13**). Acetylation of **16** gave a mixture of the diastereomeric triacetates **17** in good yield. We have not determined which of the two chiral centers in 2-hydroxygarvin B (**16**) is epimeric in the two naturally occurring diasteromers; however, the observation that garvin B (**13**) is optically active implies that **13** occurs as a single enantiomer and suggests that biological hydroxylation at C2 has occurred in a nonstereospecific fashion.

Garvalone B (**18**), an extremely minor component of the crude extracts, was isolated as a light yellow oil. In the mass spectrum, **18** showed a parent ion at m/z 328, consistent with a molecular formula of $C_{26}H_{28}O_6$. The ^{1}H nmr of **18** (Table 1) also showed a number of resonances that were doubled, again indicating the presence of two diastereomers (ratio 2:3), which we were unable to separate. The major isomer displayed signals (Table 1) that corresponded to the ^{1}H nmr resonances displayed by the functionality in the alicyclic ring of garvalone A (**8**). The remaining ^{1}H nmr resonances in the spectrum of **18** showed a close correspondence to the observed ^{1}H nmr resonances for the aromatic and lactonic portions of garvin B (**13**). Garvalone B (**18**) was quantitatively converted to the diacetate **19** in accordance with the proposed structure.

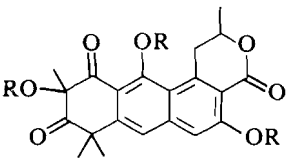

16 R = H
17 R = Ac

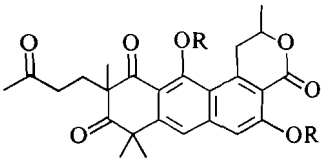

18 R = H
19 R = Ac

A synthesis of a mixture of garvalone B diastereomers (**18**) (ratio 2:3) was achieved via a Michael reaction between garvin B (**13**) and methyl vinyl ketone. The major isomer formed in the Michael reaction was the minor, naturally occurring isomer. Once again, since garvin B (**13**) occurs as a single enantiomer, it seems reasonable to assume that it is the chiral center at C2 that is epimeric in the natural garvalone B stereoisomers. This assignment is consistent with the lack of optical activity found for garvalone A (**8**) and it implies a nonstereospecific alkylation at C2 in both molecules.

Four of the new minor metabolites belong to the garveatin family. Garveatin D (**20**) was obtained as a yellow oil that showed a parent ion in its mass spectrum at m/z 354 appropriate for a molecular formula of $C_{21}H_{20}O_5$. Its ^{1}H nmr spectrum (Table 1) showed a striking resemblance to the spectrum of garveatin C (**3**) (3). The only noticeable differences were the absence of a methyl ether resonance in the region of 3.9 ppm, an upfield shift in the position of the H5 signal (**3**: 7.35; **20**: 7.05 ppm) reflecting the lack of methylation on the C8 phenol, and the appearance of two phenolic resonances (10.20, 16.15) instead of just one. These observations are consistent with the proposed structure **20** for garveatin D.

An extremely polar metabolite, 2-hydroxygarveatin A (**21**), was obtained as an orange solid that was difficult to purify and gave poor spectral data due to its low solubility in organic solvents. It was most conveniently characterized as its triacetate **22**, a colorless solid that had a molecular formula of $C_{26}H_{26}O_9$. The structure of **22** could be directly assigned by comparing its ^{1}H nmr spectrum (Table 1) to the ^{1}H nmr spectra of triacetyl garveatin A (**23**) (1) and 2-hydroxygarvin A diacetate (**24**) (3).

2-Hydroxygarveatin B (**26**) was obtained as a yellow solid that was shown by hrms to have a molecular formula of $C_{20}H_{22}O_5$. The chemical shifts of three methyl groups in the ^{1}H nmr spectrum of **26** (1.50, 1.65, 1.78) closely corresponded to the shifts of the methyl groups in the alicyclic ring of 2-hydroxygarvin A (**4**) (1.52, 1.66, 1.81) (3) and the remaining proton resonances mimicked those for the aromatic nucleus and its substituents in garveatin B (**2**), allowing a routine assignment of the structure as **26**. 2-Hydroxy garveatin B (**26**) could be converted to a mixture of the triacetate **27** (Table 1) and the diacetate **28**.

Garveatin A quinone (**29**) was isolated as a red oil that was shown by mass spectrometry to have a molecular formula of $C_{20}H_{18}O_6$. The ^{1}H nmr spectrum (Table 1) of **29** immediately

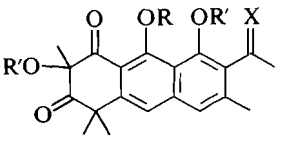

21 R = R′ = H X = O
22 R = R′ = Ac X = O
25 R = H R′ = Ac X = O
26 R = R′ = H X = H_2
27 R = R′ = Ac X = H_2

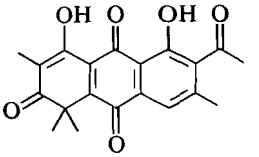

29

Can. J. Chem. Downloaded from www.nrcresearchpress.com by 80.58.250.72 on 09/07/12
For personal use only.

suggested a close relationship to garveatin A (**1**). However, in contrast to the ^{1}H nmr spectrum of 1, only one aromatic proton resonance was observed in the ^{1}H nmr of **29**, and the similarity of its chemical shift (7.55 ppm) to that observed for H5 in garvin A quinone (**5**) (7.56 ppm) (3) suggested that **29** might also be a quinone. The ^{13}C nmr resonances at 193.0 and 180.4 ppm in the spectrum of **29** confirmed the presence of the quinone functionality, and the remainder of the spectrum was in good agreement with the proposed structure. Phenolic and enolic proton resonances at 11.45 and 11.66 ppm indicated that in chloroform solution garveatin A quinone (**29**) exists as the 3-keto tautomer shown.

Garveatin A quinone (**29**) was present in fresh extracts (<48 h) of *Garveia annulata*, and we found that garveatin A (**1**) was not readily converted to the quinone by aerial oxidation in either acidic or basic solutions. Therefore, it seems likely that the quinone **29** is a true metabolite and not an oxidation artifact.

The first evidence for the presence of dimers in the *G. annulata* extracts came from the observation that ^{1}H nmr samples ($CDCl_3$) of garveatin B (**2**) developed a new set of resonances on standing and that these new resonances increased in intensity with time. Repurification of an "aged" garveatin B (**2**) nmr sample yielded, in addition to garveatin B (**2**), a less polar compound **30** whose ^{1}H nmr spectrum contained signals corresponding to the new resonances in the spectrum of "aged" **2**. Compound **30** was not formed when garveatin B (**2**) was

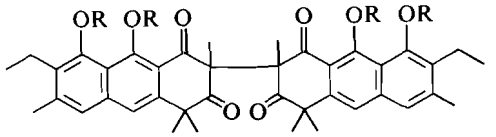

30 R = H
31 R = Ac

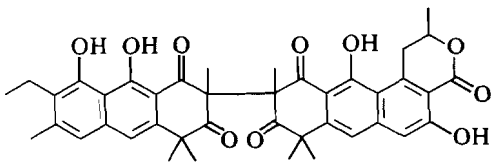

32

allowed to stand in C_6D_6 or acetone-d_6 solutions, but it was detected as a very minor constituent of the flash fraction from which garveatin B (**2**) was originally isolated.

The ^{1}H nmr spectrum of **30** (Table 3) contained resonances that could be assigned to the aromatic ethyl, aromatic methyl, H5, H10, and phenolic protons of a naphthalenic fragment identical to that found in garveatin B (**2**). All the above resonances showed small upfield shifts (range: 0.03 (C14-CH_3) – 0.40 (C9-OH) ppm) relative to the corresponding resonances in garveatin B (**2**). Methyl singlets at 1.38, 1.66, and 1.88 ppm indicated that **30** had an alicyclic ring containing an asymmetric center fused to the naphthelinic fragment. The ^{13}C nmr spectrum of **30** contained carbonyl resonances at 202.4 and 209.0 ppm that were similar in chemical shift to the resonances assigned to the C1 (205.8 ppm) and C3 (211.6 ppm) ketone functionalities in garveatin C (**3**), suggesting that the two molecules contained similarly substituted alicyclic rings. A ^{13}C nmr resonance at 63.0 ppm in the spectrum of **30** was assigned to a dialkylated carbon at C2 of the anthracenone skeleton.

The highest mass ion in the electron impact mass spectrum (EI ms) of **30** appeared at m/z 326 daltons. Acetylation of **30**, however, gave a major product **31** that gave a weak molecular ion at m/z 818 daltons in its EI ms. We concluded that **30** was a dimer formed by a 2,2′ linkage of garveatin B (**2**) monomers and that **31** was its 8,8′,9,9′ tetraacetate.

TABLE 3. ^{1}H nuclear magnetic resonance data. Chemical shifts are in ppm from TMS. All spectra were run in $CDCl_3$

Proton on carbon no.	Compound: Garveatin B dimer (**30**)	Compound: Garveatin B – Garvin B dimer (**32**)
5	6.98	6.90:6.92
10	6.98	6.90:7.02
11	1.88*	1.80:1.82*
12	1.38*	1.24:1.20*
13	1.66*	1.78:1.81*
14	2.43	2.42:—
15	2.53 (m)	2.42 (m):2.35 (dd) 2.77 (m):3.83 (dd)
16	1.07 (t)	1.00 (t):4.40 (m)
17	—	—:1.51 (d)
6OR	—	—:11.56
8OH	9.37	9.10:—
9OH	15.79	15.70:14.85

All resonances are singlets unless indicated otherwise. * indicates assignment may be reversed.

The mixed dimer **32** was obtained as an orange oil in the course of a routine work-up of a *G. annulata* crude extract. A FAB (fast atom bombardment) mass spectrum of **32** showed a molecular ion at m/z 693 (M + 1) daltons, appropriate for a molecular formula of $C_{41}H_{40}O_{10}$, and fragment ions at m/z 326/327 and 368/369 corresponding to the garveatin B (**2**) and garvin B (**13**) monomers respectively. The ^{1}H nmr spectrum of **32** (Table 3) contained resonances that could be assigned to both the garveatin B and garvin B-like fragments of the dimer, allowing a routine assignment of the structure. Once again, many of the observed ^{1}H nmr resonances of **32** show upfield shifts relative to the corresponding resonances in the ^{1}H nmr spectra of the individual monomers. Mixtures of dimers **30** and **32** form slowly in chloroform solutions containing equal parts of garveatin B (**2**) and garvin B (**13**), with or without added silica gel. It seems likely, therefore, that both the mixed dimer **32** and the symmetrical dimer **30** are artifacts formed during fractionation of the *G. annulata* extracts.

One interesting feature of the dimerization reactions leading to **30** and **32** is the apparent formation of only a single relative stereochemistry at the two new chiral centers in the products. In principle, dimerization at C2 of either of the monomers **2** or **13** can lead to the formation of either the *meso* isomer or a racemic mixture of the *R,R* and *S,S* isomers. The *meso* dimer should be separable from the *R,R* and *S,S* dimers and the two types should exhibit different spectral features. We have found no evidence for the formation of more than one type of stereoisomer. Cameron *et al.* have used chiral nmr shift reagents to identify the diasteromers of a series of 10,10′ emodin bianthrones (6). We attempted to apply this methodology to the tetraacetates of our dimers, but excessive line broadening prevented any definite conclusions. Therefore it is still not clear whether the *Garveia* monomers dimerize to give only the *meso* or a mixture of *R,R* and *S,S* isomers.

None of the other *G. annulata* metabolites spontaneously dimerize as readily as garveatin B (**2**) upon standing at room

temperature in $CDCl_3$. Garveatin A (**1**) does not dimerize at all, while garvin A (**11**) gives only a very low yield of dimer after a period of a week or longer. It is possible that the spontaneous dimerization of garveatin B (**2**) and garvin A (**11**) in chloroform solutions is related to the high percentage of diketo tautomer present for both these compounds in this solvent. In contrast, the ^1H nmr spectrum of garveatin A (**1**) ($CDCl_3$) shows it to be present exclusively as the keto-enol tautomer.

The minor *G. annulata* metabolites reported in this manuscript can be grouped into three families, the garveatins (compounds **20**, **21**, **26**, and **29**), the garvins (compounds **11**, **13**, and **16**), and the garvalones (compounds **8** and **18**). The anthracene based ring system found in all the compounds is a common feature of polyketide derived metabolites.[3] We have previously proposed that a single nonaketide precursor could lead to both the garveatins and the garvins by simply adopting different folding patterns prior to cyclization and aromatization (3). The garvalones are simply C2 alkylated garvins, although the nature of the alkylation pathway is not immediately apparent. Hydroxylation at C2 and anthraquinone formation are secondary biogenetic transformations observed in both the garveatin and garvin families.

Experimental

The ^1H nmr spectra were recorded on Bruker WP-80, Nicolet–Oxford 270, Varian XL-300, and Bruker WH-400 spectrometers. The ^{13}C nmr spectra were recorded on a Varian XL-300 spectrometer. TMS was used as an internal standard. Low resolution mass spectra were recorded on an AEI MS902 spectrometer and high resolution mass spectra on an AEI MS50 instrument. The ir spectra were recorded on a BOMEM Fourier transform spectrometer. Ultraviolet–visible spectra were recorded on a Bausch and Lomb Spectronic-2000 spectrometer. Optical rotation measurements were recorded on a Perkin–Elmer 141 polarimeter.

Merck silica gel 230–400 mesh was used for flash and preparative thin-layer chromatography and Whatman Magnum-9 Partisil-10 and Partisil-10 ODS 3 columns were used for preparative hplc. Sephadex LH-20 resin was used for molecular exclusion chromatography. The R_f values are listed for compounds in an analytical tlc system using a 1:49:49 acetic acid – ethyl acetate – hexane eluent.

Collection data

Garveia Annulata was collected by hand using SCUBA (−2 to −9 m) on exposed rocky reefs in Barkley Sound, British Columbia, during the winter and spring months.

Extraction and chromatography

Freshly collected whole specimens were immediately placed in methanol and stored at room temperature. The methanol extract was decanted and filtered. The filtrate was rotary evaporated to give an aqueous suspension that was diluted to 400 mL with distilled water and extracted successively with hexane (3 × 400 mL), methylene chloride (3 × 400 mL), and ethyl acetate (2 × 400 mL).

The hexane (600 mg) and methylene chloride (4 g) extracts were fractionated separately by step-gradient vacuum flash chromatography using a 3.5 cm thick silica pad in a sintered glass funnel (10 cm diameter). Fractions eluting with the same solvent composition from each separation were combined. Elution with 20% ethyl acetate – hexane, 50% ethyl acetate – hexane, 100% ethyl acetate, and 20% methanol – ethyl acetate gave fractions A (140 mg), B (500 mg), C (1.5 g), and D (700 mg) respectively. Chromatography of fraction B on Sephadex LH-20 (90% methanol – methylene chloride) yielded a fraction that was further purified by preparative tlc (50% ethyl acetate – hexane, 10% ethyl acetate – chloroform, and 20% ethyl acetate – hexane) to give garvalone A (**8**) (20 mg), 2-hydroxygarvin B (**16**) (9 mg), and garveatin B dimer (**30**) (3 mg). Another LH20 fraction contained a component that was purified by preparative tlc (10% ethyl acetate – hexane) and reverse phase hplc (95% acetonitrile–water) to yield garveatin B – garvin B dimer (**32**) (6 mg).

LH-20 purification of fraction C yielded garvin B (**13**) (100 mg) and 2-hydroxygarveatin B (**26**) (40 mg) as well as two other fractions that were chromatographed on preparative tlc (10% ethyl acetate – chloroform, 25% ethyl acetate – hexane, and 5% methanol–chloroform) to yield garvin A (**11**) (45 mg), garveatin D (**20**) (8 mg), and garvalone B (**18**). Fraction D contained a complex mixture of relatively polar compounds, which were separated on reversed phase tlc plates (80% methanol–water) to yield 2-hydroxygarveatin A (**21**) as the major component.

The ethyl acetate phase was subjected to vacuum flash chromatography using a 3.5-cm silica gel pad in a sintered glass funnel (10 cm diameter). Elution with an ethyl acetate – methylene chloride gradient yielded a fraction that was deep red. This fraction was further purified by preparative tlc (methanol – methylene chloride, 2:98) to give garveatin A quinone (**29**) (11 mg).

*Garvalone A (**18**):* obtained as a light yellow oil, R_f 0.42; uv (MeOH): 228 (15 000), 279 (20 100), 317 (4 900), 330 (4 100), 382 (4 400) nm; ir ($CHCl_3$): 1570, 1610, 1718, 1737 cm^{-1}; ^1H nmr (300 MHz, $CDCl_3$): 1.11 (t, 3H, J = 7 Hz), 1.47 (s, 3H), 1.55 (s, 3H), 1.59 (s, 3H), 1.75 (m, 2H), 2.04 (s, 3H), 2.23 (m, 4H), 3.15 (m, 2H), 3.93 (s, 3H), 3.96 (s, 3H), 6.93 (s, 1H), 7.13 (s, 1H), 15.10 (s, 1H) ppm; ^{13}C nmr (75 MHz, $CDCl_3$): 211.90 (s), 207.04 (s), 203.88 (s), 168.61 (s), 166.59 (s), 157.35 (s), 142.97 (s), 142.50 (s), 141.82 (s), 126.45 (s), 116.78 (s), 115.28 (d), 108.70 (s), 104.96 (d), 58.30 (s), 55.94 (q), 52.49 (q), 47.85 (s), 39.06 (t), 36.14 (t), 31.43 (t), 30.52 (q), 29.86 (q), 27.01 (q), 25.42 (t), 24.21 (q), 14.80 (q) ppm; ms m/z (relative intensity): 468 (M^+, 94), 453 (14), 437 (14), 398 (100), 397 (89), 383 (43). *Exact Mass* calcd. for $C_{27}H_{32}O_7$: 468.2149; found: 468.2162.

*Preparation of methyl garvalone A (**9**)*

Garvalone A (**8**) (20 mg), K_2CO_3 (150 mg, anhydrous), and methyl iodide (0.6 mL) were dissolved in 10 mL of acetone and the mixture was stirred at reflux overnight under an atmosphere of N_2. The reaction mixture was rotary evaporated and partitioned between water and methylene chloride. The methylene chloride phase yielded methyl garvalone A (**9**) (20 mg). Compound **9** was obtained as a pale yellow oil, R_f 0.39; uv (MeOH): 225, 263, 314 nm; ^1H nmr (400 MHz, $CDCl_3$): 0.94 (t, 3H, J = 7 Hz), 1.36 (s, 3H), 1.52 (s, 3H), 1.57 (s, 3H), 1.6 (m, 2H), 1.95–2.10 (m, 2H), 2.05 (s, 3H), 2.24 (m, 2H), 2.48 (m, 2H), 2.87 (m, 1H), 3.14 (m, 1H), 3.95 (s, 3H), 3.97 (s, 3H), 7.02 (s, 1H), 7.49 (s, 1H) ppm; ms m/z (rel. intensity): 482 (M^+, 57), 467 (11), 451 (9), 426 (23), 412 (38), 411 (37), 397 (62), 383 (18).

*Preparation of 2-(3-oxobutyl)garveatin A (**10**)*

To a solution of garveatin A (**1**) (15 mg) in benzene (7 mL) was added anhydrous K_2CO_3 (100 mg), methyl vinyl ketone (50 μL), and 18-crown-6 (one crystal). The mixture was refluxed under N_2 for 24 h after which it was filtered and the filtrate was concentrated *in vacuo*. Preparative tlc of the residue (silica gel; acetic acid – methanol–chloroform, 1:5:94) gave 2-(3-oxobutyl)garveatin A (**10**) (12 mg) and unreacted garveatin A (2 mg). Compound **10**: ^1H nmr ($CDCl_3$, 400 MHz): 1.48 (s, 3H), 1.54 (s, 3H), 1.58 (s, 3H), 2.04 (s, 3H), 2.24 (m, 4H), 2.34 (s, 3H), 2.55 (s, 3H), 6.65 (s, 1H), 7.12 (s, 1H), 10.13 (s, 1H), 16.29 (s, 1H); ^{13}C nmr ($CDCl_3$): 20.7, 24.1, 27.1, 29.9, 30.7, 31.3, 32.3, 38.9, 47.9, 58.0, 107.8, 110.8, 115.5, 120.2, 125.3, 139.5, 141.2, 142.5, 156.0, 166.1, 204.1, 204.2, 206.9, 211.3 ppm; ms m/z: M^+ 410, 341, 340, 326, 325 (100%).

*Garvin A (**11**):* obtained as a yellow solid, R_f 0.41; uv (MeOH): 220, 247, 274, 321, 383 nm; ^1H nmr (300 MHz, $CDCl_3$): 1.03 (t, 3H, J = 7 Hz), 1.64 (s, 3H), 1.73 (m, 2H), 1.99 (s, 3H), 3.18 (m, 2H), 3.95 (s, 3H), 3.97 (s, 3H), 6.91 (s, 1H), 7.17 (s, 1H), 15.14 (s, 1H), also 1.50 (d, 3H, J = 7 Hz), 4.01 (q, 1H, J = 7 Hz) due to diketo tautomer; ms m/z (rel. intensity): 398 (M^+, 100), 383 (30), 367 (21), 351 (17).

[3]For examples of anthracene based metabolites from other marine invertebrates see ref. 7.

Can. J. Chem. Downloaded from www.nrcresearchpress.com by 80.58.250.72 on 09/07/12
For personal use only.

Can. J. Chem. Downloaded from www.nrcresearchpress.com by 80.58.250.72 on 09/07/12
For personal use only.

Preparation of monomethyl garvin A (12)

Garvin A (**11**) (14 mg) was dissolved in diethyl ether (3 mL, anhydrous) and treated with diazomethane (generated by adding 0.6 mL 5 *M* NaOH to 100-mg *N*-methylnitronitrosoguanidine). After standing overnight, the reaction mixture was purified by preparative tlc (80% $CHCl_3$–hexane) to give monomethylgarvin A (**12**) (6.4 mg) as the major product. *Compound (12):* R_f 0.60; uv (MeOH): 220, 250, 275, 283 (sh), 322, 334 (sh), 390 nm; ^{1}H nmr (300 MHz, $CDCl_3$): 1.02 (t, 3H), 1.55 (s, 6H), 1.73 (m, 2H), 2.06 (s, 3H), 3.19 (m, 2H), 3.93 (s, 3H), 3.96 (s, 3H), 3.99 (s, 3H), 6.90 (s, 1H), 7.14 (s, 1H), 15.87 (s, 1H) ppm; ms *m/z* (rel. intensity): 412 (M^+, 44), 397 (32), 381 (15), 365 (24), 337 (10).

Garvin B (13): obtained as a yellow solid, R_f 0.43; uv (MeOH): 229, 256, 289, 327, 389 nm; ^{1}H nmr (300 MHz, DMSO-d_6): 1.50 (d, 3H, J = 7 Hz), 1.54 (s, 3H), 1.58 (s, 3H), 1.85 (s, 3H), 3.23 (dd, 1H, J = 19, 13 Hz), 4.35 (dd, 1H, J = 19, 3 Hz), 4.77 (m, 1H), 7.16 (s, 1H), 7.35 (s, 1H), 11.14 (s, 1H), 17.85 (s, 1H) ppm; ^{13}C nmr (75 MHz, DMSO-d_6): 191.05, 177.97, 170.58, 166.33, 159.05, 149.09, 145.56, 142.55, 115.00, 114.40, 110.53, 110.50, 107.70, 107.65, 75.40, 48.24, 33.97, 29.24, 28.93, 20.43, 7.60 ppm; ms *m/z* (rel. intensity): 368 (M^+, 6), 353 (3), 325 (3), 311 (3). *Exact Mass* calcd. for $C_{21}H_{20}O_6$: 368.1260; found: 368.1269.

Preparation of trimethyl garvin B (14)

A solution of garvin B (**13**) (15 mg), K_2CO_3 (100 mg), and methyl iodide (0.5 mL) in 10 mL acetone was refluxed under a stream of N_2 for 6 h and then partitioned between water and methylene chloride. The methylene chloride soluble material was chromatographed on silica (50% ethyl acetate – hexane) to yield trimethylgarvin B (**14**) (10 mg) as the major reaction product. *Compound (14):* obtained as a pale yellow solid, R_f 0.27; $[\alpha]_D^{22}$ +172.69° (*c* 0.26, $CHCl_3$); uv (MeOH): 232, 275, 330 nm; ^{1}H nmr (300 MHz, $CDCl_3$): 1.37 (s, 3H), 1.42 (s, 3H), 1.54 (s, 3H), 1.55 (d, 3H, J = 7 Hz), 1.57 (s, 3H), 3.27 (dd, 1H, J = 19, 13 Hz), 3.89 (s, 3H), 4.04 (s, 3H), 4.13 (dd, 1H, J = 19, 3 Hz), 4.45 (m, 1H), 7.13 (s, 1H), 7.50 (s, 1H) ppm; ms *m/z* (rel. intensity): 410 (M^+, 100), 395 (11), 377 (13), 367 (12), 340 (49), 339 (40).

Acetylation of garvin B

Garvin B (**11**) (30 mg) was acetylated at room temperature with pyridine (0.5 mL) and acetic anhydride (0.5 mL). After evaporation of the reagents, the residue was purified by preparative tlc (10% ethyl acetate – methylene chloride) and hplc (10% ethyl acetate – hexane) to give garvin B diacetate (5 mg) and garvin B triacetate (**13**) (15 mg). *Diacetate:* obtained as a light yellow oil, R_f 0.38; uv (MeOH): 245, 286, 389 nm; ^{1}H nmr (80 MHz, $CDCl_3$): 1.55 (s, 3H), 1.57 (s, 3H), 1.58 (d, 3H, J = 7 Hz), 1.88 (s, 3H), 2.38 (s, 3H), 2.41 (s, 3H), 3.40 (dd, 1H, J = 19, 13 Hz), 4.32 (dd, 1H, J = 19, 3 Hz), 4.60 (m, 1H), 7.25 (s, 1H), 7.30 (s, 1H), 15.75 (s, 1H) ppm; ms *m/z* (rel. intensity): 452 (M^+, 2), 451 (5), 409 (15), 367 (76), 352 (23). *Triacetate (15):* obtained as a pale yellow oil, R_f 0.24; uv (MeOH): 222, 237, 281, 292, 305 (sh), 345, 365 (sh), 384 nm; ^{1}H nmr (400 MHz, $CDCl_3$): 1.57 (d, 3H, J = 7 Hz), 1.58 (s, 3H), 1.64 (s, 3H), 1.81 (s, 3H), 2.36 (s, 3H), 2.40 (s, 3H), 2.57 (s, 3H), 3.28 (dd, 1H, J = 19, 13 Hz), 3.85 (dd, 1H, J = 19, 3 Hz), 4.58 (m, 1H), 7.48 (s, 1H), 7.86 (s, 1H) ppm; ms *m/z* (rel. intensity): 494 (M^+, 1), 493 (1), 451 (13), 409 (22), 367 (68), 352 (16).

2-Hydroxygarvin B (16): obtained as a yellow solid, R_f 0.35; uv (MeOH): 234, 287, 386 (neutral), 253, 310, 417 (basic) nm; ^{1}H nmr (400 MHz, $CDCl_3$): 1.50, 1.54 (s, 3H), 1.64, 1.65 (d, J = 7 Hz, 3H), 1.65, 1.66 (s, 3H), 1.80, 1.82 (s, 3H), 3.41, 3.44 (dd, J = 12, 19 Hz, 1H), 4.02 (br s, 1H), 4.38 (dd, J = 3, 19 Hz, 1H), 4.74 (m, 1H), 7.11 (s, 2H), 11.44, 11.45 (s, 1H), 14.61, 14.62 (s, 1H) ppm; ^{13}C nmr (75 MHz, $CDCl_3$): 209.83, 199.71 (199.55), 169.85 (169.80), 167.39 (167.17), 161.27 (167.16), 145.40 (145.26), 144.58 (144.54), 143.84, 116.03, 115.94, 111.81, 110.81 (110.77), 107.00 (106.88), 81.64 (81.57), 75.43 (75.35), 47.14 (47.05), 34.60 (34.36), 30.70 (30.44), 29.15 (29.04), 28.43 (27.99), 20.83 ppm; ms *m/z* (rel. intensity): 384 (M^+, 32), 368 (22), 353 (9), 342 (90), 341 (100), 327 (61), 309 (26).

Garvalone B (18): obtained as a light yellow oil (3:2 mixture of diastereomers), R_f 0.44; $[\alpha]_D$ +136.92° (*c* 0.39, $CHCl_3$); uv (MeOH): 236, 290, 385 nm; ^{1}H nmr (300 MHz, $CDCl_3$): 1.464, 1.470 (s, 3H), 1.566, 1.533 (s, 3H), 1.584, 1.611 (s, 3H), 1.646 (d, J = 7 Hz, 3H), 2.063, 2.042 (s, 3H), 2.234 (m, 4H), 3.419, 3.424 (dd, J = 18, 12 Hz, 1H), 4.387 (dd, J = 18, 3 Hz, 1H), 4.732 (m, 1H), 7.060 (s, 1H), 7.102 (s, 1H), 11.503 (s, 1H), 15.442 (s, 1H) ppm; ms *m/z* (rel. intensity): 438 (M^+, 12), 368 (10), 353 (5), 325 (3). *Garvalone B diacetate (19):* ^{1}H nmr (300 MHz, $CDCl_3$): 2.40 (s, 3H), 2.47 (s, 3H), 7.53 (s, 1H), 7.75 (s, 1H) ppm.

Synthesis of garvalone B (18)

Garvin B (**13**) (15 mg) was dissolved in benzene (8 mL) containing 100 mg of K_2CO_3 (anhydrous) and a crystal of 18-crown-6. Excess methyl vinyl ketone (100 μL) was added and the mixture was stirred at reflux overnight, under N_2. The reaction mixture was then filtered and the filtrate concentrated *in vacuo*. Preparative tlc (5% MeOH–$CHCl_3$) purification gave garvalone B (**18**) (8 mg) as a 2:3 mixture of diastereomers and unreacted garvin B (4 mg).

Garveatin D (20): obtained as a yellow solid, R_f 0.40; uv (MeOH): 238, 269, 417 nm; ^{1}H nmr (300 MHz, $CDCl_3$): 1.50 (s, 6H), 1.58 (s, 6H), 2.41 (br s, 3H), 2.63 (s, 3H), 7.05 (br s, 1H), 7.12 (s, 1H), 10.20 (s, 1H), 16.15 (s, 1H) ppm; ms *m/z* (rel. intensity): 354 (M^+, 53), 339 (59), 321 (30), 311 (15), 297 (13), 293 (16).

Preparation of 2-hydroxygarveatin A triacetate (22)

Fraction D (200 mg) obtained from flash chromatography of the methylene chloride phase of the extract was dissolved in pyridine (3 mL) and acetic anhydride (7 mL) and stirred at room temperature for 48 h. After evaporation of the reagents, the residue was purified by flash chromatography (methanol – methylene chloride gradient) and preparative tlc (50% ethyl acetate – hexane) to give 2-hydroxygarveatin A triacetate (**22**) (90 mg). *Triacetate (22):* obtained as a colourless solid, R_f 0.25; uv (MeOH): 226, 260, 303, 355 nm; ^{1}H nmr (400 MHz, $CDCl_3$): 1.45 (s, 3H), 1.57 (s, 3H), 1.79 (s, 3H), 2.20 (s, 3H), 2.34 (s, 3H), 2.41 (br s, 3H), 2.50 (s, 3H), 7.61 (s, 1H), 7.79 (s, 1H) ppm; ms *m/z* (rel. intensity): 482 (M^+, 3), 440 (25), 398 (100), 356 (20), 338 (32), 314 (83), 313 (77). *Exact Mass* calcd. for $C_{26}H_{26}O_9$: 482.1577; found: 482.1567.

Preparation of diacetate (25)

On standing in pyridine-d_6 in an nmr tube overnight, triacetate (**22**) partially decomposed to diacetate (**25**) (yield 40%) which was purified via flash chromatography (ethyl acetate – hexane gradient). *Diacetate (25):* R_f 0.40; uv (MeOH): 226, 272, 306 (sh), 385 nm; ^{1}H nmr (80 MHz, $CDCl_3$): 1.58 (s, 3H), 1.63 (s, 3H), 1.74 (s, 3H), 2.24 (s, 3H), 2.40 (s, 3H), 2.45 (br s, 3H), 2.55 (s, 3H), 7.26 (1H), 7.47 (s, 1H), 9.26 (s, 1H) ppm; ^{13}C nmr (75 MHz, $CDCl_3$): 206.5, 202.7, 198.4, 169.7, 163.7, 145.0, 142.8, 139.6, 137.9, 134.1, 126.9, 116.3, 115.1, 108.1, 82.6, 47.4, 32.0, 31.2, 29.3, 23.4, 21.1, 20.0, 19.7 ppm; ms *m/z* (rel. intensity): 440 (M^+, 14), 398 (71), 356 (9), 340 (14), 338 (25), 314 (90), 313 (100), 295 (13).

2-Hydroxygarveatin B (26): obtained as a yellow solid, R_f 0.28; uv (MeOH): 224, 275, 423 nm; ^{1}H nmr (80 MHz, $CDCl_3$): 1.18 (t, 3H, J = 7 Hz), 1.50 (s, 3H), 1.65 (s, 3H), 1.78 (s, 3H), 2.47 (br s, 3H), 2.80 (q, 2H, J = 7 Hz), 4.60 (bs, 1H), 7.08 (br s, 1H), 7.13 (s, 1H), 9.68 (s, 1H), 15.15 (s, 1H) ppm; ms *m/z* (rel. intensity): 342 (M^+, 15), 327 (5), 300 (26), 299 (30), 285 (13). *Exact Mass* calcd. for $C_{20}H_{22}O_5$: 342.1468; found: 342.1467.

Preparation of 2-hydroxygarveatin B acetates

A solution of 2-hydroxygarveatin B (**26**) (16 mg), pyridine (0.25 mL), and acetic anhydride (0.5 mL) was stirred overnight at room temperature. After removal of the reagents *in vacuo*, the residue was chromatographed on silica (2% methanol – methylene chloride) to give 2-hydroxygarveatin B diacetate (3 mg), and 2-hydroxygarveatin B triacetate (**27**) (11 mg).

Diacetate (28): R_f 0.30; uv (MeOH): 213, 250, 307 (sh), 319, 363 nm; ^{1}H nmr (80 MHz, $CDCl_3$): 1.15 (t, 3H, J = 7 Hz), 1.26 (s, 3H), 1.40 (s, 3H), 1.83 (s, 3H), 2.45 (s, 3H), 2.47 (s, 3H), 2.52 (br s, 1H), 2.71 (q, 1H, J = 7 Hz), 4.63 (br s, 1H), 7.62 (br s, 1H),

7.66 (s, 1H) ppm; ms *m/z* (rel. intensity): 426 (M^+, 10), 384 (19), 342 (47), 326 (18), 324 (33), 300 (84), 299 (100), 282 (77).

Triacetate (27): R_f 0.40; uv (MeOH): 217, 260, 304, 316, 359 nm; ^{1}H nmr (80 MHz, $CDCl_3$): 1.13 (t, 3H, J = 7 Hz), 1.44 (s, 3H), 1.55 (s, 3H), 1.78 (s, 3H), 2.22 (s, 3H), 2.45 (s, 6H), 2.50 (br s, 3H), 2.70 (q, 2H, J = 7 Hz), 7.55 (br s, 1H), 7.70 (s, 1H) ppm; ms *m/z* (rel. intensity): 468 (M^+, 4), 426 (20), 384 (100), 342 (19), 324 (28), 300 (44), 299 (82), 282 (26). *Exact Mass* calcd. for $C_{26}H_{28}O_6$: 468.1784; found: 468.1776.

Garveatin A quinone (29): obtained as a red oil, R_f 0.49; uv (MeOH): 218, 265, 280 (sh) and 410 nm; ^{1}H nmr ($CDCl_3$, 80 MHz): 1.63 (s, 6H), 1.98 (s, 3H), 2.41 (bs, 3H), 2.60 (s, 3H), 7.55 (bs, 1H), 11.45 (s, 1H), 11.66 (s, 1H); ^{13}C nmr ($CDCl_3$, 75 MHz): 202.1, 200.0, 193.0, 180.4, 159.5, 159.1, 156.2, 147.2, 136.3, 131.9, 127.7, 123.0, 118.6, 112.4, 48.3, 31.9, 26.4 (2 carbons), 20.5, 8.1. *Exact Mass* (ms) calcd. for $C_{20}H_{18}O_6$: 354.1103; found: 354.1108.

Preparation of garveatin B dimer

A solution of garveatin B (**2**) in $CDCl_3$ was allowed to stand overnight in a closed nmr tube at room temperature. The sample was then chromatographed on preparative tlc (20% ethyl acetate – hexane) to give garveatin B dimer **30** in approximately 30% yield. *Dimer 30:* obtained as an orange oil, R_f 0.66; uv (MeOH): 225, 275, 320 sh, 434 nm; ^{1}H nmr (270 MHz, $CDCl_3$): 1.07 (t, J = 7 Hz, 3H), 1.38 (s, 3H), 1.66 (s, 3H), 1.88 (s, 3H), 2.43 (s, 3H), 2.53 (m, 1H), 2.70 (m, 1H), 6.98 (s, 2H), 9.37 (s, 1H), 15.79 (s, 1H) ppm; ^{13}C nmr (75 MHz, C_6D_6): 208.9, 202.4, 167.3, 155.6, 143.5, 140.0, 137.7, 126.4, 119.9, 115.7, 110.9, 107.9, 63.0, 48.6, 33.6, 25.9, 21.2, 20.4, 19.8, 13.8 ppm; ms *m/z* (rel. intensity): 326 (57), 311 (100), 283 (20), 269 (11) (molecular ion not seen in EI spectrum).

Preparation of garveatin B dimer tetraacetate 31

Garveatin B dimer **30** (2 mg) was treated overnight with 100 μL of acetic anhydride and 100 μL of pyridine. The reaction mixture was then chromatographed on preparative tlc (50% ethyl acetate – hexane) to give the tetraacetate **31** in quantitative yield. *Tetraacetate 31:* obtained as a light yellow oil, R_f 0.60; ^{1}H nmr (300 MHz, $CDCl_3$): 1.15 (t, J = 7 Hz, 3H), 1.56 (s, 3H), 1.71 (s, 3H), 1.85 (s, 3H), 2.30 (s, 3H), 2.42 (s, 3H), 2.52 (s, 3H), 2.55 (m, 1H), 2.75 (m, 1H), 7.61 (s, 1H), 7.75 (s, 1H) ppm; ms *m/z* (rel. intensity): 818 (M^+, 0.02), 776 (0.30), 734 (0.31), 716 (0.44), 674 (2), 410 (3), 368 (12), 326 (100), 311 (67).

Garveatin B – garvin B dimer 32

Obtained as an orange oil, R_f 0.65; uv (MeOH): 283, 400 (neutral), 282, 305 (sh), 414 (basic) nm; ^{1}H nmr (400 MHz, $CDCl_3$): 1.00 (t, J = 7 Hz, 3H), 1.20 (s, 3H), 1.24 (s, 3H), 1.51 (d, J = 7 Hz, 3H), 1.78 (s, 3H), 1.80 (s, 3H), 1.81 (s, 3H), 1.82 (s, 3H), 2.35 (dd, J = 19, 12 Hz, 1H), 2.42 (s, 3H), 2.42 (m, 1H), 2.77 (m, 1H), 3.83 (dd, J = 19, 3 Hz, 1H), 4.40 (m, 1H), 6.90 (s, 2H), 6.92 (s, 1H), 7.02 (s, 1H), 9.10 (s, 1H), 14.85 (s, 1H), 15.70 (s, 1H) ppm; ms *m/z* (rel. intensity): 368 (100), 353 (53), 326 (53), 311 (88), 297 (20) (no molecular ion was seen in the EI spectrum); FAB ms (MeOH solution in thioglycerol) *m/z*: 693 (M + 1 ion), 649, 369, 368, 327, 326, 311, 297.

Acknowledgements

The authors would like to thank Mike LeBlanc and the staff of the Bamfield Marine Station for assistance with collecting *Garveia annulata*. Financial support was provided by the Natural Sciences and Engineering Research Council, the Cancer Institute of Canada, and Rohm and Haas Co.

1. (*a*) G. Cimino, S. Derosa, S. Destephano, and G. Sodano. Tetrahedron Lett. **21**, 3303 (1980); (*b*) E. Fatturoso, V. Lanzotti, S. Magno, and E. Novellino. Biochem. Syst. Ecol. **13**, 167 (1985); (*c*) E. Fatturoso, V. Lanzotti, S. Magno, and E. Novellino. J. Org. Chem. **50**, 2868 (1985).
2. E. Fahy, R. J. Andersen, H. Cun-Heng, and J. Clardy. J. Org. Chem. **50**, 1150 (1985).
3. E. Fahy, R. J. Andersen, G. D. Van Duyne, and J. Clardy. J. Org. Chem. **51**, 57 (1986).
4. E. Fahy, R. J. Andersen, C. Xu, and J. Clardy. J. Org. Chem. In press.
5. S. Ramachandran and M. S. Newman. Org. Synth. **41**, 38 (1961).
6. D. W. Cameron, J. S. Edmonds, and W. D. Raverty. Aust. J. Chem. **29**, 1535 (1976).
7. J. A. Rideout and M. D. Sutherland. Aust. J. Chem. **38**, 793 (1985), and references therein.

Can. J. Chem. Downloaded from www.nrcresearchpress.com by 80.58.250.72 on 09/07/12
For personal use only.

The temperature dependence of the Raman spectrum and *gauche* interactions of tri-*N*-butylamine: a conformational study

A. M. Amorim da Costa, L. A. E. Batista de Carvalho, and J. J. C. Teixeira-Dias[1]
Departamento de Química da Universidade, 3049 Coimbra, Portugal

AND

Ester F. G. Barbosa and Isabel M. S. Lampreia
Centro de Electroquímica e Cinética, Faculdade de Ciências da Universidade, 1294 Lisboa, Portugal

Received October 31, 1985[2]

A. M. Amorim da Costa, L. A. E. Batista de Carvalho, J. J. C. Teixeira-Dias, Ester F. G. Barbosa, and Isabel M. S. Lampreia. Can. J. Chem. **65**, 384 (1987).

Raman spectra of tri-*n*-butylamine show pairs of bands whose temperature-dependent intensities clearly suggest their assignment to different conformers in simultaneous equilibria. These spectroscopic data are interpreted and correlated with structural information obtained from statistical analysis of gauche skeletal arrangements in tri-*n*-butylamine. The average numbers of *gauche* interactions in various tri-*n*-alkylamines are used to evaluate partial molal volumes which show excellent agreement with experimental data, thus imparting statistical meaning and usefulness to the concept of "average conformation".

As the temperature decreases, the band at 904 cm^{-1} in pure liquid tri-*n*-butylamine increases in intensity at the expense of the band at 880 cm^{-1}. Both of these bands are ascribed to CH_2 and CH_3 rocking vibrations. In solution, the conformer represented by the band at 904 cm^{-1} is favoured by polar solvents, whereas the conformer represented by the 860 cm^{-1} band is favoured by non-polar solvents.

The relative intensity changes with increasing temperature of the bands at 1456 and 1440 cm^{-1} is explained by an increase in the number of CH_2 groups adjoining two *gauche* bonds and a decrease in the number of CH_2 groups adjoining a *trans* and *gauche* bond.

Temperature dependence of the relative intensities of bands in the CH stretching region suggest, by comparison with mono- and di-*n*-butylamine, that the increase in the number of alkyl chains around the nitrogen atom makes molecular packing less restrictive and unique, giving rise to mesophases, as the overall shapes of the molecules become more spherical.

A. M. Amorim da Costa, L. A. E. Batista de Carvalho, J. J. C. Teixeira-Dias, Ester F. G. Barbosa et Isabel M. S. Lampreia. Can. J. Chem. **65**, 384 (1987).

Les spectres Raman de la tri-*n*-butylamine présentent des paires de bandes dont les intensités dépendent de la température; ces observations suggèrent clairement que l'on doit les attribuer à différents conformères dans équilibres simultanés. On interprète ces données spectroscopiques et on établit une corrélation avec les informations structurales obtenues à partir d'une analyse statistique des arrangements *gauches* du squelette de la tri-*n*-butylamine. On utilise les nombres moyens d'interactions gauches dans diverses tri-*n*-alkylamines pour évaluer les volumes molales partiels qui sont en bon accord avec les données expérimentales; cette corrélation permet d'attribuer une signification statistique et de démontrer l'utilité du concept de «conformation moyenne».

Dans le cas de la tri-*n*-butylamine à l'état de liquide pur, une diminution de la température provoque une augmentation de l'intensité de la bande à 904 cm^{-1}, au détriment de la bande à 880 cm^{-1}. On attribue ces deux bandes aux vibrations de balancement des CH_2 et CH_3. En solution, le conformère représenté par la bande à 904 cm^{-1} est favorisé dans les solvants polaires alors que le conformère représenté par la bande à 860 cm^{-1} est favorisé par les solvants non polaires.

On explique les changements d'intensités relatives des bandes à 1456 et 1440 cm^{-1}, qui sont associés à une augmentation de la température, par une augmentation du nombre de groupements CH_2 dans les positions qui sont jointes directement à deux liaisons *gauches* et par une diminution du nombre de groupements CH_2 dans les positions qui sont jointes à une liaison *trans* et à une liaison *gauche*.

La relation qui existe entre la température et les intensités relatives des bandes de la région de l'élongation du CH suggère, par comparaisons avec les mono- et di-*n*-butylamines, que l'augmentation du nombre de chaînes alkyles autour de l'atome d'azote rend l'empilage moléculaire moins restrictif et moins unique; cette situation donne lieu à des mésophases au fur et à mesure que les formes globales des molécules deviennent plus sphériques.

[Traduit par la revue]

1. Introduction

Vibrational spectra have been widely used in conformational analysis (1). However, the assignment of infrared and Raman spectral lines relating to a specific molecular geometry often cannot be decided uniquely from spectra alone. Corroborative chemical or other physical evidence is usually necessary for the understanding of conformational spectral features. Moreover, assumptions regarding conformations and their relative energies cannot generally be avoided.

The role of various intramolecular effects governing conformational stability, including steric hindrance, intramolecular hydrogen bonding, the *gauche* effect and the *trans* lone-pair effect, has been experimentally considered in the conformational analysis of alcohols, amines, and their substituted derivatives (2–7).

Using the statistical thermodynamic treatment of molecular spectra, Scott (8) was able to show the statistical distribution of five conformers of *n*-propylamine in the vapour phase and reported that the observed infrared spectrum of ethylamine arose solely from the conformation with C_1 symmetry, which assumed the *gauche* orientation of the CCN group. Radom and co-workers (9) applied *ab initio* molecular orbital theory to study internal rotations in methylamine and ethylamine and

[1]To whom all correspondence should be addressed.
[2]Revision received September 26, 1986.

Printed in Canada / Imprimé au Canada

Can. J. Chem. Downloaded from www.nrcresearchpress.com by 80.58.250.72 on 09/07/12
For personal use only.

Can. J. Chem. Downloaded from www.nrcresearchpress.com by 80.58.250.72 on 09/07/12
For personal use only.

found that the staggered conformation was preferred and conformers with the vacant corner of the nitrogen tetrahedron *gauche* to C_α—C_β were the most stable. Eggert and Djerassi (10) used ^{13}C nuclear magnetic resonance to estimate the equilibrium distribution of conformers for *n*-propylamine and isobutylamine in solution and found that the rotamer distribution was quite different from that of the corresponding alkanes.

Conformational studies by Raman spectroscopy and statistical analysis of *gauche* interactions in *n*-butylamine have been previously reported by the authors (11). Also, temperature-dependent intensities of Raman bands of di-*n*-butylamine (12) suggest the occurrence of different conformers in simultaneous equilibria.

Microwave studies of tri-methylamine have shown that the molecular skeleton adopts a C_{3v} equilibrium configuration in the vapour phase with one CH bond of each methyl group *trans* to the nitrogen lone pair (13). Using this model for tri-ethylamine, Kumar (4) obtained vibrational evidence for the existence of at least two rotational isomers differing in their relative proportions between the solid, liquid, and vapour phases. Green (5) has also concluded, from vibrational spectra, that at least three forms of tri-ethylphosphine are present in the liquid. Conformational studies of other tri-alkylamines, namely NMe_2Et and $NMeEt_2$ (6, 7), were carried out by vibrational spectroscopy using the tri-methylamine model with success. In principle, there are two vibrationally distinguishable conformations of NMe_2Et (7), six of $NMeEt_2$ (6), and seven of NEt_3 (4). Conformational analysis becomes more complex with increasing number of CH_2 units. For instance, to distinguish pentane conformers, it is necessary to include six one-to-four and thirteen one-to-five different non-bonded interactions (14).

The main purpose of the present study is to interpret Raman spectra and thermodynamic information on molecular conformations of tri-*n*-butylamine (Bu_3N) in the liquid phase. Due to the existence of three butyl chains in this compound, the number of possible different conformers in equilibrium is very large, and can be determined only by systematic building of molecular models. In this work, all the vibrationally distinguishable conformations were constructed, and the average number of *gauche* interactions of each type, at various temperatures, calculated by statistical thermodynamic methods (15–17). Significant changes observed in the Raman spectra of the liquid at different temperatures and in different solvents are reported and their correlations with the average number of *gauche* interactions of each type is considered.

2. Experimental

All the compounds used in this study were of purum grade. Even so, the samples were dried and distilled by repeated fractional distillation as previously described (18), before recording the spectra and taking density measurements. Partial molal volumes were obtained from the densities of solutions. These were determined at 25 ± 0.001°C with a digital density meter Anton Parr 02D. For C_6H_6, the density was obtained with a precision of $\pm 2 \times 10^{-6}$ g cm^{-3}.

Raman spectra were recorded on a Cary 82 spectrometer using an Ar^+ Spectra Physics laser (model 164-05) whose output at 514.5 nm was adjusted to provide 200–250 mW at the sample position.

We used the photon counting mode with sensitivities adjusted in the 10^3 to 10^5 counts s^{-1} range to provide reasonable signal-to-noise ratios. The spectrometer operated with spectral slitwidths (w) of 4 cm. The pen period (τ) was set at 2.0 s and the scanning speed of the monochromator (v/cm^{-1} s^{-1}) adjusted so that $v \leq w/(4\tau)$.

Temperature variation was carried out with a continuous flow cryostat (Oxford Instruments, model CF 100) operating with liquid nitrogen. Samples were contained in 0.5 cm^3 cylindrical cells and temperature values recorded on a temperature controller.

3. Results and discussion

Conformational analysis of a compound such as Bu_3N is of great importance for the structural interpretation of its thermodynamic properties. A good example of this type of investigation was carried out by Mann and co-workers (15, 16), who related macroscopic properties, molal volumes, refractive index, and heat of combustion, with a structural parameter representing the average number of *gauche* interactions of a series of straight and branched chain alkanes. Later, Edward and co-workers (19) applied and extended these ideas to partial molal volumes.

(i) Statistical analysis of gauche *interactions in Et_3N, Pr_3N, and Bu_3N*

The evaluation of the average number of *gauche* interactions of a specific type requires the determination of all possible molecular conformations. As the number of possible conformations increases rapidly with chain length, a genealogical building of molecular models is required. Starting with three stable and spectroscopically distinguishable molecular conformations of Et_3N suggested by Kumar (4), Table 1 presents a "genealogic tree" of all possible molecular conformations, from Et_3N to Bu_3N, after the sterically hindered conformations were excluded with the help of molecular models. The statistical weight of a conformation, s, having a definite number of *gauche* interactions of a particular type, N_g, is represented by the product of statistical weights of "parent" and "son" molecules. The average numbers of *gauche* interactions, $\bar{N}_g$, can be calculated as described in ref. 15, after evaluating the mole fraction of each conformer, γ_i, using the following expression:

$$[1] \quad \gamma_i = s_i \exp(-\Delta H_i/RT)/\sum_i s_i \exp(-\Delta H_i/RT)$$

The temperature dependence of $\bar{N}_g$ is now easily evaluated as $\bar{N}_g$ is a sum of *gauche* interactions weighted by the temperature-dependent γ_i values. In particular, for Bu_3N, $\bar{N}_g$(CCNC) decreases with temperature from 3.3 at 298 K to its minimum value of 3, as ΔH(CCNC) = H(*gauche*-CCNC) − H(*trans*-CCNC) is positive (14). $\bar{N}_g$(CCCN) increases with decreasing temperature from 1.1 at 298 K to its limiting value of 3, as ΔH(CCCN) = H(*gauche*-CCCN) − H(*trans*-CCCN) is negative (14). Although the ΔH values for amines used in these calculations involve large uncertainties (14), both the above mentioned variations are consistent with the increasing influence, at lower temperatures, of the lone pair of electrons on the nitrogen atom, through the *trans* effect, with respect to the α-carbon hydrogen atoms, and the *gauche* effect, relative to the slightly polar C_α—C_β bond. Morever, $\bar{N}_g$(CCCC) decreases with temperature from 1.0 at 298 K to zero, at low temperatures, thus confirming the well-known stability of all-*trans* alkylic chains at low temperatures (20). $\bar{N}_g$(CCCN) is greater at room temperature for Pr_3N (1.4) than for Bu_3N (1.1).

In estimating the average number of *gauche* interactions in a few tri-*n*-alkylamines at 298 K, we have assumed that the $\bar{N}_g$(CCNC) and $\bar{N}_g$(CCCN) for all tertiary amines larger than tri-*n*-butylamine are equal to those of Bu_3N. For CCCC interactions $\bar{N}_g$ values were obtained by multiplying by 3 the values reported in ref. 19, for the corresponding *n*-alkanes, yielding the following results: Bu_3N, 1.0; Hex_3N, 2.9; Oct_3N, 4.6; Dec_3N, 6.4; and Dod_3N, 8.2. The value for Bu_3N has been obtained directly from the molecular models.

TABLE 1. "Genealogic tree" of most probable molecular conformations from Et_3N to Bu_3N showing the total number of *gauche* interactions, N_g, of each particular type (CCNC, CCCN, or CCCC) and the corresponding total statistical weights (s_i)

Et_3N		Pr_3N			Bu_3N			
					$s_1 \times s_2 \times s_3$			
s_1	N_g(CCNC)		$s_1 \times s_2$	N_g(CCCN)	N_g(CCCC) = 0	= 1	= 2	= 3
(G) (G) (G) 2	3	(GG′) (GG′) (GG′)	2×1	3	2×1×1	2×1×3	2×1×3	2×1×1
		(GT) (GG′) (GG′)	2×3	2	2×3×1	2×3×4	2×3×5	2×3×2
		(GT) (GT) (GG′)	2×3	1	2×3×1	2×3×5	2×3×8	2×3×4
		(GT) (GT) (GT)	2×1	0	2×1×1	2×1×6	2×1×12	2×1×8
(T) (G) (G) 6	4	(TT) (GG′) (GG′)	6×1	2	6×1×1	6×1×4	6×1×5	6×1×2
		(TT) (GT) (GG′)	6×2	1	6×2×1	6×2×5	6×2×8	6×2×4
		(TT) (GT) (GT)	6×1	0	6×1×1	6×1×6	6×1×12	6×1×8
(T) (G) (G′) 3	4	(TT) (GG′) (G′G)	3×1	2	3×1×1	3×1×4	3×1×5	3×1×2
		(TT) (GG′) (G′T)	3×2	1	3×2×1	3×2×5	3×2×8	3×2×4
		(TT) (GT) (G′T)	3×1	0	3×1×1	3×1×6	3×1×12	3×1×8

(ii) Relation between partial molal volume $\bar{V}^0$ and $\bar{N}_g$ values

A relationship between $\bar{V}^0$ and $\bar{N}_g$ was proposed by Edward and co-workers (19, 21)

$$[2] \quad \bar{V}^0 = V_c + \sum_i n_i I_i + \sum_k \delta(k)\bar{N}_g(k)$$

where V_c is the covolume (volume of the solvent molecule cavity required to accommodate a point kinetic particle of no intrinsic volume), I_i is the volume increment associated with group of type i, and n_i is the number of such groups. $\bar{N}_g(k)$ is the average number of *gauche* interactions of type k and $\delta(k)$ is the volume change associated with such an interaction.

The application of this equation to a series of compounds interacting weakly with the solvent was done with success by the same authors (21, 22). In the case of a series of tertiary amines in benzene the application of eq. [2] revealed that the volume increment associated with the amine group is not constant. The n–π specific interaction between the pair of electrons of this group and the delocalized electrons in benzene (18, 23, 24) seem to vary regularly along the series. Thus in order to evaluate this term more correctly we added to the van der Waals volume of the tertiary amine group a term proportional to its surface area fraction:

$$[3] \quad I_{:N\leq} = V_w + C(A_w/A_t)$$

V_w and A_w are the van der Waals volume and surface area (25) of the tertiary amine group, respectively, A_t is the total van der Waals surface area, and C is a constant.

In the present study, the constant C and the parameters δ(CCNC) and δ(CCCN) were obtained by a least-squares fitting of eq. [2] to the experimentally determined $\bar{V}^0$ values (18), for a few tertiary amines in benzene, using the previously determined $\bar{N}_g$ values. The CH_3 and CH_2 group contributions (I_{CH_3} = 27.40 cm^3 mol^{-1}; I_{CH_2} = 17.15 cm^3 mol^{-1}) were evaluated relating expression (2) with the linear equation $\bar{V}^0$ vs. n_C (number of carbon atoms) for the best set of experimental results of straight-clean hydrocarbons in benzene (18, 26).

The values of V_c and δ(CCCC) were taken from Edward and co-workers (26) (V_c = 11.4 cm^3 mol^{-1} and δ(CCCC) = −1.1 cm^3 mol^{-1}), although these solvent-dependent parameters were not obtained from an extensive study in benzene (26).

The $\bar{V}^0$ values for the tri-*n*-alkylamines in benzene studied at 298 K were then calculated and showed excellent agreement with experimental results (Table 2).

TABLE 2. Calculated and experimental partial molal volumes (V^0/cm^3 mol^{-1}) for a few tri-*n*-alkylamines in benzene, at 298 K

Molecule	V^0_{exp}	V^0_{calc}	$V^0_{calc} - V^0_{exp}$
Tri-*n*-ethylamine	140.27[a]	140.23	0.04
Tri-*n*-propylamine	193.51[a]	193.36	−0.15
Tri-*n*-butylamine	243.92[a]	244.02	0.10
Tri-*n*-hexylamine	344.8 [b]	345.37	0.6
Tri-*n*-octylamine	447.08[a]	446.64	−0.44
Tri-*n*-decylamine	547.6 [b]	547.78	0.2
Tri-*n*-dodecylamine	649.06[c]	648.85	−0.21

[a]From ref. 18.
[b]From ref. 36.
[c]Estimated value from a linear regression of V^0 vs. n_c with n_c varying from 9 to 30.

(iii) Spectral studies of temperature variation and solvents effects

Figure 1 shows the Raman spectrum of liquid tri-*n*-butylamine at room temperature. It is expected that some of the observed Raman bands arise from modes originating in specific conformations, whereas others result from contributions of more than one conformation.

Table 3 shows the observed Raman frequencies and their approximate descriptions based on available vibrational assignments for similar molecules.

The 650–1300 cm^{-1} region

Most of the band in this region cannot be ascribed to individual vibrational modes with a reasonable level of confidence. In fact, these vibrational modes are highly mixed, as can be inferred from previous vibrational calculations (11).

The 950–1200 cm^{-1} region contains important frequencies involving the C—C and the C—N stretching vibrations. These vibrations are expected to have very similar frequencies with appreciable coupling between C—C and C—N neighbouring oscillators. Little systematic work has yet been done to identify the bands due to these vibrational modes. However, considering the existing data, the bands at 1172 and 1185 cm^{-1} should arise mainly from C—N stretching while the bands in the 950–1128 cm^{-1} frequency region are expected to be essentially due to C—C stretching vibrations. Both C—C and C—N

Can. J. Chem. Downloaded from www.nrcresearchpress.com by 80.58.250.72 on 09/07/12
For personal use only.

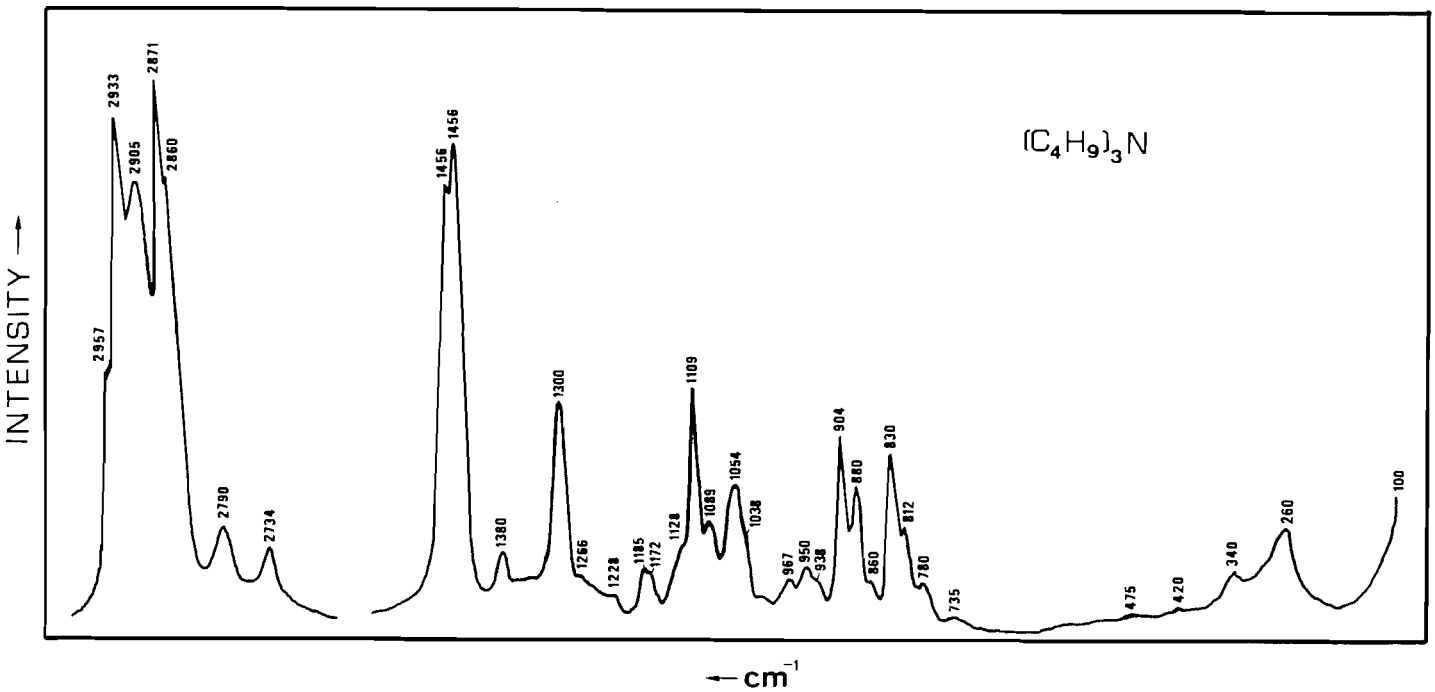

FIG. 1. The Raman spectrum of tri-*n*-butylamine, in the liquid state, at room temperature.

TABLE 3. Observed Raman frequencies and approximate descriptions for tri-*n*-butylamine

$\tilde{\nu}_{obs}/cm^{-1}$	Approximate descriptions
2957	CH_3 antisymmetric stretching
2933	Overtone CH_2 scissoring
2905	CH_2 antisymmetric stretching
2871	CH_3 symmetric stretching
2860	CH_2 symmetric stretching
1456	CH_3 antis. def. + CH_2 scissoring
1440	CH_2 scissoring
1380	CH_3 symmetric deformation
1300	CH_2 wagging
1266	CH_2 twisting
1185	C—N stretching
1172	C—N stretching
1128	C—C stretchings
1109	
1089	
1054	
1038	
967	C—C stretching + CH_3 rocking
950	C—C stretching + CH_3 rocking
938	CH_2 rocking + CH_3 rocking
904	
880	
860	
830	
812	
780	
735	CH_2 rocking
475	Skeletal deformations
420	
400	
340	
260	

vibrational motions should mix appreciably with methylene, methyl, and skeletal deformations.

Figure 2 shows the Raman spectra of tri-*n*-butylamine in the 700–1000 cm^{-1} region, at different temperatures. Temperature-dependent intensities of pairs of bands occurring at 880 and 860 cm^{-1} and at 880 and 904 cm^{-1} suggest that these bands pertain to different conformers and yield the same ΔH 2.0 kJ mol^{-1}.

As the temperature decreases, the intensity of the band at 904 cm^{-1} increases at the expense of the band at 880 cm^{-1}. At 100 K, the latter is still recognized among various neighbouring bands. However, it is clear that the band at 904 cm^{-1} dominates the bands at 880 and 860 cm^{-1} and so should probably be ascribed to the low temperature form.

In solution, the simultaneous equilibria between conformers are dependent on environmental polarity. Other things being equal, the ratio of more-polar to less-polar conformers should increase with solvent polarity. In order to assess this effect, we have determined the intensity ratios $I(880)/I(904)$ and $I(880)/I(860)$ in 1:1 solutions of tri-*n*-butylamine in various solvents (carbon tetrachloride, carbon disulphide, benzene, and chloroform). The solvent polarities were measured on the E_T scale which uses the "solvatochromic band" shifts of 4-(2,4,6-triphenylpyridinium)-2,6 diphenylphenoxide or its trimethyl derivative to probe solvent polarities (27) (E_T/kJ mol^{-1}: CCl_4 = 136.0; CS_2 = 136.4; C_6H_6 = 144.3; $CHCl_3$ = 163.6). As the medium becomes more polar, the band at 904 cm^{-1} dominates relative to the band at 860 cm^{-1}. This suggests that the conformer whose band occurs at 904 cm^{-1} is favoured by polar solvents, whereas the conformer represented by the 860 cm^{-1} band is favoured by non-polar solvents.

The 1300–1700 cm^{-1} region

The assignment of some of the observed bands in this region, where most of the CH_2 deformations occur, is fairly well

Can. J. Chem. Downloaded from www.nrcresearchpress.com by 80.58.250.72 on 09/07/12
For personal use only.

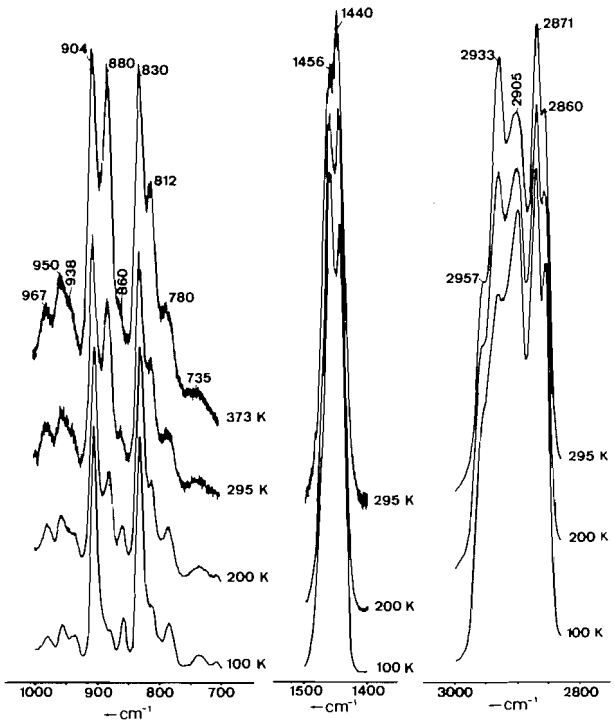

FIG. 2. The Raman spectra of tri-*n*-butylamine, at different temperatures in the liquid state.

established for hydrocarbons (28). The CH_2 scissoring vibrations occur near 1463 cm^{-1} in alkanes and are independent of the number or sequence of methylenes (29). These vibrational modes are sometimes shifted by the CH_2 wagging modes, which occur also in this region and are quite sensitive to the environment, namely, to the number of methylene sequences and to *trans* or *gauche* arrangements. The same kind of sensitivity is also known to occur for CH_2 twisting and rocking modes (29). The methyl symmetric deformation in alkanes occurs around 1350–1400 cm^{-1}.

Taking this evidence on hydrocarbons as a basis for the present assignments, the band at 1300 cm^{-1} is ascribed to the CH_2 wagging mode and the band at 1380 cm^{-1} to the symmetric deformation of the methyl groups. Bands at 1456 and 1440 cm^{-1} are associated with CH_3 and CH_2 scissoring deformations and are temperature dependent, as we shall see. On the other hand, bands at 1690 and 1645 cm^{-1} may be interpreted as combination bands involving C—C stretching modes.

Figure 2 shows also Raman spectra in the 1400 to 1500 cm^{-1} region, at different temperatures. At low temperatures, the dominating peak occurs at 1456 cm^{-1}. At about 200 K both peaks are of equal height. At higher temperatures the prominent intensity maximum occurs at 1440 cm^{-1}.

It is a striking spectral feature that the CH_2 scissoring modes have a well-defined structure which has been reported for a series of *n*-paraffins, namely for liquid *n*-paraffins longer than *n*-pentane as well as for non-crystalline solid and molten polyethylene (30). It has been previously suggested that the band at 1440 cm^{-1} should be considered as an overtone of the methylene rocking fundamental, which occurs at 720 cm^{-1} in polyethylene (31). However, the increase in the intensity of the 1440 cm^{-1} band with temperature does not conform with the expected behaviour for an overtone band. Also, the possible involvement of *gauche* methylene wagging modes should be ruled out as the 1440 cm^{-1} band would then be much weaker than the methylene wagging at 1300 cm^{-1}, which is not the case. On the other hand, the assignment of the 1440 cm^{-1} band to the scissoring vibrations of methylene groups adjoining two central bonds of *gauche* arrangements is consistent with known experimental facts (30). Namely, the temperature dependence of the band suggests that it should be associated with conformations having a higher energy than a planar chain.

Comparing the 1400–1500 cm^{-1} region in various tertiary amines, we note that the corresponding pairs of bands occur at about 1454 and 1476 cm^{-1}, for liquid tri-*n*-ethylamine, at 1448 and 1468 cm^{-1}, for liquid tri-*n*-propylamine, and at 1440 and 1456 cm^{-1}, for liquid tri-*n*-butylamine and longer alkylic chain amines. At room temperature, the higher frequency component of these pairs of bands is less intense. With increasing number of CH_2 units the high frequency component becomes more pronounced and the frequency shift of these pairs of bands reveals a small change in the force constant associated with the scissoring vibrations. On this basis, the higher frequency component of these pairs of bands should have a contribution of the scissoring mode of a methylene group adjoining a *trans* bond and a *gauche* bond, whereas, in the lower frequency component, the CH_2 oscillator should adjoin two *gauche* bonds (30). As the temperature increases, the alkylic chains become more and more fluid with an increasing number of *gauche* arrangements. Therefore, there will be an increase in the amount of CH_2 groups adjoining two *gauche* bonds and a decrease in the amount of CH_2 groups adjoining a *trans* and a *gauche* bond. This explains the relative intensity changes with increasing temperature of the 1456 and 1440 cm^{-1} bands.

The 2600–3000 cm^{-1} region

The carbon–hydrogen stretching modes of tri-*n*-butylamine can be readily assigned on the basis of group frequencies for similar molecules (6, 7, 32). The symmetric and antisymmetric stretching modes of CH_2 can be assigned to Raman lines at 2860 and 2905 cm^{-1}, respectively. The 2957 and 2871 cm^{-1} bands are assigned to CH_3 stretching vibrations, the latter frequency being ascribed to the symmetric motion. The band at 2933 cm^{-1} is essentially explained in terms of a Fermi resonance interaction between the symmetric methylene C—H stretching fundamental and binary combinations of the methylene bending vibrations of the extended chain (32).

The additional bands in this spectral region, below 2800 cm^{-1}, are believed to be due to overtones or combinations of the C—H deformations. Their intensities are largely accounted for in terms of Fermi resonance interactions with the carbon–hydrogen stretching motions.

As temperature increases, the intensity of the band at 2933 cm^{-1} increases and the intensity of the band at about 2905 cm^{-1} decreases. At about 200 K they display equal peak heights (Fig. 2). These intensity changes are consistent with a progressive elimination of extensive *trans* structure and a greater fluidity of the hydrocarbon chains. Hence, by increasing the temperature, the number of conformations increases for which the opportunity for Fermi resonance exists. Therefore, the 2933 cm^{-1} band intensity increases. On the other hand, it is known that the intensity of the CH_2 antisymmetric stretching mode is reduced when lateral interactions between hydrocarbon chains are disrupted, namely, by formation of *gauche* rotamers (32). In tri-*n*-alkylamines, lateral interactions are expected to be important, especially at low temperatures, due to antiparallel molecular alignment (33). The increase of temperature reduces these interactions drastically.

Can. J. Chem. Downloaded from www.nrcresearchpress.com by 80.58.250.72 on 09/07/12
For personal use only.

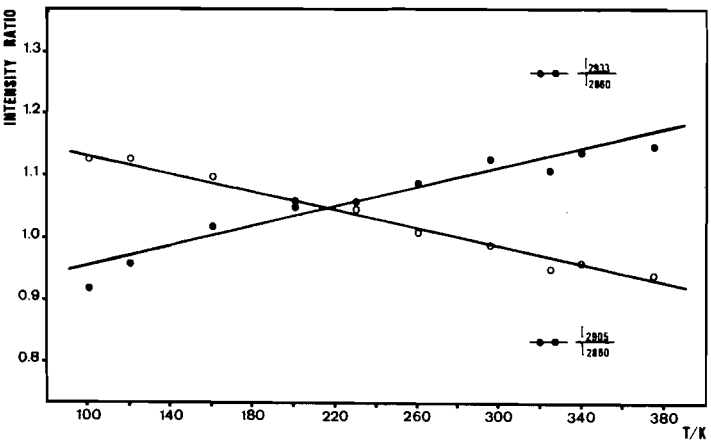

FIG. 3. Ratio of intensities vs. temperature, for pairs of Raman bands in the CH stretching region of tri-*n*-butylamine.

We have recorded Raman spectra of tri-*n*-butylamine at ten different temperatures between 100 and 373 K. At the expected solidification temperature (179 K), the crystalline solid was not obtained: the spectral lines were neither sharp nor did they show any crystal field splittings. Tri-*n*-butylamine just formed a glassy solid.

It is well known that the peak heights ratio of the methylene antisymmetric and symmetric vibrations, i.e., the ratio $I(2905)/I(2860)$, can be used to estimate the degree of order of the chains, giving intermediate values to those of the liquid and of the crystalline states after micellization (34, 35). On the other hand, the intensity ratio $I(2933)/I(2860)$ can be used as an environmental polarity parameter correlated with the polar character of the chains (34, 35).

Figure 3 shows the variation of these two parameters with temperature, for liquid tri-*n*-butylamine. As the temperature increases, the hydrocarbon chains become more disordered, as expected, with an increase in mobility of the methyl and methylene groups. At the same time, there is an increase in environmental polarity of the chains which, in turn, corresponds to a decrease in direct chain-to-chain contact. While these temperature-dependent features are expected, they nevertheless support the interpretation advanced for the relative intensity changes in the bands at 2933 vs. 2905 and 1456 vs. 1440 cm^{-1}.

When the order and polarity parameters were plotted against temperature a smooth "transition" was found below the expected solidification temperature (179 K). This is shown in Fig. 3.

4. Conclusion

Raman spectra of amines exhibit a number of features whose temperature-dependent intensities clearly sugest the occurrence of different conformers in simultaneous equilibria. These spectra provide useful vibrational information to monitor conformational changes.

In the case of tri-*n*-butylamine, where experimental data were available, the Raman spectra at different temperatures were interpreted and correlated with structural information obtained from statistical analysis of *gauche* skeletal arrangements. The average numbers of *gauche* interactions are correlated with temperature-dependent intensities of Raman bands and with the increasing influence, at lower temperatures, of the lone pair of electrons on the nitrogen atom, through the *trans* effect with respect to the α-carbon hydrogen atoms, and the *gauche* effect relative to the slightly polar $C_\alpha—C_\beta$ bond. The bands at 904 and 1456 cm^{-1} were ascribed to the low temperature form as these bands dominate at low temperatures. On the other hand, the conformer whose band occurs at 904 cm^{-1} was also favoured by polar solvents.

The introduction of the $\sum_k \delta(k)\bar{N}_g(k)$ as an additive term in eq. [2] and the correct evaluation of the volume increment associated with the amine group (eq. [3]) lead to an excellent agreement between calculated and experimental $\bar{V}^o$ values.

Temperature dependence of the relative intensities of bands in the CH stretching region suggest, by comparison with mono- (11) and di-*n*-butylamine (12), that the increase in the number of alkyl chains around the nitrogen atom makes molecular packing less restrictive and unique, giving rise to mesophases, as the overall shapes of the molecules become more spherical.

Acknowledgements

The authors thank Instituto Nacional de Investigação Científica of the Portuguese Ministry of Education for financial support.

1. P. A. PARK, R. J. D. PETHRICK, and B. H. THOMAS. Infrared and Raman band intensities change. *In* Internal rotation in molecules. *Edited by* W. J. Orville-Thomas. John Wiley and Sons, London. 1974. pp. 57–113 and references therein.
2. P. J. KRUGER and J. JAN. Can. J. Chem. **48**, 3229 (1970).
3. J. R. DURIG, G. A. GUIRGIS, and D. A. C. COMPTON. J. Phys. Chem. **83**, 1313 (1979).
4. K. KUMAR. Chem. Phys. Lett. **9**, 504 (1971).
5. J. H. S. GREEN. Spectrochim. Acta, **24A**, 137 (1968).
6. C. CROCKER and P. L. GOGGIN. J. Chem. Soc. Dalton, 388 (1978).
7. J. R. DURIG and F. O. COX. J. Mol. Struct. **95**, 85 (1982).
8. D. W. SCOTT. J. Chem. Thermodyn. **3**, 843 (1971).
9. L. RADOM, W. J. HERHE, and J. A. POPLE. J. Am. Chem. Soc. **94**, 2371 (1972).
10. E. EGGERT and C. DJERASSI. J. Am. Chem. Soc. **95**, 3710 (1973).
11. J. J. C. TEIXEIRA-DIAS, L. A. E. BATISTA DE CARVALHO, A. M. AMORIM DA COSTA, I. M. S. LAMPREIA, and E. F. G. BARBOSA. Spectrochim. Acta, **42A**, 589 (1986).
12. L. A. E. BATISTA DE CARVALHO, A. M. AMORIM DA COSTA, J. J. C. TEIXEIRA-DIAS, E. F. G. BARBOSA, and I. M. S. LAMPREIA. J. Raman Spectrosc. In press.
13. J. E. WOLLRAB and V. W. LAURIE. J. Chem. Phys. **51**, 1580 (1969).
14. J. W. H. KAO and A. CHUNG-PHILLIPS. J. Chem. Phys. **63**, 4143 (1975); **63**, 4152 (1975).
15. G. MANN. Tetrahedron, **23**, 3375 (1967).
16. G. MANN, M. MUHLSTADT, J. BRABAND, and E. DORING. Tetrahedron, **23**, 3393 (1967).
17. K. S. PITZER. Chem. Rev. **27**, 39 (1940); J. Chem. Phys. **8**, 711 (1940).
18. E. F. G. BARBOSA and I. M. S. LAMPREIA. Can. J. Chem. **64**, 387 (1986).
19. J. T. EDWARD, P. J. FARRELL, and F. SHAHIDI. J. Phys. Chem. **82**, 2310 (1978).
20. S. MIZUSHIMA and T. SIMANOUTI. J. Am. Chem. Soc. **71**, 1320 (1949).
21. F. SHAHIDI, P. G. FARRELL, and J. T. EDWARD. J. Phys. Chem. **83**, 419 (1979).
22. J. T. EDWARD, P. G. FARRELL, and F. SHAHIDI. Can. J. Chem. **57**, 2585 (1979).
23. VON R. SIEDLER, L. GROTE, E. KAUER, U. WERNER, and H. J. BITTRICH. Z. Phys. Chem. **241**, 203 (1969).
24. S. S. KERTES and G. GRAUER. J. Phys. Chem. **77**, 3107 (1973).
25. A. BONDI. J. Phys. Chem. **68**, 441 (1964).
26. J. T. EDWARD, P. G. FARRELL, and F. SHAHIDI. Can. J. Chem. **57**, 2887 (1979).

Can. J. Chem. Downloaded from www.nrcresearchpress.com by 80.58.250.72 on 09/07/12
For personal use only.

27. M. J. KAMLET, J. L. M. ABBOUD, and R. W. TAFT. Prog. Phys. Org. Chem. **13**, 485 (1981).
28. R. G. SNYDER and J. H. SCHACHTSCHNEIDER. Spectrochim. Acta, **19**, 85 (1963).
29. J. L. KOENIG. Chemical microstructure of polymer chains. John Wiley & Sons, New York. 1980. p. 185.
30. R. G. SNYDER. J. Chem. Phys. **47**, 1316 (1967).
31. S. KRIM. Fortschr. Hochpolymer Fortschr. **2**, 51 (1960).
32. R. G. SNYDER, S. L. HSU, and S. KRIM. Spectrochim. Acta, **23A**, 395 (1978).
33. F. RATKOVICS and L. DOMONKOS. Acta Chim. Acad. Sci. Hung. **89**, 325 (1976).
34. K. LARSSON and R. P. RAND. Biochim. Biophys. Acta, **326**, 245 (1973).
35. A. M. AMORIM DA COSTA, C. F. G. C. GERALDES, and J. J. C. TEIXEIRA-DIAS. J. Coll. Interf. Sci. **86**, 254 (1982).
36. C. KLOFUTAR, S. PALJK, and D. KREMSER. J. Inorg. Nucl. Chem. **37**, 1729 (1975).

Can. J. Chem. Downloaded from www.nrcresearchpress.com by 80.58.250.72 on 09/07/12
For personal use only.

Isomérisation des radicaux insaturés. IV. Les radicaux méthyl-1-, méthyl-2- et diméthyl-1,2-propène-1 yles produits dans la photolyse des tri- et tétraméthyléthylènes à 147 nm

GUY J. COLLIN[1] ET HÉLÈNE DESLAURIERS
Département des sciences fondamentales, Université du Québec à Chicoutimi, Chicoutimi (Qué.), Canada G7H 2B1

ET

GEORGE R. DE MARÉ
Laboratoire de chimie physique moléculaire, Faculté des sciences, C.P. 160, Université Libre de Bruxelles, 50 ave F.-D. Roosevelt, B-1050 Bruxelles, Belgique

Reçu le 7 juillet 1986

GUY J. COLLIN, HÉLÈNE DESLAURIERS et GEORGE R. DE MARÉ. Can. J. Chem. **65**, 391 (1987).

On a utilisé la photochimie directe à 147 nm pour générer les radicaux vinyliques C_4H_7, méthyl-1- et méthyl-2-propène-1 yles, ainsi que le radical C_5H_9, diméthyl-1,2-propène-1 yle, à partir des tri- et tétraméthyléthylènes. Dans les deux cas, la fragmentation primaire d'une liaison α(C—C) est suffisamment importante. L'excédent énergie du photon est suffisamment important pour que ces radicaux vinyliques C_4H_7 et C_5H_9 soient vibrationnellement très chauds pour pouvoir s'isomériser vers des structures allyliques avant de se fragmenter. On montre qu'à des pressions de l'ordre de quelques Torr, la majorité des radicaux vinyliques C_4H_7 (≅70%) ont atteint une structure allylique avant fragmentation et que leur temps de vie, evalué dans les présentes conditions, est inférieur à la nanoseconde. La situation est moins claire bien que très similaire dans le cas du radical vinylique C_5H_9.

GUY J. COLLIN, HÉLÈNE DESLAURIERS, and GEORGE R. DE MARÉ. Can. J. Chem. **65**, 391 (1987).

Direct photolysis at 147 nm of tri- and tetramethylethylenes has been used to produce highly excited vinylic 1-methyl- and 2-methyl-1-propene-1-yl radicals (C_4H_7), as well as the 1,2-dimethyl-1-propen-1-yl radical (C_5H_9). In both cases, the primary fragmentation of the photoexcited molecules involved the split of an α(C—C) bond with high yields. The excess energy is sufficiently important that the majority of the vinylic radicals are very hot, and are able to isomerize towards an allylic structure before the occurrence of fragmentation. At a pressure of a few Torr, most of the vinylic C_4H_7 radicals (ca. 70%) isomerize to an allylic structure, and its lifetime is estimated to be less than one nanosecond under the present conditions. Although the mechanism is less simple, the excited vinylic C_5H_9 radical exhibits similar behaviour.

Introduction

Dans les trois précédentes publications de cette série, nous avons observé l'interconversion, l'isomérisation mutuelle de radicaux allyles diversement substitués par des groupes méthyles (1). Dans ces systèmes, des radicaux allyliques vibrationnellement excités ont la possibilité de transférer un atome d'hydrogène entre les positions 1 et 4 via un intermédiaire à cinq côtés. Nous n'avons pas pu observer l'isomérisation de ces radicaux allyles vers des structures vinyliques. Par contre, dans un travail un peu plus ancien, lors de la photolyse du triméthyléthylène (3ME), nous avions proposé que les deux radicaux C_4H_7, nommément les radicaux méthyl-1- et méthyl-2-propène-1 yles, doivent s'isomériser au moins partiellement vers les formes allyliques pour rendre compte de la formation de certains produits (2, 3)

[1] 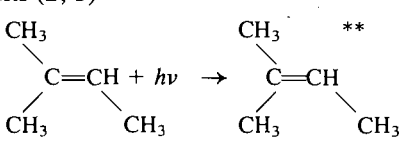

[2] 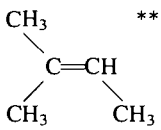 → $CH_3\dot{C}{=}CHCH_3 + CH_3$
(Méthyl-1-propène-1 yle)
$\Delta H \cong 363$ kJ mol^{-1}

[3] $CH_3\dot{C}{=}CHCH_3{}^{**} \rightarrow CH_3CH{\equiv}CH + CH_3$
$E_A = 161$ kJ mol^{-1} (4)

[4] $CH_3\dot{C}{=}CHCH_3{}^{*} \rightarrow CH_3\overline{CHCHCH_2}{}^{*}$
$\Delta H \cong -50$ kJ mol^{-1} (5)

[5] $CH_3\overline{CHCHCH_2} \rightarrow CH_2{=}CHCH{=}CH_2 + H$
$\Delta H \cong 200{,}5$ kJ mol^{-1}

[6] 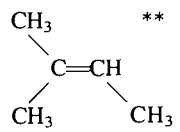 → $CH_3C(CH_3){=}\dot{C}H^* + CH_3$
(Méthyl-1-propène-1 yle)

[7] $CH_3C(CH_3){=}\dot{C}H^* \rightarrow CH_3C{\equiv}CH + CH_3$

[8] $CH_3C(CH_3){=}\dot{C}H^* \rightarrow \overline{CH_2C(CH_3)CH_2}{}^*$
$\Delta H \cong -50$ kJ mol^{-1} (5)

[9] $\overline{CH_2C(CH_3)CH_2}{}^* \rightarrow CH_3 + CH_2{=}C{=}CH_2$
$E_A = 211$ kJ mol^{-1} (6)

[10] $C_4H_7{}^* + M \rightarrow M + C_4H_7$

où M**, M* et M représentent respectivement la molécule photoexcitée, un fragment primaire radicalaire suffisamment chaud et une molécule quelconque. Le présent rapport constitue une étude systématique de l'effet de pression dans les photolyses des tri- et tétraméthyléthylènes (3ME et 4ME) à 147,0 nm afin de mesurer l'importance de ces isomérisations : processus [4] et [8], ainsi que celle impliquant le radical diméthyl-1,2-propène-1 yle.

Méthode expérimentale

Matériaux

Les 3ME et 4ME sont des produits A.P.I. contenant respectivement 0,06 ± 0,04% et 0,03 ± 0,02% d'impuretés. L'analyse chromatographique de l'échantillon de 3ME montre la présence de méthyl-2-butène-1 : 160 ppm, d'isoprène : 93 ppm, de pentène-2 (*cis* + *trans*) : 230 ppm. Quant à l'échantillon de 4ME, il ne contient que des traces de propane : 45 ppm. L'hexafluorure de soufre provient de chez

1. Auteur à qui adresser toute correspondance.

Can. J. Chem. Downloaded from www.nrcresearchpress.com by 80.58.250.72 on 09/07/12
For personal use only.

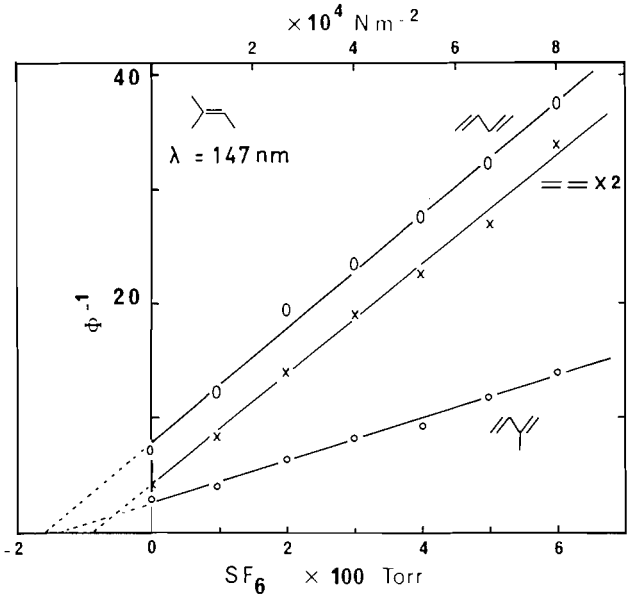

FIG. 1. Photolyse du 3ME à 147 nm. L'inverse du rendement quantique de divers produits en fonction de la pression de SF_6. Mélanges 3ME:O_2 (5:0,55 Torr). o: isoprène (r^2 = 0,996; Φ_0 = 0,39; interception axe de la pression : −140 Torr); x : allène (r^2 = 0,997; Φ_0 = 0,12; interception axe de la pression : −87 Torr); O : butadiène-1,3 (r^2 = 0,997; Φ_0 = 0,13; interception axe de la pression : −163 Torr).

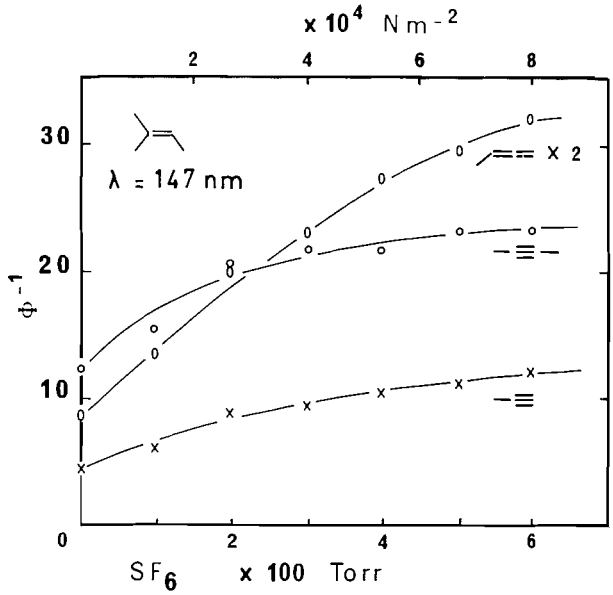

FIG. 2. Voir fig. 1; x : propyne; o : butyne-2; O : butadiène-1,2. NOTE: Les valeurs Φ(butadiène-1,2) ont été multipliées par 2.

Matheson Gas Products Canada (C.P. 99,8% min) et l'oxygène (99,995%) est acheté chez Liquid Carbonic Canada. Ces deux produits ne laissent pas voir de traces d'impuretés sur les chromatographies.

Photolyses, actinométrie, analyses

Toutes ces informations ont été récemment précisées dans la littérature (1).

Résultats

Cas du 3ME

La photolyse du 3ME à 147 nm et en présence de 10% d'oxygène moléculaire montre la formation de divers hydrocarbures. Ce sont l'isoprène, le butyne-2, les butadiène-1,3 et -1,2, le propyne et l'allène. Les rendements quantiques de ces produits décroissent avec l'ajout de quantités croissantes d'hexafluorure de soufre (figures 1 et 2). Lorsque la photolyse est réalisée en l'absence d'oxygène, d'autres produits apparaissent. Ce sont principalement l'éthane, le méthyl-2-butène-1, le méthyl-3-butène-1, l'isopentane et le diméthyl-2,2-butane (tableau 1). La formation de ces produits ainsi que celle d'autres aux rendements plus faibles a déjà été expliquée ailleurs (7).

Cas du 4ME

La photolyse du 4ME à 147 nm et en présence de 10% d'oxygène moléculaire montre la formation de diméthyl-2,3-butadiène-1,3, de méthyl-3-butadiène-1,2, de butyne-2, d'isoprène, de butadiène-1,2, de diméthyl-2,3-butène-1 et de propène avec des rendements quantiques qui décroissent avec l'augmentation de pression de l'hexafluorure de soufre (voir plus loin les figures 4 et 5).

En l'absence d'oxygène, ou d'oxyde nitrique, on observe à nouveau une formation importante d'éthane, de diméthyl-2,3- et de triméthyl-2,2,3-butane ainsi que d'un peu de divers isomères en C_6H_{12} de même qu'une formation appréciable de diméthyl-2,3-butène-1 (tableau 2).

Discussion

La photolyse du triméthyléthylène (3ME)

La photostabilité du 3ME sous rayonnement uv n'est pas inconnue. Plusieurs études partielles ont montré la complexité des mécanismes de formation des produits (2, 3, 7, 8). En plus de la double liaison, la molécule contient une liaison C—H située en position α par rapport à cette double liaison -α(C—H)-, trois liaisons α(C—C) et neuf liaisons β(C—H). Avec ce type de molécules ne disposant pas de liaisons β(C—C), la photofragmentation implique soit l'une ou l'autre des deux liaisons α(C—C) et β(C—H) avec une probabilité similaire (9). Compte tenu de l'énergie du photon à 147 nm (E = 811 kJ Einstein^{-1}), le mécanisme retenu implique les réactions [1]–[10] relatives à la scission primaire de l'une des trois liaisons α(C—C). La rupture primaire d'une liaison β(C—H) implique les réactions suivantes

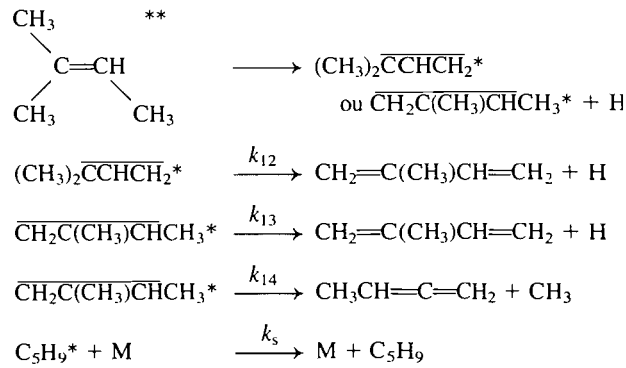

où k_{12}, k_{13} et k_{14} sont les constantes de vitesse des réactions monomoléculaires de fragmentation des radicaux activés, et k_s est la constante de vitesse de stabilisation par collision des radicaux allyles C_5H_9. Quant aux réactions engendrées par la rupture primaire de la liaison α(C—H), elle sera discutée plus en détail dans le cas de la photolyse du tétraméthyléthylène. Notons seulement que le butyne-2 sera le résultat de cette rupture α(C—H). Les réactions [1]–[15] rendent compte de la formation du propyne, de l'allène, des butadiène-1,3 et -1,2 et

Can. J. Chem. Downloaded from www.nrcresearchpress.com by 80.58.250.72 on 09/07/12
For personal use only.

TABLEAU 1. Photolyse du triméthyléthylène à 147 nm. Rendements quantiques

Monomère (Torr)[a]	4,95	4,95	4,95	4,95	4,95	4,95
SF_6 (Torr)	—	—	100	200	400	400
O_2 (Torr)	0,55	—	—	—	—	0,55
Éthane	—	0,23	0,19	0,16	$0,083_5$	—
Propyne	0,15	0,148	$0,15_5$	0,15	0,10	0,093
Allène	$0,07_6$	0,073	$0,05_4$	0,04	0,024	0,022
Butadiène-1,3	$0,09_6$	0,05	0,077	0,063	0,036	0,035
Butadiène-1,2	$0,03_8$	0,038	0,035	0,027	0,019	0,018
Butyne-2	$0,05_6$	0,054	0,06	0,06	0,047	0,044
Isoprène	0,27	0,26	0,23	0,18	$0,09_5$	0,11
Méthyl-2-butène-1	—	0,18	0,17	0,11	0,12	—
Méthyl-3-butène-1[b]	—	0,007	0,007	0,008	0,007	—
Isopentane	—	0,144	0,13	0,11	0,08	—
Diméthyl-2,2-butane	—	0,126	0,11	n.m.[d]	n.m.	—
γ_{corr}[c]	—	0,70	0,665	0,60	0,65	—

[a]1 Torr = 133 N m^{-2}.
[b]Il y a aussi formation de traces de pentène-2 (*cis* + *trans*).
[c]Voir texte.
[d]Non mesuré.

TABLEAU 2. Photolyse du tétraméthyléthylène à 147 nm. Rendements quantiques

Monomère (Torr)	4,95	4,95	5,00	4,95	4,95	4,95	4,95	4,95
SF_6 (Torr)	—	—	—	100	100	300	300	300
O_2 (Torr)	0,55	—	—	—	0,55	—	0,55	—
NO (Torr)	—	—	0,63	—	—	—	—	0,55
Éthane	—	0,205	—	0,10	—	0,08	—	—
Propène	0,07	0,04	0,02	0,025	0,06	0,016	0,03	0,008
Butadiène-1,2	0,02	0,02	0,02	0,012	0,014	0,008	0,007	0,007
Butyne-2	0,13	0,14	0,135	0,105	0,093	0,07	0,067	0,082
Isoprène	0,156	0,156	0,13	0,03	0,073	0,01	0,025	0,037
Méthyl-3-butadiène-1,2	0,025	0,035	0,028	0,012	0,014	0,008	0,006	0,007
Diméthyl-2,3-butadiène-1,3	0,25	0,15	0,145	0,04	n.m.	n.m.	n.m.	n.m.
Diméthyl-2,3-butène-1	0,070	0,34	0,05	0,11	0,023	0,11	0,013	0,01
Diméthyl-2,3-butane	—	0,136	—	0,11	—	0,08	—	—
Triméthyl-2,2,3-butane	—	0,075	—	0,05	—	0,04	—	—
C_6H_{12}[a]	—	n.m.[b]	—	0,02	—	0,02	—	—

[a]Méthyl-3-pentène-2 (*cis* + *trans*) ≅ 63%; méthyl-2-pentène-2 ≅ 30%; diméthyl-3,3-butène-1 ≅ 7%.
[b]Nom mesuré.

de l'isoprène. Compte tenu des stabilisations éventuelles par collision des intermédiaires M*, le rendement quantique de chacun de ces produits est susceptible d'un comportement de type Stern–Volmer (10, 11) : l'inverse du rendement quantique du produit X est une fonction linéaire croissante de la pression.

$$[16] \quad [\Phi(X)]^{-1} = [\Phi_0(X)]^{-1}(1 + k_s[M]/k_d)$$

où $\Phi(X)$ et $\Phi_0(X)$ sont respectivement les rendements quantiques du produit X mesuré à une pression M et extrapollé à pression nulle, k_s et k_d sont les constantes de vitesse de stabilisation (ordre deux) et de dissociation (ordre un) des intermédiaires radicalaires chauds.

La figure 1 montre l'excellente linéarité obtenue dans le cas de trois produits. La figure 2 par contre indique clairement une courbure plus ou moins négative dans le cas des rendements en propyne, butyne-2 et butadiène-1,2. Il existe plusieurs explications à ces courbures (10–12). Parmi ces explications, il y a le fait les radicaux primaires ne sont pas activés de façon monoénergétique. Les deux fragments primaires issus des réactions [2], [6] et [11] emportent chacun une part de l'énergie excédentaire. Dans le cas des fragments qui ont pour complément l'atome d'hydrogène (réaction [11]), on peut penser qu'ils ont une distribution de population en énergie plus étroite que si ce complément est le radical méthyle (réactions [2] et [6]). La courbure sera ainsi moins prononcée dans les cas de l'isoprène et du butadiène-1,2 comparativement aux cas du propyne et de l'allène. Une deuxième raison réside dans le fait que deux intermédiaires différents peuvent être à l'origine d'un même produit, mais avec des constantes de vitesse différente (cas du propyne : réactions [3] et [7]). Enfin, un produit peut être le résultat de la chimie de deux intermédiaires ou plus intervenant successivement. Par exemple, réactions [6]–[9], l'allène est le résultat de l'isomérisation du radical méthyl-2-propène-1 yle et de la fragmentation du radical β-méthallyle. Toutes ces raisons peuvent s'additionner ou se soustraire, de telle sorte que les apparentes linéarités ou courbures ne permettent pas de pousser plus avant la discussion.

On peut cependant mesurer l'importance de l'isomérisation des radicaux méthyl-1- et -2-propène-1 yles vers les structures allyliques. En effet à pression nulle, le propyne est le résultat

Can. J. Chem. Downloaded from www.nrcresearchpress.com by 80.58.250.72 on 09/07/12
For personal use only.

de la fragmentation directe de ces radicaux chauds alors que les formations d'allène et de butadiène-1,3 réclament d'abord leur isomérisation vers les formes allyliques. Si γ représente le pourcentage des radicaux vinyles isomérisés vers les formes allyliques, alors

$$[17] \quad \gamma = \frac{\Phi(\text{allène}) + \Phi(\text{butadiène-1,3})}{\Phi(\text{propyne}) + \Phi(\text{allène}) + \Phi(\text{butadiène-1,3})}$$

Cette valeur mesurée à 5 Torr de monomère est de 0,53 (colonne 1, tableau 1).

Cette relation fait cependant la supposition qu'à cette pression tous les radicaux méthyl-1- et méthyl-2-propène-1 yles d'une part et également tous les radicaux α- et β-méthallyles se fragmentent. Cela est loin d'être sûr. En effet en absence d'oxygène (tableau 1), il y a formation de quantités importantes de méthyl-2-butène-1 ($\Phi \cong 0{,}18$) via la combinaison des radicaux méthyles et β-méthyllyles et de traces de méthyl-3-butène-1 et de pentène-2 ($\Phi \cong 0{,}01$) par combinaison des radicaux méthyles et α-méthallyles. Cette observation requiert que tous les radicaux β-méthallyles ne se fragmentent pas à pression nulle, et si l'on peut admettre comme approximation que tous les radicaux α-méthallyles se décomposent à cette pression, c'est loin d'être le cas pour les radicaux β-méthallyles. Ce comportement différent des radicaux α-méthallyles se comprend aisément si l'on se souvient que dans le cas présent ils proviennent de l'isomérisation partielle des radicaux chauds méthyl-1-propène-1 yles. Il apparaît que les radicaux qui ont franchi la barrière de potentiel relative au processus [4] ont l'énergie suffisante pour se fragmenter en butadiène + H. Ce n'est pas le cas des radicaux β-méthallyles. En effet, seulement une fraction de ces radicaux issus de l'isomérisation des radicaux méthyl-2-propène-1 yles, processus [8], ont l'énergie suffisante pour donner lieu à la formation de l'allène et de radicaux méthyles. L'étude des diagrammes d'énergie potentielle est convaincante : voir figures 3 et 4 de la réf. 13. De ces considérations, il ressort que l'expression [17′] doit remplacer la précédente :

$$[17'] \quad \gamma_{corr} \cong \frac{\Phi(\text{allène}) + \Phi(\text{butadiène-1,3}) + \Phi(C_5H_{10})}{\Phi(\text{propyne}) + \Phi(\text{allène}) + \Phi(\text{butadiène-1,3}) + \Phi(C_5H_{10})}$$

Cette valeur γ_{corr} est de 0,70 sous une pression de 5 Torr (tableau 1). On peut donc conclure que les processus d'isomérisation des radicaux vinyliques vers les structures allyliques sont très importants.

La reformation du monomère par la combinaison des radicaux méthyles avec les radicaux méthylpropène-1 yles empêche l'évaluation directe de leur stabilité. Par contre le bilan complet de la fragmentation de la molécule photoexcitée incite à penser qu'il n'y en a pas, ou peu de stabilisés dans les conditions expérimentales présentes. Naturellement, si certains radicaux vinyliques sont stabilisés et, par exemple, reforment le monomère par combinaison avec les radicaux méthyles, le rapport γ_{corr} tout juste établi devrait être revue à la baisse.

Cette importante isomérisation des radicaux vinyliques chauds vers les structures allyliques doit être mise en parallèle avec le fait que les réactions inverses, les isomérisations des radicaux allyles vers les structures vinyliques, n'ont jamais été invoquées pour expliquer les formations de produits dans les photolyses de plusieurs alcènes (voir par exemple la réf. 14). La présence d'une énergie de résonance allylique de quelque 50 kJ mol^{-1} dans les radicaux allyles (5) augmente d'autant la barrière de

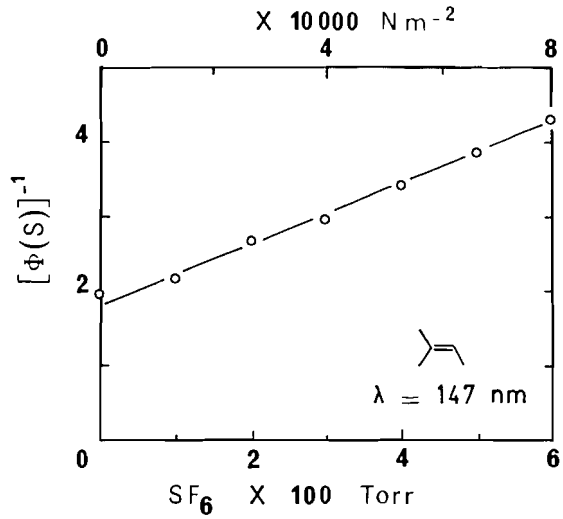

FIG. 3. Voir fig. 1; $S = \Phi(\text{propyne}) + \Phi(\text{allène}) + \Phi(\text{butadiène-1,3}) + \Phi(\text{méthyl-3-butène-1}) + \Phi(\text{méthyl-2-butène-1})$ ($r^2 = 0{,}99$; $\Phi_0 = 0{,}56$; interception axe de la pression : −420 Torr).

potentiel et que, si équilibre il y a, au facteur pré-exponentiel près, l'équilibre est nettement déplacé vers la formation des radicaux allyles (13). La variation de la valeur γ_{corr} qui semble diminuer avec l'augmentation de pression (tableau 1) est de peu d'intérêt puisque à haute pression, il y a aussi stabilisation par collision des radicaux vinyles.

Il est par contre intéresssant de noter que si l'on confond les radicaux méthyl-1- et méthyl-2-propène-1 yles, et que l'on regarde le comportement Stern–Volmer de la somme

$$[18] \quad S = \Phi(\text{propyne}) + \Phi(\text{butadiène-1,3}) + \Phi(\text{méthyl-2-butène-1}) + \Phi(\text{méthyl-3-butène-1}) + \Phi(\text{allène})$$

on obtient une linéarité presqu'exemplaire (fig. 3). Aux remarques précédentes déjà faites sur ces linéarités, on en déduit que le rapport $k_M/(k_{isom} + k_{diss})$ des radicaux vinyles C_4H_7 est voisin de 450 Torr, ou encore en traduisant en terme de fréquence de collision, le temps de vie «moyen» de ces radicaux est de l'ordre de $0{,}3–0{,}4 \times 10^{-9}$ s. Cette donnée, bien que très spéculative compte tenu des approximations faites et de la méthodologie utilisée, est quand même intéressante. En effet, on peut penser les molécules photoexcitées, M**, sont elles-mêmes susceptibles de stabilisation par collision. En supposant que toute l'énergie du photon incident réside dans le tissu vibrationnel de la molécule, nous avons déjà montré qu'en utilisant des calculs RRKM (Rice–Ramsperger–Kassel–Marcus) appropriés, le temps de la molécule pentène-1 photoexcitée à 147 nm correspond à une pression de stabilisation de 130 atm (1 atm = 101.3 kPa). Ce résultat tient compte d'un transfert d'énergie de 21 kJ mol^{-1} (5 kcal mol^{-1}) à chaque collision et une énergie de la liaison β(C—C) de 301 kJ mol^{-1} (15). Compte tenu des énergies plus rigides des liaisons individuelles du 3ME, un temps de vie «RRKM» beaucoup plus long doit être retenu pour le 3ME. Des calculs similaires ont montré que la pression de stabilisation est plutôt de l'ordre de 7 atm.[2] Il s'ensuit que l'on peut raisonnablement ignorer la réaction de stabilisation par collision du 3ME photoexcité à 147 nm.

Finalement, il est pertinent d'estimer l'importance de chacun des processus primaires de fragmentation sous faible pression (tableau 3). Bien qu'un peu d'isoprène soit aussi formé suite à la

2. G. J. Collin, résultats non publiés.

Can. J. Chem. Downloaded from www.nrcresearchpress.com by 80.58.250.72 on 09/07/12
For personal use only.

TABLEAU 3. Photofragmentation du triméthyléthylène à 147 nm

Processus primaire	Produits	Φ^a	Note
β(C—H)	Isoprène	0,32	fig. 1
	Butadiène-1,2	0,05	fig. 2
α(C—C)	Propyne Butadiène-1,3 Allène (C_5H_{10})	0,56[b]	fig. 3
α(C—H)	Butyne-2	0,08	fig. 2
	Isoprène[b]	(0,07)	
	Total	1,08	

[a]Valeurs obtenues par extrapolation des rendements à pression nulle de SF_6, donc sous une pression de TME de 5 Torr (665 N m^{-2}).
[b]Voir texte.

rupture primaire α(C—H) (voir plus loin) il est évidemment impossible ici de distinguer cette formation de celle consécutive à la rupture primaire β(C—C). On peut raisonnablement estimer que cette formation résiduaire d'isoprène est au plus similaire à celle du butyne-2 (voir plus loin). Le total des processus de fragmentation est légèrement supérieur à l'unité. Ce dépassement traduit en partie l'incertitude expérimentale ainsi que certaines subtilités de mécanismes non-discutées ici.

La photolyse du tétraméthyléthylène (4ME)

La photofragmentation du 4ME à 147 nm est relativement plus simple. Étant donné la structure symétrique de la molécule, et en l'absence d'une isomérisation de la molécule photo-excitée, celle-ci ne dispose que de deux types de liaisons disponibles pour la fragmentation. Ce sont les 12 liaisons C—H situées en position β par rapport à la double liaison -β(C—H)- et quatre liaisons α(C—C). Avec ce type de molécules ne disposant pas de liaisons β(C—C), la photofragmentation implique soit l'une ou l'autre des deux liaisons α(C—C) et β(C—H) avec une probabilité similaire (9). Compte tenu de l'énergie du photon à 147 nm ($E \cong 811$ kJ Einstein^{-1}), le mécanisme retenu est le suivant :

[19] $(CH_3)_2C{=}C(CH_3)_2 + h\nu \rightarrow (CH_3)_2C{=}C(CH_3)_2{}^{**}$

[20] $(CH_3)_2C{=}C(CH_3)_2{}^{**} \rightarrow (CH_3)_2\overline{CC(CH_3)CH_2}{}^{*} + H$
$\Delta H \cong 326$ kJ mol^{-1} (4)

[21] $(CH_3)_2\overline{CC(CH_3)CH_2}{}^{*} \rightarrow CH_2{=}C(CH_3)C(CH_3){=}CH_2 + H$
$\Delta H = 217$ kJ mol^{-1}

[22] $(CH_3)_2\overline{CC(CH_3)CH_2}{}^{*} \rightarrow (CH_3)_2C{=}C{=}CH_2 + CH_3$
$\Delta H = 222{,}5$ kJ mol^{-1}

[23] $C_6H_{11}{}^{*} + M \rightarrow M + C_6H_{11}$

[24] $(CH_3)_2C{=}C(CH_3)_2{}^{**} \rightarrow CH_3 + (CH_3)_2C{=}\dot{C}CH_3{}^{*}$

[25] $(CH_3)_2C{=}\dot{C}CH_3{}^{*} \rightarrow CH_3 + CH_3C{\equiv}CCH_3$

[26] $(CH_3)_2C{=}\dot{C}CH_3{}^{*} \rightarrow \overline{CH_2C(CH_3)CH}CH_3{}^{*}$

suivies des réactions [13]–[15]. Comme on le voit, ce mécanisme explique aisément la formation des produits observés dans la photolyse du 4ME. Il explique aussi la formation du butyne-2 dans celle du 3ME, et y ajoute de l'isoprène et du butadiène-1,2. Quantitativement, les rendements sont en accord avec le comportement de type Stern–Volmer avec les remarques déjà faites sur les courbures des droites Stern–Volmer (figures 4 et 5). En outre, dans le cas présent, il n'est pas sûr que l'on puisse ignorer la stabilisation par collision de la molécule photoexcitée. Cette dernière remarque est pertinente puisque même en présence d'oxygène moléculaire, on a toujours observé une formation de diméthyl-2,3-butène-1, un isomère

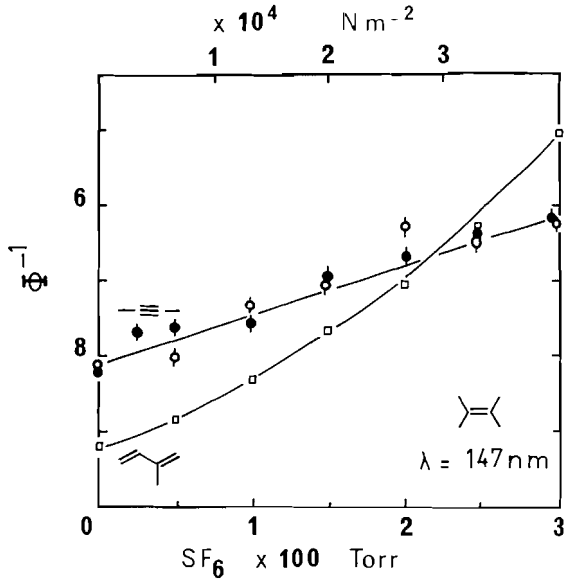

FIG. 4. Photolyse du 4ME à 147 nm. L'inverse du rendement quantique de quelques produits en fonction de la pression de SF_6. Mélanges 4ME:O_2 (5:0,55 Torr); □ : isoprène; ○ : butyne-2 (r^2 = 0,98; Φ_0 = 0,134; interception axe de la pression : −288 Torr). Mélange en l'absence d'oxygène : ● : butyne-2 (r^2 = 0,95; Φ_0 = 0,125; interception axe de la pression : −330 Torr).

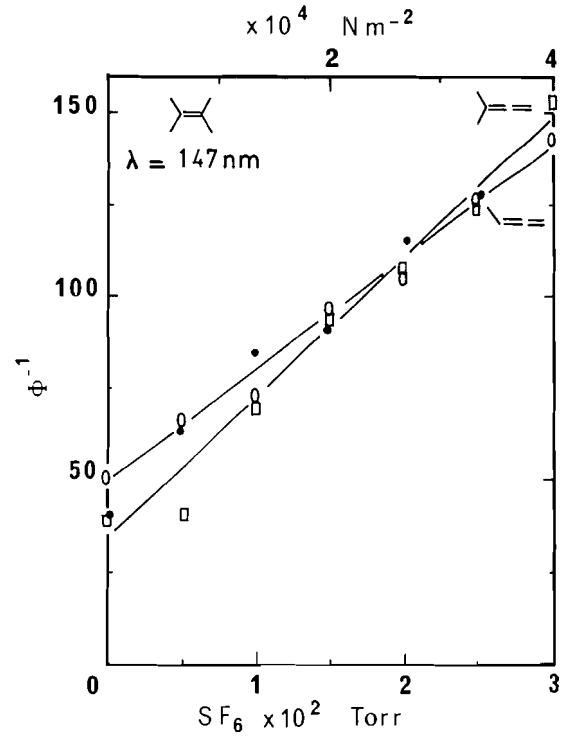

FIG. 5. Voir fig. 4. Mélange 4ME:O_2 (5:0,55 Torr). O : butadiène-1,2 (r^2 = 0,99; Φ_0 = 0,02; interception axe de la pression : −160 Torr); □ : méthyl-3-butadiène-1,2 (r^2 = 0,99; Φ_0 = 0,03; interception axe de la pression : −80 Torr). Mélange en l'absence d'oxygène : ● : butadiène-1,2 (r^2 = 0,95; Φ_0 = 0,02; interception axe de la pression : −180 Torr).

Can. J. Chem. Downloaded from www.nrcresearchpress.com by 80.58.250.72 on 09/07/12
For personal use only.

dont la formation a déjà été reportée dans la photolyse du 4ME à plus longues longueurs d'onde (16). Sans entrer dans le détail du mécanisme impliqué dans l'isomérisation, celle-ci peut bien entendu être le résultat de l'état électronique fondamental vibrationnellement chaud, mais aussi faire intervenir des états électroniques excités Rydberg (12). En l'absence de preuves suffisantes, il y a lieu seulement de ne pas écarter la possibilité de la stabilisation de la molécule fondamentale vibrationnellement très chaude.

Remerciements

Nous voulons remercier très vivement la Division des Affaires Scientifiques de l'OTAN (#85/0484) pour l'aide généreuse qu'elle a apportée à ce projet.

1. H. DESLAURIERS et G. J. COLLIN. Can. J. Chem. **63**, 3168 (1985).
2. G. J. COLLIN, H. DESLAURIERS et J. DESCHÊNES. Can. J. Chem. **57**, 870 (1979).
3. G. J. COLLIN et H. DESLAURIERS. Int. J. Chem. Kinet. **12**, 17 (1980).
4. T. GIERCZAK, J. GAWLOWSKI et J. NIEDZIELSKI. J. Photochem. **33**, 145 (1986).
5. K. W. EGGER, D. M. GOLDEN et S. W. BENSON. J. Am. Chem. Soc. **86**, 5420 (1964); A. B. TRENWITH. Trans. Faraday Soc. **66**, 2805 (1970).
6. W. TSANG. Int. J. Chem. Kinet. **5**, 929 (1973).
7. G. J. COLLIN et C. M. GAUCHER. Can. J. Chem. **52**, 34 (1974).
8. G. J. COLLIN et H. DESLAURIERS. Nouv. J. Chim. **5**, 447 (1981).
9. H. DESLAURIERS et G. J. COLLIN. J. Chim. Phys. **82**, 1033 (1985).
10. W. FORST. *Dans* Theory of unimolecular reactions. Academic Press, New York. 1973. pp. 235–245.
11. J. A. BARLTROP et J. D. COYLE. *Dans* Principles of photochemistry. J. Wiley and Sons, New York. 1975. pp. 148–155.
12. M. D. SHETLAR. Mol. Photochem. **6**, 143 (1974); **6**, 166 (1974); **6**, 191 (1974).
13. G. J. COLLIN. Rev. Chem. Intermed. **4**, 377 (1979).
14. D. HOUDE, H. DESLAURIERS et G. J. COLLIN. Can. J. Chem. **61**, 962 (1983).
15. J. GAWLOWSKI et G. J. COLLIN. J. Photochem. **23**, 241 (1983).
16. G. J. COLLIN et H. DESLAURIERS. Can. J. Chem. **61**, 1510 (1983).

Can. J. Chem. Downloaded from www.nrcresearchpress.com by 80.58.250.72 on 09/07/12
For personal use only.

Electrochemical oxidation of squaric and croconic acids on Pt and Pt surfaces modified by underpotential heavy metal monolayers in acid solutions

D. SAZOU AND G. KOKKINIDIS

Aristotelian University of Thessaloniki, Department of Chemistry, Laboratory of Physical Chemistry, Thessaloniki 54006, Greece

Received June 16, 1986

D. SAZOU and G. KOKKINIDIS. Can. J. Chem. **65**, 397 (1987).

The electrochemical oxidation of squaric and croconic acids on platinum in aqueous perchloric acid solutions has been investigated by means of cyclic voltammetry, rotating disc electrode, potentiostatic transients and controlled-potential electrolysis. The kinetic parameters (Tafel slopes, reaction orders) have been determined on the foot of the wave by varying the sweep rate, the angular velocity, depolarizer concentration, and perchloric acid concentration. A probable mechanism has been proposed for the overall oxidation processes. It involves two charge-transfer steps followed by the desorption of product, which is the rate-determining step. The oxidation product is immediately deactivated by a rapid hydration reaction. Also, the effect of underpotential Tl, Pb, and Bi monolayers on the electrochemical behaviour of squaric and croconic acids has been examined.

D. SAZOU et G. KOKKINIDIS. Can. J. Chem. **65**, 397 (1987).

Faisant appel à la voltamétrie cyclique, à l'électrode à disque tournant, aux espèces transitoires potentiostatiques et à l'électrolyse à potentiel contrôlé, on a étudié l'oxydation électrochimique des acides squarique et croconique sur le platine, dans des solutions aqueuses d'acide perchlorique. On a déterminé les paramètres cinétiques (pentes de Tafel, ordres de réaction) au pied de la vague en faisant varier la vitesse de balayage, la vitesse angulaire, la concentration du dépolarisant et la concentration de l'acide perchlorique. On propose un mécanisme probable pour l'ensemble des processus d'oxydation. Il implique deux étapes de transfert de charge qui sont suivies par la désorbtion du produit, qui est l'étape déterminante de la réaction. Le produit d'oxydation est rapidement désactivé par une réaction rapide d'hydration. De plus, on a examiné l'effet des monocouches de Tl, Pb et Bi n'ayant pas le potentiel approprié sur le comportement électrochimique des acides squarique et croconique.

[Traduit par la revue]

Introduction

Many studies have been carried out on the electrochemical oxidation of different enediol compounds like L-ascorbic, D-araboascorbic, dihydroxyfumaric and dialuric acids because of their biological importance (1–6). The oxidation studies of these enediols show a two-electron transfer followed by a pseudo-first order chemical reaction due to the carbonyl group hydration of the oxidation product.

However, the electrochemical oxidation of squaric acid (H_2SQ) and croconic acid (H_2CR) — which are also two enediols, members of a series of cyclic oxocarbon dibasic acids — has not been discussed so far. Polarographic studies were reported in the literature only for electrochemical reduction of croconic acid, as well as for the characterization of its reduction products (7–9).

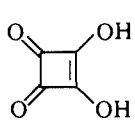

(H_2SQ)

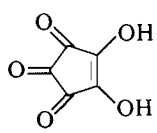

(H_2CR)

The aim of this work was first to give a detailed analysis of the kinetics of H_2SQ and H_2CR oxidation on platinum electrode in acid solutions.

On the other hand, in our previous paper (10) the influence of underpotential deposited (upd) layers of Tl. Pb, and Bi on the electrochemical behaviour of tetrahydroxy-1,4-benzoquinone and rhodizonic acid (also an enediol) on a Pt electrode has been studied in acid solutions. It was observed that the upd layers improve the reversibility of the redox system tetrahydroxy-1,4-benzoquinone/hexahydroxybenzene, as well as the oxidation of rhodizonic acid.

Thus the second purpose of this paper is to see if the electrochemical oxidation of H_2SQ and H_2CR is also catalysed by upd monolayers of certain heavy metal atoms.

The study was carried out in aqueous $HClO_4$ solutions using cyclic voltammetric and rotating disc techniques in combination with controlled-potential electrolysis and potential-step transients.

Experimental

The general experimental procedure, the activation of electrodes and the experimental set-up used have been described previously (11).

However, it must be mentioned that the roughness factor of the Pt electrodes was 1.15; this value was estimated by integration of the hydrogen adsorption–desorption current potential curves in 0.5 *M* $HClO_4$ solution, assuming that 210 $\mu C\ cm^{-2}$ of hydrogen is adsorbed on a perfectly smooth platinum electrode. The electrode potentials, E_H, given in various voltammograms and plots are referred to the normal hydrogen electrode. All the experiments were carried out at a constant temperature of 298 ± 0.1 K.

The supporting electrolyte was prepared from triply distilled water and $HClO_4$ 70% (Merck, "suprapure"). Squaric acid obtained from Fluka (Pract) was recrystallized twice from water (decomposition point, 293°C) (12). Potassium croconate was prepared according to the method of Nietzki–Benckiser (13) as reported in ref. 7. Perchlorate salts were prepared from the respective oxides or carbonates (Merck, "suprapure" or "p.a.") dissolved into the solution which contains stoichiometric quantity of $HClO_4$. Before starting any experiment, a sufficient amount of pure nitrogen was bubbled in the electrolyte solution to remove the dissolved oxygen, while during the measurements a nitrogen stream was passed above the solution.

Results

1. *Characteristics of the squaric and croconic acids oxidation on Pt electrode*

Cyclic voltammograms at different scan rates showing the oxidation of H_2SQ on Pt in 0.5 *M* $HClO_4$ are given in Fig. 1.

Can. J. Chem. Downloaded from www.nrcresearchpress.com by 80.58.250.72 on 09/07/12
For personal use only.

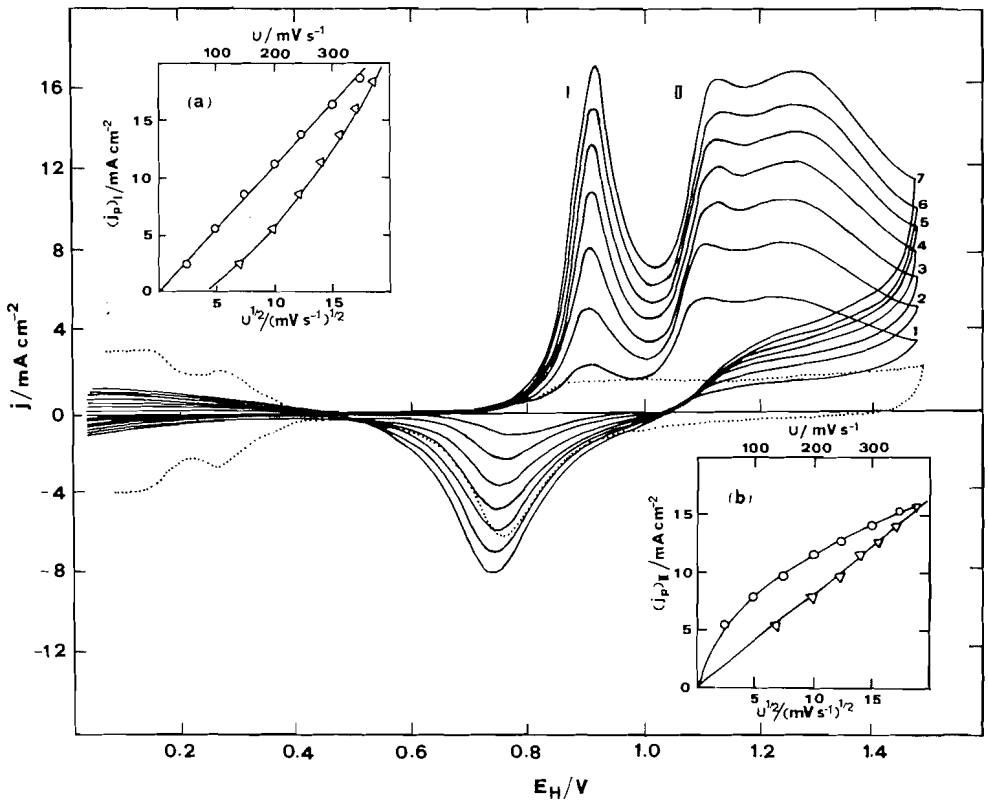

FIG. 1. Cyclic voltammograms of H_2SQ (10^{-3} *M*) on a Pt sheet in 0.5 *M* $HClO_4$ at different scan rates: (*1*) 50; (*2*) 100; (*3*) 150; (*4*) 200; (*5*) 250; (*6*) 300; (*7*) 350 mV s^{-1}. (·····) Voltammogram of the supporting electrolyte at υ = 100 mV s^{-1}. Insets: (*a*) plot of the first peak current vs. υ, (○) and $\upsilon^{1/2}$, (△); (*b*) plot of the second peak current vs. υ, (○) and $\upsilon^{1/2}$, (△).

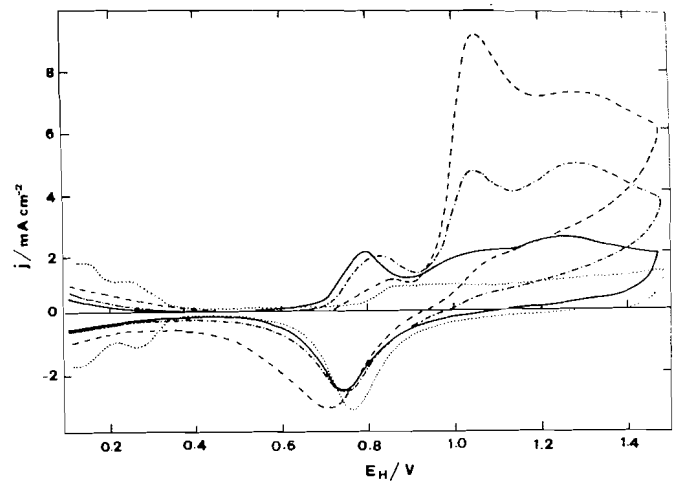

FIG. 2. Cyclic voltammograms of H_2CR (potassium croconate) on a Pt sheet in 0.5 *M* $HClO_4$ at different H_2CR concentrations: (—) 2×10^{-4} *M*; (-·-·-) 10^{-3} *M*; (---) 2.5×10^{-3} *M*; (·····) voltammogram of the supporting electrolyte; υ = 100 mV s^{-1}.

The H_2SQ oxidation commences at potentials where the electrode begins to be covered by the oxides. It is observed that two oxidation waves during the anodic sweep are obtained: a prewave (I) followed at more positive potentials by the main oxidation wave (II). Adsorption control of the prewave and diffusion control of the main wave were verified by scan rate dependence studies. The peak current density of the first wave, $(j_P)_I$, increases linearly with the scan rate, while the peak current density of the second wave, $(j_P)_{II}$, is directly proportional to the square root of the scan rate, as it is shown in the inset diagrams of Fig. 1.

The *j*–*E* curves obtained at these low scan rates ($\upsilon < 0.5$ V s^{-1}) shows an irreversible oxidation. By comparing these curves with those obtained in the same bulk solution without H_2SQ present, it can be seen that the cathodic wave at about 0.75 V is due to the reduction of formed oxides on the surface of platinum.

The other enediol, H_2CR, displays the same oxidation profile (Fig. 2) to that recorded in the case of H_2SQ differing only by the magnitude of their current densities. The current densities obtained are about twice greater for H_2SQ than for H_2CR.

The appearance of an adsorption peak at potentials more negative than the potential of the main diffusion peak indicates the strong adsorption of the reaction product (14). According to the theory of Wopschall and Shain (14), we examined only qualitatively the dependence of the scan rate on the half-peak width, ΔE_W, of the adsorption peak and the ratio, ρ, of the adsorption peak height to the diffusion peak height.

With increase of the scan rate the shape of the prepeak changes and more sharp adsorption prepeaks are obtained (Fig. 1). Also the ratio ρ varies linearly on the square root of the scan rate (Fig. 3) for different bulk concentrations of H_2SQ and H_2CR, indicating the strong adsorption of product of the oxidation process. The small deviations from the linearity of the ρ vs. $\upsilon^{1/2}$ plots observed at high concentrations of H_2SQ and H_2CR and high scan rates seem to be attributed to the small contribution of the weak adsorption of the reactants themselves.

The oxidation of H_2SQ and H_2CR has also been studied on the rotating disc electrode. Figures 4 and 5 show the current density–potential curves of H_2SQ and H_2CR, respectively, obtained on a Pt rotating disc electrode in 0.5 *M* $HClO_4$. A single oxidation wave for both H_2SQ and H_2CR appears. Note that, under rotating conditions, the adsorption prewave is very

Can. J. Chem. Downloaded from www.nrcresearchpress.com by 80.58.250.72 on 09/07/12
For personal use only.

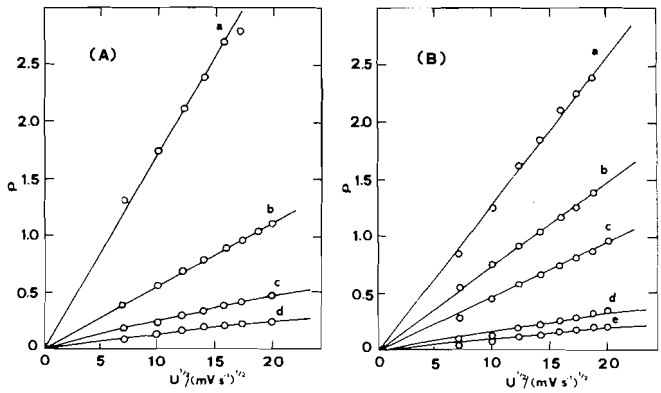

FIG. 3. Ratio of adsorption peak to diffusion peak, ρ, as a function of $v^{1/2}$ for the cyclic voltammograms at different bulk concentrations of H_2SQ (*A*): (*a*) 5×10^{-4}; (*b*) 10^{-3}; (*c*) 2.5×10^{-3}; (*d*) $5 \times 10^{-3}\,M$, and H_2CR (*B*): (*a*) 2×10^{-4}; (*b*) 5×10^{-4}; (*c*) 10^{-3}; (*d*) 2.5×10^{-3}; (*e*) $4 \times 10^{-3}\,M$.

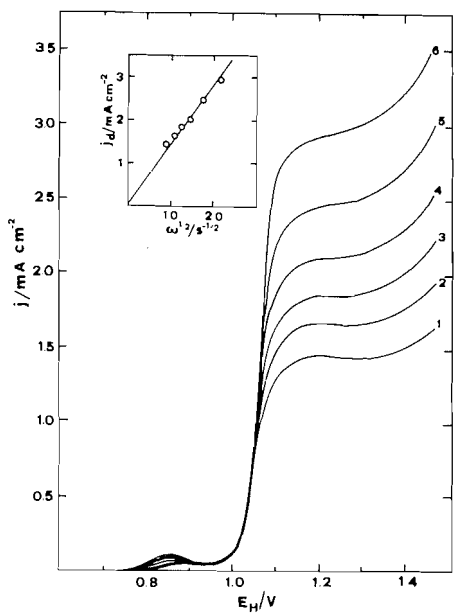

FIG. 4. Current density – potential curves for H_2SQ ($10^{-3}\,M$) oxidation on a Pt rotating disc electrode in $0.5\,M$ $HClO_4$. $|dE/dt| = 20\,mV\,s^{-1}$; rotation frequency *f*: (*1*) 12.5; (*2*) 18.3; (*3*) 25; (*4*) 35; (*5*) 50; (*6*) 75 Hz. Inset: limiting diffusion current density j_d vs. $\omega^{1/2}$ ($\omega = 2\pi f$).

small. However, it becomes more evident when the potential sweep rate increases.

The limiting current density of the oxidation waves of the two acids increases linearly with $\omega^{1/2}$ ($\omega = 2\pi f$). From the slope $dj_d/d\omega^{1/2}$ of the inset plots of Figs. 4 and 5, the diffusion coefficients of H_2SQ and H_2CR were determined by means of the corrected Levich–Riddiford equation (15, 16), after substituting for the kinematic viscosity the value $\nu = 8.929 \times 10^{-3}$ $cm^2\,s^{-1}$ and for the number of electrons consumed per molecule the value $n = 2$. The latter was estimated by controlled-potential electrolysis experiments. The calculated values are: $D_{H_2SQ} = 1.30 \times 10^{-5}\,cm^2\,s^{-1}$ and $D_{H_2CR} = 0.55 \times 10^{-5}\,cm^2\,s^{-1}$. These values agree reasonably well with those obtained from the slope of the j–$t^{1/2}$ diagrams; the j–t curves are recorded using potential-step transients (17).

Although the size of the molecules of the two compounds is about the same, comparing the values of D_{H_2SQ} and D_{H_2CR} it is

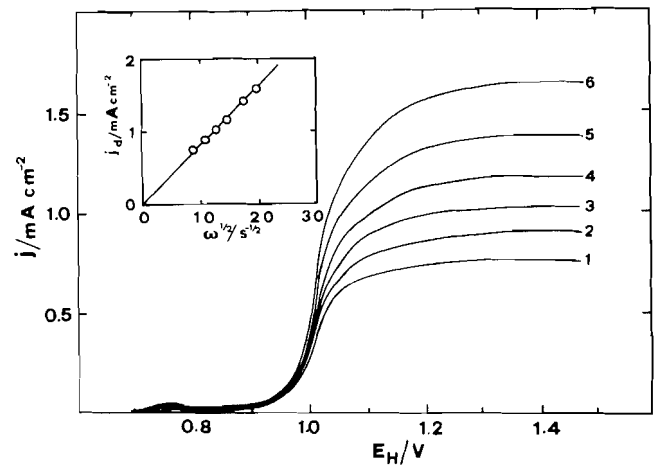

FIG. 5. Current density – potential curves for H_2CR (kalium croconate, $10^{-3}\,M$) oxidation on a Pt rotating disc electrode in $0.5\,M$ $HClO_4$. $|dE/dt| = 20\,mV\,s^{-1}$; rotation frequency *f*: (*1*) 12.5; (*2*) 18.3; (*3*) 25; (*4*) 35; (*5*) 50; (*6*) 75 Hz. Inset: limiting diffusion current density j_d vs. $\omega^{1/2}$ ($\omega = 2\pi f$).

obvious that the value of D_{H_2SQ} is about twice that of D_{H_2CR}. This difference in the diffusion coefficients may be due to the fact that H_2CR exists in aqueous solutions in its hydrated form which favors a voluminal structure of the molecule through two intramolecular hydrogen bonds, thus resulting in a lower mobility. Generally, it is known that in the case of tricarbonyl compounds, the hydration occurs in the central carbonyl group because of its high reactivity (18, 19).

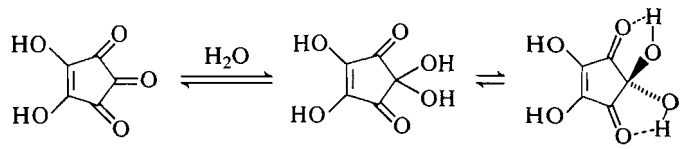

The calculated values of D allow us to evaluate the value of αz, the apparent transfer coefficient. The j_p vs. $v^{1/2}$ plots (for example Fig. 1, inset (*b*)) for low v values show a behaviour of pure diffusion, the slope of which is expressed by the following equation:

$$\frac{dj_p}{dv^{1/2}} = 3.1 \times 10^5 n(\alpha z)^{1/2} D^{1/2} c$$

In this way a value of $\alpha z = 1.42$ for H_2SQ and $\alpha z = 0.84$ for H_2CR is obtained by substituting $n = 2$, the total number of transferred electrons per depolarizer molecule.

Curves of the type shown in Figs. 4 and 5 were used to obtain $\log[j/(j_d - j)]$ vs. E plots, examples of which are given in Figs. 6 (*A*) and (*B*) for H_2SQ and H_2CR, respectively. From these diagrams the role of reactant or product adsorption becomes obvious mainly in the case of H_2CR. The slope of the $\log[j/(j_d - j)]$ vs. E plot changes with the H_2CR concentration. At low concentrations two linear parts with different slopes appear:

$$\left(\frac{dE}{d\log[j/(j_d - j)]}\right)_I = 55\,mV\,decade^{-1}$$

and

$$\left(\frac{dE}{d\log[j/(j_d - j)]}\right)_{II} = 130\,mV\,decade^{-1}$$

(for $c = 10^{-3}\,M$).

The slope of the first part in the potential range of the foot of

Can. J. Chem. Downloaded from www.nrcresearchpress.com by 80.58.250.72 on 09/07/12
For personal use only.

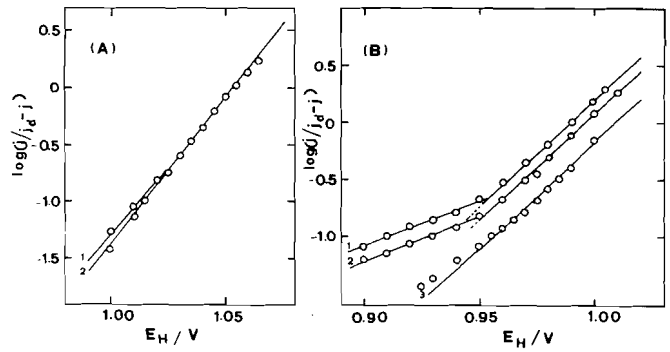

FIG. 6. $\log [j/(j_d - j)]$ vs. E plot of H_2SQ (A) and H_2CR (B) oxidation on a Pt rotating disc electrode in 0.5 M $HClO_4$. (A): (1) 10^{-3} M at 12.5 Hz; (2) 5×10^{-3} M at 12.5 Hz. (B): (1), (2) 10^{-3} M at 12.5 Hz and 25 Hz, respectively; (3) 4×10^{-3} M at 12.5 Hz.

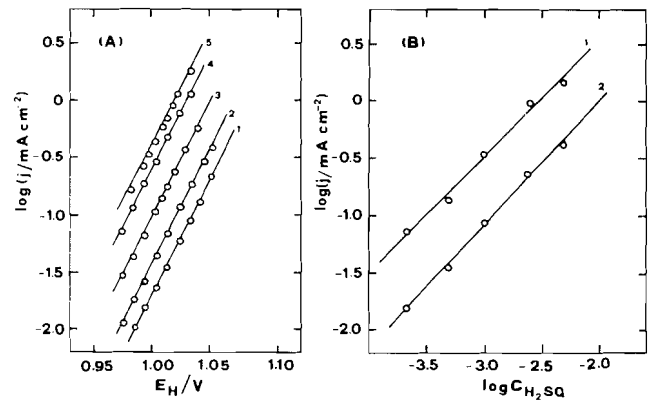

FIG. 7. (A): log j vs. E plot of H_2SQ oxidation on Pt in 0.5 M $HClO_4$ for different concentrations of H_2SQ: (1) 2×10^{-4}; (2) 5×10^{-4}; (3) 10^{-3}; (4) 2.5×10^{-3}; (5) 5×10^{-3} M. f = 25 Hz. (B): Plot of log j vs. log c_{H_2SQ} at E_H = 1.03 V (1) and E_H = 1.00 V (2).

the wave changes with the increase of H_2CR concentration, while that of the second segment remains constant. In the case of relatively low concentrations (up to 2.5×10^{-3} M) the change is negligible but at $c_{H_2CR} \simeq 4 \times 10^{-3}$ M almost one straight line with slope about equal to that of the second linear part is obtained

$$\left(\frac{dE}{d \log [j/(j_d - j)]} \simeq 65 \text{ mV decade}^{-1}\right)$$

In the case of H_2SQ (Fig. 6(A)), the change in the slope is very slight even in low concentrations of H_2SQ and it reasonably can be considered as one straight line with slope independent on H_2SQ concentration.

2. Reaction orders

Influence of H_2SQ and H_2CR concentration: From the logarithmic analysis of the raising part of the current density – potential curves under quasi-stationary conditions (dE/dt = 2 mV s^{-1}) the Tafel plots were obtained for different concentrations of H_2SQ (Fig. 7(A)). The corresponding Tafel slope is independent of the H_2SQ concentration having an average value of 40 mV $decade^{-1}$. This value is in excellent agreement with the value 42 mV $decade^{-1}$ calculated from the value of αz reported previously. The current density values at E = constant increase proportionately to the concentration of H_2SQ. The quotient (d log j/d log c) is independent of the potential at which it was measured (Fig. 7(B)), as well as of pH; it was found equal to 1.05 ± 0.1, which means first order reaction with respect to H_2SQ concentration.

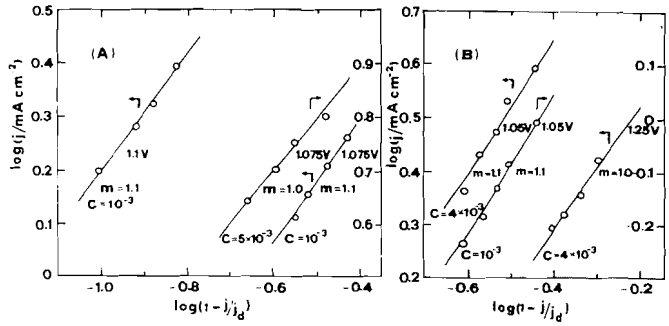

FIG. 8. Plot of log j vs. log $(1 - j/j_d)$. Data were obtained from r.d.e. experiments for H_2SQ (A) and H_2CR (B) oxidation on Pt in 0.5 M $HClO_4$. (The concentrations are expressed in molarities.)

In the case of H_2CR, the above analysis under quasi-stationary conditions also was carried out and the $(d \log j/d \log c)_E$ was found equal to 0.8 ± 0.1. The observed deviation from the unit may be attributed to the effect of H_2CR concentration on the Tafel slope value obtained at the foot of the wave. However, the reaction order with respect to H_2CR concentration can also be determined using the equation (20, 21):

$$j = kc_{Dep}^m [1 - j/j_d]^m$$

where k is the rate constant, c_{Dep} the concentration of the depolarizer in the solution, m the reaction order, j the current density at a constant potential value for different rotation frequencies and j_d the corresponding limiting current density at every rotation frequency.

According to the above equation, a plot of log j vs. log $(1 - j/j_d)$ should be linear with a slope equal to m. The reaction order obtained from this type of plots (Fig. 8(B)) for different H_2CR concentrations was equal to about 1.1.

The same equation was also applicated in the case of H_2SQ and the obtained diagram is demonstrated in Fig. 8(A). The reaction order obtained from these plots was about 1.1, which is consistent with the previous observations.

Influence of $HClO_4$ concentration: from the current density – potential curves of H_2SQ and H_2CR under quasi-stationary conditions for different $HClO_4$ concentrations at constant ionic strength, the Tafel plots were obtained which are demonstrated in Figs. 9(A) and 10(A), respectively. In these experiments the ionic strength was held constant (I = 1) by adding into the solution $NaClO_4$ the appropriate concentration. The Tafel lines shift to more positive potentials as the H^+ concentration increases. The Tafel slope obtained at the raising part of the wave is independent of pH having an average value of about 40 mV $decade^{-1}$ for H_2SQ and 110 mV $decade^{-1}$ for H_2CR. The log j vs. log c_{H^+} plots (Figs. 9(B) and 10(B)) at different constant potential values give the following reaction orders with respect to the H^+ concentration:

TABLE 1. Reaction order with respect to H^+ concentration

Substance	$\left[\frac{d \log j}{d \log c_{H^+}}\right]_{E, c_{Dep}, I=1}$
H_2SQ	−1.1 (for pH < 0.5) −0.3 (for 0.5 < pH < 2)
H_2CR	−1.1 (for pH < 0.4) −0.6 (for 0.4 < pH < 2)

Can. J. Chem. Downloaded from www.nrcresearchpress.com by 80.58.250.72 on 09/07/12
For personal use only.

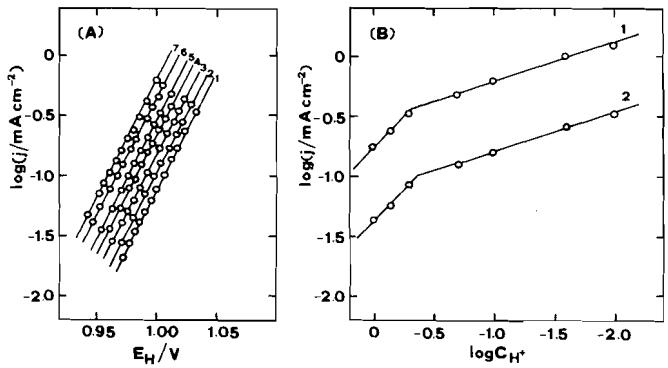

FIG. 9. (*A*): log j vs. E plot of H_2SQ ($10^{-3}M$) oxidation in different $HClO_4$ concentrations: (*1*) 1.0; (*2*) 0.7; (*3*) 0.5; (*4*) 0.2; (*5*) 0.1; (*6*) 0.02; (*7*) 0.01M and constant ionic strength (I = 1); f = 25 Hz. (*B*): plot of log j vs. log c_{H^+} at E_H = 1.03 V (*1*) and E_H = 1.00 V (*2*).

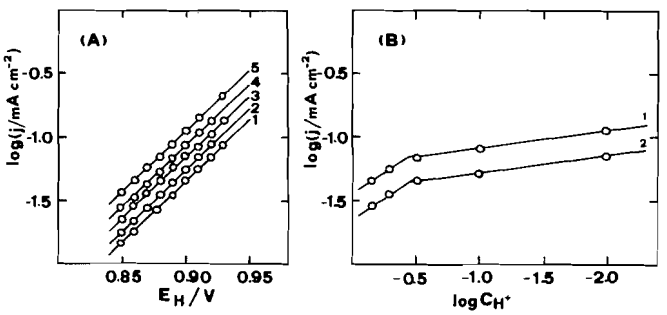

FIG. 10. (*A*): log j vs. E plot of H_2CR ($10^{-3}M$) oxidation in different $HClO_4$ concentrations: (*1*) 0.7; (*2*) 0.5; (*3*) 0.3; (*4*) 0.1; (*5*) 0.01M and constant ionic strength (I = 1); f = 25 Hz. (*B*): plot of log j vs. log c_{H^+} at E_H = 0.90 V (*1*) and E_H = 0.87 V (*2*).

The intersection of the two linear segments (Figs. 9(*B*) and 10(*B*)) reasonably coincides with the pK_{a_1} values of the two acids obtained potentiometrically: $pK_{a_1}(H_2SQ)$ = 0.52 (22, 23) and $pK_{a_1}(H_2CR)$ = 0.32 (23).

3. Mechanism proposed in acid solutions

The data collected demonstrate that the oxidation of H_2SQ and H_2CR corresponds to a two electron-transfer. Considering all the experimental results for the two electrode processes the oxidation mechanism proposed in the acid media ($pH < pK_{a_1}$) must be consistent with the following:

(*a*) Reaction order with respect to depolarizer:

$$\left(\frac{d\log j}{d\log c_{H_2SQ}}\right)_{E,c_{H^+}} = 1.1, \quad \left(\frac{d\log j}{d\log c_{H_2CR}}\right)_{E,c_{H^+}} = 1.1$$

(*b*) Reaction order with respect to H^+ for two compounds:

$$\left(\frac{d\log j}{d\log c_{H^+}}\right)_{E,c_{Dep},I=1} = -1.1$$

(*c*) Tafel slope:

40 mV for H_2SQ and 110 mV for H_2CR.

All the experimental parameters are in agreement with the theoretical ones except the reaction order with respect to H^+. The reaction orders,

$$\left(\frac{d\log j}{d\log c_{H^+}}\right)_{E,c_{Dep}}$$

measured imply that one proton intervene in the pH range where $pH < pK_{a_1}$, whereas two protons are theoretically predicted to involve in the reaction process up to the rate-determining step. This effect may be attributed to the fact that the dehydrogenation of different fuels on Pt is not an electrochemical reaction. For this phenomenon some experimental evidence exists (24) and this type of reaction seems to be plausible in light of the high adsorption enthalpy of H_{ads} on Pt. The reaction can be visualized as follows:

$$H_2SQ + 2Pt \rightarrow Pt\text{-}HSQ + Pt\text{-}H$$

$$H_2CR + 2Pt \rightarrow Pt\text{-}HCR + Pt\text{-}H$$

The adsorbed H-atom is oxidized very fast at sufficiently positive potentials.

On the other hand, the voltammetric data show the absence of a cathodic peak at low scan rates, which can be explained by the deactivation of the oxidation product caused by the hydration chemical reaction. The isolated oxidation products from the electrolyzed solution were in the case of H_2SQ the tetrahydrate of cyclobutantetrone (**I**), whereas in the case of H_2CR the leuconic acid pentahydrate (**II**). Thus the overall oxidation reactions are as follows:

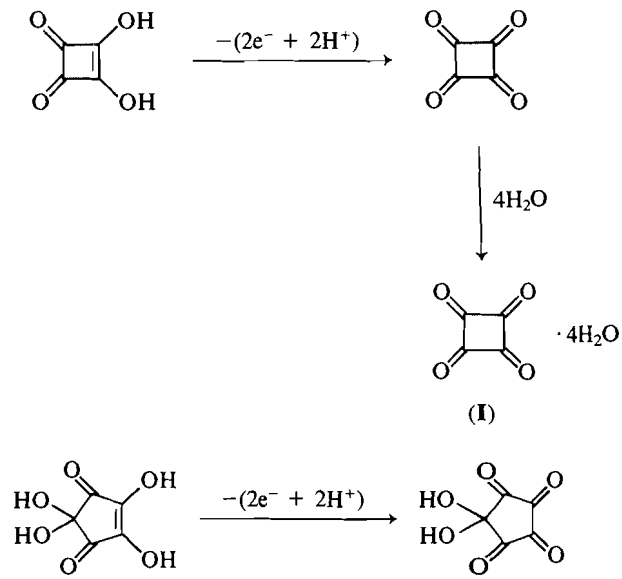

The following scheme presents a probable reaction mechanism for the oxidation of H_2SQ and H_2CR, which seems to be consistent with our experimental results.

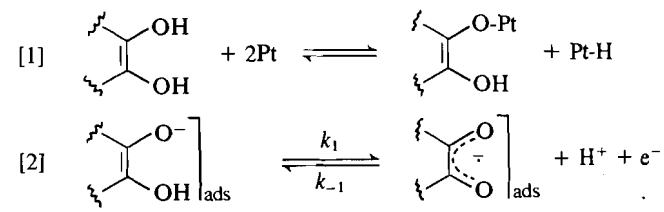

Can. J. Chem. Downloaded from www.nrcresearchpress.com by 80.58.250.72 on 09/07/12
For personal use only.

[3] 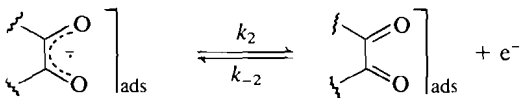

[4] 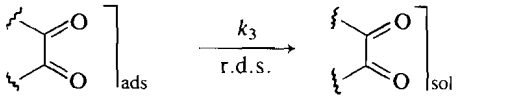

[5] 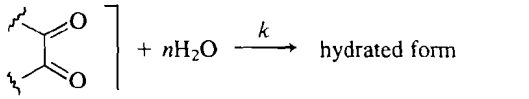

Assuming reaction [4] as being the rate-determining step and using the quasi-equilibrium approximation and a Langmuir type isotherm for depolarizer adsorption ($\vartheta \rightarrow 0$) the value of the anodic current density on the raising part of the wave can be expressed as:

$$j = 2FK_1K_2k_3c_{Dep}c_{H^+}^{-1} \exp(fE)$$

where c_{Dep} is the total concentration of H_2SQ or H_2CR in the bulk of the solution, c_{H^+} is the concentration of the H^+ ions, K_1 and K_2 are the equilibrium constants of reactions [2] and [3], k_3 is the rate constant of the r.d.s. and $f = \alpha zF/RT$. The experimental values of the Tafel slope and reaction orders are in agreement with those derived from the postulated mechanism.

4. Influence of the upd of Tl, Pb, and Bi on H_2SQ and H_2CR oxidation

The effect of the underpotential deposition of Tl on Pt on the anodic oxidation of H_2SQ is shown in Fig. 11, where the cyclic voltammograms of H_2SQ are given with and without Tl^+ ions present in the solution of the supporting electrolyte. Some change in the Pt electrode for H_2SQ oxidation is observed when Tl^+ ions are added to the solution and discharged to form the upd layer on the substrate. The adsorption peak is almost suppressed, while the peak potential of the diffusion wave appears at less positive potentials. The upd of Pb and Bi does not affect in any way the electrochemical behaviour of H_2SQ on platinum electrode.

Analogous behaviour is observed in the case of H_2CR. In Fig. 12 the cyclic voltammograms of H_2CR on Pt and Pt/M(upd) (M = Tl, Pb, and Bi) are given. For comparison the inset figure represents the cyclic voltammograms of the upd of Pb, Tl, and Bi on Pt. The concentration of Tl^+ was $10^{-3}M$, while those of Pb^{2+} and Bi^{3+} were $5 \times 10^{-5}M$. At higher concentrations complexation of H_2CR with Pb^{2+} and Bi^{3+} becomes significant. The upd of Pb and Bi causes a partial suppression of the adsorption wave and simultaneously a small increase of the current density of the diffusion wave. On the other hand, the upd of Tl causes a complete suppression of the adsorption wave with respective increase of the height of the diffusion wave. Taking into account the bounded area of the j–E curves, the increase of the diffusion wave seems to be analogous to the decrease or disappearance of the adsorption prewave.

This behaviour described above is different to that observed in the case of rhodizonic acid (10), a similar compound with six-member ring. The oxidation wave of rhodizonic acid on Pt also corresponds to a two-electron transfer. The upd ad-layers of Tl, Pb, and Bi catalyze the oxidation of this compound shifting the polarization wave towards less positive potentials and improving the reversibility of the wave not only under cyclic voltammetric conditions, but also on the Pt rotating disc electrode. Also, similar positive catalytic effect of the upd of Tl, Pb, and Bi has been reported for the oxidation of ascorbic acid (also an enediol) on the Pt electrode (25).

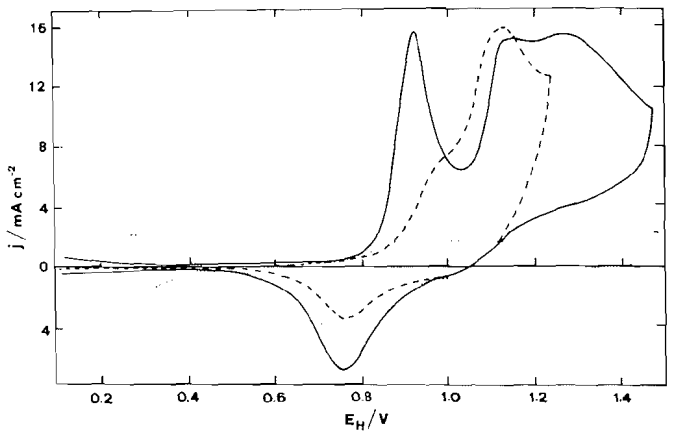

FIG. 11. Cyclic voltammograms of H_2SQ ($10^{-3}M$) on a Pt sheet in $0.5M$ $HClO_4$ in the absence (—) and presence (---) of $10^{-3}M$ $TlClO_4$. $v = 200$ mV s^{-1}. (· · · · ·) Voltammogram of the supporting electrolyte at $v = 200$ mV s^{-1}.

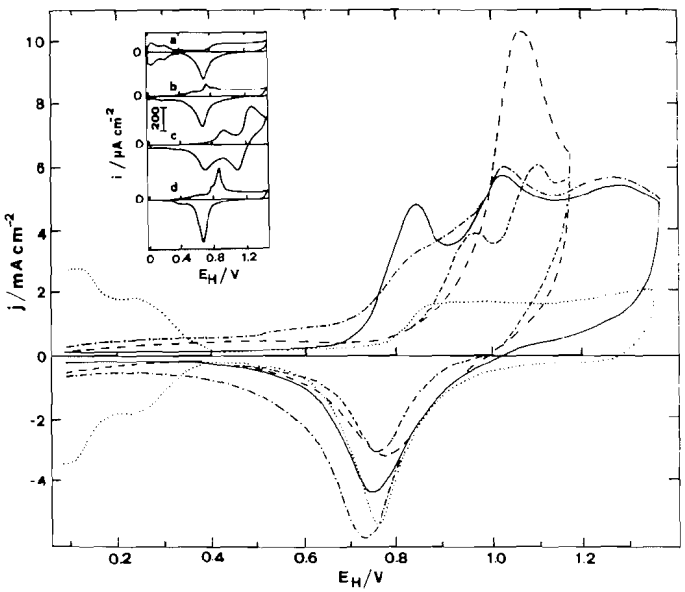

FIG. 12. Cyclic voltammograms of H_2CR (potassium croconate, $5 \times 10^{-4}M$) on a Pt sheet in $0.5M$ $HClO_4$ in the absence (—) and presence of: (---) $10^{-3}M$ $TlClO_4$; (· · · · ·) $5 \times 10^{-5}M$ $Pb(ClO_4)_2$;

The upd ad-layers of Tl, Pb, and Bi do not result in a notable increase of the catalytic activity of the Pt electrode for H_2SQ and H_2CR oxidation as in the case of rhodizonic and ascorbic acids. This difference seems to be attributed to the fact that the standard oxidation potentials of H_2SQ and H_2CR are located at more positive potentials — compared to those of rhodizonic and ascorbic acids — just on the positive boundaries of the upd ranges of the above metals on Pt, where the upd of the metals is superimposed by the upd of oxygen.

1. J. J. RUIZ, A. ALDAZ, and M. DOMINGUEZ. Can. J. Chem. **55**, 2799 (1977); **56**, 1533 (1978).
2. M. BREZINA, J. KORYTA, T. LOUCKA, D. MARSIKOVA, and J. PRADAC. J. Electroanal. Chem. **40**, 13 (1972).
3. M. DOMINGUEZ, A. ALDAZ, and E. SANCHEZ-BURGOS. J. Electroanal. Chem. **68**, 345 (1976).
4. P. KARABINAS, D. SAZOU, and D. JANNAKOUDAKIS. Bioelectroch. Bioenerg. **14**, 469 (1985).
5. D. SAZOU, P. KARABINAS, and D. JANNAKOUDAKIS. J. Electroanal. Chem. **176**, 225 (1984).

Can. J. Chem. Downloaded from www.nrcresearchpress.com by 80.58.250.72 on 09/07/12
For personal use only.

6. E. ROLDAN and M. DOMINGUEZ. Electrochim. Acta, **28**, 1215 (1983).
7. F. ARCAMONE, C. PREVOST, and P. SOUCHAY. Bull. Soc. Chim. Fr. 891 (1953).
8. M. B. FLEURY. C.R. **258**, 1512 (1964).
9. M. B. FLEURY, P. SOUCHAY, and M. GOUZERH. Bull. Soc. Chim. Fr. 2562 (1968).
10. G. KOKKINIDIS, D. SAZOU, and I. MOUMTZIS. J. Electroanal. Chem. **213**, 135 (1986).
11. G. KOKKINIDIS. J. Electroanal. Chem. **172**, 265 (1984).
12. J. D. PARK, C. M. SNOW, and J. R. LACHER. J. Am. Chem. Soc. **71**, 2337 (1949); **73**, 234 (1951).
13. NIETZKI and BENCKISER. Ber. **18**, 499 (1885); **18**, 1833 (1885).
14. R. H. WOPSCHALL and I. SHAIN. Anal. Chem. **39**, 1514 (1967).
15. W. G. LEVICH. Acta Physicochim. U.S.S.R. **17**, 257 (1964).
16. D. P. GREGORY and A. C. RIDDIFORD. J. Chem. Soc. 3756 (1956).
17. H. GERISCHER and W. VIELSTICH. Z. Phys. Chem. N.F. **3**, 16 (1955).
18. J. D. ROBERTS and M. C. CASERIO. Basic principles of organic chemistry. 2nd ed. W. A. Benjamin Inc., 1977. p. 779.
19. L. HOLLECK and O. LEHMANN. Ber. Bunsenges. Phys. Chem. **67**, 609 (1963).
20. R. W. ZURILLA, R. K. SEN, and E. YEAGER. J. Electrochem. Soc. **125**, 1103 (1978).
21. R. R. ADZIC, N. M. MARKOVIC, and V. B. VESOVIC. J. Electroanal. Chem. **165**, 105 (1984).
22. L. M. SCHARTZ and L. O. HOWARD. J. Phys. Chem. **77**, 314 (1973).
23. E. PATTON and R. WEST. J. Phys. Chem. **74**, 2512 (1970).
24. W. GÜTHER and W. VIELSTICH. Electrochim. Acta, **27**, 811 (1982).
25. K. TAKAMURA and M. SAKAMOTO. J. Electroanal. Chem. **113**, 278 (1980).

Can. J. Chem. Downloaded from www.nrcresearchpress.com by 80.58.250.72 on 09/07/12
For personal use only.

4,6-Dinitro-benzofuroxan and -benzofurazan adducts of 1,8-bis(dimethylamino)naphthalene. A conformational study by low temperature nuclear magnetic resonance

MARIE-PAULE SIMONNIN,[1] JEAN-CLAUDE HALLE, MARIE-JOSÉ POUET, AND FRANÇOIS TERRIER

Laboratoire de physicochimie des solutions, Unité Associée 403 du Centre national de la recherche scientifique, École nationale supérieure de chimie de Paris, 11 Rue Pierre et Marie Curie, 75231 Paris CEDEX 05, France

AND

DANIEL DAVOUST

Laboratoire de chimie organique structurale, Unité Associée 455 du Centre national de la recherche scientifique, Université Pierre et Marie Curie, 4 Place Jussieu, 75230 Paris CEDEX 05, France

Received July 17, 1986

MARIE-PAULE SIMONNIN, JEAN-CLAUDE HALLE, MARIE-JOSÉ POUET, FRANÇOIS TERRIER, and DANIEL DAVOUST. Can. J. Chem. **64**, 404 (1986).

Low temperature ^{1}H nuclear magnetic resonance spectra of the zwitterionic and anionic carbon-bonded adducts resulting from the addition of 4,6-dinitrobenzofuroxan (DNBF) or 4,6-dinitrobenzofurazan (DNBZ) to 1,8-bis(dimethylamino)naphthalene, the proton sponge PS, have been recorded at 500 MHz in DMF-d_7. They reveal the presence of two conformers due to restricted rotation around the C_{sp^2}—C_{sp^3} bond between C-4 of PS and the sp^3 carbon C-7′ of the negatively charged $DNBF^-$ or $DNBZ^-$ moiety. The geometry of these conformers was deduced from nuclear Overhauser enhancement difference spectra. The results show that in all systems there is a large preference for the less strained *s-trans* type of conformation, whose population lies between 80 and 90%. An interesting feature is the dependence of the chemical shift of the *peri* H5 proton on the conformation. In accordance with previously reported *peri* effects, a significant deshielding of H5 is observed in the major conformers, where this proton is spatially close to H7′. In contrast, H5 moves upfield in the minor conformers, in which it lies in the vicinity of the $DNBF^-$ or $DNBZ^-$ moiety.

MARIE-PAULE SIMONNIN, JEAN-CLAUDE HALLE, MARIE-JOSÉ POUET, FRANÇOIS TERRIER et DANIEL DAVOUST. Can. J. Chem. **64**, 404 (1986).

Les spectres rmn ^{1}H des C adduits zwitterioniques et anioniques résultant de l'addition du dinitro-4,6 benzofuroxanne (DNBF) ou du dinitro-4,6 benzofurazane (DNBZ) au bis(dimethylamino)-1,8 naphthalène, l'éponge à proton PS, ont été enregistrés, à 500 MHz, à basse température, dans le DMF-d_7. Ils indiquent la présence de deux conformères en raison d'une rotation restreinte autour de la liaison C_{sp^3}—C_{sp^2} entre le carbone C-4 de l'éponge à proton et le carbone sp^3 C-7′ de l'entité $DNBF^-$ ou $DNBZ^-$ chargée négativement. La géométrie de ces conformères a été déduite des effets nOe. Les résultats montrent que, dans tous les systèmes, une grande préférence existe pour les conformations moins encombrées de type *s-trans*, dont la population est comprise entre 80 et 90%. Le déplacement chimique du proton *peri* H5 dépend de la conformation : dans les conformères majoritaires où ce proton est proche de H7′, la résonance de H5 est déplacée vers les champs faibles, en accord avec les effets *péri*. Par contre, la résonance de ce proton est déplacée vers les champs forts dans les conformères minoritaires, dans lesquels H5 est situé au voisinage de l'entité $DNBF^-$ ou $DNBZ^-$.

Introduction

We have recently reported that 1,8-bis(dimethylamino)naphthalene, commonly known as the proton sponge (1–3),[2] behaves as a carbon nucleophile towards heteroaromatic super-electrophiles like 4,6-dinitro-benzofuroxan (DNBF) and -benzofurazan (DNBZ), yielding quantitatively the zwitterionic adducts **1**,*H* and **2**,*H* respectively in acetonitrile or dimethyl sulfoxide (Me_2SO) according to eq. [1] (5). The structure of **1**,*H* and **2**,*H* has been unambiguously established on the basis of 100-MHz ^{1}H nmr data. A particular feature was, however, the finding that the resonances of the naphthalenic H-3 and H-5 protons were broad when the nmr spectra were recorded at probe temperature, but became sharper and sharper with increasing temperature. This observation suggested restricted rotation around the C4—C7′, bond of **1**,*H* and **2**,*H* due to steric hindrance (5).

In view of the large but rather uncommon structure of **1**,*H* and **2**,*H*, we found it of interest to inspect in detail the conformations of these species at low temperature by high frequency ^{1}H nmr spectroscopy (500 MHz). During the course of this work, we observed that it was possible to deprotonate the

[1]

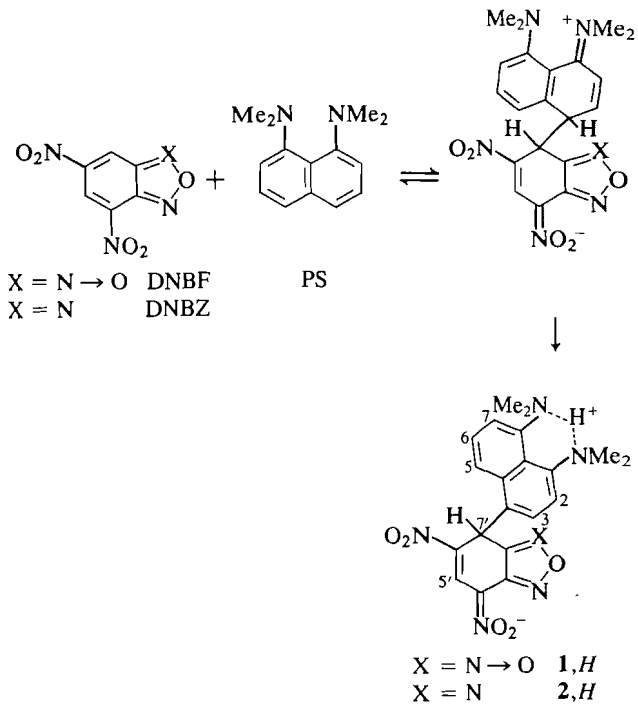

X = N → O DNBF PS
X = N DNBZ

X = N → O **1**,*H*
X = N **2**,*H*

[1]Author to whom correspondence may be addressed.

[2]Proton sponge (PS) is a trademark of Aldrich Chemical Co.

Can. J. Chem. Downloaded from www.nrcresearchpress.com by 80.58.250.72 on 09/07/12
For personal use only.

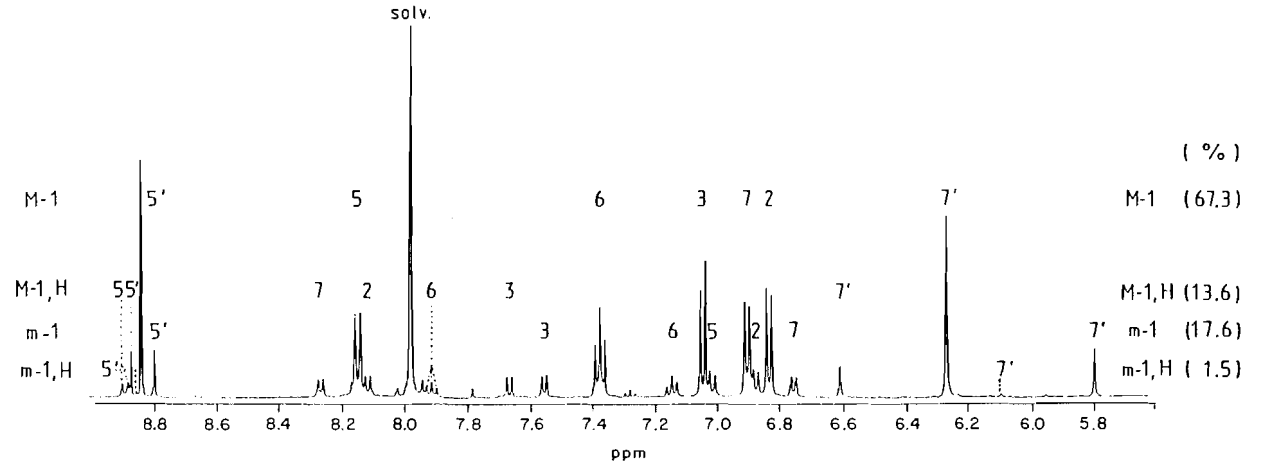

FIG. 1. The 500-MHz ^{1}H nmr spectrum (low field region) recorded at −55°C of the PS–DNBF adduct in DMF-d_7 in the presence of DABCO; the sample contains a mixture of **1** (85%) and **1**,*H* (15%). The assignments of signals belonging to each conformer are indicated on the same horizontal line.

N,*N*-dimethylamino moieties of **1**,*H* and **2**,*H*, which allowed us to extend our study to the anionic species **1** and **2**. In all cases, a full characterization of the conformers has been made by performing low temperature nOe (nuclear Overhauser enhancement) experiments. We now report our results, which also provide new data relative to rotational isomerism around a C_{sp^3}—C_{sp^2} bond in strained naphthalenic derivatives, a problem that has received particular attention in the past few years (6–11).

Results

Syntheses of **1**,*H* and **2**,*H* employed in this study have been previously detailed (5). The isolated zwitterionic adducts were dissolved in deuterated dimethylformamide (DMF-d_7). Conversion of **1**,*H* and **2**,*H* into the anionic forms **1** and **2** was achieved by *in situ* addition of diazabicyclooctane (DABCO) as the base reagent. Evidence for this conversion was provided by nmr spectra, which showed that addition of DABCO results in a decrease in the intensity of the N...$\overset{+}{\text{H}}$...N signal around 19 ppm as well as of other signals of **1**,*H* or **2**,*H*, and the appearance of a new set of signals at higher field. These are consistent with the formation of the anionic adducts **1** and **2**. In particular, the shift variations of the various protons of the naphthalenic moieties are comparable to those observed in a study of the equilibrium between the protonated and neutral forms of PS itself (1). After addition of one equivalent of DABCO to DMF-d_7 solutions of **1**,*H* or **2**,*H*, only the signals due to the anions **1** or **2** were observed.

That DABCO is a sufficiently strong base to deprotonate the proton sponge moieties of the adducts may be surprising in view of the well-known higher basicity of the proton sponge relative to DABCO in protic solvents. Significantly, nmr spectra also reveal that DABCO is more basic than the proton sponge itself in DMF-d_7 and Me_2SO-d_6, indicating that there is an inversion in the relative basicities of these two amines on transfer from water to dipolar aprotic solvents. On this ground and since the nitrogen basicity of **1**,*H* and **2**,*H* is probably lower than that of PS, due to the well-known acidifying effect exerted by the anionic moieties of DNBF and DNBZ adducts (12–14), the conversion of **1**,*H* or **2**,*H* into **1** or **2** by DABCO may be readily understood.

The 500-MHz ^{1}H nmr spectra of **1**,*H*, **2**,*H*, **1**, and **2** recorded at probe temperature (21°C) in DMF-d_7 exhibit broad signals that sharpen on decreasing the temperature. Well-resolved spectra were obtained below −50°C. These showed the presence of two sets of signals with very different intensities, which suggest the existence of two unequally populated conformers for each of the adducts (Fig. 1).

The spectrum of each conformer is expected to exhibit two singlets due to the H5′ and H7′ protons of the DNBF or DNBZ moiety, an AB and an AMX system for the H2, H3 and H5, H6, and H7 protons, respectively, of the naphthalenic ring. Two N-methyl resonances are also expected in the high field region. All these signals were actually observed and fully assigned for the major conformers that we will denote **M-1**,*H*, **M-2**,*H*, **M-1**, and **M-2**. As well, the resonances of the various protons of the minor conformers **m-1** and **m-2** of the anionic adducts could be identified, with the exception of those for the N-methyl groups. This suggests that these resonances are either the same as those for the major conformers or that they overlap with the signals due to the solvent. In the case of the minor conformers **m-1**,*H* and **m-2**,*H* of the zwitterionic adducts, only the signals of the protons belonging to the DNBF or DNBZ moiety could be observed, despite the high frequency used for this study.

Assignment of the signals was deduced from double resonance experiments. Thus, irradiation of the triplet due to the H6 proton allowed the identification of the two doublets belonging to the AMX naphthalenic system. Similarly, the AB system due to the H2 and H3 protons was identified by irradiating the A or B doublet.

Identification of the conformers was deduced from low temperature nOe experiments. The nOe difference spectra of the major conformers of the zwitterionic adducts **M-1**,*H* and **M-2**,*H* recorded while irradiating the H7′ resonance exhibited a 30% enhancement of the A part of the AMX system. Similarly, irradiation of the H7′ resonance of the major conformers of the anionic adducts **M-1** and **M-2** gave a 20% nOe enhancement of the A part of the AMX system. These results demonstrate that the low field A part of the AMX systems is due to H5 and that this proton is spatially close to H7′ in the conformers **M-1**,*H*, **M-2**,*H*, **M-1**, and **M-2**.

Despite the low population of the minor conformers **m-1** and **m-2**, nOe difference spectra show that irradiation of H7′ results in an appreciable enhancement of the low field part of the AB

Can. J. Chem. Downloaded from www.nrcresearchpress.com by 80.58.250.72 on 09/07/12
For personal use only.

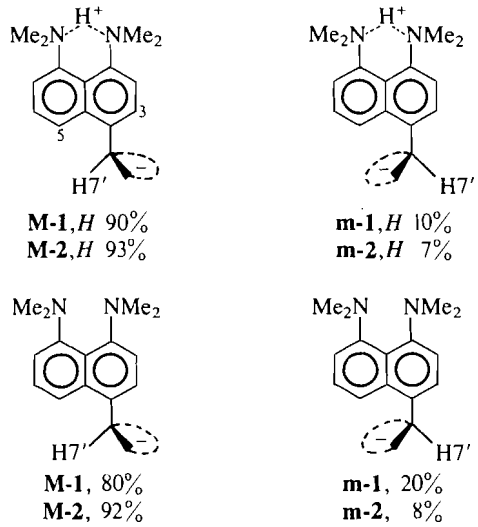

system. This effect indicates that H3 is deshielded relative to H2 and reveals that H3 lies in the vicinity of H7′ in the minor conformation of the anionic adducts.

Although the nOe experiments were carried out at −55°C, the temperature was not low enough to avoid spin saturation transfer, and small enhancements due to this effect were also observed. Thus, in the case of the conformer **M-1**, a small enhancement (~4%) was observed on the A part of the AB system, indicating that H3 is less shielded than H2, as found in the corresponding minor conformer **m-1**. Similarly, experiments involving **m-1** or **m-2** resulted in a small enhancement of one of the doublets belonging to the AMX system, which was therefore assigned to H5. This spin saturation transfer was also very useful to confirm the assignment of the H7′ signal of the minor conformers **m-1**,*H* and **m-2**,*H* whose naphthalenic protons could not be identified.

The various nmr data are summarized in Tables 1 and 2, which refer to the DNBF and DNBZ systems, respectively. For purpose of comparison, the nmr spectra of neutral and protonated forms of the proton sponge, i.e., PS and PSH^+, were recorded under similar experimental conditions as those used for the adducts. The results are given in Table 3.

Discussion

Preferred conformations around the C4—C7′ bond

The low temperature spectra indicate the presence of only two conformers in the anionic and zwitterionic adducts formed in both the DNBF–PS and DNBZ–PS systems. All major conformers have the same geometry, with the H5 proton located in the vicinity of the H7′ proton bonded to the sp^3 carbon of the adducts. This means that the negatively charged DNBF or DNBZ moiety is removed from the naphthalenic system. By analogy with the situation found in enol ethers, such a geometry can be referred to an *s-trans* conformation. In contrast, the geometry of the minor anionic conformers would be of the *s-cis* type since the $DNBF^-$ or $DNBZ^-$ moiety lies on the same side as the naphthalenic ring relative to the C4—C7′ bond. Although the naphthalenic protons of the minor zwitterionic conformers **m-1**,*H* and **m-2**,*H* could not be identified, it is reasonable to assume that they adopt a geometry similar to that of their anionic analogs.

The 180° rotation around the C4—C7′ bond has a marked influence on the chemical shifts of the naphthalenic protons. It is generally observed that the H8 proton in the *peri* position is deshielded in 1-substituted naphthalenic derivatives (15, 16). Such a situation is actually observed in the major conformers **M-1**,*H*, **M-2**,*H*, **M-1**, and **M-2**, in which the *peri*-like proton H5 is spatially close to H7′. In contrast, H5 undergoes a significant upfield shift (>1 ppm) in the minor conformers **m-1** and **m-2**, in which it is far away from the H7′ proton but close to the $DNBF^-$ or $DNBZ^-$ moieties. An opposite sequence is observed for H3; this proton is more shielded in the *s-trans* major conformers than in the *s-cis* minor ones: in these instances, H3 is the naphthalenic proton, which is the most deshielded. Finally, it is interesting to point out that an upfield shift is observed for

TABLE 1. ^1H nuclear magnetic resonance data for the major and minor conformers of the adducts **1**,*H* and **1** in DMF-d_7 at 218 K

	M-1,*H*	**M-1**	Δδ	**m-1**,*H*	**m-1**
δ_{H^+}	19.34_6				
$\delta_{H5'}$	8.87_6	8.84_4	0.03_2	8.86	8.80_2
$\delta_{H7'}$	6.61_4	6.27_4	0.34	6.10_5	5.79_8
δ_{H2}	8.12_2	6.83_6	1.28_6		6.88
δ_{H3}	7.66_9	7.04_7	0.62_6		7.55_9
δ_{H5}	8.89_6	8.15_3	0.74_3		7.01_8
δ_{H6}	7.91_6	7.37_6	0.54_0		7.14_7
δ_{H7}	8.27_1	6.90_8	1.36_3		6.75_8
δ_{NMe_2}	3.23_6 3.16_2	2.61_0 2.59_3	0.62_6 0.56_9		
J_{23}	8.0_5	8.0_5			8.0
J_{56}	8.7	8.7			8.7
J_{67}	7.5	7.5			7.5

TABLE 2. ^1H nuclear magnetic resonance data for the major and minor conformers of the adducts **2**,*H* and **2** in DMF-d_7 at 218 K

	M-2,*H*	**M-2**	Δδ	**m-2**,*H*	**m-2**
δ_{H^+}	19.42				
$\delta_{H5'}$	9.17_7	9.13_7	0.04		8.94_5
$\delta_{H7'}$	7.02_9	6.66_5	0.36_4	6.53	6.20_3
δ_{H2}	8.17_7	6.85_4	1.32_3		6.98_4
δ_{H3}	7.63_9	7.08_5	0.55_4		7.71
δ_{H5}	9.06_9	8.27_1	0.79_8		7.00_5
δ_{H6}	8.08_1	7.55_1	0.53		7.15
δ_{H7}	8.41_5	7.06_1	1.35_4		6.81_4
δ_{NMe_2}	3.29_2 3.25_2	2.70_1 2.63_1	0.59_1 0.62_1		
J_{23}	8.0	8.0			8.0
J_{56}	8.9	8.5			8.5
J_{67}	7.6	7.6			7.4

TABLE 3. ^1H nuclear magnetic resonance data for the protonated and neutral forms of the proton sponge in DMF-d_7 at 218 K

	PS,H^+	PS	Δδ
δ_{H^+}	19.01_4		
δ_{H2}	8.29_9	7.00_6	1.29_3
δ_{H3}	7.85_3	7.37_9	0.47_4
δ_{H4}	8.25_5	7.47_4	0.78_1
J_{23}	7.3_1	7.4_6	
J_{34}	8.0_3	8.2_4	

Can. J. Chem. Downloaded from www.nrcresearchpress.com by 80.58.250.72 on 09/07/12
For personal use only.

H5 or H3 only in the conformers where H5 or H3 is located above the $DNBF^-$ or $DNBZ^-$ moieties; this suggests a significant ring current in the negatively charged heterocyclic systems.

Significant nuclear Overhauser enhancements were observed for H5 in the *s-trans* major conformers and for H3 in the *s-cis* minor conformers, i.e., for the deshielded naphthalenic proton located in the vicinity of H7′. This situation is somewhat reminiscent of that observed in a recent study of imidazole adducts of 1,3,5-trinitrobenzene (TNB) (17). In this series, it was observed that the imidazolic and methyl protons are more shielded in the adducts than in the imidazoles, except for the methyl groups adjacent to a $N\text{-}TNB^-$ or $C\text{-}TNB^-$ moiety, which are deshielded relative to the parent imidazole. On the basis of nOe experiments, the deshielded methyl groups were shown to be spatially close to the H1′ or H1″ protons bonded to the sp^3 carbon of the TNB^- moiety, as depicted in structures **3**, **4**, and **5**. As previously suggested, such a deshielding effect is probably related to a proximity effect (18, 19).

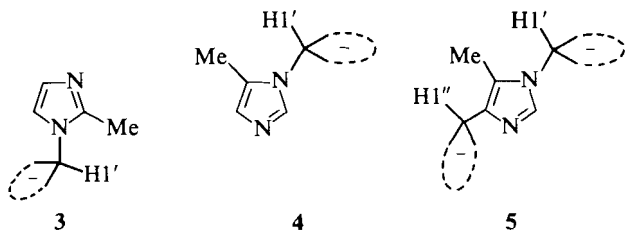

3 4 5

Although X-ray structure determinations have shown that the deformation of the naphthalenic system is greater in the neutral than in the protonated form of PS (20–22), there is no marked difference in the population of the major and minor conformers of the various anionic and zwitterionic DNBF and DNBZ adducts. In all systems, there is a large preference for the less-strained *s-trans* conformation whose population lies between 80 and 93%.

Hindered rotation around a $C_{sp^3}—C_{sp^2}$ bond has been reported in 9-(1-naphthyl) fluorenes and 1-neopentyl naphthalene and found to result in barriers of 18 and 5.15 kcal mol^{-1}, respectively (6, 7, 11). Clearly, there is some structural similarity between these molecules and our adducts but, due to the very different populations of the major and minor conformers involved in the coalescence process, a reliable estimation of the corresponding barriers is not straightforward, even at 500 MHz. To be noted, however, is that molecular mechanics calculations carried out by Anderson and Barkel (11) have shown that the *peri* interaction is of crucial importance in the barrier measured for 1-neopentyl naphthalene. It is likely that this factor also plays a significant role in the PS adducts as well as in 9-(1-naphthyl) fluorenes.

Protonation shifts

The coupling constants observed for the naphthalic protons in the various adducts show a similar trend, i.e., $J_{56} > J_{67}$. This is consistent with literature data for naphthalene (23, 24) and monosubstituted naphthalenes (25) as well as with predictions based on bond order. This also implies that J_{34} is greater than J_{23} in the case of PS and PSH^+, which agrees with results reported by Alder *et al.* for PS but not for PSH^+ (1).

The effect of protonation of the dimethylamino groups on the chemical shift of the naphthalenic protons may be measured by the equation:

$$\Delta\delta_i = \delta_i^{BH^+} - \delta_i^{B}$$

where BH^+ refers to PSH^+ or the zwitterionic adducts and B refers to PS or the anionic adducts. Comparison of the $\Delta\delta$ values in Tables 1–3 shows that the protonation shifts are very similar for PS and the major conformers of the adducts **1** and **2**. Although the positive charge is shared between two NMe_2 groups in our systems, the effect of the protonation on the *ortho* and *meta* protons is comparable to that observed by Castellano *et al.* in a study of the quaternization of *N,N*-dimethylaniline (4): $\Delta\delta_{ortho} \sim 1.39$ ppm, $\Delta\delta_{meta} \sim 0.57$ ppm. In contrast, our $\Delta\delta$ values for the *para* protons ($\Delta\delta_{para} \sim 0.7$ ppm) are weaker than the $\Delta\delta$ value reported in the *N,N*-dimethylaniline system ($\Delta\delta_{para} \sim 1$ ppm). Since the effect of the positive charge on the NR_3^+ groups is essentially to induce an inductive polarization of the π electrons in the aromatic ring(s) (4), this result is in accord with the weaker interaction between the nitrogen lone pairs and the naphthalenic ring in the neutral proton sponge moieties and therefore a weaker change in electron density at the *para* position on protonation of the N atoms. This conclusion is consistent with the known geometry of PS in the solid state (20).

Conclusion

The study has shown that the various carbon-bonded adducts resulting from the addition of the highly electrophilic DNBF and DNBZ to the C-4 carbon of the proton sponge exist as a mixture of two unequally populated conformers. Low-temperature nmr spectra indicate the existence of a twofold barrier, likely due to steric interaction between the naphthalenic *peri* proton and the negatively charged $DNBF^-$ or $DNBZ^-$ moiety. The trisubstituted nature of the naphthalenic rings in the adducts has allowed a complete assignment of the naphthalenic protons in the various conformers.

Experimental

Samples of **1**,*H* and **2**,*H* were prepared as previously described (5). About 5 mg of **1**,*H* or **2**,*H* was dissolved in 0.5 mL of DMF-d_7 (Aldrich, 99% ^2H or SST, 99.5% ^2H). These solutions were centrifuged and deoxygenated by bubbling argon just before running the nmr spectra.

Diazabicyclo octane, DABCO (Aldrich), was sublimed before use. About 12 mg of DABCO was dissolved in 0.5 mL of DMF-d_7. Increasing amounts of this DABCO solution were added to those of the zwitterionic adducts of **1**,*H* or **2**,*H* to generate the anionic adducts **1** or **2**.

The nmr spectra were run at 500 MHz on a Bruker WM 500 spectrometer equipped with an ASPECT 2000 computer. Acquisition parameters: pulse width, 4 μs (30°); spectral width, 10 000 Hz; memory size, 32 K; digital resolution, 0.6 Hz/point.

The nOe difference spectra were run using the following parameters: relaxation delay, 3.0 s; irradiation time, 1.0 s; acquisition time without irradiation, 1.6 s.

Peak positions were measured relative to the traces of CH_3CN or THF used during the synthesis of **1**,*H* or **2**,*H*, and TMS was added to the nmr tube after the low temperature experiments to determine the δ values of these solvents relative to internal TMS.

1. (*a*) R. W. Alder, P. Bowman, W. R. Steel, and D. R. Winterman. Chem. Commun. 723 (1968); (*b*) R. W. Alder and J. E. Anderson. J. Chem. Soc. Perkin Trans. 2, 2086 (1973).
2. A. Awwal and F. Hibbert. J. Chem. Soc. Perkin Trans. 2, 1589 (1977).
3. R. L. de Groot and D. J. Sikkema. Recl.: J. R. Neth. Chem. Soc. **95**, 10 (1976).
4. S. Castellano, C. Sun, and R. Kostelnik. Tetrahedron Lett. 5205 (1967).

Can. J. Chem. Downloaded from www.nrcresearchpress.com by 80.58.250.72 on 09/07/12
For personal use only.

5. F. TERRIER, J. C. HALLE, M. J. POUET, and M. P. SIMONNIN. J. Org. Chem. **51**, 409 (1986).
6. T. H. SIDDALL and W. E. STEWART. J. Org. Chem. **34**, 233 (1969).
7. K. D. BARTLE, P. M. G. BAVIN, D. W. JONES, and R. L'AMIE. Tetrahedron, **26**, 911 (1970).
8. J. E. ANDERSON, R. W. FRANCK, and W. L. MANDELLA. J. Am. Chem. Soc. **94**, 4608 (1972).
9. F. A. L. ANET, D. DONOVAN, U. SJOSTRAND, F. COZZI, and K. MISLOW. J. Am. Chem. Soc. **102**, 1748 (1980).
10. W. D. HOUNSHELL, F. A. L. ANET, F. COZZI, J. R. DAMEWOOD, C. A. JOHNSON, U. SJOSTRAND, and K. MISLOW. J. Am. Chem. Soc. **102**, 5941 (1980).
11. J. E. ANDERSON and D. J. D. BARKEL. J. Chem. Soc. Perkin Trans. 2, 1053 (1984), and quoted references.
12. F. TERRIER, F. MILLOT, and W. P. NORRIS. J. Am. Chem. Soc. **98**, 5883 (1976).
13. F. TERRIER. Chem. Rev. **82**, 77 (1982).
14. F. TERRIER, A. P. CHATROUSSE, Y. SOUDAIS, and M. HLAIBI. J. Org. Chem. **49**, 4176 (1984).
15. G. O. DUDEK. Spectrochim. Acta, **19**, 691 (1963).
16. F. GOBERT, S. COMBRISSON, and N. PLATZER. Tetrahedron, **30**, 2919 (1974).
17. M. P. SIMONNIN, J. C. HALLE, F. TERRIER, and M. J. POUET. Can. J. Chem. **63**, 866 (1985).
18. T. W. MARSHALL and J. A. POPLE. Mol. Phys. **3**, 339 (1960).
19. C. G. CARDINAS. Tetrahedron Lett. 4013 (1969).
20. H. EINSPAHR, J. B. ROBERT, R. E. MARSH, and J. D. ROBERTS. Acta Crystallogr. Sect. B, **29**, 1611 (1973).
21. D. E. FENTON, M. R. TRUTER, and B. L. VICKERY. Chem. Commun. 93 (1971).
22. M. R. TRUTER and B. L. VICKERY. J. Chem. Soc. Dalton Trans. 395 (1972).
23. J. B. PAWLICZEK and H. GUENTHER. Z. Naturforsch. B: Anorg. Chem. Org. Chem. **24**, 1068 (1969).
24. J. B. PAWLICZEK and H. GUENTHER. Tetrahedron, **26**, 1755 (1970).
25. V. LUCCHINI and P. R. WELLS. Org. Magn. Reson. **8**, 137 (1976).

Can. J. Chem. Downloaded from www.nrcresearchpress.com by 80.58.250.72 on 09/07/12
For personal use only.

Uranium(IV) trifluoromethanesulfonate and some ternary uranium(IV) trifluoromethanesulfonates

MADANMOHAN S. GILL, ANIL K. SETHI, AND RAJENDRA D. VERMA[1]
Department of Chemistry, Panjab University, Chandigarh-160 014, India

Received February 17, 1986[2]

MADANMOHAN S. GILL, ANIL K. SETHI, and RAJENDRA D. VERMA. Can. J. Chem. **65**, 409 (1987).

$U(SO_3CF_3)_4$ and $M^{II}U^{IV}(SO_3CF_3)_6$, M = Mg, Mn, Fe, Zn, have been prepared by the reaction of their respective trifluoroacetates with HSO_3CF_3 acid in CF_3COOH medium at room temperature. Infrared data indicate bidentate bridging $—SO_3CF_3$ groups in these compounds. Magnetic moments show the presence of uranium(IV) species. Diffuse reflectance spectra suggest six coordinate uranium(IV) although the presence of possible eight or higher coordinate uranium(IV) cannot be ruled out. X-ray diffraction studies reveal them to be definite entities.

MADANMOHAN S. GILL, ANIL K. SETHI et RAJENDRA D. VERMA. Can. J. Chem. **65**, 409 (1987).

Operant à température ambiante et dans un milieu de CF_3COOH, on a préparé les dérivés $U(SO_3CF_3)$ et $M^{II}U^{IV}(SO_3CF_3)_6$, dans lesquels M = Mg, Mn, Fe, Zn, en faisant réagir leurs trifluoroacétates respectifs avec du HSO_3CF_3. Les données de l'infrarouge indiquent que, dans ces composés, les groupements $—SO_3CF_3$ forment des ponts bidentates. Les moments magnétiques démontrent la présence d'espèces uranium(IV). Les spectres de réflectance diffuse suggèrent que l'uranium(IV) est hexacoordonné; toutefois, on ne peut pas éliminé la possibilité que les degrés de coordination de l'uranium(IV) soient égaux à huit ou plus. Des études par diffraction des rayons-X révèlent qu'il s'agit d'entités bien definies.

[Traduit par la revue]

Introduction

Trifluoromethanesulfonic acid and fluorosulfuric acid are isostructural and of comparable strength. The exact order of their acid strength is, however, the subject of discussion. A large number of derivatives are known for both acids (1–4). Uranium(IV) (5, 6) and uranium(V) fluorosulfates (7, 8) have been reported. $UO_2(SO_3F)_2$ and $UO(SO_3F)_2$ are also known (6). Whereas a large number of ternary fluorosulfates, such as $MU(SO_3F)_6$, M = Mg, Zn (6), $KAu(SO_3F)_4$ (9, 10), $K_2Pt(SO_3F)_6$ (11), $Ag^{II}Pt^{IV}(SO_3F)_6$ and $Ag^{II}Sn^{IV}(SO_3F)_6$ (12), $M_2[Mn(SO_3F)_5]$, M = K, Cs (13), $M_2[Pd(SO_3F)_6]$, M = Cs^+, NO^+, ClO_2^+, $M[Pd(SO_3F)_6]$, M = Ba^{II}, Pd^{II}, and $Pd^{II}[M(SO_3F)_6]$, M = Pt^{IV} and Sn^{IV} (14) are known, only a few trifluoromethanesulfonates, viz., $M^{II}UO_2(SO_3CF_3)_4$, M^{II} = Mg, Ba, Zn (15), and $K_2[Sn(SO_3CF_3)_6]$, $K[Sn(SO_3CF_3)_5]$, $Cs_2[Pt(SO_3CF_3)_6]$, $Pd^{II}[Pd^{IV}(SO_3CF_3)_6]$, and $Mn[Sn(SO_3CF_3)_6]$ (16), $Cs[Au(SO_3CF_3)_4]$ (17), and $Sn^{II}[Sn^{IV}(SO_3CF_3)_6]$ (18) have been reported. In this article, we report the preparation and characterization of $U(SO_3CF_3)_4$ and $M^{II}U^{IV}(SO_3CF_3)_6$, M = Mg, Mn, Fe, and Zn.

Experimental

$U(O_2CCH_3)_4$ and $M^{II}U^{IV}(O_2CCH_3)_6$, M = Mg, Mn, Fe, Zn were prepared according to literature methods (19). AR grade $UO_2(O_2CCH_3)_2$, $Zn(O_2CCH_3)_2$, $Mg(O_2CCH_3)_2$ and the metals were used as such. Solvents were dried and distilled before use. Trifluoromethanesulfonic acid (Aldrich) was distilled in an atmosphere of dry nitrogen. $U(O_2CCF_3)_4$ and $M^{II}U^{IV}(O_2CCF_3)_6$ were prepared by refluxing the corresponding acetates with trifluoroacetic acid.

In a typical preparation, a slight excess of trifluoromethanesulfonic acid than required on the basis of stoichiometry was added to a known amount (2–3 mmol) of the corresponding trifluoroacetate in trifluoroacetic acid (8–10 mL) and the contents were stirred at room temperature under dry N_2 atmosphere for 3–5 h. In case of $U(SO_3CF_3)_4$ and $Zn^{II}U^{IV}(SO_3CF_3)_6$ clear light green solutions were obtained, which on keeping overnight resulted in the separation of green solids. In case of $Mn^{II}U^{IV}(SO_3CF_3)_6$, a viscous light green jelly-like mass was obtained, which was triturated with petroleum ether to obtain a crystalline compound. In case of $Mg^{II}U^{IV}(SO_3CF_3)_6$ and $Fe^{II}U^{IV}(SO_3CF_3)_6$, solids remained. In all these cases, solids obtained were filtered under positive pressure of dry N_2 gas, washed with trifluoroacetic acid, followed by dry petroleum ether and finally dried *in vacuo*. The yields in all cases exceed 90%.

TABLE 1. Analytical data

Compound	% Found (calcd.) M	U	S	F	C
$U(SO_3CF_3)_4$	—	28.39 (28.53)	15.27 (15.34)	27.24 (27.33)	5.68 (5.75)
$Mg^{II}U^{IV}(SO_3CF_3)_6$	1.97 (2.10)	20.49 (20.58)	16.52 (16.60)	29.49 (29.57)	6.18 (6.22)
$Mn^{II}U^{IV}(SO_3CF_3)_6$	4.55 (4.62)	19.97 (20.05)	16.09 (16.17)	28.75 (28.81)	6.01 (6.06)
$Fe^{II}U^{IV}(SO_3CF_3)_6$	4.66 (4.70)	19.94 (20.03)	16.10 (16.16)	28.72 (28.29)	5.98 (6.06)
$Zn^{II}U^{IV}(SO_3CF_3)_6$	5.33 (5.45)	19.76 (19.87)	15.94 (16.03)	28.49 (28.56)	5.93 (6.01)

Sulfur was determined as $BaSO_4$ after fusing a known weight of the compound with fusion mixture. Fluorine was determined as described (20). Uranium, magnesium, manganese, iron, and zinc were estimated as described (19). Carbon and hydrogen were determined microanalytically by the microanalyst of the department. The analytical results are given in Table 1.

The ir spectra of the compounds were recorded as Nujol and hexachlorobutadiene mulls between silver chloride plates using a Perkin-Elmer 621 spectrophotometer. Diffuse refluctance spectra of powdered compounds were recorded on a Unicam SP-735 spectrophotometer using freshly sublimed MgO as a reflecting reference (courtesy I.I.T., New Delhi). X-ray powder diffraction data were obtained from a Philips X-ray diffraction apparatus model PW 1729 using CuK radiation and Ni filter with incorporated facilities for scintillation counting. The samples were run from 4° to 70° with 10°/min rotation. Magnetic susceptibilities were determined at room temperature using Gouy's method. $Hg[Co(NCS)_4]$ was used as calibrant. All manipulations were carried out in a dry box having dry N_2 gas atmosphere.

[1]To whom all correspondence should be addressed.
[2]Revision received September 25, 1986.

Can. J. Chem. Downloaded from www.nrcresearchpress.com by 80.58.250.72 on 09/07/12
For personal use only.

Can. J. Chem. Downloaded from www.nrcresearchpress.com by 80.58.250.72 on 09/07/12
For personal use only.

TABLE 2. X-ray powder diffraction data, d(Å) of $Mg(SO_3CF_3)_2$, $Mg^{II}U^{IV}(SO_3CF_3)_6$, and $U(SO_3CF_3)_4$

$Mg(SO_3CF_3)_2$	$Mg^{II}U^{IV}(SO_3CF_3)_6$	$U(SO_3CF_3)_4$
10.4296 vs	10.3470 s	15.8638 w
8.9888 vw	4.7469 vs	11.6882 vs
4.2311 vs	4.5357 s	6.3513 w
3.8572 s	4.3633 m	5.9358 s
3.8395 vs	4.3467 m	4.4563 s
3.8260 vs	4.2274 vs	4.4319 vs
2.5900 vs	3.8219 vs	4.0068 m
2.5376 m	3.1856 m	2.3448 w
2.4610 w	2.9920 s	1.5462 vw
1.9820 m	2.7915 m	1.5442 w
1.9576 vw	2.5887 vs	1.5401 w
1.9433 vw	2.5427 m	1.5375 m
1.4311 vw	2.2780 s	—

Results and discussion

Inorganic trifluoromethanesulfonate derivatives have largely been prepared by solvolysis (17, 21, 22) of the general type:

$$MX_n + nHSO_3CF_3 \rightarrow M(SO_3CF_3)_n + nHX$$

X = F, Cl, Br, SO_3F, carboxylates etc.

To a lesser extent, salts like $AgSO_3CF_3$ in metathetical reactions have also been used. We have observed (6, 15) the facile displacement of trifluoroacetate group at ambient temperature by SO_3X group, X = F, CF_3; in the preparation of ternary fluorosulphates or trifluoromethanesulfonates. Trifluoroacetates on the other hand are easily obtainable from the corresponding acetates by "acid exchange" method. In our opinion, solvolysis of trifluoroacetates in trifluoroacetic acid medium is a convenient method for the preparation of simple inorganic and ternary fluorosulphates as well as trifluoromethanesulfonates.

The reactions of $M^{II}U^{IV}(O_2CCF_3)_6$ with HSO_3CF_3 in trifluoroacetic acid medium may be represented as

$$M^{II}U^{IV}(O_2CCF_3)_6 + 6HSO_3CF_3 \rightarrow M^{II}U^{IV}(SO_3CF_3)_6 + 6CF_3COOH$$

These compounds are light green, hygroscopic solids and are insoluble in usual non-coordinating organic solvents. The compounds do not melt up to 200°C.

X-ray powder diffraction spectra of $Mg^{II}U^{IV}(SO_3CF_3)_6$, $Mg(SO_3CF_3)_2$, and $U(SO_3CF_3)_4$ gave well-defined diffraction lines (Table 2). The observed d(Å) values of $Mg^{II}U^{IV}(SO_3CF_3)_6$ are found to be different from those of $Mg(SO_3CF_3)_2$ or $U(SO_3CF_3)_4$. This excludes the possibility of the presence of free $Mg(SO_3CF_3)_2$ or $U(SO_3CF_3)_4$ in $Mg^{II}U^{IV}(SO_3CF_3)_6$ and suggests that the latter is real compound rather than a 1:1 stoichiometric mixture of the components. Similar X-ray diffraction studies were carried out on $M^{II}U^{IV}(O_2CCF_3)_6$, which were used as precursors for the corresponding trifluoromethanesulfonates.

Infrared spectra of $U(SO_3CF_3)_4$ and $Mg^{II}U^{IV}(SO_3CF_3)_6$ along with those of $Ag(SO_3CF_3)_2$ (17) and $(CH_3)_3SnSO_3CF_3$ (24) with their tentative assignments are given in Table 3. Six fundamental modes of vibrations ($3A'$ and $3E$ modes, all ir and Raman active) are observed for SO_3X anion (X = Cl, F, CH_3, CF_3, or CF_3SO_3) of C_{3v} symmetry. Covalent interactions result

TABLE 3

(*a*) Infrared spectral data (cm^{-1}) of $U(SO_3CF_3)_4$ and $Mg^{II}U^{IV}(SO_3CF_3)_6$ along with $Ag(SO_3CF_3)_2$ and $(CH_3)_3SnSO_3CF_3$ with their tentative assignments

$U(SO_3CF_3)_4$	$Mg^{II}U^{IV}(SO_3CF_3)_2$	$Ag(SO_3CF_3)_2$	$(CH_3)_3SnSO_3CF_3$	Tentative assignments
1300 s, b 1260 s	1305 s, b 1260 s	1310 m, sh 1274 vs	1319 s, b	νSO_3
1230 m	1225 w	1222 s, sh 1202 vs	1226 vs	νCF_3
1175 s	1180 s	1140 ms, sh 1122 vs	1170 s, b 1145 s	νCF_3
1030 vs	1030 vs	1035 s, b	1026 s	νSO_3
805 vw 760 w	805 vw 770 w	775 w	771 m	$\nu S—C$
620 w, b	630 w, b	632 ms 610 m, sh	633 ms	δSO_3
570 w	570 w	592 m 580 m, sh	577 ms	δCF_3
505 s	515 s	522 vs 455 vw, b	530 m, sh 513 ms	δSO_3

(*b*) Infrared spectra of $Mn^{II}U^{IV}(SO_3CF_3)_6$, $Fe^{II}U^{IV}(SO_3CF_3)_6$, and $Zn^{II}U^{IV}(SO_3CF_3)_6$

Compound	Infrared spectral data
$Mn^{II}U^{IV}(SO_3CF_3)_6$	1305(s, b), 1260(s), 1235(w), 1165(w), 1035(vs), 765(w), 630(w, b), 580(vw), 515(s)
$Fe^{II}U^{IV}(SO_3CF_3)_6$	1300(s, b), 1260(s, b), 1225(w), 1175(s), 1030(vs), 805(w), 770(w), 630(w), 565(w, b), 510(s)
$Zn^{II}U^{IV}(SO_3CF_3)_6$	1300(s, b), 1260(s), 1230(m), 1170(s), 1030(s), 800(w), 775(w), 625(s, b), 580(v, w), 500(s)

Can. J. Chem. Downloaded from www.nrcresearchpress.com by 80.58.250.72 on 09/07/12
For personal use only.

in splitting of all E modes. As a consequence, the number of fundamental modes increase from six to nine for covalently bonded SO_3X group. Vibrational assignments in trifluoromethanesulfonates follow the same pattern as that in fluorosulfates, but some ambiguity does exist in certain vibrational assignments due to the fact that sulfur–oxygen and carbon–fluorine vibrations of identical symmetry (A' and E) are found in the same spectral region (23) resulting in coupling. In interpreting the ir spectra of $M^{II}U^{IV}(SO_3CF_3)_6$ emphasis has been placed on the identification of the functionality of SO_3CF_3 group recognizable from the number and position of sulfur–oxygen stretching frequencies. The number of bands in the ir spectra of these compounds indicate lowering of the symmetry of SO_3CF_3 group from C_{3v} to $\hat{c}_s$. The νS—O modes around 1300 sb, 1125 s, and 1030 cm^{-1} suggest the presence of bridging bidentate SO_3CF_3 groups when compared to the corresponding SO_3CF_3 stretching bands in $Ag(SO_3CF_3)_2$ (17), $(CH_3)_3SnSO_3CF_3$ (24), and $(CH_3)_2Sn(SO_3CF_3)_2$ (25). In $(CH_3)_3SnSO_3CF_3$ and $(CH_3)_2Sn(SO_3CF_3)_2$ bridging bidentate SO_3CF_3 groups have been proposed on the basis of ^{119}Sn Mössbauer spectra and X-ray diffraction studies and a structural study on the analogous compound $(CH_3)_2Sn(SO_3F)_2$ (26). Bands around 1170–1235 cm^{-1} may be attributed to νCF_3. Weak bands around 760–775 cm^{-1} are due to νS—C. The δSO_3 (510 and 625 cm^{-1}) and δCF_3 (570 cm^{-1}) also agree with the corresponding modes in $Me_3SnSO_3CF_3$.

Diffuse reflectance spectra of uranium(IV) complexes have been studied (27) and the complexes have been divided into three classes on the basis of band intensities on the arbitrary Beckman scale of 0–2. The "weak" intensity spectra occur in six coordinate uranium(IV) complexes, whereas a "strong" and "medium" intensity spectra appear where the coordination number is higher than six. The diffuse reflectance spectra of $U(SO_3CF_3)_4$, $Mg^{II}U^{IV}(SO_3CF_3)_6$, and $Zn^{II}U^{IV}(SO_3CF_3)_6$ have been recorded. The spectra are usually not well resolved. Almost similar but not completely identical bands (28) have been observed around 400, 450, 525, 575, 700, and 1300 nm. Octahedral uranium(IV) complexes exhibit weak bands in the region 400, 590, and 630 nm as well as a weak band at 450 nm (29). The latter also appears in the spectra of 8-coordinate uranium(IV) species (30). Bands observed in the present compounds suggest six coordinate uranium(IV) species although the possibilities of eight or higher coordinate uranium(IV) cannot be ruled out because a band at 450 nm also appears in the spectra of eight coordinate uranium(IV) complexes.

The magnetic moments of the compounds having uranium(IV) centers are reported in the range 3.0–3.8 BM, having $5f^2$ configuration (31–33). The magnetic moments of the compounds at 297 K ($U(SO_3CF_3)_4$ = 3.73, $Mg^{II}U^{IV}(SO_3CF_3)_6$ = 3.80, $Mn^{II}U^{IV}(SO_3CF_3)_6$ = 9.58, $Fe^{II}U^{IV}(SO_3CF_3)_6$ = 7.38, $Zn^{II}U^{IV}(SO_3CF_3)_6$ = 3.65 BM) confirm the presence of uranium(IV) species in these compounds and also the presence of Mn^{2+} and Fe^{2+} in $Mn^{II}U^{IV}(SO_3CF_3)_6$ and $Fe^{II}U^{IV}(SO_3CF_3)_6$ according to Pascal's law of additive magnetic susceptibilities (34). Whereas the magnetic moments of these compounds at room temperature confirm the presence of uranium(IV) species, the diffuse reflectance spectra of the compounds studied suggest hexa- or higher coordination around uranium(IV).

In conclusion it may be remarked that conversion of trifluoroacetates to trifluoromethanesulfonates in trifluoroacetic acid medium at room temperature is a convenient synthetic method for the preparation of metal trifluoromethanesulfonates.

Acknowledgement

Thanks are gratefully extended to the CSIR, New Delhi, for the award of S.R.F. to one of us (M.S.G.).

1. A. W. JACHE. Adv. Inorg. Radiochem. **16**, 177 (1974).
2. R. D. HOWELLS and J. D. MCCOWN. Chem. Revs. **77**, 69 (1977).
3. A. A. WOOLF. New Pathways in Inorganic Chemistry. Cambridge University Press, New York. 1968. p. 327.
4. F. AUBKE and D. D. DESMARTEAU. J. Fluorine Chem. Rev. **8**, 73 (1974).
5. L. M. EMME and G. L. GARD. J. Fluorine Chem. **12**, 77 (1978).
6. R. C. PAUL, S. SINGH, and R. D. VERMA. J. Fluorine Chem. **16**, 153 (1980).
7. W. W. WILSON, C. NAULIN, and R. BOUGON. Inorg. Chem. **16**, 2252 (1977).
8. J. P. MASSON, C. NAULIN, P. CHARPIN, and R. BOUGON. Inorg. Chem. **17**, 1858 (1978).
9. K. C. LEE and F. AUBKE. Inorg. Chem. **18**, 389 (1979).
10. K. C. LEE and F. AUBKE. Inorg. Chem. **19**, 119 (1980).
11. K. C. LEE and F. AUBKE. Inorg. Chem. **23**, 2124 (1984).
12. P. C. LEUNG and F. AUBKE. Inorg. Chem. **17**, 1765 (1978).
13. S. P. MALLELA and F. AUBKE. Inorg. Chem. **24**, 2969 (1985).
14. K. C. LEE and F. AUBKE. Can. J. Chem. **57**, 2058 (1979).
15. I. KAPOOR, S. SINGH, and R. D. VERMA. Ind. J. Chem. **25A**, 92 (1986).
16. F. AUBKE. Private communication.
17. P. C. LEUNG, K. C. LEE, and F. AUBKE. Can. J. Chem. **57**, 326 (1979).
18. R. J. BATCHELOR, J. N. R. RUDDICK, J. R. SAMS, and F. AUBKE. Inorg. Chem. **16**, 1414 (1977).
19. D. GRDENIC and B. KORPAR-COLIG. J. Inorg. NucI. Chem. **30**, 1751 (1968).
20. G. H. CADY, R. DEV, and P. V. RADHESHWAR. J. Inorg. Nucl. Chem. **34**, 3913 (1972).
21. C. L. JENKINS and J. K. KOCHI. J. Am. Chem. Soc. **94**, 843 (1972).
22. E. H. ABBOTT, E. S. WOLF, and T. BACKSTROM. J. Coord. Chem. **3**, 255 (1974).
23. E. A. ROBINSON. Can. J. Chem. **39**, 247 (1961).
24. P. A. YEATS, J. R. SAMS, and F. AUBKE. Inorg. Chem. **10**, 1877 (1971).
25. P. A. YEATS, J. R. SAMS, and F. AUBKE. Inorg. Chem. **11**, 2634 (1972).
26. F. H. ALLEN, J. A. LERBSCHER, and J. TROTTER. J. Chem. Soc. A, 2507 (1971).
27. P. GANS, B. J. HATHAWAY, and B. C. SMITH. Spectrochim. Acta, **21**, 1589 (1965).
28. J. L. RYAN. J. Phys. Chem. **65**, 1856 (1961).
29. J. L. RYAN. Inorg. Chem. **3**, 211 (1964).
30. K. W. BAGNALL, D. BROWN, and R. COTTON. J. Chem. Soc. 2527 (1964).
31. C. A. HUTCHISON, JR., and N. ELLIOTT. J. Phys. Chem. **16**, 920 (1948).
32. N. ELLIOTT. Phys. Rev. **76**, 431 (1949).
33. J. K. DAWSON and M. W. LISTER. J. Chem. Soc. 2181 (1950).
34. L. N. MULAY. *In* Treatise on analytical chemistry. Part 1. Vol. 4. *Edited by* I. M. Kolthhoff and P. J. Elving. John Wiley and Sons, Interscience, New York. 1963. p. 1751.

The rapid synthesis of deoxyfluoro sugars using tris(dimethylamino)sulfonium difluorotrimethylsilicate (TASF)[1]

BOGDAN DOBOSZEWSKI, GEORGE W. HAY, AND WALTER A. SZAREK[2]
Department of Chemistry, Queen's University, Kingston, Ont., Canada K7L 3N6

Received March 4, 1986[3]

BOGDAN DOBOSZEWSKI, GEORGE W. HAY, and WALTER A. SZAREK. Can. J. Chem. **65**, 412 (1987).

Deoxyfluoro sugars were synthesized rapidly by the reaction of trifluoromethanesulfonyl derivatives of partially protected sugars with tris(dimethylamino)sulfonium difluorotrimethylsilicate (TASF) under mild conditions. The displacements occurred with inversion of configuration; fluorine has been introduced stereospecifically at each of the secondary alcoholic sites of aldohexopyranosides and in one example of a furanoid system. In some instances unsaturated compounds that contained no fluorine were produced.

BOGDAN DOBOSZEWSKI, GEORGE W. HAY et WALTER A. SZAREK. Can. J. Chem. **65**, 412 (1987).

On a réalisé une synthèse rapide de sucres désoxyfluorés en faisant réagir des dérivés trifluorométhanesulfonylés de sucres partiellement protégés avec du difluorotriméthylsilicate de tris(diméthylamino)sulfonium (TASF), utilisant des conditions douces. Les réactions de déplacement se font avec inversion de configuration; on a pu introduire d'une façon spécifique des atomes de fluor au niveau de chacun des sites alcooliques secondaires des aldohexopyrannosides et dans un exemple de système furannoïde. Dans quelques cas, on a obtenu des composés insaturés qui ne contenaient pas de fluor.

[Traduit par la revue]

Can. J. Chem. Downloaded from www.nrcresearchpress.com by 80.58.250.72 on 09/07/12
For personal use only.

Introduction

The expanding application of deoxyfluoro sugars for the study of carbohydrate metabolism and transport in both normal (1–5) and pathological (6–10) states has stimulated interest in their chemical (11) and biological (1*a*, 2) properties. Furthermore, it has actuated intensive efforts to develop improved methods of synthesis, and especially procedures suitable for the preparation of ^{18}F-labeled carbohydrates for use in medical imaging (12). Included in the approaches taken to this end are addition reactions of such reagents as molecular fluorine (10, 13, 14), xenon difluoride (15–17), and acetyl hypofluoride (18–22), reaction of free hydroxyl groups with (diethylamino)-sulfur trifluoride (23–25), nucleophilic ring-openings with potassium hydrogen fluoride (26–28), and nucleophilic displacement of good leaving groups by a range of fluoride salts (29–34).

We recently reported (35) in preliminary form the rapid, fluoride-ion displacement of carbohydrate triflates using tris-(dimethylamino)sulfonium difluorotrimethylsilicate (TASF) (36), a reagent that previously had been utilized (37) for the synthesis of 1-deoxy-1-fluoro-D-fructose. TASF is a hygroscopic solid, which is freely soluble in a variety of organic solvents in which it acts as an effective fluoride-ion donor when employed under rigorously anhydrous conditions; the relatively brief reaction times (35) are such that it may be of interest for the potential synthesis of ^{18}F-labeled radiopharmaceuticals for positron emission tomography. The scope and utility of the reagent are further delineated in the present report, which provides full details of the results of both the previous (35) and later studies in which TASF has been used to effect the displacement, with inversion of configuration, of triflate groups at each of C-2, C-3, C-4, and C-6 of suitably protected aldohexopyranosides, at C-6 of 1,2:3,4-di-*O*-isopropylidene-α-D-galactose (**10**), and at C-3 of 1,2:5,6-di-*O*-isopropylidene-α-D-allofuranose (**12**).

Results and discussion

The synthetic results have been summarized in Table 1. In most cases the displacement of triflate anion occurred rapidly (≦30 min) at or below reflux temperature; however, in two examples (see Table 1, compounds **4** and **13**) an elimination reaction was found to predominate.

Methyl 4,6-*O*-benzylidene-3-*O*-methyl-β-D-mannopyranoside (**1***a*) (38) was converted into the 2-*O*-triflyl derivative (**1***b*) by reaction with trifluoromethanesulfonic anhydride (39). The reaction of **1***b* with TASF[4] in dichloromethane occurred rapidly in cold solution. Examination of the reaction solution by thin-layer chromatography (tlc) 10 min after the addition of TASF failed to detect the presence of **1***b*. The reaction afforded a 64% yield of methyl 4,6-*O*-benzylidene-2-deoxy-2-fluoro-3-*O*-methyl-β-D-glucopyranoside (**14**), which was identified on the basis of its ^{13}C and ^{19}F nuclear magnetic resonance (nmr) spectra. Of particular diagnostic importance was the observation that the values of the coupling constants $J_{F,1}$ (4.2 Hz), $J_{F,2}$ (49.5 Hz), and $J_{F,3}$ (14.0 Hz) agreed closely with those reported by Adamson *et al.* (40) for 2-deoxy-2-fluoro-β-D-glucose.

The preparation of methyl 3-*O*-benzyl-4,6-*O*-benzylidene-β-D-glucopyranoside was achieved in 20% yield by benzylation of methyl 4,6-*O*-benzylidene-β-D-glucopyranoside (see ref. 41) using tetra-*n*-butylammonium hydrogen sulfate (42) under phase-transfer conditions (41, 43). Oxidation of the product, followed by reduction using sodium borohydride, afforded a high yield of methyl 3-*O*-benzyl-4,6-*O*-benzylidene-β-D-mannopyranoside (**2***a*), from which the 2-*O*-triflyl derivative **2***b* was readily obtained by reaction with triflic anhydride. Compound **2***b* underwent a rapid reaction with TASF at reflux temperature to give two compounds in an approximate ratio of 2.4:1. The main product, obtained in 45% yield, was identified as methyl 3-*O*-benzyl-4,6-*O*-benzylidene-2-deoxy-2-fluoro-β-D-glucopyranoside (**15**) on the basis of the ^{1}H, ^{13}C, and ^{19}F nmr data. The ^{1}Hmr spectrum of **15** exhibited $J_{1,2}$ = 7.5 Hz, and $J_{2,3}$ = 8.0 Hz, values indicative of a *trans* relative configuration of the protons on carbons 1, 2, and 3. Furthermore, as with compound **14**, the values for $J_{F,1}$, $J_{F,2}$, and $J_{F,3}$ corresponded to those reported by Adamson *et al.* (40) for the *gluco* configuration. The minor product (19% yield) tentatively was

[1]For a preliminary report of part of this work, see ref. 35.
[2]Author to whom correspondence may be addressed.
[3]Revision received September 29, 1986.

[4]An approximately 3-fold molar excess of reagent was employed per mole of underivatized hydroxyl group, or triflyl group, in each case.

Can. J. Chem. Downloaded from www.nrcresearchpress.com by 80.58.250.72 on 09/07/12
For personal use only.

assigned the structure of methyl 3-*O*-benzyl-4,6-*O*-benzylidene-2-deoxy-β-D-*erythro*-hex-2-enopyranoside on the basis of its ^{1}Hmr spectrum; this substance was unstable and underwent some decomposition during tlc. Base-catalyzed elimination reactions with triflyl derivatives are uncommon (44, 45), but have been observed in certain furanoid (44, 46) and, very recently, in pyranoid (34*a*,*c*) ring systems (see also Table 1). Eliminations in glycopyranosides occurred (34*a*,*c*) under conditions that decreased the ease of nucleophilic substitution (34*a*, 47).

The reaction of benzyl 3,4,6-tri-*O*-benzyl-2-*O*-trifluoromethanesulfonyl-β-D-mannopyranoside (**3***b*) with TASF, below room temperature, was complete in less than 5 min, to give a low (11%) yield of benzyl 3,4,6-tri-*O*-benzyl-2-deoxy-2-fluoro-β-D-glucopyranoside (**16**), whereas the isomeric α-D-mannopyranoside **4***b* reacted relatively slowly with TASF at room temperature to give a product that did not contain fluorine. The product obtained from **4***b* was unstable and underwent some decomposition during thin-layer or flash chromatography; the ^{1}Hmr spectrum of the product was consistent with the occurrence of an elimination reaction, and the compound was tentatively assigned the structure of **17**. The instability of this product obviated the acquisition of an elemental analysis. The reaction of **3***b* with TASF, which gave rise to **16**, was accompanied by the formation of an unidentified compound; this, by analogy with the reaction of TASF with **2***b* and **4***b*, may possibly be an unsaturated product from a competing elimination reaction.

The reactions of the β-D-glucopyranosides **5***b*, **6***b*, and **7***b* with TASF yielded results that were very different in each case, but which were fully consistent with the current understanding of nucleophilic displacements in carbohydrates (45, 47–49). The less rapid and efficient displacement of triflate anion from **6***b*, as compared with that from **5***b*, may be attributable to the increased steric hindrance occasioned by the introduction of benzyl and 2,2,2-trichloroethyl groups in place of methyl groups. Furthermore, the facile displacement of triflate from C-3 of **7***b* reflects the diminution of the steric and electronic effects that render the displacement of C-2 sulfonates in β-D-glucopyranosides much more difficult (47*b*). It is noteworthy that the product of the relatively difficult reaction of TASF with **6***b* was found to contain, in addition to **19**, two unidentified components, a result that indicates the relative increase in competing reactions as nucleophilic substitution is impeded.

The reaction of methyl 2,3,6-tri-*O*-benzyl-4-*O*-trifluoromethanesulfonyl-β-D-glucopyranoside (**8***b*) with TASF in dichloromethane at reflux temperature was monitored by tlc and was judged to be complete after 20 min, at which point the starting compound (**8***b*) no longer was detectable. The assignment of the *galacto* configuration to the product **21** was based on the nmr data; the values of the coupling constants observed for H-3 and H-4 (2.8 Hz), H-4 and H-5 (~0 Hz) (see ref. 50), H-3 and F-4 (27.5 Hz), H-4 and F-4 (49.8 Hz), and H-5 and F-4 (22.3 Hz) (see ref. 51) were in agreement with those reported in the literature for derivatives of methyl 4-deoxy-4-fluoro-β-D-galactopyranosides.

Methyl 2,3,6-tri-*O*-benzyl-4-*O*-trifluoromethanesulfonyl-α-D-galactopyranoside (**9***b*) was prepared from **9***a* (52) in the manner described for **1***b*. Compound **9***b* reacted with TASF much more rapidly than did **8***b*; the conversion was complete within 10 min after the addition of TASF to a cold solution of **9***b*. The product, methyl 2,3,6-tri-*O*-benzyl-4-deoxy-4-fluoro-α-D-glucopyranoside (**22**), was isolated in 67% yield by flash chromatography. The assignment of the *gluco* configuration to **22** followed from the nmr data. The enhanced ease of displacement of the axially oriented trifloxy group of **9***b*, as compared to that of the equatorially oriented one of **8***b*, is consistent with the suggestion (48) that a *galacto* isomer has a higher ground-state energy than the corresponding *gluco* compound.

The nucleophilic displacement by TASF of a trifloxy group located on a primary carbon atom occurred with great rapidity under mild conditions. Thus, the reaction of 1,2:3,4-di-*O*-isopropylidene-6-*O*-trifluoromethanesulfonyl-α-D-galactopyranose (**10***b*) with TASF was complete in less than 10 min at 0–20°C and afforded a 71% yield of 6-deoxy-6-fluoro-1,2:3,4-di-*O*-isopropylidene-α-D-galactopyranose (**23**) (53). In a similar manner, methyl 2,3-di-*O*-benzyl-4,6-bis-*O*-(trifluoromethanesulfonyl)-β-D-glucopyranoside (**11***b*) reacted rapidly with TASF at reflux temperature to give a 39% yield of methyl 2,3-di-*O*-benzyl-4,6-dideoxy-4,6-difluoro-β-D-galactopyranoside (**24**); this, however, was accompanied by the formation of a slightly smaller amount of a less polar, unidentified compound.

The selective introduction of fluorine into a furanose ring was demonstrated by the reaction of TASF with 1,2:5,6-di-*O*-isopropylidene-3-*O*-trifluoromethanesulfonyl-α-D-allofuranose (**12***b*), which gave a 66% yield of 3-deoxy-3-fluoro-1,2:5,6-di-*O*-isopropylidene-α-D-glucofuranose (**25**) (54). The isomeric triflate **13***b*, having the D-*gluco* configuration, reacted with TASF under the same conditions to give an 83% yield of the elimination product, 3-deoxy-1,2:5,6-di-*O*-isopropylidene-α-D-*erythro*-hex-3-enofuranose (**26**) (55), but no fluorine-containing product was detected.

The above examples have demonstrated the utility of TASF as a useful reagent for the rapid introduction of fluorine into a variety of monosaccharide triflates.

Experimental

Melting points were determined on a Fisher–Johns apparatus and are uncorrected. Optical rotations were measured with a Perkin–Elmer model 141 automatic polarimeter using chloroform as solvent in a 1-dm tube at 23 ± 3°C. The ^{1}Hmr spectra were recorded on a Bruker AM400 spectrometer at 400 MHz; ^{13}Cmr and ^{19}Fmr spectra were recorded on the same instrument at 100.6 and 476.5 MHz, respectively. Tetramethylsilane (TMS) was used as the internal standard for ^{1}Hmr and ^{13}Cmr spectra; trichlorofluoromethane was used as the external standard for the ^{19}Fmr spectra. All ^{13}Cmr spectra employed the SEFT pulse sequence (56). Thin-layer chromatography was performed on plates coated with Merck GF-254 silica gel. Flash chromatography was carried out using Merck silica gel G (230–400 mesh).

All reactions employing triflic anhydride or TASF were performed under rigorously anhydrous conditions under a constant flow of argon.

Starting compounds prepared by methods described in the literature had physical constants in agreement with the published data.

Methyl 3-O-benzyl-4,6-O-benzylidene-β-D-mannopyranoside (2a)

Methyl 4,6-*O*-benzylidene-β-D-glucopyranoside (19.2 g, 68 mmol), benzyl bromide (9.7 mL, 81.6 mmol), and tetra-*n*-butylammonium hydrogen sulfate (2 g, 5.9 mmol) in dichloromethane (150 mL) were stirred vigorously with a 10% aqueous solution of sodium hydroxide (200 mL). After 5 h the aqueous phase was replaced with a fresh solution of 10% aqueous sodium hydroxide to which tetra-*n*-butylammonium hydrogen sulfate (2 g) was added, and rapid stirring was continued overnight. The organic phase was evaporated; the residue was shown by tlc (hexanes – ethyl acetate, 2:1 (v/v)) to consist of 3 components having R_f values of 0.24, 0.48, and 0.66. The component having R_f 0.24 was isolated by flash chromatography (hexanes – ethyl acetate, gradient solution 2:1–1:1 (v/v)) and identified as methyl

Can. J. Chem. Downloaded from www.nrcresearchpress.com by 80.58.250.72 on 09/07/12
For personal use only.

TABLE 1. Summary of the results of the reactions of TASF with derivatives of aldohexo-pyranoses and -furanoses

Substrate	Reaction time (min)	Reaction temperature (°C)	Product	Proton–proton coupling constants (Hz)	Yield (%)
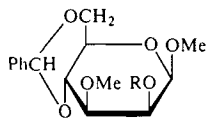 **1** *a*, R = H *b*, R = SO_2CF_3	<10	0–20	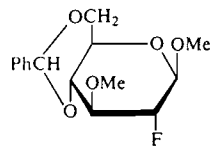 **14**	*a*	64
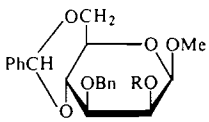 **2** *a*, R = H *b*, R = SO_2CF_3	10	~40	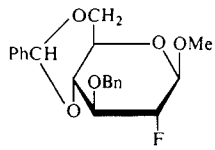 **15**	$J_{1,2}$ = 7.5 $J_{2,3}$ = 8.0	45
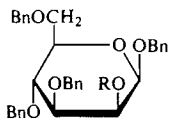 **3** *a*, R = H *b*, R = SO_2CF_3	~5	0–20	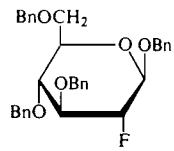 **16**	$J_{1,2}$ = 8.0 $J_{2,3}$ = 8.0	11
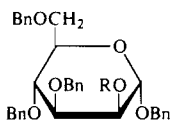 **4** *a*, R = H *b*, R = SO_2CF_3	50	23	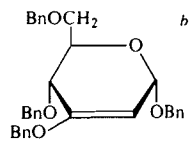 *b* **17**	*c*	~77
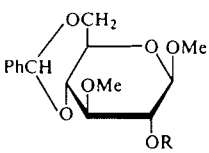 **5** *a*, R = H *b*, R = SO_2CF_3	60	~40	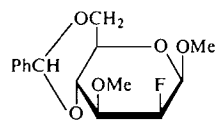 **18**	$J_{1,2}$ = ~0 $J_{2,3}$ = 2.5	65
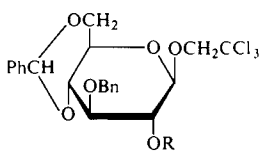 **6** *a*, R = H *b*, R = SO_2CF_3	300	~40	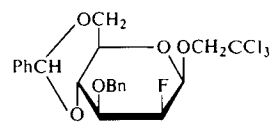 **19**	$J_{1,2}$ = ~0 $J_{2,3}$ = 2.5	23
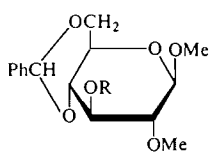 **7** *a*, R = H *b*, R = SO_2CF_3	<10	0–20	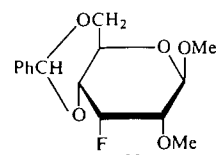 **20**	$J_{2,3}$ = 1.5 $J_{3,4}$ = 1.5	65

TABLE 1. (*concluded*)

Substrate	Reaction time (min)	Reaction temperature (°C)	Product	Proton–proton coupling constants (Hz)	Yield (%)
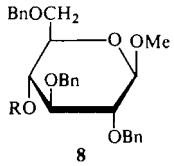 **8** *a*, R = H *b*, R = SO_2CF_3	20	~40	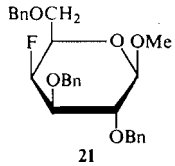 **21**	$J_{3,4}$ = 2.8 $J_{4,5}$ = ~0	77
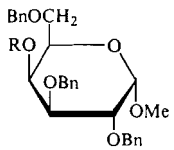 **9** *a*, R = H *b*, R = SO_2CF_3	10	0–20	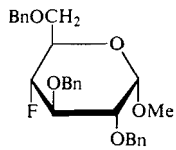 **22**	$J_{3,4}$ = 8.5 $J_{4,5}$ = 8.6	67
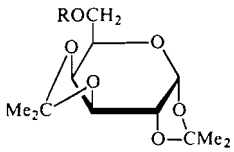 **10** *a*, R = H *b*, R = SO_2CF_3	<10	0–20	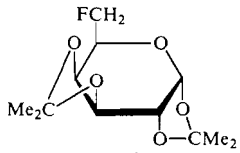 **23**	*a*	71
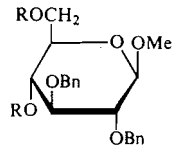 **11** *a*, R = H *b*, R = SO_2CF_3	30	~40	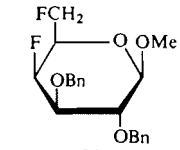 **24**	$J_{3,4}$ = 2.4 $J_{4,5}$ = ~0 $J_{5,6}$ = 6.3	39
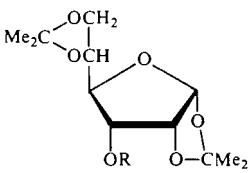 **12** *a*, R = H *b*, R = SO_2CF_3	<10	0–20	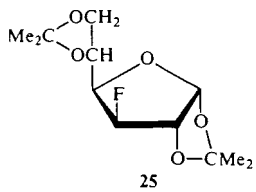 **25**	*a*	66
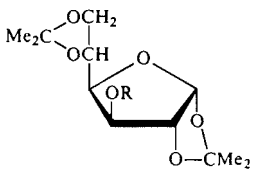 **13** *a*, R = H *b*, R = SO_2CF_3	<10	0–20	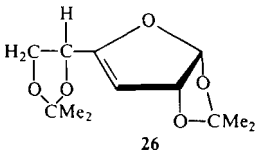 **26**	*a*	83

[a] ^{13}C and ^{19}F nmr data recorded in the Experimental.
[b] Structure is tentative and is based on ^{1}Hmr data only.
[c] See Experimental for details.

Can. J. Chem. Downloaded from www.nrcresearchpress.com by 80.58.250.72 on 09/07/12
For personal use only.

Can. J. Chem. Downloaded from www.nrcresearchpress.com by 80.58.250.72 on 09/07/12
For personal use only.

3-*O*-benzyl-4,6-*O*-benzylidene-β-D-glucopyranoside (5.0 g, 19.7%): mp 179–181°C (lit. (57) mp 181–183°C).

The product (0.3 g, 0.80 mmol) was treated with dimethyl sulfoxide (10 mL) and acetic anhydride (5 mL) for 24 h at room temperature. The solution was evaporated at ~85°C, and the residue dissolved in tetrahydrofuran (5 mL). The solution was diluted with methanol (20 mL) and sodium borohydride (0.5 g) was added in small portions. After 30 min the solvent was evaporated and the residue resolved by flash chromatography. The component having R_f 0.43 (hexanes – ethyl acetate 1:2 (v/v)) was identified as **2***a* (0.248 g, 82.7%): mp 117–118.5°C; $[\alpha]_D$ −29.8° (*c* 1.25, chloroform) (lit. (58) mp 119.5–121°C; $[\alpha]_D$ −32° (*c* 0.8, chloroform)).

*Benzyl 3,4,6-tri-*O*-benzyl-β-D-mannopyranoside (**3**a)*

3,4,6-Tri-*O*-benzyl-1,2-*O*-(1-ethoxyethylidene)-α-D-glucopyranoside (59) (0.79 g, 1.5 mmol) was treated with acetyl chloride (0.1 mL) and benzyl alcohol (10 mL) at 90°C for 4 h. Flash chromatography of the reaction product afforded benzyl 3,4,6-tri-*O*-benzyl-β-D-glucopyranoside (60) (0.33 g, 40%): mp 88–89.5°C (hexanes–ether); $[\alpha]_D$ −26.5° (*c* 0.8, chloroform). This glucopyranoside (0.253 g, 0.468 mmol) was dissolved in dichloromethane (5 mL) and dimethyl sulfoxide (0.067 mL), the solution cooled in a solid CO_2 – acetone bath, and trifluoroacetic anhydride (0.4 mL, 0.6 mmol) added dropwise during 10 min. The reaction was held in the cooling bath for 40 min. Triethylamine (0.4 mL) was added and, after 10 min, the solution was diluted with dichloromethane, washed with water, dried ($MgSO_4$), and the solvent evaporated. The residue was dissolved in ethyl ether (3 mL) and methanol (20 mL); sodium borohydride (0.5 g) was added in small portions and allowed to react for 40 min at room temperature. The solution was evaporated, the residue suspended in dichloromethane, and the mixture washed with water. The organic phase was dried ($MgSO_4$), evaporated, and the residue purified by flash chromatography using hexanes – ethyl ether (5:6 (v/v)) to give **3***a* (0.186 g, 73.5%): $[\alpha]_D$ −48.2° (*c* 4.6, chloroform) (lit. (33) $[\alpha]_D^{22}$ − 43° (*c* 1.3, chloroform); ^{1}Hmr ($CDCl_3$) δ: 4.96–4.51 (m, 8H, CH_2Ph), 4.42 (d, 1H, $J_{1,2}$ = 0.6 Hz, H-1), 4.09 (br d, 1H, $J_{2,3}$ = 2.6 Hz, H-2), 3.88 (t, 1H, $J_{4,3}$, $J_{4,5}$ = 9.5, 9.4 Hz, H-4), 3.76 (doubled AB, 2H, AB *J* = 23.0, 10.5, $J_{5,6}$ = 5.4, $J_{5,6'}$ = 2.0 Hz, H-6, H-6′), 3.52 (dd, 1H, $J_{3,2}$ = 3.2, $J_{3,4}$ = 9.0 Hz, H-3), 3.42 (dd, 1H, $J_{4,5}$ = 9.5, $J_{5,6}$ = 5.3, $J_{5,6'}$ = 2.0 Hz, H-5), 2.53 (s, 1H, OH); ^{13}Cmr ($CDCl_3$) δ: 97.97 ($J_{C\text{-}1,H\text{-}1}$ = 156.90 Hz, C-1). *Anal.* calcd. for $C_{34}H_{36}O_6$: C 75.53, H 6.71; found: C 75.11, H 6.74.

*2,2,2-Trichloroethyl 3-*O*-benzyl-4,6-*O*-benzylidene-β-D-glucopyranoside (**6**a)* (see ref. 60*a*)

2,2,2-Trichloroethyl 4,6-*O*-benzylidene-β-D-glucopyranoside (3.0 g, 7.5 mmol) was stirred with benzyl bromide (1.6 g, 9.35 mmol), tetra-*n*-butylammonium bromide (0.6 g, 1.9 mmol), and a 10% aqueous solution of sodium hydroxide (8 mL) at room temperature. After 8 h the aqueous phase was exchanged and stirring was continued for 5 h. The organic phase was separated, washed with water, evaporated, and the residual mixture resolved by flash chromatography to give **6***a* (0.48 g, 13.0%): mp 101.5–102.5°C (hexanes – ethyl ether); $[\alpha]_D$ −38.9° (*c* 1.6, chloroform). The major product has been reported (60*a*) to be the 2-*O*-benzyl isomer.

*Methyl 4,6-*O*-benzylidene-2-deoxy-2-fluoro-3-*O*-methyl-β-D-glucopyranoside (**14**)*

Methyl 4,6-*O*-benzylidene-3-*O*-methyl-β-D-mannopyranoside (38) (**1***a*) (0.133 g, 0.45 mmol) was dissolved in dichloromethane (5 mL) and pyridine (0.11 mL, 1.3 mmol) and the solution cooled in an ice–salt bath. Trifluoromethanesulfonic anhydride (0.20 mL, 1.2 mmol) was added dropwise; tlc indicated that the reaction was complete in less than 10 min. The reaction mixture was washed sequentially with ice-cold, dilute hydrochloric acid and water, dried ($MgSO_4$), and evaporated, to give the 2-*O*-triflyl derivative **1***b*, which was used immediately in the next step without further purification. TASF (0.42 g, 1.37 mmol)[5] was added in one portion to a cold (salt bath) solution of **1***b* in dichloromethane (5 mL). The reaction flask was removed from the cooling bath and after 10 min the reaction mixture was washed with water, dried ($MgSO_4$), evaporated, and purified by flash chromatography (hexanes – ethyl ether, 2:1 (v/v)) to give **14** (0.086 g, 64%): mp 107–108°C; $[\alpha]_D$ −39.6° (*c* 0.79, chloroform) (lit. (61) mp 108°C).

*Methyl 3-*O*-benzyl-4,6-*O*-benzylidene-2-deoxy-2-fluoro-β-D-glucopyranoside (**15**)*

To a cold (salt bath) solution of **2***a* (0.248 g, 0.66 mmol) in dichloromethane (7 mL) and pyridine (0.4 mL), triflic anhydride (0.45 mL, 2.7 mmol) was added dropwise during 2 min. The reaction solution was removed from the cooling bath and the reaction was monitored by tlc. After 15 min, the reaction solution was washed sequentially with ice-cold, 0.1 *M* HCl, and water (2×), dried ($MgSO_4$), evaporated, and dried under vacuum (1.33 Pa) for 1 h, to give **2***b*: ^{1}Hmr ($CDCl_3$) δ: 5.62 (s, 1H, PhCHO_2), 5.11 (d, 1H, $J_{2,1}$ = 3.0 Hz, H-2), 4.80 (AB, 2H, *J* = 13.0, 22.5 Hz, CH_2Ph), 4.51 (s, 1H, H-1), 4.33 (dd, 1H, $J_{6,5}$ = 4.7, $J_{6,6'}$ = 10.5 Hz, H-6_{eq}), 4.00 (t, 1H, $J_{4,3}$ = $J_{4,5}$ = 9.5 Hz, H-4), 3.90 (t, 1H, $J_{6',5}$, $J_{6',6}$ = 10.2, 10.5 Hz, H-6_{ax}), 3.76 (dd, 1H, $J_{3,2}$ = 3.0, $J_{3,4}$ = 9.7 Hz, H-3), 3.55 (s, 3H, OCH_3), 3.38 (ddd, 1H, $J_{5,4}$ = 9.4, $J_{5,6}$ = 5.0, $J_{5,6'}$ = 9.8 Hz, H-5). This compound was used immediately in the succeeding step.

Compound **2***b* was dissolved in cold (salt bath) dichloromethane (10 mL); TASF (0.55 g, 1.8 mmol) was added, and the solution was heated at reflux temperature for 10 min. The reaction solution was washed with water, dried ($MgSO_4$), and evaporated. The residue was shown by tlc (hexanes – ethyl ether, 1:1 (v/v)) to consist of two components having R_f values of 0.61 and 0.51. The mixture was resolved by flash chromatography (hexanes – ethyl acetate, 4:1 (v/v)) to give **15** (0.112 g, 44.9%): mp 155–158°C; $[\alpha]_D$ −45.6° (*c* 0.55, chloroform) (lit. (34*c*) mp 156–158°C; $[\alpha]_D$ −42° (*c* 0.85, chloroform)); ^{1}Hmr ($CDCl_3$) δ: 5.56 (s, 1H, PhCHO_2), 4.85 (AB, 2H, *J* = 12.0, 18.0 Hz, CH_2Ph), 4.48 (dd, 1H, $J_{1,2}$ = 7.5, $J_{1,F}$ = 4.0 Hz, H-1), 4.36 (dd, 1H, $J_{5,6'}$ = 5.0, $J_{6,6'}$ = 10.6 Hz, H-6_{eq}), 4.33 (dt, 1H, $J_{2,1}$ = $J_{2,3}$ = 8.0, $J_{2,F}$ = 49.5 Hz, H-2), 3.84 (dt, 1H, $J_{3,2}$ = 8.6, $J_{3,4}$ = 9.0, $J_{3,F}$ = 15.0 Hz, H-3), 3.78 (t, 1H, $J_{6',5}$ = 10.0, $J_{6',6}$ = 10.5 Hz, H-6_{ax}), 3.67 (t, 1H, $J_{4,3}$ = $J_{4,5}$ = 9.5 Hz, H-4), 3.57 (s, 3H, OCH_3), 3.43 (dt, 1H, $J_{5,4}$ = $J_{5,6}$ = 9.5, $J_{5,6'}$ = 5.0 Hz, H-5); ^{13}Cmr ($CDCl_3$) δ: 102.14 ($J_{C\text{-}1,F}$ = 23.8 Hz, C-1), 101.31 (PhCHO_2), 92.85 ($J_{C\text{-}2,F}$ = 186.9 Hz, C-2), 80.46 ($J_{C\text{-}4,F}$ = 8.9 Hz, C-4), 78.85 ($J_{C\text{-}3,F}$ = 19.4 Hz, C-3), 74.35, 68.56 (C-6, CH_2Ph), 66.16 (C-5), 57.37 (OCH_3); ^{19}Fmr φ: 198.27 (ddd, $J_{F,1}$ = 4.2, $J_{F,2}$ = 49.6, $J_{F,3}$ = 15.0 Hz). The second component tentatively has been designated methyl 3-*O*-benzyl-4,6-*O*-benzylidene-2-deoxy-β-D-*erythro*-hex-3-enopyranoside (0.045 g, 19.1%): ^{1}Hmr ($CDCl_3$) δ: 5.63 (s, 1H, PhCHO_2), 5.40 (t, 1H, $J_{2,1}$, $J_{2,4}$ < 1 Hz, H-2), 4.88 (AB, 2H, *J* = 12.5, 21.0 Hz, PhCH_2), 4.70 (bs, 1H, H-1), 4.50 (dt, 1H, $J_{4,2}$, $J_{4,1}$ < 1, $J_{4,5}$ = 8.4 Hz, H-4), 4.33 (dd, 1H, $J_{6,5}$ = 4.5, $J_{6,6'}$ = 10.3 Hz, H-6_{eq}), 4.00 (t, 1H, $J_{6',5}$ = 10.0, $J_{6',6}$ = 10.5 Hz, H-6_{ax}), 3.82 (ddd, 1H, $J_{5,4}$ = 8.5, $J_{5,6}$ = 4.2, $J_{5,6'}$ = 9.6 Hz, H-5).

*Benzyl 3,4,6-tri-*O*-benzyl-2-deoxy-2-fluoro-β-D-glucopyranoside (**16**)*

Compound **3***a* (0.270 g, 0.499 mmol) was converted into the corresponding triflate, **3***b*, by reaction with triflic anhydride (0.3 mL, 1.8 mmol) and pyridine (0.4 mL) in the manner described for **1***b*. TASF (0.471 g, 1.71 mmol) was added to a solution of **3***b* in cold dichloromethane (8 mL); the solution was heated at reflux temperature and the reaction was judged to be complete (tlc) after 30 min. Flash chromatography (hexanes – ethyl ether, 72:28 (v/v)) of the reaction product afforded a more polar, unstable, unidentified compound, and **16** (0.030 g, 11%): $[\alpha]_D$ −21.5° (*c* 1.57, chloroform) (lit. (33) $[\alpha]_D^{22}$ −13° (*c* 0.85, chloroform)); ^{1}Hmr ($CDCl_3$) δ: 4.98–4.51 (m, 9H, CH_2Ph, H-1), 4.43 (dt, 1H, $J_{2,1}$ = $J_{2,3}$ = 8.0, $J_{2,F}$ = 50.1 Hz, H-2), 3.80–3.61 (m, 4H, H-3, -4, -6, -6′), 3.46 (ddd, 1H, $J_{5,4}$ = 9.6, $J_{5,6}$ = 4.3, $J_{5,6'}$ = 2.0 Hz, H-5); ^{13}Cmr ($CDCl_3$) δ: 99.21 ($J_{C\text{-}1,F}$ = 22.1 Hz, C-1), 93.34 ($J_{C\text{-}2,F}$ = 187.3 Hz, C-2), 83.42 ($J_{C\text{-}3,F}$ = 15.7 Hz, C-3); ^{19}Fmr ($CDCl_3$) φ: 195.82 (ddd, $J_{F,2}$ = 50.1, *J* = 15.2, 2.0 Hz).

[5]The molar quantities of TASF reported are based on an assumed purity of 90%, as reported by the manufacturer.

Can. J. Chem. Downloaded from www.nrcresearchpress.com by 80.58.250.72 on 09/07/12
For personal use only.

*The reaction of benzyl 3,4,6-tri-O-benzyl-2-O-trifluoromethanesulfonyl-α-D-mannopyranoside (**4**b) with TASF to produce **17***

Compound **4***a* (62) (0.413 g, 0.764 mmol) was converted into **4***b* by reaction with triflic anhydride (0.45 mL, 2.7 mmol) and pyridine (0.5 mL) in dichloromethane (8 mL) in the manner described for **2***b*. The triflate **4***b*, in dichloromethane (5 mL), was treated with TASF (0.630 g, 2.29 mmol) for 50 min in the manner described for **15**. Flash chromatography of the residue from the reaction solution, using hexanes – ethyl ether (3:1 (v/v)), afforded 0.31 g (~77%) of a product that underwent some decomposition during chromatography to give two new compounds having greater polarity than the original product. The reaction product had $[\alpha]_D$ +73.90° (*c* 1, chloroform); ^{1}Hmr ($CDCl_3$) δ: 5.30 (d, 1H, $J_{2,1}$ = 3.5 Hz, H-2), 4.89 (d, 1H, $J_{1,2}$ = 3.5 Hz, H-1), 4.88–4.39 (m, 8H, C*H*$_2$Ph), 4.29 (d, 1H, $J_{4,5}$ = 9.2 Hz, H-4), 4.19 (ddd, 1H, $J_{5,4}$ = 9.2, $J_{5,6}$ = 3.8, $J_{5,6'}$ = 2.1 Hz, H-5), 3.64 (doubled AB, 2H, AB *J* = 10.5, 41.5, $J_{6,5}$ = 4.0, $J_{6',5}$ = 2.0 Hz, H-6, H-6'). These data are consistent with the product having the structure represented by **17**.

*Methyl 4,6-O-benzylidene-2-deoxy-2-fluoro-3-O-methyl-β-D-mannopyranoside (**18**)*

Methyl 4,6-*O*-benzylidene-3-*O*-methyl-β-D-glucopyranoside (**5***a*) (62) (0.273 g, 0.92 mmol) in dichloromethane (5 mL) was converted into **5***b* by reaction with triflic anhydride (0.5 mL, 3.0 mmol) and pyridine (0.7 mL) in the manner described for **1***b*. The product (**5***b*) was dissolved in cold, 1:1 (v/v) dichloromethane–acetonitrile (10 mL), TASF (0.815 g, 2.96 mmol) was added, and the solution heated at reflux temperature for 1 h. The reaction product was obtained in the manner described for **14** and was purified by flash chromatography (hexanes – ethyl acetate, 64:36 (v/v)) to give an unidentified compound (0.043 g), and **18** (0.179 g, 65.1%): mp 177–178°C (from hexanes – ethyl ether); $[\alpha]_D$ −64.8° (*c* 1.24, chloroform) (lit. (34*b*) mp 180–182°C; $[\alpha]_D$ −30° (*c* 0.3, chloroform)); ^{1}Hmr ($CDCl_3$) δ: 5.58 (s, 1H, PhC*H*O$_2$), 4.87 (dd, 1H, $J_{2,3}$ = 2.5, $J_{2,F}$ = 50 Hz, H-2), 4.45 (d, 1H, $J_{1,F}$ = 19.0 Hz, H-1), 4.35 (dd, 1H, $J_{6,5}$ = 4.8, $J_{6,6'}$ = 10.5 Hz, H-6$_{eq}$), 4.00 (dt, 1H, $J_{4,3}$, $J_{4,5}$ = 9.3, 9.6, $J_{4,F}$ = 1.6 Hz, H-4), 3.88 (t, 1H, $J_{6',5}$ = 10.2, $J_{6',6}$ = 10.5 Hz, H-6$_{ax}$), 3.58 (s, 3H, OCH_3), 3.56 (s, 3H, OCH_3), 3.48 (ddd, 1H, $J_{3,2}$ = 2.5, $J_{3,4}$ = 8.6, $J_{3,F}$ = 26.0 Hz, H-3), 3.40 (dt, 1H, $J_{5,4}$ = 10.0, $J_{5,6}$ = 5.0, $J_{5,6'}$ = 10.0 Hz, H-5); ^{13}Cmr ($CDCl_3$) δ: 101.68 (PhC*H*O$_2$), 100.37 ($J_{C\text{-}1,F}$ = 15.6 Hz, C-1), 87.50 ($J_{C\text{-}2,F}$ = 189.6 Hz, C-2), 78.38 (C-4), 72.28 ($J_{C\text{-}3,F}$ = 20.6 Hz, C-3), 68.42 (C-6), 66.99 (C-5), 58.60, 57.54 (OCH_3); ^{19}Fmr ($CDCl_3$) φ: 219.447 (ddd, $J_{F,1}$ = 18.9, $J_{F,2}$ = 50.25, $J_{F,3}$ = 26.25 Hz). *Anal.* calcd. for $C_{15}H_{19}FO_5$: C 60.39, H 6.42, F 6.37; found: C 60.20, H 6.37, F 6.25.

*2,2,2-Trichloroethyl 3-O-benzyl-4,6-O-benzylidene-2-deoxy-2-fluoro-β-D-mannopyranoside (**19**)*

Compound **6***a* (0.267 g, 0.545 mmol) was converted into the triflate **6***b* by reaction with triflic anhydride (0.25 mL, 1.5 mmol) and pyridine (0.5 mL) in dichloromethane (7 mL) in the manner described for **1***b*. The product (**6***b*) was dissolved in cold dichloromethane (7 mL), TASF (0.470 g, 1.71 mmol) was added, and the reaction solution was heated at reflux temperature for 5 h. The reaction products were isolated in the manner described for **14** and the mixture was resolved by flash chromatography (hexanes – ethyl ether, 3:1 (v/v)) to give two unidentified products, and **19** (0.061 g, 22.7%): $[\alpha]_D$ −24.6° (*c* 1.45, chloroform); ^{1}Hmr ($CDCl_3$) δ: 5.65 (s, 1H, PhC*H*O$_2$), 4.96 (dd, 1H, $J_{2,3}$ = 2.5, $J_{2,F}$ = 49.8 Hz, H-2), 4.85 (d, 1H, $J_{1,F}$ = 18.6 Hz, H-1), 4.84 (AB, 2H, *J* = 22.5, 12.0 Hz, C*H*$_2$Ph), 4.37 (dd, 1H, $J_{6,5}$ = 4.8, $J_{6,6'}$ = 10.0 Hz, H-6$_{eq}$), 4.34 (AB, 2H, *J* = 12.0, 94.5 Hz, CH_2CCl_3), 4.14 (dt, 1H, $J_{4,3}$ = $J_{4,5}$ = 9.5, $J_{4,F}$ = 1.5 Hz, H-4), 3.93 (t, 1H, $J_{6',5}$ = $J_{6',6}$ = 10.0 Hz, H-6$_{ax}$), 3.71 (ddd, 1H, $J_{3,2}$ = 2.5, $J_{3,4}$ = 9.5, $J_{3,F}$ = 25.8 Hz, H-3), 3.43 (dt, 1H, $J_{5,4}$ = $J_{5,6'}$ = 10.0, $J_{5,6}$ = 5.0 Hz, H-5); ^{13}Cmr ($CDCl_3$) δ: 101.65 (PhC*H*O$_2$), 99.55 ($J_{C\text{-}1,F}$ = 16.5 Hz, C-1), 96.06 (CH_2CCl_3), 87.89 ($J_{C\text{-}2,F}$ = 190.4 Hz, C-2), 80.43 (C*H*$_2$CCl$_3$), 77.97 (C-4), 75.60 ($J_{C\text{-}3,F}$ = 16.5 Hz, C-3), 72.60, 68.23 (C*H*$_2$Ph, C-6), 67.42 (C-5); ^{19}Fmr ($CDCl_3$) φ: 218.82 (ddd, $J_{F,1}$ = 18.5, $J_{F,2}$ = 50.0, $J_{F,3}$ = 26.0 Hz). *Anal.* calcd. for $C_{22}H_{22}Cl_3FO_5$: C 53.73, H 4.51; found: C 53.34, H 4.55.

*Methyl 4,6-O-benzylidene-3-deoxy-3-fluoro-2-O-methyl-β-D-allopyranoside (**20**)*

Methyl 4,6-*O*-benzylidene-2-*O*-methyl-β-D-glucopyranoside (**7***a*) (63) (0.27 g, 0.91 mmol) was converted into the triflate **7***b* by reaction with triflic anhydride (0.5 mL, 3.0 mmol) and pyridine (0.7 mL) in the manner described for **1***b*. The triflate **7***b* was dissolved in cold dichloromethane (8 mL) and TASF (0.75 g, 2.7 mmol) was added. The reaction flask was removed from the cooling bath and the reaction was judged (tlc) to be complete in less than 10 min. After the usual isolation procedure the product was purified by flash chromatography (hexanes – ethyl ether, 45:55 (v/v)) to give **20** (0.176 g, 64.7%): mp 157–158°C (hexanes – ethyl ether); $[\alpha]_D$ −87.2° (*c* 1.0, chloroform); ^{1}Hmr ($CDCl_3$) δ: 5.52 (s, 1H, PhC*H*O$_2$), 5.16 (dt, 1H, $J_{3,2}$ = $J_{3,4}$ = 1.5, $J_{3,F}$ = 54.0 Hz, H-3), 4.68 (dd, 1H, $J_{1,2}$ = 7.9, $J_{1,F}$ = 1.0 Hz, H-1), 4.41 (dd, 1H, $J_{6,5}$ = 5.0, $J_{6,6'}$ = 10.0 Hz, H-6$_{eq}$), 3.94 (ddt, 1H, $J_{5,4}$ = $J_{5,6'}$ = 10.0, $J_{5,6}$ = 5.0, $J_{5,F}$ = 1.0 Hz, H-5), 3.74 (dt, 1H, $J_{6',5}$ = $J_{6',6}$ = 10.0, $J_{6',F}$ = 1.5 Hz, H-6$_{ax}$), 3.61–3.49 (m, 7H, OCH_3, H-4), 3.15 (ddd, 1H, $J_{2,1}$ = 8.0, $J_{2,3}$ = 2.0, $J_{2,F}$ = 27.0 Hz, H-2); ^{13}Cmr ($CDCl_3$) δ: 102.02 (PhC*H*O$_2$), 86.90 ($J_{C\text{-}5,F}$ = 183.3 Hz, C-3), 78.99 ($J_{C\text{-}2,F}$ = 17.0 Hz, C-2), 77.30 ($J_{C\text{-}4,F}$ = 17.2 Hz, C-4), 69.01 (C-6), 62.88 ($J_{C\text{-}5,F}$ = 2.5 Hz, C-5), 58.41, 57.32 (OCH_3); ^{19}Fmr ($CDCl_3$) φ: 213.99 (quintet, $J_{F,2}$ = $J_{F,4}$ = 27.0, $J_{F,3}$ = 54.0 Hz). *Anal.* calcd. for $C_{15}H_{19}FO_5$: C 60.39, H 6.42, F 6.37; found: C 60.21, H 6.40, F 6.01.

*Methyl 2,3,6-tri-O-benzyl-4-deoxy-4-fluoro-β-D-galactopyranoside (**21**)*

A solution of methyl 2,3,6-tri-*O*-benzyl-β-D-glucopyranoside (**8***a*) (64) (0.257 g, 0.55 mmol) in pyridine (0.7 mL) and dichloromethane (6 mL) was converted into the 4-*O*-triflyl derivative **8***b* by treatment with triflic anhydride (0.3 mL, 1.78 mmol) in the manner described for **1***b*. To a solution of **8***b* in cold dichloromethane (8 mL) was added TASF (0.494 g, 1.79 mmol). The reaction was performed as described for **16** and was judged (tlc) to be complete after 20 min. The reaction product was obtained in the usual manner and purified by flash chromatography (hexanes – ethyl acetate, 3:1 (v/v)) to give **21** (0.198 g, 76.7%): $[\alpha]_D$ −10.1° (*c* 5.94, chloroform); ^{1}Hmr ($CDCl_3$) δ: 4.82 (dd, 1H, $J_{4,3}$ = 2.8, $J_{4,F}$ = 49.5 Hz, H-4), 4.91–4.69 (m, 4H, C*H*$_2$Ph), 4.56 (s, 2H, C*H*$_2$Ph), 4.29 (d, 1H, $J_{1,2}$ = 8.0 Hz, H-1), 3.77–3.59 (m, 4H, H-2, -5, -6, -6'), 3.56 (s, 3H, OCH_3), 3.49 (ddd, 1H, $J_{3,2}$ = 9.5, $J_{3,4}$ = 2.5, $J_{3,F}$ = 28.5 Hz, H-3); ^{13}Cmr ($CDCl_3$) δ: 104.52 (C-1), 85.86 ($J_{C\text{-}4,F}$ = 183.4 Hz, C-4), 78.99 (C-2), 78.89 ($J_{C\text{-}3,F}$ = 18.9 Hz, C-3), 72.06 ($J_{C\text{-}5,F}$ = 17.5 Hz, C-5), 67.74 ($J_{C\text{-}6,F}$ = 5.8 Hz, C-6), 75.22, 73.66 and 72.34 (C*H*$_2$Ph), 57.04 (OCH_3); ^{19}Fmr ($CDCl_3$) φ: 217.23 (dt, $J_{F,3}$ = 27.5, $J_{F,4}$ = 49.8, $J_{F,5}$ = 27.6 Hz). *Anal.* calcd. for $C_{28}H_{31}FO_5$: C 72.08, H 6.70, F 4.07; found: C 71.94, H 6.78, F 3.96.

*Methyl 2,3,6-tri-O-benzyl-4-deoxy-4-fluoro-α-D-glucopyranoside (**22**)*

Methyl 2,3,6-tri-*O*-benzyl-α-D-galactopyranoside (**9***a*) (52) (0.633 g, 1.36 mmol) was treated with triflic anhydride (0.55 mL, 3.3 mmol) in pyridine (0.7 mL) in the manner described for **1***b*, to form **9***b*. The product (**9***b*) was dissolved in cold dichloromethane (~15 mL) and TASF (1.061 g, 3.85 mmol) was added. The flask was removed from the ice–salt bath and allowed to warm at ambient temperature. The reaction was stopped after 10 min by the addition of water. The reaction product was isolated in the manner described for **14** and purified by flash chromatography (hexanes – ethyl ether 2:1 (v/v)) to give **22** (0.427 g, 67.1%): $[\alpha]_D$ +18.8° (*c* 3.52, chloroform);[6] ^{1}Hmr ($CDCl_3$) δ: 4.86–4.54 (m, 7H, C*H*$_2$Ph, H-1), 4.52 (dt, 1H, $J_{4,3}$, $J_{4,5}$ = 8.6, 8.5, $J_{4,F}$ = 50.2 Hz, H-4), 4.01 (dt, 1H, $J_{3,2}$ = $J_{3,4}$ = 9.0, $J_{3,F}$ =

[6]Compound **22** has been reported (1*c*) to have $[\alpha]_D^{23}$ +48.8° (*c* 1.23, chloroform); however, repetition of the reported procedure by us afforded a product established to be **22**, which has $[\alpha]_D$ +19.0° (*c* 2.3, chloroform).

Can. J. Chem. Downloaded from www.nrcresearchpress.com by 80.58.250.72 on 09/07/12
For personal use only.

15.5 Hz, H-3), 3.84 (m, 1H, H-5), 3.67 (m, 2H, H-6, H-6′), 3.50 (dd, 1H, $J_{2,1}$ = 3.3, $J_{2,3}$ = 9.5 Hz, H-2), 3.39 (s, 3H, OCH_3); ^{13}Cmr ($CDCl_3$) δ: 98.14 (C-1), 89.68 ($J_{C\text{-}4,F}$ = 183.4 Hz, C-4), 79.74 ($J_{C\text{-}3,F}$ = 17.0 Hz, C-3), 78.41 ($J_{C\text{-}2,F}$ = 8.0 Hz, C-2), 68.06 ($J_{C\text{-}5,F}$ = 24.0 Hz, C-5), 75.18, 73.64 and 73.56 (CH_2Ph), 68.02 (C-6), 55.38 (OCH_3); ^{19}Fmr ($CDCl_3$) ϕ: 194.81 (dd, $J_{F,3}$ = 15.5, $J_{F,4}$ = 50.5 Hz). *Anal.* calcd. for $C_{28}H_{31}FO_5$: C 72.08, H 6.70, F 4.07; found: C 72.05, H 6.69, F 4.12.

*6-Deoxy-6-fluoro-1,2:3,4-di-*O*-isopropylidene-α-*D*-galactopyranose (**23**)*

1,2:3,4-Di-*O*-isopropylidene-α-D-galactopyranose (**10***a*) (65) (0.481 g, 1.85 mmol) was converted into the 6-*O*-triflyl derivative **10***b* by reaction with triflic anhydride (0.77 mL, 4.63 mmol) and pyridine (0.44 mL, 5.56 mmol) in the manner described for **1***b*. Compound **10***b*, in dichloromethane (10 mL), was treated with TASF (1.79 g, 5.84 mmol) under the conditions used for **14**. The reaction product was purified by flash chromatography (toluene – ethyl ether, 19:1 (v/v)) to give **23** (0.345 g, 71%): $[\alpha]_D$ −54.8° (*c* 3.18, chloroform) (lit. (53) $[\alpha]_D$ −51.4° (*c* 1.28, chloroform); ^{13}Cmr ($CDCl_3$) δ: 95.95 (C-1), 81.84 ($J_{C\text{-}6,F}$ = 168.2 Hz, C-6), 70.39, 70.31, 70.22 (C-2, C-3, C-4), 66.49 ($J_{C\text{-}5,F}$ = 22.0 Hz, C-5); ^{19}Fmr ($CDCl_3$) ϕ: 226.57 (dt, $J_{F,5}$ = 13.0, $J_{F,6}$ = 47.5 Hz).

*Methyl 2,3-di-*O*-benzyl-4,6-dideoxy-4,6-difluoro-β-*D*-galactopyranoside (**24**)*

Methyl 2,3-di-*O*-benzyl-β-D-glucopyranoside (**11***a*) (66) (0.187 g, 0.499 mmol) was converted into the corresponding ditriflate **11***b* by treatment with triflic anhydride (0.5 mL, 3.0 mmol) and pyridine (0.5 mL) in dichloromethane (7 mL) in the usual manner. Compound **11***b* was reacted with TASF (0.850 g, 3.09 mmol) in dichloromethane (8 mL) at reflux temperature for 30 min. Flash chromatography (hexanes – ethyl ether, 60:28 (v/v)) of the reaction product afforded a less polar, unidentified compound (0.060 g), and **24** (0.074 g, 39.1%): mp 74–75°C (hexanes – ethyl ether); $[\alpha]_D$ − 13.8° (*c* 2.89, chloroform); ^{1}Hmr ($CDCl_3$) δ: 4.81 (AB, 2H, *J* = 11.1, 53.7 Hz, CH_2Ph), 4.74 (dd, 1H, $J_{4,3}$ = 2.4, $J_{4,F}$ = 49.9 Hz, H-4), 4.73 (s, 2H, CH_2Ph), 4.57 (dd, 2H, $J_{6,5}$ = 6.3, $J_{6,F}$ = 46.0 Hz, H-6, H-6′), 4.30 (d, 1H, $J_{1,2}$ = 7.7 Hz, H-1), 3.74–3.58 (m, 2H, H-2, H-5), 3.56 (s, 3H, OCH_3), 3.50 (ddd, 1H, $J_{3,2}$ = 9.5, $J_{3,4}$ = 2.5, $J_{3,F}$ = 28.5 Hz, H-3); ^{13}Cmr ($CDCl_3$) δ: 104.47 (PhCHO_2), 85.44 ($J_{C\text{-}4,F\text{-}4}$ = 181.2, $J_{C\text{-}4,F\text{-}6}$ = 4.0 Hz, C-4), 80.45 ($J_{C\text{-}6,F\text{-}4}$ = 5.9, $J_{C\text{-}6,F\text{-}6}$ = 169.1 Hz, C-6), 78.69 (C-2), 78.47 ($J_{C\text{-}3,F\text{-}4}$ = 17.7 Hz, C-3), 75.21, 72.43 (CH_2Ph), 71.29 (*J* = 17.8, 23.8 Hz, C-5); ^{19}Fmr ($CDCl_3$) ϕ: 216.86 (dt, $J_{F\text{-}4,H\text{-}3}$ = 27.8, $J_{F\text{-}4,H\text{-}4}$ = 50.3, $J_{F\text{-}4,H\text{-}5}$ = 27.7 Hz, F-4), 231.20 (dt, $J_{F\text{-}6,H\text{-}5}$ = 10.6, $J_{F\text{-}6,H\text{-}6,\text{-}6'}$ = 46.3 Hz, F-6). *Anal.* calcd. for $C_{21}H_{24}F_2O_4$: C 66.65, H 6.39, F 10.04; found: C 66.50, H 6.40, F 9.10.

*3-Deoxy-3-fluoro-1,2:5,6-di-*O*-isopropylidene-α-*D*-glucofuranose (**25**)*

1,2:5,6-Di-*O*-isopropylidene-α-D-allofuranose (**12***a*) (67) (0.428 g, 1.85 mmol) in dichloromethane (6 mL) was treated with triflic anhydride (0.76 mL, 4.54 mmol) and pyridine (0.45 mL, 5.56 mmol) as described for **1***b*. The reaction was complete in <10 min to give **12***b*, which was immediately dissolved in cold dichloromethane (10 mL) and treated with TASF (1.76 g, 5.74 mmol) in the manner described for **14**. The reaction product was purified by flash chromatography (hexanes – ethyl ether, 4:1 (v/v)) to give **25** (0.321 g, 66%): $[\alpha]_D$ −21.4° (*c* 1.15, chloroform) (lit. (54) $[\alpha]_D$ −22° (*c* 1.0, chloroform)); ^{13}Cmr ($CDCl_3$) δ: 105.15 (C-1), 93.79 ($J_{C\text{-}3,F}$ = 183.4 Hz, C-3), 82.54 ($J_{C,F}$ = 32.9 Hz, C-2 or C-4), 80.65 ($J_{C,F}$ = 19.0 Hz, C-2 or C-4), 71.88 ($J_{C\text{-}5,F}$ = 7.5 Hz, C-5), 67.16 (C-6); ^{19}Fmr ($CDCl_3$) ϕ: 207.97 (ddd, $J_{F,2}$ = 10.6, $J_{F,3}$ = 49.8, $J_{F,4}$ = 29.0 Hz).

*3-Deoxy-1,2:5,6-di-*O*-isopropylidene-α-*D*-erythro-hex-3-enofuranose (**26**)*

1,2:5,6-Di-*O*-isopropylidene-α-D-glucofuranose (**13***a*) (68) (0.114 g, 0.44 mmol) in dichloromethane (5 mL) was converted into the 3-*O*-triflyl derivative **13***b* by reaction with triflic anhydride (0.18 mL, 1.09 mmol) and pyridine (0.11 mL, 1.36 mmol) in the usual manner. Compound **13***b* was dissolved in dichloromethane (5 mL) and reacted with TASF (0.42 g, 1.37 mmol) as described for **14**. Flash chromatography (hexanes – ethyl ether, 4:1 (v/v)) of the residue from the reaction solution afforded **26** (0.088 g, 83%): $[\alpha]_D$ +15.3° (*c* 1.1 ethanol) (lit. (55) $[\alpha]_D$ +19.8° (*c* 3.03, ethanol)).

Acknowledgements

The authors are grateful to the Natural Sciences and Engineering Research Council of Canada and the Medical Research Council of Canada for financial support of this research.

1. (*a*) N. F. Taylor. *In* Carbon–fluorine compounds. Chemistry biochemistry and biological activities. A Ciba Foundation Symposium. Elsevier, Amsterdam. 1972. p. 215; (*b*) N. F. Taylor A. Romaschin, and D. Smith. Am. Chem. Soc. Symp. Ser. **28** 99 (1976); (*c*) D. P. Lopes and N. F. Taylor. Carbohydr. Res **73**, 125 (1979); (*d*) T. D'Amore and N. F. Taylor. FEBS Lett **143**, 247 (1982).
2. R. T. Schwartz and R. Datema. Trends Biochem. Sci. **5**, 6 (1980); Adv. Carbohydr. Chem. Biochem. **40**, 287 (1982).
3. J. R. Halma, J. E. Holden, J. S. Gatley, and W. J. Shaunessy J. Nucl. Med. **23**, P79 (1983).
4. A. Alavi, M. Reivich, J. Greenberg, P. Hand, A. Rosenquist, W. Rintelmann, D. Christman, J. Fowler, A. Goldman, R. MacGregor, and A. Wolf. Semin. Nucl. Med. **11**, 2 (1981); M. M. Goodman, D. R. Elmaleh, K. J. Kearfott, R H. Ackerman, B. Hoop, G. L. Brownell, N. M. Alpert, an H. W. Strauss. J. Nucl. Med. **22**, 138 (1981); E. J. Metter W. H. Reige, D. E. Kuhl, and M. E. Phelps. J. Cereb. Bloo Flow Metab. **4**, 1 (1984).
5. K. Weinhard, G. Pawlik, K. Herholz, R. Wagner, an W.-D. Heiss. J. Cereb. Blood Flow Metab. **5**, 115 (1985).
6. P. Som, H. L. Atkins, D. Bandoypadhay, J. S. Fowler, R R. MacGregor, K. Matsui, Z. H. Oster, D. F. Sacker C.-Y. Shiue, H. Turner, C.-N. Wan, A. P. Wolf, and S. V Zabinski. J. Nucl. Med. **21**, 670 (1980); K. Fukuda, T. Mat suzawa, Y. Abe, S. Endo, K. Yamada, K. Kubota, J. Hat azawa, T. Sato, M. Ito, T. Takahashi, R. Itawa, and T Ido. Eur. J. Nucl. Med. **7**, 294 (1982); Y. Yonekura, R. S Benua, A. B. Brill, P. Som, S. D. J. Yeh, N. E. Kemeny, J S. Fowler, R. R. MacGregor, R. Stamm, D. R. Christman and A. P. Wolf. J. Nucl. Med. **23**, 1133 (1982); R. C. Mar shall, J. H. Tillisch, M. E. Phelps, S.-C. Huang, R. Car son, E. Henze, and H. R. Schelbert. Circulation, **67**, 76 (1983); M. E. Phelps and H. T. Chugani. J. Nucl. Med. **26** P46 (1985).
7. G. Di Chiro, R. L. De La Paz, R. A. Brooks, L. Sokoloff, P L. Kornblith, B. H. Smith, N. J. Patronas, C. V. Kufta, R M. Kessler, G. S. Johnston, R. G. Manning, and A. P Wolf. Neurology, **32**, 1323 (1982).
8. R. P. Friedland, T. F. Budinger, E. Ganz, Y. Yano, C. A Mathis, B. Koss, B. A. Ober, R. H. Huesman, and S. E Derenzo. J. Comput. Assist. Tomogr. **7**, 590 (1983).
9. D. E. Kuhl, E. J. Metter, W. Y. Reige, and C. H. Markham Ann. Neurol. **15**, S119 (1984); D. E. Kuhl, E. J. Metter, an W. H. Reige. Ann. Neurol. **15**, 419 (1984).
10. T. Takahashi, T. Ido, M. Shinohara, R. Iwata, H. Fukuda J. Matsuzawa, M. Tada, and H. Orui. J. Labelled Compd Radiopharm. **21**, 1215 (1984), and references cited therein.
11. (*a*) P. W. Kent. *In* Carbon–fluorine compounds. Chemistry biochemistry and biological activities. A Ciba Foundation Symposium. Elsevier, Amsterdam. 1972. p. 169; (*b*) A. A. E. Penglis. Adv. Carbohydr. Chem. Biochem. **38**, 195 (1981).
12. J. P. De Kleijn. J. Fluorine Chem. **10**, 341 (1977); J. S Fowler and A. P. Wolf. Brookhaven National Laboratory Report 1981 BNL 31222 (U.S. Dept. of Energy Order No DE82012799).
13. T. Ido, C.-N. Wan, J. S. Fowler, and A. P. Wolf. J. Org Chem. **42**, 2341 (1977); T. Ido, C.-N. Wan, V. Casella, J. S

FOWLER, A. P. WOLF, M. REIVICH, and D. E. KUHL. J. Labelled Compd. Radiopharm. **14**, 175 (1978).
14. G. T. BIDA, N. SATYAMURTHY, and J. R. BARRIO. J. Nucl. Med. **25**, 1327 (1984).
15. W. KORYTNYK and S. VALENTEKOVIC-HORVAT. Tetrahedron Lett. **21**, 1493 (1980).
16. C.-Y. SHIUE, K. C. TO, and A. P. WOLF. J. Labelled Compd. Radiopharm. **20**, 157 (1983).
17. S. SOOD, G. FIRNAU, and E. S. GARNETT. Int. J. Appl. Radiat. Isot. **34**, 743 (1983).
18. C.-Y. SHIUE, P. A. SALVADORI, A. P. WOLF, J. S. FOWLER, and R. R. MACGREGOR. J. Nucl. Med. **23**, 899 (1982).
19. M. J. ADAM. J. Chem. Soc. Chem. Commun. 730 (1982); M. J. ADAM, T. J. RUTH, S. JIVAN, and B. D. PATE. Int. J. Appl. Radiat. Isot. **35**, 985 (1984).
20. M. DIKSIC and D. JOLLY. Int. J. Appl. Radiat. Isot. **34**, 893 (1983).
21. R. E. EHRENKAUFER, J. F. POTOCKI, and D. M. JEWETT. J. Nucl. Med. **25**, 333 (1984).
22. C. J. S. VAN RIJN, J. D. M. HERSCHEID, G. W. M. VISSER, and A. HOEKSTRA. Int. J. Appl. Radiat. Isot. **36**, 111 (1985).
23. M. G. STRAATMANN and M. J. WELCH. J. Labelled Compd. Radiopharm. **13**, 210 (1977).
24. P. J. CARD and G. S. REDDY. J. Org. Chem. **48**, 4734 (1983).
25. C. W. SOMAWARDHANA and E. G. BRUNNGRABER. Carbohydr. Res. **121**, 51 (1983), and references cited therein.
26. J. PACÁK, Z. TOČÍK, and M. CERNÝ. Chem. Commun. 77 (1969); A. D. BARFORD, A. B. FOSTER, J. H. WESTWOOD, L. D. HALL, and R. N. JOHNSON. Carbohydr. Res. **19**, 48 (1971).
27. P. A. BEELEY, W. A. SZAREK, G. W. HAY, and M. M. PERLMUTTER. Can. J. Chem. **62**, 2709 (1984).
28. W. A. SZAREK, G. W. HAY, B. DOBOSZEWSKI, and M. M. PERLMUTTER. Carbohydr. Res. **155**, 107 (1986).
29. D. R. CHRISTMAN, Z. ORHANOVIC, and A. P. WOLF. J. Labelled Compd. Radiopharm. **13**, 283, 555 (1977).
30. S. LEVY, D. R. ELMALEH, and E. LIVNI. J. Nucl. Med. **23**, 918 (1982).
31. A. OLESKER, A. DESSINGES, T. T. THANG, and G. LUKACS. C.R. Acad. Sci. Ser. 2, **295**, 575 (1982).
32. T. J. TEWSON. J. Org. Chem. **48**, 3507 (1983).
33. A. DESSINGES, A. OLESKER, G. LUKACS, and T. T. THANG. Carbohydr. Res. **126**, C6 (1984).
34. (*a*) T. HARADIHARA, M. MAEDA, Y. YANO, and M. KOJIMA. Chem. Pharm. Bull. **32**, 3317 (1984); (*b*) T. HARADIHARA, M. MAEDA, M. OMAE, Y. YANO, and M. KOJIMA. Chem. Pharm. Bull. **32**, 4758 (1984); (*c*) T. HARADIHARA, M. MAEDA, Y. KAI, H. OMAE, and M. KOJIMA. Chem. Pharm. Bull. **33**, 153 (1985).
35. W. A. SZAREK, G. W. HAY, and B. DOBOSZEWSKI. J. Chem. Soc. Chem. Commun. 663 (1985).
36. W. J. MIDDLETON. U.S. Patent 3,940,402 (1976).
37. P. J. CARD and W. D. HITZ. J. Am. Chem. Soc. **106**, 5348 (1984).
38. M. MILJKOVIĆ, M. GLIGORIJEVIĆ, and D. MILJKOVIĆ. J. Org. Chem. **39**, 2118 (1974).
39. P. J. STANG, M. HANACK, and L. R. SUBRAMANIAN. Synthesis, 85 (1982); P. J. STANG and M. R. WHITE. Aldrichim. Acta, **16**, 15 (1983), and references cited therein.
40. J. ADAMSON, A. B. FOSTER, L. D. HALL, R. N. JOHNSON, and R. H. HESSE. Carbohydr. Res. **15**, 351 (1970).
41. P. J. GAREGG, T. IVERSON, and S. OSCARSON. Carbohydr. Res. **50**, C12 (1976).
42. H. H. FREEDMAN and R. A. DUBOIS. Tetrahedron Lett. 3251 (1975).
43. S. CZERNECKI, C. GEORGOULIS, and C. PROVELENGHIOU. Tetrahedron Lett. 3535 (1976).
44. R. W. BINKLEY, M. G. AMBROSE, and D. G. HEHEMANN. J. Org. Chem. **45**, 4387 (1980).
45. R. W. BINKLEY and M. G. AMBROSE. J. Carbohydr. Chem. **3**, 1 (1984).
46. T. L. SU, R. S. KLEIN, and J. J. FOX. J. Org. Chem. **46**, 1790 (1981).
47. (*a*) A. C. RICHARDSON. Carbohydr. Res. **10**, 395 (1969); (*b*) M. MILJKOVIĆ, M. GLIGORIJEVIĆ, and D. GLIŠIN. J. Org. Chem. **39**, 3223 (1974).
48. C. L. STEVENS, K. G. TAYLOR, and J. A. VALICENTI. J. Am. Chem. Soc. **87**, 4579 (1965).
49. W. A. SZAREK. Adv. Carbohydr. Chem. Biochem. **28**, 225 (1973).
50. A. B. FOSTER, J. H. WESTWOOD, B. DONALDSON, and L. D. HALL. Carbohydr. Res. **25**, 228 (1972).
51. Y. ITTAH and C. P. J. GLAUDEMANS. Carbohydr. Res. **95**, 189 (1981).
52. N. MORISHIMA, S. KOTO, M. OSHIMA, A. SUGIMOTO, and S. ZEN. Bull. Chem. Soc. Jpn. **56**, 2849 (1983).
53. N. F. TAYLOR and P. W. KENT. J. Chem. Soc. 872 (1958).
54. A. B. FOSTER, R. HEMS, and J. M. WEBBER. Carbohydr. Res. **5**, 292 (1967).
55. F. WEYGAND and H. WOTZ. Chem. Ber. **85**, 256 (1952).
56. D. L. RUBENSTEIN and T. T. NAKASHIMA. Anal. Chem. **51**, 1465A (1979); D. W. BROWN, T. T. NAKASHIMA, and D. L. RUBENSTEIN. J. Magn. Reson. **45**, 302 (1981); R. BENN and H. GÜNTHER. Angew. Chem. Int. Ed. Engl. **22**, 350 (1983).
57. H. B. BORÉN, P. J. GAREGG, L. KENNE, L. MARON, and S. SVENSSON. Acta. Chem. Scand. **26**, 644 (1972).
58. P. J. GAREGG. Ark. Kem. **23**, 255 (1964).
59. N. K. KOCHETKOV, B. A. DMITRIEV, O. S. CHIZHOV, E. M. KLIMOV, N. N. MALYSHEVA, A. YA. CHERNYAK, N. E. BAYRAMOVA, and V. I. TORGOV. Carbohydr. Res. **33**, C5 (1974).
60. (*a*) B. DOBOSZEWSKI. Doctoral dissertation. Institute of Organic Chemistry, Polish Academy of Sciences, Warsaw, 1982; (*b*) B. DOBOSZEWSKI and A. ZAMOJSKI. Carbohydr. Res. **132**, 29 (1984).
61. S. LEVY, E. LIVNI, D. ELMALEH, and W. CURATOLO. J. Chem. Soc. Chem. Commun. 972 (1982).
62. H. BAUMANN, H. LÖNN, and J. LÖNNEGREN. Carbohydr. Res. **114**, 317 (1983).
63. Y. KONDO. Agric. Biol. Chem. **39**, 1879 (1975).
64. P. J. GAREGG, H. HULTBERG, and S. WALLIN. Carbohydr. Res. **108**, 97 (1982).
65. R. S. TIPSON. Methods Carbohydr. Chem. **2**, 246 (1963).
66. J. C. DENNISON and D. J. MCGILVRAY. J. Chem. Soc. 1616 (1951).
67. J. D. STEVENS. Methods Carbohydr. Chem. **6**, 163 (1972).
68. O. TH. SCHMIDT. Methods Carbohydr. Chem. **2**, 318 (1963).

Can. J. Chem. Downloaded from www.nrcresearchpress.com by 80.58.250.72 on 09/07/12
For personal use only.

Structure and magnetic exchange in poly-bis(pyrazine)bis(methanesulfonato-*O*)-copper(II). One-dimensional exchange in a two-dimensional polymer

JOHN S. HAYNES, STEVEN J. RETTIG, JOHN R. SAMS, ROBERT C. THOMPSON,[1] AND JAMES TROTTER
Department of Chemistry, University of British Columbia, 2035 Main Mall, Vancouver, B.C., Canada V6T 1Y6

Received July 14, 1986

JOHN S. HAYNES, STEVEN J. RETTIG, JOHN R. SAMS, ROBERT C. THOMPSON, and JAMES TROTTER. Can. J. Chem. **65**, 420 (1987).

Crystals of poly-bis(pyrazine)bis(methanesulfonato-*O*)copper(II) are orthorhombic, $a = 8.199(1)$, $b = 13.130(1)$, $c = 6.913(1)$ Å, $Z = 2$, space group *Pnnm*. The structure was solved by conventional heavy atom methods and was refined by full-matrix least-squares procedures to $R = 0.025$ and $R_w = 0.033$ for 1226 reflections with $I \geq 3\sigma(I)$. The complex contains parallel sheets, each sheet consisting of a square array of copper(II) ions bridged by two types of bidentate pyrazine ligands. The CuN_4O_2 chromophore is tetragonally elongated; the equatorial plane contains two pyrazine nitrogen atoms (Cu—N(1) = 2.058(2) Å) and two oxygen atoms from monodentate methanesulfonate ligands (Cu—O(1) = 1.956(1) Å); the axial sites are occupied by bridging pyrazine groups with significantly longer Cu—N bond lengths (Cu—N(2) = 2.692(2) Å). Magnetic susceptibility studies (82 to 4.2 K) reveal antiferromagnetic behaviour with a susceptibility maximum at about 6.2 K. Exchange coupling in the complex is considered to take place primarily via the more strongly bound, equatorially coordinated pyrazine ligands. Analysis of the magnetic susceptibility data according to a Heisenberg linear chain of interacting $S = 1/2$ spins yields best fit values of $J = -3.82\ cm^{-1}$ and $g = 2.13$. Vibrational and electronic spectroscopic and differential scanning calorimetric studies on the title compound and, for comparison, on the related mononuclear pyridine complex, bis(methanesulfonato)-tetrakis(pyridine)copper(II), are also reported.

JOHN S. HAYNES, STEVEN J. RETTIG, JOHN R. SAMS, ROBERT C. THOMPSON et JAMES TROTTER. Can. J. Chem. **65**, 420 (1987).

Les cristaux du poly-bis(pyrazine)bis(méthanesulfonato-*O*)cuivre(II) sont orthorhombiques et ils cristallisent dans le groupe d'espace *Pnnm* avec $a = 8{,}199(1)$, $b = 13{,}130(1)$ et $c = 6{,}913(1)$ Å et $Z = 2$. On a résolu la structure par les méthodes conventionnelles aux atomes lourds et on l'a affinée par la méthode des moindres carrés jusqu'à des valeurs de $R = 0{,}025$ et $R_w = 0{,}033$ pour 1226 réflexions avec $I \geq 3\sigma(I)$. Le complexe comporte des feuilles parallèles et chaque feuille comprend un arrangement carré d'ions de cuivre(II) qui sont pontés par deux types de ligands pyrazines bidentates. Le chromophore CuN_4O_2 est un tétragone allongé; le plan équatorial contient deux atomes d'azote de la pyrazine (Cu—N(1) = 2,058(2) Å) et deux atomes d'oxygène des ligands méthanesulfonates monodentates (Cu—O(1) = 1,956(1) Å); les sites axiaux sont occupés par des groupements pyrazines formant des ponts et ces longueurs des liaisons Cu—N sont beaucoup plus longues (Cu—N(2) = 2,692(2) Å). Des études de susceptibilité magnétique (de 82 à 4,2 K) révèlent l'existence d'un comportement antiferromagnétique avec une susceptibilité maximale à environ 6,2 K. On considère que, dans le complexe, le couplage d'échange se produit principalement par le biais des ligands pyrazines qui sont coordonnés d'une façon équatoriale et qui sont liés plus fortement. Une analyse des données de susceptibilité magnétique, en faisant appel d'une chaîne linéaire de Heisenberg des spins $S = 1/2$ qui interagissent, conduit à des valeurs de $J = -3{,}82\ cm^{-1}$ et $g = 2{,}13$. On rapporte aussi les études spectroscopiques, tant au niveau vibrationnel qu'électronique, ainsi que les études calorimétriques à balayage différentiel qui ont été faites sur le compos mentionné dans le titre et, pour fins de comparaison, sur le complexe pyridine mononucléaire apparenté, bis(méthanesulfonato)tétrakis(pyridine)cuivre(II).

[Traduit par la revue]

Introduction

Pyrazine-bridged complexes of the transition metals are of particular interest because of the potential for the propagation of magnetic exchange over extended distances, and some of the most fruitful investigations in this area have involved complexes of copper(II). Extensive structural and magnetic studies on complexes such as $Cu(pyz)_2(ClO_4)_2$ (1, 2), $Cu(pyz)(NO_3)_2$ (3) and the hexafluoroacetylacetonate analogue, $Cu(pyz)(hfac)_2$ (4) have shown that the magnitude of the exchange coupling in these systems is significantly affected by structural variations involving the bridging pyrazine network (5–7).

We report here the synthesis, X-ray structure determination, and characterization of the bis(pyrazine) complex of copper(II) methanesulfonate, $Cu(pyz)_2(CH_3SO_3)_2$. This compound bears a superficial structural resemblance to $Cu(pyz)_2(ClO_4)_2$ as both are two-dimensional pyrazine-bridged polymers, with unidentate coordinated anions. In the perchlorate, however, the anions occupy axial sites with all pyrazines in equivalent equatorial positions (1), while in the methanesulfonate the anions are bound in the equatorial plane and there are two distinct types of pyrazine bridges. In one dimension the pyrazines occupy equatorial positions with relatively short Cu—N bonds as in $Cu(pyz)(NO_3)_2$ (3) while in the other dimension the bridging pyrazines occupy more weakly bound axial positions as in $Cu(pyz)(hfac)_2$ (4). This novel pyrazine-bridge system makes $Cu(pyz)_2(CH_3SO_3)_2$ a particularly important candidate for cryomagnetic studies. To aid in the evaluation of the spectroscopic and magnetic properties of this compound we have also prepared and characterized the analogous pyridine derivative, $Cu(py)_4(CH_3SO_3)_2$.

[1]Author to whom correspondence should be addressed.

Experimental

Syntheses

The bis(pyrazine) complex of copper(II) methanesulfonate was prepared by the reaction of anhydrous copper(II) methanesulfonate (8) with an excess of pyrazine (Aldrich Chemicals, gold label) in methanol. $Cu(CH_3SO_3)_2$ (2.11 mmol) was dissolved in hot methanol (3 mL) and the solution was then added to a hot solution of pyrazine (28.7 mmol) in methanol (5 mL). A pale blue precipitate formed immediately and was removed by filtration. Overnight the filtrate yielded further product in crystalline form. Total yield 81%. *Anal.* calcd. for $CuC_{10}H_{14}N_4S_2O_6$: C 29.02, H 3.41, N 13.54; found: C 28.98, H 3.60, N 13.63. Samples left exposed to the atmosphere for several hours were found

Can. J. Chem. Downloaded from www.nrcresearchpress.com by 80.58.250.72 on 09/07/12
For personal use only.

Can. J. Chem. Downloaded from www.nrcresearchpress.com by 80.58.250.72 on 09/07/12
For personal use only.

to undergo some hydration (typically less than half a mole of water per mole of complex) as indicated by the appearance of a weak, broad absorption in the 2800 to 3500 region of the infrared spectrum and by microanalysis.

The tetrakis(pyridine) complex was made by the addition of an excess of pyridine (62 mmol) to a solution of $Cu(CH_3SO_3)_2$ (4.14 mmol) in hot methanol (8 mL). Overnight, dark blue crystals formed and these were subsequently isolated by filtration in 73% yield. *Anal.* calcd. for $CuC_{22}H_{26}N_4S_2O_6$: C 46.35, H 4.60, N 9.83; found: C 46.60, H 4.70, N 9.80.

Physical measurements

Infrared and electronic spectra and differential scanning calorimetry measurements were obtained using equipment and procedures previously described (9). Magnetic susceptibilities were measured using a P.A.R. Model 155 vibrating sample magnetometer (10) and were corrected for the diamagnetism of all atoms. These corrections were (in 10^{-6} cm^3 mol^{-1}): copper, −11; $CH_3SO_3^-$, −35; pyridine, −49; pyrazine, −45. A value of 60×10^{-6} cm^3 mol^{-1} was used to correct for the temperature-independent paramagnetism of copper(II). Analyses for C, H, and N were performed by P. Borda of this department.

X-ray crystallographic analysis of poly-bis(pyrazine)bis-(methanesulfonato-O)copper(II)

A crystal bounded by the nine faces (followed by their distances in mm from a common origin): {1 1 0}, 0.213, {0 1 1}, 0.219, (−1, −1, −3), 0.150 was mounted in a general orientation. Unit-cell parameters were refined by least-squares on 2 sin θ/λ values for 25 reflections (2θ = 47–62°) measured on a diffractometer with Mo-$K\alpha$ radiation ($\lambda(K\alpha_1)$ = 0.70930, $\lambda(K\alpha_2)$ = 0.71359 Å). Crystal data at 22°C are:

$C_{10}H_{14}CuN_4O_6S_2$ f.w. = 413.91

Orthorhombic, a = 8.199(1), b = 13.130(1), c = 6.913(1) Å, V = 744.2(1) Å^3, Z = 2, ρ_c = 1.847 Mg m^{-3}, $F(000)$ = 422, μ(Mo-$K\alpha$) = 17.74 cm^{-1}. Absent reflections: $0kl$, $k + l$ odd, and $h0l$, $h + l$ odd, space group $Pnnm$ (D_{2h}^{12}, No. 58) from structure analysis.

Intensities were measured with graphite-monochromated Mo-$K\alpha$ radiation on an Enraf-Nonius CAD4-F diffractometer. An ω–2θ scan at 1.01–10.06° min^{-1} over a range of (0.60 + 0.35 tan θ) degrees in ω (extended by 25% on both sides for background measurement) was employed. Data were measured to 2θ = 65°. The intensities of three check reflections, measured every 3600 s throughout the data collection, remained constant to within 2%. After data reduction,[2] an absorption correction was applied using the Gaussian integration method (11, 12). Transmission factors ranged from 0.521 to 0.588 for 102 integration points. Of the 1447 independent reflections measured, 1226 (84.7%) had intensities greater than or equal to 3σ(I) above background where $\sigma^2(I) = S + 2B + (0.04(S - B))^2$ with S = scan count and B = normalized background count.

The systematic absences allow space groups $Pnn2$ and $Pnnm$, the latter being suggested by both the E-statistics and the Patterson function. The coordinates of the Cu and S atoms (which both occupy special positions) were determined from the Patterson function and those of the remaining atoms were determined from subsequent difference maps. In the final stages of refinement the non-hydrogen atoms were refined with anisotropic thermal parameters and the hydrogen atoms with isotropic thermal parameters. The scattering factors of ref. 13 were used for non-hydrogen atoms and those of ref. 14 for hydrogen atoms. Anomalous scattering factors from ref. 15 were used for the Cu and S atoms. The weighting scheme $w = 1/\sigma^2(F)$, where $\sigma^2(F)$ is derived from the previously defined $\sigma^2(I)$, gave uniform average values of $w(|F_o| - |F_c|)^2$ over ranges of both $|F_o|$ and sin θ/λ and was employed in the final stages of full-matrix refinement of 82 variables. Reflections with $I < 3\sigma(I)$ were not included in the refinement. An isotropic Type I extinction correction (Thornley–Nelmes definition of mosaic anisotropy with a Lorentzian distribution) was applied (16–18). The final value of g was 1.3(2) × 10^4. Convergence was reached at R = 0.025 and R_w = 0.033 for 1226 reflections with $I \geq 3\sigma(I)$. For all 1447 reflections R = 0.034. The function minimized was $\Sigma w(|F_o| - |F_c|)^2$, $R = \Sigma||F_o| - |F_c||/\Sigma|F_o|$, $R_w = (\Sigma w(|F_o| - |F_c|)^2/\Sigma w|F_o|^2)^{1/2}$, $S = [\Sigma w\Delta^2/(m - n)]^{1/2}$ = 1.503.

On the final cycle of refinement the mean and maximum parameter shifts corresponded to 0.006 and 0.07σ, respectively. A final difference map showed maximum fluctuations of −0.93 to +0.38 e Å^{-3} (near C(4) and the midpoint of the C(2)—C(2)^1 bond, respectively). The final positional and thermal parameters appear in Tables 1 and 5, respectively.[3] Measured and calculated structure factors have been placed in the Depository for Unpublished Data.[3] Bond lengths, bond angles, and possible weak C—H···O interactions appear in Tables 2–4, respectively. Bond lengths and angles involving hydrogen (Tables 6, 7) have been deposited.

TABLE 1. Final positional (fractional × 10^5, H × 10^4) and isotropic thermal parameters ($U \times 10^3$ Å^2) with estimated standard deviations in parentheses

Atom	x	y	z	U_{eq}/U_{iso}
Cu	50000	50000	50000	23
S	54201(6)	25913(3)	50000	22
O(1)	44607(17)	35490(10)	50000	23
O(2)	63567(18)	24874(9)	32452(22)	45
N(1)	50000	50000	20228(23)	21
N(2)	17181(21)	50709(12)	50000	27
C(1)	39006(28)	16391(15)	50000	32
C(2)	40744(16)	43483(9)	10041(18)	23
C(3)	7585(26)	58949(16)	50000	30
C(4)	9358(25)	41751(15)	50000	28
H(1a)	4467(51)	851(33)	5000	67(11)
H(1b)	3239(25)	1709(15)	3882(28)	42(5)
H(2)	3471(21)	3887(13)	1702(26)	29(4)
H(3)	1236(31)	6524(22)	5000	24(6)
H(4)	1412(32)	3600(24)	5000	34(7)

TABLE 2. Bond lengths (Å) with estimated standard deviations in parentheses*

Bond	Length (Å)	Bond	Length (Å)
Cu—O(1)	1.956(1)	N(1)—C(2)	1.343(1)
Cu—N(1)	2.058(2)	N(2)—C(3)	1.338(3)
Cu—N(2)	2.692(2)	N(2)—C(4)	1.340(2)
S —O(1)	1.483(1)	C(2)—C(2)^1	1.388(2)
S —O(2)	1.442(1)	C(3)—C(4)^2	1.392(3)
S —C(1)	1.765(2)		

*Superscripts refer to symmetry operations: $^1x, y, -z$ and $^2-x, 1-y, z$.

Results and discussion

Crystal structure analysis

The crystal structure analysis of $Cu(pyz)_2(CH_3SO_3)_2$ shows that the complex contains parallel sheets (Fig. 1), each sheet consisting of an infinite square array of copper(II) ions bridged by two types of bidentate pyrazine ligands. Each copper ion

[2]The computer programs used include locally written programs for data processing and locally modified versions of the following: ORFLS, full-matrix least-squares, and ORFFE, function and errors, by W. R. Busing, K. O. Martin, and H. A. Levy; FORDAP, Patterson and Fourier syntheses, by A. Zalkin; ORTEP II, illustrations, by C. K. Johnson.

[3]The structure and factor table, Table 5 (anisotropic thermal parameters) and other material mentioned in the text may be purchased from the Depository of Unpublished Data, CISTI, National Research Council of Canada, Ottawa, Ont., Canada K1A 0S2.

TABLE 3. Bond angles (deg) with estimated standard deviations in parentheses*

Bonds	Angle (deg)	Bonds	Angle (deg)
O(1)—Cu—N(1)	90	O(2)—S —C(1)	108.0(1)
O(1)—Cu—N(2)	78.92(5)	O(2)—S —O(2)^4	114.5(1)
O(1)—Cu—O(1)^3	180	Cu —O(1)—S	134.9(1)
O(1)—Cu—N(2)^3	101.08(5)	Cu —N(1)—C(2)	121.6(1)
O(1)—Cu—N(1)^4	90	Cu —N(1)—C(2)^3	121.6(1)
N(1)—Cu—N(2)	90	C(2)—N(1)—C(2)^3	116.8(2)
N(1)—Cu—N(2)^3	90	Cu —N(2)—C(3)	128.0(1)
N(1)—Cu—N(1)^4	180	Cu —N(2)—C(4)	116.6(1)
N(2)—Cu—N(2)^3	180	C(3)—N(2)—C(4)	115.4(2)
O(1)—S —O(2)	111.3(1)	N(1)—C(2)—C(2)^1	121.6(1)
O(1)—S —C(1)	103.1(1)	N(2)—C(3)—C(4)^2	122.2(2)
O(1)—S —O(2)^4	111.3(1)	N(2)—C(4)—C(3)^2	122.4(2)

*Here and elsewhere in this report superscripts refer to the symmetry operations: $^1x, y, -z$; $^2-x, 1-y, z$; $^3 1-x, 1-y, z$; and $^4x, y, 1-z$.

TABLE 4. Possible weak C—H···O interactions*

Atoms	H···O (Å)	C···O (Å)	C—H···O (deg)
C(1)—H(1b)···O(2)^5	2.38(2)	3.271(2)	157(2)
C(2)—H(2)···O(1)^6	2.46(2)	2.972(1)	115(1)
C(2)—H(2)···O(2)^5	2.50(2)	3.323(2)	149(1)
C(4)—H(4)···O(1)^6	2.50(3)	3.005(2)	119(2)

*Superscripts refer to symmetry operations: $^5x-1/2, 1/2-y, 1/2-z$; $^6x, y, z$. Other geometrical data: H(1b)···O(2)^5···H(2) = 83.1(6)°, H(2)···O(1)···H(4) = 70.5(4)°, O(1)···H(2)···O(2)^5 = 94.9(6)°.

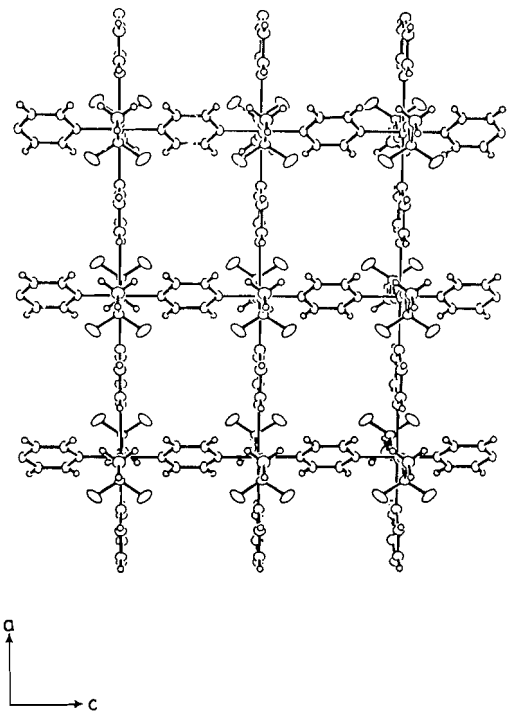

FIG. 1. View of a single layer in $Cu(N_2C_4H_4)_2(CH_3SO_3)_2$.

has tetragonally-elongated octahedral coordination (Fig. 2), the equatorial plane containing two pyrazine nitrogen atoms (Cu—N(1) = 2.058(2) Å) and two oxygen atoms from monodentate methanesulfonate ligands (Cu—O(1) = 1.956(1) Å); the axial coordination sites are occupied by bridging pyrazine groups with significantly longer Cu—N bond lengths (Cu—N(2) = 2.692(2) Å). The Cu—O bond distance is typical of an oxygen atom bound to copper in the equatorial plane; for example, in $Cu(pyz)(NO_3)_2$ the equatorial Cu—O bond distance is 2.010(4) Å (3). The Cu—N(1) distance is almost identical to the value of 2.062(3) Å found in $Cu(pyz)_2(ClO_4)_2$ (1) and only slightly longer than the Cu—N distance of 1.98 Å found in $Cu(pyz)(NO_3)_2$ (3); whereas the Cu—N(2) distance is much longer. This axial pyrazine group is even more weakly bound to copper than the axial pyrazine groups in $Cu(pyz)(hfac)_2$ (4) (Cu—N of 2.529(9) Å) and the acetate complex, $Cu_2(OAc)_4(pyz)$ (19) (Cu—N of 2.171(6) Å).

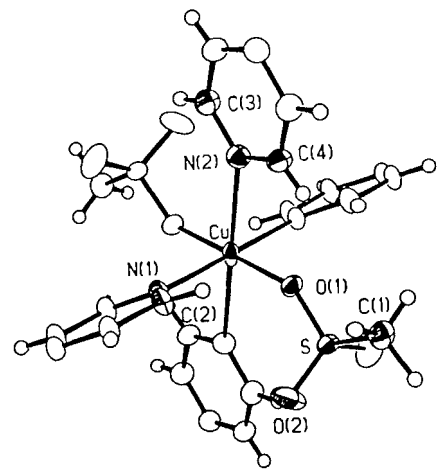

FIG. 2. Inner coordination sphere about the copper(II) ion in $Cu(N_2C_4H_4)_2(CH_3SO_3)_2$; 50% probability thermal ellipsoids are shown for the non-hydrogen atoms; crystallographically unique atoms are shaded and labelled.

In spite of being coordinated to copper at different distances, the pyrazine rings in $Cu(pyz)_2(CH_3SO_3)_2$ have similar internal bonding parameters. Both types of pyrazine ring are planar within experimental error and the bond lengths and angles within the pyrazine rings are similar to those found in free pyrazine (20). The dimensions of the pyrazine rings compare well with those reported for other metal complexes containing bidentate bridging pyrazine ligands. For example, in the Creutz–Taube (21, 22) complex the mean C—N bond length is 1.348(9) Å and the C—C distance is 1.382(10) Å; in $Cu(pyz)_2(CH_3SO_3)_2$ these distances are 1.341(2) and 1.390(3) Å, respectively. The pyrazine rings involved in the stronger bonding to copper are canted at an angle of 28.50(8)° to the $CuN_2O_2(xy)$ plane;

Can. J. Chem. Downloaded from www.nrcresearchpress.com by 80.58.250.72 on 09/07/12
For personal use only.

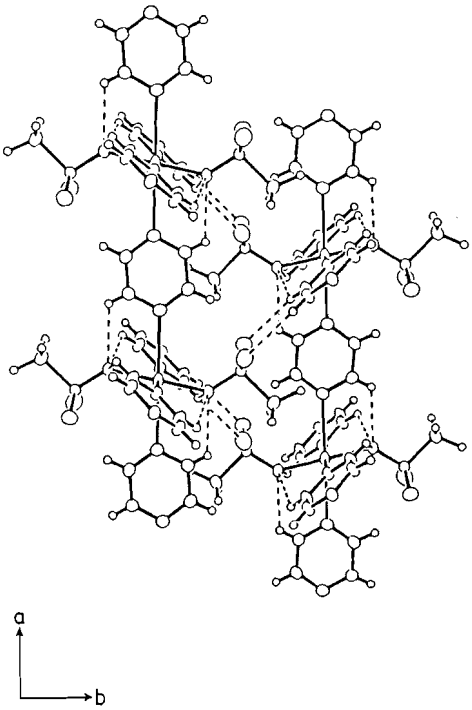

FIG. 3. Two adjacent layers in $Cu(N_2C_4H_4)_2(CH_3SO_3)_2$ viewed along the *c*-axis; hydrogen bonding interactions shown by broken lines.

whereas the pyrazine rings bonded axially lie in the $CuN_2O_2(xz)$ plane.

The $CH_3SO_3^-$ anion in $Cu(pyz)_2(CH_3SO_3)_2$ assumes a staggered-ethane configuration about the S—C bond. Repulsions between oxygen atoms on sulfur are greater than those between oxygen atoms and the methyl group; as a result, the O—S—O angles are consistently greater than the C—S—O angles. The effect of monodentate coordination on the geometry of the anion is most evident in the range of S—O bond distances observed. The S—O(1) bond involving the oxygen coordinated to copper is longest at 1.483(1) Å while the terminal S—O bonds are 1.442(1) Å. The rather long S—O(1) bond observed here compared to S to coordinated O bonding distances of 1.429–1.456 Å in $Ca(CH_3SO_3)_2$ (23), 1.445–1.462 Å in $Cu(CO)(C_2H_5SO_3)_2$ (24), 1.441 Å in $Cu(H_2O)_4(CH_3SO_3)_2$ (25), and 1.460–1.463 Å in $Cd(H_2O)_2(CH_3SO_3)_2$ (26) attest to the strength of the in-plane coordination of the $CH_3SO_3^-$ group in the pyrazine complex.

There are several C—H···O interactions which may play a role in determining the overall structure of $Cu(pyz)_2(CH_3SO_3)_2$ (Fig. 3). Intralayer C—H···O interactions between the sulfonate oxygen atom O(1) and the hydrogen atoms attached to the pyrazine rings appear to influence the canting of the pyrazine rings; H(4)···O(1) and H(2)···O(1) distances are 2.50 and 2.46 Å, respectively. The first of these interactions appears to hold the axial pyrazine group in the CuN_2O_2 plane; whereas, the second interaction may be at least partially responsible for the fact that the equatorially bound pyrazine ligand is canted at an angle of 28.5° to the CuN_2O_2 plane.

In $Cu(pyz)_2(CH_3SO_3)_2$, the layers are separated by a distance of 6.565 Å. In comparison, the interlayer separation in $Cu(pyz)_2(ClO_4)_2$ (1) is 7.012 Å. The proximity of adjacent layers in the methanesulfonate complex may result from interlayer C—H···O interactions. There appear to be two such interactions, H(1b)···O(2) (2.38 Å) and H(2)···O(2) (2.50 Å) which may be significant. Both involve the terminally bound sulfonate oxygen atom, O(2), which interacts with a hydrogen atom of a methanesulfonate anion and a hydrogen atom of the equatorially bound pyrazine ligand on an adjacent layer.

TABLE 8. Infrared spectra, anion vibrations

Assignments[b]	Infrared frequencies (cm^{-1})[a]	
	$Cu(pyz)_2(CH_3SO_3)_2$	$Cu(py)_4(CH_3SO_3)_2$
$\nu_4(E)$	1257 s 1162 s	1232 s 1183 s
$\nu_1(A_1)$	1035 s	1043 s
$\nu_2(A_1)$	778 s	773 s
$\nu_3(A_1)$, $\nu_5(E)$	572 s 542 m 529 m	559 s 532 s

[a] s = strong, m = medium.
[b] Assignments (CSO_3 part, C_{3v} symmetry) from ref. 27.

Differential scanning calorimetry (DSC)

To characterize more fully the title compound in terms of its thermal stability, particularly in view of the fact that the X-ray studies showed one of the pyrazine ligands to be relatively weakly bound, we examined the compound and the related pyridine complex, $Cu(py)_4(CH_3SO_3)_2$ by DSC. $Cu(pyz)_2(CH_3SO_3)_2$ shows an endothermic event at 188°C (ΔH = 62 kJ mol^{-1}) which, according to an approximate weight loss measurement (27), corresponds to the loss of one mole of pyrazine, presumably the more weakly bound axial ligand. Loss of the second mole of pyrazine occurs at approximately 300°C near which temperature the onset of exothermic oxidative decomposition takes place. In comparison, $Cu(py)_4(CH_3SO_3)_2$ shows two closely spaced endothermic events at 180 and 196°C. While enthalpy changes associated with these events were estimated at ~90 and 50 kJ mol^{-1}, respectively, it was not possible to establish weight changes associated with each event. Heating a sample of the compound to a temperature slightly above 196°C gave a weight loss intermediate between that expected for the loss of 2 and 3 mol of pyridine. Exothermic oxidative decomposition takes place, in this case, at temperatures above approximately 257°C. In summary, in spite of the presence of axially bound pyrazine groups, $Cu(pyz)_2(CH_3SO_3)_2$ is at least as thermally stable as its pyridine analogue, showing no measurable decomposition up to temperatures of about 167°C (onset of the first endothermic event).

Spectroscopic studies

By comparing the infrared spectra of $Cu(pyz)_2(CH_3SO_3)_2$ and $Cu(py)_4(CH_3SO_3)_2$ with those of the neutral ligands and related complexes (28–31) it is possible to identify those bands arising primarily from internal vibrations of the methanesulfonate groups. These bands are listed in Table 8. Monodentate coordination by the anion results in a lowering in symmetry of the CSO_3 moiety and a consequent splitting of the doubly degenerate (in C_{3v} symmetry) SO_3 asymmetric stretching and deformation modes, ν_4 and ν_5, are expected. In $Cu(pyz)_2(CH_3SO_3)_2$, ν_4 is split by 95 cm^{-1} and the appearance of three medium to strong bands in the deformation region ($\nu_3(A_1)$, $\nu_5(E)$) clearly indicates a splitting of ν_5. In contrast, $Cu(py)_4(CH_3SO_3)_2$ exhibits a splitting of only 49 cm^{-1} in ν_4 and there is no observable splitting of ν_5 in this complex. We interpret these differences as being a consequence of the fact that while the sulfonate anion is coordinated strongly in an equatorial position in the pyrazine complex, it is coordinated more weakly in an axial

Can. J. Chem. Downloaded from www.nrcresearchpress.com by 80.58.250.72 on 09/07/12
For personal use only.

position in the pyridine complex. Axial sulfonate coordination was proposed earlier for $Cu(py)_4(FSO_3)_2$, a complex in which ν_4 is split by 50 cm^{-1} (29). Infrared absorptions assignable to pyridine vibrations occur as expected in $Cu(py)_4(CH_3SO_3)_2$. In particular, the 8*a*, 6*a*, and 16*b* vibrations, at 1606, 641, and 440 cm^{-1} respectively, show the expected shifts to higher frequencies on coordination (29). Many of the pyrazine fundamentals are obscured by the broader and generally more intense sulfonate absorptions in the infrared spectrum of $Cu(pyz)_2(CH_3SO_3)_2$. However, little interference between anion and neutral ligand bands occurs below 900 cm^{-1} and it is possible to assign medium to strong intensity bands at 846, 813, 494, and 440 cm^{-1} to pyrazine vibrations. Pure liquid pyrazine has only two corresponding bands at 804 and 417 cm^{-1} (22, 23) and the apparent doubling of fundamentals in the complex is likely a consequence of the presence of two structurally distinct bridging pyrazine ligands in this compound.

The electronic spectrum of $Cu(py)_4(CH_3SO_3)_2$ shows a broad absorption with a maximum at 16 800 cm^{-1}. This compares favorably with the spectra reported (29, 32) for the complexes $Cu(py)_4(XSO_3)_2$ (X = CF_3, F, *p*-$CH_3C_6H_4$; abs. max. = 17 400, 17 200, and 16 900 cm^{-1}) and is consistent with all four complexes having elongated tetragonal octahedral CuN_4O_2 chromophores with axially bound sulfonates. A recent X-ray crystal structure determination has confirmed this structure for $Cu(py)_4(CF_3SO_3)_2$ (32). In contrast, the X-ray diffraction studies in the present work have revealed a rhombic distorted $CuO_2N_2N'_2$ chromophore in $Cu(pyz)_2(CH_3SO_3)_2$ and this structural difference is manifested in a shift in the electronic spectrum to lower energies. $Cu(pyz)_2(CH_3SO_3)_2$ exhibits a broad absorption with a maximum at 14 000 cm^{-1}.

Magnetic studies

Magnetic susceptibilities of both $Cu(py)_4(CH_3SO_3)_2$ and $Cu(pyz)_2(CH_3SO_3)_2$ were measured from 82 to 4.2 K; data are listed in Table 9 (deposited) and plotted as magnetic moment versus temperature in Fig. 4. Although there appears to be a slight increase in μ_{eff} with decreasing temperature for the pyridine complex, the variation with temperature is not large, and the values of μ_{eff} are of the same magnitude as reported previously for analogous fluorosulfate and paratoluenesulfonate complexes (29). In contrast, μ_{eff} for the pyrazine complex shows a strong temperature dependence with the value decreasing from 1.78 BM at 82 K to 0.85 BM at 4.2 K, suggesting the presence of relatively strong antiferromagnetic coupling in this material. The effect of magnetic concentration is more clearly seen in the magnetic susceptibility data, which exhibits a maximum at approximately 6.2 K (Fig. 5). Rather long Cu···Cu distances (6.9134(2) and 8.1991(4) Å along the *c* and *a* cell edges, Fig. 1) tend to rule out direct exchange between metal centres and the presence of pyrazine bridges suggests superexchange through the bridging ligands.

Particularly relevant to this work are the studies on $Cu(pyz)_2(ClO_4)_2$ (1, 2) where X-ray crystallography has revealed important structural similarities and differences with the compound studied here. The magnetic susceptibility of $Cu(pyz)_2(ClO_4)_2$ exhibits a maximum value at 12.1 K (2), and Darriet *et al.* (1) successfully modelled these data by using Lines' high-temperature series-expansion expression for a two-dimensional square-planar antiferromagnet in the Heisenberg limit (33). The parameters obtained by fitting the magnetic susceptibility data were $J = -5.3\ cm^{-1}$ and $g = 2.107$. Fitting the magnetic susceptibility data for $Cu(pyz)_2(CH_3SO_3)_2$ to this two-dimensional model,

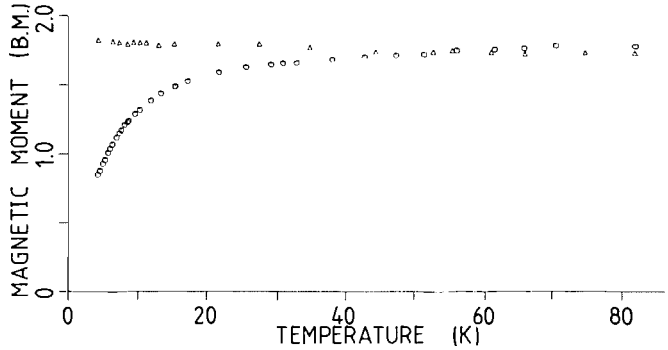

FIG. 4. Magnetic moment versus temperature for $Cu(NC_5H_5)_4(CH_3SO_3)_2$ (△) and $Cu(N_2C_4H_4)_2(CH_3SO_3)_2$ (□).

yields a best fit[4] with the parameters $J = -2.48\ cm^{-1}$ and $g = 2.15$ ($F = 0.0118$). As measured by the exchange coupling parameter, *J*, the magnitude of the magnetic exchange in the methanesulfonate complex is approximately one half of that calculated for $Cu(pyz)_2(ClO_4)_2$. Several possibilities exist to explain this relative diminution of *J* in $Cu(pyz)_2(CH_3SO_3)_2$. The first is that the methanesulfonate anion, by acting as a stronger Lewis base than the perchlorate anion towards copper, effectively decreases the acidity of the copper(II) ions towards the bridging pyrazine groups and hence, lowers the intralayer exchange interaction. A second alternative explanation is related to the fact that in the perchlorate derivative the pyrazine groups are equivalent and oriented in a way so as to interact effectively with the unpaired electron density on the copper(II) ions, resulting in an equal contribution from each pyrazine ligand to the overall exchange interaction. In $Cu(pyz)_2(CH_3SO_3)_2$, however there are two distinct pyrazine ligands and the exchange integral for each bridging pyrazine is likely to be dependent upon two factors: the degree of separation of the two copper ions (length of the bridge) and the orientation of the pyrazine π-system with respect to the copper *d*-orbitals. In $Cu(pyz)_2(CH_3SO_3)_2$ adjacent copper(II) ions are separated by either 6.9134(2) Å when the intervening pyrazine group is strongly bound in the equatorial plane, or 8.1991(4) Å, when the intervening pyrazine group is weakly bound in an axial position. Considering distances alone, it would be expected that the shorter the Cu···Cu separation is, the greater would be the magnetic exchange effect. Thus, the equatorially bound pyrazine groups may be expected to transmit exchange coupling effects more efficiently than the axially bound pyrazine groups.

It has been shown previously that for pyrazine groups bound in the equatorial, *xy*, plane the orientation of the plane of the ligand with respect to the *xy* plane of the copper chromophore also plays an important role in determining the effectiveness of exchange. Earlier research (7) has demonstrated that for copper–pyrazine complexes in which the unpaired electron is in the $d_{x^2-y^2}$ orbital (as the tetragonally elongated pseudo-octahedral environment suggests it is in $Cu(pyz)_2(CH_3SO_3)_2$) the magnitude of the antiferromagnetic exchange is determined from the overlap of the $d_{x^2-y^2}$ orbital and the pyrazine π-system. This

[4]A least-squares fitting procedure allows both *J* and *g* to vary until a minimum value is obtained for the function *F*;

$$F = \left[\frac{1}{n}\Sigma\left(\frac{\chi_i^{calcd} - \chi_i^{obs}}{\chi_i^{obs}}\right)^2\right]^{1/2}$$

where *n* is the number of data points and χ_i^{obs} and χ_i^{calcd} are the experimental and calculated molar magnetic susceptibilities.

Can. J. Chem. Downloaded from www.nrcresearchpress.com by 80.58.250.72 on 09/07/12
For personal use only.

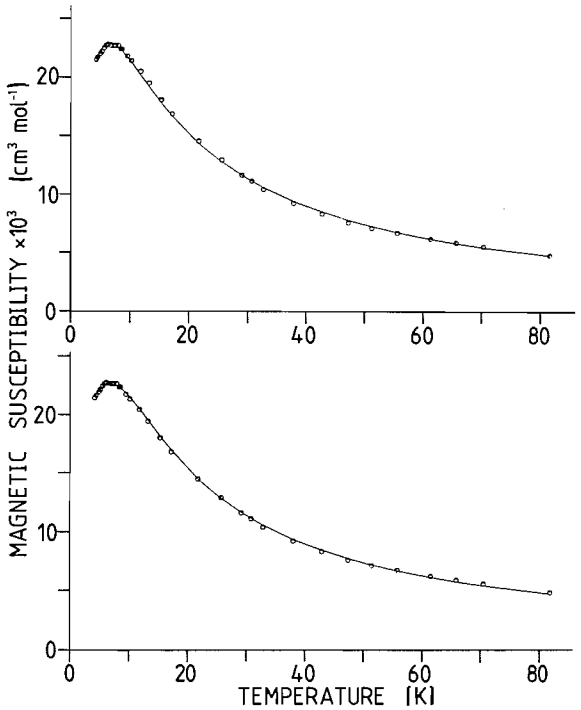

FIG. 5. Magnetic susceptibility versus temperature for $Cu(N_2C_4H_4)_2(CH_3SO_3)_2$. Upper: two-dimensional model; solid line generated with $J = -2.48\,cm^{-1}$ and $g = 2.15$. Lower: linear chain model; solid line generated with $J = -3.82\,cm^{-1}$, $g = 2.13$.

interaction, however, is only possible when the pyrazine ring is canted out of the *xy* plane. For example, the pyrazine rings in $Cu(pyz)_2(ClO_4)_2$ (1) and $Cu(pyz)(NO_3)_2$ (3) are canted out of the *xy* plane by angles of 66.1 and 50°, respectively, and significant magnetic exchange interactions are observed (1, 5). On the other hand, in $Cu(pyzA)_2(ClO_4)_2$ (where pyzA is pyrazine-2-carboxamide), the pyrazine rings lie in the *xy* plane (34) resulting in orthogonal overlap and a magnetically-dilute system (35). These previous studies and the X-ray structure results for $Cu(pyz)_2(CH_3SO_3)_2$ suggest that the equatorially bound pyrazine group in the methanesulfonate compound, which is canted out of the *xy* plane by 28.5°, is suitably oriented to present a π-pathway for magnetic interactions between copper centres.

The axially coordinated pyrazine in $Cu(pyz)_2(CH_3SO_3)_2$ is structurally similar to the bridging pyrazine group in the hexafluoroacetylacetonate complex $Cu(pyz)(hfac)_2$ (4). In both instances the Cu—N bonds are long and the plane of the pyrazine ring lies in the *xz* plane of the molecule. It was argued (7) that both the length of the Cu—N bonds and the orientation of the pyrazine ring, which did not permit effective d–π overlap with copper, accounted for the fact that no significant magnetic exchange was seen in the hfac complex. This suggests that the axial pyrazines may also be ineffective in propagating magnetic exchange in $Cu(pyz)_2(CH_3SO_3)_2$.

The above comparison of pyrazine group coordination modes in $Cu(pyz)_2(CH_3SO_3)_2$ with those in other copper(II)–pyrazine complexes suggests that the magnetic exchange interaction in the methylsulfonate derivative may proceed via two different routes, with the exchange interaction through the equatorially bound pyrazine, J_{eq}, significantly stronger than the exchange, J_{ax}, through the axially bound pyrazine. In the extreme case where $J_{eq} \gg J_{ax}$, the magnetic properties may be more closely represented by a one-dimensional linear chain model. A model has been proposed for the analysis of the magnetic susceptibility of a Heisenberg linear chain for $S = 1/2$ ions. Hall (36) and Hatfield and co-workers (37) developed the model proposed by Bonner and Fisher (38); this resulted in an expression for the molar susceptibility of a linear chain of interacting $S = 1/2$ spins as a polynomial expansion. The best fit of the data for $Cu(pyz)_2(CH_3SO_3)_2$ to this model is equally as good as the best fit to the two-dimensional model; for the one-dimensional model the parameters obtained from the best fit are $J = -3.82$ cm^{-1} and $g = 2.13$, with $F = 0.0118$. The best fit is represented by the solid line in Fig. 5. Unfortunately the magnetic exchange in $Cu(pyz)_2(CH_3SO_3)_2$ is not sufficiently strong to enable one to distinguish between one- and two-dimensional pathways on the basis of magnetic properties alone. On the basis of structural considerations discussed above, however, it seems most reasonable to consider the compound to consist of linear chains of —Cu—pyz—Cu— units, in which there are relatively strong intrachain magnetic exchange interactions and although these linear chains are crosslinked through the weakly bound axial pyrazine groups the interchain interactions are of a much smaller magnitude.

Acknowledgements

We thank the Natural Sciences and Engineering Research Council of Canada for financial support and the University of British Columbia Computing Centre for assistance. J.S.H. thanks the U.B.C. Graduate Scholarship Committee for scholarship awards.

1. J. DARRIET, M. S. HADDAD, E. N. DUESLER, and D. N. HENDRICKSON. Inorg. Chem. **18**, 2679 (1979).
2. M. S. HADDAD, D. N. HENDRICKSON, J. P. CANADY, R. S. DRAGO, and D. S. BIEKYSA. J. Am. Chem. Soc. **101**, 898 (1979).
3. A. SANTORO, A. D. MIGHELL, and C. W. REIMANN. Acta Crystallogr. Sect. B, **26**, 979 (1970).
4. R. C. E. BELFORD, D. E. FENTON, and M. R. TRUTER. J. Chem. Soc. Dalton Trans. 17 (1974).
5. J. F. VILLA and W. E. HATFIELD. J. Am. Chem. Soc. **93**, 4081 (1971).
6. P. D. W. BOYD and S. MITRA. Inorg. Chem. **19**, 3547 (1980).
7. H. W. RICHARDSON, J. R. WASSON, and W. E. HATFIELD. Inorg. Chem. **16**, 484 (1977).
8. A. L. ARDUINI, M. GARNETT, R. C. THOMPSON, and T. C. T. WONG. Can. J. Chem. **53**, 3812 (1975).
9. J. S. HAYNES, K. W. OLIVER, and R. C. THOMPSON. Can. J. Chem. **63**, 1111 (1985).
10. J. S. HAYNES, K. W. OLIVER, S. J. RETTIG, R. C. THOMPSON, and J. TROTTER. Can. J. Chem. **62**, 891 (1984).
11. P. COPPENS, L. LEISEROWITZ, and D. RABINOVICH. Acta Crystallogr. **18**, 1035 (1965).
12. W. R. BUSING and H. A. LEVY. Acta Crystallogr. **22**, 457 (1967).
13. D. T. CROMER and J. B. MANN. Acta Crystallogr. Sect. A, **24**, 321 (1968).
14. R. F. STEWART, E. R. DAVIDSON, and W. T. SIMPSON. J. Chem. Phys. **42**, 3175 (1965).
15. D. T. CROMER and D. LIBERMAN. J. Chem. Phys. **53**, 1891 (1970).
16. P. J. BECKER and P. COPPENS. Acta Crystallogr. Sect. A, **30**, 129 (1974); **30**, 148 (1974); **31**, 417 (1975).
17. P. COPPENS and W. C. HAMILTON. Acta Crystallogr. Sect. A, **26**, 71 (1970).
18. F. R. THORNLEY and R. J. NELMES. Acta Crystallogr. Sect. A, **30**, 748 (1974).

Can. J. Chem. Downloaded from www.nrcresearchpress.com by 80.58.250.72 on 09/07/12
For personal use only.

19. B. MOROSIN, R. C. HUGHES, and Z. G. SOOS. Acta Crystallogr. Sect. B, **31**, 762 (1975).
20. P. J. WHEATLEY. Acta Crystallogr. **10**, 182 (1957).
21. C. CREUTZ and H. J. TAUBE. J. Am. Chem. Soc. **91**, 3988 (1969).
22. J. K. BEATTIE, N. S. HUSH, P. R. TAYLOR, C. L. RASTON, and A. H. WHITE. J. Chem. Soc. Dalton Trans. 1121 (1977).
23. F. CHARBONNIER, R. FAURE, and H. LOISELEUR. Acta Crystallogr. Sect. B, **33**, 1478 (1977).
24. G. DOYLE, K. A. ERIKSEN, and D. VAN ENGEN. Inorg. Chem. **22**, 2892 (1983).
25. F. CHARBONNIER, R. FAURE, and H. LOISELEUR. Acta Crystallogr. Sect. B, **33**, 1845 (1977).
26. F. CHARBONNIER, R. FAURE, and H. LOISELEUR. Acta Crystallogr. Sect. B, **34**, 1504 (1978).
27. J. S. HAYNES, S. J. RETTIG, J. R. SAMS, R. C. THOMPSON, and J. TROTTER. Can. J. Chem. **64**, 429 (1986).
28. N. S. GILL, R. H. NUTTALL, D. E. SCARFE, and D. W. A. SHARP. J. Inorg. Nucl. Chem. **18**, 79 (1961).
29. C. S. ALLEYNE and R. C. THOMPSON. Can. J. Chem. **52**, 3218 (1974).
30. R. C. LORD, A. L. MARSTON, and A. F. MILLER. Spectrochim. Acta, **9**, 113 (1957).
31. M. GOLDSTEIN and W. D. UNSWORTH. Spectrochim. Acta, **27A**, 1055 (1971).
32. J. S. HAYNES. Ph.D. Thesis. University of British Columbia. 1985.
33. M. E. LINES. J. Phys. Chem. Solids, **31**, 101 (1970).
34. M. SEKIZAKI. Acta Crystallogr. Sect. B, **29**, 327 (1973).
35. R. P. ECKBERG and W. E. HATFIELD. J. Chem. Soc. Dalton Trans. 616 (1975).
36. J. W. HALL. Ph.D. Thesis. University of North Carolina. 1977.
37. W. E. ESTES, W. E. HATFIELD, J. A. C. VAN OIJEN, and J. REEDIJK. J. Chem. Soc. Dalton Trans. 2121 (1980).
38. J. C. BONNER and M. E. FISHER. Phys. Rev. **135**, A 640 (1964).

Can. J. Chem. Downloaded from www.nrcresearchpress.com by 80.58.250.72 on 09/07/12
For personal use only.

Total synthesis of the ravidomycin aglycone (defucogilvocarcin V)

JOHN A. FINDLAY, ANAND DALJEET, PETER JOHN MURRAY, AND RABINDRA N. REJ
Chemistry Department, University of New Brunswick, Fredericton, N.B., Canada E3B 6E2

Received July 24, 1986

JOHN A. FINDLAY, ANAND DALJEET, PETER JOHN MURRAY, and RABINDRA N. REJ. Can. J. Chem. **65**, 427 (1987).

The synthesis of 1-hydroxy-10,12-dimethoxy-8-vinyl-6*H*-benzo[*d*]naphtho[1,2*b*]pyran-6-one **7**, starting from vanillin and 1,5-dihydroxynaphthalene is described. This compound is the aglycone of the antitumor antibiotic ravidomycin and is identical with the recently reported antimicrobial agent, defucogilvocarcin V.

JOHN A. FINDLAY, ANAND DALJEET, PETER JOHN MURRAY et RABINDRA N. REJ. Can. J. Chem. **65**, 427 (1987).

Utilisant la vanilline et le dihydroxy-1,5 naphtalène comme produits de départ, on a synthétisé l'hydroxyl-1 diméthoxy-10,12 vinyl-8 6*H*-benzo[*d*]naphto[1,2*b*]pyrannone-6 (**7**). Ce produit est l'aglycone de l'antibiotique antitumoral, ravidomycine, et il est identique à l'agent antimicrobien rapporté récemment, défucogilvocarcine V.

[Traduit par la revue]

Introduction

Members of the chrysomycin family of antibiotics are produced by several strains of *Streptomycetes*. These compounds are yellow in colour and possess a common benzonaphthopyranone system attached to different C-glycoside moieties. The members of this family reported to date are toromycin (gilvocarcin V) **1** (1), gilvocarcin M **2** (2), and gilvocarcin E **3**, chrysomycin V **4**, chrysomycin M **5** (3), and ravidomycin **6** (4). The letters V, M, and E signify vinyl, methyl, and ethyl, respectively, the single, but important, variation in the aglycone structure among members of a category within the family. Toromycin from *Streptomyces collinus* was shown to be identical to gilvocarcin V isolated from *S. gilvotanareus* (2*e*).

This class of compounds has aroused considerable interest in view of the antibiotic and antitumor activity of its members (5). In particular, chrysomycin V **4**, gilvocarcin V **1**, and ravidomycin **6** have been shown to possess potent antitumor activity and it has been concluded, by Elespuru and Gonda (6), that the C4 vinyl group is essential for potent antitumor properties.

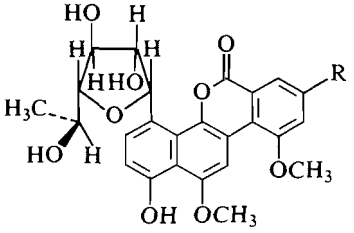

1 R = CH=CH$_2$
2 R = CH$_3$
3 R = CH$_2$CH$_3$

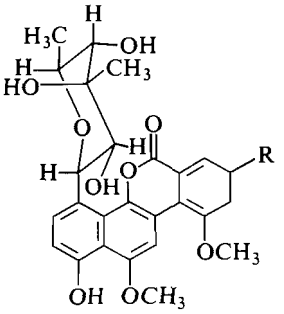

4 R = CH=CH$_2$
5 R = CH$_3$

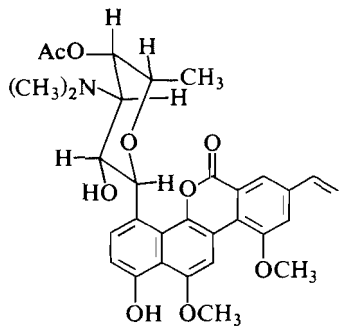

6

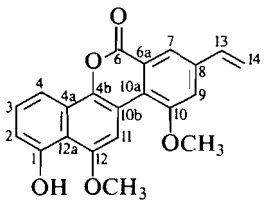

7

When we embarked on structural studies on ravidomycin in early 1980, the structures of the chrysomycins and gilvocarcins had not been published. Since ravidomycin and derivatives were not amenable to solution by X-ray methods, we deduced the complete structure and stereochemistry principally by chemical degradation studies and ^{1}H and ^{13}C nmr spectroscopy (4). A key degradation product in our work was the aglycone **7** obtained by fusion of ravidomycin **6** with potassium hydroxide. Very recently Misra *et al.* (8) have isolated **7** from the acetone extract of the mycelia of *Streptomyces arenae* 2064. They have shown it to possess antimicrobial activity and have designated it defucogilvocarcin V and suggested that its presence in the fermentation broth indicates that in the biogenesis of gilvocarcins the sugar moiety is probably attached to the chromophore **7** after it has been assembled.

In view of the importance of the aglycone in our structural elucidation of ravidomycin and the increasing interest in the chrysomycin family of antibiotics, we undertook synthetic studies targeted at 1-hydroxy-10,12-dimethoxy-8-vinyl-6*H*-benzo[*d*]naphtho[1,2*b*]pyran-6-one **7** and now present our work.

The key step in our synthetic approach involves the union of the appropriately functionalized Grignard reagent of naphthalene **10** with the protected substituted benzoic acid derivative **16** via a nucleophilic aromatic substitution producing the phenyl naphthalene **17**. The previously described (7) 5-acetoxy-2-bromo-1,4-naphthoquinone **9**, obtained in 92% yield from 1,5-dihydroxynaphthalene **8**, was reduced with sodium dithionite and immediately methylated with dimethyl sulfate/potassium hydroxide to provide the Grignard precursor **10** (43%). 3-Bromo-4,5-dimethoxybenzaldehyde **12** was prepared in 95% yield from vanillin by bromination to **11** (9), followed by methylation with iodomethane in refluxing acetone containing anhydrous potassium carbonate. A Wittig reaction on **12** afforded **13** (96% yield), which was transformed via Grignard reaction with carbon dioxide to the acid **14** in 55% yield. Attempts to protect the carboxyl group by introduction of a Δ^2-oxazoline using conditions developed by Meyers *et al.* (10) gave rise to mixtures of products, apparently due to the sensitivity of the vinyl group to the acidic medium. It was necessary then to reintroduce the vinyl group at a later stage. Catalytic reduction of the vinyl group and protection of the carbonyl group afforded the key intermediate Δ^2-oxazoline **16** in 80% yield from **14**. Thus the appropriately functionalized and protected naphthalene

Can. J. Chem. Downloaded from www.nrcresearchpress.com by 80.58.250.72 on 09/07/12
For personal use only.

Can. J. Chem. Downloaded from www.nrcresearchpress.com by 80.58.250.72 on 09/07/12
For personal use only.

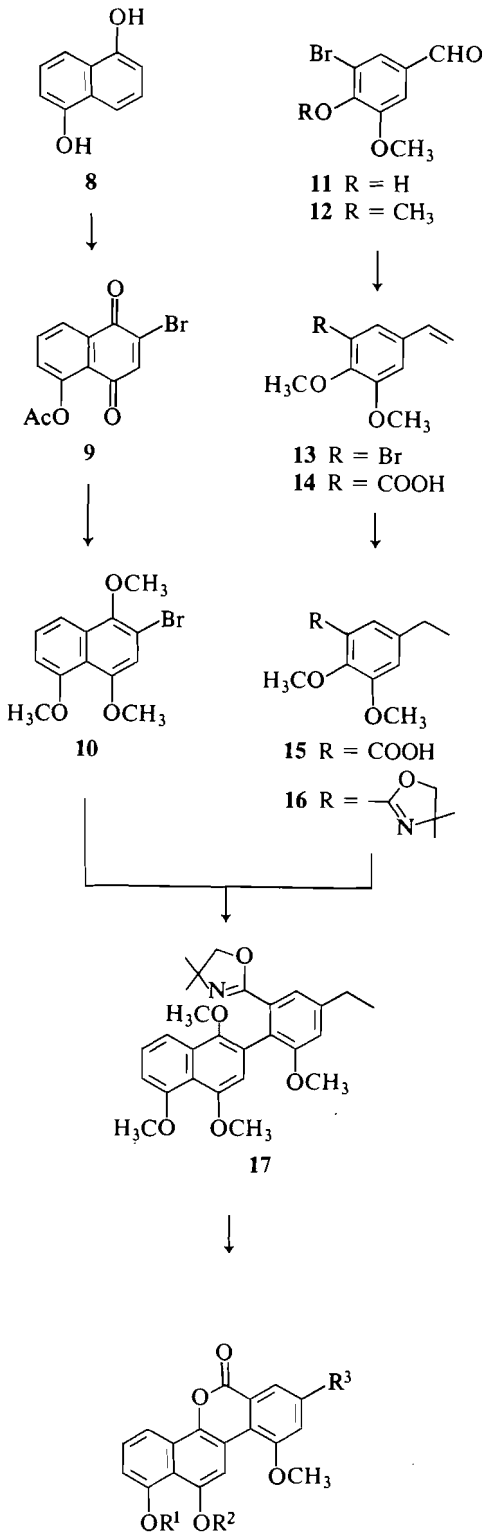

18 R^1, R^2 = H, R^3 = CH_2CH_3
19 R^1, R^2 = Ac, R^3 = CH_2CH_3
20 R^1 = Ac, R^2 = CH_3, R^3 = CH_2CH_3
21 R^1 = CH_3, R^2 = Ac, R^3 = CH_2CH_3
22 R^1, R^2 = CH_3, R^3 = CH_2CH_3
23 R^1 = Ac, R^2, R^3 = CH_3
24 R^1 = Ac, R^2 = CH_3, R^3 = $CHCH_3$ (Br)
25 R^1 = Ac, R^2 = CH_3, R^3 = $CH{=}CH_2$

10 and benzoic acid derivative **16** were prepared in simple and efficient pathways from readily available inexpensive precursors.

The convergent coupling reaction producing the phenylnaphthalene **17** in 81% yield was accomplished by adding the Δ^2-oxazoline **16** to the Grignard reagent of **10** using conditions pioneered by Meyers *et al.* (10) in other endeavours. Treatment of **17** with refluxing glacial acetic acid – hydriodic acid (1:1) effected deprotection of the carbonyl group, demethylation at three sites, and lactonization, giving **18** in 77% yield in one step.

The site of the remaining methoxyl in **18** was ascertained by comparison of the ^{1}H nmr spectra with those in its diacetate **19** (11). Thus acetylation shifts of δ +0.38, +0.46, and +0.61 ppm were noted for signals due to C11H, C2H, and C4H, while virtually no difference was noted for signals assigned to C9H and C7H. Thus the phenolic groups in **18** must be placed at C1 and C12.

Methylation of phenolic lactone **18** using one equivalent of iodomethane and anhydrous potassium carbonate in dimethylsulfoxide–acetone afforded a mixture of **20** and **21** (3:2) in 86% yield, separable by preparative thin-layer chromatography. Location of the acetate moiety in these isomers was readily accomplished by comparison of chemical shifts for the aromatic protons with those in compound **18** and its trimethoxy derivative **22**. The chemical shift assignments for monoacetate **21** are in close agreement with those for the homologous compound **23** obtained by Takahashi *et al.* (2*b*) upon treatment of the tetraacetate of gilvocarcin M **2** with HCl in refluxing methanol followed by acetylation.

Introduction of the vinyl group in **20** was effected by bromination with one equivalent of *N*-bromosuccinimide, giving the monobromide **24** in 75% yield. The latter was converted in 40% yield to the aglycone **7** via the phenyl selenoxide derivative using methodology developed by Sharpless *et al.* (12). Alternatively, the vinyl group can be introduced by treatment of **20** with two equivalents of *N*-bromosuccinimide in refluxing carbon tetrachloride containing a catalytic amount of dibenzoyl peroxide to give the acetate **25**.

1-Hydroxy-10,12-dimethyl-8-vinyl-6*H*-benzo[*d*]naphtho-[1,2*b*]pyran-6-one **7** prepared via this route was identical in all physical and spectroscopic properties with those of the aglycone obtained by alkali fusion of ravidomycin, and was consistent with those reported (8) for the antibiotic defucogilvocarcin V.

Experimental

General

All melting points were determined on a Kofler hot stage apparatus and are uncorrected. High resolution mass spectra were recorded on an AEI MS-50 spectrometer at the Mass Spectrometry Lab, University of Alberta. The infrared spectra were recorded on Perkin–Elmer 727B or 598 spectrophotometers and ultraviolet spectra were obtained with a Beckman 25 instrument.

Nuclear magnetic resonance spectra were recorded on a Varian XL-200 spectrometer using tetramethylsilane (TMS) as internal standard. Sodium 2,2-dimethyl-2-silapentane-5-sulfonate (DSS) was also used as an internal standard when DMSO-d_6 was employed as a solvent.

Column chromatograms were prepared using silica gel G or Kieselgel 60 (230–400 mesh) packed in chloroform or hexane. Analytical thin-layer chromatography (tlc) was done on precoated silica plates (silica gel 60-F-254) 20 cm × 20 cm and 0.5, 1, or 2 mm thickness.

*2-Bromo-1,4,5-trimethoxynaphthalene **10***

2-Bromo-5-acetoxy-1,4-naphthaquinone **9** (5) (1.3 g, 4.4 mmol)

Can. J. Chem. Downloaded from www.nrcresearchpress.com by 80.58.250.72 on 09/07/12
For personal use only.

dissolved in ethyl acetate – ether (1:10, 100 mL) was shaken vigorously with freshly prepared saturated aqueous sodium dithionite solution (2 × 50 mL) in a separatory funnel. The ether layer was washed with water (50 mL), saturated sodium chloride solution (50 mL), dried, and filtered immediately. The solvent was removed *in vacuo* below 15°C and the resulting dry solid dissolved in absolute ethanol (25 mL) and treated with dimethylsulfate (2.5 g). To this vigorously stirred, ice-cooled solution sodium hydroxide solution (10 mL, 40%) was added dropwise over one hour. After one more hour additional sodium hydroxide (3 mL, 40%) was added to ensure basicity and the mixture was stirred overnight. Ethanol was then removed *in vacuo* at 15°C and the resulting solution dissolved in water (200 mL) and extracted with ether (3 × 30 mL). The combined ether extract was washed with aqueous sodium hydroxide (20 mL, 20%), water (2 × 75 mL), and saturated sodium chloride solution (50 mL), and dried. After evaporation of solvent, the residue was flash chromatographed yielding 2-bromo-1,4,5-trimethoxynaphthalene **10** (0.56 g, 43%), which was recrystallized from hexane–ether to provide a white crystalline solid, mp 109–112°C; uv (CH_3OH) λ_{max} nm (log ε): 231 (4.92), 305 (4.05), 323 (4.03), 338 (4.05); ir ($CHCl_3$) ν_{max}: 1610, 1580 (aromatic) cm^{-1}; ^1H nmr ($CDCl_3$) δ: 3.91 (s, 6H, 2 × OCH_3), 3.99 (s, 3H, OCH_3), 6.86 (dd, 1H, J = 1.0 Hz, J = 7.9 Hz, C6H), 6.90 (s, 1H, C3H), 7.42 (dd, 1H, J = 7.9 Hz, J = 8.4 Hz, C7H), 7.68 (dd, 1H, J = 1.0 Hz, J = 8.5 Hz, C8H). *Exact Mass* calcd. for $C_{13}H_{13}O_3Br$: 298.0027; found: 298.0020 (M^+, 76).

3-Bromo-4,5-dimethoxybenzaldehyde 12

3-Bromo-4-hydroxy-5-methoxybenzaldehyde **11** (9) (1.0 g, 4.33 mmol) in anhydrous acetone (30 mL) was treated with anhydrous potassium carbonate (1.5 g) and excess iodomethane and the mixture was refluxed for 20 h. The solution was cooled, filtered, and evaporated, and the resulting oil dissolved in ether, washed with water and with saturated sodium chloride solution, dried, and evaporated to yield crystalline 3-bromo-4,5-dimethoxybenzaldehyde **12** (1.01 g, 95%), mp 53–54°C; uv (CH_3OH) λ_{max} nm (log ε): 210 (4.8), 218 (4.5), 272 (3.78), 302 (3.40); ir ($CHCl_3$) ν_{max}: 1690 (C=O), 1600 (aromatic) cm^{-1}; ^1H nmr ($CDCl_3$) δ: 3.95 (s, 3H, OCH_3), 3.96 (s, 3H, OCH_3), 7.40 (d, 1H, J = 1.8 Hz), 7.66 (d, 1H, J = 1.8 Hz), 9.86 (s, 1H, C*H*O). *Exact Mass* calcd. for $C_9H_9O_3Br$: 245.9715; found: 245.9716.

1-Bromo-2,3-dimethoxy-5-ethenyl benzene 13

Sodium hydride (24.6 mg, 0.82 mmol, 80% oil dispersion) and dry tetrahydrofuran (5 mL) were added to a dry three-necked flask equipped with a condenser and dry nitrogen flow. To this suspension was added methyl triphenyl phosphonium bromide (0.146 g, 0.41 mmol) and the mixture was stirred for 10 min. Then 3-bromo-4,5-dimethoxy benzaldehyde **12** (100 mg, 0.41 mmol) in tetrahydrofuran (2 mL) was added and the mixture was gently refluxed for 1.5 h, after which time tlc indicated that all starting material had been transformed. After addition of methanol (2 mL) the reaction mixture was filtered, and then poured into distilled water and extracted with ether (4 × 50 mL). The ether extract, following usual treatment, yielded a solid suspended in oil, which was taken up in hexane and introduced onto a pad of coarse silica gel in a sintered glass funnel. Elution with hexane – ethyl acetate (95:5) yielded the light-sensitive product 1-bromo-2,3-dimethoxy-5-ethenyl benzene **13** (94.3 mg, 96%), which was stored in the cold under argon until further use; uv (CH_3OH) λ_{max} nm (log ε): 218 (4.36), 256 (3.97), 296 (3.29), 306 (3.16); ir ($CHCl_3$) ν_{max}: 1630, 1590 (C=C, aromatic conj.) cm^{-1}; ^1H nmr ($CDCl_3$) δ: 3.78 (s, 3H, OCH_3), 3.79 (s, 3H, OCH_3), 5.17 (d, 1H, J_{cis} = 10.8 Hz), 5.97 (d, 1H, J_{trans} = 17.5 Hz), 6.50 (dd, 1H, J_{cis} = 10.8 Hz, J_{trans} = 17.5 Hz), 6.19 (d, 1H, J = 1.8 Hz), 7.10 (d, 1H, J = 1.8 Hz). *Exact Mass* calcd. for $C_{10}H_{11}O_2Br$: 241.9918; found: 241.9942.

2,3-Dimethoxy-5-ethenyl benzoic acid 14

To magnesium turnings (20 mg, 0.82 mmol) in dry tetrahydrofuran (3 mL) in a three-necked flask under nitrogen was added a small crystal of iodine and the mixture refluxed for 3 min with a heat gun. After cooling, the tetrahydrofuran was removed by pipette and 1-bromo-2,3-dimethoxy-5-ethenyl benzene **13** (100 mg, 0.41 mmol) in tetrahydrofuran (5 mL) was added. This mixture was refluxed for short periods with a heat gun and when there was no sign of Grignard reagent formation, a catalytic amount of iodomethane was added and refluxing initiated again. After a cloudy precipitate formed, the reaction was cooled and stirred vigorously at room temperature for 2 h. The flask was then filled cautiously with crushed Dry Ice and, after 10 h, saturated ammonium chloride solution (10 mL) was added, the solution was filtered, and the residue washed with water and then ether. The organic layer was diluted with ether (20 mL) and extracted with water (6 × 15 mL). The combined aqueous extract was washed with ether (20 mL) and then acidified with dilute sulfuric acid (5%) and extracted with ether (4 × 30 mL). The ether extract, after washing, drying, and evaporation, yielded 2,3-dimethoxy-5-ethenyl benzoic acid **14**, a solid (47 mg, 55%), mp 73–76°C; uv (CH_3OH) λ_{max} nm (log ε): 220 (3.96), 257 (3.64), 300 (3.10); ir ($CHCl_3$) ν_{max}: 3400 (OH), 1740 (COOH), 1600, 1590 (C=C, aromatic) cm^{-1}; ^1H nmr ($CDCl_3$) δ: 3.88 (s, 3H, OCH_3), 4.00 (s, 3H, OCH_3), 5.25 (d, 1H, J_{cis} = 11.0 Hz), 5.70 (d, 1H, J_{trans} = 17.5 Hz), 6.60 (dd, 1H, J_{cis} = 11.0 Hz, J_{trans} = 17.5 Hz), 7.12 (d, 1H, J = 2.0 Hz), 7.67 (d, 1H, J = 2 Hz). *Exact Mass* calcd. for $C_{11}H_{12}O_4$: 208.0735; found: 208.0731.

2,3-Dimethoxy-5-ethyl benzoic acid 15

2,3-Dimethoxy-5-ethenyl benzoic acid **14** (100 mg, 0.48 mmol) in ethanol (1.5 mL) was hydrogenated at 1 atmosphere (101.3 kPa) and room temperature in the presence of palladium-on-carbon (10 mg) overnight. The mixture was filtered through Celite and evaporated, yielding 2,3-dimethoxy-5-ethyl benzoic acid **15** as an oil (101 mg, 100%); uv (CH_3OH) λ_{max} nm (log ε): 208 (4.39), 279 (3.52); ir ($CHCl_3$) ν_{max}: 3420 (OH), 1735 (C=O), 1610, 1590 (C=C, aromatic) cm^{-1}; ^1H nmr ($CDCl_3$) δ: 1.23 (t, 3H, J = 7.6 Hz, CH_2CH_3), 2.64 (q, 2H, J = 7.6 Hz, CH_2CH_3), 3.92 (s, 3H, OCH_3), 4.04 (s, 3H, OCH_3), 7.00 (d, 1H, J = 1.7 Hz), 7.53 (d, 1H, J = 1.7 Hz). *Exact Mass* calcd. for $C_{11}H_{14}O_4$: 210.0892; found: 210.0894.

2-(2,3-Dimethoxy-5-ethylphenyl)-4,4-dimethyl-4,5-dihydro-oxazole 16

Thionyl chloride (7.6 g, 0.064 mol) was added to 2,3-dimethoxy-5-ethyl benzoic acid **15** (4.5 g, 0.0213 mol) and the mixture was refluxed for 8 h under nitrogen. Excess thionyl chloride was removed *in vacuo* yielding the acid chloride of **15** (4.6 g), which was dissolved in methylene chloride (50 mL) and added dropwise to a stirred solution of 2-amino-2-methyl-1-propanol (3.6 g, 0.04 mol) in methylene chloride (25 mL) cooled to 0°C. The reaction was stirred at room temperature overnight, then filtered and the filtrate concentrated to give a brown oil that was treated with thionyl chloride (2.64 g), by slow addition, and the solution was stirred for 2 h at room temperature. Removal of excess thionyl chloride *in vacuo* afforded an oily product that was treated with ether (75 mL) and water (150 mL). The aqueous layer was made basic by addition of aqueous sodium hydroxide (20%) and extracted with ether (3 × 100 mL). The ethereal extraction yielded a crude product (4.85 g), which was flash chromatographed affording 2-(2,3-dimethoxy-5-ethylphenyl)-4,4-dimethyl-4,5-dihydro-oxazole **16** (4.58 g, 80%); uv (CH_3OH) λ_{max} nm (log ε): 209 (4.36), 246 (3.65), 2.90 (3.32); ir ($CHCl_3$) ν_{max}: 1645 (C=N), 1580 (C=C, aromatic) cm^{-1}; ^1H nmr ($CDCl_3$) δ: 1.24 (t, 3H, J = 7.5 Hz, CH_2CH_3), 1.41 (s, 6H, $(CH_3)_2CH$), 2.62 (q, 2H, J = 7.6 Hz, CH_2CH_3), 3.85 (s, 3H, OCH_3), 3.89 (s, 3H, OCH_3), 4.14 (s, 2H, CH_2O), 6.86 (d, 1H, J = 2.2 Hz), 7.17 (d, 1H, J = 2.2 Hz). *Exact Mass* calcd. for $C_{15}H_{21}O_3N$: 263.1521; found: 263.1520.

2-[4'-Ethyl-2'-methoxy-1'-(2-{1,4,5-trimethoxynaphthalene})-phenyl]-4,4-dimethyl-2,3-dihydro-oxazole 17

To a dry three-necked flask under dry nitrogen was added magnesium (30 mg, 1.23 mmol) and 2-bromo-1,4,5-trimethoxynaphthalene **10** (108 mg, 0.36 mmol) in dry tetrahydrofuran (12 mL); the mixture was stirred vigorously and heated with a heat gun. Formation of Grignard reagent was induced by addition of a catalytic amount of iodine and the solution was then refluxed gently for 0.25 h. After

Can. J. Chem. Downloaded from www.nrcresearchpress.com by 80.58.250.72 on 09/07/12
For personal use only.

cooling to room temperature, 2-(2,3-dimethoxy-5-ethylphenyl)-4,4-dimethyl-4,5-dihydro-oxazole **16** (100 mg, 0.38 mmol) in dry tetrahydrofuran (6 mL) was added over 5 min and the solution was then stirred for 15 h at room temperature, since thin-layer chromatography (tlc) (hexane – ethyl acetate 60:40, developed twice) indicated absence of starting material and appearance of a new spot of low R_f. The reaction mixture was filtered, suspended in water, and extracted with ether (3 × 30 mL), which, after the usual treatment, afforded the product (146 mg). This product was chromatographed on a silica gel column yielding 2-[4′-ethyl-2′-methoxy-1′-(2-{1,4,5-trimethoxynaphthalene})phenyl]-4,4-dimethyl-4,5-dihydro-oxazole **17** (138 mg, 81%); uv (CH_3OH) λ_{max} (log ε): 210 (4.43), 227 (4.56), 244 (3.98), 296 (3.89), 324 (3.71), 340 (3.71); ir ($CHCl_3$) ν_{max}: 1630 (C=N), 1600, 1580 (C=C) cm^{-1}; ^1H nmr ($CDCl_3$) δ: 1.15 (s, 3H, $(CH_3)_2C$), 1.16 (s, 3H, $(CH_3)_2C$), 1.32 (t, 3H, J = 7.6 Hz, CH_2CH_3), 2.74 (q, 2H, J = 7.6 Hz, CH_2CH_3), 3.57 (s, 3H, OCH_3), 3.55 (d, 1H, J = 8.0 Hz, OCH_2), 3.64 (d, 1H, J = 8 Hz, OCH_2), 3.77 (s, 3H, OCH_3), 3.90 (s, 3H, OCH_3), 4.00 (s, 3H, OCH_3), 6.68 (s, 1H, C3H), 6.90 (d, 1H, J = 7.6 Hz, C6H), 6.96 (bs, 1H, C3′H), 7.28 (bs, 1H, C5′H), 7.42 (t, 1H, J = 7.6 Hz, C7H), 7.78 (d, 1H, J = 7.6 Hz, C8H). *Exact Mass* calcd. for $C_{27}H_{31}O_5N$: 449.2202; found: 449.2207 (M^+, 46).

*1,12-Dihydroxy-10-methoxy-8-ethyl-6*H*-benzo[*d*]naphtho[1,2*b*]-pyran-6-one* ***18***

A solution of 2-[4′-ethyl-2′-methoxy-1′-(2-{1,4,5-trimethoxynaphthalene})phenyl]-4,4-dimethyl-4,5-dihydro-oxazole **17** (100 mg, 0.22 mmol) in glacial acid acid (1.5 mL) and hydriodic acid (1.5 mL, 47%), was refluxed for 2 h, whence a solid precipitated from the solution. Acetic acid (1 mL) and hydriodic acid (1 mL) were added and refluxing continued for 7 h. After cooling, the mixture was filtered to provide the solid product 1,12-dihydroxy-10-methoxy-8-ethyl-6*H*-benzo[*d*]naphtho[1,2*b*]pyran-6-one **18** (60 mg, 77%), mp 289–290°C (dec.); uv (CH_3OH) λ_{max} nm (log ε): 242 (4.59), 264 (4.40), 273 (4.48), 314 (4.10), 324 (4.08), 340 (3.97), 380 (3.90); ir (KBr) ν_{max}: 330 (phenolic OH), 1660 (C=O), 1610, 1580 (C=C, aromatic) cm^{-1}; ^1H nmr ($(CD_3)_2SO$) δ: 1.33 (t, 3H, J = 7.6 Hz, CH_2CH_3), 2.84 (q, 2H, J = 7.6 Hz, CH_2CH_3), 4.15 (s, 3H, OCH_3), 6.96 (dd, 1H, J = 7.6 Hz, J = 1.0 Hz, C2H), 7.51 (dd, 1H, J = 8.4 Hz, J = 7.7 Hz, C3H), 7.53 (d, 1H, J = 1.7 Hz, C9H), 7.87 (d, 1H, J = 1.7 Hz, C7H), 7.88 (dd, 1H, J = 8.5 Hz, J = 1.0 Hz, C4H), 8.38 (s, 1H C11H). *Exact Mass* calcd. for $C_{21}H_{18}O_5$: 350.1154; found: 350.0996.

*1,12-Diacetoxy-10-methoxy-8-ethyl-6*H*-benzo[*d*]naphtho[1,2*b*]-pyran-6-one* ***19***

A solution of 1,12-dihydro-10-methoxy-8-ethyl-6*H*-benzo[*d*]-naphtho[1,2*b*]pyran-6-one **18** (5 mg, 0.01 mmol) in pyridine (0.5 mL) and acetic anhydride and a catalytic amount of dimethylaminopyridine was stirred overnight. Preparative thin-layer chromatography (ptlc) following evaporation of solvents provided 1,12-diacetoxy-10-methoxy-8-ethyl-6*H*-benzo[*d*]naphtho[1,2*b*]pyran-6-one **19** (6 mg, 100%), mp 211–213°C; uv (CH_3OH) λ_{max} (log ε): 224 (3.76), 243 (3.78), 263 (3.40), 272 (3.70), 315 (3.08), 335 (3.03), 357 (3.19), 365 (3.24); ir ($CHCl_3$) ν_{max}: 1762 (acetate C=O), 1725 (lactone C=O), 1615 (C=C, aromatic); ^1H nmr ($(CD_3)_2SO$) δ: 1.33 (t, 3H, J = 7.6 Hz, CH_2CH_3), 2.45 (s, 3H, $OCOCH_3$), 2.46 (s, 3H, $OCOCH_3$), 2.85 (q, 2H, J = 7.6 Hz, CH_2CH_3), 4.13 (s, 3H, OCH_3), 7.42 (dd, 1H, J = 1.1 Hz, J = 7.6 Hz, C2H), 7.55 (d, 1H, J = 1.6 Hz, C9H), 7.75 (dd, 1H, J = 7.6 Hz, J = 8.5 Hz, C3H), 7.90 (d, 1H, J = 1.6 Hz, C7H), 8.49 (dd, 1H, J = 1.1 Hz, J = 8.5 Hz, C4H), 8.76 (s, 1H, C11H); ^1H nmr ($CDCl_3$) δ: 1.35 (t, 3H, J = 7.7 Hz, CH_2CH_3), 2.43 (s, 3H, $OCOCH_3$), 2.45 (s, 3H, $OCOCH_3$), 2.86 (q, 2H, J = 7.6 Hz, CH_2CH_3), 4.07 (s, 3H, OCH_3), 7.22 (d, 1H, J = 1.0 Hz, C9H), 7.26 (d, 1H, J = 7.5 Hz, C4H), 7.62 (dd, 1H, J = 7.7 Hz, J = 8.3 Hz, C3H), 8.00 (d, 1H, J = 1.0 Hz, C7H), 8.61 (d, 1H, J = 8.2 Hz, C4H), 8.70 (s, 1H, C11H). *Exact Mass* calcd. for $C_{24}H_{20}O_7$: 420.1208; found: 420.1214.

*1-Acetoxy-10,12-dimethoxy-8-ethyl-6*H*-benzo[*d*]naphtho[1,2*b*]-pyran-6-one* ***20*** *and 12-acetoxy-1,10-dimethoxy-8-ethyl-6*H*-benzo[*d*]naphtho[1,2*b*]pyran-6-one* ***21***

1,12-Dihydroxy-10-methoxy-8-ethyl-6*H*-benzo[*d*]naphtho[1,2*b*]pyran-6-one **19** (5 mg, 0.01 mmol) in dry acetone (4 mL) and dimethylsulfoxide (2 mL) was treated with potassium carbonate (10 mg) and iodomethane and stirred at room temperature for 2 h. After filtration and removal of solvent the residue was stirred overnight with acetic anhydride (1.5 mL) and pyridine (1 mL) and a catalytic amount of dimethylaminopyridine. Evaporation followed by ptlc on silica gel (4 × chloroform) afforded the compounds **20** (3 mg), mp 223–225°C and **21** (2 mg), mp 232–238°C. 1-Acetoxy-10,12-dimethoxy-8-ethyl-6*H*-benzo[*d*]naphtho[1,2*b*]pyran-6-one **20**: uv (CH_3OH) λ_{max} nm (log ε): 241 (4.82), 265 (4.62), 273 (4.75), 298 (4.23), 311 (4.19), 324 (4.14), 331 (4.12), 368 (4.19); ir ($CHCl_3$) ν_{max}: 1750 (acetate C=O), 1720 (lactone C=O), 1610, 1590 (C=C, aromatic) cm^{-1}; ^1H nmr ($CDCl_3$) δ: 1.31 (t, 3H, J = 7.6 Hz, CH_2CH_3), 2.74 (q, 2H, J = 7.6 Hz, CH_2CH_3), 3.92 (s, 3H, OCH_3), 3.96 (s, 3H, OCH_3), 7.08 (bs, 1H, C9H), 7.17 (dd, 1H, J = 1.1 Hz, J = 7.5 Hz, C2H), 7.56 (dd, 1H, J = 7.5 Hz, J = 8.6 Hz, C3H), 7.90 (bs, 1H, C7H), 8.28 (s, 1H, C11H), 8.47 (dd, 1H, J = 1.1 Hz, J = 8.6 Hz, C4H); ^{13}C nmr ($CDCl_3$) δ: 14.97 (q, CH_3CH_2), 20.93 (q, CH_3CO), 28.8 (t, CH_2CH_3), 55.93 (q, OCH_3), 56.03 (q, OCH_3), 104.12 (d, C11), 113.68 (s, C10b), 116.92 (d, C9), 120.56 (d, C7), 120.74 (s, C12a), 120.93 (d, C4), 121.38 (d, C3), 121.71 (s, C6a), 123.03 (s, C10a), 126.23 (s, C4a), 126.66 (d, C2), 140.30 (s, C4b), 146.12 (s, C8), 146.12 (s, C1), 150.62 (s, C12), 157.06 (s, C10), 161.18 (s, C6), 170.11 (s, acetate C=O). *Exact Mass* calcd. for $C_{23}H_{20}O_6$: 392.1260 found: 392.1259. 12-Acetoxy-1,10-dimethoxy-8-ethyl-6*H*-benzo[*d*]naphtho[1,2*b*]pyran-6-one **21**: uv (CH_3OH) λ_{max} nm (log ε): 24 (4.82), 265 (4.62), 273 (4.75), 298 (4.23), 311 (4.19), 324 (4.14) 331 (4.12), 368 (4.19); ir ($CHCl_3$) ν_{max}: 1750 (acetate CO), 172((lactone C=O), 1610, 1590 (C=C, aromatic) cm^{-1}; ^1H nmr ($CDCl_3$ δ: 1.33 (t, 3H, J = 7.7 Hz, CH_2CH_3), 2.41 (s, 3H, $OCOCH_3$), 2.7 (q, 2H, J = 7.7 Hz, CH_2CH_3), 3.99 (s, 3H, OCH_3), 4.03 (s, 3H OCH_3), 6.95 (d, 1H, J = 7.6 Hz, C2H), 7.15 (bs, 1H, C9H), 7.5 (t, 1H, J = 8.2 Hz, C3H), 7.95 (bs, 1H, C7H), 8.24 (d, 1H, J = 8.3 Hz, C4H), 8.54 (s, 1H, C11H). *Exact Mass* calcd. for $C_{23}H_{20}O_6$ 392.1260; found: 392.1252.

*8-Ethyl-1,10,12-trimethoxy-6*H*-benzo[*d*]naphtho[1,2*b*]pyran-6-one* ***22***

To a solution of 1,12-dihydroxy-10-methoxy-8-ethyl-6*H*-benzo[*d*]naphtho[1,2*b*]pyran-6-one **18** (5 mg, 0.01 mmol) in dry acetone (4 mL) and dimethylsulfoxide (1 mL) was added potassium carbonate (20 mg) and the mixture was stirred at room temperature for 24 h. After the customary work-up the product was purified by ptlc, giving 8-ethyl-1,10,12-trimethoxy-6*H*-benzo[*d*]naphtho[1,2*b*]pyran-6-one **22** (5 mg 96%), mp 240–245°C; uv (CH_3OH) λ_{max} nm (log ε): 242 (4.79), 26 (4.51), 273 (4.67), 300 (4.19), 310 (4.16), 320 (4.06), 340 (4.01) 370 (4.21); ir ($CHCl_3$) ν_{max}: 1720 (lactone C=O), 1600 (C=C aromatic) cm^{-1}; ^1H nmr ($CDCl_3$) δ: 1.35 (t, 3H, J = 7.7 Hz, CH_2CH_3) 2.83 (q, 2H, J = 7.7 Hz, CH_2CH_3), 4.03 (t, 3H, OCH_3), 4.06 (s, 3H OCH_3), 4.12 (s, 3H, OCH_3), 7.01 (dd, 1H, J = 1.2 Hz, J = 7.9 Hz C2H), 7.23 (d, 1H, J = 1.3 Hz, C9H), 7.53 (dd, 1H, J = 7.9 Hz, J = 8.5 Hz, C3H), 8.03 (d, 1H, J = 1.3 Hz, C7H), 8.26 (dd, 1H, J = 1.2 Hz, J = 8.5 Hz, C4H), 8.48 (s, 1H, C11H). *Exact Mass* calcd for $C_{22}H_{20}O_5$: 364.1310; found: 364.1309.

*1-Acetoxy-10,12-dimethoxy-8-(bromoethyl)-6*H*-benzo[*d*]naphtho-[1,2*b*]pyran-6-one* ***24***

A mixture of 1-acetoxy-10,12-dimethoxy-8-ethyl-6*H*-benzo[*d*]-naphtho[1,2*b*]pyran-6-one **20** (20 mg, 0.05 mmol) in dry carbon tetrachloride was treated with *N*-bromosuccinimide (5 mg, 0.03 mmol) and a catalytic amount of dibenzoyl peroxide, and was then refluxed for 3 h. Since tlc showed the presence of starting material, additional *N*-bromosuccinimide (5 mg, 0.03 mmol) was added and refluxing was continued for 3 h, after which all starting material appeared, from tlc scrutiny, to be consumed. Evaporation of solvent and recrystallization

from chloroform–ether gave 1-acetoxy-10,12-dimethoxy-8-(bromoethyl)-6*H*-benzo[*d*]naphtho[1,2*b*]pyran-6-one **24** (18 mg, 75%), mp 178–180°C; uv (CH_3OH) λ_{max} nm (log ε): 242 (4.88), 264 (4.06), 275 (4.77), 302 (4.41), 316 (4.32), 328 (4.28), 375 (4.38); ir ($CHCl_3$) ν_{max}: 1750 (acetate C=O), 1720 (lactone C=O), 1610, 1590 (C=C, aromatic) cm^{-1}; ^1H nmr ($CDCl_3$) δ: 2.15 (d, 3H, J = 6.9 Hz, CH_3CHBr), 2.41 (s, 3H, CH_3COO), 2.77 (s, OH), 3.98 (s, 3H, OCH_3), 4.09 (s, 3H, OCH_3), 5.31 (q, 1H, J = 6.9 Hz, CH_3CHBr), 7.21 (dd, 1H, J = 1.2 Hz, J = 7.5 Hz, C2H), 7.42 (d, 1H, J = 1.7 Hz, C9H), 7.60 (dd, 1H, J = 7.5 Hz, J = 8.6 Hz, C3H), 8.16 (d, 1H, J = 1.6 Hz, C7H), 8.38 (s, 1H, C11H), 8.51 (dd, 1H, J = 1.1 Hz, J = 8.6 Hz, C4H). *Exact Mass* calcd. for $C_{23}H_{19}O_6Br$: 472.0364; found: 472.0334.

*1-Hydroxy-10,12-dimethoxy-8-vinyl-6*H*-benzo[*d*]naphtho[1,2*b*]-pyran-6-one* **7**

Sodium borohydride (3 mg) was added to diphenyl diselenide (11.8 mg) in absolute ethanol (2 mL) under a flow of argon. Diphenyl diselenide (2 mg) was added to destroy any excess sodium borohydride and the solution turned yellow. 1-Acetoxy-10,12-dimethoxy-8-(bromoethyl)-6*H*-benzo[*d*]naphtho[1,2*b*]pyran-6-one **24** (8 mg, 0.02 mmol) in dry tetrahydrofuran was added and the reaction mixture was refluxed for 2.5 h. The solution was cooled in an ice bath, hydrogen peroxide (2 mL, 30%) was added over 20 min, and the mixture was stirred for 3 h at 0°C. Dilution with water (10 mL) and extraction with ether (3 × 20 mL) provided a crude product that was purified by ptlc to give 1-hydroxy-10,12-dimethoxy-8-vinyl-6*H*-benzo[*d*]naphtho[1,2*b*]pyran-6-one **7** (2.3 mg, 40%), mp 263–265°C, identical in all physical and spectroscopic properties with compound **7** obtained by alkali fusion of ravidomycin (4).

*1-Acetoxy-10,12-dimethoxy-8-vinyl-6*H*-benzo[*d*]naphtho[1,2*b*]-pyran-6-one* **25**

1-Acetoxy-10,12-dimethoxy-8-ethyl-6*H*-benzo[*d*]naphtho[1,2*b*]-pyran-6-one **20** (16 mg, 0.04 mmol) in carbon tetrachloride (30 mL) was refluxed with *N*-bromosuccinimide (7.3 mg) and a catalytic amount of dibenzoyl peroxide for 4 h. Thin-layer chromatography showed the presence of starting material and so additional *N*-bromosuccinimide (7.3 mg) was added and refluxing was continued for 4 h, after which tlc showed the absence of starting material. After evaporation of solvent the products were purified by ptlc on silica gel (chloroform). Fractional crystallization (chloroform–hexane) of the main band gave 1-acetoxy-10,12-dimethoxy-8-vinyl-6*H*-benzo[*d*]naphtho[1,2*b*]-pyran-6-one **25** (5 mg, 31%), mp 215–218°C (the mother liquor contained the acetate monobromide **24** together with **25**); uv (CH_3OH) λ_{max} nm (log ε): 242 (4.85), 276 (4.69), 282 (4.72), 306 (4.47), 319 (4.38), 330 (4.30), 346 (4.27), 380 (4.36); ir ($CHCl_3$) ν_{max}: 1750 (acetate C=O), 1720 (lactone C=O), 1605, 1590 (C=C, aromatic) cm^{-1}; ^1H nmr ($CDCl_3$) δ: 2.42 (s, 3H, CH_3COO), 4.03 (s, 3H, OCH_3), 4.14 (s, 3H, OCH_3), 5.47 (d, 1H, J = 10.7 Hz, vinyl H), 5.98 (d, 1H, J = 17.8 Hz, vinyl H), 6.84 (dd, 1H, J = 17.8 Hz, J = 10.7 Hz, vinyl H), 7.22 (dd, 1H, J = 1.0 Hz, J = 7.5 Hz, C2H), 7.40 (d, 1H, J = 1.4 Hz, C9H), 7.61 (dd, 1H, J = 7.6 Hz, J = 8.5 Hz, C3H), 8.21 (d, 1H, J = 1.4 Hz, C7H), 8.49 (s, 1H, C11H), 8.55 (dd, 1H, J = 1.0 Hz, J = 8.5 Hz, C4H). *Exact Mass* calcd. for $C_{23}H_{18}O_6$: 390.1103; found: 390.1101.

Acknowledgements

This work was supported in part by grants from the Natural Sciences and Engineering Research Council of Canada.

1. S. Horii, H. Fukase, E. Mizuta, K. Hatano, and K. Mizuno. Chem. Pharm. Bull. **28**, 3601 (1980).
2. (*a*) H. Nakano, K. Matsuda, K. Ito, S. Ohkubo, M. Morimoto, and F. Tomita. J. Antibiot. **34**, 266 (1981); (*b*) K. Takahashi, Y. Yoshida, F. Tomita, and K. Shirahata. J. Antibiot. **34**, 271 (1981); (*c*) D. M. Balitz, F. A. O'Herron, J. Bush, D. M. Vyas, D. E. Nettleton, R. E. Grulich, W. T. Bradner, T. W. Doyle, E. Arnold, and J. Clardy. J. Antibiot. **34**, 1544 (1981); (*d*) N. Hirayama, K. Takahashi, K. Shirahata, Y. Ohashi, and Y. Sasada. Bull. Chem. Soc. Jpn. **54**, 1338 (1981); (*e*) T. C. Jain, G. C. Simolike, and L. M. Jackman. Tetrahedron, **39**, 599 (1983).
3. (*a*) F. Strelitz, H. Flon, and I. N. Asheshov. J. Bacteriol. **69**, 280 (1955); (*b*) U. Weiss and K. Yoshihira, R. J. Highet, R. J. White, and T. T. Wei. J. Antibiot. **35**, 1194 (1982).
4. (*a*) J. A. Findlay, J.-S. Liu, L. Radics, and S. Rakhit. Can. J. Chem. **59**, 3018 (1981); (*b*) J. A. Findlay, J.-S. Liu, and L. Radics. Can. J. Chem. **61**, 323 (1983).
5. (*a*) M. Morimoto, S. Okubo, F. Tomita, and H. Marumo. J. Antibiot. **34**, 701 (1981); (*b*) F. Tomita, K. Takahashi, and T. Tamaoki. J. Antibiot. **35**, 1038 (1982); (*c*) S. N. Sehgal, H. Czerkawski, Alicia Kudelski, K. Pandev, R. Saucier, and C. Vezina. J. Antibiot. **36**, 355 (1983); (*d*) S. Rakhit, C. Eng, H. Baker, and K. Singh. J. Antibiot. **36**, 1490 (1983); (*e*) K. Singh. J. Antibiot. **37**, 71 (1984); (*f*) T. T. Wei, K. M. Byrne, D. Warnick-Pickle, and M. Greenstein. J. Antibiot. **35**, 545 (1982).
6. R. K. Elespuru and S. K. Gonda. Science, **223**, 69 (1984).
7. (*a*) S. W. Heinzman and J. R. Grunwell. Tetrahedron Lett. 4305 (1980); (*b*) M. E. Jung and J. A. Hagenah. J. Org. Chem. **48**, 5359 (1983).
8. R. Misra, H. R. Tritch III, and R. C. Pandey. J. Antibiot. **38**, 1280 (1985).
9. H. A. Torrey and E. D. Clarke. J. Am. Chem. Soc. **31**, 583 (1909).
10. (*a*) A. I. Meyers, R. Gabel, and E. D. Mihelich. J. Org. Chem. **43**, 1372 (1978); (*b*) A. I. Meyers, D. L. Temple, D. Haidukewych, and E. D. Mihelich. J. Org. Chem. **39**, 2787 (1974).
11. J. B. Stothers. Carbon-13 nuclear magnetic resonance spectroscopy. Academic Press, New York. 1972.
12. K. B. Sharpless and R. F. Lauer. J. Am. Chem. Soc. **95**, 2697 (1973); K. B. Sharpless, R. F. Lauer, and A. Y. Teranishi. J. Am. Chem. Soc. **95**, 6137 (1973).

Can. J. Chem. Downloaded from www.nrcresearchpress.com by 80.58.250.72 on 09/07/12
For personal use only.

Long chain electrophilic contact poisons from the Dufour's gland of the ant *Crematogaster scutellaris* (Hymenoptera, Myrmicinae)

D. DALOZE, J. C. BRAEKMAN,[1] P. VANHECKE, J. L. BOEVÉ, AND J. M. PASTEELS

Collectif de Bio-écologie, Faculté des Sciences, C.P. 160, Université Libre de Bruxelles, Av. F. D. Roosevelt 50, B - 1050 Bruxelles, Belgium

Received July 25, 1986

D. DALOZE, J. C. BRAEKMAN, P. VANHECKE, J. L. BOEVÉ, and J. M. PASTEELS. Can. J. Chem. **65**, 432 (1987).

The Dufour's gland secretion of *C. scutellaris* contains a series of C_{23} long chain derivatives characterized by the presence of a cross-conjugated dienone linked to either a primary acetate, an aldehyde, or a carboxylic acid function. These compounds further differ from each other by the degree of unsaturation and (or) the position of an isolated double bond in the carbon atom chain. A combination of spectroscopic data and chemical degradations led to structures **1***a–c*, **2***a–c*, and **5***a–c* for the major components of the secretion. The highly electrophilic character of these compounds accounts for their efficiency as contact poisons.

D. DALOZE, J. C. BRAEKMAN, P. VANHECKE, J. L. BOEVÉ et J. M. PASTEELS. Can. J. Chem. **65**, 432 (1987).

La sécrétion de la glande de Dufour de *C. scutellaris* contient une série de dérivés à longue chaîne en C_{23} qui sont caractérisés par la présence d'une dièнone conjugée croisée liée à une fonction acétate primaire, aldéhyde ou acide carboxylique. Ces composés diffèrent aussi les uns des autres par le degré d'insaturation et (ou) par la position d'une double liaison isolée dans la chaîne carbonée. En se basant sur une combinaison de données spectroscopiques et de dégradations chimiques, on a pu attribuer les structures **1***a–c*, **2***a–c* et **5***a–c* aux principaux composants de la sécrétion. Le caractère électrophile élevé de ces composés explique leur efficacité comme poisons de contact.

[Traduit par la revue]

Introduction

The composition of the Dufour's gland secretion of ants has been the subject of several investigations. Aliphatic linear hydrocarbons in the range C_9–C_{27} are generally present, but branched-chain hydrocarbons and oxygenated compounds can also be encountered (for review see ref. 1). Among the subfamily Myrmicinae, the Dufour's gland contents of several species of the genus *Myrmica* have been investigated (2–8). Besides the linear, odd-numbered hydrocarbon theme, traces of highly volatile alcohols, aldehydes, and ketones in the C_1–C_4 range have also been reported (9). Most species of *Myrmica* also possess terpenoid hydrocarbons, identified as (*Z*,*E*)-α-farnesene, homofarnesene, and bishomofarnesene (8). Farnesene derivatives have also been identified in the Dufour's gland of several species of the genera *Atta* (10), *Solenopsis* (11–13), *Aphaenogaster* (14), and *Pheidole* (15).

Ethological studies have shown that ants of the genus *Myrmica* use their Dufour's gland contents as recruitment and home-range marking pheromone (4). In addition, some ant species utilize trace components of the Dufour's gland secretion as trail pheromone (e.g., the sesquiterpenoid aldehyde faranal in *Monomorium pharaonis* (16) and farnesene derivatives in several *Solenopsis* species (11–13)).

Ants of the genus *Crematogaster* are unique among the myrmicines in that they use their Dufour's gland secretion as a contact defensive secretion (17), instead of injecting, by stinging, a venom produced by the poison gland as in most primitive ant species.

Crematogaster species are able to swing their gasters up and over the thorax and head so that the sting is presented in a cephalad direction (18). Furthermore, while their spatulate sting is not a suitable injection device, it would function ideally as an organ for topically applying venom (18). This interpretation is supported by the observation that the venom of *Crematogaster lineolata* is very toxic when topically administered to termite workers (ref. 1*b*, p. 809). We have similarly observed that the venom of *C. scutellaris*, an aggressive Mediterranean species, is toxic to other ants. These observations prompted us to examine the chemical composition of this venom.

Results and discussion

When workers of *C. scutellaris* are immobilized with tweezers, a droplet of venom is emitted and accumulates on the spatulate portion of the sting. This secretion can be collected on bits of filter paper and stored in hexane. In this manner, the secretion of 250 ants afforded about 15 mg of a light yellow oil, after removal of the solvent (about 60 μg/ant).

Preliminary observations have shown that the constituents of the secretion are unstable and must be kept in dilute solutions under N_2, at −30°C, to avoid extensive decomposition. A tlc analysis of freshly collected material (SiO_2; eluent, hexane–acetone 8:2) indicated the presence of five spots corresponding to at least five components, numbered CS1 to CS5 in order of increasing polarity. The relative proportions of these five components vary from one collection to another.

All attempts to separate the venom constituents by adsorption chromatography on either silica gel, alumina, or Florisil failed, since most of the material (≥75%) remained on the column and could not be recovered. However, repetitive partition chromatographies on Sephadex LH-20 columns, using heptane–$CHCl_3$–MeOH (10:10:1) as eluent (20), allowed us to resolve the mixture in five fractions, corresponding to the above-mentioned tlc spots. As will be shown below, these fractions are not pure compounds but rather mixtures of derivatives differing by the number and (or) position of the double bond(s).

We first turned our attention to CS2, whose stability looked more promising than that of its companions.

Fraction CS2

The EI (electron impact) ms (mass spectrum) of CS2 shows at least three peaks attributable to molecular ions, at *m/z* 388,

[1]Maître de Recherches du Fonds National de la Recherche Scientifique.

Printed in Canada / Imprimé au Canada

Can. J. Chem. Downloaded from www.nrcresearchpress.com by 80.58.250.72 on 09/07/12
For personal use only.

Can. J. Chem. Downloaded from www.nrcresearchpress.com by 80.58.250.72 on 09/07/12
For personal use only.

390, and 392 (the intensity of the latter being very small), thus indicating that this fraction is still a mixture of compounds differing by their degree of unsaturation. High performance liquid chromatography (hplc) analysis (SiO_2, 5 μm, hexane–dioxane 99:1) of CS2 demonstrated the presence of at least six components (in order of increasing polarity): A (3.5%); B (2.5%); C (14.0%); D (44%); E (9.0%), and F (27%). These values are approximate since some of the peaks (e.g., C and D) are poorly resolved. Preparative hplc afforded very small samples of C and D (as a mixture) and of F. Interestingly, the ms of the C and D mixture displays only a small M^+ peak at m/z 390, suggesting that these compounds are isomers. High resolution ms measurements on the most intense fragment ions gave the following results: m/z 362.28244 ($C_{23}H_{38}O_3$); 330.29172 ($C_{23}H_{38}O$); 320.27248 ($C_{21}H_{36}O_2$); 302.26095 ($C_{21}H_{34}O$). This suggests that C and D have the empirical formula $C_{25}H_{42}O_3$. In the ms of F, the molecular ion (M^+ 388), and all the characteristic fragment ions appear two mass units lower than in the ms of C and D, thus indicating the molecular formula $C_{25}H_{40}O_3$ for F. The ir and uv spectra of CS2 ($\nu_{C=O}$ 1745 and 1670 cm^{-1}; $\nu_{C=C}$ 1640 and 1620 cm^{-1}; ν_{C-O} 1230 cm^{-1}; λ_{max} 235 nm, ε 30 000 (CH_3OH)) indicated the presence of acetoxy group(s) and of a conjugated ketone, probably of the cross-conjugated dienone type (21).

The ^1H nmr spectrum (Table 1, column **2***a*,*b*) fully confirmed these assignments. In particular, it showed the presence of a primary allylic acetoxy group (4.78 ppm, dd, J = 4.8 and 1.6 Hz; 2H) linked to a cross-conjugated dienone. Extensive decoupling experiments and comparison of the ^1H nmr spectrum of CS2 with those of reference cross-conjugated dienones (21, 22) established the presence of partial structure **X**:

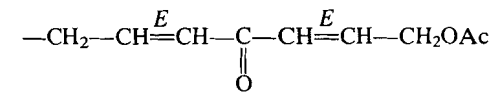

X

Bearing in mind the empirical formula $C_{25}H_{42}O_3$ for C and D, structural moiety **X** contains all the oxygen atoms and four out of the five unsaturations of the molecules. It follows that, to complete the structure of C and D, a $C_{16}H_{31}$ moiety must be linked to **X**. The ^1H nmr spectrum unambiguously demonstrated that this moiety is an unbranched carbon atom chain bearing one isolated double bond (1.25 ppm, bs, methylenes; 0.89 ppm, distorted t, 3H, methyl; and 5.34 ppm, t, 2H, olefins).

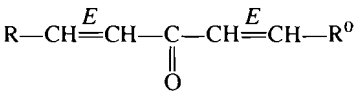

	R^0	R
1*a*	CHO	R^1
1*b*	CHO	R^2
1*c*	CHO	R^3
2*a*	CH_2OAc	R^1
2*b*	CH_2OAc	R^2
2*c*	CH_2OAc	R^3
3*a*	CH_2OAc	R^4
3*b*	CH_2OAc	R^5
5*a*	COOH	R^1
5*b*	COOH	R^2
5*c*	COOH	R^3

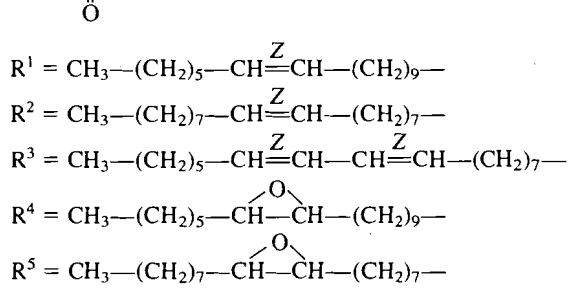

Combination of these structural elements led to the structural hypothesis **Y** for C and D, which must only differ by the location and (or) the geometry of the isolated double bond.

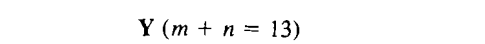

Y ($m + n = 13$)

This was proved as follows. Microozonolysis (23) of both CS2 and of the crude secretion, followed by treatment of the resulting ozonide with $P\phi_3$, afforded *n*-heptanal and *n*-nonanal in a 3:1 ratio (glc). On the other hand, treatment of CS2 with *m*-chloroperbenzoic acid yielded chiefly a monoepoxide fraction (**3***a*,*b*) which, after purification by preparative tlc, showed only one molecular ion at m/z 406 in its EI ms. This result, together with the ^1H nmr of **3***a*,*b*, demonstrated that the latter are derived from C and D and are not contaminated by any epoxide coming from the dehydro derivative F. The ms of **3***a*,*b* displays strong peaks at m/z 279.19672 ($C_{17}H_{27}O_3$) and 251.16393 ($C_{15}H_{23}O_3$) arising from cleavage α to the epoxide group in **3***a* and **3***b*, respectively.

Cleavage of **3***a*,*b* with HIO_4 (24) again led to the identification of *n*-heptanal and *n*-nonanal in a 3:1 ratio (glc). These results demonstrated that, in the major compound D, the double bond is located between C-16 and C-17, and between C-14 and C-15 in its isomer C.

Finally, the geometry of these double bonds was assigned as *Z*, on the basis of a $^1H/^{13}C$ nmr heterodecoupling experiment, allowing us to assign the signals of the allylic carbon atoms at 27 ppm (25). Since this experiment was performed on the crude secretion, the geometry of the isolated double bond must also be *Z* in all other Δ^{16} and Δ^{14} derivatives whose structures will be discussed shortly.

Compound D is thus (2*E*,5*E*,16*Z*)-4-oxotricosa-2,5,16-trien-1-ol acetate (**2***a*), whereas C is (2*E*,5*E*,14*Z*)-4-oxotricosa-2,5,14-trien-1-ol acetate (**2***b*).

In addition to the signals attributed to **2***a* and **2***b*, the ^1H nmr spectrum of CS2 also contains three signals at 5.38 ppm (dt, 2H), 6.24 ppm (bd, J = 9 Hz, 2H), and 2.12 ppm (m, 4H) attributable to a conjugated *Z*,*Z*-diene in a long chain (26). This was fully confirmed by double irradiation experiments. Consequently, compound F possess a conjugated diene, which should be located either in the $\Delta^{14,16}$ or in the $\Delta^{12,14}$ position,

TABLE 1. ^{1}H nuclear magnetic resonance spectra of compounds **1***a*,*b*–**6***a*,*b* and **7** (250 MHz, $CDCl_3$, TMS, δ, multiplicities, (*J* in Hz))

	1*a*,*b*	**2***a*,*b*	**3***a*,*b*	**4***a*,*b**	**5***a*,*b*†	**6***a*,*b*	**7** (29)‡
HC-1 or H_2C-1	9.80, d (7.3)	4.77, dd (4.8, 1.6)	4.77, dd (4.8, 1.6)	— —	— —	4.27, dd(11.4, 6.7) 4.15, dd(11.4, 5.3)	— —
HC-2	6.83, dd (16.0, 7.3)	6.84, dt (15.5, 4.8)	6.84, dt (15.5, 4.8)	6.09, d (5.5)	7.40, bd (15.5)	3.41, m	6.12, (5.6)
HC-3 or H_2C-3	7.16, d (16.0)	6.52, dt (15.5, 1.6)	6.52, dt (15.5, 1.6)	7.13, d (5.5)	6.74 bd (15.5)	2.76, dd(15.8, 6.0) 2.55, dd(15.8, 7.3)	7.44, (5.6)
HC-5	6.39, dt (15.8, 1.5)	6.31, dt (15.7, 1.0)	6.31, dt (15.7, 1.0)	—	6.30, d (15.5)	6.12, dt (15.8, 1.4)	— —
HC-6	7.05, dt (15.8, 7.0)	6.94, dt (15.7, 7.0)	6.94, dt (15.7, 7.0)	—	7.04, dt (15.5, 7.0)	6.85, dt (15.8, 7.0)	— —
H_2C-7	2.15, m	2.20, m	2.23, m		2.25, m	2.20, m	—
H_2C-15 + H_2C-18 or H_2C-13 + H_2C-16	2.0, m	2.0, m	—	2.0, m	2.05, m	2.0, m	—
HC-16 + HC-17 or HC-14 + HC-15	5.35, t (5.0)	5.34, t (5.0)	2.90, t (4.0)	5.35, t (5.0)	5.34, t (5.0)	5.35, t (5.0)	— —
H_3C-23	0.88, t§	0.88, t§	0.89, t§	0.9, t§	0.89, t§	0.88, t§	—
CH_3COO	—	2.14, s	2.12, s	—	—	2.04, s	
Morpholine protons	—	—	—	—	—	2.62, m (4H) 3.65, t (4H)	—

*Recorded at 80 MHz.
†Sensitive to concentration effects.
‡Recorded at 60 MHz.
§Distorted triplet.

according to the results of the ozonolysis reaction of CS2. On the basis of the double bond position in the monoenes, we tentatively propose that compound F could be (2*E*,5*E*,14*Z*,16*Z*)-4-oxotricosa-2,5,14,16-tetraen-1-ol acetate (**2***c*).

The structural assignments of compounds **2***a*–*c* were confirmed as follows. Treatment of CS2 with morpholine (27) in EtOH led, after silica gel column chromatography, to a mixture of adducts **6***a*–*c*. The spectral properties of the latter (EI

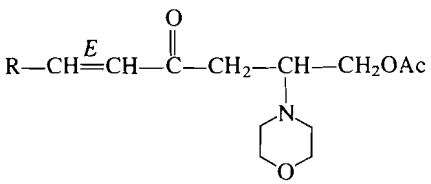

6*a* R = R^1
6*b* R = R^2
6*c* R = R^3

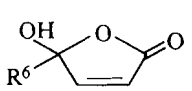

4*a* R^6 = CH_3—$(CH_2)_5$—CH=CH—$(CH_2)_{11}$— (Z)
4*b* R^6 = CH_3—$(CH_2)_7$—CH=CH—$(CH_2)_9$— (Z)
4*c* R^6 = CH_3—$(CH_2)_5$—CH=CH—CH=CH—$(CH_2)_9$— (Z, Z)
7 R^6 = CH_3—

ms: M^+ at *m*/*z* 475 and 477, CI (NH_3) ms: $(M+H)^+$ at *m*/*z* 476 and 478, leading to empirical formulae $C_{29}H_{49}NO_4$ and $C_{29}H_{51}NO_4$, respectively; ir: $\nu_{C=O}$ 1745, 1700, and 1670 cm^{-1}; $\nu_{C=C}$ 1620 cm^{-1}; uv λ_{max} 228 nm) are in agreement with the addition of one morpholine molecule to the conjugated chromophore of **2***a*–*c*. Indeed, the presence of partial structure **Z** in **6***a*–*c* was clearly demonstrated by the ^{1}H nmr spectrum (Table 1) and by extensive double irradiation experiments.

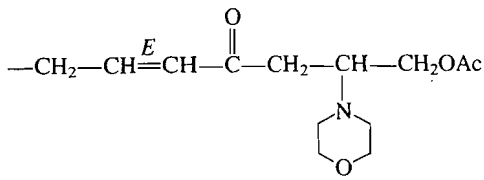

Z

The structures of the three major components of CS2 (C, D, and F) are thus unambiguously established. The three minor ones (A, B, and E) have not yet been identified. However, the presence of a small peak at *m*/*z* 392 in the ms of CS2 (*vide supra*) points to the existence of one or several dihydro derivatives of **2***a* and **2***b*, whose structures could not be more accurately defined.

Several attempts were made to correlate compounds **2***a*–*c*, in particular by homo- or heterogeneous catalytic hydrogenation, but without success, since only intractable mixtures were obtained.

Fraction CS1

This very unstable fraction also displays three molecular ions at *m*/*z* 344, 346, and 348, in a 1:3:1 ratio.

An intense fragment ion is observed at *m*/*z* 318.25534 ($C_{21}H_{34}O_2$, hrms, $M^+ - C_2H_4$). In the CI ms (isobutane) of CS1, $(M+H)^+$ peaks appear at 345, 347, and 349 with $(M+C_4H_9)^+$ peaks at *m*/*z* 401, 403, and 405. It follows from these data that

Can. J. Chem. Downloaded from www.nrcresearchpress.com by 80.58.250.72 on 09/07/12
For personal use only.

Can. J. Chem. Downloaded from www.nrcresearchpress.com by 80.58.250.72 on 09/07/12
For personal use only.

the major component of CS1 has a molecular weight of 346 daltons, and a molecular formula $C_{23}H_{38}O_2$. As in CS2, it is clearly accompanied by one (or more) dehydro (M^+ at m/z 344) and dihydro derivative(s) (M^+ at m/z 348). The ir spectrum shows the presence of conjugated carbonyl groups ($\nu_{C=O}$ 1695, 1675 cm^{-1}; $\nu_{C=C}$ 1625 cm^{-1}), whereas the ^1H nmr of CS1 (Table 1, column **1***a*,*b*) clearly shows the presence of an aldehyde function linked to the usual cross-conjugated dienone (CHO, 9.80 ppm, d, 7.3 Hz coupled to H-2; 6.83 ppm, dd, 16.0 and 7.3 Hz), and of the same mixture of monoenic (5.30 ppm, t) and dienic (5.45, dt and 6.20 ppm, bd) components. These ms and nmr data, together with our results on CS2, indicated that CS1 is a mixture of at least four derivatives, the structures of three of which may be represented by **1***a*–**1***c*. Thus, the major compound of CS1 (**1***a*) is, most probably, (2*E*,5*E*,16*Z*)-4-oxotricosa-2,5,16-trienal.

Fraction CS5

The more polar fraction of the secretion follows the same EI ms pattern as the others, with molecular ions at m/z 360, 362, and 364 (confirmed by D/CI (NH_3) ms). The most intense peak, at m/z 362, gives rise to prominent fragment ions at m/z 334.2502 ($C_{21}H_{34}O_3$, hrms, $M^+ - C_2H_4$) and 316.23925 ($C_{21}H_{32}O_2$, hrms, $M^+ - C_2H_4 - H_2O$), and corresponds to the molecular formula $C_{23}H_{38}O_3$. The uv (λ_{max} 235 nm) and ir spectra (ν_{OH} 3500–2400 cm^{-1}; $\nu_{C=O}$ 1710, 1685, 1665 cm^{-1}; $\nu_{C=C}$ 1625 cm^{-1}) suggest the presence of a carboxylic acid function and of the cross-conjugated dienone.

Two C=O groups are evident in the ^{13}C nmr spectrum of CS5 (CO, 188.5 and COOH, 170.0 ppm), whereas the ^1H nmr spectrum (Table 1) fully supports structures **5***a*–**5***c* for the major components of CS5. The major compound (**5***a*) is thus formulated as (2*E*,5*E*,16*Z*)-4-oxotricosa-2,5,16-trienoic acid. Again, all our attempts to chemically correlate **5***a*–**5***c* with other derivatives of the series failed. Esterification of the carboxylic acid was also attempted under various experimental conditions (CH_2N_2, CH_3OH/H^+, Meerwein salts), but only led to degraded material.

Fraction CS3

This minor yellow fraction suffered extensive degradation as soon as it came out of the Sephadex LH-20 column, and could not be investigated.

Fraction CS4

The EI ms spectrum of this minor fraction is very similar to that of CS5 (M^+ at m/z 360, 362, 364, 366, and 368; intense fragment ions at m/z 334 and 316), thus suggesting a close relationship between both fractions.

The ir spectrum (ν_{OH} 3350 cm^{-1}; $\nu_{C=O}$ 1775 and 1750 cm^{-1}; $\nu_{C=C}$ 1670 cm^{-1}) indicated the presence of an hydroxyl group and of an α,β-unsaturated lactone (28). After several LH-20 chromatographies, we obtained a sample of CS4, whose ^1H nmr is reported in Table 1 (column **4***a*,*b*). Comparison of this spectrum with that of pseudo *cis*-β-acetylacrylic acid (**7**) (29) points to the presence of the same structural elements in both derivatives. Further, the sole olefinic signals that appear in this spectrum are those of the $\Delta^{2(Z)}$ (*cis*) and the $\Delta^{14/16}$ double bonds. These observations lead us to propose structures **4***a*–**4***c* for the major components of CS4. These compounds probably arise by addition of the COOH group to the unsaturated C=O function of $\Delta^{2(Z)}$ dihydro isomers of **5***a*–**5***c*. Although no attempt was made to investigate this reaction in detail, we have observed that uv irradiation of CS5 (254 nm) yielded a less polar fraction with an R_f in tlc identical to that of fraction CS4.

Careful dissection of Dufour's and poison glands, followed by CH_2Cl_2 extraction and tlc analyses, have demonstrated that the compounds we have discussed originate from the Dufour's gland.

The structure and chemical reactivity of *C. scutellaris* derivatives suggest that their toxicity stems from their electrophilic character, allowing them to react with biologically important nucleophilic sites containing hydroxyl, sulfhydryl, or amino groups. Similar contact poisons from termites of the subfamilies Prorhinotermitinae and Rhinotermitinae (30) have been described, and include nitroalkenes, vinylketones, and β-ketoaldehydes. Conjugated ketoaldehydes have also been reported from defensive secretions of bugs (31) and sawflies (19).

However, to the best of our knowledge, this is the first report of this type of derivative in the defensive secretion of an ant.

Experimental

The following instruments were used to measure the physical data: ir, Pye unicam SP1000; uv, Cary 14; ^1H and ^{13}C nmr, Bruker WM 250; ms, Finnigan 3000 D and Micro-mass 7070 F. The nmr spectra were recorded in $CDCl_3$ solution. Chemical shifts are quoted in δ values downfield from TMS as internal standard. The tlc were performed on Polygram Sil G precoated plates (Macherey Nagel).

Collection of the secretion

C. scutellaris workers were seized by tweezers and the defensive secretion that appears at the tip of the sting was collected on bits of filter paper and stored in hexane at −30°C under N_2.

Thin-layer chromatography of the secretion (hexane–acetone 8:2) shows the presence of 5 well-resolved spots numbered from CS1 to CS5 in order of increasing polarity.

Isolation of the compounds

Twenty-two milligrams of the crude secretion of *C. scutellaris* were submitted to partition chromatography on a Sephadex LH-20 column (1 m) using heptane–$CHCl_3$–MeOH (10:10:1) as eluent (20). Flow rate: 0.2 mL/min. Fractions of 3 mL were collected and combined after analysis by tlc (hexane–acetone 8:2). In this manner were obtained (in order of elution from the Sephadex LH-20 column) CS3 (2.5 mg), CS2 (5.0 mg), CS1 (4.5 mg), CS4 (2.5 mg), and CS5 (7.5 mg).

Fraction CS1

Oil; ir: $\nu_{C=O}$ 1695, 1675 cm^{-1}; $\nu_{C=C}$ 1625 cm^{-1}; uv: λ_{max} 234 nm (hexane); ^1H nmr: see Table 1; EI ms: M^+ at m/z 348, 346, 344 (1:3:1); fragment ions at m/z 320, 318.25534 ($C_{21}H_{34}O_2$), 316, 304, 302, 263, 261, 123, 121, 109, 107, 97, 95. CI ms (isobutane): 405, 403, 401 $(M + C_4H_9)^+$, 349, 347, 345 $(M + H)^+$, 319 $(346 - 28 + H^+)$.

Fraction CS2

Oil; ir and uv spectra: see text; ^1H nmr: Table 1; EI ms: M^+ at m/z 392, 390, 388; fragment ions at m/z 364, 362.28244 ($C_{23}H_{38}O_3$), 360, 350, 348, 346, 330.29172 ($C_{23}H_{38}O$), 328, 320.27248 ($C_{21}H_{36}O_2$), 318, 304, 302.26095 ($C_{21}H_{34}O$), 263, 261, 163, 161, 123, 121, 109, 107.

The hplc analysis of CS2: hplc analysis of CS2 (SiO_2, 5 μm, hexane–dioxane 99:1, uv and refractive index detectors) shows the presence of six components, A–F (see text). EI ms of C–D mixture: M^+ at m/z 390; fragment ions at m/z 362, 348, 330, 320, 302, 263 ... 177, 175, 163, 161, 123, 121, 109, 107; EI ms of F: M^+ at m/z 388; fragment ions at m/z 360, 346, 328, 318, 300, 284, 256 ... 175, 163, 161, 123, 121, 109, 107.

Ozonolysis of CS2

CS2 (2 mg) in 50 μL pentane and 250 μL MeOH was ozonolyzed according to Beroza and Bierl (23) at −60°C during 5 min. Addition of $P\phi_3$ and glc analysis on a capillary OV-1 column (115°C) allowed us to identify *n*-heptanal and *n*-nonanal in a 3:1 ratio, by coinjection

with authentic samples. The same result was obtained by glc analysis on a packed 10% Carbowax 20 M column (80 and 105°C).

Ozonolysis of the crude secretion also yielded *n*-heptanal and *n*-nonanal in roughly the same ratio.

Epoxides **3**a,b

CS2 (3 mg) in CH_2Cl_2 was treated at 0°C with an excess of MCPBA under stirring for 2 h. The reaction mixture was concentrated under N_2 and purified by preparative tlc (SiO_2, 0.25 × 5 × 10 cm, hexane–acetone 7:3) affording 1.5 mg of a mixture of **3***a* and **3***b*. **3***a*,*b*: oil; ^1H nmr: see Table 1; EI ms: M^+ at *m/z* 406 ($C_{25}H_{42}O_4$); fragment ions at *m/z* 378, 364, 346, 336, 333, 318, 305, 279.19672 ($C_{17}H_{27}O_3$), 251.16393 ($C_{15}H_{23}O_3$), 249, 247, 223.16956 ($C_{14}H_{23}O_2$) and 223.13343 ($C_{13}H_{19}O_3$), 221, 219, 191, 163.

Cleavage of **3**a,b *with* HIO_4

Treatment of **3***a*,*b* in hexane–Et_2O with HIO_4 (24) followed by glc analysis under the same conditions as above allowed the identification of *n*-heptanal and *n*-nonanal in a 3:1 ratio.

Treatment of CS2 with morpholine

Fraction CS2 (5 mg) in EtOH was treated with 5 drops of freshly distilled morpholine and left at 4°C for 1 h. After evaporation of the solvent and silica gel column chromatography (hexane–dioxane 9:1), the adducts **6***a*, **6***b*, and **6***c* were obtained as a mixture giving only one spot on tlc in several solvent systems.

6*a*, **6***b*, **6***c*: oil; ir and uv spectra: see text; ^1H nmr: Table 1; EI ms: M^+ at *m/z* 479 (small), 477, and 475; fragment ions at *m/z* 449, 447, 404, 402, 390, 389, 376, 362, 350, 348, 330, 320, 302, 263; CI ms (NH_3): $(M+H)^+$ at *m/z* 478 and 476.

Fraction CS4

Oil; ir and uv spectra: see text. This sample was further purified by Sephadex LH-20 chromatography ($CHCl_3$–hexane, 7:3) affording a fraction whose ^1H nmr is described in Table 1; EI ms: M^+ at *m/z* 368, 366, 364, 362, and 360; fragment ions at *m/z* 334, 332, 317, 316, 314, 303, 289, 288, 250.

Fraction CS5

Oil; ir and uv spectra: see text; ^1H nmr: Table 1; EI ms: M^+ at *m/z* 364, 362, and 360; fragment ions at *m/z* 336, 334.2502 ($C_{21}H_{34}O_3$), 332, 316.23925 ($C_{21}H_{32}O_2$), 284, 256; CI ms (NH_3): $(M+NH_4^+)$ at *m/z* 384, 382, 380, 378; fragment ions at *m/z* 356, 354, 352 and 350 $(M+NH_4^+ - C_2H_4)$, 337, 335 and 333 $(M+H^+ - C_2H_4)$.

Acknowledgments

We thank Prof. J. F. Normant (Paris) for sending us spectroscopic data of dienone systems, Dr. R. Ottinger for the nmr spectra, and Mr. C. Moulard for the mass spectra.

1. (*a*) A. B. Attygalle and E. D. Morgan. Chem. Soc. Rev. **13**, 245 (1984); (*b*) M. S. Blum and H. R. Hermann. *In* Arthropod venoms. *Edited by* S. Bettini. Springer Verlag, New York. 1978.
2. A. B. Attygalle, M. C. Cammaerts, and E. D. Morgan. J. Insect Physiol. **29**, 27 (1983).
3. A. B. Attygalle, R. P. Evershed, E. D. Morgan, and M. C Cammaerts. Insect Biochem. **13**, 507 (1983).
4. M. C. Cammaerts, R. P. Evershed, and E. D. Morgan. J Insect Physiol. **27**, 59 (1981).
5. E. D. Morgan, K. Parry, and R. C. Tyler. Insect Biochem. **9** 117 (1979).
6. E. D. Morgan, R. C. Tyler, and M. C. Cammaerts. J. Insec Physiol. **23**, 511 (1977).
7. M. C. Cammaerts-Tricot, E. D. Morgan, R. C. Tyler, anc J. C. Braekman. J. Insect Physiol. **22**, 927 (1976).
8. E. D. Morgan and L. J. Wadhams. J. Insect Physiol. **18**, 112 (1972).
9. M. C. Cammaerts, M. R. Inwood, E. D. Morgan, K. Parry and R. C. Tyler. J. Insect Physiol. **24**, 207 (1978).
10. R. P. Evershed and E. D. Morgan. Insect Biochem. **10**, 8 (1980).
11. H. J. Williams, M. R. Strand, and S. B. Vinson. Tetrahedron, **37**, 2763 (1981).
12. R. K. Vander Meer, F. D. Williams, and C. S. Lofgren. Tetrahedron Lett. **22**, 1651 (1981).
13. M. R. Barlin, M. S. Blum, and J. M. Brand. J. Insect Physiol. **22**, 839 (1976).
14. G. W. K. Cavill, P. J. Williams, and F. B. Whitfield. Tetrahedron Lett. 2201 (1967).
15. C. Detrain, J. M. Pasteels, J. C. Braekman, and D. Daloze. Experientia. In press.
16. F. J. Ritter, I. E. M. Bruggeman-Rotgans, J. E. J. Verviel, C. J. Persoons, and E. Talman. Tetrahedron Lett. 2617 (1977).
17. U. W. J. Maschwitz and W. Kloft. *In* Venomous animals and their venoms. Vol. 3. *Edited by* W. Bücherl and E. E. Buckley. Academic Press, New York. 1971.
18. W. F. Buren. J. N.Y. Entomol. Soc. **66**, 118 (1958).
19. J. L. Boeve, J. C. Braekman, D. Daloze, M. Houart, and J. M. Pasteels. Experientia, **40**, 546 (1984).
20. E. Änggard and H. Bergkvist. J. Chromatogr. **48**, 542 (1970).
21. J. Meinwald, K. Opheim, and T. Eisner. Proc. Natl. Acad. Sci. USA, **69**, 1208 (1972).
22. N. Jabri, A. Alexakis, and J. F. Normant. Tetrahedron, **42**, 1369 (1986).
23. M. Beroza and B. A. Bierl. Anal. Chem. **39**, 1131 (1967).
24. B. A. Bierl-Leonhardt, E. D. De Vilbiss, and J. R. Plummer. J. Chromatogr. Sci. **18**, 364 (1980).
25. A. Barabas, A. A. Botar, A. Gocan, N. Popovici, and F. Hodosan. Tetrahedron, **34**, 2191 (1978).
26. T. Ando, K. Kusa, M. Uchiyama, S. Yochida, and N. Takahashi. Agric. Biol. Chem. **47**, 2849 (1983).
27. L. Ananthasubramanian, S. V. Govindan, K. D. Deodhar, and S. C. Bhattacharyya. Indian J. Chem. **16B**, 191 (1978).
28. K. Nakanishi. Infrared absorption spectroscopy. Holden–Day, San Francisco. 1962.
29. S. Seltzer and K. D. Stevens. J. Org. Chem. **33**, 2708 (1960).
30. S. G. Spanton and G. D. Prestwich. Tetrahedron, **38**, 1921 (1982).
31. T. O. Olagberimo and B. W. Staddon. J. Chem. Ecol. **9**, 1397 (1983).

Can. J. Chem. Downloaded from www.nrcresearchpress.com by 80.58.250.72 on 09/07/12
For personal use only.

Synthesis, ^1H, ^{13}C, and ^{29}Si nuclear magnetic resonance spectra and crystal structure of *trans*-1,4-diphenyldecamethylcyclohexasilane

KANTA KUMAR[1] AND MORTON H. LITT
Department of Macromolecular Science, Case Western University, Cleveland, OH 44106, U.S.A.

AND

RAJ K. CHADHA AND JOHN E. DRAKE
Department of Chemistry and Biochemistry, University of Windsor, Windsor, Ont., Canada N9B 3P4

Received June 13, 1986

KANTA KUMAR, MORTON H. LITT, RAJ K. CHADHA, and JOHN E. DRAKE. Can. J. Chem. **65**, 437 (1987).

The coupling reaction between $PhMeSiCl_2$ and Me_2SiCl_2 in the presence of Na/K alloy resulted in a variety of phenylated permethylcyclohexasilanes of which only *trans*-1,4-$Ph_2Me_{10}Si_6$ could be obtained in pure form by repeated recrystallizations. It was studied by means of nmr (^1H, ^{13}C, and ^{29}Si) and X-ray crystallography. The crystals are monoclinic, $P2_1/c$ with $a = 10.105(6)$, $b = 14.77(1)$, $c = 9.973(6)$ Å, $\beta = 94.08(5)°$, $V = 1485(2)$ Å^3, and $Z = 2$ for 1922 unique "observed" reflections and the structure refined to an R index of 0.036. The molecule has site symmetry $\bar{1}$ and the chair conformation of cyclohexane, with the two phenyl rings occupying the equatorial positions.

KANTA KUMAR, MORTON H. LITT, RAJ K. CHADHA et JOHN E. DRAKE. Can. J. Chem. **65**, 437 (1987).

La réaction de couplage du $PhMeSiCl_2$ et du Me_2SiCl_2, en présence d'un alliage de Na/K, conduit à un mélange de perméthylcyclohexasilanes phénylés duquel, des cristallisations fractionnées répétées, n'ont permis d'isoler à l'état pur que le diphényl-1,4-*trans* $Me_{10}Si_6$. On l'a étudié par rmn du ^1H, du ^{13}C et du ^{29}Si ainsi que par diffraction des rayons-X. Les cristaux sont monocliniques, $P2_1/c$, avec $a = 10{,}105(6)$, $b = 14{,}77(1)$ et $c = 9{,}973(6)$ Å, $\beta = 94{,}08(5)°$, $V = 1485(2)$ Å^3 et $Z = 2$ pour 1922 réflexions uniques observées : on a affiné la structure jusqu'à une valeur de R de 0,036. La molécule possède un site de symétrie $\bar{1}$; le cyclohexane adopte une conformation chaise et les deux groupements phényles occupent des positions équatoriales.

[Traduit par la revue]

Introduction

Phenylated permethylcyclohexasilane derivatives are generally prepared by the reaction of PhMgCl with chloropermethylcyclohexasilanes (1–3). The method is basically used to purify the chloro derivatives because the phenyl compounds are much easier to handle in air and can be quantitatively converted back to the chloro derivatives (1). For this reason we decided to prepare phenylated permethylcyclohexasilanes directly from monosilane precursors, following the procedures of Helmer and West (1). In this paper, we report the preparation of one such compound, namely *trans*-1,4-diphenyldecamethylcyclohexasilane, along with an X-ray crystallographic study which confirms the *trans* geometry and establishes the orientation of the phenyl rings in the compound.

Results and discussion

The method used to synthesize the phenyl-substituted permethylcyclohexasilanes was that of alkali metal co-condensation of one equivalent of $PhMeSiCl_2$ with two equivalents of Me_2SiCl_2.

$$PhMeSiCl_2 + 2Me_2SiCl_2 \xrightarrow[THF]{Na/K} Ph_xMe_{12-x}Si_6 + MCl$$

$x = 0$–6; M = Na or K

Though the method gave compounds with every degree of phenyl substitution, only $Me_{12}Si_6$, $PhMe_{11}Si_6$, and $Ph_2Me_{10}Si_6$ derivatives were isolated and characterized. The yield of the diphenyl derivatives was optimized by the slow addition of the mixed dihalosilanes to Na/K alloy in refluxing THF. The maximum yield of the mixture of various isomers of $Ph_2Me_{10}Si_6$ thus obtained was 32%. Table 1 shows the percent yield of various isolated derivatives. The theoretical yields were obtained by assuming that the coupling of the dimethyl and methylphenyl silyl groups was random, and by using a binomial expansion to calculate the values. There is good agreement between theory and experiment (Table 1) showing that the slow addition results in establishing a random product distribution, probably by ring opening and reshuffling reactions subsequent to coupling. In reactions where the silanes were added to the reaction flask rapidly, large amounts of $Me_{12}Si_6$ and higher phenylated compounds were obtained.

TABLE 1. Percent yield of various isolated derivatives

$Ph_xMe_{12-x}Si_6$ x	Yield wt%	Yield mol%	Theoretical yield mol%
0	8	11	8.8
1	24	27	26.3
2	32	32	32.9
3	36	30	21.9
4			8.2
5			1.6
6			0.1

The isomeric mixture of diphenyl derivatives obtained from the optimum yield reaction was further separated into the solid (A) and liquid (B) fractions by the addition of ethanol. The ^1H nmr spectra of these two fractions are shown in Fig. 1 and an hplc run showed that the solid fraction (A) was a mixture of more than five isomers. Repeated recrystallizations of the solid fraction were carried out until its chromatogram showed only a single peak. Thus, this diphenyldecamethylcyclohexasilane (mp 168–170°C) was isolated only in a small yield. Its ^1H nmr

[1]Present address: Corporate Research Laboratories, 3M Center, St. Paul, MN 55144, U.S.A.

Can. J. Chem. Downloaded from www.nrcresearchpress.com by 80.58.250.72 on 09/07/12
For personal use only.

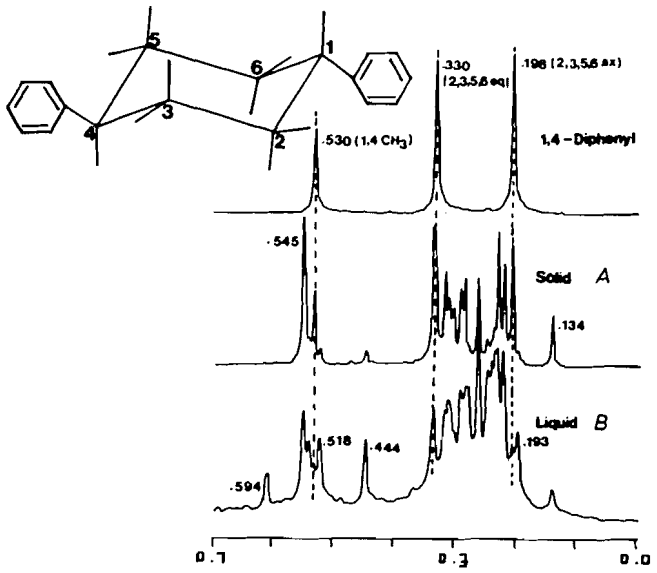

FIG. 1. ^1H nmr of diphenyldecamethylcyclohexasilanes.

TABLE 2. Final fractional co-ordinates with esd's in parentheses and equivalent isotropic thermal parameters ($\times 10^3$) for non-H atoms

Atom	x	y	z	U^*_{eq}(Å^2)
Si(1)	0.1363(1)	0.0928(1)	0.3959(1)	40.0(4)
Si(2)	−0.0665(1)	0.0455(1)	0.2885(1)	43.9(4)
Si(3)	−0.2211(1)	0.0156(1)	0.4487(1)	40.6(4)
C(1)	0.1077(3)	0.2018(2)	0.4884(3)	63(2)
C(2)	−0.0483(3)	−0.0622(2)	0.1875(3)	69(2)
C(3)	−0.1348(4)	0.1359(2)	0.1703(3)	80(2)
C(4)	−0.3739(3)	−0.0341(2)	0.3564(3)	65(2)
C(5)	−0.2704(3)	0.1224(2)	0.5353(4)	71(2)
C(11)	0.2659(3)	0.1155(2)	0.2714(2)	48(1)
C(12)	0.3558(3)	0.1868(2)	0.2908(3)	69(2)
C(13)	0.4526(4)	0.2020(3)	0.2023(5)	93(3)
C(14)	0.4604(4)	0.1494(3)	0.0912(4)	93(3)
C(15)	0.3744(4)	0.0795(4)	0.0693(3)	91(3)
C(16)	0.2783(3)	0.0633(3)	0.1597(3)	71(2)

*$U_{eq} = \frac{1}{3}\Sigma_i\Sigma_j a^*_i a^*_j a_i \cdot a_j$.

spectrum is shown in Fig. 1 and ^1H, ^{13}C, and ^{29}Si nmr data are given in the Experimental section.

If the two phenyl substituents in a 1,4-disubstituted hexasilane ring are either both equatorial or both axial, there would be two non-equivalent silicon atoms (ratio 2:4), three non-equivalent methyl groups (2:4:4), and three non-equivalent methyl protons (6:12:12). The observed number of signals clearly indicate that the diphenyl derivative possesses *trans* geometry, i.e., the two phenyl rings are indeed either both equatorial or both axial. However, it is expected that the bulkier phenyl groups, in order to minimize non-bonding interactions, should probably occupy the equatorial positions. The following assignment of the nmr signals are based on this assumption.

In the ^1H nmr spectrum, the methyl groups attached to the 1,4 silicon atoms being axial appear downfield at 0.530 ppm. As the equatorial methyl groups at positions 2, 3, 5, and 6 lie in the deshielding region of the phenyl rings, they appear at 0.330 ppm, while the axial methyl groups are shielded and appear to highfield at 0.198 ppm. In contrast with the ^1H nmr spectra, an upfield shift was observed for the 1,4 methyl groups

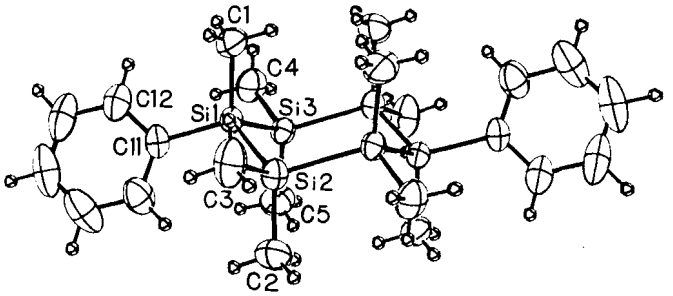

FIG. 2. ORTEP plot of *trans*-1,4-$Ph_2Me_{10}Si_6$. The atoms are drawn with the 50% probability ellipsoids. The labeling scheme is defined, unlabeled atoms are related to labeled ones by a centre of inversion at 0, 0, ½. Hydrogen atoms are drawn arbitrarily small.

in the ^{13}C nmr spectrum (−6.49 ppm). The methyl groups which are *cis* to the phenyl groups appear downfield at −4.32 ppm and those which are *trans* to the phenyl groups appear upfield at −6.71 ppm. These assignments are consistent with the results of Helmer and West (1). The 1,4-silicon resonances appear at −41.40 ppm while other silicon resonances appear at −41.08 ppm. This assignment of peaks is based on the results of Sharp *et al.* (4).

The single crystal X-ray structure determination confirms the *trans* geometry of 1,4-diphenyldecamethylcyclohexasilane. The final atomic coordinates for Si and C atoms are given in Table 2 and important distances and angles in Table 3. The compound exists as discrete molecules as shown in Fig. 2. The cyclohexasilane ring adopts a regular chair conformation with $\bar{1}$ site symmetry at 0, 0, ½. The two phenyl rings which are present at the 1,4 positions occupy equatorial sites. The average Si—Si distance of 2.350(3) Å is close to that in elemental silicon, 2.352 Å (5), $Me_{12}Si_6$, 2.338(4) Å (6), and $Ph_6Me_6Si_6$, 2.359(2) Å (7). These distances agree well with the Si—Si covalent bond length of 2.34 Å (8). The average Si—Si—Si bond angle is 110.6(6)° and average SiSiSiSi torsion angle is 57.1°. These and other torsion angles (Table 4) are closer to the ideal angles of 109.5°, 60°, and 180° for a six-membered chair conformation than the respective angles in other hexasilane structures studied so far (6, 7, 9). This indicates that the structure of *trans*-1,4-$Ph_2Me_{10}Si_6$ has the least distorted cyclohexasilane ring relative to those of $Me_{12}Si_6$ (6), all *trans*-$Ph_6Me_6Si_6$ (7), and $Ph_{12}Si_6.7C_6H_6$ (9).[2]

The average Si—C bond length is 1.890(8) Å and there is very little or no difference between the average Si—C(ax) (1.890(9) Å) and Si—C(eq) (1.889(9) Å) bond lengths. Here, the structure differs from $Me_{12}Si_6$ where a difference of 0.033 Å is reported between axial and equatorial Si—C bond distances (6). However, the difference between averaged Si—C(Me), 1.888(8) Å and Si—C(Ph) 1.897(3) Å is of the same magnitude as has been observed in $Ph_6Me_6Si_6$ (7).

Experimental

Starting materials

Me_2SiCl_2 and $MePhSiCl_2$ were obtained from Aldrich Chemical Co., and were distilled before use. Tetrahydrofuran (THF) was predried over $LiAlH_4$ and distilled from Na/benzophenone.

[2]Lists of structure factors, anisotropic thermal parameters, unit cell packing diagram, torsion angles, and fractional coordinates for H atoms may be purchased from the Depository of Unpublished Data, CISTI, National Research Council of Canada, Ottawa, Ont., Canada K1A 0S2.

Can. J. Chem. Downloaded from www.nrcresearchpress.com by 80.58.250.72 on 09/07/12
For personal use only.

TABLE 3. Interatomic distances (Å) and angles (deg)*

Atoms	Distance	Bonds	Angle
Si(1)—Si(2)	2.350(1)	Si(2)—Si(1)—Si(3)	111.3(1)
Si(1)—Si(3)	2.348(1)	Si(2)—Si(1)—C(1)	108.5(1)
Si(1)—C(1)	1.887(3)	Si(3)—Si(1)—C(1)	108.7(1)
Si(1)—C(11)	1.897(3)	Si(2)—Si(1)—C(11)	112.0(1)
Si(2)—Si(3)[1]	2.353(1)	Si(3)—Si(1)—C(11)	108.4(1)
Si(2)—C(2)	1.900(3)	C(1)—Si(1)—C(11)	107.8(1)
Si(2)—C(3)	1.880(3)	Si(1)—Si(2)—Si(3)′	110.2(1)
Si(3)—C(4)	1.890(3)	Si(1)—Si(2)—C(2)	112.1(1)
Si(3)—C(5)	1.883(3)	Si(3)′—Si(2)—C(2)	107.3(1)
Phenyl ring C(11)—C(16)*		Si(1)—Si(2)—C(3)	110.1(1)
C—C(mean)	1.376(17)	Si(3)′—Si(2)—C(3)	109.1(1)
C—C—C(mean)	119.6(17)*	C(2)—Si(2)—C(3)	107.9(2)
		Si(1)—Si(3)—Si(2)′	110.3(1)
Si(1)---Si(3)′	3.858	Si(1)—Si(3)—C(4)	107.6(1)
Si(1)---Si(2)′	3.859	Si(2)′—Si(3)—C(4)	107.6(1)
Si(2)---Si(3)	3.879	Si(1)—Si(3)—C(5)	111.4(1)
		Si(2)′—Si(3)—C(5)	111.4(1)
		C(4)—Si(3)—C(5)	108.4(2)
		Si(1)—C(11)—C(12)	121.0(2)
		Si(1)—C(11)—C(16)	122.8(2)
		C—C—C(mean)	119.6(17)†

*Symmetry equivalent position for primed atom is $-x, -y, 1-z$.
†E.S.D.'s on average values are calculated using the scatter formula: $\sigma = [\Sigma(d_i - \bar{d})^2/(N-1)]^{1/2}$.

TABLE 4. Comparison of some averaged bond angles (deg) and distances (Å) in the cyclohexasilanes and cyclohexane*

Compound (ref.)	Si—Si	∠SiSiSi	∠CSiC	Si—C	SiSiSiSi	CSiSiSi	CSiSiC
trans-1,4-$Ph_2Me_{10}Si_6$	2.350(3)	110.6(6)		1.890(8)	57.1	64.7, 177.4	55.7, 62.6, 174.0
$Me_{12}Si_6$ (6)	2.338(4)	111.9(4)	108.1(5)	1.935(6) (eq) 1.913(4) (ax)	53.5	68.6, 173.6	51.3, 66.7, 169.3
$Ph_6Me_6Si_6$ (7)	2.359(2)	111.1		1.882(5) (Me) 1.893(3) (Ph)	55.2		55.3, 66.6, 171.0
$Ph_{12}Si_67C_6H_6$ (9)	2.394	113.8	105.5	1.898	47.5		

Compound (ref.)	C—C	CCC	CCCC
C_6H_{12} (13)	1.528(5)	111.6(2)	54.5(8)

*Results obtained from electron diffraction.

Preparation of 1,4-diphenyldecamethylcyclohexasilane

Typically, K (22.9 g) and Na (3.82 g; 78% K by weight) (10) were placed in a 3-necked, 1-L round bottom flask along with THF (300 mL) and then warmed and stirred for 1 h. A mixture of $PhMeSiCl_2$ (20 g, 0.105 mol) and Me_2SiCl_2 (27 g, 0.210 mol) in THF (50 mL) was then added dropwise over 2 h. The solution was refluxed overnight, cooled, and hexane (approx. 250 mL) added. Excess of Na/K was destroyed by slow and careful addition of water. The organic layer was separated, washed with aqueous NaCl, and dried over anhydrous Na_2SO_4. After evaporation of the solvent, 24.5 g of viscous liquid was obtained.

Thin layer chromatography (silica) using hexane as solvent showed the liquid to be a mixture of at least five products. Three products, $Me_{12}Si_6$, $PhMe_{11}Si_6$, and $Ph_2Me_{10}Si_6$ were isolated with the help of flash column chromatography (6 × 18 cm, packed with 40–63 μ silica gel 60) (11) using hexane as eluent. Fractions of 125 mL were collected, which on evaporation afforded the following compounds:

Fractions 4–6: $Me_{12}Si_6$ (3.2 g, 8%); ^1H nmr ($CDCl_3$, δ ppm) 0.182 (s); mp 251–253°C (lit. (7) 254–257°C).

Fractions 14–16: $PhMe_{11}Si_6$, recrystallized from ethanol (6.2 g, 24%); mp 109–110°C (lit. (5) 110–111°C).

Fractions 17–28: The isomeric mixture of 2,3-, 1,3-, and 1,4-*cis* and *trans* derivatives of $Ph_2Me_{10}Si_6$ (8.3 g, 32%). The mixture became semi-solid after standing overnight at room temperature. A small amount of ethanol was added to it and the solid (A) and liquid (B) fractions were separated by filtration.

Repeated recrystallizations of the solid fraction (A) gave 1.2 g of pure *trans*-1,4-$Ph_2Me_{10}Si_6$ (mp 168–170°C). High performance liquid chromatography showed a single peak. *Anal.* calcd. for $Si_6H_{40}C_{22}$: C 55.85, H 8.52, Si 35.62; found: C 55.70, H 8.53, Si 35.83. Mass spectrum (m/z): 472 (M^+). ^1H nmr ($CDCl_3$, δ ppm): 0.198 (s, 12H); 0.330 (s, 12H), 0.530 (s, 6H); 7.42 (m, 10H). $^{13}C\{^1H\}$ nmr ($CDCl_3$, δ ppm): −4.32, −6.49, −6.71, 134.68(*o*), 127.86(*p*), 127.71(*m*), 146.98(*ipso*). ^{29}Si nmr ($CDCl_3$, δ ppm): −41.08, −41.40. Infrared spectrum (ν, cm^{-1}): 3060m, 3040m, 2950s, 2890s, 1420m, 1400m, 1245br,m, 1090m, 835s, 800s, 770s, 727s, 695s, 650m, 630m.

Physical measurements

The liquid chromatograph used was a Varian 8500 equipped with a Waters μ Bondapak C18 (reverse phase) column. The solvent used was 80% CH_3OH/20% THF and the flow rate was 1 mL/min. The uv

Can. J. Chem. Downloaded from www.nrcresearchpress.com by 80.58.250.72 on 09/07/12
For personal use only.

TABLE 5. Summary of crystal data, intensity collections, and structural refinement for *trans*-1,4-$Ph_2Me_{10}Si_6$

Cell constants	$a = 10.105(6)$, $b = 14.77(1)$, $c = 9.973(6)$ Å, $\beta = 94.08(5)°$
Cell volume (Å^3)	1485(2)
Space group	$P2_1/c$
Z	2
M_r	472.6
ρ(calcd), ρ(obsd) (g cm^{-3})	1.06, 1.10
Absorption coefficient (cm^{-1})	2.48
Crystal dimensions (mm)	0.18 × 0.27 × 0.34
Radiation	Mo-K_α, λ = 0.71069 Å
Temperature (°C)	22
2θ angle (deg)	3–50
Scan type	θ/2θ
Scan width (deg)	$K_{\alpha_1} - 1$ to $K_{\alpha_2} + 1$
Scan speed (deg min^{-1})	2.02–4.88
Background time/scan time	0.5
Total reflections measured	3068 ($+h, +k, \pm l$)
Unique data used	1922 ($I > 3\sigma(I)$)
No. of parameters	127
$R = (\Sigma\|\|F_o\| - \|F_c\|\|/\Sigma\|F_o\|)$	0.0361
$R_w = \Sigma w(\|F_o\| - \|F_c\|)^2/\Sigma w\|F_o\|^2]^{1/2}$	0.0414
$\Delta\rho_{max}$ (e Å^{-3})	0.33 at −0.063, 0.096, 0.0333
Shift: error (max)	0.2

absorbance detector was set at 254 nm. ^{1}H nmr spectra were run using $CDCl_3$ as solvent and CH_2Cl_2 as internal reference (δ 5.35). ^{13}C nmr spectra were referenced to the central peak of the $CDCl_3$ triplet (δ 77.0). TMS was the internal standard for ^{29}Si nmr spectra. $Cr(acac)_3$ was added for the ^{29}Si and ^{13}C nmr. Infrared spectra were recorded on a Digilab Model FT-IRS-14. Mass spectra were obtained on a Finnigan mass spectrometer. Melting points were uncorrected. Elemental analyses were done by Galbraith Laboratory. Density was measured by the flotation method in C_6H_{12}/CCl_4.

X-ray crystallographic analysis

A crystal of dimensions 0.18 × 0.27 × 0.34 mm was mounted along the largest dimension and aligned on a Syntex $P2_1$ automated diffractometer. The unit cell dimensions were calculated from the setting angles of 15 strong reflections having $15° < 2\theta < 30°$. The data were collected and processed following the procedure described previously (12). The intensities of three monitor reflections checked every 60 reflections changed only by 2% during data collection. Of the 3068 reflections measured ($3° < 2\theta < 50°$, h, $0 \rightarrow 12$; k, $0 \rightarrow 17$, l, $-11 \rightarrow 11$), 1922 independent reflections had $I > 3\sigma(I)$ and only these were used in subsequent calculations. The intensities were corrected for Lorentz and polarization effects and not for absorption, since μ was only 2.48 cm^{-1}. Systematic absences ($0k0$, $k = 2n + 1$; $h0l$, $l = 2n + 1$) indicate the space group $P2_1/c$. Details of X-ray data and refinement parameters are summarized in Table 5.

The positions of Si(1), Si(2), and Si(3) atoms were obtained from the E-map (direct methods) using SHELX, while those of carbon atoms were determined from a difference Fourier map. The structure was refined anisotropically by the full-matrix least-squares methods. A difference map at this stage showed peaks at plausible hydrogen positions. Hydrogen atoms were included in subsequent refinements in ideal positions (C—H 0.95 Å, ∠CCH 120°, ∠HCH 109.5°). Methyl hydrogen atoms were refined as a group with isotropic thermal parameters assigned 0.01 Å^2 greater than the atoms to which they are attached. Refinement gave final values of $R = 0.036$ and $R_w = 0.041$. The function $(|F_o| - |F_c|)^2$ was minimized during least-squares refinement and in the final cycles, a weighting scheme of the form $w = 1/[\alpha^2(F) + pF^2]$ was employed with a final p value of 0.0006. No evidence of secondary extinction was found. Sources of scattering factors and computer programs used have been given elsewhere (12).

Acknowledgements

K.K. and M.H.L. thank NASA Lewis Research Center for financial support. Dr. Cheng-yih Kuo of Glidden Resins and Coatings (SCM) for the hplc analyses, and Mr. Jim Gordon of Warrensville Research Center (Sohio) for mass spectra determinations.

J.E.D. thanks the Natural Sciences and Engineering Research Council of Canada for the operating grants to support this work in part.

1. B. J. HELMER and R. WEST. J. Organomet. Chem. **236**, 21 (1982).
2. M. ISHIKAWA and M. KUMADA. Synth. Inorg. Metal-Org. Chem. **1**, 191 (1971).
3. M. ISHIKAWA and M. KUMADA. Synth. Inorg. Metal-Org. Chem. **1**, 229 (1971).
4. K. G. SHARP, P. A. SUTOR, E. A. WILLIAMS, J. D. CARGIOLI, T. C. FARRAR, and K. ISHIBITSU. J. Am. Chem. Soc. **98**, 1977 (1976).
5. M. E. STRAUMANIS and E. Z. AKA. J. Appl. Phys. **23**, 330 (1952).
6. H. L. CARRELL and J. DONOHUE. Acta Crystallogr. B**28**, 1566 (1972).
7. S.-M. CHEN, L. D. DAVID, K. J. HALLER, C. L. WADSWORTH, and R. WEST. Organometallics, **2**, 409 (1983).
8. L. PAULING. Nature of chemical bond. 3rd ed. Cornell University Press. Ithaca, NY. 1960. p. 246.
9. VON M. DRAGER and K. G. WALTER. Z. Anorg. Allg. Chem. **479**, 65 (1981).
10. R. WEST, L. BROUGH, and W. WOJNOWSKI. Inorg. Synth. **XIX**, 265 (1975).
11. W. C. STILL, M. KAHN, and A. MITZ. J. Org. Chem. **43**, 2923 (1978).
12. R. K. CHADHA, J. E. DRAKE, and A. B. SARKAR. Inorg. Chem. **25**, 2201 (1986).
13. M. DAVIS and O. HASSEL. Acta Chem. Scand. **17**, 1181 (1963).

Can. J. Chem. Downloaded from www.nrcresearchpress.com by 80.58.250.72 on 09/07/12
For personal use only.

Kinetics of acid-catalyzed hydration in aqueous solution of 1-methoxy- and 1-methylthio-2-phenylethyne and some related acetylenes

N. BANAIT, M. HOJATTI, P. FINDLAY, AND A. J. KRESGE[1]

Department of Chemistry, University of Toronto, Toronto, Ont., Canada M5S 1A1

Received June 13, 1986

N. BANAIT, M. HOJATTI, P. FINDLAY, and A. J. KRESGE. Can. J. Chem. **65**, 441 (1987).

The rates of conversion of $C_6H_5C{\equiv}COCH_3$ to $C_6H_5CH_2CO_2CH_3$ were measured in dilute $HClO_4/H_2O$, $DClO_4/D_2O$, and H_3PO_4–$H_2PO_2^-/H_2O$ buffer solutions, and the rates of conversion of $C_6H_5C{\equiv}CSCH_3$ to $C_6H_5CH_2COSCH_3$, $C_6H_5C{\equiv}CH$ to $C_6H_5COCH_3$, 2,4,6-$(CH_3)_3C_6H_2C{\equiv}CH$ to 2,4,6-$(CH_3)_3C_6H_2COCH_3$, and p-$CH_3OC_6H_4C{\equiv}CCH_3$ to p-$CH_3OC_6H_4COCH_2CH_3$ were measured in concentrated $HClO_4/H_2O$ solutions, all at 25°C. The reaction of $C_6H_5C{\equiv}COCH_3$ showed general acid catalysis and gave the isotope effect $k_{H^+}/k_{D^+} = 1.59$, which indicates that it proceeds through rate-determining proton transfer from catalyst to substrate. The hydronium ion catalytic coefficient for this reaction is $k_{H^+} = 8.8 \times 10^{-2}\ M^{-1}\ s^{-1}$, and those for the other four, in the order given above, are $k_{H^+} = 1.2 \times 10^{-3}$, 2.9×10^{-7}, 1.2×10^{-4}, and $8.5 \times 10^{-6}\ M^{-1}\ s^{-1}$. Relative reactivities based on these rate constants are discussed.

N. BANAIT, M. HOJATTI, P. FINDLAY et A. J. KRESGE. Can. J. Chem. **65**, 441 (1987).

Opérant à 25°C, on a mesuré les vitesses de conversion du $C_6H_5C{\equiv}COCH_3$ en $C_6H_5CH_2CO_2CH_3$ dans des solutions diluées de $HClO_4/H_2O$ et de $DClO_4/D_2O$ et dans des solutions tampons de H_3PO_4–$H_2PO_2^-/H_2O$; on a aussi mesuré les vitesses de conversion du $C_6H_5C{\equiv}CSCH_3$ en $C_6H_5CH_2COSCH_3$, du $C_6H_5C{\equiv}CH$ en $C_6H_5COCH_3$, du $(CH_3)_3$-2,4,6 $C_6H_2C{\equiv}CH$ en $(CH_3)_3$-2,4,6 $C_6H_2COCH_3$ et du p-$CH_3OC_6H_4C{\equiv}CCH_3$ en p-$CH_3OC_6H_4COCH_2CH_3$ dans des solutions concentrées de $HClO_4/H_2O$. La réaction du $C_6H_5C{\equiv}COCH_3$ est soumise à une catalyse acide générale et l'effet isotopique $k_{H^+}/k_{D^+} = 1{,}59$; ce dernier résultat indique que la réaction procède par une étape déterminante impliquant un transfert de proton du catalyseur vers le substrat. Le coefficient catalytique de l'ion hydronium, pour cette réaction, est $k_{H^+} = 8{,}8 \times 10^{-2}\ M^{-1}\ s^{-1}$ et pour les quatre autres, dans l'ordre mentionné plus haut, ces coefficients sont respectivement $1{,}2 \times 10^{-3}$, $2{,}9 \times 10^{-7}$, $1{,}2 \times 10^{-4}$ et $8{,}5 \times 10^{-6}\ M^{-1}\ s^{-1}$. On discute des réactivités relatives en se basant sur ces constantes de vitesses.

[Traduit par la revue]

In an extensive series of investigations, Drenth and his students examined the acid-catalyzed addition of water to acetylenic ethers and thioethers (1). That work showed that these reactions occur through protonation of the triple bond in the β-position to give a vinyl cation, reaction [1] X = O, S,

$$[1]\quad CH{\equiv}CXR \xrightarrow[-A^-]{HA} CH_2{=}\overset{+}{C}XR$$

followed by hydration of this cation and tautomerization of the ensuing ester enol, reaction [2].

$$[2]\quad CH_2{=}\overset{+}{C}XR \xrightarrow[-H^+]{H_2O} CH_2{=}\overset{OH}{\overset{|}{C}}XR \rightarrow CH_3\overset{O}{\overset{\|}{C}}XR$$

We hope to use the photochemical analog of this thermal reaction to prepare ester enols in aqueous solution and to examine their chemistry in that medium. We have found it necessary for this purpose to know the stability of 1-methoxy-2-phenylethyne, **1**, and 1-methylthio-2-phenylethyne, **2**, in

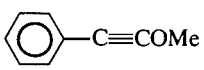

1

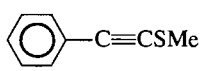

2

aqueous acids, and we have consequently measured the rates of acid-catalyzed hydration of these substances in aqueous solution. We report the results of that study here together with some information on the kinetics of acid-catalyzed hydration of the related acetylenes phenylethyne, **3**, mesitylethyne, **4**, and 1-(*p*-methoxyphenyl)-propyne, **5**.

[1]To whom correspondence should be addressed.

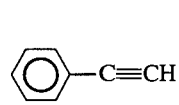

3

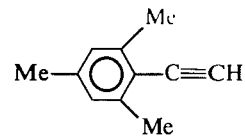

4

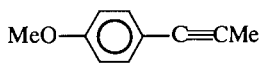

5

Experimental section

Materials

1-Methoxy-2-phenylethyne was prepared by treating 1-chloro-2-phenylethyne with sodium methoxide (2), and 1-methylthio-2-phenylethyne was prepared by treating sodium phenylacetylide first with sulfur and then with methyl iodide (3). A portion of the latter substance was converted to methyl phenylthioacetate by heating in acetic acid solution (4). Mesitylethyne was synthesized by dehydrohalogenating 1-chloro-1-mesitylethene, which in turn was obtained by treating 2,4,6-trimethylacetophenone with phosphorous pentachloride (5). 1-(*p*-Methoxyphenyl)-propyne (6) was prepared by alkylating sodium *p*-methoxyphenylacetylide with methyl iodide, and *p*-methoxyphenylacetylene (7) was made from *p*-methoxyacetophenone in a manner similar to that used for mesitylethyne. All of these substances had physical properties similar to literature values and gave spectra consistent with their structures. Other materials used in this research were best available commercial grades. Samples used for kinetic determinations were purified by gas chromatography.

Solutions were prepared from deionized H_2O purified further by distillation or from D_2O (MSD Isotopes 99.8 atom % D) as received.

Kinetics

Rates of reaction were determined spectroscopically by monitoring the decrease in absorbance of the strong uv band characteristic of

Can. J. Chem. Downloaded from www.nrcresearchpress.com by 80.58.250.72 on 09/07/12
For personal use only.

Can. J. Chem. Downloaded from www.nrcresearchpress.com by 80.58.250.72 on 09/07/12
For personal use only.

arylacetylenes with $\lambda_{max} \cong 240$ nm. Measurements were made with a Cary 118 spectrometer whose cell compartment was thermostatted at 25.0 ± 0.02°C. Runs were performed by first allowing 3.0 mL of aqueous acid or buffer solution to come to temperature equilibrium with the spectrometer cell compartment and then adding a few μL of stock solution of substrate dissolved in acetonitrile; initial substrate concentrations in the reaction mixtures were $2–6 \times 10^{-5}$ *M*. Reactions were followed to completion. The data so obtained conformed to the first-order rate law well, and observed first-order rate constants were calculated by least-squares fitting of absorbance and time values to an expontential function (8).

Results

Gas chromatographic examination of a spent reaction mixture indicated that only one product is formed in the acid-catalyzed hydration of 1-methoxy-2-phenylethyne in aqueous solution, and comparison of the uv spectrum of this product with that of an authentic sample showed this substance to be the methyl ester of phenylacetic acid, as expected. Similar spectral comparisons likewise showed the product of the hydration of 1-methylthio-2-phenylethyne to be the methanethiol ester of phenylacetic acid, and the products of the hydrolysis of phenylethyne, mesitylethyne, and 1-(*p*-methoxyphenyl)-propyne to be the corresponding aryl ketones.

Measurements of the rate of hydration of 1-methoxy-2-phenylethyne were made in perchloric acid solutions over the concentration range 0.02–0.1 *M* in H_2O solution and over the range 0.01–0.06 *M* in D_2O; these data are summarized in Table S1.[2] Observed first-order rate constants determined in both solvents were accurately proportional to acid concentration, and linear least-squares analysis gave the catalytic coefficients $k_{H^+} = (8.81 \pm 0.18) \times 10^{-2}\ M^{-1}\ s^{-1}$ and $k_{D^+} = (5.54 \pm 0.07) \times 10^{-2} M^{-1} s^{-1}$; these provide the isotope effect $k_{H^+}/k_{D^+} = 1.59 \pm 0.04$.

Rates of hydration of 1-methoxy-2-phenylethyne were also measured in phosphoric acid buffer solutions. Two series of solutions of constant buffer ratio ($[H_3PO_4]/[H_2PO_4^-] = 0.47$ and 0.92) and constant ionic strength (0.10 *M*, maintained with NaCl) were used. Within each series, buffer concentrations were varied by a factor of five. These data are summarized in Table S2.[2]

Because H_3PO_4 is a moderately strong acid, hydronium ion concentrations failed to remain constant within these buffer solution series. This "buffer failure" (9) was treated by adjusting observed first-order rate constants to values expected for a common hydronium ion concentration within each series (10); values of $[H_3O^+]$ needed for this purpose were obtained by calculation using $K_a = 7.14 \times 10^{-3}$ *M* (11) and ionic activity coefficients (for $H_2PO_4^-$ and H_3O^+) recommended by Bates (12).

Observed first-order rate constants adjusted in this way increased with increasing phosphoric acid concentration, indicating that the hydration of 1-methoxy-2-phenylethyne is subject to general acid catalysis. The relationship between k_{adj} and $[H_3PO_4]$ was accurately linear, and least-squares analysis gave $k_{H_3PO_4} = (6.00 \pm 0.15) \times 10^{-3} M^{-1} s^{-1}$ (buffer ratio = 0.47) and $(7.36 \pm 0.15) \times 10^{-3} M^{-1} s^{-1}$ (buffer ratio = 0.92). These values are in reasonable agreement with each other, and that indicates that there is no catalysis by the general base ($H_2PO_4^-$) present in these buffer solutions. The intercepts of these linear relationships provided the hydronium ion catalytic coefficients $k_{H^+} = (9.19 \pm 0.09) \times 10^{-2} M^{-1} s^{-1}$ (buffer ratio = 0.47) and $(9.06 \pm 0.08) \times 10^{-2} M^{-1} s^{-1}$ (buffer ratio = 0.92), each of which is in good agreement with the value measured directly in perchloric acid solutions, $k_{H^+} = (8.81 \pm 0.18) \times 10^{-2} M^{-1} s^{-1}$.

TABLE 1. Summary of hydrogen-ion catalytic coefficients for the hydration of acetylenes in dilute aqueous solution at 25°C

Substrate	$k_{H^+}/M^{-1} s^{-1}$
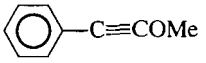	$(8.81 \pm 0.18) \times 10^{-2}$
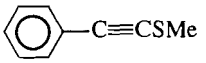	$(1.21 \pm 0.01) \times 10^{-3}$
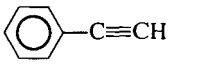	$(2.86 \pm 0.09) \times 10^{-7}$
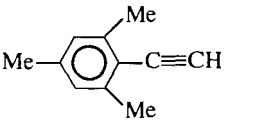	$(1.21 \pm 0.03) \times 10^{-4}$
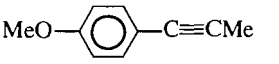	$(8.45 \pm 0.27) \times 10^{-6}$

All of the other acetylenes examined here were considerably less reactive than 1-methoxy-2-phenylethyne, and their rates of hydration were consequently measured in concentrated acid solutions: 0.5–24 wt. % $HClO_4$ for 1-methylthio-2-phenylethyne, 30–50 wt. % $HClO_4$ for 1-(*p*-methoxyphenyl)-propyne. These data are summarized in Table S3.[2] For all four substrates, observed first-order rate constants increased with increasing medium acidity much more rapidly than in direct proportion to hydronium ion concentration, and an acidity function had to be used to extrapolate the data to dilute solution. The Cox–Yates X_0 function (13) appears to be the best currently available quantity for this purpose (14), and each of the four present sets of data gave good linear relationships when treated in this way. The dilute solution hydronium ion catalytic coefficients obtained by extrapolating these relationships to $X_0 = 0$ are listed in Table 1.

The rate of hydration of one of these actylenes, phenylethyne, has been measured before in concentrated aqueous sulfuric acid solutions in two different laboratories (15), and extrapolation of those data to dilute solution using the Cox–Yates *X* function (16) gives $k = (2.31 \pm 0.15) \times 10^{-7}\ M^{-1}\ s^{-1}$ and $k = (1.77 \pm 0.32) \times 10^{-7}\ M^{-1}\ s^{-1}$. Although these values are broadly consistent with the present result, $k_{H^+} = (2.86 \pm 0.09) \times 10^{-7} M^{-1} s^{-1}$, differences in the direction of faster rates in sulfuric acid might have been expected: sulfuric acid at the concentrations used contains the additional acidic species HSO_4^-, and this is known to cause the rates of some acid-catalyzed reactions to be faster in this medium than in solutions of completely dissociated monobasic acids such as $HClO_4$ (17). In order to determine whether this unexpected behavior could be the result of unintentional differences in reaction conditions between the present and the previous studies, we made a few rate measurements in sulfuric acid solutions at three different concentrations, all in the range used by the previous studies. These data, summarized in Tables S4,[2] show good agreement with the previous results. It seems likely, therefore, that the

[2]Tables S1–S4 of rate data may be purchased from the Depository of Unpublished Data, CISTI, National Research Council of Canada, Ottawa, Ont., Canada K1A 0S2.

discrepancy comes rather from a difference in the acidity functions employed for the sulfuric acid (X) and perchloric acid (X_0) correlations, for use of the X function for perchloric acid (16) gives $k_{H^+} = (1.93 \pm 0.17) \times 10^{-7} M^{-1} s^{-1}$, which differs in the expected sense from at least one of the sulfuric acid results.

Discussion

We have found that the hydration of 1-methoxy-2-phenylethyne is a general-acid-catalyzed reaction with a hydronium-ion isotope effect in the normal ($k_H/k_D > 1$) direction. This is evidence for a rate-determining proton transfer process, which indicates that the mechanism of this reaction is the same as that established for the hydration of purely aliphatic acetylenic ethers (1), namely, slow proton transfer from the catalyst to the substrate, reaction [3] followed by rapid hydration of the vinyl

[3] $$PhC{\equiv}COMe + HA \rightarrow PhCH{=}\overset{+}{C}OMe + A^-$$

cation thus formed and tautomerization of the resulting enol of methyl phenylacetate, reaction [4]. This mechanistic assignment is supported by the fact that vinyl cations react with water rapidly, at rates near the encounter-controlled limit (18), as well as by the expectation that ester enols should be at least as reactive as the closely related ketene acetals, which are normally very labile substances (19).

[4] $$PhCH{=}\overset{+}{C}OMe \xrightarrow[-H^+]{H_2O} PhCH{=}\overset{OH}{\overset{|}{C}}OMe \rightarrow PhCH_2\overset{O}{\overset{\|}{C}}OMe$$

The fact that methyl phenylacetate and not α-methoxyacetophenone, **6**, is the product of this hydration reaction indicates that the direction of addition is as shown in reaction [3], and that a methoxyl group is better than phenyl at stabilizing the adjacent developing carbocationic center. Similarly, thiomethyl is also better than phenyl in this respect, for methyl phenylthioacetate, **7**, and not α-methanethioacetophenone, **8**, is the product of

$PhC(=O)CH_2OMe$ **6** $\quad$ $PhCH_2C(=O)SMe$ **7** $\quad$ $PhC(=O)CH_2SMe$ **8**

acid-catalyzed hydration of 1-methanethio-2-phenylethyne, **2**. This regioselectivity is similar to that found in the hydration of arylalkylthioacetylenes catalyzed by mercuric ion (3*b*, 20), and it is also consistent with the fact that the σ^+ constants of methoxy (−0.78) and methylthio (−0.60) are both stronger than that of phenyl (−0.18).

The present results show PhC≡COMe to be 70 times more reactive to carbon protonation by the hydronium ion than is PhC≡CSMe. This is an order of magnitude less than the superiority of oxygen over thio acetylenic ethers found in purely aliphatic systems (1), and the difference could be the result of initial state stabilization in the aryl systems through conjugation of the ether function with the phenyl group; the latter would be expected to be stronger in the oxygen than in the thio ether. Such conjugation may also be responsible for the much lower (900-fold) reactivity of PhC≡COMe as compared to HC≡COMe; similar effects have been found in the hydrolysis of corresponding vinyl ethers (21).

The influence of a β-methyl group on the rate of carbon-protonation of acetylenic ethers is also rate retarding, but the effect is weaker than that of phenyl. A factor of 25–40 may be estimated for this retardation from the rate constant measured here for *p*-$MeOC_6H_4C{\equiv}CMe$ and those reported for *p*-$MeO_6H_4C{\equiv}CH$ (15); this factor is similar to those found for aliphatic acetylenic ethers (1) and also for other acetylenes (22) as well as vinyl ethers (23) and alkenes (24).

Methyl substitution in the phenyl ring of arylacetylenes which are not acetylenic ethers, on the other hand, raises the rate of acid-catalyzed hydration, as expected, for now the positive charge is generated on the carbon atom adjacent to the aryl group, reaction [5]. A 17- to 20-fold rate acceleration has been

[5] $$ArC{=}CH \xrightarrow[-A^-]{HA} Ar\overset{+}{C}{=}CH_2$$

found for one methyl group in the *para* position (15), and the rate constants for phenyl- and mesitylacetylene measured here give a 420-fold acceleration for methyl substitution in all three *ortho* and *para* positions. The latter factor is similar to the rate acceleration found for mesityl- over phenylacetylene in sulfuric acid – acetic acid media at 50°C (7); it shows that the electrical effect of an *ortho* methyl group is not unlike that of a *para* methyl and that *ortho*-group steric effects are not important in the hydration of mesitylacetylene.

Acknowledgements

We are grateful to Dr. R. A. Cox for helpful discussion and to the Natural Sciences and Engineering Research Council of Canada and the Donors of the Petroleum Research Fund, administered by the American Chemical Society, for financial support of this research.

1. W. Drenth and H. Hogeveen. Rec. Trav. Chim. **79**, 1002 (1960); E. J. Stamhuis and W. Drenth. Rec. Trav. Chim. **80**, 797 (1961); H. Hogeveen and W. Drenth. Rec. Trav. Chim. **82**, 375 (1963); E. J. Stamhuis and W. Drenth. **82**, 385 (1963); **82**, 394 (1963); G. L. Hekkert and W. Drenth. Rec. Trav. Chim. **82**, 405 (1963); H. Hogeveen and W. Drenth. Rec. Trav. Chim. **82**, 410 (1963).
2. R. Tanaka and S. I. Miller. Tetrahedron Lett. 1753 (1971).
3. (*a*) L. Brandsma, H. E. Wijers, and C. Jonker. Rec. Trav. Chim. **83**, 208 (1964); (*b*) Y. A. Boiko, B. S. Kupin, and A. A. Petrov. Zhur. Org. Kh. **2**, 1923 (1966).
4. N. Miyamoto and H. Nozaki. Tetrahedron, **29**, 3819 (1973).
5. T. H. Vaughn and J. A. Nieuwland. J. Am. Chem. Soc. **56**, 1207 (1934).
6. T. Okuyama, K. Izawa, and T. Fueno. J. Org. Chem. **39**, 351 (1974).
7. R. W. Bott, C. Eaborn, and D. R. M. Walton. J. Chem. Soc. 384 (1965).
8. C. G. Swain, M. S. Swain, and L. F. Berg. J. Chem. Inf. Comput. Sci. **20**, 47 (1980).
9. J. R. Keeffe and A. J. Kresge. *In* Techniques of chemistry. Volume VI. Investigation of rates and mechanisms of reactions. *Edited by* C. F. Bernasconi. Wiley, New York. 1986. Part 1. Chap. XI.
10. A. J. Kresge, H. L. Chen, Y. Chiang, E. Murrill, M. A. Payne, and D. S. Sagatys. J. Am. Chem. Soc. **93**, 413 (1971).
11. K. S. Pitzer and L. F. Silvester. J. Soln. Chem. **5**, 269 (1976).
12. R. G. Bates. Determination of pH. Theory and practice. Wiley, New York. 1973. p. 49.
13. R. A. Cox and K. Yates. Can. J. Chem. **59**, 2116 (1981).
14. A. J. Kresge, H. J. Chen, G. L. Capen, and M. F. Powell. Can. J. Chem. **61**, 249 (1983).
15. D. S. Noyce and M. D. Schiavelli. J. Am. Chem. Soc. **90**, 1020 (1968); G. Modena, F. Rivetti, G. Scorrano, and U. Tonellato. J. Am. Chem. Soc. **99**, 3392 (1977).
16. R. A. Cox and K. Yates. J. Am. Chem. Soc. **100**, 3861 (1978).

Can. J. Chem. Downloaded from www.nrcresearchpress.com by 80.58.250.72 on 09/07/12
For personal use only.

17. W. M. SCHUBERT and P. C. MYHRE. J. Am. Chem. Soc. **80**, 1755 (1958); A. J. KRESGE, L. E. HAKKA, S. MYLONAKIS, and Y. SATO. Discuss. Faraday Soc. **39**, 75 (1965); A. J. KRESGE, Y. CHIANG, P. H. FITZGERALD, R. S. MCDONALD, and G. H. SCHMID. J. Am. Chem. Soc. **93**, 4907 (1971); Y. CHIANG and A. J. KRESGE. J. Am. Chem. Soc. **107**, 6363 (1985); J. R. KEEFFE, A. J. KRESGE, and J. TOULLEC. Can. J. Chem. **64**, 1224 (1986).
18. S. KOBAYASHI, T. KITAMURA, H. TANIGUCHI, and W. SCHNABEL. Chem. Lett. 1117 (1983).
19. A. KANKAANPERA and H. TOUMINEN. Suom. Kemistil. B, **40**, 271 (1967); B. CAPON and A. K. GOSH. J. Am. Chem. Soc. **103**, 1765 (1981); Y. CHIANG, M. HOJATTI, J. R. KEEFFE, A. J. KRESGE, N. P. SCHEPP, and J. WIRZ. J. Am. Chem. Soc. To be published.
20. Y. A. BOIKO, B. S. KUPIN, and A. A. PETROV. Zh. Org. Kh. **3**, 2102 (1967).
21. Y. CHIANG, A. J. KRESGE, and C. I. YOUNG. Can. J. Chem. **56**, 461 (1978).
22. K. YATES, G. H. SCHMID, T. W. REGULSKI, D. G. GARRATT, H.-W. LEUNG, and R. MCDONALD. J. Am. Chem. Soc. **95**, 160 (1973).
23. D. M. JONES and N. F. WOOD. J. Chem. Soc. 5400 (1964); P. SALOMAA, A. KANKAANPERA, and M. LAJUNEN. Acta Chem. Scand. **20**, 1790 (1966); T. OKUYAMA, T. FUENO, H. NAKATSUJI, and J. FURUKAWA. J. Am. Chem. Soc. **89**, 5826 (1967); A. J. KRESGE, D. S. SAGATYS, and H. L. CHEN. J. Am. Chem. Soc. **99**, 7228 (1977).
24. P. KNITTEL and T. T. TIDWELL. J. Am. Chem. Soc. **99**, 3408 (1977); W. K. CHWANG, V. J. NOWLAN, and T. T. TIDWELL. J. Am. Chem. Soc. **99**, 7233 (1977).

Can. J. Chem. Downloaded from www.nrcresearchpress.com by 80.58.250.72 on 09/07/12
For personal use only.

Ternary charge transfer complexes. IV.[1] Complexes with Fe, Nb, Ta, Mo, W, or U in the anion[2]

SYDNEY BROWNSTEIN, ERIC GABE, BRIDGET IRISH, FLORENCE LEE, BRENDA LOUIE, AND ANDREJ PIOTROWSKI
Division of Chemistry, National Research Council of Canada, Ottawa, Ont., Canada K1A 0R9

Received May 22, 1986

SYDNEY BROWNSTEIN, ERIC GABE, BRIDGET IRISH, FLORENCE LEE, BRENDA LOUIE, and ANDREJ PIOTROWSKI. Can. J. Chem. **65**, 445 (1987).

$NOMX_6$·aromatic charge transfer complexes are formed from NOX and NbX_5 or TaX_5, where X may be F or Cl and the aromatic portion is a methyl-substituted benzene. $NOMoF_6$, $NOUF_6$, $NOUF_7$, and $NOWCl_7$·aromatic complexes have been identified but only oxyfluoro species have been isolated when M is Mo, W, or U. $NOTaCl_6$·hexamethylbenzene crystallizes in the trigonal space group $P3_2$, with a = 9.822(3), c = 17.469(7) Å. $NOFeCl_4$·hexamethylbenzene·½benzene crystallizes in the orthorhombic space group *Ccmb*, with a = 14.8009(20), b = 15.7683(10), c = 17.3913(14) Å. High conductivity in these complexes appears to depend upon a long N—O bond.

SYDNEY BROWNSTEIN, ERIC GABE, BRIDGET IRISH, FLORENCE LEE, BRENDA LOUIE et ANDREJ PIOTROWSKI. Can. J. Chem. **65**, 445 (1987).

Partant de NOX et de NbX_5 ou TaX_5, on peut former des complexes de transfert de charge $NOMX_6$·aromatique dans lesquels X = F ou Cl alors que la portion aromatique = benzènes substitués par des groupements méthyles. On a pu identifier les complexes $NOMoF_6$, $NOUF_6$, $NOUF_7$ et $NOWCl_7$·aromatique; toutefois, seules les espèces oxyfluorées dans lesquelles M est égal à Mo, W ou U ont pu être isolées. Le composé $NOTaCl_6$·hexaméthylbenzène cristallise dans le groupe d'espace trigonal $P3_2$, avec a = 9,822(3) et c = 17,469(7) Å. Le composé $NOFeCl_4$, hexaméthylbenzène·½benzène cristallise dans le groupe d'espace orthorhombique *Ccmb*, avec a = 14,8009(20), b = 15,7683(10) et c = 17,3913(14) Å. La conductivité élevée de ces complexes semble dépendre de la longue liaison N—O.

[Traduit par la revue]

Introduction

The nature of the anion is found to have a large effect on the properties of charge transfer complexes of type $NO^+ \cdot MX_n^- \cdot$ aromatic, where X may be F or Cl, n may be 4 or 6, M may be B, Al, Ga, Tl, P, As, or Sb and aromatic may be benzene or a methyl substituted benzene (1, 2). In this article the properties of such complexes will be presented where the halogen is chlorine or fluorine and M is niobium or tantalum. In addition, complexes with the anion $FeCl_4^-$ and with some anions MX_n^-, where M may be Mo, W or U, n may be 6 or 7, and X may be chlorine or fluorine, as well as complexes with anions $M_2O_2F_9^-$ where M may be Mo or W, will also be discussed.

Following is a brief history of the nitrosyl salts which were used in this study. Infrared and Raman spectra have been previously recorded for $NOMCl_6$ (M = Nb, Ta) (3), $NOMF_6$ (4–7) (M = Mo, U), $NOMF_7$ (M = Mo, W, U) (6, 8), $NOM_2O_2F_9$ (M = Mo, W) (9); and $NOFeCl_4$ (10). Mixed chloro–fluoro anions have been observed for both niobium and tantalum, but not with the nitrosyl cation (11). The reaction of NOCl with $MoCl_5$ and WCl_6 has not been reported previously. $NOMF_7$ (M = Mo, W, U) is prepared from NOF and MF_6 (8). Nitric oxide itself reacts with MF_6 (M = Mo, U) to give $NOMF_6$ (7) while another route is by reduction with nitrosyl chloride (8).

Experimental

Chemicals

Nitrosyl chloride and molybdenum, tungsten, and uranium hexafluorides were used directly from the supplier's cylinders. Nitric oxide was passed through a silica gel trap in "Dry Ice", to remove NO_2, just before use. Nitrosyl fluoride was synthesized by the direct reaction of nitric oxide and fluorine at low temperature (7). Niobium and molybdenum pentachloride, ferric chloride, niobium and tantalum pentafluoride, tungsten hexachloride, hexamethylbenzene, mesitylene, *p*-xylene and toluene were used as purchased. Tantalum pentachloride was vacuum sublimed before use. Sulfur dioxide, methylene chloride, and neopentane were purified and stored as previously described (12). All manipulations were carried out under an atmosphere of dry nitrogen.

$NOTaCl_6 \cdot C_6(CH_3)_6$

An equimolar quantity of hexamethylbenzene was added, in a dry box, to $TaCl_5$ in a reaction vessel closed with a "Teflon" stopcock. One equivalent of nitrosyl chloride and sulfur dioxide as solvent were added by vacuum transfer and a reaction occurred immediately upon warming to room temperature. An equal volume of methylene chloride was added and the sulfur dioxide was very slowly pumped away while the solution was kept at 0°C. Black crystals of the $NOTaCl_6$·hexamethylbenzene adduct precipitated from the CH_2Cl_2 solution.

$NOFeCl_4 \cdot C_6(CH_3)_6 \cdot 0.5(C_6H_6)$

To 46.2 mg of $FeCl_3$ in one arm of a two armed reactor was condensed 3 mL of NOCl. After warming to room temperature all volatile materials were pumped away under vacuum to give a residue of 62.4 mg of $NOFeCl_4$ (yield = 96%). In a nitrogen-filled dry box, 41.3 mg of hexamethylbenzene was added directly onto the $NOFeCl_4$. SO_2 (3 mL) was condensed onto these solids which dissolved completely to give a clear, intensely colored brown solution. All volatile materials were pumped away under vacuum and 3 mL of CH_2Cl_2 was condensed onto the black solid. Most of the material went into solution which was carefully decanted from the residual solid into the other arm of the reactor. Approximately 1 mL of benzene was condensed onto the CH_2Cl_2 solution. After warming to room temperature and mixing, approximately half of the liquid was slowly distilled into the original arm of the reactor by cooling it gradually. Black, glossy crystals appeared on the walls of the reactor. The remaining solution was decanted into the original arm of the reactor to isolate the crystalline solid. This arm was evacuated and sealed under vacuum for storage.

$NOMF_x \cdot C_6(CH_3)_6$ (M = Mo or U, x = 6; M = Mo, W or U, x = 7)

In a typical reaction sequence 1.00 mmol of NO or NOF and an equimolar amount of MF_6 (M = Mo, W, or U) were condensed into a Monel reactor at −196°C. The reactor was gradually warmed to room temperature over a period of 0.5–1 h and then opened in a dry box. Samples of the resulting $NOMF_x$ (x = 6 or 7) salts were sealed in capillary tubes and checked for purity by Raman spectroscopy.

[1]For Part III, see ref. 2.
[2]NRC No. 26631.

Can. J. Chem. Downloaded from www.nrcresearchpress.com by 80.58.250.72 on 09/07/12
For personal use only.

TABLE 1. Parameters from X-ray structural characterization

Parameter	Value	
	$NOTaCl_6$·hexamethylbenzene	$NOFeCl_4$·hexamethylbenzene·½benzene
Crystal type	Trigonal	Orthorhombic
Space group	$P3_2$	$Ccmb$[a]
a, Å	9.822(3)	14.8009(20)
b, Å	—	15.7683(10)
c, Å	17.469(7)	17.3913(14)
$2\theta_{max}$	50°	45°
Z	3	8
D_{calcd} Mg m^{-3}	2.0	1.40
Crystal dimensions, mm	0.6 × 0.2 × 0.2	0.3 × 0.25 × 0.2
Unique reflections	3416	1379
Significant reflections	2815	710
μ mm^{-1}	6.41	1.27
R all data[b]	0.053	0.134
R significant data	0.038	0.075
R_w all data[c]	0.031	0.047
R_w significant data	0.031	0.046

[a]The transformation matrix to turn the axes of the space group $Ccmb$ into the standard setting $Cmca$ is 0,0,1/1,0,0/0,0,−1.
[b]$R = \Sigma||F_o| - |F_c||/\Sigma|F_o|$.
[c]$R_w = \Sigma w(|F_o| - |F_c|)^2/\Sigma wF_o^2$.

Assuming a 100% yield of the nitrosyl salt, a 0.5 equivalent of hexamethylbenzene was added to the reactor in the dry box. The reactor was subsequently evacuated and ~5 mL of SO_2 or CH_2Cl_2 condensed onto the reactants at −196°C. The reactor was warmed to −78°C and shaken gently at this temperature for ~5 min. The solvent was then removed *in vacuo* while keeping the reactor at −78°C. After all the volatiles were removed at this temperature, the reactor was warmed to room temperature with continual pumping and then opened in a dry box revealing red–brown (M = Mo or W) or purple (M = U), air- and moisture-sensitive powders.

Magnetic resonance spectra were obtained on a Bruker AM400 spectrometer at a magnetic field strength corresponding to 400 MHz for protons. Carbon and proton chemical shifts are reported with respect to tetramethylsilane, although neopentane was used as an internal reference since it is inert with respect to the compounds studied. A correction of 0.92 ppm was applied for protons and 31.4 ppm for ^{13}C. Fluorine resonance shifts are reported with respect to internal $CFCl_3$.

Ultraviolet–visible spectra, in CH_2Cl_2 as solvent, were obtained on a Cary 210 Spectrometer. Infrared spectra were obtained for KBr pellets by Beckman Acculab 4 and Perkin–Elmer 683 Infrared Spectrometers. Samples for conductivity measurements were prepared as pressed pellets with the same die used for KBr infrared pellets. The resistance was measured between the parallel, adjustable plates of a General Radio type 1690A conductivity cell with a 1673A automatic capacitance bridge operating at 1 kHz.

X-ray reflection intensities were measured with monochromatized MoKα radiation, (λ(MoKα_1) = 0.70932 Å). Reflections were considered significant with $I_{net} > 2.5\sigma(I_{net})$. X-ray structural data for $NOTaCl_6$·hexamethylbenzene and $NOFeCl_4$·hexamethylbenzene·½benzene are listed in Table 1.

The diffraction intensities of a crystal of $NOTaCl_6$·hexamethylbenzene were collected at 115 K using a Picker diffractometer and the $\theta/2\theta$ scan technique with profile analysis (13). The data for $NOFeCl_4$·hexamethylbenzene·½benzene were collected at room temperature using a Nonius CAD-4 diffractometer with the ω scan technique. Both structures were solved with MULTAN (14) and refined by full-matrix least-squares. All calculations were performed with the NRCVAX system of programs (15). Scattering factors including anomalous dispersion were taken from the International tables for X-ray crystallography (16).

The final atomic positional parameters, bond lengths and angles, and mean temperature factors for $NOTaCl_6$·hexamethylbenzene are given in Table 2. The anisotropic thermal parameters and the structure factors are deposited as supplementary material.[3] It is not possible to unambiguously assign the nitrogen and oxygen atoms as shown. Reversing their relative positions causes an insignificant change in the agreement indices. The present assignment is preferred since it agrees with our previously reported results (2).

The structure consists of three entities $TaCl_6$, NO, and $C_6(CH_3)_6$ as shown in Fig. 1. The Ta atom is co-ordinated to six Cl atoms to form a distorted octahedron (maximum deviation from the ideal octahedral angle is 2.1°). The distances of Ta—Cl are 2.302(4) to 2.342(4) Å. The N—O distance is 1.10(1) Å. The distances from the plane of the ring to the N atom and the O atom are 2.12(1) and 2.94(2) Å, respectively. The arrangement of the three entities in the unit cell as in Fig. 2 shows no ordered sheet or layer of any molecule, probably owing to the 32 symmetry element in the space group.

The final atomic positional parameters, bond lengths and angles, and mean temperature factors for $NOFeCl_4$·hexamethylbenzene·½benzene are listed in Table 3. The anisotropic thermal parameters and final structure factors are included as supplementary material.[3] During data collection the crystal decayed as shown by an intensity drop to 72% on the standard reflections. Sets of three standard reflections were measured after each 100 regular measurements and the average intensity ratio for each set was used in a five point smoothing process to establish an intensity correction curve. Corrections were then obtained by linear interpolation between adjacent points. It is probably because of this decay, despite the attempt to correct for it, that the thermal parameters are high and that attempts to locate hydrogen atoms from the difference Fourier synthesis were unsuccessful. The structure consists of four entities, $FeCl_4$, NO, $C_6(CH_3)_6$, and ½C_6H_6, shown in Fig. 3 as a whole molecule. The Fe atom is co-ordinated to four Cl atoms to form a distorted tetrahedron with the distances of Fe—Cl from 2.170(4) to 2.171(4) Å. The N—O distance is 1.09(2) Å. The distances and angles of $C_6(CH_3)_6$ and C_6H_6 molecules are normal. The distances from the plane of the $C_6(CH_3)_6$ ring to the N and O atoms are 2.02(3) and 2.87(3) Å, respectively.

[3]Complete set of data may be purchased from the Depository of Unpublished Data, CISTI, National Research Council of Canada, Ottawa, Ont., Canada K1A OS2.

Can. J. Chem. Downloaded from www.nrcresearchpress.com by 80.58.250.72 on 09/07/12
For personal use only.

Can. J. Chem. Downloaded from www.nrcresearchpress.com by 80.58.250.72 on 09/07/12
For personal use only.

TABLE 2. $NOTaCl_6$·hexamethylbenzene
(*a*) Atom positions

Atom	X^a	Y	Z	$B_{iso}{}^b$
Ta	0.50345(5)	0.03489(5)	0.83238	3.68
C11	0.4446(6)	0.1688(5)	0.74234(22)	6.8
C12	0.5621(5)	−0.0997(5)	0.92475(21)	5.92
C13	0.3266(5)	−0.2000(5)	0.77371(24)	6.7
C14	0.6824(5)	0.2739(4)	0.88999(22)	5.46
C15	0.3048(5)	0.0202(5)	0.9107 (3)	6.8
C16	0.7077(6)	0.0597(6)	0.75453(23)	6.8
N	0.7617(12)	0.5177(11)	0.7315 (5)	4.3
O	0.8584(13)	0.4949(12)	0.7431 (6)	6.7
C1	0.7216(16)	0.7344(15)	0.6743 (9)	4.3
C2	0.5564(15)	0.6179(13)	0.6738 (8)	5.1
C3	0.4859(14)	0.5415(13)	0.7428 (7)	4.0
C4	0.5701(13)	0.5824(14)	0.8079 (7)	3.9
C5	0.7280(16)	0.6939(14)	0.8051 (7)	4.5
C6	0.8110(14)	0.7745(14)	0.7415 (7)	4.1
C7	0.8037(17)	0.8257(18)	0.5964 (9)	6.7
C8	0.4607(17)	0.5741(18)	0.5954 (9)	6.6
C9	0.3101(14)	0.4280(15)	0.7390 (8)	5.7
C10	0.4918(14)	0.5018(14)	0.8836 (7)	4.8
C11	0.8323(16)	0.7339(17)	0.8843 (6)	6.5
C12	0.9837(14)	0.8990(16)	0.7392 (8)	5.8

(*b*) Bond lengths and angles

Bond	Length	Bonds	Angle
Ta—C11	2.302(4)	C11—Ta—C12	179.33(15)
Ta—C12	2.333(4)	C11—Ta—C13	89.39(15)
Ta—C13	2.320(4)	C11—Ta—C14	89.87(14)
Ta—C14	2.342(4)	C11—Ta—C15	89.72(17)
Ta—C15	2.328(5)	C11—Ta—C16	89.45(17)
Ta—C16	2.333(4)	C12—Ta—C13	90.94(15)
		C12—Ta—C14	89.80(13)
		C12—Ta—C15	89.70(16)
		C12—Ta—C16	91.12(16)
		C13—Ta—C14	179.20(14)
		C13—Ta—C15	90.60(17)
		C13—Ta—C16	91.35(17)
		C14—Ta—C15	89.72(16)
		C14—Ta—C16	88.32(16)
N—O	1.098(14)	C15—Ta—C16	177.87(17)
C1—C2	1.445(19)	C2—C1—C6	121.7 (13)
C1—C6	1.401(21)	C2—C1—C7	119.3 (13)
C1—C7	1.606(20)	C6—C1—C7	119.0 (12)
C2—C3	1.405(19)	C1—C2—C3	118.5 (12)
C2—C8	1.593(19)	C1—C2—C8	119.7 (13)
C3—C4	1.345(17)	C3—C2—C8	121.8 (11)
C3—C9	1.518(17)	C2—C3—C4	120.1 (11)
C4—C5	1.381(18)	C2—C3—C9	115.5 (11)
C4—C10	1.534(16)	C4—C3—C9	124.0 (11)
C5—C6	1.370(18)	C3—C4—C5	119.0 (11)
C5—C11	1.648(16)	C3—C4—C10	120.0 (10)
C6—C12	1.516(17)	C5—C4—C10	121.0 (10)
		C4—C5—C6	126.5 (11)
		C4—C5—C11	118.4 (11)
		C6—C5—C11	115.0 (11)
		C1—C6—C5	114.1 (11)
		C1—C6—C12	119.7 (12)
		C5—C6—C12	126.2 (12)

[a]Estimated standard deviations refer to the last digit printed.
[b]B_{iso} is the mean of the principal axes of the thermal ellipsoid.

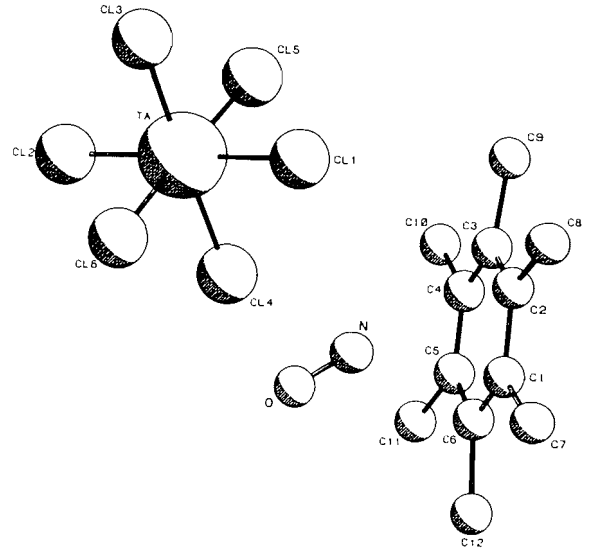

FIG. 1. The asymmetric unit of the $NOTaCl_6$·hexamethylbenzene structure.

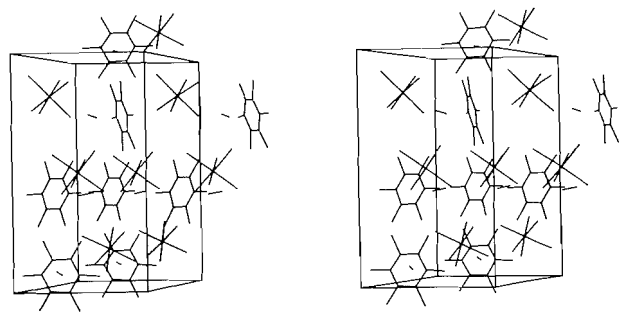

FIG. 2. Packing in the crystal of $NOTaCl_6$·hexamethylbenzene.

Results and discussion

Both the pentachlorides and pentafluorides of niobium and tantalum react with the corresponding nitrosyl halide and a methyl-substituted benzene to give a charge transfer compound of formula $NOMX_6$·aromatic. These have been identified by the physical properties listed in Table 4. The chloro compounds are thermally unstable, those of $NbCl_5$ decomposing in solution above approximately 0°C. From the characteristic red–brown color, the proton resonance spectra at −10°C, and the sharpening of the ^{93}Nb resonance from the broad lines found for $NbCl_5$ and $NONbCl_6$, the formation of charge transfer complexes is confirmed for the chloro–niobium system. Similar results are found for the niobium–fluorine complexes, with the additional evidence from fluorine resonance spectroscopy of the classical ten line pattern for NbF_6^- (17). Although $NONbF_6$ itself is insoluble in liquid SO_2 it is brought into solution upon complexing with the aromatic species. These adducts are thermally stable, in contrast to the chloro compounds. The proton resonance spectra of the aromatic portion of the fluoro compounds display somewhat smaller displacements than the chloro species relative to the uncomplexed aromatic species, suggesting less transfer of charge. With the mixed halide aromatic complexes NOCl + NbF_5 and NOCl + TaF_5 the only fluorine signals observed were from the hexafluoroanions showing that halogen disproportionation has occurred.

Vanadium trichloride with NOCl does not appear to form

TABLE 3. $NOFeCl_4 \cdot$ hexamethylbenzene $\cdot \frac{1}{2}$ benzene

(*a*) Atom positions

Atom	X^a	Y	Z	$B_{iso}{}^b$
Fe	0.73125(19)	1/4	1/4	6.18
C11	0.6489 (3)	0.29737(20)	0.15609(19)	8.51*
C12	0.81331(25)	0.35548(23)	0.28939(19)	8.62*
O	0.7128 (11)	1/2	0.1559 (12)	8.0
N	0.7851 (12)	1/2	0.1451 (12)	6.2
C1	0.9623 (12)	0.4551 (10)	0.1204 (9)	6.8*
C2	0.9035 (14)	0.4110 (13)	0.0732 (11)	8.1
C3	0.8377 (13)	0.4539 (10)	0.0269 (8)	7.6*
C4	1.0303 (11)	0.4097 (10)	0.1750 (9)	13.0
C5	0.9033 (12)	0.3130 (8)	0.0719 (10)	12.9
C6	0.7683 (12)	0.4076 (11)	−0.0218 (8)	14.0
C7	1/2	0.4130 (23)	0	10.6
C8	0.4848 (17)	0.4534 (13)	0.0658 (9)	11.5*

*Indicates that there are symmetry equivalents of these atoms. The following atoms are the symmetry equivalents

Cl(1)a	0.64891	0.20264	0.34391	X,	$0.500 - Y$,	$0.500 - Z$
Cl(2)a	0.81331	0.14452	0.21061	X,	$0.500 - Y$,	$0.500 - Z$
C(1)b	0.96231	0.54488	0.12041	X,	$1.000 - Y$,	Z
C(3)b	0.83769	0.54615	0.02689	X,	$1.000 - Y$,	Z
C(8)c	0.51516	0.45335	−0.06579	$1.000 - X$,	Y,	$-Z$
C(8)b	0.48484	0.54665	0.06579	X,	$1.000 - Y$,	Z

(*b*) Bond lengths and angles

Bond	Length	Bonds	Angle
Fe—Cl(1)	2.170(4)	Cl(1)—Fe—Cl(1)a	111.68(20)
Fe—Cl(1)a	2.170(4)	Cl(1)—Fe—Cl(2)	106.74(13)
Fe—Cl(2)	2.171(4)	Cl(1)—Fe—Cl(2)a	109.90(13)
Fe—Cl(2)a	2.171(4)	Cl(1)a—Fe—Cl(2)	109.90(13)
O—N	1.087(23)	Cl(1)a—Fe—Cl(2)a	106.74(13)
C(1)—C(1)b	1.42 (3)	Cl(2)—Fe—Cl(2)a	111.95(19)
C(1)—C(2)	1.38 (3)	C(1)b—C(1)—C(2)	120.1 (17)
C(1)—C(4)	1.559(23)	C(1)b—C(1)—C(4)	117.4 (16)
C(2)—C(3)	1.43 (3)	C(2)—C(1)—C(4)	122.5 (15)
C(2)—C(5)	1.545(24)	C(1)—C(2)—C(3)	121.6 (17)
C(3)—C(3)b	1.46 (3)	C(1)—C(2)—C(5)	120.8 (19)
C(3)—C(6)	1.517(23)	C(3)—C(2)—C(5)	117.5 (18)
C(7)—C(8)	1.33 (3)	C(2)—C(3)—C(3)b	118.1 (17)
C(7)—C(8)c	1.33 (3)	C(2)—C(3)—C(6)	123.2 (15)
C(8)—C(8)b	1.47 (4)	C(3)b—C(3)—C(6)	118.7 (17)
		C(8)—C(7)—C(8)c	122 (3)
		C(7)—C(8)—C(8)b	118.6 (19)

[a] Estimated standard deviations refer to the last digit printed.
[b] B_{iso} is the mean of the principal axes of the thermal ellipsoid.

charge transfer complexes. The solvents and aromatic compounds used in this study were rapidly fluorinated by VF_5 and VF_5 + NOF. Niobium and tantalum pentachlorides with $POCl_3$ also do not form charge transfer complexes. Niobium pentachloride and $SOCl_2$ or NSCl chlorinate hexamethylbenzene. There is some spectral evidence for a ternary charge transfer complex of NOCl, $MoCl_5$, and hexamethylbenzene, stable at low temperature, listed in Table 2. However, in the corresponding system with mesitylene the aromatic compound is chlorinated. The system WCl_6, NOCl, and hexamethylbenzene forms a slightly more stable complex but this too decomposes rapidly at room temperature.

Mixing $NOMF_7$ (M = Mo or W) with hexamethylbenzene in a Monel reactor at −78°C using CH_2Cl_2 or SO_2 as solvent results in the formation of the corresponding ternary complex where the anion is the fluorine-bridged species $OMF_4 \cdot F \cdot MF_4O$. This has been identified by the characteristic M—O and M—F absorptions in the infrared region. Similarly, in solution in a glass nmr tube at −78°C only the fluorine resonance of the oxyfluoroanion is observed. There is no evidence for the initial formation of $NOMF_7 \cdot$ hexamethylbenzene followed by a disproportionation. Pertinent spectral data are listed in Table 4. A freshly prepared KBr pellet of the reaction product of $NOUF_7$ and hexamethylbenzene initially had a single strong N—O stretching frequency at 1870 cm^{-1}. This changed with time to yield the same spectrum as previously assigned to the

Can. J. Chem. Downloaded from www.nrcresearchpress.com by 80.58.250.72 on 09/07/12
For personal use only.

TABLE 4. Physical properties of some ternary charge transfer complexes

Compound	δ^1H		$\delta^{13}C$		λ_{max} (Å)	Conductivity ($ohm^{-1}\,cm^{-1}$)	$\nu N{-}O\,cm^{-1}$	$\delta^{19}F$
	CH_3	H	CH_3	CH				
$NONbF_6$·hexamethylbenzene	2.46		17.1	148.1	3300	0.29	1850	109.5
$NONbCl_6$·hexamethylbenzene	2.49							
$NONbF_6$·mesitylene	2.41	7.18	20.7	132.9 145.5	3860			109.7
$NONbCl_6$·mesitylene	2.52	7.44						
$NONbF_6$·*p*-xylene	2.45	7.43	20.6	135.0			1810	109.3
$NONbCl_6$·*p*-xylene	2.57	7.67						
$NOTaF_6$·hexamethylbenzene	2.47		17.2	149.8	3340	3.9×10^{-4}	1800	45.6
$NOTaCl_6$·hexamethylbenzene	2.48		17.5	150.3	3320			
$NOTaF_6$·mesitylene	2.51	7.40	20.9	136.1 149.8	3880	1.5×10^{-3}		45.1
$NOTaCl_6$·mesitylene	2.58	7.57	21.2	138.9 153.4				
$NOTaF_6$·*p*-xylene	2.44	7.40	20.6	134.3 142.5	4460 2740		1810	45.5
$NOTaCl_6$·toluene	2.57	7.70→ 7.82	21.4	133.7 136.1 137.0 149.3				
$NOMoCl_6$·hexamethylbenzene	2.21		16.5	131.7				
$NOWCl_7$·hexamethylbenzene	2.46		17.7	150.5	3580			
$NOMo_2O_2F_9$·hexamethylbenzene	2.46		17.1	148.6	3230		1870	142.9 and −133.0
$NOW_2O_2F_9$·hexamethylbenzene	2.42		17.4	146.9			1878	62.1 and −145.6
$NOUF_7$·hexamethylbenzene	2.47		17.3	149.5	3250		1870	
$NOMoF_6$·hexamethylbenzene	2.40		17.1	147.9			1780	156.0
$NOUF_6$·hexamethylbenzene	2.34		17.2	143.7	3200		1880	
$NOFeCl_4$·hexamethylbenzene					3600 3250			

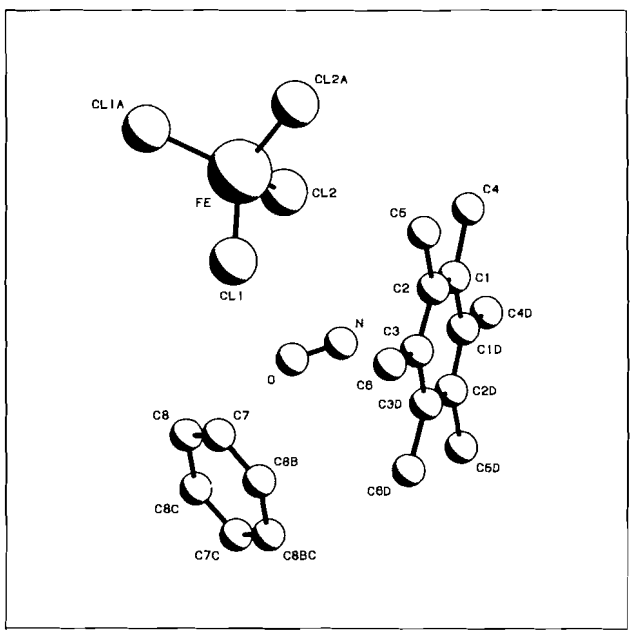

FIG. 3. The structure of $NOFeCl_4$·hexamethylbenzene·½benzene.

$UO_2F_2X_2^{2-}$ anion (X = NO_3 or F) (18, 19). No fluorine resonance signals were observed in the uranium systems.

$NOMF_6$ (M = Mo or U) reacts with hexamethylbenzene at −78°C to immediately give the adduct with the MF_6^- anion. The change in the infrared (Mo and U) and fluorine resonance (Mo) spectra with time show that these adducts again

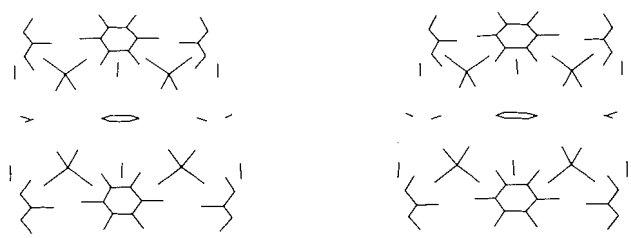

FIG. 4. A stereo drawing of the arrangement of the various entities of $NOFeCl_4$·hexamethylbenzene·½benzene. Only one half of the benzene, hexamethylbenzene, and NO entities are shown on each side of the central region.

quickly decompose to give the oxofluoroanions $Mo_2O_2F_9^-$ and $UO_2F_2X_2^{2-}$ (X = NO_3 or F), respectively.

The adduct of $NOFeCl_4$ and hexamethylbenzene is quite reactive to traces of moisture and an infrared spectrum could not be obtained without decomposition. The paramagnetic nature of the complex prevents acquisition of proton or carbon resonance spectra. The characteristic intense red–brown colour and ultraviolet spectrum, listed in Table 4, readily identify the fact that charge transfer has occurred. The crystal structure, as partially presented in the stereo drawing of Fig. 4, is rather unusual in that the benzene molecules are quite far from the other entities, suggesting negligible interaction between benzene and NO^+ in this structure. The overall structural arrangement consists of sheets perpendicular to the *Z* axis. At approximately $Z = 0 + \frac{1}{2}$ there are sheets of hexamethylbenzene and benzene moieties and at $Z = \frac{1}{4}$ and $\frac{3}{4}$ there are sheets of $FeCl_4$ anions. The NO groups are sandwiched between the two types

Can. J. Chem. Downloaded from www.nrcresearchpress.com by 80.58.250.72 on 09/07/12
For personal use only.

of layers in an arrangement which is too complex to present clearly in a diagram. Figure 4 is a simplified stereo diagram, viewed down the *Z* axis, showing the spatial relationship of the various structural elements. From an investigation of the uv spectrum of the system $NOFeCl_4$ and benzene in methylene chloride as solvent it appears that there is negligible charge-transfer complex formation between them.

It is interesting to note that both the group V and group VI transition elements form less stable complexes than the main group V elements (2). In every case where complex formation occurs the ultraviolet spectra are essentially independent of the anion. The proton and carbon resonance shifts upon charge transfer formation are somewhat anion dependent, being largest for the strongest complexes. Except for $NOSbCl_6 \cdot$ hexamethylbenzene the N—O stretching frequencies and N—O bond lengths do not vary greatly for the different anions. The conductivity varies markedly in those complexes where it may be measured. From the limited data it appears that high conductivity requires a very long N—O bond, as found previously (2).

1. S. BROWNSTEIN, A. MORRISSON, and L. TAN. Can. J. Chem. **64**, 265 (1986).
2. S. BROWNSTEIN, E. GABE, F. LEE, and A. PIOTROWSKI. Can. J. Chem. **64**, 1661 (1986).
3. J. MACCORDICK, G. KAUFMANN, and R. ROHMER. J. Inorg. Nucl. Chem. **31**, 3059 (1969).
4. J. E. GRIFFITHS, W. A. SUNDER, and W. E. FALCONER. Spectrochim. Acta, **31**A, 1207 (1975).
5. J. SHAMIR and J. G. MALM. J. Inorg. Nucl. Chem. Supp. 107 (1976).
6. W. A. SUNDER, A. L. WAYDA, D. DISTEFANO, W. E. FALCONER, and J. E. GRIFFITHS. J. Fluor. Chem. **14**, 299 (1979).
7. J. R. GEICHMAN, E. A. SMITH, S. S. TROND, and P. R. OGLE. Inorg. Chem. **1**, 661 (1962).
8. J. R. GEICHMAN, E. A. SMITH, and P. R. OGLE. Inorg. Chem. **2**, 1012 (1963).
9. R. BOUGON, T. B. HUY, and P. CHARPIN. Inorg. Chem. **14**, 1822 (1975).
10. D. W. A. SHARP and J. THORLEY. J. Chem. Soc. 3557 (1963).
11. YU. A. BUSLAEV and E. G. ILYIN. J. Fluorine Chem. **4**, 271 (1974).
12. L. K. TAN and S. BROWNSTEIN. J. Org. Chem. **48**, 302 (1983).
13. D. F. GRANT and E. J. GABE. J. Appl. Crystallogr. **11**, 114 (1978).
14. G. GERMAIN, P. MAIN, and M. M. WOOLFSON. Acta Crystallogr. **27**, 368 (1971).
15. E. J. GABE, F. L. LEE, and Y. LE PAGE. Crystallogr. Comput. **3**, 167 (1984).
16. International tables for X-ray crystallography. Vol. IV. 1974. Kynoch Press, Birmingham, England. Table 2.2B, p. 99 and Table 2.3.1, p. 149.
17. D. W. AKSNES, S. M. HUTCHISON, and K. J. PARKER. Mol. Phys. **14**, 301 (1968).
18. S. P. MCGLYNN, J. K. SMITH, and W. C. NEELY. J. Chem. Phys. **35**, 105 (1961).
19. G. L. CALDOW, A. B. VANCLEAVE, and R. L. EAGER. Can. J. Chem. **38**, 772 (1960).

Can. J. Chem. Downloaded from www.nrcresearchpress.com by 80.58.250.72 on 09/07/12
For personal use only.

The dynamics of the reaction of F atoms with *trans*-diimide[1]

R. A. BACK, P. S. NEUDORFL, J. J. SLOAN, AND P. T. WASSELL
Division of Chemistry, National Research Council of Canada, 100 Sussex Drive, Ottawa, Ont., Canada K1A 0R6

Received June 5, 1986

R. A. BACK, P. S. NEUDORFL, J. J. SLOAN, and P. T. WASSELL. Can. J. Chem. **65**, 451 (1987).

Emission from the HF product of the reaction F + N_2H_2 has been measured in an arrested-relaxation infrared chemiluminescence experiment. The vibrational distribution is inverted, peaking in HF($v' = 2$). This energy partitioning indicates that the reaction occurs without the formation of a long-lived intermediate species. The detailed shape of the primary energy distribution could not be determined due to severe difficulties in the production of N_2H_2.

R. A. BACK, P. S. NEUDORFL, J. J. SLOAN et P. T. WASSELL. Can. J. Chem. **65**, 451 (1987).

Au cours d'une expérience de chemiluminescence infrarouge par relaxation stoppée, on a mesuré l'émission de HF provenant de la réaction de F + N_2H_2. La distribution vibrationnelle est inversée et elle atteint un maximum avec HF($v' = 2$). Cette énergie de partition indique que la réaction se produit sans formation d'espèces intermédiaires de longue vie. Dû aux difficultés extrêmes rencontrées dans la production de N_2H_2, on n'a pas pu déterminer la forme détaillée de la distribution de l'énergie primaire.
[Traduit par la revue]

Can. J. Chem. Downloaded from www.nrcresearchpress.com by 80.58.250.72 on 09/07/12
For personal use only.

Introduction

Reactions of F atoms with N—H bonds have been the subject of several dynamics studies in this (1–6) and other (7, 8) laboratories. The molecular reagent, hence the molecular environment of the N—H bond, varied widely in these studies. The reagents included $HCONH_2$ and CH_3NH_2 (1), NH_3 (3, 5, 7, 8), N_2H_4 (3, 7), HN_3 (2, 8), HNCO (4), and NH_2 (6). In all cases but one, that of the NH_2 radical, the HF vibrational excitation created by the F/H—NR family of reactions is smaller than that observed for comparable F atom reactions at C—H bonds. The latter typically create HF vibrational distributions which peak sharply at a point more than half way to the maximum level permitted by the exoergicity. The F/H—NR reactions, on the other hand, produce observed HF vibrational distributions which either decrease monotonically with increasing vibrational level, as in the $HCONH_2$ and N_2H_4 cases, or peak very weakly at a low vibrational level, as in the CH_3NH_2 reaction.

These general results have been observed in many laboratories, although differences in detail exist among the various studies as to the precise extent of vibrational excitation in a few of the cases. The N_2H_4 and C_2H_4 reactions illustrate the point. The exoergicity of the N_2H_4 reaction is 237 kJ mol^{-1} whereas that of the C_2H_4 reaction is 115 kJ mol^{-1}. In the former case, the *observed* HF vibrational distribution peaks in HF($v' = 1$) (3, 7) (probably it peaks in the $v' = 0$ level) and the fraction of the exoergicity channelled into vibration, $f_v' \cong 0.34$ whereas the vibrational distribution created by the C_2H_4 reaction peaks at HF($v' = 2$), the maximum energetically-accessible level, and has $f_v' \cong 0.55$.

The N—H reactions listed above all have substantial exoergicity, ranging from 250 to about 540 kJ mol^{-1}. The observation of a low HF vibrational excitation from such a reaction implies that the energy released in the formation of the HF bond has not remained there, but has migrated elsewhere during the reactive collision. This intramolecular energy migration in the reaction intermediate can be caused, for example, by interactions between the energized fragment (the HF) and either the nuclei or nearby orbitals of the substrate molecule, which prolong the reaction and provide a pathway for energy flow. The duration and intensity of these interactions determine the amount of the exoergicity lost to the polyatomic fragment during the product-separation phase of the reaction. In particular, if a statistical HF vibrational distribution is observed (characterized by rapidly-decreasing populations with increasing vibrational level), it can be assumed that the exoergicity was distributed equally among the product degrees of freedom via the transient formation of a reaction intermediate having a relatively long lifetime. This is because statistical energy partitioning favours product modes having the highest state densities. Since translational and rotational state densities are much higher than the vibrational state density of a small diatomic such as HF, it is impossible for a reaction forming a long-lived intermediate to produce vibrational inversion in HF.

Conversely, the observation of vibrational inversion in a product such as HF indicates unequivocally that the reaction time is very short. Dynamical calculations imply that the timescale in this case is in the order of one vibrational period. The reasons for the differences in the lifetimes of the reaction intermediates have been the subject of many publications. On the simplest level, short-lived reactions occur via reaction geometries for which there is no strong bonding in the intermediate. For the F/NH_2 reaction (6), for example, short-time (direct) dynamics occur because the barrier to reaction on the lowest triplet surface is approximately zero (6), hence the reaction can occur via an F—HNH geometry without sampling the deep FNH_2 potential well on the singlet surface.

Even if a strongly-bound intermediate is formed, however, its lifetime may be short if the potential energy released is large and the reduced masses for the collision and product separation are small. This is the case with the reaction O($^1D_2$) + H_2 for which the mechanism is predominantly an insertion to form vibrationally-excited H_2O. The consequent release of about 770 kJ mol^{-1} of potential energy causes the immediate dissociation of the intermediate with the formation of vibrationally-inverted OH (9).

The F + NH_3 reaction appears to be a case where the circumstances of geometry and bonding prolong the reactive collision and produce HF which is vibrationally colder than that created by comparable F/H—CR reactions. *Ab initio* computations of the F/NH_3 potential energy surface indicate that there is a hydrogen bonded species of the form F—H—NH_2 in the exit channel which is stable with respect to the separated products by 46 kJ mol^{-1} or about one third of the exoergicity of the reaction (10). Although the analysis of the calculations is still under way, it appears that this bound species facilitates

[1]NRC No. 25869.

the intramolecular vibrational energy transfer process by which the NH_2 radical receives part of the exoergicity which would otherwise have led to vibrational inversion in the HF product.

In the present paper, we carry these studies further by measuring the energy distribution in the reaction of fluorine atoms with *trans*-diimide:

[1] $F + N_2H_2 \rightarrow HF(v') + N_2H \qquad \Delta H_0^0 = -73$ kcal mol^{-1}

In this case, the H—N_2H bond energy is low (60 kcal mol^{-1}) and the N—N bond is essentially olefinic (11). These energetics are based on the reported heat of formation of N_2H_2, $\Delta H_{f(298)}^0 = 212 \pm 8$ kJ mol^{-1} (12), combined with a calculated value for the H—NN· bond energy of -38 kJ mol^{-1} (13). The weak N—H bond and the olefinic N=N bond of N_2H_2 make it similar in these respects to N_2H_4 which produces, on reaction with F atoms, vibrationally cold HF (3, 7). We find, however, that the HF produced in reaction [1] is vibrationally inverted.

Experimental

These experiments were carried out in a conventional low pressure arrested-relaxation infrared chemiluminescence apparatus (14). The reaction chamber was a stainless steel cylinder 25 cm diameter × 30 cm high containing liquid-nitrogen-cooled vertical chevron baffles arranged radially to completely enclose the interior of the chamber except for a rectangular volume containing a multipass optical cell (Welsh cell). The cryobaffle was designed to ensure that molecules escaping from the reaction volume (at the centre of the chamber) would be efficiently trapped and would have a very small probability of re-entering the observation zone subtended by the Welsh cell. The Welsh cell mirrors were freshly gold-coated before each experiment. The infrared emission collected by this cell was focussed into a Fourier transform spectrometer by an f/2 CaF_2 lens mounted in a flange in the reaction chamber wall.

The atomic fluorine reagent was generated by a 2450 MHz plasma discharge in CF_4 flowing in a 10 mm diameter quartz tube mounted in the centre of the reaction chamber lid. The lower end of the discharge tube was located slightly above the Welsh cell mirrors on the central axis of the reaction chamber. The N_2H_2 was admitted through a second tube mounted in the wall of the reaction chamber perpendicular to the discharge tube and located slightly below it. This configuration provided good reagent mixing and had the added advantage that the molecular reagent was directed across the stream of F atoms, towards the vertical chevron cryobaffle on the opposite side of the reaction chamber. As a result, the molecules which failed to collide with F atoms in the reaction zone immediately below the F-atom inlet tube, passed through this region and entered the liquid-nitrogen-cooled cryobaffle, where they were trapped very efficiently. The average pressure in the reaction zone was in the 10^{-4} Torr range but the pressure immediately below the F-atom discharge tube could have been an order of magnitude higher than this.

The N_2H_2 was produced by the thermal decomposition of solid Na-tosylhydrazide at temperatures between about 60°C and 120°C (11, 15) and admitted to the reaction vessel via a short thermostatted tube. It has previously been shown that this method produces almost pure *trans*-N_2H_2 in the gas phase (16). This is a very unstable molecule, however, and the possibility remains for heterogeneous decomposition on surfaces such as those of the reagent inlet tube. The tube carrying the N_2H_2 was kept as short as possible in order to minimize this problem, but for this reason, no direct measurement of the flowrate was attempted. As a result, the flowrate of the N_2H_2 and hence its concentration in the reaction zone were assumed to be proportional to the temperature of the decomposition. This uncertainty precluded the unequivocal determination of the shape of the initial energy distribution, as will be described in the next section.

Before each experiment, the F-atom discharge was run for approximately one hour until this system had become stable. Then the temperature of the solid Na-tosylhydrazide was increased slowly while monitoring the reaction zone for emission. Detectable emission began when the temperature reached about 60°C: its intensity increased with the temperature of the decomposition thereafter until either the solid reagent had been consumed (a few hours) or the heater was turned off and the temperature allowed to decrease again. Spectra were recorded for various temperature ranges — hence N_2H_2 flows — at known, constant F-atom flows. Two series of observations were carried out: one at low temperatures and one at high temperatures. The CF_4 flows for these two experiments were 5.2 and 4.0 μmol s^{-1}, respectively. These flows gave a signal-to-noise ratio in the measured spectra of 50–70 for N_2H_2-generator temperatures above about 90°C. The only spectrum observed during these experiments was the $\Delta v' = -1$ fundamental of HF. Emission from all vibrational levels up to $v' = 5$ was obtained. The spectra were assigned and measured by spectral analysis programs written here for this purpose. The vibrational and rotational populations were obtained from these spectra using a standard data analysis, which has been described previously (17). In the following, the results of both series of experiments will be reported and the initial distribution which these imply will be identified.

Results

Although emission was detected from the observation zone at temperatures above about 65°C, the spectral signal-to-noise was inadequate to obtain a distribution until a temperature of about 80°C was reached. Thereafter, measurements were carried out over a temperature range from about 80 to 124°C in two separate experiments. The results are listed in Table 1. All distributions in the table are normalized to $\Sigma_{v'} P(v') = 1.0$.

Runs 67 to 70 represent the lower-temperature group of measurements. In this case, the decomposition temperature was permitted to rise only to 95°C. The heater was then switched off and the data acquisition continued while the temperature decreased (see run 70). The flowrates and consequently the signal-to-noise for these low temperature experiments were smaller than those of the high-temperature runs. The uncertainty in all vibrational populations, however, was less than ±0.03 per v' level. Table 1 shows that all the low-temperature distributions are the same within this uncertainty. Runs 33 to 45 were done in a separate experiment in which the temperature was permitted to rise to 124°C before the heater was turned off. Observations in the lower part of this temperature range gave the same distributions as listed for runs 67 to 70. As the temperature rose above 100°C, however, the population of $v' = 2$ began to increase with respect to the other levels, and some population was detected in $v' = 5$.

The absence of population in $v' = 5$ for the low-temperature runs could be attributed to poorer signal-to-noise due to the lower flowrates but the markedly higher relative population in $v' = 2$ at the higher temperature cannot be created by a change in flowrates or intensity. It is not possible to attribute the $v' = 2$ population increase to vibrational deactivation from higher levels either, since this process would cause a strong increase in the population of $v' = 1$ as well. Table 1 shows that after the temperature reaches about 105°C the distribution does not change with increasing flow, even up to the highest temperature, 124°C. (Temperatures above this were not used in order to avoid dissociating the N_2H_2 on the hot surfaces.) It must be assumed that the flowrate increased with the temperature in this range and hence that the distribution observed in runs 34, 35, and 45 is not dependent on the N_2H_2 flow. The two different distributions into which the data fall can be seen more clearly from Fig. 1, in which runs from each temperature range are plotted.

The rotational distributions observed in experiment 69 are shown in Fig. 2. These are typical of the rotational excitation

Can. J. Chem. Downloaded from www.nrcresearchpress.com by 80.58.250.72 on 09/07/12
For personal use only.

TABLE 1. Vibrational distribution

Run	Temperature	$P(v' = 1)$	$P(v' = 2)$	$P(v' = 3)$	$P(v' = 4)$	$P(v' = 5)$
67	80–81	0.24	0.32	0.27	0.16	—
68	87	0.26	0.31	0.24	0.19	—
69	90–95	0.22	0.31	0.27	0.18	—
70	82–70	0.25	0.30	0.27	0.18	—
33	101–103	0.27	0.33	0.26	0.09	0.05
34	105–106	0.27	0.44	0.22	0.05	0.02
35	111–118	0.24	0.41	0.28	0.05	0.02
45	124	0.26	0.41	0.23	0.07	0.03

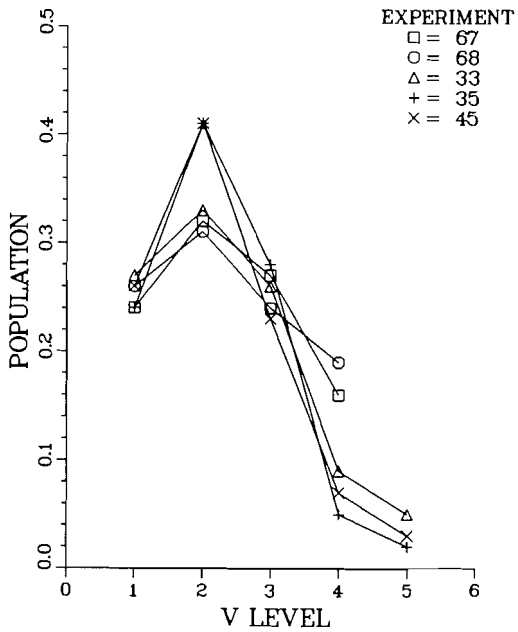

FIG. 1. The vibrational energy distributions obtained in the experiments listed in Table 1.

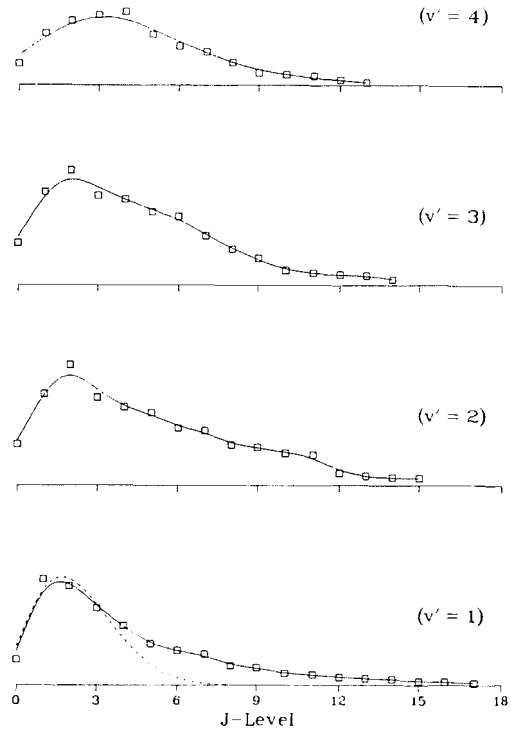

FIG. 2. The rotational distributions created in experiment 69. The dashed curve is a room-temperature Boltzmann distribution for comparison.

observed in all experiments. The solid curves are cubic splines which approximate the experimental observation (the points) to enhance the visibility of the latter. The dashed curve in the lower panel is a room-temperature Boltzmann distribution for comparison with the experimental data. This shows that all of the observed distributions have suffered partial rotational relaxation, but residual non-Boltzmann populations remain in all cases. The height of the latter suggests that the initial rotational excitation (before the partial relaxation) was not large, considering that the exoergicity of the reaction is sufficient to population $J' = 27$ of the $v' = 4$ level.

The extreme difficulty in producing stable flows of N_2H_2 which were high enough for this experimental technique, coupled with our inability to measure the flows directly, introduce unavoidable uncertainties in the interpretation of these data. The similarity of the distributions in each temperature range and the incompatibility of the observed differences with normal vibrational deactivation patterns suggest that a second process, separate from reaction [1], is responsible for these differences. In particular, the strong maximum in the population of $v' = 2$ which appears in the high-temperature experiments introduces the suspicion that a second process begins to contribute to the emission at high temperature. The simplest candidate for this process is the reaction of F atoms with H_2, which is well known to produce an HF vibrational distribution peaking in $v' = 2$. The H_2 could presumably come from the thermal decomposition of N_2H_2 before it reached the reaction zone. Although previous work (16) has suggested that the N_2H_2 produced by this method is quite pure, a contribution to the HF($v \leq 3$) populations at the highest temperature cannot be ruled out.

On the other hand, if there is no contribution from impurities such as H_2, it must be assumed that a secondary reaction is the source of the differences between the high- and low-temperature distributions. We have previously observed several primary/secondary reaction sequences of the form: $F + RH_2 \rightarrow HF_p(v') + RH$, followed by $F + RH \rightarrow HF_s(v') + R$ in this laboratory and have measured the product energy distributions in the systems: $F/H_2O/OH$ (18), $F/C_2H_4/C_2H_3$ (19), and $F/NH_3/NH_2$ (5, 6). The general behaviour observed in such cases is a change in the vibrational distribution when conditions are changed from those favouring only the primary reaction to those favouring *both* reactions. A complete discussion of this is given in ref. 6, including a numerical model of the $F/NH_3/NH_2$ system.

Can. J. Chem. Downloaded from www.nrcresearchpress.com by 80.58.250.72 on 09/07/12
For personal use only.

Can. J. Chem. Downloaded from www.nrcresearchpress.com by 80.58.250.72 on 09/07/12
For personal use only.

The most important condition for observation of a secondary reaction is a very large rate constant for the primary reaction. This ensures the creation of a high concentration of the intermediate radical and hence adequate opportunity for the secondary reaction to occur before the mixture leaves the observation zone. In the present system, the rate constant for reaction [1] (the primary reaction) is unknown, but would be expected to be at least as large as that for the reaction of F atoms with NH_3 — 3×10^{-11} cm^3 $molecule^{-1}$ s^{-1} (20). In addition to this, it is necessary for the secondary reaction to have a large rate constant as well, so the HF product will be produced in the observation zone. A simple kinetic analysis of the two-step primary/secondary sequence above, with the intermediate radical RH in steady state, shows that the rate of production of HF_s has the form:

$$k_1[F][RH_2]\cdot\frac{k_2[F]}{k_2[F] + k_p} - k_p[HF_s]$$

where k_1 and k_2 are the rate constants for the primary and secondary reactions and k_p is the rate constant for removal of all species from the observation zone by pumping. If the pumping rate is very large with respect to all other processes, the first term becomes very small and the secondary reaction cannot be observed. If $k_p \ll k_2[F]$, however, this rate expression shows that the secondary process can become appreciable with respect to the primary one.

The relative sizes of these terms is a sensitive function of the local conditions in the experiment and it is not possible to accurately determine the factors necessary for their calculation. It is possible, however, to make some rough estimates. These experiments were carried out using a 6″ diffusion pump (since replaced with a 15″ pump) which had a baffled pumping speed of about 1000 l/s. The volume of the observation zone is somewhat less than 1 L, but k_p may be taken to be about 10^3 s^{-1}. Although the average pressure observed in the reaction chamber was 10^{-4} Torr for these experiments, it is possible for the *local* pressure in the reaction zone immediately below the quartz inlet tube to be an order of magnitude higher than that. It is reasonable to assume that, on the average, about 50% of the CF_4 flow is converted to CF_2 + 2F in the discharge and thus 33% of the gas in the CF_4 reagent inlet is atomic fluorine (6). Since the observed total pressure in these experiments depended almost completely on the CF_4 flow (presumably because the N_2H_2 efficiently cryopumped on the liquid-nitrogen-cooled baffles), this indicates that the $[F] \cong 3 \times 10^{-4}$ Torr. If k_2 is approximately gas kinetic ($\cong 3 \times 10^{-10}$ cm^3 $molecule^{-1}$ s^{-1}), the value of $k_2[F]$ would therefore be about 10^3. This shows that under conditions of very high N_2H_2 flow, large F atom concentration *and* large k_2, it is possible to have seen the product of the secondary process $F + N_2H \rightarrow HF_s(v') + N_2$.

In the case where the N_2H_2 flow is low, the production rate of primary HF, given by the first term in the above expression, will be small and the pumping terms will dominate. The steady-state concentration of the radical intermediate, given by

$$[RH] = \frac{k_1[F][RH_2]}{k_2[F] + k_p}$$

will also be very small in this case. Using the rate constant for the F/NH_3 reaction with the other values estimated above, the average value of $[RH]/[RH_2]$ in the observation zone is found to be about 0.08. Under these conditions, the products of the secondary reaction might not be observable. If the higher temperature runs produced an order of magnitude increase in the N_2H_2 flow, then the production rate for HF_s will increase by the same amount, and the secondary reaction might be expected to make a detectable contribution.

The preceding paragraphs have shown that the increase in the $HF(v' = 2)$ population in the high-temperature experiments could be due to a contribution from either the $F + H_2$ reaction or the secondary $F + N_2H$ reaction. The NN—H bond energy is thought to be negative (13), although it may have a substantial barrier to dissociation (11). If the N_2H dissociates immediately after the primary reaction, the source of the added $HF(v' = 2)$ would have to be the $F + H_2$ reaction. In any case, it is clear that the distributions recorded at low temperature (and hence low N_2H_2 concentration) are least likely to be contaminated by either of these interfering reactions. Thus we regard the average of the distributions measured in runs 67–70 as the initial distribution from the N_2H_2 reaction.

Discussion

This reaction conforms to the energy partitioning patterns of other F/H—NR reactions inasmuch as it does not channel a large amount of energy into HF vibration or rotation. The suggested initial vibrational distribution — $P(v' = 1:2:3:4) = 0.25:0.31:0.26:0.18$ — represents only about 35% of the available energy. In this respect it is very similar to the F/N_2H_4 reaction, for which we have obtained $f_v' = 0.19$.[2] This may be contrasted with the F/H—CR reactions, mentioned earlier, for which this fraction (f_v') is typically in the range of 0.45–0.55. The latter reactions have similar exoergicity and the same mass combination (the transfer of a light atom between two heavier species), so the difference in the energy partitioning must be due to differences in the potential energy surface sampled during the reactive event.

The large HF vibrational excitation created by the F/H—CR reactions is understood to indicate simple abstraction dynamics in which the H atom is transferred rapidly (during approximately one C—H vibrational period) at a relatively large distance, thus preventing the migration of the exoergicity from the newly-formed HF bond back to the polyatomic product. Any influence on the reaction dynamics which facilitates this energy flow causes a reduction in the HF vibrational excitation. Thus, for example, if the F atom bonds first to the molecular reagent, forming a chemically-activated intermediate complex, the excitation of the internal modes of the reaction products from the subsequent (unimolecular) decomposition of the complex is statistical, depending only upon the density of states of each mode. In this event, the HF vibrational populations decrease rapidly and monotonically with increasing vibrational level.

The vibrational distribution from the $F/H—N_2H$ reaction does not have this extreme shape, so it must be concluded that it does not involve a long-lived intermediate complex. Its (slightly-inverted) distribution is more characteristic of a short-lived reaction, dynamically similar to the F/H—CR reactions. Its reduced f_v' and less strongly-peaked vibrational distribution suggest there are dynamical influences which enhance the energy flow from the HF back to the N_2H fragment. These could be, for example, hydrogen-bonded species such as F··H··NR, which could prolong the interaction slightly. Alternately, the F atom could preferentially interact with some part of the molecule other than the H atom, forming a transient

[2]D. W. Setser. Private communication.

bond there before reacting with the hydrogen. If this interaction were very abbreviated, the HF vibrational distribution, while inverted, would be less strongly-peaked than that from a single abstraction.

Whatever the dynamical cause, this reaction does not channel energy efficiently into the HF internal mode. The maximum vibrational excitation possible on the basis of the exoergicity is $HF(v' = 7)$ — substantially above the highest level observed in the experiment. The excess energy remaining after creation of the most-probable HF level ($v' = 2$) is 200 kJ mol^{-1}. It is likely that a large part of this energy remains in the N_2H fragment, which probably dissociates as a result of this excitation.

1. R. G. MACDONALD, J. J. SLOAN, and P. T. WASSELL. Chem. Phys. **41**, 201 (1979).
2. J. J. SLOAN, D. G. WATSON, and J. S. WRIGHT. Chem. Phys. **43**, 1 (1979).
3. D. J. DOUGLAS and J. J. SLOAN. Chem. Phys. **46**, 307 (1980).
4. J. J. SLOAN, D. G. WATSON, and J. S. WRIGHT. Chem. Phys. **63**, 283 (1981).
5. D. J. DONALDSON, J. PARSONS, J. J. SLOAN, and A. STOLOW. Chem. Phys. **85**, 47 (1984).
6. D. J. DONALDSON, J. D. GODDARD, and J. J. SLOAN. J. Chem. Phys. **82**, 4524 (1985).
7. W. H. DUEWER and D. W. SETSER. J. Chem. Phys. **58**, 2310 (1973).
8. A. S. MANOCHA, D. W. SETSER, and M. A. WICKRAMAARATCHI. Chem. Phys. **76**, 129 (1983).
9. P. M. AKER and J. J. SLOAN. J. Chem. Phys. **85**, 1412 (1986).
10. J. D. GODDARD, D. J. DONALDSON, and J. J. SLOAN. Unpublished results.
11. R. A. BACK. Rev. Chem. Intermediates, **5**, 293 (1984).
12. S. N. FONER and R. L. HUDSON. J. Chem. Phys. **68**, 3162 (1978).
13. (*a*) N. C. BAIRD and H. B. KATHPAL. Can. J. Chem. **55**, 863 (1977); (*b*) N. C. BAIRD. J. Chem. Phys. **62**, 300 (1975).
14. R. G. MACDONALD and J. J. SLOAN. Chem. Phys. **31**, 165 (1978).
15. N. WIBERG, G. FISCHER, and H. BACHHUBER. Chem. Ber. **107**, 1456 (1974).
16. P. S. NEUDORFL, R. A. BACK, and A. E. DOUGLAS. Can. J. Chem. **59**, 506 (1981).
17. R. G. MACDONALD and J. J. SLOAN. Chem. Phys. **31**, 165 (1978).
18. J. J. SLOAN, D. G. WATSON, and J. S. WRIGHT. Chem. Phys. **43**, 1 (1978).
19. D. J. DONALDSON, J. J. SLOAN, and D. G. WATSON. Chem. Phys. **68**, 95 (1982).
20. C.-D. WALTHER and H. GG. WAGNER. Ber. Bunsenges. Phys. Chem. **87**, 403 (1983).

Can. J. Chem. Downloaded from www.nrcresearchpress.com by 80.58.250.72 on 09/07/12
For personal use only.

Comment on "Thermodynamics of solvent mixtures. I. Density and viscosity of binary mixtures of *N*-methylpyrrolidinone – tetrahydrofuran and propylene carbonate – acetonitrile"

NORMAN GEE AND GORDON R. FREEMAN
Chemistry Department, University of Alberta, Edmonton, Alta., Canada T6G 2G2

AND

A. V. ANANTARAMAN
Defence Research Establishment, Ottawa, Ont., Canada K1A 0Z4

Received August 14, 1986

NORMAN GEE, GORDON R. FREEMAN, and A. V. ANANTARAMAN. Can. J. Chem. **65**, 456 (1987).

In the recent work of Anantaraman (Can. J. Chem. **64**, 46 (1986)) the conversion from kinematic viscosity to dynamic viscosity was incorrect. We calculated correct values from the tabulated data. We also give corrected values of the ideal mixture viscosity, the Grunberg–Nissan deviation parameter, and the Hind interaction parameter.

NORMAN GEE, GORDON R. FREEMAN et A. V. ANANTARAMAN. Can. J. Chem. **65**, 456 (1987).

Dans le travail récent de Anantaraman (Can. J. Chem. **64**, 46 (1986)), la conversion de la viscosité cinématique à la viscosité dynamique était incorrecte. On a recalculé les valeurs correctes à partir des données présentées dans les tableaux. On rapporte aussi les valeurs corrigées pour la viscosité du mélange idéal, pour le paramètre de déviation de Grunberg–Nissan et pour le paramètre d'interaction de Hind.

[Traduit par la revue]

Can. J. Chem. Downloaded from www.nrcresearchpress.com by 80.58.250.72 on 09/07/12
For personal use only.

In a recent work (1) values of the dynamic viscosity η were calculated from measured values of the kinematic viscosity ν and the mass density ρ using the incorrect equation [1].

[1] $\eta = \nu/\rho$

That this was done can be verified by comparing (ν/ρ) calculated from data in Table 3 of ref. 1 to η values in Fig. 4 and Table 6 of ref. 1. The correct equation is:

[2] $\eta = \nu \times \rho$

as kinematic viscosity is defined as fluid viscosity divided by fluid density (2). Values of the observed experimental viscosity η_{obs} in ref. 1 are incorrect. Correct ones calculated from the tabulated values of ν and ρ in ref. 1 are given in Table 1.

TABLE 1. Corrected dynamic viscosities and model parameters at 5.0 ± 0.05°C

x_1	η_{obs} (cP)[a]	η_{GN} (cP)[b]	ϵ[c]	η_{12} (cP)[d]
	Propylene carbonate in acetonitrile			
0.0000	0.432	0.432		
0.0920	0.512	0.528	−0.366	0.739
0.1675	0.619	0.622	−0.038	0.762
0.3043	0.854	0.838	0.087	0.688
0.3763	1.007	0.981	0.113	0.636
0.4910	1.312	1.259	0.164	0.560
0.6293	1.806	1.702	0.254	0.504
0.7795	2.390	2.361	0.071	0.145
0.7953	2.510	2.444	0.165	0.238
0.9537	3.519	3.451	0.444	0.525
1.0000	3.817	3.817		
	N-Methylpyrrolidinone in tetrahydrofuran			
0.0000	0.573	0.573		
0.1004	0.665	0.658	0.121	0.988
0.2369	0.779	0.794	−0.102	0.880
0.3418	0.911	0.917	−0.027	0.885
0.4511	1.086	1.065	0.078	0.914
0.5601	1.308	1.237	0.225	0.987
0.7055	1.562	1.511	0.160	0.926
0.8122	1.857	1.750	0.390	1.123
0.8685	2.012	1.890	0.545	1.285
0.9625	2.187	2.151	0.457	1.217
1.0000	2.265	2.265		

[a]Calculated from ν and ρ in ref. 1.
[b]Grunberg–Nissan's ideal viscosity, eq. [3].
[c]Grunberg–Nissan's deviation parameter, eq. [4].
[d]Hind interaction parameter, eq. [5].

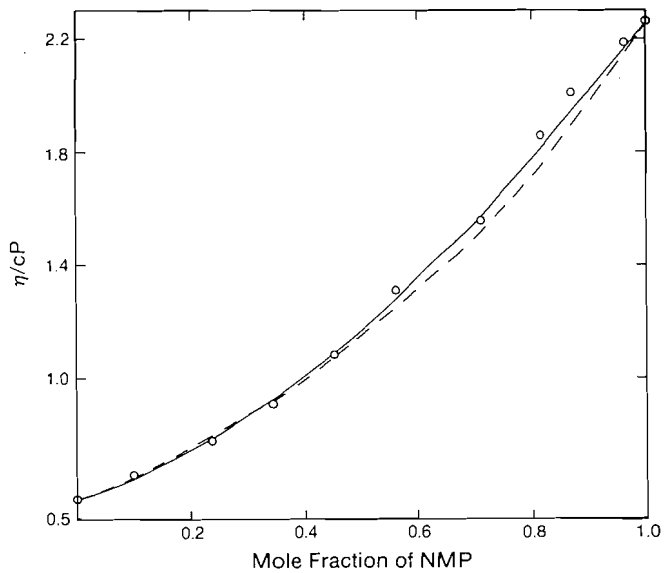

FIG. 1. Dynamic viscosity as a function of composition. System: NMP—THF; temperature: 5.0 ± 0.05°C. ○ Measured; --- ideal eq. [3]; — empirical.

The previous work analyzed η values using the Grunberg–Nissan model (3) and the Hind model (4). The ideal mixture viscosity in the Grunberg–Nissan model η_{GN} was that of Arrhenius (5) as modified by Kendall and Monroe (6) from volume to mole fraction:

[3] $\ln \eta_{GN} = x_1 \ln \eta_1 + x_2 \ln \eta_2$

where 1 and 2 refer to the two components. Values of η_{GP}

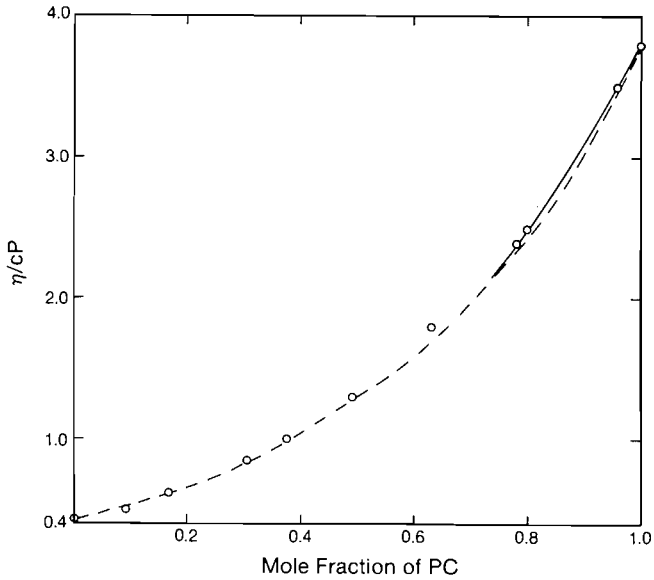

FIG. 2. Dynamic viscosity as a function of composition. System: PC—AN; temperature: 5.0 ± 0.05°C. ○ Measured; --- ideal eq. [3]; — empirical.

based on the correct η are given in Table 1; Figs. 4 and 5 of ref. 1 are redrawn in Figs. 1 and 2, respectively. Viscosities of both the binary mixtures NMP–THF and PC–AN follow the empirical Arrhenius expression, eq. [3], suggesting the absence of specific intermolecular interactions during the process of momentum transfer in these systems. Values of the Grunberg–Nissan deviation parameter ϵ defined as

$$[4] \quad \epsilon = (\ln \eta_{obs} - \ln \eta_{GN})/x_1 x_2$$

and the Hind interaction parameter η_{12} from

$$[5] \quad \eta_{12} = [\eta_{obs} - (x_1^2 \eta_1 + x_2^2 \eta_2)]/2x_1 x_2$$

for the corrected η_{obs} are also given in Table 1.

1. A. V. ANANTARAMAN. Can. J. Chem. **64**, 46 (1986).
2. W. C. MICHELS (*Editor*). The international dictionary of physics and electronics. Van Nostrand, New York. 1956. p. 966.
3. (*a*) L. GRUNBERG and A. H. NISSAN. Nature, **164**, 799 (1949); (*b*) L. GRUNBERG. Trans. Faraday Soc. **50**, 1293 (1954).
4. P. K. HIND, E. MCLAUGHLIN, and A. R. UBBELOHDE. Trans. Faraday Soc. **56**, 328 (1960).
5. S. ARRHENIUS. Z. Phys. Chem. **1**, 285 (1887).
6. J. KENDALL and K. P. MONROE. J. Am. Chem. Soc. **39**, 1777 (1917).

Can. J. Chem. Downloaded from www.nrcresearchpress.com by 80.58.250.72 on 09/07/12
For personal use only.

ADDITIONS AND CORRECTIONS/AJOUTS ET CORRECTIONS

Yasutsugu Ueda and Viviane Vinet. Can. J. Chem. **64**, 2184 (1986). Synthesis and in vitro activity of several new carbapenems.

Page 2188. In the final paragraph, for the preparation of *cis*-4-(*p*-nitrobenzyloxycarbonylaminomethyl)cyclohexylthiol (**3***e*), the third line should read: "followed by diisopropylethylamine (0.42 mL, 2.42 mmol)" instead of "by diisopropylamine."

Can. J. Chem. Downloaded from www.nrcresearchpress.com by 80.58.250.72 on 09/07/12
For personal use only.

Organometallic aspects of cytochrome P-450 metabolism

J.-I. SETSUNE
Department of Applied Chemistry, University of Osaka Prefecture, Sakai, Osaka 591, Japan
AND
D. DOLPHIN
Department of Chemistry, University of British Columbia, 2036 Main Mall, Vancouver, B.C., Canada V6T 1Y6

Received April 14, 1986

J.-I. SETSUNE and D. DOLPHIN. Can. J. Chem. **65**, 459 (1987).

Carbeneiron porphyrins, (*N,Fe*)-bridged methyleneiron porphyrins, *N*-alkyliron porphyrins and σ-alkyliron porphyrins have all been shown to occur in nature and to be interconvertible via redox reactions. The chemistry of the naturally occurring iron porphyrins and model iron, cobalt, and ruthenium porphyrins is reviewed emphasizing their organometallic chemistry.

J.-I. SETSUNE et D. DOLPHIN. Can. J. Chem. **65**, 459 (1987).

On a démontré que les porphyrines liées au carbène-fer, des porphyrines liées au méthylène-fer par une liaison *N–Fe*, les porphyrines liées à des *N*-alkyl-fer et les porphyrines liées à des σ-alkyl-fer se retrouvent toutes dans la nature et qu'elles se transforment les unes dans les autres par des réactions rédox. On passe en revue la chimie des porphyrines liées au fer ainsi que celle de porphyrines modèles liées au fer, au cobalt et au ruthénium en faisant ressortir leur chimie organométallique.
[Traduit par la revue]

Can. J. Chem. Downloaded from www.nrcresearchpress.com by 80.58.250.72 on 09/07/12
For personal use only.

I. Introduction

Until recently the only major organometallic chemistry of biological significance was that associated with coenzyme B_{12} and related systems containing cobalt–carbon bonds (1). However, the importance of organometallic chemistry of iron porphyrins and heme proteins is now being recognized.

The cytochromes P-450 (2) activate molecular oxygen by using prosthetic heme at the active site and NADPH as an electron source. One atom of dioxygen is reduced to water and the other used for the monooxygenation reactions such as hydroxylation of alkanes and arenes, epoxidation of olefins, and *N*-oxide and *S*-oxide formation of amino and sulfur compounds (2–4). Cytochrome P-450 also plays a key role in the reductive dehalogenation of polyhalogenated compounds (5–8). The oxoiron (IV) π-cation radical complex (**D**, Scheme 1), or some equivalent, is the key intermediate of the monooxygenation reaction in the catalytic cycle shown in Scheme 1 while the iron(II) complex (**B**) seems to interact directly with halogenated compounds during their reductive metabolism.

Recent studies on iron porphyrins have elucidated the chemical properties of, and the mutual relationships between,

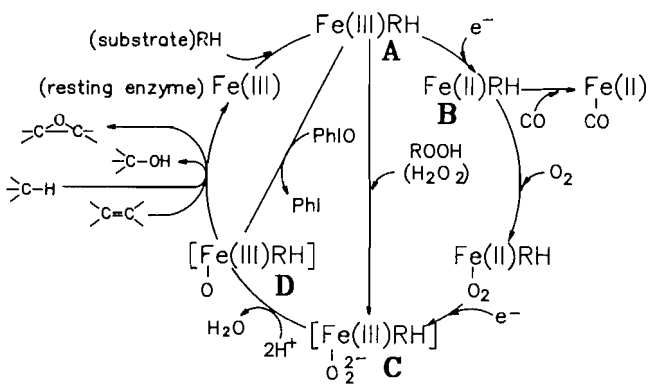

SCHEME 1

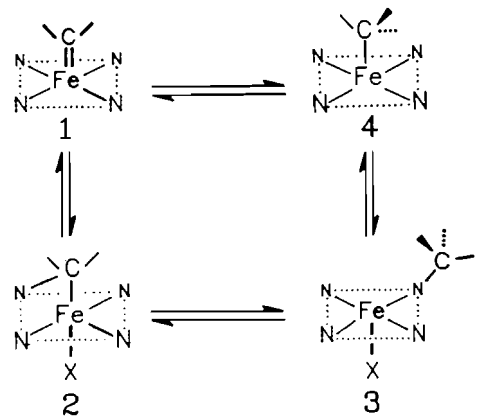

SCHEME 2

carbeneiron(II) porphyrins[1] (**1**), (*N,Fe*)-bridged methyleneiron(III) porphyrins (**2**), *N*-alkyliron(II) porphyrins (**3**), and σ-alkyliron(III) porphyrins (**4**) (Scheme 2). These four complexes may be regarded as models which can explain much of the *in vivo* chemical and biochemical reactions of cytochrome P-450. The complex (**1**) is a carbon analogue of compound II of catalases and peroxidases (3), while complex (**2**) is isoelectronic with an Fe—O—N bridged structure which is one of several structures proposed for compound I of catalase (9). Hepatic green porphyrins generated as a result of suicidal inactivation of cytochrome P-450 were shown to be *N*-alkylporphyrins (**3**) (10), and formation of a protein-stabilized σ-alkylporphyrin (**4**) has been postulated in the reaction of hemoglobin and myoglobin with phenyl hydrazine, ultimately giving rise to *N*-phenylheme (cf. **3**) (11). The carbeneiron(II) structure (**1**) was postulated for the stable 455 nm-absorbing complex of cytochrome P-450 which was observed upon oxidative metabolism of 1,3-benzodioxole known to be a potent insecticide

[1] We name these complexes as iron(II) carbene complexes cognizant of the fact that we have called the isoelectronic complexes in schemes 20 and 23 oxoiron(IV) species.

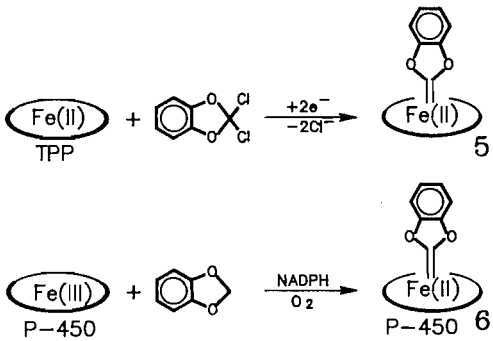

SCHEME 3

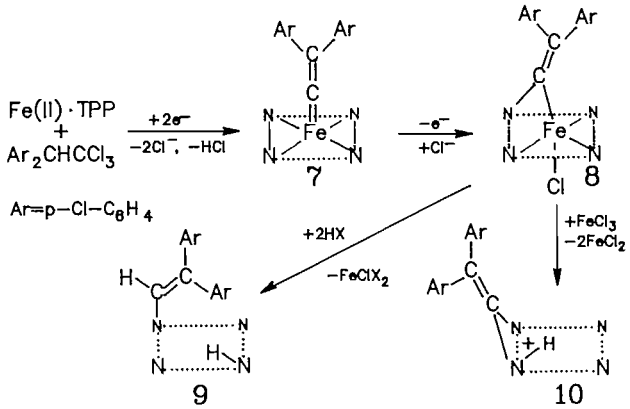

SCHEME 4

synergist (12). A 470 nm-absorbing intermediate was observed during the reductive metabolism of halothane, an inhalation anaesthetic, and ascribed to the formation of a carbeneiron(II) complex (**1**) or a σ-alkyliron(III) complex (**4**) (5–8).

In view of these observations, the organometallic chemistry of iron porphyrins may serve as an excellent basis for elucidating the mechanism of the catalytic reactions in which the cytochromes P-450 play important roles. We present here, recent advances in the field of organometalloporphyrin chemistry which will be surveyed emphasizing their biological relevance.

II. Carbeneiron(II) and σ-alkyliron(III) porphyrins

The first carbeneiron(II) porphyrin, dichlorocarbeneiron(II) tetraphenylporphyrin, was reported in 1977 (13). Various carbeneiron(II) porphyrins were prepared through the reaction of iron(II) porphyrins with polyhalogenated compounds in the presence of a reducing agent (14). The 1,3-benzodioxole-2-carbene complex (**5**) was synthesized from Fe(II)TPP (**4**) and 2,2-dichloro-1,3-benzodioxole to provide spectroscopic evidence in support of the formation of a 1,3-benzodioxole-2-carbene complex (**6**) (Scheme 3) of cytochrome P-450. These observations may explain the inhibitory action of 1,3-benzodioxole, as an insecticide synergist, on the enzymes responsible for insecticide detoxification (12).

The insecticide DDT, 2,2-bis(*p*-chlorophenyl)-1,1,1-trichloroethane, when reacted as above, followed by β-elimination of HCl, afforded a diaryl vinylidene carbene complex, $Ar_2C{=}C{=}Fe(II)TPP$ (**7**) (Scheme 4), which was found to be exceptionally stable (15) and was therefore conveniently used to investigate the general behavior of carbeneiron(II) porphyrins. Upon a one-electron oxidation of the vinylidene carbene complex (**7**), the electrophilic vinylidene ligand is no longer

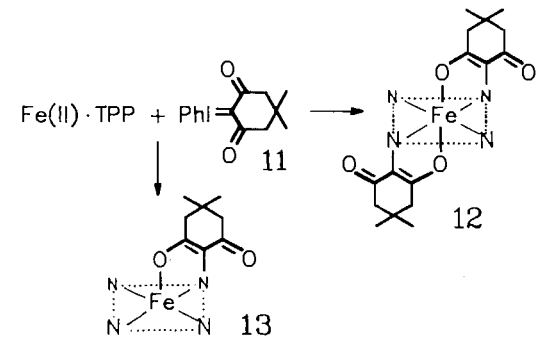

SCHEME 5

stabilized by iron in the ferric state and nucleophilic attack of the pyrrole nitrogen leads to the formation of the (*N*,*Fe*)-bridged vinylidene complex (**8**) which is transformed into the *N*-vinylporphyrin (**9**) upon protonolysis of the iron–carbon bond. The *N*,*N'*-bridged vinylidene porphyrin (**10**) is generated upon a further one-electron oxidation with $FeCl_3$ (9, 16–18).

Although it has been reported that a green porphyrin absorbing at 595 nm was transiently observed when chloro-iron(III) protoporphyrin IX dimethyl ester was allowed to react with diazomethane (19), iron carbene complexes of the type (**1**) and (**2**) have never been successfully obtained through the action of iron porphyrins with diazo compounds. Instead, the reaction of Fe(II)TPP with a phenyliodonium ylide (**11**), which is structurally analogous to iodosylbenzene, PhIO, afforded the bis(*N*-alkyl)porphyrin Fe(II) complex (**12**) which can be regarded as an analog of the bridged methylene complex (**2**) (20) (Scheme 5). The carbeneiron(II) structure and the (*N*,*Fe*)-bridged methyleneiron(III) structure were confirmed by single crystal X-ray determinations (9, 21). Under more carefully controlled conditions the mono(*N*-alkyl) complex (**13**) has also been prepared (22) (Scheme 5).

Electrochemical reduction of complex (**7**) was accompanied by spectral changes indicating the formation of a σ-vinyl-iron(II) porphyrin (**14**) which was alternately produced by a one-electron reduction of the σ-vinyliron(III) porphyrin (**15**) (23, 24). The redox relationship between the complexes (**7**) and (**15**) are shown in Scheme 6 (25).

σ-Alkyliron(III) porphyrins are obtained classically by the reaction of iron(III) porphyrins with Grignard reagents (26–28). Two other routes to σ-alkyliron(III) porphyrin reported recently are the reaction of Fe(II) porphyrins with alkyl radicals generated under pulse radiolysis conditions (29) and the reaction of an electrochemically generated Fe(I) porphyrin with alkyl halides in an S_N2 type nucleophilic substitution, oxidative addition, reaction (24, 30).

The σ-alkyliron(III)TPP complex (**16**) was detected during the catalytic reduction of *p*-nitrobenzyl chloride to *p*-nitrotoluene using a H_2O–toluene biphasic system with a phase transfer catalyst, sodium ascorbate, and Fe(III)TPP(Cl) (31). This supports the mechanism shown in Scheme 7 and also suggests that σ-alkyliron(III) complexes could be intermediates in the formation of carbeneiron(II) complexes, emphasizing the role of σ-alkyliron(III) intermediates in the metabolic reduction of halogenated compounds by cytochrome P-450. In fact, formation of the σ-alkyliron(III) porphyrin (**17**) was demonstrated when $CF_3CHClBr$, an inhalation anaesthetic, was allowed to react under the same conditions as when the carbeneiron(II)·tetraphenylporphyrin (**18**) was formed (8, 32). A unifying reaction mechanism is presented in Scheme 8 for these reactions.

Can. J. Chem. Downloaded from www.nrcresearchpress.com by 80.58.250.72 on 09/07/12
For personal use only.

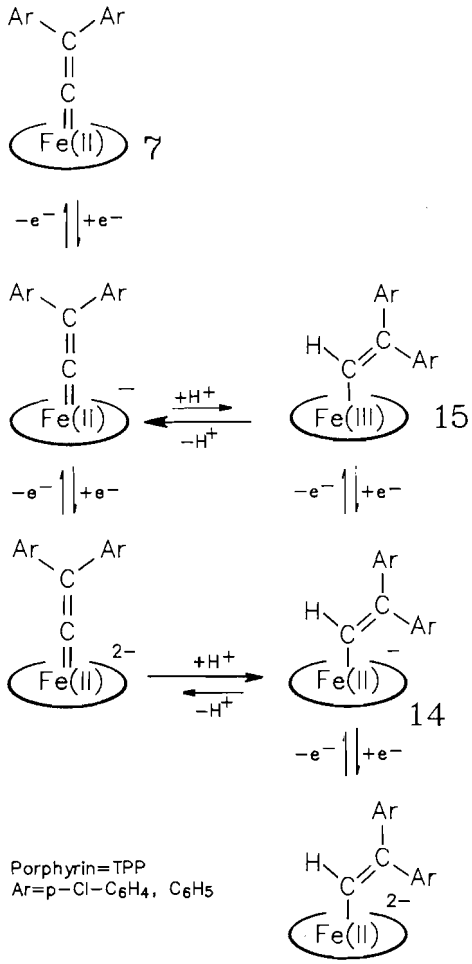

SCHEME 6

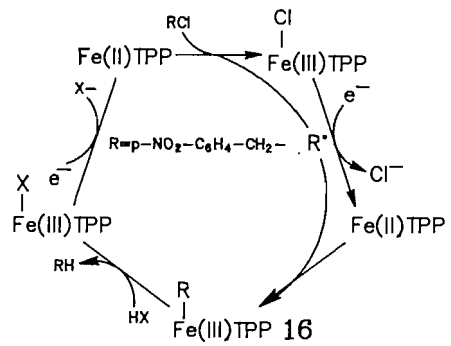

SCHEME 7

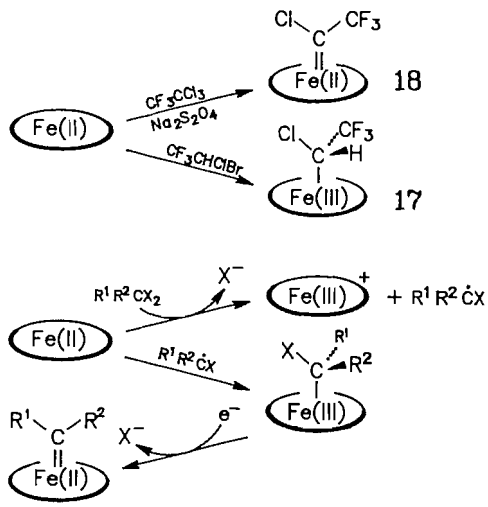

SCHEME 8

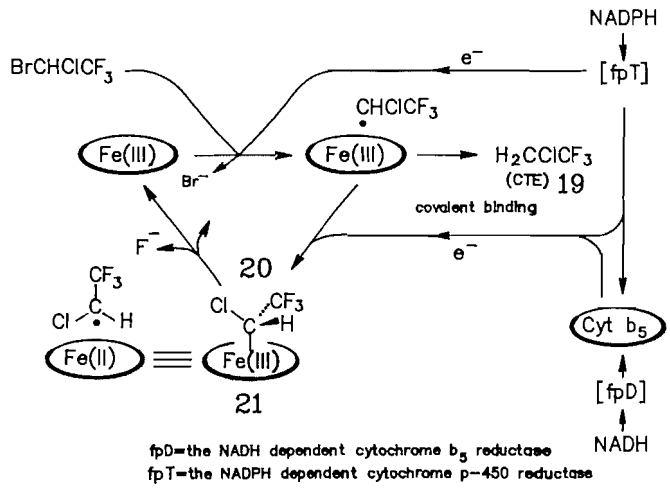

SCHEME 9

Although $CF_3CHClBr$ is metabolized in man to trifluoroacetic acid via a monooxygenase pathway, debrominated metabolites, 2-chloro-1,1,1-trifluoroethane (CTE, **19**) and 2-chloro-1,1-difluoroethylene (CDE, **20**), were detected *in vitro* accompanied by an increased covalent binding of the labelled substrate to the enzyme with decreasing dioxygen tension (5). Since the CTE/CDE ratio is shifted by addition and inhibition of cytochrome b_5, which is responsible for the second electron donation in the catalytic cycle of cytochrome P-450 system (**B** → **C**, Scheme 1), it follows that a $CF_3CHCl^{\bullet}$ radical is formed upon the first one-electron reduction which then abstracts a hydrogen atom to give CTE or attacks an amino acid residue. The Fe(III)$CHClCF_3$ σ-complex (**21**) is formed upon the second one-electron reduction and decomposes to CDE by a β-elimination mechanism (Scheme 9).

Hemoglobin and myoglobin are inactivated during the catalytic oxidation of aryl hydrazines to arenes, hydrogen peroxide, and dinitrogen (11). Nuclear magnetic resonance signals of the aryl group, which is thought to be bound directly to iron(III), are observed both with the inactivated hemoglobin and with the prosthetic heme extracted under anaerobic conditions (33). Aerobic work-up, with acid, of the inactivated hemoglobin gave *N*-arylprotoporphyrin IX dimethyl ester. Ethyl hydrazine is also oxidatively decomposed by hemoproteins to give *N*-ethylation of the prosthetic heme. Predominant *N*-ethylation on ring C of the protoporphyrin IX was observed. The globin is not necessary for *N*-arylation and *N*-alkylation to take place since hemin itself reacts analogously (34), however the protein may stabilize the intermediates which are thought to be aryl and σ-alkyliron(III) complexes.

A reversible iron-to-nitrogen shift (**22**–**23**) of alkyl, aryl, and vinyl groups was demonstrated upon a one-electron redox step with iron TPP complexes (35). The iron-to-nitrogen shift can be interpreted formally in terms of an oxidation of iron(III) to iron(IV) followed by the reductive elimination of the C and N ligands to form a C—N bond and iron(II), although earlier experiments with cobalt porphyrins (see below) have shown the involvement of the porphyrin macrocycle (37). A similar

Can. J. Chem. Downloaded from www.nrcresearchpress.com by 80.58.250.72 on 09/07/12
For personal use only.

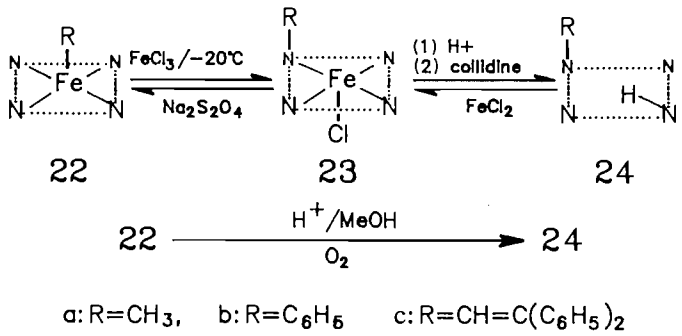

SCHEME 10

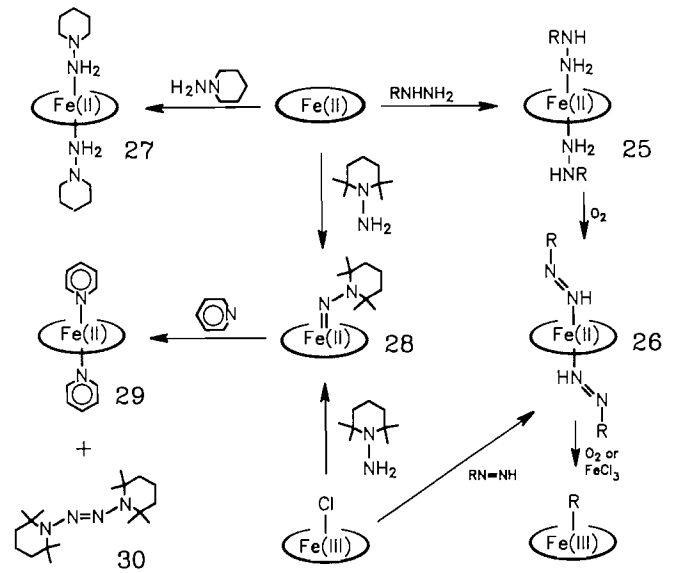

SCHEME 11

iron-to-nitrogen rearrangement of a phenyl group was shown by treatment of σ-phenyliron(III) tetraphenylporphyrin (**22***b*) with acidic methanol under aerobic conditions (36). These findings provide a rationale for the formation of σ-alkyliron(III) complexes and their transformation into *N*-alkylhemes (**24**) in the reaction of hemoproteins with alkyl hydrazines (Scheme 10).

Methyl hydrazine reduces ferric tetraphenylporphyrin to the corresponding bishydrazine hemochrome, TPP·Fe(II)$(RNHNH_2)_2$ (**25**), under anaerobic conditions, which is then oxidized to a bisdiazene hemochrome, TPP·Fe(II)$(RN{=}NH)_2$ (**26**), which upon further oxidation by $FeCl_3$ or O_2 gives the σ-methyliron(III) TPP (**19***a*) (38). A similar reaction pathway was suggested for phenyl hydrazine although the corresponding bisdiazene hemochrome proved to be too unstable to be characterized (38). The reactions of 1,1-dialkyl hydrazines toward iron porphyrin are different from those of monoalkylhydrazines. While 1-aminopiperidine reacts with TPP·Fe(III)Cl to give only the bishydrazine hemochrome, TPP·Fe(II)$(NH_2{-}NC_5H_{10})_2$ (**27**), the iron–nitrene complex, TPP·Fe(N—NC_9H_{18}) (**28**), was obtained when 1-amino-2,2,6,6-tetramethylpiperidine was used (39). The same nitrene complex (**28**) was prepared by the direct reaction of TPP·Fe(II) with pre-generated nitrene at low temperature and shown to release the nitrene ligand upon addition of excess pyridine to give TPP·Fe(II)$(py)_2$ (**29**) and the tetrazene (**30**). These results indicate that the reactions of hydrazines with iron porphyrins are strongly dependent on the nature of the substituted hydrazine (Scheme 11).

III. Organometalloporphyrins other than iron

Treatment of the *N,N'*-bridged tetraphenylporphyrin (**31**) with $Fe_3(CO)_{12}$ gave the carbene complex (**32**) (40). Similarly reaction with $Ru_3(CO)_{12}$ gave the corresponding ruthenium carbene complex (**32**). However, reaction of (**31**) with $Ni(CO)_4$ leaves one of the C—N bonds intact with formation of a σ-C—Ni bond (**33**) (40) (Scheme 12).

Ruthenium porphyrins are beginning to exhibit some rich organometallic chemistry. Thus Collman's group (41) have reported the reactions outlined in Scheme 13 where the ruthenium(II) dimers (**34**) of OEP and TPP both undergo similar reactions. Reduction, using potassium in THF, of the dimers gives the dipotassium Ru^0 porphyrin (**35**) (42) which undergoes the reactions shown in Scheme 14. The bisalkyl complexes can also be prepared by the reaction of the ruthenium(IV)

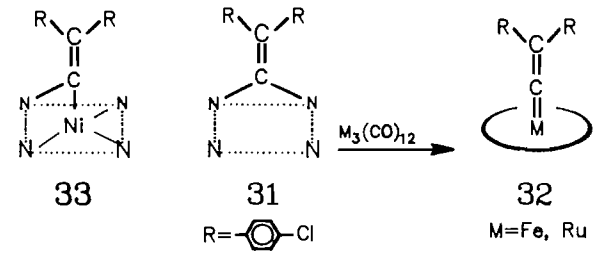

SCHEME 12

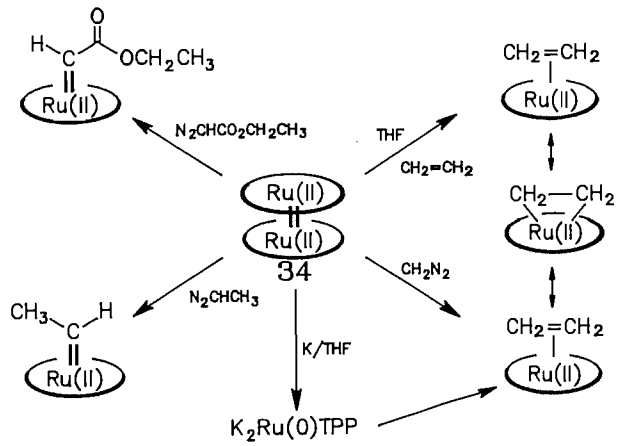

SCHEME 13

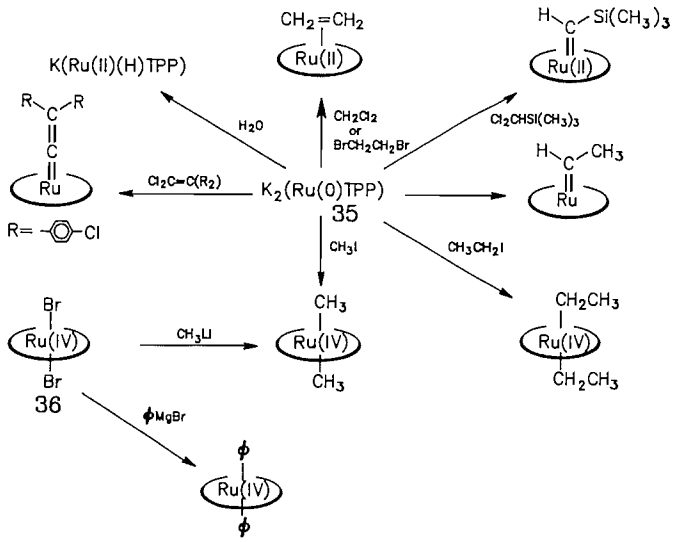

SCHEME 14

Can. J. Chem. Downloaded from www.nrcresearchpress.com by 80.58.250.72 on 09/07/12
For personal use only.

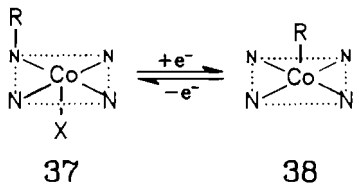

37 38

SCHEME 15

dibromide (**36**) with alkyl lithium and Grignard reagents (43) (Scheme 14).

σ-Alkyl complexes, *N*-alkyl complexes, and (*N,metal*)-bridged methylene complexes of cobalt porphyrins are known. Oxidative migration of ethyl and carboethoxy groups from cobalt to nitrogen occurs after an electrochemical oxidation to afford *N*-ethyl- and *N*-carboethoxy–TPP·Co(II) complexes (**37** ⇄ **38**, Scheme 15) (37). Spectroelectrochemical evidence showed that the initial site of oxidation was at the porphyrin ring to give a porphyrin π-cation radical intermediate. Treatment of σ-alkyl-, σ-aryl-, and σ-vinylcobalt(III) porphyrins with trifluoroacetic acid under aerobic conditions analogously brings about cobalt-to-nitrogen ligand migration (44, 45). In this case molecular oxygen, in acidic solution, seems to act as a strong oxidant to drive the reaction. Reductive nitrogen-to-metal migration of a methyl group takes place when cobalt, rhodium, and iridium complexes of *N*-methyl octaethylporphyrin are treated with sodium borohydride (46–48). These reversible metal-to-nitrogen migrations occur intramolecularly (Scheme 15), and detailed studies on the transfer of alkyl, aryl, and styryl groups between cobalt and nitrogen have been made (49, 50).

Unusual (*N,Co*)-bridged methylene complexes (**39**) of OEP·Co(III) were prepared through the reaction of divalent and trivalent cobalt OEP with ethyl diazoacetate (51, 52) and diazoacetaldehyde (53). A carbene cobalt(II) porphyrin was not detected and oxygen plays a key role in the reaction of Co(II)OEP with diazo compounds. Protonolysis of the cobalt(III)–carbon bond occurs to give *N*-substituted porphyrins (**40**) when the bridged complex (**39**) is treated with acid under conditions where Co(III) can be reduced to Co(II). The studies of Callot and Schaeffer with diazoalkanes were the first to suggest exchange of an organic fragment between metal and nitrogen proceeding via a bridged intermediate (54). Base treatment of (*N*-$CH_2CO_2C_2H_5$)Ni(II)TPPClO_4 (**41**) generates a kinetically favored (*N,C*)-bridged methylene intermediate (**42**) which gives rise to the (*N,Ni*)-bridged methylene complex (**43**) which can be further transformed into *N*-carboethoxymethyl TPP (**40**) upon addition of trifluoroacetic acid (55) (Scheme 16).

Addition of pyridine to (*N,Co*)-ethoxycarbonylmethylene Co(III)OEPCl (**39**) results in the formation of the pyridinium compound (**44**) (52). Direct formation of σ-halomethylcobalt(III) porphyrins (**45**) from the reaction of halocobalt(III) porphyrins with diazomethane involves a nucleophilic cleavage reaction of the transient bridged methylene complex, which was not isolated in this case (56). The σ-vinylcobalt(III) TPP (**46**) is generated directly when ethyl diazopropionate is allowed to react with Co(III)TPPCl (54). The N—C bond fission is facilitated if the bridgehead substituent bears a proton (56, 57).

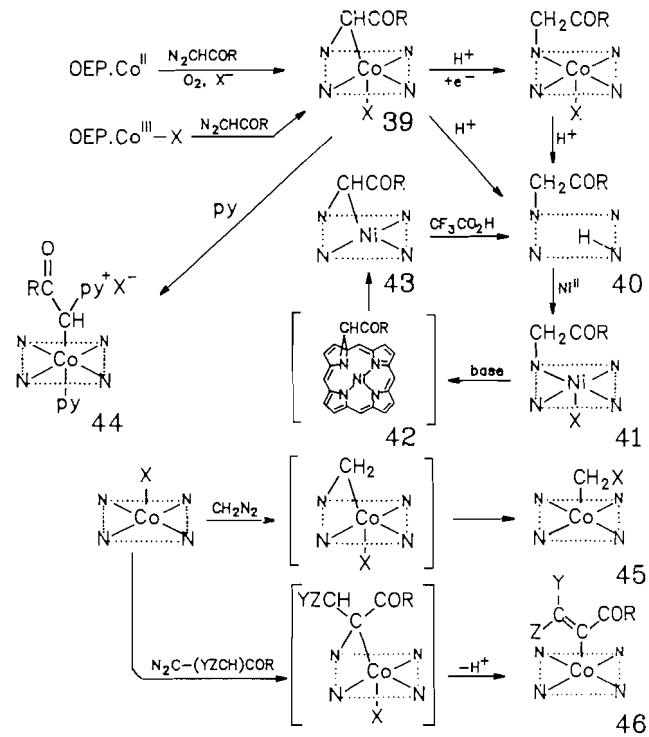

SCHEME 16

IV. Suicidal *N*-alkylation of cytochrome P-450

It has recently been reported that the prosthetic heme of cytochrome P-450 monooxygenases is converted into abnormal green porphyrins during the metabolism of 1,4-dihydropyridine derivatives (9, 58–60), cyclopropyl amines (61, 62), alkyl hydrazines (63), 1-aminobenzotriazole (64, 65), terminal olefins (66, 67), and terminal acetylenes (68–71). The hepatic porphyrin biologically modified with 3,5-dicarboethoxy-1,4-dihydrocollidine (**47**) was characterized as *N*-methylprotoporphyrin IX dimethyl ester (**49**). The *N*-methyl group was shown to be predominantly on pyrrole ring A on the basis of chemical synthesis and hplc separation of the four possible isomers of (**49**) (10, 58) (Scheme 17). *N*-Methylation of protoporphyrin IX dimethyl ester (**48**) with methyl fluorosulfonate afforded a mixture of four isomers in approximately equal amounts. The site of *N*-methylation of the four different pyrrole rings (A, B, C, and D) was determined using nmr techniques (58). The preferential ring A alkylation in the biological process seems to be controlled by the stereochemical arrangement of the protein surrounding the prosthetic heme.

Destructive activity of various 4-substituted 3,5-bis(ethoxycarbonyl)-2,6-dimethyl-1,4-dihydropyridines (**47**) as suicidal substrates in the catalytic metabolism of cytochrome P-450 enzymes was studied by using spin trapping technique to provide evidence in support of the formation of an alkyl radical derived from the 4-substituent of the substrate, which argues for the one-electron oxidation of a nitrogen lone pair of the substrate as the initial step (60). Cyclopropyl amines as suicidal substrates for cytochrome P-450 have also been reported and an aminium cation radical intermediate was postulated to form via a one-electron oxidation mechanism (61, 62). A tracer experiment showed covalent binding of the substrate to both the protein and the prosthetic heme presumably by the action of a ring-opened carbon-centered radical (**51**) formed from the aminium cation radical intermediate (**50**). Suicidal *N*-alkylation of the prosthetic heme of cytochrome P-450 was also reported in the metabolic processing of alkyl hydrazines (63) and 1-aminobenzotriazole (64, 65). *N*-(2-Phenylethyl)protoporphyrin IX dimethyl ester (**53**) was isolated from rat liver microsomes treated with 2-phenylethyl hydrazine and analyzed spectroscopically to show that *N*-alkylation had occurred on the pyrrole ring C or D. A spin trap experiment was successfully used to

Can. J. Chem. Downloaded from www.nrcresearchpress.com by 80.58.250.72 on 09/07/12
For personal use only.

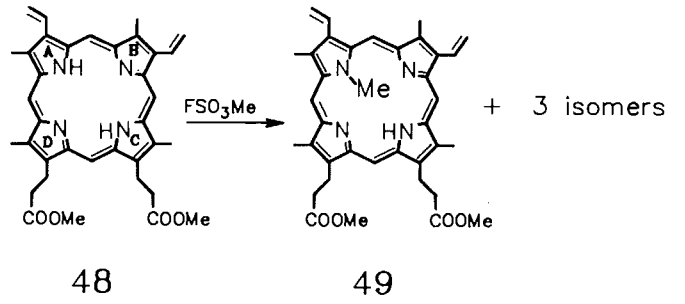

SCHEME 17

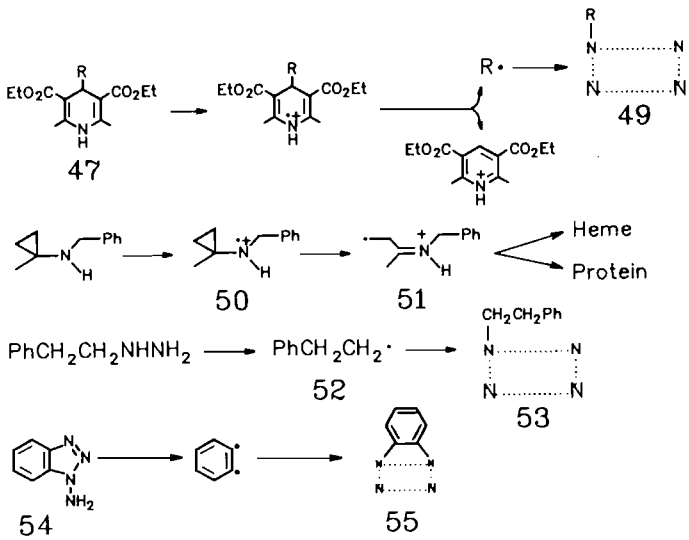

SCHEME 18

detect the 2-phenylethyl radical (**52**) in the metabolic process (63). Exceptionally high destructive ability was obtained with 1-aminobenzotriazole (**54**), which is known to yield benzyne upon mild chemical oxidation, and the hepatic porphyrin in this case was tentatively characterized as *N,N'-ortho*-phenylene bridged protoporphyrin IX dimethyl ester (**55**) on the basis of nmr, mass, and visible spectra (64, 65) (Scheme 18). More recently the total synthesis of vinylidene and phenylene bridged porphyrins have been reported (72). The catalytic metabolism of these amino compounds is believed to be initiated by a one-electron heteroatom oxidation. This parallels the cases of *N*-oxygenation and *S*-oxygenation of aminopyrine (73–75) and organosulfur compounds (76, 77) catalyzed by microsomal cytochrome P-450 enzymes. The above results indicate that suicidal inactivation by these substrates originates in the generation of a carbon-centered radical, the radical then inactivates cytochrome P-450 through an attack on either protein or the nitrogen of heme as summarized in Scheme 18. The heme alkylation can occur first at the iron atom to give a σ-bonded alkyliron complex which can rearrange to an *N*-alkylheme upon a one-electron oxidation (11, 35, 63).

The prosthetic heme of cytochrome P-450 is converted during the metabolism of terminal olefins and acetylenes into *N*-alkylporphyrins; the *N*-substituent consists of the substrate and one oxygen atom. Nuclear magnetic resonance studies showed that hydroxyethyl, 2-hydroxypropyl, and 2-hydroxyoctyl groups were bonded to the pyrrolic nitrogen of ring D of the hemes biologically modified with ethylene, propene, and 1-octene, respectively (66, 68).

We have demonstrated suicidal *N*-alkylation of an iron porphyrin model complex of cytochrome P-450 when *N*-(4,4-dimethyl-2-hydroxypentyl)-5,10,15,20-tetrakis(2,6-dichlorophenyl)porphine (**57**) was isolated from the epoxidation reaction of 4,4-dimethyl-1-pentene with iodosopentafluorobenzene catalysed by 5,10,15,20-tetrakis(2,6-dichlorophenyl)porphinatoiron(III) chloride (**56**) (78) (Scheme 19).

We have also shown (79) that *N*-alkylation of cobalt(III) porphyrin π-cation radicals occurs with alkynes. Thus cobalt(III) octaethylporphyrin π-cation radicals, prepared by the oxidation of cobaltic OEP with ferric chloride or perchlorate, reacted with acetylene, 1-hexyne, propargyl alcohol, 2-butyne-1,4-diol, and mono- and diphenyl acetylenes, to give in good yields the *N*(21),*N*(22)–etheno bridged porphyrins (**58**) (Scheme 20).

Both of the above *N*-alkylations can be considered as occurring via an initial one-electron transfer from the unsaturated hydrocarbon to the highly oxidized metalloporphyrin (Scheme 21) to generate a radical cation of the hydrocarbon (this concept is developed in more detail below).

Intermediate **59** (Scheme 21*b*) generated after formation of an initial N—C bond contains a σ-cobalt–carbon bond and an oxidized porphyrin π-cation radical. We have shown earlier that such a species may undergo a cobalt → nitrogen ligand migration. Such a migration in this case would lead to the observed etheno bridged product (**58**).

It was reported that inactivation of cytochrome P-450 with acetylene, propyne, and 1-octyne afforded *N*-(2-oxoalkyl)pro-

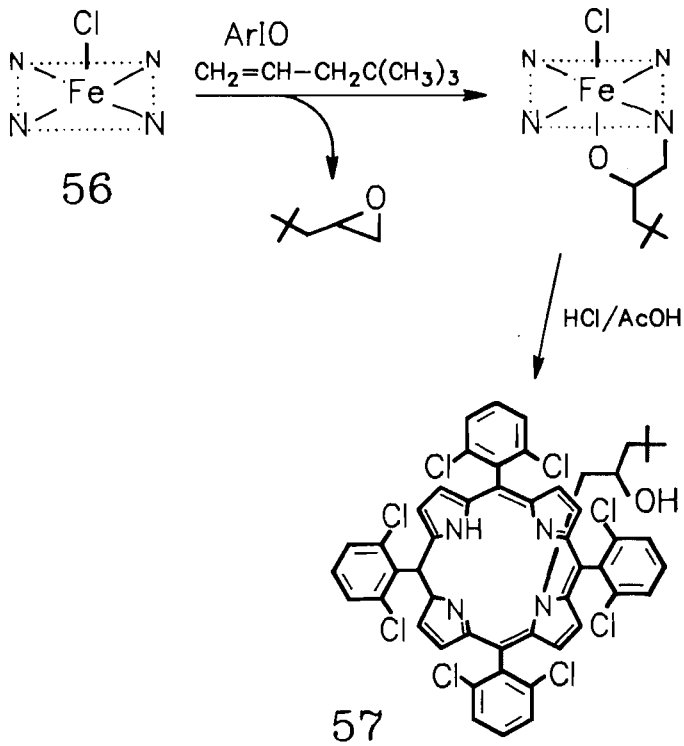

SCHEME 19

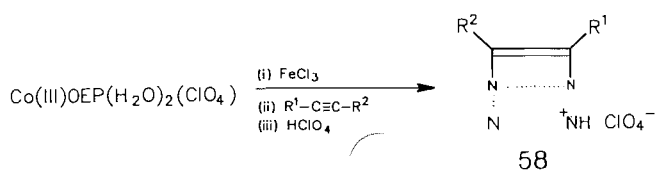

SCHEME 20

Can. J. Chem. Downloaded from www.nrcresearchpress.com by 80.58.250.72 on 09/07/12
For personal use only.

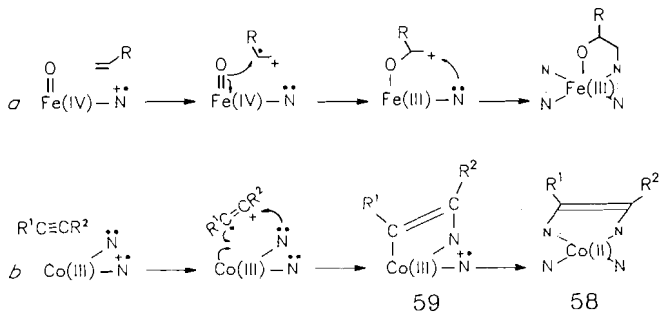

SCHEME 21

toporphyrin IX dimethyl esters with the *N*-substituents specifically on pyrrole ring A in the case of propyne and 1-octyne (68, 70). The acetylene-derived porphyrin was a mixture of two *N*-alkylprotoporphyrin IX dimethyl esters, the *N*-substituents of which were shown to be formylmethyl and the corresponding dimethyl acetal on the basis of mass spectroscopic studies. The site of the pyrrole ring bearing *N*-substituent was not determined (69). In order to provide a firm basis for the structural identification of these *N*-alkylporphyrins biologically modified with unsaturated compounds, chemical synthesis of *N*-formylmethyl- (**60**), *N*-(2,2-dimethoxyethyl)- (**61**), and *N*-(2-hydroxyethyl)protoporphyrin IX dimethyl ester (**62**) was accomplished as shown in Scheme 22 (80). Spectroscopic analysis of these synthetic *N*-alkylprotoporphyrin IX dimethyl esters showed that the site of *N*-alkylation in the biological reactions with acetylene occurred on ring C or D.

In order to isolate the hepatically modified hemes they were esterified with methanol. During this process the naturally derived and synthetic *N*-formylmethylporphyrins were partially converted into the *N*-(2,2-dimethoxyethyl)porphyrin. Unsubstituted acetylene seems to show less regiospecificity during the *N*-alkylation of cytochrome P-450 than is observed with substituted acetylenes and appears to be similar to that observed with unsubstituted ethylene.

The biological *N*-alkylation of heme takes place not only regiospecifically but also stereospecifically with respect to the plane of alkylation. The circular dichroism spectra of two ring C isomers of *N*-ethylprotoporphyrin IX dimethyl ester zinc(II) chloride, one from cytochrome P-450 inactivated with 3,5-bis(ethoxycarbonyl)-2,6-dimethyl-4-ethyl-1,4-dihydropyridine and the other from hemoglobin treated with ethyl hydrazine, are identical (81). This in combination with the hypothesis that *N*-alkylation in hemoglobin most likely occurs from the distal side of the porphyrin plane to which molecular oxygen is bound, provides a rationale for the assignment of an absolute *R*-configuration of the *N*-ethylprotoporphyrin IX obtained from hemoglobin and cytochrome P-450, since the active site geometry of hemoglobin is known X-ray crystallographically. The same absolute *R*-configuration was suggested for the *N*-alkylated porphyrins obtained with propyne and ethylene because the circular dichroism spectra of these porphyrins are virtually the same as those of the corresponding regioisomers of the biologically obtained *N*-ethyl derivative (81). The regiospecificity and stereospecificity observed in the *N*-alkylation of cytochrome P-450 with unsaturated compounds led to an active site model of the phenobarbital induced cytochrome P-450 enzymes which features the absolute orientation of the prosthetic heme, steric constraints over pyrrole ring B, and a lipophilic channel over pyrrole ring C accommodating linear alkyl substituent (68).

The stereochemical course of the catalytic epoxidation and

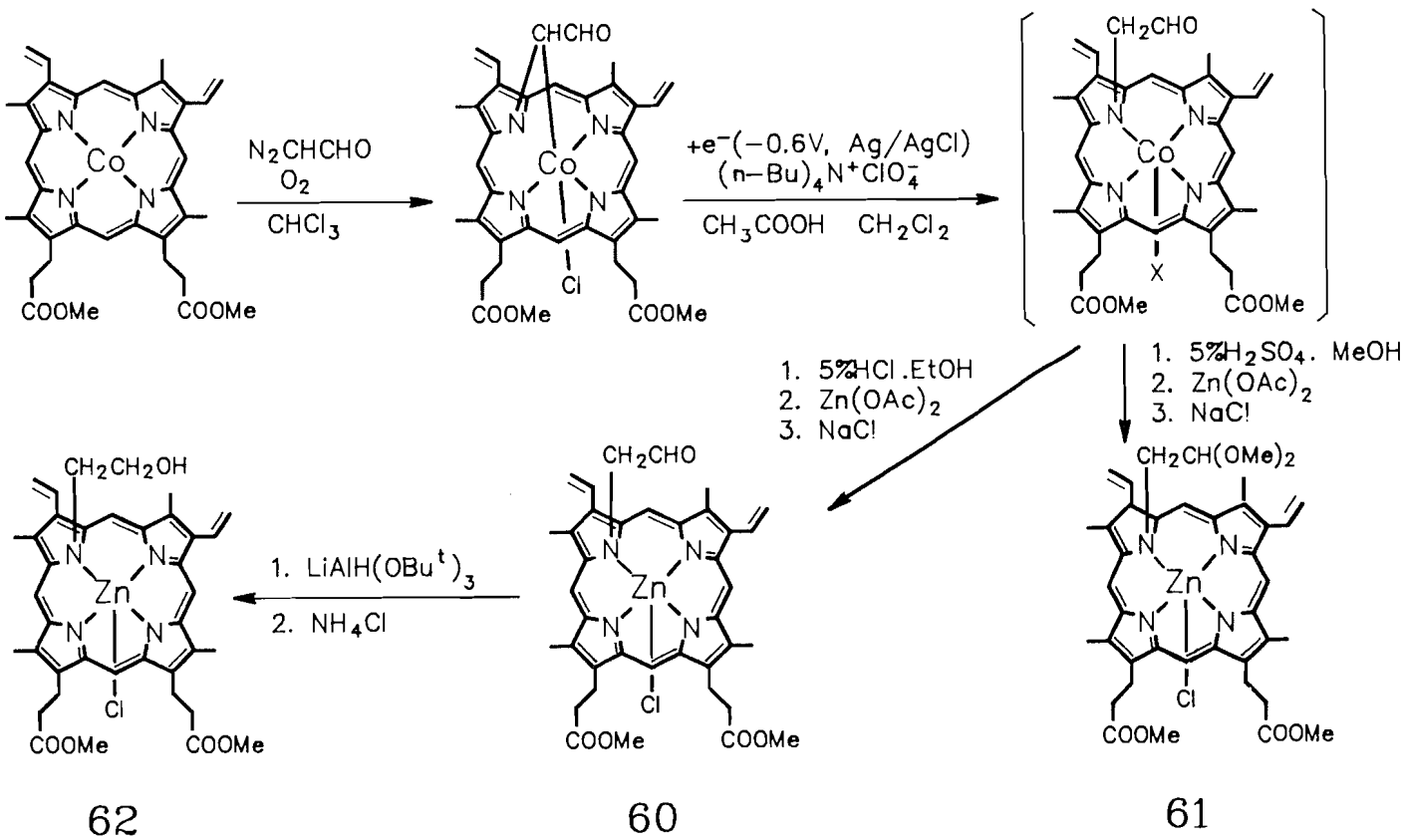

SCHEME 22

Can. J. Chem. Downloaded from www.nrcresearchpress.com by 80.58.250.72 on 09/07/12
For personal use only.

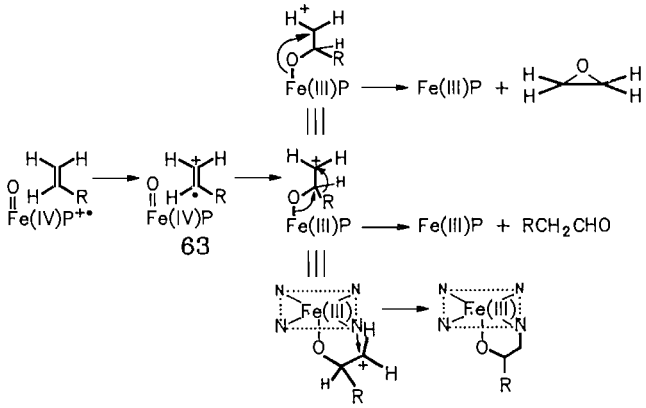

SCHEME 23

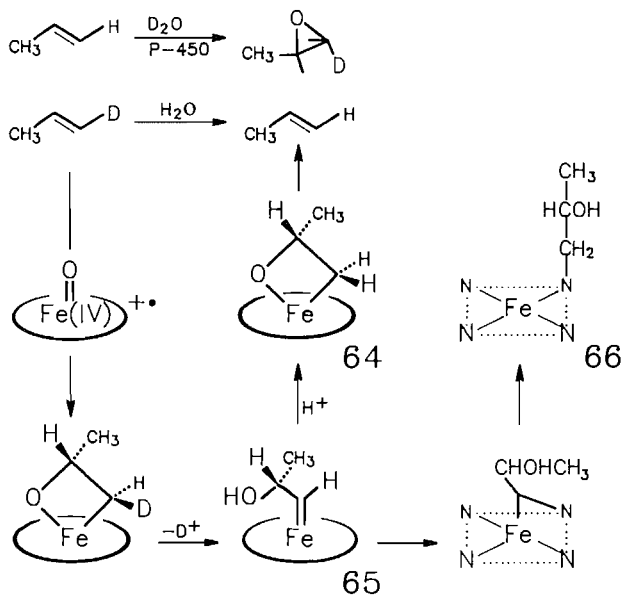

SCHEME 24

prosthetic heme alkylation during the metabolism of 1-octene has been studied to show that the olefin stereochemistry is completely retained in both transformations and that only the *re* face of the olefin undergoes *N*-alkylation whereas the *re* and the *si* face are almost equally available for epoxidation (67). The latter observation is consistent with the regiospecific ring D *N*-alkylation by 1-octene under the stereochemical control of the active site.

It is now apparent that the hemoprotein families of the catalases, peroxidases, and cytochrome P-450 are closely related and the active iron–oxygen species of cytochrome P-450 is suggested to be an oxoiron(IV) porphyrin π-cation radical (**D**, Scheme 1) comparable to that seen for catalase and horseradish peroxidase (82).

High valent oxo complexes of iron(IV) tetramesitylporphyrin (83) and ruthenium(IV) octaethylporphyrin have been prepared from the corresponding trivalent metalloporphyrins and iodosylbenzene (84). These compounds exhibit spectral properties similar to those reported for the high oxidation states of catalases and peroxidase and their reactivity towards alkanes and olefins parallels that of cytochrome P-450. Scheme 23 shows how, after an initial one electron transfer from an olefin to the electron deficient oxo-ferryl π-cation radical, an intermediate cation radical of the olefin (**63**) can account for all of the products observed both biologically (4) and in the model systems (78).

Groves *et al.* (85) have shown for the specific case of propylene, that deuterium can be both regio- and stereospecifically incorporated into the recovered alkene during a P-450 mediated epoxidation, when the reaction is run in D_2O. In addition, deuterium can be lost from deuterated propene when the reaction is carried out in water. Groves *et al.* have suggested that this reaction may proceed via a metallocycle (**64**) which reversibly gives, upon deprotonation, the metallocarbene (**65**) and which in turn would lead to the *N*-alkylheme (**66**) (Scheme 24).

Acknowledgements

This work was supported by the United States National Institute of Health (GM 29198) and the Natural Sciences and Engineering Research Council of Canada.

1. B_{12}. Vols. 1 and 2. *Edited by* D. Dolphin. Wiley Interscience, New York. 1982.
2. J. T. GROVES. *In* Metal ion activation of dioxygen. *Edited by* T. G. Spiro. John Wiley and Sons, New York. 1980. pp. 125–162.
3. R. E. WHITE and M. J. COON. Ann. Rev. Biochem. **49**, 315 (1980).
4. F. P. GUENGERICH and T. L. MCDONALD. Acc. Chem. Res. **17**, 9 (1984).
5. H. J. AHR, L. J. KING, W. NASTAINCZYK, and V. ULLRICH. Biochem. Pharm. **31**, 383 (1982).
6. C. R. WOLF, D. MANSUY, W. NASTAINCZYK, G. DEUTSCHMANN, and V. ULLRICH. Mol. Pharm. **13**, 698 (1977).
7. W. MASTAINCZYK, V. ULLRICH, and H. SIES. Biochem. Pharm. **27**, 397 (1978).
8. H. H. RUF, H. AHR, W. NASTAINCZYK, V. ULLRICH, D. MANSUY, J.-P. BATTIONI, R. MONTIEL-MONTOYA, and A. TRAUTWEIN. Biochemistry, **23**, 5300 (1984).
9. B. CHEVRIER, R. WEISS, M. LANGE, J.-C. CHOTTARD, and D. MANSUY. J. Am. Chem. Soc. **103**, 2899 (1981).
10. P. R. ORTIZ DE MONTELLANO, H. S. BEILAN, and K. L. KUNZE. Proc. Natl. Acad. Sci. U.S.A. **78**, 1490 (1981).
11. O. AUGUSTO, K. L. KUNZE, and P. R. ORTIZ DE MONTELLANO. J. Biol. Chem. **257**, 6231 (1982).
12. D. MANSUY, J.-C. CHOTTARD, and V. ULLRICH. J. Am. Chem. Soc. **101**, 3971 (1979).
13. D. MANSUY, M. LANGE, J.-C. CHOTTARD, P. GUERIN, P. MORLIER, D. BRAULT, and M. ROUGEE. J. Chem. Soc. Chem. Commun. 648 (1977).
14. D. MANSUY. Pure Appl. Chem. **52**, 681 (1980).
15. D. MANSUY, M. LANGE, and J.-C. CHOTTARD. J. Am. Chem. Soc. **100**, 3213 (1978).
16. M. LANGE and D. MANSUY. Tetrahedron Lett. **22**, 2561 (1981).
17. L. LATOS-GRAZYNSKI, R.-J. CHENG, G. N. LA MAR, and A. L. BALCH. J. Am. Chem. Soc. **103**, 4270 (1981).
18. T. J. WISNIEFF, A. GOLD, and S. A. EVANS, JR. J. Am. Chem. Soc. **103**, 5616 (1981).
19. P. S. CLEZY and D. B. MORELL. Biochim. Biophys. Acta, **71**, 150 (1963).
20. D. MANSUY, J.-P. BATTIONI, I. AKHREM, D. DUPRE, J. FISCHER, R. WEISS, and I. MORGENSTERN-BADARAU. J. Am. Chem. Soc. **106**, 6112 (1984).
21. D. MANSUY, M. LANGE, J.-C. CHOTTARD, J. F. BARTOLI, B. CHEVRIER, and R. WEISS. Angew. Chem. **90**, 828 (1978).
22. D. MANSUY. Revista Portuguera de Quim. **27** (1/2), 104 (1985).
23. D. LEXA, J.-M. SAVEANT, J.-P. BATTIONI, M. LANGE, and D. MANSUY. Angew. Chem. **93**, 585 (1981).
24. D. LEXA and J.-M. SAVEANT. J. Am. Chem. Soc. **104**, 3503 (1982).

Can. J. Chem. Downloaded from www.nrcresearchpress.com by 80.58.250.72 on 09/07/12
For personal use only.

Can. J. Chem. Downloaded from www.nrcresearchpress.com by 80.58.250.72 on 09/07/12
For personal use only.

25. J.-P. BATTIONI, D. LEXA, D. MANSUY, and J.-M. SAVEANT. J. Am. Chem. Soc. **105**, 207 (1983).
26. D. A. CLARKE, D. DOLPHIN, A. W. JOHNSON, and H. A. PINNOCK. J. Chem. Soc. C, 881 (1968).
27. D. A. CLARKE, R. GRIGG, and A. W. JOHNSON. J. Chem. Soc. Chem. Commun. 208 (1966).
28. P. COCOLIOS, E. LAVIRON, and R. GUILARD. J. Organomet. Chem. **228**, C39 (1982).
29. D. BRAULT and P. NETA. J. Am. Chem. Soc. **103**, 2705 (1981).
30. D. LEXA, J. MISPELTER, and J.-M. SAVEANT. J. Am. Chem. Soc. **103**, 6806 (1981).
31. D. MANSUY, M. FONTECAVE, and J.-P. BATTIONI. J. Chem. Soc. Chem. Commun. 317 (1982).
32. D. MANSUY and J.-P. BATTIONI. J. Chem. Soc. Chem. Commun. 638 (1982).
33. K. L. KUNZE and P. R. ORTIZ DE MONTELLANO. J. Am. Chem. Soc. **105**, 1380 (1983).
34. P. R. ORTIZ DE MONTELLANO and K. L. KUNZE. J. Am. Chem. Soc. 6534 (1981).
35. D. MANSUY, J.-P. BATTIONI, D. DUPRE, F. SARTORI, and G. CHOTTARD. J. Am. Chem. Soc. **104**, 6159 (1982).
36. P. R. ORTIZ DE MONTELLANO, K. L. KUNZE, and O. AUGUSTO. J. Am. Chem. Soc. **104**, 6159 (1982).
37. D. DOLPHIN, D. J. HALKO, and E. JOHNSON. Inorg. Chem. **20**, 4348 (1981).
38. J.-P. BATTIONI, J. P. MAHY, G. GILLET, and D. MANSUY. J. Am. Chem. Soc. **105**, 1399 (1983).
39. D. MANSUY, J.-P. BATTIONI, and J. P. MAHY. J. Am. Chem. Soc. **104**, 4487 (1982).
40. Y. W. CHAN, M. W. RENNER, and A. L. BALCH. Organometallics, **2**, 1888 (1983).
41. J. P. COLLMAN, P. J. BROTHERS, L. MCELWEE-WHITE, E. ROSE, and L. J. WRIGHT. J. Am. Chem. Soc. **107**, 4570 (1985).
42. J. P. COLLMAN, P. J. BROTHERS, L. MCELWEE-WHITE and E. ROSE. J. Am. Chem. Soc. **107**, 6110 (1985).
43. C. SISHTA, M. KE, B. R. JAMES, and D. DOLPHIN. J. Chem. Soc. Chem. Commun. 787 (1986).
44. H. J. CALLOT and E. SCHAEFFER. Tetrahedron Lett. 1335 (1980).
45. H. J. CALLOT and F. METZ. J. Chem. Soc. Chem. Commun. 947 (1982).
46. H. OGOSHI, E. WATANABE, N. KOKETSU, and Z. YOSHIDA. J. Chem. Soc. Chem. Commun. 943 (1974).
47. H. OGOSHI, J.-I. SETSUNE, T. OMURA, and Z. YOSHIDA. J. Am. Chem. Soc. **97**, 6461 (1975).
48. H. OGOSHI, J.-I. SETSUNE, and Z. YOSHIDA. J. Organomet. Chem. **159**, 317 (1978).
49. H. J. CALLOT, F. METZ, and R. CROMER. Nouv. J. Chim. **8**, 759 (1984).
50. H. J. CALLOT, R. CROMER, A. LOUATI, and M. GROSS. Nouv. J. Chim. **8**, 765 (1984).
51. A. W. JOHNSON, D. WARD, P. BATTEN, A. L. HAMILTON, G. SCHELTON, and C. M. ELSON. J. Chem. Soc. Perkin I, 2076 (1975).
52. A. W. JOHNSON and D. WARD. J. Chem. Soc. Perkin I, 720 (1977).
53. J.-I. SETSUNE and D. DOLPHIN. Organometallics, **3**, 440 (1984).
54. H. J. CALLOT and E. SCHAEFFER. Nouv. J. Chim. **4**, 307 (1980).
55. H. J. CALLOT, TH. TSCHAMBER, B. CHEVRIER, and R. WEISS. Angew, Chem. **87**, 545 (1975).
56. H. J. CALLOT and E. SCHAEFFER. J. Organomet. Chem. **145**, 91 (1978).
57. H. J. CALLOT and E. SCHAEFFER. J. Organomet. Chem. **193**, 111 (1980).
58. K. L. KUNZE and P. R. ORTIZ DE MONTELLANO. J. Am. Chem. Soc. **103**, 4225 (1981).
59. P. R. ORTIZ DE MONTELLANO, H. S. BEILAN, and K. L. KUNZE. J. Biol. Chem. **256**, 6708 (1981).
60. O. AUGUSTO, H. S. BEILAN, and P. R. ORTIZ DE MONTELLANO. J. Biol. Chem. **257**, 11288 (1982).
61. R. P. HANZLIK and H. TULLMAN. J. Am. Chem. Soc. **104**, 208 (1982).
62. T. L. MACDONALD, K. ZIRVI, L. T. BURKA, P. PEYMAN, and F. P. GUENGERICH. J. Am. Chem. Soc. **104**, 2050 (1982).
63. P. R. ORTIZ DE MONTELLANO, O. AUGUSTO, F. VIOLA, and K. L. KUNZE. J. Biol. Chem. **258**, 8623 (1983).
64. P. R. ORTIZ DE MONTELLANO and J. M. MATHEWS. Biochem. J. **195**, 761 (1981).
65. P. R. ORTIZ DE MONTELLANO, J. M. MATHEWS, and K. C. LANGRY. Tetrahedron, **40**, 511 (1984).
66. P. R. ORTIZ DE MONTELLANO, H. S. BEILAN, K. L. KUNZE, and B. A. MICO. J. Biol. Chem. **256**, 4395 (1981).
67. P. R. ORTIZ DE MONTELLANO, B. L. K. MANGOLD, C. WHEELER, K. L. KUNZE, and N. O. REICH. J. Biol. Chem. **258**, 4208 (1983).
68. K. L. KUNZE, B. L. K. MANGOLD, C. WHEELER, H. S. BEILAN, and P. R. ORTIZ DE MONTELLANO. J. Biol. Chem. **258**, 4202 (1983).
69. P. R. ORTIZ DE MONTELLANO, K. L. KUNZE, H. S. BEILAN, and C. WHEELER. Biochemistry, **21**, 1331 (1982).
70. P. R. ORTIZ DE MONTELLANO and K. L. KUNZE. Biochemistry, **20**, 7266 (1981).
71. P. R. ORTIZ DE MONTELLANO and K. L. KUNZE. J. Biol. Chem. **255**, 5578 (1980).
72. H. J. CALLOT and R. CROMER. Tetrahedron Lett. **26**, 3357 (1985).
73. B. W. GRIFFIN and P. L. TING. Biochemistry, **17**, 2206 (1978).
74. B. W. GRIFFIN C. MARTH, Y. YASUKOCHI, and B. S. S. MASTERS. Arch. Biochem. Biophys. **205**, 543 (1980).
75. B. W. GRIFFIN, D. K. DAVIS, and G. V. BRUNO. Bioorg. Chem. **10**, 177 (1981).
76. Y. WATANABE, T. IYANAGI, and S. OAE. Tetrahedron Lett. 3685 (1980).
77. Y. WATANABE, T. IYANAGI, and S. OAE. Tetrahedron Lett. 533 (1982).
78. T. MASHIKO, D. DOLPHIN, T. NAKANO, and T. G. TRAYLOR. J. Am. Chem. Soc. **107**, 3735 (1985).
79. J.-I. SETSUNE, M. IKEDA, Y. KISHIMOTO, and T. KITAO. J. Am. Chem. Soc. **108**, 1309 (1986).
80. J.-I. SETSUNE and D. DOLPHIN. J. Org. Chem. **50**, 2958 (1985).
81. P. R. ORTIZ DE MONTELLANO, K. L. KUNZE, and H. S. BEILAN. J. Biol. Chem. **258**, 45 (1983).
82. D. DOLPHIN. Phil. Trans. R. Soc. London, B**311**, 579 (1985).
83. J. T. GROVES, R. C. HAUSHALTER, M. NAKAMURA, T. E. NEMO, and B. J. EVANS. J. Am. Chem. Soc. **103**, 2994 (1981).
84. D. DOLPHIN, B. R. JAMES, and T. LEUNG. Inorg. Chim. Acta, **79**, 25 (1983).
85. J. T. GROVES, G. E. AVARIA-NEISSER, K. M. FISH, M. IMACHI, and R. L. KUZKOWSKI. J. Am. Chem. Soc. **108**, 3837 (1986).

Spectral studies on the interaction of iodine with thiazoles

REFAT ABDEL-HAMID, AHMED A. EL-SAMAHY, ABDEL-HAFIZ EL-TAHER, AND HUSSEIN EL-SAGHER
Department of Chemistry, Faculty of Science, Sohag, Egypt

Received May 2, 1986

REFAT ABDEL-HAMID, AHMED A. EL-SAMAHY, ABDEL-HAFIZ EL-TAHER, and HUSSEIN EL-SAGHER. Can. J. Chem. **65**, 468 (1987).

The electron donor–acceptor molecular complexes between thiazole and some of its derivatives and iodine in several solvents have been investigated spectrophotometrically at different temperatures. Spectral characteristics, equilibrium constants, K, extinction coefficients, ϵ, and thermodynamic functions of formation, ΔH^0, ΔG^0, and ΔS^0 have been determined. It was found that the data fit satisfactorily the 1:1 stoichiometric equilibrium: $D + I_2 = DI_2$ "outer complex". The EDA complexes obtained are of "n–σ*" type in which the nitrogen atom of thiazole is the donor center. Moreover, the effect of solvents on the K values is discussed in terms of the solute–solute and solute–solvent competing equilibria.

REFAT ABDEL-HAMID, AHMED A. EL-SAMAHY, ABDEL-HAFIZ EL-TAHER et HUSSEIN EL-SAGHER. Can. J. Chem. **65**, 468 (1987).

Opérant à plusieurs températures différentes et faisent appel à la spectrophotométrie, on a étudié les complexes moléculaires donneurs–accepteurs d'électrons entre le thiazole ainsi que quelques-uns de ses dérivés avec l'iode, dans plusieurs solvants. On a déterminé les caractéristiques spectrales, les constantes d'équilibre, K, les coefficients d'extinction, ϵ, ainsi que les fonctions thermodynamiques de formation, ΔH^0, ΔG^0 et ΔS^0. On a trouvé que les données s'accordent bien avec un équilibre stoechiométrique 1:1: $D + I_2$ = « complexe externe » DI_2. Les complexes que l'on a obtenus avec le EDA sont du type « n–σ* » dans lequel l'atome d'azote du thiazole est le centre donneur. De plus, on discute de l'effet des solvants sur les valeurs de K en fonction d'équilibres solutés–solutés et solutés–solvants qui sont en compétition.

[Traduit par la revue]

Can. J. Chem. Downloaded from www.nrcresearchpress.com by 80.58.250.72 on 09/07/12
For personal use only.

Introduction

Heterocyclic compounds form 1:1 stoichiometric electron donor–acceptor molecular complexes with iodine in aprotic solvents (1–3). It has been reported that these EDA complexes are of n-donor–acceptor type and have high thermodynamic stability. Their formation constants and enthalpies of formation put them among the strongest complexes of this type. Recently, a study on the electron donor–acceptor molecular complex equilibria of iodine and thiazoles in carbon tetrachloride using the constant activity method has been performed (4).

This article reports an attempt to study the electron donor–acceptor molecular complexes of iodine with thiazole and some of its derivatives. This was undertaken to determine the spectral and thermodynamic characteristics of such complexes to give more information about such systems. Equilibrium constants and molar extinction coefficients of these complexes are computed at different temperatures. The study is extended to include the effect of solvents on such equilibria. The results are discussed in terms of the molecular structure of the compounds and the solute–solute and solute–solvent competing equilibria. The thiazoles investigated herein are thiazole, (**I**); 4-methylthiazole, (**II**); 2,4-dimethylthiazole, (**III**); and bezothiazole, (**IV**). Solvents used are *n*-heptane, cyclohexane, carbon tetrachloride, and benzene.

Experimental

Materials

The thiazoles used were all supplied by Aldrich Chemical Co. Solvents (B.D.H. or E. Merck) spectroquality were used without further purification and stored under nitrogen atmosphere over 4A Linde molecular sieves. Fisher certified iodine was resublimed under reduced pressure.

Solutions

Stock solutions of donor and iodine were prepared by dissolving a precisely measured amount in the appropriate volume of solvent and stored in the dark. Solutions for measurements were made by mixing appropriate amounts of stock donor, stock iodine, and pure solvent and kept from moisture as far as possible. The measurements were made after about 10 h of mixing. Each set contained eight to ten solutions with the same iodine concentration and varying amounts of donor. The range of concentration for the donors was 0.01 to 0.18 mol dm^{-3} and concentration of acceptor was held constant of 5.0×10^{-4} mol dm^{-3}.

Measurements

Electronic absorption spectrophotometric measurements were made on a UNICAM SP 8-100 Recording Spectrophotometer equipped with a thermostatted cell accessories. Stoppered silica cells of 1.0 cm path length were used. The temperature of solutions was controlled within ±0.1°C using a Haake Ultrathermostat.

The conductivity measurements were carried out on a YSI Conductivity bridge at 25°C.

Calculations

The calculations were performed only for solutions with absorbance changing by no more than 1% after 24 h. The computer program fitted the experimental data (the measured absorbance and concentrations) in the form of a straight line by the linear least-squares fit method (5), based on the equations (6) obtained on the rearrangment of the Bensi–Hildebrand (7) equation. The rearranged equations enable independent evaluation of the equilibrium constant, K, as well as the extinction coefficient, ϵ, of the molecular EDA complexes. These equations are:

$$[1] \quad \left(\frac{C_A^0 + C_D^0}{C_D^0}\right) d = C_A^0 \epsilon l - \frac{d}{K C_D^0}$$

$$[2] \quad (C_A^0 + C_D^0) = \epsilon l \frac{C_A^0 \cdot C_D^0}{d} - \frac{1}{K}$$

where C_A^0, C_D^0 are the initial concentration of the acceptor (iodine) and donor, respectively (in mol dm^{-3}), d is the absorbance at the wavelength of investigation, and l (the cell thickness) = 1.0 cm. The K and ϵ values were derived from the slope and the intercept of eq. [1] and from the intercept and the slope of eq. [2]. The data for every set of solutions containing a constant acceptor concentration and varying amounts of the donor were processed separately. The K and ϵ values obtained at three wavelengths (λ_{max}, $\lambda_{max} \pm 5$ nm of the perturbed iodine) for three sets were then averaged and the results are listed in Tables 1 and 2. All calculations were performed on an Apple IIe computer.

TABLE 1. Equilibrium characteristics of iodine–thiazoles charge transfer complexes in CCl_4 and pK values of thiazoles (23)*

Compound	λ (nm)	λ_{iso} (nm)	λ (nm)	K ($dm^3\ mol^{-1}$) a	K ($dm^3\ mol^{-1}$) b	ε ($dm^3\ mol^{-1}\ cm^{-1}$) a	ε ($dm^3\ mol^{-1}\ cm^{-1}$) b	K_s	pK
IV	410	477	405	9.16	9.16	4419.0	4420.3	10.35	1.20
			410	9.24	9.24	4407.1	4405.2		
			415	9.38	9.38	4384.0	4364.1		
			av.	9.26	9.26	4403.3	4396.5		
I	415	478	410	15.57	15.25	1313.0	1329.2	18.82	2.52
			415	16.60	16.20	1300.2	1299.1		
			420	17.45	16.93	1291.3	1305.2		
			av.	16.54	16.13	1301.5	1311.1		
II	418	477	413	22.00	21.22	1416.8	1447.2	26.66	3.07
			418	22.78	21.62	1410.6	1440.8		
			423	23.20	21.89	1384.8	1422.3		
			av.	22.53	21.29	1404.9	1436.8		
III	415	470	410	64.80	65.32	1474.1	1468.3	81.23	3.98
			415	65.10	65.22	1433.2	1442.0		
			420	65.30	65.97	1465.0	1462.2		
			av.	65.07	65.50	1457.4	1457.5		

*a and b refer to eqs. [1] and [2] used for calculations; data are at 298 K; standard deviations of K, ±1.3%; ε, ±2%.

TABLE 2. Equilibrium characteristics of iodine–4-methylthiazole complexes in different solvents at 293 K*

Solvent	λ (nm)	λ_{iso} (nm)	λ (nm)	K ($dm^3\ mol^{-1}$) a	K ($dm^3\ mol^{-1}$) b	ε ($dm^3\ mol^{-1}\ cm^{-1}$) a	ε ($dm^3\ mol^{-1}\ cm^{-1}$) b
n-Heptane	425	488	420	47.39	47.00	1181.0	1188.2
			425	47.90	47.50	1194.2	1190.1
			430	48.22	47.98	1178.3	1181.4
			av.	47.85	47.49	1184.5	1186.6
Cyclohexane	430	483	425	40.80	36.02	1324.2	1380.0
			430	40.44	35.55	1340.0	1399.5
			435	40.89	35.66	1323.3	1384.1
			av.	40.71	35.74	1329.2	1387.9
CCl_4	418	477	413	25.26	23.87	1416.0	1447.2
			418	26.07	24.50	1417.2	1448.0
			423	26.50	24.90	1403.3	1437.1
			av.	25.94	24.42	1412.2	1444.1
Benzene	408	462	403	22.77	21.90	1344.0	1364.3
			408	22.79	21.56	1331.2	1353.0
			413	22.50	22.04	1301.1	1334.1
			av.	22.69	21.83	1325.4	1350.5

*a and b refer to eqs. [1] and [2] used for calculations; standard deviations of K, ±1%; ε, ±1.2%.

Results and discussion

In the present system, iodine–thiazoles, the electronic absorption spectra are recorded in the wavelength range of 350–625 nm. A typical example is shown in Fig. 1 for thiazole, (**I**). The absorption spectra of iodine with other thiazoles are of similar nature except the position of the perturbed iodine band and the isosbestic point of the complex. It is found that in carbon tetrachloride the iodine visible absorption spectrum shows a broad band with λ_{max} of 512 nm. The thiazoles visible absorption spectra, in the same solvent, exhibit practically no absorption at the 350–625 nm range. On addition of thiazole compounds to the iodine solution, the iodine absorption band at 512 nm is shifted towards shorter wavelengths and a decrease in its absorbance is observed. Further increase in donor concentration leads to an increase in the intensity of the blue-shifted iodine band (about 410 nm) at the expense of the longer wavelength one. Moreover, a sharp isosbestic point is observed near 470 nm for all iodine–thiazoles studied. A similar behaviour is observed in the case of imidazoles–iodine systems (8, 9). These results are indicative of the formation of one species of complex, between iodine and each of the subject thiazoles, and the complex species is in equilibrium with free iodine and thiazole in solution.

This behaviour can be interpreted on the basis of the valance-

Can. J. Chem. Downloaded from www.nrcresearchpress.com by 80.58.250.72 on 09/07/12
For personal use only.

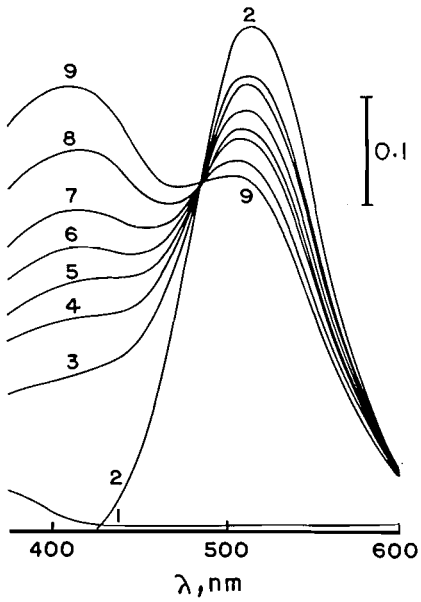

FIG. 1. Electronic absorption spectra of iodine (5.0×10^{-4} mol dm^{-3}) – thiazole – carbon tetrachloride system at different concentrations of donor: 2-C_D = 0, 3- = 0.014, 4- = 0.020, 5- = 0.027, 6- = 0.034, 7- = 0.041, 8- = 0.054, 9- = 0.068 mol dm^{-3} (1-thiazole concentration: 0.02 mol dm^{-3}).

bond theory for charge transfer interaction developed by Mulliken (10). The 512 nm band of iodine in carbon tetrachloride ($B \leftarrow X$) is mainly due to the $3\pi_{ou}^{+} \leftarrow {}^{1}\Sigma_{g}^{+}$ and $\sigma_u \leftarrow \pi_g$ transitions. The $B \leftarrow X$ transition shifts an electron from a π_g to a σ_u MO antibonding orbital. Thus, the blue-shift of the iodine band is attributed to the perturbation of iodine by repulsive interaction between the two partners of the electron donor–acceptor molecular complex (1). Herein, it seems that the complexing site of the donor is the nitrogen atom of thiazole molecule. The lone electron pair on the nitrogen atom is the most probable one, since their ionisation potential is relatively smaller than that of the sulfur atom (the ionisation potential of the lone electron pair for nitrogen is 10.40 eV and for sulfur is 12.70 eV for thiazole, (**I**) (11)). Consequently, the σ_u MO of iodine will be raised while the energy of the nonbonding orbital of the donor will be lowered. This leads to the observed blue shift of the iodine visible band (about 100 nm). This is verified from the examination of the total charge density on the nitrogen and the sulfur atoms of thiazole (−0.625 and +0.727, respectively (12)).

On plotting C_A^0/d against $1/C_D^0$, at the wavelength of the perturbed iodine band a fairly good straight line is obtained with a correlation coefficient of 0.998, in all the investigated thiazoles–iodine systems, indicating thereby the formation of 1:1 stoichiometric complexes in these systems in the concentration region of study. It is found that the thiazoles–iodine solutions show very low conductivity (below 1.0×10^{-6} ohm^{-1} cm^{-1}). These results and the observed constant isosbestic point reveal a typical equilibrium between uncharged species

[3] $D + I_2 = D—I_2$ "outer complex"

Equilibrium constants, K, and the molar extinction coefficients, ϵ, of the subject thiazoles – iodine EDA complexes in carbon tetrachloride are evaluated at three wavelengths in the range of the blue-shifted iodine band making use of eqs. [1] and [2] as described above. It is found that there is no systematic dependence of the equilibrium constants on the analytical wavelength (c.f. Tables 1 and 2). This gives a verification of the assumption that within the experimental errors, one iodine – thiazole EDA complex only is formed in the solution. The mean values of K and ϵ estimated for the three wavelengths are compiled in Table 1, along with the other spectral characteristics.

A linear least-squares fit is observed between log K and the magnitude of the blue shift, $\Delta\bar{\nu}$, except for 2,4-dimethylthiazole, with a correlation coefficient of 0.995 as with the other aza-aromatics (13) revealing that the extent of the blue shift of the iodine band is a rough measure of the strength of the complex formation between the subject thiazole and iodine.

In these systems, like the present ones the formation of I_3^- ion is inevitable, I_3^- has absorption maxima at 293 and 365 nm (14, 15). Although there is no indication of any absorption near 365 nm, slight changes of K and ϵ values with wavelength are observed as shown in Table 1. This is most likely due to I_3^- ion.

For the thiazole–iodine complexes the equilibrium constants of formation obtained (c.f. Table 1) are rather high compared with the K values for the π complexes. This supports the conclusion that these complexes are of the "n–σ^*" type.

A satisfactory linear least-squares fit is obtained between log K_{EDA} and pK_a for the iodine–thiazole system under investigation. The regression line of that fit is as follows:

$$[4] \quad \log K_{EDA} = (0.546 \pm 0.002) + (0.299 \pm 0.001)pK_a \qquad r = 0.976$$

This indicates that the complexation reaction is analogous with the protonation reaction and also that the same electrons (n electrons of the nitrogen atom) is responsible for the bond with the proton for the electron donor–acceptor interaction. This gives a further support for the conclusion that these complexes are of the "n–σ^*" type.

Introduction of a methyl group in the thiazole nucleus (compound **II**) increases the basicity of the nitrogen atom relative to the unsubstituted thiazole (compound **I**). This leads to an increase in the equilibrium constant of the EDA molecular complex. Further introduction of a methyl group (compound **III**) causes a further increase of the basicity and K value, since the effect of the electron-donating groups was noted to be additive. On the other hand, the replacement of a vinyl group in thiazole by a phenyl group (compound **IV**), decrease the basicity and hence the K value. This decrease in basicity is due to the lone pair of electrons on the nitrogen atom in benzothiazole, **IV**, being more extensively delocalized than in thiazole.

It is worth noting that the possibility of the fused phenyl group of benzothiazole acting as a π-donor to iodine is not considered since this action is much weaker than that for the nitrogen atom of the thiazole nucleus.

The equilibrium constants of the subject thiazole–iodine systems in carbon tetrachloride have been determined previously by the constant activity method (4), K_s and the values obtained are recorded in Table 1. On comparing the K_s values with that obtained herein, spectral K, it is evident that the K_s values are slightly higher than that of the spectral K values. Similar higher values of K_s have been reported by Childs *et al.* (16) for aromatic–iodine systems and by Mahmoud *et al.* (9) for imidazole-iodine systems. It has been pointed out by Christian *et al.* (17) that K_s actually includes both specific interactions (complex formation) and non-specific interactions between donor and iodine. If the correction term due to non-specific interac-

Can. J. Chem. Downloaded from www.nrcresearchpress.com by 80.58.250.72 on 09/07/12
For personal use only.

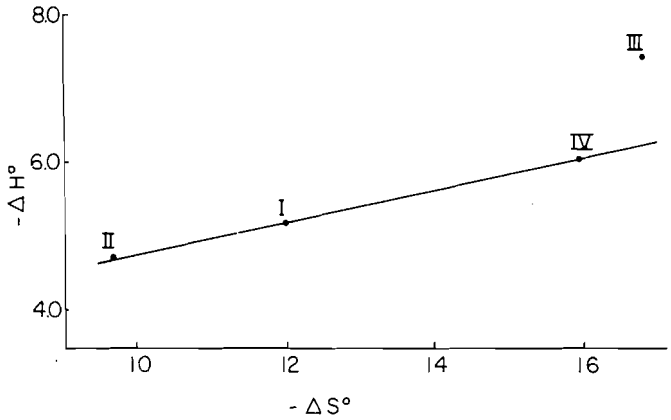

FIG. 2. The ΔH^0–ΔS^0 relationship for the thiazoles–I_2 system in CCl_4.

tions is near zero, then the K_s values may equal to the spectral K (18, 19). In the case of strong complexes like thiazole–iodine the contribution due to non-specific interaction is small.

In order to estimate the thermodynamic parameters, the enthalpy and entropy of formation, the equilibrium measurements are carried out at different temperatures. Equilibrium constants are determined and a relation between $R \ln K$ vs. $1/T$ are plotted. The enthalpies of formation, ΔH^0, and the entropies of formation, ΔS^0, are obtained from the slopes and the intercepts with abscissa, respectively, using the unweighted linear least-squares method. The values obtained are presented in Table 3. The Gibbs's free energies of formation, ΔG^0, are also calculated from eq. [5] and the values obtained are collected in Table 3.

$$[5] \quad \Delta G^0 = -RT \ln K$$

On plotting ΔH^0 versus ΔS^0, a linear relationship is obtained (Fig. 2). This behaviour is similar to the ΔS^0 dependence on ΔH^0 known for EDA complexes involving iodine. Therefore, it is evident that the most important factor affecting the magnitude of thermodynamic functions of complexation is common to ΔS^0 and ΔH^0. The increase in ΔH^0 values reflects an enhancement of the donor–acceptor interactions. This is substantiated by the examination of the values of b^2/a^2 values for such EDA complexes, where a and b are the coefficients of the dative and no-bond functions of the ground state function of the molecular electron donor–acceptor complexes (1). To get an estimate of the b^2/a^2 values, one may use the following equation (8)

$$[6] \quad b^2/a^2 = -\Delta H^0/h\bar{\nu}$$

where $\bar{\nu}$ is the wavenumber of the maximum absorption of the perturbed iodine band in cm^{-1}. The results show that the magnitude of the interaction of thiazoles as donors and iodine as acceptor is high.

Solvent effect

The electronic absorption spectra of 4-methylthiazole (**II**)–iodine solvent viz. *n*-heptane, cyclohexane, carbon tetrachloride, benzene are very similar except for the position of the λ_{max} and λ_{iso} of the complex. These spectrophotometric data are employed to calculate the equilibrium data for the 4-methylthiazole–iodine–solvent systems using the above method. The equilibrium characteristics are collected in Table 2.

The experimental results obtained for 4-methylthiazole–iodine complex in different solvents show that the values of the

TABLE 3. Thermodynamic properties of formation for iodine–thiazole complexes and b^2/a^2 values in CCl_4*

Compound	$-\Delta H^0$ (kcal mol^{-1})	$-\Delta S^0$ (cal mol^{-1})	$-\Delta G^0$ (kcal mol^{-1})	b^2/a^2
IV	6.000	15.96	1.323	0.086
I	5.168	11.99	1.655	0.075
II	4.715	9.70	1.872	0.069
III	7.405	16.83	2.475	0.107

*Standard deviations ΔH^0, ±2%; ΔS^0, ±5%; ΔG^0, ±3%. (ΔG^0 is calculated at 25°C.)

spectrophotometric properties are markedly affected by the variation of the solvent in which the measurements are carried out. The most striking feature of the data is that the effect of changing the medium on the equilibrium constants runs in the following sequence:

n-heptane > cyclohexane > carbon tetrachloride > benzene

The starting point for discussing the solvent effect on donor–acceptor equilibria should be the data referring to the gas phase reaction. Unfortunately, these data are not available. Therefore, the obtained data should be related to a medium which can be arbitrarily assumed to be a non-solvating one. As usual, a non-polar and non-reacting aliphatic hydrocarbon must be chosen (here *n*-heptane). It is, however, immediately seen that even within the aliphatic hydrocarbons the change in K values is as great as 13%. While the differences in equilibrium constants between subsequent members of this series of solvents are, within experimental error, parallel to the observed K variations for the isoquinoline– and lutidine–iodine systems (20, 21).

The lower value of the equilibrium constant, K, in cyclohexane relative to that in *n*-heptane could be due to the poorer solvation of the EDA complex by cyclohexane because of its rather rigid molecular structure.

It seems rather clear that the decrease in K values, as observed for carbon tetrachloride and benzene, must be ascribed to the solute–solute and solute–solvent competing equilibria. In carbon tetrachloride, which is a weak acceptor, the competing interactions would involve mainly the *n*-donor action of thiazoles towards iodine and the solvent. It would be expected that the specific interactions of thiazoles with carbon tetrachloride are rather weak; nevertheless, the excess of the solvent makes them important in decreasing amine activity. Furthermore, it has been reported that there is a specific interaction between carbon tetrachloride and iodine to form a 1:1 EDA complexes with equilibrium constant as great as 1.54 $dm^3\ mol^{-1}$ (22). Thus, the interactions between the complex and carbon tetrachloride should be of non-specific character and importance of dipole – induced dipole interaction in the solvation of the complex by CCl_4.

The solvation pattern in benzene is much more complicated. Even with the well-known classical iodine–benzene interactions, the quantitative interpretation of the measurements is far from being unequivocal. Moreover, one must take into account the interactions between the donor and benzene which, in contrast to the situation in CCl_4, do not seem to involve the n-donor of thiazoles. If this really is the case, the solvation of thiazole nucleus with benzene might be retained, at least partly, in the complex.

Can. J. Chem. Downloaded from www.nrcresearchpress.com by 80.58.250.72 on 09/07/12
For personal use only.

1. R. S. MULLIKEN and W. B. PERSON. Molecular complexes. John Wiley and Sons, New York. 1969.
2. R. FOSTER. Organic complexes. Academic Press, London. 1969.
3. M. TAMRES. *In* Spectroscopy and structure of molecular complexes. *Edited by* J. Yarwood. Plenum Press, London. 1973.
4. R. ABDEL-HAMID, A. A. EL-SAMAHY, M. A. ABDEL-RAHMAN, and H. EL-SAGHER. Spectrochim. Acta, In press.
5. A. C. NORRIS. Computational chemistry: an introduction to numerical methods. John Wiley and Sons, Chichester, New York. 1981. p. 261.
6. B. K. SEAL, H. SIL, and D. C. MUKHERJEE. Spectrochim. Acta, **38A**, 289 (1982).
7. H. A. BENSI and J. H. HILDEBRAND. J. Am. Chem. Soc. **71**, 2703 (1949).
8. R. A. MAHMOUD, A. A. EL-SAMAHY, and M. M. RABIA. Bull. Soc. Chim. Belg. **92**, 923 (1983).
9. R. A. MAHMOUD, A. A. EL-SAMAHY, and M. M. RABIA. J. Solution Chem. **13**, 517 (1984).
10. R. S. MULLIKEN. J. Am. Chem. Soc. **74**, 811 (1982).
11. J. V. METZGER, E-J. VINCENT, J. CHOUTEAU, and G. MILLE. *In* Thiazole and its derivatives. *Edited by* J. V. Metzger. Part One. John Wiley and Sons, New York. 1979. p. 46.
12. S. LALITHA, V. KANNAPPAN, and M. J. NAMAN. Indian J. Chem. **20A**, 714 (1981).
13. V. G. KRISHNA and M. CHOWDHURY. J. Phys. Chem. **67**, 1067 (1963).
14. A. D. AUTERLY and R. E. COUNICK. J. Am. Chem. Soc. **73**, 1842 (1951).
15. R. E. BUCKLES, J. P. YUK, and I. POPOV. J. Am. Chem. Soc. **74**, 4379 (1952).
16. J. D. CHILDS, S. D. CHRISTIAN, and J. GRUNDNES. J. Am. Chem. Soc. **94**, 5657 (1972).
17. J. D. CHILDS, S. D. CHRISTIAN, J. GRUNDNES, and S. R. ROACH. Acta Chem. Scand. **25**, 1679 (1969).
18. H. C. TSE and M. TAMRES. J. Phys. Chem. **81**, 1367 (1977); **81**, 1376 (1977).
19. S. D. CHRISTIAN and J. GRUNDNES. J. Am. Chem. Soc. **93**, 6363 (1971).
20. I. UTUSKA and H. KARACZEWSKA. J. Solution Chem. **8**, 105 (1979).
21. I. UTRUSKA and H. INEROWICZ. J. Solution Chem. **9**, 97 (1980).
22. G. B. SERGEJEW, W. W. SMIRNOV, and M. S. SYTILIN. Zh. fiz. Khim. **47**, 704 (1973).
23. J. V. METZGER. *In* Comprehensive heterocyclic chemistry. Vol. 6. *Edited by* K. T. Potts. Pergamon Press, Oxford, New York. 1984. p. 252.

Can. J. Chem. Downloaded from www.nrcresearchpress.com by 80.58.250.72 on 09/07/12
For personal use only.

Structures and stabilities of $C_2H_2F_3^+$ cations: an *ab initio* molecular orbital study

MICHELINE CHARPENTIER AND JACQUES FOSSEY
CERCOA-CNRS, 2 rue H. Dunant, 94320 Thiais, France
THOMAS T. TIDWELL
Department of Chemistry, University of Toronto, Toronto, Ont., Canada M5S 1A1
AND
SAUL WOLFE
Department of Chemistry, Queen's University, Kingston, Ont., Canada K7L 3N6

Received December 13, 1985[1]

MICHELINE CHARPENTIER, JACQUES FOSSEY, THOMAS T. TIDWELL, and SAUL WOLFE. Can. J. Chem. **65**, 473 (1987).

Eleven stationary points on the singlet $C_2H_2F_3^+$ potential energy surface have been calculated using the 3-21G basis set, and characterized as minima (four structures) or first-order saddle points (seven structures) by vibrational analysis. To check the reliability of this basis set, three of the structures have also been optimized at the 6-31G* level; although the geometries change somewhat, the relative energies and nature (maxima, minima) of the structures remain the same. For $CF_3CH_2^+$ the minimum energy structure has one C—F bond coplanar with the vacant *p*-atomic orbital at the cationic centre. The structure is 16.4 kcal/mol less stable than the lowest energy conformation of $FCH_2CF_2^+$, and the barrier for the 1,2 fluorine migration which connects the two structures is low. The cation F_2CHCHF^+ has a conformation that is a minimum on the potential energy surface that is 16.9 kcal/mol higher in energy than $FCH_2CF_2^+$; the two structures are separated by a barrier for 1,2 hydrogen migration of 23.5 kcal/mol. The electronic effects in the various structures have been studied using a quantitative PMO analysis of the interactions between the two carbon fragments of the ions. For $CF_3CH_2^+$ the net effect of the fluorine is highly destabilizing; the principal stabilizing interactions between CF_3^+ and CH_2 consist of π donation from CF_3^+ to CH_2 and homoconjugation of a fluorine lone pair with the cationic centre. No net stabilization attributable to fluorine bridging could be found.

MICHELINE CHARPENTIER, JACQUES FOSSEY, THOMAS T. TIDWELL et SAUL WOLFE. Can. J. Chem. **65**, 473 (1987).

Utilisant un ensemble 3-21G, on a calculé la surface d'énergie potentielle de onze points stationaires du singulet $C_2H_2F_3^+$ et, à l'aide d'une analyse vibrationnelle, on a caractérisé quatre structures comme minima et sept structures comme des maxima du premier ordre. Afin de vérifier la fiabilité de cet ensemble, on a aussi optimisé trois structures au niveau 6-31G*; même si les géométries changent un peu, les énergies relatives et la nature (maxima ou minima) des structures demeurent les mêmes. Pour l'ion $CF_3CH_2^+$, la structure présentant un minimum d'énergie possède une liaison C—F qui est coplanaire avec l'orbitale atomique *p* vacante du centre cationique. La structure est 16,4 kcal/mol moins stable que la conformation d'énergie minimale de l'ion $FCH_3CF_2^+$ et la barrière à la migration 1,2 du fluor qui relie les deux structures est faible. Le cation F_2CHCHF^+ possède une conformation qui est un minimum sur la surface d'énergie potentielle et qui est 16,9 kcal/mol plus riche en énergie que celle du $FCH_2CF_2^+$; les deux structures sont séparées par une barrière de 23,5 kcal/mol pour la migration 1,2 de l'hydrogène. On a étudié les effets électroniques sur les diverses structures en faisant appel à une analyse quantitative PMO des interactions entre les deux sections carbonées des ions. Pour le $CF_3CH_2^+$ l'effet de fluor est fort déstabilisant; les interactions stabilisantes principales entre le CF_3^+ et le CH_2 sont une donation π du CF_3^+ au CH_2 et une homoconjugaison de la paire libre du fluor avec le centre cationique. On n'a pas pu mettre en évidence de stabilisation nette attribuable à un pontage du fluor.

[Traduit par la revue]

Despite the strong σ-electron withdrawing effect of fluorine, CF_3^+ is *stabilized* relative to CH_3^+: the reaction $CH_3^+ + CHF_3 \rightarrow CF_3^+ + CH_4$ is exothermic by 13.2 kcal/mol (1). The infrared spectrum of matrix isolated CF_3^+ exhibits a high ν_3 fundamental and shows that the stabilization of this cation is associated with n_π–p_π bonding between fluorine lone pairs and the carbocationic centre (2).

The powerful *destabilizing* (3) effect of a CF_3 group upon an *adjacent* (4, 5) or nearby carbocationic centre (4*i*, 6) has been amply demonstrated experimentally by kinetic (4, 6), and spectroscopic (5) studies, and has also been applied to organic synthesis (7). Even in the gas phase the reaction $CF_3CH_2^+ + CH_4 \rightarrow CF_3CH_3 + CH_3^+$ is exothermic by 13 kcal/mol (3*a*).

The interaction of a CF_3 group with an adjacent carbocationic center has also been studied theoretically (8), but the conclusions of such calculations seem superficially to disagree with those based on experimental studies. For example, in solution the CF_3 group is found experimentally to be uniformly deactivating relative to hydrogen in the generation of an adjacent carbocation center, usually by very large factors (10^5 to 10^7) (4). A second electron-withdrawing substituent has a greatly diminished effect: $k(H)/k(CF_3) = 54$ for formation of the cations $PhCHCF_3^+$ and $PhC(CF_3)_2^+$ (9), respectively. There is no evidence for fluorine migration, and despite much effort (10), there is no definitive example of the fluorine bridging depicted in reaction [1] in solution.

[1] 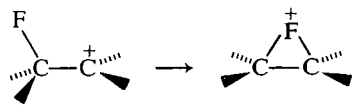

1 2

However, in the gas phase, on the basis of the isotope distribution in the fragment ions using ^2H or ^{13}C labeled precursors, a bridged ion $C_2H_4F^+$ appears to be formed (11) in the process shown in reaction [2].

[2] $p\text{-}CH_3C_6H_4OCH_2CH_2F \xrightarrow[-p\text{-}CH_3H_6H_4O]{-e^-}$ 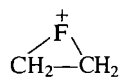

The theoretical studies suggest that there is both n-electron and π-electron donation by fluorine to an adjacent carbocation.

[1]Revision received September 15, 1986.

Can. J. Chem. Downloaded from www.nrcresearchpress.com by 80.58.250.72 on 09/07/12
For personal use only.

TABLE 1. Geometrical parameters and energies of cations $CF_3CH_2^+$ [a]

Bond	Distance (Å) for cation in 3a	3b	3c
C_1—H_2	1.0758(1.0804)	1.0791(1.0809)	1.0735(1.0750)
C_1—H_3	1.0758(1.0804)	1.0777(1.0803)	1.0735(1.0750)
C_1—C_4	1.4828(1.5285)	1.5337(1.5377)	1.4601(1.4521)
C_4—F_5	1.3978(1.3112)	1.3214(1.2915)	1.4552(1.4544)
C_4—F_6	1.3088(1.2899)	1.3308(1.2985)	1.3006(1.2636)
C_4—F_7	1.3088(1.2899)	1.3313(1.2985)	1.3006(1.2636)
Bonds	**Angle (deg) for cation in 3a**	**3b**	**3c**
C_4—C_1—H_2	118.54(119.67)	121.10(121.55)	118.71(119.24)
C_4—C_1—H_3	118.54(119.67)	117.58(118.22)	118.71(119.24)
F_5—C_4—C_1	83.29(99.16)	110.84(110.66)	74.29(69.85)
F_6—C_4—C_1	117.05(111.27)	105.59(105.55)	119.73(120.69)
F_7—C_4—C_1	117.05(111.27)	105.35(105.55)	119.73(120.69)
Bonds	**Dihedral angle (deg) for cation in 3a**	**3b**	**3c**
F_6—C_4—C_1—F_5	110.40(117.50)	120.83(120.54)	104.97(102.03)
F_7—C_4—C_1—F_5	−110.38(−117.57)	−120.66(−120.54)	−104.95(−102.03)
H_2—C_1—C_4—F_5	85.00(87.00)	−0.08(0.0)	88.04(89.97)
H_3—C_1—C_4—F_5	−85.00(−87.00)	179.99(180.0)	−88.04(−89.97)
Parameter	**Value for cation in 3a**	**3b**	**3c**
3-21G//3-21G			
E(RHF) in au	−372.772112	−372.770340	−372.772025
E(rel) in kcal/mol	0	1.11	0.05
6-31G*//3-21G			
E(RHF) in au	−374.817979	−374.820237	−374.815783
E(rel) in kcal/mol	1.53	0	2.79
6-31G*//6-31G*			
E(RHF) in au	−374.82428	−374.82364	−374.81915
E(rel) in kcal/mol	0	0.40	3.22

[a]Geometries in parentheses refer to 6-31G*//6-31G* calculations, others are 3-21G//3-21G.

In a calculation on $CF_3CH_2^+$ (**3**), which employed STO-3G calculations to optimize the geometries, and a single point 4-31G calculation to determine the energy, conformation **3***a* ($\theta = 101°$; $\phi = 4°$) was preferred (8*a*).

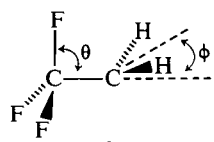

3*a*

It was argued (8*a*) that this "cation is distorted in exactly the same fashion as the ethyl cation", shows "abnormally low destabilization", and there is "no hyperconjugative stabilization by the trifluoromethyl group". Nevertheless, **3***a* shows some kind of attractive interaction between one of the fluorines and the methylene hydrogens. The origin of this effect has not been discussed.

In another study it was concluded that CF_3 could become a π-donor "in systems with relatively extreme π-electron deficiency" (8*c*).

Theoretical studies of the $C_2H_4F^+$ cation are extensive (12), and are relevant to the problem of $CF_3CH_2^+$. The best calculations (12*b*) find the bridged structure **2** to be more stable by 7.1 kcal/mol. Bridging of $C_2H_4F^+$ is also predicted by MINDO/3 (12*c*), but to an "exaggerated" (12*a*) extent.

The structures and energies of the isomeric ions $CH_3CF_2^+$, CH_2FCHF^+, and $CHF_2CH_2^+$ have been calculated recently, and used to facilitate the interpretation of the experimental photoionization of CH_3CHF_2 (12*d*); bridged structures were explicitly excluded from this latter study.

The theoretical calculations and gas phase experimental studies suggest that stabilization of an adjacent carbocation center by fluorine bridging or π-donation can be significant. This contrasts to the experimental studies in solution.

Can. J. Chem. Downloaded from www.nrcresearchpress.com by 80.58.250.72 on 09/07/12
For personal use only.

Can. J. Chem. Downloaded from www.nrcresearchpress.com by 80.58.250.72 on 09/07/12
For personal use only.

The purpose of the present work is to examine, in a more comprehensive manner, the cation **3**, and its putative rearrangement products $CH_2FCF_2^+$ (**4**) and CHF_2CHF^+ (**5**). We intend eventually to extend the study to more highly fluorinated systems. Such studies will provide a theoretical framework for ongoing experimental examinations of large polyfluorinated systems.

Method

Ab-initio molecular orbital calculations were carried out with the GAUSSIAN 80 (13) and MONSTERGAUSS (14) programs. Stationary points in the singlet $C_2H_2F_3^+$ potential energy surface were located at the Hartree–Fock (HF) level by gradient optimization techniques (15) using the 3-21G basis set (16). One point calculations were then performed on these geometries at the 6-31G* level (17) (6-31G*//3-21G). The 3-21G geometries, total energies and relative energies are displayed in Tables 1 to 3. Structures are classified as equilibrium structures or as transition structures on the basis of a vibrational analysis carried out at the HF/3-21G level.

Quantitative PMO analyses (18) were performed at the STO-3G level on standard geometries, to provide insight into the origins of the conformational preferences and the nature of the molecular distortions. In this procedure the orbitals of a molecular system A–B, which contains the functional groups A and B, are rewritten as a linear combination of the orbitals of A and B. This allows the stabilizing and destabilizing orbital interactions between A and B to be calculated explicitly. As has been discussed extensively (18), the molecular geometry relaxes so as to minimize destabilization and maximize stabilization. The standard geometries employed for the PMO analysis were, in all cases, C—C = 1.53 Å, C—H = 1.08 Å, C(+)—F = 1.26 Å, C—F = 1.35 Å, tetrahedral angle = 109.4712, trigonal angle 120°. Table 4 summarizes the total energy differences computed in this manner.

Discussion

As shown in reaction [3], **3** and **4** are related by a 1,2 F-migration; **4** and **5** are related by a 1,2 H-migration. Two transition structures connect these cations, one for the process 3 ⇄ 4 and the other for the process 4 ⇄ 5. All of these structures have been calculated.

[3] $CF_3CH_2^+ \rightarrow {}^+CF_2CH_2F \rightarrow CF_2HCHF^+$
3 **4** **5**

$CF_3CH_2^+$

For the ion **3**, only the bisected conformation **3***a*, which has one C—F bond coplanar with the *p*-atomic orbital at the carbocation center, is an energy minimum. A 90° rotation about the C—C bond affords a transition structure **3***b*, in which one C—F bond is perpendicular to the *p*-atomic orbital at the carbocation center. Both these structures have been optimized fully without constraints, and are true stationary points on the 3-21G hypersurface.

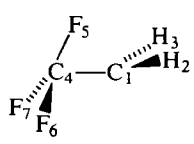

3*a*

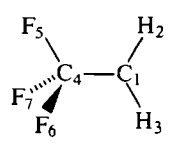

3*b*

Structure **3***a* is 1.11 kcal/mol more stable than **3***b* at the 3-21G//3-21G level. However, at the 6-31G*//3-21G level, **3***a* is found to be 1.53 kcal/mol less stable than **3***b*. Such a reversal of stabilities normally reflects a difference in geometries at the two basis set levels. Since fluorine is known to be difficult to describe adequately with a small Gaussian basis set (12*b*), it was considered desirable to extend the study of $CF_3CH_2^+$ to full optimization of the structures at the 6-31G* level (6.31G*//6-31G*). These results are included in Table 1. The C_1—C_4—F_5 angle of **3***a* increases from 83.3 to 99.2°, but **3***a* remains a minimum, more stable than **3***b* by only 0.40 kcal/mol, and **3***b* remains a first-order saddle point.

The quantitative PMO analysis of $CF_3CH_2^+$ focuses on interactions between CF_3 and CH_2 in the standard geometries **3***a*$_s$ and **3***b*$_s$. The fragment orbitals (FO's) of CF_3 are treated as linear combinations of C—F bond orbitals (i.e., σC—F, σ*C—F, and three n doublets on each F atom). In C_{3v} symmetry these linear combinations lead to three kinds of orbitals, which are shown schematically in Fig. 1.

The FO's of CH_2^+ are σCH_2, πCH_2, *p*CH_2, π*CH_2, and σ*CH_2. In Table 5, the total PMO energetic effect and the sum over all CF_3 FO's of the energetic effect associated with each CH_2 FO are given.

TABLE 2. Geometrical parameters and energies of cations $FCH_2CF_2^+$ (3-21G)

	Distance (Å) for cation in	
Bond	**4***a*	**4***d*
C_1—F_2	1.2614	1.2656
C_1—F_3	1.2614	1.2584
C_1—C_4	1.5195	1.4846
C_4—F_5	1.3961	1.3724
C_4—H_6	1.0747	1.0869
C_4—H_7	1.0747	1.0869
	Angle (deg) for cation in	
Bonds	**4***a*	**4***d*
F_2—C_1—C_4	122.56	120.89
F_3—C_1—C_4	122.56	123.66
F_5—C_4—C_1	100.27	106.72
H_6—C_4—C_1	109.81	108.40
H_7—C_4—C_1	109.81	108.40
	Dihedral angle (deg) for cation in	
Bonds	**4***a*	**4***d*
F_2—C_1—C_4—F_5	87.84	180.00
F_3—C_1—C_4—F_5	−87.84	0.00
H_6—C_4—C_1—F_5	117.31	121.21
H_7—C_4—C_1—F_5	−117.31	−121.21
	Value for cation in	
Parameter	**4***a*	**4***d*
3-21G//3-21G		
E(RHF) in au	−372.788733	−372.798231
E(rel) in kcal/mol	5.96	0
6-31G*//3-21G		
E(RHF) in au	−374.844982	−374.853998
E(rel) in kcal/mol	5.66	0

Can. J. Chem. Downloaded from www.nrcresearchpress.com by 80.58.250.72 on 09/07/12
For personal use only.

TABLE 3. Geometrical parameters and energies of cations F_2CHCHF^+ (3-21G)

	Distance (Å) for cation in					
Bond	**5***a*	**5***b*	**5***c*	**5***d*	**5***g*	**5***h*
C_1—H_2	1.0768	1.0769	1.0767	1.0754	1.0759	1.0721
C_1—F_3	1.2626	1.2635	1.2631	1.2615	1.2630	1.3052
C_1—C_4	1.5339	1.5263	1.5281	1.5219	1.5431	1.3791
C_4—H_5	1.0694	1.0701	1.0746	1.0786	1.0682	1.3236
C_4—F_6	1.3527	1.3431	1.3467	1.3525	1.3519	1.3087
C_4—F_7	1.3527	1.3661	1.3579	1.3496	1.3519	1.3034
	Angles (deg) for cation in					
Bonds	**5***a*	**5***b*	**5***c*	**5***d*	**5***g*	**5***h*
H_2—C_1—C_4	121.12	122.39	123.56	122.72	125.90	120.28
F_3—C_1—C_4	121.07	119.68	118.81	119.57	117.56	120.25
H_5—C_4—C_1	113.49	113.85	111.36	109.47	111.68	64.80
F_6—C_4—C_1	102.72	106.08	105.22	104.63	104.12	120.10
F_7—C_4—C_1	102.72	99.03	104.04	107.14	104.12	122.73
Bonds	**5***a*	**5***b*	**5***c*	**5***d*	**5***g*	**5***h*
F_6—C_4—C_1—H_5	122.26	125.36	121.87	119.37	121.44	95.34
F_7—C_4—C_1—H_5	−122.26	−119.25	−120.31	−120.96	−121.44	−99.82
F_3—C_1—C_4—H_5	0.00	−30.12	−57.67	−89.25	180.00	−93.29
H_2—C_1—C_4—H_5	180.00	153.02	121.38	89.25	0.00	86.06
Parameter	**5***a*	**5***b*	**5***c*	**5***d*	**5***g*	**5***h*
3-21G//3-21G						
E(RHF) in au	−372.770668	−372.770996	−372.770777	−372.771232	−372.765234	−372.733771
E(rel) in kcal/mol	0.35	0.15	0.29	0	3.76	23.51
6-31G*//3-21G						
E(RHF) in au	−374.826519	−374.826234	−374.825929	−374.826264	−374.822648	−374.797274
E(rel) in kcal/mol	0	0.18	0.37	0.16	2.43	18.35

TABLE 4. Total energy differences computed at the STO-3G level for various conformations of fluorine-containing carbocations in standard geometries as part of the quantitative PMO analyses

	Conformation		
Cation	**I**	**II**	$\Delta E = E(\mathbf{I}) - E(\mathbf{II})$
$CF_3CH_2^+$	$\mathbf{3}a_s$	$\mathbf{3}b_s$	0.00
	$\mathbf{3}a_{st}$	$\mathbf{3}b_{st}$	−6.82
$FCH_2CF_2^+$	$\mathbf{4}a_s$	$\mathbf{4}d_s$	3.04
F_2CHCHF^+	$\mathbf{5}a_s$	$\mathbf{5}g_s$	−1.04
	$\mathbf{5}d_s$	$\mathbf{5}a_s$	−1.60
$FCH_2CH_2^+$	$\mathbf{9}a_s$	$\mathbf{9}b_s$	8.40
$F_2CHCH_2^+$	$\mathbf{10}a_s$	$\mathbf{10}b_s$	−3.85

The same PMO effect is found for $\mathbf{3}a_s$ and $\mathbf{3}b_s$. This includes the destabilizing interaction associated with the πCH_2 FO's, and the stabilizing interaction associated with the *p* orbital at the carbocation center. The individual stabilizing interactions associated with the *p*-CH_2 FO's are examined in more detail in Table 6. Stabilization is seen to arise mainly from two specific interactions of the *p*-CH_2 FO's, viz., (*i*) interaction with the πCF_3 FO's of rotamer $\mathbf{3}a_s$, or with the $\pi' CF_3$ FO's of rotamer $\mathbf{3}b_s$, corresponding to the π-donor effect of the CF_3 fragment; (*ii*) interaction with the πnF_3 FO's of the rotamer $\mathbf{3}a_s$, or with the $\pi' nF_3$ FO's of rotamer $\mathbf{3}b_s$, corresponding to the homoconjugative interaction between the fluorine lone pairs and the cationic center. The π-donor and homoconjugative effects are almost the same (−5.22 and −5.32 kcal/mol, respectively).

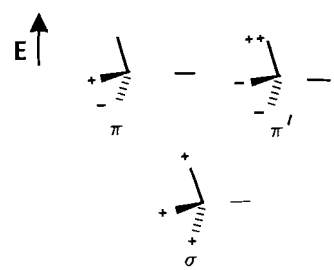

FIG. 1. The σ- and π-type orbitals of a CF_3 fragment.

The decrease in the C_1—C_4—F_5 angle seen in **3***a* parallels the observation made previously at the STO-3G level (6*a*), as does the slight bending of C_1—H_2 and C_1—H_3 towards F_5. These effects are more pronounced at the 3-21G level (83.3°) than at 6-31G* (99.2°) or STO-3G (101°).

The PMO analysis provides insights into the origins of these deformations. Structures $\mathbf{3}a_{st}$ and $\mathbf{3}b_{st}$ refer to standard geometries in which the CF_3 moiety has been tilted clockwise by 10° in the symmetry plane of the molecule (Fig. 2). This deforma-

TABLE 5. PMO analyses of various conformations of $CF_3CH_2^+$ [a]

Conformation	σ_{CH_2}	π_{CH_2}	p_{CH_2}	$\sigma^*_{CH_2}$	$\pi^*_{CH_2}$	ΔE^{PMO}_{TOTAL} [a]
$3a_s$	1.24	11.70	−10.78	−0.32	−1.16	0.68
$3b_s$	1.20	11.72	−10.78	−0.32	−1.16	0.66
$3a_{st}$	1.12	10.76	−16.50	−0.30	−0.98	−5.90
$3b_{st}$	1.20	14.60	−8.70	−0.42	−1.58	5.10
$3a$	1.74	13.84	−51.58	−0.48	−1.94	−37.52

[a] Energies are in kcal/mol.

TABLE 6. PMO analysis showing the stabilizing orbital interaction energies of the pCH$_2$ FO with donor FO's of the CF_3 fragment in $CF_3CH_2^+$ [a]

	Conformation				
Donor orbital	$3a_s$	$3b_s$	$3a_{st}$	$3b_{st}$	$3a$
$\pi' nF_3$	0	−5.56	0	−2.88	0
πnF_3	−5.56	0	−10.72	0	−40.52
σnF_3	0	0	−1.42	0	−8.96
$\pi' CF_3$	0	−5.22	0	−5.82	0
πCF_3	−5.22	0	−4.30	0	−1.98
σCF_3	0	0	−0.06	0	−0.12
$\Delta E^{PMO}_{pCH_2}$	−10.78	−10.78	−16.50	−8.70	−51.58

[a] Energies are in kcal/mol.

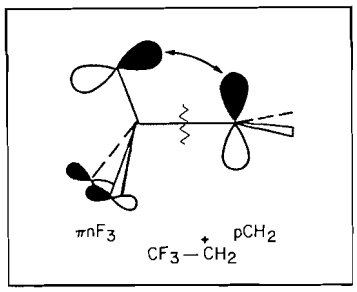

FIG. 2. An orbital interaction illustrating homoconjugation between πnF_3 and pCH$_2$ in $CF_3CH_2^+$.

tion is net stabilizing for $3a_s$ but net destabilizing for $3b_s$. The reason for this is seen in Fig. 2: $3a_{st}$ is stabilized by the interaction between the p orbital at the carbocation center and the π-combination of lone pairs on the fluorine atoms (compare interaction πnF_3–pCH$_2$ in $3a_s$ and $3a_{st}$ in Table 6).

According to the PMO formalism, the magnitude of the stabilization associated with the interaction between an unoccupied orbital (e.g., the pCH$_2$ FO) and a doubly occupied orbital (e.g., the πnF_3 FO) (see Fig. 3) is given by eq. [4], in which i = HOMO, j = LUMO, S_{ij} = overlap integral, and H_{ij} = matrix element. Equation [4] states that ΔE(PMO) is the result of three effects: (*i*) S_{ij} (overlap control); (*ii*) H_{ij} (matrix element control); (*iii*) $\Delta\epsilon = \epsilon_i = \epsilon_j$ (energy gap control).

$$[4] \quad \Delta E^{ij}_{PMO} = \frac{2S^2_{ij}(\epsilon_i - H_{ij}/S_{ij})^2}{\epsilon_i - \epsilon_j}$$

The distortion $3a_s \rightarrow 3a_{st}$ leads to net stabilization because of the overlap effect S_{ij} denoted by the double-headed arrow of Fig. 2. The corresponding deformation is unfavorable in $3b_s \rightarrow 3b_{st}$ because of the interaction between the occupied CH_2 and CF_3 fragments (cf. the interactions associated with πCH_2 in $3b_s$ and $3b_{st}$, Table 5) and the decreased stabilization associated with the pCH$_2$ FO. This analysis indicates that the deformation of the C_1—C_4—F_5 angle in $3a$ originates from homoconjugation with the lone pair on F_5.

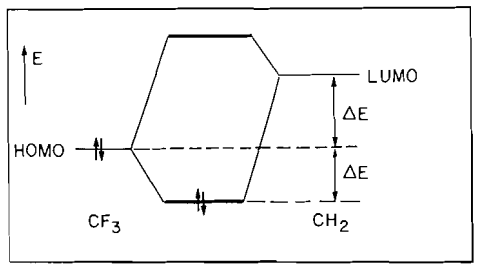

FIG. 3. The orbital interaction diagram appropriate to eq. [4].

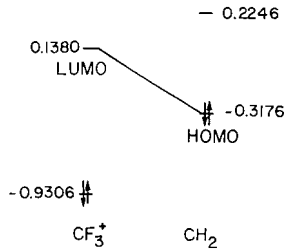

FIG. 4. Orbital interaction diagram for the reaction of CF_3^+ with CH_2 (STO-3G calculations).

A quite different interpretation of the geometry of $3a$ can be suggested, if this structure is regarded as a complex between CF_3^+ and the carbene CH_2. As seen in the Newman projection **6**, the methylene group lies above the F_5—C_4 perpendicular,

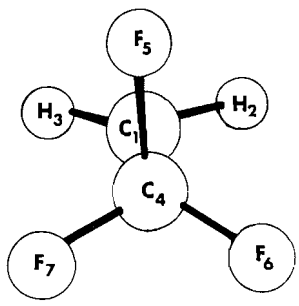

6

and is tilted towards F_5. This implies that the most favorable geometry for a cation–carbene interaction is **7**. The interaction would lead to charge transfer from the HOMO of the carbene to the LUMO of the cation or, alternatively, from the HOMO of the cation to the LUMO of the carbene. In either case, charge transfer into antibonding C—F regions or charge transfer from bonding C—F regions will lead to lengthening of C—F bonds.

These ideas were explored by computations on CF_3^+ and CH_2 at the 3-21G and STO-3G levels. At the 3-21G level the

Can. J. Chem. Downloaded from www.nrcresearchpress.com by 80.58.250.72 on 09/07/12
For personal use only.

Can. J. Chem. Downloaded from www.nrcresearchpress.com by 80.58.250.72 on 09/07/12
For personal use only.

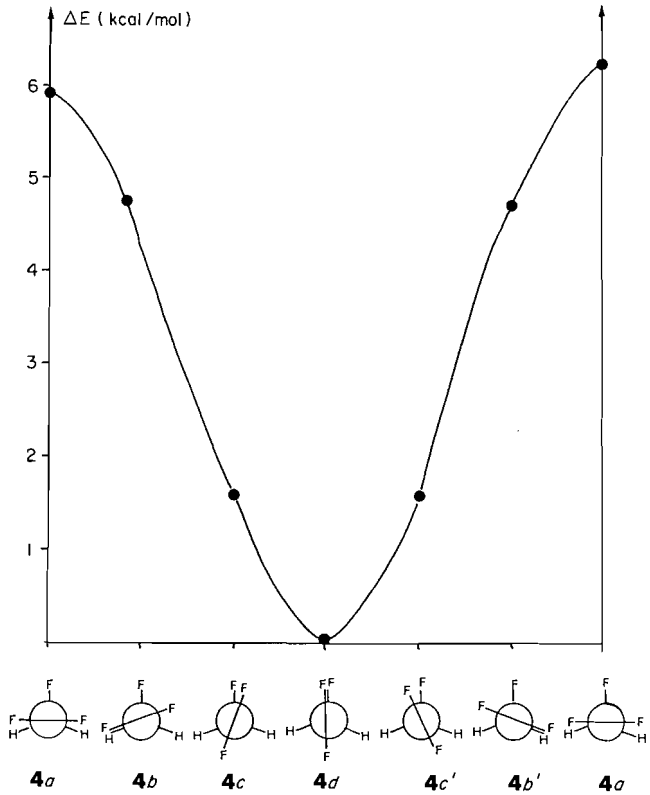

FIG. 5. Rotation about the C—C bond in $FCH_2CF_2^+$ (3-21G calculations).

C—F bond length in CF_3^+ is 1.2507 Å. Comparison of this value with the C—F bond lengths in **3***a* reveals that the putative interaction of CF_3^+ with CH_2 lengthens all three C—F bonds, and the effect is greatest on C—F_5. The STO-3G interaction diagram is shown in Fig. 4, from which it is clear that the dominant interaction would comprise charge transfer from the HOMO of CH_2 to an unoccupied orbital of CF_3^+. This interaction is depicted in **8**; the acceptor orbital is antibonding between C and F, and the out-of-phase secondary overlap (depicted by double-headed arrows) would cause the CH_2 to move towards F_5, as in structure **7**. In summary, the CF_3 group in $CF_3CH_2^+$ is strongly destabilizing, and the conformation **3***a* which maximizes the CF_3 interactions with CH_2 is only 0.40 kcal/mol more stable than **3***b* at the 6-31G*//6-31G level.

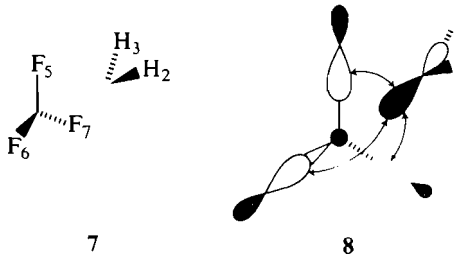

7

8

$FCH_2CF_2^+$

For the ion $FCH_2CF_2^+$ (**4**), four limiting conformations, **4***a*–**4***d*, were examined. To describe rotation about the C—C bond these were optimized in a subspace in which the C—C rotational angle was fixed (Fig. 5). Only **4***d* is an energy minimum, and **4***a* is an energy maximum. These stationary points were optimized fully without restriction with the 3-21G basis set, and their geometrical parameters and energies are given in Table 2. The barrier height is 5.96 kcal/mol at the 3-21G//3-21G level and 5.66 kcal/mol at the 6-31G*//3-21G level.

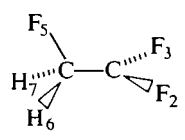

4a

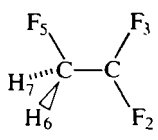

4d

In **4***a*, which has C_4—F_5 eclipsed with the vacant *p* orbital on C_1, the F_5—C_4—C_1 angle is small, as in **3***a* (**3***a*, 83.3°, **4***a*, 100.3°), but in this case no stabilization is associated with the decreased angle. That the relative stability of **4***d* is the result of hyperconjugation by H_6 and H_7 was demonstrated by a series of quantitative PMO analyses on **4**, $FCH_2CH_2^+$ (**9**) and $F_2CHCH_2^+$ (**10**). For **4** this analysis focuses on interactions between CH_2F and CF_2, and these are summarized in Table 7, for the standard structures $\mathbf{4}a_s$ and $\mathbf{4}d_s$. The FO's termed p_1CF_2, p_2CF_2, and p_3CF_2 are the result of a linear combination of the vacant *p* orbital on C_1 with the symmetry adapted *p* lone pair on the F atoms (Fig. 6).

The PMO analysis suggests that the difference in stability between $\mathbf{4}a_s$ and $\mathbf{4}d_s$ originates in the interactions associated with p_3CF_2, the lowest vacant CF_2 FO. To check this point, a PMO analysis was performed on $FCH_2CH_2^+$ (**9**) in conformations $\mathbf{9}a_s$ and $\mathbf{9}b_s$. This analysis is included in Table 8. Reference to Table 4 demonstrates that the rotational behaviour of **9** parallels that of **4**, since $\mathbf{9}b_s$ is more stable than $\mathbf{9}a_s$ (19), but the barrier is larger in **9**. According to the PMO analysis the larger barrier in **9** is associated with the interactions of the vacant pCH_2 FO.

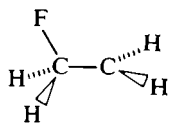

$\mathbf{9}a_s$

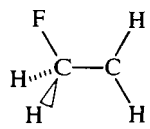

$\mathbf{9}b_s$

The vacant FO's p_3CF_2 and pCH_2 of **4** and **9**, respectively, interact with all occupied orbitals of the FCH_2 fragment. These interactions are given in Table 8, and the relevant FCH_2 FO's are shown in Fig. 7. The *s*, *p*, and σ FO's are symmetric, and the π FO's are antisymmetric with respect to the plane of the molecule. The conformational preferences in **4** and **9** result from favourable interactions between the p_3CF_2 FO of **4** and the pCH_2 of **9** with π_1FCH_2 and π_2FCH_2. The interaction with π_1FCH_2 corresponds to hyperconjugation with the two C—H bonds, while the interaction with π_2FCH_2 corresponds to homoconjugation with the symmetry-adapted lone pair on the F atom of FCH_2. These interactions are more favourable in rotamers $\mathbf{4}d_s$ and $\mathbf{9}b_s$ than the homoconjugation with the lone pair (*p*F) and the hyperconjugation with the C—F bond (σC—F) in rotamers $\mathbf{4}a_s$ and $\mathbf{9}a_s$. The effects are dominated by overlap between fragment FO's (S_{ij} in eq. [4]).

We may conclude that hyperconjugation with C—H bonds controls the conformational preferences of cations adjacent to FCH_2. In the case of the cation **10**, $F_2CHCH_2^+$, conformation $\mathbf{10}a_s$, in which C—H bond hyperconjugation is operative, is more stable than conformation $\mathbf{10}b_s$ (Table 4).

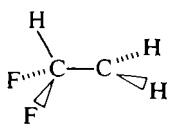

$\mathbf{10}a_s$

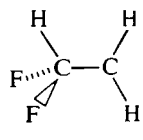

$\mathbf{10}b_s$

TABLE 7. PMO analyses of various conformations of $FCH_2CF_2^+$ and $FCH_2CH_2^+$ [a]

Structure	Fragment orbital [b]								
$FCH_2CF_2^+$	σCF_2	πCF_2	σ^*CF_2	π^*CF_2	p_1CF_2	p_2CF_2	p_3CF_2	nF_2	ΔE^{PMO}_{TOTAL}
4a_s	0.52	7.00	−0.18	−2.66	4.88	−0.02	−7.04	4.46	6.96
4d_s	0.48	5.04	−0.26	−1.92	7.00	−0.02	−11.78	3.64	2.18
$FCH_2CH_2^+$	σCH_2	πCH_2	σ^*CH_2	π^*CH_2	—	—	pCH_2	—	
9a_s	0.78	17.12	−0.10	−1.86	—	—	−12.26	—	3.68
9b_s	0.94	12.28	−0.18	−1.32	—	—	−22.26	—	−10.54

[a] Energies are in kcal/mol.
[b] All interactions associated with each FO are included.

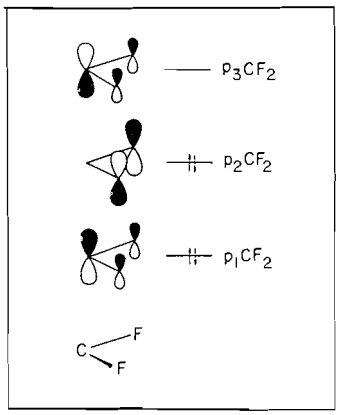

FIG. 6. Some of the CF_2 fragment orbitals.

TABLE 8. PMO analysis showing the stabilizing orbital interaction energies of the pCF_2 FO of **4** and the pCH_2 FO of **9** with the FO's of an adjacent FCH_2 fragment [a]

FO	Structure			
	4a_s	**4**d_s	**9**a_s	**9**b_s
sF	−0.04	0	−0.06	0
pF	−4.52	0	−7.18	0
$\sigma C—F$	−2.42	0	−4.92	0
σCH_2	−0.06	0	−0.10	0
π_1FCH_2	0	−6.44	0	−11.26
π_2FCH_2	0	−5.34	0	−11.00
$\Delta E^{PMO}_{pCX_2}$	−7.04	−11.78	−12.26	−22.25

[a] Energies are in kcal/mol.

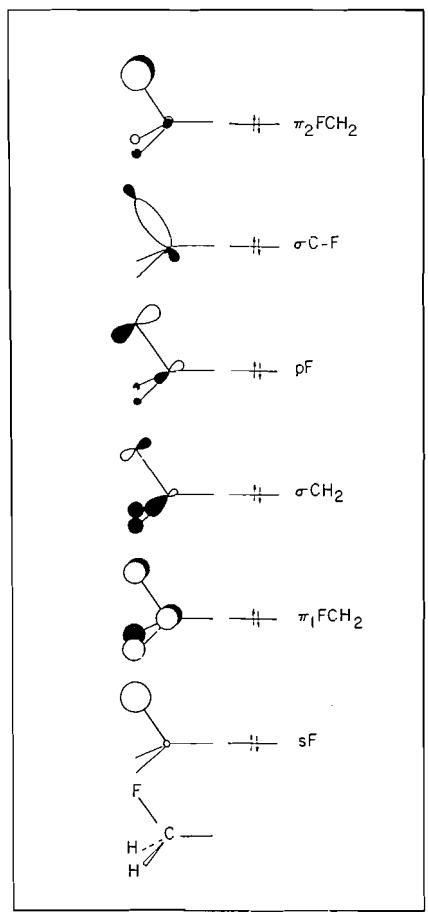

FIG. 7. The fragment orbitals of FCH_2 (see Table 8).

F_2CHCHF^+

For the ion F_2CHCHF^+ (**5**), the seven conformations **5***a*–**5***g* were optimized in a subspace in which the rotational angle about the C—C bond was fixed (Fig. 8).

Conformations **5***a*–**5***d* are close in energy, and **5***e*–**5***g* are progressively less stable.

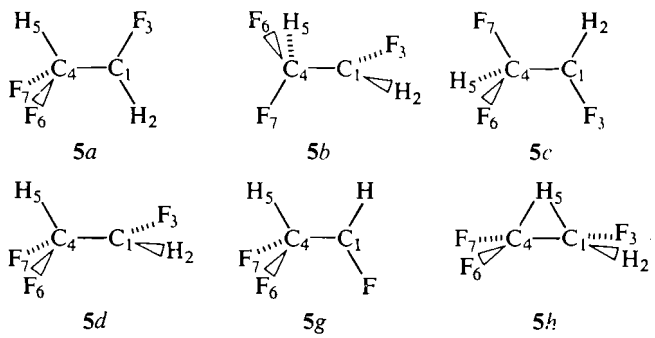

On the 3-21G//3-21G hypersurface, **5***b* and **5***d* are minima, and rotamers **5***a*, **5***e*, and **5***g* are rotational transition structures. Conformation **5***d* is the global minimum. The 6-31G*//3-21G energy differences are similar (Table 3).

As in **3***a* and **4***a*, conformations of **5** having a C—F bond eclipsed with the vacant *p* orbital exhibit a small $C_1—C_4—F$ angle (**5***b*, 99.1°; **5***f*, 98.8°). However, no stabilization is reflected in these structures in comparison to **5***d*, in which the C—H bond is eclipsed with the *p* orbital. This latter structure has a normal $C_1—C_4—H$ angle (109.5°).

Interconversion of 3–5

The chemical pathway for interconversion of the $C_2H_2F_3^+$ isomers **3**–**5** is shown in Fig. 9. The most stable ion, by a considerable margin, is **4**.

The transformation of **3***a* into **4***a* is a 1,2 F-migration. At the 3-21G//3-21G level, the transition structure for this pro-

Can. J. Chem. Downloaded from www.nrcresearchpress.com by 80.58.250.72 on 09/07/12
For personal use only.

Can. J. Chem. Downloaded from www.nrcresearchpress.com by 80.58.250.72 on 09/07/12
For personal use only.

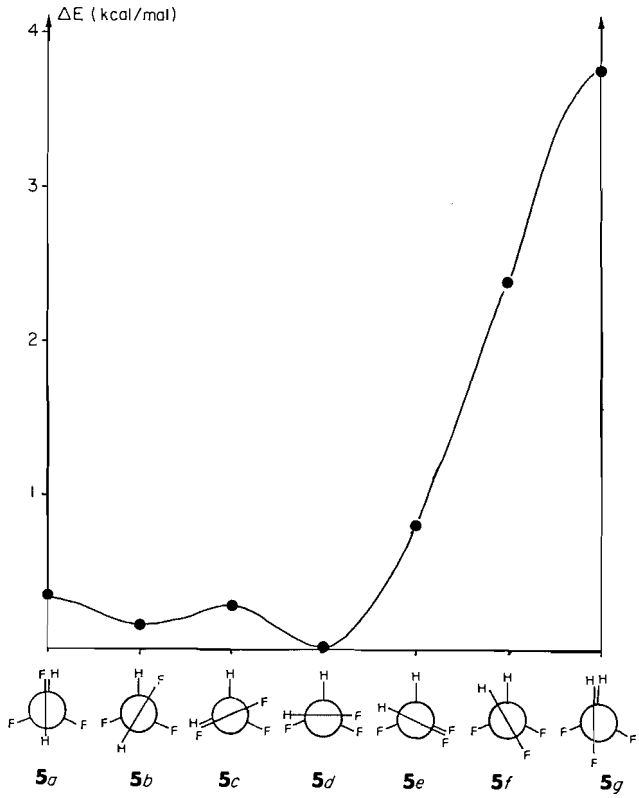

FIG. 8. Rotation about the C—C bond in F_2CHCHF^+.

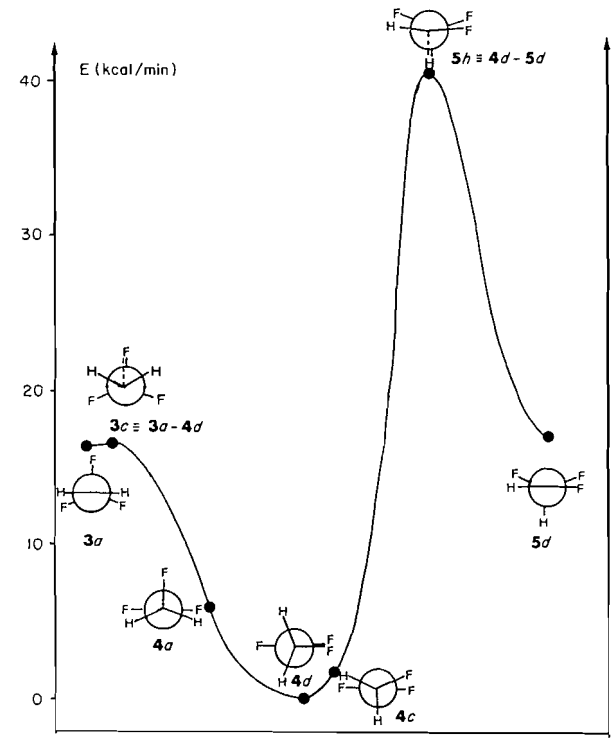

FIG. 9. Energy diagram for interconversion of $C_2H_2F_3^+$ isomers.

cess, **3***c*, is only 0.05 kcal/mol above **3***a* and the geometrical parameters of the two structures are very similar (Table 1). Moreover, **3***c* is more stable than the rotational transition state **3***b*. At the 6.31G*//3-21G level, the barrier for the rearrangement $CF_3CH_2^+ \rightarrow FCH_2CF_2^+$ is 2.79 kcal/mol. This finding is consistent with calculations on $C_2H_4F^+$, in which the bridged structure becomes relatively less stable with larger basis sets (20, 21), and with the absence of experimental evidence for fluorine migration in any well characterized system. With full optimization at 6-31G* (Table 1), **3***c* is 3.22 kcal/mol less stable than **3***a* and 2.82 kcal/mol less stable than **3***b*.

The ion **5***d* is transformed into the significantly more stable ion **4***c* by a 1,2 H-migration. At the 3-21G//3-21G level, the transition state for this process, **5***h*, is calculated to lie 23.51 kcal/mol above **5***d* (Table 3). At the 6-31G*//3-21G level, this barrier is slightly smaller (18.35 kcal/mol). The structure of **5***h* (C—C = 1.379 Å, versus C—C = 1.315 Å in ethylene at 3-21G//3-21G) resembles that of a weak $H^+\cdots CH_2{=}CHF$ complex, in contrast to **3***c* (C—C = 1.460 Å). Substitution of fluorine for hydrogen raises the barrier for 1,2 H-transfer: in $C_2H_5^+$ the bridged structure is 7.71 kcal/mol higher than the classical structure at the 3.21G//3-21G level, and is more stable than the classical structure at 6-31G**//6-31G* (20).

In conclusion the stability of $CH_2FCF_2^+$ (**4**) relative to $CF_3CH_2^+$ (**3**) and CHF_2CFH^+ (**5**) is evidently due to the stabilization associated with the CF_2^+ moiety (1, 2), and the presence of only one β-fluorine. There is strong net destabilization in **3**, but the similar energies of **3** and **5** provide evidence of some stabilizing interactions in **3**, since **5***d* benefits from both n_π–p_π donation to the cationic centre and hyperconjugative stabilization by the β-C—H bonds, but is no more stable than **3**. There is no strong conformational preference in **3**. The CF_3 group stabilizes **3** in two ways: by π-donation (hyperconjugation) and *n*-donation (homoconjugation).

The conformational preference in $FCH_2CF_2^+$ (**4**) is caused by hyperconjugation with the β-C—H bonds. The same effect explains the conformational preference in $FCH_2CH_2^+$. Hyperconjugation with a C—H bond leads to greater stabilization of a positive charge on carbon than hyperconjugation with a C—F bond combined with homoconjugation with a fluorine lone pair. In F_2CHCHF^+ the conformational preference is best explained by repulsion between the F atoms.

The absence of any reports of a solution phase fluorine migration despite the low barrier for **3***b* → **4***d* interconversion is remarkable. Even $CF_3CH_2N_2^+$ in FSO_3H gives only $CF_3CH_2O_3SF$ (22). Evidently in this system the incipient $CF_3CH_2^+$ species is so unstable that solvent capture is favoured over fluorine migration.

Acknowledgements

Final support by the Natural Sciences and Engineering Research Council of Canada (to T.T.T. and S.W.) and by a NATO collaborative research grant (to M.C. and T.T.T.) is gratefully acknowledged.

1. R. J. BLINT, T. B. MCMAHON, and J. L. BEAUCHAMP. J. Am. Chem. Soc. **96**, 1269 (1974).
2. F. T. PROCHASKA and L. ANDREWS. J. Am. Chem. Soc. **100**, 2102 (1978).
3. (*a*) T. T. TIDWELL. Angew. Chem. Int. Ed. Engl. **23**, 20 (1984); (*b*) P. G. GASSMAN and T. T. TIDWELL. Acc. Chem. Res. **16**, 279 (1983).
4. (*a*) K. M. KOSHY, D. ROY, and T. T. TIDWELL. J. Am. Chem. Soc. **101**, 357 (1979); (*b*) K. M. KOSHY and T. T. TIDWELL. J. Am. Chem. Soc. **102**, 1216 (1980); (*c*) M. P. JANSEN, K. M. KOSHY, N. N. MANGRU, and T. T. TIDWELL. J. Am. Chem. Soc. **103**, 3863 (1981); (*d*) A. D. ALLEN, M. P. JANSEN, K. M. KOSHY, N. N. MANGRU, and T. T. TIDWELL. J. Am. Chem. Soc. **104**, 207 (1982); (*e*) A. D. ALLEN, F. SHAHIDI, and T. T. TIDWELL. J. Am. Chem. Soc. **104**, 2516 (1982); (*f*) K.-T. LIU, M.-Y. KUO, and C. F. SHEU. J. Am. Chem. Soc. **104**, 211 (1982); (*g*) K.-T. LIU and C.-F. SHEU. Tetrahedron Lett. **21**,

4091 (1980); (*h*) K.-T. LIU and M.-Y. KUO. Tetrahedron Lett. **26**, 355 (1985); (*i*) K.-T. LIU and Y. W. WA. J. Chem. Res. In press; (*j*) P. G. GASSMAN and C. K. HARRINGTON. J. Org. Chem. **49**, 2258 (1984).

5. (*a*) G. A. OLAH and C. U. PITTMAN. J. Am. Chem. Soc. **88**, 3310 (1966); (*b*) G. A. OLAH, G. K. S. PRAKASH, M. ARVANAGHI, V. V. KRISHNAMURTHY, and S. C. NARANG. J. Am. Chem. Soc. **106**, 2378 (1984).
6. (*a*) D. LENOIR. Chem. Ber. **108**, 2055 (1975); (*b*) P. G. GASSMAN and J. B. HALL. J. Am. Chem. Soc. **106**, 4267 (1984); (*c*) C. D. POULTER, D. M. SATTERWHITE, and H. C. RILLING. J. Am. Chem. Soc. **98**, 3376 (1976); (*d*) W. KIRMSE, U. MROTZECK, and R. SIEGFRIED. Angew. Chem. Int. Ed. Engl. **24**, 55 (1985).
7. (*a*) S. COHEN. J. Am. Chem. Soc. **79**, 1499 (1957); (*b*) A. STREITWIESER, JR., A. P. MARCHAND, and A. H. PUDJAATMAKA. J. Am. Chem. Soc. **89**, 693 (1967); (*c*) W. D. KRAY and R. W. ROSSER. J. Org. Chem. **42**, 1186 (1977); (*d*) C. CAMBILLAU, D. BONNET-DELPON, M. CHARPENTIER, M. D. OUREVITCH, and R. JACQUOT. J. Fluorine Chem. **29**, 115 (1985).
8. (*a*) M. N. PADDON-ROW, C. SANTIAGO, and K. N. HOUK. J. Am. Chem. Soc. **102**, 6561 (1980); (*b*) M. N. PADDON-ROW, K. N. HOUK, and T. T. TIDWELL. Tetrahedron Lett. **23**, 383 (1982); (*c*) W. F. REYNOLDS, P. DAIS, D. W. MACINTYRE, R. D. TOPSOM, S. MARRIOTT, E. V. NAGY-FELSOBUKI, and R. W. TAFT. J. Am. Chem. Soc. **105**, 378 (1983); (*d*) A. C. HOPKINSON and M. H. LIEN. J. Mol. Struct. **104**, 303 (1983).
9. (*a*) A. D. ALLEN, V. M. KANAGASABAPATHY, and T. T. TIDWELL. J. Am. Chem. Soc. **105**, 5961 (1983); (*b*) V. M. KANAGASABAPATHY, J. F. SAWYER, and T. T. TIDWELL. J. Org. Chem. **50**, 503 (1985).
10. (*a*) G. A. OLAH. Halonium ions. Wiley, New York. 1975; (*b*) G. F. KOSER. *In* Chemistry of halides, pseudo-halides, azides. Suppl. D, *Edited by* S. Patai and Z. Rappoport. Wiley, New York. 1983; (*c*) P. E. PETERSON. Acc. Chem. Res. **4**, 407 (1971); (*d*) G. ANGELINI and M. SPERANZA. J. Am. Chem. Soc. **103**, 3792 (1981); (*e*) D. K. SEN SHARMA, S. M. DE HÖJER, and P. KEBARLE. J. Am. Chem. Soc. **107**, 3757 (1985); (*f*) G. A. OLAH, G. K. S. PRAKASH, and V. V. KRISHNAMURTHY. J. Org. Chem. **48**, 5116 (1983).
11. B. CIOMMER and H. SCHWARTZ. Z. Naturforsch. **38B**, 635 (1983).
12. (*a*) H. LISCHKA and H.-J. KÖHLER. J. Am. Chem. Soc. **100**, 5297 (1978); (*b*) I. RAGHAVACHARI, R. C. HADDON, and W. H. STARNES, JR. J. Am. Chem. Soc. **104**, 5054 (1982); (*c*) G. FRENKING. Tetrahedron, **40**, 377 (1984); (*d*) T. HEINIS, R. BÄR, K. BÖRLIN, and M. JUNGEN. Chem. Phys. Lett. **105**, 327 (1984).
13. J. S. BINKLEY, R. A. WHITESIDE, R. KRISHNAN, R. SEEGER, D. J. DEFREES, H. B. SCHLEGEL, S. TOPIOL, L. R. KAHN, and J. A. POPLE. QCPE, **13**, 406 (1980).
14. M. R. PETERSON and R. POIRIER. Private communication. University of Toronto, June 1981.
15. H. B. SCHLEGEL. J. Comput. Chem. **3**, 214 (1982).
16. J. S. BINKLEY, J. A. POPLE, and W. D. HEHRE. J. Am. Chem. Soc. **102**, 939 (1980).
17. P. C. HARIHARAN and J. A. POPLE. Theoret. Chim. Acta, **28**, 213 (1973).
18. (*a*) W.-H. WHANGBO, H. B. SCHLEGEL, and S. WOLFE. J. Am. Chem. Soc. **99**, 1296 (1977); (*b*) F. BERNARDI, A. BOTTONI, and J. FOSSEY. Theoret. Chim. Acta, **61**, 251 (1982).
19. R. HOFFMANN, L. RADOM, J. A. POPLE, P. V. R. SCHLEYER, W. J. HEHRE, and L. SALEM. J. Am. Chem. Soc. **94**, 6221 (1972).
20. A. C. HOPKINSON, M. H. LIEN, K. YATES, and I. G. CSIZMADIA. Theoret. Chim. Acta. **38**, 21 (1975).
21. R. A. WHITESIDE, M. J. FRISCH, J. S. BINKLEY, D. J. DEFREES, H. B. SCHLEGEL, R. KRISHNAN, and J. A. POPLE. Carnegie Mellon Quantum Chemistry Archive. 2nd ed. July 1981. Dept. of Chemistry, Carnegie Mellon University, Pittsburgh, PA 15213.
22. J. R. MOHRIG and K. KEEGSTRA. J. Am. Chem. Soc. **89**, 5492 (1967).

Can. J. Chem. Downloaded from www.nrcresearchpress.com by 80.58.250.72 on 09/07/12
For personal use only.

Preparation of 1-thio and 1-amino substituted 1,3-dihydrobenzo[*c*]thiophene 2,2-dioxides

ZAFAR KHAN AND TONY DURST

Ottawa–Carleton Chemistry Institute, Department of Chemistry, University of Ottawa, Ottawa, Ont., Canada K1S 5B6

Received April 9, 1986

ZAFAR KHAN and TONY DURST. Can. J. Chem. **65**, 482 (1987).

The 1-hydroxy substituent in 1-hydroxy-1,3-dihydrobenzo[*c*]thiophene 2,2-dioxides is readily replaced by alkoxy, alkylthio, and amino groups. These compounds serve as precursors of alkoxy, alkylthio, and amino substituted *o*-quinodimethanes. Cycloaddition reactions between a series of 1,4-disubstituted *o*-quinodimethanes bearing a phenyl group and one of the above heteroatoms, and typical dienophiles such as dimethyl fumarate and methyl crotonate were carried out. The phenyl group controlled both the regiochemistry and stereochemistry of these cycloaddition reactions, with the major products being *trans*-1-phenyl-2-carbomethoxytetrahydronaphthalenes. The amino substituted *o*-quinodimethanes were trapped only by dimethyl fumarate.

ZAFAR KHAN et TONY DURST. Can. J. Chem. **65**, 482 (1987).

Le substituant hydroxy-1 des dioxydes-2,2 de l'hydroxy-1 dihydro-1,3 benzo[*c*]thiophènes peut facilement être remplacé par des groupements alkoxy, alkylthio et amino. Ces composés servent de précurseurs pour les *o*-quinodiméthanes substitués par des groupements alkoxy, alkylthio et amino. On a effectué des réactions de cycloadditions entre, d'une part, une série de *o*-quinodiméthanes disubstitués en positions-1,4 par un groupement méthyle et l'un des hétéroatomes mentionnés ci-dessus et, d'autre part, des diénophiles typiques comme le fumarate de diméthyle et le crotonate de méthyle. Le groupement phényle contrôle tant la régiochimie que la stéréochimie de ces réactions de cycloadditions; les produits principaux sont les phényl-1 carbométhoxy-2 tétrahydronaphtalènes-*trans*. Les *o*-quinodiméthanes substitués par un groupement amino n'ont pu être piégés que par le fumarate de diméthyle.

[Traduit par la revue]

Can. J. Chem. Downloaded from www.nrcresearchpress.com by 80.58.250.72 on 09/07/12
For personal use only.

We have recently reported the preparation of 1-hydroxy-1,3-dihydrobenzo[*c*]thiophene 2,2-dioxides, **1**, via photolysis of *ortho*-substituted benzaldehydes in the presence of SO_2 (1). The hydroxyl group in **1** could readily be exchanged with a variety of alcohols leading to the formation of the alkoxy derivatives **2**. The latter have been used to generate 1-alkoxy substituted *o*-quinodimethanes **3** (2, 3), via SO_2 extrusion, and are trapped by typical dienophiles to give the tetrahydronaphthalenes **4**. Such compounds have considerable potential in the synthesis of lignan derivatives (4).

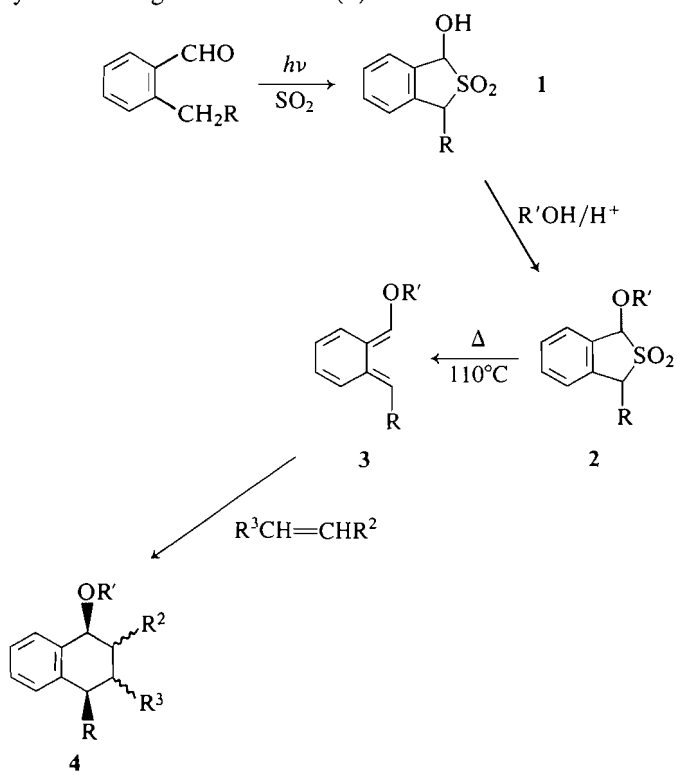

We would now like to report the preparation of derivatives of **1** in which the oxygen substituent at C-1 is replaced by other heteroatoms such as sulfur and nitrogen, e.g. **5**; the thermal extrusion of SO_2 from these derivatives to yield a new set of *ortho*-quinodimethanes, **6**; and a comparison of some cycloadditions of **6** with those of the alkoxy derivatives **3**.

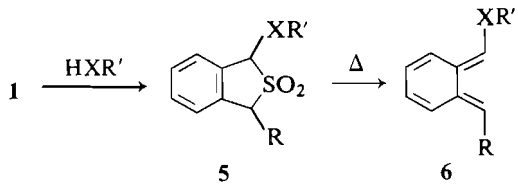

XR' = SPh, SCH_2Ph, SO_2CH_2Ph, NHPh, NPh_2, N⬭O; R = H, Ph

Preparation of 5

We had shown earlier that the hydroxyl group of **1** was readily exchanged for an alkoxy group simply by refluxing **1** in CH_2Cl_2 solution in the presence of an alcohol and a catalytic amount of TsOH (1).

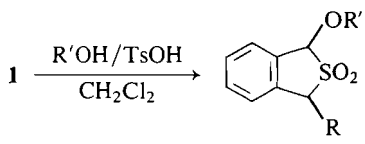

Essentially the same conditions sufficed for the preparation of the sulfides **7** and **8**. Thus, reaction of **1** (R = Ph) with an equimolar amount of benzyl of phenyl mercaptan and a catalytic amount of TsOH in CH_2Cl_2, either at reflux for several hours or room temperature for several days, afforded the sulfides **7** and **8** in about 80% crude yield (61 and 46% recrystallized yield, respectively). Under these conditions only one isomer, assigned the 1,3-*cis* configuration, was obtained. When **7***a* was exposed to 20% NaOH, isomerization to an approximately 1:1 mixture of *cis* (**7**) and *trans* (**9**) isomers occurs.

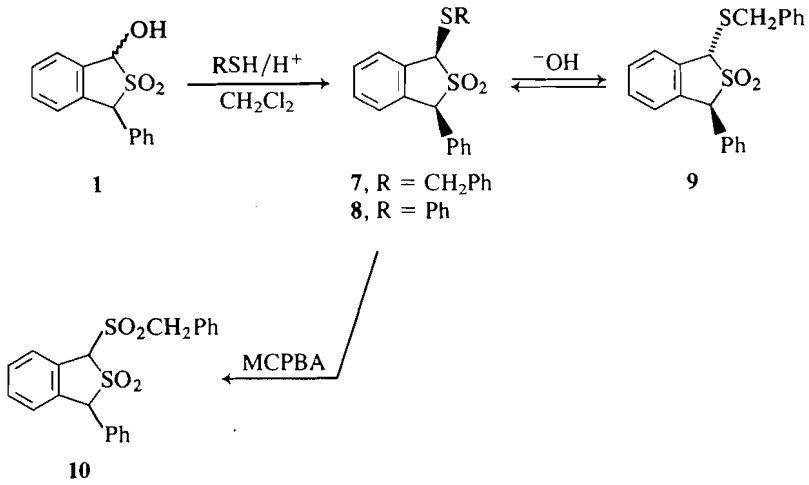

1 7, R = CH_2Ph; 8, R = Ph 9 10

The structures of **7** and **8** follow from their analytical data, spectral properties, and their reaction with dimethyl fumarate. Thus **7**, mp 124–125°C, showed two singlets at δ 5.40 and 5.18 assigned to H-1 and H-3 respectively and an AB quartet (δ_A 3.90, δ_B 4.20, J_{AB} = 13.2 Hz), in addition to 14 aromatic hydrogens. Oxidation of **7** afforded the disulfone **10** in which the proton, H-1, α to both sulfone groups, was deshielded by 0.5 ppm relative to H-1 in **7** while H-3 remained essentially unaffected. The *trans* isomer **9** was separated from the mixture of **7** and **9** by preparative tlc. Its proton nmr had peaks at δ 5.8 (H-1), 5.02 (H-3), 4.33 (d, J = 13.2 Hz), 4.01 (d, J = 13.2 Hz) in addition to a multiplet of 14 aromatic hydrogens at 7.0–7.5 ppm. The benzylic hydrogens of **8**, mp 127–128°C, were found at 5.56 and 5.44 ppm. When the reaction of **1** with PhSH and TsOH was carried out in refluxing benzene the major product was orthobenzylbenzaldehyde diphenylthioacetal **11**.

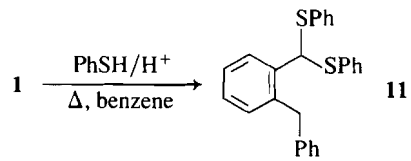

The α-aminosulfones **12–14** were formed when a solution of **1** was allowed to react with the appropriate primary or secondary amine in CH_2Cl_2 at room temperature. These aminosulfones were obtained as mixtures of isomers that were not separable on column chromatography. The isomer ratios were generally near 1:1 as determined from the integration of the pairs of singlets (H-1 and H-3) due to each isomer, appearing in the 5–6 ppm range. (See experimental section for further details.) In several cases when a primary amine was employed, e.g. *tert*-butyl amine, or when the reaction mixture was heated, desulfonylated imines, e.g. **15**, were obtained as the sole isolable product.

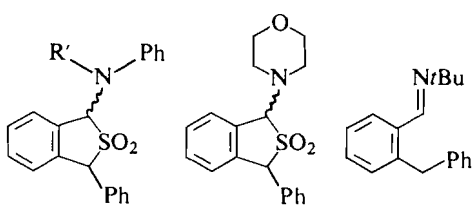

12, R′ = H; **14**, R′ = Ph **13** **15**

A plausible mechanism for the exchange reaction is shown below. Cyclic α-hydroxysulfones such as **1** can also exist in the open chain aldehyde – sulfinic acid tautomeric form, e.g., **16** (1). The latter compound is convertible into **2** or **5** (X = S) via acid-catalyzed hemiacetal or hemithiocetal formation giving **17**, followed by cyclization with concomitant loss of H_2O. The iminium ion **18** is a plausible intermediate in the formation of the α-aminosulfones.

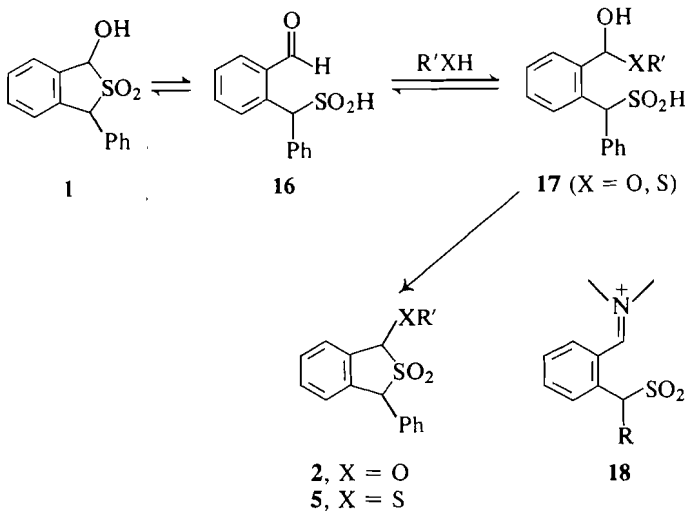

1 **16** **17** (X = O, S)

2, X = O; **5**, X = S **18**

The possible intermediacy of the benzothiophene sulfone **19** in the formation of **2** (X = O, R = CH_3) from **1** was eliminated by showing that the conversion, when carried out in CH_3OD, did not result in any deuterium incorporation at C-3.

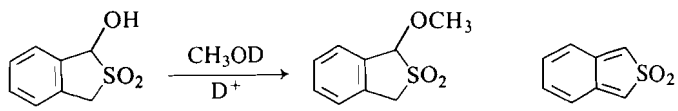

19

Cycloaddition reactions of 5

Each of the new sulfones **7**, **8**, **12–14** failed to show a molecular ion in its electron impact ms; in all cases the base peak occurred at $M^+ - 64$ suggesting a facile loss of SO_2. The exception to this behavior was the disulfone **10**, which showed a strong molecular ion peak at m/e 398 (25% of the base peak); this was reflected by the thermal stability of **10** (see below).

Can. J. Chem. Downloaded from www.nrcresearchpress.com by 80.58.250.72 on 09/07/12
For personal use only.

Can. J. Chem. Downloaded from www.nrcresearchpress.com by 80.58.250.72 on 09/07/12
For personal use only.

The ease of thermal extrusion from the various α-substituted 1,3-dihydrobenzo[*b*]thiophene 2,2-dioxides varies greatly with the nature of the substituent. Heteroatom substituents that can interact conjugatively with the newly generated 1,3-diene system of the *ortho*-quinodimethane lower significantly the temperature required for the extrusion reaction, when compared to the parent system **20** (5), or typical alkyl (6) or aryl (7) derivatives **21**, which are usually thermolyzed above 180°C.

Qualitatively, the amino substituted sulfones extrude SO_2 at convenient rates in refluxing $CHCl_3$ and even in refluxing CH_2Cl_2, while the thio and alkoxy substituted derivatives require 80–110°C (boiling cyclohexane or toluene). α-Acetoxy sulfones, e.g. **22**, lose SO_2 at similar rates when heated between 140 and 180°C (3). As expected from the ms data, the disulfone **10** was recovered unchanged after refluxing for 12 h in decalin.

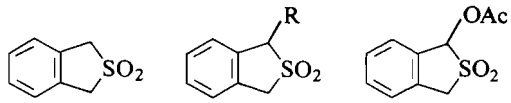

20 **21** **22**

The trapping of the thio substituted *ortho*-quinodimethane **23** was carried out in refluxing toluene with dimethyl fumarate and methyl crotonate for about 6–8 h and yielded the adducts **24** and **25**, respectively. The purified yields were 89 and 35% (31% recovery of **8**), respectively.

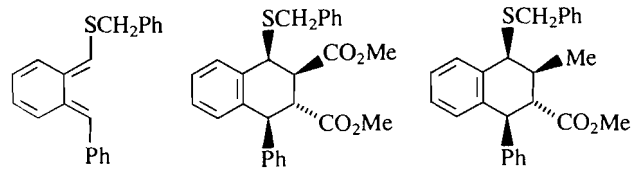

23 **24** **25**

The structures of these products were assigned on the basis of their analytical and ms data and comparison of their 300-MHz proton nmr spectra with those of the corresponding 4-methoxy (8) and 4-acetoxy (3) adducts (Table 1). In particular, the large (9–11 Hz) coupling constant for H1, H2 and the small (3–4 Hz constant for H3, H4 for **24** and **25** are consistent with a *trans* diaxial and a *gauche* arrangement for H1–H2 and H3–H4, respectively. Furthermore, oxidation of **24** with MCPBA yielded the corresponding sulfone, which eliminated phenylmethanesulfinic acid upon treatment with triethylamine to form the dihydronaphthalene **26**. This product had previously been obtained by acid-catalyzed elimination of methanol from the adduct **27** (2). Thus **24** and **25** are judged to have the *trans* arrangement between the phenyl and adjacent carbomethoxy group.

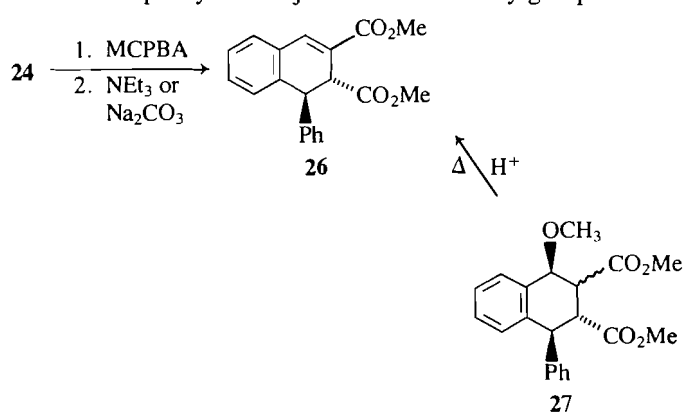

TABLE 1. Chemical shifts and coupling constants for

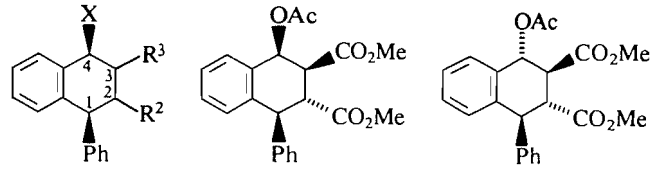

37 (ref. 3) **36** (ref. 3)

Compound	Chemical shift (δ)				Coupling constant (Hz)		
	H-1	H-2	H-3	H-4	$J_{1,2}$	$J_{2,3}$	$J_{3,4}$
24	4.08	3.45	3.55	4.33	10.8	11.8	3.5
25	4.26	3.07	2.5	3.79	11.0	11.2	3.4
27	4.09	3.61	3.30	4.70	11.0	12.1	2.9
29	4.27	3.16	2.22	3.99	11.2	11.2	2.0
34	4.02	3.3	3.31	4.32	10.6	—	3.9
35	4.37	3.31	3.49	4.35	10.5	9.3	8.3
37	4.02	3.82	3.56	6.69	11.3	12.3	3.2
36	4.37	3.48	3.60	6.80	10.7	10.8	8.9

A careful investigation of the thermolysis of the methoxy derivative **28** with methyl crotonate revealed that, in addition to **29** (31%), the adducts **30** (6%) and **31** (1.2%) having the opposite regiochemistry to **29** were also obtained. In contrast, only **25**, corresponding to **29** in the methoxy series, could be isolated from the reaction of **23** and methyl crotonate, albeit in only 35% yield. Again the relative stereochemical assignments are based on the size of the relevant coupling constants (Table 1), which are consistent with these compounds existing in conformation **A**.

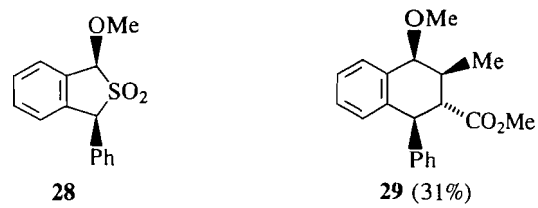

28 **29** (31%)

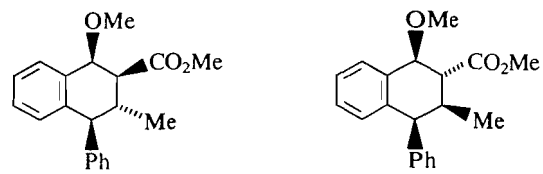

30 (6.0%) **31** (1.2%)

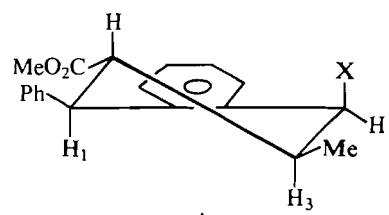

A

In agreement with the regiochemical assignment, compound **29** was converted to *trans*-2-methyl-3-carbomethoxy-4-phenyl-3,4-dihydronaphthalene in 97% yield upon heating with TsOH in benzene. In contrast, similar treatment of **30** and **31** afforded the isomeric *trans*-2-carbomethoxy-3-methyl-4-phenyl-3,4-dihydronaphthalene. Both of these naphthalenes were character-

Can. J. Chem. Downloaded from www.nrcresearchpress.com by 80.58.250.72 on 09/07/12
For personal use only.

ized by their nmr, ms, and *Exact Mass* spectra (see Experimental). As expected, the sulfone corresponding to **25** was unaffected by treatment with triethylamine, thus confirming that this compound does not have a β-ester sulfone arrangement.

It was a considerable disappointment to us that thermolysis of the aminosulfones, e.g. **13**, in refluxing cyclohexane in the presence of the very reactive dienophile, dimethyl fumarate, gave only a modest yield of the two adducts **34** (26%) and **35** (3%), along with a 24% yield of 2-benzylbenzaldehyde. The structure of the major isomer **34** was assigned the same stereochemistry as **24**, again on the basis of the large (10.6 Hz) coupling constant between H1 and H2 and a small (3.9 Hz) coupling for H3, H4. This compound presumably arises from the *exo* addition of dimethyl fumarate to *trans–trans* diene **32**. The minor adduct **35** has similar coupling constants, as does the acetoxy derivative **36** (3) (Table 1) and may be assumed to have arisen from the trapping of a *cis–trans* diene, isomeric with **33**. Since the aminosulfone **13** was obtained as a mixture of isomers, both dienes should be formed in the thermolysis reactions thereby leading to the two adducts **34** and **35**.

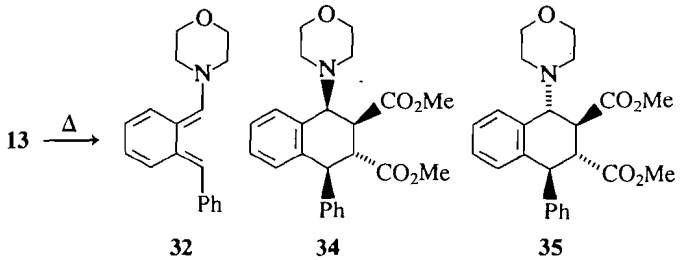

32 **34** **35**

Attempts to trap the aminosubstituted *o*-quinodimethane **32** with dimethyl maleate or methyl crotonate under a variety of conditions (refluxing $CHCl_3$, cyclohexane, toluene, no solvent, 50°C) were unsuccessful. The major product isolated in all these attempts was 2-benzylbenzaldehyde. When **13** was melted and the melt examined by tlc, the above aldehyde again appeared as the major product.

In contrast to **32**, *o*-quinodimethanes bearing urethane or amide substituents have been trapped effectively, at least intramolecularly, by relatively weak dienophiles such as terminal alkenes (10) or alkynes (9).

Experimental

General

Proton nmr spectra were determined on a Varian XL-300 spectrometer in $CDCl_3$ solution. Work-up refers to partitioning the reaction mixture between H_2O and CH_2Cl_2, drying the CH_2Cl_2 layer with Na_2SO_4, and evaporating the solvent.

1-Benzylthio-1,3-dihydrobenzo[c]thiophene 2,2-dioxide, 7

Hydroxysulfone **1** (0.5 mmol), benzyl mercaptan (0.5 mmol), and TsOH (5 mg) were dissolved in 6 mL of CH_2Cl_2. The solution was stored at room temperature for 4 d, then extracted successively with 10 mL of saturated $NaHCO_3$ and 10 mL of H_2O. Crude yield: 148 mg of semi-solid material. Recrystallization afforded 111 mg (61%) of **7**, mp 124–125°C; nmr, δ: 3.89 (d, J = 13.2 Hz, 1H), 4.20 (d, J = 13.2 Hz, 1H), 5.12 (s, 1H), 5.40 (s, 1H), 7.05–7.5 (m, 14H); ms, CI/ether (relative %): 367 (1.3), 303 (32), 243 (20), 211 (40), 179 (28), 178 (16). *Anal.* calcd. for $C_{21}H_{18}O_2S_2$: C 68.82, H 4.95; found: C 68.50, H 5.00.

A solution of **7** in CH_2Cl_2 when stirred with 20% aqueous NaOH for 1 h afforded a 1:1 mixture of **7** and **9**. The mixture was separated by preparative tlc using 4:1 hexane – ethyl acetate as eluent. The nmr spectrum of **9** had peaks at δ 4.00 (d, J = 13.2 Hz, 1H), 4.33 (d, J = 13.2 Hz, 1H), 5.02 (s, 1H), 5.68 (s, 1H), and 7.0–7.45 (m, 14H).

Oxidation of 7 to 10

To a solution of 0.25 mmol of **7** in 3 mL of CH_2Cl_2 was added 0.8 mmol of MCPBA. The reaction was kept at room temperature for 14 h, then washed successively with 5 mL of 20% $NaHSO_3$, 20% $NaHCO_3$, and saturated NaCl solutions. The yield of **10**, mp 96–101°C, was quantitative; nmr, δ: 4.55 (d, J = 13.5 Hz, 1H), 5.10 (d, J = 13.5 Hz, 1H), 5.18 (s, 1H), 5.90 (s, 1H), and 6.8–8.0 (m, 14H); ms, CI/ether (relative %): 399 (25, M + 1), 335 (63), 179 (90), 91 (100).

1-Phenylthio-1,3-dihydrobenzo[c]thiophene 2,2-dioxide (8)

A solution of 0.5 mmol of hydroxysulfone **1**, 0.5 mmol of benzenethiol, and 30 mg of TsOH was heated in 10 mL of CH_2Cl_2 for 2 h. The mixture was cooled, washed with saturated sodium bicarbonate solution (15 mL), and then with 15 mL of H_2O. The organic layer was dried and evaporated. The yield of crude product was 137 mg (5:1 mixture of **8** and **11** by nmr). Recrystallization from ether afforded **8**, 46%, mp 126–128°C; nmr, δ: 5.56 (s, 1H), 5.44 (s, 1H), and 7.05–7.76 (m, 14H); ms (rel. %): 288 (42), 179 (100). *Anal.* calcd. for $C_{20}H_{16}O_2S_2$: C 68.15, H 4.58, S 18.19; found: C 68.30, H 4.99, S 18.05.

The above procedure, using benzene as solvent and refluxing the reaction mixture for 15 h, afforded the dithioacetal **11** in 61% isolated yield as a clear oil; nmr, δ: 3.85 (s, 2H), 5.30 (s, 1H), 6.8–7.8 (m, 19H); ms (rel. %): M^+ (not observed), 289 (55), 180 (60), 179 (100).

Anilinosulfone 12

Hydroxysulfone **1** (0.2 mmol) and aniline (0.4 mmol) were stirred in 1 mL CH_2Cl_2 for 0.5 h. The reaction mixture was diluted with 20 mL of CH_2Cl_2 and washed successively with 10 mL of saturated $NaHCO_3$ and 10 mL of saturated NaCl solution. Further work-up afforded a mixture of **12** and aniline. Trituration with ether gave pure **12** in 86% yield; mp 104–105°C; nmr, δ: 4.5–4.8 (b, NH), 5.33 (s, 2/3H) 5.40 (s, 1/3H), 5.87 (d, $J \approx$ 10 Hz, 1/3H), 5.98 (d, $J \approx$ 10 Hz, 2/3H), 6.8–7.5 (m, 14H); ms (rel. %): 271 (43), 270 (29), 179 (45), 178 (100), 77 (23). *Anal.* calcd. for $C_{20}H_{17}NO_2S$: C 71.62, H 5.11, N 4.18; found: C 71.43, H 5.19, N 4.11.

Morpholinosulfone 13

Sulfone **1** (632 mg, 2.43 mmol) and morpholine (212 mg, 2.43 mmol) were dissolved in 5 mL of dry CH_2Cl_2. After 2 h the solvent was evaporated, affording **13** as a crystalline substance in 95% yield (nmr). The product was recrystallized from CH_2Cl_2–hexane at −78°C; mp 62–66°C; nmr, δ: 3.2–3.3 (m, 4H), 3.7–3.8 (m, 4H), 5.25, 5.31, 5.40, 5.43 (4s, total 2H), 7.0–7.6 (m, 9H); ms (rel. %): M^+ (329, not observed), 265 (100), 264 (22), 179 (11), 178 (29). *Anal.* calcd. for $C_{18}H_{19}NO_3S$: C 65.63, H 5.81, N 4.25, S 9.73; found: C 65.79, H 6.02, N 4.09, S 9.98.

Diphenylaminosulfone 14

A solution of 0.4 mmol of hydroxysulfone **1** and 0.8 mmol of diphenylamine in 5 mL of CH_2Cl_2 was stirred at room temperature for 2.5 h, then refluxed for an additional 45 min. At this point **1** had not been completely consumed (tlc). Triethylamine (0.4 mmol) was added and the solution was refluxed for a further 4 h. Work-up as above afforded a thick oil, which was further purified by preparative tlc. The yield of **14** was 20%; nmr, δ: 6.14 (s, 1H), 6.37 (s, 1H), 6.9–8.0 (m, 19H); ms (rel. %): 411 (M^+, not observed), 347 (26), 179 (71).

Imine 15

A solution of 0.31 mmol of hydroxysulfone **1**, 0.44 mmol of *tert*-butylamine, and 0.27 mmol of triethylamine in 5 mL of CH_2Cl_2 was stirred at room temperature for 1 h. The CH_2Cl_2 layer was evaporated. Further purification via column chromatography afforded the imine **15** in 37% yield; nmr, δ: 1.40 (s, 9H), 4.38 (s, 2H), 7.1–7.8 (m, 3H), 8.00 (d, 1H), and 10.02 (s, 1H). *Exact Mass* calcd. for $C_{18}C_{21}N$: 251.1674; found: 251.1676.

Thermolysis of 7

(a) Trapping of 23 with dimethyl fumarate

Benzylthiosulfone **7** (0.3 mmol), dimethyl fumarate (0.6 mmol), and anhydrous zinc oxide were refluxed in 5 mL of toluene for 11 h.

Can. J. Chem. Downloaded from www.nrcresearchpress.com by 80.58.250.72 on 09/07/12
For personal use only.

The zinc oxide was filtered off and the solvent evaporated. The crude product was dissolved in ether and precipitated with hexane to afford **24**, mp 46–52°C, in 89% yield; nmr, δ: 3.44 (s, 3H), 3.45 (dd, J = 10.8 and 11.8 Hz, 1H), 3.55 (dd, J = 11.8 and 3.5 Hz, 1H), 3.73 (s, 3H), 3.74 (d, J = 13.4 Hz, 1H), 4.08 (d, J = 10.8 Hz, 1H), 4.43 (d, J = 3.5 Hz, 1H), 6.70 (d, J = 7.8 Hz, 1H), 6.80 (d, J = 7.3 Hz, 1H), and 7.0–7.4 (m, 12H). *Anal.* calcd. for $C_{27}H_{26}O_4S$: C 72.62, H 5.87, S 7.18; found: C 72.49, H 6.02, S 7.38.

Compound **24** was oxidized with 3 equivalents of MCPBA in CH_2Cl_2 at room temperature for 7 h. The solution was then washed successively with saturated $NaHSO_3$, $NaHCO_3$, and NaCl solutions. Further work-up afforded a sulfone in 97% yield, mp 269–271°C. When this compound was warmed with triethylamine in CH_2Cl_2 for 1 h it was converted in quantitative yield to the alkene **26**, whose properties matched those reported by Charlton and Durst (2); nmr, δ: 3.61 (s, 3H), 3.75 (s, 3H), 4.06 (d, J = 3.0 Hz, 1H), 4.74 (d, J = 3.0 Hz, 1H), 7.0–7.4 (m, 9H), 7.72 (m, 1H). *Exact Mass* calcd. for $C_{20}H_{18}O_4$: 322.1205; found: 322.1188.

*(b) Trapping of **23** with methyl crotonate*

Benzylthiosulfone **7** (0.17 mmol), methyl crotonate (1.0 mmol), and zinc oxide (30 mg) were dissolved in 1 mL of toluene and the solution was refluxed for 16 h. The crude product, isolated after filtration and removal of most of the excess methyl crotonate, was purified by preparative tlc. The yield of **25** was 35%; in addition, 31% of **7** was recovered; nmr, δ: 1.10 (d, J = 6.6 Hz, 3H), 2.4–2.5 (m, 1H), 3.07 (t, J = 11.2 Hz, 1H), 3.49 (s, 3H), 3.78 (d, J = 3.4 Hz, 1H), 3.80 (d, J = 13.2 Hz, 1H), 3.83 (d, J = 13.2 Hz, 1H), 4.26 (d, J = 11.0 Hz, 1H), 6.68 (d, J = 7.6 Hz, 1H), 6.81 (d, J = 7.3 Hz, 1H), 7.0–7.5 (m, 12H); ms (rel. %): 412 (M^+, not observed), 311 (49), 310 (9), 279 (7), 220 (19), 219 (100), 91 (39). *Anal.* calcd. for $C_{20}H_{26}O_2S$: C 77.58, H 6.51, S 7.96; found: C 77.82, H 6.46, S 7.82.

The above sulfide was oxidized with 3 equiv. of MCPBA in CH_2Cl_2 at room temperature for 2 h. The reaction mixture was washed successively with saturated sodium sulfite, sodium bicarbonate, and sodium chloride solution. Further work-up afforded a quantitative yield of the sulfone corresponding to **25**, mp 168–171°C; nmr, δ: 1.39 (s, 3H), 2.6–2.7 (m, 1H), 3.48 (s, 3H), 3.81 (t, J = 11 Hz, 1H), 4.2–4.4 (m, 4H), 6.86 (d, J = 7 Hz, 1H), 7.0–7.6 (m, 13H). *Anal.* calcd. for $C_{26}H_{26}O_4S$: C 71.86, H 6.03, S 7.38; found: C 71.99, H 6.24, S 7.18.

The above sulfone was stable to refluxing with excess triethylamine in CH_2Cl_2 for 6 h.

*Reaction of **28** with methyl crotonate*

Methoxysulfone **28** (0.89 mmol), methyl crotonate (1.8 mmol), and zince oxide (50 mg) were refluxed in 0.5 mL of CH_2Cl_2 and 3.0 mL of cyclohexane for 3 d. The reaction mixture was diluted with an additional 30 mL of cyclohexane, filtered, and the solvents were evaporated. The crude product was separated by flash column chromatography and yielded 26% recovered **28**, 31% of **29**, 6.0% of **30**, and 1.2% of **31**.

Compound **29**: nmr, δ: 1.10 (d, J = 6.6 Hz, 3H), 2.22 (ddq, J = 11.2, 2.4, and 6.6 Hz, 1H), 3.16 (t, J = 11.2 Hz, 1H), 3.40 (s, 3H), 3.50 (s, 3H), 3.99 (d, J = 2.4 Hz, 1H), 4.27 (d, J = 11.2 Hz, 1H), 6.82 (m, 1H), 7.1–7.3 (m, J = 8 Hz); ms (rel. %): 310 (1.3, M^+), 278 (15). *Exact Mass* calcd. for $C_{20}H_{22}O_3$: 310.1569; found: 310.1557.

Compound **29** (47 mg) and TsOH (5 mg) were refluxed in 5 mL of benzene for 6 h. The reaction mixture was washed with saturated $NaHCO_3$ solution and the organic solvent dried and evaporated to yield 41 mg (97%) of *trans*-2-methyl-3-carbomethoxy-4-phenyl-3,4-dihydronaphthalene, mp 36–39°C; nmr, δ: 1.89 (s, 3H), 3.43 (d, J = 6.1 Hz, 1H), 3.59 (s, 3H), 4.54 (d, J = 6.1 Hz, 1H), 6.40 (s, 1H), 6.89 (d, J = 6.1 Hz, 1H), 7.1–7.3 (m, 8H); ms (rel. P): 278 (33), 219 (100), 218 (25). *Exact Mass* calcd. for $C_{19}C_{18}O_2$: 278.1307; found: 278.1308.

Compounds **30** and **31** were obtained as an inseparable 5:1 mixture. The major isomer **30** had nmr peaks at δ: 1.02 (d, J = 5.9 Hz, 3H), 2.69–2.73 (m, 2H), 3.36 (s, 3H), 3.49–3.51 (m, 1H), 3.76 (s, 3H), 4.50 (d, J = 2.0 Hz, 1H), 6.8 (m, 1H), 7.0 (m, 1H), 7.15–7.40 (m, 7H); ms (rel. %): 310 (6), 295 (10), 278 (83), 219 (100). *Exact Mass* calcd. for $C_{20}H_{22}O_3$: 310.1569; found: 310.1562.

The above mixture was refluxed for 0.5 h in benzene containing a catalytic amount of TsOH and yielded *trans*-2-carbomethoxy-3-methyl-4-phenyl-3,4-dihydronaphthalene in greater than 95% yield; nmr, δ: 1.12 (d, J = 7.1 Hz, 3H), 3.15 (dq, J = 1.2 and 7.1 Hz, 1H), 3.68 (s, 3H), 3.95 (bs, 1H), 6.9 (m, 2H), 7.0–7.4 (m, 7H), 7.50 (s, 1H); ms (rel. %): 278 (88), 219 (88), 218 (40), 178 (100). *Exact Mass* calcd. for $C_{19}H_{18}O_2$: 278.1307; found: 278.1314.

Evidence for the presence of a third isomer having the 3-methyl and 4-phenyl group in a *cis* relationship was also obtained from the nmr spectrum of the mixture: δ: 0.80 (d, J = 7.1 Hz, CH_3), 2.93 (quint., J ~ 7 Hz, H-3), 3.77 (OCH_3), and 4.34 (d, J ~ 6 Hz, H-4).

*Reaction of aminosulfone **13** with dimethyl fumarate*

Sulfone **13** (404 mg, 1.23 mmol), dimethyl fumarate (180 mg, 1.25 mmol), and 25 mg of ZnO were refluxed in 6 mL of cyclohexane for 8 h. The zinc oxide was filtered off, washed with additional cyclohexane, and the solvents were evaporated. The crude product was fractionated on a silica gel column to yield 26% of **34** and 3% of **35**; in addition, 15% of 2-benzylbenzaldehyde was also obtained.

The adduct **34**, mp 47–49°C, showed nmr peaks at δ: 2.45–2.55 (m, 2H), 2.65–2.75 (m, 2H), 3.3–3.4 (m, 2H), 3.41 (s, 3H), 3.5–3.6 (m, 2H), 3.6–3.7 (m, 2H), 3.71 (s, 3H), 4.02 (d, J = 10.6 Hz, 1H), 4.32 (d, J = 3.9 Hz, 1H), 6.77 (d, J = 6.9 Hz, 1H), 7.1–7.35 (m, 8H). *Anal.* calcd. for $C_{24}H_{27}NO_5$: C 70.40, H 6.65, N 3.42; found: C 70.22, H 6.97, N 3.23.

The proton nmr of **35** had key peaks at δ: 2.40–2.55 (m, 4H), 3.31 (dd, J = 9.6 and 10.5 Hz, 1H), 3.44 (s, 3H), 3.49 (t, J = 8.7 Hz, 1H), 3.64 (s, 3H), 3.6–3.7 (m, 4H), 4.35 (d, J = 8.3 Hz, 1H), 4.37 (d, J = 10.1 Hz, 1H), 6.61, (d, J = 6.9 Hz), 7.1–7.4 (m, J = 8 Hz). This compound was not further characterized.

Acknowledgement

The continued financial support of NSERC (Canada) is gratefully acknowledged.

1. J. L. CHARLTON and T. DURST. Tetrahedron Lett. **25**, 2663 (1984).
2. J. L. CHARLTON and T. DURST. Tetrahedron Lett. **25**, 5287 (1984).
3. J. L. CHARLTON, M. M. ALAUDDIN, and G. H. PENNER. Can. J. Chem. **64**, 793 (1986).
4. M. E. JUNG, P. Y-S. LAM, M. M. MANSURI, and L. M. SPELTZ. J. Org. Chem. **50**, 1087 (1985).
5. M. P. CAVA and A. A. DEANA. J. Am. Chem. Soc. **79**, 1701 (1957).
6. (*a*) T. KAMETANI, H. MATSUMOTO, H. NEMOTO, and K. FUKUMOTO. Tetrahedron Lett. 2425 (1978); (*b*) W. OPPOLZER. Heterocycles, 1615 (1980); (*c*) K. C. NICOLAOU, W. E. BARNETTE, and P. MA. J. Org. Chem. **45**, 1463 (1980); (*d*) W. OPPOLZER, D. A. ROBERTS, and G. C. BIRD. Helv. Chem. Acta, 1979, **62**, 2017 (1979); (*e*) Helv. Chem. Acta, **63**, 1703 (1980).
7. J. MANN and S. E. PIPER. J. Chem. Soc. Chem. Commun. 430 (1982).
8. T. DURST, E. E. KOZMA, and J. L. CHARLTON. J. Org. Chem. **50**, 4829 (1985).
9. W. OPPOLZER and K. KELLER. J. Am. Chem. Soc. **93**, 3836 (1971).
10. W. OPPOLZER. J. Am. Chem. Soc. **93**, 3834 (1971).

Anomalous ozone degradations of 1-chloro substituted conjugated dienes in methanol

KARL GRIESBAUM[1] AND ASHIS R. BANDYOPADHYAY
Engler-Bunte-Institut, Bereich Petrochemie, Universität Karlsruhe (TH), D-7500 Karlsruhe, Federal Republic of Germany

Received June 26, 1986

KARL GRIESBAUM and ASHIS R. BANDYOPADHYAY. Can. J. Chem. **65**, 487 (1987).

Diozonolyses in methanol of (*E*)-4-chloro-2,3-dimethyl-1,3-hexadiene (**4***a*) and of (4*E*)-5-chloro-3,4-dimethyl-2,4-heptadiene (**4***b*) resulted in complete cleavage of the double bonds and of the single bonds of the respective diene systems. The course of these anomalous cleavage reactions has been established by step-wise ozonolyses of these dienes, and by the identification of labile methoxy hydroperoxides as intermediates.

KARL GRIESBAUM et ASHIS R. BANDYOPADHYAY. Can. J. Chem. **65**, 487 (1987).

La diozonolyse du chloro-4 diméthyl-2,3 hexadiène-1,3-(*E*) (**4***a*) et du chloro-5 diméthyl-3,4 heptadiène-2,4-(*E*4) (**4***b*), dans le méthanol, conduit à une coupure complète des doubles et des simples liaisons des systèmes diéniques respectifs. On a déterminé le cours de ces réactions de coupures anormales en procédant à l'ozonolyse par étape de ces dienes ainsi qu'à l'identification des méthoxy hydroperoxydes labiles comme intermédiaires.

[Traduit par la revue]

Introduction

In previous work we obtained the chlorinated diene **1** as one of several products from the reaction of anhydrous hydrogen chloride with 2-butyne (1). In an attempt to confirm this structure by ozone degradation, we observed an anomalous ozonolysis of **1** in methanol, which resulted in the cleavage of the double bonds and of the single bond of the diene system to give fragments **2** and **3** in a ratio of 3:1 (2).

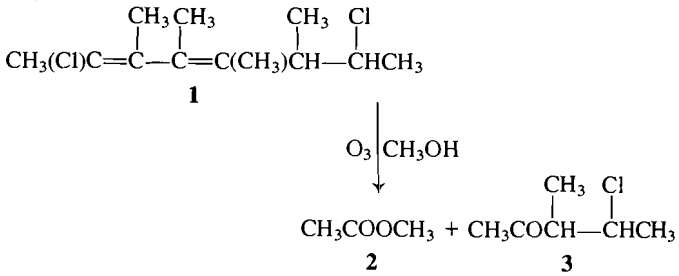

Since **1** was only available in a minute quantity, we were not in a position to follow this observation in more detail and to establish the course of this abnormal ozonolysis reaction. In the present study we have readdressed ourselves to this problem by examining the ozonolyses of the similarly structured but more readily accessible chlorinated dienes **4***a* and **4***b*.

Results and discussion

Complete ozonolysis of **4***a* and of **4***b* in methanol at ca. −60°C afforded colorless, strongly peroxidic solutions. After warming of the crude reaction products to room temperature, the peroxide contents had considerably decreased and the solutions remained colorless. Quantitative ^{1}H nmr analyses were consistent with the formation of **2** (96%), **12** (75%), **14***a* (42%), and **15** (10%) from **4***a* and with the formation of **2** (95%) and **12** (ca. 100%) from **4***b*. Compounds containing an intact $CH_3C—CCH_3$ moiety, such as **16** or **17**, could not be detected either by ^{1}H nmr or by gc (gas chromatographic) analyses. By contrast, when the freshly ozonized solutions were admixed with perdeuteriated dimethyl sulfide (DMS-d_6) and subsequently warmed up to room temperature, ^{1}H nmr and gc analyses of the yellow solutions were consistent with the formation of **16** (35%) from **4***a* and of **16** (27%) and **17** (20%) from **4***b*. Simultaneously, the yield of the abnormal cleavage product **2** was lowered from 96% after direct warm-up to 60% after DMS-d_6 treatment in the ozonolysis of **4***a* and from 95 to 18% in the ozonolysis of **4***b*.

These results demonstrated that **4***a* and **4***b* underwent anomalous ozonolysis reactions, similar to that observed for **1**, viz. by cleavage of the double bonds and of the central single bond of the respective conjugated diene systems. The fact that the extent of the abnormal cleavage could be lowered by reduction of the product mixture indicated, however, that it did not occur during the ozonolysis reaction itself, but rather by subsequent reactions of ozonolysis products in which the original central single bond of the diene system was still intact. In an attempt at identifying these ozonolysis products, we have studied the stepwise ozonolysis of **4***a* and of **4***b* with the following results:

Treatment of **4***a* in methanol with 0.8 molar equivalents of ozone afforded compounds **5***a* and **6** in yields of 93 and 87%, respectively, along with 5%, each, of **2** and of **12**. Ozonolysis of **4***b* under the same conditions gave **6** and **7** in yields of 28 and 59%, respectively, along with **8***b* and very minor proportions of **2** and **12**. The hitherto unknown hydroperoxide **6** has been isolated. In the presence of acid or triphenylphosphine it was rapidly converted into **7**, whereas in neutral media or in the presence of base, such as e.g., sodium methoxide, it was stable at room temperature.

It is apparent from these results that, in line with the known deactivating effect of chlorine substituents (3), monoozonolysis of **4***a* and of **4***b* occurred with high preference at the respective nonchlorinated double bonds to give the normal cleavage products **7** and (or) **6**, in which the central single bonds of the original diene systems were still intact. Hence, the abnormal cleavage, which was observed in the diozonolysis of **4***a* and of **4***b*, must have occurred in conjunction with the second cleavage step, i.e., the ozonolysis of the chloro substituted double bonds in **7** and (or) **6**. In an attempt at elucidating the course of this abnormal cleavage, compounds **6** and **7** have been individually ozonized in methanol/$CDCl_3$ at −60°C.

Ozonolysis of **6** and subsequent warm-up to room temperature gave a peroxidic solution, which contained **2** and **12** in yields of 82 and 79%, respectively, but no detectable amounts of compounds having an intact $CH_3C—CCH_3$ moiety. This result can be rationalized by the following sequence of reactions: In the first step the chlorinated double bond of **6** is selectively cleaved by ozone to give propionyl chloride (**10**) and the

[1]Author to whom correspondence should be addressed.

Can. J. Chem. Downloaded from www.nrcresearchpress.com by 80.58.250.72 on 09/07/12
For personal use only.

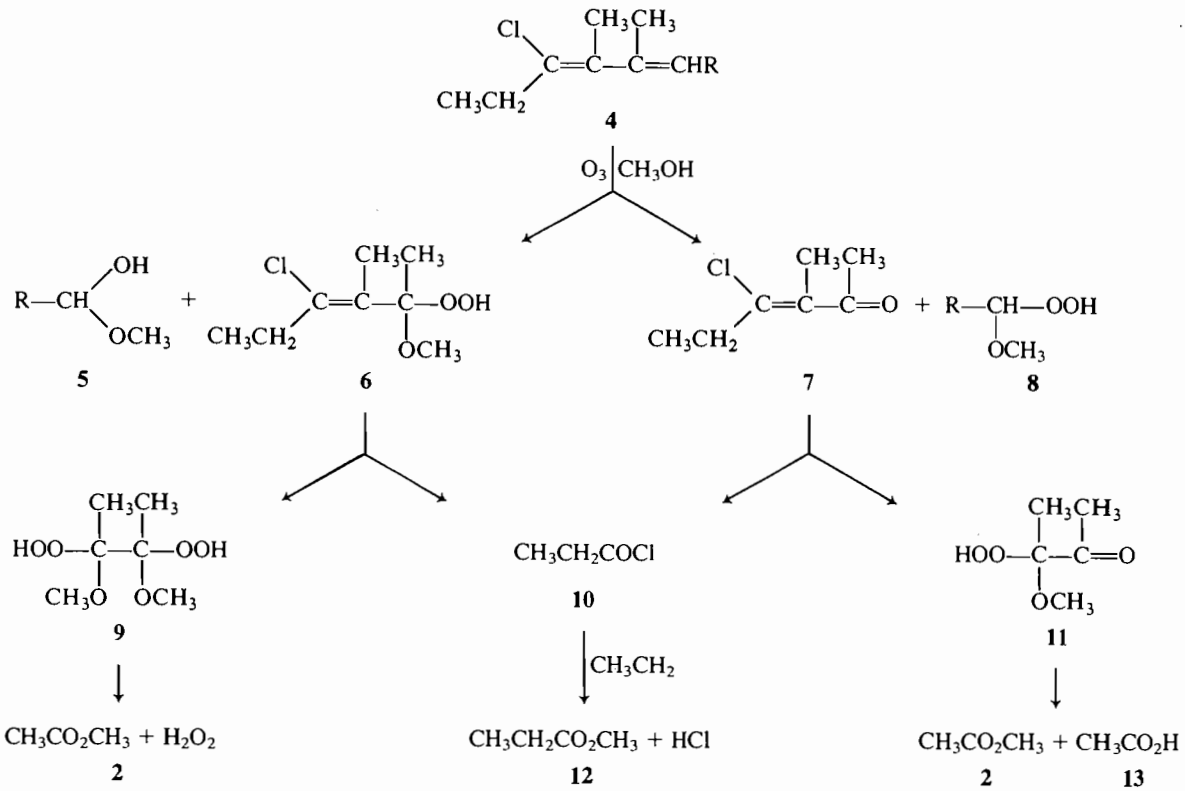

a : R=H; *b* : R=CH_3

carbonyl oxide **18**. In subsequent steps, **10** is solvolyzed by methanol to give **12** and hydrogen chloride, and **18** is eventually converted into two equivalents of **2** and hydrogen peroxide. A priori, the latter conversion could occur by fragmentation of **18** itself, possibly via **19**, by intramolecular ring closure of **18** to **20** and fragmentation of the latter, or by trapping of **18** with methanol and subsequent cleavage of the resulting vicinal bismethoxyhydroperoxide **9**. As we have shown above, reduction of a fresh ozonolysis product of **6** at −60°C with DMS afforded ca. 80% of diacetyl **16** and only ca. 20% of the abnormal cleavage product **2**. This result requires that there is a peroxidic intermediate that has a finite lifetime at −60°C and in which the central single bond of the original diene system is still intact, preconditions that cannot be met by intermediates **18** or **19**. Compounds **9** and **20** had been previously postulated by us as possible intermediates in the ozonolysis of **21** in methanol (4). In that case, the transient existence of **9** or of **20** was indicated, though not rigorously proven, by ^1H nmr analysis of the fresh ozonolysis product. It is conceivable that, in the present case, the conversion of **9** or **20** into **2** was accelerated by HCl catalysis and that for this reason these intermediates evaded detection by ^1H nmr spectroscopy.

$RCH(OCH_3)_2$ **14** HCO_2CH_3 **15**

$CH_3COCOCH_3$ **16** $CH_3COC(OCH_3)_2CH_3$ **17**

a : R=H; *b* : R=CH_3

Ozonolysis of **7** and subsequent warm-up to room temperature gave a colorless solution, which was only weakly peroxidic and which contained **2** and **12** in yields of 93 and 100%, respectively. By contrast, ^1H nmr analysis of the fresh ozonolysis product at −60°C showed the presence of **10** and **11** as the single major products. Warming of the same sample to room temperature and monitoring of the reaction by ^1H nmr spectroscopy showed, besides the formation of **12**, a gradual decrease of the signals of **11** and a concurrent increase of the signals of **2** as the temperature surpassed ca. 0°C. These observations are in line with the results of previous experiments in our laboratory (4). They had shown that **11**, which had been obtained as the major product in the ozonolysis of **21**

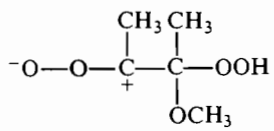

18

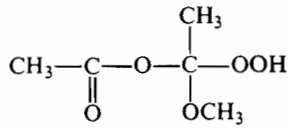

19

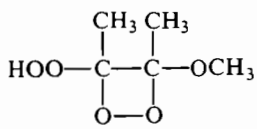

20

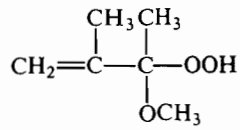

21

in methanol, underwent a spontaneous decomposition at temperatures above 0°C. In CD_2Cl_2 as a solvent, approximately equimolar amounts of **2** and **13** were formed, whereas in methanol **2** was the sole product, probably as the result of a post-esterification of **13**. The formation of **11** in the ozonolysis of **7** was further substantiated by reduction of the fresh ozonolysis product with DMS-d_6 at −60°C, which afforded **2**, **16**, and **17** in yields of 43, 15, and 36%, respectively, and 100% of **12**.

From the foregoing results we conclude that 1-chloro substi-

Can. J. Chem. Downloaded from www.nrcresearchpress.com by 80.58.250.72 on 09/07/12
For personal use only.

TABLE 1. Analytical data of products from the ozonolysis of **4***a*, **4***b*, **6**, and **7**

Compound	^{1}H nuclear magnetic resonance data δ (ppm)	Gas chromatography, t_R[a] (min)	Gas chromatography/ mass spectral data *m/e* (rel. intensity)
2	2.06 (s, 3H), 3.67 (s, 3H)	5.2	74 (37), 43 (100)
5*a*	3.45 (s, 3H), 4.76 (s, 2H)	—	—
6	1.14 (t, 3H), 1.47 (s, 3H), 1.89 (t, 3H), 2.64 (q, 2H), 3.30 (s, 3H)	—	—
7	1.16 (t, 3H), 2.03 (t, 3H), 2.28 (s, 3H), 2.53 (q, 2H)	—	—
8*a*	3.50 (s, 3H), 4.98 (s, 2H)	—	—
11	1.40 (s, 3H), 2.33 (s, 3H), 3.41 (s, 3H)	—	—
12	1.13 (t, 3H), 2.31 (q, 2H), 3.67 (s, 3H)	6.6	88 (26), 57 (36), 57 (100)
14*a*	3.36 (s, 6H), 4.58 (s, 2H)	4.1	76 (2), 75 (46), 45 (100)
14*b*	1.26 (d, 3H), 3.31 (s, 6H), 4.51 (q, 1H)	4.6	75 (93), 59 (100), 43 (49)
15	3.77 (d, 3H), 8.08 (q, 1H)	4.2	60 (100)
16	2.32 (s, 6H)	8.0	86 (8), 43 (100)
17	1.37 (s, 3H), 2.23 (s, 3H), 3.24 (s, 6H)	16.3	101 (2), 89 (4), 43 (100)

[a]Gas chromatography conditions: glass column 0.3 × 500 cm, 5% Carbowax 20 M on Chromosorb G; 60–160°C at 4°C/min.

Can. J. Chem. Downloaded from www.nrcresearchpress.com by 80.58.250.72 on 09/07/12
For personal use only.

tuted conjugated dienes are bound to give solely abnormal diozonolysis products in methanol, irrespective of the nature and the position of alkyl or aryl substituents at the diene system. This is due to the fact that monochloro substituted double bonds are selectively cleaved to give acyl chloride and nonchlorinated carbonyl oxide fragments (5). As a consequence, the second cleavage step in the diozonolysis of 1-chloro substituted dienes generates vicinal bismethoxyhydroperoxides like **9** or α-oxo-methoxyhydroperoxides like **11**, both of which are thermally labile and undergo spontaneous fragmentation at room temperature with concurrent rupture of the central single bond of the original diene system. In retrospect, this reaction course now also provides an explanation for the previously observed anomalous ozonolysis of **1**, which could not be rationalized at that time.

Experimental

Materials

Chemicals, solvents, and technical gases were of commercial grades.

Methods

The ^{1}H nmr spectra were recorded in $CDCl_3$/TMS on a Bruker WP 60 and the ir spectra on a Beckman 4260 instrument. The gc analyses were carried out on a Shimadzu model 6A and gc/ms on a Hewlett Packard instrument 5985B. Analytical data that were used for the qualitative and (or) quantitative determination of ozonolysis products are compiled in Table 1.

The yields of diozonolysis products are based on the presence of a measured amount of 1,1,2,2-tetrachloroethane as a standard. The yields of products derived from **4***a* are calculated such that the maximum attainable yields of the fragments derived from the CH_2, CH_3CH_2CCl, and $CH_3C{-}CCH_3$ moieties amounted to 100% each. The yields of products derived from **4***b* are calculated such that the maximum attainable yields of the fragments derived from the CH_3CH_2CCl moiety on the one hand, and from the combined CH_3CH and $CH_3C{-}CCH_3$ moieties on the other hand, amounted to 100% each. This is based on the fact that fragments **5***b* and **8***b* are eventually converted into **2**, viz. by HCl-catalyzed dehydration of **8***b* (6) and by HCl-catalyzed conversion of **5***b* into **14***b*, followed by ozone oxidation of the latter (7).

The yields of monoozonolysis products are calculated such that the maximum attainable yields of the moieties derived from cleavage of the nonchlorinated double bond amounted to 100% each.

Diozonolysis of **4**a

A mixture of 278 mg (1.9 mmol) of **4***a* (8), 217 mg (1.3 mmol) of 1,1,2,2-tetrachloroethane, and 381 mg (11.9 mmol) of methanol was ozonized to completion at −60°C, flushed with nitrogen, and divided into two parts. The first part was warmed up to room temperature; ^{1}H nmr analysis showed the presence of **2**, **12**, **14***a*, and **15** in yields of 96, 75, 42, and 10%, respectively. The second part was immediately admixed with DMS-d_6 and slowly warmed up to room temperature; ^{1}H nmr analysis showed the presence of **2**, **12**, **14***a*, and **16**[2] in yields of 60, 63, 58, and 35%, respectively. The assignments of the above structures have been confirmed by gc/ms analyses.

Diozonolysis of **4**b

A mixture of 163 mg (1.00 mmol) of **4***b* (8), 130 mg (0.78 mmol) of 1,1,2,2-tetrachloroethane, and 215 mg (6.70 mmol) of methanol was ozonized to completion at −60°C, flushed with nitrogen, and divided into two parts. These were treated further as described above; ^{1}H nmr analysis showed the presence of **2** and **12** in yields of 95 and 100%, respectively, in the colorless product obtained after direct warm-up, and the presence of **2**, **12**, **14***b*, **16**,[2] and **17** in yields of 18, 64, 53, 27, and 20%, respectively, in the yellow product obtained after reduction with DMS-d_6. The product identification was confirmed by gc/ms analysis.

Monoozonolysis of **4**a

(a) Isolation of **6**

A solution of 1.44 g (10 mmol) of **4***a* (8) in 20 mL of methanol was treated with 8 mmol of ozone at −78°C. The crude product was admixed with 135 mg (2.5 mmol) of sodium methoxide, warmed up to room temperature, and concentrated to ca. one-half of the original volume in a rotary evaporator at 15 Torr (1 Torr = 133.3 Pa) and room temperature. Flash chromatography (column 2 × 60 cm, 105 g of silica gel, *n*-hexane/ether 9:1) of the concentrate afforded 291 mg (15%) of **6**.

[(E)-3-Chloro-1,2-dimethyl-1-methoxy-2-pentenyl]-hydroperoxide (6): Colorless liquid; ir (film): 3380 (OOH), 1630 (C=C) cm^{-1}; ^{1}H nmr (recorded in the presence of solid potassium carbonate), δ: 1.14 (t, J = 7.5 Hz, 3H), 1.47 (s, 3H), 1.89 (t, J = 0.9 Hz, 3H), 2.64 (q, J = 7.5 Hz, 2H), 3.30 (s, 3H), 7.83 (bs, 1H).

(b) Determination of product distribution

A solution of 720 mg (5 mmol) of **4***a* (8), 750 mg (4.47 mmol) of 1,1,2,2-tetrachloroethane, and 990 mg (31 mmol) of methanol in 3 mL of $CDCl_3$ was treated with 192 mg (4.0 mmol) of ozone at −60°C, admixed with 68 mg (1.25 mmol) of sodium methoxide, and warmed up to room temperature; ^{1}H nmr analysis showed the presence of **2**, **6**, **8***a*, and **12** in yields of 5, 87, 93, and 5%, respectively.

[2]Due to overlap of the CH_3CO singlet signal of **16** with the CH_2 quartet of **12**, the yield of **16** was determined by the difference between the total intensity of these two signal groups and the intensity of the $CH_3(CH_2)$ signal of **12**.

(c) Reduction of ***6***

A solution of **6** in $CDCl_3$ (previously shaken with potassium carbonate) was admixed with 35 mg of triphenylphosphine; ^1H nmr analysis after 5 min showed the signals of **7** and no residual signals of **6**.

Monoozonolysis of ***4***b

A solution of 314 mg (2.0 mmol) of ***4b*** (8), 236 mg (1.4 mmol) of 1,1,2,2-tetrachloroethane, and 234 mg (7.3 mmol) of methanol in 2 mL of $CDCl_3$ was treated with 763 mg (1.5 mmol) of ozone at −55°C, admixed with 27 mg (0.5 mmol) of sodium methoxide, and warmed up to room temperature. The ^1H nmr analysis showed the presence of **2**, **6**, **7** (8), ***8b*** (δ: 1.32 (d, J = 5.3 Hz, 3H), 3.49 (s, 3H), 4.95 (q, 1H)), and **12** in yields of 3, 28, 59, 39, and 3%, respectively.

Ozonolysis of ***6***

A solution of 190 mg (0.98 mmol) of **6**, 249 mg (1.88 mmol) of 1,1,2,2-tetrachloroethane, and 170 mg (5.31 mmol) of methanol in 2 mL of $CDCl_3$, which had been shaken with potassium carbonate, was ozonized at −60°C and divided into two parts. One part was warmed up to room temperature; ^1H nmr analysis of the strongly peroxidic solution showed the presence of **2** and of **12** in yields of 82 and 79%, respectively. The second sample was admixed with 15 drops of DMS-d_6 and warmed up to room temperature; ^1H nmr analysis showed the presence of **2**, **12**, and **16**[2] in yields of 14, 65, and 81%, respectively. The identification of the products in the second sample was confirmed by gc/ms analysis.

Ozonolysis of ***7***

A solution of 189 mg (1.30 mmol) of **7** (8), 129 mg (0.77 mmol) of 1,1,2,2-tetrachloroethane, and 249 mg (7.78 mmol) of methanol in 2 mL of $CDCl_3$ was divided into three equal parts and each part was ozonized to completion at −60°C. The first sample was warmed up to room temperature, and the second sample was admixed with 5 drops of DMS-d_6 and subsequently warmed up to room temperature. The ^1H nmr analysis showed the presence of **2** and **12** in yields of ca. 100% each, in the first sample, and the presence of **2**, **12**, **16**, and **17** in yields of 43, 100, 15, and 36%, respectively, in the second sample. The identification of the above products was confirmed by gc/ms analyses. The third sample was immediately analyzed by ^1H nmr spectroscopy at −60°C, which showed the signals of **10** (δ: 1.24, t, J = 7.0 Hz; 2.97, q) and of **11** (6). The ^1H nmr analysis of the same sample ca. 5 min after it had reached 0°C showed the presence of **2** and **12** as the single major components.

Acknowledgment

Support of this research by the Sonderforschungsbereich 62 is gratefully acknowledged.

1. H. SCHNEIDER and K. GRIESBAUM. J. Org. Chem. **44**, 3316 (1979).
2. H. SCHNEIDER and K. GRIESBAUM. Tetrahedron Lett. 1705 (1979).
3. D. G. WILLIAMSON and R. J. CVETANOVIĆ. J. Am. Chem. Soc. **90**, 4248 (1968).
4. K. GRIESBAUM, G. ZWICK, S. AGARWAL, H. KEUL, B. PFEFFER, and R. W. MURRAY. J. Org. Chem. **50**, 4194 (1985).
5. H. KEUL and K. GRIESBAUM. Can. J. Chem. **58**, 2049 (1980).
6. K. GRIESBAUM and H. KEUL. Angew. Chem. **87**, 748 (1975).
7. P. DESLONGCHAMPS and C. MOREAU. Can. J. Chem. **49**, 2465 (1971).
8. K. GRIESBAUM, A. R. BANDYOPADHYAY, and M. MEISTER. Can. J. Chem. **64**, 1553 (1986).

Can. J. Chem. Downloaded from www.nrcresearchpress.com by 80.58.250.72 on 09/07/12
For personal use only.

A Raman spectroscopic study of the complexation of the methylmercury(II) cation by amino acids

SERGE ALEX AND RODRIGUE SAVOIE
Département de chimie et C.R.A.M., Université Laval, Québec (Qué.), Canada G1K 7P4

Received June 23, 1986

SERGE ALEX and RODRIGUE SAVOIE. Can. J. Chem. **65**, 491 (1987).

A systematic Raman spectroscopic investigation of the complexation of CH_3Hg^+ by the standard amino acids is reported. It is shown that the vibrational bands due to the ligand—Hg and Hg—CH_3 stretching modes and to the symmetric —CH_3 bending mode of the —$HgCH_3$ unit are well suited to characterize the extent of complexation and the sites of attachment of the cation. Coordination, which occurs mostly on sulfur and nitrogen atoms by substitution of a proton on the thiol group of cysteine or on amino groups in general, is best identified by the frequency of the ligand—Hg stretching vibration in the 250–550 cm^{-1} region of the spectrum.

SERGE ALEX et RODRIGUE SAVOIE. Can. J. Chem. **65**, 491 (1987).

La complexation de l'ion CH_3Hg^+ par les acides aminés usuels a été étudiée systématiquement par spectroscopie Raman. On démontre que les bandes dues aux vibrations de valence des ensembles ligand—Hg et Hg—CH_3, de même que celle attribuable au mode de déformation symétrique du groupe CH_3, réflètent bien le degré de complexation et le site de fixation du cation. La coordination, qui implique principalement les atomes de soufre et d'azote suite à une substitution d'un proton sur le groupe thiol de la cystéine ou sur les groupes aminés en général, est la mieux identifiée par la fréquence du mode de vibration de valence ligand—Hg dans la région de 250 à 550 cm^{-1} du spectre.

Can. J. Chem. Downloaded from www.nrcresearchpress.com by 80.58.250.72 on 09/07/12
For personal use only.

Introduction

The mercury (Hg^{2+}) and methylmercury (CH_3Hg^+) cations are known to react extensively with living organisms (1). The main targets for this type of complexation are thiol ligands (2–5), such as the cysteine residues in proteins, although other sites are also involved. Complex formation through the sulfur atom is easily characterized by vibrational spectroscopy (4–9) and the substitution of a proton of an amino group by a methylmercury(II) cation also gives specific vibrational bands (10–13). We have recently studied in detail several complexes of methylmercury with some amino acids (alanine and glycine) (10), a dipeptide (glycylglycine) (11), and a small polypeptide (glutathione) (14). These studies have shown that the formation of S—Hg and N—Hg bonds by substitution of a proton on a —SH or —NH_3^+ group readily occurs in these systems. These complexation processes were followed by monitoring the frequencies and intensities of the ν(Hg—ligand), ν(Hg—CH_3), and $\delta(CH_3)$ bands (ν = stretching and δ = bending), which are particularly intense in the Raman spectra.

It became obvious in the above studies that the potential of Raman spectroscopy for determining the possible sites of complexation of the CH_3Hg^+ ion by amino acids and proteins in general had not been used to its full capacity. Also lacking in certain cases was an accurate knowledge of the conditions under which complexation could occur. The present paper gives an account of a systematic Raman spectroscopic investigation of this problem, using standard amino acids and small parent molecules.

Experimental

The amino acids in the zwitterionic or salt form were purchased from the Sigma Chem. Co. and used without further purification. The source of methylmercury(II) was the hydroxide CH_3HgOH (1 *M* aqueous solution from Alfa Inorganics). The various complexes, generally at a final concentration of 0.33 *M*, were prepared by direct mixing of appropriate quantities of aqueous solutions of the reagents. The pH was adjusted with 4 *M* NaOH or HNO_3. Reagents containing the easily oxidized —SH function were dissolved in distilled water in which nitrogen had been bubbled for ca. 15 min. Raman spectra were then recorded as soon as possible after the preparation of the complexes. The solid complexes reported here (e.g. $CH_3COOHgCH_3$) were in general prepared by mixing the appropriate amounts of the reagents (assuming a specific stoichiometry) and evaporating the solvent.

The Raman spectra, excited by the 514.5 nm line from a Spectra Physics 165 argon ion laser, were recorded on a Spex Model 1400 microcomputer-controlled spectrometer. The solutions were studied in capillary cells mounted in a copper block maintained at 10°C, except in the case of the aqueous solutions of tryptophan, where a temperature of 25°C was chosen to improve the solubility of the product (1% w/w). The spectra were typically recorded with a laser power of 300 mW at the sample. The spectral resolution was 5 cm^{-1}, one data point being recorded at each 2 cm^{-1} increment, with an integration time of 2 s per point. The spectra reproduced in this paper are original (unsmoothed) spectra.

Results and discussion

Aqueous methylmercury(II)

The methylmercury cation, CH_3Hg^+, is associated with water in aqueous solution, giving the hydroxide CH_3HgOH at high pH and the charged $CH_3HgOH_2^+$ and $(CH_3Hg)_2OH^+$ species at low pH. Note that the hydroxide can be regarded as a complex formed by the substitution of a proton of a water molecule by a CH_3Hg— group, whereas the charged species are in fact oxonium ions, resulting from a mono or disubstitution on the H_3O^+ ion. The completely substituted $(CH_3Hg)_3O^+$ ion can also exist (15), but we have had no indication of its occurrence. From the known formation constant of this species (15), it can be calculated that its concentration in the conditions that prevailed in the present study should be less than ca. 10^{-3} *M* (0.5%).

The distribution of the mercuric species as a function of pH in a 0.33 *M* aqueous solution is shown in Fig. 1. These curves were calculated using the equilibrium constants given by Libich and Rabenstein (16). The predominance of only one of the three species at certain pH values has allowed the recording of the Raman spectrum of each individually (Fig. 2). The spectra are very intense in the region shown (300–1300 cm^{-1}), with characteristic bands of the CH_3Hg moiety near 1210 cm^{-1} (symmetric bending mode, $\delta(CH_3)$) and 570 cm^{-1} (Hg—CH_3 stretching mode, ν(Hg—C)). The band due to the ν(Hg—O) vibration, which differs considerably both in intensity and frequency for each species, is particularly helpful in their

Can. J. Chem. Downloaded from www.nrcresearchpress.com by 80.58.250.72 on 09/07/12
For personal use only.

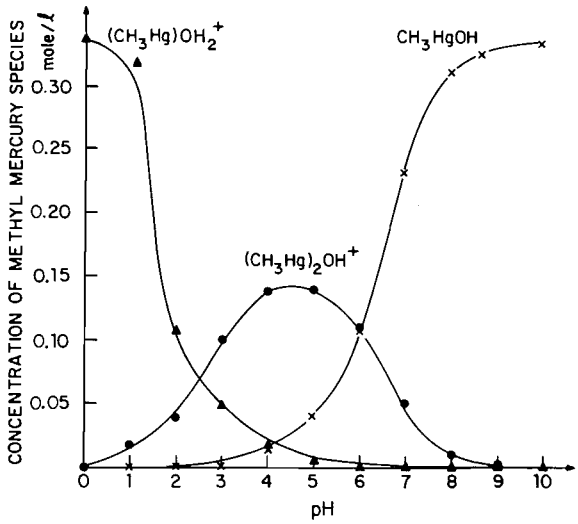

FIG. 1. Distribution of the species present in a 0.33 *M* aqueous solution of CH_3Hg^+ as a function of pH.

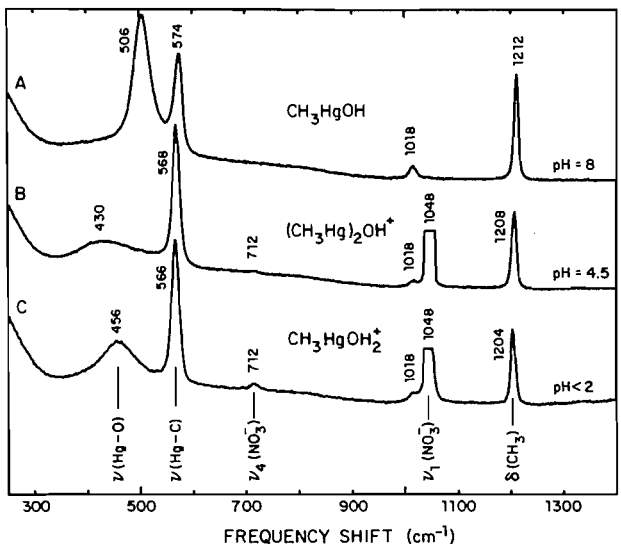

FIG. 2. Raman spectra of the species present in an aqueous solution of CH_3Hg^+ (8% w/w) as a function of pH.

identification and it can also be used to detect the presence of uncomplexed methylmercury in mixtures where complexation can occur. Also noteworthy is the hyperchromicity of the ν(Hg—C) band near 570 cm^{-1} in the charged complexes (peak-height intensity relative to the 1210 cm^{-1} band). The same effect has been found to occur following complex formation, throughout this study.

Substitution on amino groups

The charged NH_3^+ group of amino acids is a fair target for complex formation with the methylmercury cation. Rabenstein *et al.* (17) have determined by nuclear magnetic resonance spectroscopy the equilibrium constants associated with the formation of various complexes through nitrogen–mercury bonding:

$$RNH_3^+ + CH_3Hg^+ + H_2O \rightleftharpoons RNH_2HgCH_3^+ + H_3O^+$$

They showed that the complex formation constant is directly proportional to the pK_a of the NH_3^+ group, with a value of 10^7 to 10^8 at 25°C.

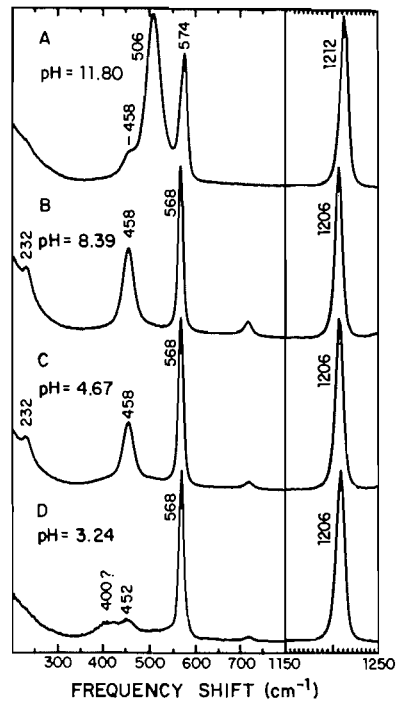

FIG. 3. Raman spectra of a 1:1 stoichiometric mixture of $CH_3NH_3^+$ and CH_3Hg^+ as a function of pH.

We have studied the simplest representative of this class of compounds, aminomethane, $CH_3NH_3^+$. The Raman spectra of equimolar aqueous mixtures of this compound and CH_3Hg^+ as a function of pH are shown in Fig. 3. The spectrum at pH 8.39 (Fig. 3 *B*) shows no sign of the 506 cm^{-1} band of CH_3HgOH, which is predominant in the spectrum of aqueous methylmercuric hydroxide at pH 8 (Fig. 2 *A*). On the other hand, a new band at 458 cm^{-1} in the spectrum can be unambiguously assigned to the ν(N—Hg) vibration of the $CH_3NH_2HgCH_3^+$ species, by comparison with similar complexes with glycine (460 cm^{-1}) (10, 12), alanine (476 cm^{-1}) (10), glycylglycine (462 cm^{-1}) (11), and even the NH_4^+ ion (468 cm^{-1}) (Table 1). This characteristic band is accompanied by a weaker peak at 232 cm^{-1}, assigned to the N—Hg—CH_3 bending mode of the complex, as this type of vibration in similar molecules has been found to occur in this region (15, 18–21).

The spectra shown in Fig. 3, together with those of aqueous methylmercuric hydroxide (Fig. 2), clearly delimitate the pH range in which complexation takes place (ca. pH 4–11). At pH ca. 3, the two bands near 400 and 450 cm^{-1} reveal the presence of uncomplexed $(CH_3Hg)_2OH^+$ and $CH_3HgOH_2^+$, with little, if any, of the complex present. At pH ca. 12, the presence of free CH_3HgOH is indicated by the strong 506 cm^{-1} band, the complex occurring in very small amount (458 cm^{-1} band). Our observations here are consistent with the nmr results (17), which showed that the methylamine complex is formed at intermediate pH values.

As can be seen in Table 1, the α-NH_3^+ group of amino acids consistently react with CH_3Hg^+, to give a complex of the —$NH_2HgCH_3^+$ type. In amino acids with no potentially reactive side chains, such as alanine, glycine, valine, leucine, isoleucine, and phenylalanine, this is the only type of complexation that should occur. The ν(N—Hg) stretching vibration of the complexes thus formed has a frequency in the range 460–475 cm^{-1} in aqueous solutions.

In the solid complexes, however, perturbations sometimes

TABLE 1. Frequencies of characteristic CH_3Hg—ligand vibrations in amino acid complexes, as a function of the attachment site (α-COO^-, side chain, and α-NH_3^+)

Complexed species	pH	Side-chain reactive group	ν(ligand—Hg)			ν(Hg—CH_3)			$\delta(CH_3)$		
			α-COO^-	Side chain	α-NH_3^+	α-COO^-	Side chain	α-NH_3^+	α-COO^-	Side chain	α-NH_3^+
NH_4^+ (SO_4^{2-})	7	—	—	—	468	—	—	570	—	—	1205
$CH_3NH_3^+$	7	—	—	—	458	—	—	568	—	—	1206
Glycine[a]	7	—	—	—	460	—	—	561	—	—	1205
Glycine[a]	(Solid)	—	—	—	470	—	—	559	—	—	1200
Alanine[a]	6–7	—	—	—	475	—	—	562	—	—	1206
Alanine[a]	(Solid)	—	—	—	546[b]	—	—	546[b]	—	—	1192
Lysine	7	NH_3^+	—	456	470	—	—	560	—	—	1205
*N*α-Acetyl-L-lysine	7	NH_3^+	—	456	—	—	560	—	—	1206	—
*N*ε-Acetyl-L-lysine	7	—	—	—	470	—	—	560	—	—	1204
Arginine (hydrochloride)	7	NH_2^+	—	—	470	—	—	564	—	—	1204
Histidine (hydrochloride)	7	NH^+	—	452	472	—	—	564	—	—	1206
Asparagine	7	$CONH_2$	—	—	472	—	—	564	—	—	1204
Tryptophan	7	NH	—	440	474	—	—	564	—	1200[b]	1210[b]
Tryptophan[d]	(Solid)	NH	—	486[b]	486[b]	—	—	560	—	—	1198
Proline (NH group)	7	—	—	—	452	—	—	560	—	—	1202
HCOOH	3–4	—	400	—	—	560	—	—	1205	—	—
CH_3COOH	4–5	—	506	—	—	566	—	—	1206	—	—
$CH_3COO^-Na^+$	(Solid)	—	498	—	—	560	—	—	1194	—	—
Aspartic acid	3–4	COO^-	—	—	472	—	—	562	—	—	1204
Glutamic acid (Glu)	7	COO^-	—	(506)	472	—	—	562	—	—	1204
Glutamic acid (Glu)	(Solid)	COO^-	—	499	542[b]	—	555	542[b]	—	—	1199
N-acetyl-L-Glu	4–6	COO^-	—	518?	—	—	562	—	—	1204	—
N-acetyl-L-Glu	(Solid)	COO^-	—	520	—	—	556	—	—	1196	—
L-Glu γ-ethyl ester	7	—	—	—	470	—	—	560	—	—	1204
L-Glu γ-ethyl ester	(Solid)	—	—	—	546[b]	—	—	546[b]	—	—	1206
Glycylglycine[c]	7	—	—	—	462	—	—	564	—	—	1206
Glycylglycine (1:1)[c]	(Solid)	—	—	—	466	—	—	558	—	—	1202
Glycylglycine (1:2)[c]	(Solid)	—	536	—	~450	572	—	560	1202	—	1220
Serine[d]	(Solid)	OH	—	—	476	—	—	560	—	—	1204
Cysteine	7	SH	—	328	460	—	544	—	—	1190	1210
Methionine	7	SCH_3	—	—	468	—	—	560	—	—	1204
Methionine	<2	SCH_3	—	285	—	—	544	—	—	1188	—

[a]Reference 10.
[b]Overlapping or superimposed bands.
[c]Reference 11.
[d]Complex prepared by M.-C. Corbeil and A. L. Beauchamp, Département de chimie, Université de Montréal.

occur and no band appears in the 470 cm^{-1} region of the spectrum. Examples of this are found in the complexes with alanine, glutamic acid, and the γ-monoethyl ester of glutamic acid (see Table 1). In these cases, it is also observed that the ν(Hg—CH_3) mode is displaced by ca. 20 cm^{-1}, at ca. 545 cm^{-1}. The likely explanation for this anomaly is an accidental coincidence of the ν(Hg—N) and ν(Hg—C) vibrations, which is likely due to structural factors in the solids. A similar effect has been observed by Wong *et al.* (6) in a complex with methionine, the spectrum of which gave a single peak at 543 cm^{-1} (ν(Hg—N) + ν(Hg—C)) in the normal compound and a doublet at 518 (ν(Hg—N)) and 534 cm^{-1} (ν(Hg—C)) in the amino deuterated compound.

The proton on the NH group of the "abnormal" amino acid proline can be substituted to some extent by CH_3Hg^+ in the pH range ca. 5–10. However, the reaction is incomplete, even in the presence of a tenfold excess of the methyl mercury cation. The weak ν(Hg—N) Raman band characterizing the complex occurs at a relatively low frequency, 452 cm^{-1}, and it is accompanied by the δ(N—Hg—C) bending mode at 186 cm^{-1}, a value which is also lower than that observed in most α-NH_3^+ substituted complexes (ca. 230 cm^{-1}).

A special effort has been made in the present study to characterize the complexation of CH_3Hg^+ by charged amino groups contained in the side chains of some amino acids (lysine, arginine, and histidine), as this type of complexation is likely to occur extensively in polypeptides and proteins containing these residues. Lysine proved to be a poor model compound for this purpose, as its charged (—NH_3^+) side chain is neutralized by a counterion which preferentially reacts with CH_3Hg^+. For example, with the bromide salt at pH ≧ 7, the spectra were dominated by strong peaks attributable to CH_3HgBr, at 118 cm^{-1} (δ(C—Hg—Br)), 206 cm^{-1} (ν(Hg—Br)), 546 cm^{-1} (ν(Hg—C)), and 1172 cm^{-1} ($\delta(CH_3)$). To circumvent this difficulty, we have used lysine derivatives in which each amino function was selectively blocked by an acetyl group. These molecules exist as zwitterionic species and do not require an extra counterion for charge neutralization. The spectra obtained with the two derivatives are shown in Fig. 4 *A* and *B*. When the side-chain amino group is blocked, complexation takes place on

Can. J. Chem. Downloaded from www.nrcresearchpress.com by 80.58.250.72 on 09/07/12
For personal use only.

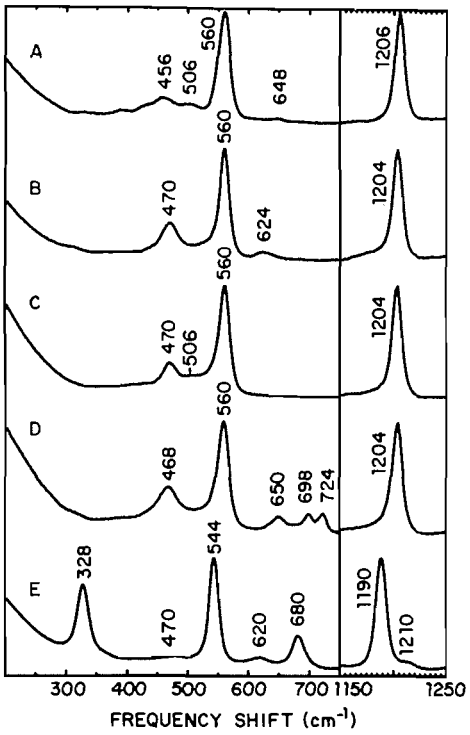

FIG. 4. Raman spectra of 1:1 stoichiometric mixtures (0.33 *M*, pH ca. 7) of CH_3Hg^+ and (*A*) *N*-α-acetyl-L-lysine, (*B*) *N*-ε-acetyl-L-lysine, (*C*) glutamic acid, (*D*) methionine, and (*E*) cysteine.

the α-NH_3^+ group and the normal ν(Hg—N) vibrational band is observed at 470 cm^{-1} (Fig. 4 *B*). On the other hand, when only the side-chain NH_3^+ group is free to react, the corresponding band is found at 456 cm^{-1} (Fig. 4 *A*). The spectrum also indicates that only partial complexation occurs, the presence of free CH_3HgOH being revealed by the 506 cm^{-1} band.

Our study of the complexation of CH_3Hg^+ by the side-chain NH_2^+ groups of arginine (hydrochloride salt) was hampered by the presence of Cl^- ions in the solutions. Although the rate constants for the formation of CH_3HgX compounds (X = Cl, Br, and I) are more important for the heavier halides (22), these constants clearly indicate that the formation of CH_3HgCl is strongly favored at low pH, whereas CH_3HgOH species should be predominant at high pH. Coordination of CH_3Hg^+ on amino groups normally occurs at intermediate pH values. Our attempts to identify specific Raman bands indicative of complexation on the side-chain —NH_2^+ groups of arginine failed, even at large CH_3Hg^+/arginine ratios. In contrast, substitution of the proton of the NH^+ group on the side chain of histidine was found to take place, giving a ν(Hg—N) vibration at 452 cm^{-1}. The negative results obtained with arginine are possibly related to the very high pK_a (ca. 12) of the side-chain group of this amino acid, which could shift the region of stability of the complex to higher pH, where the competitive reaction with OH^- species is favored.

The amide (—$CONH_2$) function on the side chain of asparagine was found to be unreactive towards the CH_3Hg^+ cation. The same conclusion is probably applicable to glutamine. On the other hand, in a solid complex obtained with tryptophan (see Table 1), complexation was indicated on the —NH group of the pyrrole unit (as well as on the α-NH_3^+ function). This was easily established from the modifications brought to the Raman spectrum of tryptophan (23), in particular from the reduced intensity of the band due to the ν(N—H) stretching mode at 3350 cm^{-1}. Only one band, at ca. 486 cm^{-1}, was found for the two expected ν(Hg—N) modes. In aqueous mixtures of tryptophan and CH_3Hg^+, the results suggested that partial complexation simultaneously occurred on both the —NH and —NH_3^+ groups, independent of the quantity of CH_3Hg^+ present. This interpretation is based on the presence in the spectra of a doublet with components at 440 and 474 cm^{-1}, respectively assigned to the ν(Hg—N) modes of the pyrrole—mercury and (α-amino)—mercury units. The value of the ν(pyrrole—Hg) vibration is comparable to that in the complex with proline (452 cm^{-1}), but it is much higher than the corresponding values proposed in similar complexes with pyridine (204–208 cm^{-1}) (24), adenine (25), and 9-methyl adenine (26) ($\nu < 300\ cm^{-1}$). The Raman spectrum of the solid complex with tryptophan also shows a band at 258 cm^{-1}, but the latter probably belongs to the δ(N—Hg—CH_3) vibration.

Coordination on carboxylate groups

The results of a proton nmr study of the complexation of the methyl mercury cation by the main organic acids (16) have indicated that the equilibrium constants of the reaction

$$RCOO^- + CH_3Hg^+ \rightleftharpoons RCOOHgCH_3$$

(10^2 to 10^3 at 25°C) are much weaker than for the substitution reaction on protonated amino groups (17). In fact, spectroscopic observations of complexes of this type have been very limited and the frequency of the ν(Hg—O) vibration is not well established. Vibrational frequencies have been reported at 279 and 295 cm^{-1} in $(CH_3COO)_2Hg$ and $(CH_3COO)_2Hg_2$, respectively (27), 300–400 cm^{-1} for Pt—glycine complexes (13), ca. 500 cm^{-1} in Zn^{2+}—glycine (28) and metal—EDTA (29) complexes, and 496 cm^{-1} for the ν(Fe—O) vibration of hemoglobin (30).

In order to better specify the frequency of the ν(Hg—O) vibration in acid—$HgCH_3$ complexes, we have studied by Raman spectroscopy the complexation of CH_3Hg^+ by formic and acetic acid. The spectra of the $CH_3COOHgCH_3$ complex in the solid phase is compared with that of the CH_3COO^- ion in Fig. 5. The interpretation of the spectrum of the solid complex is straightforward. The ν(Hg—O) vibration gives a sharp peak at 498 cm^{-1}, on the low-frequency side of the ν(Hg—C) band at 560 cm^{-1}. Also seen in the spectra are the δ(O—Hg—CH_3) band at 284 cm^{-1} and the δ(CH_3) peak at 1194 cm^{-1}. The spectrum of the ligand (31) is appreciably modified upon complex formation. In particular, one notes the disappearance of the band due to the symmetric stretching mode of the COO^- group, which is present at 1418 cm^{-1} in the spectrum of solid CH_3COONa. In aqueous solution, the spectrum (Fig. 5 *A*) shows bands due to unreacted acetic acid (894 and 1702 cm^{-1}) and to the free methylmercury ion (broad underlying band at ca. 450 cm^{-1}), which indicate that only partial complexation takes place. The characteristic bands of the complex then occur at 288, 506, 566, and 1206 cm^{-1}. The spectrum obtained upon mixing an aqueous solution of HCOOH and CH_3Hg^+ at pH 3–4 is very similar to that obtained with acetic acid, except for the ν(Hg—O) vibration which occurs at a lower frequency (400 cm^{-1}; other peaks at 274, 560, and 1205 cm^{-1}).

The ca. 500 cm^{-1} frequency for the ν(Hg—O) vibration in the complex with acetic acid is consistent with the 536 cm^{-1} value already suggested for a carboxylate-bound CH_3Hg(II) complex of glycylglycine whose structure was firmly established by X-ray diffraction (11). The fact that this vibration

Can. J. Chem. Downloaded from www.nrcresearchpress.com by 80.58.250.72 on 09/07/12
For personal use only.

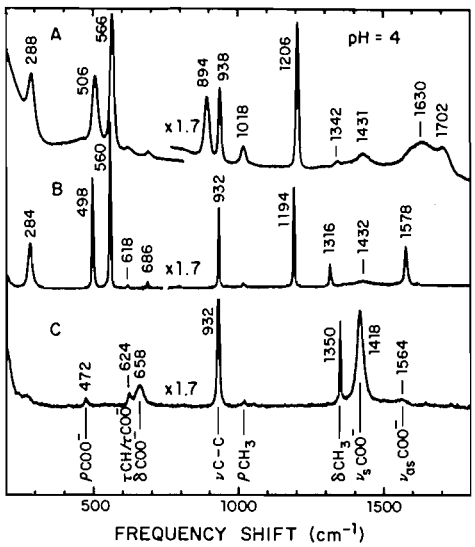

FIG. 5. Raman spectra of the $CH_3COOHgCH_3$ complex (*A*) in aqueous solution at pH 7 and (*B*) in the solid state. (*C*) Raman spectrum of CH_3COONa.

occurs at a higher frequency than that of average ν(Hg—N) vibrations (ca. 470 cm^{-1}) is unexpected as the opposite would be predicted from the relative masses of the oxygen and nitrogen atoms. The explanation for this apparent anomaly is possibly related to the relative strength of the O—Hg and N—Hg bonds, which are of different lengths (32), and to the presence of a positive charge on the nitrogen atom.

We have had no indication in the present and previous studies (10), that the α-COO^- group of amino acids reacts to any appreciable extent with CH_3Hg^+ in aqueous solution, although some solid complexes of this type have been obtained, such as the 2:1 (CH_3Hg^+:GlyGly) compound with glycylglycine (11). On the other hand, a weak band at 506 cm^{-1} in the spectrum of aqueous mixtures of glutamic acid and CH_3Hg^+ in the pH range 1 to 7 (see Fig. 4 *C*) indicates that the COO^- group on the side chain of this amino acid is slightly reactive towards the methylmercury cation. The origin of the band at 506 cm^{-1} (499 cm^{-1} in the solid complex) was ascertained from the spectra of selectively blocked glutamic acid derivatives (see Table 1). This band was not present in the spectrum of the γ-monoethyl ester of the acid, in which the side-chain carboxylate group is not available for complexation. On the other hand, in *N*-acetyl glutamic acid, where the α-NH_3^+ end is transformed into —NHC(=O)CH_3, interaction with the side-chain COO^- group took place, with resulting ν(Hg—O) band near 520 cm^{-1}. Also observed in this case was a band at 456 cm^{-1}, which had its maximum intensity at pH ca. 4, and which is believed to arise from the —$NH(HgCH_3^+)C(=O)CH_3$ complex.

It should be noted that the pK_a of the γ-COOH group of glutamic acid and of the β-COOH group of aspartic acid are quite similar (ca. 4) to that of acetic acid, which reacts appreciably with CH_3Hg^+, whereas the pK_a of the unreactive α-COOH group of amino acids are appreciably lower (ca. 2).

Coordination on sulfur atoms

Amino acids containing an OH group on their side chain (serine, threonine, and tyrosine) failed to show any side-chain complexation with CH_3Hg^+. Methionine, with —SCH_3 side group, showed the same behavior in the pH range 3 to 11 (Fig. 4 *D*). However, at very low pH (<2) metallation occurred on the sulfur atom, giving the R—$S(HgCH_3)CH_3^+$ charged species, which is characterized by the ν(Hg—S) vibrational band at 285 cm^{-1} (other peaks at 544 and 1188 cm^{-1}). Our results here are consistent with those of previous studies which indicated coordination of the thioether by Hg(II) (33) and CH_3Hg(II) (34) in very acidic solutions.

The —SH group of cysteine is known to be very reactive towards CH_3Hg^+ (35, 36), forming a very stable —$SHgCH_3$ unit (37). The vibrations of the methylmercury moiety in this complex are very characteristic on account of their relatively low frequencies: ν(Hg—S): 328 cm^{-1}, ν(Hg—C): 544 cm^{-1}, and $\delta(CH_3)$: 1190 cm^{-1} (4, 8, 9, 14). By monitoring the intensity of the ν(S—H) Raman band at 2580 cm^{-1} (38) we have confirmed that the substitution of the proton of the thiol group occurs preferentially to that on NH_3^+. The ν(S—Hg) vibrational band of the thiol-substituted complex (328 cm^{-1}) is predominant in the spectrum (Fig. 4 *E*), which also shows that both the ν(Hg—CH_3) and $\delta(CH_3)$ vibrations in this complex have frequencies which are 15 to 20 cm^{-1} lower than the usual frequencies for these modes. The very weak band at ca. 470 cm^{-1} in this spectrum indicates that some substitution has also occurred on the —NH_3^+ group in a 1:1 stoichiometric mixture of CH_3Hg^+ and cysteine. Given the much greater tendency for CH_3Hg^+ to bind to thiol groups compared to amino functions, it is unlikely that this metal ion will complex to —NH_3^+ while there are free thiol groups available. Our observations can probably be explained by a slight lowering of the concentration of cysteine in the solutions due to oxidation to cystine. A similar effect was encountered in our study of the complexation of CH_3Hg^+ by glutathione (14).

When disubstitution (—S and —N) occurred on cysteine, the resulting complex precipitated. Furthermore, when an excess of CH_3Hg^+ was present in the solutions, precipitation of L-cystine also occurred, this oxidized compound being only sparingly soluble in water at pH 1 to 8. This was followed in the Raman spectra by the appearance of a strong and sharp line at 498 cm^{-1}, attributable to the ν(S—S) vibration of the bridging unit (39). Metals are known to slowly oxidize thiols, especially at high pH (35). It is not clear, however, if the present oxidation process was due to the presence of CH_3Hg^+ alone or if it was triggered by the presence of traces of oxygen in the solution.

Summary and conclusion

Amino acids can react in a number of ways with the methylmercury cation. The reactivity of the possible coordination sites are as follows:

Terminal NH_3^+ (all amino acids): substitution of a proton readily occurs in the pH range ca. 4 to 11; ν(Hg—N): 460–475 cm^{-1} in aqueous solution, sometimes missing in solid complexes due to structural effects.

Side-chain NH_3^+ (lysine): less reactive than the α-amino end of the acid; partial substitution on this group in aqueous solution, in the same pH range as for the terminal NH_3^+ groups, but with ν(Hg—N) at a slightly lower frequency (452 cm^{-1}).

Terminal COO^- (all amino acids): no coordination detected in aqueous solution although solid complexes can be obtained; ν(Hg—O): >500 cm^{-1}.

Side-chain COO^- (glutamic acid): very slightly reactive in acid aqueous solution (aspartic acid less reactive); ν(Hg—O): >500 cm^{-1}.

Terminal NH (proline): substitution of the proton can take place to some extent in the pH range 5–10; ν(Hg—N): 452 cm^{-1}, δ(N—Hg—C): 186 cm^{-1}.

Can. J. Chem. Downloaded from www.nrcresearchpress.com by 80.58.250.72 on 09/07/12
For personal use only.

—$NHC(NH_2)_2^+$ (arginine): no reaction of this group was detected in aqueous solution.

—NH^+ (histidine): substitution of the proton in aqueous solution; ν(Hg—N): 452 cm^{-1}.

—NH (tryptophan): the reactivity of this group in aqueous solution is comparable to that of the α-NH_3^+ group and occurs at the same time; ν(Hg—N): 440 cm^{-1}?

—OH (serine, threonine, and tyrosine): no reaction of this group detected in aqueous solution.

—$C(=O)NH_2$ (asparagine and glutamine): no reaction of this group detected in aqueous solution.

—SH (cysteine): the most reactive site in amino acids. Substitution occurs preferentially to that on NH_3^+ groups; ν(Hg—S): 328 cm^{-1}, ν(Hg—C): 544 cm^{-1}, and $\delta(CH_3)$: 1190 cm^{-1}.

—SCH_3 (methionine): no reaction in the pH range 3 to 11, but some coordination on the sulfur atom at very low (<2) pH; ν(Hg—S): 285 cm^{-1}.

The results of the present spectroscopic investigation on the coordination of CH_3Hg^+ by amino acids can probably be used in similar studies on polypeptides and proteins. Attempts along that line in our laboratory have indicated that this assumption is partly justified. However, the complexation of CH_3Hg^+ by biopolymers often cause important secondary effects, such as precipitation and conformational changes, which modify the Raman spectra in a more pronounced manner than would normally be expected from the bare complexation process.

Acknowledgements

Financial support of this work by the Natural Sciences and Engineering Research Council of Canada and by the Ministère de l'Education du Québec is gratefully acknowledged. The authors also wish to thank M.-C. Corbeil and A. L. Beauchamp from the Département de chimie de l'Université de Montréal for many helpful discussions concerning this work and their involvement in the synthesis of some of the complexes studied.

1. M. J. Inskip and J. K. Piotrowski. J. Appl. Toxicol. **5**, 113 (1985).
2. L. A. AE Scuyterman and J. Wijdenes. Eur. J. Biochem. **71**, 383 (1976).
3. D. L. Rabenstein and R. S. Reid. Inorg. Chem. **23**, 1246 (1984).
4. C. Perchard, M. H. Baron, and C. de Loze. J. Mol. Struct. **112**, 247 (1984).
5. A. P. Arnold, A. J. Canty, P. W. Moors, and G. B. Deacon. J. Inorg. Biochem. **19**, 319 (1983).
6. Y. S. Wong, A. J. Carty, and P. C. Chieh. J. Chem. Soc. Dalton Trans. 1157 (1977).
7. Y. S. Wong, P. C. Chieh, and A. J. Carty. J. Chem. Soc. Chem. Commun. 741 (1973).
8. N. J. Taylor, Y. S. Wong, P. C. Chieh, and A. J. Carty. J. Chem. Soc. Dalton Trans. 438 (1975).
9. Y. K. Sze, A. R. Davis, and G. A. Neville. Inorg. Chem. **14**, 1969 (1975).
10. M.-C. Corbeil, A. L. Beauchamp, S. Alex, and R. Savoie. Can. J. Chem. **64**, 1876 (1986).
11. S. Alex, R. Savoie, M.-C. Corbeil, and A. L. Beauchamp. Can. J. Chem. **64**, 148 (1986).
12. T. V. Long, II, and C. M. Yoshida. Inorg. Chem. **7**, 1754 (1967).
13. J. A. Kieft and K. Nakamoto. J. Inorg. Nucl. Chem. **29**, 2561 (1967).
14. S. Alex and R. Savoie. J. Raman Spectrosc. In press.
15. D. L. Rabenstein, C. A. Evans, M. C. Tourangeau, and M. T. Fairhurst. Anal. Chem. **47**, 338 (1975).
16. S. Libich and D. L. Rabenstein. Anal. Chem. **45**, 118 (1973).
17. D. L. Rabenstein, R. Ozubko, S. Libich, C. A. Evans, M. T. Fairhurst, and C. Suvanprakorn. J. Coord. Chem. **3**, 263 (1974).
18. D. L. Rabenstein, M. C. Tourangeau, and C. A. Evans. Can. J. Chem. **54**, 2517 (1976).
19. J. H. S. Green. Spectrochim. Acta, Part A, **24**, 863 (1968).
20. P. L. Goggin and L. A. Woodward. Trans. Faraday Soc. **58**, 1495 (1962).
21. J. H. R. Clarke and L. A. Woodward. Trans. Faraday Soc. **64**, 1041 (1968).
22. R. B. Simpson. J. Chem. Phys. **46**, 4775 (1967).
23. A. Y. Hirakawa, Y. Nishimura, T. Matsumoto, M. Nakanishi, and M. Tsuboi. J. Raman Spectrosc. **7**, 282 (1978); R. P. Rava and T. G. Spiro. J. Am Chem. Soc. **106**, 4062 (1984).
24. K. H. Tan and M. J. Taylor. Aust. J. Chem. **33**, 1753 (1980).
25. R. Savoie, J.-J. Jutier, L. Prizant, and A. L. Beauchamp. Spectrochim. Acta, Part A, **38**, 561 (1982).
26. R. Savoie, D. Poirier, L. Prizant, and A. L. Beauchamp. J. Raman Spectrosc. **11**, 481 (1981).
27. R. P. J. Cooney and J. R. Hall. J. Inorg. Nucl. Chem. **34**, 1519 (1972).
28. K. Krishnan and R. A. Plane. Inorg. Chem. **6**, 55 (1967).
29. A. A. McConnell and R. H. Nuttall. Spectrochim. Acta, Part A, **33**, 459 (1977).
30. A. T. Tu. Raman spectroscopy in biology: principles and applications. John Wiley and Sons Inc., New York, 1982. pp. 310–312.
31. K. Nakamoto. Infrared spectra of inorganic and coordination compounds. John Wiley and Sons Inc., New York, 1963. p. 199.
32. B. Dupuy and C. Garrigou-Lagrange. J. Chim. Phys. **62**, 1359 (1965).
33. N. J. Taylor and A. J. Carty. J. Chem. Soc. Chem. Commun. 214 (1976); B. Birgersson, T. Drakenberg, and G. A. Neville. Acta Chem. Scand. **27**, 3953 (1973).
34. M. T. Fairhurst and D. L. Rabenstein. Inorg. Chem. **14**, 1413 (1975).
35. J. Yon. *In* Structure et dynamique conformationnelle des protéines. Hermann, Paris, 1969. Chap. 4.
36. D. L. Rabenstein. Acc. Chem. Res. **11**, 100 (1978).
37. R. S. Reid and D. L. Rabenstein. Can. J. Chem. **59**, 1505 (1981).
38. D. M. Byler, H. Susi, and H. M. Farrell, Jr. Biopolymers, **22**, 2507 (1983).
39. H. E. Van Hart and H. A. Scheraga. J. Phys. Chem. **80**, 1812 (1976).

Can. J. Chem. Downloaded from www.nrcresearchpress.com by 80.58.250.72 on 09/07/12
For personal use only.

Mécanisme des réactions du chlorite et du dioxyde de chlore. 5. Cinétique de la réaction chlorite–bromure

GUY SCHMITZ ET HENRI ROOZE
Université libre de Bruxelles, Faculté des sciences appliquées, 50 avenue F. Roosevelt, 1050 Bruxelles, Belgique

Reçu le 29 avril 1986

GUY SCHMITZ et HENRI ROOZE. Can. J. Chem. **65**, 497 (1987).

Dans les solutions acides de chlorite et de bromure on observe simultanément la dismutation du chlorite et une réaction autocatalytique conduisant à une production rapide de ClO_2. Les caractéristiques inhabituelles de cette réaction sont décrites. Dans ce système compliqué, il n'est pas possible de mesurer la vitesse de $HClO_2 + Br^- + H^+ \rightarrow HClO + HBrO$. C'est par contre possible en présence d'*ortho*-tolidine qui capte le HBrO et le HClO. Nous avons obtenu $r = k[HClO_2][Br^-][H^+]$ avec $k = 1{,}48 \times 10^{-2}\ M^{-2}\ s^{-1}$ à 25°C. En absence d'*ortho*-tolidine cette réaction initie la réaction autocatalytique pour laquelle nous proposons un modèle.

GUY SCHMITZ and HENRI ROOZE. Can. J. Chem. **65**, 497 (1987).

In acidic solutions of chlorite and bromide two processes occur simultaneously, the disproportionation of chlorite and an autocatalytic reaction leading to a rapid production of ClO_2. The unusual features of this reaction are described. In this complex system the rate of $HClO_2 + Br^- + H^+ \rightarrow HClO + HBrO$ cannot be measured. It can be, however, with added *ortho*-tolidine to remove the HBrO and HClO. We obtained $r = k[HClO_2][Br^-][H^+]$ with $k = 1.48 \times 10^{-2}\ M^{-2}\ s^{-1}$ at 25°C. Without added *ortho*-tolidine this reaction initiates the autocatalytic reaction for which we suggest a kinetic scheme.

Introduction

L'étape déterminante de la réaction chlorite–chlorure est [1]. Elle est suivie de réactions entre le chlorite et l'hypochlorite conduisant à la formation de chlorate et de dioxyde de chlore en proportions variables suivant les conditions (1).

[1] $\quad HClO_2 + Cl^- + H^+ \rightarrow 2\ HClO$

Nous avons obtenu $k_1 = 1{,}8 \times 10^{-3}\ M^{-2}\ s^{-1}$ à 25°C et une force ionique $I = 1\ M$.

Kern et Kim (2) ainsi que de Meeus et Sigalla (3) ont étudié la réaction chlorite–iodure dans la zone de pH 4–8. Sa première étape est [2].

[2] $\quad ClO_2^- + I^- + H^+ \rightarrow ClO^- + HIO$

Cette réaction est suivie d'un ensemble d'autres, faisant intervenir le chlorite, l'hypochlorite, l'iodite et l'hypoiodite, conduisant à une production autocatalytique d'iode. Le système est compliqué mais ses aspects principaux sont établis. Il peut conduire à des oscillations qui ont été étudiées par Epstein et Kustin (4).

Pour la réaction chlorite–bromure la seule étude antérieure à celle-ci est celle de Simoyi (5) que nous discuterons plus loin. Il s'agit également d'une réaction compliquée d'allure autocatalytique. Afin d'étudier isolément sa première étape, analogue de [1] et [2], nous avons utilisé la méthode à l'*ortho*-tolidine décrite dans l'article précédent de cette série (6).

Technique expérimentale

Le chlorite de sodium a été purifié par trois recristallisations successives. Ses solutions sont conservées dans le noir en milieu légèrement basique et standardisées par iodométrie. Les autres réactifs de la qualité «pour analyses» sont utilisés sans purification supplémentaire. La température est toujours fixée à 25,0 ± 0,1°C.

Lors des expériences en absence d'*ortho*-tolidine, les productions de ClO_2 sont mesurées par absorptiométrie à 360 nm comme indiqué antérieurement (1). Nous avons vérifié que dans les conditions des expériences discutées ici (faibles concentrations initiales en bromure), la contribution aux absorbances mesurées d'une éventuelle formation de brome serait totalement négligeable.

Pour les expériences faites en présence d'*ortho*-tolidine, les techniques et précautions expérimentales ont été entièrement décrites précédemment (1, 6). Rappelons que nous abrégeons la formule de l'*ortho*-tolidine en NH_2RNH_2 et celle de sa forme oxydée en NHRNH.

Les concentrations totales en chlorite de sodium seront désignée par $[NaClO_2]$ et celles des espèces effectivement présentés en solution par $[HClO_2]$ et $[ClO_2^-]$. On a donc:

$$[HClO_2] = \frac{[H^+]}{[H^+] + K_a}[NaClO_2]$$

À 25°C et pour $I = 1\ M$, $K_a = 2{,}4 \times 10^{-2}$ (7).

Caractéristiques de la réaction chlorite–bromure

Les figures 1–3 montrent des courbes caractéristiques de la formation de ClO_2 dans des mélanges acides de chlorite et de bromure. On y voit la contribution de deux groupes de réactions: (*1*) La dismutation du chlorite que nous avons étudiée antérieurement (8). Elle résulte d'une réaction catalysée par les traces de fer inévitablement présentes dans les réactifs et d'une réaction radicalaire d'ordre deux par rapport au chlorite. (*2*) La réaction due au bromure et comportant une période d'induction suivie d'une période d'allure autocatalytique. Ses principales caractéristiques sont les suivantes.

Assez curieusement, l'augmentation de la concentration du chlorite allonge la période d'induction (figure 1). Une augmentation de la concentration initiale en Br^- diminue ou augmente la période d'induction suivant que la concentration en chlorite est grande ou petite (figures 2 et 3).

Si on remplace le bromure par du brome on obtient le même genre de courbes mais la période d'induction est plus courte (figure 3, courbe 4). Si on remplace le brome par du HBrO la période d'induction est supprimée.

Si $[Br^-]_0 = 10^{-4}\ M$ la réaction se termine par consommation totale du chlorite et la stoéchiométrie correspond approximativement à [3].

[3] $\quad 4\ HClO_2 \rightarrow 2\ ClO_2 + ClO_3^- + Cl^- + 2\ H^+ + H_2O$

Par contre si $[Br^-]_0 = 10^{-6}\ M$ le type de comportement dépend de la concentration du chlorite. Si elle est grande la réaction autocatalytique ne démarre jamais et on n'observe que la dismutation du chlorite. Si elle est faible la réaction autocatalytique démarre très vite mais s'arrête alors qu'il reste du chlorite. Dans le cas de la courbe 3 de la figure 3 on

Can. J. Chem. Downloaded from www.nrcresearchpress.com by 80.58.250.72 on 09/07/12
For personal use only.

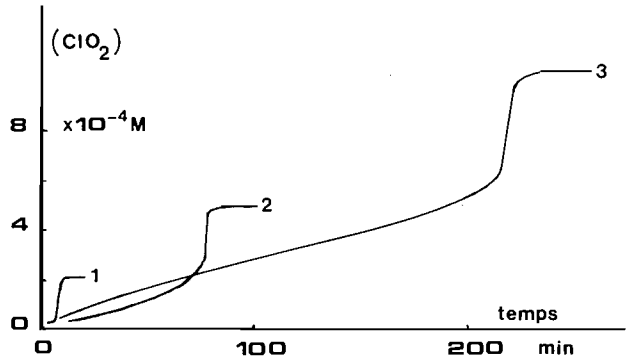

FIG. 1. La réaction chlorite–bromure : effet du chlorite. $[HClO_4] = 1\ M$; $[Br^-]_0 = 4 \times 10^{-6}\ M$; $[NaClO_2]_0 = 4{,}7 \times 10^{-4}$ (1), $9{,}4 \times 10^{-4}$ (2), $1{,}88 \times 10^{-3}\ M$ (3).

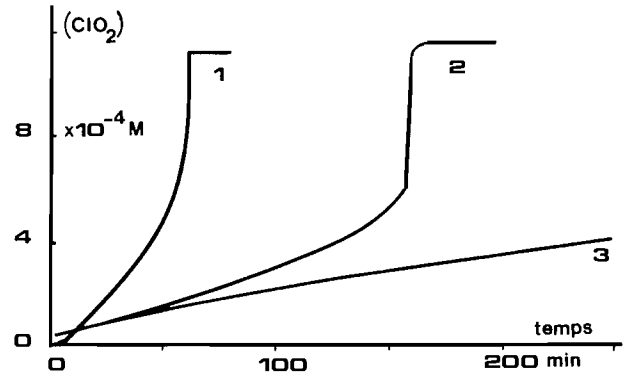

FIG. 2. La réaction chlorite–bromure : effet du bromure si $[NaClO_2]_0 = 1{,}88 \times 10^{-3}\ M$, $[HClO_4] = 1\ M$; $[Br^-]_0 = 10^{-4}$ (1), 10^{-5} (2), $10^{-6}\ M$ (3).

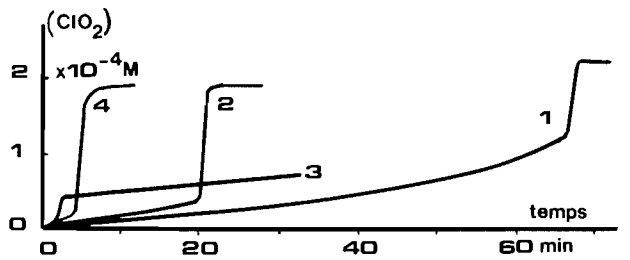

FIG. 3. La réaction chlorite–bromure : effet du bromure si $[NaClO_2]_0 = 4{,}7 \times 10^{-4}\ M$. $[HClO_4] = 1\ M$; $[Br^-]_0 = 10^{-4}$ (1), 10^{-5} (2), $10^{-6}\ M$ (3), $[Br_2] = 10^{-5}\ M$ (4).

n'a consommé que le quart du chlorite initial. Une addition de bromure fait alors redémarrer la réaction autocatalytique après une nouvelle période d'induction. Ces différents faits conduisent aux conclusions suivantes.

Des concentrations élevées en chlorite ont un effet inhibiteur sur la réaction autocatalytique.

La catalyse ne résulte pas directement du bromure et la période d'induction correspond à son oxydation en HBrO.

L'arrêt de la réaction alors qu'il reste du chlorite (figure 3) ne peut résulter que d'une oxydation totale du Br^- sous une forme inactive. Nous en déduisons qu'il est oxydé en BrO_3^-.

En milieux acides 0,1 *M* on peut également observer la réaction autocatalytique mais pour des concentrations en bromure plus élevées. Il se forme alors des quantités non négligeables de brome dont le spectre (λ_{max} = 390 nm) se superpose à celui du ClO_2 (λ_{max} = 360 nm) et il devient très difficile d'interpréter les mesures d'absorbances.

L'article de Simoyi (5) consacré à cette réaction devrait être oublié. Dans ses équations et ses calculs il confond concentrations analytiques et particulaires (avec nos notations $[NaClO_2]$ et $[ClO_2^-]$), le chlorite utilisé contenait 13% d'impuretés et surtout la stoéchiométrie n'est pas celle qu'il indique. On ne peut rien déduire de ses mesures d'absorbances. Nous avons relevé des spectres au cours de la réaction dans les conditions de sa figure 1. Ceux-ci montrent une contribution très importante du ClO_2 à 390 nm, longueur d'onde de mesures qu'il attribue au Br_2.

Étude en présence d'*ortho*-tolidine

Dans les conditions ci-dessus, il n'est pas possible d'étudier la réaction [4] :

[4] $\quad HClO_2 + Br^- + H^+ \rightarrow HClO + HBrO$

En milieux acides 1 *M* elle est masquée par la dismutation du chlorite et (ou) par la réaction autocatalytique. Diminuer l'acidité ne résoud rien car la vitesse de dismutation du chlorite augmente (8). Enfin en milieux moins acides et riches en bromure les absorbances mesurées résultent à la fois du ClO_2 et du brome.

Cette étude est par contre possible en présence d'*ortho*-tolidine. La réaction autocatalytique est supprimée et la dismutation du chlorite peut être très simplement prise en compte. La figure 4 montre qu'aux faibles conversions (inférieures à quelques pourcents), on obtient des droites dont les pentes donnent les *vitesses initiales* d'oxydation de l'*ortho*-tolidine. Nous verrons qu'elles correspondent à une somme de deux termes, l'un du à la réaction catalysée par le fer, l'autre du à la réaction [4].

D'après ce qu'on sait des réactions chlorite–chlorure et chlorite–iodure, le point de départ de la réaction autocatalytique doit être [5]. En présence d'*ortho*-tolidine cette réaction est en compétition avec [6].

[5] $\quad HClO_2 + HBrO \rightarrow BrClO_2 + H_2O$

[6] $\quad NH_2RNH_2 + HBrO \rightarrow NHRNH + Br^- + H^+ + H_2O$

Nous avons vu (1) que le HClO réagit plus rapidement avec l'*ortho*-tolidine qu'avec le chlorite. Les résultats du tableau 1 montrent qu'il en est de même du HBrO. Si on ajoute une solution de Br_2 ou de HBrO (obtenue par réaction du brome avec des ions Ag^+) à une solution acide d'*ortho*-tolidine on obtient la réaction [6], ou son homologue pour le brome. La production de NHRNH est la même que la solution d'*ortho*-tolidine contienne ou non du chlorite : le HBrO ne réagit que suivant [6] et la réaction autocatalytique est supprimée. Cette réaction apparaît par contre si on mélange le chlorite et le HBrO avant d'ajouter l'*ortho*-tolidine. La dernière ligne du tableau 1 montre que la production de NHRNH est alors nettement plus grande.

Résultats de l'étude cinétique

*Effet de l'*ortho-*tolidine*

La suppression des réactions indésirées par l'*ortho*-tolidine n'est effective que si sa concentration est suffisante. Nous avons toujours vérifié que nos vitesses sont indépendantes de cette concentration. Si $[HClO_4] = 1\ M$ et $[NaClO_2] = 5 \times 10^{-4}\ M$ cette condition est satisfaite dès $[NH_2RNH_2] = 2 \times 10^{-4}\ M$. La valeur minimale à réaliser augmente si la concentration du chlorite augmente et si l'acidité diminue.

Effet de la force ionique

Dans l'acide perchlorique 0,1 *M* les vitesses diminuent d'un facteur 1,2 si la force ionique *I* varie de 0,1 à 0,2 *M*. Entre 0,4 et

Can. J. Chem. Downloaded from www.nrcresearchpress.com by 80.58.250.72 on 09/07/12
For personal use only.

Can. J. Chem. Downloaded from www.nrcresearchpress.com by 80.58.250.72 on 09/07/12
For personal use only.

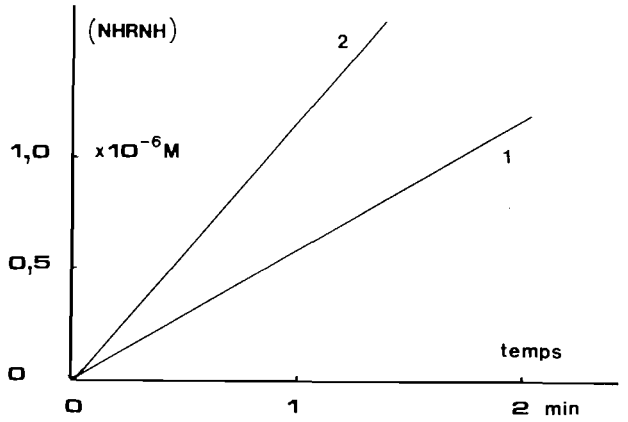

FIG. 4. La réaction chlorite–bromure en présence d'*ortho*-tolidine. $[HClO_4] = 1{,}01\ M$; $[NH_2RNH_2] = 5 \times 10^{-4}\ M$; $[NaClO_2] = 5{,}5 \times 10^{-4}\ M$; $[Br^-] = 10^{-4}$ (1), $7 \times 10^{-4}\ M$ (2).

TABLEAU 1. Oxydation de l'*ortho*-tolidine par HBrO ou Br_2 en présence de chlorite

$[NaClO_2]$ $10^{-4}\ M$	$[HBrO]_0$ $10^{-5}\ M$	[NHRNH] $10^{-5}\ M$
0	2(a)	1,93
5,5	2(a)	1,96
5,5	4(a)	3,84
0	2(b)	1,97
1,1	2(b)	1,92
1,1	2(c)	4,75

$[HClO_4] = 0{,}101\ M$; $[NH_2RNH_2]_0 = 10^{-4}\ M$. Ordre de mélange : acide, *ortho*-tolidine, chlorite, Br_2 (a) ou HBrO (b). Contre-épreuve : acide, chlorite, HBrO, *ortho*-tolidine (c).

1 *M* elles ne dépendent quasi pas de *I*. Toutes nos mesures ont été faites avec $I = 1\ M$, ajustée au besoin par du perchlorate de sodium.

Loi cinétique

La figure 4 donne un exemple de mesures des vitesses initiales d'oxydation de l'*ortho*-tolidine. Ces vitesses varient linéairement en fonction de la concentration du bromure comme le montre la figure 5.

$$\frac{d[NHRNH]}{dt} = k'[Br^-] + k''$$

Le tableau 2 donne les valeurs de k' obtenues. Elles sont proportionnelles aux concentrations $[HClO_2]$ et $[H^+]$. k'' est dû à la réaction catalysée par le fer (9). On en déduit la loi cinétique [7].

$$[7] \qquad \frac{d[NHRNH]}{dt} = k_7[HClO_2][H^+][Br^-] + r_{Fe}$$

Quelques séries de mesures ont été faites en présence d'EDTA, ce qui réduit notablement le terme r_{Fe}(9). Les valeurs de k_7 sont en parfait accord avec celles obtenues sans EDTA.

Dans l'acide 0,1 *M*, si la concentration de l'*ortho*-tolidine est inférieure à $10^{-3}\ M$ ou si celle du chlorite est supérieure à $10^{-4}\ M$ les vitesses ne sont plus indépendantes de la concentration de l'*ortho*-tolidine, ce qui explique les valeurs trop élevées du tableau 2. D'autre part si $[NH_2RNH_2]$ est supérieur à $10^{-3}\ M$ la dégradation de l'*ortho*-tolidine oxydée risque de ne plus être négligeable. Ceci limite le domaine d'acidités et de concentrations en chlorite des mesures.

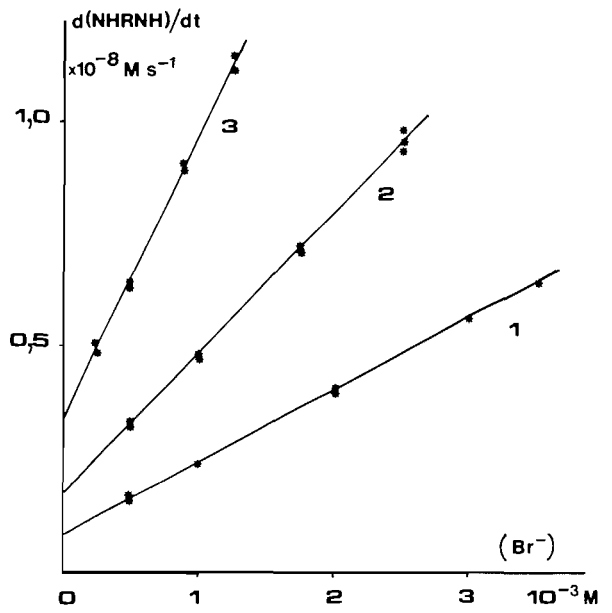

FIG. 5. Effet du bromure sur les vitesses initiales. $[HClO_4] = 1{,}01\ M$; $[NH_2RNH_2] = 5 \times 10^{-4}\ M$; $[NaClO_2] = 5{,}5 \times 10^{-5}$ (1), $1{,}1 \times 10^{-4}$ (2), $2{,}2 \times 10^{-4}\ M$ (3).

TABLEAU 2. Constantes cinétiques

$[HClO_4]$ *M*	$[NaClO_2]$ $10^{-4}\ M$	$[Br^-]$ $10^{-3}\ M$	$10^6\ k'\ s^{-1}$	$10^2\ k_7\ M^{-2}\ s^{-1}$
1,01(a)	0,55	0,5–3,5	1,62	2,99
1,01(a)	1,10	0,5–2,5	3,17	2,92
1,01(a)	2,20	0,2–1,2	6,38	2,94
1,01(a)	5,50	0,1–0,7	16,5	3,04
1,01(b)	0,55	1,0–5,0	1,57	2,90
1,01(b)	5,50	0,2–1,0	16,2	2,99
0,402(a)	0,55	4–16	0,647	3,10
0,402(a)	1,00	10–40	1,09	2,87
0,402(b)	0,55	10–50	0,594	2,85
0,201(a)	1,00	10–40	0,551	3,06
0,101(a)	0,55	10–80	0,147	3,28(c)
0,101(b)	0,275	30–100	0,064	2,85
0,101(b)	0,55	30–100	0,128	2,85
0,101(b)	1,10	10–50	0,288	3,21
0,101(b)	5,50	10–50	1,54	3,43(c)

$[NH_2RNH_2] = 5 \times 10^{-4}$ (a) ou $10^{-3}\ M$ (b). Valeurs (c) trop grandes : cf. texte.

Conclusion

En présence d'*ortho*-tolidine la réaction [4] est suivie de [6] et de son homologue pour le HClO, donnant globalement [8] :

$$[8] \qquad HClO_2 + 2\,NH_2RNH_2 \rightarrow Cl^- + H^+ + 2\,NHRNH + 2\,H_2O$$

L'étape déterminante étant [4] on obtient la loi [7] avec $k_7 = 2\ k_4$. Les valeurs du tableau 2 donnent $k_4 = (1{,}48 \pm 0{,}05) \times 10^{-2}\ M^{-2}\ s^{-1}$ à 25°C et $I = 1\ M$.

En absence d'*ortho*-tolidine le HBrO produit par [4] réagit suivant [5] et on obtient la réaction autocatalytique.

Mécanisme de la réaction autocatalytique

Idées de base

Le mécanisme que nous proposons est basé sur les faits suivants.

Can. J. Chem. Downloaded from www.nrcresearchpress.com by 80.58.250.72 on 09/07/12
For personal use only.

1. Le catalyseur est le HBrO formé pendant la période d'induction.

2. Des concentrations élevées en chlorite inhibent la réaction autocatalytique.

3. Le sens de l'effet du bromure sur la durée de la période d'induction dépend de la concentration du chlorite.

4. La stoéchiométrie de la dismutation du chlorite est approximativement [3].

5. Le bromure et le HBrO peuvent être oxydés en bromate ne catalysant pas la décomposition du chlorite.

Plusieurs variantes de notre modèle nous ont permis de reproduire l'allure des courbes expérimentales et nous avons retenu celle qui nous a donné le meilleur accord avec les valeurs numériques des temps d'induction. Il ne faut pas accorder trop d'importance à ses détails mais bien aux idées générales suivantes, sans lesquelles il ne nous semble pas possible d'expliquer les comportements observés.

Les composés du type X_2O_2 sont des intermédiaires des réactions d'oxydo-réduction des halogènes. Ce ne sont pas des complexes activés mais de véritables composés chimiques pouvant intervenir dans au moins trois types de réactions.

$$XO_3^- + X^- + 2\,H^+ = X_2O_2 + H_2O$$

$$X_2O_2 + H_2O = HXO_2 + HXO$$

$$X_2O_2 + X^- = XO_2^- + X_2$$

Dans le cas du chlore, il faut ajouter la formation de ClO_2 par réaction avec le chlorite (1).

$$Cl_2O_2 + HClO_2 \rightarrow 2\,ClO_2 + Cl^- + H^+$$

Le Cl_2O_2 est asymétrique (10), sa structure étant

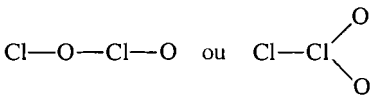

Cette asymétrie est importante car nous n'avons pu justifier les effets inhabituels des concentrations sur la période d'induction qu'en admettant l'existence de deux isomères que nous représenterons par $BrClO_2$ et $ClBrO_2$ et dont les structures sont

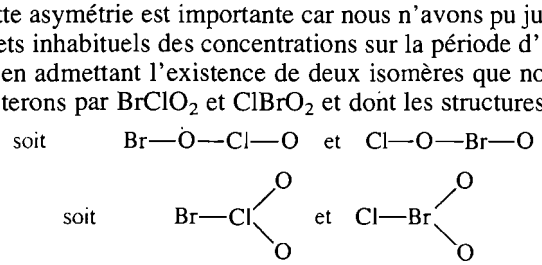

La réaction HBrO + $HClO_2$ donne le premier alors que la réaction HClO + $HBrO_2$ donnerait le second.

Composantes du modèle simplifié

1. Dismutation du chlorite

En milieux 1 *M* acides et en l'absence de chlorure, elle résulte principalement d'une réaction radicalaire d'ordre deux (8). Nous ne faisons apparaître dans le modèle que la réaction globale [M1].

[M1] $2\,HClO_2 \rightarrow HClO + ClO_3^- + H^+$

2. Réactions du HClO

Nous savons qu'au cours de la dismutation du chlorite, il réagit suivant $HClO_2 + HClO \rightarrow Cl_2O_2 + H_2O$ et que le Cl_2O_2 peut donner soit du dioxyde de chlore soit du chlorate et du chlorure (1, 8). Dans les conditions étudiées ici le premier est largement prépondérant et on peut simplifier le modèle en n'écrivant que la réaction globale [M2] :

[M2] $2\,HClO_2 + HClO \rightarrow 2\,ClO_2 + Cl^- + H^+ + H_2O$

$$r_{M2} = k_{M2}[HClO_2][HClO]$$

3. Initiation

Sa première étape est la réaction étudiée ci-dessus :

[M3] $HClO_2 + Br^- + H^+ \rightarrow HClO + HBrO$

Le HBrO peut être transformé en Br_2 suivant [M4] :

[M4] $HBrO + Br^- + H^+ \rightleftharpoons Br_2 + H_2O$

Dans certaines variantes du modèle nous avons inclu la réaction $HClO + Br^- \rightarrow HBrO + Cl^-$. Elle n'en modifie guère les propriétés et est négligée ici.

4. Réactions de $BrClO_2$

Une des bases de notre modèle est sa formation suivant [M5] :

[M5] $HBrO + HClO_2 \rightleftharpoons BrClO_2 + H_2O$

Outre la réaction inverse et l'isomérisation [M6], plusieurs réactions de consommation peuvent être envisagées. L'effet du chlorite sur la période d'induction suggère que la principale soit [M7], la somme [M5] + [M7] donnant la réduction du HBrO en Br^-.

[M6] $BrClO_2 \rightarrow ClBrO_2$

[M7] $BrClO_2 + HClO_2 \rightarrow 2\,ClO_2 + Br^- + H^+$

5. Réactions du $ClBrO_2$

Cet intermédiaire formé par [M6] peut réagir suivant [M8], [M9] et [M10], analogues de réactions connues d'autres intermédiaires du type X_2O_2.

[M8] $ClBrO_2 + H_2O \rightarrow BrO_3^- + Cl^- + 2\,H^+$

[M9] $ClBrO_2 + Br^- + H^+ \rightarrow BrCl + HBrO_2$

[M10] $ClBrO_2 + HClO_2 \rightarrow BrO_2 + ClO_2 + Cl^- + H^+$

La réaction [M8] explique l'oxydation du catalyseur sous une forme inactive lorsque [Br^-] et [$HClO_2$] sont petits. La réaction [M9] est suivie de [M11] et [M12] :

[M11] $BrCl + H_2O \rightleftharpoons HBrO + Cl^- + H^+$

[M12] $HBrO_2 + HClO_2 \rightarrow HBrO + ClO_3^- + H^+$

La somme [M5] + [M6] + [M9] + [M11] + [M12] donne l'oxydation autocatalytique du Br^- en HBrO. Le BrO_2 formé par [M10] peut réagir suivant [M13] et [M14] :

[M13] $BrO_2 + HClO_2 \rightarrow ClO_2 + HBrO_2$

[M14] $BrO_2 + ClO_2 + H_2O \rightarrow ClO_3^- + H^+ + HBrO_2$

La somme [M5] + [M6] + [M10] + [M13] + [M12] donne la décomposition du chlorite suivant la stoéchiométrie [3] catalysée par le HBrO.

D'autres réactions possibles ont été négligées car elles ne faisaient que compliquer le modèle sans en modifier les propriétés, par exemple $HBrO_2 + Br^- + H^+ \rightarrow 2\,HBrO$. Nous avons également négligé les réactions du bromate, sa concentration étant toujours très faible.

6. Valeurs des constantes cinétiques

Les valeurs suivantes sont connues :

$$k_{M1} = 5{,}1 \times 10^{-3}\ M^{-1}\ s^{-1}\ (8)$$

$$k_{M3} = 1{,}48 \times 10^{-2}\ M^{-2}\ s^{-1}\ \text{(ci-dessus)}$$

$$k_{-M4} = 110\ s^{-1}\ (11)$$

$$k_{M4}/k_{-M4} = 10^8\ M^{-2}\ (\text{estimé pour } I = 1\ M)$$

$$k_{M13}/k_{M14} = 3{,}1\ (12)$$

Il semble qu'il reste un grand nombre de constantes à ajuster.

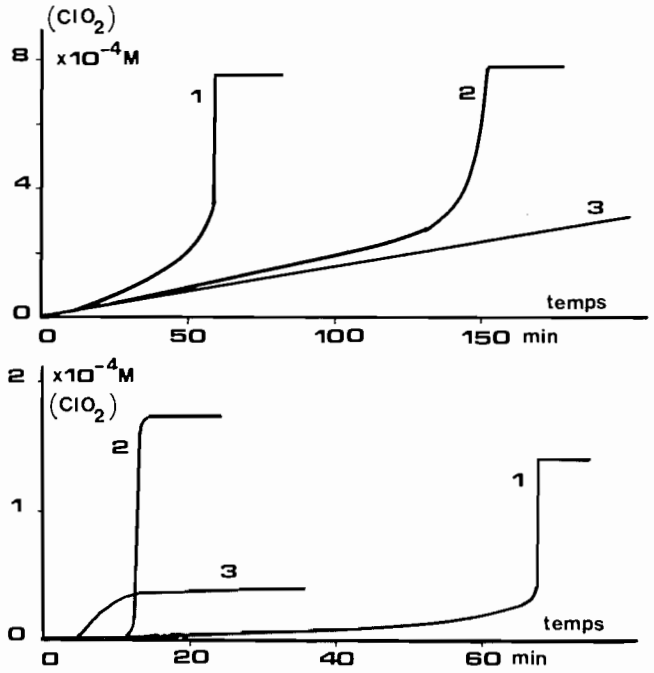

FIG. 6. Productions de ClO_2 prévues par le modèle cinétique dans les conditions des expériences des figures 2 et 3.

En fait ce nombre se réduit notablement si l'on impose que les concentrations de divers intermédiaires soient négligeables. Par exemple la valeur de k_{M2} n'est pas connue mais est certainement assez grande pour que le HClO ne s'accumule pas dans le système. Nous avons constaté que si cette condition est respectée, le choix de k_{M2} n'a aucun effet sur les consommations de $HClO_2$ et les productions de ClO_2 calculées par intégration des équations associées à notre modèle.

Cette simplification du comportement des solutions des équations différentielles est à rapprocher de l'approximation classique de la quasi-stationnarité. Considérons le cas des réactions du $ClBrO_2$. Si k_{M6} et k_{M7} sont suffisamment grands pour que $[ClBrO_2]$ soit négligeable, la valeur calculée de cette concentration est quasi-égale à celle donnée par

$$r_{M6} + r_{M7} = r_{M5}$$

Comme

$$\frac{r_{M7}}{r_{M6}} = \frac{k_{M7}}{k_{M6}}[HClO_2]$$

on voit que r_{M6} et r_{M7} ne dépendent plus des valeurs individuelles de k_{M7} et k_{M6} mais seulement de leur rapport.

Compte tenu des valeurs connues et du fait que les concentrations de HClO, $BrClO_2$, $ClBrO_2$, BrCl, $HBrO_2$ et BrO_2 sont stoéchiométriquement négligeables, il ne reste que quatre paramètres à choisir. Nous avons pris :

$$k_{M7}/k_{M6} = 500\ M^{-1}$$

$$k_{M5}k_{M6}/k_{-M5} = 3 \times 10^4\ M^{-1}\ s^{-1}$$

$$k_{M9}/k_{M10} = 400\ M^{-1}$$

$$k_{M8}/k_{M10} = 2 \times 10^{-5}\ M$$

7. Résultats

Le système d'équations différentielles associé au modèle ci-dessus a été intégré par une méthode de Gear pour les systèmes mal conditionnés. La figure 6 montre que l'accord avec les courbes expérimentales est excellent. En particulier on obtient bien une inversion du sens de l'effet du bromure sur la période d'induction pour une variation de la concentration du chlorite d'un facteur 4 seulement. Seule l'hypothèse de l'existence des deux isomères $ClBrO_2$ et $BrClO_2$ nous a permis de rendre compte de ce fait. Les détails du modèle ne pourront être précisés que quand on connaîtra mieux les réactions de $HBrO_2$ et BrO_2.

1. G. SCHMITZ et H. ROOZE. Can. J. Chem. **59**, 1177 (1981).
2. D. M. KERN et C. H. KIM. J. Am. Chem. Soc. **87**, 5309 (1965).
3. J. DE MEEUS et J. SIGALLA. J. Chim. Phys. **63**, 453 (1966).
4. I. R. EPSTEIN et K. KUSTIN. J. Phys. Chem. **89**, 2275 (1985).
5. R. H. SIMOYI. J. Phys. Chem. **89**, 3750 (1985).
6. G. SCHMITZ et H. ROOZE. Can. J. Chem. **64**, 1747 (1986).
7. C. C. HONG et W. H. RAPSON. Can. J. Chem. **46**, 2053 (1968).
8. G. SCHMITZ et H. ROOZE. Can. J. Chem. **63**, 975 (1985).
9. G. SCHMITZ et H. ROOZE. Can. J. Chem. **62**, 2231 (1984).
10. H. TAUBE et H. DODGEN. J. Am. Chem. Soc. **71**, 3330 (1949).
11. M. EIGEN et K. KUSTIN. J. Am. Chem. Soc. **84**, 1355 (1962).
12. R. C. THOMPSON. Inorg. Chem. **12**, 1905 (1973).

Can. J. Chem. Downloaded from www.nrcresearchpress.com by 80.58.250.72 on 09/07/12
For personal use only.

Side chain hydroxylation of aromatic compounds by fungi. 1. Products and stereochemistry

HERBERT L. HOLLAND, ELEANOR J. BERGEN, P. CHINNA CHENCHAIAH, SHAHEER H. KHAN, BENITO MUNOZ, RONALD W. NINNISS, AND DENISE RICHARDS

Department of Chemistry, Brock University, St. Catharines, Ont., Canada L2S 3A1

Received June 27, 1986

HERBERT L. HOLLAND, ELEANOR J. BERGEN, P. CHINNA CHENCHAIAH, SHAHEER H. KHAN, BENITO MUNOZ, RONALD W. NINNISS, and DENISE RICHARDS. Can. J. Chem. **65**, 502 (1987).

The fungus *Mortierella isabellina* can convert ethylbenzene and a number of *para*-substituted derivatives to the corresponding optically active 1-phenylethanols with enantiomeric excesses between 5 and 40% and chemical yields up to 45%. 2-Ethylnaphthalene, 2-ethylthiophene, and *n*-propylbenzene were similarly converted, as were the bicyclic compounds indane and tetralin. In most cases, the *R* absolute configuration of product predominated. The fungi *Cunninghamella echinulata* var. *elegans* and *Helminthosporium* species are also capable of performing some of these transformations. *M. isabellina* and *C. elegans* also produce 2-phenylethanols as products in some cases. The highest enantiomeric excesses during benzylic hydroxylation were obtained with *Helminthosporium* and are attributable, at least in part, to further stereoselective oxidation of the alcohol. Cross induction experiments with *M. isabellina* indicate that the same enzyme may be responsible for the benzylic hydroxylation of ethylbenzene, 2-ethylthiophene, and 2-ethylnaphthalene.

HERBERT L. HOLLAND, ELEANOR J. BERGEN, P. CHINNA CHENCHAIAH, SHAHEER H. KHAN, BENITO MUNOZ, RONALD W. NINNISS et DENISE RICHARDS. Can. J. Chem. **65**, 502 (1987).

Le champignon *Mortierella isabellina* peut transformer l'éthylbenzène et un certain nombre de ses dérivés comportant un substituant en position *para* en des phényl-1 éthanols optiquement actifs, avec des excès énantiomériques variant de 5 à 40% et avec des rendements chimiques allant jusqu'à 45%. On peut aussi transformer de la même manière l'éthyl-2 naphtalène, l'éthyl-2 thiophène, le *n*-propylbenzène ainsi que des composés bicycliques comme l'indane et la tétraline. Dans la plupart des cas, on obtient préférentiellement le produit possédant la configuration absolue *R*. Les champignons des espèces *Cunninghamella echinulata* var. *elegans* et *Helminthosporium* sont aussi capables d'effectuer les mêmes transformations. Dans quelques cas, les champignons *M. isabellina* et *C. elegans* produisent en plus des phényl-2 éthanols. Lors des hydroxylations benzyliques, les excès énantiomériques les plus élevés ont été obtenus avec le *Helminthosporium* et ces résultats sont probablement dus, au moins en partie, à une oxydation subséquente sélective de l'alcool. Des expériences d'induction croisée impliquant le *M. isabellina* indiquent que le même enzyme peut être responsable de l'hydroxylation benzylique de l'éthylbenzène, de l'éthyl-2 thiophène et de l'éthyl-2 naphtalène.

[Traduit par la revue]

Ethylbenzene, an intermediate in the manufacture of styrene, is among the highest volume organic chemicals in production, the U.S. annual output alone exceeding 2 billion kilograms. In view of its importance as an industrial chemical, ethylbenzene is a prime candidate for metabolic study. Nevertheless, data on the products of its mammalian metabolism are not extensive, being limited to reports of conversion to racemic 1-phenylethanol by rabbits (1), to predominantly *R*(+)-1-phenylethanol (ee's 33–80%) by rat liver enzymes (2–4), and to 1-phenylethanol of unspecified stereochemistry (as the first formed of a series of oxidative metabolites) in the live rat (5).

In view of the structural similarity between ethylbenzene and thioanisole, we decided to investigate the biotransformation of the former by fungi (*Mortierella isabellina* and *Helminthosporium* species) that are efficient oxidizers at the sulphur atom of thioanisole (6). The fungus *Cunninghamella echinulata* var. *elegans* was also studied, its use being suggested by the observation that it is capable of benzylic hydroxylation of methyl-substituted aromatic compounds (7). Our aim was twofold: firstly, to identify fungal systems capable of the production of benzylic alcohols directly from hydrocarbons in an asymmetric manner and, secondly, to investigate the fungal biotransformation as a model for the first step in the mammalian metabolic pathway.

There have been no reports of the fungal oxidative metabolism of ethyl benzene other than our preliminary communication (8). Studies of its bacterial metabolism have shown that oxidation occurs in the ring (9) or at the side chain terminus (10), depending on the strain of bacteria and the growth conditions. Of the substrates used in this study, only tetralin (**31**) has been previously studied as a substrate for fungal metabolism, being converted to α-tetralol (**31***a*) (of unspecified stereochemistry) and α-tetralone (**32**) by *Aspergillus niger* (11).

The results of the fungal incubations are listed in Table 1. The yields quoted are those of isolated, purified material. Absolute configurations were assigned using optical rotation data (Table 2) by comparison with literature values for compounds of known configuration (ref. 12, and references listed in Table 2). In the case of *M. isabellina*, the predominant absolute stereochemistry of hydroxylation of **1**–**4**, **6**, **8**, and **9** is the same as that observed for sulphoxidation of the analogous thioanisole derivative by this fungus (13). In two cases, **5** and **7**, however, products of opposite predominant stereochemistry were obtained. The reason for this is not clear, but may be related to the difference in steric requirements of S and $-CH_2-$, and to differences in the ways in which the reaction intermediates are influenced by the nature of the *para* substituent. The formation of 2-phenylethanols (**35**–**43**) as minor products was also observed in a number of cases.

Incubation of **1** with *M. isabellina* in the presence of the protein synthesis inhibitor cycloheximide does not lead to the production of **1***a*, indicating that the enzyme that normally carries out this transformation is inducible. By using thioanisole as an enzyme inducer during the growth period, and then subsequently performing the incubation of **1** in the presence of cycloheximide, a normal yield and stereochemistry of product was obtained. Similarly, ethylbenzene is capable of inducing an enzyme that can subsequently oxidize thioanisole in the

Can. J. Chem. Downloaded from www.nrcresearchpress.com by 80.58.250.72 on 09/07/12
For personal use only.

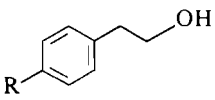

35, R = CH_3
36, R = C_2H_5
37, R = F
38, R = Cl
39, R = OCH_3
40, R = H
41, R = $CH(OH)CH_3$
42, R = CH_2CH_2OH
43, R = $COCH_3$

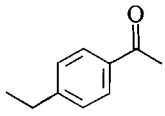

44

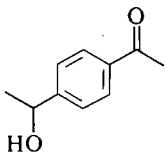

45

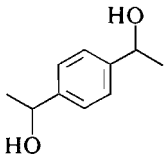

46

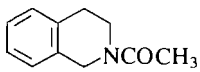

47

normal way (13). Cycloheximide also prevents the oxidation of thioanisole, 2-ethylthiophene, and 2-ethylnaphthalene by non-induced cells of *M. isabellina*. Successful cross-induction experiments, as described above for ethylbenzene/thioanisole, were also carried out with 2-ethylthiophene/thioanisole and 2-ethylnaphthalene/thioanisole combinations of inducer and substrate, suggesting that the same enzyme in *M. isabellina* is responsible for metabolizing all these substrates (14), although the induction of several (closely related) enzymes by a single substrate cannot be entirely excluded from consideration (15). In support of our hypothesis, however, it should be noted that the purified enzyme dopamine β hydroxylase, in addition to its normal function of producing norepinephrine from dopamine by benzylic hydroxylation, is also capable of converting a sulphide analogue of the normal substrate to sulphoxide with the same absolute configuration as the normal product (16).

In view of the stereochemical complications that could arise following possible stereoselective oxidation of the product alcohols and (or) stereoselective reductions of the resulting ketones by dehydrogenase enzymes, a situation that can obscure the mammalian hydroxylation of ethylbenzene (4), we have performed control incubations with *M. isabellina* using both enantiomers of 1-phenylethanol as substrate (see Table 1). In both cases, substrate was recovered whose absolute stereochemistry was unchanged. In the two cases in which ketones were incubated with *M. isabellina* (**14** and **32**), reduction occurs according to Prelog's rule (17) to give alcohol of predominantly *S* configuration.

The other two fungi used in this study, however, both gave acetophenone (**14**) in addition to 1-phenylethanol as product from ethylbenzene, suggesting that further oxidation of alcohol had occurred. Incubation of racemic α-tetralol (**31***a*) with *H.* species gave recovered substrate highly enriched in the *R* isomer, together with α-tetralone (**32**), and high enantiomeric excesses (e.e.'s) were observed for multiple oxidation products (e.g. **45**) of *p*-diethylbenzene with *C. echinulata*. These data suggest that these latter two microorganisms are capable of the stereoselective oxidation of secondary alcohols of *S* configuration (in accord with Prelog's rules) and that the relatively high enantiomeric excesses observed for monohydroxylated products such as **1***a* and **31***a* from *H.* species may be due in part to selective removal of the *S* enantiomer by its conversion to ketone. Transformations of α-tetralone (**32**) by *C. elegans* (a subspecies of *C. echinulata*) are reported not to involve carbonyl reduction (18). In the case of *M. isabellina* the absence of further oxidation products and the data presented above suggest, however, that benzylic alcohols, once produced, are configurationally stable under the conditions of the incubation. This is also confirmed by the results from the incubation of α,α-dideuteroethylbenzene, which will be presented at a later date.

One unexpected feature of our data is the absolute stereochemistry of benzylic hydroxylation by *H.* species. This fungus produces the opposite absolute stereochemistry of benzylic sulphoxide from that given by *M. isabellina* with the same substrate (6), but the same absolute stereochemistry of benzylic hydroxylation (Table 1). There is no doubt that our observations are the results of enzymic reactions, and cannot be attributed to autoxidation in a chiral environment; incubations performed with autoclaved fungus (inactivated enzymes) showed no evidence of 1-phenylethanol or α-tetralol formation from the corresponding substrate. We have considered the possibility that the observed enantiomeric enrichments may be the result of unequal transformation of the substrate by two different enzymes, each of which gives the opposite predominant stereochemistry of product, but have found that the enantiomeric excess in the conversion of **1** to **1***a* by *M. isabellina* is independent of temperature over the range 18–30°C, and also independent of substrate concentration over the range 0.3–1.0 mg/mL, ranges over which it is unlikely that two different enzymes would exhibit the same K_m and temperature dependence.

The range of substrates listed in Table 1 includes two whose bacterial metabolism has been reported (**12**, ref. 19), (**23**, ref. 20), but which were not metabolized by the fungi examined in this study. 1-Phenylethyl chloride (**13**) was incubated for control purposes in connection with future studies with deuterium labelled ethylbenzene, for which it is a synthetic precursor. The amines **10** and **33** were both acetylated at nitrogen during incubation, the corresponding amides being inert to further biotransformation. Cumene (**15**) gave a high yield of the benzylic alcohol with *M. isabellina*, which may be due, at least in part, to the ready autoxidation of this substrate. Although *n*-propylbenzene (**16**) gave a moderate yield of benzylic alcohol with *M. isabellina*, *n*-butylbenzene (**17**) gave a complex mixture of isomeric alcohols.

Fungal biotransformation of pyrrole (e.g. **18**) and furan (e.g. **20**) derivatives has not been reported, although furan rings are known to be degraded by several bacteria (21). Transformation of neither 2-ethylpyrrole (**18**) nor 2-ethylfuran (**20**) was observed in the present study, although 2-ethylthiophene (**19**) was hydroxylated. Previous reports of the fungal transformation of thiophene derivatives have been limited to carbonyl reduction (22) and S oxidation (23).

Phenylacetylene (**25**) and styrene (**24**) were studied in view of the reported oxidation of these substrates (to phenylacetic acid and styrene oxide, respectively) by hydroxylating enzymes (24), but neither was transformed by *M. isabellina*. Although *ortho*-diethylbenzene was not hydroxylated by the fungi used in this study, the bicyclic compounds indane (**30**) and tetralin (**31**) were, the former process serving as a comparison to the mammalian metabolism of indene (25). Although fungi are

Can. J. Chem. Downloaded from www.nrcresearchpress.com by 80.58.250.72 on 09/07/12
For personal use only.

TABLE 1. Summary of biotransformation of alkyl substituted aromatic compounds by *Mortierella isabellina* (*M.i.*), *Helminthosporium species* (*H.s.*), and *Cunninghamella echinulata* (*C.e.*) var. *elegans*

	Substrate	Benzylic alcohol (yield, ee, predominant configuration)			Other products yield (%), ee (%), predominant configuration		
		M.i.	*H.s.*	*C.e.*	*M.i.*	*H.s.*	*C.e.*
1		10,33, *R*	9,55, *R*	10,33, *R*	None	**14**(1)	**14**(1), **40**(0.5)
2	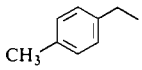	4,20, *R*	—	—	**35**(0.1)	—	—
3	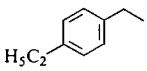	3,35, *R*	10,97, *R*	12,33, *R*	**36**(1)	**44**(15)	**36**(9) **45**(3)(97)*R* **43**(1) **46**(5)(97)*R*,*R* **41**(10)(97)*R* **42**(2)
4	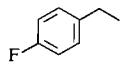	5,26, *R*	—	—	**37**(1)	—	—
5	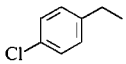	30,34, *S*	—	—	**38**(10)	—	—
6	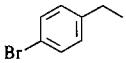	22,5, *R*	—	—	None	—	—
7	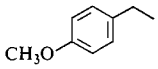	10,29, *S*	—	—	**39**(1)	—	—
8	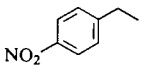	40,9, *R*	—	—	None	—	—
9	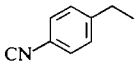	60,39, *R*	—	—	None	—	—
10	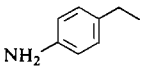	None	—	—	**11**(21)	—	—
11	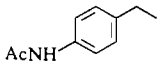	None	—	—	None	—	—
12	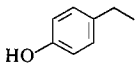	None	—	—	None	—	—
13		None	—	—	None	—	—
14		87,54, *S*	—	—	None	—	—
1*a*	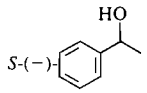	72,97, *S*	—	—	None	—	—
1*a*	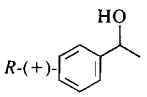	82,97, *R*	—	—	None	—	—
15		85	—	—	None	—	—
16	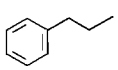	45,25, *R*	—	—	None	—	—
17	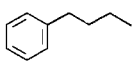	?	—	—	(19)[a]	—	—
18		None	—	—	None	—	—

Can. J. Chem. Downloaded from www.nrcresearchpress.com by 80.58.250.72 on 09/07/12
For personal use only.

TABLE 1. (*concluded*)

	Substrate	Benzylic alcohol (yield, ee, predominant configuration)			Other products yield (%), ee (%), predominant configuration		
		M.i.	*H.s.*	*C.e.*	*M.i.*	*H.s.*	*C.e.*
19		5,31, *R*	—	—	None	—	—
20		None	—	—	None	—	—
21		None	—	—	None	—	—
22	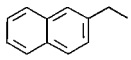	8,33, *R*	—	—	None	—	—
23		None	—	—	None	—	—
24	$PhCH{=}CH_2$	None	—	—	None	—	—
25	$PhC{\equiv}CH$	None	—	—	None	—	—
26	$PhNMe_2$	None	—	—	None	—	—
27	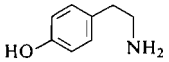	None	—	—	None	—	—
28		None	None	None	None	None	None
29		None	None	None	None	None	None
30		12,33, *R*	None	3,33, *R*	None	None	None
31		17,33, *R*	3,75, *R*	23,60, *R*	None	**32**(3)	Diol(1.5)
31*a*	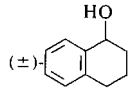	—	40,97, *R*	—	—	**32**(60)	—
32		87,30, *S*	None	See ref. 18	None	None	
33	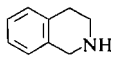	—	—	None	—	—	**47**(75)
34	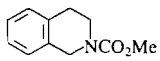	—	—	None	—	—	None

[a] ^{1}Hnmr analysis indicated to be a complex mixture of mono-alcohols; further analysis was not undertaken.

capable of hydroxylating substituted tetrahydroisoquinolines (usually at methoxyl carbon) (26), neither of the simple tetrahydroisoquinolines **33** or **34** was hydroxylated in the present study.

The enzymes involved in the hydroxylations listed in Table 1 are almost certainly monooxygenases. We have previously shown that the enzyme in *M. isabellina* that performs sulphoxidation of thioanisole has some of the properties of this class of enzymes (27), which are common in fungi (28) and are characterized by their ability to hydroxylate unactivated hydrocarbon functionality (29). It is thought that these enzymes operate by allowing an activated oxygen species to react with a substrate radical intermediate (eq. [1]) (ref. 30, and references therein). Enzymes of this type also oxidize aromatic rings, via arene oxides, to give phenols, a reaction that fungi can perform

[1] 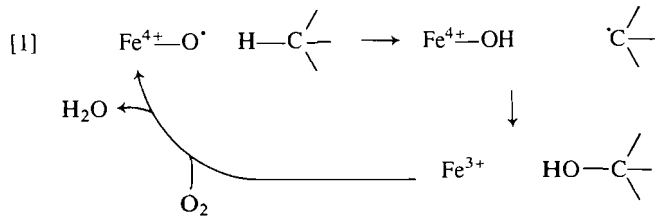

efficiently on halo-substituted aromatics (31), but no evidence for phenol formation was found during the present study.

The stereochemistry of product formation is presumably controlled by the interaction between a benzylic radical intermediate and the oxygenating species (eq. [1]). However, with a single fungus (e.g. *M. isabellina*) it appears to be largely independent of the size of the substituents (cf. **1** vs. **16** and **1** vs.

Can. J. Chem. Downloaded from www.nrcresearchpress.com by 80.58.250.72 on 09/07/12
For personal use only.

TABLE 2. Specific rotations of benzylic alcohols from Table 1[a]

Compound	$[\alpha]_D^{21}$ (°) *M.i.*	*H.s.*	*C.e.*	Reported $[\alpha]_D$ (°)	Reference
1*a* from **1**	+13.5	+23.5	+13.5	43.5 (EtOH)	33
2*a*	+7.7	—	—	—	—
3*a*	+16.2	+41.5	+11.6	—	—
41	—	—	+36.5	—	—
45	—	—	+37.4	—	—
46	—	—	+60.0	—	—
4*a*	+8.7	—	—	—	—
5*a*	−12.8	—	—	—	—
6*a*	+4.1	—	—	—	—
7*a*	−10.2	—	—	45.2 (EtOH)	34
8*a*	+8.2	—	—	—	—
9*a*	+16.5	—	—	—	—
1*a* from **14**	−22.4	—	—	43.5 (EtOH)	33
16*a*	+13.0	—	—	55.5 (EtOH)	35
19*a*	+10.1	—	—	—	—
22*a*	+12.5	—	—	41.3 (EtOH)	36
30*a*	−11.8	—	−10.9	30.8	37
31*a* from **31**	−9.6	−25.6	−20.1	32.6 ($CHCl_3$)	38
31*a* recovered	—	−31.5		32.6 ($CHCl_3$)	38
31*a* from **32**	+9.5	—	—	32.6 ($CHCl_3$)	38

[a]The "a" suffix on the arabic numeral from Table 1 is used to denote the corresponding benzylic alcohol.

19 vs. **22**) provided that they are acceptable by the enzyme, and does not exhibit the dependence upon the electronic nature of the *para* substituent (for the range **1**–**9**) shown by the stereochemistry of sulphoxides produced enzymically from the corresponding *para*-substituted thioanisoles (13). This lack of apparent correlation between ee and the size of substituent, its electronic properties (e.g. Hammett σ), or substrate polarity parameters such as the Hansch π lipophilicity term (32), precludes meaningful discussion on the magnitude of ee produced by fungal metabolism of these substrates. The observed predominance of benzylic hydroxylation with *R* absolute stereochemistry, however, may be of predictive value. A more detailed study of the hydroxylations of **1**, **3**, **30**, and **31**, using isotopically labelled substrates, is nearing completion and will be published in the near future.

Experimental

Apparatus, materials, and methods

Melting points (uncorrected) were determined on a Kofler heating stage. Infrared spectra were recorded with an Analect 6260FX spectrometer. Proton nmr spectra were recorded at 80 MHz with a Bruker WP80CW or at 200 MHz with a AC200 spectrometer, using $CDCl_3$ as solvent and TMS as internal standard. Enantiomeric ratios were determined in CCl_4 in the presence of tris[3-(heptafluoropropylhydroxymethylene)-*d*-camphorato] europium(III). Mass spectra were obtained with an AEI MS30/Kratos DS55 system. Thin-layer chromatography was performed on Merck silica gel 60 F-254 and flash column chromatography on silica gel (230–400 mesh, Merck 9385). Optical rotations were determined with a Perkin–Elmer 241MC polarimeter (at McMaster University), or with a Rudolph Autopol-III polarimeter.

Maintenance of microorganisms

Mortierella isabellina NRRL 1757 was maintained on malt agar slopes. *Helminthosporium* species NRRL 4671 was maintained on V-8 juice agar slopes (ATCC medium 343), and *Cunninghamella echinulata* var. *elegans* ATCC 26269 on potato dextrose agar slopes.

Preparation of substrates

With the exception of *N*-carbomethoxy-1,2,3,4-tetrahydroisoquinoline (**34**) all the compounds used in this study were commercial samples. Their purity was checked by nmr and gc analysis, particularly for those samples (e.g. **31**) that can undergo autoxidation. Where necessary, samples were redistilled before use. Compound **34** was prepared by treatment of 1,2,3,4-tetrahydroisoquinoline (**33**) with methyl chloroformate in pyridine solution in the normal way, and gave satisfactory spectral data.

Incubations with fungi

These are summarized in Table 1. *Mortierella isabellina* NRRL 1757 was grown as previously described (27). After 3 days growth at 28°C, incubations were carried out in distilled water at substrate concentrations of 1 mg/mL in closely stoppered 1-L Erlenmeyer flasks for 72 h at 25°C. Products were isolated from the incubation medium by continuous extraction (4 days) with CH_2Cl_2, following removal of the fungus by filtration. The crude extracts were examined by tlc and submitted to flash chromatography using a benzene–ether 10% step gradient. The yields and ee values quoted in Table 1 refer to purified, isolated material, and arise from the combination of homogeneous column fractions without further purification (e.g. crystallization) that could lead to alteration of stereochemical enrichment values. In most cases, the volatility of starting material precluded its recovery after solvent evaporation, but in all cases the presence of starting material at the end of the incubation period was evident by its aroma. *Helminthosporium* species NRRL 4671 was grown in a medium consisting of V-8 juice (200 mL) and calcium carbonate (3 g), in distilled water (1 L), adjusted to pH 7.2, and *Cunninghamella echinulata* ATCC 26269 in a commercially prepared medium of Sabouraud dextrose broth (Difco). Subsequent incubations and product isolations were carried out exactly as described above.

Isolation and structure determination of products

Following chromatography as described above, products were identified by ^1H nmr, mass spectral, infrared, and optical rotation analysis. Spectral assignments were straightforward and unambiguous in all cases. Optical rotation values are listed in Table 2. Measured values were obtained in EtOH or $CHCl_3$ as appropriate. A typical procedure is outlined in full below.

Incubation of p-*diethylbenzene with* C. echinulata

para-Diethylbenzene (1.5 g) in ethanol (30 mL, 95%) was distri-

Can. J. Chem. Downloaded from www.nrcresearchpress.com by 80.58.250.72 on 09/07/12
For personal use only.

buted over 15 1-L Erlenmeyer flasks, each containing a 3-day growth of *C. echinulata* suspended in distilled water (150 mL). The stoppered flasks were maintained on a rotary incubator (150 rpm) at 25°C for 72 h, and the contents filtered through a Buchner funnel. The filtrate was continuously extracted with CH_2Cl_2 for 96 h, and the extract evaporated to yield a residue (0.7 g). Chromatography of this residue gave, in order of elution: 1-(4′-ethylphenyl)ethanol, **3***a* (0.18 g), oil; ^{1}H nmr (δ): 1.25 (3H, t), 1.38 (3H, d), 2.6 (2H, q), 4.75 (1H, q), and 7.25 (2H, ABq) ppm; 2-(4′-ethylphenyl)ethanol, **36** (0.15 g), oil; ^{1}H nmr (δ): 1.3 (3H, t), 2.5–2.9 (total 4H, superimposed t+q), 3.75 (2H, t), and 7.2 (4H, s) ppm; 1-(4′-acetylphenyl)ethanol, **45** (0.04 g), oil; ^{1}H nmr (δ): 1.4 (3H, d), 2.6 (3H, s), 4.8 (1H, q), 7.4 and 7.8 (4H, ABq) ppm; 2-(4′-acetylphenyl)ethanol, **43** (0.015 g); ^{1}H nmr (δ): 2.6 (3H, s), 2.8 (2H, t), 3.8 (2H, t), 7.4 and 7.8 (4H, ABq) ppm; 1-[4′-(1″-hydroxyethyl)phenyl]ethanol, **46** (0.06 g), mp 92–94°C (lit. (39) mp 90–91°C or 114–115°C); ^{1}H nmr (δ): 1.45 (6H, d), 4.75 (2H, q), and 7.25 (4H, s) ppm; 1-[4′-(2″-hydroxyethyl)phenyl]ethanol, **41** (0.15 g), mp 78–81°C; ^{1}H nmr (δ): 1.45 (3H, d), 2.8 (2H, t), 3.8 (2H, t), 4.8 (1H, q), and 7.25 (4H, ABq) ppm; 2-[4′-(2″-hydroxyethyl)phenyl]ethanol, **42** (0.02 g), mp 83–86°C (lit. (40) mp 86°C; ^{1}H nmr (δ): 2.8 (4H, t), 3.75 (4H, t), and 7.2 (4H, s) ppm.

Cross-induction experiments

Induction of enzyme was carried out by the addition of a solution of thioanisole or ethylbenzene (12 mg) in ethanol (95%, 8 mL) to the initial fungal growth medium (1 L). After the normal growth period (see above), the fungus was resuspended in distilled water containing cycloheximide at a concentration of 0.1 mg/mL and subsequent incubations with substrate performed as described above. Experiments without induction of enzyme, but in which *de novo* protein synthesis during the incubation with substrate was stopped, were also carried out in the presence of cycloheximide (0.1 mg/mL).

Determination of enantiomeric ratios

Enantiomeric ratios were determined by observation of the benzylic hydrogen resonances in the presence of sufficient chiral shift reagent (ca. 0.8–1.2 molar equivalent) to cause baseline separation of the enantiomeric signals and a shift of those resonances to ca. 20 ppm. Under these conditions, the aromatic hydrogens *ortho* to the side chain were shifted to ca. 14 ppm, and the enantiomeric signals sufficiently well separated to permit use of these as an additional check on optical purity. In all cases studied, the signals from the *R* enantiomers were downfield for the CHOH pair and upfield for the *ortho*-hydrogen pair. This observation correlated with optical rotation data for the assignment of absolute configuration to the predominant enantiomer.

Acknowledgements

Financial support was provided by the Natural Sciences and Engineering Research Council of Canada. We are grateful to Frances Brown for assistance with microbiological work, to Tim Jones for assistance in obtaining spectra, and to Dr. M. G. Coombe and Mr. S. A. Haskoll of the Department of Physical Sciences, Brighton Polytechnical College, U.K., for data on tetralone conversion by *C. elegans*.

1. J. N. Smith, R. H. Smithies, and R. T. Williams. Biochem. J. **56**, 320 (1954).
2. R. E. McMahon and H. R. Sullivan. Life Sci. **5**, 921 (1966).
3. G. A. Maylin and M. W. Anders. Pharmacologist, **11**, 251 (1969).
4. G. A. Maylin, M. J. Cooper, and M. W. Anders. J. Med. Chem. **16**, 606 (1973).
5. K. Engstrom, E. Elovaara, and A. Aitio. Xenobiotica, **15**, 281 (1985).
6. E. Abushanab, D. Reed, F. Suzuki, and C. J. Sih. Tetrahedron Lett. 3415 (1978).
7. C. E. Cerniglia, K. J. Lambert, D. W. Miller, and J. P. Freeman. Appl. Environ. Microbiol. **47**, 111 (1984).
8. H. L. Holland, I. M. Carter, P. C. Chenchaiah, S. H. Khan, B. Munoz, R. W. Ninniss, and D. Richards. Tetrahedron Lett. **26**, 6409 (1985).
9. D. T. Gibson, B. Gschwendt, W. K. Yeh, and V. M. Kobal. Biochemistry, **12**, 1520 (1973).
10. J. B. Davies and R. L. Raymond. Appl. Microbiol. **9**, 383 (1961).
11. P. K. Battacharyya and K. Ganapathy. Ind. J. Biochem. **2**, 137 (1965).
12. O. Cervinka. Collect. Czech. Chem. Commun. **30**, 1684 (1965).
13. H. L. Holland, H. Pöpperl, R. W. Ninniss, and P. C. Chenchaiah. Can. J. Chem. **63**, 1118 (1985).
14. S. Orrenius and L. Ernster. *In* Molecular mechanisms of oxygen activation. *Edited by* O. Hayaishi. Academic Press, New York. 1974. p. 230.
15. M. A. Lang, J. E. Gielen, and D. W. Nebert. J. Biol. Chem. **256**, 12068 (1981).
16. S. W. May and R. S. Phillips. J. Am. Chem. Soc. **102**, 5981 (1980).
17. V. Prelog. Pure Appl. Chem. **9**, 119 (1964).
18. M. G. Coombe and S. A. Haskoll. Presented at the 30th IUPAC Congress, Manchester, UK, Sept. 1985.
19. W. McIntire, D. J. Hopper, J. C. Craig, E. T. Everhart, R. V. Webster, M. J. Causer, and T. P. Singer. Biochem. J. **224**, 617 (1984).
20. Y. Arai and K. Yamada. Agric. Biol. Chem. **33**, 63 (1969).
21. L. T. Burka and M. R. Boyd. *In* Bioactivation of foreign compounds. *Edited by* M. W. Anders. Academic Press, New York. 1985. p. 243.
22. S. Fujise. Biochem. Z. **236**, 241 (1931).
23. H. L. Holland, S. H. Khan, D. Richards, and E. Riemland. Xenobiotica, **16**, 733 (1986).
24. P. Ortiz de Montellano. *In* Bioactivation of foreign compounds. *Edited by* M. W. Anders. Academic Press, New York. 1985. p. 121.
25. T. J. R. Frances, R. J. Rick, P. Callaghan, and R. P. Hopkins. Biochem. Soc. Trans. **3**, 1244 (1975).
26. T. A. Crabb and S. L. Soilleux. J. Chem. Soc. Perkin Trans. 1, 1381 (1985).
27. H. L. Holland and I. M. Carter. Can. J. Chem. **60**, 2420 (1982).
28. H. Honeck, W.-H. Schunk, and H.-G. Muller. Pharmazie, **40**, 221 (1985).
29. R. Sato and T. Omura (*Editors*). Cytochrome P-450. Academic Press, New York. 1978.
30. H. L. Holland and E. Riemland. Can. J. Chem. **63**, 1121 (1985).
31. B. J. Auret, S. K. Balani, D. R. Boyd, R. M. E. Greene, and G. A. Berchtold. J. Chem. Soc. Perkin Trans. 1, 2659 (1984).
32. C. Hansch, A. Leo, S. H. Unger, K. H. Kim, D. Nikaitani, and E. J. Lien. J. Med. Chem. **16**, 1207 (1973).
33. E. Downer and J. Kenyon. J. Chem. Soc. 1156 (1939).
34. K. Okamoto, T. Kinoshita, Y. Takemura, and H. Yoneda. J. Chem. Soc. Perkin Trans. 2, 1426 (1975).
35. G. Vavon and B. Angelo. C. R. Acad. Sci. **224**, 1435 (1947).
36. T. A. Collyer and J. Kenyon. J. Chem. Soc. **143**, 676 (1940).
37. D. R. Boyd, N. D. Sharma, and A. E. Smith. J. Chem. Soc. Perkin Trans. 1, 2767 (1982).
38. A. G. Davies and A. M. White. J. Chem. Soc. 3300 (1952).
39. D. T. Mowry, M. Renoll, and W. F. Huber. J. Am. Chem. Soc. **68**, 1105 (1946).
40. P. Ruggli and W. Theilheimer. Helv. Chim. Acta, **24**, 899 (1941).

Can. J. Chem. Downloaded from www.nrcresearchpress.com by 80.58.250.72 on 09/07/12
For personal use only.

Étude comparative de l'adsorption d'acide déoxyribonucléique sur le chrysotile et le chrysotile phosphorylé (chrysophosphate)

JEAN-CLAUDE TOURAY ET PATRICK BAILLIF

École supérieure de l'énergie et des matériaux, Université d'Orléans, Unité associée du Centre national de la recherche scientifique n° 724, 45067 Orléans CEDEX 2, France

MARIE-CLAUDE JAURAND[1] ET JEAN BIGNON

Institut national de la santé et de la recherche médicale, Unité 139 et Unité associée du Centre national de la recherche scientifique 604, Centre hospitalier universitaire Henri Mondor, 94010 Créteil CEDEX, France

ET

LAURE MAGNE

Laboratoire d'étude des particules inhalés, 44 rue Charles Moureu, 75013 Paris, France

Reçu le 18 février 1986[2]

JEAN-CLAUDE TOURAY, PATRICK BAILLIF, MARIE-CLAUDE JAURAND, JEAN BIGNON et LAURE MAGNE. Can. J. Chem. **65**, 508 (1987).

L'adsorption d'acide déoxyribonucléique (ADN) sur un échantillon de chrysotile ainsi que sur deux échantillons de chrysophosphate a été étudiée par analyse chimique et par analyse de surface (spectrométrie de photoélectrons, XPS). Le chrysophosphate dérive du chrysotile par un traitement au $POCl_3$ en voie gazeuse; l'un des échantillons de chrysophosphate a été défibré par passage dans un défibreur Pallmann. L'analyse XPS des échantillons, avant traitement par l'ADN, a montré qu'une partie du phosphore fixé à la surface des fibres de chrysophosphate n'était pas stable puisqu'elle était solubilisée lorsque les fibres étaient dispersées dans l'eau distillée. Après traitement par l'ADN, la quantité d'ADN adsorbée par ces fibres était inférieure à celle adsorbée sur les fibres de chrysotile non phosphorylées (12,6 ± 1,7 μg/mg et 74,0 ± 4,0 μg/mg respectivement). L'échantillon défibré avait un comportement intermédiaire ce qui indiquerait qu'une partie des fibres a échappé à la phosphorylation (28,3 ± 5,6 μg/mg). Les résultats indiquent que l'adsorption d'ADN est une méthode sensible pour apprécier l'état de surface des fibres de chrysotile. On peut également formuler l'hypothèse que ce processus de phosphorylation masque ou bloque des sites superficiels, actifs dans l'adsorption d'ADN.

JEAN-CLAUDE TOURAY, PATRICK BAILLIF, MARIE-CLAUDE JAURAND, JEAN BIGNON, and LAURE MAGNE. Can. J. Chem. **65**, 508 (1987).

Deoxyribonucleic acid (DNA) adsorption on one sample of Canadian chrysotile and two samples of chrysophosphate has been studied using chemical analysis and a surface method of analysis (photoelectron spectroscopy, XPS). Chrysophosphate was obtained using a phosphorylation process applied to chrysotile fibres; one chrysophosphate sample was opened in a Pallmann device. XPS analysis of the samples before DNA adsorption has shown that some surface phosphorus was dissolved following suspension of the fibres in distilled water. After DNA treatment, the amount of DNA adsorbed at the surface of the chrysophosphate sample was lower than that adsorbed at the chrysotile surface (12.6 ± 1.7 μg/mg and 74.0 ± 4.0 μg/mg respectively). In addition, the opened sample adsorbed an intermediary DNA amount (28.3 ± 5.6 μg/mg), suggesting that the phosphorylation process has not reached all the bulk fibres. The results indicate that DNA adsorption is a sensitive method for investigation of the surface state of the fibre. Moreover, it seems that the phosphorylation process masks or blocks the reactive surface sites for DNA adsorption.

Introduction

L'usage commercial des fibres d'amiante fait peu à peu place à celui d'autres matériaux, le plus souvent fibreux, dont le potentiel toxique n'est pas toujours connu. Les données reportées dans la littérature ont montré que, in vitro, la toxicité des fibres d'amiante était caractérisée par une diminution de la viabilité cellulaire (1–4), une altération de la structure des chromosomes (5, 6), et une transformation des cellules (7, 8). Sur le plan physico-chimique, la réactivité de surface des fibres dans les phénomènes d'adsorption a été suggérée comme étant l'un des facteurs responsables de certains effets toxiques. Les fibres d'amiante montrent, en effet, une capacité à adsorber différentes molécules, aussi bien des cancérigènes chimiques exogènes tels que le benzo(*a*)pyrène (9) que des macromolécules endogènes. Bien que non absolue, une relation a pu être trouvée entre la capacité des minéraux à adsorber des membranes synthétiques et leur potentiel cytotoxique (10–12). L'adsorption d'acide déoxyribonucléique (ADN), macromolécule qui contient le matériel génétique, a été reportée par Chang *et al.* (12) qui, de plus, ont mis en évidence une modification de l'activité enzymatique de la DNAse après adsorption sur les fibres de chrysotile. Compte tenu de ces différents travaux, nous avons étudié les propriétés d'adsorption des fibres de chrysophosphate, fibres de chrysotile ayant subi un traitement de phosphorylation en voie gazeuse par $POCl_3$. Les études ont porté sur l'adsorption d'ADN analysée par la méthode de spectrométrie de photoélectrons (XPS) et par l'analyse chimique.

Méthodes

1. Matériel

Les fibres de chrysotile phosphorylé (chrysophosphates 3-4-5 et 3-13-5) et non phosphorylé (4-4-3) ont été fournies par la Société Nationale de l'Amiante, Sherbrooke, Quebec, Canada. La phosphorylation a été obtenue par traitement des fibres à l'oxychlorure de phosphore, $POCl_3$ (17). Un courant de gaz sec (air, azote) est chargé en $POCl_3$, par barbotage dans ce liquide maintenu à une température contrôlée. Le gaz porteur, chargé de $POCl_3$ en quantité variable, selon la température utilisée, est dirigé vers un cylindre rotatif contenant l'amiante à traiter. Un arrangement à contrecourant a été utilisé,

1. Auteur à qui adresser toute correspondance.
2. Révision reçue le 14 octobre 1986.

Printed in Canada / Imprimé au Canada

Can. J. Chem. Downloaded from www.nrcresearchpress.com by 80.58.250.72 on 09/07/12
For personal use only.

Can. J. Chem. Downloaded from www.nrcresearchpress.com by 80.58.250.72 on 09/07/12
For personal use only.

l'amiante arrivant par une extrémité du cylindre et le $POCl_3$ par l'autre. Les échantillons 3-4-5 et 3-13-5 se distinguent par le fait que le second échantillon a été soumis à un défibrage mécanique après phosphorylation (défibreur Pallmann).

2. Caractérisation des échantillons en XPS

Avant traitement par l'ADN, les fibres ont été caractérisées par analyse XPS. Celles-ci ont été mises en suspension dans de l'eau distillée à la température ambiante pendant 5 min, puis filtrées sur membrane Millipore. Une expérience complémentaire de plus longue durée a été réalisée en incubant les fibres à 37°C pendant 6 h dans l'eau distillée.

3. Adsorption d'ADN

Pour le traitement par l'ADN, les fibres ont été dispersées par sonication pendant 10 min (50 kHz, 20 watts); la concentration en fibres était de 2 mg/mL dans une solution de KCl/NaCl 0,145 *M*. L'ADN utilisé provenait de la Société Sigma, Saint Louis, Missouri, U.S.A. (ADN de thymus de veau). Les suspensions de fibres ont été mélangées, volume à volume, avec des solutions d'ADN à des concentrations croissantes. Le mélange était incubé à 37°C pendant 15 min.

Après incubation, le mélange était centrifugé pendant 30 min à 10 000 tours/min (12 000 × *g*) et les fibres lavées 2 fois à l'aide de la solution de KCl/NaCl 0,145 *M*. Pour l'analyse XPS, les fibres étaient recueillies, après lavage, sur un filtre, comme décrit précédemment (13).

4. Méthodes analytiques

Le tracé des isothermes d'adsorption a été effectué, pour des concentrations en ADN croissantes, par détermination de la densité optique, à 255 nm, du surnageant obtenu après centrifugation, et par référence à une courbe d'étalonnage. Les mesures ont été effectuées à l'aide d'un spectrophotomètre Beckman modèle 24 (Beckman Instruments France, Gagny, France).

L'analyse XPS a été réalisée à l'aide d'un spectromètre AEI ES 200. Les pics de photoélectrons Si_{2p} et Mg_{2s} ont été utilisés comme référence pour la matrice silicatée; les pics P_{2p} et Cl_{2p} ont été enregistrés pour mettre en évidence le traitement par $POCl_3$. Enfin, l'ADN a été caractérisé par le pic d'azote N_{1s}. La puissance de radiation (MgKα) était de 240 W. Le temps de balayage du spectre était réduit à 15 min/échantillon afin de minimiser les effets de l'irradiation sur la molécule d'ADN. Le pic N_{1s} caractéristique de la molécule d'ADN est un pic complexe qui présente 2 composantes principales qui ont pu être déterminées par ajustement en utilisant la méthode des moindres carrés à l'aide d'un microordinateur HP 85 (fig. 1).

La spectrométrie XPS, méthode d'analyse basée sur le processus photoélectronique, est quantitative lorsqu'elle est appliquée à une série d'échantillons de même nature. Pour un solide dont l'épaisseur est supérieure à 4 fois le libre parcours moyen (λ) des électrons étudiés, l'intensité du signal XPS est de la forme :

$$I = aFS\sigma C$$

où a = aire de l'échantillon, F = flux des rayons X incidents, S = facteur de transmission de l'analyseur, σ = section efficace de photoionisation, et C = concentration atomique de l'élément considéré.

Résultats et discussion

1. Analyse XPS des échantillons lessivés dans l'eau distillée

Les résultats sont présentés dans le tableau 1 où sont indiquées les intensités des pics XPS ainsi que les intensités normalisées au pic Si_{2p} qui est utilisé habituellement comme référence.

Sur les deux échantillons de chrysophosphate (3-4-5 et 3-13-5), on constate la présence de phosphore (E_l = 134,6 eV, valeur proche d'un phosphate) et de chlore (E_l = 199,2 eV, valeur observée généralement pour un chlorure). L'échantillon 3-4-5 est le plus enrichi en ces deux éléments.

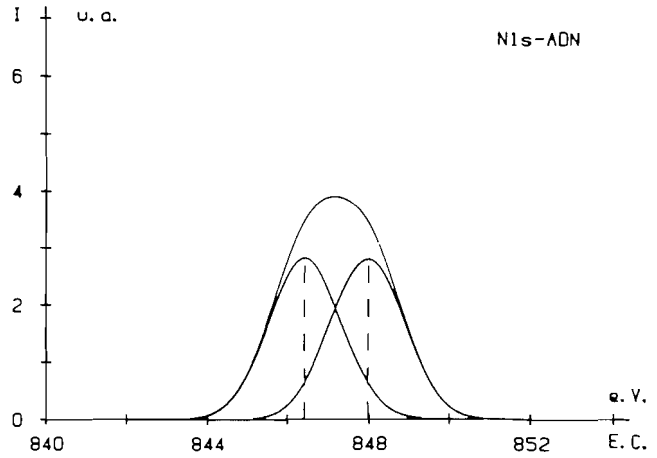

FIG. 1. Spectre N_{1s} de l'ADN. Les 2 composantes ont été déterminées par le calcul comme décrit dans le texte. u.a. : unités arbitraires; e.V. : electron volt; E.C. : Energie Cinétique.

On peut noter que l'intensité du pic Mg_{2s} normalisée au pic de silicium Si_{2p} est, pour l'échantillon 4-4-3, la même avant et après traitement dans l'eau distillée, alors que cette intensité est nettement plus faible, après lavage, pour les 2 chrysophosphates. Pour ces derniers, l'abaissement significatif du rapport Mg_{2s}/Si_{2p} s'accompagne d'une diminution importante des pics P_{2p} et Cl_{2p} ainsi que des rapports P_{2p}/Si_{2p} et Cl_{2p}/Si_{2p} qui sont diminués d'un facteur 4 et 10, respectivement. Cependant, la composition superficielle semble se stabiliser rapidement puisque l'essai 6 h à 37°C fournit des résultats très voisins de ceux obtenus après quelques minutes à la température ambiante.

Les intensités des pics Si_{2p} des échantillons avant traitement par l'ADN sont indiquées dans le tableau 2. On peut remarquer que les valeurs sont voisines pour les trois échantillons étudiés. En outre, les valeurs du rapport Mg_{2s}/Si_{2p} montrent que la surface du chrysophosphate est appauvrie en magnésium et que l'échantillon défibré (3-13-5) présente une composition intermédiaire entre le chrysophosphate non défibré (3-4-5) et le chrysotile témoin (4-4-3). Ces résultats montrent qu'une partie du phosphore fixé à la surface des fibres de chrysophosphate l'est sous forme soluble. Par ailleurs, lors du traitement par $POCl_3$, l'extraction du magnésium sous la forme probable d'un phosphate acide, mobilise essentiellement la couche brucitique externe des fibrilles de chrysotile. Un argument est apporté par la valeur théorique du rapport XPS Mg_{2s}/Si_{2p} pour une fibrille élémentaire entièrement lixiviée sur la première couche. Ce rapport s'établit à 0,69 alors qu'il est de 0,81 pour le chrysotile de référence (13, 14). La valeur 0,63 obtenue pour le chrysophosphate (3-4-5) traité dans l'eau est donc très proche de celle qui caractérise une fibre dont la couche brucitique externe aurait été lessivée.

2. Adsorption d'ADN

2.a. Isothermes d'adsorption : analyse chimique

Les résultats sont exprimés sur la figure 2. L'affinité pour l'ADN est la plus grande pour le chrysotile témoin (4-4-3) pour lequel la quantité d'ADN adsorbée au plateau est 74,0 ± 4,0 μg/mg (n = 6); elle est plus faible pour le chrysophosphate non défibré : 12,6 ± 1,7 μg/mg (n = 6); elle est intermédiaire et moins reproductible pour le chrysophosphate défibré 28,3 ± 5,6 μg/mg (n = 7), ce qui suggère que l'intérieur des fagots de fibrilles a pu échapper au traitement par $POCl_3$. En effet, on

TABLEAU 1. Effet du lessivage dans l'eau distillée, données XPS

	Échantillon[a]									
	4-4-3		3-4-5				3-13-5			
A[b]	Mg_{2s}	Si_{2p}	Mg_{2s}	Si_{2p}	P_{2p}	Cl_{2p}	Mg_{2s}	Si_{2p}	P_{2p}	Cl_{2p}
Fibres avant mise en suspension	211	206	93	114	96	83	108	143	82	81
H_2O, 20°C, 5 min	296	286	182	290	66	19	190	282	38	20
H_2O, 37°C, 6 h	284	282	178	286	52	15	194	277	36	13
B[c]	Mg_{2s}/Si_{2p}		Mg_{2s}/Si_{2p}	P_{2p}/Si_{2p}	Cl_{2p}/Si_{2p}		Mg_{2s}/Si_{2p}	P_{2p}/Si_{2p}	Cl_{2p}/Si_{2p}	
Fibres avant mise en suspension	0,83		0,83	0,83	0,74		0,75	0,57	0,57	
H_2O, 20°C, 5 min	0,82		0,63	0,23	0,06		0,67	0,13	0,07	
H_2O, 37°C, 6 h	0,84		0,63	0,19	0,06		0,70	0,13	0,06	

[a]4-4-3 Chrysotile non traité. 3-4-5 Chrysophosphate. 3-13-5 Chrysophosphate défibré Pallmann.
[b]A : Surface des pics (unité arbitraire).
[c]B : Intensité normalisée à Si_{2p}.

TABLEAU 2. Surface des pics des échantillons de référence. Les pics SFA (fibres longues et fines)[a] et FCC (fibres courtes obtenues par flottaison)[b] sont présentées à titre comparatif (unité arbitraire)

Échantillon[c]	Si_{2p}	Mg_{2s}/Si_{2p}
4-4-3	286 ± 10	0,81 ± 0,03
3-4-5	299 ± 5	0,63 ± 0,01
3-13-5	291 ± 10	0,69 ± 0,02
SFA	150 ± 15	0,76 ± 0,03
FCC	289 ± 15	0,79 ± 0,03

[a]Don de J. C. Wagner, Penarth, Wales, G.B.
[b]Don de F. Kimmerle, Quebec, Canada.
[c]4-4-3 Chrysotile non traité. 3-4-5 Chrysophosphate. 3-13-5 Chrysophosphate défibré Pallmann.

peut admettre que le défibrage Pallmann a, de manière plus ou moins aléatoire, ouvert les fagots de fibrilles, permettant ainsi d'exposer des fibres entières et (ou) des parties de fibres vierges.

2.b. Analyse XPS

Les résultats sont présentés sous la forme de courbes où le rapport N_{1s}/Si_{2p} a été reporté en fonction de la concentration initiale en ADN (fig. 3).

On peut constater, sur la figure 3, qu'il existe une dispersion variable des résultats, faible pour les échantillons 4-4-3 et 3-4-5, et maximale pour l'échantillon de chrysophosphate défibré. Ceci était également observé sur les isothermes (fig. 2). Par ailleurs, l'examen des courbes indique que la valeur au plateau est atteinte très rapidement pour le chrysophosphate alors qu'il faut des concentrations en ADN nettement supérieures dans le cas du chrysotile témoin. Le chrysophosphate défibré présente un comportement intermédiaire entre les deux autres. Toutefois, la comparaison des figures 2 et 3 montre que le rapport des hauteurs des plateaux relatifs aux échantillons 4-4-3 et 3-4-5 est d'environ 6 pour les isothermes d'adsorption alors qu'il est d'environ 3 pour les courbes XPS. Nous n'avons pas d'explication simple de ce fait qui, selon nous, pourrait traduire une différence dans la configuration des molécules adsorbées. Cette hypothèse repose sur un calcul simple qui compare les données de l'analyse XPS et de l'analyse chimique; elle est basée sur les résultats montrant que le chrysophosphate fixait 6 fois moins d'ADN que le chrysotile témoin, alors que le taux de recouvrement ne diminuait pas dans les mêmes proportions.

Si nous faisons l'hypothèse que les macromolécules d'ADN adsorbées à la surface des fibres ont une épaisseur $l > 4\lambda$, le

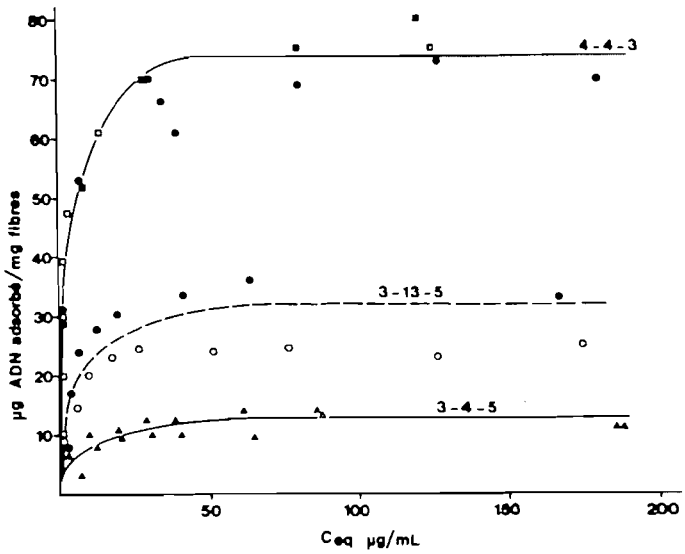

FIG. 2. Isothermes d'adsorption de l'ADN sur les différents échantillons. 4-4-3 Chrysotile non traité. 3-4-5 Chrysophosphate. 3-13-5 Chrysophosphate défibré Pallmann.

signal N_{1s}, caractéristique de l'adsorbat, sera proportionnel au taux de recouvrement θ de l'ADN, tandis que le signal Si_{2p}, caractéristique du substrat, sera proportionnel à $(1 - \theta)$. Le paramètre $R = I(N_{1s})/I(Si_{2p})$ (fig. 3) sera alors proportionnel à $\theta/(1 - \theta)$.

Par ailleurs, on peut supposer que les molécules d'ADN adsorbées sur le chrysophosphate et sur le chrysotile témoin ont le même volume moléculaire; soit n, le nombre de molécules d'ADN adsorbées sur le chrysophosphate et n', le nombre de molécules d'ADN adsorbées sur le chrysotile témoin, on aura, d'après les résultats de l'analyse chimique, $n' = 6n$. L'analyse XPS nous indique par ailleurs que $R' = 3R$; ou encore

$$[1] \quad \theta'/(1 - \theta') = 3\theta/(1 - \theta)$$

Le taux de recouvrement du chrysophosphate par l'ADN est égal au nombre n de molécules par unité de surface multiplié par s, aire d'une molécule projetée sur la surface. Il vient :

$$[2] \quad \theta = ns$$

De même pour le chrysotile témoin :

$$[3] \quad \theta' = n's' = 6ns'$$

La combinaison des relations [1], [2] et [3] permet d'obtenir une

Can. J. Chem. Downloaded from www.nrcresearchpress.com by 80.58.250.72 on 09/07/12
For personal use only.

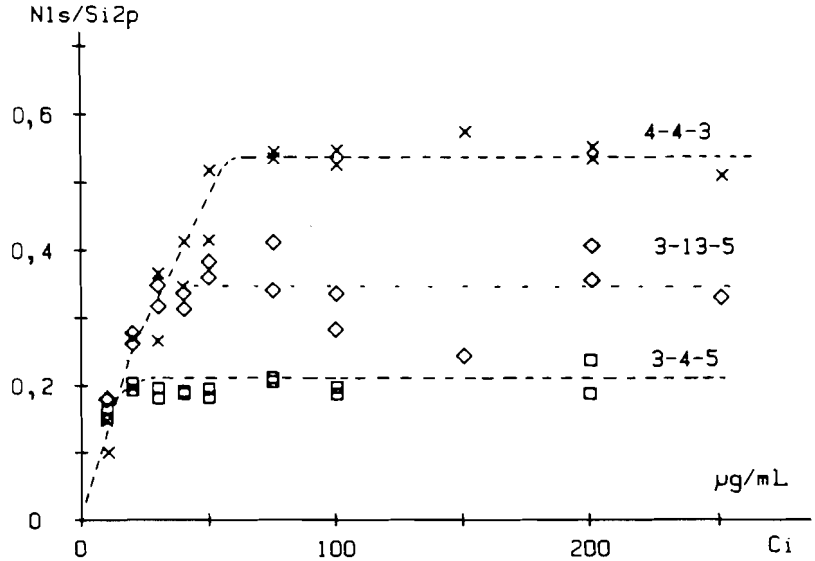

FIG. 3. Analyse XPS. Evolution du rapport d'intensité des pics N_{1s}/Si_{2p} (aire des pics) en fonction de C_i, concentration initiale en ADN. 4-4-3 Chrysotile non traité. 3-4-5 Chrysophosphate. 3-13-5 Chrysophosphate défibré Pallmann.

relation qui relie s, s' et θ' : $6s'/s + 2\theta' = 3$; par exemple, pour $\theta' = \frac{1}{2}$, on obtient $s = 3s'$ et, d'après [1], $\theta = \frac{1}{4}$.

Ce calcul simple ne permet pas de résoudre le système mais les résultats de l'analyse chimique et ceux de l'analyse XPS conduisent finalement à formuler l'hypothèse d'un plus grand étalement des macromolécules d'ADN à la surface du chrysophosphate qu'à celle du chrysotile témoin.

Conclusion

Les expériences effectuées montrent que l'adsorption d'ADN est un test sensible pour apprécier l'état de surface des fibres de chrysotile. L'interprétation complète des résultats suppose des comparaisons avec l'adsorption de molécules biologiques de plus petite taille et de forme non fibrillaire. À l'heure actuelle, les résultats relatifs à l'ADN conduisent cependant à formuler l'hypothèse d'un blocage des sites superficiels actifs par le phosphore ou par un composé phosphaté. On soulignera qu'il n'est pas indispensable que tous les sites actifs aient été bloqués par la phosphorylation pour expliquer les résultats obtenus : la possibilité de fixation d'une macromolécule organique est, en particulier, fonction de sa dimension et de sa forme. Un effet de barrière stérique (15) peut jouer un rôle pour contrôler l'adsorption de macromolécules fibrillaires telles que l'ADN.

La présence de phosphore fixé superficiellement diminue les propriétés sorptives du matériau vis-à-vis des molécules biologiques telles que l'ADN; il a été également observé une diminution des capacités d'adsorption de certains phospholipides du surfactant pulmonaire (résultats non publiés). Ces différents résultats peuvent être en relation avec la diminution de l'effet cytotoxique des fibres de chrysotile phosphaté (16). On peut par ailleurs se demander si la diminution du pouvoir clastogène (cassures de chromosomes) de ces fibres (16), comparativement au chrysotile non phosphaté, a un lien avec la diminution de l'adsorption d'ADN reportée ici.

Remerciements

Ce travail a été réalisé à l'aide de financement Société Nationale de l'Amiante, Québec, Canada et au moyen de fonds du Centre National de la Recherche Scientifique et de l'Institut National de la Santé et de la Recherche Médicale.

1. B. REISS, S. SOLOMON, J. WEISBURGER et G. M. WILLIAMS. Environ. Res. **22**, 109 (1980).
2. M. J. WADE, J. E. LIPKIN, R. W. TUCKER et A. L. FRANK. Nature, **264**, 444 (1976).
3. M. CHAMBERLAIN et R. C. BROWN. Br. J. Exp. Pathol. **59**, 183 (1978).
4. M. C. JAURAND, I. BASTIE-SIGEAC, J. BIGNON et P. STOEBNER. Environ. Res. **30**, 255 (1983).
5. A. SINCOCK et M. SEABRIGHT. Nature, **257**, 56 (1975).
6. G. K. LIVINGSTON, W. N. ROM et M. V. MORRIS. J. Environ. Pathol. Toxicol. **4**, 373 (1980).
7. T. W. HESTERBERG et J. C. BARRETT. Cancer Res. **44**, 2170 (1984).
8. M. J. PATEROUR, J. BIGNON et M. C. JAURAND. Carcinogenesis. **6**, 523 (1985).
9. H. MENARD, L. NOEL, F. KIMMERLE, L. TOUSIGNANT et M. LAMBERT. Anal. Chem. **56**, 1240 (1984).
10. M. C. JAURAND, L. MAGNE, J. L. BOULMIER et J. BIGNON. Toxicology, **21**, 323 (1981).
11. M. C. JAURAND, L. MAGNE et J. BIGNON. Toxicol. Lett. **15**, 205 (1983).
12. M. J. W. CHANG, L. B. JOSEPH, R. E. STEPHENS et R. W. HART. J. Am. Coll. Toxicol. **2**, 187 (1983).
13. M. C. JAURAND, P. BAILLIF, J. H. THOMASSIN, L. MAGNE et J. C. TOURAY. J. Colloid Interface Sci. **95**, 1 (1983).
14. J. H. THOMASSIN, J. GONI, P. BAILLIF, J. C. TOURAY et M. C. JAURAND. Phys. Chem. Miner. **1**, 385 (1977).
15. M. J. ROSEN. Surfactants and interfacial phenomena. J. Wiley and Sons, New York, Toronto. 1978.
16. M. C. JAURAND, A. RENIER, A. GAUDICHET, L. KHEUANG, L. MAGNE et J. BIGNON. Ann. NY Acad. Sci. Sous presse.
17. J. M. LALANCETTE et J. DUNNIGAN. U.S. Patent 4,356,057. 26 octobre 1982; Canadian Patent 1169230. 1984; J. M. LALANCETTE, M. COSETTE et P. DELVAUX. U.S. Patent 4,495,223. 22 janvier 1985.

Can. J. Chem. Downloaded from www.nrcresearchpress.com by 80.58.250.72 on 09/07/12
For personal use only.

Electrical breakdown phenomenon and electronic conduction during the anodic growth of Nb_2O_5

R. K. NIGAM,[1] K. C. SINGH, AND SANJEEV MAKEN

Department of Chemistry, Maharshi Dayanand University, Rohtak, Haryana, India

Received June 6, 1986

R. K. NIGAM, K. C. SINGH, and SANJEEV MAKEN. Can. J. Chem. **65**, 512 (1987).

Electrical breakdown voltage studies on Nb_2O_5 films in aqueous solutions of weak organic acid as a function of concentration, temperature, and applied field are carried out under galvanostatic conditions. Electronic conduction measurement through the Nb_2O_5 film as a function of temperature and applied field are also determined so as to examine the validity of Ikonopisov theory of electrical breakdown quantitatively.

R. K. NIGAM, K. C. SINGH et SANJEEV MAKEN. Can. J. Chem. **65**, 512 (1987).

Opérant dans des conditions galvanostatiques, on a examiné l'influence de la concentration, de la température et du champ appliqué sur le voltage lors de pannes électriques d'acides organiques. Dans le but d'évaluer quantitativement la validité de la théorie d'Ikonopisov sur les pannes électriques, on a aussi déterminé la conduction électronique à travers le film de Nb_2O_5 en fonction de la température et du champ appliqué.

[Traduit par la revue]

Can. J. Chem. Downloaded from www.nrcresearchpress.com by 80.58.250.72 on 09/07/12
For personal use only.

Introduction

A considerable interest has been witnessed in recent years in the studies of electrical breakdown during the anodization of valve metals. The phenomenon is important both for electrolytic capacitor industry (1–3) and for anodization in general. But the difficulties lie both in the definition of breakdown and in the interpretation of the process.

A number of criteria (4), namely, the appearance of visible sparking, the slowing down of the potential rise, the reaching of a maximum voltage, the occurrence of audible crackling, the rapid voltage fluctuation, and the abrupt increase in the number of high frequency pulses in the anode circuit have been used for detecting breakdowns. Local crystallization (5) or fissure formation in oxide or electronic impact ionization and avalanching (6) are some of the breakdown mechanisms proposed by a number of investigators (7). Kardary and Klein (8) have interpreted the breakdown process by applying the stochastic succession of avalanche breakdown (9) while Ikonopisov (10) based his avalanche breakdown theory on the Forlani and Minnaja (11) model. The latter has been further supported by the experimental observations of Van Geel *et al.* (12), Fritzsche (13), and Montero and co-workers (14, 15).

In this paper a systematic study of the electrical breakdown on Nb_2O_5 film as a function of temperature, concentration, and composition of electrolyte, and current density and other experimental conditions has been made. Electronic current measurements through the oxide film as a function of temperature and applied field are also carried out. The Ikonopisov's theory of electrical breakdown has been examined critically.

Experimental

Niobium specimens (2 cm^2 in area) with a short tag were cut by a die from a sheet of niobium (99.9% purity). The edges of the specimens were abraded with fine emery paper to make them smooth. The specimen was then dipped in KOH melt to clean the surface and finally washed with distilled water. The chemical polishing of the specimen was done by dipping in a freshly prepared etching mixture of 98% H_2SO_4 + 70% HNO_3 + 48% HF (5:2:2, v/v) for 3–5 s and then washed with distilled water. It was then placed in boiling water for about 10 min to remove thin film of unknown compound from the surface of specimen. The tag of the specimen was covered with a thick anodic film formed in 0.1 *N* citric acid at room temperature. The specimen thus prepared was placed in a glass cell and was surrounded by a platinum gauze which served as a cathode during the production of oxide. The glass cell was placed in water thermostat (controlled to ±0.01 K).

Anodic polarization of the specimen was carried out at constant current, adjusted through an electronically operated constant current generator (General Electronics, Ambala Cantt.) designed specially for this purpose. The supply of current was cut off by an electronic control after the desired voltage of formation was reached. The time for the passage of current for film formation through successive intervals of voltages was recorded by an electronic timer (ET5302, Electronics Corporation of India Limited, Hydrabad) which could read ±0.01 s. The experiments under galvanostatic conditions were carried up to the breakdown voltage with A.R. grade tartaric, citric, and oxalic acids as electrolytes at temperatures ranging from 273.15 to 348.15 K and at different concentrations. Current density employed for anodic growth was varied from 1 to 100 mA/cm^2. Each reading was repeated at least five times and the breakdown voltage data show a very good reproducibility as mean values of breakdown voltage (U_B) for each set is not very much different from the lowest and the highest value of breakdown.

Thickness of the oxide film was determined by the Faraday law method. The density of niobium oxide (Nb_2O_5) was taken to be 4.36 g/cm^2 as suggested by Holtzberg *et al.* (16) and the temperature coefficient of density between 0 to 70°C has been assumed zero. The thickness was also measured using ellipsometer (Model Gaertner Production Ellipsometer L117 manufactured in USA). In electronic current (J_e) measurements, "adapted" electrolytes (17) were used. The method for the determination of stationary electronic current was the same as described by Ikonopisov *et al.* (17, 18). The film formation and the measurements of J_e as a function of temperature and applied field (E) were done under identical conditions in all electrolytes. The anodization was carried out in two stages. Initially through galvanostatic anodization at a current density of 10 mA/cm^2, a formation voltage of 200 V was reached and then maintained for 4 h. The highest values of the applied field strength were low enough (electropotentials less than 75% of the voltage at which the film was formed), thus ensuring a negligible ionic component of the current through the film. It was further supported by a negligible change in the thickness of the oxide film (measured with ellipsometer) at different intervals of time (say 1 h).

Results and discussion

Criteria of breakdown voltage

A number of criteria are used by different workers to define breakdown quantities. The particular phenomenon appearing at

[1]To whom all correspondence should be addressed.

Can. J. Chem. Downloaded from www.nrcresearchpress.com by 80.58.250.72 on 09/07/12
For personal use only.

breakdown depends upon the nature of the metal, concentration, composition, and temperature of electrolyte and the current applied for the anodic growth of the film. In case of niobium metal, breakdown is observed by the evolution of gas at the surface. Rate of gas evolution goes on increasing with time and the voltage becomes static for sometime (say 100 s). This particular voltage is taken as the breakdown voltage (U_B) for our investigations. No sparking or crackling sounds are observed at low current densities but at high current densities, say at 50 to 100 mA/cm^2, visible sparks are observed on the film. If the current is passed for a longer period the white crystalline solid is formed on the film. Once the solid is formed the voltage suddenly falls by 100 to 150 V below the breakdown voltage, then rises gradually to any maximum value. This maximum value is dependent on the quantity of the white solid formed. The formation of white solid is easier at higher concentrations of electrolyte and for larger applied current densities.

Effect of concentration

The dependence of U_B on the electrolyte resistivity ($\rho, \Omega m$) can be represented by a well known relation (1–3, 6, 19)

[1] $$U_B = a_B + b_B \log \rho$$

Here a_B and b_B are empirical constants, depending on the nature of the electrolyte. These are calculated by the method of least squares.

Electrolyte	a_B, V	b_B, V
Tartaric acid	212	46
Citric acid	160	60
Oxalic acid	143	56

In all observations, temperature of each electrolyte was set at 298.15 K and current density employed for anodization was 10 mA/cm^2. The data have been plotted in Fig. 1. The variation of log ρ from 2 to 4 was achieved by varying the molar concentrations of oxalic, citric, and tartaric acids from 0.04 to 0.0003 *M*, 0.482 to 0.00030 *M*, and 0.574 to 0.00030 *M*, respectively.

Effect of stirring

A considerable effect of stirring on U_B in fairly dilute solutions of electrolytes has been observed. This is in contradiction with the observation of many investigators (1, 2, 7, 20) who found U_B values independent of stirring. We could not explore the effect in concentrated solutions because of the formation of a white crystalline solid on the film. The values of U_B were (Fig. 2) always found to be higher when the solution was stirred than when the experiment was carried without stirring. As the concentration of solution increases the effect of stirring on U_B decreases. It seems possible that under the influence of field (when solution was not stirred) the anions density of electrolyte near the film surface becomes higher than their density in bulk. Thus the value of log ρ near the film surface will be lower than the experimentally measured value. Therefore, the measured U_B will be lower than the U_B corresponding to the bulk concentration (log ρ). But because of stirring, the concentration of anions near the surface of film and in bulk remains the same, and thus higher values of U_B are obtained in stirring solution. In concentrated solution, the number of ions near film surface become more or less maximum

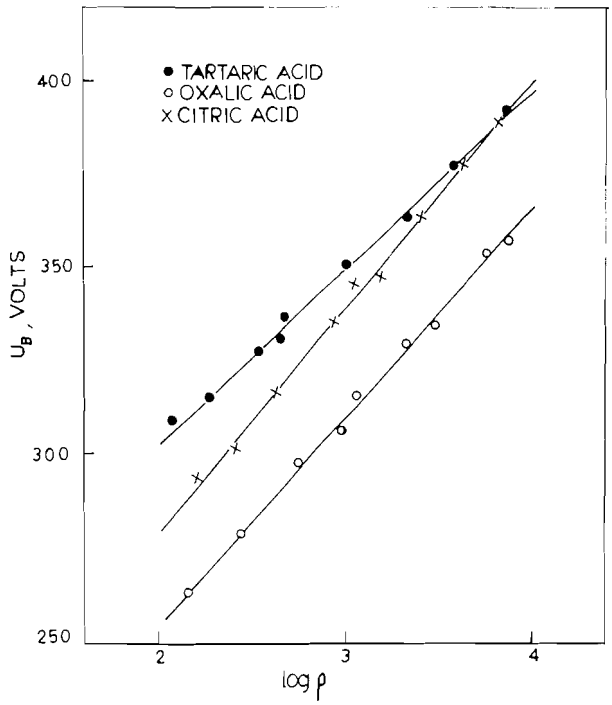

FIG. 1. Variation of breakdown voltage (U_B) with resistivity of electrolyte (ρ) at 288.15 K.

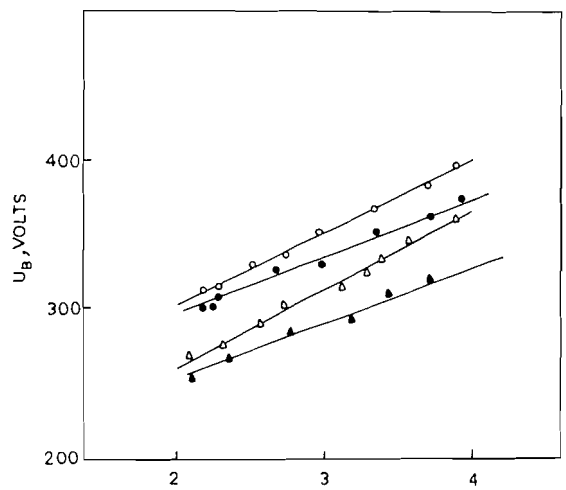

FIG. 2. Plot of U_B vs. log ρ at 298.15 K: ○ tartaric acid and △ oxalic acid (with stirring) and ● tartaric acid and ▲ oxalic acid (without stirring).

and the ions attracted by applied field do not find sufficient space near the surface. Thus further increase of concentration will not increase the ion concentration near the surface. Therefore, the effect of stirring goes on decreasing with the increase of concentration (Fig. 2).

Effect of current density (j)

The effect of current density (j) on U_B could only be measured between 1 to 100 mA/cm^2 due to experimental restrictions. The anodization at very low current densities proceeds so slowly that U_B can not be reached for a reasonable duration of the experiment. On the other hand, the abrupt potential rise and the formation of white solid at the surface of the film at sufficiently high current densities impede the accurate

Can. J. Chem. Downloaded from www.nrcresearchpress.com by 80.58.250.72 on 09/07/12
For personal use only.

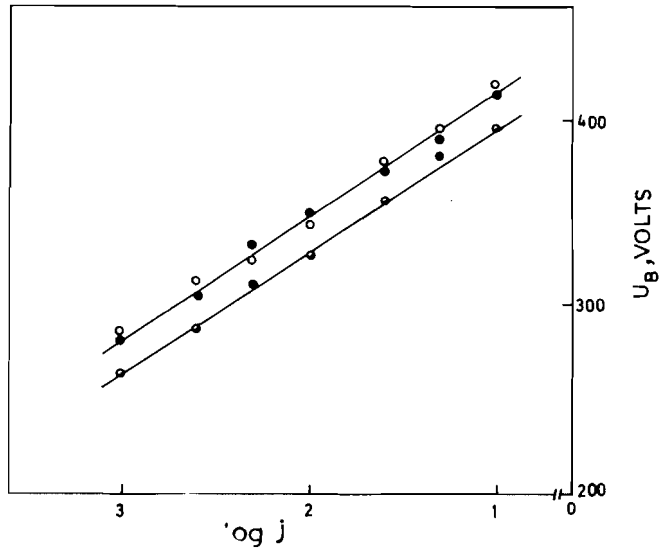

FIG. 3. Plot of U_B vs. log j, j in A/cm^2: ◒ oxalic acid, ● tartaric acid, ○ citric acid.

detection of U_B. Nevertheless, a reliable measurements of U_B can be carried out for the above stated range of current densities. At low current densities, the criterion for observation of U_B was the evolution of gas and at high current densities the evolution of gas was accompanied by the sparks at the film surface. Plots of U_B vs. log j are found to be linear (Fig. 3). With a 100-fold increase of j the increase in U_B for all three systems studied is 120 V. The 100-fold change of j changes the field strength ($E^{1/2}$) only to 18%. Thus U_B is very sensitive to the applied field. This observation is in contradiction with the observations of other workers (1, 2, 21–23). In tantalum and aluminium oxide film, the effect of current density on U_B is very small (21, 23, 24). Our data can be fitted well to the equation

$$[2] \quad U_B = A_B + B_B \log j$$

where A_B and B_B are the empirical constants dependent on the nature of metal, and the composition and concentration of the electrolyte in contact.

The following values of constants A_B and B_B are obtained:

Electrolyte	A_B, V	B_B, V
Tartaric acid	483.3	66.6
Citric acid	483.3	66.6
Oxalic acid	461.6	65.7

Here the electrolyte temperature was maintained at 298.15 K and the resistivity of solution was set at log $\rho = 3.0$ in each case. Approximately the same value of B_B in all the three electrolytes predicts that B_B is independent of the composition of electrolyte and it is only a function of the nature of metal. A_B, however, depends on the nature and concentration of the electrolyte.

Effect of temperature

Effect of temperature on U_B has been explored between the temperatures 273.15 to 348.15 K in electrolytes tartaric, oxalic, and citric acid. The resistivity of each electrolyte was set (log $\rho = 3.0$) at 298.15 K and the current density was 10 mA/cm^2. As the experimental temperature changes so does the resistivity of the solution. Thus the observed U_B values at

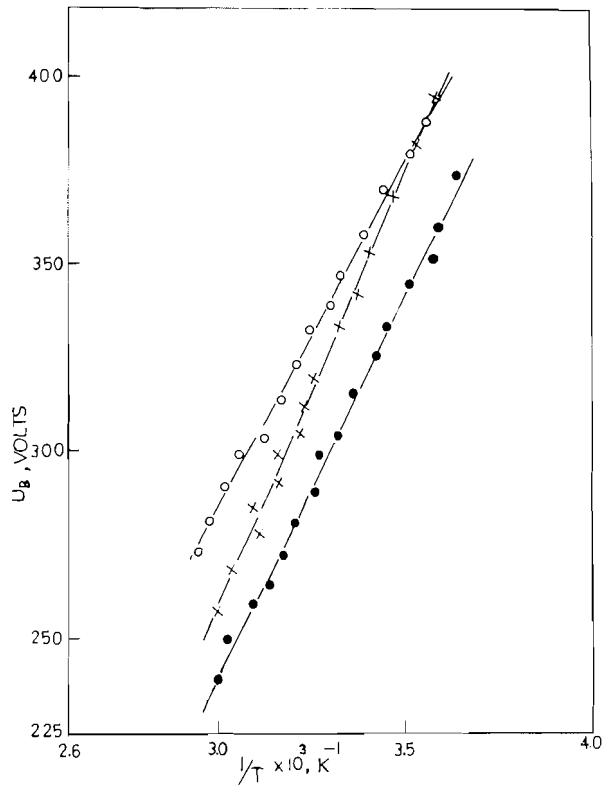

FIG. 4. Plot of U_B vs. $1/T$, ● oxalic acid, × citric acid, ○ tartaric acid.

different temperatures not only reflect the effect of temperature but also that of resistivity. In order to obtain the effect of temperature on U_B, the experimental values of U_B were corrected as follows:

$$[3] \quad U_T = U_B(T,\rho_2) - U_B(\rho_2) + U_B(25, \rho)$$

where U_T = calculated breakdown voltage at temperature T when log $\rho = 3$; $U_B(T, \rho_2)$ = experimentally measured breakdown voltage at temperature T, with solution resistivity ρ_2; $U_B(\rho_2)$ = breakdown voltage calculated from eq. [1] with resistivity ρ_2; $U_B(25, \rho)$ = breakdown voltage at temperature 25°C and log $\rho = 3.0$. Clearly the last two terms in the right hand side of eq. [3] give the change in breakdown voltage at 25°C when the resistance of solution changes from (log $\rho = 3$) to log ρ_2. Data before and after applying correction have been plotted in Figs. 4 and 5 and can be represented by the equation

$$[4] \quad U_B = \alpha_B + \beta_B/T$$

Here α_B and β_B are constants. Their values are calculated and given below:

Electrolyte	α_B, V	β_B, V K
Oxalic acid	−461.8	230.8×10^3
Tartaric acid	−366.05	214.3×10^3
Citric acid	−533.15	260.9×10^3

Here a change in temperature from 273.15 to 343.15 K changes U_B to 134, 115, 146 V in oxalic, tartaric, and citric acid, respectively. The change in field (E) within the film with the same change of temperature is calculated by employing eq. [16] and the change of E corresponding to the change in U_B was

calculated from eq. [15] and presented below

Electrolyte	Temperature changes	Change in $E^{1/2}$	Change in U_B
Oxalic acid	From 273.15 to 343.15 K	10.65%	27.62%
Citric acid	"	10.71%	36.47%
Tartaric acid	"	9.82%	26.63%

Thus the temperature change affects U_B in many ways: it changes the resistivity of the solution, field "E" within the film, and perhaps other characteristic breakdown parameters such as impact-ionization constant, primary electronic current density etc.

Ikonopisov's theory of breakdown voltage

According to Ikonopisov (10), during anodization the electrolytic contact not only provides ions for the oxidation, but also injects electrons into the conduction band of the oxide. The high field strength in it can accelerate these electrons to an energy which is sufficient to free other electrons by impact ionization so that an avalanche multiplication occurs. The avalanching effect causes the density (j_e) of the electronic current to increase with distance (x) within the anodic film.

$$[5] \quad j_e(x) = j_e(0)P \exp\left[\frac{eE}{\epsilon_m}\left(\frac{1}{x} - \frac{1}{x_r}\right)^{-1}\right]$$

where $j_e(0)$ = primary current density, injected at the electrolyte/oxide interface (at $x = 0$); e = electronic charge; x_r = recombination length; P = probability for an electron to reach the unstable energy required for surmounting the phonon scattering.

The general equation for breakdown voltage is given by

$$[6] \quad U_B = \frac{\epsilon_m}{re}[\ln j_B - \ln j_e(0)]$$

where U_B = breakdown voltage, r = recombination constant.

$$r = \frac{a_r}{a_r + 1} < 1$$

ϵ_m = difference between the mean energy of an electron necessary for ionization and the mean energy of the electrons emerging from an ionization event.

The temperature dependence of $j_e(0)$ can be described by the expression (25)

$$[7] \quad \ln j_e(0) = \ln \alpha_e + \beta_e/T$$

where α_e and β_e are constants. Substituting eq. [7] in eq. [6] and putting

$$[8] \quad \frac{\epsilon_m}{re}[\ln j_B - \ln \alpha_e] = \text{constant} = \alpha_B$$

$$[9] \quad \frac{\epsilon_m}{re}\beta_e = \text{constant} = \beta_B$$

we obtain eq. [4]

$$U_B = \alpha_B + \beta_B/T$$

The validity of above equation has already been proved

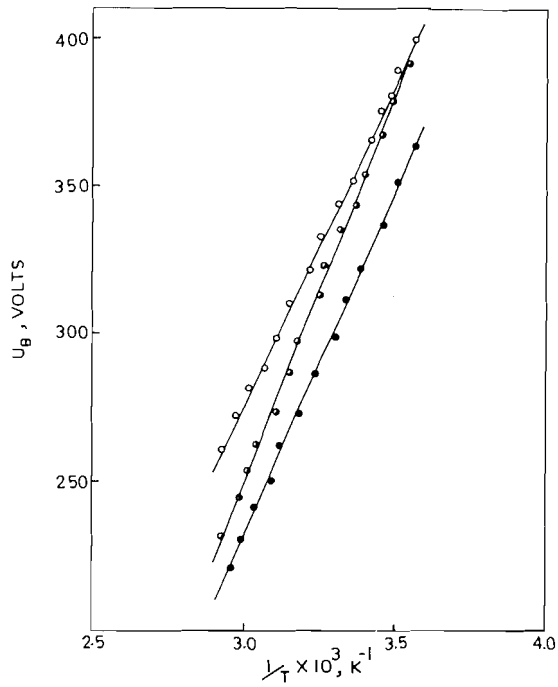

FIG. 5. Variation of U_B with $1/T$ after applying correction for log ρ: ● oxalic acid, ◒ citric acid, ○ tartaric acid.

(Fig. 5). A more intrinsic test to the theory can be derived from eq. [9].

$$[10] \quad \left(\frac{\beta_B}{\beta_e}\right) = \frac{\epsilon_m}{re}$$

Here e is the electronic charge ϵ_m and r are constants specific only for the anodized metal, and β_e is a quantity which characterizes the electron injection from the electrolyte into the oxide and depends on the electrolyte composition and nature of metal.

Consequently, the ratio β_B/β_e is determined only by the nature of the anodized metal.

For a given metal and two electrolytes with different compositions (ϵ_1 and ϵ_2) at the same conductivity

$$[11] \quad \left(\frac{\beta_B}{\beta_e}\right)_{\epsilon_1} = \left(\frac{\beta_B}{\beta_e}\right)_{\epsilon_2} = \frac{\epsilon_m}{re}$$

β_e values for all the three electrolytes are calculated from the electronic conduction experiments (Fig. 6). The slope of the line gives value of β_e; the ratio β_B/β_e for all three electrolytes are as follows:

Electrolyte	β_B	β_e	β_B/β_e
Oxalic acid	230.8	4.3×10^3	53.67
Tartaric acid	214.3	3.70	57.92
Citric acid	260.9	3.23	80.77

Similarly the dependence of $j_e(0)$ on the field strength can be described by the relation (25–27)

$$[12] \quad j_e(0) = A_e \exp[\beta_e E^{1/2}]$$

Can. J. Chem. Downloaded from www.nrcresearchpress.com by 80.58.250.72 on 09/07/12
For personal use only.

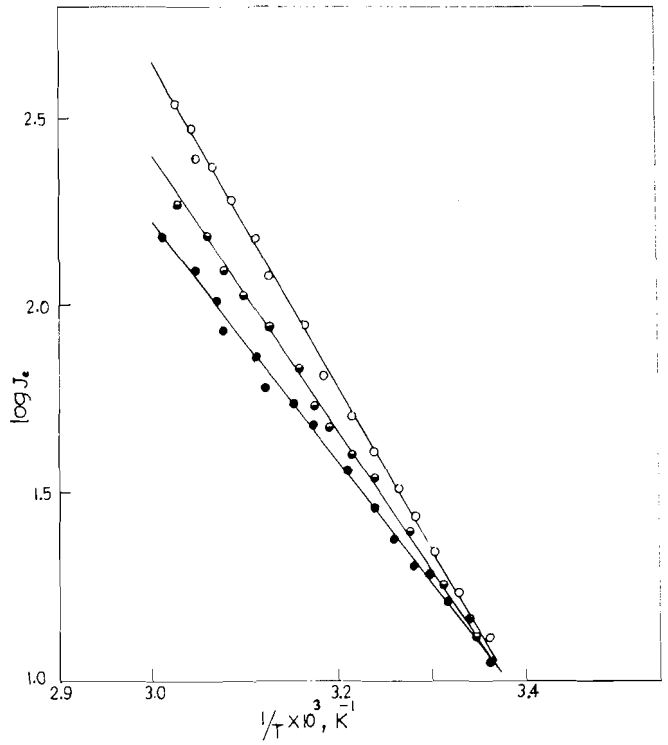

FIG. 6. Variation of electronic current (log j_e) with temperature ($1/T$): ○ oxalic acid, ◒ tartaric acid, ● citric acid.

Substituting eq. [12] in eq. [6] and putting

$$[13] \quad \frac{\epsilon_m}{re}[\ln j_B - \ln A_e) = \text{constant} = A_B'$$

$$[14] \quad \frac{\epsilon_m}{re}\beta_e = \text{constant} = B_B'$$

we obtain,

$$[15] \quad U_B = A_B' - B_B' E^{1/2}$$

The calculations of E were done using the equation of Young (28, 29)

$$[16] \quad j_i = A_i \exp\left(-\frac{B_i}{kT}\right) \exp\left(\frac{\alpha_i E - \beta_i E^2}{kT}\right)$$

where k is the Boltzmann constant, and the constants A_i, B_i, α_i, and β_i are determined only by the nature of anodized metal.

Plots of U_B vs. $E^{1/2}$ (Fig. 7) are linear, when the contacting electrolytes were tartaric, oxalic, and citric acids. A similar relation of type [11] can be obtained from eq. [14].

$$[17] \quad \left(\frac{B_B'}{B_e}\right)_{\epsilon_1} = \left(\frac{B_B'}{B_e}\right)_{\epsilon_2}$$

Again the values of B_e are obtained from the plot of $\ln j_e$ vs. $E^{1/2}$ (Fig. 8), the ratio B_B'/B_e are compared below:

Electrolyte	B_B'	B_e	B_B'/B_e
Oxalic acid	2.35×10^{-3}	0.73	3.196×10^{-3}
Tartaric acid	2.35×10^{-3}	0.78	3.008×10^{-3}
Citric acid	1.95×10^{-3}	0.80	2.418×10^{-3}

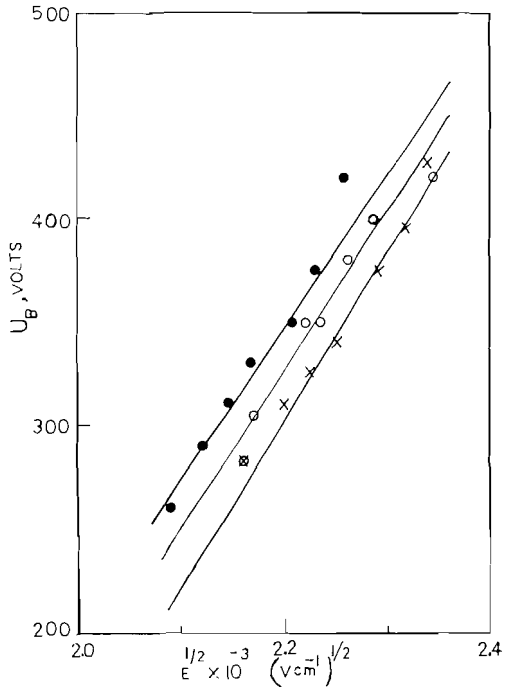

FIG. 7. Plot of U_B vs. $E^{1/2}$: ● oxalic acid, ○ tartaric acid, × citric acid.

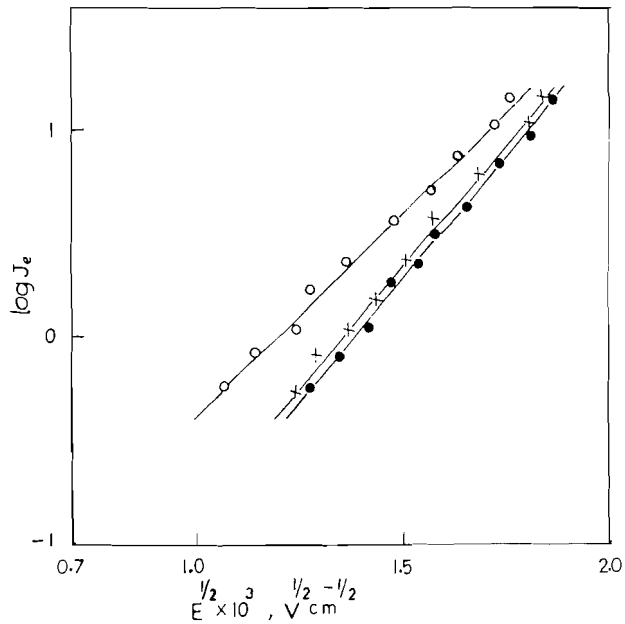

FIG. 8. Plot of j_e vs. $E^{1/2}$ at 298.15 K for various conducting electrolytes: ○ citric acid, × oxalic acid, ● tartaric acid.

Here again the ratio for oxalic and tartaric acids are the same but that for citric acid is different. Thus Ikonopisov's theory of breakdown voltage provides a theoretical justification to the effect of temperature, concentration, composition, and applied field on the breakdown voltage. However, the quantitative estimation of the various constants from experiments are different from those calculated. This may be due to the fact that the dependence of $J_e(0)$ on E, T, M, ρ have been studied at sufficiently low electric fields and the same relations have been used at high electric fields. The main limitation of the theory

Can. J. Chem. Downloaded from www.nrcresearchpress.com by 80.58.250.72 on 09/07/12
For personal use only.

is for not knowing the exact mechanism of the introduction of electron from the electrolyte to the oxide film. Recently Montero *et al.* (14, 15) have suggested that electron injection into the conduction band of oxide takes place from the anions incorporated in the film lattice. Thus the higher the concentration of anions in the film, the higher the primary electron current density ($J_e(0)$) and field (E); and therefore the lower the breakdown voltage. Incorporation of oxalate ions in film are known to be negligible. It has further been shown that the $J_e(0)$ and E remain almost constant during the concentration variation of oxalic acid electrolyte, but the impact ionisation coefficient changes, which is further responsible for the change of U_B with concentration.

As U_B in citric and tartaric electrolyte at particular concentration is always higher than the U_B values in oxalic acid electrolyte at the same concentration. This indirectly suggests that the concentration of citrate and tartrate ions incorporated in the film is less than that of oxalate ions. It is also obvious that the size of citrate and tartrate ions are quite large compared to the size of the oxalate ions. Thus a smaller number of larger ions will be able to penetrate in the film as compared to small-sized ions. The results of the above discussion can now be summarized. U_B depends upon the concentration, composition, and temperature of the contacting electrolyte and the current density employed for anodization. The criteria for observing U_B is the evolution of gas at the oxide film surface which makes the applied voltage static for some time. The Ikonopisov theory of electrical breakdown is able to explain all the observed effects qualitatively but its quantitative success is not certain.

Acknowledgements

The authors would like to thank the Head of the Chemistry Department for providing laboratory facilities. S.M. acknowledges C.S.I.R., New Delhi, for the award of a Junior Research Fellowship.

1. A. GUNTHERSCHULZE and H. BETZ. Elektrolytkondernzatoren. 2nd ed. Herbert Cram, Berlin. 1952.
2. I. N. ZAKZEIM. Elektroliticheskie kondensatory, Energiya, Leningrad. 1969.
3. V. T. RENNE. Elektroliticheskie kondensatory, Energiya, Leningrad. 1969.
4. S. IKONOPISOV, A. GIRGINOV, and M. MACHKOVA. Electrochim. Acta, **24**, 451 (1979).
5. N. N. AXELROD and N. SCHWARTZ. J. Electrochem. Soc. **116**, 460 (1969).
6. J. YAHOLOM. *In* Oxide–electrolyte interface. *Edited by* R. S. Alwitt. Princeton. 1973. p. 288.
7. A. K. VIJH. Corros. Sci. **11**, 411 (1971).
8. V. KADARY and N. KLEIN. J. Electrochem. Soc. **127**, 139 (1980).
9. N. KLEIN. Adv. Phys. **21**, 605 (1972).
10. S. IKONOPISOV. Electrochim. Acta, **22**, 1077 (1977).
11. F. FORLANI and N. MENNAJA. Phys. Status Solid. **4**, 311 (1964); F. FORLANI and N. MENNAJA. J. Vac. Sci. Tech. **6**, 518 (1969).
12. W. CH. VAN GEEL, A. C. PISTORIUS, and B. C. BOUMA. Philips Res. Rep. **12**, 6 (1957).
13. C. R. FRITZSCHE. J. Phys. Chem. Solids, **30**, 1885 (1969).
14. J. M. ALBELLA, I. MONTERO, and J. M. MARTINEZ. Duart J. Electrochem. Soc. **131**, 1101 (1984).
15. I. MONTERO, J. M. ALBELLA, and J. M. MARTINEZ. Duart J. Electrochem. Soc. **132**, 814 (1985).
16. F. HOLTZBERG, A. REISMAN, M. BERRY, and M. BERKENBLIT. J. Am. Chem. Soc. **79**, 2039 (1957).
17. S. IKONOPISOV. J. Electroanal. Chem. **86**, 105 (1978).
18. S. IKONOPISOV and N. ELENKOV. J. Electroanal. Chem. **88**, 417 (1978).
19. D. A. VERMILYEA. Anodic films. *In* Advances in electrochemistry and electrochemical engineering. Vol. 3. *Edited by* P. Delahay and C. W. Tobias. Interscience, New York. 1963.
20. G. C. WOOD and C. PEARSON. Corros. Sci. **7**, 119 (1967).
21. J. YAHALOM and T. P. HOAR. Electrochim. Acta, **15**, 877 (1970).
22. W. BAR. Z. Phys. **98**, 3 (1935).
23. J. ZAHAVI and J. YAHALOM. Electrochim. Acta, **16**, 89 (1971).
24. S. IKONOPISOV. Electrodeposition Surf. Treat. **2**, 303 (1973/74).
25. L. L. ODYNETS and S. S. CHEKMASOVA. Elektrokhimiya, **9**, 1177 (1973).
26. S. IKONOPISOV. Electrochim. Acta, **14**, 761 (1969).
27. V. P. MALINENKO, L. L. ODYNETS, S. S. CHEKMASOVA, and E. YA. HANINA. Elektrokhimiya, **7**, 1846 (1971).
28. M. J. DIGNAM. *In* Oxide and oxide films. Vol. 1. *Edited by* John W. Diggle. Marcel Dekker, Inc., New York. 1972. p. 91.
29. C. J. DELL'OCA, D. L. PULFREY, and L. YOUNG. Anodic oxide films. *In* Physics of thin films. Vol. 6. Academic Press, New York. 1971.

Can. J. Chem. Downloaded from www.nrcresearchpress.com by 80.58.250.72 on 09/07/12
For personal use only.

New nitrogenous sesquiterpenes based on alloaromadendrane and *epi*-eudesmane skeletons from the marine sponge *Axinella cannabina*[1]

PATRIZIA CIMINIELLO, ERNESTO FATTORUSSO,[2] SILVANA MAGNO, AND LUCIANO MAYOL

Dipartimento di Chimica delle Sostanze Naturali, Università di Napoli, Via L. Rodinò 22, I-80138 Napoli, Italy (081-207014)

Received August 8, 1986

PATRIZIA CIMINIELLO, ERNESTO FATTORUSSO, SILVANA MAGNO, and LUCIANO MAYOL. Can. J. Chem. **65**, 518 (1987).

Six new nitrogenous sesquiterpenes (**1–6**), which form two new isocyanide-isothiocyanate-formamide series, have been isolated from the marine sponge *Axinella cannabina*. The structure elucidation of these compounds is based upon spectral data, including 2D-nmr, and chemical interconversions. The complete assignment of all proton and carbon resonances in nmr spectra of axisonitrile-2 (**7**), an isonitrile previously isolated from the same source, is also reported, along with its complete relative stereochemistry.

PATRIZIA CIMINIELLO, ERNESTO FATTORUSSO, SILVANA MAGNO et LUCIANO MAYOL. Can. J. Chem. **65**, 518 (1987).

De l'éponge marine *Axinella cannabina* ont été isolés six nouveaux sesquiterpènes azotés (**1–6**) qui constituent deux nouvelles séries de trois composés voisins : isonitrile, isothiocyanate et formamide. Se basant sur leurs intercorrélations chimiques et faisant appel à la rmn, y compris la rmn ^{1}H-2D, on a déterminé les structures. On a aussi donné l'attribution complète des résonances de tous les protons et de tous les carbones, dans la rmn du composé axisonitrile-2, un isonitrile déjà isolé de la même éponge, avec sa complète configuration relative.

Can. J. Chem. Downloaded from www.nrcresearchpress.com by 80.58.250.72 on 09/07/12
For personal use only.

Numerous bioactive natural products carrying rare functionalities have been isolated from marine sponges. Among these, novel sesqui- and di-terpenoid isocyanides, isothiocyanates, and formamides represent a group of closely related compounds, none of which is yet known to be produced by any other marine organism (1). Undoubtedly, the mediterranean *Axinella cannabina* is the most prolific source of these unusual metabolites since its chemical investigation resulted in the isolation of isocyanides always accompanied by the corresponding isothiocyanates and formamides (2), most likely biogenetically deriving from them (3, 4).

In this paper we amplify on our earlier work by reporting the presence in this organism of two further isocyanide-isothiocyanate-formamide series based on the *epi*-eudesmane (**1–3**) and alloaromadendrane (**4–6**) carbon skeletons. Compound **4** is epimeric at C-1 to the co-occurring axisonitrile-2 whose structure had been previously established devoid of the chirality of the 10-carbon atom (5), which is here described.

Isolation of sesquiterpenes **1–6** from the $CHCl_3$ soluble material of the methanolic extract of the animals was carried out by chromatography on SiO_2 columns followed by reversed phase high performance liquid chromatographies.

Spectral (nmr and ms) examination of the pure constituents thus obtained made it apparent that each of the two terpenoid series was based on a single carbon skeleton and that the members of each series differed only in the nature of the functional groups. This was confirmed by conversion of the isocyanides into the formamides, by treatment with aqueous AcOH, and into the isothiocyanates, by heating with sulphur.

epi-*Eudesmane compounds (1–3)*

Compound **1** (11-isocyano-7β*H*-eudesm-5-ene), an oil, showed $[\alpha]_D$ −85.7 and was analyzed for $C_{16}H_{25}N$ by high resolution mass spectroscopy. The ir spectrum showed the typical absorption for the -N⁺≡C⁻ functionalities (ν_{max} 2135 cm^{-1}). Consideration of ^{1}H and ^{13}C nmr data (Table 1) indicated that the five degrees of unsaturation inherent in the molecular formula consisted of a trisubstituted double bond and two rings in addition to the isonitrile group. The ^{1}H nmr spectrum ($CDCl_3$) indicated the presence in **1** of a secondary (δ 1.14) and a tertiary (δ 1.10) methyl. Two further CH_3 existed as a $(CH_3)_2C(\text{—}N^+\equiv C^-)$ group as seen by a 6H broad singlet at δ 1.36. The structural hypothesis for compound **1** was supported by an accurate analysis of the 500-MHz ^{1}H nmr spectrum, involving double resonance techniques and by the ^{13}C–^{1}H correlated 2D-nmr spectrum. Comparison of the ^{1}H nmr spectrum of **1** in C_6D_6 vs. $CDCl_3$ revealed that the proton resonances were more resolved in C_6D_6 and hence these values (Table 1) are recorded around structure **1** for discussion. The ^{13}C nmr spectrum revealed the presence in **1** of only two methine carbons (δ 39.25 and 44.12), the pertinent protons resonating at δ 2.42 and 1.90 as indicated by the 2D-correlated spectrum. These two methine groups were shown to delimit the segment C4 to C7 by

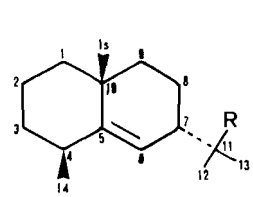

1 R = −N⁺≡C⁻

2 R = −N=C=S

3 R = −NHCHO

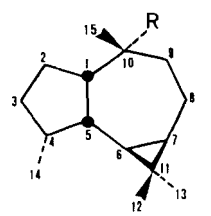

4 R = −N⁺≡C⁻

5 R = −N=C=S

6 R = −NHCHO

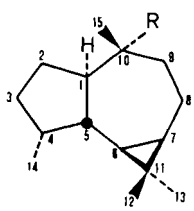

7 R = −N⁺≡C⁻

8 R = −N=C=S

9 R = −NHCHO

[1]This work was supported by the National Research Council of Italy (CNR) under "Progetto Finalizzato Chimica Fine e Secondaria" and M.P.I.

[2]Author to whom correspondence may be addressed.

TABLE 1. ^1H and ^{13}C nuclear magnetic resonance data in C_6D_6 for **1**

^{13}C chemical shift	Assignment	^1H chemical shift
	1ax	1.14 (ddd, J = 12.5, 12.5, 3.5 Hz)
41.31		
	1eq	1.36 (bd, J = 12.5)
	2ax	1.74 (m)
18.14		
	2eq	1.38 (m)
	3ax	
33.84		1.49 (m)
	3eq	
39.25	4	2.42 (m)
151.62	5	
129.19	6	5.38 (bd, J = 3.6 Hz)
44.12	7	1.90 (ddd, J = 3.6, 4.5, 4.5 Hz)
	8ax	1.57 (dddd, J = 13.0, 13.5, 4.5, 3.8 Hz)
20.64		
	8eq	1.44 (bddd, J = 13.5, 4.5, 3.8 Hz)
	9ax	1.29 (ddd, J = 13.5, 13.0, 3.8 Hz)
39.47		
	9eq	1.19 (bdd, J = 13.5, 3.8 Hz)
34.78	10	
60.46	11	
26.94*	12	1.05 (s)
27.04*	13	1.05 (s)
27.31*	14	1.14 (d, J = 7.0 Hz)
22.38	15	1.05 (s)
157.88	16	

*These resonances may be interchanged.

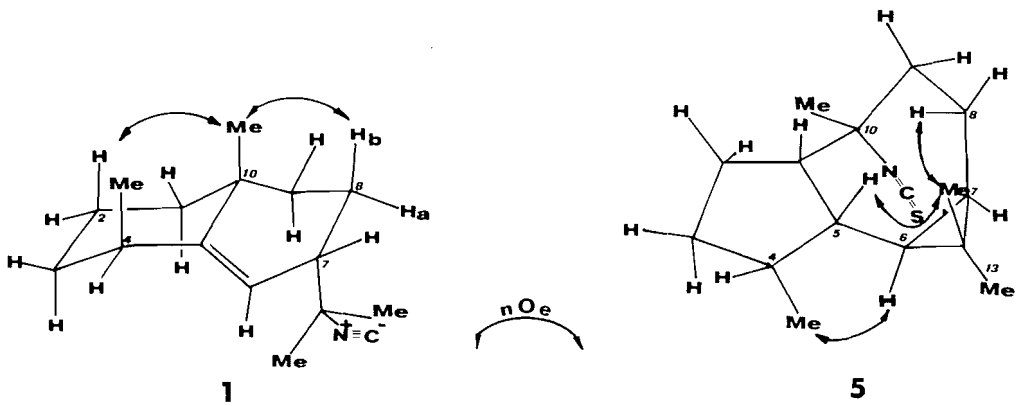

FIG. 1

the proton interactions shown by the following decoupling experiments. Irradiation at δ 5.38 (6-H) simplified the signal at δ 1.90 (7-H) into a bdd, whereas irradiation at δ 2.42 (4-H) removed the long range coupling between 4-H and 6-H and caused the doublet at δ 1.14 (15-H3) to collapse into a singlet. The extension of the above partial structure from C7 to C9 and from C4 to C1 was accomplished by further double resonance experiments assisted by 2D-correlation and spin decoupling difference techniques, which allowed us to assign all the proton resonances in **1** as reported in Table 1. At this stage the only way to accommodate the quaternary carbon atom (C-10) resonating at δ 34.78 was its incorporation among C14, C1, C9, and C5 and consequently the -$\overset{+}{N}\equiv\overset{-}{C}$ carrying isopropyl group must be located at C7.

To determine the relative spatial arrangements of all substituents we employed ^1H nmr data including nuclear Overhauser enhancement (nOe) difference spectroscopy. The equatorial nature of 4-H was established from the value of the coupling constant with 3-H_{ax} (deduced after irradiation at δ 1.14, which simplified the 4-H signal into a double doublet (J = 3.6 and 3.6 Hz)). On the other hand, the coupling constant values (J_{7-8a} and J_{7-8b}) required a *gauche* relationship of 7-H to both the C8 protons, thus indicating that the substituted isopropyl group should be either pseudo-axial α or pseudo-axial β. The latter possibility could be discarded on the grounds that the bulky β-substituent is sterically incompatible with the C-10 β-Me group. Furthermore the stereostructure **1** fully accounts for the observed nOe's between 10-Me and 2-H_{ax} and between 10-Me and 8-H_b (Fig. 1).

The molecular formula of the compound **2** (11-isothiocyano-7β*H*-eudesm-5-ene) was determined as $C_{16}H_{25}NS$ from hrms on the molecular ion at m/z 263. The presence of an

Can. J. Chem. Downloaded from www.nrcresearchpress.com by 80.58.250.72 on 09/07/12
For personal use only.

TABLE 2. ^1H and ^{13}C nuclear magnetic resonance data for **4**, **5**, and **7** ($CDCl_3$)

	5		**4**		**7**	
Assignment	^{13}C	^1H	^{13}C	^1H	^{13}C	^1H
1	53.15	2.13 (ddd)	52.33	2.19 (ddd)	55.80	2.17 (ddd)
2a						1.47 (m)
	26.80	1.81 (m)	26.67	[a]	27.71	
2b						1.9*
3a		1.68 (dddd)				1.22*
	30.95		30.72	[a]	34.30	
3b		1.39*				1.68 (dddd)
4	38.24	1.94 (b sextet)	38.24	2.00 (b sextet)	37.05	2.05 (m)
5	41.19	1.86 (bdd)	41.19	1.85 (bdd)	39.02	1.25*
6	23.58	0.43 (dd)	24.05	0.47 (dd)	29.41	0.53 } Further coupled
7	23.91	0.79 (ddd)	24.86	0.81 (ddd)	26.62	0.59 } B System
8a		1.86*				0.93*
	20.28		20.38	[a]	19.83	
8b		1.31*				1.8*
9a		2.07 (ddd)				1.97 } Further
	39.26		39.00	[a]	43.54	} coupled
9b		1.78 (ddd)				1.89 } AB System
10	64.95		64.86			
11	19.16		19.21		20.63	
12 }	28.58	1.06 (s)	28.61	1.03 (s)	28.55	0.99 (s)
13 }	15.21	0.97 (s)	15.39	0.94 (s)	15.71	0.95 (s)
14	15.72	0.95 (d)	15.82	0.93 (d)	15.99	0.91 (d)
15	31.24	1.36 (s)	31.89	1.36 (s)	19.54	1.28 (bs)
16	152.98		154.78			

*Submerged by other signals.

[a]Overlapped with other signals in the region 2.10–1.65 δ.

J values (Hz) for **4** and **5**: 1–2a = 7; 1–2b = 7; 1–5 = 7; 2a–3a = 7; 2b–3a = 7; 3a–3b = 13.5; 3a–4 = 7; 3b–4 = 7; 4–5 = very small; 4–15 = 7; 5–6 = 9.5; 6–7 = 9.0; 7–8a = 11.5; 7–8b = 6.0; 8a–9a = 7.5; 8b–9a = 12.0; 8a–9b = 3.0; 8b–9b = 7.5; 9a–9b = 15.0.

J values (Hz) for **7**: 1–2a = 8; 1–2b = 8; 1–5 = 8; 2a–3b = 5.5; 2b–3b = 5.5; 3a–3b = 12; 3b–4 = 5.5; 4–15 = 7.

isothiocyanate function was indicated by a strong absorption at ν_{max} 2100 cm^{-1} in the ir spectrum. A clear structural relationship between **1** and **2** exists, as indicated by comparison of their ^1H and ^{13}C nmr spectra (Experimental). This was proved by conversion of **1** into **2** by treatment with sulphur at 120°C.

The third *epi*-eudesmane sesquiterpene was the formamide **3** (11-formamido-7β*H*-eudesm-5-ene, $C_{16}H_{27}NO$ from hrms), which exists as a mixture of the two rotational isomers of the NHCHO group in the ratio 2(*cis*):3(*trans*) as indicated by ^1H nmr features in $CDCl_3$ (*trans* isomer: δ 8.20 (d, *J* = 12.0 Hz, H—C(=O)), 5.33 (d, *J* = 3.5 Hz, 6-H), 1.30 (s, 12-H3 or 13-H3), 1.29 (s, 13-H3 or 12-H3), 1.12 (d, *J* = 7.0 Hz, 14-H3), 1.06 (s, 15-H3); *cis* isomer: δ 8.06 (d, *J* = 2.0 Hz, H—C(=O)), 5.33 (d, *J* = 3.5 Hz, 6-H), 1.35 (s, 12-H3 or 13-H3), 1.32 (s, 13-H3 or 12-H3), 1.12 (d, *J* = 7.0 Hz, 14-H3), 1.06 (s, 15-H3)).

Its structure was rapidly assigned by the synthesis starting from **1** with aqueous AcOH in Et_2O.

Alloaromadendrane compounds (4–6)

A minor metabolite **5** (10α-isothiocyanoalloaromadendrane) was isolated from fraction A by reversed phase hplc. This new compound was analyzed for $C_{16}H_{25}NS$ (by hrms) and this formula was substantiated by its ^{13}C nmr features (Table 2). The presence of an isothiocyanate group was concluded on the basis of an ir band at ν_{max} 2100 cm^{-1} and of a facile loss of HNCS (*m/z* 204) from the molecular ion in the mass spectrum. The determination of the gross structure of **5** was made by ^1H nmr decoupling experiments supported by ^{13}C–^1H shift-correlated 2D spectroscopy, which allowed all protons and carbons to be assigned. These data clearly indicated that **5** must possess an aromadendrane-like skeleton with the isothiocyanate group linked to C-10; therefore the compound under investigation should differ only for stereochemical details from axisothiocyanate-2 (**8**), a sesquiterpene isothiocyanate previously isolated from the same source (5).

Proof for the stereostructure **5** was obtained from nOed data and by using a shift reagent ($Eu(fod)_3$) (5, 6) in obtaining a series of nmr spectra of the corresponding isocyanide **4** (10α-isocyanoalloaromadendrane), isolated from fraction B by hplc, which gave **5** by treatment with sulphur at 120°C.

The cyclopropyl hydrogens experience a large paramagnetic shift (80% of 10-Me) on complexation with $Eu(fod)_3$. Inspection of molecular models showed that the close proximity of these atoms with the $\overset{+}{N}\equiv\overset{-}{C}$ group can occur only if compound **4** is based on an alloaramodendrane skeleton with the isocyanide function in a *cis* relationship with 6-H and 7-H. On the other hand, the intramolecular nuclear Overhauser effects observed in **5** between 6-H and 4-Me, as well as between 12-H3 and the protons linked to C-5 and C-8, accord with this postulation and indicate the relative stereochemistry at C-4 in the above related compounds (Fig. 1).

The remaining metabolite **6** (10α-formamidoalloaromadendrane), isolated from fraction C by hplc, was identified as the amide corresponding to the isocyanide and isothiocyanate described above. Amide **6** was analyzed for $C_{16}H_{27}NO$ by high

Can. J. Chem. Downloaded from www.nrcresearchpress.com by 80.58.250.72 on 09/07/12
For personal use only.

resolution mass measurement of its parent ion at m/z 263. Structure **6** was assigned as the more plausible by studies of ^{1}H nmr features including decoupling experiments, which revealed a 2(*trans*):1(*cis*) ratio of the rotational isomers at the formylamino group (*trans* isomer, δ: 8.22 (d, J = 12.0 Hz, H—C(=O)—NH), 5.20 (bm, NH), 1.33 (s, 15-H3), 1.01 (s, 12-H3 or 13-H3), 0.94 (s, 13-H3 or 12-H3), 0.89 (d, J = 7.0 Hz, 14-H3), 0.69 (ddd, J = 11.5; 9.0; 6.0 Hz, 7-H), 0.25 (dd, J = 9.5; 9.0 Hz, 6-H); *cis* isomer, δ: 8.00 (d, J = 2 Hz, H—C(=O)—NH), 5.47 (bm, NH), 1.46 (s, 15-H3), 1.00 (s, 12-H3 or 13-H3), 0.92 (s, 13-H3 or 12-H3), 0.88 (d, J = 7.0 Hz, 14-H3), 0.63 (ddd, J = 11.5; 9.0; 6.0 Hz, 7-H), 0.16 (dd, J = 9.5; 9.0 Hz, 6-H)).

This attribution was secured by conversion of **4** into **6** by hydration following the usual work-up.

Axisonitrile-2 (**7**) and the related compounds **8–9** were isolated about ten years ago from the same source and their structures, including the relative stereochemistries apart from the chirality at C-10, were determined (5).

The assignment of the stereochemistry of the above chiral center has been now determined by an accurate analysis of ^{1}H and ^{13}C nmr spectra, including extensive ^{1}H decoupling studies and two-dimensional ^{13}C–^{1}H shift-correlated spectroscopy, which led to the assignment of all proton and carbon atoms in **7**, as reported in Table 2.

The ^{13}C nmr frequency of 10-Me (δ 19.54) established the *trans* relationship between this group and 1-H when compared with the corresponding carbon atom in aromadendrane derivatives (7). Further proof was obtained by the ^{1}H nmr spectrum of **7** measured in the presence of varying amounts of Eu(fod)$_3$. The 1-H proton suffered a remarkable europium shift, thus confirming its *cis* relationship with the isocyanide group.

The correct assignment of stereostructure **7** to axisonitrile-2 was secured by nOed data, which showed that 1-H and 6-H are in the nOe proximity, whereas no detectable effect was observed, as expected, between 10-Me and the cyclopropyl protons.

Experimental

The ^{1}H nmr spectra, including spin decoupling and nOe difference experiments, were recorded on a Bruker 500 WM spectrometer. The ^{13}C spectra and 2D-nmr experiments were recorded on a Bruker WM 250 spectrometer; all chemical shifts are reported in ppm, using TMS as internal standard (δ = 0). Nuclear Overhauser effects were determined with the aid of an Aspect 2000 microprogram using samples previously degassed by bubbling argon through the solution for 40 min. ^{13}C–^{1}H shift-correlated 2D-nmr spectra were obtained using a Bruker microprogram. The shift correlation with polarization transfer via J-coupling experiments were performed by adjusting the fixed delays to give maximum polarization for J_{C-H} = 135 Hz.

Low resolution mass spectra were recorded at 70 eV on an AEI MS 30 instrument. High resolution mass spectra were obtained on a Kratos spectrometer.

Optical rotations were measured in $CHCl_3$ using a Perkin Elmer 141 polarimeter with a 10-cm microcell.

The ir spectra were measured on a Perkin Elmer 157 spectrophotometer.

The hplc separations were carried out using Lichrosorb Si60 5-μm silica gel and μ-Bondapak C_{18} preparative columns (1.0 × 25 cm) with a Varian 5000 apparatus equipped with a differential refractometer detector.

Extraction

The sponge (*Axinella cannabina*) was collected in the spring of 1984, off the coast of Taranto near Porto Cesareo (Italy). The fresh material (600 g dry weight after extraction) was homogenized and extracted with MeOH (3 L × 3) and then with $CHCl_3$ (2 L × 2) at room temperature. The methanolic extracts were evaporated *in vacuo* to give an aqueous phase, which was extracted with Et_2O. Evaporation of the combined Et_2O and $CHCl_3$ extracts afforded 25 g of an oily residue, which was chromatographed under a slight N_2 pressure, on an SiO_2 column (using as eluent solvent of increasing polarity from hexane to Et_2O through C_6H_6). Early fractions (eluent hexane–C_6H_6 8:2) gave a mixture (2 g) of isothiocyanates (fraction A); middle fractions (eluent hexane–C_6H_6 2:8) yielded a mixture (11 g) of isonitriles (fraction B), and the later fractions (eluent Et_2O) afforded a mixture (700 mg) of amides (fraction C). Fractions A–C were used for the isolation of compounds **1–6** as described below.

Isolation of 2 and 5

Fraction A, obtained as above, was further separated by a silica gel column (500 g) under pressure, eluent *n*-hexane, to give an oily residue (600 mg) containing **2** and **5**. Pure **2** and **5** were obtained by hplc by using a 5-μm C_{18} reversed phase column with MeOH–H_2O 95:5 as eluent.

2, 22 mg, $[\alpha]_D$ −89.7 (*c* 0.8 in $CHCl_3$); ν_{max}: 2100 cm^{-1}; ^{1}H nmr ($CDCl_3$) δ: 5.34 (d, J = 3.5 Hz, 6-H), 2.43 (m, 4-H), 1.38 (s, 12-H3 or 13-H3), 1.36 (s, 13-H3 or 12-H3), 1.13 (d, J = 7.0 Hz, 14-H3), 1.09 (s, 15-H3); ^{13}C nmr ($CDCl_3$) δ: 158.33 (C-16), 152.66 (C-5), 119.69 (C-6), 64.83 (C-11), 45.07 (C-7), 40.93 (C-1), 39.19 (C-9), 39.06 (C-4), 34.65 (C-10), 33.32 (C-3), 27.28 (C-14), 27.18 (C-12 and C-13), 22.24 (C-15), 20.64 (C-8), 17.70 (C-2); hrms, m/z calcd. for $C_{16}H_{25}NS$: 263.1709; found: 263.1704.

5, 35 mg, $[\alpha]_D$ −6.95 (*c* 0.9 in $CHCl_3$); ν_{max}: 2100 cm^{-1}; ^{1}H nmr and ^{13}C nmr data are reported in Table 2; hrms, m/z calcd. for $C_{16}H_{25}NS$: 263.1709; found: 263.1703.

Isolation of 1 and 4

Fraction B, obtained as above, was chromatographed over silica gel (900 g), again with *n*-hexane–C_6H_6 (2:8) as eluent.

The fractions containing **1** and **4** were pooled and resolved into the single components by hplc by using a 5-μm C_{18} column (eluent 10% aqueous MeOH).

1, 31 mg, $[\alpha]_D$ −85.7 (*c* 0.8, $CHCl_3$); ν_{max}: 2135 cm^{-1}; ^{1}H nmr and ^{13}C nmr are reported in Table 1; hrms, m/z calcd. for $C_{16}H_{25}N$: 231.1988; found: 231.1986.

4, 28 mg, $[\alpha]_D$ −17.21 (*c* 0.7, $CHCl_3$); ν_{max}: 2135 cm^{-1}; ^{1}H nmr and ^{13}C nmr data are reported in Table 2; hrms, m/z calcd. for $C_{16}H_{25}N$: 231.1988; found: 231.1989.

Isolation of 3 and 6

Fraction C, obtained as above, permeated through an SiO_2 column (200 g), *n*-hexane eluent, to give 200 mg of an oil containing **3** and **6**. Final purification of amides **3** and **6** was achieved by hplc (silica gel column, eluent EtOAc–*n*-hexane 9:1).

3, 6 mg; ν_{max}: 3440 and 1680 cm^{-1}; hrms, m/z calcd. for $C_{16}H_{27}NO$: 249.2094; found: 249.2090. *cis* Isomer δ: 8.06 (d, J = 2.0 Hz, H—C(=O)—), 5.33 (d, J = 3.5 Hz, 6-H), 1.35 (s, 12-H3 or 13-H3), 1.32 (s, 13-H3 or 12-H3), 1.12 (d, J = 7.0 Hz, 14-H3), 1.06 (s, 15-H3); *trans* isomer δ: 8.20 (d, J = 12.0 Hz, H—C(=O)—), 5.33 (d, J = 3.5 Hz, 6-H), 1.30 (s, 12-H3 or 13-H3), 1.29 (s, 13-H3 or 12-H3), 1.12 (d, J = 7.0 Hz, 14-H3), 1.06 (s, 15-H3).

6, 5 mg; ν_{max}: 3440 and 1680 cm^{-1}; hrms, m/z calcd. for $C_{16}H_{27}NO$: 249.2094; found: 249.2089. *cis* Isomer δ: 8.00 (d, J = 2.0 Hz, H—C(=O)—), 5.47 (bm, NH), 1.00 (s, 12-H3), 0.92 (s, 13-H3), 0.88 (d, J = 7.0 Hz, 15-H3), 0.63 (ddd, J = 11.5; 9.0; 6.0 Hz, 7-H), 0.16 (dd, J = 9.5; 9.0 Hz, 6-H); *trans* isomer δ: 8.22 (d, J = 12.0 Hz, H—C(=O)—), 5.20 (bm, NH), 1.01 (s, 12-H3), 0.94

Can. J. Chem. Downloaded from www.nrcresearchpress.com by 80.58.250.72 on 09/07/12
For personal use only.

(s, 13-H3), 0.89 (d, J = 7.0 Hz, 15-H3), 0.69 (ddd, J = 11.5; 9.0; 6.0 Hz, 7-H), 0.25 (dd, J = 9.5; 9.0 Hz, 6-H).

*Treatment of **1** with sulphur to obtain **2***

A mixture of **1** (6 mg) and excess of sulphur was heated at 120°C for 16 h. After addition of 40–70° light petroleum and filtration, the solution, taken to dryness, was purified by tlc (silica gel, *n*-hexane, uv). The band with R_f 0.6, scraped and eluted with Et_2O, afforded 4 mg of an oily product, identical to the natural **2** on the basis of their chromatographic and spectral properties.

*Treatment of **4** with sulphur to obtain **5***

Compound **4** (8 mg) was treated with sulphur by the procedure used for **1**, thus obtaining 4.5 mg of **5**, identical to the natural **5**.

*Hydration of **1** to obtain **3***

To **1** (6 mg) in anhydrous Et_2O (6 mL), glacial AcOH was added and the solution allowed to stand at room temperature for 2 h. After washing with 10% Na_2CO_3 solution and then with H_2O, the organic phase, dried and taken to dryness, was purified by tlc (SiO_2, Et_2O) to give 3.5 mg of **3**, identical to **3** isolated from *A. cannabina*.

*Hydration of **4** to obtain **6***

Compound **4** (6 mg) was treated in the analogous way used for the synthesis of **3**, thus obtaining 4 mg of **6**, identical to natural **6** on the basis of their chromatographic and spectral properties.

*Dehydrogenation of **4***

A mixture of 15 mg of **4** and 30 mg of Se was heated at 280°C for 30 min. After cooling, 40–70° light petroleum was added and the filtered solution was extracted with 60% aqueous H_2SO_4. The acid phase was diluted with water and extracted with 40–70° light petroleum. After washing with H_2O the organic phase was taken to dryness to give guaiazulene, identified by comparison of its properties with those of an authentic specimen.

Acknowledgments

The authors wish to thank Professor M. Sarà (University of Genova) for identifying the sponge. Mass spectra were provided by "Servizio di Spettrometria di Massa del C.N.R. e dell'Università di Napoli". The assistance of the staff is gratefully acknowledged.

1. D. J. Faulkner. Nat. Prod. Rep. 551 (1984).
2. P. Ciminiello, E. Fattorusso, S. Magno, and L. Mayol. Experientia, **42**, 625 (1986), and literature cited therein.
3. M. R. Hagadone, P. J. Scheuer, and A. Holm. J. Am. Chem. Soc. **106**, 2447 (1984).
4. M. J. Garson. J. Chem. Soc. Chem. Commun. 35 (1986).
5. E. Fattorusso, S. Magno, L. Mayol, C. Santacroce, and D. Sica. Tetrahedron, **30**, 3911 (1974).
6. P. Ciminiello, E. Fattorusso, S. Magno, and L. Mayol. Experientia, **42**, 625 (1986).
7. C. M. Beechan, C. Djerassi, and H. Eggert. Tetrahedron, **34**, 2503 (1978).

Can. J. Chem. Downloaded from www.nrcresearchpress.com by 80.58.250.72 on 09/07/12
For personal use only.

Hydrodésazotation de l'indole sur catalyseur fer supporté sur amiante

ROGER ZALMA, LIONEL BONNEAU, JEANINE FOURNIER, JOËLLE GUIGNARD, FRANÇOISE BORG[1] ET HENRI PEZERAT[2]

Laboratoire de réactivité de surface et structure, Unité associée 1106, Centre national de la recherche scientifique, Université Pierre et Marie Curie, 4 Place Jussieu, Tour 54–55, 75252 Paris CEDEX 05, France

Reçu le 15 juillet 1986

ROGER ZALMA, LIONEL BONNEAU, JEANINE FOURNIER, JOËLLE GUIGNARD, FRANÇOISE BORG et HENRI PEZERAT. Can. J. Chem. **65**, 523 (1987).

Dans ce travail, la réaction de désazotation de l'indole a été testée en présence de deux variétés d'amiante (chrysotile et crocidolite) sous pression d'hydrogène. Cette réaction s'effectue suivant deux voies compétitives dont les principales étapes ont été déterminées. Les produits de désazotation sont essentiellement l'éthylcyclohexane et le méthylcyclohexane. L'augmentation de la température et de la pression et la préréduction des matériaux favorisent la désazotation. La présence de particules de Fe^0 en surface de fibres, formées à partir du matériau de départ, joue un rôle dans la première coupure des liaisons C—N et dans l'hydrogénation des cycles.

ROGER ZALMA, LIONEL BONNEAU, JEANINE FOURNIER, JOËLLE GUIGNARD, FRANÇOISE BORG, and HENRI PEZERAT. Can. J. Chem. **65**, 523 (1987).

The aim of this study is to examine hydrodenitrogenation (HDN) of indole on asbestos catalysts (chrysotile and crocidolite) under hydrogen pressure. HDN is carried out according to two competitive pathways, either via *ortho*-ethylaniline or via *ortho*-toluidine. This reaction is assisted by increase of temperature and pressure and by pre-reduction of the asbestos. Particles of Fe^0 on the fibre surface are formed from the original material. Their presence plays a role in the initial breaking of the C—N bond and in the hydrogenation reaction.

Le processus d'hydrotraitement catalytique a pour but d'éliminer les hétéroatomes (S, N, O) à partir des fractions lourdes du pétrole en effectuant l'hydrodésulfuration (HDS) et l'hydrodésazotation (HDN) qui s'avère être l'étape la plus difficile.

L'hydrodésazotation des hydrocarbures azotés est un processus catalytique entraînant la formation de NH_3 dont la présence conduit à un empoisonnement des sites actifs des catalyseurs acides utilisés en craquage, réformage et isomérisation.

Actuellement, l'HDN est effectuée à partir de catalyseurs hétérogènes tels CoMo, NiMo sulfurés supportés sur alumine. Plusieurs auteurs étudiant les mécanismes des réactions d'HDN sur ces catalyseurs (1, 2) ont avancé l'intervention de plusieurs espèces de sites actifs.

Nos précédents travaux sur les amiantes ont mis en évidence la présence dominante de sites donneurs d'électrons sur ces matériaux. Ces sites sont des groupements OH en basse coordination, situés en frontière de la phase solide (3, 4). De plus, nous avons révélé le caractère catalytique des amiantes, notamment dans l'oxydation d'un hydrocarbure polyaromatique, le fluorène (5). Aussi, était-il intéressant de tester ces solides comme catalyseurs en HDN.

Pour cette étude, nous avons utilisé deux minéraux, le chrysotile et la crocidolite (une amphibole ferrifère) représentatifs des deux familles d'amiante. Ces deux minéraux contiennent de la magnétite comme impureté principale (3–4%). Lors des opérations de réduction, la magnétite est réduite en Fe^0 ce qui conduit à un solide qu'on peut considérer comme un catalyseur fer supporté sur amiante. Dans la majorité de nos travaux, l'indole a été choisi comme molécule de départ.

Le but de ce travail n'est pas de fournir des mécanismes détaillés des réactions en cause, mais plutôt de mettre en évidence l'activité catalytique de matériaux simples pour l'HDN de certains hétérocycles.

Méthodes expérimentales

Les réactions ont été réalisées dans un autoclave Prolabo (volume de 250 mL) avec un système d'agitation oscillant (environ une oscillation par seconde, non modulable). Le volume de solution est inférieur à 100 mL et la vitesse maximale de montée en température est de 4°C/min. L'inertie du four est telle que le refroidissement s'effectue avec une vitesse de l'ordre de 1°C/min. Un tube central muni d'une crépine et d'un robinet permet des prises d'essai au cours du temps.

Le solvant utilisé est l'hexadécane, sauf dans quelques expériences où nous avons employé l'hexane.

Les matériaux testés sont un chrysotile et une crocidolite commerciaux. Le chrysotile est très proche des échantillons canadiens, en particulier parce qu'il contient les mêmes contaminants minéraux : magnétite et némalite (brucite fibreuse). Le taux de fer total exprimé en Fe_2O_3 est de 5,85%, celui de Fe^{2+} exprimé en FeO, de 1,58%. La crocidolite, en provenance d'Afrique du Sud, a une composition proche de la formule théorique, soit $Na_2Fe_3Si_8O_{22}(OH)_2$, avec à peu près le même taux de Fe^{2+} et de Fe^{3+}.

Ces amiantes ont d'abord été séchés à 60°C puis broyés 30 s dans un broyeur à anneau. Ils sont ensuite lavés deux fois avec du benzène à l'ébullition pour éliminer les impuretés susceptibles d'être préadsorbées, puis séchés sous courant d'azote à 70°C. Ces matériaux, suivant les expériences, peuvent ensuite subir d'autres traitements que nous préciserons ultérieurement.

La réaction est effectuée avec 75 mL de solvant, 2,25 g d'amiante et 225 mg de produit organique à désazoter. Certaines expériences ont été réalisées avec une préréduction du solide, consistant en un traitement dans l'autoclave avec 50 mL de solvant sous une pression d'hydrogène de 7 MPa et à une température de 350°C pendant 6 h. Après refroidissement on ajoute 25 mL de solvant et le produit organique à traiter.

Les produits de la réaction sont analysés en chromatographie phase vapeur (cpv) sur un chromatographe Girdel E 330 (colonne Chromosorb W à 10% de silicone OV 17).

Après réaction, les fibres sont séparées par filtration et la solution est analysée.

Nos résultats sont exprimés en pourcentage par rapport à l'ensemble des produits provenant de la réaction d'HDN de l'indole. L'analyse chromatographique et, dans quelques cas, la spectrographie de masse ont permis de déterminer les produits formés.

1. TOTAL-Compagnie Française de Raffinage, Centre de recherches, B.P. 27, 76700 Harfleur, France.
2. Auteur à qui adresser toute correspondance.

Printed in Canada / Imprimé au Canada

Can. J. Chem. Downloaded from www.nrcresearchpress.com by 80.58.250.72 on 09/07/12
For personal use only.

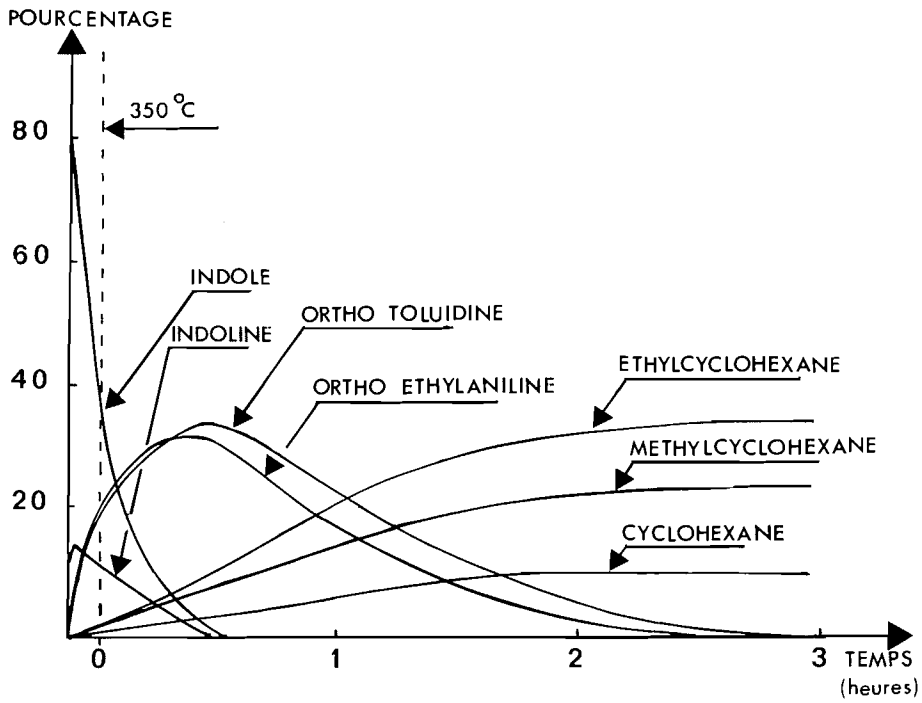

FIG. 1. Evolution du pourcentage des différents produits en fonction du temps à partir du chrysotile préréduit (350°C, 7 MPa H_2).

L'inertie du four utilisé ne permet pas de considérer comme négligeable l'intervalle de temps nécessaire à l'établissement des conditions expérimentales choisies. Ceci nous a conduit à utiliser trois modes opératoires afin de mieux appréhender les processus réactionnels :

(a) Des réactions avec palier de température

Un temps de 6 h est compté entre l'instant de mise en marche du four et celui de son arrêt. La vitesse de montée en température est de 4°C/min. L'analyse des produits contenus dans le réacteur a lieu après refroidissement complet. Le choix d'un temps relativement long de 6 h permet de négliger les éventuels problèmes de diffusion. Nous verrons d'ailleurs (fig. 1) que l'équilibre réactionnel est atteint pour un temps de 3–4 h.

(b) Des réactions sans palier de température

L'expérience est menée comme dans le cas précédent si ce n'est que le four est arrêté dès qu'il atteint la température choisie.

(c) Des réactions avec prélèvements (1 mL) au cours du temps réalisées dans les mêmes conditions opératoires qu'en (*a*). Dans ce cas le refroidissement est très rapide ce qui permet d'admettre que les réactions sont stoppées instantanément.

Dans les trois cas, la pression d'hydrogène annoncée est la pression initiale à froid, la pression finale étant évidemment plus élevée compte tenu de l'augmentation de la température.

Nous avons limité volontairement la température maximale à 380°C pour éviter une altération structurale des solides utilisés.

Le chrysotile et la crocidolite utilisés contiennent en faible quantité de la magnétite Fe_3O_4 que l'on met en évidence par diffraction des rayons X après extraction à l'aide d'un barreau aimanté (agitation dans le benzène). La formation de particules de Fe^0 lors des opérations est suivie par le même méthode.

Résultats

(a) Etudes préliminaires

À 350°C sous 7 MPa d'hydrogène et en absence des catalyseurs, nous avons constaté la formation de 0,8% d'indoline, 99% de l'indole étant conservé. Dans une expérience effectuée en palier de température à 380°C sous 7 MPa d'hydrogène et sans catalyseur, 1% de l'indole est consommé. Seulement des traces de produits désazotés ont pu être décelées.

En présence d'amiante et en absence d'indole on observe un début de craquage du solvant, l'héxadécane, à 350°C sous pression d'hydrogène. Huit *n*-alcanes (de C_5 à C_{12}) sont mis en évidence. On les retrouve dans toutes les réactions et on ne les prend pas en considération dans les résultats.

Quelques expériences en palier de température à 250, 300 et 350°C, avec chrysotile et crocidolite, permettent d'identifier, dans tous les cas, les trois grandes étapes ci-dessous :

$$\text{Indole} \xrightarrow{\text{(I)}} \text{indoline} \xrightarrow{\text{(II)}} \begin{matrix}\textit{ortho}\text{-éthylaniline}\\ \textit{ortho}\text{-toluidine}\end{matrix}$$

$$\xrightarrow{\text{(III)}} \begin{matrix}\text{éthylcyclohexane}\\ \text{méthylcyclohexane}\\ \text{cyclohexane}\end{matrix}$$

(b) Evolution des produits formés en fonction du temps

Cette étude, en palier de température, a été réalisée à partir de chrysotile préréduit et en effectuant des prélèvements au cours du temps.

Nous avons représenté sur la figure 1 l'évolution du pourcentage des différents produits de la réaction en fonction du temps. Sur le graphique nous avons choisi comme origine des temps l'instant où le four atteint 350°C. Les réactions en cause débutent aux environs de 250°C, donc avant le point choisi comme origine des temps.

Nos conditions expérimentales ne nous permettent pas d'accéder aux constantes de vitesse de chacune des réactions, mais on peut cependant observer que les vitesses apparentes de disparition de l'indoline, de l'*ortho*-éthylaniline et de l'*ortho*-toluidine sont plus lentes que celles d'apparition.

Au delà de 30 min, à chaque instant la somme S_E de l'*ortho*-éthylaniline et de l'éthylcyclohexane d'une part et la somme S_T de l'*ortho*-toluidine, du méthylcyclohexane et du cyclohexane sont sensiblement constantes.

Les chemins réactionnels probables sont donnés dans la figure 2.

Au début de la réaction, l'indole est réduit en indoline, qui,

Can. J. Chem. Downloaded from www.nrcresearchpress.com by 80.58.250.72 on 09/07/12
For personal use only.

Can. J. Chem. Downloaded from www.nrcresearchpress.com by 80.58.250.72 on 09/07/12
For personal use only.

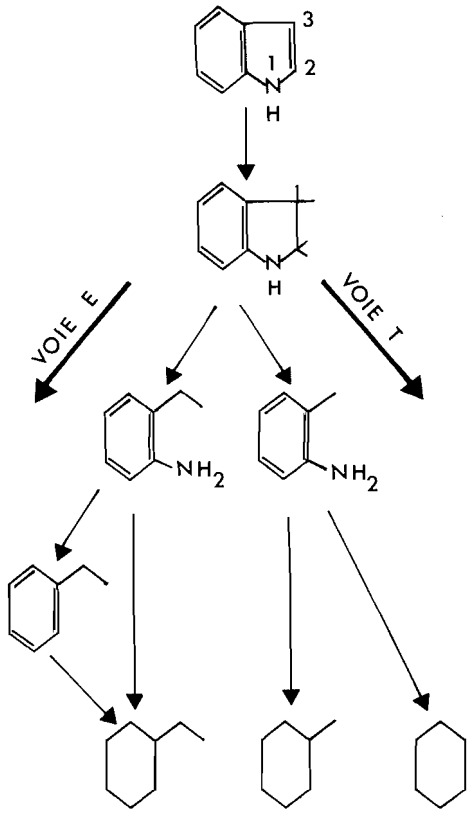

FIG. 2. Schéma des chemins réactionnels.

au delà d'une demi-heure, est totalement transformée en *ortho*-éthylaniline et en *ortho*-toluidine selon des réactions compétitives comme nous le montrerons ci-dessous. L'*ortho*-éthylaniline conduit ensuite à l'éthylcyclohexane (avec peut-être l'éthylbenzène comme phase intermédiaire) d'où la quasi-constance de la somme S_E. De même, nous pouvons déduire que l'*ortho*-toluidine est désazotée en méthylcyclohexane. Le cyclohexane provient directement de l'*ortho*-toluidine sans passer par le méthylcyclohexane, comme nous le montrerons ci-après.

(c) Influence de divers paramètres

Influence de la pression

Les expériences H_{33} et H_{26} (tableau 1) ont été réalisées à 380°C sans palier (notées ↗380°C↘) sous des pressions de 3 et 7 MPa, avec du chrysotile préréduit.

L'examen du tableau 1 révèle que la diminution de la pression (de 7 à 3 MPa) abaisse le taux de désazotation de l'indole. À faible pression on obtient une teneur élevée en *ortho*-éthylaniline et *ortho*-toluidine, ce qui confirme qu'il s'agit bien de produits intermédiaires dans la formation de l'éthylcyclohexane et du méthylcyclohexane. Sur ce même tableau on observe aussi qu'une diminution de pression favorise la voie T au détriment de la voie E. Par exemple, la somme *ortho*-toluidine plus méthylcyclohexane (voie T) passe de 25,6 à 41% alors que la somme *ortho*-éthylaniline plus éthylcyclohexane (voie E) passe de 54 à 33%.

Nous avons désigné par G un produit non identifié qui a un temps de rétention en chromatographie gazeuse proche de celui de l'éthylbenzène. Il apparaît en faible quantité et les expériences complémentaires ci-dessous nous font penser qu'il s'agit de l'éthylcyclohexène, composé déjà mis en évidence par Stern (6) dans l'HDN de l'indole. Ce composé serait intermédiaire, dans la voie E, entre éthylbenzène et l'éthylcyclohexane.

TABLEAU 1. Influence de la pression

	Chrysotile préréduit	
	H_{33}, ↗380°C↘ 3 MPa (%)[a]	H_{26}, ↗380°C↘ 7 MPa (%)
Indole	0	0
Indoline	0	0
ortho-Éthylaniline	13	0,5
ortho-Toluidine	24	0,5
Ethylbenzène	3,4	1,9
G	5	4,4
Ethylcyclohexane	20,1	53,5
Méthylcyclohexane	17	25,1
Cyclohexane	17,5	14,1

[a]% : pourcentage par rapport à la somme des produits issus de l'indole.

Influence de la température

L'influence de la température a été étudiée d'une part avec le chrysotile préréduit (H_{25}, H_{27}, H_{26}) sans palier de température, d'autre part avec la crocidolite (H_{18}, H_{21}) sans préréduction et avec palier de température (noté $\overrightarrow{300°C}$ et $\overrightarrow{380°C}$).

L'examen du tableau 2 dans le cas du chrysotile préréduit fait apparaître, d'une part que le taux de désazotation varie dans le même sens que la température (37% à 350°C, 60,6% à 365°C, 99% à 380°C), et d'autre part que la variation de température ne favorise pas sélectivement une voie de désazotation (E ou T).

Dans le cas de la crocidolite, à 300°C (H_{18}) sans préréduction du catalyseur, on observe une hydrogénation de l'indole en indoline et formation d'éthylaniline. À 350°C (H_{21}) l'indole est complètement transformé en produits désazotés. La voie T est très favorisée par rapport à la voie E quand on passe de 300 à 350°C.

Influence de la préréduction

Le tableau 3 permet de mettre en évidence le rôle de la préréduction à diverses températures (250, 350 et 380°C). À 250°C, sans préréduction, la transformation de l'indole est faible (<5%). À cette température, la préréduction entraîne la transformation de 93% de l'indole avec prédominance de la voie E (58% d'*ortho*-éthylaniline). À 350°C, les expériences effectuées sans préréduction montrent que la désazotation reste faible (10%). La transformation de l'indole est cependant quasi totale avec prédominance de la voie T (60% contre 30% pour la voie E). Par contre, lors de l'utilisation de catalyseurs préréduits, on observe que la désazotation (>35%) et la voie E (60%) sont nettement favorisées.

Les expériences H_{29} et H_{30} réalisées avec la crocidolite à 380°C sans et avec préréduction font apparaître une évolution dans le même sens. En effet, sans préréduction on a 21,3% pour la voie E contre 30% pour la voie T alors qu'avec préréduction on obtient 65,3% pour la voie E contre 23,6% pour la voie T.

Il est nécessaire de préciser que nos conditions expérimentales entraînent l'apport de particules de Fe^0 en surface de nos matériaux dès la température de 300°C en particulier dans les expériences de préréduction à 350°C. Ce Fe^0 provient de la réduction des contaminants minéraux des deux variétés d'amiante (en particulier de la magnétite) et peut être d'une fraction des couches octaèdriques de surface des « I-beam » dans le cas de la crocidolite. Les expériences rapportées dans le tableau 3

TABLEAU 2. Influence de la température

	Chrysotile préréduit			Crocidolite	
	H_{25}, ↗350°C↘ 7 MPa (%)[a]	H_{27}, ↗365°C↘ 7 MPa (%)	H_{26}, ↗380°C↘ 7 MPa (%)	H_{18}, $\overrightarrow{300°C}$ 7 MPa (%)	H_{21}, $\overrightarrow{350°C}$ 7 MPa (%)
Indole	1,8	0	0	58,2	0,11
Indoline	0	0	0	17,4	0
ortho-Éthylaniline	37,6	19,4	0,5	21,4	0
ortho-Toluidine	23,6	20	0,5	0	0
Éthylbenzène	0,7	1,3	1,9	0	0,66
G	0	5,9	4,4	0	0,34
Éthylcyclohexane	22,8	31,7	53,5	0,53	32,7
Méthylcyclohexane	6	13,1	25,1	2,41	45,1
Cyclohexane	7,5	8,6	14,1	0	21,1
S_E	61,1	58,3	60,3		
S_T	37,1	41,7	39,7		

[a]% : pourcentage par rapport à la somme des produits issus de l'indole.

TABLEAU 3. Influence de la préréduction

	Chrysotile				Crocidolite	
	H_{14}, $\overrightarrow{250°C}$ 7 MPa (%)[a]	H_{15} préréduit, $\overrightarrow{250°C}$ 7 MPa (%)	H_{24}, ↗350°C↘ 7 MPa (%)	H_{25} préréduit, ↗350°C↘ 7 MPa (%)	H_{29}, ↗380°C↘ 7 MPa (%)	H_{30} préréduit, ↗380°C↘ 7 MPa (%)
Indole	95,9	7,37	0,5	1,8	19,2	0
Indoline	2,70	27,37	0	0	3,6	0
ortho-Éthylaniline	0	57,89	29,5	37,6	17	0,5
ortho-Toluidine	0	5,16	60	23,6	43,6	0,6
Éthylbenzène	0	0,16	0	0,7	0	1,8
G	0	1,26	1	0	0,7	1,5
Éthylcyclohexane	0	0,37	3,2	22,8	4,3	64,8
Méthylcyclohexane	1,4	0,42	3,2	6	6,4	23
Cyclohexane	0	0	2,6	7,5	5,2	7,8

[a]% : pourcentage par rapport à la somme des produits issus de l'indole.

montrent que la présence de Fe^0 et la température élevée favorisent l'étape hydrogénante.

(d) Expériences complémentaires

En vue de préciser les étapes de transformation de l'indole, nous avons réalisé des expériences en partant de différents produits intermédiaires. Toutes ces réactions, en palier de température, ont été effectuées à 350°C sous une pression de 7 MPa d'hydrogène avec du chrysotile préréduit comme catalyseur et en effectuant plusieurs prélèvements au cours du temps. Sur la figure 2 nous avons noté les différents produits mis en évidence au cours de nos analyses. Il est possible sinon probable qu'il existe d'autres produits intermédiaires mais trop instables pour qu'on ait pu les caractériser.

Afin de vérifier que la formation de l'indoline est une étape intermédiaire dans la réaction de désazotation de l'indole, qu'elle se fasse par la voie E ou la voie T, nous avons réalisé une réaction en partant de l'indoline. Un prélèvement, effectué dès que la température de l'autoclave atteignait 350°C, montrait la formation d'*ortho*-éthylaniline et d'*ortho*-toluidine, dans des proportions voisines de celles obtenues à partir de l'indole dans des conditions comparables.

Par ailleurs, afin de vérifier que l'*ortho*-toluidine n'était pas formée à partir de l'*ortho*-éthylaniline, nous avons réalisé une réaction en partant de l'*ortho*-éthylaniline. Des prélèvements effectués toutes les heures ont montré que la désazotation a bien lieu sans formation ni d'*ortho*-toluidine, ni de méthylcyclohexane, ni de cyclohexane. Seuls apparaissent l'éthylcyclohexane, un peu d'éthylbenzène et un peu de produit G qui apparaît bien comme un composé se formant dans la voie E. La quantité de G diminue en fonction du temps.

Une réaction effectuée, dans les mêmes conditions, à partir de l'éthylbenzène ne produit que de l'éthylcyclohexane.

En partant de l'*ortho*-toluidine, on forme essentiellement du méthylcyclohexane, et un peu de cyclohexane. Par contre, en partant du méthylcyclohexane on n'observe pas de transformation. Il semble donc que le cyclohexane puisse être obtenu à partir de l'*ortho*-toluidine sans passer par le méthylcyclohexane.

Afin d'examiner ce qui se passe dans le cas où le carbone en α de l'azote appartient à un cycle, nous avons essayé la réaction sur l'acridine avec le chrysotile et la crocidolite comme catalyseurs. Les produits de la réaction ont été identifiés par spectrographie de masse.

Les seuls produits mis en évidence sont des produits d'hydrogénation de l'acridine : les octahydroacridine et les tétradécahydroacridines. Des prélèvements successifs au cours de la réaction ont montré que les octahydroacridines sont une étape intermédiaire de la formation des tétradécahydroacridines. Nous

Can. J. Chem. Downloaded from www.nrcresearchpress.com by 80.58.250.72 on 09/07/12
For personal use only.

n'avons observé aucune coupure de la molécule. Le chrysotile et la crocidolite ne semblent pas être capables d'assurer la désazotation de l'acridine dans nos conditions expérimentales.

Discussion

Les étapes de l'HDN de l'indole sur amiante révèlent des points communs et des différences avec celles présentées par l'HDN de la même molécule sur des catalyseurs à base de sulfure de molybdène et de sulfure de cobalt ou de nickel supportés sur alumine ou silice (6–8).

Les points communs sont : (*i*) le passage par l'indole, c'est-à-dire l'hydrogénation de la liaison 2–3, C_α–C_β, à peu près dans les mêmes conditions de température et de pression. Ceci confirme les observations faites par de nombreux auteurs (par exemple, réf. 9) sur la nécessité d'hydrogéner cette liaison avant de pouvoir réaliser la désazotation; (*ii*) le passage probable par l'éthylbenzène entre les étapes *ortho*-éthylaniline et éthylcyclohexane (6, 8).

La différence principale entre la catalyse sur amiante et la catalyse sur sulfures de Mo et Ni, est l'existence, dans le premier cas, d'une seconde voie d'hydrogénolyse de l'indoline (voie T sur la figure 2), puisque nous avons montré que l'*ortho*-toluidine ne provenait pas de l'éthylaniline. Cette voie conduit à la formation de méthylcyclohexane et de cyclohexane.

La présence de cette seconde voie de dégradation de l'indoline (voie T) nous amène à discuter sur la nature des sites responsables de la coupure de la liaison C_α—C_β, non constatée avec d'autres catalyseurs classiques d'HDN. Si les fibres d'amiantes sont à l'origine, du moins pour une part, de cette coupure, nous ne pouvons pas exclure le rôle du Fe^0. En effet, nous avons testé comme catalyseur, un oxyde de fer noir Prolabo qui est un mélange d'hématite et de magnétite. Préréduit dans les conditions habituelles (350°C), il donne également du Fe^0. Testé en palier à 350°C sous 7 MPa d'hydrogène, après réduction, il conduit à 43% d'indoline, 22% d'*ortho*-éthylaniline et 7% d'*ortho*-toluidine. Dans cette expérience, on n'arrive pas au stade de la désazotation proprement dite. On constate donc que le Fe^0 seul est capable d'une part de permettre la première coupure des liaisons C—N et d'autre part de conduire aux deux voies d'hydrogénolyse en favorisant la voie E par rapport à la voie T.

Le fait que la première coupure de la liaison C—N soit liée à la présence de Fe^0 dans nos matériaux tendrait à confirmer les propositions de Laine (10) sur le rôle des métaux. Cet auteur fait appel à la formation transitoire de complexes où le métal M se lie à l'azote et au carbone situé en α. Ce mécanisme est voisin de celui proposé par Guttieri et Maier (11) qui utilise le platine supporté sur silice comme catalyseur d'HDN.

À partir de toutes les expériences où nos matériaux sont préréduits, nous avons constaté que la présence du Fe^0 favorise la formation de phases hydrogénées. Aussi est-il quasi certain que le Fe^0 joue également un rôle dans l'hydrogénation du cycle benzénique pouvant conduire à partir de l'éthylaniline et de l'*ortho*-toluidine aux amines saturées correspondantes, très réactives.

Si l'on se réfère aux mécanismes catalytiques proposés par Nelson et Levy (9), la coupure des liaisons C—N sur les catalyseurs NiMo et CoMo sulfurés serait un mécanisme basique. Cette proposition est cohérente avec le fait que Ni_3S_2 est l'une des phases actives dans les catalyseurs NiMo (12) et avec le fait que cette phase a un caractère donneur d'électrons (12, 13). De même, Laine (10) fait appel à ce mécanisme pour expliquer la très nette augmentation d'activité des catalyseurs CoMo et NiMo en présence de H_2S et même d'H_2O. En effet, il fait référence à une attaque nucléophile sur le carbone situé en α, ce qui revient à faire jouer un rôle important à des entités à caractère donneur.

Dans notre cas, les sites en cause peuvent être ceux des deux variétés d'amiante puisque nous avons montré précédemment que ces matériaux avaient essentiellement un caractère donneur d'électrons (3, 4).

Conclusion

Les présents travaux indiquent que le chrysotile et la crocidolite réduits constituent des catalyseurs d'HDN avec l'indole. Par contre, avec des molécules azotées où les deux carbones en α de l'azote sont engagés dans des cycles, l'hydrogénolyse de l'hétérocycle devient très difficile.

À 380°C, sans palier de température et sous 7 MPa d'hydrogène, l'HDN de l'indole est quasi complète avec les deux minéraux préréduits. Les premières étapes confirment le fait déjà noté (6, 7) que les carbones en α et en β de l'azote doivent être saturés avant qu'il y ait hydrogénolyse. Par rapport aux catalyseurs sulfurés de molybdène et de nickel, nos catalyseurs présentent l'originalité d'une voie particulière dans l'hydrogénolyse du cycle à cinq atomes, avec perte d'un méthane, cette voie intéressant environ 50% des molécules d'indole de départ.

Les sites donneurs de l'amiante peuvent jouer un rôle dans la coupure des liaisons C—N des amines intermédiaires, les sites des particules de Fe^0 participant selon le plus probable aussi bien à la coupure des liaisons C—N qu'à celle des liaisons C—C. Si les catalyseurs bifonctionnels contenant des métaux supportés sur des solides présentant des sites acides ont été bien étudiés, il n'en est pas de même pour les catalyseurs ayant des supports à caractère basique. La présente étude est un exemple de réactivité catalytique mettant en jeu ces deux types de sites.

Comme on pouvait s'y attendre, notre étude a montré que pression et température favorisaient l'HDN, la pression semblant également favoriser la voie passant par l'*ortho*-éthylaniline par rapport à celle passant par l'*ortho*-toluidine.

Remerciements

Les auteurs tiennent à remercier la Société TOTAL-CFR pour son aide financière et technique, et notamment Mr Philippe Doligez pour les analyses en spectrographie de masse.

1. J. Maternova. Appl. Catal. **3**, 3 (1982).
2. S. H. Yang et C. N. Satterfield. Ind. Eng. Chem. Process Des. Dev. **23**, 20 (1984).
3. L. Bonneau et H. Pezerat. J. Chim. Phys. **80**, 275 (1983).
4. L. Bonneau, H. Suquet, C. Malard et H. Pezerat. Environ. Res. **41**, 251 (1986).
5. R. Zalma, J. Guignard, E. Copin et H. Pezerat. Environ. Res. **41**, 296 (1986).
6. E. W. Stern. J. Catal. **57**, 390 (1979).
7. J. L. Olive, S. Biyoko, T. Jei et P. Geneste. Amélioration des procédés d'hydroraffinage. Document DGRST. Mai 1981. (AR 9218).
8. L. D. Rollmann. J. Catal. **46**, 243 (1977).
9. N. Nelson et R. B. Levy. J. Catal. **58**, 485 (1979).
10. R. M. Laine. Catal. Rev. **25**, 459 (1983).
11. M. J. Guttieri et W. F. Maier. J. Org. Chem. **49**, 2875 (1984).
12. K. C. Pratt, J. V. Sanders et N. Tamp. J. Catal. **66**, 82 (1980).
13. O. Weisser et S. Landa. Sulfide catalysts. Their properties and applications. Pergamon, New York. USA. 1983.

Can. J. Chem. Downloaded from www.nrcresearchpress.com by 80.58.250.72 on 09/07/12
For personal use only.

Étude des complexes fluorés et chlorés du plomb dans les mélanges eau–HF

RÉJEAN BEAUDOIN ET HUGUES MÉNARD

Département de chimie, Faculté des sciences, Université de Sherbrooke, Sherbrooke (Qué.), Canada J1K 2R1

Reçu le 24 juin 1986

RÉJEAN BEAUDOIN et HUGUES MÉNARD. Can. J. Chem. **65**, 528 (1987).

L'étude des complexes fluorés et des complexes chlorés du plomb dans les mélanges eau–HF a été effectuée par polarographie. La diminution de l'ordre des complexes fluorés de PbF_2 à PbF^+ est en accord avec la diminution de l'activité en ions fluorure, $R_0(F)$, mesurée en augmentant la concentration en HF. L'obtention de deux formes cristallines du PbF_2 selon le domaine de concentration en HF vient appuyer l'existence de deux complexes fluorés. L'observation du PbFCl confirme la présence de complexe mixte fluorure–chlorure dans les mélanges eau–HF.

RÉJEAN BEAUDOIN and HUGUES MÉNARD. Can. J. Chem. **65**, 528 (1987).

The polarographic study of lead fluoride and of lead chloride complexes has been done in water – hydrogen fluoride solutions. The successive formation of PbF_2 and of PbF^+ is in agreement with the reduction of the fluoride ion activity, $R_0(F)$, measured with the augmentation of the HF content of the solution. The formation of two crystalline structures of PbF_2 is in accord with the existence of two complexes in solution. The formation of PbFCl shows the existence of mixed fluoride–chloride complexes in water–HF solutions.

Can. J. Chem. Downloaded from www.nrcresearchpress.com by 80.58.250.72 on 09/07/12
For personal use only.

Introduction

La polarographie dans des milieux extrêmement corrosifs pour le verre, comme les mélanges HF–H_2O, est maintenant accessible à l'aide de capillaires protégés du milieu (1). Il est possible par cette technique d'analyser la formation de complexes métalliques. Une bonne connaissance des espèces dans les mélanges HF–H_2O (2–5) permet de calculer les constantes de formation des divers complexes du fluor en solution. L'utilisation d'un système de référence indépendant du solvant est une condition (6) nécessaire car il ne s'agit plus de solutions aqueuses diluées mais de mélanges de force ionique variable et d'acidité très élevée.

Mesaric et Hume (7) ont étudié les complexes fluorés du plomb en solution aqueuse. Le complexe PbF^+ se forme à faible concentration en ions fluorure ($\beta_1 = 18$) et le PbF_2 ($\beta_2 = 356$) existe à plus grande concentration en ions fluorure dans l'eau. D'autres auteurs (8) ont obtenu les mêmes résultats avec l'ion fluorure et ont démontré que le plomb forme trois complexes avec le chlore et le brome (9, 10).

La formation de complexes chlorés en solution aqueuse a été étudiée par Bond et Hefter (8, 9). Ils ont observé trois complexes avec l'ion chlorure alors que l'ion fluorure ne conduit qu'à deux complexes dans les mêmes conditions.

Nous allons déterminer les complexes fluorés du plomb dans les mélanges eau–HF jusqu'à une concentration de 55% en poids et nous allons examiner la formation des complexes chlorés dans ces mêmes solutions. Le calcul des constantes de formation permettra de préciser les zones où on retrouve les différents complexes.

Partie expérimentale

Appareils

Un potentiostat modèle PAR174A (Princeton Applied Research) a été utilisé avec un système à trois électrodes. L'électrode au calomel saturé est séparée de la solution par une jonction en Teflon poreux. Le capillaire polarographique est recouvert de polyéthylène (1) et l'électrode auxiliaire est faite d'un fil de platine. La cellule a été fabriquée dans nos ateliers à partir de Ke1F et de Teflon. La diffraction des rayons-X a été effectuée avec un appareil Philips PW1140/1139.

Produits

Les solutions ont été préparées à partir de HF 48% en poids (J. T. Baker) et à partir de HF 100% (Matheson) dilué à la concentration voulue avec de l'eau distillée. Les autres produits utilisés sont le grade ACS.

La méthode expérimentale consiste à mesurer le potentiel de demi-vague du plomb par rapport à l'électrode de référence au calomel saturé. Le potentiel de demi-vague du système de référence indépendant du solvant, le système ferricinium/ferrocène, est ensuite mesuré dans la même solution lorsque c'est possible. Si les vagues polarographiques sont trop près l'une de l'autre, on prend les mesures séparément mais l'une après l'autre.

L'étude du plomb en présence d'ions chlorure se fait en ajoutant du KCl à une solution de 10^{-3} *M* en plomb. L'activité en ions chlorure est mesurée à l'aide d'une électrode sélective Ag/AgCl, de façon à s'assurer que l'activité est près de la concentration. Jusqu'à 55% en HF, la correspondance est suffisamment bonne pour assumer l'activité égale à la concentration.

Résultats et discussion

Pour faire les calculs concernant les complexes fluorés, nous avons besoin des mesures de l'activité en ions fluorure, $R_0(F)$, et du potentiel de l'électrode au trifluorure de lanthane E_{F^-} mesuré par rapport au système de référence ferricinium/ferrocène (Fc^+/Fc). Les valeurs de $R_0(F)$ et E_{F^-} sont les mêmes que celles publiées par Vaillant *et al.* (3).

Les complexes fluorés évoluent en fonction de l'activité en ions fluorure libres. Du point de vue expérimental, on observe un déplacement du potentiel de demi-vague, $E_{\frac{1}{2}}$, selon le milieu fluoré. On peut calculer à partir de l'équation de Nernst, les pentes que l'on devrait mesurer pour des complexes fluorés d'ordre croissant. Les calculs sont faits par rapport à l'électrode réversible aux ions fluorure libres.

Le potentiel de l'électrode réversible aux ions fluorure s'exprime selon l'équation [1]

$$[1] \quad E_{F^-} = E^0_{F^-} - E_{ECS} - 0{,}059 \log a_{F^-}$$

où a_{F^-} est l'activité des ions fluorure libres. Si on mesure l'écart $\Delta E_{\frac{1}{2}}$ entre le potentiel de demi-vague du plomb et le potentiel de l'électrode réversible aux ions fluorure, on peut définir les équations suivantes pour les complexes fluorés du plomb. On choisit comme exemple un complexe bifluoré :

$$[2] \quad PbF_2 + 2e \leftrightarrows Pb_{Hg} + 2F^-$$

$$[3] \quad E_{Pb} = E^{0\prime}_{Pb} - E_{ECS} - \frac{0{,}059}{2} \log \frac{(a_{F^-})^2}{K_d[PbF_2]}$$

Can. J. Chem. Downloaded from www.nrcresearchpress.com by 80.58.250.72 on 09/07/12
For personal use only.

En combinant les équations [1] et [3]:

$$[4] \quad \Delta E_{\frac{1}{2}} = E^{0\prime}_{Pb} - E^{0}_{F^-} + 0{,}059 \log a_{F^-} - \frac{0{,}059}{2} \log \frac{(a_{F^-})^2}{K_d}$$

$$[5] \quad \Delta E_{\frac{1}{2}} = \text{cte} + 0{,}059 \log a_{F^-} - 0{,}059 \log a_{F^-}$$

$$[6] \quad \Delta E_{\frac{1}{2}} = \text{cte} + 0 \log a_{F^-}$$

L'équation [6] montre clairement que pour le complexe PbF_2, la pente du potentiel de demi-vague en fonction du log a_{F^-} est de 0 volt. De la même façon on peut démontrer que le complexe PbF^+ produira une pente de +0,029 volt et le PbF_3^- produira une pente de −0,029 volt.

Les constantes de formation obtenues en présence d'ions chlorure ont été calculées à partir de la théorie de DeFord et Hume (11). Pour un ion métallique complexé dont le métal est soluble dans le mercure, la réduction à l'état métallique peut s'exprimer par l'équilibre suivant, [7]:

$$[7] \quad MX_J^{+(n-Jb)} + ne \leftrightarrows M_{Hg} + JX^{-b}$$

Le terme X^{-b} représente l'espèce complexante et J représente le nombre de ligands sur le métal.

Les constantes de formation cumulatives peuvent être évaluées à partir des équations [8] et [9].

$$[8] \quad F_0(X) = \Sigma \beta_J C_X^J$$

$$[9] \quad F_0(X) = \text{antilog} \left\{ 0{,}434 \frac{nF}{RT} (E_{\frac{1}{2}})_S - (E_{\frac{1}{2}})_c + \log \frac{(i_d)_S}{(i_d)_c} \right\}$$

Le terme $F_0(X)$ est introduit pour représenter la quantité mesurable du côté droit de l'équation. Le terme β_J représente la constante de formation du complexe J et C_X la concentration de l'espèce complexante. Les termes $(E_{\frac{1}{2}})$ et $(i_d)_S$ font référence au potentiel de demi-vague et au courant de diffusion de l'ion en solution sans l'espèce complexante alors que $(E_{\frac{1}{2}})_c$ et $(i_d)_c$ réfèrent à l'ion en présence de l'espèce complexante.

On introduit par la suite la fonction $F_1(X)$, [10], où

$$[10] \quad F_1(X) = (F_0(X) - \beta_0)/c_X$$

β_0 est la constante de formation du complexe zéro. Sa valeur est donc de l'unité. Si on porte en graphique $F_1(X)$ en fonction de la concentration en ligand, c_X, l'extrapolation à $c_X = 0$ de la fonction $F_1(X)$ nous donne la constante de formation β_1. De la même façon, on peut obtenir les autres constantes de formation par l'équation générale suivante, [11]:

$$[11] \quad F_n(X) = (F_{n-1}(X) - \beta_{n-1})/c_X$$

Pour le dernier complexe, le graphique de $F_n(X)$ en fonction de c_X donnera une droite parallèle à l'abscisse. Ceci permet de déterminer le nombre de complexes possible dans le mélange.

Shaap et McMaster (12) ont mis au point une méthode pour l'étude de complexes mixtes. On peut calculer les constantes de formation des complexes mixtes en autant que l'on connaisse les constantes de formation de chacun des complexes simples à la même force ionique et dans le même solvant. Dans notre étude, il n'est pas possible de faire ce calcul car le solvant est lui-même une espèce complexante. On connaît les constantes de formation des complexes fluorés sur le domaine de concentration en HF jusqu'à 60%. Il n'est cependant pas possible de connaître les constantes de formation des complexes chlorés pour chaque concentration en HF. La force ionique change peu avec l'addition de KCl, mais d'une concentration en HF à l'autre la différence devient très importante. Les concentrations en HF varient de 2 à 40 mol/L.

TABLEAU 1. Potentiel de réduction du plomb

% HF (Poids)	$E_{\frac{1}{2}}Pb^{+2}/Pb$ Fc^+/Fc (Volt)	$R_0(F)$	$E_{\frac{1}{2}}Pb^{+2}/Pb$ E_{F^-} (Volt)	E_{F^-} Fc^+/Fc (Volt)
2	−0,550	2,1	−0,494	−0,056
5	−0,533	2,4	−0,493	−0,040
10	−0,505	2,9	−0,494	−0,011
15	−0,480	3,4	−0,499	+0,018
20	−0,450	4,0	−0,501	+0,051
25	−0,425	4,5	−0,504	+0,079
30	−0,395	5,0	−0,504	+0,109
35	−0,365	5,6	−0,507	+0,142
40	−0,339	6,2	−0,516	+0,177
45	−0,310	7,3	−0,550	+0,240
50	−0,275	9,0	−0,610	+0,335
55	−0,225	9,8	−0,607	+0,382
60	−0,187	10,3	−0,593	+0,406
65	−0,160	10,7	−0,585	+0,425

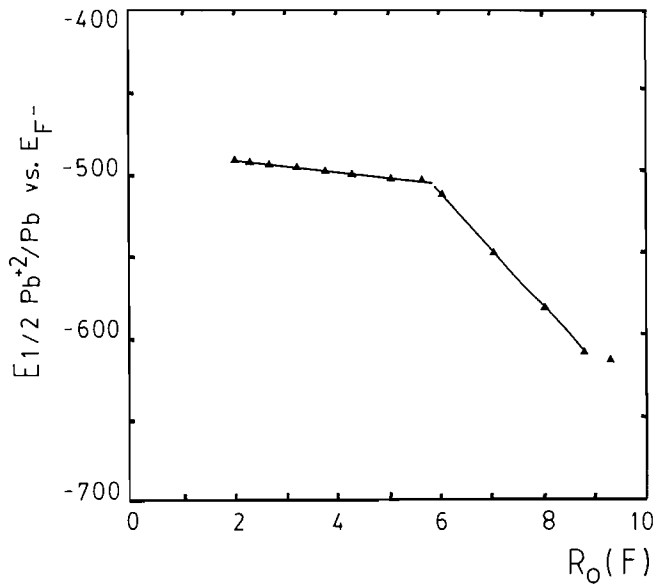

FIG. 1. Potentiel de réduction du plomb vs. E_{F^-} en fonction de l'activité en ions fluorures libres.

On ne peut pas calculer les constantes de formation des complexes mixtes contenant l'ion fluorure et l'ion chlorure mais on peut intuitivement comprendre qu'en solution l'ion chlorure remplacera successivement les ions fluorure sur le métal. Si on considère un mélange où on a le complexe MF_2, l'addition d'ions chlorure conduira aux complexes MFCl, $MFCl_2^-$ et MCl_3^-, selon la concentration en ions chlorure.

Les potentiels de réduction du plomb en fonction de la concentration en HF sont présentés au tableau 1. Le tableau 1 montre les mesures par rapport au système ferricinium/ferrocène et les résultats calculés par rapport au potentiel de l'électrode réversible aux ions fluorure.

La figure 1 présente le graphique du potentiel de demi-vague réversible aux ions fluorure en fonction de $R_0(F)$. On peut calculer la pente de $E_{\frac{1}{2}}$ versus $R_0(F)$ et déterminer les complexes fluorés en solution.

TABLEAU 2. Pentes tirées du graphique de la réduction du plomb

Domaine de % en HF (Poids)	Pente (Volt)	Complexe	Pente calculée (Volt)
2–35	+0,003	PbF_2	0
35–55	+0,032	PbF^+	+0,029

TABLEAU 3. Constantes d'équilibre et de formation successives des complexes fluorés du plomb

	log K	log β
PbF^+	9,3	9,3
PbF_2	5,8	15,1

Les complexes fluorés du plomb

L'interprétation des résultats se fait à partir de la pente du graphique de $E_{\frac{1}{2}}$ versus $R_0(F)$ ($R_0(F) = -\log a_{F^-}$). Le tableau 2 donne les résultats pour les complexes du plomb obtenus en solution.

La pente du potentiel de demi-vague en fonction de l'activité en ions fluorure nous permet de dire que dans le domaine de 2 à 35% en HF, le complexe en solution est le PbF_2. Dans le domaine de 35 à 55% en HF, le complexe est le PbF^+. On peut écrire les équilibres [12] et [13]:

[12] $PbF_2 + 2é \leftrightarrows Pb_{Hg} + 2F^-$

[13] $PbF^+ + é \leftrightarrows Pb_{Hg} + F^-$

Dans les solutions aqueuses, le complexe existant est PbF_2. Lorsque la concentration diminue, on passe à PbF^+. On observe le même comportement dans les solutions aqueuses de HF. On peut noter que le changement de PbF_2 à PbF^+ se fait entre 35 et 40% en HF.

Il est possible d'évaluer les constantes de formation des complexes fluorés à partir du changement de pente du potentiel de demi-vague réversible aux ions fluorure en fonction de l'activité en ions fluorure, $R_0(F)$ (13). Si on établit l'équilibre suivant:

[14] $PbF^+ \overset{K_1}{\rightleftarrows} Pb^{+2} + F^-$ et $PbF_2 \overset{K_2}{\rightleftarrows} PbF^+ + F^-$

la constante d'équilibre K_2 s'établit comme suit:

$$[15] \quad K_2 = \frac{[a_{F^-}][a_{PbF^+}]}{[a_{PbF_2}]}$$

Au point d'inflection, à la figure 1, on peut faire l'approximation que la concentration des deux complexes fluorés est équivalente. L'équilibre est alors contrôlé par l'activité en ions fluorure du milieu. La constante d'équilibre du complexe peut alors être exprimée de la façon suivante:

[16] $K_2 = 1/a_{F^-}$

[17] $\log K_2 = -\log a_{F^-} = R_0(F)$

Une approche similaire nous permet de calculer K_1. Le tableau 3 montre les constantes d'équilibre K_1 et K_2 et le log des constantes de formation β_1 et β_2.

La figure 2 présente la distribution des complexes fluorés du plomb jusqu'à 60% en HF calculée à partir des constantes successives de formation.

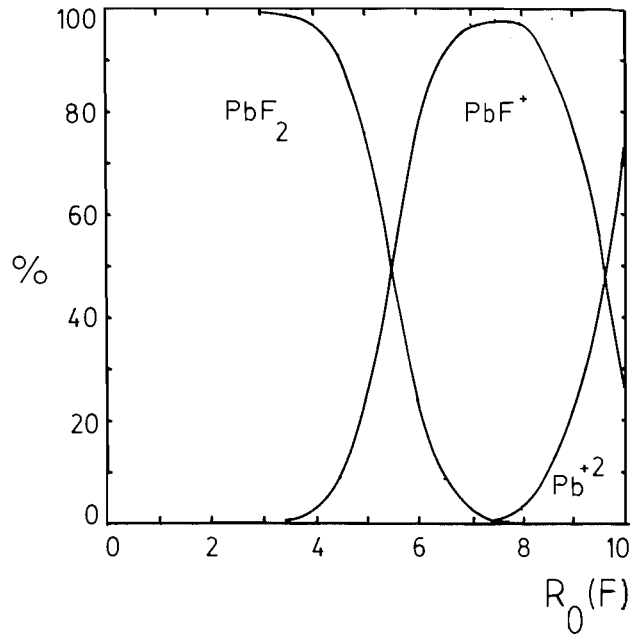

FIG. 2. Distribution des complexes fluorés du plomb en fonction de l'activité en ions fluorure libres.

D'autre part, en diffraction des rayons-X, on a analysé l'espèce formée à la surface d'une plaque de plomb oxydée dans les mélanges eau–HF. Le fluorure de plomb PbF_2 a la particularité de cristalliser sous deux formes dont les plans de diffraction sont très différents.

On a la forme orthorhombique appelée αPbF_2 et la forme cubique appelée βPbF_2 (14). La forme orthorhombique a la même structure que le $PbCl_2$ et le $PbBr_2$. Il y a quatre groupements PbF_2 par maille. La distance Pb—F varie de 2,49 à 2,85 Å. Cette structure est stable à basse température. Le αPbF_2 (orthorhombique) est préparé en dissolvant du PbO dans du HF 39%. La solution est évaporée puis le résidu est séché sous atmosphère inerte à une température de 80 à 100°C. L'analyse par rayons-X a démontré que l'échantillon n'est pas contaminé par du βPbF_2 cubique (15). Kennedy *et al.* (16) ont rapporté que la précipitation rapide de PbF_2 à partir d'une solution de $Pb(NO_3)_2$ et NH_4F donne majoritairement du αPbF_2. Cependant, si la précipitation se fait lentement, la forme cubique sera prédominante. Ceci implique que la forme cubique est la plus stable à la température de la pièce.

La forme cubique a la même structure que le CaF_2. Il y a deux groupements PbF_2 par maille. La distance Pb—F est de 2,57 Å. Cette structure est stable à haute température. Le PbF_2 sous forme cubique est transparent à température et pression normale. La phase cubique se transforme en phase orthorhombique sous l'influence de la pression. La phase orthorhombique a un volume environ 10% inférieur à la phase cubique. Cette transition avec la pression est non réversible (17, 18).

Nos mesures de diffraction des rayons-X ont montré que le PbF_2 sur les plaques de plomb oxydées dans les mélanges eau–HF se retrouve sous les deux formes cristallines. À faible concentration en HF, on trouve du αPbF_2 comme dans les solutions aqueuses concentrées en ions fluorure (7). Les analyses montrent que dans les mélanges jusqu'à 30% en HF on retrouve du αPbF_2. À 5, 10 et 20% en HF, on note la présence d'une très petite quantité de βPbF_2. La hauteur des pics est dans un rapport de 1 à 100. À 30% en HF, le αPbF_2 et le βPbF_2 sont présents en quantité comparable. À 40% en HF, on retrouve exclusivement la forme cubique du PbF_2.

Can. J. Chem. Downloaded from www.nrcresearchpress.com by 80.58.250.72 on 09/07/12
For personal use only.

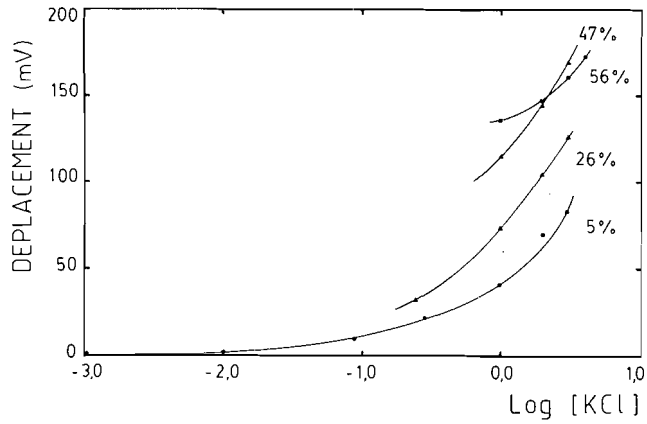

FIG. 3. Déplacement du potentiel de demi-vague du plomb en fonction du log de la concentration en KCl pour différentes concentrations en HF.

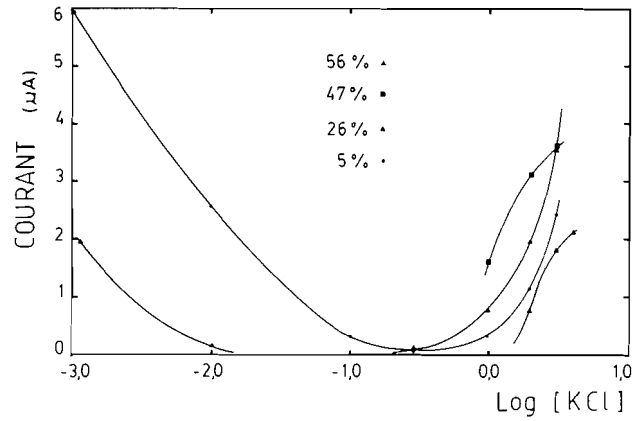

FIG. 4. Evolution du courant de diffusion du plomb en fonction du log de la concentration en KCl pour différentes concentrations en HF.

La transition de αPbF_2 à βPbF_2 aux concentrations entre 30 et 40% en HF correspond très bien à la brisure dans la relation du potentiel de demi-vague en fonction de l'activité en ions fluorure R_0(F). La relation à la figure 1 change de pente à R_0(F) d'environ 5,5. Ceci correspond à une concentration en HF de 35%. À moins de 35% en HF, le PbF_2 cristallise sous la forme orthorhombique, comme en solution aqueuse. On peut donc conclure que le complexe en solution est PbF_2 et la précipitation ou cristallisation est rapide. La pente à la figure 1 est de 0,0 volt, ce qui avait permis de conclure au complexe PbF_2 en solution.

À 40% en HF, on retrouve seulement du βPbF_2. Pour toutes les concentrations subséquentes, l'espèce cubique est la seule retrouvée à la surface du plomb.

La forme cubique du PbF_2 occupe un volume environ 10% plus élevé que la forme orthorhombique. Dans le domaine de concentration en HF entre 35 et 55%, l'espèce en solution est PbF^+. Cette espèce chargée est sûrement stabilisée par le solvant. Dans les solutions concentrées en HF, il y aura aussi stabilisation par le solvant. Il est donc raisonnable de penser que le complexe chargé est stabilisé en solution par le solvant et que l'évaporation ou la désolvatation soit responsable de la cristallisation lente sous la forme la plus volumineuse. Dans ce cas, on obtient la forme cubique du PbF_2.

Les complexes chlorés de plomb

Le déplacement anodique du potentiel de demi-vague a été relié à la formation de complexes chlorés en solution. Nous

TABLEAU 4. Constantes de formation successives des complexes chlorés du plomb

% HF (Poids)	β_1	β_2	β_3
56	30 000±10 000	10 000±3000	~4 000
47	3 700±200	5 000±200	10 000±2000
26	100±10	140±20	100±50
5	11,5±0,2	12,0±0,2	~10
	$PbCl^+$	$PbCl_2$	$PbCl_3^-$

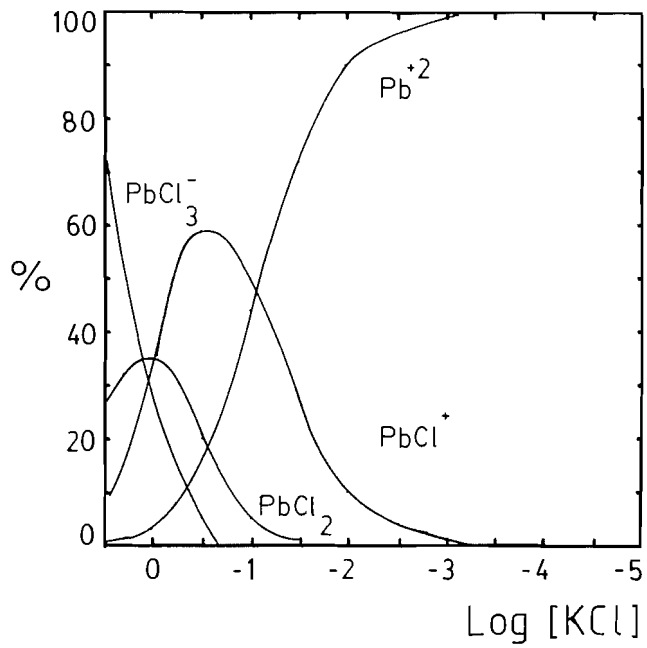

FIG. 5. Distribution des complexes chlorés dans HF 5% en fonction de la concentration en KCl.

allons calculer les constantes de formation à partir de la théorie de DeFord et Hume (11). Les déplacements du potentiel de demi-vague sont présentés à la figure 3 et l'évolution du courant de diffusion est montrée à la figure 4.

La diminution du courant de diffusion est due à la précipitation du plomb sous forme du complexe mixte PbFCl. Le précipité a été identifié par diffraction des rayons-X.

Les écarts entre nos valeurs et celles fournies par ASTM sont à l'intérieur des limites de l'appareil que nous avons utilisé.

À partir des constantes de formation données au tableau 4, on peut calculer la proportion de chaque complexe chloré dans les mélanges eau–HF. Les figures 5–8 montrent les proportions de chaque complexe en fonction de la concentration en KCl dans la solution. La figure 9 montre la distribution des complexes chlorés en solution aqueuse calculée à partir des constantes de formation de Bond et Hefter (9).

En solution aqueuse, le plomb donne trois complexes chlorés. Dans les mélanges eau–HF on a aussi trois complexes chlorés. À 5 et 26% en HF, le complexe fluoré en solution est le PbF_2. La distribution des complexes chlorés ressemble beaucoup à ce qu'on observe en solution aqueuse. Le complexe $PbCl_3^-$ apparaît à des concentrations en KCl élevées et dans la même région que $PbCl_2$. Les constantes de formation dans l'eau et dans HF 5% sont du même ordre de grandeur. Dans HF, le complexe $PbCl^+$ forme le PbFCl qui est non soluble et on

Can. J. Chem. Downloaded from www.nrcresearchpress.com by 80.58.250.72 on 09/07/12
For personal use only.

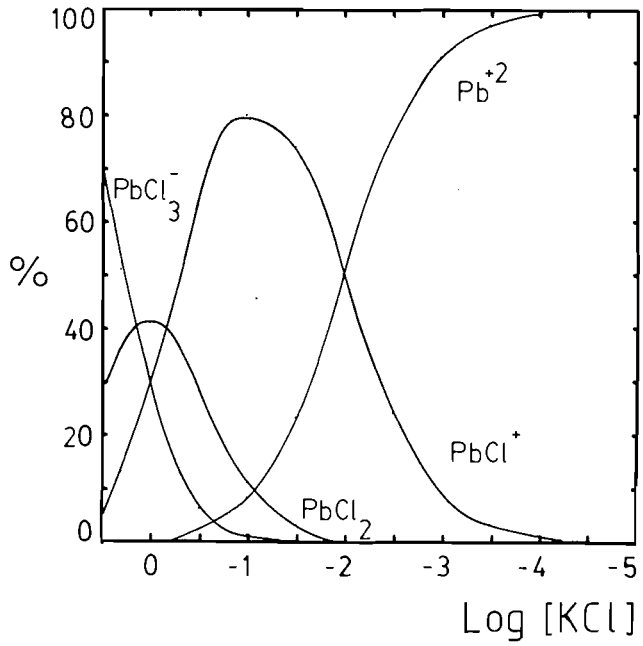

FIG. 6. Distribution des complexes chlorés dans HF 26% en fonction de la concentration en KCl.

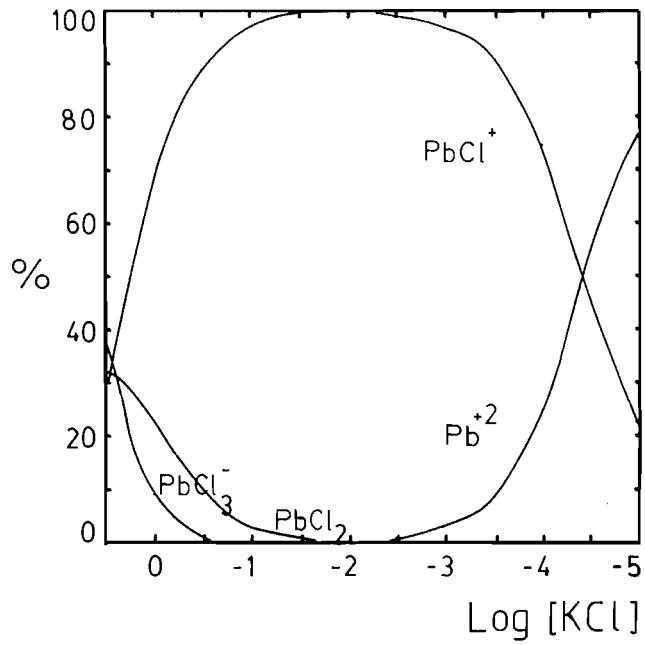

FIG. 8. Distribution des complexes chlorés dans HF 56% en fonction de la concentration en KCl.

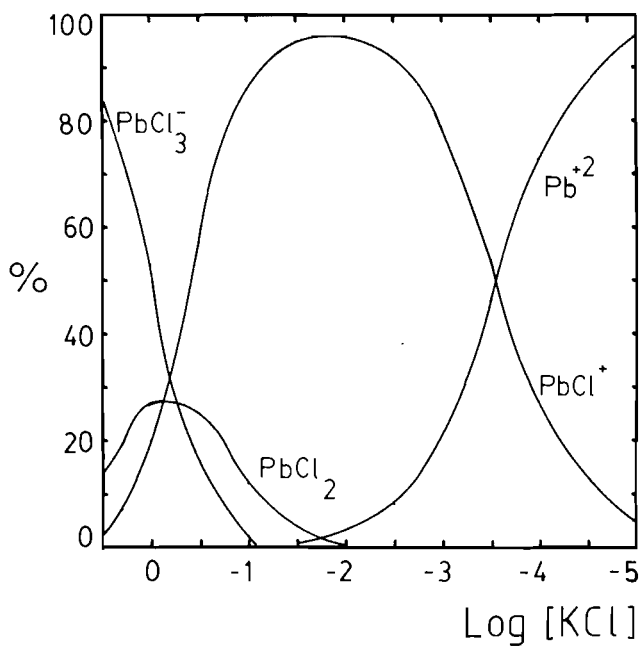

FIG. 7. Distribution des complexes chlorés dans HF 47% en fonction de la concentration en KCl.

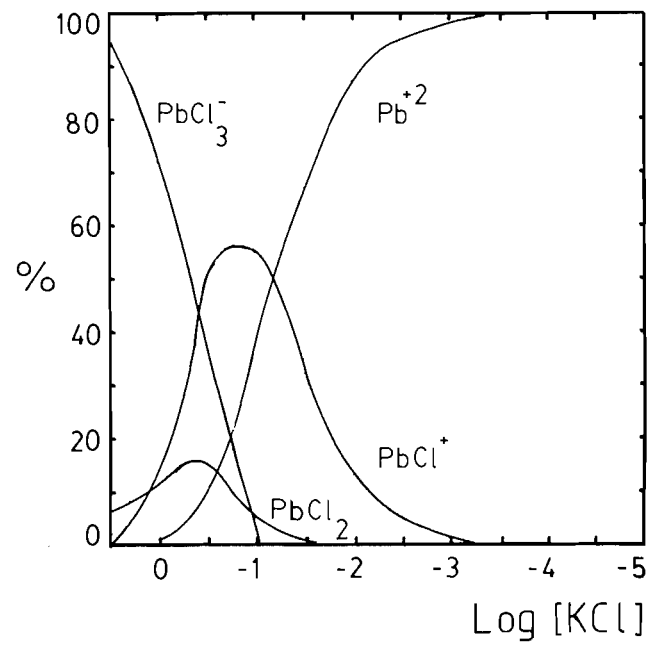

FIG. 9. Distribution des complexes chlorés en solution aqueuse en fonction de la concentration en KCl.

observe une diminution importante du courant de diffusion en polarographie.

[18] $PbF^+ + Cl^- \rightleftarrows PbFCl$ (précipité)

À 47 et 56% en HF, le complexe fluoré en solution est le PbF^+. L'addition d'un ion chlorure à cette espèce devrait être facile. En effet, la constante de formation β_1 augmente de façon très importante et le courant de diffusion chute à zéro à cause de la formation de PbFCl insoluble. Aux figures 7 et 8, on voit que le plomb est totalement sous forme de complexe $PbCl^+$ pour un important domaine de concentrations en ions chlorure.

La formation du complexe insoluble PbFCl vient appuyer l'hypothèse de la formation de complexes mixtes. Dans le domaine de concentration en HF où le complexe fluoré est PbF_2, on a remplacement des ions fluorure par des ions chlorure mais de façon successive. Dans la région où on a PbF^+, l'addition d'un ion chlorure est largement facilitée. Cependant le remplacement de l'ion fluorure semble aussi difficile qu'à plus faible concentration en HF, si on considère la proportion de complexes chlorés de degrés supérieurs. En effet, le complexe $PbCl_3^-$ apparaît toujours vers un molaire en ion chlorure. Le complexe $PbCl_2$ est peu représenté à toutes les concentrations en HF de même qu'en solution aqueuse.

Can. J. Chem. Downloaded from www.nrcresearchpress.com by 80.58.250.72 on 09/07/12
For personal use only.

Conclusion

L'étude de la vague polarographique du plomb à différentes concentrations en HF a permis de déterminer la présence de deux complexes fluorés. Le PbF_2 est présent jusqu'à 35% en poids de HF et le PbF^+ est présent de 35 à 60% en HF. L'ion chlorure déplace l'ion fluorure et on a formation de complexes mixtes chlorure–fluorure.

Remerciements

Les auteurs sont reconnaissants des octrois de recherche du Conseil de recherche en sciences naturelles et en génie du Canada et du Ministère de l'éducation du Québec qui ont rendu ce travail possible.

1. H. MÉNARD et F. LEBLOND-ROUTHIER. Anal. Chem. **50**, 687 (1980).
2. A. VAILLANT, J. DEVYNCK et B. TREMILLON. Anal. Lett. **6**, 1095 (1973).
3. A. VAILLANT, J. DEVYNCK et B. TREMILLON. J. Electroanal. Chem. **57**, 219 (1974).
4. H. MÉNARD, J. P. MASSON, J. DEVYNCK et B. TREMILLON. J. Electroanal. Chem. **63**, 163 (1975).
5. P. A. GIGUERE et S. TURRELL. J. Am. Chem. Soc. **102**, 5473 (1980).
6. H. STREHLOW. *Dans* The chemistry of nonaqueous solvents. Vol. 1. *Edité par* J. J. Lagowski. Academic Press, New York, NY. 1966. Chap. 4.
7. S. S. MESARIC et D. N. HUME. Inorg. Chem. **2**, 788 (1963).
8. A. M. BOND et G. HEFTER. Inorg. Chem. **9**, 1021 (1970).
9. A. M. BOND et G. HEFTER. J. Electroanal. Chem. **31**, 477 (1971).
10. A. M. BOND et G. HEFTER. J. Electroanal. Chem. **42**, 1 (1973).
11. D. D. DEFORD et D. N. HUME. J. Am. Chem. Soc. **73**, 5321 (1951).
12. W. B. SHAAP et D. L. MCMASTER. J. Am. Chem. Soc. **83**, 4699 (1961).
13. J. DEVYNCK, A. VAILLANT, B. TREMILLON, F. LEBLOND-ROUTHIER et H. MÉNARD. J. Electrochem. Soc. **100**, 885 (1979).
14. R. FAIVRE et R. WEISS. *Dans* Nouveau traité de chimie minérale. Tome VIII. *Edité par* P. Pascal. Masson et Cie., 1963. pp. 522, 552.
15. P. BOLDRINI et B. O. LOOPSTRA. Acta Crystallogr. **22**, 744 (1967).
16. J. H. KENNEDY, R. MILES et J. HUNTER. J. Electrochem. Soc. **123**, 1441 (1973).
17. G. A. SAMARA. Phys. Rev. B: Solid State, **13**, 4529 (1976).
18. G. A. SAMARA. J. Phys. Chem. Solids, **40**, 509 (1979).

Can. J. Chem. Downloaded from www.nrcresearchpress.com by 80.58.250.72 on 09/07/12
For personal use only.

Solvent and α-substituent perturbations of the $^2H/^1H$ isotope shifts in the ^{13}C nuclear magnetic resonance of toluene-α-d_3

TED SCHAEFER, JAMES PEELING,[1] AND RUDY SEBASTIAN
Department of Chemistry, University of Manitoba, Winnipeg, Man., Canada R3T 2N2

Received August 12, 1986

TED SCHAEFER, JAMES PEELING, and RUDY SEBASTIAN. Can. J. Chem. **65**, 534 (1987).

The $^2H/^1H$ isotope effect on ^{13}C nmr chemical shifts, $^n\Delta$, n being the number of intervening bonds between ^2H and ^{13}C nuclei, in toluene-α-d_3 is solvent dependent. For example, $^1\Delta$ ranges from 817 ppb in CD_3OH to 869 ppb in acetone-d_6 solutions, a positive number indicating increased shielding in the deuterated species. $^1\Delta$ is linearly dependent on a function of the refractive index, n_D, of the solvent, allowing extrapolation to $n_D = 1$. The hyperconjugative model, in which the C—D bond is a poorer electron donor to the aromatic system than is a C—H bond, is tested for the substituents CH_2D, CHD_2, CD_3, $CHDCH_3$, CD_2CH_3, $CD(CH_3)_2$, C_6H_5CHD, and $(C_6H_5)_2CD$. For these substituents, the negative $^5\Delta$ is linearly related to the expectation value of $\sin^2\theta$; θ is the angle by which the C—D bond twists out of the benzene plane. The model fails quantitatively for $C_6H_5CD_2X$ (X = Cl, COOH, CN, OH). For X = OH, very large negative $^5\Delta$ and $^3\Delta$ values are observed. $^n\Delta$ is also reported for 4-ethyltoluene-α-d_3 and benzaldehyde-α-d_1. For the latter, all $^n\Delta$ values are positive other than $^5\Delta$, which vanishes in acetone-d_6 solution.

TED SCHAEFER, JAMES PEELING et RUDY SEBASTIAN. Can. J. Chem. **65**, 534 (1987).

Dans le toluène-α-d_3, l'effet isotopique $^2H/^1H$ sur les déplacements chimiques en rmn du ^{13}C, $^n\Delta$, dans lequel n est égal au nombre de liaisons intervenant entre les noyaux de ^2H et de ^{13}C, dépend du solvant. Par exemple, la valeur de $^1\Delta$ varie de 817 ppb pour des solutions dans de CD_3OH à 869 ppb pour des solutions dans l'acétone-d_6; une valeur positive indique une augmentation du blindage dans les espèces deutérées. La valeur de $^1\Delta$ varie d'une façon linéaire avec l'indice de réfraction, n_D, du solvant; cette propriété permet d'extrapoler jusqu'à une valeur de $n_D = 1$. On a vérifié l'efficacité du modèle comportant de l'hyperconjugaison, dans lequel la liaison C—D donne moins facilement des électrons au système aromatique qu'une liaison C—H pour les substituants CH_2D, CHD_2, CD_3, $CHDCH_3$, CD_2CH_3, $CD(CH_3)_2$, C_6H_5CHD et $(C_6H_5)_2CD$. Pour ces substituants, la valeur négative de $^5\Delta$ présente une corrélation linéaire avec la valeur attendue de $\sin^2\theta$; θ est l'angle de torsion de la liaison C—D par rapport au plan du benzène. D'un point de vue quantitatif, le modèle n'est pas approprié pour $C_6H_5CD_2X$ (X = Cl, COOH, CN, OH). Pour X = OH, on observe des valeurs de $^3\Delta$ et $^5\Delta$ qui sont très importantes et négatives. On rapporte aussi les valeurs de $^n\Delta$ pour l'éthyl-4 toluène-α-d_3 et pour le benzaldéhyde-α-d_1. Dans ce dernier composé, toutes les valeurs de $^n\Delta$ sont positives, à l'exception de $^5\Delta$ qui disparait en solution dans l'acétone-d_6.

[Traduit par la revue]

Can. J. Chem. Downloaded from www.nrcresearchpress.com by 80.58.250.72 on 09/07/12
For personal use only.

Introduction

In general, nuclear shielding (a low frequency shift in nmr) increases with decreasing bond distances in polyatomic molecules (1). Because of anharmonic vibrations and centrifugal distortion a shorter average bond length ensues on replacement of a lighter by a heavier atom in a bond (2). In particular, it becomes qualitatively clear why $^1\Delta$, the $^2H/^1H$ isotope effect on ^{13}C nmr chemical shifts, is positive (increasing shielding) when ^2H replaces ^1H in the C—H bond.[2] For longer range isotope effects $^n\Delta$, n being the number of bonds intervening between ^{13}C and ^2H, complexities arise. According to Jameson (2), there is a primary dynamic effect at the substitution site, which is transmitted by a secondary electronic effect on the shielding at ^{13}C. In addition, there is a secondary dynamic effect on the bond lengths at the ^{13}C site with a concomitant primary electronic effect on the shielding. The computation of such long-range isotope shifts in larger molecules is not easy (8) and various models have been proposed to account for the observed shifts, which can be of either sign.

For conjugated systems, the hyperconjugative model is useful in some instances (9). The model entails a breakdown of the Born–Oppenheimer approximation and assumes less efficient hyperconjugative electron donation by a C—D than a C—H bond.

An additional complication comes from possible solvent-induced changes in isotope effects on nuclear shielding. Intrinsic effects are characteristic of an isolated molecule (10). Extrinsic contributions to isotope shifts should be quite general in solution because, for example, the hydrogen atom in a C—H bond has a larger amplitude of motion than the deuterium atom in a C—D bond. Therefore a difference in their interactions with solvent molecules should be present. Solvent-induced changes in isotope effects on nuclear shielding are thought (6) to be important where inter- or intramolecular hydrogen bonding occurs or, more generally, when isotopic substitution shifts the position of an equilibrium and the latter is solvent dependent.

In this paper we reexamine $^n\Delta$ values for some α-deuterated toluene derivatives in terms of the hyperconjugative model, show that solvent induced changes in $^n\Delta$ can be important for a molecule as inert as toluene-α-d_3, and demonstrate that the hyperconjugative model is of limited quantitative utility when applied to toluene derivatives with polar substituents on the side chain.

Results and discussion

The hyperconjugative model

The original suggestion (11), that $^5\Delta$ for the *para* ^{13}C nucleus in toluene-α-d_1, ethylbenzene-α-d_1, and cumene-α-d_1 depends on the angle θ, was elaborated (12) to eq. [1]. In [1], $\langle\sin^2\theta\rangle$ is the expectation value of $\sin^2\theta$, which can be obtained from

$$[1] \quad {}^5\Delta\ (\text{ppb}) = a\langle\sin^2\theta\rangle + b$$

$^6J_p^{H,CH}$ (13). The latter is the long-range spin–spin coupling constant between the α proton on the side chain and the *para* proton. Knowing $\langle\sin^2\theta\rangle$, it follows that the preferred conformation of the side chain and the barrier to internal rotation

[1]University of Petroleum and Minerals, Saudia Arabia.

[2]See refs. 3–7 for early discussions, as well as for recent tabulations and descriptions of isotope effects on chemical shifts.

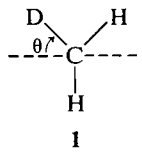

I

about the exocyclic C_{sp^2}—C_{sp^3} can be ascertained (13). Now, the measurement of $\langle \sin^2 \theta \rangle$ via $^5\Delta$ is easier than via $^6J_p^{H,CH}$ because the latter has to be extracted from complex ^{1}H nmr spectra arising from large spin systems. If relationships like [1] hold in general, then quantitative information about internal rotational barriers is available via an easy chemical shift measurement (given a high-field instrument, of course, and the requisite deuterated molecule).

Table 1 contains the observed and calculated $^5\Delta$ values for eight side chains, all measured in $CDCl_3$ solution. The calculated values come from eqs. [2] or [3], which are equivalent, of course.

$$[2] \quad {}^5\Delta \text{ (ppm)} = -13.1n\langle \sin^2 \theta \rangle + 5.1n\langle \cos^2 \theta \rangle$$

$$[3] \quad {}^5\Delta \text{ (ppm)} = -18.2n\langle \sin^2 \theta \rangle + 5.1n$$

In these equations, n is the number of α C—D bonds and $\langle \sin^2 \theta \rangle$ is 0.5 for toluene, containing a negligible internal barrier (16). For ethylbenzene, $\langle \sin^2 \theta \rangle$ is 0.385, as derived from $^6J_p^{H,CH}$ (13). A recent unpublished analysis of the ^{1}H nmr spectrum of cumene in this laboratory gave $\langle \sin^2 \theta \rangle$ as 0.229, the value used in Table 1. For diphenylmethane, $\langle \sin^2 \theta \rangle$ is taken as 0.39 ± 0.03, also deduced in this laboratory from $^6J^{H,CH}$, $^6J^{F,CH}$, and $^6J^{F,CC}$ for a number of its derivatives.

The agreement between calculated and observed $^5\Delta$ values is rather good, given the precision of about 0.4 ppb in the measurements. Note that $^5\Delta$ contains negative, presumably arising from the hyperconjugative mechanism, as well as positive components. The latter, having the same sign as $^1\Delta$, could be considered "normal," perhaps arising from the primary dynamic effect mentioned above. Equation [2] implies that this effect depends on $\langle \cos^2 \theta \rangle$, does not prove this, of course, and may be erroneous.

Solvent perturbations of $^n\Delta$ in toluene-α-d_3

Table 2 displays solvent-dependent $^n\Delta$ numbers for toluene-α-d_3, illustrating the importance of a common solvent when making comparisons of the kind given in Table 1. $^1\Delta$ increases by 51 ppb in passing from CD_3OH to CH_2I_2 as solvent. The larger $^1\Delta$ values in the more polarizable solvents are plausibly attributable to larger van der Waals interactions, which, however, cause larger deshielding in the undeuterated molecule. Solvent effects (17) for toluene display the largest deshielding of the ^{13}C nuclei in CH_2I_2 solution and are assigned to repulsive intermolecular orbital overlap effects occurring during molecular collisions. In that event, it appears sensible that C—H bonds, with their larger vibrational amplitudes, undergo larger perturbations due to collisions with solvent molecules than do C—D bonds and, therefore, that the apparent upfield shift of ^{13}C in the deuterated molecule is a consequence of the larger downfield shift in the toluene molecule itself.

Whatever the merits of the postulate (17) of a repulsive interaction as a cause of ^{13}C deshielding by solvent molecules, it may be noted that for the solvents in Table 1 a linear relation, eq. [4], exists between $^1\Delta$ and $\{(n^2 - 1)/(2n^2 + 1)\}^2 \equiv W$. The latter quantity is a measure (18) of the average squared

$$[4] \quad {}^1\Delta \text{ (ppb)} = 946.3W + 789.1$$

TABLE 1. Observed[a] and calculated[b] ^{2}H/^{1}H isotope effects on ^{13}C-4 chemical shifts in some toluene derivatives in $CDCl_3$ solution

	$^5\Delta$/ppb			$^5\Delta$/ppb	
Side chain	obsd.	calcd.	Side chain	obsd.	calcd.
CH_2D	−3.9	−4.0	CD_2CH_3	−3.8	−3.8
CHD_2	−8.0	−8.0	$CD(CH_3)_2$[c]	0	0.9
CD_3	−12.1	−12.0	C_6H_5CHD	−2.6	−2.0(5)
$CHDCH_3$	−2.1	−1.9	$(C_6H_5)_2CD$	0	0.5[d]
					−0.2[d]

[a] All but CD_2CH_3 are from refs. 9 and 11; $^5\Delta$ for CD_2CH_3 was measured in this laboratory.

[b] Calculated from $^5\Delta = -13.1n\langle \sin^2 \theta \rangle + 5.1n\langle \cos^2 \theta \rangle$ or, equivalently, from $^5\Delta = -18.2n\langle \sin^2 \theta \rangle + 5.1n$; $\langle \sin^2 \theta \rangle$ is the expectation value for $\sin^2 \theta$, θ being the angle by which the C—H bond twists out of the benzene plane; n is the number of α C—D bonds.

[c] For CH_2D, CHD_2, CD_3, $\langle \sin^2 \theta \rangle = 0.5$; for $CHDCD_3$ and CD_2CH_3, $\langle \sin^2 \theta \rangle$ is 0.385; $\langle \sin^2 \theta \rangle$ is 0.229 for $CD(CH_3)_3$ and is 0.39(3) for C_6H_5CHD (21).

[d] Deduced from $\sin^2 \theta$ for θ values given from Kerr constants (15) and infrared intensities (14); but note that these are not expectation values.

TABLE 2. ^{2}H/^{1}H isotope effects on ^{13}C nmr shifts, $^n\Delta$, of toluene-α-d_3 for a number of solvents at 300 K

Solvent	$^1\Delta$[a]	$^2\Delta$	$^3\Delta_o$	$^4\Delta_m$	$^5\Delta_p$
CD_3OH[b]	817.3	104.0	−1.9	4.7	−10.6
$(CD_3)_2C{=}O$[c]	820.1	100.2	−3.4	6.4	−9.7
$CDCl_3$[d]	825.5	104.9	−1.6	0	−12.1
$CHBr_3$[e]	—[i]	107.2	−1.2	0	−13.3
C_6D_6[f]	837.0	108.3	−1.4	3.0	−13.9
CCl_4[g]	831.3	109.2	−1.0	2.7±1	−12.6
CH_2I_2[h]	868.9	109.5	0	0	−13.0

[a] In ppb (parts per billion), a positive number representing increased shielding in the presence of ^{2}H, with a precision of 0.4 ppb.

[b] 7.1 mol% d_3 and 8.3 mol% h_3.

[c] 5.1 mol% d_3 and 7.5 mol% h_3.

[d] From ref. 11, ca. 3:1 d_3 to h_3 (1 molar in $CDCl_3$).

[e] Less than 3 mol% of each isotopomer and 10 mol% C_6D_{12}.

[f] 6.5 mol% d_3 and 7.5 mol% h_3.

[g] 7.1 mol% d_3 and 8.3 mol% h_3 and ca. 10 mol% C_6D_{12}.

[h] Ca. 2.2 mol% of each isotopomer and 10 mol% C_6D_{12}.

[i] Not observed.

electrical fields at the solute molecule, used in models for the van der Waals contribution to gas-to-liquid medium ^{1}H nmr shifts, particularly for hydrocarbons. Equation [4] implies a $^1\Delta$ of 789.1 ± 1.5 ppb for the isolated molecule if a reasonably short extrapolation is made to a refractive index, n_D, of unity. Because of the additivity observed for successive deuterations, $^1\Delta$ values for isolated toluene-α-d_1 and toluene-α-d_2 molecules can be estimated from the available data (11) as 263 and 526 ppb, respectively.[3]

The trend in $^2\Delta$ in Table 2 is quite similar to that of $^1\Delta$, with the exception of CD_3OH as solvent, and is presumably indicative of the same mechanism as postulated for $^1\Delta$ above. The longer range Δ values are harder to rationalize. $^5\Delta$ displays a rough trend towards more *positive* values in the solvents of *lower* polarizability (refractive indices). According to eqs. [2] or [3], $^5\Delta$ consists of two contributions, so that a solvent

[3] It is anticipated that $^1\Delta$ values for deuterated methanes in the gas phase could be estimated by procedures of this kind, of obvious interest in their computation from first principles.

Can. J. Chem. Downloaded from www.nrcresearchpress.com by 80.58.250.72 on 09/07/12
For personal use only.

TABLE 3. $^2H/^1H$ isotope effects on ^{13}C nmr shifts, $^n\Delta$, for a number of toluene derivatives at 300 K

Compound	$^1\Delta$[a]	$^2\Delta$	$^3\Delta_o$	$^4\Delta_m$	$^5\Delta_p$
$C_6H_5CHD_2$[b]	550.8	69.2	−1.1	0	−8.0
$C_6H_5CD_2CH_3$[c]	702.8	60.5[n]	3.5	0	−3.8
$C_6H_5CD_2OH$	675.0[d]	116.5	−46.9	−2.8	−27.9
	684.3[e]	100.3	−56.5	~0	−23.8
$C_6H_5CD_2Cl$[f]	521.4	104.8	−2.4	1.4	−7.8
$C_6H_5CD_2CN$[g]	401.6	76.1	−5.9(−13.7)[p]	3.3	−13.0
$C_6H_5CD_2COOH$[h]	546.5	50.8	38.6	−6.4	−10.1
$CH_3CH_2C_6H_4CD_3$	829.6[i]	107.4	−2.5	3.1	−9.4
	823.3[j]	101.6	−2.9	6.0	−3.7[o]
$C_6H_5CD_3$	820.1[k]	100.2	−3.4	6.4	−9.7
	825.5[l]	104.9	−1.6	0	−12.1
C_6H_5CDO[m]	290.8	72.4	9.2	4.9	0.0

[a]In ppb, as described in Table 2.
[b]In $CDCl_3$, from ref. 11.
[c]5.9 mol% d_2 and 6.7 mol% h_2 in $CDCl_3$.
[d]4.0 mol% d_2 and 5.4 mol% h_2 in $CDCl_3$.
[e]3.8 mol% d_2 and 4.7 mol% h_2 in acetone-d_6.
[f]3.2 mol% d_2 and 3.8 mol% h_2 in acetone-d_6.
[g]4.1 mol% d_2 and 5.1 mol% h_2 in acetone-d_6.
[h]2.8 mol% d_2 and 3.7 mol% h_2 in acetone-d_6.
[i]~4 mol% d_2 and ~5 mol% h_2 in $CDCl_3$.
[j]2.9 mol% d_2 and 4.3 mol% h_2 in acetone-d_6.
[k]In acetone-d_6, see Table 1.
[l]In $CDCl_3$, ref. 11.
[m]5.6 mol% d_2 and 6.1 mol% h_2 in acetone-d_6.
[n]$^2\Delta$ to CH_3 is 163.6 ppb.
[o]$^6\Delta$ to CH_2 is −0.3 ppb.
[p]Depending on how the partially resolved multiplet structure in the deuterated molecule is interpreted.

perturbation of either one or both of them is possible. It is interesting that $^4\Delta$, previously observed as zero for the compounds in Table 1 in $CDCl_3$ solution, becomes as large as 6.4 ppb for toluene-α-d_3 in acetone-d_6 solution. It is reasonable to hypothesize that $^4\Delta$ consists of terms similar in nature and equal in sign[4] to those in eqs. [2] and [3] for $^5\Delta$. Such a statement appears to hold for $^3\Delta$, in which the hyperconjugative term is nearly cancelled by the "normal" positive term (20). The latter is ca. 55 ppb for toluene-α-d_3, compared to the +15.3 ppb for $^5\Delta$. However, the data in Table 2 do not allow a decision as to the solvent dependence of either of such terms of opposite sign (see Table 3 for negative $^4\Delta$ values). Similar remarks apply to $^3\Delta$ in Table 2.

Polar α substituents

The importance of a common solvent if $^n\Delta$ values are to be compared for a set of related molecules can also be inferred from the data in Table 3. These data also demonstrate that, in the presence of polar substituents on the side chain, $\langle\sin^2\theta\rangle$ values are not ascertainable in the straightforward way found to be successful for alkyl groups in Table 1.

For the CD_2Cl, CD_2CN, and CD_2COOH side chains in Table 3, values of $\langle\sin^2\theta\rangle$ are available in acetone solution (21–23) and are 0.318, 0.51(1), and 0.33(2), respectively. It is immediately clear that eq. [3] will not reproduce the $^5\Delta$ values in acetone solution. However, on the arbitrary assumption that the hyperconjugative contribution is reduced by a factor of 9.7/12.1 (the ratio of $^5\Delta$ values for toluene-α-d_3 in acetone-d_6 and $CDCl_3$ solutions), and that the positive "normal" term is also reduced, one may write eq. [5]. This equation reproduces

$$[5]\quad {}^5\Delta\ (\text{ppb}) = -14.7n\langle\sin^2\theta\rangle + 0.7n \qquad (n = 2)$$

the observed $^5\Delta$ values to within an average deviation of 0.4 ppb. Although somewhat encouraging, this result also demonstrates that quantitative values for the internal rotational potential are not available directly from $^5\Delta$ values for arbitrary substituents on the α methyl group. A striking value of near −24 ppb is found for the CD_2OH group, for which data from this laboratory yield a $\langle\sin^2\theta\rangle$ of 0.54 in acetone solution. This value is accompanied by an equally striking $^3\Delta$ of −56.5 ppb in acetone-d_6 solution. In terms of the hyperconjugative model, the hydroxyl group causes an extraordinary decrease in the electron-donating ability of the C—D bond relative to the C—H bond.[5] Another peculiarity of $^3\Delta$ values in Table 3 is the +39 ppb observed for the CD_2COOH group, accompanied by a relatively large $^4\Delta$ of −6.4 ppb. No simple model appears to meet the requirements of such diverse values of these long-range isotope effects.

A comparison of $^n\Delta$ values for 4-ethyltoluene-α-d_3 and toluene-α-d_3 (compare for the same solvents in Table 3) suggests the rationalization that the ethyl group, being a hyperconjugative donor to the aromatic ring, decreases the donation by the methyl group and therefore leads to smaller negative (hyperconjugative) components of $^n\Delta$.

Finally, $^1\Delta$–$^4\Delta$ are all positive for benzaldehyde and $^5\Delta$

[4]Note that all ring protons in toluene are more shielded than those in benzene (19), although the *meta* protons *are* less shielded than the *ortho* and *para* protons, as expected.

[5]Of course, self-association in $CDCl_3$ solution and hydrogen bonding to solvent molecules in acetone-d_6 solution occur for benzyl alcohol, but it appears unlikely that these large values of $^3\Delta$ and $^5\Delta$ are solely attributable to such causes.

Can. J. Chem. Downloaded from www.nrcresearchpress.com by 80.58.250.72 on 09/07/12
For personal use only.

vanishes, compatible with a "normal" isotope effect that drops off rapidly as n increases. Because the barrier to internal rotation of benzaldehyde in solution is at least 30 kJ/mol (24), $\langle \sin^2 \theta \rangle$ is very small, ca. 0.05 at 300 K, so that the C—D or C—H bonds spend very little time out of the benzene plane. Furthermore, there is evidence (25) that the C=O group strongly inhibits hyperconjugative interactions of the C—H bond. These considerations are compatible with the $^n\Delta$ values in Table 3.

Experimental

Small quantities of toluene-α-d_3, benzyl alcohol-α-d_2, benzyl chloride-α-d_2, benzyl cyanide-α-d_2, phenylacetic acid-α-d_2, 4-ethyltoluene-α-d_3, ethylbenzene-α-d_2, and benzaldehyde-α-d_1 were obtained from MST Isotopes. The concentrations of undeuterated and their isotopically substituted derivatives in various solvents are given in Tables 1–3. Samples were degassed by the freeze–pump–thaw procedure and were flame-sealed. $^{13}C\{^1H\}$ nmr spectra were accumulated on an AM300 nmr spectrometer at a probe temperature of 300 K. ^1H decoupling involved the WALTZ16 pulse sequence (26). In a typical experiment, 32 FIDS were stored in 64K of memory, using a spectral window of 1064 Hz, an acquisition time of 30.8 s, and a digital resolution of 0.03 Hz/point. The precision of measurement of $^n\Delta$ was 0.4 ppb.

Caveat

A referee points out that the linear correlation between $^5\Delta$ and $^6J_p^{H,CH}$ does not necessarily support a hyperconjugative mechanism for $^5\Delta$. It may simply means that $^6J_p^{H,CH}$ and the dependence of $^5\Delta$ on the change in bond length (C—D versus C—H), at the methyl site, both depend on the same electronic transmission mechanisms. Thus, it has been shown (27, 28) that some long-range Δ values for ^{13}C and ^{19}F nuclei can be interpreted as arising from a change in electron density at the carbon and fluorine atoms, caused by a change in the bond length of the remote C—H bond. This is an interesting suggestion, although it should be noted that, while $^6J_p^{H,CH}$ in toluene is transmitted via the π electrons, it is insensitive to the presence of ring substituents (19, 29), whereas the electron densities at the various sites in the ring are markedly dependent on the nature of the substituents.

Acknowledgments

We are grateful to the Natural Sciences and Engineering Research Council of Canada for financial support.

1. B. T. HAMDI, D. J. REYNOLDS, and G. A. WEBB. Org. Magn. Reson. **22**, 90 (1984).
2. C. J. JAMESON. Prog. Nucl. Magn. Reson. Spectrosc. **14**, 1 (1985).
3. H. BATIZ-HERNANDEZ and R. A. BERNHEIM. Prog. Nucl. Magn. Reson. Spectrosc. **3**, 63 (1967).
4. C. J. JAMESON. J. Chem. Phys. **66**, 4983 (1977).
5. W. T. RAYNES. Prog. Nucl. Magn. Reson. Spectrosc. **8**, 1 (1979).
6. P. E. HANSEN. Annu. Rep. NMR Spectrosc. **15**, 105 (1983).
7. D. A. FORSYTH. *In* Isotopes in organic chemistry. Vol. 6. *Edited by* E. Buncel and C. C. Lee. Elsevier, Amsterdam. 1984. Chap. 1.
8. H.-J. OSTEN and C. J. JAMESON. J. Chem. Phys. **82**, 4595 (1985).
9. J. R. WESENER, D. MOSKAU, and H. GÜNTHER. J. Am. Chem. Soc. **107**, 7307 (1985), and references therein.
10. C. J. JAMESON. Prog. Nucl. Magn. Reson. Spectrosc. **11**, 1 (1982).
11. J. R. WESENER and H. GÜNTHER. Tetrahedron Lett. **23**, 2845 (1982).
12. T. SCHAEFER, J. PEELING, and T. A. WILDMAN. Can. J. Chem. **61**, 2777 (1983).
13. W. J. E. PARR and T. SCHAEFER. Acc. Chem. Res. **13**, 400 (1980).
14. S. HIGUCHI, H. TSUYAMA, S. TANAKA, and H. KAMADA. Spectrochim. Acta, Part A, **30**, 463 (1974).
15. M. J. ARONEY, R. J. LEFÉVRE, G. L. D. RITCHIE, and A. N. SINGH. J. Chem. Soc. 5810 (1965).
16. H. D. RUDOLPH, H. DREIZLER, A. JAESCHKE, and P. WENDLING. Z. Naturforsch. Teil A, **22**, 940 (1967).
17. K. JACKOWSKI. Org. Magn. Reson. **22**, 263 (1984).
18. F. H. A. RUMMENS. Can. J. Chem. **54**, 254 (1976).
19. T. SCHAEFER, R. SEBASTIAN, and G. H. PENNER. Can. J. Chem. **63**, 2597 (1985).
20. L. ERNST. J. Am. Chem. Soc. **105**, 4469 (1983).
21. T. SCHAEFER, J. PEELING, G. H. PENNER, A. LEMIRE, and R. SEBASTIAN. Can. J. Chem. **63**, 24 (1985).
22. T. SCHAEFER, R. SEBASTIAN, and G. H. PENNER. Can. J. Chem. **64**, 1372 (1986).
23. T. SCHAEFER and G. H. PENNER. Can. J. Chem. **64**, 2013 (1986).
24. F. A. L. ANET and M. AHMAD. J. Am. Chem. Soc. **86**, 119 (1964).
25. T. SCHAEFER, J. PEELING, G. H. PENNER, A. LEMIRE, and R. LAATIKAINEN. Can. J. Chem. **64**, 1859 (1986).
26. A. J. SHAKA, J. KEELER, T. FRENKEL, and R. FREEMAN. J. Magn. Reson. **52**, 335 (1983).
27. K. L. SERVIS and R. L. DOMENICK. J. Am. Chem. Soc. **108**, 2211 (1986).
28. D. A. FORSYTH and J-R. YANG. J. Am. Chem. Soc. **108**, 2157 (1986).
29. T. SCHAEFER, R. SEBASTIAN, R. P. VEREGIN, and R. LAATIKAINEN. Can. J. Chem. **61**, 29 (1983).

Can. J. Chem. Downloaded from www.nrcresearchpress.com by 80.58.250.72 on 09/07/12
For personal use only.

Conformational preference and internal rotation about the C_1—C_α bond in phenylacetaldehyde and some benzyl alkyl ketones from ^1H nuclear magnetic resonance and *ab initio* molecular orbital calculations

GLENN H. PENNER

Department of Chemistry, University of Manitoba, Winnipeg, Man., Canada R3T 2N2

Received August 20, 1986

GLENN H. PENNER. Can. J. Chem. **65**, 538 (1987).

Analysis of the ^1H nuclear magnetic resonance spectra of the benzyl moieties in phenylacetaldehyde, benzyl methyl ketone, benzyl ethyl ketone, benzyl isopropyl ketone, and 3,5-dichlorobenzyl *tert*-butyl ketone yields the long-range couplings between ring and α protons. These stereospecific couplings change very little upon replacement of the aldehydic hydrogen by various alkyl groups. The couplings for all the molecules studied fall within the ranges $^4J(CH_2, H_o) = -0.566 \pm 0.008$ Hz, $^5J(CH_2, H_m) = 0.278 \pm 0.002$ Hz, and $^6J(CH_2, H_p) = -0.409 \pm 0.010$ Hz, suggesting that in the ketones the alkyl group prefers to be *trans* to the phenyl ring and does not interfere with rotation about the C_1—C_α bond. The long-range couplings are consistent with a potential function $V(\theta) = 8.4 \pm 1.2 \sin^2\theta$ for two-fold rotation about the C_1—C_α bond; θ is the angle between the carbonyl and benzene ring plane. *Ab initio* molecular orbital calculations on phenylacetaldehyde at the STO-3G level with the C=O bond *cis* to the phenyl group yield a potential of $V(\theta) = (8.65 \pm 0.73) \sin^2\theta + (1.27 \pm 0.80) \sin^2 2\theta$, rather close to the experimental potential but with a small fourfold component. The spin–spin coupling constant between the aldehydic and α protons displays a solvent dependence consistent with previously reported values. The insensitivity of $^4J(CH_2, H_o)$, $^5J(CH_2, H_m)$, and $^6J(CH_2, H_p)$ to solvent suggests that $\langle\sin^2\theta\rangle$ is very weakly dependent on the rotation of the aldehyde group.

GLENN H. PENNER. Can. J. Chem. **65**, 538 (1987).

Une analyse des spectres rmn du ^1H de la portion benzylique du phénylacétaldéhyde, de la benzyl méthyl cétone, de la benzyl éthyl cétone, de la benzyl isopropyl cétone et de dichloro-3,5 benzyl *tert*-butyl cétone permet de déterminer les couplages à longue distance entre les protons du cycle et ceux en α. Ces couplages stéréospécifiques ne varient que peu lorsqu'on change l'hydrogène aldéhydique pour divers groupements alkyles. Les couplages pour chacune des molécules étudiées se situent tous dans les intervalles $^4J(CH_2, H_o) = -0{,}566 \pm 0{,}008$ Hz, $^5J(CH_2, H_m) = 0{,}278 \pm 0{,}002$ Hz et $^6J(CH_2, H_p) = -0{,}409 \pm 0{,}010$ Hz; ces résultats suggèrent que, dans les cétones, le groupement alkyle préfère la conformation *trans* par rapport au noyau phényle et qu'il n'interfère pas avec la rotation autour de la liaison C_1—C_α. Les couplages à longue distance sont en accord avec une fonction de potentiel qui serait exprimé par l'équation $V(\theta) = 8{,}4 \pm 1{,}2 \sin^2\theta$ pour une rotation binaire autour de la liaison C_1—C_α; θ est l'angle formé par le groupement carbonyle et le plane du cycle benzénique. Si l'on effectue des calculs OM *ab initio*, au niveau STO-3G, sur le phénylacétaldéhyde en faisant l'hypothèse que la liaison C=O est *cis* par rapport au groupement phényle, le potentiel est alors représenté par l'équation $V(\theta) = (8{,}65 \pm 0{,}73) \sin^2\theta + (1{,}27 \pm 0{,}80) \sin^2 2\theta$; cette équation est assez proche du potentiel expérimental, mais elle comporte une petite composante quaternaire. Il existe une corrélation entre la constante de couplage spin–spin du proton aldéhydique avec les protons en α, et le solvant, qui est en accord avec les données rapportées anterieurement. Le fait que les valeurs de $^4J(CH_2, H_o)$, $^5J(CH_2, H_m)$ et $^6J(CH_2, H_p)$ ne varient pas avec la nature du solvant suggère que $\langle\sin^2\theta\rangle$ ne dépend que faiblement sur la rotation du groupement aldéhydique.

[Traduit par la revue]

Introduction

The vicinal spin–spin coupling constants between the aldehydic and α protons in phenylacetaldehyde and several of its derivatives have been reported as a function of temperature and solvent (1). The observed coupling provides information on the conformational preference of the aldehydic group in phenylacetaldehyde.

The long-range spin–spin coupling constants between the ring and α protons in α-substituted toluene derivatives have afforded much useful information on the conformational preference of the CH_2X moiety and the rotational barrier about the C_1—C_α bond (2–4). In particular, the six-bond coupling constant between the α and the *para* ring protons takes the form

[1] $$^6J(CH_2, H_p) = {}^6J_{90}\langle\sin^2\theta\rangle_H$$

where $\langle\sin^2\theta\rangle_H$ is the expectation value of $\sin^2\theta_H$, θ_H being the angle between the C—H_α bond and the phenyl ring plane. The observed ^6J in toluene (X = H), where $\langle\sin^2\theta\rangle_H$ is 0.5, yields a $^6J_{90}$ value of −1.20 Hz (5) and eq. [1] becomes

[2] $$^6J\,(\text{Hz}) = -1.20\langle\sin^2\theta\rangle_H$$

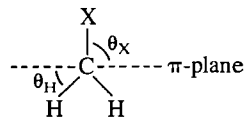

1

The relationship between $\langle\sin^2\theta\rangle$ for the X nucleus (see **1**) and $\langle\sin^2\theta\rangle$ for the α protons is

[3] $$\langle\sin^2\theta\rangle_X = 1.5 - 2\langle\sin^2\theta\rangle_H$$

The expectation value of $\sin^2\theta$ can be related to the barrier to rotation about the C_1—C_α bond by a hindered rotor model (2).

With the availability of a high-field nmr spectrometer in this laboratory, analysis of the rather tightly coupled spectra of benzylic systems has become possible (3, 4). In this paper the long-range couplings between the ring and α protons in phenylacetaldehyde, **2**, and several benzyl alkyl ketones, **2**, **4**, **5**, and **6**, are measured and related to the conformation of the side chain and to the barrier to rotation about the C_1—C_α bond.

Can. J. Chem. Downloaded from www.nrcresearchpress.com by 80.58.250.72 on 09/07/12
For personal use only.

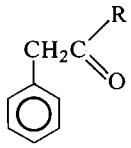

2 R = H
3 R = CH_3
4 R = CH_2CH_3
5 R = $CH(CH_3)_2$
6 R = $C(CH_3)_3$, 3,5-diCl

Results and discussion

Molecular orbital calculations

Molecular orbital calculations at the STO-3G level were performed with geometry optimization on phenylacetaldehyde as a model compound. The internal angles discussed below are shown in Fig. 1.

First, the angle θ was held at 0° while φ was rotated through 180° by 30° intervals. This was repeated for θ = 90°. The lowest energy was found for that conformation in which θ = 90° and φ = 120°, with local minima at φ = 0 and 60°, φ = 0° having the lower of the latter two energies. Energies were then calculated for rotation of θ from 0 to 90° by 15° increments while φ was held at 120°. The calculations were repeated with φ held at 0 and 180°. The energies for the last three rotations were fit to potentials of the form

[4] $V(\theta) = V_2 \sin^2 \theta + V_4 \sin^2 2\theta$

The V_2 and V_4 values, together with calculated values of $\langle \sin^2 \theta \rangle_C$, are given in Table 1. The classical expectation values are calculated, numerically, using the expression

$$[5] \quad \langle \sin^2 \theta \rangle_C = \frac{\int_{-\pi}^{\pi} (\sin^2 \theta) \exp\left[\frac{-V(\theta, \phi)}{RT}\right] d\theta}{\int_{-\pi}^{\pi} \exp\left[\frac{-V(\theta, \phi)}{RT}\right] d\theta}$$

Although $V(\theta, 120°)$, $V(\theta, 180°)$, and $V(\theta, 0°)$ are different, they yield very similar $\langle \sin^2 \theta \rangle_C$ values, suggesting that, for phenylacetaldehyde, the conformation of the aldehyde group has very little effect on $\langle \sin^2 \theta \rangle_C$, the quantity obtainable from $^6J(CH_2, H_p)$.

$^3J(CH_2, CHO)$

Reported measurements of $^3J(CH_2, CHO)$ in phenylacetaldehyde range from 2.48 Hz in *trans*-decalin to 2.09 Hz in dimethylformamide (1). The coupling appears to increase as the solvent dielectric constant increases, indicating a concomitant increase in the stability of the rotamer in which the phenyl group eclipses the C=O bond (φ = 0°). The values of $^3J(CH_2, CHO)$ given in Table 2 follow this trend.

$^6J(CH_2, H_p)$

Equations [2] and [3] yield $\langle \sin^2 \theta \rangle_H$ and $\langle \sin^2 \theta \rangle_C$ values for the molecules of interest. These values are collected in Table 2. All the ^6J values fall in the range $^6J(CH_2, H_p) = -0.409 \pm 0.010$ Hz and the corresponding $\langle \sin^2 \theta \rangle_C$ values satisfy 0.818 ± 0.017. Assuming the potential function for internal rotation about the C_1—C_α bond is twofold, a hindered rotor model (2) yields V_2 as 8.4 ± 1.2 kJ/mol.

Although STO-3G calculations for phenylacetaldehyde yield potential functions, $V(\theta)$, which are not purely twofold, the expectation values of $\sin^2 \theta_C$ derived from the calculated potentials are rather close to those deduced from ^6J.

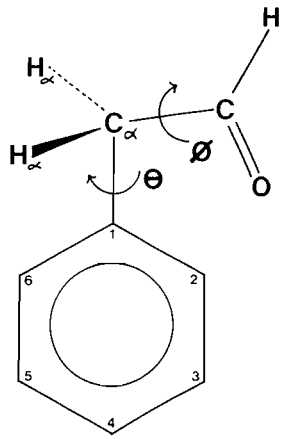

FIG. 1. The numbering system for phenylacetaldehyde. The conformation shown has θ = 0° and φ = 0°.

TABLE 1. The potential functions and $\langle \sin^2 \theta \rangle_C$ values obtained for rotation about the C_1—C_α bond in phenylacetaldehyde using the STO-3G basis set

φ[a](deg)	V_2[b](kJ/mol)	V_4[b]	$\langle \sin^2 \theta \rangle_C$
0	−11.15(33)	−1.96(33)	0.829
120	−8.65(73)	−1.27(80)	0.849
180	−14.90(15)	−4.36(15)	0.829

[a]θ and φ are defined in Fig. 1. φ is fixed at these angles as θ is varied.
[b]From a statistical best fit of the energies (seven values) to eq. [4]. The errors given in parentheses are at the 95% confidence level.
[c]$\langle \sin^2 \theta \rangle_C$ values are obtained from $V(\theta)$ using eq. [5].

The fact that $^3J(CH_2, CHO)$ changes with solvent, whereas $^6J(CH_2, H_p)$, does not, suggests that $\langle \sin^2 \theta \rangle_C$ is not strongly dependent on the conformation of the aldehyde group. *Ab initio* MO calculations agree with this suggestion.

Turning to the benzyl alkyl ketones, the independence of $^6J(CH_2, H_p)$ (and hence of $\langle \sin^2 \theta \rangle_C$) of the size of the alkyl substituent implies a conformation in which the alkyl group lies *trans* to the phenyl ring (φ = 0°) and therefore does not interfere with rotation about the C_1—C_α bond.

$^4J(CH_2, H_o)$ and $^5J(CH_2, H_m)$

The four-bond coupling constant between the α and the *ortho* protons has been written as (5, 6)

[6] $^4J(CH_2, H_o)/\text{Hz} = -1.08\langle \sin^2 \theta \rangle_H - 0.32\langle \cos^2 \theta \rangle_H$

The equation may be recast into the form

[7] $^4J(CH_2, H_o)/\text{Hz} = -0.76\langle \sin^2 \theta \rangle_H - 0.32$

It has been proposed (7) that ^5J is given by eq. [8].

[8] $^5J(CH_2, H_m)/\text{Hz} = 0.336\langle \sin^2 \theta \rangle_H + 0.322\langle \sin^2 \theta/2 \rangle_H$

For molecules with $2n$-fold barriers to internal rotation, $\langle \sin^2 \theta/2 \rangle_H$ is 0.5 (8) and eq. [8] becomes

[9] $^5J(CH_2, H_m)/\text{Hz} = 0.336\langle \sin^2 \theta \rangle_H + 0.161$

The $\langle \sin^2 \theta \rangle_H$ value obtained from $^6J(CH_2, H_p)$, using eq. [2], can be substituted into eqs. [7] and [8] to yield $^4J(CH_2, H_o) =$

Can. J. Chem. Downloaded from www.nrcresearchpress.com by 80.58.250.72 on 09/07/12
For personal use only.

TABLE 2. α Proton coupling constants[a] and derived $\langle \sin^2 \theta \rangle_H$ and $\langle \sin^2 \theta \rangle_C$ values for phenylacetaldehyde in various solvents and for benzyl alkyl ketones

R	Solvent[b]	$^3J(CH_2, CHO)$	$^4J(CH_2, H_o)$	$^5J(CH_2, H_m)$	$^6J(CH_2, H_p)$	$\langle \sin^2 \theta \rangle_H$	$\langle \sin^2 \theta \rangle_C$
H	Acetone-d_6	2.164(1)	−0.564(1)	0.279(1)	−0.405(1)	0.338	0.825
H[c]	C_6D_6	2.357(1)					
			−0.564(1)	0.282(1)	−0.399(2)	0.333	0.835
H	CCl_4/C_6D_{12}	2.489(1)	−0.563(1)	0.280(1)	−0.409(1)	0.341	0.818
CH_3	C_6D_6	—	−0.559(2)	0.278(2)	−0.401(2)	0.334	0.832
CH_2CH_3	C_6D_6	—	−0.572(1)	0.276(1)	−0.409(1)	0.341	0.818
$CH(CH_3)_2$	C_6D_6	—	−0.572(2)	0.280(2)	−0.419(3)	0.349	0.802
$C(CH_3)_3$[d]	CCl_4/C_6D_{12}	—	−0.558(7)	—	−0.403(7)	0.336	0.828

[a]Coupling constants in Hz, standard deviations (from NUMARIT analysis) in the last decimal place are given in parentheses.
[b]All solutions are between 3 and 5 mol%.
[c]For a full analysis of phenylacetaldehyde in C_6D_6 see ref. 5.
[d]The 3,5-dichloro derivative was used.

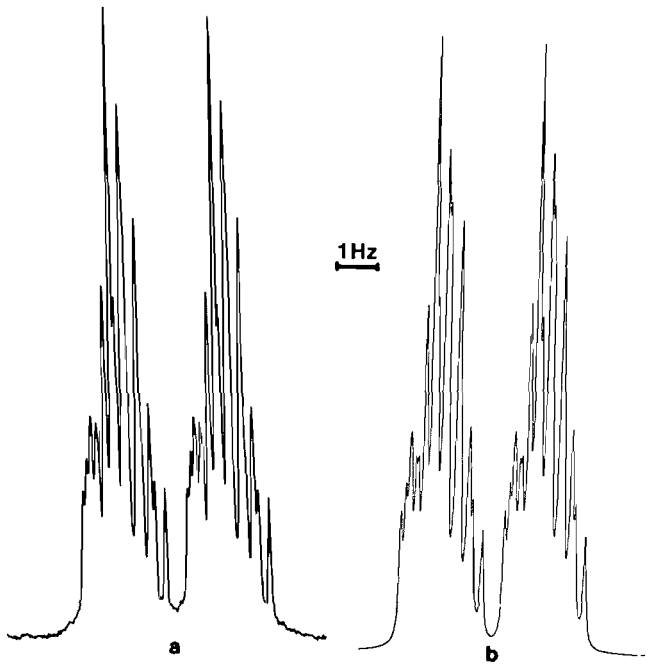

FIG. 2. The experimental (a) and computer simulated (b) spectrum of the α-protons of phenylacetaldehyde in C_6D_6 solutions. Note that the second-order nature of the spectrum does not allow simple measurement of the splittings due to long-range couplings.

-0.579 ± 0.006 Hz and $^5J(CH_2, H_m) = 0.278 \pm 0.002$ Hz. The measured values fall into the ranges $^4J(CH_2, H_o) = -0.566 \pm 0.008$ Hz and $^5J(CH_2, H_m) = 0.278 \pm 0.002$ Hz. The agreement is quite good considering the possible effects of the α carbonyl group on the coupling mechanisms involved.

Experimental

Compounds **2**, **3**, **4**, and **5** were commercially available. Compound **6** was made by reaction of the 3,5-dichlorobenzylmagnesium chloride Grignard with *tert*-butylcyanide (trimethylacetonitrile) followed by hydrolysis of the imine (9). Compound **6** was prepared with *meta* chlorine substituents to simplify the initial 90-MHz spectrum.

Samples (5.0 mol%) of the compounds together with a small amount of TMS were transferred to 5-mm od nmr tubes, were degassed by the freeze–pump–thaw method, and were flame-sealed under vacuum.

Spectra were recorded on a Bruker AM300 spectrometer at a probe temperature of 300 K. Typically 8–32 scans were acquired. Sweep-widths and data regions were adjusted to give acquisition times of approximately 30 s. The digital resolution was typically 0.03 Hz/point. After a small amount of Gaussian multiplication to improve resolution, the FID's were then transformed.

The benzyl portions of the spectra were analyzed as an AA'BB'CM_2R system for **2** and as AA'BB'CM_2 systems for **3**, **4**, **5**, and **6** using the program NUMARIT (10). Due to many small couplings to the alkyl group protons in compounds **3**, **4**, **5**, and **6**, transitions for the M_2 part of the spectra were not assigned. Linewidths of the ring proton peaks were usually less than 0.12 Hz. The experimental and simulated spectra of the M_2 part of the spectrum of phenylacetaldehyde in C_6D_6 solution are shown in Fig. 2.

Molecular orbital calculations on phenylacetaldehyde at the STO-3G level employed the program MONSTERGAUSS (11) and were run on an Amdahl 470 system. During the calculations the benzene ring nuclei were held coplanar and the ring carbons were constrained to a hexagonal geometry while allowing all ring C—C bond lengths to vary simultaneously. All other bond lengths and angles were allowed to vary independently while holding angles θ and φ constant to define a given conformation.

Acknowledgements

Part of this work was done during the tenure of an NSERC postgraduate scholarship and was also supported by grant A1296 to T. Schaefer.

1. G. J. KARABATOS and P. W. BUSHMAN. Tetrahedron, **31**, 1471 (1975).
2. W. J. E. PARR and T. SCHAEFER. Acc. Chem. Res. **13**, 400 (1980).
3. T. SCHAEFER, J. PEELING, and R. SEBASTIAN. Can. J. Chem. **63**, 3219 (1985).
4. T. SCHAEFER, R. SEBASTIAN, and G. H. PENNER. Can. J. Chem. **64**, 1372 (1980).
5. T. SCHAEFER, R. SEBASTIAN, and G. H. PENNER. Can. J. Chem. **63**, 2597 (1985).
6. M. BARFIELD, C. J. FALLICK, K. HATA, S. STERNHELL, and P. W. WESTERMAN. J. Am. Chem. Soc. **105**, 2178 (1983).
7. T. SCHAEFER and R. LAATIKAINEN. Can. J. Chem. **61**, 2785 (1983).
8. T. SCHAEFER, T. A. WILDMAN, and R. SEBASTIAN. Can. J. Chem. **60**, 1924 (1982).
9. E. HORN (*Editor*). Org. Synth. Coll. Volume **III**. J. Wiley & Sons, New York. 1955. p. 562.
10. A. R. QUIRT and J. S. MARTIN. J. Magn. Reson. **5**, 318 (1971); J. S. MARTIN, A. R. QUIRT, and K. E. WARNILL. The NMR program library. Daresbury Laboratory, Daresbury, U.K.
11. M. R. PETERSEN and R. A. POIRIER. MONSTERGAUSS, Department of Chemistry, University of Toronto, Toronto, Ontario. 1981.

Can. J. Chem. Downloaded from www.nrcresearchpress.com by 80.58.250.72 on 09/07/12
For personal use only.

Calculations of the energetics of silane–N_2O_2 exciplexes

THOMAS N. BELL
Department of Chemistry, Simon Fraser University, Burnaby, B.C., Canada V5A 1S6
AND
KATHRYN A. PERKINS AND PETER G. PERKINS
Department of Pure and Applied Chemistry, University of Strathclyde, Glasgow G1 1XL, Scotland

Received December 4, 1985[1]

THOMAS N. BELL, KATHRYN A. PERKINS, and PETER G. PERKINS. Can. J. Chem. **65**, 541 (1987).

Calculations have been made on the enthalpies of the singlet and triplet N_2O_2 species generated from $^2\pi NO + {}^4\pi NO$, and the exciplexes which result from reaction of N_2O_2 with some methyl fluorosilanes. Both the ground-state singlet and the first excited triplet of the latter systems have been studied and are discussed in relation to the mechanism for the decomposition of NO after initial excitation with $Hg(6^3P_1)$ atoms.

THOMAS N. BELL, KATHRYN A. PERKINS et PETER G. PERKINS. Can. J. Chem. **65**, 541 (1987).

On a effectué des calculs sur les enthalpies des espèces singulet et triplet du N_2O_2 qui sont générées par la réaction $^2\pi NO + {}^4\pi NO$ ainsi que sur les exciplex qui proviennent de la réaction du N_2O_2 avec quelques méthyl fluorosilanes. On a aussi étudié tant l'état singulet fondamental que le premier triplet excité de ces derniers systèmes et on en discute en relation avec le mécanisme de décomposition du NO après une excitation initiale avec des atomes de $Hg(6^3P_1)$.

[Traduit par la revue]

Can. J. Chem. Downloaded from www.nrcresearchpress.com by 80.58.250.72 on 09/07/12
For personal use only.

Introduction

The mercury-photosensitized decomposition of NO leading to N_2O, NO_2, N_2, and O_2 has been proposed (1) to occur through the intermediate N_2O_2 formed by:

$$NO^4\pi + NO \rightarrow N_2O_2 \rightarrow \text{products}$$

Silanes of general formula Me_xSiF_{4-x} enhance the rate of decomposition of NO. Mechanistic proposals involving the intial formation of the exciplexes Si—NO and Si—ON followed by further reaction of these species with NO have been advanced (2) in order to explain the observed enhancement, i.e.

$$\begin{aligned} \text{Sil} + NO^4\pi \rightarrow \text{Sil}\,NO^{\dagger} &\xrightarrow{NO} \text{Sil} + N_2 + O_2 \\ \searrow \text{Sil}\,NO^{\dagger\dagger} &\xrightarrow{NO} \text{Sil}(NO)_2 \\ &\xrightarrow{NO} \text{Sil} + N_2O + NO_2 \end{aligned}$$

This present work is concerned with a theoretical examination of the enthalpies and geometries of the species proposed in order to develop and further illuminate the mechanistic proposals for the NO decomposition.

Methods and results

The methodology relating to the theoretical calculations of the systems of this type has been described in a previous paper (3). The present work also combines the quantitative power of the MOBI method with the geometry-optimising qualities of the MNDO approach.

In the previous paper (3), calculations of a similar type dealing with the formation of the SiNO and SiON exciplexes from silane—$^4\pi$NO were discussed. In an experimental paper (2) detailing the effect of silanes on the decomposition of NO, it was suggested that these exciplexes react further with NO leading to products, though no opinion was advanced with regard to which exciplex leads to N_2 and O_2 and which to N_2O and NO_2. An examination of these experimentally based proposals is now possible as a result of our new calculations on the energetics of the various species proposed in the mechanism.

(a) N_2O_2

Since we are concerned with molecules and exciplexes formed between silanes and N_2O_2, it was first relevant to study the N_2O_2 molecule itself. Naively, one could envisage the mutual approach of two doublet NO molecules which, at bonding distances, would form an N—N single bond using the two odd electrons present in the whole system. One might expect that, on this basis, N_2O_2 would be very stable, since the single unpaired electron of each NO molecule (which is antibonding in NO) would be brought into a bonding situation. However, it appears that, experimentally, N_2O_2, although known, is not as stable as this naive picture would predict. The heat of dimerisation (4) of two NO molecules is only 8–12 kJ mol^{-1}. Hence, the simple bonding approach is unlikely to be a correct interpretation of the experimental facts. To complicate the matter, we in the present study are concerned with the interaction of a $^4\pi$NO molecule with a doublet ground-state NO molecule which would yield either a lower triplet N_2O_2 molecule (the lower energy state generated from the spin combination) or an excited quintet N_2O_2 molecule. Even the lower energy state, the triplet, of these combinations is an excited state of N_2O_2 lying above a singlet ground state which, clearly, the molecule can assume according to its (even) total number of electrons. We shall concern ourselves in this study only with the lowest singlet and the first excited triplet of N_2O_2.

We first made a calculation of the geometry of the singlet N_2O_2 molecule by optimising its energy using the MNDO method. The geometry obtained from this method was then passed into the MOBI program in order to determine the heat of formation of the N_2O_2 molecule. In order to do this, one needs a unit bond-energy parameter for the N—N bond. That for the N—O bond was taken from the previous paper (3). One can obtain the N—N bond parameter by calibrating from the hydrazine molecule. Thermodynamic data for the heat of formation of hydrazine are available (5) and a combination of this data plus a MOBI calculation of both hydrazine and ammonia yielded a bond parameter of 220.5 kJ mol^{-1} for N—N. We can now calculate the heat of reaction for the process

$$2NO \rightarrow N_2O_2$$

$$\Delta H^0_{298} = -8.4 \text{ kJ mol}^{-1}$$

[1]Revision received October 20, 1986.

Can. J. Chem. Downloaded from www.nrcresearchpress.com by 80.58.250.72 on 09/07/12
For personal use only.

This value is in excellent agreement with that contained in the review by Heicklen and Cohen (4). The geometry of the singlet N_2O_2 molecule shows an N—O bond length equal to 1.337 Å and an N—N bond length of 1.29 Å. The molecule is cisoid and the N—N—O bond angle is 90.7°. A calculation on the transoid molecule of similar geometry showed it to be much less stable. Since the NO and N_2O_2 molecules are small, *ab initio* calculations using an ST631G gaussian basis set were carried out. The calculated energy of *cis* N_2O_2 was −258.2682 hartree whilst that for two NO molecules, using the same basis set, is −258.3498 hartree (6). Hence the dimerisation is calculated by this method to be endothermic (214.2 kJ mol^{-1}). This has the opposite sign to that of the quoted experimental value (4) and we believe that *ab initio* methods at this SCF level of sophistication are not usefully applicable to estimating small heats of reaction as in the NO/N_2O_2 system (7).

Using the MNDO program, it is also possible to optimize the geometry of the triplet state of the N_2O_2. Similar treatment of this molecule resulted in an N—O bond length of 1.162 Å, an N—N bond length of 1.768 Å, and an N—N—O angle of 106.5°. In the triplet N_2O_2 system, it is clear that the double bond has been destroyed and the N—N bond is essentially a single bond.

Next, a calculation of the excited states of the N_2O_2 singlet molecule was carried out using a configuration–interaction routine which extends the MOBI program. These states were calculated using a geometry based on that of the ground-state singlet. A total of six bonding orbitals and six antibonding orbitals was included in the configuration interaction and both singlet-excited and triplet-excited states were calculated. The results showed that the optical excitation of the lowest singlet N_2O_2 molecule to the lowest triplet state required 1.83 eV (177.0 kJ mol^{-1}). Using this linking value, it is now possible to construct a cycle for the formation and decomposition of N_2O_2 in these two different spin states. Figure 1 shows such a cycle and, using this cycle, it is possible to cross-check the thermochemistry. Hence, if we enter all the figures calculated for N_2O_2 states into the cycle, leaving as unknown the stage in which singlet N_2O_2 decomposes into N_2 and O_2, we obtain, from the small inner cycle, the value for this stage (shown as A in Fig. 1) as −172.1 kJ mol^{-1} whereas if it is calculated from the large outer cycle, we obtain a figure of −202.7 kJ mol^{-1}. There is only 30 kJ difference between these and this difference almost certainly stems from the error in the calculation of the singlet–triplet optical excitation energy, given as 177.0 kJ mol^{-1} in the cycle. The cycle as a whole, however, is gratifyingly self-consistent. The heat of atomisation, to the relevant states of the atoms, of the triplet N_2O_2 molecule is 1251.0 kJ mol^{-1}.

(b) Silane N_2O_2 complexes

When one considers the complexes formed between the silane and N_2O_2, one sees immediately that two types of complex can be formed, i.e., between the silane and N_2O_2 and the silane and O_2N_2. Within these two types, there are singlet complexes and triplet complexes corresponding to the singlets and triplets of N_2O_2 itself. Whilst a large number of geometries in general could be suggested for the complexes it seems reasonable, bearing in mind that the N_2O_2 complex will be formed from the NO complex, that the geometries will be based on those of the simpler NO type. Hence, the geometries selected for the silane—N_2O_2 exciplexes were based on the minimised geometry of the silane—NO exciplex which has quasi trigonal bipyramidal site symmetry around silicon. The

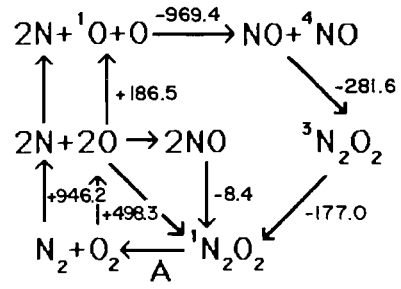

FIG. 1. Thermodynamic enthalpy cycle for $^1N_2O_2$ and $^3N_2O_2$ systems (kJ mol^{-1}).

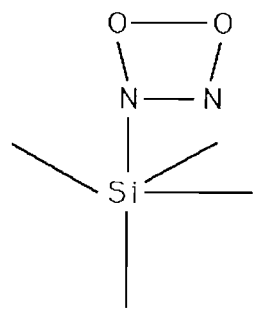

FIG. 2. Basic geometry of the Si—(N_2O_2) exciplex.

Si—NO or Si—ON axis is not exactly linear, of course, in the N_2O_2 complex, since the N—N—O angle is not 90° in either the singlet or the triplet form of N_2O_2.

The basic geometry is shown in Fig. 2. Table 1 contains heats of atomisation (to the relevant atomic states) from calculations on the singlet states of the silane—N_2O_2 species. The first three sets of data refer to the complex $SiF_4O_2N_2$ and it can be seen from the heats of atomisation that the result obtained by optimising (*i*) none of the geometrical data, (*ii*) that of the N_2O_2 moiety only, and (*iii*) all of the geometry to be optimised, affords heats of atomisation which differ only by 7.1 kJ between the extremes. Hence, in considering the rest of the singlets, only the geometry of the N_2O_2 moiety in the exciplex was optimised. The results for the heats of atomisation (to the relevant atomic states) of the triplet exciplexes are also recorded in Table 1 and in this case, there was no optimisation of any of the geometry. In the singlet complexes, the N—N link shows very strong π bond characteristics, whilst there is only an incipient O—O single bond in the complex. On this basis, we suggest that the products N_2 and O_2 stem from direct decomposition of the Si—O_2N_2 complex in the singlet state. We further suggest that N_2O and NO_2 arise from the Si—N_2O_2 complex, through reaction with a further NO molecule. These proposals are outlined in Fig. 3.

These suggestions require the decomposition of a singlet N_2O_2 complex and thus they involve the kinetics of relaxation from the triplet N_2O_2 complex or O_2N_2 complex to the singlet complexes. Hence, overall, from a mechanistic point of view, we envisage that quartet nitric oxide reacts with the silane to give the quartet silane – nitric oxide exciplex: this then interacts with a further doublet NO molecule to give the triplet N_2O_2 complex. This latter then relaxes to the singlet N_2O_2 complex which reacts to give products that depend on the orientation of N_2O_2 in the N_2O_2 exciplex. All the heats of

TABLE 1. $XSi—O_2N_2$ and $XSiN_2O_2$ systems*

	Singlets		ΔH_{atom}(kJ mol^{-1})	
X = F_4	$SiF_4O_2N_2$	no geometry optimisation	3710.0	
	$SiF_4O_2N_2$	all geometry optimised	3704.1	
	$SiF_4O_2N_2$	N_2O_2 moiety optimised	3702.8	6.2
	$SiF_4N_2O_2$	N_2O_2 moiety optimised	3696.6	
= F_3Me	$SiF_3MeO_2N_2$	N_2O_2 moiety optimised	4525.4	−1.3
	$SiF_3MeN_2O_2$	N_2O_2 moiety optimised	4526.7	
= F_2Me_2	$SiF_2Me_2O_2N_2$	N_2O_2 moiety optimised	5438.8	0.9
	$SiF_2Me_2N_2O_2$	N_2O_2 moiety optimised	5437.9	
	Triplets (no optimisation in any case)		ΔH_{atom}(kJ mol^{-1})	
X = F_4	$SiF_4O_2N_2$		3611.2	23.4
	$SiF_4N_2O_2$		3587.8	
= F_3Me	$SiF_3MeO_2N_2$		4451.8	33.9
	$SiF_3MeN_2O_2$		4417.9	
= F_2Me_2	$SiF_2Me_2O_2N_2$		5366.0	39.3
	$SiF_2Me_2N_2O_2$		5326.7	

*ΔH atomisation relates to the processes:

Singlet exciplex → Si + 4F + 2N + 2(O^3P)

Triplet exciplex → Si + 4F + 2N + O(^3P) + O(^1D).

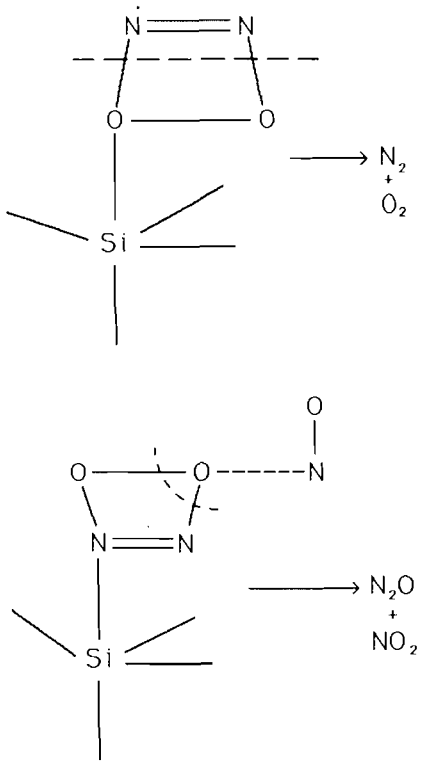

FIG. 3. Mechanistic proposals for product formation for the silane-catalysed decomposition of NO.

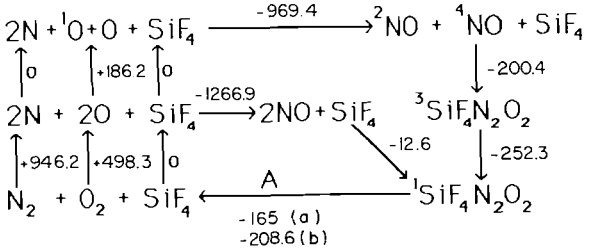

(a) Calcd. from inner cycle

(b) Calcd. from outer cycle.

All values in kJ

FIG. 4. Thermodynamic enthalpy cycle for the $Si—N_2O_2$ triplet and singlet exciplex system (kJ mol^{-1}).

atomisation calculated are shown in Table 1 and we can distill the following conclusions from that table: (*i*) There is little difference between the enthalpies of the members of a pair of singlet exciplexes derived from a particular silane, whether they be of the N_2O_2 or the O_2N_2 variety. (*ii*) For the triplet systems, the silane—O_2N_2 complex has a greater (21–38 kJ mol^{-1}, depending upon the particular silane) heat of atomisation than the corresponding triplet silane N_2O_2 isomer. Thermochemically, all species of general formula "silane—N_2O_2" for a particular silane shows that the triplet system lies some 96 kJ mol^{-1} lower in energy (i.e., less stable) than the singlet state. That is, the energy sequence is triplet silane–O_2N_2 < triplet silane–N_2O_2 < singlet silane–O_2N_2 = singlet silane–N_2O_2.

In order to construct a consistent thermochemical cycle, we also calculated the optical excitation energy of the singlet–triplet transition for each species. This was effected by using again the configuration-interaction program with six mutually interacting occupied orbitals and six antibonding orbitals. The values obtained are also shown in Table 2 and all are in the region of 2.5 eV (243 kJ). These can be correlated with the thermochemical difference in enthalpies using a cycle similar to that effective for the relationship between NO, $NO^4\pi$, and N_2O_2. This is shown in Fig. 4 and as before, we calculate the energy for stage A from an inner cycle and an outer cycle. The

Can. J. Chem. Downloaded from www.nrcresearchpress.com by 80.58.250.72 on 09/07/12
For personal use only.

TABLE 2. Excited state properties of $SiF_xMe_{4-x}N_2O_2$ or O_2N_2 complexes

System	ΔE (kJ) singlet → triplet	Orbitals* involved	Oscillator strength	Si coefficients (*d* orbitals)
$SiF_4N_2O_2$	252.3	2 ← 3	0.17	0.59; orb (3) small; orb (2)
O_2N_2	235.6	2 ← 3	0.16	No Si
$SiF_3MeN_2O_2$	250.6	1 ← 4	0.17	No Si
O_2N_2	243.9	1 ← 4	0.16	No Si
$SiF_2Me_2N_2O_2$	250.6	1 ← 6	0.17	No Si
O_2N_2	243.9	1 ← 6	0.16	No Si

*The left-hand number is the antibonding orbital and the right the bonding orbital chiefly involved in the transition. In all cases this was the dominant configuration.

difference between the two values in the exemplary case of SiF_4 is ca. 40 kJ mol^{-1} and, clearly, this difference stems mainly from error in the calculated singlet–triplet optical excitation energy of $SiF_4N_2O_2$. Actually, since the value obtained for stage A accumulates all the errors in the cycle together, then the agreement may be considered satisfactory.

Finally, we suggest that the species designated as silane—$(NO^{\dagger})$ in the experimental paper (2) corresponds to silane—(ON), whilst the species silane—$(NO^{\dagger\dagger})$ corresponds to silane—(NO).

1. O. P. STRAUSZ and H. E. GUNNING. Can. J. Chem. **39**, 2549 (1961).
2. T. N. BELL, G. SOTO-GARRIDO, and A. G. SHERWOOD. Can. J. Chem. **61**, 946 (1983).
3. T. N. BELL, K. A. PERKINS, and P. G. PERKINS. Can. J. Chem. **65**, 000 (1987).
4. J. HEICKLEN and N. COHEN. Advances in photochemistry. Vol. 5. Interscience, John Wiley, New York. 1968. p. 157.
5. J. Phys. Chem. Ref. Data, Vol. II, Supp. 2 (1982).
6. D. R. ARMSTRONG and G. D. WALKER. Private communication.
7. H. F. SCHAEFFER, III. The electronic structure of atoms and molecules. Addison Wesley. 1972. p. 273.

Can. J. Chem. Downloaded from www.nrcresearchpress.com by 80.58.250.72 on 09/07/12
For personal use only.

Calculations on the relative energies of complexes of silanes with $^2\pi$ and $^4\pi$NO

THOMAS N. BELL
Department of Chemistry, Simon Fraser University, Burnaby, B.C., Canada V5A 1S6
AND
KATHRYN A. PERKINS AND PETER G. PERKINS
Department of Pure and Applied Chemistry, University of Strathclyde, Glasgow G1 1XL, Scotland

Received December 4, 1985[1]

THOMAS N. BELL, KATHRYN A. PERKINS, and PETER G. PERKINS. Can. J. Chem. **65**, 545 (1987).

A theoretical study is presented of the relative enthalpies (calculated through heats of atomisation) of complexes of the silanes SiF_4, SiF_3Me, and SiF_2Me_2, with ground state $^2\pi$NO, and exciplexes with excited state $^4\pi$NO. The calculations favour an increasing relative stability of the complexes and exciplexes with silanes in the order $SiF_4 < F_3SiMe < F_2SiMe_2$ with, in each particular case, a geometry favouring the $\gtrless$SiON over the $\gtrless$SiNO arrangement.

THOMAS N. BELL, KATHRYN A. PERKINS et PETER G. PERKINS. Can. J. Chem. **65**, 545 (1987).

On rapporte une étude théorique sur les enthalpies relatives (calculées en faisant appel aux chaleurs d'atomisation) de complexes des silanes SiF_4, SiF_3Me et SiF_2Me_2 avec l'état fondamental du $^2\pi$NO et les exciplex de l'état excité $^4\pi$NO. Les calculs suggèrent que la stabilité relative des complexes et des exciplex avec les silanes augmente dans l'ordre $SiF_4 < F_3SiMe < F_2SiMe_2$: de plus, dans chacun des cas, la géométrie favoris $\gtrless$SiON par rapport à l'arrangement $\gtrless$SiNO.
[Traduit par la revue]

Can. J. Chem. Downloaded from www.nrcresearchpress.com by 80.58.250.72 on 09/07/12
For personal use only.

Introduction

Sensitisation of NO by $Hg(6^3P_1)$ atoms leads to $^4\pi$NO which provides a route to decomposition into the observed (1) products N_2, O_2, and N_2O. The decomposition quantum yields are markedly enhanced (2) by the methylfluorosilanes with the order of enhancement

$$Me_2SiF_2 > MeSiF_3 \gg SiF_4$$

The mechanism proposed (2) to explain the enhancement envisaged the formation of two different distinct and non-interchangeable exciplexes (designated $SiNO^\dagger$ and $SiNO^{\dagger\dagger}$) resulting from the reaction of silane with $^4\pi$NO. It was suggested that these two types of exciplex differed as a result of either the O or N of the NO bonding to the silane, i.e., Si—ON or Si—NO. No conclusion was made as to which exciplex led to N_2 and O_2 and which to N_2O because it was extremely difficult to evince direct evidence from the experiments as to the nature and structures of such complexes, since they are of essentially transient nature. However, such a study is well suited to investigation from a theoretical point of view and, hence, we have pursued this in order to determine if, based on enthalpy considerations, complexes of the type proposed would be stable relative to the separate molecules.

Methods, results and discussion

The molecular orbital – bond index method (MOBI) has been formulated and extensively used in studies of the reactions of hydrocarbons and of the thermodynamics of silane derivatives (3–7). The technique starts from a rotationally invariant quantity, the *bond index*. This latter is compounded from the relevant elements of the Coulson bond order – density matrix, in turn obtained from some quantum mechanical self consistent field molecular calculation on the system of interest. The bond index is given by

$$B_{AB} = \sum_{\sigma \epsilon A} \sum_{\lambda \epsilon B} P_{\lambda\sigma}^2$$

where the $P_{\mu\nu}$ are the Coulson density matrix elements.

Bond indices for simple molecules such as hydrocarbons follow a pattern which correlates with the chemist's concept of multiplicity of bonds; thus, for ethane, ethylene, and acetylene the C—C bond indices are, respectively, 1.023, 2.032, and 2.998. Following this trend we have suggested that such bond indices may be used, in conjunction with experimental standard-state heats of atomisation, to obtain a set of standard energy terms for a range of bonds. These terms we call the *bond energy parameters*. Thus the bond energy parameter for a bond X—Y is the intrinsic enthalpy associated with an X—Y of unit bond index. Since the bond index reflects minor variations in the intrinsic bond strength with the environment of the bond in question, the concept should be appropriate for the direct calculation of heats of formation for molecules.

A set of bond indices may be calculated for any system and can thus afford, in principle, the heat of formation for that system in the standard state. Thus, in the case of one or more species undergoing reaction, a grid of points on an energy surface can be set up, the heat of atomisation for the system computed for each, and the reaction followed along a coordinate and over a saddle. Even without following the whole reaction hypersurface it is possible to examine a limited part of such a surface by investigating directly the geometries of transition state complexes.

The calibration process uses experimental heats of atomisation of selected compounds in the standard state at 298 K. One then takes a weighted sum of the bond indices for each interaction in the molecule and sets this equal to the experimental standard state heat of atomisation for the system. The approach depends essentially on the assumption that the energies of separate bonds in molecules and radicals are additive.

Having calibrated the bond energy parameters in this way we can then transfer them to systems of unknown thermochemistry and in our case this means the transition-state complexes in the reactions between silanes and nitric oxide. In conclusion it can be said that the MOBI method is a fast, accurate, and computer-wise efficient way of obtaining thermodynamic information on systems built from first and second row atoms. The MOBI method is thus now well established (4–7) as a quantitative tool for the investigation of the bond energies and

[1]Revision received October 20, 1986.

Can. J. Chem. Downloaded from www.nrcresearchpress.com by 80.58.250.72 on 09/07/12
For personal use only.

heats of formation of systems. Moreover, the method has been shown to be valid even when bond lengths and angles are not "normal", e.g., when the former are stretched (6). The discussion of the present implementation of the method will be carried out under several headings.

(a) The silanes

The first step was to determine heats of atomisation of the three silanes SiF_4, SiF_3Me, and SiF_2Me_2. Since the intermediate species and complexes in the Si—NO reaction were to be geometry-optimised using the MNDO method (8) (which involves Fletcher–Powell minimisation) the geometries of the silane molecules were also minimised using the same program in order to give consistency between the results. The heats of formation produced from MNDO were then discarded and the new optimised coordinates produced by the MNDO minimisation were transferred to the MOBI program which, as forestated, calculates heat of atomisation for these molecules. The SCF technique which forms the basis of the MOBI method has been fully described elsewhere (9). For molecules such as NO and the complexes a Restricted Hartree–Fock treatment was applied. Bond energy parameters are already available for F—F (3) and for the moieties involving silicon and the methyl group (4). The Si—F parameter was obtained by calibration from SiF_4. The experimental standard-state heat of formation at 298 K for SiF_4 was taken from ref. 10. A list of the bond energy parameters used is given in Table 1. The derived values of ΔH^0_{atom} are in Table 2 and it can be seen that the heat of atomisation of SiF_4 differs from its experimental value of 2387.0 kJ mol^{-1} because of the use of the "MNDO" internal coordinates.

(b) The nitric oxide molecule

The experimental heat of formation (11) of NO is 90.4 kJ mol^{-1}, which yields ΔH^0_{atom} = 631.4 kJ mol^{-1}. The NO bond index is 2.017 in nitric oxide and, hence, the unit bonding parameter for N—O is 313.0 kJ mol^{-1}. In this calculation the experimental bond length for NO was taken. If the bond length in nitric oxide is minimised with respect to the bond energy using the MNDO method, however, the optimum bond length is 1.1232 Å. Use of this "MNDO" bond length with MOBI yields a heat of atomisation for the molecule of 633.5 kJ mol^{-1}. This does not differ significantly from the standard heat of atomisation which can be deduced from experiment.

(c) Nitric oxide in the excited quartet state, $^4\pi$NO

In the series of reactions under consideration, the nitric oxide is believed to react not in its doublet ground state, but in an excited quartet state. Certainly there appears to be no decomposition of nitric oxide unless the molecule is excited by the Hg(6^3P_1) atom. The NO molecule contains eleven electrons and in the ground state, ten electrons lie in the five lowest energy levels whilst the remaining electron is described by a linear combination of the degenerate 6th and 7th π levels. We can construct a zeroth approximation configuration for the quartet state by assuming that the first four levels are filled, whilst one electron lies in each of the 5th, 6th, and 7th levels. This yields the $^4\pi$ state. The MNDO program is capable of handling calculations on quartet nitric oxide and the minimisation calculation by MNDO yields a bond length of 1.2745 Å and, directly from this method a ΔH^0_f of 377.4 kJ mol^{-1}. We can also carry out the same calculation using MOBI since the basis method for the MOBI calculation also includes an algorithm which will deal with quartet states. In this calculation, it is possible to preselect a particular configuration before performing the SCF cycles in this program. This yields an SCF solution for a single configuration determinant. If, now, the "MNDO" quartet bond length obtained as above (1.2745 Å) is used in the MOBI program, we obtain ΔH^0_{atom} = 336.8 kJ mol^{-1}, i.e., ΔH^0_f = 384.9 kJ mol^{-1} for $^4\pi$NO. This is the value we shall adopt and it concurs very well with the value obtained directly from MNDO. This implies that the bond energy parameter derived from the doublet molecule is also appropriate to the quartet state. Later, we shall confirm that this is, indeed, the case. We therefore retain the bonding parameter appropriate to a ground-state NO distance of 1.123 Å, i.e., 313.0 kJ mol^{-1}, throughout all the calculations.

In comparing ΔH^0_f values calculated as above with spectroscopically derived data on nitric oxide, it is necessary to consider the calculated atomic states of the dissociative products. The data can then be analysed by constructing a thermocycle which correlates thermodynamic and spectroscopic data. Accordingly the MOBI calculations on $^4\pi$NO were next repeated using a series of bond lengths in which the separation of the N and O atoms was increased. Thus the electron distribution throughout the orbitals of the separated atoms was determined at large N—O separation distances and it was found that these distributions correspond to the states N(^4S) and O(^1D). The NO molecule exhibits numerous excited states (12) which can be designated as Σ, Π, and Δ. Some of the potential curves for these have been calculated by Gilmore (13) and only quartet spin states can arise from a combination of the N(^4S) and O(^1D) states of the atoms. Since the ground state of oxygen is ^3P the O atom excitation energy to ^1D must be taken into account in determining ΔH^0_f from the calculated cycle. This ΔH^0_f is then compared with that estimated from the value of

TABLE 1. Bond energy parameters (kJ mol^{-1})

Description	Bond	Energy
	C—C	334.8
	C—H	420.7
	Si—F	623.0
	Si—C	306.4
	Si—N	322.2
	Si—O	472.8
	N—N	220.5
	O—O	249.2
	N—O	313.0
Distant	Si—H	298.9
Distant	F—F	291.6
Distant	H—F	140.2
Distant	N—H	389.5
Distant	O—H	462.8
Distant	C—F	130.0
Distant	C—N	259.4
Distant	C—O	337.1
Distant	F—N	279.1

TABLE 2. ΔH^0_{atom} values for silanes

Molecule	ΔH^0_{atom}(kJ mol^{-1})
SiF_4	2417.1
SiF_3Me	3247.2
SiF_2Me_2	4163.1

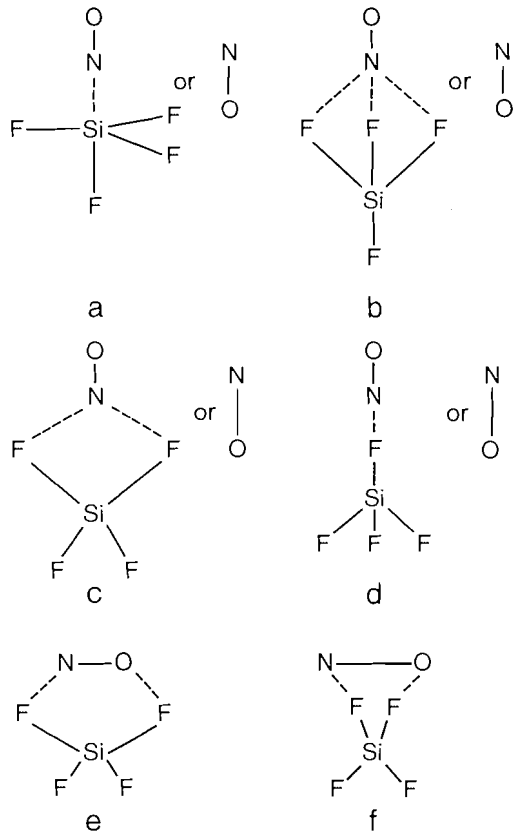

FIG. 1. Investigated geometries for Si—NO and Si—ON species.

ΔH_f^0 ($^2\pi$NO) and the spectroscopic excitation energy $^2\pi$NO → $^4\pi$NO. Thus

$$\begin{array}{ccc} N(^4S) + O(^1D) & \xrightarrow{d} & {}^4\pi NO \\ \uparrow & & \\ N(^4S) \quad O(^3P) & & \downarrow y \\ \uparrow \quad \uparrow & & \\ \tfrac{1}{2}N_2 + \tfrac{1}{2}O_2 & \xleftarrow{x} & {}^2\pi NO \end{array}$$

$$\Delta H_f^0(^4\pi NO) = a + b + c + d$$
$$= (1/2)D_{N_2} + (1/2)D_{O_2} + E_{(O^3P \rightarrow O^1D)} - D^4\pi NO$$

(Calculated) $473 \pm 4 + 249.4 + 188.7 - 336.8 = 574.3 \pm 4\,\text{kJ mol}^{-1}$

$$\Delta H_f^0(^4\pi NO) = -(x + y)$$
$$= \Delta H_f^0(^2\pi NO) + E(^2\pi NO \rightarrow {}^4\pi NO)$$

(Literature) $90.4 + 452 \pm 19 = 542.4 \pm 19\,\text{kJ mol}^{-1}$

The satisfactory agreement here confirms that the N—O bonding parameter derived for the $^2\pi$NO ground state is also appropriate for the quartet state of NO.

(d) The silane—NO doublet complexes

We first investigated the doublet complex formed by the interaction of a silane and $^2\pi$NO. It was first necessary to decide what basic geometry of approach of the NO to the silane moiety would be favoured and, having made a primary selection of the mode, then to investigate this in detail using minimisation techniques. The geometries shown in Fig. 1 were initially investigated by the MOBI method in order to decide which of them should be studied in detail. For brevity, the detailed results are not given here but we can state that five coordinate geometry around the silicon atom was favoured strongly over all other geometries and, indeed, it is intuitively reasonable that a five-coordinate geometry which is based closely on the trigonal bipyramidal symmetry around the silicon atom would be favoured. Although it is realised that a full global search using MNDO and calculation of a second derivative matrix is the most comprehensive and reliable route to a minimum, we believe that in practice our short cut to the favoured five-coordinate complex is acceptable. Many intermediates in reactions such as the hydrolysis of the silicon halides have a trigonal bipyramidal transition state, and this geometrical arrangement is invoked to explain many mechanistic processes.

TABLE 3. ΔH^0_{atom} values for the SiF_4NO complexes

Si—N (Å)	ΔH^0_{atom}(kJ mol^{-1})
5.0	3056.0
4.0	3060.6
3.7	3061.4
3.5	3061.9
2.8	3055.2
2.0	3035.5

We next investigated in detail the intermediates formulated as Si—NO by varying the Si—N distances over a range, whilst at each point optimising the remainder of the internal coordinates using the MNDO program. These optimised coordinates were then transferred to the MOBI program and the heat of atomisation calculated at each of the Si—N distances. We first studied SiF_4 and have selected (for brevity) the results for the complex SiF_4NO given in Table 3.

The figures in Table 3 show that the heat of atomisation of the SiF_4NO system leads to maximum enthalpy at Si—N = 3.5 Å. A similar series of calculations was carried out for (SiF_3Me)—NO and for (SiF_2Me_2)—NO where corresponding minima in the Si—N bond lengths occurred at 3.4 Å and 3.0 Å, respectively. Examination of the results for the above series of calculations showed that internal coordinates other than the Si—N bond length were little changed by the geometry optimisation. The optimised geometry shows that the silane moiety has a shape which is intermediate between a true trigonal bipyramid and a tetrahedron, e.g., in $^2SiF_4NO$ the bonds in the axial plane are 17.5° bent towards the NO group. Hence, in our further investigation of the complexes of type silane—ON, we did not minimise all the internal coordinates but performed calculations in which the Si—O bond lengths were taken as those for the corresponding Si—NO complexes.

From the heats of atomisation of the combined versus the non-combined systems, the enthalpy difference, $\Delta H^0_{comb} - \Delta H^0_{non\text{-}comb}$ was obtained. These results are given in Table 4, together with those for the —Si—ON systems. All show that the complexes were stable relative to the separated components, and the stabilisation enthalpies range between 10.5–18.8 kJ mol^{-1}, with Si—ON compounds showing greater stability than Si—NO compounds. The latter generalisation is weakest for the complexes of SiF_3Me and SiF_4 where the enthalpy differences are quite small.

In the ground state $^2\pi$NO the NO bond index is 2.017 (*vide supra*) and it diminishes to 2.00 in, say, the SiF_4NO complex. Thus little perturbation of this bond results from complexation of the doublet state to SiF_4.

Can. J. Chem. Downloaded from www.nrcresearchpress.com by 80.58.250.72 on 09/07/12
For personal use only.

TABLE 4. ΔH^0 values for silane complexes (kJ mol^{-1})

System	$\Sigma\Delta H^0_{atom}$ (separate components)	ΔH^0_{atom}(SiNO)	ΔH^0_{atom}(SiON)	Stabilisation enthalpy: Column 2 − column 1 Si—NO	Stabilisation enthalpy: Column 3 − column 1 Si—ON
SiF_4 + $^2\pi$NO	3050.6	3061.9	3062.7	11.3	12.1
SiF_3Me + $^2\pi$NO	3880.7	3890.7	3894.9	10.0	14.2
SiF_2Me_2 + $^2\pi$NO	4796.5	4807.8	4815.4	11.3	18.9
SiF_4 + $^4\pi$NO	2753.9	2751.4	2763.5	−2.5	9.6
SiF_3Me + $^4\pi$NO	3584.0	3582.8	3604.9	−1.2	20.9
SiF_2Me_2 + $^4\pi$NO	4499.9	4548.8	4588.2	48.9	88.3

(e) The silane—NO quartet exciplexes

The experimental work on silanes plus NO involves the $^4\pi$ state of NO and thus the silane—$^4\pi$NO exciplexes are of immediate interest. The mechanistic proposal (2) requires consideration of both exciplexes Si—NO and Si—ON. Hence, the SCF method mentioned previously, which allows quartet configurations to be selected and studied has also been used to investigate the nature, bonding, and energetics of the quartet exciplexes. These nitric oxide exciplexes with SiF_4, SiF_3Me, and SiF_2Me_2 were studied for a series of Si—N and Si—O bond lengths (i.e., both NO and ON exciplexes were studied) ranging from 1.7 to 2.5 Å. The heats of atomisation were calculated in each case using the unit bond energy parameter for NO, as described in the last section.

In order to consider the stability of the exciplexes with respect to the separated components, we must compare the heats of atomisation of these exciplexes with those of the parent silane and with the heat of atomisation of quartet NO to N(^4S) and O(^1D). The heat of formation for each exciplex as a function of Si—N or Si—O distance falls on a smooth curve and each curve can be extrapolated to a minimum point; hence, an Si—O or Si—N bond length corresponding to the maximum heat of atomisation of that exciplex can be found. The minima in the enthalpy curves for the complexes were, in all cases, found by quadratic fitting of the enthalpy versus Si—N or Si—O bond length and differentiation of the equation of the line given. All the Si—O, Si—N bond lengths thus determined fall below 3 Å. In all cases, quadratic fitting was very accurate, the points on the line being reproduced to ±0.4 kJ by the equation. All the data for the complexes calculated are given in Table 4. A measure of the complex and exciplex stability is given by the difference in the heats of atomisation, i.e., ΔH^0_{atom} (combined system) − ΔH^0_{atom} (separate components).

These results show that, in all cases, the Si—NO system is somewhat less stable than the Si—ON system. Somewhat surprisingly the ground state NO system shows that the complexes have some stability. With the exciplex system resulting from $^4\pi$NO, the Me_2SiF_2 system shows considerable stability with both configurations, that for Si—ON being more stable than Si—NO. It is interesting that only in this case is the calculated Si—O bond length (1.7 Å) near to that of a normal Si—O bond length and it is this feature which adds considerably to the stability of this particular complex. In all other cases both the Si—ON and Si—NO lengths are considerably greater than those for normal covalent bonds. With SiF_4 and $MeSiF_3$, the SiNO exciplex systems have a stability similar to the separated molecules, while the corresponding SiON systems show stabilities of 10 and 21 kJ, respectively. Promotion of NO to the excited quartet level diminishes the NO bond index and this is further lowered, e.g., in the SiF_2Me_2—ON complex, to 1.18. Excitation and complex formation therefore brings about a considerable weakening of the NO bond and produces an incipient tendency in that moiety to bonding with a second molecule of NO to give the N_2O_2 complex. This latter complex, as we will show, constitutes the next step in the decomposition of NO.

The calculations reported support the mechanistic proposal (2) that exciplexes of $^4\pi$NO with the methyfluorisilanes may indeed be formed and participate in providing a means for enhancement of the decomposition of NO. In this regard, the greatest enhancement is observed with Me_2SiF_2, i.e., the silane where exciplex formation is calculated to be most stable. Further work will examine the thermodynamics of the subsequent exciplexes which are proposed to account for the decomposition products.

1. O. P. STRAUSZ and H. E. GUNNING. Can. J. Chem. **39**, 2549 (1961).
2. T. N. BELL, G. SOTO-GARRIDO, and A. G. SHERWOOD. Can. J. Chem. **61**, 946 (1983).
3. T. N. BELL and P. G. PERKINS. J. Phys. Chem. **81**, 2012 (1977).
4. T. N. BELL, K. A. PERKINS, and P. G. PERKINS. J. Chem. Soc. Faraday Trans. 1, **77**, 1779 (1981).
5. T. N. BELL, K. A. PERKINS, and P. G. PERKINS. J. Phys. Chem. **86**, 3922 (1982).
6. T. N. BELL, K. A. PERKINS, and P. G. PERKINS. J. Phys. Chem. **81**, 2610 (1977).
7. T. N. BELL, A. F. KIERAN, K. A. PERKINS, and P. G. PERKINS. J. Phys. Chem. **88**, 1334 (1984).
8. M. J. S. DEWAR and W. THIEL. J. Am. Chem. Soc. **99**, 4899 (1977).
9. D. R. ARMSTRONG, P. G. PERKINS, and J. J. P. STEWART. J. Chem. Soc. A, 3654 (1971).
10. J. B. PEDLEY and B. S. ISEARD. CATCH tables for silicon compounds. University of Sussex, England. 1972.
11. J. Phys. Chem. Ref. Data, Vol. II, Supp. 2 (1982).
12. J. HEICKLEN and N. COHEN. Advances in photochemistry. Vol. 5. Interscience, John Wiley, New York. 1968. p. 157.
13. F. R. GILMORE. J. Quant. Spectrosc. Radiat. Transfer, **5**, 369 (1965).

Can. J. Chem. Downloaded from www.nrcresearchpress.com by 80.58.250.72 on 09/07/12
For personal use only.

Réduction électrochimique de dérivés carbonylés en milieu non aqueux en présence de $EuCl_3 \cdot 6H_2O$

JAMAÂ DOUCH ET GUY MOUSSET

Laboratoire d'électrochimie organique, Unité Associée Centre national de la recherche scientifique, 434 Université de Clermont II, 24, Avenue des Landais, BP 45, 63170 - Aubière, France

Reçu le 13 mai 1986

JAMAÂ DOUCH et GUY MOUSSET. Can. J. Chem. **65**, 549 (1987).

Dans ce travail, nous avons réalisé l'étude de la réduction électrochimique en milieu non aqueux (DMF) de cétones aromatiques ou α,β éthyléniques aromatiques en présence de $EuCl_3 \cdot 6H_2O$. Une étude préalable par infra-rouge et par voltammétrie cyclique a mis en évidence l'échange de ligands H_2O–DMF et la libération de trois ions Cl^-. Un examen détaillé des interactions entre le cation métallique et le dérivé carbonylé met en évidence la formation de complexes de type 1–1 ou 1–2 selon le site de complexation. La stéréochimie des produits d'hydro-dimérisation est en accord avec la formation à l'électrode d'un complexe de stoechiométrie 1 Eu(II) – 2 >C=O.

JAMAÂ DOUCH and GUY MOUSSET. Can. J. Chem. **65**, 549 (1987).

The electrochemical reduction of aromatic or α,β ethylenic aromatic ketones in nonaqueous solvent (DMF) has been performed in the presence of $EuCl_3 \cdot 6H_2O$. Ligand exchange between DMF and water molecules of the europium salt was first studied. A voltammetric study shows that complexation involving electrogenerated Eu(II) and ketone may occur at the electrode interface or in solution, leading respectively to 1 Eu(II) – 2 >C=O and 1 Eu(II) – 1 >C=O stoichiometries. The stereochemistry of hydrodimerization products is studied.

Le chrome(II) a été fréquemment utilisé en chimie organique comme agent réducteur, par exemple, dans le cas de dérivés nitrés, halogénés ou carbonylés (1, 2). Sa génération « *in situ* » par voie électrochimique en milieu non aqueux et son rôle dans les processus de réduction ont fait l'objet de quelques travaux (3–7). Le comportement électrochimique des cétones aromatiques simples ou substituées a été très étudié aussi bien en milieu aqueux (8–10) qu'en milieu organique (11–14). Leur réduction dans le diméthyl formamide (DMF) en présence de cations métalliques et la stéréosélectivité de la réaction d'hydrodimérisation ont été particulièrement développées récemment (15, 16) en relation avec la nature du cation présent dans le milieu, son caractère acide selon Lewis et son pouvoir complexant.

Les complexes de l'europium sont très utilisés en spectroscopie (17) ou en synthèse organique (18). Dans le cadre du travail que nous avions réalisé avec les sels de chrome et dans un but comparatif, nous avons consacré cet article à l'étude de la réduction électrochimique de dérivés carbonylés en présence d'europium(II) électrogénéré. Les sels d'europium hexahydratés (en particulier $EuCl_3 \cdot 6H_2O$) présentent deux étapes cathodiques séparées par un intervalle de potentiel beaucoup plus important que pour le chrome. Ce fait peut être avantageux pour l'étude de substrats difficilement réductibles (aryl alkyl cétones) si on désire s'affranchir de processus mettant en cause une réduction par un film de métal colloïdal déposé sur l'électrode (7) ou la formation d'amalgames avec le mercure (19) lorsque l'étape M(II)/M(0) est présente. Pour qu'une interaction entre l'europium(II) et la fonction carbonyle puisse être observée, il faut que la première étape de réduction de la cétone aromatique se situe entre les potentiels $E(A_1)$ de l'étape Eu(III)/Eu(II) et $E(A_2)$ de Eu(II)/Eu(0). Nous nous sommes volontairement limités, afin de comparer la nature et la stéréochimie des produits formés, à l'étude de la réduction des cétones **1–5** qui avaient fait l'objet de travaux antérieurs en présence de sels de chrome ou d'autres métaux.

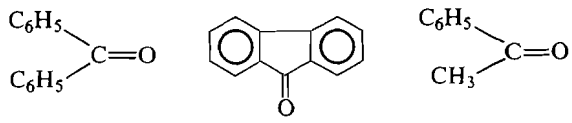

1 **2** **3**

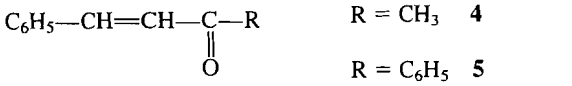

4 **5**

Résultats expérimentaux et discussion

1. Réduction de $EuCl_3 \cdot 6H_2O$

La réduction électrochimique de sels d'europium en milieu aqueux ou non aqueux a été décrite dans quelques travaux (20–23). Dans le DMF, les courbes intensité–potentiel de $EuCl_3 \cdot 6H_2O$ montrent la présence de deux étapes de réduction $E_{1/2}(A_1) = -0{,}250$ V et $E_{1/2}(A_2) = -1{,}530$ V (référence $Ag/AgI/I^-$ 0,1 *M* DMF) correspondant respectivement à des échanges de 1 et 2 électrons par molécule. En voltammétrie cyclique (fig. 1) on peut noter la présence de deux pics cathodiques (A_1 et A_2) et de deux pics anodiques (A_1') correspondant à la réoxydation de l'espèce formée en A_1 ($\Delta E_p = 95$ mV) et A_2' assez mal défini en relation avec les espèces formées en A_2. Il est généralement admis (24, 25) qu'un amalgame peut se former à la seconde étape de réduction selon :

[1] $Eu^{II} + Hg + 2e^- \rightarrow Eu\,(Hg)$

La différence de potentiel ($\Delta E_p \simeq 1$ Volt) existant entre A_2 et A_2' laisse penser que ce dernier traduit la réoxydation d'espèces formées par action de l'amalgame sur des impuretés du milieu plutôt que celle de l'amalgame lui-même. Nous nous sommes toujours efforcés d'éviter la formation de Eu(0) et nous n'avons pas cherché à élucider l'origine de A_2'.

La mise en solution dans un solvant donneur S, d'un sel hexahydraté, entraîne des échanges de ligands au niveau de la sphère interne de complexation se traduisant par l'équation

Printed in Canada / Imprimé au Canada

Can. J. Chem. Downloaded from www.nrcresearchpress.com by 80.58.250.72 on 09/07/12
For personal use only.

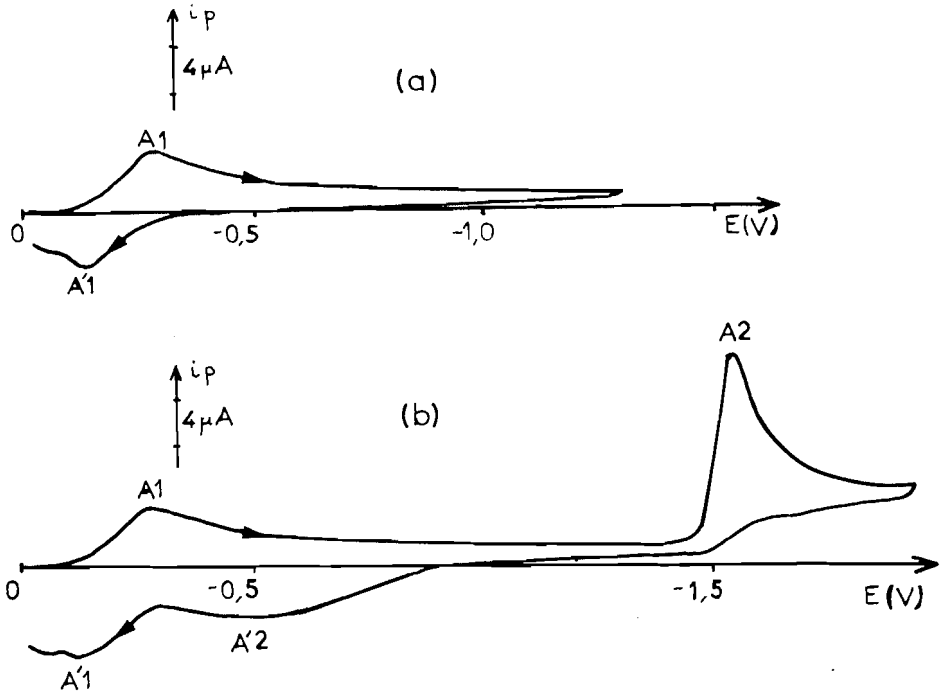

FIG. 1. Réduction voltammétrique du $EuCl_3 \cdot 6H_2O$ ($c = 2 \times 10^{-3} M$) sur électrode à goutte de mercure stationnaire $v = 0{,}1\ V\ s^{-1}$. (*a*) : Balayage 0–1,3 V. (*b*) : Balayage 0–2,0 V.

générale :

[2] $(M(H_2O)_{6-n}Cl_n)^{(3-n)^+} + mS \rightarrow (M(S)_m(H_2O)_{6-(m+n)}Cl_n)^{(3-n)^+} + mH_2O$

Afin de définir la nature du complexe final, nous avons réalisé une étude spectroscopique et voltammétrique sur $EuCl_3 \cdot 6H_2O$. La vibration dans l'infra-rouge de la liaison OH de l'eau « libre » dans le DMF fournit une bande d'absorption présentant un maximum situé à $3545\ cm^{-1}$ alors que les molécules complexées absorbent entre 3100 et $3200\ cm^{-1}$ (26). Le DMF, que nous avons utilisé, a une teneur en eau initiale de 0,15% (dosage par chromatographie en phase vapeur et par infrarouge). L'échange H_2O–DMF peut être traduit par l'équation

[3] $(Eu(H_2O)_{6-n}Cl_n)^{(3-n)^+} + (6 - n)\ DMF \rightarrow (Eu(DMF)_{6-n}Cl_n)^{(3-n)^+} + (6 - n)H_2O$

Une courbe d'étalonnage réalisée pour des solutions contenant des quantités d'eau connues permet de montrer que les six molécules d'eau de $EuCl_3 \cdot 6H_2O$ sont libérées dans le milieu lors de la mise en solution dans le DMF (fig. 2). Ceci implique que dans l'équation [3] nous ayons $n = 0$ donc que la mise en solution libère également de la sphère de complexation trois ions Cl^-.

L'oxydation de l'eau libérée par la réaction d'échange, ou contenue initialement dans le solvant, est repoussée vers des valeurs de potentiel plus anodiques en raison du phénomène de solvatation par le DMF. Il est alors possible comme dans le cas du chrome(III) (27) d'enregistrer la courbe d'oxydation des ions Cl^- libres (fig. 3) et d'en déduire la quantité présente en solution grâce à un étalonnage réalisé avec LiCl ($k_{d(DMF)} = 2{,}9 \times 10^{-2} M\,L^{-1}$) (28). La courbe voltammétrique fournie par $EuCl_3 \cdot 6H_2O$ a une morphologie tout à fait semblable à celles obtenues en absence d'ions Eu^{3+}, ce qui laisse penser que ces derniers ne perturbent pas le système. Elle permet effectivement de mettre en évidence la libération de trois ions Cl^-. L'ensemble de ces résultats nous semble apporter des arguments en faveur de l'équation d'échange :

[4] $Eu(H_2O)_6Cl_3 \xrightarrow{DMF} Eu(DMF)_6^{3+} + 6H_2O + 3Cl^-$

2. Réduction de cétones aromatiques en présence de $EuCl_3 \cdot 6H_2O$

(a) Modification du processus d'électroréduction

Lorsqu'on ajoute des quantités croissantes d'une cétone activée **1–5** à une solution de chlorure d'europium on constate : (*i*) que la présence de cétone ne modifie pratiquement pas la partie cathodique du premier pic de réduction (A_1) de l'europium(III) alors que sa partie anodique disparait progressivement. De plus, il apparait une nouvelle étape (B) irréversible située à un potentiel E(B) moins cathodique que celui du premier pic de réduction de la cétone en son radical anion (C_1) (fig. 4) (tableau 1); et (*ii*) que l'intensité de B croit avec la concentration en cétone et devient maximum pour un rapport de concentrations :

$$m = \frac{[\rangle C{=}O]}{[EuIII]} = 2$$

Jusqu'à l'équimolécularité ($m = 1$) les voltammogrammes ne présentent que deux pics (A_1 et B). Au-delà, ceux correspondant à la réduction de la cétone (C_1 et C_2) apparaissent. On peut constater également que la seconde étape (A_2) relative à la réduction de Eu(II) en Eu(0) disparait dès la première addition de cétone. Des additions successives de chlorure d'europium à une solution de cétone entraînent parallèlement à l'apparition de B, une diminution des pics de réduction C_1 et C_2 du dérivé carbonylé ainsi que des pics correspondant à la réoxydation du radical anion $\rangle C{=}O^{\cdot -}$ (C_1') ou de Eu(II) en Eu(III) (A_1'). Le potentiel du pic B est nettement moins cathodique que celui correspondant à la formation de l'europium métallique. L'ensemble des faits expérimentaux suggère l'hypothèse, déjà for-

Can. J. Chem. Downloaded from www.nrcresearchpress.com by 80.58.250.72 on 09/07/12
For personal use only.

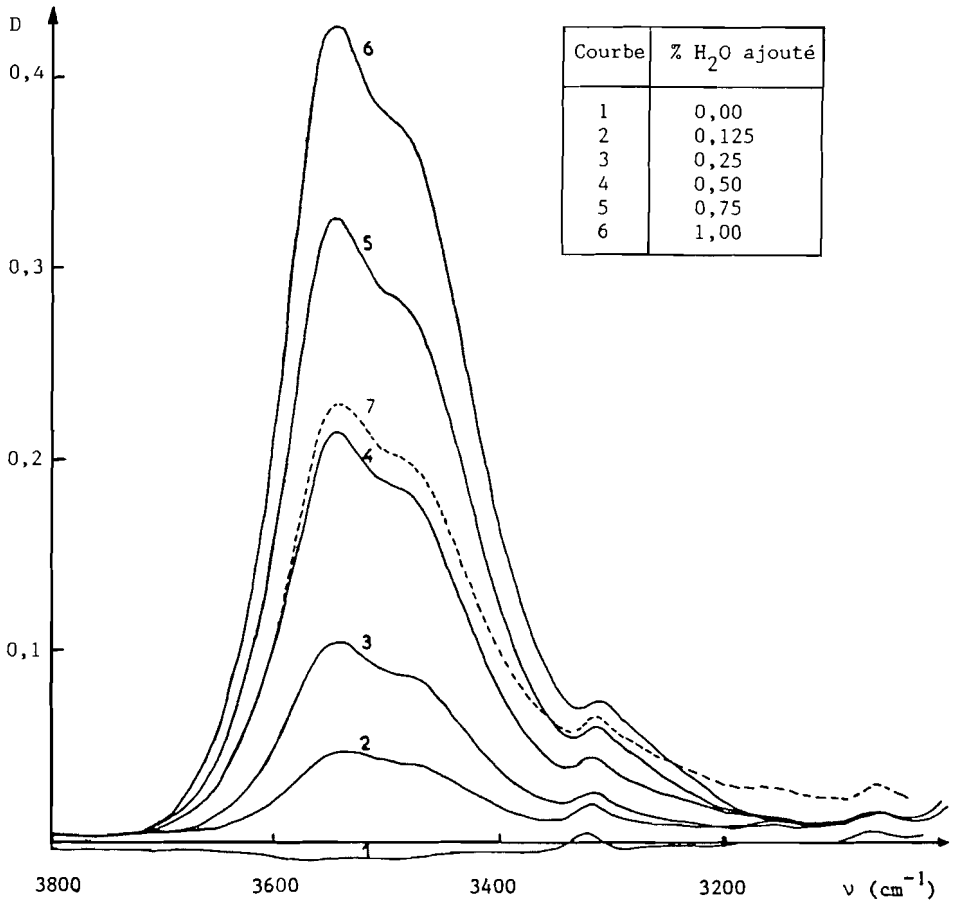

FIG. 2. Dosage de l'eau dans le DMF par spectroscopie infra-rouge. (—) (1) à (6) courbes d'étalonnage. (...) (7) DMF + $EuCl_3 \cdot 6H_2O$ ($5 \times 10^{-2} M$). Les expériences sont réalisées avec une cellule de compensation contenant du DMF.

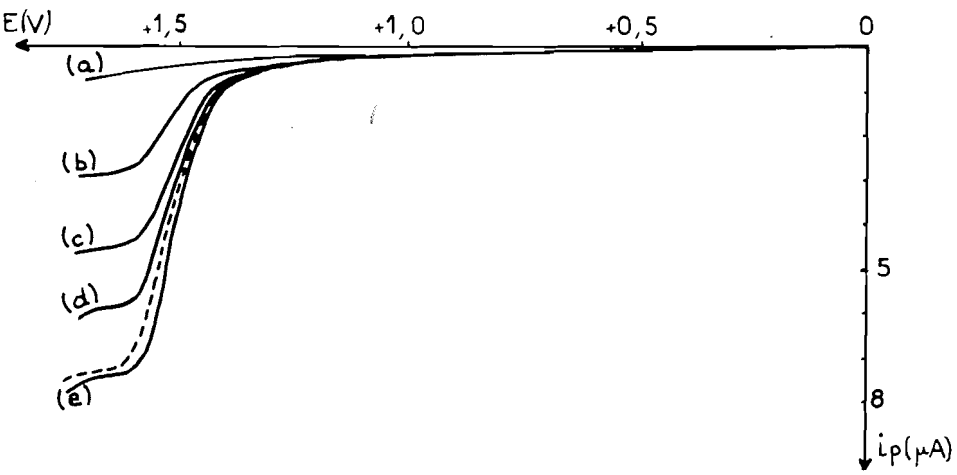

FIG. 3. Oxydation des ions Cl^- sur électrode de platine pour différentes concentrations en LiCl (—) (*a*) : 0; (*b*) : $2 \times 10^{-3} M$; (*c*) : $4 \times 10^{-3} M$; (*d*) : $6 \times 10^{-3} M$; (*e*) : $8 \times 10^{-3} M$. (---) : oxydation de $EuCl_3 \cdot 6H_2O$ $2 \times 10^{-3} M$. $v = 0{,}1\ V\ s^{-1}$. Electrolyte TBA BF_4 0,2 *M* (DMF). Electrode de référence Ag/AgI/I^- (0,1 *M* DMF).

mulée pour d'autres systèmes (4, 5), que l'espèce réduite en B résulte de l'association de molécules de cétone avec des ions divalents Eu(II).

En absence de sel métallique, des additions d'eau ou une modification de la nature de l'électrolyte support ne provoquent pas l'apparition de nouveaux pics de réduction du dérivé carbonylé. Un travail récent (29) fait état d'une possibilité de réduction indirecte de la benzophénone et du benzaldéhyde par l'ion ytterbium(II). Dans cet exemple le couple Yb^{3+}/Yb^{2+} se situe à un potentiel beaucoup plus cathodique que celui de Eu^{3+}/Eu^{2+}.

(b) Stoechiométrie du complexe et site de complexation

La figure 5 montre l'évolution de l'intensité du pic B pour une solution d'europium(III) à laquelle on ajoute des quantités croissantes de benzophénone. La proximité de la première

Can. J. Chem. Downloaded from www.nrcresearchpress.com by 80.58.250.72 on 09/07/12
For personal use only.

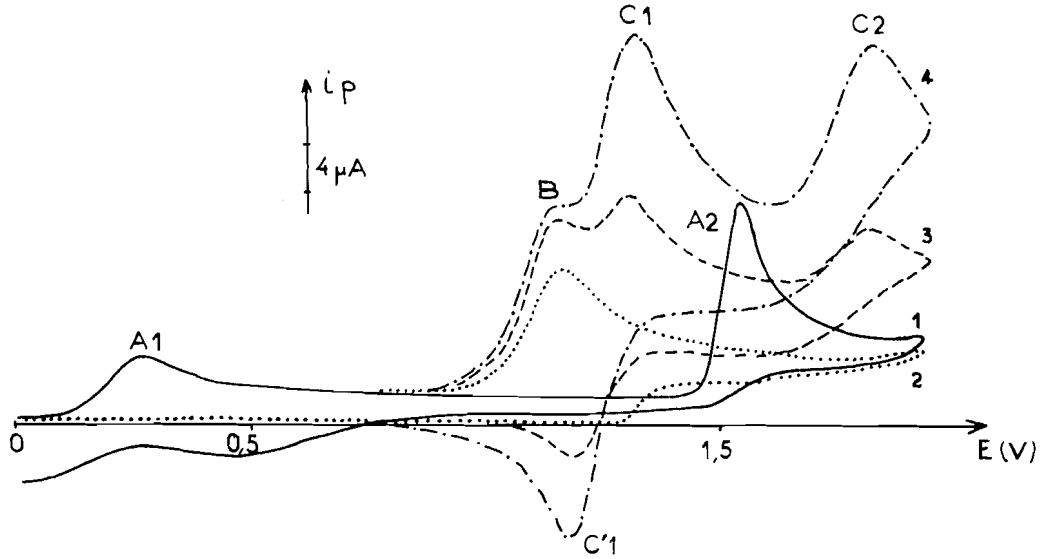

FIG. 4. Réduction de $EuCl_3 \cdot 6H_2O$ ($c = 2 \times 10^{-3} M$) en présence de benzophénone sur électrode à goutte stationnaire de mercure. (Benzophénone) : (1) $c = 0$; (2) $c = 2 \times 10^{-3} M$; (3) $c = 4 \times 10^{-3} M$; (4) $c = 7 \times 10^{-3} M$.

TABLEAU 1. Potentiels de réduction de cétones aromatiques en présence de $EuCl_3 \cdot 6H_2O$

Cétone ($4 \times 10^{-3} M$) + $EuCl_3 \cdot 6H_2O$	m	$E_p(B)$ (Volt)	$E_p(C_1)$ (Volt)	$\Delta E = E_p(C_1) - E_p(B)$ (Volt)
Benzophénone	2	−1,15	−1,25	0,10
	1	−1,15	−1,25	0,10
Fluorénone	2	−0,65	−0,77	0,12
	1	−0,65	−0,77	0,12
Acétophénone	2	−1,34	−1,52	0,18
	1	−1,34	−1,52	0,18
Benzalacétophénone	2	−0,80	−0,91	0,11
	1	−0,80	−0,91	0,11
Benzalacétone	2	−0,95	−1,15	0,20
	1	−0,95	−1,15	0,20

étape de réduction de la cétone rend délicate, en polarographie, la mesure de l'intensité de diffusion de la vague B, aussi avons nous choisi comme pour les sels de chrome (4) d'utiliser la voltammétrie cyclique qui permet de mesurer plus facilement le courant du pic (i_p). On peut constater une augmentation rapide de i_p jusqu'à ce que le rapport des concentrations m atteigne la valeur 2, contrairement à ce que l'on observe en présence d'ions Cr^{2+} où le maximum d'intensité est atteint pour $m = 1$. La stabilisation du courant de pic observée pour $m = 2$ laisse supposer la formation d'un complexe europium–cétone de stoechiométrie 1–2. Cependant l'intensité du pic B pour $m = 2$ n'est pas exactement le double de celle observée pour $m = 1$. De plus, la réapparition des pics de réduction de la cétone dès que m est supérieur à 1 indique que la formation du complexe 1–2 n'est pas complète pour ces concentrations. Pour expliquer ce phénomène nous envisageons l'hypothèse d'une destruction partielle du sel d'europium par hydrolyse en raison du milieu rendu fortement basique au voisinage de l'électrode par l'excés de radicaux anions, ce que nous pourrons vérifier lors des électrolyses préparatives. Nous avons de plus réalisé une étude des variations de i_p (B) en fonction de la concentration en mélange sel d'europium – cétone pour une même valeur de m (fig. 6). L'intensité du pic B augmente proportionnellement à la concentration en mélange lorsque celle-ci est faible puis tend vers une limite correspondant aux concentrations de $2 \times 10^{-3} M$ en $EuCl_3 \cdot 6H_2O$ et $2 \times 10^{-3} M$ en benzophénone si $m = 1$ et de $2 \times 10^{-3} M$ en $EuCl_3 \cdot 6H_2O$ et $4 \times 10^{-3} M$ en benzophénone si $m = 2$. Cette limitation peut être due à un phénomène d'adsorption des produits de réaction (pinacol ou pinacolate) (30) à la surface de la goutte de mercure.

Afin de déterminer si la complexation peut intervenir avec l'europium(II) en solution, nous avons réalisé une réduction partielle ($0{,}8\ F\ mol^{-1}$) du sel métallique au potentiel de −0,60 V préalablement à l'introduction de la cétone. L'évolution de la solution est suivie par voltammétrie sur électrode tournante de carbone vitreux. La benzophénone **1** est ajoutée dès l'arrêt de l'électrolyse et des voltammétries de contrôle sont réalisées à divers intervalles de temps sur la même solution. Pour un rapport de concentrations $m = 0{,}5$, on observe que le pic B défini précédemment et attribué à la réduction du complexe Eu(II) – cétone est accompagné d'une étape supplémentaire (B′) située à un potentiel moins cathodique que B (fig. 7). Pour une même concentration initiale en $EuCl_3 \cdot 6H_2O$ ($4 \times 10^{-3} M$) l'intensité de B′ comparée à celle de B est fonction de la concentration en benzophénone ajoutée. Ainsi, pour une faible valeur ($10^{-3} M$) c'est le pic B′ qui est prépondérant; par contre, si la concentration augmente, l'intensité de B′ diminue par rapport à celle de B. On peut constater également que pour des conditions données, l'intensité de B′ diminue en fonction du temps au profit de B qui finalement subsiste seul. L'intensité finale est alors égale à $i_p(B') + i_p(B)$ initiales. Il est connu que les sels d'europium peuvent donner des complexes de stoechiométrie 1–1 ou 1–2 (31, 32), ces derniers étant les plus stables. Lorsque la concentration en cétone est faible comparée à celle en europium, le complexe 1–1 est favorisé. Si la concentration en dérivé carbonylé est importante, c'est le complexe 1–2 qui devient prépondérant. La modification du pic B′ avec le temps traduit l'évolution du complexe 1–1.

Si la benzophénone et le sel d'europium sont introduits simultanément, le pic B′ n'est pas observé. Les coefficients de diffusion respectifs des deux espèces étant $D_{Eu^{3+}} = 4{,}05 \times$

Can. J. Chem. Downloaded from www.nrcresearchpress.com by 80.58.250.72 on 09/07/12
For personal use only.

Can. J. Chem. Downloaded from www.nrcresearchpress.com by 80.58.250.72 on 09/07/12
For personal use only.

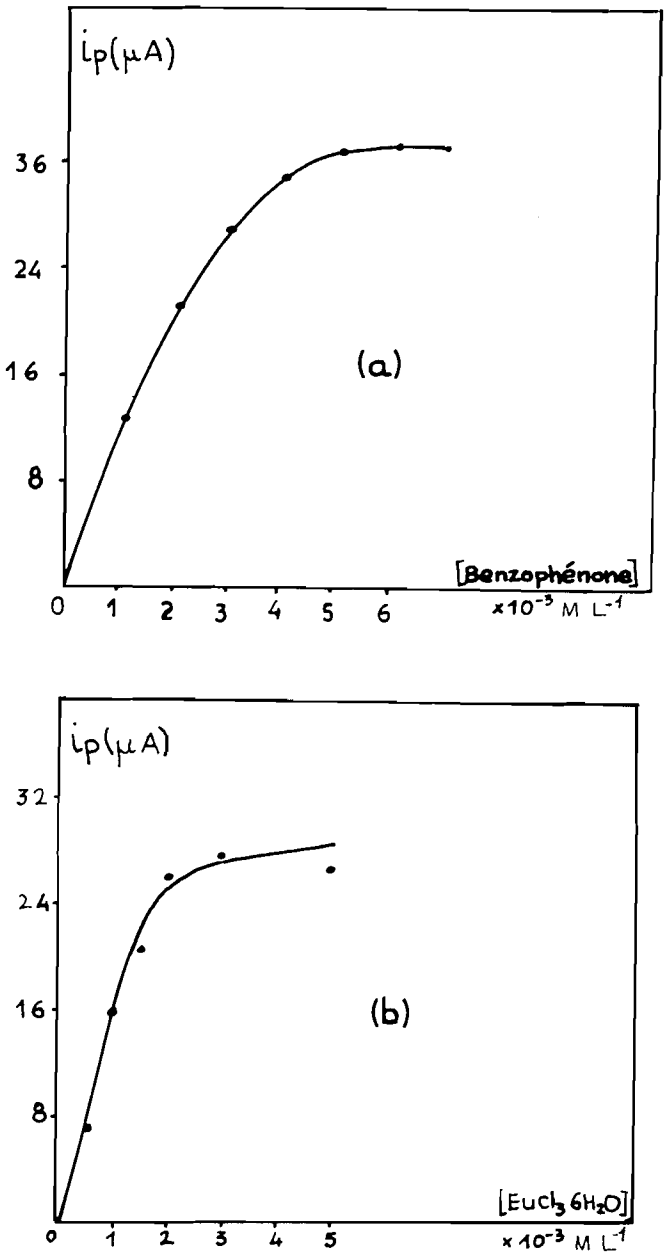

FIG. 5. Evolution de l'intensité du pic B en fonction des concentrations en $EuCl_3 \cdot 6H_2O$ ou en benzophénone. (a) $c = 2 \times 10^{-3} M$ en $EuCl_3 \cdot 6H_2O$; (b) $c = 4 \times 10^{-3} M$ en benzophénone.

$10^6 cm^2 s^{-1}$ et $D_{>C=O} = 8{,}1 \times 10^6 cm^2 s^{-1}$, on peut penser qu'à l'électrode les conditions de concentration respectives des deux espèces seront toujours plus favorables à la formation du complexe 1–2.

Après l'électrolyse partielle de l'europium(III) à −0,6 V, la comparaison des intensités de pic obtenues en voltammétrie

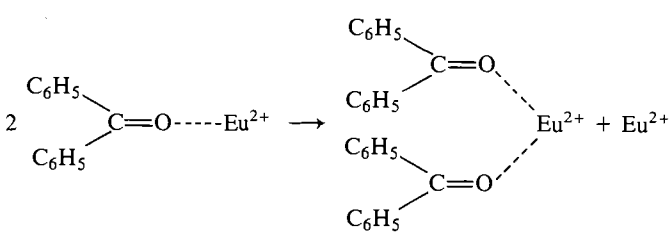

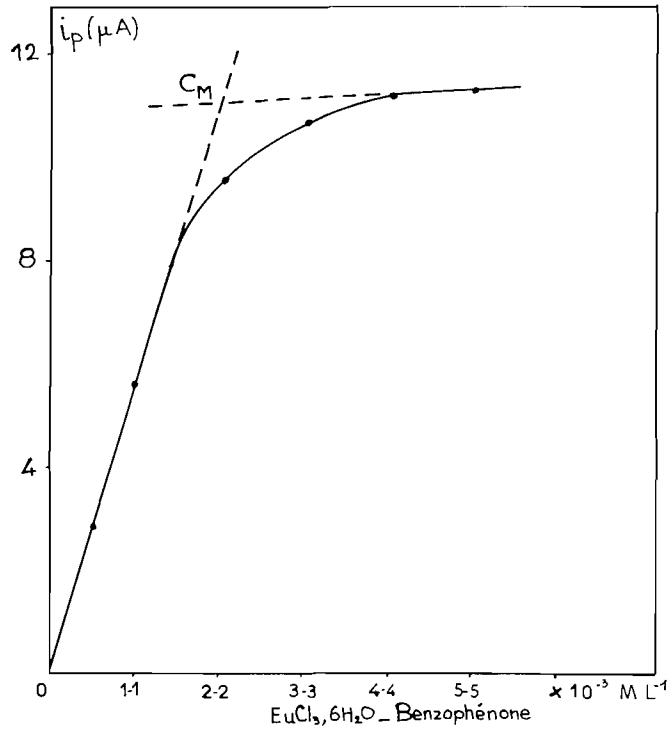

FIG. 6. Evolution de l'intensité du pic B en fonction de la concentration du mélange $EuCl_3 \cdot 6H_2O$–benzophénone pour $m = 1$.

cyclique sur goutte stationnaire de mercure donne la valeur de 3,5 pour le rapport

$$q = \frac{i_p(B') + i_p(B)}{i_p(A_1)}$$

lorsque la cétone est introduite seulement à l'arrêt de l'électrolyse. S'il y a introduction simultanée de la cétone et du sel d'europium dans la solution (sans electrolyse préalable) on obtient $q = 1{,}6$. Les mêmes expériences réalisées dans le cas de $CrCl_3 \cdot 6H_2O$ conduisent respectivement aux valeurs $q = 1{,}77$ et $q = 1{,}75$. Comme l'ont prouvé Sopher et Utley (5), ce résultat montre que l'intermédiaire clef dans le cas du chrome est Cr(III). Par contre, dans le cas de l'europium, le rapport des intensités obtenu après électrolyse préalable de Eu(III) indique que la complexation peut également intervenir avec Eu(II) en solution.

3. *Étude des produits de réduction*

Nous avons réalisé des macroélectrolyses au potentiel du pic B pour les cétones **1**, **2**, **3** et **5** afin de déterminer la nature et éventuellement la stéréochimie des produits formés. Nous distinguerons deux cas selon la valeur de m:

(i) Cas où m = *1*

Les cétones **1**, **2** et **3** donnent essentiellement les glycols par duplication. Pour l'acétophénone **3**, un seul diastéréoisomère est obtenu; il s'agit du diol racémique. Sa stéréochimie a été attribuée à partir de ses constantes physiques et de ses caractéristiques spectroscopiques (rmn ^1H des groupements méthyle) (33–35). Avec la benzalacétophénone **5**, la réduction ne fournit pas l'ε dicétone attendue mais un cétol. Là encore, la réaction est stéréospécifique et conduit au cétol chélaté *cis* (tableau 2). Sa stéréochimie a été définie par comparaison de ses constantes physiques et de sa courbe voltammétrique avec celle d'un échantillon authentique (13). La rmn ^{13}C montre un seul signal $>C=O$ à 204,9 ppm ($CDCl_3$).

Can. J. Chem. Downloaded from www.nrcresearchpress.com by 80.58.250.72 on 09/07/12
For personal use only.

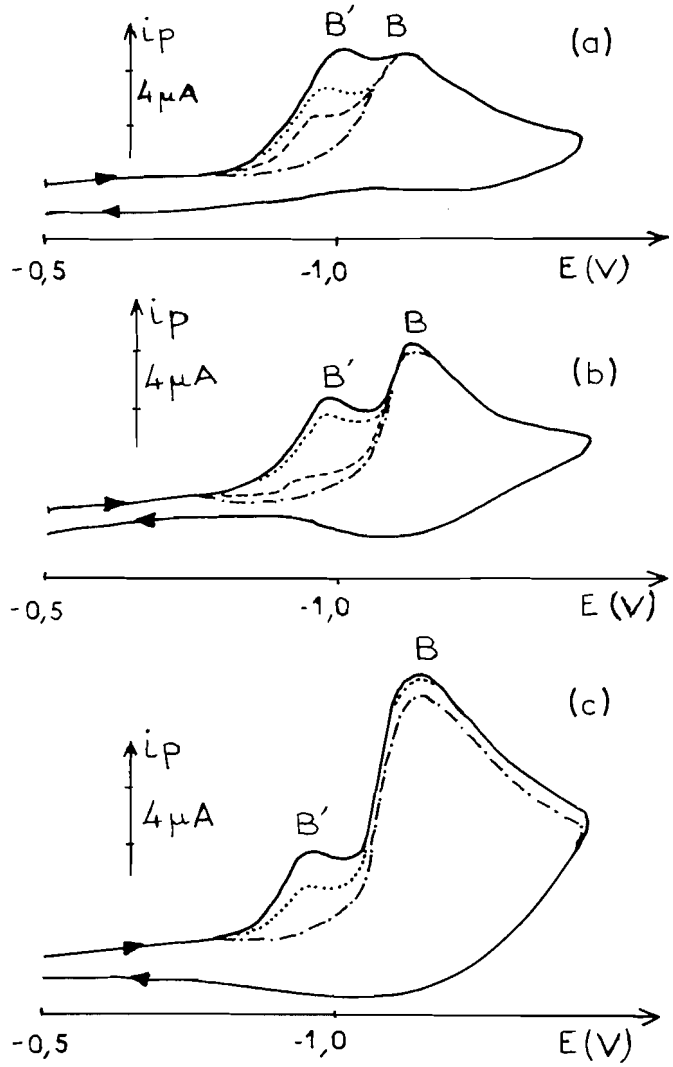

FIG. 7. Voltammogrammes obtenus après addition de benzophénone à une solution de $EuCl_3 \cdot 6H_2O$ ($c = 4 \times 10^{-3} M$) partiellement electrolysée au potentiel de $-0,6$ V, 0,8 F mol^{-1}, $v = 0,1$ V s^{-1}. Evolution en fonction du temps. (a) : (benzophénone) = $10^{-3} M$; (—) : t_0, (---) : t_0 + 60 min; (b) : (benzophénone) = $2 \times 10^{-3} M$; (—) : t_0, (---) : t_0 + 30 min; (c) : (benzophénone) = $4 \times 10^{-3} M$; (—) : t_0, (---) : t_0 + 20 min.

En présence de sel de chrome, la réduction de l'acétophénone est rendue délicate en raison de la proximité de l'étape Cr(II)/Cr(0). Nous avons réalisé une électrolyse au potentiel de $-1,04$ V (Ag/AgI/I$^-$ 0,1 *M* DMF). Elle nous a fourni les deux glycols diastéréoisomères dans un rapport *méso*-50%/*dl*-50% assez voisin de celui cité dans la littérature (16). Avec la benzalacétophénone, bien que le cétol *trans* s'isomérise dans $CDCl_3$ (15), deux pics sont obtenus en rmn ^{13}C à 204,9 et 205,8 ppm.

(ii) Cas où m = 2

Dans ces conditions, si des voltammétries de contrôle sont réalisées en cours d'électrolyse, on peut constater que l'intensité du pic de réduction A_1 de Eu(III) décroit rapidement pour ne plus représenter qu'environ 15% de la valeur initiale après consommation de 1 F mol^{-1}. Cette diminution qui peut correspondre à une réduction rapide de Eu(III) en Eu(II) (5, 15) est accompagnée d'une diminution importante du pic du complexe (40% de la valeur initiale) alors que les pics de réduction de la cétone libre ne sont pratiquement pas affectés. Dans le cas de la fluorénone, par exemple, une coloration rouge se développe également à la surface de l'électrode de travail. Parallèlement à ces modifications, on note l'apparition d'un précipité dans le milieu. Après filtration, celui-ci se révèle avoir les caractéristiques d'un produit minéral amorphe ne donnant pas de diffractogramme de rayons X. Les courbes thermogravimétriques mettent en évidence une première perte de masse dès 20°C suivie d'une seconde à 850°C. Nous n'avons pas fait de déterminations quantitatives en raison de difficultés rencontrées lors de la pesée initiale des échantillons (instabilité due vraisemblablement à une absorption d'eau ou de CO_2). Après chauffage à 850°C sous vide, le diffractogramme montre la présence de Eu_2O_3 sous ses deux formes cristallines (cubique : 3,13–2,71–2,56–2,31–2,20–2,13–1,92–1,80–1,76–1,70–1,63 Å; monoclinique : 3,18–3,04–2,98–2,89 Å). Le produit recueilli en cours d'électrolyse correspond certainement à la formation d'un hydroxy carbonate résultant de la fixation de gaz carbonique par l'hydroxyde d'europium (36). La première perte de masse est attribuée à un départ d'eau, la seconde à celui de CO_2. La forte coloration de la solution, dans le cas de la fluorénone, indique la formation du radical-anion ou du dianion. Ceci peut résulter soit de la présence à l'électrode de molécules de cétone non complexées (excés par rapport à Eu(II)), soit d'une réaction de rétropinacolisation rapide dans le cas où l'europium(II) est en défaut ($m = 2$). L'obtention des alcools (tableau 2) dans ces conditions serait en accord avec la seconde hypothèse.

La protonation, par les molécules d'eau, des formes réduites contribue à augmenter la basicité du milieu provoquant ainsi l'hydrolyse du sel d'europium :

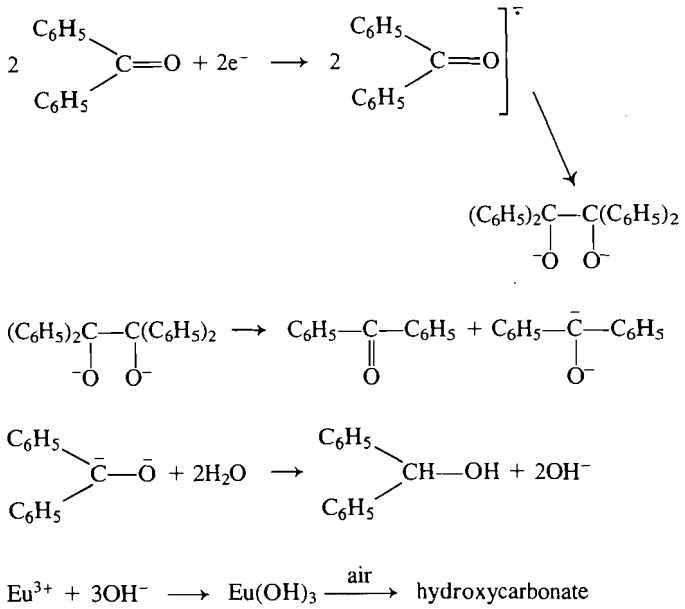

Ce phénomène peut expliquer le fait que l'intensité maximum de i_p (B) pour un rapport $m = 2$ ne soit jamais le double de celle obtenue pour $m = 1$ (fig. 4). Seules les électrolyses préparatives des composés **1** et **2** ont été réalisées dans ces conditions. Elles fournissent beaucoup de cétone de départ non réduite et une faible quantité d'alcool résultant de la réaction de rétropinacolisation.

L'étude stéréochimique de la duplication de l'acétophénone a déjà donné lieu à des travaux (37, 38) mettant en évidence l'influence de la nature de l'électrolyte et des paires d'ions susceptibles de se former. En présence de sels d'europium, il parait établi que le complexe formé possède une stoechiomé-

TABLEAU 2. Electroréduction de cétones aromatiques en présence de $EuCl_3 \cdot 6H_2O$ ou de $CrCl_3 \cdot 6H_2O$. Stéréochimie des produits de dimérisation

Cétones	*m*	Potentiel imposé Ag/AgI/I⁻ (V)	Nombre de F mol⁻¹	Produit d'électrolyse	Rendement (%)	Stéréochimie en présence de sel d'europium	Produits d'électrolyse en présence de sel de chrome	(réf.)
Benzophénone	1	−1,17	2	Alcool Diol	3 83	— —	Alcool 10% Diol 70%	(5)
Benzophénone	2	−1,20	1	Alcool	15	—	—	
Fluorénone	1	−0,67	1,5	Diol	94	—	Diol 38% Alcool 48%	(7)
Fluorénone	2	−0,75	1	Alcool	14	—	—	
Acétophénone	1	−1,40	1,8	Diol	97	*dl* 100%	Diol 20% (*dl* 10%, *méso* 10%) Cétone 80%	(*)
Benzalacétophénone	1	−0,80	1,6	Cétol	94	*cis* 100%	Cétone saturée 4% Dicétone 20% Cétols 59% (*trans* 45%, *cis* 14%)	(15)

*Résultats personnels.

trie préférentielle correspondant à 1 Eu(II) – 2 cétones. Si on admet comme Bewick et Brown (37) que la configuration privilégiée est celle où l'encombrement stérique entre les noyaux aromatiques est minimum :

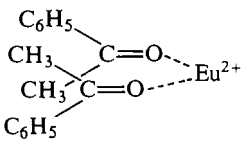

La dimérisation conduit dans ces conditions au diastéréoisomère racémique (*dl*). En présence de chrome, le complexe de stoechiométrie 1–1 peut présenter les deux configurations

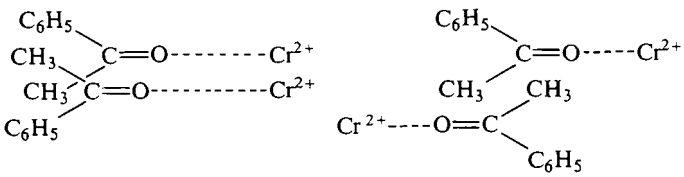

qui conduisent après duplication au mélange *méso* + racémique.

Une électrolyse au potentiel du pic B de la benzalacétophénone **5** (E_p = −0,80 V) avec m = 1 conduit à la formation d'un seul produit. La comparaison de sa température de fusion, de son spectre ir et de son voltammogramme avec les résultats obtenus pour des échantillons authentiques (13) montre qu'il s'agit du cétol *cis*. La même réaction effectuée en présence de sel de chrome conduit aux isomères *cis* et *trans* (15). À l'issue du transfert electronique intervenant au potentiel du pic B, l'addition nucléophile d'un carbanion sur l'une des fonctions carbonyles conduit au cétol *cis*.

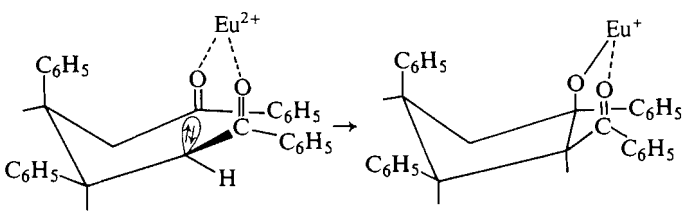

En présence de sel de chrome, les deux structures **A** et **B** sont possibles et conduisent aux isomères *cis* et *trans*.

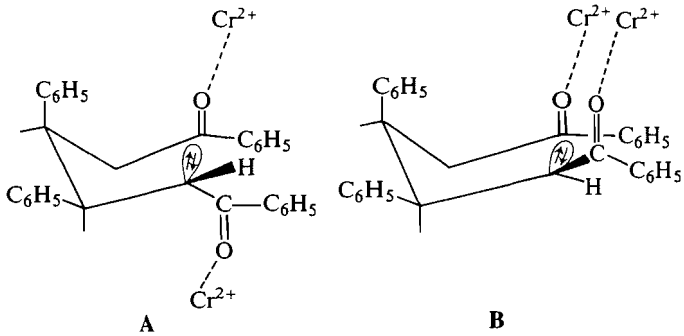

Une étude semblable effectuée sur la benzalacétone **4** ne nous a pas donné de résultats exploitables. Les électrolyses préparatives permettent d'isoler des produits présentant des fonctions alcool et carbonyle sans qu'il soit possible de les purifier. Il est connu (39) que dans ce cas les cétols sont instables et sujets à une réaction d'ouverture avec régénération de la dicétone.

Partie expérimentale

1. Techniques électrochimiques

Le dimethylformamide (DMF) est distillé sous pression réduite après avoir été séché sur carbonate de sodium. L'électrolyte indifférent est le perchlorate de tétrabutylammonium à la concentration de 0,1 *M*. Les tensions sont indiquées par rapport à l'électrode de référence Ag/AgI/I⁻ (Bu_4NI 0,1 *M* dans le DMF). L'électrode de travail est une goutte de mercure stationnaire. Toutes les mesures ont été réalisées à la température ambiante après désaération par un courant d'azote.

L'étude voltammétrique a été faite avec un ensemble Tacussel comprenant un potentiostat type PRT 20-2X équipé d'un générateur de signaux triangulaires et d'un amplificateur différentiel type ADTP.

Les déterminations coulométriques ont été réalisées dans une cellule contenant une nappe de mercure agitée pendant toute la durée de l'électrolyse. L'installation comprend un potentiostat PRT 100 et un intégrateur Tacussel IG5 N.

2. Electrolyses préparatives. Caractéristiques des produits

Les électrolyses préparatives ont été effectuées dans une cellule à trois compartiments. L'électrode auxiliaire est constituée dans ce cas

Can. J. Chem. Downloaded from www.nrcresearchpress.com by 80.58.250.72 on 09/07/12
For personal use only.

d'une plaque de graphite. Après électrolyse, le catholyte est repris par l'eau et les produits extraits à l'éther. Ces derniers sont identifiés par comparaison de leur point de fusion et de leurs caractéristiques spectroscopiques avec les données de la littérature : benzopinacol (F = 182–184°C); benzhydrol (F = 69–70°C); fluoropinacol (F = 186–187°C); fluorénol (F = 154–155°C); diphényl-2,3 butane diol-2,3 (*dl*) (F = 126°C); triphényl-1,3,4 benzoyl-2 hydroxy-1 cyclopentane *cis* (F = 196°C), *trans* (F = 210°C).

Les diffractogrammes ont été réalisés à l'aide d'un appareil Siemens composé d'un goniomètre de type 501 et d'un générateur de rayons X Kristalloplex 710. La radiation K_α du cuivre (λ = 1,5405 Å) a été utilisée. L'analyse thermogravimétrique a été faite avec une thermobalance Ugine Eyraud type 60 B commandée par un appareil de régulation et de programmation de la température RT 64. Les spectres infra-rouge ont été enregistrés sur un appareil Perkin Elmer série 18 avec des cellules en fluorure de calcium pour le dosage de l'eau.

Remerciements

Les auteurs remercient le CNRS (U.A. 434) pour son aide financière grâce à laquelle la réalisation de ce travail a été possible.

1. R. Hanson. Synthesis, 1 (1974).
2. T. J. Ho et G. A. Olah. Synthesis, 808 (1976); 815 (1976).
3. P. Pouillen, M. Perrin et P. Martinet. C.R. Seances Acad. Sci. Sér. C, **284**, 955 (1977).
4. M. Perrin, P. Pouillen, G. Mousset et P. Martinet. Tetrahedron, **36**, 221 (1980).
5. D. W. Sopher et J. H. P. Utley. J. Chem. Soc. Perkin Trans. 2, 1361 (1984).
6. F. Fournier, J. Berthelot et Y. L. Pascal. C.R. Acad. Sci. Sér. II, **294**, 849 (1982).
7. F. Fournier, J. Berthelot et Y. L. Pascal. Tetrahedron, **40**, 339 (1984).
8. E. Laviron. Collect. Czech. Chem. Commun. **30**, 4219 (1965).
9. P. Martinet et J. Simonet. Bull. Soc. Chim. Fr. 3533 (1967).
10. P. Zuman, O. Exner, R. F. Bekker et W. T. Navta. Collect. Czech. Chem. Commun. **33**, 3123 (1968).
11. M. Baizer. Organic electrochemistry: an introduction and a guide. Dekker, New York. 1973. p. 347 et références citées.
12. L. Nadjo et J. M. Saveant. J. Electroanal. Chem. **30**, 41 (1971).
13. J. Simonet et A. Albisson. Bull. Soc. Chim. Fr. 1125 (1971).
14. C. P. Andrieux et J. M. Saveant. Bull. Soc. Chim. Fr. 2090 (1973).
15. F. Fournier, J. Berthelot et J. J. Basselier. Tetrahedron, **41**, 5667 (1985).
16. F. Fournier et M. Fournier. Can. J. Chem. **64**, 881 (1986).
17. A. F. Cockerill, G. L. O. Davies, R. C. Harden et D. M. Rackman. Chem. Rev. **73**, 553 (1973).
18. H. Schumann. Angew. Chem. Int. Ed. Engl. **23**, 474 (1984).
19. E. N. Wise et E. J. Cockal. Anal. Chem. **32**, 1417 (1960).
20. O. Ikeda, K. Tsuura et H. Tamura. Bull. Chem. Soc. Jpn. **54**, 661 (1981).
21. F. Sanz, E. Valles et J. Virgili. An. Quim. Ser. A, **79**, 33 (1983).
22. T. Rabockai et I. Jordan. Anal. Lett. **7**, 647 (1974).
23. A. Albalat, E. Valles, F. Sanz et J. Virgili. Electrochim. Acta, **30**, 653 (1985).
24. M. Kohlthof et J. F. Coetzee. J. Am. Chem. Soc. **79**, 1852 (1957).
25. A. Leveque et R. Rosset. Bull. Soc. Chim. Fr. **11**, 4205 (1971).
26. A. B. F. Duncan, F. A. Matsen, W. Gordy, C. Sandorfy, R. N. Jones et W. West. Chemical application of spectroscopy. Interscience, New York. 1956.
27. M. Perrin et P. Martinet. C.R. Seances Acad. Sci. Sér. C, **285**, 511 (1977).
28. J. E. Prue et P. H. Sheringson. Trans. Faraday Soc. **57**, 1795 (1961).
29. Yu P. Skobochina et Z. N. Timofeeva. Sov. Electrochem. (Engl. Transl.), **16**, 1208 (1980).
30. E. Laviron. Bull. Soc. Chim. Fr. **4**, 1637 (1970).
31. O. M. Parkash, S. K. Bhasin et D. S. Jain. J. Less-Common Met. **60**, 179 (1978).
32. M. Shivare et M. Singh. Ind. J. Chem. Sect. A, **23**, 458 (1984).
33. J. H. Stocker, D. H. Kern et R. M. Jenevein. J. Org. Chem. **33**, 412 (1968).
34. J. H. Stocker et R. M. Jenevein. J. Org. Chem. **33**, 2145 (1968).
35. J. H. Stocker et R. M. Jenevein. J. Org. Chem. **34**, 2807 (1969).
36. R. C. Vickery. Nature, **164**, 787 (1949).
37. A. Bewick et D. J. Brown. J. Chem. Soc. Perkin Trans. 2, 99 (1977).
38. A. Bewick et H. P. Cleghorn. J. Chem. Soc. Perkin Trans. 2, 1410 (1973).
39. J. Kossanyi. Bull. Soc. Chim. Fr. **3**, 722 (1965).

Can. J. Chem. Downloaded from www.nrcresearchpress.com by 80.58.250.72 on 09/07/12
For personal use only.

Determination of polyacrylamides by maximum suppression

BYRON R. WENTZELL, TRUIS SMITH-PALMER,[1] AND JOHN C. DONINI
Chemistry Department, St. Francis Xavier University, Antigonish, N.S., Canada B2G 1C0

Received January 31, 1986[2]

BYRON R. WENTZELL, TRUIS SMITH-PALMER, and JOHN C. DONINI. Can. J. Chem. **65**, 557 (1987).

The use of polarographic maximum suppression methods for determining polyacrylamides and polyacrylic acid-based polymers was investigated. Using the oxygen, Co^{2+}, and Hg^{2+} maxima these polymers were determined at the low ppm level. The effectiveness of polymers as maximum suppressors was dependent on the charge of the polymer and that of the electrode at the potential at which the polarographic wave occurred. The maximum suppression of various binary mixtures of polyacrylamides indicated that in some mixtures suppression was additive while in other mixtures, particularly those containing both anionic and cationic polymers, the suppression was greatly reduced. Aqueous extracts of chosen coals contained various interfering substances which could be removed most efficiently using Sephadex G-75, although this resin was only compatible with anionic and neutral polymers.

BYRON R. WENTZELL, TRUIS SMITH-PALMER et JOHN C. DONINI. Can. J. Chem. **65**, 557 (1987).

On a étudié la possibilité d'utiliser les méthodes de suppression polarographiques maximales pour déterminer les polyacrylamides ainsi que les polymères dérivés de l'acide polyacrylique. En utilisant les maxima de l'oxygène, du Co^{2+} et du Hg^{2+}, on a déterminé ces polymères à des niveaux de ppm. L'efficacité des polymères comme suppresseurs maximaux dépend de la charge du polymère ainsi que de celle de l'électrode au potentiel de laquelle la vague polarographique se produit. La suppression maximale de divers mélanges binaires de polyacrylamides indique que, dans quelques mélanges, la suppression est additive; toutefois, dans d'autres mélanges et particulièrement dans ceux contenant à la fois des polymères anioniques et des polymères cationiques, la suppression est fortement réduite. Les extraits aqueux de charbons choisis contiennent diverses substances qui interfèrent et qui peuvent être éliminées efficacement en utilisant du Sephadex G-75; toutefois, cette résine n'est compatible qu'avec les polymères anioniques ou neutres.

[Traduit par la revue]

Introduction

Polyacrylamides and polyacrylic acid-based polymers (pam) have many industrial applications. A variety of these polymers with cationic or anionic functional groups is commercially available in a wide range of molecular weights. One of their uses is as a flocculating agent in coal-washing operations. In these operations modern practice dictates the recycling of the wash water after sedimentation of suspended solids. Thus the residual concentration of flocculating agent should be known before additional polymer is added to the recycled water. Since these polymers are generally used at the ppm level, methods for their determination must have a low detection limit. Unfortunately there are only a few analytical methods available to determine these polymers at such low levels.

Many of the methods described in the literature are based on chemical reactions of the amide group and are not applicable to polyacrylic acid and its esters. Most of these methods are also time consuming, often involving lengthy hydrolysis steps. Scoggins and Miller (1) developed a method involving the oxidation of amide groups to a product which oxidized I^- to I_2. The I_2 was then determined spectrophotometrically as the starch–triiodide complex. Hendrickson and Neuman (2) converted the amide groups of polyacrylamide to amine groups via the Hofmann rearrangement, and then determined the polyamine fluorometrically after derivatizing with *o*-phthalaldehyde. Crummet and Hummel (3) hydrolyzed polyacrylamide in hot acid, and then distilled off the ammonia under alkaline conditions for determination with Nessler's reagent. Similarly, Hawn and Talley (4) derivatized ammonia released by alkaline hydrolysis of polyacrylamide and quantified the derivative by gas chromatography.

Several turbidimetric methods have also been described. In a method developed by Michaels and Morelos (5), and improved by Crummett and Hummell (3), benzethonium chloride, a cationic detergent, is mixed with partially hydrolyzed polyacrylamide to form a colloidally suspended complex which is determined turbidimetrically. In addition to the hydrolysis step, an ion exchange step to remove interferences and an evaporation step to concentrate dilute samples are necessary (3). Attia and Rubio (6) measured the turbidity produced when tannic acid is added to solutions of neutral and cationic polyacrylamides. While this method is relatively simple, it cannot determine strongly anionic polymers.

Electrochemical methods which measure effects due to adsorption of molecules at an electrode surface offer simple, rapid means of determining the concentration of many surface-active substances. Methods based on the measurement of changes in capacitance currents by phase-sensitive ac polarography (7) and the Kalousek commutator technique (8) have been described. Measurement of peaks due to adsorption–desorption of surfactants in ac polarography (9) and in differential pulse polarography (10) has also been used to determine surfactant concentrations. Another electrochemical method which has been used involves measuring the suppression of polarographic maxima by surfactants. In conventional dc polarography some polarographic waves are distorted by large peaks which can be many times greater than the actual diffusion current. These "maxima" are caused by convective streaming (11) and are suppressed by the addition of surface active substances such as polyacrylamide. Methods based on the suppression of the polarographic maxima of oxygen (12), Co^{2+} (13) and Hg^{2+} (14) have been described. In this paper, we describe our investigation into the use of polarographic maximum suppression as a means of determining polyacrylamides and related polymers, with particular attention being paid to determining these polymers in coal washings.

Experimental

The polyacrylamides used are listed in Table 1. They were provided by the Coal Research Lab., Energy, Mines and Resources, Edmonton, Alberta. Praestol 2810/73 is a simple polyacrylamide while in Praes-

[1]To whom all correspondence should be addressed.
[2]Revision received October 23, 1986.

Can. J. Chem. Downloaded from www.nrcresearchpress.com by 80.58.250.72 on 09/07/12
For personal use only.

TABLE 1. Polymers used in this study

Polymer	Charge	Charge density	Molecular weight
Praestol 2810/73	Non-ionic	—	$(0.5–1) \times 10^7$
Polyacrylamide	Non-ionic	—	—
Praestol 2900/73	Anionic	25%	$(0.5–1) \times 10^7$
Praestol 2830/72	Anionic	12.5%	—
Praestol 444k	Cationic	100%	$<5 \times 10^6$
Praestol 411k	Cationic	25%	—

tol 2900/73 approximately 25% of the amide groups of the polyacrylamide structure have been hydrolyzed to carboxyl groups, i.e., it has a charge density of 25%. Praestol 444k is a cationic polymer prepared from acrylic acid esterified with a cationic alcohol: $HOCH_2CH_2N^+R_3Cl^-$. Stock solutions of 200 ppm of these polymers were prepared in 10 megohm-cm resistivity water which was used throughout. Humic acid was purchased from Aldrich Chemical Company Inc. Polarograms were obtained using a Princeton Applied Research Model 174A Polarographic Analyzer and a Model 303 SDME. The analog output of the polarograph was digitized using an Apple IIe microcomputer with Interactive Microware software (Lab Data Manager, Scientific Plotter) and hardware (ADALAB Interface Card, ADA-AMP Instrumentation Amplifier). All potentials reported are relative to a silver – silver chloride reference electrode.

The polarograph was operated in the current-sampled dc mode with a scan rate of 2 mV/s and a drop time of 2 s. Oxygen maxima were measured in 10 m*M* KCl. Samples were bubbled with medical grade air for 4 min prior to analysis. Co^{2+} maxima were measured in solutions containing 10 m*M* KCl plus 1 m*M* Co^{2+} and samples were bubbled with N_2 for 4 min prior to analysis to remove dissolved O_2. Hg^{2+} maxima were measured in unpurged solutions containing 1 m*M* Hg^{2+} plus 0.25 *M* KCl.

Four different raw coal samples were used. Three of these, Quinsam, CRL-82-11, and Alb-X, were weathered Albertan bituminous samples. The fourth, Lingan, was a weathered Cape Breton coal. Samples were ground using a Brinkman Centrifugal Grinding Mill ZM-1 using a 0.08 mm screen size. Over 80% of the coal in these samples passed through a 200 mesh sieve. Coal extracts were prepared by shaking ground coal suspensions (10% w/v) on a wrist action shaker overnight and filtering through a sintered glass filter.

Size exclusion chromatography was performed using Sephadex G-75 gel (Pharmacia Ltd.). this gel provides an effective fractionation range for globular proteins of 5 000 to 40 000 Daltons. A 0.9 cm × 30 cm column was used and unless otherwise specified the eluent was water. A head pressure of 75 cm of water produced a flow rate of approximately 0.5 mL/min. Samples of 2.5 mL volume were chromatographed and 5.0 mL fractions were collected. Polyacrylamides (MW 5×10^6) were eluted in the void volume (fraction 2).

Amberlite XAD-2 nonionic polymeric adsorbent was cleaned by soxlet extractions with methanol. The washed and dried resin was wetted with methanol and resuspended in dilute HCl pH 2.4. Columns were packed in Pasteur pipettes and were approximately 9 cm × 0.5 cm. Samples were adjusted to pH 2.4 and 8.0 mL aliquots were chromatographed. The column was then rinsed with 2.0 mL dilute HCl.

Cation exchange chromatography was performed using Rexyn 101 strong acid cation exchanger (Fisher Scientific Company). The resin was cleaned by an 8 h soxlet extraction in methanol, followed by resuspension in 1 *N* HCl and rinsing with water. Columns were packed in Pasteur pipettes and were approximately 9 cm × 0.5 cm. Eight (8.0) mL samples were chromatographed and the columns then rinsed with 2.0 mL water. The columns were reused after regeneration with 1 *N* HCl.

Anion exchange chromatography was performed using Rexyn 201 strong anion exchange resin (Fisher Scientific Company). The resin was washed with methanol and 1 *M* KCl. Columns were packed in Pasteur pipettes. Eight (8.0 mL) samples were chromatographed and the columns then rinsed with 2.0 mL of water. The columns were regenerated by washing with 1 *M* KCl.

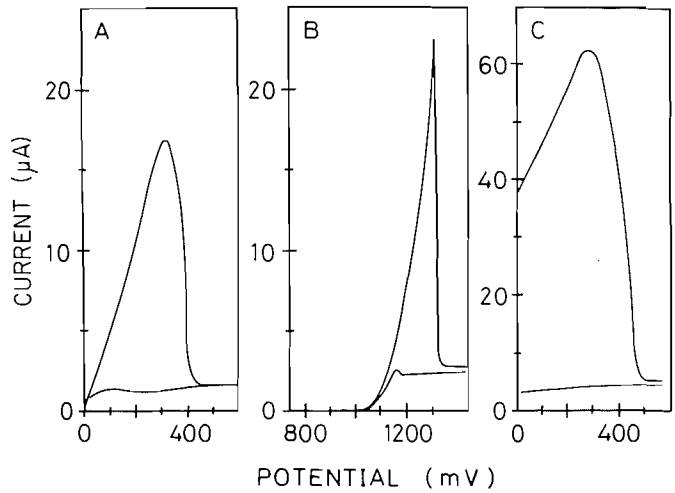

FIG. 1. Unsuppressed and suppressed polarographic waves for O_2 (*A*), Co^{2+} (*B*), and Hg^{2+} (*C*). The suppressed waves were recorded in the presence of 100 ppm polyacrylamide.

Flocculation experiments were carried out using cleaned Quinsam coal and a Kaolin powder (J. T. Baker Chemical Co.). Slurries were prepared to give a final coal concentration of 3% (w/v) and a final clay concentration of 2% (w/v) in 100 mL graduated cylinders. These slurries also contained 2 m*M* $CaCl_2$, 2 m*M* Na_2SO_4, and 2 m*M* $NaHCO_3$. Following the addition of polyacrylamides, the cylinder contents were mixed by inverting four times and the settling times then determined.

Results and discussion

In Fig. 1 are shown the unsuppressed and the suppressed polarographic waves for O_2, Co^{2+}, and Hg^{2+}. The O_2 and Co^{2+} maxima are observed only in relatively dilute salt solutions and are suppressed by increasing salt concentrations. To determine surfactants in solutions of higher or undetermined salt concentrations it would be necessary to isolate the surfactants first. By contrast the Hg^{2+} maximum is pronounced in solutions of much higher salt concentration (14). Calibration plots for the suppression of the oxygen maximum by the three Praestol polymers are shown in Fig. 2. The plots are not linear but have the general shape of adsorption isotherms, reflecting the fact that maximum suppression is due to adsorption of suppressor onto the surface of the mercury drop. This is in contrast to the standard curves reported by Dunsch *et al.* (15) which are fitted as two-piece linear graphs. The three polymers are not equally effective in suppressing the O_2 maximum. The effectiveness of a maximum suppressor depends on the strength of its adsorption onto the mercury surface and this can be influenced by such factors as polymer solubility and charge. As seen in Fig. 2, Praestol 444k is less effective than the other two polymers in suppressing the O_2 maximum. This is probably due to electrostatic repulsion of the cationic polymer from the electrode surface since the electrode is positively charged at the potential of O_2 reduction (16), or it could be due to the greater solubility of this highly charged polymer. The minimum concentrations which can be determined are approximately 2 ppm for Praestol 2810/73 and Praestol 2900/73 and 4 ppm for Praestol 444k.

Figure 3 shows the calibration plots for the suppression of the Co^{2+} maximum by the three polymers. The anionic Praestol 2900/73 is much less effective than the other two polymers.

Can. J. Chem. Downloaded from www.nrcresearchpress.com by 80.58.250.72 on 09/07/12
For personal use only.

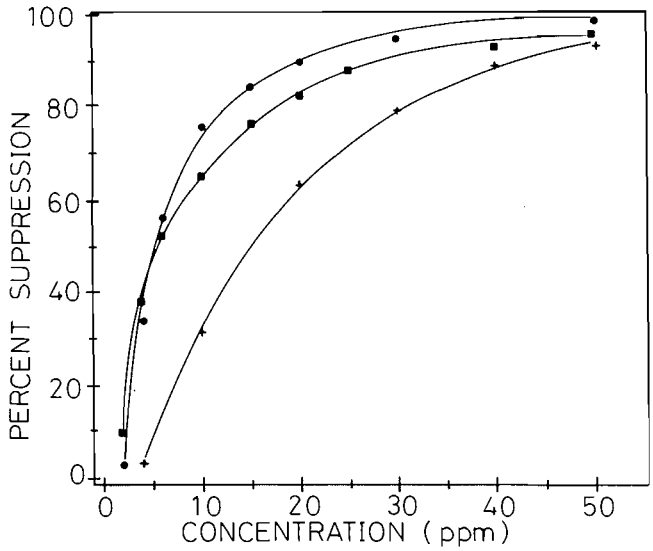

FIG. 2. Calibration curves for suppression of the O_2 maximum by Praestol 2810/73 (●), Praestol 2900/73 (■), and Praestol 444k (+).

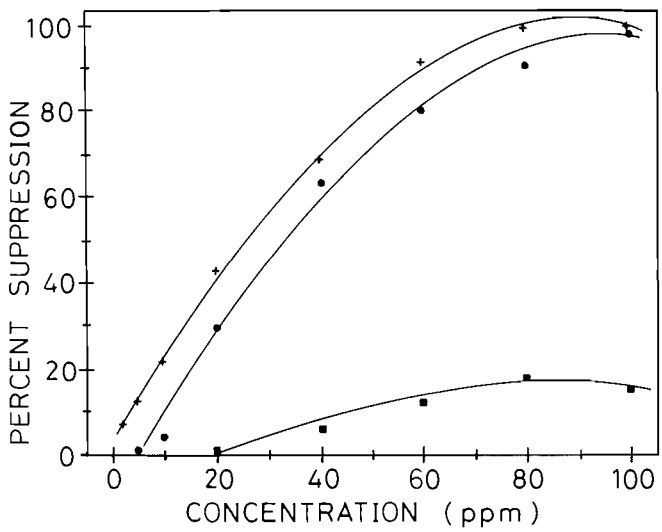

FIG. 3. Calibration curves for suppression of the Co^{2+} maximum by Praestol 2810/73 (●), Praestol 2900/73 (■), and Praestol 444k (+).

This is undoubtedly a charge effect. The mercury electrode is negatively charged at the potential of the Co^{2+} reduction and the anionic polymer should be less strongly adsorbed than the non-ionic or cationic polymers. Although these methods are basically nonspecific, a comparison of the O_2 and Co^{2+} maxima suppression should indicate whether or not a polymer is anionic.

In Fig. 4 are shown the calibration plots for the determination of the three Praestol polymers by suppression of the Hg^{2+} maximum in unpurged solutions. The minimum concentration of each polymer which can be detected is about 1 ppm. At higher concentrations Praestol 444k is the most effective while Praestol 2810/73 is the least effective. The cationic Praestol 444k would be expected to be the least effective due to its repulsion from the positively charged electrode. In samples which have been purged with N_2 to remove dissolved O_2 this is in fact observed (results not shown). The presence of O_2, however, affects the size and shape of the maxima as well as

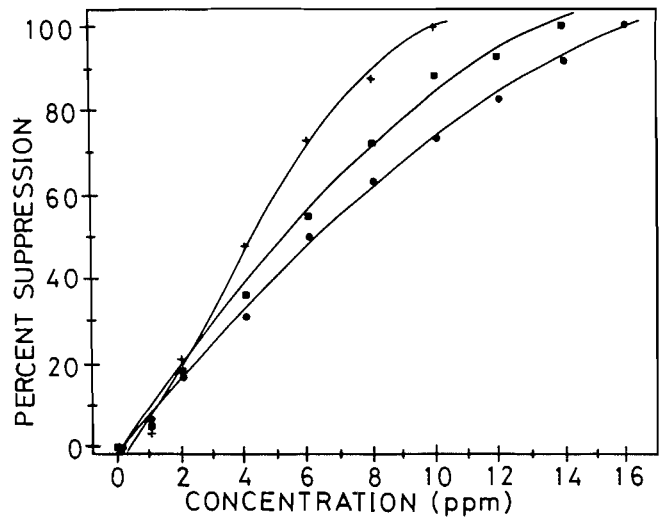

FIG. 4. Calibration curves for suppression of the Hg^{2+} maximum by Praestol 2810/73 (●), Praestol 2900/73 (■), and Praestol 444k (+).

TABLE 2. Maximum suppression by Praestol mixtures

Praestol mixture	% Suppression Obsd	Calcd
2 ppm 2810/73 + 2 ppm 2900/73	31.5	33.9
4 ppm 2810/73 + 2 ppm 2900/73	50.8	51.0
2 ppm 2810/73 + 4 ppm 2900/73	45.0	44.4
2 ppm 2810/73 + 2 ppm 444k	30.3	36.4
2 ppm 2810/73 + 4 ppm 444k	64.2	63.0
4 ppm 2810/73 + 2 ppm 444k	45.7	53.5
2 ppm 2900/73 + 2 ppm 444k	21.7	36.3
2 ppm 2900/73 + 4 ppm 444k	23.8	62.9
4 ppm 2900/73 + 4 ppm 444k	29.6	46.8
2 ppm 2900/73 + 2 ppm 444k	16.4	23.5
2 ppm 2900/73 + 2 ppm 444k	19.5	54.2

the relative effectiveness of the polymers in suppressing the maxima.

Experiments were carried out to observe the effect of mixtures of these polymers on maximum suppression. The concentrations used were from the lower, approximately linear portion of the calibration plots in Fig. 4. In Table 2 are listed the observed suppressions of mixtures of the polymers as well as the theoretical suppression of the mixtures, assuming strict additivity. The observed suppression of mixtures of non-ionic Praestol 2810/73 and anionic Praestol 2900/73 was very close to that predicted. For mixtures of Praestol 2810/73 and the cationic Praestol 444k, the observed suppression was somewhat less than predicted when the concentration of the former was greater than or equal to that of the latter, suggesting some interaction between these polymers resulting in reduced surface activity, perhaps through the formation of molecular aggregates. With mixtures of Praestol 2900/73 and Praestol 444k the observed suppression was much less than the predicted, indicating extensive interaction between these polymers through ion pair formation.

However, when mixtures of cationic and anionic pams are used in flocculation processes, they are not added together,

Can. J. Chem. Downloaded from www.nrcresearchpress.com by 80.58.250.72 on 09/07/12
For personal use only.

TABLE 3. Interferences in the Hg^{2+} maximum method

Substance	Concentration	% Suppression
NaCl	50 m*M*	18.6
$MgCl_2$	50 m*M*	20.9
$MgSO_4$	50 m*M*	16.8
$CaCl_2$	50 m*M*	21.5
KH_2PO4	50 m*M*	19.7
K_2HPO4	50 m*M*	19.9
Fe^{2+}	1.0 ppm	4.3
	10.0 ppm	50.9
Fe^{3+}	10.0 ppm	0.0
Cu^{2+}	0.1 ppm	74.0
	1.0 ppm	100.0
Zn^{2+}	1.0 ppm	2.2
	10.0 ppm	67.8
SO_3^{2-}	10.0 ppm	67.7
Benzoic acid	10.0 ppm	100.0
Propionic acid	10.0 ppm	34.3
Humic acid	10.0 ppm	33.5

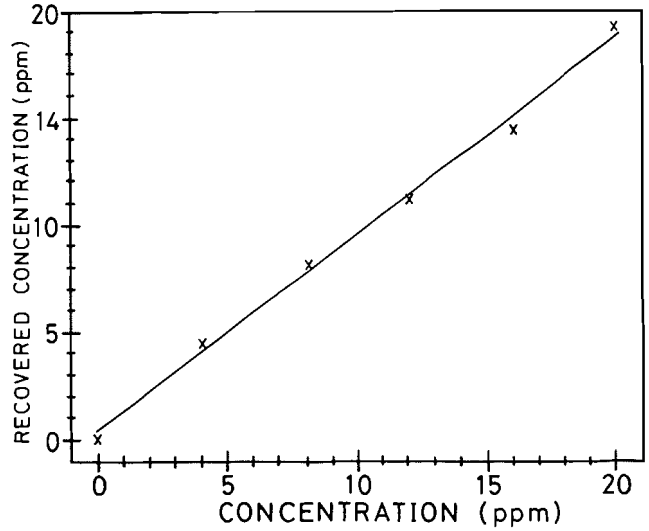

FIG. 5. Plot of measured concentration of P2830/73 in Quinsam coal washings after chromatography on Sephadex G-75, versus original concentration.

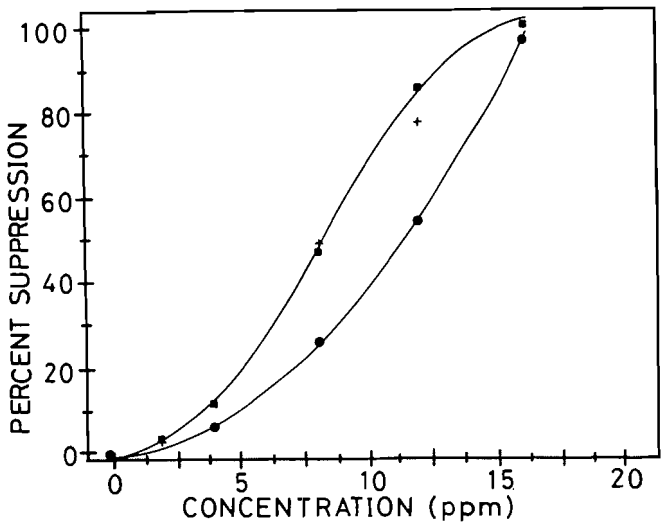

FIG. 6. Calibration curves for suppression of the Hg^{2+} maximum by P444k before chromatography (■), after chromatography in pure water (+), and after chromatography with 10 ppm humic acid (●) on XAD-2.

but, rather, sequentially (17). We have found that the cationic polymers are very strongly adsorbed onto coal/clay mixtures and thus contribute little to the final polymer mixture to be determined (see later).

These methods are not specific for polyacrylamides and other surface-active substances will interfere. Thus we investigated the determination of the pams in a number of coal washings prepared from a sampling of Canadian coals. The washings from the different coals contained different interferences. Table 3 lists these and other possible interferences along with a measure of their strength. Although none of the coal washings contained humic acid, it was felt to be worth consideration as it is often present in tap water while our coal washings were prepared with, and experiments done in, purified water. Table 4 lists the effects of various clean-up columns on the washings. A Sephadex G-75 column was the only single column able to completely remove the interferences from all of the coal washings tested and therefore was the method of choice. After passage through a Sephadex column, the recovery of the anionic polymer P2830/72 was about 90%, and a similar result was found for polyacrylamide. If the polymers were dissolved in coal washings before being passed through the column, the effect on the recovery depended on the source of the coal washings, with the greatest effect being found in washings of Quinsam coal. In this case, a plot of recovered polymer concentration (after passage through a Sephadex column) versus actual concentration yields a straight line graph with a slope of 0.92 (Fig. 5). Thus if the standards are prepared in coal washings similar to those that the unknowns are in, and are chromatographed in like fashion, analysis of neutral and anionic polymers should present no problems. However, the cationic polymers bound strongly to the Sephadex even with eluants of high salt concentration, and for their analysis in coal washings an ion exchange and/or XAD column would have to be used for the clean-up step. P444k, which is cationic with a charge density of 100%, was found to be effectively 100% recovered from XAD columns when chromatographed by itself, but in the presence of 10 ppm humic acid exhibited a markedly reduced recovery (Fig. 6). Use of this procedure would thus also require that the standards be prepared and chromatographed in the same washings that the unknowns are to be determined in. In contrast, P411k, which is also cationic but with a lower charge density, is only 90% recovered after passage through XAD, but humic acid is not found to have a significant effect on this recovery (Fig. 7). P444k was not retained on the cation exchange resin, but the recovery of P411k from it was down to about 70%.

We are using these methods in studies on flocculation rates in various systems. Some typical results are shown in Figs. 8 and 9. Cationic polymers such as P411k do not cause nearly such rapid settling as do the anionic species, but the supernatant is much clearer. Figure 8 shows that the most cost-effective concentration of P411k to use for this particular system would be approximately 10 ppm. From Fig. 9 we see that this corresponds to the point below which almost all the polymer added is bound. For the anionic polymer the situation is quite different. The settling rate curve does not show a

Can. J. Chem. Downloaded from www.nrcresearchpress.com by 80.58.250.72 on 09/07/12
For personal use only.

TABLE 4. Percent suppression by coal extracts

Resin	Coal				
	Alberta X	CRL82-11	Quinsam	Lingam	Tap
Unchromatographed	29	28	100	100	100
XAD-2	27	—	100	100	82
Cation exchange	29	—	100	56	72
Anion exchange	0	—	0	100	100
Cation exchange + XAD	—	—	—	37	3
Sephadex G 75	1	0	2	0	—

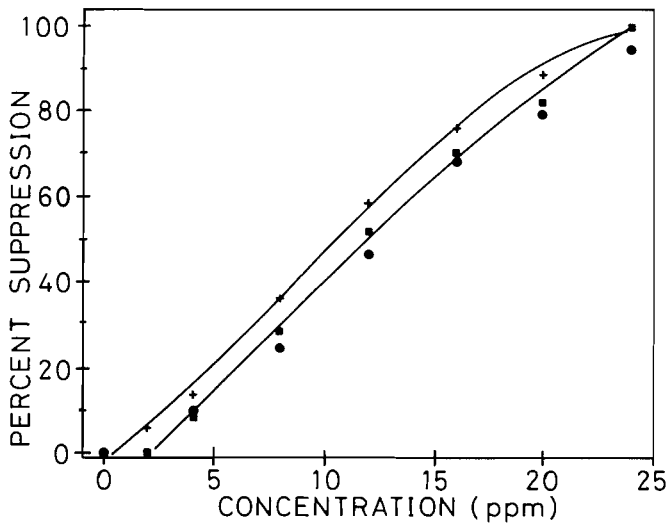

FIG. 7. Calibration curves for suppression of the Hg^{2+} maximum by P444k before chromatography (+), after chromatography (■), and after chromatography with 10 ppm humic acid (●) on XAD-2.

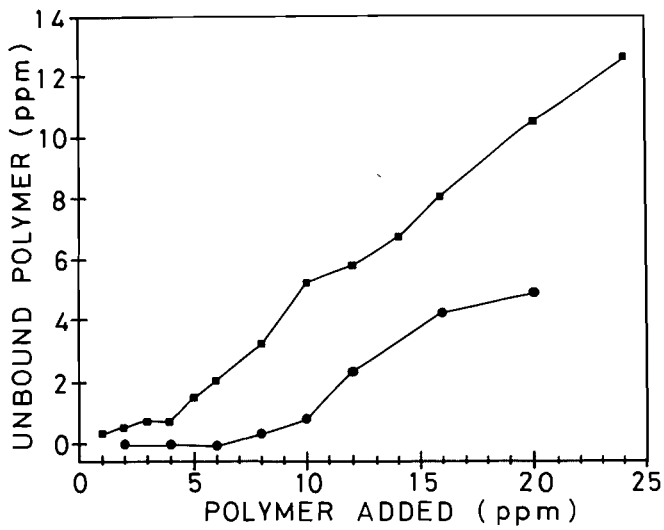

FIG. 9. Concentration of flocculant remaining in solution after flocculation versus the concentration of polymer added for P2830/72 (■) and P411k (●).

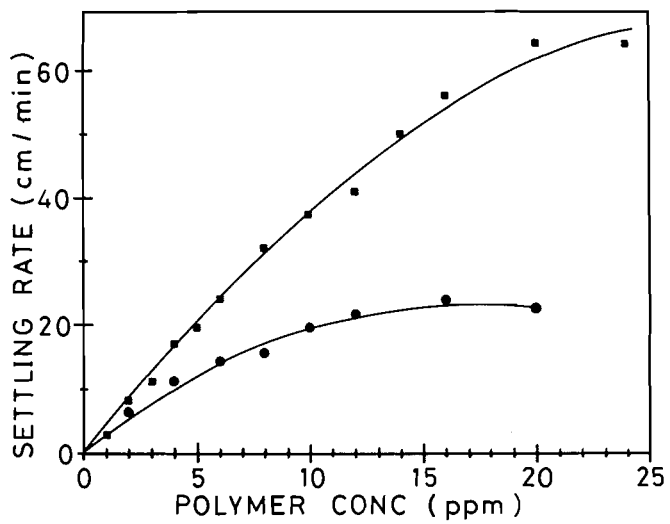

FIG. 8. Settling rate versus flocculant concentration for P2830/72 (■) and P411k (●).

plateau in the concentration region used, yet there are relatively large amounts of free polymer even for low concentrations of total added polymer.

In summary, the polarographic maximum suppression methods described here provide simple, rapid means for determining polyacrylamides and related polymers at the low ppm level. A number of common interferences have been identified and can typically be removed using a Sephadex G-75 resin before analysis of neutral or anionic polymers, or with XAD-2 and/or ion exchange resins for cationic polymers. The method involving the Hg^{2+} maximum is our method of choice as it does not require any purge time, it is the most sensitive, and it also permits the use of higher electrolyte concentrations where necessary.

Acknowledgement

This work was supported by grants from Energy, Mines and Resources, Canada.

1. M. W. SCOGGINS and J. W. MILLER. Soc. Pet. Eng. J. **19**, 151 (1979).
2. E. R. HENDRICKSON and R. D. NEUMAN. Anal. Chem. **56**, 354 (1984).
3. W. B. CRUMMETT and R. A. HUMMEL. J. Am. Water Works Assoc. **55**, 209 (1963).
4. G. G. HAWN and C. P. TALLEY. Anal. Chem. **53**, 731 (1981).
5. A. S. MICHAELS and O. MORELOS. Ind. Eng. Chem. **47**, 1801 (1955).
6. Y. A. ATTIA and J. RUBIO. Br. Polym. J. **7**, 135 (1975).
7. B. COSOVIC and V. VOJVODIC. Limnol. Oceanogr. **27**, 361 (1982).
8. Z. KOZARAC, B. COSOVIC, and M. BRANICA. J. Electroanal. Chem. **68**, 75 (1976).
9. B. BREYER and H. H. BAUER. Alternating current polarography and tensammetry. Interscience, New York. 1963.

Can. J. Chem. Downloaded from www.nrcresearchpress.com by 80.58.250.72 on 09/07/12
For personal use only.

10. D. R. CANTERFORD and R. J. TAYLOR. J. Electroanal. Chem. **98**, 25 (1979).
11. I. M. KOLTHOFF, Y. OKINAKA, and T. FUJINAGA. Anal. Chim. Acta, **18**, 295 (1958).
12. K. LINHART. Tenside Deterg. **9**, 241 (1972).
13. E. LADANYI, E. ZUGRAVU, and M. TOMOAIA. Int. Arch. Arbeitsmed. **33**, 245 (1974).
14. Z. KOZARAC, V. ZUTIC, and B. COSOVIC. Tenside Deterg. **13**, 260 (1976).
15. L. DUNSCH, U. FEIST, and J. MORGENSTERN. Acta Polymerica, **34**, 73 (1983).
16. D. C. GRAHAME. Chem. Rev. **41**, 441 (1947).
17. P. SOMASUNDARAN. Fine particles processing. Proc. Int. Symp. on Fine Particles Processing, Las Vegas, Nevada, 1980. *Edited by* P. Somasundaran. 1980. p. 947.

Can. J. Chem. Downloaded from www.nrcresearchpress.com by 80.58.250.72 on 09/07/12
For personal use only.

The reactivity of aliphatic amines and morpholines in dioxane–water solvent systems

SABRINA KALSI, RITA LAFRAMBOISE, AND RONALD M. SCOTT[1]
Department of Chemistry, Eastern Michigan University, Ypsilanti, MI 48197, U.S.A.

Received August 18, 1986

SABRINA KALSI, RITA LAFRAMBOISE, and RONALD M. SCOTT. Can. J. Chem. **65**, 563 (1987).

Using the titration of tertiary aliphatic amines as a model a linear relationship for the log equilibrium constant versus the log dielectric constant over a broad range of dioxane–water mixtures is established. Primary and secondary amines are less responsive to changes in dielectric constant, producing linear data of shallower slope. A study of morpholine and *N*-alkylmorpholines produces curves that plateau in high dielectric constant regions and display decreasing slope as water concentrations approach zero. Similar behavior for morpholines is observed in low water mixtures where they form proton transfer complexes with *p*-nitrophenol. Possible reasons for the behavior are discussed.

SABRINA KALSI, RITA LAFRAMBOISE et RONALD M. SCOTT. Can. J. Chem. **65**, 563 (1987).

En utilisant la titration d'amines aliphatiques tertiaires comme modèle, nous avons établi une relation linéaire entre le logarithme de la constante d'équilibre et le logarithme de la constante diélectrique valable pour une large plaque des compositions de mélanges dioxan–eau. Les amines primaires et secondaires sont moins sensibles aux changements de constante diélectrique ce qui conduit une relation linéaire de pente plus faible. L'étude de la morpholine et de *N*-alkylmorpholines donne des courbes qui forment un plateau pour les constantes diélectriques élevées et dont la pente décroit lorsque la concentration de l'eau tend vers zero. Un comportement semblable est observé avec les morpholines dans les mélanges à faible teneur en eau lesquelles forment des complexes de transfert de protons avec le *p*-nitrophénol. Les raisons possibles de ce comportement sont discutées.

Can. J. Chem. Downloaded from www.nrcresearchpress.com by 80.58.250.72 on 09/07/12
For personal use only.

Introduction

The effects of the solvent on the reactions of dissolved substances can be classified into two categories. Long range solvation forces relate to the relative ability of the solvent to facilitate charge separation by virtue of the polarity of the solvent molecules. A variety of measures have been used to describe or measure this solvent property. Some such as dielectric constant are based on the measurement of a physical property of the pure solvent or solvent mixture, while others such as Taft's π value are based on the observation of the relative equilibria of model reactions in a variety of solvent systems (1). Short range solvation forces depend on a specific interaction usually by hydrogen bonding between the solute and a solvent molecule. Tendencies to interact in this fashion have been measured by such constants as the α and β values of Taft (1, 2).

Previous studies of solvation effects usually have been based on comparisons of equilibrium constants obtained in a series of different pure solvents whose polarity and possibly whose tendency to form hydrogen bonds have been independently assessed (1, 3). Mixed solvent systems are often used in studies attempting to assess the effect on some system of a change in dielectric constant, the experimental conditions being varied simply by altering the proportions of the polar and non-polar solvent component. However, such solvents clearly present a special case. For example, if one solvent component, probably the more polar one, engages in short range interactions with a solute, then the solvation shell of the reactant will be enriched in that component beyond the level of its proportion in the solvent. This circumstance has been termed preferential solvation (4). This results not only in the effect on the reactivity of the solute brought about by the short range interaction, but also in a departure from the behavior one would predict based on the long range forces due to the creation of an artificially high polarity environment.

We have selected for study the dioxane–water mixed solvent system. Because it provides a range of dielectric constant from approximately 2.2 to 78 at 25°C, it has frequently been used for studies in which the effect of dielectric constant on a system is to be assessed (5). However, it is a complex system not only for the reasons already stated, but also because water and dioxane are both proton acceptors and water is a proton donor. A pattern of hydrogen bonding between solvent molecules is therefore to be anticipated.

A first concern is whether in such a mixed solvent a reaction proceeds predictably, that is linearly, with respect to some solvent parameter. Providing a model to test effects of long range forces in isolation is difficult since the reactive centers of the model would be very likely to interact directly with dioxane, water, or both and such short range interactions distort the behavior. However, tertiary amines have only the unshared electrons of the nitrogen. By choosing a strong acid as the other reactant, and by never eliminating water from the system, our acidic species is the hydrated hydronium ion which may be reproducibly hydrated across the range of solvent mixtures. Although short range solvation has not been eliminated, it may now be considered to be non-varying across the range of study. Extending the study beyond simple tertiary aliphatic amines and observing deviation from the patterns set by these structures provides insights into the effects of short range solvation on other amines.

A system that we have studied previously in this solvent mixture involves the reacting of *p*-nitrophenol (*p*NP) and amines to form proton transfer complexes, structures in which the phenylate and ammonium ions are joined by a hydrogen bond (5). A detailed study of this reaction is only possible in the lower water content solvent mixtures, since in high water content solutions the complex tends to break into individual ions. Data from these studies are useful to confirm and extend observations of amines with strong acids.

Materials and methods

The chromophore, *p*-nitrophenol (*p*NP), was Aldrich reagent grade, and was purified twice by recrystallization from benzene. All amines were Aldrich reagent grade, were purified by fractional vacuum distillation twice, and were stored under a nitrogen atmosphere. Dioxane was Aldrich Gold Label Spectrophotometric Grade and was used

[1]To whom all correspondence should be addressed.

directly from freshly opened bottles. Water was distilled, then run through a mixed bed ion exchange resin cartridge.

Titrations were performed using a Sargent Model DG Titration apparatus employing a combination pH electrode. Dioxane–water mixtures were prepared by volume rather than by weight in order to reproduce the conditions of an earlier report (6). Accurately weighed amounts of amines in the range of 0.5 mmol were dissolved in the dioxane–water mixture, which was then titrated with 0.0100 *M* HCl dissolved in the same dioxane–water mixture.

For proton-transfer studies dioxane–water mixtures were prepared by weight. The solutions for a specific equilibrium constant determination were prepared so that the phenol concentration was constant and the amine concentration was varied. All determinations included a no amine solution and five different amine concentrations. A series of such determinations were made in solvent systems varying from 0 to 30 wt.% water in dioxane. Spectrophotometric reference solutions were prepared exactly as the sample solutions but with the phenol stock solution omitted. All solutions were made the day of use.

The spectra from 550 to 350 nm were obtained using 1 cm quartz cells in a Beckman DK-2A spectrophotometer. The sample temperature was maintained at a constant 25°C by circulating water from a constant temperature bath through a brass cell holder.

Absorbances were read at three wavelengths and were analyzed by two methods to determine the equilibrium constant. In one method the Rose–Drago equation was employed (7), generating an array of ten values for the equilibrium constant at each wavelength. These values were subjected to Chauvenet's criterion to reject extreme values, and the remaining values were averaged. In the other method of calculation, the iterative technique, a somewhat low value for the extinction coefficient of the *p*NP proton transfer complex at each specific wavelength was estimated. From the absorbance at that wavelength and the estimated extinction coefficient the concentrations of all reactants and products in the reaction mixtures were calculated, and from these five equilibrium constants were determined for each set of absorbances. The estimated value for the extinction coefficient was then incremented and the process repeated. The extinction coefficient and average equilibrium constant for the set of constants displaying the greatest self-consistency was then selected. In practice a very satisfactory convergence on a best value for the equilibrium constants is observed. This method was first used by us on this project, and is favored by us over other methods at this time. It resembles the Rose–Drago calculation in that determination of the equilibrium constant depends on first determining a value for the extinction coefficient of the complex, however the iterative testing of possible extinction coefficient values allows selection of the optimum value and provides an easy visual check as to whether the resulting values for the equilibrium constant are reasonable, reproducible, and consistent with one another. Good correspondence was obtained for the final values generated for the constants by the two methods.

The data were also treated by calculating the ratio of the concentrations of proton transfer complex to non-complexed *p*NP. The log of this ratio was plotted against the log of amine concentration. In such a plot the slope of the best straight line through the points indicates the number of amine molecules associated with each phenol in the complex, while the *X* intercept provides an approximate log *K* value. In every case the slope indicated a 1:1 complex between the participants and the estimated log *K* was close to the values obtained by the two methods described above.

Results

Figure 1 presents $-\log K$ values for the reaction of the various amines with hydrochloric acid versus solvent dielectric constant. Non-linear response is demonstrated, with values dropping sharply in the low water solutions. Similarly, in Fig. 2 decidedly non-linear plots result form plotting $-\log K$ versus the Onsager coefficient. However, in Fig. 3, $-\log K$ versus $\log \epsilon$, the data plot as a series of straight lines.

Figures 1–3 also present data for a primary and a secondary

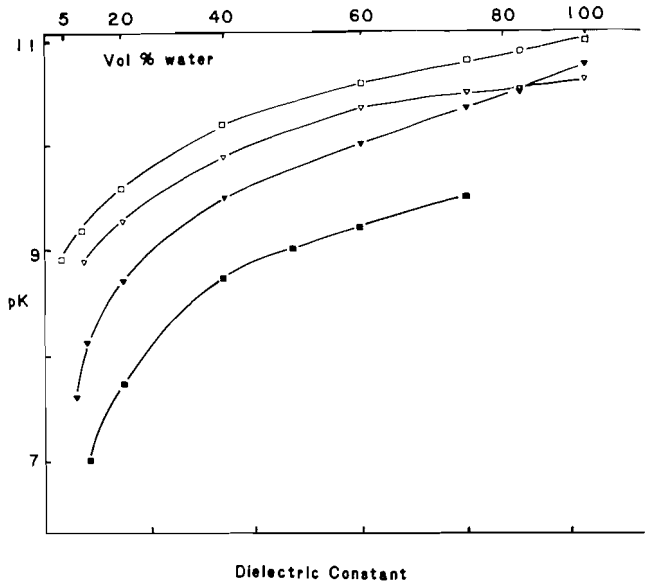

FIG. 1. The titration of aliphatic amines in mixtures of dioxane and water. Here and in Figs. 2 and 3 the solid triangles are TEA, solid squares are tributylamine, open triangles are *n*BA, and open squares are DEA. Data are plotted versus dielectric constant, with wt.% water indicated at the top of the figure.

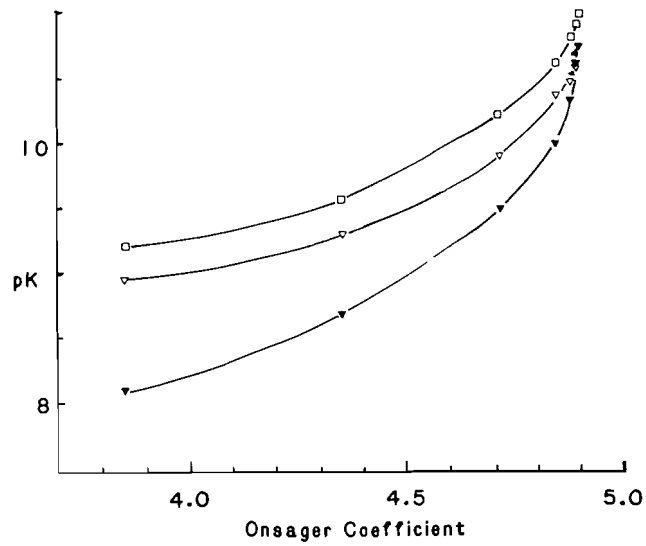

FIG. 2. These are the same data as in Fig. 1, here plotted versus Onsager coefficient $(\epsilon - 1)/(2\epsilon + 1)$.

amine. In Fig. 3 these data display linear response to $\log \epsilon$, but the slopes are more shallow. It is difficult to interpret the shallower slope as inferring other than a reduced dependence on long range forces. The linearity indicates an invariance in short range forces across the range of mixtures studied. The nitrogen protons of these amines can hydrogen bond to the oxygen unshared electrons of either dioxane or water, more likely the latter as was first predicted by Trotman–Dickenson (8). Such bonding would create an unchanging segment in the solvation shell of the amine. To the degree that this occurs the magnitude of response to changes in dielectric constant is reduced.

By contrast the data obtained when morpholine and *N*-methylmorpholine were titrated were non-linear plotting against any parameter including $\log \epsilon$ (Fig. 4). Morpholine compounds tended initially to remain at a constant equilibrium constant as

Can. J. Chem. Downloaded from www.nrcresearchpress.com by 80.58.250.72 on 09/07/12
For personal use only.

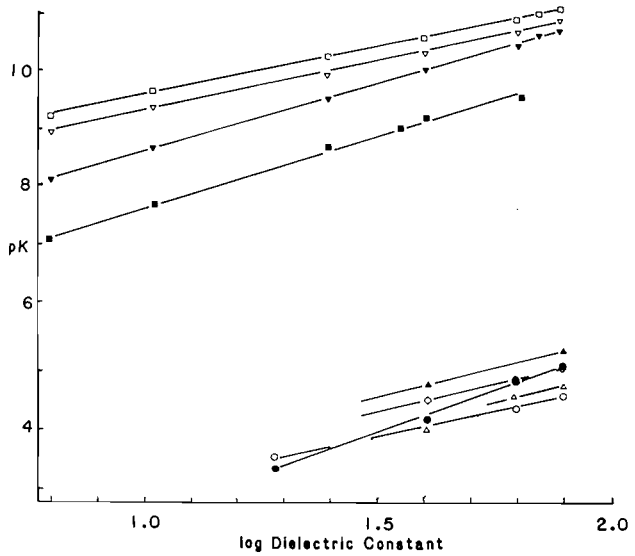

FIG. 3. These include the data in Fig. 1 plus the titration data for some aniline derivatives including aniline (open circles), *N*-methylaniline (inverted open triangles), *p*-toluidine (diamonds), *p*-anisidine (inverted solid triangles), and *N*,*N*-dimethylaniline (solid circles); aniline data from ref. 17.

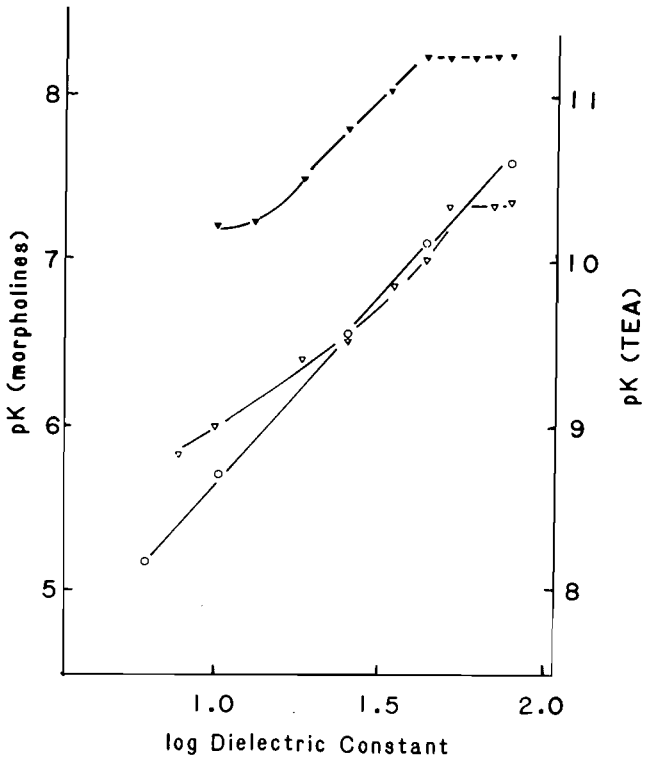

FIG. 4. The p*K* values for morpholine (solid triangles) and *N*-methylmorpholine (open triangles) as determined by titration in a variety of mixtures of dioxane and water are plotted versus log dielectric constant for the solvent mixture. Values for triethylamine are plotted for comparison (open circles).

water concentration is reduced, to drop with about the same slope as simple aliphatic amines through the middle range of water concentration, then finally to display a slower reduction in dielectric constant with loss of water at lower water concentrations than would be predicted by the behavior of simple aliphatic amines.

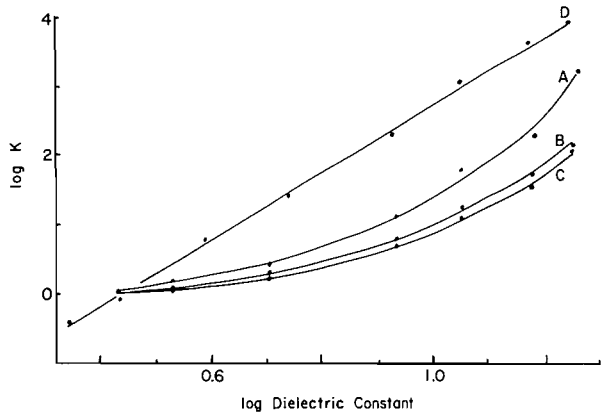

FIG. 5. The log *K* values for the formation of the proton transfer complex between *p*-nitrophenol and morpholine (*A*), *N*-methylmorpholine (*B*), and *N*-butylmorpholine (*C*) are plotted versus the log dielectric constant of the various dioxane–water solvent mixtures used. Data obtained for *n*-butylamine in the same system is plotted for comparison (*D*).

In Fig. 5 we find the log *K* for the formation of the proton transfer complex between *p*NP and various morpholines versus log ϵ. The actual values of the constants are listed in Table 1.

Discussion

Attempts to relate solvent dielectric to a number of reactions involving changes in dipole moment such as formation of quaternary ammonium ions (9), solvolysis (10), and proton transfer (11) have related a parameter of the reaction to a number of functions of dielectric constant including the constant itself, the inverse of the constant, log of the constants, and the Onsager coefficient. In previous studies using a variety of pure solvents, log ϵ was most frequently the parameter that produced linear plots. We interpret this result as an indication that under circumstances where composition-dependent interference by short range solvation forces is minimized or is invariant with solvent composition the dioxane–water mixed solvent system produces the same sort of long range solvation effects previously reported for single solvent systems.

Whether or not the linear plots obtained by the titration of tertiary amines with a strong acid in dioxane–water mixtures represent a simple response of the reaction to change in long range solvation, they certainly represent a baseline of behavior against which similar systems may be compared. With this in mind consider first the change in slope displayed by primary or secondary amines when compared to tertiary amines (Fig. 1). The only difference in the systems is the presence of hydrogen attached to the amine nitrogen in primary and secondary amines. We propose the attachment of a solvent component, probably water, to this hydrogen by a hydrogen bond, in the fashion proposed in earlier papers (12) and later validated using a dimethylsulfoxide–benzene solvent system (13). In this fashion a portion of the solvation shell of the amine becomes fixed so that the amine becomes less responsive to changes in solvent composition, finally resulting in the shallower slopes observed for primary and secondary amines in Fig. 3. In support of this concept is the observation that in very non-polar non-hydrogen bonding solvents tertiary and secondary amines are more basic than primary amines (14) while in aqueous systems the basicities of simple aliphatic amines are very similar (approximately 9.6–11.3; ref. 15). Withdrawing the proton somewhat in form-

Can. J. Chem. Downloaded from www.nrcresearchpress.com by 80.58.250.72 on 09/07/12
For personal use only.

TABLE 1. Equilibrium constants for *p*-nitrophenol with morpholine and alkylmorpholines*

	Morpholine		Methylmorpholine		Butylmorpholine	
Wt.% water	A	B	A	B	A	B
2.5	0.08±0.05	0.12			0.12±0.01	0.13
	0.04±0.14	1.03				1.02
5	0.33±0.04	0.37	0.07±0.02	0.09	0.14±0.07	0.11
	0.29±0.06	1.06		1.05		1.00
10	0.49±0.04	0.59	0.38±0.05	0.43	0.34±0.01	0.35
	0.34±0.03	1.16		1.10	0.43±0.07	1.03
15	0.92±0.03	1.03	0.65±0.04	0.77	0.74±0.01	0.75
	0.72±0.04	1.12		1.23	0.68±0.11	1.00
20	1.70±0.03	1.73	1.11±0.02	1.14	1.05±0.01	1.01
	1.68±0.03	1.02	1.11±0.05	1.02	1.00±0.10	1.06
25	1.87±0.03	1.96	1.64±0.01	1.70	1.29±0.02	1.33
	1.85±0.01	1.06	1.55±0.02	1.06	1.35±0.62	1.03
30	3.18±0.05	3.35	2.09±0.01	2.44	2.10±0.01	2.20
	3.16±0.12	1.03	1.85±0.05	1.21	1.91±0.01	1.04

*In column A the top number is calculated by the iterative program, and the bottom by the Rose–Drago calculation. In column B the top number is approximate log K and the bottom is the ratio of amine-to-phenol in the proton transfer complex.

Can. J. Chem. Downloaded from www.nrcresearchpress.com by 80.58.250.72 on 09/07/12
For personal use only.

ing the hydrogen bond with the solvent raises the electron density around the amine nitrogen much as the inductive effect of the alkyl groups does in the tertiary amines.

Turning to the titration data for the morpholines (Fig. 4), two features of the curve require explanation. The plateau in the water-rich region of the data represents an almost complete insensitivity to changes in solvent composition. In the middle region log K values decrease with a slope similar to that displayed by the simple aliphatic amines and would appear to be a normal response to changing solvent composition. At the dioxane-rich end of the data, however, we see once again a leveling of the curve, indicating a lowered sensitivity to changes in solvent composition.

The special feature of the morpholine structure is the ring oxygen with its two pairs of unshared electrons. Water can hydrogen bond to these electrons, fixing a portion of the solvation shell of morpholine and rendering it less sensitive to changes in solvent composition. In water-rich mixtures long chains of water hydrogen bonded together are proposed to exist. This for example is cited as the cause of the quenching of fluorescence in this region (16). Tying the morpholine to water would lock it into this extended water chain making the solvation shell even less changeable with solvent composition. However, in the region where this structure disappears in favor of water–dioxane hydrogen-bonded complexes, the reaction begins to respond to changing solvent composition.

At the dioxane-rich end of the solvent composition continuum we present not only titration data, but also the equilibrium constants for morpholine–*p*NP proton transfer complex formation (Fig. 5). In every case we see a lowered sensitivity to the reduction of water concentration. Once again the formation of hydrogen-bonded complexes between water and the morpholine-ring oxygen unshared electrons stabilizing a portion of the increasingly rare water in the solvation shell of the morpholine. In Fig. 5 the data for the formation of an *n*-butylamine–*p*NP proton-transfer complex[2] is superimposed on the morpholine data for contrast. The similarity to the titration data is apparent.

Summary

Studies are performed on the reaction behavior of aliphatic amines and morpholines in dioxane–water solvent mixtures of varying composition. The titration of simple aliphatic amines with a strong acid is shown to produce log K values that vary linearly with log ϵ of the solvent mixture in all cases. Shallower slopes observed with primary and secondary amines as compared to tertiary amines are explained as being due to the hydrogen bonding of water to amine protons where present, making the solvation shell of the amine less responsive to changes in solvent composition. Morpholine data show a plateau in water-rich regions and a shallower slope in water-poor regions. This is ascribed to hydrogen bonding between solvent water and the unshared electrons of the morpholine-ring oxygen.

1. M. J. KAMLET, J. L. M. ABBOUD, and R. W. TAFT. Progress in physical organic chemistry. Vol. 13. Wiley-Interscience, NY. 1981. p. 485; M. J. KAMLET and R. W. TAFT. J. Chem. Soc. Perkin II, 349 (1979).
2. R. W. TAFT and M. J. KAMLET. J. Am. Chem. Soc. **98**, 2886 (1976); M. J. KAMLET, A. SOLOMONOYICI, and R. W. TAFT. J. Am. Chem. Soc. **101**, 3734 (1979).
3. H. SUHR. Ber. Bunsenges. Phys. Chem. **67**, 893 (1963).
4. K. REMERIE and J. B. F. N. ENGBERTS. J. Phys. Chem. **87**, 5449 (1983).
5. R. SCOTT and S. VINOGRADOV. J. Phys. Chem. **73**, 1890 (1969).
6. P. RUMPT, G. GIRAULT-VEXLEARSCHI, and R. SCHALL. Bull. Soc. Chim. Fr. 554 (1955).
7. N. J. ROSE and R. S. DRAGO. J. Am. Chem. Soc. **81**, 6138 (1959).

[2]N. Duriaswamy and R. M. Scott. Unpublished data.

8. A. F. TROTMAN-DICKENSON. J. Chem. Soc. 1923 (1949).
9. C. LUSSAN and J. C. JUNGERS. Bull. Soc. Chim. Fr. 2678 (1968); V. VANEVEN and M. C. HAULAIT-PIRSON. J. Solution Chem. **6**, 757 (1977); P. L. HUYSKENS, M. C. HAULAIT-PIRSON, and F. KAPUKU. Bull. Soc. Chim. Belg. **89**, 505 (1981).
10. S. G. SMITH, A. H. FAINBERY, and S. WINSTEIN. J. Am. Chem. Soc. **83**, 618 (1961).
11. B. BRZEZINSKI and G. ZUNDEL. J. Phys. Chem. **87**, 5461 (1983); J. FRITSCH and G. ZUNDEL. J. Phys. Chem. **85**, 556 (1981); J. JADZYN and J. MAYECKI. Acta Phys. Pol. A, **41**, 599 (1972).
12. R. SCOTT, D. DEPALMA, and S. N. VINOGRADOV. J. Phys. Chem. **72**, 3192 (1968).
13. A. REYES and R. M. SCOTT. J. Phys. Chem. **84**, 3600 (1980).
14. J. W. BAYLES and A. F. TAYLOR. J. Chem. Soc. 417 (1961); R. G. PEARSON and D. C. VOGELSONG. J. Am. Chem. Soc. **80**, 1038 (1957).
15. D. D. PERRIN. Dissociation constants of organic bases in aqueous solution. Butterworth, London. 1965.
16. A. B. MILLER and R. M. SCOTT. Spectrochim. Acta, **30**A, 459 (1980).
17. H. MARSHALL and E. GRUNWALD. J. Am. Chem. Soc. **76**, 2000 (1954).

Can. J. Chem. Downloaded from www.nrcresearchpress.com by 80.58.250.72 on 09/07/12
For personal use only.

Relations entre les tungstophosphates apparentés à l'anion $PW_{12}O_{40}^{3-}$. Synthèse et propriétés d'un nouveau polyoxotungstophosphate lacunaire $K_{10}P_2W_{20}O_{70}\cdot 24H_2O$

ROLAND CONTANT

Laboratoire de physicochimie inorganique, Tours 54/55, Université Pierre et Marie Curie, 4 place Jussieu, 75252 Paris CEDEX 05, France

Reçu le 18 août 1986

ROLAND CONTANT. Can. J. Chem. **65**, 568 (1987).

Les relations entre toutes les espèces apparentées aux anions $PW_{12}O_{40}^{3-}$ et $P_2W_{21}O_{71}^{6-}$ ont été établies. Un nouveau composé $K_{10}P_2W_{20}O_{70}$ a été synthétisé et caractérisé par spectroscopie infra-rouge et Raman. L'ensemble de ses propriétés et plus particulièrement les spectres de résonance magnétique nucléaire (^{31}P et ^{183}W) permettent d'en proposer la structure. C'est une espèce lacunaire qui réagit sur le cobalt(II) pour donner deux complexes 1–1, probablement des isomères de coordination. En solution, en présence de Co^{2+}, l'isomérisation A-PW_9 → B-PW_9 se fait en plusieurs étapes qui ont été précisées. Les isomères β des tungstophosphates sont moins stables que les tungstosilicates ou germanates correspondant et β-PW_{12} n'a été identifié que sous forme réduite.

ROLAND CONTANT. Can. J. Chem. **65**, 568 (1987).

The relationship between all the polyoxotungstophosphates related to $PW_{12}O_{40}^{3-}$ and $P_2W_{21}O_{71}^{6-}$ anions was established. A new compound $K_{10}P_2W_{20}O_{70}$ was synthesized and characterized by infrared and Raman spectroscopy. These properties, and especially the ^{31}P and ^{183}W nuclear magnetic resonance spectra, allowed us to propose the structure. It is a lacunary species that reacts with Co(II) to give two 1–1 complexes, probably coordination isomers. In the presence of Co(II) the A-type → B-type PW_9 isomerization occurs in several steps, which are specified. The tungstophosphate β isomers are less stable than the corresponding tungstosilicates or germanates, and β-PW_{12} was only identified as a reduced species $PW_{12}O_{40}^{4-}$.

Introduction

Le phosphore(V) est certainement, parmi les éléments connus pour former des hétéropolyoxotungstates, celui qui donne le plus grand nombre d'espèces (1). La plupart peuvent être regroupées en « famille », une famille comprenant un polyanion « saturé » et éventuellement ses isomères, par exemple α et β $P_2W_{18}O_{62}^{6-}$, et tous les composés qui en dérivent par le départ d'un ou de plusieurs atomes de tungstène, ou par le remplacement de ces atomes de tungstène par d'autres atomes métalliques, par exemple $P_2W_{17}O_{61}^{10-}$, $P_2W_{17}MoO_{62}^{6-}$, $P_2W_{15}O_{56}^{12-}$, etc. Les trois principales familles de polyoxotungstophosphates dérivent formellement de $P_2W_{18}O_{62}^{6-}$, $PW_{12}O_{40}^{3-}$ et $P_2W_{21}O_{71}^{6-}$.

La famille de $P_2W_{18}O_{62}^{6-}$ (en abrégé P_2W_{18}) a été étudiée précédemment (2, 3). Longtemps réduite à $P_2W_{21}O_{71}^{6-}$ dont la structure a été décrite par Weakley (4), la famille de P_2W_{21} s'est enrichie récemment de $P_2W_{19}O_{69}^{14-}$ (5), de $KP_2W_{20}O_{72}^{13-}$ dont la synthèse et la structure ont été décrites par Fuchs et Palm (6) et de plusieurs composés mixtes $P_2W_{19}M_2$ et $P_2W_{18}M_3$ (7, 8). La famille de PW_{12} est plus nombreuse en raison de l'existence de plusieurs isomères. Outre α-$PW_{12}O_{40}^{3-}$ qui possède la structure bien connue, dite « de Keggin » (9), elle comprend α-$PW_{11}O_{39}^{7-}$ A,α- et A,β-$PW_9O_{34}^{9-}$ (10), γ-$PW_{10}O_{36}^{7-}$ (11) et de nombreux composés mixtes de formule générale $PW_{11}M$, $PW_{10}M_2$, PW_9M_2 (12) et PW_9M_3. Les complexes $PW_{11}M$ existent avec pratiquement tous les métaux, alors que les autres ne sont connus qu'avec des métaux à l'état d'oxydation IV, V ou VI. À cette famille, il faut ajouter B,α-$P_2W_{18}M_4O_{68}(H_2O)_2^{10-}$ (M = Co, Cu, Zn, etc.) (13) correspondant à un anion B,α-$PW_9O_{34}^{9-}$ identifié seulement à l'état solide (7).

La plupart de ces espèces ont été décrites de façon ponctuelle sans que les relations entre elles soient bien établies. Nous nous sommes attachés ici à préciser les différentes étapes conduisant du mélange tungstate–phosphate aux anions saturés $PW_{12}O_{40}^{3-}$ et $P_2W_{21}O_{71}^{6-}$. Ceci a notamment permis la synthèse d'un nouveau composé $K_{10}P_2W_{20}O_{70}\cdot 24H_2O$.

Partie expérimentale

Préparations et analyses

Les méthodes d'analyse ont été décrites dans un article précédent (2). L'acide $H_3PW_{12}O_{40}\cdot xH_2O$ (14) et $K_{14}P_2W_{19}O_{69}\cdot 24H_2O$ (5) ont été préparés suivant les méthodes décrites dans la littérature. A,β-$Na_9PW_9O_{34}\cdot 17H_2O$ a été préparée suivant la méthode décrite (12) pour la forme protonée. Ce composé n'est pas recristallisable, la précipitation est brutale et il est possible que dans certains échantillons une partie de la forme protonée en équilibre soit entraînée. B,α-$K_{10}P_2W_{18}Co_4\cdot 24H_2O$ a été préparé suivant la méthode de Weakley, Tourné et coll. (13) en augmentant légèrement l'acidité pour améliorer le rendement.

$K_{10}P_2W_{20}O_{70}\cdot 24H_2O$

Un mélange de 100 mL de tungstate de potassium molaire et 10 mL d'acide phosphorique molaire est acidifié lentement par 51 mL d'acide chlorhydrique 3 *M*. Le précipité blanc qui apparaît immédiatement est redissous en portant la solution à ébullition. La solution est abandonnée à la température ambiante et les cristaux blancs qui commencent à apparaître au bout d'une journée sont filtrés, essorés et recristallisés dans le minimum d'eau. *Anal.* calc. pour $K_{10}P_2W_{20}O_{70}\cdot 24H_2O$: K 6,88; W 64,7; P 1,09; H_2O 7,60; trouvé: K 7,08; W 64,6; P 1,09; H_2O 7,53.

La détermination de la masse molaire par ultracentrifugation a donné la valeur de 5 400, ce qui correspond à deux atomes de phosphore par mole.

$K_{14}P_2W_{20}O_{70}\cdot xH_2O$

Un mélange de 250 mL de tungstate de potassium molaire et de 25 mL d'acide phosphorique molaire est acidifié par 108 mL d'acide chlorhydrique 3 *M* et porté à ébullition. Les cristaux apparaissent au refroidissement. *Anal.* calc. pour $K_{14}P_2W_{20}O_{72}\cdot 27H_2O$: K 9,24; W 62,1; P 1,05; H_2O 8,20; trouvé: K 9,26; W 62,3; P 1,04; H_2O 8,07.

Ce composé est identique (spectres ir et Raman) à celui obtenu par Fuchs et Palm (6) à partir de $K_3PW_{12}O_{40}$. Ce sel s'effleurit facilement et l'état d'hydratation varie d'un échantillon à l'autre.

$K_6P_2W_{21}O_{71}\cdot 32H_2O$

Un échantillon de 37 g de $K_{14}P_2W_{20}O_{72}\cdot 27H_2O$ est dissous dans 70 mL d'acide chlorhydrique molaire et porté à ébullition. La partie insoluble est filtrée à chaud. Dans la solution abandonnée à température ambiante, les aiguilles blanches apparaissent au bout de 24 h et sont filtrées essorées. *Anal.* calc. pour $K_6P_2W_{21}O_{71}\cdot 32H_2O$: K 4,00;

Can. J. Chem. Downloaded from www.nrcresearchpress.com by 80.58.250.72 on 09/07/12
For personal use only.

W 65,8; P 1,06; H_2O 9,81; trouvé : K 4,12; W 66,0; P 1,06; H_2O 9,87. On peut utiliser dans les mêmes conditions $K_{10}P_2W_{20}O_{70}\cdot 24H_2O$.

α-$K_{7-x}Na_xPW_{11}O_{39}\cdot 14H_2O$

À une solution de 181,5 g de $Na_2WO_4\cdot 2H_2O$ dans 300 mL d'eau, on ajoute successivement 50 mL d'acide phosphorique molaire et 88 mL d'acide acétique. La solution est portée une heure à reflux, puis après addition de 60 g de chlorure de potassium solide, il apparaît un fin précipité qui est filtré, essoré et séché à l'air. *Anal.* calc. pour $K_{6,4}Na_{0,6}PW_{11}O_{39}\cdot 14H_2O$: K 7,84; Na 0,43; W 63,3; P 0,97; H_2O 7,89; trouvé : K 7,90; Na 0,50; W 63,6; P 0,97; H_2O 8,06.

La proportion de sodium peut varier d'un échantillon à l'autre, et en reprécipitant plusieurs fois par le chlorure de potassium on peut obtenir le sel pratiquement exempt de sodium.

A,α-$K_9PW_9O_{34}\cdot 16H_2O$

$K_{7-x}Na_xPW_{11}O_{39}$ (64 g) est dissous dans 200 mL d'eau, puis versé dans 60 mL de solution de carbonate de potassium 2 *M*. La précipitation est instantanée. Le précipité est filtré, lavé à l'éthanol et séché à l'air. *Anal.* calc. pour $K_9PW_9O_{34}\cdot 16H_2O$: K 12,28; W 57,7; P 1,08; H_2O 10,03; trouvé : K 12,02; W 57,4; P 1,08; H_2O 9,85.

A,β-$K_8HPW_9O_{34}\cdot 18H_2O$

Un échantillon de 40 g de α-$K_9PW_9O_{34}\cdot 16H_2O$ est dissous dans 100 mL d'eau bouillante. Le précipité apparaît au refroidissement. Il est filtré, lavé à l'alcool et séché à l'air. *Anal.* calc. pour $K_8HPW_9O_{34}\cdot 18H_2O$: K 10,91; W 57,7; P 1,08; H_2O 11,30; trouvé : K 10,87; W 57,5; P 1,06; H_2O 11,33.

$K_{12}P_2W_{18}Co_3(H_2O)_3O_{68}\cdot 24H_2O$

À une solution de 1,8 g de $Co(NO_3)_2\cdot 6H_2O$ dans 80 mL d'eau sont ajoutés 11 g de α-$K_9PW_9O_{34}\cdot 16H_2O$. Le précipité bleu cristallin qui apparaît est filtré immédiatement et séché à l'air. *Anal.* calc. pour $K_{12}P_2W_{18}Co_3(H_2O)_3O_{68}\cdot 24H_2O$: K 8,39; Co 3,16; W 59,2; P 1,11; H_2O 8,69; trouvé : K 8,30; Co 3,25; W 59,0; P 1,09; H_2O 8,68.

Anions β_n-$PW_{11}O_{39}^{7-}$, β-$PW_{12}O_{40}^{4-}$ et β_n-$PW_{11}Co(OH_2)O_{39}^{5-}$

Il n'a pas été possible d'isoler des sels purs de ces complexes, mais ils peuvent être préparés en solution diluée : à 100 mL d'une solution de tungstate 2×10^{-2} mol L^{-1} sont ajoutés successivement, à froid, 2 mL d'acide chlorhydrique molaire, 2,82 g de A,β-$Na_9PW_9O_{34}\cdot 17H_2O$, puis 4 mL d'acide molaire. Le pH doit être inférieur à 5 et la formation de l'anion β_n-$PW_{11}O_{39}^{7-}$ est alors quantitative. On obtient β_n-$PW_{11}Co(H_2O)O_{39}^{5-}$ et β-$PW_{12}O_{40}^{4-}$ en ajoutant respectivement à la solution précédente 1 mL de nitrate de cobalt molaire ou 20 mL d'une solution de W(V) (5×10^{-2} mol L^{-1}) dans l'acide chlorhydrique concentré obtenue par électrolyse. Tous ces anions sont caractérisé par polarographie.

Mésures physiques

Les spectres ultraviolet et visible ont été obtenus sur un spectrophotomètre Perkin–Elmer 500, les spectres ir sur un spectrophotomètre Perkin–Elmer 283 et le spectre Raman sur un Coderg PHO utilisant la ligne à 514,5 nm d'un laser à argon Spectra Physics.

Les spectres rmn ont été obtenus sur un appareil Bruker WM 250 à 101 MHz pour ^{31}P et à 10,4 MHz pour ^{183}W. Les déplacements chimiques du ^{31}P ont été mesurés par rapport à H_3PO_4 85% externe, et ceux du ^{183}W par rapport à une solution externe de Na_2WO_4 2 *M* dans D_2O alcalinisé.

Pour la mesure de spectre de ^{183}W, la solution a été obtenue en ajoutant 6 g de $K_{10}P_2W_{20}O_{70}\cdot H_2O$ dans 10 mL de $LiClO_4$ saturé. Après filtration de perchlorate de potassium, 1 mL de D_2O a été ajouté.

Les spectres du ^{31}P ont été obtenus dans des solutions contenant 10% de D_2O de concentration $2,5\times 10^{-2}$ mol L^{-1} en phosphore. La solution de $K_6P_2W_{21}O_{71}$ est stabilisée en milieu acide (HCl 0,1 mol L^{-1}). Les autres espèces à l'exception de $K_{10}P_2W_{20}O_{70}$ sont solubilisées dans le chlorure de lithium molaire.

Les polarogrammes ont été enregistrés sur un polarographe Radiometer PO_4 avec une électrode à goutte de mercure ou une électrode de carbon tournante.

TABLEAU 1. Potentiels de demi-vague (volts E.C.S.) de quelques polyoxotungstophosphates

Espèce	$E_{1/2}$ (nombre d'électrons)		
α-PW_{12}[a]	+0,01 (1)	−0,28 (1)	−0,70 (2)
β-PW_{12}[a]	+0,11 (1)	−0,18 (1)	−0,58 (2)
α-PW_{11}[b]	−0,74 (2)	−0,86 (2)	
β_n-PW_{11}[b]	−0,61 (2)	−0,79 (2)	
α-P_2W_{20}[b]	−0,74 (4)	−0,88 (4)	
A,α-PW_9[b]	−0,77 (4)		
A,β-PW_9[b]	−0,77 (2)	−0,87 (2)	
α-$PW_{11}Co$[b]	−0,72 (2)	−0,89 (2)	
β_n-$PW_{11}Co$[b]	−0,64 (2)	−0,80 (2)	
B,α-$P_2W_{18}Co_4$[b]	−0,85 (4)	−1,00 (4)	

[a]Electrode de carbone tournante; pH 1 HCl 0,1 *M*/NaCl 0,9 *M*.
[b]Electrode à goutte de mercure; pH 4,6 acide acétique/acétate de lithium 1 *M*.

Résultats et discussion

Polarographie

Les hétéropolyanions stables en solution diluée ou dont la décomposition est suffisamment lente, peuvent être caractérisés par polarographie (tableau 1). Comme pour une protonation donnée, le processus de réduction dépend essentiellement de la structure et n'est que peu influencé par la nature de l'hétéroatome central; il est possible de comparer les tungstophosphates aux tungstosilicates (15, 16). Ainsi ont pu être identifiés A,α-PW_9 et A,β-PW_9, de même que β_n-PW_{11} et β-PW_{12} plus oxydants que les isomères α correspondants. Il existe théoriquement trois isomères β_n-PW_{11} correspondant à trois positions différentes de la lacune (15). Un seul a été observé et il s'agit probablement de l'isomère β_1, mais les polarogrammes des trois isomères β_n-SiW_{11} ne sont pas suffisamment différents pour permettre une identification sur ce seul critère.

Spectres rmn de ^{31}P

Le spectre des solutions de $P_2W_{20}O_{70}^{10-}$ présente un seul pic à −12,3 ppm, ce qui correspond à un seul type d'atome de phosphore. Le déplacement chimique est intermédiaire entre celui de $P_2W_{21}O_{71}^{6-}$ (−13,3 ppm) et celui de $PW_{11}O_{39}^{7-}$ (−11,0 ppm). Toutes les espèces plus basiques présentent en solution diluée ($P = 2,5\times 10^{-2}$ mol L^{-1}) 2 pics de hauteurs inégales. Le premier à −11,0 ppm est présent dans tous les spectres, il correspond à PW_{11}. Le second varie de +2,56 pour la solution de $KP_2W_{20}O_{72}^{13-}$ à +3,18 ppm pour la solution de α-$PW_9O_{34}^{9-}$. Ces valeurs correspondent à des mélanges en proportion variable de $H_2PO_4^-$ et HPO_4^{2-}. Pour la solution de P_2W_{19}, les deux pics sont dans le rapport 2:1 correspondant à la réaction de décomposition :

$$P_2W_{19}O_{69}^{14-} \rightarrow 4/3PW_{11}O_{39}^{7-} + 0,62W_7O_{24}^{6-} + 0,28HPO_4^{2-} + 0,39H_2PO_4^-$$

En solution très concentrée, il apparaît d'autres espèces, mais toujours en très faible proportion.

Spectres infra-rouge et Raman

Dans le tableau 2 sont présentés quelques pics sélectionnés des spectres ir des tungstophosphates. On peut noter : (*i*) une grande similitude entre les composés de la famille P_2W_{21}; (*ii*) le déplacement important de la bande P—O pour les deux isomères PW_9; (*iii*) l'absence de dédoublement de la bande P—O dans B,α-$P_2W_{18}Co_4$.

Can. J. Chem. Downloaded from www.nrcresearchpress.com by 80.58.250.72 on 09/07/12
For personal use only.

TABLEAU 2. Bandes sélectionnées des spectres infra-rouges de quelques polyoxotungstophosphates

Composé	ν_{as}(P—O)		ν_{as}(W—O) terminal	ν_{as} ponts W—O—W
$K_6P_2W_{21}O_{71}$[a]	1095, 1085	1030	972, 940	890, 790, 750, 700, 670
$K_{10}P_2W_{20}O_{70}$	1090, 1078	1020	955, 925	860, 795, 748, 660
$K_{14}P_2W_{20}O_{72}$[b]	1080	1025	940	890, 855, 755, 640
$K_{14}P_2W_{19}O_{69}$[a]	1075, 1065	1025	960 ép.	888, 825, 770, 750, 715
		1015	940	
$K_7PW_{11}O_{39}$[a]	1085	1040	950	900, 865, 810, 725
A,α-$K_9PW_9O_{34}$	1056	1002	931, 909	815, 728
A,β-$K_8HPW_9O_{34}$	1054	1008	935, 918	875, 828, 755
A,β-$Na_9PW_9O_{34}$	1058	1015	937	886, 820, 763
$K_{10}P_2W_{19}Co_2O_{69}$[a]	1095, 1080	1020	960 ép.	890, 825, 740, 715, 700
			940	
$K_{12}P_2W_{18}Co_3O_{68}$	1080, 1072	1022	935	895, 800, 705
B,α-$K_{10}P_2W_{18}Co_4O_{68}$		1037	960, 940	880, 770, 735

[a]Référence 5.
[b]Référence 6.

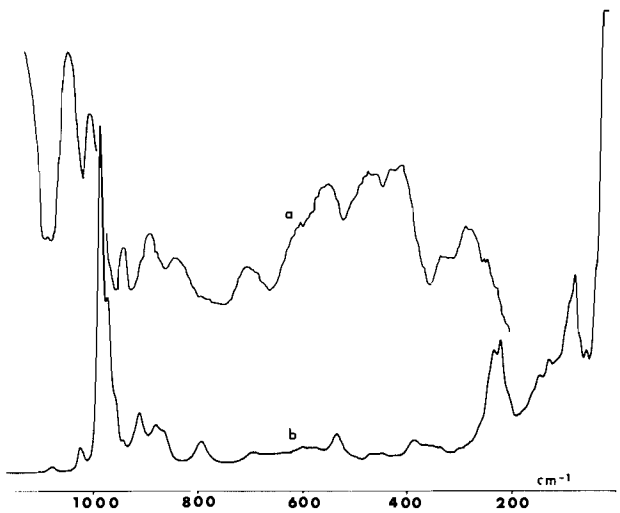

FIG. 1. Spectre infra-rouge (a) et Raman (b) de $K_{10}P_2W_{20}O_{70}\cdot 24H_2O$.

Les spectres ir et Raman de $K_{10}P_2W_{20}O_{70}$ (fig. 1) sont nettement différents de ceux de $K_{14}P_2W_{20}O_{70}$ décrits par Fuchs et Palm (6).

Action des acides et des bases : stabilité

Alors que α-$PW_{12}O_{40}^{3-}$, α-$PW_{11}O_{39}^{7-}$ et $P_2W_{20}O_{70}^{10-}$ sont stables en solution, $P_2W_{21}O_{71}^{6-}$ se décompose en quelques heures, mais peut être stabilisé par addition d'acide. Sur la courbe d'alcalinisation d'une solution fraîche de $K_6P_2W_{21}O_{71}$, il apparaît un premier saut de pH (fig. 2) correspondant à la réaction :

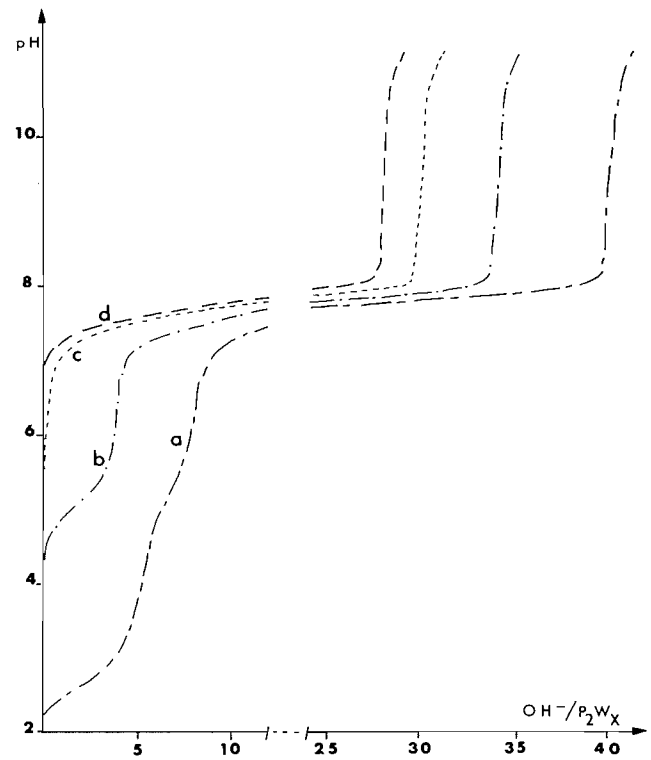

FIG. 2. Courbes d'alcalinisation de $P_2W_{21}O_{71}^{6-}$ (a), $P_2W_{20}O_{70}^{10-}$ (b), $P_2W_{20}O_{72}^{14-}$ (c) et $P_2W_{19}O_{69}^{14-}$ (d). Solutions $10^{-2}M$ dans $NaNO_3$ 0,2 M.

$$P_2W_{21}O_{71}^{6-} + 5OH^- \rightarrow 1/2P_2W_{20}O_{70}^{10-} + HPW_{11}O_{39}^{6-} + 2H_2O$$

$K_{10}P_2W_{20}O_{70}$ peut être isolé dans ces conditions à partir de $K_6P_2W_{21}O_{71}$. Le deuxième saut de pH correspond à la réaction :

$$P_2W_{20}O_{70}^{10-} + 4OH^- \xrightarrow{(1)} 3/2P_2W_{19}O_{69}^{14-} + 2/3PW_{11}O_{39}^{7-} + 2H_2O$$

$$P_2W_{20}O_{70}^{10-} + 4OH^- \xrightarrow{(2)} KP_2W_{20}O_{72}^{13-} + 2H_2O$$

$$KP_2W_{20}O_{72}^{13-} \xrightarrow{(3)} 3/2P_2W_{19}O_{69}^{14-} + 2/3PW_{11}O_{39}^{7-} + 2H_2O$$

Can. J. Chem. Downloaded from www.nrcresearchpress.com by 80.58.250.72 on 09/07/12
For personal use only.

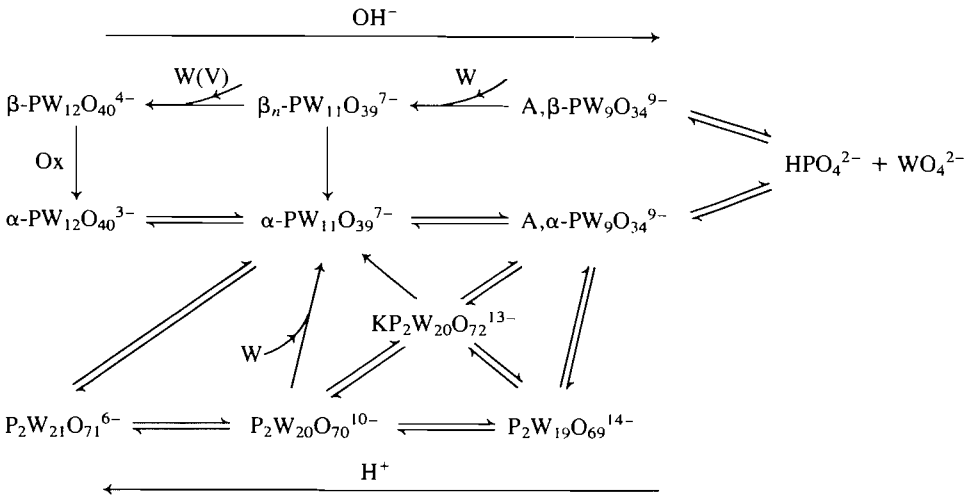

SCHÉMA 1

P_2W_{19} se décompose ensuite rapidement sans modification du pH suivant la réaction donnée plus haut, mais sa présence instantanée peut être mise en évidence par la formation du complexe $P_2W_{19}Co_2O_{71}H_4^{10-}$ (5). Comme la réaction (3) est instantanée, il n'est pas possible de mettre en évidence $KP_2W_{20}O_{72}^{13-}$ et par conséquent de choisir entre les séquences (1) ou (2) + (3). En tout état de cause, la décomposition de $P_2W_{20}O_{70}^{10-}$ est relativement lente et ne correspond pas à une simple déprotonation.

Au dessus de pH 7, toutes les courbes d'alcalinisation sont identiques et le palier de pH correspond en solution diluée à l'équilibre de l'anion α-$PW_{11}O_{39}^{7-}$ avec le paratungstate, puis le tungstate. Toutefois, la décomposition de α-PW_{11} se fait par l'intermédiaire de α-PW_9, comme le montre la préparation de ce dernier. En effet, en acidifiant un mélange tungstate–phosphate, on peut obtenir, soit A,β-PW_9 seul, soit un mélange de A,α-PW_9 et de A,β-PW_9, mais jamais l'isomère α seul.

À partir de A,α-K_9PWO_{34}, en ajoutant les quantités stoechiométriques de tungstate de potassium et d'acide, il est possible de préparer, outre α-PW_{11} et α-PW_{12} toutes les espèces de la famille de P_2W_{21}. Comme il a été signalé pour certains d'entre eux (5, 6), la présence de potassium, ou de rubidium, est indispensable pour la formation de toutes les espèces de cette famille.

À partir de A,β-$K_8HPW_9O_{34}$ ou A,β-$Na_9PW_9O_{34}$, on obtient β_n-$PW_{11}O_{39}^{7-}$ qui s'isomérise d'autant plus rapidement qu'il est plus concentré, mais jamais β-$PW_{12}O_{40}^{3-}$. Ce dernier n'est pas stable et l'anion β-$PW_{12}O_{40}^{4-}$ se transforme instantanément en α-$PW_{12}O_{40}^{3-}$ quand il est oxydé.

Les relations entre les différentes espèces sont résumés dans le schéma 1.

Finke *et al.* (17) ont les premiers signalés que le sel A,β-$Na_9PW_9O_{34}$ se transformait, à l'état solide, sous l'action de la chaleur, en B,α-$Na_9PW_9O_{34}$. Les résultats du traitement thermique sont erratiques et pour notre part, nous n'avons jamais obtenu d'échantillons contenant plus de 30% de l'isomère B. Cette transformation ne se produit ni avec A,α-$K_9PW_9O_{34}$, ni avec A,β-$K_8HPW_9O_{34}$. Il semble donc que comme avec $P_2W_{15}O_{56}^{12-}$ (2), la présence de sodium soit indispensable pour stabiliser les espèces dans lesquelles il existe un atome d'oxygène lié seulement au phosphore.

Action du cobalt(II) sur les tungstophosphates lacunaires monovacants

Il est bien connu (1) que la plupart des hétéropolyoxotungstates lacunaires complexent de nombreux ions métalliques. Nous avons pris ici l'exemple du Co(II).

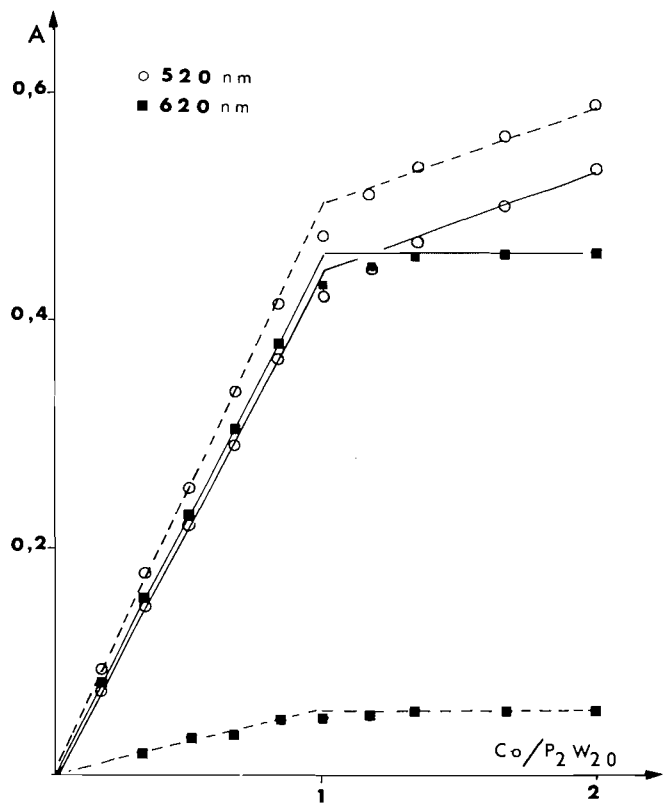

FIG. 3. Addition de Co(II) à des solutions de $P_2W_{20}O_{70}^{10-}$ $10^{-2}M$ en milieu eau–diméthylformamide à 50% : en pointillé mesures rapides de l'absorbance à 10°C; en trait plein mesures à l'équilibre à 25°C. (l = 1 cm).

Comme celle de α-$PW_{11}O_{39}^{7-}$, la solution de β_n-$PW_{11}O_{39}^{7-}$ réagit quantitativement et instantanément sur le Co(II) pour former β_n-$PW_{11}CoO_{40}H_2^{5-}$. La structure β est stabilisée, mais toutefois l'isomérisation est totale au bout de quelques jours.

L'addition de Co(II) à $P_2W_{20}O_{70}^{10-}$ montre qu'il s'agit bien d'une espèce lacunaire. Dans l'eau, il se forme un complexe peu stable rose, qui, chauffé, devient reversiblement vert entre 50 et 70°C. À partir de solutions concentrées et chaudes, il est possible d'isoler un solide de composition $P_2W_{20}Co_n$ ($n < 1$) qui redevient lentement rose lorsqu'il est refroidi. Il s'agit probablement d'un mélange de P_2W_{20} et $P_2W_{20}Co$. En utilisant un mélange eau–diméthylformamide à 50% comme solvant, il est possible de montrer (fig. 3) que le complexe rose et

Can. J. Chem. Downloaded from www.nrcresearchpress.com by 80.58.250.72 on 09/07/12
For personal use only.

TABLEAU 3. Spectres électroniques de quelques cobalto-tungstophosphates

Espèce	λ_{max} (absorptivité molaire)		
α-$PW_{11}Co$	505 ép. (61)	529 (71)	539 (71)
β_n-$PW_{11}Co$	502 ép. (67)	525 (75)	535 (74)
A,α-$P_2W_{20}Co$ (rose)	480 ép. (29)	520 (48)	620 ép. (7)
A,α-$P_2W_{20}Co$ (vert)	517 (43)	540 ép. (38)	624 (46)
A,α-$P_2W_{19}Co_2$	505 (54)	538 (52)	622 (83)
A,α-$P_2W_{18}Co_3$	496 (73)	540 (70)	622 (101)
B,α-$P_2W_{18}Co_4$	500 ép. (68)	515 (86)	578 (176)

le complexe vert correspondent tous les deux au rapport 1–1. Dans ces conditions, le composé rose se forme quantitativement et instantanément en dessous de 25°C, puis se transforme irréversiblement pour donner l'isomère vert en quelques heures. De tels composés intermédiaires roses avaient déjà été observés au cours de la formation de $As_2^{III}W_{20}Co$ (18) et de $P_2{}^{V}W_{19}Co_2$ (5), mais ils n'avaient pas été identifiés comme des isomères du complexe vert.

Ces deux isomères peuvent correspondre à différentes coordinations pour l'atome de cobalt. Dans le complexe rose, l'atome de cobalt serait hexacoordiné comme dans $Co(H_2O)_6^{2+}$ ou $PW_{11}CoO_{40}H_2^{5-}$ (tableau 3), tandis que dans le complexe vert, il serait pentacoordiné. L'étape lente correspondrait alors au départ d'une molécule d'eau, déshydratation favorisée par l'élévation de température ou la présence de diméthylformamide.

Action du cobalt(II) sur les tungstophosphates lacunaires multivacants

Tourné *et al.* (5) ont décrit la formation de $P_2W_{19}Co_2$ vert; cette réaction peut être utilisée pour détecter la présence de $P_2W_{19}O_{69}^{14-}$ comme l'apparition, en présence de cobalt(II), d'une coloration verte à chaud permet d'identifier $P_2W_{20}O_{70}^{10-}$. Par contre, $KP_2W_{20}O_{72}^{13-}$ ne donne pas de complexes avec les ions métalliques, ce qui est cohérent avec sa structure (6) (fig. 4*a*). En effet, il ne possède que des sites bidentés. L'addition de $K_{14}P_2W_{20}O_{72}$ solide à des solutions de cobalt(II) conduit à un mélange équimoléculaire $P_2W_{19}Co_2$–$PW_{11}Co$ ou à $PW_{11}Co$ seul, si le cobalt est en défaut.

L'action de A,α ou A,β-PW_9, ou d'une solution de synthèse équivalente, sur une solution de Co(II), conduit toujours à α-$PW_{11}Co$ ou B,α-$P_2W_{18}Co_4$ qui sont les seules espèces stables pour $Co/P < 2{,}5$, mais il existe plusieurs étapes intermédiaires qui dépendent de la nature de l'isomère ou du contre-ion.

A,α-$K_9PW_9O_{34}$ forme d'abord quantitativement A,α-$P_2W_{18}Co_3$. Cette espèce est instable en solution et évolue lentement pour conduire presque quantitativement à B,α-$P_2W_{18}Co_4$. Cette transformation dont la vitesse dépend fortement de la température et de la concentration se fait en 3 étapes, les intermédiaires (I et II) peuvent être caractérisés par leurs spectres visibles. Le premier (λ_{max} : 484 nm et 509 nm) a été isolé sous forme de sel de potassium correspondant à la formule $K_7PW_9Co_2$. Le second (λ_{max} : 510 nm et 532 nm), bien que plus stable, n'a pas été isolé. Ces deux espèces donnent α-$PW_{11}Co$ lorsqu'elles sont acidifiées. Avec A,β-$Na_9PW_9O_{34}$ il apparaît une nouvelle espèce. En effet, en mesurant immédiatement l'absorbance d'une série de solutions obtenues par addition d'une même quantité de A,β-$Na_9PW_9O_{34}\cdot 17H_2O$ dans des solutions de cobalt(II) de concentrations croissantes, on observe qu'à toute longueur d'onde elle croit jusqu'à $Co/P = 2$, ce qui indique la formation d'un complexe de formule $(PW_9Co_2)_n$ (λ_{max} : 475, 495 et 510 nm). À partir des solutions de ce complexe très

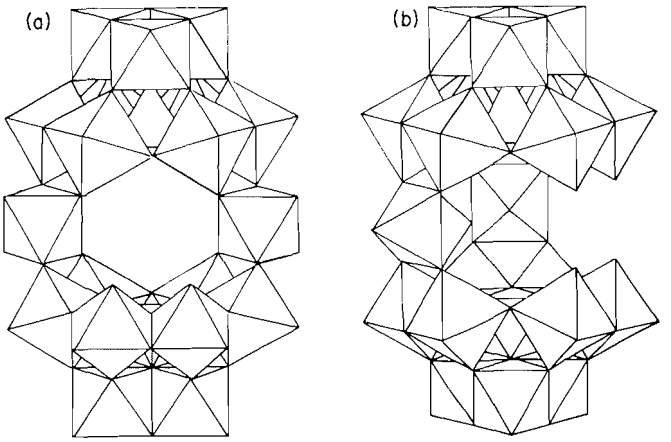

FIG. 4. Structures idéalisées des deux anions P_2W_{20}: (*a*) structure de $P_2W_{20}O_{72}^{14-}$ déterminée par Fuchs et Palm (6); (*b*) structure proposée pour $P_2W_{20}O_{70}(H_2O)_2^{10-}$.

instable, on peut obtenir : (*i*) β_n-$PW_{11}Co$ par addition de tungstate et d'acide; (*ii*) α-$P_2W_{18}Co_3$ par addition d'ions potassium, cette propriété a été utilisé pour préparer (7) ce dernier; (*iii*) α-PW_9Co_2 signalé plus haut par simple évolution. Il existerait donc deux isomères PW_9Co_2 correspondant aux formes A,α et A,β.

À partir de A,β-$K_8HPW_9O_{34}$, il se forme avec Co(II) un sel insoluble qui peut conduire à β_n-$PW_{11}Co$ par addition de tungstate et d'acide.

Les solutions de synthèse obtenues en mélangeant H_3PO_4, Co^{2+}, H_3O^+ et WO_4^{2-} ($2Na^+$) dans les proportions 2:4:18:18 conduisent dans un premier temps à un mélange des deux isomères PW_9Co_2 qui évoluent comme décrit ci-dessus pour donner principalement B,α-$P_2W_{18}Co_4$. De même, l'alcalinisation ménagée de α-$PW_{11}Co$ conduit à B,α-$P_2W_{18}Co_4$ en passant par les deux étapes intermédiaires. L'ensemble de ces relations est résumé dans le schéma 2. On peut noter qu'il existe deux voies pour la transformation A-PW_9 → B-PW_9, le traitement thermique du solide (17) ou l'isomérisation en solution en présence de Co(II) ou d'un autre ion métallique. Le cobalt(II) ne permet donc de caractériser B-PW_9 qu'à froid.

Les polyoxocobalto-tungstophosphates décrits ici ne représentent que les espèces prépondérantes. Il existe plusieurs autres complexes se formant en moindre proportion, comme par exemple $Na_{14}P_5W_{27}Co_5O_{119}H_{27}$ décrit par Weakley (19).

Considérations structurales. Résonance magnétique nucléaire de ^{183}W

Weakley (4) a déterminé la structure de $K_4P_2W_{21}O_{73}H_6\cdot 21H_2O$. Il contient deux entités A,α-PW_9 reliées entre elles par un atome de tungstène pentacoordiné et deux atomes de tungstène hexacoordinés dont les atomes d'oxygènes terminaux ou

Can. J. Chem. Downloaded from www.nrcresearchpress.com by 80.58.250.72 on 09/07/12
For personal use only.

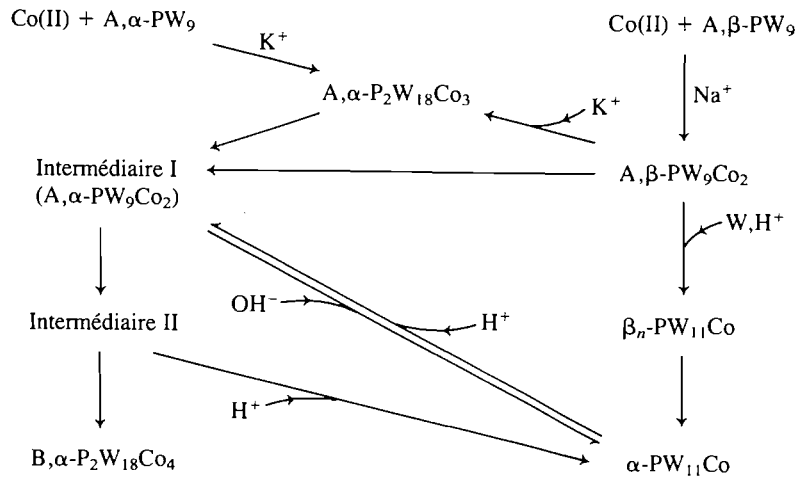

SCHÉMA 2

les molécules d'eau de coordination sont en position *trans*. La structure de $K_{14}P_2W_{20}O_{72}\cdot xH_2O$ décrite par Fuchs et Palm (6) correspond à deux entités A,α-PW_9 reliées par deux atomes de tungstène dont les oxygènes terminaux sont en *cis* (fig. 4*a*). Étant donné la filiation entre ces deux complexes et $K_{10}P_2W_{20}O_{70}\cdot 24H_2O$, on peut raisonnablement postuler que ce dernier est formé de deux entités A,α-PW_9 reliés par deux atomes de tungstène. L'existence de complexes $P_2W_{20}M$, exclut la possibilité qu'il s'agisse d'une forme protonée du complexe de Fuchs et Palm (6). Le spectre rmn du ^{183}W présente six pics d'intensité relative 2:4:4:4:4:2 à 75,6; −116,1; −142,9; −164,3; −166,3 et −201,1 ppm. Sur les cinq premiers pics on observe les couplages $^2J_{W-P}$ avec des valeurs de 1 Hz pour le premier, 2 Hz pour le second et 1,5 Hz pour chacun des trois suivants. Seul le dernier pic à 201,1 ppm ne présente pas de couplage P–W. Ce spectre est en accord avec la structure proposée (fig. 4*b*) et permet d'attribuer le dernier pic à −201,1 ppm aux tungstènes de jonction. Ceux-ci peuvent être soit pentacoordinés, soit hexacoordinés, avec une molécule d'eau occupant la sixième position. En comparant avec $As^{III}W_{21}$ dans lequel il existe des tungstènes de jonction penta- et hexacoordiné, et où le pic correspondant au plus grand déplacement chimique a été attribué au tungstène hexacoordiné (20), ce qui est en accord avec un blindage important, nous sommes amené à proposer deux tungstènes de jonction hexacoordiné. Comme sur $As_2^{III}W_{21}$, il est probable que les atomes d'oxygènes (liaison courte) sont dirigés vers l'intérieur de la cavité (21).

On peut penser que la structure de $P_2W_{19}O_{69}(H_2O)^{14-}$ se déduit de celle de $P_2W_{20}O_{70}(H_2O)_2^{10-}$ par le départ d'un tungstène de jonction.

Dans un article récent (8), Knoth *et al.* signalent la formation, par dégradation acide des complexes $M_2P_2W_{19}$, de $K_{14}P_2W_{20}O_{72}$, un isomère *trans* du composé de Fuchs. Les seules caractéristiques données sont les spectres rmn. Les déplacements chimiques sont identiques au notre pour le ^{31}P et très légèrement différents pour le ^{183}W. Il devrait s'agir de la forme déprotonée de $P_2W_{20}O_{70}(H_2O)_2^{10-}$, mais nous avons montré qu'elle est instable. Étant donné les conditions opératoires décrites, il est possible que la solution rmn acidifiée vers pH 2 contienne notre composé, et que le solide isolé vers pH 7 soit celui de Fuchs. La même ambiguïté existe d'ailleurs entre $K_4P_2W_{21}O_{72}H_6$ (4) et $K_6P_2W_{21}O_{72}H_4$ qui est la forme usuelle (1) que nous avons préparée, le passage d'une espèce à l'autre n'étant sans doute pas un simple échange de proton.

Remerciements

L'auteur remercie Martine Richet pour sa collaboration technique et le Dr. René Thouvenot qui a enregistré les spectres rmn, pour ses conseils avisés.

1. M. T. POPE. Inorganic chemistry concepts 8. Springer Verlag, Berlin. 1983.
2. R. CONTANT et J. P. CIABRINI. J. Chem. Res. (S), 222 (1977); (M), 2601 (1977); J. Inorg. Nucl. Chim. **43**, 1525 (1981).
3. R. CONTANT et A. TÉZÉ. Inorg. Chem. **24**, 4610 (1985).
4. T. J. R. WEAKLEY. Atelier des polyoxométallates. St. Lambert des Bois, France. juillet, 1983.
5. C. TOURNÉ, A. REVEL et G. TOURNÉ. Rev. Chim. Min. **14**, 537 (1977).
6. J. FUCHS et R. PALM. Z. Naturforsch. Teil B, **39**, 757 (1984).
7. W. H. KNOTH, P. J. DOMAILLE et R. D. FARLEE. Organometallics, **4**, 62 (1985).
8. W. H. KNOTH, P. J. DOMAILLE et R. L. HARLOW. Inorg. Chem. **25**, 1577 (1986).
9. J. F. KEGGIN. Proc. R. Soc. A, **144**, 75 (1934).
10. R. CONTANT, J. M. FRUCHART, G. HERVÉ et A. TÉZÉ. C.R. Acad. Sci. Paris, Sér. C, **278**, 199 (1974).
11. W. H. KNOTH et R. L. HARLOW. J. Am. Chem. Soc. **103**, 1865 (1981).
12. R. MASSART, R. CONTANT, J. M. FRUCHART, J. P. CIABRINI et M. FOURNIER. Inorg. Chem. **16**, 2916 (1977).
13. T. J. R. WEAKLEY, H. T. EVANS, J. S. SHOWELL, G. F. TOURNÉ et C. M. TOURNÉ. J. Chem. Soc. Chem. Commun. 139 (1973).
14. P. SOUCHAY. Ions minéraux condensés. Masson, Paris. 1969. p. 92.
15. A. TÉZÉ et G. HERVÉ. J. Inorg. Nucl. Chem. **39**, 999 (1977).
16. F. ROBERT et A. TÉZÉ. Acta Crystallogr. Sect. B, **37**, 318 (1981).
17. R. G. FINKE, M. DROEGE, J. R. HUTCHINSON et O. GANSOW. J. Am. Chem. Soc. **103**, 1587 (1981).
18. M. LEYRIE, J. MARTIN-FRÈRE et G. HERVÉ. C.R. Acad. Sci. Paris, Sér. C, **279**, 895 (1974).
19. T. J. R. WEAKLEY. J. Chem. Soc. Chem. Commun. 1406 (1984).
20. M. LEYRIE. Thèse d'État, Paris. 1984.
21. Y. JEANNIN et J. MARTIN-FRÈRE. J. Am. Chem. Soc. **103**, 1664 (1981).

Can. J. Chem. Downloaded from www.nrcresearchpress.com by 80.58.250.72 on 09/07/12
For personal use only.

Preparation of chiral allylic alcohols using *Rhizopus nigricans*. Use of the Harada–Nakanishi exciton chirality method for verifying configurational assignments of allylic alcohols

SATORU ITO,[1] MASAJI KASAI,[2] AND HERMAN ZIFFER[3]

Laboratory of Chemical Physics, National Institute of Diabetes and Digestive and Kidney Diseases, National Institutes of Health, Bethesda, MD 20892, U.S.A.

AND

J. V. SILVERTON[3]

Laboratory of Chemistry, National Heart, Lung, and Blood Institute, National Institutes of Health, Bethesda, MD 20892, U.S.A.

Received June 2, 1986

SATORU ITO, MASAJI KASAI, HERMAN ZIFFER, and J. V. SILVERTON. Can. J. Chem. **65**, 574 (1987).

A series of (*R*) acyclic and cyclic allylic alcohols was prepared by enantioselective hydrolysis of acetates using *Rhizopus nigricans*. The configurations of the alcohols formed were established by chemical methods and, in the case of 1,2-benzocyclohepta-1,3-dien-5-yl camphanate, by X-ray crystallography. In conjunction with the Harada–Nakanishi rule, the chiroptical properties of the *p*-bromobenzoate esters were used to verify configurations tentatively assigned from their method of preparation.

SATORU ITO, MASAJI KASAI, HERMAN ZIFFER et J. V. SILVERTON. Can. J. Chem. **65**, 574 (1987).

Faisant appel au *Rhizopus nigricans*, on a effectué des hydrolyses énantiosélectives d'acétates qui ont permis de préparer une série d'alcools allyliques cycliques et acycliques de configuration (*R*). On a déterminé ces configurations en faisant appel à des méthodes chimiques et, dans le cas du camphanate de benzo-1,2 cycloheptadiène-1,3 yle-5, à la diffraction des rayons-X. En relation avec la règle de Harada–Nakanishi, on a utilisé les propriétés chiroptiques des esters *p*-bromobenzoates pour vérifier les configurations qui avaient été attribuées provisoirement en se basant sur les méthodes de préparation.

[Traduit par la revue]

The emergence of chiral allylic alcohols as critical and versatile intermediates for the synthesis of natural products, metabolites, and drugs (1) makes this class of compounds a logical target for testing our recently developed method of preparing chiral secondary alcohols of a predictable absolute stereochemistry (2, 3). The method employs the mold, *Rhizopus nigricans*, for the hydrolysis of racemic acetates to yield chiral alcohols enriched in one enantiomer and unhydrolyzed acetates derived from the antipodal alcohol. Predictions of the absolute stereochemistry of the alcohol formed are based on a rule that the enantiomer shown in Fig. 1 is the one more rapidly hydrolyzed, where R^1 is the effectively larger substituent. The results of some 50 hydrolyses were used to assign the effective sizes of a number of substituents; the observed ordering in their sizes was found to be identical with that employed in a chemical method developed by Horeau (4) for determining the configurations of secondary alcohols.

Our earlier studies provided no information on the relative size of a carbon–carbon double bond versus a methylene group; consequently, no a priori prediction about the stereochemical course of the hydrolysis of allylic acetates was possible. We describe here the results of hydrolyzing a number of acyclic and cyclic allylic acetates using *R. nigricans* and compare the predicted configurations of the resulting alcohols with those established by chemical or crystallographic methods. While these hydrolyses have consistently yielded optically active alcohols, the absolute stereochemistry of one of the approximately ten alcohols, predicted from the above rule, was found to be in error. In an effort to identify other possible exceptions to the rule, we have determined the chiroptical properties of the allylic alcohols and their *p*-bromobenzoates. The cd (circular dichroism) curves of the latter were used in conjunction with the Harada–Nakanishi rule (5) for relating the signs of these curves to their configurations. When the configurations deduced from the optical and microbial methods differed, additional work was necessary to establish the configuration of the alcohol.

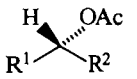

Where $R^1 > R^2$

FIG. 1. Enantiomer more rapidly hydrolyzed (where R^1 is effectively larger than R^2).

Results and discussion

Partial hydrolysis of racemic 3-cyclopentenyl (**1***b*), 3-cyclohexenyl (**2***b*), and 3-cycloheptenyl (**3***b*) acetates using the mold, *Rhizopus nigricans*, yielded alcohols enriched in the (*R*) enantiomer. The results summarized in Table 1 can be accounted for by our rule (Fig. 1) and the assumption that a carbon–carbon double bond is effectively larger than a methylene group. This assignment of the relative size of these groups agrees with that used in Horeau's chemical method (6) of assigning configurations of secondary alcohols.

The enantiomeric excesses (ee's) obtained in these hydrolyses were low; we have therefore examined two methods of increasing these values. The first approach simply involves reacetylating the chiral alcohol obtained from one hydrolysis, and subjecting the resulting ester to a second hydrolysis. There are data in the literature from the work of Sih and co-workers (7) and results by us (3) on other alcohols to indicate that this

[1]Current address: Fujirebio Inc., Research Laboratory, 51 Komiya-cho, Hachioji, Tokyo 192, Japan.

[2]On leave from Kyowa Hakko Kogyo Co., Ltd., Tokyo Research Laboratory, 3-6-6 Asahi-machi Machida-shi, Tokyo 194, Japan.

[3]Authors to whom correspondence may be addressed.

Can. J. Chem. Downloaded from www.nrcresearchpress.com by 80.58.250.72 on 09/07/12
For personal use only.

TABLE 1. Summary of data on the hydrolysis of allylic acetate by *Rhizopus nigricans*

Substrate	% Hydrolysis	% Recovery*	Configuration of alcohol formed	Specific rotation in $CHCl_3$ (ee)
1*b*	24	45	*R*	+5.7(14)
2*b*	28	51	*R*	+18.4(15)
3*b*	51	98	*R*	+7.9(25)
4*b*	43	93	*R*	+32(51)
5*b*	52	79	*R*	+16.6(29)
6*b*	40	52	*R*	+28.9(40)
7*b*	18	72	*R*	+8.3†
8*b*	37	68	*R*	+16.1(22)
10*b*	19	48	*R**	+9.9†
11*b*	38	57	*R**	+39.5(31)
13*b*	—	—	*R*	+31.2(98)
14*b*	28	64	*S*	−99.7(28)
15*b*	20	46	*R*	+98.5(74)
16*b*	44	68	*R*	−164(97)
17*b*	40	69	*R*	+28(58)
18*b*	46	34	*R*	+14.5(41)
20*b*	59	—	*S*	−8.6(51)

*Configurational assigned based on the cd of the *p*-bromobenzoate and the Harada–Nakanishi exciton chirality method.

†Optical purity unknown.

approach is successful. The second approach followed logically from an earlier observation that alcohols with large ee's were obtained from substrates in which substituents on the carbinol carbon differed greatly in their effective sizes. If the larger ee values were related to large differences in the relative sizes of substituents, then a further increase in the effective size of the double bond should result in an increase in the ee of the carbinol formed. One method of increasing the effective size of the double bond is to introduce a substituent on either olefinic carbon. To be able to prepare unsubstituted alcohols, the added substituent should be readily replaceable by a hydrogen. We therefore prepared racemic acetates of several 2- and 3-substituted allylic alcohols (see Scheme 1) and determined the configurations and ee's of alcohols obtained from their enantioselective hydrolysis. To better understand the effect of substituents on the double bond we also prepared and examined the products from the hydrolysis of 2-methyl-, 2-chloro-, 2-phenyl-, and 2-*tert*-butyl-2-cyclohexenyl acetates. Data on the results of these hydrolyses are included in Table 1; they

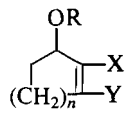

a R = H
b R = Ac
c R = camphanate

1 *n* = 1 X = Y = H
2 *n* = 2 X = Y = H
3 *n* = 3 X = Y = H
4 *n* = 1 X = Br, Y = H
5 *n* = 2 X = Br, Y = H
6 *n* = 3 X = Br, Y = H
7 *n* = 1 X = H, Y = Br
8 *n* = 2 X = H, Y = Br
9 *n* = 2 X = ϕ, Y = H
10 *n* = 2 X = CH_3, Y = H
11 *n* = 2 X = Cl, Y = H
12 *n* = 2 X = *t*-Bu, Y = H

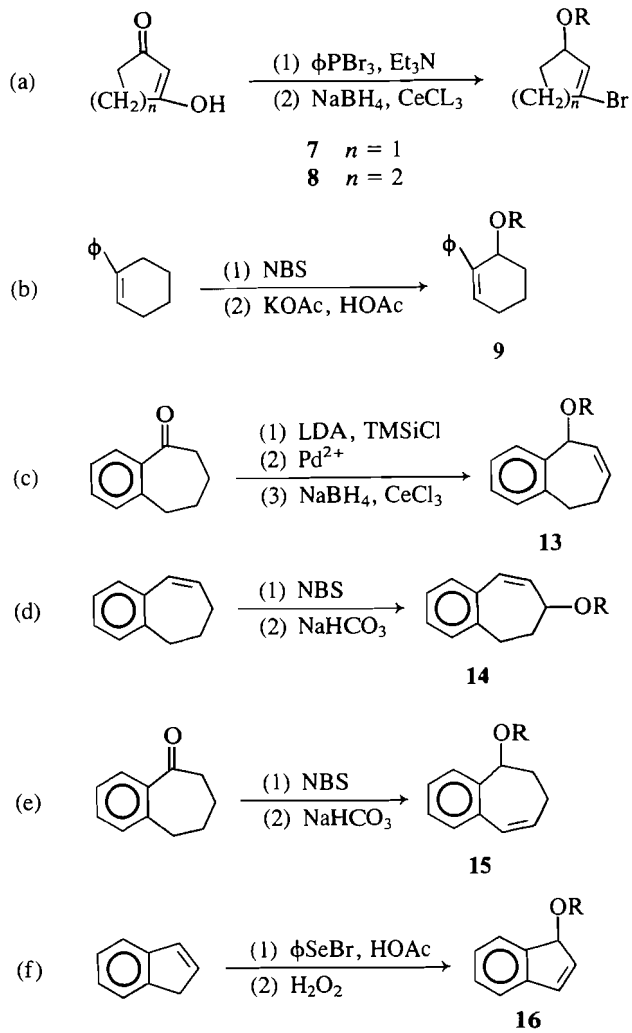

a R = H *b* R = Ac

SCHEME 1

Can. J. Chem. Downloaded from www.nrcresearchpress.com by 80.58.250.72 on 09/07/12
For personal use only.

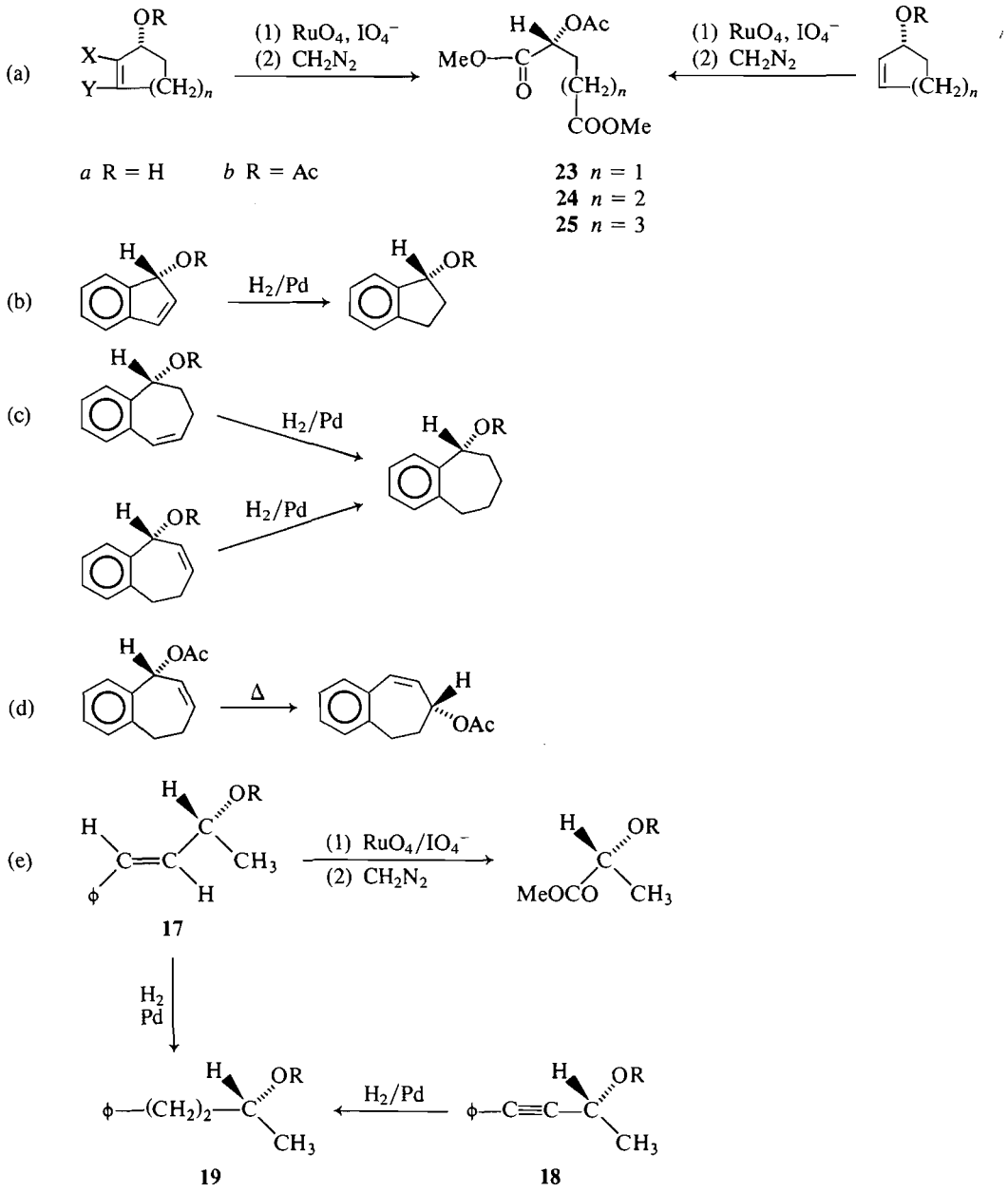

SCHEME 2

show that very bulky groups, 2-phenyl and 2-*tert*-butyl, hinder or severely retard the enzymic hydrolysis of the ester.

Each of the brominated allylic alcohols obtained in these hydrolyses had the same (*R*) configuration as the unsubstituted alcohol. The ee's of the 2-substituted five-, six-, and seven-membered cyclic compounds were equal to or greater than those of the unsubstituted ones. The presence of a substituent two bonds away from the acetate did not significantly increase the ee of the resulting alcohol.

Since the results of these hydrolyses establish that carbon–carbon double bonds are effectively larger than the methylene group and since earlier studies had shown that a fused aromatic ring was likewise larger (3), we were interested in determining the relative size of an aromatic ring and carbon–carbon double bond. Compounds **13***b* and **16***b* were prepared (Scheme 1, (c) and (f)) and the absolute stereochemistries of the alcohols formed were established as (*R*) by the reaction sequence shown in Scheme 2. While hydrolysis of **13***b* yields a small quantity of (+)-**13***a*, the major hydrolysis product was the rearranged alcohol (−)-**14***a*. In the process of establishing the configuration of the latter, the hydrolysis of **14***b* was also examined and found to yield (−)-**14***a*, i.e. the same enantiomer as was obtained from **13***b*. As converting (−)-**14***b* into a compound of established absolute stereochemistry proved to be difficult, we elected to convert (*R*)-**13***b* into **14***b*. This rearrangement was achieved by heating a sample of (−)-**13***b* at 145°C for 20 min to yield (+)-**14***b* (Scheme 2(d)). Since (−)-**13***b* has an (*R*) configuration and similar 1,3-rearrangements proceed in a suprafacial manner, the product (+)-**14***b* (which yields (+)-**14***a* on hydrolysis) should have an (*R*) configuration. The enantioselective hydrolysis of (±)-**14***b* was expected to yield the (*R*) enantiomer, (+)-**14***a*, from our rule. The observation that (−)-**14***a* was formed required its configuration to be assigned in an unequivocal manner. That assignment was made by an X-ray structure determination of the camphanate ester **14***c*, which yields (+)-**14***a* on hydrolysis. The structure determination, Fig. 2, confirmed an (*S*) configuration for (−)-**14***a*.

In addition to cyclic allylic acetates, the enantioselective

Can. J. Chem. Downloaded from www.nrcresearchpress.com by 80.58.250.72 on 09/07/12
For personal use only.

Can. J. Chem. Downloaded from www.nrcresearchpress.com by 80.58.250.72 on 09/07/12
For personal use only.

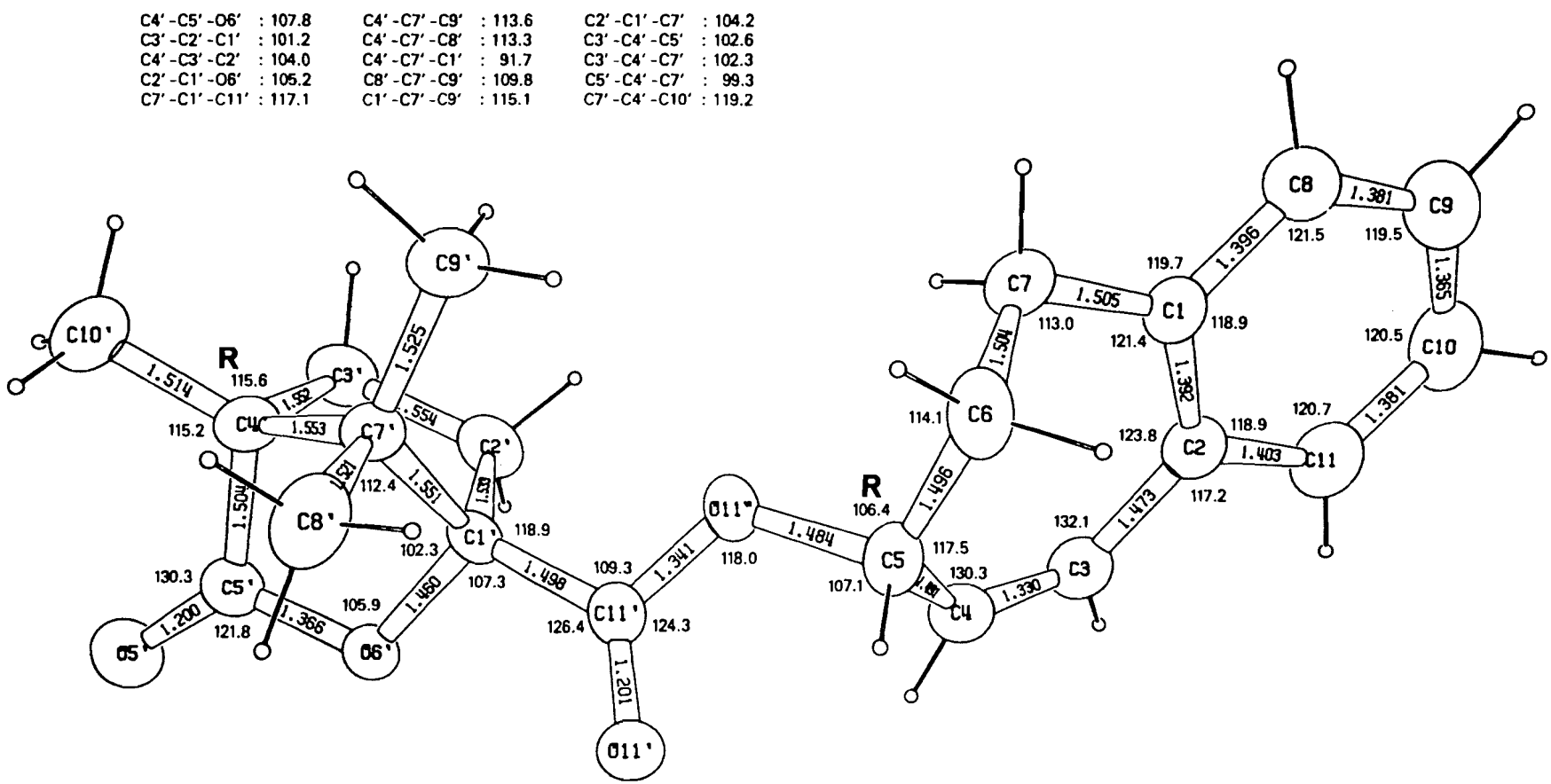

FIG. 2. Crystal structure of (+)-**14***c*.

TABLE 2. Summary of data on chiroptical properties of the corresponding acetates and *p*-bromobenzoates of allylic alcohols

Alcohol	Absolute stereochemistry	Circular dichroism of acetate $\Delta\epsilon$	Sign of cd of *p*-bromobenzoates $\Delta\epsilon$ (λ_{max})
1*a*	*R*		+
2*a*	*R*		+
3*a*	*R*		+
4*a*	*R*		+
5*a*	*R*		+
6*a*	*R*		+
7*a*	*R*		+
8*a*	*R*		+
9*a*	*R*	+6.0(233)	+
10*a*	*R*		+
11*a*	*R*		+
14*a*	*S*	+21.3(250) +27.4(250)*	−114(255) +51.5(238)
15*a*	*R*	+9.7(249)	+21.2(256) −12.3(235)
16*a*	*R*	−4.74(264)	−10.4(259) 5.3(230)
17*a*	*R*	+8.5(251)	−12.8(255) +9.24(238)

*Camphanate ester.

hydrolyses of an acyclic allylic acetate **17***b* and an acetylenic ester **18***b* were also examined. The (*R*)-alcohols (see Table 1) were obtained in each case. The result is consistent with the rule and the assumption that a carbon–carbon double or triple bond is effectively larger than a methyl group. Data on the chiroptical properties of the corresponding *p*-bromobenzoates are given in Table 2.

Data on the hydrolysis of an acyclic phenyl acetylenic acetate, **20***b*, had previously been reported (3); the configuration of the alcohol formed was accounted for by our rule and the assumption that a phenyl group was effectively larger than a carbon–carbon triple bond.

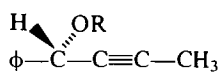

20

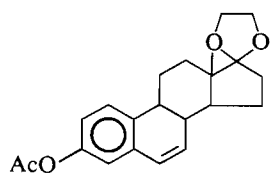

21

a R = H
b R = Ac
c R = camphanate

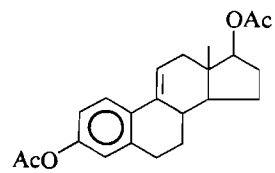

22

Synthesis of racemic substrates and determination of the absolute stereochemistry of the alcohols formed in R. nigricans *mediated hydrolyses*

Samples of the racemic substrates used in these studies were prepared by standard literature methods and by those outlined in Scheme 1.

Although the absolute stereochemistry of most of the unsubstituted cyclic allylic alcohols was known, that of the corresponding brominated derivatives was not. The groups of compounds were interrelated by oxidizing the olefinic carbons in each compound to carboxylic acid groups as shown in Scheme 2(a). A comparison of the specific rotations of the dimethyl esters, **23**–**25**, derived from the allylic acetates and their halogenated derivatives (Scheme 2(a) and Table 3), was used in assigning the absolute stereochemistry of the latter.

The configuration of (−)-**16***a* was determined by reduction to (*R*)-indanol (Scheme 2(b)).

The absolute stereochemistries of (+)-**13***b* and (−)-**15***b* were established by reducing each to (*R*)-benzocyclohepten-3-yl acetate (**15**) (Scheme 2(c)).

*X-ray crystallographic structure and stereochemical assignment of (+)-**14**c*

A sample of racemic **14***a* was converted to diastereomeric camphanate esters, which were separated by fractional crystallization. The structure and absolute stereochemistry of the (+)-camphanate, **14***c*, were determined crystallographically; the results given in the experimental section of this paper show an (*R*) configuration at the carbinol carbon. Since hydrolysis of the (+)-camphanate yields (+)-**14***a*, the configuration of (−)-**14***a* formed in the enantioselective hydrolysis of **13***b* and **14***b* was (*S*). This assignment confirms the earlier one based on the thermal rearrangement of (−)-**13***b*.

While determining absolute stereochemistry by X-ray crystallographic methods is usually unambiguous, we have found the assignment of (*R*) and (*S*) designations from visual inspection of crystallographic diagrams or display screens to be a process fraught with error. Common molecular display programs usually allow the rapid calculation of torsion angles and the calculation can be extended to nonbonded atoms for unambiguous determination of stereochemistry. If a chiral atom has four prioritized substituents 1, 2, 3, and 4 and the atoms directly attached to the chiral atom are 1a, 2a, 3a, and 4a, we define the chiral angle χ as the 1a–2a–3a–4a dihedral angle (it

Can. J. Chem. Downloaded from www.nrcresearchpress.com by 80.58.250.72 on 09/07/12
For personal use only.

TABLE 3. Summary of data on the specific rotations of dimethyl 2-acetoxydicarboxylates from 3-cycloalkenyl and 2-bromo-3-cycloalkenyl acetates

Compound	Specific rotation (ee)	Specific rotation corrected to 100% ee
23 (from **1***b*)	−1.43(6)	−24
23 (from **4***b*)	−12.6(51)	−25
23 (from **7***b*)	−5.36(23)	−23
24 (from **2***b*)	−5.14(20)	−26
24 (from **5***b*)	−7.11(27)	−26
24 (from **8***b*)	−3.64(15)	−24
25 (from **3***b*)	−6.00(25)	−24
25 (from **6***b*)	−3.00(13)	−24

is not strictly a torsion angle since the atoms are not directly connected). Since probable errors in dihedral angles are of the order of 2–3° and since the χ value for a chiral atom with substituents at the corners of a regular tetrahedron is +70.53° for an (*R*) and −70.53° for an (*S*) configuration, χ is usually definitive. In real structures, the magnitude of χ is normally 60–80°. One might also note that only the order of the substituents is required since $\chi(1\text{–}2\text{–}3\text{–}4) = \chi(4\text{–}3\text{–}2\text{–}1)$.

The chiroptical properties of p-*bromobenzoates of allylic alcohols*

Since the configuration of (−)-**14***a* obtained from **13***b* and **14***b* was not the one predicted from its method of preparation, it became important to have another method of independently assigning the configurations of small quantities of chiral allylic alcohols that were not optically pure. Since many such compounds are oils and are available in relatively small quantities, we elected to investigate an optical method developed by Harada and Nakanishi (H–N) (5*b*). Their method has proven to be reliable in assigning the absolute stereochemistry of *p*-substituted benzoates of allylic alcohols from data on the signs of their cd curves. The H–N rule states that if one looks down the carbon–carbon bond from the carbinol carbon toward the carbon–carbon double bond, a positive cd band (at approximately 240–245 nm) is predicted for the molecule if the benzoate group has to be rotated in a clockwise direction to eclipse the double bond. A counterclockwise rotation is associated with a negative cd band (see Fig. 3). For five-, six-, and seven-membered rings these predictions are independent of the conformation of the molecule. In acyclic compounds the predicted sign is dependent upon the rotamer under consideration. Thus, as a distribution of rotamers exists in solution, the observed cd band, which is the algebraic sum of the curves of all rotamers, can only be related to the absolute stereochemistry of acyclic allylic esters when there is some information on the rotamer distribution in solution along with an estimate of the rotational strengths of the various rotamers.

p-Bromobenzoates of the alcohols obtained in these studies were prepared and data on their chiroptical properties are summarized in Table 2. Inspection of the table shows that all esters of cyclic (*R*)-alcohols, except for (−)-**16***b*, exhibit positive cd bands at 240–245 nm. Thus, the negative cd curve observed for the *p*-bromobenzoate of (−)-**14***a* serves as a warning that the configuration based on its method of preparation might be incorrect.

As data for the relation between the signs of the cd curves of the acyclic allylic alcohols are limited, it is premature to interpret those data. Since the exciton chirality model relates the

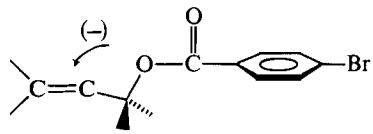

FIG. 3.

interaction of the transition moment along the carbon–carbon double bond with the transition moment of the *p*-substituted benzoate along its long axis, the presence of a halogen on the carbon–carbon double bond of cyclic allylic esters should not alter the direction of the transition moment of that carbon–carbon double bond. Indeed, the observed signs of the cd curves of the brominated derivatives are the same as those of the unsubstituted compounds. The signs of three (*R*)-alcohol derivatives in which the double bond is conjugated to an aromatic ring differ. Thus, in at least one case, the presence of a conjugated aromatic ring has changed the direction of the transition moment of the carbon–carbon double bond.

Chiroptical properties of conjugated allylic alcohols

While the cd curves of the conjugated allylic alcohols or acetate esters cannot be analyzed by the exciton chirality method, Crabbe (8*a*) suggested a relationship between the signs of the chiroptical effects of these compounds and their absolute stereochemistry. That analysis classified skewed styrenes as dissymmetric chromophores and suggested that the skew sense of the chromophore is related to the sign of the longest wavelength cd band. Our measurement of the cd curves of the camphanate and acetate esters of (−)-**14***a* shows them to have very strong positive cd bands, as would be expected from dissymmetric chromophores. The X-ray structure determination of (+)-**14***c* established a left-handed skew sense for the styrene chromophore in the crystal. Molecular models of the compounds **21** and **22**, which Crabbe reported as exhibiting positive cd bands for the longest wavelength transition, have a left-handed skew sense. The Crabbe analysis and the observed positive sign for the cd band of (+)-**14***b* are consistent with the left-handed skew sense found crystallographically. However, molecular models show that the skew sense of **14***a* and derivatives varies with their conformations. Furthermore, the critical assumption that *only* dissymmetric chromophores (e.g., skewed dienes) exhibit large cd curves for the longest wavelength transition is *not* consistent with recent observations for planar dienes. Duraisamy and Walborsky (8*b*) reported that the planar dienes that are not dissymmetric chromophores also show very strong chiroptical effects. To collect data on the chiroptical properties of additional styrene derivatives, we have measured the cd curves of compounds **9***b*, **15***b*, and **17***b* and summarized those results in Table 2.

Conclusion

Enantioselective hydrolysis of esters by *R. nigricans* can be used to prepare a wide variety of chiral allylic alcohols. The order of the effective sizes of substituents used in predicting the configurations of these alcohols is identical with that employed in Horeau's method. While the configurational assignments of allylic alcohols formed in these hydrolyses can usually be assigned from their method of preparation, they should be verified using information on the signs of the cd bands of the corresponding *p*-bromobenzoates and the Harada–Nakanishi rule. The microbially based method thus complements existing chemical methods of preparing chiral samples of this class of

Can. J. Chem. Downloaded from www.nrcresearchpress.com by 80.58.250.72 on 09/07/12
For personal use only.

molecules and provides an additional method of assigning their configurations.

Experimental

General methods

All melting points were determined using a hot-stage apparatus and are uncorrected. Proton magnetic resonance spectra were recorded on a Varian HR-220 instrument in $CDCl_3$. Chemical shifts are reported in parts per million (ppm) downfield from tetramethylsilane. Coupling constants are given in Hz. Optical rotations were recorded on a Perkin–Elmer 241MC polarimeter. Circular dichroism measurements were made using a Jasco J-500A spectropolarimeter. Preparative and analytical tlc work was performed on plates coated with silica gel F-254. The enantiomeric excesses (ee's) were usually obtained by comparing observed and reported specific rotations.

Microbial hydrolyses

The potato-dextrose medium for growing *R. nigricans* was prepared as previously described (3). A 1-L Erlenmeyer flask containing 250 mL of this medium was inoculated with *Rhizopus nigricans* (ATCC 6227b) grown in liquid culture, and shaken for 6–7 days at 25°C. The substrate (460 mg) in 1 mL of THF was added and the flask was shaken for 16–24 h. The mycelium and medium were extracted with ethyl acetate (3 × 100 mL) and the combined extracts were dried and concentrated. The area under the protons on the carbinol carbon in an nmr spectrum of the crude extract was used to determine percent hydrolysis. The recovered acetate and the alcohol formed were separated by column chromatography on silica gel with *n*-hexane and ethyl acetate as eluants. Data on recoveries, configurations of the alcohols formed, and specific rotations are summarized in Table 1.

Synthesis

Compounds **1***b*, **2***b*, and **3***b* were prepared from the corresponding unsaturated ketones by reduction with sodium borohydride in the presence of an equivalent of cerium trichloride as described by Gemal and Luche (10). The allylic alcohols were acetylated with acetic anhydride in pyridine in the usual manner. The 2-bromo derivatives **4***a* and **5***a* were prepared from the corresponding α,β-unsaturated ketones by bromination in the presence of triethylamine and purified by column chromatography on silica gel. Data on their proton nmr spectra were identical to that reported in the literature (9). The 2-bromo α,β-unsaturated ketones were reduced to allylic alcohols with sodium borohydride in the presence of an equivalent of cerium trichloride (10). A sample of **6***b* was prepared from dibromo[6.1.0]heptane by a silver acetate catalyzed solvolysis (11).

The 3-bromo α,β-unsaturated compounds **7***a* and **8***a* were prepared from the corresponding 1,3-diketone by reaction with triphenylphosphine dibromide (Scheme 1(a)) as described by Piers and Nagakura (12*a*), followed by reduction with sodium borohydride in the presence of cerium chloride as described above.

The absolute stereochemistry of compounds **1***a* (19), **2***a* (20), and **3***a* (15) is known. The corresponding acetates were oxidized, using ruthenium tetroxide (15), to the corresponding dicarboxylic acids (Scheme 2(a)), which were methylated with diazomethane. The esters were purified by column chromatography to yield known esters, and data on their specific rotations are summarized in Table 3. Compounds **4***b*, **5***b*, **6***b*, **7***b*, and **8***b* were also oxidized with ruthenium tetroxide and the resulting dicarboxylic acids esterified with diazomethane. After purification (column chromatography on silica gel), a comparison of the specific rotations of the dimethyl esters with those obtained from the unsubstituted allylic acetates showed them to have the same sign, see Table 3. A sample of racemic **9***a* was prepared by allylic bromination (NBS), in carbon tetrachloride, of 1-phenylcyclohexene followed by solvolysis of the resulting allylic bromide in aqueous THF containing sodium bicarbonate. A sample of the chiral alcohol, **9***a*, was prepared from (*R*, *S*) *trans* 2-phenylcyclohexanol, $[\alpha]_D$ −46.3° (*c* 3.1, C_6H_6), obtained by hydrolysis of the corresponding acetate by *R. nigricans*. The alcohol was reacetylated to yield **9***b*, $[\alpha]_D$ −14.0° (*c* 3.1, $CHCl_3$). Allylic bromination in CCl_4 with NBS and benzoylperoxide gave, after the standard work-up, an oil that was dehydrohalogenated with DBU in THF at room temperature. The mixture was extracted with ether, concentrated, and the acetate hydrolyzed by refluxing for 20 min in aqueous THF containing KOH. After the standard work-up, chromatography on silica gel yielded **9***a* as a colorless oil; $[\alpha]_D$ +114.5° (*c* 1.6, $CHCl_3$); ^{1}H nmr: 1.50–2.02 (m, 5H), 2.09–2.35 (m, 2H), 4.70 (br s, 1H), 6.15 (t, *J* = 4, 1H), 7.14–7.75 (m, 5H). The *p*-bromobenzoate was prepared by reaction with *p*-bromobenzoyl chloride in the usual manner.

Compounds **10***b*, **11***b*, and **12***b* were prepared by chlorinating the appropriately 2-substituted cyclohexanones with sulfuryl chloride in CCl_4 at room temperature. The reaction mixtures were then washed with water, aqueous $NaHCO_3$, saturated aqueous NaCl, dried, and distilled *in vacuo*. The 2-chloro derivatives were dehydrohalogenated with LiCl in DMF at 140°C for 1 h. The reaction mixtures were diluted with water, extracted into ether, and the ether extract was washed with dilute H_2SO_4, dried, and concentrated. The unsaturated ketones were isolated by vacuum distillation and purified by column chromatography. The unsaturated ketones were converted to allylic acetates by reduction and acetylation as described above.

An optically active sample of **10***a* was prepared by Tanno and Terashima (21) but they were unable to assign its configuration. A configuration has been assigned to the alcohol, based on the observation of a positive cd curve for its *p*-bromobenzoate and the Harada–Nakanishi rule (5). An (*R*) configuration was also assigned to (+)-**11***a*, based on the finding of a positive cd curve of the *p*-bromobenzoate ester.

*1,2-Benzocyclohepta-1,4-diene-3-ol (**13**a)*

A solution of benzosuberone in ether (8 g in 5 mL) was added dropwise to an ether solution of LDA in 60 mL of ether at −78°C (Scheme 1(c)). After 2 h, a solution of triethylamine (2.5 mL) in ether (5 mL) was added followed by a solution of trimethylsilyl chloride (10 mL) in ether (15 mL). The mixture was warmed to room temperature after 30 min and poured into water (100 mL). The solution was extracted with hexane and the hexane solution washed with aqueous sodium bicarbonate, dried, and concentrated. The trimethylsilyl enol ether was distilled as a colorless oil (10.0 g, bp 102–103°C/0.85 Torr (1 Torr = 133.3 Pa)). It was next added dropwise to a mixture of palladium acetate (3.25 g) and benzoquinone (1.23 g) in acetonitrile (50 mL) at room temperature (14), stirred for 4 h, and filtered. The filtrate was concentrated under reduced pressure and purified by column chromatography on silica gel to yield 2.41 g of 1,2-benzocyclohepta-1,4-diene-3-one as a colorless oil; ^{1}H nmr: 2.56 (td, *J* = 5.5, 5.0, 2H), 3.03 (t, *J* = 5.5, 2H), 6.25 (d, *J* = 11.5, 1H), 6.71 (td, *J* = 11.5, 5.0, 1H), 7.07–7.46 (m, 3H), 7.72 (d, *J* = 7, 1H). The unsaturated ketone was reduced with sodium borohydride (587 mg) in methanol (40 mL) containing cerium trichloride heptahydrate (5.67 g) at 0°C for 15 min. The resulting alcohol **13***a* was extracted with ether and purified by column chromatography on silica gel to yield colorless needles, mp 84–86°C; ^{1}H nmr: 2.07–2.37 (m, 2H), 2.46 (s, 1H), 2.70–3.13 (m, 2H), 5.46 (dt, *J* = 9.5, 4.0, 1H), 5.66 (s, 1H), 5.69 (dd, *J* = 9.5, 2.0, 1H), 7.02–7.25 (m, 3H), 7.30–7.43 (m, 1H). The empirical formula and molecular weight were established by mass spectroscopy as $C_{11}H_{12}O$; calcd.: 160.0888; found: 160.0887.

The acetate, **13***b*, was obtained from **13***a*, as a colorless oil; ^{1}H nmr: 2.14 (s, 3H), 2.34 (m, 2H), 2.95 (dt, *J* = 14.6, 1H), 3.17 (dt, *J* = 14.0, 6.0, 1H), 5.64 (dt, *J* = 12.0, 2.8, 1H), 5.75 (dd, *J* = 12.0, 4.2, 1H), 6.48 (dd, *J* = 1.8, 4.2, 1H), 7.07–7.31 (m, 4H).

Hydrolysis of **13***b* (543 mg) using *R. nigricans* (7 h at room temperature) yielded a crude mixture of **13***a*, **14***a*, and **14***b*. These were separated by column chromatography on silica gel to yield **13***a* (116 mg, 28%), $[\alpha]_D$ +31.2° (*c* 2.9, $CHCl_3$); **14***a* (111 mg, 26%), $[\alpha]_D$ −67.5° (*c* 2.8, $CHCl_3$); **14***b* (11 mg, 2%), $[\alpha]_D$ +63.5° (*c* 0.90, $CHCl_3$).

A sample of (−)-**13***b* (91 mg, $[\alpha]_D$ −14.5° ($CHCl_3$)) in DMSO-d_6 (1 mL) was heated to 145°C for 25 min. Chromatography of the yellow solution on silica gel ((ethyl acetate:hexane, 3:97) yielded **14***b* (17 mg, $[\alpha]_D$ +43.0° (*c* 0.60, $CHCl_3$)).

Configurational assignments

A sample of (−)-**13***a* ($[\alpha]_D$ −25.2°) was hydrogenated in ethyl

Can. J. Chem. Downloaded from www.nrcresearchpress.com by 80.58.250.72 on 09/07/12
For personal use only.

Can. J. Chem. Downloaded from www.nrcresearchpress.com by 80.58.250.72 on 09/07/12
For personal use only.

acetate over PtO_2 to yield, after chromatography, 78 mg of (*R*) 1,2-benzocyclohepten-3-ol ($[\alpha]_D$ +33.8°) (15).

A sample of (3*S*) 1,2-benzocycloheptenol ($[\alpha]_D$ −32.2°) was acetylated in the usual manner to yield (3*S*) acetoxy-1,2-benzocycloheptene ($[\alpha]_D$ −76.8°).

*1,2-Benzocyclohepta-1,3-dien-5-ol (**14**a)*

A solution of 1,2-benzocyclohepta-1,3-diene (4.3 g) in CCl_4 (70 mL) was refluxed with NBS (6.297 g) and benzoylperoxide (596 mg) for 20 min. The crude mixture of allylic bromides was isolated and hydrolyzed with sodium bicarbonate (10.8 g) in 100 mL THF–H_2O for 6 h. The solution was extracted several times with ether and the ether solution concentrated. The crude reaction product was chromatographed on silica gel to yield **14***a* (2.52 g) as a colorless oil; ^{1}H nmr: 1.92–2.29 (m, 3H), 2.31–2.63 (m, 2H), 4.85 (br d, J = 4.5, 1H), 5.89 (td, J = 4.6, 12.4, 1H), 6.37 (d, J = 12.4, 1H), 7.08–7.30 (m, 3H), 7.38 (d, J = 6.5, 1H). *Mol. Wt.* calcd. for $C_{11}H_{12}O$: 160.0888; found: 160.0874.

The acetate, **14***b*, was prepared by acetylation of **14***a* in the usual manner. The empirical formula and molecular weight were established by mass spectroscopy as $C_{13}H_{14}O_2$; calcd.: 202.0994; found: 202.1003.

Acetylation of (−)-**14***a* ($[\alpha]_D$ −67.46°) yielded (−)-**14***b* ($[\alpha]_D$ −80.5° (*c* 0.026, $CHCl_3$).

*Preparation of **14**c, the (+)-camphanate of **14**a*

A solution of the racemic alcohol in pyridine was reacted with 1.1 equivalents of camphanic acid chloride at room temperature overnight. The camphanate was purified by column chromatography; repeated fractional crystallization from hexane – ethyl acetate yielded colorless plates, mp 120–121°C; $[\alpha]_D$ +286° (*c* 1.3, $CHCl_3$). *Anal.* calcd. for $C_{21}H_{24}O_4$: C 74.12, H 7.06; found: C 74.45, H 7.36.

The (+)-camphanate was hydrolyzed in refluxing aqueous THF (1:1) containing 2 equiv. of KOH. The solution was diluted with water and extracted with ether. The alcohol was purified by column chromatography on silica gel to yield (+)-**14***a*; $[\alpha]_D$ +361° (*c* 1.5, $CHCl_3$).

*1,2-Benzocyclohepta-1,3-dien-7-ol (**15**a)*

The crude reaction product obtained by allylic bromination of benzosuberone in carbon tetrachloride with one equivalent of NBS was dehydrohalogenated in DMF with calcium hydrogen phosphate at 80°C. The reaction mixture was poured into water, extracted into ether, and the ether solution concentrated to yield a mixture of benzosuberone and 1,2-benzocyclohepta-1,3-dien-7-one. The mixture was separated by column chromatography on silica gel; ^{1}H nmr: 2.51 (q, 2H), 2.95 (t, J = 6, 2H), 6.11–6.25 (m, 1H), 6.48 (d, J = 11, 1H), 7.16–7.30 (m, 3H), and 7.91 (d, J = 7, 1H). The empirical formula and molecular weight were established by mass spectroscopy as $C_{11}H_{10}O$; calcd.: 158.0732; found: 158.0735. Reduction of the ketone with sodium borohydride in the presence of one equivalent of cerium chloride in methanol yielded **15***a*, which was purified by chromatography on silica gel; ^{1}H nmr: 2.05–2.23 (m, 2H), 2.41–2.55 (m, 2H), 4.84 (br s, 1H), 5.84–5.98 (m, 2H), 6.39 (d, J = 11, 1H), 7.09–7.25 (m, 3H), and 7.39 (d, 1H).

Acetylation of **15***a* yielded **15***b*; ^{1}H nmr: 1.82–2.32 (m, 2H), 2.48 (m, 2H), 5.82–5.98 (m, 2H), 6.39 (br d, J = 11, 1H), 7.50–7.73 (m, 3H), and 7.72 (d, J = 7, 1H). The empirical formula and molecular weight were established by mass spectroscopy as $C_{13}H_{14}O_2$: calcd.: 202.9938; found: 202.1003.

Hydrogenation of the optically active acetate, (−)-**15***b* ($[\alpha]_D$ −14.8° ($CHCl_3$) in ethyl acetate with PtO_2 yielded (−)-(3*S*) acetoxybenzocycloheptene ($[\alpha]_D$ −6.30° (*c* 4.3, $CHCl_3$)) (15).

*Indenol (**16**a)*

Diphenyl diselenide (6.9 g) was added to a solution of bromine (3.5 g) in acetic acid (50 mL); after 30 min indene (5.2 g) was added, followed by potassium acetate (8.5 g). The mixture was stirred for 2 h, poured into water (100 mL), and extracted with ethyl acetate. The ethyl acetate solution was washed with aqueous sodium bicarbonate and water, dried over sodium sulfate, and concentrated *in vacuo*. The crude product in THF (100 mL) was cooled to 0°C and oxidized with 30% H_2O_2 (20 mL). The reaction mixture was extracted with ethyl acetate and the organic layer concentrated. Distillation yielded **16***b* as a pale yellow oil (bp 113–114°C/3.3 Torr.). The empirical formula and molecular weight of **16***b* were established by mass spectroscopy. *Mol. Wt.* calcd. for $C_{11}H_{10}O_2$: 174.06808; found: 174.06879.

A sample of (−)-**16***a*, $[\alpha]_D$ −164° (*c* 2.8, $CHCl_3$), obtained by *R. nigricans* mediated hydrolysis, was hydrogenated with PtO_2 to yield (*R*)-indanol ($[\alpha]_D$ −21.8° (*c* 3.1, $CHCl_3$)) (16).

*(E) 4-Phenyl-3-buten-2-ol (**17**a)*

The desired alcohol was prepared by the reaction of 1.1 equiv. of methyl lithium with cinnamaldehyde at −78°C. After 30 min the mixture was poured into cold 2*N* HCl and extracted with ether. The ether solution was washed with aqueous sodium bicarbonate, dried, and concentrated. The crude reaction product was acetylated in the usual way to give **17***b*; ^{1}H nmr: 1.41 (d, J = 5.5, 3H), 2.06 (s, 1H), 5.51 (qd, J = 5.5, 6.0, 3H), 6.16 (dd, J = 15.5, 6.0, 1H), 6.59 (d, J = 15.5, 1H), 7.16–7.41 (m, 5H). The empirical formula and molecular weight were established by mass spectroscopy as $C_{12}H_{14}O_2$; *Mol. Wt.* calcd.: 190.09938; found: 190.09944.

The absolute stereochemistry of the acetate recovered from the enantioselective hydrolysis using *R. nigricans* was established as (*S*) by oxidizing the acetate (131 mg, $[\alpha]_D$ −13.7°) in acetonitrile–CCl_4 (3 mL)–H_2O (6 mL) with a catalytic quantity of RuO_4 in CCl_4 in the presence of $NaIO_4$ (758 mg) at room temperature for 8 h. The mixture was poured into cold 2*N* HCl, extracted with ethyl acetate, and the organic solution was concentrated to give the crude acid (143 mg), which was methylated with excess diazomethane. Chromatography on silica gel gave (*S*)-acetoxy methyl lactate (39 mg, 48%), $[\alpha]_D$ −2.5° (*c* 2.6, $CHCl_3$)).

*4-Phenyl-3-butyn-2-ol (**18**a)*

A solution of 1.1 equiv. of methyl lithium was added to an ether solution of phenylpropargyl aldehyde at −78°C. After 30 min the mixture was poured into cold 2*N* HCl and extracted with ether. The ether solution was washed with aqueous sodium bicarbonate, dried, and concentrated. The crude alcohol was acetylated with Ac_2O in pyridine. After the usual work-up the acetate, **18***b*, was purified by column chromatography on silica gel; ^{1}H nmr: 1.58 (d, J = 6.0, 3H), 2.11 (s, 3H), 5.67 (q, J = 6.0, 1H), 7.23–7.34 (m, 3H), 7.36–7.48 (m, 2H). The empirical formula and molecular weight were established by mass spectroscopy as $C_{12}H_{12}O_2$; *Mol. Wt.* calcd.: 188.08373; found: 188.08473.

Hydrolysis of **18***b* using *R. nigricans* yielded **18**a, $[\alpha]_D$ +14.5°.

The absolute stereochemistry of the recovered acetate, **18***b*, $[\alpha]_D$ −25.7° (*c* 0.033, $CHCl_3$), was determined by hydrogenation over PtO_2 in ethyl acetate to yield (2*S*) acetoxy-4-phenylbutane, **19***b*, as a colorless oil ($[\alpha]_D$ −2.27° (*c* 0.030, $CHCl_3$)). The empirical formula and molecular weight of **19***b* were established by mass spectroscopy as $C_{12}H_{16}O_2$; *Mol. Wt.* calcd.: 192.11503; found: 192.11475.

*X-ray crystallography of (+)-**14**c*

Crystals of **14***c* were irregular plates and preliminary X-ray investigation indicated an orthorhombic unit cell. The crystal used for data collection was cut to a maximum dimension of 0.25 mm. From 15 reflections measured at ±θ angles between 20 and 30°, a least-squares refinement produced a cell with dimensions a = 9.601(1), b = 12.129(1), c = 15.854(1) Å (assumed wavelength for CuKα: 1.5418 Å). The space group was uniquely determined as $P2_12_12_1$. Assuming 4 molecules in the cell, the calculated crystal density of 1.282 g cm^{-3} was reasonable.

The phase problem was solved with MITHRIL (17). The distribution of intensities was acentric and all heavy atoms of the molecule were visible in the E map. The structure was refined by standard methods using the programs XRAY72 (18) (isotropic followed by anisotropic refinement of heavy atoms, finding H atoms in a difference map, and finally refinement of all atoms with isotropic H thermal parameters). The anisotropic temperature factor used had the form: $\exp(-(2\pi^2(\Sigma_i\Sigma(U_{ij}h_ih_ja^*_ia^*_j)))$. With 2132 observations (1483

with $I > \sigma(I)$) and a maximum sin θ/λ of 0.6233 $Å^{-1}$, the final conventional R factor was 3.9%.

The final molecular dimensions (Tables 1 through 4) are given as supplemental depository material.[4] The configuration at C-5 has been deduced as R from the known R configuration of C-4′ in the camphanate portion of the molecule and the conformation of the molecule shown in Fig. 2. There are no unusual close contacts in the crystal and no hydrogen bonds.

1. K. B. SHARPLESS, C. H. BEHRENS, T. KATSUKI, A. W. M. LEE, V. S. MARTIN, M. TAKATANI, S. M. VITTI, F. J. WALKER, and S. S. WOODWARD. Pure Appl. Chem. **55**, 589 (1983).
2. H. ZIFFER, K. KAWAI, M. KASAI, M. IMUTA, and C. FROUSSIOS. J. Org. Chem. **48**, 3017 (1983).
3. (*a*) M. KASAI, K. KAWAI, M. IMUTA, and H. ZIFFER. J. Org. Chem. **49**, 675 (1984); (*b*) K. KAWAI, M. IMUTA, and H. ZIFFER. Tetrahedron Lett. **22**, 2527 (1981).
4. A. HOREAU. Stereochemistry: Fundamentals and methods. Vol. 2. George Thieme, Stuttgart. 1977. pp. 52–94.
5. (*a*) N. HARADA, J. IWABUCHI, Y. YOKOTA, H. UDA, and K. NAKANISHI. J. Am. Chem. Soc. **103**, 5590 (1981); (*b*) N. HARADA and K. NAKANISHI. Circular dichroism spectroscopy; exciton coupling in organic chemistry. University Science Books, Mill Valley, CA. 1983. pp. 260–274.
6. R. WEIDMANN, A. SCHOOFS, and A. HOREAU. Bull. Soc. Chim. Fr. 1645 (1976).
7. C.-S. CHEN, Y. FUJIMOTO, G. GIRDAUKAS, and C. J. SIH. J. Am. Chem. Soc. **104**, 7294 (1982).
8. (*a*) P. CRABBE. Optical rotatory dispersion and circular dichroism in organic chemistry. Holden–Day, San Francisco. 1965. pp. 253–254; (*b*) M. DURAISAMY and H. M. WALBORSKY. J. Am. Chem. Soc. **105**, 3264 (1983); **105**, 3270 (1983).
9. C. J. KOWALSKI, A. E. WEBER, and K. W. FIELDS. J. Org. Chem. **47**, 5088 (1982).
10. A. L. GEMAL and J.-L. LUCHE. J. Am. Chem. Soc. **103**, 5454 (1981).
11. S. ITO, H. ZIFFER, and A. BAX. J. Org. Chem. **51**, 1130 (1986).
12. (*a*) E. PIERS and I. NAGAKURA. Synth. Commun. **5**, 193 (1975); (*b*) E. PIERS, J. R. GRIERSON, C. K. LAU, and I. NAGAKURA. Can. J. Chem. **60**, 210 (1982).
13. C. BEARD, C. DJERASSI, T. ELLIOT, and R. C. C. TAO. J. Am. Chem. Soc. **84**, 874 (1962).
14. Y. ITOH, T. HIRAO, and T. SAEGUSA. J. Org. Chem. **43**, 1011 (1978).
15. M. KASAI and H. ZIFFER. J. Org. Chem. **48**, 712 (1983).
16. D. R. BOYD, N. D. SHARMA, and A. E. SMITH. J. Chem. Soc. Perkin Trans. 1, 2767 (1982).
17. C. J. GILMORE. MITHRIL. A computer program for the automatic solution of crystal structures from X-ray data. University of Glasgow. 1983.
18. J. M. STEWART, G. J. KRUGER, H. L. AMMON, C. DICKINSON, and S. R. HALL. XRAY system–version of June 1972. Tech. Report TR-192, University of Maryland.
19. R. K. HILL and A. G. EDWARDS. Tetrahedron Lett. 3239 (1964).
20. H. WYNBERG and B. MARSMAN. J. Org. Chem. **45**, 158 (1980).
21. N. TANNO and S. TERASHIMA. Chem. Pharm. Bull. **31**, 837 (1983).

[4]These tables may be purchased from the Depository of Unpublished Data, CISTI, National Research Council of Canada, Ottawa, Ont., Canada K1A 0S2.

Can. J. Chem. Downloaded from www.nrcresearchpress.com by 80.58.250.72 on 09/07/12
For personal use only.

Acid–base behaviour of the ferrocyanide ion in perchloric acid media potentiometric and spectrophotometric study

PEDRO L. DOMINGO, BEGOÑA GARCIA, AND JOSE M. LEAL[1]

Universidad de Valladolid, Departamento de Química Física, Colegio Universitario Integrado, Burgos, Spain

Received December 9, 1985[2]

PEDRO L. DOMINGO, BEGOÑA GARCIA, and JOSE M. LEAL. Can. J. Chem. **65**, 583 (1987).

Ferrocyanide ion behaves as a tetravalent Brønsted base and can react with four protons, forming ferrocyanic acid. By potentiometric and spectrophotometric techniques it is shown that the first two protonation equilibria overlap, as do the third and fourth equilibria. The two techniques yield identical results when processed with the inclusion of non-ideality terms. The method of "separation of equilibria" is proposed to allow separate study of each of the overlapping equilibria. Values of $pK_1 = -2.54 \pm 0.10$, $pK_2 = -1.08 \pm 0.03$, $pK_3 = 2.65 \pm 0.02$, and $pK_4 = 4.19 \pm 0.02$ were obtained.

PEDRO L. DOMINGO, BEGOÑA GARCIA et JOSE M. LEAL. Can. J. Chem. **65**, 583 (1987).

L'ion ferrocyanure se comporte comme une base de Brønsted et il peut réagir avec quatre protons pour former de l'acide ferrocyanique. Faisant appel à des techniques potentiométriques et spectrophotométriques, on démontre que les deux premiers équilibres de la protonation se recouvrent comme le font les troisième et quatrième équilibres. Les deux techniques conduisent à des résultats identiques lorsqu'on les traite avec l'inclusion de termes qui tiennent compte de la non-idéalité. On propose une méthode de « séparation des équilibres » pour permettre d'étudier séparément chacun des équilibres qui se recoupent. On a obtenu les valeurs de $pK_1 = -2{,}54 \pm 0{,}10$, $pK_2 = -1{,}08 \pm 0{,}03$, $pK_3 = 0{,}02$ et $pK_4 = 4{,}19 \pm 0{,}02$.

[Traduit par la revue]

Can. J. Chem. Downloaded from www.nrcresearchpress.com by 80.58.250.72 on 09/07/12
For personal use only.

I. Introduction

In 1820 Berzelius (1) reported the isolation of a white solid, identified as $Fe(CN)_6H_4$, from an aqueous acid solution of potassium ferrocyanide. It was later established by Kolthoff (2) that the ferrocyanide ion could be protonated as a tetravalent Brønsted base in aqueous solution. The successive protonation equilibria may be expressed in the following simplified notation:

$$[1] \quad Fe(CN)_6H_3^- + H^+ \overset{K_1}{\rightleftharpoons} Fe(CN)_6H_4$$

$$[2] \quad Fe(CN)_6H_2^{2-} + H^+ \overset{K_2}{\rightleftharpoons} Fe(CN)_6H_3^-$$

$$[3] \quad Fe(CN)_6H^{3-} + H^+ \overset{K_3}{\rightleftharpoons} Fe(CN)_6H_2^{2-}$$

$$[4] \quad Fe(CN)_6^{4-} + H^+ \overset{K_4}{\rightleftharpoons} Fe(CN)_6H^{3-}$$

Here K_4, K_3, K_2, and K_1 are the thermodynamic ionization constants of the mono, bi, tri, and tetraprotonated species, which will be designated BH^{3-}, BH_2^{2-}, BH_3^-, and BH_4; B^{4-} refers to the non-protonated species.

Kolthoff and Tomsicek (3), Nekrasov and Zotor (4), and Lanford and Kiehl (5) were the first to estimate K_3 and K_4. Jordan and Ewing (6), using a potentiometric technique, obtained values for pK_3 and pK_4 of 2.22 and 4.17. They also deduced that $K_1 > K_2 > 0.1$. Other values recently published (7) are $pK_3 = 2.57$ and $pK_4 = 4.35$. Of the four possible acid–base equilibria, only values for K_3 and K_4 have been reported. In this investigation a complete study is carried out of all four equilibria by means of potentiometric and spectrophotometric techniques.

II. Results

It has been verified that the decomposition of ferrocyanide ion in perchloric acid is negligible under the conditions of these experiments. Various authors (11–14) have studied the thermal and photochemical dissociation of the ferrocyanide ion over the 0–14 pH interval; when exposed to uv light, the pH of the solutions increases due to hydrolysis of the cyanide ion formed. In darkness, this reaction is reversible. Also, in darkness decomposition is very slow; Gaspar and Beck (14) showed that thermic and photochemical conversion is small, 0.112% and 0.045%, respectively, and that the quantum yield becomes smaller as the pH increases.

Our experiments were carried out at 25°C and with light excluded. Ultraviolet–visible measurements have shown that oxidation of ferrocyanide by perchloric acid does not occur; the ferrocyanide ion shows no noticeable absorption above 270 nm, whereas the ferricyanide ion displays absorption maxima at 301 and 416 nm regardless of the acidity of the medium. Within the acidity range 0.0 to 8.0 mol dm^{-3} of perchloric acid, no absorption bands appear above 270 nm, which provides proof of the absence of any oxidising effect. For levels above 8.0 mol dm^{-3} if the concentration of ferrocyanide is sufficiently high, a white solid consisting of a mixture of $KClO_4$ and ferrocyanic acid, $Fe(CN)_6H_4$, precipitates. Identification was carried out by means of comparison with a sample of this acid prepared according to Brauer's method (8). Figure 1 shows the most characteristic ir peaks for both samples; these coincide with those indicated in the literature (15).

(A) Potentiometric study

Equilibria [3] and [4] occur within the pH 0–14 range and overlap one another (6). The calculation of constants of overlapping equilibria from potentiometric measurements can be made by Pritz's elimination method (16) or by Speakman's method of linear extrapolation (17), the latter being used in this investigation. The thermodynamic constants of ionic dissociation for these equilibria are:

$$[5] \quad K_4 = \frac{C_{B^{4-}}}{C_{BH^{3-}}} \frac{f_4}{f_3} a_{H^+}$$

$$[6] \quad K_3 = \frac{C_{BH^{3-}}}{C_{BH_2^{2-}}} \frac{f_3}{f_2} a_{H^+}$$

where f_4, f_3, and f_2 are the activity coefficients of the B^{4-}, BH^{3-}, and BH_2^{2-} species, respectively. These two equations,

[1]To whom all correspondence is to be addressed.

[2]Revision received November 3, 1986.

Can. J. Chem. Downloaded from www.nrcresearchpress.com by 80.58.250.72 on 09/07/12
For personal use only.

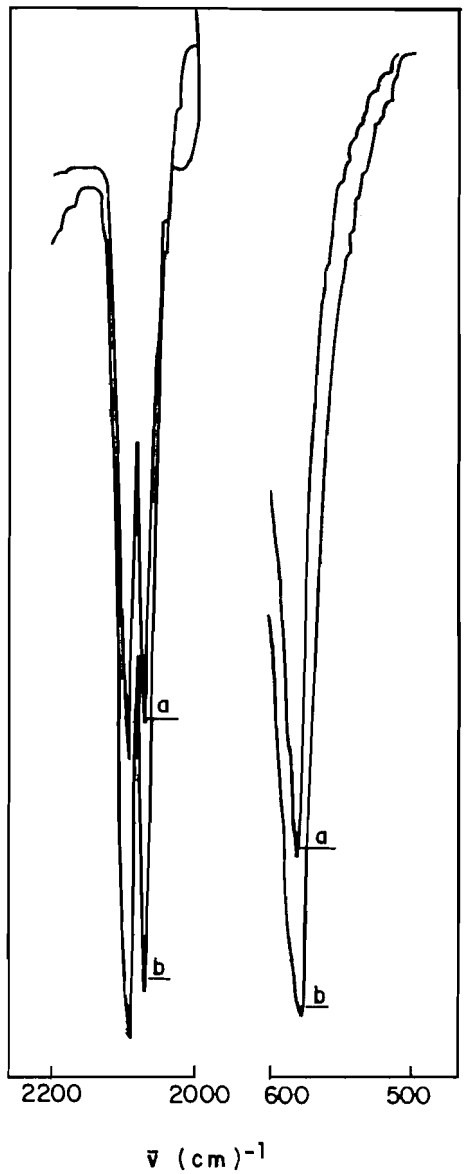

FIG. 1. Characteristic ir bands of (*a*) ferrocyanic acid prepared according to ref. 6, and (*b*) the white precipitate obtained from concentrated potassium ferrocyanide solutions (perchloric acid above 8 mol dm^{-3}).

together with a mass balance ($C_{BH_3^-} = C_{BH_4} = 0$ in this region) and a charge balance, enable us to write:

$$[7] \quad (1 - C_A/L)a_{H^+}10^{7FI_0} = 1/K_3(2C_A/L - 1)a_{H^+}^2 10^{12FI_0} - K_4$$

where C_A is the analytical concentration of potassium ferrocyanide, $L = [ClO_4^-] + [OH^-] + [H^+]$, and FI_0 is a function of the ionic strength (7), which can be calculated from

$$[8] \quad FI_0 = -\frac{AI_0^{1/2}}{1 + \mathring{a}BI_0^{1/2}}$$

where $\mathring{a} = 5 \times 10^{-8}$ cm for the ferrocyanide ion (18). Equation [7] can be written as:

$$[9] \quad y = x/K_3 - K_4$$

x and y being functions which can be determined for each pair of values V_A (the added volume of titrant)/pH. So far the treatment is analogous to that of Jordan (6), but expressions are introduced for the calculation of activity coefficients and there is also included an iterative process for a successive refining of the constants K_3 and K_4 similar to that described by Albert and Serjeant (7). This process begins by postulating initial values for K_3 and K_4; for each pair V_A/pH, the value of I_0 is postulated and, without eliminating at any time the activity coefficients, the relative concentrations C_0, C_1, and C_2 are determined for the species B^{4-}, BH^{3-}, and BH_2^{2-}, respectively. Equation [10] enables calculation of the ionic strength; if the value obtained does not coincide within a margin of ±0.1% with the postulated I_0, the process is repeated with the introduction of the calculated value of I_0, which is taken as correct, until a self-consistent value is obtained.

$$[10] \quad I_0 = ([ClO_4^-] + [OH^-] + [H^+] + C_A(16C_0 + 9C_1 + 4C_2 + 4)) \times 0.5$$

Finally, regression [9] is carried out and K_3 and K_4 are determined. If the values obtained do not coincide with those initially postulated, the process is iterated until self-consistent results are achieved. This treatment of data was programmed in BASIC. A similar, more generalized program, applicable to diacid bases, diprotic acids, and ampholites, has been developed in FORTRAN IV (7). If the program is designed so as to introduce initially the value of I_0 calculated for the first V_A/pH pair, self-consistent results are rapidly achieved. Values obtained were $K_3 = (2.22 \pm 0.04) \times 10^{-3}$, $K_4 = (6.48 \pm 0.15) \times 10^{-5}$, r_{xy} (linear correlation coeff.) = 0.9942, θ (degrees of freedom) = 18. These results are in good agreement with recent results (7).

Equilibria [1] and [2] occur at levels of acidity above 0.1 mol dm^{-3}. To obtain differential readings for a mixture of such weak bases dipolar aprotic solvents such as acetonitrile (19, 20) and acetone (21) are best; acetic anhydride also widens the range of titrations with bases as weak as the anions of strong acids (22, 23). However, potassium ferrocyanide is practically insoluble in these solvents. Dipolar aprotic solvents, such as acetonitrile, methylisobutyl ketone, etc. (24) are also best for differentiating titrations of strong acids. However, the acid $Fe(CN)_6H_4$ is very difficult to dissolve in these solvents. Dimethylsulfoxide (DMSO), which has a much higher dielectric constant, was found satisfactory. Figure 2 shows the curve obtained on titration of ferrocyanic acid in DMSO with NaOH in isopropanol. Only three inflections are observed, indicating that two of the four acid species have become leveled; this complicates quantitative treatment since each equilibrium is decomposed into at least two other equilibria:

$$[11] \quad AH + S \rightleftharpoons SH^+\text{---}A^-$$

$$[12] \quad SH^+\text{---}A^- \rightleftharpoons SH^+ + A^-$$

where AH is the acid species and S the solvent; if the solvent is water, the ion-pair cannot be detected and the dissociation is reduced to a single step.

(B) Spectrophotometric study

Figures 3 and 4 show the absorption uv spectra of the ferrocyanide ion as a function of acidity in water. The appearance of an isosbestic point indicates the presence of at least two species in equilibrium (25). A computational method for working out the number of species in equilibrium, based on the calculation of the range of a matrix of absorbances ($N \times N$), with readings at N wavelengths in N solutions of different

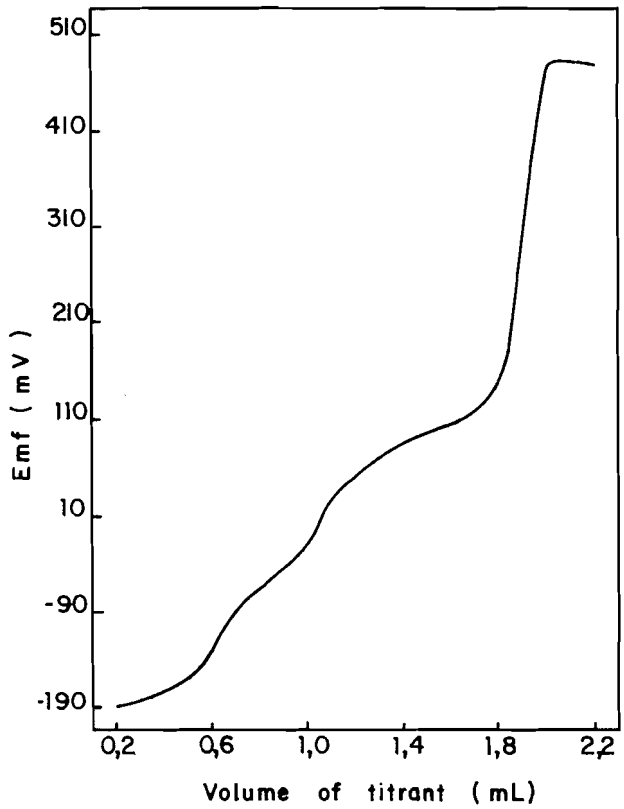

FIG. 2. Titration curve of ferrocyanic acid ($2.13 \times 10^{-3} N$) in dimethyl sulfoxide (20 mL) using NaOH ($0.022 N$) in isopropyl alcohol as titrant.

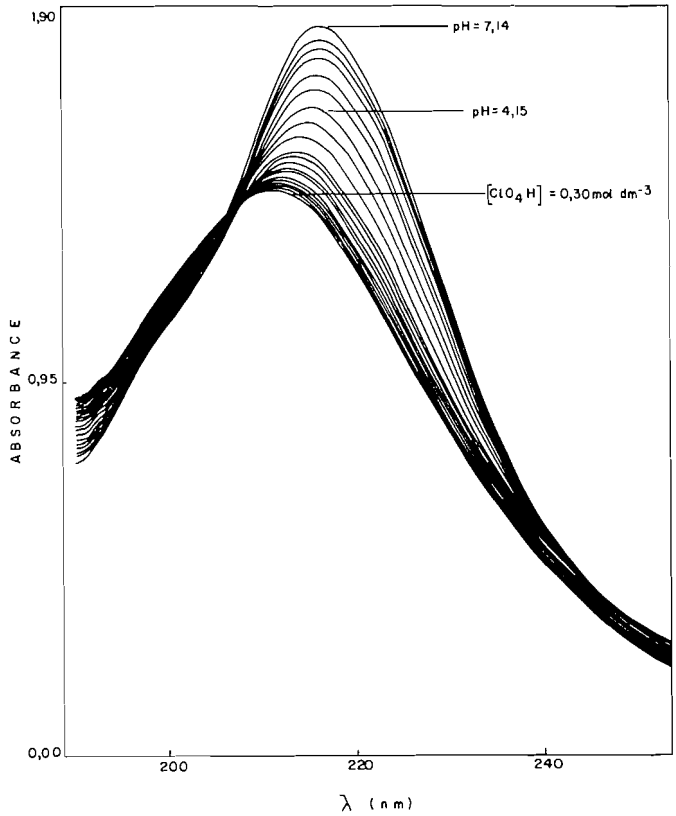

FIG. 3. Absorption uv spectra of potassium ferrocyanide (7.89×10^{-5} mol dm^{-3}) in aqueous perchloric acid solutions of pH = 7.14, 6.65, 6.20, 5.79, 4.80, 4.48, 4.15, 3.91, 3.65, 3.41, 3.33, 3.19, 3.01, 2.86, 2.55, 2.34, 2.13, 2.00, 1.85, 1.72, and $[HClO_4]$ = 0.30 mol dm^{-3}.

composition, originally written in FORTRAN (26) was rewritten in BASIC and applied separately to Figs. 3 and 4. In Fig. 3, pH range 0–14, there are three absorbing species, which match the potentiometric result: B^{4-}, BH^{3-}, and BH_2^{2-}; in Fig. 4, the high acidity region, the number of absorbing species is also three: BH_2^{2-}, BH_3^-, and BH_4. An absorbance matrix (6×6) which includes concentrations within the range 0.3–8.0 mol dm^{-3} of $HClO_4$ was used to verify this point. The error in the experimental reading of absorbances used in constructing the initial matrix of errors is estimated at 0.004. The thermodynamic constants for equilibria [1] and [2] can be written as:

$$[13] \quad pK_2 = \log I_2 - \log C_{H^+} - \log (f_{BH_2^{2-}} f_{H^+}/f_{BH_3^-})$$

$$[14] \quad pK_1 = \log I_1 - \log C_{H^+} - \log (f_{BH_3^-} f_{H^+}/f_{BH_4})$$

where I is the ionization ratio

$$(I_2 = C_{BH_3^-}/C_{BH_2^{2-}},\ I_1 = C_{BH_4}/C_{BH_3^-})$$

which, for an independent equilibrium, can be estimated by means of Gold-Hawe's equation (27):

$$[15] \quad I = \Sigma_i (1/n)(A_B - A)/(A - A_A))_{\lambda_i}$$

where A_B is the absorbance of the basic species and A_A that of the conjugate acid, each corresponding to the limits of acidity in which the equilibrium takes place; A is the absorbance value corresponding to intermediate acidity.

(1) Study in high acidity media

In media containing a high concentration of mineral acid, the terms of the activity coefficients in [13] and [14] cannot be calculated by means of the Debye–Hückel equation, so we need to resort to one of general alternative methods.

The Hammett–Deyrup general equation (28, 29) states:

$$[16] \quad \log I = -mH_x + pK$$

where H_x is Hammett's acidity function, which is particular to the type of the species under discussion. A wide collection of acidity functions have been reported (29); according to eq. [16], pK is obtained as the ordinate of the log I/H_x linear regression, and the slope, m, enables us to verify if the function H_x has been correctly chosen. If $m = 1$, then the function H_x is correct since Hammett's postulation is satisfied (28).

The Bunnett–Olsen equation (30) states:

$$[17] \quad \log I + H_0 = \Phi(H_0 + \log C_{H^+}) + pK$$

where H_0 is the Hammett acidity function for the primary aromatic amines (31, 32). As before, pK is obtained as the ordinate of a linear regression and the slope can be interpreted in terms of solvation (33).

The Cox–Yates equation (10) states:

$$[18] \quad \log I - \log C_{H^+} = m^*X + pK$$

where X, the excess acidity function, which is the same for all bases in a single system, is calculated by an iterative method based on the ionization of a large number of different bases. For aqueous perchloric acid, used in this investigation, the function X is determined by starting from the percentage of mineral acid (10). The pK is obtained as the ordinate of the linear regression $(\log I - \log C_{H^+})/X$, while from the slope we obtain the parameter m^*, which is particular to each base and can be interpreted in terms of hydration.

Can. J. Chem. Downloaded from www.nrcresearchpress.com by 80.58.250.72 on 09/07/12
For personal use only.

TABLE 1. Planes of regression obtained by Mongay's method (see text for details)

Plane	1	2
Equation	$Z = A_3^{-1} - A_3^{-1}K_2U - A_3^{-1}K_1^{-1}V$	$Z = A_3 - K_1^{-1}U - K_2V$
Z	A^{-1}	A
U	$(C_{H^+}10^{m_2^*X})^{-1}(A_2 - A)/A$	$C_{H^+}10^{m_1^*X}(A - A_4)$
V	$C_{H^+}10^{m_1^*X}(A_4 - A)/A$	$(C_{H^+}10^{m_2^*X})^{-1}(A - A_2)$

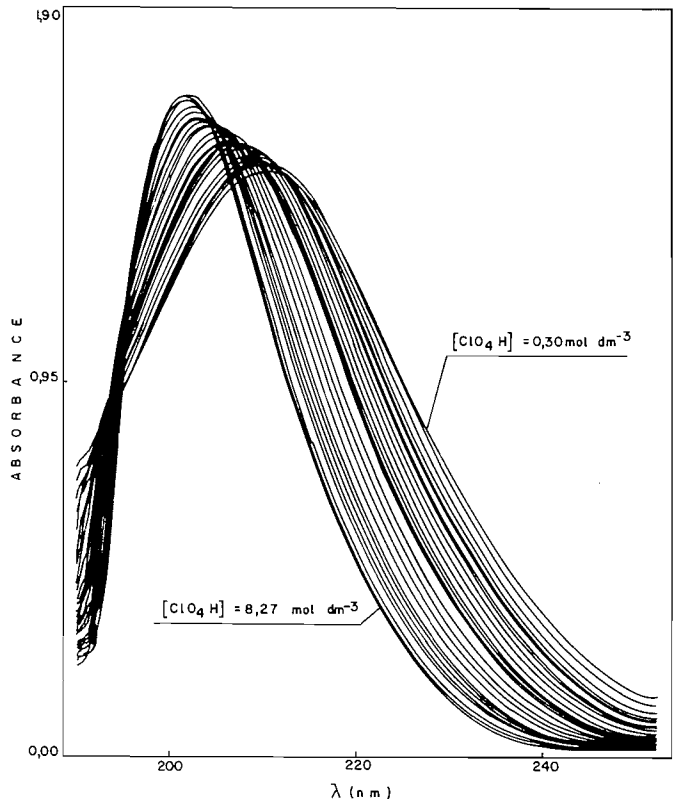

FIG. 4. Absorption uv spectra of potassium ferrocyanide (7.89×10^{-5} mol dm^{-3}) in aqueous perchloric acid solutions of concentration: 0.300, 0.810, 1.120, 1.431, 1.741, 1.974, 2.284, 2.594, 2.905, 3.215, 3.525, 3.836, 4.058, 4.379, 4.378, 5.000, 5.309, 5.619, 5.930, 6.240, 6.473, 6.783, 7.094, 7.404, 7.714, 8.000, and 8.270.

(a) Extension of Mongay's method. The isosbestic area in Fig. 4 indicates the co-existence of the species BH_2^{2-}, BH_3^-, and BH_4, that is to say, equilibria [1] and [2] overlap one another ($pK_2 - pK_1 < 3$). Mongay's method for determining constants of overlapping equilibria was developed for regions of low acidity, with activity coefficients being taken as 1 for all species (34). In this work we shall use the method without eliminating the terms related to the non-ideality of the system. Any one of the eqs. [16], [17], or [18] could be used for the investigation in strongly acid media, but we shall limit ourselves to the Cox–Yates equation for reasons which will be discussed later.

The following scheme is used. Equation [18] is applied to [1] and [2]:

$$[19] \quad K_2 = \frac{C_{BH_2^-}C_{H^+}}{C_{BH_3^-}} 10^{m_2^*X}$$

$$[20] \quad K_1 = \frac{C_{BH_3^-}C_{H^+}}{C_{BH_4}} 10^{m_1^*X}$$

These equations and those numbered [13] and [14] are equivalent (10). If we take into account the additivity of absorbances,

$$[21] \quad A = A_{BH_2^-} + A_{BH_3^-} + A_{BH_4} = A_2 + A_3 + A_4$$

and apply a mass balance:

$$[22] \quad C = C_{BH_2^-} + C_{BH_3^-} + C_{BH_4}$$

the following expression is arrived at:

$$[23] \quad A = \frac{A_2 + A_3C_{H^+}10^{m_2^*X}/K_2 + A_4C_{H^+}^2 10^{(m_1^* + m_2^*)X}/K_1K_2}{1 + C_{H^+}10^{m_2^*X}/K_2 + C_{H^+}^2 10^{(m_1^* + m_2^*)X}/K_1K_2}$$

this equation can be rearranged and written as the equation of a plane:

$$[24] \quad Z = a_0 + a_1U + a_2V$$

where Z, U, and V are functions dependent on previously known parameters and can therefore be worked out. Coefficients a_0, a_1, and a_2 contain the three values K_1, K_2, and A_3. The problem can therefore be solved using a multiple linear regression by the method of least squares. Although eq. [24] leads to several planes, for greater precision we have only chosen those appearing in Table 1. The procedure is straightforward. Using values of A/C_{H^+} such as those obtained from an expansion of Fig. 4, we look in Table V of ref. 10 for the values of m_1^* and m_2^* which are most appropriate to the type of compound being studied (since we are dealing with species of the same type it is reasonable to take $m_1^* = m_2^*$). Then for each pair of A/C_{H^+} values Z, U, and V are determined and the multilinear regression is carried out; in our case the optimum value according to ref. 10 is in the space corresponding to the anions, $m^* = 1.18 \pm 0.25$. Where this interval is narrow there is only a small error in m^*, but here the error is large and it was found advisable to develop a new method which functions in a way comparable to modern methods of iterative refining. This method is described in the next section.

(b) The separation method for overlapping equilibria. Equations [20] and [21], together with a mass balance, enable us to obtain C_2, C_3, and C_4 expressions corresponding to relative quantities of the species BH_2^{2-}, BH_3^-, and BH_4:

$$[25] \quad C_4 = (1 + (C_{H^+}10^{(m_1^*X + pK_1)})^{-1} + (C_{H^+}^2 10^{(m_1^* + m_2^*)X + pK_1 + pK_2})^{-1})^{-1}$$

$$[26] \quad C_3 = C_4(C_{H^+}10^{(m_1^*X + pK_1)})^{-1}$$

$$[27] \quad C_2 = 1 - (C_3 + C_4)$$

We postulate initial values for pK_1, pK_2, m_1^*, and m_2^* (in this case $pK_1 < pK_2 < 1$ (6) and $0.20 \leqslant m_1^* = m_2^* \leqslant 2.60$ (10)). For each acidity value the value of the function X is determined (10) as are the quantities C_2, C_3, and C_4. If we already know at the same wavelength A_2 (for 0.30 mol dm^{-3} $HClO_4$), A_4 (for 8.0 mol dm^{-3} $HClO_4$) and A (for any interme-

Can. J. Chem. Downloaded from www.nrcresearchpress.com by 80.58.250.72 on 09/07/12
For personal use only.

diate level of acidity), by means of [28] we can obtain a value for A_3 for each value of acidity.

$$[28] \quad A_3 = \frac{A - C_2A_2 - C_4A_4}{C_3}$$

Once A_3 has been obtained it is possible to eliminate the contribution of BH_4 to the total absorbance A and to calculate by means of [29] values for A_c (corrected absorbance) which would correspond to the system if the only species existing in equilibrium were BH_2^{2-} and BH_3^-.

$$[29] \quad A_c = \frac{A - C_4A_4}{C_2 + C_3}$$

This process can be applied independently to a single wavelength or to several different ones, in such a way that by means of [15] the ionization ratio for each level of acidity can be determined, starting from the A_c values obtained previously. Equation [18] can then be used to obtain m_2^* and pK_2. In a similar fashion we eliminate the contribution made by the BH_2^{2-} species to the total absorption and, by means of [30], A_c' values can be obtained corresponding to the system where species BH_3^- and BH_4 are the only ones involved in the equilibrium.

$$[30] \quad A_c' = \frac{A - C_2A_2}{C_3 + C_4}$$

In this way equilibrium [1] can be studied independently and, by means of [15] and [18], values are obtained for m_1^* and pK_1. If the values now calculated for m_1^*, m_2^*, pK_1, and pK_2 do not match those postulated originally, the process is repeated until self-consistent results are achieved. The advantage of this method lies in the way it allows comparison of the m_1^* and m_2^* values at the end of the process. All data processing was carried out by computer. By using the data of absorbances (Fig. 4) at six different wavelengths (227, 223, 219, 204, 202, and 200 nm), the ionization ratio values of equilibria [1] and [2], (eq. [15]), as well as the values ($\log I - \log C_{H^+}$) and X (eq. [18]), were obtained (Table 2). Table 3 summarizes the average values of pK_1 and pK_2 obtained at the six wavelengths and the regression planes (Table 1) by means of Mongay's method, using $m_1^* = m_2^* = 0.85$ obtained by means of the separation method. It will be noted that the values $m_1^* = m_2^* = 0.850 \pm 0.044$ do not fall within the margin of 1.18 ± 0.25 assigned to the anions (10), a fact explained by these latter values having been obtained exclusively from anions of cyanocarbon acids, which differ in structure from the ferrocyanide ion and its protonated forms. Moreover, protonation does not affect the same atom in cyanides (35) as in cyanocarbon acids (36). The difference in the values of m^* shows that the function H_- is not able to explain the acid–base behaviour of the ferrocyanide system, and confirms that the m^* value obtained for one base is only valid for another if it is structurally similar and the functional group is the same (37).

(2) Study in low acidity media

Within the pH range 0–14, for the equilibrium

$$[31] \quad B + H^+ \rightleftharpoons BH^+$$

the thermodynamic pK_{BH^+} can be calculated empirically (31):

$$[32] \quad pK_{BH^+} = \lim_{C_{MA} \to 0} (\log I + pH) = \lim_{C_{MA} \to 0} (pK_{BH^+} + \log (f_B/f_{BH^+}))$$

with the value ($\log I$ + pH) vs. C_{MA} (mineral acid concentration) being extrapolated at infinite dilution.[3] It has recently been shown (38) that this empirical relation is not acceptable and that more satisfactory results can be obtained with the equation:

TABLE 2. Ionization ratio values for regression [18]

Equilibrium	C_{H^+} (mol dm^{-3})	I	$\log I - \log C_{H^+}$	X
[2]	1.120	0.128	−0.940	0.233
	1.431	0.213	−0.827	0.318
	1.741	0.340	−0.709	0.412
	1.974	0.473	−0.620	0.487
	2.284	0.619	−0.567	0.595
	2.594	0.929	−0.446	0.711
	2.905	1.297	−0.350	0.834
	3.215	1.750	−0.264	0.964
	3.525	2.260	−0.192	1.100
[1]	5.000	0.570	−0.943	1.817
	5.309	0.706	−0.876	1.981
	5.619	1.039	−0.733	2.149
	5.930	1.502	−0.596	2.322
	6.240	2.237	−0.446	2.499
	6.473	3.201	−0.306	2.634
	6.783	5.395	−0.099	2.819

$$[33] \quad \log I = -n\text{p}H + n\text{p}K_{BH^+}$$

where n is a measurement of the non-ideal behaviour of the system.

The separation method

The basic equations [33] are applied to equilibria [3] and [4], with the additional introduction of mass balance. The relative quantities C_0, C_1, and C_2 are obtained for the species B^{4-}, BH^{3-}, and BH_2^{2-}:

$$[34] \quad C_0 = (1 + a_{H^+}^{n_4}K_4^{-n_4} + a_{H^+}^{(n_3+n_4)}K_3^{-n_3}K_4^{-n_4})^{-1}$$

$$[35] \quad C_1 = C_0a_{H^+}^{n_4}K_4^{-n_4}$$

$$[36] \quad C_2 = 1 - (C_0 + C_1)$$

Applying the iterative procedure for the separation of equilibria similar to that described for the high acidity region, we postulate values for n_3, n_4, pK_3, and pK_4 which, by means of equations similar to [28], [29], and [30], enable the determination of A_1 (absorbance of BH^{3-}), A_c and A_c'. Using [15] we arrive at I and n_3, n_4, pK_3, and pK_4 can be determined by means of [33]. With the data of absorbances (Fig. 3) at three different wavelengths (216, 222, and 228 nm), the ionization ratios (eq. [15]) of [3] and [4] are determined (Table 4). Table 5 shows the results obtained.

The poorer correlation in the latter case is due to three wavelengths chosen being to the right of the isosbestic point (Fig. 3); since the absorption maximum is shifted, three wavelengths should also have been chosen to the left of this point, but this did not prove to be useful because the differences are very small.

III. Discussion

Although potentiometric methods have been considered superior to spectrophotometric methods in speed, precision, and

[3]The data of absorbances used in low and high acidity media as well as the data of the titration of potassium ferrocyanide may be purchased from the Depository of Unpublished Data, CISTI, National Research Council of Canada, Ottawa, Ont., Canada K1A 0S2.

Can. J. Chem. Downloaded from www.nrcresearchpress.com by 80.58.250.72 on 09/07/12
For personal use only.

TABLE 3. Thermodynamic ionization constants of equilibria [1] and [2]

Equilibrium	Separation method: Initial	Separation method: Final	Mongay's Method
[1]	$m_1^* = 0.85$ $pK_1 = -2.55$	$m_1^* = 0.849 \pm 0.043$ $pK_1 = -2.538 \pm 0.101$ $\theta = 5$ $r_{xy} = 0.9935$	$pK_1 = -2.539 \pm 0.146$ $\theta = 11$
[2]	$m_2^* = 0.85$ $pK_2 = -1.08$	$m_2^* = 0.851 \pm 0.044$ $pK_2 = -1.080 \pm 0.030$ $\theta = 7$ $r_{xy} = 0.9905$	$pK_2 = -1.002 \pm 0.148$ $\theta = 11$

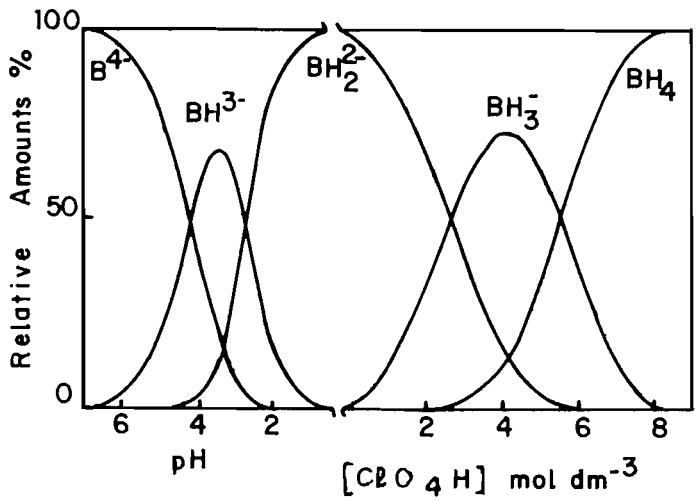

FIG. 5. Distribution of the various protonated forms of ferrocyanide ion as a function of aqueous perchloric acid concentration.

TABLE 4. Ionization ratio values used for regression [33]

Equilibrium	I	log I	pH
[4]	0.368	−0.434	4.80
	0.530	−0.276	4.48
	0.950	−0.022	4.15
	1.423	0.153	3.91
	2.294	0.361	3.65
	3.891	0.590	3.41
[3]	1.418	0.152	2.55
	1.871	0.272	2.34
	2.557	0.408	2.13
	4.311	0.634	2.00
	7.023	0.846	1.85

accuracy (26, 39) for the study of ionic equilibria in solution, this is only true in aqueous solutions and within the pH 0–14 range. The complexity and lack of development of theoretical models for potentiometric study in non-aqueous media mean that this technique has only a very limited use for quantitative measurements of ionic dissociation in strong acids or bases. In this investigation, the potentiometric technique yielded better results than the spectrophotometric for [3] and [4], but the opposite was true for [1] and [2].

Although the method developed for high acidity media has been based on eq. [18], also eqs. [16] or [17] could have been used just as well to design other methods. However, eq. [18] does provide a simpler way, because it is similar in form to [13] or [14] and is also more general, since the function X is valid for all bases in the same system.

TABLE 5. Thermodynamic ionization constants of equilibria [3] and [4] obtained by means of the separation method

Equilibrium	Thermodynamic ionization constant: Initial	Thermodynamic ionization constant: Final
[3]	$n_3 = 0.97$ $pK_3 = 2.65$	$n_3 = 0.97 \pm 0.13$ $pK_3 = 2.65 \pm 0.30$ $\theta = 3$ $r_{xy} = 0.9712$
[4]	$n_4 = 0.74$ $pK_4 = 4.16$	$n_4 = 0.74 \pm 0.03$ $pK_4 = 4.15 \pm 0.13$ $\theta = 4$ $r_{xy} = 0.9958$

Finally, it must be stressed that when engaged in the study of a system, it is advisable to use a real system without eliminating such terms as activity coefficients, m^*X, etc., since they provide information about non-ideal behaviour; this entails using iterative methods, which are becoming increasingly frequent in this type of calculation (7, 26). Most methods for studying overlapping equilibria are designed with the ideal model in mind and it seems clear that they can be developed with the use of a real model. Examples of the latter methods are provided by Ang (40) and Albelda *et al.* (41); because of their lesser accuracy, these methods have not proved useful in the present investigation.

IV. Experimental

Reactants

All reagents were analytical grade. Twice distilled deionized water was used throughout; in the low acidity range, water was boiled and then cooled in a closed beaker to avoid CO_2. Titrations of potassium ferrocyanide in aqueous media were carried out on 100 mL portions (0.005 mol dm^{-3}), using perchloric acid (0.999 mol dm^{-3}) as titrant. Titrations in non-aqueous media were carried out on 20 mL portions of ferrocyanic acid (0.03 mol dm^{-3}), using as titrant a solution of NaOH in isopropyl alcohol. A nitrogen atmosphere was maintained over the solutions during titrations. In the high acidity range, C_{H^+} values were calculated directly from molar concentrations of perchloric acid, since this species is fully ionized at least up to 60% w/w (9,

Can. J. Chem. Downloaded from www.nrcresearchpress.com by 80.58.250.72 on 09/07/12
For personal use only.

10). It was not necessary to control the ionic strength since this factor is included in the excess acidity function method,[4] as stated in eq. [18].

Equipment

In the potentiometric experiments, titrant was added by microburet (±0.001 mL); pH readings were made with a Crison pH-meter (±0.01) and titration curves were plotted with a Radiometer REC 61 recorder. Spectrophotometric measurements were made with a Bodenseewerk Perkin Elmer 554 model with double beam, 1 nm slit and 1 cm optical path. The reference cell contained the same solvent as the sample under measurement. The temperature of all solutions were kept constant at 25°C ± 0.01 with a P-Selecta thermostat.

Acknowledgements

Thanks are due to P. Mitchell for his contribution to the English version of the text. The comments of the Editor and one of the referees are gratefully acknowledged.

1. J. J. Berzelius. Schu. J. **30**, 44 (1820).
2. I. M. Kolthoff. Z. Anorg. Allgem. Chem. **110**, 143 (1920).
3. I. M. Kolthoff and W. J. Tomsicek. J. Phys. Chem. **39**, 928 (1935).
4. B. Nekrasov and G. Zotor. J. Appl. Chem. USSR, **14**, 234 (1941).
5. O. F. Lanford and S. J. Kiehl. J. Phys. Chem. **45**, 300 (1941).
6. J. Jordan and G. I. Ewing. Inorg. Chem. **1**, 587 (1962).
7. A. Albert and E. P. Serjeant. The determination of ionization constants. Chapman and Hall, New York. 1984. p. 57.
8. G. Brauer. Química inorgánica preparativa. Ed. Reverté. Barcelona. 1958. p. 907.
9. R. W. Duerst. J. Chem. Phys. **48**, 2275 (1968).
10. R. A. Cox and K. Yates. J. Am. Chem. Soc. **100**, 3861 (1978).
11. A. G. McDiarmid and N. F. Hall. J. Am. Chem. Soc. **75**, 5204 (1953).
12. G. Emschwiller. Comp. Rend. **236**, 72 (1953).
13. S. Asperger, I. Murati, and D. Paulovic. J. Chem. Soc. 730 (1960).

[4]R. A. Cox. Private communication.

14. V. Gaspar and M. T. Beck. Polyhedron, **2**, 387 (1983).
15. J. B. Ayers and W. H. Waggoner. J. Inorg. Nucl. Chem. **33**, 721 (1971).
16. M. Pritz. Z. Anorg. Allgem. **172**, 147 (1928).
17. J. C. Speakman. J. Chem. Soc. 855 (1940).
18. N. A. Lange. Handbook of chemistry. 11th ed. McGraw-Hill, New York. 1973. Table 5.2.
19. J. S. Fritz. Anal. Chem. **29**, 437 (1953).
20. H. K. Hall. J. Phys. Chem. **60**, 63 (1956).
21. J. S. Fritz and C. A. Burgett. Anal. Chem. **44**, 1673 (1972).
22. C. A. Streuli. Anal. Chem. **30**, 997 (1958).
23. D. C. Wimer. Anal. Chem. **30**, 77 (1958).
24. D. C. Bruss and G. E. Wyld. Anal. Chem. **39**, 232 (1957).
25. M. D. Cohen and E. Fischer. J. Chem. Soc. 3044 (1962).
26. F. Hartley, C. Burgess, and R. Alcoch. Solution equilibria. Wiley, Chichester. 1980. p. 313.
27. V. Gold and B. W. V. Hawes. J. Chem. Soc. 2102 (1951).
28. L. P. Hammett and A. J. Deyrup. J. Am. Chem. Soc. **54**, 2721 (1932).
29. S. Geribaldi, A. G. Luciano, P. C. Maria, and M. Azzaro. J. Chim. Phys. **79**, 103 (1982).
30. J. F. Bunnett and F. P. Olsen. Can. J. Chem. **44**, 1899 (1966).
31. M. A. Paul and F. A. Long. Chem. Rev. **57**, 1 (1957).
32. M. J. Jørgenson and D. R. Hartter. J. Am. Chem. Soc. **85**, 878 (1963).
33. A. Levi, G. Modena, and G. Scorrano. J. Am. Chem. Soc. **96**, 6585 (1974).
34. C. Mongay, G. Ramiro, and M. C. Garcia. Spectrochim. Acta, **38A**, 247 (1982).
35. A. N. Garg and P. S. Goel. J. Inorg. Nucl. Chem. **32**, 1547 (1970).
36. R. H. Boyd. J. Phys. Chem. **67**, 737 (1963).
37. R. A. Cox and R. Stewart. J. Am. Chem. Soc. **98**, 488 (1976).
38. B. Garcia. Doctoral Thesis. Valladolid University, Spain. 1984.
39. H. Rossotti. Talanta, **21**, 809 (1974).
40. K. P. Ang. J. Phys. Chem. **62**, 1109 (1958).
41. M. L. Albelda, V. Cerda, and C. Mongay. Bull. Soc. Chim. Fr. 19 (1982).

Can. J. Chem. Downloaded from www.nrcresearchpress.com by 80.58.250.72 on 09/07/12
For personal use only.

Structural studies of organoboron compounds. XXV. Synthesis and structure of (maltolato)diphenylboron

CHRIS ORVIG, STEVEN J. RETTIG, AND JAMES TROTTER

Department of Chemistry, University of British Columbia, 2036 Main Mall, Vancouver, B.C., Canada V6T 1Y6

Received July 17, 1986

CHRIS ORVIG, STEVEN J. RETTIG, and JAMES TROTTER. Can. J. Chem. **65**, 590 (1987).

The reaction of maltol (3-hydroxy-2-methyl-4-pyrone) with diphenylborinic acid affords a high yield of the title compound. Crystals of (maltolato)diphenylboron are monoclinic, $a = 14.3481(6)$, $b = 8.3994(3)$, $c = 12.6657(5)$ Å, $\beta = 100.892(4)°$, $Z = 4$, space group $P2_1/n$. The structure was solved by direct methods and was refined by full-matrix least-squares procedures to $R = 0.041$ and $R_w = 0.052$ for 2052 reflections with $I \geq 3\sigma(I)$. The molecule contains a five-membered C_2O_2B ring having a flattened *B*-envelope conformation, the B atom being displaced 0.081(2) Å from the C_2O_2 plane. Structural and spectroscopic data are consistent with weak binding of the maltolate oxygen atoms to boron. Bond distances (corrected for libration) are O—B = 1.533(2) and 1.600(3), B—C = 1.600(3) and 1.605(3) Å.

CHRIS ORVIG, STEVEN J. RETTIG et JAMES TROTTER. Can. J. Chem. **65**, 590 (1987).

La réaction du maltol (hydroxy-3 méthyl-2 pyrone-4) avec l'acide diphénylborinique conduit, avec un excellent rendement, au composé mentionné dans le titre. Les cristaux du (maltolato)diphénylbore sont monocliniques avec $a = 14,3481(6)$, $b = 8,3994(3)$ et $c = 12,6657(5)$ Å, $\beta = 100,892(4)°$, $Z = 4$ et groupe d'espace $P2_1/n$. On a résolu la structure par des méthodes directes et on a l'a affinée par la méthode des moindres carrés jusqu'à des valeurs de $R = 0,041$ et $R_w = 0,052$ pour 2052 réflexions avec $I \geq 3\sigma(I)$. La molécule contient un anneau à cinq chaînons de C_2O_2B qui adopte une conformation enveloppe *B* aplatie; l'atome de B se trouve à 0,081(2) Å du plan des C_2O_2. Les données de structure et spectroscopiques sont en accord avec une liaison faible entre les atomes d'oxygène du maltolato et le bore. Les longueurs de liaison (corrigées pour la libration) sont : O—B = 1,533(2) et 1,600(3), B—C = 1,600(3) et 1,605(3) Å.

[Traduit par la revue]

Can. J. Chem. Downloaded from www.nrcresearchpress.com by 80.58.250.72 on 09/07/12
For personal use only.

Introduction

(Maltolato)diphenylboron, **1**, has been synthesized and its molecular structure determined both as part of a continuing study of the structures of organoboron compounds[1] and in parallel with studies of neutral water-soluble aluminum complexes of neurological interest (1) and related gallium analogs (2). The neutral complex tris(maltolato)aluminum has been shown to be a potent neurotoxin (3). The natural product maltol (3-hydroxy-2-methyl-4-pyrone) is commonly used as a food additive. Since ir data indicate weak binding of the maltol oxygen atoms to boron in the title compound relative to that in the tris(maltolato) complexes of Al and Ga (2), comparison of the ligand geometries is of interest.

Experimental

(Maltolato)diphenylboron ((3-hydroxy-2-methyl-4-pyronato)-diphenylboron)

A solution of diphenylborinic acid was prepared by the acid hydrolysis (60 mL 0.10 *M* HCl) of (2-aminoethanolato)diphenylboron (1.319 g, 5.86 mmol) and extraction with diethylether (4 × 50 mL). To the organic layer was added ethanol (50 mL) followed by a solution of maltol (0.740 g, 5.87 mmol, Aldrich Chemical) in 30 mL ethanol. White flakes appeared within 10 min and the product was isolated after cooling (−20°C) overnight. Yield 1.506 g (90%). Analytically pure flakes were obtained by recrystallization from acetone/water, mp 195–196.5°C (uncorrected). *Anal.* calcd. for $C_{18}H_{15}BO_3$: C 74.52, H 5.21; found: C 74.95, H 5.28. Ir (KBr, all strong): 1640 cm^{-1} (CO); 1570, 1560 (C=C). ^1H nmr (d_6-acetone, 25°C, 80 MHz): δ 2.63 (s, 3H, CH_3); 7.25 (m, 11H, $2C_6H_5$ and $CHC(O)$); 8.62 (d, 5.4 Hz, OC*H*CH).

The ir spectrum was recorded on a Perkin-Elmer 783 from 4000–200 cm^{-1} and the ^1H nmr spectrum on a Bruker WP-80. Crystals suitable for X-ray analysis were obtained by slow evaporation of an acetone solution.

[1]For Part XXIV, see ref. 23.

X-ray crystallographic analysis

A crystal bounded by the six faces (followed by their distances in mm from a common origin): {1 0 1}, 0.12, {1 0 −1}, 0.05, (−1 ±1 1), 0.11 was mounted in a general orientation. Unit-cell parameters were refined by least-squares on 2 sin θ/λ values for 25 reflections (2θ = 70–94°) measured on a diffractometer with Cu-*K*α radiation (λ(*K*α$_1$) = 1.540562, λ(*K*α$_2$) = 1.544390 Å). Crystal data at 22°C are:

$C_{18}H_{15}BO_3$ fw = 290.1

Monoclinic, $a = 14.3481(6)$, $b = 8.3994(3)$, $c = 12.6657(5)$ Å, $\beta = 100.892(4)°$, $V = 1498.9(1)$ $Å^3$, $Z = 4$, $\rho_c = 1.285$ Mg m^{-3}, $F(000) = 608$, μ(Cu-*K*α) = 6.52 cm^{-1}. Absent reflections: $h0l$, $h + l$ odd, and $0k0$, k odd, uniquely indicate the space group $P2_1/n$ (alternate setting of $P2_1/c$, C_{2h}^5, No. 14).

Intensities were measured with nickel-filtered Cu-*K*α radiation on an Enraf-Nonius CAD4-F diffractometer. An ω–2θ scan at 1.18–10.06° min^{-1} over a range of (0.60 + 0.14 tan θ) degrees in ω (extended by 25% on both sides for background measurement) was employed. Data were measured to 2θ = 150°. The intensities of three check reflections, measured every 3600 s throughout the data collection, remained constant to within 4%. After data reduction,[2] an absorption correction was applied using the analytical method (4, 5). Transmission factors ranged from 0.724 to 0.896. Of the 3067 independent reflections measured, 2052 (66.9%) had intensities greater than or equal to $3\sigma(I)$ above background where $\sigma^2(I) = S + 2B + (0.04(S - B))^2$ with S = scan count and B = normalized background count.

The structure was solved by direct methods, all non-hydrogen atoms being positioned from an *E*-map. Hydrogen atoms were positioned from a subsequent difference map. In the final stages of

[2]The computer programs used include locally written programs for data processing and locally modified versions of the following: MULTAN 80, multisolution program by P. Main, S. J. Fiske, S. E. Hull, L. Lessinger, G. Germain, J. P. Declercq, and M. M. Woolfson; ORFLS, full-matrix least-squares, and ORFFE, function and errors, by W. R. Busing, K. O. Martin and H. A. Levy; FORDAP, Patterson and Fourier syntheses, by A. Zalkin; ORTEP II, illustrations, by C. K. Johnson.

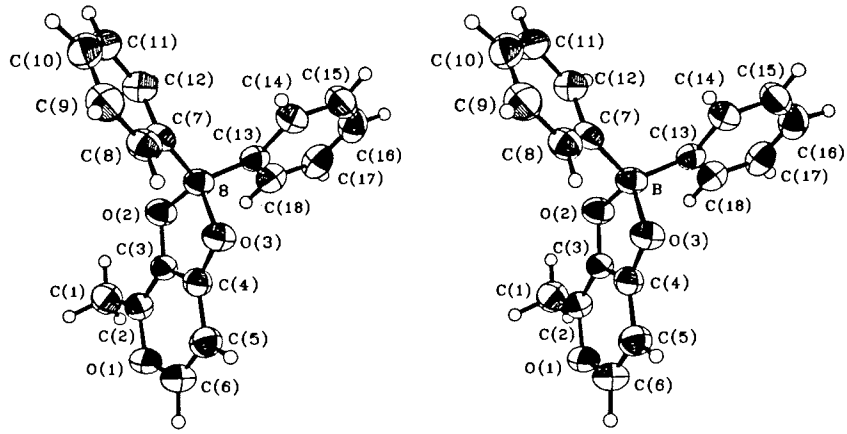

FIG. 1. Stereoscopic view of the (maltolato)diphenylboron molecule; 50% probability thermal ellipsoids are shown for the non-hydrogen atoms. Hydrogen atoms have been assigned arbitrary thermal parameters for the sake of clarity.

TABLE 1. Final positional (fractional × 10^4, H × 10^3) and isotropic thermal parameters ($U \times 10^3$ Å^2) with estimated standard deviations in parentheses

Atom	x	y	z	U_{eq}/U_{iso}
O(1)	5685(1)	4279(2)	6781(1)	60
O(2)	3229(1)	3125(2)	6068(1)	51
O(3)	3804(1)	1959(2)	4598(1)	52
C(1)	4562(2)	4948(4)	7857(2)	67
C(2)	4763(1)	4160(3)	6888(2)	51
C(3)	4162(1)	3350(2)	6116(2)	44
C(4)	4479(1)	2658(2)	5248(2)	48
C(5)	5444(2)	2772(3)	5169(2)	56
C(6)	5999(2)	3588(3)	5957(2)	67
C(7)	2059(1)	2997(2)	4253(2)	47
C(8)	2202(2)	3617(3)	3279(2)	55
C(9)	1503(2)	4462(3)	2602(2)	66
C(10)	635(2)	4677(3)	2871(2)	69
C(11)	458(2)	4061(3)	3815(2)	67
C(12)	1160(1)	3236(3)	4495(2)	58
C(13)	2614(1)	330(2)	5429(1)	45
C(14)	2080(1)	−724(3)	4699(2)	55
C(15)	1928(2)	−2283(3)	4974(2)	66
C(16)	2294(2)	−2838(3)	5991(2)	69
C(17)	2802(2)	−1828(3)	6732(2)	65
C(18)	2961(2)	−280(3)	6456(2)	53
B	2860(1)	2086(3)	5087(2)	46
H(1a)	499(3)	462(5)	851(3)	143(13)
H(1b)	476(3)	613(5)	783(3)	141(13)
H(1c)	390(2)	481(3)	778(2)	90(9)
H(5)	570(2)	232(3)	457(2)	68(7)
H(6)	669(2)	381(3)	602(2)	76(7)
H(8)	281(2)	351(3)	307(2)	63(7)
H(9)	168(2)	482(3)	193(2)	93(9)
H(10)	17(2)	537(3)	240(2)	79(8)
H(11)	−13(2)	427(3)	401(2)	93(9)
H(12)	104(1)	278(3)	514(2)	60(6)
H(14)	180(1)	−32(3)	398(2)	54(6)
H(15)	155(2)	−296(3)	451(2)	78(8)
H(16)	218(2)	−394(4)	620(2)	89(8)
H(17)	304(2)	−216(3)	751(2)	76(7)
H(18)	330(2)	45(3)	698(2)	60(6)

refinement the non-hydrogen atoms were refined with anisotropic thermal parameters and the hydrogen atoms with isotropic thermal parameters. The scattering factors of ref. 6 were used for non-hydrogen atoms and those of ref. 7 for hydrogen atoms. The weighting scheme $w = 1/\sigma^2(F)$, where $\sigma^2(F)$ is derived from the previously defined $\sigma^2(I)$, gave uniform average values of $w(|F_o| - |F_c|)^2$ over ranges of both $|F_o|$ and $\sin\theta/\lambda$ and was employed in the final stages of full-matrix refinement of 260 variables. Reflections with $I < 3\sigma(I)$ were not included in the refinement. An isotropic Type I extinction correction (Thornley–Nelmes definition of mosaic anisotropy with a Lorentzian distribution) was applied (8–10). The final value of g was $0.74(13) \times 10^4$. Convergence was reached at $R = 0.041$ and $R_w = 0.052$ for 2052 reflections with $I \geq 3\sigma(I)$. For all 3067 reflections $R = 0.073$. The function minimized was $\Sigma w(|F_o| - |F_c|)^2$, $R = \Sigma||F_o| - |F_c||/\Sigma|F_o|$ and $R_w = (\Sigma w(|F_o| - |F_c|)^2/\Sigma w|F_o|^2)^{1/2}$.

On the final cycle of refinement the mean and maximum parameter shifts corresponded to 0.009 and 0.117σ, respectively. The mean error in an observation of unit weight was 2.130. A final difference map showed maximum fluctuations of −0.40 to +0.28 e Å^{-3}, both near O(2), and was essentially featureless elsewhere. The final positional and thermal parameters appear in Tables 1 and 6[3], respectively. Measured and calculated structure factors have been placed in the Depository of Unpublished Data.[3] The ellipsoids of thermal motion for the non-hydrogen atoms are shown in Fig. 1. The thermal motion has been analysed in terms of the rigid-body modes of translation, libration, and screw motion (11). The rms standard error in the temperature factors σU_{ij} (derived from the least-squares analysis) is 0.0012 Å^2. The subunits PhB and (maltolato)B were analysed separately (rms $\Delta U_{ij} = 0.0016$–0.0031 Å^2). The appropriate bond distances have been corrected for libration (11, 12), using shape parameters q^2 of 0.08 for all atoms involved. Corrected bond lengths appear in Table 2 along with the uncorrected values; corrected bond angles do not differ by more than 1σ from the uncorrected values given in Table 3. Intra-annular torsion angles defining the conformation of the five-membered chelate ring are listed in Table 4. Bond lengths and angles involving hydrogen and a complete listing of torsion angles (Tables 7–9) are included as supplementary material.

Results and discussion

The crystal structure of (maltolato)diphenylboron consists of discrete molecules separated by normal van der Waals distances. The shortest intermolecular contact between non-hydrogen atoms is C···C = 3.295(4) Å. The molecule (Fig. 1) has as its central feature a fused-ring system which is planar to within 0.054(2) Å. Each of the three six-membered rings in the molecule is slightly, but significantly, non-planar (maximum deviation from the mean plane = 0.010(3) Å), while the five-membered C_2O_2B ring has a flattened B-envelope conformation with the boron

[3]The structure factor table, Table 6 (anisotropic thermal parameters) and other material mentioned in the text may be purchased from the Depository of Unpublished Data, CISTI, National Research Council of Canada, Ottawa, Ont., Canada K1A 0S2.

Can. J. Chem. Downloaded from www.nrcresearchpress.com by 80.58.250.72 on 09/07/12
For personal use only.

TABLE 2. Bond lengths (Å) with estimated standard deviations in parentheses

Bond	Length		Bond	Length	
	Uncorr.	Corr.		Uncorr.	Corr.
O(1)—C(2)	1.359(2)	1.363	C(7)—B	1.601(3)	1.605
O(1)—C(6)	1.344(3)	1.348	C(8)—C(9)	1.386(3)	1.390
O(2)—C(3)	1.343(2)	1.347	C(9)—C(10)	1.364(4)	1.372
O(2)—B	1.529(2)	1.533	C(10)—C(11)	1.369(4)	1.379
O(3)—C(4)	1.288(2)	1.292	C(11)—C(12)	1.381(3)	1.385
O(3)—B	1.595(3)	1.600	C(13)—C(14)	1.399(3)	1.407
C(1)—C(2)	1.470(3)	1.474	C(13)—C(18)	1.398(3)	1.405
C(2)—C(3)	1.358(3)	1.362	C(13)—B	1.596(3)	1.600
C(3)—C(4)	1.394(3)	1.398	C(14)—C(15)	1.383(3)	1.387
C(4)—C(5)	1.410(3)	1.415	C(15)—C(16)	1.377(4)	1.384
C(5)—C(6)	1.340(3)	1.344	C(16)—C(17)	1.369(4)	1.377
C(7)—C(8)	1.390(3)	1.400	C(17)—C(18)	1.377(3)	1.381
C(7)—C(12)	1.395(3)	1.404			

TABLE 3. Bond angles (deg) with estimated standard deviations in parentheses

Bonds	Angle (deg)	Bonds	Angle (deg)
C(2)—O(1)—C(6)	121.4(2)	C(8)—C(9)—C(10)	120.1(3)
C(3)—O(2)—B	107.83(14)	C(9)—C(10)—C(11)	119.7(2)
C(4)—O(3)—B	108.24(15)	C(10)—C(11)—C(12)	120.1(2)
O(1)—C(2)—C(1)	113.5(2)	C(7)—C(12)—C(11)	122.0(2)
O(1)—C(2)—C(3)	117.5(2)	C(14)—C(13)—C(18)	115.9(2)
C(1)—C(2)—C(3)	129.0(2)	C(14)—C(13)—B	121.7(2)
O(2)—C(3)—C(2)	126.6(2)	C(18)—C(13)—B	122.2(2)
O(2)—C(3)—C(4)	112.1(2)	C(13)—C(14)—C(15)	121.6(2)
C(2)—C(3)—C(4)	121.3(2)	C(14)—C(15)—C(16)	120.4(2)
O(3)—C(4)—C(3)	112.1(2)	C(15)—C(16)—C(17)	119.4(3)
O(3)—C(4)—C(5)	128.0(2)	C(16)—C(17)—C(18)	120.2(2)
C(3)—C(4)—C(5)	119.9(2)	C(13)—C(18)—C(17)	122.4(2)
C(4)—C(5)—C(6)	115.7(2)	O(2)—B —O(3)	99.49(13)
O(1)—C(6)—C(5)	124.1(2)	O(2)—B —C(7)	111.0(2)
C(8)—C(7)—C(12)	116.0(2)	O(2)—B —C(13)	111.52(15)
C(8)—C(7)—B	123.7(2)	O(3)—B —C(7)	109.5(2)
C(12)—C(7)—B	120.2(2)	O(3)—B —C(13)	107.0(2)
C(7)—C(8)—C(9)	122.0(2)	C(7)—B —C(13)	116.9(2)

atom displaced 0.081(2) Å from the C_2O_2 plane (see Table 4). The conformation of the C_2O_2B ring in **1** is intermediate between the essentially planar rings in **2** (13) and **3** (14) and the more folded envelopes observed in **4***a* and **4***b* (15).

The O—B and B—C distances in **1** are relatively long and short, respectively, when compared with those observed in other O,O-chelates of "Ph_2B^+" (compounds **2**–**9**, see Table 5), consistent with weak binding of the maltolate oxygen atoms to boron. The O(3)—B distance of 1.600(3) Å[4] is the longest O—B bond yet observed for a Ph_2BO_2 compound. Other long O—B distances occur in **4***a* (15), for the pyridinic oxygen atom in **9** (16), and for the aldehyde oxygen atom in **8** (17). In general the two O—B distances in **1**–**9** differ significantly from one another, by as much as 0.100(6) Å in **9**. Only in compound **3** are the two O—B bond lengths equal within experimental error. Despite the sometimes considerable differences between the two O—B bond lengths, the average O—B distance is a good indicator of the binding strength of the *O*,*O*-chelating ligand to the Ph_2B moiety. The B—C distances, which differ by a maximum of 0.020(7) Å in **9**, also reflect this property. In fact, the sum of all bond lengths involving the boron atom is essentially constant for a given chelate ring size: 6.328(7) Å for five-membered (**1**–**5**[5]) and 6.28(1) Å for the six-membered chelates **7**–**9**. Compounds **1**–**9** fall into three

TABLE 4. Intra-annular torsion angles (deg) standard deviations in parentheses

Atoms	Torsion angle (deg)
B —O(2)—C(3)—C(4)	3.2(2)
O(2)—C(3)—C(4)—O(3)	0.0(2)
B —O(3)—C(4)—C(3)	−3.0(2)
C(4)—O(3)—B —O(2)	4.5(2)
C(3)—O(2)—B —O(3)	−4.4(2)

[4]Libration corrected bond lengths (esd's assumed equal to those of the uncorrected values) are employed in the discussion of the geometry of the boron atom and are compared with similarly treated distances unless otherwise stated.

[5]Compound **6** with a distance sum of 6.283(6) Å is anomalous as a result of O—B bond shortening to compensate for a sterically lengthened intra-annular N—C bond (18).

Can. J. Chem. Downloaded from www.nrcresearchpress.com by 80.58.250.72 on 09/07/12
For personal use only.

TABLE 5. Comparison of selected structural parameters

(*a*) Ph_2BO_2 moieties (distances in Å)*

Compound	O—B	C—B	Mean O—B	Mean C—B	Sum at B
1	1.533(2), 1.600(2)	1.600(3), 1.605(3)	1.567	1.603	6.340
2	1.544(2), 1.565(2)	1.599(2), 1.611(3)	1.555	1.605	6.320
3	1.548(2), 1.552(2)	1.609(2), 1.609(2)	1.550	1.609	6.328
4	1.557(3)–1.580(3)	1.595(3)–1.604(4)	1.565	1.600	6.330
5	1.506(7), 1.556(8)	1.624(7), 1.639(8)	1.531	1.632	6.326
6	1.507(3), 1.534(3)	1.618(3), 1.624(3)	1.521	1.621	6.284
7	1.530(2)–1.547(2)	1.601(2)–1.610(3)	1.538	1.606	6.288
8	1.500(4), 1.574(4)	1.603(5), 1.610(5)	1.537	1.607	6.288
9	1.478(4), 1.578(4)	1.596(5), 1.618(5)	1.528	1.607	6.270

*

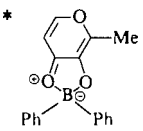

1

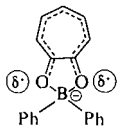

2

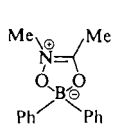

3

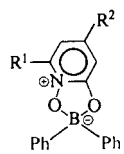

4

(*a*: $R^1 = R^2 = H$;
b: $R^1 = C_6H_{11}$, $R^2 = Me$)

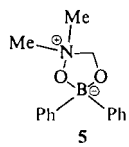

5

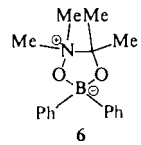

6

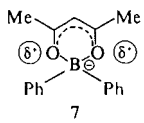

7

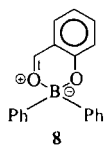

8

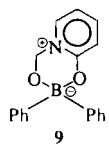

9

(*b*) Maltolate ligand and related structures (distances in Å, angles in deg)

	1	Tris(maltolato)-aluminum*	2,6-Dimethyl-4-pyrone HBr H_2O	4-Pyrone
O(2)—C(3)	1.343(2)	1.330(2)		
O(3)—C(4)	1.288(2)	1.271(4)	1.32(2)	1.248
O(1)—C(2)	1.359(2)	1.369(13)	1.34	1.355
O(1)—C(6)	1.344(3)	1.343(1)	1.39	1.355
C(2)—C(3)	1.358(3)	1.350(7)	1.35	1.356
C(3)—C(4)	1.394(3)	1.423(9)	1.41	1.440
C(4)—C(5)	1.410(3)	1.418(8)	1.39	1.440
C(5)—C(6)	1.340(3)	1.313(1)	1.31	1.356
O(2)—C(3)—C(2)	126.6(2)	125.0(6)		
O(2)—C(3)—C(4)	112.1(2)	115.1(6)		
C(2)—C(3)—C(4)	121.3(2)	120.0(2)		
O(3)—C(4)—C(3)	112.1(2)	117.0(6)	117	122.9
O(3)—C(4)—C(5)	128.0(2)	124.6(2)	126	122.9
C(3)—C(4)—C(5)	119.9(2)	118.4(8)	117	115.1

*Average values for the two ordered ligands.

groups. The weakest O—B binding occurs for compounds **1**–**4**, which all possess unsaturated five-membered chelate rings. The longest mean O—B distances for this group occur in **1** and **4**, which both contain strained ring systems consisting of planar six-membered rings fused to nearly planar five-membered rings. Compounds **5** (19) and **6** (18) contain fully saturated five-membered chelate rings, these particular ligands being among the best donors known for the "Ph_2B^+" cation. Compounds **7** (13), **8** (17), and **9** (16) all contain less strained six-membered chelate rings.

The ν_{CO} band in the ir spectrum of **1** at 1640 cm^{-1} suggests that O(3) is less strongly bound to the boron atom than are the corresponding oxygen atoms to Al in tris(maltolato)aluminum (ν_{CO} = 1617 cm^{-1}) (1). The relative weakness of the O(3)—B bond with respect to chemically similar bonds has been discussed above. The ratios of the long and short bond distances to the maltolate O atoms in the B and Al complexes (1.044 and 1.029, respectively) further support a stronger interaction of the keto oxygen atom with aluminum. In apparent contradiction to the ir data, the (uncorrected) C(4)—O(3) distance in **1** is 0.016(4) Å longer than the corresponding mean (for the two ordered ligands) in tris(maltolato)aluminum. This may result from the greater ring strain in **1** (see below).

In general, the bond lengths in the 4-pyrone moieties in **1** and tris(maltolato)aluminum are similar to one another and to those in 2,6-dimethyl-4-pyrone hydrobromide monohydrate (20) (see Table 5), the C—O distance involving the protonated keto oxygen atom in the latter structure being slightly longer

Can. J. Chem. Downloaded from www.nrcresearchpress.com by 80.58.250.72 on 09/07/12
For personal use only.

than the corresponding distances in the maltolate complexes. Although the structure of maltol itself has not been determined, the related structures of 4-pyrone (21) and 2,6-dimethyl-4-thiopyrone (22) indicate that upon coordination the keto C—O distance increases relative to that in 4-pyrone while the adjacent ring C—C distances decrease slightly. The remaining bond lengths are essentially unchanged.

There are some significant differences between the maltolate ligands of **1** and tris(maltolato)aluminum. The most prominent of these is the difference in the ligand bite (O(2)···O(3)) which is reduced from an average value of 2.562(8) Å in the Al complex to 2.384(2) Å in **1**. The O···O distance in the free ligand would be expected to be approximately 2.75 Å. This change is achieved primarily by angular deformations about the ring junction atoms C(3) and C(4); angles in the chelate ring decrease with compensatory increases in the exocyclic O—C—C and (to a lesser extent) the C—C—C angles in the six-membered heterocycle. Both C—O distances in the chelate ring of **1** are longer, and the C(3)—C(4) bond shorter than the corresponding mean values in tris(maltolato)aluminum. This could result from partial electron delocalization and/or the increased ring strain in **1**.

Acknowledgments

We thank the Natural Sciences and Engineering Research Council of Canada for financial support and the University of British Columbia Computing Centre for assistance. We also thank Mr. P. Borda for the C,H analysis.

1. M. M. FINNEGAN, S. J. RETTIG, and C. ORVIG. J. Am. Chem. Soc. **108**, 5033 (1986).
2. M. M. FINNEGAN, T. G. LUTZ, W. O. NELSON, A. SMITH, and C. ORVIG. To be published.
3. D. R. MCLACHLAN and C. ORVIG. In preparation.
4. P. COPPENS, L. LEISEROWITZ, and D. RABINOVICH. Acta Crystallogr. **18**, 1035 (1965).
5. J. D. MEULENAER and H. TOMPA. Acta Crystallogr. **19**, 1014 (1965).
6. D. T. CROMER and J. B. MANN. Acta Crystallogr. Sect. A, **24**, 321 (1968).
7. R. F. STEWART, E. R. DAVIDSON, and W. T. SIMPSON. J. Chem. Phys. **42**, 3175 (1965).
8. P. J. BECKER and P. COPPENS. Acta Crystallogr. Sect. A, **30**, 129 (1974); **30**, 148 (1974); **31**, 417 (1975).
9. P. COPPENS and W. C. HAMILTON. Acta Crystallogr. Sect. A, **26**, 71 (1970).
10. F. R. THORNLEY and R. J. NELMES. Acta Crystallogr. Sect. A, **30**, 748 (1974).
11. V. SCHOMAKER and K. N. TRUEBLOOD. Acta Crystallogr. Sect. B, **24**, 63 (1968).
12. D. W. J. CRUICKSHANK. Acta Crystallogr. **9**, 747 (1956); **9**, 754 (1956); **14**, 896 (1961).
13. S. J. RETTIG and J. TROTTER. Can. J. Chem. **60**, 2957 (1982).
14. S. J. RETTIG, J. TROTTER, W. KLIEGEL, and D. NANNINGA. Can. J. Chem. **56**, 1676 (1978).
15. W. KLIEGEL, D. NANNINGA, S. J. RETTIG, and J. TROTTER. Can. J. Chem. **61**, 2493 (1983).
16. W. KLIEGEL, H.-W. MOTZKUS, D. NANNINGA, S. J. RETTIG, and J. TROTTER. Can. J. Chem. **64**, 507 (1986).
17. S. J. RETTIG and J. TROTTER. Can. J. Chem. **54**, 1168 (1976).
18. W. KLIEGEL, H.-W. MOTZKUS, S. J. RETTIG, and J. TROTTER. Can. J. Chem. **62**, 838 (1984).
19. S. J. RETTIG, J. TROTTER, and W. KLIEGEL. Can. J. Chem. **52**, 2531 (1974).
20. H. HOPE. Acta Chem. Scand. **19**, 217 (1965).
21. C. L. NORRIS, R. C. BENSON, P. BEAK, and W. H. FLYGARE. J. Am. Chem. Soc. **95**, 2766 (1973).
22. J. TOUSSAINT. Bull. Soc. Chim. Belg. **65**, 213 (1956).
23. W. KLIEGEL, L. PREU, S. J. RETTIG, and J. TROTTER. Can. J. Chem. **64**, 1855 (1986).

Can. J. Chem. Downloaded from www.nrcresearchpress.com by 80.58.250.72 on 09/07/12
For personal use only.

Lanostane to cucurbitane transformations[1,2]

O. E. EDWARDS[3] AND R. J. KOLT

Division of Chemistry, National Research Council of Canada, Ottawa, Ont., Canada K1A 0R6

Received June 27, 1986

O. E. EDWARDS and R. J. KOLT. Can. J. Chem. **65**, 595 (1987).

Transformation of 3,7,9,11-tetraoxygenated lanostane derivatives into 3,7,11-trioxygenated cucurbit-1(10)-enes and cucurbit-5(10)-enes has been achieved. Attempts to convert the latter in good yield into cucurbit-5-enes are documented. The steric and electronic factors influencing the course of dehydration, under Westphalen conditions, of 9α-hydroxylanostane derivatives are discussed. Unusual autooxidation and dehydrogenation promoted by rhodium trichloride and iron pentacarbonyl are described.

O. E. EDWARDS et R. J. KOLT. Can. J. Chem. **65**, 595 (1987).

On a réalisé la transformation de lanostanes tétraoxygénes en 3, 7, 9 et 11 en cucurbitènes-1(10) (ou -5(10)) trioxygénés en 3, 7 et 11. On présente des exemples d'essais de transformation, avec de bons rendements, de ces derniers en cucurbitènes-5. On discute des facteurs stériques et électroniques qui influencent le cours de la déshydratation, utilisant les conditions de Westphalen, de dérivés de l'hydroxy-9α lanostane. On décrit des réactions inhabituelles d'autooxydation et de déshydrogénation qui sont favorisées par le trichlorure de rhodium et le pentacarbonyle de fer.

[Traduit par la revue]

Can. J. Chem. Downloaded from www.nrcresearchpress.com by 80.58.250.72 on 09/07/12
For personal use only.

Work of Edwards and Paryzek (1) on the Westphalen-type dehydration of 3β-acetoxy-9α-hydroxylanostan-11-one **1** showed that this produced a pair of cucurbitenes[4] **2** and **3** with 1(10) and 5(10) double bonds respectively. The problem of how to convert these into the desired cucurbitacins with 5,6 double bonds (e.g., 25-deoxybryogenin acetate **4**), and the hope of improving the yields of products of migration of C-19 from C-10 to C-9, led us to place an additional carbonyl at C-7. We anticipated facile migration of any 5(10) double bond into conjugation with the 7-carbonyl. In addition, as has been pointed out by Paryzek (2) and Baddeley *et al.* (3), this carbonyl might suppress backbone rearrangement involving a transient positive charge on C-8, thus increasing the yield of 19(10→9β) *abeo*-products. On the other hand, we faced the possibility that the leaving group on C-9 might eliminate to give a large proportion of the 8-en-7-one derivatives.

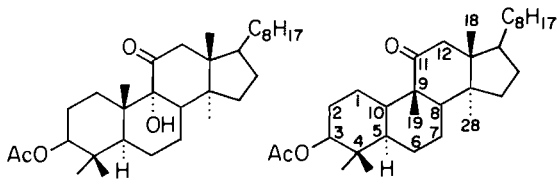

1

2 5αH, 1(10) double bond
3 5(10) double bond
4 10αH, 5(6) double bond

Work by Hartshorn and co-workers (4) and Jones and Marples (5) on the Westphalen dehydration–rearrangement showed that an acetoxy group on the carbon adjacent to the tertiary hydroxyl group being eliminated was effective in promoting methyl group migration. This was borne out in our earlier work (1). It also seemed possible that the electron-withdrawing action of a 7-acetoxy group might suppress backbone rearrangement (see above) without promoting simple elimination of water from a 9α-hydroxy compound. Hence the work developed into a study of Westphalen-type rearrangements of 9α-hydroxy-lanostanes with various combinations of carbonyl and acetoxy groups on C-7 and C-11.

Results

An efficient route to 3,7,9,11-tetraoxygenated lanostanes proved to be through chromic acid oxidation of the readily available 3β-acetoxy-7,9(11)-diene (dihydroagnosteryl acetate) to 3β-acetoxy-5α-lanost-9(11)-en-7-one **5** (6) followed by osmium tetroxide oxidation to the 9α,11α-diol **6*a***. Attempts to do the hydroxylation using catalytic amounts of osmium tetroxide with other oxidants (7) failed. Modified Moffatt oxidation (8) of the diol gave the 9α-hydroxy-7,11-dione **7**. However, purer **7** was obtained directly from **5** by addition of a molar equivalent of osmium tetroxide followed by oxidation of the osmate ester with hydrogen peroxide in a tetrahydrofuran–pyridine mixture. In the latter reaction full advantage was taken of the susceptibility of *cis*-diols to further oxidation under Milas-type conditions (7, 9).

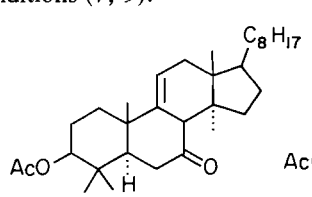

5

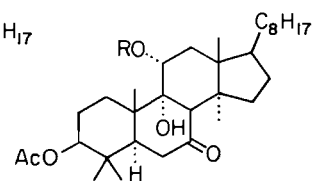

6*a* R = H
b R = Ac
c R = CH_2SCH_3

The desired variations in functionality at C-7 and C-11 were achieved as shown in Flowsheets I and II and eq. [1] using (*a*) lithium aluminohydride reduction of the 7-carboxyl of **5** to give the 7β-alcohol, (*b*) metal hydride reduction of 11-carbonyl groups to give the 11β-alcohols, (*c*) catalytic reduction of a 7-carbonyl to give the 7α-alcohol, (*d*) lithium aluminohydride reduction of the 7,11-dione **7** giving a reasonable yield of the 3β- and 7β,11β-triol, and (*e*) selective acetylation of 3β- and 7β-hydroxyl groups in the presence of an 11β-hydroxyl group.

[1]Issued as NRCC No. 25872.

[2]Presented in part at the Chemical Institute of Canada Conference, Calgary, June 1983, and the IUPAC symposium on Natural Products, Poznan, July 1984. See Natural Products Chemistry 1984. Elsevier Science Publishers, B.V., Amsterdam. 1985. pp. 51–60.

[3]Author to whom correspondance may be addressed at Department of Chemistry, Carleton University, Ottawa, Ont., Canada K1S 5B6.

[4]Alternative names: 9β-methyl-19-*nor*-lanostenes; 19(10→9β) *abeo*-lanostenes.

FLOWSHEET 1

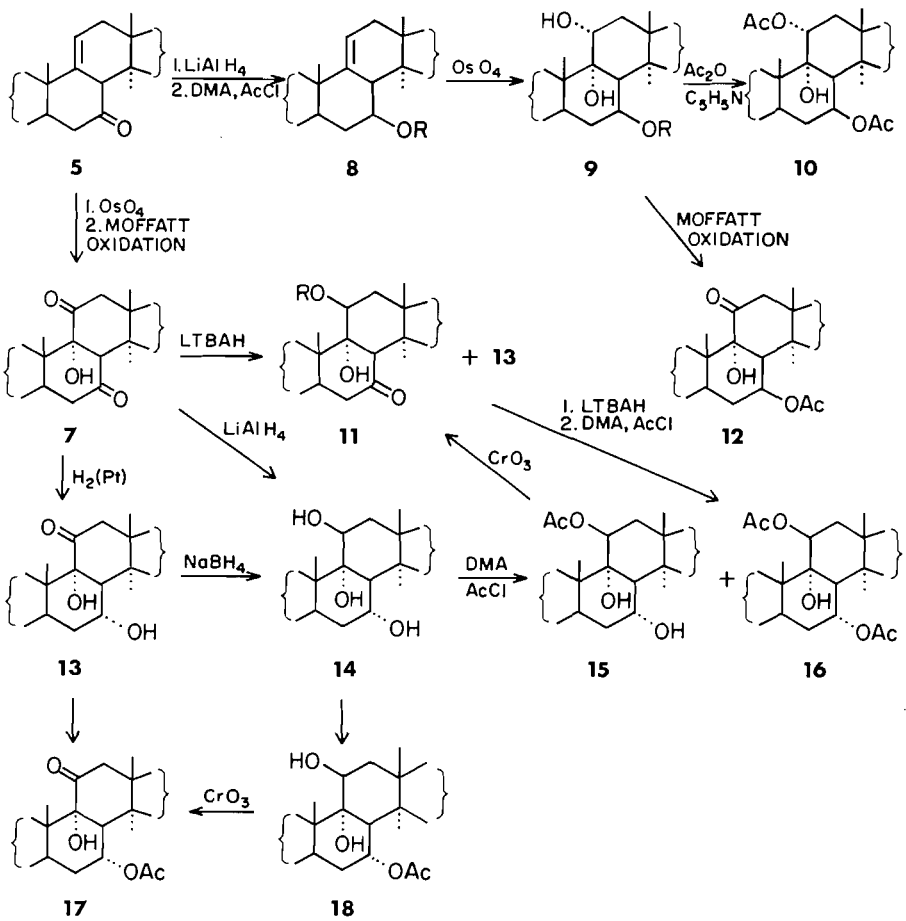

The Westphalen dehydration studies were all done using the same sulfuric acid – acetic acid – acetic anhydride mixture. The results are summarized in Table 1.

It is noteworthy that the compounds with 11β-acetoxy groups gave no significant amount of cucurbitenes. The outstanding yields of 9-methyl products were in the reaction of the 7α-acetoxy-11-one **17** (78% based on unrecoverable starting material) and the 7β-acetoxy-11-one **12** (90%). A dramatic reversal of the ratios of 1(10)-ene to 5(10)-ene occurred in the change from 11-one to 11α-acetate. Since at present the 5(10)-enes are more useful for conversion to cucurbitacins, via the 5-en-7-one derivatives (2), this makes the 11α-acetoxy-7-one ***6b*** the most valuable substrate despite the lower yield (49%) of 9-methyl

FLOWSHEET 2

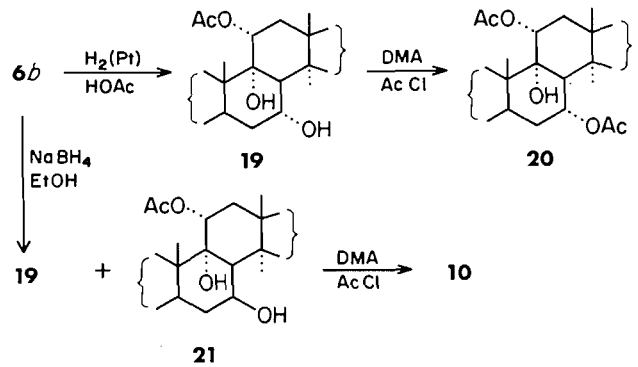

[1] **7** $\xrightarrow[2.\,DMA\text{-}AcCl]{1.\,LiAlH_4}$ **16** + **22**

products. Although the ratio of olefins was even better for the 7β,11α-diacetoxy compound **10**, the gain was more than offset by the extra steps needed to obtain a 5-en-7-one.

By-products in which no C-19 migration had taken place were identified for five of the substrates. These were as follows:

From ***6b***, 3β-11α-diacetoxy-5α-lanost-8-en-7-one ***24b*** (10%); 3β-acetoxy-18(13→12β) *abeo*-5α-lanosta-8,13(17)-dien-7-one **30** (5%); 3β-acetoxy-18(13→12β) *abeo*-5α-lanosta-8,11,13(17)-trien-7-one **35** (0.5%); 3β-acetoxy-5α-lanostana-7,11-dione **33** (8%); and 3β,11β-diacetoxy-5α-lanost-8-en-7-one ***24a*** (1.5%)

From **7**, 3β,9α-diacetoxy-5α-lanostana-7,11-dione **25** (23%) and 3β-acetoxy-5α-lanost-8-en-7,11-dione (12%)

From **11**, 3β,7,11-triacetoxy-5α-lanosta-7,9(11)-diene **29** (24%); 3β-acetoxy-5α-lanostana-7,11-dione **33** (32%); and 3β,11β-diacetoxy-5α-lanost-8-en-7-one ***24a*** (6%)

From **16**, 3β,7α-diacetoxy-5α-lanostan-11-one **28** (R^1 = H, R^2 = OAc) (57%)

From **22**, 3β,7α-diacetoxy-5α-lanostan-11-one **28** (R^1 = OAc, R^2 = H) (47%) and 3β,7β,11-triacetoxy-5α-lanost-9(11)-ene **43** (11%)

It was of interest to study other leaving groups at C-9. Indeed,

Can. J. Chem. Downloaded from www.nrcresearchpress.com by 80.58.250.72 on 09/07/12
For personal use only.

TABLE 1. Westphalen yields (%)

Substrate	(10)-ene	5(10)-ene	9α-OAc	Other*	Time (h)	Corrected† yield
7-one-11-one **7**	31	10	28	12	6	78
7α-OAc-11-one **17**	47	26	7	—	0.5	78
7β-OAc-11-one **12**	61	29	—	—	1	90
7-one-11α-OAc ***6b***	2	46	—	25	1	48
7α-OAc-11α-OAc **20**	1	7	—	—	Slow	39
7β-OAc-11α-OAc **10**	6	59	—	—	4	51
7-one-11β-OAc **11**	—	—	—	62	1.5	
7α-OAc-11β-OAc **16**	—	—	—	57	9	
7β-OAc-11β-OAc **22**	—	—	—	58	0.5	

*Well-characterized products not involving C-19 migration.
†Based on unrecoverable starting material.

the initial intention was to prepare and deaminate 9α-amino compounds (1, 10). The 9α-acetoxy-7,11-dione **25** was obtained as a by-product of the Westphalen dehydration of **7**, and as the product of acetylation of **7** using perchloric acid in acetic anhydride. Attempts to prepare the corresponding mesylate directly using methanesulfonyl chloride, or indirectly via the methanesulfinate (11), failed.

The 9α-acetoxy compound was quite stable. Slow decomposition took place at 195°C. The only product characterized was the 8-en-7,11-dione.

In view of the success of Paryzek (2) and Baddeley *et al.* (3) in the use of boron trifluoride in acetic anhydride, we examined its use as a dehydrating agent for our 9α-hydroxy compounds ***6a***. However, the reagent mainly acetylated the 9-hydroxyl group giving 46% of **27**. Only a small amount (9%) of the acetoxydiene **32** was produced.

Initial attempts to isomerize the 5(10)-en-7-one **45** to the conjugated 5-en-7-one **47** using potasssium hydroxide in methanol resulted in oxidation and hydrolysis to 3β,6,11α-trihydroxycucurbit-1(10),5-dien-7-one **48** (R = H). This had λ_{max} 337 nm, shifting to 383 nm in alkali. The corresponding triacetate had λ_{max} 305 nm with a weaker maximum at 240 nm and nmr spectra in accord with the assigned structure (**48**, R = Ac). A comparable 6-acetoxy dienone **49** was formed by the action of alkali on the 5(10)-en-7,11-dione **44**, followed by reacetylation.

When solutions of the enol acetate **32** or the 5(10)-en-7-one

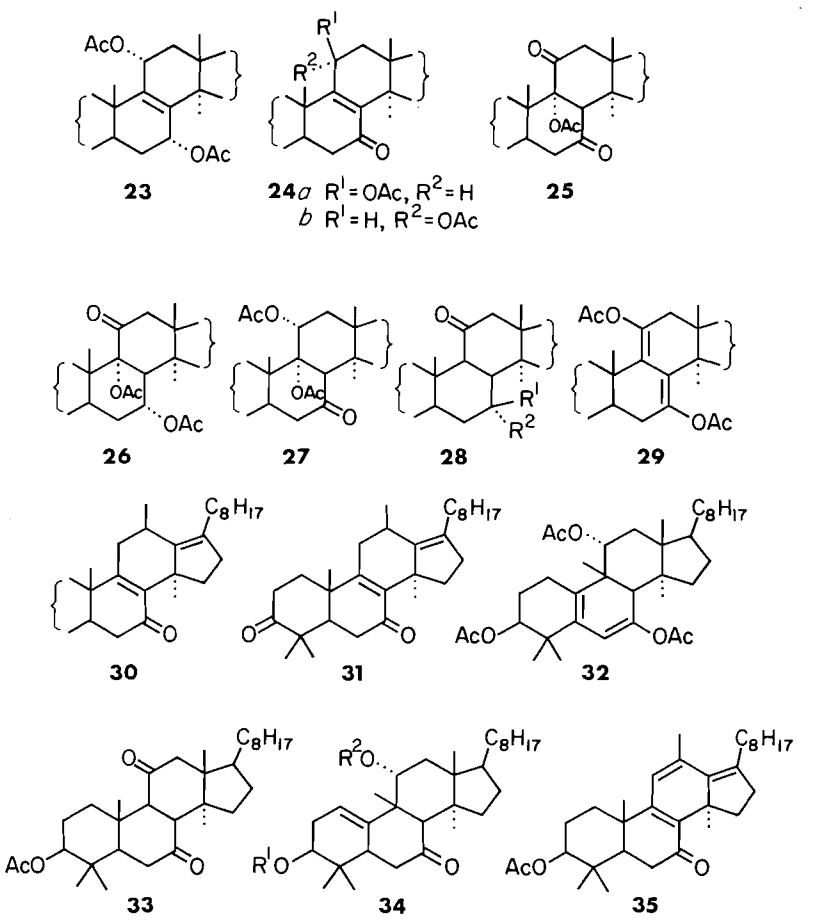

Can. J. Chem. Downloaded from www.nrcresearchpress.com by 80.58.250.72 on 09/07/12
For personal use only.

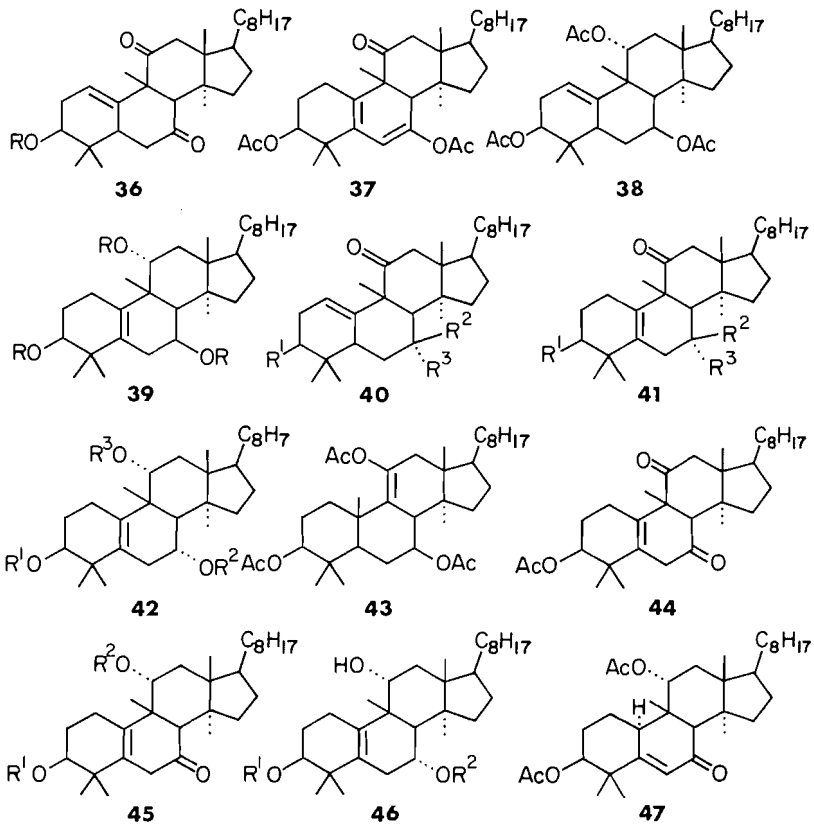

45 in 95% ethanol were degassed by boiling under argon, and a similarly degassed solution of potassium hydroxide in the same solvent was added, a maximum at 300 nm appeared followed by one at 240 nm. We attribute these to the enolate anion **48**, $R^1 = R^2 = Ac$, $R^3 = O^-$, and the 5-en-7-one **47** respectively. Again a slow development of a maximum at 380 nm occurred. After acid work-up and separation on silical gel, fractions with λ_{max} 255 and 335 nm were obtained. Thus simple conjugation had not been achieved.

The action of dilute perchloric acid in 95% ethanol at 65°C on the enol acetate **32** or 5(10)-en-7-one **45** produced mixtures containing some product with λ_{max} near 245 nm. Since the yield of this was low, this approach was abandoned.

The best method found for producing the conjugated enone **47** from the enol acetate **32** was the use of a refluxing solution of sodium carbonate in aqueous methanol, followed by reacetylation. In this way a modest 12% conversion to **47**, identical to a previously prepared sample (12), was achieved. Two other isomers of **47** were characterized and presence of a fourth possible isomer detected.

A different approach to production of the conjugated enone **47** was based on the work of Edward and Alper (13). It was hoped that complexation of the homoannular diene of **32** with iron pentacarbonyl would mobilize the double bonds and effect isomerization to the corresponding 5,7-diene. This enol acetate would presumably hydrolyse to the 5-en-7-one **47**. In actuality, dehydrogenation and hydrolysis took place when **32** was heated with iron pentacarbonyl in diglyme, leading to 3β,11α-diacetoxycucurbita-1(10),5-dien-7-one **50** (79% based on unrecovered **32**).

The dienone **50** has recently been described as a product of the action of $BF_3 \cdot Et_2O$ in acetic anhydride on 3β-acetoxy-9α,11α-epoxy-lanost-5-en-7-one (14). Its uv, ir, and ^1H nmr spectra correspond reasonably well with those reported, as did those of the corresponding diol.

In a related attempt to rearrange the 5(10)-en-7-one to the 5-en-7-one, **45** (R = Ac) was heated in alcohol with rhodium trichloride. This reagent is known to isomerize double bonds (15). However, the same dehydrogenation resulted, producing **50** as major product. Palladium-on-charcoal in refluxing benzene also catalysed the same dehydrogenation.

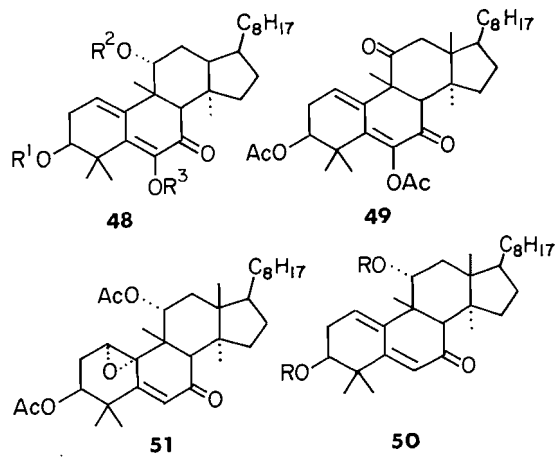

Samples of the dienol acetate **32** oxidized when left in air as a gum or froth for several months. Analysis and spectroscopic evidence showed that this was an α,β-unsaturated ketone, with the 3- and 11-acetate groups intact and a new ether oxygen. The evidence was consistent with it being 3β,11α-diacetoxy-1α,10α-epoxycucurbit-5-en-7-one **51**. Paryzek and Wydra (12) had assigned this structure to an autooxidation product of **32** obtained from 3β-acetoxy-9α,11α-epoxy-5α-lanostan-7-one, and the properties were identical.

Discussion

A good body of evidence exists that cyclic carbocations are destabilized by the presence of an adjacent carbonyl group (1,

Can. J. Chem. Downloaded from www.nrcresearchpress.com by 80.58.250.72 on 09/07/12
For personal use only.

10, 11, 16, 17) and that they are usually only formed with the aid of charge delocalization by σ-bond participation or other neighboring group participation. It also appears that when σ-bond participation is involved, corner- and edge-protonated cyclopropanes are either intermediates or transition states on the way to products (18, 19). Thus the methyl migrations encountered in this work and other Westphalen rearrangements likely involve the methyl-bridged ion (corner-protonated cyclopropane) **52** or a transition state closely resembling this. The same applies to methyl migrations during deamination of 9α-amino- and 12α-amino-11-keto steroids (10). Our anticipation that intermediates such as **52** would lead to some cyclopropanes (in the present work, cycloartane derivatives) was not realized. This may be due to the high proton acidity of the medium, suppressing proton loss from **52**.

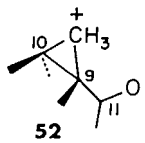

52

In harmony with the observations of Hartshorn and co-workers (4) and Jones and Marples (5), an α-acetoxy group on C-11 was nearly as effective as an 11-carbonyl in inducing methyl migration. However, the presence of an 11β-acetoxy group blocked methyl migration. Two factors could be involved in this. One is steric interference with methyl movement toward C-9, thus blocking formation of the methyl-bridged ion. The other is acetate participation in the ionization of the C-9 oxygen bond, taking the place of the 10-methyl group participation.

Most of the other results shown in the table can be rationalized on the basis of a few assumptions:

(*a*) That mixed anhydride (acetylsulfate) formation was rapid in all cases, as suggested by Hartshorn and co-workers (4) and that in all the cases studied except that of the 7α,11α-diacetoxy compound **20** this hydrolysed rapidly in contact with a tlc plate. Thus remaining mixed anhydride showed up as starting material.

(*b*) That the rate-determining step in the reactions was the ionization of the C(9)—O bond. This was slow in the case of the 7,11-dione **7** because of the two powerful electron-withdrawing groups, but was more rapid in the cases of **12** and **17** where one of the carbonyls had been replaced by an acetoxyl group.

(*c*) That protonation of the mixed anhydride was needed to initiate the C—O bond rupture in the mixed anhydride. This is the only way in which we can account for the exceedingly slow rate for the 7α,11α-diacetoxy compound **20**. We argue that the two bulky acetoxy groups block approach of solvated protons to the anhydride and also act as competing bases.

(*d*) That acetylation of the 9α-hydroxy group could only occur when crowding of the α-face was minimal (e.g., for the 7,11-dione), and it results from acetic acid attack on the acetylsulfate with O—SO_2 bond rupture.

(*e*) The dramatic change in ratio 1(10)-ene to 5(10)-ene in going from the 11-one **7** to the 11α-acetate **6*b*** can be explained if the 11α-acetate blocks removal of the 1α-hydrogen by external bases, or if the 11-carbonyl acts as internal base assisting removal of the 1-hydrogen, or if both factors operate.

The most unusual observation is the slow reaction of the 7α,11β-diacetoxy compound **16**. A conformational change due to the interaction of the 11β function with the 10- and 13-methyl groups may make the 9α-substituent less accessible to solvated protons (see point (*c*)).

The opening of saturated 9,11-epoxides with boron trifluoride in any medium but acetic anhydride failed to give 10-methyl migration (2, 3, 20). This suggests that the attacking species in the anhydride medium is the acylium ion. Thus the different behavior in acetic anhydride could be a consequence of the difference between zwitterions **53** and the more isolated cations represented by **54** (see also ref. 14). We can only reconcile our observations on the 11β-acetates with the results for 9β,11β-epoxides (2, 3) if the cationic carbon of **54** is free to form a methyl bridged ion (**52**), while in our cases the ionization of the 9-O bond leads (with participation of the 11β-acetate) directly to the delocalized ion **55**. We postulate that **55** would give no methyl migration. Instead, elimination of protons on C-8 or C-11 would lead to 8-enes or 9(11)-enes respectively. Both types of product were actually observed, in addition to the 11-ketones arising by hydrolysis of the enol acetates.

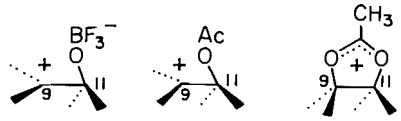

53 **54** **55**

Although the yield of the β,γ-unsaturated ketone **45** was good, conversion of this to the desired conjugated stereoisomer **47** was low. Since it was accompanied, depending on the time of heating in base, by one or two stereoisomers, it appears that the rate of isomerization is comparable to that of epimerization at C-8 and C-10. It has been assumed that the first center to be inverted is C-10 (2, 3). However, this has not been rigorously established, hence we reserve judgement on the configuration of our new isomers.

Since we were unable to form **47** by acid-catalysed isomerization of **45** or by the action of transition metals or palladium-on-charcoal on **45** or **32**, further research is needed in the Westphalen route is to be an efficient one to cucurbitacins (8β,10α-cucurbit-5-enes).

The facile dehydrogenation of the 5(10)-ene-7-one **45** to the 1(10),5-dien-7-one **50** must reflect a relief of nonbonded interactions as rings A and B are flattened. A similar dehydrogenation had been observed earlier in oxidation of cucurbitacins having a carbonyl on C-2 (21).

The very facile Barton-type oxidation (22) of the 5(10)-en-7-one derivatives **44** and **45** to 6-hydroxydienones, even in as weak a base as sodium carbonate in aqueous methanol, reflects the acidity of the proton on C-6.

The formation of the dienone **31** and trienone **35** from the 11α-acetoxy-9α-hydroxy-7-one **6*b*** was unexpected. The formation of **31** from the corresponding 9α,11α-epoxide has been described by Paryzek and Wydra (12) who have discussed possible mechanisms for its formation. Under our reaction conditions, formation of the conjugated dienone by double elimination, followed by proton-catalysed rearrangement as shown in **56**, is a plausible possibility. (See, however, ref. 12.) The dehydrogenation to **35** must be produced by oxygen.

The autooxidation of the enol acetate **32** is remarkable. Two possible mechanisms for the air oxidation are shown in Flow-

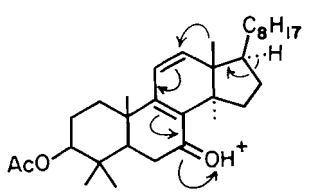

56

Can. J. Chem. Downloaded from www.nrcresearchpress.com by 80.58.250.72 on 09/07/12
For personal use only.

FLOWSHEET 3

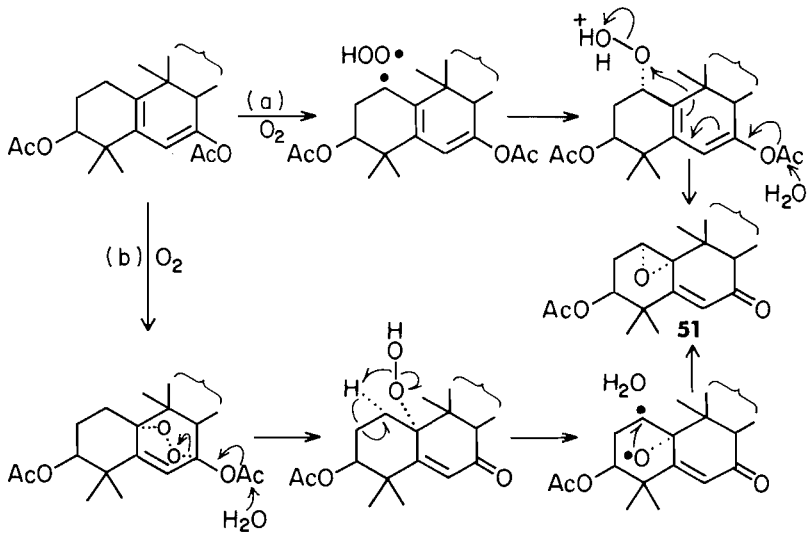

sheet 3. In view of the well-known epidioxide formation from ergosterol (23), mechanism (b) is attractive. Mechanism (a) has also been proposed by Paryzek and Wydra (12), who observed the same phenomenon.

Nuclear magnetic resonance spectra

The ^{13}C nmr spectra of compounds prepared in this work are listed in Tables 2–5. The assignments are based on multiplicity, known substituent effects, and assignments previously made by Baddeley and co-workers (3) and Paryzek and Wydra (12) for related compounds. However, the availability of good quantities of 3β-acetoxycucurbit-1(10)-en-7,11-dione **36** and the distinctive chemical shifts due to its functional groups prompted us to use it to check these assignments by using other nmr techniques.

It seemed likely that the proximity of the 1- and 19-hydrogens would give rise to significant nuclear Overhauser effects. However, irradiation of any of the methyl signals (δ 0.7–1.25) failed to produce a noticeable intensity change for the 1-hydrogen signal, and conversely irradiation of the 1-hydrogen gave no effect on the methyl signal intensities.

The use of ^1H COSY spectra, especially with emphasis on long range couplings ($J \sim 1$ Hz) coupled with ^1H–^{13}C correlations, made it possible to assign shifts to hydrogens on C-18 (δ 0.71, coupled to the lowest field 12-hydrogen), C-28 (δ 1.25, coupled with the 8-hydrogen and a 15-hydrogen near δ 1.42), C-29 (0.88, coupled with the 3-hydrogen), and C-30 (0.78, coupled with the 3-hydrogen). Thus the signal at δ 1.05, which had long range coupling with the 8-hydrogen, could be assigned to the 19-hydrogens. The ^1H–^{13}C correlation then gave a ^{13}C shift for C-19 of 20.2 ppm. It followed also that C-30 had the highest chemical shift (13.3) but that C-28 resonated at 30.8 ppm. Thus it appears that many of the C-19, C-28, and C-29 assignments in our tables and those of other workers (3, 12) should be revised. However, since we are unable to provide nmr evidence comparable to that for **36** we have not altered the original assignments for the other compounds.

Experimental

The instrumentation and separation techniques were as described previously (1). Abbreviations used are LAH (lithium aluminum hydride, LTBAH (lithium tri-*tert*-butoxyaluminohydride), DMA (dimethylaniline). Unless otherwise stated, rotations were of chloroform solutions, infrared spectra were taken in chloroform, and ultraviolet spectra in 95% ethanol.

Substrates and reference compounds

3β-Acetoxy-5α-lanostan-9(11)en-7-one (5). The enone **5** was prepared by chromium trioxide oxidation of either 24,25-dihydrolanosteryl acetate (**6***a*) or 24,25-dihydroagnosteryl acetate (**6***b*). The yield was better in the latter case (ca. 23%). The major impurity in both cases was 3β-acetoxy-5α-lanost-8-en-7,11-dione.

Compound **5** gave ^1H nmr signals at δ 5.41 (m, 1H, 11), 4.49 (t, J = 5 Hz, 3α), 2.87 (m, 1H, 8β), 2.35 (s, part of signals for H-6), 2.06 (s, 3H, CH_3CO), 1.12, 0.93, 0.90, 0.83, 0.76, and 0.68 (singlets, 3H, CH_3's).

3β-Acetoxy-9α,11α-dihydroxy-5α-lanostan-7-one (6a). A solution of 1.9 g of enone **5** and 1 g of osmium tetroxide in 12 mL of dry pyridine was stirred in the dark under argon for two days. A Solution of 3.6 g of sodium metabisulfate in 60 mL of water and 50 mL of pyridine was added. The dark viscous mixture was stirred for 2 h, by which time it became an orange solution. This was extracted three times with dichloromethane, then the dichloromethane solutions washed successively with water, 2*N* hydrochloric acid, saturated sodium carbonate solution, and water. The dried organic layers yielded a product that crystallized from methanol–chloroform mixtures, giving 1.7 g of dihydroxy ketone **6***a*, mp 218–220°C; $[\alpha]_D$ +33° (*c* 1.0); ν_{max}: 3610, 3520 (br), 1725 and 1710 cm^{-1}; ^1H nmr, δ: 4.41 (m, 1H, 3α), 4.24 (m, 1H, 11β), 3.28 (s, 1H, OH), 2.60 (s, 1H, 8β), 2.31 (s, 2H, 6), 2.04 (s, 3H, CH_3CO), 1.27, 1.19, 0.90, 0.86, 0.82, and 0.78 (CH_3 groups). *Anal.* calcd. for $C_{32}H_{54}O_5$: C 74.09, H 10.49; found: C 74.15, H 10.48.

Attempts to oxidize **5** using partial molar equivalents of osmium tetroxide with *N*-methylmorpholine *N*-oxide (24) or $Ba(ClO_3)_2$ (7) as oxidants only produced small amounts of **6***a*. Hydroxylation of the double bond by potassium permanganate under basic (basic potassium permanganate, ref. 25) or neutral (using water instead of 40% sodium hydroxide as the aqueous phase) phase transfer conditions, or by barium permanganate in pyridine gave mainly 3β-acetoxylanost-8-ene-7,11-dione.

3β,11α-Diacetoxy-5α-lanostan-9α-ol-7-one (6b). One gram of diol **6***a* in 5 mL of acetic anhydride and 5 mL of pyridine was left at room temperature overnight. The solution was poured into 20 mL of saturated aqueous sodium bicarbonate, then the product extracted into benzene. After removal of the benzene **6***b* crystallized from hexane, yield 1 g, mp 174–176°C; $[\alpha]_D$ +40° (*c* 1.2); ν_{max} 3600 and 1725 cm^{-1}; ^1H nmr, δ: 5.40 (dd, J_1 = 6.5 Hz, J_2 = 10 Hz, 1H, 11β), 4.42 (t, J = 6 Hz, 1H, 3α), 2.74 (s, 1H, OH), 2.64 (s, 1H, 8β), 2.31 (d, 2H, 6), 2.05 (s, 6H, CH_3CO's), 1.29, 1.22, 1.16, 0.89, 0.86, and 0.82 (CH_3's). *Anal.* calcd. for $C_{34}H_{56}O_6$: C 72.82, H 10.06; found: C 72.95, H 9.89.

Can. J. Chem. Downloaded from www.nrcresearchpress.com by 80.58.250.72 on 09/07/12
For personal use only.

TABLE 2. ^{13}C nuclear magnetic resonance spectra

	Compound													
					9		11							
Carbon	6*a*	6*b*	6*c*	7	R = Ac	10	R = H	R = Ac	12	13	14	15	16	17
1	30.9	29.7	30.9	28.9	31.6	30.4	28.7	28.6	29.2	29.3	29.5	29.4	29.4	29.0
2	23.9	23.8	24.0	23.6	23.9	23.9	23.6	23.5	23.6	23.8	23.8	23.7	23.6	23.8
3	80.1	79.5	79.9	80.1	80.3	79.9	80.3	80.0	80.3	80.4	80.8	80.4	79.9	79.9
4	37.7	37.6	37.8	38.1	37.6	37.5	37.7	37.7	38.0	37.9	37.5	37.5	37.4	37.8
5	44.3	44.1	44.3	45.3	42.4	42.3	44.4	43.9	43.8	40.7	40.7	40.5	41.3	41.5
6	39.3	39.0	39.3	39.3	28.4	28.2	39.8	39.3	28.7	31.8	32.2	32.1	37.7	27.8
7	210.1	208.5	209.3	208.5	72.4	71.7	211.3	210.6	71.3	71.2	71.1	70.9	74.0	74.2
8	55.3	55.3	55.5	55.9	45.1	45.4	55.0	55.1	46.4	43.6	42.9	42.8	42.4	43.6
9	80.1	80.2	80.7	83.1	77.9	78.3	81.0	80.4	81.2	82.4	81.2	80.6	79.9	81.4
10	43.8	43.9	43.9	42.3	43.7	43.7	42.5	42.3	41.8	43.3	43.8	43.6	43.5	43.0
11	66.5	70.0	72.3	208.8	67.4	71.0	76.7	76.6	208.8	209.6	76.6	76.8	76.1	207.0
12	40.7	36.4	35.5	49.4	40.3	36.4	36.2	35.3	48.6	50.1	40.3	36.2	35.9	49.3
13	46.1*	45.9*	45.8*	48.9*	46.4*	46.3*	46.3*	46.1*	49.4*	47.9*	45.7*	45.3*	45.6*	48.2*
14	45.3*	45.2*	45.2*	45.6*	46.6*	46.5*	45.3*	45.3*	47.0*	47.8*	48.4*	48.1*	47.7*	47.6*
15	33.9	33.8	33.9	33.8	36.3	36.0	34.7	34.7	36.2	33.5	34.3	34.3	34.1	33.6
16	28.2	28.2	28.2	28.4	28.4	28.4	28.4	28.2	28.3	28.0	28.0	28.0	28.1	28.0
17	49.2	49.1	49.3	48.7	49.1	49.0	49.7	49.6	48.6	49.6	50.4	50.3	50.3	49.3
18	15.5	15.3	15.5	16.0	15.4	15.3	16.8	16.9	15.7	16.4	17.0	17.1	16.8	15.9
19	17.0	17.1	17.3	16.3	17.1	17.1	17.1	17.4	16.5	16.8	17.8	18.2	18.5	16.5
20	35.9	35.8	35.9	35.8	35.9	35.8	35.9	35.8	35.7	36.1	36.3	36.2	36.1	36.0
21	18.2	18.2	18.2	18.4	18.3	18.3	18.3	19.0	18.6	18.4	18.8	18.8	18.7	18.3
22	36.4	36.4	36.5	36.2	36.4	36.2	36.5	36.4	36.2	36.3	36.6	36.5	36.4	36.3
23	24.0	23.9	24.0	23.9	24.0	23.9	24.0	24.0	23.9	24.1	24.1	24.1	24.1	24.0
24	39.5	39.4	39.5	39.4	39.5	39.5	39.4	39.5	39.5	39.5	39.6	39.5	39.5	39.4
25	27.9	27.9	28.0	27.9	28.0	27.9	28.0	28.0	28.0	28.0	28.0	28.0	28.0	28.0
26	22.8	22.7	22.8	22.8	22.8	22.8	22.8	22.8	22.8	22.8	22.9	22.9	22.8	22.8
27	22.5	22.5	22.5	22.5	22.6	22.5	22.5	22.5	22.5	22.6	22.6	22.6	22.5	22.5
28	18.7	18.6	19.2	19.0	18.9	18.8	18.9	19.2	18.8	19.8	19.9	19.8	19.2	19.4
29	27.7	27.6	28.0	27.7	28.0	27.9	28.0	27.8	28.1	28.3	28.5	28.5	28.3	28.2
30	16.0	15.8	16.2	16.0	16.3	16.2	16.2	16.2	16.2	16.5	16.5	16.2	16.2	16.1

*Assignments indicated by an asterisk may be interchanged.

Can. J. Chem. Downloaded from www.nrcresearchpress.com by 80.58.250.72 on 09/07/12
For personal use only.

Dehydration of **6***b* using thionyl chloride in pyridine gave 3β,11α-diacetoxy-5α-lanost-8-en-7-one (**24***b*).

3β-Acetoxy-9α-hydroxy-5α-lanosta-7,11-dione (7)

(a) By osmium tetroxide – hydrogen peroxide oxidation of **5** *(7, 9).* Two grams of osmium tetroxide was added to a solution of 3.8 g of 9,11-olefin **5** in 25 mL of dry pyridine. The mixture was stirred in the dark under argon for 3 days, then the bulk of the pyridine removed *in vacuo* at 50°C. The residue was dissolved in 50 mL of tetrahydrofuran, then 40 mL of 30% hydrogen peroxide was added slowly with stirring while cooling in an ice bath. After 1 h in the ice bath 5 g of sodium metabisulfite was added and the mixture stirred for 2 h at room temperature. The product was recovered as described for the hydroxylation of **5**. Crystallization from methanol–dichloromethane gave 2.4 g (59%) of hydroxy-dione **7**.

(b) By dimethylsulfonium chloride oxidation of **6***a (26).* Dimethylsulfide (0.24 mL, 3.19 mmol) was added under argon to a solution of 319 mg (2.39 mmol) of *N*-chlorosuccinimide in 10 mL of dichloromethane at −25°C. After 15 min at −25°C a solution of 331 mg (0.64 mmol) of diol **6***a* in 2 mL of dichloromethane was added. The cooling bath was removed, then after 15 min 50 mL of ether was added. The solution was washed with 0.2 *N* hydrochloric acid, water (3 times), then dried over magnesium sulfate. The 295 mg of crude product was separated on silica gel plates using 5:1 benzene – ethyl acetate, giving 151 mg of hydroxydione **7** and 102 mg of the slightly less polar methylthiomethyl ether **6***c*.

(c) By modified Moffatt oxidation of **6***a (8).* A mixture of 2.0 g of diol **6***a*, 400 mg of pyridine, 320 mg of dichloroacetic acid, 2.64 g of dicyclohexylcarbodiimide, 15 mL of dimethylsulfoxide, and 10 mL of benzene was stirred in a stoppered flask for 22 h at room temperature. A solution of 4 g of oxalic acid in 5 mL of methanol was added carefully, then the mixture stirred for 2 h. Water and benzene were added, then the precipitate removed by filtration, and the solid washed well with benzene. The benzene layers were washed with saturated aqueous oxalic acid, 5% sodium carbonate solution, dried, and distilled. The product crystallized from acetone–water giving 1.65 g (92%) of crude hydroxydione **7**, mp 195–205°C. This was contaminated with a small amount of the methylthiomethyl ether **6***c*, which could be removed by recrystallization or separation on silica gel.

The 9α-hydroxy-7,11-dione **7** had mp 215–218°C; $[\alpha]_D$ +55° (*c* 1.2); ν_{max} 3575, 3440, and 1712 cm^{-1}; ^1H nmr, δ: 4.48 (t, J = 7.5 Hz, 1H, 3α), 3.39 (s, 1H, OH), 3.25 and 3.07 (singlets, 1H, part of d of d for the 12-hydrogens), 2.88 (s, 1H, 8β), 2.4–2.1 (m, ca. 2H, 6), 2.03 (s, 3H, CH_3CO), 1.38, 1.29, 0.93, 0.90, 0.85, 0.83, and 0.76 (CH_3s). *Anal.* calcd. for $C_{32}H_{52}O_5$: C 74.37, H 10.14; found: C 74.66, H 10.34.

3β-Acetoxy-9α-hydroxy-11α(methyl thiomethoxy)-5α-lanosta-7-one (6c). Thiomethyl ether **6***c* crystallized as plates from hexane–dichloromethane. It had mp 209–212°C; $[\alpha]_D$ +6.5° (*c* 0.5); ν_{max}: 3550, 1720, and 1710 cm^{-1}; ^1H nmr, δ: 4.67 (s, 2H, S—CH_2—O), 4.47 (m, 1H, 3α), 4.09 (dd, 1H, J_1 = 6.3 Hz, J_2 = 10 Hz, 11β), 3.09 (d, 1H, J = 2 Hz, OH), 2.60 (d, 1H, J = 1.5 Hz, C-8), 2.31 (s, 2H, 6), 2.18 (s, 3H, S—CH_3), 2.05 (s, 3H, CH_3CO), 1.28, 1.21, 0.92, 0.90, 0.877, 0.83, and 0.76 (CH_3CO). *Anal.* calcd. for $C_{34}H_{58}O_5S$: C 70.55, H 10.10, S 5.53; found: C 70.55, H 10.18, S 5.71.

Dehydration of 3β-acetoxy-9α-hydroxy-5α-lanosta-7,11-dione (7)

Twenty-five microliters of thionyl chloride was added to an ice-

TABLE 3. ^{13}C nuclear magnetic resonance spectra

	Compound													
											28			
Carbon	18	19	20	21	22	24*a*	24*b*	25	26	27	R^1 = OH R^2 = H	R^1 = OAc R^2 = H	R^1 = H R^2 = OH	R^1 = H R^2 = OAc
1	29.5	30.1	30.3	30.5	29.2	32.2	32.6	29.8	30.6	31.2	36.2	36.1	36.8	36.8
2	23.7	24.1	23.8	23.9	23.5	23.8	23.9	23.6	23.6	24.0	24.0	23.8	24.0	24.0
3	80.3	80.2	78.8	80.0	80.2	79.3	79.6	79.7	80.2	79.5	80.5	80.3	80.7	80.3
4	37.4	37.3	37.3	37.6	37.6	38.0	38.0	38.2	37.7	38.0	37.9	38.0	37.7	37.7
5	41.5	39.7	40.4	42.9	42.7	48.3	50.1	46.2	41.5	45.7	47.7	44.4	43.4	42.5
6	27.7	31.9	27.8	32.3	28.3	36.5	36.7	39.1	28.0	38.6	31.5	27.6	31.1	27.3
7	74.4	70.4	73.4	71.3	72.1	199.8	199.4	202.2	71.6	203.5	72.3	73.4	68.5	71.4
8	42.4	43.4	42.9	48.3	43.9	142.3	144.5	55.6	43.7	53.4	51.5	51.0	45.9	47.1
9	80.3	80.4	79.7	78.6	79.0	157.6	156.0	89.5	87.9	92.5	59.6	59.5	55.6	56.5
10	43.7	44.5	44.5	43.8	42.3	39.5	40.5	43.8	44.0	45.7	36.8	36.6	38.5	38.3
11	75.8	70.2	70.3	69.3	76.4	69.6	68.2	206.9	203.6	70.1	210.7	210.0	213.1	211.8
12	40.1	36.5	36.4	36.9	34.8	39.3	41.3	51.5	52.3	36.5	52.3	52.3	53.3	53.1
13	45.9*	45.8*	46.3*	46.4*	45.4*	43.1*	47.2*	49.6*	49.2*	46.4*	47.5*	47.2*	47.9*	47.5*
14	48.0*	47.8*	47.4*	46.8*	47.0*	48.9*	48.2*	45.6*	47.5*	45.6*	49.7*	49.5*	48.0*	48.0*
15	34.1	33.8	33.7	36.1	36.4	33.7	32.7	33.7	33.4	34.1	35.8	34.7	33.2	33.4
16	28.1	28.0	28.0	28.6	28.0	28.8	28.1	28.4	28.0	28.3	29.0	28.8	28.1	28.0
17	50.4	49.9	49.8	48.9	49.7	50.7	50.1	48.7	49.4	48.8	49.0	49.0	49.6	49.5
18	16.8	15.3	15.4	15.3	16.8	19.8	19.6	15.7	15.9	16.2	15.6	15.6	16.4	16.4
19	18.0	17.0	17.0	17.2	18.1	25.4	24.7	16.4	16.8	17.2	14.6	14.4	14.0	14.0
20	36.3	36.1	36.1	35.8	35.8	36.3	36.3	35.6	35.9	35.8	35.8	35.8	36.1	36.1
21	18.7	18.7	18.6	18.3	18.8	18.9	18.7	18.3	18.2	18.1	18.6	18.5	18.3	18.3
22	36.5	36.5	36.4	36.5	36.4	36.3	36.3	36.2	36.2	36.4	36.4	36.3	36.4	36.3
23	24.1	24.1	24.1	24.1	23.9	24.1	24.1	23.9	23.9	24.0	24.0	23.9	24.0	24.0
24	39.5	39.5	39.5	39.5	39.5	39.5	39.5	39.4	39.5	39.5	39.5	39.5	39.5	39.5
25	28.0	28.0	28.0	28.0	28.0	28.0	28.1	27.9	28.0	27.9	28.0	28.0	28.0	28.0
26	22.8	22.8	22.8	22.8	22.8	22.8	22.9	22.7	22.8	22.8	22.8	22.8	22.8	22.8
27	22.5	22.6	22.5	22.6	22.5	22.5	22.6	22.5	22.5	22.5	22.6	22.5	22.5	22.5
28	19.3	19.4	19.2	18.9	19.0	17.0	17.2	18.9	19.0	18.7	17.3	17.3	19.6	19.2
29	28.3	28.3	28.2	28.0	28.3	27.6	27.5	28.1	28.4	28.3	28.2	28.1	28.3	28.2
30	16.5	16.7	16.4	16.2	16.6	16.4	16.4	16.2	16.4	16.5	16.8	16.6	16.9	16.6

*Assignments indicated by an asterisk may be interchanged.

Can. J. Chem. Downloaded from www.nrcresearchpress.com by 80.58.250.72 on 09/07/12
For personal use only.

cold solution of 40 mg of **8** in 0.5 mL of pyridine. After 0.5 h crushed ice was added to the mixture. The resulting solid was collected on a sintered glass funnel and washed with water. It was dissolved in chloroform. The dried solution yielded 32 mg of 3β-acetoxy-5α-lanost-8-ene-7,11-dione, identical (ir, uv, ^1H nmr) with authentic material.

*3β,7β-Diacetoxy-5α-lanost-9(11)-ene (**8**, R = Ac).* This was prepared by reduction of **5** using lithium aluminum hydride in refluxing ether (27) followed by acetylation of **8** (R = H) in 1:1 acetic anhydride – pyridine at 85°C for 1 h, then 16 h at room temperature. It had mp 210–212°C (lit. (27) mp 213–214°C) and gave ^1H nmr signals at δ 5.36 (br s, $W_{\frac{1}{2}}$ = 10 Hz, 1H, 11), 4.93 (ddd, J_1 = 5 Hz, J_2 = 11 Hz, J_3 = 16 Hz, 1H, 7α), 4.47 (m, 1H, 3α), 2.03 (two CH_3CO), 1.12, 0.89, 0.83, 0.78, and 0.68 (CH_3 signals).

*3β,7β-Diacetoxy-5α-lanosta-9α,11α-diol (**9**, R = Ac).* The action of 1.2 molar equivalents of osmium tetroxide in dry pyridine on **8** (R = Ac) during 40 h and work-up as for **7** gave crude **9**. This was purified by flash chromatography on silica gel using 5:1 benzene – ethyl acetate for elution, giving a quantitative yield of **9** (R = Ac). It crystallized from acetone–hexane as fine needles, mp 118–121°C; $[\alpha]_D$ +37.5° (*c* 1.08); ν_{max}: 3500 and 1728 cm^{-1}. Its ^1H nmr spectrum had signals at δ 5.36 (ddd, J_1 = 4.5 Hz, J_2 = 10 Hz, J_3 = 15.5 Hz, 1H, 7α), 4.40 (m, 1H, 3α), 4.10 (m, 1H, 11β), 3.10 (s, 1H, OH), 2.00 and 2.02 (CH_3CO groups), 1.12, 1.00, 0.90, 0.87, and 0.81 (CH_3 groups). *Anal.* calcd. for $C_{34}H_{58}O_6$: C 72.56, H 10.39; found: C 72.70, H 10.26.

No catalytic osmylations or permanganate oxidations were attempted on substrate **8**.

*3β,11α-Diacetoxy-5α-lanosta-7β,9α-diol (**21**).* Sodium borohydride (225 mg) was added in small portions during 7 min to a solution of 113 mg of 3β,11α-diacetoxy-9α-hydroxy-5α-lanostan-7-one (**6***b*) in 6 mL of ethanol at 50°C. The solution was maintained at 50°C for 1 h, then the bulk of the solvent removed under reduced pressure. The products were distributed between 5 mL of water and dichloromethane. The dried organic layer yielded 117 mg of a mixture, which was separated on two 1000-μm silica gel plates using 6:1 benzene – ethyl acetate. A higher R_f zone yielded 32 mg of **21** while a lower R_f zone contained 68 mg of the 7α isomer **19**. In other experiments the ratio **21**:**19** varied between 1:2 and 1:3.

The diacetoxydiol **21** was not obtained crystalline. It had $[\alpha]_D$ +26.5° (*c* 1.5) and ν_{max} 3590, 3450, and 1725 cm^{-1}. Its ^1H nmr spectrum had signals at δ 5.29 (dd, J_1 = 6.5 Hz, J_2 = 10.5 Hz, 1H, 11), 4.38 (m, 1H, 3α), 4.12 (dd, J_1 = 4 Hz, J_2 = 10 Hz, 1H, 7α), 2.42 (s, 1H, OH), 2.02 and 2.04 (CH_3CO groups), 1.12, 0.90, 0.81, and 0.82 (CH_3 groups). *Anal.* calcd. for $C_{34}H_{58}O_6$: C 72.56, H 10.39; found: C 72.28, H 10.42.

*Acetylation of **21***

Acetylation of 155 mg of **21** in 10 mL of dichloromethane containing 1 mL of dimethylaniline and 0.5 mL of acetyl chloride was complete at room temperature in two days. After purification on two 500-μm silica gel plates (6:1 benzene – ethyl acetate) the product gave 151 mg of **10**, mp 212–213°C, identical to the product from **9** (R = Ac).

*3β,7β,11α-Triacetoxy-5α-lanostan-9α-ol (**10**).* Acetylation of **9** (R = Ac) in 1:1 acetic anhydride – pyridine for 16 h gave the triacetate

Can. J. Chem. Downloaded from www.nrcresearchpress.com by 80.58.250.72 on 09/07/12
For personal use only.

TABLE 4. ^{13}C nuclear magnetic resonance spectra

	Compound														
			34					39		40					
Carbon	29	32	$R^1=R^2=H$	$R^1=R^2=Ac$	35	36 R = Ac	37	R = H	R = Ac	$R^1=R^2=OAc$ $R^3=H$	$R^1=R^2=OH$ $R^3=H$	$R^1=OAc$ $R^2=H$ $R^3=OH$	$R^1=R^3=OAc$ $R^2=H$	41 $R^1=R^2=OAc$ $R^3=H$
1	33.7	24.0	121.5	120.4	35.6	121.5	24.0	23.1	23.4	120.1	120.6	120.0	120.6	23.8
2	24.5	24.0	33.9	30.4	23.8	29.6	24.0	26.1	23.6	29.4	32.7	29.4	29.4	24.5
3	79.6	76.9	75.0	76.6	79.9	75.9	77.3	74.7	76.9	76.4	74.7	76.6	76.4	77.3
4	38.0	37.0	37.7	36.3	37.7	36.2	37.2	39.2	37.9	36.3	37.5	36.2	36.3	38.3
5	49.5	133.4	43.7	43.4	51.4	43.1	132.4	135.2	134.6	51.1	48.5	48.5	47.0	131.5
6	27.0	113.3	37.9	37.4	35.9	37.4	112.6	33.9	30.5	25.2	30.0	29.8	26.9	29.5
7	145.0	148.1	214.7	213.2	193.2	210.2	148.0	69.6	71.8	71.0	67.4	67.2	68.4	70.5
8	129.8	48.3	59.8	59.7	141.0	60.1	49.5	55.3	51.2	43.3	42.0	41.8	42.1	50.8
9	126.3	44.5	42.7	42.6	172.6	51.1	53.5	44.2	43.1	51.6	51.9	51.8	51.6	51.6
10	39.1	130.9	138.0	137.5	36.2	135.7	127.3	130.2	129.9	137.0	138.2	138.1	137.3	130.3
11	143.0	77.7	78.2	78.7	116.1	212.3	213.2	77.7	78.3	212.5	213.0	213.0	212.0	215.0
12	42.0	37.5	39.9	36.2	122.3	48.6	51.2	41.4	37.7	49.6	48.8	48.8	48.6	51.8
13	44.4*	46.9*	47.4*	47.6*	169.9	49.0*	48.0*	46.7*	46.5*	47.7*	48.1*	48.1*	48.0*	48.5*
14	49.6*	48.4*	50.1*	49.9*	49.7	49.1*	48.3*	49.7*	49.5*	48.4*	49.9*	49.8*	49.8*	47.6*
15	35.2	32.6	33.9	33.6	34.3	34.3	33.8	32.7	32.5	33.0	35.9	35.8	35.0	33.4
16	28.3	28.3	27.9	28.0	25.5	27.8	28.2	27.6	27.6	27.7	28.8	28.8	28.5	27.5
17	49.6	50.4	49.8	49.6		48.9	49.7	51.0	50.7	50.1	49.1	49.1	48.6	49.9
18	16.9	16.1	17.6	17.0	14.2	16.6	16.5	16.7	16.3	16.6	16.7	16.7	16.7	16.8
19	23.0	17.5	23.8	23.8	19.5	20.2	17.1	20.7	21.0	23.8	23.7	23.7	21.8	21.8
20	36.2	35.8	36.2	36.1	30.5	36.0	35.9	36.0	35.9	36.1	36.0	36.0	35.9	36.0
21	18.7	18.7	18.6	18.7	19.9	18.5	18.5	18.6	18.4	18.4	18.6	18.5	18.6	18.4
22	36.3	36.4	36.5	36.4	34.9	36.2	36.3	36.4	36.4	36.3	36.4	36.4	36.4	36.3
23	24.1	24.0	24.1	24.1	22.4	24.0	24.0	24.0	24.0	24.1	24.0	24.1	24.0	24.0
24	39.5	39.4	39.5	39.4	39.1	39.4	39.4	39.5	39.5	39.4	39.5	39.5	39.5	39.5
25	28.0	28.0	28.0	28.0	27.8	27.9	28.0	28.0	28.0	28.0	28.0	28.0	28.0	28.0
26	22.8	22.8	22.8	22.8	22.6	22.8	22.8	22.8	22.8	22.8	22.8	22.8	22.8	22.8
27	22.5	22.5	22.6	22.5	22.6	22.5	22.5	22.5	22.6	22.5	22.5	22.5	22.5	22.5
28	19.6	22.6	20.3	20.2	20.0	30.8	21.6	23.1	22.8	19.3	20.0	20.1	20.1	19.5
29	28.1	26.4	32.6	31.7	27.6	23.3	25.3	26.9	26.1	31.2	29.1	29.1	28.8	24.7
30	16.5	26.1	12.3	13.4	16.2	13.3	21.9	25.7	25.3	13.7	12.6	14.0	13.9	24.0

*Assignments indicated by an asterisk may be interchanged.

Can. J. Chem. Downloaded from www.nrcresearchpress.com by 80.58.250.72 on 09/07/12
For personal use only.

TABLE 5. ^{13}C nuclear magnetic resonance spectra

	Compound												
	41					**45**				**47**	**48**		
Carbon	$R^1=R^3=OH$ $R^2=H$	$R^1=R^3=OAc$ $R^2=H$	$R^1=OAc$ $R^2=H$ $R^3=OH$	**42**	**44**	$R^1=R^2=H$	$R^1=R^2=Ac$	**46** $R^1=R^2=H$	**47**	Isomer B	$R^1=R^2=R^3=Ac$	**50** R = Ac	**51**
1	25.6	24.0	24.0	23.8	23.6	23.2	23.4	25.1	25.8	28.0	126.6	126.6	57.5
2	27.4	25.4	25.4	24.5	24.1	26.1	23.5	26.8	26.4	27.8	28.4	29.7	27.2
3	75.4	77.5	77.6	77.4	76.7	74.3	76.4	75.2	78.7	78.8	75.1	33.3	75.0
4	39.9	38.6	38.6	38.1	38.0	38.8	37.6	39.5	39.7	42.7	39.3	39.4	39.7
5	135.1	134.3	134.7	134.1	131.5	135.2	134.5	134.8	168.0	168.6	143.0	162.0	161.8
6	36.8	29.4	36.8	28.9	38.9	40.3	40.0	35.1	125.3	123.3	145.9	123.1	131.4
7	68.2	70.2	68.2	69.9	211.5	214.2	212.8	68.0	201.0	201.5	192.3	200.6	200.3
8	49.9	46.3	49.9	45.0	59.8	59.0	58.9	48.2	59.4	57.1	57.7	58.5	59.9
9	53.7	53.3	53.7	44.6	52.3	43.7	43.3	45.2	41.9	39.4	43.7	44.2	40.3
10	128.1	128.7	128.4	131.8	129.7	128.4	128.8	131.9	38.8	43.5	137.4	137.0	61.3
11	214.2	213.3	214.0	78.2	212.8	76.7	77.6	77.6	79.2	77.5	77.3	77.4	77.1
12	50.7	50.6	50.7	37.6	51.2	41.3	37.6	41.6	36.0	36.8	36.2	36.2	37.1
13	48.5*	48.6*	48.5*	47.9*	48.8*	47.3*	47.3*	48.0*	46.9*	47.2*	47.6*	47.6*	47.2*
14	49.5*	49.4*	49.6*	48.7*	49.1*	49.6*	49.6*	48.7*	48.3*	47.6*	50.4*	49.6*	48.1*
15	33.0	36.1	32.8	34.5	33.5	32.8	32.7	33.7	33.7	35.2	33.2	33.5	33.3
16	28.9	28.6	28.9	29.8	27.6	27.9	27.9	29.2	28.0	29.1	28.0	28.1	27.9
17	48.0	49.3	48.1	49.1	49.2	50.0	49.9	48.9	50.0	49.6	50.0	50.1	49.9
18	16.5	16.5	16.5	16.4	16.8	17.1	16.6	16.8	16.4	16.6	16.6	16.7	16.5
19	20.6	21.7	21.6	19.3	21.7	21.1	21.1	19.3	24.9	21.2	23.7	23.2	25.3
20	36.0	36.0	36.0	35.8	35.9	36.0	35.9	36.0	36.0	35.9	35.9	36.0	35.9
21	18.7	18.6	18.7	18.8	18.5	18.7	18.7	18.8	18.9	18.9	18.8	18.8	18.6
22	36.5	36.4	36.5	36.5	36.2	36.4	36.3	36.6	36.4	36.5	36.3	36.4	36.3
23	24.0	24.0	24.0	24.0	23.9	24.0	24.0	24.1	24.1	24.1	24.0	24.1	24.0
24	39.5	39.5	39.5	39.5	39.4	39.5	39.5	39.4	39.5	39.5	39.5	39.5	39.4
25	28.0	28.0	28.0	28.0	28.0	28.0	28.0	28.0	28.0	28.0	28.0	28.1	27.9
26	22.8	22.8	22.8	22.8	22.7	22.8	22.8	22.8	22.8	22.9	22.8	22.8	22.8
27	22.5	22.5	22.5	22.5	22.5	22.5	22.5	22.5	22.6	22.6	22.5	22.6	22.5
28	18.3	18.3	18.3	22.8	19.6	22.9	22.9	22.3	19.3	20.9	20.8	20.5	19.9
29	26.2	26.0	26.2	29.0	24.5	28.4	27.5	30.2	26.8	34.3	28.4	28.3	27.0
30	24.2	24.0	24.0	24.9	24.5	25.3	25.1	24.8	25.6	24.4	16.8	17.5	25.6

*Assignments indicated by an asterisk may be interchanged.

Can. J. Chem. Downloaded from www.nrcresearchpress.com by 80.58.250.72 on 09/07/12
For personal use only.

10. After purification on silica gel plates it crystallized from hexane–dichloromethane mixtures; mp 212–213°C; $[\alpha]_D$ +37° (*c* 0.47); ν_{max}: 3590 and 1725 cm^{-1}. It gave ^1H nmr signals at δ 5.30 (m, 3H, 7α and 11β), 4.39 (m, 1H, 3α), 2.45 (s, 1H, OH), 2.02 (6H, CH_3CO), 2.03 (CH_3CO), 1.14, 1.04, 0.89, 0.87, and 0.82 (CH_3 groups). *Anal.* calcd. for $C_{36}H_{60}O_7$: C 71.48, H 10.00; found: C 71.26, H 10.17.

*3β-Acetoxy-9α,11β-dihydroxy-5α-lanostan-7-one (**11**, R = H).* Lithium tri-*tert*-butoxyaluminohydride (1.2 g) was added to 632 mg of hydroxydione **7** in 30 mL of ice-cold tetrahydrofuran. The mixture was then stirred at room temperature under argon for 3.5 h. The bulk of the tetrahydrofuran was removed under reduced pressure. Water (10 mL) was added cautiously to the residue (ice cooling). A precipitate was dissolved by addition of 2*N* hydrochloric acid, then the product extracted into dichloromethane. The organic layer was washed with 5% sodium carbonate solution, then with brine, dried, and distilled. The crude product was separated on 1000-μm silica gel plates using 10% ethyl acetate in dichloromethane, giving, in order of increasing R_f, 406 mg of **11** (R = H) and 132 mg of 3β-acetoxy-7α,9α-dihydroxy-5α-lanostan-11-one (**13**). 3β-Acetoxy-9α,11β-dihydroxy-5α-lanostan-7-one **11** (R = H) crystallized from methanol as needles with mp 228–230°C; $[\alpha]_D$ +36.5 (*c* 0.5); ν_{max}: 3520, 3450, 1720, and 1700 cm^{-1}; ^1H nmr, δ: 4.49 (t, *J* = 7 Hz, 1H, 3α), 3.85 (m, 1H, 11α), 2.93 (s, 1H, 8β), 2.30 (s superimposed on a mult, 2H, 12), 2.05 (s, 3H, CH_3CO), 1.47, 1.10, 0.98, 0.95, 0.90, 0.86, and 0.83 (CH_3 groups). *Anal.* calcd. for $C_{32}H_{54}O_5$: C 74.09, H 10.49; found: C 74.21, H 10.40.

*3β,11β-Diacetoxy-9α-hydroxy-5α-lanostan-7-one (**11**, R = Ac).* The ketodiol **11** (R = H) was acetylated during 5 days by a dimethylaniline – acetyl chloride mixture as described for preparation of **10**. The diacetate **11** (R = Ac) crystallized from hexane–dichloromethane as rods with mp 220–223°C; $[\alpha]_D$ +68° (*c* 0.15); ν_{max}: 3510, 1725 with shoulders at 1735 and 1700 cm^{-1}; ^1H nmr, δ: 4.86 (br d, *J* = 2 Hz, 1H, 11α), 4.48 (t, *J* = 7 Hz, 1H, 3α), 2.97 (s, 1H, 8β), 2.32 (s, 2H, 6), 2.05 and 2.07 (two CH_3CO groups), 1.88 (s, 1H, OH), 1.41, 1.12, 0.94, 0.89, 0.87, and 0.82 (CH_3 groups). *Anal.* calcd. for $C_{34}H_{56}O_6$: C 72.82, H 10.06; found: C 72.96, H 10.20.

*3β,11β-Diacetoxy-5α-lanost-8-en-7-one (**24**a).* Dehydration of **11** (R = Ac) with thionyl chloride in pyridine at 0°C gave ***24a***, which was not obtained crystalline. It had ν_{max} 1725 and 1660 cm^{-1} and λ_{max} 251 nm (ε 9400). It gave ^1H nmr signals at δ 5.64 (d, *J* = 5.5 Hz, 1H, 11α), 4.52 (m, 1H, 3α), 2.60–2.25 (m, including a singlet at 2.44, 2H, 6), 2.08, 2.05 (s, 3H, CH_3CO's), 1.35, 0.97, 0.90, 0.88, and 0.83 (CH_3 groups).

*3β,7β-Diacetoxy-9α-hydroxy-5α-lanostan-11-one (**12**).* A solution of 250 mg of diol **9** (R = Ac) and 30 mg of dicyclohexylcarbodiimide in 1 mL of benzene was prepared. To this was added 1.5 mL of dry dimethylsulfoxide followed by a solution of 50 mg of pyridine and 49 mg of dichloroacetic acid in 1 mL of benzene. After 4 h a further 190 mg of DCC was added, followed by a solution of 55 mg of pyridine and 32 mg of dichloroacetic acid in 1 mL of benzene. Thin-layer chromatography (tlc) (25% ethyl acetate in benzene) showed disappearance of most of the starting material after one more hour. The mixture was left overnight, then 0.5 g of oxalic acid in 2 mL of methanol was added cautiously. After 2 h stirring, 5 mL of hexane and 5 mL of water were added. The solid was removed by filtration and washed with 1:1 benzene–hexane mixture. The organic layer was washed with aqueous oxalic acid, then with sodium carbonate solution, dried, and distilled. More crystals were filtered from a concentrated solution of the products in 1:1 benzene–hexane. The 360 mg of residue after removal of the solvents was separated on four 1000-μm silica gel plates using 20% ethyl acetate in benzene, giving 201 mg of pure ketol **12** and 36 mg of slightly impure ketol. Ketol **12** did not crystallize. It had $[\alpha]_D$ +49.5° (*c* 0.5) and ν_{max} 3689, 3450, 1728 and 1710 (shoulder cm^{-1}. It gave ^1H nmr signals at δ 5.35 (m, 1H, 7α), 4.45 (t, *J* = 7.5 Hz, 3α), 3.19, 2.27 (pair of doublets 2H, *J* = 13 Hz, 12), 2.92 (s, 1H, OH), 2.03 (6H, CH_3CO), 1.21, 1.16, 0.89, 0.88, 0.82, and 0.77 (CH_3 groups). *Anal.* calcd. for $C_{34}H_{56}O_6$: C 72.82, H 10.05; found: C 72.53, H 9.88. A small amount of what appeared (^1H nmr) to be the methylthiomethyl ether of **9** moved on the plate just ahead of the ketol.

*3β-Acetoxy-7α,9α-dihydroxy-5α-lanostan-11-one (**13**).* A solution of 1 g of the 7,11-dione **7** and 230 mg of Adams platinum oxide catalyst in 30 mL of acetic acid was shaken under hydrogen for 1 h. The catalyst was removed by filtration through a bed of Celite, which was then washed with 200 mL of chloroform. The filtrate was shaken with enough 5% sodium carbonate solution to remove the acetic acid, then with water. The dried solution was concentrated and the residue crystallized by addition of methanol. The 853 mg of **13** had mp 231–234°C; $[\alpha]_D$ +45° (*c* 0.46), and gave ν_{max}: 3610, 3450, 1720, and 1700 cm^{-1}. It gave ^1H nmr signals at δ 4.56 (t, *J* = 7 Hz, 1H, 3α), 4.31 (s, OH), 4.24 (m, 1H, 7β), 3.05, 2.31 (pair of doublets, 2H, *J* = 15 Hz, 12), 2.40 (s, 1H, 8β), 2.05 (s, 3H, CH_3CO), 1.49, 1.08, 0.90, 0.83, and 0.77 (CH_3 groups). *Anal.* calcd. for $C_{32}H_{54}O_5$: C 74.09, H 10.49; found: C 74.23, H 10.49.

*3β-Acetoxy-5α-lanosta-7α,9α,11β-triol (**14**).* One gram of sodium borohydride was added in small portions to a refluxing solution of 370 mg of the 7α-hydroxy-11-ketone **13** in 30 mL of methanol during 4 h. The solution was cooled, then 100 mL of 1:1 benzene–ether was added. The benzene–ether layer was washed with water, dried, and distilled. The crude product was purified by repeated chromatography on silica gel plates using 4:1 benzene – ethyl acetate for development. Starting material (19 mg) was followed by a zone containing 232 mg of **14**. This had ν_{max}: 3630, 3450, and 1720 cm^{-1}; ^1H nmr, δ: 4.56 (t, *J* = 7 Hz, 1H, 3α), 4.19 (s, 2H, OH), 3.78 (m, 1H, 11α), 2.04 (s, 3H, CH_3CO), 1.32, 1.29, 0.93, 0.90, and 0.83 (CH_3 groups).

*3β,11β-Diacetoxy-5α-lanosta-7α,9-diol (**15**).* (*a*) Lithium tri-*tert*-butoxyaluminohydride (300 mg) was added to a solution of 110 mg of 3β,11β-diacetoxy-9α-hydroxy-5α-lanostan-7-one (**11**, R = Ac) in 10 mL of tetrahydrofuran. The mixture was stirred under argon for 20 h. Water (10 mL) was added, then the product extracted into dichloromethane. After purification on a 1000-μm silica gel plate using 6:1 benzene – ethyl acetate, 100 mg of **15** was obtained. It crystallized from methanol–dichloromethane as needles, mp 242–243°C; $[\alpha]_D$ +39° (*c* 0.5); ν_{max}: 3610, 3450, and 1725 cm^{-1}; ^1H nmr, δ: 4.80 (d, *J* = 3 Hz, 1H, 11α), 4.65 (s, 1H, OH), 4.65 (m, 1H, 3α), 4.27 (br s, $W_{\frac{1}{2}}$ = 10 Hz, 7β), 2.65 (s, 1H, OH), 2.26 (br d, *J* = 4 Hz, 8β), 2.04 and 2.01 (CH_3CO), 1.35, 1.23, 0.90, 0.88, and 0.83 (CH_3 groups). *Anal.* calcd. for $C_{34}H_{58}O_6$: C 72.56, H 10.56; found: C 72.32, H 10.23.

(*b*) Dimethylaniline (1.5 mL) and 0.7 mL of acetyl chloride were added to a cold solution of 108 mg of triol **14** in 11 mL of dichloromethane. The mixture was stirred under argon for 20 h, then worked up as described for **10**. Repeated separation on silica gel plates using 6:1 benzene – ethyl acetate gave 35 mg of triacetate **10** and 108 mg of diacetate **15**.

Oxidation of **15** with Jones' reagent in acetone gave a high yield of **11** (R = Ac).

*3β,7α,11β-Triacetoxy-9α-hydroxy-5α-lanostane (**16**).* (*a*) This was obtained as a by-product of acetylation of **14** to produce **15** (see above). (*b*) Reduction of 533 mg of the 7,11-dione **7** with 700 mg of lithium aluminium hydride in 40 mL of refluxing ether for 3 h under argon, followed by acetylation in dichloromethane using dimethyl aniline and acetyl chloride (see preparation of **15**), gave, after plate separation, 141 mg of **16** and 193 mg of the 7β isomer **22**.

Triacetate **10** crystallized from hexane as needles, mp 166–168°C; $[\alpha]_D$ +10° (*c* 0.5); ν_{max}: 3560, 1735, and 1725 cm^{-1}; ^1H nmr, δ: 5.34 (br s, $W_{\frac{1}{2}}$ = 6 Hz, 1H, 7β), 4.90 (br d, *J* = 4 Hz, 1H, 11α), 4.58 (t, *J* = 7.5 Hz, 1H, 3α), 3.32 (s, 1H, OH), 2.33 (m, 1H, 8β), 2.08, 2.04, 2.02 (CH_3CO), 1.24, 1.11, 0.90, and 0.81 (CH_3 groups). *Anal.* calcd. for $C_{36}H_{60}O_7$: C 71.48, H 10.00; found: C 71.48, H 9.88.

*3β,7α-Diacetoxy-9α-hydroxy-5α-lanostan-11-one (**17**).* Acetyl chloride (3 mL) was added to a cold solution of 853 mg of 7α-hydroxy-11-ketone **13** and 6 mL of dimethylaniline in 15 mL of dichloromethane. The solution, which turned violet in a few minutes, was stirred at room temperature for 5 days. It was then washed with 2*N* hydrochloric acid, 5% sodium carbonate solution, then water, dried, and distilled. The residue crystallized from methanol giving 591 mg of **17**, mp 157–160°C; $[\alpha]_D$ +3° (*c* 1.0); ν_{max}: 3670, 1738, 1725, and 1710 cm^{-1}; ^1H nmr, δ: 5.32 (br s, $W_{\frac{1}{2}}$ = 7 Hz, 1H, 7β), 4.58 (t, *J* = 7.5 Hz, 1H, 3α), 3.45 (OH), 3.07 (d, *J* = 14 Hz, half of a pair of

Can. J. Chem. Downloaded from www.nrcresearchpress.com by 80.58.250.72 on 09/07/12
For personal use only.

doublets for the 12-hydrogens), 2.42 (s, 1H, 8β), 2.12 (7-CH_3CO), 2.05 (3-CH_3CO), 1.30, 1.11, 0.90, 0.82, and 0.76 (CH_3 groups).

Jones' oxidation of **18** in acetone gave a nearly quantitative yield of **17**.

3β,7α-Diacetoxy-5α-lanosta-9α-11β-diol (18). A solution of 400 mg of triol **14** in 1 mL of acetic anhydride and 1 mL of pyridine was heated at 75°C for 72 h. The mixture was cooled, then poured into 20 mL of saturated sodium bicarbonate solution. After one hour stirring, the product was extracted into dichloromethane; then the organic phase was washed with 2*N* hydrochloric acid, bicarbonate solution, dried, and distilled, giving 26 mg of **18**. This was not obtained crystalline. It had ν_{max} 3590, 1735, and 1725 cm^{-1}. It gave ^1H nmr signals at δ 5.31 (br s, $W_{\frac{1}{2}}$ = 6 Hz, 1H, 7β), 4.60 (t, J = 7.5 Hz, 1H, 3α), 3.86 (m, 1H, 11α), 3.26 (s, 1H, 11α), 2.25 (s, ca. 1H, 8β), 2.07 and 2.05 (CH_3CO), 1.30, 1.09, 0.99, 0.91, and 0.82 (CH_3 groups).

3β,11α-Diacetoxy-5α-lanostan-7α,9α-diol (19). Adam's platinum oxide catalyst (75 mg) was added to a solution of 261 mg of 11α-acetoxy-7-one **6*b*** in 15 mL of acetic acid. The mixture was shaken under hydrogen for 4 h, then worked up as described for **13**. The crude product crystallized from methanol–dichloromethane to give 185 mg of **19**, mp 224–226°C; $[\alpha]_D$ +15° (*c* 0.5); ν_{max}: 3590, 3510, and 1725 cm^{-1}; ^1H nmr, δ: 5.31 (dd, J_1 = 7 Hz, J_2 = 10 Hz, 1H, 11β), 4.46 (t, J = 7 Hz, 1H, 3α), 3.96 (m, 1H, 7β), 3.89 (s, OH), 3.19 (s, OH), 2.25 (m, ca. 1H, 8β), 2.05 and 2.07 (CH_3CO), 1.41, 1.13, 0.90, and 0.82 (CH_3 groups). *Anal.* calcd. for $C_{34}H_{58}O_6$: C 72.56, H 10.39; found: C 72.70, H 10.19.

3β,7α,11α-Triacetoxy-5α-lanostan-9α-ol (20). A solution of 147 mg of diol **19** in 3 mL of 1:1 acetic anhydride – pyridine was kept at 65°C for 6 days. The solution was concentrated *in vacuo* to a syrup. This crystallized from hexane–dichloromethane giving 127 mg of **20**, mp 201–204°C; $[\alpha]_D$ −6° (*c* 0.5); ν_{max}: 3570 and 1723 cm^{-1}; ^1H nmr, δ: 5.37 (t, J = 8 Hz, 1H, 11β), 5.27 (m, 1H, 7β), 4.53 (dd, J_1 = 6 Hz, J_2 = 9.5 Hz, 1H, 3α), 3.30 (s, OH), 3.33 (br s, ca. 1H, 8β), 2.08, 2.04, 2.04 (CH_3CO), 1.19, 1.15, 0.89, 0.85, and 0.83 (CH_3 groups). *Anal.* calcd. for $C_{36}H_{60}O_7$: C 71.48, H 10.00; found: C 71.20, H 10.10.

3β,7β,11β-Triacetoxy-5α-lanostan-7α-ol (22). This product of reduction of **7** followed by acetylation (see preparation of **16**) crystallized from hexane as needles, mp 166–168°C; $[\alpha]_D$ +57° (*c* 1.2); ν_{max}: 3510 and 1725 cm^{-1}; ^1H nmr, δ: 5.32 (m, 1H, 7α), 4.78 (br s, $W_{\frac{1}{2}}$ = 8 Hz, 1H, 11α), 4.47 (br t, $J \simeq$ 7 Hz, 1H, 3α), 2.24 (s, OH), 2.04 (two CH_3CO), 2.02 (CH_3CO), 1.25, 1.01, 0.90, and 0.82 (CH_3 groups). *Anal.* calcd. for $C_{36}H_{60}O_7$: C 71.48, H 10.00; found: C 71.53, H 10.08.

3β,7α,11α-Triacetoxy-5α-lanost-8-ene (23). Triacetate **20** was dehydrated at 0°C using thionyl chloride in pyridine. The amorphous product had ν_{max} 1725 cm^{-1} and gave ^1H nmr signals at δ 5.28 (m, 2H, 7β and 11β), 4.55 (m, 1H, 3α), 2.05 (3 × CH_3CO), 1.16, 1.02, 0.89, 0.87, 0.82, and 0.62 (CH_3 groups).

3β,11α-Diacetoxy-5α-lanost-8-en-7-one (24b). Diacetate **6*b*** was dehydrated at 0°C using thionyl chloride in pyridine. The product crystallized from methanol containing a trace of pyridine, mp 131–133°C (lit. (28) mp 133–135°C); $[\alpha]_D$ +39° (*c* 1.0); λ_{max}: 248 nm (ε 9700); ν_{max}: 1730 and 1672 cm^{-1}; ^1H nmr, δ: 5.51 (dd, J_1 = 4.5 Hz, J_2 = 9 Hz, 1H, 11β), 4.54 (m, 1H, 3α), 2.75–2.35 (2H, 6), 2.07, 2.06 (CH_3CO), 2.07, 2.06 (6H), 1.25, 1.11, 0.96, 0.90, 0.82, and 0.67 (CH_3 groups). *Anal.* calcd. for $C_{34}H_{54}O_5$: C 75.23, H 10.03; found: C 75.13; H 9.89.

3β,9α-Diacetoxy-5α-lanosta-7,11-dione (25). Perchloric acid (0.1 mL, 60%) was added to a solution of 100 mg of dione **7** in 5 mL of acetic acid and 2 mL of acetic anhydride. After 5 h of stirring at room temperature the solution was added to ice water, then the products extracted into benzene. The benzene layers were washed successively with 2*N* sodium hydroxide solution and water, dried, and distilled, giving 103 mg of **25**. This crystallized from methanol–acetone, mp 169–170°C; $[\alpha]_D$ +43° (*c* 1.1); ν_{max}: 1710 and 1725 (shoulder) cm^{-1}; ^1H nmr, δ: 4.44 (t, J = 8 Hz, 3α), 2.91 (s, 1H, 8β), 3.30 and 3.03 (singlets, part of a dd, 1H, 12), 2.47 (dd, ca. 2H, J_1 = 8 Hz, J_2 = 13 Hz, 6), 2.11 (s, 3H, 9α-CH_3CO), 2.06 (s, 3H, 3β-CH_3CO), 1.39, 1.22, 0.94, 0.89, 0.87, 0.82, and 0.73 (CH_3 groups). *Anal.* calcd. for $C_{34}H_{54}O_6$: C 73.08, H 9.74; found: C 73.21, H 9.72.

3β,7α-Diacetoxy-5α-lanostan-11-one (28, R^1 = H, R^2 = OAc). Acetylation of 3β-acetoxy-7α-hydroxy-5α-lanostan-11-one (28) R^1 = H, R^2 = OH) overnight in 1:1 acetic anhydride – pyridine gave this diacetate. It crystallized as needles from hexane with mp 182–185°C; $[\alpha]_D$ +12° (*c* 1.0); ν_{max}: 1725 and 1692 cm^{-1}; ^1H nmr, δ: 5.22 (br s, $W_{\frac{1}{2}}$ = 7 Hz, 1H, 7β), 4.56 (t, J = 7 Hz, 1H, 3α), 2.98 (br d, J = 13 Hz, 1H, 9α), 2.42 (d, J = 3 Hz, 2H, 12), 2.07 and 2.04 (CH_3CO), 1.11, 1.09, 0.90, 0.85, 0.83, 0.75, and 0.73 (CH_3 groups). *Anal.* calcd. for $C_{34}H_{56}O_5$: C 74.95, H 10.36; found: C 74.72, H 10.26.

3β,7β-Diacetoxy-5α-lanostan-11-one (28, R^1 = OAc, R^2 = H). This was prepared by acetylation of 3β-acetoxy-7β-hydroxy-5α-lanostan-11-one (29) using 1:1 acetic anhydride – pyridine at room temperature. It crystallized as prisms from hexane, mp 173–174°C; $[\alpha]_D$ +46° (*c* 1.10); ν_{max}: 1727 and 1702 (shoulder) cm^{-1}; ^1H nmr, δ: 4.97 (ddd, J_1 = 5 Hz, J_2 = 10 Hz, J_3 = 14 Hz, 1H, 7α), 4.47 (dd, J_1 = 7 Hz, J_2 = 9 Hz, 1H, 3α), 2.78 (br d, J = 14 Hz, 1H, 9α), 2.43 (d, J = 4 Hz, 2H, 12), 2.03 (two CH_3CO), 1.14, 0.90, 0.87, 0.82, and 0.73 (CH_3 groups). *Anal.* calcd. for $C_{34}H_{56}O_5$: C 74.95, H 10.36; found: C 74.70, H 10.47.

3β,7,11-Triacetoxy-5α-lanosta-7,9(11)-diene (29). Perchloric acid (0.05 mL, 60%) was added to a solution of 50 mg of 3β-acetoxy-5α-lanosta-7,11-dione (**31**) in 2 mL of acetic anhydride and 1 mL of acetic acid. The yellow solution was stirred under argon at room temperature for 6 days. Ice water was added, then the products extracted into 1:1 benzene–ether. The dark-colored residue from evaporation of the solvents was separated on two 500-μm silica gel plates using 3% ethyl acetate in dichloromethane. The main zone gave 28 mg of **29** identical to the product from Westphalen reaction of **11** (R = Ac). It was not obtained crystalline. It had $[\alpha]_D$ +73° (*c* 0.33); λ_{max}: 240 nm (ε 10 000); ν_{max}: 1735 (shoulder), 1722, and 1610 cm^{-1}. Its ^1H nmr spectrum had signals at δ 4.50 (t, J = 7 Hz, 3α), 2.85–2.30 (m, 4H, 6 and 12), 2.12 and 2.11 (singlets, 6H, CH_3CO), 2.04 (s, 3H, 3-CH_3CO), 1.17, 1.01, 0.90, 0.83, and 0.72 (CH_3 groups). *Anal.* calcd. for $C_{36}H_{56}O_6$: C 73.93, H 9.65; found: C 74.07, H 9.79.

Westphalen dehydrations and related reactions

Sulfuric acid reagent

A stock solution was prepared by diluting 5 mL of concentrated sulfuric acid to 10 mL with acetic acid. This could be kept for months without deterioration.

Westphalen reaction of 3β,11α-diacetoxy-9α-hydroxy-5α-lanostan-7-one (6b)

Sulfuric acid solution (5 mL) was added to a solution of 5 g of **6*b*** in 75 mL of acetic anhydride and 150 mL of acetic acid. The solution soon turned red. After 1 h at room temperature **6*b*** could no longer be detected by tlc (silica, 5:1 benzene – ethyl acetate). It was poured into 250 mL of water, then the products extracted into 1:1 benzene ether (2 × 250 mL). The organic layers were washed free of acetic acid using 2*N* sodium hydroxide solution, then washed with saturated brine, dried (Na_2SO_4), and distilled. The product (ca. 5 g) was separated by medium pressure liquid chromatography on silica gel using 12% ethyl acetate in hexane, giving four major fractions in order of elution. Fraction A contained 248 mg of 3β-acetoxy-18(13→12β)-*abeo*-lanosta-8,13(17)-dien-7-one **30**. Fraction B (2.73 g) was a mixture of mainly 3β,7,11α-triacetoxycucurbita-5(10),6-diene **31**, and a small amount of 3β-acetoxy-5α-lanosta-7,11-dione **33**, which could be separated on silica gel using 3% ethyl acetate in dichloromethane. Fraction C was a mixture of six components. These were roughly separated, on silica gel plates using 10:1 benzene – ethyl acetate, then completely by a second separation using 5% ethyl acetate in dichloromethane. This gave (in order of decreasing R_f), 74 mg of 7-acetoxydiene **32**, 113 mg of 3β,11α-diacetoxy-cucurbita-1(10)-en-7-one **34** (R = Ac), 69 mg of 3β,11β,5α-lanost-8-en-7-one **24*a***, 80 mg of 3β,11α-diacetoxy-5α-lanost-8-en-7-one **24*b***, and 25 mg of 3β-acetoxy-18(13→12β)-*abeo*-lanosta-8,11,13(17)-trien-7-one (**35**). Fraction D contained another 398 mg of **24*b*** for a total of 478 mg.

To confirm the role of the acetic anhydride, compound **6*b*** was left

Can. J. Chem. Downloaded from www.nrcresearchpress.com by 80.58.250.72 on 09/07/12
For personal use only.

in sulfuric acid in acetic acid of comparable concentration to the above Westphalen reaction. No change occurred in 17 h. Addition of acetic anhydride to reproduce the Westphalen conditions then gave complete reaction in 1 h, with product ratios comparable to those described above.

3β-Acetoxy-18(13→12β)-abeo-*5α-lanosta-8,13(17)-dien-7-one (30).* This was produced from **6*b*** in 5% yield. It crystallized from methanol as needles with mp 134°C and λ_{max} 251 nm (ε 10 000). These properties and its nmr spectra agreed with those previously reported (3).

18[13→12β]-abeo-*5α-Lanosta-8,13(17)-dien)3,7-dione (31).* The acetate **30** (29 mg) was hydrolysed by potassium hydroxide in refluxing ethanol. After purification on a 500-μm silica gel plate using 5% methanol in chloroform, 22 mg of product was isolated from the main zone (R_f 0.45). This gave 6 mg of needles from aqueous methanol, with unknown structure, and 17 mg of amorphous hydroxy ketone **30** (3β-hydroxy) with λ_{max} 252 nm (ε 9000). This was oxidized in acetone using Jones' reagent diluted with acetone. The product was purified on a 500-μm silica gel plate using 5% methanol in chloroform, giving 13 mg of the 3,7-dione **31** in Zone 1 (R_f 0.7). This had λ_{max} 248 nm (ε 7400) and ν_{max} (CH_2Cl_2) 1704 and 1661 cm^{-1}. Its ^1H nmr spectrum showed the presence of ca. 10% of impurity, giving singlets at δ 7.0 and 6.6. Aside from a 1H multiplet at δ 3.0 ($W_{\frac{1}{2}}$ = 11 Hz) the spectrum was complex.

3β,7,11α-Triacetoxycucurbita-5(10),6-diene (32). This was produced from **6*b*** in 46% yield. It was not obtained crystalline. It had $[\alpha]_D$ −34° (*c* 1.4); ν_{max}: 1740 and 1723 cm^{-1}; λ_{max}: 273 nm (ε 5550). Its ^1H nmr spectrum gave signals at δ 5.89 (s, 1H, 6), 5.22 (t, J = 8.5 Hz, 1H, 11β), 4.73 (t, J = 5 Hz, 1H, 3α), 2.30 (s, 1H, 8β), 2.12, 2.09, 2.05 (CH_3CO), 1.22, 1.02, 0.98, 0.90, and 0.83 (CH_3 groups). *Anal.* calcd. for $C_{36}H_{56}O_6$: C 73.93, H 9.65; M^+ 584.4077; found: C 73.83, H 9.69; M^+ 584.4060.

3β-Acetoxy-5α-lanosta-7,11-dione **33**. The yield from **6*b*** was 8%. Its properties corresponded to those reported (27).

3β,11α-Diacetoxycucurbit-1(10)-en-7-one (34, R = Ac). This was produced from **6*b*** in 2% yield. It crystallized from methanol as needles with mp 160–161°C; $[\alpha]_D$ −25° (*c* 1.0); ν_{max}: 1725 and 1695 cm^{-1}; ^1H nmr, δ: 6.46 (m, 1H, 1), 5.23 (dd, J_1 = 4 Hz, J_2 = 8.5 Hz, 1H, 11β), 4.83 (dd, J_1 = 8 Hz, J_2 = 10.5 Hz, 1H, 3α), 2.9–2.5 (m, 2H, 2), 2.11, 2.00 (CH_3CO), 1.14, 1.04, 0.96, 0.89, 0.86, and 0.82 (CH_3 groups). Irradiation between δ 2.65 and 2.80 made the vinyl hydrogen signal approach a singlet while simultaneously affecting the multiplet from the 3α-hydrogen.

3β-Acetoxy-18-(13→12)-abeo-*5α-lanosta-8,11,13(17)-trien-7-one (35).* This was not obtained crystalline. It had λ_{max}: 368 (ε 8250) and 232 nm (ε 10 500); ν_{max}: 1725 and 1620 cm^{-1}; ^1H nmr, δ: 6.03 (s, 1H, 11), 4.57 (dd, J_1 = 5.5 Hz, J_2 = 9.5 Hz, 1H, 3α), 2.07 (CH_3CO), 1.26, 1.22, 1.11, 1.00, 0.92, 0.88, and 0.81 (CH_3 groups).

Action of $BF_3 \cdot Et_2O$ in acetic anhydride on **6***b*

After addition of 0.25 mL of $BF_3 \cdot Et_2O$ to a solution of 121 mg of 3β,11α-diacetoxy-9α-hydroxylanostan-7-one in 3 mL of acetic anhydride, a slow reaction ensued (tlc using 6:1 benzene – ethyl acetate). Further 0.25-mL volumes of reagent were added after 70 and 120 min. The reaction was ended after 6 h by addition to 10 mL of water. The product was extracted into 1:1 benzene–ether. The organic layers were washed with sodium bicarbonate solution, then with water, dried, and distilled. The residue was separated on two 1000-μm tlc plates using 10:1 benzene – ethyl acetate, giving 15 mg of unknown, closely followed by 11 mg of dienol acetate. The main zone, with lower R_f, gave 56 mg of 9α-acetoxy compound **27**.

3β,9α,11α-Triacetoxy-5α-lanostan-7-one (27). The amorphous product from the action of $BF_3 \cdot Et_2O$ on **6*b*** had $[\alpha]_D$ +46° (*c* 0.46) and ν_{max} 1725, 1690 cm^{-1}. It gave ^1H nmr signals at δ 5.58 (t, J = 8 Hz, 1H, 11β), 4.39 (dd, J_1 = 5 Hz, J_2 = 8.5 Hz, 1H, 3α), 2.72 (s, 1H, 8β), 2.6–2.2 (m, ca. 2H, 6), 2.11 (9α-CH_3CO), 2.05 and 2.04 (CH_3CO), 1.33, 0.93, 0.89, 0.86, and 0.82 (CH_3 groups). *Anal.* calcd. for $C_{36}H_{58}O_7$: C 71.72, H 9.70; found: C 71.93, H 9.52.

Westphalen reaction of 3β-acetoxy-9α-hydroxy-5α-lanostan-7,11-dione (8)

Reaction of 1 g of **7** was carried out exactly as for **6*b***. The mixtures had become dark red after 15 min but starting material did not disappear until 5 h reaction time (tlc). The crude product was separated on eight 1000-μm silica gel plates using 10:1 benzene – ethyl acetate. Three zones, A–C (in order of decreasing R_f), were isolated, followed by a zone yielding 21 mg of unreacted **7**.

Zone A was separated on two 1000-μm plates using 2% ethyl acetate in dichloromethane, then a front zone further on two 1000-μm plates using 10% ethyl acetate in hexane. In this way 119 mg of 3β-acetoxy-5α-lanostan-8-en-7,11-dione (12%), 305 mg of 3β-acetoxy-cucurbit-1(10)-en-7,11-dione **36** (31%), 102 mg of 3β,7-diacetoxycucurbita-5(10),6-diene-11-one **37** (10%), and 284 mg of 3β,9α-diacetoxy-5α-lanostan-7,11-dione **25** (28%) were obtained in order of decreasing R_f.

3β-Acetoxycucurbit-1(10)-en-7,11-dione (36, R = Ac). This crystallized from methanol as needles with mp 104–107°C; $[\alpha]_D$ +41° (*c* 1.0); ν_{max}: 1725 and 1695 cm^{-1}; ^1H nmr, δ: 5.39 (m, 1H, 1), 4.80 (dd, J_1 = 7 Hz, J_2 = 10 Hz, 1H, 3α), 2.93 and 2.74 (singlets, 1H, part of a dd for the 12-hydrogens), 2.58 (s, ca. 1H, 8β), 2.49 (s, ca. 2H, 6) (these two signals superimposed on the other branch of the H-12 dd), 2.65–2.35 (m, 2H, 2), 2.07 (CH_3CO), 1.29, 1.09, 0.92, 0.90, 0.83, and 0.74 (CH_3 groups). *Anal.* calcd. for $C_{32}H_{50}O_4$: C 77.06, H 10.11; found: C 76.89, H 9.90.

3β,7-Diacetoxycucurbita-5(10),6-dien-11-one (37). This did not crystallize. It had $[\alpha]_D$ +35° (*c* 0.9); λ_{max}: 272 nm (ε 5610); ν_{max}: 1740 (shoulder), 1720, and 1690 cm^{-1}; ^1H nmr, δ: 5.91 (s, 1H, 6), 4.67 (dd, J_1 = 4 Hz, J_2 = 9 Hz, 1H, 3β), 2.58 (s, 2H, 12), 2.42 (s, 1H, 8β), 2.13 (s, 3H, 7-CH_3CO), 2.05 (s, 3H, 3-CH_3CO), 1.24, 1.13, 1.02, 0.99, 0.90, 0.82, and 0.72 (CH_3 groups). *Anal.* calcd. for $C_{34}H_{52}O_5$: C 75.51, H 9.69; found: C 75.33, H 9.89.

Westphalen reaction of 3β,7β,11α-triacetoxy-9α-hydroxy-5α-lanostane (10)

Stock sulfuric acid in acetic acid solution (0.1 mL) was added to a solution of 90 mg of **10** in 1 mL of acetic anhydride and 2 mL of acetic acid. The starting material was no longer evident (tlc) after 4.5 h stirring at room temperature. Work-up as for **6*b*** followed by separation on three 500-μm silica gel plates using 6:1 benzene – ethyl acetate gave 5 mg of 3β,7β,11β-triacetoxycucurbit-5(10)-ene **38**, 53 mg of 3β,7β,11α-triacetoxycucurbit-5(10)-ene **39**, and 19 mg of starting material **10**, in order of decreasing R_f.

3β,7β,11α-Triacetoxycucurbit-1(10)-ene (38). Because of the small amount isolated, this was only characterized by its ^1H nmr spectrum. This had signals at δ 5.30 (br s, $W_{\frac{1}{2}}$ = 9 Hz, 1H, 1), 5.20 (m, 2H, 7α and 11β), 4.75 (t, J = 7 Hz, 3α), 2.10, 2.06, and 2.04 (CH_3CO), 1.24, 1.03, 0.96, and 0.81 (CH_3 groups).

3β,7β,11α-Triacetoxycucurbit-5(10)-ene (39). This was not obtained crystalline. It had $[\alpha]_D$ +43.5° (*c* 0.5); ν_{max}: 1725 cm^{-1}; ^1H nmr, δ: 5.09 (m, 2H, 7α and 11β), 4.75 (t, J = 4 Hz, 1H, 3), 2.09, 2.05, and 2.04 (CH_3CO), 1.12, 1.03, 0.89, 0.82, and 0.62 (CH_3 groups). *Anal.* calcd. for $C_{36}H_{58}O_6$: C 73.68, H 9.95; found: C 73.85, H 10.08.

Westphalen reaction of 3β,11β-diacetoxy-9α-hydroxy-5α-lanostan-7-one (11, R = Ac)

A solution of 75 mg of **11** (R = Ac) in 1 mL of acetic anhydride, 2 mL of acetic acid, and 0.075 mL of stock sulfuric acid solution only developed a yellow color. Starting material could not be detected (tlc) after 90 min. Working up as for **7**, followed first by separation on silica gel plates using 6:1 benzene – ethyl acetate, then by replating of the major zones using 2% ethyl acetate in chloroform, gave (in order of decreasing R_f) 24 mg of 3β-acetoxy-5α-lanostan-7,11-dione **33** (2), 18 mg of 3β,7,11-triacetoxy-5α-lanosta-7,9(11)-diene **29**, and 4.5 mg of 3β,11β-diacetoxy-5α-lanost-8-en-7-one **24*a***.

Westphalen reaction of 3β,7β-diacetoxy-9α-hydroxy-5α-lanostan-11-one (12)

A solution of 110 mg of **12** in 1 mL of acetic anhydride, 2 mL of acetic acid, and 0.1 mL of stock sulfuric acid solution was stirred for 1 h at room temperature. It remained yellow, but the starting material was not detectable (tlc) at the end of this time. After work-up as for **7** and separation on two 1000-μm silica gel plates using 5% ethyl acetate in dichloromethane, two main products were isolated; 67 mg

Can. J. Chem. Downloaded from www.nrcresearchpress.com by 80.58.250.72 on 09/07/12
For personal use only.

(61%) of 3β,7β-diacetoxycucurbit-1(10)-en-11-one **40** (R^1 = R^2 = OAc, R^3 = H) and 32 mg (29%) of 3β,7β-diacetoxy-cucurbit-5(10)-en-11-one **41**, (R^1 = R^2 = OAc, R^3 = H) in order of increasing R_f.

*3β-7β-Diacetoxycucurbit-1(10)-en-11-one (**40**, R^1 = R^2 = OAc, R^3 = H).* This was not obtained crystalline. It had $[\alpha]_D$ +103° (*c* 1.5) and ν_{max} 1730 and 1690 cm^{-1}. Its ^1H nmr spectrum had signals at δ 5.25 (m, 2H, 1 and 7α), 4.73 (dd, J_1 = 6.5 Hz, J_2 = 10 Hz, 1H, 3α), 2.57 (d, *J* = 9 Hz, 2H, 12), 2.05 (2 × CH_3CO), 1.38, 1.08, 0.94, 0.90, 0.83, and 0.76. *Anal.* calcd. for $C_{34}H_{54}O_5$: C 75.23, H 10.03; found: C 75.46, H 9.80.

*3β-7β-Diacetoxycucurbit-5(10)-en-11-one (**41**, R^1 = R^2 = Ac, R^3 = H).* This was amorphous, with ν_{max} 1725 and 1693 cm^{-1}; ^1H nmr, δ: 5.18 (m, 1H, 7α), 4.65 (m, 1H, 3α), 2.72 (half a pair of doublets, *J* = 14 Hz, 12), 2.53 (s, 1H, 8), 2.05 (2-CH_3CO), 1.25, 1.01, 0.97, 0.93, 0.90, 0.82, and 0.74 (CH_3 groups); ms, *m/e* calcd. for $C_{34}H_{54}O_5$: M^+ 542; found: M^+ at 542 only 0.35% of the base peak; strong signals at *m/e* 482 (*M* − 60) and 422 (*M* − 120) (base peak).

*Westphalen reaction on 3β,7α,11β-triacetoxy-9α-hydroxy-5α-lanostane (**16**)*

A stirred solution of 46 mg of **16** in 0.5 mL of acetic anhydride, 1 mL of acetic acid, and 0.05 mL of stock sulfuric acid solution was left for 9 h at room temperature. The yellow solution was worked up as usual (see **7**), then the products separated on two 500-μm silica gel plates using 3% ethyl acetate in dichloromethane. The only product characterized was 26 mg of 3β,7α-diacetoxy-5α-lanostan-11-one **28** (R^1 = H, R^2 = OAc).

*Westphalen reaction of 3β,7α-diacetoxy-9α-hydroxy-5α-lanostan-11-one (**17**)*

A solution of 300 mg of **17** in 3.75 mL of acetic anhydride, 7.5 mL of acetic acid, and 0.3 mL of stock sulfuric acid solution was stirred at room temperature for 45 min. The red solution no longer contained starting material (tlc). It was worked up as for **7**. The products were partially separated on four 1000-μm silica gel plates using 5:1 benzene – ethyl acetate, giving 229 mg of a mixture of cucurbitenes **40** (R^1 = R^3 = OAc, R^2 = H) and **41** (R^1 = R^3 = OAc, R^2 = H) (from ^{13}C nmr evidence) and 23 mg of 3β,7α,9α-triacetoxy-5α-lanostan-11-one **26**.

The major zone was hydrolysed using 295 mg of potassium hydroxide in 10 mL of methanol and 0.5 mL of water at room temperature (11.5 h). The resulting diols were separated on three 1000-μm silica gel plates using 1:1 benzene – ethyl acetate. Two major zones were isolated, 86 mg of **40** (R^1 = R^3 = OH, R^2 = H) and 57 mg of **41** (R^1 = R^3 = OH, R^2 = H) in order of decreasing R_f. These could be acetylated in 1:1 pyridine – acetic anhydride at room temperature to the corresponding diacetates. Subsequently it was found that the original mixture of acetates from the Westphalen reaction could be separated on silica using 4% ethyl acetate in dichloromethane.

*3β,7α-Diacetoxycucurbit-1(10)-en-11-one (**40**, R^1 = R^3 = OAc, R^2 = H).* This was amorphous, with $[\alpha]_D$ +58° (*c* 0.49) and ν_{max} 1722 and 1690 cm^{-1}. Its ^1H nmr spectrum had signals at δ 5.62 (ddd, J_1 = 3 Hz, J_3 = 1 Hz, 7β), 5.24 (dd, J_1 = 3 Hz, J_2 = 7 Hz, 1H, 1), 4.77 (dd, J_1 = 6.5 Hz, J_2 = 10 Hz, 1H, 3α), 2.82, 2.44 (pair of doublets 2H, *J* = 14.5 Hz, 12), 2.55 (d, *J* = 10 Hz, 1H, 8β), 2.08 (7-CH_3CO), 2.06 (3-CH_3CO), 1.28, 0.90, 0.83, 0.75, and 0.74 (methyl groups). *Anal.* calcd. for $C_{34}H_{52}O_5$: C 75.23, H 10.03; found: C 75.26, H 9.90.

*3β,7α-Dihydroxycucurbit-1(10)-en-11-one (**40**, R^1 = R^3 = OH, R^2 = H).* This was amorphous with ν_{max} 3620, 3470, and 1685 cm^{-1}. It gave ^1H nmr signals at δ 5.22 (dd, J_1 = 3 Hz, J_2 = 8 Hz, 1H, 1), 4.58 (ddd, J_1 = 3 Hz, J_2 = 7 Hz, J_3 = 9 Hz), 3.65 (s, 1H, OH), 2.82, 2.42 (pair of doublets, 2H, *J* = 14.5 Hz, 12), 2.45 (d, *J* = 10 Hz, 1H, 8β), 1.27, 1.23, 1.04, 0.90, 0.82, 0.75, and 0.68 (methyl groups).

*3β,7α-Diacetoxycucurbit-5(10)-en-11-one (**41**, R^1 = R^3 = OAc, R^2 = H).* This was amorphous, with $[\alpha]_D$ +144° (*c* 0.16) and ν_{max} 1722 and 1695 cm^{-1}. It gave ^1H nmr signals at δ 5.57 (ddd, J_1 = 6 Hz, J_2 = 10 Hz, J_3 = 10 Hz, 1H, 7β), 4.67 (m, 1H, 3α), 2.54 (s, 2H, 12), 2.31 (d, *J* = 7 Hz, H, 8β), 2.07 (s, 3H, 7α-CH_3CO), 2.05 (s, 3H, 3β-CH_3CO), 1.31, 1.03, 0.97, 0.90, 0.83, and 0.68 (methyl groups). *Anal.* calcd. for $C_{34}H_{54}O_5$: C 75.23, H 10.03; found: C 75.38, H 10.04.

*3β,5α-Diacetoxycucurbit-5(10)-en-11-one (**41**, R^1 = R^3 = OH, R^2 = H).* This was amorphous, with ν_{max} 3620 and 1690 cm^{-1}. It gave ^1H nmr signals at δ 2.54 (s, 2H, 12), 2.17 (d, *J* = 6 Hz, 8β), 1.28, 1.25, 1.07, 0.98, 0.90, 0.83, and 0.72 (methyl groups).

*3β,7α-Triacetoxy-5α-lanostan-11-one (**26**).* This was amorphous, with ν_{max} 1725 cm^{-1}; ^1H nmr, δ: 5.26 (dd, J_1 = 3 Hz, J_2 = 6 Hz, 1H, 7β), 4.46 (dd, J_1 = 7 Hz, J_2 = 9 Hz, 1H, 3α), 2.99, 2.52 (pair of doublets, *J* = 13.5 Hz, 2H, 12), 2.18 (s, 3H, 9α-CH_3CO), 2.08 (s, 3H, 7α-CH_3CO), 2.05 (s, 3H, 3β-CH_3CO), 1.21, 0.89, 0.82, and 0.73 (methyl groups); ms *m/e* calcd. for $C_{36}H_{58}O_7$: M^+ 601.9; found: M^+ 601.9.

*Westphalen reaction of 3β,7α,11α-triacetoxy-9α-hydroxy-5α-lanostane (**20**)*

A solution of 100 mg of triacetate **20** in 1.25 mL of acetic anhydride, 2.5 mL of acetic acid, and 0.1 mL of stock sulfuric acid solution was left at room temperature. It soon became reddish-orange. After 70 h, tlc indicated that over half the material had been converted to products. In the usual work-up (as for **6*b***) a major component with R_f near that of the starting material disappeared, apparently being reconverted to **20**. Separation of the products on two 500-μm plates using 6:1 benzene – ethyl acetate gave 77 mg of recovered **20**, 8 mg of 3β,7α,11α-triacetoxycucurbit-5(10)-ene **42** (R = Ac), and 1 mg of the corresponding 1(10)-ene **38** (but 7α-acetoxy). Tripling the sulfuric acid concentration or heating at 60°C did not increase the yield of **42** and resulted in poorer recovery of starting material.

*3β,7α,11α-Triacetoxycucurbit-1(10)-ene (**42**, R = Ac).* This was amorphous, with $[\alpha]_D$ +21° (*c* 0.2); ν_{max}: 1725 cm^{-1}; ^1H nmr, δ: 5.70 (dd, J_1 = 9 Hz, J_2 = 15.5 Hz, 1H, 7β), 5.25 (t, 8 Hz, 1H, 11β), 4.71 (dd, J_1 = 4 Hz, J_2 = 7 Hz, 1H, 3α), 2.6–2.2 (m, ca. 2H, 6), 2.07 and 2.05 (CH_3CO), 1.19, 1.00, 0.90, and 0.82 (CH_3 groups). *Anal.* calcd. for $C_{36}H_{58}O_6$: C 73.68, H 9.96; found: C 73.39, H 10.02.

*3β,7α,11α-Triacetoxycucurbit-1(10)-ene (**38**, but 7α-OAc).* Because of the small quantity produced, this was only identified by its ^1H nmr spectrum. It gave signals at δ 6.17 (m, 1H, 1), 5.58 (m, 1H, 7β), 5.20 (m, 1H, 11β), and 2.07 and 2.04 (CH_3CO).

*Westphalen reaction on 3β,7β,11β-triacetoxy-9α-hydroxy-5α-lanostane (**22**)*

Triacetate **22** was treated with the same ratio of solvents and acid as for **20**. The red solution contained no starting material after 15 min at room temperature. After 0.5 h the mixture was poured into water and worked up as for **7**. The products were separated as for **20**, giving, in order of decreasing R_f, 47 mg of 3β,7β-diacetoxy-5α-lanostan-11-one **28** (R^1 = OAc, R^2 = H) and 11 mg of 3β,7β,11-triacetoxy-5α-lanost-9(11)-ene **43**.

Extending the reaction time to 2.5 h resulted in little change in the product ratio.

*3β,7β,11-Triacetoxy-5α-lanost-9(11)-ene (**43**).* This was not obtained crystalline; ^1H nmr, δ: 4.94 (m, 1H, 7α), 4.46 (br t, *J* = 7 Hz, 1H, 3α), 1.96 (α, *J* = 11.5 Hz, 1H, 8β), 2.06, 2.06, and 2.04 (CH_3CO), 1.24, 0.89, 0.82, and 0.78 (CH_3 groups).

*Thermolysis of 3β,9α-diacetoxy-5α-lanosta-7,11-dione (**35**)*

A solution of 103 mg of **24** in 1 mL of decalin was heated at 195°C for 7 h, then the bulk of the decalin removed under reduced pressure. Only 3β-acetoxy-5α-lanost-8-en-7,11-dione (29 mg) and starting material (37 mg) were recovered after separation of the product on silica gel plates using 5:1 benzene – ethyl acetate. Several minor zones were not identified.

*Action of Westphalen reagent on 3β,9α-diacetoxy-5α-lanosta-7,11-dione (**25**)*

Diacetate **25** was recovered unchanged after 3 days in the same ratio of acetic anhydride – acetic acid – sulfuric acid as was used for the Westphalen dehydrations and the normal work-up (see reaction of **6*b***). Other attempts to esterify the 9α-hydroxyl group of **7**:

1. No mesylate was obtained using methanesulfonyl chloride in

Can. J. Chem. Downloaded from www.nrcresearchpress.com by 80.58.250.72 on 09/07/12
For personal use only.

pyridine. Methane sulfonic acid containing methanesulfonic anhydride converted **7** to the 8-en-7,11-dione. Attempts to make the 9α-methanesulfinate, following Creary (12), failed.

2. Attempts to make a 9α-triflate by the method of Blunt *et al.* (4) gave a complex mixture.

3. A carbamate appeared to form when **7** was treated in $CDCl_3$ with trichloromethyl isocyanate (30). However, this hydrolysed back to **7** when purification on silica gel plates was attempted or when the crude product was heated in xylene.

4. The action of phosgene in 100:1 benzene–pyridine at 60°C for 2 h converted **7** mainly to the 8-en-7,11-dione.

*Partial acetylation of 3β,7α-dihydroxycucurbit-1(10)-en-11-one (**40**, $R^1 = R^3 = OH$, $R^2 = H$)*

The diol **40** ($R^1 = R^3 = OH$, $R^2 = H$) (89 mg) was left in 1.5 mL of pyridine and 90 mg of acetic anhydride at 0°C for four days. Excess anhydride was destroyed using methanol, then the mixture evaporated to dryness *in vacuo*. Separation of the residue on two 500-μm plates using 6:1 benzene – ethyl acetate gave, in order of decreasing R_f, 43 mg of diacetate **40** ($R^1 = R^3 = OAc$, $R^2 = H$), 39 mg of 3β-acetoxy-7α-hydroxycucurbit-1(10)-en-11-one **40** ($R^1 = OAc$, $R^2 = H$, $R^3 = OH$), 5 mg of 7α-acetoxy-3β-hydroxycucurbit-1(10)-en-11-one **40** ($R^1 = OH$, $R^2 = H$, $R^3 = OAc$), and 3 mg of parent diol.

*3β-Acetoxy-7α-hydroxycucurbit-1(10)-en-11-one (**40**, $R^1 = OAc$, $R^2 = H$, $R^3 = OH$).* This had ν_{max}: 3620, 1720, and 1685 cm^{-1}; ^1H nmr, δ: 5.22 (dd, $J_1 = 3$ Hz, $J_2 = 8$ Hz, 1H, 1), 4.77 (dd, $J_1 = 7$ Hz, $J_2 = 10$ Hz, 1H, 3α), 4.58 (ddd, $J_1 = 3$ Hz, $J_2 = 7$ Hz, $J_3 = 9$ Hz, 1H, 7β), 2.82, 2.42 (pair of doublets, $J = 14.5$ Hz, 2H, 12), 2.45 (d, $J = 10$ Hz, 1H, 8β), 2.05 (CH_3CO), 1.28, 1.25, 0.95, 0.90, 0.83, and 0.76 (CH_3 groups).

*7α-Acetoxy-3β-hydroxycucurbit-1(10)-en-11-one (**40**, $R^1 = OH$, $R^2 = H$, $R^3 = OAc$).* This gave ^1H nmr signals at δ 5.62 (m, 1H, 7β), 5.24 (m, 1H, 1), 3.63 (OH), 3.57 (m, 1H, 3α), 2.84 and 2.42 (pair of doublets, $J = 14$ Hz, 2H, 12), 2.55 (d, $J = 10$ Hz, 8β), 2.09 (CH_3CO), 1.27, 1.26, 1.01, 0.90, 0.82, 0.72, and 0.63 (CH_3 groups).

*Oxidation of **40** ($R^1 = OAc$, $R^2 = H$, $R^3 = OH$)*

This alcohol was oxidized in acetone at 0°C using a small excess of Jones' reagent diluted with acetone. The product was 3β-acetoxycucurbit-1(10)-en-7,11-dione **36** (R = Ac), identical (^1H nmr, ir) with the product of Westphalen reaction on 9α-hydroxy-7,11-dione **7**.

*3β-Hydroxycucurbit-1(10)-en-7,11-dione (**36**, R = H).* A solution of 104 mg of 3β-acetoxycucurbit-1(10)-en-7,11-dione (**35**, R = H) in 5 mL of methanol containing 100 mg of KOH was refluxed under argon for 1 h. The recovery after work-up and purification on a 500-μm silica gel plate was only 43 mg of **36** (R = H); ν_{max}: 3620 and 1692 cm^{-1}; ^1H nmr, δ: 5.50 (m, 1H, 1), 3.53 (dd, $J_1 = 6$ Hz, $J_2 = 11$ Hz, 1H, 3α, 2H, 12), 2.52 (s, 2H, 6), 1.72 (s, OH), 1.26, 1.13, 1.02, 0.92, 0.82, and 0.73 (CH_3 groups).

Addition of $Eu(DPM)_3$ to the $CDCl_3$ solution resulted in comparable moderate downfield shifts of the vinyl hydrogen, and the 5α and 6α and 6β hydrogens.

*Hydrolysis of 3β,-11α-diacetoxycucurbit-1(10)-en-7-one (**34**, $R^1 = R^2 = Ac$)*

A solution of 34 mg of **34** ($R^1 = R^2 = Ac$) in 2 mL of 10% KOH in methanol was left under argon for 20 h at room temperature. Separation on a 500-μm silica gel plate using 6:1 benzene – ethyl acetate gave 4 mg of 11α-acetoxy-3β-hydroxycucurbit-1(10)-en-7-one (**34**, $R^1 = H$, $R^2 = Ac$) followed by 20 mg of 3β,11α-dihydroxycucurbit-1(10)-en-7-one (**34**, $R^1 = R^2 = H$).

*11α-Acetoxy-3β-hydroxycucurbit-1(10)-en-7-one (**34**, $R^1 = H$, $R^2 = Ac$).* This was not obtained crystalline. It had ν_{max} 3620 and 1695 cm^{-1} and gave ^1H nmr signals at δ 6.46 (m, 1H, 1), 5.23 (dd, $J_1 = 4$ Hz, $J_2 = 11$ Hz, 1H, 11β), 3.63 (t, $J = 9$ Hz, 1H, 3α), 2.12 (CH_3CO), 1.27, 1.20, 1.14, 0.96, 0.90, 0.83, 0.77, and 0.71 (CH_3 groups).

*3β,11α-Dihydroxycucurbit-1(10)-en-7-one (**34**, $R^1 = R^2 = H$).* This was not obtained crystalline. It had ν_{max} 3620, 3420, and 1685 cm^{-1} and gave ^1H nmr signals at δ 6.73 (m, 1H, 1), 4.00 (dd, $J_1 = 5$ Hz, $J_2 = 11.5$ Hz, 1H, 11β), 3.59 (dd, $J_1 = 7.5$ Hz, $J_2 = 10$ Hz, 1H, 3α), 2.45 (s, 2H, 6), 2.38 (5, 1H, 8β), 1.30, 0.97, 0.93, 0.90, 0.82, and 0.77 (CH_3 groups).

*3β-Acetoxy-11α-hydroxycucurbit-1(10)-en-7-one (**34**, $R^1 = Ac$, $R^2 = H$).* A solution of 20 mg of diol **34** ($R^1 = R^2 = H$) in 0.5 mL of pyridine and 30 mg of acetic anhydride was stirred at 0°C for 48 h. Another 30 mg of anhydride was added and stirring continued for 24 h. The product was separated on a 500-μm silical gel plate using 6:1 benzene – ethyl acetate, giving (in order of decreasing R_f) 5 mg of diacetate (**34**, $R^1 = R^2 = Ac$), 9 mg of monoacetate (**34**, $R^1 = Ac$, $R^2 = H$), and 5 mg of unchanged diol.

This monoacetate had ν_{max} 3620, 1720, and 1685 cm^{-1} and gave ^1H nmr signals at δ 6.73 (dd, $J_1 = 3$ Hz, $J_2 = 7.5$ Hz, 1H, 1), 4.81 (dd, $J_1 = 7.5$ Hz, $J_2 = 10.5$ Hz, 1H, 3α), 4.00 (dd, $J_1 = 3$ Hz, $J_2 = 9$ Hz, 1H, 11β), 2.8–2.3 (m, 2H, 2), 2.45 (s, 2H, 6), 2.24 (s, 1H, 8β), 2.07 (CH_3CO), 1.30, 1.25, 0.97, 0.93, 0.90, 0.86, and 0.83 (CH_3 groups).

Oxidation of monoacetate **34** ($R^1 = Ac$, $R^2 = H$) with Jones' reagent in acetone gave a high yield of 7,11-dione **36** (R = Ac), identical (^1H nmr, ir) with samples described above.

*3β,11α-Diacetoxycucurbit-5(10)-en-7-one (**45**, $R^1 = R^2 = Ac$).* 3β,7,11α-Triacetoxycucurbit-5(10),6-diene **32** (153 mg) was dissolved in 10 mL of a saturated solution of sodium carbonate in aqueous methanol (35:15 v/v) under argon. The reaction was complete in 1 h. The 142 mg of crude products was purified using three 1000-μm silica gel plates and 6:1 benzene – ethyl acetate, giving 110 mg of **45** ($R^1 = R^2 = Ac$), as a gum; ν_{max}: 1725 and 1695 (shoulder) cm^{-1}; ^1H nmr, δ: 5.15 (t, $J = 8$ Hz, 1H, 11β), 4.81 (t, $J = 3.5$ Hz, 1H, 3α), 2.89 (br s, 2H, 6), 2.44 (s, 1H, 8β), 2.11 (11α-CH_3CO), 2.05 (3β-CH_3CO), 1.07, 1.05, 0.95, 0.90, 0.82, and 0.78 (CH_3 groups); ms *m/e* calcd. for $C_{34}H_{54}O_5$: M^+ 542.4307; found: 542.4703.

*Acid hydrolysis of 3β,7,11α-triacetoxycucurbita-5(10),6-diene (**32**)*

A solution of 10 mg of **32** in 6 mL of methanol containing 1 mg of *p*-toluenesulfonic acid was left under argon for 22 h. The bulk of the methanol was evaporated, the product was extracted into dichloromethane, and this solution washed with sodium carbonate solution, dried, and distilled. The product was 9 mg of 3β,11α-diacetoxycucurbit-5(10)-en-7-one **45** ($R^1 = R^2 = Ac$) identical to the product of mild basic hydrolysis.

*3β,11α-Dihydroxycucurbit-5(10)-en-7-one (**45**, $R^1 = R^2 = H$).* A 1.4 molar solution of lithium aluminium hydride in ether (2.3 mL) was added to a solution of 200 mg of triacetoxy-diene **32** in 20 mL of ether at 0°C under argon. After 15 min at 0°C ammonia gas was used to destroy excess hydride, (22), then 8 mL of 2 *N* hydrochloric acid added cautiously. Fifty millilitres of 1:1 benzene–ether was added; the aqueous layer was separated and then washed with 50 mL of 1:1 benzene–ether. The organic layers were extracted with 5% sodium bicarbonate solution, dried, and distilled. The crude product (158 mg) was purified using three 1000-μm plates with 3:2 benzene – ethyl acetate. The 120 mg of **45** ($R^1 = R^2 = OH$) crystallized from hexane–ether mixtures with mp 156–158°C; $[\alpha]_D$ +32° (*c* 1.1); ν_{max}: 3620, 3470 and 1690 cm^{-1}; ^1H nmr, δ: 3.86 (dd, $J_1 = 6$ Hz, $J_2 = 10$ Hz, 1H, 11β), 3.53 (t, $J = 4$ Hz, 1H, 3α), 2.88 (br s, 2H, 6), 2.44 (s, 1H, 8β), 1.20, 1.00, 0.94, 0.89, 0.82, and 0.75 (CH_3 groups). *Anal.* calcd. for $C_{30}H_{50}O_3$: C 78.55, H 10.99; found: C 78.5, H 11.20.

*Vigorous reduction of 3β,11α-diacetoxycucurbit-5(10)-en-7-one (**45**, $R^1 = R^2 = Ac$)*

A mixture of 90 mg of **45** ($R^1 = R^2 = Ac$) and 90 mg of lithium aluminum hydride in 15 mL of ether was heated under reflux under argon for 2 h. After addition of a further 50 mg of hydride, refluxing was continued for 3 h. Saturated aqueous sodium sulfate was added, followed by enough anhydrous magnesium sulfate to give a filtrable solid. This was removed on sintered glass, and the solid washed with dichloromethane.

The organic layers gave 65 mg of product, which was separated on two 500-μm silica gel plates using 10% methanol in chloroform. The products obtained were 3β,11α-dihydroxycucurbit-5(10)-en-7-one (**45**, $R^1 = R^2 = H$) (11 mg), 3β,7α,11α-trihydroxy-cucurbit-5(10)-ene (**46**, $R^1 = R^2 = H$) (31 mg), and 3β,7β,11α-trihydroxy-cucurbit-5(10)-ene (**39**, R = H) (10 mg).

*3β,7α,11α-Trihydroxycucurbit-5(10)-ene (**46**, $R^1 = R^2 = H$).* This was not obtained crystalline. It had ν_{max} 3620 and 3450 cm^{-1} and gave ^1H nmr signals at δ 4.68 (dd, J_1 = 8 Hz, J_2 = 12 Hz, 1H, 7β), 3.88 (t, J = 8.5 Hz, 1H, 11β), 3.45 (dd, J_1 = 3.5 Hz, J_2 = 8 Hz, 1H, 3α), 1.29, 1.03, 1.00, 0.95, 0.90, and 0.83 (CH_3 groups).

*3β,7β,11α-Trihydroxycucurbit-5(10)-ene (**39**, R = H).* This was not obtained crystalline. It had ν_{max} 3610 and 3450 cm^{-1} and gave ^1H nmr signals at δ 3.91 (apparent t, $J \simeq$ 8 Hz, 2H, 7α and 11β), 3.49 (t, J = 3.5 Hz, 1H, 3α), 1.32, 1.16, 1.02, 1.00, 0.95, 0.89, 0.62, and 0.56 (CH_3 groups).

*Acetylation of 3β,11α-dihydroxycucurbit-5(10)-en-7-one (**45**, $R^1 = R^2 = H$)*

Ten microlitres of 60% perchloric acid was added to a stirred solution of 10 mg of diol **45** ($R^1 = R^2$ = H) in 0.5 mL of acetic anhydride and 0.25 mL of acetic acid. After 10 min at room temperature the reaction was quenched with water. The product was extracted into dichloromethane, then washed free of acid with sodium carbonate solution and the solution dried and distilled. This gave 11 mg of nearly pure 3β,7,11α-triacetoxycucurbita-5(10),6-diene **32**. Diol **45** (R = H) could not be acetylated using acetic anhydride and pyridine to give diacetate **45** (R = Ac). Instead a complex mixture containing no trace of the desired compound was obtained.

*Acetylation of 3β,7α,11α-trihydroxycucurbit-5(10)-ene (**42**, $R^1 = R^2 = R^3 = H$)*

A solution of 31 mg of triol **42** (R = H) in 1 mL of pyridine and 150 mg of acetic anhydride was kept at 0°C for 48 h. The excess anhydride was destroyed using methanol, then the solution evaporated *in vacuo*. The products were separated on two 500-μm silica gel plates using 5:1 benzene – ethyl acetate. Only the 7- and 11-monoacetates required further separation using 10% ethyl acetate in dichloromethane on a 500-μm plate. The compounds obtained, in order of decreasing R_f, and their characteristic low-field ^1H nmr shifts are collected in Table 6.

Jones' oxidation in acetone converted 3β,7α-diacetoxy-11α-hydroxycucurbit-5(10)-ene (**42***b*) into **41** (R^1 = OAc, R^2 = H, R^3 = OAc), 3β,11α-diacetoxy-7α-hydroxycucurbit-5(10)-ene (**42***c*) into **45** ($R^1 = R^2$ = Ac), and 3β-acetoxy-7α,11α-dihydroxycucurbit-5(10)-ene (**42***d*) into 3β-acetoxy-cucurbit-5(10)-en-7,11-dione (**44**), identified in each case by ir and ^1H nmr spectra with samples described above.

*Acetylation of 3β,7β,11α-trihydroxycucurbit-5(10)ene (**38**, R = H)*

This product of lithium aluminium hydride reduction of **45** ($R^1 = R^2$ = Ac) was left for 16 h in 1:1 acetic anhydride – pyridine. The product gave a ^1H nmr spectrum coincident with that of 3β,7β,11α-triacetoxycucurbit-5(10)-ene **38** (R = Ac) obtained by Westphalen reaction of **10**.

*Controlled acetylation of 3β,7α-dihydroxycucurbit-5(10)-ene-11-one (**41**, $R^1 = R^3 = OH$, $R^2 = H$)*

A solution of 41 mg of **41** ($R^1 = R^3$ = OH, R^2 = H) in 1 mL of pyridine and 40 mL of acetic anhydride was left at 0°C for three days. The excess anhydride was destroyed with methanol, then the product isolated as usual. Separation on a 500-μm silica gel plate using 6:1 benzene – ethyl acetate gave (in order of decreasing R_f) 9 mg of the 3β,7α-diacetate (**41**, $R^1 = R^3$ = OAc, R^2 = H), 11 mg of 3β-acetoxy-7α-hydroxycucurbit-5(10)-en-11-one (**41**, R^1 = OAc, R^2 = H, R^3 = OH), 6 mg of 7α-acetoxy-3β-hydroxycucurbit-5(10)-en-11-one (**41**, R^1 = OH, R^2 = H, R^3 = OAc), and 12 mg of starting diol.

*3β-Acetoxy-7α-hydroxycucurbit-5(10)-en-11-one (**41**, R^1 = OAc, R^2 = H, R^3 = OH).* This had ν_{max} 3610, 1720, and 1692 cm^{-1} and gave ^1H nmr signals at δ 4.80–4.35 (m, 2H, 3α and 7β), 2.54 (s, 2H, 12), 2.17 (d, J = 6Hz, 8β), 2.05 (CH_3CO), 1.28, 1.25, 1.03, 0.98, 0.90, 0.83, and 0.72 (CH_3 groups).

Oxidation of 11 mg **41** (R^1 = OAc, R^2 = H, R^3 = OH) in 1 mL of acetone using a small excess of Jones' reagent diluted with acetone gave 11 mg of 3β-acetoxycucurbit-5(10)-en-7,11-dione **44**.

*7α-Acetoxy-3β-hydroxycucurbit-5(10)-en-11-one (**41**, R^1 = OH, R^2 = H, R^3 = OAc).* This gave ^1H nmr signals at δ 5.56 (m, 1H, 7β), 3.38 (m, 1H, 3α), 2.52 (s, 2H, 12), 2.31 (d, J = 8 Hz, 1H, 8β), 2.07 (CH_3CO), 1.30, 1.26, 1.06, 0.96, 0.90, 0.82, and 0.68 (CH_3 groups).

*3β-Acetoxycucurbit-5(10)-en-7,11-dione (**44**).* A solution of 74 mg of **37** in 7.5 mL of a saturated solution of sodium carbonate in aqueous methanol (15:35 v/v) was stirred at room temperature for 20 min. Most of the methanol was removed under reduced pressure, then the product extracted into dichloromethane. The 57 mg of **44** so obtained did not crystallize readily; ν_{max}: 1720 and 1690 cm^{-1}; ^1H nmr, δ: 4.75 (m, 1H, 3α), 2.96 (br s, 2H, 6), 2.64 (s, 2H, 12), 2.54 (s, 1H, 8β), 2.05 (CH_3CO), 1.11, 1.03, 0.98, 0.90, 0.82, and 0.74 (CH_3 groups).

*Hydrolysis and isomerization of **32***

A saturated solution of sodium carbonate in a 35:15 v/v methanol–water mixture was prepared and degassed by boiling under argon. To 90 mL of this solution was added a solution of 180 mg of **32** in 25 mL of methanol, prepared under argon. The mixture was refluxed under argon for 16 h. The bulk of the methanol was removed under reduced pressure, then the products extracted into dichloromethane. The extracts were dried over magnesium sulfate, then distilled to give 147 mg of residue. This contained no acetoxy group (^1H nmr). It was acetylated at room temperature in 1:1 acetic anhydride – pyridine, giving 182 mg of acetates. These were separated on five 500-μm silica gel plates using 3% ethyl acetate in dichloromethane. In order of decreasing R_f the zones contained: A, 27 mg of **32**, B, 29 mg of a diacetoxy α,β-unsaturated ketone; C, 15 mg of a mixture; D, 14 mg of 3β,6,11α-triacetoxy-cucurbita-1(10),5-dien-7-one **48** (R = Ac); E, 7 mg of a conjugated ketone; F, 22 mg of 3β,11α-diacetoxycucurbit-5-en-7-one **47**; G, 2 mg of conjugated ketone. Zones E and G were incompletely characterized.

*Zone B; stereoisomer of **47**.* This amorphous acetate had ν_{max} 1725 and 1648 cm^{-1}. Its ^1H nmr spectrum had signals at δ 6.02 (s, 1H, 6), 5.24 (dd, J_1 = 6 Hz, J_2 = 12 Hz, 1H, 11β), 4.61 (m, 1H, 3α), 2.45 (s, 1H, 8), 2.11, and 2.09 (CH_3CO groups). This and its ^{13}C nmr spectrum (Table 5) are consistent with it being an isomer of **47**.

*3β,11α-Diacetoxy-10α,8β-cucurbit-5-en-7-one (**47**)*

This had ν_{max} 1725, 1650, and 1620 cm^{-1} and λ_{max} 243 nm. It gave ^1H nmr signals at δ 6.0 (s, 1H, 6), 5.18 (t, J = 7 Hz, 1H, 11β), 4.68 (br, 1H, 3α), 3.04 (br d, J = 8 Hz, 1H, 10α), 2.46 (s, 1H, 8β), 2.08 and 2.02 (CH_3CO groups). This and its ^{13}C nmr signals show it to be identical to the compound assigned this structure by Paryzek and Wydra (12). See, however, revised ^{13}C assignment in Table 5.

Briefer hydrolysis of **33** (2 h reflux) under the same conditions followed by acetylation gave, in addition to **47**, another apparent isomer of **47** with λ_{max} 242 nm; ^1H nmr, δ: 6.13 (s, 1H, 6), 5.17 (dd, J_1 = 9 Hz, J_2 = 6.6 Hz, 11β), 4.57 (m, 1H, 3α), 2.95 (br d, J = 12 Hz, 1H, 10), 2.44 (s, 1H, 8), 2.08 (two CH_3CO groups).

Attempts to induce conjugation by acid hydrolysis of **32** (*p*-toluenesulfonic acid in methanol) failed.

*Alkaline autooxidation of 3β-acetoxycucurbit-5(10)-en-7,11-dione (**44**)*

Ten milligrams of **44** was dissolved in 10 mL of methanol and 2 mL of a saturated sodium carbonate solution in 35:15 methanol–water mixture. This was refluxed under argon for 2 h. The solvent was removed under reduced pressure, then the products distributed between dichloromethane and dilute sulfuric acid. The dichloromethane solution was washed with 5% sodium carbonate solution, dried, and distilled. The residue was acetylated during 16 h in 1:1 acetic anhydride – pyridine. The usual work-up gave a product that was separated on a 500-μm silica gel plate using 6:1 benzene – ethyl acetate. The main zone yielded 6 mg of 3β,6-diacetoxycucurbita-1(10),5-dien-7,11-dione **49**.

*Alkaline autooxidation of **45** ($R^1 = R^2$ = Ac)*

(*a*) A solution of 10 mg of 3β,11α-diacetoxycucurbit-5(10)-en-7-one **45** ($R^1 = R^2$ = Ac) in 10 mL of methanol and 2 mL of a saturated solution of sodium carbonate in 35:15 methanol–water mixture was refluxed under argon for 1.5 h. The bulk of the methanol was removed under reduced pressure, then the product extracted into dichloromethane. The 9 mg of product was separated on a 500-μm silica gel plate using 1:1 benzene – ethyl acetate. The main zone gave 5 mg of the sensitive triol **48** (R = H).

(*b*) A stock solution of 1 g of potassium hydroxide in 95 mL of

Can. J. Chem. Downloaded from www.nrcresearchpress.com by 80.58.250.72 on 09/07/12
For personal use only.

TABLE 6. Partial acetylation of **42** (R = H)

Compound	Weight (mg)	Substituent effects on geminal ^{1}H nmr shifts					
		7α-OAc	11α-OAc	3β-OAc	7α-OH	11α-OH	3β-OH
42*a*, triacetate	6	5.66m	5.16t	4.69m	—	—	—
42*b*, 3,7-diacetate	6	5.70m	—	4.68m	—	3.82t	—
42*c*, 3,11-diacetate	6	—	5.18t	4.7m	4.7m	—	—
42*d*, 3-acetate	5	—	—	4.7m	4.7m	3.79t	—
42*e*, 7,11-diacetate	4	5.70m	5.15t	—	—	—	3.45m
42*f*, 11-acetate	2	—	5.18t	—	4.70m	—	3.45m
42*g*, 7-acetate	2	5.66m	—	—	—	3.80t	3.45m
42, triol	4	—	—	—	4.68m	3.88t	3.45m

methanol and 5 mL of water was prepared. One millilitre of this was added to a solution of 37 mg of **45** (R^1 = R^2 = Ac) in 3 mL of methanol. The mixture was stirred under argon for 90 min, then concentrated *in vacuo*. The products were extracted into 1:1 benzene–ether, then the organic layers washed successively with 2*N* hydrochloric acid, 5% sodium carbonate solution, then saturated brine, dried, and distilled. The residue was acetylated at room temperature in 1 mL of acetic anhydride and 1 mL of pyridine for 16 h. The acetate produced was purified on a 1000-μm silica gel plate using 10:1 benzene – ethyl acetate to give 24 mg of 3β,6,11α-triacetoxycucurbita-1(10),5-dien-7-one (**48**, R = Ac), which did not crystallize.

*Partial acetylation of **48** (R = H)*

The triol **48** (R = H) was produced as in (*a*) or by hydrolysis of **48** (R = Ac) using potassium hydroxide in methanol as in (*b*), but for 16 h at room temperature under argon. Crude triol (20 mg) was acetylated during 90 min at room temperature in 0.4 mL of pyridine and 0.4 mL of acetic anhydride. The product was separated on a 500-μm silica gel plate to give 5 mg of triacetate **48** (R = Ac) and 5 mg of 3β,6-diacetoxy-11α-hydroxycucurbita-1(10),5-diene-7-one (**48**, R^1 = R^3 = Ac, R^2 = H).

*3β,6,11α-Trihydroxycucurbita-1(10),5-dien-7-one (**48**, R = H).* This was amorphous, and gave λ_{max} 330 nm (accurate intensity not available because of decomposition) and ν_{max} 3620, 3420, 1650, and 1605 cm^{-1}. It gave ^{1}H nmr signals at δ 6.75 (s, 1H, 6-hydroxyl), 6.74 (t, J = 4.5 Hz, 1H, 1), 4.07 (dd, J_1 = 3 Hz, J_2 = 10 Hz, 1H, 11β), 3.52 (t, J = 3 Hz, 1H, 3α), 2.48 (s, 1H, 8β) superimposed on a multiplet between 2.5 and 2.3 (2H, 2), 1.43, 1.36, 1.30, 1.26, 0.96, 0.89, and 0.82 (methyl groups).

*3β,6-Diacetoxy-11α-hydroxycucurbita-1(10),5-diene-7-one (**48**, R^1 = R^3 = Ac, R^2 = H).* This was amorphous, with λ_{max}: 308 nm (ε 9000) and a weak maximum at 235 nm; ν_{max}: 3620, 1760, 1735 (shoulder), 1720, 1665, 1620, and 1585 cm^{-1}; ^{1}H nmr, δ: 6.97 (t, J = 4 Hz, 1H, 1), 4.79 (t, J = 5 Hz, 1H, 3α), 4.07 (dd, J_1 = 3 Hz, J_2 = 10 Hz, 11β), 2.43 (s, 1H, 8β) superimposed on a multiplet at 2.55–2.45 (2H, 2), 2.27 (s, 6-CH_3CO), 2.03 (s, 3H, 3β-CH_3CO), 1.42, 1.26, 1.05, 0.95, 0.89, and 0.82 (methyl groups).

*3β,6,11α-Triacetoxycucurbita-1(10),5-dien-7-one (**48**, R = Ac).* This was amorphous, with λ_{max} 306 nm (ε 8500) and a weak maximum at 1585 cm^{-1}. It gave ^{1}H nmr signals at δ 6.67 (t, J = 4.5 Hz, 1H, 1), 5.30 (dd, J_1 = 4 Hz, J_2 = 10 Hz, 1H, 11β), 4.79 (t, J = 4.5 Hz, 1H, 3α), 2.56 (s, 1H, 8β) superimposed on a multiplet at 2.6–2.35 (2H, 2), 2.28 (6-CH_3CO), 2.09 (11α-CH_3CO), 2.02 (3β-CH_3CO), 1.27, 1.26, 1.05, 0.89, and 0.82 (methyl groups). Irradiation at δ 2.53 caused the signals at 6.67 and 4.79 to collapse to singlets.

*3β,6-Diacetoxycucurbita-1(10),5-dien-7,11-dione (**49**).* This was amorphous, with ν_{max}: 1760, 1735, 1720, 1695, 1665, 1615, and 1585 cm^{-1}; ^{1}H nmr, δ: 5.56 (t, J = 4.5 Hz, 1H, 1), 4.76 (dd, J_1 = 4.5 Hz, J_2 = 6 Hz, 1H, 3α), 2.76 (s, 1H, 8β), 2.70 (s, 2H, 12), 2.30 (6-CH_3CO), 2.03 (3β-CH_3CO), 1.32, 1.20, 0.90, 0.82, and 0.78 (methyl groups); ms *m/e* calcd. for $C_{34}H_{50}O_6$: M^+ 554.3607; found: M^+ 554.3602.

*Dehydrogenation of 3β,11α-diacetoxycucurbit-5(10)-en-7-one (**45**)*

(*a*) A mixture of 21 mg of **45** (R^1 = R^2 = Ac) and 10 mg of rhodium trichloride trihydrate in 1 mL of 95% ethanol was refluxed for 2 h. A dark precipitate formed. The ethanol was evaporated, the product dissolved in dichloromethane, then this solution washed with dilute sulfuric acid followed by dilute sodium carbonate solution. The 30 mg of product was separated on a 500-μm silica gel plate using 6:1 benzene – ethyl acetate. Four zones were detected. The main product (14 mg) had R_f 0.5 and λ_{max} 296 nm, and was shown to be 3β,11α-diacetoxycucurbita-1(10),5-dien-7-one (**50**, R = Ac).

(*b*) A solution of 10 mg of diol **45** (R = H) in 5 mL of benzene containing 10 mg of 30% palladium-on-charcoal was refluxed under argon for 24 h. A further 10 mg of catalyst was added and refluxing continued for 3 days. The product (13 mg) was purified on a 500-μm silica gel plate using 1:1 benzene – ethyl acetate, giving 5 mg of amorphous dienone **50** (R = H).

Acetylation of the diol during 60 h in 1:1 acetic anhydride – pyridine at room temperature gave the amorphous diacetate **50** (R = Ac).

*Dehydrogenation of 3β,7,11α-triacetoxycucurbita-5(10),6-diene (**32**)*

The enol acetate **32** (45 mg) and 68 mg of iron pentacarbonyl in 3 mL of dry diglyme under an argon atmosphere was heated in a bath at 148°C for 26 h. The solvent was evaporated *in vacuo*, then the residue dissolved in 1 mL of ethanol. A solution of 393 mg of ferric chloride in 3 mL of 95% ethanol was added, and the mixture was stirred for 1.5 h at room temperature. The solvent was removed under reduced pressure, then the product distributed between dichloromethane and dilute sulfuric acid. The dichloromethane was washed with sodium carbonate solution, dried, and distilled. The residue gave four main zones when separated on a 1000-μm silica gel plate using 6:1 benzene – ethyl acetate. One zone (R_f 0.6) yielded 12 mg of parent **32**. The main zone (R_f 0.5) contained 26 mg (79% based on unrecovered **32**) of conjugated dienone **50** (R = Ac). This was further purified by passage of a hexane solution through a short column of Activity 1 neutral alumina. The 21 mg of amorphous product was used to obtain spectra.

*3β,11α-Dihydroxycucurbita-1(10),5-dien-7-one (**50**, R = H).* This had λ_{max} 302 nm (ε 6700) with a weak maximum at 2.35 nm, and ν_{max}: 3630, 3470, 1640, and 1585 cm^{-1}. It gave ^{1}H nmr signals at δ 6.94 (t, J = 3.5 Hz, 1H, 1), 6.02 (s, 1H, 6), 4.07 (dd, J_1 = 5 Hz, J_2 = 11 Hz, 1H, 11β), 3.62 (dd, J_1 = 7 Hz, J_2 = 9 Hz, 1H, 3α), 2.33 (s, 1H, 8β), 2.6–2.2 (m, 2H, 2), 1.28, 1.26, 1.22, 1.03, 0.95, 0.90, and 0.82 (CH_3 groups).

*3β,11α-Diacetoxycucurbita-1(10),5-dien-7-one (**50**, R = Ac).* The amorphous diacetate from acetylation of **50** (R = H) or dehydrogenation of **45** (R = H) and **32** had λ_{max} 296 nm (ε 11 300) with a weak maximum at 237 nm, and ν_{max}: 1725, 1645, and 1585 cm^{-1}. It gave ^{1}H nmr signals at δ 6.65 (br t, J = 3.2 Hz, 1H, 1), 6.03 (s, 1H, 6), 5.30 (dd, J_1 = 11.5 Hz, 1H, 11β), 4.81 (dd, J_1 = 6 Hz, J_2 = 11 Hz, 1H, 3α), 2.9–2.25 (m, 2H, 2), 2.46 (s, 1H, 8β), 2.11, 2.09 (CH_3COO groups), 1.15, 1.14, 1.10, 1.06, 0.94, 0.90, and 0.82 (CH_3 groups). Irradiation at 2.67 ppm collapsed the 1H triplet to a singlet, the signals for the 3α-H approached a singlet, and the splitting pattern for the 6-hydrogen changed. Its mass spectrum had a weak peak at *m/e* 540 (M^+) and strong peaks *m/e* 480 (M − 60) and 420 (M − 120).

*Autooxidation of 3β,7,11α-triacetoxycucurbita-5(10),6-diene (**32**)*

A 632-mg sample of the acetoxydiene **32** was stored as a froth at room temperature for 15 months. It now contained major impurities.

Can. J. Chem. Downloaded from www.nrcresearchpress.com by 80.58.250.72 on 09/07/12
For personal use only.

Separation on six 1000-μm plates using 6:1 benzene – ethyl acetate gave, in order of decreasing R_f, 296 mg of **32**, 169 mg of 3β,11α-diacetoxy-1α,10α-epoxycucurbit-5-en-7-one **51**, and 24 mg of unidentified product.

3β,11α-Diacetoxy-1α,10α-epoxycucurbit-5-en-7-one (51). This amorphous product had ν_{max}: 1730, 1655, and 1615 cm^{-1}. It gave ^1H nmr signals at δ 6.35 (s, 1H, 6), 5.10 (dd, J_1 = 3.5 Hz, J_2 = 12.5 Hz, 1H, 11β), 4.85 (t, J = 4 Hz, 1H, 3β), 4.26 (d, J = 1 Hz, 1H, 1), 3.47 (s, 1H, 8β), 2.10 (11α-CH_3COO), 2.01 (3β-CH_3COO), 1.21, 1.15, 1.06, 1.03, 0.89, and 0.82 (CH_3 groups). On irradiation at 2.30 ppm the signals for the 1-H collapsed to a singlet and the 3-H and 11-H signals became less complex. Mass spectrum, m/e calcd. for $C_{34}H_{52}O_7$: M^+ 556.3764; found: M^+ 556.3751.

Acknowledgements

We thank Dr. Z. Paryzek for communicating his results prior to publication, Dr. J. L. Holmes and associates for mass spectra, and Mr. H. Séguin for microanalyses. We are grateful to Dr. B. Blackwell for nuclear Overhauser enhancement and COSY ^1H nmr studies, ^1H–^{13}C nmr correlations, and help with interpretation.

1. O. E. Edwards and Z. Paryzek. Can. J. Chem. **61**, 1973 (1983).
2. Z. Paryzek. J. Chem. Soc. Perkin Trans. 1, 1222 (1979).
3. G. V. Baddeley, H. J. Samaan, J. J. H. Simes, and Tu Hoa Ai. J. Chem. Soc. Perkin Trans. 1, 7 (1979).
4. J. W. Blunt, A. Fischer, M. P. Hartshorn, F. W. Jones, D. N. Kirk, and S. W. Yoong. Tetrahedron, **21**, 1567 (1965).
5. J. G. Ll. Jones and B. A. Marples. J. Chem. Soc. (C), 572 (1971).
6. (*a*) R. B. Boar, J. F. McGhie, and D. A. Lewis. J. Chem. Soc. Perkin Trans. 1, 2590 (1972); (*b*) E. V. Lassak, J. T. Pinhey, and J. J. H. Simes. Aust. J. Chem. **26**, 1051 (1973).
7. M. Schröder. Chem. Rev. **80**, 187 (1980).
8. K. E. Pfitzner and J. G. Moffatt. J. Am. Chem. Soc. **87**, 5661 (1965).
9. N. A. Milas and S. Sussmann. J. Am. Chem. Soc. **56**, 1302 (1936).
10. O. E. Edwards and T. Sano. Can. J. Chem. **47**, 3489 (1969).
11. X. Creary and C. C. Geiger. J. Am. Chem. Soc. **104**, 4151 (1982).
12. Z. Paryzek and R. Wydra. Can. J. Chem. **63**, 1280 (1984).
13. H. Alper and J. T. Edward. J. Organomet. Chem. **14**, 411 (1968).
14. Z. Paryzek. Bull. Acad. Pol. Sci. **26**, 583 (1978).
15. J. Andrieux, D. H. R. Barton, and H. Patin. J. Chem. Soc. Perkin Trans. 1, 359 (1977).
16. J. P. Bégné and M. Charpentier-Morize. Acc. Chem. Res. **13**, 207 (1980).
17. P. Yates and R. J. Crawford. J. Am. Chem. Soc. **88**, 1561 (1966); R. A. Blattel and P. Yates. Tetrahedron Lett. 1073 (1972).
18. O. E. Edwards, J. Dixon, J. W. Elder, R. J. Kolt, and M. Lesage. Can. J. Chem. **59**, 2096 (1981).
19. N. H. Werstiuk. Can. J. Chem. **53**, 26 (1975).
20. J. W. ApSimon and J. M. Rosenfeld. Chem. Commun. 1271 (1970).
21. W. T. DeKock, P. R. Enslin, K. B. Norton, D. H. R. Barton, B. Sklarz, and A. A. Bothner-By. J. Chem. Soc. 3828 (1963); D. Lavie, Y. Shvo, O. R. Gottlieb, and E. Glotter. Tetrahedron Lett. 615 (1961).
22. D. H. R. Barton, R. H. Hesse, C. Wilshire, and M. M. Pechet. J. Chem. Soc. Perkin Trans. 1, 1075 (1977).
23. W. Bergmann, F. B. Hirschmann, and E. L. Skau. J. Org. Chem. **4**, 29 (1939).
24. S. D. Larsen and S. A. Monti. J. Am. Chem. Soc. **99**, 8015 (1977).
25. W. P. Weber and J. P. Shepherd. Tetrahedron Lett. 4907 (1972).
26. E. J. Corey and C. U. Kim. J. Am. Chem. Soc. **94**, 7586 (1972).
27. J. F. Cavalla and J. F. McGhie. J. Chem. Soc. 834 (1951).
28. M. V. Mijovic, W. Voser, H. Heuser, and O. Jeger. Helv. Chim. Acta, **35**, 964 (1952).
29. O. E. Edwards and Z. Paryzek. Can. J. Chem. **51**, 3866 (1973), and references therein.
30. I. R. Trehan, C. Monder, and A. K. Bose. Tetrahedron Lett. 67 (1968).

Can. J. Chem. Downloaded from www.nrcresearchpress.com by 80.58.250.72 on 09/07/12
For personal use only.

Mixed anhydrides in peptide synthesis. A study of urethane formation with a contribution on minimization of racemization

FRANCIS M. F. CHEN, YOUNG LEE, RENE STEINAUER,[1] AND N. LEO BENOITON[2]
Department of Biochemistry, University of Ottawa, Ottawa, Ont., Canada K1H 8M5

Received July 3, 1986

FRANCIS M. F. CHEN, YOUNG LEE, RENE STEINAUER, and N. LEO BENOITON. Can. J. Chem. **65**, 613 (1987).

A study of the factors contributing to urethane formation during the coupling of *N*-alkoxycarbonylamino acids with an amino acid ester by the mixed carboxylic–carbonic acid anhydride method has been carried out, using nuclear magnetic resonance spectroscopy and high-performance liquid chromatography for the quantitation of products. Urethane formation is associated primarily with reactions of activated hindered residues such as isoleucine and *N*-methylamino acids. Of prime importance in dictating the amount of urethane generated is the tertiary amine/solvent combination. *N*-Methylpiperidine/dichloromethane is the best combination for minimizing urethane formation, *N*-methylmorpholine/tetrahydrofuran is a good combination, while triethylamine/dichloromethane is a particularly bad one. In dimethylformamide, the differences between these amines are marginal. Aqueous dimethylformamide is a good solvent for mixed anhydride generation and coupling. A small excess of substrate reduces the amount of urethane. Less racemization accompanies the coupling of peptide acids in tetrahydrofuran than in halogen-containing solvents, *N*-methylpiperidine being the superior base in these solvents, but not in dimethylformamide. Racemization is reduced by one half when menthyl chloroformate instead of isobutyl chloroformate is used in the couplings.

FRANCIS M. F. CHEN, YOUNG LEE, RENE STEINAUER et N. LEO BENOITON. Can. J. Chem. **65**, 613 (1987).

Faisant appel à la rmn et la chromatographie liquide à haute performance pour quantifier les produits formés, on a effectué une étude des facteurs qui contribuent à la formation d'uréthane lors du couplage, par la méthode des anhydrides mixtes d'acides carboxylique et carbonique, d'acides *N*-alkoxycarbonylamino avec un ester d'acide aminé. La formation d'uréthane est principalement associée avec les réactions de résidus activés empêchés, comme l'isoleucine et les acides *N*-méthylaminés. La combinaison amine tertiaire/solvant est d'importance capitale dans la quantité d'uréthane formée. Le couple *N*-méthylpipéridine/dichlorométhane correspond à la meilleure combinaison pour minimiser la formation d'uréthane; la combinaison *N*-méthylmorpholine/tétrahydropyranne est bonne alors que la combinaison triéthylamine/dichlorométhane est particulièrement mauvaise. Dans le diméthylformamide, les différences entre ces amines sont marginales. Le diméthylformamide aqueux est un bon solvant pour générer des anhydrides mixtes et pour leur couplage. Un léger excès de substrat réduit la quantité d'uréthane. Il y a moins de racémisation lors du couplage de peptides dans le tétrahydrofuranne que dans des solvants contenant des halogènes; la *N*-methylpipéridine est la base la meilleure dans ces solvants, mais pas dans le diméthylformamide. La racémisation est réduite de moitié lorsqu'on utilise du chloroformate de menthyle au lieu du chloroformate d'isobutyle hors de ces couplages.

[Traduit par la revue]

Can. J. Chem. Downloaded from www.nrcresearchpress.com by 80.58.250.72 on 09/07/12
For personal use only.

The mixed anhydride method of coupling used in peptide synthesis involves reaction of a protected amino or peptide acid **1** with an alkyl chloroformate **2** in the presence of a tertiary amine base to give the mixed carboxylic acid – carbonic acid anhydride **3**. The anhydride is then reacted with an amine nucleophile **4**, which is either an amino acid ester **4***a* or a peptide ester, giving the protected peptide **5** (1, 2). Three side reactions may accompany the coupling reaction. An inversion of configuration may occur at the activated residue when **1** is a peptide acid, and a second acylation product, urethane **6**, may be produced by aminolysis at the carbonyl of the carbonate moiety of the anhydride or aminolysis of unconsumed chloroformate **2**, or both. Conditions for minimizing the racemization have been defined (3, 4), and protocols for obtaining maximum coupling yields have been recommended (2–4). But little is known about the urethane-forming reaction except that more urethane is generated when the activated residue is valyl or isoleucyl (5), and when the incoming nucleophile is a secondary amine (Pro, MeXxx) (2). In the course of studies on the coupling of *N*-methylamino acids (6), it became apparent to us that many questions about the mixed anhydride method of coupling remained unanswered, in particular regarding the factors contributing to the formation of the urethane side product. We therefore began a systematic investigation of this side reaction, the results of which are reported in this communication. Preliminary reports on some of the work have appeared (7, 8). Emerging from this study was the realization that mixed anhydrides are not immediately destroyed by contact with water, and consequently can be isolated from the mixture in which they are generated by washing the solution with water (9). This and the information derivable therefrom is described in the accompanying communication (10).

Results and discussion

Representative *N*-alkoxycarbonylamino acids **1***a* were coupled with an amino acid ester **4***a* under various conditions and the proportions of peptides **5***a* and urethanes **6***a* present in the neutral fractions were determined by 60-MHz ^{1}H nmr spectroscopy after the usual work-up. The combination of Boc-Ile-OH,[3] a derivative of a hindered residue, and H-Lys(Z)-OMe, which gives unique singlet resonances in the nmr spectrum, was selected as the standard system for examining the effect of parameters external to the coupling components. Reactions were carried out initially under conditions recommended for achieving optimum results except for the tempera-

[1]Present address: Novabiochem, CH-4448 Läufelfingen, Switzerland.

[2]Author to whom correspondence may be addressed.

[3]Abbreviations: Boc, *tert*-butoxycarbonyl; Bzl, benzyl; Mn, menthyl; Ms, methylsulfonylethyl; Z, benzyloxycarbonyl; NMM, *N*-methylmorpholine; NMP, *N*-methylpiperidine; DMF, dimethylformamide; THF, tetrahydrofuran. Amino-acid symbols represent the L isomer, except for glycine. A substituent in parentheses indicates side-chain substitution.

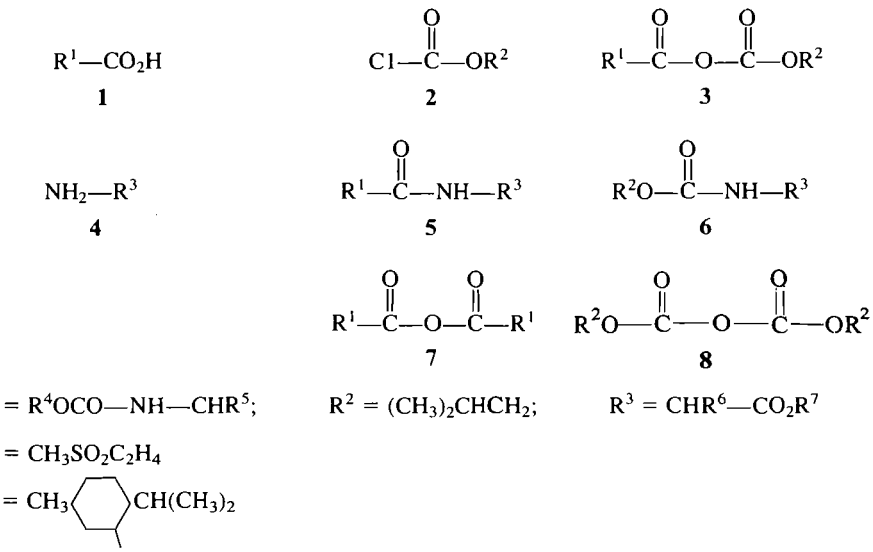

a: $R^1 = R^4OCO—NH—CHR^5$; $R^2 = (CH_3)_2CHCH_2$; $R^3 = CHR^6—CO_2R^7$

b: $R^2 = CH_3SO_2C_2H_4$

c: $R^2 =$

ture, namely activation for 90 s in tetrahydrofuran using isobutyl chloroformate in the presence of *N*-methylmorpholine, followed by addition of the nucleophile in the same solvent (2–4). For ease of operation, −5°C instead of the recommended −15°C was chosen as temperature. After considerable data had been acquired it became obvious that an analytical method more sensitive than nmr spectroscopy was required for us to arrive at reliable conclusions. The products of the reactions were then determined by high-performance liquid chromatography (hplc). Representative results are collated in Tables 1–6, and are discussed in different sections, not necessarily in the order obtained. Only selected data from the preliminary communications (7, 8) have been reproduced. Data on racemization are given in Tables 7 and 8. In view of the novel information that has been acquired with the isolated mixed anhydrides (9), the discussion in the present communication is limited in scope to avoid duplication.

Effect of the amount of acid ***1***

One postulated source of urethane **6** is reaction of nucleophile **4** with unconsumed chloroformate **2**. The effect of using a 5% excess of **1***a* to promote complete consumption of **2***a* is shown in Table 1. The extent of the effect varied, depending on the nature of **1***a*, but it was beneficial in all cases, eliminating the formation of iBuOCO-Lyz(Z)-OMe for Boc-Pro-OH, decreasing its yield by six times for Boc-Leu-OH and by 23% for Boc-Ile-OH. These results are significant enough to conclude that the use of a small excess of **1***a* reduces the amount of urethane produced by promoting consumption of the chloroformate. Excess substrate obviously cannot be expected to eliminate the urethane generated by aminolysis at the carbonate moiety of the anhydride. Others have employed this tactic of using a small excess of substrate (11), but it has not been included in the general recommendations (2, 3, 12). In fact, it has been reported that the use of a 100% excess of substrate had no effect on the amount of **6** generated when Boc-amino acids were coupled with amino acid β-naphthylamides (5).

Effect of the nature of the base, and the activation time

Couplings were carried out using various tertiary amines selected on the basis of frequency of use and availability, bearing in mind the desirability that the amine should contain at least one *N*-methyl group (2, 3). The yields of **5***a* and **6***a* obtained are given in Table 2. The recovery of material was high

TABLE 1. Effect of the amount of substrate on urethane formation[a]

Substrate	1.00 equiv.	1.05 equiv.
Boc-Leu-OH[b]	1.48	0.24
Boc-Pro-OH	1.1	<0.05
Boc-Ile-OH	6.5	5.0

[a]Yield (%) of urethane **6***a*, determined by hplc. Substrate coupled with H-Lys(Z)-OMe using iBuOCOCl and NMM in THF at −5°C with an activation time of 90 s.
[b]Data from ref. 7.

TABLE 2. Effect of the nature of the tertiary amine on urethane formation[a]

Amine	Peptide (%)	Urethane (%)
N-Methylpiperidine	83	4.3
N-Methylmorpholine	82	5.2
N-Methylpyrrolidine	70	7.1
Triethylamine	54	34
N-Methylimidazole	24	59
N-Methylpyrrole	5	
1,2,5-Trimethylpyrrole	0	
Diisopropylethylamine	0	90

[a]Boc-Ile-OH (1.05 equiv.) coupled with H-Lys(Z)-OMe using iBuOCOCl in THF at −5°C with an activation time of 90 s. Results determined by weighing and nmr.

and approximately the same in all cases. There was an inverse relationship between the amount of urethane produced and the yield of peptide. Best results in terms of the amount of urethane generated were obtained with the saturated six-membered ring amines, with *N*-methylpiperidine being slightly superior to *N*-methylmorpholine. Triethylamine was definitely inferior as it gave only a 54% yield of peptide. Since all other factors were identical in the experiments, one must conclude that most of the urethane formed in the latter case, as well as with *N*-methylimidazole as base, originated from the reaction of ester **4***a* with unconsumed chloroformate. This suggests that the anhydride

Can. J. Chem. Downloaded from www.nrcresearchpress.com by 80.58.250.72 on 09/07/12
For personal use only.

TABLE 3. Effect of the temperature and activation time on urethane formation and coupling yield[a]

Base	−5°C/ 2 min		−5°C/ 10 min		23°C/ 10 min	
	% P	% U	% P	% U	% P	% U
N-Methylpiperidine	83	4.3	83	3.9	79	6.1
N-Methylpyrrolidine	70	7.1	73	5.2	75	6.8

[a]Boc-Ile-OH (1.05 equiv.) coupled with H-Lys(Z)-OMe using iBuOCOCl in THF. P = peptide; U = urethane. Results determined by weighing and nmr.

TABLE 4. Effect of the amine/solvent combination on urethane formation[a]

Substrate	Amine	Solvent	Peptide:urethane
Z-Leu-OH	TEA	THF	70:30
	TEA	DCM	39:62
	NMM	THF	>100
Z-MeLeu-OH	TEA	THF	65:35
Z-MeVal-OH[b]	NMM	THF	60:40
	NMP	THF	78:22
	NMP	DCM	90:10
Z-MeVal-OH[c]	NMM	THF	40:60
Boc-Ile-OH[b]	TEA	DMF	93.0:7.0
	NMM	DMF	94.5:5.5
	NMP	DMF	94.5:5.5
	NMM	THF	94.3:5.7
	NMP	THF	95.1:4.9
Boc-MeLeu-OH[c]	TEA	THF	57:43
	NMM/TEA[d]	THF	>100
	TEA/NMM[d]	THF	60:40
Boc-MeVal-OH	NMM	THF	67:33
	NMM	DCM	76:24
Boc-MeVal-OH[e]	NMM	THF	50:50
Z-Gly-Val-OH[c]	NMM	THF	>100
	TEA	THF	50:50

[a]Substrate (1.0 equiv.) coupled with H-Lys(Z)-OMe using iBuOCOCl at −5°C with an activation time of 90 s. Results determined by nmr. TEA = triethylamine; DCM = CH_2Cl_2.
[b]Data from ref. 7, 1.05 equiv. substrate. Results determined by hplc.
[c]EtOCOCl.
[d]Used to neutralize the ester hydrochloride salt.
[e]−70°C.

is formed considerably faster in the presence of *N*-methylmorpholine than in the presence of triethylamine.[4] In support of this are the data in Table 3 showing the beneficial effects of extending the time of activation when *N*-methylpiperidine and *N*-methylpyrrolidine were used as bases. That the tertiary amine exerts its effect at the anhydride generation stage, and not at the coupling step, emerges from the results with Boc-MeLeu-OH as substrate (Table 4). When *N*-methylmorpholine was used to generate the anhydride and triethylamine was used to neutralize the hydrochloride of the ester, no urethane was detectable. But when the bases were interchanged, two thirds of the product was urethane. No peptide whatsoever was obtained from the couplings involving the two highly hindered amines. This is essentially in agreement with the literature (3).

Effect of the solvent

The course of the mixed anhydride reactions was examined in tetrahydrofuran and in dichloromethane, despite allusions to the unsuitability of the latter as a solvent (2), because of its popularity for carbodiimide-mediated reactions. The ratios of peptide to urethane obtained for several hindered substrates are given in Table 4. It is seen that when the amine was *N*-methylmorpholine or *N*-methylpiperidine, a higher ratio was obtained in dichloromethane than in tetrahydrofuran. But when the base was triethylamine, the ratio obtained in dichloromethane was much lower than in tetrahydrofuran. The conclusion is that dichloromethane is a poor solvent only when triethylamine is the base, and it is a superior solvent when *N*-methylmorpholine or *N*-methylpiperidine is used as base. On the other hand, when the solvent was dimethylformamide, there was only a slight difference in the results for the three amines. In Table 5 is shown the effect of the solvent on the yields of peptide obtained for several substrates that give rise to minimal amounts of urethane. It is seen that there was no significant difference between tetrahydrofuran, dimethylformamide, and the halogen-containing solvents. In addition, it was found that dimethylformamide to which had been added 25% of water, a solvent used successfully for couplings of symmetrical anhydrides **7***a* (13), served as well for mixed anhydride reactions as the anhydrous solvent. These results are contradictory to the generally held notions that halogen-containing solvents are poor solvents, and that anhydrous solvents are essential, for mixed anhydride reactions. The previous conclusions that halogen-containing solvents are not suitable for mixed anhydride reactions were based on results obtained using triethylamine as the base.

TABLE 5. Effect of the solvent on the yield (%) of peptide[a]

Substrate	THF	DMF	DMF–H_2O (4:1)
Boc-Val-OH	92	82	80
Boc-Pro-OH	83		91
Boc-MeLeu-OH	82	73	75
Z-Gly-Pro-OH	84		80

[a]Substrate (1.0 equiv.) coupled with H-Lys(Z)-OMe using EtOCOCl and NMM at −5°C with an activation time of 90 s; $CHCl_3$, 88%; $CHCl_2$, 84%. No urethane was detectable by nmr.

Effect of the temperature

Mixed anhydride reactions have traditionally been carried out at −15°C to minimize racemization and to avoid disproportionation of the anhydride to the symmetrical anhydride **7***a* and the dialkyl pyrocarbonate **8**. A comparison of the amounts of urethane obtained at −5°C and 23°C for our standard system in the presence of two different tertiary amines is given in Table 3. Substantially more urethane was generated at the higher temperature. This is consistent with the notion that the higher temperature promotes disproportionation, thus providing an additional source of urethane, namely the pyrocarbonate, which is a good acylating agent. An experiment with Boc-MeVal-OH at −70°C (Table 4) showed a moderate increase in urethane formation, which can be attributed to the slower formation of the anhydride. But one cannot be sure that this is the correct explanation, in view of the demonstrated effect of temperature on the aminolysis (10). Regardless, the results show that a mixed anhydride still can be coupled efficiently at a very low temperature.

Effect of the nature of the nucleophile **4**

Boc-Ile-OH was coupled with different amino acid esters **4***a* and the peptide-to-urethane ratio was determined. The results in

[4]That this is so has been unequivocally demonstrated (10).

Can. J. Chem. Downloaded from www.nrcresearchpress.com by 80.58.250.72 on 09/07/12
For personal use only.

TABLE 6. Effect of the nature of the nucleophile on urethane formation[a]

Substrate	Nucleophile	Peptide:urethane
Boc-Ile-OH	H-Gly-OBzl	97.4:2.6
Boc-Ile-OH	H-Leu-OBzl	96:4
Boc-Ile-OH	H-Val-OBzl	95:5
Boc-Ile-OH	H-Lys(Z)-OMe	93.5:6.5
Boc-Ile-OH	H-Pro-OBzl	51:49
Boc-Gly-OH	H-Gly-OBzl	>100
Boc-Leu-OH	H-Leu-OBzl	99.7:0.3
Boc-Pro-OH	H-Lys(Z)-OMe	>100
Boc-Pro-OH	H-Pro-OBzl	58:42
Boc-Pro-OH	H-Pro-OBzl	67:33[b]

[a]Substrate (1.05 equiv.) coupled using iBuOCOCl and NMM in THF at −5°C with an activation time of 90 s. Results determined by hplc.
[b]NMP in CH_2Cl_2.

Table 6 show that the side chain of **4***a* had very little influence on the extent of urethane formation except in the case of proline, for which the ratio was one. The propensity of the imino group of proline to generate urethane from the mixed anhydride reaction is well known (2). Selectivity during aminolysis is eliminated because of the higher basicity of the secondary amino group.

Effect of the addition of 1-hydroxybenzotriazole (HOBt)

A recent publication reports that the side reaction of urethane formation is suppressed when HOBt is added to the mixed anhydride before the addition of the amine nucleophile (14). The rationale is that aminolysis is preceded by transformation of the mixed anhydride into the activated ester. Boc-Ile-OH was coupled with H-Lys(Z)-OMe in an acetonitrile–dimethylformamide mixture at −15°C using isobutyl chloroformate and *N*-methylmorpholine exactly as described by Prasad *et al.* (14) with and without the addition of one equivalent of HOBt. The results were 85 and 3.0% yields of peptide and urethane, respectively, in the absence of the additive, and 90 and 2.0% yields in the presence of the additive. We conclude that the tactic of adding HOBt is beneficial, but it does not eliminate the formation of urethane.

Effect of the nature of the solvent on racemization

In view of the success achieved with the mixed anhydride reaction in dichloromethane, the extent of stereomutation accompanying the coupling of some dipeptide acids was examined in halogen-containing solvents as well as in tetrahydrofuran. A dipeptide ester, H-Lys(Z)-Gly-OBzl, was selected as the amino component. The results appear in Table 7. With alanyl and valyl as the activated residues, racemization in either tetrahydrofuran, chloroform, or dichloromethane did not exceed the limits of detection of the analytical method. With phenylalanyl as the activated residue, less racemization occurred in tetrahydrofuran than in the halogen-containing solvents. Toluene gave rise to more racemization than the other solvents. Other data in Table 8 show that more racemization occurred in dimethylformamide than in dichloromethane. Though it is stated above that anhydrous solvents are not essential for efficient coupling, the presence of water did cause considerable racemization (Table 7). The results are thus in agreement with the original contention (2, 3) that tetrahydrofuran is the best solvent for minimizing racemization.

Effect of the nature of the chloroformate on racemization

In the accompanying communication, it is reported that a 2-alkoxy-5(4*H*)-oxazolone is formed more quickly from the mixed anhydride of an *N*-alkoxycarbonylamino acid when the alkyl group is methylsulfonylethyl than when it is isobutyl, and less quickly when the alkyl group is menthyl (10). Since the racemization accompanying the coupling of peptide acids results from the formation and tautomerism of the 2-alkyl-5(4*H*)-oxazolone, it was reasoned that the racemization associated with mixed anhydride reactions might depend on the chloroformate use. Indeed this is the case. The results in Table 8 show that menthyl chloroformate (**2***c*) consistently gave rise to less racemization than isobutyl chloroformate, and in some cases less than half as much. Methylsulfonylethyl chloroformate (**2***b*) (15) led to more than 50% racemization. The results therefore can be correlated with the ease of formation of the 2-alkoxy-5(4*H*)-oxazolone from anhydride **3***a* (10). To our knowledge, this is the first time anyone has addressed the possibility that the nature of the chloroformate might have some bearing on the racemization associated with mixed anhydride reactions. The use of menthyl chloroformate can thus be considered as an option for trying to minimize racemization when coupling peptide acids. The yields of peptide product **5** were satisfactory with the model system examined (Table 8). However, the benefits of using menthyl chloroformate must be weighed against the associated disadvantages, namely that menthyl alcohol is difficult to get rid of because it is insoluble in aqueous sodium hydrogen carbonate, and the higher tendency of the mixed anhydride to generate urethane (10).

On the coupling of N*-alkoxycarbonylamino acids*

The data in Tables 1, 4, and 6 and in ref. 7 are in agreement with the notion that urethane formation is of major concern during the couplings of the hindered residues valyl and isoleucyl (2, 5) (but not leucyl as indicated in ref. 2), which led to 10–20 times more urethane than the other residues. The *N*-methylamino acid derivatives generated about five times more urethane (MeLeu vs. Leu) than the corresponding unmethylated derivatives. Whether the small amounts (0.0–0.3%) observed for the other residues resulted from incomplete consumption of chloroformate or from aminolysis at the carbonate of the anhydride cannot be established by the present approach. It should be emphasized, however, that more than minor amounts of urethane can result from the couplings of unhindered residues if an unsuitable solvent/base combination such as dichloromethane/triethylamine is used. In this regard, the results in Tables 4 and 6 and in ref. 7 indicate that the best combination for minimizing urethane formation is *N*-methylpiperidine/dichloromethane. The difficult case of Boc-Pro-OH coupled with H-Pro-OBzl improved from a peptide–urethane ratio of 58:42 for *N*-methylmorpholine/tetrahydrofuran to a ratio of 67:33 for *N*-methylpiperidine/dichloromethane (Table 6). The recommendation in the original study that *N*-methylmorpholine was the most suitable tertiary amine for mixed anhydride reactions was based on chirality considerations and on the yield of peptide without making a distinction between the two types of substrate that might be implicated (3). We suggest that careful distinction between *N*-alkoxycarbonylamino acids and peptide acids should be made in any discussion on the mixed anhydride reaction. It is not at all as critical to have a short activation time of 90 s as recommended (3) when coupling *N*-alkoxycarbonylamino acids as it is when coupling peptide acids where racemization becomes pertinent. In fact, it is probably wiser to extend the time to 2 or 3 minutes for the *N*-alkoxycarbonylamino acids to ensure complete consumption of the chloroformate, especially for the more difficult cases.

Can. J. Chem. Downloaded from www.nrcresearchpress.com by 80.58.250.72 on 09/07/12
For personal use only.

TABLE 7. Effect of the solvent on racemization[a]

Substrate	Amine	THF	$CHCl_3$	CH_2Cl_2	$PhCH_3$
Z-Gly-Phe-OH	NMP	0.61	2.16	2.5 (5)[b]	5.58
	NMM	1.87	2.77	3.0 (4)[b]	
Z-Gly-Val-OH	NMP	<<0.6	<<0.6	<0.6 (3)[b]	2.9 (1)[b]
	NMM	<0.6		<0.6 (2)[b]	
Z-Gly-Ala-OH	NMP	0.74		<0.7	
Z-Gly-Phe-OH	NMP	8[c]		6[c]	

[a]% D–L isomer formed during coupling with H-Lys(Z)-Gly-OBzl using iBuOCOCl at −5°C with an activation time of 2 min. No coupling occurred in CCl_4.
[b]Amount of urethane produced estimated by hplc to be (1) >> (2) ≥ (3) = 5% > (4) ≥ (5).
[c]2% water added.

TABLE 8. Effect of the nature of the chloroformate on racemization[a]

Substrate	Solvent	Amine	MnOCOCl	iBuOCOCl	MsOCOCl
Z-Gly-Phe-OH	CH_2Cl_2	NMM	1.7	3.0	
	CH_2Cl_2	NMP	0.6, 1.9	2.5	29 (48)
	DMF	NMM	(74) 2.0	5.3	
	DMF	NMP	(77) 5.3		
	THF	NMP	[b]		[b]
Z-Gly-Val-OH	CH_2Cl_2	NMP	<<0.6	<0.6	33
	CH_2Cl_2	NMM	<<0.6		
	DMF	NMM	1.1	1.5	
	DMF	NMP	1.7	4.9	42 (25)

[a]% D–L isomer formed during coupling with H-Lys(Z)-Gly-OBzl at −5°C with an activation time of two min. ( ) = % yield of peptide.
[b]Couplings in THF did not work.

When prolyl is the nucleophile, or a hindered residue is activated, it is impossible to avoid urethane formation. Recognizing this, it occurred to us that one way to surmount the difficulty might to be generate a urethane that could be removed by its selective destruction before continuing on with the synthesis. The benzyloxycarbonyl groups came to mind, but using benzyl chloroformate for the coupling would not allow us to prepare our standard peptide. We therefore examined the use of methylsulfonylethyl chloroformate (**2***b*) (15), the MsOCO-*N* group being sensitive to cleavage by nucleophiles. Boc-Ile-OH was coupled with H-Lys(Z)-OMe in dichloromethane by the standard procedure using MsOCOCl instead of iBuOCOCl. A 90% yield of Boc-Ile-Lys(Z)-OMe containing 2.7% of MsOCO-Lys(Z)-OMe was obtained. The mixture was left in acetonitrile containing sodium methoxide for 5 min. Work-up gave an 80% yield of pure Boc-Ile-Lys(Z)-OMe. A small amount of deesterification had accompanied the cleavage. It should be noted that it is not possible to obtain this compound pure by the conventional mixed anhydride reaction without some form of fractionation, which could be tedious or inefficient. We recommend consideration of this approach. The alternative for circumventing the urethane problem with prolyl as the nucleophile is to insert the prolyl residue through the activated dipeptide (e.g., Boc-Xxx-Pro-OH), which is not susceptible to racemization (16).

On the coupling of peptide acids

A possible source of urethane in the coupling of peptide acids is aminolysis of unconsumed chloroformate, which accounts for the results with Z-Gly-Val-OH/TEA in Table 4. Optimum conditions to promote complete anhydride formation are therefore obviously desirable. Some indication of the amount of urethane produced during couplings under favourable conditions is given in Table 7; however, even here, one cannot be sure that all the chloroformate had been consumed before the addition of the peptide ester nucleophile. Completion of the reaction might have been assured by extending the time of activation; however, in practice, this is counter-productive as it promotes racemization (3). Consequently, the issue was not pursued, and we make no conclusions here on the generation of urethane by aminolysis at the carbonate moiety of mixed anhydrides of peptide acids. With regards to chiral preservation during couplings, the results in Table 7 are in agreement with the original contention (2, 3) that tetrahydrofuran is the best solvent for minimizing racemization. On the other hand, the results in Tables 7 and 8 suggest that the superior base for achieving the same purpose in either tetrahydrofuran or dichloromethane is *N*-methylpiperidine and not *N*-methylmorpholine. The superiority of *N*-methylpiperidine does not seem to hold in dimethylformamide (Table 8), despite our initial claim that it does (7). We have no explanation for the discrepancy in the data, and suspect that the unusually high values for racemization reported earlier (7) were obtained for couplings carried out in improperly preserved solvent.

Experimental

General

Tertiary amines and alkyl chloroformates (Aldrich products) were purchased from Terochem Laboratories, Edmonton, except for methylsulfonylethyl chloroformate, which was a gift from Professor G. I. Tesser (15). Menthyl chloroformate was the *levo* isomer. Solvents (Fisher Scientific) were dried (CH_2Cl_2 over K_2CO_3; THF over $LiAlH_4$) and distilled. Dimethylformamide was used within 72 h of distillation. Amino acid and peptide derivatives were purchased from Sigma Chemical Company or obtained by synthesis, H-Lys(Z)-OMe.HCl (17), Z-Gly-Xxx-OH (18), H-Xxx-OBzl.HCl (19), ROCO-MeXxx-

Can. J. Chem. Downloaded from www.nrcresearchpress.com by 80.58.250.72 on 09/07/12
For personal use only.

Can. J. Chem. Downloaded from www.nrcresearchpress.com by 80.58.250.72 on 09/07/12
For personal use only.

OH (20). All amino acid esters were hydrochlorides, which were neutralized by the addition of an equivalent of the pertinent tertiary amine. Solvents were removed at room temperature using a rotary evaporator. Reference compounds **6** were obtained as oils by reaction of iBuOCOCl with the appropriate amino acid ester in CH_2Cl_2 followed by aqueous washes and removal of the solvent. Proton nmr spectra were determined in deuterochloroform using a Varian EM-360 60-MHz instrument. The high-performance liquid chromatograph was a basic Waters Scientific instrument incorporating a variable-wavelength detector, a data module, and a 30 cm × 3.9 mm id stainless-steel column with 10-μm μBondapak-C_{18} packing as previously described (21).

Representative coupling procedure

To 10 mL of a stock solution of THF containing 1 mmol of *N*-methylmorpholine was added 1 mmol of H-Lys(Z)-OMe.HCl; the mixture was stirred at 23°C for 30 min and then cooled to −5°C. One or 1.05 mmol of Boc-Ile-OH was added to 10 mL of the same stock solution in a second flask, and the solution was cooled to −5°C. To this stirred solution was added 1 mmol of iBuOCOCl followed, 90 s later, by the first solution of ester. After 1 h at −5°C, and 3 or more h at room temperature, the solvent was removed and the residue was dissolved in CH_2Cl_2. The solution was washed with dilute citric acid, aqueous $NaHCO_3$, water, and dried ($MgSO_4$); the solvent was removed by evaporation and the residue was weighed. When DMF was used as solvent for couplings, it was not removed before the addition of CH_2Cl_2. In a few cases, products were separated by passage through a silica-gel column with ethyl acetate – light petroleum as solvent.

*Quantitation of peptides **5** and urethanes **6***

When not indicated, the proportions of **5** and **6** in the products were determined by comparing the intensities of appropriate signals in the nmr spectra. Otherwise, the amounts of **5** and **6** were determined by hplc using acetonitrile–water (1:1) as solvent at a flow rate of 1 mL/min with absorbance monitoring at 215 nm. The molar absorbance of Boc-Ile-Lys(Z)-OMe was 1.1% greater than that of iBuOCO-Lys(Z)-OMe. Compounds **5** and **6** for other pairs of products were assumed to have the same absorbance. The elution times (min) were: iBuOCO-Gly-OBzl, 11.2; iBuOCO-Lys(Z)-OMe, 13.4; iBuOCO-Val-OBzl, 24.5; iBuOCO-Leu-OBzl, 33.5; Boc-Pro-Lys(Z)-OMe, 9.0; Boc-Ile-Gly-OBzl, 14.0; Boc-Ile-Lys(Z)-OMe, 17.3; Boc-Leu-Lys(Z)-OMe, 18.9; Boc-Ile-Val-OBzl, 29.8; Boc-Leu-Leu-OBzl, 40.5.

Extent of racemization

This was determined by hplc of the diastereomeric H-Gly-D/L-Xxx-Lys-Gly-OH peptides on the C-18 column after deprotection of the coupling products (Z-Gly-Xxx-Lys(Z)-Gly-OBzl) by catalytic hydrogenation as described (18). The solvents, at flow rates of 1 mL/min, were 0.01 *M* ammonium acetate, pH 6.6 for Xxx = Ala, pH 4.0 for Xxx = Val, and pH 4.0 containing 4% acetonitrile for Xxx = Phe, with monitoring at 208 nm.

Preparation of H-Lys(Z)-Gly-OBzl.HCl

To an equimolar solution of Boc-Lys(Z)-OH (10 mmol), H-Gly-OBzl.HCl, 1-hydroxybenzotriazole, and *N*-methylmorpholine in CH_2Cl_2 (50 mL) at 0°C was added *N*,*N*′-dicyclohexylcarbodiimide (10 mmol) and the mixture was stirred at 0°C for 3 h. The urea was removed by filtration, the filtrate was washed with dilute citric acid and aqueous $NaHCO_3$, dried, and the solvent was removed. The residue was taken up in ethyl acetate, the solution was filtered, and the solvent was evaporated to give an oil (5.2 g, 93%). To this oil (Boc-Lys(Z)-Gly-OBzl, 4.56 g) dissolved in tetrahydrofuran at 0°C was added anhydrous diethyl ether (30 mL), which had been saturated with HCl at 0°C. After 1 h at 0°C, the solvent was removed, the residue was triturated in ether (30 mL), and the crystals that formed were collected. Recrystallizatio from ethanol–ether gave H-Lys(Z)-Gly-OBzl.HCl (3 g, 75%), m 153–154°C, $[\alpha]_D^{22}$ + 8.0° (*c* 1.0, 0.1 *N* HCl). *Anal.* calcd. fo $C_{23}H_{30}N_3O_5Cl$: C 59.40, H 6.52, N 9.06; found: C 59.26, H 6.48 N 9.04.

Acknowledgements

We are grateful to the Medical Research Council of Canad for financial support of this research and to Dr. G. I. Tesse for the gift of methylsulfonylethyl chloroformate. N.L.B. is Career Investigator of the M.R.C.C.

1. R. A. Boissonnas. Helv. Chim. Acta, **34**, 874 (1951); J. R Vaughan. J. Am. Chem. Soc. **73**, 3547 (1951); J. R. Vaughai and R. L. Osata. J. Am. Chem. Soc. **74**, 676 (1952); T Wieland and H. Bernhardt. Justus Liebigs Ann. Chem. **572** 190 (1951). N. F. Albertson. Org. React. (N.Y.), **12**, 15 (1962); D. S. Tarbell. Acc. Chem. Res. **2**, 296 (1969).
2. J. Meienhofer. *In* The peptides. Vol. 1. *Edited by* E. Gross an J. Meienhofer. Academic Press, New York. 1979. p. 263.
3. G. W. Anderson, J. E. Zimmerman, and F. M. Callahan J. Am. Chem. Soc. **89**, 5012 (1967); G. W. Anderson. *I* Peptides: chemistry and biochemistry. *Edited by* B. Weinstei and S. Lande. Marcel Dekker, New York. 1970. p. 255.
4. T. Wieland, J. Faesel, and W. Konz. Justus Liebigs Ann Chem. **722**, 197 (1969); T. Wieland, H. Faulstich, an F. Fahrenholz. Justus Liebigs Ann. Chem. **743**, 77 (1971).
5. M. Bodanszky and M. Tolle. Int. J. Pept. Protein Res. **10**, 38 (1977).
6. R. Steinauer, F. M. F. Chen, and N. L. Benoiton. Int. J. Pep Protein Res. **26**, 109 (1985), and references therein.
7. F. M. F. Chen, R. Steinauer, and N. L. Benoiton. J. Org Chem. **48**, 2939 (1983).
8. F. M. F. Chen, R. Steinauer, and N. L. Benoiton. *I* Peptides. Structure and function. *Edited by* V. J. Hruby an D. Rich. Pierce Chemical Co., Rockport, IL. 1983. p. 123.
9. F. M. F. Chen, R. Steinauer, and N. L. Benoiton. *In* Peptide 1984. *Edited by* U. Ragnarsson. Almqvist and Wiksell Int. Stockholm. 1984. p. 105.
10. F. M. F. Chen and N. L. Benoiton. Can. J. Chem. **65**, 61 (1987).
11. A. van Zon and H. C. Beyerman. Helv. Chim. Acta, **56**, 172 (1973).
12. M. Bodanszky and A. Bodanszky. The practice of peptid synthesis. Springer Verlag, Berlin. 1984. p. 103.
13. N. L. Benoiton and F. M. F. Chen. FEBS Lett. **125**, 10 (1981).
14. K. U. Prasad, M. A. Iqbal, and D. W. Urry. Int. J. Pep Protein Res. **25**, 408 (1985).
15. G. I. Tesser and I. C. Balvert-Geers. Int. J. Pept. Protein Re **7**, 295 (1975).
16. H. C. Beyerman, E. W. B. de Leer, and J. Floor. Recl. Tra Chim. Pays-Bas, **92**, 481 (1973).
17. J. R. Coggins, R. Demayo, and N. L. Benoiton. Can. J. Chem **48**, 385 (1970).
18. N. L. Benoiton, K. Kuroda, S. T. Cheung, and F. M. F Chen. Can. J. Biochem. **57**, 776 (1979).
19. F. M. F. Chen and N. L. Benoiton. Int. J. Pept. Protein Res. **27** 221 (1986).
20. J. R. McDermott and N. L. Benoiton. Can. J. Chem. **51**, 191 (1973); S. T. Cheung and N. L. Benoiton. Can. J. Chem. **5** 906 (1977).
21. R. Steinauer, F. M. F. Chen, and N. L. Benoiton. Chromatogr. **325**, 111 (1985).

The preparation and reactions of mixed anhydrides of *N*-alkoxycarbonylamino acids

FRANCIS M. F. CHEN AND N. LEO BENOITON[1]

Department of Biochemistry, University of Ottawa, Ottawa, Ont., Canada K1H 8M5

Received July 3, 1986

FRANCIS M. F. CHEN and N. LEO BENOITON. Can. J. Chem. **65**, 619 (1987).

Pure mixed anhydrides $R^1OCO\text{-}Xxx\text{-}O\text{-}COOR^2$ (Xxx = NHCHRCO) have been obtained by reaction of *N*-alkoxycarbonylamino acids $R^1OCO\text{-}Xxx\text{-}OH$ with alkyl chloroformate R^2OCOCl (R^2 = methyl, ethyl, isobutyl, menthyl) in the presence of *N*-methylmorpholine or *N*-methylpiperidine (NMP) in dichloromethane at −5°C, followed by washing the mixtures with aqueous solutions and removal of the solvent. $R^1OCO\text{-}Xxx\text{-}O\text{-}COOR^2$ (R^2 = ethyl, *tert*-butyl) have been obtained by reaction of $R^1OCO\text{-}Xxx\text{-}O^-.{}^+HNMP$ with the corresponding dialkyl dicarbonates followed by the same work-up. Mixed anhydride generation is much slower when triethylamine is used as base. The initial reaction in the decomposition of mixed anhydrides is cyclization to the 2-alkoxy-5(4*H*)-oxazolone (R^1O-oxazolone) followed by release of alcohol R^2OH. Symmetrical anhydride $(R^1OCO\text{-}Xxx)_2O$ and ester $R^1OCO\text{-}Xxx\text{-}OR^2$ are also formed. The ease of cyclization depends on R^2, and is in the order methylsulfonylethyl (Ms) ≫ methyl/ethyl/isobutyl ≫ menthyl. $R^1OCO\text{-}Xxx\text{-}O\text{-}COOMs$ preparations contained a substantial amount of R^1O-oxazolone. Attempts to use this reaction as a preparative procedure for obtaining R^1O-oxazolones failed because they are too sensitive to hydrolysis and react too quickly with the product, forming the symmetrical anhydride. The effect of various parameters on the amount of urethane generated by aminolysis at the carbonate moiety of $R^1OCO\text{-}Xxx\text{-}O\text{-}COOR^2$ was examined without the uncertainty that any urethane arose from aminolysis of unconsumed chloroformate.

FRANCIS M. F. CHEN et N. LEO BENOITON. Can. J. Chem. **65**, 619 (1987).

En faisant réagir les acides *N*-alkoxycarbonylaminés $R^1OCO\text{-}Xxx\text{-}OH$ avec les chloroformates d'alkyles R^2OCOCl (R^2 = méthyle, éthyle, isobutyle et menthyle) dans le dichlorométhane, à −5°C et en présence de *N*-méthylmorpholine ou de *N*-méthylpipéridine (NMP), puis en lavant les mélanges avec des solutions aqueuses et en enlevant les solvants, on a obtenu les anhydrides mixtes $R^1OCO\text{-}Xxx\text{-}O\text{-}COOR^2$ (Xxx = NHCHRCO) à l'état pur. On a obtenu les anhydrides mixtes $R^1OCO\text{-}Xxx\text{-}O\text{-}COOR^2$ (R^2 = éthyle et *tert*-butyle) en faisant réagir $R^1OCO\text{-}Xxx\text{-}O^-.{}^+HNMP$ avec les dicarbonates de dialkyles correspondants et en les purifiant ensuite de la manière plus haut. La formation des anhydrides mixtes est beaucoup plus lente lorsqu'on utilise la triéthylamine comme base. La réaction initiale lors de la décomposition des anhydrides mixtes est la cyclisation en l'alkoxy-2 5(4*H*)-oxazolone (R^1O-oxazolone) qui est suivie par l'élimination de l'alcool R^2OH. L'anhydride symétrique $(R^1OCO\text{-}Xxx)_2O$ et l'ester $R^1OCO\text{-}Xxx\text{-}OR^2$ se forment aussi. La facilité de cyclisation dépend de R^2, dans l'ordre suivant : méthylsulfonyléthyl (Ms) ≫ méthyl/éthyl/isobutyl ≫ menthyl. Les $R^1OCO\text{-}Xxx\text{-}O\text{-}COOMs$ qui ont été obtenus contenaient des quantités importantes de R^1O-oxazolone. Des essais effectués dans le but d'utiliser cette réaction comme une méthode de préparer des R^1O-oxazolones n'ont pas donné les résultats escomptés parce que ces composés sont trop sensibles à l'hydrolyse et qu'ils réagissent trop rapidement avec le produit qui conduit à l'anhydride symétrique. On a étudié l'effet de divers paramètres sur la quantité d'uréthane qui se forme par aminolyse de la portion carbonate des $R^1OCO\text{-}Xxx\text{-}O\text{-}COOR^2$ sans se soucier de la possibilité que l'uréthane puisse provenir d'une aminolyse du chloroformate qui n'a pas réagi.

[Traduit par la revue]

A well-known method of preparing amides or phenolic esters from carboxylic acids involves activation of the acid as the mixed carboxylic–carbonic acid anhydride **3** followed by reaction with the pertinent nucleophile (1, 2). The anhydride is generated by the action of an alkyl chloroformate **2** in the presence of a tertiary amine, and is not isolated before the subsequent reaction. The activation is carried out at low temperature in anhydrous solvents, and is usually of only one or two minutes duration, to avoid decomposition of the anhydride and, when pertinent, the production of stereomuted product. In the course of a study on the side reaction of urethane formation, which is associated with mixed anhydride reactions, it was found that dichloromethane is a good solvent for mixed anhydride reactions if the tertiary amine used is *N*-methylmorpholine (3) or *N*-methylpiperidine, and that aqueous dimethylformamide could also serve as solvent for both the generation and the aminolysis steps of the reaction (4). The latter suggested to us that mixed anhydrides might be stable enough to allow their purification by washing solutions of the anhydrides in a water-immiscible solvent with water in the same way that the symmetrical anhydrides **8** of *N*-alkoxycarbonylamino acids can be purified (5). Indeed, this proved to be the case. This communication describes the preparation of mixed anhydrides of *N*-alkoxycarbonylamino acids **1** using the conventional reaction in dichloromethane, followed by washing the reaction mixture with aqueous solutions and removal of solvent. In addition, a study of the properties and reactions of mixed anhydrides is presented. A preliminary report of this work has appeared (6).

Results and discussion

Mixed anhydrides from alkyl chloroformates

Reaction of *N*-alkoxycarbonylamino acids **1** with an equivalent of methyl, ethyl, or isobutyl chloroformate in dichloromethane at −5°C in the presence of a 5% deficiency of NMM or NMP for 20 min, followed by washing the mixture with cold aqueous citric acid and sodium hydrogen carbonate and removal of solvent, gave the mixed anhydrides in 80–90% yields (eq. [1]). Some of the compounds prepared appear

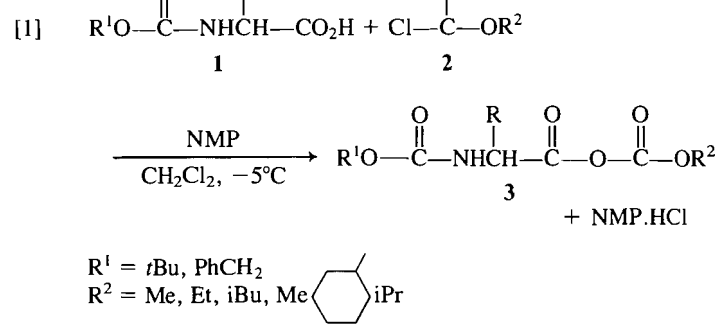

[1]Author to whom correspondence may be addressed.

Can. J. Chem. Downloaded from www.nrcresearchpress.com by 80.58.250.72 on 09/07/12
For personal use only.

TABLE 1. Nuclear magnetic resonance chemical shifts of alkoxy protons[a]

		CH_3O	$(CH_3)_3CO$
R^2 in chloroformate	**2**	3.93	
R^2 in mixed anhydride	**3**	3.90	1.55
R^2 in dialkyl dicarbonate	**4**		1.51
R^2 in dialkyl carbonate		3.77	
R^2 in ester	**7**	3.70	
R^2 in alcohol	**6**	3.45	1.28
R^1 in oxazolone	**5**	4.00	1.58
R^1 in compounds	**3**, **7**, **8**[b]	3.79	1.48

[a]In ppm in $CDCl_3$ relative to $(CH_3)_4Si$. There were corresponding differences in the chemical shifts of the CH_3CH_2O quartets for compounds with R^2 = Et and the $(CH_3)_2CHCH_2O$ doublets for compounds with R^2 = iBu.

[b]See ref. 8 for a different δ, 3.83, for methoxy protons in urethane —CO—N(COOCH_3)—CHR—.

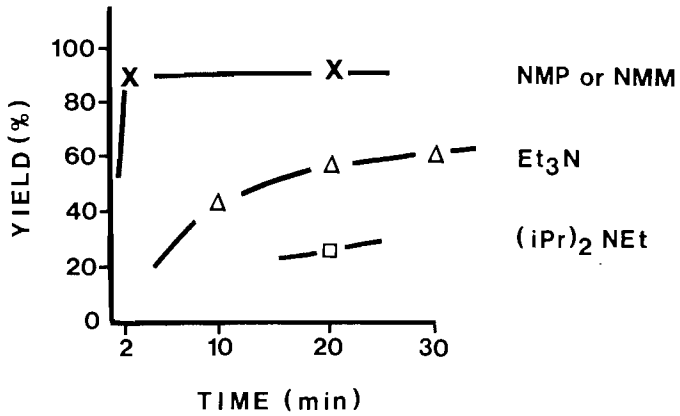

FIG. 1. Graph showing the amount of Boc-Ile-O-COOiBu isolated at various times from the reaction of Boc-Ile-OH with iBuOCOCl in dichloromethane at −5°C in the presence of different tertiary amines.

in Tables 2 and 3. They were obtained as oils except for Z-DL-Ala-O-COOEt,[2] mp 50–52°C, which crystallized on evaporation of the solvent. A few anhydrides of Boc-amino acids contained a small amount of 2-alkoxy-5(4*H*)-oxazolone **5** identifiable by the unique chemical shifts of the $(CH_3)_3CO$-protons in the nmr spectra (7), Table 1. In these cases, a shorter reaction time of 2 min gave the pure anhydrides in slightly lower yields. Comparable yields were obtained from reactions effected in ethyl acetate, in which the NMP.HCl precipitated, or in moist dichloromethane. The anhydrides are identifiable by their proton nmr spectra, which resemble those of the corresponding esters **7**, i.e., Boc-Ile-O-COOR[2] vs. Boc-Ile-OR[2], except that the alkoxy protons in the anhydrides are shifted slightly downfield, Table 1. Their identities as activated forms of substrates were confirmed by their immediate reaction with amines. The compounds were stable for several hours at −5°C, or in solution in dichloromethane at 25°C. Only after 6 h did the nmr spectrum of Boc-Gly-O-COOiBu in $CDCl_3$ show a change. The solution contained 5% of 2-alkoxy-5(4*H*)-oxazolone but no other obvious contaminant after 30 h. Boc-Ile-O-COOiBu was stable in *tert*-butanol at 23°C for 24 h. There were no signs of fulvene or FmOH in the nmr curve of Fmc-Val-O-COOiBu that had been kept at −5°C for 2 weeks.

The work-up procedure destroys methyl and ethyl chloroformates, therefore an excess of reagent was used to promote complete reaction of the substrate. Moreover, any contamination of the anhydride by the chloroformate is detectible by nmr, Table 1. Isobutyl chloroformate cannot be detected by the same method, and it is more stable to hydrolysis, so it was not used in excess.

Menthyl chloroformate reacted more slowly, but produced high yields of anhydrides from Boc-Ile-OH (89%) and Boc-Val-OH (96%) after 1 h at 23°C. The products were stable for at least 2 weeks. Pure anhydrides could not be obtained from methylsulfonylethyl chloroformate (see below).

Attempts to prepare the anhydrides of derivatives of the trifunctional amino acids met with varied success depending on the reactivity of the functional group on the side chain. Z-Asp(OBzl)-OH behaved normally (see below). Z-Gln-OH, after a 4-min reaction, gave a 60% yield of anhydride containing a small amount of oxazolone and some iBuOH. Z-Asn-OH gave a 10% yield of impure anhydride. Z-Tyr-OH gave no product, but coupled efficiently when the anhydride was not isolated (Table 2). Boc-Ser-OH gave a product that decomposed, probably by polymerization. Z-Asp-OH gave the internal anhydride in moderate yield.

The accompanying communication concluded that the tertiary amine/solvent combination has a marked effect on the mixed anhydride reaction, and that the poor performance of the Et_3N/dichloromethane combination was probably due to slow generation of the anhydride (4). To prove the latter, the rate of formation of anhydride in dichloromethane in the presence of various bases was examined by isolating the anhydride at appropriate times. The results are given in Fig. 1. It is seen indeed that in the presence of Et_3N, formation of anhydride was still incomplete after 30 min. In the presence of NMM or NMP, the maximum yield of anhydride had been attained within 2 min. With diisopropylethylamine as base, the yield after 2 min was nil. This explains why the product was exclusively urethane when diisopropylethylamine had been the base in a reaction (4). The results demonstrate why the amine/solvent combination is of critical importance. It has a marked effect on the rate at which the anhydride is generated.

Mixed anhydrides from dialkyl dicarbonates

The availability of *t*BuOCO-O-COO*t*Bu (9) and the intriguing possibility that it might provide entry to mixed anhydrides that were previously inaccessible because of the unavailability of *tert*-butyl chloroformate prompted an examination of the reaction of dialkyl dicarbonates with *N*-alkoxycarbonylamino acids. Diethyl dicarbonate did not react with Boc-Ile-OH in dichloromethane at 23°C (eq. [2]), but gave a high yield of mixed anhydride after 1 h at 23°C in the presence of one equivalent of NMP (eq. [3]). A 10% excess of reagent was used. The reagent is not destroyed by the work-up, but it is readily eliminated from the product under vacuum. $(t\text{BuOCO})_2O$ reacted more slowly with the carboxylate anion, but gave a 90% yield of anhydride after 3 h. In this case an excess of reagent could not be used because the reagent is not readily eliminated under vacuum. The same yield was obtained starting from Boc-Ile-OH.$\frac{1}{2}H_2O$. No reaction occurred between $(t\text{BuOCO})_2O$ and Boc-Ile-O-$^-$.$^+$HNMP at −5°C. Compounds **3** (R = $PhCH_2$,

[2]Abbreviations: Boc, *tert*-butoxycarbonyl; Bzl, benzyl; Fmc, 9-fluorenylmethoxycarbonyl; Mn, menthyl; Ms, methylsulfonylethyl; NMM, *N*-methylmorpholine; NMP, *N*-methylpiperidine; DMF, dimethylformamide; THF, tetrahydrofuran. Amino-acid symbols represent the L-isomer. A substituent in parentheses indicates side-chain substitution.

Can. J. Chem. Downloaded from www.nrcresearchpress.com by 80.58.250.72 on 09/07/12
For personal use only.

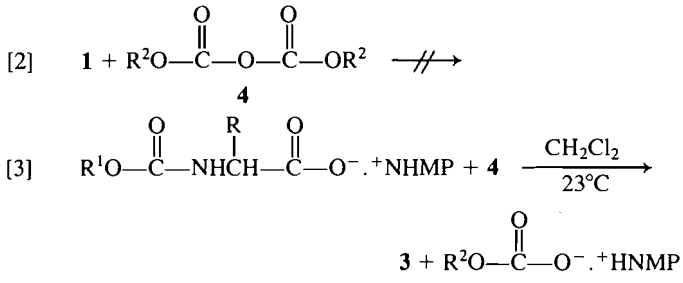

R^2 = Et, *t*Bu

iPr) obtained from **4** were demonstrated to be stereochemically pure. This approach using dialkyl dicarbonates, eq. [3], thus allows preparation of mixed anhydrides without cooling, provides an attractive alternative to the use of ethyl chloroformate, and allows access to the heretofore undescribed mixed anhydrides containing the *tert*-butyl carbonate moiety.

Mixed anhydrides using N*-ethoxycarbonyl-2-ethoxy-1,3-dihydroquinoline (EEDQ)*

EEDQ is a peptide-bond forming reagent recognized to effect coupling through the intermediate mixed anhydride (10). The feasibility of preparing mixed anhydrides using EEDQ was examined. The addition of EEDQ to one equivalent of Boc-Val-OH in dichloromethane gave, after 2 h at 23°C and subsequent work-up, a 95% yield of Boc-Val-O-COOEt, identical with that prepared using EtOCOCl. The use of *N*-alkoxycarbonyl-2-alkoxy-1,3-dihydroquinolines (10, 11) thus allows the preparation of mixed anhydrides without the addition of a tertiary amine. Our results also demonstrate unequivocally for the first time that the mechanism proposed for the action of these reagents (10) is correct.

*Decomposition of mixed anhydrides by cyclization to the 2-alkoxy-5(4*H*)-oxazolone*

An additional source of decomposition of the mixed anhydride is cyclization to the 2-alkoxy-5(4*H*)-oxazolone **5** accompanied by release of the alkoxy group of the carbonate moiety as the alcohol (eq. [4]). The rate of this reaction depends on the nature of the two alkyl groups R and R^1, and is higher for the unpurified anhydride. The amounts of oxazolone and alcohol originating from purified Boc-Phe-O-COOMe in $CDCl_3$ at 23°C were at their maxima at 60 min, after which the nmr spectrum became complex. A pure anhydride undergoes the same reaction, but the identifiable product is the ester **7**. After 3 weeks at −5°C, 20% of Z-Val-O-COOMe had been converted to Z-Val-OMe. The nmr spectrum showed no other peaks. Formation of ester is attributed to the reaction of the alcohol with the oxazolone (eq. [5]). The cyclization is promoted by

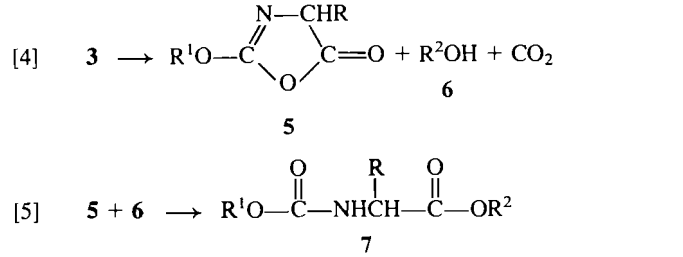

tertiary amines, iBuOH being visible in the nmr spectrum of Z-Val-O-COOiBu within 20 min of the addition of Et_3N. The spectrum of Fmc-Ile-O-COOiBu in the presence of Et_3N showed 5–10% of FmOH, but no fulvene, at 30 min.

With regard to the alkyl group of the carbonate moiety, the order of stability is menthyl ≫ methyl/ethyl/isobutyl ≫ methylsulfonylethyl. Half of a sample of Boc-Ile-O-COOMn in dichloromethane remained intact after 20 h at 23°C in the presence of Et_3N. Oxazolone accounted for most of the anhydride that had disappeared. On the other hand, Boc-Ile-O-COOMs could not be obtained free of oxazolone, giving more oxazolone than anhydride. The lesser tendency of anhydrides containing menthyl to cyclize to the oxazolone suggested that less racemization would accompany the coupling of peptide acids if activation were carried out using MnOCOCl instead of iBuOCOCl. The validity of this deduction has been confirmed (4). The reaction of cyclization of the mixed anhydride promoted by base is analogous to that of the cyclization of a symmetrical anhydride (12). Together with the *O*-acylisourea generated with *N*,*N*′-dialkylcarbodiimides (7), this is the third activated form of *N*-alkoxycarbonylamino acids that has been shown to give rise to 2-alkoxy-5(4*H*)-oxazolones.

*Attempted preparation of 2-alkoxy-5(4*H*)-oxazolones from mixed anhydrides containing the methylsulfonylethyl moiety*

A previous paper reported that the reaction of *N*-alkoxycarbonylamino acids with one equivalent of soluble *N*,*N*′-dialkylcarbodiimide produced the 2-alkoxy-5(4*H*)-oxazolone **5** as well as the expected symmetrical anhydride **8** (7). The amounts were substantial only for valine and isoleucine derivatives, and only for Boc-Val-OH and Z-Val-OH could the oxazolones be isolated pure. The ease with which 2-alkoxy-5(4*H*)-oxazolones were generated by the anhydrides containing the MsOCO- moiety prompted us to examine the possibility of using them as a source of pure oxazolones. We failed, because oxazolone is generated before complete consumption of the MsOCOCl and substrate. Liberated MsOH reacts with the oxazolone producing the ester, eq. [5], and probably with unconsumed MsOCOCl, since we isolated $(MsO)_2CO$, mp 114°C, in one instance. The oxazolones from leucine and phenylalanine derivatives are formed more rapidly and are more reactive than those from valine and isoleucine derivatives. They are readily hydrolyzed, the liberated R^1OCO-Xxx-OH reacting with oxazolone to produce symmetrical anhydride **8**. Manipulation of oxazolone and symmetrical anhydride mixtures enriched the solutions with anhydride at the expense of the oxazolone. We conclude that it will be difficult to obtain pure 2-alkoxy-5(4*H*)-oxazolones from derivatives other than those of valine and isoleucine because they are sensitive to moisture and react so quickly with the product of their hydrolysis.

Reaction of mixed anhydrides with carboxylic acids. The synthesis of symmetrical anhydrides

We have previously observed that scrambling occurs when an *N*-alkoxycarbonylamino acid is added to a symmetrical anhydride (unpublished). A solution of $(Boc\text{-}Val)_2O$ and Z-Val-OH in dichloromethane, after being washed with aqueous $NaHCO_3$, contained the $PhCH_2O$- group (nmr) presumably belonging to the unsymmetrical anhydride Boc-Val-O-Val-Z. We therefore examined the reaction of a mixed anhydride **3** with its parent acid **1**, entertaining the possibility that this might be a source for symmetrical anhydrides, eq. [6]. Z-Val-O-COOMe

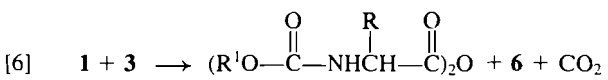

was left with 2 equiv. of Z-Val-OH in dichloromethane at 23°C for 20 h. After work-up, the neutral fraction contained $(Z\text{-}Val)_2O$, Z-Val-O-COOMe, and Z-Val-OMe in a ratio of 9:1:1. A similar result was obtained with Z-Val-O-COOiBu,

Can. J. Chem. Downloaded from www.nrcresearchpress.com by 80.58.250.72 on 09/07/12
For personal use only.

Can. J. Chem. Downloaded from www.nrcresearchpress.com by 80.58.250.72 on 09/07/12
For personal use only.

and Boc-Ile-O-COOiBu. The reaction does take place, but relatively slowly, and even more slowly with Boc-Xxx-anhydrides, and the liberated alcohol begins to esterify the parent acid before all of the anhydride has been consumed. Pure symmetrical anhydride was obtained in one case because of the fortuitous fact that it was the only one of the three products that precipitated out of light petroleum. The method therefore can be used to obtain symmetrical anhydrides; however, its efficiency depends on the ease with which the product can be separated from the ester and in some cases the starting mixed anhydride. An option for speeding up the reaction between the mixed anhydride and the parent acid is to use the carboxylate anion instead of the carboxylic acid. However, this implies the presence of a tertiary amine, which promotes cyclization of the mixed anhydride to the oxazolone (eq. [4]) thus complicating the issue further.

Decomposition of mixed anhydrides by disproportionation

Any discussion on mixed anhydrides mentions that they should be handled quickly at low temperature to avoid disproportionation to the symmetrical anhydride and the dialkyl dicarbonate, eq. [9] (2). The fate of Boc-Ile-O-COOiBu was examined by leaving a sample in dichloromethane at −5°C for 24 h. Methylamine in anhydrous ether was added and, after an hour, the Boc-Ile-O^-.$^+H_3NCH_3$ that had precipitated was collected by filtration. The yield corresponded to <1%. On the basis that the reaction of $(Boc\text{-}Ile)_2O$ with CH_3NH_2 liberates 1 equiv. of the salt, the result showed that <1% of disproportionation had occurred. A control experiment indicated that a 1% contamination could indeed be detected by this method. In a second experiment, Boc-Ile-O-COOMe was left in $CDCl_3$ at 23°C for 16 h. Inspection of the nmr spectrum revealed that the solution contained the substrate, the 2-alkoxy-5(4*H*)-oxazolone, $(Boc\text{-}Ile)_2O$, and Boc-Ile-OMe in the proportions of 21:52:23:4. In addition to the substrate and ester, the methoxy moiety was present as MeOH (53%) and MeOCO- (12%, δ = 3.77 ppm) of unestablished identity. These results are not compatible with the notion that a pure mixed anhydride undergoes simple disproportionation, eq. [9]. One could argue that if a mixed anhydride has not been purified, decomposition could be initiated by attack of a carboxylate anion, eq. [7], which in effect would result in disproportionation, eqs. [7]–[9].

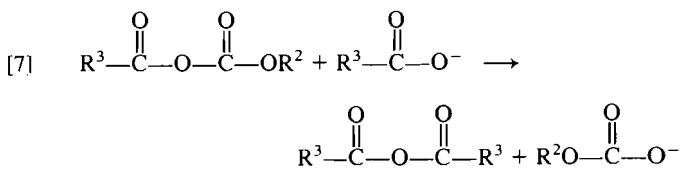

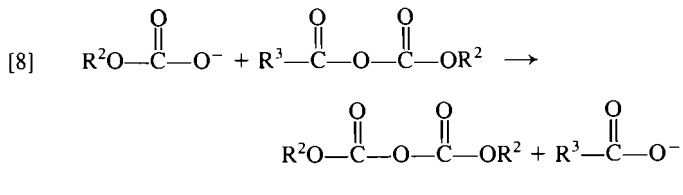

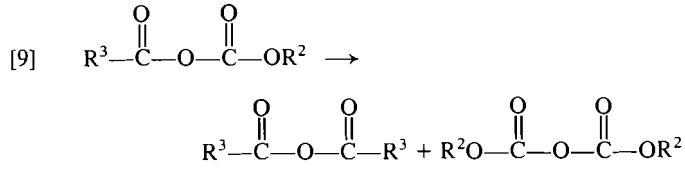

$R^3 = R^1OCO—NHCHR—$

However, we have shown above that in the presence of the tertiary amine required to initiate reaction [7], 2-alkoxy-5(4*H*)-oxazolone **5** is formed. Moreover, this oxazolone reacts quickly with the parent acid or acid anion to give symmetrical anhydride **8**. In fact, the addition of 5% of Boc-Ile-O^-.$^+$HNMP to Boc-Ile-O-COOMe in $CDCl_3$ resulted in the immediate release of MeOH (5%), with MeOH being formed continuously thereafter. We conclude that a mixed anhydride by itself does not undergo disproportionation upon storage at low temperature, and that what obtains when decomposition occurs is not disproportionation as commonly written, eq. [9], but a series of reactions subsequent to the initial cyclization to oxazolone **5**.

Aminolysis of mixed anhydrides at the carbonate moiety. Urethane formation

The major side reaction attending the coupling of *N*-alkoxycarbonylamino acids by the mixed anhydride method is the formation of urethane resulting from aminolysis at the carbonate moiety and (or) aminolysis of unconsumed alkyl chloroformate (2, 3, 14). The availability of isolated anhydrides allowed for the first time a study of the factors implicated in urethane formation by aminolysis at the carbonate moiety of the anhydride, eq. [10], without the uncertainty that some of the

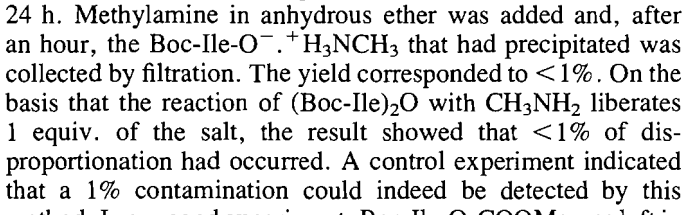

$R^3 = R^1OCO—NHCHR—$

product might have originated from aminolysis of unconsumed chloroformate. The amounts of peptide **9** and urethane **10** produced from various anhydrides by the same amino acid ester under various conditions are given in Tables 2–4. Products were determined by high performance liquid chromatography (4) (hplc). Some of the results are expressed also as the ratio of the amount of urethane over the amounts of the two products. It is seen in Table 2 that the presence of NMP.HCl resulting from the use of the amino acid ester hydrochloride instead of the amino acid ester had a small positive or no effect on the generation of urethane in dichloromethane. Since it made little difference and was more convenient, all other experiments were carried out using H-Lys(Z)-OMe.HCl neutralized with NMP as the nucleophile. Dichloromethane was used as the test solvent because of its superior performance. The nature of the *N*-protector had a marked effect on the amount of urethane, benzyloxycarbonyl leading to 3–4 times as much as Boc- with Fmc- being intermediate. For the same alkyl group R^2, isoleucyl generated 12–14 times as much as leucyl. It is significant that the value for leucyl was not zero (see below).

The influence of the alkyl group R^2 of the carbonate moiety is given in Table 3. Ethyl led to slightly more urethane than isobutyl, which agrees with the generally held notion that attack at the carbonyl group is hindered by the latter. *tert*-Butyl led to three times as much as ethyl, which is inconsistent with this notion, and also contrary to what might be expected on the basis of the electron-donating property of methyl groups. Generation of urethane therefore cannot be rationalized on the basis of the size and electronic nature of the alkyl group. Methylsulfonylethyl was intermediate between the two butyl groups, and menthyl led to five times as much urethane as was obtained

TABLE 2. Influence of various parameters on the amount of urethane **10** produced by the aminolysis of a mixed anhydride[a]

Anhydride	*N*-Methylpiperidine.HCl		
	Absent[b]	Present[c]	Present[c,d]
Boc-Leu-O-COOiBu	0.13	0.17	0.17
Boc-Ile-O-COOiBu	1.8	2.1 (81)	2.5 (87)
Fmc-Ile-O-COOiBu		3.5±0.5[e]	
Z-Ile-O-COOiBu	7.0	6.9[f]	
Z-Tyr-O-COOiBu			0.15 (75)
Z-Gly-Pro-O-COOiBu		0.6 (77)	
Boc-Ile-O-COCCMe$_3$		10.3[g] (80)	12.2[g,h] (78)

[a]Yield (%) of iBuOCO-Lys(Z)-OMe produced in dichloromethane at −5°C. ( ) yield of peptide.
[b]H-Lys(Z)-OMe used as the nucleophile.
[c]H-Lys(Z)-OMe.HCl neutralized with NMP used as the nucleophile.
[d]Anhydride not isolated. Conventional mixed anhydride reaction, with an activation time of 90 s.
[e]A second unknown product was also formed.
[f]Mean of three experiments. Values differed by <0.5%.
[g]Yield (%) of Me$_3$CCO-Lys(Z)-OMe.
[h]Activation time of 2 h.

TABLE 3. Influence of the alkyl group R^2 on the chemoselectivity of the aminolysis of Boc-Ile-O-COOR^2

R^2	Peptide (% yield)	Urethane (% yield)	(100×%U)/(%P+%U)
Isobutyl	81	2.1	2.5
Ethyl	82	2.8	3.3
Methyl-SO$_2$-ethyl	73	4.4	5.6
tert-Butyl	80	7.0	8.1
Menthyl	55	11	16

[a]Aminolysis by H-Lys(Z)-OMe.HCl neutralized with NMP in dichloromethane at −5°C. P = peptide = Boc-Ile-Lys(Z)-OMe. U = urethane = R^{2}OCO-Lys(Z)-OMe.

from the commonly used chloroformates. This seemingly undesirable feature of the menthyl-containing anhydrides must be taken into consideration when MnOCOCl is substituted for iBuOCOCl for mixed anhydride reactions to minimize racemization (4). However, it should be considered in the proper context, that the activated moiety is a peptide acid that generates less urethane than an activated *N*-alkoxycarbonyl-amino acid.

The influence of temperature and the nature of the solvent are shown in Table 4. The solvents are listed in the order of increasing ratios, which corresponds roughly with the increase in the polarity of the solvents. The halogen-containing solvents and toluene gave the lowest ratios, but the yields of peptide in CCl_4 and $CHCl_3$ were significantly lower. The best compromise as solvent is therefore dichloromethane or toluene. Toluene has been recommended in the past, but dichloromethane has been considered an undesirable solvent for mixed anhydride reactions (2). Tetrahydrofuran performed surprisingly poorly in this test, probably in part because of the insolubility of the NMP.HCl. Diminution of the temperature from −5°C to −20°C reduced the amount of urethane formed in the halogen-containing solvents by 38–48%, but had no effect on the amount in DMF, though more was generated in DMF at 23°C. Use of low temperatures as traditionally recommended (2, 3) therefore minimizes the amount of urethane formed by aminolysis at the carbonate moiety.

Impurities in alkyl chloroformates as a minor source of urethane

In carrying out the experiments described in Table 1, it was found impossible to obtain reproducible results for the small amount of urethane generated from Boc-Leu-O-COOiBu/OEt until the chloroformates had been freshly distilled. Yields ranging from 0.25 to 1.1% were obtained. A second alkoxy peak was visible in the nmr spectra of some samples of MeOCOCl and EtOCOCl. The residue after distilling MeOCOCl was enriched in impurity, which did not react with dimethylamino-propylamine. We conclude it was dimethyl carbonate (see Table 1). EtOCOCl was enriched in impurity after being washed with aqueous acid and $NaHCO_3$. The impurity disappeared in 1 min when dimethylaminopropylamine was added, which coincided with the behavior of $(EtOCO)_2O$. The latter is more resistant to hydrolysis than is EtOCOCl. We conclude that the impurity in old samples of EtOCOCl is $(EtOCO)_2O$, which arises from the reaction of EtOCOCl with EtOCOOH that originates from the hydrolysis of EtOCOCl. It is our experience that chloroformates stored at +5°C are stable for at least one month.

Mixed anhydrides from pivaloyl chloride

An alternative to activation of an *N*-alkoxycarbonylamino acid as the anhydride R^{1}OCO-Xxx-O-COOR^2 is activation as the mixed carboxylic–carboxylic anhydride R^{1}OCO-Xxx-O-COCMe$_3$ formed by its reaction with Me$_3$CCOCl (15). These anhydrides are more reactive, and their aminolysis is considered to be more chemoselective for the -COCMe$_3$ moiety. The preparation and aminolysis of Boc-Ile-O-COCMe$_3$ (COC(CH_3)$_3$, nmr, δ = 1.28 ppm) were examined. It was found that the reaction of Boc-Ile-OH with Me$_3$CCOCl in dichloromethane at −5°C was still incomplete after 30 min. The pure anhydride was eventually obtained in 60% yield based on the amount of acid chloride by the use of an excess of Boc-Ile-OH and a reaction time of 2 h. The amounts of peptide and pivaloyl derivative generated by aminolysis of the anhydride are given in Table 2. The amount of undesired aminolysis product (10.3%) was much greater than that produced by Boc-Ile-O-COOiBu, and slightly less than that generated when the anhydride had not been isolated. We conclude that aminolysis of anhydrides containing the pivaloyl moiety is less chemoselective than aminolysis of mixed carboxylic–carbonic acid anhydrides.

Mixed anhydrides for synthetic purposes

As an example of the value of isolated mixed anhydrides for synthetic purposes, we chose the preparation of Z-Asp(OBzl)-NH$_2$, the immediate precursor of isoasparagine in a synthesis published by one of us (16). It had been brought to our attention that the method, involving coupling of Z-Asp(OBzl)-OH with ammonia via the mixed anhydride, occasionally gave erratic results. Z-Asp(OBzl)-O-COOEt was obtained in 90% yield using a 20% excess of EtOCOCl as described above. Ammonia dissolved in dichloromethane was added to the ester at −5°C. The ammonia solution had been prepared by extracting ammonium hydroxide with dichloromethane at −5°C, and adding $MgSO_4$. Filtration, evaporation of the solvent, and collection of the residue with the aid of ethyl acetate – light petroleum gave Z-Asp(OBzl)-NH$_2$ (two crops, 82%) with the appropriate nmr spectrum and the same mp as reported (16). With respect to their use for synthetic purposes, we do not suggest that isolated anhydrides are to be preferred in all cases, but the possibility that their use might prove advantageous should be kept in mind.

Miscellaneous

When the substrate in eq. [1] was an acylamino or a peptide

Can. J. Chem. Downloaded from www.nrcresearchpress.com by 80.58.250.72 on 09/07/12
For personal use only.

TABLE 4. Effect of the solvent and the temperature on the chemoselectivity of the aminolysis of Boc-Ile-O-COOiBu[a]

Solvent	Peptide (% yield)		Urethane (% yield)		(100×%U)/(%P+%U)	
	−20°C	−5°C	−20°C	−5°C	−20°C	−5°C
CCl_4	51.6	71.3	0.80	1.3	1.53	1.79
$CHCl_3$	57.5	64.5	0.98	1.5	1.68	2.24
CH_2Cl_2	72.9	81.0	1.1	2.1	1.49	2.53
$PhCH_3$		87.4		2.3		2.56
DMF–CH_2Cl_2 (1:4)		83.0		3.7		4.27
THF		68.3		3.2		4.49
$CH_3CO_2C_2H_5$		65.0		3.6		5.24
DMF	66.0	75.7	4.2	4.3	6.0	5.38
	77.0[b]		9.2[b]		10.6[b]	
CH_3CN–DMF (1:2)		67.2		3.8		5.35
CH_3CN–DMF (2:1)		73		4.3		5.56
$(CH_3)_3COH$–CH_2Cl_2 (40:1)	71[b]		10[b]		12.3[b]	
CH_3CN		58.3		12.7		17.9
$(CH_3)_2CHOH$		27.8		5.7		17.0
$(CH_3)_2SO$	45[b]		11.7[b]		20.7[b]	

[a]Aminolysis by H-Lys(Z)-OMe.HCl neutralized with NMP. P = peptide = Boc-Ile-Lys(Z)-OMe. U = urethane = iBuOCO-Lys(Z)-OMe.
[b]+23°C.

acid (**1**, R^1CO instead of R^1OCO), the neutral fraction after work-up contained no mixed anhydride except when the activated residue was prolyl. The major product isolated from the reactions was the 2-alkyl-5(4*H*)-oxazolone. Details will be presented in another publication. Z-Gly-Pro-O-COOiBu (Table 2) was obtained in the same yield as the anhydrides **3**. Aminolysis of this anhydride with H-Lys(Z)-OMe.HCl/NMP gave a 77% yield of peptide, 0.6% of iBuOCO-Lys(Z)-OMe, and 5% of a third unidentified product. No racemization (<0.05%; hplc as in ref. 4) accompanied the coupling. When the substrate in eq. [1] was Boc-MeVal-OH, the products were the mixed anhydride and *N*-methylvaline *N*-carboxyanhydride in a 5:1 ratio. We intend to do further work on anhydrides of this type of substrate.

Experimental

General

Tertiary amines, alkyl chloroformates, dialkyl dicarbonates, and pivaloyl chloride (Aldrich products) were purchased from Terochem Laboratories, Edmonton, except for methylsulfonylethyl chloroformate, which was a gift from Dr. G. I. Tesser (13). Menthyl chloroformate was the *levo* isomer. Solvents (Fisher Scientific) were dried (4) and distilled. Amino acid derivatives were purchased from Sigma Chemical Company. Proton nmr spectra were determined in deuterochloroform using a Varian EM-360 60-MHz instrument. With one exception, no attempt was made to secure elemental analyses for the anhydrides since it is our experience that such activated forms of amino acids are too unstable to send through the mails. The presence of contaminants in the mixed anhydrides and chloroformates and the composition of mixtures resulting from their decomposition were established by comparing the intensities and chemical shifts of the appropriate signals in the nmr spectra with those of reference compounds (Table 1). Products from the aminolysis of mixed anhydrides were determined by reversed phase hplc after washing the mixture with aqueous solutions as described in the accompanying paper (4). Me_3CCO-Lys(Z)-OMe (oil, 45% yield) was obtained by reaction of Me_3CCOCl with H-Lys(Z)-OMe.HCl/NMP in dichloromethane at 23°C for 1 h. The mixture was washed many times with aqueous solutions before removing the solvent. The absorbance of the compound at 215 nm (hplc) was 80% of that of Boc-Ile-Lys(Z)-OMe.

Preparation of mixed anhydrides 3

To acid **1** (1 mmol) and NMP or NMM (0.95 equiv.) in 10 mL of dichloromethane at −5°C was added chloroformate **2** (1.1 equiv. for R^2 = Me, Et; 1.0 equiv. otherwise), and the mixture was left at −5°C for 20 min (23°C for 1 h for R^2 = Mn). The solution was washed with cold dilute citric acid, aqueous $NaHCO_3$, and water, and the solvent was dried ($MgSO_4$) and removed at room temperature with a rotary evaporator. Z-DL-Ala-O-COOEt, mp 50–52°C. *Anal.* calcd. for $C_{14}H_{17}NO_6$: C 56.94, H 5.08, N 4.74; found: C 56.68, H 5.56, N 4.84.

In the alternative procedure, dialkyl dicarbonate **4** (1.1 equiv. for R^2 = Et, 1.0 equiv. for R^2 = *t*Bu) was added to a mixture of acid **1** (1 mmol) and NMP or NMM (1 mmol) in dichloromethane and the solution was left at room temperature for 1 h for R^2 = Et and 3 h for R^2 = *t*Bu.

Acknowledgements

We are grateful to the Medical Research Council of Canada for financial support of this research, to Dr. G. I. Tesser for the gift of methylsulfonylethyl chloroformate, to Mr. Hector Seguin of the National Research Council for the elemental analyses, and to Mrs. Y. Lee for the data in Table 3. N.L.B. is a Career Investigator of the M.R.C.C.

1. R. A. BOISSONNAS. Helv. Chim. Acta, **34**, 874 (1951); J. R. VAUGHAN. J. Am. Chem. Soc. **73**, 3547 (1951); J. R. VAUGHAN and R. L. OSATA. J. Am. Chem. Soc. **74**, 676 (1952); T. WIELAND and H. BERNHARDT. Justus Liebigs Ann. Chem. **572**, 190 (1951); N. F. ALBERTSON. Org. React. (N.Y.), **12**, 157 (1962); D. S. TARBELL. Acc. Chem. Res. **2**, 296 (1969).
2. J. MEIENHOFER. *In* The peptides. Vol. 1. *Edited by* E. Gross and J. Meienhofer. Academic Press, New York. 1979. p. 263.
3. G. W. ANDERSON, J. E. ZIMMERMAN, and F. M. CALLAHAN. J. Am. Chem. Soc. **89**, 5012 (1967); G. W. ANDERSON. *In* The peptides: chemistry and biology. *Edited by* B. Weinstein and S. Lande. Marcel Dekker, New York. 1970. p. 255.
4. F. M. F. CHEN, Y. LEE, R. STEINAUER, and N. L. BENOITON. Can. J. Chem. **65**, 613 (1987).
5. F. M. F. CHEN, K. KURODA, and N. L. BENOITON. Synthesis, 928 (1978); 232 (1979).

Can. J. Chem. Downloaded from www.nrcresearchpress.com by 80.58.250.72 on 09/07/12
For personal use only.

6. F. M. F. CHEN, R. STEINAUER, and N. L. BENOITON. *In* Peptides 1984. *Edited by* U. Ragnarsson. Almqvist and Wiksell Int., Stockholm. 1984. p. 105.
7. N. L. BENOITON and F. M. F. CHEN. Can. J. Chem. **59**, 384 (1981).
8. F. H. AHMED, F. M. F. CHEN, and N. L. BENOITON. Can. J. Chem. **64**, 1396 (1986).
9. L. MORODER, A. HALLETT, E. WÜNSCH, O. KELLER, and G. WERSIN. Hoppe-Seyler's Z. Physiol. Chem. **357**, 1651 (1976).
10. B. BELLEAU and G. MALEK. J. Am. Chem. Soc. **90**, 1651 (1968).
11. Y. KISO and H. YAJIMA. J. Chem. Soc. Chem. Commun. 942 (1972).
12. N. L. BENOITON and F. M. F. CHEN. J. Chem. Soc. Chem. Commun. 1225 (1981).
13. G. I. TESSER and I. C. BALVERT-GEERS. Int. J. Pept. Protein Res. **7**, 295 (1975).
14. M. BODANSZKY and M. TOLLE. Int. J. Pept. Protein Res. **10**, 380 (1977).
15. M. ZAORAL. Collect. Czech. Chem. Commun. **27**, 5439 (1962).
16. L. BENOITON. Can. J. Chem. **40**, 570 (1962).

Can. J. Chem. Downloaded from www.nrcresearchpress.com by 80.58.250.72 on 09/07/12
For personal use only.

Synthesis and properties of phenyl substituted derivatives of 2-phenyl-1,1,3,3-tetramethylguanidine

PRZEMYSLAW PRUSZYNSKI
Department of Chemistry, Adam Mickiewicz University, 60-780 Poznan, Poland

Received July 31, 1986

PRZEMYSLAW PRUSZYNSKI. Can. J. Chem. **65**, 626 (1987).

A series of 17 phenyl substituted derivatives of 2-phenyl-1,1,3,3-tetramethylguanidine was synthesized. The structure and purity of these compounds were checked by means of elemental analyses, mass spectrometry, ultraviolet spectrophotometry, and ^{1}H nuclear magnetic resonance. The pK_a values were determined and are discussed in terms of substituent effects using Hammett substituent constants. The Hammett reaction constant $\rho = 1.84 \pm 0.05$ was found to be much lower for *para* and *meta* substituted compounds than for anilines, even though the phenyl ring is attached directly to the basic centre in both cases.

PRZEMYSLAW PRUSZYNSKI. Can. J. Chem. **65**, 626 (1987).

On a synthétisé une série de 17 phényl-2 tétraméthyl-1,1,3,3 guanidines substituées par des groupements phényles. On a vérifié la structure et la pureté de ces composés à l'aide d'analyses élémentaires, de spectrométrie de masse, de spectrophotométrie ultraviolette et de résonance magnétique nucléaire de ^{1}H. On a déterminé les valeurs des pK_a et on en discute en fonction des effets de substituants en faisant appel aux constantes de Hammett pour les substituants. On a déterminé que la constante de réaction de Hammett, $\rho = 1{,}84 \pm 0{,}05$, pour les composés substitués en positions *méta* et *para* est beaucoup plus faible que pour les anilines, même si, dans chaque cas, le groupement phényle est attaché directement au centre basique.

[Traduit par la revue]

Introduction

In most kinetic studies the opportunity of using series of closely related compounds is of great importance. The series of phenyl substituted derivatives of 2-phenyl-1,1,3,3-tetramethylguanidine (**1**) may be very useful when strong bases are

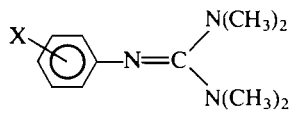

1

required. There are several papers concerned with the influence of substituent effects on the strength of guanidine bases, but they are generally concerned with substitution on one of the terminal nitrogen atoms and with alkyl substituents (1–6).

The relation between the observed pK_a values and Taft's substituent constants σ^* was found to be $pK_a = 14.0 - 3.60\sigma^*$ (1). There is no relationship present in the literature concerned with the influence of a substituent on a benzene ring that is attached to the nitrogen in a guanidine base. Values of $pK_a = 10.8$ for 1-phenyl-guanidine (2) together with $pK_a = 10.6$ for 1-(4-chlorophenyl)-guanidine (3) may give some rough idea about the sensitivity of base strength to the substituent present in the molecule. It seemed worthwhile to check the wider relationship for the case of phenyl ring attached to the nitrogen atom that undergoes protonation. Compounds presented in this paper, except for 2-phenyl-1,1,3,3-tetramethylguanidine and 2-(4′-methylphenyl)-1,1,3,3-tetramethylguanidine previously synthesized by Bredereck and Bredereck (7), have not been reported in the literature. They have been synthesized for use as bases in kinetic studies of proton transfer reactions from carbon acids. The kinetic results will be presented elsewhere.

This work gives a general procedure of synthesis, and the properties of a series of new bases. The method of Bredereck (7) is applied with some modifications. This method is based on the condensation reaction of 1,1,3,3-tetramethylurea with an appropriate aniline derivative in the presence of $POCl_3$, eq. [1], and makes it possible to synthesize various compounds by changing the aniline derivative used for synthesis.

[1]

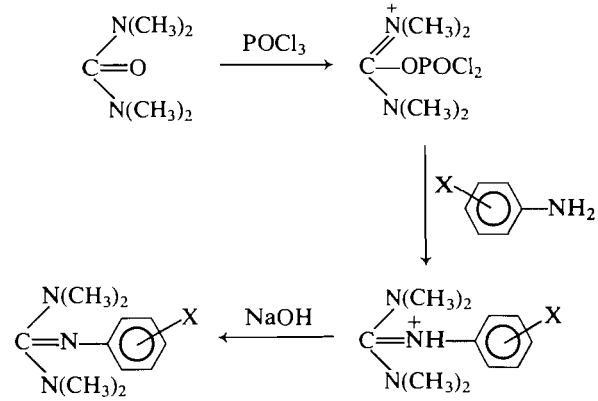

Results and discussion

The pK_a values of the synthesized compounds together with the value for unsubstituted 2-phenyl-1,1,3,3-tetramethylguanidine are presented in Table 1, which also gives the literature values of the pK_a of the corresponding anilines and the values of Hammett's substituent constants.

Figure 1 shows a plot of the measured values of pK_a of *meta* and *para* substituted 2-phenyl-1,1,3,3-tetramethylguanidines (2-Ph-TMG) against the Hammett's $\sigma_{m,p}$ values.

The relation shown in Fig. 1 is described by eq. [2]:

[2] $$pK_{a\,\text{2-Ph-TMG}} = (12.12 \pm 0.02) - (1.84 \pm 0.05)^*\sigma_{m,p}$$

with a correlation coefficient 0.997. This equation gives the Hammett reaction constant $\rho = 1.84 \pm 0.05$. The equation for the dissociation reaction of anilinium ions is $pK_{a\,\text{aniline}} = 4.58 - 2.88\sigma$ (9). When anilines with the same substituents as reported for 2-phenyl-1,1,3,3-tetramethylguanidines are taken into account, eq. [3] is obtained, with correlation coefficient 0.998:

[3] $$pK_{a\,\text{aniline}} = (4.59 \pm 0.03) - (2.85 \pm 0.06)^*\sigma_{p,m}$$

In both correlations the special value of $\sigma = 1.26$ for the *p*-NO_2

Can. J. Chem. Downloaded from www.nrcresearchpress.com by 80.58.250.72 on 09/07/12
For personal use only.

TABLE 1. The pK_a values for 2-phenyl-1,1,3,3-tetramethylguanidines and the corresponding aniline derivative

Base no.	Substituent	$\sigma_{m,p}$[a]	pK_a 2-Ph-TMG	pK_a aniline[b]
—[c]	H	0	12.18+0.02	4.62
1	2-CH_3	—	12.28+0.03	4.42
2	3-CH_3	−0.06	12.25+0.04	4.70
3	4-CH_3	−0.14	12.37+0.01	5.11
4[c]	2,4-diCH_3	—	12.50+0.03	4.89
5	2-OCH_3	—	12.19+0.04	4.52
6	3-OCH_3	0.11	11.96+0.04	4.23
7	4-OCH_3	−0.28	12.57+0.03	5.34
8	2,4-diOCH_3	—	12.54+0.04	—
9	2-Cl	—	11.16+0.10	2.64
10	3-Cl	0.37	11.47+0.09	3.52
11	4-Cl	0.24	11.70+0.02	3.98
12	2,4-diCl	—	10.46+0.23[d]	2.00
13	2,5-diCl	—	10.14+0.25[d]	1.57[e]
14	2-Br	—	10.97+0.04	2.53
15	3-Br	0.39	11.47+0.10	3.58
16	4-Br	0.22	11.60+0.10	3.86
17	4-NO_2	1.26	9.78+0.09[f]	0.99

[a]From ref. 1.
[b]From ref. 8.
[c]Previously synthesized by Bredereck (7).
[d]In dilute NaOH solution.
[e]At 22°C.
[f]In Na_2CO_3–$NaHCO_3$ buffer.

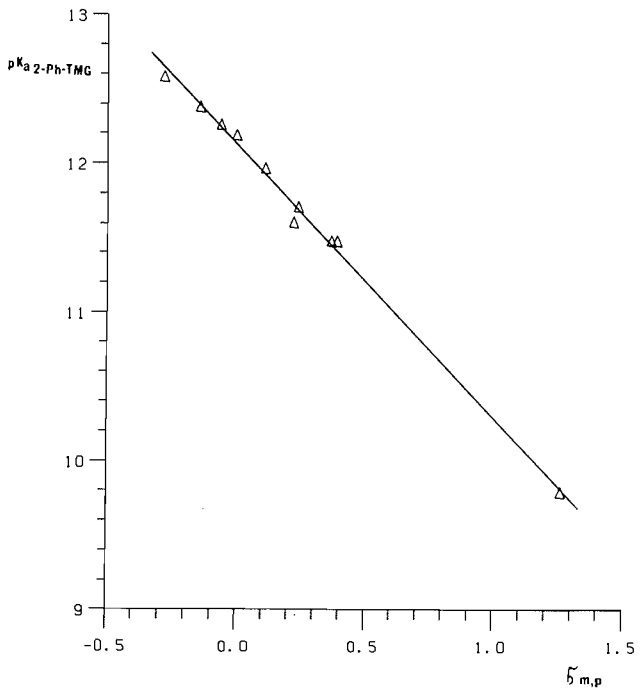

FIG. 1. The plot of the relation of pK_a of *meta* and *para* substituted derivatives of 2-phenyl-1,1,3,3-tetramethylguanidine (2-Ph-TMG) and Hammett $\sigma_{m,p}$ constants.

substituent, reported by Perrin *et al.* (1) as the best for anilines, was used. This value provides a good fit of experimental data for both series of compounds. This proves that the -N=C[$N(CH_3)_2$]$_2$ substituent is a group capable of strong resonance electron donation to the phenyl ring. It can undergo resonance interaction with the *p*-NO_2 group stabilizing the

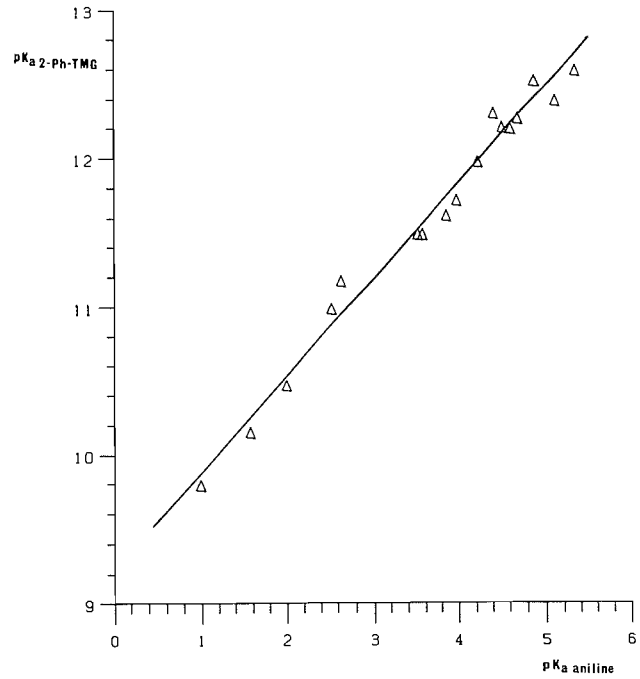

FIG. 2. The plot of pK_a of 2-phenyl-1,1,3,3-tetramethylguanidines (2-Ph-TMG) against pK_a of the corresponding anilines.

unprotonated form, which is reflected in much lower pK_a value (Table 1). This strong mesomeric interaction may be explained by the unique possibility of the -N=C[$N(CH_3)_2$]$_2$ group spreading the positive charge over all three nitrogens. According to our ^{35}Cl nqr measurements (10) this group can donate electrons mesomerically stronger than the -NH_2 group. This observation agrees with the larger bathochromic shift of the uv peak observed in the case of 2-(4-nitrophenyl)-1,1,3,3-tetramethylguanidine (λ_{max} = 400 nm) than in the case of *p*-nitroaniline (λ_{max} = 381 nm). Nevertheless the same values of σ for the *p*-NO_2 substituent show good correlations with pK_a values for anilines and 2-phenyl-1,1,3,3-tetramethylguanidines.

Equations [2] and [3] demonstrate that the base strength of aniline is more sensitive to the presence of a particular substituent than that of guanidine compounds. Figure 2 presents the relation between the pK_a value of the derivatives of aniline and the pK_a value found for the corresponding 2-phenyl-1,1,3,3-tetramethylguanidines.

Equation [4] presents the relationship between the pK_a values of anilines and appropriate derivatives of 2-phenyl-1,1,3,3-tetramethylguanidine:

$$[4]\quad pK_{a\,\text{2-Ph-TMG}} = (9.21 \pm 0.09) + (0.65 \pm 0.02) * pK_{a\,\text{aniline}}$$

with correlation coefficient 0.998.

In both cases the phenyl ring is attached directly to the nitrogen atom being protonated and the value of ρ = 2.85 for anilines is typical for such compounds. The ρ = 1.84 for guanidine derivatives indicates much lower sensitivity of their strength to the nature and position of substituent on the phenyl ring. This observation may be reasonably explained by taking into account, as mentioned above, general behaviour of the guanidines, e.g., resonance delocalization of the positive charge of their cation over three nitrogen atoms. The resonance effect causes properties of both free base and its conjugate base to be less sensitive to the substituent effect. The electron-

Can. J. Chem. Downloaded from www.nrcresearchpress.com by 80.58.250.72 on 09/07/12
For personal use only.

withdrawing substituents, for example, destabilize the anilinium cation to a higher extent than they do in the case of 2-phenyl-1,1,3,3-tetramethylguanidinium cations, which bear a significant part of the positive charge on two nitrogens that are three bonds away from the benzene ring.

It is also interesting (Table 1) that a methyl group in the *ortho* position to the amino group in aniline causes a decrease of the strength of *o*-toluidine when compared to aniline (pK_a 4.42 and 4.62 respectively). In the case of guanidine derivatives this substitution leads to a small increase of the pK_a value (12.18 for the unsubstituted compound and 12.28 for 2-methyl substituted, Table 1). According to our ^{35}Cl nqr measurements (10) there is steric interaction between the *ortho* substituent and $-N{=}C[N(CH_3)_2]_2$ substituent. This interaction must lead to an increase in the energy of the unprotonated form of the base. There is a change of the hybridization of nitrogen during protonation, which allows reduced interaction of both substituents. This effect would give additional stabilization to the protonated form, leading to an increase in pK_a value.

These studies, concerned with synthesis and properties of further phenyl substituted derivatives of 2-phenyl-1,1,3,3-tetramethylguanidines, are being continued.

Experimental

The synthetic procedure was common for all compounds synthesized: a solution of 0.1 mol of 1,1,3,3-tetramethylurea (TMU, dried over molecular sieve 4A) in 100 mL of dry benzene was treated dropwise with a solution of 0.2 mol of $POCl_3$ in 20 mL of dry benzene. The reaction mixture was stirred for 1–2 h at a temperature not exceeding 25°C and left overnight at room temperature. A solution of 0.15 mol of the appropriate derivative of aniline in 50 mL of benzene was added and the reaction mixture was then stirred for 7 h at 70°C. The lower oily phase was then separated and washed several times with benzene. The pH was fixed at 7–9 with 2 *M* NaOH and the extraction with benzene was repeated. The aqueous phase was then made strongly alkaline (pH > 14) and the 2-phenyl-tetramethylguanidine derivative was extracted with benzene. These benzene extracts were collected and dried over anhydrous sodium sulphate, and the benzene was then evaporated. Usually the crude product was fractionally distilled under reduced pressure unless it solidified after removal of benzene, in which case it was recrystallized from cyclohexane. The amounts of $POCl_3$ and aniline derivative used were larger than reported by Bredereck (7). The introduction of an additional extraction at pH 7–9 allowed for easy separation of product from the unreacted aniline. An excess of $POCl_3$ and aniline increased the yield of reaction calculated against the amount of TMU used.

The picrates were obtained by mixing equimolar amounts of 2-phenyl-1,1,3,3-tetramethylguanidine derivative and picric acid in 95% ethanol. This mixture was refluxed for 15 min, cooled to room temperature, and poured into a threefold excess of water. The fine yellow crystals obtained were then recrystallized from 95% ethanol.

Melting points were measured using a Boetius apparatus and were uncorrected. The ^1H nmr spectra were obtained using a Varian EM-360 spectrometer with TMS as internal reference in $CDCl_3$. The mass spectra were recorded on a JEOL JMS D-100 spectrometer. Elemental analyses were obtained on a Perkin–Elmer 240 apparatus. In the case of oily products only very freshly distilled samples showed satisfactory results; increasing water content was observed after some time. The uv measurements were performed with a Specord M-40 spectrophotometer equipped with a thermostatic device. The pK_a measurements were done spectrophotometrically in water at 25°C and at ionic strength 0.1 mol dm^{-3} maintained by addition of KCl. Measurements were performed using NaOH solution for all compounds excepting the *p*-NO_2 derivative, where Na_2CO_3–$NaHCO_3$ buffer was used. The procedure was identical to that described by Hibbert (11) for 1,8-bis(dimethylamino)naphthalene, a base of comparable strength. The pK_a values for dichlorosubstituted compounds had to be measured in very dilute NaOH solution. This was the reason for bigger scatter of results for these two bases than in the case of other compounds. More individual measurements were done in these cases. The mean value is probably more accurate than the standard deviations show.

*2-(2'-Methylphenyl)-1,1,3,3-tetramethylguanidine (**1**)*

Yield 50%; bp 200°C/22 Torr (1 Torr = 133.3 Pa); uv, λ_{max}, nm (ε, dm^3 mol^{-1} cm^{-1}): free amine B 258.8 (10 640); protonated amine BH^+ 235.1 (14 750); ^1H nmr δ: 7.00–5.83 (m, 4H), 2.55 (s, 12H), 2.10 (s, 3H); mass spectrum, *m/e* (rel. intensity, %): 205 (93), 190 (46), 161 (60), 44 (100). *Anal.* calcd. for $C_{12}H_{19}N_3$: C 70.20, H 9.33, N 20.47; found: C 69.93, H 9.38, N 20.33. Picrate: mp 131.5–132.5°C; uv, λ_{max} (ε): 358.4 (15 600).

*2-(3'-Methylphenyl)-1,1,3,3-tetramethylguanidine (**2**)*

Yield 56%; bp 175°C/15 Torr; uv, λ_{max} (ε): B 270.7 (14 600), BH^+ 236.9 (16 400); ^1H nmr δ: 7.17–6.38 (m, 4H), 2.58 (s, 12H), 2.23 (s, 3H); mass spectrum, *m/e* (rel. intensity, %): 205 (45), 190 (13), 161 (100). *Anal.* calcd. as for **1**; found: C 70.03, H 9.30, N 20.21. Picrate: mp 134.5–135°C; uv, λ_{max} (ε): 358.4 (15 400).

*2-(4'-Methylphenyl)-1,1,3,3-tetramethylguanidine (**3**)*[1]

Yield 80%; bp 174°C/30 Torr; uv, λ_{max} (ε): B 269.3 (12 200); BH^+ 237.3 (12 360); ^1H nmr δ: 7.03–6.83 (m, 4H), 2.58 (s, 12H), 2.20 (s, 3H); mass spectrum, *m/e* (rel. intensity, %): 205 (55), 190 (17), 161 (100). *Anal.* calcd. as for **1**; found: C 69.94, H 9.39, N 20.24. Picrate: mp 156–157°C (lit. (7) mp 156–158°C); uv, λ_{max} (ε): 358.4 (16 000).

*2-(2',4'-Dimethylphenyl)-1,1,3,3-tetramethylguanidine (**4**)*

Yield 64%; bp 157°C/15 Torr; uv, λ_{max} (ε): B 259.5 (12 540), BH^+ 235.1 (16 300); ^1H nmr δ: 6.78–6.25 (m, 3H), 2.48 (s, 12H), 2.20 (s, 3H), 1.98 (s, 3H); mass spectrum, *m/e* (rel. intensity, %): 219 (74), 204 (44), 175 (49). *Anal.* calcd. for $C_{13}H_{21}N_3$: C 71.19, H 9.65, N 19.16; found: C 71.02, H 9.79, N 18.89. Picrate: mp 144–145°C; uv, λ_{max} (ε): 358.4 (16 100).

*2-(2'-Methoxyphenyl)-1,1,3,3-tetramethylguanidine (**5**)*

Yield 80%; bp 176°C/23 Torr; uv, λ_{max} (ε): B 260.9 (12 600), BH^+ 235.0 (15 500); ^1H nmr δ: 7.00–6.65 (m, 4H), 3.76 (s, 3H), 2.70 (s, 12H); mass spectrum, *m/e* (rel. intensity, %): 221 (75), 190 (86), 177 (80). *Anal.* calcd. for $C_{12}H_{19}N_3O$: C 65.13, H 8.65, N 18.99; found: C 64.80, H 8.77, N 18.70. Picrate: mp 125–126°C; uv, λ_{max} (ε) 358.4 (15 800).

*2-(3'-Methoxyphenyl)-1,1,3,3-tetramethylguanidine (**6**)*

Yield 74%; bp 186°C/15 Torr; uv, λ_{max} (ε): B 267.7 (13 500), BH^+ 241 (16 500); ^1H nmr δ: 7.13–6.13 (m, 4H), 3,61 (s, 3H), 2.54 (s, 12H); mass spectrum, *m/e* (rel. intensity, %): 221 (56), 177 (100). *Anal.* calcd. as for **5**; found: C 64.91, H 8.71, N 18.81. Picrate: mp 117–118°C; uv, λ_{max}(ε): 358.4 (15 300).

*2-(4'-Methoxyphenyl)-1,1,3,3-tetramethylguanidine (**7**)*

Yield 77%; bp 189°C/21 Torr; uv, λ_{max} (ε): B 269.3 (12 200), BH^+ 237.3 (12 400); ^1H nmr δ: 7.00–6.65 (m, 4H), 3.78 (s, 3H), 2.72 (s, 12H); mass spectrum, *m/e* (rel. intensity, %): 221 (75), 190 (86), 177 (80). *Anal.* calcd. as for **5**; found: C 64.87, H 8.83, N 18.63. Picrate: mp 122–123°C; uv, λ_{max} (ε) 358.4 (15 300).

*2-(2',4'-Dimethoxyphenyl)-tetramethylguanidine (**8**)*

Yield 90%; bp 210°C/27 Torr; uv, λ_{max} (ε): B 254.9 (14 300), spectrum for BH^+ without sharp maximum in the region over 200 nm. ^1H nmr δ: 6.58–6.23 (m, 3H), 3.66 (s, 6H), 2.57 (s, 12H); mass spectrum, *m/e* (rel. intensity, %): 251 (100), 236 (42), 220 (50), 207 (75). *Anal.* calcd. for $C_{13}H_{21}N_3O_2$: C 62.13, H 8.42, N 16.51; found: C 61.83, H 8.56, N 16.51. Picrate: mp 116.5–118°C; uv, λ_{max} (ε) 358.4 (15 700).

*2-(2'-Chlorophenyl)-1,1,3,3-tetramethylguanidine (**9**)*

Yield 50%; bp 175°C/16 Torr; mp 39–41°C; uv, λ_{max} (ε): B 263.3 (12 500), BH^+ 237.5 (18 810); ^1H nmr δ: 7.20–6.80 (m, 4H), 2.57

[1]Previously synthesized by Bredereck (7).

Can. J. Chem. Downloaded from www.nrcresearchpress.com by 80.58.250.72 on 09/07/12
For personal use only.

(s, 12H); mass spectrum, *m/e* (rel. intensity, %): 227 (13), 225 (40), 190 (27), 183 (33), 181 (100). *Anal.* calcd. for $C_{11}H_{16}N_3Cl$: C 58.53, H 7.14, N 18.62; found: C 58.26, H 7.07, N 18.60. Picrate: mp 122.5–123°C; uv, λ_{max} (ε): 358.4 (15 500).

*2-(3'-Chlorophenyl)-1,1,3,3-tetramethylguanidine (**10**)*

Yield 90%; bp 187°C/21 Torr; uv, λ_{max} (ε): B 272 (16 000), BH^+ 240.0 (17 600); ^1H nmr δ: 7.63–6.62 (m, 4H), 2.75 (s, 12H); mass spectrum, *m/e* (rel. intensity, %): 227 (13), 225 (42), 183 (33), 181 (100). *Anal.* calcd. as for **9**; found: C 58.40, H 7.21, N 18.41. Picrate: mp 158.5–159.5°C; uv, λ_{max} (ε): 358.4 (15 500).

*2-(4'-Chlorophenyl)-1,1,3,3-tetramethylguanidine (**11**)*

Yield 90%; mp 55–56°C; uv, λ_{max} (ε): B 273.8 (18 100), BH^+ 253.0 (19 500); ^1H nmr δ: 7.17–6.53 (m, 4H), 2.63 (s, 12H); mass spectrum, *m/e* (rel. intensity, %): 227 (14), 225 (40), 183 (34), 181 (100). *Anal.* calcd. as for **9**; found: C 58.40, H 7.21, N 18.51. Picrate: mp 141–142°C; uv, λ_{max} (ε): 358.4 (16 000).

*2-(2',4'-Dichlorophenyl)-1,1,3,3-tetramethylguanidine (**12**)*

Yield 80%; bp 198°C/18 Torr; mp 37–39°C; uv, λ_{max} (ε): B 269.9 (15 200), BH^+ 244.2 (19 500); ^1H nmr δ: 7.13–6.47 (m, 3H), 2.55 (s, 12H); mass spectrum, *m/e* (rel. intensity, %): 261 (27), 259 (39), 217 (60), 215 (100). *Anal.* calcd. for $C_{11}H_{15}N_3Cl_2$: C 50.78, H 5.81, N 16.15; found: C 50.60, H 5.83, N 16.02. Picrate: mp 128.5–129°C; uv, λ_{max} (ε): 358.4 (15 400).

*2-(2',5'-Dichlorophenyl)-1,1,3,3-tetramethylguanidine (**13**)*

Yield 50%; bp 206°C/19 Torr; mp 45.5–46°C; uv, λ_{max} (ε): B 268.6 (10 850), BH^+ 240 (14 200); ^1H nmr δ: 7.47–6.75 (m, 3H), 2.83 (s, 12H); mass spectrum, *m/e* (rel. intensity, %): 261 (24), 259 (42), 217 (62), 215 (100). *Anal.* calcd. as for **12**; found: C 50.49, H 5.47, N 16.07. Picrate: mp 163.5–164.5°C; uv, λ_{max} (ε): 358.4 (15 600).

*2-(2'-Bromophenyl)-1,1,3,3-tetramethylguanidine (**14**)*

Yield 42%; bp 179°C/15 Torr; mp 48.5–50°C; uv, λ_{max} (ε): B 256.6 (13 500), BH^+ 233.9 (18 550); ^1H nmr δ: 7.40–6.43 (m, 4H), 2.53 (s, 12H); mass spectrum, *m/e* (rel. intensity, %): 271 (41), 269 (42), 227 (98), 225 (100). *Anal.* calcd. for $C_{11}H_{16}N_3Br$: C 48.90, H 5.97, N 15.55; found: C 48.63, H 5.97, N 15.57. Picrate: mp 119–120.5°C; uv, λ_{max} (ε): 358.4 (16 000).

*2-(3'-Bromophenyl)-1,1,3,3-tetramethylguanidine (**15**)*

Yield 75%; bp 198°C/14 Torr; uv, λ_{max} (ε): B 273.7 (12 600), BH^+ 239.5 (15 100); ^1H nmr δ: 7.06–6.42 (m, 3H), 2.59 (s, 12H); mass spectrum, *m/e* (rel. intensity, %): 271 (45), 269 (43), 227 (86), 225 (100). *Anal.* calcd. as for **14**; found: C 48.66, H 5.99, N 15.38. Picrate: mp 152–153°C; uv, λ_{max} (ε): 358.4 (16 200).

*2-(4'-Bromophenyl)-1,1,3,3-tetramethylguanidine (**16**)*

Yield 71%; bp 197°C/19 Torr; mp 53–54°C; uv, λ_{max} (ε): B 276.3 (17 900), BH^+ 254.7 (18 900); ^1H nmr δ: 7.28–6.42 (m, 3H), 2.59 (s, 12H); mass spectrum, *m/e* (rel. intensity, %): 271 (50), 269 (52), 256 (24), 254 (25), 227 (96), 225 (100). *Anal.* calcd. as for **14**; found: C 48.81, H 5.99, N 15.43. Picrate: mp 154–155°C; uv, λ_{max} (ε): 358.4 (15 600).

*2-(4'-Nitrophenyl)-1,1,3,3-tetramethylguanidine (**17**)*

Yield 46%; mp 80–82°C; uv, λ_{max} (ε): B 400 (14 500), BH^+ 319.7 (12 250). ^1H nmr δ: 7.85–6.47 (m, 4H), 2.73 (s, 12H); mass spectrum, *m/e* (rel. intensity, %): 236 (73), 221 (22), 192 (100). *Anal.* calcd. for $C_{11}H_{16}N_4O_2$: C 55.92, H 6.82, N 23.71; found: C 55.67, H 6.91, N 23.81.

*2-(2'-Methoxy-4'-nitrophenyl)-1,1,3,3-tetramethylguanidine (**18**)*

Yield 46%; bp 262°C/18 Torr; uv, λ_{max} (ε): B 412 (14 100), BH^+ 344 (8700); ^1H nmr δ: 7.85–6.47 (m, 3H), 3.83 (s, 3H), 2.67 (s, 12H); mass spectrum, *m/e* (rel. intensity, %): 266 (72), 251 (31), 235 (79), 222 (99). *Anal.* calcd. for $C_{12}H_{18}N_4O_3$: C 54.12, H 6.81, N 21.04; found: C 54.03, H 6.96, N 20.93. Picrate: mp 188–189°C; uv, λ_{max} (ε): 350.4 (20 800).

Acknowledgements

I am grateful to Professor A. Jarczewski for helpful discussions and to Ms. M. Pawlak for extensive help. The financial support of the Polish Academy of Sciences is gratefully acknowledged.

1. D. D. PERRIN, B. DEMPSEY, and E. P. SERJEANT. pK_a Prediction for organic acids and bases. Chapman and Hall, London, New York. 1981.
2. R. C. HIRT, F. HALVERSON, and F. T. KING. Spectrochim. Acta, 962 (1959).
3. R. GEBORIAUD, J. MENTRE, and R. SCHALL. C. R. Acad.Sci. Ser. C, **268**, 1093 (1969).
4. N. F. HALL and M. R. SPRINKLE. J. Am. Chem. Soc. **54**, 3469 (1932).
5. J. P. GREENSTEIN. J. Biol. Chem. **101**, 603 (1933).
6. J. C. GAGE. J. Chem. Soc. 221 (1949).
7. H. BREDERECK and K. BREDERECK. Ber. **94**, 2278 (1961).
8. D. D. PERRIN. *In* Dissociation constants of organic bases in aqueous solution. IUPAC, London. 1965.
9. A. J. BIGGS and R. A. ROBINSON. J. Chem. Soc. 388 (1961).
10. B. NOGAJ, P. PRUSZYNSKI, and M. MACKOWIAK. *In* Radio and microwave spectroscopy. Proceedings of RAMIS-85 International Conference, Poznan, Poland. 1985. pp. 605–609; B. NOGAJ and P. PRUSZYNSKI. Magn. Reson. Chem. In press.
11. F. HIBBERT. J. Chem. Soc. Perkin Trans. 2, 1862 (1974).

Can. J. Chem. Downloaded from www.nrcresearchpress.com by 80.58.250.72 on 09/07/12
For personal use only.

Synthesis of yomogin, 1-deoxyivangustin, and 1-deoxy-8-epiivangustin

JUAN ALBERTO MARCO[1] AND MANUEL ARNO
Departamento de Química Orgánica, Facultad de Químicas, Universidad de Valencia, Burjasot, Valencia, Spain

AND

MIGUEL CARDA
Departamento de Química Orgánica, Colegio Universitario de Castellón, Castellón, Spain

Received June 25, 1986

JUAN ALBERTO MARCO, MANUEL ARNO, and MIGUEL CARDA. Can. J. Chem. **65**, 630 (1987).

The chemical transformation of (−)-artemisin **1** into the natural sesquiterpene lactones yomogin **2**, 1-deoxyivangustin **3**, and 1-deoxy-8-epiivangustin **4** is described.

JUAN ALBERTO MARCO, MANUEL ARNO et MIGUEL CARDA. Can. J. Chem. **65**, 630 (1987).

On décrit la transformation chimique du sesquiterpène (−)-artémisine **1** dans les lactones sesquiterpéniques yomogine **2**, déoxy-1 ivangustine **3** et déoxy-1 épi-8 ivangustine **4**.

[Traduit par la revue]

Can. J. Chem. Downloaded from www.nrcresearchpress.com by 80.58.250.72 on 09/07/12
For personal use only.

Introduction

α,β-Unsaturated lactones have always aroused very much interest in medicine because of their remarkable biological properties, mainly as cytotoxic, antitumor, and bactericidal agents. Among these compounds, sesquiterpene α-methylene-γ-lactones have been intensively studied (1) from both the medicinal and chemical points of view. Numerous synthetic methods for the α-methylene-γ-lactone grouping have been designed and both total and partial syntheses of this class of compounds have been published (2, 3). Our efforts have focused on the transformation of readily available artemisin **1** into other natural sesquiterpene lactones (4). We now wish to report on our studies concerning the chemical transformation of (−)-artemisin into the natural eudesmanolides yomogin **2**, 1-deoxyivangustin **3**, and 1-deoxy-8-epiivangustin **4**.

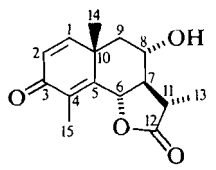

1

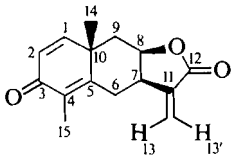

2

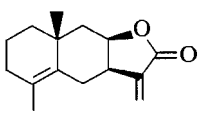

3

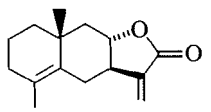

4

Yomogin was first isolated by Geissman from *Artemisia princeps* Pamp. (5). The racemic form has been obtained by total synthesis (6), while the natural (−)-form was prepared by Yamakawa *et al.* (7) starting from α-santonin. This last synthesis, however, implied the loss of the stereochemistry of the santonin molecule at C-7, which had to be recreated in a later step, and gave an overall yield of ca. 0.8%. On the other hand, 1-deoxyivangustin and 1-deoxy-8-epiivangustin were isolated for the first time by Bohlmann *et al.* from *Inula helenium* L. and *Artemisia pectinata* Pall., respectively (8, 9). 1-Deoxyivangustin has also been called alloalantolactone (10). Its enantiomeric (−)-form had been isolated even earlier (11) from the liverworts *Diplophyllum albicans* and *D. taxifolium*, and was named diplophyllin.

Apart from the partial conversion of isoalantolactone into **3** by acid isomerization (11), no stereodirected syntheses of **3** or **4** have been published in the literature. Artemisin **1**, which already possesses an oxygen function at C-8 and the appropriate stereochemical configuration at C-7 and C-10, should serve as a very adequate precursor for these and many other eudesman-12,8-olides with either *cis* or *trans* junction between the cyclohexane and lactone rings. According to this expectation, we have synthesized eudesmanolides **2**, **3**, and **4** from (−)-artemisin **1** in, respectively, 7, 10, and 8 steps. Overall yields were 7.5, 2, and 28%, respectively. Since artemisin had already been obtained by total synthesis (12), our syntheses can be formally considered as total syntheses of the above-mentioned compounds.

Results and discussion

A key step for the creation of the 12,8-lactone ring is the reductive cleavage of the C6—O bond in artemisin with subsequent relactonization to C-8. This reaction had already been described for α-santonin (13) and requires epimerization at C-6 prior to reduction with Zn dust. Indeed, artemisin **1** could be easily epimerized at C-6 (4*b*) by a modification of Sumi's method (14), giving **5** in ca. 60% yield. Zn reduction and esterification afforded the 8α-hydroxyester **6**, which could be lactonized almost quantitatively to lactone **7** (12*a*). By hydrogenation in the presence of Wilkinson catalyst, **7** gave **11** (15) in 95% yield. The overall yield of **11** from **1** was thus 33–35% (Scheme 1). Since epimerization at C-6 of 1,2-dihydro-α-santonin takes place with much better yields (16) than that of α-santonin, we also examined this alternative. Lactone **11** was obtained via 1,2-dihydroartemisin **8** in an overall yield of 58–60% from **1**.

Compound **11** was converted into the normal eudesmanolide **4** in a straightforward manner. By reaction with ethanedithiol, **11** gave the thioketal **12**, which yielded, by treatment with active Raney nickel, the unsaturated lactone **13** (17), contaminated with a small percentage (ca. 5%) of a double-bond isomer (16). Phenylselenylation and subsequent oxidation afforded **4** in an overall yield of ca. 49% from **11** (Scheme 2). The compound had physical and spectral properties identical with those reported by Bohlmann *et al.* (9).

For the synthesis of the eudesman-12,8β-olides **2** and **3**, an

[1]Author to whom correspondence may be addressed.

Printed in Canada / Imprimé au Canada

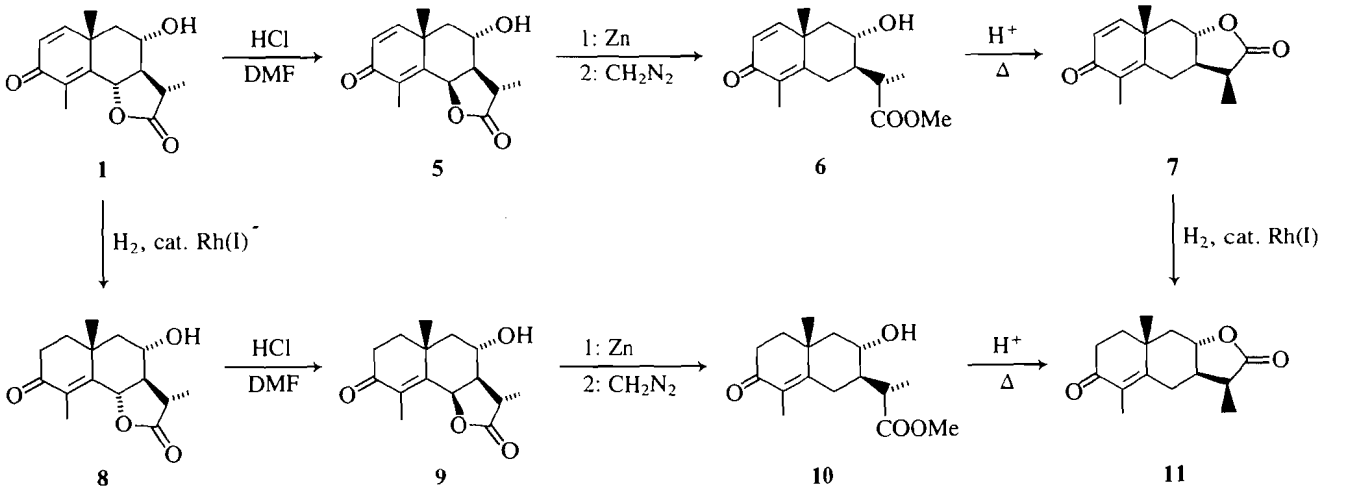

SCHEME 1

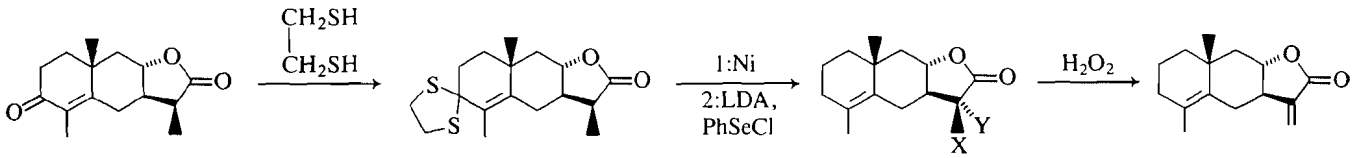

SCHEME 2

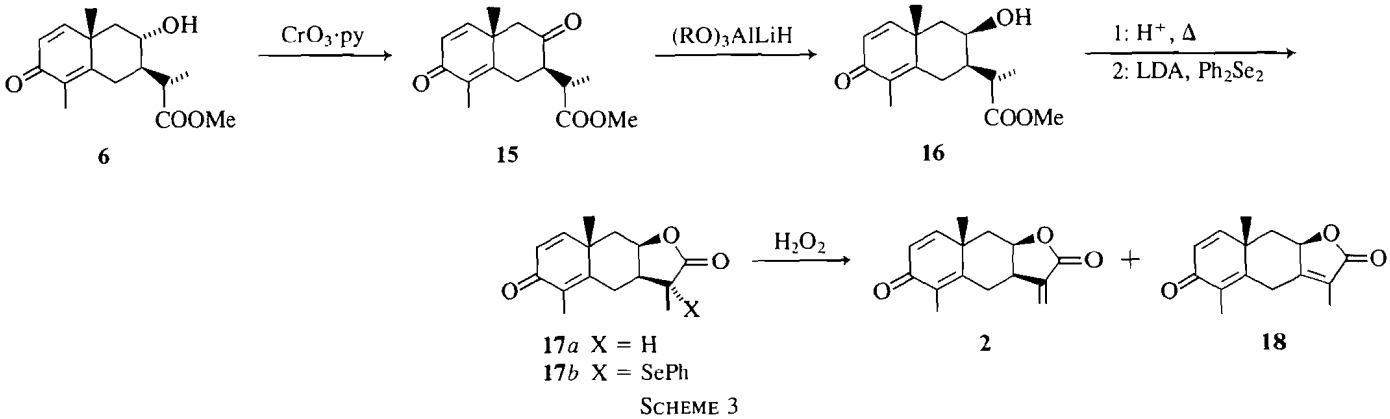

SCHEME 3

inversion of the configuration at C-8 is necessary. This was achieved via oxidation–reduction of the hydroxyester **6**. Oxidation with a modified Collins reagent (18) yielded the diketone **15**, which was subsequently reduced with $LiAlH(OBu^t)_3$. The 8β-hydroxyester **16** (80% overall yield from **6**) cyclized quantitatively to the *cis*-lactone **17***a* by brief heating in benzene with catalytic amounts of camphorsulfonic acid. Compound **17***a*, an 11,13-dihydroyomogin, had been already obtained from α-santonin by Yamakawa *et al.* (7*a*) and converted to yomogin **2** and the endocyclic double-bond isomer **18** by the phenylselenylation–oxidation procedure (Scheme 3).

The same sequence of hydrogenation, thioketalization, and desulfurization that had been utilized for the synthesis of lactone **13** proved useful for the preparation of the *cis*-isomer **21** (Scheme 4) in an overall yield of 47% from **17***a*. As in the former case (**12** → **13**), the desulfurization reaction gave not only the desired Δ^4-eudesmanolide **21** (17) but also a certain amount (ca. 13%) of the Δ^3-isomer **22**, which could be separated by chromatography. No other by-products were noted. A secure stereochemical assignment for **22** could be made from a 500-MHz ^1H nmr spectrum, in which the signals of H-5, H-6α, and H-6β were resolved. The enantiomers of compounds **21** and **22** have been described in the literature (11, 19).

By selenylation under rather strict conditions (4*b*), **21** gave **23**, in which attack of the selenylating agent proceeded from the less hindered convex α-face. As a consequence, the phenylselenyl group was located in a *syn* relationship to H-7 and the oxidative elimination step took place toward both H-7 and H-13, giving a mixture of two double-bond isomers, as in the case of yomogin (7*a*). The less abundant reaction product was shown to be identical in its spectral properties with 1-deoxy-

Can. J. Chem. Downloaded from www.nrcresearchpress.com by 80.58.250.72 on 09/07/12
For personal use only.

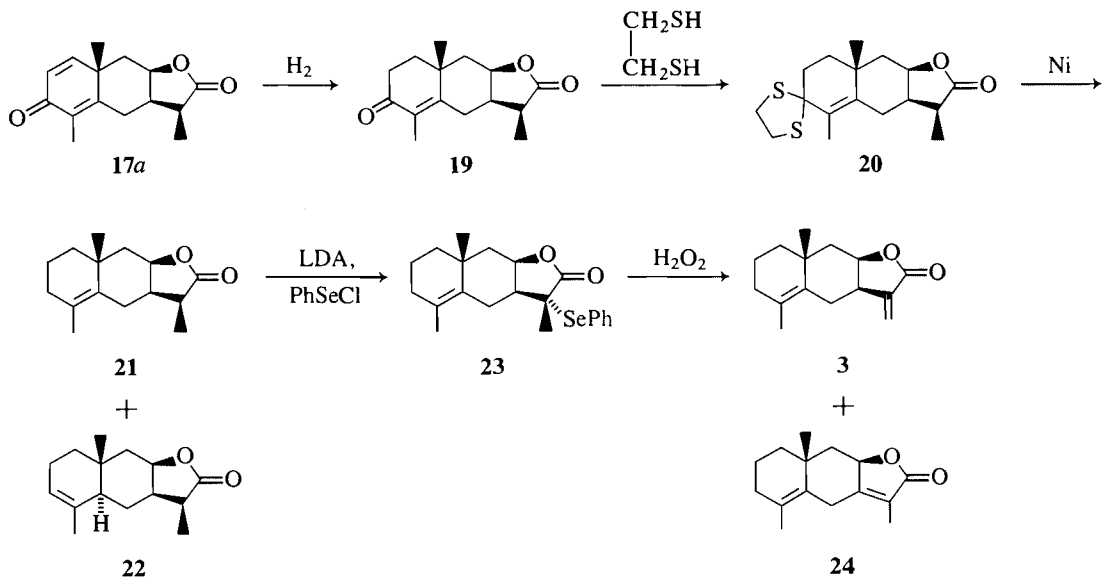

SCHEME 4

ivangustin **3** (8). The main reaction product was the unstable endocyclic double-bond isomer **24**.

Experimental

Data have been taken in part from the Ph.D. Thesis of M. Carda. Infrared spectra were recorded as KBr pellets (solids) or as films (oils) on a Perkin Elmer model 281 spectrophotometer. The uv spectra were measured in EtOH solution. Mass spectra were run by electron impact (70 eV) on a Varian MAT-311A spectrometer. The ^{1}H nmr spectra were registered, unless otherwise stated, at 200.13 MHz ($CDCl_3$ solution) on a Bruker AC-200 spectrometer. The signals of the hydrogen atoms were assigned with the aid of decoupling experiments and 2D-nmr spectroscopy (COSY). Melting points were determined on a Büchi melting point apparatus and are not corrected. Optical rotations were measured in $CHCl_3$ solutions (*c* 0.1–0.3 g/100 mL).

THF was distilled under Ar from $LiAlH_4$ and used immediately. DMF was distilled from CaH_2, benzene and CH_2Cl_2 were distilled from anhydrous $CaCl_2$, and all were kept over molecular sieves. MeOH and AcOH (Merck analytical grades) were used as received.

6-Epiartemisin, 5

Artemisin (1.3 g, ca. 5 mmol) was dissolved in 20 mL of dry DMF containing 5% hydrogen chloride. The solution was heated under Ar for 4 h at 90°C, then poured into water (50 mL) and extracted with CH_2Cl_2 (5 × 30 mL). The organic layer was then washed with 5% aqueous $NaHCO_3$ and water, dried over anhydrous Na_2SO_4, filtered, and concentrated *in vacuo*. The oily residue obtained was then chromatographed on silica gel. Elution with hexane–EtOAc 1:4 gave 728 mg (56%) of 6-epiartemisin **5** as white needles, mp 159–160°C (from hexane–CH_2Cl_2) (lit. (14) mp 156–157°C); $[\alpha]_D^{25}$ −191° (lit. (14) $[\alpha]_D^{25}$ −198°), with the expected spectroscopic properties; ^{1}H nmr, δ (ppm): 6.77 (d, *J* = 9.8 Hz, H-1), 6.27 (d, *J* = 9.8 Hz, H-2), 5.62 (d, *J* = 5.5 Hz, H-6), 3.99 (ddd, *J* = 11.7, 9.9, and 4.3 Hz, H-8), 2.99 (q, *J* = 7.7 Hz, H-11), 2.08 (s, 3H, H-15), 2.03 (dd, *J* = 12.5 and 4.3 Hz, H-9β), 2.02 (dd, *J* = 9.9 and 5.5 Hz, H-7), 1.50 (dd, *J* = 12.5 and 11.7 Hz, H-9α), 1.45 (d, 3H, *J* = 7.7 Hz, H-13), 1.32 (s, 3H, H-14).

Further elution enabled the recovery of 81 mg of unreacted artemisin. The yield of **5** thus amounts to ca. 60%, based on consumed **1**.

Methyl (11S)-3-oxo-8α-hydroxy-7αH-eudesma-1,4-dien-12-oate, 6

Activated Zn dust (1.7 g) and anhydrous AcOH (0.3 mL) were added to a solution of lactone **5** (700 mg, 2.67 mmol) in anhydrous MeOH (12 mL). After refluxing under Ar for 15 min, the reaction mixture was cooled to room temperature and directly treated with a great excess of ethereal diazomethane, until persistence of a pale yellow colour. The resulting cloudy solution was then filtered and concentrated *in vacuo*, yielding an oily residue, which was chromatographed on silica gel. Elution with hexane–EtOAc 1:1 gave 475 mg (64%) of a colorless oil, $[\alpha]_D^{25}$ −14°, which was identified as **6** by its spectral properties; ir (film), ν_{max}: 3600–3300 (br s), 1727 (s), 1655 (s) cm^{-1}; uv, λ_{max} (log ε_{max}): 240 nm (4.07); ^{1}H nmr, δ (ppm): 6.73 (d, *J* = 9.8 Hz, H-1), 6.23 (d, *J* = 9.8 Hz, H-2), 4.05 (ddd, *J* = 11, 10.5, and 4.5 Hz, H-8), 3.73 (s, 3H, COOMe), 2.96 (qd, *J* = 7.2 and 2.8 Hz, H-11), 2.82 (dd, *J* = 14.1 and 3.8 Hz, H-6α), 2.19 (ddq, *J* = 14.1, 13.6, and 1.1 Hz, H-6β), 2.10 (dd, *J* = 12.5 and 4.5 Hz, H-9β), 1.92 (d, 3H, *J* = 1.1 Hz, H-15), 1.69 (dddd, *J* = 13.6, 10.5, 3.8, and 2.8 Hz, H-7), 1.30 (d, 3H, *J* = 7.2 Hz, H-13), 1.30 (dd, *J* = 12.5 and 11 Hz, H-9α), 1.24 (s, 3H, H-14); ms *m/z* (% rel. int.): 278 (M^+, 13), 260 (28), 246 (18), 218 (10), 200 (22), 185 (44), 173 (100). *Anal.* calcd. for $C_{16}H_{22}O_4$: C 69.06, H 7.91; found: C 69.29, H 7.77.

3-Oxo-7,11α,8βH-eudesma-1,4-dien-12,8-olide, 7

A solution of hydroxyester **6** (100 mg, 0.36 mmol) and camphorsulfonic acid (CSA) (10 mg) in dry benzene (8 mL) was heated at reflux for 90 min. After evaporation of the solvent *in vacuo*, the oily residue was chromatographed on silica gel. Elution with hexane–EtOAc 1:1 gave 86 mg (97%) of lactone **7** as white needles, mp 108–109°C (from hexane–CH_2Cl_2) (lit. (12*a*) mp 151–154°C); $[\alpha]_D^{25}$ −144°; and the expected ir, uv, and mass spectra; ^{1}H nmr, δ (ppm): 6.77 (d, *J* = 9.8 Hz, H-1), 6.27 (d, *J* = 9.8 Hz, H-2), 4.49 (td, *J* = 11.6 and 4.2 Hz, H-8), 2.99 (dd, *J* = 13.6 and 3.2 Hz, H-6α), 2.79 (quintuplet, *J* = 7.6 Hz, H-11), 2.37 (dd, *J* = 11.6 and 4.2 Hz, H-9β), 2.28 (tq, *J* = 13.6 and 1.1 Hz, H-6β), 1.98 (dddd, *J* = 13.6, 11.6, 7.6, and 3.2 Hz, H-7), 1.94 (d, 3H, *J* = 1.1 Hz, H-15), 1.62 (t, *J* = 11.6 Hz, H-9α), 1.33 (s, 3H, H-14), 1.30 (d, 3H, *J* = 7.6 Hz, H-13).

1,2-Dihydro-6-epiartemisin, 9

1,2-Dihydroartemisin **8** (4*e*) (630 mg, 2.38 mmol) was treated as above (**1** → **5**) by heating for 45 min in 5% HCl/DMF. After work-up, column chromatography (elution with hexane–EtOAc 3:7) yielded 598 mg (95%) of lactone **9** as colorless needles, mp 172–173°C (from ether), $[\alpha]_D^{25}$ −71°; ir (KBr), ν_{max}: 3600–3300 (br s), 1775 (s), 1666 (s) cm^{-1}; uv, λ_{max} (log ε_{max}): 242 nm (3.96); ^{1}H nmr, δ (ppm): 5.54 (d, *J* = 5.6 Hz, H-6), 3.90 (ddd, *J* = 11.8, 9.9, and 3.8 Hz, H-8), 2.98 (q, *J* = 7.7 Hz, H-11), 2.72 (ddd, *J* = 18, 14.1, and 5.9 Hz, H-2β), 2.51 (ddd, *J* = 18, 5.1, and 2.4 Hz, H-2α), 2.00–1.90 (m, 1H, overlapped; H-1α), 2.05 (dd, *J* = 9.9 and 5.6 Hz, H-7), 1.93 (s, 3H, H-15), 1.85 (dd, *J* = 13 and 3.8 Hz, H-9β), 1.80 (ddd, *J* = 13.3, 5.9, and 2.4 Hz, H-1β), 1.45 (dd, *J* = 13 and 11.8 Hz, H-9α), 1.43 (d, 3H, *J* = 7.7 Hz, H-13), 1.28 (s, 3H, H-14); ms *m/z* (% rel. int.): 264

Can. J. Chem. Downloaded from www.nrcresearchpress.com by 80.58.250.72 on 09/07/12
For personal use only.

Can. J. Chem. Downloaded from www.nrcresearchpress.com by 80.58.250.72 on 09/07/12
For personal use only.

(M^+, 100), 249 (41), 246 (5), 231 (13), 221 (20), 191 (26), 137 (42). *Anal.* calcd. for $C_{15}H_{20}O_4$: C 68.18, H 7.57; found: C 68.25, H 7.68.

Methyl (11S)-3-oxo-8α-hydroxy-7αH-eudesm-4-en-12-oate, ***10***

In a similar procedure as above (**5** → **7**), 600 mg (2.27 mmol) of lactone **9** was allowed to react with activated Zn dust (1.45 g) and acetic acid (0.25 mL) in anhydrous MeOH (10 mL). After refluxing under Ar for 15 min, the reaction mixture was cooled to room temperature, treated with excess of ethereal diazomethane, filtered, concentrated *in vacuo*, and chromatographed on silica gel. Elution with hexane–EtOAc 1:1 gave **10** (410 mg, 65%) as colorless needles, mp 120–121°C (from ether); $[\alpha]_D^{25}$ +58°; ir (KBr), ν_{max}: 3600–3300 (br s), 1735 (s), 1660 (s), 1612 (m) cm^{-1}; uv, λ_{max} (log ε_{max}): 244 nm (3.95); ^1H nmr, δ (ppm): 3.93 (ddd, J = 11.1, 10.5, and 4.2 Hz, H-8), 3.71 (s, 3H, COOMe), 2.90 (qd, J = 7.2 and 2.7 Hz, H-11), 2.71 (dd, J = 14.9 and 3.6 Hz, H-6α), 2.50 (ddd, J = 17.5, 12, and 7 Hz, H-2β), 2.38 (ddd, J = 17.5, 5.3, and 3.5 Hz, H-2α), 2.03 (tq, J = 14.9 and 1.3 Hz, H-6β), 1.93 (dd, J = 12.7 and 4.2 Hz, H-9β), 1.90–1.70 (m, 3H, overlapped; H-1α/β and H-7), 1.77 (d, 3H, J = 1.3 Hz, H-15), 1.37 (dd, J = 12.7 and 11.1 Hz, H-9α), 1.25 (d, 3H, J = 7.2 Hz, H-13), 1.20 (s, 3H, H-14); ms, *m/z* (% rel. int.): 280 (M^+, 49), 262 (84), 248 (15), 247 (34), 234 (18), 219 (7), 215 (7), 202 (100), 187 (48), 175 (83), 159 (33), 147 (76). *Anal.* calcd. for $C_{16}H_{24}O_4$: C 68.57, H 8.57; found: C 68.69, H 8.43.

3-Oxo-7,11α,8βH-eudesm-4-en-12,8-olide, ***11***

(A) By hydrogenation of **7**: Freshly prepared Wilkinson catalyst (15 mg, 16.2 μmol) was suspended in dry benzene (1 mL) and stirred under H_2 atmosphere until complete dissolution (20–30 min). A solution of lactone **7** (70 mg, 0.28 mmol) in dry C_6H_6–EtOH 1:1 (4 mL) was then added via syringe. After stirring for 12 h at room temperature, the hydrogenation mixture was concentrated *in vacuo* and the brownish oily residue was chromatographed on silica gel. Elution with hexane–EtOAc 7:3 gave 67 mg (95%) of compound **11** as white needles, mp 136–137°C (from hexane–CH_2Cl_2) (lit. (15) mp 142°C); $[\alpha]_D^{25}$ +21° (lit. (15) $[\alpha]_D^{18}$ +19.4°), with the expected ir, uv, and mass spectra; ^1H nmr, δ (ppm): 4.44 (ddd, J = 11.9, 10.5, and 4 Hz, H-8), 2.90 (dd, J = 13.7 and 2 Hz, H-6α), 2.76 (quintuplet, J = 7.6 Hz, H-11), 2.58 (ddd, J = 17.5, 13.7, and 5.5 Hz, H-2β), 2.46 (ddd, J = 17.5, 5.2, and 3.1 Hz, H-2α), 2.24 (dd, J = 11.9 and 4 Hz, H-9β), 2.16 (tq, J = 13.7 and 1.2 Hz, H-6β), 2.15–1.80 (m, 3H, H-1α/1β and H-7), 1.80 (d, 3H, J = 1.2 Hz, H-15), 1.62 (t, J = 11.9 Hz, H-9α), 1.31 (s, 3H, H-14), 1.26 (d, 3H, J = 7.6 Hz, H-13).

(B) By lactonization of **10**: By the same procedure as in the transformation **6** → **7**, 56 mg of lactone **10** (0.2 mmol) and CSA (5 mg) were refluxed in dry benzene (4 mL) for 90 min. Column chromatography on silica gel (elution with hexane–EtOAc 7:3) gave 48.5 mg (98%) of compound **11**.

3,3-Ethanedithio-7,11α,8βH-eudesm-4-en-12,8-olide, ***12***

A modification of the published procedure (15) was utilized: Lactone **11** (57 mg, 0.23 mmol), ethanedithiol (0.15 mL, 1.78 mmol), and $BF_3 \cdot OEt_2$ (40 μL) were dissolved in glacial acetic acid (1 mL) and stirred for 9 h at room temperature. The reaction mixture was then poured into water (10 mL) and extracted with CH_2Cl_2 (3 × 10 mL). The organic layer was washed with 5% aqueous $NaHCO_3$ and water, dried over anhydrous Na_2SO_4, filtered, and concentrated *in vacuo*. Column chromatography on silica gel (elution with hexane–EtOAc 19:1) of the residue yielded **12** (61 mg, 82%) as white needles, mp 170–171°C (from hexane–ether) (lit. (15) mp 158°C); $[\alpha]_D^{25}$ +22° (lit. (15) $[\alpha]_D^{19}$ +43.6°), with the expected ir, uv, and mass spectra; ^1H nmr, δ (ppm): 4.37 (ddd, J = 11.7, 10.7, and 4.1 Hz, H-8), 3.50–3.15 (m, 4H, thioketal hydrogens), 2.80–2.60 (m, 1H, overlapped; H-6α), 2.68 (quintuplet, J = 7.7 Hz, H-11), 2.32 (ddd, J = 14, 12, and 3.4 Hz, H-2β), 2.21 (ddd, J = 14, 4.8, and 3.5 Hz, H-2α), 2.11 (dd, J = 11.7 and 4.1 Hz, H-9β), 1.91 (s, 3H, H-15), 1.85 (ddd, J = 13.5, 12, and 3.5 Hz, H-1α), 1.67 (ddd, J = 13.5, 4.8, and 3.4 Hz, H-1β), 1.47 (t, J = 11.7 Hz, H-9α), 1.21 (d, 3H, J = 7.7 Hz, H-13), 1.15 (s, 3H, H-14).

7,11α,8βH-Eudesm-4-en-12,8-olide, ***13***

Approximately 1 g active W-2 Raney nickel was added at once to a solution of thioketal **12** (50 mg, ca. 0.15 mmol) in MeOH (3 mL). The mixture was stirred for 8 min at room temperature and rapidly quenched by addition of ethanedithiol (0.1 mL). The reaction mixture was then filtered through a pad of silica gel (elution with EtOAc). The organic solution was then concentrated *in vacuo* and chromatographed on silica gel. Elution with hexane–EtOAc 8:2 gave **13** as a colorless oil (30 mg, 83%), homogeneous by tlc, which was shown by nmr to contain a small percentage (ca. 5%) of a double-bond isomer, probably the Δ^3-isomer (16). Elimination of this minor impurity took place in the chromatographic separation after the next step. The compound gave the expected ir and mass spectra; ^1H nmr, δ (ppm): 4.39 (ddd, J = 11.5, 10.5, and 4 Hz, H-8), 2.75–2.60 (m, 2H, H-6α and H-11), 2.06 (dd, J = 11.5 and 4 Hz, H-9β), 2.10–1.80 (m, 4H, H-3α/3β, H-6β, and H-7), 1.61 (br s, 3H, H-15), 1.70–1.40 (m, 4H, H-1α/1β and 2α/2β), 1.39 (t, J = 11.5 Hz, H-9α), 1.19 (d, 3H, J = 7.7 Hz, H-13), 1.08 (s, 3H, H-14).

11β-Phenylseleno-7α,8βH-eudesm-4-en-12,8-olide, ***14***

A solution of *n*BuLi (0.14 mL of a 1.6 *M* solution in hexane, 0.22 mmol) was added at room temperature under Ar via syringe to a solution of diisopropylamine (33 μL, 0.23 mmol) in dry THF (0.2 mL). After stirring for 15 min, the mixture was cooled to −78°C (Dry Ice – acetone bath). Lactone **13** (26 mg, 0.11 mmol) was dissolved in dry THF (0.5 mL) and added dropwise (5 min) to the cooled LDA solution. After stirring for 1 h at −78°C, a solution of Ph_2Se_2 (68 mg, 0.22 mmol) and HMPT (40 μL) in dry THF (0.5 mL) was added dropwise via syringe (5 min). The reaction mixture was stirred for 40 min at −78°C, then for a further 40 min at −40°C, and was quenched at this temperature with 0.5 *N* HCl (0.7 mL). The reaction mixture was then poured into water (5 mL) and extracted with EtOAc (3 × 5 mL), and the organic layer was washed with brine and dried over anhydrous Na_2SO_4. Filtration and evaporation *in vacuo* yielded a yellowish oil, which was chromatographed on silica gel. Elution with hexane–EtOAc 19:1 gave **14** (34 mg, 79%) as colorless needles, mp 154–155°C (from MeOH); ir (KBr), ν_{max}: 1770 (s), 1580 (m), 1475 (m), 736 (m), 689 (m) cm^{-1}; ^1H nmr, δ (ppm): 7.70–7.25 (m, 5H, aromatic hydrogens), 4.60 (ddd, J = 11.8, 10.6, and 4.2 Hz, H-8), 2.80 (dd, J = 13.5 and 3.5 Hz, H-6α), 2.07 (dd, J = 11.8 and 4.2 Hz, H-9β), 2.10–1.90 (m, 4H, H-3α/3β, H-6β, and H-7), 1.80–1.40 (m, 4H, H-1α/1β and H-2α/2β), 1.65 (br s, 3H, H-15), 1.54 (s, 3H, H-13), 1.38 (t, J = 11.8 Hz, H-9α), 1.13 (s, 3H, H-14). *Anal.* calcd. for $C_{21}H_{26}O_2Se$: C 64.79, H 6.68, Se 20.30; found: C 64.91, H 6.80, Se 20.10.

1-Deoxy-8-epiivangustin, ***4***

Hydrogen peroxide (90 μL of a 30% aqueous solution, ca. 0.8 mmol) was added at 0°C to a solution of **14** (31 mg, ca. 0.08 mmol) and AcOH (10 μL) in THF (0.5 mL). After stirring for 1 h at 0°C, the reaction mixture was poured into 5% aqueous $NaHCO_3$ (5 mL) and extracted with EtOAc (3 × 5 mL). The organic layer was washed several times with brine, dried over anhydrous Na_2SO_4, concentrated *in vacuo*, and chromatographed on silica gel. Hexane–EtOAc 8:2 eluted a colorless oil (17.5 mg, 94%), $[\alpha]_D^{25}$ −46°, with spectral properties coincident with those reported by Bohlmann *et al.* (9) for 1-deoxy-8-epiivangustin **4**; ir (film), ν_{max}: 1770 (s), 1670 (w), 983 (m) cm^{-1}; ^1H nmr, δ (ppm): 6.09 (d, J = 3.2 Hz, H-13′), 5.44 (d, J = 3 Hz, H-13), 4.11 (ddd, J = 12.1, 10.9, and 3.9 Hz, H-8), 3.00 (dd, J = 13.6 and 3.3 Hz, H-6α), 2.29 (ddq, J = 12.3, 10.9, and 3.1 Hz, H-7), 2.09 (dd, J = 11.5 and 3.9 Hz, H-9β), 2.20–1.80 (m, 3H, H-3α/3β and H-6β), 1.66 (br s, 3H, H-15), 1.70–1.40 (m, 4H, H-1α/1β and H-2α/2β), 1.51 (dd, J = 12.1 and 11.5 Hz, H-9α), 1.10 (s, 3H, H-14); ms, *m/z* (% rel. int.): 232 (M^+, 33), 217 (100), 204 (3), 199 (4), 189 (7), 123 (67). High resolution molecular weight determination, *Mol. Wt.* calcd. for $C_{15}H_{20}O_2$: 232.1463; found: 232.1456.

Methyl (11S)-3,8-dioxo-7αH-eudesma-1,4-dien-12-oate, ***15***

CrO_3 (2.57 g, 25.7 mmol) was added at 0°C portionwise (**slow addition!**) under Ar to a mixture of dry pyridine (5.5 mL) and dry CH_2Cl_2 (30 mL). After stirring this mixture for 4–5 min at 0°C, a solution of **6** (360 mg, 1.3 mmol) in dry CH_2Cl_2 (15 mL) was added. Stirring was then maintained for 6 h at 0°C, after which the reaction

Can. J. Chem. Downloaded from www.nrcresearchpress.com by 80.58.250.72 on 09/07/12
For personal use only.

mixture was filtered, washed successively with 0.1 *N* HCl, water, 5% aqueous $NaHCO_3$, and brine, and dried over anhydrous Na_2SO_4. Filtration, evaporation of the solvent *in vacuo*, and column chromatography on silica gel (elution with hexane–EtOAc 1:1) yielded **15** (340 mg, 95%) as a colorless oil, lit. (*7a*) solid mp 95–97°C; $[\alpha]_D^{25}$ −100°, with the expected ir, uv, and mass spectra; ^{1}H nmr, δ (ppm): 6.67 (d, J = 9.8 Hz, H-1), 6.30 (d, J = 9.8 Hz, H-2), 3.72 (s, 3H, COOMe), 3.17 (dd, J = 13.6 and 6.2 Hz, H-6α), 3.01 (qd, J = 7.2 and 5.2 Hz, H-11), 2.83 (tq, J = 13.6 and 1 Hz, H-6β), 2.70–2.60 (m, 1H, H-7), 2.49 (d, J = 13.8 Hz, H-9β), 2.35 (d, J = 13.8 Hz, H-9α), 2.01 (d, 3H, J = 1 Hz, H-15), 1.31 (d, 3H, J = 7.2 Hz, H-13), 1.30 (s, 3H, H-14).

Methyl (11S)-3-oxo-8β-hydroxy-7αH-eudesma-1,4-dien-12-oate, ***16***

Diketoester **15** (330 mg, 1.19 mmol) was dissolved in dry THF (30 mL) and treated at 0°C with $LiAlH(OBu^t)_3$ (960 mg, 3.77 mmol). After stirring for 3 h under Ar at this temperature, the reaction was carefully quenched by addition of 0.5 *N* HCl (25 mL), diluted with brine, and extracted with EtOAc (3 × 40 mL). The organic layer was then washed with water, dried over anhydrous Na_2SO_4, filtered, concentrated *in vacuo*, and chromatographed on silica gel. Elution with hexane–EtOAc 1:1 gave **16** (280 mg, 84%) as white needles, mp 160–161°C (from hexane–CH_2Cl_2) (lit. (*7a*) oil); $[\alpha]_D^{25}$ −138°, with the expected ir, uv and mass spectra; ^{1}H nmr, δ (ppm): 6.75 (d, J = 9.8 Hz, H-1), 6.17 (d, J = 9.8 Hz, H-2), 4.20 (apparent q, average J = 2.7 Hz, H-8), 3.74 (s, 3H, COOMe), 2.74 (dq, J = 9.3 and 7 Hz, H-11), 2.60–2.40 (m, 2H, H-6α and H-6β), 2.07 (dd, J = 14.4 and 2.4 Hz, H-9β), 1.89 (br s, 3H, H-15), 1.67 (dddd, J = 11.1, 9.3, 5, and 2.7 Hz, H-7), 1.46 (dd, J = 14.4 and 3.4 Hz, H-9α), 1.44 (s, 3H, H-14), 1.23 (d, 3H, J = 7 Hz, H-13).

Further elution led to the recovery of ca. 1.5 mg (4.5%) of the 8α-hydroxyester **6**.

3-Oxo-7,8,11αH-eudesma-1,4-dien-12,8-olide, ***17***a

The hydroxyester **16** (270 mg, 0.97 mmol) was lactonized as described above (**6** → **7** and **10** → **11**) by refluxing in benzene (15 mL) in the presence of CSA (25 mg) for 90 min. Work-up and column chromatography on silica gel (elution with hexane–EtOAc 1:1) yielded ***17a*** (236 mg, 99%) as a white solid, mp 178–179°C (from hexane–CH_2Cl_2) (lit. (*7a*) mp 180–180.5°C); $[\alpha]_D^{25}$ −136° (lit. (*7a*) $[\alpha]_D^{23}$ −117.5°), with the expected ir, uv, and mass spectra; ^{1}H nmr, δ (ppm): 6.77 (d, J = 9.8 Hz, H-1), 6.22 (d, J = 9.8 Hz, H-2), 4.49 (td, J = 4.4 and 1.9 Hz, H-8), 2.92 (quintuplet, J = 6.9 Hz, H-11), 2.79 (dd, J = 13.6 and 5.8 Hz, H-6α), 2.50 (dddd, J = 13.6, 6.9, 5.8, and 4.4 Hz, H-7), 2.48 (dd, J = 15.3 and 1.9 Hz, H-9β), 2.04 (br t, J = 13.6 Hz, H-6β), 1.94 (br s, 3H, H-15), 1.58 (dd, J = 15.3 and 4.4 Hz, H-9α), 1.30 (s, 3H, H-14), 1.29 (d, 3H, J = 6.9 Hz, H-13). Several signals in the reported spectrum (*7a*) appear to have been misassigned.

3-Oxo-11α-phenylseleno-7,8αH-eudesma-1,4-dien-12,8-olide, ***17***b

The published procedure (*7a*) was exactly repeated. It yielded ***17b*** in 49% yield as colorless crystals, mp 214–215°C (from EtOAc) (lit. (*7a*) mp 215–218°C), with the expected ir, uv, and mass spectra; ^{1}H nmr, δ (ppm): 7.70–7.30 (m, 5H, aromatic hydrogens), 6.80 (d, J = 9.9 Hz, H-1), 6.25 (d, J = 9.9 Hz, H-2), 5.08 (m, 1H, H-8), 2.89 (dd, J = 13.5 and 5.7 Hz, H-6α), 2.54 (dd, J = 15.4 and 1.9 Hz, H-9β), 2.46 (ddd, J = 13.5, 5.7, and 4.1 Hz, H-7), 2.16 (br t, J = 13.5 Hz, H-6β), 1.95 (br s, 3H, H-15), 1.64 (s, 3H, H-13), 1.63 (dd, J = 15.4 and 4.7 Hz, H-9α), 1.33 (s, 3H, H-14).

Yomogin, ***2***

The oxidation of ***17b*** was carried out according to the described procedure (*7a*). After crystallization from EtOAc, yomogin **2** was obtained in 33% yield as colorless cubes, mp 206–207°C (lit. (*7a*) mp 210–211°C), with the expected ir, uv, and mass spectra; ^{1}H nmr, δ (ppm): 6.81 (d, J = 9.9 Hz, H-1), 6.28 (d, J = 1 Hz, H-13′), 6.26 (d, J = 9.9 Hz, H-2), 5.76 (d, J = 1 Hz, H-13), 4.51 (apparent q, average J = 4.2 Hz, H-8), 3.20–3.05 (m, 1H, H-7), 3.00 (dd, J = 13.6 and 7 Hz, H-6α), 2.46 (dd, J = 15.3 and 2.6 Hz, H-9β), 2.31 (ddq, J = 13.6, 11, and 1.2 Hz, H-6β), 1.98 (d, 3H, J = 1.2 Hz, H-15), 1.70 (dd, J = 15.3 and 4.7 Hz, H-9α), 1.35 (s, 3H, H-14).

3-Oxo-7,8,11αH-eudesm-4-en-12,8-olide, ***19***

Lactone ***17a*** (210 mg, 0.85 mmol) was dissolved in benzene–ethanol 1:1 (15 mL) and hydrogenated for 14 h under the same conditions as **7** in the presence of Wilkinson catalyst (40 mg). Work-up and column chromatography (elution with hexane–EtOAc 7:3) afforded **19** (201 mg, 95%) as a white solid, mp 103–104°C (from hexane–CH_2Cl_2) (lit. (*7a*) mp 111–112°C); $[\alpha]_D^{25}$ +92° (lit. (*7a*) $[\alpha]_D^{23}$ +130.4°), with the expected ir, uv, and mass spectra; ^{1}H nmr, δ (ppm): 4.52 (apparent q, average J = 2.7 Hz, H-8), 2.90 (quintuplet, J = 7 Hz, H-11), 2.67 (dd, J = 13.9 and 5.8 Hz, H-6α), 2.54 (dddd, overlapped; H-7), 2.55–2.40 (m, 2H, H-2α and H-2β), 2.30 (dd, J = 15.5 and 2.5 Hz, H-9β), 1.96 (tq, J = 13.9 and 1.3 Hz, H-6β), 1.90–1.75 (m, 2H, H-1α/1β), 1.82 (d, 3H, J = 1.3 Hz, H-15), 1.72 (dd, J = 15.5 and 4.4 Hz, H-9α), 1.30 (s, 3H, H-14), 1.28 (d, 3H, J = 7 Hz, H-13).

3,3-Ethanedithio-7,8,11αH-eudesm-4-en-12,8-olide, ***20***

A modification of the published procedure (*7b*) was utilized: Lactone **19** (180 mg, 0.72 mmol), ethanedithiol (0.45 mL, 5.34 mmol), and $BF_3 \cdot OEt_2$ (40 μL) were dissolved in glacial acetic acid (3 mL) and stirred for 4 h at room temperature. The reaction mixture was then poured into water (20 mL) and extracted with CH_2Cl_2 (4 × 10 mL). The organic layer was washed with 5% aqueous $NaHCO_3$ and water, dried over anhydrous Na_2SO_4, filtered, and concentrated *in vacuo*. Column chromatography on silica gel (elution with hexane–EtOAc 19:1) yielded **20** (206 mg, 87%) as white needles, mp 138–139°C (from hexane–CH_2Cl_2) (lit. (*7b*) mp 141–143°C); $[\alpha]_D^{25}$ +51° (lit. (*7b*) $[\alpha]_D^{23}$ +50.3°), with the expected ir and mass spectra; ^{1}H nmr, δ (ppm): 4.45 (m, 1H, H-8), 3.40–3.20 (m, 4H, thioketal hydrogens), 2.81 (qd, J = 7.2 and 6.2 Hz, H-11), 2.44 (dd, J = 14.2 and 5.8 Hz, H-6α), 2.37 (m, 1H, overlapped, H-7), 2.25–2.10 (m, 2H, H-2α/2β), 2.18 (dd, J = 15.4 and 1.8 Hz, H-9β), 1.93 (d, 3H, J = 1.1 Hz, H-15), 1.80–1.60 (m, 3H, H-1α/1β and H-6β), 1.57 (dd, J = 15.4 and 4.4 Hz, H-9α), 1.22 (d, 3H, J = 7.2 Hz, H-13), 1.14 (s, 3H, H-14).

7,8,11αH-Eudesm-4-en-12,8-olide, ***21****, and 5,7,8,11αH-eudesm-3-en-12,8-olide,* ***22***

Approximately 4 g active W-2 Raney nickel were added at once to a solution of thioketal **20** (195 mg, 0.6 mmol) in 6 mL MeOH. The mixture was stirred for 10 min at room temperature and the reaction was quenched by rapid addition of ethanedithiol (0.2 mL). Work-up as above (**12** → **14**) and column chromatography on silica gel (elution with hexane–EtOAc 9:1) yielded first **21** (81 mg, 57%) as a colorless oil, lit. (17) solid mp 59–62°C; $[\alpha]_D^{25}$ +47° (lit. (17) $[\alpha]_D^{20}$ +29.7°); its enantiomer has been reported to be an oil, $[\alpha]_D$ −53° (11, 19); ^{1}H nmr, δ (ppm): 4.45 (td, J = 4 and 2 Hz, H-8), 2.78 (qd, J = 7.2 and 6.2 Hz, H-11), 2.46 (dd, J = 13.9 and 5.8 Hz, H-6α), 2.29 (dddd, J = 12.2, 6.2, 5.8, and 4 Hz, H-7), 2.13 (dd, J = 15.3 and 2 Hz, H-9β), 2.00–1.65 (m, 3H, H-3α/3β and H-6β), 1.64 (br s, 3H, H-15), 1.54 (dd, J = 15.3 and 4 Hz, overlapped; H-9α), 1.22 (d, 3H, J = 7.2 Hz, H-13), 1.11 (s, 3H, H-14). High resolution molecular weight determination, *Mol. Wt.* calcd. for $C_{15}H_{22}O_2$: 234.1620; found: 234.1618.

Further elution with the same solvent mixture gave 18 mg (13%) of a solid compound, mp 106–107°C (from hexane–EtOAc); $[\alpha]_D^{25}$ +7°, which was assigned structure **22** on the basis of its spectral properties: ir (KBr), ν_{max}: 1765 (s), 1755 (s), 1165 (s) cm^{-1}; ^{1}H nmr at 500 MHz, δ (ppm): 5.36 (m, 1H, H-3), 4.48 (td, J = 4.3 and 1.8 Hz, H-8), 2.79 (quintuplet, J = 7.1 Hz, H-11), 2.39 (dddd, J = 12.4, 7.1, 6.2, and 4.3 Hz, H-7), 2.12 (dd, J = 15.3 and 1.8 Hz, H-9β), 2.10–1.90 (m, 2H, H-2α/2β), 1.88 (br d, $J \simeq$ 13.6 Hz, H-5), 1.74 (ddd, J = 13.6, 6.2, and 2.6 Hz, H-6α), 1.63 (br s, 3H, H-15), 1.44 (dd, J = 12.6 and 6.4 Hz, H-1β), 1.39 (dd, J = 15.3 and 4.3 Hz, H-9α), 1.30 (td, J = 12.6 and 6.5 Hz, H-1α), 1.20 (d, 3H, J = 7.1 Hz, H-13), 1.01 (td, J = 13.6 and 12.4 Hz, H-6β), 0.87 (s, 3H, H-14); ms, m/z (% rel. int.): 234 (M^+, 28), 219 (59), 173 (21), 161 (38), 145 (100). High resolution molecular weight determination, *Mol. Wt.* calcd. for $C_{15}H_{22}O_2$: 234.1620; found: 234.1612. *Anal.* calcd. for $C_{15}H_{22}O_2$: C 76.92, H 9.40; found: C 76.76, H 9.51.

11α-Phenylseleno-7,8αH-eudesm-4-en-12,8-olide, ***23***

A solution of *n*BuLi (0.75 mL of a 1.6 *M* solution in hexane,

1.2 mmol) was added at room temperature under Ar via syringe to a solution of diisopropylamine (0.18 mL, 1.26 mmol) and TMEDA (0.55 mL, 3.61 mmol) in dry THF (2 mL). After stirring for 5 min, the mixture was cooled to −23°C (Dry Ice – CCl_4 bath). Lactone **21** (70 mg, 0.3 mmol) was dissolved in dry THF (2 mL) and added dropwise (5 min) to the cooled LDA/TMEDA solution. After stirring for 1 h at −23°C, a solution of PhSeCl (230 mg, 1.2 mmol) and HMPT (0.2 mL) in dry THF (2 mL) was added dropwise (10 min) via syringe. The reaction mixture was stirred for 1 h at −23°C and quenched at this temperature with 0.5 *N* HCl (2 mL). The reaction mixture was then poured into water (15 mL) and extracted with EtOAc (4 × 15 mL). The organic layer was washed twice with brine, dried over anhydrous Na_2SO_4, filtered, and concentrated *in vacuo*. Column chromatography of the yellowish oily residue (elution with hexane–EtOAc 19:1) yielded **23** (71 mg, 66% based on recovered **21**) as almost colorless crystals, mp 134–135°C (from hexane–CH_2Cl_2); ir (KBr), ν_{max}: 1765 (s), 1170 (m), 740 (m), 690 (m); ^{1}H nmr, δ (ppm): 7.65–7.25 (m, 5H, aromatic hydrogens), 5.01 (m, 1H, H-8), 2.54 (dd, J = 13.6 and 5.9 Hz, H-6α), 2.27 (ddd, J = 12.4, 5.9, and 4.1 Hz, H-7), 2.16 (dd, J = 15.4 and 4.1 Hz, H-9β), 2.00–1.80 (m, 2H, H-3α/3β), 1.81 (dd, J = 13.6 and 12.4 Hz, H-6β), 1.62 (br s, 3H, H-15), 1.59 (dd, J = 15.4 and 4.4 Hz, H-9α), 1.55 (s, 3H, H-13), 1.10 (s, 3H, H-14). *Anal.* calcd. for $C_{21}H_{26}O_2Se$: C 64.79, H 6.68, Se 20.30; found: C 64.88, H 6.58, Se 20.12.

Further elution with the same solvent mixture led to the recovery of unreacted **21** (7 mg).

1-Deoxyivangustin, 3 and 8αH-eudesma-4,7(11)-dien-12,8-olide, 24

Hydrogen peroxide (0.18 mL of a 30% aqueous solution, ca. 1.6 mmol) was added at 0°C to a solution of **23** (63 mg, 0.16 mmol) and AcOH (20 μL) in THF (1.5 mL). After stirring for 1 h at 0°C, the reaction mixture was poured into 5% aqueous $NaHCO_3$ (8 mL) and extracted with EtOAc (4 × 5 mL). The organic layer was washed several times with brine, dried over anhydrous Na_2SO_4, filtered, and concentrated *in vacuo*. Column chromatography on silica gel (elution with hexane–EtOAc 9:1) gave first 5 mg of a colorless oil (13%), $[\alpha]_D^{25}$ +46°, identified with 1-deoxyivangustin **3** (lit. (8) $[\alpha]_D^{24}$ +35.2°); lit. $[\alpha]_D$ for the enantiomer (11) is surprisingly different in its absolute value (−119°); ir (film), ν_{max}: 1760 (s), 1260 (m), 1115 (m) cm^{-1}; ^{1}H nmr, δ (ppm): 6.23 (d, J = 2.6 Hz, H-13′), 5.60 (d, J = 2.4 Hz, H-13), 4.49 (apparent q, average J = 6.9 Hz, A-part of a strongly coupled AXX′Y-system; H-8), 3.05 (dtt, J = 10, 7.3, and 2.5 Hz, H-7), 2.80 (dd, J = 13.2 and 7.3 Hz, H-6α), 2.10–1.90 (m, 3H, H-3α/3β and H-6β), 1.74 (d, 2H, J = 6.9 Hz, XX′ part of a AXX′Y-system; H-9α/9β), 1.66 (br s, 3H, H-15), 1.08 (s, 3H, H-14); ms, m/z (% rel. int.): 232 (M^+, 36), 217 (100), 199 (12), 171 (55), 145 (53). High resolution molecular weight determination, *Mol. Wt.* calcd. for $C_{15}H_{20}O_2$: 232.1463; found: 232.1456.

Further elution with the same solvent mixture gave 23 mg (61%) of an unstable colorless oil, $[\alpha]_D^{25}$ −76°, which was assigned structure **24** on the basis of its spectral properties; ir (film), ν_{max}: 1750 (s), 1685 (m), 1680 (m), 1025 (m) cm^{-1}; uv, λ_{max} (log ε_{max}): 216 (3.99), 272 (3.76); ^{1}H nmr, δ (ppm): 4.70 (ddq, J = 9.3, 8.2, and 1.9 Hz, H-8), 3.35 (dq, J = 19.8 and 1 Hz, H-6α), 3.25 (dq, J = 19.8 and 1.9 Hz, H-6β), 2.24 (dd, J = 13.3 and 9.3 Hz, H-9β), 2.05–1.85 (m, 2H, H-3α/3β), 1.83 (td, J = 1.9 and 1 Hz, H-13), 1.65 (q, J = 1 Hz, H-15), 1.41 (dd, J = 13.3 and 8.2 Hz, H-9α), 0.94 (s, 3H, H-14); ms, m/z (% rel. int.): 232 (M^+, 39), 217 (100), 199 (9), 189 (15), 171 (12), 161 (22). High resolution molecular weight determination, *Mol. Wt.* calcd. for $C_{15}H_{20}O_2$: 232.1463; found: 232.1460.

Acknowledgements

We are deeply indebted to Professor D. H. R. Barton, Gif-sur-Yvette, for a generous supply of artemisin and to Professors F. Bohlmann, Berlin, and D. S. Caine, Alabama, for the sending of spectra of natural eudesmanolides. We also thank Dr. M. Spraul, Bruker Company, Karlsruhe, West Germany, for recording an ^{1}H nmr spectrum at 500 MHz.

1. H. M. R. Hoffmann and J. Rabe. Angew. Chem. **97**, 96 (1985); Angew. Chem. Int. Ed. Engl. **24**, 94 (1985).
2. C. H. Heathcock. *In* The total synthesis of natural products. Vol. 2. *Edited by* J. ApSimon. John Wiley & Sons, New York. 1973. Chapt. 2.
3. C. H. Heathcock, S. L. Graham, M. C. Pirrung, F. Plavac, and C. T. White. *In* The total synthesis of natural products. Vol. 5. *Edited by* J. ApSimon. John Wiley & Sons, New York. 1983.
4. (*a*) M. Arno, B. Garcia, J. R. Pedro, and E. Seoane. Tetrahedron Lett. 1741 (1983); (*b*) M. Arno, M. Carda, J. A. Marco, and E. Seoane. Chem. Lett. 1021 (1984); (*c*) M. Arno, B. Garcia, J. R. Pedro, and E. Seoane. Tetrahedron, **40**, 5243 (1984); (*d*) M. Arno, B. Garcia, J. R. Pedro, and E. Seoane. An. Quím. Ser. C, **80**, 277 (1984); (*e*) M. Carda, M. Arno, and J. A. Marco. Tetrahedron, **42**, 3655 (1986).
5. T. A. Geissman. J. Org. Chem. **31**, 2523 (1966).
6. D. S. Caine and G. Hasenhuettl. J. Org. Chem. **45**, 3278 (1980).
7. (*a*) K. Yamakawa, K. Nishitani, A. Murakami, and A. Yamamoto. Chem. Pharm. Bull. **31**, 3397 (1983); (*b*) K. Yamakawa, K. Nishitani, and A. Murakami. Chem. Pharm. Bull. **31**, 3411 (1983).
8. F. Bohlmann, P. K. Mahanta, J. Jakupovic, R. C. Rastogi, and A. A. Natu. Phytochemistry, **17**, 1165 (1978).
9. F. Bohlmann, C. Trinks, J. Jakupovic, and S. Huneck. Phytochemistry, **24**, 995 (1985).
10. P. Bhandari and R. P. Rastogi. Indian J. Chem. Sect. B, **22**, 286 (1983).
11. Y. Ohta, N. H. Andersen, and C.-B. Liu. Tetrahedron, **33**, 617 (1977).
12. (*a*) M. Nakazaki and K. Naemura. Tetrahedron Lett. 2615 (1966); (*b*) Bull. Chem. Soc. Jpn. **42**, 3366 (1969).
13. E. Piers and K. F. Cheng. Can. J. Chem. **46**, 377 (1968).
14. M. Sumi. J. Am. Chem. Soc. **80**, 4869 (1958).
15. W. Cocker and M. A. Nisbet. J. Chem. Soc. 534 (1963).
16. A. E. Greene, J.-C. Muller, and G. Ourisson. J. Org. Chem. **39**, 186 (1974).
17. K. Naemura and M. Nakazaki. Tetrahedron Lett. 33 (1969).
18. R. W. Ratcliffe. Org. Synth. **55**, 84 (1976).
19. Y. Asakawa, M. Toyota, T. Takemoto, and C. Suire. Phytochemistry, **18**, 1007 (1979).

Can. J. Chem. Downloaded from www.nrcresearchpress.com by 80.58.250.72 on 09/07/12
For personal use only.

Isomeric 6*H*,8*H*-naphthyridino-1,3-benzothiazin-8-ones

LAJOS FODOR[1] AND DAVID B. MACLEAN[2]

Department of Chemistry, McMaster University, Hamilton, Ont., Canada L8S 4M1

Received July 21, 1986

LAJOS FODOR and DAVID B. MACLEAN. Can. J. Chem. **65**, 636 (1987).

The synthesis of the ring system present in two of the four possible isomeric 6*H*,8*H*-naphthyridino-1,3-benzothiazines is reported here for the first time. 2,3-Dimethoxy-6*H*,8*H*-[2,7]naphthyridino[2,3-*c*][1,3]benzothiazin-8-one (**5**) and several related compounds have been prepared by both chemical and photochemical methods. 2,3-Dimethoxy-6*H*,8*H*-[1,6]naphthyridino[6,7-*c*][1,3]benzothiazin-8-one (**9**) has been isolated in 15% yield along with **5** in 38% yield on irradiation of 6,7-dimethoxy-3-nicotinoyl-4-methylidene-2*H*-1,3-benzothiazine (**8**).

LAJOS FODOR et DAVID B. MACLEAN. Can. J. Chem. **65**, 636 (1987).

On rapporte la première synthèse du système cyclique que l'on retrouve dans deux des quatre isomères possibles des 6*H*,8*H*-naphtyridinobenzothiazines-1,3. Utilisant des méthodes tant chimiques que photochimiques, on a préparé la diméthoxy-2,3 6*H*,8*H*-[2,7]naphtyridino-[2,3-*c*][1,3]-benzothiazinone-8 (**5**) et plusieurs composés apparentés. On a isolé la diméthoxy-2,3 6*H*,8*H*-[1,6]naphtyridino-[6,7-*c*][1,3]-benzothiazinone-8 (**9**) avec un rendement de 15% aux côtés de 38% du composé **5** lorsqu'on a effectué l'irradiation de la diméthoxy-6,7 nicotinoyl-3 méthylène-4 2*H*-benzothiazine-1,3 (**8**).

[Traduit par la revue]

There are four possible isomeric 6*H*,8*H*-naphthyridino[1,3]-benzothiazines (**I**–**IV**) as illustrated in the accompanying formulas. To our knowledge, the synthesis of these ring systems has not been reported. The four six-membered rings present in **I**–**IV** have the same array as the 8*H*-dibenzo[*a*,*g*]quinolizines (**V**), the 6*H*,8*H*-isoquino[2,3-*c*][1,3]benzothiazines (**VI**), and the 6*H*,8*H*-isoquino[2,1-*b*][2,7]naphthyridines (**VII**). A general route to ring systems **V** (1, 2), **VI** (3), and **VII** (4, 5) has been developed in this laboratory, involving the condensation of a bicyclic imine (a 3,4-dihydro-isoquinoline in the case of **V** and **VII** and a 2*H*-1,3-benzothiazine in the case of **VI**) with a phthalide anion in the case of **V** and **VI** and an azaphthalide anion in the case of **VII**. Another general approach to ring systems **V** and **VII** has been developed by Lenz (6, 7) and by Ninomiya and co-workers (8, 9), involving the photochemical cyclization of enamides such as **VIII** and **IX**, respectively. Here we report the application of these general procedures to the synthesis of compounds containing ring systems **II** and **IV**.

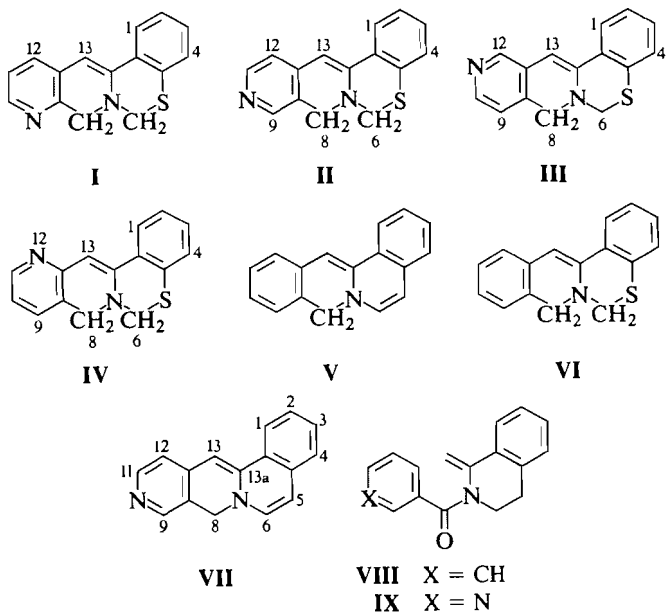

I **II** **III**

IV **V** **VI**

VII **VIII** X = CH; **IX** X = N

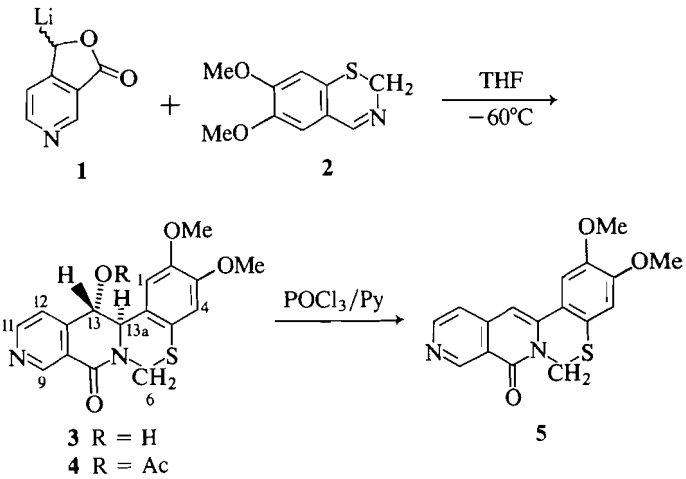

1 **2**

3 R = H; **4** R = Ac

5

SCHEME 1

Compounds of structure **II** have been prepared as shown in Scheme 1. A solution of the lithium salt of azaphthalide **1** (4, 5) in tetrahydrofuran (THF) at −60°C was treated with a solution of 6,7-dimethoxy-2*H*-1,3-benzothiazine (**2**) in THF at −60°C for 2 h and for a longer period at 20°C. The product of reaction isolated on work-up was the racemic, crystalline lactam alcohol (**3**). The relative stereochemistry of **3** at C-13 and C-13a is similar to that observed for compounds prepared in related condensations (1–5) and was established through nmr examination of **3** and its *O*-acetate (**4**). Dehydration of **3** through treatment with $POCl_3$ in pyridine yielded **5**. The spectroscopic properties of compounds **3**–**5** are compatible with the assigned structures.

The ^1H nmr spectra of **3** and **4** show three aromatic singlets, the two at highest field being assigned to hydrogen atoms at C-1 and C-4 and that at lowest field to the hydrogen atom at C-9. An AB quartet in the aromatic region present in each spectrum is attributed to signals for hydrogen atoms at C-11 and C-12, the former being at lower field. In each spectrum the hydrogen atoms at C-6 appear as an AB quartet. In the case of the alcohol (**3**) the signals are centered at δ 4.20 and δ 5.77, and in the case of the acetate at δ 4.08 and δ 5.85; the lower field proton in each case was assigned to the equatorial proton. The signals for the methoxy groups are in the usual position for aromatic methoxy groups. The protons at C-13 and C-13a appear, respectively, at

[1]Present address: Central Laboratory, County Hospital, H-5701, Gyula, POB 46, Hungary.

[2]Author to whom correspondence may be addressed.

Can. J. Chem. Downloaded from www.nrcresearchpress.com by 80.58.250.72 on 09/07/12
For personal use only.

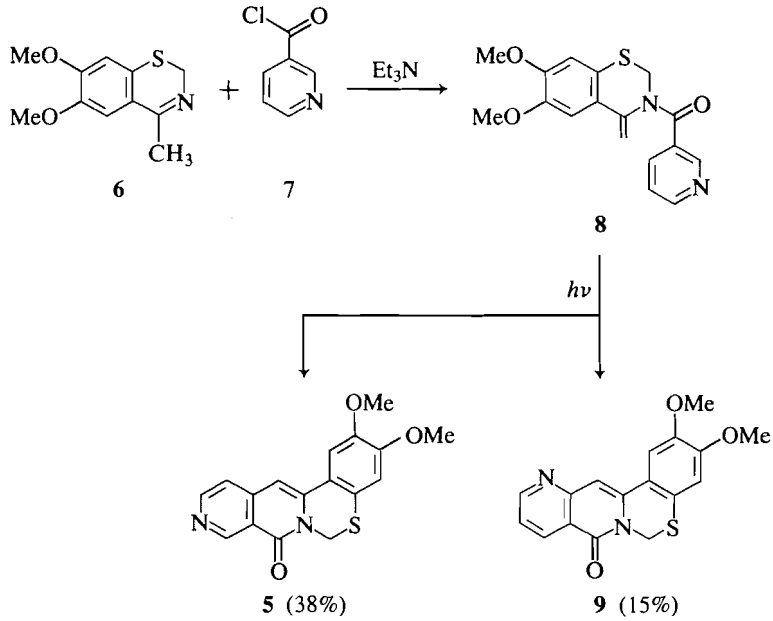

6 7 8

5 (38%) 9 (15%)

SCHEME 2

δ 4.79 and 4.95 in **3** and at δ 6.24 and 5.02 in **4**. The coupling constants, $J = 9.3$ Hz for **3** and $J = 9.5$ Hz for **4**, indicate that the vicinal hydrogen atoms are *trans* to one another.

The ^{1}H nmr spectrum of **5**, aside from the signals of the two methoxy groups and the two hydrogen atoms at C-6, shows signals only in the aromatic region. Noteworthy is the presence of a signal at δ 7.24 assigned to C-13 H.

The ^{13}C nmr spectra of **3** and **5** were also recorded and agree with the structures assigned.

The mass spectrum of **3** is very similar to the spectra observed for analogous compounds of ring systems **V** (2), **VI** (3), and **VII** (5). Compound **4** suffers loss of acetic acid on electron ionization yielding an ion of m/z 326, which corresponds to the molecular ion of **5**. In the case of both **4** and **5** the ion of m/z 326 loses SH to form a fragment ion of m/z 293, which is the base peak in each spectrum. This behaviour is similar to that observed for analogous compounds of ring system **VI** (3).

We also examined a photochemical route to the preparation of compounds of ring systems **II** and **IV**. To this end we prepared the enamide **8** by condensation of 4-methyl-2*H*-1,3-benzothiazine (**6**) with nicotinoyl chloride (**7**) in the presence of triethylamine. The enamide was then irradiated in methanol solution, in a water-cooled apparatus, with a low pressure mercury lamp for 5 h. On work-up of the reaction mixture, compound **5** was isolated in 38% yield and its isomer **9** in 15% yield (see Scheme 2). In accord with previous experience in related systems (6–9), none of the dihydro derivatives of **5** and **9** were detected, although they might be expected to be the initial products of the photochemical reaction.

The structure of **9**, like that of **5**, rests upon a spectroscopic analysis. The major difference between the ^{1}H nmr spectrum of **9** and that of **5** lies in the signals associated with the hydrogen atoms of the pyridine ring. In compound **5** the three signals were observed as a singlet and an AB quartet; in **9** the three protons are contiguous and the three signals are observed as multiplets appearing at δ 7.40, 8.71, and 8.90. The lowest field signal in **5** appeared at δ 9.56, a consequence of its position adjacent to both the pyridine nitrogen and the lactam. There is no proton similarly situated in **9**, where the lowest field proton appears at δ 8.90.

In this investigation we have effected the synthesis of two (**II** and **IV**) of the four possible ring systems present in the isomeric naphthyridino-1,3-benzothiazines. The two remaining ring systems (**I** and **III**) should be obtainable by application of one or other of the general methods applied in this study provided that the requisite starting materials may be prepared. Ring system **II** is a thia analogue of the ring system present in several alkaloids of *Alangium lamarckii Thw.* (9*b*, and references therein).

Experimental

The ^{1}H nmr spectra were recorded on a Bruker AM500 at 500 MHz and the ^{13}C nmr spectra on the same instrument at 125.8 MHz. The samples were dissolved in $CDCl_3$ using tetramethylsilane (TMS) as internal standard; chemical shifts are reported in ppm (δ) downfield from TMS. The symbols, s (singlet), d (doublet), t (triplet), q (quartet), m (multiplet), and br (broadened), are used to report the multiplicity and shape of the signals. EI mass spectra were recorded either on a VG Micromass 7070F or a VG ZAB E mass spectrometer at an ionizing voltage of 70 eV. Infrared spectra were recorded on a Perkin–Elmer 283 infrared spectrometer. Melting points were determined using a Gallenkamp apparatus and are uncorrected.

6,7-Dimethoxy-2*H*-1,3-benzothiazine (**2**) (10, 11), 6,7-dimethoxy-4-methyl-2*H*-1,3-benzothiazine (**6**) (10, 11), and furo[3,4-*c*]-pyridin-3-(1*H*)-one (azaphthalide) (4, 5) were prepared as described in the literature. Nicotinic acid was obtained commercially.

*(13*R*,*13a*R*)-13,13a-Dihydro-13-hydroxy-2,3-dimethoxy-6*H,*8*H-*[2,7]naphthyridino[2,3-c][1,3]benzothiazino-8-one (3)*

A stirred solution of 1,1,1,3,3,3-hexamethyldisilazine (0.38 mL, 1.78 mmol) in dry THF (5 mL) at −20°C was treated with *n*BuLi (1.78 mmol) (1.202 mL of 1.48 *M* solution in hexane). The mixture was then cooled to −60°C and a solution of azaphthalide (0.200 g, 1.48 mmol) in dry THF (5 mL) was added dropwise, producing an orange solution that was stirred for another 15 min at −60°C. 6,7-Dimethoxy-2*H*-1,3-benzothiazine (0.30 g, 1.48 mmol) in dry THF (5 mL) was added dropwise and, when addition was complete, the stirring was continued for another 2 h. The temperature was allowed to rise to 20°C and the reaction mixture was left overnight before work-up. The solvent was evaporated, water was added, and the mixture extracted several times with $CHCl_3$. The extract was dried over Na_2SO_4 and evaporated, yielding a yellow oil that was recrystallized from ethanol (0.316 g, 62.1%), mp 259–262°C; ir, ν_{max}($CHCl_3$):

Can. J. Chem. Downloaded from www.nrcresearchpress.com by 80.58.250.72 on 09/07/12
For personal use only.

Can. J. Chem. Downloaded from www.nrcresearchpress.com by 80.58.250.72 on 09/07/12
For personal use only.

3600, 1655 cm^{-1}; ^1H nmr (500 MHz, $CDCl_3$), δ: 3.77 (3H, s, OMe), 3.80 (3H, s, OMe), 4.20 (1H, d, J = 12.3 Hz, C-6 H_{ax}), 4.79 (1H, m, C-13 H), 4.95 (1H, d, J = 9.3 Hz, C-13a H), 5.77 (1H, d, J = 12.3 Hz, H-6_{eq}), 6.28 (1H, d, J = 7.4 Hz, OH), 6.95 (1H, s, C-1 H or C-4 H), 7.06 (1H, s, C-4 H or C-1 H), 7.67 (1H, d, J = 5.0 Hz, C-1), 8.8 (1H, d, J = 5.0 Hz, C-10 H), 9.00 (1H, s, C-9 H); ^{13}C nmr (125.8 MHz, DMSO-d_6), δ: 43.2 (C-6), 55.6 and 55.7 (2 × OMe), 61.4 (C-13a), 67.6 (C-13), 112.0, 114.9, 119.8, 122.3, 123.5, 124.7, 146.1, 148.0, 148.3, 150.2, 153.1 (aromatic C's), 160.8 (C-8); ms (EI), m/z (rel. int.): 344 (44) $M^{+\cdot}$, 326 (11), 293 (15), 210 (100), 135 (13). *Mol. Wt.* (hrms) calcd. for $C_{17}H_{16}N_2O_4S$: 344.0830; found: 344.0819.

O-*Acetyl derivative (3)*

Compound (**3**) (50 mg) was dissolved in pyridine and treated with an excess of acetic anhydride (2 mL). The mixture was kept in a stoppered flask for 8 h, the excess reagent removed under vacuum, and water (5 mL) added to the residue. The aqueous suspension was extracted with $CHCl_3$, the extract dried over Na_2SO_4, and evaporated to dryness. The *O*-acetate (**4**) (49 mg, 88%) crystallized from methanol, mp 243–245°C; ^1H nmr (500 MHz, $CDCl_3$), δ: 2.10 (3H, s, CH_3CO), 3.86, 3.88 (6H, 2 × s, 2 × OMe), 4.08 (1H, d, J = 12.3 Hz, C-6 H_{ax}), 5.02 (1H, d, J = 9.5 Hz, C-13a), 5.85 (1H, d, J = 12.3 Hz, C-6 H_{eq}), 6.24 (1H, d, J = 9.5 Hz, C-13 H), 6.70 (1H, s, C-1 or C-4 H), 6.84 (1H, s, C-1 or C-4 H), 7.28 (1H, d, J = 5.0 Hz, C-12 H), 8.79 (1H, d, J = 5.0 Hz, C-11 H), 9.24 (1H, s, C-9 H); ms (EI), m/z (rel. int.): 386 (10)$M^{+\cdot}$, 326 (71), 293 (100). *Mol. Wt.* (hrms) calcd. for $C_{19}H_{18}N_2O_5S$: 386.0934; found: 386.0927.

*2,3-Dimethoxy-6*H,*8*H-*[2,7]naphthyridino[2,3-c][1,3]benzothiazin-8-one (5)*

The lactam (**3**) (150 mg), in dry pyridine (5 mL) was treated with freshly distilled $POCl_3$ (1.5 mL) and the mixture left at room temperature for 3 h. The volatile reagents were evaporated under reduced pressure, the residue taken up in H_2O (20 mL), the solution made alkaline with sodium carbonate, and the mixture extracted with $CHCl_3$. The extract was taken to dryness under reduced pressure and the last traces of pyridine removed from the residue by codistillation with benzene. The residue, freed of pyridine, was crystallized from ethanol. The product (114 mg, 80.2%) melted at 246–248°C; ir, ν_{max}($CHCl_3$): 1660; ^1H nmr (500 MHz, $CDCl_3$), δ: 3.95 (3H, s, OMe), 4.00 (3H, s, OMe), 5.35 (2H, br s, C-6 H's), 6.69 (1H, s, C-1 or C-4 H), 6.89 (1H, s, C-1 or C-4 H), 7.24 (1H, s, C-13 H), 7.39 (1H, d, J = 5.1 Hz, C-12 H), 8.69 (1H, d, J = 5.1 Hz, C-11 H), 9.56 (1H, s, C-9 H); ^{13}C nmr (125.8 MHz, $CDCl_3$), δ: 42.6 (C-6), 56.4, 56.5 (2 × OMe), 101.8, 110.6, 111.2, 119.5, 119.6, 122.5, 129.2, 142.7, 143.0, 148.8, 149.3, 150.6, 151.7 (aromatic C's), 160.4 (*C*=O); ms (EI), m/z (rel. int.): 326 ($M^{+\cdot}$) (77), 293 (100), 277 (8). *Mol. Wt.* (hrms) calcd. for $C_{17}H_{14}N_2O_3S$: 326.0715; found: 326.0720. *Anal.* calcd. for $C_{17}H_{14}N_2O_3S$: C 62.6, H 4.3, N 8.6; found: C 62.3, H 4.2, N 8.4%.

*4-Methylidene-6,7-dimethoxy-3-nicotinoyl-2*H-*1,3-benzothiazine (8)*

A mixture of nicotinic acid (1.77 g, 0.01 mol) and thionyl chloride was heated under reflux in a nitrogen atmosphere for 3 h. The excess thionyl chloride was removed by distillation. The remaining traces of $SOCl_2$ were removed by codistillation with benzene (20 mL) and the process was repeated twice more. To the white solid remaining in the flask were added CH_2Cl_2 (50 mL) and triethylamine (10 mL) and the mixture was stirred under an atmosphere of dry nitrogen. A solution of 6,7-dimethoxy-4-methyl-2*H*-1,3-benzothiazine (0.557 g, 0.0025 mol) dissolved in CH_2Cl_2 (20 mL) was then added and the solution was heated under reflux for 2 h. The solvent was removed, yielding a brown oil that crystallized from ethanol (0.762 g, 92.9%), mp 154–155°C; ir, ν_{max}($CHCl_3$): 1665 cm^{-1}; ^1H nmr (500 MHz, $CDCl_3$), δ: 3.88 (3H, s, OMe), 3.90 (3H, s, OMe), 4.52 (1H, d, J = 1.5 Hz, vinyl H), 5.20 (2H, s, C-2 H's), 5.42 (1H, d, J = 1.5 Hz, vinyl H), 6.67 (1H, s, C-5 H or C-8 H), 7.04 (1H, s, C-5 H or C-8 H), 7.29 (1H, m, C-4′ or C-5′ H), 7.76 (1H, m, C-4′ or C-5′ H), 8.61 (2H, m, C-2′ H and C-6′ H); ^{13}C nmr (125.8 MHz, $CDCl_3$), δ: 44.6 (C-2), 56.2 (2 × OMe), 108.5, 108.6, 110.4, 119.5, 123.1, 124.6, 131.5, 135.9, 141.4, 147.6, 148.9, 150.5, 150.9 (aromatic vinylic C-atoms), 166.7 (C=O); ms (EI), m/z (rel. int.): 328 (41) $M^{+\cdot}$, 327 (32), 300 (76), 299 (38), 194 (83), 106 (81), 78 (100). *Mol. Wt.* (hrms) calcd. for $C_{17}H_{16}N_2O_3S$: 328.0881; found: 328.0896. *Anal.* calcd. for $C_{17}H_{16}N_2O_3S$: C 62.2, H 4.9, N 8.5; found: C 62.5, H 5.4, N 8.3%.

*Irradiation of 6,7-dimethoxy-3-nicotinoyl-4-methylidene-2*H-*1,3-benzothiazine (8)*

A solution of compound **8** (0.566 g) in methanol (80 mL) deoxygenated with bubbling N_2 was irradiated for 5 h with a 10-watt Osram low pressure mercury lamp using a Vycor filter in a water cooled immersion well vessel. The reaction mixture was evaporated to dryness, dissolved in a minimum amount of $CHCl_3$, and chromatographed on a silica column. The column was developed with a 1% solution of MeOH in $CHCl_3$. The first compound to be eluted (0.212 g, 37.7%) was identical with **5** described above. The identity was established by a comparison of its spectroscopic properties (^1H nmr, ms), its mp, and its tlc behaviour. The second compound eluted from the column (0.083 g, 14.8%) melted at 234–237°C (ethanol); ^1H nmr (500 MHz, $CDCl_3$), δ: 3.95 (3H, s, OMe), 3.97 (3H, s, OMe), 5.37 (2H, brs, C-6 H), 6.89 (1H, s, C-1 or C-4 H), 7.15 (1H, s, C-1 or C-4 H), 7.34 (1H, s, C-13 H), 7.40 (1H, m, C-10 H), 8.71 (1H, m, C-9 H), 8.90 (1H, m, C-11 H); ^{13}C nmr (125.8 MHz, $CDCl_3$), δ: 43.0 (C-6), 56.5 (2 × OMe), 104.2, 110.5, 111.1, 120.8, 121.4, 122.7, 127.4, 138.3, 141.9, 148.9, 151.5, 152.1 (aromatic and vinylic C-atoms), 166.8 (*C*=O); ms (EI), m/z (rel. int.): 326 (85) $M^{+\cdot}$, 293 (100), 277 (7); *Mol. Wt.* (hrms) calcd. for $C_{17}H_{14}N_2O_3S$: 326.0726; found: 326.0726.

Acknowledgements

We gratefully acknowledge financial support from the Natural Sciences and Engineering Research Council of Canada through an International Scientific Exchange Award and an Operating Grant. We thank Dr. W. J. Leigh of this Department for making available to us his photochemical equipment and Mr. B. Sayer for recording the nmr spectra.

1. R. Marsden and D. B. MacLean. Tetrahedron Lett. 2036 (1983).
2. R. Marsden and D. B. MacLean. Can. J. Chem. **62**, 1392 (1984).
3. R. Marsden, D. B. MacLean, and L. Fodor. Can. J. Chem. **62**, 2682 (1984).
4. D. B. MacLean. *In* Stud. Org. Chem. (Amsterdam), *Edited by* R. I. Zalewski and J. J. Skolik. Elsevier, Amsterdam. 1985. p. 113.
5. Jahangir, D. B. MacLean, and H. L. Holland. Can. J. Chem. **64**, 1031 (1986).
6. G. R. Lenz. Synthesis, 489 (1978).
7. G. R. Lenz. J. Heterocycl. Chem. **16**, 433 (1979).
8. I. Ninomiya, T. Naito, and H. Takasugi. J. Chem. Soc. Perkin Trans. 1, 1720 (1975).
9. (*a*) T. Naito and I. Ninomiya. Heterocycles, **14**, 959 (1980); (*b*) T. Naito, O. Miyata, I. Ninomiya, and S. C. Pakrashi. Heterocycles, **16**, 725 (1981).
10. J. Szabo, L. Fodor, I. Varga, E. Vinkler, and P. Sohar. Acta Chim. Acad. Sci. Hung. **92**, 317 (1977).
11. J. Szabo, L. Fodor, I. Varga, and P. Sohar. Acta. Chim. Acad. Sci. Hung. **88**, 149 (1976).

Raman and far-infrared spectra of triphenyltin isochalcocyanates and their adducts with *O*- and *N*-donor ligands: the crystal and molecular structure of isocyanato-triphenyl(pyridine-*N*-oxide)tin[1]

IVOR WHARF, LARS PIEHLER, BRUCE M. SAILOFSKY, AND MARIO ONYSZCHUK[2]
Department of Chemistry, McGill University, Montreal, Que., Canada H3A 2K6

AND

MICHEL G. SIMARD
Département de Chimie, Université de Montréal, Montréal (P.Q.), Canada H3C 3V1

Received July 14, 1986

Can. J. Chem. Downloaded from www.nrcresearchpress.com by 80.58.250.72 on 09/07/12
For personal use only.

IVOR WHARF, LARS PIEHLER, BRUCE M. SAILOFSKY, MARIO ONYSZCHUK, and MICHEL G. SIMARD. Can. J. Chem. **65**, 639 (1987).

Solid state infrared and Raman data (350–100 cm^{-1}) are reported for Ph_3SnNCY (Y = O, S, Se) and their 1:1 adducts with hexamethylphosphoramide (HMPA), pyridine-*N*-oxide (pyO), 4-picoline-*N*-oxide (4-picO), triphenylphosphine oxide (Ph_3PO), and pyridine (py), as well as for $Ph_3SnNCSe \cdot L$ where L = β-pic (β-picoline) or γ-pic (γ-picoline), and assignments are given. The crystal structure of $Ph_3SnNCO \cdot pyO$ was determined by single crystal X-ray analysis. The compound crystallizes in space group *Pbca* with $a = 14.443(3)$, $b = 16.676(4)$, $c = 17.523(6)$ Å (−110°C); $Z = 8$. The structure was solved by the direct method and refined by full-matrix least-squares methods to $R = 0.024$ for 2086 observed reflections. The tin atom has distorted trigonal bipyramidal coordination with the isocyanate group and pyridine-*N*-oxide at the apices of the bipyramid and phenyl rings in the equatorial positions. Changes in ν(Sn—NCY) on adduct formation are correlated with either increased coordination at tin (Y = O) or breaking of strong chalcocyanate bridges with tin remaining five-coordinate (Y = S, Se).

IVOR WHARF, LARS PIEHLER, BRUCE M. SAILOFSKY, MARIO ONYSZCHUK et MICHEL G. SIMARD. Can. J. Chem. **65**, 639 (1987).

On a déterminé les spectres infrarouges et Raman (350–100 cm^{-1}), à l'état solide, des dérivés Ph_3SnNCY (Y = O, S, Se) et de leurs adduits 1:1 avec la pyridine, l'hexaméthylphosphoramide (HMPA) et avec les oxydes de la pyridine, de la picoline-4 et de la triphénylphosphine ainsi que des complexes $Ph_3SnNCSe \cdot L$ dans lesquels L = β-pic (β-picoline) ou γ-pic (γ-picoline) et on rapporte les attributions des bandes. On a déterminé la structure cristalline du composé $Ph_3SnNCO \cdot pyO$ par diffraction des rayons-X sur un cristal unique. Le composé cristallise dans le groupe d'espace *Pbca*, avec $a = 14{,}443(3)$, $b = 16{,}676(4)$ et $c = 17{,}523(6)$ Å (à −110°C) et $Z = 8$. On a résolu la structure par la méthode directe et on l'a affinée par les méthodes des moindres carrés jusqu'à une valeur de $R = 0{,}024$ pour 2086 réflexions observées. La coordination de l'étain est bipyramidale trigonale déformée, avec les groupements isocyanate et *N*-oxyde de la pyridine dans les positions apicales de la bipyramide et les noyaux phényles dans les positions équatoriales. On a établi une corrélation entre les changements dans les ν(Sn—NCY) qui se produisent lors de la formation de l'adduit avec soit une augmentation de la coordination au niveau de l'étain (Y = O) soit un bris des puissants ponts chalcocyanates avec l'étain penta-coordonné qui reste (Y = S, Se).

[Traduit par la revue]

Introduction

Triphenyltin compounds, principally the hydroxide and acetate, are used as agricultural fungicides (1), while Ph_3SnNCX (X = O, S, Se) and their adducts have also been tested for biological activity (2–5), following earlier studies of adducts formed by Ph_3SnNCS (6). Our knowledge of the vibrational spectra of triphenyltin pseudohalides is incomplete (7) and structures of their adducts have not yet been determined. Following our recent report on the mid-infrared spectra of $Ph_3SnNCSe$ and its adducts (8), we now present complete vibrational data (in the skeletal region) for Ph_3SnNCX (X = O, S, Se) and their adducts with some O— and N—donor ligands. In addition, one adduct, $Ph_3SnNCO \cdot pyO$, was chosen for X-ray analysis so that its structure could be compared with that of the parent Ph_3SnNCO (9). Our purpose is to obtain vibrational and structural data which would be useful in organotin chemistry, especially in evaluating the biological activity of pseudohalide derivatives.

[1]Presented in part by I.W. at the 69th Canadian Chemical Conference, Saskatoon, Sask., June 1–4, 1986, paper IN-A1-5.

[2]To whom correspondence should be addressed.

Experimental

Solvents and liquid ligands were stored over molecular sieves before use, while solid ligands were used as received as was triphenyltin chloride (Alfa). Other experimental details, e.g. microanalyses, and Raman (powder) and infrared (Nujol mull) spectral methods were as described elsewhere (10). Triphenyltin isoselenocyanate and its adducts were those prepared earlier (8), as was triphenyltin isothiocyanate (6) and its HMPA adduct (14).

Preparations

Triphenyltin isocyanate (A)

Potassium cyanate (7.0 g; 0.086 mol) was added to a solution of triphenyltin chloride (20 g; 0.05 mol) in methanol (500 mL) and the mixture was stirred at room temperature for 2 h. The mixture was poured into ice-cold water to give a white precipitate. After further stirring (20 min) the white *product* was filtered and recrystallized from toluene; yield, 31%, mp 95–97°C (lit. 98–99°C (11), 100–103°C (12), 73–75°C (13): ν(CN) 2219 cm^{-1} (ir). *Anal.* calcd. for $C_{19}H_{15}NOSn$: C 58.2, H 3.9, N 3.7; found: C 58.0, H 3.9, N 4.1.

Triphenyltin isocyanate – pyridine-N-oxide

A mixture of pyridine-*N*-oxide (0.13 g; 1.37 mmol) and **A** (0.50 g; 1.28 mmol) was stirred in dry pentane (30 mL) for 22 h at room temperature. The *product* was filtered and recrystallized from carbon

Can. J. Chem. Downloaded from www.nrcresearchpress.com by 80.58.250.72 on 09/07/12
For personal use only.

tetrachloride; yield, 71%, mp 120–122°C; ir data, ν(CN) 2205, ν(NO) 1213 cm^{-1}. *Anal.* calcd. for $C_{24}H_{20}N_2O_2Sn$: C 59.2, H 4.1, N 5.75; found: C 59.2, H 4.2, N 5.8.

*Triphenyltin isocyanate – 4-picoline-*N*-oxide*

A mixture of 4-picoline-*N*-oxide (0.15 g; 1.37 mmol) and **A** (0.50 g; 1.28 mmol) was stirred in toluene (35 mL) at room temperature for 24 h. The fine suspension obtained was filtered and dried in a vacuum for 1 h; yield, 62%, mp 149–152°C; ir data, ν(CN) 2202, ν(NO) 1225 cm^{-1}. *Anal.* calcd. for $C_{25}H_{22}N_2O_2Sn$: C 59.9, H 4.4, N 5.6; found: C 60.0, H 4.6, N 5.3.

*Triphenyltin isothiocyanate – 4-picoline-*N*-oxide*

Triphenyltin isothiocyanate (2.0 g; 4.9 mmol) was stirred with a toluene (80 mL) solution of 4-picoline-*N*-oxide (0.75 g; 6.9 mmol) until dissolved. An oil slowly formed and this was redissolved by warming the mixture. *Slow* cooling gave crystals of the adduct; yield, 89%, mp 135–136°C; ν(CN) 2057 (ir) 2056 (R), ν(NO) 1221 cm^{-1} (ir). *Anal.* calcd. for $C_{25}H_{22}N_2OSSn$: C 58.05, H 4.3, N 5.4; found: C 58.1, H 4.1, N 5.35.

Triphenyltin isocyanate – pyridine

A mixture of **A** (1.0 g; 2.6 mmol), pyridine (14 mL), and carbon tetrachloride (15 mL) was stirred for 22 h. *Dropwise* addition of pentane to the stirred ice-cold solution precipitated the *adduct*; yield, 41%, mp 89–90°C; ir data, ν(CN) 2185, pyridine modes [8*a*] 1595, [8*b*] 1576, [14] 1405 cm^{-1}. *Anal.* calcd. for $C_{24}H_{20}N_2OSn$: C 61.2, H 4.3, N 5.95; found: C 61.0, H 4.1, N 5.8.

Procedures similar to those given above or in the literature were used to prepare *$Ph_3SnNCO \cdot HMPA$*, mp 142–145°C (lit. 130°C (3)), *$Ph_3SnNCO \cdot Ph_3PO$*, mp 142–144°C (lit. 134°C (3)), *$Ph_3SnNCS \cdot Ph_3PO$*, mp 179–180°C (lit. 180°C (6)), *$Ph_3SnNCS \cdot pyO$*, mp 164–166°C (lit. 169°C (6)), and *$Ph_3SnNCS \cdot py$*, mp 158–161°C (lit. 162°C (6)).

X-ray analysis of $Ph_3SnCO \cdot pyO$

Crystal data

$C_{24}H_{20}N_2O_2Sn$ fw = 487.13

Orthorhombic, space group *Pbca*, a = 14.444(3), b = 16.676(4), c = 17.523(6) Å, V = 4220.7 Å^3, Z = 8, ρ_c = 1.533 g cm^{-3}, (−110°C; MoK$\bar{\alpha}$, λ = 0.71069 Å, graphite monochromator) and μ(MoKα) = 12.3 cm^{-1}; crystal dimensions, 0.15 (100, $\bar{1}$00) × 0.35 (010, 0$\bar{1}$0) × 0.48 (001, 00$\bar{1}$) mm, transmission range 0.66–0.83.

A well-formed crystal was mounted on an Enraf-Nonius CAD-4 diffractometer. A set of 25 reflections was collected using the automatic SEARCH routine of the CAD4 software and the unit cell was obtained by running the INDEX program. The Niggli parameters clearly showed a primitive orthorhombic space group. Oscillation photographs, taken along the three axes, showed mirror symmetry on the three films as expected, and the layer line separations corresponded to the lengths of the chosen axes. Reflections in the range $10° \leq \theta \leq 15°$ were used for the final centering and determining the orientation matrix. Fast pre-collection over the $hk0$, $h0l$, and $0kl$ planes showed the systematic absences, $hk0$, $h \neq 2n$, $h0l$, $l \neq 2n$, and $0kl$, $k \neq 2n$, which are consistent with the space group *Pbca*.

The selenium analogue, $Ph_3SnNCSe \cdot pyO$, was also studied at room temperature using the same techniques. The crystal data[3] show the two compounds are isostructural.

The intensity data were collected using the $\omega/2\theta$ technique at low temperature to augment the intensity of high angle reflections. A fixed slit of 4.0 mm was used and the scan range was ω = (1.00 + 0.35 tan θ)°, extended 25% on either side for background measurement. All reflections were collected at the same rate of 1.7 min^{-1}. Seven standards were measured every hour and a variation of ≤2% was observed for their intensities. Crystal orientation was checked every 100 measurements. A set of 3555 reflections (hkl, $2\theta \leq 45°$) was collected and 2086 reflections with $I \geq 3\sigma(I)$ were retained for structural resolution. Net intensities and standard deviations were obtained as described elsewhere (17). The data were corrected for both Lorentz and polarisation effects and the absorption correction was done using a Gaussian integration (grid 10 × 10 × 10).

The structure was solved by the direct method (EEES) and refined by full-matrix least-squares using the SHELX programme (18). The three phenyl groups were refined as rigid groups using idealised hexagons (d(C—C) = 1.395 Å). Isotropic refinement of all nonhydrogen atoms gave $R = [\Sigma(||F_o| - |F_c||)/\Sigma|F_o|] = 0.047$; further refinement using absorption-corrected data and introduction of the hydrogen atoms at their ideal coordinates (d(C—H) = 1.08 Å and U = 0.05 Å^2) gave R = 0.041. The hydrogen parameters were not refined but the coordinates were recalculated after each cycle. In the final cycles individual weights ($w = 1/\sigma^2(F)$) based on counting statistics were applied. Convergence gave R = 0.024 with $R_w = [\Sigma w(|F_o| - |F_c|)^2/\Sigma w|F_o|^2]^{1/2} = 0.027$ and a goodness-of-fit of 1.25. The last ΔF map showed only a background of 0.3e$^-$/Å^3 except for one peak of 0.5e$^-$/Å^3 at 1.2 Å from tin.

N-bonding of cyanate was assumed in the above refinement. The refinement was repeated assuming O-bonding, in which case R = 0.027, R_w = 0.037, and the goodness-of-fit was 1.42. The fact that these values are significantly higher than those for N-bonding confirms that the cyanate group is indeed N-bonded.

Scattering curves were taken from Cromer and Waber (19) except those for hydrogen (20). Anomalous dispersion factors f' and f'' were applied to the non-hydrogen scattering curves (21). Anisotropic thermal parameters (Table SI) together with observed and calculated structure factors (Table SII) and least-squares planes calculations (Table SIII), as well as the stereo view of the unit cell (Fig. SI), have been placed in the Depository of Unpublished Data.[4]

Results

(a) Vibrational spectra (350–100 cm^{-1})

(i) Ph_3SnNCY (Y = O, S, Se)

Vibrational data in the skeletal region are reported in Table 1 for Ph_3SnNCY (Y = O, S, Se) with assignments following those for the triphenyltin halides. Mössbauer data (13) suggest Ph_3SnNCO contains 4-coordinate tin in the solid state consistent with its relatively low melting point and solubility in benzene, where in solution ν(CN) is observed at 2218 cm^{-1}. Unfortunately ν(CN) values do not allow the bonding mode (Sn—N or Sn—O) of the cyanate ligand to be determined. However, the X-ray analysis of Ph_3SnNCO (9) shows it is indeed almost molecular with primary tin—nitrogen bonding and weak tin—oxygen bonding, enabling ν(Sn—NCO) and δ(Sn—NCO) to be assigned to peaks not present in the spectra of triphenyltin halides. The assignment of ν(Sn---O) to the infrared absorption at 138 cm^{-1} is consistent with the weakness of the interaction (d(Sn---O) = 2.81 Å).

Triphenyltin isothiocyanate is polymeric using thiocyanate bridges to join 5-coordinate tin atoms with strong axial primary (Sn—N) and secondary (Sn—S) bonding (23), while ν(CN) and ν(CSe) values show $Ph_3SnNCSe$ is also polymeric (8). Thus ν(Sn—NCY) is assigned to distinct infrared absorptions at ~200 cm^{-1}, while broad peaks in the region 100–130 cm^{-1} may be assigned to overlapping ν(Sn---YCN) and δ(Sn—NCY) modes. Since Ph_3SnNCS has four molecules in the asymmetric unit, crystal lattice splitting may also account for the broad character of these low frequency peaks. Where modes are

[3]Crystal data for $C_{24}H_{20}N_2O_2Sn$ at 25°C: orthorhombic, space group *Pbca*, a = 14.570(5), b = 16.738(6), c = 17.578(11) Å, V = 4287.0 Å^3; crystal data for $C_{24}H_{20}N_2OSeSn$ at 25°C: orthorhombic, space group *Pbca*, a = 14.080(7), b = 17.841(7), c = 18.379(5) Å, V = 4616.3 Å^3.

[4]Tables SI–SIII and Fig. SI are available at a nominal charge from the Depository of Unpublished Data, CISTI, National Research Council of Canada, Ottawa, Ont., Canada K1A 0S2.

TABLE 1. Skeletal frequencies[a] (350–100 cm^{-1}) for Ph_3SnNCY

Y = O		Y = S		Y = Se		
IR	R	IR	R	IR	R	Assignment
326 mbr						ν(Sn—NCO)
303 w	294 vw				305 w	
		281 vs	276 sh	279 vs	278 w	$\nu_{as}(SnPh_3)(t)^b$
277 vs		272 vs	270 w			
250 w	268 w	253 vw				
231 s, sp		235 m	233 sh	239 msp	236 vw	
220 sh		227 s	229 wm			(u)
214 m		220 m		221 m		
205 m, sp						δ(Sn—NCO)
	208 vs		213 vs		212 vs	$\nu_s(SnPh_3)(t')$
		199 s	198 sh	201 mbr	200 sh	ν(Sn—NCY)
190 sh	192 w				194 w	
182 m	183 wm				178 m	(x)
153 w	154 wm	148 w	156 w, br	159 w	149 m	
138 m						ν(Sn---OCN)
				125 sm, br		ν(Sn---YCN)
		117 s, br				+
				105 m, br		δ(Sn—NCY)

[a]IR, Nujol mull; Raman, powder, 488.0 nm radiation.
[b]Whiffen's notation (22) for phenyl ring modes.

both Raman and infrared active for Ph_3SnNCS ((t), (u), and ν(Sn—NCS)), their almost complete coincidence (within experimental error, ±2 cm^{-1}) is consistent with the space group ($P2_1$–C_2^2) of this compound.

(ii) $Ph_3SnNCY \cdot L$ (L = O—donor ligand)

Tables 2(*a*)–(*d*) list vibrational data in the skeletal region (350–100 cm^{-1}) for $Ph_3SnNCY \cdot L$ (L = HMPA, Ph_3PO, pyO, and 4-picO, respectively); not included are weak-to-medium, mainly infrared-active peaks (~350, ~250 cm^{-1}) due to internal HMPA modes (14) and peaks associated with Ph_3PO (24), i.e. ~300–310 cm^{-1} (δ(P=O)), ~250–260 cm^{-1} ((u)(PPh_3)), and ~200–210 cm^{-1} ((x)(PPh_3)).[5] Assignments follow the conventional pattern with ν(Sn—NCY) and δ(Sn—NCY) modes identified by comparing the spectra with those of the analogous halide adducts[5] in the same region. No specific assignment of ν(Sn—O) is given since the axial tin—oxygen stretching mode can interact with the equatorial tin—phenyl deformations (u) in the same region.

Complete data are given for $Ph_3SnNCY \cdot L$ (L = pyO, 4-picO) with the skeletal modes, including ν(Sn—NCY) and δ(Sn—NCY), assigned after inspection of the spectra of the corresponding halide complexes.[6] Pyridine-*N*-oxide itself has an infrared peak at ~230 cm^{-1} (γ(N—O) (25, 26) while the coordinated ligand has a vibration corresponding to twisting of the ring against the donor oxygen (τ(N—O)), as well as the expected ν(Sn—O) and δ(Sn—O) modes (27, 28). The assignment of ν(Sn—O) for $Ph_3SnNCY \cdot pyO$ (~320 cm^{-1}) is consistent with that given earlier for $Ph_3SnNO_3 \cdot pyO$, 325 cm^{-1} (29) and for a number of organotin halide – pyridine-*N*-oxide adducts (30, 31).

There does not appear to be any definite assignments in the skeletal region (≤350 cm^{-1}) for 4-picoline-*N*-oxide complexes in the literature. The assignments given here by analogy with those for the pyridine-*N*-oxide adducts, must be regarded as tentative. The higher values for ν(Sn—O) may reflect the stronger donor power of 4-picoline-*N*-oxide compared with that of pyridine-*N*-oxide.

(iii) $Ph_3SnNCY \cdot L$ (L = py, β-pic, γ-pic)

Complete data for the skeletal region are given in Table 3 for the adducts with pyridine as well as for $Ph_3SnNCSe \cdot L$ (L = β-pic, γ-pic). Although most skeletal modes were readily assigned, no definite values have been given for those involving the ligands; however, assignment of ν(Sn—N_L) to 150–200 cm^{-1} (perhaps the peak of medium intensity at ~150 cm^{-1}) is consistent with the earlier assignment for $Ph_2SnX_2Py_2$ (X = Cl, Br) (32). Only by using per-deuterated ligands following Hutton *et al.* (28, 33) will it be possible to identify these tin—ligand modes clearly.

(b) Crystal and molecular structure of $Ph_3SnNCO \cdot pyO$

A conventional ORTEP drawing of the adduct is shown in Fig. 1 (top), while Fig. 1 (bottom) shows the view down the N—Sn—O axis. The refined coordinates are listed in Table 4 with bond lengths and bond angles for the non-hydrogen atoms in the adduct given in Table 5. The compound is molecular with the tin atom having a slightly distorted trigonal bipyramidal geometry in which phenyl groups occupy the equatorial positions and the isocyanate and pyridine-*N*-oxide ligands are at the apices of the bipyramid. The cell representation (Fig. S1) clearly shows the monomeric nature of the adduct and the shortest intermolecular contacts (Table 6) are consistent with only van der Waals interactions between adjacent molecules with no stacking interactions in the structure.

There is some departure from the ideal geometry as can be seen by the unequal tin—carbon bond lengths and the bond angles around the tin. The tin atom is 0.167 Å above the equatorial plane formed by C(21)—C(31)—C(41) towards the isocyanate group (2.335 Å above the plane), while the pyridine-*N*-oxide molecule is 2.182 Å below the plane. The staggered

[5]Complete Raman and infrared spectral data (350–100 cm^{-1}) for $Ph_3SnNCY \cdot L$ (Y = O, S, Se; L = HMPA, Ph_3PO) are available on request from the authors (I.W.).

[6]I. Wharf, unpublished data and ref. 14.

Can. J. Chem. Downloaded from www.nrcresearchpress.com by 80.58.250.72 on 09/07/12
For personal use only.

Can. J. Chem. Downloaded from www.nrcresearchpress.com by 80.58.250.72 on 09/07/12
For personal use only.

TABLE 2. Skeletal frequencies[a] (350–100 cm^{-1}) for $Ph_3SnNCY \cdot L$ (L = O-donor ligand)

(*a*) L = HMPA						(*b*) L = Ph_3PO					
Y = O		Y = S		Y = Se		Y = O[b]	Y = S		Y = Se		
IR	R	IR	R	IR	R	IR	IR	R	IR	R	Assignment
(277 vs)						297 sm					ν(Sn—NCO)
277 vs	273 wm	281 vs 278	281 vw 277	282 sh 278 vs	282 w	277 vs	279 vs	279 sh 274 w	281 vs 276	279 w	$_{as}(SnPh_3)^c(t)$
236 vs	235 vw	228 s	229 vw	227 vs		235 s	235 s	233 sh	232 s 224 sh		ν(Sn—O) + (u)
221 sm 209 m	219 sh	219 s	219 sh	219 sh		221 wm	219 m	224 m	219 sh	217 sh	
197 sm						199 sm					δ(Sn—NCO)
	210 vs		212 vs		213 vs			212 vs		211 vs	$\nu_s(SnPh_3)(t')$
		190 s, br		196 m			197 vs		204 sm		ν(Sn—NCY)
171 w						186 sh	170 vw	181 vw	194 w	199 brsh	(x)
150 wm	151 w	152 wm 129 m	153 vw 125 vw	159 sh 143 m, br		154 w	154 w 143 wm	156 wm 141 wm	184 m 139 s, br	150 m	δ(Sn—NCY)?
139 w	125 w			131 w		139 w	123 w				

Can. J. Chem. Downloaded from www.nrcresearchpress.com by 80.58.250.72 on 09/07/12
For personal use only.

TABLE 2. (*Concluded*)

(*c*) L = pyO						(*d*) L = 4-picO[d]						
Y = O		Y = S		Y = Se		Y = O		Y = S		Y = Se		
IR	R	IR	R	IR	R	IR	R	IR	R	IR	R	Assignment
307 sh	311 wbr	320 vs	319 w, br	323 vs	327 w, br	379 m	374 vw, br	382 s		384 s		ν(Sn—O)
						321 sh		329 wm		340 sm		$\delta(H_3C—C)$
289 sh						307 sm						ν(Sn—NCO)
279 vs, br	274 wbr	281 277 vs	275 w	282 276 vs	278 wm	278 w	274 w	281 vs	278 w	279 vs	280 w	$\nu_{as}(SnPh_3)^c$(t)
255 vw		254 vw				251 w		256 wm	254 m	258 wm	257 wm	
235 s, sp		230 vs	230 m	230 vs	231 s	238 s		230 sh	231 m	230 vs	230 m, sp	(u) + γ(N—O)
	223 s											
221 wm	218 s	213 m				225 w		222 vs	220 sm	221 sm	220 sm	
209												
203 m						202 s	204 sh					δ(Sn—NCO)
	207 vs		214 vs		217 vs		211 vs					$\nu_s(SnPh_3)$(t′)
							207 vs		205 vs		203 vs	
		203 s	207 sh	201 s	209 sh			213 s	214 sh	210 m	213 m	ν(Sn—NCY)
		199 sh	201 m									
182 w		176 sh		178 vs	177 m	182 w		195 vs	196 sh	195 s	197 sh	(x) + τ(N—O)
162 m	163 sh	170 m	170 w			160 w		165 wm	160 sh	170 m	163 m, br	+ δ(Sn—O)?
153 w	156 m	150 w	154 m	152 w	156 s	153 w	153 m		151 m	153 m	153 sm, br	
141 sm	137 w	141 m	141 wm	138 wm	140 m	144 w		138 sm	139 m			δ(Sn—O)?
126 m	126 w	125 m				125 wm	122 m, sp	128 m		129 m, br		+ δ(Sn—NCY)
				113 m					114 vs			

[a]IR, Nujol mull; Raman, powder, 488.0 nm radiation.
[b]Sample gave excessive fluorescence so no Raman spectrum could be observed.
[c]Whiffen's notation (22) for phenyl ring modes.
[d]Range, 400–100 cm^{-1}.

TABLE 3. Skeletal frequencies[a] (350–100 cm^{-1}) for $Ph_3SnNCY \cdot L$ (L = N-donor ligand)

Y = O, L = py		Y = S, L = py		Y = Se, L = py		Y = Se, L = β-pic		Y = Se, L = γ-pic[b]	Assignment
IR	R	IR	R	IR	R	IR	R	IR	
316 sbr	~310 vw								ν(Sn—NCO)
279 vs	276 vw	280 vs	278 w	283 vs		282 vs		283 vs	$\nu_{as}(SnPh_3)$[c](t)
				277 sh	277 w	277	275 w	278 sh	
233 ssp	230 w	235 s	239 m	237 s		234 s		235 s	
			229 sm	222 sm					
212 wm	218 sh	224 sh	223 s	219 sm		216 wm			(u)
						209 vw	220 wm		
205 m									δ(Sn—NCO)
		204 s	210 vw?	203 s		202 s		204 sm	ν(Sn—NCY)
	290 vs		204 vs		216 vs		210 vs		$\nu(SbPh_3)$(t′)
183 wm	203 sh	178 vw		180 sm		186 wm			
						163 m		164 wm	(x) +
	160 wm	164 w	172 m	168 wm		158 vw			ν(Sn—N_L)
151 m		152 wm	151 wm			153 m			
								148 smbr	
140 w	143 w	141 w	142 wm	146 w		146 m			δ(Sn—N_L)?
	129 w	121 m	122 w	234 sm		125 wm		132 sh	+ δ(Sn—NCY)
109 m	114 m					106 vw			

[a]IR, Nujol mull; Raman, powder, 488.0 nm radiation.
[b]Decomposed in the laser beam.
[c]Whiffen's notation (22) for phenyl ring modes.

orientation of the ligand ring with respect to the equatorial phenyl groups, as is also observed in the structure of $Ph_3SnNO_3 \cdot pyO$ (29), suggests weak inter-ring repulsions may influence the structures of these adducts. Twisting of the phenyl rings may also minimise interactions between them. These rings are differently oriented to the equatorial plane, being twisted out of the plane defined by C(21)—C(31)—C(41) by 73.0° (C(21)—C(26)), 30.2° (C(31)—C(36)), and 94° (C(41)—C(46)); reciprocal orientations of the rings are given by the dihedral angles (φ1Λφ2, 59.2°; φ1Λφ3, 80.4°; φ2Λφ3, 39.1°).

Discussion

(a) Vibrational spectra and adduct formation

The small, random changes in ν(Sn—NCY) values on adduct formation by Ph_3SnNCY (Y = S, Se) (Table 7) are consistent with the picture of strong chalcocyanate bridges being broken by the coordinating ligand with the tin atom (in the Ph_3Sn moiety) being five-coordinate in both the Lewis acids and the adducts. Mixing of axial stretching modes with each other or tin—phenyl deformations may account for the small variations observed in the ν(Sn—NCY) frequencies. It is, in fact, the chalcocyanate group which is more affected by adduct formation, with ν(CN) and ν(CY) reflecting the change from the bridging to terminal (Sn—N) bonding mode.

In contrast, the Ph_3SnNCO system shows the decrease in ν(Sn—NCO) on adduct formation that is expected with the change from mainly four to five coordination at tin. However, comparison with the change in ν(Sn—X) (X = Cl, Br) on adduct formation by Ph_3SnX (Table 7) suggests this picture is overly simplistic. For the adducts, the trend ν(Sn—NCO) ≥ ν(Sn—Cl) is consistent with other isocyanate–chloride comparisons of ν(M—X) frequencies, e.g. Me_3SiX; X = NCO, 521 cm^{-1} (34); X = Cl, 470 cm^{-1} (35); and Ph_3GeX; X = NCO, 450 cm^{-1} (36); X = Cl, 375 cm^{-1} (37), where each pair is structurally similar. The fact that Ph_3SnNCO has *ν(Sn—NCO) ≤ ν(Sn—Cl)*, and that crystalline triphenyltin

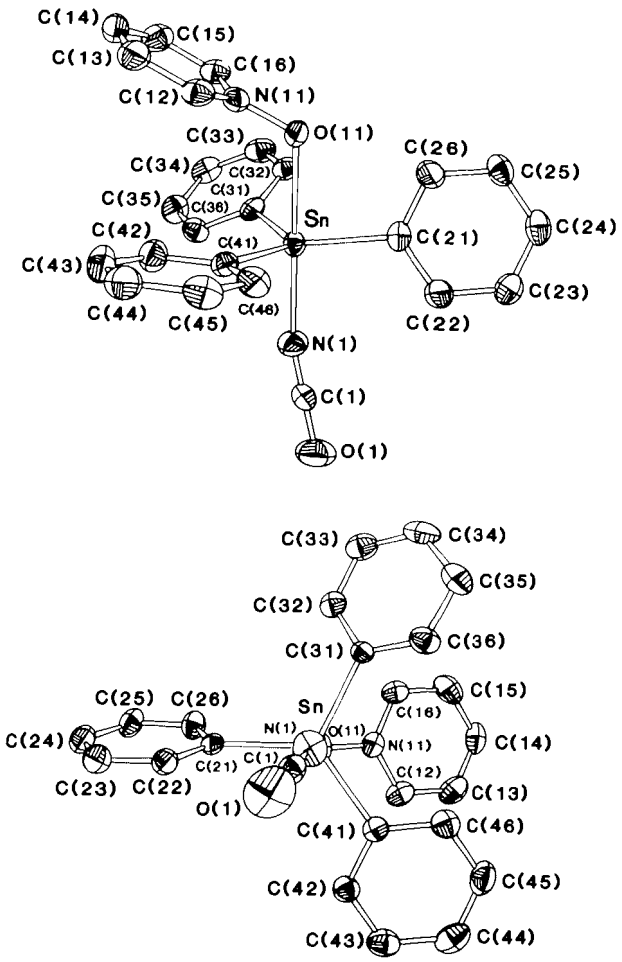

FIG. 1. ORTEP drawing of $Ph_3SnNCO \cdot pyO$, hydrogen atoms omitted for clarity. The ellipsoids correspond to 50% probability level. Conventional side-view (top), view down N—Sn—O oxide (bottom).

Can. J. Chem. Downloaded from www.nrcresearchpress.com by 80.58.250.72 on 09/07/12
For personal use only.

Can. J. Chem. Downloaded from www.nrcresearchpress.com by 80.58.250.72 on 09/07/12
For personal use only.

TABLE 4. Refined coordinates ($\times 10^4$; Sn $\times 10^5$) and isotropic temperature factors ($U_{eq} \times 10^3$)

Atom	x	y	z	U_{eq} (Å^2)
Sn	22714(2)	−2463(2)	8188(1)	24
O(1)	3829(3)	−2396(2)	1555(2)	66
O(11)	1125(2)	678(2)	446(1)	31
N(1)	3269(3)	−1160(2)	1134(2)	39
N(11)	1233(2)	1066(2)	−211(2)	28
C(1)	3537(3)	−1771(3)	1336(2)	29
C(12)	831(3)	785(3)	−850(2)	35
C(13)	939(3)	1190(3)	−1529(3)	40
C(14)	1452(3)	1883(3)	−1552(3)	40
C(15)	1857(3)	2164(3)	−890(3)	41
C(16)	1731(3)	1754(2)	−218(2)	32
C(21)	1470(2)	−331(1)	1846(1)	26
C(22)	1579(2)	−993(1)	2323(1)	30
C(23)	1083(2)	−1040(1)	3005(1)	37
C(24)	477(2)	−425(1)	3209(1)	38
C(25)	368(2)	238(1)	2731(1)	37
C(26)	864(2)	284(1)	2049(1)	33
C(31)	3269(2)	695(1)	790(1)	24
C(32)	3161(2)	1360(1)	1264(1)	31
C(33)	3816(2)	1975(1)	1251(1)	40
C(34)	4577(2)	1925(1)	764(1)	40
C(35)	4685(2)	1259(1)	290(1)	42
C(36)	4031(2)	644(1)	303(1)	33
C(41)	1927(2)	−817(2)	−234(1)	27
C(42)	1180(2)	−1346(2)	−255(1)	31
C(43)	892(2)	−1672(2)	−949(2)	40
C(44)	1351(2)	−1469(2)	−1621(1)	43
C(45)	2099(2)	−940(2)	−1601(1)	46
C(46)	2387(2)	−614(2)	−907(1)	37
H(12)	424(3)	242(3)	−830(2)	50
H(13)	620(3)	963(3)	−2043(3)	50
H(14)	1538(3)	2205(3)	−2082(3)	50
H(15)	2271(3)	2703(3)	−900(3)	50
H(16)	2030(3)	1980(2)	305(2)	50
H(22)	2048(2)	−1470(1)	2166(1)	50
H(23)	1167(2)	−1553(1)	3375(1)	50
H(24)	92(2)	−461(1)	3736(1)	50
H(25)	−102(2)	714(1)	2888(1)	50
H(26)	779(2)	797(1)	1679(1)	50
H(32)	2572(2)	1399(1)	1641(1)	50
H(33)	3732(2)	2491(1)	1618(1)	50
H(34)	5084(2)	2401(1)	754(1)	50
H(35)	5275(2)	1220(1)	−87(1)	50
H(36)	4114(2)	129(1)	−64(1)	50
H(42)	824(2)	−1504(2)	266(1)	50
H(43)	313(2)	−2081(2)	−965(1)	50
H(44)	1128(2)	−1721(2)	−2159(1)	50
H(45)	2455(2)	−782(2)	−2122(1)	50
H(46)	2966(2)	−204(2)	−891(1)	50

chloride is monomeric (38) implies that the weak tin–oxygen interaction (2.807 Å) in Ph_3SnNCO is sufficient to render the tin atom quasi-five-coordinate and the tin—nitrogen bond slightly weaker. Thus, Ph_3SnNCO is structurally between monomeric Ph_3GeNCO (39) and polymeric Ph_3PbNCO (40).

Since the decrease in ν(Sn—NCO) on adduct formation indicates a further weakening of the tin—nitrogen bond, the crystal structure of $Ph_3SnNCO \cdot pyO$ was determined. The structure of this adduct can also be compared with that of $Ph_3SnNO_3 \cdot pyO$ (29) which has almost trigonal bipyramidal geometry.

Formation of the pyridine-*N*-oxide adduct by Ph_3SnNCO causes an increase in d(Sn—N) from 2.122 to 2.169 Å, paralleling the change in ν(Sn—NCO) from 326 to 289 cm^{-1}, but almost no change in the cyanate group is observed. When comparing $Ph_3SnNCO \cdot pyO$ with $Ph_3SnNO_3 \cdot pyO$, the d(Sn—O_L) values, 2.355 and 2.227 Å, respectively, are consistent with the increase in ν(Sn—O_L) from 309 to 325 cm^{-1}, and suggest an order of Lewis acid strength $Ph_3SnNO_3 \geq Ph_3SnNCO$ with respect to pyridine-*N*-oxide. Although the three triphenyltin compounds considered here do not have exactly trigonal Ph_3Sn moieties, the adducts are clearly five-coordinate, but the nature of triphenyltin isocyanate requires more detailed consideration.

(b) Triphenyltin isocyanate; four- or five-coordinate?

While the degree of coordination of a metal atom or ion is often discussed in terms of the number of nearest neighbours leading to assignments of integral coordination numbers, for adduct formation by Ph_3SnX it is more appropriate to consider the changes in the angles of a trigonal unit Ph_3SnX (**I**) due to attachment of a ligand L *trans* to X.

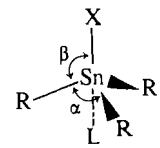

$$\sin\beta = \sqrt{\frac{4}{3}}\sin\left(\frac{\alpha}{2}\right)$$

I

In the absence of ligand L, four-coordinate Ph_3SnX should have quasi-tetrahedral geometry with $\alpha = \beta = 109.5°$. When X and L are identical (or have equivalent donor power), the system is five-coordinate with $\alpha = 90°$ and $\beta = 120°$. These extremes may be equated with tin using sp^3 and sp^2 hybridisation schemes, respectively (10). In the solid state, no triphenyltin structure obtained to date shows ideal trigonal symmetry and tin and usually the distortion is such that all tin—carbon bonds as well as the three bond angles (α) are different. Thus, average $\angle$CSnC(α) and $\angle$CSnX(β) as well as $\angle$XSnL values are given in Table 8 for selected $Ph_3SnX \cdot L$ as a measure of the degree of coordination of tin in these compounds.

X-ray diffraction studies show Ph_3SnCl and Ph_3SnBr are monomeric having four-coordinate tin with $\alpha = 113°$ ($\beta = 106°$) indicating increased *s*-character in the tin—carbon bonds in agreement with Bent's rule. Full five coordination with both Sn—X and Sn—L bonds of equal or comparable strength is shown by $Ph_3SnNCS \cdot L^-$ (L^- = 2-pyridinium carboxylate), $Ph_3SnCl_2^-$ and Ph_3SnNCS ($\alpha = 120°$), while $Ph_3SnNO_3 \cdot L$ (L = pyO, Ph_3PO) and $Ph_3SnCl \cdot L^-$ are five-coordinate within experimental error. With $\alpha \leq 119.5°$ and $\beta \sim 95°$, $Ph_3SnNCO \cdot pyO$, as well as the adducts of Ph_3SnCl with neutral O-donor ligands, while still five-coordinate, have unequal Sn—X and Sn—L bonds with the bond order being Sn—X $\geq$ Sn—L.

Triphenyl isocyanate ($\alpha = 118°$, $\beta = 98°$) lies between the two extremes, $\alpha = 113°$, $\beta = 106°$, and $\alpha = 120°$, $\beta = 90°$. Since no exact values of α and β can be given for the boundary between four or five coordination, Ph_3SnNCO is best described as an intermediate form. However, ν(Sn—NCO) for this compound favours the description of its structure as quasi-five-coordinate with the weak tin—oxygen interaction sufficient to influence the geometry around the tin atom and weaken the *trans* tin—nitrogen bond.

The correlation of quadrupole splitting parameters (Δ mm s^{-1}) for triorganotin systems with the degree of coordination at tin

Can. J. Chem. Downloaded from www.nrcresearchpress.com by 80.58.250.72 on 09/07/12
For personal use only.

TABLE 5. Bond distances and bond angles

(*a*) Bond distances (Å)

Bond	Distance	Bond	Distance	Bond	Distance
Sn—O(11)	2.355(3)	Sn—N(1)	2.169(4)	Sn—C(21)	2.145(3)
Sn—C(31)	2.131(2)	Sn—C(41)	2.135(2)	O(1)—C(1)	1.188(6)
N(1)—C(1)	1.146(6)	O(11)—N(11)	1.330(4)	N(11)—C(12)	1.346(5)
C(12)—C(13)	1.377(6)	C(13)—C(14)	1.373(6)	C(14)—C(15)	1.381(6)
C(15)—C(16)	1.374(6)	C(16)—N(11)	1.354(5)		

(*b*) Bond angles (deg)

Bonds	Angle	Bonds	Angle
O(11)—Sn—N(1)	176.23(12)	O(11)—Sn—C(21)	84.05(9)
O(11)—Sn—C(31)	89.24(9)	O(11)—Sn—C(41)	83.58(9)
N(1)—Sn—C(21)	95.66(12)	N(1)—Sn—C(31)	94.26(12)
N(1)—Sn—C(41)	93.54(12)	C(21)—Sn—C(31)	115.67(9)
C(21)—Sn—C(41)	124.76(9)	C(31)—Sn—C(41)	117.74(9)
Sn—N(1)—C(1)	158.1 (4)	O(1)—C(1)—N(1)	178.6 (5)
Sn—O(11)—N(11)	118.4 (2)	O(11)—N(11)—C(12)	120.0 (3)
O(11)—N(11)—C(16)	118.8 (3)	C(12)—N(11)—C(16)	121.1 (4)
N(11)—C(12)—C(13)	120.0 (4)	C(12)—C(13)—C(14)	120.0 (4)
C(13)—C(14)—C(15)	119.3 (4)	C(14)—C(15)—C(16)	119.7 (4)
C(15)—C(16)—N(11)	119.7 (4)		

TABLE 6. Intermolecular contacts (Å) less than 3.60 Å*

Atoms	Distance	Atoms	Distance
O(1)—C(14[a])	3.450(6)	O(1)—C(16[b])	3.509(6)
O(1)—C(32[b])	3.581(4)	O(1)—C(43[c])	3.525(4)
O(11)—C(42[d])	3.527(4)	O(11)—C(43[d])	3.466(4)
C(34)—C(43[e])	3.563(4)		

*$a, \frac{1}{2} - x, \bar{y}, \frac{1}{2} + z$; $b, \frac{1}{2} - x, -\frac{1}{2} + y, z$; $c, \frac{1}{2} + x, -\frac{1}{2} - y, \bar{z}$; $d, \bar{x}, \bar{y}, \bar{z}$; $e, \frac{1}{2} - x, \frac{1}{2} + y, z$.

TABLE 7. Comparison of ν(Sn—X)[a] (cm^{-1}) values for triphenyltin isochalcocyanates or halides and their adducts ($Ph_3SnX \cdot L$)

	ν when ligand (L) is					
X	Ph_3SnX	HMPA	pyO	4-picO	Ph_3PO	py
—NCSe	201	196	205	212	204	203
—NCS	199	190	203	213	197	204
—NCO	326	277	289	307	297	313
—Cl	335	251	250	251	265	[b]
—Br	252	161	161	159	172	[b]

[a]Average of solid state Raman and infrared data.
[b]Not measured.

is well known (41), with Ph_3SnCl (Δ = 2.550) and Ph_3SnBr (Δ = 2.480) being quasi-tetrahedral, while Ph_3SnNCS (Δ = 3.538), $Ph_3SnNCS \cdot pyO$ (Δ = 3.144), $Ph_3SnNCS \cdot Ph_3PO$ (Δ = 3.478), and $Ph_3SnCl \cdot Ph_3PO$ (Δ = 3.228) are five-coordinate with the phenyl rings occupying the equatorial positions in a trigonal bipyramidal structure. Thus, Δ = 2.47 for Ph_3SnNCO (13) was taken to indicate a quasi-tetrahedral structure for this compound. However, Δ values are very dependent on the nature of the groups attached to the tin since alkyl and phenyl groups have large partial quadrupole splittings (pqs), e.g. alkyl, pqs(tet) = −1.37, pqs(eq) = 1.13, or phenyl, pqs(tet) = −1.26, pqs(eq) = −0.98, while anions (X) and O-donor ligands (L) such as those given in Table 8 have small pqs, e.g. Cl or Br, pqs = 0 (by definition); NCS, pqs(tet) = +0.21, pqs(ax) = +0.065; Ph_3PO, pqs(ax) = +0.12; pyO, pqs(ax) = 0.00 (42). Thus, a decrease in ∠CSnC from 120° alone will cause Δ to vary without great changes in stereochemistry

TABLE 8. Average bond angles (deg) for some $Ph_3SnX \cdot L$ (X = unidentate anion; L = unidentate ligand)

Compound	∠CSnC	∠CSnX	∠XSnL
Ph_3SnCl[a]	113	106	—
Ph_3SnBr[b]	113.4	105.2	—
Ph_3SnNCO[c]	118	98	(173)
$Ph_3SnNCO \cdot pyO$[d]	119.4	94.5	176.2
$Ph_3SnCl \cdot L'$[e]	119.2	95.1	173.0
$(Ph_3SnCl)_2 \cdot L''_2$[f]	119.3	95.0	178.7
$Ph_3SnCl \cdot L^-$[g]	119.7	93.5	172.8
$Ph_3SnNO_3 \cdot Ph_3PO$[h]	119.8	92.3	174.1
$Ph_3SnNO_3 \cdot pyO$[i]	119.9	91.5	171.4
Ph_3SnNCS[j]	120	92	175
$Ph_3SnCl_2^-$[k]	120	91	178
$Ph_3NCS \cdot L^-$[l]	120.0	90.3	175.8

[a]Reference 38.
[b]Reference 15.
[c]Reference 9.
[d]This work.
[e]Reference 16. L′ = *cis*-$Ph_2P(O)CHCHP(O)Ph_2$, only one oxygen coordinates.
[f]Reference 43. L''_2 = *rac*-$Pr^nS(O)CHCHS(O)Pr^n$, the ligand coordinates to two Ph_3SnCl molecules.
[g]Reference 44. L^- ≡ 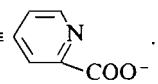 .
[h]Reference 45.
[i]Reference 29.
[j]Reference 23.
[k]Reference 46; anion found in $[Ph_3AsCH_2COPh]^+[Ph_3SnCl_2]^-$.
[l]Reference 47.

or the degree of coordination of ligand L being required. Therefore, Mössbauer data must be used with caution in judging subtle changes from four to five coordination in triorganotin compounds.

Acknowledgement

We thank le Gouvernement de Quebec, Ministère de l'Education (Fonds FCAR), for financial support.

1. C. J. Evans and S. Karpel. J. Organomet. Chem. Libr. **16**, 1 (1985) and references therein.
2. T. N. Srivastava and P. C. Kamboj. J. Indian Chem. Soc. **56**, 857 (1979).
3. T. N. Srivastava and P. C. Kamboj. Indian J. Chem. **19**A, 167 (1980).
4. T. N. Srivastava, P. C. Srivastava, and S. K. Srivastava. Indian J. Chem. **20**A, 443 (1981).
5. T. N. Srivastava, P. C. Srivastava, S. K. Srivastava, and O. P. Srivastava. J. Antibact. Antifung. Agents, **9**, 439 (1981).
6. J. H. Holloway, G. P. McQuillan, and D. S. Ross. J. Chem. Soc. (A), 1935 (1971).
7. T. N. Srivastava and S. K. Tandon. Spectrochim. Acta, **27**A, 593 (1971).
8. I. Wharf, R. Wojtowski, and M. Onyszchuk. J. Indian Chem. Soc. **60**, 800 (1985).
9. T. N. Tarkhova, E. V. Chuprunov, M. A. Simonov, and N. V. Belov. Sov. Phys. – Cryst. **22**, 571 (1977).
10. I. Wharf, R. Cuenca, and M. Onyszchuk. Can. J. Spectrosc. **29**, 31 (1984).
11. T. N. Srivastava and S. K. Tandon. Indian J. Appl. Chem. **26**, 171 (1963).
12. A. S. Mufti and R. C. Poller. J. Chem. Soc. 5055 (1965).
13. K. L. Leung and R. H. Herber. Inorg. Chem. **10**, 1020 (1971).
14. I. Wharf, M. Onyszchuk, D. M. Tallett, and J. M. Miller. Can. J. Spectrosc. **24**, 123 (1979).
15. H. Preut and F. Huber. Acta Crystallogr. B**35**, 745 (1979).
16. C. Pelizzi and G. Pelizzi. Inorg. Nucl. Chem. Lett. **16**, 451 (1980).
17. F. Belanger-Gariepy and A. L. Beauchamp. J. Am. Chem. Soc. **102**, 3461 (1980).
18. G. M. Sheldrick. SHELX. Programme for Structure Determination. University of Cambridge, England. 1976.
19. D. T. Cromer and J. T. Waber. Acta Crystallogr. **18**, 104 (1965).
20. R. F. Stewart, E. R. Davidson, and W. T. Simpson. J. Chem. Phys. **42**, 3175 (1965).
21. D. T. Cromer. Acta Crystallogr. **18**, 17 (1965).
22. D. H. Whiffen. J. Chem. Soc. 1350 (1956).
23. A. M. Domingos and G. M. Sheldrick. J. Organomet. Chem. **67**, 257 (1974).
24. G. B. Deacon and J. H. S. Green. Spectrochim. Acta, **25**A, 355 (1969).
25. H. D. Best and J. S. Parchar. Chem. Phys. Lett. **32**, 244 (1975).
26. A. Gambi and S. Ghersetti. Spectrosc. Lett. **8**, 627 (1977).
27. A. D. van Ingen Schenau, C. Romers, D. Kretsch, and W. L. Groeneveld. Spectrochim. Acta, **33**A, 859 (1977).
28. A. T. Hutton and D. A. Thornton. J. Mol. Struct. **39**, 33 (1977).
29. C. Pelizzi, G. Pelizzi, and P. Tarasconi. J. Organomet. Chem. **124**, 151 (1977).
30. B. V. Liengme, R. S. Randall, and J. R. Sams. Can. J. Chem. **50**, 3212 (1972).
31. Y. Kawasaki, M. Hori, and K. Venaka. Bull. Chem. Soc. Jpn. **40**, 2463 (1967).
32. R. C. Poller, J. N. R. Ruddick, M. Theverasa, and W. R. McWhinnie. J. Chem. Soc. (A), 2327 (1969).
33. A. T. Hutton and D. A. Thomton. Spectrosc. Lett. **10**, 57 (1977).
34. J. S. Thayer and D. P. Strommen. J. Organomet. Chem. **5**, 383 (1966).
35. A. L. Smith. J. Chem. Phys. **21**, 1997 (1953).
36. T. N. Srivastava and S. K. Tandon. Bull. Chem. Soc. Jpn. **45**, 633 (1972).
37. J. W. Durig, C. W. Sink, and J. B. Turner. Spectrochem. Acta, **25**A, 629 (1969).
38. N. G. Bokü, G. N. Zakharova, and Yu. T. Struckhov. J. Struct. Chem. **11**, 828 (1970).
39. T. N. Tarkhova, L. E. Nikolaeva, E. V. Chuprunov, M. A. Simonov, and N. V. Belov. Sov. Phys-Cryst. **21**, 216 (1976).
40. T. N. Tarkhova, E. V. Chuprunov, L. E. Nikolaevea, M. A. Simonov, and N. V. Belov. Sov. Phys-Cryst. **23**, 281 (1978).
41. J. Ensling, Ph. Gütlich, K. M. Hassellbach, and B. W. Fitzsimmons. J. Chem. Soc. (A), 1940 (1971).
42. G. M. Bancroft, V. G. Kumar Das, T. K. Sham, and M. G. Clark. J. Chem. Soc. (A), 643 (1976), and references therein.
43. C. A. L. Filgueiras, P. R. Holland, B. F. G. Johnson, and P. R. Raithby. Acta Crystallogr. B**38**, 2684 (1982).
44. L. Prasad, E. J. Gabe, and F. E. Smith. Acta Crystallogr. B**38**, 1325 (1982).
45. M. Nardelli, C. Pelizzi, and G. Pelizzi. J. Organomet. Chem. **112**, 263 (1976).
46. P. G. Harrison, K. Molloy, R. C. Phillips, P. J. Smith, and A. J. Crowe. J. Organomet. Chem. **160**, 421 (1978).
47. E. J. Grabe, F. L. Lee, L. E. Khoo, and F. E. Smith. Inorg. Chim. Acta, **112**, 41 (1986).

Can. J. Chem. Downloaded from www.nrcresearchpress.com by 80.58.250.72 on 09/07/12
For personal use only.

Nouveaux modèles du NADH en série oxazolyl-3 dihydro-1,4 pyridine : synthèse, réactivité, rôle de la complexation dans la réactivité

P. BINAY, G. DUPAS, J. BOURGUIGNON[1] ET G. QUEGUINER

Institut national des sciences appliquées, Institut de recherches en chimie organique fine, B.P. 08-76130 Mont-Saint-Aignan, France

Reçu le 7 avril 1986

P. BINAY, G. DUPAS, J. BOURGUIGNON et G. QUEGUINER. Can. J. Chem. **65**, 648 (1987).

Une nouvelle classe de modèles du NADH est décrite : ils contiennent la structure oxazolyl-3 dihydro-1,4 pyridine. Ils ont été préparés à la suite de l'addition régiosélective en 4 de dérivés organométalliques (dont un possède un groupe chiral), sur la (diméthyl-4,4 oxazolyl-2)-3 pyridine. La structure dihydro-1,4 pyridine est obtenue après quaternarisation et réduction par le dithionite de sodium. La quaternarisation par l'intermédiaire de la réaction de Zincke a permis d'obtenir des modèles porteurs d'une copule chirale sur l'atome d'azote pyridinique. Cette chiralité est indispensable pour induire une asymétrie au niveau du carbone en 4 dans la dihydro-1,4 pyridine correspondante. Cette asymétrie joue un rôle prépondérant dans la faible énantiosélectivité de la réduction d'un substrat prochiral tel le benzoylformiate de méthyle. La réactivité chimique des modèles préparés a été étudiée en effectuant la réduction du paranitrobenzaldéhyde en présence de perchlorate de magnésium. Tous les modèles permettent d'atteindre des rendements quantitatifs. Cependant les réactions sont plus lentes que celles effectuées, dans les mêmes conditions, avec le *N*-benzyl dihydro-1,4 nicotinamide (BNAH). Une étude en rmn de ^{13}C a montré que ce comportement est sans doute une conséquence de la forte complexation exercée par le groupe oxazolinique sur le magnésium.

P. BINAY, G. DUPAS, J. BOURGUIGNON, and G. QUEGUINER. Can. J. Chem. **65**, 648 (1987).

A new class of NADH models is described: they contain the 3-oxazolyl-1,4-dihydropyridine structure. They have been synthesized by regioselective addition at the 4 position of organometallic derivatives (one of them bearing a chiral group) on 3-(4,4-dimethyl-2-oxazolyl)pyridine. The 1,4-dihydropyridine structure is obtained after quaternarization and reduction by sodium dithionite. Quaternarization through Zincke's reaction leads to models having a chiral group at the pyridine nitrogen. This chirality is necessary to induce asymmetry at the 4 carbon in the corresponding 1,4-dihydropyridine. This asymmetry plays an important role in the low enantioselectivity of reduction of a prochiral substrate such as methyl benzoylformate. The chemical reactivity of the models has been studied by performing the reduction of *p*-nitrobenzaldehyde in the presence of magnesium perchlorate. All models gave quantitative yields. However, reactions are slower than those performed, in the same conditions, with *N*-benzyl-1,4-dihydronicotinamide (BNAH). A ^{13}C nmr study shows that this behaviour is probably a consequence of the high complexation of magnesium with the oxazoline moiety.

Can. J. Chem. Downloaded from www.nrcresearchpress.com by 80.58.250.72 on 09/07/12
For personal use only.

Le nicotinamide adénine dinucléotide est l'un des coenzymes les plus importants : il joue un rôle essentiel dans les processus d'oxydo-réduction qui se produisent dans l'organisme. Il a été établi depuis longtemps que la partie active du coenzyme sous sa forme réduite (NADH) était constituée par la fraction dihydro-1,4 nicotinamide.

Rapidement les chimistes ont préparé des «modèles» du NADH contenant la structure dihydro-1,4 pyridine, qui ont permis de développer une famille de réducteurs spécifiques, d'étudier le mécanisme des réductions biomimétiques ou de réaliser des réductions asymétriques, certaines avec des très forts excès énantiomériques. Des centaines de références rapportent les résultats obtenus dans ces divers domaines (1).

Les modèles de NADH qui ont été les plus utilisés peuvent se rattacher à deux types principaux : (*i*) ceux dérivés de la dihydro-1,4 nicotinamide tels le *N*-benzyl dihydro-1,4 nicotinamide (BNAH); (*ii*) ceux dérivés de l'ester de Hantzsch.

Ces modèles possèdent la caractéristique de comporter au moins un substituant électroattracteur en position 3, ce qui a pour conséquence de conférer une certaine stabilité à la structure dihydropyridinique (stabilité indispensable pour envisager une utilisation en synthèse) tout en lui conservant un pouvoir réducteur suffisant.

1. Auteur à qui adresser toute correspondance.

Nous décrivons ici un nouveau type de modèle du NADH comprenant le groupe oxazolinique en position 3. Ce substituant possède un bon effet électroattracteur et il est susceptible, en plus, de complexer les métaux.

Dans un premier temps nous exposerons la préparation de ces composés et de dérivés comprenant un substituant alkyle en 4. Ce substituant doit nous permettre d'étudier l'influence électronique et l'influence stérique d'un tel groupement sur le pouvoir réducteur du modèle.

Nous avons ensuite précisé les facteurs qui gouvernent la réactivité de ces modèles (appelés par la suite en abrégé OPH pour oxazoline pyridinique hydrogénée), lors de la réduction du *p*-nitrobenzaldéhyde. Nous avons à cette occasion réalisé une étude comparative des pouvoirs réducteur et complexant de la *N*-benzyl OPH (BOPH) et du BNAH.

Dans un dernier temps, la méthode utilisée pour accéder aux dérivés du type OPH a permis d'introduire une copule chirale sur le sommet 4. Nous avons pu ainsi obtenir un modèle asymétrique qui n'est pas self-immolatif et nous l'avons testé dans la réduction de substrats prochiraux.

I. Synthèse des (dimethyl-4,4 oxazolyl-2)-3 dihydro-1,4 pyridines

Nous avons suivi le schéma suivant :

TABLEAU 1. Addition des organométalliques sur la (diméthyl-4,4 oxazolyl-2)-3 pyridine

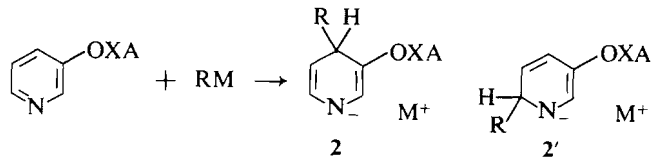

Entrée	R–M	Solvant	Température (°C)	Durée (h)	2/2*	Rdt global (%)
1	CH_3Li	Éther	−78	2	100/0	99
2	CH_3Li	THF	+20	1	48/52	95
3	CH_3Li	THF	−78	1	100/0	99
4	CH_3MgI	Éther	−78	1	100/0	99
5	CH_3MgI	THF	−78	1	100/0	99
6	C_4H_9Li	THF	−78	15	100/0	94
7	CH_3, C_2H_5 $CHCH_2MgCl$†	THF	−78	15	100/0	90

*Le pourcentage d'intermédiaires **2** et **2'** a été déterminé par examen du spectre de rmn ^1H du mélange brut enregistré immédiatement après hydrolyse du complexe organométallique.

†Le magnésien du chloro-1 méthyl-2 butane a été préparé à partir du dérivé chloré lui-même obtenu à partir de l'alcool correspondant (5).

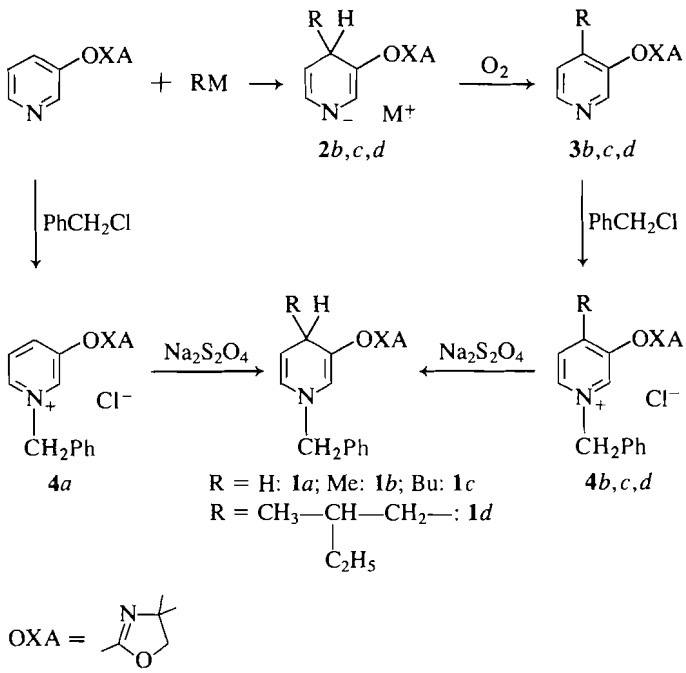

SCHÉMA 1

1. Addition d'un organométallique sur la (diméthyl-4,4 oxazolyl-2)-3 pyridine

L'addition régiosélective des organométalliques sur la (diméthyl-4,4 oxazolyl-2)-3 pyridine ou oxazolyl-3 pyridine a été étudiée par Hauck et Giam (3) et par Meyers et coll. (4). Ces auteurs ont montré que les facteurs déterminant la régiosélectivité de l'attaque sur le cycle pyridinique étaient la température, la durée de réaction, la nature du solvant.

Pour notre part, nous avons obtenu les résultats résumés dans le tableau 1.

Nos résultats sont en général très proches de ceux observés par Meyers et Gabel dans des conditions voisines (comparer entrées 2, 6 et réf. 4*a*). Par contre, on peut noter des différences dans la régiosélectivité de l'attaque de l'organométallique sur l'oxazoline pyridinique entre nos résultats et ceux obtenus par Hauck et Giam (comparer entrées 1 et 2 et réf. 3*a*). Nous n'avons pas observé pour notre part d'attaque notable sur le sommet 2.

Par ailleurs, les résultats décrits dans les entrées 4, 5 et 7 sont originaux. On peut remarquer que les rendements globaux sont toujours excellents, même s'il faut augmenter nettement le temps de la réaction avec des groupements R encombrants (entrées 6 et 7), et que la température joue un rôle prépondérant sur cette régiosélectivité (entrées 2 et 3).

2. Alkylation et passage aux structure dihydropyridiniques

L'alkylation directe des intermédiaires de type **2** par le chlorure de benzyle conduit à des mélanges difficiles à exploiter probablement à cause des divers sites nucléophiles apparaissant sur les composés **2** par suite de la délocalisation de la charge négative.

Nous avons choisi d'oxyder directement les composés **2** par l'oxygène sec (6). Les produits **3** sont ainsi obtenus avec d'excellents rendements variant de 85 à 90% en produit brut.

Le passage aux dihydropyridines a été réalisé par deux méthodes différentes :

(*i*) préparation des sels de pyridinium **4** puis réduction en dérivés dihydro-1,4 pyridiniques par le dithionite de sodium selon la méthode classique (7).

(*ii*) préparation des sels de pyridinium **4** par l'intermédiaire d'une réaction de Zincke (8) suivie d'une réduction par le dithionite de sodium.

Cette seconde méthode donne des rendements comparables à ceux obtenus par la première, mais elle est plus délicate à mettre en oeuvre; en particulier, il est nécessaire d'opérer avec un sel de Zincke de très bonne pureté.

On peut remarquer que dans les deux méthodes la quaternari-

Can. J. Chem. Downloaded from www.nrcresearchpress.com by 80.58.250.72 on 09/07/12
For personal use only.

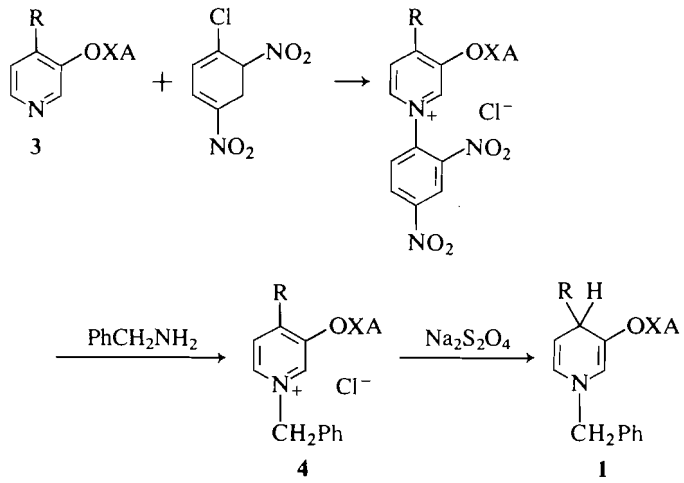

SCHÉMA 2

sation affecte l'atome d'azote du cycle pyridinique plutôt que celui du cycle oxazolinique. Le fort déblindage des protons en 2 et 6 des composés de type **4** par rapport aux déplacements chimiques des protons correspondants dans les composés du type **3** prouve sans ambiguité que l'on a préparé des sels de pyridinium.

Un calcul de chimie quantique nous a permis de confirmer la réactivité nettement plus élevée de l'azote pyridinique. En effet, la quaternarisation est une substitution nucléophile qui a lieu sous contrôle orbitalaire. Le calcul effectué par la méthode CNDO IV nous a fourni les résultats suivants concernant les coefficients orbitalaires des atomes d'azote pyridinique ou oxazolinique dans les orbitales σ occupées de plus haute énergie qui sont celles qui interviennent dans la réaction.

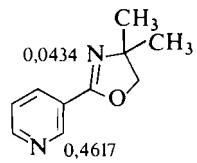

FIG. 1. Coefficients orbitalaires des atomes d'azote de la (diméthyl-4,4 oxazolyl-2)-3 pyridine.

II. Réactivité des modèles

1. Réactivité : réduction du p*-nitrobenzaldéhyde*

La réduction peut être schématisée ainsi avec le modèle **1***a* que nous avons étudié en premier (schéma 3).

Le choix du paranitrobenzaldéhyde (pNBA) est guidé par le

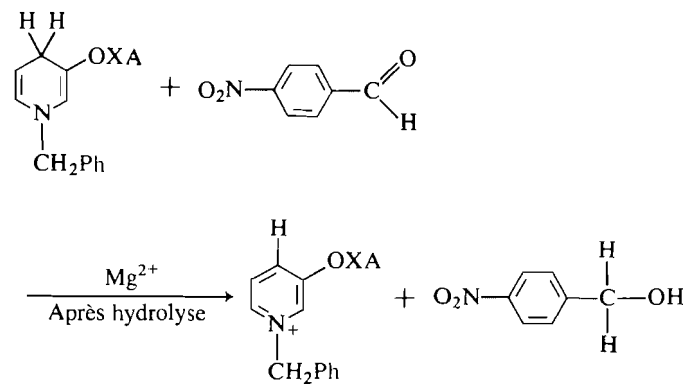

SCHÉMA 3

fait qu'il est facilement réduit par les modèles du type BNAH et que l'analyse rmn ^1H du mélange brut réactionnel est facile.

En travaillant dans des rapport 1:1:1, modèle:substrat:Mg^{2+}, nous avons obtenu avec les produits **1***a*, *b*, *c*, les résultats suivants (tableau 2) :

TABLEAU 2. Réduction du pNBA par divers modèles OPH*

Entrée	Réducteur	Durée (h)	Rapport réducteur/substrat	Rendement en alcool (%)
1	BNAH	18	1	100
2	BOPH **1***a*	18	1	33
3	BOPH **1***a*	25	1	56
4	BOPH **1***a*	43	1	61
5	BOPH **1***a*	68	1	61
6	BOPH **1***a*		2,5	100
7	Me4 BOPH **1***b*	18	1	27
8	Me4 BOPH **1***b*	43	1	59
9	Me4 BOPH **1***b*	68	1	60
10	Me4 BOPH **1***b*		2,5	100
11	Bu4 BOPH **1***c*	36	1	41
12	Bu4 BOPH **1***c*	68	1	41
13	Bu4 BOPH **1***c*	240	2,5	100

*pNBA : paranitrobenzaldéhyde. OPH : oxazolines pyridiniques hydrogénées.

On peut observer que le groupe oxazolyle rend le cycle dihydropyridinique moins réactif qu'il ne l'est avec un groupe carbamoyle dans les mêmes conditions (entrées 1 et 2). Ce résultat sera discuté plus loin.

Les composés **1***a* et **1***b* ont des réactivités assez proches (entrées 2, 4, 5 et 7, 8, 9) alors que dans le cas de **1***c* l'encombrement stérique du groupement butyle est sans doute responsable de la nette baisse de réactivité observée (entrées 11 et 12).

Nous avons alors décidé d'opérer avec un excès de modèle. En utilisant 2,5 équivalents de composé **1** pour 1 équivalent d'aldéhyde, la réduction est quantitative quel que soit le substituant en 4 (entrée 6, 10 et 13). Nous avons travaillé systématiquement en excès de réducteur par la suite.

2. Réduction avec des modèles chiraux

Au départ du sel de pyridinium **4***d* nous espérions que la présence d'une chiralité dans le groupement R induirait une asymétrie en 4 lors de la réduction par $Na_2S_2O_4$. Malheureusement cela n'a pas été le cas : les deux diastéréoisomères **1′***d* et **1″***d* sont obtenus en quantités sensiblement équivalentes (détermination par hplc). La réduction du benzoylformiate de méthyle par ce mélange nous a fourni l'alcool correspondant avec un rendement chimique de 100% et comme attendu, un rendement optique pratiquement nul.

Malgré la présence d'un carbone asymétrique sur la chaine latérale portée par le sommet 4 on constate que cette chiralité n'induit pas une réduction asymétrique du benzoylformiate. Ce résultat confirme le rôle prépondérant joué par la présence d'une chiralité sur le sommet à partir duquel s'effectue le transfert d'hydrogène (9).

Dans le but de tenter d'induire une asymétrie au niveau de ce carbone lors de la réduction par le dithionite de sodium, nous avons alors préparé des modèles portant un substituant chiral sur l'atome d'azote du cycle pyridinique.

Can. J. Chem. Downloaded from www.nrcresearchpress.com by 80.58.250.72 on 09/07/12
For personal use only.

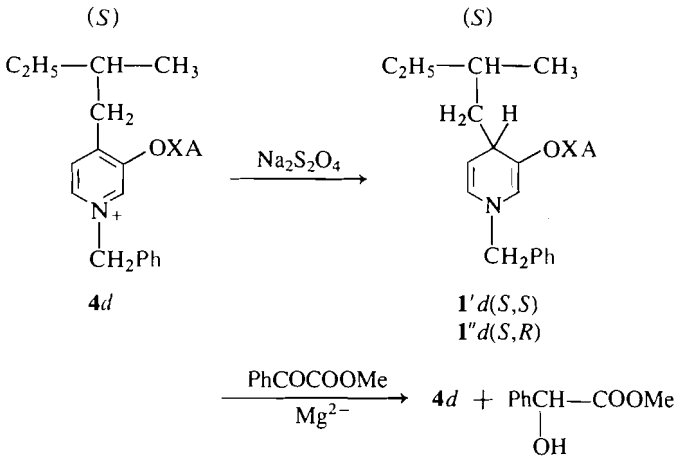

SCHÉMA 4

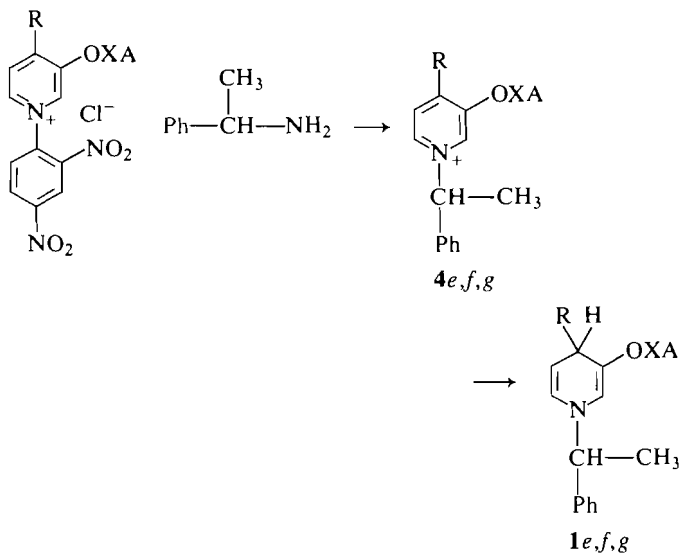

SCHÉMA 5

La réduction de PhCOCOOMe avec ces modèles a donné les résultats indiquées dans le tableau 3.

On observe cette fois une faible induction asymétrique lors de la réduction du benzoylformiate de méthyle par les modèles **1***e*, **1***f* et **1***g*. Avec **1***e* l'induction observée lors de la réduction est due à la chiralité portée par le substituant de l'azote pyridinique. Cette chiralité étant éloignée du site réactif du réducteur il n'est pas étonnant que le rendement optique soit faible.

Cependant la présence de cette chiralité dans le sel de pyridinium **4***f* permet d'obtenir majoritairement l'un des diastéréoisomères de structure **1***f* puisque la réduction du benzoylformiate de méthyle fournit un excès de l'alcool de configuration *S* inverse de celui obtenu avec **1***e*. Ce résultat est incontestablement dû à une induction issue de l'asymétrie présente sur le carbone en 4 de **1***f*.

Dans le cas de **1***g* on peut penser que le changement de configuration sur le substituant de l'azote pyridinique annule et contrarie l'induction exercée par la chiralité en 4 et justifie que l'on obtienne un faible excès enantiomérique de l'alcool *R*.

3. Étude de la réactivité du modèle **1** a

La réduction du paranitrobenzaldéhyde par le BNAH ou par le BOPH **1***a* en présence de Mg^{2+} s'est révélée plus facile avec le BNAH (entrées 1 et 2, tableau 2).

TABLEAU 3. Réduction de PhCOCOOMe par des OPH chirales

Modèle	R (configuration)	R′ (configuration)	Alcool e.e.* (configuration)
1*e*	H	—CH—CH_3 (*R*) Ph	2,4% (*R*)
1*f*	CH_2—CH—C_2H_5 CH_3 (*S*)	—CH—CH_3 (*R*) Ph	8,9% (*S*)
1*g*	CH_2—CH—C_2H_5 CH_3 (*S*)	—CH—CH_3 (*S*) Ph	1,6% (*R*)

*L'excès enantiomérique (e.e.) est calculé à partir de la valeur mesurée du pouvoir rotatoire du mandélate de méthyle comparée à celle du mandélate enantiomériquement pur (12).

TABLEAU 4. Spectres de résonance magnétique nucléaire (*a*) de ^1H et (*b*) de ^{13}C : déplacements chimiques pour le BNAH et le BOPH en solution dans CD_3CN

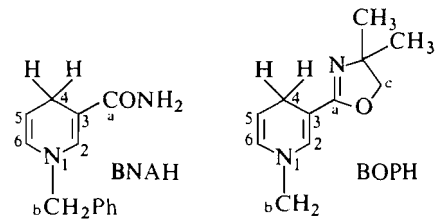

1*a*

(a)

	H(2)	H(4)	H(5)	H(6)	H_b	H_c
BNAH	6,96	3,05	4,70	5,84	4,29	—
BOPH **1***a*	6,76	3,03	4,70	5,90	4,29	3,83

(b)

	C(2)	C(4)	C(5)	C(6)	C_a	C_b	C_c
BNAH	138,4	22,2	102,5	127,3	169,0	56,4	—
BOPH **1***a*	136,4	22,7	102,0	127,4	162,0*	56,4	77,9

* Valeur sujette à caution.

Nous avons mesuré le potentiel de demi-vague du BNAH et du BOPH[2] et obtenu la même valeur de 0,4 V. Cela signifie que le cycle dihydropyridinique est aussi facile à oxyder dans les deux cas.

Nous avons ensuite enregistré les spectres de rmn du BNAH et du BOPH **1***a* en présence de Mg^{2+}. Cette méthode a permis d'obtenir des informations sur la complexation exercée par le métal divalent sur le BNAH (10).

On constate que les déplacements chimiques des protons portés par le carbone 4 ou de ce carbone 4 lui-même sont proches les uns des autres. D'une manière générale il n'existe pas de différences notables entres les atomes correspondants de l'un ou l'autre modèle.

2. Valeur mesurée sur électrode de graphite dans le milieu CH_3CH + 0,1 mol L^{-1} de Bu_4NBF_4 au laboratoire du Professeur M. Devaud à l'INSA.

Can. J. Chem. Downloaded from www.nrcresearchpress.com by 80.58.250.72 on 09/07/12
For personal use only.

TABLEAU 5. Alkyl-4 (diméthyl-4,4 oxazolyl-2)-3 pyridines **3**

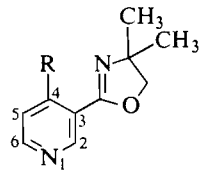

Composé	Rdt* (%)	*E*	Litterature ou microanalyses (voir tableau 8)	Résonance magnétique nucléaire de ^1H ($CDCl_3$)					
				H(2)	H(5)	H(6)	CH_2	CH_3	Autres protons
R = CH_3 **3***b*	70	$E_{0,3}$ = 60	$C_{11}H_{14}N_2O$ (4)	8,90	7,08	8,45	4,00	1,38	CH_3 : 2,53
R = C_4H_9 **3***c*	65	$E_{0,3}$ = 80	$C_{14}H_{20}N_2O$ (4)	8,90	7,07	8,43	4,02	1,35	$CH_3CH_2CH_2$—CH_2— 0,83 à 1,77 3,06
R = CH_3—CH(CH_2CH_3)—CH_2 **3***d* (S)	63	$E_{0,3}$ = 114	$C_{15}H_{22}N_2O$	8,95	7,10	8,50	4,02	1,35	0,85 à 2,0 CH_3, CH_3CH_2, CH—CH_2—

*Rendement en produit pur calculé par rapport à la (diméthyl-4,4 oxazolyl-2)-3 pyridine.

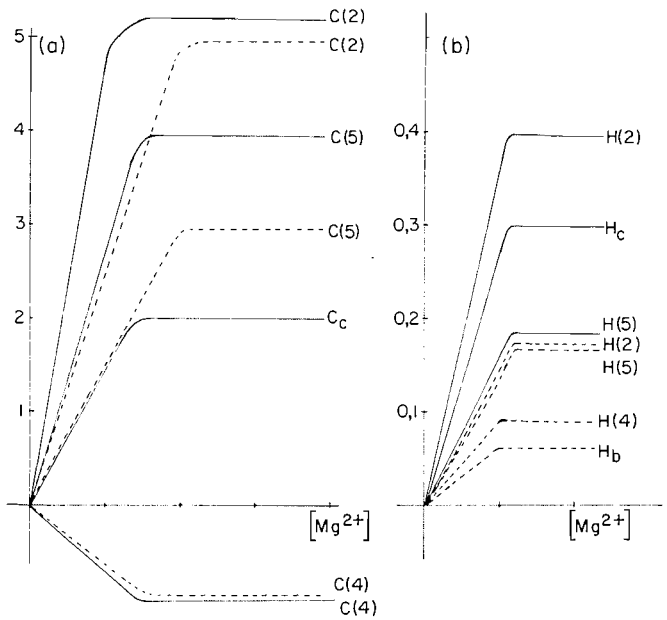

FIG. 2. Δδ en rmn (*a*) de ^{13}C et (*b*) de ^1H en présence de Mg^{2+} (en trait plein, BOPH; en trait pointillé, BNAH).

Si l'on examine maintenant les différences de déplacement chimique engendrées par addition de Mg^{2+} aux deux modèles, on obtient les résultats résumés dans la courbe ci-dessus (fig. 2).

On observe en rmn de ^1H et de ^{13}C que les protons et carbones 2, 5, 6 et c du modèle **1***a* sont déblindés alors que les protons ou carbone en 4 sont blindés par addition de $Mg(ClO_4)_2$.

On peut remarquer en particulier que le carbone méthylènique (C_c) du cycle oxazolinique subit un déblindage important en présence de Mg^{2+}. Ceci indique que la complexation affecte essentiellement le groupe oxazolinique et justifie les variations importantes de déplacements chimiques observées pour les atomes en 2, 4 et 5 situés au voisinage du site de complexation.

On peut noter que les déplacements chimiques des atomes liés au sommet 6 sont peu affectés par addition de Mg^{2+}, ce qui semble exclure une participation de l'atome d'azote du cycle dihydropyridinique dans la complexation.

On observe une différence importante dans les variations de déplacement chimique des carbones 2 et 5 de **1***a* et du BNAH en présence de Mg^{2+}. Les déblindages subis par les carbones de **1***a* sont supérieurs d'environ 1 ppm. On peut penser que la complexation par Mg^{2+} a pour effet de diminuer plus la densité électronique dans le cas du BOPH par rapport à la situation dans le BNAH : le groupement oxazolyle complexé exerce un effet attracteur plus fort sur le cycle dihydropyridinique que ne le fait le groupement carbamoyle complexé dans le BNAH. Ce phénomène ne facilite pas le départ d'un ion hydrure en polarisant la liaison C(4)—H un peu plus vers le carbone comme le montre le blindage un peu plus important pour le C(4) observé dans **1***a* par rapport au BNAH.

Lors de la réduction d'un composé carbonylé le magnésium permet d'établir un complexe ternaire : substrat/Mg^{2+}/modèle dihydropyridinique (BNAH ou BOPH). Si le magnésium est fortement complexé par le modèle dihydropyridinique il est alors moins disponible pour se lier au substrat et assurer son activation.

Ces hypothèses justifient que lors de la réduction du para-nitrobenzaldéhyde le BOPH soit moins réactif que le BNAH.

Partie expérimentale

Les points de fusion ont été déterminés sur un banc de Kofler et n'ont pas été corrigés.

Les spectres ir ont été enregistrés soit avec un spectrographe Perkin–Elmer 237 soit avec un spectrographe Beckman IR 4350; les solides sont dispersés dans du KBr sous forme de pastilles et les liquides sont insérés dans des fenêtres de NaCl sous forme de film.

Les spectres de rmn de ^1H ont été enregistrés sur un appareil Varian A60 ou Varian T60, les spectres de rmn de ^{13}C sur un appareil Brucker WH 90 D.

Les microanalyses ont été effectuées sur un appareil Carlo Erba 1106. Dans les tableaux récapitulatifs les produits pour lesquels la formule brute est donnée ont fourni des résultats corrects à l'analyse.

Les pouvoirs rotatoires ont été mesurés sur un micropolarimètre Perkin–Elmer type 241.

Can. J. Chem. Downloaded from www.nrcresearchpress.com by 80.58.250.72 on 09/07/12
For personal use only.

TABLEAU 6. Sels de pyridinium **4**

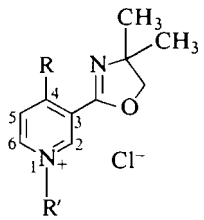

R (configuration)	R′ (configuration)		Méthode*	Analyse (voir tableau 8)	$[\alpha]_D^{25}$†	Résonance magnétique nucléaire de ^1H des protons pyridiniques ($CDCl_3$)‡ H(2)	H(5)	H(6)	H(4)
H	Ph CH_2	**4***a*	a, b	$C_{17}H_{19}N_2OCl$		9,8	8,4	9,9	9,0
CH_3	Ph CH_2	**4***b*	a	$C_{18}H_{21}N_2OCl$		9,6	8,0	10,2	
C_4H_9	Ph CH_2	**4***c*	a	$C_{21}H_{27}N_2OCl$		9,6	8,0	10,2	
CH_3 $CHCH_2$ C_2H_5 (*S*)	Ph CH_2	**4***d*	a, b	$C_{22}H_{29}N_2OCl$		9,6	8,0	10,2	
H	Ph—CH (*R*) CH_3	**4***e*	b	$C_{18}H_{21}N_2OCl$		10,0	8,4	9,7	9,0
CH_3 $CHCH_2$ C_2H_5 (*S*)	Ph—CH (*R*) CH_3	**4***f*	b	$C_{23}H_{31}N_2OCl$§		9,5	8,0	10,3	
CH_3 $CHCH_2$ C_2H_5 (*S*)	Ph—CH (*S*) CH_3	**4***g*	b	$C_{23}H_{31}N_2OCl$§	+14,66°	9,5	8,0	10,3	

*Le sel de pyridinium a été préparé par la méthode au chlorure de benzyle (a) ou la méthode de Zincke (b).
†Le pouvoir rotatoire a été déterminé lorsque la solution chloroformique du sel de pyridinium possède une transparence suffisante.
‡Les déplacements chimiques sont donnés avec un seul chiffre après le virgule car ils varient avec la concentration dans $CDCl_3$.
§Ces produits n'ont pu être obtenus analytiquement purs. Il ont cependant fournis, dans l'étape suivante, les produits **1***f* et **1***g* purs.

A. Synthèse des modèles dihydropyridiniques

1. Addition d'un organométallique sur la (diméthyl-4,4 oxazolyl-2)-3 pyridine

La (diméthyl-4,4 oxazolyl-2)-3 pyridine est obtenue par action de l'amino-2 méthyl-2 propanol sur le chorure de nicotinoyle (11).

Dans un ballon d'un litre balayé par un courant d'argon, muni d'une agitation mécanique, d'un réfrigérant protégé de l'humidité atmosphérique par une garde à chlorure de calcium et d'un septum, on introduit 52,8 g (0,3 mol) de l'oxazoline ci-dessus et 400 mL de tetrahydrofuranne sec. On refroidit à −78°C puis on siphonne goutte à goutte 0,3 mol du dérivé organométallique en solution dans l'éther ou le THF. L'addition dure en générale 20 min. On maintient ensuite à basse température, puis on laisse remonter à température ambiante avant de procéder à l'oxydation.

*2. Oxidation : obtention des alkyl-4 (diméthyl-4,4 oxazolyl-2)-3 pyridines **3** (tableau 5)*

L'intermédiaire organométallique en solution dans l'éther ou le THF obtenu à l'étape précédente est oxydé par barbottage d'oxygène sec pendant 15 min. On concentre en éliminant la majeure partie du solvant à l'évaporateur rotatif. Le résidu est hydrolysé avec précautions, puis extrait à l'éther. La phase éthérée est séchée sur $MgSO_4$, évaporée sous vide et purifiée aussitôt par distillation sous vide. (Le produit brut se dégrade rapidement au cours du temps.)

3. Quaternarisation : passage aux chlorures de N*-benzyl alkyl-4 (diméthyl-4,4 oxazolyl-2)-3 pyridiniums : **4**a, b, c, d, e, f, g*

(a) Méthode au chlorure de benzyle. Dans un ballon muni d'un réfrigérant à reflux, on dissout 0,05 mol de composé **3** et 9,5 g (0,075 mol) de chlorure de benzyle fraîchement distillé dans 50 mL d'acétonitrile. On porte à reflux pendant trois jours, puis concentre sous vide. Le résidu est dissous dans le minimum d'éthanol chaud. On verse dans un large excès d'éther. Le sel de pyridinium se sépare généralement sous forme d'huile. Sa pureté est suffisante pour passer à l'étape suivante.

(b) Méthode par le sel de Zincke. Cette méthode a été utilisée au départ des alkyl-4 (diméthyl-4,4 oxazolyl-2)-3 pyridines **3***a* et **3***d*.

Dans un ballon muni d'un réfrigérant à reflux on introduit 0,05 mol de composé **3***a* ou **3***d* et 50 g (0,25 mol) de chloro-1 dinitro-2,4 benzène. On chauffe le mélange progressivement de 20 à 90°C en 30 min. On maintient à cette température pendant 2 h. On laisse refroidir, puis reprend le mélange dans un minimum de méthanol et verse ensuite dans un large excès d'éther. Le sel de Zincke précipite. Il est purifié par dissolution dans l'eau à ébullition en présence de noir animal. La solution est filtrée à chaud, puis évaporée. Le solide obtenu est recristallisé dans le méthanol. Rendement 80%.

Le sel de Zincke (4,5 g soit environ 0,01 mol) et 1,1 g (0,01 mol) de benzylamine ou 1,2 g (0,01 mol) d'α-méthylbenzylamine (*R* ou *S*) sont dissous dans le méthanol. On porte à reflux pendant 24 h. Le sel

Can. J. Chem. Downloaded from www.nrcresearchpress.com by 80.58.250.72 on 09/07/12
For personal use only.

TABLEAU 7. Dihydro-1,4 pyridines **1**

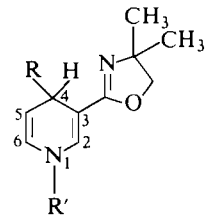

R (configuration)	R′ (configuration)		Analyse (voir tableau 8)	$[\alpha]_D^{25}$ ($CDCl_3$)	Résonance magnétique nucléaire de ^1H ($CDCl_3$) H(2)	H(4)	H(5)	H(6)
H	Ph CH_2	**1***a*	$C_{17}H_{20}N_2O$	—	6,77	3,20	4,72	5,74
CH_3	Ph CH_2	**1***b*	$C_{18}H_{22}N_2O$	—	6,85	3,50	4,77	5,76
nC_4H_9	Ph CH_2	**1***c*	$C_{21}H_{28}N_2O$	—	6,90	3,45	4,70	5,83
CH_3 \ $CHCH_2$ (*S*) / C_2H_5	Ph CH_2	**4***d*	$C_{22}H_{30}N_2O$	+21,2° (*c* 1,75)	6,87	3,55	4,73	5,82
H	Ph—CH (*R*) CH_3	**4***e*	$C_{18}H_{22}N_2O$	+12,65° (*c* 0,63)	6,83	3,21	4,62	5,70
CH_3 \ $CHCH_2$ (*S*) / C_2H_5	Ph—CH (*R*) CH_3	**4***f*	$C_{23}H_{32}N_2O$	+27,81° (*c* +1,14)	6,97	3,53	4,73	5,83
CH_3 \ $CHCH_2$ (*S*) / C_2H_5	Ph—CH (*S*) CH_3	**4***g*	$C_{23}H_{32}N_2O$	+15,92° (*c* +2,42)	6,97	3,53	4,73	5,83

de pyridinium est précipité dans un large excès d'éther et isolé par filtration. Les caractéristiques des produits préparés sont décrites dans le tableau 6.

NOTA : Le mélange brut obtenu après le reflux peut être repris dans l'eau. Dans ces conditions la dinitro-2,4 aniline précipite et la solution résiduelle peut être utilisée directement pour effectuer la réduction en dihydro-1,4 pyridine.

4. Réduction : obtention des N*-benzyl alkyl-4 dihydro-1,4 (diméthyl-4,4 oxazolyl-2)-3 pyridines :* **1** a, b, c, d, e, f, g

Dans un ballon muni d'une agitation et maintenu sous atmosphère d'argon, on dissout 3 g (environ 0,01 mol) de sel de pyridinium **4**) dans 10 mL d'eau (préalablement désoxygénée par bullage d'argon). On porte à 40°C et on ajoute sous agitation un mélange fraîchement préparé de 5 g de dithionite de sodium et de 5 g de $CO_3Na_{2,10}H_2O$ (ce qui correspond à un large excès). Après 30 min d'agitation, on extrait l'huile en suspension par 4 × 30 mL de chloroforme. Le solvant est éliminé, puis le résidu est purifié par flash chromatographie sur silice en éluant au chloroforme.

Les produits obtenus qui se présentent tous sous forme d'huile sont décrits dans le tableau 7.

B. Réduction de substrats

1. Réduction du paranitrobenzaldéhyde (pNBA)

La réactivité des modèles de type **1** vis-à-vis du pNBA a été étudiée en suivant l'évolution de la réaction par rmn de ^1H. Dans un tube de rmn sec on introduit le modèle, le perchlorate de magnésium et le pNBA dans les proportions décrites dans la partie théorique. On dissout dans l'acétonitrile deutérié. On maintient à 60°C et on enregistre le spectre rmn du mélange à intervalles réguliers.

Nous décrivons, par ailleurs, le mode opératoire suivi pour réaliser la réduction dans des conditions préparatives : dans un tube sec, purgé à l'argon, on introduit 0,151 g (0,001 mol) de pNBA, 0,001 mol ou 0,0025 mole de modèle **1***a*, **1***b* ou **1***c* et 0,446 g (0,002 mol) de perchlorate de magnésium anhydre, le mélange est mis en solution dans 2 mL d'acétonitrile parfaitement anhydre. Le tube est scellé et on maintient à 60°C (durée : voir partie théorique). Après refroidissement, on ouvre le tube, hydrolyse avec 2 mL d'eau et extrait à l'éther. Après séchage on évapore le solvant et récupère l'alcool *p*-nitrobenzylique par avec un rendement quasi quantitatif.

2. Réduction du benzoylformiate de méthyle

Dans un ballon sec, muni d'un septum, on mélange 0,0025 mol de modèle **1** fraîchement préparé, 0,446 g (0,002 mol) de perchlorate de magnésium et 0,164 g (0,001 mol) de benzoylformiate de méthyle. On purge à l'argon et on introduit, par le septum, 10 mL d'acétonitrile parfaitement anhydre.

La solution est agitée et chauffée au bain d'huile pendant trois jours. Chaque essai est hydrolysé en traitant le milieu réactionnel par un mélange de 2 mL d'eau et 100 mL de chloroforme. La phase organique est séparée. La phase aqueuse est extraite par 2 × 50 mL de chloroforme. Les extraits sont rassemblés, séchés sur $MgSO_4$, évaporés sous vide. On reprend le résidu par 1 mL d'éthanol absolu, puis on dilue par 100 mL d'éther. On sépare le sel de pyridinium qui a précipité et le filtrat est recueilli dans un ballon préalablement taré. On évapore à sec et on pèse le résidu.

On connait ainsi le rendement de la réduction qui est généralement quasi quantitatif. Le résidu est ensuite purifié par chromatographie sur silice en éluant par un mélange éther–hexane (1:2). Les fractions contenant le mandélate de méthyle pur (vérifié en ccm) sont évaporées à sec. Le mandélate cristallisé est mis à sécher pour mesurer ensuite son pouvoir rotatoire (mandélate de méthyle *d* ou *l* : $[\alpha]_D^{25}$ = 167° dans le chloroforme (12)).

Can. J. Chem. Downloaded from www.nrcresearchpress.com by 80.58.250.72 on 09/07/12
For personal use only.

TABLEAU 8. Microanalyses des produits nouveaux

Composé	Valeurs calculées			Valeurs trouvées		
	% C	% H	% N	% C	% H	% N
3*d* $C_{15}H_{22}N_2O$	73,17	8,94	11,38	72,9	8,9	11,3
4*a* $C_{17}H_{19}N_2OCl$	67,44	6,28	9,26	67,3	6,1	9,1
4*b* $C_{18}H_{21}N_2OCl$	68,24	6,63	8,84	67,8	6,5	8,7
4*c* $C_{21}H_{27}N_2OCl$	70,29	7,53	7,81	69,9	7,7	7,6
4*d* $C_{22}H_{29}N_2OCl$	70,87	7,78	7,52	70,8	7,8	7,4
4*e* $C_{18}H_{21}N_2OCl$	68,24	6,63	8,84	67,9	6,8	8,6
1*a* $C_{17}H_{20}N_2O$	76,12	7,46	10,45	76,1	7,4	10,3
1*b* $C_{18}H_{22}N_2O$	76,60	7,80	9,93	76,5	7,8	9,9
1*c* $C_{21}H_{28}N_2O$	77,78	8,64	8,64	77,6	8,5	8,5
1*d* $C_{22}H_{30}N_2O$	78,10	8,87	8,28	78,0	8,9	8,2
1*e* $C_{18}H_{22}N_2O$	76,60	7,80	9,93	76,6	7,5	9,8
1*f* $C_{23}H_{32}N_2O$	78,41	9,09	7,96	78,2	9,0	7,6
1*g* $C_{23}H_{32}N_2O$	78,41	9,09	7,96	78,1	9,0	7,6

Mise en oeuvre des calculs de chimie quantique

La géométrie de la pyridine est celle rapportée dans la littérature (13). La géométrie de la partie oxazoline a été optimisée par la méthode MINDO III : Pour des raisons liées aux capacités de calcul de ce programme, les deux méthyles 4 ont été supprimés.

Le tableau ci-dessous contient la géométrie complète en coordonnées internes de GAUSS. Les coefficients orbitalaires ont été calculés par la méthode CNDO IV.

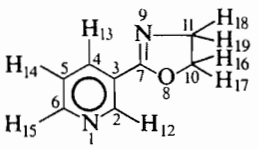

N	At	Réf.	Long.	Réf.	Angle	Réf.	Dièdre
1	7	0	0,0	0	0,0	0	0,0
2	6	1	1,34	0	0,0	0	0,0
3	6	2	1,40	1	123,90	0	0,0
4	6	3	1,39	2	118,50	1	0,0
5	6	4	1,39	3	118,50	2	0,0
6	6	5	1,40	4	118,50	3	0,0
7	6	3	1,47	2	120,75	1	180,00
8	8	7	1,34	3	121,00	2	0,00
9	7	7	1,28	3	121,00	2	180,00
10	6	8	1,38	7	107,60	3	180,00
11	6	9	1,46	7	105,00	3	180,00
12	1	2	1,08	1	115,90	6	180,00
13	1	4	1,08	3	120,80	2	180,00
14	1	5	1,08	6	121,30	1	180,00
15	1	6	1,08	1	115,90	2	180,00
16	1	10	1,12	8	110,18	7	120,00
17	1	10	1,12	8	110,18	7	240,00
18	1	11	1,12	9	112,20	7	120,00
19	1	11	1,12	9	112,20	7	240,00

1. (*a*) D. M. STOUT et A. I. MEYERS. Chem. Rev. **82**, 223 (1982); (*b*) R. J. KILL et D. A. WIDDOWSON. Bioorganic chemistry. Vol. IV. *Editeur*: E. E. Van Tamelen. Academic Press, Inc., New York. 1978. p. 239.
2. A. J. DE KONING, H. J. ALBERTS-JANSEN, J. BEERSMA et G. J. M. VAN DER KERK. Recl. J. R. Neth. Chem. Soc. **99**, 316 (1980).
3. (*a*) A. E. HAUCK et C. S. GIAM. J. Chem. Soc. Perkin Trans. 1, 2227 (1984); (*b*) G. E. DUBEY, E. KNAUS et C. S. GIAM. Heterocycles, **22**, 1091 (1984).
4. (*a*) A. I. MEYERS et R. A. GABEL. J. Org. Chem. **47**, 2633 (1982); (*b*) N. REUMAN et A. I. MEYERS. Tetrahedron Report N° 181. Tetrahedron, **41**, 837 (1985).
5. H. C. BROWN et C. GROOT. J. Am. Chem. Soc. **64**, 2563 (1942).
6. R. A. ABRAMOVITCH et J. G. SAHA. Adv. Heterocycl. Chem. **6**, 229 (1966).
7. D. MAUZERALL et F. H. WESTHEIMER. J. Am. Chem. Soc. **77**, 2261 (1955).
8. V. H. LETTRE, W. HAEDE et E. RUHBAUM. Ann. Chem. **579**, 123 (1953).
9. A. OHNO, M. IKEGUCHI, T. KIMURA et S. OKA. J. Am. Chem. Soc. **101**, 7036 (1979).
10. M. HUGHES, R. H. PRINCE et P. WYETH. J. Inorg. Nucl. Chem. **40**, 714 (1978).
11. A. I. MEYERS et R. GABEL. Heterocycles, **11**, 133 (1978).
12. W. H. PIRKLE et S. D. BEARE. Tetrahedron Lett. 2579 (1968).
13. W. COHRAN. Physical methods in heterocyclic chemistry. Vol. I. Academic Press, New York. 1963. 164 ff.

Can. J. Chem. Downloaded from www.nrcresearchpress.com by 80.58.250.72 on 09/07/12
For personal use only.

The potassium permanganate oxidation of steroidal homoannular dienes

ZBIGNIEW BOŃCZA-TOMASZEWSKI
Department of Chemistry, Warsaw University, 02-093 Warszawa, ul. Pasteura 1, Poland

Received June 19, 1986

ZBIGNIEW BOŃCZA-TOMASZEWSKI. Can. J. Chem. **65**, 656 (1987).

The oxidation of 3β-acetoxycholesta-5,7-diene (**1**) with potassium permanganate – sodium periodate reagent gave epoxy-diol **2** with almost quantitative yield. Similar oxidation of cholesta-2,4-diene (**3**) afforded, as well as epoxy-diols **5** and **6**, products of cleavage of the double bonds. These results show that formation of epoxy-diols predominates in the case of hindered steroidal dienes (e.g., diene **1**), whereas oxidation of unhindered steroidal dienes (e.g., diene **2**) gives, in addition to epoxy-diols, products of cleavage of the double bonds.

ZBIGNIEW BOŃCZA-TOMASZEWSKI. Can. J. Chem. **65**, 656 (1987).

L'oxydation de l'acétoxy-3β cholestadiène-5,7 (**1**) par le couple permanganate de potassium – periodate de sodium conduit à l'époxy-diol **2** avec un rendement pratiquement quantitatif. Une oxydation semblable du cholestadiène-2,4 (**3**) conduit, en plus des époxy-diols **5** et **6**, aux produits de rupture des doubles liaisons. Ces résultats démontrent que la formation des époxy-diols est la réaction prédominante dans les cas des dienes stéroïdaux empêchés (comme le diène **1**) alors que l'oxydation des dienes stéroïdaux non-empêchés (comme le diène **2**) conduit, en plus des époxy-diols, à des produits provenant de la scission des doubles liaisons.

[Traduit par la revue]

A few years ago we undertook some studies on extensive degradation of steroids as a possible route for the preparation of intermediates required for the synthesis of heterocyclic steroids. The oxidative cleavage of double bonds in steroidal homoannular dienes should lead to γ-dicarbonyl compounds, which could be very useful in the synthesis of diazasteroids. Recently we described the utilization of ruthenium tetroxide for oxidation of steroidal conjugated dienes (1). In continuing the search for better oxidative methods we turned our attention to potassium permanganate – sodium periodate mixture (2). This reagent has been used especially for cleavage of double bonds and in many cases was found to be superior to ozonolysis.

We observed that hindered homoannular dienes (e.g. 3β-acetoxycholesta-5,7-diene (**1**)) were resistant to degradation with potassium permanganate – sodium periodate mixture. Instead of cleavage of conjugated double bonds we found that less hindered C(5)—C(6) double bonds underwent hydroxylation, whereas more hindered C(7)—C(8) bonds underwent epoxidation, and epoxy-diol **2** was obtained (3, 4).[1]

These results prompted us to establish whether oxidation of homoannular dienes with potassium permanganate – sodium periodate mixture had general character or if it was limited to hindered ring B in the steroid system. Therefore we investigated a reaction of cholesta-2,4-diene (**3**) with potassium permanganate.

When diene **3** was treated with neutral or alkaline potassium permanganate four products were isolated from the neutral fraction: the known lactol **4***a* (5)[2] (12% yield), epoxy-diol **5** (31% yield), epoxy-diol **6** (2.5% yield), and epoxy-lactol **7***a*[2] (1.5% yield). From the acidic fraction, after methylation with diazomethane, acetal ester **8***b* (2% yield) and hydroxy-lactone ester **9***b* (21% yield) were isolated (Scheme 1).

Structures of compounds **6**, **7**, and **8***b* followed from their analytical and spectral data (cf. Experimental). However, no definitive stereochemical assignment of epoxy-diol **5** and hydroxy-lactone ester **9***b* could be made on the basis of nmr evidence alone. In the case of epoxy-diol **5** it was not possible to establish unequivocally the configuration of the 2,3-epoxide ring and C-4 and C-5 hydroxyl groups. The only signal of 19-H (at δ 0.93 ppm) suggested their α configuration. In the case of β substituents at C-2, C-3, C-4, and C-5, these protons would be strongly deshielded (6). In the ^{13}C nmr spectrum of epoxy-diol **5** the observed shieldings were in good agreement with those calculated for an α configuration of the 2,3-epoxide and the C-4 and C-5 hydroxyl groups. The calculation was made by the addition of substituent effects listed by Blunt and Stothers for certain steroids (7) (see Table 1). Further evidence for an α configuration of 4-OH, 5-OH, and the 2,3-epoxide ring was obtained by reduction of epoxy-diol **5** with lithium aluminum hydride and lithium aluminum deuteride to triols **10***a* and **10***b*, respectively. The ^1H nmr spectrum of **10***a* showed (after shaking with D_2O) a narrow one-proton multiplet at δ 3.97 ppm ($W/2$ = 10.5 Hz) and a one-proton doublet at δ 3.49 ppm (J_{ae} = 3.5 Hz) corresponding to a β-equatorial proton at C-3 and a β-axial proton at C-4, respectively. The comparison of the ^1H nmr spectra of **10***a* and **10***b* exhibited one difference: instead of a multiplet at 3.97 ppm, a triplet was observed ($J_{ae} = J_{ee}$ = 3.5 Hz). It indicated that coupling constant $J_{2a,3e}$ = 3.5 Hz disappeared. The ^{13}C nmr spectrum of **10***a* strongly supported an α configuration of the 3-OH, 4-OH, and 5-OH hydroxyl groups. The observed shieldings were in good agreement with those calculated by the addition of substituent effects (7) (see Table 1). Hence triols **10***a* and **10***b* must arise by diaxial opening of the 2,3-α-epoxide ring during nucleophilic attack of hydride (or deuteride) ion from the β-side of the molecule (8). It showed that the 2,3-epoxide ring and C-4, C-5 hydroxyl groups had an α configuration.

Most of the assignments for hydroxy-lactone ester **9***b* followed from their analytical and spectral data (cf. Experimental). However, no definitive assignment of the lactone and ring B junction and the configuration at C-4 could be made. Evidence for five-membered lactone and B-ring *trans* fusion was obtained from a comparison of ^1H nmr of **9***b* (free OH group at C-4) and **9***c* (with an acetoxy group at C-4). In the ^1H nmr spectrum of **9***a* the magnitude of shielding of 19-H protons (at δ 1.20 ppm) was almost the same as in the spectrum of **9***c* (at δ 1.18 ppm). It

[1]In communication 3 compound **2** was erroneously described as tetrol. The correct structure was established after reinvestigation (cf. ref. 4).

[2]The lactols **4***a* and **7***a* are tautomers of seco-keto-acids **4***b* and **7***b*, respectively.

Can. J. Chem. Downloaded from www.nrcresearchpress.com by 80.58.250.72 on 09/07/12
For personal use only.

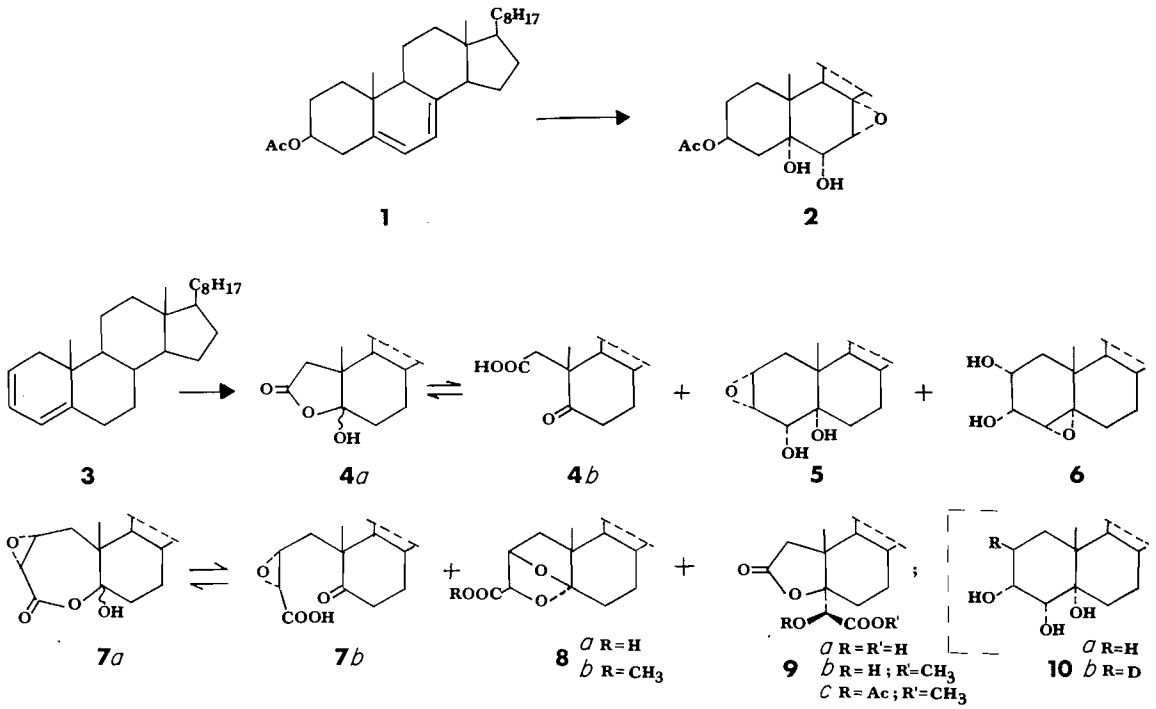

SCHEME 1

TABLE 1. Comparison of calculated and observed ^{13}C shieldings[a] in epoxy-diol **5** and triol **10***a*

Epoxy-diol **5**[b]			Triol **10***a*		
C	Calculated	Observed	C	Calculated	Observed
1	39.2	39.8	1	23.8	23.9
2	47.2	51.4	2	25.9	25.4
3	57.8	57.4	3	69.9	70.5
4	69.5	69.8[c]	4	77.3	77.0
5	75.5	75.5[c]	5	72.4	71.1[c]
6	27.2	28.0	6	27.7	28.0
7	25.2	25.7	7	25.7	25.4
8	34.4	35.0	8	34.5	34.4
9	45.0	46.3	9	45.8	45.6
10	37.8	36.5	10	40.5	40.4
11	21.1	20.7	11	21.0	20.9
12	39.9	39.6	12	40.1	40.1
13	42.5	42.4	13	42.7	42.7
14	56.0	55.9	14	56.2	56.2
15	24.1	24.1	15	24.1	24.1
16	28.3	28.2	16	28.2	28.2
17	56.2	56.3	17	56.1	56.1
18	11.9	12.0	18	12.2	12.2
19	17.9	16.9	19	16.5	15.8

[a]δ_C ppm from TMS. Original data converted using $\delta_C^{CHCl_3}$ 77.2.
[b]The reference steroid here is 2α,3-epoxy-5α-androstan, the shieldings for which were obtained by subtracting the effects for the 17β-OAc group from the shieldings for 2α,3-epoxy-5α-androstan-17β-yl acetate.
[c]Assigned by off-resonance decoupling.

suggested that the substituent at C-5 occupied the opposite (α) position to 19-CH_3, hence fusion of five-membered lactone and B-ring should be *trans*. "*S*" configuration at C-4 in hydroxy-lactone ester **9***b* followed from the mechanism of its formation.

To gain further information about the oxidation reaction, diene **3** was subjected to potassium permanganate – sodium periodate mixture oxidation. We observed that the yield of hydroxy-lactone ester **9***b* was slightly increased (to 25%) and the yield of epoxy-diol **6** was decreased (to 1.5%). From these results it appears that sodium periodate is not necessary for degradation of diene **3** and the permanganate is effecting both hydroxylation (or epoxydation) and cleavage of conjugated double bonds.

To obtain evidence for the formation of compounds **8***a* and **9***a*, independent syntheses of acetal ester **8***b* and hydroxy-lactone ester **9***b* were carried out. When epoxy-diol **5** was oxidized with potassium permanganate – sodium periodate mixture for three days, after methylation with diazomethane, acetal ester **8***b* was obtained with a poor yield (3.75%). Epoxy-diol **6** was subjected to the same reaction conditions. In this instance the hydroxy-lactone ester **9***b* was formed in 6% yield (after methylation with diazomethane). It indicated that the epoxy-acid **7***b* and epoxy-diacid **11** could be intermediates in the formation of acetal **8***a* and hydroxy-lactone acid **9***a*, respectively (Scheme 2).

The simplest mechanism that explains this rearrangement is a nucleophilic attack by the carbonyl group at C-5 in epoxy-acid **7***b* concerted with epoxide bond rupture, leading to an acetal bridged structure **8***a*. Similarly, epoxide cleavage concerted with a nucleophilic attack by oxygen from the carbonyl group in epoxy-diacid **11** leads to hydroxy-lactone acid **9***a* (Scheme 2).

On the basis of data presented in this paper it was possible to draw the following conclusions: (a) the oxidation of homo-annular steroidal dienes with potassium permanganate – sodium periodate reagent gives epoxy-diols resistant to further oxidation, instead of cleavage products.[3] Small amounts of degraded and cyclized products are formed in the case of unhindered

[3]Certain vicinal glycols, for example, those having one or two tertiary hydroxyls, are known to be somewhat resistant to C—C bond cleavage with periodate. This is ascribed to difficulties in the formation of the cyclic transition state encompassing the two hydroxyls and periodic ion (9).

Can. J. Chem. Downloaded from www.nrcresearchpress.com by 80.58.250.72 on 09/07/12
For personal use only.

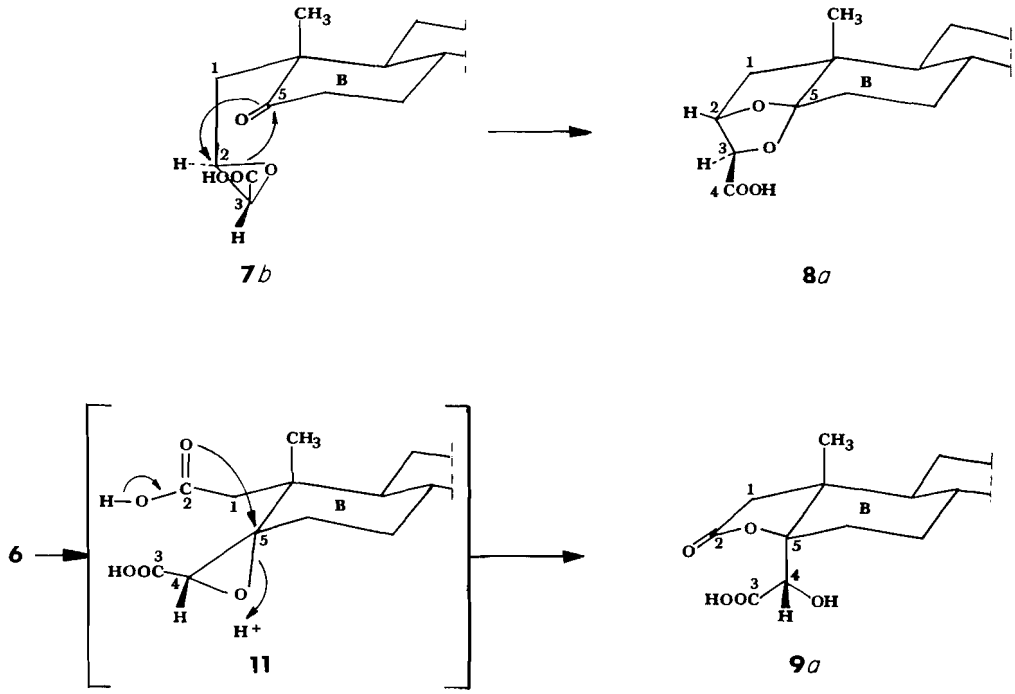

SCHEME 2

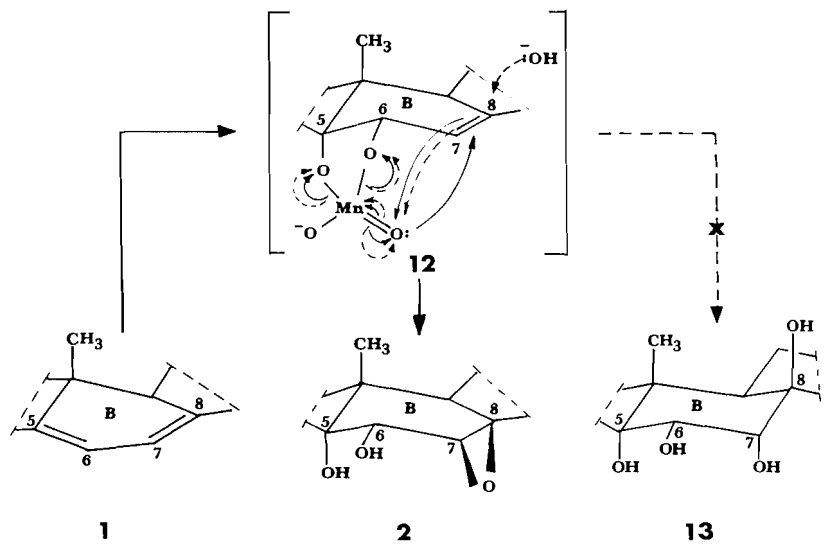

SCHEME 3

dienes (e.g., diene **3**); (b) the unhindered double bonds (Δ^5 in the diene **1** and Δ^6 in the diene **3**) undergo hydroxylation, whereas relatively hindered double bonds (Δ^7 in the diene **1** and Δ^3 in the diene **3**) are epoxydized; (c) the formation of epoxy-diol **2** occurs by a mechanism proposed by Sable *et al.* (10), with only one difference: the reactive intermediate **12** is converted only to epoxy-diol **2**, not to tetrol **13**, as indicated in Scheme 3. It is evident that the mechanism of oxidation of the diene **3** to epoxy-diols **5** and **6** should be the same.

Experimental

The melting points were determined on a Boetius micro melting apparatus and were uncorrected. Analyses were by Dr. J. Wasiak and Associates, Microanalytical Laboratories, Department of Chemistry, Warsaw University. Thin-layer chromatography (tlc) was carried out with DC-Alufolien plates (Merck) coated with Kieselgel 60. The plates were eluted with various solvent systems and visualized with 50% sulfuric acid after heating. The flash column chromatography was performed on silica gel (Kieselgel 60, 230–400 mesh Merck), packed in benzene, and the samples were put on the column in benzene. The infrared spectra were recorded on a UR-20 (Jena) spectrophotometer. The ^{1}H nmr spectra were taken with a 100-MHz Brucker WP-100 SY spectrophotometer, and the ^{13}C nmr spectra with a 22.5-MHz JEOL FX 90 Q spectrophotometer in deuterochloroform with TMS as an internal standard. Optical rotations were measured on a Perkin–Elmer 241 polarimeter in $CHCl_3$ (*c* 1.000). All solvents were dried and freshly distilled prior to use. The known cholesta-2,4-diene (**3**) was prepared according to the procedures described in ref. 11.

Oxidation of cholesta-2,4-diene (3) with potassium permanganate

To a solution of 5.00 g (13.6 mmol) of cholesta-2,4-diene (**3**) in 250 mL of *tert*-butanol was added 5.60 g of potassium permanganate in 100 mL of water and the resulting mixture was stirred for 3 h at room

Can. J. Chem. Downloaded from www.nrcresearchpress.com by 80.58.250.72 on 09/07/12
For personal use only.

Can. J. Chem. Downloaded from www.nrcresearchpress.com by 80.58.250.72 on 09/07/12
For personal use only.

temperature under nitrogen. The reaction was terminated with 20 mL of 40% sodium bisulfite solution, then extracted thoroughly with ether. The extract was washed with water, 50% bicarbonate solution, again with water, and dried (Na_2SO_4). Ether was evaporated to give 2.75 g of solid neutral fraction. The sodium bicarbonate wash was acidified with hydrochloric acid and extracted with ether. The extract was washed with water, dried (Na_2SO_4), and evaporated to give 1.58 g of a mixture of acids that was methylated with diazomethane.

The neutral fraction was chromatographed on silica, and elution with 9:1 benzene–ether gave 0.088 g (1.5%) of epoxy-lactol **7***a* and 0.635 g (12%) of lactol **4***a*. Elution with 4:1 benzene–ether gave 1.790 g (31%) of epoxy-diol **5** and 0.142 g (2.5%) of epoxy-diol **6**.

The acid fraction was chromatographed on silica, and elution with 9:1 benzene–ether gave 0.123 g (2%) of acetal ester **8***b* and 1.320 g (21%) of hydroxy-lactone ester **9***b*.

Similar results were obtained when potassium permanganate (5.60 g) and magnesium sulfate (5.00 g of $MgSO_4 \cdot 7H_2O$) mixture was used.

The samples were recrystallized twice for analysis. Spectral and analytical data are as follows.

Lactol **4**a: mp 165–166°C; $[\alpha]_D^{24}$ +29.8° (lit. (5) mp 165–166°C, $[\alpha]_D^{24}$ +28.8°); ir ν_{max}(KBr): 3355, 1770, 1250, 1145 cm^{-1}; ^1H nmr δ (100 MHz): 0.69 (s, 3H, 18-H), 1.12 (s, 3H, 19-H), 4.65 (s, 1H, 5ξ-O*H*, disappears on the addition of D_2O). *Anal.* calcd. for $C_{25}H_{42}O_3$: C 76.87, H 10.84; found: C 76.89, H 10.84.

Epoxy-diol **5***:* mp 181–182°C (acetone); $[\alpha]_D^{25}$ −4.3°; ir ν_{max}(KBr): 3555, 3480, 845, 835 cm^{-1}; ^1H nmr δ (100 MHz): 0.65 (s, 3H, 18-H), 0.93 (s, 3H, 19-H), 3.16 (s, 4α and 3α-O*H*, disappears on the addition of D_2O), 3.43 (s, 2H, 2β-H and 3β-H), 3.76 (s, 1H, 4β-H). *Anal.* calcd. for $C_{27}H_{46}O_3$: C 77.44, H 11.11; found: C 77.39, H 11.18.

Epoxy-diol **6***:* foam; $[\alpha]_D^{24}$ −2.7°; ir ν_{max}(KBr): 3590, 3580, 1058, 945, 869 cm^{-1}; ^1H nmr δ (100 MHz): 0.69 (s, 3H, 18-H), 1.06 (s, 3H, 19-H), 3.15 (d, 1H, 4β-H, J = 5 Hz), 3.60 (m, 1H, 2β-H, $W/2$ = 20 Hz), 3.98 (t, 1H, 3β-H, J = 5 Hz). *Anal.* calcd. for $C_{27}H_{46}O_3$: C 77.44, H 11.11; found: C 77.35, H 11.23.

Epoxy-lactol **7**a: mp 182–183°C (hexane – methylene chloride); $[\alpha]_D^{25}$ +40.9°; ir ν_{max}(KBr): 3525, 1725 cm^{-1}; ^1H nmr δ (100 MHz): 0.63 (s, 3H, 18-H), 0.90 (s, 3H, 19-H), 3.38 (d, 1H, 3β-H, J = 3.2 Hz), 3.59 (t, 1H, 2β-H, $J_1 = J_2$ = 3.2 Hz); ^{13}C nmr δ (22.5 MHz): 56.2 (C-2), 57.5 (C-3), 203.9 (C-4), 79.5 (C-5). *Anal.* calcd. for $C_{27}H_{44}O_4$: C 74.95, H 10.25; found: C 74.92, H 10.30.

Acetal ester **8**a: oil; $[\alpha]_D^{24}$ +42.1°; ir ν_{max}(KBr): 1735, 1085, 1010, 980 cm^{-1}; ^1H nmr δ (100 MHz): 0.68 (s, 3H, 18-H), 1.04 (s, 3H, 19-H), 3.76 (s, 3H, CH_3OOC), 3.85 (s, 1H, 3α-H), 3.65 (q, 1H, 2β-H, J = 2.5 Hz, J = 6 Hz); ^{13}C nmr δ (22.5 MHz): 175.65 (C-4), 107.55 (C-5), 74.12 (C-3), 72.06 (C-2). *Anal.* calcd. for $C_{28}H_{48}O_4$: C 74.95, H 10.78; found: C 74.89, H 10.70.

Hydroxy-lactone ester **9**b: mp 173–175°C (hexane – methylene chloride); $[\alpha]_D^{24}$ +38.7°; ir ν_{max}(KBr): 3560, 3472, 1785, 1735, 1085 cm^{-1}; ^1H nmr δ (100 MHz): 0.68 (s, 3H, 18-H), 1.20 (s, 3H, 19-H), 2.31 (d, 1H, 1α-H, J = 17.5 Hz), 3.28 (d, 1H, 4-O*H*, J = 7.5 Hz, disappears on the addition of D_2O), 3.84 (s, 3H, CH_3OOC-), 4.29 (d, 1H, J = 7.5 Hz); ^{13}C nmr δ (22.5 MHz): 177.2 (C-2), 172.3 (C-3), 88.6 (C-4), 76.7 (C-5). *Anal.* calcd. for $C_{28}H_{46}O_5$: C 72.69, H 10.02; found: C 72.72, H 10.08.

Acetoxy-lactone ester **9**c

Hydroxy-lactone ester **9***b* (30 mg) was acetylated with acetic acid anhydride (1 mL) in pyridine (3 mL) at room temperature for 24 h. Then 2 mL of methanol was added. The usual work-up gave 32 mg (95%) of a product, which upon crystallization from ether–hexane afforded 28 mg of acetoxy-lactone ester **9***c*, mp 238–240°C; $[\alpha]_D^{25}$ +40.2°; ir ν_{max}(KBr): 1785, 1735, 1725, 1085 cm^{-1}; ^1H nmr δ (100 MHz): 0.68 (s, 3H, 18-H), 1.16 (s, 3H, 19-H), 2.17 (s, 3H, 4-CH_3COO), 2.38 (d, 1H, 1α-H, J = 7.5 Hz), 2.75 (d, 1H, 1β-H, J = 7.5 Hz), 3.76 (s, 3H, CH_3OOC-), 4.93 (s, 1H, 4-H). *Anal.* calcd. for $C_{30}H_{48}O_6$: C 71.39, H 9.59; found: C 71.45, H 9.63.

*Oxidation of cholesta-2,4-diene (***3***) with potassium permanganate – sodium periodate reagent*

To a solution of 5.000 g (13.6 mmol) of cholesta-2,4-diene (**3**) in 250 mL of *tert*-butanol was added 5.60 g of potassium permanganate in 100 mL of water, followed by 18 g sodium periodate in 50 mL of water. The reaction mixture was stirred at room temperature under nitrogen for 3 h and worked up as in the previous oxidation to give 2.78 g of neutral material and 1.82 g of acidic material. Chromatography of the neutral fraction as before gave lactol **4***a* (0.740 g, 14% yield), epoxy-lactol **7***a* (0.110 g, 1.7% yield), epoxy-diol **5** (1.55 g, 25.2% yield), and epoxy-diol **6** (0.085 g, 1.5% yield). Chromatography of the acid fraction gave acetal ester **8***b* (0.123 g, 2% yield) and hydroxy-lactone ester **9***b* (1.567 g, 25% yield).

Acetal ester **8**b *by direct oxidation of epoxy-triol* **5**

To a solution of 0.300 g (0.72 mmol) of epoxy-diol **5** in 60 mL of *tert*-butanol was added 0.300 g of potassium permanganate in 50 mL of water, followed by 1.000 g of sodium periodate in 15 mL of water. The reaction mixture was stirred at room temperature under nitrogen for 3 days. After the usual work-up, 0.220 g of neutral material and 0.020 g of acidic material were obtained. The neutral fraction was chromatographed on silica and elution with 9:1 benzene–ether gave 0.080 g (25.5% yield) of epoxy-lactol **7***a*, identified in the usual fashion by comparison with an authentic sample. Elution with 4:1 benzene–ether gave 0.120 g of starting material. The acidic fraction, after methylation with diazomethane, was chromatographed on silica and elution with 9:1 benzene–ether gave 0.012 g (3.74% yield) of acetal ester **8***b*. The product was found identical in all respects with that described in the previous experiment.

Hydroxy-lactone ester **9**b *by direct oxidation of epoxy-diol* **6**

To a solution of 0.300 g (0.72 mmol) of epoxy-diol **6** in 50 mL of *tert*-butanol was added 0.28 g of potassium permanganate in 20 mL of water, followed by 0.90 g of sodium periodate in 10 mL of water. The reaction mixture was stirred at room temperature under nitrogen for 3 days. Work-up in the usual manner gave 0.250 g of neutral fraction and 0.070 g of acidic material. The neutral fraction was chromatographed on silica and elution with 4:1 benzene–ether gave 0.098 g of starting material and 0.080 g (28.6% yield) of lactol **4***a*. The acidic fraction, after methylation with diazomethane, was chromatographed on silica and elution with 9:1 benzene–ether gave 0.020 g (6%) of hydroxy-lactone ester **9***b*, identical in all respects with that obtained in the previous experiment.

Triol **10**a

To a suspension of 0.050 g of $LiAlH_4$ in 100 mL of dry tetrahydrofuran was added 0.200 g (0.48 mmol) of epoxy-diol **5** in 100 mL of dry tetrahydrofuran. After stirring at room temperature for 15 min and heating under reflux for 2 h, water was added and the precipitate was filtered through Celite and was thoroughly washed with tetrahydrofuran. Evaporation of the solvent gave crude triol **10***a* (0.185 g, 92.5%), mp 210–215°C. The analytical sample was obtained by two recrystallizations from ether – methylene chloride, mp 216–218°C; $[\alpha]_D^{25}$ +20.2° (*c* 1.000, dioxane); ir ν_{max}(KBr): 3360 cm^{-1}; ^1H nmr δ (100 MHz): 0.65 (s, 3H, 18-H), 0.95 (s, 3H, 19-H), 3.16 (m, 2H, O*H*, disappears on the addition of D_2O), 3.49 (d, 1H, 4β-H, J = 3.5 Hz), 3.97 (m, 1H, 3β-H, $W/2$ = 10.5 Hz). *Anal.* calcd. for $C_{27}H_{48}O_3$: C 77.07, H 11.32; found: C 77.00, H 11.55.

Deuteration of the 2β-position by reduction of epoxy-diol **5** *with lithium aluminum deuteride*

A solution of epoxy-diol **5** (0.200 g, 0.48 mmol) in anhydrous tetrahydrofuran (100 mL) was treated with lithium aluminum deuteride (0.059 g) and the resulting mixture was heated under reflux for 3 h. Then work-up as in the previous reduction gave 0.170 g (85% yield) of 2β-d_1-triol **10***b*; ir ν_{max}(KBr): 3360, 2185 cm^{-1} (C-D); ^1H nmr δ: 0.65 (s, 3H, 18-H), 0.95 (s, 3H, 19-H), 3.18 (m, 2H, O*H*, disappears on the addition of D_2O), 3.49 (d, 1H, 4β-H, J = 3.5 Hz), 3.97 (t, 1H, 3β-H, $J_{2e,3e} = J_{3e,4a}$ = 3.5 Hz).

Acknowledgments

Sincere thanks are extended to Dr. M. Kabat for some experiments. The author is grateful to Professor W. J. Rodewald, Dr. R. Siciński, and Dr. J. Morzycki for their helpful comments

and for fruitful discussion. This work was supported by the Polish Academy of Sciences.

1. W. J. RODEWALD and Z. BOŃCZA-TOMASZEWSKI. Tetrahedron Lett. 3119 (1979).
2. R. U. LEMIEUX and E. VON RUDLOFF. Can. J. Chem. **33**, 1714 (1955).
3. W. J. RODEWALD and Z. BOŃCZA-TOMASZEWSKI. Polish J. Chem. **54**, 405 (1980).
4. M. ANASTASIA, A. FIECCHI, and A. SCALA. J. Org. Chem. **44**, 3657 (1979).
5. R. J. CONCA and W. BERGMAN. J. Org. Chem. **18**, 1184 (1953).
6. N. S. BHACCA and D. H. WILLIAMS. Application of NMR spectroscopy in organic chemistry. Holden–Day, San Francisco. 1966. p. 101; W. ARNOLD, W. MEISTER, and G. ENGLERT. Helv. Chim. Acta, **57**, 1559 (1974).
7. J. W. BLUNT and J. B. STOTHERS. Org. Magn. Reson. **9**, 339 (1977).
8. D. N. KIRK and M. P. HARTSHORN. Steroids reaction mechanism. Elsevier Publishing Company, Amsterdam, London, New York. 1968. p. 112.
9. R. STEWART. Oxidation mechanism. W. A. Benjamin, Inc., New York. 1964. p. 97.
10. H. Z. SABLE, K. A. POWELL, H. KATCHIAN, C. A. NIEWOCHNER, and S. KADLEC. Tetrahedron, **26**, 1509 (1970).
11. W. G. DAUBEN, M. E. LORBER, N. D. VIETMEYER, R. H. SHAPIRO, J. H. DUNCAN, and K. TOMER. J. Am. Chem. Soc. **90**, 4762 (1968).

Can. J. Chem. Downloaded from www.nrcresearchpress.com by 80.58.250.72 on 09/07/12
For personal use only.

Protonation of a conjugated Schiff base by weak to strong acids: a ^{13}C and ^{15}N nuclear magnetic resonance study

DANIEL COSSETTE AND DANIEL VOCELLE[1]

Département de chimie, Université du Québec à Montréal, C.P. 8888 Succ. A, Montréal (Qué.), Canada H3C 3P8

Received July 24, 1986

DANIEL COSSETTE and DANIEL VOCELLE. Can. J. Chem. **65**, 661 (1987).

The interactions (mostly protonation) between several carboxylic and mineral acids and *trans,trans*-2,4-heptadienylidene *tert*-butylamine (HBA) were determined by ^{13}C and ^{15}N nuclear magnetic resonance spectroscopies. Results indicate that protonation is only partial with weak acids in both polar and nonpolar solvents. No interaction between polar groups located on the acids and the polyenic chain of HBA seems to occur. The chemical shifts of all carbon atoms and also of the Schiff base nitrogen are linearly correlated with the acidity strength of the carboxylic acids.

DANIEL COSSETTE et DANIEL VOCELLE. Can. J. Chem. **65**, 661 (1987).

Les interactions (surtout la protonation) entre plusieurs acides carboxyliques et minéraux avec la *trans,trans*-heptadiényli-dène-2,4 *tert*-butylamine (HBA) ont été déterminées par la résonance magnétique nucléaire du ^{13}C et du ^{15}N. Les résultats indiquent que la protonation est partielle pour les acides faibles aussi bien pour les solvants polaires que non-polaires. Aucune interaction entre les groupes polaires des acides et la chaîne polyénique de HBA n'a pu être décelée. Les déplacements chimiques de tous les atomes de carbone et aussi de l'azote de la base de Schiff sont linéairement corrélés avec la force de l'acidité des acides carboxyliques.

Can. J. Chem. Downloaded from www.nrcresearchpress.com by 80.58.250.72 on 09/07/12
For personal use only.

Introduction

High-resolution nuclear magnetic resonance is a technique that has been widely used in the examination of structural and dynamic properties of molecules in solution and in the solid state. In particular, ^{13}C and ^{15}N nmr spectra have yielded important information in biological systems. Among these, two membrane proteins, rhodopsin (1) and bacteriorhodopsin (2–6), have been studied with a certain amount of success, using both nuclei as a probe for measuring the interactions of the chromophore with the proteins. However, to be able to study pigments by nmr, they need first to be isolated from the biological milieu by using different techniques, and the end results usually consist of a purified protein dispersed in a detergent or lyophilized to a thin film. Whatever the method used, the pigment has been perturbed to some degree and the nmr data obtained on these proteins must reflect this new situation. This being the case, the true state of the chromophore in rhodopsin and bacteriorhodopsin in intact membranes cannot be determined with complete accuracy. A rapid survey of recent literature on this subject indicates that different spectra are obtained depending on the state of the sample examined (5, 7). Because of this fact and since conjugated Schiff bases have not been fully studied by ^{13}C and ^{15}N nmr spectroscopies, we have devised a model system where spectra of both conjugated imines and their interactions with carboxylic acids could be evaluated. This model consists of a Schiff base, *trans,trans*-2,4-heptadienylidene *tert*-butylamine (HBA) (**1**), and different halogenated carboxylic acids in chloroform or methanol solutions. It represents the first ^{13}C and ^{15}N nmr study of a model of rhodopsin where carboxylic acids having pK_as similar to, or in the same region as, glutamic and aspartic acids are interacting with a conjugated Schiff base resembling the retinal chromophore. In particular, the extent of protonation of the Schiff base in the presence of weak to strong acids in a nonpolar ($CHCl_3$) or a more polar solvent (CH_3OH) will be investigated, since this question is still controversial, especially with visual pigments (8). Our system has already been studied using uv (9) and ^1H nmr spectroscopies (10).

[1]Author to whom correspondence may be addressed.

Experimental

For our study we used equimolar concentrations of HBA and of one of the halogenated carboxylic acids of Table 1 in $CDCl_3$ or CD_3OD solution. Solutions were of the order of 0.07 *M* for the ^{13}C experiments and between 0.6 and 1.0 *M* for the ^{15}N spectra. The acids used are listed in Table 1 and numerotation of the carbon atoms of HBA is shown in Fig. 1. Spectra were obtained on a WH-400 pulse Fourier transform instrument (Bruker Co.) at frequencies of 100.0 MHz for ^{13}C and 40.4 MHz for ^{15}N. Typically, the ^{13}C proton noise-decoupled spectra were taken with rf pulses of 5 μs with a pulse angle of 45° and at intervals of 3.2 s; usually 400–600 scans were collected. Assignation of the different peaks with the proper carbon atoms was done using two well-known methods: selective proton decoupling centered at H5 using the same parameters as before, and 2D proton–carbon correlation. The chemical shifts were determined using TMS as an internal standard. The ^{15}N nmr spectra were determined using two different techniques. For the unprotonated Schiff base, proton noise-decoupled spectra in the gated decoupled mode, for nOe (nuclear Overhauser effect) suppression, were obtained using rf pulses of 12 μs with an angle of 90° and a pulse delay of 1.6 s; the acquisition time was 0.4 s and 2000–5000 scans were necessary. For the protonated Schiff base, the sequence called INEPT (11) was used and only 200–400 scans were then necessary. The chemical shifts reported in this paper are calculated from formamide. *trans,trans*-2,4-Heptadienylidene *tert*-butylamine was synthesized by using *trans,trans*-2,4-heptadienal and *tert*-butylamine according to a procedure that has already been described elsewhere (9).

Results and discussion

^{13}C nuclear magnetic resonance results

Table 1 shows the chemical shifts of C3, C4, C5, C6, and C7 of HBA in deuterated chloroform solution (first line) and when in equimolar concentrations with different carboxylic acids (all subsequent lines). It shows also the deshielding (or shielding) experienced by these carbon atoms and these values (in parentheses in Table 1) are calculated by subtracting the chemical shifts of unprotonated HBA from the chemical shifts of HBA in the presence of the acids. Deshielding is indicated by a positive value while shielding is expressed by a negative value. Table 2 gives the results obtained in deuterated methanol.

In $CDCl_3$, as expected, the most deshielded carbon atom is C7. Its chemical shift varies from 157.17 ppm for the pure imine to a value of 165.05 ppm in the presence of the strong acid HI.

TABLE 1. Chemical shifts of HBA in presence of acids in deuterated chloroform at 25°C

System studied	pK_a	C7	C6	C5	C4	C3
HBA		157.17	130.68	141.22	128.61	140.73
HBA/CH_3CH_2COOH	4.90	158.80	128.02	144.29	128.42	143.15
		(+1.63)[a]	(−2.66)	(+3.07)	(−0.19)	(+2.42)
HBA/$NO_2CH_2CH_2COOH$	3.90	159.69	126.84	146.94	128.54	145.46
		(+2.52)	(−3.84)	(+5.72)	(−0.07)	(+4.73)
HBA/ICH_2COOH	3.15	161.26	124.33	150.75	128.36	148.52
		(+4.09)	(−6.35)	(+9.53)	(−0.25)	(+7.80)
HBA/$BrCH_2COOH$	2.95	161.27	124.38	150.81	128.37	148.61
		(+4.10)	(−6.30)	(+9.59)	(−0.24)	(+7.88)
HBA/$ClCH_2COOH$	2.85	162.08	123.23	152.71	128.33	150.20
		(+4.91)	(−7.45)	(+11.49)	(−0.28)	(+9.47)
HBA/$NCCH_2COOH$	2.45	162.52	122.49	153.96	128.28	151.27
		(+5.35)	(−8.19)	(−12.74)	(−0.33)	(+10.54)
HBA/HCCCOOH	1.85	162.79	122.51	154.12	128.21	151.11
		(+5.62)	(−8.17)	(+12.90)	(−0.40)	(+10.38)
HBA/Cl_3CCOOH	0.66	163.63	121.25	156.57	128.22	153.48
		(+6.46)	(−9.43)	(+15.35)	(−0.39)	(+12.75)
HBA/F_3CCOOH	0.23	164.10	120.68	157.71	128.18	154.36
		(+6.93)	(−10.00)	(+16.49)	(−0.43)	(+13.63)
HBA/HCl	−6.90	163.76	120.81	157.32	128.28	154.04
		(+6.59)	(−9.87)	(+16.10)	(−0.33)	(+13.31)
HBA/HBr	−8.90	164.84	120.06	158.76	128.24	154.75
		(+7.67)	(−10.62)	(+17.54)	(−0.37)	(+14.02)
HBA/HI	−9.20	165.05	118.93	160.39	128.29	156.62
		(+7.88)	(−11.75)	(+19.17)	(−0.32)	(+15.89)

[a]In parentheses, the difference in chemical shifts betwen HBA and HBA/acids.

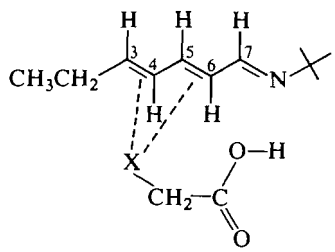

1

FIG. 1. Interaction between HBA and some substituted carboxylic acids.

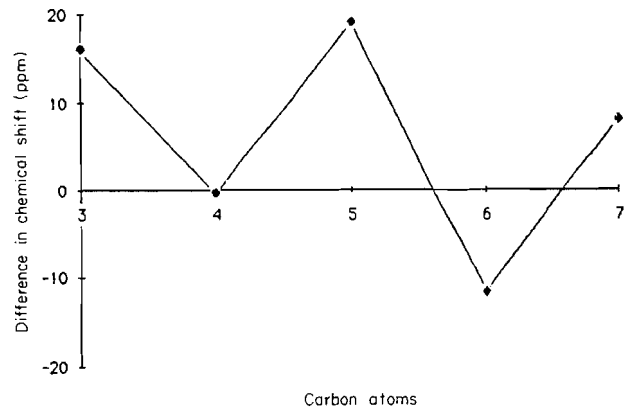

FIG. 2. Zigzag pattern of the differences in chemical shifts for C3–C7.

Table 1 also reports the pK_as, in water, of the acids. It would have been more appropriate to use pK_a values measured in chloroform since it is in that solvent that the nmr spectra were taken; however, in the absence of these values, it is still relevant to use the pK_as measured in water since Rumeau (12) has shown that in chloroform the ordering of all carboxylic acids of Table 1 is the same as in water. There exists a good linear correlation (with values exceeding 0.95) between the pK_as of all carboxylic acids and the differences in chemical shifts of C7, C6, C5, C3; it signifies that the polar groups located on the acids (such as Cl, Br, I, NO_2, CN, etc.) do not interact directly with the polyene chain except by increasing the acidity of the acids. The mineral acids behave differently: their acidity strengths are linearly correlated to C7 only, while affording a poor relationship with C6 and C5. This fact can be explained by the size of the counterions (Cl^-, Br^-, I^-), which varies considerably, while with the carboxylate anions the size remains constant. This also occurred in the ^1H nmr spectra of these systems, as for example between the pK_a of the acids and H6 (10*a*).

From Table 1, it is important to note a zigzag pattern: Fig. 2 shows an example of this using HBA and HI. This pattern is obtained for all acids used and in both solvents ($CDCl_3$ and CD_3OD). It has already been noted by Harbison *et al.* (5*b*), Inoue *et al.* (13), and by Pattaroni and Lauterwein (14), who report a similar behavior for all-*trans*-retinylidene *n*-butylamine (NRBA) and strong acids. It can be rationalized by the fact that all odd-numbered carbon atoms have a partial positive charge while those that are even numbered are in a nonresonance position. The first are deshielded while the others are shielded. The deshieldings are more important at carbon 5, then decrease slowly along the chain. Normally, because C7 is adjacent to the nitrogen of the azomethine function, it should be highly deshielded (it is in a resonance position), but the weak deshielding as shown in Tables 1 and 2 can be explained by the same argument already given by Sharma and Roels (15) for the weak deshielding value of the aldimine proton of NRBA. The

Can. J. Chem. Downloaded from www.nrcresearchpress.com by 80.58.250.72 on 09/07/12
For personal use only.

TABLE 2. Chemical shifts of HBA in presence of acids in deuterated methanol at 25°C

System studied[a]	pK_a	C7	C6	C5	C4	C3
HBA		160.84	129.95	145.06	129.95	143.88
n-HBA[b]		165.33	129.21	144.67	129.64	143.72
HBA/CH_3CH_2COOH	4.90	162.93	127.58	149.27	129.71	147.30
		(+2.09)	(−2.37)	(+4.21)	(−0.24)	(+3.42)
HBA/C_6H_5COOH	4.11	164.53	125.40	152.93	129.66	150.17
		(+3.69)	(−4.55)	(+7.87)	(−0.29)	(+3.42)
HBA/$NO_2CH_2CH_2COOH$	3.90	165.42	124.42	154.88	129.66	151.75
		(+4.86)	(−5.55)	(+9.24)	(−0.29)	(+6.29)
HBA/ICH_2COOH	3.15	167.23	122.95	158.30	129.66	154.55
		(+6.39)	(−7.00)	(+13.24)	(−0.29)	(+10.67)
HBA/$ClCH_2COOH$	2.85	168.01	121.66	160.05	129.67	155.97
		(+7.17)	(−8.29)	(+14.99)	(−0.28)	(+12.19)
HBA/Cl_3CCOOH	0.66	168.56	121.44	161.03	129.78	156.64
		(+7.72)	(−8.51)	(+15.97)	(−0.17)	(+12.76)
HBA/F_3CCOOH	0.23	168.45	121.09	161.08	129.78	156.70
		(+7.61)	(−8.86)	(+16.02)	(−0.17)	(+12.82)
HBA/HCl	−6.90	168.59	121.18	161.20	129.78	156.77
		(+7.75)	(−8.77)	(+16.14)	(−0.17)	(+12.89)
HBA/HBr	−8.90	168.61	121.18	161.34	129.77	156.82
		(+7.77)	(−8.77)	(+16.28)	(−0.18)	(+12.94)
HBA/HI	−9.20	168.56	121.11	161.48	129.77	156.99
		(+7.72)	(−8.84)	(+16.42)	(−0.18)	(+13.11)

[a]In parentheses, the difference in chemical shifts between HBA and HBA/acids.
[b]*trans,trans*-2,4-Heptadienylidene *n*-butylamine.

effect of being in a resonance position just beside nitrogen (high deshielding) is counterbalanced by the fact that resonance decreases the double bond character of the azomethine function, which in turn decreases the anisotropy of such a bond thus causing a shielding effect. Combination of both effects means that deshielding for carbon 7 is less important. The case of C6 is also rather interesting. Proton nmr indicates that H6 is highly deshielded (9, 10) while this work shows that C6 is quite shielded (the system and conditions being identical). Again it must be pointed out that H6, being close to the carboxylate anion, should feel strongly the anisotropy of the counterion, while C6 is less affected since it lies further away. In fact, the effects on H6 and C6 of the electric field generated by the counterion can be easily calculated using the following relation: the field on C6 is proportional to $1/R^2 \cos \phi$ where ϕ is the angle between the chain axis and the anion; R is the distance between the carbon atom C6 (or H6) and the anion (16). Using a distance of 3 Å between the anion and the Schiff base nitrogen, simple trigonometry indicates that R is 3.7 Å for C6 and 2.9 Å for H6. The field then encountered by C6 is approximately half the one felt by H6.

To summarize briefly, in deuterated chloroform the chemical shifts of HBA are related to the acidity strength of the carboxylic acids, and no secondary interactions between the polar function (X in Fig. 1) of the acids and HBA could be found.

The results obtained in deuterated methanol appear in Table 2. The first thing to note is that the chemical shifts are more deshielded, by around 3 ppm, in CD_3OD than in $CDCl_3$. Also, Table 2 shows the shielding effect of a *tert*-butyl group since there is a shielding of around 4.5 ppm for C7 on passing from an *n*-butyl to a *tert*-butyl group. Models of rhodopsin usually consist of an *n*-butyl group since lysine is the anchor by which the chromophore is attached to the protein. In our studies, we prefer a *tert*-butyl group since it affords a more stable compound than its counterpart and because the presence of the *syn* isomer is held at a minimum (less than 5%). The effect resides mostly in C7 since C3–C6 chemical shifts are roughly the same for both Schiff bases. The same zigzag patterns discussed previously are also obtained in deuterated methanol. From Table 2 it can readily be seen that strong acids (from TCA to HI) are able to perturb HBA in the same way, giving almost identical chemical shift differences. This is not surprising since methanol is known as a levelling solvent (17). The weaker acids act somewhat the same way as in deuterated chloroform except that deshielding (and shielding) is more important. Linear correlation curves between the pK_as of the weaker acids and the chemical shift differences show good linear correlations for C7, C6, C5, and C3, again indicating that there is no secondary interaction between the polar function and the polyenic chain of HBA.

Degrees of protonation of the Schiff base

As we have stated before, it is important to investigate the degree of protonation of a conjugated Schiff base when the protonating agent is a weak acid. Data given in Tables 1 and 2 allow the calculation of the degrees of protonation. However, it appears important to define some terms before discussing the protonating ability of the weak acids. Protonation is defined by the following equation:

[1] $R—CH=N—R' + HX \rightleftharpoons [R—CH=N^+H—R']X^-$

There is no doubt that the very strong mineral acids like HCl, HBr, and HI protonate HBA completely, so that in the above equation the equilibrium lies entirely to the right. That this is the case has been shown by several groups (principally by Blatz and Mohler (17)) and the subject has recently been reviewed by us (8). In a previous paper (10*b*), we have shown by ^1H nmr that HBA was 100% protonated by the strong mineral acids. Complete protonation was proven since alkylidene iminium hydrochlorides, in chloroform solution, show a doublet of doublets for the aldimine proton, while for the unprotonated Schiff base, as expected, only a doublet is present. Protonation

Can. J. Chem. Downloaded from www.nrcresearchpress.com by 80.58.250.72 on 09/07/12
For personal use only.

Can. J. Chem. Downloaded from www.nrcresearchpress.com by 80.58.250.72 on 09/07/12
For personal use only.

was also proven by ir spectroscopy. In three recent papers (18), Sandorfy and our group used FTIR to investigate the protonation of different Schiff bases. By using the same systems as the one described here, infrared spectra indicated 100% protonation when mineral acids were used: for *trans,trans*-2,4-heptadienylidene isopropylamine the pertinent bands were located at 2530 (N^+–H stretching), 1668 (ν(C=N^+), 1625 (ν(C=C), and 1069 cm^{-1} (N^+–H out-of-plane bending). In the same paper (18*b*), the degree of protonation of the Schiff base was also measured for weak carboxylic acids: propionic acid gave about 10% protonation, chloroacetic acid around 65%, and trichloroacetic acid 95–100%. These percentages were only estimated since overlap between the carboxylate band and the ν(CV=N^+) precluded a more precise treatment. Reversibility of the system was also shown to be occurring since varying amounts of carboxylic acids were able to shift the equilibrium (10).

The degree of protonation was calculated as follows. In methanol all strong acids affect HBA in the same fashion. Table 2 shows that with trichloro (TCA) and trifluoro acetic acids (TFA), HCl, HBr, and HI, the data are all very similar. This is due to a levelling effect caused by the solvent (17). Since the chemical shifts of HBA are linearly correlated with the pK_as of the acids, it can be safely presumed that deshielding (or shielding) values are indicative of the degrees of protonation. Considering, from Table 2, that strong acids cause a deshielding on C5 of some 16.2 ppm, then the extent of protonation can be easily calculated for the weaker acids. The protonation percentages are as follows: for propionic acid, 26%; benzoic acid, 49%; 3-nitropropanoic acid, 57%; iodoacetic acid, 82%; and chloroacetic acid, 93%. Protonation in chloroform solutions is somewhat more difficult to assess. Table 1 shows that the chemical shifts are all different since, in that solvent, there is no levelling effect. However, the chemical shifts are linearly correlated with the pK_as only for the carboxylic acids, while for the hydrohalides it is the size of the counterion that regulates the deshielding of HBA (14, 17). Since it has been demonstrated by ir (18*b*) and by nmr (10, 14) that TFA was protonating HBA completely (100%), the same procedure as described before can be used. Table 1 shows that for TFA, C5 is deshielded by some 16.5 ppm. Then, the degrees of protonation for the other acids are, for propionic acid, 19%; 3-nitropropanoic acid, 35%; iodo and bromoacetic acids, 58%; chloroacetic acid 70%; cyanoacetic acid, 77%; propiolic acid, 78%; and TCA, 93%. These last results compare very well with those obtained by ir (18*b*). Furthermore, it is important to note that protonation of HBA by weak acids is more favored in methanol than in chloroform. One would then expect from these data that an environment more polar than methanol is required in order to have 100% protonation by acids with pK_as of 4.

^{15}N nuclear magnetic resonance results

Roberts and co-workers (19) have studied Schiff bases, protonated and unprotonated, and have reported considerable chemical shift differences between the two. Thus ^{15}N nmr is a technique well suited to study the interaction between a conjugated Schiff base and carboxylic acids at the nitrogen site. Data from our study are reported in Table 3 for both $CDCl_3$ and CD_3OD. From this table it is readily seen that the chemical shifts vary by more than 160 ppm in deuterated chloroform and 130 ppm in deuterated methanol between protonated and unprotonated HBA. In $CDCl_3$, there exists a good linear correlation between the chemical shifts of the nitrogen of HBA and the acidity strength of the carboxylic acids (correlation coefficient of 0.932). The effect of the counterion can be best judged by considering the systems HBA–HCl and HBA–HI. The Cl^- anion induces a chemical shift of 96.89 ppm while I^- gives 75.28 ppm. The difference is more than 20 ppm while the pK_as vary by only 2.2. Passing from TCA to HCl, there is a small chemical shift difference of some 3 ppm for a large pK_a change of 7.5. In deuterated chloroform then, only the carboxylic acids correlate well with the pK_as, while for the mineral acids the size of the counterion is the prime factor that influences the chemical shifts. In CD_3OD, the situation is again quite different, as noted previously by ^1H and ^{13}C nmr. All strong acids give somewhat the same chemical shifts. For the weaker acids (propionic to chloroacetic acids), the chemical shifts vary according to the pK_as of the acids (correlation coefficient of 0.97) and, judging by the values obtained, protonation is far more extensive. As an example, propionic acid, the weakest acid used in our model system, shields HBA by some 29 ppm in $CDCl_3$ while CD_3OD shielding reaches roughly 90 ppm. The fact that acids shield the Schiff base nitrogen atom has been explained by Roberts and co-workers (19) on the basis of paramagnetic effects due to perturbations of the lone pair of nitrogen electrons by protonation. Table 3 reports also the chemical shifts obtained in a mixed solvent composed of 90% CH_3OH and 10% CD_3OD. This experiment was done to measure the impact on protonation by using CD_3OD instead of CH_3OH. Using deuterated methanol as solvent (for the purpose of obtaining a good lock) implies that HBA is protonated by a deuteron rather than a proton since there is a rapid exchange between the solvent and the acid. Table 3 shows that the chemical shifts did not vary significantly. The interaction between the polyenic chain and the polar functions of the substituted acetic acids was also investigated by measuring the chemical shifts of the nitrogen of the cyano group of cyanoacetic acid. If there exists a strong interaction between the two, the chemical shift of the cyano group should be particularly affected. Table 3 shows that the nitrogen of the cyano function has a chemical shift of 131.5 ppm in deuterated chloroform for cyanoacetic acid and 125.08 ppm for its carboxylate salt. With HBA, the cyano group has a value of 129 ppm, a value

TABLE 3. ^{15}N Chemical shifts of HBA in presence of acids in deuterated chloroform and deuterated methanol at 25°C

System studied	pK_a	Chloroform	Methanol
HBA		237.10	222.03
HBA/CH_3CH_2COOH	4.90	208.22	186.02
HBA/$NO_2CH_2CH_2COOH$	3.90	184.75	120.32
HBA/ICH_2COOH	3.15	156.75	107.31
HBA/$BrCH_2COOH$	2.95	138.42	
HBA/$ClCH_2COOH$	2.85	137.42	93.47
HBA/$NCCH_2COOH$[a]	2.45	110.74	
HBA/$NCCH_2COOH$[b]	2.45	129.00	
$(NCCH_2COO^-)Mg^{2+}$		125.08	
$NCCH_2COOH$	2.45	131.53	
HBA/HCCCOOH	1.85	106.20	
HBA/Cl_3CCOOH	0.66	100.15	92.10
HBA/F_3CCOOH	0.23	97.52	91.95
HBA/HCl	−6.90	96.89	91.66
HBA/HCl[c]	−6.90		92.00
HBA/HI	−9.20	75.8	90.26

[a]Chemical shifts of imino function.
[b]Chemical shifts of cyano function.
[c]With 90% methanol-h_4 and 10% methanol-d_4.

intermediate between the protonated and unprotonated form of cyanoacetic acid. This value does not rule out completely some form of interaction between the polyenic chain and the acid but it seems to indicate that if such an interaction is present, it has a weak effect on the chemical shift of the cyano group. Again we tried to calculate the percentage of protonation in CD_3OD. Since strong acids induce a chemical shift of approximately 92 ppm, HBA was considered 100% protonated. Simple calculations give 28% protonation for propionic acid, 78% for 3-nitropropanoic acid, 88% for iodoacetic acid, and more than 98% for chloroacetic acid. These protonation percentages compare well with those calculated previously by ^{13}C nmr. If we follow the same reasoning as before for the data obtained in deuterated chloroform and accept that a chemical shift of some 100 ppm (which means a shielding of some 137 ppm) does indicate 100% protonation, then we have the following protonation percentages: propionic acid, 21%; 3-nitropropanoic acid, 38%; iodoacetic acid, 58%; chloro and bromoacetic acids, 70%; cyanoacetic acid, 92%; and propiolic acid, 95%. These percentages again compare quite well with those obtained by ^{13}C nmr.

Finally, some mention must be made of the fact that we use a *tert*-butyl group instead of the customary *n*-butyl function. Mateescu and co-workers (1) found a value of 83 ppm (adjusted to formamide) for all-*trans*-2,4-hexadienylidene *n*-butylamine hydrochloride. Since we used all-*trans*-2,4-heptadienylidene *tert*-butylamine hydrochloride and found a value of 97 ppm (both salts in deuterated chloroform), we can say that a *tert*-butyl group creates a deshielding of some 14 ppm. For the unprotonated imine, Mateescu found 219 ppm (adjusted to formamide) while we found 237 ppm, a difference of 18 ppm. Again it must be said that a difference of a few ppm is not very important since full protonation gives shielding of more than 100 ppm. The greater stability of a *tert*-butyl Schiff base compared to an *n*-butyl group is reason enough to use it.

In conclusion, we can safely say that weak carboxylic acids in both polar and nonpolar solvents can only partially protonate HBA and that polar groups such as those used here (Cl, Br, I, NO_2, CN) do not seem to interact with the polyenic chain. Also, it is important to note that when the protonating agent is a weak acid, the chemical shifts of most carbon atoms of HBA as well as for the Schiff base nitrogen differ markedly from a nonpolar solvent to a more polar one and that these differences could possibly be used in the visual pigment field as an indicator of the polarity of the milieu surrounding the chromophore.

Acknowledgements

The authors wish to express their sincere thanks to Professor Camille Sandorfy for helpful discussions and to the Laboratoire régional de RMN à haut champ (Dr. Phan Viet Minh Tan) of Université de Montréal for all ^{13}C and ^{15}N nmr spectra. It is a pleasure to acknowledge the financial help of the National Research Council of Canada (grant A0943) and of the Université du Québec à Montréal.

1. D. D. Muccio, W. G. Copan, E. W. Abrahamson, and G. D. Mateescu. Org. Magn. Reson. **22**, 121 (1984).
2. G. S. Harbison, S. O. Smith, J. A. Pardoen, C. Winkel, J. Lugtenburg, J. Herzfeld, R. Mathies, and R. G. Griffin. Proc. Natl. Acad. Sci. USA, **81**, 1706 (1984).
3. G. S. Harbison, J. Herzfeld, and R. G. Griffin. Biochemistry, **22**, 1 (1983).
4. A. Yamaguchi, T. Unemoto, and A. Ikegami. Photochem. Photobiol. **33**, 511 (1981).
5. (*a*) G. S. Harbison, S. O. Smith, J. A. Pardoen, P. P. J. Mulder, J. Lugtenburg, J. Herzfeld, R. Mathies, and R. G. Griffin. Biochemistry, **23**, 2662 (1984); (*b*) G. S. Harbison, S. O. Smith, J. A. Pardoen, P. P. J. Mulder, J. Lugtenburg, J. Herzfeld, R. Mathies, and R. G. Griffin. J. Am. Chem. Soc. **107**, 4809 (1985).
6. J. Lugtenburg, M. Muradin-Szweykowska, C. Heeremans, J. A. Pardoen, G. S. Harbison, J. Herzfeld, R. G. Griffin, S. O. Smith, and R. A. Mathies. J. Am. Chem. Soc. **108**, 3104 (1986).
7. (*a*) G. D. Mateescu, D. V. Waterhous, M. Iqbal, W. G. Copan, D. D. Muccio, and E. W. Abrahamson. Biochemistry, **22**, 22 A (1983); (*b*) G. D. Mateescu, W. G. Copan, D. D. Muccio, D. V. Waterhous, and E. W. Abrahamson. *In* Proceedings of the International Symposium on Synthesis and Applications of Isotopically Labeled Compounds. Elsevier, Amsterdam. 1983. pp. 123–132.
8. (*a*) C. Sandorfy and D. Vocelle. Can. J. Chem. **64**, 2251 (1986); (*b*) N. J. Barboy and A. Warshel. J. Am. Chem. Soc. **104**, 1469 (1982).
9. (*a*) M. Bissonnette and D. Vocelle. Spectrosc. Int. J. **2**, 120 (1983); (*b*) M. Bissonnette, H. Le Thanh, and D. Vocelle. Can. J. Chem. **62**, 1459 (1984).
10. (*a*) M. Bissonnette, H. Le Thanh, and D. Vocelle. Can. J. Chem. **63**, 2298 (1985); (*b*) Can. J. Chem. **63**, 1480 (1985).
11. R. K. Harris. *In* Nuclear magnetic resonance spectroscopy. Marshfield (Mass.), U.S.A. 1983. pp. 173–175, and references therein.
12. M. Rumeau. Ann. Chim. **2**, 131 (1973).
13. Y. Inoue, Y. Hanafusa, M. Toda, and R. Chûjô. J. Am. Chem. Soc. **99**, 5592 (1979).
14. C. Pattaroni and J. Lauterwein. Helv. Chim. Acta, **64**, 1969 (1981).
15. G. M. Sharma and O. A. Roels. J. Org. Chem. **38**, 3648 (1973).
16. F. W. Wehrli and T. Wirthlin. *In* Interpretation of carbon-13 NMR spectra. Heiden, London. 1978. p. 30.
17. (*a*) P. E. Blatz and J. H. Mohler. Biochemistry, **14**, 2304 (1975); (*b*) Biochemistry, **11**, 3240 (1972).
18. (*a*) L. S. Lussier, A. Dion, C. Sandorfy, H. Le Thanh, and D. Vocelle. Photochem. Photobiol. **44**, 629 (1986); (*b*) L. S. Lussier, C. Sandorfy, H. Le Thanh, and D. Vocelle. Photochem. Photobiol. Submitted for publication; (*c*) L. S. Lussier, C. Sandorfy, H. Le Thanh, and D. Vocelle. J. Phys. Chem. In press.
19. (*a*) M. Allen and J. D. Roberts. J. Org. Chem. **45**, 130 (1980); (*b*) J. Org. Chem. **43**, 2590 (1978); (*c*) M. Allen, J. D. Roberts, and R. O. Dutheler. J. Am. Chem. Soc. **100**, 3882 (1978).

Can. J. Chem. Downloaded from www.nrcresearchpress.com by 80.58.250.72 on 09/07/12
For personal use only.

An improved route to pregna-5,20-dien-3β-ol (muricin aglycone): Carbon and proton nuclear magnetic resonance assignments for the aglycone and a number of related pregnene derivatives[1]

R. D. DAWE AND J. L. C. WRIGHT[2]

National Research Council of Canada, Atlantic Research Laboratory, 1411 Oxford Street, Halifax, N.S., Canada B3H 3Z1

Received August 11, 1986

R. D. DAWE and J. L. C. WRIGHT. Can. J. Chem. **65**, 666 (1987).

Carbon and proton assignments for muricin aglycone (**5**) and a number of related pregnenes, carried out with the aid of two-dimensional homo- and heteronuclear chemical shift correlation experiments, have resulted in previously reported carbon assignments for the aglycone being revised. An improved route to muricin aglycone is also reported.

R. D. DAWE et J. L. C. WRIGHT. Can. J. Chem. **65**, 666 (1987).

Sur la base de l'attribution des carbones et des protons de l'aglycone muricine (**5**) et d'un certain nombre de pregnènes apparentés, qui a été effectuée en faisant appel à des expériences de corrélation de déplacements chimiques homo- et hétéronucléaires bidimensionnelles, on a été amené à reviser des attributions faites antérieurement pour un certain nombre de carbones de l'aglycone. On rapporte aussi une méthode améliorée d'obtenir l'aglycone muricine.

[Traduit par la revue]

Can. J. Chem. Downloaded from www.nrcresearchpress.com by 80.58.250.72 on 09/07/12
For personal use only.

Introduction

Several pregnene derivatives have been isolated from marine invertebrates. The pregnene derivative **1** was identified as aglycone from a complex saponin mixture from 3 species of starfish (1–3). The free pregnene derivatives **2**–**4** were isolated from the sponge *Haliclona rubens* (4), two others (**5** and **6**), were extracted from the soft coral *Gersemia rubiformis* (5), and steroid **6** together with **7** and **8** were isolated from an unidentified Pacific soft coral (6). More recently the vinyl steroid **5** was identified as the aglycone of muricin (**9**) as well as several other galactosamine saponins, from the Pacific gorgonian *Muricea fruticosa* (7), which displayed antifungal activity. With the exception of the latter compounds no ^{13}C nmr data have been reported for these steroids. Before the synthesis of muricin and other related saponins containing the C_{21} pregnene nucleus was attempted, it was necessary to develop a more efficient preparation of the aglycone **5** and at the same time obtain unambiguous proton and carbon data for these C_{21} steroids.

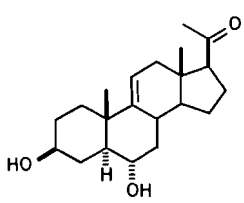

1

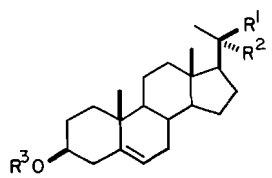

2 R^1 R^2 = O, R^3 = H
3 R^1 = OH, R^2 = H, R^3 = H
4 R^1 = H, R^2 = OH, R^3 = H
11 R^1 R^2 = O, R^3 = Ac
13 R^1 = OH, R^2 = H, R^3 = Ac
14 R^1 = OAc, R^2 = H, R^3 = Ac
15 R^1 = OMs, R^2 = H, R^3 = Ac

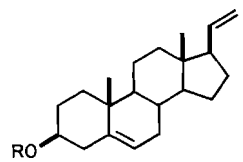

5 R = H
16 R = Ac

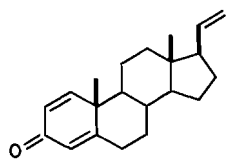

6

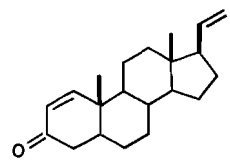

7

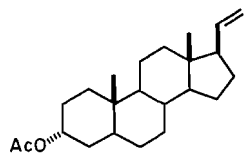

8

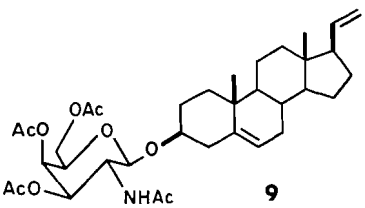

9

Results and discussion

Two syntheses of the C_{21} vinyl steroid **5** have been reported. In the original synthesis (8), the vinyl side chain was generated by Hofmann degradation of the appropriate C-21 amine in 3 steps and approximately 53% overall yield starting from the cholenic acid derivative **10**. More recently (5), a two-step synthesis from **2** in overall yield ca. 31% was accomplished by desulphurization of the C-20 thioacetal over deactivated Raney nickel. The synthesis reported here uses the commercially available keto-acetate **11**, which is converted to **5** in three steps and an overall yield of ca. 83%. In this short route, borohydride reduction of **11** gave **13**, which, after conversion to the mesylate **15**, was smoothly converted to **5** with potassium *tert*-butoxide.

The many reports concerning the assignment of ^{13}C resonances of steroids have been thoroughly reviewed (9), but only a few have been studied using modern pulse sequences. To establish a reliable set of data at the start of this short synthetic sequence, nmr assignments of **11** were secured as follows. The easily identified resonances for H-3 and H-6 are well separated from the methylene envelope and were used to assign signals for neighbouring protons (H-2, H-3, H-4 and H-6, H-7, H-8) by homonuclear 2-D chemical shift correlation experiments. These assignments were then used to identify the signals for carbons bonded to these protons by heteronuclear 2-D chemical shift correlation studies. Generally speaking, most resonances of the sterol nucleus are unaffected by variations in the side chain, and the converse is also true (10). Consequently the remaining

[1]NRCC No. 26731.

[2]Author to whom correspondence may be addressed.

TABLE 1. Carbon chemical shifts of C_{21} steroids

Carbons	2	5	11	12*	13	14	15	18	20
1	37.32	37.40	37.16	35.6	37.06	37.08	36.97	37.34	37.27
2	31.78	31.70	27.68	33.8	27.76	27.84	27.73	31.70	31.96
3	71.41	71.76	73.69	198.5	73.95	73.94	73.81	71.80	71.31
4	42.10	42.35	38.02	123.7	38.13	38.18	38.09	42.34	38.24
5	140.97	140.84	139.61	169.8	139.72	139.81	139.76	140.87	44.89
6	121.19	121.57	122.20	32.6	122.47	122.45	122.21	121.58	28.74
7	31.89	32.05	31.74	31.8	31.94	31.92	31.92	31.84	31.56
8	31.46	32.05	31.42	35.4	31.73	31.82	31.82	31.50	31.56
9	50.04	50.30	49.86	53.5	50.13	50.18	49.98	50.72	54.47
10	36.55	36.65	36.51	38.5	36.61	36.66	36.57	36.74	35.10
11	21.11	20.75	20.91	21.0	21.03	21.48	21.34	21.11	21.49
12	39.28	37.46	38.73	38.5	39.74	39.22	39.65	36.04	37.02
13	44.06	43.41	43.84	43.7	42.31	42.23	42.16	43.50	44.38
14	56.94	56.01	56.76	55.9	56.23	56.14	56.08	55.11	56.29
15	24.51	24.91	24.42	24.2	24.56	24.36	24.14	24.42	24.41
16	22.86	27.27	22.81	22.8	25.70	25.51	25.43	110.33	31.96
17	63.73	55.36	63.55	63.3	58.41	55.11	55.43	152.51	150.4
18	13.21	12.75	13.16	13.2	12.26	12.41	11.90	18.97	13.06
19	19.39	19.45	19.24	17.3	19.31	19.32	19.27	19.43	16.91
20	195.49	139.75	196.42	208.3	70.24	72.83	81.41	26.35	113.23
21	31.46	114.56	31.94	31.3	23.70	19.96	21.02	13.80	12.31

*These values for progesterone were reported in ref. 9.

unidentified carbon resonances were assigned from their multiplicities and by comparison with published data (9, 11–13). It should be noted that acetylation of the 3β-hydroxy group results in shielding (ca. 4 ppm) of C-2 and C-4, whereas C-3 is deshielded by about 2 ppm (9) (Table 1). Furthermore the chemical shifts for C-15 and C-16 in steroids containing a 17β-acetyl group such as **12** have been unequivocally assigned by two groups (9, 14) using ^2H isotope effects. These experiments also confirmed the assignments for C-17 through C-21 and by comparison were used to assist in the assignment of these resonances in **2** and **11**. (For convenience, the published ^{13}C nmr data for **12** are reproduced in Table 1.)

Stereospecific reduction of the ketone **11** to the 20*R* alcohol **13** using borohydride resulted in predictable chemical shift changes: compared with **11**, the ring D carbons C-13 through C-15 of **13** were essentially unaffected, the resonance for C-16 was somewhat deshielded (+2.89 ppm), but the C-17 resonance was considerably shifted upfield (−5.14 ppm) upon reduction of the α-keto function. The new resonances at δ_C 70.24 and 23.70 were consistent with a methyl carbinol side chain and were assigned by comparison with 3-methyl-2-butanol (15). The remaining resonances displayed chemical shifts consistent with a 3β-acetoxy Δ^5 steroid nucleus and once again several of these assignments (C-1 through C-8 and C-17 through C-21) were confirmed by COSY and heteronuclear correlation experiments in the manner already described for **11**.

Acetylation of the methyl carbinol to yield the diacetate **14** resulted in the usual deshielding (ca. 2.5 ppm) of C-20 and shielding (ca. 3–4 ppm) of the adjacent carbons C-17 and C-21. Using the diacetate, the stereochemistry of C-17 and C-20 was confirmed by comparison with an authentic sample. In the mesylate **15**, the downfield shift of C-20, observed upon formation of the acetate, is more marked (ca. 11 ppm). However, the differences are less marked at the adjacent positions where C-17 is shielded by approximately the same amount as in the acetate, but C-21 is only shielded by about half. The resonance for C-18 is a little more shielded (ca. 0.5 ppm)

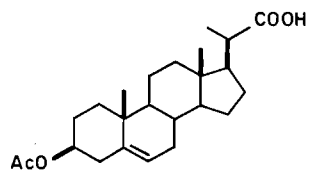

10

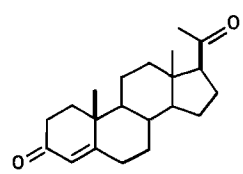

12

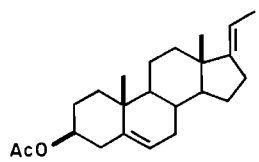

17

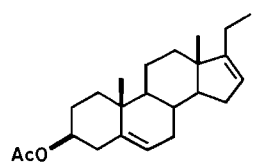

18

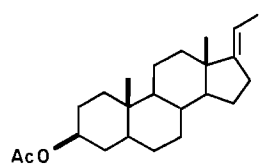

19

in the mesylate than the acetate, but the remaining resonances, which are removed from the side chain, are essentially unchanged.

Gas chromatographic analysis of the mesylate **15** resulted in decomposition and showed a mixture of three components with retention times 0.67, 0.68, 0.69 (relative to cholesterol) in the ratio 1:2.5:1.5. This mixture was obtained, in approximately the same ratio, upon elimination of methanesulphonic acid from **15** in refluxing pyridine. The olefinic region of the ^{13}C nmr spectrum of this mixture contained signals attributable to the vinyl sterol **16** (δ_C 114.51(t) and 139.7(d)) as well as two other

Can. J. Chem. Downloaded from www.nrcresearchpress.com by 80.58.250.72 on 09/07/12
For personal use only.

TABLE 2. Proton chemical shift assignments of selected C_{21} steroids obtained by 2D heteronuclear correlation experiments

Proton	5	11	13	15	18
1	1.07, 1.84	1.16, 1.88	1.15, 1.86	1.13, 1.84	1.08, 1.84
2	1.53, 1.83	1.58, 1.86	1.60, 1.83	1.58, 1.83	1.55, 1.82
3	3.53	4.60	4.62	4.60	3.53
4	2.27	2.33	2.33	2.31	2.30
6	5.36	5.37	5.37	5.37	5.36
7	1.62, 1.96	1.63, 1.96	1.58, 1.93	1.63, 1.93	1.55, 2.00
8	1.44	1.47	1.49	1.47	1.49
9	0.94	1.03	0.94	0.96	0.98
11	1.37, 1.56	1.39, 1.61	1.49 (br)	1.45 (br)	1.46, 1.62
12	1.65, 1.88	1.45, 2.07	1.23, 2.04	1.20, 2.04	1.22, 1.80
14	1.01	1.16	0.97	1.03	1.00
15	1.17, 1.65	1.29, 1.72	1.13, 1.62	1.15, 1.66	1.70
16	1.52, 1.75	1.68, 2.20	1.13, 1.62	1.26, 1.75	5.05
17	1.95	2.52	1.35	1.62	—
18	0.61	0.64	0.77	0.77	0.76
19	1.02	1.03	1.03	1.00	1.03
20	5.76	—	3.73	4.82	2.25
21	4.96	2.13	1.14	1.39	1.54

sets of signals ascribed to the sterols **17** (δ_C 113.55(d) and 150.12(s)) and **18** (δ_C 110.33(d) and 152.51(s)), as determined by comparison with an authentic sample of **18** and the pregnene derivative **19** (Table 1).

Elimination of methanesulphonic acid with potassium *tert*-butoxide simultaneously removed the acetate group and yielded the naturally occurring steroid **5** as the sole product. The ^{13}C nmr spectrum of this material contained an olefinic methylene resonance at δ_C 114.56 assigned to C-21, and another new resonance at δ_C 139.75 assigned to the olefinic methine at C-20. The two remaining olefinic resonances were consistent with Δ^5 substitution. Only two resonances in the sterol nucleus were significantly perturbed upon conversion of the mesylate **15** to the vinyl steroid **5** (Table 1): the resonances for C-13 and C-16 are shifted downfield (by 1.25 ppm and 1.84 ppm respectively), and the slight chemical shift differences for C-2, C-3, and C-4 are entirely consistent with hydrolysis of the acetate grouping (9). The assignments for C-1 through C-8 were confirmed by performing homonuclear and heteronuclear two-dimensional correlation experiments. Furthermore, the readily characterized resonances for H-20 (δ_H 5.74) and H-21 (δ_H 4.96) of the vinyl side chain were used to identify the ^1H–^1H connectivities H-21, H-20, H-17, and thus establish the assignment of C-17. Finally, the heteronuclear correlation data that yielded the ^1H resonance assignments in Table 2 were used to cross-check the assignment of the remaining ^{13}C resonances. The data listed in Table 1 show several discrepancies in the previously published ^{13}C nmr data (7) for **5**. In particular, the resonance at δ_C 37.3, assigned to C-4, is too low for a 3β-hydroxy sterol; the resonance is more appropriate for C-12. The resonance at δ_C 32.0 assigned to C-12 should be assigned to C-2. The resonance at δ_C 29.7 assigned to C-2 is incorrect, and is probably due to an impurity.

The muricins are an interesting group of metabolites that may account for the antifouling properties of the gorgonian *M. fruticosa*. The short high-yield synthesis of the aglycone **5** allows ready access to muricin and details of this, as well as the syntheses of other related saponins, will be reported later.

Experimental

The following steroids were purchased from Steraloids Inc., Wilton, NH: 5-pregnene-3β-ol-20-one 3-acetate (**11**) (Catalogue No. Q5501); pregna-5,16-diene-3β-ol (P1420) (**18**); 5α-pregn-17(20)-ene (**19**) (Q6790).

Optical rotations were measured using a Perkin–Elmer polarimeter, and infrared spectra were recorded with a Perkin–Elmer 283B spectrophotometer. Nuclear magnetic resonance spectra were obtained with a Bruker MSL-300 spectrometer using 5-mm tubes and ^2H lock as follows: ^1H spectra at 300 MHz, spectral width 4.5 kHz, data size 16 K zero-filled to 32 K (0.26 Hz/pt), 45 deg pulses (6 μs), repetition rate 6.8 s, temperature 20°C, sample amount in the 10–25 mg range in 0.7 mL $CDCl_3$: ^{13}C spectra (variables in same order): 75.4 MHz, 16.7 kHz, 16 K, 32 K (1.0 Hz/pt), 30 deg (2 μs), 1 s, 23°C, broadband [^1H]-decoupling; ^1H *J*-correlated "COSY" spectra (16); spectral width 1859 Hz, 512 × 128 word data table zero-filled in both dimensions giving data resolution 7.3 Hz/pt, data multiplication by squared sine-bell in both dimensions; $^{13}C/^1H$ heteronuclear *J*-correlated spectra (17); ^{13}C dimension 11 628 Hz, 1 K zero-filled, 11.4 Hz/pt, line broadening 10 Hz; ^1H dimension 2491 Hz, 128 words zero-filled, 9.7 Hz/pt, squared sine-bell. Mass spectra were obtained with a VG Analytical ZAB-EQ spectrometer operating in the EI mode (8 kV accelerating voltage, 70 eV ionizing energy). Gas–liquid chromatographic analyses were performed using a Varian 3400 chromatograph and a Varian series 600 chromatography data system. Operating conditions were as follows: fused silica capillary column (30 m × 0.25 mm) coated with DB5, injector port 310°C, detector 310°C, oven programmed from 150 to 270°C at 5°/min, helium carrier gas, flow 3 mL/min.

Pregn-5-ene-3β, 20R-diol, 3-acetate

The crystalline ketoacetate (**11**, 5.40 g, 15.1 mmol) was dissolved in methanol (150 mL), cooled to 0°C, and sodium borohydride was added slowly with stirring. After complete reduction (followed by tlc) excess borohydride was destroyed with acetic acid and the mixture was extracted twice with dichloromethane. The combined organic extracts were washed with saturated sodium bicarbonate, brine, and evaporated to yield the alcohol **13** as a white solid (5.40 g, 99%). Material that crystallized from methanol had the following characteristics: mp 152–155°C; $[\alpha]_D^{20}$ −76.4° (*c* 0.432, $CHCl_3$); ir (CCl_4): 3600 and 1720 cm^{-1}; ^1H nmr (300 MHz), δ_H: 0.77 (s, 3H), 1.03 (s, 3H), 1.14

Can. J. Chem. Downloaded from www.nrcresearchpress.com by 80.58.250.72 on 09/07/12
For personal use only.

(d, J = 6.1 Hz, 3H), 2.04 (s, 3H), 3.73 (m, 1H), 4.62 (m, 1H), 5.37 (bd, J = 4.86 Hz, 1H).

The alcohol **13** (25 mg, 0.069 mmol) was acetylated in the usual manner to yield the diacetate **14** (25 mg, 89%), which had the same physical characteristics as authentic pregn-5-ene-3β,20β-diacetate (Steraloids), mp 126–128°C; $[\alpha]_D^{20}$ −36° (*c* 2.78, $CHCl_3$).

*Pregn-5-ene-3β, 20*R*-diol, 3-acetate, 20-methanesulphonate*

The secondary alcohol (**13**, 5.40 g, 15.0 mmol) was dissolved in dichloromethane (100 mL) and pyridine (15 mL) and treated with methanesulphonyl chloride (10 mL). When the reaction was complete (18 h), saturated aqueous sodium bicarbonate (100 mL) was added, the mixture was extracted with dichloromethane (200 mL), washed with water and brine, dried, and evaporated to yield a yellow solid (5.7 g). This solid was filtered through a short pad of Florosil using ethyl acetate/hexane (1:1) as eluant. Evaporation of the solvent yielded the mesylate **15** as an off-white solid (5.6 g, 85%), mp 125–127°C; $[\alpha]_D^{23}$ −37.5 (*c* 1.02, $CHCl_3$); ir (CCl_4): 1725 and 1330 cm^{-1}; ^1H nmr (80 MHz), δ_H: 0.79 (s, 3H), 1.01 (s, 3H), 1.40 (d, J = 6.0 Hz, 3H), 2.01 (s, 3H), 3.0 (s, 3H), 4.6 (bm, 2H (H-3, H-20)), 5.40 (bd, J = 4 Hz, 1H).

Pregna-5,20-diene-3β-ol

The mesylate **15** (0.5 g, 1.14 mmol), in dry toluene (6 mL) with potassium *tert*-butoxide (0.3 g, 2.7 mmol) added, was refluxed under nitrogen for 1.5 h. After cooling to room temperature the mixture was extracted twice with dichloromethane. The combined organic extracts were washed with water and brine, dried, and evaporated to yield the diene **5** as a white solid (0.35 g, 99%) that was homogeneous by tlc, ^1H and ^{13}C nmr spectral analysis. The material crystallized from methanol as needles, mp 136.5–138°C (lit. (8) mp 138–139°C); $[\alpha]_D^{23}$ −83.6° (*c* 0.616, $CHCl_3$) (lit. (8) $[\alpha]_D^{23}$ −85° (*c* 0.91, $CHCl_3$)); ir (CCl_4): 3450 and 1600 cm^{-1}; ^1H nmr (360 MHz), δ_H: 0.61 (s, 3H), 1.02 (s, 3H), 3.53 (m, 1H), 4.96 (dd, 2H), 5.36 (m, 1H), 5.76 (ddd, J = 8, 16, and 11 Hz, 1H); m/z (rel. intensity): 300.2557 (75) (M^+ calcd. for $C_{21}H_{32}O$: 300.2567), 285 (25) [M − 15], 282 (25) [M − 18], 267 (100) [M − (15 + 18)], 213 (50) [M − (33 + 54)].

*Treatment of mesylate **15** with refluxing pyridine*

The mesylate (50 mg, 0.11 mmol) was refluxed in dry pyridine (3 mL) for 3 h, after which time analysis of the mixture by tlc showed complete conversion to a new less polar spot. After extraction, analysis of the product by ^{13}C nmr (20 MHz) showed it to be a 2.5:1.5:1 mixture of the dienes **18**, **16**, and **17**. The olefinic resonances were δ_C 152.39(s), 150.12(s), 139.75(s), 139.75(d), 122.52(d), 114.56(t), 113.55(d), and 110.37(d).

Acknowledgements

We thank Cheryl Craft for technical assistance and Dr. John Walter for assistance in obtaining the nmr spectra. One of us (RDD) is grateful to the Natural Sciences and Engineering Research Council of Canada for financial assistance.

1. Y. M. Sheikh, B. M. Tursch, and C. Djerassi. J. Am. Chem. Soc. **94**, 3278 (1972).
2. Y. Shimizu. J. Am. Chem. Soc. **94**, 4051 (1972).
3. S. Ikegami, Y. Kamiya, and S. Tamura. Tetrahedron Lett. 1601 (1972).
4. J. A. Ballantine, K. Williams, and B. A. Burke. Tetrahedron Lett. 1547 (1977).
5. J. F. Kingston, B. Gregory, and A. G. Fallis. J. Chem. Soc. Perkin Trans. 1, 2064 (1979).
6. M. D. Higgs and D. J. Faulkner. Steroids, **30**, 397 (1977).
7. M. M. Bandurraga and W. Fenical. Tetrahedron, **41**, 1057 (1985).
8. P. L. Julian, E. W. Meyer, and H. C. Printy. J. Am. Chem. Soc. **70**, 887 (1948).
9. J. W. Blunt and J. B. Stothers. Org. Magn. Reson. **9**, 439 (1977).
10. J. L. C. Wright, A. G. McInnes, S. Shimizu, D. G. Smith, J. A. Walter, D. Idler, and W. Khalil. Can. J. Chem. **56**, 1898 (1978).
11. H. J. Reich, M. Jautelet, M. T. Messe, F. J. Weigert, and J. D. Roberts. J. Am. Chem. Soc. **91**, 7445 (1969).
12. J. W. ApSimon, H. Beierbeck, and J. K. Saunders. Can. J. Chem. **51**, 3874 (1973).
13. G. Popjak, J. Edmond, F. A. L. Anet, and N. R. Easton. J. Am. Chem. Soc. **99**, 931 (1977).
14. D. J. Kim, L. D. Colebrook, and T. J. Adley. Can. J. Chem. **54**, 3766 (1976).
15. E. Breitmaier and W. Voelter. Carbon-13 NMR spectroscopy. Verlag Chemie GmbH, Weinheim. 1974.
16. A. Bax and R. Freeman. J. Magn. Reson. **44**, 542 (1981).
17. A. Bax and G. A. Morris. J. Magn. Reson. **42**, 501 (1981).

Can. J. Chem. Downloaded from www.nrcresearchpress.com by 80.58.250.72 on 09/07/12
For personal use only.

Synthesis of functionalized bicyclo[3.2.1]octa-2,6-dienes by thermal rearrangement of substituted 6-*exo*-(1-alkenyl)bicyclo[3.1.0]hex-2-ene systems

EDWARD PIERS, GRACE L. JUNG, AND EDWARD H. RUEDIGER

Department of Chemistry, University of British Columbia, 2036 Main Mall, University Campus, Vancouver, B.C., Canada V6T 1Y6

Received September 2, 1986

EDWARD PIERS, GRACE L. JUNG, and EDWARD H. RUEDIGER. Can. J. Chem. **65**, 670 (1987).

Thermolysis of each of the enol silyl ethers **31**–**35** affords, cleanly and efficiently, the bicyclo[3.2.1]octadienes **36**–**40**, respectively. Similarly, thermal rearrangement of the enol silyl ether **50** provides the diene **51**. Hydrolysis of **36**, **37**, and **39**, and decarbomethoxylation of the resultant keto esters **41**, **42**, and **44**, gives the ketones **46**–**48**, respectively. The ketone **46** is also obtained by acid hydrolysis of **51**. Conversion of 6-methyl-1-hepten-4-yn-3-ol (**56**) into the enol ether **63** is described. Thermolysis of **63** gives **64**, which, upon acid hydrolysis, affords **65**. Thermolysis of the enones **68** and **69** produces the bicyclic dienones **70** and **71**, respectively. On the other hand, thermolysis of **73** and **74**, derived from the enone **69**, provides the C-8 *exo* substituted bicyclo[3.2.1]octa-2,6-dienes **75** and **76**, which are transformed smoothly, by acid hydrolysis, into the ketones **77** and **78**, respectively.

EDWARD PIERS, GRACE L. JUNG et EDWARD H. RUEDIGER. Can. J. Chem. **65**, 670 (1987).

Les thermolyses de chacun des éther énoliques silylés **31**–**35** conduisent respectivement, d'une manière propre et efficace, aux bicyclo[3.2.1]octadiènes **36**–**40**. De la même manière, la transposition thermique de l'éther énolique silylé **50** conduit au diène **51**. L'hydrolyse des composés **36**, **37** et **39** et la decarbométhoxylation des céto-esters **41**, **42** et **44** qui en résultent conduisent respectivement aux cétones **46**–**48**. On a aussi obtenu la cétone **46** par hydrolyse acide du composé **51**. On décrit la transformation du méthyl-6 heptène-1 yne-4 ol-3 (**56**) en son éther énolique **63**. La thermolyse du composé **63** conduit au produit **64** qui, par hydrolyse, conduit au composé **65**. La thermolyse des énones **68** et **69** conduit respectivement aux diénones bicycliques **70** et **71**. Par ailleurs, la thermolyse des composés **73** et **74**, qui proviennent du composé **69**, conduit aux bicyclo[3.2.1]octadiènes-2,4 (**75** et **76**) portant des substituants dans la positions C-8 *exo* qui se transforment respectivement, par hydrolyse acide, en cétones **77** et **78**.

[Traduit par la revue]

Can. J. Chem. Downloaded from www.nrcresearchpress.com by 80.58.250.72 on 09/07/12
For personal use only.

Introduction

More than twenty years ago, Cupas, Watts, and Schleyer (1) reported that reaction of the bicyclic aldehyde **1** with methylenetriphenylphosphorane in refluxing tetrahydrofuran (THF) gives directly bicyclo[3.2.1]octa-2,6-diene (**3**). Thus, under these conditions, the initially formed 6-*endo*-vinylbicyclo[3.1.0]hex-2-ene (**2**) undergoes a facile [3,3]-sigmatropic (Cope) rearrangement to provide **3**. Subsequently, Brown (2) was able to isolate **2** and to show that this substance has a half-life of approximately one day at 25°C. In contrast, 6-*exo*-vinylbicyclo[3.1.0]hex-2-ene (**4**), like other *trans*-1,2-divinylcyclopropane systems,[1] is stable at ambient temperatures. However, **4** rearranges smoothly at 195°C to afford the bicyclic diene **3**. In

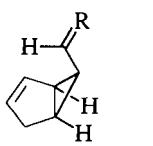

1 R = O
2 R = CH_2

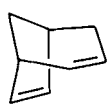

3

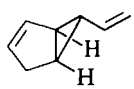

4

an elegant study (6), the latter transformation was shown to proceed via a one-center epimerization at C-6. Presumably, this epimerization occurs via a diradical intermediate (5*a*) to produce the *endo* vinyl isomer **2**, which then undergoes rapid bond reorganization to yield **3** (5*b*).

Interestingly, the rearrangement of 6-(1-alkenyl)bicyclo-[3.1.0]hex-2-enes has received relatively little attention from a synthetic point of view (7–11). Since many natural products, particularly members of the terpenoid family, possess structures that incorporate the bicyclo[3.2.1]octane carbon skeleton, we have carried out a study aimed at the synthesis of functionalized bicyclo[3.2.1]octanes via Cope rearrangement of *trans*-divinylcyclopropane systems derived from 6-*exo*-(1-alkenyl)bicyclo[3.1.0]hexan-2-enes. We report herein the details of some of our work in this area.[2]

Results and discussion

(a) Preparation of the diene bromides 15–17

Of the diene bromides **14**–**17** (see Chart 1) required for this study, the "parent" (*E*)-5-bromo-1,3-pentadiene **14** was a known substance (14). The others, **15**–**17**, were prepared via relatively straightforward chemistry. Treatment of 2-methylpropanal with (carboethoxymethylene)triphenylphosphorane in

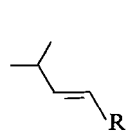

5 R = CO_2Et
6 R = CH_2OH
7 R = CHO

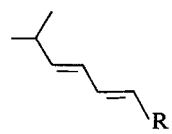

8 R = CO_2Et
9 R = CH_2OH

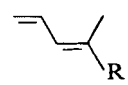

10 R = CO_2Et
11 R = CH_2OH

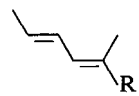

12 R = CO_2Et
13 R = CH_2OH

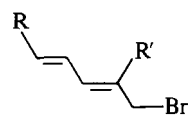

14 R = R′ = H
15 R = *i*-Pr, R′ = H
16 R = H, R′ = Me
17 R = R′ = Me

CHART 1

[1]For general discussions of the Cope rearrangement of 1,2-divinylcyclopropane systems, see refs. 3–5.

[2]For preliminary reports regarding some of the work described herein, see refs. 12 and 13.

Can. J. Chem. Downloaded from www.nrcresearchpress.com by 80.58.250.72 on 09/07/12
For personal use only.

dichloromethane provided, highly stereoselectively, the enoate **5**. Reduction (diisobutylaluminum hydride) of **5**, followed by oxidation (pyridinium chlorochromate on alumina (15)) of the resultant alcohol **6**, gave the aldehyde **7**. The latter substance was transformed into the diene alcohol **9** via a two-step sequence very similar to that used for the conversion of 2-methylpropanal into **6**. Treatment of **9** with phosphorus tribromide in ether containing a small amount of pyridine (16) produced the bromide **15**.

Reaction of propenal and (*E*)-2-butenal with (carboethoxyethylidene)triphenylphosphorane in dichloromethane afforded the dienoates **10** and **12**, respectively. Reduction of the latter materials with lithium ethoxyaluminohydride (17) gave the alcohols **11** and **13**, which were converted into the corresponding bromides **16** and **17** by reaction with triphenylphosphine dibromide in acetonitrile containing one equivalent of triethylamine (18).

The allylic bromides **15**–**17** were rather unstable and tended to darken on standing. They were generally stored under argon at low temperatures (−20°C) and were distilled just prior to use.

*(b) Preparation of the 2-(*tert*-butyldimethylsiloxy)-6-*exo*-(1-alkenyl)bicyclo[3.1.0]hex-2-enes **31**–**35***

The β-keto esters **18**–**21** (see Chart 2) were prepared conveniently by use of the method developed by Huckin and Weiler (19). Successive treatment of methyl acetoacetate with 1.1 equivalents of each of sodium hydride and *n*-butyllithium, followed by alkylation of the resultant dianion with the bromide **15**, provided the β-keto ester **19** in 53% yield. In similar fashion, compounds **18**, **20**, and **21** were obtained by alkylation of $Li_2(CH_2COCHCO_2Me)$[3] with the bromides **14**, **16**, and **17**, respectively. The best yields for the latter alkylations were obtained when the reactions were carried out at 0°C for short periods of time (~5 min). Longer reaction times increased significantly the formation of undesired by-products.

Treatment of each of the β-keto esters **18**–**21** with *p*-toluenesulfonyl azide in acetonitrile containing one equivalent of triethylamine (20) afforded, in essentially quantitative yields, the corresponding diazo compounds **22**–**25**, respectively. The latter substances exhibited, in their infrared spectra, an absorption band in the region 2120–2125 cm^{-1}, typical of the diazo function.

Carbenoid ring closure (21) of the diazo dienes **22**–**25** was effected by treatment of these substances with copper(II) acetylacetonate (**22**–**24**) or copper-bronze (**25**) in refluxing benzene (**23**) or toluene (**22**, **24**, **25**). The yields of the bicyclic products **26**–**29** varied from 50 to 78%. Since it is well known (21) that carbenoid cyclizations of this type are stereospecific with respect to the stereochemistry of the double bond involved, only the expected 6-*exo*-alkenyl isomers were formed. Methylation (LDA, THF; MeI, THF–hexamethylphosphoramide) of the keto ester **26** provided the alkylated material **30**.

Treatment of each of the ketones **26**–**30** with 1.1 equivalents of LDA (THF, −78°C), followed by trapping of the resultant enolate anion with *tert*-butyldimethylsilyl chloride (THF–hexamethylphosphoramide, −78°C to room temperature), produced cleanly and efficiently the corresponding enol silyl ethers **31**–**35**, respectively. The stage was thus set for an investigation

[3]This species was prepared by reaction of methyl acetoacetate with 2.1 equivalents of lithium diisopropylamide (LDA) (19) or lithium 2,2,6,6-tetramethylpiperidide. In general, the yields of alkylations involving the bromides **14**–**17** were higher with $Li_2(CH_2COCHCO_2Me)$ than with $LiNa(CH_2COCHCO_2Me)$.

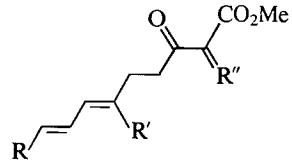

18 R = R′ = H, R″ = H_2
19 R = *i*-Pr, R′ = H, R″ = H_2
20 R = H, R′ = Me, R″ = H_2
21 R = R′ = Me, R″ = H_2
22 R = R′ = H, R″ = N_2
23 R = *i*-Pr, R′ = H, R″ = N_2
24 R = H, R′ = Me, R″ = N_2
25 R = R′ = Me, R″ = N_2

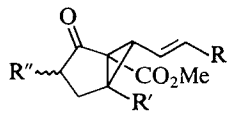

26 R = R′ = R″ = H
27 R = *i*-Pr, R′ = R″ = H
28 R = R″ = H, R′ = Me
29 R = R′ = Me, R″ = H
30 R = R′ = H, R″ = Me

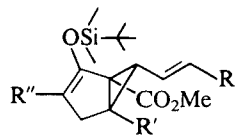

31 R = R′ = R″ = H
32 R = *i*-Pr, R′ = R″ = H
33 R = R″ = H, R′ = Me
34 R = R′ = Me, R″ = H
35 R = R′ = H, R″ = Me

CHART 2

of the thermal rearrangement of these functionalized 6-*exo*-alkenylbicyclo[3.1.0]hex-2-enes.

*(c) Thermal rearrangement of the 6-*exo*-(1-alkenyl)bicyclo[3.1.0]hex-2-enes **31**–**35** and **50***

When a solution of the divinylcyclopropane **31** in dry xylene was refluxed for 2.5 h, the bicyclo[3.2.1]octa-2,6-diene **36** (see Chart 3) was obtained in nearly quantitative yield. In similar fashion, thermolysis of the more highly substituted substrates **32** (benzene, sealed tube, 200°C, 2 h), **33** (refluxing xylene, 6 h), **34** (refluxing mesitylene, 4 h), and **35** (refluxing mesitylene, 1 h) provided the Cope rearrangement products **37**–**40**, respectively, in high yields (>90%). In each case, the reaction was clean and the progress of the rearrangement process could be followed conveniently by gas–liquid chromatography (glc).

Presumably, the rearrangement of compounds **31**–**35** takes place via a mechanism outlined in general terms in Scheme 1 (3–6). Thus, one-center epimerization (6) of the substrates **31**–**35** to the corresponding *endo* isomers **B** by way of the diradical intermediate **A** (5*a*), followed by [3,3]-sigmatropic rearrangement of **B** via boat-like transition states **C** (3–5), would afford the bicyclic products **36**–**40**. Implicit in this mechanistic scheme is the prediction that substrates **32** and **34**, which possess a *trans*-1-alkenyl group at C-6, would produce bicyclo[3.2.1]octa-2,6-diene products (**37**, **39**, respectively) in which the R group at C-4 would have an *endo* (pseudoequatorial) orientation. Indeed, thermolysis of **32** and **34** provided exclusively the products **37** and **39**, respectively. Evidence in

Can. J. Chem. Downloaded from www.nrcresearchpress.com by 80.58.250.72 on 09/07/12
For personal use only.

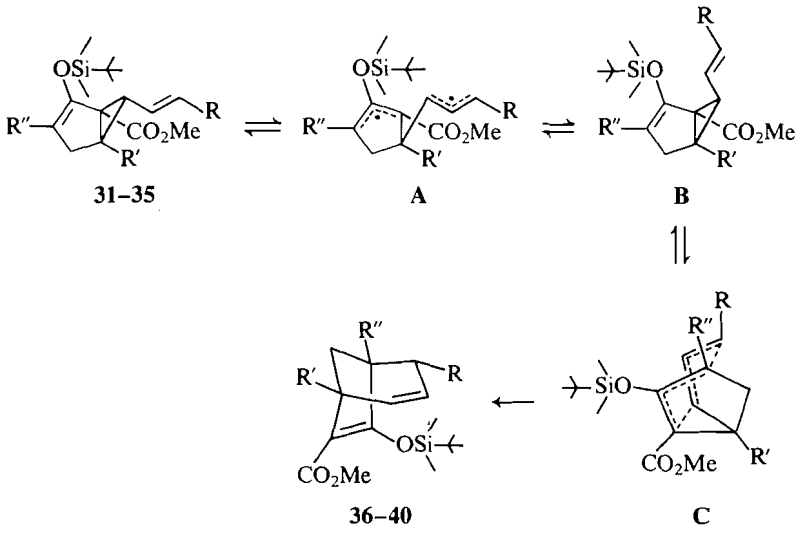

31–35 A B

36–40 C

SCHEME 1

support of the expectation that **37** possesses an *endo* oriented isopropyl group was obtained from an examination of the ^{1}H nmr spectrum of this material. Appropriate decoupling experiments showed that the coupling constant J_{AB} associated with the signals due to H_A and H_B is about 5 Hz. For example, irradiation at δ 5.44 (signal due to H_D) caused partial collapse of the resonance (δ 2.06) due to H_B, which changed from an "octet" (overlapped dddd, J_{BC} = 8.5 Hz, J_{AB} = 5 Hz, J_{BD} = J_{BE} = 2.5 Hz) to a "heptet" (overlapped ddd) with J_{BC} = 8.5 Hz, J_{AB} = 5 Hz, and J_{BE} = 2.5 Hz. Had the isopropyl group possessed an *exo* orientation, the dihedral angle between H_A and H_B would have been close to 90°C and a much smaller coupling constant would have been anticipated. This expectation was confirmed later in this study when a bicyclo[3.2.1]octa-2,6-diene bearing an *exo* isopropyl group at C-4 was prepared (*vide infra*).

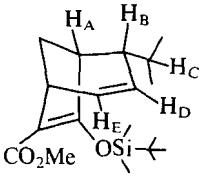

37

The mechanism shown in Scheme 1 would also lead one to predict that the thermal rearrangement of **31–35** would be assisted by the angular carbomethoxy group. Normally, the rate-determining step of the Cope rearrangement of *trans*-divinylcyclopropane systems (e.g. **31–35**) is the epimerization of the *trans* compound to the corresponding *cis*-divinylcyclopropane (e.g. **B**) (3–5).[4] Presumably, the CO_2Me group would assist in stabilizing the diradical **A** (and, in turn, the transition state leading to this intermediate) and would thus be instrumental in facilitating the rate of the overall rearrangement of substrates **31–35** to the products **36–40**. This conclusion is qualitatively supported by comparison of the thermal rearrangements of the structurally similar substrates **31** and **50**[5] (Chart 3). When a solution of compound **31** in xylene (bp 138°C) was

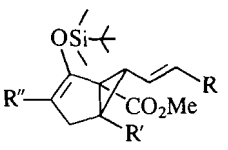

31 R = R′ = R″ = H
32 R = *i*-Pr, R′ = R″ = H
33 R = R″ = H, R′ = Me
34 R = R′ = Me, R″ = H
35 R = R′ = H, R″ = Me

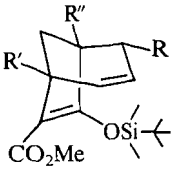

36 R = R′ = R″ = H
37 R = *i*-Pr, R′ = R″ = H
38 R = R″ = H, R′ = Me
39 R = R′ = Me, R″ = H
40 R = R′ = H, R″ = Me

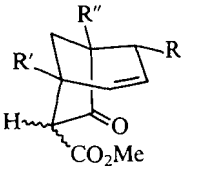

41 R = R′ = R″ = H
42 R = *i*-Pr, R′ = R″ = H
43 R = R″ = H, R′ = Me
44 R = R′ = Me, R″ = H
45 R = R′ = H, R″ = Me

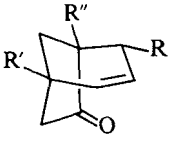

46 R = R′ = R″ = H
47 R = *i*-Pr, R′ = R″ = H
48 R = R′ = Me, R″ = H

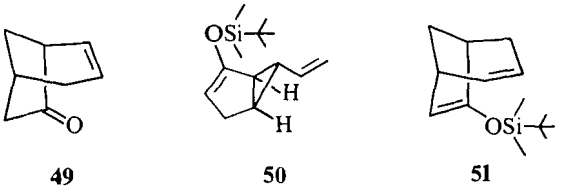

49 **50** **51**

CHART 3

refluxed, rearrangement to **36** was complete within a period of 2 h. On the other hand, complete transformation of **50** into **51** required a temperature of ~200°C (neat, sealed tube) for the same length of time. Nevertheless, the latter conversion was very clean and efficient (97% yield).

The rearrangement products **36–40** could be converted readily into the corresponding β-keto esters **41–45**, respectively. For example, treatment of **36** and **39** with potassium fluoride in methanol (0°C, 1 h) and **37** with tetra-*n*-butylammonium fluoride in dry THF (room temperature, 1 h) afforded, efficiently, the β-keto esters **41**, **44**, and **42**, respectively. In each case, the product consisted of a mixture of

[4]Exceptions to this generalization are known (see, for example, refs. 22 and 23).

[5]This substance is readily prepared (LDA, THF; *t*-BuMe$_2$SiCl, THF–hexamethylphosphoramide) from 6-*exo*-vinylbicyclo[3.1.0]hexan-2-one (24).

Can. J. Chem. Downloaded from www.nrcresearchpress.com by 80.58.250.72 on 09/07/12
For personal use only.

epimers associated with the carbomethoxy-bearing carbon. Acid hydrolysis – decarboxylation of **41** and **42** provided the bicyclic ketones **46** and **47**, respectively, while base hydrolysis of **44** gave **48**. Bicyclo[3.2.1]oct-2-en-6-one (**46**), which could also be obtained by treatment of the enol silyl ether **51** with dilute hydrochloric acid in THF, was shown to be identical (glc retention times, ^{1}H nmr spectrum) with a sample of the same substance obtained by preparative glc from an independently prepared mixture of the two isomeric keto alkenes **46** and **49** (25, 26).[6] Thus, the fact that the rearrangement products **36** and **51** possessed the bicyclo[3.2.1]octa-2,6-diene carbon skeleton was conclusively established.

The work summarized above demonstrated the utility of the Cope rearrangement of functionalized 6-*exo*-(1-alkenyl)bicyclo[3.1.0]hex-2-enes (e.g. **31**–**35**, **50**) for the preparation of substances possessing the bicyclo[3.2.1]octane carbon skeleton. The reactions employed for the preparation of the substrates **31**–**35** and **50** were relatively straightforward and the thermal rearrangement reactions were clean and efficient. The latter processes led to the preparation of bicyclo[3.2.1]octa-2,6-dienes with alkyl substituents at either bridgehead position (see **38**, **40**) and on C-4 with an *endo* orientation (see **37**, **39**). Furthermore, the rearrangement products contain on the 3-carbon and 2-carbon bridges functional groups (carbon–carbon double bond, "hidden" β-keto ester, enol silyl ether) suitable for further synthetic manipulations.

From a synthetic point of view, particularly as related to the possible use of the above-described methods in natural product synthesis, two additional goals remained. First, it was of considerable interest to test the viability of the Cope rearrangement of compounds of general structure **52**. Mechanistic considerations (see Scheme 1) would lead to the prediction that successful Cope rearrangement in these cases would afford bicyclo[3.2.1]octa-2,6-diene products **53** that possess at C-4 an *exo*, pseudoaxially oriented R group. However, if the R group is quite bulky (e.g. isopropyl), the presumed transition state for the Cope rearrangement would be destabilized considerably by steric and, perhaps, torsional strain involving the R group and the C-3 methylene group on the five-membered ring (see **D**). Therefore, it would not be unreasonable to conjecture that thermolysis of **52**, particularly if R is bulky, could result in bond reorganization processes different from the desired Cope rearrangement.

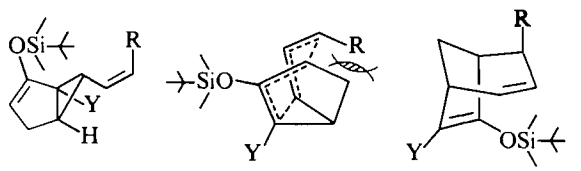

52 **D** **53**

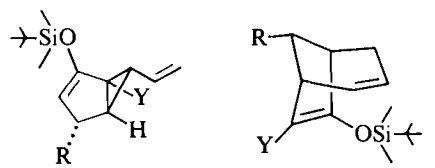

54 **55**

A second extension to the work described thus far was related to our desire to prepare bicyclo[3.2.1]octadienes that contain functional groups on the 1-carbon bridge (C-8). Specifically, we wished to prepare substrates of general structure **54**. It is evident that successful Cope rearrangements of **54**, which would produce products of general structure **55**, would significantly enhance the synthetic utility of the method under investigation.

The results of our studies as related to the preparation and thermolysis of substances of general structure **52** and **54** are summarized in the next two sections of this paper.

(d) Preparation and thermolysis of 2-(tert-*butyldimethylsiloxy)*-6-exo-*[(Z)-3-methyl-1-butenyl]bicyclo[3.1.0]hex-2-ene (63)*

Treatment of a THF solution of 1-lithio-3-methyl-1-butyne with propenal provided (86%) the alcohol **56** (see Chart 4). Subjection of the latter substance to an orthoester-based Claisen rearrangement (27) afforded, in 66% yield, the ester **57**. The expectation (27) that the newly formed double bond would possess a *trans* configuration was verified by the ^{1}H nmr spectrum of **57**, which showed that the mutual coupling constant associated with the two olefinic protons is 15.5 Hz. Conversion of the ester **57** into the diazoketone **60**, via the acid **58** and the acid chloride **59**, was accomplished by means of standard reactions. Copper(II) acetylacetonate-catalyzed carbenoid ring closure of **60** in refluxing benzene provided the bicyclic ketone **61** (49% from the ester **57**). Hydrogenation of the alkyne **61** in the presence of Lindlar's catalyst gave, in 94% yield, the corresponding *cis* alkene **62**. The ^{1}H nmr spectrum of **62** revealed that the olefinic protons are mutually coupled with a coupling constant of 10.5 Hz. The latter value is typical of *cis* disubstituted alkenes.

It was gratifying to find that thermolysis (240°C, benzene, sealed tube, 4.5 h) of the enol silyl ether **63** (derived from the ketone **62**) provided, in 93% yield, a single product that proved to be the bicyclic diene **64**. The presumption that **64** would possess an *exo*, pseudoaxially oriented isopropyl group was substantiated by its ^{1}H nmr spectrum. An appropriate

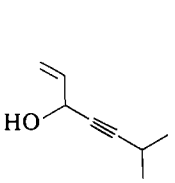

56

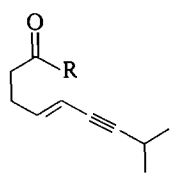

57 R = OEt
58 R = OH
59 R = Cl
60 R = CHN_2

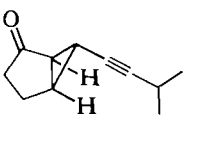

61

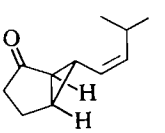

62

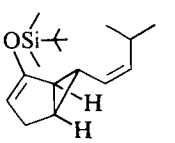

63

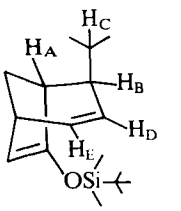

64

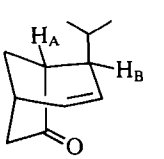

65

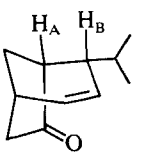

47

CHART 4

[6]We are grateful to Professor Stephen Monti for a sample of a mixture of the two ethylene ketals corresponding to the ketones **46** and **49** (25). The ^{1}H nmr spectrum of **49** (26) is significantly different from that of **46**.

Can. J. Chem. Downloaded from www.nrcresearchpress.com by 80.58.250.72 on 09/07/12
For personal use only.

decoupling experiment showed that J_{AB} (see **64**) is ≤ 1 Hz. Thus, irradiation of the broad doublet at δ 2.38 (H_A) did not alter the width-at-half-height associated with the multiplet at δ 1.88–1.94 (H_B), although the latter resonance did change to a clean 6-line signal (overlapped ddd, $J_{BC} = 7$ Hz, $J_{BD} \approx 3$ Hz, $J_{BE} \approx 2$ Hz). Molecular models indicate that the dihedral angle between H_A and H_B in **64** is close to 90°, and thus a small coupling constant would be expected. Furthermore, acid-promoted hydrolysis of the enol ether function in **64** furnished the ketone **65**, which, on the basis of spectral data, is clearly epimeric with the previously prepared ketone **47** (*vide supra*). In particular, suitable decoupling experiments similar to those described previously for the enol silyl ethers **64** and **37** (*vide supra*) showed that, in the ^{1}H nmr spectra of **65** and **47**, J_{AB} is ≤ 1 Hz and 5 Hz, respectively (see Chart 4). These observed coupling constants fully support the stereochemical assignments.

It is evident from the successful, efficient conversion of **63** into **64** that Cope rearrangements of 6-*exo*-(1-alkenyl)bicyclo[3.1.0]hex-2-enes possessing relatively bulky, *cis*-oriented alkyl groups on the 6-*exo*-(1-alkenyl) side chain are, in fact, viable processes. Thus, our initial misgivings concerning the viability of this type of transformation were unfounded. As implied previously, the success of the transformation of **63** into **64** is of importance for the possible application of this method to the synthesis of natural products.

(e) Preparation and thermolysis of compounds 68, 69, 73, and 74. Synthesis of bicyclo[3.2.1]octa-2,6-dienes functionalized at C-8

Conversion of the keto ester **26** into the enone **68** (see Chart 5) was effected by means of a selenenylation-selenoxide elimination method (28). Thus, reaction of the lithium enolate of **26** with phenylselenenyl chloride gave the α-phenylseleno ketones **66** (mixture of epimers). Oxidation of **66** with hydrogen peroxide provided the enone **68**, although the overall yield of this material from **26** was low (32%). Transformation of 6-*exo*-vinylbicyclo[3.1.0]hexan-2-one (24) into the corresponding enone **69** was accomplished more efficiently (88%) by use of a one-pot procedure (28, 29) in which the intermediate α-phenylseleno ketones **67** were not isolated.

It is evident from an examination of the structures of the enones **68** and **69** that these substances contain a *trans* divinylcyclopropane system in which one of the "vinyl" groups consists of the enone carbon–carbon double bond. Thus, although the functional group pattern in **68** and **69** is somewhat different from that present in the substrates (**31–35**, **50**, **63**) studied earlier, it might be expected that thermolysis of **68** and **69** would also lead to successful Cope rearrangement.

When a solution of compound **68** in xylene was refluxed for 18 h, the bicyclic keto ester **70** was obtained in 73% yield. Similarly, thermolysis (160°C, benzene, sealed tube, 4 h) of **69** provided bicyclo[3.2.1]octa-2,6-dien-8-one (**71**) in 68% yield. These interesting rearrangement reactions reveal that one solution to the problem of producing C-8 functionalized bicyclo[3.2.1]octadienes involves the preparation and thermolysis of 6-*exo*-(1-alkenyl)bicyclo[3.1.0]hex-3-en-2-ones (e.g. **68**, **69**). Presumably, suitable functional group manipulations of the C-8 carbonyl group in the resultant products (e.g. **70**, **71**) would produce substances with a variety of substituents on the 1-carbon bridge of the bicyclo[3.2.1]octadiene system.

Copper(I)-catalyzed conjugate addition of vinylmagnesium bromide to the enone **69** gave, in 80% yield, a single product[7]

[7]Treatment of the enone **68** with cuprate reagents gave complex mixtures of products.

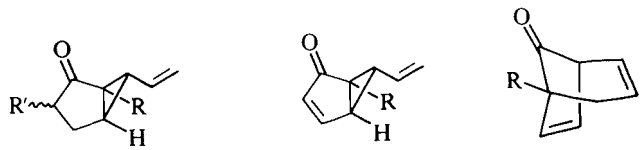

26 R = CO_2Me, R′ = H
66 R = CO_2Me, R′ = SePh
67 R = H, R′ = SePh

68 R = CO_2Me
69 R = H

70 R = CO_2Me
71 R = H

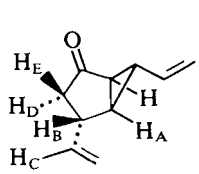

72

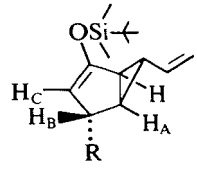

73 R = CH = CH_2
74 R = CH_2CO_2Et

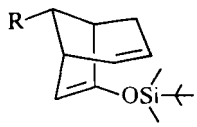

75 R = CH = CH_2
76 R = CH_2CO_2Et

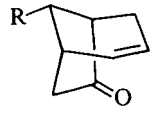

77 R = CH = CH_2
78 R = CH_2CO_2Et

CHART 5

that, on the basis of steric considerations (approach of the vinylcopper(I) reagent from the less hindered side of the enone), was expected to possess the stereochemistry depicted in **72**. This expectation was verified by the ^{1}H nmr spectrum of the reaction product. Molecular models show that the dihedral angles between H_A and H_B and between H_B and H_D (see **72**) are close to 90° and therefore J_{AB} and J_{BD} would be expected to be small. Indeed, in a decoupling experiment, irradiation at δ 3.02 (overlapped dd, $J = 8, 8$ Hz, H_B) led to no change in the signals at δ 1.87–1.94 (which included H_D) and 2.04 (H_A, overlapped dd, $J = 5, 4$ Hz), while the anticipated simplifications occurred at δ 2.36 (H_E, dd, $J_{DE} = 18.5$ Hz, $J_{BE} = 8$ Hz to d, $J_{DE} = 18.5$ Hz) and δ 5.84 (H_C, ddd, $J = 17.5, 10, 8$ Hz to dd, $J = 17.5, 10$ Hz).

Transformation of the ketone **72** into the enol silyl ether **73** was accomplished by means of standard reactions. Interestingly, in the ^{1}H nmr spectrum of **73**, the coupling constant J_{AB} was found to be ~2.5 Hz. Thus, in a decoupling experiment, irradiation at δ 4.31 (H_C, br s) caused the signal at δ 3.13 (H_B, br unresolved d) to sharpen to a dd, with coupling constants 7.5 and 2.5 Hz (J_{AB}).

In an attempt to prepare a 2-(*tert*-butyldimethylsiloxy)-6-*exo*-vinylbicyclo[3.1.0]hex-2-ene containing a functionalized C-4 *exo* substituent different from a vinyl group, the reaction of the enone **69** with 1-(*tert*-butyldimethylsiloxy)-1-ethoxyethene (30) in warm acetonitrile (31) was investigated. Although this process was quite sluggish, it produced cleanly, after a reaction time of 12 h, a 33% yield (>95% based on consumed **69**) of the enol silyl ether **74**. A decoupling experiment similar to that described above for compound **73** showed that, in the ^{1}H nmr spectrum of **74**, $J_{AB} = 2.5$ Hz. Therefore, it is evident that substances **73** and **74** possess the same relative stereochemistry.

It was pleasing to find that thermal rearrangement (200°C, benzene, sealed tube) of compounds **73** and **74** proceeded smoothly to produce, in each case, a single product (**75**, **76**, respectively) in high yield. Acid hydrolysis of **75** and **76** under mild conditions provided the corresponding bicyclic ketones **77**

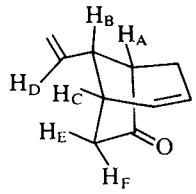

77

(97%) and **78** (94%), respectively. The expectation that the vinyl and carboethoxymethyl groups of **77** and **78**, respectively, would possess an *exo* orientation was corroborated by the ^{1}H nmr spectra of these substances. For example, in a decoupling experiment, irradiation of the signal due to H_D (δ 5.90) in the ^{1}H nmr spectrum of **77** caused the resonance at δ 2.91 (H_B) to sharpen to a broad s, ($w_{1/2}$ = 5 Hz). This experiment showed that H_B is only weakly coupled to the two bridgehead protons H_A and H_C. Furthermore, irradiation at δ 2.91 (H_B) changed the signal due to H_F (δ 2.22) from a dd (J_{EF} = 17.5 Hz, J_{BF} = 2 Hz) to a clean d (J_{EF} = 17.5 Hz). Thus, as expected, J_{CF} is very small (the dihedral angle between H_C and H_F is ~90°). However, there is long range coupling between H_B and H_F, indicating that these two protons, along with the two intermediate carbon–carbon single bonds, have a W-configuration (32). These spectral data show clearly that the vinyl group in **77** is in an *exo* orientation. In similar fashion, it was shown that the C-8 proton in the bicyclic ketone **78** couples only weakly to the two adjacent bridgehead protons. Therefore, the CH_2CO_2Et group in **78** also has an *exo* stereochemistry.

It is evident from the work summarized above that bicyclo[3.2.1]octa-2,6-dienes possessing a C-8 functional group (e.g. **70**, **71**) or containing a C-8 *exo* substituent (e.g. **75**, **76**) can be obtained readily by thermolysis of the requisite 6-*exo*-vinylbicyclo[3.1.0]hex-3-en-2-ones (e.g. **68**, **69**) or the C-4 *exo* substituted 6-*exo*-vinylbicyclo[3.1.0]hex-2-enes (e.g. **73**, **74**), respectively. These results demonstrate further the utility and versatility of the methods that formed the subject of the present study.

Experimental

General information

Melting points, boiling points, and air-bath temperatures (short-path Kugelrohr distillations) are uncorrected. Infrared (ir) spectra were recorded on a Perkin–Elmer model 710B spectrophotometer and were calibrated using the 1601 cm^{-1} band of polystyrene film. Proton nuclear magnetic resonance (^{1}H nmr) spectra were recorded on deuteriochloroform solutions using tetramethylsilane as the internal standard. In cases of compounds with *tert*-butyldimethylsilyl groups, the resonance positions were determined relative to the chloroform signal (δ 7.25). Microanalyses were carried out in the Microanalytical Laboratory, University of British Columbia. Analytical gas–liquid chromatography (glc) was performed with a Hewlett–Packard model 5832A gas chromatograph (columns: 6 ft × 0.125 in., 5% OV-17 on 80–100 mesh Chromosorb W(HP), 6 ft × 0.125 in., 5% OV-210 on 80–100 mesh on Chromosorb W(HP), or 10 ft × 0.125 in., 10% SE-30 on 80–100 mesh Chromosorb W(HP)) or with a Hewlett–Packard model 5880 gas chromatograph (column: 25 m × 0.21 mm fused silica column coated with cross-linked SE-54). Thin-layer chromatography (tlc) was accomplished with commercial aluminum-backed silica gel plates (E. Merck, Type 5539). Preparative tlc was carried out on 20 × 20 cm glass plates coated with 0.9 mm of silica gel (E. Merck, Silica Gel 60). Conventional column chromatography was performed using 70–230 mesh silica gel (E. Merck), while flash column chromatography was done using 230–400 mesh silica gel (E. Merck).

Note. All reactions requiring dry conditions were done using glassware that had been flame-dried under an argon flow. Unless otherwise stated, all reactions were done under an atmosphere of argon.

Note. In experiments producing volatile products, the extraction and (or) chromatography solvent(s) were removed from the desired product by careful (fractional) distillation at atmospheric pressure.

Note. All compounds for which exact masses (high resolution mass spectrometry) are reported gave clean ^{1}H nmr spectra and exhibited essentially one peak by glc and one spot by tlc analyses.

*Ethyl (*E*)-4-methyl-2-pentenoate (**5**)*

To a stirred solution of (carboethoxymethylene)triphenylphosphorane (40 g, 114.9 mmol) in dry dichloromethane (100 mL) was added dropwise 10.4 mL (114.9 mmol) of 2-methylpropanal, and the resultant mixture was refluxed for 4 h. Removal of most of the solvent by distillation (atmospheric pressure) left a white residue that was triturated with pentane. The mixture was filtered through a short column of silica gel and the column was washed with pentane. Removal of the solvent from the eluate and distillation (air-bath temperature 45–50°C/0.1 Torr; 1 Torr = 133.3 Pa) of the residual yellow oil gave 15.0 g (92%) of the ester **5**, which exhibited ir (film): 1715, 1648 cm^{-1}; ^{1}H nmr (80 MHz), δ: 1.06 (d, 6H, J = 7 Hz), 1.30 (t, 3H, J = 7 Hz), 2.46 (overlapped dd septet, 1H, J = 7, 1, 7 Hz), 4.20 (q, 2H, J = 7 Hz), 5.76 (dd, 1H, J = 16, 1 Hz), 6.95 (dd, 1H, J = 16, 7 Hz). *Exact Mass* calcd. for $C_8H_{14}O_2$: 142.0994; found: 142.0991.

*(*E*)-4-Methyl-2-penten-1-ol (**6**)*

To a cold (−78°C), stirred solution of the ester **5** (1.0 g, 7.04 mmol) in dry pentane (15 mL) was added dropwise a hexane solution of diisobutylaluminum hydride (17.6 mmol). The mixture was stirred at −78°C for 1 h and at 0°C for 1 h. Saturated aqueous ammonium chloride (1 mL) was added and the mixture was poured into 5% hydrochloric acid. The organic phase was washed with 5% hydrochloric acid, brine, and saturated aqueous sodium bicarbonate and then was dried ($MgSO_4$). Removal of the solvent (distillation at atmospheric pressure) gave the allylic alcohol **6** (0.668 g, 95%) as a colorless oil; ir (film): 3300, 1660 cm^{-1}; ^{1}H nmr (80 MHz), δ: 1.00 (d, 6H, J = 7 Hz), 1.47 (br s, 1H), 2.10–2.60 (m, 1H), 4.04–4.17 (m, 2H), 5.38–5.87 (m, 2H). *Exact Mass* calcd. for $C_6H_{12}O$: 100.0888; found: 100.0887.

*(*E*)-4-Methyl-2-pentenal (**7**)*

To a stirred solution of the alcohol **6** (200 mg, 2.0 mmol) in dry dichloromethane (10 mL) was added pyridinium chlorochromate (3.2 mmol) supported on alumina (15). The mixture was stirred at room temperature for 3 h and then was filtered through a short column of silica gel (70–230 mesh). The column was eluted with dry ether. Removal of the solvent from the eluate (distillation at atmospheric pressure) gave a brown oil. Subjection of this material to flash distillation (air-bath temperature ~30°C/0.1 Torr, receiver cooled to −78°C) afforded the aldehyde **7** (194 mg, 99%) as a colorless oil; ir (film): 1675, 1622 cm^{-1}; ^{1}H nmr (80 MHz), δ: 1.13 (d, 6H, J = 7 Hz), 2.37–2.85 (m, 1H), 6.10 (ddd, 1H, J = 16, 8, 1 Hz), 6.86 (dd, 1H, J = 16, 7 Hz), 9.55 (d, 1H, J = 8 Hz). *Exact Mass* calcd. for $C_6H_{10}O$: 98.0732; found: 98.0732.

*Ethyl (2*E*,4*E*)-6-methyl-2,4-heptadienoate (**8**)*

This compound was prepared by reaction of the aldehyde **7** (1.78 g, 18.1 mmol) with (carboethoxymethylene)triphenylphosphorane (6.32 g, 18.1 mmol) in refluxing (5 h) dichloromethane (19 mL) via a procedure very similar to that described above for the preparation of the ester **5**. Distillation (air-bath temperature 68–75°C/0.1 Torr) of the crude yellow oil produced 1.34 g (44%) of the diene ester **8**, which exhibited ir (film): 1700, 1635, 1612 cm^{-1}; ^{1}H nmr (400 MHz), δ: 1.05 (d, 6H, J = 7 Hz), 1.30 (t, 3H, J = 7 Hz), 2.43 (overlapped d septet, 1H, J = 6, 7 Hz), 4.22 (q, 2H, J = 7 Hz), 5.80 (d, 1H, J = 14 Hz), 6.09 (dd, 1H, J = 15, 6 Hz), 6.13 (dd, 1H, J = 15, 9 Hz), 7.26 (dd, 1H, J = 14, 9 Hz). *Exact Mass* calcd. for $C_{10}H_{16}O_2$: 168.1150; found: 168.1151.

*(2*E*,4*E*)-6-Methyl-2,4-heptadien-1-ol (**9**)*

Reduction of the ester **8** (386 mg, 2.3 mmol) with diisobutylaluminum hydride (5.0 mmol) in dry pentane (7 mL) (−78°C, 1 h; 0°C, 3 h) was carried out via a procedure very similar to that employed for the preparation of the alcohol **6** (*vide supra*). Distillation (air-bath

Can. J. Chem. Downloaded from www.nrcresearchpress.com by 80.58.250.72 on 09/07/12
For personal use only.

Can. J. Chem. Downloaded from www.nrcresearchpress.com by 80.58.250.72 on 09/07/12
For personal use only.

temperature 60–65°C/0.1 Torr) of the crude product afforded 280 mg (96%) of the alcohol **9**; ir (film): 3300, 1650 cm^{-1}; ^1H nmr (270 MHz), δ: 1.00 (d, 6H, J = 7 Hz), 1.57 (br s, 1H), 2.34 (overlapped d septet, 1H, J = 7, 7 Hz), 4.15 (d, 2H, J = 6 Hz), 5.68 (dd, 1H, J = 15, 7 Hz), 5.74 (dt, 1H, J = 15, 6 Hz), 6.02 (dd, 1H, J = 15, 10 Hz), 6.22 (dd, 1H, J = 15, 10 Hz). *Exact Mass* calcd. for $C_8H_{14}O$: 126.1045; found: 126.1043.

(2E,4E)-1-Bromo-6-methyl-2,4-heptadiene (15)

To a cold (0°C), stirred solution of the alcohol **9** (1.0 g, 7.93 mmol) and pyridine (32 μL, 0.4 mmol) in dry ether (2 mL) was added dropwise a solution of phosphorus tribromide (0.23 mL, 3.2 mmol) in ether (1 mL). The mixture was stirred at 0°C for 4 h and then was poured into ice-water. The organic phase was washed successively with brine, 5% aqueous sodium bicarbonate, and brine and then was dried ($MgSO_4$). Careful removal of the solvent under reduced pressure, followed by flash distillation (air-bath temperature ~30°C/0.1 Torr, receiver cooled to −78°C) of the residual oil, yielded 1.17 g (78%) of the diene bromide **15**. This material, a pale yellow oil, darkened on standing at room temperature. It was stored under argon at low temperatures and was distilled immediately prior to use. Compound **15** exhibited ir (film): 1643, 990 cm^{-1}; ^1H nmr (80 MHz), δ: 1.00 (d, 6H, J = 7 Hz), 2.10–2.60 (m, 1H), 4.04 (d, 2H, J = 8 Hz), 5.55–6.50 (m, 4H). *Exact Mass* calcd. for $C_8H_{13}{}^{79}Br$: 188.0200; found: 188.0200.

Ethyl (E)-2-methyl-2,4-pentadienoate (10)

To a stirred solution of (carboethoxyethylidene)triphenylphosphorane (40 g, 0.11 mmol) in dry dichloromethane (150 mL) was added dropwise propenal (6.2 g, 0.11 mol). An exothermic reaction ensued and the mixture was heated to maintain gentle reflux for an additional 2 h. Most of the solvent was removed under reduced pressure, the residue was diluted with pentane to precipitate triphenylphosphine oxide, and the mixture was filtered. The collected material was washed with pentane. Removal of the solvent from the combined filtrate, followed by flash distillation (air-bath temperature ~50°C/0.1 Torr, receiver cooled to −78°C) of the residual oil, provided the ester **10** (12.3 g, 80%) as a colorless liquid that exhibited ir (film): 1715, 1635, 1600 cm^{-1}; ^1H nmr (100 MHz), δ: 1.32 (t, 3H, J = 7 Hz), 1.97 (d, 3H, J = 2 Hz), 4.24 (q, 2H, J = 7 Hz), 5.46 (dd, 1H, J = 10, 2 Hz), 5.58 (dd, 1H, J = 17, 2 Hz), 6.68 (ddd, 1H, J = 17, 12, 10 Hz), 7.19 (dq, 1H, J = 12, 2 Hz). *Exact Mass* calcd. for $C_8H_{12}O_2$: 140.0837; found: 140.0841.

(E)-2-Methyl-2,4-pentadien-1-ol (11)

To a stirred solution–suspension of lithium aluminum hydride (2.55 g, 67 mmol) in 200 mL of dry ether at 0°C was added dropwise a solution of anhydrous ethanol (3.9 mL, 67 mmol). After the mixture had been stirred for 15 min, a solution of the ester **10** (12.3 g, 89 mmol) in 30 mL of dry ether was added and stirring was continued at 0°C for 1 h. Solid $Na_2SO_4 \cdot 10H_2O$ was added and stirring was maintained until a white granular precipitate formed. The mixture was filtered and the collected material was washed thoroughly with ether. Concentration of the combined filtrate and distillation (air-bath temperature ~60°C/0.1 Torr, receiving bath cooled to −78°C) gave 8.6 g (99%) of the alcohol **11**, a colorless liquid that exhibited ir (film): 3300, 1660, 1600 cm^{-1}; ^1H nmr (100 MHz), δ: 1.68 (s, 1H), 1.80 (s, 3H), 4.08 (s, 2H), 5.08–6.31 (m, 2H), 6.09 (br d, 1H, J = 10 Hz), 6.63 (ddd, 1H, J = 16, 10, 10 Hz). *Exact Mass* calcd. for $C_6H_{10}O$: 98.0731; found: 98.0730.

(E)-5-Bromo-4-methyl-1,3-pentadiene (16)

To a mixture of triphenylphosphine (23.6 g, 90 mmol) in 100 mL of dry acetonitrile at 0°C was added bromine (4.6 mL, 90 mmol) and the solution was stirred until triphenylphosphine dibromide precipitated as a flocculent white solid. To this suspension was added successively triethylamine (12.5 mL, 90 mmol) and a solution of the alcohol **11** (8.0 g, 81 mmol) in 15 mL of dry acetonitrile. The mixture was stirred at room temperature for 30 min and then was filtered. The collected material was washed thoroughly with petroleum ether and then filtered again. Removal of the solvent from the filtrate, followed by flash distillation (air-bath temperature ~40°C/0.1 Torr, receiver cooled to −78°C) of the residual oil gave 10 g (71%) of the bromide **16** as a pale yellow liquid; ir (film): 1645, 1600, 1210, 995, 920 cm^{-1}; ^1H nmr (80 MHz), δ: 1.92 (s, 3H), 4.05 (s, 2H), 5.15–5.43 (m, 2H), 6.13–6.68 (m, 2H). *Exact Mass* calcd. for $C_6H_9{}^{79}Br$: 159.9888; found: 159.9890.

Ethyl (2E,4E)-2-methyl-2,4-hexadienoate (12)

To a solution of (carboethoxyethylidene)triphenylphosphorane (10.86 g, 30 mmol) in 30 mL of dry dichloromethane was added dropwise 2.1 g (30 mmol) of freshly distilled (*E*)-2-butenal. The solution was refluxed for 20 h. Approximately 20 mL of solvent was removed under reduced pressure, the residual mixture was diluted with pentane, and the resultant mixture was filtered. The collected material was washed with pentane. Removal of the solvent from the combined filtrate and distillation (air-bath temperature 40°C/0.1 Torr, receiver cooled to −78°C) afforded 3.94 g (85%) of the ester **12**, which exhibited ir (film): 1710, 1640, 1615 cm^{-1}; ^1H nmr (100 MHz), δ: 1.31 (t, 3H, J = 8 Hz), 1.89 (d, 3H, J = 6 Hz), 1.94 (br s, 3H), 4.22 (q, 2H, J = 8 Hz), 6.10 (dq, 1H, J = 15, 6 Hz), 6.40 (dd, 1H, J = 15, 10 Hz), 7.21 (br d, 1H, J = 10 Hz). *Exact Mass* calcd. for $C_9H_{14}O_2$: 154.0994; found: 154.0992.

(2E,4E)-2-Methyl-2,4-hexadien-1-ol (13)

This alcohol was obtained by reduction of the ester **12** via a procedure very similar to that described for the preparation of **11** (see above). From 3.64 g (23.6 mmol) of the ester **12** there was obtained 2.6 g (98%) of the alcohol **13**; distillation temperature ~50°C/0.1 Torr (receiver cooled to −78°C); ir (film): 3325 cm^{-1}; ^1H nmr (80 MHz), δ: 1.58 (s, 1H), 1.80 (s, 3H), 1.83 (d, 3H, J = 7 Hz), 4.05 (s, 2H), 5.70 (dq, 1H, J = 15, 7 Hz), 6.00 (br d, 1H, J = 10 Hz), 6.30 (br dd, 1H, J = 15, 10 Hz). *Exact Mass* calcd. for $C_7H_{12}O$: 112.0888; found: 112.0892.

(2E,4E)-1-Bromo-2-methyl-2,4-hexadiene (17)

This substance was obtained from the alcohol **13** via a procedure similar to that outlined above for the preparation of the bromide **16**, except that the reaction time was 1 h rather than 30 min. Flash distillation (air-bath temperature 40–45°C/0.1 Torr, receiver cooled to −78°C) of the crude product provided 1.67 g (71%) of the bromide **17** as a pale yellow oil that darkened even when stored at −20°C in the dark. This material, which was routinely distilled immediately prior to being used, exhibited ir (film): 1650, 1610, 1445, 1215, 960 cm^{-1}; ^1H nmr (100 MHz), δ: 1.80 (d, 3H, J = 6 Hz), 1.87 (s, 3H), 4.05 (s, 2H), 5.70–6.42 (m, 3H). *Exact Mass* calcd. for $C_7H_{11}{}^{79}Br$: 174.0044; found: 174.0040.

Methyl (6E,8E)-10-methyl-3-oxo-6,8-undecadienoate (19)

To a cold (−78°C), stirred suspension of sodium hydride (0.15 g, 6.8 mmol) in dry THF (30 mL) was added a solution of methyl acetoacetate (0.719 g, 6.19 mmol) in dry THF (2 mL) and the mixture was stirred at 0°C for 10 min. A solution of *n*-butyllithium (6.81 mmol) was added and stirring was maintained at 0°C for an additional 15 min. A solution of the allylic bromide **15** (1.17 g, 6.19 mmol) in dry THF (3 mL) was added and the mixture was stirred at room temperature for 2 h. The mixture was diluted with ether and then was acidified with 5% hydrochloric acid. The layers were separated, the aqueous phase was washed with ether, and the combined organic extract was washed three times with brine and then dried ($MgSO_4$). Removal of the solvent and flash column chromatography (100 g of silica gel, elution with 5:1 petroleum ether – ethyl acetate) of the residual material afforded the β-keto ester **19** (0.743 g, 53%) as a colorless oil; ir (film): 1740, 1710, 1650, 1620, 993 cm^{-1}; ^1H nmr (400 MHz), δ: 1.00 (d, 6H, J = 7 Hz), 2.31 (overlapped d septet, 1H, J = 7, 7 Hz), 2.37 (overlapped dt, 2H, J = 7, 7 Hz), 2.65 (t, 2H, J = 7 Hz), 3.46 (s, 2H), 3.76 (s, 3H), 5.57 (overlapped dt, 1H, J = 14.5, 7 Hz), 5.61 (dd, 1H, J = 15, 7 Hz), 5.98 (dd, 1H, J = 15, 10 Hz), 6.06 (dd, 1H, J = 14.5, 10 Hz). *Exact Mass* calcd. for $C_{13}H_{20}O_3$: 224.1412; found: 224.1411.

Methyl (E)-3-oxo-6,8-nonadienoate (18)

To a solution of lithium diisopropylamide (LDA) (10.5 mmol) in 25 mL of dry THF at −5°C was added methyl acetoacetate (539 μL, 5.0 mmol), and the resulting yellow solution was stirred at 0°C for 20 min. The bromide **14** (735 mg, 5.0 mmol) was added and stirring

Can. J. Chem. Downloaded from www.nrcresearchpress.com by 80.58.250.72 on 09/07/12
For personal use only.

was continued at 0°C for 5 min. The reaction mixture was poured into a mixture of 1 *N* hydrochloric acid and ether. The layers were separated and the aqueous phase was extracted with ether. The combined organic extract was washed once with 1 *N* hydrochloric acid and three times with brine and then was dried ($MgSO_4$). Removal of the solvent, followed by distillation (air-bath temperature 81–85°C/0.1 Torr) of the residual oil, gave the desired product **18** (766 mg, 84%); ir (film): 1755, 1715, 1650, 1630, 1600 cm^{-1}; ^1H nmr (100 MHz), δ: 2.28–2.74 (m, 4H), 3.46 (s, 2H), 3.74 (s, 3H), 4.92–5.20 (m, 2H), 5.52–5.80 (m, 1H), 5.90–6.60 (m, 2H). *Exact Mass* calcd. for $C_{10}H_{14}O_3$: 182.0943; found: 182.0948.

*Methyl (*E*)-6-methyl-3-oxo-6,8-nonadienoate (**20**)*

This substance was prepared via a procedure very similar to that described above (preparation of **18**). From 712 μL (6.6 mmol) of methyl acetoacetate and 1.06 g (6.6 mmol) of the bromide **16** there was obtained a crude product that was subjected to flash column chromatography (silica gel, elution with 1:4 ether – petroleum ether). Distillation (air-bath temperature 88–92°C/0.1 Torr) of the oil thus obtained provided the keto ester **20** (920 mg, 71%); ir (film): 1750, 1720, 1655 cm^{-1}; ^1H nmr (100 MHz), δ: 1.78 (s, 3H), 2.34 (t, 2H, J = 8 Hz), 2.62–2.80 (m, 2H), 3.47 (s, 2H), 3.75 (s, 3H), 4.90–5.22 (m, 2H), 5.86 (br d, 1H, J = 10 Hz), 6.57 (overlapped ddd, 1H, J = 17, 10, 10 Hz). *Exact Mass* calcd. for $C_{11}H_{16}O_3$: 196.1099; found: 196.1102.

*Methyl (6*E*,8*E*)-6-methyl-3-oxo-6,8-decadienoate (**21**)*

This material was obtained from methyl acetoacetate (2.46 mL, 22.8 mmol) and the bromide **17** (4.0 g, 22.8 mmol) via a procedure very similar to that described for the preparation of **18** (see above). Purification of the crude product by flash column chromatography (silica gel, 3:1 pentane–ether) and distillation (air-bath temperature 103–108°C/0.1 Torr) afforded 2.87 g (60%) of the β-keto ester **21**; ir (film): 1750, 1720, 1650, 1630 cm^{-1}; ^1H nmr (80 MHz), δ: 1.73 (s, 3H), 1.76 (s, 3H), 2.20–2.80 (m, 4H), 3.48 (s, 2H), 3.75 (s, 3H), 5.58 (dq, 1H, J = 15, 6 Hz), 5.80 (d, 1H, J = 10 Hz), 6.25 (dd, 1H, J = 15, 10 Hz). *Exact Mass* calcd. for $C_{12}H_{18}O_3$: 210.1256; found: 210.1256.

*1-Carbomethoxy-6-*exo*-[(*E*)-3-methyl-1-butenyl]bicyclo[3.1.0]hexan-2-one (**27**)*

To a stirred solution of the β-keto ester **19** (200 mg, 0.89 mmol) and *p*-toluenesulfonyl azide (176 mg, 0.89 mmol) in dry acetonitrile (4 mL) was added triethylamine (0.89 mmol) and the mixture was stirred at room temperature for 24 h. Removal of the solvent under reduced pressure furnished a yellow residue, which was dissolved in a minimum amount of ether. Dilution of this solution with pentane precipitated *p*-toluenesulfonamide. The mixture was filtered through a layer of Celite. Removal of the solvent from the filtrate gave a yellow oil. The latter material was treated with pentane and the resultant mixture was refiltered to remove any residual insoluble material. Solvent removal (reduced pressure) provided 216 mg (97%) of the diazo compound **23** (ir (film): 2120, 1715, 1650 cm^{-1}), which showed a single spot on tlc analysis and was used without further purification.

To a stirred suspension of copper(II) acetylacetonate [$Cu(acac)_2$] (26 mg, 0.1 mmol) in dry, refluxing benzene (16 mL) was added dropwise a solution of the diazo keto ester **23** (180 mg, 0.72 mmol) in dry benzene (3 mL). The mixture was refluxed for 6 h, cooled to room temperature, and filtered through a layer of Celite. Removal of the solvent from the filtrate (reduced pressure) gave a dark yellow oil, which was subjected to preparative tlc (5:1 petroleum ether – ethyl acetate). Distillation (air-bath temperature 90–95°C/0.1 Torr) of the material thus obtained provided 125 mg (78%) of the desired compound **27**; ir (film): 1750, 1720 cm^{-1}; ^1H nmr (400 MHz), δ: 0.95, 0.96 (d, d, 3H each, J = 7 Hz), 2.00–2.34 (m, 6H), 2.67 (overlapped dd, 1H, J = 5.5, 5.5 Hz), 3.76 (s, 3H), 5.21 (ddd, 1H, J = 15.5, 8.5, 1 Hz), 5.71 (dd, 1H, J = 15.5, 7 Hz). *Exact Mass* calcd. for $C_{13}H_{18}O_3$: 222.1256; found: 222.1251.

*1-Carbomethoxy-6-*exo*-vinylbicyclo[3.1.0]hexan-2-one (**26**)*

Conversion of 3.03 g (16.6 mmol) of the β-keto ester **18** into 3.42 g (99%) of the corresponding diazo compound **22** (ir (film): 2125, 1720, 1655 cm^{-1}) was carried out as described above (preparation of **27**). Cyclization of **22** was accomplished as described above, except that the reaction medium was refluxing toluene instead of benzene, and the reaction time was 3 h. From 1.01 g (48.5 mmol) of **22** there was obtained, after purification of the crude product by flash column chromatography (4:1 petroleum ether – ethyl acetate) and distillation (air-bath temperature 100–110°C/0.1 Torr), 557 mg (64%) of the bicyclic keto ester **26**; ir (film): 1730 (br), 1635 cm^{-1}; ^1H nmr (100 MHz), δ: 2.0–2.4 (m, 5H), 2.64–2.77 (m, 1H), 3.78 (s, 3H), 5.12–5.86 (m, 3H). *Exact Mass* calcd. for $C_{10}H_{12}O_3$: 180.0787; found: 180.0787.

*1-Carbomethoxy-5-methyl-6-*exo*-vinylbicyclo[3.1.0]hexan-2-one (**28**)*

Treatment of 3.32 g (17 mmol) of the β-keto ester **20** with *p*-toluenesulfonyl azide (3.33 g, 17 mmol), as described above, provided 3.68 g (97%) of the diazo compound **24** (ir (film): 2125, 1720, 1665 cm^{-1}). Cyclization of the latter substance (3.68 g, 16.6 mmol) with $Cu(acac)_2$ in refluxing toluene (2 h) (see above), followed by purification of the crude product by flash column chromatography (4:1 petroleum ether – ethyl acetate) and distillation (air-bath temperature 83–88°C/0.1 Torr), afforded 1.84 g (57%) of the keto ester **28**. This material solidified on standing and exhibited mp 38–40°C; ir ($CHCl_3$): 1750, 1720, 1635 cm^{-1}; ^1H nmr (100 MHz), δ: 1.48 (s, 3H), 1.94–2.40 (m, 5H), 3.78 (s, 3H), 5.25 (dd, 1H, J = 10, 2 Hz), 5.32 (dd, 1H, J = 17, 2 Hz), 5.91 (overlapped ddd, 1H, J = 17, 10, 10 Hz). *Exact Mass* calcd. for $C_{11}H_{14}O_3$: 194.0943; found: 194.0949.

*1-Carbomethoxy-5-methyl-6-*exo*-[(*E*)-1-propenyl]bicyclo[3.1.0]-hexan-2-one (**29**)*

Conversion of the β-keto ester **21** (530 mg, 2.52 mmol) into the diazo compound **25** (595 mg, 100%; ir (film): 2125, 1720, 1655 cm^{-1}) was accomplished as described above (preparation of **27**). Copper-bronze (200 mg) catalyzed cyclization of **25** (595 mg) in refluxing toluene (25 mL, 2.5 h), followed by work-up as described above, gave a dark yellow oil. Purification of this material by preparative tlc (3:1 pentane–ether) and distillation (air-bath temperature 105–112°C/0.1 Torr) gave 259 mg (50%) of **29** as a colorless oil that solidified on standing. Recrystallization from pentane gave colorless crystals, mp 84–86°C; ir ($CHCl_3$): 1720 (br), 970 cm^{-1}; ^1H nmr (80 MHz), δ: 1.48 (s, 3H), 1.75 (d, 3H, J = 5 Hz), 1.9–2.6 (m, 5H), 3.79 (s, 3H), 5.3–6.1 (m, 2H). *Exact Mass* calcd. for $C_{12}H_{16}O_3$: 208.1100; found: 208.1105.

*1-Carbomethoxy-3-methyl-6-*exo*-vinylbicyclo[3.1.0]hexan-2-one (**30**)*

To a cold (−78°C), stirred solution of LDA (1.04 mmol) in 10 mL of dry THF was added a solution of the bicyclic keto ester **26** (156 mg, 0.87 mmol) in 2 mL of dry THF. The solution was stirred for 30 min. After addition of a mixture of iodomethane (108 μL, 1.74 mmol) and hexamethylphosphoramide (302 μL, 1.74 mmol), the reaction mixture was allowed to warm to room temperature and then was stirred for an additional 1 h. The solution was poured into brine and the resultant mixture was extracted thoroughly with pentane. The combined organic extract was washed with brine and dried ($MgSO_4$). Removal of the solvent, followed by distillation (air-bath temperature 110–115°C/0.1 Torr) of the residual yellow oil, gave 121 mg (72%) of compound **30**; ir (film): 1750, 1725, 1640 cm^{-1}; ^1H nmr (80 MHz), δ: 1.10 (d, 3H, J = 6 Hz), 1.68–2.60 (m, 5H), 3.80 (s, 3H), 5.08–5.85 (m, 3H). *Exact Mass* calcd. for $C_{11}H_{14}O_3$: 194.0943; found: 194.0946.

*2-(*tert*-Butyldimethylsiloxy)-1-carbomethoxy-6-*exo*-[(*E*)-3-methyl-1-butenyl]bicyclo[3.1.0]hex-2-ene (**32**)*

To a cold (−78°C), stirred solution of LDA (0.5 mmol) in dry THF (3 mL) was added a solution of the ketone **27** (100 mg, 0.45 mmol) in dry THF (1 mL) and the mixture was stirred for 30 min. After addition of a solution of freshly sublimed *tert*-butyldimethylsilyl chloride (98 mg, 0.65 mmol) and hexamethylphosphoramide (0.9 mmol) in dry THF (1 mL), the reaction mixture was stirred at −78°C for 30 min and at room temperature for 2 h. The solution was poured into saturated aqueous sodium bicarbonate and the layers were separated. The aqueous phase was extracted with ether. The combined extract was

Can. J. Chem. Downloaded from www.nrcresearchpress.com by 80.58.250.72 on 09/07/12
For personal use only.

washed three times with brine and dried ($MgSO_4$). Removal of the solvent under reduced pressure gave a yellow oil that, upon purification by column chromatography on neutral alumina (80–100 mesh, petroleum ether) and distillation (air-bath temperature 149–152°C/0.1 Torr), afforded 131 mg (87%) of the enol silyl ether **32**; ir (film): 1720, 1620 cm^{-1}; ^1H nmr (400 MHz), δ: 0.16 (s, 6H), 0.95 (s, 9H), 0.97, 0.98 (d, d, 3H each, J = 7 Hz), 1.73 (dd, 1H, J = 9, 5 Hz), 2.11 (dd, 1H, J = 7, 5 Hz), 2.23 (dd, 1H, J = 16, 3 Hz), 2.24–2.34 (m, 1H), 2.58 (ddd, 1H, J = 16, 7, 2 Hz), 3.69 (s, 3H), 4.38 (br s, 1H), 5.48 (dd, 1H, J = 15, 9 Hz), 5.59 (dd, 1H, J = 15, 6 Hz). *Exact Mass* calcd. for $C_{19}H_{32}O_3Si$: 366.2121; found: 366.2122.

*2-(*tert*-Butyldimethylsiloxy)-6-*exo*-vinylbicyclo[3.1.0]hex-2-ene (**50**)*

Conversion of 6-*exo*-vinylbicyclo[3.1.0]hexan-2-one (24) (122 mg, 1.0 mmol) into the enol silyl ether **50** (224 mg, 95%; distillation temperature 50–54°C/0.2 Torr) was carried out via a procedure identical with that described above (preparation of **32**). Compound **50** exhibited ir (film): 1627, 1250, 1210, 840 cm^{-1}; ^1H nmr (400 MHz), δ: 0.15 (s, 6H), 0.93 (s, 9H), 1.14 (overlapped ddd, 1H, J = 9, 2, 2 Hz), 1.57–1.63 (m, 1H), 1.67–1.72 (m, 1H), 2.29 (overlapped ddd, 1H, J = 17, 3, 3 Hz), 2.52 (ddd, 1H, J = 17, 8, 2 Hz), 4.30 (br s, 1H), 4.86 (dd, 1H, J = 10, 2 Hz), 5.01 (dd, 1H, J = 16, 2 Hz), 5.41 (ddd, 1H, J = 16, 10, 9 Hz). *Exact Mass* calcd. for $C_{14}H_{24}OSi$: 236.1596; found: 236.1592.

*2-(*tert*-Butyldimethylsiloxy)-1-carbomethoxy-6-*exo*-vinylbicyclo-[3.1.0]hex-2-ene (**31**)*

To a solution of LDA (1.87 mmol) in 20 mL of dry THF at −78°C was added a solution of the ketone **26** (300 mg, 1.7 mmol) in 2 mL of dry THF and the solution was stirred for 20 min. Solid, freshly sublimed *tert*-butyldimethylsilyl chloride (385 mg, 2.55 mmol) and dry hexamethylphosphoramide (3.4 mmol) were added successively and the reaction mixture was stirred at −78°C for 30 min and at room temperature for 1 h. The solvent was removed under reduced pressure and the residual material was triturated several times with pentane. The combined pentane solution was washed with a small amount of brine and then was passed through a short column of Florisil (elution with 2:1 pentane–ether). Removal of the solvent from the eluate, followed by distillation (air-bath temperature 115–120°C/0.1 Torr) of the residual oil, gave 476 mg (97%) of the desired product **31**; ir (film): 1720, 860, 840, 780 cm^{-1}; ^1H nmr (100 MHz), δ: 0.08 (s, 6H), 0.88 (s, 9H), 1.72 (dd, 1H, J = 10, 6 Hz), 2.05–2.26 (m, 2H), 2.55 (ddd, 1H, J = 17, 6.5, 2.5 Hz), 3.64 (s, 3H), 4.33 (dd, J = 4.5, 2.5 Hz), 4.99 (dd, 1H, J = 10, 2.5 Hz), 5.12 (dd, J = 17, 2.5 Hz), 5.88 (overlapped ddd, 1H, J = 17, 10, 10 Hz). *Exact Mass* calcd. for $C_{16}H_{26}O_3Si$: 294.1652; found: 294.1657.

*2-(*tert*-Butyldimethylsiloxy)-1-carbomethoxy-5-methyl-6-*exo*-vinylbicyclo[3.1.0]hex-2-ene (**33**)*

Conversion of the ketone **28** (594 mg, 3.06 mmol) into the silyl enol ether **33** (888 mg, 94%; distillation temperature 94–98°C/0.1 Torr) was accomplished via a procedure very similar to that described above (preparation of **31**). Compound **33** exhibited ir (film): 1730, 1640, 840, 790 cm^{-1}; ^1H nmr (80 MHz), δ: 0.15 (s, 6H), 0.89 (s, 9H), 1.33 (s, 3H), 1.81 (d, 1H, J = 10 Hz), 2.43 (d, 2H, J = 2.5 Hz), 3.72 (s, 3H), 4.43 (t, 1H, J = 2.5 Hz), 5.13 (dd, 1H, J = 10, 2.5 Hz), 5.23 (dd, 1H, J = 17, 2.5 Hz), 6.25 (overlapped ddd, 1H, J = 17, 10, 10 Hz). *Exact Mass* calcd. for $C_{17}H_{28}O_3Si$: 308.1808; found: 308.1826.

*2-(*tert*-Butyldimethylsiloxy)-1-carbomethoxy-5-methyl-6-*exo*-[(*E*)-1-propenyl]bicyclo[3.1.0]hex-2-ene (**34**)*

This substance was prepared from the ketone **29** by the procedure described above (preparation of **31**). From 500 mg (2.4 mmol) of **29** there was obtained 717 mg (93%) of **34**; ir (film): 1730, 1640, 845 cm^{-1}; ^1H nmr (80 MHz), δ: 0.08 (s, 6H), 0.84 (s, 9H), 1.23 (s, 3H), 1.5–1.8 (m, 1H), 1.68 (d, 3H, J = 5 Hz), 2.33 (d, 2H, J = 2 Hz), 3.63 (s, 3H), 4.33 (t, 1H, J = 2 Hz), 5.40–5.97 (m, 2H). *Exact Mass* calcd. for $C_{18}H_{30}O_3Si$: 322.1964; found: 322.1985.

*2-(*tert*-Butyldimethylsiloxy)-1-carbomethoxy-3-methyl-6-*exo*-vinylbicyclo[3.1.0]hex-2-ene (**35**)*

Conversion of the ketone **30** (98 mg, 0.51 mmol) into the enol silyl ether **35** (102 mg, 65%; distillation temperature 105–110°C/0.1 Torr) was accomplished as described above (preparation of **31**). Compound **35** exhibited ir (film): 1725, 1675, 1635, 845, 785 cm^{-1}; ^1H nmr (100 MHz), δ: 0.04–0.07 (s, s, 3H each), 0.92 (s, 9H), 1.47 (br s, 3H), 1.4–2.8 (m, 4H), 3.66 (s, 3H), 4.90–6.05 (m, 3H). *Exact Mass* calcd. for $C_{17}H_{28}O_3Si$: 308.1808; found: 308.1802.

*6-(*tert*-Butyldimethylsiloxy)-7-carbomethoxy-4-*endo*-isopropylbicyclo[3.2.1]octa-2,6-diene (**37**)*

A solution of the enol silyl ether **32** (123 mg; 0.37 mmol) in dry benzene (2.5 mL) was placed in a pyrolysis tube[8] and was then degassed. The tube was cooled with liquid nitrogen, sealed under vacuum (0.1 Torr), and then was heated (200°C, 2 h) in a steel container (packed with sand). The tube was cooled to room temperature and unsealed. Removal of the solvent and distillation (air-bath temperature 131–136°C/0.1 Torr) of the remaining oil afforded 117 mg (95%) of the desired product **37**; ir (film): 1700, 1610, 1215, 850 cm^{-1}; ^1H nmr (400 MHz), δ: 0.19, 0.21 (s, s, 3H each), 0.91, 1.00 (d, d, 3H each, J = 7 Hz), 0.97 (s, 9H), 1.64 (d septet, 1H, J = 8.5, 7 Hz), 1.78 (d, 1H, J = 9.5 Hz), 2.06 (overlapped dddd, 1H, J = 8.5, 5, 2.5, 2.5 Hz), 2.20 (overlapped dddd, 1H, J = 9.5, 5, 4, 1 Hz), 2.73 (overlapped dd, 1H, J = 5, 4 Hz), 2.92 (overlapped dd, 1H, J = 6, 5 Hz), 3.66 (s, 3H), 5.44 (br d, J = 9.5 Hz), 6.30 (overlapped dddd, 1H, J = 9.5, 6, 2.5, 1 Hz). *Exact Mass* calcd. for $C_{19}H_{32}O_3Si$: 336.2121; found: 336.2128.

*6-(*tert*-Butyldimethylsiloxy)bicyclo[3.2.1]octa-2,6-diene (**51**)*

Thermolysis (200°C, 2 h) of compound **50** (112 mg, 0.47 mmol) was carried out via a procedure identical with that described above (preparation of **37**) except that no solvent was used. Distillation (air-bath temperature 79–82°C/0.1 Torr) of the thermolysate furnished 109 mg (97%) of the bicyclic diene **51** as a colorless oil; ir (film): 1615, 1245, 880 cm^{-1}; ^1H nmr (400 MHz), δ: 0.14, 0.16 (s, s, 3H each), 0.93 (s, 9H), 1.77 (d, 1H, J = 9.5 Hz), 2.06–2.23 (m, 3H), 2.46–2.54 (m, 2H), 5.11 (d, 1H, J = 2.5 Hz), 5.27–5.32 (m, 1H), 6.16–6.22 (m, 1H). *Exact Mass* calcd. for $C_{14}H_{24}OSi$: 236.1596; found: 236.1595.

*6-(*tert*-Butyldimethylsiloxy)-7-carbomethoxybicyclo[3.2.1]octa-2,6-diene (**36**)*

A solution of the silyl enol ether **31** (300 mg, 1.02 mmol) in 20 mL of dry, degassed xylene was heated to reflux for 2.5 h. The solution was cooled to room temperature and the solvent was removed under reduced pressure. The remaining oil was dissolved in pentane and the solution was passed through a short column of Florisil. The column was eluted with 5:1 pentane–ether. Removal of the solvent from the eluate provided 296 mg (99%) of compound **36**; ir (film): 1710, 1615, 840, 790 cm^{-1}; ^1H nmr (100 MHz), δ: 0.16 (s, 6H), 0.91 (s, 9H), 1.5–1.75 (m, 1H), 1.9–2.3 (m, 3H), 2.5–2.7 (m, 1H), 2.89 (br t, 1H, J = 5 Hz), 3.62 (s, 3H), 5.27 (m, 1H), 6.27 (m, 1H). *Exact Mass* calcd. for $C_{15}H_{23}O_3Si$ (M − CH_3): 279.1417; found: 279.1424.

*6-(*tert*-Butyldimethylsiloxy)-7-carbomethoxy-1-methylbicyclo[3.2.1]-octa-2,6-diene (**38**)*

Thermal rearrangement of **33** (440 mg, 1.43 mmol) in 50 mL of dry, refluxing xylene (6 h), followed by work-up as described above and distillation (air-bath temperature 100–105°C/0.1 Torr) of the oil thus obtained, afforded 410 mg (93%) of the product **38**; ir (film): 1700, 1600, 850, 790 cm^{-1}; ^1H nmr (80 MHz), δ: 0.21 (s, 6H), 0.98 (s, 9H), 1.30 (s, 3H), 1.55–2.80 (m, 5H), 3.69 (s, 3H), 5.29 (ddt, 1H, J = 10, 4, 2 Hz), 6.13 (br d, 1H, J = 10 Hz). *Exact Mass* calcd. for $C_{17}H_{28}O_3Si$: 308.1808; found: 308.1801.

*6-(*tert*-Butyldimethylsiloxy)-7-carbomethoxy-1,4(*endo*)-dimethylbicyclo[3.2.1]octa-2,6-diene (**39**)*

Thermolysis (4 h) of the enol silyl ether **34** (715 mg, 2.22 mmol) in

[8]The pyrolysis tubes (2-mm wall thickness) used in this study were treated as follows: (*a*) washed with detergent and water; (*b*) soaked (15 min) in 1% aqueous KOH; (*c*) washed with dry methanol and then with dry toluene; (*d*) soaked (15 min) in a 5% solution of *N*,*N*-bis(trimethylsilyl)acetamide in dry toluene; (*e*) rinsed with dry methanol, oven-dried, cooled, and stored in a desiccator.

Can. J. Chem. Downloaded from www.nrcresearchpress.com by 80.58.250.72 on 09/07/12
For personal use only.

75 mL of dry, refluxing mesitylene, followed by work-up as described above (preparation of **36**), furnished 700 mg (98%) of the bicyclic diene **39**; ir (film): 1700, 1600, 840, 785 cm^{-1}; ^1H nmr (100 MHz), δ: 0.11, 0.14 (s, s, 3H each), 0.88 (s, 9H), 0.92 (d, 3H, J = 6 Hz), 1.20 (s, 3H), 1.50–2.58 (m, 4H), 3.60 (s, 3H), 5.07 (ddd, 1H, J = 10, 3, 2 Hz), 6.01 (br d, 1H, J = 10 Hz). *Exact Mass* calcd. for $C_{17}H_{27}O_3Si$ ($M - CH_3$): 307.1729; found: 307.1713.

*6-(*tert*-Butyldimethylsiloxy)-7-carbomethoxy-5-methylbicyclo[3.2.1]-octa-2,6-diene (40)*

A solution of 79 mg (0.26 mmol) of compound **35** in 10 mL of dry mesitylene was refluxed for 1 h. Work-up as described previously (preparation of **36**) gave 77 mg (97%) of the diene **40**; ir (film): 1700, 1600, 840, 790 cm^{-1}; ^1H nmr (100 MHz), δ: 0.06, 0.24 (s, s, 3H each), 0.88 (s, 9H), 1.07 (s, 3H), 1.5–2.8 (m, 4H), 2.88 (br t, 1H, J = 5 Hz), 3.60 (s, 3H), 5.33 (dt, 1H, J = 10, 3 Hz), 6.26 (m, 1H). *Exact Mass* calcd. for $C_{16}H_{25}O_3Si$ ($M - CH_3$): 293.1573; found: 293.1555.

*4-*endo*-Isopropylbicyclo[3.2.1]oct-2-en-6-one (47)*

To a stirred solution of the silyl enol ether **37** (150 mg, 0.45 mmol) in dry THF (5 mL) was added a THF solution of tetra-*n*-butylammonium fluoride (1.34 mmol) and the resulting mixture was stirred at room temperature for 1 h. The mixture was diluted with 1:1 ether – petroleum ether and then was poured into saturated aqueous ammonium chloride. The aqueous layer was extracted with ether and the combined extract was washed with brine and dried ($MgSO_4$). Removal of the solvent gave 100 mg of the β-keto ester **42** (mixture of epimers) as a pale yellow oil. A solution of this material in THF (7 mL) was treated with 5% hydrochloric acid (11 mL), the mixture was refluxed for 23 h, cooled to 0°C, and poured into saturated aqueous sodium bicarbonate. The aqueous phase was extracted with ether and the combined extract was washed with brine and dried ($MgSO_4$). Removal of the solvent and purification of the residual oil by flash column chromatography (18 g silica gel, 1:12 ether – petroleum ether) gave 37 mg (50%) of the bicyclic ketone **47**; ir (film): 1730 cm^{-1}; ^1H nmr (400 MHz), δ: 0.95, 1.06 (d, d, 3H each, J = 7 Hz), 1.43 (d septet, 1H, J = 10, 7 Hz), 2.00 (dd, 1H, J = 11.5, 3 Hz), 2.09 (dddd, 1H, J = 11.5, 5.5, 4, 1.5 Hz), 2.12 (overlapped dddd, 1H, J = 10, 5, 2.5, 2.5 Hz), 2.22 (dd, 1H, J = 17.5, 3 Hz), 2.28 (dd, 1H, J = 17.5, 5.5 Hz), 2.69–2.77 (m, 2H), 5.63 (ddd, 1H, J = 10, 2.5, 1.5 Hz), 6.05 (dddd, 1H, J = 10, 6, 2.5, 1.5 Hz). *Exact Mass* calcd. for $C_{11}H_{16}O$: 164.1201; found: 164.1197.

Bicyclo[3.2.1]oct-2-en-6-one (46)

(a) From the enol silyl ether 36

To a cold (0°C) solution of the enol silyl ether **36** (111 mg, 0.38 mmol) in 7 mL of spectrograde methanol was added 66 mg (1.14 mmol) of anhydrous potassium fluoride and stirring was continued for 1 h at 0°C. Most of the solvent was removed (reduced pressure), the residue was treated with saturated aqueous ammonium chloride, and the resultant mixture was extracted with petroleum ether. The combined extract was washed with 1 *N* hydrochloric acid and twice with brine, and dried (Na_2SO_4). Removal of the solvent and distillation (air-bath temperature 85–88°C/0.1 Torr) of the residual oil gave 56 mg (82%) of the β-keto ester **41**, the ^1H nmr spectrum of which showed that this material consisted of a mixture of epimers (ratio ≈ 3:1). This material was dissolved in a mixture of THF (2 mL) and 1 *N* hydrochloric acid (5 mL) and the solution was refluxed for 4 h. The reaction mixture was poured into brine and the resultant mixture was extracted with pentane. The combined extract was washed with brine and dried ($MgSO_4$). Removal of the solvent, followed by distillation (air-bath temperature 40–45°C/0.1 Torr, receiver cooled to −78°C) of the remaining oil, gave 33 mg (88%) of the bicyclic ketone **46**; ir (film): 1730, 1640, 735 cm^{-1}; ^1H nmr (400 MHz), δ: 2.03 (d, 1H, J = 11 Hz), 2.08 (overlapped ddd, 1H, J = 11, 4.5, 4.5 Hz), 2.20 (br d, 1H, J = 18 Hz), 2.29 (dd, 1H, J = 17.5, 5 Hz), 2.34 (overlapped ddd, 1H, J = 17.5, 3, 1.5 Hz), 2.43 (overlapped dddd, 1H, J = 18, 5, 2.5, 2.5 Hz), 2.57–2.62 (m, 1H), 2.73–2.80 (m, 1H), 5.47 (overlapped ddd, 1H, J = 9.5, 3, 3 Hz), 6.01–6.09 (m, 1H). *Exact Mass* calcd. for $C_8H_{10}O$: 122.0732; found: 122.0732.

(b) From the enol silyl ether 51

A mixture of compound **51** (179 mg, 0.76 mmol), 5% hydrochloric acid (3 mL), and THF (3 mL) was stirred at room temperature for 6 h. The mixture was diluted with ether and poured slowly into saturated aqueous sodium bicarbonate. The layers were separated, the aqueous phase was extracted twice with ether, and the combined extract was washed with brine and dried. Removal of the solvent and distillation of the remaining oil gave 81 mg (88%) of the ketone **46**.

*1,4(*endo*)-Dimethylbicyclo[3.2.1]oct-2-en-6-one (48)*

The conversion of the enol silyl ether **39** into the β-keto ester **44** was accomplished via a procedure identical with that described above for the transformation of **36** into **41**. From 652 mg (2.0 mmol) of **39** there was obtained 347 mg (83%) of **44** (distillation temperature 92–96°C/0.1 Torr), which, on the basis of its ^1H nmr spectrum, consisted of a mixture of epimers in a ratio of about 1:1.

A solution of this material in methanol (20 mL) and 2 *N* aqueous potassium hydroxide (10 mL) was refluxed for 5 h. The solution was poured into aqueous ammonium chloride and the mixture was extracted thoroughly with 1:1 ether–pentane. The combined extract was washed with brine and dried ($MgSO_4$). Removal of the solvent and distillation (air-bath temperature 40–50°C/0.1 Torr, receiver cooled to −78°C) of the residual oil afforded 122 mg (50%) of the bicyclic ketone **48**; ir (film): 1730, 745, 700 cm^{-1}; ^1H nmr (100 MHz), δ: 1.01 (d, 3H, J = 7 Hz), 1.24 (s, 3H), 1.92–1.98 (m, 2H), 2.10–2.25 (m, 2H), 2.37–2.82 (diffuse m, 2H), 5.39 (overlapped ddd, 1H, J = 10, 2, 2 Hz), 5.77 (dd, 1H, J = 10, 2 Hz). *Exact Mass* calcd. for $C_{10}H_{14}O$: 150.1045; found: 150.1044.

6-Methyl-1-hepten-4-yn-3-ol (56)

To a cold (−78°C), stirred solution of 3-methyl-1-butyne (1.5 mL, 14.7 mmol) in dry THF (25 mL) was added a hexane solution of *n*-butyllithium (16.1 mmol). The mixture was stirred at −30°C for 1 h and then a solution of propenal (1.08 mL, 16.1 mmol) in 5 mL of dry THF was added dropwise. After the reaction mixture had been allowed to warm to room temperature over a period of 1 h, it was diluted with ether and then was poured into saturated aqueous ammonium chloride. The organic phase was separated, washed (saturated aqueous sodium bicarbonate, brine), and dried ($MgSO_4$). Removal of the solvent, followed by distillation (air-bath temperature 65–68°C/0.1 Torr) of the residual oil, gave 1.57 g (86%) of the alcohol **56** as a colorless oil that exhibited ir (film): 3350 (br), 3050, 2215, 1630, 992, 930 cm^{-1}; ^1H nmr (80 MHz), δ: 1.18 (d, 6H, J = 7 Hz), 1.95 (br s, 1H, exchanges with D_2O), 2.62 (septet, 1H, J = 7 Hz), 4.87 (br s, 1H $w_{1/2}$ = 6 Hz), 5.20 (overlapped ddd, 1H, J = 10, 1.5, 1.5 Hz), 5.43 (overlapped ddd, 1H, J = 17, 1.5, 1.5 Hz), 6.00 (ddd, 1H, J = 17, 10, 5 Hz). *Exact Mass* calcd. for $C_8H_{12}O$: 124.0888; found: 124.0881.

*Ethyl (*E*)-8-methyl-4-nonen-6-ynoate (57)*

A stirred mixture of the alcohol **56** (1.82 g, 14.7 mmol), propanoic acid (0.066 mL, 0.88 mmol), and triethyl orthoacetate (13.4 mL) was heated at 130–135°C for 40.5 h. Most of the triethyl orthoacetate was removed by fractional distillation of the mixture at atmospheric pressure and the residual oil was subjected to flash chromatography (125 g of silica gel, 1:9 ether – petroleum ether). Distillation (air-bath temperature 91–104°C/0.1 Torr) of the oil obtained from the appropriate fractions provided 1.88 g (66%) of the ester **57** as an odoriferous, colorless oil that exhibited ir (film): 3000, 2190, 1730, 960 cm^{-1}; ^1H nmr (400 MHz), δ: 1.17 (d, 6H, J = 7 Hz), 1.25 (t, 3H, J = 7 Hz), 2.35–2.44 (m, 4H), 2.64 (septet, 1H, J = 7 Hz), 4.12 (q, 2H, J = 7 Hz), 5.49 (br d, 1H, J = 15.5 Hz), 5.95–6.04 (m, 1H). *Exact Mass* calcd. for $C_{12}H_{18}O_2$: 194.1307; found: 194.1316.

*(*E*)-8-Methyl-4-nonen-6-ynoic acid (58)*

A stirred mixture of methanol (20 mL), water (0.5 mL), potassium hydroxide (0.4 g, 7.1 mmol), and the ester **57** (1.15 g, 5.94 mmol) was refluxed for 3.5 h. The cooled solution was washed with petroleum ether and then was acidified (at 0°C) with 10% hydrochloric acid. The resulting mixture was extracted with ether and the combined extract was washed with brine and dried ($MgSO_4$). Removal of the solvent and distillation (air-bath temperature 139–143°C/0.1 Torr) of the residual material gave 0.77 g (78%) of the acid **58** as a colorless oil that solidified on standing. Recrystallization from heptane provided an analytical sample that exhibited mp 65.5–67.5°C; ir ($CHCl_3$): 3200–

Can. J. Chem. Downloaded from www.nrcresearchpress.com by 80.58.250.72 on 09/07/12
For personal use only.

2500, 1701, 960 cm^{-1}; ^1H nmr (80 MHz), δ: 1.17 (d, 3H, J = 7 Hz), 2.32–2.52 (m, 4H), 2.65 (septet, 1H, J = 7 Hz), 5.53 (br d, 1H, J = 15.5 Hz), 5.85–6.30 (m, 1H). *Anal.* calcd. for $C_{10}H_{14}O_2$: C 72.25, H 8.49; found: C 72.09, H 8.40. *Exact Mass* calcd.: 166.0994; found: 166.0988.

*6-exo-(3-Methyl-1-butynyl)bicyclo[3.1.0]hexan-2-one (**61**)*

A stirred solution of the acid **58** (0.648 g, 3.9 mmol) and oxalyl chloride (1.02 mL, 11.7 mmol) in dry hexane (17 mL) was refluxed for 1 h. Removal of solvent and excess oxalyl chloride under reduced pressure, followed by distillation (air-bath temperature 70–75°C/0.1 Torr) of the residual oil, gave 0.60 g (83%) of the acid chloride **59** as a pungent, colorless oil. This material, which exhibited ir (film): 3000, 2190, 1790, 960 cm^{-1}, was dissolved in dry ether (4 mL) and the resultant solution was added, dropwise, to a cold (0°C), stirred solution of diazomethane (0.81 g, 19.3 mmol) in dry ether (30 mL). The solution was stirred at 0°C for 30 min and then was warmed to room temperature over a period of 1 h. Excess diazomethane was removed by passing argon, via a flame-polished pipette, through the solution for 30 min. Removal of the solvent afforded 0.60 g (97%) of the diazoketone **60**, a viscous yellow oil (ir (film): 3070, 2085, 1634, 960 cm^{-1}) that was used immediately for the next reaction.

To a stirred, refluxing suspension of copper(II) acetylacetonate (0.064 g) in dry benzene (16 mL) was added a solution of the diazoketone **60** (0.60 g) in 8 mL of dry benzene. The mixture was refluxed for 1 h and then was cooled to room temperature. Careful removal of the solvent under reduced pressure gave an oil that was subjected to flash chromatography (70 g of silica gel, 1:5 ether – petroleum ether). Distillation (air-bath temperature 74–80°C/0.1 Torr) of the oil thus obtained yielded 0.40 g (63% from the acid **58**) of the bicyclic ketone **61** as a colorless oil. This material exhibited ir (film): 3030, 1725, 1180, 882 cm^{-1}; ^1H nmr (400 MHz), δ: 1.12 (d, 6H, J = 6.5 Hz), 1.70–1.75 (m, 1H), 1.94–2.18 (m, 5H), 2.24 (dd, 1H, J = 10.5, 4.5 Hz), 2.49 (d septet, 1H, J = 6.5, 1.5 Hz). *Exact Mass* calcd. for $C_{11}H_{14}O$: 162.1045; found: 162.1044.

*6-exo-[(Z)-3-Methyl-1-butenyl]bicyclo[3.1.0]hexan-2-one (**62**)*

To a stirred, prehydrogenated suspension of Lindlar's catalyst (5% Pd on $CaCO_3$, 10 mg) in dry pentane (15 mL) containing 4 μL of quinoline was added a solution of the keto alkyne **61** (0.20 g, 1.23 mmol) in pentane (2 mL) and the mixture was stirred under hydrogen (1 atmosphere (101.3 kPa)) at room temperature. Reaction progress was monitored by glc, which indicated the absence of starting material after 2.5 h. The reaction mixture was filtered through Celite. Removal of the solvent from the filtrate gave a pale yellow oil that was shown (glc) to consist of the desired product **62** (>95%), along with a small amount of corresponding *trans* isomer. Subjection of this mixture to column chromatography (20 g of silica gel impregnated with 5 g of silver nitrate, 1:12 ether – petroleum ether), followed by distillation (air-bath temperature 75–80°C/0.1 Torr) of the oil thus obtained, furnished 190 mg (94%) of the keto alkene **62** as a colorless oil. This material exhibited ir (film): 3000, 1722 cm^{-1}; ^1H nmr (400 MHz), δ: 0.99, 1.01 (d, d, 3H each, J = 6.5, 6.5 Hz), 1.75 (dd, 1H, J = 5, 2.5 Hz), 2.00–2.21 (m, 6H), 2.70 (dd, septet, 1H, J = 9, 1, 6.5 Hz), 4.65 (overlapped ddd, 1H, J = 10.5, 9.5, 1 Hz), 5.24 (overlapped ddd, 1H, J = 10.5, 9.0, <1 Hz). *Exact Mass* calcd. for $C_{11}H_{16}O$: 164.1201; found: 164.1203.

*2-(tert-Butyldimethylsiloxy)-6-exo-[(Z)-3-methyl-1-butenyl]bicyclo-[3.1.0]hex-2-ene (**63**)*

Conversion of the ketone **62** (160 mg, 0.98 mmol) into the enol silyl ether **63** (266 mg, 98%; distillation temperature 110–115°C/0.1 Torr) was carried out via a procedure identical with that described previously for the preparation of **32**. Compound **63**, a colorless oil, exhibited ir (film): 3030, 1625, 1255, 960, 787 cm^{-1}; ^1H nmr (400 MHz), δ: 0.17, 0.18 (s, s, 3H each), 0.94 (s, 9H), 0.99 (d, 6H, J = 6.5 Hz), 1.28 (br d, 1H, J = 10 Hz), 1.50–1.55 (m, 1H), 1.59–1.64 (m, 1H), 2.30 (overlapped ddd, 1H, J = 16.5, 3, 3 Hz), 2.52 (ddd, 1H, J = 16.5, 7, 2 Hz), 2.73 (dd septet, 1H, J = 9.5, <1, 6.5 Hz), 4.31 (br s, 1H, $w_{1/2}$ = 5.5 Hz), 4.64 (overlapped dd, 1H, J = 10.5, 10 Hz), 5.14 (overlapped dd, 1H, J = 10.5, 9.5 Hz). *Exact Mass* calcd. for $C_{17}H_{30}OSi$: 278.2066; found: 278.2073.

*6-(tert-Butyldimethylsiloxy)-4-exo-isopropylbicyclo[3.2.1]octa-2,6-diene (**64**)*

Thermal rearrangement (240°C, 4.5 h) of compound **63** (100 mg, 0.36 mmol) in dry benzene (2.5 mL) was carried out via a procedure similar to that described previously for the thermolysis of **32** (preparation of **37**). Distillation (air-bath temperature 89–93°C/0.1 Torr) of the crude product afforded 93 mg (93%) of the bicyclic diene **64** as a colorless oil that exhibited ir (film): 3050, 3010, 1620, 841, 785 cm^{-1}; ^1H nmr (400 MHz), δ: 0.13, 0.15 (s, s, 3H each), 0.92 (s, 9H), 0.96, 0.99 (d, d, 3H each, J = 7, 7 Hz), 1.68 (d septet, 1H, J = 7, 7 Hz), 1.75 (d, 1H, J = 9.5 Hz), 1.88–1.94 (m, 1H), 1.97 (overlapped dddd, 1H, J = 9.5, 5, 3, 1 Hz), 2.38 (br d, 1H, J = 5 Hz), 2.52–2.57 (m, 1H), 5.11 (d, 1H, J = 3 Hz), 5.33 (overlapped ddd, 1H, J = 9.5, 3, 2 Hz), 6.21 (overlapped dddd, 1H, J = 9.5, 6, 2, 1 Hz). *Exact Mass* calcd. for $C_{17}H_{30}OSi$: 278.2066; found: 278.2067.

*4-exo-Isopropylbicyclo[3.2.1]oct-2-en-6-one (**65**)*

A mixture of the enol silyl ether **64** (158 mg, 0.57 mmol), 5% hydrochloric acid (14 mL), and THF (6 mL) was stirred at room temperature for 3 h. The reaction mixture was cooled, diluted with ether, and then was poured into saturated aqueous sodium bicarbonate. The layers were separated and the aqueous phase was extracted thoroughly with ether. The combined ether extract was dried ($MgSO_4$) and concentrated to afford a pale yellow oil that was subjected to flash chromatography on silica gel (18 g; 1:9 ether – petroleum ether). Distillation (air-bath temperature 98–101°C/0.1 Torr) of the oil thus obtained gave 53 mg (57%) of the ketone **65** as a colorless oil; ir (film): 3013, 1735, 741 cm^{-1}; ^1H nmr (400 MHz), δ: 0.97, 0.98, (d, d, 3H each, J = 6.5, 6.5 Hz), 1.68 (d septet, 1H, J = 8, 6.5 Hz), 1.85–1.93 (m, 2H), 2.06 (br d, 1H, J = 11.5 Hz), 2.23 (dd, 1H, J = 16.5, 5 Hz), 2.28 (overlapped ddd, 1H, J = 16.5, 2.5, 1.5 Hz), 2.59 (br d, 1H, J = 5.5 Hz), 2.73–2.79 (m, 1H), 5.55 (ddd, 1H, J = 9.5, 3.5, 1.5 Hz), 6.07 (overlapped dddd, 1H, J = 9.5, 6.5, 2, 1.5 Hz). *Exact Mass* calcd. for $C_{11}H_{16}O$: 164.1201; found: 164.1205.

*1-Carbomethoxy-6-exo-vinylbicyclo[3.1.0]hex-3-en-2-one (**68**)*

To a cold (−78°C), stirred solution of LDA (1.2 mmol) in 10 mL of dry THF was added a solution of the keto ester **26** (180 mg, 1 mmol) in 2 mL of dry THF, and the solution was stirred at −78°C for 30 min. A solution of phenylselenenyl chloride (230 mg, 1.2 mmol) and hexamethylphosphoramide (348 μL, 2.0 mmol) in 2 mL of dry THF was added, stirring was continued for 5 min, and the cold reaction mixture was poured into a mixture of 1 *N* hydrochloric acid and pentane–ether (1:1). The layers were separated and the aqueous phase was extracted with 1:1 pentane–ether. The combined organic extract was washed (saturated aqueous sodium bicarbonate), dried (Na_2SO_4), and concentrated. The remaining yellow oil was purified by preparative tlc (silica gel, chloroform) to afford 230 mg (69%) of the α-phenylseleno ketones **66** as a viscous yellow oil (ir (film): 1720, 745 cm^{-1}).

To a cold (0°C), stirred solution of the α-phenylseleno ketones **66** (428 mg, 1.28 mmol) in 25 mL of dichloromethane was added a solution of 30% hydrogen peroxide (0.35 mL) in 2 mL of water and the resulting two-phase system was stirred vigorously at room temperature for 30 min. The layers were separated and the aqueous phase was extracted with dichloromethane. The combined organic extract was washed twice with brine, dried ($MgSO_4$), and concentrated. Distillation (air-bath temperature 98–102°C/0.1 Torr) of the remaining yellow oil afforded 106 mg (47%) of the enone **68**, a colorless oil that exhibited ir (film): 1740, 1705, 1575 cm^{-1}; ^1H nmr (100 MHz), δ: 2.51 (dd, 1H, J = 10, 4 Hz), 3.12 (dd, 1H, J = 4, 3 Hz), 3.83 (s, 3H), 5.22 (dd, 1H, J = 10, 2 Hz), 5.32 (dd, 1H, J = 18, 2 Hz), 5.81 (d, 1H, J = 6 Hz), 5.86 (overlapped ddd, 1H, J = 18, 10, 10 Hz), 7.66 (dd, 1H, J = 6, 3 Hz). *Exact Mass* calcd. for $C_{10}H_{10}O_3$: 178.0629; found: 178.0629.

*6-exo-Vinylbicyclo[3.1.0]hex-3-en-2-one (**69**)*

To a cold (−78°C), stirred solution of LDA (4.9 mmol) in 10 mL of dry THF was added a solution of 6-*exo*-vinylbicyclo[3.1.0]hexan-2-one (500 mg, 4.1 mmol) in 7 mL of dry THF, and the resultant solution was stirred at −78°C for 30 min. A solution of phenylselenenyl chloride (940 mg, 4.9 mmol) in 6 mL of dry THF was added dropwise (syringe). After the mixture had been stirred at 0°C for 30 min, a

Can. J. Chem. Downloaded from www.nrcresearchpress.com by 80.58.250.72 on 09/07/12
For personal use only.

solution of acetic acid (0.47 mL, 8.2 mmol) in water (0.5 mL) was added. Subsequently, 30% hydrogen peroxide (2.3 g, 20.5 mmol) was added dropwise and the mixture was stirred at 0°C for 1 h. The mixture was diluted with 1:1 ether – petroleum ether and then was poured into saturated aqueous sodium bicarbonate. The layers were separated, the aqueous phase was extracted with ether, and the combined organic extract was washed with brine and dried ($MgSO_4$). Removal of the solvent, followed by distillation (air-bath temperature 78–83°C/0.1 Torr) of the remaining oil, provided 430 mg (88%) of the enone **69** as a colorless oil; ir (film): 3070, 3050, 1690, 1640 cm^{-1}; ^1H nmr (400 MHz), δ: 2.17 (overlapped ddd, 1H, J = 9, 2.5, 2.5 Hz), 2.27–2.32 (m, 1H), 2.59 (overlapped ddd, 1H, J = 4, 3, 2.5 Hz), 5.06 (dd, 1H, J = 10, 1 Hz), 5.20 (dd, 1H, J = 17, 1 Hz), 5.45 (ddd, 1H, J = 17, 10, 9 Hz), 5.70 (d, 1H, J = 5.5 Hz), 7.64 (ddd, 1H, J = 5.5, 2.5, 1 Hz). *Exact Mass* calcd. for C_8H_8O: 120.0575; found: 120.0574.

*1-Carbomethoxybicyclo[3.2.1]octa-2,6-dien-8-one (**70**)*

A stirred solution of the enone **68** (15 mg, 0.08 mmol) in 5 mL of dry xylene was refluxed for 18 h. The solution was cooled and the solvent was removed under reduced pressure. Bulb-to-bulb distillation (air-bath temperature 76–80°C/0.1 Torr) of the residual oil afforded 11 mg (73%) of the bicyclic ketone **70**, a colorless oil that exhibited ir (film): 1770, 1730 cm^{-1}; ^1H nmr (100 MHz), δ: 2.35–3.05 (m, 2H), 2.9–3.0 (m, 1H), 3.82 (s, 3H), 5.58 (br dt, 1H, J = 10, 3 Hz), 6.28 (dd, 1H, J = 7, 3 Hz), 6.30 (m, 1H), 6.70 (d, 1H, J = 7 Hz). *Exact Mass* calcd. for $C_{10}H_{10}O_3$: 178.0629; found: 178.0629.

*Bicyclo[3.2.1]octa-2,6-dien-8-one (**71**)*

Thermolysis (160°C, 4 h) of the enone **69** (40 mg, 0.33 mmol) in dry benzene (3 mL) was accomplished via a procedure similar to that employed for the thermolysis of **32** (*vide supra*, preparation of **37**). Distillation (air-bath temperature 47–51°C/0.1 Torr) of the crude product gave 27 mg (68%) of the ketone **71** as a colorless oil that exhibited ir (film): 3050, 1755, 1622, 680 cm^{-1}; ^1H nmr (400 MHz), δ: 2.45–2.53 (m, 1H), 2.73–2.82 (m, 3H), 5.46–5.53 (m, 1H), 6.04 (overlapped dddd, 1H, J = 9, 7, 3, 2 Hz), 6.21 (dd, 1H, J = 7, 3 Hz), 6.69 (dd, 1H, J = 7, 3 Hz). *Exact Mass* calcd. for C_8H_8O: 120.0575; found: 120.0563.

*4-exo-6-exo-Divinylbicyclo[3.1.0]hexan-2-one (**72**)*

To a cold (−30°C), stirred solution of vinylmagnesium bromide (1.4 mmol) in 3 mL of dry THF was added copper(I) bromide – dimethyl sulfide complex (3.0 mg, 0.013 mmol) and the mixture was stirred at −30°C for 10 min. A solution of the enone **69** (95 mg, 0.79 mmol) in dry THF (3 mL) was added dropwise over a period of 10 min. After the reaction mixture had been allowed to warm to 0°C over a period of 40 min, it was diluted with ether and then poured into saturated aqueous ammonium chloride. The aqueous phase was extracted with ether and the combined organic extract was washed (once with saturated aqueous sodium bicarbonate, twice with brine), dried ($MgSO_4$), and concentrated. Distillation (air-bath temperature 80–85°C/0.1 Torr) of the residual oil furnished 93 mg (80%) of the ketone **72** as a colorless oil that exhibited ir (film): 3050, 1718, 1635, 990, 915 cm^{-1}; ^1H nmr (400 MHz), δ: 1.87–1.94 (m, 2H), 1.97 (overlapped ddd, 1H, J = 8.5, 4, 4 Hz), 2.04 (overlapped dd, 1H, J = 5, 4 Hz), 2.36 (dd, 1H, J = 18.5, 8 Hz), 3.02 (overlapped dd, 1H, J = 8, 8 Hz), 5.01 (dd, 1H, J = 10.5, 1 Hz), 5.04 (overlapped ddd, 1H, J = 10, 1, 1 Hz), 5.12 (overlapped ddd, 1H, J = 17.5, 1, 1 Hz), 5.15 (ddd, 1H, J = 17, 1, <1 Hz), 5.36 (ddd, 1H, J = 17, 10.5, 8.5 Hz), 5.84 (ddd, 1H, J = 17.5, 10, 8 Hz). *Exact Mass* calcd. for $C_{10}H_{12}O$: 148.0888; found: 148.0886.

*2-(tert-Butyldimethylsiloxy)-4-exo-6-exo-divinylbicyclo[3.1.0]hex-2-ene (**73**)*

Conversion of the ketone **72** (140 mg, 0.94 mmol) into the enol silyl ether **73** (240 mg, 97%; distillation temperature 130–135°C/0.1 Torr) was accomplished via a procedure identical with that employed for the transformation of **27** into **32** (*vide supra*). Compound **73**, a colorless oil, exhibited ir (film): 3060, 3015, 1618 cm^{-1}; ^1H nmr (400 MHz), δ: 0.18 (s, 6H), 0.95 (s, 9H), 1.23 (overlapped ddd, 1H, J = 8.5, 3.5, 2.5 Hz), 1.51 (ddd, 1H, J = 6.5, 3.5, 1.5 Hz), 1.75 (overlapped ddd, 1H, J = 6.5, 2.5, 2.5 Hz), 3.13 (br d, 1H, J = 7.5 Hz), 4.31 (br s, 1H, $w_{1/2}$ = 5 Hz), 4.88 (dd, 1H, J = 10.5, 1.5 Hz), 4.94 (ddd, 1H, J = 10, 2, 1 Hz), 5.03 (dd, 1H, J = 17, 1.5 Hz), 5.05 (ddd, 1H, J = 17, 2, 1 Hz), 5.41 (ddd, 1H, J = 17, 10.5, 8.5 Hz), 5.75 (ddd, 1H, J = 17, 10, 7.5 Hz). *Exact Mass* calcd. for $C_{16}H_{26}OSi$: 262.1753; found: 262.1759.

*2-(tert-Butyldimethylsiloxy)-4-exo-carboethoxymethyl-6-exo-vinylbicyclo[3.1.0]hex-2-ene (**74**)*

A stirred mixture of the enone **69** (157 mg, 1.3 mmol), 1-*tert*-butyldimethylsiloxy-1-ethoxyethene (397 mg, 1.96 mmol), and dry acetonitrile (3 mL) was heated at 55°C for 12 h. The solvent was removed and the residual oil was distilled. The colorless oil (140 mg, 33%) with distillation temperature 103–106°C/0.1 Torr proved to be the enol silyl ether **74**, which exhibited ir (film): 3050, 1730, 1620, 1255, 787 cm^{-1}; ^1H nmr (400 MHz), δ: 0.16 (s, 6H), 0.94 (s, 9H), 1.21 (overlapped ddd, 1H, J = 9, 3.5, 2.5 Hz), 1.26 (t, 3H, J = 7.5 Hz), 1.49 (overlapped ddd, 1H, J = 6.5, 3.5, 1.5 Hz), 1.73 (overlapped ddd, 1H, J = 6.5, 2.5, 2.5 Hz), 2.29 (dd, 1H, J = 15, 8 Hz), 2.34 (dd, 1H, J = 15, 7 Hz), 2.88–2.94 (m, 1H), 4.14 (q, 2H, J = 7 Hz), 4.35 (br s, 1H, $w_{1/2}$ = 5 Hz), 4.87 (dd, 1H, J = 10, 1.5 Hz), 5.20 (dd, 1H, J = 17, 1.5 Hz), 5.40 (ddd, 1H, J = 17, 10, 9 Hz). *Exact Mass* calcd. for $C_{18}H_{30}O_3Si$: 322.1964; found: 322.1957.

*6-(tert-Butyldimethylsiloxy)-8-exo-vinylbicyclo[3.2.1]octa-2,6-diene (**75**)*

Thermolysis (200°C, 5 h) of the divinylcyclopropane **73** (118 mg, 0.45 mmol) in dry benzene (2.5 mL) was carried out via a procedure similar to that used for the conversion of **32** into **37** (*vide supra*). Distillation (air-bath temperature 80–85°C/0.1 Torr) of the crude product gave 105 mg (89%) of the bicyclic compound **75**, a colorless oil that exhibited ir (film): 3050, 3010, 1624, 1245, 790 cm^{-1}; ^1H nmr (400 MHz), δ: 0.14, 0.15 (s, s, 3H each), 0.92 (s, 9H), 2.14–2.28 (m, 2H), 2.31–2.35 (m, 1H), 2.38 (dd, 1H, J = 6, 2.5 Hz), 2.65 (d, 1H, J = 7.5 Hz), 4.95–5.01 (m, 2H), 5.08 (ddd, 1H, J = 17.5, 2, 1 Hz), 5.33 (br d, 1H, J = 9.5 Hz), 6.03 (ddd, 1H, J = 17.5, 10, 7.5 Hz), 6.25 (dddd, 1H, J = 9.5, 6, 2, 2 Hz). *Exact Mass* calcd. for $C_{16}H_{26}OSi$: 262.1753; found: 262.1752.

*6-(tert-Butyldimethylsiloxy)-8-exo-(carboethoxymethyl)bicyclo-[3.2.1]octa-2,6-diene (**76**)*

Thermolysis (200°C, 2.5 h) of compound **74** (68 mg, 0.21 mmol) in dry benzene (3 mL) was accomplished via a procedure similar to that employed for the rearrangement of **32** to **37** (*vide supra*). Distillation (air-bath temperature 131–135°C/0.1 Torr) of the crude product afforded 65 mg (95%) of compound **76** as a colorless oil; ir (film): 3050, 3010, 1725, 1620, 790 cm^{-1}; ^1H nmr (400 MHz), δ: 0.14, 0.16 (s, s, 3H each), 0.92 (s, 9H), 1.26 (t, 3H, J = 7 Hz), 2.15 (br dd, 1H, J = 5.5, 2.5 Hz), 2.43–2.52 (m, 3H), 4.13 (q, 2H, J = 7 Hz), 4.97 (d, 1H, J = 2.5 Hz), 5.28–5.33 (br d, 1H, J = 10 Hz), 6.20–6.26 (m, 1H). *Exact Mass* calcd. for $C_{18}H_{30}O_3Si$: 322.1964; found: 322.1963.

*8-exo-Vinylbicyclo[3.2.1]oct-2-en-6-one (**77**)*

A mixture of the enol silyl ether **75** (96 mg, 0.37 mmol), 5% hydrochloric acid (9 mL), and THF (5 mL) was stirred at room temperature for 5.5 h, was diluted with 1:1 ether – petroleum ether, and then was poured slowly into saturated aqueous sodium bicarbonate. The layers were separated and the aqueous phase was extracted with ether. The combined organic extract was washed with brine, dried ($MgSO_4$), and concentrated. Distillation of the residual oil provided 50 mg (93%) of the ketone **77** as a colorless oil that exhibited ir (film): 3052, 3010, 1730, 1630, 998, 920, 730 cm^{-1}; ^1H nmr (400 MHz), δ: 2.20 (dd, 1H, J = 17.5, 2 Hz), 2.30 (overlapped dddd, 1H, J = 18, 3.5, 2, 2 Hz), 2.43 (dd, 1H, J = 17.5, 6 Hz), 2.52 (overlapped dddd, 1H, J = 18, 5.5, 2, 2 Hz), 2.59–2.63 (m, 1H), 2.66 (overlapped dd, 1H, J = 6.5, 6 Hz), 2.91 (br d, 1H, J = 5.5, 2 Hz), 5.08 (overlapped ddd, 1H, J = 17.5, 1.5, 1 Hz), 5.14 (overlapped ddd, 1H, J = 10.5, 1.5, 1.5 Hz), 5.53 (overlapped ddd, 1H, J = 9.5, 3.5, 2 Hz), 5.90 (ddd, 1H, J = 17.5, 10.5, 5.5 Hz), 6.14 (dddd, 1H, J = 9.5, 6.5, 2, 2 Hz). *Exact Mass* calcd. for $C_{10}H_{12}O$: 148.0888; found: 148.0887.

*8-exo-(Carboethoxymethyl)bicyclo[3.2.1]oct-2-en-6-one (**78**)*

Hydrolysis of the enol silyl ether **76** (54 mg, 0.168 mmol) with 5%

hydrochloric acid (2 mL) in THF (2 mL) was carried out via a procedure very similar to that described above (**75** → **77**). The keto ester **78** (33 mg, 94%), a colorless oil, exhibited ir (film): 3000, 1740, 1730, 1625 cm^{-1}; ^1H nmr (400 MHz), δ: 1.27 (t, 3H, J = 7 Hz), 2.22–2.45 (m, 6H), 2.54 (overlapped dddd, 1H, J = 18, 5.5, 2.5, 2 Hz), 2.60 (overlapped ddd, 1H, J = 7, 6, 1 Hz), 2.70 (overlapped dd, 1H, J = 8, 7.5 Hz), 4.15 (q, 2H, J = 7 Hz), 5.51 (overlapped ddd, 1H, J = 9.5, 3.5, 2.5 Hz), 6.11 (overlapped dddd, 1H, J = 9.5, 7, 2, 2 Hz). *Exact Mass* calcd. for $C_{12}H_{16}O_3$: 208.1099; found: 208.1096.

Acknowledgements

We are grateful to the Natural Sciences and Engineering Research Council of Canada for financial support and for Postgraduate Scholarships (to G.L.J. and E.H.R.).

1. C. Cupas, W. E. Watts, and P. von R. Schleyer. Tetrahedron Lett. 2503 (1964).
2. J. M. Brown. Chem. Commun. 226 (1965).
3. S. J. Rhoads and N. R. Raulins. Org. React. **22**, 1 (1975).
4. E. M. Mil'vitskaya, A. V. Tarakanova, and A. V. Plate. Russ. Chem. Rev. **45**, 469 (1976).
5. J. J. Gajewski. Hydrocarbon thermal isomerizations. Academic Press, Inc., New York, NY. 1981; (*a*) pp. 215–216; (*b*) pp. 258–260.
6. J. E. Baldwin and K. E. Gilbert. J. Am. Chem. Soc. **98**, 8283 (1976).
7. J. M. Brown. Chem. Commun. 638 (1967).
8. G. W. Klumpp, J. W. F. K. Barnick, A. H. Veefkind, and F. Bickelhaupt. Recl. Trav. Chim. Pays-Bas, **88**, 766 (1969).
9. B. C. C. Cantello, J. M. Mellor, and G. Scholes, J. Chem. Soc. (C), 2915 (1971).
10. W. Adam, O. De Lucchi, and D. Scheutzow. J. Org. Chem. **46**, 4130 (1980).
11. G. W. Klumpp and M. Schakel. Tetrahedron Lett. **24**, 4595 (1983).
12. E. Piers and E. H. Ruediger. J. Org. Chem. **45**, 1725 (1980).
13. E. Piers, G. L. Jung, and N. Moss. Tetrahedron Lett. **25**, 3959 (1984).
14. C. Prevost, P. Miginiac, and L. Miginiac-Groizeleau. Bull. Soc. Chim. Fr. 2485 (1964).
15. Y.-S. Cheng, W.-L. Liu, and S.-H. Chen. Synthesis, 223 (1980).
16. R. B. Miller. Synth. Commun. **2**, 267 (1972).
17. R. S. Davidson, W. H. H. Gunther, S. M. Waddington-Feather, and B. Lythgoe. J. Chem. Soc. 4907 (1964).
18. L. Horner, H. Oediger, and H. Hoffmann. Liebigs Ann. Chem. **626**, 26 (1959).
19. S. N. Huckin and L. Weiler. J. Am. Chem. Soc. **96**, 1082 (1974).
20. M. Regitz. Angew. Chem. Int. Ed. Engl. **6**, 733 (1967).
21. S. D. Burke and P. A. Grieco. Org. React. **26**, 361 (1979).
22. T. Sasaki, S. Eguchi, and M. Ohno. J. Org. Chem. **37**, 466 (1972).
23. M. P. Schneider and A. Rau. J. Am. Chem. Soc. **101**, 4426 (1979).
24. T. Hudlicky, F. J. Koszyk, T. M. Kutchan, and J. P. Sheth. J. Org. Chem. **45**, 5020 (1980).
25. S. A. Monti and S.-S. Yuan. J. Org. Chem. **36**, 3350 (1971).
26. S. A. Monti and G. L. White. J. Org. Chem. **40**, 215 (1975).
27. W. S. Johnson, L. Werthemann, W. R. Bartlett, T. J. Brocksom, T. Li, D. J. Faulkner, and M. R. Peterson. J. Am. Chem. Soc. **92**, 741 (1970); K. A. Parker and R. W. Kosley, Jr. Tetrahedron Lett. 691 (1975).
28. H. J. Reich, J. M. Renga, and I. L. Reich. J. Am. Chem. Soc. **97**, 5434 (1975).
29. H. J. Reich, I. L. Reich, and J. M. Renga. J. Am. Chem. Soc. **95**, 5813 (1973).
30. M. W. Rathke and D. F. Sullivan. Synth. Commun. **3**, 67 (1973).
31. Y. Kita, J. Segawa, J. Haruta, T. Fujii, and Y. Tamura. Tetrahedron Lett. **21**, 3777 (1980); Y. Kita, J. Segawa, J. Haruta, H. Yasuda, and Y. Tamura. J. Chem. Soc. Perkin Trans. 1, 1099 (1982).
32. L. M. Jackman and S. Sternhell. Applications of nuclear magnetic resonance spectroscopy in organic chemistry. 2nd ed. Pergamon Press, New York, NY. 1969. pp. 334–335.

Can. J. Chem. Downloaded from www.nrcresearchpress.com by 80.58.250.72 on 09/07/12
For personal use only.

The He(I) photoelectron spectra of the propenoyl halides

DIETER KLAPSTEIN[1] AND ROBERT T. O'BRIEN
Department of Chemistry, St. Francis Xavier University, Antigonish, N.S., Canada B2G 1C0

Received September 5, 1986

DIETER KLAPSTEIN and ROBERT T. O'BRIEN. Can. J. Chem. **65**, 683 (1987).

The He(I) photoelectron spectra of propenal and the propenoyl halides, CH_2=CHCOX, X = H, F, Cl, Br, were measured and interpreted with the aid of semi-empirical MO calculations, comparison with results for structurally related species, and a sum-rule for the out-of-plane orbital energies. Information concerning the identities and relative energies of the higher occupied molecular orbitals of the neutral molecules could be deduced from the spectra.

DIETER KLAPSTEIN et ROBERT T. O'BRIEN. Can. J. Chem. **65**, 683 (1987).

On a mesuré les spectres photoélectroniques He(I) du proènal et des halogénures de propènoyles, CH_2=CHCOX dans lesquels X = H, F, Cl et Br, et on les interprète à l'aide de calculs d'OM semi-empiriques, de comparaisons avec des résultats obtenus avec des espèces qui leur sont apparentées par la structure et d'une règle des sommes pour les énergies des orbitales hors-plan. L'information relative aux identités et aux énergies relatives des orbitales moléculaires hautes occupées des molécules neutres peut être déduite des spectres.

[Traduit par la revue]

Introduction

Valence-shell photoelectron spectroscopy is a powerful tool for studying the electronic structure of molecules through the approximation of Koopmans' Theorem (1), which equates an MO eigenvalue with the experimentally observed (vertical) ionization energy, $IE_v(i) = -\epsilon(i)$. Each band in a spectrum corresponds to ionization from a specific MO, and the IE is directly related to the MO energy. This paper reports the He(I) photoelectron spectra of a series of α,β-unsaturated carbonyl compounds of the general structure:

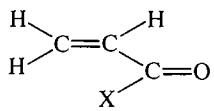

The specific members are propenal (acrolein), X = H, and the propenoyl halides, X = F, Cl, and Br. The spectra were interpreted by comparison with the spectra of structurally related molecules and by the use of semi-empirical molecular orbital calculations. The PE spectrum of propenal has been presented and interpreted elsewhere (2), but is included here to aid in the interpretation of the spectra of the propenoyl halides, reported here for the first time.

The primary goal of this study was to determine the identities and relative energies of some of the least-bound, occupied, MOs and their energy variation with the carbonyl substituent X. These MOs are expected to be the oxygen lone-pair, the ethenyl π-, and the carbonyl π-orbitals. Also, the degree of interaction between the out-of-plane π-orbitals, and the out-of-plane "lone-pair" orbital of the halogens, is of interest. We have previously studied similar trends and interactions in a similar series of ethynyl carbonyl compounds (3).

Experimental

The spectra were obtained with a photoelectron spectrometer incorporating a helium high voltage dc discharge lamp and a 127° cylindrical electron energy analyzer (32 mm mean radius) operated with a constant bandpass. The signals were gathered with a Nicolet 1170 Signal Averager and Apple IIe microcomputer data acquisition system. The working resolution of the full spectra scans was 30 meV, and was increased to 20 meV for scans of bands displaying fine structure. The ionization energy scale was calibrated with argon, nitrogen, and iodomethane. The band positions have an uncertainty of ±0.02 eV.

Commercial samples of propenal and propenoyl chloride (Aldrich) were used following vacuum distillation. Propenoyl fluoride was prepared by refluxing propenoyl chloride with potassium hydrogen fluoride, the acid fluoride being distilled off as it was formed, and purified by vacuum distillation. Propenoyl bromide was prepared by refluxing a mixture of propenoic (acrylic) acid and phosphorus tribromide, the acid bromide being distilled off as it was formed, and purified by vacuum distillation. The bromide was found to be quite sensitive to light. The purities of all samples were checked by gas-phase infrared and uv absorption spectroscopies, and for the bromide by ^{13}C nmr spectroscopy.

Semi-empirical molecular orbital calculations were carried out using CNDO/2 (4) and HAM/3 (5) programs adapted for use on a VAX 11/780 computer. The HAM/3 program was not parameterized for chlorine and neither program could handle bromine. The CNDO/2 eigenvalues have been divided by 1.35 to give better agreement with the observed IEs. The structural parameters used in the calculations were those assumed in the analyses of the microwave spectra (6).

Results and discussion

The molecules of this ethenyl carbonyl series may exist as rotational isomers by rotation about the ethenyl–carbonyl σ-bond. While propenal exists almost exclusively as the s-*trans* form in the gas-phase (at 25°C), the propenoyl halides exist as mixtures of two isomers, s-*trans* and s-*cis*. By studying the temperature-dependent ir (7, 8) and nmr (9) spectra, it has been concluded that the major form is s-*trans*. Of the two SCF-MO programs available to us, CNDO/2 and HAM/3, the latter predicts ionization energies in better agreement with experiment. The HAM/3 program was applied to propenoyl fluoride which has the highest percentage of s-*cis*, 40% at 25°C (7), to see how the individual ionization energies behaved in converting from one isomeric form to another. The energy differences were predicted to be quite small, on the PES energy scale, so that the analyses of the spectra were carried out using the dominant s-*trans* configuration for all species.

In the planar molecular geometry, the ethenyl carbonyls of this study have the symmetry classification C_s. As a consequence, the molecular orbitals may be described as a' (in-plane) or a'' (out-of-plane). The π-type orbitals associated with the ethenyl (π''_{CC}) and carbonyl (π''_{CO}) groups belong to the latter group. For the carbonyl halogen substituents there is another

[1]Author to whom correspondence should be addressed.

Can. J. Chem. Downloaded from www.nrcresearchpress.com by 78.46.186.204 on 09/07/12
For personal use only.

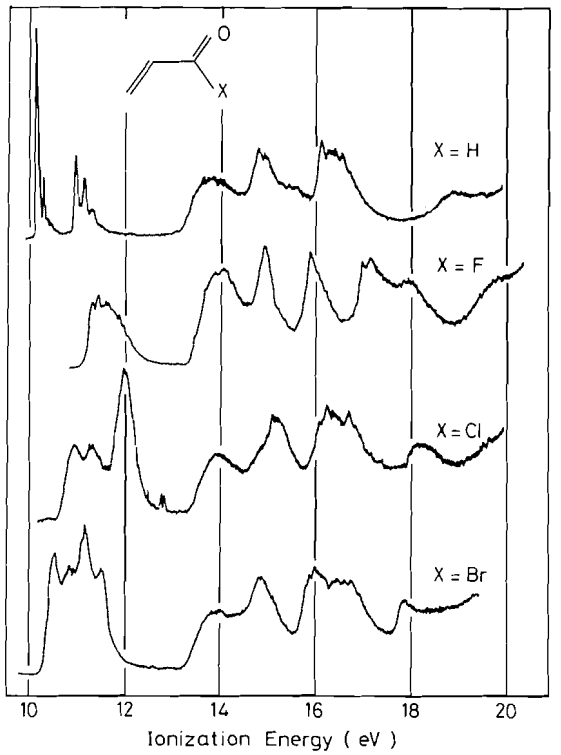

FIG. 1. The He(I) photoelectron spectra of propenal and propenoyl fluoride, chloride, and bromide.

TABLE 1. Results and assignments for propenal, CH_2=CHCHO

IE_v (eV)	Vibrational structure (cm^{-1})	Assignment	CNDO/2	HAM/3
10.11	1510, 320	$13a'$, n'_O	10.13	9.86
10.93	1460, 1200, 260	$2a''$, π''_{CC}	10.63	10.85
13.67		$12a'$, σ(C—H)	12.83	13.76
		$1a''$, π''_{CO}	15.36	13.89
14.73	1150	$11a'$, σ	13.06	14.76
15.4		$10a'$, σ	16.93	15.40
16.05		$9a'$, σ	17.70	15.83
18.75		$8a'$, σ	21.56	19.01

orbital of a'' symmetry: the out-of-plane "lone-pair" orbital of the halogen atom (n''_X).

Figure 1 shows the He(I) photoelectron spectra. The band ionization energies, vibrational structure, MO eigenvalues, and band assignments for each of the species are given in Tables 1 to 4. It can be seen from Fig. 1 that the higher IE region of the spectra contain many overlapping bands due to the accessible σ-type MOs. Although many of the σ-bonding MOs are delocalized over most of the structures, the MO calculations predict some to have appreciable densities in specific internuclear regions, as noted in the tables.

A very useful aid for identifying the PE bands arising from the out-of-plane orbitals of planar molecules is the sum-rule of Kimura (10). The completely localized orbital energies are obtained from the PE spectra of simple molecules (for example, an orbital energy of -14.38 eV for π''_{CO} from the spectrum of formaldehyde (11)). The sum of the orbital energies of the completely localized orbitals should remain constant even after interaction of the orbitals takes place. This method has been successfully applied to many types of planar species, where the

TABLE 2. Results and assignments for propenoyl fluoride, CH_2=CHCOF

IE_v (eV)	Vibrational structure (cm^{-1})	Assignment	CNDO/2	HAM/3
11.42[a]	1120	$3a''$, π''_{CC}	10.83	10.99
11.7		$16a'$, n'_O	11.13	11.10
14.03	1730	$2a''$, π''_{CO}	13.82	13.44
		$15a'$, σ	12.96	14.06
14.91		$14a'$, n'_F	15.41	14.90
15.84		$13a'$, σ	13.34	15.60
16.93	1300	$1a''$, n''_F	17.92	17.32
17.89		$12a'$, σ	16.82	16.32
			18.32	17.41

[a]Adiabatic IE = 11.09 eV.

TABLE 3. Results and assignments for propenoyl chloride, CH_2=CHCOCl

IE_v (eV)	Vibrational structure (cm^{-1})	Assignment	CNDO/2
10.90		$20a'$, n'_O	9.64
11.23		$3a''$, π''_{CC}	11.63
11.95		$19a'$, n'_{Cl}	10.56
		$2a''$, n''_{Cl}	10.53
13.90		$18a'$, σ(C—H)	12.52
14.85		$1a''$, π''_{CO}	16.52
15.11		$17a'$, σ	13.56
16.22	1270	$16a'$, σ(C—C=O)	16.79
16.67	1100	$15a'$, σ	16.85
18.12		$14a'$, σ(C—H)	19.21

TABLE 4. Results and assignments for propenoyl bromide, CH_2=CHCOBr

IE_v (eV)	Vibrational structure (cm^{-1})	Assignment
10.51		$29a'$, n'_O
10.85		$3a''$, π''_{CC}
11.16		$2a''$, n''_{Br}
11.49		$28a'$, n'_{Br}
13.80		$27a'$, σ(C—H)
14.5		$1a''$, π''_{CO}
14.83		$26a'$, σ
15.96		$25a'$, σ(C—C=O)
16.70	1100	$24a'$, σ
17.83		$23a'$, σ

out-of-plane orbitals form a small subset and are all usually accessible with He(I) radiation. It is particularly useful for identifying the higher IE out-of-plane orbital bands since they usually overlap with σ-type bands. Table 5 presents the calculated orbital energy sum, using the parameters given, and the sum taken from the band assignments and measured IEs of Tables 1 to 4. The agreement is satisfactory.

The following outlines of the band assignments focus on the low IE region where the bands due to ionization from the chemically interesting orbitals, n'_O (in-plane oxygen lone pair), n'_X, n''_X, π''_{CC}, and π''_{CO}, are expected. These band assignments are more conclusive because the bands are better resolved and

Can. J. Chem. Downloaded from www.nrcresearchpress.com by 78.46.186.204 on 09/07/12
For personal use only.

TABLE 5. Calculated and experimental sums for the out-of-plane orbital energies for CH_2=CHCOX

X	$\Sigma\epsilon(i)^a$ (eV)	$\Sigma(-IE_v(i)$ (eV)
H	−24.89	−24.60
F	−42.30	−42.05
Cl	−37.67	−38.43
Br	−36.71	−36.5

[a]Using the localized orbital energies (in eV): π''_{CC} = −10.51 from ethene (11), π''_{CO} = −14.38 from formaldehyde (11), n''_F = −17.41 eV from F_2 (21) and F (22), n''_{Cl} = −12.78 from HCl (17), and n''_{Br} = −11.82 from HBr (17).

comparisons with photoelectron bands arising from similarly localized orbitals in structurally related molecules are straightforward.

Propenal

The measured ionization energies, observed vibrational fine-structure, and band assignments for propenal are gathered in Table 1. The values agree with those of previous studies on this species (2), as do the band assignments, which are also consistent with the other members of this series.

Of importance to this study are the two sharp bands in the low IE region. The intensity of the adiabatic component of the transition between the neutral ground state and the cationic states imply that electrons have been removed from MOs which are weakly- or nonbonding in nature. The 10.11 eV band is assigned to the $(n'_O)^{-1}$ ionization process, and corresponds to the bands of acetaldehyde (12) and propynal (3) appearing at IEs of 10.24 and 10.70 eV, respectively. The relative inductive effects of the aldehyde substituents are ethynyl > ethenyl > methyl. The second band of the spectrum, IE_v = 10.93 eV, corresponds to ionization from the π''_{CC} MO ($2a''$). The π-orbital of ethene itself has an IE of 10.51 eV (11). Thus, the major effect on the energy of the π''_{CC} orbital on adding the carbonyl group is a stabilization due to the inductive effect of the carbonyl group. On the other hand, conjugation between π''_{CC} and π''_{CO}, with a higher IE, would result in a destabilization of π''_{CC} relative to its energy in ethene. The $(\pi''_{CO})^{-1}$ band is one of the two overlapping bands at 14.03 eV. The corresponding bands of formaldehyde (11) and propynal (3) appear at 14.38 and 14.37 eV, respectively.

Propenoyl fluoride

Figure 1 shows that the low IE region of the spectrum contains only one distinct band. This must be assigned to overlap of the n'_O and π''_{CC} bands. Closer examination of the region, Fig. 2, shows what appears to be a fairly sharp band, adiabatic IE = 11.09 eV and vertical IE = 11.42 eV, with vibrational intervals of about 1120 cm^{-1}, overlapping with a broader band estimated to lie at 11.7 eV. Both MO calculations predict π''_{CC} to have a lower ionization energy than n'_O. Consideration of the energy shifts of the n'_O band of acetyl fluoride compared to acetaldehyde, +1.56 eV (12), and of propynoyl fluoride compared to propynal, +1.11 eV (3), leads to the prediction of the corresponding band of propenoyl fluoride to lie in the region 11.2–11.7 eV. The 11.42 and 11.7 eV bands (Fig. 2) are thus assigned as $(\pi''_{CC})^{-1}$ and $(n'_O)^{-1}$, respectively. The shifts to higher ionization energies, relative to propenal, reflect the strong inductive effect of the fluorine substituent. However, the energy of π''_{CC} is not stabilized as much as that of n'_O since the former may interact

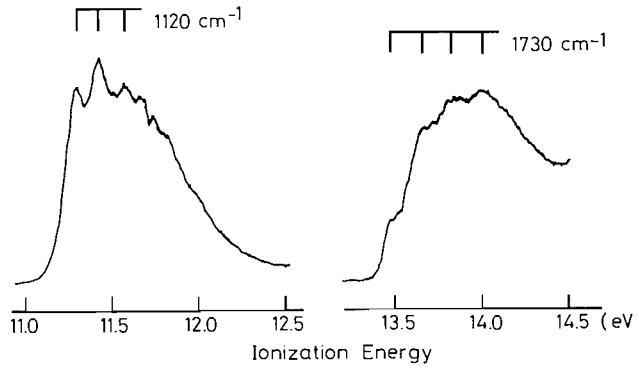

FIG. 2. Details of the first two bands in the spectrum of propenoyl fluoride.

with the other out-of-plane orbitals, π''_{CO} and n''_F, lying at higher IEs, which destabilizes it. Of the two opposing effects, inductive and resonance, the former is slightly more important since the π''_{CC} band is at a slightly higher IE compared to its position for propenal.

The 1120 cm^{-1} interval on the $(\pi_{CC})^{-1}$ band cannot be unambiguously assigned. This frequency is likely too low for the cationic ν(C=C) stretching mode (1636 cm^{-1} for the neutral (13)). For the $(\pi''_{CC})^{-1}$ bands of related species the following reductions from the ν(C=C) values of the neutrals are observed: 330 cm^{-1} for ethene (14), 310 cm^{-1} for propene (15), and 165 cm^{-1} for propenal. The 1120 cm^{-1} structure could be excitation of the ν(C—C) stretching mode (1002 cm^{-1} for the neutral (13)). The MO calculations, and the positions of the $(\pi''_{CO})^{-1}$ and $(n''_F)^{-1}$ bands (see below), suggest a substantial resonance interaction between the three out-of-plane orbitals with a node in the C—C internuclear region. Removal of an electron from the $3a''$ MO, which is antibonding in the C—C region, results in a slightly increased C—C bond strength and vibrational frequency.

The broad profile of the $(n'_O)^{-1}$ band is consistent with the observations for acetyl fluoride (12) and propynoyl fluoride (3), and is probably the result of some delocalization of this in-plane orbital over the entire —COF group. The MO calculations also predict this.

It is difficult to assign the other a'' bands, $(\pi''_{CO})^{-1}$ and $(n''_F)^{-1}$, since they lie in the congested part of the spectrum. They are assigned to the bands at 14.03 and 16.93 eV, respectively, by analogy with the spectra of propenal, propynoyl fluoride (3), and formyl fluoride (16). These assignments are also consistent with the sum-rule for the out-of-plane orbital energies. A broad vibrational progression of 1730 cm^{-1}, which could be the cationic ν(C=O) mode, is observed on the 14.03 eV band (Fig. 2). It should be noted that the energy separation of the $(n''_F)^{-1}$ and $(n'_F)^{-1}$ bands is quite large, about 2 eV, due to the substantial interaction of the out-of-plane lone-pair orbital with π''_{CO}.

Propenoyl chloride

In addition to the n'_O and π''_{CC} bands, the low IE region of the propenoyl chloride spectrum is expected to exhibit bands due to ionization from the in- and out-of-plane chlorine lone-pair orbitals (for example, these orbitals give rise to a band centered at 12.78 eV for HCl (17)). Only three bands are observed in the spectrum (Fig. 1). The intense band at 11.95 eV is due to the chlorine lone-pair electrons, the energy difference between the n'_{Cl} and n''_{Cl} orbitals being small, by analogy with formyl chloride (18) and acetyl chloride (12). Note that the CNDO/2

Can. J. Chem. Downloaded from www.nrcresearchpress.com by 78.46.186.204 on 09/07/12
For personal use only.

MO calculation (Table 3) predicts the chlorine orbitals to have much lower IEs; this seems to be a result of the parameterization of the program. The lowest IE band in the spectrum, 10.90 eV, is assigned as $(n'_O)^{-1}$, the position being intermediate to the corresponding bands of the aldehyde and acid fluoride. Ionization from the π''_{CC} orbital gives rise to the band at 11.23 eV. The π''_{CO} band is located at 14.85 eV and can only be identified by comparison with the spectra of formyl chloride (18) and propynoyl chloride (3), and use of the sum-rule.

Propenoyl bromide

Figure 1 shows that the spectrum of the bromide is very similar to that of the chloride, with a general shift to lower IEs due to the decreased inductive effect of bromine. For example, both the n'_O and π''_{CC} bands are shifted by 0.4 eV. It is at first glance surprising, in view of the results for the chloride, that the bromine lone-pair orbitals gave rise to distinct bands at 11.16 and 11.49 eV. This energy difference is equal to the spin–orbit splitting of the doubly-degenerate bromine lone-pair orbital band in HBr (17). It has been demonstrated that this magnitude of splitting also occurs in alkyl bromides of C_s symmetry and is insensitive to the degree of conjugation of n''_{Br} with other a'' orbitals (19). This behaviour has been explained with the use of a simple orbital model which showed that two opposing trends, increased splitting with increased conjugation of n''_{Br} and increased spin–orbit splitting with increased localization on the halogen atom, compensated each other (20). A similar situation is believed to hold in the case of propenoyl bromide. The lower IE band is assigned as $(n''_{Br})^{-1}$ as this orbital should be destabilized by any interaction with the higher IE π''_{CO} orbital. Conversely, n'_{Br} would be stabilized by interaction with n'_O.

Summary

The photoelectron spectra of the propenoyl halides were interpreted by comparison with propenal and other related compounds. Semi-empirical MO calculations were carried out for some species and, where applicable, the HAM/3 method gave better agreement with measured ionization energies than the CNDO/2 method. The HOMO for the chloride and bromide was found to be n'_O while the penultimate occupied MO is π''_{CC}. For the fluoride this ordering must be reversed. Extensive delocalization of the out-of-plane orbitals was found only for the fluoride, and is due to the favourable π-type overlap of n''_F with the other π-orbitals. No specific features of the spectra could be assigned to the two rotational isomers of the acid halides owing to the overlap of the bands and the small orbital energy differences predicted by the HAM/3 MO calculation. At best, rotational isomerism gives rise to the broadness of the bands.

Acknowledgements

This work was supported by the Natural Sciences and Engineering Research Council of Canada and the St. Francis Xavier University Council for Research.

1. T. KOOPMANS. Physica, **1**, 104 (1933).
2. D. W. TURNER, C. BAKER, A. D. BAKER, and C. R. BRUNDLE. Molecular photoelectron spectroscopy. Wiley, New York. 1970. p. 250; H. VAN DAM and A. OSKAM. J. Electron Spectrosc. Relat. Phenom. **13**, 273 (1978).
3. D. KLAPSTEIN. J. Electron Spectrosc. Relat. Phenom. In press.
4. P. DOBOSH and N. S. OSTLUND. QCPE, **11**, 281 (1975).
5. L. ÅSBRINK, C. FRIDH, and E. LINDHOLM. QCPE, **13**, 393 (1981).
6. R. WAGNER, J. FINE, J. W. SIMMONS, and J. H. GOLDSTEIN. J. Chem. Phys. **26**, 634 (1957); J. J. KEIRNS and R. F. CURL, JR. J. Chem. Phys. **48**, 3773 (1968); R. KEWLEY, D. C. HEMPHILL, and R. F. CURL, JR. J. Mol. Spectrosc. **44**, 443 (1972).
7. G. L. CARLSON, W. G. FATELEY, and R. E. WITKOWSKI. J. Am. Chem. Soc. **89**, 6437 (1967).
8. J. E. KATON and W. R. FEAIRHELLER, JR. J. Chem. Phys. **47**, 1248 (1967).
9. D. F. KOSTER. J. Am. Chem. Soc. **88**, 5067 (1966).
10. K. KIMURA, S. KATSUMATA, T. YAMAZAKI, and H. WAKABAYASHI. J. Electron Spectrosc. Relat. Phenom. **6**, 41 (1975).
11. A. D. BAKER, C. BAKER, C. R. BRUNDLE, and D. W. TURNER. Int. J. Mass Spectrom. Ion Phys. **1**, 285 (1968).
12. D. CHADWICK and A. KATRIB. J. Electron Spectrosc. Relat. Phenom. **3**, 39 (1974).
13. R. L. REDINGTON. J. Chem. Phys. **62**, 4927 (1975).
14. C. R. BRUNDLE and D. B. BROWN. Spectrochim. Acta, **27A**, 2491 (1971).
15. A. KATRIB and J. W. RABALAIS. J. Phys. Chem. **77**, 2358 (1973).
16. K. WITTEL. J. Electron Spectrosc. Relat. Phenom. **8**, 245 (1976).
17. H. J. LEMPKA, T. R. PASSMORE, and W. C. PRICE. Proc. R. Soc. London, Ser. A, **304**, 53 (1968).
18. D. C. FROST, C. A. MCDOWELL, and N. P. C. WESTWOOD. Chem. Phys. Lett. **51**, 607 (1977).
19. J. A. HASHMALL and E. HEILBRONNER. Angew. Chem. Int. Ed. **9**, 305 (1970); K. KIMURA, S. KATSUMATA, Y. ACHIBA, H. MATSUMOTO, and S. NAGAKURA. Bull. Chem. Soc. Jpn. **46**, 373 (1973).
20. F. BROGLI and E. HEILBRONNER. Helv. Chim. Acta, **54**, 1423 (1971).
21. A. W. POTTS and W. C. PRICE. Trans. Faraday Soc. **67**, 1242 (1971); A. B. CORNFORD, D. C. FROST, C. A. MCDOWELL, J. L. RAGLE, and I. A. STENHOUSE. J. Chem. Phys. **54**, 2651 (1971).
22. S.-T. LEE. Ph.D. Dissertation, University of British Columbia. 1974. p. 74.

Can. J. Chem. Downloaded from www.nrcresearchpress.com by 78.46.186.204 on 09/07/12
For personal use only.

Synthesis and structural study of aminals derived from 8-aminoquinoline and 1-aminonaphtalene

ENRIQUE GALVEZ, ISABEL IRIEPA, AND ANTONIO LORENTE
Departamento de Química Orgánica, Universidad de Alcalá de Henares, Alcalá de Henares, Madrid, Spain

AND

JOSE MIGUEL MOHEDANO, FELICIANA FLORENCIO, AND SEVERINO GARCIA-BLANCO
Instituto "Rocasolano", Departamento de Rayos-X, C.S.I.C., Serrano 119 28006 Madrid, Spain

Received August 18, 1985[1]

ENRIQUE GALVEZ, ISABEL IRIEPA, ANTONIO LORENTE, JOSE MIGUEL MOHEDANO, FELICIANA FLORENCIO, and SEVERINO GARCIA-BLANCO. Can. J. Chem. **65**, 687 (1987).

Reaction of 8-aminoquinoline with pyridine-2-carboxaldehyde (**2**), pyridine-3-carboxaldehyde (**3**), pyridine-4-carboxaldehyde (**4**), and benzaldehyde (**5**) yields the corresponding aminals or Schiff's bases according to reaction conditions; analogous results are obtained from the reaction of 1-amino-naphtalene with pyridine-2-carboxaldehyde (**6**). On the other hand, reaction of 8-aminoquinoline with thiophene-2-carboxaldehyde or pyrrole-2-carboxaldehyde yields neither the aminal nor the Schiff's base. Crystals of **4** ($C_{24}H_{19}N_5$) belong to the triclinic space group $P\bar{1}$. Cell dimensions are a = 11.547(3), b = 11.759(2), c = 15.687(5) Å, α = 98.50(2)°, β = 101.61(2)°, γ = 107.28(2)°, V = 1942.6(9) Å^3. Final R = 0.077 and R_w = 0.064; 3160 reflections were observed. The ir, ^{1}H nmr of **2–6**, the mass spectra of **4** and **5** and the X-ray analysis of **4** are described and discussed. Preparative features, ir, ^{1}H nmr, analyses and crystal structure indicate that the formation of **2–6** are governed mainly by the nucleophilicity at the aldehyde carbon atom and the existence of the hydrogen bonds in the aminal.

ENRIQUE GALVEZ, ISABEL IRIEPA, ANTONIO LORENTE, JOSE MIGUEL MOHEDANO, FELICIANA FLORENCIO et SEVERINO GARCIA-BLANCO. Can. J. Chem. **65**, 687 (1987).

La réaction de l'amino-8 quinoléine avec le benzaldéhyde (**5**) ou avec les pyridinecarboxaldéhydes-2, -3 ou -4 (**2**, **3** ou **4**) conduit, suivant les conditions réactionnelles, soit aux aminals correspondants ou aux bases de Schiff; on obtient des résultats analogues lors de la réaction de l'amino-1 naphtalène avec le pyridinecarboxaldéhyde (**2**). Par ailleurs, lors de la réaction de l'amino-8 quinoléine avec le thiophènecarboxaldéhyde-2 ou avec le pyrrolecarboxaldéhyde-2, on n'obtient ni l'aminal ni la base de Schiff. Les cristaux du composé **4** ($C_{24}H_{19}N_5$) appartiennent au groupe d'espace $P\bar{1}$ et les dimensions de la maille sont: a = 11,547(3), b = 11,759(2) et c = 15,687(5) Å, avec α = 98,50(2), β = 101,61(2) et γ = 107,28(2)° et V = 1942,6(9) Å^3. La structure a été affinée jusqu'à des valeurs finales de R = 0,077 et R_w = 0,064 pour 3160 réflexions observées. On rapporte et on discute des spectres ir et rmn du ^{1}H des composés **2–6**, des spectres de masse des composés **4** et **5** et de la diffraction par les rayons-X du composé **4**. Les caractéristiques de la préparation, les spectres ir et rmn du ^{1}H, les analyses et les structures cristallines indiquent que la formation des composés **2–6** est gouvernée principalement par le caractère nucléophile de l'atome de carbone de l'aldéhyde par l'existence de liaisons hydrogènes dans l'aminal.

[Traduit par la revue]

Introduction

In a previous paper (1) we reported the preparation and spectroscopic features of 6M-PQUAM (**1**) and PQUAM (**2**). In the same line, and because of the chelating properties shown by these aminals for transition metals (1), we report in this paper the synthesis and structural studies, by several methods, of the aminals formed by condensation of 8-aminoquinoline with pyridine-3-carboxaldehyde (**3**), pyridine-4-carboxaldehyde (**4**), benzaldehyde (**5**), and the aminal obtained by condensation of 1-aminonaphtalene with pyridine-2-carboxaldehyde (**6**). Our objective is to establish the main structural stabilizing requirements for these compounds.

Applying the procedure for **1** and **2** (1) to **3–6** yielded neither the aminals nor the Schiff's bases. By condensing 8-aminoquinoline with the appropriate aldehyde and by removing water through azeotropic distillation with benzene, we were able to synthesize the aminals in good yields (Table 1). By addition to the reaction mixture of *p*-toluene – sulfonic acid, only the Schiff's base was isolated. Finally, it is interesting to remark that, in the reaction of 8-aminoquinoline with thiophene-2-carboxaldehyde or pyrrole-2-carboxaldehyde, neither the aminal nor the Schiff's base was isolated. These facts and the yields obtained for **2–6** (Table 1) show that the nucleo-

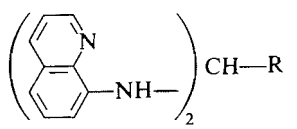

1 R = 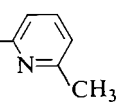

2 R =

3 R =

4 R =

5 R =

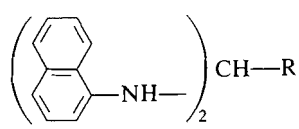

6 R =

[1]Revision received August 19, 1986.

Can. J. Chem. Downloaded from www.nrcresearchpress.com by 78.46.186.204 on 09/07/12
For personal use only.

TABLE 1. Physical data and spectral properties of **1–6**

Compound	Yield %	Melting point (°C)	Crystal solvent	Formula	Analysis % Calcd	Analysis % Found	MS, *m/e*
1[a]	30	119–121	Ethanol	$C_{25}H_{21}N_5$	C 76.70 H 5.40 N 17.88	76.69 5.33 17.65	
2	67	109–112	Ethanol	$C_{24}H_{19}N_5$	C 76.38 H 5.07 N 18.56	76.60 4.79 18.70	
3	76	107	Ether	$C_{24}H_{19}N_5$	C 76.38 H 5.07 N 18.56	76.67 5.13 18.49	
4	80	122	Ether–ethanol	$C_{24}H_{19}N_5$	C 76.38 H 5.07 N 18.56	76.66 5.27 18.77	
5[b]	49	88		$C_{25}H_{19}N_4$			233, 232, 155, 129 144, 104, 103, 78, 77
6	11	208	Ethanol	$C_{26}H_{21}N_3$	C 83.17 H 5.64 N 11.19	83.23 5.37 11.40	

[a]Reference 1.
[b]This product is very unstable and cannot be purified by recrystallization.

philicity at the carbonyl carbon is the main factor affecting the condensation.

Experimental

Synthesis

General procedure for compounds 2–6

The appropriate aldehyde (2.08 mmol) was added to a solution of 8-aminoquinoline (or 1-aminonaphtalene) (1.04 mmol) in benzene (10 mL). The reaction mixture was warmed at reflux for 5 h, and water was removed by azeotropic distillation in a Dean-Stark apparatus. After cooling to room temperature, the reaction mixture was concentrated up to dryness under reduced pressure, and the oil obtained was treated with ether. The resulting solid was recrystallized. Melting points and elemental analyses are given in Table 1.

Methods

All melting points were measured in open capillary tubes in a Büchi SMP-20 apparatus and are uncorrected.

Infrared spectra were recorded on a Perkin Elmer 599 spectrophotometer. All compounds were compressed into KBr pellets.

^{1}H nmr spectra were obtained in DMSO-d_6 at 80 MHz with a Varian FT-80 spectrometer using TMS as internal standard.

The mass spectra were measured at 70 eV on a Varian MAT 711 or on a Hitachi-Perkin Elmer RMU-6M spectrometers.

The elemental analyses were performed in a Carlo Erba analyzer.

Crystallography

Preliminary cell dimensions and the possible space group of the compound 4-pyridyl-*N*,*N*-di((8-quinolyl)amino)methane (**4**) were determined from Weissenberg and precession photographs. Accurate cell parameters were determined by least-squares methods from the setting angles of 25 reflections measured on an automatic Nonius CAD4 four circle diffractometer on the range of $8 < \theta < 20°$ with graphite-monochromated MoKα radiation. Crystal data are as follows: $C_{24}H_{19}N_5$ mw = 377.447
Space group $P\bar{1}$, a = 11.547(3), b = 11.759(2), c = 15.687(5) Å, α = 98.50(2), β = 101.61(2), γ = 107.28(2)°, V = 1942.6(9) Å^3, d_0 = 1.3, d_x = 1.291(2) g cm^{-3}, Z = 4, λ(MoKα) = 0.71069 Å, $F(000)$ = 729, μ(MoKα) = 0.0074 mm^{-1}.

Experimental density was measured by flotation method using an aqueous KBr solution. There are two independent molecules, **A** and **B** in a unit cell.

Intensities were measured from a crystal of 0.18 × 0.20 × 0.40 mm on the same automatic Nonius CAD4 four circle diffractometer, for $2 < \theta < 28.5°$. The ω–2θ scan technique was used. $\Delta\omega = (1 + 0.3 \tan\theta)°$. Two reflections were used as standard and remeasured after every 100 reflections, with a variation <12%, due to the presence of some unstableness in the crystal, of the 6700 independent reflections measured on the range $\bar{15} < h < 15$, $\bar{15} < k < 15$, $0 < l < 21$, 3160 were considered observed with $I > 2\sigma(I)$, σ being determined from counting statistics. R_{int} = 0.01. Lorentz and polarization corrections were applied, but no correction was made for absorption.

The phase problem was solved by direct methods with MULTAN-80 programs (2). An E map generated from the phase set of 466 reflections with the highest combined figure of merit, located one of the two independent molecules and a fragment of the other one; the remaining atoms were found from difference Fourier syntheses.

Further least-squares refinements with isotropic and anisotropic temperature factors reduced R to 0.09. A difference Fourier map revealed the positions of all H atoms which were included with isotropic temperature factors. The process of refining was stopped when the averaged Δ/σ = 0.10, the maximum Δ/σ = 0.27 and the maximum residual peak = 0.20 e Å^{-3}. The function minimized was $\Sigma w(|F_o| - |F_c|)^2$ with $w = k/\sigma_1^2\sigma_2^2$, $\sigma_1 = a_1 + b_1(F_o)$, $\sigma_2 = a_2 + b_2(\sin\theta/\lambda)$, and k = 0.543 (3).

The final R values are $R = \Sigma(|F_o| - |F_c|)/\Sigma|F_o| = 0.077$ and $R_w = [\Sigma w\Delta^2/\Sigma w|F_o|^2]^{1/2} = 0.064$. $S = \Sigma[w\Delta F^2/(m - n)]^{1/2} = 1.15$.

The scattering factors were taken from the International tables for X-ray crystallography (4). The computations were made with programs of the X-RAY 70 system (5), PARST (6), and PESOS (3) on a VAX 11/750 computer.

The coordinates are listed in Table 2.[2]

[2]Tables of coordinates of H atoms, anisotropic temperature parameters, deviations of atoms from the mean plane and the structure factors may be purchased from the Depository of Unpublished Data, CISTI, National Research Council of Canada, Ottawa, Ont., Canada K1A 0S2.

Can. J. Chem. Downloaded from www.nrcresearchpress.com by 78.46.186.204 on 09/07/12
For personal use only.

TABLE 2. Coordinates and thermal parameters as $U_{eq} = \frac{1}{2}\Sigma_i\Sigma_j U_{ij} a^*_i a^*_j a_i a_j \cos(a_i, a_j) \times 10^3$

	Molecule **A**				Molecule **B**			
Atom	x	y	z	U_{eq}	x	y	z	U_{eq}
N1	0.2035(4)	0.2761(3)	0.5283(3)	53(2)	1.0892(5)	0.3935(4)	1.1790(3)	68(3)
C2	0.2328(6)	0.3928(5)	0.5698(3)	61(3)	1.0672(7)	0.3735(6)	1.2557(4)	78(3)
C3	0.3547(7)	0.4743(6)	0.5941(4)	74(3)	1.1467(8)	0.3359(6)	1.3162(4)	79(3)
C4	0.4485(7)	0.4376(5)	0.5769(4)	70(3)	1.2503(7)	0.3199(5)	1.2977(4)	73(3)
C5	0.4216(5)	0.3144(5)	0.5311(3)	54(2)	1.2803(6)	0.3425(4)	1.2182(3)	62(2)
C6	0.5140(6)	0.2700(6)	0.5062(4)	71(3)	1.3873(6)	0.3301(5)	1.1943(4)	73(3)
C7	0.4816(6)	0.1500(6)	0.4626(4)	72(3)	1.4091(6)	0.3531(6)	1.1151(4)	78(3)
C8	0.3563(6)	0.0715(5)	0.4427(4)	64(3)	1.3237(6)	0.3867(6)	1.0561(4)	75(3)
C9	0.2632(5)	0.1114(4)	0.4633(3)	50(2)	1.2153(6)	0.3965(5)	1.0746(3)	68(3)
C10	0.2970(5)	0.2373(4)	0.5098(3)	46(2)	1.1930(6)	0.3783(4)	1.1591(3)	62(2)
N11	−0.2753(4)	−0.2578(4)	0.2545(3)	59(2)	0.7496(6)	0.2917(5)	0.7719(3)	90(3)
C12	−0.3900(7)	−0.3241(6)	0.2067(4)	78(3)	0.6348(9)	0.2591(10)	0.7219(5)	103(5)
C13	−0.4561(8)	−0.2975(8)	0.1320(5)	87(4)	0.5423(10)	0.1455(13)	0.7118(6)	120(6)
C14	−0.3958(7)	−0.1969(8)	0.1052(4)	87(4)	0.5741(11)	0.0641(9)	0.7560(7)	121(6)
C15	−0.2716(6)	−0.1211(5)	0.1512(4)	70(3)	0.6954(9)	0.0928(6)	0.8110(5)	97(4)
C16	−0.1973(9)	−0.0153(7)	0.1278(5)	95(4)	0.7376(14)	0.0132(8)	0.8593(7)	125(6)
C17	−0.0791(7)	0.0475(6)	0.1738(5)	91(2)	0.8584(14)	0.0488(11)	0.9090(7)	127(7)
C18	−0.0237(7)	0.0117(5)	0.2499(4)	77(3)	0.9463(9)	0.1642(8)	0.9136(5)	98(4)
C19	−0.0894(6)	−0.0866(4)	0.2781(3)	60(3)	0.9069(7)	0.2439(7)	0.8695(3)	80(3)
C20	−0.2146(5)	−0.1568(5)	0.2276(3)	56(2)	0.7812(7)	0.2086(5)	0.8156(4)	79(3)
N21	−0.0398(4)	−0.1210(4)	0.3542(3)	57(2)	0.9872(6)	0.3599(5)	0.8708(3)	81(3)
N22	0.1397(4)	0.0425(3)	0.4429(3)	57(2)	1.1251(6)	0.4234(5)	1.0178(3)	86(3)
C23	0.0914(5)	−0.0858(4)	0.3947(4)	55(2)	1.1149(6)	0.4078(7)	0.9215(3)	80(3)
N24	0.1531(5)	−0.3359(5)	0.5603(4)	85(3)	−0.3046(6)	−0.7392(6)	0.1546(6)	109(4)
C25	0.1650(6)	−0.2214(6)	0.5948(4)	77(3)	−0.2869(8)	−0.7380(9)	0.0743(6)	102(5)
C26	0.1475(5)	−0.1379(5)	0.5452(4)	64(3)	−0.2292(8)	−0.6366(8)	0.0443(5)	92(4)
C27	0.1162(4)	−0.1720(4)	0.4536(3)	49(2)	−0.1837(6)	−0.5237(6)	0.1046(4)	73(3)
C28	0.1070(6)	−0.2903(5)	0.4166(4)	65(3)	−0.2020(7)	−0.5231(8)	0.1839(4)	83(4)
C29	0.1254(6)	−0.3672(6)	0.4712(5)	78(3)	−0.2595(8)	−0.6285(9)	0.2124(6)	99(4)

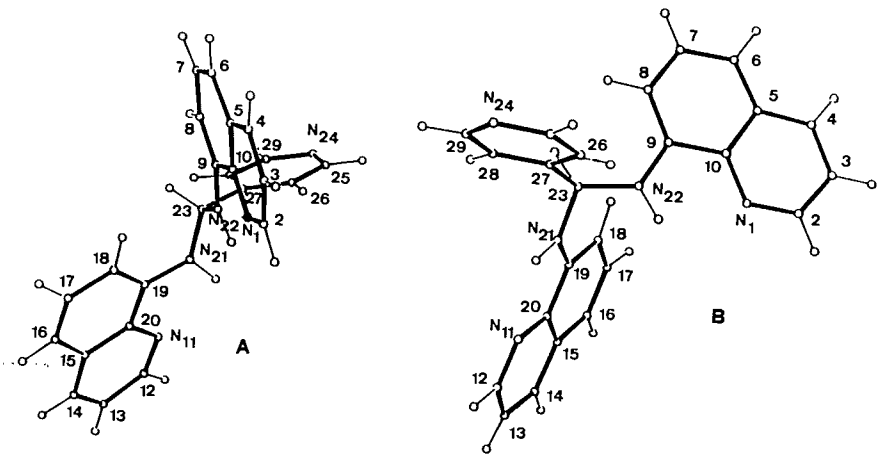

FIG. 1. A view of two independent molecules.

Results and discussion

Description of the structure of 4

Figure 1 shows a view of two independent molecules with the atomic labelling and Fig. 2 displays a projection along the *b* axis, with the intermolecular H bonds represented by dashed lines. Bonds lengths and bond angles with their esd's are given in Table 3. These values are very similar for the two independent molecules and are also in good agreement with that of **2** (7).

In molecule **A**, average torsion angles for the two 8-aminoquinolyl groups are 1.3(5)° and 1.5(6)°, and that for the pyridine ring is 1.2(6)°. In molecule B, the corresponding values are 1.7(6)°, 1.4(5)°, and 1.0(6)° respectively. That is to say, both 8-aminoquinolyl groups and pyridine rings are planar.

The dihedral angle between the two 8-aminoquinolyl planes are 75.6(2)° and 64.3(2)° in molecules **A** and **B**. The dihedral angles between the 8-aminoquinolyl planes and the pyridine ring are 92.7(1)° and 119.7(3)° in molecule **A**, and 64.3(2)° and 117.9(2)° in molecule **B**. These values are quite different and also different from those found for **2** (7) as a result of different molecular packing. In the former case intra- and interhydrogen bonds and short contacts are possible.

Can. J. Chem. Downloaded from www.nrcresearchpress.com by 78.46.186.204 on 09/07/12
For personal use only.

Can. J. Chem. Downloaded from www.nrcresearchpress.com by 78.46.186.204 on 09/07/12
For personal use only.

TABLE 3. Bond lengths, angles, and torsion angles

(*a*) Bond length

Bond	Distance (Å) Mol. **A**	Mol. **B**	Bond	Distance (Å) Mol. **A**	Mol. **B**
N1—C2	1.340(7)	1.318(9)	C15—C16	1.430(10)	1.420(15)
N1—C10	1.356(8)	1.352(9)	C15—C20	1.428(8)	1.407(9)
C2—C3	1.384(9)	1.398(11)	C16—C17	1.333(11)	1.359(19)
C3—C4	1.340(11)	1.345(13)	C17—C18	1.418(11)	1.414(14)
C4—C5	1.431(8)	1.400(9)	C18—C19	1.368(8)	1.373(13)
C5—C6	1.416(10)	1.403(10)	C19—C20	1.428(7)	1.427(10)
C5—C10	1.395(7)	1.429(9)	C19—N21	1.386(7)	1.398(9)
C6—C7	1.377(9)	1.367(10)	N21—C23	1.426(7)	1.423(8)
C7—C8	1.408(8)	1.398(10)	N22—C23	1.468(6)	1.470(7)
C8—C9	1.370(10)	1.374(11)	C23—C27	1.519(8)	1.519(10)
C9—C10	1.448(6)	1.435(8)	N24—C25	1.331(9)	1.318(14)
C9—N22	1.359(6)	1.373(9)	N24—C29	1.337(10)	1.358(11)
N11—C12	1.318(7)	1.308(11)	C25—C26	1.375(10)	1.381(14)
N11—C20	1.360(7)	1.367(9)	C26—C27	1.376(7)	1.396(10)
C12—C13	1.395(11)	1.404(15)	C27—C28	1.389(8)	1.386(9)
C13—C14	1.355(12)	1.354(19)	C28—C29	1.365(10)	1.360(13)
C14—C15	1.417(9)	1.404(14)			

(*b*) Bond angles

Bonds	Angle (deg) Mol. **A**	Mol. **B**	Bonds	Angle (deg) Mol. **A**	Mol. **B**
C2—N1—C10	118.4(5)	118.6(6)	C15—C16—C17	122.2(7)	120.4(9)
N1—C2—C3	122.3(6)	122.2(7)	C16—C17—C18	120.1(7)	121.8(11)
C2—C3—C4	120.3(6)	120.3(6)	C17—C18—C19	121.4(7)	118.8(9)
C3—C4—C5	119.5(7)	120.2(7)	C18—C19—N21	122.9(6)	122.7(7)
C4—C5—C10	116.9(6)	116.1(6)	C18—C19—C20	118.9(5)	120.7(7)
C4—C5—C6	123.1(6)	124.0(6)	C20—C19—N21	118.2(5)	116.6(6)
C6—C5—C10	120.0(5)	120.0(6)	C15—C20—C19	120.1(5)	119.6(6)
C5—C6—C7	120.0(7)	120.2(6)	N11—C20—C19	117.6(5)	117.4(6)
C6—C7—C8	120.0(7)	120.5(7)	N11—C20—C15	122.3(6)	123.1(7)
C7—C8—C9	121.9(6)	122.0(6)	C19—N21—C23	123.8(5)	123.0(6)
C8—C9—N22	125.2(5)	124.7(6)	C9—N22—C23	122.5(5)	122.2(6)
C8—C9—C10	188.3(6)	118.7(6)	N21—C23—N22	109.9(5)	111.4(6)
C10—C9—N22	116.4(5)	116.7(6)	N22—C23—C27	113.0(4)	113.4(5)
C5—C10—C9	119.7(5)	118.7(6)	N21—C23—C27	110.1(5)	110.3(5)
N1—C10—C9	117.6(5)	118.7(6)	C25—N24—C29	115.7(6)	115.2(9)
N1—C10—C5	122.6(5)	122.6(6)	N24—C25—C26	124.3(6)	126.5(9)
C12—N11—C20	117.6(5)	117.4(7)	C25—C26—C27	119.4(6)	117.4(7)
N11—C12—C13	125.4(7)	124.2(9)	C23—C27—C26	122.1(5)	121.1(6)
C12—C13—C14	117.0(7)	118.0(11)	C26—C27—C28	116.9(5)	116.9(7)
C13—C14—C15	121.7(7)	121.1(10)	C23—C27—C28	121.0(5)	122.0(6)
C14—C15—C20	116.0(6)	116.2(8)	C27—C28—C29	119.7(6)	121.1(7)
C14—C15—C16	126.8(6)	125.1(9)	N24—C29—C28	124.0(7)	122.9(8)
C16—C15—C20	117.3(6)	118.7(8)			

(*c*) Some torsion angles

Bonds	Torsion angle (deg) Mol. **A**	Mol. **B**	Bonds	Torsion angle (deg) Mol. **A**	Mol. **B**
C8—C9—N22—C23	−0.4(9)	19.4(9)	C9—N22—C23—C27	78.1(7)	−94.6(8)
C18—C19—N21—C23	−20.4(9)	−3.3(9)	N22—C23—C27—C26	17.2(8)	−11.9(9)
C19—N21—C23—C27	−159.6(5)	169.0(8)	C20—C19—N21—H21	−8(4)	13(5)
C19—N21—C23—N22	75.3(7)	−64.1(9)	C10—C9—N22—H22	3(5)	−10(6)
C9—N22—C23—N21	−158.5(5)	140.2(8)			

TABLE 4. Intra- and intermolecular contacts

	N—H	H---N	N---N	N—H—N	H---H
N22A—H---N1A (x, y, z)	0.87(7)Å	2.37(5)Å	2.682(5)Å	102(4)°	
N22B—H---N1B (x, y, z)	0.94(9)	2.37(8)	2.701(7)	100(5)	
N21A—H---N11A (x, y, z)	0.97(6)	2.40(5)	2.715(6)	98(4)	
N21B—H---N11B (x, y, z)	0.87(8)	2.27(6)	2.682(8)	109(5)	
N21A—N22A (x, y, z)			2.369(5)		
N21B—N22B (x, y, z)			2.391(6)		
H21A---H22A (x, y, z)					2.98(7)Å
H21B---H22B (x, y, z)					2.81(7)
N21A—H---N1A ($-x$, $-y$, $1-z$)	0.97(6)	2.33(6)	3.262(6)	161(5)	
H21B—H---N1B ($2-x$, $1-y$, $2-z$)	0.87(8)	2.60(11)	3.421(9)	157(5)	

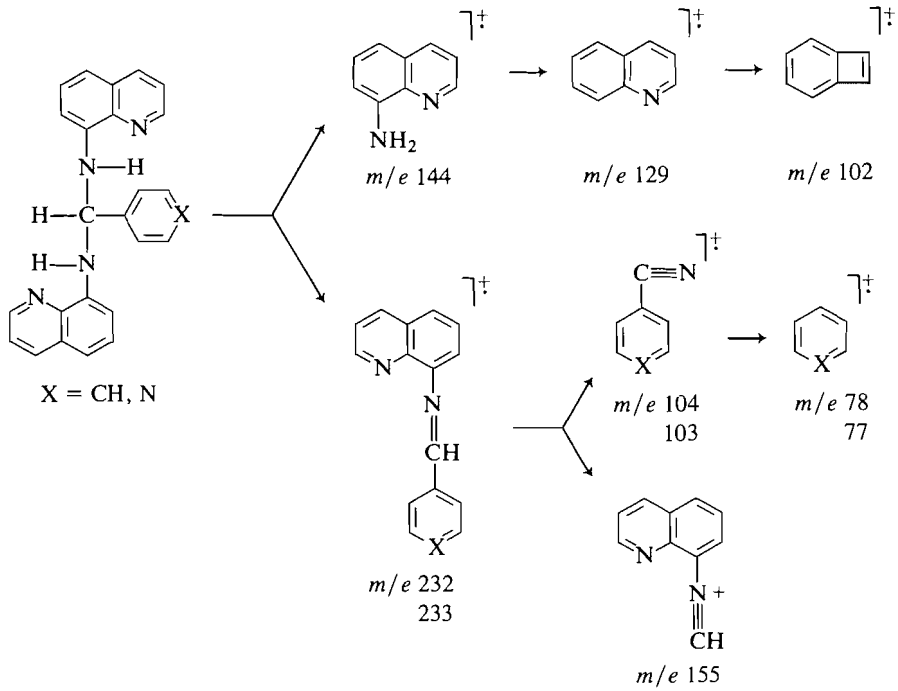

SCHEME 1

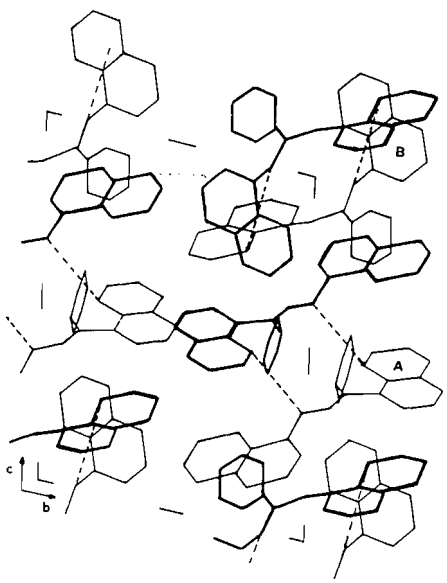

FIG. 2. A view of the relative positions of the two independent molecules, with the intermolecular H-bonds represented by dashed lines.

There is a short intramolecular N21...N22 contact and two intramolecular H-bonds in N22—H...N1 and N21—H...N11 for each **A** and **B** molecules.

There are also clear intermolecular interactions between each pair of molecules related by an inversion center, although the N...N distances are rather large. The corresponding distances and angles are shown in Table 4.

By comparing these distances with that of the compound **2**, it can be deduced that in compounds **2** and **4** the N amine is bonded to N quinoline through an intramolecular H-bond and the N amine...N amine is a short intramolecular contact. In compound **2**, there are two intramolecular H-bonds N amine—H...N pyridine and as this kind of H-bond can not be found in compound **4**, an intermolecular interaction, N amine—H...N quinoline, takes place between each two symmetrical molecules.

Infrared spectra

In compounds **2** and **4**, the bands at 3405 cm^{-1} and 3400 cm^{-1} are assigned respectively to the ν(N—H...N) single intramolecular hydrogen bonds, whereas the bands at 3370 cm^{-1} and 3355 cm^{-1} are assigned to the ν(N—H:::$^{N}_{N}$) bifurcated hydrogen bonds. These structural facts are in good

Can. J. Chem. Downloaded from www.nrcresearchpress.com by 78.46.186.204 on 09/07/12
For personal use only.

agreement with the results obtained by X-ray diffraction. For the ν(N—H) bands of compounds **3**, **5**, and **6**, the corresponding bands appear at 3410, 3410, —cm^{-1} and 3368, 3378, 3378 cm^{-1}, respectively, the conclusions seem to be similar to those deduced for compounds **2** and **4**.

Nuclear magnetic resonance spectra

The triplets at $\delta \simeq 6.5$ ppm which convert into singlets on deuteration are assigned to the methine protons coupled to the amine protons, as previously described for **2** (1).

The sequence δH_α (**2**) (6.57 ppm) $\simeq \delta H_\alpha$ (**3**) (6.59 ppm) > δH_α (**4**) (6.52 ppm) > δH_α (**5**) (6.33 ppm) is consistent with the increased electron-withdrawing effect exerted by the pyridine nitrogen atom. Finally, it is interesting to remark, that on dissolution of **1**–**6** in DMSO-d_6 a N—H free signal appears at $\delta \simeq 5.9$ ppm; and, as a consequence of deuteration, compounds **1**–**6** begin to hydrolyze, giving an aldehyde proton signal at $\delta \simeq 10$ ppm.

Mass spectra

The proposed fragmentation pathways of **4** and **5** are given in Scheme 1.

The cleavage of the C—N linkage in M^+ gives rise to the peaks at *m/e* 144, 233, and 232. From the aminoquinolinium ion, the peaks at *m/e* 129 (base peak) and *m/e* 102 are obtained. The fragmentation of the ions at *m/e* 233 and 232 originated the ions at *m/e* 104, 103, and 155. These fragmentation patterns are similar to those described for **2** and **3** (1).

Conclusions

From the preparative features, ir, and ^{1}H nmr data of **2**–**6** and the crystal structure of **2** and **4**, it was inferred that the syntheses of **1**–**6** are governed mainly by (*a*) the nucleophilicity at the carbonyl carbon of the appropriate aldehyde; and (*b*) the presence of intra- and intermolecular hydrogen bonds, which stabilize the aminal.

1. J. Bellanato, E. Galvez, R. Escobar, and J. M. Cano-Pavon. Can. J. Chem. **60**, 1775 (1982).
2. P. Main, S. J. Fiske, S. E. Hull, L. Lessinger, G. Germain, J. P. Declerq, and M. M. Woolfson. MULTAN 80. A system of computer programs for the automatic solution of crystal structures from X-ray diffraction data. University of York, Gt. Britain and Louvain, Belgium. 1980.
3. M. Martinez-Ripoll and F. H. Cano. PESOS. A computer program for the automatic treatment of weighting schemes. Instituto Rocasolano. C.S.I.C. Serrano 119 Madrid, Spain. 1975.
4. International tables for X-ray crystallography. Vol. IV. Kynoch Press. Birmingham. 1974.
5. J. M. Stewart, F. A. Kundell, and J. C. Baldwin. The X-ray 70 system. Computer Science Center, University of Maryland. College Park, MD. 1970.
6. M. Nardelli and M. Parst. A computer program. University of Parma, Italy. 1982.
7. J. M. Mohedano, F. Florencio, and S. Garcia-Blanco. Z. Kristallogr. **70**, 297 (1985).

Can. J. Chem. Downloaded from www.nrcresearchpress.com by 78.46.186.204 on 09/07/12
For personal use only.

Syntheses of model oligosaccharides of biological significance. 9.[1] Syntheses of trideuteriomethyl di-3,6-*O*-(2-acetamido-2-deoxy-β-D-glucopyranosyl)-β-D-galactopyranoside: the I antigen branch-point trisaccharide and related disaccharides[2]

DENNIS M. WHITFIELD[3] AND CAROLINE J. RUZICKA[4]

Ludwig Institute for Cancer Research, Toronto Branch, 9 Earl Street, Toronto, Ont., Canada M4Y 1M4, and Department of Medical Genetics, University of Toronto, Toronto, Ont., Canada M5S 1A8

JEREMY P. CARVER

Departments of Medical Genetics and Medical Biophysics, University of Toronto, Toronto, Ont., Canada M5S 1A8

AND

JIRI J. KREPINSKY[5]

Ludwig Institute for Cancer Research, Toronto Branch, 9 Earl Street, Toronto, Ont., Canada M4Y 1M4, and Departments of Medical Genetics and Medical Biophysics, University of Toronto, Toronto, Ont., Canada M5S 1A8

Received July 29, 1986

DENNIS M. WHITFIELD, CAROLINE J. RUZICKA, JEREMY P. CARVER, and JIRI J. KREPINSKY. Can. J. Chem. **65**, 693 (1987).

The title trisaccharide, **13***c*, was synthesized, as well as its two component disaccharides, **10***c* and **11***c*. Four disaccharides, **3***c*, **4***c*, **5***c*, and **7***c*, were also prepared to serve as model compounds for the investigation of the 3-dimensional structure of more complex oligosaccharides. The β-1,3 linkage was formed in 75% yield by coupling 3,4,6-tri-*O*-acetyl-2-deoxy-2-phthalimido-β-D-glucopyranosyl bromide (**9**) with trideuteriomethyl 2-*O*-benzoyl-4,6-benzylidene-β-D-galactopyranoside (**2***a*), using silver trifluoromethanesulphonate as a promoter in the presence of the base 2,6-di-*tert*-butyl-4-methylpyridine. Using a silver zeolite as a promoter under a variety of conditions, both α-1,3 and β-1,3 linkages were formed. The β-1,6 linkages were prepared in high yield using **9** and silver zeolite with either trideuteriomethyl 2,3-di-*O*-benzoyl-β-D-galactopyranoside (**8***b*) or trideuteriomethyl 2-*O*-benzoyl-3-*O*-(3,4,6-tri-*O*-acetyl-2-deoxy-2-phthalimido-β-D-glucopyranosyl)-β-D-galactopyranoside (**11***b*). 2,3,4-Tri-*O*-benzyl-α-L-fucopyranosyl bromide (**1***b*) was used in the halide ion catalyzed fucosylation of **2***a* or its 3-*O*-benzoyl isomer **2***b*. The glycosylations of 3,6-di-*O*-acetyl-4-*O*-(2,3,4,6-tetra-*O*-acetyl-β-D-galactopyranosyl)-2-deoxy-2-phthalimido-β-D-glucopyranosyl bromide (**6***b*) and 4-*O*-(2,3,4,6-tetra-*O*-acetyl-β-D-galactopyranosyl)-2,3,6-tri-*O*-acetyl-α-D-glucopyranosyl bromide (**5***a*) by heptadeuterioisopropanol used silver zeolite as promoter.

DENNIS M. WHITFIELD, CAROLINE J. RUZICKA, JEREMY P. CARVER et JIRI J. KREPINSKY. Can. J. Chem. **65**, 693 (1987).

On a synthétisé le trisaccharide mentionné dans le titre (**13***c*) ainsi que les deux disaccharides qui le forment (**10***c* et **11***c*). On a aussi préparé les quatre disaccharides **3***c*, **4***c*, **5***c* et **7***c* comme composés modèles pour l'étude de la structure tridimensionnelle d'oligosaccharides plus complexes. On a formé la liaison β-1,3 avec un rendement de 75% en procédant au couplage du bromure de tri-*O*-acétyl-3,4,6 déoxy-2 phtalimido-2 β-D-glycopyrannosyle (**9**) avec le *O*-benzoyl-2 benzylidène-4,6 β-D-galactopyrannoside de trideutérométhyle (**2***a*), sous l'influence du trifluorométhanesulfonate d'argent comme promoteur de la réaction et en présence de di-*tert*-butyl-2,6 méthyl-4 pyridine comme base. Si on utilise le zéolite d'argent comme promoteur, sous diverses conditions, il y a formation des liaisons α-1,3 ainsi que β-1,3. On a préparé les liaisons β-1,6 avec de bons rendements en faisant réagir le composé **9**, en présence de zéolite d'argent comme promoteur, avec soit le di-*O*-benzoyl-2,3 β-D-galactopyrranoside de trideutérométhyle (**8***b*) soit le *O*-benzoyl-2 *O*-(tri-*O*-acétyl-3,4,6 déoxy-2 phtalimido-2 β-D-glucopyrannosyl)-3 β-D-galactopyrannoside de trideutérométhyle (**11***b*). On a utilisé le bromure de tri-*O*-benzyl-2,3,4 α-L-fucopyrannosyle (**1***b*) pour la fucosylation, catalysée par les ions halogénures, du composé **2***a* ou de son isomère *O*-benzoyle-3 (**2***b*). Les glycosylations des bromures de di-*O*-acétyl-3,6 *O*-(tétra-*O*-acétyl-2,3,4,6 β-D-galactopyrannosyl)-4 déoxy-2 phtalimido-2 β-D-glucopyrannosyle (**6***b*) et de *O*-(tétra-*O*-acétyl-2,3,4,6 β-D-galactopyrannosyl)-4 tri-*O*-acétyl-2,3,6 α-D-glucopyrannosyle (**5***a*) par l'heptadeutéro-isopropanol se font sous l'influence du zéolite d'argent comme promoteur.

[Traduit par la revue]

As part of our program of studies of complex oligosaccharides, in particular those structures related to neoplasia (1), we have synthesized trisaccharide **13***c* and several related disaccharides **3***c*, **4***c*, **5***c*, **7***c*, and **10***c* as their β-glycosides. These anomerically pure oligosaccharides are suitable for the elucidation of their 3-dimensional structures by nmr spectroscopic techniques (2).

It is our premise that to understand the biological functions of cell surface oligosaccharides it is necessary to have detailed knowledge of their 3-dimensional structures. For example, the origin of the specificities of antibodies directed against tumour associated carbohydrate antigens (1) probably resides in the antigen's shape. Furthermore, it has been suggested that the conformations of N-linked oligosaccharides, glycoproteins with carbohydrates linked to the amidic nitrogen of asparagine residues, regulate the processing pathways for their biosynthesis. The conformational analyses of N-linked oligosaccharides has relied extensively on chemically synthesized component oligosaccharides, which have allowed for the examination of each component linkage separately (3). Of particular interest are branch points, since these are points of potential flexibility and interchain interactions.

In O-linked oligosaccharides, trisaccharide **13***c* represents the branch point of "I antigen" structures, GlcNAc-β-1,3-[GlcNAc-β-1,6-]-Gal-β-. Branching resulting from the glyco-

[1]For Part 7, see ref. 1; for Part 8, see ref. 36.

[2]Presented in part at the Conference of the Chemical Institute of Canada, Kingston, Ontario, June 1985.

[3]D.M.W. is a recipient of an NSERC postdoctoral fellowship.

[4]A participant in the honours program, Ryerson Institute of Technology, Toronto, Ontario.

[5]Author to whom correspondence may be addressed.

Can. J. Chem. Downloaded from www.nrcresearchpress.com by 78.46.186.204 on 09/07/12
For personal use only.

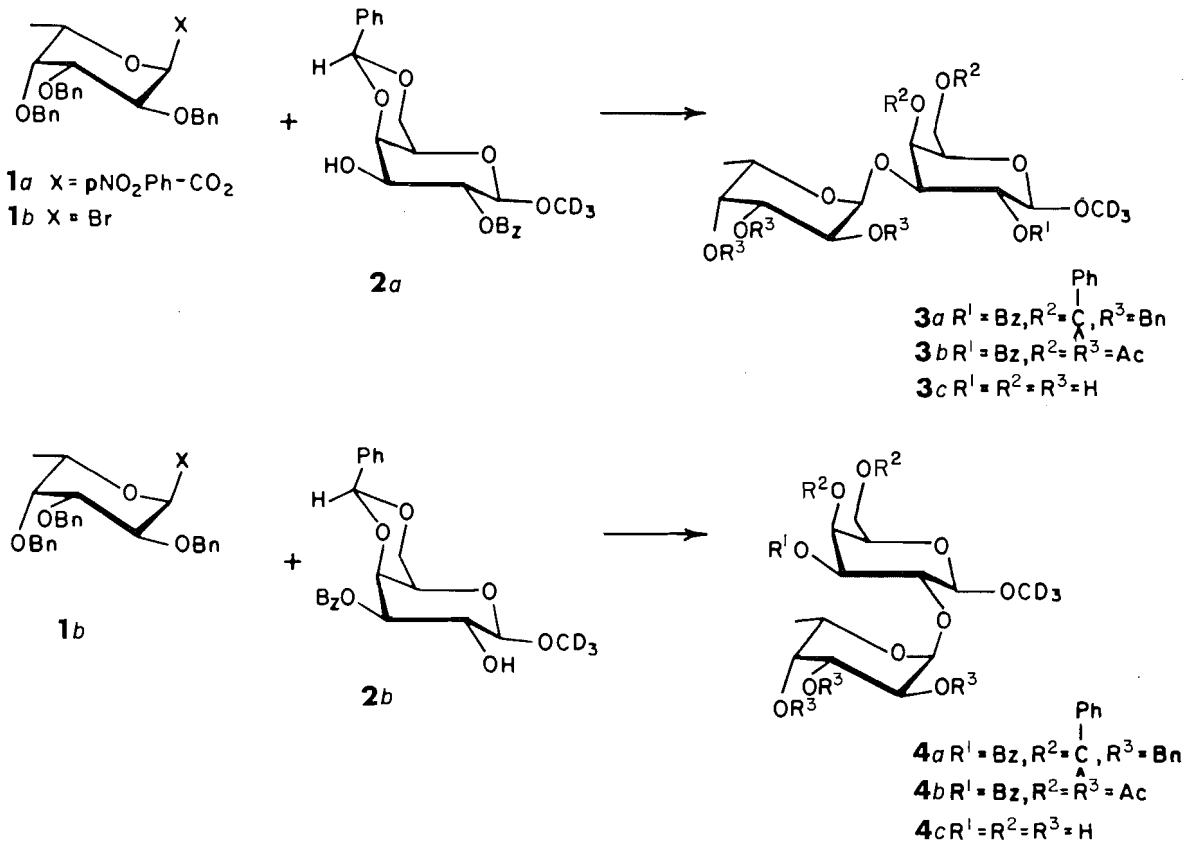

SCHEME 1. Syntheses of fucose disaccharides.

sylation of O-6 of the galactose residue of an "i" disaccharide fragment by another GlcNAc residue is responsible for the oncofetal differentiation from "i to I" structures. In fact, the previously prepared disaccharide **11***c* (4), GlcNAc-β-1,3-Gal-β-OCD_3, is an excellent acceptor for the GlcNAc transferase associated with this transformation (5, 6). A synthesis of the reducing trisaccharide related to **13** has been previously reported by Veyrières and co-workers (7) using a different synthetic design. The procedure described in this communication represents a simplification resulting in a better yield (75 vs. 40%) (4) of the β-1,3-linked β-disaccharide, **11***a*, and its subsequent elaboration into the β-trisaccharide **13***c*. This methodology applied to a galactose derivative, **8***a* (4), afforded the disaccharide **10***c*, GlcNAc-β-1,6-Gal-β-OCD_3.

Fucose containing disaccharides **3***c*, Fuc-α-1,3-Gal-β-OCD_3, and **4***c*, Fuc-α-1,2-Gal-β-OCD_3, are usually found at the non-reducing termini of oligosaccharides; for example the blood group H is associated with the structure Fuc-α-1,2-Gal-β-1,4-GlcNAc-β- and the grouping Fuc-α-1,3-Gal-β-1,4-Glc- has been found among the milk oligosaccharides (8). Syntheses of closely related derivatives of **4***c* have been reported by several groups (9, 10) and the 3-dimensional structure of this linkage has been elucidated by Lemieux and co-workers (11, 12).

The lactose disaccharides **5***c*, Gal-β-1,4-Glc-β-OC_3D_7, and **7***c*, Gal-β-1,4-GlcNAc-β-OC_3D_7, were prepared to investigate their conformations. They are ubiquitous structural elements of oligosaccharides found in glycoproteins and glycolipids. Syntheses of similar derivatives have been reported previously (13, 14). The solution conformations of the Gal-β-1,4-GlcNAc linkage have been studied (15–17) with reported values of ϕ (H1—C1—O—C4′) ranging from 40° to 55° and ψ (C1—O—C4′—H4′) from 0° to 20° in qualitative agreement with each other. The related Gal-β-1,4-Glc linkage has also been studied in solution (18, 19) with similar results. The reported solid state (20) conformation for β-lactose as determined by X-ray diffraction studies is $\phi \cong 50°$ and $\psi = 10°$, in qualitative agreement with the solution studies. However, the solid state conformation for β-lactosamine is $\phi \cong 30°$ and $\psi = -20°$, significantly different from the solution studies (21). Furthermore, Kochetkov and co-workers, studying related β-1,4 linkages, have presented evidence that a model considering a single predominant conformer (22), as in the studies above, is not sufficient to account for the experimental data and so the conformational preference(s) of these β-1,4 linkages still requires further investigations.

Synthesis of fucose disaccharides

The fucose containing β-disaccharides **3***c* and **4***c* were prepared by glycosylation of the galactose derivatives **2***a* and **2***b* (4) at O3 and O2 respectively (see Scheme 1) with bromide **1***b*, using the halide ion catalyzed method (8), to yield fully protected β-disaccharides **3***a* and **4***a*. The ^1H nmr spectra for these and all subsequent protected oligosaccharides are summarized in Table 1. It is interesting to note that the resonances of the benzoate group were very useful in assessing both the outcome and the purity of individual synthetic transformations.

The benzyl and the benzylidene groups were removed by hydrogenation in glacial acetic acid employing palladium black as catalyst (4).[6] Subsequent acetylation afforded the fully acylated derivatives **3***b* and **4***b*, which were purified by silica gel

[6]It should be noted that the benzoate groups at O2 (**3***b*) or O3 (**4***b*) were not removed during hydrogenolysis, cf. ref. 4.

Can. J. Chem. Downloaded from www.nrcresearchpress.com by 78.46.186.204 on 09/07/12
For personal use only.

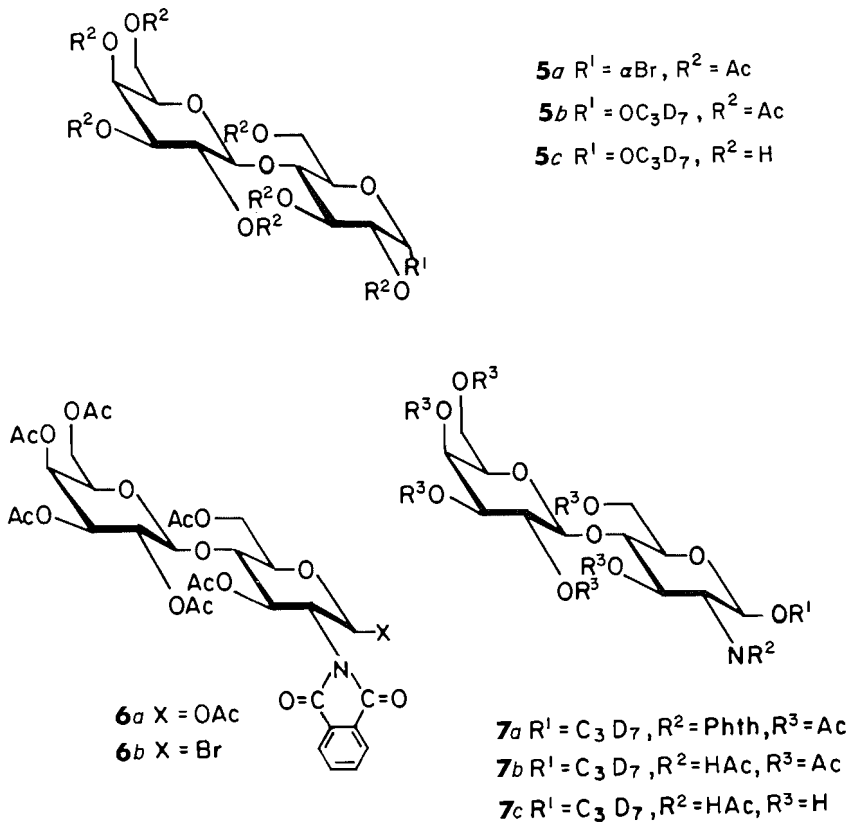

SCHEME 2. Syntheses of lactose derivatives.

column chromatography (23), and then deprotected to **3***c* and **4***c* by Zemplen transesterification in 28 and 40% overall isolated yields from **2***a* and **2***b* respectively. The physical data for **4***c* agree well with the reported values (see Experimental) (9). The ^{13}C and ^{1}H nmr spectra are summarized in Tables 2 and 3.

Syntheses of lactose derivatives

The disaccharide Gal-β-1,4-Glc-β-OC_3D_7, **5***c*, was prepared from peracetylated bromide **5***a*, silver zeolite, and a slight excess of heptadeuterioisopropanol (24, 25) (see Scheme 2). Peracetylated glycoside **5***b* was purified by silica gel chromatography and subsequently deprotected under Zemplen conditions to give **5***c*. The β-disaccharide **7***a* was prepared in an analogous manner from the bromide **6***b* (26) generated from the accessible acetate **6***a*. The peracetate **7***b* was obtained by treatment with hydrazine hydrate at 70°C for 30 min, followed by complete acetylation. Zemplen transesterification gave **7***c* in 57% overall isolated yield from **6***a*.

Synthesis of I antigen branch point trisaccharide

The β-1,6-linked β-disaccharide **10***c* was prepared from the trideuteriomethyl 2,3-di-*O*-benzoyl-β-D-galactopyranoside (**8***b*) accessible from the 4,6-benzylidene derivative **8***a* (4) by hydrogenation on palladium black in acetic acid. The primary 6-OH was sufficiently more reactive than the 4-OH that it reacted regiospecifically with 3,4,6-tri-*O*-acetyl-2-deoxy-2-phthalimido-β-D-glucopyranosyl bromide (**9**), using silver zeolite, to give the required β-1,6-linked β-disaccharide in 79% yield (see Scheme 3). The deprotected β-disaccharide **10***c* was obtained in 78% yield from **10***a* by the hydrazine hydrate, acetylation, and Zemplen transesterification sequence. The nmr spectral data summarized in Tables 2 and 3 agree with the data reported for this linkage in other small oligosaccharides (27, 28).

The formation of the β-1,3 linkage in β-disaccharide **11***a* using silver zeolite (40% yield) as promoter from alcohol **2***a* and bromide **9** was previously reported (4). A subsequent attempt to increase the yield, by adding more bromide **9** and continuing the room temperature stirring for up to a week, did result in an apparent increase in yield (about 60%). The reaction product consisted of an approximately 2:3 α:β mixture of **11***a* and undesired **12***a* as determined from ^{1}H nmr analysis of the crude reaction product (see Scheme 4). This mixture could be completely separated by preparative hplc. The ^{1}H and ^{13}C nmr data clearly show the compound **12***a* to be the α-1,3-linked isomer of **11***a* (e.g. H1 GlcNPhth: δ = 5.225, J_{1-2} = 3.6 Hz; and C1 GlcNPhth: δ = 93.7, J_{C1-H1} = 172 Hz). This result was surprising since reports using bromide **9** or the similar bromide **6***b* describe the exclusive formation of β linkages (29, 30). Systematic variations of reaction conditions using freshly prepared aglycon **2***a*, bromide **9**, or silver zeolite led to similar mixtures. Further experiments, using 2 equivalents of bromide **9** and either overnight ultrasonic agitation or heating at 55–60°C, always resulted in similar mixtures with a reproducible crude yield (90%) of 1:2 α:β using ultrasonic agitation or (80%) of 4:3 α:β without ultrasound agitation. The heating experiment was performed as a control since the propylene glycol used in the ultrasonic bath reached 55–60°C. We originally thought that acid was produced under these conditions, which would then lead to a Fischer-like equilibrium. This explanation was ruled out by the following observations: an addition of the soluble bases 2,4,6-trimethylpyridine (*s*-collidine) or tetramethylurea led to almost complete suppression of product formation (about

Can. J. Chem. Downloaded from www.nrcresearchpress.com by 78.46.186.204 on 09/07/12
For personal use only.

TABLE 1. ^{1}H nuclear magnetic resonance spectra of synthetic intermediates

Sugar	H1 (J_{12})	H2 (J_{23})	H3 (J_{34})	H4 (J_{45})	H5 (J_{56})	H6 ($J_{66'}$)	H6′ ($J_{56'}$)
				3*a*			
Fuc	4.805 d (3.45)	3.78 dd[(1)a] (10.2)	3.889 dd (2.7)	3.489 brd	4.09 m[(2)]	0.910 d[b] (6.5)	
Gal	4.628 d (8.3)	5.650 dd (10.0)	3.79 dd[(1)] (3.1)	4.343 dd (<0.5)	3.523 brs (<0.5)	4.353 brd (−12.6)	4.250 brd (<0.5)
Aromatics	Bz(o) 8.05 dd(2), remainder 7.54–6.98 m(18) (7.2, 1.2)						
Benzyl	CH_2 4.868 d(1), 4.623 d(1), 4.551 d(1), 4.514 d(1), 4.09 m[(2)] (2) (−11.5) (−11.3) (−11.9) (−11.5)						
Benzylidene	PhCHO$_2$ 5.511 s(1)						
				3*b*			
Fuc	5.177 d (3.7)	4.976 dd (11.0)	5.183 dd (3.3)	5.247 brd (<0.5)	4.377 brq	1.157 d[b] (6.4)	
Gal	4.416 d (8.0)	5.479 dd (9.1)	4.206 dd (3.0)	5.391 brd (<0.5)	3.951 brdd (6.4)[c]	4.203 dd (2.1)	4.130 dd (7.1)
Acetates	2.254, 2.105, 2.084, 2.045, 1.918 5 × s(3)						
Aromatics	Bz(o) 7.978 brd(2), Bz(p) 7.595 brt(1), Bz(m) 7.453 brt(2) (8.0) (7.5) (7.6)						
				4*a*			
Fuc	5.427 d (3.7)	3.952 dd (10.1)	3.873 dd (2.6)	3.670 brd (<0.5)	4.28 m[(5)]	1.140 d[b] (6.4)	
Gal	4.533 d (7.8)	4.398 dd (9.8)	5.354 dd (3.7)	4.29 m[(5)] (<0.5)	3.578 brs (<0.5)	4.359 dd (−12.2)	4.086 dd (1.1)
Aromatics	Bz(o) 8.005 brd(2), Bz(p) 7.533 brt(1), 7.45 m(2), Bz(m) 7.363 brt(2) (7.4) (7.4) (7.8) 7.32–7.20 m(13), 7.122 brt(1), 7.055 brt(2), 6.933 brd(2) (7.1) (7.3) (7.2)						
Benzyls	CH_2 4.931 d(1), 4.735 d(1), 4.630 d(2), 4.537 d(1), 4.28 m[(5)] (1) (−11.6) (−11.6) (−11.6) (−12.3)						
Benzylidene	PhCHO$_2$ 5.485 s(1)						
				4*b*			
Fuc	5.247 d (1.8)	5.268 dd (10.4)	5.086 dd (3.8)	5.288 brd (<0.5)	4.515 brq	1.142 d[b] (6.5)	
Gal	4.486 d (7.7)	4.075 dd (10.0)	5.309 dd (3.5)	5.512 dd (0.6)	3.987 brt (7.7)	4.215 dd (−11.8)	4.137 dd (6.6)
Acetates	2.124, 2.060, 2.052, 1.931, 1.597 5 × s(3)						
Aromatics	Bz(o) 7.881 dd(2), Bz(p) 7.594 tt(1), Bz(m) 7.363 brt(2) (7.7, 1.4) (7.6, 1.1) (7.7)						
				5*b*			
Gal	4.413 d (7.9)	5.039 dd (10.4)	4.882 dd (3.4)	5.274 brd (<0.5)	3.804 brt (6.5)	4.05 m[(6)] —	4.05 m[(6)] —
Glc	4.439 d (8.1)	4.776 dd (9.6)	5.123 dd (9.4)	3.700 dd (9.8)	3.524 ddd (2.0)	4.399 dd (−12.0)	4.05 m[(6)] (5.3)
Acetates	2.082 s(3), 2.041 s(3), 1.991 s(3), 1.975 brs(6), 1.961 s(3), 1.895 s(3)						
				7*a*			
Gal	4.536 d (7.9)	5.128 dd[(7)] (10.4)	4.956 dd (3.5)	5.333 brd (<0.5)	3.848 m[(8)] (4.8)	4.068 m[(9)] (−11.2)	4.037 m[(9)] (7.5)
GlcNPhth	5.414 d (8.5)	4.174 m[(9)] (10.4)	5.739 dd (10.6)	3.846 dd[(8)] (8)	3.805 m[(8)] (1.6)	4.509 m[(7)] (−11.9)	4.156 m[(9)] (4.9)
Acetates	2.137 brs(6), 2.070 s(3), 2.042 s(3), 1.966 s(3), 1.902(3)						
Aromatics	Phth(o) 7.847 m(2), Phth(m) 7.731 m(2)						
				7*b*			
Gal	4.494 d (7.7)	5.13 m[(10)] (10.7)	4.967 dd (3.6)	5.354 brd (<0.5)	3.9 m[(11)] —	4.1 m[(12)] —	3.9 m[(11)] —
GlcNAc	4.542 d (7.7)	4.15 m[(12)] —	5.13 m[(10)] —	3.754 dd (8.7)	3.616 m (2.7)	4.483 dd (−11.6)	4.1 m[(12)] —
N—H	5.486 d (8.8)						
Acetates	2.153 s(3), 2.107 s(3), 2.073 s(3), 2.058 brs(6), 1.971 s(3), 1.957 s(3)						

Can. J. Chem. Downloaded from www.nrcresearchpress.com by 78.46.186.204 on 09/07/12
For personal use only.

TABLE 1 (*Concluded*)

Sugar	H1 (J_{12})	H2 (J_{23})	H3 (J_{34})	H4 (J_{45})	H5 (J_{56})	H6 ($J_{66'}$)	H6′ ($J_{56'}$)
				8*b*			
Gal	4.647 d	5.767 dd	5.307 dd	4.413 brt	3.79 brt	4.0 m[13]	4.0 m[13]
	(7.9)	(10.3)	(3.2)	(<0.5)	—	—	—
Aromatics	Bz(o) 7.95 m(4), Bz(p) 7.48 m(2), Bz(m) 7.34 m(4)						
Hydroxyls	OH4 3.219 d (4.3), OH6 2.71 brt						
				10*a*			
GlcNPhth	5.488 d	4.31 dd[14]	5.785 dd	5.147 dd	3.88 m[15]	4.31 m[14]	4.167 dd
	(8.5)	(10.6)	(9.2)	(9.9)	—	(−12.2)	(4.9)
Gal	4.460 d	5.651 dd	5.202 dd	4.240 brd	3.742 brt	3.88 m[15]	4.070 dd
	(7.9)	(10.3)	(3.1)	(<0.5)	(6.1)	(−10.3)	(6.3)
Acetates	2.032, 2.026, 1.863 3 × s(3)						
Aromatics	Bz(o) 7.949, 7.929 2 × brdd(4), Bz(p) 7.48 m(2), Bz(m) 7.35 brt(4)						
	(2 × 7.0, 1.1)				(7.5)		
	Phth(o) 7.852 brdd (2), Phth(m) 7.725 brdd (2)						
	(5.3, 3.0)						
				10*b*			
GlcNAc	4.865 brd	3.594 ddd	5.39 m[16]	5.031 dd	3.72 m[17]	4.130 dd	4.257 dd
	(8.3)	(10.6)	(9.7)	(9.7)	(2.2)	(−12.2)	(4.3)
N—H	5.673 d (7.9)						
Gal	4.389 d	5.180 dd	4.975 dd	5.39 m[16]	3.73 m[17]	3.85 m[18]	3.85 m[18]
	(7.9)	(10.4)	(2.9)	(<0.5)	—	—	—
Acetates	2.137, 2.091, 2.064, 2.027, 2.023, 1.971, 1.954 7 × s(3)						
				12*a*			
GlcNPhth	5.225 d	4.452 dd	6.384 dd	4.912 dd	3.9 m[19]	4.787 dd	3.9 m[19]
	(3.6)	(11.5)	(9.4)	(10.1)	(2.9)	(−12.2)	—
Gal	4.618 d	5.567 dd	4.037 dd	4.081 brd	3.425 brs	4.241 brd	3.9 m[19]
	(7.9)	(10.0)	(2.9)	(2.9)	(<0.5)	(−12.2)	(<0.5)
Acetates	2.072, 1.776, 1.700 3 × s(3)						
Aromatics	Bz(o) 8.153 brd(2), Bz(p) 7.599 brt(1), Bz(m) 7.501 brt(2), 7.408 brs(4), 7.199 m(1), 7.115 brd(4)						
	(7.2)		(7.2)	(7.2)		(4.3)	(4.3)
Benzylidene	PhC*H*O$_2$ 4.955 s(1)						
				13*a*			
GlcNPhth	5.483 d	4.36 m[20]	5.782 dd	5.188 dd	3.89 m[21]	4.36 m[20]	4.18 m[22]
(1,3)	(8.4)	(10.6)	(9.3)	(9.8)	—	—	—
GlcNPhth	5.360 d	4.267 dd	5.558 dd	5.020 dd	3.499 m	4.18 m[22]	4.08 m[23]
(1,6)	(8.5)	(10.6)	(9.3)	(9.8)	—	—	—
Gal	4.188 d	5.194 dd	3.685 dd	3.955 brd	3.56 brt	3.89 m[21]	4.08 m[23]
	(7.8)	(10.0)	(3.2)	(<0.5)	(5.9)	—	—
Acetates	2.144, 2.105, 2.040, 2.020, 1.865, 1.754 6 × s(3)						
Aromatics	Phth 7.8 vbrm(4), Phth(o) 7.425 dd(2), Phth(m) dd 7.330(2)						
	—		(5.4, 3.1)		(5.4, 3.1)		
	Bz(o) 7.543 dd(2), Bz(p) 7.391 m(1), Bz(m) 7.125 brt						
	(7.7, 1.2)		—		(7.7)		
				13*b*			
GlcNAc	5.036 d[24]	3.350 ddd	5.48 m[25]	5.07 m[24]	3.68 m[26]	4.135 dd	4.264 dd
(1,3)	(8.1)	(10.5)	(9.1)	—	(2.2)	(−12.2)	(4.5)
N—H	5.558 d (7.9)						
GlcNAc	4.822 d	3.567 m[27]	5.45 m[25]	5.05 m[24]	3.72 m[26]	4.413 dd	4.039 dd
(1,6)	(8.2)	(10.1)	(9.1)	—	(2.2)	(−12.2)	(3.5)
N—H	6.227 d (8.2)						
Gal	4.277 d	5.05 m[24]	3.809 dd	5.342 brd	3.889 brdd	3.72 m[26]	3.58 m[27]
	(7.9)	(10.0)	(3.4)	(<0.5)	(5.5)	—	(10.3)
Acetates	2.131 s(3), 2.104 s(3), 2.101 s(3), 2.086 s(3), 2.022 s(9), 2.015 s(3), 1.934 s(3), 1.912 s(3)						

[a](1),(2),(5),(6)–(27) Resonances overlapped with resonances marked with the same superscript number.
[b]Methyl of fucose with (J_{H5-CH_3}).
[c]Spin system is not first order.
NOTE: In most cases it was possible to assign all resonances by conventional decoupling techniques. All chemical shifts and coupling constants are from a first-order analysis, i.e., from peak separations. Overlapping resonances are marked with the same superscript numbers, e.g. (1), (2), etc.

Can. J. Chem. Downloaded from www.nrcresearchpress.com by 78.46.186.204 on 09/07/12
For personal use only.

TABLE 2. ^{13}C nuclear magnetic resonance spectra of oligosaccharides

Sugar	C1	C2	C3	C4	C5	C6	C=O	CH_3
				Fuc-α-1,3-Gal-β-OCD_3, **3***c*				
Fuc	101.55	69.02	69.96	72.33	67.77			15.92
Gal	104.02	70.58	81.60	69.24	75.62	61.48		
				Fuc-α-1,2-Gal-β-OCD_3, **4***c*				
Fuc	100.75	69.14	70.29	72.60	67.54			15.89
Gal	103.33	78.91	73.94	69.45	75.56	61.62		
				Gal-β-1,4-Glc-β-OC_3D_7, **5***c*				
Gal	103.77	71.78	73.37	69.38	76.15	61.87		
Glc	101.09	73.69	75.30	79.34	75.51	61.01		
				Gal-β-1,4-GlcNAc-β-OC_3D_7, **7***c*				
Gal	104.21	72.25	73.81	69.84	76.62	62.35		
GlcNAc	100.90	56.60	73.76	79.82	76.00	61.40	175.69	23.50
				GlcNAc-β-1,6-Gal-β-OCD_3, **10***c*				
GlcNAc	102.36	56.33	74.45	70.54	76.53	61.53	175.30	23.00
Gal	104.47	71.50	73.50	69.53	74.37	69.72		
				GlcNAc-β-1,3-Gal-β-OCD_3, **11***c*				
GlcNAc	103.55	56.57	74.45	70.54	76.53	61.34	175.80	23.00
Gal	104.67	70.59	83.05	69.20	75.55	61.76		
				GlcNAc-β-1,3-[GlcNAc-β-1,6]-Gal-β-OCD_3, **13***c*				
GlcNAc-1,3	103.51	56.53	74.40	70.45	76.48	61.28	175.78	22.97
GlcNAc-1,6	102.28	56.29	74.54	70.70	76.62	61.48	175.24	22.97
Gal	104.44	70.47	82.83	69.35	74.22	70.15		

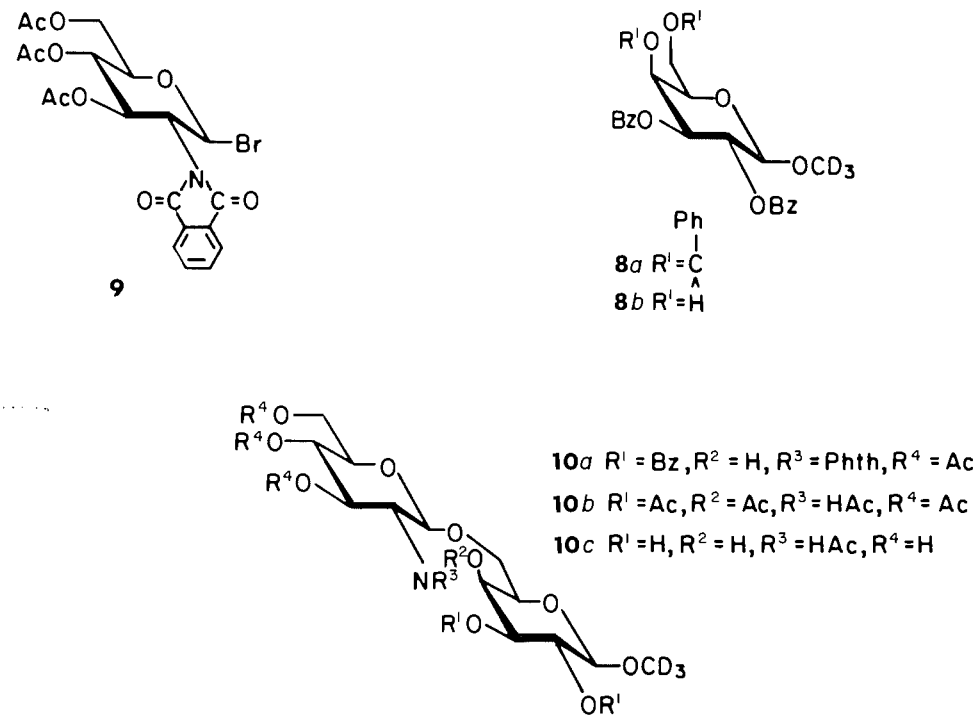

SCHEME 3. Synthesis of GlcNAc-β-1,6 disaccharide.

5% after 7 days of heating), while an addition of the insoluble silver carbonate and subsequent heating or ultrasonic agitation led to a similar α:β mixture, and an addition of the non-nucleophilic base 2,6-di-*tert*-butyl-4-methylpyridine (31) led to a high yield of a similar mixture. The desired β-disaccharide **11***a* was finally obtained using the last mentioned base and silver triflate in a 75% isolated yield. These results strongly support Paulsen's proposals that the glycosylation mechanism(s) using insoluble catalysts like silver zeolite or silver silicate are fundamentally different from soluble promoters

Can. J. Chem. Downloaded from www.nrcresearchpress.com by 78.46.186.204 on 09/07/12
For personal use only.

TABLE 3. ^{1}H nuclear magnetic resonance spectra of oligosaccharides

Sugar	H1 (J_{12})	H2 (J_{23})	H3 (J_{34})	H4 (J_{45})	H5 (J_{56})	H6 ($J_{66'}$)	H6′ ($J_{56'}$)
				Fuc-α-1,3-Gal-β-OCD_3, **3***c*			
Fuc	5.152 d	3.776 dd	3.928 dd	3.824 brd	4.191 brq	1.206[a] d	
	(4.0)	(10.4)	(3.3)	(<0.5)		(6.4)	
Gal	4.375 d	3.670 dd	3.678 dd	4.023 brd	3.695 m[(2)b]	3.754 m[(2)]	3.723 m[(2)]
	(7.9)	(10.4)	(2.9)	(<0.5)	—	—	—
				Fuc-α-1,2-Gal-β-OCD_3, **4***c*			
Fuc	5.117 d	3.778 dd	3.854 dd	3.799 brd	4.248 brq	1.204[a] d	
	(3.9)	(10.3)	(3.2)	(<0.5)		(6.6)	
Gal	4.407 d	3.513 dd	3.822 m	3.906 brd	3.676 ddd	3.769 m	3.748 m
	(7.8)	(9.6)	(3.4)	(0.6)	(7.8)	(−11.8)	(4.4)
				Gal-β-1,4-Glc-β-OC_3D_7, **5***c*			
Gal	4.438 d	3.536 dd	3.638 dd	3.918 brd	3.699 brd	3.789 dd	3.734 dd
	(7.8)	(9.9)	(3.4)	(<0.5)	(7.2)	(−12.2)	(3.6)
Glc	4.552 d	3.255 m[c]	3.644 m[c]	3.628 m[c]	3.593 m[c]	3.957 dd	3.768 dd
	(8.0)	—	—	—	(1.9)	(−12.4)	(4.7)
				Gal-β-1,4-GlcNAc-β-OC_3D_7, **7***c*			
Gal	4.470 d	3.535 dd	3.666 dd	3.924 brd	3.718 brdd	3.762 dd	3.752 dd
	(7.8)	(10.0)	(3.4)	(<0.5)	(3.1)	(−11.8)	(6.4)
GlcNAc	4.602 dd[d]	3.674 m[(5)]	3.688 m[(5)]	3.685 m[(5)]	3.546 m	3.972 dd	3.819 dd
	(7.6)	—	—	—	(1.9)	(−12.2)	(5.1)
				GlcNAc-β-1,6-Gal-β-OCD_3, **10***c*			
GlcNAc	4.544 d	3.713 dd	3.553 m[(6)]	3.468 m[(7)]	3.461 m[(7)]	3.937 dd	3.765 dd
	(8.4)	(10.2)	(9.8)	—	(1.5)	(−12.2)	(6.5)
$NHCOCH_3$	2.033						
Gal	4.292 d	3.486 dd	3.628 dd	3.889 brd	3.778 m[e]	4.026 m[e]	3.774 m[e]
	(7.9)	(9.9)	(3.4)	(<0.5)	(5.0)	(−12.0)	(7.5)
				GlcNAc-β-1,3-Gal-β-OCD_3, **11***c* (4)			
GlcNAc	4.690 d	3.729 dd	3.523 dd	3.47 m[(9)]	3.45 m[(9)]	3.80 m[(10)]	3.90 dd
	(8.4)	(10.2)	(9.8)	—	—	(−12.2)	(6.5)
$NHCOCH_3$	2.030						
Gal	4.298 d	3.541 dd	3.69 m[(11)]	4.138 brd	3.69 m[(11)]	3.8 m[(10)]	3.8 m[(10)]
	(8.0)	(8.0)	(3.2)	(<0.5)	(4.1)	—	—
				GlcNAc-β-1,3-[GlcNAc-β-1,6]-Gal-β-OCD_3, **13***c*			
GlcNAc-1,3	4.685 d	3.729 dd	3.548 dd	3.462 m[(12)]	3.433 m[(12)]	3.890 dd	3.737 dd
	(8.5)	(10.2)	(9.2)	(8.9)	(0.4)	(−12.2)	(5.1)
$NHCOCH_3$	2.030						
GlcNAc-1,6	4.531 d	3.708 dd	3.540 dd	3.440 m[(12)]	3.456 m[(12)]	3.926 dd	3.744 dd
	(8.4)	(10.2)	(9.2)	(8.9)	(<0.5)	(−12.2)	(5.1)
$NHCOCH_3$	2.030						
Gal	4.274 d	3.537 dd	3.691 dd	4.112 dd	3.775 m[f]	4.033 dd[f]	3.754 m[f]
	(7.9)	(9.8)	(3.3)	(<0.5)	(4.5)	(−12.0)	(7.5)

[a]Methyl of fucose with (J_{H5-CH_3}).
[b](2),(5)–(7) and (9)–(12) Resonances overlapped with resonances marked with the same superscript number.
[c]These resonances (Glc H2, H3, H4, and H5) are not a first-order spin system and Glc H2 shows at least 8 lines due to the overlap of H3 and H4.
[d]This resonance shows virtual coupling due to overlap of GlcNAc H2, H3 and H4.
[e]These resonances form a non-first-order spin system. The assignments were made by simulations.
[f]These resonances form a non-first-order spin system. The assignments were made by simulations.

(32). It has been suggested (24) that some type of solid surface carbonium ion pair is the reactive species, with the aglycon approaching from the opposite face leading in some cases to the thermodynamically unfavorable isomer (20).

This easy access to compound **11***a* made it a good starting material for the synthesis of trisaccharide **13***c* by the following sequence of reactions. The benzylidene group of **11***a* was cleaved (4) by hydrogenolysis using palladium black in acetic acid and the resulting diol **11***b* was treated with bromide **9** using silver zeolite as promoter to give protected trisaccharide **13***a* in 63% yield after purification. The deprotected trisaccharide **13***c* was obtained by a hydrazine hydrate, acetylation, and Zemplen transesterification sequence as described above in 67% yield from **13***a*. The nmr spectral data summarized in Tables 2 and 3 agree well with the values for β-disaccharides **10***c* and **11***c*. The analysis of the nmr data in our study of the 3-dimensional structure of these compounds will be published in a separate communication.

Can. J. Chem. Downloaded from www.nrcresearchpress.com by 78.46.186.204 on 09/07/12
For personal use only.

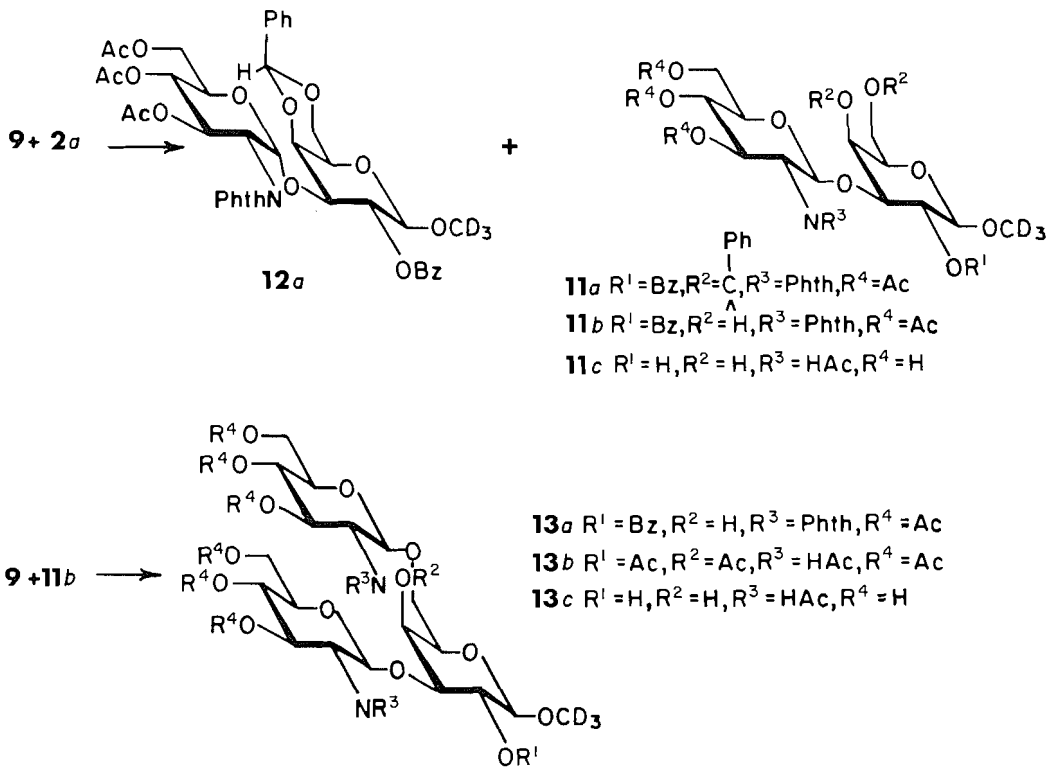

SCHEME 4. Synthesis of I antigen branchpoint trisaccharide.

Experimental

General methods

Melting points were determined on a Reichert Thermovar melting point apparatus and are uncorrected. Optical rotations were measured with a Perkin–Elmer polarimeter (Model 243 B) at 26 ± 1°C. Microanalyses were performed by the Microanalytical Laboratory Ltd., Markham, Ontario. The ^{1}H nmr spectra were recorded at 360.06 MHz with a Nicolet spectrometer at the NMR Spectroscopy laboratory of the Centre for the Determination of Carbohydrate Structures, University of Toronto. The ^{13}C nmr spectra were recorded at 100.566 MHz with a Varian XL-400 spectrometer at the Chemistry Department, University of Toronto. Spectra were obtained at 19 ± 2°C either in $CDCl_3$ containing a trace of TMS (0 ppm, ^{1}H and ^{13}C) as the internal standard or in D_2O (99.996%, Aldrich) containing a trace of acetone (2.225 ppm relative to internal DSS, ^{1}H) as the internal standard. The ^{13}C spectra in D_2O were referenced to external dioxane (67.4 ppm relative to TMS). Chemical shifts are cited in δ (ppm) scale and coupling constants are in Hz. Samples for nmr analyses in D_2O were passed through a Chelex 100 (Bio-Rad) ion-exchange resin in doubly distilled H_2O to remove paramagnetic impurities, lyophilized, and then lyophilized three times with D_2O. The ir spectra were recorded on a Perkin–Elmer (Model 1430) spectrometer using thin film on NaCl plates. Fast Atom Bombardment mass spectra (FAB-MS) were recorded with a VG Analytical ZAB HF reverse geometry instrument (for general conditions cf. ref. 33) at the Institute of Physiological Chemistry, University of Bonn, through the courtesy of Dr. H. Egge.

Thin-layer chromatography (tlc) was performed on silica gel $60F_{254}$ (Merck) plastic plates and visualized by spraying with 50% sulfuric acid and (or) 1% orcinol acidic ferric chloride (34) and heating at 200°C. Silica gel (230–400 mesh; Toronto Research Chemicals) was used for flash chromatography. All starting materials were dried overnight under vacuum (10^{-3} Torr; 1 Torr = 133.3 Pa) prior to use and the solvents were distilled from appropriate drying agents. Solutions were concentrated at water aspirator pressure.

*Trideuteriomethyl 2-O-benzoyl-4,6-O-benzylidene-3-O-(2,3,4-tri-O-benzyl-α-L-fucopyranosyl)-β-D-galactopyranoside (**3**a)*

Activated molecular sieves 3A (5 g), tetraethylammonium bromide (7.5 g; 35 mmol), alcohol **2***a* (1.5 g; 3.85 mmol), and dichloromethane (50 mL) were mixed and stirred for 1 h. Then tribenzyl fucosyl bromide (35) **1***b* prepared from *p*-nitrobenzoate **1***a* (3.5 g; 6.2 mmol) in dichloromethane (50 mL) was added and the resulting mixture was left to stir for 6 days in the dark under an argon atmosphere. The mixture was diluted with dichloromethane (50 mL), filtered through Celite, rinsed with dichloromethane (50 mL), washed with cold water (2 × 200 mL), dried over Na_2SO_4, filtered, and evaporated to dryness. The disaccharide **3***a* was purified by flash chromatography (silica gel, hexane:ethyl acetate 60:40) as eluant to yield 1.4 g (45%); mp 68–70°C; $[\alpha]_D$ +47.0° (*c* 0.99, chloroform); ir (neat): 1720 (CO) cm^{-1}; ^{13}C nmr ($CDCl_3$) δ: 165.3 (CO), 101.72 ($PhCHO_2$[(1)],[7] $^2J_{C-H}$ 158), 101.3 (C1-Gal[(1)], $^2J_{C-H}$ 161), 100.5 (C1-Fuc, $^2J_{C-H}$ 166). *Anal.* calcd. for $C_{48}H_{47}D_3O_{11}$ (805.89): C 71.54, H 5.88; found: C 71.33, H 5.68.

*Trideuteriomethyl 4,6-di-O-acetyl-2-O-benzoyl-3-O-(2,3,4-tri-O-acetyl-α-L-fucopyranosyl)-β-D-galactopyranoside (**3**b)*

Hydrogenolysis of the disaccharide **3***a* (1.0 g; 1.24 mmol) in glacial acetic acid (30 mL) on Pd black (350 mg; Strem) at room temperature overnight gave, after removal of the solids by filtration through Celite, rinsing with ethyl acetate (50 mL) and toluene (50 mL), and evaporation, a syrupy residue. The residue was dissolved in toluene (2 × 50 mL) and the solvent was evaporated. To this residue was added pyridine (12 mL) and acetic anhydride (6 mL) and the mixture was stirred under argon overnight. Toluene (25 mL) was added and the mixture evaporated. The residue was taken up in dichloromethane (50 mL) and washed with water (3 × 50 mL), dried over Na_2SO_4, filtered, and the solvents evaporated. This yielded, after purification by flash chromatography (silica gel, ethyl acetate:hexane 50:50), disaccharide **3***b* (540 mg; 66%); mp 102–104°C; $[\alpha]_D$ −46.5° (*c* 1.84, chloroform); ir (neat): 1750 and 1720 sh (CO) cm^{-1}. *Anal.* calcd. for $C_{30}H_{35}D_3O_{16}$ (657.60): C 54.79, H 5.36; found: C 54.83, H 5.43.

*Trideuteriomethyl 3-O-α-L-fucopyranosyl-β-D-galactopyranoside (**3**c)*

Protected disaccharide **3***b* (125 mg; 0.19 mmol) was dissolved in methanol (20 mL), 1 *M* methanolic NaOMe (0.4 mL) was added, and

[7]Assignments may be interchanged with resonances marked with the same superscript number, e.g. (1).

Can. J. Chem. Downloaded from www.nrcresearchpress.com by 78.46.186.204 on 09/07/12
For personal use only.

Can. J. Chem. Downloaded from www.nrcresearchpress.com by 78.46.186.204 on 09/07/12
For personal use only.

the solution was stirred under argon for 14 h. After neutralization with Dowex 80W-8X H^+ ion exchange resin, filtration, and evaporation of the solvent, the residue was crystallized from methanol/benzene/hexane to yield **3***c* (61 mg; 94%); mp 218–221°C; $[\alpha]_D$ −123.1° (*c* 0.67, $CH_3OH:H_2O$, 9:1); ir (neat): 3300 (br, OH) cm^{-1}. *Anal.* calcd. for $C_{13}H_{21}D_3O_{10}$ (343.31): C 45.40, H 6.16; found: C 45.53, H 6.36.

*Trideuteriomethyl 3-O-benzoyl-4,6-O-benzylidene-2-O-(2,3,4-tri-O-benzyl-α-L-fucopyranosyl)-β-D-galactopyranoside (**4**a)*

Compound **4***a* was prepared as for compound **3***a* using tetraethylammonium bromide (15 g; 71 mmol), alcohol **2***b* (3.0 g; 7.7 mmol), molecular sieves 3A (10 g), and tribenzyl fucosyl bromide **1***b* (12.4 mmol). The disaccharide **4***a* was purified by flash chromatography (silica gel, hexane:ethyl acetate 65:35) to yield 4.1 g (66%); mp 149–152°C; $[\alpha]_D$ +2.3° (*c* 0.64, $CHCl_3$); ir (neat): 1730 (CO) cm^{-1}; ^{13}C nmr ($CDCl_3$) δ: 165.9 (CO), 102.6 ($PhCHO_2$[(2)],[8] $^3J_{C-H}$ 158), 100.7 (C1–Gal[(2)],[8] $^2J_{C-H}$ 161), 97.2 (C1-Fuc, $^2J_{C-H}$ 170). *Anal.* calcd. for $C_{48}H_{47}D_3O_{11}$ (805.89): C 70.51, H 5.88; found: C 71.38, H 5.76.

*Trideuteriomethyl 4,6-di-O-acetyl-3-O-benzoyl-2-O-(2,3,4-tri-O-acetyl-α-Lfucopyranosyl)-β-D-galactopyranoside (**4**b)*

Compound **4***a* (3.5 g; 4.34 mmol) was hydrogenated using the same conditions as for compound **3***a* and subsequently acetylated in the same manner. The disaccharide **4***b* was purified by flash chromatography (silica gel, ethyl acetate:hexane 50:50) to yield 2.2 g (66%); mp 71–73°C; $[\alpha]_D$ −48.7° (*c* 1.02, $CHCl_3$); ir (neat): 1750 and 1720 sh (CO) cm^{-1}; ^{13}C nmr δ ($CDCl_3$): 169.4–170.4 (4 × CH_3CO), 165.0 (Ph*C*O), 102.2 (C1-Gal, $^2J_{C-H}$ 161), 96.9 (C1-Fuc, $^2J_{C-H}$ 174). *Anal.* calcd. for $C_{30}H_{35}D_3O_{16}$ (657.60): C 54.79, H 5.36; found: C 55.16, H 5.34.

*Trideuteriomethyl 2-O-α-L-fucopyranosyl-β-D-galactopyranoside (**4**c)*

The ester protecting groups were removed from **4***b* (200 mg; 0.3 mmol) under Zemplen conditions as described for compound **3***b*. The residue was crystallized from methanol/benzene/hexane to yield **4***c* (95 mg; 91%); mp 123–126°C; $[\alpha]_D$ −102.1° (*c* 1.24, $CH_3OH:H_2O$ 3:1); ir (neat): 3300 (br, OH) cm^{-1}. *Anal.* calcd. for $C_{13}H_{21}D_3O_{10}$ (343.31): C 45.40, H 6.16; found: C 45.54, H 6.19.

*Heptadeuterioisopropyl 4-O-β-D-galactopyranosyl-β-D-glucopyranoside (**5**c)*

The crude bromide **5***a* (prepared from lactose peracetate (15 g; 22 mmol)) in dry dichloromethane (50 mL) was added to a stirred suspension of silver zeolite 13X (25 g), dichloromethane (25 mL), and heptadeuterioisopropanol (2.0 mL; 25 mmol) under an argon atmosphere. The stirring was continued for 16 h at room temperature. The solids were removed by filtration, washed twice with dichloromethane, and the combined washings and filtrates were evaporated to dryness. The residue was purified by flash chromatography on silica gel (hexane:ethyl acetate 50:50) to yield peracetylated glycoside **5***b*. This product (6.3 g; 1.5 mmol) was dissolved in dry methanol (200 mL), 1 *M* methanolic NaOMe (2 mL) was added, and the mixture stirred for 4 h. After neutralization with Dowex mixed bed resin Ag-501-X8 and Dowex 80W-8X H^+ (3:1), the combined filtrates and washings were evaporated to dryness and the residue purified by flash chromatography on silica gel (isopropanol:water 95:5) to yield **5***c* (1.9 g; 22%), mp 189–191°C; $[\alpha]_D$ −15.0° (*c* 0.66, CH_3OH); ir (neat): 3350 (br, OH) cm^{-1}. *Anal.* calcd. for $C_{15}H_{21}D_7O_{11}$ (391.33): C 46.04, H 5.41; found: C 45.83, H 5.82.

*Heptadeuterioisopropyl 3,6-di-O-acetyl-2-deoxy-2-phthalimido-4-O-(2,3,4,6-tetra-O-acetyl-β-D-galactopyranosyl)-β-D-glucopyranoside (**7**a)*

The crude bromide **6***b* (from acetate **6***a*, 0.87 g; 1.14 mmol; cf. ref. 25) in dry dichloromethane (5 mL) was added to a stirred suspension of silver zeolite 13X (4 g), dry dichloromethane (10 mL), and heptadeuterioisopropanol (0.25 mL; 2.9 mmol) under argon, and the stirring was continued for 16 h at room temperature. The solids were removed by filtration, washed twice with dichloromethane, and the combined washings and filtrates were evaporated to dryness. The residue was purified by flash chromatography on silica gel (hexane:ethyl acetate 6:4) to give **7***a* (604 mg; 68%); mp 253–255°C; $[\alpha]_D$ +3.9° (*c* 0.96, $CHCl_3$); ir (neat): 1780 sh, 1750, 1720 (CO) cm^{-1}; ^{13}C nmr ($CDCl_3$) δ: 169.0–170.4 (6 × CH_3CO), 167.9, 167.6 (*CONCO*), 101.0 (C1-Gal, $^2J_{C-H}$ 161), 99.6 (C1-Glc, $^2J_{C-H}$ 163). *Anal.* calcd. for $C_{35}H_{36}D_7NO_{18}$ (722.67): C 54.41, H 4.70, N 1.81; found: C 54.36, H 4.82, N 1.72.

*Heptadeuterioisopropyl 2-acetamido-2-deoxy-3,6-di-O-acetyl-4-O-(2,3,4,6-tetra-O-acetyl-β-D-galactopyranosyl)-β-D-glucopyranoside (**7**b)*

Compound **7***a* (350 mg; 0.76 mmol) was dissolved in ethanol (8 mL) and hydrazine hydrate (85%, 4 mL) and heated at 70°C for 30 min. After concentration of the reaction mixture *in vacuo*, toluene was added (2 × 50 mL) and the solvent evaporated. The resulting residue was stirred in acetic anhydride (4 mL) and pyridine (8 mL) for 16 h under argon. Crude peracetylated disaccharide **7***b* was obtained after distilling off the reagents at reduced pressure, last traces being removed by codistillation with toluene (3 × 50 mL). The residue yielded, after flash chromatography (silica gel, dichloromethane:methanol 25:1), crystalline **7***b* (454 mg; 87%); mp 155–160°C; $[\alpha]_D$ −17.6° (*c* 0.64, $CHCl_3$:CH_3OH 10:1); ir (neat): 3360, 3300, 3080 (NH), 1750 (COO), 1670, 1550 (CON) cm^{-1}; ^{13}C nmr ($CDCl_3$) δ: 169.9–170.6 (7 × CH_3CO), 101.0 (C1-Gal, $^2J_{C-H}$ 160), 99.5 (C1-Glc, $^2J_{C-H}$ 159). *Anal.* calcd. for $C_{29}H_{36}D_7NO_{17}$ (684.60): C 50.88, H 5.30, N 2.05; found: C 50.92, H 5.41, N 2.08.

*Heptadeuterioisopropyl 2-acetamido-2-deoxy-4-O-(β-D-galactopyranosyl)-β-D-glucopyranoside (**7**c)*

Peracetylated disaccharide **7***b* (454 mg; 0.66 mmol) was dissolved in dry methanol (10 mL), 1 *M* methanolic NaOMe (0.1 mL) was added, and the resulting reaction mixture was stirred under argon for 16 h. After neutralization with a mixture of Dowex mixed bed resin Ag-501-X8 and Dowex 80W-8X H^+ (3:1), the resin was removed by filtration, washed with methanol (35 mL), and the combined filtrates evaporated to dryness. The residue was taken up in methanol (10 mL), toluene (30 mL) was added, and the mixture concentrated to about 5 mL and then precipitated with hexane to yield **7***c* (279 mg; 97%); mp 189–191°C; $[\alpha]_D$ −15.0° (*c* 0.66, CH_3OH); ir (neat): 3300 (br, OH, NH), 1650, 1550 (CON) cm^{-1}; ms *m/e*: 455 (MNa^+), 366 (MH − HOCD $(CD_3)_2^+$). *Anal.* calcd. for $C_{17}H_{24}D_7NO_{11}$ (432.38): C 47.22, H 5.59, N 3.24; found: C 47.02, H 5.32, N 3.34.

*Trideuteriomethyl 2,3-di-O-benzoyl-β-D-galactopyranoside (**8**b)*

Compound **8***a* (1.2 g; 2.43 mmol) prepared according to ref. 4, was hydrogenated in glacial acetic acid (25 mL) over Pd black (300 mg; Strem). The solids were filtered off through a Celite bed, washed with ethyl acetate (50 mL) and toluene (50 mL), and the combined filtrates evaporated to dryness. Toluene (2 × 50 mL) was added and evaporated to remove the residual acetic acid. The residue was purified by flash chromatography (silica gel, chloroform:acetone 5:1) to yield **8***b* (0.81 g; 82%); mp 70–72°C; $[\alpha]_D$ +98.2° (*c* 0.85, $CHCl_3$); ir (neat): 3350 (OH), 1720 (COO) cm^{-1}. *Anal.* calcd. for $C_{21}H_{19}D_3O_8$ (405.38): C 62.22, H 4.72; found: C 61.95, H 4.65.

*Trideuteriomethyl 2,3-di-O-benzoyl-6-O-(3,4,6-tri-O-acetyl-2-deoxy-2-phthalimido-β-D-glucopyranosyl)-β-D-galactopyranoside (**10**a)*

A solution of the diol **8***b* (213 mg; 0.53 mmol) in dry dichloromethane (5 mL) was added to silver zeolite 13X (2 g), which was cooled in an ice bath, and the suspension was stirred under an argon atmosphere for 30 min. A solution of bromide **9** (Toronto Research Chemicals; 0.275 mg; 0.55 mmol) in dichloromethane (5 mL) was added and the stirring was continued for 16 h. The solids were removed by filtration, washed with dichloromethane (25 mL), and the combined filtrates were evaporated to dryness. The residue was purified by flash chromatography (silica gel, dichloromethane:isopropanol 25:1) to yield **10***a* (343 mg; 79%); mp 122–126°C; $[\alpha]_D$ +58.0° (*c* 1.84, $CHCl_3$); ir (neat): 3500 (OH), 1780 sh, 1750, 1720 (CO) cm^{-1}; ^{13}C nmr ($CDCl_3$) δ: 169.4–170.7 (3 × CH_3CO), 167.5 (br, *CONCO*), 165.6, 165.3 (Ph*C*O), 101.7 (C1-Gal, $^2J_{C-H}$ 159), 98.1 (C1-Glc,

[8]Assignments may be interchanged with resonances marked with the same superscript number.

Can. J. Chem. Downloaded from www.nrcresearchpress.com by 78.46.186.204 on 09/07/12
For personal use only.

$^2J_{C-H}$ 161). *Anal.* calcd. for $C_{41}H_{38}D_3NO_{17}$ (822.75): C 59.85, H 4.66, N 1.70; found: C 59.63, H 4.71, N 1.62.

*Trideuteriomethyl 2,3,4-tri-*O*-acetyl-6-*O*-(2-acetamido-2-deoxy-3,4,6-tri-*O*-acetyl-β-*D*-glucopyranosyl)-β-*D*-galactopyranoside (**10**b)*

Disaccharide **10***a* (343 mg; 0.41 mmol) was converted into the peracetate as described for compound **7***a*. Purification by flash chromatography (silica gel, dichloromethane:isopropanol 20:1) yielded pure **10***b* (221 mg; 83%); mp 216–222°C; $[\alpha]_D$ −17.1° (*c* 0.99, $CHCl_3$); ir (neat): 3290, 3070 (NH), 1750 (COO), 1660, 1550 (CON) cm^{-1}; ^{13}C nmr ($CDCl_3$) δ: 169.4–171.0 (7 × CH_3CO), 101.7 (C1-Gal, $^2J_{C-H}$ 160), 99.7 (C1-Glc, $^2J_{C-H}$ 163); ms *m/e*: 675 (MNa^+), 330 (PerAcGlcNAc − H^+). *Anal.* calcd. for $C_{27}H_{35}D_3NO_{17}$ (651.63): C 61.04, H 4.75, N 1.74; found: C 60.92, H 4.68, N 1.79.

*Trideuteriomethyl 6-*O*-(2-acetamido-2-deoxy-β-*D*-glucopyranosyl)-β-*D*-galactopyranoside (**10**c)*

Zemplen transesterification of **10***b* (105 mg; 0.61 mmol) using the same procedure as for compound **7***b* gave **10***c* (60 mg; 94%); mp 230–246°C; $[\alpha]_D$ −20.83° (*c* 0.85, $CH_3OH:H_2O$ 3:1); ir (neat): 3300 (br, OH, NH), 1650, 1550 (CON) cm^{-1}; ms *m/e*: 423 (MNa^+), 204 (GlcNAc − H^+). *Anal.* calcd. for $C_{15}H_{24}D_3NO_{11}$ (400.35): C 45.00, H 6.04, N 3.50; found: C 44.72, H 5.82, N 3.34.

*Trideuteriomethyl 2-*O*-benzoyl-4,6-*O*-benzylidene-3-*O*-(3,4,6-tri-*O*-acetyl-2-deoxy-2-phthalimido-β-*D*-glucopyranosyl)-β-*D*-galactopyranoside (**11**a)*

The bromide **9** (10 g; 20 mmol) in dry dichloromethane (25 mL) was added to a stirred mixture of alcohol **2***a* (3.63 g; 9.3 mmol), silver trifluoromethanesulphonate (5.2 g; 20 mmol), 2,6-di-*tert*-butyl-4-methylpyridine (4.1 g; 20 mmol), molecular sieves 3A (5 g), and dry dichloromethane (100 mL) at 0–5°C under an atmosphere of argon. The stirring was continued for 3 h and then the temperature was allowed to rise to room temperature. The solids were removed by filtration through a Celite bed, washed with dichloromethane, and the combined filtrates evaporated to dryness. The residue was purified by flash chromatography on silica gel (chloroform:acetone 98:2) to yield pure **11***a* (5.6 g; 75%); ^{13}C nmr ($CDCl_3$) δ: 169.3–170.5 (3 × CH_3CO), 167.5 (br, *C*O*N*C*O*), 164.5 (Ph*C*O), 101.7 (C1-Gal[3],[9] $^2J_{C-H}$ 158), 100.8 (PhCO_2[3], $^2J_{C-H}$ 159), 99.3 (C1-Glc[3], $^2J_{C-H}$ 162).

*Trideuteriomethyl 2-*O*-benzoyl-4,6-*O*-benzylidene-3-*O*-(3,4,6-tri-*O*-acetyl-2-deoxy-2-phthalimido-α-*D*-glucopyranosyl)-β-*D*-galactopyranoside (**12**a)*

Prepared as described for the β-isomer **11***a* (cf. ref. 4) except that a total of 4 equivalents of bromide **9** were added in 3 portions and the stirring continued for 5 days. The total disaccharide fractions accounted for about 80% of starting alcohol **2***a* and contained approximately a 2:1 α:β mixture of isomers. Pure α-disaccharide **12***a* was obtained by preparative hplc (μPorasil, hexane:ethyl acetate 1:1); mp 253–258°C; $[\alpha]_D$ +186.5° (*c* 1.15, $CHCl_3$); ir (neat): 1780 sh, 1750, 1720 (CO) cm^{-1}; ^{13}C nmr ($CDCl_3$) δ: 168.8–170.3 (3 × CH_3CO), 167.5 (br, *C*O*N*C*O*), 164.6 (Ph*C*O), 101.5 (C1-Gal, $^2J_{C-H}$ 162), 99.9 (PhCO_2, $^2J_{C-H}$ 156), 93.7 (C1-Glc, $^2J_{C-H}$ 172). *Anal.* calcd. for $C_{41}H_{38}D_3NO_{16}$ (806.75): C 61.04, H 4.75, N 1.74; found: C 60.92, H 4.68, N 1.79.

*Preparation of **12**a using ultrasound or heating*

The procedure described above was used except that 1,2-dichloroethane was used as solvent, 2 equivalents of bromide **9** to 1 equivalent of **2***a* (typically using 0.5 mmol), and 2 equivalents of added bases (2,4,6-trimethylpyridine or tetramethylurea or silver carbonate or 2,6-di-*tert*-butyl-4-methylpyridine (26)) were added and ultrasonic agitation, using a Bransonic 220 with propylene glycol as the bathing solution or heating to 55–60°C with an oil bath, was provided. The progress of the reactions was monitored by tlc (ethyl acetate:hexane 50:50) and the crude reaction mixtures were analyzed by ^1H nmr.

*Trideuteriomethyl 2-*O*-benzoyl-3,6-di-*O*-(3,4,6-tri-*O*-acetyl-2-deoxy-2-phthalimido-β-*D*-glucopyranosyl)-β-*D*-galactopyranoside (**13**a)*

Compound **13***a* was prepared as described for disaccharide **10***a* except that diol **11***b* (235 mg; 0.33 mmol) prepared as for diol **8***b* (cf. ref. 4) was used as aglycon. The trisaccharide **13***a* was ultimately purified by flash chromatography (silica gel, dichloromethane:isopropanol 25:1) to yield pure **13***a* (236 mg; 63%); mp 153–156°C; $[\alpha]_D$ +48.4° (*c* 1.01, $CHCl_3$); ir (neat): 3400 (OH), 1780 sh, 1750, 1720 (CO) cm^{-1}; ^{13}C nmr ($CDCl_3$) δ: 169.9–170.7 (6 × CH_3CO), 167.5 (br, *C*O*N*C*O*), 164.3 (Ph*C*O), 101.3 (C1-Gal, $^2J_{C-H}$ 160), 98.4 (C1, 3-Glc[4],[10] $^2J_{C-H}$ 160), 98.0 (C1, 6-Glc[4], $^2J_{C-H}$ 163). *Anal.* calcd. for $C_{54}H_{53}D_3N_2O_{25}$ (1136.15): C 57.09, H 4.70, N 2.47; found: C 57.52, H 4.62, N 2.32.

*Trideuteriomethyl 2,4-di-*O*-acetyl-3,6-di-*O*-(3,4,6-tri-*O*-acetyl-2-deoxy-2-acetamido-β-*D*-glucopyranosyl)-β-*D*-galactopyranoside (**13**b)*

Trisaccharide **13***a* (171 mg; 0.16 mmol) was converted into the peracetate **13***b* by exactly the procedure described for disaccharide **7***a*. The product was purified by flash chromatography (silica gel, chloroform:methanol 20:1) to yield pure **13***b* (124 mg; 85%); mp 252–255°C; $[\alpha]_D$ +1.7° (*c* 0.88, $CHCl_3$); ir (neat): 3285, 3090 (NH), 1750 (COO), 1650, 1540 (CON) cm^{-1}. *Anal.* calcd. for $C_{39}H_{53}D_3N_2O_{24}$ (939.85): C 49.84, H 5.68, N 2.98; found: C 50.22, H 5.42, N 3.03.

*Trideuteriomethyl 3,6-di-*O*-(2-acetamido-2-deoxy-β-*D*-glucopyranosyl)-β-*D*-galactopyranoside (**13**c)*

The acetates of **13***b* (85 mg; 0.09 mmol) were transesterified following the procedure used for compound **7***a* to yield pure trisaccharide **13***c* (43 mg; 79%); mp 263–273°C; $[\alpha]_D$ −4.6° (*c* 0.98, $CH_3OH:H_2O$ 3:1); ir (neat): 3300 (br, OH, NH), 1650, 1550 (CON) cm^{-1}. *Anal.* calcd. for $C_{19}H_{17}D_3N_2O_{16}$ (603.54): C 45.77, H 6.18, N 4.64; found: C 45.62, H 6.25, N 4.53.

Acknowledgements

This work was supported in part by the Medical Research Council (Canada) through grants (to J.P.C.). D.M.W. is grateful to the Natural Sciences and Engineering Research Council of Canada for a postdoctoral fellowship. The authors would also like to thank Dr. D. W. Hughes for running the ^{13}C nmr spectra, Dr. H. Egge for measurement of the mass spectrum, and Mr. J. Baptista for the hplc separations as well as the optical rotation measurements.

1. H. H. Lee, D. A. Schwartz, J. F. Harris, J. P. Carver, and J. J. Krepinsky. Can. J. Chem. **64**, 1912 (1986).
2. J. R. Brisson and J. P. Carver. Biochemistry, **22**, 1362 (1983).
3. J. P. Carver and D. A. Cumming. Pure Appl. Chem. In press.
4. D. M. Whitfield, J. P. Carver, and J. J. Krepinsky. J. Carbohydr. Chem. **4**, 369 (1985).
5. H. Schachter. Biochem. Cell. Biol. **64**, 163 (1986).
6. B. Andersson, J. Dahmen, T. Frejd, H. Leffler, G. Magnusson, G. Noori, and C. S. Eden. J. Exp. Med. **158**, 559 (1983).
7. C. Augé, S. David, and A. Veyrières. Nouv. J. Chim. **3**, 491 (1979).
8. T. Takamura, T. Chiba, and S. Tejima. Chem. Pharm. Bull. **29**, 1076 (1981).
9. R. U. Lemieux, D. R. Bundle, and D. A. Baker. J. Am. Chem. Soc. **97**, 4076 (1975).
10. K. L. Matta, S. S. Rana, C. F. Piskorz, and S. A. Abbas. Carbohydr. Res. **131**, 247 (1984).
11. R. U. Lemieux, K. Bock, L. T. J. Delbaere, S. Koto, and V. S. Rao. Can. J. Chem. **58**, 631 (1980).
12. H. Thøgersen, R. U. Lemieux, K. Bock, and B. Meyer. Can. J. Chem. **60**, 44 (1982).

[9]Assignments may be interchanged with resonances marked with the same superscript number.

[10]Assignments may be interchanged with resonances marked with the same superscript number.

13. T. C. WONG and R. U. LEMIEUX. Can. J. Chem. **62**, 1207 (1984).
14. S. S. RANA, J. J. BARLOW, and K. L. MATTA. Carbohydr. Res. **113**, 257 (1983).
15. R. BARKER, H. A. NUÑEZ, P. ROSEVAR, and A. S. SERIANNI. Methods Enzymol. **83**, 58 (1982).
16. H. PAULSEN, T. PETERS, V. SINNWELL, R. LEBUHN, and B. MEYER. Liebigs Ann. Chem. 489 (1985).
17. K. BOCK, J. ARNARP, and J. LÖNNGREN. Eur. J. Biochem. **129**, 175 (1983).
18. M. L. HAYES, A. S. SERIANNI, and R. BARKER. Carbohydr. Res. **100**, 87 (1982).
19. K. J. NEUROHR, D. R. BUNDLE, N. M. YOUNG, and H. H. MANTSCH. Eur. J. Biochem. **123**, 305 (1982).
20. K. HIROTSU and A. SHIMADA. Bull. Chem. Soc. Jpn. **47**, 1872 (1974).
21. F. LONGCHAMBON, J. OHANESSIAN, H. GILLIER-PANDRAUD, D. DUCHET, J. C. JACQUINET, and P. SINAY. Acta Crystallogr. Sect. B**37**, 601 (1981).
22. G. M. LIPKIND, A. S. SHASHKOV, and N. K. KOCHETKOV. Carbohydr. Res. **141**, 191 (1985).
23. R. N. SHAH, D. A. CUMMING, A. A. GREY, J. P. CARVER, and J. J. KREPINSKY. Carbohydr. Res. **53**, 155 (1986).
24. P. J. GAREGG and P. OSSOWSKI. Acta Chem. Scand. Ser. B, **37**, 249 (1983).
25. D. M. WHITFIELD, R. N. SHAH, J. P. CARVER, and J. J. KREPINSKY. Synth. Commun. **15**, 737 (1985).
26. J. ARNARP, H. HARALDSSON, and J. LÖNNGREN. J. Chem. Soc. Perkin Trans. 1841 (1982).
27. T. TAKAMURA, T. CHIBA, and S. TEJIMA. Chem. Pharm. Bull. **29**, 1027 (1981).
28. (*a*) R. U. LEMIEUX and M. H. BURZYNSKA. Can. J. Chem. **60**, 76 (1982); (*b*) R. U. LEMIEUX, T. C. WONG, and H. THØGERSEN. Can. J. Chem. **60**, 81 (1982).
29. H. PAULSEN, W. RAUWALD, and R. LEBUHN. Carbohydr. Res. **138**, 29 (1985).
30. J. ARNARP and J. LÖNNGREN. J. Chem. Soc. Perkin Trans. 1, 2070 (1981).
31. R. W. BINKLEY and M. G. AMBROSE. J. Org. Chem. **48**, 1777 (1983).
32. H. PAULSEN. Chem. Soc. Rev. **13**, 15 (1984).
33. H. EGGE, J. PETER-KATALINIĆ, J. PAZ-PARENTE, G. STRECKER, J. MONTREUIL, and B. FOURNET. FEBS Lett. **156**, 357 (1983).
34. J. C. TOUCHSTONE and M. F. DOBBINS. Practice of thin layer chromatography. Wiley, New York. 1983.
35. R. U. LEMIEUX, K. B. HENDRIKS, R. V. STICK, and R. JAMES. J. Am. Chem. Soc. **97**, 4056 (1975).
36. D. S. DIME, E. RACHAMAN, C. E. DIME, A. A. GREY, J. P. CARVER, and J. J. KREPINSKY. J. Labelled Compd. Radiopharm. In press.

Can. J. Chem. Downloaded from www.nrcresearchpress.com by 78.46.186.204 on 09/07/12
For personal use only.

Enzymes in organic synthesis. 36.[1]
Synthesis of optically active civet constituent from an enzyme-generated chiral synthon

J. Bryan Jones and R. Scott Hinks
Department of Chemistry, University of Toronto, Toronto, Ont., Canada M5S 1A1

Received September 11, 1986

J. Bryan Jones and R. Scott Hinks. Can. J. Chem. **65**, 704 (1987).

A synthesis of the civet constituent, (+)-(*S*,*S*)-(*cis*-6-methyltetrahydropyran-2-yl)acetic acid, is described, in which the key stereochemistry of the chiral starting material is set by an enantiotopically selective, porcine pancreatic lipase-catalyzed, hydrolysis of a *meso* diester.

J. Bryan Jones et R. Scott Hinks. Can. J. Chem. **65**, 704 (1987).

On décrit une synthèse du constituant du civet, l'acide (+)-(méthyl-6-*cis* tétrahydropyrannyl-2) acétique-(*S*,*S*), dans laquelle la stéréochimie clé du produit de départ chiral est obtenue par une hydrolyse énantiosélective d'un diester *méso* qui est effectuée par la catalyse d'une lipase pancréatique du porc.

[Traduit par la revue]

Can. J. Chem. Downloaded from www.nrcresearchpress.com by 78.46.186.204 on 09/07/12
For personal use only.

The broad spectrum of new asymmetric synthetic opportunities opened up by the exploration of the chiral catalytic properties of enzymes is now well documented (1). Stereospecific transformations on symmetrical substrates are particularly attractive in this regard, with the commercially available porcine pancreatic lipase (PPL) being one of the most widely applied of the enzymes in current use for this purpose (2). In this paper we report a new synthesis of the optically active civet constituent **8** from a PPL-generated chiron.

(+)-(*S*,*S*)-(*cis*-6-methyltetrahydropyran-2-yl)acetic acid (**8**) is a constituent of a glandular secretion of the civet cat (3), whose synthesis, both of the optically active (4) and racemic (5) forms, has attracted considerable attention. Of these syntheses, only the latest one of Keinan *et al.* (4*d*), which exploits alcohol dehydrogenase stereospecificity, has been based on an enzymically generated chiron. Our current PPL-based approach is outlined in Scheme 1.

The *meso* diester **1** starting material was readily prepared from 4*H*-pyran-2,6-dicarboxylic acid (**9**) (6) in 69% overall yield by the method summarized in Scheme 2.

The key stereochemistry of the starting chiron for the synthesis was set by stereoselective PPL-catalyzed hydrolysis of **1** to give the alcohol-ester (−)-**2** of 55% e.e. (enantiomeric excess) in 77% isolated yield. Oxidation of **2** → **3** proceeded smoothly in 94% yield. Homologation of **3** was effected in 41% yield by the Arndt–Eistert procedure, a reaction that is known to proceed with retention of configuration at the α-position of the carboxyl function (7). The remaining steps of transesterification (**4** → **5**), tosylation (**5** → **6**), reduction (**6** → **7**), and oxidation (**7** → **8**) were achieved in quantitative, 88%, 68%, and 76% yields respectively. The overall yield of the civet constituent **8** from **2** was 18%, with the target product having the same e.e. as the starting chiron **2**. The enantiomeric excesses of **2** and **8** were determined directly. The alcohol-ester **2** was oxidatively converted to its corresponding lactone, and hence to the (*R*,*R*)-butane-2,3-diol orthoester, for e.e. measurement by the standard glc method (8). The e.e. of **8** was established by its conversion to the methyl ester with diazomethane, followed by ^{1}H nmr examination of the methoxyl protons in the presence of Eu(hfc)$_3$ (9).

Since the stereoisomeric integrity of the enzymically generated chiron **2** is retained throughout the synthesis, it is evident that enantiomerically pure **8** would result from optically pure **2** as the starting material. For hydrolytic enzymes such as pig liver esterase and PPL, the stereospecificities of hydrolyses of *meso* diester and related substrates can be dramatically improved by manipulation of the reaction conditions (10, 11). This aspect is being pursued further and protocols for improving the stereospecificities of PPL-catalyzed hydrolyses will be reported shortly.

[1]For Part 35, see ref. 10.

Experimental

Porcine pancreatic lipase (PPL, EC 3.1.1.3, Type II, Sigma L-3126, Lot # 82F-0636) was obtained from Sigma Chemical Co. All enzymic reactions were monitored using a Radiometer RTS 822 pH-stat. The ^{1}H nmr spectra were recorded on Varian T60 or XL 200 instruments and ^{13}C nmr spectra on a Varian CFT-20 spectrometer, both in $CDCl_3$ unless noted otherwise. The ir spectra were recorded on a Nicolet 5DX FT-IR system, optical rotations on a Perkin–Elmer 141 polarimeter, and glc analyses on a Hewlett–Packard HP 57/019 chromatograph. Melting points were determined on an Electrothermal capillary apparatus and are uncorrected. Chromatotron separations were performed with a Harrison Research model 7924 using Merck 7749 silica gel on 8-inch rotors with 4 mm thickness of adsorbent.

Preparation of substrate: cis-*2,6-bis(butanoxymethyl)tetrahydropyran (**1**)*

The 4*H*-pyran-2,6-dicarboxylic acid (**9**) starting material was prepared from diethyl oxaloacetate in 22% yield, mp >360°C (lit. (6) mp >300°C). The diacid **9** (39.2 g, 0.23 mol) and trimethylorthoformate (50.5 mL, 48.9 g, 0.46 mol) in dry MeOH (200 mL) containing concentrated H_2SO_4 (1 mL) was heated under reflux for 3 h. The dark mixture was then cooled and kept at 20°C for 2 days. The crystalline product was filtered and the mother liquors concentrated to give a second crop. The combined crystalline products were washed with cold (0°C) MeOH (3 × 50 mL) and then sublimed at 85°C/0.1 Torr (1 Torr = 133.3 Pa). Recrystallization from MeOH yielded 2,5-dicarbomethoxy-4*H*-pyran (38.6 g, 84%), mp 122–123°C; ir (KBr) ν: 1750, 1721, 1702, 1687, 1642 cm^{-1}; ^{1}H nmr δ: 3.09 (t, 2H, J = 4 Hz), 3.86 (s, 6H), and 6.10 (t, 2H, J = 4 Hz) ppm; ^{13}C nmr δ: 21.31, 52.11, 109.53, 141.61, and 161.16 ppm. *Anal.* calcd. for $C_9H_{10}O_5$: C 54.55, H 5.09; found: C 54.78, H 5.00%.

This unsaturated diester (36.8 g, 0.186 mol) in MeOH (250 mL) containing 5% Rh–C (0.4 g) was hydrogenated in a Parr apparatus at 50 psi (1 psi = 6.9 kPa) for 4 h. The mixture was then filtered through Celite and rotoevaporated. The crude product (37.8 g, 100%) was recrystallized from diethyl ether (20 mL) to give *cis*-2,6-dicarbomethoxytetrahydropyran (**10**, 30.8 g, 82%), mp 52–54°C (lit. (12) mp 54°C); ir (molten film) ν: 1749 cm^{-1}; ^{1}H nmr δ: 1.30–2.20 (m, 6H), 3.81 (s, 6H), and 3.90–4.25 (m, 2H) pm; ^{13}C nmr δ: 22.07, 27.20, 51.32, 75.89, and 170.04 ppm.

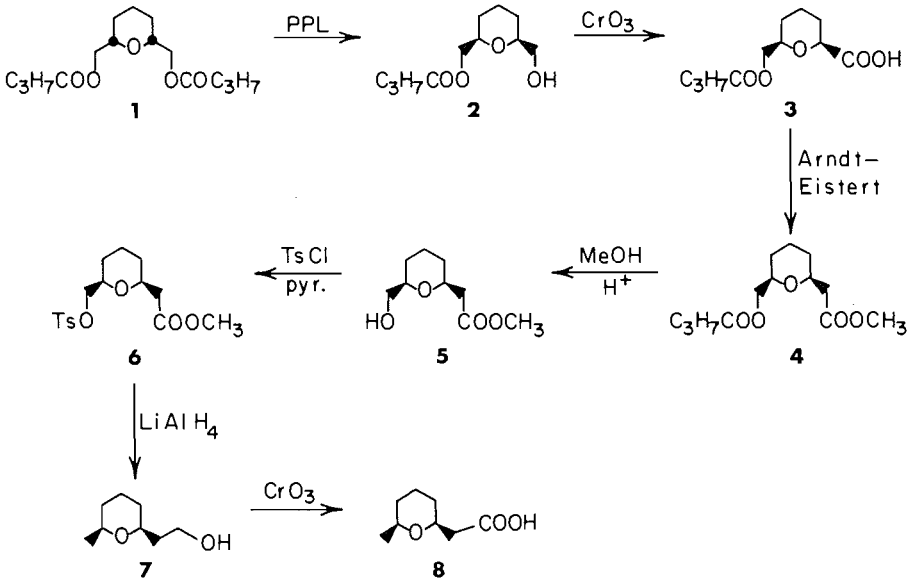

SCHEME 1

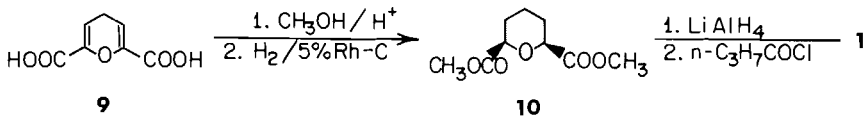

SCHEME 2

The dimethyl ester **10** (15.0 g, 74.3 mmol) in dry THF (100 mL) was added dropwise with stirring during 30 min to a suspension of $LiAlH_4$ (8.5 g, 220 mmol) in dry THF (200 mL) at 25°C. The mixture was then heated under reflux for 30 min, cooled, and then quenched with saturated aqueous sodium potassium tartrate. Rotoevaporation of the dried ($MgSO_4$) THF solution followed by Kugelrohr distillation and then recrystallization from diethyl ether afforded *cis*-2,6-dihydroxymethyltetrahydropyran (9.26 g, 85%), bp 90°C/0.1 Torr, mp 44–46°C (lit. (6) mp 45.7–46.4°C); ir (molten film) ν: 3350 (br) cm^{-1}; ^1H nmr δ: 1.20–2.00 (m, 6H), 2.90–3.70 (m, 8H) ppm; ^{13}C nmr δ: 22.38, 26.71, 65.80, and 78.08 ppm.

To the above diol (3.01 g, 20.6 mmol) in dry THF (50 mL) and dry pyridine (8.3 mL, 103 mmol) at 20°C was added, with stirring and via a syringe, butanoyl chloride (3.4 mL, 41.2 mmol) during 2 min. After stirring for a further hour, the mixture was rotoevaporated and the residue dissolved in water (50 mL) and acidified with concentrated HCl to pH 1. This solution was extracted with diethyl ether (2 × 50 mL) and the ether solution washed with saturated aqueous $NaHCO_3$ (2 × 10 mL) and then with brine (10 mL). The ether solution was then decolorized with Norit (1 g), dried ($MgSO_4$), and rotoevaporated. Kugelrohr distillation of the residue yielded *cis*-2,6-dibutanoyloxymethyltetrahydropyran (**1**, 5.7 g, 96%), bp 105°C/0.15 Torr; ir (film) ν: 1738 cm^{-1}; ^1H nmr δ: 0.95 (t, 6H, J = 6 Hz), 1.18–2.03 (m, 10H), 2.23 (t, 2H, J = 7 Hz), 3.40–3.83 (br m, 2H), and 4.08 (apparent d, 4H, J(app) = 5 Hz) ppm; ^{13}C nmr δ: 13.43, 18.25, 22.45, 27.32, 35.94, 66.69, 75.34, and 173.25 ppm. *Anal.* calcd. for $C_{15}H_{26}O_5$: C 62.91, H 9.15; found: C 62.96, H 9.06%.

Preparation of hydroxyester 2 via PPL-catalyzed hydrolysis of 1

The diester **1** (3.30 g, 11.5 mmol) was suspended at 25°C in buffer solution (30 mL) of pH 7.0 consisting of 0.01 *M* KH_2PO_4, 0.1 *M* NaCl, and 0.0025 *M* $CaCl_2$. PPL (104 mg, 12 U/mg) was then added and the reaction maintained at 25°C, and at pH 7.0 by pH-stat controlled titration of the liberated acid with 0.5 *M* NaOH. After 9 h, when one equivalent of base had been taken up, the mixture was filtered through Celite and extracted with diethyl ether (3 × 70 mL). The combined ether extracts were washed with saturated aqueous $NaHCO_3$, then with brine, and finally dried ($MgSO_4$) and rotoevaporated. The mixture obtained was purified by Chromatotron separation (pentane:diethyl ether gradient = 1:1 (150 mL), 0:1 (250 mL)). The central fractions were Kugelrohr distilled to give (−)-(2*R*,6*S*)-2-butanoyloxymethyl-6-hydroxymethyltetrahydropyran (**2**, 2.09 g, 84%, 55% e.e.), bp 80°C/0.05 Torr; $[\alpha]_D^{25}$ −4.3° (*c* 4.4, $CHCl_3$); ir (film) ν: 3460 (br), 1738 cm^{-1}; ^1H nmr δ: 0.96 (t, 3H, J = 6 Hz), 1.13–2.15 (m, 8H), 2.26 (br s, 1H), 2.32 (t, 2H, J = 6 Hz), 3.26–3.86 (m, 4H), and 4.10 (d, 2H, J = 5 Hz) ppm; ^{13}C nmr δ: 13.28, 18.10, 22.29, 26.66, 27.37, 35.75, 65.64, 66.16, 75.16, 77.97, and 173.17 ppm. *Anal.* calcd. for $C_{11}H_{20}O_4$: C 61.09, H 9.32; found: C 60.84, H 9.22%.

The enantiomeric excess determination for (−)-**2** was performed via its oxidation (50-mg scale) with CrO_3 (see below) followed by esterification with CH_2N_2 to the corresponding methyl ester. This was then heated under reflux with (*R*,*R*)-butane-2,3-diol (2 equiv.) in benzene (25 mL) containing *p*-TsOH (10 mg). Following an initial lactonization to (−)-(1*S*,5*R*)-3,9-dioxabicyclo[3.3.1]nonan-2-one, the orthoester formed in the usual (8) way and was analyzed by glc (8) using the orthoester from (±)-**2** as reference standard. With a Supelcowax capillary column, 6 psi (41.4 kPa), 140°C, the diastereomeric peak retention times were 12.98 min (22.5%) and 13.81 min (77.5%), for an e.e. of 55 ± 3%.

Synthesis of the civet constituent (+)-(2S,6S)-8

To the PPL-derived alcohol-butyrate (−)-(2*R*,6*S*)-**2** (1.83 g, 8.46 mmol, 55% e.e.) in acetone (100 mL) at 20°C was added Jones reagent until a yellow colour persisted. At this point, a 50% excess of Jones reagent was added and the mixture stirred at 20°C for 15 min. The reaction was then quenched by the dropwise addition of 2-propanol, then filtered, and the residue was washed with acetone (3 × 20 mL). The combined acetone solutions were rotoevaporated and the residual oil dissolved in 0.5 *M* hydrochloric acid (25 mL) and extracted with diethyl ether (3 × 50 mL). Rotoevaporation of the dried ($MgSO_4$) extract followed by Kugelrohr distillation gave (−)-(2*S*,6*R*)-*cis*-butanoyloxymethyltetrahydropyran-2-carboxylic acid (**3**, 1.84 g, 94%), bp 110°C/0.05 Torr; $[\alpha]_D^{25}$ −21.3° (*c* 3.7, $CHCl_3$); ir (film) ν: 3400–2500, 1735, and 1718 cm^{-1}; ^1H nmr δ: 0.95 (t, 3H, J = 6 Hz),

Can. J. Chem. Downloaded from www.nrcresearchpress.com by 78.46.186.204 on 09/07/12
For personal use only.

Can. J. Chem. Downloaded from www.nrcresearchpress.com by 78.46.186.204 on 09/07/12
For personal use only.

1.20–2.20 (m, 8H), 2.33 (t, 2H, J = 7 Hz), 3.51–4.28 (m, 4H), and 9.41 (s, 1H) ppm; ^{13}C nmr δ: 13.44, 18.25, 22.51, 26.70, 27.96, 35.91, 66.26, 75.54, 75.96, 173.59, and 173.82 ppm. *Anal.* calcd. for $C_{11}H_{18}O_5$: C 57.38, H 7.88; found: C 56.93, H 7.90%.

The acid-butyrate (−)-**3** (689 mg, 3.03 mmol) in benzene (30 mL) was dried by distillation of part (10 mL) of the benzene under N_2. After cooling the remaining solution to 20°C, oxalyl chloride (5 mL) was added and the mixture stirred for 2 h at 20°C. The solvent and excess oxalyl chloride were distilled off at 14 Torr and dry diethyl ether added to the residual oil. The ether solution was cooled to −78°C and, via cannula, a Na-dried solution of CH_2N_2 (1 g, 24 mmol) in diethyl ether (75 mL) containing Et_3N (2 mL, distilled from $LiAlH_4$) was added slowly. The mixture was warmed to 20°C during 30 min and then stirred at this temperature for 1 h. The reaction solution was then washed successively with water (30 mL), 10% aqueous acetic acid (50 mL), water (30 mL), saturated aqueous $NaHCO_3$ (20 mL), and brine (20 mL). The dried (Na_2SO_4, **not** $MgSO_4$) ether solution was rotoevaporated, with final solvent traces removed at 20°C/0.05 Torr, to afford (2*S*,6*R*)-*cis*-6-butanoyloxymethyl-2-diazoketotetrahydropyran (758 mg, 98%); ir (film) ν: 3132, 2109, 1737, and 1644 cm^{-1}; ^{1}H nmr δ: 0.96 (t, 3H, J = 7 Hz), 1.13–2.25 (m, 11H), and 3.50–4.20 (m, 2H) ppm; ^{13}C nmr δ: 13.62, 18.46, 22.60, 27.05, 28.37, 36.10, 52.37, 66.44, 75.73, 80.97, 173.55, and 181.02 ppm.

The above diazoketone (732 mg, 2.88 mmol) in dry MeOH (10 mL) was brought to reflux under N_2 and 1 mL of catalyst (prepared from silver benzoate (1 g) in dry Et_3N (10 mL)) was added. N_2 was evolved immediately and the reaction was completed by refluxing for a further 45 min, with two further additions of 1-mL aliquots of catalyst during this period after 5 and 15 min respectively. The mixture was then cooled to 20°C, filtered through Celite, and rotoevaporated. The residue was dissolved in diethyl ether (50 mL), washed with 1 *M* hydrochloric acid, then with saturated aqueous $NaHCO_3$ (20 mL), and finally with brine (20 mL). The dried ($MgSO_4$) ether solution was rotoevaporated and the residue purified by flash chromatography on silica (30 g, pentane:diethyl ether:MeOH 79:20:1 (200 mL) elution). Kugelrohr distillation then yielded (−)-methyl (2*S*,6*R*)-*cis*-(6-butanoyloxymethyltetrahydropyran-2-yl)acetate (**4**, 287 mg, 42%), bp 85°C/0.025 Torr; $[\alpha]_D^{25}$ −2.8° (*c* 8.5, $CHCl_3$); ir (film) ν: 1739 and 1733 cm^{-1}; ^{1}H nmr δ: 0.96 (t, 3H, J = 7 Hz), 1.13–2.16 (m, 8H), 2.16–2.63 (m, 4H), 3.69 (s, 3H), and 3.50–4.20 (m, 4H) ppm; ^{13}C nmr δ: 13.31, 18.12, 22.60, 27.06, 30.62, 35.79, 41.01, 51.13, 66.51, 73.99, 75.36, 171.19, and 173.00 ppm. *Anal.* calcd. for $C_{13}H_{22}O_5$: C 60.45, H 8.58; found: C 60.34, H 8.39%.

The methyl-butanoate diester **4** (226 mg, 0.89 mmol) in MeOH (50 mL) containing *p*-TsOH (20 mg) was heated under reflux for 24 h, when conversion to the hydroxyester **5** was shown by tlc to be complete. The solution was then rotoevaporated, with the final traces of solvent being removed at 25°C/0.05 Torr. Dry pyridine (10 mL) was then added and the solution cooled to 0°C. *p*-Toluenesulfonyl chloride (340 mg, 1.78 mmol) was added and the mixture kept for 20 h at 0–5°C. Ice-water was then added and, after 20 min, the mixture was extracted at 0°C with diethyl ether (75 mL). The cold ether extract was washed at 0°C with cold 1 *M* hydrochloric acid (2 × 40 mL) and then with ice-water (20 mL). The ether layer was dried ($MgSO_4$) and rotoevaporated to yield methyl (2*S*,6*R*)-(*cis*-6-tosyloxymethyltetrahydropyran-2-yl)acetate (**6**, 268 mg, 88%) as a pale yellow oil; ir (film) ν: 1738 cm^{-1}; ^{1}H nmr δ: 1.10–2.00 (m, 6H), 2.20–2.56 (m, 2H), 2.46 (s, 3H), 3.35–4.12 (m, 4H), 3.68 (s, 3H), 7.36 (d, 2H, J = 8 Hz), and 7.79 (d, 2H, J = 8 Hz) ppm.

$LiAlH_4$ (600 mg, 15 mmol) was added with stirring to the tosylate **6** (265 mg, 0.78 mmol) in dry THF (50 mL) at 0°C. After stirring for 10 min at 0°C, the mixture was stirred for 10 min at 20°C and finally refluxed for 1 h. The cooled (20°C) reaction mixture was then quenched with saturated aqueous sodium potassium tartrate and the THF solution rotoevaporated. The residue was dissolved in diethyl ether, dried ($MgSO_4$), rotoevaporated, and finally Kugelrohr distilled to give (+)-(*S*,*S*)-cis-2-(2′-hydroxyethyl)-6-methyltetrahydropyran (**7**, 77 mg, 68%), bp 30°C/0.05 Torr (lit. (5*c*) (±-**7**) bp 45–47°C/12 Torr); $[\alpha]_D^{25}$ +15.3° (*c* 5, $CHCl_3$) (lit. (4*b*) $[\alpha]_D^{25}$ +24.6° ($CHCl_3$)); ir (film) ν: 3400 (br) cm^{-1}; ^{1}H nmr δ: 1.16 (d, 3H, J = 6 Hz), 1.10–1.93 (m, 8H), 2.78 (br s, 1H), 3.25–3.66 (m, 2H), and 3.78 (t, 2H, J = 5.5 Hz) ppm; ^{13}C nmr δ: 22.06, 23.36, 31.17, 32.96, 61.51, 73.95, and 78.41 ppm.

Jones reagent was added dropwise with stirring at 20°C to the above alcohol **7** (46 mg, 0.32 mmol) in acetone (25 mL) until the yellow color persisted, then 50% excess of Jones reagent was added and the mixture stirred for 30 min at 20°C. The reaction was then quenched by the dropwise addition of 2-propanol until colorless, and the mixture rotoevaporated. The residue was then dissolved in water (25 mL), the solution brought to pH 1 with 12 *M* hydrochloric acid, and then extracted with diethyl ether (6 × 50 mL). The dried ($MgSO_4$) ether extracts were rotoevaporated to yield the civet constituent (+)-(*S*,*S*)-(*cis*-6-methyltetrahydropyran-2-yl)acetic acid (**8**, 39 mg, 76%, 58% e.e.); $[\alpha]_D^{25}$ +24.5° (*c* 3.3, C_6H_6) (lit. (4*a*) $[\alpha]_D^{22}$ +32.86° (*c* 1.05, C_6H_6); (4*b*) $[\alpha]_D^{25}$ +46.8° (C_6H_6); (4*d*) $[\alpha]_D^{22}$ +43.85° (*c* 2.52, C_6H_6); ir (film) ν: 2500–3500 cm^{-1}; ^{1}H nmr δ: 1.08 (d, 3H, J = 6 Hz), 1.05–2.00 (m, 6H), 2.55 (d, 2H, J = 6.5 Hz), 3.30–4.00 (m, 2H), 9.46 (br s, 1H) ppm; ^{13}C nmr δ: 21.93, 23.18, 30.76, 32.75, 41.30, 73.96, 74.43, and 175.50 ppm.

The e.e. of (+)-**8** was determined via its esterification with diazomethane, followed by 200-MHz ^{1}H nmr examination of the methoxyl protons (ΔΔδ 0.014 ppm in the presence of Eu(hfc)$_3$ (0.4 equiv.) (9). An e.e. value of 58 ± 3% was measured.

Acknowledgements

We are grateful to the Natural Sciences and Engineering Research Council of Canada for support of this work and to the University of Toronto and the Province of Ontario for the award of Scholarships (to R.S.H.).

1. C.-H. Wong and G. M. Whitesides. Angew. Chem. Int. Ed. Engl. **24**, 617 (1985); J. B. Jones. Tetrahedron, **42**, 3351 (1986).
2. Y.-F. Wang, C.-S. Chen, G. Girdaukas, and C. J. Sih. J. Am. Chem. Soc. **106**, 3695 (1984); Y.-F. Wang and C. J. Sih. Tetrahedron Lett. **25**, 4999 (1984); B. Cambou and A. M. Klibanov. J. Am. Chem. Soc. **106**, 2687 (1984); Appl. Biochem. Biotech. **9**, 255 (1984); W. E. Ladner and G. M. Whitesides. J. Am. Chem. Soc. **106**, 7250 (1984); S. Hamaguchi, J. Hasegawa, K. Kawahara, and K. Watanabe. Agric. Biol. Chem. **48**, 2055 (1984); T. Kitazume, T. Sato, and N. Ishikawa. Chem. Lett. 1811 (1984); W. Kasel, P. G. Hultin, and J. B. Jones. J. Chem. Soc. Chem. Commun. 1563 (1985); C. Marlot, G. Langrand, C. Triantaphylides, and J. Baratti. Biotechnol. Lett. **7**, 647 (1985); G. Langrand, M. Secchi, G. Buono, J. Baratti, and C. Triantaphylides. Tetrahedron Lett. **26**, 1857 (1985); K. Laumen and M. Schneider. Tetrahedron Lett. **26**, 2073 (1985); G. Kirchner, M. P. Scollar, and A. M. Klibanov. J. Am. Chem. Soc. **107**, 7072 (1985); A. Zaks and A. M. Klibanov. Proc. Natl. Acad. Sci. (U.S.), **82**, 3192 (1985); B. de Jeso, S. Drouillard, C. Lafarge, and B. Maillard. Tetrahedron Lett. **26**, 6063 (1985); K. Takahashi, Y. Kodera, T. Yoshimoto, A. Ajima, A. Matsushima, and Y. Mada. Biochem. Biophys. Res. Commun. **131**, 532 (1985); J. P. Rosazza, S. Reeg, and L. M. Yang. Enzyme Microb. Technol. **8**, 161 (1986); G. Langrand, J. Baratti, G. Buono, and C. Triantophylides. Tetrahedron Lett. **27**, 29 (1986); Q.-M. Gu, C.-S. Chen, and C. J. Sih. Tetrahedron Lett. **27**, 1736 (1986); S. Hamaguchi, T. Ohashi, and K. Watanabe. Agric. Biol. Chem. **50**, 1629 (1986); G. Eichberger, G. Penn, K. Faber, and H. Griengl. Tetrahedron Lett. **27**, 2843 (1986).
3. (*a*) B. Maurer, A. Grieder, and W. Thommen. Helv. Chim. Acta, **62**, 44 (1979); B. Maurer and W. Thommen. Helv. Chim. Acta, **62**, 1096 (1979); (*b*) D. A. Van Dorp and J. P. Ward. Experientia, **37**, 917 (1981).
4. (*a*) D. Seebach and M. Pohmakotr. Helv. Chim. Acta, **62**, 843 (1979); D. Seebach, M. Pohmakotr, C. Schregenberger, B.

WEIDMANN, R. S. MALI, and S. POHMAKOTR. Helv. Chim. Acta, **65**, 419 (1982); (*b*) Y. MASAKI, Y. SERIZAWA, K. NAGATA, and K. KAJI. Chem. Lett. 1601 (1983); (*c*) F. W. LICHTENTHALER, F. D. KLINGLER, and P. S. JARGLIS. Carbohydrate Res. **132**, c1 (1984); (*d*) E. KEINAN, K. K. SETH, and R. LAMED. J. Am. Chem. Soc. **108**, 3474 (1986).

5. (*a*) M. F. SEMMELHACK and C. J. BODUROW. J. Am. Chem. Soc. **106**, 1496 (1984); (*b*) H. A. BATES and P. N. DENG. J. Org. Chem. **48**, 4479 (1983); (*c*) Y. KIM and B. P. MUNDY. J. Org. Chem. **47**, 3556 (1982); (*d*) S. V. LEY, B. LYGO, H. MOLINES, and J. A. MORTON. J. Chem. Soc. Chem. Commun. 1251 (1982).
6. A. C. COPE and A. FOURNIER, JR. J. Am. Chem. Soc. **79**, 3896 (1957).
7. H. MEIER and K.-P. KELLER. Angew. Chem. Int. Ed. Engl. **14**, 32 (1975); J. F. LANE and E. S. WALLIS. J. Org. Chem. **6**, 443 (1941).
8. G. SAUCY, R. BORER, D. P. TRULLINGER, J. B. JONES, and K. P. LOK. J. Org. Chem. **42**, 3206 (1977).
9. R. R. FRASER, M. A. PETIT, and J. K. SAUNDERS. Chem. Commun. 1450 (1971).
10. L. K. P. LAM, R. A. H. F. HUI, and J. B. JONES. J. Org. Chem. **51**, 2047 (1986).
11. G. M. WHITESIDES. 5th IUPAC Organic Synthesis Conference, Freiburg, FRG. 1984.
12. W. CZORNODOLA. Rocz. Chem. **16**, 459 (1936).

Can. J. Chem. Downloaded from www.nrcresearchpress.com by 78.46.186.204 on 09/07/12
For personal use only.

Trans to *cis* photoisomerization of *N,N'*-disubstituted indigo dyes via excited singlet states; a laser flash photolysis and steady state irradiation study

HELMUT GÖRNER
Max Planck Institut fur Strahlenchemie, Stiftstrasse 34–36, D-4330 Mülheim a.d. Ruhr, Federal Republic of Germany

AND

JOSEPH POULIQUEN AND JEAN KOSSANYI[1]
Laboratoire de photochimie solaire, Équipe de recherche 241 du Centre national de la recherche scientifique, 2–8 rue Henry Dunant, 94320 – Thiais, France

Received July 14, 1986

HELMUT GÖRNER, JOSEPH POULIQUEN, and JEAN KOSSANYI. Can. J. Chem. **65**, 708 (1987).

The relaxation pathways of excited *trans-N,N'*-diacylindigo dyes (*trans*-**1**–*trans*-**4**) and of the rigid *trans* (**5**) and *cis* (**6**) indigo analogues have been studied by nanosecond flash photolysis and steady state measurements. In fluid solution the *trans* to *cis* photoisomerization of **1**–**4** occurs via a singlet excited state mechanism on direct excitation, and the triplet state appears to be reached only by sensitized reaction. The lower quantum yield for *trans* → *cis* isomerization of **2**–**4** at room temperature, as compared to **1**, is due to a thermally activated internal conversion step leading to the *trans* ground state. This pathway competes with fluorescence and twisting of the molecule around the central double bond in the excited singlet state. Increasing the viscosity of the medium decreases the twisting of the flexible molecules and, as a consequence, increases the population of the lowest triplet state. A triplet transient, the intensity of which increases with the viscosity of the medium, could be characterized at low temperature under direct excitation. A transient species, which can be assigned to a triplet state on the basis of quenching experiments and on the fact that the same transient could be found under sensitized conditions, also has been observed at room temperature for the rigid **5** and **6** molecules. Quenching measurements of triplet sensitizers by **5**, *trans*-**1**, and *trans*-**2** enables the localization of the triplet energy at around 40 kcal/mol.

HELMUT GÖRNER, JOSEPH POULIQUEN et JEAN KOSSANYI. Can. J. Chem. **65**, 708 (1987).

Les différentes voies de désactivation des états excités du *trans N,N'*-diacétylindigo (*trans*-**1**) et des *N,N'*-dibenzoylindigos substitués (*trans*-**2**–*trans*-**4**), ainsi que leurs analogues rigides *trans* (**5**) et *cis* (**6**), ont été étudiés par photolyse laser nanoseconde et par irradiation continue. En solution fluide, la photoisomérisation *trans* → *cis* obtenue par irradiation directe se produit à partir du seul état excité singulet, l'état triplet n'étant atteint que par sensibilisation. La plus faible valeur du rendement quantique d'isomérisation *trans* → *cis* observée pour **2**–**4** à la température ambiante, est attribuable à une étape activée de la conversion interne qui mène à l'état fondamental *trans*. Cette voie est en compétition avec la fluorescence et la rotation autour de la double liaison centrale dans l'état excité singulet. L'augmentation de la viscosité du milieu permet d'accéder à l'état triplet *trans* avec une efficacité croissante, et un transitoire triplet, dont l'intensité augmente précisemment avec la viscosité de ce milieu, a pu être caractérisé pour les indigos flexibles **1**–**4**. Pour les composés **5** et **6**, à la température ambiante, un transitoire analogue est obtenu qui a été attribué à l'état triplet à l'aide d'expériences de sensibilisation et d'inhibition (par l'azulène, le ferrocène et l'oxygène). L'inhibition de l'état triplet d'une série de sensibilisateurs par le composé bloqué **5** permet de localiser son énergie de triplet autour de 40 kcal/mol.

Introduction

Thioindigo and substituted indigo dyes in *cis* ⇄ *trans* isomerization (1–4) show interesting photochemical behaviour, which has been proposed for solar energy conversion and storage (5). A triplet mechanism, postulated by Wyman and co-workers (1, 6), is now generally accepted for the *trans* → *cis* photoisomerization of thioindigo and its derivatives (7–12), while the *cis* → *trans* pathway is still under debate (9, 12). *N,N'*-Diacetyl indigo **1** and *N,N'*-dibenzoyl substituted indigo dyes **2**–**4** undergo *trans* → *cis* photoisomerization from the singlet excited state and no evidence for participation of a triplet excited state (13) could be put forward. In any case, since a transient could be characterized as a triplet state for *trans*-**1** (8),[2] an isomerization that would involve this triplet can still be questioned. On the other hand, unsubstituted indigo itself does not isomerize due to an efficient intramolecular hydrogen transfer from the nitrogen atom to the carbonyl group (14).

The purpose of the present work is to describe the photophysical and photochemical properties of trans-**1** and of three

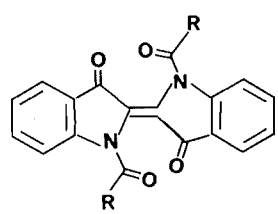

1-4

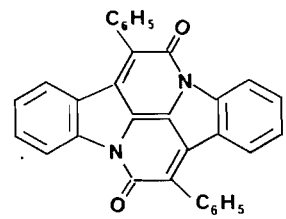

5

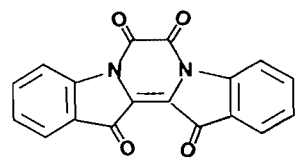

6

trans-**1** R = CH_3
trans-**2** R = C_6H_5
trans-**3** R = *p*-ClC_6H_4
trans-**4** R = *p*-$MeOC_6H_4$

N,N'-disubstituted indigo dyes (**2**–**4**). In addition, two rigid analogues (**5** and **6**) were studied. Due to their longer lifetime, the excited states of the latter two should be more readily accessible by nanosecond laser flash photolysis than those of the flexible dyes, since rotation around the central C=C double bond is for them impossible. Evidence for a singlet pathway for direct *trans* → *cis* photoisomerization is further established.

[1]Author to whom correspondence may be addressed.

[2]Note: "dimethyl" and "diacetyl" in Table 1 of this reference had been erroneously interchanged and λ_2 for *N,N'*-dimethylindigo is 740 nm, not 470 nm.

Can. J. Chem. Downloaded from www.nrcresearchpress.com by 78.46.186.204 on 09/07/12
For personal use only.

Can. J. Chem. Downloaded from www.nrcresearchpress.com by 78.46.186.204 on 09/07/12
For personal use only.

Experimental

Laser excitation was carried out with a neodymium laser (λ_{exc} = 353 and 530 nm, pulse width ~ 15 ns) (8, 15). If not otherwise indicated, 530-nm light was used and the samples were purged with argon. Concentrations of (0.3–1) × 10^{-4} *M* for **5** and (0.5–3) × 10^{-4} *M* for *trans*-**1**–*trans*-**4** were used for experiments under direct excitation while higher concentrations were generally used for sensitized excitation (λ_{exc} = 353 nm). Low temperature measurements were carried out in a 1 × 1 or 0.6 × 0.6 cm^2 rectangular cell placed in a cooled Dewar for steady state and pulsed measurements, respectively.

Fluorescence spectra at +25 and −196°C were recorded on a Spex–Fluorolog (corrected spectra), and at various temperatures on Perkin–Elmer MPF44-B or LS-5 spectrofluorimeters. Since ϕ_f is only slightly quenched by oxygen for **1**–**4** at +25°C (<10% in air- versus argon-saturated dichloromethane solution), the fluorescence spectra of the flexible dyes were recorded in air-saturated solutions. The concentrations were kept small, corresponding to an absorption of 0.1–0.4 in 1-cm cells at λ_{exc} = 530 nm. Values for ϕ_f were determined by using 9,10-diphenylanthracene (from EGA) as reference (cf. ref. 16). Singlet lifetimes were measured by excitation at 354 nm with an Applied Photophysics SP-1 single-photon counting fluorimeter, which was connected to an Ortec multichannel analyzer and a VAX 11/780 computer system.

Steady state irradiation measurements were carried out with a 1000-W xenon–mercury lamp combined with a monochromator (12-nm bandwidth, λ_{irr} = 546 nm unless otherwise indicated). For the direct excitation measurements in argon-saturated solutions, indigo concentrations of (4–6) × 10^{-5} *M* were used. Low temperature measurements were performed by irradiating the sample in a Dewar. Values for $\phi_{t\rightarrow c}$ were obtained by analysis of the visible absorption spectra (Perkin–Elmer 554) using as reference the absolute values in chloroform (13).

The *trans* isomers were prepared according to the procedure of Ross and Blanc (3*b*) for **1** and by Posner's method for **2**–**4** (17); the *cis* isomers of **1**–**3** were the same as described previously (13). The rigid molecule **5** was prepared using a procedure adapted from the one described by Engi (18). Oxalylindigo **6** was obtained according to the procedure of Heller (19). The compounds were purified by repetitive recrystallization in benzene (**1**–**5**) or in chloroform (**6**).

Ferrocene (Merck) was recrystallized from methanol while azulene (Aldrich) was used as received. The sensitizers were purified by recrystallization except for benzophenone, which was zone-refined. The solvents (Merck) were of p.A. quality (toluene, dichloromethane, glycerol triacetate (GT), acetone, *N*,*N*-dimethylformamide, and ethanol), Uvasol (acetonitrile), gold label (benzene, Aldrich); 2-methyltetrahydrofuran (MTHF, free of peroxides), ethyl iodide, and butyronitrile were purified by distillation.

The poly(methyl methacrylate) (PMMA) samples were prepared by dissolving 0.05–0.1% (by weight of the monomer) of the dye in 18 mL of methyl methacrylate at room temperature. Quantities of 5–6 mL of the solution were placed in a 16 mm diameter Pyrex tube with 0.075% by weight (based on methyl methacrylate) of 2,2-azobis(2-methyl propionitrile). The contents of the tubes were frozen by means of Dry Ice; the tubes were flushed with argon for several minutes and then sealed. The sealed tubes were placed in a sand bath, the temperature of which was gradually raised from 40 to 60°C, and subsequently were held at this temperature for 24 h. The polymerization was completed by heating further for 2 h at 120°C. The solidified samples were then cut and polished to make rectangular blocks (ca. 10 × 10 × 25 mm^3).

Results

A. *Transients at room temperature*

Rigid trans *compound 5*

On excitation (λ_{exc} = 530 nm) of compound **5** in ethyl iodide at 25°C, a transient absorption spectrum with two maxima (λ_{max} = 415 and 590 nm) and a bleaching zone in the range of the main ground state absorption band (maxima: λ_b = 510, 550 nm) were observed (Fig. 1*a*). The recovery at λ_b and the

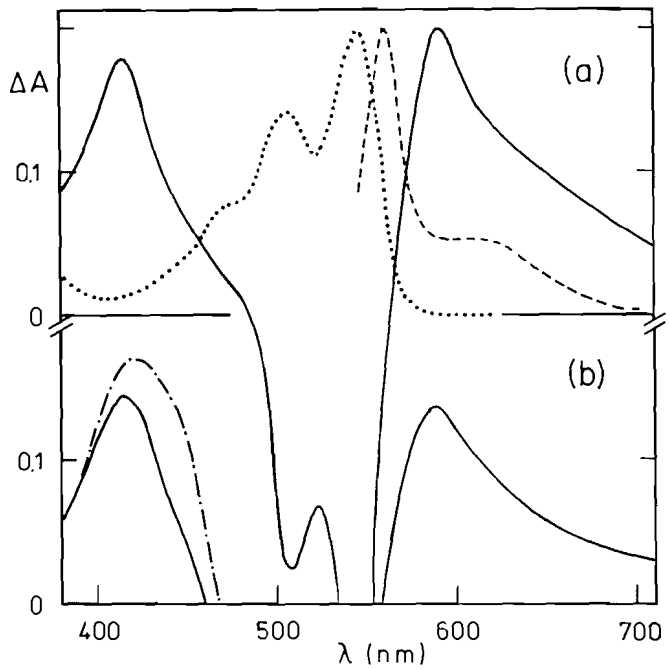

FIG. 1. Transient absorption spectra of compound **5** at 25°C; (*a*) in ethyl iodide (full line) 200 ns after the laser pulse; ground state absorption (dotted line) and fluorescence spectra (dashed lines); (*b*) in PMMA at the pulse end (broken line) and after 200 ns (full line).

decay at λ_{max} show the same time dependence; the main component of the transient (Tr_3) decays at both λ_{max} by first-order kinetics with a rate constant $k_{obs} = \tau^{-1} < 2 \times 10^5\ s^{-1}$. Similar absorption spectra and lifetimes in the μs range were recorded for the transient in dichloromethane solution and in a PMMA matrix (Fig. 1*b* and Table 1). In addition to Tr_3, a short-lived transient (Tr_1) was found in PMMA around 430 nm with a lifetime shorter than 50 ns; due to the strong fluorescence of **5** during the laser pulse, Tr_1 would escape our observation at $\lambda > 550$ nm. The transient absorbance (ΔA) at λ_{max}, as a measure of the relative yield of Tr_3, is about three times larger in ethyl iodide than in dichloromethane.

The lifetime of Tr_3 of **5** is reduced by addition of oxygen whereas ΔA (at the end of the laser pulse) remains constant. From linear plots of k_{obs} versus the concentration of oxygen (argon-, air-, oxygen-saturated solutions), rate constants for quenching by oxygen of $k_{ox} = 1.3 \times 10^9$ and $1.8 \times 10^9\ M^{-1}\ s^{-1}$ in dichloromethane and ethyl iodide, respectively, were obtained, using a solubility of $[O_2] = 8 \times 10^{-3}\ M$ for saturation. Tr_3 is also quenched by ferrocene and azulene but not by perylene (rate constant $< 10^7\ M^{-1}\ s^{-1}$). The rate constant for quenching by ferrocene in dichloromethane and by azulene in ethyl iodide (λ_{exc} = 353 nm in the latter case) is about 0.8 × 10^9 and 0.4 × $10^9\ M^{-1}\ s^{-1}$, respectively. No attempt was made to evaluate other effects on k_{obs} (e.g. concentrations of ground and (or) excited states). On the basis of these results, the short-lived transient Tr_1 has been attributed to the singlet excited state and the long-lived Tr_3 to the triplet excited state.

Rigid cis *compound 6*

With compound **6**, the following results were found on excitation at 353 nm: the transient absorption spectrum (Fig. 2*a*) shows maxima around 350, 500–600, and 700 nm and a bleaching zone around 420 nm, with the same rate constant for recovery as the k_{obs} observed for the decay of the transient absorption at longer wavelengths. The triplet lifetime τ_T is in the

TABLE 1. Absorption maxima and lifetime of the triplet transients Tr_3[a]

Indigo	Solvent	λ_{max} (nm)			λ_b (nm)		Temperature (°C)	τ_T (μs)
trans-**1**	PMMA	~380		570			25	5[b]
	MTHF–DCM	≦380		575			−160	
	GT	≦370		570			−75	
trans-**2**	PMMA	≦370	510	610			25	4[b]
	MTHF–DCM	<370	510	≦640	580		−160	
trans-**3**	PMMA	≦370	500	610			25	5[b]
	MTHF–DCM	≦370	500	620	580		−160	
	GT	~370	510	620			−80	
trans-**4**	MTHF–DCM	<390	500	620	600		−160	
	GT	≦370	500	620	590		−70	
5	PMMA	415		585	505	546	25	5[b]
	Ethyl iodide	415		590	510	550	25	>5
	Dichloromethane	410		580	500	540	25	>10
	Benzene[c]	415		580	510	560	25	≧10
6[d]	PMMA		540		≦430		25	≧100
	Benzene	340	530		425		25	~5
	Benzene[c]		540		~430		25	>3
	Acetonitrile	340	530		420		25	6

PMMA: poly(methyl methacrylate). GT: glycerol triacetate. MTHF–DCM: 2-methyltetrahydrofuran/dichloromethane (1:1, vol.).

[a]In argon-saturated solutions, λ_{exc} = 530 nm, unless indicated otherwise.

[b]The lifetime is probably reduced by oxygen.

[c]Benzophenone sensitized, λ_{exc} = 353 nm.

[d]λ_{exc} = 353 nm.

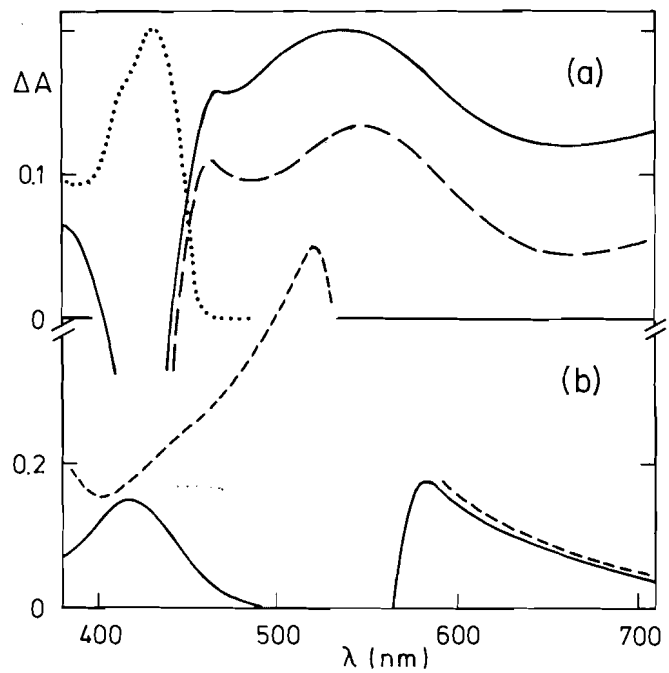

FIG. 2. Transient absorption spectra at 25°C using laser excitation at 353 nm of (*a*) **6** in acetonitrile solution (——) at the end of the pulse and (---) in the presence of benzophenone 0.5 μs after the pulse; (····) ground state absorption; (*b*) **5** in benzene solution with benzophenone sensitization (---) 20 ns after the laser pulse and (——) 1 μs after the pulse.

μs range when taken in fluid solution but much higher, in the ms range, when **6** is inserted in a PMMA matrix (Table 1). The rate constants for quenching of Tr_3 by oxygen (ferrocene) are about 2×10^9 (8×10^9) M^{-1} s^{-1} in benzene solution and 2×10^9 (10×10^9) M^{-1} s^{-1} in acetonitrile solution, but 5×10^9 M^{-1} s^{-1} for quenching by azulene in dichloromethane solution.

Flexible molecules ***1–4***

Two transients, a short-lived one Tr_1 ($\tau < 30$ ns, λ_{max} = 430 nm) and a longer-lived one Tr_3 with two maxima (λ_{max} around 380 and 570 nm), were recorded for *trans*-**1** in a PMMA matrix at 25°C. Analogous spectra were recorded for *trans*-**2** and *trans*-**3** (Table 1); here, Tr_3 has three maxima. However, the singlet transient Tr_1 could be detected with low absorbance only in some specific cases, e.g. for *trans*-**1** in benzene (6, 8) or dichloromethane solutions (with λ_{max} around 450 nm). At room temperature and in the solvents used here, no triplet transient that would have a lifetime longer than 20 ns could be observed for *trans*-**1**–*trans*-**4**.

B. Transients at low temperatures

Similar to the results in PMMA matrix, a short-lived transient (Tr_1, λ_{max} around 440 nm and $\tau < 50$ ns) was found at low temperature in some cases (Fig. 3*b*). Tr_1 is assigned to the lowest excited *trans* singlet state $^1t^*$ as already proposed for *trans*-**1** (6, 8), on the basis of its short lifetime even in rigid matrices. An $S_1 \rightarrow S_n$ absorption transition also has been reported for *trans* thioindigo (12). It is noteworthy that the singlet lifetime (τ_S) deduced from the fluorescence decay is around 5 ns for *trans*-**1**–*trans*-**3** in PMMA at 20°C and around 12 ns in MTHF glass at −196°C (13). For **5** in dichloromethane at 25°C, τ_S was found to be around 6 ns.

In contrast to measurements in fluid solution at ambient temperature, a long-lived transient (Tr_3) was observed for *trans*-**1**–*trans*-**4** in several viscous media at lower temperatures. Examples are shown for *trans*-**1** in GT at −70°C (Fig. 3*a*) and for *trans*-**3** in a 1:1 mixture of 2-methyltetrahydrofuran and dichloromethane (MTHF–DCM) at −170°C (Fig. 3*b*). In both glassy solvents, *trans*-**2**–*trans*-**4** show triplet transient absorption ($Tr_3 = {}^3t^*$) with λ_{max} at about 370, 500, and 620 nm, and λ_b around 580 nm (Table 1).

Can. J. Chem. Downloaded from www.nrcresearchpress.com by 78.46.186.204 on 09/07/12
For personal use only.

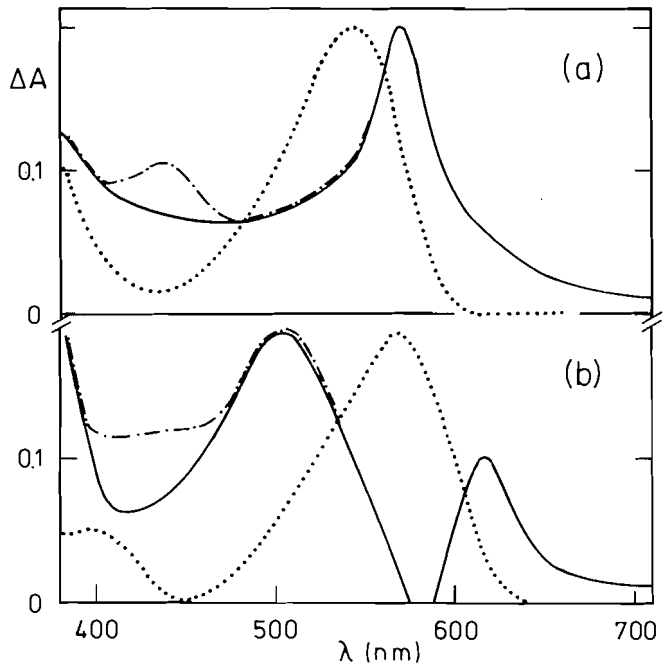

FIG. 3. Transient absorption spectra in rigid media: (*a*) of *trans*-**1** in GT at −70°C (·····) at the end of the pulse and (—) after 200 ns; (*b*) of *trans*-**3** in MTHF–DCM at −170°C (·····) at the pulse end and (—) after 200 ns; (····) ground state absorption at 25°C.

The temperature dependence of the transient absorption at 570 nm, ΔA_{570}, is shown for *trans*-**1** in MTHF–DCM and GT (Figs. 4 and 5). The following general trend was found for *trans* indigos: on going from 25°C to lower temperatures, $^3t^*$ was first observed (around λ_{max}) at the temperature t_m; on decreasing the temperature further, ΔA_{570} increases and reaches a maximum value at about −70°C in GT and at about −180°C in MTHF–DCM. The ratio of ΔA_{570} values (*trans*-**1**) and ΔA_{550} (**5**) in GT at −70°C is ≧3 under identical excitation conditions.

In the accessible temperature range (Table 2), the absorption of the triplet $^3t^*$ of *trans*-**1** decays at its maximum λ_{max} by first-order kinetics. As shown in Figs. 4 and 5, k_{obs} decreases from about $\tau^{-1} = 1 \times 10^7\ s^{-1}$ (at $t_m = -30$°C in GT and −135°C in MTHF–DCM) to values smaller than $10^5\ s^{-1}$ below a certain temperature t_0 (−70°C in GT and −175°C in MTHF–DCM). Below t_0, k_{obs} is virtually constant, with small variations when observed at around 400 and 600 nm.

For *trans*-**2**–*trans*-**4** in GT, plots of k_{obs} versus T^{-1} are similar to that of *trans*-**1** but, in MTHF–DCM and in a certain temperature range between t_m and t_0, the decay is no longer first order. Due to small ΔA values no kinetic analysis was performed.

C. Quenching of sensitizers by the trans *isomers*

To obtain some information about the triplet energy (E_T) of the *N,N'*-disubstituted indigo dyes, the effect of triplet quenching of several aromatic compounds (sensitizer: Sens) by *trans*-**1**, *trans*-**2**, and **5** was studied in dichloromethane solution at room temperature using $\lambda_{exc} = 353$ nm. On increasing the indigo concentration, the rate constant for decay of a given aromatic triplet (k_{obs}^{Sens}) increases linearly (up to a limit of $5 \times 10^6\ s^{-1}$ corresponding to a lifetime of 200 ns). The rate constant for triplet quenching (k_q), obtained from the slope of this dependence, is around $3 \times 10^9\ M^{-1}\ s^{-1}$ for several high energy triplet donors ($E_T > 42$ kcal/mol) and decreases on going to lower E_T values (Table 3).

TABLE 2. Lifetime of the triplet transient Tr_3 at low temperature[a]

Indigo	Solvent	t_m[b] (°C)	τ_T^{min} (μs)	t_0 (°C)	τ_T^{max} (μs)
trans-**1**	MTHF–DCM	−135	0.1	−165	~13 (20)
	GT	−30	0.1	−65	~12 (18)
trans-**2**	MTHF–DCM	−90	0.2	−150	≧4
	GT	−15	0.1	−50	~5
trans-**3**	MTHF–DCM	−80	0.3	−150	≧10
	GT	−7	0.1	−45	≧5
trans-**4**	MTHF–DCM	−100	0.6	−160	≧3
	GT	0	0.1	−60	~6

[a]Observed in the 400–430 nm and (or) 580 nm range; values in parentheses refer to $\lambda_{max} = 580$ nm; for **2**–**4** no wavelength dependence (400 vs. 580 nm) of k_{obs} is found.
[b]t_m is the highest temperature at which the triplet transient could be observed.

When benzophenone is used as triplet sensitizer of **5** in benzene solution, it is observed that the remaining spectrum after decay of ^{3}Sens* is very similar to that obtained for Tr_3 on direct excitation (compare Figs. 2*b* and 1). This confirms the triplet nature of Tr_3. Using $\varepsilon_{TT} = 7.6 \times 10^3\ M^{-1}\ cm^{-1}$ for benzophenone in benzene solution (20) and assuming 100% energy transfer, the absorption coefficient of Tr_3 of **5** (at 580 nm) is $5 \times 10^3\ M^{-1}\ cm^{-1}$. Under the same conditions, the rigid *cis* molecule **6** shows also a triplet transient for which ε_{TT} was estimated to be $\leqq 2 \times 10^3\ M^{-1}\ cm^{-1}$ at its maximum (530 nm). Similar experiments at room temperature with the *trans* isomers showed a permanent (>1 ms) increase in ΔA in the range between the isosbestic points (e.g. 410 nm and 516 nm for **1**, where the ground state of the *cis* isomer absorbs and where the triplet is expected to absorb as well) and a permanent decrease in ΔA above 516 nm, where mainly the ground state of the *trans* isomers absorbs. Such a result is typical for *cis* ⇄ *trans* isomerization (7, 9). However, no transient was found after 200 ns that could be assigned to an indigo triplet state.

At high indigo concentrations, corresponding to $k_{obs}^{Sens} > 5 \times 10^6\ s^{-1}$, the yield of ^{3}Sens* is markedly reduced due to the increasing absorption of the *trans* isomer at 353 nm and (or) (benzophenone excepted) to fluorescence quenching of the sensitizer by the indigo dye. Dynamic fluorescence quenching of Sens should be of minor importance since under the conditions used here (indigo concentration $< 2 \times 10^{-3}\ M$) only a few per cent of ^{1}Sens* ($\tau_S < 10$ ns) can react with a quencher even under diffusion-controlled conditions.

D. Fluorescence quantum yield and singlet lifetime

While **6** shows virtually no emission throughout in fluid media at ambient temperature, compound **5** exhibits fluorescence with maxima at 515 and 525 nm in dichloromethane and ethyl iodide solutions, respectively (Fig. 1*a*). Its quantum yield of fluorescence (ϕ_f) in several solvents at room temperature is close to unity and is significantly smaller only in the heavy atom solvent ethyl iodide (Table 4). On the other hand, changing the temperature (e.g. in GT from 25 to −75°C) has virtually no effect on ϕ_f.

For *trans*-**1**–*trans*-**4** the substituent R, the temperature, and the nature of the solvent have remarkable effects on ϕ_f (Table 4). While the fluorescence maximum is only little affected by the solvent (610 nm in MTHF–DCM and butyronitrile, 620 nm

Can. J. Chem. Downloaded from www.nrcresearchpress.com by 78.46.186.204 on 09/07/12
For personal use only.

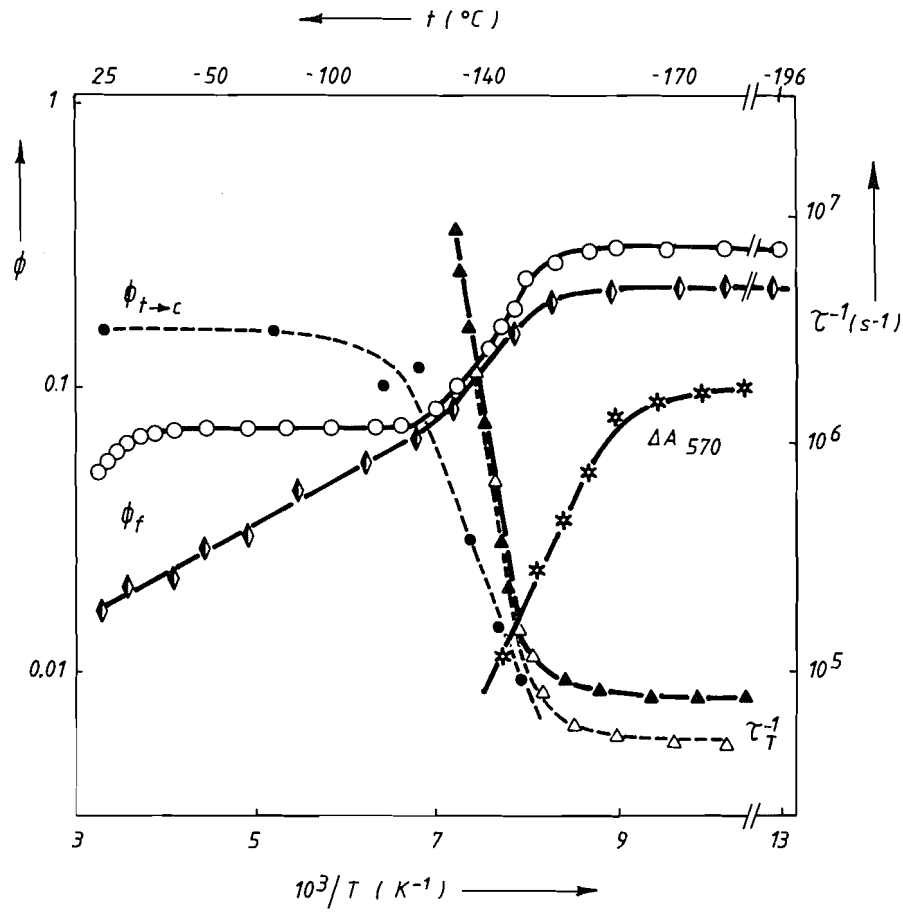

FIG. 4. Semilogarithmic plots versus T^{-1} for *trans*-**1** in MTHF–DCM: (—○—○—○—) ϕ_f at 530 nm; (—●--●--●—) $\phi_{t\to c}$ at 546 nm; (—▲—▲—) k_{obs} at 400 nm; (—△—△—) k_{obs} at 570 nm; (*—*—*) ΔA_{570}; (—◆—◆—) ϕ_f in butyronitrile.

TABLE 3. Rate constant for quenching of the triplet state of aromatic compounds[a]

Sensitizer	E_T (kcal/mol)	$10^{-9} \times k_q$ (M^{-1} s^{-1})			
		trans-**1**	*trans*-**2**	**5**	**6**
Benzophenone	68.5	(5)[b]	(5)	(4)	
2-Nitronaphthalene	56.8	4	3	3.5	2
Acridine	45.3	4	3	2	2
9,10-Dibromoanthracene	41	4	3	1.2	<1
Tetraphenylporphin	37		1.5	1	
Perylene	36		≦0.01		
Methylene blue	33	≥2	≥2	<0.5	

[a]At 25°C. λ_{exc} = 353 nm in argon-saturated dichloromethane unless indicated otherwise.
[b]Values in parentheses refer to benzene solution.

in ethanol for **1**, and 620 nm for **4** in MTHF–DCM), in a given solvent, ϕ_f decreases in the order **1**–**4**. For **2**–**4**, ϕ_f depends only slightly on solvent properties while for **1** it decreases when the solvent polarity increases. At low temperatures and corresponding high viscosities, ϕ_f is strongly enhanced but the values remain well below unity.

The temperature dependence of ϕ_f is shown for the flexible *trans* isomers in GT and MTHF–DCM (Figs. 4–6). ϕ_f increases monotonously on lowering the temperature. From the linear parts of log ϕ_f versus T^{-1} (at higher temperatures) activation energies (E_a) of about 1 kcal/mol (**2** in MTHF–DCM) to 5 kcal/mol (**4** in GT) were determined (Table 5). An exception is *trans*-**1** in MTHF–DCM, where ϕ_f changes only slightly at the beginning when going down to −130°C but exhibits a steep increase in the −130 to −150°C temperature range where the viscosity increases strongly (Fig. 4). This viscosity-induced increase is also indicated for **1** (Fig. 4) in butyronitrile and for **2** in MTHF–DCM (Fig. 6).

Data reported in the previous work (13) already indicate that the singlet lifetime τ_s of the flexible *trans* molecules increases to a smaller extent than the corresponding fluorescence quantum yields when going from 25 to −196°C. To verify this important observation τ_S was now determined in the same solvent at these temperatures. For the flexible *trans* isomers, values of τ_s are

Can. J. Chem. Downloaded from www.nrcresearchpress.com by 78.46.186.204 on 09/07/12
For personal use only.

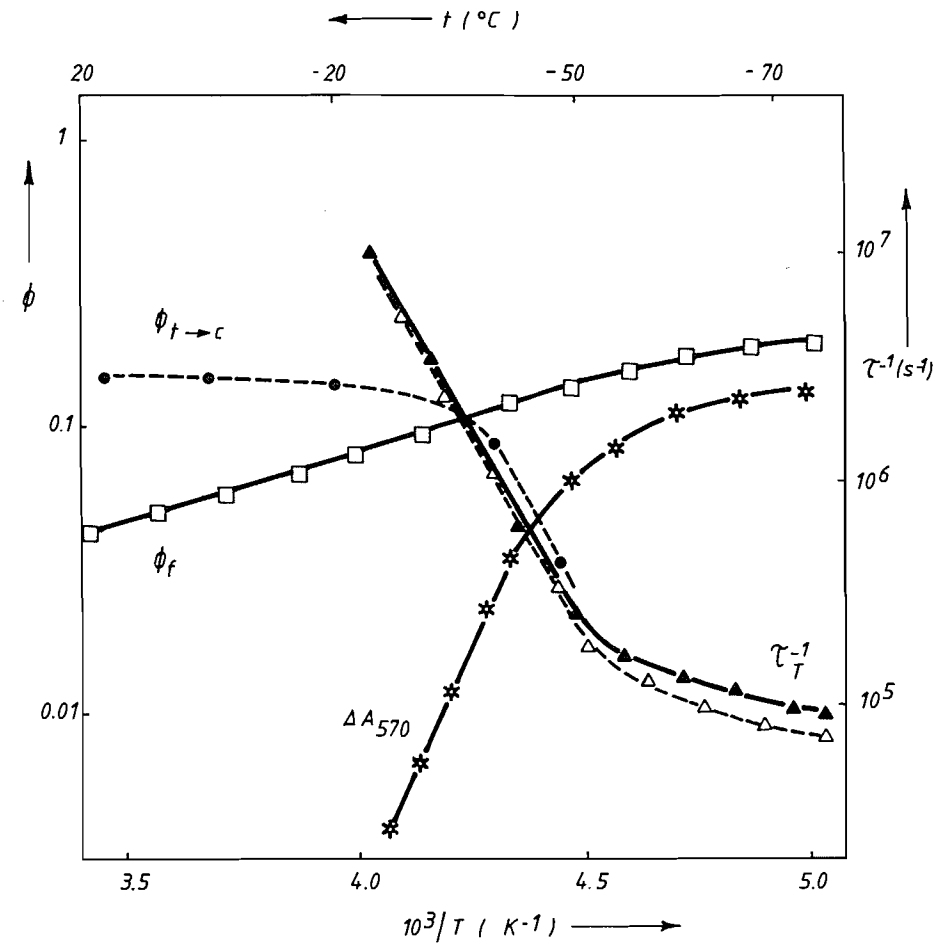

FIG. 5. Semilogarithmic plots versus T^{-1} for *trans*-**1** in GT: (—□—□—□—) ϕ_f; (—●--●--●—) $\phi_{t\rightarrow c}$; (*—*—*) ΔA_{570}; (—▲—▲—) k_{obs} at 400 nm; (—△—△—) k_{obs} at 570 nm.

TABLE 4. Quantum yield of fluorescence of *trans* isomers in fluid and rigid media[a]

Solvent	ϕ_f				
	1	**2**	**3**	**4**	**5**
Benzene	0.10	0.012	<0.009	0.006	
Toluene	0.10	0.012	0.009	0.007	
GT	0.04	0.010	0.008	0.006	0.9
	(0.2)	(0.08)	(0.1)	(0.1)	(0.9)
MTHF–DCM	0.05	0.015	0.008	0.004	0.95
	(0.3)	(0.4)	(0.3)	(0.3)	(≧0.8)
Chloroform[b]	0.022	0.005	0.0045	0.004	
Acetone	0.03	0.004	0.003	0.002	
Dimethylformamide	0.015	0.002	0.002	0.001	
Acetonitrile[b]	0.015	0.002	<0.003	≦0.001	
Butyronitrile[b]	0.016	0.004	0.003		
	(0.24)	(0.29)	(0.42)		
Ethanol	≦0.005	0.004	0.002		
	(0.2)	(≦0.2)	(0.2)		
Ethyl iodide	0.06	0.009			0.12

[a]λ_{exc} = 530 nm at 25°C unless otherwise indicated; values in parentheses refer to measurements at −75°C in GT and at −196° in all the other solvents.
[b]Taken from ref. 13, λ_{exc} = 580 nm.

Can. J. Chem. Downloaded from www.nrcresearchpress.com by 78.46.186.204 on 09/07/12
For personal use only.

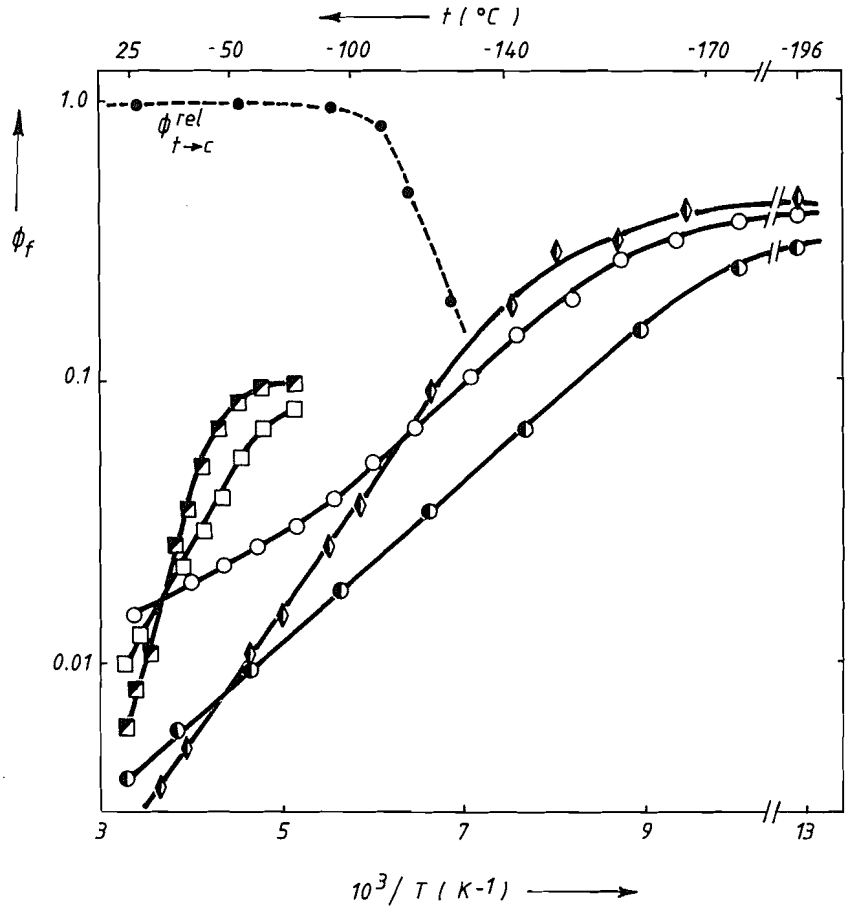

FIG. 6. Semilogarithmic plots versus T^{-1}: (—○—○—○—) ϕ_f for *trans*-**2** in MTHF–DCM; (—□—□—□—) ϕ_f for *trans*-**2** in GT; (—◆—◆—) ϕ_f for *trans*-**3** in butyronitrile; (—◐—◐—) ϕ_f for *trans*-**4** in MTHF–DCM; (—◩—◩—) ϕ_f for *trans*-**4** in GT; (—●--●--●—) $\phi^{rel}_{t\to c}$ for *trans*-**2** in MTHF–DCM.

TABLE 5. Data obtained from the temperature dependence of ϕ_f[a]

Indigo	Solvent	E_a (kcal/mol)	A/k_f	A[b] (s^{-1})
trans-**1**	MTHF–DCM	≧0.1[c]		
	Butyronitrile	0.8[d]	2×10^2	3×10^9
	GT	2.4	1×10^3	2×10^{10}
trans-**2**	MTHF–DCM	1.1	4×10^2	8×10^8
	GT	3.0	1×10^4	2×10^{10}
trans-**3**	MTHF–DCM	1.6	2×10^3	5×10^9
	Butyronitrile	2.1	1×10^4	3×10^{10}
	GT	4.0	1×10^5	2×10^{11}
trans-**4**	MTHF–DCM	2.0	7×10^3	1×10^{10}
	GT	4.9	6×10^5	1×10^{12}

[a]λ_{exc} = 530 nm; E_a and A/k_f were obtained from the linear dependence of log ϕ_f^{-1} versus T^{-1} at high temperatures where, according to eq. [1], $[1 + (k_{ic} + k_{isc})/k_f] \ll (A/k_f)\exp(-E_a/RT)$.
[b]Taking k_f values from ref. 13 and assuming k_f being solvent independent.
[c]Range: −20 to −130°C.
[d]Below −130°C.

TABLE 6. Fluorescence lifetimes of *trans* isomers in fluid and rigid media (in argon-saturated solutions)[a]

Solvent	Temperature (°C)	τ_S (ns) **1**	**2**	**3**	**4**	**5**
2-MTHF	25	3.6	5.5	3.9		6.5
	−196	11.0	15.0	14.0		7.3
Butyronitrile	25	2.0	2.3	1.6	3.1	
	−196	11.0	15.0	14.0	15.0	
PrCN–BA[b]	−196	6.6	7.0	6.4		
Ethanol	−196	10.0	14.0	14.0	15.0	
Ethyl iodide	25					≦1.0

[a]λ_{exc} = 354 nm. 2-MTHF: 2-methyltetrahydrofuran.
[b]Taken from ref. 13. PrCN–BA: butyronitrile (95%) – butyl acetate (5%).

typically 2–5 ns at 25°C and show no pronounced dependence on the substituent R or on the solvent properties (Table 6). Moreover, in rigid media τ_S is only prolonged by a factor of less than 10. This is in striking constrast to the behaviour of the ϕ_f values (Table 4).

For the rigid compound **5** in MTHF solution τ_S changes only little between +25 and −196°C, but it decreases at room temperature (Table 6) in a similar manner to ϕ_f (Table 4) when changing MTHF to ethyl iodide as solvent.

E. Steady-state irradiation measurements

Depending on λ_{irr}, a photostationary state is formed from both isomers. In a given solvent and at ambient temperature, the quantum yield of *trans* → *cis* photoisomerization ($\phi_{t\to c}$), which is larger for **1** than for **2** and **3** (Table 7), shows a trend to decrease with increasing solvent polarity (as it already has been observed for *N,N'*-dimyristoylindigo; see ref. 4*c*). The photostationary state depends on λ_{irr} and is shifted towards the *trans* side in the order **1**, **2**, **3** for λ_{irr} = 546 nm.

Can. J. Chem. Downloaded from www.nrcresearchpress.com by 78.46.186.204 on 09/07/12
For personal use only.

TABLE 7. Quantum yield of *trans* to *cis* photoisomerization and % *cis* in the photostationary state[a]

Solvent	λ_{irr} (nm)	1		2		3	
		$\phi_{t\rightarrow c}$	% *cis*	$\phi_{t\rightarrow c}$	% *cis*	$\phi_{t\rightarrow c}$	% *cis*
Benzene	366	0.25	55	0.05	40	0.03	24
	546	0.25	86	0.05	55	0.04	42
Chloroform[b]	>400	0.25	50	0.06	25	0.04	16
Dichloromethane	546	0.16	75				
Acetone	546		>60[c]	0.03	40	<0.02	<20
Dimethylformamide	546	[c]		[c]		[c]	
Acetonitrile	546	[c]		0.015	20	<0.02	<20

[a]In argon-saturated solution at 25°C.
[b]Taken from ref. 13.
[c]Thermal *cis* → *trans* isomerization during the irradiation time (10 min).

$\phi_{t\rightarrow c}$ decreases also with temperature: for **1** and **2** in MTHF–DCM, it changes only little above −100°C and decreases on going to lower temperatures (Figs. 4 and 6). A similar dependence was observed for **1** in GT with a marked change below −30°C (Fig. 5). Measurements at higher temperatures were unsuccessful because of the occurrence of thermal *cis* → *trans* isomerization (13, 21).

Discussion

A. Triplet state

For the rigid *trans* analogue **5**, Tr_3 is assigned to a triplet state due to the following. First, the kinetics are independent of the wavelength, indicating the formation of a single species. Second, Tr_3 is efficiently quenched by azulene (E_T = 39 kcal/mol), ferrocene (E_T = 39.5 kcal/mol (22)), and by oxygen. Third, the triplet yield is enhanced in a heavy atom solvent. Fourth, energy transfer measurements from the triplet state of aromatic compounds (^{3}Sens*), with $E_T > 41$ kcal/mol, to **5** show that ^{3}Sens* is quenched in solution at room temperature with a rate constant k_q (Table 3) that is a factor of 3–7 below the diffusion-controlled limit (10^{10} M^{-1} s^{-1} for benzene and 1.5×10^{10} M^{-1} s^{-1} for dichloromethane). Finally, the spectrum of the remaining transient under sensitized excitation conditions is similar to that of Tr_3 (compare Figs. 1 and 2*b*). On the basis of energy transfer and quenching measurements the triplet energy of **5** is placed at about 40 kcal/mol. A similar value is estimated for *trans*-**1** and *trans*-**2** (Table 3). The rigid *cis* analogue **6** also shows a long-lived transient (Table 1) after excitation with the 353-nm laser beam. Quenching of this transient by ferrocene and azulene occurs with a rate constant close to the diffusion controlled limit; in addition, **6** quenches the triplet state of aromatic compounds (^{3}Sens*). These results are in agreement with the assignment of the transient to a triplet species the energy of which, E_T, would be slightly higher than that of **5** or of the *trans* isomers.

For the flexible indigo dyes, Tr_3 is assigned to a triplet state with *trans* configuration ($^3t^*$) on the following basis. First, the transient absorption spectra of a *trans* isomer in PMMA at 25°C and in glassy media at low temperatures are more or less similar (Table 1). This confirms the identity of the transient. Second, Tr_3 was observed for *trans*-**1**–*trans*-**4** only in viscous media (Fig. 3 and Table 1), i.e., under conditions where the *trans* to *cis* photoisomerization is strongly reduced. Third, the increase of the transient absorption at 570 nm (ΔA_{570}) as the temperature is decreased (Figs. 4 and 5) is in line with the proposal that the triplet is populated by intersystem crossing at the *trans* side (8). Analogous temperature and viscosity dependences were also found for *trans*-stilbenes (16, 23) and other dyes that can twist around a C=C double bond, e.g. azobenzenes (15).

That the donor triplet with $E_T > 40$ kcal/mol could be quenched to a rate constant limit of about 5×10^6 s^{-1} and that the triplet state of the *trans* isomers, in contrast to that of **5**, was not spectroscopically observed at ambient temperature, places the triplet lifetime of the flexible dyes at a value smaller than 200 ns. An estimate of ≦100 ns would be expected from the temperature dependences under direct excitation (Figs. 4 and 5). The maximum yield for triplet formation ϕ_{isc}^{max} is probably smaller than $(1 - \phi_f)$ since, even at −196°C, ϕ_f remains significantly smaller than 0.5 (Table 4); consequently, the triplet yield would remain smaller than 0.5. This agrees with estimates based on the relative values of the transient absorption ΔA_{570} obtained for *trans*-**1** and **5** in GT at −70°C assuming $\phi_{isc} = 1 - \phi_f \leqq 0.1$ for **5**.

B. Excited trans *singlet state*

The emission of compounds **1**–**5** is attributed to fluorescence from the lowest excited *trans* singlet state ($^1t^*$) on the basis of the short lifetime. This is in agreement with the previous conclusion that the *cis* isomers of **1**–**4** exhibit no fluorescence even in rigid media and that both isomers show no phosphorescence (13). Only recently has the very weak fluorescence emission ($\phi_f < 10^{-5}$) for matrix isolated *cis* thioindigo been reported (24). For **5** in MTHF–DCM (as an example of a solvent without heavy atom effect), ϕ_f is close to unity (Table 4). This shows that fluorescence is the major deactivation step of excited **5** in fluid and rigid media. A minor step is intersystem crossing (≦0.1).

For the *trans* isomers of **1**–**4**, the temperature dependence of ϕ_f (Figs. 4–6) indicates that a temperature induced activated step ($A \times \exp(-E_a/RT)$) competes with the radiative decay (k_f). Assuming that k_f is independent of temperature, at least one radiationless, nonactivated step should be involved since ϕ_f is markedly smaller than unity even if the activated step is frozen out (Table 4). One possibility for this nonactivated step is intersystem crossing (k_{isc}) at the *trans* configuration. Indeed, a transient was observed (Fig. 3) that can be assigned to a triplet state. However, the maximum yield for triplet formation (ϕ_{isc}^{max}) is small, as indicated above. Therefore, we propose the involvement of internal conversion at the *trans* form (k_{ic}) as a second nonactivated, radiationless step.

According to this minimum number of decay channels of the

Can. J. Chem. Downloaded from www.nrcresearchpress.com by 78.46.186.204 on 09/07/12
For personal use only.

trans singlet excited state $^1t^*$, the effect of temperature on ϕ_f may be described by eq. [1] (in a simplified manner, e.g. assuming that k_f and k_{isc} are independent of the temperature):

$$[1] \quad \phi_f = \frac{k_f}{k_f + k_{ic} + k_{isc} + A \times \exp(-E_a/RT)}$$

Although **1**–**4** show similar temperature dependence in both GT and butyronitrile solution, a net difference is observed in MTHF–DCM solution: an activated step is found for *trans*-**2**–*trans*-**4** (Fig. 6), while two activated steps (a temperature- and a viscosity-induced one) seem to occur for *trans*-**1** (Fig. 4). Twisting around the central double bond seems to depend on the viscosity of the medium, as demonstrated by the absence of isomerization in GT at −70°C or in th PMMA matrix at room temperature. The temperature activated step is less simple and will be discussed with the photoisomerization mechanism in the next section. In any case, distinction between the two activation steps is difficult and the Arrhenius expression in eq. [1] includes both of them. At high temperature

$$[2] \quad [1 + (k_{ic} + k_{isc})/k_f] \ll (A/k_f) \exp(-E_a/RT)$$

and consequently one can write

$$[3] \quad \log \phi_f = \log k_f - \log A + E_a/2.3RT$$

showing that $\log \phi_f$ is proportional to T^{-1}. The E_a values obtained from the slope are generally larger in GT than in MTHF–DCM and increase in the order **1** < **2** < **3** < **4**. The use of known k_f values (13) yields A factors in the order of 10^9–10^{10} s^{-1} in MTHF–DCM (Table 5). The lower ϕ_f values for **2**–**4**, as compared to **1**, are due to the differences in k_f, A, and E_a. Solvent properties may have further influence on ϕ_f, as claimed for *N,N'*-dimyristoylindigo (4*d*) and as observed here for **1** (Table 4). Nevertheless, the properties of the excited *trans* singlet state are still not fully understood and need further study. For example, the ratio ϕ_f/τ_S seems not to be independent of temperature and increases significantly on going from fluid to rigid media (Tables 4 and 6).

C. Mechanism of trans *to* cis *photoisomerization*

For *trans*-**2**–*trans*-**4**, as compared to *trans*-**1**, the following differences were found: first, $\phi_{t\rightarrow c}$ is significantly larger (~0.25) for *trans*-**1** than for the benzoylindigos (Table 7). Second, ϕ_f also is markedly larger for *trans*-**1** than for *trans*-**2**–*trans*-**4** at room temperature (Table 4). Third, a step with a pronounced activation energy (E_a) competes for **2**–**4** with fluorescence between −20 and −130°C in MTHF–DCM solution (Table 5). Finally, the temperature t_m at which $^3t^*$ is first observed is lower for *trans*-**1** than for *trans*-**2**–*trans*-**4** (Table 2). The origin of these differences will be discussed tentatively as follows.

(a) N,N'-*Diacetylindigo* ***1***

At room temperature an important pathway for *N,N'*-diacetylindigo is *trans* to *cis* photoisomerization since ϕ_f is small (Table 4) and $\phi_{t\rightarrow c}$ is substantial (Table 7). Twisting in the excited singlet state to the twisted configuration ($^1p^*$) rather than in the triplet state is suggested since the triplet state is observed only at high viscosities (Table 2). The main reason for the lack of *T–T* absorption at room temperature in fluid solution is probably the small ϕ_{isc} (cf. ref. 8) rather than a too short triplet lifetime. Furthermore, the temperature dependence of the triplet transient absorption $\Delta A(Tr_3)$ and of ϕ_f show no evident correlation below t_m (Figs. 4 and 5).

A *trans* → *cis* photoisomerization could occur via an upper excited triplet state, not involving an activation barrier at the *trans* side, and such an upper excited triplet pathway has been already suggested for *trans*-4-bromostilbene (16, 23). However, if such an upper excited triplet pathway were the only one involved, then ϕ_f would remain constant even in the high viscosity media. Since ϕ_f still increases in MTHF–DCM between −130 and −160°C (Fig. 4), this disagrees with a nonactivated pathway at the *trans* side and with an increase of the triplet transient absorption as the temperature is reduced. Obviously, $^3t^*$ is populated only in the high viscosity range, i.e., in the range where the molecule can no longer rotate around the C=C double bond in the excited state. The singlet decay can be interpreted by two processes: intersystem crossing at only the *trans* configuration below the temperature t_0 for which the rate constant k_0 for recovery of the transient is virtually constant, and twisting, which is important above t_0 (8).

We suggest that the step $^1t^* \rightarrow {}^1p^*$ has to overcome only a small activation barrier in fluid solution. This, together with a small ϕ_f value and a certain contribution of internal conversion at the *trans* side, leads to moderate $\phi_{t\rightarrow c}$ values unless a high viscosity of the medium hinders the twisting process; then $\phi_{t\rightarrow c}$ decreases while both ϕ_f and ϕ_{isc} increase. The high temperature (> −20°C) dependence of ϕ_f in MTHF–DCM (Fig. 4) indicates another activated step. Whether or not this step leads to the *cis* form is as yet unknown. If a second *trans* to *cis* pathway were operating, $\phi_{t\rightarrow c}$ should increase at higher temperatures. Unfortunately, these measurements failed due to the occurrence of thermal *cis* → *trans* isomerization above room temperature (13, 21).

(b) Substituted N,N'-*dibenzoylindigos* ***2–4***

A triplet route for *trans* to *cis* photoisomerization of the benzoylindigos is also excluded on the basis of the arguments presented above. In addition, the photostationary state obtained from direct excitation is different (Table 7). The lower values for ϕ_f and $\phi_{t\rightarrow c}$ (for instance, 0.012 and 0.05 respectively for **2** in benzene solution as compared to 0.10 and 0.25 for **1** in the same solvent) are at least partly due to an activated step competing with fluorescence. In the simplest cases this activated step could lead to a twisted excited configuration (p^*) and finally to the *cis* and *trans* forms in the ratios α and $(1 - \alpha)$, respectively. This would imply that α is ca. 0.05 since the activated step is the main process for deactivation of $^1t^*$ at room temperature and since $\phi_{t\rightarrow c}$ is 0.05 in benzene and 0.06 in chloroform (Table 7). On the other hand, $\phi_{c\rightarrow t}$ is also small (0.12 and 0.09 for **2** and **3**, respectively) (13). Thus, α should be of the order of 0.88 if the *cis* → *trans* photoisomerization also occurs via the same intermediate p^*. This is inconsistent with the small value obtained above for α.

A more likely possibility is that the $^1t^*$ state decays on the one hand via $^1p^*$ to *trans* and *cis* ground states ($^1t + {}^1c$) as a minor route and, on the other hand, to the *trans* ground state through an activated step, which leads to an A^* excited state with essentially transoid configuration (Scheme 1). Such a scheme has already been suggested in the case of the *trans* to *cis* photoisomerization of 4-nitro-4'-dimethylaminostilbene in toluene solution (25).

Formation of A^* may involve an intrinsic as well as a viscosity-induced activation barrier. The effect of viscosity is indicated by a comparison of the temperature dependence of ϕ_f in MTHF–DCM and GT (Fig. 6). Thus, at the same temperature between +25 and −50°C, ϕ_f is ca. ten times higher in the more viscous solvent GT than in MTHF–DCM. The nature of A^* may

Can. J. Chem. Downloaded from www.nrcresearchpress.com by 78.46.186.204 on 09/07/12
For personal use only.

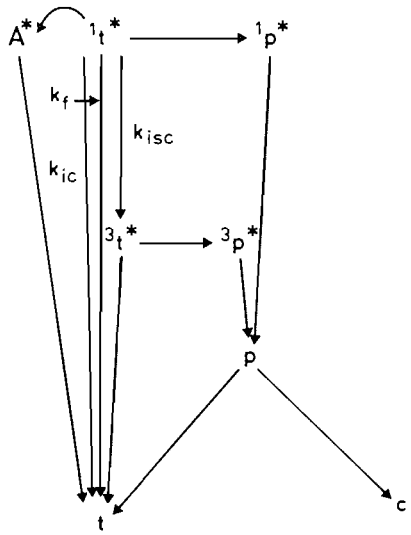

SCHEME 1. Pathways for deactivation of $^1t^*$ for **1** (essentially not involving A^*) and for **2–4** (mainly via A^*).

be related to the process of rotation of the benzoyl groups around the N—C single bond (thermally activated free rotor effect). Differences in τ_S, for the compounds inserted in PMMA matrices at room temperature as compared to fluid solution, have already been ascribed to this rotation (13).

Acknowledgements

We thank Professor D. Schulte-Frohlinde for stimulating discussions, and Mrs. C. Husken and Mr. L. J. Currell for technical assistance.

1. A. D. KIRSCH and G. M. WYMAN. J. Phys. Chem. (*a*) **79**, 543 (1975); (*b*) **81**, 413 (1977).
2. (*a*) J. WEINSTEIN and G. M. WYMAN. J. Am. Chem. Soc. **78**, 4007 (1956); (*b*) G. M. WYMAN and A. F. ZENHAUSERN. Ber. Bunsenges. Phys. Chem. **72**, 326 (1968).
3. (*a*) J. BLANC and D. L. ROSS. *In* Photochromism. *Edited by* G. H. Brown. John Wiley, New York. 1971. p. 471 ff; (*b*) D. L. ROSS and J. BLANC. J. Phys. Chem. **72**, 2817 (1968).
4. (*a*) C. R. GIULIANO, L. D. HESS, and J. M. MARGERUM. J. Am. Chem. Soc. **90**, 587 (1968); (*b*) G. HAUCKE and R. PAETZOLD. J. Prakt. Chem. **321**, 978 (1979); (*c*) G. R. SEELY and E. R. SHAW. J. Photochem. **24**, 383 (1984); (*d*) G. R. SEELY and E. R. SHAW. J. Photochem. **28**, 559 (1985).
5. R. A. NATHAN, R. E. SCHWERZEL, A. H. ALDEMAN, and R. E. WYANT. U.S. Patent No. 4,004,572; Jan. 25 (1977)/June (1975), and others cited in ref. 13.
6. D. SCHULTE-FROHLINDE, H. HERRMANN, and G. M. WYMAN. Z. Phys. Chem. Neue Folge, **101**, 115 (1976).
7. K. H. GRELLMANN and P. HENTZSCHEL. Chem. Phys. Lett. **53**, 545 (1978).
8. H. GÖRNER and D. SCHULTE-FROHLINDE. Chem. Phys. Lett. **66**, 363 (1979).
9. (*a*) T. KARSTENS, K. KOBS, and R. MEMMING. Ber. Bunsenges. Phys. Chem. **83**, 504 (1979); (*b*) R. MEMMING and K. KOBS. Ber. Bunsenges. Phys. Chem. **85**, 238 (1981); (*c*) C. P. KLAGES, K. KOBS, and R. MEMMING. Chem. Phys. Lett. **90**, 46 (1982).
10. Y. MAEDA, T. OKADA, N. MATAGA, and M. IRIE. J. Phys. Chem. **88**, 1117 (1984).
11. (*a*) S. A. KRYSANOV and M. V. ALFIMOV. Chem. Phys. Lett. **76**, 221 (1980); (*b*) R. MEMMING and K. KOBS. Chem. Phys. Lett. **80**, 475 (1981).
12. S. A. KRYSANOV and M. V. ALFIMOV. (*a*) J. Photochem. **23**, 329 (1983); (*b*) Laser Chem. **4**, 121 (1984).
13. J. POULIQUEN, V. WINTGENS, V. TOSCANO, B. BEN JAAFAR, S. TRIPATHI, J. KOSSANYI, and P. VALAT. Can. J. Chem. **62**, 2478 (1984).
14. (*a*) W. R. BRODE, E. G. PEARSON, and G. M. WYMAN. J. Am. Chem. Soc. **76**, 1034 (1954); (*b*) T. KOBAYASHI and P. M. RENTZEPIS. J. Chem. Phys. **70**, 886 (1979).
15. H. GÖRNER, H. GRÜN, and D. SCHULTE-FROHLINDE. J. Phys. Chem. **84**, 3031 (1980).
16. H. GÖRNER and D. SCHULTE-FROHLINDE. J. Phys. Chem. **83**, 3107 (1979).
17. T. POSNER. Ber. Dtsch. Chem. Ges. **59**, 1977 (1926).
18. G. ENGI. Z. Angew. Chem. **27**, 146 (1914).
19. G. HELLER. Chem. Ber. B, **77**, 163 (1944).
20. R. BENSASSON and E. J. LAND. Trans. Faraday Soc. **67**, 1904 (1971).
21. Y. SUEISHI, K. OHTANI, and N. NISHIMURA. Bull. Chem. Soc. Jpn. **58**, 810 (1985).
22. W. G. HERKSTROETER. J. Am. Chem. Soc. **97**, 4161 (1975).
23. J. SALTIEL and J. L. CHARLTON. *In* Rearrangements in ground and excited states. Vol. 3. *Edited by* P. de Mayo. Academic Press, New York. 1980. p. 25.
24. A. CORVAL and H. P. TROMMSDORF. J. Phys. (Les Ulis, Fr.), **46** (C7), 447 (1985).
25. H. GÖRNER and D. SCHULTE-FROHLINDE. J. Mol. Struct. **84**, 227 (1982).

Can. J. Chem. Downloaded from www.nrcresearchpress.com by 78.46.186.204 on 09/07/12
For personal use only.

The fast atom bombardment mass spectra of some N-substituted pyrimidinium salts

CLEMENT W. KAZAKOFF[1]
Department of Chemistry, University of Ottawa, 365 Nicholas Street, Ottawa, Ont., Canada K1N 9B4

AND

ROBIN T. B. RYE[1] AND OSWALD S. TEE
Department of Chemistry, Concordia University, 1455 de Maisonneuve Blvd. W., Montreal (Que.), Canada H3G 1M8

Received August 22, 1986

CLEMENT W. KAZAKOFF, ROBIN T. B. RYE, and OSWALD S. TEE. Can. J. Chem. **65**, 718 (1987).

The fast atom bombardment mass spectra of selected 1,2-dihydro-1,3-disubstituted-2-oxo-pyrimidinium salts are presented. Loss of N-substituents from the solute cation is the principal fragmentation observed in the positive ion spectra. Several concentration dependent features of the spectra are identified; these are thought to result from the interaction of the solute cation with bombardment-induced matrix fragments. Cluster ions are observed in both positive and negative ion spectra. In a mixed solute system cluster ions resulting from extensive cation and anion mixing are observed; the concentration dependence of these mixed cluster ion peaks can be approximately described in terms of conventional solution equilibria.

CLEMENT W. KAZAKOFF, ROBIN T. B. RYE et OSWALD S. TEE. Can. J. Chem. **65**, 718 (1987).

On rapporte les spectres de masse par bombardement avec des atomes rapides (FAB) de sels de dihydro-1,2 oxo-2 pyrimidinium disubstitués dans les positions 1 et 3. Dans le spectre des ions positifs, la principale fragmentation observée correspond à la perte des substituants du cation dissous. On a identifié plusieurs caractéristiques qui dépendent de la concentration; on croit que ces variations proviennent de l'interaction du cation dissous avec les fragments de matrice induits par le bombardement. On a observé des agrégats d'ions tant dans les spectres des ions positifs que ceux des ions négatifs. Dans un système de solutés mixtes, on observe des agrégats d'ions provenant d'un important échange des anions et des cations; pour décrire la relation qui existe entre la concentration et les pics de ces agrégats mixtes d'ions, on peut faire appel aux équilibres conventionnels en solution.

[Traduit par la revue]

Can. J. Chem. Downloaded from www.nrcresearchpress.com by 78.46.186.204 on 09/07/12
For personal use only.

Introduction

Since the 1981 publication of the work of Barber *et al.* (1) fast atom bombardment (FAB) has become a widely-used ionization method, with particular application to the mass spectrometric study of thermally fragile and nonvolatile compounds. Several recent reviews have surveyed the development of the technique and the increasingly wide range of its applications (2).

As part of a continuing study of the mass spectra of 2-pyrimidinones and related compounds (3), we have examined the FAB mass spectra of selected pyrimidinium salts (Table 1). Preliminary measurements showed that the FAB spectra of many of these compounds exhibited cluster ion peaks of significant intensity. These observations suggested that the FAB technique might be used for the study of ion pairing in solutions of the pyrimidinium salts. Ion pairing in solutions of *N*-alkylpyridinium salts has received considerable attention (4).

Experimental

The 1,2-dihydro-1,3-disubstituted-2-oxo-pyrimidinium salts used in this work were stable samples remaining from earlier solution studies (5). Fast atom bombardment mass spectra were taken on a VG-7070E instrument, with 9-keV xenon atoms as bombarding particles at a beam current of 1.5 mA. The accelerating voltage was 6 kV. Data were acquired using the VG DEC PDP8A data system except for the B/E linked scans, in which spectra were taken on a Visicorder. Samples for quantitative measurement were prepared by weight, using glycerol as the liquid matrix. The long term stability of the solutions was confirmed by the excellent reproducibility of the spectra over a period of several months.

Results and discussion

Single solute

The positive ion FAB spectra of the quaternary salts **1**–**7** are given in Table 2. The effect of solute concentration on the spectra was investigated for **1** and **3**. With **1** at a solute concentration of 25 mg/mL (0.11 *M*) the protonated glycerol dimer gave the base peak in the spectrum at *m/z* 185. The solute cation peak (*m/z* 125) was clearly observable at this concentration, and at concentrations as low as 4 mg/mL (0.02 *M*). At concentrations greater than ca. 0.15 *M* the base peak in the spectrum of **1** was due to the solute cation. At the higher solute concentrations cluster ions C_nA_{n-1} (C = cation, A = anion) of low (<5%) relative intensities are observed. The intensities of these cluster ion peaks, particularly for $n > 3$, were found to depend markedly on the N substituents. For **1**–**3**, clusters up to $n = 5$ could be observed under appropriate conditions, whereas for **4**–**7** the $n = 2$ cluster was barely detectable. The unimolecular fragmentation of the $n = 2$ cluster from **1** was examined by B/E linked scan. Losses of $A - 1$, A, $A + 1$, and $CA + 1$ were observed. There was some evidence for very minor losses of methyl radical and water from the cluster ion, but identification of these processes is only tentative because of the poor S/N ratio at the high gain used.

TABLE 1. Compounds studied

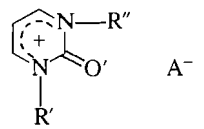

Compound	R′	R″	A
1	CH_3	CH_3	HSO_4^-
2	$CH(CH_3)_2$	CH_3	HSO_4^-
3	C_2H_5	C_2H_5	I^-
4	Phenyl	CH_3	I^-
5	Cyclohexyl	CH_3	I^-
6	Benzyl	CH_3	HSO_4^-
7	Benzyl	Benzyl	HSO_4^-

[1]Authors to whom correspondence may be addressed.

TABLE 2. Positive ion FAB spectra of **1–7** in glycerol[a]

Compound	m/z (relative intensity %)
1	97 (2), 111 (5), 125 (C^+, 100), 126 (10), 139 (*, 13), 347 (**, 3)
2	97 (3), 111 (59), 139 (3), 153 (C^+, 100), 154 (11), 167 (*, 9), 307 (**, 3), 349 (**, 2), 403 (**, 6)
3	97 (7), 125 (6), 153 (C^+, 100), 154 (11), 167 (*, 1), 185 (8), 307 (**, 1), 433 (**, 2)
4	97 (.5), 111 (4), 173 (3), 187 (C^+, 100), 188 (15), 201 (*, 4), 219 (*, 6), 249 (*, 2)
5	97 (4), 111 (50), 179 (2), 193 (C^+, 100), 194 (14), 207 (*, 12), 225 (*, 66), 239 (*, 9), 417 (**, 2)
6	91 (100), 111 (8), 201 (C^+, 44), 202 (7), 215 (*, 8), 233 (*, 2)
7	91 (100), 92 (37), 277 (C^+, 70), 278 (16), 291 (*, 7)

[a]Concentrations: **1**, 180 mg/mL; **3**, 107 mg/mL; **2**, **4–7**, 50 mg/mL.
* = adduct ion of cation plus glycerol or glycerol-derived fragment; ** = solute cluster ion.

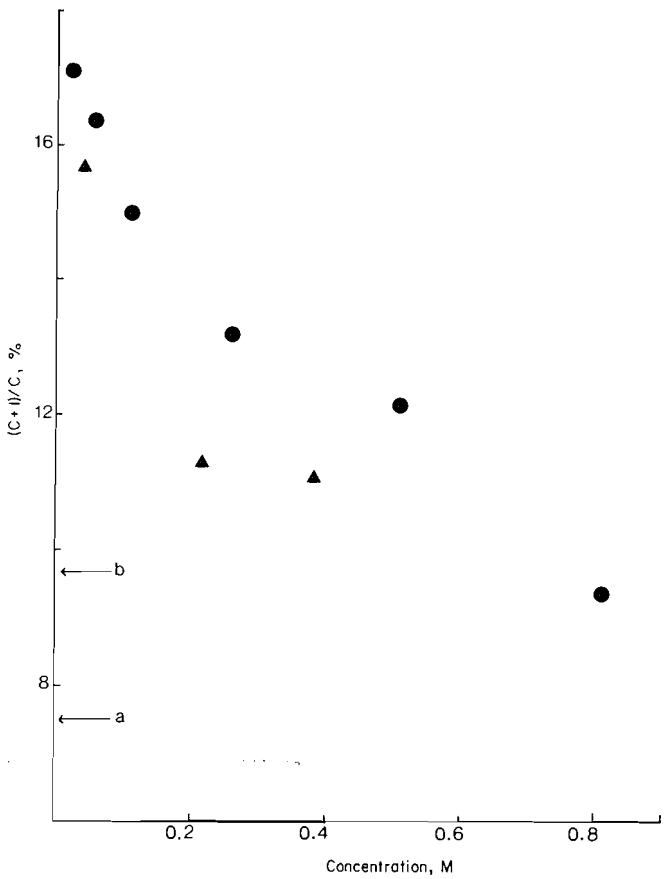

FIG. 1. Variation of $(C + 1)C$ ratio for **1** (●) and **3** (▲). Calculated values (based on natural isotopic abundances) indicated by horizontal lines as *a* (**1**, 7.5%) and *b* (**3**, 9.7%).

Concentration effects related to reactions of the solute cation with bombardment-induced matrix fragments are also observed. The variation of the $(C + 1)/C$ peak intensity ratio with concentration, as shown in Fig. 1, has obvious analytical implications. Similar enhancement effects in the FAB spectra of dyestuffs have been explained in terms of oxidation–reduction reactions in the matrix (6), but the mechanism of such reactions has not been established. While the enhancement of the $C + 1$ peak intensity in our case is small compared to that reported for organic dyestuffs (6), it is sufficiently large to preclude

TABLE 3. Variation of selected ion abundances with solution composition for mixtures of **1** and **3** in glycerol

	Composition			
1, moles × 10^5	2.75	7.75	10.0	14.7
3, moles × 10^5	9.36	7.64	5.11	3.60
Total solute, M	0.38	0.42	0.37	0.42
m/z	Peak abundance[a]			
Positive ion				
125	1 491	2 111	5 196	8 864
153	10 000	10 000	10 000	10 000
307	108	138	164	169
375	37	92	124	211
403	136	198	115	113
405	23	26	—	32
433	64	49	—	—
Negative ion				
97	4 708	10 000	10 000	10 000
127	10 000	5 680	2 644	1 441
319	17	65	168	317
349	33	59	48	78
377	236	176	69	61
407	403	86	—	—

[a]Normalized to base peak = 10 000.

use of natural isotopic abundance ratios as a means of solute characterization. Adduct ions of nominal masses $C + 14$ and $C + 32$ daltons were also observed in all the positive ion spectra. The abundance of these ions, relative to that of the solute cation, decreased as solute concentration increased. Thus, for **1**, the $C + 14/C$ ratio dropped from ca. 0.4 to ca. 0.08 as the solute concentration was increased from 0.06 M to 0.81 M. The effect of solute concentration on the fragmentation pattern is discussed below.

Compounds **1**, **2**, and **4–6** constitute a convenient series for examination of substituent effects in the fragmentation of the solute cations. In agreement with the even-electron rule (7) the fragment ion $C_5H_7N_2O$ (m/z 111) is observed in all the spectra. For **2** and **5** this peak can be rationalized in terms of hydrogen transfer from the N(1) substituent to the pyrimidine ring followed by loss of the substituent as the unsaturated neutral molecule. For **1** and **4**, however, this pathway would be energetically unfavourable compared to loss of the N(1) substituent as the neutral radical from the $C + 1$ ion. In the case of **1** this alternative mechanism is given support by the observation that the relative abundance of m/z 111 shows a variation with concentration similar to that observed for the $C + 1$ peak. Because of the particular stability of the tropyl cation, **6** fragments almost exclusively by inductive cleavage to give m/z 91 as the base peak in the spectrum. This mode of fragmentation is observed to only a limited extent in **4** (m/z 77, relative intensity = 7%) and **5** (m/z 83, rel. int. = 7%); for **1** and **2** the poor S/N ratio in the appropriate regions of the spectra precluded reliable measurements. Limited fragmentation of the pyrimidinium ring was observed for **1**; in the B/E linked scan of the m/z 125 peak minor losses of 28, 29, 41, and 42 daltons were noted. Unambiguous identification of the corresponding peaks in the conventional spectrum was complicated by matrix interference below m/z 100.

The negative ion spectra are characteristically simple and relatively free from background interference. The solute anion

Can. J. Chem. Downloaded from www.nrcresearchpress.com by 78.46.186.204 on 09/07/12
For personal use only.

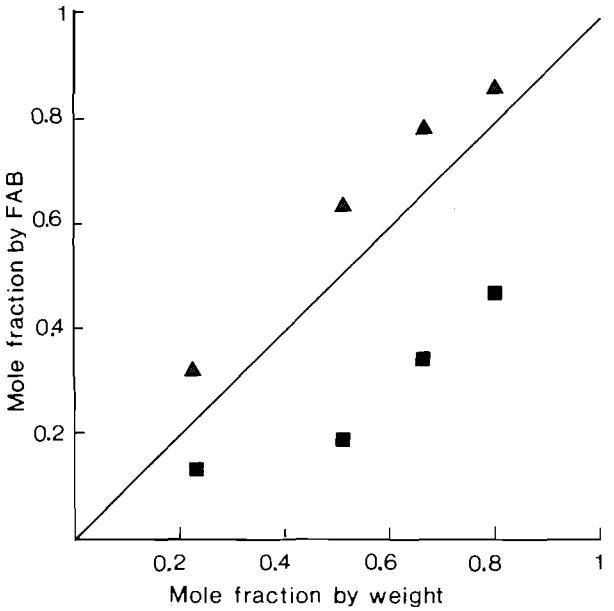

FIG. 2. Actual vs. experimental mole fraction of **1** in mixtures of **1** and **3**; positive (■) and negative (▲) ion FAB.

gave the base peak in all cases. Peaks of moderate intensity corresponding to A + glycerol were observed (**1**, m/z 189, rel. int. = 7%; **3**, m/z 219, rel. int. = 7%), but peaks for more highly solvated anions were of negligible intensity. As described above for the positive ion FAB, cluster ion peaks of significant intensity were observed. In the spectrum of **1** peaks at m/z 195 (rel. int. = 16%) and m/z 319 (rel. int. = 6%) were assigned to AHA and ACA, respectively. At higher gain A_nC_{n-1} cluster ions were observable up to $n = 4$ (m/z 763), with peak intensity decreasing rapidly with increasing n. The AHA peak (m/z 255) was not observed in the spectrum of **3**, but peaks corresponding to $n = 2$ (m/z 407) and $n = 3$ (m/z 687) were seen. Analogous results were obtained for the other salts.

Mixed solutes

Several reports have emphasized the application of FAB mass spectrometry to the study of solution equilibria. Caprioli (8) showed that the pK_a of weak acids in glycerol–water mixtures could be determined by FAB, and concluded that the FAB spectra accurately reflect the ionic equilibria in the matrix. The SIMS spectra of mixed organic salts in an ammonium chloride matrix showed cluster ions with all possible combinations of cation and anion (9); these authors also cite unpublished FAB experiments that gave similar results.

In the present work solutions of **1** and **3**, containing from 0.2 to 0.8 mole fraction of **1**, were examined in both positive and negative ion mode. As a simple test of the degree to which the FAB spectra reflected solution composition, the mole fraction of **1** in each of the mixtures was calculated from the negative ion spectra, using the m/z 97 (HSO_4^-) and m/z 127 (I^-) absolute peak area (Table 3). Analogous calculations were done from the positive ion data, using absolute peak areas for the cations (**1**, m/z 125; **3**, m/z 153). The results are shown in Fig. 2. Agreement between theoretical and experimental mole fractions was as expected, but it is not clear why the negative ion results were superior to those based on the cation spectra, particularly in view of the similarity of the two cations **1** and **3**. Inspection of the $n = 2$ cluster ion regions of both the positive and negative ion spectra (Fig. 3) reveals extensive cation and anion mixing

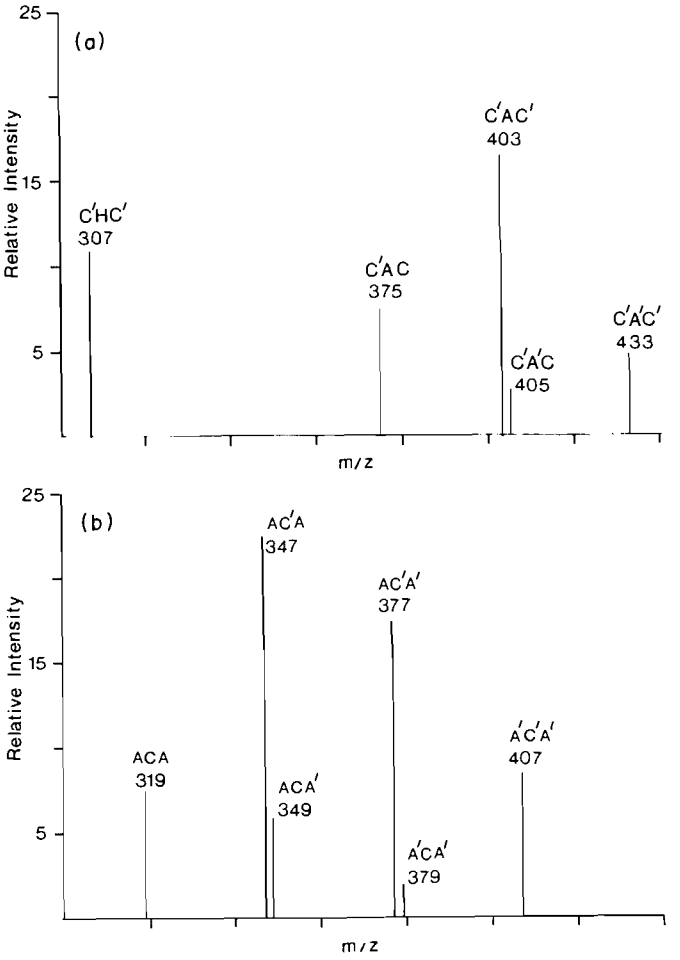

FIG. 3. Expanded (×10) cluster ion region of the FAB spectrum of a mixture of **1** and **3** containing 0.5 mole fraction of **1**. (*a*) Positive ion; (*b*) negative ion. Anion and cation of **1** and **3** denoted by A, C and A′C′, respectively.

in this system. The spectra in Fig. 3 were obtained from an approximately equimolar mixture (mole fraction of **1** = 0.504). It is evident from the negative ion spectra (Fig. 3*b*) that the cation of **3** confers greater stability to the cluster ions (peaks at m/z 347, 377, and 407) than does the cation of **1** (peaks at m/z 319, 349, and 379). Selectivity in favour of HSO_4^- as the cluster anion is also indicated by a decrease in relative abundance with an increase in I^- content, regardless of the cation involved. In an attempt to quantify the interactions involved in these effects, the peaks at m/z 319, 349, 377, and 407 in the negative ion spectrum were taken as convenient probes of ionic equilibria. Denoting the anion and cation of **1** as A and C, and of **3** as A′ and C′, respectively, these cluster ions can be identified as ACA (m/z 319), ACA′ (m/z 349), A′C′A (m/z 377), and A′C′A′ (m/z 407). A detailed analysis of this multiequilibrium system is not feasible, but rough calculations have shown that the concentration dependence of these cluster ion peaks can be approximately described in terms of conventional solution equilibria. While concentrations of neutral or cationic species cannot be estimated from the negative ion FAB spectra, ratios of dissociation constants can be estimated from the ion peak intensity data. Thus, for the equilibria

$$\begin{aligned} \text{ACA} &\rightleftharpoons \text{AC} + \text{A} & K_1 \\ \text{A'C'A'} &\rightleftharpoons \text{A'C'} + \text{A'} & K_2 \\ \text{A'C'A} &\rightleftharpoons \text{A'C'} + \text{A} & K_3 \end{aligned}$$

we estimate $K_3/K_2 < 1$ and, setting [AC]/[A′C′] = [**1**]/[**3**]

Can. J. Chem. Downloaded from www.nrcresearchpress.com by 78.46.186.204 on 09/07/12
For personal use only.

for the equimolar mixture, $K_1/K_2 > 1$. The value of K_3/K_2 reflects the fact that the interaction between A′C′ and HSO_4^- is stronger than the interaction between the ion pair and I^-.

The predominant effect of the cation in determining cluster ion stability is reflected in the comparison of the dissociation constants for ACA and A′C′A′, with $K_1 > K_2$. Given the many approximations made in these calculations, the ratios are, at best, rough estimates. The results are consistent with the observed spectra, and indicate the potential of this approach for the study of ion pairing in this type of system.

Acknowledgement

We thank Professor J. L. Holmes for making the mass spectrometry facilities of the University of Ottawa available to us.

1. M. BARBER, R. S. BORDOLI, R. D. SEDGWICK, and A. N. TYLER. J. Chem. Soc. Chem. Commun. 325 (1981).
2. A. J. BURLINGAME and J. O. WHITNEY. Anal. Chem. **56**, 417R (1984); J. M. MILLER. Adv. Inorg. Chem. Radiochem. **28**, 1 (1984).
3. E. M. KAZDAN, R. T. B. RYE, and O. S. TEE. Can. J. Chem. **60**, 1800 (1982); R. T. B. RYE, O. S. TEE, and E. M. KAZDAN. Can. J. Chem. **62**, 2340 (1984).
4. M. PAL and S. BAGCHI. J. Chem. Soc. Faraday Trans. 1, **81**, 2323 (1985), and references cited therein.
5. O. S. TEE and M. ENDO. J. Heterocycl. Chem. **11**, 441 (1974); Can. J. Chem. **54**, 2681 (1976).
6. P. J. GALE, B. L. BENTZ, B. T. CHAIT, F. H. FIELD, and R. J. COTTER. Anal. Chem. **58**, 1070 (1986).
7. M. KARNI and A. MANDELBAUM. Org. Mass Spectrom. **15**, 53 (1980).
8. R. M. CAPRIOLI. Anal. Chem. **55**, 2387 (1983).
9. K. L. BUSCH, B. H. HSU, Y.-X. XIE, and R. G. COOKS. Anal. Chem. **55**, 1157 (1983).

Can. J. Chem. Downloaded from www.nrcresearchpress.com by 78.46.186.204 on 09/07/12
For personal use only.

A conductometric study of dissociation of picric acid in 2-methoxyethanol and 1,2-ethanediol from −10 to 80°C

GIANCARLO FRANCHINI, ELENA ORI, CARLO PRETI, LORENZO TASSI, AND GIUSEPPE TOSI[1]
University of Modena, Department of Chemistry, Via G. Campi, 183 41100 Modena, Italy

Received September 18, 1986

GIANCARLO FRANCHINI, ELENA ORI, CARLO PRETI, LORENZO TASSI, and GIUSEPPE TOSI. Can. J. Chem. **65**, 722 (1987).

Dissociation constants of 2,4,6-trinitrophenol (picric acid) in 2-methoxyethanol and 1,2-ethanediol were measured by a conductance method at temperatures ranging from −10 to 80°C. The determined constants in the two solvents are discussed and are compared on the basis of the physical properties of the solvents, which have been measured at the various temperatures. The dissociation constants show different behaviour with the temperature in the investigated range and they are fitted by equations of the type $\ln K = A+BT+C/T+D \ln T$. Furthermore, the thermodynamic functions have been evaluated and discussed.

GIANCARLO FRANCHINI, ELENA ORI, CARLO PRETI, LORENZO TASSI et GIUSEPPE TOSI. Can. J. Chem. **65**, 722 (1987).

Opérant à des températures allant de −10 à 80°C et faisant appel à la conductimétrie, on a mesuré les constantes de dissociation du trinitro-2,4,6 phénol (acide picrique) dans le méthoxy-2 éthanol et dans l'éthanediol-1,2. On discute des constantes déterminées dans ces deux solvants et on les compare entre elles en fonction des propriétés physiques de ces solvants qui ont été mesurées aux diverses températures. Dans la fourchette des températures examinées, les constantes de dissociation présentent des comportements différents que l'on peut toutefois représenter par des équations du type $\ln K = A + BT + C/T + D \ln T$. De plus, on a évalué et on discute des fonctions thermodynamiques.

[Traduit par la revue]

Introduction

This work is to study the effect of solvent on dissociation constants of weak acids and the influence of temperature.

Although alcohols have received much attention as solvents for acid–base determinations (1, 2) there are not many studies on the use of 2-methoxyethanol (hereafter abbreviated Gliem) and 1,2-ethanediol (Gliet) as solvents in acid–base titrations and on the determination of dissociation constants of weak acids. Our previous works (3–6) have reported on the feasibility of conductometric titrations of monoprotic and diprotic acids, phenols and aromatic nitroderivatives in the above solvents using *N*,*N*′-diphenylguanidine as titrant. The results indicated the possibility of also performing differential titrations of acid mixtures in cases where such determinations are impossible in aqueous solutions.

Preliminary studies have shown that temperature plays an important role in the shape of the conductometric titrations curves and that the effect is different for different solvents.

Continuing our conductometric studies, the dissociation constants of picric acid in Gliet and Gliem have been determined at different temperatures and the data obtained are discussed. The reaction under study in the two solvents is

[1] $HA + Solv \rightleftarrows (SolvH^+A^-) \rightleftarrows SolvH^+ + A^-$

In addition, in view of the importance of the solvents employed in this study, dipolar and amphiprotic in nature, it would also be desirable to have more data on ionization enthalpies and entropies. These thermodynamic data can contribute to an understanding of solute–solvent interactions as well as problems specifically involving acidity in solvents or solvents mixtures other than water.

The conductometric rather than the potentiometric method is chosen because there are limitations in using hydrogen or glass electrodes in nonaqueous solvents, i.e. (*i*) if the emf of the hydrogen electrode is taken to be zero in all the solvent systems, quite a large number of unrelated pH or emf scales will be generated (7), and it is difficult to correlate the values of dissociation constants; (*ii*) liquid junction potentials and responses of the glass electrodes change with solvent system composition (8).

Results and discussion

The experimental data of conductance measurements, performed at nineteen temperatures in the −10 to 80°C range for six different concentrations in the two solvents, are reported in the Tables 1 and 2. All data were corrected at each temperature with the specific conductances of the solvents. The corrected values were analyzed by means of the method of Fuoss and Shedlovsky (9). The equation

$$\frac{1}{\Lambda S} = \frac{1}{\Lambda_0} + \frac{c\Lambda Sf^2}{K\Lambda_0^2}$$

was used, where the symbols have the usual significance. If $1/\Lambda S$ is plotted vs. $c\Lambda Sf^2$, the intercept is $1/\Lambda_0$ and the slope is $1/K\Lambda_0^2$. In practice an initial value of Λ_0 is estimated from a plot of Λ vs. $c^{1/2}$ and then an iterative method allows us to calculate K and Λ_0; usually only a few iterations are necessary.

The values of Λ_0 and K at different temperatures are reported in Tables 3 and 4 for picric acid in 1,2-ethanediol and 2-methoxyethanol, respectively.

For the purpose of calculating the thermodynamic functions, the experimental data for K at the various temperatures were fitted to an equation of the type

[2] $\ln K = A + BT + C/T + D \ln T$

by the method of least-squares to yield, using standard equations, the thermodynamic data, also reported in Tables 3 and 4.

By examining the behaviour of the K values with temperature in the two solvents, we may note that although the same equation fits the data, the trend in the temperature range investigated is different. Figure 1 shows this behaviour: the curves are plotted using eq. [2] ($A = 317.2531$, $B = 0.04648$, $C = -11683.34$, $D = -52.2908$ for Gliet; $A = -2148.1026$, $B = -0.6903$, $C = 54518.42$, $D = 379.1845$ for Gliem). While in the case of Gliet the dissociation constant of picric acid shows a maximum, estimated by setting the derivative of eq.

[1]Author to whom all correspondence should be addressed.

Printed in Canada / Imprimé au Canada

Can. J. Chem. Downloaded from www.nrcresearchpress.com by 78.46.186.204 on 09/07/12
For personal use only.

TABLE 1. Molar concentrations and conductances of picric acid solutions in Gliet

	Λ (cm² S mol⁻¹)					
t (°C)	$c = 65.602 \times 10^{-4}$ (mol dm^{-3})	$c = 35.634 \times 10^{-4}$ (mol dm^{-3})	$c = 15.861 \times 10^{-4}$ (mol dm^{-3})	$c = 3.5791 \times 10^{-4}$ (mol dm^{-3})	$c = 1.2396 \times 10^{-4}$ (mol dm^{-3})	$c = 1.1697 \times 10^{-4}$ (mol dm^{-3})
−10	2.95	3.80	4.86	6.12	6.26	6.61
− 5	3.55	4.36	5.33	6.95	7.50	7.80
0	4.06	4.88	6.17	7.68	8.46	8.64
5	5.11	5.95	7.52	9.45	10.26	10.90
10	6.08	7.19	9.06	11.00	11.81	12.98
15	7.40	8.65	10.78	13.75	14.33	15.32
20	8.75	10.25	12.70	16.25	17.18	17.60
25	10.16	11.96	15.08	18.53	19.69	20.60
30	12.05	13.82	17.62	22.00	22.90	24.35
35	13.83	15.96	20.53	25.55	26.61	27.01
40	15.85	18.20	23.48	28.95	30.02	31.58
45	17.95	20.70	26.50	33.00	34.05	35.75
50	20.22	23.29	29.24	36.34	38.29	41.50
55	22.25	26.12	32.90	40.40	42.76	45.70
60	24.36	29.29	36.00	44.71	47.42	50.42
65	26.55	32.00	39.28	48.78	51.98	55.76
70	28.78	34.76	42.65	53.12	56.92	61.10
75	31.08	37.56	46.13	58.55	61.31	67.04
80	33.85	40.72	49.81	64.95	67.21	72.94

TABLE 2. Molar concentrations and conductances of picric acid solutions in Gliem

	Λ (cm² S mol⁻¹)					
t (°C)	$c = 50.439 \times 10^{-4}$ (mol dm^{-3})	$c = 33.661 \times 10^{-4}$ (mol dm^{-3})	$c = 15.259 \times 10^{-4}$ (mol dm^{-3})	$c = 7.3589 \times 10^{-4}$ (mol dm^{-3})	$c = 3.8235 \times 10^{-4}$ (mol dm^{-3})	$c = 1.1959 \times 10^{-4}$ (mol dm^{-3})
−10	1.99	2.46	3.39	4.51	5.77	8.44
− 5	2.12	2.64	3.65	4.87	6.23	9.20
0	2.27	2.82	3.91	5.23	6.73	10.05
5	2.41	2.99	4.17	5.62	7.26	11.00
10	2.55	3.17	4.43	5.99	7.77	11.92
15	2.68	3.32	4.65	6.31	8.22	12.66
20	2.79	3.46	4.86	6.61	8.65	13.46
25	2.89	3.58	5.06	6.91	9.06	14.27
30	2.98	3.69	5.21	7.14	9.42	14.99
35	3.05	3.78	5.35	7.36	9.72	15.55
40	3.12	3.85	5.48	7.54	10.03	16.20
45	3.16	3.92	5.58	7.72	10.27	16.72
50	3.21	3.97	5.67	7.86	10.49	17.16
55	3.24	4.00	5.72	7.96	10.65	17.51
60	3.25	4.02	5.76	8.02	10.76	17.86
65	3.28	4.04	5.79	8.10	10.90	18.28
70	3.31	4.06	5.83	8.17	11.05	18.69
75	3.33	4.08	5.86	8.24	11.20	19.18
80	3.36	4.09	5.90	8.36	11.40	19.73

[2] equal to zero, ($K_{max} = 2.49 \times 10^{-3}$) in the investigated temperature range at 34.4°C, in the case of Gliem a continuous decrease of the K value is observed.

The value for K_{max} calculated to best fit eq. [2] is quite in good agreement both with the results obtained by a method suggested by Harned (10) ($K_{max} = 2.46 \times 10^{-3}$ at $t = 38.4$°C) and with those evaluated by a correlation of pK vs. $1/\epsilon$. In fact, knowing the relationship between ϵ and t, the above correlation provides two straight lines (one of negative slope, $r = 0.923$, and the other of positive slope, $r = 0.980$) intersecting in a point whose ordinate and abscissa give pK_{max} and the temperature of K_{max}, respectively ($K_{max} = 2.61 \times 10^{-3}$, $t = 34.3$°C).

A further difference in the behaviour of experimental data in the two solvents comes by examining the relation between Λ_0 and viscosity. We observe (Tables 3 and 4) that in the case of Gliem the Walden rule $\Lambda_0\eta$ = constant is substantially obeyed, while for Gliet $\Lambda_0\eta$ decreases as the temperature increases. Such behaviour, observed by Fuoss (11), has been attributed to a decrease in dielectric constant. On the contrary, for Gliet our results are better reproduced by a modified Walden product as

Can. J. Chem. Downloaded from www.nrcresearchpress.com by 78.46.186.204 on 09/07/12
For personal use only.

TABLE 3. Dissociation constants, limiting molar conductances, and thermodynamic functions of picric acid in Gliet solution

t (°C)	ϵ_{Gliet}	$K \times 10^3$	$\Delta G°$ (cal mol^{-1})	$\Delta H°$ (cal mol^{-1})	$\Delta S°$ (cal mol^{-1} deg^{-1})	Λ_0	$\Lambda_0\eta$	$\Lambda_0\eta^{0.7}$
−10	49.11	1.79±0.01	3302±4	2258±51	−4.0±0.2	7.1±0.1	6.94	7.00
− 5	47.87	1.96±0.02	3325±3	1987±39	−5.0±0.1	8.1±0.1	5.66	6.31
0	46.60	2.10±0.01	3352±3	1721±27	−6.0±0.1	9.0±0.1	4.71	5.72
5	45.48	2.21±0.01	3385±3	1458±18	−6.9±0.1	11.0±0.1	4.41	5.80
10	44.33	2.29±0.008	3421±2	1200±10	−7.8±0.1	13.0±0.2	4.08	5.78
15	43.21	2.37±0.01	3463±3	946±13	−8.7±0.1	15.6±0.2	3.87	5.88
20	42.12	2.41±0.01	3509±2	696±13	−9.6±0.1	18.3±0.2	3.65	5.92
25	41.06	2.45±0.01	3559±2	450±13	−10.4±0.5	21.2±0.2	3.43	5.92
30	40.02	2.47±0.01	3613±2	209±12	−11.2±0.1	24.8±0.3	3.28	6.02
35	39.01	2.48±0.01	3671±2	−29±11	−12.0±0.1	28.5±0.3	3.12	6.05
40	38.03	2.48±0.01	3733±2	−262± 9	−12.8±0.1	32.6±0.4	2.97	6.10
45	37.07	2.46±0.01	3799±2	−492± 6	−13.5±0.1	37.0±0.4	2.85	6.14
50	36.13	2.43±0.01	3868±2	−717± 7	−14.2±0.1	41.6±0.5	2.73	6.18
55	35.22	2.38±0.01	3940±3	−938±15	−14.9±0.1	46.5±0.5	2.63	6.22
60	34.33	2.33±0.01	4016±2	−1155±24	−15.5±0.1	51.6±0.6	2.53	6.26
65	33.46	2.26±0.01	4096±3	−1368±35	−16.2±0.2	56.7±0.6	2.44	6.27
70	32.62	2.19±0.01	4178±4	−1577±47	−16.8±0.2	62.0±0.7	2.36	6.30
75	31.79	2.10±0.02	4263±4	−1781±59	−17.4±0.2	67.9±0.9	2.30	6.36
80	31.31	2.03±0.01	4352±6	−1982±74	−17.9±0.2	74.5±0.9	2.26	6.45

TABLE 4. Dissociation constants, limiting molar conductances, and thermodynamic functions of picric acid in Gliem solution

t (°C)	ϵ_{Gliem}	$K \times 10^5$	$\Delta G°$ (cal mol^{-1})	$\Delta H°$ (cal mol^{-1})	$\Delta S°$ (cal mol^{-1} deg^{-1})	Λ_0	$\Lambda_0\eta$	$\Lambda_0\eta^{0.7}$
−10	20.03	7.40±0.11	4958±11	−5040±287	−38.0±1.1	16.0±0.2	0.54	1.49
− 5	19.56	6.45±0.10	5147± 7	−4916±202	−37.5±0.7	18.2±0.2	0.54	1.54
0	19.09	5.59±0.08	5334± 6	−4861±125	−37.3±0.4	20.1±1.0	0.52	1.55
5	18.64	4.59±0.07	5521± 7	−4875± 54	−37.4±0.1	24.3±0.3	0.55	1.72
10	18.20	3.88±0.06	5708± 7	−4957± 36	−37.7±0.2	27.8±0.4	0.56	1.81
15	17.77	3.47±0.26	5898± 8	−5108± 66	−38.2±0.3	30.8±0.8	0.56	1.86
20	17.35	2.96±0.06	6091±10	−5327±117	−38.9±0.5	34.5±0.5	0.56	1.94
25	16.94	2.42±0.07	6288±12	−5615±160	−39.9±0.6	39.4±0.7	0.58	2.06
30	16.54	2.07±0.05	6490±14	−5971±197	−41.1±0.7	43.8±0.8	0.58	2.14
35	16.15	1.75±0.05	6699±16	−6397±225	−42.5±0.8	48.6±1.0	0.59	2.23
40	15.76	1.44±0.05	6915±19	−6890±249	−44.1±0.8	54.4±1.2	0.60	2.35
45	15.39	1.18±0.04	7140±22	−7452±265	−45.9±0.9	61.1±1.4	0.62	2.48
50	15.03	0.996±0.049	7374±26	−8083±273	−47.8±1.0	67.2±1.9	0.63	2.58
55	14.67	0.855±0.036	7619±30	−8783±275	−50.0±0.9	73.0±2.0	0.64	2.65
60	14.32	0.691±0.034	7874±35	−9551±270	−52.3±0.9	81.3±2.4	0.66	2.80
65	13.99	0.581±0.031	8142±39	−10387±259	−54.8±0.9	89.1±2.9	0.67	2.92
70	13.65	0.466±0.029	8423±43	−11292±261	−57.5±0.9	99.8±3.7	0.71	3.11
75	13.33	0.355±0.026	8717±47	−12266±271	−60.3±0.9	114.8±4.8	0.76	3.42
80	13.02	0.227±0.018	9026±52	−13309±279	−63.2±0.9	144.2±6.6	0.90	4.11

suggested by Stokes (12) for high density aqueous solutions: $\Lambda_0\eta^{0.7}$ = constant; the better fitting of this empirical relation suggests that this unusual behaviour is probably a consequence of the high viscosity of the medium.

Tables 3 and 4 report the thermodynamic data calculated by the usual equations from the best fitting equation [2]. Many difficulties and uncertainties are associated with these calculations which derive from the inevitable experimental errors in K values and partly from the calculator's choice of the function which represents the dependance on the temperature. However, $\Delta H°$, and especially $\Delta S°$ values, have proved useful in yielding structural information about solute species and solute–solvent interactions.

When considering the entropy of dissociation in detail, we are concerned with entropy changes due to differences "within" the acid and its anion and also with entropy changes due to differences in solute–solvent interactions. As a consequence, by using the same solute in two different solvents in this work, our thermodynamic data, in particular the $\Delta S°$ values, could be useful in investigating the properties of the media.

The factors that define $\Delta S°$ values in the two solvents are many and sometimes opposite. The entropies of ionization here reported (Tables 3 and 4) indicate that the solute species orienting neighbouring molecules are more effective in Gliem than in Gliet.

Bearing in mind that dielectric constant decreases as temperature increases, an increase in temperature should play an important role in stabilizing ion pairs of reaction [1], particu-

Can. J. Chem. Downloaded from www.nrcresearchpress.com by 78.46.186.204 on 09/07/12
For personal use only.

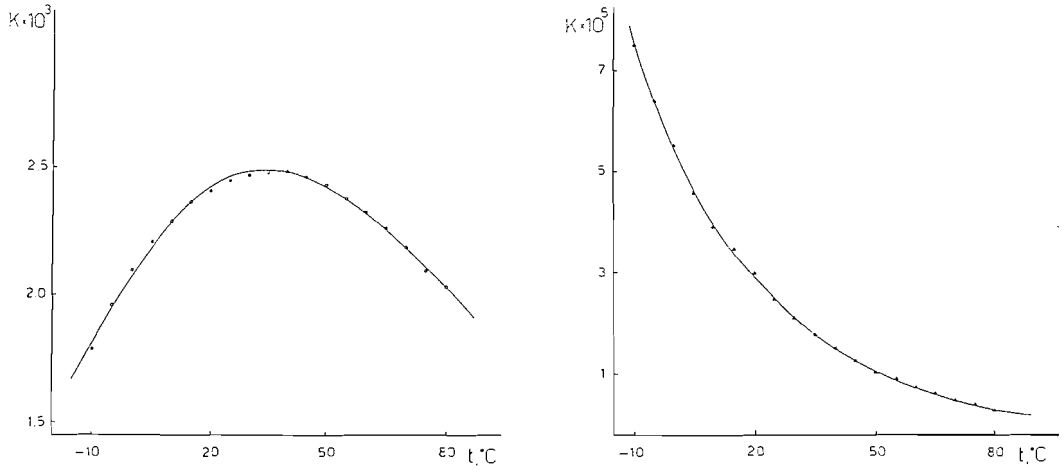

FIG. 1. The dissociation constant of picric acid in Gliet (left) and Gliet (right) as a function of the temperature.

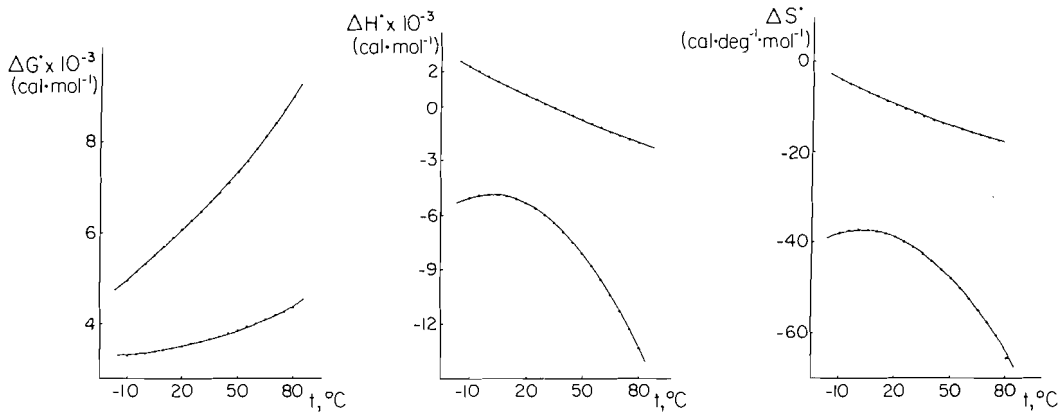

FIG. 2. The dependance on the temperature of $\Delta G°$, $\Delta H°$, and $\Delta S°$ of dissociation for picric acid in Gliet (●) and Gliem (▲).

larly in the case of Gliem. In fact we may think that the species ($SolvH^+A^-$) can orient solvent molecules in its immediate neighbourhood with increasing ease as the dielectric constant decreases. Consequently, $\Delta S°$ values are always more negative for Gliem ($\epsilon_{25°C}$ = 16.94) than for Gliet ($\epsilon_{25°C}$ = 41.06) (but other factors may play a role, see below) and the $\Delta S°$ vs. t curves show a negative temperature coefficient, except for Gliem in the temperature range between −10 and 0°C (Fig. 2).

In the case of the solvent Gliet we need further considerations in addition to the ones above mentioned. We must consider the viscosity effect; in fact the greater value of η suggests a highly polymerized structure of this solvent especially at the lower temperatures. This structure is quickly depolymerized as the temperature increases and this fact is supported by the sudden decrease of η (from 97.12 cP at −10°C to 3.04 cP at 80°C). Thus we may think of a positive contribution to the entropy of the system; a more positive contribution would be expected also by considering the increase in the K values of our solute in Gliet up to 34.4°C. The actual negative $\Delta S°$ values for the Gliet system indicate that probably the importance of these two last contributions is small if compared to the importance of the opposite effect produced by the charged species (ions or ion pairs) on the neighbour solvent molecules.

Experimental

Materials

2,4,6-Trinitrophenol (picric acid), supplied by Fluka (reagent grade), was used without further purification. The solvents 1,2-ethanediol and 2-methoxyethanol (containing less than 0.10 and 0.05% water, respectively, found by Karl Fischer titration) were supplied by Carlo Erba in high purity grade.

Apparatus

Conductances of the solutions were measured with an Amel Mod. 123 conductivity bridge and platinized platinum electrodes (cell constant equal to 0.98 cm), operating in the 0.1 μS to 0.3 S f.s.; the instrument, for the conductance range studied, has a sensitivity of ±1.0%.

The temperature control was provided by a Lauda K2R thermostatic bath maintained to ±0.02°C.

Viscosity measurements were performed by a AVS 400 viscosity measuring system Schott-Geräte, equipped with a series of Ubbelhode viscometers.

Densities at the different temperatures were determined with calibrated Hg densimeters (sensitivity ±0.0005 g cm^{-3}).

The dielectric constants were measured using a WTW-DM01 Dipolmeter equipped with two stainless-steel cylindrical cells: MFL2 ($7 < \epsilon < 21$) was calibrated with dichloromethane (ϵ = 9.08 at 20°C), pyridine (ϵ = 12.30 at 25°C), 1-butanol (ϵ = 17.80 at 20°C), and acetone (ϵ = 20.70 at 25°C) (13); MFL3 ($21 < \epsilon < 90$) was calibrated with ethanol (ϵ = 24.30 at 25°C), methanol (ϵ = 32.63 at 25°C), glycerol (ϵ = 42.50 at 25°C), and water (ϵ = 80.37 at 20°C) (13).

Karl Fischer titrations were performed with an automatic titration system Crison Mod. KF431 equipped with a digital burette Crison Mod. 738.

Procedure

The solutions of picric acid at different concentrations were obtained by successive dilution of stock solutions, freshly prepared by weight

Can. J. Chem. Downloaded from www.nrcresearchpress.com by 78.46.186.204 on 09/07/12
For personal use only.

corrected to the vacuum values; concentration in volume was then calculated from weight concentration and density. Conductance readings were recorded when they became invariant with time; this took about 30 min for each measurement. Solvent conductance corrections were applied to all data at different temperatures.

Acknowledgments

We thank the "Centro di Calcolo Elettronico" of Modena University for the computing facilities and the "Ministero della Pubblica Istruzione" of Italy for the financial support.

1. M. K. CHANTOONI, JR. and I. M. KOLTHOFF. J. Phys. Chem. **82**, 994 (1978) and references therein.
2. I. M. KOLTHOFF and M. K. CHANTOONI, JR. Anal. Chem. **50**, 1440 (1978) and references therein.
3. C. PRETI and G. TOSI. Anal. Chem. **53**, 48 (1981).
4. C. PRETI, L. TASSI, and G. TOSI. Anal. Chem. **54**, 796 (1982).
5. E. NEVIANI GILIBERTI, C. PRETI, L. TASSI, and G. TOSI. Ann. Chim. (Rome), **73**, 527 (1983).
6. C. PRETI, L. TASSI, and G. TOSI. Ann. Chim. (Rome), **75**, 201 (1985).
7. O. POPOVYCH. Anal. Chem. **46**, 2009 (1974).
8. P. ZUMAN and S. WAWZONEK. *In* The chemistry of nonaqueous solvents. *Edited by* J. J. Lagowski. Academic Press, New York, NY 1978. Chapt. 3.
9. R. M. FUOSS and T. SHEDLOVSKY. J. Am. Chem. Soc. **71**, 1496 (1949).
10. H. S. HARNED and I. KAZANIJIAN J. Am. Chem. Soc. **58**, 1912 (1936).
11. R. M. FUOSS. Proc. Natl. Acad. Sci. U.S. **45**, 807 (1959).
12. J. M. STOKES and R. H. STOKES. J. Phys. Chem. **62**, 497 (1958).
13. R. C. WEAST (*Editor*). Handbook of chemistry and physics. 63rd ed. The Chemical Rubber Co., Cleveland (OH). 1982–1983. p. E-50.

Can. J. Chem. Downloaded from www.nrcresearchpress.com by 78.46.186.204 on 09/07/12
For personal use only.

Preparation of 8-methylberberines and aza analogues: Synthesis of (±)-alamaridine

JAHANGIR AND DAVID B. MACLEAN[1]
Department of Chemistry, McMaster University, Hamilton, Ont., Canada L8S 4M1
AND
HERBERT L. HOLLAND[1]
Department of Chemistry, Brock University, St. Catharines, Ont., Canada L2S 3A1

Received September 18, 1986

JAHANGIR, DAVID B. MACLEAN, and HERBERT L. HOLLAND. 1987. Can. J. Chem. **65**, 727 (1987).

Methyllithium reacted with oxyberberine, affording on alkaline work-up a compound with an exomethylene group at C-8 that was transformed in acidic media into an 8-methylberberinium salt. The iminium salt was reduced to a mixture of racemic α- and β-8-methylcanadine. 5,6-Dihydro-8*H*-isoquino[2,1-*b*][2,7]naphthyridin-8-ones were similarly transformed into 8-exomethylene and 8-methyl derivatives, which were subjected to further reduction. These reactions have been employed in a synthesis of the *Alangium* alkaloid, (±)-alamaridine.

JAHANGIR, DAVID B. MACLEAN et HERBERT L. HOLLAND. 1987. Can. J. Chem. **65**, 727 (1987).

La réaction du méthyl-lithium avec l'oxyberbérine conduit, après récupération en milieu alcalin, à un composé contenant un groupement exométhylène en position C-8 qui se transforme, en milieu acide, en un sel de méthyl-8 berbérinium. On a réduit le sel d'iminium en un mélange racémique des méthyl-8α (ainsi que 8β) canadines. De la même manière, on a transformé les dihydro-5,6 8*H*-isoquino [2,1-*b*][2,7] naphtyridinones-8 en dérivés exométhylène-8 et méthyl-8 que l'on a soumis à des réductions subséquentes. On a utilisé ces réactions pour synthétiser la (±)-alamaridine, un alcaloïde de l'*Alangium*.
[Traduit par la revue]

Can. J. Chem. Downloaded from www.nrcresearchpress.com by 78.46.186.204 on 09/07/12
For personal use only.

Alamaridine **1** was isolated a few years ago as a minor constituent of *Alangium lamarckii* Thw. (1) and the synthesis of the racemic base and its relative stereochemistry has since been reported (2). We have recently described general methods (3, 4) for the synthesis of the ring system found in alamaridine and related *Alangium* alkaloids (5) that provide ready access to compounds of type **2** and **3**. The conversion of these lactams into 8-methyl derivatives, of which **1** is an example, and the related conversion of 8-oxyberberine (**4**) (6) into 8-methylberberines is described here.

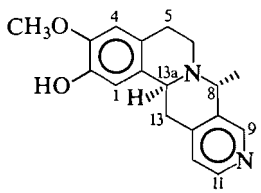

1

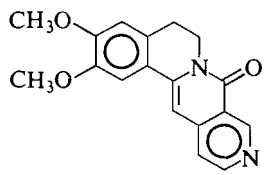

2

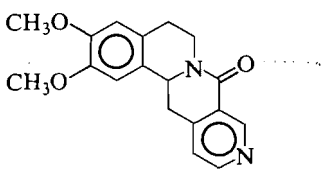

3

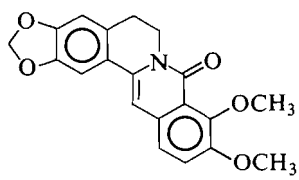

4

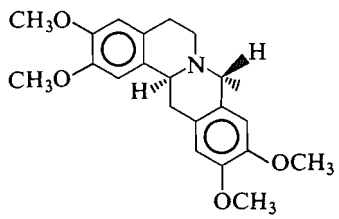

9

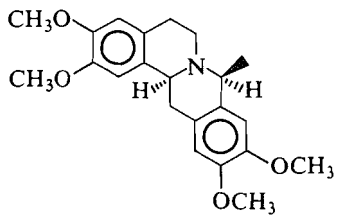

10

8-Oxyberberine, because of its availability, was used as a model substance to investigate the reaction of methyllithium with a lactam function at C-8 as a means of introducing a methyl group at C-8 of a berberine system. As outlined in Scheme 1, treatment of **4** with MeLi at −40°C followed by work-up of the reaction mixture under alkaline conditions afforded the exomethylene compound **5**. The presence of two singlets in the ^{1}H nmr spectrum of **5** at δ 4.20 and δ 5.35 was indicative of the presence of the $>C=CH_2$ group. Compound **5** was transformed as expected in acidic media into the iminium salt **6**, which showed a signal (3H) at 3.60 in the region expected of a methyl group α to a quaternary nitrogen atom in an iminium system (7). Reduction of **6** with sodium borohydride in ethanol afforded a separable mixture of (8*R**,13a*S**)- and (8*S**,13a*S**)-8-methylcanadine, **7** and **8**, respectively, in a ratio of ca. 1:3. The ratio is similar to that observed in the borohydride reduction of 8-methylberberinium salts that have oxygen substituents at C-10 and C-11 (8). Oxyberberine could also be converted into a mixture of **7** and **8**, without isolation of intermediates, in a "one-pot" process.

The assignment of the relative stereochemistry of **7** and **8** is based upon spectroscopic examination of the two isomers and a comparison of their ir and nmr spectra with those of *O*-methylcorytenchirine **9** and coralydine **10** (8, 9) whose relative stereochemistry has been established by X-ray analysis (10). The ir spectrum of **8**, like that of coralydine, displays Bohlmann bands but these are absent in the spectra of **7** and *O*-methylcorytenchirine. Thus **8**, like coralydine, has a *trans* quinolizidine ring fusion, and **7**, like *O*-methylcorytenchirine, a *cis* fusion at the N-13a bond.[2]

The reaction of **2** (3) (Scheme 2) with methyllithium proceeded analogously to that of **4**. The methylene compound (**11**), isolated on alkaline work-up, was readily converted in acidic media into iminium salt **12**. Reduction of **12** with sodium borohydride in ethanol afforded a separable 1:3 mixture of the (8*R**,13a*S**)- and (8*S**,13a*S**)-8-methyl compounds **13** and

[1]Authors to whom correspondence may be addressed.

[2]Nuclear magnetic resonance data in support of these assignments is discussed below.

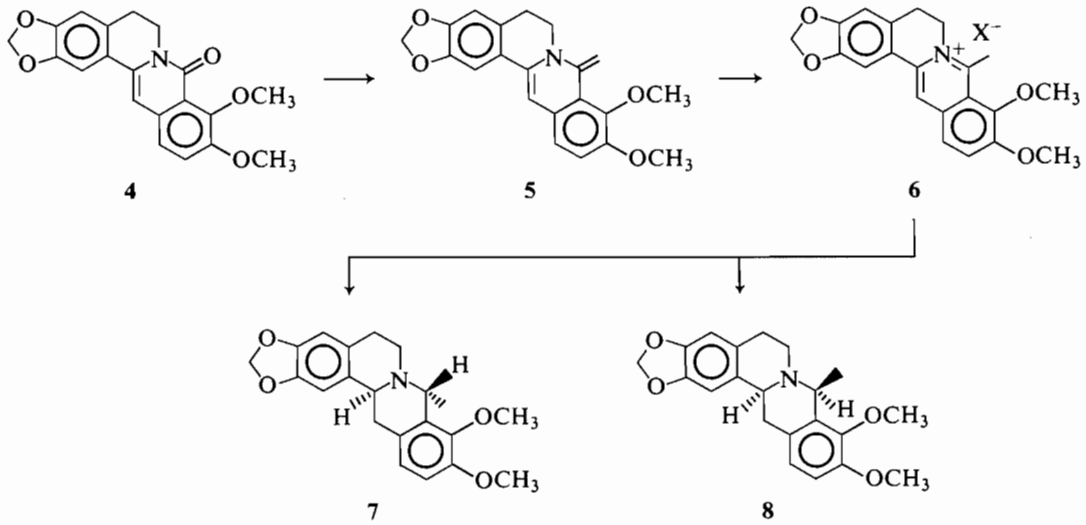

SCHEME 1

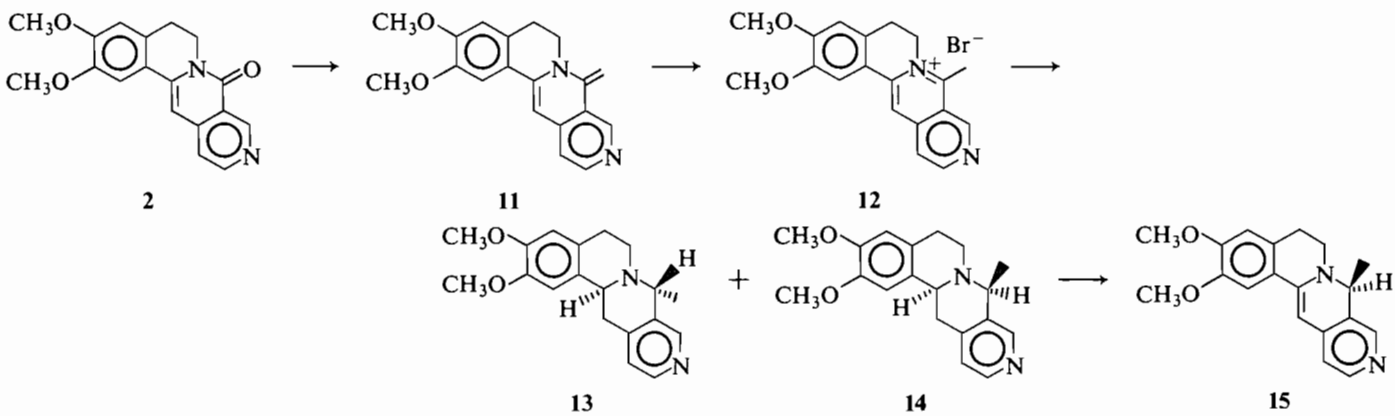

SCHEME 2

14, respectively, the former corresponding in structure to (±)-*O*-methylalamaridine. The assignment of relative stereochemistry to **13** and **14** is based on their spectroscopic properties. Of special importance is the fact that **14** shows Bohlmann bands in its ir spectrum but **13** does not. Compounds **13** and **14** may also be prepared without isolation of the intermediates in a "one-pot" reaction.

The tetrahydro compounds **13** and **14** were highly susceptible to aerial oxidation, which was a complicating factor in their isolation and purification. The product of aerial oxidation, **15**, was a 13,13a didehydro compound that was strongly fluorescent. A related oxidation of tetrahydro-2,7-naphthyridines has been reported (11). It should be noted that (±)-alamaridine (*vide infra*) does not undergo a similar facile oxidation.

The treatment of **15** with sodium borohydride in ethanol afforded, as expected, the same ratio of products as that obtained in the reduction of **12**.

The *O*-benzyl analogue of **2**, compound **16** (3), was converted without isolation of intermediates into a mixture of **17** and **18** in a ratio of 1:3 (Scheme 3) but only **18** was isolated in pure form. The mixture of **17** and **18**, like the mixture of compounds **13** and **14**, was highly susceptible to aerial oxidation. As a result, the separation and purification of the isomers was only partially successful. Debenzylation of the mixture of **17** and **18** was effected by hydrogenolysis, affording a separable mixture of (±)-8-epialamaridine (**19**) and (±)-alamaridine (**1**). The ir and ^{1}H nmr spectra of **1** in solution correspond with the spectra of natural (1) and synthetic alamaridine (2), which were kindly sent to us by Dr. S. C. Pakrashi. The ^{1}H nmr spectra of Pakrashi were recorded in $CDCl_3$ at 100 MHz and ours in the same solvent at 500 MHz. Our measured chemical shifts for the aromatic signals, the *O*-methyl signal, and the *C*-methyl signal agree with those of Pakrashi within experimental error. The aliphatic protons of the ring, which occur as complex multiplets, are much better resolved at 500 MHz but are situated in each spectrum within the same range of δ values. The ir spectrum of **19** had Bohlmann bands typical of a *trans* quinolizidine system but these bands were absent in the spectrum of (±)−**1**.

We also examined the reaction of **3** with methyllithium, and the subsequent treatment of the addition product with borohydride and hydrogen to determine the ratio (8α to 8β) of reduction products (Scheme 4). Compound **3** was prepared in two steps by treatment of 3,4-dihydro-6,7-dimethoxyisoquinoline (**20**) with the lithium salt of 3-cyano-4-methylpyridine (**21**) at −40°C in THF in the manner already described (4). The initial product, amidine (**22**), was hydrolysed in aqueous base to **3**. Treatment of **3** with MeLi afforded a product on alkaline work-up, presumably **23**, that was hydrogenated over a Pd catalyst. The reaction product, which was homogeneous by tlc,

Can. J. Chem. Downloaded from www.nrcresearchpress.com by 78.46.186.204 on 09/07/12
For personal use only.

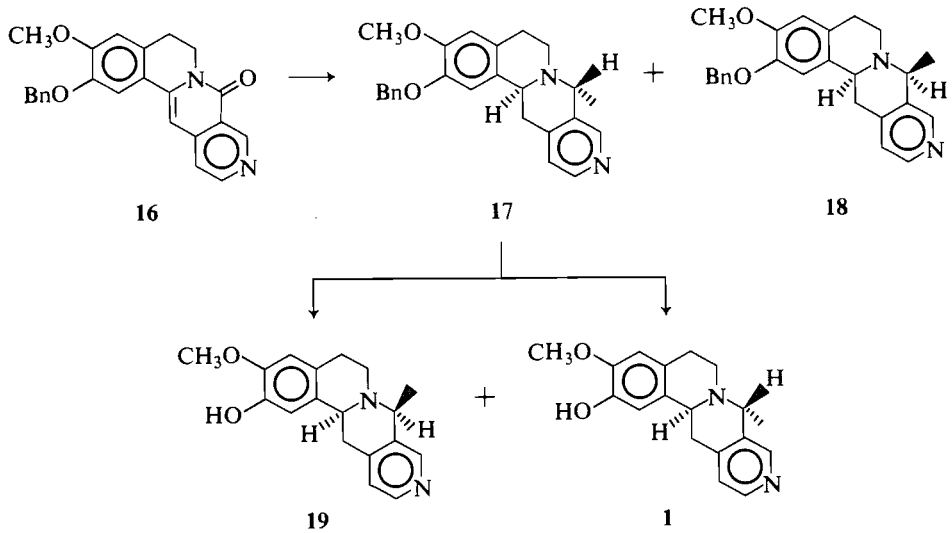

SCHEME 3

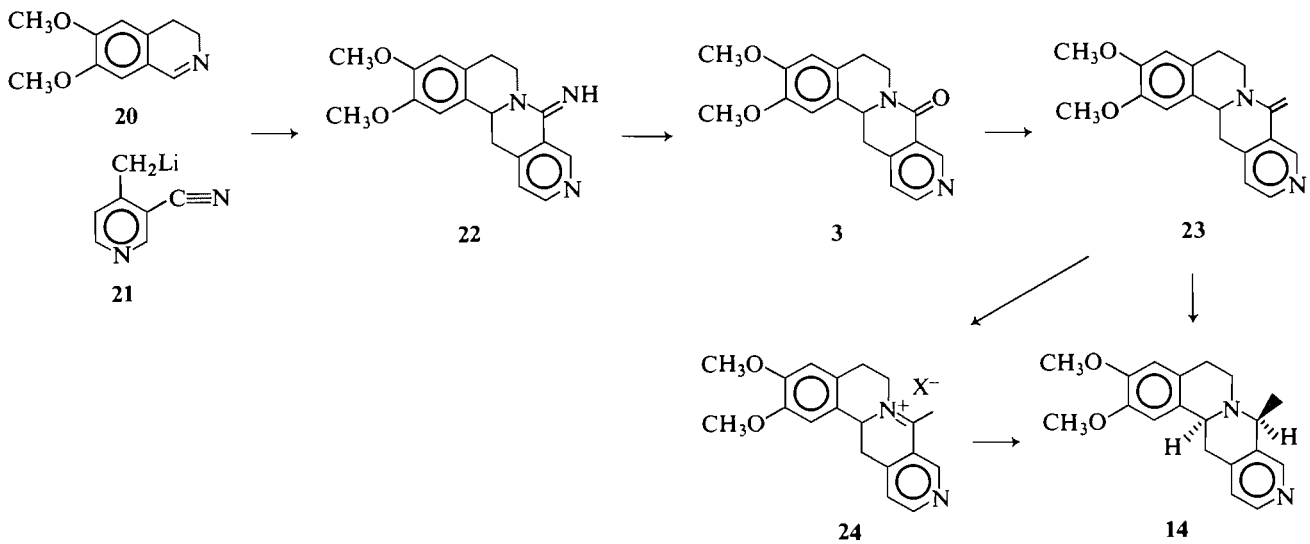

SCHEME 4

was identical with **14**. In another experiment the crude reaction product from the methyllithium reaction was taken up in glacial acetic acid, in which **23** would be expected to be converted into **24**, and then treated with sodium cyanoborohydride. Again, only **14** was isolated. In the cyanoborohydride reduction of **24** the iminium bond undergoing reduction is the N—C-8 double bond. In the other cases examined that involved reduction of berberinium salts, and in the case of **15**, the last bond to be reduced would be an iminium bond between C-13a and N. It is apparent that the reductions of the two bonds are subject to different steric constraints. The stereospecific reduction of an N—C-8 bond has also been observed in a recently reported asymmetric synthesis of coralydine (7).

Tourwé *et al.* (9) have reported that nmr spectroscopy may be used effectively to ascertain the conformation of dibenzo[*a*,*g*]-quinolizidines. In an examination of the spectra of coralydine (**10**) and *O*-methylcorytenchirine (**9**) they have noted along with other observations that the chemical shift of the protons of C-8 H, C-8 CH_3, and C-13a H and the coupling constant between C-8 H and C-8 CH_3 are diagnostic of the conformation and configuration of the molecules. In the *trans* quinolizidine, coralydine (**10**), the methyl group at C-8 is deshielded and the protons at C-8 and C-13a are shielded relative to the corresponding signals in *O*-methylcorytenchirine (**9**), which has been assigned a *cis* quinolizidine conformation and which is a diastereomer of coralydine. The coupling constant between C-8 H and C-8 CH_3 also differs in the two systems, as shown in Table 1. In the same table the relevant data for the isomeric pairs of 8-methyl compounds prepared in this investigation are collated. It is evident that there is an excellent correlation between the conformation (as ascertained by ir examination) and the ^1H nmr of the signals examined. It may be inferred therefore that the conclusions drawn by Tourwé *et al.* (9) regarding the use of ^1H nmr spectroscopy in assigning the conformation of the quinolizine ring in 8-methylberberines substituted at C-10 and C-11 are generally valid for berberines and apply equally well to the related systems prepared in this investigation.

An examination of the ^{13}C spectra of the 8-methylberberines has revealed a correlation between the chemical shifts of selected carbon atoms and the stereochemistry. These data, collated in Table 2, show that the signals at C-8, C-8 CH_3, and C-13a are diagnostic of the stereochemistry. Signals at C-6 and C-13, which have been used in assigning conformation in other

Can. J. Chem. Downloaded from www.nrcresearchpress.com by 78.46.186.204 on 09/07/12
For personal use only.

TABLE 1. Correlation between stereochemistry and ^1H nmr signals of 8-methylberberines and 8-methylazaberberines

Compound	Signal 8β *Me*	8α *H*	13a *H*	$J_{8H,Me}$	Compound	Signal 8α *Me*	8β *H*	13a *H*	$J_{8H,Me}$
Coralydine (**10**)[a]	1.54	3.72	3.71	6.2	*O*-Methylcorytenchirine (**9**)[a]	1.40	4.10	4.24	6.6
8β-Methylcanadine (**8**)	1.50	3.81	3.53	6.1	8α-Methylcanadine (**7**)	1.37	4.30	4.19	6.7
8-*epi*-*O*-Methylalamaridine (**14**)	1.60	3.83	3.75	6.4	*O*-Methylalamaridine (**13**)	1.42	4.23	4.27	6.9
8-*epi*-Alamaridine (**19**)	1.60	3.79	3.71	6.4	Alamaridine (**1**)	1.41	4.24	4.21	6.9

[a]Data on Tourwé *et al.* (9).

TABLE 2. Correlation between stereochemistry and ^{13}C nmr signals of 8-methylberberines and 8-methylazaberberines

Compound	Signal C-8	C-13a	C-8 CH_3	Compound	Signal C-8	C-13a	C-8 CH_3
Coralydine (**10**)[a]	58.9	58.6	21.3	*O*-Methylcorytenchirine (**9**)[a]	58.8	50.0	17.7
8β-Methylcanadine (**8**)[b]	57.3	59.1	23.0	8α-Methylcanadine (**7**)[b]	50.7	55.6	15.9
8-*epi*-*O*-Methylalamaridine (**14**)	57.6	58.3	21.2	*O*-Methylalamaridine (**13**)	49.9	56.7	17.7
(±)-*epi*-Alamaridine (**19**)	57.8	58.4	21.4	(±)-Alamaridine (**1**)	49.7	57.0	17.3

[a]Data from ref. 8.
[b]The assignment of signals to C-8 and C-13a in **7** and **8** was made on the basis of a hetero-COSY experiment. The assignment of signals to these two centres in **9** was made prior to the development of 2D techniques and probably should be reversed in view of our results.

protoberberine systems (12), are not appreciably different in the isomeric pairs examined in this investigation and the signals have not been tabulated. Tourwé and Van Binst (12) have noted that differences between the ^{13}C spectra of **9** and **10** may not be a reliable criterion for the assignment of conformation to the two systems. However, there is no doubt that ^{13}C nmr may be used to differentiate between diastereomers. Nevertheless, ir and ^1H nmr appear to be more reliable measures of conformation.

In summary, it has been shown that 8-oxoberberines react readily with methyllithium. The products isolated on alkaline work-up are enamines with an 8-exomethylene group. The enamines are transformed to iminium salts in acidic media and the latter undergo facile reduction to 8-methylberberines. (±)-Almaridine has been synthesized from the readily available lactam (**2**) using these procedures.

Experimental

Apparatus, materials, and methods

The continuous wave ^1H nmr spectra were recorded on a Varian EM 390 spectrometer and the Fourier transform spectra on either a Bruker WP 80 (80 MHz), WM 250 (250 MHz), or WM 500 (500 MHz) spectrometer. Unless otherwise specified, the samples were dissolved in chloroform-*d* using tetramethylsilane (TMS) as internal standard. Chemical shifts, quoted as δ values, were measured in relation to TMS. The symbols s, singlet, d, doublet, t, triplet, q, quartet, br, broad, and m, multiplet are used in reporting spectra. The ^{13}C nmr spectra were recorded at 62.9 MHz on a Bruker WM 250 FT or at 125.76 MHz on a WM 500 FT spectrometer at ambient temperature.

EI mass spectra were recorded at 70 eV with a source temperature of ca. 200°C either on a VG Micromass 7070 F mass spectrometer equipped with a data system comprised of a PDP 8A with VG 2000 software or a VG analytical ZAB E mass spectrometer equipped with a VG 11-250 data system. High resolution mass spectra (hrms) were recorded on either of the above instruments. CI mass spectra were recorded on a VG Micromass 7070 F mass spectrometer using NH_3 at ca. 1 Torr (133.3 Pa) as reagent gas and DCI mass spectra were recorded under similar conditions on a VG analytical ZAB E mass spectrometer. Infrared spectra were run on a Perkin–Elmer 283 spectrometer in $CHCl_3$ solution or $CHCl_3$ film. Melting points were determined using a Gallenkamp apparatus and are uncorrected. The microanalyses were performed by the Guelph Chemical Laboratories Ltd., Guelph, Ontario.

Thin-layer chromatography (tlc) was performed using Polygram Sil G/UV_{254} and Polygram Alox N/UV_{254} plates. For flash column chromatography (13) Kieselgel 60 (230–400 mesh) was used.

All reactions involving lithiation steps were carried out in flame-dried apparatus under a blanket of argon, using septa and syringes for transfer of reagents. Diisopropylamine and 1,1,1,3,3,3,-hexamethyldisilazane were heated under reflux over calcium hydride and distilled onto activated molecular sieves (4A) for storage. THF was dried by distillation from Na/benzophenone under a nitrogen atmosphere just prior to use.

5,6-Dihydro-9,10-dimethoxy-2,3-methylenedioxy-8H-dibenzo[a,g]-quinolizin-8-one (oxyberberine) **4**

Oxyberberine **4** was prepared by the procedure of Perkin (6) from berberine chloride by refluxing with 30% NaOH solution (aqueous) for 3 h; mp 204°C (EtOAc) (lit. (15) mp 200°C, lit. (16) mp 192–195°C); ^1H nmr (90 MHz), δ: 2.85 (2H, t, J=6.0 Hz, C-5 H's), 3.95 (3H, s, $-OCH_3$), 4.00 (3H, s, $-OCH_3$), 4.25 (2H, t, J=6.0 Hz, C-6 H's), 5.97 (2H, s, $-OCH_2O-$), 6.70 (2H, s, C-1 and C-4 H's), 7.20 (1H, apparent s, C-13 H), 7.30 (2H, apparent s, C-11 and C-12 H's); ms (EI), *m/z* (%): 351 (100)$M^{+\cdot}$, 336 (84), 321 (33), 308 (28), 291 (25), and 83 (14).

(8α)- and (8β)-8-methylcanadine, 7 and 8, respectively, from 4

(a) Without isolation of intermediates

To a stirred solution of oxyberberine (**4**) (0.526 g, 1.5 mmol) in dry THF (100 mL) at −40°C was added a solution of MeLi (5 mL, 1.5 *M* in hexane, 7.5 mmol) under an argon atmosphere. The reaction mixture was stirred at −40°C for 3 h and then the temperature was raised slowly to ca. 20°C and stirring was continued for a further 2–3 h. The excess of MeLi was destroyed by adding water (1 mL) at 0°C and a few drops of concentrated HCl solution (aqueous). The reaction mixture was then stirred for another 15 min at room temperature. Sodium borohydride (0.57 g, 15 mmol) was added in portions to the above stirred reaction mixture and stirring continued for 1 h. At this point the solution became clear and the solvent was evaporated *in vacuo*. The excess $NaBH_4$ was cautiously destroyed with glacial acetic acid; the resulting reaction mixture was basified with concentrated NH_3 solution (aq.) to pH 10 and

Can. J. Chem. Downloaded from www.nrcresearchpress.com by 78.46.186.204 on 09/07/12
For personal use only.

Can. J. Chem. Downloaded from www.nrcresearchpress.com by 78.46.186.204 on 09/07/12
For personal use only.

then thoroughly extracted with $CHCl_3$. The combined $CHCl_3$ extracts were washed with brine, dried over Na_2SO_4 (anhydrous), and evaporated *in vacuo*, affording in nearly quantitative yield a mixture of isomeric 8-methylcanadines in a ratio (8α:8β = 1:3) as estimated by nmr. The crude product on crystallization from EtOH (95%) gave the 8β isomer **8** (0.2 g). The ethanolic mother liquor was evaporated and the residue subjected to flash chromatography on silica gel (eluting with cyclohexane and EtOH in a ratio of 10:3), affording an additional 0.163 g of the 8β isomer (8*S**,13a*S**) and the 8α isomer (8*R**,13a*S**) **7** (0.13 g).

8β *Isomer* (**8**): 0.363 g (69%); R_f 0.70 (silica; EtOAc–cyclohexane (1:1)); mp 166–167°C (EtOH); ir ($CHCl_3$), ν_{max}: 2820–2740 cm^{-1} (Bohlmann bands); ^1H nmr (500 MHz), δ: 1.50 (3H, d, J=6.1 Hz, C-8 CH_3), 2.52 (1H, m, C-6 H_{ax}), 2.65 (1H, apparent d, J=16.0 Hz, C-5 H_{ax}), 2.80 (1H, m, C-13 H_{ax}), 3.10 (2H, m, C-5 H_{eq} and C-13 H_{aq}), 3.30 (1H, m, C-6 H_{eq}), 3.53 (1H, d, J=10.8 Hz, C-13a H), 3.81 (1H, q, J=6.1 Hz, partially overlapped by OCH_3 signals, C-8 H), 3.85 (3H, s, -OCH_3), 3.86 (3H, s, -OCH_3), 5.88 (2H, m, OCH_2O), 6.58 (1H, s, C-4 H), 6.75 (1H, s, C-1 H), 6.78 (1H, A part of AB, J=8.3 Hz, C-11 H), 6.86 (1H, B part of AB, J=8.3 Hz, C-12 H); ^{13}C nmr (125.76 MHz), δ: 23.0 (q, C-8 CH_3), 30.8 (t, C-5), 37.8 (t, C-13), 49.3 (t, C-6), 56.0 (q, OCH_3), 57.3 (d, C-8), 59.1 (d, C-13a), 60.4 (q, OCH_3), 100.8 (t, OCH_2O) 105.8 (d, C-4), 108.6 (d, C-1), 110.8 (d, C-12), 123.6 (d, C-11), 128.5, 129.1, 131.6, 134.0, 146.0, 146.1 146.2, 151.1 (s's, Ar C's); ms(EI), *m/z* (%): 353 (10)$M^{+\cdot}$, 338 (100), 336 (20), 178 (45), and 163 (18). *Exact Mass* (hrms) calcd. for $C_{21}H_{23}NO_4$: 353.163; found: 353.163.

8α *Isomer* (**7**): 0.13 g (25%); R_f 0.52 (silica; EtOAc–cyclohexane (1:1)); mp 138°C (EtOAc–hexane); ir ($CHCl_3$), ν_{max}: no Bohlmann bands; ^1H nmr (500 MHz), δ: 1.37 (3H, d, J=6.7 Hz, C-8 CH_3), 2.71–3.10 (6H, complex m, C-5, C-6, and C-13 H's), 3.83 (3H, s, OCH_3), 3.85 (3H, s, OCH_3), 4.19 (1H, dd, J=11.3 and 4.2 Hz, C-13a H), 4.30 (1H, q, J=6.7 Hz, C-8 H), 5.88 (2H, s, OCH_2O), 6.57 (1H, s, C-4 H), 6.67 (1H, s, C-1 H), 6.76 (1H, A part of AB, J=8.4 Hz, C-11 H), 6.80 (1H, B part of AB, J=8.4 Hz, C-12 H); ^{13}C nmr (125.76 MHz), δ: 15.9 (q, C-8 CH_3), 30.0 (t, C-5), 35.2 (t, C-13), 47.2 (t, C-6), 50.7 (d, C-8), 55.6 (d, C-13a), 55.9 (q, OCH_3), 60.6 (q, OCH_3), 100.8 (t, OCH_2O), 106.3 (d, C-1), 108.7 (d, C-4), 111.3 (d, C-11), 124.1 (d, C-12), 126.6, 127.6, 132.2, 133.7, 145.4, 146.0, 146.1, and 150.5 (s's, Ar C's); ms (EI), *m/z* (%): 353 (12)$M^{+\cdot}$, 338 (100), 178 (72), 163 (26), and 135 (10). *Exact mass* (hrms) calcd. for $C_{21}H_{23}NO_4$: 353.163; found: 353.160.

(b) With isolation of intermediates

8-Methylene-5,6-dihydro-9,10-dimethoxy-2,3-methylenedioxy-8H-dibenzo[a,g]quinolizine (**5**): The reaction was carried out using oxyberberine **4** (1.5 mmol) as described previously. After an appropriate reaction time, the excess MeLi was destroyed by adding a saturated solution of Na_2SO_4 (2 mL aq.). The reaction mixture was diluted with $CHCl_3$ (100 mL), dried over Na_2SO_4 (anhyd.), and filtered. The residue was washed several times with $CHCl_3$ and the combined $CHCl_3$ filtrates were evaporated *in vacuo* to give the exomethylene compound as an oil in almost quantitative yield; ^1H nmr (90 MHz), δ: 2.87 (2H, t, J=6.0 Hz, C-5 H's), 3.48 (2H, q, J=6.0 Hz, C-6 H's), 3.80 (3H, s, OCH_3), 3.86 (3H, s, OCH_3), 4.20 and 5.35 (1H each, s's, methylene protons), 5.90 (2H, s, OCH_2O), 6.00 (1H, s, C-13 H), 6.63 (1H, s, C-4 H), 6.87 (2H, s, C-11 and C-12 H's), 7.10 (1H, s, C-1H).

5,6-Dihydro-9,10-dimethoxy-2,3-methylenedioxydibenzo[a,g]quinolizinium bromide (**6**)

To a methanolic solution of the crude exomethylene compound was added 48% HBr solution (1 mL, aq.). The reaction mixture was stirred for 5 min at room temperature and then evaporated to dryness *in vacuo* to give the quaternary bromide (0.6 g), which was crystallized from MeOH (0.405 g, 63%), mp 220–223°C (dec.); ^1H nmr (90 MHz, TFA), δ: 3.25 (2H, t, J=6.0 Hz, C-5 H's), 3.60 (3H, s, C-8 CH_3), 4.20 (6H, s, 2×OCH_3), 4.88 (2H, t, J=6.0 Hz, C-6 H's), 6.12 (2H, s, OCH_2O), 6.95 (1H, s, C-4 H), 7.48 (1H, s, C-1 H), 8.04 (2H, s, C-11 and C-12 H's), 8.37 (1H, s, C-13 H); ms (EI), *m/z* (%): 350 (19) (M^+), 349 (35), 334 (100), 318 (25), 290 (34), 167 (24), 148 (36), and 135 (32).

Sodium borohydride reduction of the iminium salt (**6**)

To a stirred solution of the salt **6** (0.3 g) in EtOH (50 mL) was added $NaBH_4$ (0.3 g) in small portions with cooling and the reaction mixture was stirred for 1 h at room temperature. The excess $NaBH_4$ was carefully destroyed with glacial acetic acid at 0°C, the solution was made basic with concentrated NH_3 solution (aq.), and then the product was thoroughly extracted into $CHCl_3$. The combined $CHCl_3$ extracts were washed with brine and evaporated *in vacuo*. The crude product, containing an isomeric mixture of 8-methylcanadines **7** and **8**, was subjected to flash chromatography on silica gel, eluting with EtOAc–cyclohexane (3:10) to give the 8β isomer (0.17 g, 73%) and the 8α isomer (0.056 g, 23%), identical with the samples described above (mp, tlc, ^1H nmr, and mass spectra).

(8S,13aS*)-5,6-13,13a-Tetrahydro-2,3-dimethoxy-8-methyl-8H-isoquino[2,1-b][2,7]naphthyridine* (**14**) *and its epimer at C-8* (**13**)

(a) Without isolation of intermediates

To a solution of the lactam (**2**) (0.39 g, 1.27 mmol) in dry THF (25 mL) was added a solution of MeLi (6 mL, 1.5 *M* in hexane) dropwise at −78°C and the mixture was then stirred for ca. 3 h. The excess MeLi was destroyed with saturated Na_2SO_4 solution (2 mL), a few drops of 48% HBr (aq.) were added, and the solution was stirred for 10 min. Excess $NaBH_4$ (0.4 g) was added to the reaction mixture, which was stirred for a further 3 h, and then the solvent was removed *in vacuo*. The excess $NaBH_4$ was destroyed with glacial acetic acid, the resulting solution basified with concentrated NH_3 (aq.), and the solution thoroughly extracted with $CHCl_3$. The combined $CHCl_3$ extracts were washed successively with water and brine, and then dried over Na_2SO_4 (anhyd.). Evaporation of the solvent *in vacuo* gave the crude product (0.378 g), which was approximately a 3:1 mixture of **14** and **13** as estimated by ^1H nmr of the crude product. The reduced product undergoes rapid aerial oxidation, giving a highly fluorescent green-coloured solution, and therefore it must be immediately chromatographed after work-up. Flash chromatography on silica gel using 1–5% MeOH in $CHCl_3$ enabled the two isomers to be separated.

8β *Isomer* (**14**): 213 mg (54%); mp 158–159°C (EtOAc); R_f 0.30 (alumina; EtOAc–hexane (1:1)); ir ($CHCl_3$ film), ν_{max}: 2820–2740 cm^{-1} (Bohlmann bands); ^1H nmr (500 MHz), δ: 1.60 (3H, d, J=6.4 Hz, C-8 CH_3), 2.48 (1H, d of t, J=11.2 and 3.5 Hz, C-6 H_{ax}), 2.73 (1H, br d, J=16.0 Hz, C-5 H_{eq}), 2.91 (1H, dd, J=16.5 and 11.2 Hz, C-13 H_{ax}), 3.06 (1H, m, C-5 H_{ax}), 3.18 (1H, dd, J=16.5 and 3.1 Hz, C-13 H_{eq}), 3.39 (1H, complex m, C-6 H_{eq}), 3.75 (1H, apparent d, J=10.0 Hz, C-13a H), 3.83 (1H, q, J=6.4 Hz, C-8 H), 3.87 (3H, s, OCH_3), 3.89 (3H, s, OCH_3), 6.63 (1H, s, C-4 H), 6.71 (1H, s, C-1 H), 7.07 (1H, d, J=5.0 Hz, C-12 H), 8.35 (1H, d, J=5.0 Hz, C-11 H), 8.49 (1H, s, C-9 H); ^{13}C nmr (125.76 MHz), δ: 21.2 (C-8 CH_3), 29.6 (C-5), 36.6 (C-13), 46.5 (C-6), 55.9 (OCH_3), 56.2 (OCH_3), 57.6 and 58.3 (C-8 and C-13a), 109.0, 111.5, 123.0 and 127.1, 129.7, 135.6, 143.6, 146.7, 147.6, 147.8, and 148.4 (Ar C's); ms (EI), *m/z* (%): 310 (41)$M^{+\cdot}$, 309 (43), 295 (100), 191 (25), 190 (39), 176 (17), and 118 (11). *Exact Mass* (hrms) calcd. for $C_{19}H_{22}N_2O_2$: 310.168; found: 310.168.

8α *Isomer* (**13**): 97 mg (25%); glassy solid; R_f 0.23 (alumina; EtOAc–hexane, (1:1)); ir ($CHCl_3$), ν_{max}: no Bohlmann bands; ^1H nmr (500 MHz), δ: 1.42 (3H, d, J=6.9 Hz, C-8 CH_3), 2.90–3.10 (5H, complex m, C-5 H, C-6 H and C-13 H_{ax}), 3.13 (1H, dd, J=17.2 and 4.2 Hz, C-13 H_{eq}), 3.87 (3H, s, OCH_3), 3.89 (3H, s, OCH_3), 4.23–4.27 (2H, m, C-8 and C-13a H's), 6.63 (1H, s, C-4 H), 6.69 (1H, s, C-1 H), 7.03 (1H, d, J=5.0 Hz, C-12 H), 8.33 (1H, d, J=5.0 Hz, C-11 H), and 8.35 (1H, s, C-9 H); ^{13}C nmr (125.76 MHz), δ: 17.7 (C-8 CH_3), 29.7 (C-5), 35.9 (C-13), 47.5 (C-6), 49.9 (C-8), 56.1 (C-13a), 56.3 (OCH_3), 57.2 (OCH_3), 109.4, 111.8, 123.8, 126.9, 130.2, 136.4, 143.1, 147.1, 147.7, 147.8, and 148.9 (Ar C's); ms (EI), *m/z* (%): 310 (45)$M^{+\cdot}$, 309 (40), 295 (100), 192 (13), 191 (35), 190 (49), 176 (20), 120 (8), 119 (9), and 118 (12). *Exact Mass* (hrms) calcd. for $C_{19}H_{22}N_2O_2$: 310.168; found: 310.167.

Can. J. Chem. Downloaded from www.nrcresearchpress.com by 78.46.186.204 on 09/07/12
For personal use only.

(*b*) *With isolation of intermediates*

(*i*) *8-Methylene-5,6-dihydro-2,3-dimethoxy-8*H*-isoquino[2,1-*b*][2,7]naphthyridine* (***11***): To a solution of lactam (**2**) (0.2 g) in dry THF (12 mL) was added a solution of MeLi (5 mL, 1.5 *M* in hexane) dropwise at −78°C as described previously. The reaction mixture was stirred under argon at −78°C for 3–4 h (reaction monitored by tlc). The excess MeLi was destroyed with saturated Na_2SO_4 (2 mL, aq.). The reaction mixture was diluted with $CHCl_3$, filtered through a pad of Na_2SO_4 (anhyd.), and the residue washed several times with $CHCl_3$. Evaporation of the $CHCl_3$ filtrate *in vacuo* afforded an oil (0.187 g, 94%); ^{1}H nmr (90 MHz), δ: 2.90 (2H, t, *J*=6.0 Hz, C-5 H's), 3.45 (2H, t, *J*=6.0 Hz, C-6 H's), 3.90 (3H, s, OCH_3), 3.93 (3H, s, OCH_3), 4.65 and 5.95 (1H each, s's, methylene protons), 6.68 (1H, s, C-4 H), 6.93 (1H, d, *J*=5.5 Hz, C-12 H), 7.00 (1H, s, C-1 H), 7.17 (1H, s, C-13 H), 8.35 (1H, d, *J*=5.5 Hz, C-11 H), and 8.83 (1H, s, C-9 H).

*(ii) 5,6-Dihydro-2,3-dimethoxy-8-methylisoquino[2,1-*b*][2,7]naphthyridinium bromide* (***12***): The crude product **11** obtained above was taken into EtOH (5 mL), 48% HBr solution (1 mL, aq.) added, and the reaction mixture was stirred for 15 min. The solvent was evaporated *in vacuo* and the last traces of water were removed by codistillation with benzene. The crude product **12** was crystallized from EtOH–EtOAc (0.12 g, 51%), mp 190–198°C (dec.); ^{1}H nmr (90 MHz), δ: 2.95 (2H, t, *J*=6.0 Hz, C-5 H's), 3.95 (6H, s, OCH_3 and NCH_3), 4.00 (3H, s, OCH_3), 4.34 (2H, t, *J*=6.0 Hz, C-6 H's), 6.76 (2H, s, C-1 and C-4 H's), 7.30 (1H, s, C-13 H), 7.39 (1H, d, *J*=5.4 Hz, C-12 H), 8.68 (1H, d, *J*=5.4 Hz, C-11 H), 9.61 (1H, s, C-9 H); ms (EI), *m/z* (%): 307 (23)M^+, 306 (100), 305 (75), 291 (68), 289 (30).

(±)-*5,6-Dihydro-2,3-dimethoxy-8-methyl-8*H*-isoquino[2,1-*b*][2,7]-naphthyridine* (***15***)

A chloroform solution of a mixture of **13** and **14** undergoes rapid aerial oxidation, producing a highly fluorescent green solution. A sample of the mixture, when left open to air for ca. 48 h at room temperature, was found completely oxidized to **15**. The crude product was purified on neutral alumina (EtOAc), yielding a glassy solid; ^{1}H nmr (90 MHz), δ: 1.28 (3H, d, *J*=6.5 Hz, C-8 CH_3), 2.80–3.05 (2H, m, C-5 H's), 3.30–3.63 (2H, m, C-6 H's), 3.90 (3H, s, OCH_3), 3.95 (3H, s, OCH_3), 4.65 (1H, q, *J*=6.5 Hz, C-8 H), 5.76 (1H, s, C-13 H), 6.76 (1H, s, C-4 H), 6.88 (1H, d, *J*=5.2 Hz, C-12 H), 7.25 (1H, s, C-1 H), 8.18 (1H, s, C-9 H), 8.30 (1H, *J*=5.2 Hz, C-11 H); ms (EI), *m/z* (%): 308 (14)$M^{+\cdot}$, 293 (100), and 277 (20). This compound was reduced with $NaBH_4$ to give an isomeric mixture of **13** and **14** in a ratio of ca. 1:3.

(8S,13aS*)-2-Benzyloxy-5,6,13,13a-tetrahydro-3-methoxy-8-methyl-8*H*-isoquino[2,1-*b*][2,7]naphthyridine* (***18***)

To a solution of lactam **16** (0.3 g, 0.78 mmol) in dry THF (20 mL) (3) was added dropwise a solution of MeLi (4 mL, 1.5 *M* in hexane) and the resulting solution was stirred for 3.5 h at −78°C. The excess MeLi was then decomposed with a saturated Na_2SO_4 solution (2 mL aq.). The resulting mixture was treated with an excess of $NaBH_4$ (0.4 g) and stirred for ca. 3 h at room temperature. After removal of the solvent *in vacuo*, the excess $NaBH_4$ was carefully destroyed with glacial acetic acid. The mixture was basified with concentrated NH_3 solution and thoroughly extracted with $CHCl_3$. The $CHCl_3$ extract was washed with brine, dried over Na_2SO_4 (anhyd.), and the solvent recovered *in vacuo*, affording a crude product (0.293 g, 97%) that was a mixture of (8*S**,13a*S**) isomer **18** and (8*R**,13a*S**) isomer **17** as shown by ^{1}H nmr of the crude product.

The reduced product in solution oxidizes rapidly in air, forming a highly fluorescent green-coloured mixture, and must be chromatographed immediately.

The reduced product was separated into two fractions by flash chromatography on silica gel ($CHCl_3$-EtOAc, 8:1) but only the (8*S**,13a*S**) isomer **18** was obtained in pure form (167 mg, 55%); mp 137–141°C (EtOAc–hexane); R_f 0.65 (silica; $CHCl_3$–EtOAc (2:1)); ir ($CHCl_3$), ν_{max}: 2840–2740 cm^{-1} (Bohlmann bands); ^{1}H nmr (500 MHz), δ: 1.59 (3H, d, *J*=6.4 Hz, C-8 CH_3), 2.47 (1H, d of t, *J*=11.0 and 3.6 Hz, C-6 H_{ax}), 2.71–3.01 (3H, complex m, C-5 and C-13 H_{ax} H's), 3.05 (1H, dd, *J*=17.3 and 3.1 Hz, C-13 H_{eq}), 3.31 (1H, complex m, C-6 H_{eq}), 3.71 (1H, m, C-13a H), 3.79 (1H, q, *J*=6.4 Hz, C-8 H), 3.88 (3H, s, OCH_3), 5.13 (2H, m, OCH_2Ar), 6.66 and 6.67 (1H each, s's, C-1 and C-4 H's), 7.18 (1H, d, *J*=5.8 Hz, C-12 H), 7.32–7.44 (5H, complex m, Ar H's), 8.31 (1H, d, *J*=5.8 Hz, C-11 H), and 8.44 (1H, s, C-9 H); ms (EI), *m/z* (%): 386 (53)$M^{+\cdot}$, 385 (38), 371 (95), 295 (33), 280 (21), 279 (27), 267 (14), 266 (25), 120 (21), 119 (12), 118 (16), and 91 (100). *Exact Mass* (hrms) calcd. for $C_{25}H_{26}N_2O_2$: 386.199; found: 386.199.

(±)-*8*-epi-*Alamaridine* (***19***) *and* (±)-*alamaridine* (***1***)

The crude mixture of **17** and **18**, obtained from the reaction of 300 mg of lactam **16** and excess MeLi under conditions described above, was dissolved in MeOH (15 mL) and glacial acetic acid (1 mL), 10% Pd–C (0.1 g) was added, and the reaction mixture was treated with H_2 for ca. 12 h at 30 psi (1 psi = 6.9 kPa). The catalyst was removed by filtration through Celite and the residue washed with $CHCl_3$. The filtrate was diluted with water (25 mL), basified with 20% Na_2CO_3 (aq.), and thoroughly extracted with $CHCl_3$. The combined $CHCl_3$ extracts were washed with brine, dried over Na_2SO_4 (anhyd.), and evaporated *in vacuo* to give a mixture (0.167 g, 72%) containing **1** and **19**, which was subjected to flash chromatography (silica gel; eluting with 5–10% MeOH in $CHCl_3$), yielding two components.

(*a*) (±)-*8*-epi-*Alamaridine* (**19**): 93 mg (40%); mp 197-200°C (dec.) (EtOAc–hexane); R_f, 0.26 (silica; $CHCl_3$–MeOH (10.1)); ir ($CHCl_3$), ν_{max}: 3550 cm^{-1}, 2820–2740 cm (Bohlmann bands); ^{1}H nmr (500 MHz), δ: 1.60 (3H, d, *J*=6.4 Hz, C-8, CH_3), 2.46 (1H, d of t, *J*=11.3 and 3.5 Hz, C-6 H_{ax}), 2.71 (1H, apparent d, *J*=15.8 Hz, C-5 H_{ax}), 2.89 (1H, dd, *J*=16.5 and 11.2 Hz, C-13 H_{ax}), 3.05 (1H, m, C-5 H_{eq}), 3.13 (1H, dd, *J*=16.5 and 2.8 Hz, C-13 H_{eq}), 3.39 (1H, m, C-6 H_{eq}), 3.71 (1H, d, *J*=10.9 Hz, C-13a H), 3.79 (1H, q, *J*=6.4 Hz, C-8 H), 3.87 (3H, s, OCH_3), 5.55 (1H, br s, phenolic -OH), 6.61 (1H, s, C-4 H), 6.80 (1H, s, C-1 H), 7.05 (1H, d, *J*=4.9 Hz, C-12 H), 8.34 (1H, d, *J*=4.9 Hz, C-11 H), and 8.48 (1H, s, C-9 H); ^{13}C nmr (125.76 MHz), δ: 21.4 (C-8, CH_3), 29.8 (C-5), 36.7 (C-13), 47.0 (C-6), 56.1 (OCH_3), 57.8 (C-8), 58.4 (C-13a), 110.8 (C-1), 111.7 (C-4), 123.4, 126.4, 130.6, 135.8, 144.0, 144.2, 145.5, 146.8, and 148.4 (Ar C's); ms (EI), *m/z* (%): 296 (33)$M^{+\cdot}$, 295 (36), 281 (100), 279 (25), 178 (18), 177 (20), 176 (32), 162 (13), 120 (18), 119 (11), and 118 (12). *Exact Mass* (hrms) calcd. for $C_{18}H_{20}N_2O_2$: 296.152; found: 296.152.

(*b*)(±)-Alamaridine (***1***): 46 mg (20%); mp 178–182°C; R_f 0.20 (silica; $CHCl_3$–MeOH (10:1)); ^{1}H nmr (500 MHz), δ: 1.41 (3H, d, *J*=6.9 Hz, C-8, CH_3), 2.76–3.14 (5H, complex m, C-5, C-6, and C-13 H_{ax} H's), 3.12 (1H, dd, *J*=17.5 and 4.5 Hz, C-13 H_{eq}), 3.88 (3H, s, OCH_3), 4.21 (1H, dd, *J*=11.0 and 4.5 Hz, C-13a H, partially overlapped with q of C-8 H), 4.24 (1H, q, *J*=6.9 Hz, C-8 H), 5.20 (1H, br s, phenolic OH), 6.60 (1H, s, C-4 H), 6.77 (1H, s, C-1 H), 7.02 (1H, d, *J*=4.9 Hz, C-12 H), 8.32 (1H, d, *J*=4.9 Hz, C-11 H), and 8.37 (1H, s, C-9 H); ^{13}C nmr (125.76 MHz), δ: 17.3 (C-8 CH_3), 29.7 (C-5), 35.8 (C-13), 47.4 (C-6), 49.7 (C-8), 56.0 (OCH_3), 57.0 (C-13a), 110.9 (C-1), 111.9 (C-4), 123.7, 126.0, 130.9, 136.2, 143.0, 144.1, 145.2, 146.9, and 148.6 (Ar C's); ms (EI), *m/z* (%): 296 (36)$M^{+\cdot}$, 295 (29), 281 (100), 237 (4), 178 (38), 177 (19), 176 (29), 163 (11), 162 (16), 120 (18), 119 (11), and 118 (5). *Exact Mass* (hrms) calcd. for $C_{18}H_{20}N_2O_2$: 296.153; found: 296.150. The ir spectrum of the synthetic sample was identical with that of natural alamaridine. The ^{1}H nmr (500 MHz) spectrum of our synthetic sample and the ^{1}H nmr (100 MHz, $CDCl_3$) spectra of natural alamaridine (1) and synthetic alamaridine (2) of Pakrashi had chemical shifts for C-methyl, O-methyl, and aromatic protons that agreed within experimental error. Other signals that appeared as multiplets fell within the same range of δ values.

(±)-*5,6,13,13a-Tetrahydro-2,3-dimethoxy-8*H*-isoquino[2,1-*b*]-[2,7]naphthyridine-8-imine* (***22***)

A solution of imine **20** (0.6 g, 3.15 mmol) in dry THF (4 mL) was treated dropwise with trimethylsilyl triflate (0.75 mL, 3.83 mmol) at −78°C under an argon atmosphere. The resulting cloudy suspension was stirred first at −78°C for 1 h, then at 0°C for an additional 1 h. Meanwhile a solution of *n*-BuLi (2.33 mL, 1.55 *M* in hexane, 3.6 mmol) was added dropwise to a stirred solution of 1,1,1,3,3,3-hexa-

Can. J. Chem. Downloaded from www.nrcresearchpress.com by 78.46.186.204 on 09/07/12
For personal use only.

methyldisilazane (0.76 mL, 3.6 mmol) in dry THF (3 mL) at −78°C. The lithium bistrimethylsilylamide (LHS) solution so generated was stirred for an additional 10 min at −20°C and then cooled to −78°C. A solution of 3-cyano-4-methylpyridine **21** (0.354 g, 3 mmol) in dry THF (2 mL) was added dropwise to the above LHS solution at −78°C and the golden anion solution generated was stirred for a further 15 min at −78°C. The anion solution was then added dropwise to the imine – TMS triflate complex at −78°C and, when the addition was complete, the mixture was stirred for a further 4 h at −40°C. The reaction mixture was allowed to warm slowly to room temperature and stirred for ca. 12 h. The mixture was quenched with saturated NH_4Cl solution (1 mL, aq.) and the resulting mixture was evaporated to dryness, water added, and the contents extracted with $CHCl_3$. The $CHCl_3$ extract was dried over Na_2SO_4 (anhyd.) and the solvent evaporated *in vacuo*. The crude product was filtered through a short neutral alumina column, eluting first with $CHCl_3$ and then with $CHCl_3$–MeOH (3:1), affording the amidine **22** (0.904 g, 97.5%); mp 160–163°C (EtOAc); ir ($CHCl_3$ film), ν_{max}: 1615 cm^{-1}; ^1H nmr (500 MHz), δ: 2.79–2.82 (1H, m, C-6 H_{ax}), 2.92–3.05 (3H, complex m, C-5 and C-13 H_{ax} H's), 3.16 (1H, dd, J=16.0 and 2.6 Hz, C-13 H_{eq}), 3.90 (6H, s, 2×OCH_3), 4.63 (1H, dd, J=12.4 and 2.6 Hz, C-13a H), 4.85 (1H, m, C-6 H_{eq}), 6.68 (1H, s, C-4 H), 6.71 (1H, s, C-1 H), 7.20 (1H, d, J=4.9 Hz, C-12 H), 8.60 (1H, d, J=4.9 Hz, C-11 H), and 9.13 (1H, s, C-9 H); ^{13}C nmr (125.76 MHz), δ: 29.2 (C-5), 38.3 (C-13), 39.9 (C-6), 54.4 (C-13a), 56.1 (OCH_3), 56.4 (OCH_3), 109.1, 111.6, 122.5, 147.8, and 150.8 (15 × Ar CH's), 125.5, 144.9, 148.2, 148.3, and 150.8 (Ar C's),[3] and 159.6 (>C=NH); ms (EI), m/z (%): 309 (100)$M^{+\cdot}$, 294 (58), 255 (18), 192 (40), 190 (24), 176 (59), 149 (40), and 118 (47). *Exact Mass* (hrms) calcd. for $C_{18}H_{19}N_2O_3$: 309.148; found: 309.146.

*(±)-5,6,13,13a-Tetrahydro-2,3-dimethoxy-8*H*-isoquino[2,1-*b*]-[2,7]naphthyridin-8-one (**3**)*

Amidine **22** (250 mg) was dissolved in a mixture of dioxane (15 mL) and 20% KOH solution (10 mL, aq.) and the mixture was gently heated under reflux for 2 days. The solution was then evaporated to dryness *in vacuo*, acidified with concentrated HCl (aq.), and heated under reflux for an additional 30 min. Evaporation of the acidified solution was followed by basification with saturated Na_2CO_3 solution (aq.) and extraction with $CHCl_3$. The combined $CHCl_3$ extracts were washed with brine and dried over $MgSO_4$ (anhyd.). Removal of the solvent *in vacuo* and crystallization from EtOAc gave lactam **3** (231 mg, 92%); mp 173–175°C (EtOAc); R_f 0.34 (alumina; EtOAc); ir ($CHCl_3$ film), ν_{max}: 1655 cm^{-1}; ^1H nmr (500 MHz), δ: 2.78–2.80 (1H, C-6 H_{ax}), 2.93–3.00 (3H, complex m, C-5 and C-13 H_{ax} H's), 3.24 (1H, dd, J=16.2 and 3.3 Hz, C-13 H_{eq}), 3.90 (3H, s, OCH_3), 3.91 (3H, s, OCH_3), 4.85 (1H, dd, J=13.3 and 3.3 Hz, C-13a H), 4.98–5.00 (1H, m, C-6 H_{eq}), 6.70 and 6.72 (1H each, s's, C-1 and C-4 H's), 7.21 (1H, d, J=4.7 Hz, C-12 H), 8.66 (1H, d, J=4.7 Hz, C-11 H), and 9.27 (1H, s, C-9 H); ^{13}C nmr (125.76 MHz), δ: 29.1 (C-5), 37.4 (C-13), 38.8 (C-6), 54.5 (C-13a), 56.1 (OCH_3), 56.4 (OCH_3), 108.9, 111.8, 121.7, 150.3 and 152.3 (5 × Ar CH's), 124.9, 126.9, 127.4, 145.8, 148.4 and 148.4 (6 × Ar C's), and 163.3 (>C=O); ms (EI), m/z (%): 310 (100)$M^{+\cdot}$, 295 (46), 279 (42), 190 (48), 176 (20), 149 (21), and 119 (51). *Exact Mass* (hrms) calcd. for $C_{18}H_{18}N_2O_3$: 310.132; found: 310.130.

*Reaction of lactam **3** with MeLi followed by reduction with $NaCNBH_3$ in glacial acetic acid*

To a solution of lactam **3** (0.1 g, 0.323 mmol) in dry THF (10 mL) was added dropwise with stirring a solution of MeLi (1.5 mL, 1.5 *M* in hexane, 2.26 mmol) at −78°C under an argon atmosphere. The stirring was continued for ca. 4 h after which the excess MeLi was decomposed at −78°C with saturated Na_2CO_3 solution (1 mL, aq.). The reaction mixture was diluted with $CHCl_3$ (50 mL), filtered, and the residue washed several times with $CHCl_3$. The combined $CHCl_3$ extracts were washed with brine and then dried over Na_2SO_4 (anhyd). Removal of the solvent *in vacuo* provided a crude product, which was a mixture of 8-exomethylene compound **23** and iminium salt **24** (by ^1H nmr).

The crude material obtained above was dissolved in glacial acetic acid (3 mL), an excess of $NaCNBH_3$ was added, and the reaction mixture was stirred for ca. 30 min at 5–10°C. The mixture was then evaporated to dryness *in vacuo*, basified with concentrated NH_3 solution (aq.), and thoroughly extracted with $CHCl_3$. The $CHCl_3$ extracts were washed with brine, dried over Na_2SO_4 (anhyd.), and evaporated to dryness, yielding 85 mg of product homogeneous on tlc. It proved to be identical with the (8*S**,13a*S**) isomer **14** (tlc, ^1H nmr, and mass spectra).

*Reaction of lactam **3** with MeLi followed by catalytic reduction of the 8-exomethylene compound (**23**)*

Lactam **3** (100 mg) was heated with excess of MeLi in the manner already described. The reaction mixture was treated with a saturated Na_2CO_3 solution (1 mL) at −78°C, and extracted with $CHCl_3$ as in the previous experiment. The crude exomethylene compound so obtained was dissolved in EtOH (10 mL) and a few drops of concentrated NH_3 solution. It was then treated with H_2 over 10% Pd–C (50 mg) at room temperature for ca. 12 h. The catalyst was removed by filtration and the residue was washed with $CHCl_3$. Evaporation of the combined filtrate *in vacuo* gave a compound (88 mg, 88%) homogeneous by tlc that proved to be identical with the (8*S**,13a*S**) isomer **14** (tlc, ^1H nmr, and mass spectra).

[3]Five signals were observed for the six aromatic quaternary C atoms.

Acknowledgements

We thank the Natural Sciences and Engineering Research Council of Canada for financial support through grants to D. B. M. and H. L. H. We are indebted to Dr. Pakrashi for ir and ^1H nmr spectra of natural alamaridine and (±)-alamaridine and to Mr. B. Sayer and Mr. F. Ramelan for recording the nmr and mass spectra.

1. S. C. Pakrashi, R. R. Sinha, A. Bhattacharjya, R. Mukhopadhyay, and E. Ali. Heterocycles, **21**, 557 (1984).
2. A. Bhattacharjya, R. Mukhopadhyay, and S. C. Pakrashi. Tetrahedron Lett. **27**, 1215 (1986).
3. Jahangir, D. B. MacLean, and H. L. Holland. Can. J. Chem. **64**, 1031 (1986).
4. Jahangir, D. B. MacLean, M. A. Brook, and H. L. Holland. J. Chem. Soc. Chem. Commun. 1608 (1986).
5. S. C. Pakrashi, B. Achari, E. Ali, P. P. G. Dastidar, and R. R. Sinha. Tetrahedron Lett. **21**, 2667 (1980); S. C. Pakrashi, R. Mukhopadhyay, R. R. Sinha, P. P. G. Dastidar, B. Achari, and E. Ali. Indian J. Chem. **24B**, 19 (1985).
6. W. H. Perkin, Jr. J. Chem. Soc. 722 (1918).
7. Z. Czarnocki, D. B. MacLean, and W. A. Szarek. Bull. Soc. Chim. Belg. **95**, 749 (1986).
8. T. Kametani, A. Ujiie, M. Ihara, K. Fukumoto, and S.-T. Lu. J. Chem. Soc. Perkin Trans. 1, 1218 (1976).
9. D. Tourwé, G. Van Binst, and T. Kametani. Org. Magn. Reson. **9**, 341 (1977).
10. H. Bruderer, J. Metzger, A. Brossi, and J. J. Daly. Helv. Chim. Acta, **59**, 2793 (1976).
11. N. Ikekawa. Chem. Pharm. Bull. **6**, 269, (1958); **6**, 408 (1958).
12. D. Tourwé and G. Van Binst. Heterocycles, **9**, 507 (1978).
13. W. C. Still, M. Kahn, and A. Mitra. J. Org. Chem. **43**, 2923 (1978).

Facile calculations of select eigenvalues and the characteristic polynomial of small molecular graphs containing heteroatoms

JERRY RAY DIAS
Department of Chemistry, University of Missouri, Kansas City, MO 64110, U.S.A.

Received September 17, 1986

JERRY RAY DIAS. 1987. Can. J. Chem. **65**, 734 (1987).

Determination of common eigenvalues by embedding smaller subgraphs onto larger ones is illustrated. A nearly universal expression of the sixth coefficient of the characteristic polynomial valid for all conjugated hydrocarbon polyenes is presented. Its use in a graph theoretical determination of the Hückel MO characteristic polynomial of molecular graphs possessing heteroatoms is detailed.

JERRY RAY DIAS. 1987. Can. J. Chem. **65**, 734 (1987).

On illustre comment on peut déterminer les valeurs propres communes en incorporant des petits graphiques dans des plus grands. On présente une expression qui est pratiquement universelle pour la détermination du sixième coefficient du polynome caractéristique qui est valide pour tous les hydrocarbures polyéniques conjugés. On présente les détails de son utilisation dans la détermination, dans la théorie des graphs, du polynôme caractéristique des OM de Hückel des graphiques moléculaires possédant des hétéroatomes.

[Traduit par la revue]

Can. J. Chem. Downloaded from www.nrcresearchpress.com by 80.58.250.72 on 09/07/12
For personal use only.

Introduction

Previously the author derived less comprehensive versions of the following general equations for the fourth and sixth coefficients of the characteristic polynomial

$$[1]\quad a_4 = (1/2)(q^2 - 9q + 6N_c) - 2r_4 - d_1 - d_4 - 3d_5 - 6d_6 - \ldots$$

$$[2]\quad a_6 = -(1/6)(q^3 - 27q^2 + 116q) - N_c(3q - 16) - e(3,3) - 2r_6 + (q - 6)e(2,1) + (q - 5)e(3,1) + 2(q - 4 - \alpha_4)r_4 + r_3$$

where q = number of C—C σ bonds, N_c = number of carbon vertices, r_n = number of rings of size n, d_i = number of carbon vertices of degree i, $e(i, j)$ = number of edges (C—C σ bonds) with end points of degree i and degree j, and α_4 = number of attachments or branches on the tetragonal ring (1). Equation [1] is valid for all graphs and eq. [2] now, for the first time, presented in a more universal form is valid for all graphs having vertices of degree 1 to 3 and having no more than one trigonal or/and one tetragonal ring. With eq. [1] and eq. [2] the characteristic polynomial of small molecules can be quickly generated by inspection.

The following equation for the characteristic polynomial is valid for all conjugated polyenes having no more than one trigonal ring

$$P(G;X) = X^N - qX^{N-2} - 2r_3X^{N-3} + a_4X^{N-4} - [2r_5 - 2(q - 3 - \alpha_3)r_3]X^{N-5} + a_6X^{N-6} + \ldots$$

where a_4 is given by eq. [1], a_6 is given by eq. [2], α_3 is the number of attachments or branches on the trigonal ring, and $X = (E - \alpha)/\beta$. With this equation one can compute by inspection the characteristic polynomial of polyene molecules with seven or less carbon vertices. Polyene molecules with 8, 9, or 10 carbon vertices can be determined also if one or more eigenvalues are known via embedding or by its alternant or symmetry characteristics (2, 3). The method presented in this paper expands the scope of those previously published (4–6).

All the eigenvalues of a graph are collectively called the spectrum of the graph. If the eigenvalues of a smaller graph are contained among the eigenvalues of a larger graph, then the smaller graph is said to be subspectral to the larger one (3). This paper will show how to identify subspectral components by a process called embedding. Embedding along with the above equations allows one to quickly determine the Hückel MO energy levels of many molecules without the aid of a computer.

Throughout this paper only the σ-bond graph will be drawn where the carbon and hydrogen atoms and the C—H and p π bonds are omitted (1). A graph edge (line) and σ bond are synonymous, and a vertex (point) is equivalent to a carbon atom (carbon vertex). A primary carbon has a degree of one, a secondary carbon has a degree of two, and a tertiary carbon has a degree of three. Both benzene and cyclohexane have the same σ-bond molecular graph which is a hexagon that consists of only second degree vertices joined by $e(2,2)$-type edges. In this paper a 3(2)-valent polycyclic graph, denoted as a 3(2)-polycyclic graph, is a polycyclic molecular σ-bond graph consisting of only degree-2 and degree-3 carbon vertices with no internal second degree vertices, i.e., a polycyclic graph containing third degree vertices with some second degree vertices on its outer boundary that can be contracted to give a simple 3-polycyclic graph which is 3-connected and 3-valent.

Results and discussion

Identifying select eigenvalues in alternant hydrocarbons through embedding

In a series of papers, Hall provided the basis for recognition of the HMO eigenvalues of $\epsilon = \pm 1.0$ and $\pm 2.0\beta$ by inspection of the molecular topology of alternant hydrocarbons (7). His rules derive immediately from the eigenvector equations themselves and were translated into descriptive form called embedding that will now be reviewed (8). To repetitively embed a fragment into a molecule the following rules must be followed: (1) all atoms connected directly to the fragment must be nodes; (2) on the other side of each of these nodes will be the repetition of the fragment with the opposite sign; and (3) other branches at these nodes will also be nodes since at all nodes the sum of nearest neighbor fragments must be zero in regard to their signs (8). Ethene, allyl, butadiene, and benzene are the most common fragments embedded in benzenoid hydrocarbons. All nodes are designated in the figures by open circles.

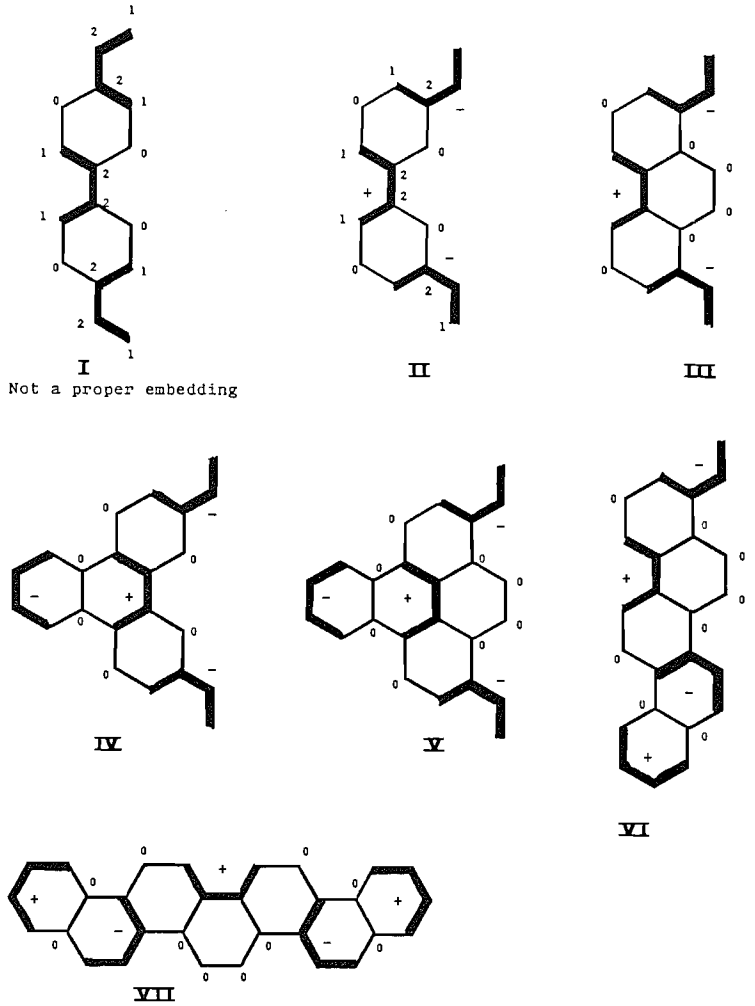

FIG. 1. 1,3-Butadiene embedding of 3,3′-divinylbiphenyl and related structures.

A number of aspects associated with embedding are illustrated by the structures presented in Fig. 1. Structure **I** illustrates an improper embedding of 1,3-butadiene fragments where corresponding fragment positions through the node positions do not match whereas those in structure **II** do. Since structures **II** to **VII** are embeddable by butadiene fragments, they all have eigenvalues of $\epsilon = \pm(\sqrt{5} + 1)/2$ and $\pm(\sqrt{5} - 1)/2$; butadiene is subspectral to **II** to **VII**. Molecule **II**, 3,3′-divinylylbiphenyl, is the principal structure from which the others can be derived. Placement of a heteroatom or polyene substituent at a node position in **II** does not change the butadiene embedding in the molecule thus obtained. Therefore **III** has the same butadiene embedding as **II**, and **V** has the same embedding pattern as **IV**. Structure **IV** was constructed from **II** by connecting a butadiene fragment through nodes onto nonnode positions of **II**. Similarly, **V** and **VI** were constructed from **III**, and **VII** was constructed from **VI** by this same process. In these constructions, the butadiene fragments were added on in such a manner as to always have corresponding butadiene positions match up through the new node positions.

Figure 2 presents a number of structures embedded by allyl that can be constructed from styrene or *m*-quinodimethane, and Fig. 3 illustrates benzene embedding of pentaphene-related structures produced by a similar construction. Mixed embedding with more than one type of substructure without common eigenvalues is not allowed. Embedding is a sufficient but not a necessary requirement for the presence of a set of eigenvalues. For example, 1,2-diethenylcyclobutadiene has $\epsilon = \pm 1.0\beta$ but cannot be embedded by ethene. The embedding of fragments other than methyl, ethene, or benzene must be done so as to always have corresponding fragment positions align through each node position. This requirement makes mixed embedding less *a priori* predictable and embedding of more complicated fragments increasingly more difficult. The construction process shown in Figs. 1 to 3 has features making it similar to Dixon's construction method which appears to be equivalent to retro-embedding (9). Since both benzene and trivinylmethyl radical have the same eigenvalues of $\epsilon = \pm 1, \pm 1$, and $\pm 2\beta$, Dixon showed that the following structure could be constructed from one benzene, two methyl, and two trivinylmethyl fragments where the methyl fragments become node positions (9, 10).

$\epsilon = \pm 1, \pm 1$, and $\pm 2\beta$

Since benzene can be embedded by ethene and naphthalene by butadiene, it should be noted that every benzenoid in Fig. 3 can be embedded by ethene and in Fig. 4 by butadiene. These observations suggest that whenever a benzenoid can be embed-

Can. J. Chem. Downloaded from www.nrcresearchpress.com by 80.58.250.72 on 09/07/12
For personal use only.

Can. J. Chem. Downloaded from www.nrcresearchpress.com by 80.58.250.72 on 09/07/12
For personal use only.

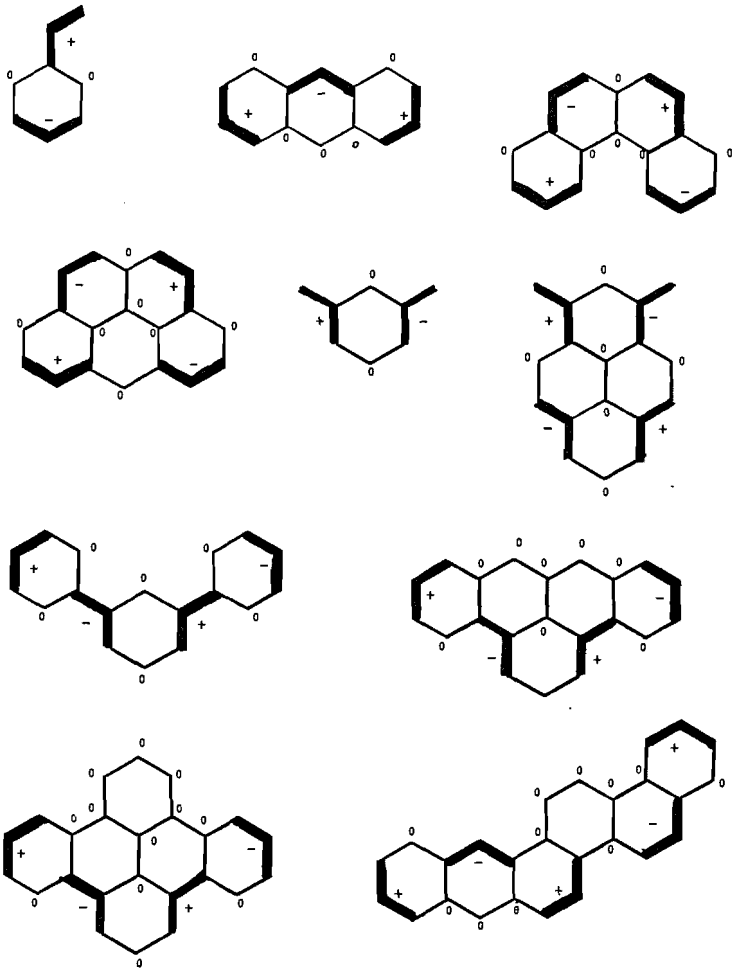

FIG. 2. Representative allyl embedding where all the above structures have eigenvalues of $\pm \sqrt{2}\beta$.

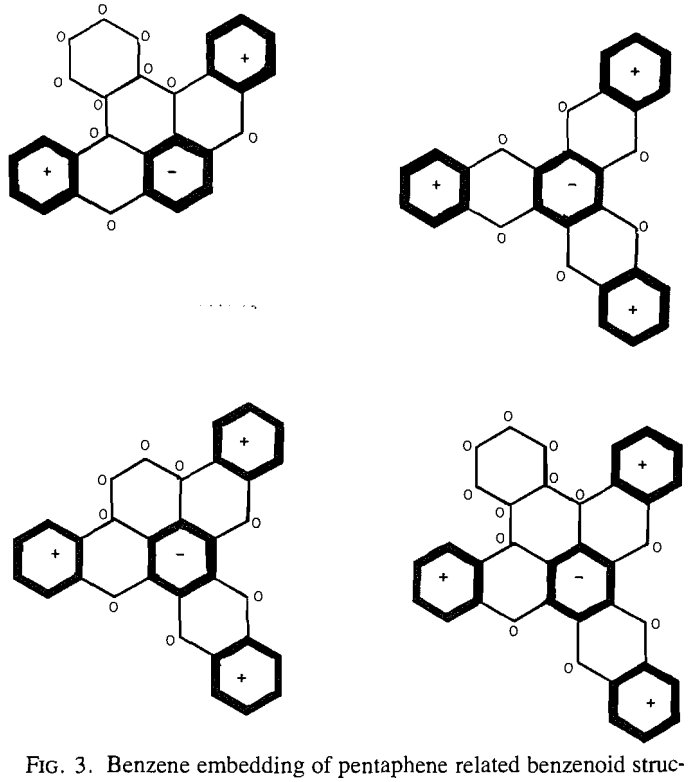

FIG. 3. Benzene embedding of pentaphene related benzenoid structures which have eigenvalues of ± 1, ± 1, and $\pm 2\beta$.

ded by ethene or butadiene, one should check to see if it can be embedded by the larger benzene or naphthalene substructures, respectively.

Examples of naphthalene embedding are presented in Fig. 4. Both ovalene and tetrabenzo[*a*,*c*,*h*,*j*]anthracene can be embedded by phenanthrene, and both these molecules have phenanthrene as a mirror plane fragment. The following benzenoid hydrocarbon has no mirror plane benzenoid fragments but can be embedded by phenanthrene as shown and therefore has the eigenvalues of phenanthrene in its spectrum.

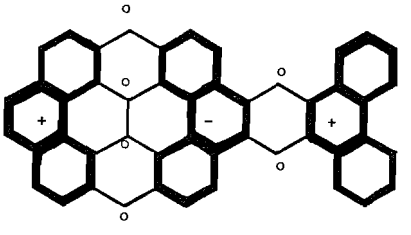

Characteristic polynomials of small molecular graphs with one heteroatom

If one wishes to compute the characteristic polynomial of a small molecular graph possessing one heteroatom utilizing eq. [1] and eq. [2], the following relationship presented here for the first time will be needed

$$[3]\quad P(G_x; X) = XP(G_x - \nu_x; X) - hP(G_x - \nu_x; X) - k^2[XP(G_x - \nu_x; X) - P(G; X)]$$

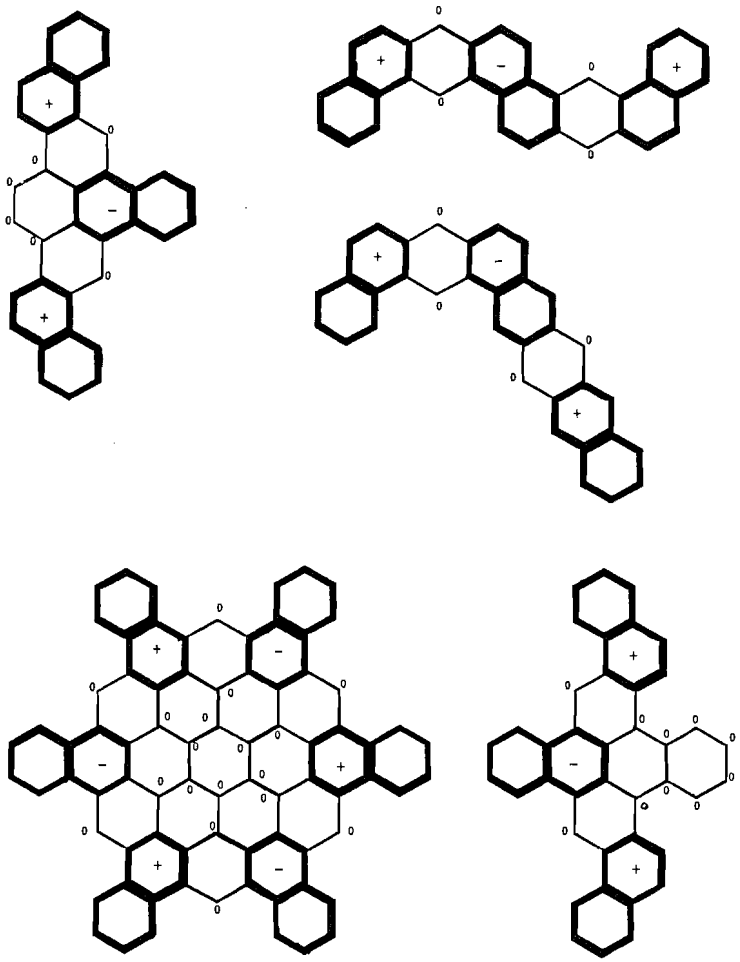

FIG. 4. Benzenoid hydrocarbons that have naphthalene eigenvalues.

where G_x is the graph containing the heteroatom, G is its isoconjugate graph, $G_x - \nu_x$ is the graph obtained upon deletion of the heteroatom vertex with its adjacent edges, h comes from $\alpha_x = \alpha_c + h\beta$, k comes from $\beta_{cx} = k\beta_{cc}$, and $X = (E - \alpha)/\beta$. Equation [3] is valid for both the acyclic and characteristic polynomials. The application of eq. [3] will be illustrated with the molecular graphs in Fig. 5. Computation of the HMO characteristic polynomial for the pyridine-like structure **3** is equivalent to the graph theoretical determination of the charcteristic polynomial of the following edge/vertex weighted molecular graph.

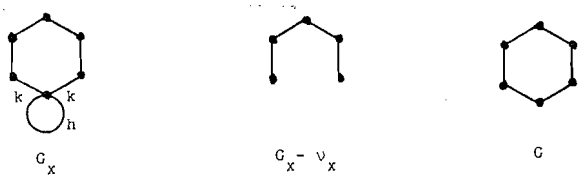

The characteristic polynomial of both $G_x - \nu_x$ and G can be easily computed using eq. [1] and eq. [2] giving

$$P(G_x - \nu_x; X) = X^5 - 4X^3 + 3X$$

$$P(G; X) = X^6 - 6X^4 + 9X^2 - 4$$

which when combined according to eq. [3] gives

$$P(G_x; X) = (X^6 - 4X^4 + 3X^2) - h(X^5 - 4X^3 + 3X) - k^2(2X^4 - 6X^2 + 4)$$

Note that if $h = 0$ and $k = 1$, this latter equation gives $P(C_6H_6;X) = X_6 - 6X^4 + 9X^2 - 4$ which is the characteristic polynomial for benzene. Computation of the characteristic polynomial of the quinoline-like structure **4** is achieved as follows.

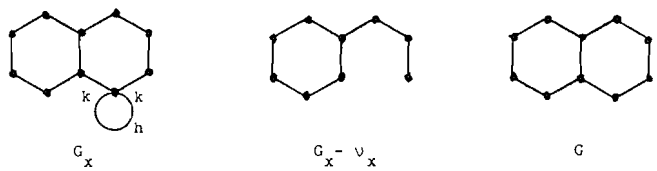

From eq. [1] and eq. [2] and ethene embedding of $G_x - \nu_x$ and G, it is determined that

$$P(G_x - \nu_x; X) = X^9 - 9X^7 + 26X^5 - 29X^3 + 11X$$

$$P(G; X) = X^{10} - 11X^8 + 41X^6 - 65X^4 + 43X^2 - 9$$

where when combined per eq. [3] gives

$$P(G_x; X) = (X^{10} - 9X^8 + 26X^6 - 29X^4 + 11X^2) - h(X^9 - 9X^7 + 26X^5 - 29X^3 + 11X) - k^2(2X^8 - 15X^6 + 36X^4 - 32X^2 + 9).$$

The $G_x - \nu_x$ subgraph of the isoquinoline-like structure **5** can be embedded by allyl fragments as shown by the following.

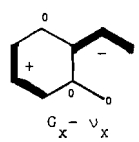

Can. J. Chem. Downloaded from www.nrcresearchpress.com by 80.58.250.72 on 09/07/12
For personal use only.

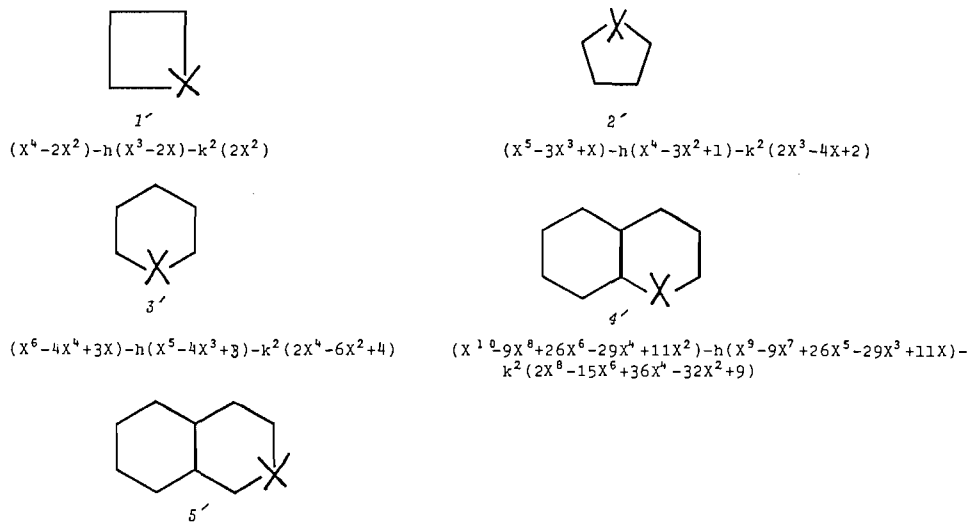

FIG. 5. The HMO characteristic polynomials for several heterocyclic molecular graphs where $\alpha_x = \alpha_c + h\beta$, $\beta_{cx} = k\beta_{cc}$, and $X = (E - \alpha)/\beta$.

Thus from eq. [1] and eq. [2], we get

$$P(G_x - \nu_x; X) = X^9 - 9X^7 + 25X^5 - 26X^3 + 8X$$

which, when combined with eq. [3], gives

$$P(G_x; X) = (X^{10} - 9X^8 + 25X^6 - 26X^4 + 8X^2) - h(X^9 - 9X^7 + 25X^5 - 26X^3 + 8X) - k^2(2X^8 - 16X^6 + 39X^4 - 35X^2 + 9)$$

From these examples, it is evident that a weighted graph vertex makes no contribution to the even terms of a characteristic polynomial. Since in a set of Sach's graphs a weighted vertex (h) in G_x excludes a K_2 component from the same two edge sites as excluded when the number of non-edge-weighted K_2 and C_n combinations are counted in $G_x - \nu_x$, then the combinatorial possibilities for both cases become identical and, therefore, the two associated polynomial parts will have the same set of coefficients. This observation is key to the formulation of eq. [3] which represents a distinct improvement over the recursive pair of equations used by Trinajstić where the latter are valid only for acyclic polynomial computations (11).

Characteristic polynomials of small molecular graphs with multiple heteroatoms

Successive use of eq. [3] on molecular graphs possessing multiple heteroatoms will be illustrated. Consider the pyrazine-like structure G_{xx} and its subgraphs.

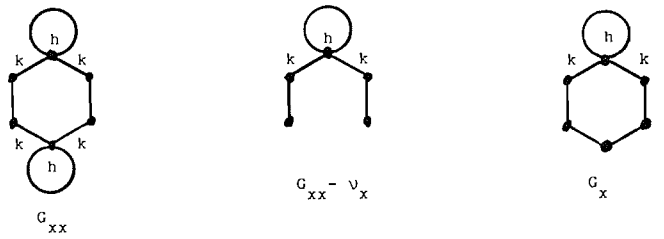

To compute $P(G_{xx}; X)$ using eq. [3], one needs to know $P(G_{xx} - \nu_x; X)$ and $P(G_x; X)$ which are obtained per the method outlined above for molecular graphs containing a single heteroatom. Thus,

$$P(G_{xx} - \nu_x; X) = (X^5 - 2X^3 + X) - h(X^4 - 2X^2 + 1) - k^2(2X^3 - 2X)$$

$$P(G_x; X) = (X^6 - 4X^4 + 3X^2) - h(X^5 - 4X^3 + 3X) - k^2(2X^4 - 6X^2 + 4)$$

Incorporation of these latter quanties into eq. [3] leads to

$$P(G_{xx}; X) = [(X^6 - 2X^4 + X^2) - h(X^5 - 2X^3 + X) - k^2(2X^4 - 2X^2)] - h[(X^5 - 2X^3 + X) - h(X^4 - 2X^2 + 1) - k^2(2X^3 - 2X)] - k^2[(2X^4 - 2X^2) - h(2X^3 - 2X) - k^2(4X^2 - 4)]$$

For $h = 1$ and $k = 1$, this latter equation becomes

$$P(G_{xx}; X) = X^6 - 2X^5 - 5X^4 + 8X^3 + 7X^2 - 6X - 3$$

having eigenvalues of $\epsilon = \pm\sqrt{3}, \pm 1, 1 - \sqrt{2}$ and $1 + \sqrt{2}\beta$. Although the weighted vertices in this example both had the same values of h and k, this method is still valid for molecular graphs having multiple heteroatoms with different values for h and k. Successive use of eq. [3] per this procedure will yield the characteristic polynomial of molecular graphs having multiple heteroatoms of different kinds.

These results lead us to the conclusion that if embedding of a fragment can be accomplished on a molecular graph such that all the heteroatoms are located at node positions, then the eigenvalues of the fragment will also be eigenvalues of the heteroatom containing molecular graph. Consider anthracene which can be embedded by allyl, benzene, and ethene substructures giving it eigenvalues of $\epsilon = \pm 1, \pm 1, \pm\sqrt{2}$, and $\pm 2\beta$; if a carbon atom is substituted by a heteroatom at position 9, then these eigenvalues remain unchanged while the others change (Fig. 6). If a carbon atom at position 1 in anthracene is substituted by a heteroatom, then the resulting stucture can be embedded only by allyl and ethene substructures where the heteroatom is located at a node position giving eigenvalues of $\epsilon = \pm 1$ and $\pm\sqrt{2}\beta$. If a heteroatom is located at position 2 in the anthracene skeleton, then the resulting structure can only be embedded by ethene where the heteroatom is located at a node position giving $\epsilon = \pm 1\beta$.

From eq. [3] it is apparent that the two kinds of roots exist for vertex-edge weighted graphs. The roots of the first kind are those that remain unchanged regardless of the values of h and k, whereas roots of the second kind depend on the values of h and k. The greatest common divisor of polynomials $P(G_x - \nu_x; X)$ and $P(G; X)$ is a polynomial, $R_f(X)$, composed of all the roots of the first kind. This latter polynomial is the last nonzero

Can. J. Chem. Downloaded from www.nrcresearchpress.com by 80.58.250.72 on 09/07/12
For personal use only.

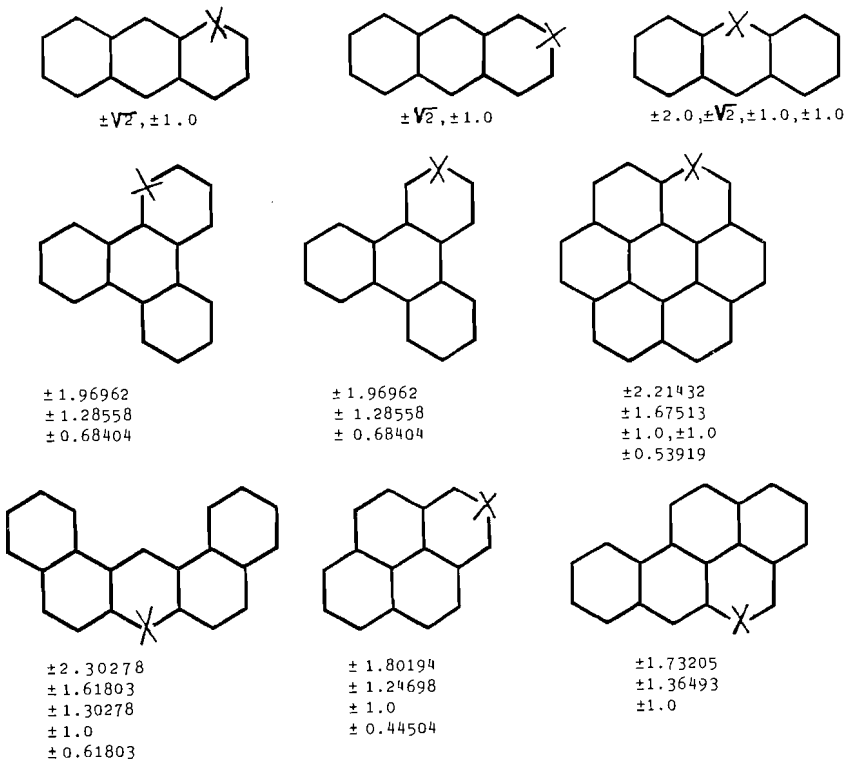

FIG. 6. Eigenvalues for representative heterocyclic molecular graphs.

remainder $R_l(X)$ obtained after l iterations of the Euclidean division algorithm. Figure 6 presents some representative molecular graphs with a single heteroatom along with their roots of the first kind; many of these roots can be obtained via embedding. Coronene has 1,4-diethenylbenzene as a mirror plane fragment and is doubly degenerate in the eigenvalues of this fragment because of its three-fold summetry. Taking the appropriate linear combination of these molecular orbitals one can obtain a node at position 1 in coronene, and thus the vertex–edge weighted graph shown in Fig. 6 will have the eigenvalues of 1,4-diethenylbenzene regardless of the values assigned to the parameters of h and k in eq. [3].

Conclusion

The nearly universal expression for a_6 derives quite naturally from our a_6 (PAH6) expression previously published (1). Since 2-dimensional 3(2)-polyhexagonal structures represent a fundamental type of structure of nature that results in minimization of energy, the ramification of our topological studies of this structural class should find applicability beyond benzenoid hydrocarbons.

Embedding is possible on molecules with a high to low degree of symmetry. Placement of heteroatoms or polyene substituents at node positions of an embedded molecular graph does not alter its associated eigenvalues. Use of the equations presented in this paper allows one to determine the characteristic polynomial of many small molecules without having to solve a secular determinant.

The study of molecular topology in-itself and by-itself is a worthwhile endeavor. In this study we have found that the ultimate graphical invariants of q, N_c, r, $e(i,j)$, and d_i can be interrelated to transmit information regarding other properties such as a_4 and a_6. Embedding is shown to be invariant with the node positions possessing special properties. Determination of select eigenvalues by embedding is applicable to both Hückel and extended Hückel molecular orbital models. Symmetrical polyene molecules having a mirror plane bisecting only vertices can be embedded by the mirror fragment where the vertices on the mirror plane become nodes. Less symmetrical alternant polyene molecules can frequently be embedded by smaller fragments. Embedding combined with equations for a_4 and a_6 provides a powerful method for computing the characteristic polynomial of many small polyene molecules. These calculations are easily performed by a novice without a computer.

Acknowledgement

The author wishes to thank Professor Ivan Gutman for bringing to his attention ref. 12 which deals with the relationship of $P(G_x; X) = P(G; X) - hP(G_x - \nu_x; X)$ that is a less comprehensive form of eq. [3].

1. J. R. DIAS. Theoret. Chim. Acta, **68**, 107 (1985); Acc. Chem. Res. **18**, 241 (1985).
2. J. V. KNOP, K. SZYMANSKI, G. JASHARI, and N. TRINAJSTIC'. Croat. Chem. Acta, **56**, 443 (1983); B. DZONOVA-JERMAN-BLAZIC and N. TRINAJSTIC'. Comput. Chem. **6**, 121 (1982).
3. S. S. D'AMATO, B. M. GIMARC, and N. TRINAJSTIC'. Croat. Chem. Acta, **54**, 1 (1981).
4. M. RANDIC'. J. Comput. Chem. **3**, 421 (1982).
5. K. BALASUBRAMANIAN. J. Comput. Chem. **5**, 387 (1984).
6. Y. KIANG and A. TANG. Int. J. Quantum Chem. **29**, 229 (1986).
7. G. G. HALL. Trans. Faraday Soc. **53**, 573 (1957); Mol. Phys. **33**, 551 (1977).
8. G. G. HALL. Bull. Inst. Math. Appl. **17**, 70 (1981).
9. W. DIXON. Faraday Trans. 2, **72**, 282 (1976).
10. I. GUTMAN and J. KRUSZEWSKI. Nouv. J. Chim. **9**, 669 (1985).
11. N. TRINAJSTIC'. Croat. Chem. Acta, **49**, 593 (1977); Chemical graph theory. CRC Press, Boca Raton, FL. 1983.
12. I. GUTMAN. Bull. Soc. Beograd, **49**, 157 (1984); R. DAUDEL, R. LEFEBVRE, and C. MOSHER. Quantum chemistry Interscience Publishers Inc., NY. 1959. pp. 539–546.

Can. J. Chem. Downloaded from www.nrcresearchpress.com by 80.58.250.72 on 09/07/12
For personal use only.

The direct electrochemical synthesis of some transition metal carboxylates

N. KUMAR, DENNIS G. TUCK, AND KATHERINE D. WATSON
Department of Chemistry and Biochemistry, University of Windsor, Windsor, Ont., Canada N9B 3P4

Received July 14, 1986

N. KUMAR, DENNIS G. TUCK, and KATHERINE D. WATSON. Can. J. Chem. **65**, 740 (1987).

The transition metal carboxylates $M(O_2CR)_n$ (M = Cr, R = C_2H_5, C_6H_5, n = 3; M = Mn, Fe, Ni, R = CH_3, C_2H_5, C_6H_5, n-C_7H_{15}, n = 2, not all combinations) have been prepared by oxidising suitable metal anodes electrochemically in solutions of RCOOH in acetonitrile. With Co and Cu, a wide range of carboxylic acids (R = C_2H_5, c-C_3H_5, c-C_5H_9, C_6H_5, n-C_4H_9, n-C_7H_{15}, 2-ethylhexanoic, oleic, linoleic) has been used successfully to give $M(O_2CR)_2$. The advantages of the method are discussed. The preparation of $Cu(O_2CR)_2$ involves the prior formation of CuO_2CR at the anode, followed by oxidation by the solvent.

N. KUMAR, DENNIS G. TUCK et KATHERINE D. WATSON. Can. J. Chem. **65**, 740 (1987).

On a préparé les carboxylates des métaux de transition $M(O_2CR)_n$ (M = Cr, R = C_2H_5, C_6H_5, n = 3; M = Mn, Fe, Ni, R = CH_3, C_2H_5, C_6H_5, n-C_7H_{15}, n = 2; toutefois, toutes les combinaisons n'ont pas été préparées) en oxydant électrochimiquement des anodes métalliques appropriées dans des solutions de RCOOH dans l'acétonitrile. Avec le Co et le Cu, on a utilisé avec succès un grand nombre d'acides carboxyliques (R = C_2H_5, c-C_3H_5, c-C_5H_9, C_6H_5, n-C_4H_9, n-C_7H_{15}, éthyl-2 hexanoïque, oléique et linoléique) pour préparer des dérivés $M(O_2CR)_2$. On discute des avantages de la méthode. La préparation des composés $Cu(O_2CR)_2$ implique la formation préalable de CuO_2CR à l'anode qui est suivie d'une oxydation par le solvant.

[Traduit par la revue]

Introduction

Previous papers from this laboratory have described the synthesis of metallic derivatives of weak acids by the oxidation of a sacrificial anode in a non-aqueous solution of the acid. Typical examples include neutral and anionic derivatives of alkyl and aryl thiolates (1–3), thiocyanates (4), phenylacetylene (5), and β-diketonates (6, 7). An obvious extension of these studies to include derivatives of carboxylic acids has now been carried out, and we show below that a variety of transition metal salts are easily prepared from the parent element. We have also used two metals, cobalt and copper, in studies of the synthesis of salts of acids with both cyclic and long chain groups. As emphasized below, the electrochemical method offers distinct advantages in the latter systems in particular, since conventional methods do not easily yield clean products.

Experimental

General

Acetone was dried by refluxing over anhydrous magnesium sulphate, and was stored over this reagent. Acetonitrile was refluxed over calcium hydride and stored over molecular sieves. Carboxylic acids were used as supplied (Aldrich). All metals were used as foils, usually 0.1–1.0 mm thick.

Products were characterised by metal analysis (atomic absorption spectrophotometry), by infrared spectroscopy, and in some cases by molecular weight, determined by mass spectrometry using a Varian MAT CH-5DF instrument operating in the field desorption mode. Elemental analysis (C, H) on selected compounds was by Guelph Chemical Co. Ltd.

Electrochemical

The electrochemical preparation followed essentially the same procedure in each case, with the metal forming the anode of a simple cell

$$Pt_{(-)}/CH_3CN + RCOOH/M_{(+)}$$

Acetone replaced acetonitrile in a number of cases. The solution composition and electrochemical conditions are shown in Table 1.

Product isolation

(*i*) Propionates. The propionates of all the metals used were soluble in the electrolyte solution, and the mixture was therefore filtered at the end of the experiment to remove the metallic particles which occasionally broke away from the anode, and the solvent removed at 60°C *in vacuo*. This procedure yielded solids which were collected, washed with diethyl ether, and dried at 110°C. These products, as others produced in this work, were characterised by metal analysis, and by infrared spectroscopy which confirmed the presence of the RCOO ligand. Results are given in Table 2.

In the case of cobalt and chromium propionates, removal of solvent precipitated an oil which was collected and triturated with acetone to give solid $Co(O_2CEt)_2 \cdot H_2O$ (**1**) and $Cr(O_2CEt)_3 \cdot 2H_2O$ (**2**), respectively (*Anal.* calcd. for **1**: Co 26.4, C 32.3, H 5.4; found: Co 25.6, C 32.5, H 5.3. *Anal.* calcd. for **2**: Cr 16.9, C 34.3, H 6.2; found: Cr 17.2, C 35.2, H 6.6). The cobalt compound lost H_2O on heating (80°C, 15 h, 15 mm pressure) to give $Co(O_2CEt)_2$, changing color from red–violet to deep violet in the process. Extended heating of **2** did not remove water, and the solid was therefore dissolved in benzene and reprecipitated by the addition of petroleum ether (35–60°C) to give $Cr(O_2CEt)_3$ as a green solid, which was washed with petroleum ether and dried *in vacuo*.

(*ii*) Benzoates. Chromium(III) and cobalt(II) benzoates precipitated in the cell and were collected, washed, and dried in the manner just described.

(*iii*) Octanoates. All but one of the metal derivatives of $C_8H_{17}COOH$ precipitated during the electrolysis and were subsequently collected, washed with acetonitrile, and dried *in vacuo* for 3–4 h at room temperature. The copper(II) derivative is soluble in the reaction mixture, but was thrown down as a blue solid when the volume of the solution was reduced by 50% *in vacuo*.

(*iv*) Cobalt(II) salts. Most of the cobalt(II) carboxylates precipitated directly during the electrochemical oxidation in either acetone or acetonitrile media (see Table 1*b*). The exceptions were the *o*-toluate, where the addition of acetonitrile was needed to precipitate the salt, and 2-ethylhexanoate, for which the addition of diethyl ether, or removal of solvent *in vacuo*, lead to the formation of solid. The cobalt compounds are all pink–red, free-flowing powders, and are generally air-stable, although the benzoate and 2-ethylhexanoate compounds are slightly hygroscopic.

(*v*) Copper(II) salts. The electrochemical oxidation of copper was carried out in acetone solutions of carboxylic acids (see Table 1*c*) producing in each case a blue solution. The solution was removed from the cell, and solvent partially evaporated *in vacuo*; with cyclopropanoic or oleic acids the blue copper(II) salt precipitated at this stage. For the remainder, evaporation was taken to dryness, and the copper salt dissolved in diethyl ether, leaving behind Et_4NClO_4. The ether extract was itself taken to dryness, and the salt recrystallised from solvents

Can. J. Chem. Downloaded from www.nrcresearchpress.com by 78.46.186.204 on 09/07/12
For personal use only.

TABLE 1. Experimental conditions for the direct electrochemical synthesis

(*a*) carboxylates of Cr, Mn, Fe, and Ni

Metal	R in RCOOH	Mass[a] RCOOH (g)	Initial voltage (V)[b]	Time of electrolysis (h)	Metal dissolved (mg)	Product[c]	Yield[d] (%)
Cr	C_2H_5	2	23	4.3	80	$CrL_3 \cdot 2H_2O$	68
	C_6H_5	1	26	3	76	CrL_3	67
Mn	CH_3	2	50	4.5	150	MnL_2	95
	C_2H_5	1.5	40	6.5	220	MnL_2	85
	C_6H_5	1	28	3	140	MnL_2	45
	n-C_7H_{15}	2	30	3.8	130	MnL_2	70
Fe	C_2H_5	2	24	4	110	FeL_2	[e]
	n-C_7H_{15}	2	40	4	110	FeL_2	88
Ni	C_2H_5	2	40	5	196	NiL_2	87
	n-C_7H_{15}	2	30	4	115	NiL_2	98

[a]In 50 mL CH_3CN containing 40 mg Et_4NClO_4.
[b]Voltage required to produce an initial current of 30 mA.
[c]L = $RCOO^-$.
[d]Based on metal dissolved.
[e]Not recorded.

(*b*) Cobalt(II) carboxylates

R in RCOOH	Mass RCOOH (g)[a]	Initial voltage (V)[b]	Time of electrolysis (h)	Metal dissolved (mg)
C_2H_5	2[c]	16[d]	5	210
c-C_3H_5	0.1	44	2	44
c-C_4H_9	0.1	26	1	22
C_6H_5	0.15	12	2	42
o-$CH_3C_6H_4$	0.44	40	4.5	126
n-C_4H_9	0.1	30	1.7	38
n-C_7H_{15}	2.0[c]	32[e]	2	61
$CH_3(CH_2)_3CH(C_2H_5)$ (2-ethylhexanoic)	0.1	46	3.5	76
$CH_3(CH_2)_7CH{=}CH(CH_2)_7$ (oleic)	0.1	36	0.75	17
$CH_3(CH_2)_4CH{=}CHCH_2CH{=}CH(CH_2)_7$ linoleic)	0.1	25	0.75	18

[a]In 50 mL acetone containing 40 mg Et_4NClO_4.
[b]Voltage required to produce an initial current of 20 mA.
[c]Current 40 mA.
[d]Current 30 mA.

(*c*) Copper(II) carboxylates

R in RCOOH	Mass RCOOH (g)[a]	Initial voltage (V)[b]	Time of electrolysis (h)	Metal dissolved (mg)
C_2H_5	2.0[c]	45[d]	3.5	130
c-C_3H_5	0.1	20	1.25	52
c-C_4H_9	1.0	22	1.4	58
C_6H_5	0.15	10	5	171
o-$CH_3C_6H_4$	0.07	30	1.25	53
n-C_4H_9	1.0	12	2	69
n-C_7H_{15}	2.0[c]	50[e]	5	135
2-Ethylhexanoic	0.1	18	1.9	82
Oleic	1.0	24	1.2	44
Linoleic	0.1	20	2	87

[a]In 50 mL acetone containing 40 mg Et_4NClO_4.
[b]Voltage required to produce an initial current of 20 mA.
[c]Acetonitrile used as solvent.
[d]Current 30 mA.
[e]Current 25 mA.

Can. J. Chem. Downloaded from www.nrcresearchpress.com by 78.46.186.204 on 09/07/12
For personal use only.

TABLE 2. Analytical results for transition metal carboxylates, ML_n (L = $RCOO^-$) (found/calcd values)

R in RCOOH	CrL_3	MnL_2	FeL_2	CoL_2	NiL_2	CuL_2
C_2H_5	19.4(19.2)	27.2(27.3)	27.1(27.7)	28.5(28.8)	29.4(28.7)[a]	29.8(30.3)[b]
c-C_3H_5				25.4(25.7)		27.7(27.2)[c,e]
c-C_5H_9				21.3(20.7)		21.4(21.9)[e]
C_6H_5	12.7(12.5)	19.3(18.5)		19.6(19.6)		20.3(20.8)
o-$CH_3C_6H_4$				18.3(17.9)		18.7(19.0)[e]
n-C_4H_9				22.1(22.6)		24.4(23.9)
n-C_7H_{15}			16.8(16.3)	17.4(17.1)	17.4(17.2)	17.7(18.2)
2-Ethylhexanoic				16.1(17.1)		18.3(18.2)[e]
Oleic				10.0(9.5)		10.7(10.1)[d]
Linoleic				9.3(9.5)		10.9(10.2)

[a]C 35.1 (34.3), H 4.9 (5.9).
[b]C 34.6 (34.3), H 5.2 (4.8).
[c]C 41.5 (41.1), H 4.5 (4.3).
[d]C 67.9 (69.0), 10.7 (10.6).
[e]Prominant molecular ion of calculated m/e observed in mass spectrum.

such as ethanol (R = C_6H_5), diethyl ether + acetone (2-ethylhexanoic, linoleic), diethyl ether + petroleum ether (c-C_5H_9), or diethyl ether + CH_3CN + petroleum ether (n-C_4H_9). The products were all air-stable, light blue powders. The results of studies of the mechanism of the formation of copper(II) salts are discussed below.

The electrochemical synthesis of copper(II) carboxylates can also be carried out in acetonitrile, but the significant deposition of copper metal on the cathode is a major problem.

Hydrogen formation

The production of H_2 (g) at the cathode was monitored directly by mounting a gas burette, total volume 10 mm, directly above the platinum cathode, which in these experiments was fused through the bottom of the cell. Visual observation confirmed that all the gas formed at the cathode was collected by virtue of the widened mouth of the burette. The results of these measurements are discussed below.

Results and discussion

General

The preparative studies show that the technique of direct electrochemical oxidation is a convenient and simple route to a variety of transition metal carboxylates. The results include the salts of both short- and long-chain carboxylic acids and of benzoic acid for the range chromium–copper, and an extended series of acids for cobalt and copper, including the C_{17}-chain oleic and linoleic acid. In view of the range of compounds prepared under a wide variety of conditions, it seems reasonable to suggest that the method is a general one for the synthesis of metal carboxylates.

The methods generally recommended for preparing metal carboxylates of (say) copper are based on dissolving the metal hydroxide or carbonate in an aqueous solution of the appropriate carboxylic acid. Crystallisation may yield either anhydrous or hydrated materials (8). For the higher molecular weight acids, which are relatively insoluble in water, mixing alcoholic solutions of the acetate and RCOOH leads to precipitation of $Cu(O_2CR)_2$. For the high molecular weight metal carboxylates which find use as driers in the paint industry, or as co-catalysts in polymerisation, reactions involving aqueous solutions of $Na^+ \cdot RCOO^-$ and a soluble metal mineral salt give a better commercial product that is obtained by fusing a metal salt with the parent carboxylic acid (9). The present method appears to offer substantial advantages, both in simplicity of experiment and in purity of product, over the techniques otherwise available, and we have shown that the electrochemical method is readily adapted to continuous production if so desired.

Electrochemical efficiency

Following our standard procedure, we have measured the electrochemical efficiency, defined as the number of moles of metal dissolved per Faraday of electricity, using cells with a constant current of 20 mA and weighed anodes. For reactions leading to the M^{II} derivatives of Mn, Fe, and Ni, $E_F = 0.51 \pm 0.03$ mol F^{-1} (10 systems), and for the ten Co^{II} compounds listed in Table 1*b*, $E_F = 0.49 \pm 0.01$ mol F^{-1}. The results for copper compounds are discussed below.

The evolution of H_2(g) was measured for a series of solvents, taking the Co/*o*-toluic acid system as a standard, and using $E_F = 0.5$ mol F^{-1} for anionic dissolution as an internal measure of total charge. With both *N*,*N*-dimethylformamide and acetone, the production of H_2, corrected for temperature, atmospheric pressure, and solvent vapor pressure, gave $E_F(H_2) = 0.5$ mol F^{-1} as expected. With acetonitrile, the initial (theoretical) value dropped with time of electrolysis, suggesting some reduction of CH_3CN (cf. ref. 10 for the aqueous phase reduction of CH_3CN). Gas production was much below theoretical with *N*-methyl pyrrolidinone, and was close to zero with nitromethane and propylene carbonate, all of which are readily reduced electrochemically.

The combination of these E_F determinations confirms the mechanism proposed for other weak acid systems in non-reducible solvents, namely

[1] cathode: $n\text{RCOOH} + ne \rightarrow \frac{n}{2}\text{H}_2(\text{g}) + n\text{RCOO}^-$

[2] anode: $n\text{RCOO}^- + \text{M} \rightarrow \text{M}(\text{O}_2\text{CR})_n + ne$

One preparative advantage which follows from these results is that a precise relationship exists between total current and quantity of product.

Copper carboxylates

The behaviour of Cu/RCOOH systems has been investigated in some detail because of two significant differences from those discussed so far. The most obvious factor is that although the final products were always $Cu(O_2CR)_2$, E_F was not 0.5 mol F^{-1}; in acetonitrile, $E_F = 1.02 \pm 0.02$ for eight different acids, while for the same acids in acetone the average value was 0.85 ± 0.08 F^{-1}, within a range of 0.72 (R = n-C_4H_9) and 0.93 (2-ethylhexanoic). In addition, we observed that the reaction developed a blue color as soon as current began to flow, that copper deposited as the cathode after about 15 min, and that small

Can. J. Chem. Downloaded from www.nrcresearchpress.com by 78.46.186.204 on 09/07/12
For personal use only.

quantities of a yellow solid precipitated on the anode and subsequently fell to the bottom of the cell. The only systems for which a copper(I) product was isolated were with *c*-C_3H_5COOH and *c*-C_5H_9COOH in acetone, where small quantities of white solid (approximately 40 mg) were recovered.

In the case of *o*-toluic acid in acetone, we showed that the yellow substance is Cu_2O (calcd.: Cu 88.8, found: 79.0) mixed with RCOOH (infrared spectroscopy). Bubbling oxygen gas through the solution inhibited the formation of this yellow substance, while the addition of 1 mL of water increased both the rate of formation and the quantity produced. These observations are consistent with the properties of Cu_2O, which is known to be formed by the hydrolysis of copper(I) carboxylates and is readily oxidised to copper(II) by oxygen. The presence of traces of H_2O in the acetone, which is notoriously difficult to dry completely, may be responsible for the formation of Cu_2O in the present experiments. When appropriate allowance is made for the production of Cu_2O, the electrochemical efficiency for the dissolution of copper is close to 1.0 mol F^{-1}.

It is clear that in both acetone and acetonitrile, the sequence of electrode reactions is

[3] cathode: $RCOOH + e \rightarrow RCOO^- + (1/2)H_2(g)$

[4] anode: $RCOO^- + Cu \rightarrow Cu(OOCR) + e$

but that eq. [4] must be followed by an electroless process to produce $Cu(O_2CR)_2$. Since hydrogen formation was not observed in the bulk solution phase, the process

[5] $Cu(O_2CR) + RCOOH \rightarrow Cu(O_2CR)_2 + (1/2)H_2$

or the equivalent sequence beginning with disproportionation

[6] $2\,Cu(O_2CR) \rightarrow Cu(O_2CR)_2 + Cu$

[7] $Cu + RCOOH \rightarrow Cu(O_2CR) + (1/2)H_2$

can be ruled out. We suggest that in acetone solution, the oxidation of CuO_2CR to $Cu(O_2CR)_2$ involves reaction of the former with solvent. This conclusion is based on the results of an extended (7 h) electrolysis of copper in an acetone solution of octanoic acid. The solvent phase was stripped from the final solution in a rotary evaporator, and acetone then removed by distillation to give about 0.5 mL of a pale yellow liquid. Gas–liquid chromatography (10% Carbowax) established the presence of acetone, *i*-propanol, and two minor components, one of which could not be clearly separated from acetone, and the other of which had $m/e = 204$ as the main peak in an EI mass spectrum, and is probably a derivative of octanoic acid and solvent. The presence of *i*-propanol implies that the oxidation of CuO_2CR involves the sequence

[8] $CuO_2CR + RCOOH + Me_2CO \rightarrow Cu(O_2CR)_2 + Me_2COH$

[9] $Me_2COH \xrightarrow{H} Me_2C(H)OH$

We have not attempted to establish the source of the hydrogen atom in eq. [9]. Pinacol, diacetone alcohol, and mesityl oxide were not detected in the glc spectrum. The overall reaction is apparently similar to the Meerwein–Pondorf–Verley reduction. A similar sequence can be written for the oxidation of CuO_2CR in acetonitrile via $CH_3C{=}NH$, but since the main thrust of the present work was the electrochemical synthesis of metal carboxylates, these mechanistic problems have not been investigated in any detail.

Acknowledgements

This work was supported in part by Operating Grants (to D.G.T.) from the Natural Sciences and Engineering Research Council of Canada. We thank Mr. C. Geloso for the results on hydrogen formation, and Dr. J. M. McIntosh for a discussion on the reduction of acetone.

1. F. F. Said and D. G. Tuck. Inorg. Chim. Acta, **59**, 1 (1982).
2. J. L. Hencher, M. A. Khan, F. F. Said, R. Sieler, and D. G. Tuck. Inorg. Chem. **21**, 2787 (1982).
3. J. L. Hencher, M. A. Khan, F. F. Said, and D. G. Tuck. Polyhedron, **4**, 1263 (1985).
4. C. Oldham, M. J. Taylor, and D. G. Tuck. Inorg. Chim. Acta, **100**, L9 (1985).
5. R. Kumar and D. G. Tuck. J. Organomet. Chem. **281**, C47 (1985).
6. J. J. Habeeb, D. G. Tuck, and F. H. Walters. J. Coord. Chem. **8**, 27 (1978).
7. L. Matassa, N. Kumar, and D. G. Tuck. Inorg. Chim. Acta, **109**, 19 (1985).
8. R. L. Martin and H. Waterman. J. Chem. Soc. 2545 (1957).
9. H. F. Payne. Organic coating technology. Vol. I. Wiley, New York. 1964. p. 230.
10. L. Eberson. Organic electrochemistry. *Edited by* M. M. Baizer. Marcel Dekker Inc., New York. 1973. pp. 423, 424.

Can. J. Chem. Downloaded from www.nrcresearchpress.com by 78.46.186.204 on 09/07/12
For personal use only.

Mechanism of electroreduction of 9-anthraldehyde

ANDRZEJ LASIA AND ABDELHAQ RAMI

Department of Chemistry, University of Sherbrooke, Sherbrooke, Que., Canada J1K 2R1

Received July 15, 1986

ANDRZEJ LASIA and ABDELHAQ RAMI. 1987. Can. J. Chem. **65**, 744 (1987).

The electroreduction of 9-anthraldehyde (ANCHO) and 10-methyl-9-anthraldehyde (MeANCHO) has been studied in aprotic solvents. The anion free radicals of both compounds undergo subsequent dimerization reaction with $ANCHO^{\cdot}$ being more reactive than $MeANCHO^{\cdot}$. The rate constant of the dimerization reaction depends on the solvent and for $ANCHO^{\cdot}$ in HMPA is equal to $2 \times 10^4 M^{-1} s^{-1}$. Using spectroscopic measurements it has been shown that the dimerization takes place at position 10.

ANDRZEJ LASIA et ABDELHAQ RAMI. 1987. Can. J. Chem. **65**, 744 (1987).

L'électroréduction du 9-anthraldéhyde (ANCHO) et du 10-méthyl-9-anthraldéhyde (MeANCHO) a été étudiée dans les solvants aprotiques. Les anions radicaux de ces composés se dimérisent et $ANCHO^{\cdot}$ est beaucoup plus réactif que $MeANCHO^{\cdot}$. La constante de vitesse de dimérisation dépend du solvant et pour $ANCHO^{\cdot}$ dans le HMPA cette constante égale $2 \times 10^4 M^{-1} s^{-1}$. La structure de dimère a été étudiée par la spectroscopie rmn et on a trouvé que la dimérisation a lieu à la position 10.

Can. J. Chem. Downloaded from www.nrcresearchpress.com by 78.46.186.204 on 09/07/12
For personal use only.

Introduction

The electroreduction of aromatic aldehydes has been studied extensively (1, 2). In protic solvents they are reduced in two one-electron or one two-electron processes. In aprotic solvents aromatic aldehydes form two one-electron polarographic waves (1, 3). The most detailed studies have been carried out for benzaldehyde (4–8) and it was found that the product of the one-electron reduction of aldehydes is a radical ion which is not stable and undergoes subsequent dimerization (9–12). The reactivity of the ion radicals in aprotic solvents is influenced by the ion-pair formation with the supporting electrolyte cations and the rate of the dimerization reaction increases with the decrease in the radius of the cation (9). The reactivity of the radical anions of the aromatic aldehydes depends strongly on the structure of the aldehydes and increases in the order: 1-naphthaldehyde ≤ 2-naphthaldehyde ≤ 3-benzaldehyde ≤ 9-anthraldehyde (9).

The structure of the dimer was studied in detail in the case of benzaldehyde which, upon one-electron reduction, forms hydrobenzoin (4, 5). The structure of a dimer formed by 9-anthraldehyde (ANCHO) has not been studied chemically but it has been suggested (without proof) that it does not form a glycol but instead forms a dimer by coupling in position 10 (10, 11). The mechanism of the electroreduction of similar compounds: 9-cyano and 9-nitroanthracene has also been studied (10–16). In the case of 9-cyanoanthracene it was found that the dimerization process is reversible and two mechanisms have been proposed: formation of a non-bonded dimer followed by a C—C bond formation (14) and a reversible formation of the C—C dimer (16).

The structure of the dimers has been studied by chemical and spectroscopic techniques. It was established that 9-cyanoanthracene forms dimer **I** (16) and that 9-nitroanthracene forms initially compound **II** which, upon reaction with methyl iodide, forms bianthronyldioxime **III** (11) (isolated product). We have undertaken studies of the electrodimerization of 9-anthraldehyde (ANCHO) and 10-methyl-9-anthraldehyde (MeANCHO) in order to explain the mechanism of the reaction and a structure of the dimer.

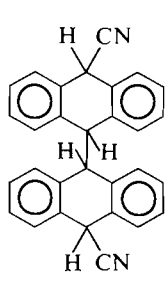

I

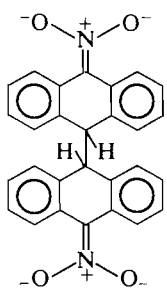

II

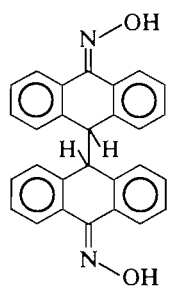

III

Experimental

Chemicals

9-anthraldehyde (Aldrich) was purified by column chromatography using silica gel (60–200 mesh, J. T. Barker) and an eluting mixture of 1:1 hexane–dichloromethane. The purity of the product was verified using thin layer chromatography. 10-Methyl-9-anthraldehyde (Aldrich) was used as received.

Dimethylsulfoxide (DMSO) (Anachema) and dimethylfornamide (DMF) (Fisher) were dried by calcium hydride, stored over activated molecular sieves type 4A (Fisher), and distilled at reduced pressure under nitrogen. Hexamethylphosphoramide (HMPA) (Aldrich) was dried over molecular sieves 4A and distilled under reduced pressure before use. DMSO-d_6 (99.9% MSD isotopes) was dried using molecular sieves.

Tetraethylammonium perchlorate (TEAP) was prepared from tetraethylammonium bromide and perchloric acid, recrystallized three times from water, and then dried *in vacuo* over P_2O_5 at 60°C.

Lithium perchlorate (BDH) was dried *in vacuo* over P_2O_5 at 140°C.

All products were stored in a controlled atmosphere chamber (Vacuum Atmospheres) before use.

Apparatus

The apparatus for electrochemical measurement consisted of a PAR Model 173 potentiostat, PAR Model 175 wave form generator, and IBM PC microcomputer equipped with a data translation DT 2801-A interface. Positive feedback compensation was used with the fast scan rate.

The working electrode was a dropping mercury electrode with a drop time 1–5 s in dc polarography and 20 s for fast cyclic voltammetric measurements. In slow voltammetric measurements the working electrode was a mercury drop attached to a platinum disk (9). The reference electrode was a silver wire in 0.05 *M* $AgNO_3$ + 0.05 *M* TEAP in a given solvent but in the fast voltammetric experiments a tungsten wire was used as a pseudoreference electrode (9). Electrochemical measurements were carried out in a dry box (Vacuum Atmospheres). Marcoelectrolyses were performed in the H-type cell (volume ~ 70 mL) and electrolyses in deutered DMSO in a smaller cell (volume ~ 4 mL) on a mercury pool electrode. The concentration of the depolariser used for the electrolyses in DMSO-d_6 was ~ 4 mg/mL.

Infrared spectra were recorded using a Perkin-Elmer 621 instrument and nmr spectra were obtained using Brucker WM 250 MHz instrument.

Results and discussion

ANCHO in non-aqueous solvents forms two one-electron

polarographic waves. In DMF the half-wave potentials obtained in the presence of 0.1 *M* TEAP are −1.646 and −2.229 V vs. Ag/Ag^+ reference electrode and in DMSO −1.433 and −1.974 V, respectively. The logarithmic analysis of the first polarographic wave in DMF gives a slope of 49 mv. However, the analysis according to an equation describing a reversible process with the fast subsequent irreversible dimerization (19)

$$E = E^\circ_{\frac{1}{2}} + \frac{RT}{3nF}\ln\frac{\pi k_d C^*_{Ox} t}{7} + \frac{RT}{nF}\ln\frac{2^{\frac{1}{3}}(i_l - i)}{i^{\frac{2}{3}} i_l^{\frac{1}{3}}}$$

gives a slope of 59 mV, which is in agreement with the theoretical value expected for that mechanism. The half-wave potential of MeANCHO is more negative (−1.522 V in DMSO) which reflects an inductive effect of the methyl group at position 10.

Radical anions of ANCHO are not stable in solution. In DMF values of k_d of $10^5 M^{-1}$ s^{-1} (0.1 *M* TEAP) (9) and $3.1 \times 10^5 M^{-1}$ s^{-1} (0.1 *M* Bu_4NBF_4) (11) are reported in the literature. We have found no anodic peak in cyclic voltammetry at slow sweep rates which means that the dimerization reaction is not reversible, contrary to 9-cyanoanthracene (14, 16). However, voltammetric measurements of MeANCHO show that at sweep rates of 0.02–0.1 V s^{-1} the anodic peak is well formed and the radical anion is stable. The methyl substituent in position 10 makes the dimerization process less favored.

If the supporting electrolyte is changed from 0.1 *M* TEAP to 0.1 *M* $LiClO_4$ a shift of ~16 mV towards a positive direction is observed for the half-wave potential of the first wave which may be explained by ion-pair formation and a consequent increase in rate of the dimerization process.

The cyclic voltammetric measurements performed in HMPA in the presence of 0.1 *M* $LiClO_4$ indicate that the dimerization reaction is slower than in DMF or DMSO. Using sweep rates between 10 and 20 *V* s^{-1} the kinetics of dimerization was determined by measuring the ratio of the absolute values of the anodic $(i_{ap})_o$ to cathodic i_{cp} peak currents according to data presented in ref. 17. The second order rate constant obtained equals to $2 \times 10^4 M^{-1} s^{-1}$ in 2×10^{-3} *M* ANCHO solution. The decrease in rate of dimerization in HMPA may be explained by the stronger solvating power of that solvent towards cations (donor number of HMPA: 38.8, DMF: 26.6) (18). In HMPA cations are very well solvated and the probability of the formation of the contact ion pairs is negligible which means that the measured rate constant is that of dimerization of the free anion radicals.

We have also carried out macroelectrolyses in order to study the structure of the dimer. Figure 1 shows polarograms of ANCHO in 0.1 *M* TEAP in DMF before (*A*), during (*B*), and after electroreduction (*C*) at the potentials of the plateau of the first polarographic wave. During electrolysis the wave height of the first and the second polarographic wave decreases while the anodic wave at −1.21 V is formed. At the beginning of the anodic wave a large maximum is formed. The addition of a proton donor (acetic acid) to the dimer after electrolysis causes shift of the anodic wave to more positive potentials (of ~0.49 V), making the electrooxidation process more difficult and causing the maximum to disappear. During electrolysis one electron per molecule is consumed. Electrochemical oxidation of the dimer at potentials at the plateau of the anodic wave gives the initial product ANCHO. The electroreduction of MeANCHO proceeds in a similar way, that is, dimer is also formed but the kinetics of the dimerization is much slower than ANCHO (it can be observed only during macroelectrolysis, not during cyclic voltammetric experiments).

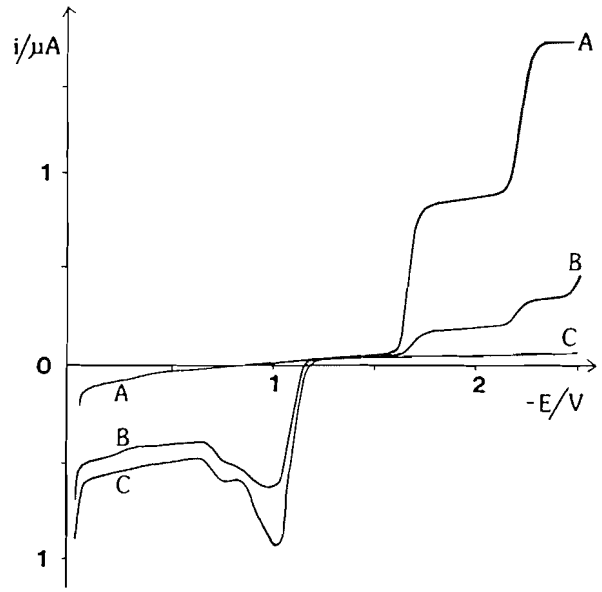

FIG. 1. Direct current polarograms of $6 \times 10^{-4} M$ ANCHO in 0.1 *M* TEAP in DMF; *A*, before, *B*, during, and *C* after electrolysis at −1.8 V.

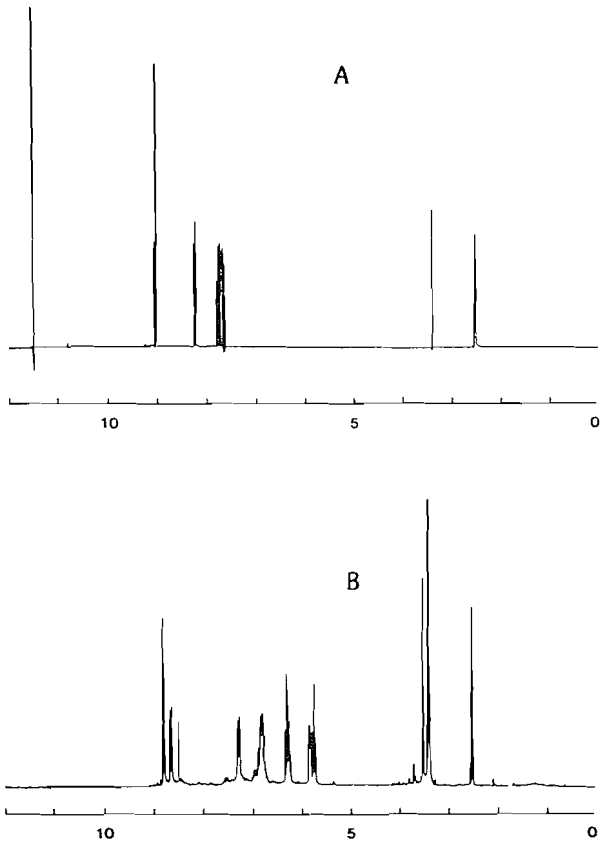

FIG. 2. ^1H nmr spectra of ANCHO (*A*) and dimer (*B*) in DMSO-d_6. Peaks at 2.5 ppm and 3.4 ppm are caused by DMSO and HDO, respectively.

We have tried to isolate the dimer of ANCHO but it was immediately oxidized by the air. Because of that we have used spectroscopic techniques to determine the structure of the dimer formed in solution. Infrared measurements show that during electrolysis in DMSO, the C—O band of ANCHO at 1645 cm^{-1} disappears which means that the carboxyl group is reduced.

Nuclear magnetic resonance measurements after electrore-

Can. J. Chem. Downloaded from www.nrcresearchpress.com by 78.46.186.204 on 09/07/12
For personal use only.

Can. J. Chem. Downloaded from www.nrcresearchpress.com by 78.46.186.204 on 09/07/12
For personal use only.

duction in DMSO-d_6 in the presence of $LiClO_4$ (to avoid interferences of protons of tetraalkylammonium salts) were performed (see Figs. 2 and 3). ^1H nmr of ANCHO shows the carbonyl proton at 11.47 ppm and aromatic signals between 7.6 and 9 ppm. ^{13}C nmr shows the carbonyl group at 193.8 ppm with the aromatic protons between 123.3 and 143.9 ppm. The nmr spectrum of the product of electrolysis is more complex. The ^1H spectrum shows that the signal of the carbonyl proton disappears. There are seven groups of protons with ratio 1:2:2:2:1:1:1 at 3.49 ppm (d), 5.70–5.83 ppm (m), 6.21–6.33 ppm (m), 6.74–6.86 ppm (m), 7.24–7.28 ppm (m), 8.61–8.65 ppm (d), and 8.76–8.79 (d). The ^{13}C *J*-modulated spectrum of the dimer shows C–H carbons with negative phase at 51.70–51.52 ppm (d), 118.03–118.97 ppm (m), 123.84 ppm (s), 124.28–124.45 ppm (m), 127.90 ppm (s), 128.57–128.71 ppm (d), and 163.11–163.26 ppm (d). The quaternary carbons appear between 102.4–140.7 ppm with positive phase. The ^1H–^{13}C correlation spectrum shows that the carbon ^{13}C 51.6 ppm is linked with ^1H 3.49 ppm, ^{13}C 163.2 ppm with ^1H 8.78 ppm, and ^{13}C 128.6 ppm with ^1H 8.63 ppm.

From the point of view of the reactivity of the radical three structures of the dimer are probable:

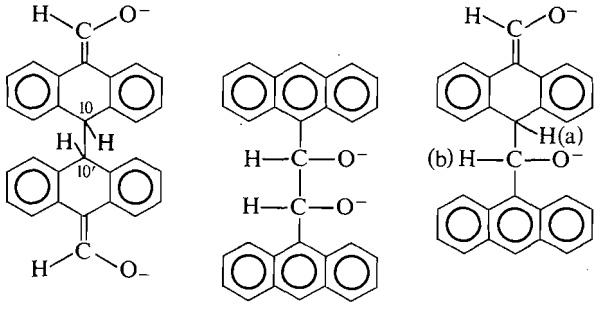

IV **V** **VI**

In structure **VI** two types of aliphatic protons, (*a*) and (*b*), exist and should give two different signals in the aliphatic region, each having an intensity 1/20 the total intensity of all protons. Since only one aliphatic proton is observed, this structure must be eliminated. For compound **V** one signal of two carbons of the glycol group should be observed in the aliphatic region and all the other carbons of the anthryl groups should be similar to those found in ANCHO. That structure cannot explain the appearance of the carbon signal at 163.2 ppm.

On the other hand, structure **IV** is in agreement with the obtained spectra. The carbons 10 and 10′ having configuration sp^3 appear at 51.6 ppm and the corresponding protons at 3.49 ppm, both in the aliphatic region. The hydrogen and the carbon of the —CHO^- group appear at 8.78 ppm and 163.2 ppm, respectively. The shift of the carbon signal to lower fields (higher ppm values) may be connected with the negative charge on oxygen atom and the possibility of existence of the mesomeric structures:

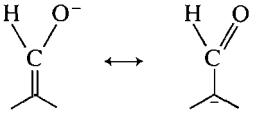

The anions are probably stabilized by the ion-pair formation with lithium cations. All other C—H carbons of anthryl groups appear between 118.0–128.7 ppm and are shifted to higher field as compared with ANCHO. It should be noted in passing that the ^1H resonance at 3.49 ppm is a doublet with a very small splitting which might suggest that the product is a 1:1 mixture of isomers.

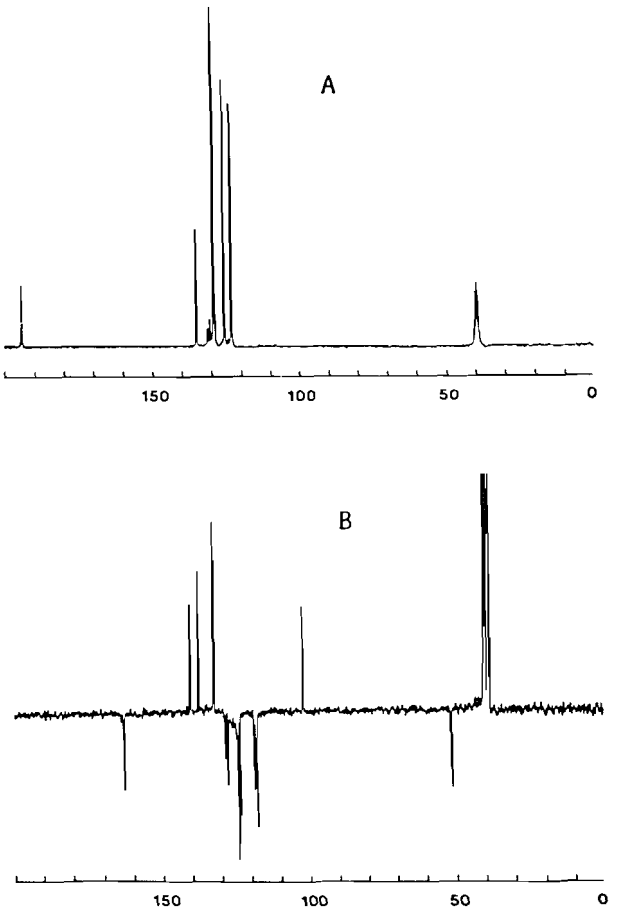

FIG. 3. ^{13}C nmr spectra of ANCHO (*A*) and dimer (*B*) in DMSO-d_6. *J*-modulated spectrum *B* shows C—H carbons with negative and quaternary carbons with positive phase. Peaks at 38.5–40.5 ppm are caused by DMSO.

We have also carried out semiempirical quantum-chemical calculations of the anion radical of ANCHO using an open shell restricted Longuet–Higgins–Pople method in π-approximation (PPP-like method) (20). We have found that the highest spin density in the radical is on carbon 10, $\rho_{10} = 0.2257$ and the spin density on the carbonyl carbon atom is 0.0863. This observation is in agreement with our supposition that the dimerization reaction takes place at position 10. Our previous calculations using simple HMO technique (9) gave $\rho_{10} = 0.3833$ which seems to be too high.

The study of MeANCHO shows that the initially formed dimer is not stable and undergoes subsequent reactions, probably polymerization.

Conclusions

The study of the electroreduction of 9-anthraldehyde shows that the radical ion formed undergoes subsequent dimerization reaction. Dimer is stable in the absence of oxygen but may be electrochemically oxidized to ANCHO. The kinetics of the dimerization reaction depend on the solvent and in HMPA in the presence of 0.1 *M* $LiClO_4$ the second order rate constant is $2 \times 10^4 M^{-1}\ s^{-1}$.

From spectroscopic studies, the dimer has been shown to be that of structure **IV** (and does not form glycols). The proposed structure is supported by the quantum-chemical calculations

which show the highest spin density in the radical at position 10. It is also in agreement with the structure found for the dimers of 9-cyano and 9-nitroanthracenes but is different from the structure of the dimers of benzaldehyde. Also the comparison of the reactivity of the radical of ANCHO and its 10-Me derivative shows that, the MeANCHO radical anion is much more stable in solution, the methyl substituent at position 10 sterically hindering dimerization.

Acknowledgements

This research was supported by the Natural Sciences and Engineering Research Council of Canada.

The authors wish to thank Dr. S. Lacelle and Dr. L. Magdzinski of University of Sherbrooke for helpful discussion on nmr specta.

1. D.H. EVANS. *In* Encyclopedia of electrochemistry of the elements. vol. 12. *Edited by* A. J. Bard and H. Lund. Marcel Dekker, New York. 1978.
2. L. FEOKTISTOV and H. LUND. *In* Organic electrochemistry. *Edited by* M. M. Baizer. Marcel Dekker, New York. 1973.
3. G. ANTHOINE, J. NASIELSKI, and B. WILMET-DEVOS. Bull. Soc. Chim. Belg. **78**, 465 (1969).
4. S. WAWZONEK and A. GUNDERSEN. J. Electrochem. Soc. **107**, 537 (1960).
5. P. H. GIVEN and M. E. PEOVER. J. Chem. Soc. 385 (1961).
6. L. N. VYKHODTSEVA and L. N. NEKRASOV. Elektrokhimiya, **14**, 1439 (1978).
7. N. R. ARMSTRONG, R. K. QUINN, and N. E. VANDERBORGH. Anal. Chem. **46**, 1759 (1974).
8. N. R. ARMSTRONG, N. E. VANDERBORGH, and R. K. QUINN. J. Electrochem. Soc. **122**, 615 (1975).
9. W. R. FAWCETT and A. LASIA. Can. J. Chem. **59**, 3256 (1981).
10. A. YILDIZ and H. BAUMGÄRTEL. Ber. Buns. Ges. **81**, 1177 (1977).
11. O. HAMMERICH and V. D. PARKER. Acta Chem. Scand. B**35**, 341 (1981).
12. C. AMATORE, J. PINSON, and J. M. SAVÉANT. J. Electroanal. Chem. **137**, 143 (1982).
13. C. AMATORE, J. PINSON, and J. M. SAVÉANT. J. Electroanal. Chem. **139**, 193 (1982).
14. O. HAMMERICH and V. D. PARKER. Acta Chem. Scand. B**37**, 379 (1983).
15. V. D. PARKER. Acta Chem. Scand. B**37**, 871 (1983).
16. C. AMATORE, D. GARREAU, M. HAMMI, J. PINSON, and J. M. SAVÉANT. J. Electroanal. Chem. **184**, 1 (1985).
17. A. LASIA. J. Electroanal. Chem. **146**, 413 (1983).
18. V. GUTMANN, G. RESCH, and W. LINERT. Coord. Chem. Rev. **43**, 133 (1982).
19. C. P. ANDRIEUX, L. NADJO, and J. M. SAVÉANT. J. Electroanal. Chem. **42**, 223 (1973).
20. S. MIERTUS, D. KYSEL', and P. MACH. Coll. Czechoslov. Chem. Commun. **45**, 339 (1980).

Can. J. Chem. Downloaded from www.nrcresearchpress.com by 78.46.186.204 on 09/07/12
For personal use only.

Metabolites produced by the scleroderris canker fungus, *Gremmeniella abietina*. Part 2. The structure of scleroderolide

WILLIAM A. AYER, YUMIKO HOYANO, AND M. SOLEDADE PEDRAS
Department of Chemistry, University of Alberta, Edmonton, Alta., Canada T6G 2G2

AND

JON CLARDY AND EDWARD ARNOLD
Department of Chemistry, Baker Laboratory, Cornell University, Ithaca, NY 14853, U.S.A.

Received August 8, 1986

WILLIAM A. AYER, YUMIKO HOYANO, M. SOLEDADE PEDRAS, JON CLARDY, and EDWARD ARNOLD. Can. J. Chem. **65**, 748 (1987).

Scleroderolide, a yellow pigment produced by the Scleroderris canker fungus *Gremmeniella abietina* (Lagerb.) Morelet, is shown to possess structure **1**. The structure was determined by an X-ray crystallographic study of the racemic monoacetate **1***a*. The crystal of **1***a* belongs to the triclinic system space group, $P\bar{1}$, the *R*-factor converged to 0.047 for the 1957 observed reflections. Scleroderolide occurs mainly as the levorotatory enantiomer (*S* configuration at C-2′) although on one occasion it was obtained in partially racemic form. The absolute stereochemistry of the levorotatory form was determined by transformation of (−)-sclerodione (**5**) of known absolute configuration into (−)-scleroderolide. The absolute configuration of (−)-sclerodione was established by correlation with (−)-sclerodin (**3**). The diacetyl derivative of scleroderolide (**1***b*) shows interesting temperature dependent nuclear magnetic resonance spectral properties due to restricted rotation of the C-4 O-acetyl group. Oxidation of the red pigment sclerodione (**5**) with *m*-chloroperbenzoic acid provides both sclerodin (**3**) and scleroderolide (**1**). Scleroderolide (**1**) is the first natural product to be reported that contains a phenylglyoxylate lactone functionality.

WILLIAM A. AYER, YUMIKO HOYANO, M. SOLEDADE PEDRAS, JON CLARDY et EDWARD ARNOLD. Can. J. Chem. **65**, 748 (1987).

On démontre que le sclérodérolide, un pigment jaune qui est produit par le champignon nécrosant Scleroderris *Gremmeniella abietina* (Lagerb.) Morelet, possède la structure **1**. On a déterminé la structure grâce à une étude cristallographique à l'aide de rayons-X effectuée sur le monoacétate **1***a*, à l'état racémique. Le cristal de **1***a* appartient au groupe d'espace triclinique $P\bar{1}$ et le facteur *R* converge vers une valeur de 0,047 pour les 1957 réflexions observées. On retrouve le sclérodérolide principalement sous la forme de l'énantiomère lévogyre (configuration *S* au niveau du C-2′) même si, à une occasion, on l'a obtenu sous une forme partiellement racémique. On a déterminé la stéréochimie absolue de la forme lévogyre en se basant sur une transformation de la (−)-sclérodione (**5**) de configuration absolue connue en (−)-sclérodérolide. On a établi la configuration absolue de la (−)-sclérodione par une corrélation avec la (−)-sclérodine (**3**). Les propriétés spectrales rmn du dérivé diacétylé (**1***b*) du sclérodérolide varient d'une façon intéressante avec la température à cause d'une rotation empêchée du groupement O-acétyle attaché en position C-4. L'oxydation du pigment rouge sclérodione (**5**) par l'acide *m*-chloroperbenzoïque conduit à la sclérodine (**3**) ainsi qu'au sclérodérolide (**1**). Le sclérodérolide (**1**) est le premier produit naturel pour lequel on rapporte la présence d'une fonctionnalité phénylglyoxylate lactone.

[Traduit par la revue]

In Part 1 of this series (1) we have reported on the isolation of several colored metabolites produced by the Scleroderris canker causing fungus *Gremmeniella abietina*. In addition to the compounds already reported, one strain of *G. abietina* (C699) produces a bright yellow metabolite that possesses the biogenetically novel internal phenylglyoxylate lactone structure, **1**.

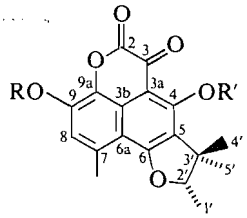

1 R = R′ = H
1*a* R = Ac R′ = H
1*b* R = R′ = Ac

In this article we describe the isolation, structure determination, and some of the chemical properties of this unusual compound.

Gremmeniella abietina (strain C-699) was grown in still culture, at 16–17°C on a medium of 10% V-8 juice containing 1% added glucose (2). Chromatographic separation of the crude mycelium extract gave Scleroderris blue (**2**), sclerodin (**3**), *ent*-atrovenetinone (**4**), sclerodione (**5**), and the yellow metabolite (**1**), for which we propose the name scleroderolide.

Scleroderolide (mp 239–240°C) is isomeric with sclerodin (**3**, $C_{18}H_{16}O_6$) and initially we suspected it to be the isomeric ether **6**. The ^{1}H nmr spectrum of scleroderolide is similar to that of **3** except for the OH hydrogens (δ 6.65 and 13.73 vs. δ 11.43 and 11.64). Scleroderolide readily forms a monoacetate on treatment with acetic anhydride – pyridine, whereas **3** forms the

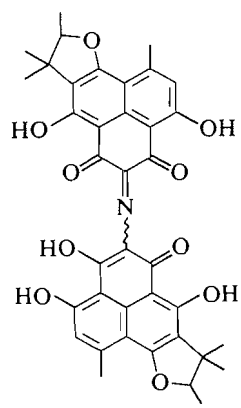

2

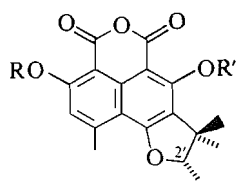

3 R = R′ = H
3*a* R = Ac R′ = H
3*b* R = H R′ = Ac
3*c* R = R′ = Ac
3*d* R = R′ = Me

Can. J. Chem. Downloaded from www.nrcresearchpress.com by 78.46.186.204 on 09/07/12
For personal use only.

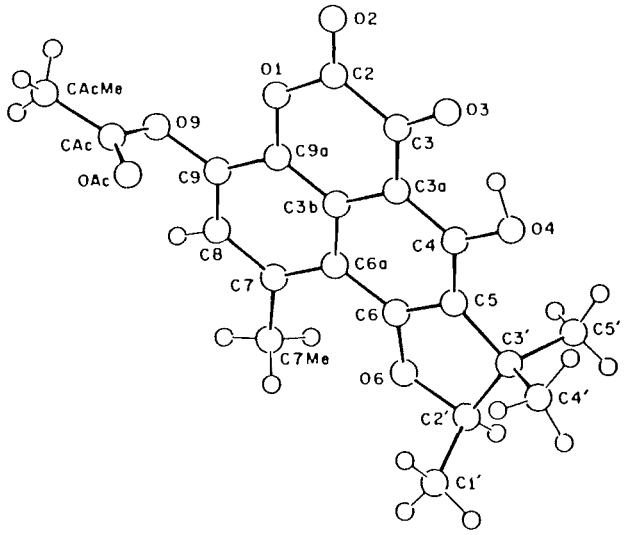

FIG. 1. A perspective drawing of the structure of scleroderolide monoacetate.

diacetate **3***c* (1). This is consistent with structure **6**, since an OH group at carbon 6 would be expected to be sterically hindered. However, the ^{13}C nmr spectrum of **1** shows carbonyl absorption at δ 170.1 and 155.7, which is not in good agreement with the anhydride structure (δ 165.4 and 164.9 in **3**). Also the ir spectrum shows carbonyl absorption at 1750 cm^{-1} while that of the anhydride **3** appears at 1705 cm^{-1}.

The monoacetate of scleroderolide crystallizes from dichloromethane – petroleum ether in the form of beautiful red-orange crystals, well suited for an X-ray cyrstallographic study. Figure 1 shows a computer generated perspective drawing of the X-ray model of scleroderolide monoacetate, which reveals that it possesses structure **1***a*.

To our surprise, the sample used for X-ray analysis proved to be racemic, though the parent compound (**1**) had an optical rotation of −22.3°. Several hypotheses may be entertained to explain these unusual results: 1, scleroderolide was not optically pure (i.e., both enantiomers are produced by *G. abietina*); 2, scleroderolide was racemized during isolation; 3, scleroderolide was racemized during acetylation. Hypothesis 1 was tested in two ways: using a chiral shift reagent (3, 4); using an optically active acylating agent.

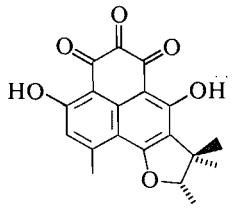

4

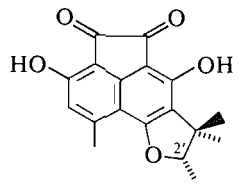

5

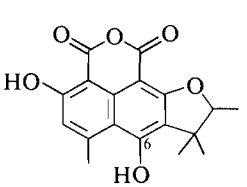

6

In the first instance, tris[3-(trifluoromethylhydroxymethylene)-*d*-camphorato]europium(III) ($Eu(tfc)_3$) was added to scleroderolide in $CDCl_3$ in successively increasing amounts (up to 1 equiv.) and the ^1H nmr spectra were obtained; however, no significant shifts were observed although there was a considerable amount of broadening of the spectral lines. This result is probably due to the lack of effective complexation of the shift reagent with scleroderolide.

We then acylated **1** with the Mosher reagent (−)-α-methoxy-α-trifluoromethyl-α-phenylacetic acid (5); the ^{19}F nmr spectrum of the resulting monoester **7** (no diester was formed) showed a single peak at δ −72.17 (internal standard $CFCl_3$). Although we did not observe two ^{19}F signals (indicating two diastereomeric products), this result may be due to the large distance (approximately 9.9 Å) between the two asymmetric centers in **7**.

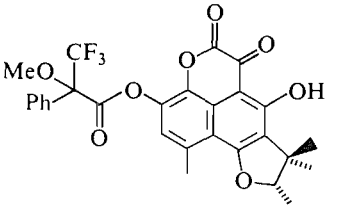

7

Sclerodin (**3**) and sclerodione (**5**) were used to test hypothesis 2.[1] Sclerodione was dissolved in chloroform – trifluoroacetic acid (several ratios) at room temperature (up to 15 days) and at 60°C (1 h); the optical rotation ($[\alpha]_D$ −115.3°) of the recovered material was unchanged. In the case of sclerodin (**3**) we used deuterated solvents (C_6D_6–CF_3CO_2D) at 80°C (sealed tube) and monitored the reaction by ^1H nmr spectroscopy. After 24 h the aromatic hydrogen was exchanged for deuterium. Prolonged treatment (7 days) led to no further changes. The optical rotation ($[\alpha]_D$ −72.6°) of the recovered compound was unchanged. Thus racemization is not likely to have occurred during the isolation of these metabolites.

To test hypothesis 3 scleroderolide was isolated from a fresh culture of *G. abietina*. Surprisingly, this sample of scleroderolide (mp 232–233°C) had a much higher optical rotation ($[\alpha]_D$ −116°) than the previous sample. The monoacetate from this new preparation showed the same optical rotation ($[\alpha]_D$ −69°)[2] regardless of its method of formation (acetic anhydride, and either pyridine or 4-*N*,*N*-dimethylaminopyridine or sulfuric acid as catalyst). These results were not due to the selective crystallization of one enantiomer, as demonstrated in the following manner: acylation of the combined mother liquors from recrystallization of scleroderolide (**1**) gave a monoacetate with the same optical rotation as obtained previously. The optical rotation was unchanged after crystallization. These results seem to indicate that *G. abietina* (strain C-699) produces scleroderolide in high optical purity and that scleroderolide is not racemized during acylation.

Scleroderolide is closely related to atrovenetin, a metabolite of *Penicillium atrovenetum* (6) and *P. herquei* (7). The structure of atrovenetin (**8**) was established by X-ray crystallographic analysis (8) and the configuration (*R*) at C-2′ was determined by chemical correlation with (*S*)-ethyl lactate (9). Interestingly, atrovenetin isolated from *P. herquei* has a lower optical rotation ($[\alpha]_D$ +54.6°) than atrovenetin isolated from *P. atrovenetum* ($[\alpha]_D$ +100.6°) (10). Thus in the case of

[1] Scleroderolide is produced by the fungus in smaller amounts and is difficult to purify.

[2] Scleroderolide isolated as its monoacetate from other later cultures showed the same optical rotation.

Can. J. Chem. Downloaded from www.nrcresearchpress.com by 78.46.186.204 on 09/07/12
For personal use only.

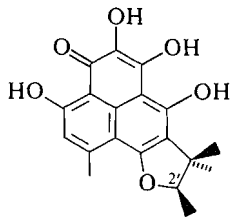

8

P. herquei, it is possible that both enantiomers of atrovenetin are produced (10). In our case, the low optical purity (ca. 20% e.e. enantiomeric excess) of the initially isolated scleroderolide might be due to the use of a mutant strain on that occasion, although we cannot completely exclude the possibility that the strain used initially was incorrectly labelled.

Scleroderolide (**1**) is readily converted to the monoacetate **1***a* by treatment with acetic anhydride in the presence of pyridine or 4-*N*,*N*-dimethylaminopyridine. Utilizing longer reaction times, we attempted to prepare the diacetate **1***b*. A major product was obtained, the ^{1}H nmr spectrum of which was very similar to that of **1***a* except that the phenolic OH resonance at δ 13.75 was replaced by a signal at δ 6.94 (not D_2O exchangeable). The hrms of this product displayed a molecular ion at *m/z* 394 ($C_{22}H_{18}O_7$). The ir spectrum shows carbonyl absorption at 1774 and 1738 cm^{-1}. These data are consistent with structure **9**. Compound **9** presumably is formed by base catalyzed cyclization of the initially formed diacetate **1***b*.

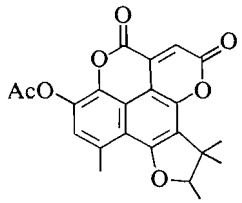

9

The diacetate **1***b* is readily formed under acidic conditions (e.g., acetic anhydride – trifluoroacetic acid). Remarkably, its ^{1}H and ^{13}C nmr spectra are temperature dependent. For example, the ^{1}H nmr spectrum of **1***b* (in toluene-d_8) exhibits broad signals for the C-2′, C-4′, and C-5′ hydrogens at room temperature. At 60°C these signals are sharp, whereas at 0°C they appear as resolved pairs. Further cooling to −60°C induces broadening in the signals for the C-1′, C-8, and $ArCH_3$ hydrogens as well as the acetate methyl group at C-9. Interestingly, the acetate methyl at C-4 remains relatively unchanged with temperature. Similarly, the ^{13}C nmr spectrum ($CDCl_3$) shows several broad signals at room temperature, which are sharp at 55°C and are resolved into pairs at −60°C. Since the ^{1}H and ^{13}C nmr spectra of **1***a* do not show this temperature dependence, it appears that the acetate group at C-4 in **1***b* is the structural feature responsible for these unusual results. The effect could, in principle, be due to acetyl migration from the C-4 to the C-3 oxygen (Scheme 1) or to restricted rotation of the acetate group (Scheme 2). To examine this further, we investigated the nmr spectra of several derivatives of sclerodin (**3**).

Sclerodin diacetate (**3***c*) and sclerodin dimethyl ether (**3***d*) have previously (1) been prepared. The monoacetate **3***a* was obtained from **3** by treatment with acetic anhydride – pyridine, while monoacetate **3***b* may be obtained either from **3** by treatment with acetic anhydride – trifluoroacetic acid (along with the diacetate **3***c*) or from **3***c* by hydrolysis ($NaHCO_3$).

The ^{1}H nmr spectra of **3***d* (1) and **3***a* do not show temperature dependence, but the spectra of **3***b* and **3***c* exhibit temperature dependent features very similar to those of **1***b*. Since the propensity for acetyl migration is expected to be similar for **3***a* and **3***b*, we concluded that it is restricted rotation of the acetate group at C-4 which is responsible for the temperature dependent nmr spectra in these compounds.

Sclerodione (**5**), a metabolite of *G. abietina* (1), on standing in solution is oxidized to sclerodin (**3**). Treatment of **5** with hydrogen peroxide gives **3**, along with lactone **10** (1).

Reasoning that the lactone **10** may be derived from scleroderolide (**1**) by peroxide oxidation of the corresponding α-keto

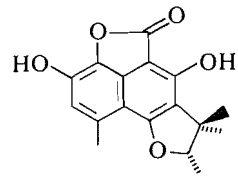

10

acid, we decided to investigate the reaction of sclerodione (**5**) with *m*-chloroperbenzoic acid. To our satisfaction, we found that this reaction led to the formation of both sclerodin (**3**) and scleroderolide (**1**), isolated as its monoacetate **1***a*.

The *S* configuration at C-2′ has been established (1) for some metabolites of *G. abietina*. The (+)-form ($[\alpha]_D$ +75°) of sclerodin (**3**) has been shown to have the *R* configuration at C-2′ by X-ray crystallography (11). Consequently sclerodin (**3**, $[\alpha]_D$ −72.6°) from *G. abietina* is assigned the *S* configuration. *Ent*-atrovenetinone (**4**) and sclerodione (**5**) from *G. abietina*, on oxidation gave sclerodin (**3**, $[\alpha]_D$ −72.6°), establishing the *S* configuration for **4** and **5**. Similarly, scleroderolide (**1**, $[\alpha]_D$ −116°) can be prepared, as mentioned above, from sclerodione (**5**), thus allowing the assignment of the *S* configuration at C-2′ for **1**.

To the best of our knowledge, scleroderolide (**1**) is the first natural product possessing the interesting phenylglyoxylate lactone structure. Its biosynthesis is discussed in Part 4 of this series.

Experimental

All solvents except diethyl ether were distilled prior to use. ACS quality anhydrous diethyl ether was used without purification. Petroleum ether refers to Skelly Oil Company light petroleum (Skellysolve B), bp 62–70°C. Pyridine was distilled from CaH_2 and stored over molecular sieves; acetic anhydride was dried over P_2O_5 and distilled from sodium acetate.

Analytical thin-layer chromatography (tlc) was carried out on aluminum sheets (75 × 25 or 75 × 50 mm) precoated (0.2 mm) with silica gel $60F_{254}$ (E. Merck, Darmstadt). Preparative thin-layer chromatography (ptlc) was carried out on glass plates (20 × 20 cm) precoated (0.25 mm) with the same adsorbent. Materials were detected by visualization under an ultraviolet (uv) lamp (254 or 350 nm), or by spraying with a solution of phosphomolybdic acid (5%) containing a trace of ceric sulfate in aqueous sulfuric acid (5%, v/v), followed by charring on a hot plate. Flash column chromatography (12) was performed with Merck Silica Gel 60 (40–63 μm).

High resolution mass spectra (hrms) were recorded on an A.E.I. MS-50 mass spectrometer coupled to a DS 50 computer. Chemical ionization mass spectra (cims) were recorded on an A.E.I. MS-9 mass spectrometer. Ammonia was used as reagent gas. Data are reported as *m/z* (relative intensity). Unless diagnostically significant, peaks with intensities less than 20% of the base peak are omitted. Infrared (ir) spectra were recorded on a Nicolet 7199 FT interferometer. Optical rotations were measured on a Perkin Elmer Model 141 polarimeter.

Can. J. Chem. Downloaded from www.nrcresearchpress.com by 78.46.186.204 on 09/07/12
For personal use only.

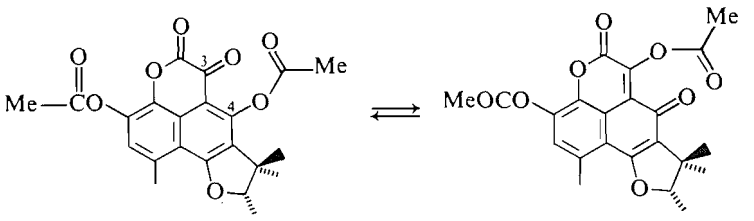

1*b*

SCHEME 1

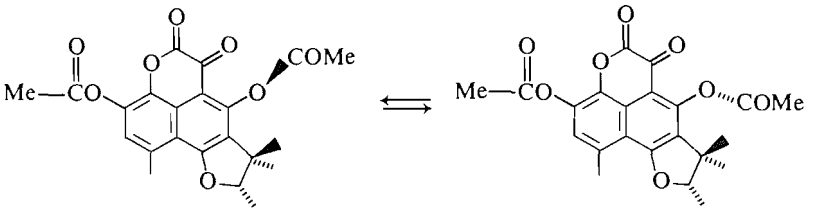

1*b*

SCHEME 2

^{1}H nuclear magnetic resonance (^{1}H nmr) spectra were measured on a Bruker WH-200 spectrometer on a Bruker WH-400 spectrometer. ^{13}C nuclear magnetic resonance (^{13}C nmr) spectra were measured on a Bruker WH-400 spectrometer. For ^{1}H nmr, residual $CHCl_3$ in $CDCl_3$ was employed as the internal standard (assigned as 7.26 ppm downfield from tetramethylsilane (TMS)) and measurements are reported in ppm downfield from TMS (δ). For ^{13}C nmr, $CDCl_3$ was employed as the internal standard (assigned as 77.0 ppm downfield from TMS) and measurements are reported in ppm downfield from TMS (δ). Melting points were recorded on a Fisher–Johns melting point apparatus and are uncorrected.

Growth of Gremmeniella abietina *and extraction of metabolites*

Stock cultures of *Gremmeniella abietina* (strain C-699, Northern Forest Research Centre, Canadian Forestry Service, Edmonton) were maintained in slant tubes on potato dextrose agar at 4°C. To initiate large scale cultures, small fragments of agar containing the mycelium were aseptically transferred to Erlenmeyer flasks (5 × 300 mL) containing a sterile culture medium (200 mL) composed of 10% (v/v) clarified V-8[3] juice and 1% (w/v) glucose. The cultures were shaken for 10 days at 15–17°C. The content of each inoculation flask was transferred to two 2.8-L Fernbach flasks containing the same liquid medium (900 mL) and the flasks (ten) were kept at 15–17°C. After 4 weeks the mycelium was separated from the broth by filtration through cheesecloth. The wet mycelium was extracted with diethyl ether or dichloromethane (24 h), and twice with methanol (24 h), in a Soxhlet extractor. The ether (or dichloromethane) and methanol extracts were dried over sodium sulfate and the solvents evaporated *in vacuo* at 30°C.

Isolation of scleroderolide (1)

Pure scleroderolide (**1**) was obtained from crude mycelium extracts from *G. abietina* strain C-699. The dichloromethane extract (700 mg) was fractionated by flash column chromatography (dichloromethane–methanol – acetic acid, 47:2:1, 2 L) and the fractions (100 mL) were coevaporated with toluene. Fractions 5–7 were refractionated using the same process. After evaporation of the solvent the residue was dissolved in dichloromethane and petroleum ether was added to the solution (brownish) until precipitation occurred. The precipitate was filtered and crystallized from ethanol – petroleum ether to give scleroderolide (**1**, mp 232–233°C); tlc: R_f 0.26 (dichloromethane – petroleum ether – acetic acid, 10:10:1, double elution), yellow spot; $[\alpha]_D$ −116.0° (*c* 0.30, $CHCl_3$); ir ($CHCl_3$, solution): 3500 (br), 2920, 1750, 1610, 1470, 1380, 1365, 1205, 1030 cm^{-1}; ^{1}H nmr ($CDCl_3$) δ: 1.34 (3H, s, C-3′ CH_3), 1.51 (3H, d, 6.5 Hz, C-2′ CH_3), 1.56 (3H, s, C-3′ CH_3), 2.75 (3H, s, ArCH_3), 4.77 (1H, q, 6.5 Hz, C-2′ H), 6.65 (1H, br s, OH), 6.92 (1H, s, C-8 H), 13.73 (1H, s, OH); ^{13}C nmr ($CDCl_3$)[4] δ: 14.6 (C-1′), 20.6 (C-5′), 22.3 (ArCH_3), 25.6 (C-4′), 43.1 (C-3′), 92.8 (C-2′), 107.2 (C-3a), 109.1 (C-6a), 117.1 (C-8), 119.4 (C-5), 122.2 (C-3b), 129.9 (C-9a), 137.1 (C-7), 144.5 (C-9), 155.7 (C-2), 167.4 (C-4), 169.6 (C-6), 170.1 (C-3); hrms, *m/z* calcd. for $C_{18}H_{16}O_6$ (M^+): 328.0947; found: 328.0950 (50), 300 (61), 285 (100), 270 (9), 267 (11), 257 (14); cims, *m/z*: 346 (*M* + 18, 46), 329 (*M* + 1, 100).

Scleroderolide monoacetate (1a)

Pure scleroderolide (**1**, 10 mg) was dissolved in dichloromethane (5 mL), and acetic anhydride (excess) and 4-*N*,*N*-dimethylaminopyridine were added at room temperature. After 30 min the reaction mixture was diluted with dichloromethane (20 mL) and washed successively with 5% aqueous hydrochloric acid (10 mL) and then water (10 mL). The dichloromethane layer was dried (Na_2SO_4), filtered, and concentrated to give the crude product (13 mg). Crystallization from dichloromethane – petroleum ether gave scleroderolide monoacetate (**1***a*, mp 183–186°C, 85% yield); tlc: R_f 0.32 (benzene–acetone – acetic acid, 90:10:0.1), yellow spot; $[\alpha]_D$ −69.3° (*c* 0.28, $CHCl_3$); ir ($CHCl_3$, solution): 3500 (br), 3000, 1760, 1620, 1590, 1470, 1420, 1370, 1300, 1225, 1195, 1030 cm^{-1}; ^{1}H nmr ($CDCl_3$) δ: 1.35 (3H, s, C-3′ CH_3), 1.52 (3H, d, 6.5 Hz, C-2′ CH_3), 1.57 (3H, s, C-3′ CH_3), 2.43 (3H, s, OOCCH_3), 2.79 (3H, s, ArCH_3), 4.80 (1H, q, 6.5 Hz, C-2′ H), 7.01 (1H, s, C-8 H), 13.77 (1H, s, OH); ^{13}C nmr ($CDCl_3$) δ: 14.6 (C-1′), 20.5 (C-5′), 20.6 (OOC*C*H_3), 22.3 (ArCH_3), 25.6 (C-4′), 43.4 (C-3′), 93.0 (C-2′), 107.6 (C-3a), 113.5 (C-6a), 121.1 (C-5), 122.2 (C-3b), 122.3 (C-8), 135.0 (C-9a), 135.8 (C-7), 137.9 (C-9), 155.1 (C-2), 167.8 (C-4), 168.2 (OO*C*CH_3), 169.0 (C-6), 170.7 (C-3); hrms, *m/z* calcd. for $C_{20}H_{18}O_7$ (M^+): 370.1052; found: 370.1050 (26), 328 (64), 300 (100), 285 (96).

Scleroderolide diacetate (1b)

Pure scleroderolide (**1**, 10 mg) was dissolved in dichloromethane (5 mL), and acetic anhydride (excess) and trifluoroacetic acid (0.5 mL) were added at room temperature. After 24 h the reaction mixture was diluted with toluene and concentrated to give the crude product (14 mg). Crystallization from dichloromethane – petroleum ether gave pure scleroderolide diacetate (**1***b*, mp 200–202°C, 80% yield); tlc: R_f 0.22 (benzene–acetone – acetic acid, 90:10:0.1), yield spot; $[\alpha]_D$ −44.6° (*c* 0.28, $CHCl_3$); ir ($CHCl_3$, cast): 2970, 1760, 1670, 1625, 1580, 1530, 1460, 1410, 1360, 1180, 1040 cm^{-1}; ^{1}H nmr (toluene-d_8)

[3]Clarified V-8 juice refers to V-8 (eight garden vegetables, Campbell Soup Company Ltd.) juice filtered through a pad of Celite.

[4]Details of the assignment are reported in Part 4 of this series.

Can. J. Chem. Downloaded from www.nrcresearchpress.com by 78.46.186.204 on 09/07/12
For personal use only.

Can. J. Chem. Downloaded from www.nrcresearchpress.com by 78.46.186.204 on 09/07/12
For personal use only.

at 60°C, δ: 1.0 (3H, s, C-3′ CH_3), 1.06 (3H, d, 6.5 Hz, C-2′ CH_3), 1.17 (3H, s, C-3′ CH_3), 1.82 (3H, s, $OOCCH_3$), 2.20 (3H, s, $OOCCH_3$), 2.60 (3H, s, $ArCH_3$), 4.21 (1H, q, 6.5 Hz, C-2′ H), 6.78 (1H, s, C-8 H); ^{13}C nmr ($CDCl_3$) at 55°C, δ: 14.3 (br),[5] 20.5, 21.0, 21.5, 22.4, 25.7 (br), 44.0, 92.4, 112.7, 115.9, 123.8, 124.8, 127.9, 134.7, 135.4, 137.6, 152.8, 153.4, 166.8, 168.0, 176.2; hrms, *m/z* calcd. for $C_{22}H_{20}O_8$ (M^+): 412.1158; found: 412.1164 (6), 384 (7), 370 (6), 342 (21), 328 (12), 300 (100), 285 (50).

*Sclerodin monoacetate (**3**a)*

Sclerodin (**3**, 3 mg) was dissolved in dichloromethane, and acetic anhydride (excess) and 4-*N*,*N*-dimethylaminopyridine (catalytic amount) were added at room temperature. After 30 min the reaction mixture was diluted with dichloromethane, then washed successively with 5% aqueous hydrochloric acid and water. The dichloromethane layer was dried (Na_2SO_4), filtered, and concentrated. Preparative thin-layer chromatography (benzene–acetone, 95:5) gave **3***a* (3 mg); tlc: R_f 0.44 (benzene–acetone, 95:5), blue fluorescence under uv light; ir ($CHCl_3$, cast): 2980, 1780, 1750, 1670, 1610, 1420, 1290, 1180, 1015 cm^{-1}; ^1H nmr ($CDCl_3$) δ: 1.28 (3H, s, C-3′ CH_3), 1.49 (3H, d, 6.5 Hz, C-2′ CH_3), 1.53 (3H, s, C-3′ CH_3), 2.42 (3H, s, $OOCCH_3$), 2.86 (3H, s, $ArCH_3$), 4.73 (1H, q, 6.5 Hz, C-2′ H), 6.97 (1H, s, C-8 H), 12.14 (1H, s, OH); hrms, *m/z* calcd. for $C_{20}H_{18}O_7$ (M^+): 370.1052; found: 370.1045 (9), 328 (37), 313 (100), 285 (6), 269 (6).

*Sclerodin monoacetate (**3**b) and sclerodin diacetate (**3**c)*

Sclerodin (**3**, 10 mg) was dissolved in dichloromethane, and acetic anhydride (excess) and trifluoroacetic acid (0.5 mL) were added at room temperature. After 12 h the reaction mixture was diluted with dichloromethane and washed with water. The dichloromethane layer was dried (Na_2SO_4), filtered, and coevaporated with toluene. Preparative thin-layer chromatography (benzene–acetone, 95:5) gave **3***b* (2 mg) and **3***c* (8 mg). Monoacetate **3***b* was also prepared by hydrolysis ($NaHCO_3$, H_2O, MeOH; room temperature; 6 h) of diacetate **3***c*. Sclerodin monoacetate (**3***b*) showed the following properties: tlc: R_f 0.35 (benzene–acetone, 95:5), blue fluorescence under uv light; ir ($CHCl_3$, cast): 2980, 1780, 1750, 1670, 1610, 1300, 1180, 1030, 860 cm^{-1}; ^1H nmr ($CDCl_3$) at 55°C, δ: 1.26 (3H, br s, C-3′ CH_3), 1.45 (3H, br s, C-3′ CH_3), 1.50 (3H, d, 6.5 Hz, C-2′ CH_3), 2.47 (3H, s, $OOCCH_3$), 2.87 (3H, s, $ArCH_3$), 4.69 (1H, q, 6.5 Hz, C-2′ H), 6.98 (1H, s, C-8 H), 11.88 (1H, s, OH); ^1H nmr (toluene-d_8) at 65°C, δ: 1.0 (3H, s, C-3′ CH_3), 1.05 (3H, d, 6.5 Hz, C-2′ CH_3), 1.16 (3H, s, C-3′ CH_3), 2.17 (3H, s, $OOCCH_3$), 2.52 (3H, s, $ArCH_3$), 4.21 (1H, q, 6.5 Hz, C-2′ H), 6.56 (1H, s, C-8 H), 12.0 (1H, s, OH); hrms, *m/z* calcd. for $C_{20}H_{18}O_7$ (M^+): 370.1052; found: 370.1058 (12), 328 (33), 313 (100), 285 (5), 269 (5).

Sclerodin diacetate (**3***c*) showed the following properties: tlc: R_f 0.26 (benzene–acetone, 95:5), blue fluorescence under uv light; ir ($CHCl_3$, cast): 2980, 1778, 1760, 1724, 1605, 1600, 1290, 1015 cm^{-1}; ^1H nmr (toluene-d_8) at 65°C, δ: 1.0 (3H, s, C-3′ CH_3), 1.07 (3H, d, 6.5 Hz, C-2′ CH_3), 1.16 (3H, s, C-3′ CH_3), 2.13 (3H, s, $OOCCH_3$), 2.16 (3H, s, $OOCCH_3$), 2.55 (3H, s, $ArCH_3$), 4.23 (1H, q, 6.5 Hz, C-2′ H), 6.68 (1H, s, C-8 H); hrms, *m/z* calcd. for $C_{22}H_{20}O_8$ (M^+): 412.1158; found: 412.1161 (11), 370 (26), 328 (64), 313 (100).

*Scleroderolide α-methoxy-α-trifluoromethyl-α-phenylacetate (**8**)*

Pure scleroderolide (**1***a*, ca. 3 mg) was dissolved in dichloromethane (1 mL) containing 4-*N*,*N*-dimethylaminopyridine (excess) and the solution was added to α-methoxy-α-trifluoromethyl-α-phenylacetyl chloride (prepared from the corresponding (−)-acid and oxalyl chloride – dimethylformamide) at room temperature. After 20 min the reaction mixture was diluted with dichloromethane and washed successively with 5% aqueous hydrochloric acid and water. The dichloromethane layer was dried (Na_2SO_4), filtered, and concentrated to give the crude product. Preparative thin-layer chromatography (benzene–acetone – acetic acid, 90:10:0.1) gave **7** (2.4 mg); tlc: R_f 0.38 (benzene–acetone – acetic acid, 90:10:0.1), yellow spot; ^1H nmr ($CDCl_3$) δ: 1.36 (3H, s, C-3′ CH_3), 1.53 (3H, d, 6.5 Hz, C-2′ CH_3), 1.58 (3H, s, C-3′ CH_3), 2.80 (3H, s, $ArCH_3$), 3.81 (3H, s, OCH_3), 4.81 (1H, q, 6.5 Hz, C-2′ H), 6.95 (1H, s, C-8 H), 7.53 (3H, m, Ph H's), 7.80 (2H, m, Ph H's), 13.71 (1H, s, OH); hrms, *m/z* calcd. for $C_{28}H_{23}F_3O_8$ (M^+): 544.1345; found: 544.1348 (6), 342 (6), 314 (7), 189 (100).

*Anhydroscleroderolide diacetate (**9**)*

Pure scleroderolide (**1**, 6 mg) was dissolved in dichloromethane (4 mL), and acetic anhydride (excess) and 4-*N*,*N*-dimethylaminopyridine (excess) were added at room temperature. After 2 h the reaction mixture was diluted with dichloromethane and washed successively with 5% aqueous hydrochloric acid (10 mL) and water (10 mL). The dichloromethane layer was successively dried (Na_2SO_4), filtered, and concentrated. Preparative thin-layer chromatography (benzene–acetone – acetic acid, 90:10:1, double elution) gave **9** (45% yield); tlc: R_f 0.37 (benzene–acetone – acetic acid, 90:10:0.1), yellow spot; $[\alpha]_D$ −21.2° (*c* 0.17, $CHCl_3$); ir ($CHCl_3$, cast): 2980, 1774, 1738, 1590, 1570, 1188, 1032 cm^{-1}; ^1H nmr ($CDCl_3$) δ: 1.39 (3H, s, C-3′ CH_3), 1.52 (3H, d, 6.5 Hz, C-2′ CH_3), 1.65 (3H, s, C-3′ CH_3), 2.44 (3H, s, acetyl CH_3), 2.84 (3H, s, $ArCH_3$), 4.76 (1H, q, 6.5 Hz, C-2′ H), 6.94 (1H, s, vinylic H), 7.09 (1H, s, C-8 H); hrms, *m/z* calcd. for $C_{22}H_{18}O_7$ (M^+): 394.1052; found: 394.1050 (18), 352 (100), 337 (67), 300 (20); cims, *m/z*: 412 (*M* + 18, 14), 394 (100).

*Preparation of scleroderolide (**1**) from sclerodione (**5**)*

Sclerodione (**5**, 4.3 mg) was dissolved in dichloromethane (3 mL) and *m*-chloroperbenzoic acid (3.4 mg) in dichloromethane (1 mL) was added at room temperature. After 5 h the reaction mixture was diluted with dichloromethane and washed with aqueous sodium bicarbonate. The dichloromethane layer was dried and concentrated to give a mixture of sclerodin (**3**) and scleroderolide (**1**). The aqueous layer was extracted several times with dichloromethane; the dichloromethane extracts were combined, and evaporated to dryness. Thin-layer chromatography of the residue showed a major yellow spot corresponding to scleroderolide. Acetylation (acetic anhydride – 4-*N*,*N*-dimethylaminopyridine) of this residue gave, after work-up (*vide supra*), scleroderolide monoacetate **1***a* (2 mg, 40% yield from **5**), identical with an authentic sample (tlc, ir, ^1H nmr, and hrms).

*Aerial oxidation of sclerodione (**5**)*

Sclerodione (**5**, 5 mg) was dissolved in dichloromethane (5 mL) in a loosely stoppered flask. After 5 weeks, separation of the reaction mixture by ptlc (dichloromethane–methanol, 49:1, double elution), gave sclerodin (**3**, 1 mg) and recovered sclerodione (3 mg). Sclerodin (**3**) was identical with an authentic sample (tlc, ir, ^1H nmr, and hrms).

X-ray crystallographic study of racemic scleroderolide monoacetate

Red-orange single crystals of racemic scleroderolide monoacetate suitable for X-ray diffraction analysis were obtained from CH_2Cl_2 – Skellysolve B. The crystal was roughly cubic with edges of 0.4 mm. Preliminary X-ray photographs showed triclinic symmetry. Precise lattice constants of a = 11.027 (2), b = 9.716 (1), c = 9.300 (1) Å, α = 77.44 (1), β = 91.34 (1), and γ = 117.97 (1)°, were determined by a least-squares analysis of the diffractometrically measured angular positions of 15 reflections. The results of the X-ray analysis show the space group for the crystals to be $P\bar{1}$, in which one molecule of scleroderolide monoacetate ($C_{20}H_{28}O_7$, M.Wt. = 370.44, V = 855.4 (2) Å^3, ρ_{calc} = 1.44 g/cm^3), μ = 8.8 cm^{-1}, forms the asymmetric unit. All unique diffraction data with $2\theta < 114°$ were surveyed using nickel-filtered CuK radiation (λ = 1.54178 Å) and a variable-speed ω-scan (1° scan width, 1.0°/min ≤ speed ≤ 29.3°/min) on a Syntex $P2_1$ diffractometer. After correction for Lorentz, polarization, and background effects, 1957 of a total of 2300 unique data (85.1%) were considered observed ($|F_o| > 3\sigma_F$) and used for the ensuing structure solution and refinement.[6]

[5]These signals are sharp at 75°C in toluene-d_8.

[6]All crystallographic computations and formulae are given in the Ph.D. thesis of Edward Van Dyke Arnold, Cornell University, 1982.

The structure of scleroderolide monoacetate was solved by standard multisolution direct methods.[7] All hydrogens were located by a difference synthesis following partial refinement. Block-diagonal least-squares refinement, with anisotropic oxygens and carbons and isotropic hydrogens, converged to a residual of 0.047 for the observed data.

Figure 1 shows a computer-generated perspective drawing of the final X-ray model of one enantiomer of scleroderolide monoacetate. The five-membered ring of scleroderolide monoacetate is in the C_2 conformation with the two-fold axis bisecting the C-5—C-6 bond. There is an intramolecular hydrogen bond between O-4 (H) and O-3 with an O-4—(H)—O-3 distance of 1.57 Å and OHO angle of 156°. The best least-squares plane through the 13 atoms of the three six-membered rings shows a maximum deviation of 0.095 Å from the plane for atom C-9. Although the substituents O-3, O-4, O-6, and C-3′ are also within 0.09 Å of this plane, O-2, C-7 Me, and O-9 are respectively 0.20, 0.16, and 0.18 Å away from this plane.

Tables of fractional coordinates and thermal parameters, bond distances, bond angles, torsion angles, and observed and calculated structure factors are available.[8]

Acknowledgements

The work at the University of Alberta was financially supported by the Natural Sciences and Engineering Research Council of Canada and that at Cornell University by the National Institutes of Health. To both of these agencies we extend our thanks. We also wish to thank Dr. Y. Hiratsuka for providing cultures of *G. abietina* and Dr. D. E. Ward for his interest and helpful advice.

[7]All crystallographic calculations were done on a PRIME 850 computer, operated by the Cornell Chemistry Computing Facility. Principal programs employed were REDUCE and UNIQUE (13); MULTAN78, A System of Computer Programs for the Automatic Solution of Crystal Structures from X-ray Diffraction Data, direct methods programs and Fast Fourier Transform routine (locally modified to perform all Fourier calculations including Patterson syntheses) (14); NQEST, CYBER 173 version, negative quartets figure of merit calculation (15); BLS78A, anisotropic block-diagonal least squares refinement (16); ORTEP, crystallographic illustration program (17). For a summary description of MULTAN, see ref. 18. For a summary of NQEST, refer to ref. 19.

[8]These tables may be purchased from the Depository of Unpublished Data, CISTI, National Research Council of Canada, Ottawa, Ont., Canada K1A 0S2.

1. W. A. Ayer, Y. Hoyano, M. S. Pedras, and I. van Altena. Can. J. Chem. **64**, 1585 (1986).
2. C. E. Dorworth and Y. Krywienczyk. Can. J. Bot. **53**, 2506 (1975).
3. K. A. Kine and R. E. Sievers. Aldrichimica Acta, 54 (1977).
4. G. R. Sullivan. Top. Stereochem. **10**, 287 (1978).
5. J. A. Dale and H. S. Mosher. J. Am. Chem. Soc. **95**, 512 (1973).
6. K. G. Neill and H. Raistrick. Biochem. J. **65**, 166 (1957).
7. N. Narashimhachari and L. C. Vining. Can. J. Chem. **41**, 641 (1963).
8. I. C. Paul and G. A. Sim. J. Chem. Soc. 1097 (1965).
9. J. S. Brooks and G. A. Morrison. Chem. Commun. 1359 (1971).
10. D. A. Frost, D. D. Halton, and G. A. Morrison. J. Chem. Soc. Perkin Trans. 1, 2443 (1977).
11. K. Homma, K. Fukuyama, Y. Katsube, Y. Kimura, and T. Hamasaki. Agric. Biol. Chem. **44**, 1333 (1980).
12. W. C. Still, M. Kahn, and A. Mitra. J. Org. Chem. **43**, 1923 (1978).
13. M. E. Leonowicz. REDUCE and UNIQUE, data reduction programs. Cornell University. 1978.
14. P. Main, S. E. Hull, L. Lessinger, G. Germain, J.-P. Declercq, and M. M. Woolfson. MULTAN78. University of York, England. 1978.
15. C. M. Weeks. NQEST, CYBER 173. Medical Foundation of Buffalo, Inc. August, 1976.
16. K. Hirotsu and E. Arnold. BLS78A. Cornell University. 1980.
17. C. K. Johnson. ORTEP, ORNL-3794. Oak Ridge, TN.
18. G. Germain, P. Main, and M. M. Woolfson. Acta Crystallogr. Sect. B, **26**, 274 (1970); M. M. Woolfson. Acta Crystallogr. Sect. A, **33**, 219 (1977).
19. G. T. DeTitta, J. W. Edmonds, D. A. Langs, and H. Hauptman. Acta Crystallogr. Sect. A, **31**, 472 (1975).

Can. J. Chem. Downloaded from www.nrcresearchpress.com by 78.46.186.204 on 09/07/12
For personal use only.

Metabolites produced by the Scleroderris canker fungus, *Gremmeniella abietina*. Part 3. Some further metabolites

WILLIAM A. AYER AND M. SOLEDADE PEDRAS

Department of Chemistry, University of Alberta, Edmonton, Alta., Canada T6G 2G2

Received August 8, 1986

WILLIAM A. AYER and M. SOLEDADE PEDRAS. Can. J. Chem. **65**, 754 (1987).

This article describes the metabolites of a strain of *Gremmeniella abietina* (Lagerb.) Morelet indigenous to Alberta. This strain does not produce the phenalenone derived metabolites isolated from the other strains of *G. abietina* examined to date. Only fatty acids and esters, glycerides, and sterol esters were produced. This raises a question regarding the identity of this particular strain. A greenish-yellow metabolite named Scleroderris green, isolated from a New Brunswick strain of *G. abietina*, is shown to have structure **12**. Scleroderris green (**12**) is structurally related to Scleroderris blue (**4**) and is produced when the latter compound is reduced with sodium bisulfite. Air oxidation of Scleroderris green (**12**) gives rise to Scleroderris blue (**4**). The structure of compound **12** was established by a study of the ^{13}C nmr spectra of the three pentamethyl derivatives (**8**, **9**, and **10**) produced when **12** is treated with ethereal diazomethane. It is suggested that the greenish discoloration of the wood of Scleroderris infected pine may be due to the presence of compound **12**.

WILLIAM A. AYER et M. SOLEDADE PEDRAS. Can. J. Chem. **65**, 754 (1987).

Dans ce travail, on décrit les métabolites d'une souche de *Gremmeniella abietina* (Lagerb.) Morelet qui est indigène à l'Alberta. Cette souche ne produit pas les métabolites dérivés de la phénalénone qui ont été isolés des autres souches de *G. abietina* qui ont été examinées jusqu'à maintenant. Il ne se produit que des acides gras et des esters, des glycérides ainsi que des esters de stérols. On démontre qu'un métabolite jaune-verdâtre, nommé le vert de Scléroderris et qui a été isolé d'une souche de *G. abietina* du Nouveau Brunswick, possède la structure **12**. Le vert de Scléroderris (**12**) possède une structure apparentée à celle du bleu de Scléroderris (**4**) et il se transforme en ce dernier lorsqu'on le réduit par du bisulfite de sodium. Une oxydation par de l'air du vert de Scléroderris (**12**) conduit au bleu de Scléroderris (**4**). On a déterminé la structure du composé **12** grâce à une étude des spectres rmn du ^{13}C des trois dérivés pentaméthylés (**8**, **9** et **10**) qui sont formés lorsqu'on traite le composé **12** par une solution éthérée de diazométhane. On suggère que la décoloration verdâtre du bois des pins infectés par le Scléroderris pourrait être du à la présence du composé **12**.

[Traduit par la revue]

In Parts 1 and 2 of this series (1, 2) we have described several metabolites produced in liquid culture by the Scleroderris canker fungus *Gremmeniella abietina* (Lagerb.) Morelet. The fungus *G. abietina* has been subdivided serologically into two races, the European and the North American.[1] The strain of the fungus used in the previous studies (1, 2), Canadian Forestry Service strain C-699, isolated in New Brunswick, is a member of the so-called European race. As part of our study of this plant disease we have compared the metabolites produced by different strains of this fungus collected in different parts of the world.[2] While most of these strains showed a similar chromatographic profile to that of strain C-699, the chromatographic profile of strain C-656, collected in Alberta, was distinctly different.[3] This report describes the metabolites of *G. abietina* strain C-656 as well as the isolation of a new metabolite from strain C-699.

Gremmeniella abietina strain C-656 was grown in still culture at 16–17°C on a medium of 10% V-8 juice containing added glucose. After four weeks the mycelium was harvested and extracted in a Soxhlet apparatus to give a brownish oily material, which was then fractionated by silica gel chromatography. The most polar fraction was readily identified, by its ir and ^1H nmr spectra, as a mixture of fatty acids. The high resolution mass spectrum (hrms) of the methylated (ethereal diazomethane) mixture revealed molecular ions corresponding to stearic ($C_{19}H_{38}O_2$), oleic ($C_{19}H_{36}O_2$), linoleic ($C_{19}H_{34}O_2$), and palmitic ($C_{17}H_{34}O_2$) acid methyl esters. The relative amount of each acid was estimated by integration of the ^1H nmr spectrum as follows (5): the resonance at δ 2.77 is due to the two doubly allylic hydrogens (C-11 H's) of linoleic acid. Since it integrates for 0.5 units and the total methyl groups (δ 0.89) for 3.0 units, this acid constitutes approximately 25% ($3/2 \times 0.5/3.0 \times 100$) of the mixture. The resonance at δ 5.30 (*CH*=*CH*), due to oleic and linoleic acids, integrates for 2.0 units, indicating that oleic acid comprises about 50% ($3/2 \times (2.0 - 1.0)/3.0 \times 100$) of the mixture. The remaining 25% is a mixture of stearic and palmitic acids.

The least polar fraction was similarly identified as a mixture of methyl linoleate (ca. 40%), methyl stearate, and methyl palmitate (ca. 35%).

The fractions of intermediate polarity contained di- and triglycerides, which were identified by means of their ^1H nmr, hrms, and chemical ionization mass spectra (cims). The ^1H nmr spectrum of the triglyceride fraction shows the characteristic signals of a triacylglycerol (5): δ 4.20 (2H, dd, 6, 12 Hz), 4.30 (2H, dd, 4.5, 12 Hz), and 5.36 (m, C-2 H) corresponding to five hydrogens of the glyceryl moiety, as well as the resonances due to the fatty acid residues (the signal at δ 5.36 overlaps with those of the olefinic protons). Although the hrms of this fraction did not reveal a molecular ion, analysis of the observed fragmentation pattern (6) provided evidence for the fatty acid composition of the triglycerides. Five major tetraoxygenated ion peaks, which represent the loss of an acyloxy group ($[M - RCOO]^+$ or $[M - RCOOH]^+$) were observed: m/z 604 ($C_{39}H_{72}O_4$), 603 ($C_{39}H_{71}O_4$), 602 ($C_{39}H_{70}O_4$), 600 ($C_{39}H_{68}O_4$), and 577 ($C_{37}H_{70}O_4$). These peaks indicate the presence of at least four different fatty acid residues in the triglyceride molecules. The acyl ions ($[RCO]^+$ or $[RCOH]^+$) detected (m/z 265 ($C_{18}H_{33}O$), 264 ($C_{18}H_{32}O$), 263 ($C_{18}H_{31}O$), 262

[1] For a good summary of all aspects of this disease see ref. 3.

[2] Canadian Forestry Service strains C-656 (Alberta), C-659 (Ontario), C-704 (Japan), C-706 (Sweden), C-707 (New York), C-708 (Vermont) provided by Y. Hiratsuka, Northern Forest Research Centre, Canadian Forestry Service, Edmonton.

[3] For details of this study, see ref. 4.

Can. J. Chem. Downloaded from www.nrcresearchpress.com by 78.46.186.204 on 09/07/12
For personal use only.

Can. J. Chem. Downloaded from www.nrcresearchpress.com by 78.46.186.204 on 09/07/12
For personal use only.

($C_{18}H_{30}O$), 239 ($C_{16}H_{31}O$)) indicate the presence of oleic, linoleic, linolenic, and palmitic acid residues. Thus this material is a mixture of triglycerides, which may be represented by the general structural formulae:

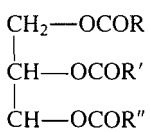

R, R′, R″ = $C_{17}H_{35}$, $C_{17}H_{33}$, $C_{17}H_{31}$, $C_{17}H_{29}$, $C_{15}H_{31}$

The 1,3-diglycerides can be distinguished from the 1,2-diglycerides by ^{1}H nmr (5). The ^{1}H nmr spectrum of the 1,3-diglycerides shows all of the glyceryl resonances in one multiplet (δ 4.18), whereas the ^{1}H nmr spectrum of 1,2-diglycerides shows four resonances (δ 3.76, 4.25, 4.35, and 5.10) for the glyceryl moiety. The cims of the 1,3-diglyceride fraction revealed it to be a complex mixture: *m/z* (relative intensity) 640 (16), 638 (72), 636 (87), 634 (51), 612 (73), 610 (79). These results indicate the presence of at least four different acyl residues corresponding to stearic, oleic, linoleic, linolenic, and palmitic acids. The general structural formulae of the components of the 1,3-diglyceride fraction may be represented as follows:

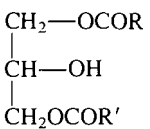

R, R′ = $C_{17}H_{35}$, $C_{17}H_{33}$, $C_{17}H_{31}$, $C_{17}H_{29}$, $C_{15}H_{31}$

Similar results were obtained with the 1,2-diglycerides. The cims clearly showed that this fraction was a mixture: *m/z* (relative intensity) 640 (13), 638 (16), 612 (88), 610 (18). The presence of stearic, oleic, linoleic, linolenic, and palmitic acid residues is consistent with these results. The general structural formulae of the components of the 1,2-diglyceride fraction may be represented as follows:

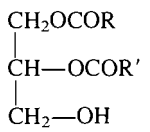

R, R′ = $C_{17}H_{35}$, $C_{17}H_{33}$, $C_{17}H_{31}$, $C_{17}H_{29}$, $C_{15}H_{31}$

Finally, the least abundant of the metabolites produced by strain C-656 was tentatively identified as a mixture of three sterol esters. The hrms of this fraction indicated two molecular ions: *m/z* 662 ($C_{46}H_{78}O_2$) and 660 ($C_{46}H_{76}O_2$) (confirmed by cims). The base peak at *m/z* 380 ($C_{28}H_{44}$) and a peak at *m/z* 382 ($C_{28}H_{46}$) suggested the loss of the same fragment ($C_{18}H_{32}O_2$) from the two molecular ions. This fragment is consistent with the loss of linoleic acid (7):

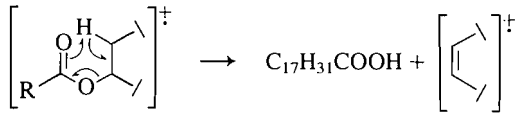

m/z 660 or 662 *m/z* 382 or 380

The ^{1}H nmr spectrum of this material is complex. It shows all the resonances attributable to a double unsaturated fatty acid (e.g., linoleic acid), as well as the following signals: δ 0.55 (s), 0.60 (s), 0.70 (s), 0.84 (vt), 0.92 (d), 0.98 (s), 4.64 (m), 5.2 (m). The ir shows carbonyl absorption at 1736 cm^{-1}.

The hrms of the neutral portion of the hydrolyzed (8) mixture (methanolic potassium hydroxide) showed a prominent peak at *m/z* 398 ($C_{28}H_{46}O$). A detailed analysis of the fragmentation pattern is precluded by the complexity of the spectrum. However, the major fragments support the hypothesis that it is a C_{28} sterol (8–10): *m/z* 383 (M − CH_3), 300 (M − C_7H_{14}), 271 (M − side chain − 2H), 255 (M − side chain − H_2O), 213 (M − side chain − H_2O − C_3H_6). The ^{1}H nmr spectrum of this hydrolyzed material is also consistent with a sterol mixture (11). It shows resonances at δ 0.54 (s), 0.61 (s), 0.70 (ca. 3H, s), 0.83 (ca. 6H, ap t, 6.5 Hz), 0.90 (ca. 3H, d, 6.5 Hz), 0.94 (s), 0.98–1.02 (m), 3.54 (m), 3.62 (m), 4.68 (<1H, br s); 4.72 (<1H, br s), 5.20 (ca. 2H, m), 5.37 (ca. 1H, m). On acetylation (12) (acetic anhydride – pyridine) the resonances at δ 3.54 and 3.62 shifted to δ 4.62 and 4.70 (acetyl methyls at δ 2.03 and 2.04).

A search of the literature revealed a similarity in the ^{1}H nmr chemical shifts between some 24-methylsterols (C_{28}) and our mixture. The major component in the mixture is a doubly unsaturated sterol: $C_{28}H_{46}O$, olefinic hydrogens at δ 5.20 (m) and 5.37 (m). The C-18 and C-19 hydrogens of $\Delta^{7,22}$ sterols are shifted upfield in relation to $\Delta^{5,22}$ isomers (e.g., δ 0.54 and 0.81 vs. δ 0.69 and 1.02) (11). Therefore the three singlets at δ 0.54, 0.61, and 0.70 (relative intensity 3:5:10) observed in the ^{1}H nmr spectrum of the mixture could be due to the C-18 hydrogens of three different sterols. The chemical shifts for the major component are consistent with those published (11, 13) for ergosta-5,22-diene-3β-ol (**1**). Although the resonances for the other components cannot be clearly assigned, the presence of signals at δ 4.68 (br s) and 4.72 (br s) (second major component) indicates the presence of a terminal methylene group (14). The second major component (C-18 hydrogens at δ 0.61) is consistent with ergosta-8,24(28)-diene-3β-ol (**2**) (14). A more definite assignment would require the separation of the components, which was not attempted because of the small quantities available.

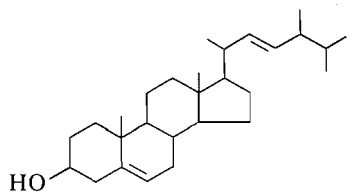

1

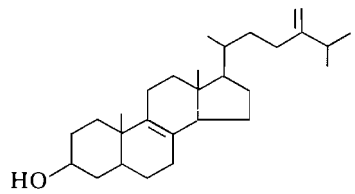

2

The strains of *G. abietina* previously studied (1, 2) (C-699 and C-708) produce metabolites possessing the phenalenone skeleton. We could not detect phenalenone metabolites in strain C-656 (Alberta). This raises a question regarding the identification of this strain. It is possible that the western fungus (C-656), which is only mildly pathogenic (15), represents a race (species?) different from those which occur in Eastern North America (C-699 and C-708) (15).

During the isolation of scleroderolide (**3**) (2) from the mycelium extract of *G. abietina* strain C-699, we observed that the thin-layer chromatograms (tlc) of some of the fractions obtained from column chromatography had a blue component,

Can. J. Chem. Downloaded from www.nrcresearchpress.com by 78.46.186.204 on 09/07/12
For personal use only.

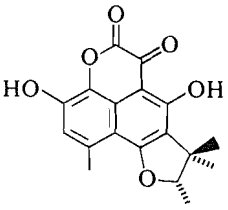

3

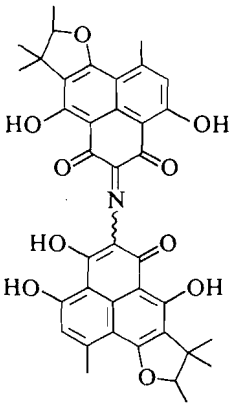

4

which seemed to increase in concentration with time. This blue component had an R_f identical with Scleroderris blue (**4**). This was unexpected since **4** is the least polar of the metabolites (1) isolated from *G. abietina*. We thus set about to isolate the compound responsible for this behaviour.

The mycelium methanolic extract from strain C-699 was washed with cold dichloromethane and the residue was vacuum dried to afford an amorphous greenish-yellow powder (mp > 350°C). This material, upon standing in solution, was transformed into blue material, which was identical with Scleroderris blue (**4**) by tlc comparison. Efforts to crystallize the greenish powder led to decomposition. The ^{1}H nmr spectrum of this material shows resonances consistent with the presence of fragment **5** (underlined hydrogens), as well as four downfield

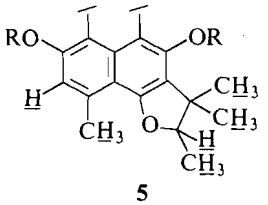

5

signals (δ 12–15, D_2O exchangeable). The hrms showed a prominent peak at *m/z* 326 ($C_{19}H_{18}O_5$) and a base peak at *m/z* 311 ($C_{18}H_{15}O_5$); the cims showed a base peak at *m/z* 327. These data suggested the molecular formula $C_{19}H_{18}O_5$, which would be consistent with a deoxyatrovenetin structure. Consideration of the biosynthesis of atrovenetin (**6**) (16) led us to consider structure **7** as a possibility. However, in the ^{1}H nmr

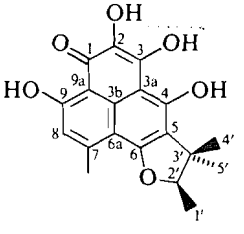

6

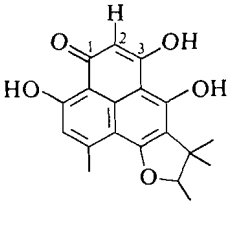

7

spectrum, we were unable to assign a signal attributable to the hydrogen at C-2. A structure such as **7** can exist in several tautomeric forms (the ^{1}H nmr is temperature dependent, indicating a dynamic equilibrium). To further study this material and to try at the same time to render it more stable, it was treated with an excess of ethereal diazomethane. After 12 h, the tlc of the reaction mixture showed three prominent spots. Preparative tlc of the crude reaction mixture yielded the three components. The hrms of each product indicated the presence of one nitrogen and suggested the molecular formula $C_{43}H_{45}NO_{10}$ (mol. wt. 735). Analysis of the ^{1}H and ^{13}C nmr spectra allowed the assignment of the "dimeric" structures **8**, **9**, and **10** to these derivatives.

The ^{1}H nmr spectrum of the most polar component, **8**, showed all of the characteristic signals of fragment **5**. However, to be consistent with a molecular formula of $C_{43}H_{45}NO_{10}$, the signals must represent twice the number of hydrogens, i.e., it must be a dimeric structure. The remaining protons appear as follows: δ 3.68 (3H, s), 3.90 (6H, s), 4.03 (6H, s), 18.50 (2H, s). The diazomethane treatment had apparently led to the introduction of five methyl groups. Except for small differences in chemical shifts, the ^{1}H nmr spectrum of the least polar compound (**10**) is the same as that for **8**. The compound of

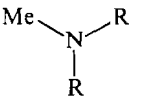

8

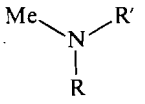

9

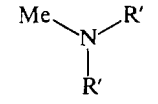

10

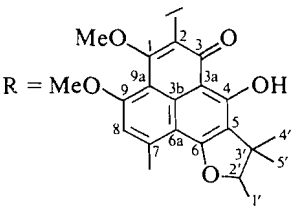

11*a*

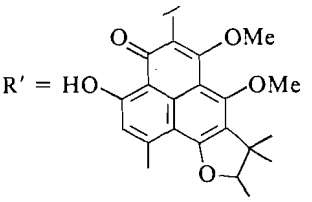

11*b*

intermediate polarity (**9**) has a different ^{1}H nmr spectrum. Instead of showing signals of double intensity for fragment **5**, each signal is paired. The remaining protons are observed as follows: δ 3.68 (3H, s), 3.80 (3H, s), 3.87 (3H, s), 3.91 (3H, s), 4.04 (3H, s), 17.91 (1H, s), 18.45 (1H, s). It is noteworthy that this ^{1}H nmr spectrum is simulated by superimposing the spectra of compounds **8** and **10**. The ^{1}H nmr spectra of these three derivatives suggest that two of them have an element of symmetry that renders two fragments of type **5** equivalent, while in the third the symmetry element does not exist. This hypothesis is supported by the ^{13}C nmr spectrum: compound **8** shows 22 signals while compound **9** shows 43 signals (the spectrum of **10** was not obtained because of a lack of sufficient material).

From these symmetry considerations several conclusions may be drawn: (1) the nitrogen atom must be involved in linking two identical fragments; (2) the point of attachment in each fragment must be identical; (3) each fragment must contain two OCH_3 groups and the fifth methyl group must be an N-CH_3 group; (4) each fragment must have an internally hydrogen-bonded OH group. Thus the structures may be represented as $(C_{21}H_{21}O_5)_2NCH_3$. The fragments ($C_{21}H_{21}O_5$) must each have two OCH_3 groups, an OH group, and the structural features inherent in **5**. These requirements are satisfied by an atrovenetin-like structure (**6**) in which one of the oxygens (at C-1, 2, 3, 4, or 9) is replaced by nitrogen, while two others are methylated. Since there are two different symmetrical derivatives, as well as an unsymmetrical one, the site of N-substitution must be such as to leave an arrangement of OH groups whereby dimethylation can occur in two ways, leaving two different hydrogen-bonded OH groups. The chemical shifts (δ 18.50 and 17.91) and the sharpness of the OH signals in the ^{1}H nmr spectra suggest an *ortho*-acyl phenol unit. Only nitrogen substitution at C-2 can provide a structure in which this feature may appear in two

Can. J. Chem. Downloaded from www.nrcresearchpress.com by 78.46.186.204 on 09/07/12
For personal use only.

TABLE 1. ^{13}C chemical shifts[a] of Scleroderris green derivatives

	Compound		
		9	
Carbon	8	R	R′
C-1	157.2	157.4	178.2[x]
C-2	133.7	133.6	132.4
C-3	177.2[x]	177.0[x]	156.9[y]
C-3a	107.7	107.6	109.9
C-3b	127.6	127.5	128.0
C-4	175.7[x]	175.9[x]	159.3[y]
C-5	119.3	119.4	126.2
C-6	166.5	166.6	162.2
C-6a	109.3	109.4	108.1
C-7	143.0	143.1	149.2
C-8	110.4	110.4	121.5
C-9	160.5	160.3	176.5[x]
C-9a	110.7	110.5	109.7
$ArCH_3$	23.9	24.0	24.4
C-1′	14.7	14.7	14.4
C-2′	91.1	91.1	90.2
C-3′	43.4	43.4	44.3
C-4′	25.9	25.9	26.2
C-5′	20.5	20.5	22.0
OCH_3	56.4	56.5	61.9
OCH_3	61.3	61.1	64.1
NCH_3	41.1	41.2	

[a]In $CDCl_3$. [x,y]Carbon assignments may be interchanged.

different ways. Thus structures **8**, **9**, and **10** may be proposed for the three derivatives.

The structures were confirmed by a thorough analysis of the ^{13}C nmr spectra. The proton decoupled ^{13}C nmr spectrum of compound **8** shows 22 signals. All except one (δ 41.1, NCH_3) of the signals represent a pair of equivalent carbons. The signals may be divided into three groups: 5 sp^2 carbons bound to oxygen (δ 150–180); 8 other sp^2 carbons (δ 107–150); 9 sp^3 carbons (δ 14–91). The 9 sp^3 carbons (C-1′, 2′, 3′, 4′, 5′, $ArCH_3$, 2 × OCH_3, and NCH_3) and C-8 are readily assigned based on chemical shift and (or) multiplicity as well as by analogy to other metabolites (17). The remaining carbons were assigned by analysis of the 2-, 3-, and 4-bond $^{13}C-^1H$ coupling observed in the fully coupled spectrum (confirmed by selective ^1H decoupling) as follows. Since the C-8 hydrogen should have large (ca. 6 Hz) (18) coupling to both C-6a and C-9a and small (ca. 2 Hz) coupling (16) to C-7 and C-9, and since only C-6a and C-7 should be coupled to the $ArCH_3$, the assignment of C-6a, C-7, C-9, and C-9a can be made unambiguously. Because of the $^3J_{CH}$ coupling, the assignment of the carbons bearing the OCH_3 and CH_3 groups is possible by irradiation of the appropriate CH_3 hydrogens (δ 3.68, 3.90, and 4.03). Similarly the carbon bearing the OH group (C-3, 4)[4] is identified by its $^2J_{CH}$ coupling (ca. 3 Hz), while the $^3J_{CH}$ coupling serves to locate the α carbons. The C-6 assignment is made on the basis of chemical shift and is confirmed by a small (< 1 Hz) coupling to the C-2′ hydrogen. Of the three remaining carbons (3a, 3b, and 5), C-3b is assigned on the basis of chemical shift as well as its lack of long range coupling. Finally, C-5 is a multiplet due to $^3J_{CH}$ coupling to the C-4′ and C-5′ hydrogens, while C-3a appears as a doublet if an OH is present at C-4 (or C-3).

The complete ^{13}C nmr assignments for compound **8** are shown in Table 1. The following observations are pertinent with respect to the proposed structure. Since the resonance at δ 160.3 is coupled to both the C-8 hydrogen (δ 6.82) and to the lower field OCH_3 hydrogens (δ 4.03), a methoxyl substituent at C-9 is indicated. Significantly, the OH hydrogen (δ 18.50) shows coupling to four resonances: δ 107.7 (C-3a), 119.4 (C-5), 175.7, and 177.2. The resonances at δ 177.2 and 175.7 are not coupled to the OCH_3 hydrogens and therefore must represent a carbonyl carbon and an sp^2 carbon bearing an OH group. This strongly indicates nitrogen substitution at C-2 and thus structure **8**.

The proton decoupled ^{13}C nmr spectrum of **9** exhibits 43 signals. The presence of fragment **11***a* was assumed, since 22 of the signals are very close to the 22 signals observed for **8**, with respect to chemical shift (within 0.2 ppm), multiplicity, and long range coupling (confirmed by selective proton decoupling of the NCH_3 (δ 3.68), the lower field OH (δ 18.45), the lower field C-8 H (δ 6.83), and the lower field $ArCH_3$ (δ 2.88)). That the remaining 21 resonances are due to a fragment of structure **11***b* was confirmed by analysis of the long range $^{13}C-^1H$ coupling (selective proton decoupling of the NCH_3 (δ 3.68), the higher field OH (δ 17.91), the higher field C-8 H (δ 6.79), and the higher field $ArCH_3$ (δ 2.78)), as described above for compound **8**. In this case the OH (δ 17.91) is coupled to four resonances: δ 109.2 (C-9a), 121.5 (C-8), 176.5, and 178.2. The δ 178.2 and 176.5 signals are also coupled to the C-8 hydrogen, thus confirming their assignment as C-1 and C-9. This coupling is uniquely consistent with fragment **11***b*. The complete assignment for **9** is given in Table 1.

The structures **8** and **9** are unambiguously confirmed and that of **10** may be inferred since its ^1H nmr spectrum is in agreement with that of fragment **11***b* in **9**. Thus the structure of the parent compound, for which we suggest the trivial name Scleroderris green, must be **12** (several tautomers possible).

Structure **12** is closely related to the structure proposed (1) for Scleroderris blue (**4**). This structural relationship was confirmed as follows. Scleroderris blue was treated with sodium bisulphite (the blue colour gradually changed to violet, green, and then yellow). After 18 h the tlc of the crude reaction mixture showed a major spot corresponding to **12**. Treatment of the crude reaction mixture with diazomethane (excess) gave, after ptlc (petroleum ether – ethyl acetate, 4:1), three products identical with authentic samples of **8** (tlc, ir, ^1H nmr, hrms), **9** (tlc, ir, ^1H nmr, hrms), and **10** (tlc). In addition, a solution of **12**

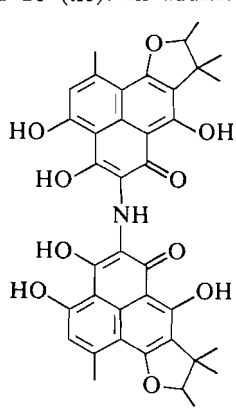

12

[4]Because of strong intramolecular hydrogen bonding, C-3 and C-4 are indistinguishable.

(dichloromethane–methanol), on standing, gives a blue compound identical (tlc) with Scleroderris blue (**4**).

The wood of Scleroderris infected pine shows a characteristic yellowish green coloration (19). It is possible that compound **12** causes this discoloration.

Experimental

For general experimental details see part 2 (2).

Growth of Gremmeniella abietina *strain C-656 and extraction of metabolites*

Gremmeniella abietina (strain C-656) was grown in liquid still culture at 16–17°C, as reported previously (2). After 4 weeks the mycelium was separated from the broth, washed with cold methanol, and dried. The dry mycelium was extracted with ethyl ether (24 h) and twice with methanol (24 h each) in a Soxhlet apparatus. The ether and methanol extracts were separately concentrated *in vacuo* at 30°C.

Isolation of metabolites from G. abietina *strain C-656*

The crude mycelium ether extract of *G. abietina* C-656 gave ca. 0.1 g/L of crude metabolites and the combined crude methanol extracts gave 0.4 g/L. Both extracts were brownish oils (similar by tlc). The crude mycelium ether extract (0.8 g) was fractionated by flash column chromatography (20) on Merck Silica Gel 60 (40–63 μm) with the following solvent system: dichloromethane–methanol (49:1, 1.5 L), dichloromethane–methanol (46:2, 1 L), and methanol (0.5 L). Fractions of 125 mL were collected. Fractions 2–4 and 15 were further purified as indicated for the individual components.

Fatty acids

The fatty acids were eluted in the most polar fractions. Fractions 19–21 (50 mg) gave a single spot on tlc; tlc: R_f 0.16 (dichloromethane–methanol, 49:1); ir ($CHCl_3$, cast): 2925, 2855, 1711, 1460, 1280, 938, 720 cm^{-1}; ^1H nmr ($CDCl_3$), δ: 0.89 (vt, 6.5 Hz, CH_3), 1.26–1.32 (m, $CH_2)_n$), 6.64 (m, CH_2CH_2CO), 2.0–2.08 (m, $CHCH$=), 2.34 (t, 8.0 Hz, CH_2CO), 2.77 (t, 6.5 Hz, =$CHCH_2CH$=), 5.30–5.42 (m, CH=CH); hrms, *m/z*: 97 (21), 95 (30), 83 (39), 82 (26), 81 (50), 69 (65), 68 (29), 67 (61), 57 (49), 56 (25), 55 (100); cims, *m/z*: 300 (*M* + 18 for 282, 26), 298 (*M* + 18 for 280, 74), 296 (*M* + 18 for 278, 87).

Methylation of fatty acids: the mixture of fatty acids (5 mg) was dissolved in dichloromethane (1 mL) and treated with excess ethereal diazomethane to give fatty acid methyl esters (5 mg); tlc: R_f 0.60 (petroleum ether – ethyl acetate, 9:1); hrms, *m/z*: 298 (25), 296 (27), 294 (34), 270 (13), 264 (95), 262 (14), 55 (100).

Fatty acid methyl esters

The fatty acid methyl esters were eluted in fractions 2–4 (80 mg). Preparative tlc (petroleum ether – ethyl acetate, 19:1, double elution) of these combined fractions gave a mixture of fatty acid methyl esters (10 mg); tlc: R_f 0.60 (petroleum ether – ethyl acetate, 9:1); ir ($CHCl_3$, cast): 3100, 2925, 2854, 1743, 1460, 1430, 1165, 720 cm^{-1}; ^1H nmr ($CDCl_3$), δ: 0.89 (vt, 6.5 Hz, CH_3), 1.26–1.32 (m, $CH_2)_n$), 1.64 (m, CH_2CH_2CO), 2.0–2.08 (m, CH_2CH=), 2.28 (t, 8.0 Hz, CH_2CO), 2.75 (t, 6.5 Hz, =$CHCH_2CH$=), 3.67 (s, OCH_3), 5.30–5.40 (m, CH=CH); hrms, *m/z*: 298 (3), 296 (2), 294 (2), 270 (12), 264 (7), 74 (100).

Triglycerides

The triglycerides were eluted in fractions 2–4 (80 mg). Preparative tlc (petroleum ether – ethyl acetate, 19:1) of these combined fractions gave a mixture of triglycerides (30 mg); tlc: R_f 0.36 (petroleum ether – ethyl acetate, 9:1); ir ($CHCl_3$, cast): 3010, 2925, 2854, 1745, 1463, 1163, 720 cm^{-1}; ^1H nmr ($CDCl_3$), δ: 0.89 (vt, 6.5 Hz, CH_3), 1.28–1.32 (m, $CH_2)_n$), 1.62 (m, CH_2CH_2CO), 2.05 (m, CH_2CH=), 2.32 (t, 7.0 Hz, CH_2CH_2CO), 2.78 (br t, 6.0 Hz, =$CHCH_2CH$=), 4.18 (dd, 6.0, 12 Hz, $OCH_2CH(O)CH_2O$), 4.30 (dd, 4.5, 12 Hz, $OCH_2CH(O)CH_2O$), 5.36 (m, CH=CH, $OCH_2CH(O)CH_2O$); hrms, *m/z*: 604 (45), 603 (80), 602 (63), 601 (40), 600 (43), 577 (78), 576 (39), 574 (25), 341 (7), 339 (28), 337 (8), 313 (19), 265 (24), 264 (36), 263 (32), 262 (89), 239 (11), 55 (100).

1,3-Diglycerides

The 1,3-diglycerides were eluted in fractions 6–10. Fraction 8 (10 mg) gave a single spot on tlc; tlc: R_f 0.45 (dichloromethane–methanol, 49:1); ir ($CHCl_3$, cast): 3460 (br), 2925, 2854, 1743, 1465, 1170, 720 cm^{-1}; ^1H nmr ($CDCl_3$), δ: 0.90 (vt, 6.5 Hz, CH_3), 1.28–1.32 (m, $(CH_2)_n$), 1.62 (m, CH_2CH_2CO), 2.04 (m, CH_2CH=), 2.37 (t, 7.0 Hz, CH_2CH_2CO), 2.48 (d, 4.5 Hz, OH), 2.78 (br t, 6.0 Hz, =$CHCH_2CH$=), 4.18 (m, $OCH_2CH(OH)CH_2O$), 5.36 (m, CH=CH); hrms, *m/z*: 602 (2), 600 (2), 576 (2), 339 (39), 313 (27), 265 (23), 264 (26), 262 (35), 239 (15), 55 (100); cims, *m/z*: 640 (*M* + 18 for 622, 16), 638 (*M* + 18 for 620, 72), 636 (*M* + 18 for 618, 87), 634 (*M* + 18 for 616, 51), 612 (*M* + 18 for 594, 74), 610 (*M* + 18 for 592, 80).

1,2-Diglycerides

The 1,2-diglycerides were eluted in fractions 12–16 (50 mg). Preparative tlc (dichloromethane–methanol, 97:3) of fraction 15 gave a mixture of 1,2-diglycerides (6 mg); tlc: R_f 0.33 (dichloromethane–methanol, 49:1); ir ($CHCl_3$, cast): 3440 (br), 2925, 2854, 1740, 1463, 1170, 720 cm^{-1}; ^1H nmr ($CDCl_3$), δ: 0.90 (vt, 6.5 Hz, CH_3), 1.28–1.32 (m, $(CH_2)_n$), 1.63 (m, CH_2CH_2CO), 2.03–2.08 (m, CH_2CH=, OH), 2.34 (m, CH_2CH_2CO), 2.79 (br t, 6.0 Hz, =$CHCH_2CH$=), 3.76 (t, 5.0 Hz, CH_2OH), 4.25 (dd, 6.0, 12 Hz, $OCH_2CH(O)CH_2OH$), 4.35 (dd, 4.5, 12 Hz, $OCH_2CH(O)CH_2OH$), 5.10 (m, $OCH_2CH(O)CH_2OH$), 5.36 (m, CH=CH); hrms, *m/z*: 604 (4), 602 (4), 576 (19), 341 (16), 339 (39), 313 (75), 265 (26), 264 (40), 262 (16), 239 (32), 55 (100); cims, *m/z*: 640 (*M* + 18 for 622, 13), 638 (*M* + 18 for 620, 16), 612 (*M* + 18 for 594, 88), 610 (*M* + 18 for 592, 18).

Sterol esters

The sterol esters were eluted in fractions 2–4. Preparative tlc (petroleum ether – ethyl acetate, 97:3, double elution) of these combined fractions gave a mixture of sterol esters (5 mg); tlc: R_f 0.55 (petroleum ether – ethyl acetate, 9:1); ir ($CHCl_3$, cast): 2954, 2928, 1736, 1460, 1175, 720 cm^{-1}; ^1H nmr ($CDCl_3$): see text; hrms, *m/z*: 662 (1), 660 (2), 535 (1), 382 (24), 381 (42), 380 (100), 337 (4), 282 (5), 255 (36), 253 (6); cims, *m/z*: 678 (*M* + 18 for 660, 69), 398 (100).

Hydrolysis of sterol esters: the mixture of sterol esters (4 mg), was dissolved in dichloromethane and 10% methanolic potassium hydroxide (excess) was added. After refluxing for 1 h, the reaction mixture was cooled, diluted with dichloromethane, washed with 5% hydrochloric acid, and concentrated. The resulting residue was fractionated by ptlc (petroleum ether – ethyl acetate, 4:1, double elution) to give a mixture of sterols (2 mg); tlc: R_f 0.26 (petroleum ether – ethyl acetate, 4:1); ir ($CHCl_3$, cast): 3400 (br), 2955, 2924, 2853, 1728 (w), 1460, 1370, 1060, 980 cm^{-1}; ^1H nmr ($CDCl_3$): see text; hrms, *m/z*: 400 (11), 298 (68), 396 (14), 383 (16), 363 (12), 314 (12), 300 (20), 271 (52), 255 (28), 69 (90), 55 (100).

Acetylation of sterols: the sterol mixture (2 mg) was dissolved in dichloromethane (1 mL) and acetic anhydride (excess) and pyridine (excess) were added at room temperature. After 24 h the reaction mixture was diluted with dichloromethane, washed with 5% hydrochloric acid, dried (Na_2SO_4), and concentrated to give a mixture of sterol acetates; tlc: R_f 0.70 (petroleum ether – ethyl acetate, 4:1); ir ($CHCl_3$, cast): 2955, 2860, 1730 (s), 1460, 1375, 1240, 1040, 970 cm^{-1}; ^1H nmr ($CDCl_3$): see text; hrms, *m/z*: 440 (16), 398 (16), 382 (20), 380 (100), 313 (19), 255 (38).

*Isolation of Scleroderris green (**12**)*

Scleroderris green (**12**) was isolated from the second methanol extract from *G. abietina* C-699. The crude mycelial extract was washed several times with cold dichloromethane and the residue was vacuum dried to afford ca. 200 mg of an amorphous greenish-yellow powder (mp > 340°C). Attempts at crystallization (CH_2Cl_2, EtOAc, MeOH, etc.) led to decomposition; tlc: R_f: 0.65 (benzene–acetone, 9:1), yellowish spot (with streaking), which turns blue on standing; uv (MeOH) λ_{max}: 214 (0.79), 259 (0.48), 396 (0.29) nm; ir ($CHCl_3$, cast): 3320 (br), 2920, 1617, 1380, 1280, 1060 cm^{-1}; ^1H nmr ($CDCl_3$) at 50°C, δ: 1.33 (6H, br s, C-3′ CH_3), 1.48 (6H, d, 6.6 Hz, C-2′ CH_3),

Can. J. Chem. Downloaded from www.nrcresearchpress.com by 78.46.186.204 on 09/07/12
For personal use only.

1.56 (6H, br s, C-3′ CH_3), 2.84 (6H, s, $ArCH_3$), 4.69 (2H, q, 6.6 Hz, C-2′ H), 6.88 (2H, s, C-8 H), 12.44, 13.28, 13.42, 14.26 (ca. 4H, D_2O exchangeable); hrms, *m/z*: 340 (15), 326 (38), 311 (100), 269 (24); cims, *m/z*: 327 (100).

Methylation of Scleroderris green

Scleroderris green **12** (ca. 40 mg) was suspended in dichloromethane (10 mL) and was treated with excess ethereal diazomethane. After 12 h, the crude reaction mixture was evaporated to dryness and fractionated by ptlc (petroleum ether – ethyl acetate, 4:1, multiple elution), to give compounds **8** (8 mg), **9** (8 mg), and **10** (3 mg). Compounds **8** (orange crystals, mp 282–283°C) and **9** (red crystals, mp 275–277°C) were crystallized from dichloromethane–methanol.

Compound 8: tlc: R_f 0.29 (petroleum ether–ethyl acetate, 3:1), yellow spot; $[\alpha]_D$ −36.4° (*c* 0.44, $CHCl_3$); ir ($CHCl_3$, cast): 3400 (br), 2920, 1607, 1580, 1452, 1354, 1300, 1223 cm^{-1}; ^1H nmr ($CDCl_3$), δ: 1.32 (6H, s, C-3′ CH_3), 1.46 (6H, d, 6.5 Hz, C-2′ CH_3), 1.54 (6H, s, C-3′ CH_3), 2.87 (6H, s, $ArCH_3$), 3.68 (3H, s, NCH_3), 3.90 (6H, s, OCH_3), 4.03 (6H, s, OCH_3), 4.64 (2H, q, 6.5 Hz, C-2′ H), 6.82 (2H, s, C-8 H), 18.50 (2H, s, OH); ^{13}C nmr ($CDCl_3$): see Table 1; hrms, *m/z* calcd. for $C_{43}H_{45}NO_{10}$ (M^+): 735.3043; found: 735.3035 (71), 704 (100); cims, *m/z*: 736 (100).

Compounds 9: tlc: R_f 0.35 (petroleum ether – ethyl acetate, 3:1), orange spot; $[\alpha]_D$ −78.6° (*c* 0.15, $CHCl_3$); ir ($CHCl_3$, cast): 3400 (br), 2920, 1607, 1580, 1455, 1354, 1299 cm^{-1}; ^1H nmr ($CDCl_3$), δ: 1.27 (3H, s, C-3′ CH_3), 1.33 (3H, s, C-3′ CH_3), 1.46 (3H, d, 6.5 Hz, C-2′ CH_3), 1.47 (3H, d, 6.5 Hz, C-2′ CH_3), 1.52 (3H, s, C-3′ CH_3), 1.56 (3H, s, C-3′ CH_3), 2.78 (3H, s, $ArCH_3$), 2.88 (3H, s, $ArCH_3$), 3.68 (3H, s, NCH_3), 3.80 (3H, s, OCH_3), 3.87 (3H, s, OCH_3), 3.91 (3H, s, OCH_3), 4.04 (3H, s, OCH_3), 4.55 (1H, q, 6.5 Hz, C-2′ H), 4.64 (1H, q, 6.5 Hz, C-2′ H), 6.79 (1H, s, C-8 H), 6.83 (1H, s, C-8 H), 17.91 (1H, s, OH), 18.45 (1H, s, OH); ^{13}C nmr ($CDCl_3$): see Table 1; hrms, *m/z* calcd. for $C_{43}H_{45}NO_{10}$ (M^+): 735.3043; found: 735.3061 (100), 704 (80), 366 (24), 341 (29); cims, *m/z*: 736 (100).

Compound 10: tlc: R_f 0.48 (petroleum ether – ethyl acetate, 3:1), red spot; ir ($CHCl_3$, cast): 3400 (br), 2925, 1609, 1586, 1458, 1318, 1296 cm^{-1}; ^1H nmr ($CDCl_3$), δ: 1.27 (6H, s, C-3′ CH_3), 1.46 (6H, d, 6.5 Hz, C-2′ CH_3), 1.52 (6H, s, C-3′ CH_3), 2.80 (6H, s, $ArCH_3$), 3.67 (3H, s, NCH_3), 3.75 (6H, s, OCH_3), 3.86 (6H, s, OCH_3), 4.56 (2H, q, 6.5 Hz, C-2′ H), 6.82 (2H, s, C-8 H), 17.91 (2H, s, OH); hrms, *m/z* calcd. for $C_{43}H_{45}NO_{10}$ (M^+): 735.3043; found: 735.3054 (100), 704 (69), 367 (39), 366 (44), 341 (26); cims, *m/z*: 736 (100).

Reduction of Scleroderris blue (4)

Scleroderris blue (**4**, 3 mg) was dissolved in dichloromethane–methanol (1:1, 2 mL) and aqueous sodium bisulfite (ca. 20 mg) was added with stirring at room temperature (the color of the reaction mixture changed from blue to violet, then green, and finally light yellow). After 18 h the reaction mixture was diluted with dichloromethane, washed with water (twice), dried, and concentrated. The tlc (benzene–acetone – acetic acid, 90:10:0.1) of the residue showed a major spot corresponding to Scleroderris green (**12**). To the residue (3 mg) in dichloromethane (1 mL) was added ethereal diazomethane (excess) at room temperature. After 12 h the solvents were evaporated and the residue was fractionated by ptlc (petroleum ether – ethyl acetate, 4:1, multiple elution) to give compounds **8** (0.5 mg), **9** (0.5 mg), and **10** (<0.3 mg). Compounds **8** and **9** were identical with authentic samples by tlc, ir, ^1H nmr, and hrms comparison; compound **10** was identical with an authentic sample by tlc.

Acknowledgements

We acknowledge with thanks the financial support of the Natural Sciences and Engineering Research Council of Canada. We also thank Dr. Y. Hiratsuka, Northern Forest Research Centre, Edmonton, for cultures of *G. abietina* and for his interest, and Mrs. Anna Szenthe for maintaining and growing the cultures. Thanks are also due to Drs. L. M. Browne and D. E. Ward for helpful discussion and assistance.

1. W. A. Ayer, Y. Hoytano, M. S. Pedras, and I. van Altena. Can. J. Chem. **64**, 1585 (1986).
2. W. A. Ayer, Y. Hoytano, M. Soledade Pedras, J. Clardy, and E. Arnold. Can. J. Chem. **65**, 000 (1987).
3. P. D. Manion (*Editor*). Scleroderris canker of conifers. Martinus Nijhoff, Dr. W. Junk Publishers, The Hague. 1984.
4. M. S. Pedras. The Ph.D. Thesis, University of Alberta, Edmonton. 1986. pp. 127–133.
5. C. Y. Hopkins. Prog. Chem. Fats Other Lipids, **8**, 215 (1965).
6. Carter Litchfield. Analysis of triglycerides. Academic Press, New York. 1972. pp. 207–210.
7. M. Ohnishi and Y. Fujino. Agric. Biol. Chem. **44**, 681 (1980).
8. Y. Fayret, L. Lacoste, Y. Alais, A. Lablache-Combier, A. Maquestiau, Y. van Harverbeke, R. Flammang, and H. Mispreuve. Phytochemistry, **18**, 431 (1979).
9. S. G. Wyllie and C. D. Djerassi. J. Org. Chem. **33**, 305 (1968).
10. H. Budzikiewicz, C. Djerassi, and D. H. Williams. Structure elucidation of natural products by mass spectrometry. Vol. II. Holden–Day Inc., San Francisco. 1964. pp. 94–101.
11. I. Rubinstein, L. J. Goad, A. D. H. Clague, and L. J. Mulheirn. Phytochemistry, **15**, 195 (1976).
12. F. de Simone, F. Senatore, D. Sica, and F. Zollo. Phytochemistry, **18**, 1572 (1979).
13. Y. M. Sheikh and C. Djerassi. Tetrahedron, **30**, 4095 (1974).
14. D. H. R. Barton, U. M. Kempe, and D. A. Widdowson. J. Chem. Soc. Perkin Trans. 1, 513 (1972).
15. Y. Hiratsuka and A. Funk. Plant. Dis. Rep. **60**, 631 (1976).
16. A. Quick, R. Thomas, and D. J. Williams. J. Chem. Soc. Chem. Commun. 1051 (1980).
17. T. J. Simpson. J. Chem. Soc. Perkin Trans. 1, 1233 (1979).
18. J. L. Marshall. Carbon–carbon and carbon–proton NMR couplings: Applications to organic stereochemistry and conformational analysis. Verlag Chemie International, Deerfield Beach, FA. 1983. pp. 42–51.
19. D. D. Skilling, J. T. O'Brien, and J. A. Beil. Forest Insect and Disease Leaflet 130, U.S. Dept. of Agric., Forest Service.
20. W. C. Still, M. Kahn, and A. Mitra. J. Org. Chem. **43**, 2923 (1978).

Can. J. Chem. Downloaded from www.nrcresearchpress.com by 78.46.186.204 on 09/07/12
For personal use only.

Metabolites produced by the Scleroderris canker fungus, *Gremmeniella abietina*. Part 4.[1] Biosynthetic studies

WILLIAM A. AYER, M. SOLEDADE PEDRAS, AND DALE E. WARD
Department of Chemistry, University of Alberta, Edmonton, Alta., Canada T6G 2G2

Received August 8, 1986

WILLIAM A. AYER, M. SOLEDADE PEDRAS, and DALE E. WARD. Can. J. Chem. **65**, 760 (1987).

The biosynthetic origin of the carbon atoms of the most highly oxidized, polyketide derived, ring (carbons 1–3) of the *Gremmeniella abietina* metabolites sclerodione (**3**), scleroderolide (**4**), sclerodin (**5**), and Scleroderris green (**6**) has been studied. It is shown that both C-1 and C-3 of **3** and **4** are derived from C-1 of acetate, and that C-2 of scleroderolide (**4**) is derived from C-2 of acetate while C-3 is derived from C-1 of acetate. As expected, C-1 and C-3 of Scleroderris green (**6**) originate from the carboxyl carbon of acetate, while C-2 originates from the methyl carbon of acetate. Complete ^{13}C and ^{1}H nuclear magnetic resonance spectra of these metabolites are reported. It has also been shown that *ent*-atrovenetin (*ent*-**7***a*) is a metabolite of *G. abietina*.

WILLIAM A. AYER, M. SOLEDADE PEDRAS et DALE E. WARD. Can. J. Chem. **65**, 760 (1987).

On a étudié l'origine biosynthétique des atomes de carbone du cycle le plus oxydé (carbones 1–3) et dérivé d'un polycétide des métabolites du *Gremmeniella abietina* suivants : la sclérodione (**3**), le sclérodérolide (**4**), la sclérodine (**5**) et le vert de Sclérodérris (**6**). On a démontré que les carbones C-1 ainsi que C-3 des composés **3** et **4** sont dérivés du carbone C-1 de l'acetate et que le C-2 du sclérodérolide (**4**) est dérivé du C-2 de l'acétate alors que le C-3 est dérivé du C-1 de l'acétate. Comme on pouvait s'y attendre, les carbones C-1 et C-3 du vert de Scleroderris (**6**) ont leur origine dans le groupement carboxyle de l'acétate alors que le C-2 provient du carbone méthylique de l'acétate. On rapporte les spectres de résonance magnétique nucléaire ^{13}C et ^{1}H complets de ces métabolites. On démontre aussi que le *ent*-atrovenétine (**7***a*-*ent*) est un métabolite du *G. abietina*.

[Traduit par la revue]

We have previously reported (1–3) the isolation from *Gremmeniella abietina* of several metabolites, which contain a phenalenone nucleus fused to a dihydrofuran ring. Several structurally related metabolites have been isolated from other fungi.[2] Biosynthetic studies on metabolites of *Penicillium herquei* (e.g., atrovenetin (**1**)) have revealed a heptaketide origin for the phenalenone nucleus, whereas the dihydrofuran ring is mevalonate derived (Scheme 1) (5). The metabolites of *G. abietina* are expected to have a similar biosynthetic origin. Three of the metabolites (**3**, **4**, and **5**) have one carbon atom less than the parent phenalenones (e.g., **1** and **2**). In principle such a degradation could involve the loss of C-1, C-2, or C-3. We have previously speculated (6) that *ent*-atrovenetinone (**2**) could be a precursor of sclerodione (**3**), by loss of C-2. A possible pathway from **2** to **3** is illustrated in Scheme 2. Oxidation of **3** could lead to both sclerodin (**5**) and scleroderolide (**4**) (Scheme 3).

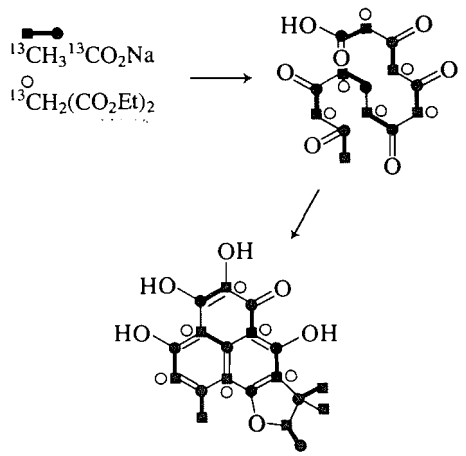

1

SCHEME 1

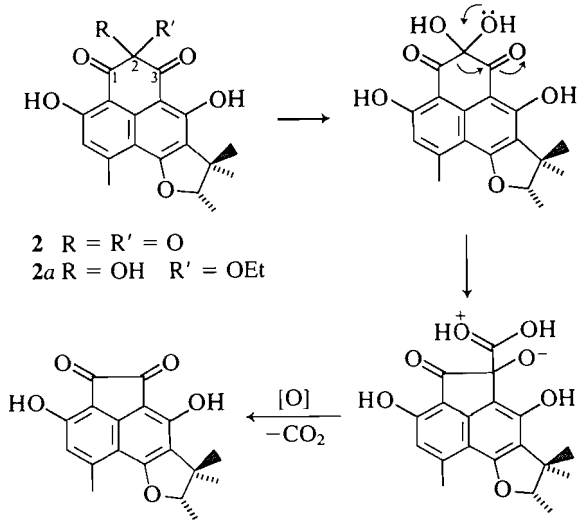

SCHEME 2

To examine the nature of this transformation we have studied the incorporation of [1-^{13}C]- and [2-^{13}C]acetate by *G. abietina* into compounds **3**, **4**, and **5**, as well as into the recently described Scleroderris green (**6**).

To follow the labelling pattern of ^{13}C enriched metabolites, it was first necessary to assign the ^{13}C chemical shifts for the metabolites. Since *ent*-atrovenetinone (**2**) is produced in small amounts, is unstable in solution (1), and since the stable ethanolate **2***a* is a mixture of epimers at C-2, we were prompted to utilize compound **6***a* rather than *ent*-atrovenetinone to represent metabolites with the intact phenalenone skeleton. Scleroderolide (**4**) was most conveniently isolated as the monoacetate **4***a*.

The ^{13}C nmr and ^{1}H nmr chemical shifts of **3**, **4***a*, **5**, and **6***a* are summarized in Tables 1 and 2. The ^{13}C nmr spectrum of **6***a* was assigned previously (3). Assignment of the ^{13}C nmr spectrum of sclerodin (**5**) was accomplished as follows. The

[1]For part 3, see preceding paper.

[2]For a recent review, see ref. 4.

Can. J. Chem. Downloaded from www.nrcresearchpress.com by 78.46.186.204 on 09/07/12
For personal use only.

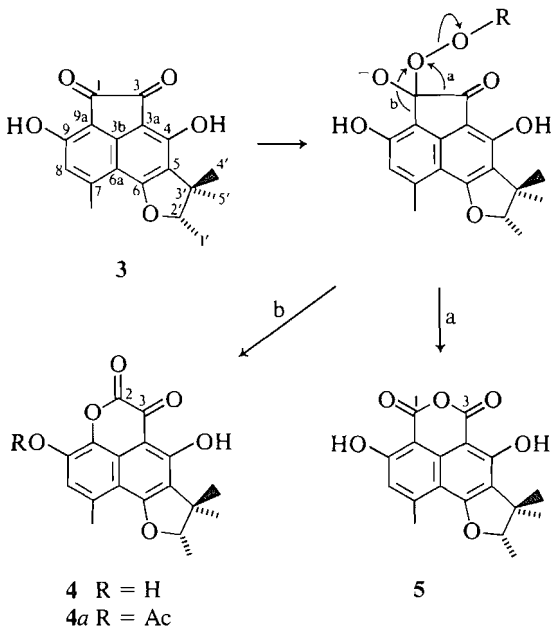

SCHEME 3

carbon shieldings in the proton decoupled spectrum may be subdivided into three groups: 5 sp^2 carbons bound to oxygen (δ 164–167); 7 other sp^2 carbons (δ 150–193); 6 sp^3 carbons (δ 14–93). The sp^3 carbons (C-1′, C-2′, C-3′, C-4′, C-5′, and $ArCH_3$) and C-8 are readily assigned on the basis of chemical shift, multiplicity, and by analogy to other metabolites (5). The remaining carbons of the phenalenone ring system are assigned by analysis of the 2-, 3-, and 4-bond $^{13}C-^1H$ coupling observed in the fully coupled spectrum (confirmed by selective proton decoupling experiments). Since the C-8 hydrogen should have

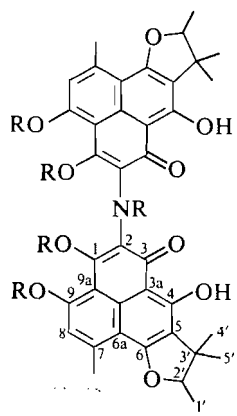

large (ca. 6 Hz) (7) coupling to both C-6a and C-9a and small (ca. 2 Hz) (7) coupling to C-7 and C-9, while only C-6a and C-7 should be coupled to the $ArCH_3$, the assignment of C-6a, C-7, C-9, and C-9a can be made unambiguously. The phenolic hydrogens at C-9 and C-4 are strongly hydrogen bonded and show coupling to C-1, C-9a, C-9 and C-3, C-3a, C-4, respectively. The previous assignment of C-9a allows unambiguous assignment of the phenolic hydrogens (C-9 OH, δ 11.43; C-4 OH, δ 11.64). Of the carbons coupled to the C-4 OH group, C-3a is assigned on the basis of chemical shift while C-4 is distinguished from C-3 on the basis of the magnitude of the coupling constants ($^2J_{CH}$ = 5 Hz, $^4J_{CH}$ = 2 Hz). Similarly, for the carbons coupled to the C-9 OH group the previous

TABLE 1. ^{13}C Chemical shifts[a] of some metabolites and derivatives of *G. abietina*

	Compound				
Carbon	**3**	**4*a***	**5**	**6*a***	
C-1	189.8[x]		165.4	157.2	
C-2		155.1		133.7	
C-3	186.3[x]	170.7	164.9	177.2[x]	
C-3a	106.2	107.6	93.5	107.7	
C-3b	150.9	122.2	135.4	127.6	
C-4	154.8	167.8	164.2	175.7[x]	
C-5	119.6	121.1	119.1	119.3	
C-6	164.3	169.0	166.1	166.5	
C-6a	109.2	113.5	108.5	109.3	
C-7	146.4	135.8	149.8	143.0	
C-8	117.4	122.3	117.3	110.4	
C-9	154.3	137.9	166.0	160.5	
C-9a	107.2	135.0	97.3	110.7	
$ArCH_3$	22.0	22.3	23.6	23.9	
C-1′	14.5	14.6	14.5	14.7	
C-2′	92.0	93.0	92.1	91.1	
C-3′	43.3	43.4	43.5	43.4	
C-4′	25.8	25.6	15.6	25.9	
C-5′	21.0	20.5	20.7	20.5	
$OOCCH_3$		168.2			
$OOCCH_3$		20.6			
OCH_3				56.4	61.3
NCH_3				41.1	

[a]In $CDCl_3$. [x]These assignments may be interchanged.

TABLE 2. ^1H nuclear magnetic resonance data[a] for some metabolites and derivatives of *G. abietina*

	Compound			
Proton	**3**	**4*a***	**5**	**6*a***
H-4′ (5′)	1.29	1.35	1.32	1.32
H-1′	1.48 (d, 8.0)	1.52 (d, 6.5)	1.51 (d, 7.0)	1.46 (d, 6.5)
H-5′ (4′)	1.54	1.57	1.55	1.54
$ArCH_3$	2.75	2.79	2.84	2.87
H-2′	4.67 (q, 8.0)	4.80 (q, 6.5)	4.72 (q, 7.0)	4.64 (q, 6.5)
H-8	6.66	7.01	6.85	6.82
OH	7.48, 7.79	13.77	11.43, 11.64	18.50
Other		2.43 ($OCCH_3$)		3.68 (NCH_3), 3.90 (OCH_3), 4.03 (OCH_3)

[a]Shift (δ), (multiplicity, *J*(Hz), in $CDCl_3$).

assignment of C-9a and C-9 leads to the recognition of C-1 (confirmed by the magnitude of the coupling constants $^2J_{CH}$ = 5 Hz, $^4J_{CH}$ = 2 Hz). The remaining sp^2 carbon bound to oxygen is thus assigned as C-6 (confirmed by $^3J_{CH}$ to the C-2′ H). Of the two remaining carbons, C-3b is assigned due to its lack of long range coupling, whereas C-5 appears as a multiplet in the coupled spectrum.

The assignment of the ^{13}C nmr spectrum of sclerodione (**3**) was made in a similar fashion. However, in this case the phenolic hydrogens appear as very broad signals in the ^1H nmr spectrum (δ 7.48 and 7.79, $W_{1/2}$ = 16 Hz), precluding selective decoupling. Thus C-1 and C-3 are distinguished from C-4 and

Can. J. Chem. Downloaded from www.nrcresearchpress.com by 78.46.186.204 on 09/07/12
For personal use only.

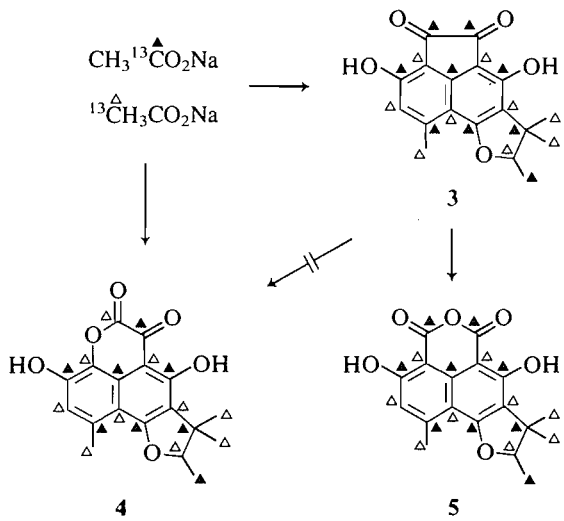

SCHEME 4

C-9 on the basis of chemical shift. While the assignment of C-9 (as with **5**) allows the assignment of C-4, C-1 and C-3 cannot be assigned unambiguously.

The assignment of the ^{13}C nmr spectrum of scleroderolide acetate (**4***a*) was made in a similar manner as for sclerodin (**5**). The acetate carbonyl (δ 168.2) is assigned by its two-bond $^{13}C-^{1}H$ coupling to the acetyl methyl hydrogens (δ 2.43). The C-2 carbonyl is assigned on the basis of its chemical shift (8) and its lack of long range coupling.

Gremmeniella abietina was grown in liquid still culture in the presence of sodium[1-^{13}C]acetate and, separately, in the presence of sodium[2-^{13}C]acetate. Compounds **3**, **4***a*, **5**, and **6***a* were isolated by chromatography.

Examination of the proton decoupled ^{13}C nmr spectrum of compound **6***a*, isolated from the culture containing [1-^{13}C]-labelled acetate, showed enrichment (about 5% incorporation) at carbons 1, 3, 3b, 4, 6, 7, 9, 1′, and 3′ relative to the natural abundance spectrum. The use of [2-^{13}C]-labelled acetate led to enrichment at the remaining carbons (C-2, C-3a, C-5, C-6a, C-8, C-9a, $ArCH_3$, C-2′, C-4′, and C-5′). These results are consistent with those obtained with *P. herquei* (5) and confirm the polyketide–mevalonate origin of these metabolites.

Examination of the proton decoupled ^{13}C nmr spectrum of sclerodione (**3**), isolated from the culture containing [1-^{13}C]acetate, revealed the same labelling pattern as that of **6***a*; again carbons[3] 1, 3, 3b, 4, 6, 7, 9, 1′, and 3′ were enriched (about 3% incorporation) relative to the natural abundance spectrum. When sclerodione (**3**) was isolated from the culture containing [2-^{13}C]acetate, carbons 3a, 5, 6a, 8, 9a, $ArCH_3$, 2′, 4′, and 5′ were enriched. These results are fully consistent with the hypothesis of formation of sclerodione (**3**) by loss of C-2 from an intact phenalenone skeleton.

According to Scheme 3, oxidation of sclerodione (**3**), enriched at C-1 and C-3, would lead to sclerodin (**5**) also enriched at C-1 and C-3 (path a) and to scleroderolide (**4**) enriched at C-2 and C-3 (path b). The ^{13}C nmr spectrum of sclerodin (**5**), isolated from the culture containing [1-^{13}C]acetate, showed the same labelling pattern as that for **3** and **6***a* (i.e., C-1 and C-3 are enriched). The ^{13}C nmr spectrum for scleroderolide acetate (**4***a*) isolated from the same culture, however, failed to show the expected enrichment at C-2. These results were confirmed by incorporation of [2-^{13}C]acetate (C-2 of **4***a* is derived from C-2 of acetate). Thus sclerodione (**3**) may be a biosynthetic precursor to sclerodin (**5**) but not to scleroderolide (**4**) (Scheme 4). The pathway leading to scleroderolide (**4**) must involve oxidation at an earlier stage, perhaps prior to cyclization of the heptaketide chain. Interestingly, in vitro oxidation of sclerodione (**3**) with *m*-chloroperbenzoic acid gives both scleroderolide (**4**) and sclerodin (**5**) (2); however, air oxidation gives only sclerodin (**5**) (2).

The oxidation of atrovenetin (**7**) to atrovenetinone (*ent*-**2**) (9) and **5** (10), as well as other unidentified products (**11**), has been reported. In our hands a dichloromethane–methanol solution of atrovenetin (**7**),[4] after standing for five weeks in the presence of air, gave rise to the enantiomers of compounds **2**, **3**, and **5** as the major products.

Examination of the hrms of crude methanol extracts of *G. abietina* revealed the presence of an ion corresponding to atrovenetin ($C_{19}H_{18}O_6$). Methylation (excess diazomethane) of the crude extract, followed by repeated chromatography, provided the enantiomer (*ent*-**7***a*) of atrovenetin trimethyl ether, indistinguishable by tlc, ir, ^{1}H nmr, ^{13}C nmr, and hrms from an authentic sample of **7***a*.[5]

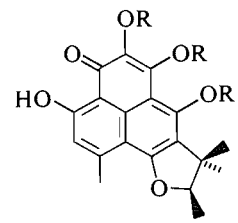

7 R = H
7*a* R = Me

The presence of the enantiomer of atrovenetin in cultures of *G. abietina* raises the possibility that **2**, **3**, and **5** are produced by in vitro aerial oxidation. The possibility that the anhydride **5** is an isolation artifact has been mentioned previously (13), although in other cases (14) it seems to be of biological origin. Although the formation of some of compounds **2**, **3**, and **5** during the isolation process cannot be excluded, it seems unlikely that this is the only source of these substances; the air oxidation of **3** or **7** is a relatively slow process. It would

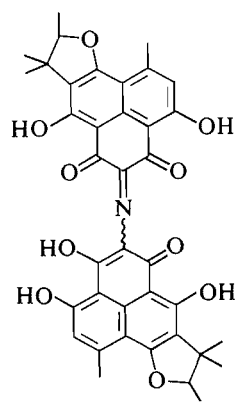

8

[3]For biogenetic reasons (see below) the ketonic carbonyls are numbered 1 and 3.

[4]Sample kindly provided by Professor L. C. Vining.

[5]Prepared by methylation of atrovenetin (12). This reaction gives two isomers of atrovenetin trimethyl ether (see Experimental). Structures **7***a* and **9** were assigned by analysis of ^{13}C nmr spectra, as described for **6***a*.

Can. J. Chem. Downloaded from www.nrcresearchpress.com by 78.46.186.204 on 09/07/12
For personal use only.

appear that *G. abietina* catalyzes the oxidation of atrovenetin to other metabolites.

Another point that deserves consideration is the biogenesis of compound **6**. According to Narasimhachari and Vining (9) the blue green pigments of *P. herquei* did not form when sodium sulphite was present in the culture medium. This blue pigment possesses structure **8** (1), which may be formed by a ninhydrin-like reaction between atrovenetinone (**2**) and amino acids (1). Compound **6**, a reduced form of **8**, might be formed from *ent*-atrovenetin and *ent*-atrovenetinone (**2**), via atrovenetinone transamination. At this stage we do not know whether both **6** and **8** are produced in vivo by *G. abietina*. It is possible that **8** is an artifact derived from **6**.

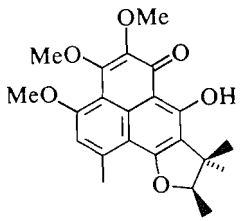

9

Experimental

For general experimental details see part 2 of this series (2).

Nuclear magnetic resonance spectra

^{1}H nuclear magnetic resonance (^{1}H nmr) spectra and ^{13}C nuclear magnetic resonance (^{13}C nmr) spectra were measured on a Bruker WH-400 spectrometer. Solutions of 0.5–5% (w/v) in $CDCl_3$ (0.5 mL, 5-mm tube) were employed depending on availability of sample. For ^{1}H nmr, residual $CHCl_3$ in $CDCl_3$ was employed as the internal standard (assigned as 7.26 ppm downfield from tetramethylsilane (TMS)) and measurements are reported in ppm downfield from TMS (δ). For ^{13}C nmr, $CDCl_3$ was employed as the internal standard (assigned as 77.0 ppm downfield from TMS) and measurements are reported in ppm downfield from TMS (δ).

Incorporation of ^{13}C-labelled acetate

G. abietina C-699 was grown in liquid still culture (10 mL) in a medium of 10% V-8 juice and 1% glucose (15) in 2.8-L Fernbach flasks (1 liter of medium/flask), as reported previously (2). After 15 days of growth, a sterile solution of sodium [1-^{13}C]acetate (0.082 g, 1 mmol) in water (5 mL) was injected into each flask. After a further 7, and then 14 days, an additional 1.0 mmol of labelled acetate was injected into each flask. After a total of 38 days of growth the mycelium was removed by filtration (through cheesecloth), washed with cold methanol, and air dried in the dark (2 days). The dried mycelium was extracted in a Soxhlet extractor, twice with dichloromethane (12 and 24 h) and then twice with methanol (24 h each). The crude extracts were evaporated to dryness *in vacuo*, at room temperature. Compounds **3**, **4***a*, and **5** were isolated from the first crude dichloromethane extract (ca. 6.0 g), whereas compounds **6***a* and *ent*-**7***a* were isolated from the second crude methanol extract (ca. 250 mg).

The dichloromethane extract (700 mg) was fractionated by flash column chromatography (dichloromethane–methanol – acetic acid, 48:1:1, 3 L) and the fractions (125 mL) were coevaporated with toluene. The fractions were further purified as indicated for the individual components.

The second crude methanol extract showed two major components on tlc, one component corresponding to Scleroderris green (**6**) (higher R_f) and the other to atrovenetin (**7**).

The experiments with sodium [2-^{13}C]acetate were carried out in the same way as described above for sodium [1-^{13}C]acetate. The yields of the crude extracts were ca. 50% of the yields reported above.

Isolation of sclerodione (3)

Sclerodione (**3**) was eluted in fraction 5 (200 mg from 2.1 g of crude extract). Flash column chromatography (dichloromethane–methanol – acetic acid, 48:1:1) of this fraction gave crude sclerodione. Recrystallization from dichloromethane – petroleum ether gave sclerodione (20 mg), identical in all respects with an authentic sample.

*Isolation of scleroderolide monoacetate (4*a*)*

Scleroderolide (**4**) was more conveniently isolated as its monoacetate derivative **4***a*. Scleroderolide was eluted in fractions 6 and 7 in a very crude form. Flash column chromatography (dichloromethane–methanol – acetic acid, 48:1:1) of these combined fractions (300 mg, from 2.1 g of crude extract) gave crude scleroderolide (25 mg). Acetylation (acetic anhydride/pyridine/4-*N*,*N*-dimethylaminopyridine), followed by ptlc (benzene–acetone – acetic acid, 90:10:0.1, double elution) gave scleroderolide monoacetate (5 mg), identical in all respects with an authentic sample.

Isolation of sclerodin (5)

Sclerodin (**5**) was eluted in fractions 2 and 3. Flash column chromatography (petroleum ether – ethyl acetate, 4:1) of these combined fractions (600 mg, from 1.4 g of crude extract) gave crude sclerodin. Recrystallization from dichloromethane – petroleum ether gave sclerodin (20 mg), identical in all respects with an authentic sample.

*Isolation of pentamethyl Scleroderris green (6*a*)*

Pentamethyl Scleroderris green (**6***a*) was obtained on methylation (ethereal diazomethane) of the methanol extract. After 12 h the crude reaction mixture was evaporated to dryness and fractionated twice by ptlc (petroleum ether – ethyl acetate, 4:1, multiple elution) to give compound **6***a* (ca. 2 mg from 100 mg of crude extract), identical in all respects with an authentic sample.

Isolation of ent*-atrovenetin trimethyl ether (*ent*-7*a*)*

ent-Atrovenetin trimethyl ether (*ent*-**7***a*) was obtained on methylation (excess ethereal diazomethane) of the methanol extract. Fractionation of the crude reaction mixture by ptlc (petroleum ether – ethyl acetate, 4:1, multiple elution) gave a yellow residue (yellow fluorescence under uv light). Further purification by ptlc (benzene–acetone, 1:1) gave compound *ent*-**7***a* ($[\alpha]_D$ −103°), indistinguishable from authentic **7***a* (prepared from atrovenetin as follows) by tlc, ir, ^{1}H nmr, ^{13}C nmr, and hrms comparison.

Methylation of atrovenetin (7)

Atrovenetin (ca. 16 mg) was suspended in dichloromethane and excess ethereal diazomethane was added at room temperature. After 12 h the reaction mixture was evaporated and fractionated by ptlc (benzene–acetone, 19:1, double elution), to afford two major products **7***a* (ca. 4 mg, 22% yield) and **9** (ca. 8 mg, 44% yield).

*Atrovenetin trimethyl ether (7*a*):* tlc: R_f 0.35 (benzene–acetone, 19:1), yellow spot (yellow fluorescence under uv light); ir ($CDCl_3$, cast): 3240 (br), 2920, 1610, 1585, 1460, 1320, 1285 cm^{-1}; ^{1}H nmr ($CDCl_3$), δ: 1.28 (3H, s, C-3′ CH_3), 1.45 (3H, d, 7.0 Hz, C-2′ CH_3), 1.54 (3H, s, C-3′ CH_3), 2.80 (3H, s, $ArCH_3$), 3.85 (3H, s, OCH_3), 4.03 (3H, s, OCH_3), 4.09 (3H, s, OCH_3), 4.60 (1H, q, 7.0 Hz, C-2′ H), 6.84 (1H, s, C-8 H), 17.67 (1H, s, OH); ^{13}C nmr ($CDCl_3$), δ: 14.4 (C-1′), 22.1 (C-4a′), 26.2 (C-5′), 24.5 ($ArCH_3$), 44.3 (C-3′), 61.0, 62.3, 64.4 (3 × OCH_3), 90.5 (C-2′), 108.4 (C-6a), 109.3 (C-9a), 109.9 (C-3a), 121.3 (C-8), 126.9 (C-5), 127.8 (C-3b), 140.3 (C-2), 149.9 (C-7), 157.6 (C-4), 160.5 (C-3), 163.3 (C-6), 174.7 (C-9), 177.3 (C-1);[6] hrms, *m/z* calcd. for $C_{22}H_{24}O_6$: 384.1572; found: 384.1560 (100), 369 (79), 341 (67), 311 (13).

Atrovenetin trimethyl ether (9): tlc: R_f 0.32 (benzene–acetone, 19:1), yellow spot; ir ($CHCl_3$, cast): 3240 (br), 2920, 1610, 1585, 1455, 1355, 1300, 1260, 1220 cm^{-1}; ^{1}H nmr ($CDCl_3$), δ: 1.33 (3H, s, C-3′ CH_3), 1.48 (3H, d, 7.0 Hz, C-2′ CH_3), 1.57 (3H, s, C-3′ CH_3), 2.90 (3H, s, $ArCH_3$), 4.05 (6H, s, OCH_3), 4.11 (3H, s, OCH_3), 4.68 (1H, q, 7.0 Hz, C-2′ H), 6.88 (1H, s, C-8 H), 18.10 (1H, s, OH); ^{13}C nmr ($CDCl_3$), δ: 14.6 (C-1′), 20.5 (C-4′), 25.9 (C-5′), 24.1

[6]Assignments for C-3 and C-4 as well as C-1 and C-9 may be interchanged.

Can. J. Chem. Downloaded from www.nrcresearchpress.com by 78.46.186.204 on 09/07/12
For personal use only.

($ArCH_3$), 43.3 (C-3′), 56.5, 60.8, 61.4 (3 × OCH_3), 91.4 (C-2′), 108.2 (C-3a), 109.4 (C-6a), 109.6 (C-9a), 110.7 (C-8), 119.4 (C-5), 127.3 (C-3b), 142.4 (C-2), 144.7 (C-7), 157.3 (C-1), 161.2 (C-9), 166.9 (C-6), 173.9 (C-3), 176.0 (C-4); hrms, *m/z* calcd. for $C_{22}H_{24}O_6$: 384.1572; found: 384.1577 (50), 369 (100), 351 (9), 341 (8).

Aerial oxidation of atrovenetin (7)

Atrovenetin (**7**, 20 mg) was suspended in chloroform–methanol (1:1) and exposed to sunlight in a loosely stoppered flask. After 5 weeks, separation of the reaction mixture by ptlc (dichloromethane–methanol, 49:1, double elution) gave three major fractions: R_f 0.90 (3 mg, 16%), R_f 0.55 (5 mg, 25%), and R_f 0.12 (4 mg, 22%). The R_f 0.90 compound was indistinguishable from sclerodin (**5**) by tlc, ^1H nmr, and hrms comparison. The R_f 0.55 compound was indistinguishable from atrovenetinone (**2**) by tlc and hrms comparison; its ethanolate (hot ethanol) was also indistinguishable from atrovenetinone ethanolate (**2***a*) by ir comparison. The R_f 0.12 compound was identical with sclerodione (**3**) by tlc, ^1H nmr, ^{13}C nmr, and hrms comparison.

Acknowledgements

We gratefully acknowledge the financial support provided by the Natural Sciences and Engineering Research Council of Canada. We thank Dr. Y. Hiratsuka, Northern Forest Research Centre, Edmonton, for his interest and for providing cultures of *G. abientina*, and Prof. L. C. Vining for a sample of atrovenetin. We also wish to thank Dr. L. M. Browne and Mrs. A. Szenthe for their help in various aspects of this work.

1. W. A. Ayer, Y. Hoyano, M. S. Pedras, and I. van Altena. Can. J. Chem. **64**, 1585 (1986).
2. W. A. Ayer, Y. Hoyano, S. M. Pedras, J. Clardy, and E. Arnold. Can. J. Chem. **65**, 748 (1986).
3. W. A. Ayer and S. M. Pedras. Can. J. Chem. **65**, 754 (1986).
4. R. G. Cooke and J. M. Edwards. Prog. Chem. Org. Nat. Prod. **40**, 153 (1981).
5. T. J. Simpson. J. Chem. Soc. Perkin Trans. 1, 1233 (1979).
6. W. A. Ayer, Y. Hoyano, I. van Altena, and Y. Hiratsuka. Rev. Latinoamer. Quim. **13**, 84 (1982).
7. J. L. Marshall. Carbon–carbon and carbon–proton NMR couplings: Applications to organic stereochemistry and conformational analysis. Verlag Chemie International, Deerfield Beach, FA. 1983. pp. 42–51.
8. T. Winkler, P. G. Ferrini and G. Haas. Org. Magn. Reson. **12**, 101 (1979).
9. N. Narasimhachari and L. C. Vining. Can. J. Chem. **41**, 641 (1963).
10. D. H. Barton, P. de Mayo, G. A. Morrison, and H. Raistrick. Tetrahedron, **6**, 48 (1959).
11. N. Narasimhachari, V. B. Joshi, and S. Krishnan. Experientia, **24**, 528 (1968).
12. J. S. Brooks and G. A. Morrison. J. Chem. Soc. Perkin Trans. 1, 4421 (1972).
13. R. Thomas. Pure Appl. Chem. **34**, 515 (1973).
14. C. Rossi and R. Ubaldi. Ann. Ist. Super. Sanita, **9**, 320 (1973).
15. C. E. Dorworth and Y. Krywiewczyk. Can. J. Bot. **53**, 2506 (1975).

Can. J. Chem. Downloaded from www.nrcresearchpress.com by 78.46.186.204 on 09/07/12
For personal use only.

The chemistry of the blue stain fungi. Part 3.[1] Some metabolites of *Ceratocystis minor* (Hedgcock) Hunt

WILLIAM A. AYER, SAMUEL K. ATTAH-POKU, LOIS M. BROWNE, AND HELENA ORSZANSKA
Department of Chemistry, The University of Alberta, Edmonton, Alta., Canada T6G 2G2

Received August 22, 1986

WILLIAM A. AYER, SAMUEL K. ATTAH-POKU, LOIS M. BROWNE, and HELENA ORSZANSKA. Can. J. Chem. **65**, 765 (1987).

The metabolites formed in still cultures by *Ceratocystis minor*, one of the fungal species associated with the blue stain disease of pine, have been isolated and identified as ceratenolone (**5**), 6,8-dihydroxy-3-methylisocoumarin (**2**), 8-hydroxy-6-methoxy-3-methylisocoumarin (**8**), 3,4-dihydro-6,8-dihydroxy-3-methylisocoumarin (**10**), 3,4-dihydro-3-methyl-3,6,8-trihydroxy-3-methylisocoumarin (**12**), 3,4-dihydro-3-methyl-3,4,6,8-tetrahydroxyisocoumarin (**13**), and succinic acid. Ceratenolone (**5**), a new type of natural product, forms an intensely blue chelate with ferric ions. This chelate may be responsible for the blue coloration of the wood of pine infected by *Ceratocystis minor*.

WILLIAM A. AYER, SAMUEL K. ATTAH-POKU, LOIS M. BROWNE et HELENA ORSZANSKA. Can. J. Chem. **65**, 765 (1987).

On a isolé les métabolites qui se forment dans les milieux de culture du *Ceratocystis minor*, une des espèces de champignons reliés à la maladie des taches bleues du pin, et on les a identifiés comme étant la cératénolone (**5**), la dihydroxy-6,8 méthyl-3 isocoumarine (**2**), l'hydroxy-8 méthoxy-6 méthyl-3 isocoumarine (**8**), la dihydro-3,4 dihydroxy-6,8 méthyl-3 isocoumarine (**10**), la dihydro-3,4 méthyl-3 trihydroxy-3,6,8 isocoumarine (**12**), la dihydro-3,4 méthyl-3 tétrahydroxy-3,4,6,8 isocoumarine (**13**) et l'acide succinique. La cératénolone (**5**), un nouveau type de produit naturel, forme un chélate bleu intense avec les ions ferriques. Ce chélate pourrait être responsable de la coloration bleue du bois de pin infecté par le *Ceratocystis minor*.

[Traduit par la revue]

Introduction

The blue stain disease of conifers is a serious disease of pine that currently causes the death of over 40 million pine trees per year in Western Canada (1–3). The disease is spread by the mountain pine beetle (*Dendroctonus ponderosae* Hopk.), which lives symbiotically with a variety of microorganisms (1). Four species of blue stain fungi have consistently been isolated from diseased wood, including *Ceratocystis clavigera*, *C. huntii*, *C. ips*, and *C. minor*. In part 1 of this series we described the metabolites produced in liquid culture by the first three mentioned *Ceratocystis* species. The metabolites of *C. minor* were not included in our initial study since they had been the subject of an earlier investigation (4, 5). As a part of our earlier study we investigated the rate at which the various *Ceratocystis* species caused the blue staining of pine chips and pine bolts. We found that *C. minor* was the most active in this respect followed by *C. huntii*, then *C. clavigera*. 2,3-Dihydroxybenzoic acid (**1**), which forms an intensely blue complex with ferric ions and which induces blue staining of lodgepole pine shavings and debarked sapwood (1), was isolated as one of the metabolites of *C. huntii*. It was postulated that the blue stain associated with the fungal infection might be due to metal complexes of compound **1** (1). Since 2,3-dihydroxybenzoic acid was not reported as a metabolite of *C. minor* (4, 6), and since this fungus stains pine most rapidly, we decided to reexamine the metabolites produced by the fungus. The metabolites reported earlier (4–6), 6,8-dihydroxy-3-methylisocoumarin (**2**), 6,8-dihydroxy-3-hydroxymethylisocoumarin (**3**), and 3,6,8-trihydroxy-α-tetralone (**4**), although phenolic in nature, do not contain the 2,3-dihydroxybenzoyl unit found in many strongly iron-chelating compounds (7) often referred to as siderophores (8). In this article we report the isolation of several metabolites, including a new natural product that chelates very strongly with ferric ions, produced in liquid culture by *C. minor*.

Results and discussion

Ceratocystis minor (Hedgcock) Hunt was grown in liquid still culture using a modified malt extract medium. Extraction of the pale yellow culture broth with ethyl acetate gave a pale blue extract, which was separated into "neutral" and "acidic" fractions using sodium bicarbonate solution. The blue coloration disappeared during the bicarbonate treatment but reappeared when the alkaline solution was acidified. The pale blue acidic fraction could be decolorized by dissolution in dilute sodium hydroxide solution followed by reacidification. The colorless extract, however, showed a pale blue spot on thin-layer chromatography (tlc) when eluted with chloroform–acetone – acetic acid in the ratio 23:1:1. When the ratio was 97:2:1, no blue coloration was observed until the plate was sprayed with ferric chloride solution. The compound responsible for this behavior, which we have named ceratenolone, was separated by flash chromatography using the $CHCl_3$:Me_2CO:AcOH (23:1:1) solvent system and collecting the "blue" fraction, which was decolorized by treatment with dilute sodium hydroxide.

Ceratenolone, obtained as a viscous oil, has the molecular formula $C_{14}H_{20}O_3$, as determined by high resolution mass spectrometry (hrms). The ultraviolet (uv) spectrum shows maxima at 312 and 396 nm, shifted to 317 and 400 nm by the addition of base. The infrared (ir) spectrum shows H-bonded hydroxyl absorption in the 2600–3400 cm^{-1} region and absorption at 1662 and 1616 cm^{-1} in the double bond region. The ^1H nmr spectral data (see Experimental for details) revealed the presence of a methyl, an ethyl, and a *sec*-butyl group, all linked to fully substituted carbons. The methine proton of the *sec*-butyl group appears considerably downfield (δ 2.62), suggesting this group is linked to unsaturated carbon. The remaining hydrogens of ceratenolone appear as a singlet at δ 5.90, a doublet at δ 8.44 (J = 9.0 Hz), and a doublet at δ 16.36 (J = 9.0 Hz). On treatment with D_2O, the peak at δ 16.36 disappears and the signal at δ 8.44 becomes a singlet, suggesting the presence of an H-bonded hydroxymethylene group. The ^{13}C nmr spectrum shows signals for the alkyl groups mentioned above, a quaternary carbon (δ 58.6), and sp^2 carbons as doublets at δ 116.6 and 173.5 and as singlets at δ 109.4, 159.2, 199.8, and 206.2. The appearance of a strong peak at m/z 208 in the mass spectrum of ceratenolone, corresponding to the loss of ethylene from the molecular ion, suggested that the ethyl group is located

[1]For parts 1 and 2, see refs. 1 and 2.

Can. J. Chem. Downloaded from www.nrcresearchpress.com by 80.58.250.72 on 09/07/12
For personal use only.

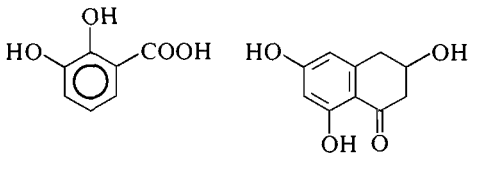

1 4 5 5*a* 6

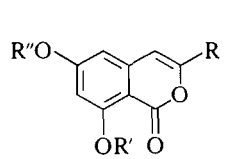

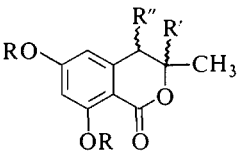

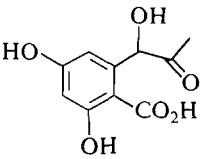

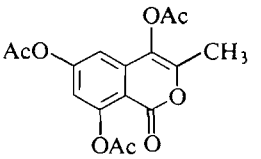

2 R = CH_3; R′ = R″ = H
3 R = CH_2OH; R′ = R″ = H
7 R = CH_3; R′ = R″ = $COCH_3$
8 R = CH_3; R′ = H; R″ = CH_3
9 R = CH_3; R′ = $COCH_3$; R″ = CH_3

10 R = R′ = R″ = H
11 R = $COCH_3$; R′ = R″ = H
12 R = R″ = H; R′ = OH
13 R = H; R′ = R″ = OH
16 R = $COCH_3$; R′ = R′ = $OCOCH_3$

14 **15**

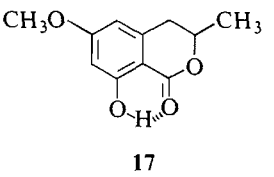

17

α to a carbonyl group (leading to loss by McLafferty rearrangement). At this stage it was possible to define the structural units present in ceratenolone (an enolized β-ketoaldehyde, an α,β-unsaturated ketone carrying a *sec*-butyl group, a quaternary carbon carrying a methyl and an ethyl group, one ring) but it was not possible to unambiguously determine their arrangement. The X-ray crystallographic study described below establishes the carbon skeleton and permits the assignment of structure **5** (the absolute configuration was not determined) to ceratenolone. The hydroxymethylene ketone form **5** is believed to be the major tautomer, rather than the aldo enol form **5***a*, because of the relatively large coupling constant (9 Hz) observed for the enolic hydrogen (9).

Treatment of ceratenolone with acetic anhydride – pyridine gave rise to a colorless, crystalline compound $C_{20}H_{28}O_7$, resulting from the incorporation of an acetoxyl and two acetyl groups. This derivative, which does not give a color reaction with ferric chloride, was shown by a single crystal X-ray diffraction study to possess structure **6**. Compound **6** presumably arises by acetylation of the enolic hydroxyl of **5** and 1,6-addition of acetic anhydride to the unsaturated carbonyl system. Diacetylacetoxyceratenolone (**6**) crystallizes from Skellysolve B as colorless prisms, mp 103–104°C. Figure 1 is a computer generated perspective drawing of the final X-ray model of diacetylacetoxyceratenolone (**6**).[2]

Ceratenolone represents a new structural type among natural products. Biogenetically, it may arise by condensation of two 4-methyltriacetic acid equivalents as illustrated in Scheme 1, with subsequent adjustment of the oxidation level. The enolized β-ketoaldehyde functionality presumably accounts for the iron chelating ability of ceratenolone. This chelate may be responsible for the blue coloration of the wood of pine infected with *C. minor*.

[2]The X-ray crystallographic study was carried out by R. G. Ball, Structure Determination Laboratory, Department of Chemistry, University of Alberta, Edmonton, Alberta T6G 2G2. Inquiries regarding the crystallographic results should be directed to Dr. Ball at the above address quoting report number SR:012505-03-84.

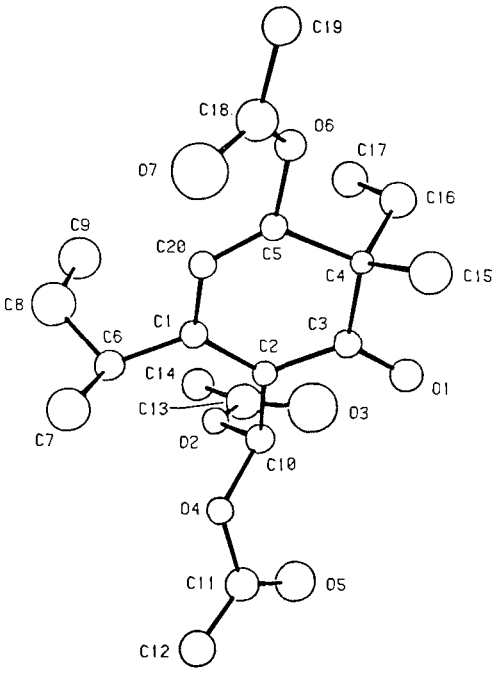

FIG. 1. Computer generated perspective drawing of compound **6**.

In addition to ceratenolone, several phenolic compounds and succinic acid are present in the acidic fraction of the broth extract. The previously reported metabolite of *C. minor*, 6,8-dihydroxy-3-methylisocoumarin (**2**), was isolated and identified by comparison of its spectral properties and those of its diacetyl derivative **7** with those reported (4–6). Four related methylisocoumarins were also isolated. The structures were established by comparison of the spectral data for the metabolite and its acetyl derivative with those of compounds **2** and **7** as follows. The least polar compound, **8**, is an O-methyl derivative of **2**. Since the ir spectrum of **8** shows the weak hydroxyl and low frequency carbonyl absorption (1683 cm^{-1}) characteristic

Can. J. Chem. Downloaded from www.nrcresearchpress.com by 80.58.250.72 on 09/07/12
For personal use only.

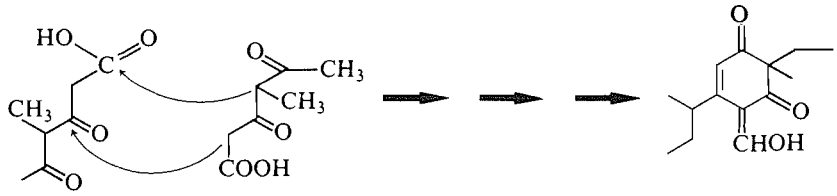

SCHEME 1

of 8-hydroxyisocoumarins, it is the C-6 hydroxyl that is methylated. Acetylation of **8** afforded a monoacetyl derivative **9**. Compound **8**, which has previously been isolated from *C. fimbriata* (10), displays behavior on silica gel somewhat similar to that described earlier for ceratenolone. When a colorless ethyl acetate solution of **8** is adsorbed on silica gel it forms a pale pink band and elutes as a pale pink solution.

The second isocoumarin metabolite **10** is the dihydro derivative of **2**. In the ^{1}H nmr spectrum of **10** no signals characteristic of a vinyl proton or vinyl methyl are present; instead, a low-field methine (δ 4.68) coupled to a methyl group (δ 1.45) and two benzylic methylene protons (δ 2.85, 2.88) are observed. The spectral properties of compound **10**, which readily forms the diacetyl derivative **11** (acetic anhydride – pyridine), are identical with those reported (11–14).

A more polar metabolite, $C_{10}H_{10}O_5$ (**12**), is an hydrated derivative of **2** (11). The ^{1}H nmr spectrum of **12** shows the presence of a low-field methyl singlet (δ 1.65) and a benzylic methylene singlet (δ 3.09). Acetylation of **12** occurs with loss of acetic acid to give 6,8-diacetoxy-3-methylisocoumarin (**7**). The properties of **12**, which has been isolated previously from *Alternaria kikuchiana* (15), are identical with those reported (15–17).

The most polar component of the acidic fraction, $C_{10}H_{10}O_6$, was also the major component produced by *C. minor*. It was isolated as an inseparable mixture of epimers and was shown to be a dihydroxylated derivative (**13**) of compound **2**. Its tautomeric form **14** has previously been reported as a metabolite of *C. ulmi* (18). The ir spectrum of **13** shows intense hydroxyl (3400, 3300, 3055 cm^{-1}) and low frequency carbonyl (1635 cm^{-1}) absorption bands. The ultraviolet spectrum of **13** shows absorption maxima at 300, 267, 216, and 214 nm. Comparison of this data with that of tautomer **14** (18) and compound **17** (described below) supports the assignment of an isocoumarin structure to **13**. The ^{1}H nmr spectrum of **13** clearly shows two sets of signals for the major and minor epimer of the mixture (ratio 2:1). The major isomer shows four D_2O exchangeable protons (δ 5.92, 7.55, 10.60, 11.12), two *meta*-related aromatic protons (δ 6.22, 6.38), a low-field benzylic methine (δ 4.20), and a low-field methyl group (δ 1.52). The minor isomer shows similar proton resonances at δ 5.84, 7.38, 10.58, 11.10 (hydroxyl), 6.18, 6.50 (aromatic protons), 4.61 (benzylic methine), and 1.58 (methyl protons). The ^{13}C nmr spectrum of **13** confirmed that it was isolated as an epimeric mixture of lactols rather than as its keto acid tautomer. The lowest field signal (δ 168.4) in the spectrum is that arising from the lactol carbonyl. No signal characteristic of a ketone carbon is observed. Signals of a lactol carbon (δ 100.7), a benzylic carbinol carbon (69.1), six aromatic carbons, and a methyl carbon (δ 22.9, 24.4 indicating the isomeric mixture) are also present. The chemical shift assignments (see Experimental) are based on calculations using the principle of additivity of substituents. The observed values compare well with the calculated values. Acetylation of compound **13** gave a single triacetate derivative **15** in quantitative yield. Compound **15**, which is the only product formed, apparently results from the loss of acetic acid from tetraacetate **16**. The spectral properties of **15**, including its ^{13}C nmr spectrum, are consistent with its assigned structure.

The structures of compounds **2**, **8**, **10**, and **12** were further secured by correlation with the known compound **17** (19, 20). Catalytic hydrogenation of **8** afforded 3,4-dihydro-8-hydroxy-6-methoxy-3-methylisocoumarin (**17**). The ^{1}H nmr spectrum of **17** shows the presence of an intramolecular H-bonded phenolic proton (δ 11.26), two *meta*-related aromatic protons (δ 6.26 and 6.38), two benzylic protons (δ 2.88), an acyloxy proton (δ 4.69), a methoxyl group (δ 3.84), and a methyl doublet (δ 1.54). Nuclear Overhauser enhancement (nOe) studies confirm the placement of the substituents in **17**. Thus, irradiation of the benzylic methylene enhances the aromatic signal at δ 6.28 (H-5), and irradiation of the methoxyl protons causes enhancement of both aromatic hydrogen signals. The phenolic OH must then be located at C-8, in agreement with its H-bonded nature. The lactone carbonyl absorbs at 1655 cm^{-1}, confirming that it is also H-bonded. Treatment of compound **10** with ethereal diazomethane at −10°C gives compound **17**. Acetylation of **10** provides compound **11**, which may also be obtained by catalytic hydrogenation of compound **7**. Compound **7**, in turn, is prepared by acetylation of **2** and of **12**.

Examination of the neutral fraction of the broth extract of *C. minor* led to the isolation of methylisocoumarins **2**, **8**, and **10**. The mycelium of *C. minor* was extracted and separated into acidic and neutral fractions. Chromatographic separation of each of the fractions led to the isolation of small amounts of ceratenolone (**1**) along with compound **8** and appreciable amounts of triglycerides. The separation and characterization of the triglycerides was not pursued.

Experimental

High resolution mass spectra were recorded on an A.E.I. MS-50 mass spectrometer coupled to a DS 50 computer. Unless diagnostically significant, only peaks greater than 20% of the base peak are reported. Infrared spectra were recorded on a Nicolet 7199 FT spectrometer. High field ^{1}H nmr spectra were recorded on a Bruker WH-200 or WH-400 spectrometer with an Aspect 2000 computer system. Optical rotations were obtained on a Perkin Elmer 141 polarimeter. Melting points were determined on a Fisher–Johns melting point apparatus and are uncorrected. E. Merck silica gel 60 (230–400 mesh) was used for flash chromatography. Analytical thin-layer chromatography (tlc) was carried out on BDH precoated plates of silica gel 60 PF 254, with visualization by ultraviolet light or 5% phosphomolybdic acid in 5% sulfuric acid, followed by careful charring on a hot plate. All solvents were distilled prior to use. Skellysolve B refers to Skelly Oil Company light petroleum, bp 62–70°C.

Fungal cultures

The blue stain fungi used in this study were obtained from Y. Hiratsuka, Northern Forest Research Centre, Edmonton, and deposited with L. Sigler, Curator, The University of Alberta Microfungus Collection (UAMH). *Ceratocystis minor* (Hedgcock) Hunt strain

Can. J. Chem. Downloaded from www.nrcresearchpress.com by 80.58.250.72 on 09/07/12
For personal use only.

Can. J. Chem. Downloaded from www.nrcresearchpress.com by 80.58.250.72 on 09/07/12
For personal use only.

C-839 (UAMH 4820) was isolated by A. Tsuneda from *Pinus contorta* growing in southern Alberta in June 1983.

Ceratocystis minor was maintained at 4°C in slant tubes containing 0.2% yeast extract in Difco potato dextrose agar. An aqueous suspension of mycelium was used to inoculate two potato dextrose – yeast extract agar plates. After 7–10 days at 17°C the culture was blended in a Waring blender with approximately 200 mL of sterile medium, and 20-mL aliquots were used to innoculate 10 × 1-L sterile modified malt extract medium in 2-L Fernbach flasks. (Modified malt extract medium: Difco malt extract 20 g, dextrose 20 g, peptone 1 g in water 1 L.) After inoculation, the still cultures were kept at room temperature for 8 weeks. The culture broth was decanted from the mycelium, concentrated *in vacuo* to about 1 L, and extracted by stirring with an equal volume of ethyl acetate for 24 h. The extraction procedure was repeated three times. The combined ethyl acetate extract was dried and concentrated to give crude broth extract. The mycelium was air dried, pulverized, and subjected to Soxhlet extraction with ethyl acetate. The ethyl acetate was dried and concentrated to give crude mycelial extract.

Isolation of metabolites

The broth extract (2.3 g) was redissolved in ethyl acetate (200 mL) and extracted with saturated sodium bicarbonate (3 × 15 mL). The bicarbonate extract was washed with ethyl acetate (3 × 20 mL), cooled with ice, acidified to pH 3 with 6 *N* hydrochloric acid, and extracted with ethyl acetate (3 × 50 mL). The ethyl acetate extract was dried (anhydrous sodium sulfate), filtered, and evaporated to give a viscous oil (1.6 g). The ethyl acetate extract left after bicarbonate extraction was washed with brine, dried, filtered, and concentrated to give neutral material (0.65 g). The acidic viscous oil (1.6 g) was dissolved in hot ethyl acetate (40 mL) and chloroform (10 mL) was added. The solution was allowed to cool and stored at 10°C for 48 h. The precipitate (0.560 g) was collected by filtration and dried *in vacuo*. Repeated precipitation from hot ethyl acetate afforded a solid material (0.200 g, **13**). Component **13** is an inseparable mixture of isomers (2:1 ratio) and the major component produced by *C. minor*. The mother liquor, obtained after precipitation of the major metabolite, was concentrated and subjected to flash column chromatography on silica gel. The following metabolites were obtained.

Ceratenolone (5)

Elution of the column with 5% ethyl acetate in Skellysolve B afforded a purple colored solution as the least polar fraction. Evaporation of the solvent afforded a purple oil, which was decolorized in the following way. Extraction with 5% aqueous sodium hydroxide, acidification of the aqueous extract with dilute hydrochloric acid, extraction with diethyl ether, and evaporation of the solvent gave a colorless oil. The oil was identified as the "blue compound" ceratenolone (**5**) (40 mg); R_f 0.80 ($CHCl_3$:acetone:acetic acid, 23:1:1); $[\alpha]_D$ 0; $[\alpha]_{360}$ +210° (*c* 0.33, MeOH); uv λ_{max} (MeOH): 312 (ε = 1920), 396 (ε = 755) nm; λ_{max} (MeOH + few drops aqueous NaOH): 317 (ε = 1359), 400 (ε = 1877) nm; λ_{max} (acidification (aqueous HCl) of previous alkaline solution): 300 ($\varepsilon \approx$ 1800) nm; λ_{max} (MeOH + $FeCl_3$): 550 nm; ir ($CHCl_3$ cast): 3400–2400 (weak, broad), 2968, 1662, 1616 cm^{-1}; ^1H nmr ($CDCl_3$, 400 MHz) δ: 0.78 (t, *J* = 7 Hz, 3H), 0.96 (t, *J* = 7 Hz, 3H), 1.24 (d, *J* = 7 Hz, 3H), 1.38 (s, 3H), 1.56 (m, 1H), 1.68 (m, 1H), 1.98 (m, 2H), 2.62 (m, 1H), 5.90 (s, 1H), 8.44 (d, *J* = 8 Hz, 1H), 16.36 (d, *J* = 8 Hz, 1H, exchanges D_2O); ^{13}C nmr ($CDCl_3$, 50 MHz) δ: 9.8 (q), 11.3 (q), 19.9 (q), 21.4 (q), 28.8 (t), 33.1 (t), 35.6 (d), 58.6 (s), 109.4 (s), 116.6 (d), 159.2 (s), 173.5 (d), 199.8 (s), 206.2 (s); hrms, *m/z* calcd. for $C_{14}H_{20}O_3$: 236.1429; found: 236.1421 (75), 221 (10), 208 (79), 193 (52), 190 (26), 179 (100); cims, NH_3, *m/z*: 237 (M^+ + 1).

Ceratenolone (10 mg) was dissolved in a mixture of acetic anhydride (1 mL) and pyridine (0.5 mL) and left at room temperature for 4 h. The reaction mixture was poured into water (5 mL) and the aqueous solution extracted with ethyl acetate. Evaporation of the ethyl acetate gave a semicrystalline residue (13 mg), which was triturated with cold Skellysolve B. The residue was crystallized from Skellysolve B to give compound **6** (6 mg); R_f 0.51 ($CHCl_3$:acetone:acetic acid, 23:1:1); mp 103–104°C; uv (MeOH) λ_{max}: 323 (ε = 8269) nm; ir ($CHCl_3$ cast): 2960, 1768, 1640, 1570 cm^{-1}; ^1H nmr ($CDCl_3$, 400 MHz) δ: 0.68 (t, *J* = 7 Hz, 3H), 0.87 (t, *J* = 7 Hz, 3H), 1.14 (d, *J* = 7 Hz, 3H), 1.28 (s, 3H), 1.54 (d, q, *J* = 7.7 Hz, 2H), 1.68 (d, q, *J* = 7.7 Hz, 1H), 1.93 (dq, *J* = 7, 7 Hz, 1H), 2.06 (s, 3H), 2.07 (s, 3H), 2.25 (s, 3H), 3.33 (ddq, *J* = 7, 7, 7 Hz, 1H), 6.27 (s, 1H), 7.89 (s, 1H); ^{13}C nmr (C_6D_6, 100 MHz) δ: 9.1 (q), 12.1 (q), 19.1 (q), 20.1 (q), 20.2 (q), 20.4 (q), 23.3 (q), 28.0 (t), 33.1 (t), 37.4 (d), 53.5 (s), 86.2 (d), 109.8 (d), 124.7 (s), 160.5 (s), 162.5 (s), 167.7 (s), 168.3 (s), 199.2 (s); hrms, *m/z* calcd. for $C_{20}H_{28}O_7$: 380.1836; found: 380.1834 (6), 338 (6), 278 (12), 236 (100).

8-Hydroxy-6-methoxy-3-methylisocoumarin (8)

Elution with 10% ethyl acetate in Skellysolve B afforded a waxy material. Crystallization of this material from diethyl ether – Skellysolve B afforded **8** (10 mg). This compound was also isolated from the neutral broth extract (40 mg) and from the mycelium extract (20 mg); R_f 0.8 (chloroform:acetone:acetic acid, 23:1:1); mp 128–129°C (lit. (10) mp 128–129°C); ir ($CHCl_3$ cast): OH is almost absent, very broad, 1683, 1644, 1620, 1165 cm^{-1}; ^1H nmr ($CDCl_3$, 200 MHz) δ: 2.25 (d, *J* = 0.5 Hz, 3H), 3.86 (s, 3H), 6.28 (d, *J* = 2 Hz, 1H), 6.46 (d, *J* = 2 Hz, 1H), 6.18 (q, *J* = 0.5 Hz, 1H), 11.12 (sharp s, 1H, D_2O exchanges); hrms, *m/z* calcd. for $C_{11}H_{10}O_4$: 206.0576; found: 206.0577 (100), 191 (33), 177 (11), 135 (35).

Compound **8** was treated with acetic anhydride in pyridine for 6 h at room temperature. Purification of the isolated crude product by filtration through a short column of silica gel in a pipette (6 in. long × 1/4 in. diameter), followed by crystallization from 10% ethyl acetate in Skellysolve B, afforded crystalline 8-acetoxy-6-methoxy-3-methylisocoumarin (**9**); R_f 0.75 (chloroform:acetone:acetic acid, 23:1:1); mp 167–168°C; ir ($CHCl_3$): 1765, 1755, 1719, 1665, 1610, 1365, 1152, 1180, 1050 cm^{-1}; ^1H nmr ($CDCl_3$, 200 MHz) δ: 2.20 (d, *J* = 1 Hz, 3H), 2.40 (s, 3H), 3.90 (s, 3H), 6.18 (d, *J* = 1 Hz, 1H), 6.62 (d, *J* = 2 Hz, 1H), 6.67 (d, *J* = 2 Hz, 1H); hrms, *m/z* calcd. for $C_{13}H_{12}O_5$: 248.0681; found: 248.0688 (12), 206 (100), 191 (18), 135 (10).

6,8-Dihydroxy-3-methylisocoumarin (2)

Elution of the column with 20% ethyl acetate in Skellysolve B and evaporation of the solvent, followed by crystallization from ethyl acetate – Skellysolve B, afforded pure compound **2** (10 mg). Compound **2** (20 mg) was also isolated from the neutral broth extract, R_f 0.5 (chloroform:methanol:acetone:acetic acid, 16:2:1:1); mp 241–242°C (lit. (4–6) mp 240–242°C); ir (CH_3OH cast): 3250, 1679, 1645, 1629, 1382, 1253, 1184 cm^{-1}; ^1H nmr (CD_3CN, 200 MHz) δ: 2.20 (d, *J* = 0.5 Hz, 3H), 6.32, 6.34, and 6.30 (m, 3H), 6.28 (d, *J* = 0.5 Hz, 1H), 11.6 (s, 1H); hrms, *m/z* calcd. for $C_{10}H_8O_4$: 192.0410; found: 192.0424 (100), 177 (49), 163 (5), 150 (10), 121 (27).

The acetyl derivative of **2** was prepared and purified as described above to afford pure 6,8-diacetoxy-3-methylisocoumarin (**7**); R_f 0.80 (chloroform:acetone:acetic acid, 23:1:1); mp 126–127°C; ir ($CHCl_3$ cast): 1774, 1730, 1665, 1614, 1367, 1354, 1189, 1163, 1135 cm^{-1}; ^1H nmr ($CDCl_3$, 200 MHz) δ: 2.24 (d, *J* = 0.8 Hz, 3H), 2.32 (s, 3H), 2.40 (s, 3H), 6.22 (d, *J* = 0.8 Hz, 1H), 6.90 (d, *J* = 2 Hz, 1H), 7.04 (d, *J* = 2 Hz, 1H); hrms, *m/z* calcd. for $C_{14}H_{12}O_6$: 276.0619; found: 276.0632 (8), 234 (32), 192 (100), 177 (10).

Hydrogenation of **7** in ethyl acetate over 10% palladium on carbon at room temperature and 1 atmosphere (101.3 kPa) pressure afforded the dihydro derivative, which is identical in all respects with compound **11** described below.

3,4-Dihydro-6,8-dihydroxy-3-methylisocoumarin (10)

Further elution of the column with 20% ethyl acetate in Skellysolve B gave a single compound, which was crystallized to afford pure compound **10** (10 mg). Compound **10** (10 mg) was also isolated from the neutral broth extract; R_f 0.42 (chloroform:methanol:acetone:acetic acid, 16:2:1:1); $[\alpha]_D$ +19.4° (*c* 0.35, CH_3OH); mp 214–215°C (lit. (11) mp 214–215°C); ir (Nujol mull): 3208, 1652, 1632, 1477, 1385, 1257, 1211 cm^{-1}; ^1H nmr (CD_3CN, 200 MHz) δ: 1.45 (d, *J* = 6 Hz, 3H), 2.85 (d, *J* = 4 Hz, 1H), 2.88 (d, *J* = 2 Hz, 1H), 4.68 (ddq, *J* = 2 Hz, *J'* = 4 Hz, *J''* = 6 Hz, 1H), 6.22 (s, 2H), 7.85 (br s, 1H, CD_3OD exchanges), 11.25 (s, 1H, CD_3OD exchanges);

Can. J. Chem. Downloaded from www.nrcresearchpress.com by 80.58.250.72 on 09/07/12
For personal use only.

hrms, m/z calcd. for $C_{10}H_{10}O_4$: 194.0576; found: 194.0582 (100), 176 (21), 150 (87).

The diacetyl derivative of compound **10**, 6,8-diacetoxy-3,4-dihydro-3-methylisocoumarin (**11**), was prepared and purified in the usual manner; R_f 0.85 (chloroform:acetone:acetic acid, 23:1:1); $[\alpha]_D$ +58° (c 0.20, CH_3OH); mp 115–116°C; ir ($CHCl_3$ cast): 1772, 1719, 1615, 1367, 1252, 1186, 1131, 1113, 1086, 1061 cm^{-1}; ^1H nmr ($CDCl_3$, 200 MHz) δ: 1.48 (d, J = 4 Hz, 3H), 2.32 (s, 3H), 2.38 (s, 3H), 2.92 (d, J = 3 Hz, 1H), 2.95 (d, J = 6 Hz, 1H), 4.65 (m, 1H), 6.86 (d, J = 2 Hz, 1H), 6.97 (d, J = 2 Hz, 1H); hrms, m/z calcd. for $C_{14}H_{14}O_6$: 278.0786; found: 278.0788 (1), 236 (34), 194 (100), 150 (39).

Treatment of **10** with diazomethane in ether at −10°C for 1 h afforded the monomethyl derivative, which is identical in all respects with compound **17** described below.

*3,4-Dihydro-3-methyl-3,6,8-trihydroxyisocoumarin (**12**)*

Elution of the column with 40% ethyl acetate in Skellysolve B afforded an impure solid material. Preparative thin-layer chromatography of this material on silica gel (type 60 F-254; 0.25 mm thickness), followed by crystallization from ethyl acetate in Skellysolve B, afforded pure compound (**12**) (7.8 mg); R_f 0.20 (chloroform:methanol:acetone:acetic acid, 16:2:1:1); $[\alpha]_D$ 0° (c 0.25, CH_3OH); mp 160–161°C (lit. (15) mp 155–157°C); ir (Nujol cast): 3400, 3237, 1660, 1620, 1372, 1232, 1116, 1065 cm^{-1}; ^1H nmr (CD_3CN, 200 MHz) δ: 1.65 (s, 3H), 3.09 (br s, 2H), 5.15 (v br s, 1H, CD_3OD exchanges), 7.85 (br s, 1H, CH_3OD exchanges), 6.25 (s, 2H), 10.22 (br s, 1H, CD_3OD exchanges); hrms, m/z calcd. for $C_{10}H_{10}O_5$: 210.0545; found: 210.0529 (21), 192 (11), 150 (100), 122 (8), 43 (77).

Compound **12** was acetylated in the usual manner with acetic anhydride in pyridine and the product purified to afford a diacetate derivative, whose physical and spectral properties are identical with those of compound **7**.

*3,4-Dihydro-3-methyl-3,4,6,8-tetrahydroxyisocoumarin (**13**)*

Elution with 40% ethyl acetate, 0.5% acetic acid in Skellysolve B, followed by precipitation of the product from ethyl acetate and cooling at 10°C overnight, afforded a solid component (**13**) (50 mg), identical with the component obtained earlier from the acidic fraction by precipitation from ethyl acetate – chloroform solution. Component **13** exists as a mixture of two inseparable isomers (2:1 ratio by ^1H nmr); R_f 0.3 (chloroform:methanol:acetone:acetic acid, 14:4:1:1); mp 208–212°C; ir (Nujol cast): 3400, 3300, 3055, 1635, 1622, 1465, 1321, 1164 cm^{-1}; uv λ_{max} (MeOH): 214 (ε 13 541), 216 (ε 11 121), 267 (ε 6012), 300 (ε 3730) nm; ^1H nmr (DMSO-d_6, 200 MHz), major isomer, δ: 1.52 (s, 3H), 4.20 (d, J = 3 Hz, 1H, collapses to a singlet on addition of D_2O), 5.92 (d, J = 3 Hz, 1H, D_2O exchanges), 6.22 (d, J = 2 Hz, 1H), 6.38 (d, J = 2 Hz, 1H), 7.55 (s, 1H, D_2O exchanges), 10.60 (s, 1H, D_2O exchanges), 11.12 (s, 1H, D_2O exchanges); minor isomer, δ: 1.58 (s, 3H), 4.61 (d, J = 6 Hz, 1H, collapses to a singlet on addition of D_2O), 5.84 (d, J = 6 Hz, 1H, D_2O exchanges), 6.18 (d, J = 2 Hz, 1H), 6.50 (d, J = 2 Hz, 1H), 7.38 (s, 1H, D_2O exchanges), 10.58 (s, 1H, D_2O exchanges), 11.10 (s, 1H, D_2O exchanges); ^{13}C nmr (DMSO-d_6) δ: 168.4 (C-1), 164.2 (C-6), 162.8 (C-8), 143.9 (C-10), 107.9 (C-5), 104.9 (C-9), 101.5 (C-7), 100.7 (C-3), 69.1 (C-4), 24.4, 22.9 (CH_3); hrms, m/z calcd. for $C_{10}H_{10}O_6$: 226.0474; found: 226.0477 (9), 210 (15), 183 (25), 181 (44), 165 (100), 150 (58), 137 (59).

Acetylation of the epimeric mixture of component **13** with acetic anhydride in pyridine afforded only one product in quantitative yield. The triacetyl derivative was identified as 3-methyl-4,6,8-triacetoxyisocoumarin (**15**); R_f 0.70 (chloroform:acetone:acetic acid, 23:1:1), mp 175–176°C; ir ($CHCl_3$ cast): 1764, 1690, 1620, 1371, 1180, 1032, 1015, 915 cm^{-1}; ^1H nmr ($CDCl_3$, 200 MHz) δ: 2.32 (s, 3H), 2.34 (s, 3H), 2.36 (s, 3H), 2.42 (s, 3H), 6.90 (d, J = 2 Hz, 1H), 7.45 (d, J = 2 Hz, 1H); ^{13}C nmr ($CDCl_3$) δ: 168.2, 168.1, 167.9 ($COCH_3$), 162.4 (C-1), 156.5 (C-6), 149.1 (C-8), 113.9 (C-9), 139.0 (C-10), 138.2 (C-4), 137.0 (C-3), 116.8 (C-5), 112.9 (C-7), 21.2, 21.0, 20.6 ($COCH_3$), 16.3 (CH_3); hrms, m/z calcd. for $C_{16}H_{14}O_8$: 334.0684; found: 334.0683 (2), 292 (22), 250 (43).

Finally, elution with 40% ethyl acetate, 0.5% acetic acid in Skellysolve B, followed by crystallization from ethyl acetate, gave succinic acid.

*3,4-Dihydro-8-hydroxy-6-methoxy-3-methylisocoumarin (**17**)*

Catalytic hydrogenation of **8** (5 mg) in ethanol (2 mL) over 10% palladium on carbon at room temperature and 1 atmosphere pressure for 3 h gave a single product. Crystallization of the product from hexane gave compound **17**; R_f 0.75 (chloroform:acetone:acetic acid, 23:1:1); mp 75–76°C (lit. (20) mp 75–76°C); ir ($CHCl_3$): 1655, 1629, 1583, 1379, 1250, 1157, 1033, 803 cm^{-1}; uv λ_{max} (CH_3OH), 216 (ε 19 860), 267 (ε 12 580), 302 (ε 4890) nm; ^1H nmr ($CDCl_3$, 400 MHz) δ: 1.54 (d, J = 7 Hz, 3H), 2.88 (d, J = 6 Hz, 2H), 3.84 (s, 3H), 4.69 (m, 1H), 6.26 (d, J = 2 Hz, 1H), 6.38 (d, J = 2 Hz, 1H), 11.26 (s, 1H); nOe: irradiation of δ 1.54 (C-3 CH_3) gives 24% enhancement at δ 4.69 (H-3), irradiation of δ 2.88 ($ArCH_2$) gives 16% enhancement at δ 4.69 (H-3) and 26% enhancement at δ 6.26 (H-5), irradiation or δ 3.84 ($ArOCH_3$) gives 12% enhancement at δ 6.26 (H-5) and 5% enhancement at δ 6.38 (H-7); hreims, m/z calcd. for $C_{11}H_{12}O_4$: 208.0732; found: 208.0736 (100), 190 (20), 164 (89).

Acknowledgements

The financial support of the Natural Sciences and Engineering Research Council of Canada is gratefully acknowledged. We also thank Dr. Y. Hiratsuka, Northern Forest Research Centre, Canadian Forestry Service, Edmonton, for his interest and for cultures of *C. minor*, Dr. R. Ball for the X-ray crystallographic analysis, and Mrs. A. Szenthe for technical assistance.

1. W. A. Ayer, L. M. Browne, M. C. Feng, H. Orszanska, and H. Saeedi-Ghomi. Can. J. Chem. **64**, 904 (1986).
2. W. A. Ayer, B. Kratochvil, E. Allen, L. M. Browne, C. Dufresne, D. Figueroa Villar, and A. Szenthe. Can. J. Chem. **64**, 910 (1986).
3. (*a*) B. H. Moody and H. F. Cereske. Northern Forest Research Centre, Canadian Forestry Service, Information Report NOR-X-261. 1984; (*b*) C. S. Wood, G. A. van Sickle, and T. L. Shore. Pacific Forest Research Centre, Canadian Forestry Service, Information Report BC-X-259. 1984.
4. G. W. McGraw and R. W. Hemingway. Phytochemistry, **16**, 1315 (1977).
5. R. W. Hemingway, G. W. McGraw, and S. J. Barras. J. Agric. Food Chem. **25**, 717 (1977).
6. J. D. DeAngelis, J. D. Hodges, and T. E. Nebeker. Can. J. Bot. **64**, 151 (1986).
7. Subcommittee on Iron, Committee on Medical and Biologic Effects of Environmental Pollutants. *In* Iron. Division of Medical Sciences, National Research Council, University Park Press, Baltimore. 1979.
8. J. B. Neilands. Microbiol. Sci. **1**, 1 (1984).
9. E. W. Garbisch. J. Am. Chem. Soc. **85**, 1696 (1963).
10. A. Stoessl. Biochem. Biophys. Res. Commun. **35**, 186 (1969).
11. R. F. Curtis, P. C. Harris, C. H. Hassall, J. D. Levi, and D. M. Phillips. J. Chem. Soc. (C), 168 (1966).
12. R. H. Carter, R. M. Colyer, R. A. Hill, and J. Staunton. J. Chem. Soc. 1438 (1976).
13. R. A. Hill, R. H. Carter, and J. Staunton. J. Chem. Soc. Perkin Trans. 1, 2570 (1982).
14. G. B. Henderson and R. A. Hill. J. Chem. Soc. Perkin Trans. 1, 3037 (1982).
15. K. Kiyoshi, A. Hiroo, T. Hiroshi, and N. Mitsuo. Agric. Biol. Chem. **37**, 2137 (1973).
16. A. E. Oxford and H. Raistrick. Biochem. J. **27**, 634 (1933).
17. R. F. Curtis, P. C. Harries, and C. H. Hassall. J. Chem. Soc. 5382 (1964).
18. N. Claydon, J. F. Grove, and M. Hosken. Phytochemistry, **13**, 2567 (1974).
19. W. J. McGahren and L. A. Mitscher. J. Org. Chem. **33**, 1577 (1968).
20. E. Sondheimer. J. Am. Chem. Soc. **79**, 5036 (1957).

Kinetic study of the reaction between cystine and sulfide in alkaline solutions

DAVID K. LIU AND S. G. CHANG

Applied Science Division, Lawrence Berkeley Laboratory, University of California, Berkeley, CA, U.S.A. 94720

Received September 12, 1986

DAVID K. LIU and S. G. CHANG. Can. J. Chem. **65**, 770 (1987).

The reaction between cystine (CySSCy) and hydrogen sulfide ion (HS^-) in alkaline solutions has been studied by amino acid analysis and uv–visible spectroscopy. The reaction occurs in two reversible steps to form cysteine (CySH), *S*-thiocysteine ($CySS^-$), and disulfide (S_2^{2-}), as represented by the reactions $CySSCy + HS^- \underset{k_{-1}}{\overset{k_1}{\rightleftharpoons}} CySH + CySS^-$ and $CySS^- + HS^- \underset{k_{-2}}{\overset{k_2}{\rightleftharpoons}} CySH + S_2^{2-}$. The equilibrium and rate constants were pH dependent due to the presence of various charge types of reactants and products. The rate constants at 25°C, pH 10.0, and $\mu = 0.17$ *M* were determined to be: $k_1 = 3.7 \pm 0.4\ M^{-1}\ min^{-1}$, $k_{-1} = 5.5 \pm 0.6\ M^{-1}\ min^{-1}$, $k_2 = 6.1 \pm 0.5\ M^{-1}\ min^{-1}$, and $k_{-2} = 122 \pm 20\ M^{-1}\ min^{-1}$. When the rate constant k_1 is expressed as $k_1 = A \exp(-E_a/RT)$, values of $A = (4.7 \pm 0.3) \times 10^{11}\ M^{-1}\ min^{-1}$ and $E_a = 15.8 \pm 0.9$ kcal mol^{-1} were obtained. The ionic strength and pH dependence of k_1 were also studied.

DAVID K. LIU et S. G. CHANG. Can. J. Chem. **65**, 770 (1987).

Utilisant l'analyse des acides aminés et la spectroscopie uv–visible, on a étudié la réaction de la cystine (CySSCy) et les ions hydrosulfures (HS^-), en milieu alcalin. La réaction se produit en deux étapes réversibles conduisant à la cystéine (CySH), la *S*-thiocystéine ($CySS^-$) et le disulfure (S_2^{2-}) par les réactions représentées par les équations suivantes : $CySSCy + HS^- \underset{k_{-1}}{\overset{k_1}{\rightleftharpoons}} CySH + CySS$ et $CySS^- + HS^- \underset{k_{-2}}{\overset{k_2}{\rightleftharpoons}} CySH + S_2^{2-}$. Dû à la présence de divers types de réactifs et de produits, les équilibres et les constantes de vitesse varient avec le pH. A 25°C, avec un pH = 10,0 et $\mu = 0{,}17$ *M*, on a déterminé que les constantes de vitesses sont les suivantes : $k_1 = 3{,}7 \pm 0{,}4\ M^{-1}\ min^{-1}$, $k_{-1} = 5{,}5 \pm 0{,}6\ M^{-1}\ min^{-1}$, $k_2 = 6{,}1 \pm 0{,}5\ M^{-1}\ min^{-1}$ et $k_{-2} = 122 \pm 20\ M^{-1}\ min^{-1}$. Lorsqu'on exprime la constante de vitesse par l'équation $k_1 = A \exp(-E_a/RT)$, on obtient les valeurs suivantes : $A = (4{,}7 \pm 0{,}3) \times 10^{11}\ M^{-1}\ min^{-1}$ et $E_a = 15{,}8 \pm 0{,}9$ kcal mol^{-1}. On a aussi étudié la relation qui existe entre la valeur de k_1 et la force ionique et le pH.

[Traduit par la revue]

Introduction

The reaction between cystine and sulfide has been the subject of various investigations. Kuster and Irion (1) reported the isolation of a new amino acid when wool was treated with sodium sulfide, the identity of which was subsequently confirmed by Horn *et al.* (2) to be that of lanthionine. More recently, Rao and Gorin (3) and Gattner and Zahn (4) studied the same reaction under milder conditions and found cysteine and *S*-thiocysteine produced in two equilibrium steps. However, the equilibrium constants for the individual steps were not determined and little kinetic information was given in their accounts. Our interest in this system stems from recent discovery in our laboratory that ferrous–cysteine complex can effectively remove NO from flue gas (5). We have also demonstrated that the cystine formed in the process can be efficiently converted back to cysteine with HS^-/SO_3^{2-} under appropriate conditions (unpublished experiments). Therefore, a more complete understanding of the cystine–sulfide system is desirable both from a theoretical and practical viewpoint. In this paper we report the equilibrium and rate constants of the reaction between cystine and sulfide at various pH, temperatures, and ionic strengths.

Experimental

Materials

L-(−)-Cystine (Kodak) and L-(+)-cysteine hydrochloride monohydrate (MCB) were used as received. Sodium citrate dihydrate (Mallinckrodt), $Na_2S \cdot 9H_2O$ (Mallinckrodt) and $Na_2B_4O_7 \cdot 10H_2O$ (Baker) were used without further purification. Ninhydrin, stannous chloride, and ethylene glycol monomethyl ether were purchased from Pierce Chemical Co. and were used as received. Electronic absorption spectra were obtained on a Varian Cary 219 spectrophotometer.

Amino acid analysis

The concentrations of cystine, cysteine, and *S*-thiocysteine were determined by a combination of ion-exchange chromatography and quantitative photometric ninhydrin method, first developed by Moore and Stein (6). The amino acid analyzer used in this study was built in-house with the following components: A Rheodyne Model 7010 sample injection valve with a 500 μL sample loop, Eldex Model B-100-S and E-120-S high pressure single piston pumps, a Technicon Model 1 colorimeter with a 570 mm filter, and a Hewlett-Packard 680M strip chart recorder. The jacketed column (9 mm id) was packed with a sulfonated cation exchange resin (16 ± 2 μm) to a height of 13 cm and was thermostated at 55°C. The eluant employed was a pH 3.25 citrate buffer (0.2 *M* Na^+) with a flow rate of 1.5 mL min^{-1}, whereas the flow rate of the ninhydrin solution was set at 0.7 mL min^{-1}. The amino acid analyzer generally operated at a pressure of ~100 psi, and under such conditions the analysis time for each sample was ~30 min.

General procedure

In a typical kinetic experiment, cystine (0.0481 g; 0.2 mmol) was dissolved in 90.0 mL pH 10.0 borate buffer (0.05 *M* Na^+) and the solution was subjected to uv–visible spectroscopic and amino acid analyses. A 0.2 *M* Na_2S stock solution (10.0 mL) was then added to the above cystine solution and the reaction mixture was stirred under a N_2 atmosphere. The reaction mixture (1.0 mL) was taken out at designated time intervals and diluted ten times with the pH 3.25 citrate buffer for uv–visible spectroscopic and amino acid analyses. In the equilibrium studies, the reaction was allowed to proceed until no change in reactant and product concentrations was observed (generally less than 3 h). The concentrations of the amino acids were determined by comparing their peak areas to those of standard samples. The retention times for $CySS^-$, CySH, and CySSCy under present conditions were about 9, 21, and 28 min, and their relative sensitivities were 1.0:1.6:30.8, respectively.

In the temperature dependence experiments, the reaction mixtures

Printed in Canada / Imprimé au Canada

Can. J. Chem. Downloaded from www.nrcresearchpress.com by 80.58.250.72 on 09/07/12
For personal use only.

TABLE 1. Composition of equilibrium mixtures and equilibrium constant of reactions [3] and [4] at various pH at 25°C[a]

pH[b]	[CySSCy]	[CySH]	[CySS$^-$]	[HS$^-$]	[S_2^{2-}]	K_1	K_2
8.0	0.51	2.40	0.58	17.60	0.91	0.16	0.21
9.0	0.30	2.25	1.15	17.75	0.50	0.49	0.06
10.0	0.24	2.25	1.27	17.75	0.49	0.65	0.05
11.0	0.20	2.20	1.40	17.80	0.40	0.87	0.04
12.0	~0.05[c]	2.20	1.70	17.80	0.25	~4.2[c]	0.02

[a]All concentrations are in m*M*. Initial concentration of CySSCy and HS$^-$ are 2.0 and 20 m*M*, respectively. Results shown here are averages of at least two separate runs.
[b]pH attained by addition of HCl or NaOH to a 0.05 *M* Na^+ borate buffer.
[c]The equilibrium concentration of CySSCy is too low to be accurately determined (see Fig. 1; inset curve *2*); therefore the value of K_1 reported here is only approximate.

were kept in a controlled-temperature water bath. For ionic strength dependence studies, less concentrated borate buffers were used for $\mu < 0.17$ *M* whereas for $\mu = 0.01$ *M*, the solutions were not buffered but were adjusted to pH 10.0 by dropwise addition of 0.5 *M* NaOH. pH other than 10.0 were obtained by addition of concentrated HCl or 1 *M* NaOH to a 0.05 *M* Na^+ borate buffer.

Results and discussion

Previous works by Rao and Gorin (3) and Gattner and Zahn (4) established that the reaction between cystine (CySSCy) and sulfide in 0.1–0.2 *M* NaOH solution yielded cysteine (CyS$^-$), *S*-thiocysteine (CySS$^-$), and disulfide (S_2^{2-}) in two reversible steps:

$$[1] \quad \text{CySSCy} + \text{S}^{2-} \underset{k_{-1}}{\overset{k_1}{\rightleftharpoons}} \text{CyS}^- + \text{CySS}^-$$

$$[2] \quad \text{CySS}^- + \text{S}^{2-} \underset{k_{-2}}{\overset{k_2}{\rightleftharpoons}} \text{CyS}^- + \text{S}_2^{2-}$$

However, the only kinetic information given in these reports were the approximate half-lives (3) and the approximate rate constant (4) of the forward reaction in reaction [1]. Our discovery that cystine can be quantitatively converted to cysteine by HS^-/SO_3^{2-} prompted us to undertake a more detailed kinetic study of the above equilibria. Since in the pH range (7.8 to 12.0) of our study the predominant form of sulfide in solution would be HS$^-$ (7), reactions [1] and [2] should be rewritten as:

$$[3] \quad \text{CySSCy} + \text{HS}^- \underset{k_{-1}}{\overset{k_1}{\rightleftharpoons}} \text{CySH} + \text{CySS}^-$$

$$[4] \quad \text{CySS}^- + \text{HS}^- \underset{k_{-2}}{\overset{k_2}{\rightleftharpoons}} \text{CySH} + \text{S}_2^{2-}$$

It should be pointed out that different charge forms of CySSCy, CySH, and CySS$^-$ are also present under such conditions (8). This problem will be addressed below.

The reaction between CySSCy and HS$^-$ has been monitored by a combination of uv–visible spectroscopy and amino acid analysis (ion-exchange chromatography), as shown in Fig. 1. The absorption maximum at 332 nm associated with the equilibrium mixture starting with 2.0 m*M* CySSCy and 10.0 m*M* HS$^-$ at 25°C and pH 10.0 (curve *1*) had been previously ascribed to CySS$^-$ (3, 4). Our result here is consistent with their finding since neither CySSCy (curve *0*), CySH, or HS$^-$ (not shown) absorb appreciably at 332 nm. Furthermore, the fact that the magnitude of A_{332} at pH 10.0 and 12.0 correlates well with

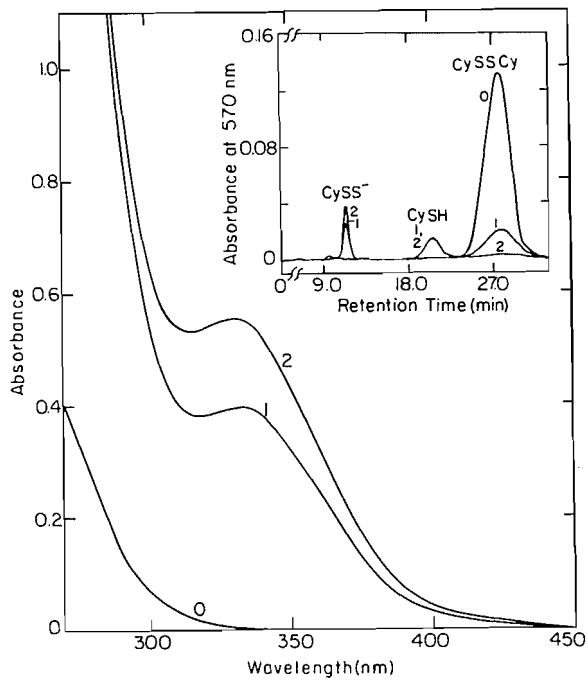

FIG. 1. Ultraviolet–visible spectral changes upon reaction of CySSCy with HS$^-$ at 25°C and $\mu = 0.17$ *M*. Curve *0*: 2.0 m*M* CySSCy in pH 10.0 borate buffer (0.05 *M* Na^+). Curve *1*: upon reaching equilibrium with 20.0 m*M* HS$^-$ at 3.0 h. Curve *2*: equilibrium mixture at pH 12.0. Inset shows the ion chromatograms corresponding to curves *0*, *1*, and *2*.

the equilibrium concentrations of CySS$^-$ as shown in the ion chromatograms (Fig. 1; inset) but not those of S_2^{2-} (Table 1) establishes that the absorption maxima at 332 nm is in fact due to CySS$^-$. From the known equilibrium concentrations of CySS$^-$ (Table 1), one can calculate using Beer's law the molar absorptivity of CySS$^-$ at 332 nm to be $370 \pm 15\ M^{-1}\,\text{cm}^{-1}$.

Determination of equilibrium constants K_1 *and* K_2 *at various pH*

The equilibrium concentrations of CySSCy and CySH in a given mixture can be determined by comparison of the peak areas in the ion chromatograms with those of standard samples. Since CySS$^-$ has not been isolated in a pure state, the equilibrium concentration can be calculated by mass balance using eq. [5]. We generally found a good agreement between the calculated value for $[\text{CySS}^-]_{eq}$ and the observed value from uv–visible spectroscopy (using $\epsilon_{332} = 370\ M^{-1}\,\text{cm}^{-1}$) or using

Can. J. Chem. Downloaded from www.nrcresearchpress.com by 80.58.250.72 on 09/07/12
For personal use only.

amino acid analysis (assuming a sensitivity factor 1/1.6 that of CySH). The equilibrium concentrations for HS^- and S_2^{2-} are calculated using eqs. [6] and [7], respectively.

$$[5] \quad [CySS^-]_{eq} = 2\{[CySSCy]_0 - [CySSCy]_{eq}\} - [CySH]_{eq}$$

$$[6] \quad [HS^-]_{eq} = [HS^-]_0 - \{([CySSCy]_0 - [CySSCy]_{eq}) + \tfrac{1}{2}([CySH]_{eq} - [CySS^-]_{eq})\}$$

$$[7] \quad [S_2^{2-}]_{eq} = \tfrac{1}{2}\{[CySH]_{eq} - [CySS^-]_{eq}\}$$

The composition of equilibrium mixtures at various pH are listed in Table 1. We have studied equilibria [3] and [4] in the pH range of 7.8 to 12.0 because (*i*) of the low solubility of CySSCy between pH 2 and 8 (9); and (*ii*) both CySSCy and CySH are known to decompose in strongly alkaline medium (10). Stricks and Kolthoff reported that CySSCy is stable in pH 11 to 13 solutions for at least 1 h between 12 and 37°C such that polarographic measurements were possible (8). However, we detected the decomposition of CySSCy within 15 min after preparation of the solution at pH 13.0 and 25°C by amino acid analysis. Therefore, determination of equilibrium and rate constants at pH $\geq$ 13 by the present analytical method is not feasible.

The equilibrium constants of reactions [3] and [4], K_1 and K_2, are calculated from eqs. [8] and [9], respectively,

$$[8] \quad K_1 = \frac{[CySH][CySS^-]}{[CySSCy][HS^-]}$$

$$[9] \quad K_2 = \frac{[CySH][S_2^{2-}]}{[CySS^-][HS^-]}$$

and their values at different pH are listed in Table 1. The equilibrium constant K_1 increases whereas K_2 decreases with increasing pH. The fact that the apparent equilibrium constants vary with pH can be explained by the presence of different charge forms of CySSCy, CySH, $CySS^-$, and HS^- at different pH. In order to determine the equilibrium constants due to specific charge forms, the absolute equilibrium constants would first have to be measured at pH ~ 14, where only a single charge form of each species is present. Equilibrium constants involving other charge forms could then be calculated from the absolute equilibrium constants at pH ~ 14 and the apparent equilibrium constants at other pH (8). Unfortunately, such procedure is not feasible here because of the rapid decomposition of CySSCy at pH $\geq$ 13.

Determination of rate constants k_1, k_{-1}, k_2, *and* k_{-2}

Method I

For two parallel reversible reactions such as [3] and [4], it can be shown (11) that the reaction rate can be expressed as

$$[10] \quad V = -\frac{d[CySSCy]}{dt} = \frac{k_1k_2[CySSCy][HS^-]^2 - k_{-1}k_{-2}[S_2^{2-}][CySH]^2}{k_{-1}[CySH] + k_2[HS^-]}$$

At the onset of the reaction, $[S_2^{2-}]$ and [CySH] are negligible compared to [CySSCy] and $[HS^-]$. Therefore the k_{-2}-containing term can be ignored and eq. [10] can be simplified to

$$[11] \quad V = \frac{k_1k_2[CySSCy][HS^-]^2}{k_{-1}[CySH] + k_2[HS^-]}$$

Inverting and multiplying eq. [11] by [CySSCy], one obtains

$$[12] \quad \frac{[CySSCy]}{V} = \frac{k_{-1}[CySH]}{k_1k_2[HS^-]^2} + \frac{1}{k_1[HS^-]}$$

The term on the left hand side of eq. [12] can be written as the reciprocal of the pseudo first-order initial-rate constant if HS^- is present in excess compared to CySSCy. Therefore eq. [12] becomes

$$[13] \quad \frac{1}{k_i} = \frac{k_{-1}[CySH]_0}{k_1k_2[HS^-]_0^2} + \frac{1}{k_1[HS^-]_0}$$

where k_i represents the pseudo first-order initial-rate constant, and $[CySH]_0$ and $[HS^-]_0$ are the initial concentrations of CySH and HS^-, respectively. The value of k_i at a given $[CySH]_0$ can be obtained from the initial slope of a plot of log $([CySSCy]_0/[CySSCy]_t)$ vs. t. Finally, a plot of $1/k_i$ vs. $[CySH]_0$ at constant $[HS^-]_0$ should yield a straight line with a slope of $k_{-1}/k_1k_2[HS^-]_0^2$ and an intercept of $1/k_1[HS^-]_0$, as shown in Fig. 2. From the slope and intercept of the plot and the values of K_1 and K_2 (Table 1), we have obtained $k_1 = 3.7 \pm 0.4\ M^{-1}\ min^{-1}$, $k_{-1} = 5.5 \pm 0.6\ M^{-1}\ min^{-1}$, $k_2 = 6.1 \pm 0.5\ M^{-1}\ min^{-1}$, and $k_{-2} = 122 \pm 20\ M^{-1}\ min^{-1}$ at 25°C, pH 10.0 and ionic strength (μ) of 0.17 *M*. Gattner and Zahn (4) reported $k_1 = 0.8\ M^{-1}\ min^{-1}$ at 20°C and unspecified μ in an unbuffered 0.1 *M* NaOH solution, whereas k_{-1}, k_2, and k_{-2} were all omitted in their approximation method.

Method II

Since $K_1 \gg K_2$ at pH $\geq$ 9 (Table 1), the values of k_1 and k_{-1} can alternately be determined by a method which only consider the first equilibrium (reaction [3]) and ignores the effect of the second equilibrium (reaction [4]). For an opposing reaction of second order such as reaction [3], it has been shown (12) that the reaction rate

$$[14] \quad \frac{dx}{dt} = \alpha + \beta x + \gamma x^2$$

where $x = [CySSCy]_0 - [CySSCy]_t$, $\alpha = k_1[CySSCy]_0[HS^-]_0$, $\beta = -k_1([CySSCy]_0 + [HS^-]_0)$, and $\gamma = k_1 - k_{-1}$. For $k_1 < k_{-1}$ ($K_1 = 0.65$ at pH 10.0; Table 1), the solution takes the form (13)

$$[15] \quad -\tanh^{-1}\frac{2\gamma x + \beta}{q^{1/2}} = \frac{q^{1/2}}{2}t - \theta$$

where $q = \beta^2 - 4\alpha\gamma$, and θ can be determined by the condition $x = 0$ at $t = 0$, or $\theta = \tanh^{-1}(\beta/q^{1/2})$. Therefore, from our knowledge of $[HS^-]_0$, $[CySSCy]_0$, $[CySSCy]_t$, and K_1, we can determine the values of k_1 and k_{-1} from the slope of a plot of $-\tanh^{-1}\left(\frac{2\gamma x + \beta}{q^{1/2}}\right)$ vs. t (since there is a k_1 term in the slope $(q^{1/2}/2)$.

Figure 3 shows plots of eq. [15] at different $[HS^-]_0$. The fact that all the data fit well as straight lines is consistent with (*i*) the reaction is first-order in CySSCy and HS^-, and (*ii*) the first equilibrium can be effectively separated from the second in the determination of k_1 and k_{-1}. The average values of k_1 and k_{-1} at 25°C, pH 10.0, and $\mu = 0.17\ M$ determined by this method are 3.2 ± 0.3 and 4.8 ± 0.5 $M^{-1}\ min^{-1}$, respectively, in good agreement to those determined by Method 1 under the same conditions. As a result, this simpler approach (eq. [14]) can be employed to study the effect of temperature, pH and ionic strength on the rate constant k_1.

Can. J. Chem. Downloaded from www.nrcresearchpress.com by 80.58.250.72 on 09/07/12
For personal use only.

Can. J. Chem. Downloaded from www.nrcresearchpress.com by 80.58.250.72 on 09/07/12
For personal use only.

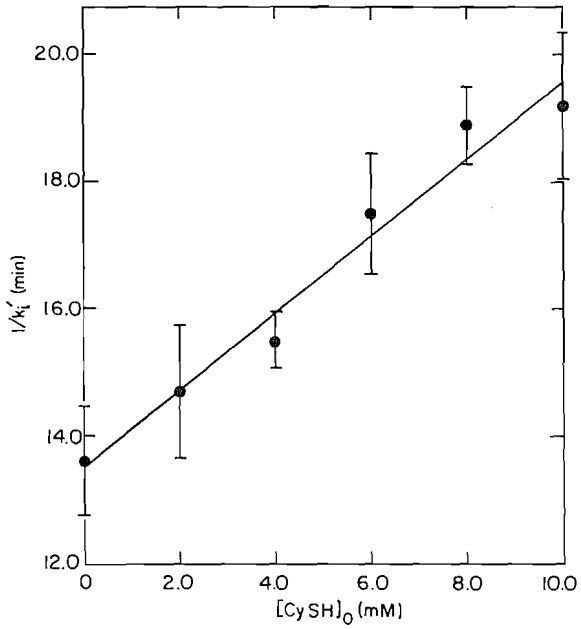

FIG. 2. Plot of $1/k_i$ vs. $[CySH]_0$ at constant $[HS^-]_0$. Reaction conditions are: $[CySSCy]_0 = 2.0$ mM and $[HS^-]_0 = 20.0$ mM, $T^0 = 25$°C, pH = 10.0, and $\mu = 0.17$ M.

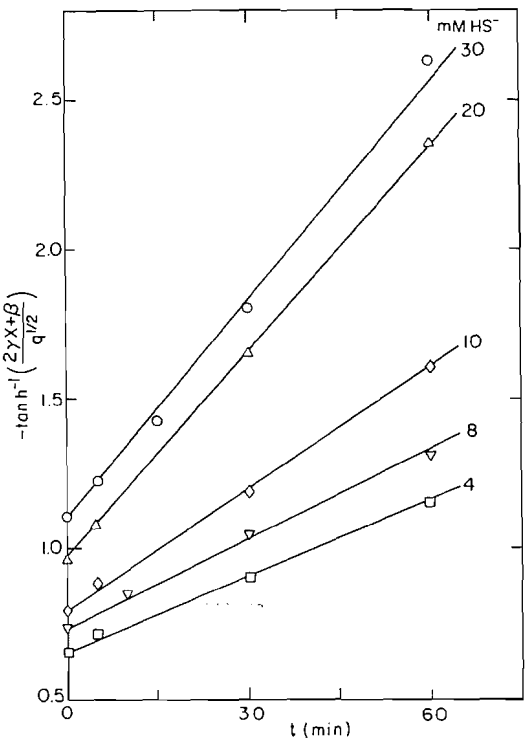

FIG. 3. Plot of $-\tanh^{-1}\left(\dfrac{2\gamma x + \beta}{q^{1/2}}\right)$ vs. t at different $[HS^-]_0$. Reaction conditions are $[CySSCy]_0 = 2.0$ mM, $T^0 = 25$°C, pH = 10.0, and $\mu = 0.17$ M.

Temperature, pH, and ionic strength dependence of k_1

The temperature dependence of the reaction between CySSCy and HS^- was studied in the range of 25 to 50°C, and an Arrhenius plot of the data is shown in Fig. 4(*a*). If the rate constant is expressed as $k_1 = A\exp(-E_a/RT)$, then least-square fit of the data yields $A = (4.7 \pm 0.3) \times 10^{11}$ M^{-1} min^{-1} and $E_a = 15.8 \pm 0.9$ kcal mol^{-1}. The value of E_a we obtained is slightly higher that of 12.8 kcal mol^{-1} obtained by Gattner and Zahn (4).

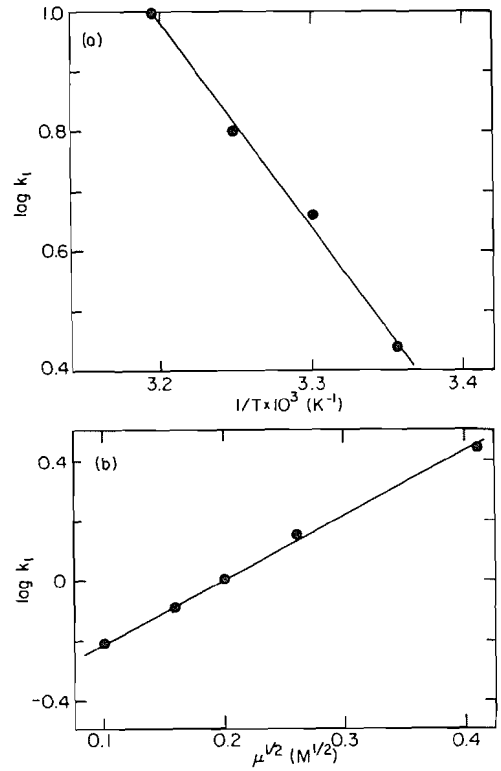

FIG. 4. (*a*) Arrhenius plot for k_1 at pH 10.0 and $\mu = 0.17$ M. (*b*) Ionic strength dependence of k_1 at pH 10.0 and 25°C.

The effect of ionic strength on k_1 was examined over the range of $\mu = 0.01$ to 0.17 M Brønsted's equation for the influence of ionic strength on reaction rate at 25°C in H_2O (12) can be expressed as

$$[16] \quad \log\frac{k_1}{k_1^0} = 1.02\, Z_A Z_B \mu^{1/2}$$

where k_1^0 is the limiting rate constant at $\mu = 0$, and Z_A and Z_B are the charges of the reactants. A plot of log k_1 vs. $\mu^{1/2}$ is shown in Fig. 4(*b*). The best fit of the data is a straight line with a slope of 2.11 ± 0.05 and an intercept of −0.42 ± 0.01, from which one can obtain $Z_A Z_B = 2.07 \pm 0.05$ and $k_1^0 = 0.38 \pm 0.01$ M^{-1} min^{-1}. Hence our result indicates that $CySSCy^{2-}$ react with HS^- at pH 10.0, which is consistent with predictions based on their acid dissociation constants (Fig. 5).

Finally, the effect of pH on k_1 has been studied over a pH range of 7.8 to 12.0, and the results are shown in Fig. 5. It is clear from the experimental results at k_1 does not have a simple $[H^+]$ dependence but is determined by the charge types of both cystine and sulfide at a given pH. To determine the contribution to k_1 from each pair of charged reactants, the absolute rate constant would first have to be determined at pH ~ 14 where only $CySSCy^{2-}$ and S^{2-} are present. The absolute rate constant for $CySSCy^{2-}$ and HS^- can then be calculated from the measured absolute rate constant at pH ~ 14 and the apparent rate constant measured at pH ~ 12, and so on. However, the rapid decomposition of cystine at pH ≥ 13 precludes such a systematic determination of absolute rate constants from being undertaken. However, some qualitative conclusions can be

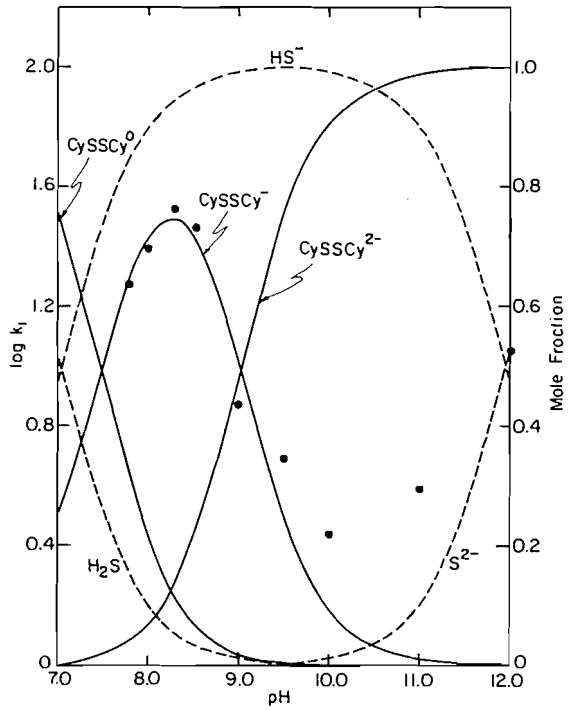

FIG. 5. pH dependence of k_1 at 25°C and μ = 0.17 *M*. The experimental data are represented by closed circles. The curves showing the mole fractions of various charge types of cystine and sulfide were computed using acid dissociation constants from refs. 13 and 14.

drawn from the results shown in Fig. 5. Since the value of k_1 at pH 12.0 (where $CySSCy^{2-}/S^{2-}$ and $CySSCy^{2-}/HS^-$ are present in roughly equal amounts) is greater than that at pH 10.0 (where the reactant pair $CySSCy^{2-}/HS^-$ is predominant), the rate constant for $CySSCy^{2-}/S^{2-}$ must be greater than that for $CySSCy^{2-}/HS^-$. Similarly, by comparing the values of k_1 at pH 10.0 and 8.7 (~70% $CySSCy^-/HS^-$ and ~20% $CySSCy^{2-}/HS^-$), and at pH 12.0 and 8.7, one can conclude that the rate constants for the charged reactant pairs are in the order: $CySSCy^{2-}/S^{2-} \sim CySSCy^-/HS^- > CySSCy^{2-}/HS^-$.

Acknowledgements

This work was supported by the Assistant Secretary for Fossil Energy, Office of Coal Research, Advanced Environment Control Division of the U.S. Department of Energy under contract number DE-AC03-76SF00098 through the Pittsburgh Energy Technology Center, Pittsburgh, PA. We thank Andrew Yee for a gift of the cation exchange resin and helpful discussions.

1. W. KUSTER and W. IRION. Z. Physiol. Chem. **184**, 255 (1929).
2. M. J. HORN, D. B. JONES, and S. J. RINGEL. J. Biol. Chem. **138**, 141 (1940).
3. G. S. RAO and G. GORIN. J. Org. Chem. **24**, 749 (1959).
4. H.-G. GATTNER and H. ZAHN. Proc.-Int. Wooltextil-Forschungskonf. 5th, **3**, 154 (1975); Chem. Abstr. **87**, 24577r (1977).
5. M. TU and S. G. CHANG. AIChE Environ. Progr. In press.
6. S. MOORE and W. H. STEIN. Science, **80**, 458 (1973).
7. W. GIGGENBACH. Inorg. Chem. **10**, 1333 (1971).
8. W. STRICKS and I. M. KOLTHOFF. J. Am. Chem. Soc. **73**, 4569 (1951).
9. K. SANO. Biochem. Z. **168**, 14 (1926).
10. A. L. LEHNINGER. Biochemistry. Worth Publishers, New York. 1975.
11. R. G. WILKINS. The study of kinetics and mechanisms of reactions of transition metal complexes. Allyn and Bacon, Boston. 1974. pp. 26–31.
12. S. W. BENSON. The foundations of chemical kinetics. McGraw-Hill, New York. 1960.
13. R. C. WEAST (*Editor*). CRC handbook of chemistry and physics. 60th ed., CRC Press, Boca Raton, FL. 1980. pp. A49–50.
14. A. MEISTER (*Editor*). Biochemistry of the amino acids. Vol. I. 2nd ed. Academic Press, New York. 1965.

Can. J. Chem. Downloaded from www.nrcresearchpress.com by 80.58.250.72 on 09/07/12
For personal use only.

Synthesis of taxodione

ROBERT H. BURNELL,[1] MICHEL JEAN, AND DONALD POIRIER
Département de chimie, Université Laval, Québec (Qué.), Canada G1K 7P4

Received September 26, 1986

ROBERT H. BURNELL, MICHEL JEAN, and DONALD POIRIER. Can. J. Chem. **65**, 775 (1987).

Two syntheses of taxodione are described, as well as some of the model experiments that preceded them. The yields are low but comparable to most other syntheses of this extended quinone.

ROBERT H. BURNELL, MICHEL JEAN et DONALD POIRIER. Can. J. Chem. **65**, 775 (1987).

Deux synthèses de la taxodione sont présentées avec quelques séquences réactionnelles qui ont servi comme modèles. Les rendements globaux sont plutôt faibles mais ils sont comparables à ceux de synthèses déjà publiées.

Can. J. Chem. Downloaded from www.nrcresearchpress.com by 78.46.186.204 on 09/07/12
For personal use only.

As an extension of certain diterpene syntheses under investigation in our laboratory (1), we were tempted to add our efforts to the several previous taxodione **1** syntheses (2). This extended

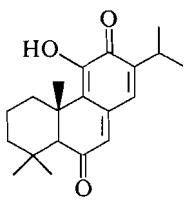

1

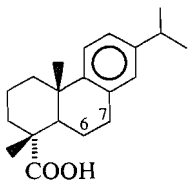

2

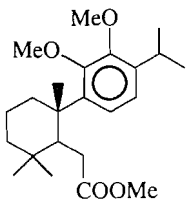

3

quinone showed interesting biological (3) activity, which precipitated the flurry of methods leading to its synthesis, but in most of the schemes the yields have been low.

During our synthesis and structure correction of 5-dehydronellionol trimethyl ether (1), we converted dehydroabietic acid **2** to the B-seco ester **3** but, for economy of time and effort, we had actually performed the original experimentation without reducing the carboxyl function at C.4 to the methyl. We now describe these transformations because some of the compounds also served as models in the taxodione field. By established procedures, methyl dehydroabietate was oxidized to the C.7 ketone, which, when subjected to Baeyer–Villiger conditions, afforded a 7-membered lactone and the latter, on acid catalysed methanolysis, gave the phenol diester **4**.

As in the previously reported sequence, a second oxygen function was introduced on the aromatic ring by oxidation with phenyl seleninic anhydride (4), which gave mainly the red *o*-quinone **5** and a small quantity of the *p*-quinone **6**. Catalytic hydrogenation of the *o*-quinone **5** gave an intermediate, which was immediately methylated *in situ* (Me_2SO_4, NaOH) under hydrogen to afford the di-*O*-methyl catechol derivative **7***a*. Of the four *O*-methyl groups in the latter, the two ethers and the pivalic type ester at C.4 are stable to aqueous base but the other ester was readily hydrolysed to the acid **7***b*.

Cyclization of the latter in trifluoroacetic anhydride led to the ketone **8***a*. As a taxodione model, the molecule still lacked an oxygen function at C.6, which we intended to introduce by oxygenation in strong base, but, on attempting this reaction on **8***a*, the newly introduced enol, as in **9**, cyclized spontaneously to the lactone **10***a*.

In our original scheme for this synthesis, we had hoped to force the cyclization of the acid **11***c* despite the unfavorable disposition of the substituents and to oxidize the aromatic ring to the *o*-quinone at a later stage. The cyclization, for which several literature equivalents exist (5), gave only the rearranged

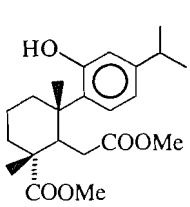

4

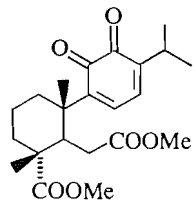

5

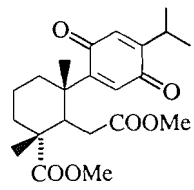

6

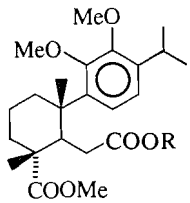

7*a* R = Me
7*b* R = H

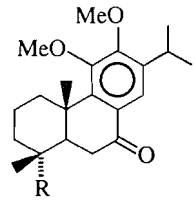

8*a* R = COOMe
8*b* R = Me

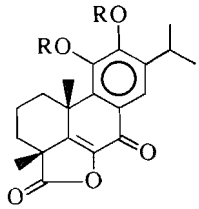

10*a* R = Me
10*b* R = H

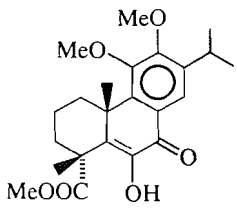

9

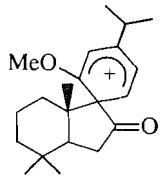

14

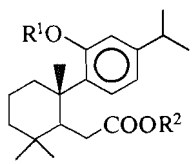

11*a* R^1 = H, R^2 = Me
11*b* R^1 = R^2 = Me
11*c* R^1 = Me, R^2 = H

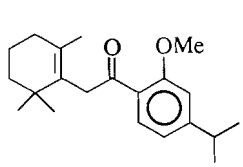

12

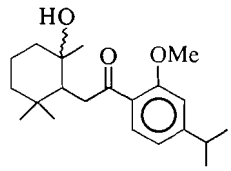

13

products **12** and **13**, presumably via the *ipso* substituted intermediate **14** (or its equivalent). The double bond in compound **12** resisted conjugation.

The preparation of the dimethoxy ketone **15**, which we published earlier (1), represented a formal synthesis of taxodione, since this was an intermediate that Matsumoto used to prepare the corresponding $\Delta^{6,7}$-olefin, which in turn was transformed by Mori into taxodione in four steps (2). We felt that this sequence could be improved. Stirring the ketone **15** under oxygen in the presence of potassium *tert*-butylate

[1]Author to whom correspondence should be addressed.

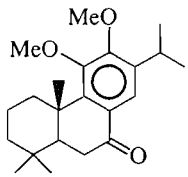

15

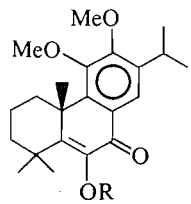

16*a* R = H
16*b* R = Me

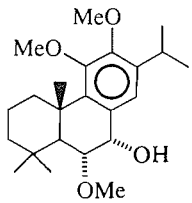

17

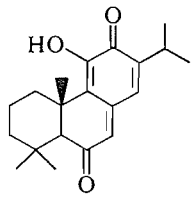

1

afforded the enolized α-diketone **16***a*. We had previously found that hydrogenation of such diketones gives several products, including appreciable quantities of the compound where both oxygen functions are lost by hydrogenolysis, but that this difficulty can be avoided to a large extent by methylation of the enolic carbonyl group (6). So after protecting this hydroxyl group as the methyl ether **16***b*, the product was catalytically hydrogenated to give the 6-methoxy-7-hydroxy compound **17** in which the configurations were assigned using the proton nmr vicinal coupling constants. Upon demethylating this material with boron tribromide and chromatographing the product slowly over silica gel, we obtained taxodione **1** directly in about 20% yield.

Another synthesis of a taxodione analogue described by Ohtsuka and Tahara (7) involves the transformation of an abietatriene type ester by an arduous route into an *o*-quinone, which on slow silica gel chromatography was oxidized directly to the taxodione chromophore in low but interesting yield (14%, see Scheme 1). The authors added that they were unable to prepare the appropriate *o*-quinone (*gem*-dimethyls at C.4) for the synthesis of taxodione itself.

This fortuitous synthesis was appealing so, as a trial system, we demethylated the ester **18***a*, which we had on hand from previous model studies, and subjected the acid **18***b* to oxidation by phenyl seleninic anhydride, which gave an excellent yield of the *o*-quinone **19** (87%). The latter was not too stable so, following the procedure suggested by Tahara *et al.*, we chromatographed it very slowly over silica gel, which caused the colour to change from red to orange to yellow. After further purification, we isolated a 58% yield of the lactone **20**, which showed the same uv absorption as taxodone **21** (8).

When ferruginol **22** was oxidized with phenyl seleninic anhydride the *o*-quinone **23** was isolated in 40% yield accompanied by the quinol **24** (13%). The latter could be dehydrated by refluxing in methanol containing hydrochloric acid but the probable intermediate **28***a* enolized to afford the conjugated olefin **25***a*. It was hoped to integrate the quinol **24** into the synthesis via the olefin **25***a* or the ketone **26**, prepared from it by rearrangement of the 6,7-diol, but their oxidation with phenyl seleninic anhydride led to intractable mixtures, even at low temperature. The *o*-quinone **23** was reduced catalytically and methylated while still under hydrogen, affording both the dimethoxy compound **27***a* and the monomethoxy **27***b*. Of course, the latter gave the former upon further methylation.

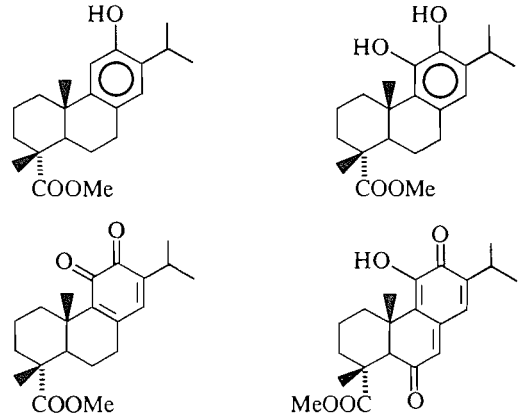

SCHEME 1

In their synthesis of taxodione, Mori and Matsui bypassed compound **27***a*, which was prepared in a completely different fashion (2*a*).

When the *o*-quinone **23** was slowly chromatographed following the Tahara method, we obtained up to 14% taxodione, but the yield was variable. In an effort to understand this oxidation of the quinone, which must be quite complex, we followed the uv–vis absorption as a function of time. Freshly dissolved in ethanol, the *o*-quinone absorbs at 264 and 424 nm; however, in chloroform there is an intense stable peak at 311 nm, which is exactly like that shown by taxodone **21**. In methanol solution, the 311-nm band diminishes over a period of a few days to the advantage of a peak at 278 nm but, after evaporation, the residue showed only the 311-nm peak, so no irreversible change had occurred. Taxodione has two very intense peaks at 320 and 332 nm (EtOH, ε = 25 000 and 26 000 respectively).

During the slow chromatography the first product we noticed was that showing the peak at 311 nm, and we could isolate this intermediate as a yellow oil in 69% yield after adsorbing the *o*-quinone on a small quantity of silica gel by evaporation of the solvent and then eluting the material from a conventional column. The uv spectrum suggests the taxodone chromophore while absorptions in the ir at 3300 and 1650 cm^{-1} confirmed the presence of a hydroxyl group and a highly conjugated carbonyl. The molecular ion in the mass spectrum at 300 *m/z* showed the new product to be isomeric with the original *o*-quinone, and only the mono-enolized structure **28***b* adequately fits the physical data. The other enol **29** would not only show a different uv absorption but the methyl groups in the sidechain would be displaced from their observed positions of δ 1.13 and 1.14. The stabilizing effect of the hydrogen bonding in **28***b* precludes enolization to the fully aromatic **25***b*. The intermediate **28***b* also gave taxodione on repeated slow chromatography in carbon tetrachloride in yields comparable to those obtained directly from the *o*-quinone.

Experimental

Unless otherwise stated, the conditions and instruments used to characterize the products were melting points, Electrothermal, uncorrected; ultraviolet spectra, ethanol solutions (log ε in parentheses), Hewlett Packard 8450 A; infrared spectra, carbon tetrachloride solutions, Beckman 4250 and Perkin Elmer 457; proton magnetic resonance spectra, deuteriochloroform solutions, TMS internal standard (multiplicity, integrated peak areas, coupling constants, and assignments in parentheses), Bruker HX 90; carbon-13 magnetic resonance spectra, deuteriochloroform solutions, TMS internal standard, Bruker WP 80; mass spectra, Hewlett Packard 5992. Elemental analyses were by Galbraith Laboratories, Knoxville. The high resolution mass spectra were recorded on an A.E.I. MS-30. Unless otherwise stated, dry

Can. J. Chem. Downloaded from www.nrcresearchpress.com by 78.46.186.204 on 09/07/12
For personal use only.

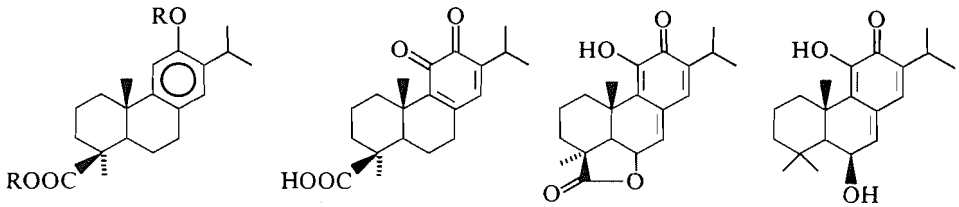

18*a* R = Me
18*b* R = H

19 **20** **21**

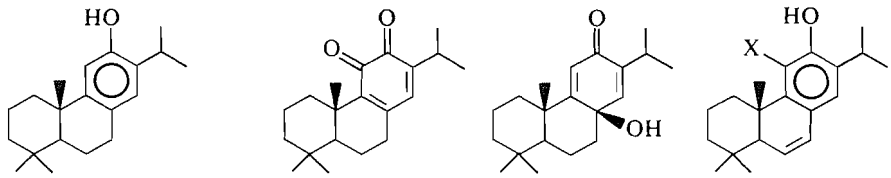

22 **23** **24**

25*a* X = H
25*b* X = OH

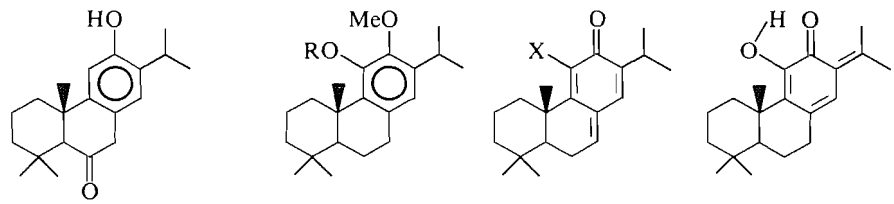

26

27*a* R = Me
27*b* R = H

28*a* X = H
28*b* X = OH

29

column chromatography implies the use of Merck Kieselgel 60F (70–230 mesh) and elution with hexane – ethyl acetate (proportions determined by prior thin-layer chromatography using Machery–Nagel Polygram precoated plastic sheets).

Ortho-quinone **5**

The phenol diester **4** (1.24 g, prepared following essentially the procedure described by Pelletier and Ohtsuka (9)) was dissolved in anhydrous THF (50 mL) and this solution was added dropwise to a suspension of freshly sublimed phenyl seleninic anhydride (2.60 g) in THF (50 mL) warmed to 50–60°C. After 60 min the mixture was poured into ice-water and extracted with ether, which was then well washed with a saturated sodium bicarbonate solution. The reddish crude product was chromatographed (silica gel; benzene – ethyl acetate 9:1) affording diphenyl diselenide (730 mg, yellow solid, mp 50–55°C), the *p*-quinone **6** (270 mg; 21%), and the *o*-quinone **5** (900 mg; 70%) as a viscous dark red oil; uv λ_{max}: 275 (sh), 414 (1800), and 580 (weak) nm; ir (CCl_4): 1730, 1685, 1675, and 1660 cm^{-1}; ^1H nmr δ: 1.11 (d, J = 7 Hz, iso-Pr methyls), 1.18 and 1.23 (2s, C.4-Me and C.10-Me), 2.26 and 2.28 (d, J = 5 Hz, CH_2—COOMe), 2.94 (sept, J = 7 Hz, iso-Pr CH), 3.51 (dd, J = 6 and 5 Hz, C.5-H), 3.59 and 3.75 (2s, COOMe), 6.72 (s, 2H, =CH); ^{13}C nmr: see Table 1; mass spectrum, m/z: 392 (M + 2), 390 (M^+), 362, 360, 332, and 181 (base). *Exact Mass* (hrms) calcd. for $C_{22}H_{30}O_6$: 390.2042; found: 390.2034.

The yellow *p*-quinone **6** was identified by comparison with a sample prepared in another context: ^{13}C nmr, see Table 1.

Reduction and methylation

The *o*-quinone (900 mg) in methanol (20 mL) was added to prehydrogenated Adams catalyst (40 mg) in methanol (10 mL) and hydrogenated at atmospheric pressure. When the red solution had become colorless, without opening to the atmosphere, sodium hydroxide (30% aqueous solution, total 18 mL) and dimethyl sulfate (total 7 mL) were added 1 mL at a time at intervals over a period of 50 h. After filtering and washing the catalyst, the organic solvent was evaporated to give the crude product **7***a*, which was purified by dry column chromatography (705 mg; 70%); ir (CCl_4): 1740 cm^{-1}; ^1H nmr δ: 1.18 (d, J = 7 Hz, iso-Pr methyls), 1.26 and 1.32 (2s, C.4-Me and C.10-Me respectively), 2.22 (d, J = 6 Hz, -CH_2COOMe), 3.28 (sept, J = 7 Hz, iso-Pr CH), 3.36 and 3.47 (2s, COOMe), 3.66 (t, J = 6 Hz, C.5-H), 3.79 and 4.09 (2s, Ar-OMe), 6.89 (ABq, Δν = 11.7, J = 8.5 Hz, arom. H); ^{13}C nmr, see Table 1; mass spectrum, m/z: 420 (M^+), 405, and 389. *Anal.* calcd. for $C_{24}H_{36}O_6$: C 68.54, H 8.63; found: C 68.26, H 8.02.

Hydrolysis ester **7**a → **7**b

To the ester **7***a* (570 mg) in methanol (25 mL) was added potassium hydroxide solution (25 mL of 10% aqueous) and the mixture was refluxed for 140 min. Most of the methanol was then evaporated under vacuum and the aqueous solution washed with ether to remove neutral materials. After acidification (concentrated HCl), ether extraction afforded the acid **7***b* as a yellow solid (538 mg; 97%), mp 112–114°C; ir (KBr): 3600–2400 (v br), 1730, and 1710 cm^{-1}; ^1H nmr δ: 1.17 (d, J = 7 Hz, iso-Pr Me), 1.24 and 1.29 (2s, C.4-Me and C.10-Me respectively), 2.25 (d, J = 6 Hz, -CH_2COOMe), 3.26 (sept, J = 7 Hz, iso-Pr CH), 3.36 (s, COOMe), 3.60 (t, J = 6 Hz, C.5-H), 3.76 and 4.00 (2s, Ar-OMe), 6.88 (ABq, Δν = 12.1, J = 8 Hz, arom. H), 9.80 (bs, D_2O, COOH); ^{13}C nmr, see Table 1; mass spectrum, m/z: 406 (M^+), 374, and 160 (base). *Anal.* calcd. for $C_{23}H_{34}O_6$: C 67.95, H 8.43; found: C 68.41, H 8.74.

Cyclization to the ketone **8**a

The acid **7***b* (300 mg) was stirred in trifluoroacetic anhydride (3 mL) for 12 h at room temperature. The mixture was poured into ice-water and the ether extract was washed with sodium bicarbonate solution until neutral, then evaporated and taken up in methanol (30 mL) and aqueous potassium hydroxide (3 mL of 10%). After 2 h at room temperature the product was obtained by adding water and extracting with ether. The ketone **8***a* was obtained as a wax (253 mg; 83%); ir (CCl_4): 1730 and 1690 cm^{-1}; uv λ_{max}: 272 (8000) nm; ^1H nmr δ: 1.22 and 1.25 (two d, J = 7 Hz, iso-Pr Me), 1.34 and 1.42 (2s, C.4-Me and C.10-Me respectively), 2.69 (d, J = 11 Hz, —CH_2—C(=O)—), 3.28 (sept, J = 7 Hz, iso-Pr CH), 3.68 and 3.87 (2s, Ar-OMe), 7.79

Can. J. Chem. Downloaded from www.nrcresearchpress.com by 78.46.186.204 on 09/07/12
For personal use only.

Can. J. Chem. Downloaded from www.nrcresearchpress.com by 78.46.186.204 on 09/07/12
For personal use only.

TABLE 1. ^{13}C nuclear magnetic resonance data[a]

Carbon	Compound															
	4	**5**	**7***a*	**7***b*	**10***a*	**11***c*	**12**	**13**	**16***a*	**16***b*	**18***b*	**20**	**23**	**24**	**25***a*	**28***b*
1	34.8	34.4	36.2	35.7	37.8	36.1	39.5	40.0	29.6	29.4	40.4	35.6	36.1	39.9	36.2	36.9
2	19.2	18.6	18.9	19.0	18.7	19.5	19.7	20.7	18.3	18.2	20.8	18.1	18.1	17.1	19.1	18.5
3	32.9	33.1	35.2	34.5	36.7	41.5	43.4	43.5	36.7	37.5	38.5	43.1	33.4	37.9	29.7	41.9
4	46.5	46.8	46.8	46.2	47.6	34.6	32.7	35.3	36.7	37.5	44.3	31.5	41.6	41.9	47.0	33.0
5	40.0	40.2	41.1	41.0	44.5	44.4	130.7	52.0	142.4	142.2	53.7	48.7	51.4	55.0	51.1	50.7
6	34.1	33.5	33.5	33.1	36.5	33.1	34.2	41.5	143.9	144.0	22.2	73.0	20.0	20.3	124.8	26.8
7	175.0	173.9	173.9	179.6	197.5	181.0	200.1	204.2	180.1	181.0	31.8	132.8	33.4	34.3	127.5	136.2
8	128.6	134.9	119.5	119.6	128.3	128.3	130.5	130.9	124.0	125.0	126.7	143.8	145.1	69.4	127.3	144.1
9	131.0	148.8	141.6	141.7	145.5	134.4	127.6	127.2	145.6	144.0	147.2	123.2	146.9	169.0	147.4	127.5
10	41.3	42.3	42.2	42.2	40.2	42.7	131.6	73.2	41.4	42.4	39.1	43.1	38.1	41.9	41.2	38.9
11	155.4	181.3	153.1	153.1	151.5	158.8	158.6	158.6	151.0	150.8	112.5	144.4	181.5	122.1	109.7	140.7
12	115.9	180.6	151.5	151.5	156.8	111.0	110.0	110.0	156.1	155.5	153.4	191.9	180.5	187.5	167.1	181.6
13	148.5	147.8	139.0	139.0	141.7	148.5	154.8	155.0	143.4	144.3	133.0	132.9	147.9	142.2	131.1	131.9
14	118.0	133.0	123.4	123.4	121.5	118.1	119.0	119.0	118.0	119.8	127.3	136.0	137.9	145.5	125.0	148.9
15	33.4	27.4	26.9	26.9	27.1	33.7	34.6	34.5	27.2	27.3	26.9	26.4	26.9	25.7	26.9	26.0
16	23.9	21.5	23.5	23.5	23.4	23.9	23.8	23.7	23.6	23.6	23.0	21.4	21.4	21.8	22.7	21.5
17	23.9	21.5	23.5	23.5	23.1	23.9	23.8	23.7	23.3	23.3	23.0	21.4	21.4	21.8	22.7	21.9
18	21.7	178.2	178.5	178.5	178.1	33.7	28.2	32.7	31.8	31.7	32.0	32.3	33.8	33.5	33.1	33.4
19	178.5	21.5	20.2	20.2	16.7	21.4	28.2	22.8	28.1	29.4	179.4	181.9	21.7	21.4	20.3	22.2
20	23.9	23.9	23.5	23.9	20.4	22.8	20.6	21.6	29.9	29.4	23.7	21.8	18.9	18.7	37.9	19.0
Other	51.7	52.2	51.7	51.4	52.2	55.1	55.5	55.6	59.9	59.6						
	51.6	51.8	51.1	59.6	60.0				60.3	59.9						
			59.6	59.9	60.2					60.3						
			60.0													

[a]In ppm from TMS.

Can. J. Chem. Downloaded from www.nrcresearchpress.com by 78.46.186.204 on 09/07/12
For personal use only.

(s, arom. H at C.14); ^{13}C nmr, see Table 1; mass spectrum, *m/z*: 388 (M^+, 100%), 373, 358, 329, and 313. *Anal.* calcd. for $C_{23}H_{32}O_5$: C 70.33, H 8.08; found: C 70.10, H 8.30.

Formation of the lactone ***10****a*

At room temperature the ketone ***8a*** (240 mg) in *tert*-butanol (20 mL) was added to the solution resulting from dissolving potassium (1.5 g) in *tert*-butanol (40 mL). Oxygen was bubbled through the solution for 4 h, the reaction mixture was then acidified with 10% hydrochloric acid, and the product obtained by ether extraction. The ester **9** and the lactone ***10a*** are both present at this stage (tlc and spectra) in the ratio 3:7 but during the silica gel chromatography (benzene–EtOAc 9:1) the former disappears and only lactone ***10a*** was isolated (165 mg; 72%) as a white solid, mp 182–183°C: uv λ(EtOH): 251 (9600), 269 (11 600), and 306 (10 000) nm; ir (KBr): 1810 (lactone), 1680, 1660, and 1600 cm^{-1}; ^{1}H nmr δ: 1.27 and 1.29 (2d, total 6H, J = 7 Hz, nonequivalent iso-Pr Me), 1.67 and 1.69 (2s, C-Me at C.4 and C.10), 3.35 (sept, J = 7 Hz, iso-Pr CH), 3.89 and 3.95 (2s, Ar-OMe), 8.03 (s, arom. H at C.14); ^{13}C nmr, see Table 1; mass spectrum, *m/z*: 370 (M^+), 342 (100%), and 327. *Anal.* calcd. for $C_{22}H_{26}O_5$: C 71.33, H 7.08; found: C 71.50, H 7.12.

Demethylation of ***10****a to give* ***10****b*

A solution of boron tribromide (0.4 mL) in dichloromethane (1.0 mL) was added very slowly (during 3 h), with stirring, to the lactone ***10a*** (20 mg) in dichloromethane (2 mL) at room temperature. After 11 h, the solvent was removed by evaporation, the residue taken up in water, and ether extracted. Chromatography (silica gel; hexane – ethyl acetate 6:4) gave some starting material (3 mg) and then the catechol ***10b*** (14 mg; 76%), mp 268–270°C (yellow crystals); uv: 262 (9400), 340 (2700), and 424 (3600) nm; ir (KBr): 3470, 3420, 1800, 1670, 1645, and 1610 cm^{-1}; ^{1}H nmr δ: 1.25 (d, J = 7 Hz, iso-Pr Me), 1.59 and 1.67 (2s, C-Me), 3.1 (m, iso-Pr CH), 6.6 (br, 2H, D_2O), and 7.84 (s, arom. H); (in acetone-d_6: 1.26, 1.66, 1.78, 3.3, and 7.82); mass spectrum, *m/z*: 342 (M^+), 314, 299, 298, and 286 (100%). *Exact Mass* (hrms) calcd. for $C_{20}H_{22}O_5$: 342.1467; found: 342.1466.

Preparation of the acid ***11****c*

The phenol ester ***11a*** (described earlier (*1c*), 0.86 g), dimethyl sulfate (8.4 g), and anhydrous potassium carbonate (9.0 g) were refluxed in acetone (100 mL) for 20 h. Water was added to destroy excess dimethyl sulfate and most of the acetone was then evaporated before extracting the solution with ether. Chromatography (silica gel; hexane – ethyl acetate 9:1) afforded the methoxy ester ***11b*** (0.71 g; 80%); ir: 1740 cm^{-1}; ^{1}H nmr δ: 3.20 ($COOCH_3$) and 3.89 (Ar-OCH_3); ^{13}C nmr, see Table 1; mass spectrum, *m/z*: 346 (M^+), 315, 303, and 117 (100%), which was hydrolysed without further purification.

To the methoxy ester ***11b*** (2.44 g) in methanol (85 mL) was added sodium hydroxide (85 mL, 10% aqueous) and the mixture was refluxed for 20 h. Most of the methanol was evaporated and the product obtained by ether extraction. Chromatography (silica gel; hexane – ethyl acetate 4:1) gave the acid ***11c*** as a low-melting solid (1.78 g; 79%), mp 46–50°C; ir: 3200–2500 (acid), 1710, and 1610 cm^{-1}; ^{1}H nmr δ: 0.89, 0.97 and 1.31 (3s, Me-C), 1.20 (d, J = 7 Hz, iso-Pr Me), 1.89 (dd, J = 16 and 5 Hz, -C*H*—CO), 2.17 (dd, J = 16 and 6 Hz, CH—CO), 2.70 (sept, J = 7 Hz, iso-Pr CH), 3.50 (dd, J = 6 and 5 Hz, C.5-H), 3.84 (s, Ar, OMe), 6.7 and 7.16 (arom. H), 11.4 (bs, COO*H*, D_2O); ^{13}C nmr, see Table 1; mass spectrum, *m/z*: 332 (M^+, 100%), 317, and 289. *Anal.* calcd. for $C_{21}H_{32}O_3$: C 75.86, H 9.70; found: C 75.95, H 9.94.

ipso *Cyclization of acid* ***11****c*

The methoxy acid (308 mg) was stirred in trifluoroacetic anhydride (4 mL) at room temperature for 6 h. The mixture was decomposed with ice-water and the product obtained by ether extraction and well washed with aqueous potassium hydroxide. Chromatography (silica gel; hexane – ethyl acetate 4:1) afforded two products:

Nonconjugated enone ***12*** (162 mg; 56%); uv λ_{max}: 253 (10 000) and 304 (5200) nm; ir (film): 1680 and 1600 cm^{-1}; ^{1}H nmr δ: 0.91 and 1.49 (2s, Me-C), 1.23 (d, J = 7 Hz, iso-Pr Me), 2.85 (sept, iso-Pr CH), 3.64 (s, 2H, C═C—CH_2—C═O), 3.83 (s, Ar, OMe), 6.88, 6.94 (m), and 7.61 (d, J = 8 Hz, arom. H); ^{13}C nmr, see Table 1; mass spectrum, *m/z*: 314 (M^+), 299, 287, 272 and 177 (100). *Exact Mass* (hrms) calcd. for $C_{21}H_{30}O_2$: 314.2246; found: 314.2244.

Tertiary alcohol ***13*** (44 mg; 14%); uv λ_{max}: 253 (14 700) and 302 (6000) nmr; ir: 3460, 1670, and 1600 cm^{-1}; ^{1}H nmr δ: 0.86 (6H), 1.14 (2s, 3 × Me-C), 1.24 (d, J = 7 Hz, iso-Pr Me), 2.12 (dd, J = 6 and 5 Hz, C.5-H), 2.24 (s, OH, D_2O), 2.86 (sept, J = 7 Hz, iso-Pr CH), 3.83 (s, Ar-OMe), 6.84, 6.92 (m), and 7.59 (d, J = 8 Hz) (3 × arom. H); ^{13}C nmr, see Table 1; mass spectrum, *m/z*: 332 (M^+), 317, 314, 299, 289, and 177 (100). *Anal.* calcd. for $C_{21}H_{32}O_3$: C 75.86, H 9.70; found: C 76.02, H 9.89.

NOTE: When the alcohol **13** (91 mg) was refluxed in methanol (20 mL) containing hydrochloric acid (5 mL, 50%) for 5 h, the product was the tetraene **12** (83 mg; after chromatography: 96%).

Oxygenation of the ketone ***15*** *(→ diosphenol* ***16****a)*

Potassium (2.0 g) was dissolved in *tert*-butanol (50 mL) and stirred for 12 h. The ketone **15** (290 mg) dissolved in *tert*-butanol (25 mL) was then added at room temperature and oxygen was bubbled through the solution for 2 h. The mixture was then acidified with dilute hydrochloric acid (5%) and the weak acid product was extracted into ether and finally crystallized from hexane, affording the diosphenol ***16a*** (253 mg; 84%), mp 115–117°C (colorless plates, hexane); uv λ_{max}: 243 (8000), 279 (9600), and 322 (10 500) nm; ir: 3370, 3340, 1640, 1625, and 1585 cm^{-1}; ^{1}H nmr δ: 1.25, 1.29 (two d, J = 7 Hz, iso-Pr Me), 1.48 (6H) and 1.66 (3s, Me-C at C.4 and C.10 respectively), 3.33 (sept, J = 7 Hz, iso-Pr CH), 3.87, 3.94 (2s, Ar-OMe), 7.14 (s, enol OH, D_2O), 7.92 (s, arom. H); ^{13}C nmr, see Table 1; mass spectrum, *m/z*: 358 (M^+), 343, 330, 327, 315, and 273 (100). *Anal.* calcd. for $C_{22}H_{30}O_4$: C 73.71, H 8.44; found: C 73.75, H 8.31.

Methylation of the diosphenol ***16****a (→* ***16****b)*

The diosphenol (159 mg) was dissolved in ethanol (10 mL) and water (10 mL), and aqueous sodium hydroxide (8.0 mL of 30%) was added, followed by dimethyl sulfate (4.0 mL, dropwise). The mixture was stirred for 21 h and then more sodium hydroxide (4 mL of 30%) and dimethyl sulfate (2.0 mL) were added. After 26 h the solution was diluted with water and the product obtained by ether extraction. Chromatography (silica gel; hexane – ethyl acetate 19:1) gave some starting material (29 mg; 18%) and then the methylated product ***16b*** (89 mg; 54%), mp 104–106°C (from hexane): uv λ_{max}: 243 (20 000), 274 (30 000), and 299 (27 000) nm; ir: 1650 and 1600 cm^{-1}; ^{1}H nmr δ: 1.23, 1.26 (two d, J = 7 Hz, iso-Pr Me), 1.43 (6H) and 1.65 (2s, 3 × Me-C), 3.30 (sept, iso-Pr CH), 3.85 (6H) and 3.92 (2s, 3 × OMe), 7.92 (s, arom. H); ^{13}C nmr, see Table 1; mass spectrum, *m/z*: 372 (M^+), 357, 341, 329, and 287 (100). *Anal.* calcd. for $C_{23}H_{32}O_4$: C 74.16, H 8.66; found: C 74.01, H 8.76.

Hydrogenation of the methylated enol ***16****b (→* ***17****)*

The methylated product ***16b*** (22 mg) in methanol (15 mL) was introduced into a hydrogenation apparatus containing prehydrogenated 10% palladium on carbon (25 mg) in methanol (10 mL). After stirring under hydrogen for 12 h, the catalyst was filtered off, and the solution diluted with water and extracted with ether. After chromatography (silica gel; carbon tetrachloride – ethyl acetate 9:1) the colorless solid **17** was crystallized from hexane, mp 92–95°C (19.5 mg; 88%); ir: 3620, 3380, and 1615 cm^{-1}; ^{1}H nmr δ: 1.03, 1.17, and 1.60 (3s, C-Me), 1.21 (d, J = 7 Hz, iso-Pr Me), 2.28 (d, J = 12 Hz, C.5-H), 3.24 (sept, J = 7 Hz, iso-Pr CH), 3.58 (s, OMe at C.6), 3.74, 3.82 (2s, Ar-OMe), 3.98 (d, J = 5 Hz, C*H*OH), 4.56 (dd, J = 12 and 5 Hz, C*H*-OMe), 7.30 (s, arom. H); mass spectrum, *m/z*: 376 (M^+, 100), 361, 358, and 343. *Anal.* calcd. for $C_{23}H_{36}O_4$: C 73.36, H 9.64; found: C 73.11, H 9.64.

Taxodione ***1*** (demethylation and oxidation of **17**)

To the trimethoxy derivative **17** (27 mg) in dry dichloromethane (5 mL) cooled to 0°C was added boron tribromide (0.5 mL of 1 *M* solution in dichloromethane). After 2 h, more boron tribromide solution (0.5 mL) was added and the reaction stirred for 12 h at room temperature. The reaction mixture was poured into ice-water and extracted with ether that was well washed with saturated sodium

Can. J. Chem. Downloaded from www.nrcresearchpress.com by 78.46.186.204 on 09/07/12
For personal use only.

bicarbonate solution. The crude oily orange product (26 mg) was slowly chromatographed over silica gel in carbon tetrachloride, twice, affording a fraction of pure taxodione (3.0 mg; 13%); ir: 3320, 1675, 1640, 1628, 1618, and 1600 cm^{-1}; mass spectrum, *m/z*: 314 (M^+), 299, 286, 271, and 149 (100). *Exact Mass* (hrms) calcd. for $C_{20}H_{26}O_3$: 314.1882; found: 314.1875.

Comparison of the product with an authentic sample obtained from Prof. Takashi Matsumoto (Hiroshima University) showed the two to be identical (ir, tlc; two solvent systems).

*Synthesis of lactone **20** (via o-quinone **19**)*

The methyl *O*-methyl-13-isopropylpodocarpate **18***a* (323 mg, prepared as described previously (1*a*) was dissolved in methylene chloride (20 mL) and, at −10°C and under nitrogen, boron tribromide (5 mL) in methylene chloride (10 mL) was rapidly added. After stirring for 1 h, water was added and the volatile solvent removed *in vacuo*. Ether extraction gave a brownish oil from which chromatography (silica gel; ethyl acetate) gave the substituted podocarpic acid **18***b* (256 mg; 83%), mp 252°C (colorless needles); ir: 3600–2400 (very br), 1690, 1600, 1575, and 1500 cm^{-1}; ^1H nmr, acetone-d_6, δ: 1.12 and 1.30 (2s, 2 × Me-C), 1.21 (d, *J* = 7 Hz, iso-Pr Me), 3.23 (sept, *J* = 7 Hz, iso-Pr CH), 6.81 and 6.86 (2s, arom. H at C.11 and C.14); ^{13}C nmr, see Table 1; mass spectrum, *m/z*: 316 (84, M^+), 301 (54), 255 (73), 213 (100), 199 (23), 185 (22), 171 (39), 157 (59), and 147 (55). *Anal.* calcd. for $C_{20}H_{28}O_3$: C 75.91, H 8.92; found: C 75.79, H 9.02.

Phenyl seleninic anhydride (466 mg) was suspended in anhydrous THF (50 mL) and warmed to 50°C. The phenol **18***b* (200 mg) in anhydrous THF (20 mL) was added drop by drop and stirring was continued for 2 h. The reaction mixture was diluted with chloroform (200 mL) and the solution washed many times with aqueous sodium bicarbonate and then with brine. The organic phase gave a red oil, which was chromatographed rapidly over silica gel to give the unstable red *o*-quinone **19** (182 mg; 87%); ^1H nmr δ: 1.12 and 1.19 (2d, 6H, *J* = 7 Hz, iso-Pr Me), 1.17 and 1.32 (2s, Me-C), 2.29 (m, iso-Pr CH), 6.46 (s, C.14-H).

The *o*-quinone **19** (182 mg) was adsorbed on a small quantity of silica gel by evaporation, introduced at the top of a silica gel column, and, very slowly, the product was eluted with carbon tetrachloride. The color changed from red to orange to dark yellow. This slow chromatography was repeated a second time and gave the lactone **20** (105 mg; 58%), mp 100–104°C (yellow needles, ethanol–water); uv: 268 (13 000), 311 (26 500), and 378 (2900) nm; ir: 3340, 1765 (lactone), 1645, 1625, and 1615 cm^{-1}; ^1H nmr δ: 1.16 and 1.18 (2d, 6H, *J* = 7 Hz, iso-Pr Me), 1.22 and 1.38 (2s, Me-C), 2.13 (d, *J* = 5 Hz, C.5-H), 3.08 (sept, *J* = 7 Hz, iso-Pr CH), 5.19 (dd, *J* = 5 and 5 Hz, C.6-H), 6.61 (d, *J* = 5 Hz, C.7-H), 6.92 (s, C.14-H), and 7.22 (s, OH, D_2O); ^{13}C nmr, see Table 1; mass spectrum, *m/z*: 328 (29, M^+), 300 (49), 285 (51), 272 (35), 257 (93), 229 (38), and 218 (100). *Anal.* calcd. for $C_{20}H_{24}O_4$: C 73.14, H 7.37; found: C 73.21, H 7.70.

*Oxidation of ferriginol **22** to o-quinone **23***

Ferruginol (300 mg) in anhydrous THF (20 mL) was oxidized by adding to a suspension of phenyl seleninic anhydride (760 mg) in THF (40 mL) warmed to 50°C as described above. Chromatography over silica gel afforded first the *o*-quinone **23** (127 mg; 40%), mp 143–144°C (dark red needles from hexane); uv: 264 (6100) and 424 (1750) nm; ir: 1670 and 1655 cm^{-1}; ^1H nmr δ: 0.90 and 0.94 (2s, *gem* Me), 1.11 (d, *J* = 7 Hz, iso-Pr Me), 1.24 (s, Me-C.10), 2.83 (sept, *J* = 7 Hz, iso-Pr CH), 6.42 (s, olefinic H); ^{13}C nmr, see Table 1; mass spectrum, *m/z*: 302 (8, *M* + 2), 300 (11, M^+), 258 (8), 257 (25), 231 (31), 229 (44), 217 (43), and 204 (65). *Anal.* calcd. for $C_{20}H_{20}O_2$: C 79.95, H 9.39; found: C 80.12, H 9.52.

A second fraction from the column contained the quinol **24** (40 mg; 13%), mp 177–179°C (lit. (2*c*) mp 181–182°C); ^{13}C nmr, see Table 1.

*Dehydration of the quinol **24***

The quinol (90 mg) was gently refluxed in methanol (50 mL) containing concentrated hydrochloric acid (1 mL) for 3 h. Dilution with water, removal of most of the methanol by evaporation, and then ether extraction afforded some starting material (10 mg) and then the olefin **25***a* (42 mg; oil, 50%, identical with the product obtained by boron tribromide demethylation of the known methyl ether); ir: 3600, 3385, 3030, 1650, and 1610 cm^{-1}; uv: 278 (10 500) nm; ^1H nmr δ: 0.97 and 1.04 (2s, *gem* Me), 1.20 and 1.24 (2d, *J* = 7 Hz, iso-Pr Me), 1.27 (s, Me-C), 3.17 (m, iso-Pr CH), 5.88 (dd, *J* = 9 and 3 Hz, olefinic H at C.6), 6.60 (s, arom. H at C.11), 6.88 (dd, *J* = 9 and 3 Hz, olefinic H at C.7), and 6.91 (s, arom. H at C.14); ^{13}C nmr, see Table 1.

*Formation of the ketone **26***

Following the Défaye–Duchateau procedure (10), a solution of the olefin **25***a* (84 mg) in acetone (30 mL) was treated with osmic acid (50 mg) in carbon tetrachloride (5 mL). The mixture was protected from light with aluminium foil and stirring was continued at room temperature for 1.5 days. The solvents were then evaporated and the black residue taken up in methanol (30 mL) and reduced by adding excess sodium borohydride and stirring for 24 h. After dilution with water and acidification with concentrated hydrochloric acid, the crude product (mixture of *cis*-diols) was obtained by ether extraction. The residue was taken up in dry benzene (35 mL) containing *p*-toluenesulfonic acid (4 mg) and then refluxed for 2 h. Extraction and chromatography gave the ketone **26** (43 mg; 48% from the olefin **25***a*): ir (film): 3380, 1690, and 1620 cm^{-1}; ^1H nmr δ: 1.12 and 1.18 (2s, *gem* Me), 1.28 (d, *J* = 7 Hz, iso-Pr Me), 1.34 (s, Me-C), 2.43 (s, C.5-H), 3.22 (m, iso-Pr CH), 3.61 (s, 2H, C.7-H), 5.08 (s, OH, D_2O), 6.81 and 6.92 (2s, arom. H); mass spectrum, *m/z*: 300 (100, M^+), 285 (92), 257 (36), 240 (63), 217 (22), 215 (36), and 201 (63).

NOTE: Attempts to oxidize this phenolic ketone **26** and the preceding olefin **25***a* with phenyl seleninic anhydride led to the complete destruction of the substrates.

*Reduction and methylation of the o-quinone **23***

The *o*-quinone **23** (59 mg) in methanol (50 mL) was introduced into an atmospheric hydrogenation apparatus containing prehydrogenated palladium on charcoal (20%, 50 mg) suspended in methanol (25 mL). Agitation under hydrogen rapidly changed the solution from red to colorless and then, without opening to the air, sodium hydroxide (2 mL of 30%) was added, followed by dimethyl sulfate (1 mL). The addition of base and dimethyl sulfate was repeated every half hour (total 8 mL and 4 mL respectively). After 24 h the reaction mixture was filtered, diluted with water, concentrated, and extracted with ether. Chromatography gave two products, first the *dimethoxy compound* **27***a* (15 mg; 23%); ir: 1615, 1570, and 1500 cm^{-1}; ^1H nmr δ: 0.95 (s, 6H, *gem* Me), 1.15 (d, *J* = 7 Hz, iso-Pr Me), 1.30 (s, Me-C), 3.75 and 3.80 (2s, O-Me), 6.68 (s, arom. H); mass spectrum: 330 (M^+). These properties are identical with those given by Mori and Matsui (2*a*).

The second fraction was the *monomethylated compound* **27***b* (28 mg; 45%); ir: 3500, 1615, and 1495 cm^{-1}: ^1H nmr δ: 0.97 (s, 6H, *gem* Me), 1.18 (d, *J* = 7 Hz, iso-Pr Me), 1.30 (s, Me-C), 3.75 (s, O-Me), 5.83 (s, OH, D_2O), 6.33 (s, arom. H); mass spectrum: 316 (M^+).

Methylation of **27***b* (NaOH, dimethyl sulfate) afforded **27***a*.

Formation of taxodione by slow chromatography

The *o*-quinone **23** (35 mg) was adsorbed by evaporation of the solvent onto a small quantity of silica gel and then introduced to the top of a conventional column of silica gel and slowly eluted with carbon tetrachloride. Evaporation of the eluate afforded a yellow oil, **28***b* (24 mg; 69%) uv:316 (7000) and 370 (1600) nm; ir (film): 3300, 1650, 1620, 1610, and 1560 cm^{-1}; ^1H nmr δ: 0.92 and 0.97 (s, 6H, *gem* Me), 1.13 and 1.14 (2d, 6H, *J* = 7 Hz, iso-Pr Me), 1.18 (s, Me-C), 3.07 (m, iso-Pr CH), 6.81 (m, 2H, C.7-H and C.14-H), and 7.48 (s, OH, D_2O); ^{13}C nmr, see Table 1; mass spectrum, *m/z*: 300 (35, M^+), 232 (35), 231 (50), 229 (70), 218 (45), 215 (40), and 204 (90).

When either the *o*-quinone **23** or the mono-enolized form **28***b* was subjected to repeated, slow chromatography (as described above), taxodione (identical with that described above) was formed in yields up to 15%. Attempts to accelerate this process by bubbling air through a solution of the *o*-quinone for 2 days produced no permanent change. Although the uv–vis spectrum of the solution showed an intense peak

at 311 nm, upon evaporation of the methanol only the *o*-quinone chromophore was evident. Bubbling oxygen through a methanol solution of the *o*-quinone led to its complete and rapid decomposition.

Acknowledgments

We thank the Natural Sciences and Engineering Research Council of Canada and the Ministère de l'éducation du Québec for operating and equipment grants. A graduate bursary (F.C.A.R., Québec) is also gratefully acknowledged (D.P.).

1. (*a*) R. H. BURNELL, A. ANDERSEN, M. NERON-DESBIENS, and S. SAVARD. Can. J. Chem. **59**, 2820 (1981); (*b*) R. H. BURNELL, M. JEAN, and S. SAVARD. Can. J. Chem. **61**, 2461 (1983); (*c*) R. H. BURNELL, M. JEAN, D. POIRIER, and S. SAVARD. Can. J. Chem. **62**, 2822 (1984); (*d*) R. H. BURNELL, A. ANDERSEN, M. NERON, and S. SAVARD. Can. J. Chem. **63**, 2769 (1985); (*e*) R. H. BURNELL and J.-M. DUFOUR. Can. J. Chem. **65**, 21 (1987).
2. (*a*) K. MORI and M. MATSUI. Tetrahedron, **26**, 3467 (1970); (*b*) T. MATSUMOTO, Y. TACHIBANA, J. UCHIDA, and K. FUKUI. Bull. Chem. Soc. Jpn. **44**, 2766 (1971); (*c*) T. MATSUMOTO, Y. OSHUGA, S. HARADA, and K. FUKUI. Bull. Chem. Soc. Jpn. **50**, 266 (1977); (*d*) T. MATSUMOTO, S. USUI, and T. MORIMOTO. Bull. Chem. Soc. Jpn. **50**, 1575 (1977); (*e*) T. MATSUMOTO, T. OHMURA, and S. USUI. Bull. Chem. Soc. Jpn. **52**, 1957 (1979); (*f*) D. L. SNITMAN, R. J. HIMMELSBACH, R. C. HALTIWANGER, and D. S. WATT. Tetrahedron Lett. 2477 (1979); (*g*) R. V. STEVENS and G. S. BISACCHI. J. Org. Chem. **47**, 2396 (1982); (*h*) A. K. BANNERJEE and M. C. CARRASCO. Synth. Commun. **13**, 281 (1983).
3. F. MARLETTI, F. D. MONACHE, G. B. MARINI-BETTOLO, M. D. C. M. DE ARAUJO, M. D. S. B. CAVALCANTI, I. L. D'ALBUQUERQUE, and O. G. DE LIMA. Gazz. Chim. Ital. **106**, 119 (1976).
4. D. H. R. BARTON, A. G. BREWSTER, S. V. LEY, C. M. READ, and M. N. ROSENFELD. J. Chem. Soc. Perkin Trans. **1**, 1473 (1981).
5. Y. OHTSUKA and A. TAHARA. Chem. Pharm. Bull. **21**, 643 (1973); **21**, 653 (1973).
6. R. H. BURNELL and M. JEAN. Synth. Commun. **14**, 1229 (1984).
7. Y. OHTSUKA and A. TAHARA. Chem. Pharm. Bull. **26**, 2007 (1978).
8. S. M. KUPCHAN, A. KARIM, and C. MARCKS. J. Org. Chem. **34**, 3912 (1969).,
9. S. W. PELLETIER and Y. OHTSUKA. Tetrahedron, **33**, 1021 (1977).
10. G. DEFAYE-DUCHATEAU. Bull. Soc. Chim. Fr. 1469 (1964).

Can. J. Chem. Downloaded from www.nrcresearchpress.com by 78.46.186.204 on 09/07/12
For personal use only.

Synthesis, characterization, and crystal and molecular structures of the coordination compounds, $[Me_2Ga\cdot O(C_5H_3N)CH_2NMe_2]$ and $[Me_2Ga\cdot O(C_9H_6N)]_2$

EMMANUEL C. ONYIRIUKA, STEVEN J. RETTIG, ALAN STORR,[1] AND JAMES TROTTER[1]

Department of Chemistry, University of British Columbia, 2036 Main Mall, Vancouver, B.C., Canada V6T 1Y6

Received August 18, 1986

EMMANUEL C. ONYIRIUKA, STEVEN J. RETTIG, ALAN STORR, and JAMES TROTTER. Can. J. Chem. **65**, 782 (1987).

Crystals of (2-dimethylaminomethyl-3-pyridolato)dimethylgallium are monoclinic, a = 13.443(3), b = 6.7563(3), c = 13.046(2) Å, β = 100.38(1)°, Z = 4, space group $I2/m$, and those of bis[(8-quinolinolato)dimethylgallium] are monoclinic, a = 9.7340(4), b = 12.7135(5), c = 9.6843(4) Å, β = 117.014(3)°, Z = 2, space group $P2_1/c$. Both structures were solved by conventional heavy atom methods and were refined by full-matrix least-squares procedures to R = 0.044 and 0.032 for 1485 and 1567 reflections with $I \geq 3\sigma(I)$, respectively. The structure of $[Me_2Ga\cdot O(C_5H_3N)CH_2NMe_2]$ consists of discrete monomeric molecules which contain tetrahedrally coordinated gallium atoms. The bidentate anionic 2-dimethylaminomethyl-3-pyridolate ligand coordinates Ga via the oxygen and amino nitrogen atoms (Ga—O = 1.892(3), Ga—N = 2.127(4), Ga—C = 1.950(5) and 1.939(6) Å). The structure of $[Me_2Ga\cdot O(C_9H_6N)]_2$ consists of centrosymmetric dimers which contain a nearly planar system of seven fused rings. The Ga atoms are five-coordinate, having distorted trigonal bipyramidal coordination geometry. The dimerization occurs via the formation of a central, planar, four-membered $(Ga—O)_2$ ring in which each asymmetrically bridging oxygen atom occupies an equatorial coordination site on one gallium atom and an axial site on the other. Important geometrical parameters for $[Me_2Ga\cdot O(C_9H_6N)]_2$ are Ga—O(eq) = 1.937(3), Ga—O(ax) = 2.297(3), Ga—N(ax) = 2.211(3), Ga—C(eq) = 1.948(6) and 1.945(5) Å, O(ax)—Ga—N(ax) = 149.7(1)°.

EMMANUEL C. ONYIRIUKA, STEVEN J. RETTIG, ALAN STORR et JAMES TROTTER. Can. J. Chem. **65**, 782 (1987).

Les cristaux du (diméthylaminométhyl-2 pyridolato-3) diméthylgallium sont monocliniques, avec a = 13,443(3), b = 6,7563(3) et c = 13,046(2) Å et β = 100,38(1)°, Z = 4 et groupe d'espace $I2/m$ alors que ceux du bis[(quinolinolato-8) diméthylgallium] sont monocliniques, avec a = 9,7340(4), b = 12,7135(5) et c = 9,6843(4) Å et β = 117,014(3)°, Z = 2 et groupe d'espace $P2_1/c$. On a résolu les deux structures par les méthodes conventionnelles aux atomes lourds et on les a affinées par la méthode des moindres carrés jusqu'à des valeurs de R = 0,044 et 0,032 pour respectivement 1485 et 1576 réflexions avec $I \geq 3\sigma(I)$. La structure du $[Me_2Ga\cdot O(C_5H_3N)CH_2NMe_2]$ consiste en molécules monomères discrètes qui contiennent des atomes de gallium coordonnés d'une façon tétraédrique. Le ligand anionique bidentate diméthylaminométhyl-2 pyridolate-3 se coordonne au Ga par le biais des atomes d'azote et d'oxygène (Ga—O = 1,892(3), Ga—N = 2,127(4), Ga—C = 1,950(5) et 1,939(6) Å). La structure du $[Me_2Ga\cdot O(C_9H_6N)]_2$ consiste en des dimères centrosymétriques qui contiennent un système pratiquement planaire de sept cycles fusionnés. Les atomes de Ga sont pentacoordonnés et ils possèdent une géométrie de coordination bipyramide trigonale déformée. La dimérisation se produit par le biais de la formation d'un cycle central, planaire et à quatre chaînons $(Ga—O)_2$ dans lequel chaque atome d'oxygène formant un pont asymétrique occup un site de coordination équatorial sur un atome de gallium et un site axial sur l'autre. Les paramètres géométriques importants pour le $[Me_2Ga\cdot O(C_9H_6N)]_2$ sont: Ga—O(eq) = 1,937(3), Ga—O(ax) = 2,297(3), Ga—N(ax) = 2,211(3), Ga—C(eq) = 1,948(6) et 1,945(5) Å et O(ax)— Ga—N(ax) = 149,7(1)°.

[Traduit par la revue]

Introduction

The complex bis(2-methyl-8-quinolinolato)chlorogallium, $GaCl(C_{10}H_8NO)_2$, was characterized as the first crystallographic example of a trigonal bipyramidal, five-coordinate gallium complex (1, 2). In a previous report (3), the *N*-methyldiethanolaminogallane dimer $[MeN(CH_2CH_2O)_2GaH]_2$ was characterized as the second such example. The related derivatives, $[Me_2NCH_2CH_2O\cdot GaH_2]_2$ and $[Me_2NCH_2CH_2O\cdot GaMe_2]_2$ (4), both dimeric five-coordinate gallium species, and the monomeric four-coordinate gallium complex $[H_2NCH_2CH_2O\cdot GaMe_2]$ (5) have subsequently been structurally characterized. Recently the study was extended to include derivatives incorporating a pyridyl "aromatic" ring, resulting in the structure analysis of the $[Me_2Ga\cdot OCH_2(C_5H_4N)]_2$ dimer (6). As part of our continued interest in four- and five-coordinate gallium compounds, we have extended our study to include the sterically more bulky quinolyl and 2-dimethylaminomethylpyridyl ring systems in these gallium complexes. The present account details the synthesis, characterization, and crystal structure determinations of (2-dimethylaminomethyl-3-pyridolato)dimethylgallium, $[Me_2Ga\cdot O(C_5H_3N)CH_2NMe_2]$, and bis[(8-quinolinolato)-dimethylgallium], $[Me_2Ga\cdot O(C_9H_6N)]_2$.

[1]Authors to whom correspondence may be addressed.

Experimental

Air-sensitive materials were handled in a glove box under oxygen-free dry nitrogen or on a high-vacuum line. Tetrahydrofuran (THF) was dried by refluxing over Na/benzophenone and was used immediately following distillation. Benzene was dried by refluxing over molten potassium followed by distillation. Trimethylgallium was prepared as described previously (7). 2-Dimethylaminomethyl-3-hydroxypyridine (Aldrich), and 8-quinolinol (Eastman Organic Chemicals) were used as supplied.

Preparation of $[Me_2Ga\cdot O(C_5H_3N)CH_2NMe_2]$

To a solution of trimethylgallium (1.01 g, 8.8 mmol) in THF was added an equimolar amount of 2-dimethylaminomethyl-3-hydroxypyridine in the same solvent. The reaction mixture was refluxed overnight (~24 h) until cessation of methane gas evolution.

$$Me_3Ga + HO(C_5H_3N)CH_2NMe_2 \xrightarrow[\Delta]{THF} [Me_2Ga\cdot O(C_5H_3N)CH_2NMe_2] + MeH$$

The solvent was removed *in vacuo* and the colorless residue was extracted with benzene followed by filtration. The desired compound was isolated as air- and moisture-sensitive pale-yellow crystals in ~80% yield. Mp ~62°C. *Anal.* calcd. for $[Me_2Ga\cdot O(C_5H_3N)CH_2NMe_2]$: C 47.85, H 6.83, N 11.16; found: C 48.05, H 6.76, N 10.96. ^{1}H nmr (C_6D_6, 400 MHz, $\tau(C_6H_6)$ = 2.84 ppm): τ 10.29 s ($GaMe_2$), 8.39 s

Can. J. Chem. Downloaded from www.nrcresearchpress.com by 80.58.250.72 on 09/07/12
For personal use only.

TABLE 1. Crystallographic data[a]

Compound	$Me_2Ga\cdot O(C_5H_3N)CH_2NMe_2$	$[Me_2Ga\cdot O(C_9H_6N)]_2$
Formula	$C_{10}H_{17}GaN_2O$	$C_{22}H_{24}Ga_2N_2O_2$
fw	250.98	487.88
Crystal system	Monoclinic	Monoclinic
Space group	$I2/m$[b]	$P2_1/c$
a	13.443(3)	9.7340(4)
b	6.7563(3)	12.7135(5)
c (Å)	13.046(2)	9.6843(4)
β (deg)	100.38(1)	117.014(3)
V (Å^3)	1165.5(3)	1067.7(1)
Z	4	2 (dimers)
ρ_c (g/cm^3)	1.430	1.518
$F(000)$	520	496
Radiation	Mo	Cu
μ cm^{-1}	23.2	32.2
Crystal dimensions (mm)	0.23 × 0.40 × 0.63	0.26 × 0.31 × 0.55
Transmission factors	0.389–0.602	0.403–0.545
Scan type	ω–2θ	ω–2θ
Scan range (deg in ω)	0.90 + 0.35 tan θ	0.65 + 0.14 tan θ
Scan speed (deg/min)	1.18–10.06	1.18–10.06
$2\theta_{max}$ (deg)	60	150
Data collected	$+h, +k, \pm l$	$\pm h, +k, +l$
Unique reflections	1827	2182
Reflections with $I \geq 3\sigma(I)$	1485	1567
Number of variables	124	176
R	0.044	0.032
R_w	0.048	0.041
S	2.245	1.716
Mean Δ/σ (final cycle)	0.03	0.02
Max Δ/σ (final cycle)	0.29	0.18
Residual density (e/Å^3)	−2.6 to +2.1 (near Ga)	−0.73 to +0.64

[a]Temperature 22°C, Enraf-Nonius CAD4-F diffractometer, graphite-monochromated Mo-K_α($\lambda_{K\alpha1}$ = 0.70930, $\lambda_{K\alpha2}$ = 0.71359 Å) or nickel-filtered Cu-K_α radiation ($\lambda_{K\alpha1}$ = 1.540562, $\lambda_{K\alpha2}$ = 1.544390 Å), takeoff angle 2.7°, aperture (2.00 + tan θ) × 4.00 mm at a distance of 173 mm from the crystal, scan range extended by 25% on both sides for background measurement, $\sigma^2(I) = S + 2B + [0.04(S - B)]^2$ (S = scan count, B = normalized background count), function minimized $\Sigma w(|F_o| - |F_c|)^2$ where $w = 1/\sigma^2(F)$, $R = \Sigma||F_o| - |F_c||/\Sigma|F_o|$, $R_w = (\Sigma w(|F_o| - |F_c|)^2/\Sigma w|F_o|^2)^{1/2}$, $S = (\Sigma w(|F_o| - |F_c|)^2/(m - n))^{1/2}$. Values given for R, R_w, and S are based on those reflections with $I \geq 3\sigma(I)$.

[b]Non-standard setting of $C2/m$. Equivalent positions in $I2/m$: (0, 0, 0), (1/2, 1/2, 1/2) ± [x, y, z; $-x$, y, $-z$].

(NMe$_2$), 6.40 s (—CH$_2$), ring protons appeared at 3.14 dd (J = 4.0, 8.0 Hz), 2.74 d (J = 8.0 Hz), and 1.94 dd (J = 2.0, 4.0 Hz).

The mass spectrum displayed strong signals corresponding to the parent P$^+$, and P − Me$^+$ ions at m/e 250 and 235, respectively. The most intense peaks in the spectrum (100%) were those attributable to the $[Me_2Ga\cdot O(C_5H_3N)]^+$ fragment ion signal at 192 (m/e values based on ^{69}Ga isotope).

Preparation of $[Me_2Ga\cdot O(C_9H_6N)]_2$

$$Me_3Ga + HO(C_9H_6N) \xrightarrow[\Delta]{THF} (1/2)[Me_2Ga\cdot O(C_9H_6N)]_2 + MeH$$

The coordination compound $[Me_2Ga\cdot O(C_9H_6N)]_2$ was prepared by an identical procedure to that described above, using 8-hydroxyquinoline as the active-hydrogen containing starting material. The air-sensitive lemon–yellow needles of the product were isolated in ~85% yield. Mp ~63°C. *Anal.* calcd. for $[Me_2Ga\cdot O(C_9H_6N)]_2$: C 54.16, H 4.92, N 5.74; found: C 54.58, H 4.61, N 5.97. ^{1}H nmr (C_6D_6, 400 MHz, τ(C_6H_6) = 2.84 ppm) τ 9.90 s ($GaMe_2$), ring protons at 3.58 dd (J = 4.0, 8.0 Hz), 3.31 dd (J = 2.0, 8.0 Hz), 2.71 m, 2.61 dd (J = 2.0, 4.0 Hz), and 2.57 dd (J = 2.0, 8.0 Hz).

The mass spectrum displayed a moderately strong signal corresponding to the monomer ion at m/e 243. Strong signals were displayed for P − Me$^+$ and P − 2Me$^+$ ions at 228 and 213, respectively, the former being the most intense signal (100%) in the spectrum.

X-ray crystallographic analyses

Crystallographic data for $[Me_2Ga\cdot O(C_5H_3N)CH_2NMe_2]$ and $[Me_2Ga\cdot O(C_9H_6N)]_2$ appear in Table 1. Unit-cell parameters were refined by least-squares on 2 sin θ/λ for 25 reflections with 2θ = 40–45° for $[Me_2Ga\cdot O(C_5H_3N)CH_2NMe_2]$ and 2θ = 70–90° for $[Me_2Ga\cdot O(C_9H_6N)]_2$. The intensities of three check reflections, measured each hour of X-ray exposure time throughout the data collections, showed only small random variations in each case. The data were reduced[2] and corrected for absorption using the Gaussian integration method (8, 9).

Both structures were solved by conventional heavy atom methods. The gallium coordinates were determined from the Patterson functions and those of the remaining non-hydrogen atoms from subsequent difference maps. Non-hydrogen atoms were refined with anisotropic thermal parameters. Hydrogen atoms were included as fixed contribu-

[2]The computer programs used include locally written programs for data processing and locally modified versions of the following: ORFLS, full-matrix least-squares, and ORFFE, function and errors, by W. R. Busing, K. O. Martin, and H. A. Levy; FORDAP, Patterson and Fourier syntheses, by A. Zalkin; ORTEP II, illustrations, by C. K. Johnson.

Can. J. Chem. Downloaded from www.nrcresearchpress.com by 80.58.250.72 on 09/07/12
For personal use only.

Can. J. Chem. Downloaded from www.nrcresearchpress.com by 80.58.250.72 on 09/07/12
For personal use only.

TABLE 2. Final positional (fractional × 10^4, Ga × 10^5, H × 10^3) and isotropic thermal parameters ($U \times 10^3$ Å^2) with estimated standard deviations in parentheses

Atom	x	y	z	U_{eq}/U_{iso}
		$[Me_2Ga\cdot O(C_5H_3N)CH_2NMe_2]$		
Ga	22241(3)	0	39(3)	35
O	1026(3)	−1167(5)	−731(3)	43
N(1)	24(4)	2569(10)	−2616(4)	51
N(2)	1733(3)	2970(5)	−299(3)	35
C(1)	415(3)	1668(9)	−1732(4)	37
C(2)	596(3)	−393(6)	−1639(3)	35
C(3)	290(5)	−1548(11)	−2520(5)	50
C(4)	−155(10)	−572(13)	−3457(10)	56
C(5)	−223(9)	1426(14)	−3446(9)	58
C(6)	636(3)	2920(7)	−771(4)	40
C(7)	2337(5)	−447(7)	1497(4)	54
C(8)	3303(4)	−485(9)	−771(6)	66
C(9)	2304(4)	4001(8)	−1006(5)	50
C(10)	1844(4)	4130(9)	677(5)	55
		$[Me_2Ga\cdot O(C_9H_6N)]_2$		
Ga	51303(5)	40217(4)	38326(5)	48
O	6421(3)	4883(2)	5600(3)	54
N	7459(4)	3440(2)	4364(4)	46
C(1)	7932(6)	2696(4)	3731(6)	60
C(2)	9493(6)	2478(4)	4230(6)	64
C(3)	10575(6)	3049(4)	5402(5)	59
C(4)	10139(4)	3848(3)	6136(4)	46
C(5)	11152(5)	4466(4)	7377(5)	55
C(6)	10576(5)	5200(4)	8008(6)	59
C(7)	8985(5)	5361(3)	7436(5)	54
C(8)	7952(4)	4781(3)	6215(5)	45
C(9)	8530(4)	4012(3)	5557(4)	41
C(10)	4565(8)	4693(6)	1839(7)	68
C(11)	4359(7)	2760(4)	4383(8)	69
H(1)	725(5)	239(4)	302(5)	59(14)
H(2)	964(8)	201(6)	363(8)	123(23)
H(3)	1157(6)	294(4)	574(6)	62(13)
H(5)	1215(6)	449(5)	767(6)	85(17)
H(6)	1126(7)	563(5)	876(7)	86(17)
H(7)	869(7)	587(4)	792(6)	77(16)
H(10a)	473(12)	528(9)	191(11)	160(40)
H(10b)	524(8)	443(6)	150(7)	105(21)
H(10c)	360(8)	459(5)	146(7)	85(20)
H(11a)	325(9)	272(5)	403(9)	113(22)
H(11b)	457(10)	229(7)	402(9)	140(31)
H(11c)	446(13)	265(8)	545(14)	190(39)

tors to the structure in idealized positions (based on observed positions with C(sp^2)—H = 0.97, C(sp^3)—H = 0.98 Å) for $[Me_2Ga\cdot O(C_5H_3N)CH_2NMe_2]$ and were refined with isotropic thermal parameters for $[Me_2Ga\cdot O(C_9H_6N)]_2$. Neutral atom scattering factors for all atoms and anomalous scattering corrections for Ga were taken from ref. 10. An isotropic Type I extinction correction (Thornley–Nelmes definition of mosaic anisotropy with a Lorentzian distribution) was applied for $[Me_2Ga\cdot O(C_9H_6N)]_2$ (11–13). The final value of g was 0.20(4) × 10^4.

Space group symmetry and structural considerations indicate that the $[Me_2Ga\cdot O(C_5H_3N)CH_2NMe_2]$ molecule must reside on a crystallographic mirror plane in the space group $I2/m$. It was immediately apparent that apart from the Ga atom, which does reside on the mirror plane, all remaining atoms are 1:1 disordered with respect to the mirror plane. Refinement was then attempted in the non-centrosymmetric space groups $I2$ and Im (both consistent with the systematic absences observed from film and diffractometer data: hkl, $h + k + l$ odd) in the hope that an ordered structure would result. In each case a similar disorder persisted. The refinement was carried out in the space group $I2/m$, all atoms in general positions being assigned occupancy factors of 0.5. The maximum parameter shift was associated with U_{33} for C(5), all other shifts being less than 0.2σ. The relatively large residual density near Ga may be due in part to imperfect modelling of the thermal motion for the superimposed Ga atoms.

Final positional and thermal parameters appear in Tables 2 and 8, respectively.[3] Bond lengths and angles involving non-hydrogen atoms are given in Tables 3 and 4, respectively, and intra-annular torsion angles in Table 5. Calculated hydrogen parameters, bond lengths and angles involving hydrogen, and a complete listing of torsion angles (Tables 7, 9–11), and measured and calculated structure factors have been placed in the Depository of Unpublished Data.[3]

TABLE 3. Bond lengths (Å) with estimated standard deviations in parentheses*

Bond	Length (Å)	Bond	Length (Å)
	$[Me_2Ga\cdot O(C_5H_3N)CH_2NMe_2]$		
Ga —O	1.892(3)	N(2)—C(9)	1.477(6)
Ga —N(2)	2.127(4)	N(2)—C(10)	1.480(6)
Ga —C(7)	1.950(5)	C(1)—C(2)	1.415(8)
Ga —C(8)	1.939(6)	C(1)—C(6)	1.498(7)
O —C(2)	1.328(5)	C(2)—C(3)	1.389(8)
N(1)—C(1)	1.325(7)	C(3)—C(4)	1.423(14)
N(1)—C(5)	1.324(13)	C(4)—C(5)	1.353(15)
N(2)—C(6)	1.492(6)		
	$[Me_2Ga\cdot O(C_9H_6N)]_2$		
Ga —O	1.937(3)	C(2)—C(3)	1.356(7)
Ga —N	2.211(3)	C(3)—C(4)	1.411(6)
Ga —C(10)	1.948(6)	C(4)—C(5)	1.400(6)
Ga —C(11)	1.945(5)	C(4)—C(9)	1.419(5)
Ga —O′	2.297(3)	C(5)—C(6)	1.367(7)
O —C(8)	1.336(5)	C(6)—C(7)	1.403(6)
N —C(1)	1.319(5)	C(7)—C(8)	1.369(5)
N —C(9)	1.362(5)	C(8)—C(9)	1.415(5)
C(1)—C(2)	1.397(7)		

*Here and elsewhere in this report, primed atoms are related to those in Table 2 by inversion through the centre of symmetry at (1/2, 1/2, 1/2).

Results and discussion

Gallium alkyls are known to eliminate methane on reaction with active-hydrogen containing compounds. In a previous study, the dimeric complex $[Me_2NCH_2CH_2OGaMe_2]_2$ was structurally characterized as the product of the reaction of trimethylgallium with *N,N*-dimethylethanolamine (4). In a later study, the reaction of Me_3Ga with ethanolamine, a compound containing active hydrogen at both the oxygen and nitrogen ends of the molecule, resulted in preferential elimination of the hydroxyl hydrogen to yield the complex $H_2NCH_2CH_2OGaMe_2$ (5). This selectivity was not surprising since it is known that O—H groups coordinated to gallium alkyls eliminate alkanes much more rapidly at lower temperatures than do similarly coordinated N—H groups which require elevated temperatures for alkane elimination (14). With the notable exception of $H_2NCH_2CH_2OGaMe_2$, which has a structure consisting of monomeric molecules containing tetrahedrally coordinated gallium atoms (5), monomer units of similar Me_2Ga systems have been shown by X-ray crystallographic analysis to dimerize in the solid state

[3]The structure factor table, Table 8 (anisotropic thermal parameters), and other material mentioned in the text may be purchased from the Depository of Unpublished Data, CISTI, National Research Council of Canada, Ottawa, Ont., Canada K1A 0S2.

Can. J. Chem. Downloaded from www.nrcresearchpress.com by 80.58.250.72 on 09/07/12
For personal use only.

TABLE 4. Bond angles (deg) with estimated standard deviations in parentheses

Bonds	Angle (deg)	Bonds	Angle (deg)
	$[Me_2Ga\cdot O(C_5H_3N)CH_2NMe_2]$		
O —Ga —N(2)	95.2(2)	C(6)—N(2)—C(10)	107.8(4)
O —Ga —C(7)	110.3(2)	C(9)—N(2)—C(10)	107.7(4)
O —Ga —C(8)	108.3(2)	N(1)—C(1)—C(2)	124.2(5)
N(2)—Ga —C(7)	107.3(2)	N(1)—C(1)—C(6)	117.2(6)
N(2)—Ga —C(8)	107.4(2)	C(2)—C(1)—C(6)	118.6(5)
C(7)—Ga —C(8)	124.3(3)	O —C(2)—C(1)	120.3(4)
Ga —O —C(2)	118.8(3)	O —C(2)—C(3)	122.2(5)
C(1)—N(1)—C(5)	116.5(7)	C(1)—C(2)—C(3)	117.4(5)
Ga —N(2)—C(6)	107.8(3)	C(2)—C(3)—C(4)	117.8(7)
Ga —N(2)—C(9)	112.4(3)	C(3)—C(4)—C(5)	118.2(12)
Ga —N(2)—C(10)	111.1(3)	N(1)—C(5)—C(4)	125.7(13)
C(6)—N(2)—C(9)	109.8(4)	N(2)—C(6)—C(1)	113.0(4)
	$[Me_2Ga\cdot O(C_9H_6N)]_2$		
O —Ga —N	78.4(1)	N —C(1)—C(2)	122.4(5)
O —Ga —C(10)	114.0(2)	C(1)—C(2)—C(3)	119.6(4)
O —Ga —C(11)	113.6(2)	C(2)—C(3)—C(4)	120.7(4)
O —Ga —O′	71.3(1)	C(3)—C(4)—C(5)	125.5(4)
N —Ga —C(10)	100.1(2)	C(3)—C(4)—C(9)	115.9(4)
N —Ga —C(11)	98.2(2)	C(5)—C(4)—C(9)	118.5(4)
N —Ga —O′	149.7(1)	C(4)—C(5)—C(6)	119.7(4)
C(10)—Ga —C(11)	131.5(3)	C(5)—C(6)—C(7)	121.7(4)
C(10)—Ga —O′	92.9(2)	C(6)—C(7)—C(8)	120.6(4)
C(11)—Ga —O′	93.2(2)	O —C(8)—C(7)	124.4(4)
Ga —O —C(8)	118.9(2)	O —C(8)—C(9)	117.2(3)
Ga —O —Ga′	108.7(1)	C(7)—C(8)—C(9)	118.3(4)
C(8)—O —Ga′	132.3(2)	N —C(9)—C(4)	122.6(3)
Ga —N —C(1)	132.0(3)	N —C(9)—C(8)	116.3(3)
Ga —N —C(9)	109.1(2)	C(4)—C(9)—C(8)	121.1(3)
C(1)—N —C(9)	118.9(4)		

TABLE 5. Intra-annular torsion angles (deg) standard deviations in parentheses

Atoms	Value (deg)
$[Me_2Ga\cdot O(C_5H_3N)CH_2NMe_2]$	
N(2)—Ga —O —C(2)	41.7(3)
Ga —O —C(2)—C(1)	−49.5(5)
C(6)—C(1)—C(2)—O	−5.0(7)
C(2)—C(1)—C(6)—N(2)	64.9(6)
Ga —N(2)—C(6)—C(1)	−56.1(5)
O —Ga —N(2)—C(6)	9.8(3)
$[Me_2Ga\cdot O(C_9H_6N)]_2$	
N —Ga —O —C(8)	2.8(3)
Ga —O —C(8)—C(9)	−2.3(5)
Ga —N —C(9)—C(8)	2.8(4)
O —C(8)—C(9)—N	−0.7(5)
O —Ga —N —C(9)	−3.0(2)

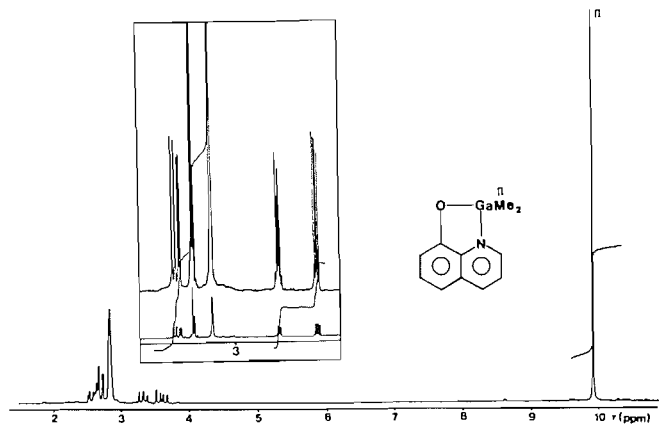

FIG. 1. 80 MHz ^1H nmr spectrum of $[Me_2Ga\cdot O(C_9H_6N)]_2$ in C_6D_6 solution (400 MHz spectrum inset).

via the formation of four-membered $(Ga—O)_2$ rings giving distorted trigonal bipyramidal arrangements about each five-coordinate gallium atom (3, 4, 6, 15–18).

The reaction of 8-hydroxyquinoline with trimethylgallium afforded the coordination compound "$[Me_2GaO(C_9H_6N)]$". The ^1H nmr spectrum of this quinolinato complex in C_6D_6 solution (Fig. 1) is in accord with an overall planar structure for the complex in solution. In this configuration, the two methyl groups on gallium lie above and below the plane, hence a sharp singlet is observed for the —$GaMe_2$ group.

The crystal structure of $[Me_2Ga\cdot O(C_9H_6N)]_2$ consists of discrete centrosymmetric dimeric units (Fig. 2) which are separated by normal van der Waals distances. Although the mass spectrum shows the complex to be monomeric in the gas phase, the solid state structure reveals that dimerization via the formation of a four-membered $(Ga—O)_2$ ring has taken place. The resulting structure contains a system of seven fused rings which is planar to within 0.053(5) Å. Taken individually, only

Can. J. Chem. Downloaded from www.nrcresearchpress.com by 80.58.250.72 on 09/07/12
For personal use only.

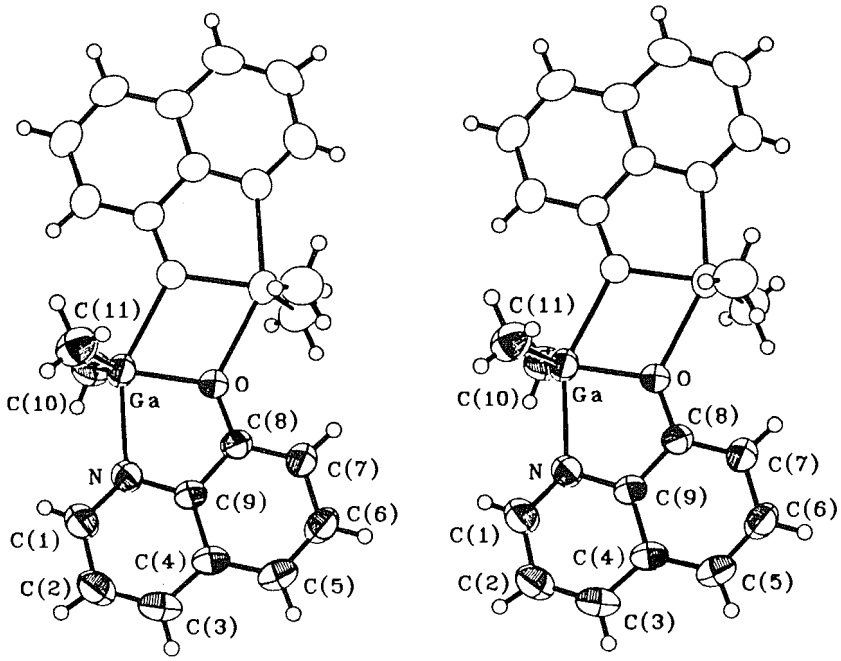

FIG. 2. Stereoscopic view of the bis[(8-quinolinolato)dimethylgallium] molecule; 50% probability thermal ellipsoids are shown for the non-hydrogen atoms. Hydrogen atoms have been assigned arbitrary thermal parameters for the sake of clarity. Shaded atoms comprise the asymmetric unit.

the two symmetry-related five-membered chelate rings are significantly non-planar (maximum deviation from the mean plane 0.027(3) Å), and have flattened Ga—envelope conformations. The quinoline moiety is slightly folded with an angle of 1.4(3)° between the normals to the mean planes of the two six-membered rings. The coordination about each Ga atom is trigonal bipyramidal, distorted primarily by the steric requirements imposed by the existence of the fused ring system. The Ga—N and Ga—O distances in $[Me_2Ga{\cdot}O(C_9H_6N)]_2$ are compared with those observed for other five-coordinate gallium complexes (1–4, 6, 15–25) in Table 6. The axial Ga—N distance is 2.211(3) Å, while those previously reported range from 2.104(3) to 2.779(3) Å with an average value of 2.361 Å. The equatorial and axial Ga—O distances, which occur in the central $(Ga—O)_2$ ring, are 1.937(3) and 2.297(3) Å, respectively. The corresponding ranges and averages for the seven other complexes which contain the same type of central $(Ga—O)_2$ ring are 1.911(3)–1.963(2) (mean 1.935 Å) for equatorial, and 2.012(6)–2.545(2) (mean 2.190 Å) for the axial Ga—O bonds. Those complexes with longer than average intracyclic axial Ga—O bonds all contain nearly planar, extended, fused-ring systems.

The coordination compound $[Me_2Ga{\cdot}O(C_5H_3N)CH_2NMe_2]$ was isolated as the product of the reaction of 2-dimethylamino-3-hydroxypyridine with trimethylgallium. The ^1H nmr spectrum of this compound in C_6D_6 solution (Fig. 3) is again consistent with an overall planar structure in solution, displaying singlets for the $—GaMe_2$, $—NMe_2$, and $—CH_2—$ groupings.

The mass spectrum of the compound $[Me_2Ga{\cdot}O(C_5H_3N)CH_2NMe_2]$ displayed as its highest mass peaks, a moderately strong parent ion (P^+) signal as well as a very strong $P - Me^+$ signal, suggestive of a monomeric species in the gas phase. The most intense signals were those corresponding to the loss of the "CH_2NMe_2" moiety from the monomer species.

The monomeric nature of $[Me_2Ga{\cdot}O(C_5H_3N)CH_2NMe_2]$ in the solid state was confirmed by the X-ray crystallographic analysis, which shows the structure to consist of discrete monomeric molecules containing tetrahedrally coordinated gallium

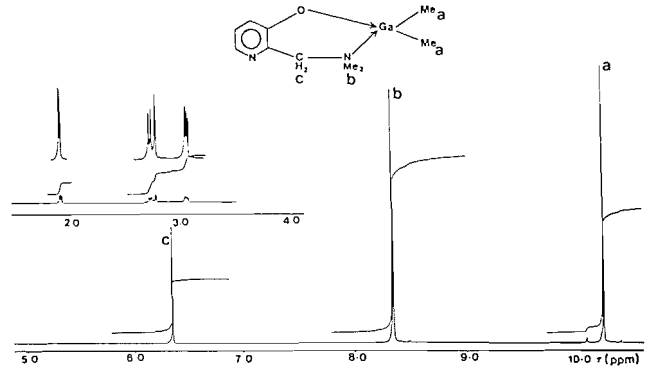

FIG. 3. 400 MHz ^1H nmr spectrum of $[Me_2Ga{\cdot}O(C_5H_3N)CH_2NMe_2]$ in C_6D_6 solution.

atoms (Fig. 4). This is somewhat surprising since similar dimethylamino compounds have been shown to dimerize in the solid state (4). The monomeric nature of the present compound is probably related to the steric constraints imposed by the unsaturation of the pyridine ring. Since the pyridine substituent atoms O and C(6) are constrained to lie approximately in the plane of the pyridine ring, four atoms of the six-membered chelate must be roughly coplanar. In order to minimize angular strain, the chelate ring adopts a steep and slightly twisted boat conformation in which the NMe_2 and $GaMe_2$ groups are nearly eclipsed. The partial staggering about the Ga—N bond which would be required for dimerization most likely results in too high a degree of ring strain. It is noteworthy that the presence of extensive $N—H\cdots O$ hydrogen bonding was sufficient to prevent the dimerization of $H_2NCH_2CH_2OGaMe_2$ (5) and $H_2NCH_2CO_2GaMe_2$ (26) in the solid state.

The Ga—N distance of 2.127(4) Å in $[Me_2Ga{\cdot}O(C_5H_3N)CH_2NMe_2]$ is as expected: longer than the bonds of 2.056(6) and 2.072(6) Å in the tetrahedral complex $H_2NCH_2CH_2OGaMe_2$ (5), similar to the values of 2.139(17) and 2.138(9) Å in (hexamethylenetetramine)bis(dimethylgallium) (27), and shorter than the bonds of 2.20(3) Å in Me_3GaNMe_3 (28) and 2.241(9) Å in

Can. J. Chem. Downloaded from www.nrcresearchpress.com by 80.58.250.72 on 09/07/12
For personal use only.

TABLE 6. Comparison of Ga—N and Ga—O bond lengths in five-coordinate gallium compounds*

Compound	Coordination geometry	Bond distances (Å)		Reference
		Ga—N	Ga—O	
$GaCl(C_{10}H_8NO)$	TBP	ax 2.104(5), 2.108(5)	eq 1.86(1), 1.88(1)	1, 2
$[MeN(CH_2CH_2O)_2GaH]_2$	TBP	ax 2.184(7), 2.193(7)	eq 1.843(7), 1.839(7) eq 1.945(6), 1.960(6) ax 2.012(6), 2.016(6)	3
$[Me_2NCH_2CH_2OGaMe_2]_2$	TBP	ax 2.471(4)	eq 1.913(3) ax 2.078(3)	4
$[Me_2NCH_2CH_2OGaH_2]_2$	TBP	ax 2.279(3)	eq 1.911(3) ax 2.053(3)	4
$C_{24}H_{72}Ga_8N_{12}O_2$	TBP	eq 1.945(3), 1.996(3) ax 2.778(3)	ax 1.957(3)	19
$[Me_2Ga(C_5H_7O_2)]_2$	TBP		eq 1.927(3) ax 2.120(3), 2.462(3)	15
$Me_2GaCl(C_{12}H_8N_2)$	TBP	eq 2.119(6) ax 2.433(6)		20
$Me_2Ga(C_5H_8NO_2)$	TBP	eq 2.027(3)	ax 2.036(3), 2.695(3)	21
$MeGa(O_2CCH_3)_2$	TBP		eq 1.873(3), 1.942(3) ax 2.086(3), 2.219(3)	22
$GaCl(C_{16}H_{14}N_2O_2)$	SP	ba 2.014(6), 2.030(5)	ba 1.863(4), 1.879(4)	23
$[Me_2Ga(C_7H_5O_2)]_2$	TBP		eq 1.963(2) ax 2.020(2), 2.545(2)	16, 17
$GaCl_3(C_4H_8O_2)$	TBP		ax 2.210(4)	24
$GaCl(C_{32}H_{20}N_8)$	SP	ba 1.979(4)–1.988(4)		25
$[Me_2GaOCH_2(C_5H_4N)]_2$	TBP	ax 2.271(3)	eq 1.925(3) ax 2.073(3)	6
$[Me_2Ga(C_9H_{13}O_7)]_2$	TBP		eq 1.950(3) ax 2.103(3), 2.395(3)	18
$[Me_2GaO(C_9H_6N)]_2$	TBP	ax 2.211(3)	eq 1.937(3) ax 2.297(3)	This work

*TBP = trigonal-bipyramidal, SP = square-pyramidal, eq = equatorial, ax = axial, ba = basal.

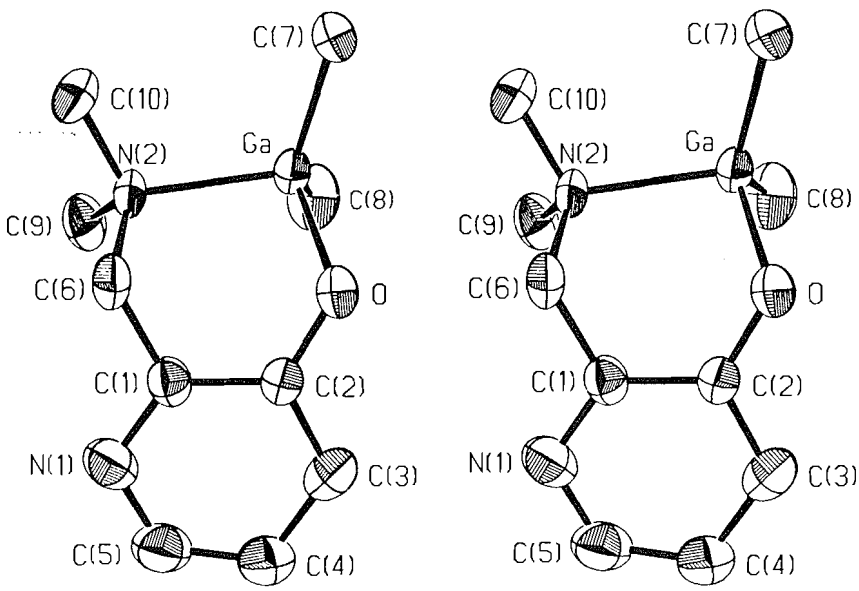

FIG. 4. Stereoscopic view of the (2-dimethylaminomethyl-3-pyridolato)dimethylgallium molecule; 50% probability thermal ellipsoids are shown for the non-hydrogen atoms.

$(Me_2NCH_2CH_2NMe_2)Ga(CH_2SiMe_3)_2$ (29). The Ga—O and Ga—C distances are normal. The pyridine ring is planar to within 0.03(1) Å, the substituent atoms O and C(6) being displaced 0.035(4) and −0.139(5) Å, respectively, from the pyridine ring mean plane.

Acknowledgements

We thank the Natural Sciences and Engineering Research Council of Canada for financial support and the University of British Columbia Computing Centre for assistance. We also would like to thank Mr. P. Borda for the C, H, N analyses.

1. M. Shiro and Q. Fernando. Anal. Chem. **43**, 1222 (1971).
2. K. Dymock and G. J. Palenik. J. Chem. Soc. Chem. Commun. 884 (1973).
3. S. J. Rettig, A. Storr, and J. Trotter. Can. J. Chem. **52**, 2206 (1974).
4. S. J. Rettig, A. Storr, and J. Trotter. Can. J. Chem. **53**, 58 (1975).
5. K. S. Chong, S. J. Rettig, A. Storr, and J. Trotter. Can. J. Chem. **57**, 586 (1979).
6. S. J. Rettig, A. Storr, J. Trotter, and K. Uhrich. Can. J. Chem. **62**, 2788 (1984).
7. A. Storr and B. S. Thomas. Can. J. Chem. **48**, 3667 (1970).
8. P. Coppens, L. Leiserowitz, and D. Rabinovich. Acta Crystallogr. **18**, 1035 (1965).
9. W. R. Busing and H. A. Levy. Acta Crystallogr. **22**, 457 (1967).
10. International tables for X-ray crystallography. Vol. IV. Kynoch Press, Birmingham. 1974. pp. 99–102 and 149.
11. P. J. Becker and P. Coppens. Acta Crystallogr. Sect. A, **30**, 129 (1974); **30**, 148 (1974); **31**, 417 (1975).
12. P. Coppens and W. C. Hamilton. Acta Crystallogr. Sect. A, **26**, 71 (1970).
13. F. R. Thornley and R. J. Nelmes. Acta Crystallogr. Sect. A, **30**, 748 (1974).
14. G. E. Coates and K. Wade. Organometallic compounds; the main group elements. Vol. 1. 3rd ed. Methuen, London. 1967.
15. S. J. Rettig, A. Storr, and J. Trotter. Can. J. Chem. **54**, 1278 (1976).
16. I. Waller, T. Halder, W. Schwarz, and J. Weidlein. J. Organomet. Chem. **232**, 99 (1982).
17. S. J. Rettig, A. Storr, and J. Trotter. Can. J. Chem. **62**, 1705 (1984).
18. G. A. Banta, S. J. Rettig, A. Storr, and J. Trotter. Can. J. Chem. **63**, 2545 (1985).
19. S. J. Rettig, A. Storr, and J. Trotter. Can. J. Chem. **53**, 753 (1975).
20. A. T. McPhail, R. W. Miller, C. G. Pitt, G. Gupta, and S. C. Srivastava. J. Chem. Soc. Dalton Trans. 1657 (1976).
21. K. R. Breakell, S. J. Rettig, A. Storr, and J. Trotter. Can. J. Chem. **55**, 4174 (1977).
22. H. Koster, D. Theonnes, and E. Weiss. J. Organomet. Chem. **160**, 1 (1978).
23. K. S. Chong, S. J. Rettig, A. Storr, and J. Trotter. Can. J. Chem. **59**, 94 (1981).
24. A. Boardman, S. E. Jeffs, R. W. H. Small, and I. J. Worrall. Inorg. Chim. Acta, **87**, L27 (1984).
25. K. J. Wynne. Inorg. Chem. **23**, 4658 (1984).
26. S. J. Rettig, A. Storr, and J. Trotter. Can. J. Chem. In press.
27. H. Krause, K. Sille, H.-D. Hausen, and J. Weidlein. J. Organomet. Chem. **235**, 253 (1982).
28. L. M. Golubinskaya, A. V. Golubinskii, V. S. Mastryukov, L. V. Villkov, and V. I. Bregadze. J. Organomet. Chem. **117**, C4 (1976).
29. R. B. Hallock, W. E. Hunter, J. L. Atwood, and O. T. Beachley, Jr. Organometallics, **4**, 547 (1985).

Can. J. Chem. Downloaded from www.nrcresearchpress.com by 80.58.250.72 on 09/07/12
For personal use only.

^{13}C magnetic resonance studies. 129.[1] Homoenolization in the camphenilone system. Examination of some 7-substituted derivatives

SRIYAWATHIE PEIRIS, ARTHUR J. RAGAUSKAS,[2] AND J. B. STOTHERS
Department of Chemistry, University of Western Ontario, London, Ont., Canada N6A 5B7

Received October 7, 1986

SRIYAWATHIE PEIRIS, ARTHUR J. RAGAUSKAS, and J. B. STOTHERS. Can. J. Chem. **65**, 789 (1987).

The behavior of the 7,7-dimethyl, 7-spirocyclopropyl, and 7-isopropylidene derivatives of camphenilone under strongly basic conditions (*t*-BuO$^-$/*t*-BuOH/185°C) has been investigated to examine substituent effects on β-enolization in the [2.2.1] system. In each case, an equilibrium mixture of the initial ketone and its corresponding 5-substituted isomer was obtained, with the latter increasingly favored through the series. In each case the $^1H/^2H$ exchange processes were examined by experiments utilizing *t*-BuO$^-$/*t*-BuOD to establish the individual sites of deuterium incorporation in these ketones with ^2H and ^{13}C magnetic resonance. These data provide the stereoselectivities and relative rates of the exchange processes. The ^2H-induced effects in the ^{13}C spectra are discussed.

SRIYAWATHIE PEIRIS, ARTHUR J. RAGAUSKAS et J. B. STOTHERS. Can. J. Chem. **65**, 789 (1987).

Dans le but d'évaluer les effets des substituants sur la β-énolisation dans les systèmes [2.2.1], on a étudié le comportement des dérivés diméthyl-7,7, spirocyclopropyl-7 et isopropylidène-7 de la camphénoline dans des conditions fortement basiques (*tert*-BuO$^-$/*tert*-BuOH/185°C). Dans chacun des cas, on a obtenu un mélange à l'équilibre contenant de la cétone initiale et de son isomère correspondant substitué en position 5; la quantité de ce dernier augmente dans la série des composés étudiés. Dans chacun des cas, on a étudié les processus d'échange $^1H/^2H$ sous l'influence du *tert*-BuO$^-$/*tert*-BuOD; on a pu établir les sites individuels d'incorporation du deutérium dans ces cétones en faisant appel à la rmn du ^2H et du ^{13}C. Ces données nous ont permis d'établir les stéréosélectivités et les vitesses relatives des processus d'échange. On discute des effets du ^2H sur les spectres rmn du ^{13}C.

[Traduit par la revue]

Introduction

The discovery of β-enolization by Nickon and Lambert (1) arose from their examination of the fate of optically active camphenilone (**1***a*, 3,3-dimethylbicyclo[2.2.1]heptan-2-one) upon treatment with *t*-BuO$^-$/*t*-BuOH(D) at elevated temperatures. At 185°C, **1***a* was found to racemize (69% after 36 h, 88% after 48 h) and, in *t*-BuOD, racemization is accompanied by deuterium exchange at C-1 and -6 such that up to three deuterium atoms are incorporated in short reaction times, <48 h. Furthermore, the initial rate of deuterium incorporation is the same as the rate of racemization, establishing that proton abstraction leads to an intermediate that is symmetrical, or becomes symmetrical, before deuteration by solvent. This β-enolate intermediate may be represented as **2***a*, resulting from proton abstraction from C-6 in **1***a*. Ketonization of **2***a* can occur by cleavage (**a**) or (**b**) to yield **1***a* or its enantiomer **3***a*, respectively, which, in *t*-BuOD would pick up deuterium at C-6. In the early work, Nickon *et al.* (2) also studied the stereochemistry of the homoketonization process by examination of the cleavage of nor-**2***a*, generated from 1-acetoxynortricyclene at room temperature. In *t*-BuO$^-$/*t*-BuOD, deuteration occurred with high stereoselectivity (>94%) favoring the *exo* orientation, thereby signalling opening with inversion of configuration. Subsequently, the stereochemistry of ketonization of several β-enolates has been investigated and a general tendency for opening with inversion established (3).

The regioselectivity of β-enolate ketonization has been established for many systems (3) and the major governing factors appear to be relief of strain, product stability, and the stability of the incipient carbanion. Since the half-life for racemization of **1***a* is ca. 25 h at 185°C, this constitutes one of the more efficient isomerizations known to proceed through a β-enolate and, consequently, seemed to be a good system for an examination of substituent effects on the equilibrium **1** ⇌ **3**. For 7-

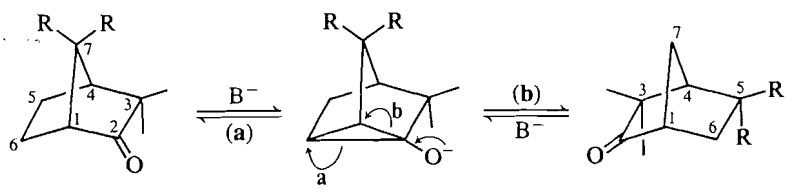

1 **2** **3**

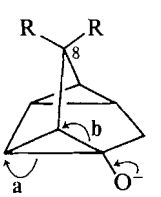

4

a R = H
b R = Me
c R, R = $(CH_2)_2$
d R, R = Me_2C=

[1]For Part 128 see ref. 18; for Part 127 see ref. 19.

[2]Present address: Department of Chemistry, Colorado State University, Fort Collins, Colorado 80523, U.S.A.

Can. J. Chem. Downloaded from www.nrcresearchpress.com by 80.58.250.72 on 09/07/12
For personal use only.

TABLE 1. ^{13}C shieldings[a] for **1***b–d*, **3***b–d*, and their precursors

Compound	C-1	C-2	C-3	C-4	C-5	C-6	C-7	Spirocyclopropyl	Methyl
5	60.8	212.7	38.3	46.0	142.0	129.4	46.1	6.0, 7.0	
6[b]	54.8	213.6	46.0	41.6	27.7	24.3	33.9	5.3, 5.7	
1*c*	51.2	221.8	49.5	55.5	23.6	24.7	32.3	3.8, 8.9	22.1, 23.2
7	58.1	217.5	44.1	43.3	27.6	22.7	45.2		20.7, 21.6
1*b*	59.4	224.2	47.0	53.2	23.5	23.3	45.0		22.9, 25.2, 26.4, 27.4
3*b*	(50.9)	223.7	49.0	(58.1)	38.2	41.4	35.6		24.3, 27.7, 29.2, 34.6
3*c*	51.9	222.8	48.0	54.3	22.4	35.4	35.8	11.0, 13.9	23.0, 23.4
10	57.8	219.8	46.2	47.9	(35.3)	21.4	(35.7)	10.8, 13.6	21.4, 23.5
11	50.0	74.7	41.7	38.6	41.0	19.6	38.5	9.2, 11.6	
12	44.6	72.3	31.6	45.9	25.9	(38.1)	(38.3)	8.9, 16.2	
18	59.4	79.0	40.9	43.9	38.2	(34.5)	(35.0)		22.8, 29.2, 34.1, 34.9
								C-8	
14	57.8	213.4	44.3	48.5	143.0	131.3	117.6	145.0	16.0, 19.4, 19.9
15	52.0	217.0	43.7	51.3	27.1	24.0	121.2	136.4	15.2, 20.3, 20.7
1*d*	51.9	219.7	50.8	48.1	22.2	24.9	120.0	137.0	20.0 (*endo*-3), 24.4 (*exo*-3) 20.3, 20.6
3*d*	50.4	222.9	47.9	50.8	123.4	32.1	35.4	131.4	21.8 (*endo*-3), 22.5 (*exo*-3) 20.2, 21.0

[a]In ppm from internal TMS for $CDCl_3$ solutions; similar values in parentheses may be interchanged.
[b]Unequivocal assignments obtained from an INADEQUATE spectrum of a C_6D_6 solution.

substituted derivatives the regioselectivity of β-enolate cleavage could be biased toward formation of the 5-substituted isomers, thereby providing a viable preparative route to these derivatives; for example, 3,3,5,5-tetramethylnorcamphor (**3***b*) had not been described in the literature. We have recently found (4) that the 8-isopropylidene substituent in **4***d* gives regiospecific ketonization via path **b**, whereas **4***a* and **4***c* open exclusively by path **a**, demonstrating that conjugative stabilization of one of the incipient carbanionic centres can have a marked effect on the regiochemistry of homoketonization. For the camphenilone system, we have studied the fate of the 7,7-dimethyl (**1***b*), 7-spirocyclopropyl (**1***c*), and 7-isopropylidene (**1***d*) derivatives under typical homoenolization conditions and we wish to report our observations in this paper together with the results of an examination of the $^1H/^2H$ exchange processes in **1***b–d*.

Results and discussion

Preparation of materials

From an earlier study (4) 7-spirocyclopropylnorbornenone (**5**) was available and was readily hydrogenated over Pd/C to give 7-spirocyclopropylnorbornanone (**6**), which afforded 7,7-dimethylnorbornanone (**7**) upon hydrogenation over PtO_2, as described by Turro and Farrington (5). Both **6** and **7** were converted to their 3,3-dimethyl analogs **1***c* and **1***b*, respectively, by treatment with $NaNH_2/Et_2O/MeI$, and characterized by their ^{13}Cmr spectra (Table 1) and mass spectrometry. The ^{13}C assignments for **6** were established from the results of an INADEQUATE spectrum (6). In anticipation of the results of homoenolization of **1***c*, an alternative route to **3***c* was explored (Scheme 1). Treatment of 2-methyl-3-chloropropene with $NaNH_2$ in *t*-BuOH/THF gave methylene cyclopropane, which was reacted with cyclopentadiene to furnish the known olefin **8** (7). Hydroboration of **8** with borane – methyl sulfide complex furnished a 1:1 mixture of isomeric alcohols, which was oxidized quantitatively to the corresponding mixture of ketones **9** with pyridinium chlorochromate (PCC), but these mixtures were inseparable by gas liquid chromatography (glc) and thin-layer chromatography (tlc). Treatment of the ketone mixture

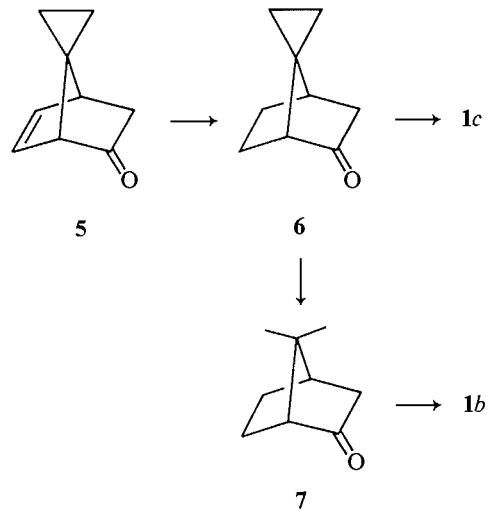

5 6 7

with $NaNH_2/Et_2O/MeI$, however, afforded a 1:1 mixture of **3***c* and **10**, which was readily separated by preparative glc. It may be noted that reduction of mixture **9** with LAH furnished a 1:1 mixture of the *endo*-alcohols **11** and **12**, which were easily separated by glc.

For the preparation of **1***d*, 7-isopropylidenenorbornenone (**13**), available from earlier work (4), was employed. Since hydrogenation of **13** has been reported to occur at both double bonds (8), it was anticipated that *exo*-3-methylation of **13** could render hydrogenation of the 5-double bond more favorable. Hence, **13** was converted to the corresponding enolate with LDA and quenched with methyl iodide to generate **14**, which was quantitatively hydrogenated over Pd/C to furnish **15**. Methylation of **15** using $NaNH_2/Et_2O/MeI$ gave **1***d* in 94% yield.

The ^{13}C shielding data for the compounds involved in the preparative procedures are collected in Table 1.

Homoenolization experiments

Initially the behavior of **1***b* under homoenolization conditions was examined following our usual procedures (9); **1***b*

Can. J. Chem. Downloaded from www.nrcresearchpress.com by 80.58.250.72 on 09/07/12
For personal use only.

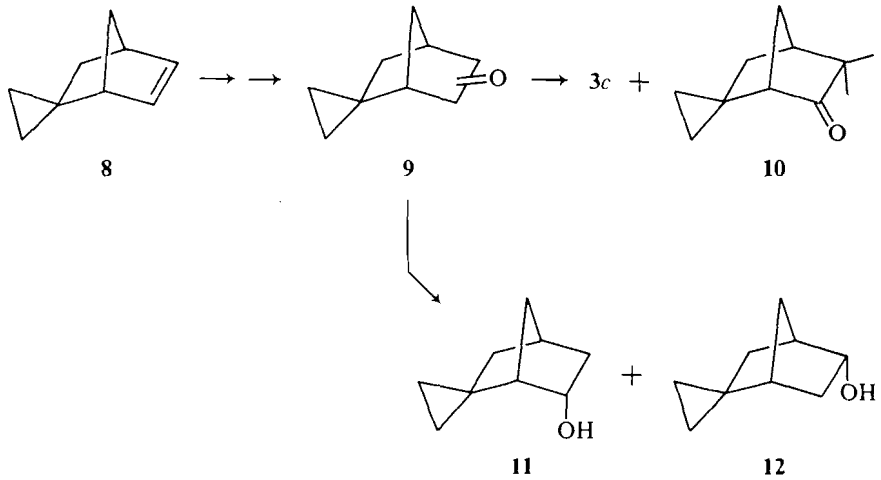

8 9 10 11 12

SCHEME 1

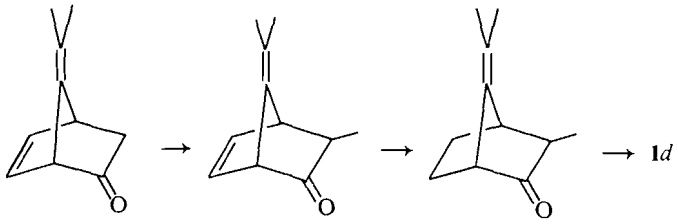

13 14 15 → 1d

was dissolved in anhydrous *t*-BuO$^-$/*t*-BuOH and aliquots were transferred to predried glass tubes under nitrogen, which were sealed and heated at 185°C for varying periods of time. The neutral product was isolated (>80% recovery) and analyzed by glc and ^{13}Cmr. While the chromatograms contained a single major band, the ^{13}C spectra clearly showed that the product is a mixture of two ketones with **1***b* as the major component. The minor compound was tentatively assigned structure **3***b*, the isomer expected from β-enolization of **1***b* via **2***b*, and the ^{13}C data offered permissive support for this structure. Confirmation of the identity of **3***b* was obtained later (see below). The proportions of each ketone in the neutral product, as a function of time, are listed in Table 2, from which it is apparent that **3***b* reaches a maximum concentration of ~16% after ~100 h at 185°C, which is presumably the equilibrium value. For additional evidence that the 5:1 ratio of **1***b* to **3***b* is the equilibrium mixture, two tubes containing a 1:1 mixture of **1***b* and **16** were heated at 200°C for 245 and 345 h. Under these conditions **16** is cleanly isomerized to **17** in 90% yield (10). The neutral

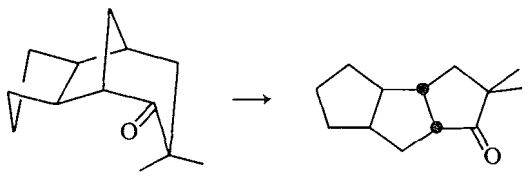

16 17

product in each case was the same, within experimental error, 42% (**1***b*), 8% (**3***b*), 5% (**16**), and 45% (**17**), which confirmed the initial results for **1***b* ⇌ **3***b* equilibration.

Under the same conditions, a series of experiments with **1***c* as the initial ketone gave a neutral product (>90% recovery) whose ^{13}C spectra contained two sets of signals attributable to **1***c* and **3***c* but the components of the mixture could not be separated by glc or tlc. Attempts to separate the mixture obtained by LAH reduction of the product were uniformly unsuccessful. Hence the relative proportions of the two ketones in the original product mixtures were determined from the ^{13}C spectra (Table 2). To confirm the 3:7 equilibrium distribution observed in these experiments, a series of runs with **3***c* was also carried out; these results are listed in Table 2. The behavior of the isomeric ketone **10** was also examined under these conditions but gave no indication of isomerization even after >400 h at 185°C, with >90% recovery of **10**.

With the proof that **1***c* and **3***c* are interconvertible under strongly basic conditions, attention was turned to the interconversion of **3***c* → **3***b*. Hydrogenation of the equilibrium mixture of **1***c* and **3***c* over PtO_2 in glacial acetic acid furnished a 37:63 mixture (by glc) of **1***b* and an alcohol exhibiting four methyl signals and lacking cyclopropyl absorption in its ^{1}H and ^{13}C spectra. Hence it could be concluded that hydrogenolysis of the spirocyclopropyl function occurred, as expected, together with reduction of the carbonyl group in **3***b*, which is much less hindered than that in **1***b*, and structure **18** was assigned to this

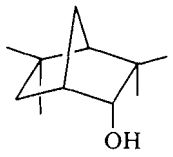

18

alcohol. Oxidation of **18** with PCC gave ketone **3***b* in 89% yield, having the identical ^{13}C spectrum as the isomerized product from **1***b*. Furthermore, this ketone was treated with *t*-BuO$^-$/*t*-BuOH at 185°C following our usual procedure and, after 85 h, gave a neutral product (>90% recovery) consisting of a 1:1 mixture of the same components found in the experiments with **1***b*, described above. These results confirm structure **3***b* for the isomeric ketone formed from **1***b* and illustrate a viable synthetic route from **1***c* → **3***b*.

The fate of **1***d* under strongly basic conditions was next examined and, from a series of experiments at 185°C, the neutral product, isolated in >90% yield, was found to contain two major components (>95% of the total product) that were readily separable by preparative glc. The relative proportions of **1***d* and the new component in the product were determined, as a function of time, by analytical glc and these results are

Can. J. Chem. Downloaded from www.nrcresearchpress.com by 80.58.250.72 on 09/07/12
For personal use only.

TABLE 2. Neutral product composition from β-enolization of **1***b–d* and **3***c*

Compound	Temperature (°C)	Time (h)	Products[a] (%) **1***b*	**3***b*
1*b*	185	12	95	5
		24	90	10
		50	85	15
		120	84	16
		256	83	17
	200	245	82[b]	18[b]
		345	84[b]	16[b]
			1*c*	**3***c*
1*c*	185	2.5	70	30
		5	47	53
		10	36	64
		20	33	67
		90	30	70

Compound	Temperature	Time	Products[a] **1***c*	**3***c*
3*c*	185	10	10	90
		20	15	85
		30	23	77
		45	30	70
		108	30	70
			1*d*[c]	**3***d*[c]
1*d*	185	2.5	27	73
		4	20	80
		6	9	91
		44	6	94
		98	5	95

[a]Unless otherwise indicated, relative proportions determined by ^{13}Cmr (±5%).
[b]Mixtures also contained **16** and **17** (see text).
[c]Relative proportions determined by glc (FFAP), ±3%.

collected in Table 2. Precise mass measurements showed that the new component has the molecular formula $C_{12}H_{18}O$ and, therefore, is isomeric with **1***d*. The carbonyl carbon signal, δ_C 222.9, is 3.2 ppm downfield from that of **1***d*, indicative of reduced interaction with the double bond, as is the reduced shielding difference exhibited by the fully substituted olefinic carbons, 8.0 ppm vs. 17 ppm for **1***d*. These data are entirely consistent with isomerization of **1***d* → **3***d* and the carbon signals were readily assigned to **3***d*. The ^{1}Hmr spectrum provided further support for this structural assignment. Two sharp methyl singlets at δ 0.94 and 1.10, readily ascribed to the 3-methyl groups, were accompanied by the methyl signals of the isopropylidene group, δ 1.64 (bs), 1.73 (dd. J = 1.7 Hz). The latter are coupled to methylene patterns at δ 2.03 (*endo*-H-6, bd, J ~ 16 Hz), and 2.43 (*exo*-H-6, bd, J ~ 16 Hz) as shown by double irradiation experiments, which also revealed that irradiation of the δ 2.43 pattern collapsed a 4.5-Hz coupling in a one-proton multiplet, δ 2.73 (H-1, m, $\nu_{1/2}$ ~ 8 Hz). Irradiation of a one-proton multiplet at δ 2.92 (H-4, $\nu_{1/2}$ ~ 4 Hz) affected only the methylene patterns at δ 1.60 (*anti*-H-7, "dt", J ~ 10, 2 Hz) and 2.09 (*syn*-H-7, bd, J ~ 10 Hz). The ^{13}C shieldings are listed in Table 1; the individual assignments were confirmed by a series of experiments in *t*-BuOD.

These results show that derivatives **1***b–d* isomerize reversibly under strongly basic conditions in a manner analogous to that found for the racemization of camphenilone (**1***a*), presumably via an intermediate β-enolate that can be represented as **2**. In contrast to **2***a*, however, **2***b–d* are not symmetric and, consequently, different incipient carbanions are generated by cleavage of bonds **a** and **b**. For **2***d* it is evident that cleavage proceeds mainly via mode **b**, which furnishes an allylic carbanion. However, the cleavage is not regiospecific as is the case for **4***d* (4). The 5:95 equilibrium mixture of **1***d* and **3***d* shows that the latter is the more stable entity. It is interesting that a single isomer is generated by cleavage **b** since, upon formation of **3***d*, hydrogens at C-6 and the isopropylidene methyl carbons are the most acidic in the molecule and various allylic carbanions can form, as established by ^{1}H/^{2}H exchange experiments described below. Nevertheless, significant amounts of other double bond isomers of **3***d* were not detected. The presence of trace amounts of other isomers cannot be entirely discounted because two very small bands were visible by glc in the neutral product but were not investigated. The generation of some of the 5-isopropenyl isomer(s) was anticipated since sp^3 hybridization of C-5 in the [2.2.1] system will reduce the C-4,5,6 bond angle, but the interactions encountered by an 5-isopropenyl group must preclude its formation in significant amounts.

An inspection of molecular models of **1***b* and **3***b* suggests that the nonbonded interactions between closely lying methyl groups will be appreciably less for **1***b*. Consequently the marked preference for **1***b* in the equilibrium mixture seems reasonable and indicates an energy difference of ca. 1.5 kcal/mol for these two isomers at 185°C. While nonbonded interactions also appear to be less in **1***c* relative to those in **3***c*, the bond angle strain introduced by the spirocyclopropyl group at C-7 in the former may be expected to be greater than that produced by the corresponding substitution at C-5 in **3***c*. The 30:70 ratio of **1***c*:**3***c* at equilibrium indicates that **3***c* is the more stable by ca. 0.8 kcal/mol at 185°C. The preferential formation of **3***c* and its efficient separation from **1***c* by hydrogenation to the alcohol, which is readily oxidized to **3***b* in high yield, provided a preparative route (60% yield from **1***c*) to the latter. This was of interest since **3***b* was one of the tetramethylnorbornanones that had not been prepared heretofore.

H/D exchange experiments

To obtain additional information on the proton abstraction processes occurring in these systems, a series of experiments with each of **1***b–d* was carried out in *t*-BuO$^-$/*t*-BuOD at 185°C. The ^{13}C spectra of the recovered deuterated materials reveal the sites of H/D exchange through the characteristic ^{2}H-induced effects (11). Typically, in saturated systems, a deuterated carbon exhibits an upfield shift ($^1\Delta$) of 300–600 ppb (1 ppb = 0.001 ppm) with J_{CD} ~ 20 Hz, while geminal carbons (^{13}C–C-^{2}H) undergo two-bond shifts ($^2\Delta$) of 50–150 ppb with $J_{CCD} \leq 0.5$ Hz. Vicinal shifts are generally smaller, $^3\Delta$

Can. J. Chem. Downloaded from www.nrcresearchpress.com by 80.58.250.72 on 09/07/12
For personal use only.

Can. J. Chem. Downloaded from www.nrcresearchpress.com by 80.58.250.72 on 09/07/12
For personal use only.

10–20 ppb, but it has been recently recognized (11) that these exhibit a dependence on the dihedral angle (θ) relating the ^{13}C and ^{2}H nuclei extending the range of $^{3}\Delta$ to ~80 ppb for θ ~ 0°. The well-known angular dependence of vicinal couplings often provides a distinction between $^{2}\Delta$ and $^{3}\Delta$ shifts near 80 ppb since periplanar vicinal $^{13}C-^{2}H$ interactions generally exhibit resolvable couplings of ca. 1 Hz.

Samples of **1***d*-d_x and **3***d*-d_x were obtained from runs with **1***d*. The ^{2}H and ^{13}C spectra of **1***d*-d_x recovered after 0.5 and 1.5 h treatment only showed that extensive exchange occurred at the isopropylidene methyl sites. The ^{13}C spectra of the **3***d*-d_x samples (0.5, 1.5, 6, and 20 h) were more informative since the presence of deuterium at C-1 and -6 was clearly revealed, in addition to that at the isopropylidene methyl carbons. Generation of **3***d* via **2***d* in *t*-BuOD leads directly to deuterium incorporation at C-6, which becomes allylic, resulting in increased acidity of the 6-hydrogens and their ready exchange. This was confirmed by the C-6 absorption at 32 ppm, which consisted of a weak signal at δ_C 32.1 (CH_2) as well as a triplet and a barely discernible quintet arising from CHD and CD_2 species, respectively, with J = 20.5 Hz and $^{1}\Delta$ = 330 ppb/D. For the 6- and 20-h samples, a second set of these lines was apparent to signal the presence of deuterium at C-1 with $^{2}\Delta$ = 95 ppb. The C-1 pattern confirmed mono- and dideuteration at C-6 through its appearance as a four-line pattern with isotope-shifted components 70, 90, and 160 ppb upfield from the weak signal at δ_C 50.4 for the protio material. For the 0.5-h sample, the relative intensities were, in order of increasing field, 1:8:2:8, indicating that the initial incorporation at C-6 is stereoselective, presumably favoring *exo* deuteration, as is usual in related systems (3). Supporting evidence for this suggestion was provided by the C-7 absorption in which the δ_C 35.4 signal was accompanied by a prominent singlet, 18 ppb upfield, and a weak triplet, J ~ 0.9 Hz, 21 ppb upfield. The relative intensities of these components were approximately equal for the 1.5-h sample. These lines must be induced by *exo*- and *endo*-6-deuterons, respectively; since the latter is antiperiplanar to C-7, a resolvable vicinal coupling is expected (11). The relative intensities of these isotope-shifted components in the spectrum of the 0.5-h sample confirm the predominance of *exo*-6-deuteration initially, i.e., via cleavage of **2***d*. For the 6- and 20-h samples, a second set of the shifted components appeared 95 ppb upfield from the first set, arising from species bearing deuterium at C-1. Although the triplet for deuterated C-1 was indistinguishable from the noise in the 50-ppm pattern, the appearance of the second set of shifted components in the patterns for each of C-6 and C-7 established the occurrence of bridgehead exchange. The relatively rapid equilibration and allylic exchange, with the consequent rapid diminution of the deuterium pool, precluded the extraction of meaningful quantitative data on the rates and stereoselectivity of the processes involving **2***d*.

Although the mixtures of **1***b*-d_x and **3***b*-d_x obtained from the treatment of **1***b* with *t*-BuO^-/*t*-BuOD at 185°C could not be separated by glc, the individual signals for each carbon are nicely separated in the ^{13}Cmr spectra (Table 1) and the major sites of exchange in **1***b*-d_x could be identified. From the spectra of the products recovered after 4, 8, 16, and 32 h there was clear evidence of deuterium incorporation at C-1 and -6. After 4 h, a characteristic CHD triplet, J = 20.6 Hz, with $^{1}\Delta$ = 300 ppb, accompanied the original C-6 signal at δ_C 23.3, while the C-1 and -5 patterns, δ_C 59.4 and 23.5, respectively, each contained an isotope-shifted component, 60 and 115 ppb upfield. After longer reaction times, a second, less intense component appeared in each of the C-1 and -5 patterns with $^{2}\Delta$ = 85 and 90 ppb, respectively. In the spectra of the 16- and 32-h samples the C-6 absorption included a second, weak triplet, $^{2}\Delta$ = 105 ppb shifted by deuterium at C-1, which was also evidenced by the appearance of a shifted component in the C-7 absorption, δ_C 45.0, $^{2}\Delta$ = 85 ppb. The CD triplet for C-1 was, unfortunately, indistinguishable from the noise. The relative intensities of these various isotope-shifted components for C-1, -5, -6, and -7 indicated that incorporation at C-6 is stereoselective, favoring, presumably, *exo* exchange by ca. 6:1 over *endo* exchange, with the latter about three times slower than bridgehead exchange. To obtain better estimates of the relative rates of exchange and to check for lower incorporation levels at other centres, it was necessary to obtain pure samples of **1***b*-d_x. Hydrogenation of each of the mixtures over PtO_2 in HOAc afforded mixtures of **1***b*-d_x and **18**-d_x that were readily separated by flash chromatography to provide the requisite pure samples of **1***b*-d_x for examination by mass spectrometry, to determine the total deuterium content, and by ^{2}Hmr, to assess the incorporation level at the individual sites. The ^{2}Hmr spectrum of **1***b*-d_x that was recovered after 16 h with *t*-BuO^-/*t*-BuOD exhibited five signals at δ 2.08, 1.95, 1.50. 1.24, and 1.04. The two highest field signals coincide with two of the four methyl singlets in the proton spectrum of **1***b* and, by analogy with several related systems (3) can be assigned to the geminal 3-methyls, with that at highest field arising from the *endo*-methyl group since the rate of ^{2}H uptake was found to be slowest. For several related systems, it has been established (3) that β-methyl exchange is regioselective, favoring *exo* incorporation. The lowest field ^{2}H signal at δ 2.08 coincides with a broadened doublet, J ~ 5 Hz, in the proton spectrum and is readily assigned to the bridgehead H-1. The remaining pair of signals, therefore, arises from the 6-methylene deuterons. Both signals coincide with multiplets in the proton spectrum in which the lower field pattern is the more complex and is, therefore, attributable to the *exo*-6 proton since its *endo*-6 counterpart lacks significant coupling to H-1. The relative intensities of the 1- and 6-deuterium signals confirmed the relative rates of deuterium incorporation tentatively deduced from the ^{13}C spectra, as noted above, and in combination with the total ^{2}H content determined by mass spectrometry permitted estimates of the first-order rate constants for exchange at the various sites as: $7.5 \times 10^{-7}\,s^{-1}$ (C-1), $2 \times 10^{-5}\,s^{-1}$ (*exo*-6), $3 \times 10^{-6}\,s^{-1}$ (*endo*-6), $1 \times 10^{-7}\,s^{-1}$ (*exo*-3-Me), and $5 \times 10^{-8}\,s^{-1}$ (*endo*-3-Me).

As in the preceding case, the mixtures of **1***c*-d_x and **3***c*-d_x obtained upon homoenolization in *t*-BuOD could not be separated but there is little overlap of the ^{13}C signals from each in the mixtures and considerable information could be extracted. From the ^{13}C spectra of the mixtures recovered after 2, 4, 8, and 16 h at 185°C, there was clear evidence of deuterium incorporation at C-1 and -6 in **1***c*-d_x. The signal for C-7 at δ_C 32.3 was accompanied by an upfield component, $^{2}\Delta$ 75 ppb, whose intensity increased with reaction time and is attributable to deuterium incorporation at C-1. Similarly, the δ_C 23.6 pattern for C-5 contained an isotope-shifted signal, $^{2}\Delta$ 115 ppb, which grew more rapidly and arose from deuterium exchange at C-6. In the spectrum of the 2-h sample, the C-6 pattern consisted of the normal signal δ_C 24.7 and a shifted component, $^{2}\Delta$ 105 ppb, due to deuterium at C-1. For the later samples, characteristic triplets, $^{1}\Delta$ 310 ppb, J = 21.0 Hz, were increasingly apparent for species bearing deuterium at C-6 and at both C-1 and -6

Can. J. Chem. Downloaded from www.nrcresearchpress.com by 80.58.250.72 on 09/07/12
For personal use only.

such that, after 16 h, these triplets constituted virtually the entire absorption for C-6. Thus, although there is extensive deuterium incorporation at C-6, there was no evidence of a resolvable $^3\Delta$-shifted component in the absorption for C-7; this indicated that most of the deuterium at C-6 is *exo*, which is consistent with inversion of configuration upon cleavage of **2***c* via bond **a**. The ^{13}C patterns for **3***c*-d_x also provided clear evidence of deuterium incorporation at C-1 and -6. In each case, the C-7 absorption contained the original signal at δ_C 35.8 together with a $^2\Delta$ component 100 ppb upfield indicative of deuterium at C-1. In the later samples a third component appearing as a closely spaced triplet, $J \sim 0.8$ Hz, $^3\Delta$ 20 ppb, became evident. The spectrum of the 2-h sample revealed that >95% of the absorption for C-1, δ_C 51.9, was the isotope-shifted component, $^2\Delta$ 66 ppb, signifying nearly complete mono-deuteration at C-6. In addition, 95% of the absorption for one of the spirocyclopropyl methylene carbons, δ_C 13.9, was a triplet, $J \sim 0.8$ Hz, 90 ppb, upfield from the normal signal while the second spirocyclopropyl methylene signal, δ_C 11.0, was unaffected. However, in the later samples, a distinctly broadened ($\nu_{1/2}$ 1.6 Hz) component, $^3\Delta$ 70 ppb, became increasingly intense; in fact, the growth of this component was similar to that found for the closely spaced triplet in the C-7 absorption, noted above. These spectral changes shed light on the stereoselectivity of deuterium incorporation at C-6. After 2 h, the *exo*-6 proton is nearly completely exchanged and the large vicinal isotope shift and coupling exhibited by one of the spirocyclopropyl methylene carbons identifies that which is synperiplanar, i.e., *exo*. After longer reaction times, the incorporation of *endo*-6-deuterium is manifest in the appearance of vicinal effects in the absorptions for C-7 and the second spirocyclopropyl methylene carbon to which this deuterium is antiperiplanar and synperiplanar, respectively. These results are consistent with preferential cleavage of **2***c* via **b** proceeding with inversion of configuration. The spectrum of the 2-h sample contained a prominent triplet, $J = 20.5$ Hz, $^1\Delta$ 375 ppb, together with a weak singlet (<5% of the total intensity) at δ_C 35.4 for C-6. With increasing time, a second triplet, $^2\Delta$ 100 ppb, became increasingly prominent and was due to deuterium exchange at C-1. After 16 h, the latter triplet constituted >60% of the total intensity in the C-6 pattern. It should be noted that the absorption for fully deuterated C-6 species was not distinguishable from the noise.

To obtain estimates of the relative rates of exchange in **1***c*-d_x, the mixtures of **1***c*-d_x and **3***c*-d_x were hydrogenated over PtO_2 in HOAc to furnish mixtures of **1***b*-d_x and **18**-d_x, which were readily separated by flash chromatography. The ^2H content of the resulting pure samples of **1***b*-d_x was assessed by mass spectrometry and ^{2}Hmr as described above for the analogous samples from the experiments with **1***b*. With the assumption that the hydrogenolysis of **1***c*-d_x to **1***b*-d_x did not alter the ^2H distribution, approximate first-order rate constants for exchange at the various sites in **1***c* were estimated and these data are collected in Fig. 1 together with those for **1***b*, **19** (9), **20** (16), and **21** (17). From these results it is apparent that the rates of exchange at C-6 are comparable in **1***b*, **1***c*, and **19**, with *exo* exchange favored. It is interesting that bridgehead exchange at C-1 is significantly enhanced in **1***c* relative to that in **1***b* by a factor of 25, while this process proceeds at comparable rates in **1***b* and **20**. Bridgehead exchange in **1***c* approaches the rate found for **21**, indicating that the three-membered ring in each enhances the acidity of the 1-hydrogen in each case. Finally, it may be noted that the rates of deuterium exchange at

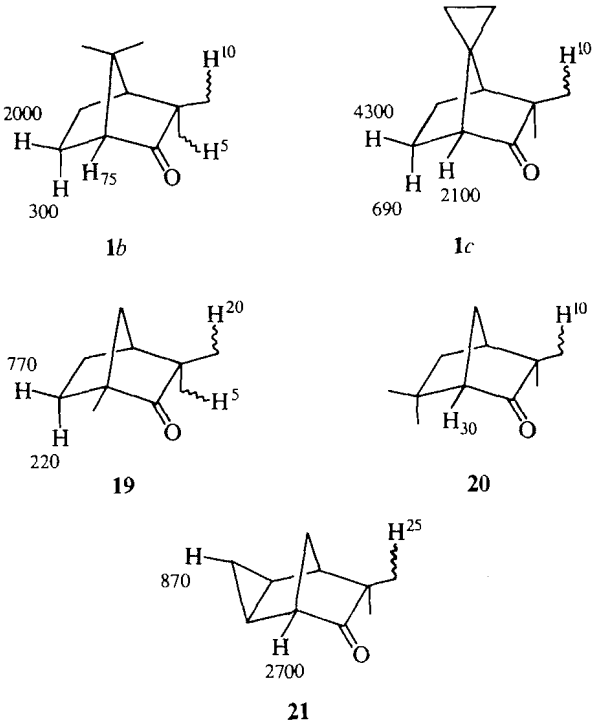

FIG. 1. Deuterium exchange rates ($k \times 10^8\ s^{-1}$) at the various sites in **1***b*, **1***c*, and **19–21** by β-enolization at 185°C in *t*-BuO$^-$/*t*-BuOD. The data for **1***c* were obtained by examination of samples of **1***b* from hydrogenolysis of **1***c* (see text).

the *exo*-methyl carbon are similar in the five systems. There was no evidence of γ-exchange at the cyclopropylmethylene sites in **1***c* although such hydrogens may be expected to be more acidic than their alicyclic counterparts. This contrasts sharply with the results for **21**, which exhibits deuterium incorporation at the less hindered of the two cyclopropylmethylene hydrogens, with $k \sim 8.7 \times 10^{-6}\ s^{-1}$, i.e., at a rate comparable to that found for the *endo*-6-hydrogen in **1***c* (17). This suggests that the carbonyl group in **21** enhances the acidity of the cyclopropylmethylene hydrogen due to the orientation of the three-membered ring relative to the carbonyl π system, which differs from that in **1***c*. It may be noted that the *endo* isomer of **21** also exhibits γ-exchange at the less hindered of the cyclopropylmethylene sites $k \sim 1.6 \times 10^{-5}\ s^{-1}$. Clearly the effect of the carbonyl group is dependent on the geometry of the system. Work is in progress to obtain more data on the reactivity of exchange in related systems, which may permit more definitive interpretation of the trends for both β- and γ-exchange.

Experimental

Gas–liquid chromatography was carried out on Varian 920 and 3700 instruments using columns of 10% Carbowax 20 M, 6% FFAP or 10% SE-30 in Chromosorb W, as indicated. Tetrahydrofuran (THF) and ether were dried over sodium and freshly distilled before use. Diisopropyl amine was distilled from CaH_2 and stored over 4A molecular sieves; methyl iodide was dried over 4A sieves. The ketones, 7-spirocyclopropylnorbornenone (**5**) and 7-isopropylidenenorbornenone (**13**), were employed as the starting materials for the preparation of **1***b–d* and have been described previously (4).

Infrared spectra were recorded with a Beckman 4250 instrument and mass spectra were obtained on a Varian MAT-311A system at 70 eV (direct inlet). Routine ^{1}Hmr spectra were recorded with a Varian EM-360 instrument while data for pure samples were collected with a Varian XL-200 spectrometer. The ^2H and ^{13}Cmr spectra were

Can. J. Chem. Downloaded from www.nrcresearchpress.com by 80.58.250.72 on 09/07/12
For personal use only.

obtained using a Varian XL-300 system and comparison of the fully decoupled ^{13}C spectra with those recorded with either the APT (12) or DEPT (13) sequences identified the methyl, methylene, methine, and fully-substituted carbon signals. The INADEQUATE spectrum of **6** was obtained using the C13SAT sequence of the XL software with the XL-200 instrument: 3000 Hz sweep width (sp^3 carbons only), 12 s repetition rate, 32 000 points, and a 32K transform.

7-Spirocyclopropylnorbornanone (6)

To a solution of **5** (1.89 g) in 95% EtOH (24.2 mL) was added 10% Pd/C (73 mg) and the mixture hydrogenated in a Parr shaker (50 psi, H_2 pressure (1 psi = 6.9 kPa)) for 6 h. After removal of the catalyst by filtration, the solution was concentrated by evaporation and the residue taken up in *n*-pentane (30 mL), before washing with H_2O (2 × 15 mL) and drying over $MgSO_4$. Removal of the solvent gave **6** (1.80 g, 94% yield) as an oil, >99% pure by glc (Carbowax), which crystallized on standing, mp 65–66°C (lit. (14) mp 64°C); ir (film): 3070, 2960, 1750 cm^{-1}; ^{1}Hmr agreed with the literature (5); ^{13}Cmr (see Table 1). *Exact Mass* calcd. for $C_9H_{12}O$: 136.0888; found: 136.0890.

7,7-Dimethylnorbornanone (7)

The mixture composed of **6** (300 mg) in glacial acetic acid (11.5 mL) and Pt_2O (70 mg) was hydrogenated in a Parr shaker (50 psi, H_2 pressure) for 16.5 h. After the addition of H_2O (6 mL) the catalyst was removed by filtration and the acid neutralized by the addition of solid $NaHCO_3$. Extraction with *n*-pentane (4 × 30 mL), washing the combined extracts with 10% aqueous NaCl solution (2 × 40 mL), and drying over $MgSO_4$ before evaporation of the solvent afforded crude **7** as an oil, which was purified by flash chromatography (ether – petroleum ether, 10:90) to furnish **7** (300 mg, 98% yield); ir ($CHCl_3$): 2940, 1740 cm^{-1}; ^{1}Hmr agreed with the literature (5); ^{13}Cmr (see Table 1). *Exact Mass* calcd. for $C_9H_{14}O$: 138.1045; found: 138.1050.

3,3-Dimethyl-7-spirocyclopropylnorbornan-2-one (1c)

Ketone **6** (500 mg) in Et_2O (4 mL) was added to a stirred suspension of $NaNH_2$ (0.8 g) in Et_2O (20 mL) under nitrogen and the mixture stirred for 2 h under reflux. Methyl iodide (0.46 mL) was added slowly and then equivalent amounts of MeI were added at intervals of 2, 4, and 11 h. The mixture was refluxed for 2 h before cooling to 0°C and dilution with H_2O (12 mL). Pentane extraction in the usual fashion gave a yellow oil, which was purified by flash chromatography (Et_2O – petroleum ether, 5:95) to furnish **1***c* (320 mg, 52% yield); ir (CCl_4): 3070, 2960, 1742 cm^{-1}; ^{1}Hmr ($CDCl_3$) δ: 0.27–0.52 (m, 2H), 0.73–0.97 (m, 2H), 1.06 (s, 3H, Me), 1.20 (s, 3H, Me), 1.45–1.65 (m, 2H), 1.75–2.15 (m, 4H); ^{13}Cmr (see Table 1). *Exact Mass* calcd. for $C_{11}H_{16}O$: 164.1201; found: 164.1201.

3,3,7,7-Tetramethylnorbornornan-2-one (1b)

Following the general procedure described for the preparation of **1***c*, **7** (300 mg) in Et_2O (4 mL) was reacted with $NaNH_2$ (0.5 g) in Et_2O (11 mL) at reflux for 2.5 h before the addition of MeI (0.5 mL). Further additions after 10 and 2.5 h followed by reflux for 7 h furnished a product (250 mg) after pentane extraction, which appeared by glc (Carbowax) to be a 4:1 mixture of **1***b* and 3,7,7-trimethylnorbornanone. This mixture was recycled through the methylation sequence to afford oily **1***b* (80 mg), which glc indicated to be >95% pure. Preparative glc provided pure **1***b* for characterization and for homoenolization studies; ir (film): 2960, 1850 cm^{-1}; ^{1}Hmr ($CDCl_3$) δ: 1.04 (s, 3H, Me), 1.09 (s, 3H, Me), 1.13 (s, 3H, Me), 1.23 (s, 3H, Me), 1.47 (m, 1H), 1.68–2.10 (m, 5H); ^{13}Cmr (see Table 1). *Exact Mass* calcd. for $C_{11}H_{18}O$: 166.1358; found: 166.1356.

3,3-Dimethyl-5-spirocyclopropylnorbornan-2-one (3c)

(i) 5-Spirocyclopropylnorbornene (8)

Methylenecyclopropane (3.27 g), prepared from methallyl chloride and $NaNH_2$ in *t*-BuOH/THF as described by Conia and co-workers (15), cyclopentadiene (4.9 g), and hydroquinone (12 mg) were combined and aliquots were transferred to a series of thick-walled glass tubes (tube volume:solution volume, 5:1) that were sealed under vacuum. These were placed in an oil bath at 100°C and the temperature increased to 190°C over 3.5 h. After 19 h at 190°C the tubes were removed from the bath and cooled to room temperature before opening. The contents of the tubes were recovered by washing with pentane. Bulb-to-bulb distillation gave **8**, bp 28–30°C/18 Torr (1 Torr = 133.3 Pa), 3.98 g, 55% yield, whose physical properties were identical to those found by Adam *et al.* (7).[3]

(ii) 5- and 6-Spirocyclopropyl-3,3-dimethylnorbornan-2-ones (3c and 10)

Upon cooling a solution of **8** (3.9 g) in *n*-hexane (11 mL) to 0°C, 10 *M* borane – methyl sulfide solution (1.33 mL) was added dropwise, after which the ice bath was removed and the reaction mixture stirred for 6 h. Excess borane was destroyed by the slow addition of EtOH (12.7 mL) followed by the addition of 3 *M* NaOH aqueous solution (4.7 mL). The solution was cooled to 0°C before 30% H_2O_2 solution (4.7 mL) was slowly added. Then the reaction mixture was refluxed for 1.5 h. Upon cooling, the solution was diluted with H_2O (50 mL) and the organic layer removed by decantation. The aqueous phase was extracted with pentane (3 × 60 mL) and the combined extracts washed with brine before drying over $MgSO_4$ and evaporation of solvent. Distillation of the residue afforded a 1:1 mixture (by ^{13}Cmr) of two alcohols, bp 49–50°C/0.4 Torr, 3.05 g, 68% yield, which could not be separated by glc (Carbowax, FFAP, SE-30) or tlc. Precise mass measurement of the mixture indicated the expected molecular formula, $C_9H_{14}O$. *Exact Mass* calcd.: 138.1045; found: 138.1047.

The mixture of alcohols (1.0 g) in CH_2Cl_2 (9.6 mL) was added to a slurry of PCC (2.33 g), sodium acetate (0.18 g), Celite (2.33 g), and CH_2Cl_2 (9.6 mL), which was stirred for 3 h before isolation of the product by our usual pentane extraction. Removal of the solvent gave an oil (0.99 g, quantitative yield) whose ^{13}C spectrum indicated the presence of two isomeric ketones **9** but, again, glc and tlc failed to separate the two components. The expected molecular formula for the product, $C_9H_{12}O$, was obtained by precise mass measurement. *Exact Mass* calcd.: 136.0888; found: 136.0885.

Dimethylation of this mixture of ketones was accomplished following the general procedure described above. A slurry of $NaNH_2$ (1.9 g), Et_2O (30 mL), and mixture **9** (0.83 g) was refluxed for 2 h. Methyl iodide (0.76 mL) was then added and three further additions were made after 2 h (0.76 mL), 4 h (1.52 mL), and 11 h (1.52 mL). Before work-up, the mixture was refluxed for 5 h; however, the ^{13}Cmr spectrum of this product indicated the presence of both mono- and dimethylated material. Two additional cycles were required before a product consisting of a 1:1 mixture of two components (0.77 g, 77% yield) was obtained, which was readily separated by preparative glc (FFAP) to furnish pure samples of each dimethylated ketone.

3*c*: ir ($CHCl_3$): 3080, 2990, 1740 cm^{-1}; ^{1}Hmr ($CDCl_3$) δ: 0.26 (m, 1H), 0.74 (m, 1H), 0.76 (m, 2H), 1.02 (s, 3H, Me), 1.17 (s, 3H, Me), 1.66 (bd, *J* = 12.4, *endo*-H-6), 1.79 (dd, *J* = 12.4, 5.3 Hz, *exo*-H-6), 2.67 (d″q″, *J* = 5.3, 1.8 Hz, H-1), 1.48 (m, H-4), 1.99 (dt, 11.4, 1.8 Hz, *anti*-H-7), 2.02 (d″q″, *J* = 11.4, 1.8 Hz, *syn*-H-7); ^{13}Cmr (see Table 1). *Exact Mass* calcd. for $C_{11}H_{16}O$: 164.1201; found: 164.1197.

10: ir (CCl_4): 3030, 2920, 1737 cm^{-1}; ^{1}Hmr ($CDCl_3$) δ: 0.47 (m, 2H), 0.57 (m, 1H), 0.68 (m, 1H), 1.08 (s, 3H, Me), 1.10 (s, 3H, Me), 1.62 (dd, *J* = 12.2, 2.5 Hz, *endo*-H-5), 1.81 (dd, *J* = 12.2, 3.9 Hz, *exo*-H-5), 1.75 (t, *J* = 1.5 Hz, H-1), 1.89 (dt, *J* = 10.5, 1.5 Hz, *anti*-H-7), 2.02 (ddt, *J* = 10.5, 2.5, 1.5 Hz, *syn*-H-7), 2.30 (m, H-4); ^{13}Cmr (see Table 1). *Exact Mass* calcd. for $C_{11}H_{16}O$: 164.1201; found: 164.1201.

*5- and 6-Spirocyclopropyl-*endo*-2-norbornanols (11 and 12)*

To a slurry of LAH (42 mg) in Et_2O (4 mL) was added the 1:1 mixture of ketones **9** (100 mg), described above, in Et_2O (2 mL) and the reaction mixture was stirred overnight. Excess LAH was destroyed by the cautious addition of H_2O and the product isolated by ether extraction to yield a 1:1 mixture of alcohols **11** and **12** (70 mg, 70% yield), which was readily separated by preparative glc (Carbowax).

[3]The ^{13}C data, ir, mass, and ^{1}Hmr spectra for authentic **8** were kindly provided by Professor Adam for comparison with our material.

Can. J. Chem. Downloaded from www.nrcresearchpress.com by 80.58.250.72 on 09/07/12
For personal use only.

11: ir (CCl_4): 3620, 3080, 2980, 1050, 1025 cm^{-1}; ^{1}Hmr ($CDCl_3$) δ: 4.26 (bdddd, J = 9.6, 6.3, 6.1, 3.6 Hz, H-2), 2.37 (m, H-1), 1.95 (ddd, J = 12.7, 9.6, 4.5 Hz, 1H), 1.81 (dd, J = 12.3, 2.4 Hz, 1H), 1.71 (dddd, J = 9.8, 3.6, 1.7, 1.7 Hz, 1H), 1.30–1.64 (m, 4H), 1.19 (ddd, J = 12.7, 3.6, 3.6 Hz, 1H), 0.21–0.38 (m, 4H); ^{13}Cmr (see Table 1). *Exact Mass* calcd. for $C_9H_{14}O$: 138.1045; found: 138.1044.

12: ir (CCl_4): 3602, 3080, 2940, 1045 cm^{-1}; ^{1}Hmr ($CDCl_3$) δ: 4.26 (bdddd, J = 9.8, 9.8, 3.6, 3.6 Hz, H-2), 2.32 (m, H-1), 2.00–2.15 (m, 2H), 1.645–1.75 (m, 2H), 1.58 (m, 1H), 1.32–1.42 (m, 2H), 1.15 (ddd, J = 13.1, 3.4, 3.4 Hz, 1H), 0.69–0.85 (m, 2H), 0.40 (m, 1H), 0.12 (m, 1H); ^{13}Cmr (see Table 1). *Exact Mass* calcd. for $C_9H_{14}O$: 138.1045; found: 138.1048.

Separation of mixtures of ***1****c*/***3****c and* ***1****b*/***3****b by hydrogenation to* ***1****b and* ***18***

The 32:68 mixture of **1***c* and **3***c* (210 mg) from homoenolization of **1***c* for 187 h at 185°C was placed in a pressure vessel containing glacial acetic acid (7 mL) and PtO_2 catalyst (100 mg) and the mixture hydrogenated under 50 psi of H_2 for 33 h. After the addition of H_2O (10 mL), the mixture was neutralized with solid $NaHCO_3$ and the catalyst removed by filtration. The neutral solution was saturated with NaCl and extracted with pentane (3 × 20 mL) in the usual manner. Removal of the solvent gave an oil (200 mg), which glc analysis (FFAP) and ^{13}Cmr indicated to be a mixture of **1***b* and **18**. Flash chromatography (Et_2O – petroleum ether, 10:90) furnished pure samples of each, **1***b* (70 mg) and **18** (120 mg); ir (film): 3360, 2945, 1073 cm^{-1}. ^{1}Hmr ($CDCl_3$) δ: 3.74 (d, J = 4.5 Hz, H-2), 2.31 (bt, J = 4.5 Hz, H-1), 1.60 (m, 3H), 1.25 (m, 2H), 1.22, 1.11, 1.05, 1.03 (4 × Me); ^{13}Cmr (see Table 1). *Exact Mass* calcd. for $C_{11}H_{20}O$: 168.1514; found: 168.1517.

The same procedure was employed to separate the mixtures of **1***b*-d_x and **3***b*-d_x obtained upon homoenolization of **1***b* in *t*-BuO^-/*t*-BuOD at 185°C.

*3,3,5,5-Tetramethylnorbornan-2-one (****3****b)*

To a slurry of PCC (190 mg), sodium acetate (15 mg), Celite (190 mg), and CH_2Cl_2 (1.0 mL) was added a solution of **18** (100 mg) in CH_2Cl_2 (1.0 mL) and the reaction mixture was stirred for 3 h. The crude product was isolated by pentane extraction and purified by column chromatography on silica (eluent: ether – petroleum ether, 5:95) to give **3***b* (88 mg, 89% yield); ir (film): 2940, 1745 cm^{-1}; ^{1}Hmr ($CDCl_3$) δ: 2.52 (d″q″, J = 5.8, 1.6 Hz, H-1), 2.00 (dt, J = 11.2, 1.8 Hz, *anti*-H-7), 1.94 (dq, J = 11.2, 1.8 Hz, *syn*-H-7), 1.83 (m, H-4), 1.76 (ddd, J = 13.2, 5.8, 1.2 Hz, *exo*-H-6), 1.39 (dd, J = 13.2, 1.8 Hz, *endo*-H-6), 1.23 (s, 6H), 1.17 (s, 3H, Me), 1.14 (s, 3H, Me); ^{13}Cmr (see Table 1). *Exact Mass* calcd. for $C_{11}H_{18}O$: 166.1358; found: 166.1362.

*3,3-Dimethyl-7-isopropylidenenorbornan-2-one (****1****d)*

*(i) 3-*exo*-Methyl-7-isopropylidenenorborn-5-en-2-one (****14****)*

To a stirred solution of LDA, prepared from diisopropyl amine (0.53 mL), THF (6 mL), and *n*-butyllithium in hexane (1.3 mL, 2.5 *M*) at −78°C, under an N_2 atmosphere was added dropwise a solution of 7-isopropylidenenorbornenone (400 mg) in THF (2 mL) and stirring was continued for 35 min before the addition of methyl iodide (0.35 mL). After stirring overnight at room temperature, the reaction mixture was diluted with 10% aqueous NaCl solution (10 mL) and the product extracted with pentane (4 × 15 mL). The combined extracts were washed with the NaCl solution (2 × 15 mL) and H_2O (15 mL) before drying over $MgSO_4$. Removal of the solvent afforded **14** (430 mg, 98% yield), which was pure by glc analysis (FFAP); ir (CCl_4): 3080, 2940, 1748 cm^{-1}; ^{1}Hmr ($CDCl_3$) δ: 6.66 (dd, J = 5.8, 3.0 Hz, H-5), 6.24 (dddd, J = 5.8, 3.3, 1.2, 0.6 Hz, H-6), 3.53 (bdd, J = 3.3, 1.8 Hz, H-1), 3.32 (m, $\nu_{1/2}$ ~ 6 Hz, H-4), 2.14 (q, J = 7.4 Hz, *endo*-H-3), 1.68 (s, 3H, Me), 1.63 (s, 3H, Me), 1.04 (d, J = 7.4 Hz, *exo*-3-Me); ^{13}Cmr (see Table 1). *Exact Mass* calcd. for $C_{11}H_{14}O$: 162.1045; found: 162.1039.

*(ii) 3-*exo*-Methyl-7-isopropylidenenorboran-2-one (****15****)*

To a solution of **14** (220 mg) in 95% EtOH (3.26 mL) was added 10% Pd/C (80 mg) and the mixture hydrogenated in a Parr shaker at 760 Torr for 6 h. The catalyst was removed by filtration and the product isolated by pentane extraction (3 × 8 mL). The combined extracts were washed with 10% aqueous NaCl (2 × 10 mL) and H_2O (10 mL) and the aqueous fractions were reextracted with pentane (20 mL). After drying over $MgSO_4$, the pentane solution was concentrated to yield **15** (220 mg, 99% yield), which was pure by glc analysis (FFAP); ir (CCl_4): 2960, 1745 cm^{-1}; ^{1}Hmr ($CDCl_3$) δ: 3.05 (m, H-1), 2.75 (m, H-4), 2.09 (q, J = 7.4 Hz, H-3), 1.75–1.90 (m, 2H), 1.73 (s, 3H, Me), 1.69 (s, 3H, Me), 1.48–1.58 (m, 2H), 1.02 (d, J = 7.4 Hz, *exo*-3-Me); ^{13}Cmr (see Table 1). *Exact Mass* calcd. for $C_{11}H_{16}O$: 164.1201; found: 164.1201.

A mixture of **15** (420 mg), $NaNH_2$ (840 mg), and Et_2O (8.4 mL) was heated under reflux for 2.5 h. Methyl iodide (1.0 mL) was then added and four further additions were made after 8 h (0.5 mL), 4 h (0.5 mL), 3 h (0.5 mL), and 2 h (0.3 mL). After refluxing for an additional 17 h, the reaction mixture was worked up to furnish an oil (430 mg, 94% yield) by pentane extraction, and glc analysis (FFAP) indicated purity of >98%. Preparative glc (FFAP) provided pure **1***d* for characterization and for homoenolization experiments; ir (CCl_4): 2970, 1747 cm^{-1}; ^{1}Hmr ($CDCl_3$) δ: 3.05 (dd, J = 5.0, 1.5 Hz, H-1), 2.62 (dd, J = 4.5, 1.5 Hz, H-4), 1.5–1.9 (m, 4H), 1.72 (s, 3H, Me), 1.66 (s, 3H, Me), 1.07 (s, 3H, Me), 1.01 (s, 3H, Me); ^{13}Cmr (see Table 1). *Exact Mass* calcd. for $C_{12}H_{18}O$: 178.1358; found: 178.1361.

Homoenolization experiments

The general procedures for the rearrangement and exchange experiments, reported previously (9), were followed as illustrated for **1***b*. To a solution of *t*-BuO^-/*t*-BuOH (1.27 *M*, H_2O content = 50 μg/mL) was added **1***b*, to give a solution that was 0.26 *M* in ketone. To a series of 5-mL predried, thick-walled glass tubes were transferred 0.5-mL aliquots of the reaction solution; the tubes were degassed and sealed before immersion in an oil bath at 185°C. Tubes were removed at various times, cooled before opening, and the contents removed by washing with H_2O (10 mL). The organic product was isolated by pentane extraction (3 × 15 mL) and the combined extracts backwashed with H_2O (3 × 10 mL). The aqueous washings were reextracted with pentane (2 × 15 mL) and the pentane extracts dried over $MgSO_4$. Removal of the solvent by distillation afforded a neutral organic product, representing 80–90% yields from the various tubes, which consisted of two components according to the ^{13}C spectra, although only a single band was evident upon glc analysis (FFAP, Carbowax SE-30). The major component was the initial ketone and the minor component was **3***b*, identified by the synthesis of an authentic sample (see above). From the various runs, the results showed that a 6:1 mixture of **1***b*:**3***b* represented the equilibrium value. An 85-h run at 185°C with **3***b* as starting material gave a 1:1 mixture of **1***b* and **3***b* (>90% recovery), confirming the identity of the latter.

Analogous experiments with **1***c* also gave a neutral two-component product (>90% yield) inseparable by glc (FFAP, Carbowax, SE-30) but whose ^{13}C spectra showed the presence of **1***c* and **3***c*, which was identified by comparison with an authentic sample (see above). The same mixture of **1***c* and **3***c* resulted upon base treatment of either as the initial ketone showing the equilibrium mixture to be 30:70 (**1***c*:**3***c*). The isomeric ketone **10** was found to be stable under the strongly basic conditions. With >90% recovery after >300 h there was no evidence of isomerization. Homoenolization experiments with **1***d* resulted in a 95% conversion to **3***d*, which was identified on the basis of its spectroscopic properties (see text).

The results of these homoenolization runs are collected in Table 2.

For the exchange experiments, *tert*-butyl alcohol-*O*-d_1 (99% deuterated and <0.005 *M* in water) was employed and a series of runs for each of the ketones **1***b–d* was carried out: **1***b*, 4, 8, 16, and 32 h; **1***c*, 2, 4, 8, 16 h; **1***d*, 0.5, 1.5, 6, and 20 h, using the same batch of *t*-BuO^-/*t*-BuOD for each. The products from each run were examined by ^{13}Cmr to determine the ^{2}H-induced effects. To assess the deuterium incorporation as a function of reaction time, samples of the initial ketones were required for analysis by mass spectrometry and ^{2}Hmr. While preparative glc afforded the requisite samples of **1***d*-d_x from the **1***d*-d_x/**3***d*-d_x mixtures, a different method was required for the others. Pure samples of **1***b*-d_x were obtained from the mixtures of

1*b*-d_x/**3***b*-d_x and **1***c*-d_x/**3***c*-d_x by hydrogenation over PtO_2/HOAc, followed by flash chromatography as described above. Mass spectrometric analysis of each sample provided the overall deuterium content while integration of the ^{2}Hmr spectra gave the proportions of ^{2}H at the individual sites. From these results approximate rate constants for ^{2}H incorporation at each site were determined, as discussed in the text.

Acknowledgements

We are grateful for the financial support provided by the Natural Sciences and Engineering Research Council of Canada.

1. A. NICKON and J. L. LAMBERT. J. Am. Chem. Soc. **84**, 4604 (1962); **88**, 1905 (1966).
2. A. NICKON, J. H. HAMMONS, J. L. LAMBERT, and R. O. WILLIAMS. J. Am. Chem. Soc. **85**, 3713 (1963).
3. N. H. WERSTIUK. Tetrahedron, **39**, 205 (1983).
4. A. J. RAGAUSKAS and J. B. STOTHERS. Can. J. Chem. **63**, 2961 (1985).
5. N. J. TURRO and G. L. FARRINGTON. J. Am. Chem. Soc. **102**, 6056 (1980).
6. A. BAX, R. FREEMAN, and S. P. KEMPSELL. J. Am. Chem. Soc. **102**, 4849 (1980).
7. W. ADAM, N. CARBALLEIRA, E-M. PETERS, K. PETERS, and H. G. v. SCHNERING. J. Am. Chem. Soc. **105**, 5132 (1983).
8. C. H. DEPUY and P. R. STORY. J. Am. Chem. Soc. **82**, 627 (1960).
9. A. L. JOHNSON, J. B. STOTHERS, and C. T. TAN. Can. J. Chem. **53**, 212 (1975).
10. B. A. DAWSON, A. K. GHOSH, J. L. JURLINA, A. J. RAGAUSKAS, and J. B. STOTHERS. Can. J. Chem. **62**, 2521 (1984).
11. Z. MAJERSKI, M. ZVANIC, and B. METELKO. J. Am. Chem. Soc. **107**, 1721 (1985), and references therein.
12. S. L. PATT and J. N. SHOOLERY. J. Magn. Reson. **46**, 535 (1982).
13. D. M. DODDRELL, D. T. PEGG, and M. R. BENDALL. J. Magn. Reson. **48**, 323 (1982).
14. K. ALDER, H. J. ACHE, and F. H. FLOCK. Chem. Ber. **93**, 1888 (1960).
15. J. R. SALAUN, J. CHAMPION, and J. M. CONIA. Org. Synth. **57**, 36 (1977).
16. N. H. WERSTIUK, S. YEROUSHALMI, and G. TIMMINS. Can. J. Chem. **61**, 1945 (1983).
17. A. K. CHENG, A. K. GHOSH, and J. B. STOTHERS. Can. J. Chem. **62**, 1385 (1984).
18. J. P. WIEBE, V. DAVE, and J. B. STOTHERS. Steroids. In press.
19. J. L. JURLINA, H. A. PATEL, S. PEIRIS, and J. B. STOTHERS. Magn. Reson. Chem. In press.

Can. J. Chem. Downloaded from www.nrcresearchpress.com by 80.58.250.72 on 09/07/12
For personal use only.

Complexes of hybrid ligands. The synthesis of a thioanisole-substituted fluoro-alcohol and its complexes with Pd^{2+} and Pt^{2+}; the structure of a palladium(II) complex containing alkoxide, phosphine, thioether, and chloride donors

RENÉ T. BOERÉ, DAVID E. ESSER, AND CHRISTOPHER J. WILLIS
Department of Chemistry, The University of Western Ontario, London, Ont., Canada N6A 5B7
AND
DOUGLAS W. STEPHAN AND TARAS W. OBAL
Department of Chemistry, The University of Windsor, Windsor, Ont., Canada N9B 3P4

Received August 6, 1986

RENÉ T. BOERÉ, DAVID E. ESSER, CHRISTOPHER J. WILLIS, DOUGLAS W. STEPHAN, and TARAS W. OBAL. Can. J. Chem. **65**, 798 (1987).

The compound 2-thioanisole-1,1,1,3,3,3-hexafluoro-2-propanol, $CH_3S—C_6H_4—C(CF_3)_2OH$, HL^2, has been prepared, and shown to act (in the ionized form) as a hybrid, chelating, ligand. Neutral bis-complexes $M(L^2)_2$ are formed with Pd^{2+} and Pt^{2+}; the former reacts with $PdCl_4^{2-}$ to give the Cl-bridged dinuclear complex $(L^2)Pd(\mu\text{-}Cl)_2Pd(L^2)$, which may in turn be cleaved by PPh_3 or PPh_2Me to give $PdCl(L^2)(PR_3)$.

A complete structural determination has been made for $PdCl(L^2)(PPh_2Me)$; $C_{23}H_{20}ClF_6OPPdS$. Crystals are monoclinic, space group $P2_1/n$, a = 15.526(5), b = 12.966(9), c = 12.900(8) Å, β = 101.84°, V = 2542(2) Å^3, Z = 4. Least-squares refinement on F of 198 variables using 2801 observations converged at R_1 = 0.0434, R_2 = 0.0559. The complex consists of discrete square-planar molecules with phosphine and alkoxide *trans*-disposed. Bond lengths are Pd—O, 2.053(3); Pd—P, 2.242(1); Pd—Cl, 2.323(2); Pd—S, 2.252(2) Å. In the six-membered chelate ring, all atoms with the exception of Pd are close to coplanarity; there is a dihedral angle of 127.9° between the O—Pd—S plane and that of the aromatic ring.

Multinuclear nmr measurements are used to show that both *cis*- and *trans*-forms of complexes $PdCl(L^2)(PR_3)$ are present in solution, with inversion at coordinated sulfur occurring much more rapidly in the latter.

RENÉ T. BOERÉ, DAVID E. ESSER, CHRISTOPHER J. WILLIS, DOUGLAS W. STEPHAN et TARAS W. OBAL. Can. J. Chem. **65**, 798 (1987).

On a préparé le composé thioanisole-2 hexafluoro-1,1,1,3,3,3 propanol, $CH_3S—C_6H_4—C(CF_3)_2OH$, HL^2 et on a démontré qu'il peut agir (sous la forme ionisée) comme un ligand hybride et chélatant. Avec le Pd^{2+} et le Pt^{2+}, il se forme des bis-complexes neutres $M(L^2)_2$; le premier réagit avec le $PdCl_4^{2-}$ pour donner le complexe dinucléaire ponté par des Cl $[(L^2)Pd(\mu\text{-}Cl)_2Pd(L^2)]$ qui peut être clivé à son tour par le PPh_3 ou le PPh_2Me pour donner le complexe $PdCl(L^2)(PR_3)$.

On a déterminé complètement la structure du composé $PdCl(L^2)(PPh_2Me)$; $C_{23}H_{20}ClF_6OPPdS$. Les cristaux sont monocliniques, groupe d'espace $P2_1/n$, avec a = 15,526(5), b = 12,966(9) et c = 12,900(8) Å et β = 101,84°, V = 2542(2) Å^3 et Z = 4. Un affinement de 198 variables, par la méthode des moindres carrés sur F et utilisant 2801 réflexions, converge à R_1 = 0,0434 et R_2 = 0,0559. Le complexe consiste en des molécules discrètes plan-carré de phosphine et d'alcoolate disposé en *trans*. Les longueurs des liaisons sont: Pd—O, 2,053(2); Pd—P, 2,242(1); Pd—Cl, 2,323(2); Pd—S, 2,252(2) Å. Dans le cycle à 6 chaînons du chélate, tous les atomes, à l'exception du Pd, sont pratiquement coplanaires; l'angle dièdre entre le plan O—Pd—S et celui du cycle aromatique est égal à 127,9°.

On a fait appel à des mesures rmn multinoyaux pour démontrer que les formes tant *cis* que *trans* des complexes $PdCl(L^2)(PR_3)$ sont présentes en solution et que l'inversion au niveau du soufre coordonné se produit beaucoup plus rapidement dans le dernier.

[Traduit par la revue]

Introduction

We have previously reported the synthesis of some fluorinated alcohols containing a thioether function, $RS—CH_2—C(CF_3)_2—OH$ (**1**), and their use (in the ionized form) as hybrid ligands to form neutral complexes $[M\{RSCH_2C(CF_3)_2O\}_2]$ (M = Pd, Pt; R = Me, Ph) (1) and cationic complexes $[M\{RSCH_2C(CF_3)_2O\}(PPh_3)_2]^+$ (2, 3). Five-membered chelate rings are formed, and the presence of the soft thioether stabilizes the bond from the hard alkoxide group to the soft transition-metal ions. The related diarylphosphino fluoro-alcohol $PPh_2CH_2C(CF_3)_2OH$ behaves similarly (4).

The conformations of the highly-substituted chelate rings in complexes of these ligands show a remarkable consistency, with four atoms (including the metal) coplanar and the fifth significantly out of plane (3, 4). We now report the preparation of a similar hybrid ligand with an aryl backbone, which coordinates through oxygen and sulfur to form six-membered chelate rings. Ligand alcohol **2**, 2-thioanisole-1,1,1,3,3,3-hexafluoro-2-propanol, (abbreviated HL^2) is prepared by the reaction sequence:

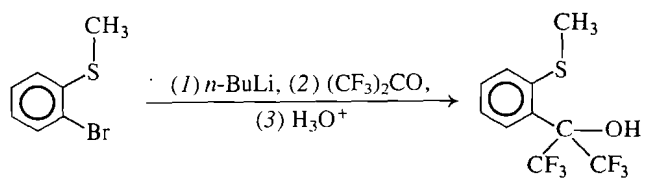

2

We have prepared Pd^{2+} and Pt^{2+} complexes of the ionized form of this alcohol and find it to be generally similar to alcohol **1**. However, the use of nmr data in conjunction with a solid-state X-ray structure on the palladium complex $[Pd(L^2)Cl(PPh_2Me)]$ shows that differences in the type and proportions of the isomers observed in solution may be related to the distinctly different chelate ring conformations adopted by **1** and **2**.

Experimental section

General experimental conditions have been described previously (1). New complexes were characterized by elemental analysis (data in Table 1, deposited)[1] and nmr spectra (Table 5, below). *n*-Butyl lithium and *o*-aminothiophenol were commercial samples (Aldrich).

Can. J. Chem. Downloaded from www.nrcresearchpress.com by 78.46.186.204 on 09/07/12
For personal use only.

TABLE 2. Summary of crystal and data collection parameters

Molecular formula	$C_{23}H_{20}ClF_6OPPdS$
Formula weight	631.27
Crystal class	Monoclinic
a	15.526(5) Å
b	12.966(9) Å
c	12.900(8) Å
β	101.84°
V	2542(2) Å^3
Z	4
d(calcd.)	1.65 g cm^{-3}
Space group	$P2_1/n$
Diffractometer	Syntex $P2_1$, four-circle
Radiation	Mo Kα, graphite monochromatized, λ = 0.71069 Å
Data collected	2θ of 4.5–45° ($\pm h$, $+k$, $+l$)
Temperature	24°C
θ Range	$4.5 \leq 2\theta \leq 45°$
Scan speed	2.0–5.0 deg min^{-1} (θ/2θ scan)
Scan range	1.0° below $K\alpha_1$; 1.1° above $K\alpha_2$
Crystal dimensions	0.35 × 0.37 × 0.44 mm
μ	9.35 cm^{-1}
Reflections collected	3689
No. unique data where $F_o > 3\sigma(F_o)$	2801
Variables	198
Final R_1[a]	0.0434
Final weighted R_2[b]	0.0559

[a] $R_1 = \Sigma||F_o| - |F_c||/\Sigma|F_o|$.
[b] $R_2 = \{\Sigma w(|F_o| - |F_c|)^2/\Sigma wF_o^2\}^{1/2}$.

Ligand synthesis

o-Bromothioanisole (16 g, 0.078 mol, prepared from *o*-aminothiophenol) (6) was dissolved in ether (20 mL) in a 250 mL three-necked flask attached to a vacuum/argon line and equipped with a serum-capped dropping funnel, magnetic stirrer, and serum cap. The solution was cooled to 0°C under ~10 cm Ar pressure and *n*-BuLi (50 mL of 1.55 *M* solution in hexane, 0.078 mol) introduced by syringe into the dropping funnel, then added dropwise over 2 h. Continuous stirring was necessary as the organolithium reagent precipitated. A separate vacuum flask equipped with serum cap was charged with anhydrous ether (50 mL) and hexafluoroacetone (13 g, 0.078 mol; and held at −78°C. The organolithium reagent was transferred in as a slurry using a double-ended stainless steel needle. After stirring 2 h at −78°C, the mixture was poured onto concentrated HCl (100 mL) on ice, extracted with ether, dried ($MgSO_4$), and distilled to yield 2-thioanisole-1,1,1,3,3,3-hexafluoro-2-propanol, HL^2, **2**, 17.5 g (78%), bp 80°C/1 mm, mass spectrum *m/e* 290 (parent ion). Nuclear magnetic resonance ($CDCl_3$ solution): δ(CH_3S) s, 2.45 ppm; δ(aromatic) m, 7.0–7.8 ppm; δ(CF_3) s, −74.96 ppm.

Complex preparation

(*i*) $Pt(L^2)_2$, **3**. K_2PtCl_4 (0.42 g, 1.0 mmol) was dissolved in water and HL^2 (0.58 g, 2.0 mmol) added, followed by KOH (2.0 mmol. In this and subsequent reactions, it was convenient to measure KOH by use of a standardized solution.) After stirring 48 h, solvent was removed by rotary evaporation and the residue extracted with CH_2Cl_2. Recrystallization from $CHCl_3$ gave $Pt(L^2)_2$, **3** (87% yield), colorless, mp 157–159°C.

(*ii*) $Pd(L^2)_2$, **4**. Starting from K_2PdCl_4 ($PdCl_2$ in aqueous KCl), the same route as that used for **3** gave the palladium analog **4**, orange, mp 278–281°C.

(*iii*) $Pd_2Cl_2(L^2)_2$, **5**. Attempts to prepare the Cl-bridged dinuclear complex by direct reaction of ligand with $PdCl_2$ in 1:1 molar ratio lead only to mixtures containing the bis-complex **4**. Successful synthesis was achieved by dissolving **4** in excess acetone, heating to reflux, and adding the stoichiometric amount of $PdCl_2$, dissolved in a minimum volume of aqueous KCl, dropwise under reflux. After reflux 1 h, acetone was removed by distillation until crystallization began, at which point an excess of water was added and the solution cooled to 0°C, when the bridged complex **5** precipitated in essentially quantitative yield; orange crystals from $CHCl_3$, mp 260–262°C.

(*iv*) Cleavage reactions of **5** using PPh_3: Bridged complex **5** (0.10 g, 0.12 mmol) and PPh_3 (0.073 g, 0.28 mmol) were stirred together in toluene (40 mL) at 20°C for 3 h, then slowly heated with stirring until solution was complete. After cooling to 0°C, the greenish-yellow precipitate was filtered off and washed quickly with hexanes, yielding $PdCl(L^2)(PPh_3)$, **6**, mp 190–195°C. Analytical data indicated a small degree of impurity, but attempts at recrystallization led to disproportionation.

Using PPh_2Me, the bridged complex **5** (0.42 g, 0.48 mmol) was dissolved in acetone and PPh_2Me (0.19 g, 0.97 mmol) added at 25°C; an immediate darkening in color was seen. Solvent was removed by rotary evaporation and the residue recrystallized from 60–80 petroleum ether/$CHCl_3$ to give $PdCl(L^2)(PPh_2Me)$, **7**, mp 192°C. Using $PPhMe_2$ in a similar reaction sequence led only to disproportionation reactions and formation of a mixture containing $Pd(L^2)_2$ and $PdCl_2(PPhMe_2)_2$. A similar result was obtained using $AsPh_3$.

Structure determination: X-ray data collection and reduction

Yellow blocks of compound **7**, chloro(2-thioanisole-1,1,1,3,3,3-hexafluoro-2-propoxy)(methyldiphenylphosphine)palladium(II), were obtained by slow evaporation from 60–80 petroleum ether/chloroform and a suitable crystal mounted in a capillary tube. Diffraction experiments were performed with a four-circle Syntex $P2_1$ diffractometer using graphite-monochromatized Mo Kα radiation. The initial orientation matrix was obtained from 15 machine-centered reflections selected from a rotation photograph, and these data used to determine the crystal system. Partial rotation photographs around each axis were consistent with a monoclinic crystal system. A total of 40 high-angle reflections ($15° < 2\theta < 25°$) were used to obtain the final lattice parameters and the orientation matrix. Machine parameters, crystal data, and data collection conditions are summarized in Table 2.

Observed extinctions were consistent with the space group $P2_1/n$, and $\pm h$, $+k$, and $+l$ data were collected in one shell. Three standard reflections were recorded every 197 reflections, and analysis of their intensity showed that no appreciable crystal decomposition occurred during data collection. The data were processed using the SHELX-76 package (7) on the computing facilities at the University of Windsor.

Can. J. Chem. Downloaded from www.nrcresearchpress.com by 78.46.186.204 on 09/07/12
For personal use only.

Can. J. Chem. Downloaded from www.nrcresearchpress.com by 78.46.186.204 on 09/07/12
For personal use only.

TABLE 3. Positional parameters ($\times 10^4$)

Atom	x	y	z
Pd	962(1)	1261(1)	38(1)
S	2223(1)	1052(1)	1243(1)
C(1)	−273(1)	1571(1)	−1282(1)
P	318(1)	2091(1)	1201(1)
O	1607(2)	434(3)	−927(3)
F(21)	1228(3)	1213(3)	−2875(3)
F(22)	1714(3)	2455(3)	−1820(4)
F(23)	2510(3)	1813(4)	−2852(3)
F(31)	3317(3)	5(4)	−2313(5)
F(32)	2040(3)	−653(3)	−2493(4)
F(33)	2966(3)	−847(4)	−1042(4)
C(1)	2304(4)	783(5)	−1314(5)
C(2)	1933(5)	1547(6)	−2227(6)
C(3)	2663(5)	−166(6)	−1805(6)
C(4)	2387(4)	−320(5)	1377(6)
C(5)	−866(4)	2013(5)	981(5)
C(11)	3060(4)	1454(5)	571(5)
C(12)	3062(4)	1320(5)	−520(5)
C(13)	3780(6)	1715(7)	−883(7)
C(14)	4480(7)	2193(8)	−185(8)
C(15)	4469(6)	2342(7)	863(8)
C(16)	3740(4)	1961(6)	1230(6)
C(21)	584(4)	3484(4)	1215(4)
C(22)	117(5)	4156(6)	1703(6)
C(23)	326(5)	5211(6)	1660(6)
C(24)	953(5)	5542(6)	1183(6)
C(25)	1422(5)	4857(6)	728(7)
C(26)	1233(5)	3804(5)	738(6)
C(31)	679(4)	1635(4)	2549(5)
C(32)	324(5)	725(5)	2857(6)
C(33)	639(5)	325(7)	3862(6)
C(34)	1268(5)	831(6)	4561(6)
C(35)	1627(5)	1720(6)	4294(6)
C(36)	1345(4)	2140(6)	3264(5)

A total of 2801 reflections having $F_o^2 > 3\sigma(F_o^2)$ were used in the refinement. No absorption correction was applied to the data.

Structure solution and refinement

Neutral atom scattering factors were taken from Cromer and Waber (8). The Pd position was determined by the heavy-atom Patterson technique, and the remaining non-hydrogen atoms were located from successive difference-Fourier map calculations. Refinement was carried out by full-matrix least-squares techniques on F, minimizing the function $\Sigma w(|F_o| - |F_c|)^2$, where the weight w is defined as $4|F_o|/\sigma^2(F_o^2)$ and F_o and F_c are the observed and calculated structure-factor amplitudes. Refinement with all non-hydrogen atoms assigned isotropic temperature factors gave $R_1 = 8.01\%$. Hydrogen-atom contributions for both methyl and phenyl were included, assuming C—H bond lengths of 0.95 Å, and hydrogen-atom temperature factors were fixed at 1.10× the isotropic temperature factor of the bonded carbon atom.

In the final cycles of full-matrix least-squares refinement, all non-hydrogen and non-carbon atoms were assigned anisotropic temperature factors and hydrogen-atom contributions were included but not refined. Final values of R_1 and R_2 were 4.34% and 5.59%, and maximum shift on any of the parameters in the final cycle was 0.003σ. A final difference-Fourier map showed no peaks of chemical significance, the largest peak being 0.95 eÅ^{-3} associated with the Pd atom.

Final atomic positions of non-hydrogen atoms for compound **7** are given in Table 3.

Anisotropic temperature factors are given in supplementary Table S-I, hydrogen-atom positions and temperature factors in Table S-II, bond angles and distances associated with the phenyl rings and the trifluoromethyl groups in Table S-III, and values of $10|F_o|$ and $10|F_c|$ in Table S-IV.[1]

TABLE 4. Selected bond distances and angles

Bond	Distances (Å)	Bond	Distances (Å)
Pd—S	2.252(2)	P—C(21)	1.827(6)
Pd—Cl	2.323(2)	P—C(31)	1.814(6)
Pd—P	2.242(1)	O—C(1)	1.359(7)
Pd—O	2.053(3)	C(1)—C(2)	1.578(10)
S—C(4)	1.800(7)	C(1)—C(3)	1.540(9)
S—C(11)	1.783(6)	C(1)—C(12)	1.557(9)
P—C(5)	1.803(6)		

Bonds	Angle (deg)	Bonds	Angle (deg)
S—Pd—Cl	175.2(1)	C(2)—C(1)—C(3)	108.7(5)
S—Pd—P	92.3(1)	O—C(1)—C(2)	117.2(5)
Cl—Pd—P	89.6(1)	C(2)—C(1)—C(12)	108.1(5)
S—Pd—O	83.8(1)	C(3)—C(1)—C(12)	109.9(5)
Cl—Pd—O	94.5(1)	S—C(11)—C(12)	126.6(5)
P—Pd—O	175.4(1)	S—C(11)—C(16)	120.9(6)
Pd—S—C(4)	105.8(2)	C(1)—C(12)—C(11)	123.6(5)
Pd—S—C(11)	104.3(2)	C(1)—C(12)—C(13)	119.5(6)
C(4)—S—C(11)	103.4(3)	P—C(21)—C(22)	119.8(5)
Pd—P—C(5)	116.6(2)	P—C(21)—C(26)	119.9(5)
Pd—P—C(21)	110.1(2)	P—C(31)—C(32)	119.1(5)
C(5)—P—C(21)	106.1(3)	P—C(31)—C(36)	121.5(5)
Pd—P—C(31)	113.1(2)	F(21)—C(2)—C(1)	111.8(6)
C(5)—P—C(31)	103.7(3)	F(22)—C(2)—C(1)	110.3(6)
C(21)—P—C(31)	106.4(3)	F(23)—C(2)—C(1)	114.0(6)
Pd—O—C(1)	125.0(3)	F(31)—C(3)—C(1)	116.4(6)
O—C(1)—C(2)	107.1(5)	F(32)—C(3)—C(1)	112.2(6)
O—C(1)—C(3)	105.5(5)	F(33)—C(3)—C(1)	109.1(6)

Structure description

Selected interatomic distances and bond angles for compound **7** are shown in Table 4.

An ORTEP view of the molecule is shown as Fig. 1. (The phenyl ring in the ligand contains carbon atoms 11–16; phenyl rings on phosphorus contain carbon atoms 21–26 and 31–36.) The metal atom is in essentially square-planar coordination, with the two soft ligands, phosphine and thioether, *cis* to each other; we will therefore refer to the overall conformation as *cis*.[2] The bond angles at the metal are close to 90°, except for the S—Pd—O angle within the chelate ring, which is reduced to 83.8(1)°. Five of the atoms in the six-membered chelate ring are close to coplanarity, the exception being the Pd atom. The ring may therefore be described as "hinged" at the O—S axis with a dihedral angle of 127.9° between the plane defined by O—Pd—S and that containing O, C(1), S, and the aromatic ring; the CF_3 groups are disposed on opposite sides of the latter.

The effect of this ring conformation on the geometry at the coordinated sulfur atom is to swing the methyl group away from the phosphine coligand, making the S—Pd—P bond angle 92.3(1)°. In the platinum complexes $[Pt(PR_3)_2\{CH_3SCH_2C(CF_3)_2O\}]^+$, where the five-membered chelate is closer to planarity, the bite angle of the ligand is essentially the same as in **7** but the greater repulsion between the phosphine and S—CH_3 group increases the S—Pt—P angles to 94.6(1)° ($PR_3 = PPh_2Me$) and 97.28(7)° (PPh_3).

[1]Complete set of data may be purchased from the Depository of Unpublished Data, CISTI, National Research Council of Canada, Ottawa, Ont., Canada K1A 0S2.

[2]In terms of CIP priority rules, it has the *Z* configuration.

Can. J. Chem. Downloaded from www.nrcresearchpress.com by 78.46.186.204 on 09/07/12
For personal use only.

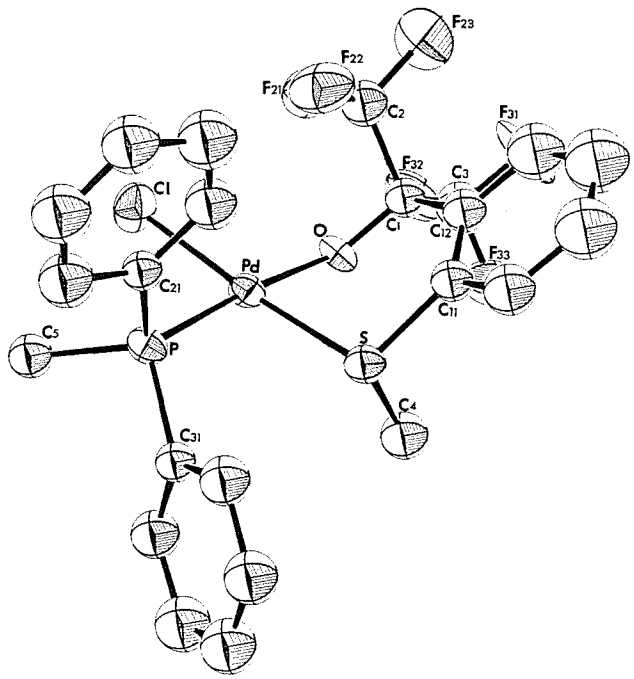

FIG. 1. An ORTEP view of **7**, $\{\overline{OC(CF_3)_2C_6H_4SMe}\}PdCl(PPh_2Me)$.

Results and discussion

Synthesis of complexes

The synthesis of ligand **2** proceeded smoothly, in accordance with our previous experience with compounds of this type. Neutral bis-complexes $M(L^2)_2$ were readily prepared with M = Pt^{2+} (**3**) or Pd^{2+} (**4**), but could not be isolated with Ni^{2+} or Co^{2+}; this also is consistent with precedent, since the hybrid ligands **1**, containing the same donor set, preferentially complex with the softer transitional-metal ions. In order to extend the range of complexes of **2** available for study, we then prepared the chloro-bridged dinuclear palladium complex **5** by the reaction of **4** with $PdCl_4^{2-}$ in acetone, an established route in palladium chemistry (10).

$$Pd(L^2)_2 + PdCl_2 \xrightarrow[H_2O/Me_2CO]{KCl}$$

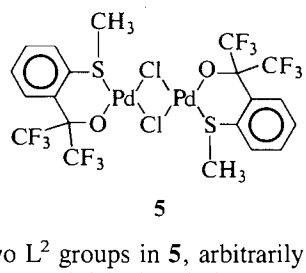

5

(The relative orientation of the two L^2 groups in **5**, arbitrarily shown as *trans* above, has not been established.) Limited success was achieved in preparing other palladium complexes by cleavage of **5** with other ligands. With tertiary phosphines, PPh_3 gave *cis*-$PdCl(L^2)(PPh_3)$, **6**, and PPh_2Me gave *cis*-$PdCl(L^2)$-(PPh_2Me), **7**. However, disproportionation generally accompanied recrystallization. Using $PPhMe_2$, disproportionation to $(PPhMe_2)_2PdCl_2$ and $Pd(L^2)_2$ was rapid, and $AsPh_3$ behaved similarly. Use of thioethers in cleavage reactions also led to disproportionation.

These results are essentially parallel to those reported a number of years ago by Livingstone for Pd^{2+} complexes of *o*-methylthiobenzoic acid, HL^3. This ligand forms bis-complexes $Pd(L^3)_2$ in a single geometric isomer (11, 12) and halo-bridged complexes $(L^3)Pd((\mu\text{-}X)_2Pd(L^3)$ (X = Cl, Br) (10, 12). Mixed-ligand complexes could not be isolated in the solid state, the product being $M(L^3)_2$ (10) and disproportionation was assumed to be rapid.

The structure of **7** (Fig. 1) shows the metal to be in square-planar coordination with the two soft ligands, phosphine and thioether, in *cis*-conformation. Metal–ligand bond lengths are within normal limits, with the mutually *trans* Pd—P and Pd—O bonds having the values 2.242(1) and 2.053(3) Å, respectively. A very similar situation is found in the perfluoropinacolato complex $(PEt_3)_2Pd(PFP)$ (14), where the respective bond lengths to Pd from phosphine and *trans* fluorinated alkoxide are 2.237 and 2.043 Å.[3] The C—O bond in the six-membered chelate ring in **7** is 1.359(7) Å, within the range of 1.34(1) (16), 1.341 and 1.388 Å (14), and 1.365(3) Å (17) found where a fluorinated alkoxide is chelated to Pd in five-membered rings, and in accord with the usual trend toward short C—O linkages in metal alkoxides.

The conformation adopted by the ligand may be compared with that observed in the $PdCl_2$ complex of the endocyclic thioether 5-methyl-1-thia-5-azacyclooctane (TACO) (18):

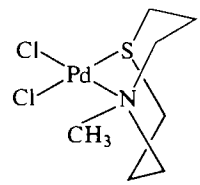

The geometry at sulfur and nitrogen in this complex is essentially identical to that in **7**, with the non-bonding pair on sulfur lying close to the coordination plane and bent in toward the metal in each, as is the *N*-methyl substituent in the TACO complex. A further consequence for **7** is that one of the CF_3 groups is directed toward the chloride coordination site, which it might be said to overhang.

Solution structures: nuclear magnetic resonance studies

The ^1H, ^{19}F, and ^{31}P nmr data for complexes **3–7** are shown in Table 5. We have previously demonstrated the power of using a combination of ^1H and ^{19}F data in identifying the constituents of isomeric mixtures of fluorinated alkoxides (2), and the same approach is used here.

For the ML_2 complexes **3** and **4**, *cis* and *trans* isomers are possible, and with slow inversion at the pyramidal coordinated sulfur, each of these may exist in solution as "*syn*" or "*anti*" diastereomers with respect to the disposition of the two CH_3—S substituents about the coordination plane of the metal (15). Interestingly, the proton spectra of $Pt(L^2)_2$, **3**, show that the product first isolated is a mixture of two isomeric species, **3***a* and **3***b*, which do not interconvert in solution. Fractional crystallization gives pure **3***a*. The equivalence of the ^{195}Pt coupling constants and the similarity in chemical shift of the two isomers agree with their being *syn* and *anti* forms of the *same* geometrical isomer, a situation we found for the analogous complex $[Pt\{CH_3SCH_2C(CF_3)_2O\}_2]$ (1). However, while in the latter case thioether inversion re-establishes an equilibrium population of diastereomers when the complex is redissolved, inversion for $[Pt(L^2)_2]$ is a higher-energy process, and equilibrium is not established after several days in solution at ambient temperature in the nmr tube. We attribute this lack of dynamic equilibration to the greater rigidity and steric bulk of the aromatic ligand, discussed below.

Each of the Pd^{2+} complexes of L^2, **4** and **5**, shows only a

[3]B. R. Penfold. Private communication.

TABLE 5. Nuclear magnetic resonance data on complexes[a]

Compound	CF_3 group			CH_3—S group		^{31}P
	δ, ppm[b]	Δ_{AB}, Hz	J_{AB}, Hz	δ, ppm[c]	J, Hz	δ, ppm[d]
3, $Pt(L^2)_2$[e] (*a*)	−73.6	130	8.5	2.76	47.6[f]	—
(*b*)	−72.9	300	8.5	2.74	47.6[f]	—
4, $Pd(L^2)_2$	−73.6	s (w = 10 Hz)[g]		2.68	—	—
5, $Pd_2Cl_2(L^2)_2$[h]	−72.6	s (w = 4 Hz)		2.74	—	—
6, *cis*-$PdCl(L^2)(PPh_3)$	−73.3	112 (br doublet)		2.54	1.0[i]	+27.5
trans-$PdCl(L^2)(PPh_3)$	(not identified)			2.83	4.3[i]	+13.5
7, *cis*-$PdCl(L^2)(PPh_2Me)$	−73.5	105 (br doublet)		2.54	1.0[i]	+16.7[j]
trans-$PdCl(L^2)(PPh_2Me)$	−73.6	s (w = 3 Hz)		2.83	4.1[i]	+9.9[k]

[a]At 30°C in $CDCl_3$, unless otherwise specified. Positive shifts are downfield.
[b]At 94.1; from $CFCl_3$.
[c]At 100.1 MHz; from TMS.
[d]From $(MeO)_3PO$(ext); all ^{31}P spectra proton decoupled.
[e]At 0°C.
[f]$^3J(^{195}Pt, H)$.
[g]w = peak width at half-height.
[h]In $(CD_3)_2CO$.
[i]$^4J(P, H)$.
[j]δ(CH_3—P) = 2.24 ppm; $^2J(P, H)$ = 12.2 Hz.
[k]δ(CH_3—P) = 1.97 ppm; $^2J(P, H)$ = 12.3 Hz.

single species in solution at all times, and the CF_3 groups show only a single ^{19}F resonance. Equivalence of CF_3 groups on the nmr time-scale may occur through rapid thioether inversion, but this is unlikely because of the observed rigidity of the Pt^{2+} complex. More probable with this sterically crowded complex is a mechanism involving dissociation of the Pd—S bond. In strong contrast, the Pd^{2+} complexes of the more flexible ligand **1** show complex isomerism and inversion behaviour in solution (1, 2).

The mixed-ligand complexes **6** and **7** can exist as two geometric isomers, which we will designate as *cis* and *trans* with respect to the two soft ligands, CH_3—S and R_3P:

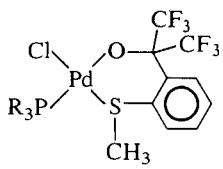

cis

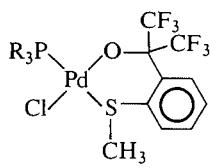

trans

Since only one pyramidal sulfur atom is found in each complex, diastereomerism does not occur, but slow inversion at coordinated sulfur could lead to inequivalent CF_3 signals (9). In $CDCl_3$ solution, nmr signals attributable to the two geometric isomers are in fact observed for both **6** and **7**. The major species, comprising ~95% for **6** and ~80% for **7**, has a CH_3—S signal at 2.54 ppm split by about 1 Hz through coupling to ^{31}P. Selective decoupling of the major ^{31}P signal in each case collapses this doublet, as well as that due to the CH_3—P in the PPh_2Me complex **7**. The ^{19}F nmr spectrum shows inequivalent CF_3 groups, with the typical doublet-of-quartet pattern we have observed in such complexes with slow or stopped thioether inversion. The minor species in **6** and **7** have CH_3—S resonances at significantly lower field (2.83 ppm), with much larger coupling to ^{31}P. Selective decoupling of the minor ^{31}P signals again confirmed the coupling in these species. Their ^{19}F signals consist of a sharp singlet in **7** and a singlet (overlapping the signal from the major species) in **7**, indicating that the CF_3 groups are dynamically equivalent through rapid inversion at coordinated sulfur. We have previously demonstrated (2) that such spectral parameters are consistent with the major components of **6** and **7** in solution being the *cis*-isomers, the minor the *trans*-isomers. In particular, the lower barrier to inversion with R_3P, rather than Cl^-, *trans* to the thioether confirms this assignment.

We note again that, for the *cis*-isomer, anisotropic ring-current effects from the phenyl substituents on the adjacent phosphine cause an upfield shift in δ(CH_3—S) (2, 5). However, the proportions of the two isomers differ dramatically from those found for the complex $PdCl\{CH_3SCH_2C(CF_3)_2O\}(PPh_3)$, for which the *trans*-isomer predominates in $CDCl_3$ solution (2), and this may be attributed to the differing ring conformations in the two hybrid ligands. In the solid state, $PdCl(L^2)(PPh_2Me)$, **7**, has the *cis*-geometry corresponding to the major solution species. The unusual conformation adopted by the ligand (Fig. 1) causes the site *trans* to the thioether to be sterically crowded by an overhanging CF_3 group, and this may account for the predominance of the *cis*-isomers in both **6** and **7**.

An additional, surprising, point of difference is that the nmr spectra of **6** and **7** show the proportions of the isomers to be invariant with temperature and the nature of the solvent, whereas with the compound $PdCl\{CH_3SCH_2C(CF_3)_2O\}(PPh_3)$ the proportions of the isomers present are very sensitive to changes in temperature or solvent. It appears that the *cis*- and *trans*-forms of **6** and **7** are generated in the initial cleavage reactions of **5**, but are not sufficiently labile to undergo subsequent equilibration in solution. Their relative proportions are therefore fixed by kinetic, rather than thermodynamic, factors, and the isolation of pure crystals of *cis*-**7** for the structural determination is the result of an adventitious fractionation during recrystallization to give the major component of the mixture.

Acknowledgements

We thank the Natural Sciences and Engineering Research Council of Canada for financial support of this work, in the form of operating grants to D.W.S. and C.J.W. and scholar-

Can. J. Chem. Downloaded from www.nrcresearchpress.com by 78.46.186.204 on 09/07/12
For personal use only.

ships to R.T.B. and D.E.E., and Professor B. R. Penfold for communication of unpublished structural data.

1. R. T. BOERÉ and C. J. WILLIS. Can. J. Chem. **63**, 3530 (1985).
2. R. T. BOERÉ and C. J. WILLIS. Can. J. Chem. **64**, 492 (1986).
3. R. T. BOERÉ, N. C. PAYNE, and C. J. WILLIS. Can. J. Chem. **64**, 1474 (1986).
4. R. T. BOERÉ, C. D. MONTGOMERY, N. C. PAYNE, and C. J. WILLIS. Inorg. Chem. **24**, 3680 (1985).
5. C. R. GREEN and R. J. ANGELICI. Inorg. Chem. **11**, 2095 (1972).
6. D. W. MEEK, G. DYER, and M. O. WORKMAN. Inorg. Synth. **16**, 168 (1976).
7. G. M. SHELDRICK. Shelx-76, Programme for crystal structure determination. University of Cambridge: Cambridge, England, 1976.
8. D. T. CROMER and J. T. WABER. International table for X-ray crystallography. Kynoch Press, Birmingham, England. 1974.
9. J. W. EMSLEY, L. PHILLIPS, and V. WRAY. Progr. NMR Spectrosc. **10**, 85 (1977).
10. S. E. LIVINGSTONE. J. Chem. Soc. 1989 (1956).
11. S. E. LIVINGSTONE, R. A. PLOWMAN, and J. SORENSEN. Proc. R. Soc. of N.S.W. **84**, 28 (1950).
12. S. E. LIVINGSTONE. J. Chem. Soc. 437 (1956).
13. S. E. LIVINGSTONE and R. A. PLOWMAN. Proc. R. Soc. of N.S.W. **84**, 188 (1950).
14. H. D. EMPSALL, M. GREEN, and F. G. A. STONE. J. Chem. Soc. Dalton Trans. 96 (1972).
15. E. W. ABEL *et al.* J. Chem. Soc. Dalton Trans. 42 (1977); 47 (1977); 1994 (1979); Polyhedron, **1**, 289 (1982).
16. A. MODINOS and P. WOODWARD. J. Chem. Soc. Dalton Trans. 2065 (1977).
17. C. D. MONTGOMERY, N. C. PAYNE, and C. J. WILLIS. Inorg. Chim. Acta, **117**, 103 (1986).
18. A. S. HIRSCHON, W. K. MUSKER, M. M. OLMSTEAD, and J. L. DALLAS. Inorg. Chem. **20**, 1702 (1981).

Can. J. Chem. Downloaded from www.nrcresearchpress.com by 78.46.186.204 on 09/07/12
For personal use only.

Coordination compounds of indium. Part 43. Indium(III) derivatives of benzenethiol, and the crystal structure of tetraphenylphosphonium bromotris(benzenethiolato)-indate(III), $Ph_4P[BrIn(SPh)_3]$

RAJ K. CHADHA, PETER C. HAYES, HASSAN E. MABROUK, AND DENNIS G. TUCK
Department of Chemistry and Biochemistry, University of Windsor, Windsor, Ont., Canada N9B 3P4

Received July 25, 1986

RAJ K. CHADHA, PETER C. HAYES, HASSAN E. MABROUK, and DENNIS G. TUCK. Can. J. Chem. **65**, 804 (1987).

$In(SPh)_3$ is readily prepared by the reaction of $InCl_3$ and NaSPh in methanol. The compound is a Lewis acid, forming 1:1 adducts with 2,2′-bipyridine, 1,10-phenanthroline, *N,N,N′,N′*-tetramethylethanediamine, bis(diphenylphosphino)ethane, and dimethylsulphoxide, and 1:2 adducts with pyridine, trimethylamine, and triphenylphosphine. Reaction with R_4NX (X = Cl, Br, I) or similar salts gives $R_4N[XIn(SPh)_3]$ salts, which are 1:1 electrolytes. The structure of $Ph_4P[BrIn(SPh)_3]$ has been determined by X-ray methods. The crystals are monoclinic, space group $P2_1/c$, with cell dimensions a = 9.964(3) Å, b = 13.477(3) Å, c = 30.359(7) Å, α = 98.30(2)°, Z = 4, R = 0.0622 for 2924 unique observed reflections. The anion has distorted tetrahedral symmetry in the $InBrS_3$ kernel, with In—Br = 2.527(2) Å, and In—S(av) = 2.450 Å. The vibrational spectra of $In(SPh)_3$ and its derivatives in the region 500–200 cm^{-1} are discussed.

RAJ K. CHADHA, PETER C. HAYES, HASSAN E. MABROUK et DENNIS G. TUCK. Can. J. Chem. **65**, 804 (1987).

On prépare facilement le composé $In(SPh)_3$ en faisant réagir le $InCl_3$ et le NaSPh dans le méthanol. Le composé est un acide de Lewis qui forme des adduits 1:1 avec la bipyridine-2,2′, la phénanthroline-1,10, la *N,N,N′,N′*-tétraméthyléthanediamine, le bis(diphénylphosphino)éthane et le diméthylsulfoxyde et qui forme des adduits 1:2 avec la pyridine, la triméthylamine et la triphénylphosphine. Sa réaction avec les composés R_4NX (X = Cl, Br ou I) ou des sels semblables conduit à des sels du type $R_4N[XIn(SPh)_3]$ qui sont des électrolytes 1:1. On a déterminé la structure du $Ph_4P[BrIn(SPh)_3]$ par diffraction des rayons-X. Les cristaux sont monocliniques, groupe d'espace $P2_1/c$, avec a = 9,964(3), b = 13,477(3) et c = 30,359(7) Å et α = 98,30(2)°, Z = 4 et R = 0,0622 pour 2924 réflexions uniques qui ont été observées. L'anion possède une symétrie tétraédrique déformée au niveau du noyau $InBrS_3$ et on a déterminé les distances In—Br = 2,527(2) et In—S(moyenne) = 2,450 Å. On discute des spectres vibrationnels du $In(SPh)_3$ et de ses dérivés dans la région de 500 à 200 cm^{-1}.

[Traduit par la revue]

Can. J. Chem. Downloaded from www.nrcresearchpress.com by 78.46.186.204 on 09/07/12
For personal use only.

Introduction

The alkyl and arylthiolato derivatives of the Main Group metals have not been studied as extensively as have those of the transition elements, but there is nevertheless a significant literature on these compounds. The chemistry of $Sn(SR)_4$ and $R_nSn(SR')_{4-n}$, of tin(II) thiolates, and of the corresponding lead compounds, has been reviewed (1–4). The complexes formed with organomercury cations have also been investigated especially in terms of their solution chemistry (5–8). There is an absence of information on the complexes of gallium, indium, and thallium, although here, as with the other elements mentioned above, dithiolato complexes have been thoroughly studied. We have now investigated the preparation and properties of $In(SPh)_3$, which is a Lewis acid, giving rise to adducts with both neutral and anionic ligands. The crystal structure of the salt of one of these derivatives, $Ph_4P[BrIn(SPh)_3]$, has been determined by X-ray crystallography and the results are compared with those of related compounds.

Experimental section

General

All solvents were distilled and stored over appropriate drying agents. Benzenethiol and neutral ligands were used as supplied; tetraalkyl ammonium and other halides were dried at 110°C before use.

Indium analysis was by atomic absorption spectrophotometry, and halide analysis by Volhard titration. Microanalysis was by Guelph Chemical Laboratories Ltd. Spectroscopic methods were those described in previous papers (9).

Indium trichloride was prepared by passing a stream of chlorine gas and nitrogen over heated metal.

Preparation of $In(SPh)_3$

A solution of NaSPh (7.1 g, 54 mmol) in 50 mL methanol was added dropwise over 1 h to a refluxing solution of $InCl_3$ (4.00 g, 18 mmol) in 50 mL of the same solvent. A white solid, subsequently identified as NaCl, precipitated. Refluxing was continued for a further 2 h, and the solution allowed to cool to room temperature, during which time more NaCl precipitated. After filtration, the filtrate was taken to dryness *in vacuo* to yield a colourless oil which was dissolved in 50 mL hot benzene leaving a white residue. A white solid deposited when the benzene extract cooled, and was re-crystallized from *n*-pentane as a white powder (yield 4.8 g, 10.8 mmol, 60% based on $InCl_3$). *Anal.* calcd. C 48.9, H 3.4, S 21.7, In 26.0; found: C 47.8, H 3.6, S 20.5, In 26.3. The ^1H nmr spectrum (d_6-dimethylsulphoxide) showed a multiplet in the aromatic region (6.8–7.4 ppm from Me_4Si; cf. a much sharper multiplet at 7.0 ppm for PhSH in the same solvent, and the absence of RS*H* at 3.3 ppm. The strongest peak in the field-desorption mass spectrum is a manifold at m/e = 441–445, with the strongest peak at 442 corresponding to $^{115}In(SPh)_3$. Other ions of significance were at m/e = 333 ($In(SPh)_2^+$), 218 ($Ph_2S_2^+$), 109 (PhS^+), and 130 + 131 (not identified).

Tris(benzenethiolato)indium(III) is an air-stable white solid, mp 240–245°C, soluble in dimethylsulphoxide, pyridine, or methanol at room temperature, and in refluxing benzene, slightly soluble in acetonitrile or methylene dichloride, but insoluble in diethyl ether, petroleum ether, nitromethane, hexane, or cold benzene. A number of attempts were made to obtain crystals from various solvent mixtures, but without success. Sublimation *in vacuo* onto a cold finger gave a powder which analysed as $In(SPh)_3$.

Neutral adducts of $In(SPh)_3$

A series of adducts involving various neutral donors was prepared by a standard method exemplified by the case of 2,2′-bipyridine (bpy). When 0.18 g of bpy (1.15 mmol) was added to a stirred solution of $In(SPh)_3$ (0.5 g, 1.13 mmol) in methanol (30 mL), the solution became green. After further stirring for 4 h under dry nitrogen, the solution was filtered and the filtrate taken to dryness *in vacuo*. The residue was a yellow–green oil, which was triturated with diethyl ether to give a yellow solid which was washed twice with diethyl ether and then with benzene. Analysis (see Table 1) and nmr spectra

TABLE 1. Analytical and related data for neutral adducts of $In(SPh)_3$

Compound[a]	Colour	Yield[b] %	% In(found/calcd)	^1H nmr[c] Solvent	Aromatic	Other
$In(SPh)_3 \cdot bpy$	Yellow	89	26.3/26.0	d_6-dmso	7.2–8.8 (m)	—
$In(SPh)_3 \cdot phen$	Yellow	95	19.4/19.2	d_6-dmso	7.3–8.7 (m)	—
$In(SPh)_3 \cdot tmen$	White	88	20.4/20.6	$CDCl_3$	7.3–7.5, m (15)	2.9, s (4), CH_2; 2.5, s (12), NMe
$In(SPh)_3 \cdot dppe$	White	87	13.5/13.7	d_6-dmso	6.8–7.4, m (35)	1.9, s (4), CH_2
$In(SPh)_3 \cdot 2py$	Yellow	88	19.1/19.1	CD_3CN	7.0–8.6, m	—
$In(SPh)_3 \cdot 2Et_3N$	Pale yellow	86	17.7/17.8	CD_3CN	6.9–7.3, m (15)	3.0, q (6) CH_2; 1.1, t (9) CH_3
$In(SPh)_3 \cdot 2Ph_3P$	Green	82	12.1/11.9	d_6-dmso	7.2–7.7	—
$In(SPh)_3 \cdot dmso$	White	83	21.9/22.1	$CDCl_3$	7.3–7.6, m (15)	2.9, s (6), CH_3

[a]See text for abbreviations.
[b]Relative to quantity of $In(SPh)_3$.
[c]Relative integrated intensities in parentheses; s = singlet, t = triplet, q = quartet, m = multiplet.

TABLE 2. Analytical and related results for salts of $[XIn(SPh)_3]^-$ and $[In(SPh)_4]^-$

Salt	Yield (%)	Analysis (found/calcd) In	Halogen	^1H nmr[c] Solvent	Aromatic	Other
$Et_4N[ClIn(SPh)_3]$	79	18.8/18.9	5.9/5.8	CD_3OD	7.0–7.4, m (15)	3.1, q (8) CH_2; 1.2, t (12) CH_3
$Et_4N[BrIn(SPh)_3]$	81	17.5/17.6	12.1/12.3	d_6-dmso	7.2–7.5, m (15)	3.2, q (8) CH_2; 1.3, t (12) CH_3
$Et_4N[IIn(SPh)_3]$	84	16.3/16.4	17.9/18.1	CD_3OD	7.1–7.3, m (15)	3.3, q (8) CH_2; 1.3, t (12) CH_3
$Ph_4P[BrIn(SPh)_3]$[a]	82	13.1/13.3	9.5/9.3	$CDCl_3$	6.8–7.6, m	
$Ph_4As[ClIn(SPh)_3]$	77	13.0/13.3	4.3/4.1	CD_3CN	6.7–7.7, m	
$Na[In(SPh)_4]$	65	19.8/20.0	—	d_6-dmso/$CDCl_3$	7.3–7.8, m	
$Et_4N[In(SPh)_4]$	77	17.0/16.8	—	CD_3OD	6.9–7.2, m (20)	3.3, q (8) CH_2; 1.4, t (12) CH_3

[a]Found C 58.2, H 4.11, S 12.3, P 3.00; calcd C 58.5, H 4.07, S 11.2, P 3.60.
[b]Abbreviations, etc., as in Table 1.

showed that this solid is $In(SPh)_3 \cdot bpy$ (yield 0.6 g, 1.00 mmol, 89% yield).

Similar methods gave 1:1 adducts of $In(SPh)_3$ with 1,10-phenanthroline (phen) *N,N,N′,N′*-tetramethylethanediamine (tmen) and bis-(diphenylphosphino)ethane (dppe), and 1:2 adducts with pyridine, triethylamine, and triphenylphosphine. With dimethylsulphoxide in three-fold excess the product was $In(SPh)_3 \cdot dmso$. Analytical and nmr results are given in Table 1; infrared spectroscopy confirmed the presence of the neutral ligand in each case.

Anionic complexes

(*i*) $[XIn(SPh)_3]^-$ (X = Cl, Br, I). In a typical experiment, Ph_4PBr (0.20 g, 0.48 mmol) in methanol was added to a solution of $In(SPh)_3$ (0.21 g, 0.48 mmol) in the same solvent. A colourless precipitate immediately formed, and was collected, washed twice with methanol, and dried *in vacuo* (yield 0.34 g of $Ph_4P[BrIn(SPh)_3]$, 0.39 mmol, 82%). This material was recrystallized from either methanol/chloroform or diethyl ether/chloroform by slow evaporation of solvent to give well-formed colourless crystals which were dried *in vacuo*. Analytical and nmr results for this salt, and for other $[XIn(SPh)_3]^-$ salts prepared by similar methods, are given in Table 2.

(*ii*) $[In(SPh)_4]^-$. A solution of NaSPh (0.12 g, 0.90 mmol) in methanol (20 mL) was added dropwise over 30 min to a solution of $In(SPh)_3$ (0.40 g, 0.9 mmol) in benzene (50 mL). The resultant suspension was refluxed for 24 h and then filtered; the pale yellow filtrate was taken to dryness *in vacuo* to yield a yellow solid which was washed with benzene and dried *in vacuo*. This material, identified as $Na[In(SPh)_4]$, is soluble in hot methanol, and a solution of 0.50 g (0.88 mmol) and Et_4NCl (0.14 g, 0.88 mmol) in boiling methanol (50 mL) was stirred for 4 h, after which the precipitated NaCl was removed by filtration. Evaporation of the filtrate gave a white solid which was washed with benzene and dried *in vacuo*; this product is $Et_4N[In(SPh)_4]$.

Crystallographic analysis

A suitable crystal of $Ph_4P[BrIn(SPh)_3]$ (1), prepared by the method described above, was sealed in a capillary tube and mounted along the largest dimension in a Syntex $P2_1$ diffractometer. The cell dimensions (Table 3) were obtained from the least-squares refinement of the setting angles of 15 high angle reflections ($15° < 2\theta < 30°$). The density was determined by flotation in CCl_4/benzene mixtures.

Relevant information on the X-ray crystallographic experiment is given in Table 3. The intensities of three monitor reflections did not change significantly during the data collection. The results were corrected for Lorentz and polarization effects, and analytical absorption corrections were applied by the use of ABSORB. Details of the collection and reduction of the experimental data, and the sources of the scattering factors and computer programmes used have been described previously (10).

The systematic absences $h0l$ ($l = 2n + 1$) and $0k0$ ($k = 2n + 1$) identify the space group $P2_1/c$ unambiguously. The position of the indium atom was determined by a sharpened Patterson synthesis using SHELX, and the remaining atoms were revealed by subsequent difference maps. The structure was refined by blocked-matrix least-squares methods using 163 parameters in one block, and 169 in the other. The indium and bromine atoms were common to the two blocks, one of which contained P, the three S atoms, twelve C atoms, and a scale factor, and the other contained the remaining C atoms and a scale factor. The carbon atoms of the Ph_4P^+ cation were refined isotropically, and the remainder anisotropically. Hydrogen atoms were included in the final refinements in ideal positions (C—H = 0.95 Å, CCH = 120°), with isotropic U values set at 0.1 $Å^2$ greater than those found for the corresponding carbon atoms in the first refinement cycles. The refinement converged at $R = 0.0622$, and $R_w = 0.0628$. The function minimized in the initial least squares refinement was $(|F_o| - |F_c|)^2$; a weighting scheme of the form $w = 1/[\sigma^2(F) + \rho F^2]$

Can. J. Chem. Downloaded from www.nrcresearchpress.com by 78.46.186.204 on 09/07/12
For personal use only.

TABLE 3. Summary of crystal data, intensity collection, and structural refinement for $[(C_6H_5)_4P][BrIn(SC_6H_5)_3]$

Cell constants (a, b, c, α)	9.964(3), 13.477(3), 30.359(7) Å, 98.30(2)°
Cell volume (Å^3)	4034(2)
Crystal system	Monoclinic
Space group	$P2_1/c$
Molecular weight	860.7
Z	4
ρ_c, ρ_o (g cm^{-3})	1.42, 1.44
Crystal dimension (mm)	0.13 × 0.22 × 0.60
Absorption coefficient, μ(cm^{-1})	17.03
Minimum absorption correction	1.013
Maximum absorption correction	1.023
Radiation	MoKα, λ = 0.71069 Å
Monochromator	Highly oriented graphite
T (°C)	21 ± 1
2θ angle (°)	4–50
Scan type	Coupled θ (crystal)/2θ (counter)
Scan width	K_{α_1} − 1° to K_{α_2} + 1°
Scan speed (°min^{-1})	Variable, 2.02–4.88
Background time/scan time	0.5
Total reflections measured	8300 ($+h$, $+k$, $\pm l$)
Unique data used	2924 [$I > 3\sigma(I)$]
Number of parameters (NP)	163, 169
$R = (\Sigma\|\|F_o\| - \|F_c\|\|/\Sigma\|F_o\|)$	0.0622
$R_w = [\Sigma\omega(\|F_o\| - \|F_c\|)^2/\Sigma\omega\|F_o\|^2]^{1/2}$	0.0628
$\Delta\rho_{max}$(e Å^{-3})	0.6
Shift:error (max)	0.3

was used, with a final p-value of 0.0001, in calculating R_w. No evidence of secondary extinction was found.

The final coordinates for the non-hydrogen atoms are given in Table 4, and important bond distances and angles in Table 5. Tables of fractional coordinates and thermal parameters for hydrogen atoms, of anisotropic thermal parameters, and of observed and calculated structure factors have been deposited, as has a packing diagram of the unit cell.[1]

Results and discussion

Tris(benzenethiolato)indium(III)

The preparation of $In(SPh)_3$ follows a conventional route and calls for no comment. The compound is clearly a Lewis acid, forming derivatives with both monodentate and bidentate donor ligands, and with halide anions. The structure of $In(SPh)_3$ could not be determined by X-ray methods, since it proved impossible to obtain crystals, but by analogy with other indium(III) compounds with sulphur ligands, it is probable that there is an InS_3 planar kernel which then leads to cross-linking through In---S′ interactions to give InS_3S_2', where S′ is a sulphur atom on a neighbouring $In(SPh)_3$ unit. This type of interaction has been invoked to explain the behaviour of indium(III) complexes with bidentate sulphur donor ligands (11–13), where the parent molecule shows evidence of cross-linking which is broken down by the formation of adducts, and is a consequence of the tendency of indium(III) to expand its coordination number from three to four, five, or six with relatively small donor atoms such as oxygen or sulphur (14).

The neutral donors derived from $In(SPh)_3$ are, with one exception, of the type InS_3N_2 or InS_3P_2, and these are reasonably formulated as mononuclear five-coordinate species. An obvious analogue for the Ph_3P adduct is $InCl_3 \cdot 2Ph_3P$, which has been shown to have D_{3h} stereochemistry (15). The exception is $In(SPh)_3 \cdot$dmso, which is the only adduct we have been able to prepare with an oxygen donor. There are a number of possible structures for this compound, and it does not seem reasonable to opt for any one of these on the present evidence.

The salts of $[XIn(SPh)_3]^-$ are 1:1 electrolytes in various solvents, as shown by the conductivities (16) (see Table 6), and the anions are readily formulated as having InS_3X kernels. This has been confirmed by X-ray methods for $Ph_4P[BrIn(SPh)_3]$ (see below). The anion $[In(SPh)_4]^-$ presumably has a tetrahedral InS_4 core, being isoelectronic with $Sn(SPh)_4$, and may well also be a Lewis acid. This mode of four-coordination has already been reported for anionic complexes of indium with the bidentate dithiolate ligands 1,2-dicyanoethylene-1,2-dithiolato (= MNT^{2-}) and toluene-3,4-dithiolate (17).

Structure of $Ph_4P[BrIn(SPh)_3]$

Figure 1 shows the structure of both cationic and anionic units. The cation has the conventional distorted tetrahedral stereochemistry at phosphorus, with bond lengths and angles within the normal range for such molecules.

The anion also has pseudo-tetrahedral symmetry in the $InBrS_3$ kernel, with the sum of the bond angles being 656.3° (average 109.4°). The In—Br bond length of 2.572(2) Å is greater than that (18) of 2.479(3) Å in $InBr_4^-$, but less than the values (19) of 2.644(3) and 2.635(2) Å in $Me_2InBr_2^-$ (C_{2v} symmetry) or in the five-coordinate (20) $EtInBr_2 \cdot$tmen (2.531(2), 2.688(2) Å). Given the effect of both coordination number and neighbouring ligands, it is not possible to discuss these values in any detail. The three In—S bonds in $[BrIn(SPh)_3]^-$ give an average value of 2.450 Å, with one bond apparently longer at 2.470(4) Å than the other two. No other monodentate In—SR systems appear to have been studied, but results are available for a number of six-coordinate complexes involving bidentate

[1]Complete set of data may be purchased from the Depository of Unpublished Data, CISTI, National Research Council of Canada, Ottawa, Ont., Canada K1A 0S2.

Can. J. Chem. Downloaded from www.nrcresearchpress.com by 78.46.186.204 on 09/07/12
For personal use only.

Can. J. Chem. Downloaded from www.nrcresearchpress.com by 78.46.186.204 on 09/07/12
For personal use only.

TABLE 4. Final fractional coordinates and isotropic thermal parameters for non-hydrogen atoms of $[(C_6H_5)_4P][BrIn(SC_6H_5)_3]$ with standard deviations in parentheses ($U_{eq} = (1/3)\Sigma_i\Sigma_j U_{ij} a_i^* a_j^* a_i \cdot a_j$)

Atom	x	y	z	U_{eq} (Å × 10^3)
In	0.20116(9)	0.13232(7)	0.36636(3)	51.3(6)
Br	0.0290(2)	0.2604(1)	0.3348(1)	87(1)
S(1)	0.1389(4)	−0.0223(3)	0.3270(1)	70(3)
S(2)	0.4106(4)	0.2186(3)	0.3583(1)	71(2)
S(3)	0.1639(4)	0.0866(3)	0.4429(1)	53(2)
P	0.4665(4)	0.1344(2)	0.1344(1)	53(2)
C(11)	0.2606(14)	−0.0507(9)	0.2926(4)	54(8)
C(12)	0.3979(15)	−0.0449(10)	0.3056(5)	68(9)
C(13)	0.4874(16)	−0.0747(11)	0.2755(6)	80(11)
C(14)	0.4382(22)	−0.1122(10)	0.2349(6)	86(13)
C(15)	0.2970(22)	−0.1192(11)	0.2235(5)	89(13)
C(16)	0.2117(16)	−0.0888(10)	0.2512(5)	69(10)
C(21)	0.3479(13)	0.1417(10)	0.3815(5)	61(9)
C(22)	0.5436(15)	0.0757(12)	0.4152(5)	74(10)
C(23)	0.6605(19)	0.0161(12)	0.4314(5)	89(12)
C(24)	0.7739(17)	0.0246(15)	0.4153(8)	127(18)
C(25)	0.7773(19)	0.0950(17)	0.3822(10)	173(22)
C(26)	0.6666(17)	0.1445(13)	0.3641(8)	140(18)
C(31)	0.1294(17)	0.1961(15)	0.4686(5)	89(12)
C(32)	0.1793(13)	0.2939(16)	0.4572(7)	111(15)
C(33)	0.1524(24)	0.3755(17)	0.4819(9)	139(19)
C(34)	0.0721(30)	0.3636(24)	0.5178(9)	163(25)
C(35)	0.0242(32)	0.2720(23)	0.5251(10)	166(25)
C(36)	0.0558(20)	0.1898(17)	0.5035(7)	123(17)
C(41)[a]	0.5280(13)	0.2197(9)	0.0961(4)	55(3)
C(42)	0.4484(15)	0.2339(10)	0.0547(5)	73(4)
C(43)	0.4992(16)	0.2973(11)	0.0244(5)	85(5)
C(44)	0.6188(17)	0.3440(12)	0.0364(6)	98(5)
C(45)	0.6973(17)	0.3309(12)	0.0774(6)	96(5)
C(46)	0.6476(14)	0.2671(10)	0.1070(5)	71(4)
C(51)	0.3936(12)	0.0281(9)	0.1026(4)	53(3)
C(52)	0.4639(15)	−0.0116(11)	0.0704(5)	79(4)
C(53)	0.4093(18)	−0.0970(12)	0.0470(6)	101(5)
C(54)	0.2980(18)	−0.1352(14)	0.0575(6)	105(6)
C(55)	0.2229(13)	−0.1022(12)	0.0870(6)	99(5)
C(56)	0.2777(14)	−0.0138(11)	0.1118(5)	77(4)
C(61)	0.3399(13)	0.1923(10)	0.1621(4)	58(4)
C(62)	0.2616(14)	0.2706(11)	0.1424(5)	75(4)
C(63)	0.1600(16)	0.3070(12)	0.1644(5)	36(5)
C(64)	0.1304(16)	0.2698(11)	0.2023(5)	85(5)
C(65)	0.2065(16)	0.1929(12)	0.2222(6)	88(5)
C(66)	0.3125(14)	0.1555(10)	0.2027(5)	72(4)
C(71)	0.6028(12)	0.0973(9)	0.1762(4)	54(3)
C(72)	0.6543(13)	0.1596(10)	0.2092(4)	62(4)
C(73)	0.7660(14)	0.1332(11)	0.2404(5)	72(4)
C(74)	0.8247(17)	0.0429(13)	0.2381(6)	98(5)
C(75)	0.7747(16)	−0.0204(13)	0.2050(6)	100(5)
C(76)	0.6641(13)	0.0032(10)	0.1722(5)	70(4)

[a]C(41)–C(76) are refined isotropically.

TABLE 5. Interatomic distances (Å) and angles (deg) for $[(C_6H_5)_4P][BrIn(SC_6H_5)_3]$

In—Br	2.527(2)	Br—In—S(1)	106.4(1)
In—S(1)	2.445(4)	Br—In—S(2)	100.2(1)
In—S(2)	2.435(4)	S(1)—In—S(2)	120.9(1)
In—S(3)	2.470(4)	Br—In—S(3)	110.2(1)
S(1)—C(11)	1.75(2)	S(1)—In—S(3)	100.9(1)
S(2)—C(21)	1.78(1)		
S(3)—C(31)	1.73(2)	S(2)—In—S(3)	117.7(1)
P—C(41)	1.80(1)	In—S(1)—C(11)	109.5(4)
P—C(51)	1.82(1)	In—S(2)—C(21)	107.6(5)
P—C(61)	1.79(1)	In—S(3)—C(31)	106.0(6)
P—C(71)	1.79(1)	C(41)—P—C(51)	107.8(6)
		C(41)—P—C(61)	110.6(6)
Ring C(11)—C(16)*		C(51)—P—C(61)	109.7(6)
Mean C—C	1.38(2)	C(41)—P—C(71)	110.0(6)
Mean C—C—C	120(1)	C(51)—P—C(71)	111.1(6)
Ring C(21)—C(26)		C(61)—P—C(71)	107.7(7)
Mean C—C	1.39(2)	S(1)—C(11)—C(12)	124(1)
Mean C—C—C	120(1)	S(1)—C(11)—C(16)	116(1)
Ring C(31)—C(36)		S(2)—C(21)—C(22)	125(1)
Mean C—C	1.38(2)	S(2)—C(21)—C(26)	119(1)
Mean C—C—C	120(1)	S(3)—C(31)—C(32)	124(1)
Ring C(41)—C(46)		S(3)—C(31)—C(36)	117(2)
Mean C—C	1.38(2)	P—C(41)—C(42)	118(1)
Mean C—C—C	120(2)	P—C(41)—C(46)	121(1)
Ring C(51)—C(56)		P—C(51)—C(52)	118(1)
Mean C—C	1.39(2)	P—C(51)—C(56)	121(1)
Mean C—C—C	120(1)	P—C(61)—C(62)	121(1)
Ring C(61)—C(66)		P—C(61)—C(66)	120(1)
Mean C—C	1.39(2)	P—C(71)—C(72)	121(1)
Mean C—C—C	120(1)	P—C(71)—C(76)	119(1)
Ring C(71)—C(76)			
Mean C—C	1.39(2)		
Mean C—C—C	119(2)		

*Esd's on mean values have been calculated with the use of the scatter formula

$$\sigma = [\Sigma(d_i - \bar{d})^2/(N-1)]^{1/2}$$

where d_i is the ith and $\bar{d}$ the mean of N equal measurements.

dithio ligands. In the anion (21) $[In(MNT)_3]^{3-}$, the average In—S distance is 2.604 Å, within a range of 2.626(8)–2.585(8) Å, while in $In(S_2COEt)_3$ the corresponding values are 2.622(1) and 2.574(1) Å, distances which are comparable to those in other 1,1-dithiolate derivatives (22). The values for $In[S_2P(OEt)_2]_3$ are in the range (23) 2.59(11)–2.633(9) Å, and those for $In[S_2C{=}N(CH_2)_5]_3$ cluster closely around an average (24) of 2.588 Å. All of these results then give longer In—S bonds than those now reported, but any detailed comparison is obviously placed in question by the differences in both coordination number and ligand type. This caveat is strengthened by more recent results (25) for the compound In(dithizonate)$_3$, in which the local geometry at the metal is trigonal bipyramidal, with two bidentate and one monodentate ligand giving a InS_2N_2S' kernel. In this compound the In—S bond lengths are 2.477(3), 2.467(3), and 2.468(3), close to the distances found in the present work.

Structural parameters have also been reported (26) for $Sn(SPh)_4bpy$, in which the Sn^{IV}—S bond distances are 2.497(1)–2.502(1) Å, but again changes in coordination number apparently affect the bond length since in species with SnC_3S kernels, values of 2.420(8) Å and 2.44(2) Å have been reported for compounds with arylthiolate ligands (27). The general conclusion is that the present In—S bond distances are clearly compatible with those in other In^{III}—S compounds and in Sn^{IV}—S (and Cd^{II}—S) (28) structures, although no exactly comparable set of results is available.

The remaining structural features reported in Table 5 are very similar to those found in other benzenethiolate derivatives, and call for no discussion.

Vibrational spectroscopy

As noted above, we recorded the infrared spectrum of all products over the range 3500–600 cm^{-1} in order to establish

TABLE 6. Conductivity results for salts of $[XIn(SPh)_3]^-$ and $[In(SPh)_4]^-$

Salt	Solvent	Molar conductivity/ohm^{-1} cm^2
$Et_4N[ClIn(SPh)_3]$	CH_3OH	92
$Et_4N[BrIn(SPh)_3]$	dmso	56
$Et_4N[IIn(SPh)_3]$	CH_3OH	102
$Ph_4P[BrIn(SPh)_3]$	CH_3CN	147
$Ph_4As[ClIn(SPh)_3]$	CH_3CN	142
$Et_4N[In(SPh)_4]$	CH_3OH	97

[a]Standard ranges for 1:1 electrolytes in these solvents are CH_3OH 80–115, CH_3CN 120–160, dmso 50–70 ohm^{-1} cm^2 (cf. ref. 16).

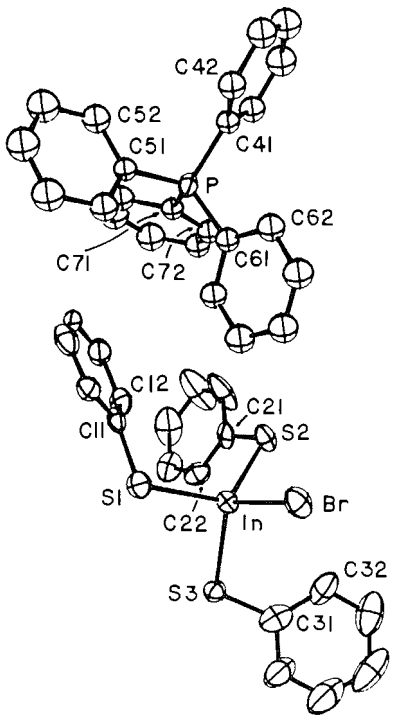

FIG. 1. Structure of cationic and anionic units in $Ph_4P[BrIn(SPh)_3]$.

the presence of the appropriate ligand, cation, etc. These results call for no comment, but the infrared and Raman spectra over the range 600–100 cm^{-1} do contain significant information. For the compound $In(SPh)_3$ there are only two bands in the infrared spectrum, at 332 m and 150 m, br, other than those readily identified as arising from vibrations of the SPh group. The Raman spectrum also shows features arising from the ligand together with emissions at 330 m and 317 s; no features could be identified below approximately 180 cm^{-1} due to the high background scatter in this region. We assign the vibrations in the 300–350 cm^{-1} region to ν_{as} (330) and ν_s (317) of In—$(SPh)_3$, with the lower frequency infrared band tentatively identified as a bending mode. The values for the stretching modes are in good agreement with earlier studies of indium complexes with —SR ligands (17, 29). These results do not permit any vigorous analysis in terms of local symmetry at the indium atom.

The vibrational spectra of the adducts of $In(SPh)_3$ with neutral ligands are too complex for analysis, but the situation is more favorable for the $[XIn(SPh)_3]^-$ anions. The relevant values are shown in Table 7, with assignments which are again in agreement with the results for $In(SPh)_3$, and with the earlier work noted above. The interpretation of the far infrared and Raman spectrum of $Ph_4As[ClIn(SPh)_3]$ and $Ph_4P[BrIn(SPh)_3]$ is hindered by the presence of cation bands, but we again observe ν(In—Cl) at 286(ir), 287(R) cm^{-1}, and ν(In—Br) at 198(ir), 200(R) cm^{-1}. In general, the vibrational spectra confirm the isostructural relationships between the anions of these salts.

TABLE 7. Metal–ligand vibrations in $Et_4N[XIn(SPh)_3]^-$ salts (in cm^{-1})

Compound	Infrared	Raman	Assignment
X = Cl	358 s	361 w	
		341 w	ν(In—S)
	330 s	330 w	
	286 s	283 w	ν(In—Cl)
X = Br	346 s	361 w	
	335 s	339 w	ν(In—S)
		320 w	
	199 s, br	204	ν(In—Br)
X = I	358 s	[a]	
	340 s		ν(In—S)
	320 s		
	156 s		ν(In—I)

[a]No Raman spectrum observed because of strong fluorescence.

Acknowledgements

This work was supported in part by Operating Grants (to D.G.T.) from the Natural Sciences and Engineering Research Council of Canada. We thank Dr. M. J. Taylor (University of Auckland, New Zealand) for a helpful discussion of the vibrational spectrum of $In(SPh)_3$.

1. E. W. ABEL and D. A. ARMITAGE. Adv. Organomet. Chem. **5**, 1 (1967).
2. H. SCHUMANN, I. SCHUMANN-RUDISCH, and M. SCHMIDT. Organotin compounds. Vol. 2. *Edited by* A. K. Sawyer. Marcel Dekker, New York. 1971. p. 297.
3. P. G. HARRISON and S. R. STOBART. Inorg. Chim. Acta, **7**, 306 (1973) and references therein.
4. E. W. ABEL. Comprehensive inorganic chemistry. Vol. 2. *Edited by* A. F. Trotman-Dickenson. Pergamon Press, Oxford. 1973. p. 134.
5. A. J. CANTY. Am. Chem. Soc. Symposia, **82**, 327 (1978); **82**, 339 (1978).
6. A. J. CANTY, R. KISHIMOTO, G. B. DEACON, and G. J. FARQUAHARSON. Inorg. Chim. Acta, **20**, 161 (1976).
7. P. A. W. DEAN. Can. J. Chem. **59**, 3221 (1981).
8. G. K. CARSON, P. A. W. DEAN, and M. J. STILLMAN. Inorg. Chim. Acta, **56**, 59 (1981).
9. R. C. STEEVENSZ, D. G. TUCK, H. A. MEINEMA, and J. G. NOLTES. Can. J. Chem. **63**, 755 (1985).
10. M. A. KHAN, R. C. STEEVENSZ, D. G. TUCK, J. G. NOLTES, and P. W. R. CORFIELD. Inorg. Chem. **19**, 3407 (1980).
11. A. F. BERNIAZ, G. HUNTER, and D. G. TUCK. J. Chem. Soc. A, 3254 (1971).
12. A. F. BERNIAZ and D. G. TUCK. J. Organomet. Chem. **46**, 243 (1972).
13. A. F. BERNIAZ and D. G. TUCK. J. Organomet. Chem. **51**, 113 (1973).
14. A. J. CARTY and D. G. TUCK. Prog. Inorg. Chem. **19**, 245 (1975).
15. M. V. VEIDIS and G. J. PALENIK. Chem. Commun. 1182 (1970).
16. W. J. GEARY. Coord. Chem. Rev. **7**, 81 (1971).
17. D. G. TUCK and M. K. YANG. J. Chem. Soc. A, 214 (1971).

Can. J. Chem. Downloaded from www.nrcresearchpress.com by 78.46.186.204 on 09/07/12
For personal use only.

18. M. A. KHAN and D. G. TUCK. Acta Crystallogr. **B38**, 803 (1982).
19. W. SCHWARTZ, H. J. GUDER, R. PREWO, and H. D. HANSEN. Z. Naturforsch. **B31**, 1427 (1976).
20. M. A. KHAN, C. PEPPE, and D. G. TUCK. J. Organomet. Chem. **280**, 17 (1985).
21. (*a*) F. W. B. EINSTEIN, G. HUNTER, D. G. TUCK, and M. K. YANG. Chem. Commun. 423 (1968); (*b*) F. W. B. EINSTEIN and R. D. G. JONES. J. Chem. Soc. A, 2762 (1971).
22. B. F. HOSKINS, E. R. T. TIEKINK, R. VECCHIET, and G. WINTER. Inorg. Chim. Acta, **90**, 197 (1984).
23. P. COGGON, J. D. LEBEDDA, A. T. MCPHAIL, and R. A. PALMER. Chem. Commun., 78 (1970).
24. P. J. HAUSER, J. BORDNER, and A. F. SCHREINER. Inorg. Chem. **12**, 1347 (1973).
25. J. M. HARROWFIELD, C. PAKOWATCHAI, and A. H. WHITE. J. Chem. Soc. Dalton Trans. 1109 (1983).
26. J. L. HENCHER, M. A. KHAN, F. F. SAID, R. SIELER, and D. G. TUCK. Inorg. Chem. **21**, 2787 (1982).
27. N. G. BOKII, YU. T. STRUCHKOV, D. N. KRAUTSOV, and E. M. ROKHLINA. J. Struct. Chem. **15**, 424 (1974).
28. D. G. TUCK. Rev. Inorg. Chem. **1**, 209 (1979).
29. C. PEPPE and D. G. TUCK. Can. J. Chem. **62**, 2798 (1984).

Can. J. Chem. Downloaded from www.nrcresearchpress.com by 78.46.186.204 on 09/07/12
For personal use only.

Ultrasonic velocity, excess adiabatic compressibility, apparent molar volume, and apparent molar compressibility properties of binary liquid mixtures containing 2-butoxyethanol

N. P. RAO[1] AND RONALD E. VERRALL[2]

Department of Chemistry, University of Saskatchewan, Saskatoon, Saskatchewan, Canada S7N 0W0

Received July 4, 1986

N. P. RAO and RONALD E. VERRALL. Can. J. Chem. **65**, 810 (1987).

Ultrasonic velocity and density data of binary systems of water–2-butoxyethanol (BE), 2-butoxyethanol–benzene, and 2-butoxyethanol–decane are reported for temperatures of 25, 40, and 55°C. Adiabatic compressibility coefficients, apparent molar volumes, and apparent molar compressibilities were calculated from these data. Excess adiabatic compressibility properties were evaluated using volume fraction weighting of the individual component properties to estimate ideal mixture behavior. These results are compared with the data obtained based on the use of mole fraction weighting of the individual component properties for the ideal behavior value. A sharp ultrasonic velocity maximum and compressibility minimum is observed at low BE concentration in mixtures of water–BE at all temperatures. These maxima in ultrasonic velocity and minima in adiabatic compressibility are attributed to the formation of "clathrate-like" structures of water and alcohol. A shift of the velocity maximum towards lower concentrations of BE was observed with increase of temperature. A minimum in the ultrasonic velocity and a maximum in adiabatic compressibility coefficient values are observed in systems of BE–benzene and BE–decane. These results are discussed in terms of the breakdown of associated alcohol structures and the interstitial location of hydrocarbon molecules in alcohol aggregates.

N. P. RAO et RONALD E. VERRALL. Can. J. Chem. **65**, 810 (1987).

Opérant à des températures de 25, 40 et 55°C, on a mesuré les vitesses ultrasoniques et les densités des systèmes binaires eau/butoxy-2 éthanol (BE), butoxy-2 éthanol/benzène et butoxy-2 éthanol/décane. A partir de ces données, on a calculé les coefficients de compressibilité adiabatique, les volumes molaires apparents et les compressibilités molaires apparentes. Utilisant les poids relatifs des fractions du volume des propriétés des composantes individuelles pour évaluer le comportement du mélange idéal, on a évalué les propriétés de compressibilité adiabatique en excès. On compare ces résultats avec les données obtenues en se basant sur l'usage des poids relatifs des fractions molaires des propriétés des composantes individuelles pour évaluer le comportement du mélange idéal. A toutes les températures, on observe un maximum important de la vitesse ultrasonique et une compressibilité minimale à des faibles concentrations de BE dans les mélanges eau/BE. On attribue ces maxima dans la vitesse ultrasonique et ces minima dans la compressibilité adiabatique à la formation de structures de l'eau et de l'éthanol "ressemblant à des chlathrates". Lorsqu'on augmente la température, on observe un déplacement du maximum de la vitesse vers les concentrations plus basses de BE. Dans les systèmes BE/benzène et BE/décane, on observe un minimum dans la vitesse ultrasonique et un maximum dans les valeurs des coefficients de compressibilité adiabatique. On discute de ces résultats en fonction d'un bris des structures associées de l'alcool et de la position des molécules interstitielles d'hydrocarbures dans les agrégats d'alcool.

[Traduit par la revue]

Introduction

It has been shown that microphase structures occur in mixtures of water, alcohol, and oil (1–3). Water and alcohol mixtures themselves show unique minima and maxima in their thermodynamic properties at low alcohol concentrations (4–10). The formation of "clathrate-like" structures is believed to be the cause of these unusual properties in the case of alcohols having alkyl groups with 3- or 4-carbon atoms. The formation of such structures also are apparent in mixtures of water and other organic solvents (11–18). It has been observed that the addition of a hydrocarbon component changes the "clathrate-like" structures of the binary water–alcohol systems and gives rise to stable microphase structures (1–3). For example, surfactants have been found to have a large stabilizing effect on these microphase structures and they give rise to the formation of microemulsions and emulsions of relatively larger size (19). However, the formation and stability of these large aggregates are not well understood. A systematic study of these systems using ultrasonic techniques has been undertaken in our laboratory. Improved instrumentation for the measurement of ultrasonic velocity and density properties enables the accurate determination of adiabatic compressibility coefficients which can be used to provide qualitative information about the physical nature of the aggregates occurring in the liquid phase. As a preliminary step in this work, binary systems of water (W) – 2-butoxyethanol (BE), BE–benzene (BNZ), and BE–decane (DEC) have been investigated. Because of the unique miscibility behavior of BE and water at temperatures below 49°C, BE was used as the alcoholic component.

Excess adiabatic compressibility coefficients, ($\Delta\beta$), which are a measure of deviations from ideal solution behavior of a mixture, were evaluated by considering ideal solution behavior values based on both mole fraction and volume fraction weighted averaging of the individual component properties. However, closer examination of the physical nature of compressibilities suggests that, while many thermodynamic and physical properties of ideal solutions are represented by the mole fraction weighted averages of component properties, it is more appropriate to use volume fraction weighted averages of compressibility coefficients of pure solution components to estimate ideal behavior of this property (20–24). Large differences occur between the values of excess compressibility coefficients estimated by these two methods, especially when the molar volumes of the individual component differ considerably. Under these circumstances it would appear useful to consider correlating the excess ultrasonic velocity and compressibility properties as a function of volume fraction.

Apparent molar volumes and apparent molar adiabatic com-

[1]On leave from the Department of Physics, Sri Venkateswara University Post Graduate Centre, Kavali 524 202, India.

[2]To whom all correspondence should be addressed.

Can. J. Chem. Downloaded from www.nrcresearchpress.com by 80.58.250.72 on 09/07/12
For personal use only.

Can. J. Chem. Downloaded from www.nrcresearchpress.com by 80.58.250.72 on 09/07/12
For personal use only.

pressibilities also have been calculated from density and ultrasonic velocity measurements over the complete composition range of these binary systems. These quantities are very sensitive to interactions between solute and solvent and to changes induced in the solvent by the solute as the concentration of the latter tends to zero. Trends in these properties with changes in temperature and composition can also offer some qualitative assessment of solution behavior in the intermediate composition range. A comparison of these properties for the three binary systems studied is presented and discussed.

Experimental section

Density measurements

The solution densities were measured with a SODEV flow digital densimeter Model 02D. This instrument, described by Picker *et al.* (25), is capable of measuring densities with an accuracy of 1 part in 10^6 g cm^{-3}. The densimeter was thermostated to ±0.001°C using a SODEV (Model-CT-C) temperature controller.

Ultrasonic velocity measurements

The ultrasonic velocities were measured at 4 MHz using a NUSONIC (Mapco, Model 6080) velocimeter based on the sing-around technique (26). The sample container is an insulated double-walled glass cell. The sample temperature was maintained to within ±0.001°C by circulating water from a SODEV (Model CT-L) temperature controller through the thermostating chamber of the cell. The ultrasonic velocities, u, in units of m s^{-1} are obtained from the average round-trip period of the ultrasonic wave in the fixed path length between the piezoelectric transducer and reflector. The period is expressed as a frequency, f, and the following relation is used to calculate u

$$[1] \quad u = fA(1 + \alpha' t)/(7 - (fB \times 10^{-6}))$$

where A is the sonic path length in meters, B is the electronic time delay in microseconds, f is the frequency in Hertz, α' is the coefficient of thermal expansion of the transducer holder, and t is the solution temperature in degrees Celsius. The constants A and B were obtained by calibrating the transducer probe with distilled water and aqueous sodium chloride solutions using the data of Del Grosso and Mader (27) and Sakurai *et al.* (28). The ultrasonic velocity measurements are accurate to ±0.02 m s^{-1}.

A region of high ultrasonic absorption is observed in binary mixtures of W–BE and the sing-around unit employed was unable to provide accurate ultrasonic velocity measurements in this range. Instead, a single crystal interferometer working at a frequency of 4 MHz was used to obtain ultrasonic velocities in this region. The accuracy in the interferometric velocity measurements is ±0.1 m s^{-1}.

The ultrasonic velocity obtained in the present work for 2-butoxyethanol at 25°C is 1305.37 m s^{-1}, a value 3.41 m s^{-1} higher than the value of 1301.96 m s^{-1} reported by Lara and Desnoyers (10). The purified (see below) alcohol was analyzed for water and other impurities using Karl Fischer and gas chromatographic techniques, respectively. The water content was found to be <0.03 wt.% and was accounted for when solutions with water were prepared. Its contribution to the ultrasonic velocity of BE would be to increase it by ca. 0.15 m s^{-1}, considerably less than the observed discrepancy reported above. A Tractor 222 gas chromatograph with dual FID/ECD detector was used to examine for the presence of other organic impurities. The glass column was packed with 10% carbowax 20M on 100/120 mesh supelcoport. No other impurities were detected with this unit, in particular 2-isobutoxyethanol, which has a different retention time on this column, was not observed. Furthermore, any presence of 2-isobutoxyethanol as an impurity can be ruled out because its presence should reduce the ultrasonic velocity since it has a reported (29) value of 1260 m s^{-1}. Notwithstanding the difference between the ultrasonic velocity of pure BE obtained in this work and that reported previously (10), there was good agreement with previously reported (10) ultrasonic velocity data for solutions of W–BE, particularly in the region of the ultrasonic velocity maximum (see Results section).

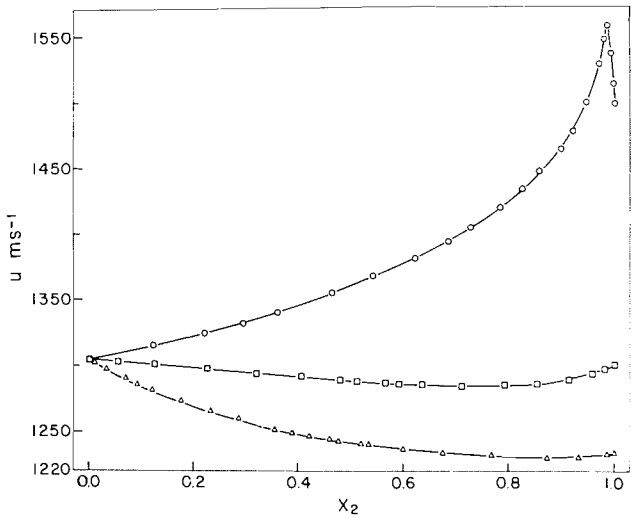

FIG. 1. Variation of ultrasonic velocity as a function of mole fraction of nonalcoholic component (2) in mixtures of (○) BE–W, (□) BE–BNZ, and (△) BE–DEC at 25°C (for the sake of clarity not all data points have been shown.)

Chemicals

2-Butoxyethanol (BE) and decane (DEC) were obtained from Aldrich Chemical Co. BE was further purified by fractional distillation under vacuum and kept over molecular sieves prior to use. Spectral grade benzene (BNZ) (BDH Chemicals) was used without further purification. All solutions were made on a weight basis using water obtained from a Millipore Super-Q system.

Results and discussion

Ultrasonic velocity and density data measured for the systems W–BE, BE–BNZ, and BE–DEC at 25, 40 and 55°C are given elsewhere.[3] A typical plot of the variation of ultrasonic velocity at 25°C as a function of mole fraction content of the nonalcoholic component is shown in Fig. 1. Adiabatic compressibility coefficients, β, are calculated from the relation

$$[2] \quad \beta = 100/(u^2 d)$$

where β is in units of bar^{-1}, d is the solution density (g cm^{-3}), and u is the ultrasonic velocity (m s^{-1}). The variation of β as a function of the mole fraction of the second component is shown in Fig. 2*A*–*C*. The W–BE system has a lower consolute temperature of 49°C. Because of this, a two phase region exists at higher temperatures and at 55°C extends over the concentration range $0.016 < X_{BE} < 0.13$. This region is shown as a dashed line in Fig. 2*A*. At 25°C, a velocity maximum and compressibility minimum is observed at $X_{BE} = 0.015$. This composition is in good agreement with the previously reported results of Lara and Desnoyers (10). Furthermore, the value of 1556.18 m s^{-1} obtained for the ultrasonic velocity maximum is in good agreement with the value of 1556.02 m s^{-1} obtained by the above authors.

The origin of this maximum at low alcohol concentration is believed to be due to long range order in water giving rise to hydrogen bonded structures which have numerous cavities that can accommodate other species. As the alcohol is added to water, alcohol molecules are assumed to occupy the cavities in the framework of the water aggregates. A denser packing of the molecules results in an increase in the ultrasonic velocity and a decrease in the compressibility of these solutions. This

[3]The supplementary tables may be purchased from the Depository of Unpublished Data, CISTI, National Research Council of Canada, Ottawa, Ontario, Canada K1A 0S2.

Can. J. Chem. Downloaded from www.nrcresearchpress.com by 80.58.250.72 on 09/07/12
For personal use only.

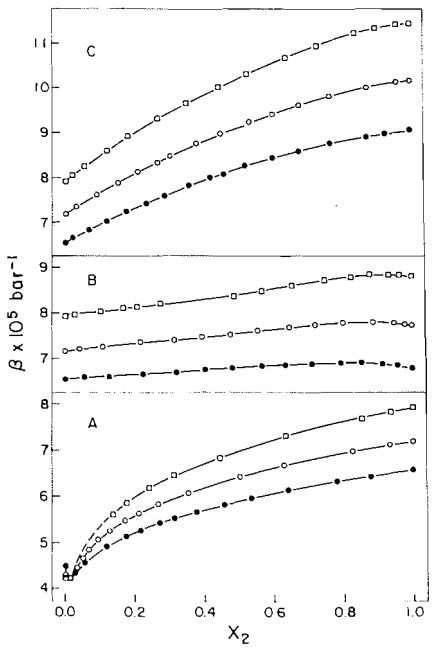

FIG. 2. Variation of the adiabatic compressibility coefficient as a function of mole fraction of component (2) in mixtures of (*A*) W–BE (2), (*B*) BE–BNZ (2), and (*C*) BE–DEC (2) ((●) 25, (○) 40, (□) 55°C).

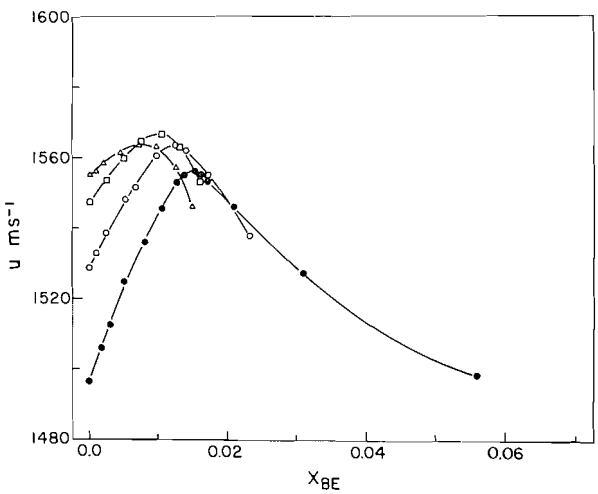

FIG. 3. Variation of ultrasonic velocity as a function of mole fraction of BE in mixtures of W–BE: (●) 25, (○) 40, (□) 55, (△) 70°C.

process continues until a concentration is reached at which all cavities are filled. A simpler argument for the increase in ultrasonic velocity is that the addition of alcohol to water causes a breakdown of the less dense hydrogen bonded structures of water. However, the results of inelastic light scattering experiments (30, 31) and ultrasonic relaxation and photon correlation spectroscopic studies (32) strongly suggest that "clathrate-like" structures are present in W–BE systems and therefore these structures are believed to contribute to the observed compressibility behavior at low BE concentrations rather than a decrease in the concentration of low density structures of water.

Figure 3 shows the variation of ultrasonic velocity as a function of mole fraction of BE at low alcohol concentrations in the binary system W–BE in the temperature range 25–70°C. A shift of the ultrasonic velocity maximum towards lower BE concentrations with increasing temperature is clearly illustrated. These maxima are postulated to correlate with the compositions at which "clathrate-like" structures of alcohol and water of well defined stoichiometry are found. This shift of the maximum to lower concentrations of BE implies that the number of possible cavities decreases at higher temperatures. It is consistent with the general view that the degree of hydrogen bonding in water decreases at higher temperatures and fewer "clathrate-like" structures would be expected to form.

The variation of the magnitude of the peak ultrasonic velocity also shows unusual behavior. It first increases with increasing temperature to above ca. 55°C and then decreases beyond this value. This trend is similar to that observed for water itself in which the creation of more compact structures with increasing temperature first produces an increase in sound velocity but, at some high temperature, the usual volume expansion property tends to dominate and thus leads to a decrease in the ultrasonic velocity. The same qualitative arguments can be used to describe the sound velocity maxima observed for the W–BE systems between 55 and 70°C.

In binary mixtures of BE–BNZ a velocity minimum and compressibility maximum (Fig. 2*B*) are observed at lower concentrations of BE. In the case of BE–DEC a velocity minimum is observed at all temperatures while, a compressibility maximum is apparent only at 55°C. The behavior of these systems can be better explained in terms of the excess adiabatic compressibility coefficients.

The usual procedure for obtaining the ideal isothermal solution property (β^{ideal}) is to take the mole fraction weighted contribution of the pure component properties represented by

$$[3] \quad \beta^{ideal} = \Sigma X_i \beta_i$$

where the suffix i represents the ith component.

However, from the fundamental definition of isothermal compressibility, it can be readily shown that the ideal solution value of this property is properly derived by taking the volume fraction (ϕ_i) weighted contributions of the isothermal compressibilities of the pure components. Considering the relationship between the isothermal and adiabatic compressibility coefficients, it has been shown (20–24) that the adiabatic compressibility coefficient of an ideal mixture can be expessed as

$$[4] \quad \beta^{ideal} = \Sigma\phi_i[\beta_i + TV_i\alpha_i^2/C_{p,i}] - T[\Sigma X_i V_i][\Sigma\phi_i\alpha_i]^2/[\Sigma X_i C_{p,i}]$$

where β_i, V_i, α_i, and $C_{p,i}$ are the adiabatic compressibility coefficient, molar volume, coefficient of thermal expansion, and heat capacity at constant pressure, respectively, of the pure i components and T is the absolute temperature. The excess adiabatic compressibility coefficients are defined as

$$[5] \quad \Delta\beta = \beta^{real} - \beta^{ideal}$$

which represents the excess of the given property of a real mixture over the value for an ideal mixture at the same temperature, pressure, and composition.

In the present work excess compressibility coefficients were calculated using both mole fraction weighted averaging (eqs. [3] and [5]) and volume fraction weighted averaging (eqs. [4] and [5]) for comparison. These data and the thermodynamic constants used in eq. [4] are given elsewhere.[3] Considerable differences are observed between the magnitudes of $\Delta\beta$ obtained from these two weighting methods. Figure 4*A* and *B* show a comparison of the excess adiabatic compressibility

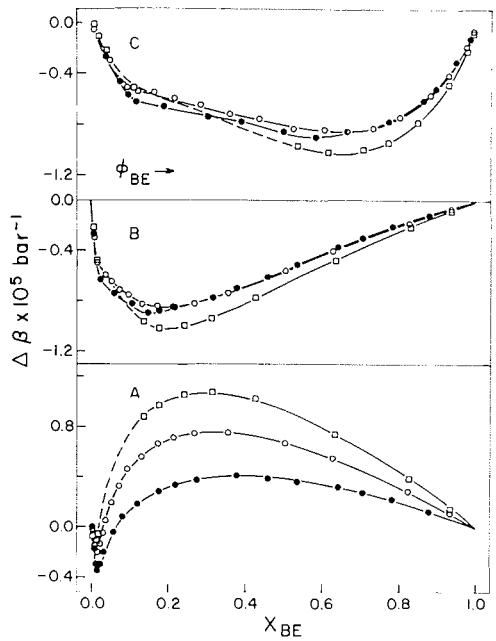

FIG. 4. Variation of excess adiabatic compressibility coefficient as a function of concentration of BE in mixtures of W–BE ((*A*) calculated from eqs. [3] and [5]; (*B* and *C*) calculated from eqs. [4] and [5]): (●) 25, (○) 40, (□) 55°C.

coefficients, calculated from mole fraction and volume fraction weighting, respectively, of the ideal solution behavior as a function of mole fraction of BE in W–BE binary solutions at 25, 40, and 55°C. Figure 4*C* shows the variation of $\Delta\beta$ obtained from the use of volume fraction weighting for the ideal solution as a function of volume fraction of BE. The dashed line in the 55°C curve for W–BE illustrates the extent of the two phase region encountered when working above the lower consolute temperature. The excess compressibility properties derived from the use of ideal solution properties based on mole fraction weighting (Fig. 4*A*) are generally positive with the exception of the low alcohol concentration range, i.e., $X_{BE} < 0.04$. However, excess compressibility coefficients derived from the use of volume fraction weighting of the ideal component contributions are negative throughout the complete composition range. The negative values of $\Delta\beta$ at very low BE concentrations in Fig. 4*A* and *B* are consistent with the view that BE molecules can occupy cavities in a hydrogen bonded framework of water molecules leading to decreased solution compressibility relative to the pure components.

The variation in $\Delta\beta$ values shown in Fig. 4 *A* and *B* exhibit considerable differences above $X_{BE} = 0.04$. In Fig. 4*A*, the values increase rapidly and eventually become positive at $X_{BE} > 0.07$ at all temperatures studied. This latter behavior is not in accordance with what would be expected for solutions containing such a high content of water. Generally, water compressibility is supposed to decrease with increasing temperature up to 64°C. It is also difficult to explain the rather sharp change in $\Delta\beta$ as being due to the positive contribution of the alcohol in conjunction with a sudden breakdown of "clathrate-like" structures of relatively lower compressibility. One would expect a gradual transformation of these well organized aggregates into merged types of aggregates leading to an increase in $\Delta\beta$, but extending over a wider alcohol composition range.

The variation of $\Delta\beta$ values (Fig. 4*B*) derived from use of eqs. [4] and [5] show a pattern more consistent with the formation and transformation of "clathrate-like" aggregates as the BE concentration is increased. The rapid decrease in $\Delta\beta$ values at low alcohol concentrations is consistent with the postulated (30, 31) "clathrate-like" structure of alcohols in water. However, the negative trend continues beyond this point ($X_{BE} = 0.015$) albeit with a reduced slope indicating that less compressible aggregates are being produced beyond the "clathrate-like" composition. Ito *et al.* (31) have proposed that in the composition range $0.015 < X_{BE} < 0.20$ both clathrate and water–alcohol aggregates with stoichiometric composition W_4BE exist. Presumably the latter structures become more prevalent as the BE concentration increases and the compressibility results reported here would appear to indicate that these W_4BE aggregates are compact and less compressible. Minima in $\Delta\beta$, depending upon temperature, are observed in the range $0.14 < X_{BE} < 0.20$. Beyond this range the increase in $\Delta\beta$ is almost linear with increasing alcohol concentration reflecting the increasing contribution of the more compressible alcohol component.

Since the compressibility coefficient is a measure of the relative change in volume with pressure, it seems appropriate to examine the variation of $\Delta\beta$ as a function of the volume fraction of BE in the binary mixtures. The results shown in Fig. 4*C* illustrate apparent differences in behavior from those exhibited in Fig. 4 *A* and *B*. However, on closer examination the results in Fig. 4 *B* and *C* are seen to be generally similar except that using ϕ_{BE} as the independent variable appears to more clearly illustrate the change in slope and the position of the minima in $\Delta\beta$ as compared to Fig. 4*B*. The excess compressibility coefficients are negative throughout the volume fraction range. A moderation of the decrease in slope of $\Delta\beta$ with ϕ_{BE} occurs at ca. $\phi_{BE} = 0.10$. Further decrease in $\Delta\beta$ continues to ca. $\phi_{BE} = 0.55$. Beyond this region the $\Delta\beta$ values become less negative as the influence of the more compressible alcohol component dominates the solution behavior. This result is consistent with the interpretation given previously with regard to the variation of $\Delta\beta$ as a function of X_{BE}.

The temperature variation of $\Delta\beta$ is unusual in the W–BE system. It is not so readily apparent in Fig. 4*B* but Fig. 4*C* shows that there is an inversion in the trend of $\Delta\beta$ with increasing temperature as the magnitude of ϕ_{BE} increases. Unfortunately, rather large ultrasonic absorption values at concentrations near the "clathrate-like" region prevented measurements of the ultrasonic velocity with the sing-around equipment. However, interferometric measurements were made to provide a few data points in this region. It is seen that at low BE concentrations $\Delta\beta$ values become less negative as temperature increases. This is in accordance with the expectations based on our discussion of Fig. 3. On the other hand, at $\phi_{BE} \geq 0.55$, $\Delta\beta$ becomes more negative with increasing temperature in the range 25–55°C. The trend is more pronounced at 55°C and suggests that the molecular arrangement of the molecules at higher temperatures is occurring with considerable economy of space leading to a reduction of compressibility relative to the ideal solution approximation.

Specific heat (33) and enthalpy of mixing (34) studies also have indicated the occurrence of clathrate structures at ca. 0.02 X_{BE}. Beyond this concentration microphase aggregates are predicted to occur and it is only at very high concentrations of BE that clathrate and microphase structures cease to exist. The variation of excess molar heat capacities and excess molar enthalpies of some normal alcohol–water and alkoxyethanol–water systems (35–38) are consistent with the variation of excess

Can. J. Chem. Downloaded from www.nrcresearchpress.com by 80.58.250.72 on 09/07/12
For personal use only.

adiabatic compressibility coefficients for BE(alkoxyethanol)–water observed in this work. The excess molar specific heat goes through a maximum at $X_{BE} = 0.2$ and then slowly decreases. The excess enthalpies, like the excess compressibility coefficients, show negative values that decrease sharply to a mole fraction of either alcohol or alkoxyethanol $\simeq 0.2$ and then slowly rise toward zero. The variation of the excess enthalpy of the 2-ethoxyethanol–water system with composition is exactly the same as the variation of the excess compressibility coefficient in the BE–W system (38). Both the excess enthalpies of 2-ethoxyethanol–water and the excess compressibilities of BE–W, at lower alcohol concentrations, decrease with increase of temperature. The results of the specific heat and enthalpy studies were interpreted as indicating that small additions of solute (alcohol or alkoxyethanol) are accommodated within the cavities in the hydrogen bonded network of water. In the intermediate compostion range stronger hydrogen bonding is believed to occur between water molecules as opposed to weaker bonding between the alcohols and water. Hence, a greater state of order exists within water in these systems as opposed to pure water itself. This is supported by light scattering studies (8) of water–*t*-butylalcohol (TBA) from which it is predicted that solvent-shared association complexes $[(H_2O)_{105}(TBA)_5]$ occur. The discussion of the behavior of the excess compressibility coefficient of BE–W systems obtained in this work is consistent with the conclusions drawn from the above studies.

Figure 5*A* shows the variation of $\Delta\beta$ calculated from the ideal solution approximation based on the use of eqs. [3] and [5] as a function of mole fraction of BNZ in the mixture BE–BNZ. The $\Delta\beta$ values are always positive and show a decrease with increasing temperature. Such temperature variation is unusual as generally organic liquids show an increase in compressibility with increase in temperature. Consequently the $\Delta\beta$ values would be expected to increase with increasing temperature. $\Delta\beta$ values (Fig. 5*B* and *C*) derived from ideal solution approximations based on volume fraction weighting (eqs. [4] and [5]) show negative values at lower BNZ concentration and an increase in the solution compressibility with increase in temperature, a result more in agreement with the expectation stated above. The negative values of $\Delta\beta$ observed in the BE rich region are believed to arise from BNZ occupying interstitial sites within associated structures of alcohol and to the structural change caused by the interaction between BNZ and BE. At higher concentrations of BNZ the associated alcohol structures no longer can exist and there is an increase in solution compressibility. At higher temperatures the association of alcohols is less favoured and consequently the occupation of interstitial sites by BNZ occurs to a lesser degree. This is reflected by the very shallow minimum in the $\Delta\beta$ curve at 55°C (Fig. 5*B*).

At low BE concentrations a maximum in the $\Delta\beta$ curve is observed at all temperatures. The peak value of the excess compressibility coefficient increases in magnitude and appears to shift to lower BNZ concentrations with increasing temperature. A graph of $\Delta\beta$ vs. ϕ_{BNZ} (Fig. 5*C*) shows this trend more clearly. This maximum in $\Delta\beta$ conceivably reflects the breakdown of self-associated alcohol aggregates of different association number. The shift of this peak to lower BNZ concentrations with increasing temperature indicates the greater disruptive effect of BNZ on the alcohol aggregates with increasing temperature. The discussion of the results of $\Delta\beta$ obtained from eqs. [4] and [5] for the BE–BNZ system are consistent with the

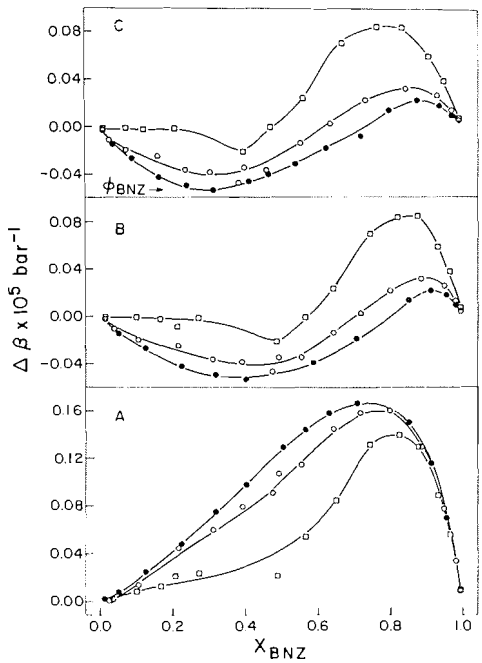

FIG. 5. Variation of excess adiabatic compressibility coefficient as a function of concentration of BNZ in mixtures of BE–BNZ ((*A*) calculated from eqs. [3] and [5]; (*B* and *C*) calculated from eqs. [4] and [5]): (●) 25, (○) 40, (□) 55°C.

interpretation of the variation of excess volume and excess compressibility coefficient property reported for 2-ethoxyethanol–hydrocarbon systems (39, 40).

The variation of $\Delta\beta$ calculated using eqs. [3] and [5] as a function of mole fraction of DEC in mixtures of BE–DEC is shown in Fig. 6*A*. All $\Delta\beta$ values are positive and show a normal increase with increase in temperature. $\Delta\beta$ values calculated from eqs. [4] and [5] (Fig. 6*B* and *C*) also are positive throughout the composition range but the maxima occur in the DEC-rich region. The reasons for the maxima are similar to those noted above for the case of BE–BNZ solutions, however, contrary to the results obtained with BE–BNZ, there is no minimum in the graphs of $\Delta\beta$ vs. X_{DEC}. This suggests that DEC does not fit interstitially into alcohol structures at lower DEC concentrations, possibly, because of the relatively larger size of the decane molecule.

The apparent molar volume ($\phi_{V,A}$) and apparent molar compressibility ($\phi_{K,A}$) properties of a solute component A defined in terms of mole fraction concentration units are calculated from the relations

$$[6] \quad \phi_{V,A} = M_0(X_0/X_A dd_0)(d_0 - d) + M_A/d$$

$$[7] \quad \phi_{K,A} = \beta\phi_{V,A} + X_0M_0(\beta - \beta_0)/(X_A d_0)$$

where d_0, X_0, M_0, and β_0 are the density, mole fraction, molecular weight, and adiabatic compressibility of the solvent, respectively, X_A and M_A are the mole fraction and molecular weight of the solute component; and d and β are the density and adiabatic compressibility of the solution mixture. Values of these properties calculated using eqs. [6] and [7] are given in the supplementary material. Typical results for the systems W–BE and BE–DEC are shown in Figs. 7–9. Figures 7 and 8 show the variation of apparent molar compressibilities and apparent molar volumes, respectively, of BE and water with composition.

Can. J. Chem. Downloaded from www.nrcresearchpress.com by 80.58.250.72 on 09/07/12
For personal use only.

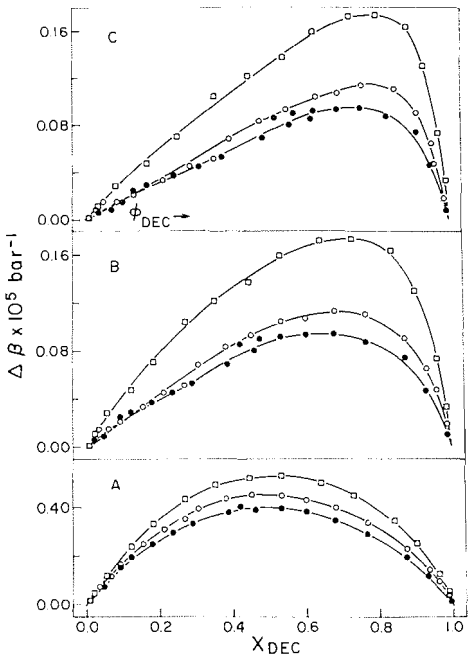

FIG. 6. Variation of excess adiabatic compressibility coefficient as a function of concentration of DEC in mixtures of BE–DEC ((*A*) calculated from eqs. [3] and [5]; (*B* and *C*) calculated from eqs. [4] and [5]): (●) 25, (○) 40, (□) 55°C.

From Fig. 7 it is seen that the change in apparent molar compressibility of water over the entire composition range is about five times smaller than that of BE. However, virtually all of this difference in magnitude between $\phi_{K,BE}$ and $\phi_{K,W}$ occurs at $X_{BE} < 0.05$. Thereafter the monotonic increase in $\phi_{K,BE}$ and $\phi_{K,W}$ as a function of their respective mole fraction contents are approximately the same over a wide composition range. Almost similar behavior arises with respect to the apparent molar volumes, Fig. 8. The sharp changes that occur in these properties at low BE mole fractions are consistent with the view that "clathrate-like" structures of BE in water are present at these low concentrations. This argument appears to be best supported by the rather sharp drop in the magnitude of $\phi_{V,BE}$ at $X_{BE} < 0.01$. The BE molecules appear to be occupying void space thereby giving rise to a marked decrease in their apparent molar volume property. As well, at high concentrations of BE, $\phi_{K,W}$ is negative showing that there is a breakdown of water aggregates and the water is being dispersed in linear and 2-dimensional hydrogen-bonded alcohol clusters leading to a reduction in the molar compressibility property of water.

A further comparison of Figs. 7 and 8 shows an interesting difference in behavior with respect to the variation of apparent molar volume and apparent molar compressibility with temperature at fixed compositions. The apparent molar volumes of both BE and water increase with increasing temperature. On the other hand the apparent molar compressibility of BE increases whereas that of water decreases with increasing temperature. It would appear that increasing temperature affects the molecular organization in these systems so as to increase the amount of free water and hence contribute to a closer packing of the molecules and a lower compressibility of the water component. The volumes show a trend expected on the basis of simple thermal expansion characteristics. On balance, it would appear that the temperature dependence of the adiabatic compressibility coefficient may be a better probe of "structural" characteristics of these solutions.

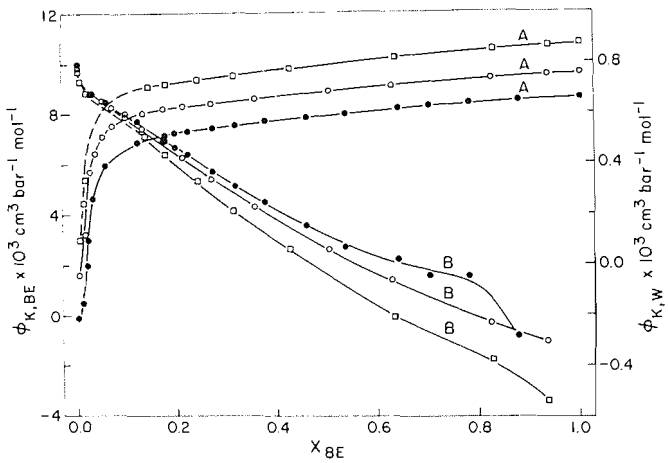

FIG. 7. Variation of apparent molar compressibility of BE (*A*) and W (*B*) in mixtures of W–BE: (●) 25, (○) 40, (□) 55°C.

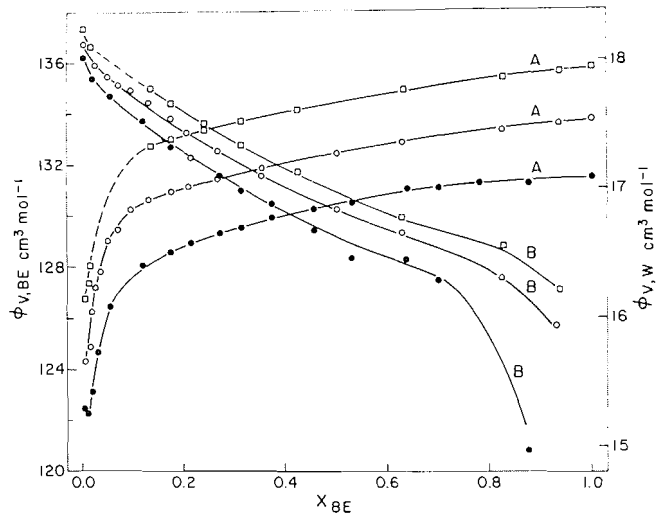

FIG. 8. Variation of apparent molar volume of BE (*A*) and W (*B*) in mixtures of W–BE: (●) 25, (○) 40, (□) 55°C.

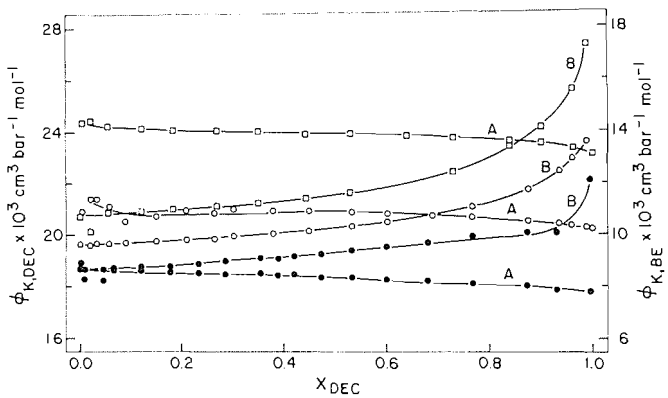

FIG. 9. Variation of apparent molar compressibility of DEC (*A*) and BE (*B*) in mixtures of BE–DEC: (●) 25, (○) 40, (□) 55°C.

The trends in the variation of apparent molar volumes and apparent molar compressibilities of BNZ in BE, BE in BNZ, DEC in BE and BE in DEC are similar at all temperatures. A typical example is shown in Fig. 9 for $\phi_{K,DEC}$ and $\phi_{K,BE}$. The magnitudes of these properties for the oil component are rela-

Can. J. Chem. Downloaded from www.nrcresearchpress.com by 80.58.250.72 on 09/07/12
For personal use only.

tively constant across the entire composition range. Variations in the apparent molar properties of BE occur at lower compositions of BE, the variations being greater at the highest solution temperatures. The higher apparent molar compressibilities of BE at low BE concentrations, $X_{BE} < 0.20$, may reflect the breakdown of associated alcohol clusters in the bulk phase creating conditions of less efficient packing and hence relatively higher compressibility. The apparent molar volumes also show a similar behavior. The conclusions reached from an assessment of the behavior of apparent molar volume and apparent molar compressibility properties are consistent with those presented to describe the peaks observed in $\Delta\beta$ curves at low BE concentrations.

Conclusions

The presence of "clathrate-like" aggregates at low concentrations of BE in W–BE mixtures and changes in these aggregates as a function of temperature appear to correlate well with the variation of ultrasonic velocity maximum in these solutions. A more consistent interpretation of molecular association process can be made from the excess compressibilities obtained on the basis of using volume fraction weighted averaging of the individual component properties to evaluate ideal solution compressibility data. The transformation from "clathrate-like" to other types of alcohol–water aggregates can be described by the slope changes in the excess adiabatic compressibilities as a function of solution composition. The occupation of interstitial sites in alcohol aggregates by BNZ at high BE concentrations gives rise to minima in the excess compressibilities of BE–BNZ solutions. The breakdown of associated alcohol aggregates at lower BE concentrations by BNZ and DEC lead to maxima in the $\Delta\beta$ values. The apparent molar volume and compressibility behavior of the components of these solutions are also consistent with these qualitative conclusions.

Acknowledgements

The authors thank the Government of Canada and the Government of Saskatchewan for their financial support of this project under the Canada–Saskatchewan Heavy Oil Fossil Fuels Agreement. They also thank Dr. Joe Boison for carrying out gc analysis of BE samples. N.P.R. thanks Sri Venkateswara University for allowing a leave of absence to perform this work.

1. C. D. Smith, C. E. Dorulam, and R. E. Barden. J. Coll. Interface. Sci. **60**, 488 (1977).
2. J. Lara, G. Perron, and J. E. Desnoyers. J. Phys. Chem. **85**, 1600 (1981).
3. J. Lara, L. Avedikian, G. Perron, and J. E. Desnoyers. J. Solution Chem. **10**, 301 (1981).
4. F. Franks and J. E. Desnoyers. Water Sci. Rev. **1**, 171 (1985).
5. F. Franks and D. J. Reid. *In* Water, a comprehensive treatise. Vol. 2. *Edited by* F. Franks. Plenum Press, New York. 1973. Chap. 5.
6. K. Tamura, M. Mackawa, and T. Yasunaga. J. Phys. Chem. **81**, 2122 (1977).
7. N. Muller. J. Magn. Reson. **28**, 203 (1977).
8. N. Iwasaki and T. Fujiyama. J. Phys. Chem. **81**, 1908 (1977); **83**, 463 (1979).
9. G. Roux, D. Roberts, G. Perron, and J. E. Desnoyers. J. Solution Chem. **9**, 629 (1980).
10. J. Lara and J. E. Desnoyers. J. Solution Chem. **10**, 465 (1981).
11. M. J. Blandamer and D. Waddington. Adv. Mol. Relaxation Processes, **2**, 1 (1970).
12. E. K. Baumgartner and G. Atkinson. J. Phys. Chem. **75**, 2336 (1971).
13. E. K. Baumgartner and G. Atkinson. Z. Phys. Chem. Leipzig, **252**, 392 (1973).
14. H. Endo. Bull. Chem. Soc. Jpn. **16**, 1586 (1973).
15. G. G. Malenkov. Zur. Strukt. Kim. **3**, 220 (1962); **7**, 331 (1966).
16. A. A. Ennan and W. A. Lapshin. Zhur. Fiz. Kim. **49**, 2295 (1975).
17. S. Ernst and J. Glinski. Mater. Sci. **3**, 69 (1977).
18. K. M. Swamy and P. S. Swamy. Acustica, **54**, 61 (1983).
19. G. Perron, R. DeLisi, I. Davidson, S. Genereux, and J. E. Desnoyers. J. Coll. Interface Sci. **79**, 432 (1981).
20. G. Douheret, C. Moreau, and A. Viallard. Fluid Phase Equilibr. **22**, 277 (1985).
21. G. L. Betrand and L. E. Smith. J. Phys. Chem. **74**, 4171 (1970).
22. O. Kiyohara and G. C. Benson. J. Chem. Thermodyn. **11**, 861 (1979).
23. G. C. Benson and O. Kiyohara. J. Chem. Thermodyn. **11**, 1061 (1979).
24. W. E. Acree, Jr. J. Chem. Eng. Data, **28**, 215 (1983).
25. P. Picker, E. Tremblay, and C. Jolicoeur. J. Solution Chem. **3**, 377 (1974).
26. R. Garnsey, R. Mahoney, and J. A. Litovitz. J. Chem. Phys. **64**, 2073 (1964).
27. V. A. Del Grasso and C. W. Mader. J. Acoust. Soc. Am. **52**, 1442 (1972).
28. M. Sakurai, T. Nakajima, T. Komatsu, and T. Nakagawa. Chem. Lett. 971 (1975).
29. R. J. Fanning and P. Kruus. Can. J. Chem. **48**, 2052 (1970).
30. N. Ito, K. Saito, T. Kato, and T. Fujiyama. Bull. Chem. Soc. Jpn. **54**, 991 (1981).
31. N. Ito, T. Fujiyama, and Y. Udagawa. Bull. Chem. Soc. Jpn. **56**, 379 (1983).
32. S. Kato, D. Jobe, N. P. Rao, C. H. Ho, and R. E. Verrall. J. Phys. Chem. To be published.
33. G. Roux, G. Perron, and J. E. Desnoyers. J. Solution Chem. **7**, 639 (1978).
34. J. E. Desnoyers. Personal communication.
35. J. A. Larkin. J. Chem. Thermodyn. **7**, 137 (1975).
36. G. C. Benson, P. J. D'Arcy, and O. Kiyohara. J. Solution Chem. **9**, 931 (1980).
37. H. Nakayama and K. Shinoda. J. Chem. Thermodyn. **3**, 401 (1971).
38. A. K. Kalasy, G. D. Nageshwar, and P. S. Mene. J. Chem. Thermodyn. **7**, 101 (1975).
39. G. C. Benson, C. J. Halpin, and A. J. Treszczanowicz. J. Chem. Thermodyn. **13**, 1175 (1981).
40. K. S. Reddy. J. Chem. Thermodyn. **16**, 597 (1984).

Can. J. Chem. Downloaded from www.nrcresearchpress.com by 80.58.250.72 on 09/07/12
For personal use only.

Étude des mélanges eau–HF par spectroscopie infrarouge à transformée de Fourier

JALEH KHORAMI, RÉJEAN BEAUDOIN ET HUGUES MÉNARD[1]

Département de chimie, Faculté des sciences, Université de Sherbrooke, Sherbrooke (Qué.), Canada J1K 2R1

Reçu le 28 juillet 1986

JALEH KHORAMI, RÉJEAN BEAUDOIN et HUGUES MÉNARD. Can. J. Chem. **65**, 817 (1987).

L'analyse des spectres infrarouges des mélanges HF–H_2O entre 10 et 97% en HF nous a permis de déterminer l'évolution des espèces ioniques de HF. Les résultats obtenus montrent la présence des ions $H_3O^+F^-$, H_3O^+, F^- ainsi que H_2O dans des solutions HF–H_2O à moins de 46% en poids de HF. À partir de 50% HF en poids, on a constaté l'apparition des bandes caractéristiques de HF_2^- dont les intensités augmentent avec la concentration jusqu'à 90% en HF. D'autre part, nous avons mis en évidence l'existence des polymères $(HF)_n$ dans les solutions à haute concentration en HF. Ces résultats expliquent le comportement électrochimique des solutions HF–H_2O que nous avons entreprises.

JALEH KHORAMI, RÉJEAN BEAUDOIN, and HUGUES MÉNARD. Can. J. Chem. **65**, 817 (1987).

An analysis of the ir spectra of HF–H_2O mixtures containing from 10 to 97% of HF has been used to determine the evolution of the ionic species of HF. The results indicate that water and the ions $H_3O^+F^-$, H_3O^+, and F^- are present in the solutions containing less than 46% w/w of HF. In the solutions containing at least 50% w/w of HF, bands characteristic of the ion HF_2^- start appearing and their intensity increases with the concentration of HF, up to a concentration of 90%. As well, polymers of $(HF)_n$ have been detected in the solutions containing the highest concentration of HF. These results can be used to explain the electrochemical behaviour of solutions of HF–H_2O.

[Journal translation]

Introduction

Les propriétés des mélanges eau–HF mesurées par voie électrochimique indiquent des changements importants au niveau de l'ionisation en solution (1–3) en passant des solutions diluées aux mélanges très concentrés. En particulier dans la région de 45 à 75% en poids de HF, plusieurs propriétés passent par un maximum ou une transition. La température d'ébullition (4), la conductivité (1), l'activité en ions fluorure (2, 3) et la densité (1) en sont des exemples.

L'étude des mélanges eau–HF par spectroscopie infrarouge effectuée par Giguère et Turrell (5, 6) permet d'établir de façon claire les espèces présentes jusqu'à 46% en HF. À plus grande concentration en HF, la compréhension des propriétés électrochimiques et physiques nécessite la connaissance des espèces ioniques et moléculaires en solution.

L'utilisation de la spectroscopie infrarouge nous permet donc de mettre en évidence l'évolution des espèces formées en solution avec la concentration croissante en HF de 10 à 90%. Par ces études, on mettra en évidence les espèces ioniques H_3O^+, HF_2^- et la probabilité de la formation des espèces polymériques du fluorure d'hydrogène. Ces résultats confirment et expliquent les propriétés particulières des mélanges eau–HF observées lors des études en électrochimie.

Partie expérimentale

Les solutions de HF sont préparées à l'avance. Les spectres ont été enregistrés à la température ambiante à l'aide d'un appareil infrarouge à transformée de Fourier Nicolet MX1 avec une résolution de 2 cm^{-1}. Le temps de balayage se situe entre 30 et 60 secondes.

Pour les mélanges eau–HF contenant moins de 46% en poids de HF, nous avons utilisé un film capillaire formé en pressant une fine goutte de liquide entre deux pastilles de KBr. À plus grande concentration en HF, nous avons utilisé la même technique avec des pastilles de AgCl à cause de la réactivité de la solution vis-à-vis le KBr. Le spectre est enregistré rapidement à cause de la haute pression partielle du HF.

Résultats et discussion

La figure 1 montre une superposition des spectres qui permet de voir l'évolution des bandes attribuées aux différentes espèces en solution.

1. Auteur à qui adresser toute correspondance.

Les tableaux 1–4 résument les attributions des bandes entre 4000 et 2500 cm^{-1}, 2500 et 1600 cm^{-1}, 1600 et 800 cm^{-1} et 800 et 400 cm^{-1}.

Région de 4000 à 2500 cm^{-1}

Lorsqu'on ajoute du HF à l'eau, on peut remarquer l'apparition d'un épaulement vers 2700 cm^{-1}.

L'intensité de cet épaulement augmente jusqu'à une concentration de HF 51% en poids et se déplace légèrement vers les fréquences plus élevées. À partir de 61% de HF, on observe une diminution de l'intensité pour cet épaulement par rapport au pic situé vers 3500 cm^{-1}.

Les deux bandes forment un ensemble qui s'étend entre 3700 et 2500 cm^{-1} pour les solutions plus concentrées en HF. Giguère et Turrell (5, 6) ont attribué cette bande vers 2700 cm^{-1} à une vibration ν_3 de H_3O^+ pour les mélanges contenant moins que 46% de HF. Cette bande qui est due à une liaison hydrogène très forte entre H_3O^+ et l'ion de fluorure en solution se déplace vers les fréquences plus basses en comparaison avec les mélanges similaires de HCl et l'eau qui se trouve vers 2900 cm^{-1}.

Pour ces mélanges, la force de liaison hydrogène entre les ions de Cl^- et H_3O^+ est considérée très faible.

Dans nos études, le déplacement et la diminution de l'intensité de la bande vers 2700 cm^{-1} sont peut-être dus respectivement à une baisse de la force de liaison hydrogène entre H_3O^+ et l'ion de fluorure et la décroissance des espèces ioniques H_3O^+ dans les solutions concentrées de HF.

D'autre part, on a remarqué que les bandes ν_1 et ν_3 de l'eau située dans cette région vers 3500 cm^{-1} persistent toujours et même augmentent d'intensité à partir des solutions contenant 61% de HF.

D'après les études suivantes qui montrent la disparition quasi totale des bandes caractéristiques de l'eau sur les spectres ir à partir de 61% en HF, cette bande vers 3500 cm^{-1} ne peut pas appartenir à l'eau.

Si on se réfère aux travaux de Couzi (7) qui ont été effectués pour HF gazeux et les travaux de Gennick *et al.* (8) pour HF dans un milieu aqueux en présence des ions d'alkylammonium ainsi que les études de Desbat et Huong (9) qui comparent

Can. J. Chem. Downloaded from www.nrcresearchpress.com by 78.46.186.204 on 09/07/12
For personal use only.

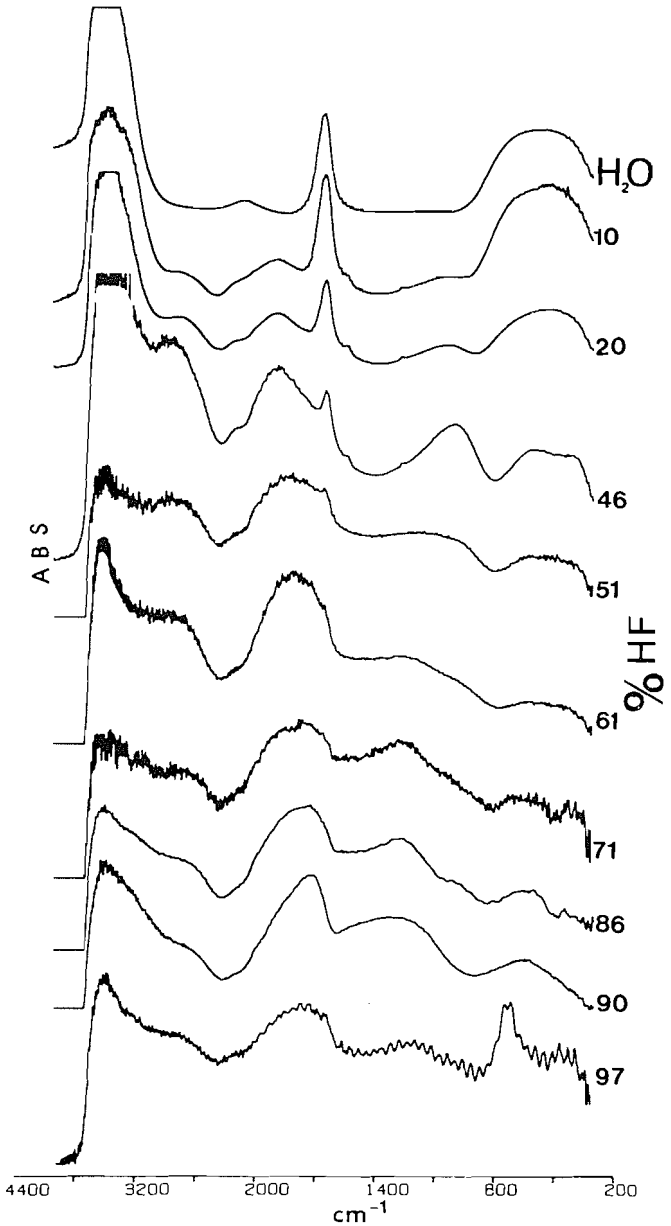

FIG. 1. Spectre infrarouge des mélanges HF–H_2O en poids.

les spectres ir des mélanges concentrés en HF et ceux de HF gazeux, on est convaincu que cette bande large située vers 3500 cm^{-1} est due à la formation des espèces de polymères ioniques de HF.

D'autre part, les études précédentes (10, 11) confirment nos résultats et montrent que les spectres infrarouges des mélanges concentrés en HF sont comparables à ceux du HF gazeux.

La région de 2500 à 1600 cm^{-1}

La comparaison des spectres infrarouges de l'eau (12) et des mélanges eau–HF jusqu'à 97% montre les points suivants :

1. Les vibrations de l'eau situées vers 1645 et 2125 cm^{-1} diminuent d'intensité avec l'augmentation de la concentration en HF à partir de 61% en HF; ces bandes caractéristiques disparaissent complètement pour donner leurs places à une bande de vibration large située entre 1600 et 2000 cm^{-1}. L'intensité de cette bande augmente et son maximum se trouve vers 1730 cm^{-1} aux hautes concentrations en HF.

2. On peut noter que, pour les solutions de 10 à 50% en HF, la disparition des deux bandes caractéristiques de l'eau est

TABLEAU 1. Les bandes de vibration observées dans la région entre 4000 et 2500 cm^{-1}

	3480 cm^{-1}		2770 cm^{-1}	
% Poids HF/H_2O	Intensité relative	Attribution	Intensité relative	Attribution
H_2O	TF	ν_1 et ν_3 H_2O	—	—
10	TF d ↓	ν_1 et ν_3 H_2O	(2720) ep	ν_3 $H_3O^+ \cdot F^-$
20	TF d ↓	ν_1 et ν_3 H_2O	(2750) f	ν_3 $H_3O^+ \cdot F^-$
46	F d ↓	ν_1 et ν_3 H_2O	F	ν_3 $H_3O^+ \cdot F^-$
51	F	ν_1 et ν_3 H_2O	F	ν_3 $H_3O^+ \cdot F^-$
		ν H_nF_n		ν H_nF_n
61	F	ν H_nF_n	F	ν_3 $H_3O^+ \cdot F^-$
				ν H_nF_n
71	F	ν H_nF_n	F d ↓	ν_3 $H_3O^+ \cdot F^-$
78	TF	ν H_nF_n	F d ↓	ν_3 $H_3O^+ \cdot F^-$
				ν H_nF_n
86	TF d ↑	ν H_nF_n	M d ↓	ν_3 $H_3O^+ \cdot F^-$
				ν H_nF_n
90	TF d ↑	ν H_nF_n	ep d ↓	ν_3 $H_3O^+ \cdot F^-$
				ν H_nF_n
97	TF d ↑	ν H_nF_n	ep d ↓	ν_3 $H_3O^+ \cdot F^-$
				ν H_nF_n
HF[a]	TF L	ν H_nF_n	—	—

[a]Référence 9. TF = très forte; F = forte; M = moyen; f = faible; tf = très faible; ep = épaulement; L = large; d ↑ = déplacement vers les fréquences plus élevées; d ↓ = déplacement vers les fréquences plus basses.

suivie par l'apparition d'une bande dont le maximum est situé vers 1880 cm^{-1}.

Dans les solutions aqueuses de HF, la bande de vibration centrée à 1880 cm^{-1} est symétrique. Par analogie avec le spectre des autres acides minéraux (11), Giguère et Turrell (5, 6) ont attribué cette bande au pliage (bending mode) ν_4 de l'ion H_3O^+. Cette fréquence, beaucoup plus élevée que dans l'acide chlorhydrique (1750 cm^{-1}), a été attribuée à la formation de paires d'ions liés par liaison hydrogène. On peut représenter ces ions à partir de l'équilibre suivant :

$$H_2O + HF \rightleftarrows [H_3O^+ \cdot F^-] \rightleftarrows H_3O^+ + F^-$$

Cette fréquence, très élevée pour un pliage hors plan, est indicatrice d'une très grande force de rappel.

À partir de 50% en HF, on note un élargissement et le déplacement du pic à 1800 cm^{-1} vers 1730 cm^{-1}. La bande devient non symétrique et s'étend encore de 200 à 1600 cm^{-1}. Le maximum à 1730 cm^{-1} apparaît d'abord comme un épaulement et augmente d'intensité avec la concentration en HF jusqu'à 90%.

D'après les études effectuées par Emsley (12) sur les spectres infrarouges de HF_2^- et qui fait intervenir les résultats de recherches de différents auteurs, il est fort probable que l'apparition de l'épaulement vers 1730 cm^{-1} et le déplacement de la bande de vibration à 1880 cm^{-1} vers 1730 cm^{-1} sont dus à la formation de l'espèce ionique HF_2^- selon les équilibres suivants :

$$HF + F^- \rightleftarrows HF_2^-$$

$$[H_3O^+ \cdot F^-] + HF \rightleftarrows H_3O^+ + HF_2^-$$

La bande de vibration ν_3 de HF_2^- peut être retrouvée entre 1450 et 1900 cm^{-1}. Harmond *et al.* (13) ont observé cette bande à 1740 cm^{-1}.

D'après nos résultats de spectroscopie infrarouge, il est possible de prévoir les conclusions suivantes sur les espèces

Can. J. Chem. Downloaded from www.nrcresearchpress.com by 78.46.186.204 on 09/07/12
For personal use only.

TABLEAU 2. Les bandes de vibration observées dans la région entre 2500 et 1600 cm^{-1}

	2140 cm^{-1}		1645 cm^{-1}		1880–1730 cm^{-1}	
% HF (poids)	Intensité relative	Attribution	Intensité relative	Attribution	Intensité relative	Attribution
H_2O	(2125) f	$\nu_2 + \nu_L$ H_2O	TF	ν_2 H_2O	—	—
10	ep	$\nu_2 + \nu_L$ H_2O	TF	ν_2 H_2O	(1800) M	ν_4 $H_3O^+ \cdot F^-$
20	ep	$\nu_2 + \nu_L$ H_2O	M	ν_2 H_2O	(1880) M	ν_4 $H_3O^+ \cdot F^-$
46	ep	$\nu_2 + \nu_L$ H_2O	tf	ν_2 H_2O	(1880) M, L	ν_4 $H_3O^+ \cdot F^-$
51	ep	$\nu_2 + \nu_L$ H_2O	tf	ν_2 H_2O	(1805) TF, L	ν_4 $H_3O^+ \cdot F^-$ ν_3 HF_2^-
61	—	—	tf	ν_2 H_2O	(1790) TF, L	ν_4 $H_3O^+ \cdot F^-$ ν_3 HF_2^-
71	—	—	—	—	(1775) TF, L	ν_4 $H_3O^+ \cdot F^-$ ν_3 HF_2^-
78	—	—	—	—	(1730) TF, L	ν_4 $H_3O^+ \cdot F^-$ ν_3 HF_2^-
86	—	—	—	—	(1730) TF, L	ν_3 HF_2^-
90	—	—	—	—	(1730) TF, L	ν_3 HF_2^-
97	—	—	—	—	(1730) TF, L	ν_3 HF_2^-
HF[a]	—	—	—	—	(1700) ep, L	H_nF_n

[a]Référence 9. TF = très forte; F = forte; M = moyen; f = faible; tf = très faible; ep = épaulement; L = large; d ↑ = déplacement vers les fréquences plus élevées; d ↓ = déplacement vers les fréquences plus basses.

ioniques et moléculaires dans les mélanges eau–HF:

1. La diminution à partir de 10% en HF et la disparition quasi-totale de l'eau «libre» à partir de 60% en HF.
2. L'apparition et l'augmentation de la concentration de la paire d'ions $H_3O^+ \cdot F^-$ de 10 à 50% en HF.
3. L'apparition à partir de 50% en HF et l'augmentation de la concentration de HF_2^- jusqu'à 85% en HF.

La région de 1600 à 800 cm^{-1}

Dans cette région de vibration, l'eau ne possède aucune bande en infrarouge. Par contre, on peut constater sur le spectre des mélanges eau–HF l'apparition d'un épaulement situé vers 1035 cm^{-1}. D'autre part, on peut noter qu'avec l'augmentation de la concentration en HF jusqu'à 50%, l'épaulement à 1030 cm^{-1} se transforme en un pic large dont le maximum se situe à 1000 cm^{-1}. À plus de 50% en HF, ce pic diminue d'intensité et on voit apparaître vers les fréquences plus élevées une bande large. À partir de 60% en HF, on observe une bande large centrée à 1260 cm^{-1} et dont l'intensité augmente jusqu'à 90% en HF. Le tableau 3 résume l'évolution des différentes bandes.

Les observations ci-dessus ainsi que les interprétations citées pour les bandes de vibration situées entre 1600 et 2500 cm^{-1} nous conduisent aux conclusions suivantes:

1. On peut interpréter l'apparition de l'épaulement à 1035 cm^{-1} dont l'intensité suit celle du pic à 1800 cm^{-1} à une bande de vibration de l'ion H_3O^+. Giguère (5) a attribué la faiblesse et la largeur anormalement élevée de cette bande au complexe $H_3O^+ \cdot F^-$. Dans les autres acides minéraux, ν_2 de H_3O^+ est beaucoup plus intense et centré à 1200 cm^{-1}. Cette particularité est consistante du point de vue du moment dipolaire de $H_3O^+ \cdot F^-$.
2. La diminution d'intensité de la bande centrée à 1035 cm^{-1} suivie de l'apparition de la bande à 1260 cm^{-1} qui augmente d'intensité avec la concentration en HF de la même façon que la bande à 1730 cm^{-1} doit être due à la formation et à l'augmentation de concentration de l'espèce HF_2^-. Selon Emsley (12), la bande ν_2 de HF_2^- est un mode de vibration dégénéré. Ceci pourrait expliquer la largeur importante de la bande à 1260 cm^{-1}.

TABLEAU 3. Les bandes de vibration observées dans la région entre 1600 et 800 cm^{-1}

	1260 cm^{-1}		1035 cm^{-1}	
% HF (poids)	Intensité relative	Attribution	Intensité relative	Attribution
Eau	—	—	—	—
10	—	—	ep	ν_2 $H_3O^+ \cdot F^-$
20	—	—	f, L	ν_2 $H_3O^+ \cdot F^-$
46	—	—	F, L	ν_2 $H_3O^+ \cdot F^-$
51	tf, L	ν_1 HF_2^-	ep	ν_2 $H_3O^+ \cdot F^-$
61	f, L	ν_2 HF_2^-	ep	ν_2 $H_3O^+ \cdot F^-$
71	F, L	ν_2 HF_2^-	—	—
78	TF, L	ν_2 HF_2^-	—	—
86	TF, L	ν_2 HF_2^-	—	—
90	TF, L	ν_2 HF_2^-	—	—
97	f, L	ν_2 HF_2^-	—	—
HF	ep	ν_L H_nF_n	—	—

La région de 800 à 400 cm^{-1}

Dans cette région de vibration, l'eau possède une bande large située entre 300 et 700 cm^{-1} avec un maximum centré à 500 cm^{-1}.

Sur les spectres infrarouges des mélanges eau–HF, on peut constater une diminution de l'intensité de ce pic et un élargissement avec l'augmentation de la concentration en HF. À partir de 46% en HF, on observe aussi l'apparition d'un épaulement puis d'un pic vers les fréquences plus élevées. On observe encore un maximum vers 650 cm^{-1} pour des concentrations de 78 à 90% en HF. Le tableau 4 résume l'évolution des bandes dans cette région.

Par ailleurs, on peut remarquer que l'apparition de l'épaulement et l'augmentation de ce pic, déplacé vers les fréquences plus élevées, suivent de façon évidente la présence et l'augmentation d'intensité des deux bandes vers 3500 et 2770 cm^{-1}. Ces deux bandes de vibration avaient été attribuées à la formation des espèces polymériques de HF avec l'augmentation de la concentration de HF jusqu'à 90%. Ces observations nous

Can. J. Chem. Downloaded from www.nrcresearchpress.com by 78.46.186.204 on 09/07/12
For personal use only.

TABLEAU 4. Les bandes de vibration observées dans la région entre 800 et 400 cm^{-1}

	650 cm^{-1}		475 cm^{-1}	
% HF (poids)	Intensité relative	Attribution	Intensité relative	Attribution
Eau	(550) TF, L	ν_L H_2O		
10	(550) TF, L	ν_L H_2O		
20	(550) F, L	ν_L H_2O		
46	(600) F	ν_L H_nF_n	F	ν_L H_2O
51	(610) M	ν_L H_nF_n	M	ν_L H_2O
61	(620) M	ν_L H_nF_n	f	ν_L H_2O
71	M	ν_L H_nF_n	—	—
78	M	ν_L H_nF_n	—	—
86	M	ν_L H_nF_n	—	—
90	F	ν_L H_nF_n	—	—
97	F	ν_L H_nF_n	—	—
HF	(700) F	ν_L H_nF_n	—	—

poussent à croire que l'apparition de cette bande de vibration à 650 cm^{-1} doit être liée à la formation des espèces polymériques en solution (14). D'autre part, dans HF gazeux, on observe des vibrations de déformation à 800 cm^{-1} attribuées aux multimètres du fluorure d'hydrogène.

Conclusion

À partir des mesures de spectroscopie infrarouge sur le système eau–HF, on peut déduire le points suivants :

1. Dans les mélanges eau–HF jusqu'à 50% en poids de HF, l'espèce ionique dominante est le H_3O^+ fortement lié à l'ion fluorure.

2. À partir de 50% en HF, la concentration de HF_2^- augmente pour atteindre au maximum entre 80 et 90% en HF.

3. Ces travaux nous ont montré aussi la probabilité de formation des espèces polymériques dans le système aqueux de HF, comme c'est le cas pour HF gazeux (7, 9) et en présence d'ions alkylammonium (8).

Il faut noter que les conclusions déduites de la spectroscopie infrarouge confirment les travaux effectués en électrochimie. La conductivité reste élevée jusqu'à 65% en HF; l'activité en ions fluorure baisse rapidement entre 45 et 65% en HF; le potentiel de réduction des métaux est affecté par une espèce en solution différente de l'ion fluorure entre 50 et 100% en HF.

Remerciements

Les auteurs remercient pour l'appui financier le Conseil de recherches en sciences naturelles et en génie du Canada, le Ministère de l'Éducation du Québec et l'Institut de l'Amiante.

1. E. G. HILL et A. P. SIRKAR. Proc. R. Soc. London, A, **83**, 130 (1909).
2. A. VAILLANT, J. DEVYNCK et B. TRÉMILLON. J. Electroanal. Chem. **57**, 219 (1974).
3. H. MÉNARD, J. P. MASSON, J. DEVYNCK et B. TRÉMILLON. J. Electroanal. Chem. **63**, 163 (1975).
4. H. H. HYMAN et J. J. KATZ. *Dans* Non-aqueous solvent systems. T. C. Waddington (*Rédacteur*). Academic Press, New York. 1965.
5. P. A. GIGUERE. Chem. Phys. Lett. **41**, 598 (1976).
6. P. A. GIGUERE et S. TURRELL. J. Am. Chem. Soc. **102**, 5473 (1980).
7. M. COUZI. Thèse de doctorat. Bordeaux, France. 1970.
8. I. GENNICK, K. M. HARMON et M. M. POTVIN. Inorg. Chem. **16**, 2033 (1977).
9. B. DESBAT et P. V. HUONG. J. Chem. Phys. **78**, 6377 (1983).
10. J. G. BAYLY, V. B. KARTHA et W. H. STEVENS. Infrared Phys. **3**, 211 (1963).
11. M. FALK et P. A. GIGUERE. Can. J. Chem. **35**, 1195 (1957).
12. J. EMSLEY. Chem. Soc. Rev. **9**, 91 (1980).
13. K. M. HARMOND, S. L. MADEIRA et R. W. CARLING. Inorg. Chem. **13**, 1260 (1974).
14. P. V. HUONG et M. COUZI. J. Chim. Phys. Phys. Chim. Biol. **66**, 1309 (1969).

Can. J. Chem. Downloaded from www.nrcresearchpress.com by 78.46.186.204 on 09/07/12
For personal use only.

On the interaction of copper with tris(hydroxymethyl)aminomethane

M. F. COLOMBO
Instituto de Biociências, Letras e Ciências Exatas – UNESP, 15.100 S. José do Rio Preto, SP, Brasil

AND

L. AUSTRILINO, O. R. NASCIMENTO, E. E. CASTELLANO, AND M. TABAK
Instituto de Física e Química de São Carlos – USP, 13.560 S. Carlos, SP, Brasil

Received July 17, 1986

M. F. COLOMBO, L. AUSTRILINO, O. R. NASCIMENTO, E. E. CASTELLANO, and M. TABAK. Can. J. Chem. **65**, 821 (1987).

The interaction of copper with tris(hydroxymethyl)aminomethane (TRIS) has been studied by optical and esr spectroscopic techniques. In solution, three different copper complexes are obtained as a function of pH. At pH 10 the room temperature esr parameters are $g_0 = 2.135$, $A_0 = 82$ G and nitrogen superhyperfine structure $A_N = 9.5$ G, characteristic of two nitrogen ligands; at pH 6.5, $g_0 = 2.147$, $A_0 = 65$ G and at pH 5.0, $g_0 = 2.180$, $A_0 = 44$ G. The high pH complex was crystallized and its molecular structure determined by X-ray methods. Space group and cell dimensions are $C2/c$, $a = 12.955(2)$ Å, $b = 10.793(1)$ Å, $c = 10.091(2)$ Å, $\beta = 116.62(1)°$, $V = 1261.4(6)$ Å^3, $Z = 4$, $D_c = 1.694$ g cm^{-3}, $R = 0.034$ for 938 reflections with $I > 3\sigma(I)$. The Cu^{2+} ion is located on the two-fold axis and coordinated to the oxygen and nitrogen atoms of two TRIS moieties; these ligand atoms form the rectangular base of a pyramid structure in which oxygen from a water molecule acts as the fifth ligand.

M. F. COLOMBO, L. AUSTRILINO, O. R. NASCIMENTO, E. E. CASTELLANO et M. TABAK. Can. J. Chem. **65**, 821 (1987).

Faisant appel à des techniques de spectroscopie optique ou rpe, on a étudié l'interaction entre le cuivre et le tris(hydroxyméthyl)aminométhane (TRIS). En solution, trois types différents de complexes de cuivre sont obtenus en fonction du pH : à un pH de 10 et à la température ambiante, les paramètres rpe sont les suivants : $g_0 = 2,135$, $A_0 = 82$ G et une structure hyperfine de l'azote $A_N = 9,5$ G qui sont caractéristiques de deux ligands azotés; à un pH de 6,5, $g_0 = 2,147$ et $A_0 = 65$ G et à un pH de 5,0, $g_0 = 2,180$ et $A_0 = 44$ G. On a cristallisé le complexe qui se forme à un pH élevé et on a déterminé sa structure par diffraction des rayons-X. Le produit cristallise dans le groupe d'espace $C2/c$, avec $a = 12,955(2)$ Å, $b = 10,793(1)$ Å et $c = 10,091(2)$ Å et $\beta = 116,62(1)°$, $V = 1261,4(6)$ Å^3, $Z = 4$, $D_c = 1,694$ g cm^{-3} et $R = 0,034$ pour 938 réflexions avec $I > 3\sigma(I)$. L'ion Cu^{2+} est situé sur l'axe binaire et il est coordonné aux atomes d'azote et d'oxygène des deux portions TRIS; les atomes de ces ligands forment la base rectangulaire d'une structure pyramidale dans laquelle l'oxygène d'une molécule d'eau agit comme cinquième ligand.

[Traduit par la revue]

Introduction

Due to the importance of the biological complexes of Cu(II) and its presence as an integral part of a number of proteins, several techniques have been used to obtain information about the binding structure and biological function of this ion. Because of the intrinsic complexity of high molecular weight systems, many model studies have been made of Cu(II) with aminoacids, small peptides and organic compounds (1).

Electron spin resonance and optical absorption spectroscopies have proved to be very useful in establishing the ligands bonded to the metallic ion, the bond symmetry and the degree of covalence in these complexes (2–4). These data are always more completely explained when the complexes formed in solution are also obtained and investigated in the solid state; in solution the copper ion often forms more than one complex for a given free ligand concentration. It is often extremely difficult to separate the complexes due to their labile character and this is why most of the work appearing in the literature is restricted to the discussion of data for samples prepared at high free ligand concentration, when the metallic ion is found as the most stable complex (5, 6).

The quantitative description and concentrations of the complexes formed in solution is made through the determination of equilibrium constants and formation curves. However, the equilibrium constants only give indirect structural information of the complexes; solid state epr and X-ray diffraction data can give a complete structural characterization (7).

In the present work the interaction of tris(hydroxymethyl)-aminomethane (TRIS) with copper is investigated with use of the epr and optical spectroscopies as well as X-ray crystallography. The choice of this compound was motivated first by its wide use as biochemical buffer and our detection of its ability to make quite strong copper complexes in competition with some biological molecules. This compound also has quite interesting properties in the solid state, where a transition is observed with the formation of a plastic crystal phase (8, 9). Further, the equilibrium constants were obtained for the Cu^{2+}—TRIS complexes in solution based on the experimental titration data and the assumption of several reaction equilibria (10). An attempt is made to characterize the complexes in solution by comparing the spectroscopic and titration data, and also to identify the complex obtained in the crystalline form by using epr and X-ray crystallography.

Experimental

Sample preparation

TRIS and $CuClO_4$ were obtained from Merck Co. and used without further purification. A solution of 0.05 *M* TRIS and 0.005 *M* $CuClO_4$ in distilled water has a characteristic blue color and the original pH value is around 8.5. The pH values in the range 3.0–12.0 (Corning Model 130 pH-meter) were adjusted with the use of concentrated solutions of NaOH and HCl so that dilution was avoided. Equal 0.5 mL aliquots at each pH value were collected from a stock of 50 mL for the measurements, and the samples were used both for electronic optical absorption and epr measurements at room temperature and at low temperature in the frozen state.

Single crystals were obtained from solutions of 1 *M* TRIS and 0.1 *M* $CuClO_4$. Generally, good crystals were obtained if the solution was maintained around pH 10.0.

Optical and esr spectroscopy

For the optical absorption measurements (350–700 nm) a spectro-

Can. J. Chem. Downloaded from www.nrcresearchpress.com by 78.46.186.204 on 09/07/12
For personal use only.

Can. J. Chem. Downloaded from www.nrcresearchpress.com by 78.46.186.204 on 09/07/12
For personal use only.

photometer Shimadzu UV-180 was used. Electron spin resonance measurements were performed in a Varian E-109 spectrometer at X-band (9.3 GHz). A rectangular cavity E-248 together with the temperature control accessory E-257 was used to obtain the spectra at room temperature and at −150°C. The signal modulation at 100 kHz was 4 G peak-to-peak and microwave power 10 mW, the power being adjusted to improve the resolution of the superhyperfine nitrogen lines. Single crystal spectra were obtained with the use of a Varian goniometer, measuring the spectra in three orthogonal crystal planes as a function of orientation of the magnetic field at room temperature.

Crystallography

A prismatic crystal with dimensions 0.52 × 0.10 × 0.10 mm was mounted on an Enraf Nonius CAD-4 diffractometer. Unit cell dimensions and the orientation matrix for data collection were obtained by least squares from 25 centered reflections. Crystal data are as follows

$Cu(TRIS)_2 \cdot H_2O$ fw = 321.81

Monoclinic, space group $C2/c$, a = 12.955(2), b = 10.793(1), c = 10.091(2) Å, β = 116.62(1)°, V = 1261.4(6) Å^3, Z = 4, D_c = 1.694 g cm^{-3}, μ(MoKα) = 1.68 mm^{-1}, λ(MoKα) = 0.71073 Å, T = 296 K.

Intensities were measured by the ω–2θ scan technique at a rate between 2.5 and 10.0° min^{-1}; the ω scan angle was (0.80 + 0.35 tan θ)°, extended at each side by 25% for background determination. From 1701 reflections measured, 1108 unique, 938 having $I > 3\sigma(I)$ ($\sigma(I)$ estimated from counting statistics) were used for structure determination and refinement. The intensity of one standard reflection ($3\bar{1}\bar{5}$) was essentially constant (variation of ±2%) over the duration of the experiment. Data were corrected for Lorentz, polarization, and absorption effects (maximum and minimum transmission factors 0.908 and 0.816).

The copper atom was readily located from a Patterson map and the rest of the structure was determined by alternate cycles of isotropic least squares and difference synthesis. The structure was refined by full-matrix least-squares, including H-atom coordinates, to final R factors R = 0.034 and R_w = 0.030. The function minimized was $\Sigma w(|F_o| - |F_c|)^2$, with $w = 1/\sigma^2(F_o)$. Hydrogen atoms were assigned a common B factor which refined to a final value of 1.2(2) Å^2. All other atoms were treated anisotropically. A total of 118 parameters were refined, including χ in the extinction correction formula $F(\text{corrected}) = F_c[1.0 - \chi F_c^2/\sin\theta]$, which converged to the value $\chi = 1.46 \times 10^{-6}$. Complex scattering factors for non-H atoms (11, 12) and bonded H-atom scattering factors (13) were employed. Most calculations were carried out with the programs SHELX-76 (14) and ORTEP (15).

Results

The formation curves for the complex in solution were calculated using the equilibrium constants and reactions proposed in the work of Bai and Martell (10). These curves predicted eight possible different complexes as a function of pH (Table 1).

Optical absorption measurements

The optical spectra for the Cu^{2+}—TRIS system as a function of pH are presented in Fig. 1. A shift of the band to lower wavelengths occurs with the increase of pH. At pH 8.1 a splitting of the absorption band into two is apparent. Figure 2 presents the dependence of the wavelength of maximum absorption of the pH. The decrease of λ with increasing pH and a splitting above pH 8.0–8.5 are clearly observed.

In order to follow the appearance of the electronic bands the intensity of absorption at two different wavelengths as a function of pH was plotted (Fig. 3). The selection of the wavelengths was made using the fact that the high pH spectrum shows two bands at approximately 630 and 530 nm. Figure 3*a* shows that the maximum intensity at 630 nm occurs at pH 7.0, while above pH 9.5 the absorption intensity remains constant.

TABLE 1. Equilibrium constants for the complexes of Cu^{2+} with TRIS in solution at 25°C, 0.10 M ionic strength (10)

Complex	Equilibrium constant	log K	pH_{max}	Maximum* concentration (%)
ML^{2+}	K_1	3.95	5.4	31
ML_2^{2+}	K_2	3.68	5.8	22
ML_3^{2+}	K_3	3.47	6.4	29
ML_4^{2+}	K_4	3.0	7.6	75
$MH_{-1}L^{+}$	K_{1a}	−6.0	5.9	13
$(MH_{-1}L)_2^{2+}$	K_{ad}	2.2	6.5	16
$ML(H_{-1}L)^{+}$	K_{2a}	−6.32	6.0	2
$M(H_{-1}L)_2$	K_{2b}	−7.90	>9	>60

*The maximum concentrations were calculated from the formation curves and are given together with the corresponding pH value.

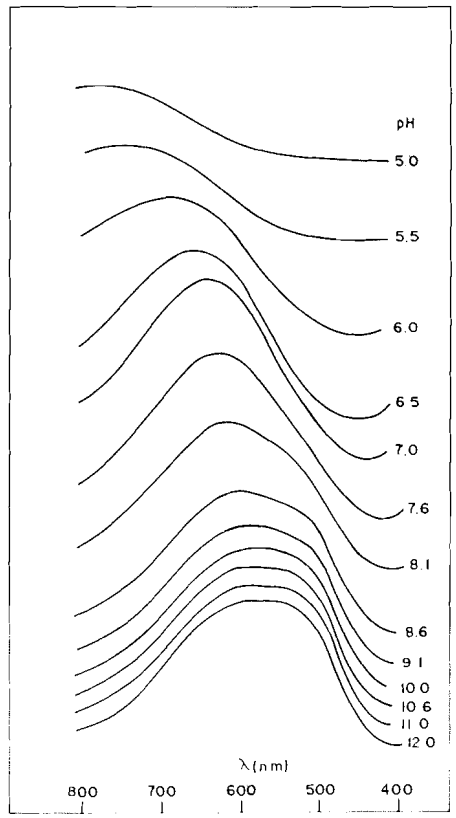

FIG. 1. Optical absorption spectra for the complexes Cu^{2+}—TRIS in solution as a function of pH.

From Fig. 3*b* the absorption at 530 nm increases with pH up to pH 9.0 and then it remains constant at approximately the intensity of the 630 nm band.

Electron spin resonance measurements

Figure 4 shows the room temperature esr spectra for the Cu^{2+}—TRIS system as a function of pH. At pH values above 8.0 a predominant spectrum is apparent with a superhyperfine splitting of the high field line into five lines probably due to two nitrogen ligands on the metal ion. From Fig. 4*b* it is evident that lowering the pH towards pH 7.0 leads to less of this complex and an increase in a second one where nitrogen structure is not resolved. This second complex has a greater value of g_0 and smaller value of A_0. We shall denote the different complexes starting from high pH so that the complex appearing above pH

Can. J. Chem. Downloaded from www.nrcresearchpress.com by 78.46.186.204 on 09/07/12
For personal use only.

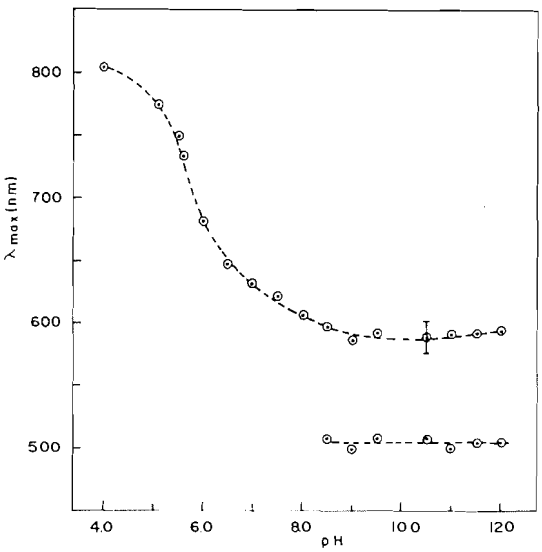

FIG. 2. Dependence of the wavelength for maximum absorption λ_{max} on the pH for the solution of Cu^{2+}—TRIS.

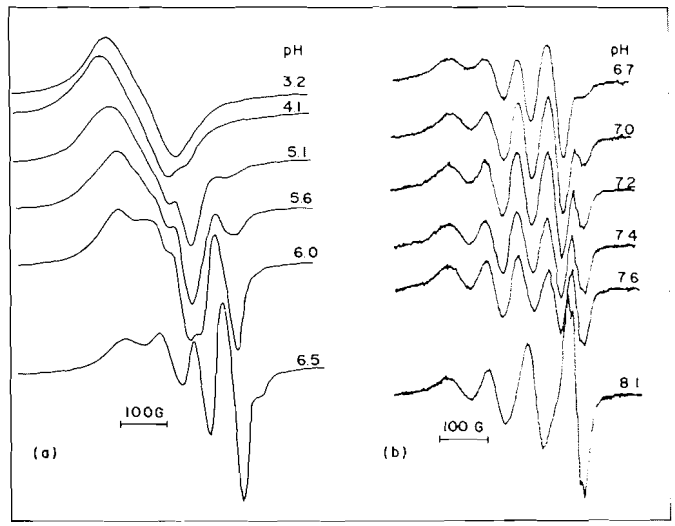

FIG. 4. Electron spin resonance spectra for the Cu^{2+}—TRIS solution as a function of pH at room temperature: (*a*) low pH range 3.2–6.5; (*b*) high pH range 6.7–8.1. Spectra above 8.1 do not change.

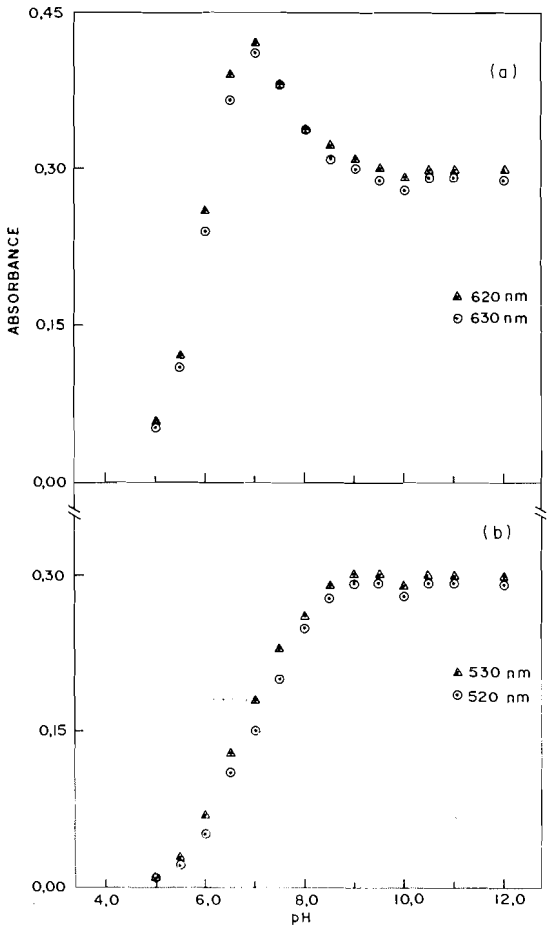

FIG. 3. Dependence of the intensity of the absorption at two different wavelengths which characterize the optical bands as a function of pH for the solution of Cu^{2+}—TRIS.

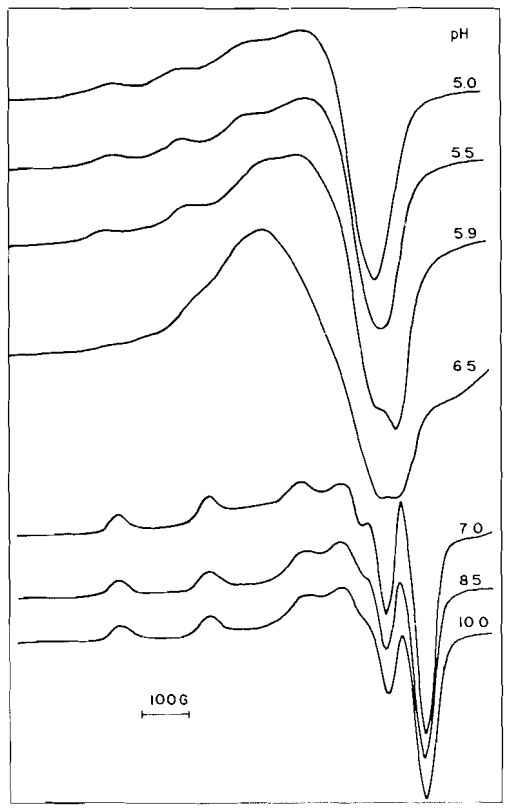

FIG. 5. Electron spin resonance spectra for the Cu^{2+}—TRIS frozen solution as a function of pH at −150°C.

8.0 will be **1**; the second complex around pH 7.0 will be **2**, etc.

Below pH 6.5, complex **1** disappears completely and the concentration of complex **2** is reduced; in fact, the amount of this complex is reduced dramatically at pH 5.6 (Fig. 4*a*). It is clear that at pH 6.0 and specially pH 5.6 there exists a complex **2** (small amount) and another lower pH complex (**3**). Further lowering of pH gives the hydrated copper ion as the predominant species. In order to further characterize the observed complexes esr spectra were taken at low temperature (Fig. 5). In the pH range 7.5–12.0 the spectrum practically does not change, this being a characteristic for the high pH species. The nitrogen hyperfine structure is not resolved at this low temperature. Complex **2** starts to show up near pH 7.0 and at pH 6.5 the contribution of complex **1** is very small (Fig. 5). The very broad line with poorly resolved hyperfine structure is probably due to the fact that complex **2** is highly charged and precipitates at low temperature or, alternatively, to dimer

TABLE 2. Electron paramagnetic resonance parameters for the complexes of Cu^{2+} with TRIS in solution as a function of pH

Complex	pH	g_0	A_0 (G)	A_N (G)	λ_{max} (nm)
1	10	2.135	82	9.5	587 508
2	6.5	2.147	65	—	650
3	5.0	2.180	44	—	775
Solvated ion	3.2	2.220	—	—	~800

*The parameters correspond to those for the pure complexes obtained through spectral subtraction (complexes **2** and **3**). The wavelength for maximum absorption was also included.

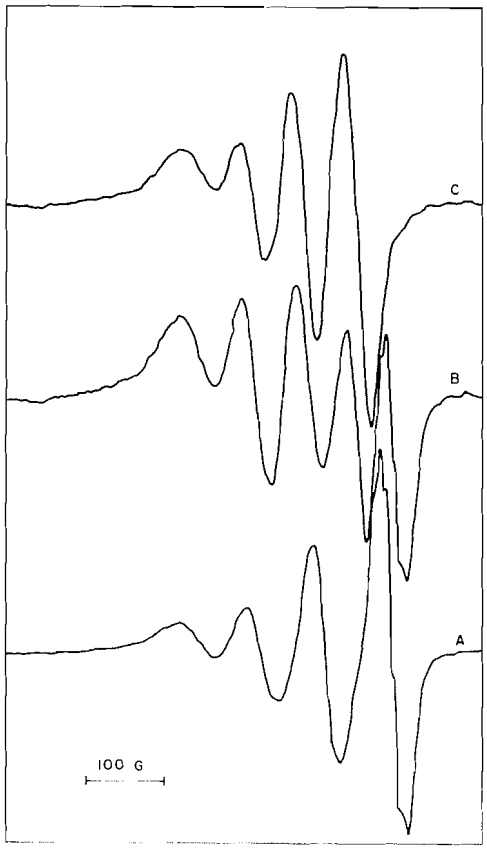

FIG. 6. Electron spin resonance spectrum for complex **2** (*C*) obtained through spectral subtraction using the experimental spectra at pH 10.0 (complex **1**, *A*) and at pH 7.6 (mixture of complexes **1** and **2**, *B*).

formation for complex **2**. It is interesting that the loss of resolution of copper hyperfine structure occurs in a very narrow pH range since both at pH 6.0 and pH 7.0 this structure again becomes resolved. The esr parameters for the complexes of Cu^{2+} with TRIS are listed in Table 2. From the spectra in Figs. 4 and 5 it is clear that the esr spectrum for **1** is pure and the parameters can be obtained with great accuracy. However, the parameters for complexes **2** and **3** can not be directly obtained due to the superposition of spectra for several complexes. To obtain the pure spectra of complexes **2** and **3**, a spectral subtraction was performed based on the relation $C = A - BX$, where *A* and *B* refer to spectra of the mixture of **1** and **2** and of pure **1**, respectively. The factor *X* is adjusted to obtain the best reproduction of the experimental spectrum (Fig. 6). The spectrum at pH 10.0 corresponds to pure complex **1** while at

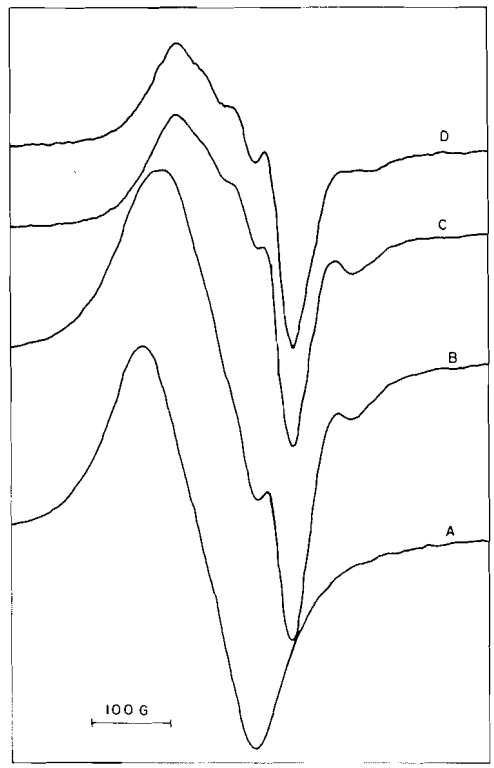

FIG. 7. Electron spin resonance spectrum for complex **3** (*D*) obtained through spectral subtraction using the experimental spectra at pH 3.2 (solvated ion *A*) and at pH 5.1 (mixture of solvated ion, complex **3** and small amount of complex **2**, *B*). The spectrum *C* was obtained from a subtraction of spectrum *A* from *B*; spectrum *D* takes in account the small amount of complex **2** in the spectrum *C*.

pH 7.6 corresponds to a contribution of both complexes. *X* turns out to be 0.45 for this case.

To obtain the spectrum of pure **3**, again the relation $C = A - BX$ was used where now *A* is the experimental spectrum at pH 5.1 and *B* is the experimental spectrum at pH 3.2, which corresponds to solvated free copper ion in solution. The result is shown in Fig. 7 ($X = 0.6$) from which it is clear that there is still a small contribution from complex **2**.

Single crystals for the high pH complex were obtained; the esr spectra and the angular variations in three orthogonal planes were measured (Fig. 8). A single esr line with no hyperfine structure is observed.

The angular variation was adjusted by the Zeeman Hamiltonian. The principal values for the g tensor are shown in Table 3. All these values are different, showing a small rhombic distortion in the symmetry of the complex.

Crystallography

Final atomic coordinates for non-hydrogen atoms and equivalent isotropic temperature factors are given in Table 4. The list of structure factors, anisotropic thermal parameters and hydrogen fractional coordinates have been deposited.[1] Bond distances and angles for the tris(hydroxymethyl)aminomethane moiety and for the coordination around the copper atom are given in Table 5.

The copper atom is located on a two-fold axis and is coordinated by an oxygen atom of a water molecule located on

[1]These tables are available from the Depository of Unpublished Data, CISTI, National Research Council of Canada, Ottawa, Ont., Canada K1A 0S2.

Can. J. Chem. Downloaded from www.nrcresearchpress.com by 78.46.186.204 on 09/07/12
For personal use only.

Can. J. Chem. Downloaded from www.nrcresearchpress.com by 78.46.186.204 on 09/07/12
For personal use only.

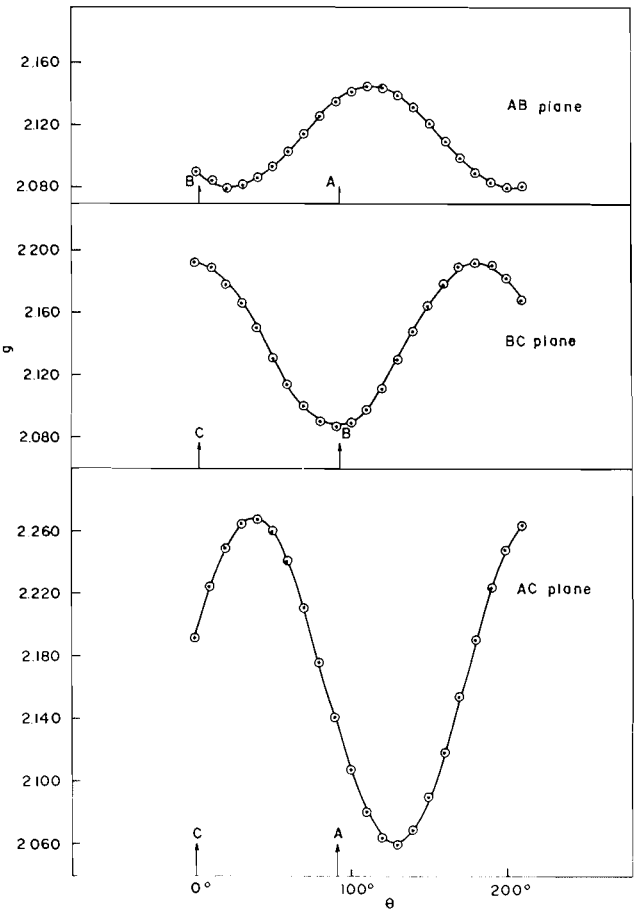

FIG. 8. Angular variations of the position of the esr spectra for the single crystal of Cu^{2+}·TRIS in three orthogonal crystal planes.

TABLE 3. Electron paramagnetic resonance parameters for the high pH complex (**1**) in solution (frozen), single crystal, and powder samples

Complex	g_1	g_2	g_3	$A_\parallel$ (G)	$A_\perp$ (G)
pH = 10 (−150°C)	2.255	2.101	2.071	190	28
Powder	2.268	2.102	2.060	—	—
Single crystal	2.268(9)	2.092(8)	2.053(6)	—	—

TABLE 4. Fractional coordinates and thermal parameters (Å^2), with standard deviations in parentheses

Atom	x/a	y/b	z/c	B_{eq}*
CU	0.0	0.2315(1)	0.25	1.63(2)
C(1)	0.1047(3)	0.2081(3)	0.0605(5)	1.8(1)
O(1)	−0.0069(2)	0.2180(2)	0.0527(3)	1.68(7)
C(2)	0.3124(3)	0.1514(4)	0.2260(5)	1.9(1)
D(2)	0.3909(2)	0.0935(2)	0.3596(3)	2.40(9)
C(3)	0.1538(3)	0.0056(3)	0.2012(5)	1.8(1)
O(3)	0.1698(2)	−0.0611(3)	0.0912(3)	2.40(9)
C(4)	0.1879(3)	0.1414(3)	0.2021(4)	1.3(1)
N	0.1716(3)	0.2027(3)	0.3235(4)	1.6(1)
O(W)	0.0	0.4343(4)	0.25	3.9(2)

*$B_{eq} = \frac{4}{3}\sum_{ij}(a_i a_j)B_{ij}$ (16).

TABLE 5. Relevant interatomic bond distances (Å) and angles (deg) for coordination around copper atom and the TRIS group

Atoms	Distance
Cu—O(1)	1.958(2)
Cu—N	2.028(4)
Cu—O(W)	2.189(4)
C(1)—O(1)	1.416(6)
C(1)—C(4)	1.530(6)
C(2)—O(2)	1.419(5)
C(2)—C(4)	1.524(6)
C(3)—O(3)	1.414(5)
C(3)—C(4)	1.530(5)
C(4)—N	1.488(5)

Bonds	Angle
O(1)—Cu—N	84.5(1)
O(1)—Cu—O(W)	94.3(1)
N—Cu—O(W)	98.8(1)
O(1)—C(1)—C(4)	111.2(3)
O(2)—C(2)—C(4)	112.1(3)
O(3)—C(3)—C(4)	110.4(3)
C(1)—C(4)—C(2)	111.5(3)
C(1)—C(4)—C(3)	111.4(3)
C(1)—C(4)—N	105.0(3)
C(2)—C(4)—C(3)	110.6(3)
C(2)—C(4)—N	111.6(3)
C(3)—C(4)—N	106.5(3)

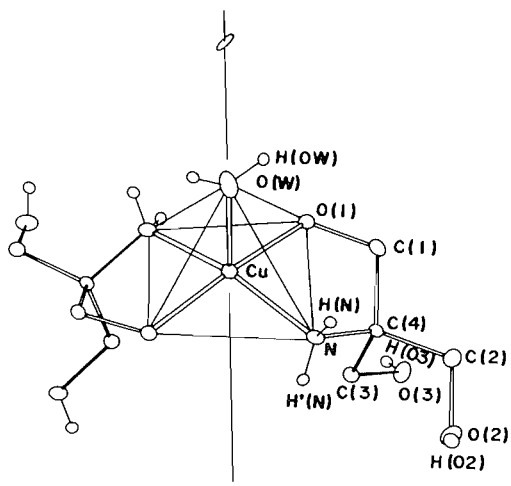

FIG. 9. Projection of the coordination around the copper atom. The atoms not named are related to the named atoms through a two-fold axis.

the same two-fold axis. Five atoms coordinate the copper atom forming an approximate pyramid with a rectangular basis as depicted in Fig. 9, which has its base formed by a pair of oxygen and nitrogen atoms. The atoms of each pair are related by a two-fold axis and belong to two symmetrically related tris(hydroxymethyl)aminomethane groups. The vertex of the pyramid is formed by the oxygen atom located on the two-fold axis. In a unit cell there are four coordination complexes linked to one another by a system of hydrogen bonds (Fig. 10).

Discussion

The formation curves were obtained on the basis of the

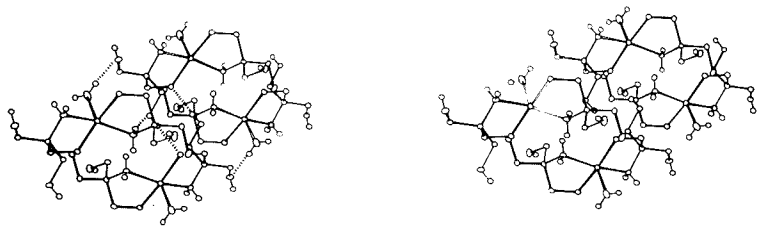

FIG. 10. Projection of the molecular packing showing the interaction through hydrogen bonds between four groups of the type depicted in Fig. 9.

TABLE 6. Relevant distances (Å) and angles (deg) in hydrogen bonds

Atoms	Distance O...O	Distance H...O	Angle O—H...O
O(3)—H(03)...O(1)	2.585(4)	0.72(4)	165.(1)
O(2)—H(02)...O(1)	2.716(4)	0.67(4)	175.(1)
O(W)—H(0W)...O(2)	2.752(4)	0.75(4)	162.(1)
N—H(N)...O(3)	3.113(5)	0.79(3)	168.(1)

equilibrium constants and reaction steps proposed for the Cu^{2+}—TRIS system (10).

The equilibrium analysis is rather complicated since eight different species are present in solution. Three species will be very predominant at different pH values: (*1*) the chelate complex $M(H_{-1}L)_2$ which above pH 9.5 is the only species present in solution; (*2*) the species ML_4 which near pH 7.6 is predominant and (*3*) the free solvated copper ion below pH 4.0. Together with the epr data, this analysis suggests that the highest pH complex observed by epr (complex **1**) could be assigned to the chelate since two nitrogen ligands show themselves in the room temperature spectrum. Our epr data show that the presence of this complex is significant down to pH 7.6 while the formation curves predict that at this low pH only ML_4 species would be significant. Therefore, our epr data seem to indicate that the formation curves in the region of pH above 7.2 should be displaced to lower pH, so that at pH 7.6 approximately 50% of the chelate species is present in the solution. This would require values for K_4 and K_{2b} to be lower and higher, respectively, than those given in ref. 10. Martell (10) considered the complete deprotonation of the hydroxyl groups, this leading to the structure corresponding to an uncharged species $M(H_{-1}L)_2$. This structure is essentially the same as the one obtained from X-ray crystallography except for the water molecule (see Fig. 9).

The epr results with the frozen solution suggest the occurrence of a rhombic distortion which is also observed for the high pH complex in the single crystal.

With regard to the optical spectra obtained at high pH it should be mentioned that similar complexes of aminoacids, where nitrogen and oxygen (carboxylate) ligands are involved, usually show a single broad band. In our case the splitting of the optical band is quite unusual; this could be explained alternatively in one of the following ways: (*a*) at high pH there is a coexistence of two different species, which have exactly the same epr spectrum, namely, $M(H_{-1}L)_2$ and $M(H_{-1}LL)^+$; the two optical bands are due to these different species and the formation curve for complex $(MH_{-1}LL)^+$ is wrong. (*b*) At high pH there is a single species with an optical band split in two bands. We believe this hypothesis should be preferred because upon freezing the splitting in the epr spectrum is not observed. Also, it is in closer agreement with the formation curves.

In the pH range between 6.0 and 7.5 the species which is predominant corresponds to our complex **2**. The equilibrium constant K_4 has to be corrected so that its maximum intensity would be shifted to pH 6.7 as indicated by the optical data (Fig. 4*a*).

Acknowledgements

We thank the Brazilian Agencies CNPq, FINEP, CAPES for partial financial support through research grants. We also appreciate the effective assistance from Mr. Valdeci Massaro for computer spectral analysis.

1. H. C. FREEMAN. *In* Inorganic biochemistry. *Edited by* G. I. Eichorn. Elsevier, Amsterdam. 1973. Chap. 4.
2. J. F. BOAS, J. R. PILBROW, and T. D. SMITH. Biological magnetic resonance. *Edited by* L. J. Berliner and J. Reuben. Plenum Press. 1978.
3. D. J. E. INGRAM. Biological and biochemical applications of ESR. Adam Hilger Ltd., London. 1969.
4. B. J. HATHAWAY and B. E. BILLING. Coordin. Chem. Rev. **5**, 143 (1970).
5. L. SPORTELLI, H. NEUBACHER, and W. LOHMANN. Biophys. Struct. Mechanism. **3**, 317 (1977).
6. H. KOZLOWSKI and B. J. TREZEBIATOWSKA. J. Mol. Struct. **45**, 159 (1978).
7. O. R. NASCIMENTO and M. TABAK. J. Inorg. Biochem. **23**, 13 (1985).
8. S. HARKEMA, J. W. BATS, A. M. WEYENBERG, and D. FEIL. Acta Crystallogr. B**29**, 143 (1973).
9. R. RUDMAN, D. EHNERMAN, and S. J. LA PLACE. Science, **200**, 531 (1978).
10. K. S. BAI and A. F. MARTELL. J. Inorg. Nucl. Chem. **31**, 1697 (1969).
11. D. T. CROMER and J. B. MANN. Acta Crystallogr. **24**, 321 (1968).
12. D. T. CROMER and D. LIBERMAN. J. Chem. Phys. **53**, 1891 (1970).
13. R. F. STEWART, E. R. DAVIDSON, and W. T. SIMPSON. J. Chem. Phys. **42**, 3175 (1965).
14. G. M. SHELDRICK. SHELX-76 program for crystal structure determination. University of Cambridge. 1976.
15. C. K. JOHNSON. ORTEP. Report ORNL-3794, Oak Ridge National Laboratory, TN. 1965.
16. W. C. HAMILTON. Acta Crystallogr. **12**, 609 (1959).

Can. J. Chem. Downloaded from www.nrcresearchpress.com by 78.46.186.204 on 09/07/12
For personal use only.

Complexes of W(VI) and Mo(VI) with glycolic, lactic, chloro- and phenyl-lactic, mandelic, and glyceric acids studied by ^1H and ^{13}C nuclear magnetic resonance spectroscopy

M. Madalena Caldeira, M. Luisa Ramos, and Victor M. S. Gil
Department of Chemistry, University of Coimbra, 3049 Coimbra, Portugal

Received August 8, 1986

M. Madalena Caldeira, M. Luisa Ramos, and Victor M. S. Gil. Can. J. Chem. **65**, 827 (1987).

A proton and carbon-13 nuclear magnetic resonance study is reported on the number, stoichiometry, geometry, and stability of the complexes that form when sodium tungstate or sodium molybdate is mixed with each one of the following α-hydroxyacids in aqueous solution at pH values in the range 3–8: glycolic, lactic, chloro-3- and phenyl-3-lactic, mandelic, and glyceric acids. The predominant complexes have 1:2 composition and pK of formation of the order of −15 to −16.

M. Madalena Caldeira, M. Luisa Ramos et Victor M. S. Gil. Can. J. Chem. **65**, 827 (1987).

On rapporte une étude par rmn du ^1H et du ^{13}C sur le nombre, le stoechiométrie, la géométrie et la stabilité des complexes qui se forment lorsqu'on mélange du tungstate ou du molybdate de sodium avec l'un des α-hydroxyacides suivants, dans des solutions aqueuses dont le pH se situe entre 3 et 8 : acides glycolique, lactique, chloro-3 et phényl-3 lactiques, mandélique et glycérique. La composition des complexes prédominats est 1:2 et les pK de leurs formations sont de l'ordre de −15 à −16.
[Traduit par la revue]

Introduction

Very stable complexes are well known to form when α-hydroxycarboxylic acids are mixed with molybdate or tungstate salts in aqueous solution. Frequently, more than one complex can form, depending on the experimental conditions, namely the molar ratio of the complexing species and the pH of the solution. This explains most of the contradictory reports often found in the literature. In addition, the classical techniques used (potentiometry, conductimetry, polarimetry, spectrophotometry, cryoscopy) measure bulk properties that must somehow be separated into individual contributions.

Taking advantage of the fact that, at ordinary temperatures, ligand exchange is usually slow enough to enable distinct nmr spectra to be obtained for free and bound ligand in the various complexes, we have been carrying out a systematic study of such complexation reactions (the most recent paper in the series, ref. 1), as well as of complexes involving other oxo-ions: uranyl (2) and vanadate ions (3). The previous study with malic (CO_2H—CH_2—$CHOH$—CO_2H) (4), thiomalic (CO_2H—CH_2—$CHSH$—CO_2H) (1, 5), and tartaric (CO_2H—$CHOH$—$CHOH$—CO_2H) (6) acids is now extended to the following ligands:

A. Glycolic acid	$CH_2(OH)$—CO_2H
B. (L)-Lactic acid	CH_3—$CH(OH)$—CO_2H
C. (L)-Phenyl-lactic acid	C_6H_5—CH_2—$CH(OH)$—CO_2H
D. (D,L)-Chloro-lactic acid	CH_2Cl—$CH(OH)$—CO_2H
E. (L)-Mandelic acid	C_6H_5—$CH(OH)$—CO_2H
F. (D,L)-Glyceric acid	$CH_2(OH)$—$CH(OH)$—CO_2H

The system Mo(VI) + lactic acid will be only briefly mentioned in comparison with the tungsten counterpart, as the former was already included in ref. 1.

Experimental

Analytical grade sodium tungstate and sodium molybdate and commercially available hydroxyacids were used (unavailability of the optically active forms in two cases and failure in attempts to resolve the racemic mixtures preclude us from also using one of the optical isomers in such cases). To reduce the intensity of the OH nmr signal, the salts were dried at 120°C, the acids were lyophilized from a solution in deuterium oxide, and D_2O solutions were used throughout. Previous to use, lactic, chloro-lactic, and glyceric acid solutions in D_2O were heated in boiling water for 2 hours to accomplish depolymerization. The concentrations of the tungstate and molybdate solutions were established by weight and the acid solutions were standardized by potentiometry. The pH was adjusted by addition of solutions of DCl and NaOD: the pH* values quoted are the direct pH-meter readings (room temperature) after standardization with aqueous (H_2O) buffers. Whenever necessary, the ionic strength was kept approximately constant by making the solution 1 M in NaCl.

The ^1H and ^{13}C spectra were obtained on a Varian XL-200 nmr spectrometer at probe temperature (21 ± 1°C). The latter were recorded using proton-decoupling techniques with suppression of the nuclear Overhauser effect; in this manner, temperature fluctuations of the sample were reduced to ca. ±1°C. Dioxane and DSS were used as internal references, respectively, for ^{13}C and ^1H shifts. Typically, spectral widths of 10 000 Hz, acquisition times of 1.5 s, pulse delays of 8–12 s, and 2000 pulses were used when recording ^{13}C spectra.

Results and discussion

Proton and carbon-13 nmr spectra were obtained for D_2O solutions of various concentrations (in the range 0.02–1.0 M for ^1H spectra and 0.2–1.0 M for ^{13}C spectra) and of different molar ratios (3:1 to 1:3 or 1:4) of complexing species and of different pH* values. Since at low pH the signals are usually broad, suggesting extensive polymerization, and at pH > 8 complexation is almost nonexistent, the pH range covered was 3–7.5. The number and intensity of ligand (free and bound) signals, together with their changes with molar ratio and pH, enable the number of complexes to be established. Job's plots based on ^1H spectral intensities give the stoichiometry of the dominant complex in each case. When only one complex is formed, a formation constant is determined.

The ^{13}C and ^1H chemical shifts observed on complexation indicate the groups by which the ligand binds to the metal. Finally, vicinal proton–proton coupling constants are measured to give information on the conformation of the bound ligands C, D, and F.

We shall now briefly present the results obtained with each acid as ligand, dealing with the first ligand in the series (glycolic acid) in more detail, and compare with results in the literature, whenever existent, provided by other techniques.

(a) Glycolic acid

The ^1H nmr spectrum of glycolic acid is just one line (δ_H = 4.02 at pH* = 5.1) (apart from the contribution of the OH groups to the common OH signal), which gives rise to an AB spectrum when complexation to tungsten occurs; the center of

Printed in Canada / Imprimé au Canada

Can. J. Chem. Downloaded from www.nrcresearchpress.com by 80.58.250.72 on 09/07/12
For personal use only.

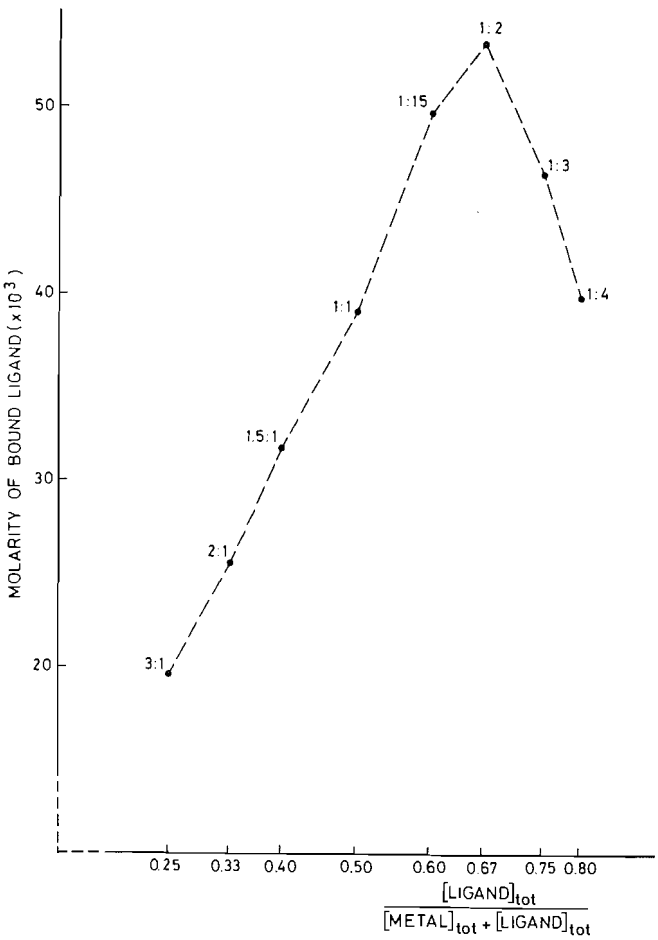

FIG. 1. Job's curve based on proton nmr spectral intensities for the system W(VI) + glycolic acid. Total concentration of complexing species 0.10 *M* (D_2O solutions, 1 *M* in NaCl, pH* = 5.1).

this spectrum is shifted by 1.08 ppm (to high frequency) with respect to free ligand (at pH* = 5.1) with $|\nu_A - \nu_B| = 0.17$ ppm and J_{AB} = 17.2 Hz. Only one complex is detected for the whole range of concentrations, pH, and molar ratios covered. The Job's plot given in Fig. 1 clearly shows that this is a 1:2 (metal:ligand) species.

A p*K* of formation of -15.7 ± 0.2 is obtained (from the measured concentrations of free and bound ligand for the various molar ratios, at pH* = 5.1, the ionic strength being kept approximately constant with NaCl 1 *M*) for the equilibrium

$$WO_4^{2-} + 2HY^- + 2H^+ \rightleftarrows WO_2Y_2^{2-} + 2H_2O$$

where the hydroxyacid is represented by H_2Y. In the calculation, due account was taken of the main equilibrium of polymerization of WO_4^{2-} for the conditions used (7)

$$12WO_4^{2-} + 18H^+ \rightleftarrows W_{12}O_{39}^{6-} + 9H_2O$$

with p*K* = −132.5; this is especially important for solutions having a higher content of metal ion.

That both the carboxylate and the hydroxyl groups are involved in chelation, with likely deprotonation of the OH group, is revealed by the proton and the carbon shifts. In particular, there is a big shift of the methylenic ^{13}C signal to high frequency on complexation. The δ_C values for the free ligand at pH* = 5.0 and the $\Delta\delta_C$ values upon complexation ($\Delta\delta$ = δ(complex) − δ(acid at same pH) are given in Table 1. At pH* = 7.2 similar shifts are observed (11.77 and 4.61) but at pH* = 3.0 they become 13.36 and 7.63, respectively, because the free ligand (pK_a = 3.8 (8)) is then almost entirely in the acid form (ionization of glycolic acid causes high frequency shifts of 1.42 and 3.22 ppm for the CH_2 and CO_2H groups, respectively).

TABLE 1. Carbon δ_C-values (in brackets) for α-hydroxycarboxylic acids A–F and shifts on complexation with W(VI) and Mo(VI) (pH* = 5.0 ± 0.1)

	R	CH(OH)	CO_2H
(A) R:H		(61.99)	(181.21)
+ W(VI)		11.61	4.29
+ Mo(VI)		12.72	3.82
(B) R: CH_3	(20.48)	(69.23)	(183.80)
+ W(VI)	−1.61	11.22	4.04
+ Mo(VI)	−1.82	12.04	3.91
(C) R:$CH_2\phi$	(40.84)	(73.76)	(180.80)
+ W(VI)	−0.99	10.74	5.17
+ Mo(VI)	−1.19	11.73	4.77
(D) R:CH_2Cl	(48.57)	(72.97)	(178.41)
+ W(VI)	0.0(*a*)	10.76(*a*)	5.09(*a*)
	−0.10(*b*)	12.09(*b*)	4.45(*b*)
+ Mo(VI)	0.0	10.66	4.45
(E) R:C_6H_5	(141.67)*	(76.00)	(180.30)
+ W(VI)	−0.32	10.50(*a*)	4.77(*a*)
		11.93(*b*)	4.29(*b*)
+ Mo(VI)	0.0	11.45	4.14
(F) R:$CH_2(OH)$	(64.80)	(74.12)	(179.71)
+ W(VI)	1.2	12.48(a_1)	4.02(a_1)
		12.21(a_2)	4.31(a_2)
	1.0	11.87(b_1)	4.49(b_1)
		11.50(b_2)	4.79(b_2)
+ Mo(VI)	0.2	12.09(*a*)	3.61(*a*)
		12.48(*b*)	3.30(*b*)

*Carbon 1 in the phenyl ring.

From the magnetic equivalence of the two ligand molecules we can conclude that the structure of a 1:2 monomeric pseudo-octahedral complex is either **I** or **II**.

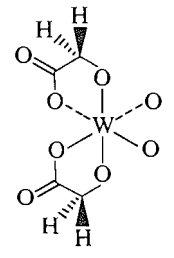

I

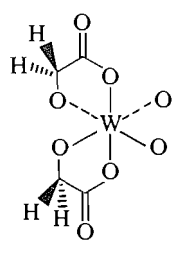

II

If an analogy with the 1:2 complex of Mo(VI) with malic acid is allowed, for which the crystal structure was recently determined (9), then **I** is to be preferred. In both **I** and **II**, the two methylenic H nuclei become nonequivalent. It is noted that this nonequivalence is a result of the *cis*-MoO_2 arrangement and would not occur for a 1:2 *trans* dioxo species.

The effect of pH on the formation of the complex is illustrated by the following concentrations measured approximately by the nmr spectral intensities in a 0.003 *M*:0.067 *M* (metal:ligand) solution (1 *M* in NaCl): 6.0×10^{-2} *M* at pH* = 3.4, 5.4×10^{-2} *M* at pH* = 5.1, and 1.9×10^{-2} *M* at pH* = 7.2.

Only one complex is also detected in the case of molyb-

Can. J. Chem. Downloaded from www.nrcresearchpress.com by 80.58.250.72 on 09/07/12
For personal use only.

Can. J. Chem. Downloaded from www.nrcresearchpress.com by 80.58.250.72 on 09/07/12
For personal use only.

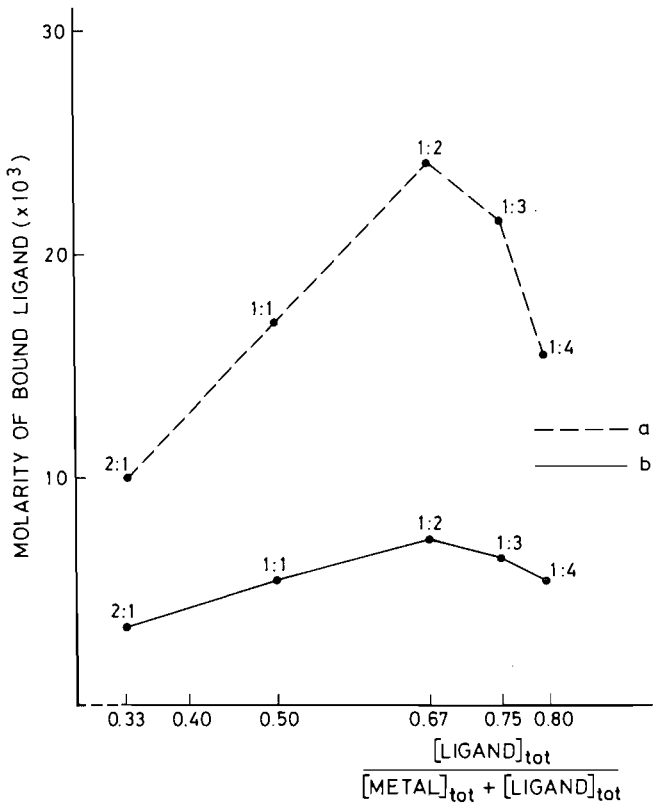

FIG. 2. Job's plots based on proton nmr spectral intensities for the system W(VI) + (L)-lactic acid: complexes *a* and *b*. Total concentration of complexing species 0.05 *M* (D_2O solutions, 1 *M* in NaCl, pH* = 5.0).

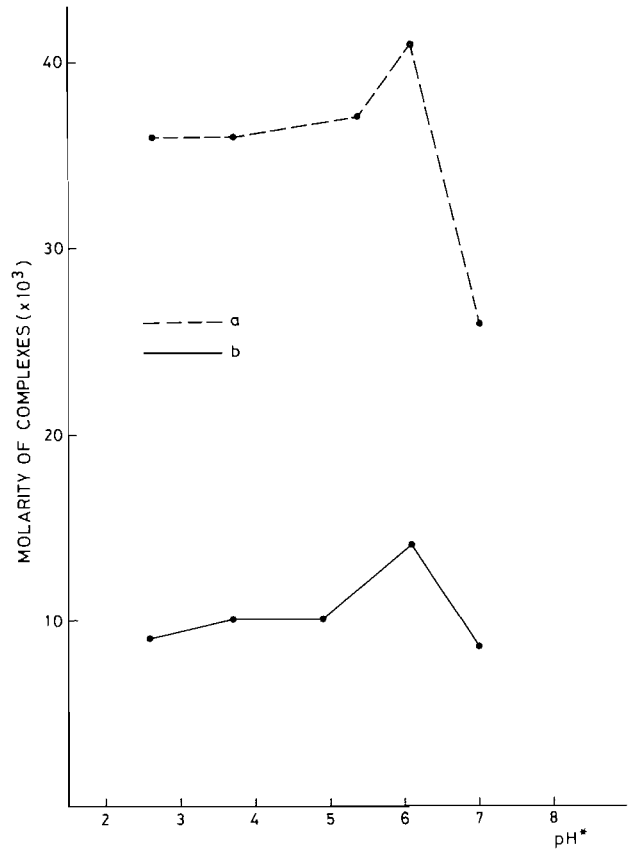

FIG. 3. Effect of pH on the concentration of the complexes (*a* and *b*) W(VI) + (L)-lactic acid (0.033 *M* : 0.067 *M* D_2O solution 1 *M* in NaCl).

denum. The proton nmr spectrum is broader than with tungsten and, instead of an AB pattern, a broad singlet (close to the OH residual signal) is observed. This broadening is due to partial reduction of Mo(VI) to paramagnetic lower oxidation states and (or) to more rapid exchange processes. The proton shift on complexation is 0.80 ppm; the carbon shifts are shown in Table 1.

Reliable integration of the signals in order to draw a Job's plot in this case was not feasible. But from qualitative inspection of the spectra and by analogy with W(VI), it seems safe to infer that the complex is again 1:2.

The formation of a 1:2 complex both with W(VI) and Mo(VI) was previously shown by the conductimetric and polarimetric studies of Brown (10), corroborated, in the case of Mo(VI), by Cadiot and Viossat using potentiometry (11) and, in the case of W(VI), by Wünsch and Nagen using uv spectrophotometry (12).

(b) Lactic, phenyl- and chloro-lactic, and mandelic acids

For lactic acid, both free and bound ligand give rise to A_3X spectra. In the case of W(VI), two complexes are formed, one being always dominant. The A doublet is almost not shifted upon complexation, but the X quartets are shifted by 0.94 and 1.08 ppm to high frequency, respectively, for the more and less abundant complex, at pH* = 5.0 (J_{AX} = 6.40 Hz and J_{AX} = 7.00 Hz, respectively); at this pH*, the δ_H values for free lactic acid are 1.34(A) and 4.12(X). Job's plots are shown in Fig. 2; the dominant complex is clearly a 1:2 species, but no stoichiometry can be unequivocally established for the weaker complex from these curves.

The effect of pH on the concentrations of the complexes is shown in Fig. 3; maximum complexation occurs at pH* $\simeq$ 6 for both cases.

The carbon shifts, at pH* = 5.0, for the most stable complex are presented in Table 1.

The structure of the complex is probably similar to that of the 1:2 complex of W(VI) with glycolic acid. We note, however, that the substitution of H in CH_2 by CH_3 leads to the possibility of formation of diastereomers. This may be the reason for the occurrence of two complexes in this case.

As expected, the use of (D,L)-lactic acid leads to additional signals of bound ligand due to the simultaneous involvement of D and L forms in the same complex.

For the system molybdenum + lactic acid only one complex is formed and its stoichiometry given by Job's method is 1:2 (1). A p*K* of formation of -14.7 ± 0.4 is calculated in the same way as done for tungsten + glycolic acid.

The proton shifts on complexation, at pH* = 5.1, are 0.07 and 0.74 ppm for CH_3 and CH, respectively; the carbon shifts are included in Table 1.

Complexation of W(VI) with lactic acid was previously mentioned in the literature (13, 14) but no quantitative study was reported. More abundant is the literature on the Mo(VI) + lactic acid system (15–17). Evidence for 1:2 complexation is found by applying various techniques. Cervilla and co-workers (17) suggested, in addition, the formation of 1:1 species at pH < 4.7 on the basis of spectrophotometry and cryoscopy; we could not corroborate those findings by nmr.

The results obtained with phenyl- and chloro-lactic acids and with mandelic acid are very similar to those for lactic acid as ligand, namely one complex with Mo(VI) of composition 1:2

TABLE 2. ^{1}H nuclear magnetic resonance parameters for W(VI) + phenyl-lactic acid and W(VI) + chloro-lactic acid (couplings in Hz)

		δ_A	δ_B	δ_X	$\lvert J_{AB}\rvert$	J_{AX}	J_{BX}
(L)-Phenyl-lactic acid (pH* = 5.3)	Free ligand	2.75	2.96	4.27	14.0	8.2	3.9
	Complex *a* (dominant)	3.07	3.04	5.14	13.0	7.7	3.5
	Complex *b*	—	—	5.31	—	$J_{AX} + J_{BX}$ = 14.2	
(D,L)-Chloro-lactic acid (pH* = 5.2)	Free ligand	3.81	3.85	4.35	11.7	2.5	4.6
	Complex *a* (dominant)	3.87	4.00	5.17	12.1	2.6	4.2
	Complex *b*	—	—	5.29	—	$J_{AX} + J_{BX}$ = 9.3	

($pK = 16.0 \pm 0.3$ for (L)-phenyl-lactic acid, $pK = 14.8 \pm 0.6$ for (L)-mandelic acid as ligands) and two complexes with W(VI), one of composition 1:2 being largely dominant ($pK = 15.8 \pm 0.3$ for (L)-phenyl-lactic acid).

The tungsten(VI) – mandelic acid system had been previously studied by Richardson using potentiometry and conductimetry (19), by Brown using conductimetry and polarimetry (10), and by Banerjee and Bhattacharya using conductimetry and potentiometry (20); Richardson concludes that there is formation of a 1:3 complex and the others propose 1:2 complexation. The authors of refs. 10 and 20 show the formation of a 1:2 complex between Mo(VI) and mandelic acid, a result earlier pointed out by Souchay on the basis of a potentiometric study (21).

The carbon shifts are included in Table 1. The proton spectra of phenyl- and chloro-lactic acids are of the ABX type (plus the aromatic signals in the case of the former). The proton nmr parameters are given in Table 2 (due to overlap of the AB signals, only partial data could be obtained for the weaker complex).

The vicinal HH coupling constants of phenyl-lactic acid are not significantly altered by complexation, which points to a conformation of the bound ligand similar to the mean conformation of free ligand. A typical *gauche* coupling ($J_{BX} = 3.85$ Hz) and a typical *trans* coupling affected by an electronegative substituent, i.e., OH ($J_{AX} = 8.15$ Hz), suggest that the preferred staggered conformer of the acid is either

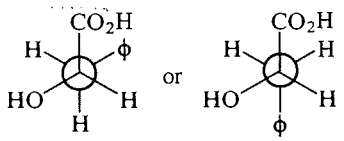

different from the conformation in the crystal (18).

The vicinal HH coupling constants for both free and bound chloro-lactic acid are particularly low, suggesting a conformation close to

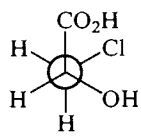

in the complex and an important contribution of such a conformer in the rapidly rotating free ligand molecule.

TABLE 3. ^{1}H nuclear magnetic resonance parameters for W(VI) + (D,L)-glyceric acid (pH* = 5.2)

	δ_A	δ_B	δ_X	$\lvert J_{AB}\rvert$	J_{AX}	J_{BX}
Free ligand	3.71	3.81	4.14	12.1	6.4	2.8
Complexes: a_1	—	—	5.26	—	$J_{AX} + J_{BX}$ = 8.2	
a_2	—	—	5.24	—	$J_{AX} + J_{BX}$ = 8.2	
b_1	3.89	3.83	5.04	12.0	5.8	2.4
b_2	—	—	5.01	—	$J_{AX} + J_{BX}$ = 8.0	

Apart from the second-order pattern arising from the aromatic ring, which is little affected by complexation, the proton spectrum of mandelic acid is just one line, due to the C*H*(OH) group ($\delta_H = 5.02$ at pH* = 5.0). This shifts by 0.71 ppm on complexation to Mo(VI) and by 0.90 and 1.04 ppm respectively on formation of the more and the less stable complex with W(VI).

(c) (D,L)-Glyceric acid

There is now an additional OH group as potential coordinating site. Also, due to the use of the racemic mixture of glyceric acid, more complexes can form. In fact, two pairs of complexes a_1,a_2 and b_1,b_2 are detected with W(VI), the chemical shifts being very similar in each pair.

The ^{1}H nmr spectra are of the ABX type and the corresponding parameters are given in Table 3.

Since separate integration of the a_1 and a_2 signals and of b_1 and b_2 was not possible, Job's plots for $a_1 + a_2$ and for $b_1 + b_2$ were constructed; maximum intensity occurs in both cases for 1:2 composition.

Only one pair a,b of spectra (broader than with W(VI)) is observed with molybdenum(VI), also due to 1:2 complexes.

The carbon shifts are given in Table 1. The big difference between the shifts of CH_2OH and $CHOH$ on complexation is a clear indication that only the α OH group, together with CO_2H, is bound to the metal.

The vicinal HH coupling constants of bound and free ligand are not significantly different. One of the values is typical of a *gauche* coupling whereas the other is intermediate between a *trans* and a *gauche* coupling constant. For the free ligand, this means an about equal contribution of conformers **III**′ and **I**′ or

Can. J. Chem. Downloaded from www.nrcresearchpress.com by 80.58.250.72 on 09/07/12
For personal use only.

TABLE 4. Complexes of W(VI) and Mo(VI) with α-hydroxycarboxylic acids as revealed by nuclear magnetic resonance

	CH_2OH CO_2H	CH_3 $CHOH$ CO_2H	$CH_2\phi$ $CHOH$ CO_2H	CH_2Cl $CHOH$ CO_2H	ϕ $CHOH$ CO_2H	CH_2OH $CHOH$ CO_2H	CO_2H CH_2 $CHOH$ CO_2H
W(VI)	1:2 ($pK = -15.7$)	1:2	1:2 ($pK = -15.8$)	1:2	1:2	1:2	1:2
	—	1:2 ?*	*	*	1:2 ?*	1:2 ?	1:2 ?* 1:1
Mo(VI)	1:2	1:2 ($pK = -14.7$)	1:2 ($pK = -16.0$)	1:2	1:2 ($pK = -14.8$)	1:2	1:2
	—	—	—	—	—	1:2 ?	1:2 ?* 1:1 ? 2:1

*Weaker complex.

III′ and **II′**:

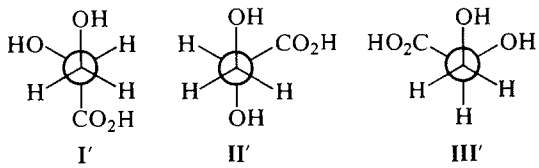

However, the undecoupled $^{13}CO_2H$ signal (the Y part of a ABMY system) shows that $^3J_{CH(A)} + {}^3J_{CH(B)} + |^2J_{CH(X)}| = 9.0$ Hz, which, in view of the typical values for *trans*, *gauche*, and *geminal* ^{13}CH coupling constants in similar compounds (22), requires a significant contribution of **I′** (for which the carboxylic group is *gauche* to both H(A) and H(B)). We may, therefore, conclude in favour of the pair I′,III′.

The values of J_{AX} and J_{BX} for the bound ligand in b_1 and the sum $J_{AX} + J_{BX}$ in the other complexes are slightly smaller than for free ligand. This suggests a conformation intermediate between **I′** and **III′**, with stabilization of **III′** with respect to the free ligand.

Conclusion

Table 4 summarizes our findings relative to the number, composition, and, in some cases, approximate formation constants of the complexes formed between W(VI) or Mo(VI) and α-hydroxycarboxylic acids in aqueous solution (pH range 3–7.5).

Malic acid, with its second carboxylic group, was also included for comparison. The data were taken from refs. 4 and 23, after confirmation at 200 MHz and for dilute solutions (Fig. 4) of the results for W(VI) + malic acid previously obtained at ~1 *M* concentrations in a continuous wave 100 MHz spectrometer (23).[1]

[1]The new data requires that two corrections should be made to the initial work (23). Firstly, it was found that the position of the X signal of complex *b* (Fig. 4) is very sensitive to pH, shifting to higher frequency in acidic media, that being the real reason for the evolution of the spectrum with time reported in ref. 23. Secondly, carbon spectra were recorded and the shifts observed on complexation (10–12 ppm for *C*HOH, 5–6 ppm for the α CO_2H group, −1 to 0 ppm for the β CO_2H group) clearly show it is the α and not the β carboxyl group that is involved in chelation, together with the OH group (see also ref. 5).

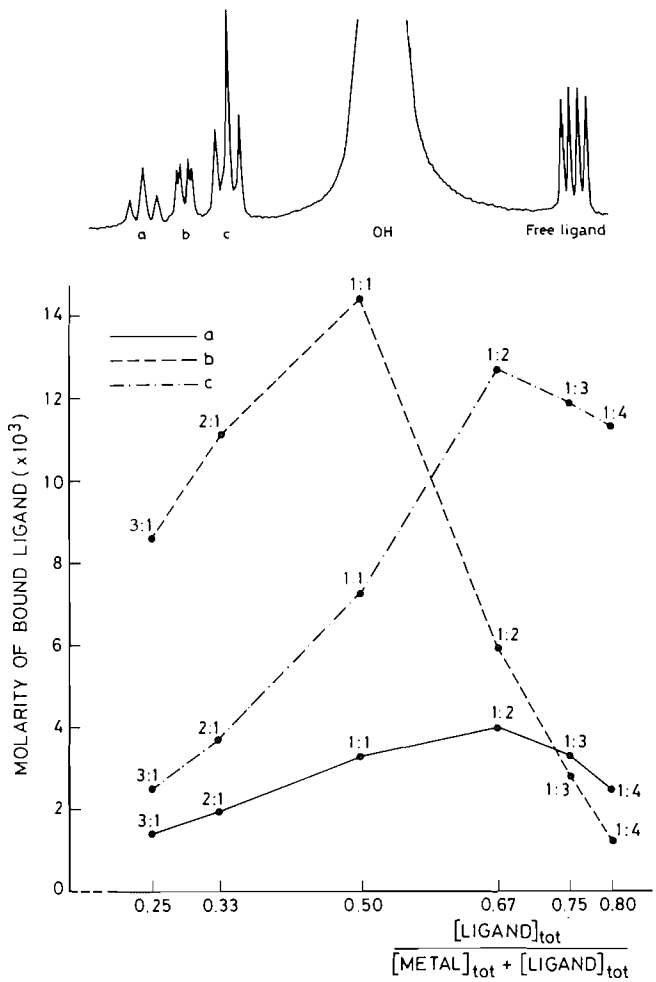

FIG. 4. The 200-MHz proton nmr *C*HOH signals for bound (complexes *a*, *b*, *c*) and free ligand in a 0.017 *M*:0.033 *M* WO_4^{2-} + (L)-malic acid solution in D_2O, and Job's plots as in Fig. 2 (pH* = 4.4).

The question marks in Table 4 refer to complexes of maximum concentration for the ratio indicated, in Job's plots, but which are not predominant in those conditions; in such cases, no stoichiometry can be directly inferred from the Job's method. Thus, for example, the weaker W(VI) + malic acid

Can. J. Chem. Downloaded from www.nrcresearchpress.com by 80.58.250.72 on 09/07/12
For personal use only.

complex might be one of the 1:1 (or 2:2) complexes suggested by Cervilla *et al.* (24).

We note the occurrence of predominant 1:2 complexation in all cases (together with 1:1 complexation for malic acid). The weaker complexes indicated in Table 4 are presumably 1:2 diastereomers of the dominant complexes arising because of the asymmetric carbon atom; in accordance with this, glycolic acid leads to only one complex. The weaker complex is usually not detected when the metal is molybdenum.

A curious observation regarding the ^{13}C shifts on complexation of the acids to the metals is that $\Delta\delta_C$ for CO_2H is larger with W(VI), whereas $\Delta\delta_C$ for $CHOH$ is in general larger with Mo(VI). On the other hand, $\Delta\delta_H$ for $CHOH$ is smaller with Mo(VI).

Acknowledgements

This work is a contribution of the Centro de Investigação em Química, Coimbra, supported by the Instituto Nacional de Investigação Cientifica (Portuguese Ministry of Education).

1. M. M. CALDEIRA and V. M. S. GIL. Polyhedron, **5**, 381 (1986).
2. M. T. NUNES and V. M. S. GIL. Inorg. Chim. Acta, **115**, 107 (1986), and references therein.
3. M. M. CALDEIRA, N. C. OLIVEIRA, V. M. S. GIL, and C. F. G. GERALDES. Rev. Port. Chim. **27**, 344 (1985).
4. M. M. CALDEIRA, M. E. SARAIVA, and V. M. S. GIL. Inorg. Nucl. Chem. Lett. **17**, 295 (1981).
5. M. M. CALDEIRA and V. M. S. GIL. Can. J. Chem. **62**, 2094 (1984).
6. A. M. CAVALEIRO, V. M. S. GIL, J. PEDROSA JESUS, R. D. GILLARD, and P. A. WILLIAMS. Transition Met. Chem. **9**, 62 (1984).
7. C. F. BAES, JR. and R. E. MESMER. The hydrolysis of cations. J. Wiley, New York. 1976.
8. L. G. SILLÉN and A. E. MARTELL. Stability constants of metal ion complexes. Chemical Society, London. 1964.
9. C. B. KNOBLER, A. J. WILSON, R. N. HIDER, I. W. JENSEN, B. R. PENFOLD, W. T. ROBINSON, and C. J. WILKINS. J. Chem. Soc. Dalton Trans. 1299 (1983).
10. D. H. BROWN. J. Chem. Soc. 4732 (1961).
11. M. CADIOT and B. VIOSSAT. Rev. Chim. Miner. **6**, 727 (1969).
12. G. WUNSCH and K. NAGEN. Fresenius Z. Anal. Chem. **295**, 119 (1979).
13. D. H. BROWN and D. NEUMANN. J. Inorg. Nucl. Chem. **37**, 330 (1975).
14. D. A. SHISHKOV. Dokl. Bolg. Akad. Nauk, **22**, 1149 (1969); Chem. Abstr. 4816a, 1970.
15. W. VOELTER, E. BAYER, G. BARTH, E. BUNNENBERG, and C. DJERASSI. Chem. Ber. **102**, 2003 (1969), and references therein.
16. L. DAVIES and R. RICHARDSON. J. Less-Common Met. **4**, 109 (1962).
17. A. BELTRÁN-PORTER, A. CERVILLA, F. CATURLA, and M. J. VILLA. Transition Met. Chem. **8**, 324 (1983).
18. M. CESARIO and J. GUILHEM. Cryst. Struct. Commun. **4**, 245 (1975).
19. E. RICHARDSON. J. Inorg. Nucl. Chem. **13**, 84 (1960).
20. S. P. BANERJEE and A. K. BHATTACHARYA. Curr. Sci. **30**, 380 (1961).
21. P. SOUCHAY. Bull. Soc. Chim. Fr. 122 (1949).
22. V. M. S. GIL. Org. Magn. Reson. **15**, 96 (1981).
23. V. M. S. GIL, M. E. SARAIVA, M. M. CALDEIRA, and A. M. D. PEREIRA. J. Inorg. Nucl. Chem. **42**, 389 (1980).
24. A. CERVILLA, J. A. RAMIREZ, and E. LLOPIS. Can. J. Chem. **63**, 1041 (1985).

Can. J. Chem. Downloaded from www.nrcresearchpress.com by 80.58.250.72 on 09/07/12
For personal use only.

Densities and apparent molar volumes of aqueous NaCl–KBr mixtures at 298.15 K. An alternative treatment

ALAN A. HUMFFRAY

Department of Physical Chemistry, University of Melbourne, Parkville, 3052, Victoria, Australia

Received September 2, 1986

ALAN A. HUMFFRAY. Can. J. Chem. **65**, 833 (1987).

In estimating properties of mixtures of electrolytes from those of the individual components, it is better to calculate the density directly using a mixing rule, rather than from the derived quantity, the apparent molar volume. Each component contributes to the density in proportion to its ionic strength fraction in the mixture; this simple mixing rule gives better agreement for NaCl–KBr mixtures than do Pitzer's equations, incorporating up to sixteen parameters. Some discrepancies in Kumar's published data (Can. J. Chem. **63**, 3200 (1985)) on NaCl–KBr mixtures are discussed.

ALAN A. HUMFFRAY. Can. J. Chem. **65**, 833 (1987).

Lorsqu'on évalue les propriétés de mélanges d'électrolytes par rapport à celles des composantes individuelles, il est avantageux de calculer la densité directement, en faisant appel à une règle de mélange, plutôt que d'utiliser une quantité qui est dérivée, comme le volume molaire apparent. Chaque composante contribue à la densité en proportion avec sa fraction de force ionique dans le mélange; cette règle de mélange simple conduit à une meilleure correspondance, pour des mélanges de NaCl/KBr, que les équations de Pitzer qui incorporent jusqu'à seize paramètres. On discute de quelques anomalies dans les données publiées par Kumar (Can. J. Chem. **63**, 3200 (1985)) pour des mélanges de NaCl/KBr.

[Traduit par la revue]

Introduction

Recently Kumar (1) has applied Pitzer's equations (2, 3) to the evaluation of the densities and apparent molar volumes of aqueous mixtures of NaCl and KBr, as well as to NaCl–$CaCl_2$ (4) and KCl–$CaCl_2$ (5). In the former case, with no common ion, a total of *sixteen* parameters was required for the calculations. These are the apparent molar volumes Φ_V^0 at infinite dilution, for NaCl and KBr, and the pressure derivatives of Pitzer's parameters $\beta^{(0)}$, $\beta^{(1)}$ and C^Φ, i.e. $(\partial\beta^{(0)}/\partial P)_T$, $(\partial\beta^{(1)}/\partial P)_T$, and $(\partial C^\Phi/\partial P)_T$ not only for NaCl and KBr, *but also for KCl and NaBr*, and the binary interaction parameters θ_{NaK} and θ_{ClBr} for interactions between ions of like charge. Although the total contribution to the apparent molar volume of the mixture from all the Pitzer parameters (i.e. the last fourteen listed above) is often not great, ranging from 0.6% at $I = 1$ *m*, $y_B = 1$ to 11.5% at $I = 4$ *m*, $y_B = 0$, the successful application of a treatment with so many parameters is a tribute to the essential soundness and usefulness of Pitzer's theory. (y_B is the ionic strength fraction of B, in this case KBr, in the mixture.) Unfortunately, for application to such a binary mixture with no common ion, measurements or tabulations of density as a function of concentration for *all four* electrolytes, NaCl, KBr, NaBr, and KCl are required, for evaluation of the parameters.

Young and Smith (6) showed previously that Wirth's results (7) for NaCl–KBr mixtures, at ionic strength up to 1 *m*, were well-fitted by eq. [1]

$$[1] \quad \Phi_V = \frac{n_A\Phi_A + n_B\Phi_B}{n_A + n_B}$$

where Φ_V, Φ_A, and Φ_B are the apparent molar volumes of the mixture (containing n_A mole of NaCl and n_B mole of KBr), and of NaCl and KBr, respectively, all at the same ionic strength. Since apparent molar volumes of individual electrolytes can be adequately represented as functions of (molar) concentration using only two (8, 9) or three (6) parameters, eq. [1] significantly reduces the number of parameters required, and, in particular, eliminates the need for data on NaBr and KCl. Equation [1] is shown below to fit the apparent molar volumes of mixtures with a precision comparable to that claimed by Kumar. In the process of comparison, some discrepancies were revealed in his data; these are discussed below.

Since the primary experimental results are the densities, or Δd ($= d - d_0$, where d and d_0 are the densities of the solution and water, respectively), it is surprising that so much emphasis in the past has been placed on the derived quality, apparent molar volume. Apart from Celeda (9), few workers have sought to utilise densities (or Δd) directly. Equation [1] implies a direct relationship between the density of a mixture and the densities of the component electrolytes at the same ionic strength, as outlined below. Application of this relationship avoids the inherent loss of precision in converting experimental densities into apparent molar volumes (10); as an example, Kumar's NaCl–$CaCl_2$ and KCl–$CaCl_2$ data show, at an ionic strength of 0.5 *m*, $y_B = 1$, Δd values of 15.01 (4) and 14.948 (5) mg cm^{-3} corresponding to Φ_V values of 20.40 (4) and 20.787 (5) cm^3 mol^{-1}, respectively, i.e. a variation of 0.4% in Δd leads to a 1.8% change in Φ_V.

Equation [1] may be written as

$$[2] \quad \Phi_V = \Sigma c_i\Phi_i/\Sigma c_i$$

where Φ_i is the apparent molar volume of component i at (molar) concentration c_i, and (molar) ionic strength $I = Q_i c_i$ ($Q = 1$ for 1:1, 3 for 2:1 electrolytes, etc.). The treatment is given in terms of molarities; if more convenient, molalities may be substituted, with appropriate changes in the equations where necessary. The relation between Φ_i and Δd_i is (10)

$$[3] \quad \Phi_i = \frac{1}{d_0}\left\{M_i - \Delta d_i \Big/ c_i\right\}$$

$$[4] \quad = \frac{1}{d_0}\left\{M_i - Q_i\Delta d_i \Big/ I\right\}$$

where M_i is the molecular weight of component i, and Δd_i ($= d_i - d_0$) is the density increment at ionic strength I. For a mixture, (increment Δd) eq. [3] becomes

$$[5] \quad \Phi_V = \frac{1}{d_0\Sigma c_i}\left\{\Sigma c_i M_i - \Delta d\right\}$$

Printed in Canada / Imprimé au Canada

Can. J. Chem. Downloaded from www.nrcresearchpress.com by 78.46.186.204 on 09/07/12
For personal use only.

Substitution of eq. [4] into eq. [2] gives

$$[6] \quad \Phi_V = \frac{1}{d_0 \Sigma c_i}\left\{\Sigma c_i M_i - \frac{1}{I}\left(\Sigma c_i Q_i \Delta d_i\right)\right\}$$

and, comparing [5] and [6],

$$\Delta d = \frac{1}{I}\left(\Sigma c_i Q_i \Delta d_i\right)$$

or

$$[7] \quad \Delta d = \Sigma y_i \Delta d_i$$

where $y_i = c_i Q_i / I$ is the ionic strength fraction of component i. Thus, the mixture rule for densities resembles that for apparent molar volumes (eq. [2]), with ionic strength fraction replacing mole fraction.

Equation [7] is shown below (Table 1) to fit Kumar's density measurements more precisely than eq. [1] fits the molar volumes, and significantly more precisely than Pitzer's equations, utilising all sixteen parameters.

Discussion

Inspection of Kumar's data on NaCl–KBr mixtures reveals that, although the densities and apparent molar volumes for KBr alone are in good agreement with those of Isano (11), the agreement of the tabulated densities for NaCl alone (at $y_B = 0$) is less satisfactory, both with results of other workers (3, 12), and with values calculated using the NaCl parameters quoted by Kumar in his Table 2 (1). For example, at $I = 4\ m$, $y_B = 0$, the observed Δd/mg cm^{-3} is 138.445, whereas Roger and Pitzer (3) quote a specific volume of 0.879457 cm^3 g^{-1} corresponding to $\Delta d = 140.018$, Romanklw and Chou (12) quote 139.793, and the value calculated from Kumar's parameters is 139.814. Evaluation of Φ_V from the first and last of these values leads to a difference of 0.33 cm^3 mol^{-1}, i.e. thirty three times the standard deviation of fit claimed. The observed densities at $I = 1\ m$ and 3 m are also too low, suggesting an error in a stock solution, but that at $I = 2\ m$ is too high!

For this reason, eqs. [1] and [7] were tested for conformity with Kumar's data, not by evaluating Φ_A, Φ_B and Δd_A, Δd_B from equations empirically fitted to experimental data (3, 6, 7, 10, 11), but by taking Φ_A and Δd_A, Φ_B and Δd_B from the tabulations at $y_B = 0$ and 1, respectively, and comparing calculated Φ_V for other values of y_B with the tabulated ones. Standard deviations for the difference between calculated and observed values are listed in Table 1, columns 2 and 4; in evaluating the standard deviations, calculations at $y_B = 0$ and 1 were not included.

Table 1, column 2 shows the fit for Φ_V is better at $I = 4\ m$, but somewhat poorer at $I = 1$ to 3 m than the fit claimed by Kumar (values in column 3, Table 1). This claimed precision, however, is not readily verified, because the parameters for KBr quoted in Kumar's Table 2 (1) are erroneous. The KBr densities from the reference (11) quoted by Kumar lead to the following values of the parameters with their standard deviations (Kumar's tabulated values in parentheses):

$$\Phi_V^0 = 33.94 \pm 0.27\ (34.08),\ 10^5\ (\partial\beta^0/\partial P)_T\ 1.35 \pm 0.66\ (4.93),\ 10^5\ (\partial\beta^1/\partial P)_T\ -1.22 \pm 3.83\ (9.18),\ 10^6\ (\partial C^\Phi/\partial P)_T\ -2.00 \pm 1.84\ (28.15)$$

The large standard deviations for the parameters, and the large standard deviation of fit (0.37 cm^3 mol^{-1}) arise from fitting a four parameter equation to only seven data points. Table 2 illustrates the improvement in calculating the apparent molar volume for KBr alone using these, rather than Kumar's published values.

TABLE 1. Standard deviations of fit for Φ_V and Δd*

	$\sigma(\Phi_V)$/ cm^3 mol^{-1}		$\sigma(\Delta d)$/mg cm^{-3}		
I/m	(*a*)	(*b*)	(*c*)	(*d*)	(*e*)
1	0.040	0.034	0.035	0.092	0.061
2	0.069	0.056	0.029	0.255	0.143
3	0.16	0.092	0.020	0.401	0.169
4	0.11	0.210	0.064	0.675	0.254

*(*a*), from eq. [1]; (*b*), Kumar's results (1); (*c*), from eq. [7]; (*d*), Kumar's results without mixing parameters θ_{ik}; (*e*) Kumar's results with mixing parameters θ_{ik}.

TABLE 2. Apparent molar volume of KBr solutions*

	Φ_V/cm^3 mol^{-1}		
I/m	(*a*)	(*b*)	(*c*)
1	35.59	35.61	39.81
2	36.42	36.40	45.07
3	36.98	37.00	51.41
4	37.47	37.46	59.00

*(*a*), calculated from measured density (11), by eq. [3]; (*b*), calculated from re-evaluated Pitzer parameters; (*c*), calculated from Kumar's parameters (Table 2, ref. 1).

Kumar's tabulated experimental density increments Δd correlate well (Table 1, column 4) with eq. [7]; columns 5 and 6 in Table 1 give Kumar's claimed standard deviations for comparison, column 5 without, and column 6 with, the mixing parameters θ_{ik}. Equation [7] gives a significantly better fit; the standard deviations are lower than those claimed by Kumar when the binary mixing parameters are included. The larger standard deviations for Kumar's procedure is undoubtedly at least partly attributable to the discrepancies discussed above.

A further test of equation [7], on systems for which $I \neq \Sigma c_i$, was performed on Kumar's data for KCl–$CaCl_2$ (5) and NaCl–$CaCl_2$ (4) mixtures. The agreement for KCl–$CaCl_2$ was excellent, the largest standard deviation in Δd being 0.025 mg cm^{-3} at $I = 3\ m$, for which Kumar's values were 0.258 mg cm^{-3} without θ_{KCa} and 0.101 mg cm^{-3} with θ_{KCa} (5). For NaCl–$CaCl_2$ mixtures, the agreement was less satisfactory, but at each ionic strength, the standard deviation was smaller than that quoted by Kumar.

Pitzer's equations incorporating the pressure derivatives have a useful role to play in dealing with mixed electrolyte solutions under elevated pressures, but, for calculating densities at atmospheric pressure, a simple mixture rule dependent on ionic strength fraction is more precise, and requires fewer parameters.

1. A. KUMAR. Can. J. Chem. **63**, 3200 (1985).
2. K. S. PITZER. J. Phys. Chem. **77**, 268 (1973).
3. P. S. Z. ROGERS and K. S. PITZER. J. Phys. Chem. Ref. Data, **11**, 15 (1982).

Can. J. Chem. Downloaded from www.nrcresearchpress.com by 78.46.186.204 on 09/07/12
For personal use only.

4. A. KUMAR, G. ATKINSON, and R. D. HOWELL. J. Soln. Chem. **11**, 857 (1982).
5. A. KUMAR. J. Chem. Eng. Data, **31**, 21 (1986).
6. T. F. YOUNG and M. B. SMITH. J. Phys. Chem. **58**, 716 (1959).
7. H. E. WIRTH. J. Am. Chem. Soc. **59**, 2549 (1937).
8. O. MASSON. Phil. Mag. **8**, 218 (1929).
9. J. CELEDA. Coll. Czech. Chem. Commun. **48**, 1538 (1983).
10. H. S. HARNED and B. B. OWEN. The physical chemistry of electrolytic solutions. 3rd ed. Reinhold, New York. 1958. p. 358.
11. T. ISANO. J. Chem. Eng. Data, **29**, 45 (1984).
12. L. A. ROMANKLW and I.-M. CHOU. J. Chem. Eng. Data, **28**, 300 (1983).

Can. J. Chem. Downloaded from www.nrcresearchpress.com by 78.46.186.204 on 09/07/12
For personal use only.

Cyclic nitronates from the diastereoselective addition of 1-trimethylsilyloxycyclohexene to nitroolefins. Starting materials for stereoselective Henry reactions and 1,3-dipolar cycloadditions[1]

MICHAEL A. BROOK[2] AND DIETER SEEBACH

Laboratorium für Organische Chemie der Eidgenössischen Technischen Hochschule, Universitätstr. 16, ETH-Zentrum, CH-8092, Zürich, Switzerland

Received September 11, 1986

MICHAEL A. BROOK and DIETER SEEBACH. Can. J. Chem. **65**, 836 (1987).

Induced by a stoichiometric excess of dichloro(diisopropoxy)-titanium, 1-trimethylsilyloxycyclohexene and (*E*)-nitroolefins (R—CH=CHNO$_2$, R = C_6H_5, *p*-$C_6H_4CH_3$, *p*-$C_6H_4OCH_3$, *p*-C_6H_4CN, CH_3) combine in CH_2Cl_2 solution at −90°C *preferentially* with relative topicity *ul*, opposite to the corresponding reaction of enolates or enamines. The primary products are the epimeric bicyclic nitronates **4–6**, which can be separated, and which are converted by KF in MeOH to the alkyl or aryl (nitroethyl)-substituted cyclohexanones **1** and **2** (Table 1). Instead of being solvolysed, the cyclic nitronates **4–6** can be used for nitroaldol additions to give the trisubstituted hexahydrobenzopyranols **15–19**. Alternatively, **4–6** can be used in 1,3-dipolar cycloadditions with acrylates to furnish the tricyclic compounds **22–31**. In either case, products with four asymmetric carbon atoms (not including acetal centres) are produced diastereoselectively. The addition described here is yet another example of an *ul* combination of trigonal centres induced by Lewis acids, overriding the influence of the configuration of the donor component.

MICHAEL A. BROOK et DIETER SEEBACH. Can. J. Chem. **65**, 836 (1987).

À −90°C et sous l'influence d'un excès stoechiométrique de dichloro(diisopropylate) de titane, le triméthylsilyloxy-1 cyclohexène et les nitrooléfines-(*E*) (R—CH=CHNO$_2$, R = C_6H_5, *p*-$C_6H_4CH_3$, *p*-$C_6H_4OCH_3$, *p*-C_6H_4CN et CH_3) en solution dans le CH_2Cl_2 se combinent avec une topicité relative *préférentielle ul* qui est opposée à celle observée au cours des réactions correspondantes des énolates ou des énamines. Les produits primaires sont les nitronates bicycliques épimères (**4–6**) qui peuvent être séparés et qui, sous l'influence du KF dans le méthanol, peuvent être transformés en nitroéthyl cyclohexanones substituées par des groupements alkyles ou aryles (composés **1** et **2** du tableau 1). Si on ne les solvolyse pas, les nitronates cycliques **4–6** peuvent être utilisés lors d'additions nitroaldoliques conduisant aux hexahydrobenzopyranols trisubstitués (**15–19**). Par ailleurs, les composés **4–6** peuvent être utilisés dans des cycloadditions dipolaires-1,3 avec les acrylates pour donner les composés tricycliques **22–31**. Dans chacun des cas, les produits contenant quatres atomes de carbone asymétriques (en ne comptant pas les centres des acétals) sont obtenus avec une diastéréosélectivité. L'addition décrite ici n'est qu'un autre exemple d'une combinaison *ul* de centres trigonaux qui est induite par des acides de Lewis et qui a plus d'importance que l'influence de la configuration des composantes du donneur.

[Traduit par la revue]

Introduction

Extensive investigations of the properties of compounds containing the nitro group have been undertaken (2). Their use in organic synthesis has been somewhat limited. This situation has been changing recently, as the utility of these compounds in selective carbon–carbon bond forming processes becomes apparent. One obvious limitation is the paucity of nitro group containing natural products. Presently, however, there are more and more methods available for cleanly converting the nitro group into the common functional groups (3).[3]

One particularly versatile type of nitro containing compounds are the nitroolefins (5). Our interest in these compounds stemmed from previous work, which showed that highly diastereo- (6, 7) and enantioselective Michael additions (8) of enamines (3, 6, 7) or of lithium enolates (9) to nitroolefins are possible.

Risaliti and co-workers (6) have demonstrated in a series of papers that enamines add to nitroolefins with relative topicity *lk*.[4,5] This preference is also observed, albeit to a somewhat lesser extent, with lithium enolates (2, 9) (Scheme 1). While the stereochemical course of the addition of lithium cyclohexenolate to 1-nitropropene can be reversed by changing the nitroolefin configuration (9*a*), this is not possible with β-nitrostyrene (9*b*; also D. Seebach and Th. Laube, ETH-Zürich, unpublished results). However, enantioselection in this Michael addition to nitroolefins can be achieved by choosing an appropriate chiral auxiliary (12; also T. Mukhopadyay, ETH-Zürich, unpublished results). In addition, enamines derived from prolinol ethers gave Michael adducts with up to 95% e.e. (enantiomeric excess) (8).

The other isomer, formally derived from an *ul* addition of the enamine to β-nitrostyrene, is accessible by acid-catalyzed equilibration of the *lk* product. This process is not synthetically useful, however, both because the isomerization is not complete (**1** → **1/2**, 2:1) and the separation of the products is relatively difficult (ΔR_f (silica gel, petroleum ether/ether) ca. 0.04). In an independent study, Mukaiyama and Stevens have found that *ul* addition occurs with the Sn(II) enolate of cyclohexanone and β-nitrostyrene (11).

The use of nitroolefins as a^2 reagents is of interest for synthesis because of the high stereoselectivity achievable in Michael reactions to them. However, the utility would be further increased if the inherent d^1 reactivity of the nitronates **3**, formed upon the addition of a nucleophile to a nitroolefin, could be exploited (Scheme 2). In this way, the nitroolefin functionality would be used for selective formation of two carbon–carbon bonds. Only a few examples of the combination of a^2 and d^1 reactions of nitroolefins have hitherto been described (14).

[1]For a preliminary report of this work, see ref. 1.

[2]Current address: Department of Chemistry, McMaster University, 1280 Main Street West, Hamilton, Ont., Canada L8S 4M1.

[3]Recent developments in the methodology of the Nef reaction have extended the utility of molecules containing the nitro group. For some selected examples, see ref. 4.

[4]For the definition of the *like*(*l*,*lk*) and *unlike*(*u*,*ul*) descriptors, see ref. 10.

[5]The relative configuration of the products was established in one case by an X-ray analysis (6*a*).

Can. J. Chem. Downloaded from www.nrcresearchpress.com by 78.46.186.204 on 09/07/12
For personal use only.

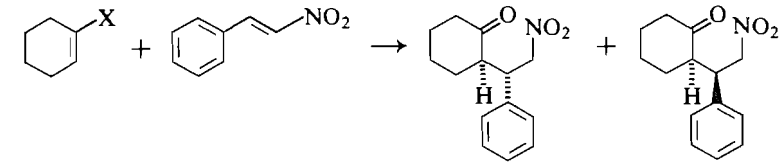

	X = NR_2	99	: 1	
	X = OLi	75	: 25	
		u	*l*	relative configuration
		lk	*ul*	relative topicity of addition

like (*lk*) addition

SCHEME 1

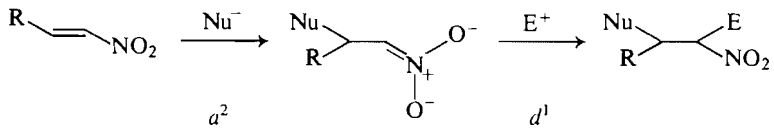

3

SCHEME 2

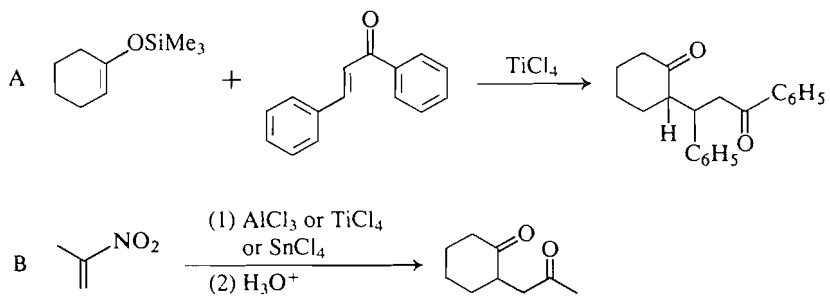

SCHEME 3

Our goal at the outset of this work was to develop both the a^2 and d^1 reactions of nitroolefins such that they occur diastereoselectively and enantioselectively. The present report describes our efforts to achieve diastereoselection.

The a^2 reaction

Results

It was hoped that the sense of diastereoselectivity of the reaction between nitroolefins and carbonyl compounds could be changed by switching from basic to acidic conditions. In place of Li enolates or enamines as nucleophiles, trialkylsilyl enol ethers would be used, with activation by Lewis acids.

Mukaiyama and co-workers first showed that silyl enol ethers will undergo the Michael addition with a variety of electrophiles in the presence of Lewis acids (15, 16) (Scheme 3A). Yoshikoshi and co-workers have demonstrated that 2-nitropropene, in the presence of a variety of Lewis acids, is also a good electrophile for the reaction (17) (Scheme 3B). In neither case was the stereochemical course of the reaction discussed.[6]

Our investigation of the Lewis acid mediated addition of silyl enol ethers to nitroolefins shows that the stereochemical course of the reaction depends strongly on the Lewis acid: the addition of 1-trimethylsilyloxycyclohexene to β-nitrostyrene at −90°C, in the presence of one equivalent of $TiCl_4$, gives rise to both diastereomeric Michael adducts **1** and **2**. In addition, however, two diastereomeric cyclic nitronates **4** and **5**, formally arising from a cycloaddition process, are isolated (Scheme 4). There was no overall discrimination between *lk* addition (**1** + **4**) and *ul* addition (**2** + **5**). These results contrast with the above-mentioned selective additions of the lithium enolate or morpholinoenamine of cyclohexanone to β-nitrostyrene (6, 9), which occur with relative topicity *lk* (up to >99:1). We chose to look optimistically at this apparently negative result, as an indication that further modification of the Lewis acid would lead to higher proportions of the hitherto less readily accessible product arising from an *ul* addition of the reactants. Systematic variation of the Lewis acid led to the discovery that the use of three equivalents[7] of $Cl_2Ti(O\text{-}iPr)_2$ resulted in the suppression of the formation of the Michael adducts **1** and **2**; instead, three silylated nitronates **4**, **5**, and **6** were isolated in good

[6]Heathcock has recently described stereochemical results for a variety of related Michael additions of silyl enol ethers (and ketene acetals) to α,β-unsaturated carbonyl compounds (18). The steric course of the reaction is governed by the nature of the silyl enol ether, by the nature of the Lewis acid, and not by the geometry of the silyl enol ether.

[7]Three equivalents were used to force the reaction to completion. While the reaction will take place with smaller quantities of the Lewis acid, it is more sluggish and some equilibration occurs, favouring the formation of the product of *lk* addition.

Can. J. Chem. Downloaded from www.nrcresearchpress.com by 78.46.186.204 on 09/07/12
For personal use only.

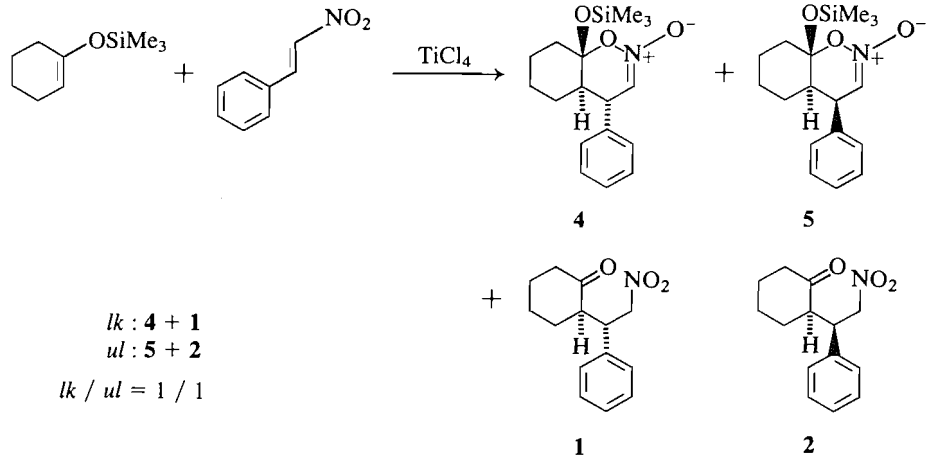

SCHEME 4

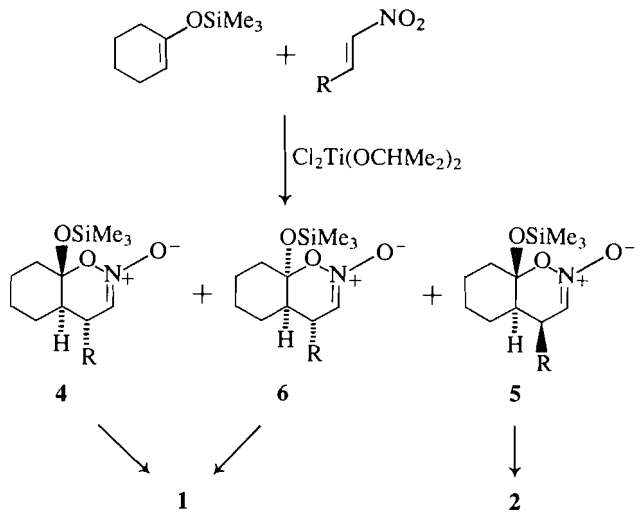

a: R = C_6H_5 *b*: R = *p*-$H_3CC_6H_4$ *c*: R = *p*-$H_3COC_6H_4$
d: R = *p*-NCC_6H_4 *e*: R = CH_3

SCHEME 5

yield (Scheme 5). The products are easily separable,[8] mostly crystalline materials, which are indefinitely stable (**4***a*, **5***a* for more than 8 months at reduced temperatures in the absence of moisture).

The survival of the O—Si bond to exposure to an aqueous work-up and flash chromatography (19) is surprising in light of the facility with which trimethylsilyl ethers normally undergo hydrolytic cleavage (20). In fact, it is this instability to aqueous conditions that obviates their use as a protecting group. More interesting, however, is the diastereoselectivity of the reaction.

Table 1 shows the results of the addition of 1-trimethylsilyloxycyclohexene to five nitroolefins in the presence of three equivalents of $Cl_2Ti(O\text{-}i\text{Pr})_2$: with the exception of 1-nitropropene, the *ul* product **5** is favoured over the *lk* products **4** and **6**, by as much as 4:1. Dichloro(diisopropoxy)-titanium led to the highest selectivity for the *ul* addition of the Lewis acids tested. Varying the size of the alkoxy group on the titanium (OMe, OEt, O-*t*Bu), the alkyl group on silicon (Et), or the size of the R group of the nitroolefin (R = *i*Pr) led to *decreased* diastereoselectivities.

Hydrolysis of the three products **4**, **5**, and **6**, with KF/methanol, led to the known Michael adducts **1** and **2** (**4** and **6** → **1**, **5** → **2**, Scheme 5).[9] This proves the relative configuration at the newly formed carbon–carbon bond. The assignment of the *trans* ring junction (**4** and **5**) was made using nuclear Overhauser effect (nOe) measurements: irradiation with the frequency of the trimethylsilyl hydrogens led to a large enhancement of the phenyl signal with compounds **5***a* and **6***a*, but no enhancement with **4***a*. Knowing the relative configuration at the newly formed carbon–carbon bond, the ring junction must be *trans* for both **4***a* and **5***a*, and *cis* for **6***a*. By analogy, the *para*-substituted derivatives **4***b–d*, **5***b–d*, and **6***b–d* are assumed to have the same relative configurations at the bridgehead position.

The configuration of products **4***e*, **5***e*, and **6***e* was assigned by hydrolysis to the known Michael products (6, 9) and by spectroscopic comparison with the aromatic nitronates. All physical and spectroscopic data are consistent with the assigned structures.

Finally, it was possible to obtain crystals of **4***a* suitable for X-ray structure analysis. The *trans* fusion of the rings and the

TABLE 1. Products of the reaction between 1-trimethylsilyloxycyclohexene and substituted nitroolefins induced by $(i\text{-PrO})_2TiCl_2$

Series	R in **4**, **5**, **6**	Isolated yield (%)[a] **4**	**6**	**5**	Total yield (%)	Ratio *ul*/*lk*[b]
a	C_6H_5	11	5	65	81[c]	3:1
b	*p*-$H_3CC_6H_4$	10	7	50	67	4:1
c	*p*-$H_3COC_6H_4$	20	4	50	74	2:1
d	*p*-NCC_6H_4	17	17	29	55	8:3
e	CH_3	27	5	27	60	2:3

[a]After flash chromatography.
[b]Determined from the ^1H nmr of the crude product mixture: **4** and **6** are formed in a *lk* addition, **5** in an *ul* addition.
[c]The only reaction for which the yield was optimized.

[8]For **4***a* and **5***a*, the ΔR_f (petroleum ether/ether) is ca. 0.25.

[9]With the nitropropene derived compounds (**4***e*, **5***e*, **6***e*), even when milder conditions were used (KF/methanol/water), a small amount of epimerization took place at the α-keto position (Risaliti has shown that such epimerization does not occur at the β-keto position (6*c*)). The products **4***a–d*, **5***a–d*, and **6***a–d* with aryl substitution were only epimerized when more basic fluoride sources were used, such as Bu_4NF in THF.

Can. J. Chem. Downloaded from www.nrcresearchpress.com by 78.46.186.204 on 09/07/12
For personal use only.

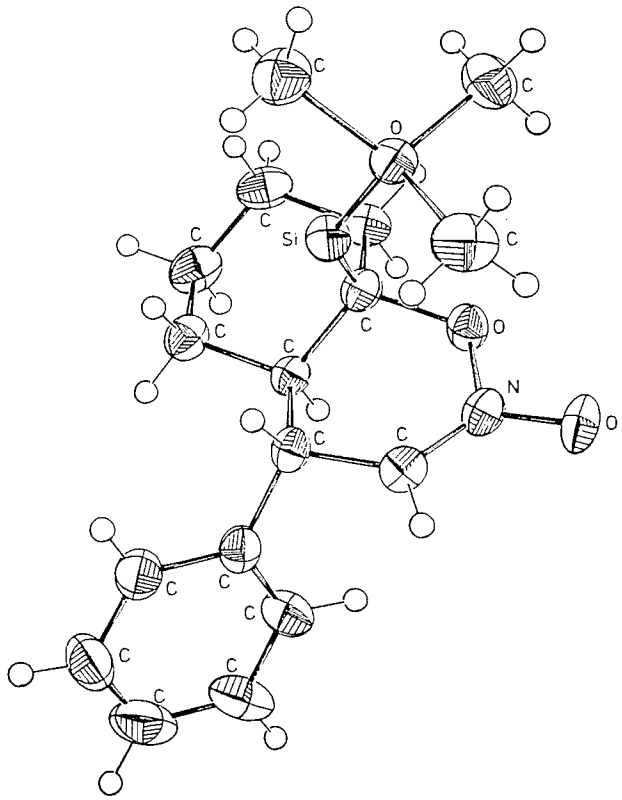

FIG. 1. ORTEP drawing of **4***a* with thermal ellipsoids shown at the 50% probability level. The X-ray crystallographic data will be published elsewhere (Acta Crystallogr., submitted).

trans configuration of the $OSiMe_3$ and phenyl groups are clearly evident from Fig. 1.

Discussion

The configuration of the isomer formed upon the addition of a metal enolate (M = Li, BR_2) to an electrophile (aldehydes, nitroolefins, etc.) is dependent on the geometry of the enolate: with (*E*)-enolates the trigonal centres combine with relative topicity *lk*; with (*Z*)-enolates, with relative topicity *ul* (21, 22). So many examples of such a geometrical dependence on diastereoselectivity exist that this relationship has become the standard by which related aldol and Michael reactions are judged (21–24*a*).

However, over the last five years a series of reactions has been described for which this geometrical relationship does not hold. When other elements of the periodic table are employed in the aldol reaction, such as $OB(OR)_2$ (24, 25), Si (26), Sn (27), Ti (28), Zr (29), and $S[(Me_2N)_3S^+$, TAS] (30), products arising from an *ul* addition are obtained *regardless of the geometry of the enolate*. Complementarily, allyl derivatives of Si (31) and Sn (32, 33) add to aldehydes in an *ul* approach, again regardless of the geometry of the allylic double bond. To this series, and there are many other examples, can be added the Michael addition to aromatic nitroolefins presently under consideration; contrary to the "rule", an (*E*)-enolate (1-trimethylsilyloxycyclohexene) preferentially adds to the nitroolefin in an *ul* fashion, to varying extents (cf. the above-mentioned addition of Sn enolates to nitrostyrene (11)).[10]

[10]With 1-trimethylsilyloxycyclohexene, the alkyl nitroolefin, 1-nitropropene, reacted to give predominantly the *lk* addition product, but to a far lesser extent than is the case of Li cyclohexenolate (9*a*) or enamines (6*b*) as the nucleophiles.

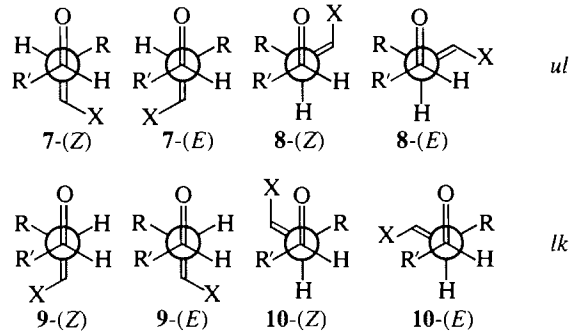

SCHEME 6

Reactions in which diastereomeric starting materials lead to the same diastereomeric product can be useful for synthesis and are interesting mechanistically. Possible explanations for the *ul* preference that has been observed in the examples cited (1, 24–33) will be discussed below.

Lewis acid

Most of the reactions that are independent of the enolate/allylic double bond geometry are performed in the presence of a Lewis acid, either the metal on the donor itself, or one specifically added. The nature of the Lewis acid is critical in determining the steric course of the reaction. As described above, the change from $TiCl_4$ to $Cl_2Ti(O\text{-}iPr)_2$ in the Michael addition under discussion led to a change from no selectivity to *ul* selectivity. Keck *et al.* (34) have observed a complete reversal of diastereoselectivity in the addition of crotylstannanes to aldehydes, depending on the Lewis acid. In addition, Danishefsky and co-workers (35) have described a relationship between the Lewis acid strength and the diastereoselectivity of the hetero Diels–Alder reaction between (*E*,*Z*)-2,4-dimethyl-1-methoxy-3-trimethylsilyloxy-1,3-butadiene and benzaldehyde. With the stronger Lewis acid $TiCl_4$, a moderate *lk* selectivity is observed (Mukaiyama reaction, refs. 15, 16, 36). With the weaker Lewis acid $MgBr_2$, *ul* addition is preferred; cf. the present case: nonselective with $TiCl_4$, *ul* selective with the weaker Lewis acid $Cl_2Ti(O\text{-}iPr)_2$. At this point it appears to us difficult to assess the nature of the electronic interactions of the Lewis acid in the transition state.

Steric effects

A variety of transition state models has been proposed for those reactions in which an *ul* approach is observed. All of these fall into one of two classes; the open transition state (addition to aldehydes of allylsilanes (31), allylstannanes (32), TAS enolates (30*b*), or the Michael addition to α,β-unsaturated carbonyl compounds of silyl enol ethers and silyl ketene acetals (18*b*)) and the synclinal transition state (addition to aldehydes of allyl stannanes (33), of bulky lithium ester enolates (37), of trichlorotitanium enolates (tilt boat, 28*b*), of bis-cyclopentadienylchlorozirconium enolates (twist boat, 29*a*), and of enol boronates (24, 25)).

Arguments (30*b*, 31, 32) for an "open" transition state suggest that minimizing the steric interaction between R and R′ is the most important feature of the approach trajectory (i.e., **7**, **10** more favourable than **8**, **9**) (Scheme 6). The "open" *ul* transition state **7** was favoured over *lk*-**10** by the corresponding authors either for reasons that were not given (32) or because it was thought to involve a minimization of electrostatic repulsion between two oxygen atoms (30*b*). Let us consider these two factors separately.

The importance of the steric interaction between R and R′ is

Can. J. Chem. Downloaded from www.nrcresearchpress.com by 78.46.186.204 on 09/07/12
For personal use only.

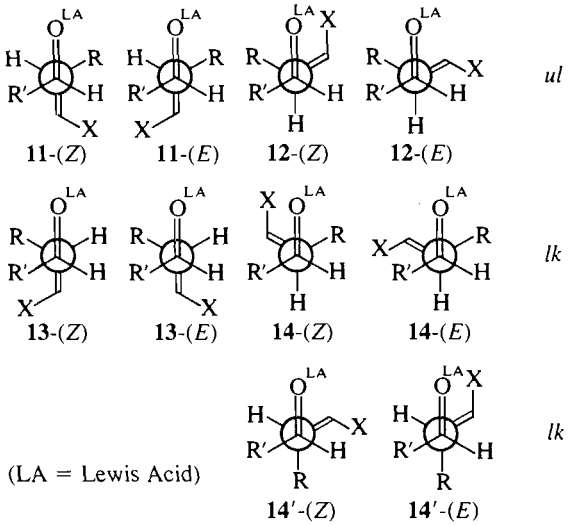

SCHEME 7

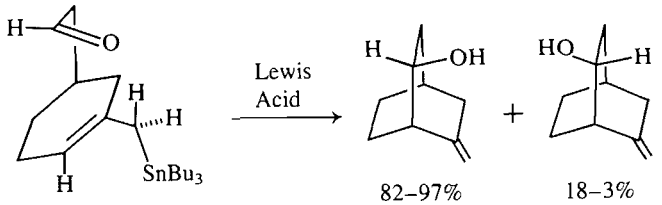

SCHEME 8

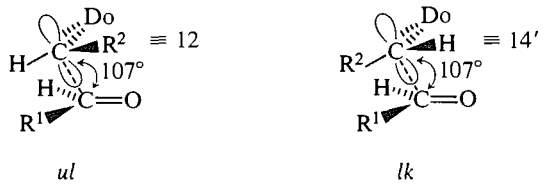

Priority sequence: =O > R^1 > H, Do > R^2 > H, =CX > R^2 > H
(Do = Donor)

SCHEME 9

overemphasized in our view. Taking butane as a model system, for example, a destabilization of only 0.8 kcal/mol occurs on going from the *anti* to the *gauche* orientation (38). Although the R, R′, and C=CHX groups are more sterically demanding than the methyl group of the model system, the forming carbon–carbon bond will also be longer in the transition state and these interactions will be less severe. Only when R or R′ is very bulky, for example, with α-substituted enolates or α,α,α-trisubstituted aldehydes, will the R/R′ steric interaction dominate the relative topicity of the approach of the donor and acceptor. Such interactions will favour a return to the "normal" reactivity in which (*E*)-enolates undergo *lk* addition and (*Z*)-enolates undergo *ul* addition to aldehydes.

In most cases in which the "open-chain" transition state was postulated, the Lewis acid was ignored. The location of the Lewis acid, particularly when its size is relatively large such as with TiX_4, will likely have a critical bearing on the relative energies of the transition states. Current evidence is compatible with a Lewis acid chelation to the aldehyde (in the aldol reaction) *trans* to the R′ group for steric reasons (33*b*, 39; see also ref. 15 cited in ref. 25*a*).[11] If one now compares the steric interactions, including the presence of the Lewis acid (Scheme 7), it seems likely that transition states **11** and **14** should be destabilized with respect to **12** and **13**.

In reactions for which chelation can occur between X (the donor) and the Lewis acid, for example with $TiCl_3$ enolates (28*b*), the synclinal transition state **12** should be favoured over **13**. However, even when this is not the case, as with allyl metal derivatives (31, 33), there is good evidence that a synclinal transition state is favoured.

In the transition state, partial charge will build up or disappear at the acceptor and donor ends. In nonpolar solvents, a common feature of the geometry independent reactions, solvation of these charges will not be efficient and the open transition state should be disfavoured. In support of this statement are the observations that the steric course of some aldol reactions (41, 42) changes from synclinal to open-chain on going from aprotic to protic solvents, the latter being better able to solvate charges.

Convincing evidence for a synclinal transition state comes from the work of Denmark and Weber (33). The Lewis acid catalyzed cyclization of an allylstannane to an aldehyde takes place with very high synclinal (*ul*) selectivity (Scheme 8). The authors (33*b*) concluded that the origin of the preference for a synclinal approach is not related to steric factors, but deferred further explanation.

Bürgi–Dunitz approach

Assuming that the reactants follow a synclinal approach for the reasons just given, it is still necessary to discriminate between an *ul*-**12** or *lk*-**14′** approach.[12] Bürgi and Dunitz have shown that nucleophiles attacking a carbonyl group approach the CO plane not at 90°, but canted at ca. 107° (43–45). When it is a nucleophile with enantiotopic faces, as is the present case, the closest approach of the reacting partners will occur when the proton, the smallest substituent on the trigonal centre of the donor, is antiperiplanar to the acceptor C=O bond (Scheme 9), the "antiperiplanar hydrogen rule" (7, 9). Based on the ability of the reactants to approach more closely in **12** than **14′**, the former should be the more favourable transition state.

Recently, Gennari and co-workers have performed semi-empirical calculations (MNDO) that have allowed an estimation of the energy difference between the *ul* and *lk* approaches (25*a*). By fixing the distance between the two bond forming carbon atoms at 2 Å, and assuming a synclinal approach, they have "modelled" the transition state of the aldol reaction of (*E*)- and (*Z*)-enolborates (dialkoxyenolboranes) and (*E*)-enolborinates (dialkylenolboranes) with benzaldehyde.

The calculations indicate that for the (*Z*)-enolborate, the *ul* approach (Scheme 7, **12**-(*Z*)), a twist boat, is favoured by 2.1 kcal/mol over the *lk* approach (Scheme 7, **14**-(*Z*) or **14′**-(*Z*)). For the (*E*)-enolborate, the half-chair, *ul* approach (Scheme 7, **12**-(*E*)) was more favourable by 2–3 kcal/mol than the *lk* approach (Scheme 7, **14**-(*E*) or **14′**-(*E*)). In contrast, the half-boat, *lk* approach was favoured by 1.2 kcal/mol over the *ul* approach for the (*E*)-enolborinate. This mechanistic

[11]X-ray analyses of boron (40*a*) and tin (S.E. Denmark, Illinois-Urbana, private communication) complexes with aromatic aldehydes show that the Lewis acid lies *trans* to the Ar group in the C—C=O plane. With titanium derivatives, the titanium is not forced to lie in the C—C=O plane. Helmchen and co-workers (40*b*) have shown, by the X-ray analysis of a $TiCl_4$-chelated ester, that there is a torsional angle (C—C=O—Ti) of >60°.

[12]Transition state **14** was discounted on steric grounds (*vide supra*), therefore its rotamer **14′** will be considered.

Can. J. Chem. Downloaded from www.nrcresearchpress.com by 78.46.186.204 on 09/07/12
For personal use only.

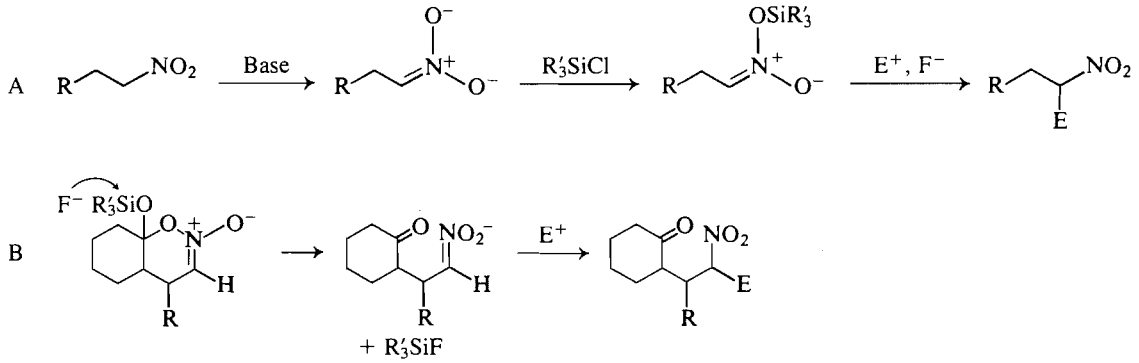

SCHEME 10

changeover, which correlates nicely with experimental observations, was ascribed by the authors to transannular interactions between the hydrogens and alkyl groups on the boron atom in the twist-boat *ul* approach.

Thus, the preference for a synclinal, *ul* approach of two trigonal centres, when the steric outcome does not display a dependence on the geometry of the nucleophile, can be traced to: (*i*) minimization of steric interactions, the most important of these being C=O-Lewis acid/R′ interactions; (*ii*) minimization of charge separation in nonpolar solvents (synclinal transition state); (*iii*) general preference for a synclinal approach (7, 33*b*) in the presence of Lewis acids, and (*iv*) optimization of the Bürgi–Dunitz trajectory.

The d^1 reaction

Results

While nitroolefins are among the most reactive electrophiles (a^2 reagents), nitronates are nucleophiles (d^1 reagents). They are typically generated by treatment of nitroalkanes with base. A convenient alternative is the use of silyl nitronates from which nitronates may be generated by fluoride ion and combined *in situ* with suitable electrophiles (Scheme 10A) (46, 47).

Nucleophilic nitronate anions should be generated by fluoride ion from the O-silyl substituted cyclic nitronates **4–6**, as indicated in Scheme 10B. There is an additional way by which elaboration of the skeleton of cyclic nitronates could be achieved: they can react as 1,3-dipoles in cycloaddition reactions (48–50). These two types of reactivity have been tested with our cyclic nitronates and are described in the following sections.[13,14]

Henry reaction

The reaction of the cyclic nitronate **4***a* with benzaldehyde in the presence of a source of fluoride ion as catalyst, such as *n*-Bu_4NF (TBAF), results in the formation in high yield of the cyclic hemiacetal **15** (Scheme 11). The reaction is highly diastereoselective (95% ds); only traces of a second unstable isomer could be detected in the ^1H nmr spectrum.

The structure of **15** was established by ^1H nmr spectroscopy, which clearly shows the *trans,trans,trans* relationship of the three protons in the 2-, 3-, and 4-positions of the heterocyclic

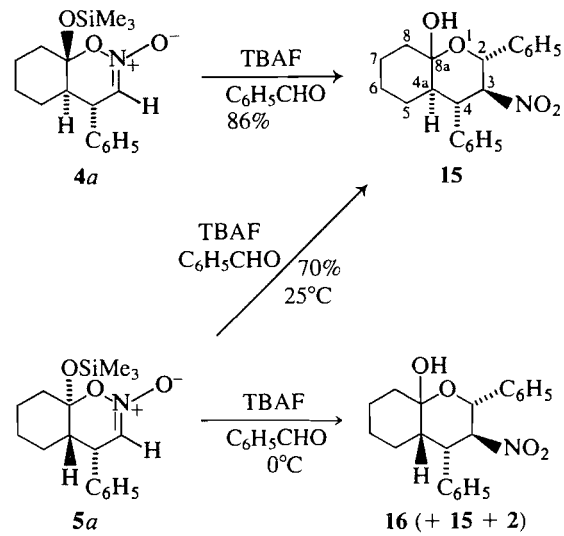

SCHEME 11

ring. It is not clear whether the formation of the hemiacetal takes place during the reaction or upon work-up and purification. In the event, no open-chain products were detected. The relative configuration of the bridgehead positions was not assigned.

The diastereomeric nitronate **5***a* did not react as cleanly. There were two kinds of problems: (*i*) fluoride ion is a sufficiently strong base to epimerize the α-keto position at room temperature, and (*ii*) hydrolysis of the starting material; at lower temperatures the most reactive electrophile is the water present in TBAF solutions[15] (Scheme 11). The latter hydrolytic reaction is clearly uninteresting. The former reaction occurring with epimerization (**16** → **15**) would be of interest if the diastereomer with *u* configuration at C(4) and C(4a) were desired (for the numbering of **15**, see Scheme 11).[16,17] It should be possible in a single step to form the most stable product **15** from the mixture of cyclic nitronates **4***a*, **5***a*, and **6***a* and benzaldehyde.

[13]Many examples of cyclic nitronic esters are known, most of which result from the additions of enamines to substituted nitroolefins (for selected examples see ref. 51). In all cases for which the diastereoselectivity is known, the products of a *lk* addition are favoured and the rings are *cis*-fused.

[14]Although the cyclic nitronates derived from enamines[13] have the potential to undergo 1,3-dipolar cycloadditions, it is less likely that conditions could be found for their participation in the Henry reaction.

[15]TBAF was used in the following forms: (*i*) commercial (Aldrich) solution, 1 *M* in THF; (*ii*) dried by azeotropic removal of water (benzene) and made up to 1 *M* solution in THF; (*iii*) dried at 100°C under high vacuum and made up to 1 *M* solution in THF; (*iv*) dried in the THF (1 *M* solution) over molecular sieves 3Å; and (*v*) supported on Kieselgel (Fluka).

[16]The product **16** of kinetic control was very labile, isomerizing to **15** under a variety of conditions. Therefore, analytically pure **16** could not be obtained.

[17]The epimerization must take place with an intermediate that has a free carbonyl group.

Can. J. Chem. Downloaded from www.nrcresearchpress.com by 78.46.186.204 on 09/07/12
For personal use only.

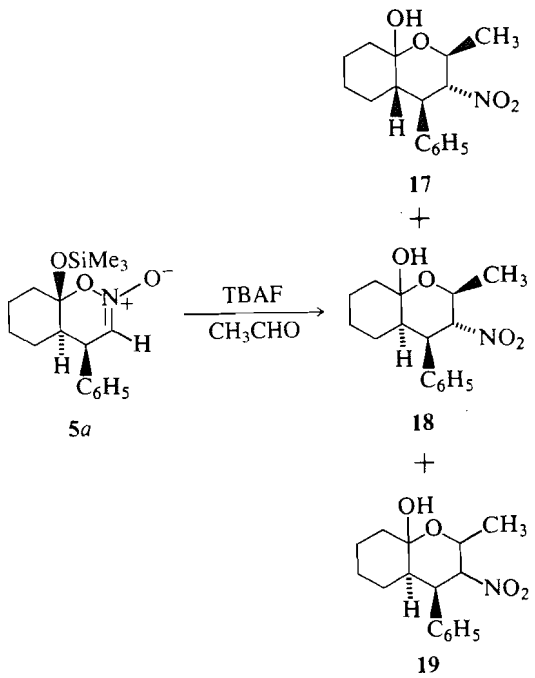

SCHEME 12

Several attempts were made to modify the conditions such that hydrolysis and epimerization could be avoided. However, a variety of other fluoride sources which are "dry", for example $(Me_2N)_3SF\cdot(TMSF)$ or KF/DMF, did not lead to improved results.

When acetaldehyde and the nitronate **5***a* were allowed to react, both epimerized (**17**) and nonepimerized (**18**)[18] products were obtained (Scheme 12). A third isomer **19** was also isolated.

The reactions take place with preferential coupling of the trigonal centres with relative topicity *ul* as is usual in the silyl nitronate modification of the Henry reaction[19] (47*a*), see **20** in Scheme 13. It is also remarkable that there appears to be a strong influence on the steric course of the reaction by the stereogenic centre adjacent to the nitronate double bond (47*b*), see the relative topicity *ul*-1,2 as depicted in **21** of Scheme 13. In two simple steps, a stereoselective construction of four new, adjacent, stereogenic centres, not including acetal centres, has been achieved!

1,3-Dipolar cycloadditions

Torssell and co-workers (49) have shown that silyl nitronates, like other nitronic acid esters, undergo 1,3-dipolar cycloadditions with a variety of olefins. This is also expected of the cyclic nitronates **4**, **5**, and **6**. Indeed, upon reaction of any of the three cyclic nitronates **4***a*, **5***a*, and **6***a* with acrylic acid derivatives, cycloadducts are formed in moderate to good yields and with good diastereoselectivities. Thus methyl acrylate, the most reactive of the dipolarophiles tested, reacted with **4***a*, **5***a*, and **6***a*, respectively, within 4–6 hours at room temperature to form the tricyclic compounds **22**, **24**, and **25** with the yields and diastereoselectivities given in Scheme 14. *p*-Bromophenyl acrylate reacted with **4***a* to give the crystalline material **23**.

The products **4***e*, **5***e*, and **6***e*, derived from 1-nitropropene, also react readily and stereoselectively with methyl acrylate

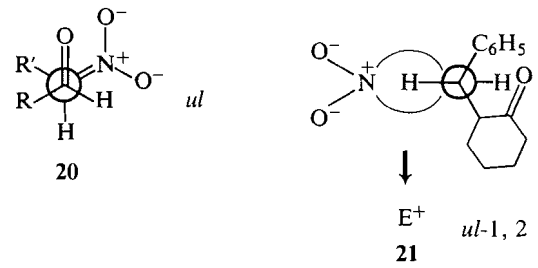

SCHEME 13

to give the tricyclic products **26**, **27**, and **28**, respectively (Scheme 15).

Although some modifications of the acrylic acid derivative are tolerated, β-substituted α,β-unsaturated esters do not yield the desired products; methyl crotonate and methyl cinnamate failed to react.[20] Acrylamide, however, will add to the nitronates **4***a* and **5***a* to give the tricyclic products **29** and **30**, respectively. Substitution at the α-position of the α,β-unsaturated ester is also possible: methyl methacrylate reacts with **5***a* to form the geminally disubstituted derivative **31** as a 1:1 mixture of diastereomers (Scheme 16).

Discussion

1,3-Dipolar cycloadditions are thought to be concerted processes (48) although a mechanism involving diradical intermediates has also been postulated (52). Like all dipolar cyloadditions, the reactions with nitrones generally take place with high stereoselectivity (53). In the case under consideration, there are four different approaches between the methyl acrylate and the bicyclic nitronate (*endo* or *exo*, α- or β-face, as drawn[21]). However, products arising from only two of these were isolated, with a pronounced preference (up to 13:1 or 93% ds) for one of the two.

In establishing the steric course of the reaction, it is first necessary to ascertain that isomerization does not occur during the reaction at the three stereogenic centres present in the starting material. The ^1H nmr measurements indicate that such isomerization does not take place. On going from **4***a* to **22** or **5***a* to **24**, the C(4)/C(4a) proton coupling constants (see Scheme 14 for numbering) changed from 11.1 to 12.2 Hz and from 9.2 to 6.9 Hz, respectively, about what is to be expected upon the loss of the double bond in the 6-membered ring. No information about the acetal centre could be obtained.

Subsequently, the relative configuration must be determined at the two stereogenic centres formed in the reaction. All attempts to establish this using nuclear Overhauser effect measurements failed. However, the configuration was assigned from the X-ray crystal structure analysis of **23** (Fig. 2). It can be seen that **23** arises from the *exo* addition of the acrylate to the diastereotopic face of the nitronate opposite to the $OSiMe_3$ group (α-face as drawn), an *lk*,*ul*-1,2 combination.

As the ^1H nmr spectra of **22** and **23** are virtually identical, with the exception of the protons of the ester functionality, it can be concluded that **22** has the same relative configuration as **23**. On the basis of the similarities of the ^1H nmr spectra, the relative configurations of the related products derived from **4***a* (**26** and **29**) are also assumed to be the same as **23**.

[18]In contrast to the product formed from benzaldehyde, the two bicyclic compounds **17** and **18** were stable crystalline materials.

[19]In the previous work (47), however, trimethylsilyl nitronates were found to add nonselectively to aldehydes.

[20]1-Nitropropene gave a complex mixture of products.

[21]The *lk*/*ul* nomenclature may be used to describe the approach of the reactants even though the new bond is not formed between the two centres with heterotopic faces: the four possible combinations are described (*lk*, *lk*-1,2), (*ul*, *lk*-1,2), (*ul*, *ul*-1,2), and (*lk*, *ul*-1,2), respectively.

Can. J. Chem. Downloaded from www.nrcresearchpress.com by 78.46.186.204 on 09/07/12
For personal use only.

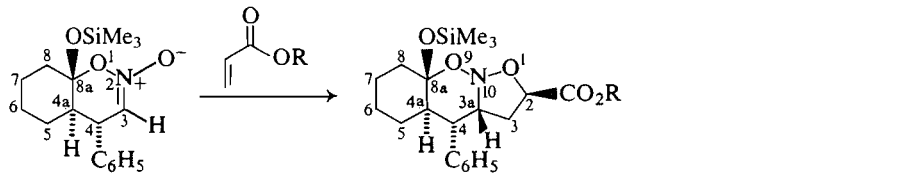

96% yield, >95% ds
87% yield, >95% ds

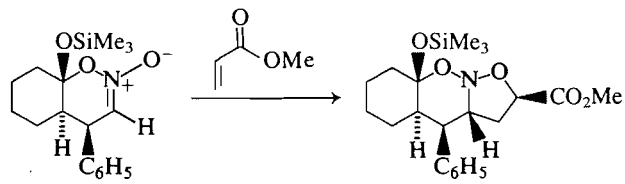

89% yield, 93% ds

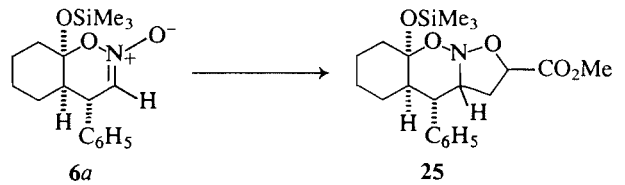

49% yield, 81% ds

SCHEME 14

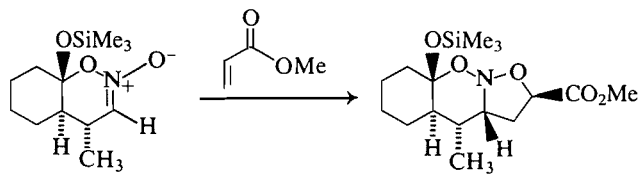

95% yield, 94% ds

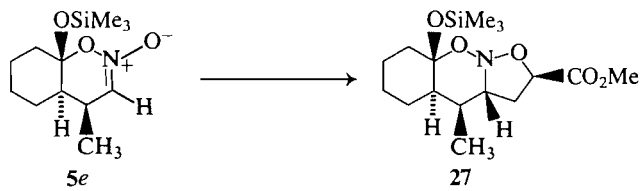

49% yield, >95% ds

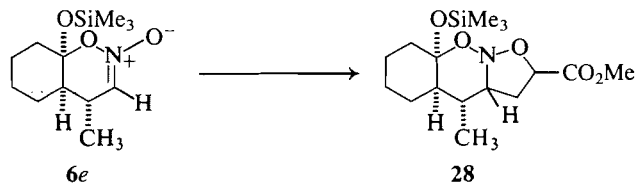

63% yield, 86% ds

SCHEME 15

The cycloadduct arising from the other diastereomer **24** is assumed also to have been formed via an *exo* α-face attack of the acrylate, as the steric shielding of the β-face of the starting material **5***a* is even more pronounced than in the case of **4***a*; both the OTMS and phenyl groups are axially disposed on the β-face. Analogously, the products **27** and **30**, derived from **5***a*, are assumed to have the same relative configuration as **24**. It was not possible to assign the configurations at the newly formed stereogenic centres in products **25** and **28**, which are derived from **6***a* and **6***e*, respectively.

A preference for an *exo* approach has also been observed in 1,3-dipolar cycloadditions of acrylates to nitronates in the work of Tartakovskii and co-workers (54), Carrié and co-workers (55), and Denmark *et al.* (14). The high selectivity for α-face attack, which is also common in reactions of this type, has been ascribed (14) to the kinetic anomeric effect (55*b*, 56). While such electronic effects are undoubtedly operating here, steric effects are also quite important. The crystal structure of the starting material **4***a* shows the β-face to be shielded by the OTMS group. In the case of the other diastereomer **5***a*, this shielding will be more pronounced as both the OTMS and phenyl groups will block the β-face. Therefore, on both steric

Can. J. Chem. Downloaded from www.nrcresearchpress.com by 78.46.186.204 on 09/07/12
For personal use only.

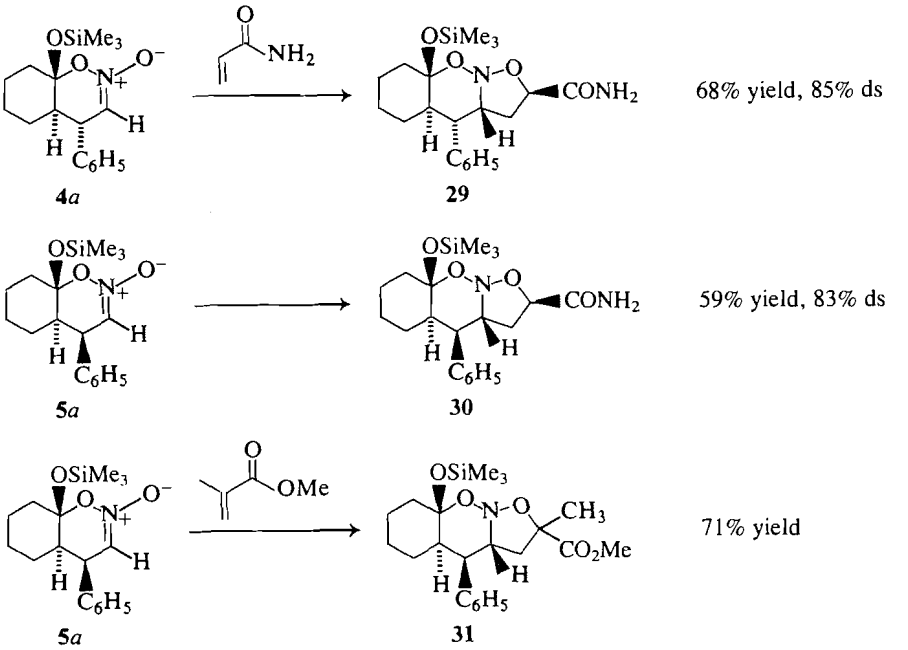

SCHEME 16

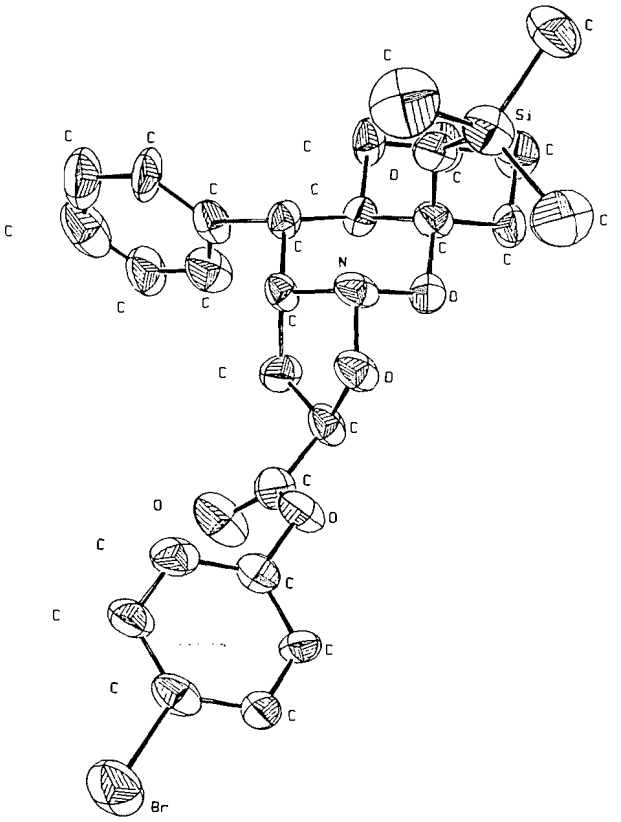

FIG. 2. ORTEP drawing of **23** with the hydrogens omitted for clarity. Thermal ellipsoids are shown at the 50% probability level. The X-ray crystallographic data will be published elsewhere (Acta Crystallogr., submitted).

and electronic grounds the selectivity for α-face attack is very reasonable.

The tricyclic products **22–31** are formed in two steps from the nitroolefins. The overall diastereoselectivity with which the four stereogenic centres are formed is high and therein lies the utility of the sequence.

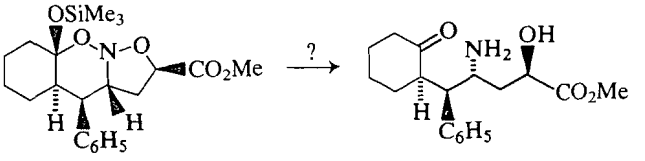

24

SCHEME 17

Reduction of the tricyclic compounds

It was hoped that the tricyclic compounds could be reduced to give useful polyfunctional starting materials for total synthesis (Scheme 17, shown for **24**). In the event, the N—O bonds proved much more rugged than anticipated and relatively severe conditions were required before any reduction was observed to take place. Using Raney nickel/KF as catalyst (49), the tricyclic compounds **24** and **27** (nitroso acetals) were reduced to the bicyclic lactams **33** and **34**, respectively (Scheme 18). The reduction of **24**, derived from β-nitrostyrene, was somewhat capricious, and in some cases the secondary amine **32** was isolated. This could be converted to the lactam **33** by potassium carbonate in methanol. The ^{1}H nmr spectra of compounds **32–35** indicate that no change occurs in the relative configuration of the stereogenic centres that were present in the starting material. The assignment of the *cis* ring junction in products **32–34** was based on the small coupling constants of the bridgehead hydrogens.

Surprisingly, the isomers **22** and **26** were not reduced under the same conditions. When the former was reduced with the more powerful reductant $LiAlH_4$, the N—O bonds remained untouched; only the ester was reduced, and after acetylation and chromatography over silica gel, the bicyclic derivative **35** was isolated (Scheme 19). Currently, other reagents are being sought that might achieve the desired reduction to the lactams in all cases.

Conclusion

The addition of silyl enol ethers to nitroolefins is a promising alternative to the traditional Michael addition. Firstly, it preferentially takes place with relative topicity *ul*, leading, after

Can. J. Chem. Downloaded from www.nrcresearchpress.com by 78.46.186.204 on 09/07/12
For personal use only.

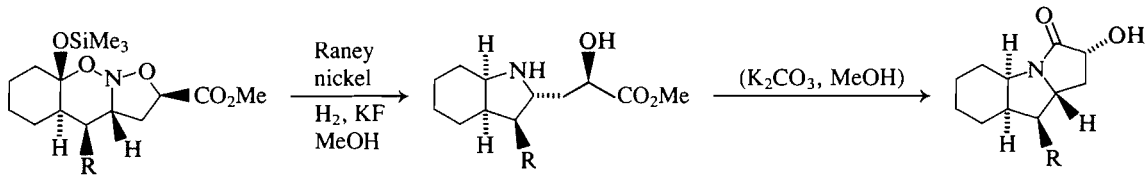

24 R = C_6H_5
27 R = CH_3

32 R = C_6H_5

33 R = C_6H_5
34 R = CH_3

SCHEME 18

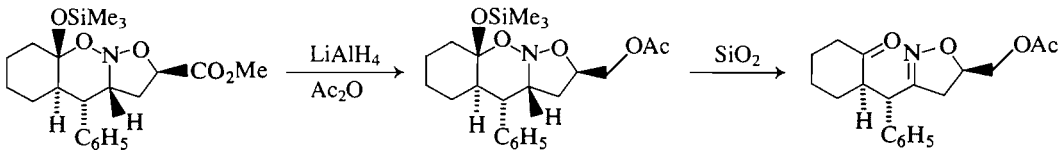

22 **35**

SCHEME 19

hydrolysis, to the diastereomeric nitroalkylated ketone **2**, which is difficult to obtain by other means. Secondly, it results in the primary formation of the isolable, novel, silylated cyclic nitronates **4–6**. These can be used in Henry reactions or 1,3-dipolar cycloadditions to give highly functionalized species in which the relative configuration of four stereogenic centres, not including acetal centres, is set. Further work to extend the utility of these processes, and to make them enantioselective as well, is under investigation.

Experimental

General remarks

Tetrahydrofuran (THF) was purified by distillation from potassium–benzophenone. Except for the 1,3-dipolar cycloadditions and reductions, all reactions were carried out in a dry Ar atmosphere. For column chromatography, Merck or Fluka silica gel 60 (70–230 mesh) was used. Melting points (mps) were determined using a Büchi 510 apparatus. All mps are uncorrected. The following instruments were used: for ir, Perkin–Elmer 297 spectrophotometer, data in cm^{-1}; for ^1H nmr, Varian EM-390 (90 MHz) and Bruker WM 300-WB (300 MHz) spectrometers; unless otherwise indicated the reported spectra were recorded at 300 MHz; chemical shifts are given in parts per million (ppm) with the tetramethylsilane (TMS) signal at 0.0 ppm as the internal standard; multiplicities as s (singlet), d (doublet), t (triplet), qa (quartet), qi (quintet), sept (septet), m (multiplet); coupling constants (J) in Hz; for mass spectra, Varian MAT311 spectrometer (70 eV, electron impact).

Preparation of nitroolefins: General procedure 1 (ref. 57)[22]

To a mixture of the aromatic aldehyde (0.20 mol) and nitromethane (0.20 mol) in methanol (200 mL) at −10°C was added aqueous KOH (0.20 mol in 60 mL H_2O) at a rate such that the temperature remains below −5°C (+5°C for *p*-cyanobenzaldehyde). The mixture was poured into cooled 2 *N* HCl (150 mL, 10°C). The bright yellow precipitate was filtered, air dried, and recrystallized from hexanes–chloroform.

p-Methyl-β-nitrostyrene: yield, 53%; mp 102.0–102.5°C; ^1H nmr (90 MHz, $CDCl_3$): 2.40 (s, 3H), 7.25, 7.46 (ABqa, $4H_{arom}$, J = 8), 7.54 (d, 1H, J = 13), 8.02 (d, 1H, J = 13).

p-Methoxy-β-nitrostyrene: yield, 48%; mp 86.6–87.0°C; ^1H nmr (90 MHz, $CDCl_3$): 3.89 (s, 3H), 6.98, 7.55 (ABqa, $4H_{arom}$, J = 10), 7.55 (d, 1H, J = 14), 8.02 (d, 1H, J = 14).

p-Cyano-β-nitrostyrene: yield, 50%; mp 179.8–186.8°C (dec); ^1H nmr (90 MHz, $CDCl_3$): 7.62 (d, 1H, J = 13), 7.68, 7.84 (ABqa, $4H_{arom}$, J = 8), 8.04 (d, 1H, J = 13).

[22]β-Nitrostyrene is commercially available; 1-nitropropene was prepared using the method described in (37).

Michael additions of silyl enol ethers to nitroolefins: General procedure 2

To a solution of titanium tetraisopropoxide ($Ti(O\text{-}iPr)_4$, 15.0 mmol) in methylene chloride (400 mL) was added titanium tetrachloride ($TiCl_4$, 15.0 mmol). After stirring for 1/2 h, the solution was cooled to ca. −40°C and the nitroolefin (10.0 mmol) was added. The coloured solution (varying from light yellow to deep red depending on the nitroolefin) was cooled to −90°C and 1-trimethylsilyloxycyclohexene (11.0 mmol) was added. The now lighter coloured solution was allowed to react for 20 min – 1 h at which time it was poured into an ether/water bilayer (4:1, 800 mL), shaken, neutralized with saturated $NaHCO_3$ solution, extracted with ether, washed with water (2 × 500 mL, brine should be avoided), and the combined organic phases were dried under an argon atmosphere at 0°C with a 1:1 mixture of $NaHCO_3/MgSO_4$. The solvents were evaporated at 10 and then 0.1 Torr (1 Torr = 133.3 Pa) to give the crude oil, which was purified by flash chromatography (ether/petroleum ether mixtures as eluent).[23,24] The three compounds isolated, **4**, **5**, and **6**, were further purified by recrystallization from hexanes/chloroform.

Series a, β-nitrostyrene. Overall yield, 81%. ul:lk *addition, 3:1*

Data of *u,l*-4a,5,6,7,8,8a-hexahydro-4-phenyl-8a-[(trimethylsilyl)-oxy]-4*H*-1,2-benzoxazine-2-oxide, **4***a*: yield, 11%; mp 125.5–126.2°C; ir (KBr): 1622; ^1H nmr ($CDCl_3$): 0.29 (s, 9H), 1.12–1.23 (m, 2H), 1.43–1.74 (m, 6H), 1.99–2.04 (m, 1H), 3.42 (dd, 1H, J = 2.8, 11.1), 6.29 (d, 1H, J = 2.8), 7.20–7.26, 7.31–7.37 (m, $5H_{arom}$); nOe, upon irradiation at δ 0.29, there was no enhancement of the phenyl signal, therefore the *trans* ring junction was assigned; ms *m/z*: 319 (1%, M^+), 170 (100%). *Anal.* calcd. for $C_{17}H_{25}NO_3Si$, *Mol. Wt.* 319.47: C 63.91, H 7.89, N 4.38; found: C 63.69, H 7.96, N 4.70.

Data of *l,l*-4a,5,6,7,8,8a-hexahydro-4-phenyl-8a-[(trimethylsilyl)-oxy]-4*H*-1,2-benzoxazine-2-oxide, **5***a*: yield, 65%; mp 110–112°C (dec.); ir (KBr): 1639, 1612; ^1H nmr ($CDCl_3$): 0.29 (s, 9H), 0.82 (dqa, 1H, J = 3.9, 12.9), 1.26–1.44 (m, 2H), 1.54–1.72 (m, 4H), 2.01–2.07 (m, 1H), 2.20 (ddd, 1H, J = 3.9, 9.2, 21.8), 3.77 (dd, 1H, J = 4.1, 9.2), 6.52 (d, 1H, J = 4.1), 7.27 (s, $5H_{arom}$); nOe, irradiation at δ 0.29 led to enhancement of the phenyl signal, therefore a *trans* ring

[23]Usually, a 2:1 petroleum ether/ether eluent was used until the first uv-active fraction eluted from the column (**4**), and then a 1:2 mixture was used to elute the two remaining components of the mixture, **6** and **5**, respectively.

[24]For efficient separation to take place, the crude residues (**4***b*, **5***b*, **6***b* and **4***c*, **5***c*, **6***c*) were dissolved in methylene chloride to which 2 g of silica gel had been added, and the solvent evaporated at 10 Torr. The solid material was then placed, without aid of solvent, at the head of a prepacked column and eluted as normal. Due to the sensitivity of **4***d*, **5***d*, **6***d*, the flash column was packed with methanol and eluted with petroleum ether/ether/methanol, 15:5:2.

Can. J. Chem. Downloaded from www.nrcresearchpress.com by 78.46.186.204 on 09/07/12
For personal use only.

Can. J. Chem. Downloaded from www.nrcresearchpress.com by 78.46.186.204 on 09/07/12
For personal use only.

junction was assigned; ms *m/z*: 319 (<1%, M^+), 170 (100%). *Anal.* calcd. for $C_{17}H_{25}NO_3Si$, *Mol. Wt.* 319.47: C 63.91, H 7.89, N 4.38; found: C 63.88, H 7.69, N 4.27.

Data of *u,u*-4a,5,6,7,8,8a-hexahydro-4-phenyl-8a-[(trimethylsilyl)-oxy]-4*H*-1,2-benzoxazine-2-oxide, **6***a*: yield, 5%; oil; ir ($CHCl_3$): 1622; ^1H nmr ($CDCl_3$): 0.14 (s, 9H), 1.20–1.39 (m, 1H), 1.26–1.71 (m, 4H), 1.71–1.83 (m, 1H), 1.83–1.94 (m, 1H), 2.05–2.22 (m, 2H), 3.47 (d, 1H, J = 4.1), 6.59 (d, 1H, J = 4.1), 7.14–7.38 (m, $5H_{arom}$); nOe, irradiation at δ 0.14 led to enhancement of the phenyl signal, therefore a *cis* ring junction was assigned; ms *m/z*: 319 (<1%, M^+), 170 (5%), 75 (100%).

Series b, p-*methyl-β-nitrostyrene. Overall yield, 68%;* ul:lk *addition, 4:1*

Data of *u,l*-4a,5,6,7,8,8a-hexahydro-4-(4-methylphenyl)-8a-[(trimethylsilyl)oxy]-4*H*-1,2-benzoxazine-2-oxide, **4***b*: yield, 10%; mp 124.9–125.2°C; ir (KBr): 1618; ^1H nmr ($CDCl_3$): 0.28 (s, 9H), 1.11–1.26 (m, 2H), 1.43–1.74 (m, 6H), 2.00 (ddd, 1H, J = 0.9, 2.0, 11.1), 2.34 (s, 3H), 3.38 (dd, 1H, J = 2.8, 11.1), 6.27 (d, 1H, J = 2.8), 7.06, 7.14 (ABqa, $4H_{arom}$, J = 8.0); ms *m/z*: 333 (<1%, M^+), 170 (100%). *Anal.* calcd. for $C_{18}H_{27}NO_3Si$, *Mol. Wt.* 333.505: C 64.83, H 8.16, N 4.20; found: C 64.62, H 7.91, N 4.04.

Data of *l,l*-4a,5,6,7,8,8a-hexahydro-4-(4-methylphenyl)-8a-[(trimethylsilyl)oxy]-4*H*-1,2-benzoxazine-2-oxide, **5***b*: yield, 50%; mp 98.8–99.2°C; ir (KBr): 1621; ^1H nmr ($CDCl_3$): 0.29 (s, 9H), 0.76–0.89 (m, 1H), 1.25–1.47 (m, 2H), 1.51–1.71 (m, 4H), 2.02–2.06 (m, 1H), 2.16 (ddd, 1H, J = 3.5, 9.1, 12.7), 2.33 (s, 3H), 3.74 (dd, 1H, J = 4.1, 9.1), 6.51 (d, 1H, J = 4.1), 7.08, 7.16 (ABqa, $4H_{arom}$, J = 8.2); ms *m/z*: 333 (<1%, M^+), 170 (100%). *Anal.* calcd. for $C_{18}H_{27}NO_3Si$, *Mol. Wt.* 333.505: C 64.83, H 8.16, N 4.20; found: C 64.88, H 8.23, N 4.19.

Data of *u,u*-4a,5,6,7,8,8a-hexahydro-4-(4-methylphenyl)-8a-[(trimethylsilyl)oxy]-4*H*-1,2-benzoxazine-2-oxide, **6***b*: yield, 8%; oil; ir ($CHCl_3$): 1626; ^1H nmr ($CDCl_3$): 0.14 (s, 9H), 1.24–1.37 (m, 1H), 1.48–1.77 (m, 5H), 1.81–1.89 (m, 1H), 2.02–2.08 (m, 1H), 2.12–2.18 (m, 1H), 2.32 (s, 3H), 3.40 (dd, 1H, J = 1.3, 4.1), 6.54 (dd, 1H, J = 0.7, 4.1), 7.10, 7.14 (ABqa, $4H_{arom}$, J = 8.5); ms *m/z*: 202 (18%), 147 (69%), 105 (100%). *Anal.* calcd. for $C_{18}H_{27}NO_3Si$, *Mol. Wt.* 333.505: C 64.83, H 8.16, N 4.20; found: C 64.93, H 8.04, N 4.08.

Series c, p-*methoxy-β-nitrostyrene. Overall yield, 74%,* ul:lk *addition, 2:1*

Data of *u,l*-4a,5,6,7,8,8a-hexahydro-4-(4-methoxyphenyl)-8a-[(trimethylsilyl)oxy]-4*H*-1,2-benzoxazine-2-oxide, **4***c*: yield, 20%; mp 135.2–135.8°C; ir (KBr): 1620, 1610; ^1H nmr ($CDCl_3$): 0.28 (s, 9H), 1.14–1.21 (m, 2H), 1.45–1.69 (m, 6H), 1.95–2.05 (m, 1H), 3.36 (dd, 1H, J = 2.8, 11.1), 3.80 (s, 3H), 6.27 (d, 1H, J = 2.8), 6.87, 7.09 (ABqa, $4H_{arom}$, J = 8.7); ms *m/z*: 349 (<1%, M^+), 170 (100%). *Anal.* calcd. for $C_{18}H_{27}NO_4Si$, *Mol. Wt.* 349.505: C 61.86, H 7.79, N 4.01; found: C 61.78, H 7.74, N 3.98.

Data of *l,l*-4a,5,6,7,8,8a-hexahydro-4-(4-methoxyphenyl)-8a-[(trimethylsilyl)oxy]-4*H*-1,2-benzoxazine-2-oxide, **5***c*: yield, 67%; mp 133.1–137.2°C; ir (KBr): 1610; ^1H nmr ($CDCl_3$): 0.30 (s, 9H), 0.85 (dqa, 1H, J = 3.8, 12.8), 1.26–1.71 (m, 6H), 2.00–2.06 (m, 1H), 2.15 (ddd, 1H, J = 3.6, 9.0, 12.8), 3.72 (dd, 1H, J = 4.2, 9.0), 3.80 (s, 3H), 6.50 (d, 1H, J = 4.2), 6.81, 7.18 (ABqa, $4H_{arom}$, J = 8.7); ms *m/z*: 349 (<1%, M^+), 170 (100%). *Anal.* calcd. for $C_{18}H_{27}NO_4Si$, *Mol. Wt.* 349.505: C 61.86, H 7.79, N 4.01; found: C 61.78, H 7.86, N 3.90.

Data of *u,u*-4a,5,6,7,8,8a-hexahydro-4-(4-methoxyphenyl)-8a-[(trimethylsilyl)oxy]-4*H*-1,2-benzoxazine-2-oxide, **6***c*: yield, 4%; mp 120.7–121.3°C; ir (KBr): 1633, 1625; ^1H nmr ($CDCl_3$): 0.16 (s, 9H), 1.25–1.36 (m, 1H), 1.47–1.77 (m, 5H), 1.80–1.89 (m, 1H), 2.00–2.06 (m, 1H), 2.13–2.19 (m, 1H), 3.39 (dd, 1H, J = 1.3, 4.1), 3.79 (s, 3H), 6.53 (dd, 1H, J = 0.7, 4.1), 6.83, 7.16 (ABqa, $4H_{arom}$, J = 8.5); ms *m/z*: 170 (100%). *Anal.* calcd. for $C_{18}H_{27}NO_4Si$, *Mol. Wt.* 349.505: C 61.86, H 7.79, N 4.01; found: C 61.51, H 7.55, N 3.82.

Series d, p-*cyano-β-nitrostyrene. Overall yield, 55%,* ul:lk *addition, 8:3*

Data of *u,l*-4-[4a,5,6,7,8,8a-hexahydro-8a-[(trimethylsilyl)oxy]-4*H*-1,2-benzoxazin-4-yl]-benzonitrile-*N*-oxide, **4***d*: yield, 17%; mp 164.6–165.2°C; ir (KBr): 1622; ^1H nmr ($CDCl_3$): 0.29 (s, 9H), 1.17–1.26 (m, 2H), 1.37–1.38 (m, 1H), 1.52–1.77 (m, 5H), 2.01–2.06 (m, 1H), 3.51 (dd, 1H, J = 2.8, 11.1), 6.20 (d, 1H, J = 2.8), 7.32, 7.64 (ABqa, $4H_{arom}$, J = 8.5); ms *m/z*: 170 (58%), 73 (100%). *Anal.* calcd. for $C_{17}H_{24}N_2O_3Si$, *Mol. Wt.* 332.476: C 62.76, H 7.02, N 8.13; found: C 62.39, H 6.65, N 8.08.

Data of *l,l*-4-[4a,5,6,7,8,8a-hexahydro-8a-[(trimethylsilyl)oxy]-4*H*-1,2-benzoxazin-4-yl]-benzonitrile-*N*-oxide, **5***d*: yield, 29%; mp 154.8–156.6°C (dec.); ir (KBr): 2226, 1620; ^1H nmr ($CDCl_3$): 0.29 (s, 9H), 0.73–0.79 (m, 1H), 1.32–1.43 (m, 2H), 1.54–1.75 (m, 4H), 2.02–2.08 (m, 1H), 2.25 (ddd, 1H, J = 3.6, 9.0, 12.7), 3.80 (dd, 1H, J = 4.1, 9.0), 6.45 (d, 1H, J = 4.1), 7.40, 7.56 (ABqa, $4H_{arom}$, J = 8.6); ms *m/z*: 170 (100%). *Anal.* calcd. for $C_{17}H_{24}N_2O_3Si$, *Mol. Wt.* 332.476: C 62.76, H 7.02, N 8.13; found: 62.55, H 7.04, N 7.97.

Data of *u,u*-4-[4a,5,6,7,8,8a-hexahydro-8a-[(trimethylsilyl)oxy]-4*H*-1,2-benzoxazin-4-yl]-benzonitrile-*N*-oxide, **6***d*: yield, 17%; oil; ir ($CHCl_3$): 1621; ^1H nmr ($CDCl_3$): 0.15 (s, 9H), 1.36 (m, 1H), 1.48–1.77 (m, 5H), 1.80–1.89 (m, 1H), 2.01–2.07 (m, 1H), 2.13–2.18 (m, 1H), 3.39 (dd, 1H, J = 1.0, 4.0), 6.53 (dd, 1H, J = 1.0, 4.0), 7.42, 7.59 (ABqa, $4H_{arom}$, J = 8.5); ms *m/z*: 170 (100%).

Series e, 1-nitropropene (25-mmol scale). Overall yield, 60%. ul:lk *addition, 2:3*

Data of *l,l*-4a,5,6,7,8,8a-hexahydro-4-methyl-8a-[(trimethylsilyl)-oxy]-4*H*-1,2-benzoxazine-2-oxide, **4***e*: yield, 27%; mp 51.7–52.3°C; ir (KBr): 1627; ^1H nmr ($CDCl_3$): 0.22 (s, 9H), 1.08 (d, 3H, J = 7.2), 1.17 (dt, 1H, J = 3.0, 11.8), 1.20–1.37 (m, 2H), 1.44–1.63 (m, 2H), 1.71–1.84 (m, 3H), 1.94–1.98 (m, 1H), 2.37 (ddqa, 1H, J = 2.7, 7.2, 7.5), 6.15 (d, 1H, J = 2.7); ms *m/z*: 257 (<1%, M^+), 227 (11%), 170 (100%). *Anal.* calcd. for $C_{12}H_{23}NO_3Si$, *Mol. Wt.* 257.408: C 55.99, H 9.01, N 5.44; found: C 55.72, H 8.94, N 5.32.

Data of *u,l*-4a,5,6,7,8,8a-hexahydro-4-methyl-8a-[(trimethylsilyl)-oxy]-4*H*-1,2-benzoxazine-2-oxide, **5***e*: yield, 27%; mp 53.7–54.3°C; ir (KBr): 1631; ^1H nmr ($CDCl_3$): 0.24 (s, 9H), 1.16 (d, 3H, J = 7.4), 1.24–1.40 (m, 1H), 1.46–1.63 (m, 4H), 1.71–1.96 (m, 4H), 2.53 (dqi, 1H, J = 4.5, 7.4), 6.30 (d, 1H, J = 4.5); ms *m/z*: 257 (<1%, M^+), 170 (100%, $M^+ - CH_3CHCHNO_2$). *Anal.* calcd. for $C_{12}H_{23}NO_3Si$, *Mol. Wt.* 257.408: C 55.99, H 9.01, N 5.44; found: C 55.71, H 8.87, N 5.38.

Data of *l,u*-4a,5,6,7,8,8a-hexahydro-4-methyl-8a-[(trimethylsilyl)-oxy]-4*H*-1,2-benzoxazine-2-oxide, **6***e*: yield, 5%; mp 61.3–66.1°C (dec.); ir (KBr): 1628; ^1H nmr ($CDCl_3$): 0.22 (s, 9H), 1.25–1.40 (m, 1H), 1.30 (d, 3H, J = 7.3), 1.56–1.71 (m, 7H), 2.12–2.19 (m, 2H), 6.25 (dd, 1H, J = 0.5, 4.2); ms *m/z*: 257 (<1%, M^+), 170 (73%, $M^+ - CH_3CHCHNO_2$), 75 (100%). *Anal.* calcd. for $C_{12}H_{23}NO_3Si$, *Mol. Wt.* 257.408: C 55.99, H 9.01, N 5.44; found: C 55.77, H 9.00, N 5.38.

Hydrolysis of the silylated cyclic nitronate: General procedure 3

To a solution of the nitronate **4**, **5**, or **6** (0.5 mmol) in methanol (10 mL) was added KF (2.5 mg, 40 μmol). After stirring at room temperature for 10 min – 3 h, the reaction mixture was extracted with ether, and washed with water (2×) and brine. The combined organic phases were dried over $MgSO_4$ and the solvents removed at 10 and then 0.1 Torr. The crude residue was purified by flash chromatography (petroleum ether/ether mixtures as eluent).

Data of *u*-2-(2-nitro-1-phenylethyl)-cyclohexanone, **1***a* (refs. 6*b*, 58, from **4***a*): yield, 86%; mp 106.1–106.4°C; ir (KBr): 1700, 1552, 1387; ^1H nmr ($CDCl_3$): 1.17–1.30 (m, 1H), 1.49–1.63 (m, 1H), 1.63–1.81 (m, 3H), 2.03–2.11 (m, 1H), 2.32–2.52 (m, 2H), 2.64–2.73 (m, 1H), 3.76 (dt, 1H, J = 4.5, 9.7), 4.64 (dd, 1H, J = 9.7, 12.5), 4.92 (dd, 1H, J = 4.5, 12.5), 7.1–7.2, 7.2–7.4 (m, $5H_{arom}$); ms *m/z*: 247 (<1%, M^+), 171 (100%).

Data of *l*-2-(2-nitro-1-phenylethyl)-cyclohexanone, **2***a* (from **5***a*): yield, 96%; mp 71.2–71.4°C; ir ($CHCl_3$): 1704, 1552, 1377; ^1H nmr ($CDCl_3$): 1.1–2.9 (m, 9H), 3.92 (dt, 1H, J = 5.0, 7.5), 4.79 (d, 2H, J = 7.5), 7.21 (bs, $5H_{arom}$); ms *m/z*: 171 (100%).

Data of *u*-2-[1-(4-methylphenyl)-2-nitroethyl]-cyclohexanone, **1***b* (from **4***b*): yield, 99%; mp 114.2–114.8°C; ir (KBr): 1700, 1554,

Can. J. Chem. Downloaded from www.nrcresearchpress.com by 78.46.186.204 on 09/07/12
For personal use only.

1387; ^{1}H nmr ($CDCl_3$): 1.18–1.26 (m, 1H), 1.53–1.81 (m, 4H), 2.03–2.09 (m, 1H), 2.31 (s, 3H), 2.36–2.49 (m, 2H), 2.62–2.71 (m, 1H), 3.71 (dt, 1H, J = 4.6, 9.8), 4.61 (dd, 1H, J = 9.7, 12.4), 4.89 (dd, 1H, J = 4.6, 12.4), 7.04, 7.11 (ABqa, $4H_{arom}$, J = 8.1); ms m/z: 261 (<1%, M^+), 185 (100%). *Anal.* calcd. for $C_{15}H_{19}NO_3$, *Mol. Wt.* 261.326: C 68.94, H 7.32, N 5.36; found: C 68.85, H 7.33, N 5.36.

Data of *l*-2-[1-(4-methylphenyl)-2-nitroethyl]-cyclohexanone, **2***b* (from **5***b*): yield, 94%; oil; ir ($CHCl_3$): 1709, 1557, 1380; ^{1}H nmr ($CDCl_3$): 1.36–1.48 (m, 1H), 1.52–1.65 (m, 3H), 1.86–1.91 (m, 1H), 2.00–2.12 (m, 2H), 2.22–2.43 (m, 1H), 2.30 (s, 3H), 2.67–2.75 (m, 1H), 3.94 (dt, 1H, J = 5.4, 9.5), 4.79 (dd, 1H, J = 9.5, 12.8), 4.87 (dd, 1H, J = 5.9, 12.8), 7.09, 7.13 (ABqa, $4H_{arom}$, J = 8.5); ms m/z: 261 (<1%, M^+), 185 (100%). *Anal.* calcd. for $C_{15}H_{19}NO_3$, *Mol. Wt.* 261.326: C 68.94, H 7.32, N 5.36; found: C 69.01, H 7.35, N 5.21.

Data of *u*-2-[1-(4-methoxyphenyl)-2-nitroethyl]-cyclohexanone, **1***c* (ref. 13, from **4***c*): yield, 93%; mp 124.9–125.9°C; ir (KBr): 1700, 1553, 1390; ^{1}H nmr ($CDCl_3$): 1.21–1.29 (m, 1H), 1.53–1.81 (m, 4H), 2.03–2.09 (m, 1H), 2.36–2.49 (m, 2H), 2.60–2.69 (m, 1H), 3.71 (dt, 1H, J = 4.6, 9.8), 3.78 (s, 3H), 4.59 (dd, 1H, J = 9.8, 12.3), 4.89 (dd, 1H, J = 4.6, 12.3), 6.84, 7.07 (ABqa, $4H_{arom}$, J = 8.7); ms m/z: 277 (7%, M^+), 201 (89%), 134 (100%). *Anal.* calcd. for $C_{15}H_{19}NO_4$, *Mol. Wt.* 277.324: C 64.97, H 6.91, N 5.05; found: C 64.78, H 7.03, N 5.08.

Data of *l*-2-[1-(4-methoxyphenyl)-2-nitroethyl]-cyclohexanone, **2***c* (from **5***c*): yield, 83%; oil; ir ($CHCl_3$): 1710, 1554, 1310; ^{1}H nmr ($CDCl_3$): 1.36–1.44 (m, 1H), 1.56–1.65 (m, 2H), 1.87–1.91 (m, 1H), 2.00–2.12 (m, 2H), 2.27–2.43 (m, 2H), 2.66–2.74 (m, 1H), 3.77 (s, 3H), 3.90 (dt, 1H, J = 5.4, 9.4), 4.78 (dd, 1H, J = 9.4, 12.7), 4.87 (dd, 1H, J = 5.9, 12.7), 6.83, 7.17 (ABqa, $4H_{arom}$, J = 8.6); ms m/z: 277 (11%, M^+), 201 (100%). *Anal.* calcd. for $C_{15}H_{19}NO_4$, *Mol. Wt.* 277.326: C 64.97, H 6.91, N 5.05; found: C 64.97, H 7.10, N 5.00.

Data of *u*-4-[2-nitro-1-(2-oxycyclohexyl)ethyl]-benzonitrile, **1***d* (from **4***d*): yield, 81%; mp 124.8–126.2°C; ir (KBr): 2228, 1703, 1555; ^{1}H nmr ($CDCl_3$): 1.19–1.32 (m, 1H), 1.56–1.74 (m, 3H), 1.79–1.85 (m, 1H), 2.07–2.14 (m, 1H), 2.32–2.51 (m, 2H), 2.64–2.73 (m, 1H), 3.85 (dt, 1H, J = 4.5, 9.8), 4.67 (dd, 1H, J = 9.8, 12.9), 4.94 (dd, 1H, J = 4.5, 12.9), 7.32, 7.62 (ABqa, $4H_{arom}$, J = 8.5); ms m/z: 272 (<1%, M^+), 196 (100%). *Anal.* calcd. for $C_{15}H_{16}N_2O_3$, *Mol. Wt.* 272.325: C 66.16, H 5.92, N 10.29; found: C 65.96, H 6.11, N 10.20.

Data of *l*-4-[2-nitro-1-(2-oxycyclohexyl)ethyl]-benzonitrile, **2***d* (from **5***d*): yield, 92%; mp 110.0–111.0°C; ir (KBr): 2233, 1708, 1443; ^{1}H nmr ($CDCl_3$): 1.33–1.43 (m, 1H), 1.55–1.68 (m, 2H), 1.90–1.96 (m, 1H), 2.05–2.13 (m, 2H), 2.26–2.35 (m, 1H), 2.39–2.46 (m, 1H), 2.77 (ddt, 1H, J = 1.1, 5.6, 13.0), 3.97 (dt, 1H, J = 5.6, 7.5), 4.85 (d, 2H, J = 7.5), 7.40–7.60 (ABqa, $4H_{arom}$, J = 8.5); ms m/z: 279 (<1%, M^+), 196 (100%).

For the e series, general procedure 3 was followed with two exceptions: (*i*) the solvent system was methanol/water 3:4 (7 mL) and (*ii*) the products were not purified by flash chromatography. Both of these modifications were made to limit epimerization at the α-keto position.

Data of *l*-2-(2-nitro-1-propyl)-cyclohexanone, **1***e* (from **4***e*): yield, 100%; oil; ir ($CHCl_3$): 1710, 1550, 1380; ^{1}H nmr ($CDCl_3$): 1.03 (d, 3H, J = 6.9), 1.47 (dqa, 1H, J = 3.5, 12.7), 1.54–1.78 (m, 2H), 1.91–1.99 (m, 1H), 2.04–2.19 (m, 2H), 2.26–2.48 (m, 3H), 2.76 (sept, 1H, J = 6.7), 4.41 (d, 2H, J = 6.5); ms m/z: 155 (3%, M^+ – NO), 95 (44%). *Anal.* calcd. for $C_9H_{15}NO_3$, *Mol. Wt.* 185.225: C 58.36, H 8.16, N 7.56; found: C 58.54, H 8.42, N 7.43.

Data of *u*-2-(2-nitro-1-propyl)-cyclohexanone, **2***e* (from **5***e*): yield, 95%; oil; ir ($CHCl_3$): 1710, 1551, 1381; ^{1}H nmr ($CDCl_3$): 1.08 (d, 3H, J = 6.9), 1.46 (dd, 1H, J = 3.6, 12.0), 1.54 (dd, 1H, J = 3.2, 12.0), 1.63–1.72 (m, 2H), 1.93–1.97 (m, 1H), 2.04–2.12 (m, 2H), 2.28–2.45 (m, 2H), 2.63–2.68 (m, 1H), 4.34 (dd, 1H, J = 8.3, 12.1), 4.57 (dd, 1H, J = 5.7, 12.1); ms m/z: 155 (4%, M^+), 95 (45%). *Anal.* calcd. for $C_9H_{15}NO_3$, *Mol. Wt.* 185.225: C 58.36, H 8.16, N 7.56; found: C 58.43, H 8.17, N 7.45.

The Henry reaction: General procedure 4

To a cooled solution (0°C) of the aldehyde (0.2–0.4 mmol) and cyclic nitronate **4** or **5** (0.1–0.25 mmol) in THF (5–30 mL) was added TBAF in THF (5–10 mol%).[25]

After stirring for 6–16 h, the solution was allowed to warm to room temperature over 1 h. Following extraction with hexanes or ether, and washing with water (10×), the combined organic phases were dried over $MgSO_4$ and evaporated at 10 and then 0.1 Torr. The crude product (**4***a* → **15**, **5***a* → **15**–**19**) was purified by flash chromatography (petroleum ether/ether) and recrystallized from hexanes/chloroform.

Data of *u*,*l*,*u*-octahydro-3-nitro-2,4-diphenyl-8a*H*-1-benzopyran-8a-ol, **15** (from **4***a*, or from **5***a* at 25°C, 70% yield): yield, 88%; mp 220–224°C (dec.); ir (KBr): 3572, 3500, 1550; ^{1}H nmr ($CDCl_3$): 1.15–1.31 (m, 3H), 1.62–1.93 (m, 6H), 1.99 (s, 1H, OH), 3.72 (t, 1H, J = 11.5), 4.76 (dd, 1H, J = 9.9, 11.4), 5.54 (d, 1H, J = 9.9), 7.13–7.39 (m, $10H_{arom}$); ms m/z: 353 (<1%, M^+), 200 (50%), 105 (46%), 91 (100%). *Anal.* calcd. for $C_{21}H_{23}NO_4$, *Mol. Wt.* 353.421: C 71.37, H 6.56, N 3.96; found: C 71.24, H 6.55, N 3.92.

Data of *u*,*l*,*l*-octahydro-3-nitro-2,4-diphenyl-8a*H*-1-benzopyran-8a-ol, **16** (from **5***a*): yield, 23%; oil; ir ($CHCl_3$): 3420, 1550; ^{1}H nmr ($CDCl_3$): 1.01–1.16 (m, 1H), 1.39–1.49 (m, 2H), 1.56–1.69 (m, 3H), 1.70–1.82 (m, 1H), 1.94–2.06 (m, 2H), 2.39 (s, 1H, OH), 4.53 (dd, 1H, J = 4.3, 12.2), 5.21 (dd, 1H, J = 9.7, 12.2), 5.49 (d, 1H, J = 9.7), 7.19–7.39 (m, $10H_{arom}$); ms m/z: 353 (<1%, M^+), 200 (52%), 171 (66%), 105 (46%), 91 (100%).

Data of *u*,*l*,*u*-octahydro-3-nitro-2-methyl-4-phenyl-8a*H*-1-benzopyran-8a-ol, **17** (from **5***a*): yield, 33%; mp 205.4–205.9°C; ir (KBr): 3440, 1548; ^{1}H nmr ($CDCl_3$): 1.08–1.23 (m, 3H), 1.26 (d, 3H, J = 6.1), 1.59–1.76 (m, 6H), 1.80 (d, 1H, J = 1.5), 3.54 (t, 1H, J = 11.5), 4.48 (dd, 1H, J = 9.7, 11.2), 4.63 (dqa, 1H, J = 6.1, 9.7), 7.11–7.21, 7.23–7.32 (m, $5H_{arom}$); ms m/z: 291 (6%, M^+), 147 (64%), 129 (62%), 91 (100%).

Data of *u*,*l*,*l*-octahydro-3-nitro-2-methyl-4-phenyl-8a*H*-1-benzopyran-8a-ol, **18** (from **5***a*): yield, 20%; mp 164.2°C, sublimes; ir (KBr): 3458, 1548; ^{1}H nmr ($CDCl_3$): 0.97–1.03 (m, 1H), 1.20–1.30 (m, 2H), 1.32 (d, 3H, J = 6.1), 1.43–1.70 (m, 4H), 1.85–1.93 (m, 2H), 2.21 (s, 1H, OH), 4.34 (dd, 1H, J = 4.4, 12.2), 4.59 (dqa, 1H, J = 6.1, 9.7), 4.96 (dd, 1H, J = 9.7, 12.3), 7.17–7.33 (m, $5H_{arom}$); ms m/z: 291 (2%, M^+), 147 (61%), 91 (100%). *Anal.* calcd. for $C_{16}H_{21}NO_3$, *Mol. Wt.* 275.879: C 65.96, H 7.27, N 4.81; found: C 65.90, H 7.34, N 4.61.

Data of 4,4a-*l*-octahydro-3-nitro-2-methyl-4-phenyl-8a*H*-1-benzopyran-8a-ol, **19** (from **5***a*): yield, 26%; oil; ir (KBr): 3465, 1550; ^{1}H nmr ($CDCl_3$): 1.02–1.20 (m, 1H), 1.25 (d, 3H, J = 6.4), 1.30–1.48 (m, 2H), 1.52–1.82 (m, 4H), 1.74 (s, 1H, OH), 1.87 (dqa, 1H, J = 4.7, 13.3), 2.84 (tqa, 1H, J = 1.5, 3.2, 12.2 (after D_2O exchange: dt, 1H, J = 3.2, 12.2)), 3.41 (dd, 1H, J = 4.2, 12.2), 4.61–4.72 (m, 2H), 7.11–7.18, 7.22–7.39 (m, $5H_{arom}$); ms m/z: 291 (9%, M^+), 217 (20%), 129 (54%), 117 (53%), 91 (100%).

1,3-Dipolar cycloadditions: General procedure 5

To a solution of the acrylate derivative (0.3–1.0 mmol) in CH_2Cl_2[26] at room temperature was added the cyclic nitronate (0.25–0.35 mmol). After stirring for 4–18 h, the solvents were removed at 10 and then 0.1 Torr. The crude residue was submitted to flash chromatography (petroleum ether/ether mixtures) to give the mixture of diastereomers. In the case of crystalline adducts, with the exception of **23**, recrystallization provided diastereomerically pure samples with sharp melting points.

Data of *l*,*u*,*u*,*l*-decahydro-4-phenyl-8a-[(trimethylsilyl)oxy]-isoxazolo[2,3-*b*][1,2]2-carbomethoxybenzoxazine, **22** (>95% ds, from **4***a*): yield, 96%; oil; ir ($CHCl_3$): 1740, 1249, 1168, 1078; ^{1}H nmr ($CDCl_3$): 0.27 (s, 9H), 1.05–1.29 (m, 3H), 1.49–1.65 (m, 4H), 1.75–1.86 (m, 2H), 1.94 (dt, 1H, J = 3.0, 11.6), 2.78 (dt, 1H, J = 10.6, 11.6), 3.52 (dd, 1H, J = 4.6, 12.2), 3.68 (s, 3H), 3.68–3.76

[25]Generally, commercial TBAF/THF (1 *M* Aldrich) was used without modification.

[26]With acrylamide, toluene was used as the solvent at 110°C. The compounds were purified by recrystallization.

Can. J. Chem. Downloaded from www.nrcresearchpress.com by 78.46.186.204 on 09/07/12
For personal use only.

(m, 1H), 5.02 (dd, 1H, J = 3.4, 10.6), 7.15–7.34 (m, 5H$_{arom}$); ms m/z: 391 (<1%), 75 (100%). *Anal.* calcd. for $C_{21}H_{31}NO_5Si$, *Mol. Wt.* 405.569: C 62.19, H 7.70, N 3.45; found: C 62.42, H 7.81, N 3.28.

Data of *l,u,u,l*-2-[(4-bromophenoxy)-carboxy]-decahydro-4-phenyl-8a-[(trimethylsilyl)oxy]-isoxazolo[2,3-*b*][1,2]-benzoxazine, **23** (>95% ds, from **4***a*): yield, 87%; mp 114–123°C (it was impossible to avoid solvent inclusion (petroleum ether) in the crystal); ir (KBr): 1753, 1480, 1244, 1198, 1060, 988, 835; ^{1}H nmr ($CDCl_3$): 0.22 (s, 9H), 0.80–1.02 (m, 1H), 1.05–1.29 (m, 3H), 1.43–1.72 (m, 4H), 1.78–2.02 (m, 2H), 2.83 (dt, 1H, J = 10.6, 11.6), 3.51 (dd, 1H, J = 4.5, 12.1), 3.64–3.85 (m, 1H), 6.91, 7.47 (ABqa, 4H, J = 8.2), 7.18–7.42 (m, 5H$_{arom}$); ms m/z: 517 (6%), 515 (5%), 170 (100%).

Data of *l,l,l,l*-decahydro-4-phenyl-8a-[(trimethylsilyl)oxy]-isoxazolo[2,3-*b*][1,2]2-carbomethoxybenzoxazine, **24** (93% ds, from **5***a*): yield, 89%; oil; ir ($CHCl_3$): 1741, 1252, 1160, 1080, 1028; ^{1}H nmr ($CDCl_3$): 0.19 (s, 9H), 0.87–1.01 (m, 1H), 1.24–1.35 (m, 1H), 1.39–1.57 (m, 4H), 1.66–1.77 (m, 2H), 1.92 (ddd, 1H, J = 3.0, 6.9, 12.5), 2.41 (ddd, 1H, J = 3.4, 7.4, 11.8), 2.80 (dt, 1H, J = 10.4, 11.8), 3.17 (d, 1H, J = 6.9), 3.75 (s, 3H), 4.00 (dd, 1H, J = 7.8, 11.6), 5.04 (dd, 1H, J = 3.4, 10.4), 7.15–7.25, 7.49–7.53 (m, 5H$_{arom}$); ms m/z: 405 (<1%, M$^+$), 205 (41%), 170 (100%). *Anal.* calcd. for $C_{21}H_{31}NO_5Si$, *Mol. Wt.* 405.569: C 62.19, H 7.70, N 3.45; found: C 62.34, H 7.71, N 3.42.

Data of 4,4a-*u*-4a,8a-*u*-decahydro-4-phenyl-8a-[(trimethylsilyl)-oxy]-isoxazolo[2,3-*b*][1,2]2-carbomethoxybenzoxazine, **25** (81% ds, from **6***a*): yield, 49%; mp 94.0–95.6°C; ir (KBr): 1751, 1249, 1210, 1168, 1079; ^{1}H nmr ($CDCl_3$): 0.24 (s, 9H), 1.05–1.14 (m, 2H), 1.21–1.29 (m, 1H), 1.38–1.47 (m, 2H), 1.52–1.66 (m, 2H), 1.74–1.79 (m, 1H), 2.41–2.58 (m, 3H), 2.79 (dd, 1H, J = 6.8, 13.3), 3.70 (s, 3H), 3.69–3.83 (m, 1H), 5.07 (dd, 1H, J = 4.5, 9.3), 7.18–7.36 (m, 5H$_{arom}$); ms m/z: 405 (<1%, M$^+$), 205 (64%), 170 (100%).

Data of *l,l,l,l*-decahydro-4-methyl-8a-[(trimethylsilyl)oxy]-isoxazolo[2,3-*b*][1,2]2-carbomethoxybenzoxazine, **26** (94% ds, from **4***e*): yield, 95%; mp 63.2–65.1°C; ir ($CHCl_3$): 1742, 1260, 1250, 996; ^{1}H nmr ($CDCl_3$): 0.21 (s, 9H), 0.89 (d, 3H, J = 7.0), 1.13–1.24 (m, 3H), 1.35 (dt, 1H, J = 5.5, 12.0), 1.53–1.74 (m, 5H), 2.13 (ddd, 1H, J = 3.2, 7.5, 12.0), 2.31–2.38 (m, 1H), 2.52 (dt, 1H, J = 10.7, 11.5), 3.58 (ddd, 1H, J = 4.7, 7.5, 11.3), 3.76 (s, 3H), 4.99 (dd, 1H, J = 3.6, 10.4); ms m/z: 343 (<1%, M$^+$), 170 (36%), 75 (100%). *Anal.* calcd. for $C_{16}H_{29}NO_5Si$, *Mol. Wt.* 343.498: C 55.95, H 8.51, N 4.08; found: for C 55.87, H 8.54, N 3.95.

Data of *l,u,u,l*-decahydro-4-methyl-8a-[(trimethylsilyl)oxy]-isoxazolo[2,3-*b*][1,2]2-carbomethoxybenzoxazine, **27** (>95% ds, from **5***e*): yield, 49%; mp 94.9–95.9°C; ir (KBr): 1752, 1261, 1248, 1210; ^{1}H nmr ($CDCl_3$): 0.21 (s, 9H), 1.26 (d, 3H, J = 7.5), 1.21–1.30 (m, 2H), 1.37 (dt, 1H, J = 5.0, 12.0), 1.49–1.67 (m, 5H), 1.73–1.78 (m, 1H), 1.97–2.02 (m, 1H), 2.22 (ddd, 1H, J = 3.4, 7.5, 11.9), 2.64 (dt, 1H, J = 10.4, 11.7), 3.54 (ddd, 1H, J = 1.2, 7.4, 11.7), 3.76 (s, 3H), 4.99 (dd, 1H, J = 3.4, 10.4); ms m/z: 343 (<1%, M$^+$), 170 (74%), 75 (67%), 73 (100%). *Anal.* calcd. for $C_{16}H_{29}NO_5Si$, *Mol. Wt.* 343.498: C 55.95, H 8.51, N 4.08; found: C 56.06, H 8.51, N 3.96.

Data of 4,4a-*l*-4a,8a-*u*-decahydro-4-phenyl-8a-[(trimethylsilyl)-oxy]-isoxazolo[2,3-*b*][1,2]2-carbomethoxybenzoxazine, **28** (86% ds, from **6***e*): yield, 63%; oil; ir ($CHCl_3$): 1740, 1248, 1093; ^{1}H nmr ($CDCl_3$): 0.20 (s, 9H), 1.02 (d, 3H, J = 6.7), 1.25–1.76 (m, 9H), 1.95–2.03 (m, 1H), 2.32 (dt, 1H, J = 9.5, 12.0), 2.56 (ddd, 1H, J = 4.0, 7.8, 16.0), 3.25–3.33 (m, 1H), 3.76 (s, 3H), 5.03 (dd, 1H, J = 4.0, 9.9); ms m/z: 343 (<1%, M$^+$), 170 (77%), 75 (76%), 73 (100%).

Data of *l,u,u,l*-decahydro-4-phenyl-8a-[(trimethylsilyl)oxy]-isoxazolo[2,3-*b*][1,2]benzoxazine-2-carboxamide, **29** (85% ds, from **4***a*): yield, 68%; mp 139.6–150.0°C (dec.); ir (KBr): 3480, 1690, 1258, 1080; ^{1}H nmr ($CDCl_3$): 0.28 (s, 9H), 0.88–1.28 (m, 3H), 1.51–1.67 (m, 4H), 1.75–1.80 (m, 1H), 1.91–2.01 (m, 2H), 2.57 (dt, 1H, J = 10.8, 11.9), 3.47–3.60 (m, 2H), 4.98 (dd, 1H, J = 3.1, 10.8), 5.38 (bs, 1H), 6.34 (bs, 1H), 7.14–7.17, 7.20–7.32 (m, 5H$_{arom}$); ms m/z: 390 (<1%, M$^+$), 186 (35%), 170 (86%), 117 (65%), 91 (60%), 75 (89%), 73 (100%). *Anal.* calcd. for $C_{20}H_{30}N_2O_4Si$, *Mol. Wt.* 390.53: C 61.51, H 7.74, N 7.17; found: C 61.59, H 7.63, N 7.02.

Data of *l,l,l,l*-decahydro-4-phenyl-8a-[(trimethylsilyl)oxy]-isoxazolo[2,3-*b*][1,2]benzoxazine-2-carboxamide, **30** (83% ds, from **5***a*): yield, 59%; mp 147.2–148.6°C (dec.); ir (KBr): 3435, 1665, 1250, 1158, 1080, 1030, 1000; ^{1}H nmr ($CDCl_3$): 0.20 (s, 9H), 0.93 (dqa, 1H, J = 3.7, 12.5), 1.27–1.58 (m, 5H), 1.65–1.78 (m, 2H), 1.94 (ddd, 1H, J = 2.9, 6.9, 12.3), 2.46 (ddd, 1H, J = 3.3, 7.3, 12.0), 2.89 (dt, 1H, J = 10.8, 12.0), 3.17 (d, 1H, J = 6.9), 3.82 (dd, 1H, J = 7.3, 12.0), 5.00 (dd, 1H, J = 3.3, 10.8), 5.44 (bs, 1H), 6.42 (bs, 1H), 7.18–7.27, 7.49–7.52 (m, 5H$_{arom}$); ms m/z: 390 (<1%), 259 (53%), 147 (100%). *Anal.* calcd. for $C_{20}H_{30}N_2O_4Si$, *Mol. Wt.* 390.53: C 61.51, H 7.74, N 7.17; found: C 61.26, H 7.62, N 7.07.

Data of 3,4-*l*-4,4a-*l*-4a,8a-*l*-decahydro-4-phenyl-8a-[(trimethylsilyl)oxy]-isoxazolo[2,3-*b*][1,2]2-carbomethoxy-2-methylbenzoxazine, **31** (1:1 mixture of isomers at C2, from **5***a*): yield, 71%; oil; ir ($CHCl_3$): 1732, 1250, 1160, 1080, 1010; ^{1}H nmr (both isomers, $CDCl_3$): 0.16 (s, 9H), 0.18 (s, 9H), 1.92 (dqa, 2 × 1H, J = 3.8, 12.8), 1.19–1.78 (m, 2 × 7H), 1.52 (s, 3H), 1.57 (s, 3H), 1.89–1.99 (m, 2 × 1H), 2.07 (dd, 1H, J = 8.2, 12.5), 2.56 (t, 1H, J = 12.2), 2.67 (dd, 1H, J = 7.0, 11.5), 3.11 (t, 2H, J = 7.8), 3.19 (dd, 1H, J = 11.0, 12.0), 3.72 (s, 3H), 3.77 (s, 3H), 3.98–4.09 (m, 2 × 1H), 7.14–7.28, 7.47–7.54 (m, 2 × 5H$_{arom}$); ms m/z: 419 (<1%, M$^+$), 259 (17%), 170 (100%). *Anal.* calcd. for $C_{22}H_{33}NO_5Si$, *Mol. Wt.* 419.596: C 62.97, H 7.93, N 3.34; found: C 62.85, H 7.79, N 3.23.

Reduction of cyclic nitronates: General procedure 6

Raney nickel was prepared according to ref. 47 (p. 1117, procedure A). To a suspension of the activated Raney nickel (0.5 g) in methanol (40 mL) was added the cyclic nitronate (0.8–0.9 mmol) and KF (5 mg). The solution stirred overnight under an atmosphere of H_2 (1–20 atm; 1 atm = 101.3 kPa) at elevated temperatures (25–120°C). The solution was filtered through Celite (2×) and evaporated at 10 and then 0.1 Torr. The residue was recrystallized from ethyl acetate or $CHCl_3$/methanol.

Data of methyl *l,l,l,l*-octahydro-1*H*-indole-3-phenyl-2-[2-hydroxy]-propanoate **32** (H_2, 20 atm, 50°C, from **23**): yield, 88%; mp 192.1–192.6°C; ir (KBr): 3325, 1744, 1210, 1204, 1094; ^{1}H nmr ($CDCl_3$): 1.04–1.09 (m, 1H), 1.18–1.30 (m, 2H), 1.60–1.66 (m, 1H), 1.72–1.88 (m, 4H), 2.12 (ddd, 1H, J = 1.3, 9.2, 14.6), 2.28–2.33 (m, 2H), 2.49 (ddd, 1H, J = 3.6, 10.1, 15.1), 3.46 (dd, 1H, J = 3.1, 5.8), 3.69 (s, 3H), 4.11 (bs, 1H, OH), 4.56 (t, 1H, J = 10.1), 4.74 (dd, 1H, J = 3.6, 9.2), 7.18–7.36 (m, 6H); ms m/z: 303 (13%, M$^+$), 200 (100%).

Data of *l,l,l,l*-decahydro-2-hydroxy-9-phenyl-3*H*-pyrrolo[1,2-*a*]-indol-3-one, **33** (H_2, 1 atm, 25°C, from **23**): yield, 78%; mp 192.1–192.6°C; ir (KBr): 3355, 1676; ^{1}H nmr ($CDCl_3$): 1.01–1.26 (m, 4H), 1.49–1.64 (m, 3H), 1.75 (dt, 1H, J = 9.1, 11.2), 2.45 (d, 1H, J = 15.0), 2.57 (dt, 1H, J = 10.5, 12.5), 2.87 (ddd, 1H, J = 5.6, 7.6, 12.5), 2.98 (d, 1H (OH), J = 2.2), 3.07 (dd, 1H, J = 5.5, 10.5), 4.10 (bs, 1H), 4.41 (ddd, 1H, J = 5.5, 9.2, 10.2), 4.69 (dddd, 1H, J = 1.2, 2.2, 7.5, 10.5 (after D_2O exchange: ddd, 1H, J = 1.2, 7.5, 10.5)), 7.13–7.38 (m, 5H$_{arom}$); ms m/z: 271 (26%, M$^+$). *Anal.* calcd. for $C_{17}H_{21}NO_2$, *Mol. Wt.* 271.360: C 75.24, H 7.80, N 5.16; found: C 75.11, H 7.64, N 5.08.

Data of *l,u,u,l*-decahydro-2-hydroxy-9-methyl-3*H*-pyrrolo[1,2-*a*]-indol-3-one, **34** (H_2, 19 atm, 120°C, from **26**): yield, 61%; oil; ir ($CHCl_3$): 3520, 3360, 1687; ^{1}H nmr ($CDCl_3$): 0.96 (d, 3H, J = 6.9), 1.03–1.21 (m, 2H), 1.44–1.88 (m, 7H), 2.18 (m, 1H), 2.38 (d, 1H, J = 13.5), 3.02 (bs, 1H (OH)), 3.58 (dt, 1H, J = 5.5, 9.5), 3.87 (bs, 1H), 4.57 (ddd, 1H, J = 1.1, 7.4, 11.1); ms m/z: 209 (100%, M$^+$).

*Conversion of **32** to **33***

To a solution of K_2CO_3 (3 mg) in methanol (10 mL) was added **34** (10.0 mg, 0.03 mmol). After 24 h at room temperature, the solvent was evaporated at 10 Torr and the residue recrystallized from ethyl acetate to give **33** (83% yield).

*Reduction of **22** to the alcohol **35**, protected as the acetate*

To a suspension of $LiAlH_4$ (0.03 g, 0.8 mmol) in THF (10 mL) under

an argon atmosphere at 25°C was added **22** (0.164 g, 0.4 mmol). After 18 h, acetic anhydride (0.5 mL, 5.3 mmol) was added and the mixture stirred for 4 h. The solution was evaporated at 10 Torr. The ^{1}H nmr spectrum (90 MHz) of the crude residue showed the presence of the OTMS group in the product. The residue was submitted to flash chromatography (petroleum ether/ether, 1:1).

Data of 2-[(5-(acetoxymethyl)-2-isoxazolidin-3-yl)-phenylmethyl]-cyclohexanone, **35**: yield, 65%; oil; ir ($CHCl_3$): 1738, 1707, 1220, 1128; ^{1}H nmr ($CDCl_3$): 1.06–1.20 (m, 1H), 1.54–1.80 (m, 5H), 2.12 (s, 3H), 2.36–2.54 (m, 2H), 2.87 (d, 2H, J = 8.7), 3.36 (ddd, 1H, J = 5.0, 10.8, 13.0), 3.78 (d, 1H, J = 10.9), 4.11 (dd, 1H, J = 5.3, 12.0), 4.16 (dd, 1H, J = 4.8, 12.0), 4.63 (ddt, 1H, J = 4.8, 5.3, 8.7), 7.20–7.37 (m, $5H_{arom}$); ms m/z: 329 (32%, M^+), 256 (90%), 130 (77%).

Acknowledgements

We would like to thank Frl. B. Brandenberg (ETH) for conducting the nmr measurements, and Mr. R. Faggiani (McMaster) for performing, and Dr. C. J. L. Lock (McMaster) for helpful discussions regarding, the X-ray crystal structure analysis. The awarding of an N.S.E.R.C. Canada Postdoctoral Fellowship (1984–1985) to M.A.B. is gratefully acknowledged.

1. D. Seebach and M. A. Brook. Helv. Chim. Acta, **68**, 319 (1985).
2. R. G. Coombes. Nitro and Nitroso Compounds. *In* Comprehensive organic chemistry. Vol. II. *Edited by* I. O. Sutherland. Pergamon Press, London. 1979. pp. 303–382; The chemistry of the nitro and the nitroso group. Parts 1 and 2. *Edited by* S. Patai. Wiley–Interscience, New York (1969–1970).
3. D. Seebach, E. W. Colvin, F. Lehr, and Th. Weller. Chimia, **33**, 1 (1979).
4. G. A. Olah, M. Arvanaghi, Y. D. Vankar, and G. K. S. Prakash. Synthesis, 662 (1980); D. H. R. Barton, W. B. Motherwell, and S. Z. Zard. Tetrahedron Lett. 5227 (1983); M. R. Galobardes and H. W. Pinnick. Tetrahedron Lett. 5235 (1981); G. A. Olah and B. G. B. Gupta. Synthesis, 44 (1980); J. H. Clark and D. G. Cork. J. Chem. Soc. Perkin Trans. 1, 2253 (1983).
5. G. M. Barratt and G. G. Graboski. Chem. Rev. In press.
6. (*a*) A. Risaliti, M. Forchiassin, and E. Valentin. Tetrahedron Lett. 6331 (1966); (*b*) E. Valentin, G. Pitacco, F. P. Colonna, and A. Risaliti. Tetrahedron, **30**, 2741 (1974); (*c*) F. P. Colonna, E. Valentin, G. Pitacco, and A. Risaliti. Tetrahedron, **29**, 3011 (1973); (*d*) A. Risaliti, M. Forchiassin, and E. Valentin. Tetrahedron, **24**, 1889 (1968); (*e*) S. Daneo, G. Pitacco, A. Risaliti, and E. Valentin. Tetrahedron, **38**, 1499 (1982).
7. D. Seebach and J. Goliński. Helv. Chim. Acta, **64**, 1413 (1981).
8. S. J. Blarer and D. Seebach. Chem. Ber. **116**, 3086 (1983); **116**, 2250 (1983); S. J. Blarer, W. B. Schweizer, and D. Seebach. Helv. Chim. Acta, **65**, 1637 (1982).
9. (*a*) R. Häner, Th. Laube, and D. Seebach. Chimia, **38**, 255 (1984); (*b*) D. Seebach, A. K. Beck, J. Goliński, J. N. Hay, and Th. Laube. Helv. Chim. Acta, **68**, 162 (1985).
10. D. Seebach and V. Prelog. Angew. Chem. **94**, 696 (1982); Angew. Chem. Int. Ed. Engl. **21**, 654 (1982).
11. R. W. Stevens and T. Mukaiyama. Chem. Lett. 851 (1985).
12. D. Seebach. *In* The Robert A. Welch Foundation Conferences on Chemical Research. XXVII. Stereospecificity in Chemistry and Biochemistry. Houston, Texas, Nov. 7–9, 1983. Published in the proceedings of the above conference, Welch Foundation, Houston, 1984.
13. M. C. Moorjani and G. K. Trevidi. Ind. J. Chem. Sect. B, **16**, 405 (1978).
14. S. E. Denmark, M. S. Dappen, and C. J. Cramer. J. Am. Chem. Soc. **108**, 1306 (1986).
15. K. Narasaka, K. Soai, and T. Mukaiyama. Chem. Lett. 1223 (1974).
16. K. Saigo, M. Osaki, and T. Mukaiyama. Chem. Lett. 163 (1976).
17. A. Yoshikoshi and M. Miyashita. Acc. Chem. Res. **18**, 284 (1985); M. Miyashita, T. Yanami, T. Kumazawa, and A. Yoshikoshi. J. Am. Chem. Soc. **106**, 2149 (1984); M. Miyashita, T. Kumazawa, and A. Yoshikoshi. Chem. Lett. 1043 (1980); Org. Synth. **60**, 117 (1981); J. Am. Chem. Soc. **98**, 4679 (1976); A. Yoshikoshi. J. Synth. Org. Chem. Jpn. **40**, 427 (1982).
18. C. H. Heathcock and D. E. Uehling. J. Org. Chem. **51**, 279 (1986); C. H. Heathcock, M. H. Norman, and D. E. Uehling. J. Am. Chem. Soc. **107**, 2797 (1985).
19. W. C. Still, M. Khan, and A. Mitra. J. Org. Chem. **43**, 2923 (1978).
20. E. W. Colvin. Silicon in organic synthesis. Butterworths, London. 1981. pp. 178–184.
21. D. A. Evans, J. V. Nelson, and T. R. Taber. *In* Topics in stereochemistry. Vol. 13. *Edited by* N. L. Allinger, E. L. Eliel, and S. H. Wilen. Wiley–Interscience, New York. 1982.
22. C. H. Heathcock. *In* Asymmetric synthesis. Vol. 3. *Edited by* J. P. Morrison. Academic Press, New York. 1984; *In* Comprehensive carbanion chemistry. Vol. 2. *Edited by* E. Buncel and T. Durst. Elsevier, Amsterdam. 1984.
23. S. Masamune, W. Choy, J. S. Petersen, and L. R. Sita. Angew. Chem. **97**, 1 (1985); Angew. Chem. Int. Ed. Engl. **24**, 1 (1985); S. Masamune, S. A. Ali, D. L. Snitman, and D. S. Garvey. Angew. Chem. **92**, 573 (1980); Angew. Chem. Int. Ed. Engl. **19**, 557 (1980); S. Masamune and W. Choy. Aldrichimica Acta, **15**, 47 (1982).
24. (*a*) R. W. Hoffmann. Angew. Chem. **94**, 569 (1982); Angew. Chem. Int. Ed. Engl. **21**, 555 (1982); (*b*) R. W. Hoffmann and K. Ditrich. Tetrahedron Lett. 1781 (1984).
25. (*a*) C. Gennari, R. Todeschini, M. G. Beretta, G. Favini, and C. Scolastico. J. Org. Chem. **51**, 612 (1986); (*b*) C. Gennari, L. Colombo, C. Scolastico, and R. Todeschini. Tetrahedron, **40**, 4051 (1984); (*c*) C. Gennari, S. Cardani, L. Colombo, and C. Scolastico. Tetrahedron Lett. 2283 (1984).
26. S. Murata, M. Suzuki, and R. Noyori. J. Am. Chem. Soc. **102**, 3248 (1980).
27. (*a*) Y. Yamamoto, H. Yatagai, and K. Maruyama. J. Chem. Soc. Chem. Commun. 162 (1981); (*b*) E. Nakamura and I. Kuwajima. Tetrahedron Lett. 3347 (1983); (*c*) I. Kuwajima and E. Nakamura. Acc. Chem. Res. 181 (1985).
28. (*a*) M. T. Reetz and R. Peter. Tetrahedron Lett. 4691 (1981); (*b*) E. Nakamura and I. Kuwajima. Tetrahedron Lett. 3343 (1983).
29. (*a*) D. A. Evans and L. R. McGee. Tetrahedron Lett. 3975 (1980); (*b*) Y. Yamamoto and K. Maruyama. Tetrahedron Lett. 4607 (1980).
30. (*a*) R. Noyori, I. Nishida, and J. Sakata. J. Am. Chem. Soc. **105**, 1598 (1983); (*b*) J. Am. Chem. Soc. **103**, 2106 (1981); (*c*) Tetrahedron Lett. 2085 (1981); (*d*) R. Noyori, I. Nishida, J. Sakata, and M. Nishizawa. J. Am. Chem. Soc. **102**, 1223 (1980).
31. T. Hayashi, M. Konishi, and M. Kumada. J. Am. Chem. Soc. **104**, 4963 (1982).
32. Y. Yamamoto, H. Yatagai, Y. Ishihara, N. Maeda, and K. Maruyama. Tetrahedron, **40**, 2239 (1984).
33. S. E. Denmark and E. J. Weber. (*a*) Origins of the stereoselectivity in the reactions of allylsilanes and allylstannanes with aldehydes. Presented at the Fifth International Conference on Organic Synthesis, Freiburg im Breisgau, August 1984; (*b*) J. Am. Chem. Soc. **106**, 7970 (1984); (*c*) Helv. Chim. Acta, **66**, 1655 (1983).
34. G. E. Keck, D. E. Abbott, E. P. Boden, and E. J. Enholm. Tetrahedron Lett. 3927 (1984); G. E. Keck and E. P. Boden. Tetrahedron Lett. 1879 (1984).

Can. J. Chem. Downloaded from www.nrcresearchpress.com by 78.46.186.204 on 09/07/12
For personal use only.

35. S. J. DANISHEFSKY, E. LARSON, D. ASKIN, and N. KATO. J. Am. Chem. Soc. **107**, 1246 (1985); S. J. DANISHEFSKY, W. H. PEARSON, and D. F. HARVEY. J. Am. Chem. Soc. **106**, 2456 (1984); E. R. LARSON and S. DANISHEFSKY. Tetrahedron Lett. 1975 (1982); S. DANISHEFSKY, J. F. KERWIN, JR., and S. KOBAYASHI. J. Am. Chem. Soc. **104**, 358 (1982); S. DANISHEFSKY, E. R. LARSON, and D. ASKIN. J. Am. Chem. Soc. **104**, 6457 (1982).
36. T. H. CHAN, T. AIDA, P. W. K. LAU, V. GORYS, and D. N. HARPP. Tetrahedron Lett. 4029 (1979).
37. R. HÄNER, W. B. SCHWEIZER, P. SEILER, and D. SEEBACH. Chimia, **40**, 97 (1986).
38. J. MARCH. Advanced organic chemistry: Reactions, mechanisms and structure. Wiley–Interscience, New York. 1985. p. 122; J. DALE. Stereochemistry and conformational analysis. Verlag Chemie, New York. 1978.
39. E. R. LARSON and S. DANISHEFSKY. J. Am. Chem. Soc. **104**, 6458 (1982); J. S. HARTMAN, P. STILBS, and S. FORSEN. Tetrahedron Lett. 3497 (1975); J. TORRI and M. AZZARO. Bull. Soc. Chim. Fr. **2**, 283 (1978).
40. (*a*) M. T. REETZ, M. HÜLLMAN, W. MASSA, S. BERGER, P. RADEMACHER, and P. HEYMANNS. J. Am. Chem. Soc. **108**, 2405 (1986); (*b*) T. POLL, J. O. METTER, and G. HELMCHEN. Angew. Chem. **97**, 116 (1985); Angew. Chem. Int. Ed. Engl. **24**, 112 (1985).
41. E. FUJITA, M. SHIBUYA, S. NAKAMURA, Y. OKADA, and T. FUJITA. J. Chem. Soc. Perkin Trans. 1, 165 (1974); Z. G. HAJOS and D. R. PARRISH. J. Org. Chem. **39**, 1612 (1974).
42. A. LUBINEAU. J. Org. Chem. **51**, 2142 (1986).
43. H.-B. BÜRGI. Angew. Chem. **87**, 461 (1975); Angew. Chem. Int. Ed. Engl. **14**, 460 (1975); H.-B. BÜRGI and J. D. DUNITZ. Acc. Chem. Res. **16**, 153 (1983).
44. H. J. BESTMANN. Pure Appl. Chem. **52**, 771 (1980).
45. N. T. AHN and O. EISENSTEIN. Nouv. J. Chimie, **1**, 61 (1977).
46. E. W. COLVIN and D. SEEBACH. J. Chem. Soc. Chem. Commun. 689 (1978).
47. (*a*) D. SEEBACH, A. K. BECK, T. MUKHOPADYAY, and E. THOMAS. Helv. Chim. Acta, **65**, 1101 (1982); (*b*) M. EYER and D. SEEBACH. J. Am. Chem. Soc. **107**, 3601 (1985).
48. R. HUISGEN. *In* 1,3-Dipolar cycloaddition chemistry. Vol. 1. *Edited by* A. Padwa. Wiley–Interscience, New York. 1984. pp. 1–176; J. Org. Chem. **41**, 403 (1976); Angew. Chem. **80**, 329 (1968); Angew. Chem. Int. Ed. Engl. **7**, 321 (1968).
49. N. B. DAS and K. B. G. TORSSELL. Tetrahedron, **39**, 2227 (1983); **39**, 2247 (1983); S. K. MUKERJI and K. B. G. TORSSELL. Acta Chem. Scand. Ser. B, **35**, 643 (1981).
50. V. A. TARTAKOVSKII. Izv. Akad. Nauk SSSR, Ser. Khim. (Engl. Transl.), 165 (1984).
51. E. B. HODGE and R. ABBOTT. J. Org. Chem. **27**, 2254 (1962); G. BARBARELLA, S. BRÜCKNER, G. PITACCO, and E. VALENTIN. Tetrahedron, **40**, 2441 (1984); H. W. SCHEEREN and A. E. FRISSEN. Synthesis, 794 (1983); G. BARBARELLA, G. PITACCO, C. RUSSO, and E. VALENTIN. Tetrahedron Lett. 1621 (1983); P. BRADAMANTE, G. PITACCO, A. RISALITI, and E. VALENTIN. Tetrahedron Lett. 2683 (1982); P. NITTI, G. PITACCO, V. RINALDI, and E. VALENTIN. Croat. Chem. Acta, **59**, 165 (1986).
52. R. A. FIRESTONE. Tetrahedron, **33**, 3009 (1977).
53. J. TUFARIELLO. *In* 1,3-Dipolar cycloaddition chemistry. Vol. 2. *Edited by* A. Padwa. Wiley–Interscience, New York. 1984. pp. 83–168; D. ST. C. BLACK, R. F. CROZIER, and V. C. DAVIS. Synthesis, 205 (1975).
54. M. SHITKIN, V. I. KHUDAK, I. E. CHLENOV, and V. A. TARTAKOVSKII. Izv. Akad. Nauk SSSR, Ser. Khim. (Engl. Transl.), 1836 (1974); V. M. SHITKIN, I. E. CHLENOV, and V. A. TARTAKOVSKII. Izv. Akad. Nauk SSSR, Ser. Khim. (Engl. Transl.), 187 (1977).
55. (*a*) R. GRÉE, F. TONNARD, and R. CARRIÉ. Tetrahedron, **32**, 675 (1976); (*b*) R. GRÉE and R. CARRIÉ. Tetrahedron, **32**, 683 (1976); (*c*) R. GRÉE and R. CARRIÉ. J. Heterocycl. Chem. **14**, 965 (1977).
56. M. PETRIZILKA, D. FELIX, and A. ESCHENMOSER. Helv. Chim. Acta, **56**, 2950 (1973); A. VASELLA. Helv. Chim. Acta, **60**, 1273 (1977).
57. P. A. ONGLEY (*Editor*). Organicum, Practical Handbook of Organic Chemistry. English Translation B. J. Hazzard. Pergamon, Oxford. 1973. p. 480.
58. M. E. KUEHNE and L. FOLEY. J. Org. Chem. **30**, 4280 (1965).

Can. J. Chem. Downloaded from www.nrcresearchpress.com by 78.46.186.204 on 09/07/12
For personal use only.

Structure cristalline et moléculaire de l'acétoxy-3β ursane olide-28,20βa

DANIELLE DRUET ET LOUIS CLAUDE COMEAU
Laboratoire de chimie biologique appliquée, Faculté des sciences et techniques, 3 place Victor Hugo, 13331-Marseille CEDEX, France

ROBERT VIANI
Laboratoire de biophysique, Université de Nice, 06034 Nice CEDEX, France

ET

ANDRÉ BALDY, JACQUES ESTIENNE ET MARCEL PIERROT
Service de cristallochimie, Faculté des sciences et techniques, Centre de Saint-Jérôme, 13397-Marseille CEDEX 13, France

Reçu le 9 juillet 1986

DANIELLE DRUET, LOUIS CLAUDE COMEAU, ROBERT VIANI, ANDRÉ BALDY, JACQUES ESTIENNE et MARCEL PIERROT. Can. J. Chem. **65**, 851 (1987).

L'étude cristallographique du triterpène $C_{32}H_{50}O_4$, extrait d'*Opilia celtidifolia*, confirme l'approche chimique de la structure moléculaire. Les cycles A, B, C et D adoptent une conformation chaise alors que le cycle E, du fait de la présence d'un groupement lactone ponteur entre les atomes de carbone C(17) et C(20), s'observe dans une conformation bateau. Les cinq cycles à six chaînons présentent des jonctions *trans*.

DANIELLE DRUET, LOUIS CLAUDE COMEAU, ROBERT VIANI, ANDRÉ BALDY, JACQUES ESTIENNE, and MARCEL PIERROT. Can. J. Chem. **65**, 851 (1987).

An X-ray crystallographic study of the triterpene $C_{32}H_{50}O_4$, isolated from *Opilia celtidifolia*, confirms the chemical analysis of the molecular structure. The rings A, B, C, and D are in the chair conformation, but ring E, due to a bridging lactone between the C(17) and C(20) carbon atoms, adopts a boat conformation. All five six-membered rings are *trans*-fused.

Can. J. Chem. Downloaded from www.nrcresearchpress.com by 78.46.186.204 on 09/07/12
For personal use only.

Introduction

Au cours de travaux effectués sur *Opilia Celtidifolia*, une Olacale de l'Afrique de l'ouest très utilisée en pharmacopée locale, nous avons isolé, après hydrolyse des glycosides, plusieurs aglycones triterpéniques. Aux côtés de l'hédéragénine (1) et de l'acide oléanique (2), nous avons pu caractériser un premier composé mineur dont nous avons établi la structure (3). Nous reportons ici l'étude chimique et structurale d'un second composé mineur : l'acétoxy-3β ursane olide-28,20βa **1***a*.

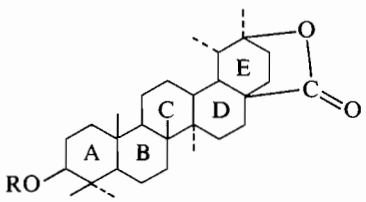

1 *a*: R = Ac
b: R = H

Résultats et discussion

Le composé **1***a* est isolé par chromatographie sur colonne de silice du mélange d'aglycones acétylées provenant de l'hydrolyse des glycosides d'*Opilia Celtidifolia*. **1***a* cristallise en aiguilles dans le mélange dichlorométhane–hexane (F = 314–321°C).

Les cristaux répondent positivement aux tests caractéristiques des triterpènes et négativement au test au tétranitrométhane. Une fraction des cristaux est hydrolysée par la potasse méthanolique afin d'établir les constantes physico-chimiques du composé **1***b*. Recristallisé du mélange dichlorométhane–hexane, celui-ci présente un point de fusion de 277–281°C.

Les analyses spectroscopiques ont été effectuées, pour plus de commodité, sur le derivé acétylé **1***a*. Le résultat de l'analyse centésimale et la présence en spectrométrie de masse d'un pic d'ion moléculaire à m/z = 498 conduisent à la formule brute $C_{32}H_{50}O_4$. La spectrométrie infrarouge montre qu'il s'agit d'un acétate (1725–1250 cm^{-1}) comportant vraisemblablement un pont lactone (1725–1160–1098 cm^{-1}). En spectrométrie de masse, le composé **1***a* donne la fragmentation caractéristique des triterpènes pentacycliques hydroxylés en 3 : les pics à m/z = 189 et 204 proviennent d'une coupure au niveau du cycle C (4, 5). D'autres fragments sont intéressants et notamment celui à m/z = 249 ($M^+ - 44$) venant confirmer la présence d'un pont lactone. Celui à m/z = 249, dont dérive le fragment à m/z = 204 par perte d'un groupement -CO_2H, permet de fixer une des positions du pont lactonique sur le carbone C(17) (5). La rmn du ^{1}H à 100 MHz, effectuée sur **1***a*, montre la présence de 6 groupements angulaires et d'un groupement méthyle porté par un carbone tertiaire. À δ = 2,04 ppm, un singulet (3H) dû au méthyle d'un groupement acétyle indique que le composé **1***a* ne possède qu'un seul hydroxyle acétylable. Le déplacement chimique du quadruplet à δ = 4,47 ppm (^3J = 10 Hz, ^3J = 6 Hz), correspondant au proton en α de la fonction acétyle, situe celle-ci en position 3β équatoriale. On n'observe aucun signal correspondant à un hydrogène en α de la fonction lactone, ce qui permet de conclure que celle-ci est portée par des carbones quaternaires. Le spectre du ^{13}C a été enregistré sur l'acétate **1***a* en utilisant la technique DEPT pour déterminer la nature des carbones présents dans la molécule. L'attribution des différents glissements chimiques figure dans le tableau 1, établi après détermination de la structure du composé par diffraction des rayons X.

La présence en rmn du ^{1}H d'un méthyle porté par un carbone tertiaire nous a orienté vers les dérivés de l'ursane dont l'un des méthyles en 19 ou 20 serait porté par un carbone rendu quaternaire, probablement par la présence d'un pont lactone. Une comparaison des caractéristiques physico-chimiques de notre composé **1***a* et de dérivés de l'ursane hydroxylés en 3 et comportant un cycle lactonique (6, 7) a permis de conclure que l'acétoxy-3β ursane olide-28,20 présentait de grandes similitudes avec notre composé : points de fusion identiques et

TABLEAU 1. En rmn du ^{13}C, glissements chimiques de l'acétoxy-3β ursane olide-28,20 (**1***a*)

Carbone	δ	Carbone	δ
C(1)	38,50	C(17)	34,53
C(2)	23,66	C(18)	48,38
C(3)	80,92	C(19)	42,86[b]
C(4)	37,78	C(20)	84,15
C(5)	55,49	C(21)	27,28[c]
C(6)	18,12	C(22)	27,56[d]
C(7)	33,84	C(23)	27,92
C(8)	40,54	C(24)	16,46
C(9)	50,51	C(25)	16,34
C(10)	37,07	C(26)	15,68
C(11)	20,97	C(27)	14,19
C(12)	25,16	C(28)	185,76
C(13)	41,99[a]	C(29)	23.98
C(14)	41,99	C(30)	18,72
C(15)	27,06	$CH_3—CO_2—$	21,31
C(16)	32,23	$CH_3—CO_2—$	171,01

a et *b*, *c* et *d* peuvent être interchangées. Les valeurs de δ sont données en ppm avec le TMS comme référence interne.

valeurs des glissements chimiques des différents signaux en rmn du ^1H très proches.

La configuration absolue de la molécule n'a pas été déterminée dans cette étude. Toutefois, la connaissance de la configuration observée dans divers composés analogues de la même famille de triterpènes pentacycliques, et, notamment, celle du *p*-bromobenzoate-3 méthyl ursolate (8), permet la détermination de la stéréochimie de l'ensemble de la molécule. Cette configuration, à laquelle correspondent les coordonnées des atomes non hydrogènes mentionnés dans le tableau 3, se trouve portée sur la figure 1.

Les liaisons simples $C_{sp^3}—C_{sp^3}$ varient entre 1,487 et 1,593 Å, avec des limites paraissant anormales au regard de la valeur classique de 1,54 Å pour une liaison de ce type. En fait, dans la mesure où le rayon de van der Waals associé à un groupement méthyle est de l'ordre de 2,0 Å (9) et que les contacts de non liaison C(24)...C(25) et C(25)...C(26) sont respectivement de 3,25(1) et 3,11(1) Å, il existe dans la région des cycles A et B du noyau triterpénique une importante interaction stérique. Il s'observe en conséquence un allongement de certaines liaisons C—C, associé tout naturellement à un raccourcissement compensateur pour d'autres.

Les angles de valence varient de 107,1 à 118,3° avec une valeur moyenne de 111,2°. Les cycles A, B, C et D, en jonctions *trans*, présentent une conformation chaise avec respectivement pour meilleur plan moyen, les groupes d'atomes [C(1), C(3), C(4), C(10)], [C(6), C(7), C(9), C(10)], [C(8), C(9), C(12), C(13)] et [C(13), C(18), C(15), C(16)]. Le cycle E, également en jonction *trans*, s'observe dans une conformation bateau résultant du pontage de type lactone entre les atomes de carbone C(17) et C(20) situés respectivement à 0,757(7) et 0,640(7) Å au-dessus du plan moyen défini par le groupe d'atomes [C(18), C(19), C(21), C(22)].

L'existence d'une structure bicyclique ne semble pas en fait une condition nécessaire à l'adoption pour le cycle E de la conformation la moins favorable. En effet, les résultats relatifs à la structure du taraxasterol (10) semblent montrer que l'interaction stérique entre $C(12)H_2$ et $C(29)H_3$ est suffisante pour imposer la conformation bateau.

Aucune interaction intermoléculaire particulière au regard

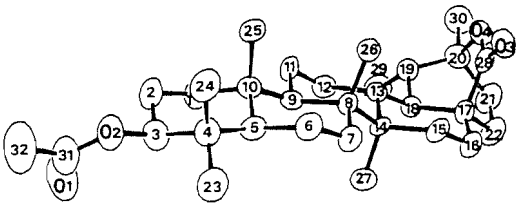

FIG. 1. Vue de la molécule (ellipsoïdes thermiques à 50% de probabilité) et indexation des atomes.

de la somme des rayons de van der Waals des atomes n'est à signaler.

Conclusion

D'après la littérature, l'hydroxy-3β ursane olide-28,20βa n'a jamais été isolé à l'état naturel dans une fraction aglycone provenant de végétaux, mais a été préparé à des fins analytiques (7) ou synthétisé par oxydation du formyl-3β époxy-28,20 ursane (6).

Certains auteurs (11–13) ont remarqué qu'une lactonisation pouvait se produire au cours de l'hydrolyse acide de glycosides dont l'aglycone possédait une fonction carboxylique en C(17) et une double liaison ou un groupement hydroxyle proche du -COOH.

Ces résultats doivent nous conduire à vérifier si l'aglycone **1***a* n'est pas issue d'une autre aglycone ayant subi une transformation chimique au cours de l'hydrolyse acide.

La conformation bateau du cycle E constitue un facteur déterminant pour une réaction d'estérification interne et les composés **2**, **3**, **4** ou **5**, **6** nous paraissent être de possibles précurseurs.

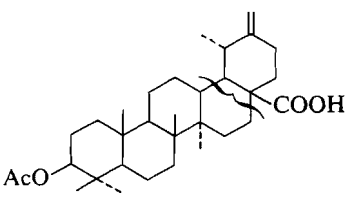

2

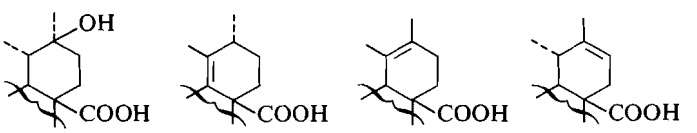

3 **4** **5** **6**

Partie expérimentale

Les points de fusion ont été pris sur microscope à platine chauffante de Reichert. Les spectres ir ont été effectués sur un appareil Leitz. Les spectres de rmn du ^1H et du ^{13}C ont été enregistrés sur Bruker AM 100 en solution dans le deutérochloroforme avec le TMS comme référence interne. Le spectre de masse a été déterminé sur L.K.B.

La fraction glycosidique (340 g) d'*Opilia Celtidifolia* est hydrolysée par 500 mL de mélange de Kiliani (eau – acide acétique – HCl, 275:175:50 v/v/v) à 100°C pendant 3 h. Les aglycones brutes (79 g) obtenues sont extraites au soxhlet pendant 72 h par de l'oxyde d'éthyle. Après évaporation du solvant, on récupère 40 g de résidu que l'on acétyle par 80 mL d'anhydride acétique en présence de 400 mL de pyridine anhydre, à température ambiante, pendant 48 h. Les réactifs sont ensuite éliminés sous pression réduite et la phase organique est reprise au dichlorométhane, lavée successivement au Na_2CO_3, à l'eau, par HCl 2 *N*, à nouveau à l'eau jusqu'à neutralité. Après séchage sur Na_2SO_4 et élimination du solvant, on obtient 41,2 g d'acétates

Can. J. Chem. Downloaded from www.nrcresearchpress.com by 78.46.186.204 on 09/07/12
For personal use only.

TABLEAU 2. En rmn du ^1H, glissements chimiques comparés des méthyles de **1***a* et de l'acétoxy-3β ursane olide-28,20 (réf. 7)

Composé	δ*				
	Me 23, 24, 25	Me 26	Me 27	Me 29	Me 30
Acétoxy-3β ursane olide	0,836 (×3)	0,90	0,93	0,98 (d)	1,31
Composé **1***a*	0,835 (×2) – 0,846	0,90	0,93	0,99 (d)	1,31

*Les valeurs des déplacements chimiques sont données en partie par million avec le TMS comme référence interne (d = doublet).

TABLEAU 3. Paramètres de position et facteur d'agitation thermique isotrope équivalent des atomes non hydrogènes

Atome	*x*	*y*	*z*	B_{eq} (Å^2)*
C1	0,5676(6)	0,013	0,2647(5)	4,1
C2	0,6464(7)	−0,052(1)	0,3539(5)	4,6
C3	0,7181(6)	0,090(1)	0,4074(4)	4,2
C4	0,6421(6)	0,240(1)	0,4230(4)	4,0
C5	0,5566(6)	0,297(1)	0,3330(4)	3,2
C6	0,4764(6)	0,450(1)	0,3367(5)	4,0
C7	0,4227(6)	0,532(1)	0,2477(4)	3,8
C8	0,3504(6)	0,4084(9)	0,1771(4)	3,0
C9	0,4247(5)	0,2419(9)	0,1793(4)	2,9
C10	0,4813(6)	0,1567(9)	0,2714(4)	3,3
C11	0,3571(6)	0,1175(9)	0,1080(4)	3,3
C12	0,3206(6)	0,199(1)	0,0179(4)	3,5
C13	0,2503(5)	0,3651(9)	0,0139(4)	3,1
C14	0,3231(5)	0,4931(9)	0,0832(4)	3,0
C15	0,2464(6)	0,6591(9)	0,0776(4)	3,7
C16	0,2022(6)	0,734(1)	−0,0136(5)	4,3
C17	0,1341(6)	0,608(1)	−0,0822(4)	3,5
C18	0,2047(5)	0,440(1)	−0,0802(4)	3,1
C19	0,1249(6)	0,309(1)	−0,1457(4)	3,3
C20	0,0096(6)	0,397(1)	−0,1992(4)	3,9
C21	0,0303(7)	0,562(1)	−0,2428(5)	4,9
C22	0,1060(7)	0,685(1)	−0,1745(5)	5,0
C23	0,7284(8)	0,389(1)	0,4629(5)	5,4
C24	0,5772(7)	0,190(1)	0,4887(5)	4,7
C25	0,3840(6)	0,071(1)	0,3051(5)	4,1
C26	0,2309(6)	0,368(1)	0,1951(4)	3,6
C27	0,4400(6)	0,547(1)	0,0651(5)	4,2
C28	0,0135(6)	0,5574(9)	−0,0729(4)	3,3
C29	0,1931(7)	0,227(1)	−0,2028(5)	5,0
C30	−0,0803(7)	0,280(1)	−0,2625(5)	5,0
C31	0,8933(7)	−0,053(1)	0,4966(5)	5,9
C32	0,9522(9)	−0,123(2)	0,5840(6)	8,6
O1	0,9317(5)	−0,065(1)	0,4382(3)	8,1
O2	0,7898(4)	0,0235(8)	0,4919(3)	5,0
O3	−0,0277(4)	0,6044(7)	−0,0184(3)	4,2
O4	−0,0506(4)	0,4495(8)	−0,1358(3)	3,9

*$B_{eq} = (4/3)[a^2 \cdot B(1,1) + b^2 \cdot B(2,2) + c^2 \cdot B(3,3) + ab \cos\gamma \cdot B(1,2) + ac \cos\beta \cdot B(1,3) + bc \cos\alpha \cdot B(2,3)]$.

d'aglycones. Ceux-ci sont fractionnés par chromatographie sur colonne de silice (50 g de silice/1 g d'aglycones) avec comme éluant le mélange hexane – oxyde d'éthyle (90:10 v/v). À partir de 5 g d'aglycones acétylées, on isole en moyenne 55 mg de composé **1***a*. Après cristallisation dans le mélange dichlorométhane–hexane, l'acétate **1***a* présente les caractéristiques suivantes : *F* : 314–321°C; ir (KBr) : 1730, 1725, 1370, 1250, 1160, 1098, 1075, 1030, 980, 955, 950 cm^{-1}; rmn $^1H(CDCl_3)$ δ : 0,835 (s, 3H, CH_3); 0,846 (s, 6H, CH_3 × 2); 0,90 (s, 3H, CH_3); 0,93 (s, 3H, CH_3); 0,99 (d, 3H, ^3J = 7 Hz, —CH—CH_3); 1,31 (s, 3H, CH_3); 2,05 (s, 3H, CH_3—C(=O)—O—); 4,47 (q, 1H, ^3J = 10 Hz, ^3J = 6 Hz, —CH—OAc); rmn $^{13}C(CDCl_3)$: tableau 2; masse *m/z* : 498 (17), 470 (36), 454 (30), 438 (60), 423 (25), 395 (100), 249 (44), 233 (10), 234 (10), 204 (13), 189 (28). *Anal.* calc. pour $C_{32}H_{50}O_4$: C 77,11; H 10,04; O 12,85%; tr. : C 77,20; H 10,29; O 12,51%.

Quinze milligrammes d'acétate **1***a* sont hydrolysés pendant trois heures à reflux par 7 mL de potasse 2 *N* méthanolique. Après dilution, la fraction hydroalcoolique est extraite au dichlorométhane. L'extrait organique est lavé à l'eau, séché sur Na_2SO_4 et le solvant est éliminé. Le résidu (12 mg) est recristallisé du mélange dichlorométhane–hexane; *F* : 277–281°C; ir (KBr) : 1750, 1500, 1450, 1370, 1080, 1060, 950 cm^{-1}; rmn $^1H(CDCl_3)$ δ : 0,75 (s, 3H, CH_3); 0,82 (s, 3H, CH_3); 0,90 (s, 3H, CH_3); 0,93 (s, 3H, CH_3); 0,96 (s, 3H, CH_3); 0,98 (d, 3H, —CH—CH_3); 1,31 (s, 3H, CH_3); 3,20 (q, 1H, ^3J = 11 Hz, ^3J = 5,5 Hz, —CH—OH). *Anal.* calc. pour $C_{30}H_{48}O_3$: C 78,95; H 10,53; O 10,53%; tr. : C 78,82; H 10,50; O 10,68%.

Données cristallographiques

$C_{32}H_{50}O_4$ M_r = 498,7

Monoclinique, groupe spatial $P2_1$ avec *a* = 11,709(4), *b* = 7,774(4), *c* = 16,186(4) Å et β = 108,53(2)°, *U* = 1397(2) Å^3, D_c = 1,19 g cm^{-3}, *Z* = 2, MoKα radiation (λ = 0,71073 Å), μ = 0,71 cm^{-1}.

Les paramètres de la maille cristalline ont été déterminés à partir d'un affinement par moindres carrés des positions angulaires en θ de 25 réflexions dans l'intervalle 5,3–14,6°. La mesure des intensités a été effectuée sur diffractomètre CAD-4 Enraf–Nonius équipé d'un monochromateur au graphite, à température ambiante (293 K). Technique de scan ω/2θ de 0,91 à 10,06°min^{-1} sur un intervalle de (0,90 + 0,35 tg θ) degrés en ω avec un angle de balayage dans le rapport de 1/4 entre fond continu et pic de diffraction.

Aucune variation significative des intensités de trois réflexions standards ($70\bar{3}/1\bar{2}0/027$) mesurées toutes les heures n'a été observée lors de l'enregistrement des 3069 réflexions ($2\theta_{max}$ = 52°) effectué sur un cristal incolore de forme en aiguille (0,15 × 0,15 × 0,30 mm^3), h_{max} = ±14, k_{max} = 9, l_{max} = 20. Répondant au critère $I > 3\sigma(I)$, 1791 réflexions sont utilisées pour la résolution structurale.

Tous les calculs ont été effectués sur PDP 11/44, programmes SDP d'Enraf–Nonius (14). Correction des facteurs de Lorentz polarisation et résolution de la structure par méthodes directes (MULTAN (15)). Après affinement en matrice totale avec des facteurs d'agitation thermique anisotrope pour le atomes de carbone et d'oxygène, isotrope fixé à B = 5 Å^2 pour les atomes d'hydrogène aux positions calculées (C—H : 0,950 Å) non affinées, les facteurs de reliabilité *R* et R_w (pondération unitaire) prennent respectivement les valeurs finales de 0,046 et 0,047. Une valeur de 0,86 pour le facteur de reliabilité *S* corrobore le choix de la pondération. Les facteurs de diffusion sont ceux donnés par Cromer et Waber (16) corrigés de la dispersion anomale (17).

Une fonction Fourier différence ne présente alors pas de pic supérieur à 0,16 e Å^{-3}. Les tables relatives aux positions des atomes d'hydrogène, aux facteurs d'agitation thermique anisotrope des atomes

Can. J. Chem. Downloaded from www.nrcresearchpress.com by 78.46.186.204 on 09/07/12
For personal use only.

non hydrogènes, aux angles dièdres, aux longueurs et angles de liaisons, aux calculs des plans moyens et aux listes des facteurs de structure ainsi qu'une vue de l'empilement cristallin, ont été déposées.[1]

1. R. ROQUES, D. DRUET et L. C. COMEAU. Acta Crystallogr. Sect. B, **34**, 1634 (1978).
2. D. DRUET et L. C. COMEAU. Ann. Univ. Abidjan. Ser. C, **14**, 57 (1978).
3. D. DRUET, L. C. COMEAU et J. P. ZAHRA. Can. J. Chem. **64**, 295 (1986).
4. H. BUDZIKIEWICZ, J. M. WILSON et C. DJERASSI. J. Am. Chem. Soc. **85**, 3688 (1963).
5. C. DJERASSI, H. BUDZIKIEWICZ et J. M. WILSON. Tetrahedron Lett. **7**, 263 (1962).
6. A. VYSTRCIL et J. KLINOT. Collect. Czech. Chem. Commun. **24**, 3273 (1959).
7. J. M. LEHN et A. VYSTRCIL. Tetrahedron, **19**, 1733 (1963).
8. W. F. PATON et I. C. PAUL. Cryst. Struct. Commun. **8**, 207 (1979).
9. L. PAULING. The nature of the chemical bond. 3e éd. Cornell University Press, Ithaca, NY. 1960.
10. W. F. REYNOLDS, J. F. SAWYER, R. G. ENRIQUEZ, L. I. ESCOBAR, M. A. CHAVEZ et J. N. SHOOLERY. Can. J. Chem. **63**, 1048 (1985).
11. P. POTIER, B. C. DAS, A. M. BUI, M. M. JANOT, A. POURRAT et H. POURRAT. Bull. Soc. Chim. Fr. **11**, 3458 (1966).
12. D. H. R. BARTON, H. T. CHEUNG, P. L. J. DANIELS, K. G. LEWIS et J. F. MCGHIE. J. Chem. Soc. 5163 (1962).
13. K. W. MERZ et H. TSCHUBEL. Ber. **72**, 1017 (1939).
14. B. A. FRENZ *et al.* Enraf–Nonius structure determination package. College Station, Texas. 1981.
15. P. MAIN *et al.* MULTAN 11/82 system of programs for the automatic solution of crystal structures from X-ray diffraction data. University of York, England. 1982.
16. D. T. CROMER et J. T. WABER. Acta Crystallogr. **18**, 104 (1965).
17. D. T. CROMER. Acta Crystallogr. **18**, 17 (1965).

1. On peut acheter les données mises en dépôt en s'adressant au Dépôt de données non publiées, ICIST, Conseil National de recherches du Canada, Ottawa (Ont.), Canada K1A 0S2.

Can. J. Chem. Downloaded from www.nrcresearchpress.com by 78.46.186.204 on 09/07/12
For personal use only.

Dimerisation of mononuclear and binuclear cobalt phthalocyanines

W. A. NEVIN, WEI LIU,[1] AND A. B. P. LEVER[2]
Department of Chemistry, York University, North York, Ont., Canada M3J 1P3

Received August 25, 1986

W. A. NEVIN, WEI LIU, and A. B. P. LEVER. Can. J. Chem. **65**, 855 (1987).

The aggregation of mononuclear [2,9,16,23-tetra(neopentoxy)phthalocyanato]cobalt(II) and of some related binuclear cobalt(II) phthalocyanine derivatives, in *o*-dichlorobenzene, has been studied by electronic absorption spectroscopy. Dimerisation constants and the calculated aggregate dimer spectra are reported.

W. A. NEVIN, WEI LIU et A. B. P. LEVER. Can. J. Chem. **65**, 855 (1987).

Faisant appel à la spectroscopie d'absorption électronique et opérant dans le *o*-dichlorobenzène, on a étudié l'aggrégation du [tétra(néopentylate)-2,9,16,23 phtalocyanato]cobalt(II) mononucléaire et de quelques dérivés apparentés binucléaires de la phtalocyanine de cobalt(II). On rapporte les constantes de dimérisation et les spectres calculés des dimères sous formes d'aggrégats.

[Traduit par la revue]

Can. J. Chem. Downloaded from www.nrcresearchpress.com by 78.46.186.204 on 09/07/12
For personal use only.

Introduction

Extensive studies on the water-soluble tetrasulphonated phthalocyanines (TsPc) (1–10) have shown a tendency for these complexes to dimerise in aqueous solution, the extent of dimerisation depending strongly upon the nature of the central substituent in the phthalocyanine ring. Typically, the dimer has a Q band absorption at ca. 30–50 nm to the blue of the monomer Q band, due to exciton coupling between the two halves of the aggregate (11). At high concentrations, higher aggregates form which absorb in the same region as the dimer Q band, but with broader, lower intensity bands (1–3, 5, 6).

These aggregation phenomena are of considerable interest since coupling interactions between the Pc rings have important biological significance as models for similar porphyrin behaviour and may also have a direct influence on properties such as semiconductivity, photo- and electrocatalytic efficiency, and electrochromism. In particular there is intense interest in designing multi-electron redox catalysts by the purposeful construction of polynuclear species which are often prepared by difficult, time consuming, and low yield routes. Aggregation offers a facile procedure for generating multinuclear species which may prove to have useful properties different from their mononuclear components.

A major difficulty in evaluating dimerisation processes in aqueous solution is that the strong solvent–solvent interaction, rather than the dye–dye interaction is the dominant force causing the molecules to aggregate (12, 13). Hence, studies in solvents of low dielectric constant are desirable to maximise the Pc–Pc interactions. However, few studies have been carried out on Pc dimerisation in organic solvents. Monahan *et al.* (12–14) have shown that the degree of dimerisation of tetraalkyl phthalocyanines (PcX_4) increases in the order of central substituent: Cu ≪ Zn < VO in benzene, which is in contrast to the results for TsPc species in aqueous solution (Zn ≈ VO < Cu (3–5)).

We have recently reported a series of binuclear and tetranuclear phthalocyanines (15–18) based upon the organic-solvent soluble [2,9,16,23-tetra(neopentoxy)phthalocyanato]cobalt(II) (Co(II)TNPc). The complexes can exist in various conformations depending upon the nature of the bridging unit. For example, the EtMeO(5) and Cat(4) species (the latter linked by an O—O catecholate group) can close in a "clamshell"-like fashion (11, 15) while other binuclear phthalocyanines are constrained by the geometry of the bridge to have an open conformation. We present here data for the mononuclear control phthalocyanine, Co(II)TNPc, for an example of a "clamshell" (EtMeO(5)) and for an open conformation binuclear phthalocyanine (C(2)) (the number in parentheses is the number of bridging atoms). The binuclear species are EtMeO(5)-$[Co(II)TrNPc]_2$ (trineopentoxyphthalocyanine rings linked via $—OCH_2C(Me)(Et)CH_2O—$) and C(2)$[Co(II)TrNPc]_2$ (trineopentoxyphthalocyanine rings linked via $—CH_2CH_2—$).

Experimental

Electronic spectra were recorded with a Hitachi – Perkin Elmer Microprocessor model 340 spectrometer. Cobalt phthalocyanines were prepared following literature routes (15, 16). *N,N*-Dimethylformamide (DMF) was supplied by Aldrich (Gold Label). Tetrabutylammonium perchlorate (TBAP) (Kodak) was recrystallised from absolute ethanol and dried at 50°C under vacuum for 2 days. Solutions in *o*-dichlorobenzene (DCB, Aldrich Gold Label) were prepared by dilution of a freshly prepared stock solution of phthalocyanine. Spectra were run immediately after each dilution and solutions were shielded from room light to minimise any photodecomposition of the phthalocyanine.

Results and discussion

Figure 1 shows that for Co(II)TNPc in DCB solution, Beer's law was obeyed for the band at 678 nm (monomer Q band) up to a concentration of 2×10^{-5} *M*, above which the results show considerable deviation from linearity. Increasing the concentration of Co(II)TNPc caused an increase in intensity at 612 nm relative to 678 nm, indicating the formation of aggregates. The values of the molar absorptivities of the monomeric form of Co(II)TNPc, calculated from the linear portion of the Beer's law plot, are given in Table 1.

In the presence of 0.3 *M* TBAP, deviation from Beer's law occurred at lower concentrations of Co(II)TNPc and to a greater extent than for pure DCB solution (Fig. 1), while the absorbance at 612 nm increased further relative to 678 nm. This shows a greater tendency for aggregation as the ionic strength of the solution is increased, which was also noted for phthalocyanines in aqueous solution (3, 5–10). Figure 2*a* shows the variation of the spectrum of Co(II)TNPc in DCB with 0.3 *M* added TBAP, at concentrations of between 9×10^{-5} and 7×10^{-4} *M*. The spectrum of monomeric Co(II)TNPc is included for comparison. Note that the electronic spectrum, in DCB, of the monomeric species (ca. 5×10^{-6} *M*) is unperturbed in the presence of 0.3 *M* TBAP, indicating that no strong

[1]Present address: Department of Chemistry, Yangzhou Teachers' College, Yangzhou, Jiangsu, People's Republic of China.

[2]To whom all correspondence should be addressed.

TABLE 1. Electronic spectra of the monomeric phthalocyanine species in DCB

Species	λ_{max} nm ($\epsilon \times 10^{-4}\ M^{-1}\ cm^{-1}$)				
Co(II)TNPc	330 (6.54)	382 (2.49)	612 (3.45)	645 sh	678 (13.5)
EtMeO(5)[Co(II)TrNPc]$_2$	322 (10.8)	380 sh	626 (9.25)		674 (9.38)
C(2)[Co(II)TrNPc]$_2$	334 (9.67)	380 sh	628 (6.96)	645 sh	682 (10.3)

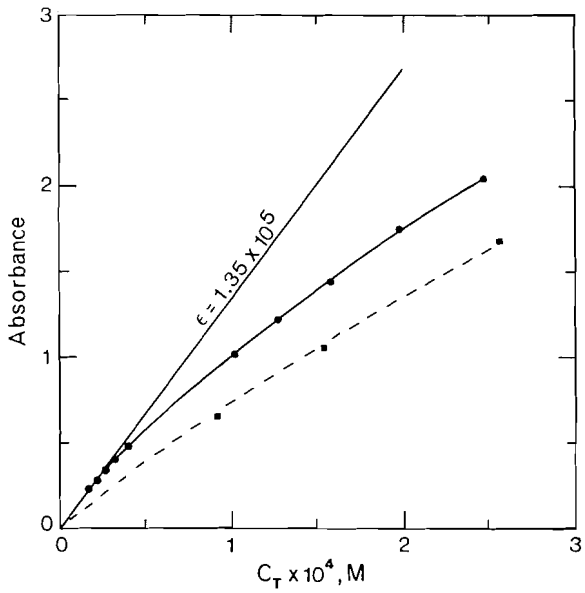

FIG. 1. Beer's law experiment (678 nm absorbance) for Co(II)TNPc in DCB solution (●) and DCB solution containing 0.3 M TBAP (■). The line marked $\epsilon = 1.35 \times 10^5$ defines Beer's law behaviour for Co(II)TNPc.

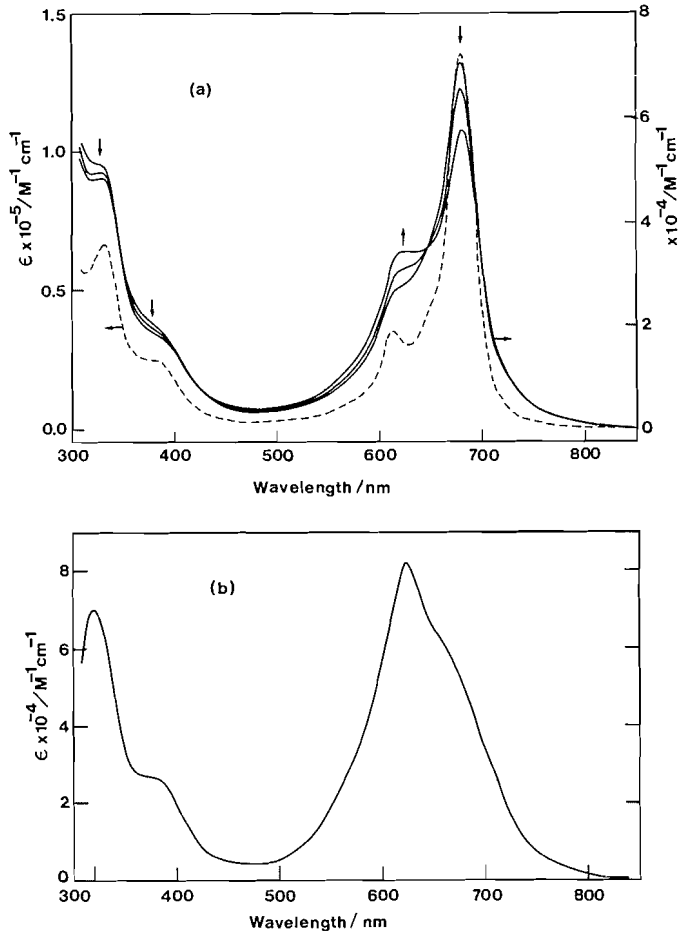

FIG. 2. (*a*) Electronic absorption spectra of Co(II)TNPc in DCB solution containing 0.3 M TBAP at concentrations of $9.2 \times 10^{-5}\ M$, $2.6 \times 10^{-4}\ M$, and $6.6 \times 10^{-4}\ M$ (—), and monomeric Co(II)TNPc in DCB solution (----). (*b*) Calculated spectrum of the aggregate dimer of Co(II)TNPc in DCB. ϵ_D(max) (625 nm) = $8.2 \times 10^4\ M^{-1}\ cm^{-1}$.

CoTNPc–TBAP interactions occur. The increased aggregation is probably due to a polarisation effect of the added electrolyte.

Addition of DMF to a solution of Co(II)TNPc in DCB reduces the aggregation, in agreement with previous work on metalloPcX$_4$ complexes in organic solvents (14), where the degree of aggregation was found to decrease with increasing dielectric constant of the solvent (DCB = 9.93, DMF = 36.7 (19)).

The dimerisation constant, K_D, for Co(II)TNPc in DCB was calculated from the uv–visible spectra using a computer program based upon the approximation method of West and Pearce (20), taking the spectrum at $< 2 \times 10^{-5}\ M$ to be that of the pure monomer. Data are given in Table 2. A plot of $\log_{10} C_M$ versus $\log_{10} C_D$, where C_M and C_D are the concentrations of monomer and aggregate dimer, respectively, at a given total concentration, C_T, of phthalocyanine, gave a straight line with a slope of 2 (statistical R coefficient > 0.99). This confirms the existence of a monomer(M)–dimer(D) (1) equilibrium excluding significant formation of trimers etc. at the concentrations studied.

$$[1] \quad 2\,M \rightleftharpoons^{K_D} D$$

An average value of $K_D = 2.57\ (\pm 0.05) \times 10^3\ M^{-1}$ was obtained.

Dimerisation constants of the binuclear complexes EtMeO(5)-[Co(II)TrNPc]$_2$ and C(2)[CoTrNPc]$_2$ in DCB were measured using phthalocyanine concentrations of 10^{-7}–10^{-4} and 10^{-6}–$10^{-4}\ M$, respectively. The spectra measured at $< 5 \times 10^{-6}\ M$ were taken as those of the pure monomeric forms. Absorption data used for calculation of the dimerisation constants are given in Tables 3 and 4, respectively. Plots of $\log_{10} C_M$ versus $\log_{10} C_D$ are shown in Fig. 3. In each case a straight line with a slope of 2 is obtained, showing that an equilibrium exists

TABLE 2. Dimerisation constant, K_D, of Co(II)TNPc in DCB at 20°C[a]

$C_T \times 10^4$ (M)	OD_{obs} (678 nm)	OD_M	$C_M \times 10^4$ (M)	$C_D \times 10^5$ (M)	$K_D \times 10^{-3}$ (M^{-1})
2.48	2.04	1.95	1.44	5.18	2.49
1.98	1.71	1.65	1.22	3.82	2.58
1.59	1.44	1.39	1.03	2.78	2.62
1.27	1.22	1.18	0.874	1.97	2.58
1.01	1.01	1.00	0.735	1.40	2.59

[a]Cell pathlength = 0.1 cm; OD_{obs} = observed optical density; OD_M = corrected optical density of the monomeric species. $C_D = (C_T - C_M)/2$; $K_D = C_D/C_M^2$.

Can. J. Chem. Downloaded from www.nrcresearchpress.com by 78.46.186.204 on 09/07/12
For personal use only.

TABLE 3. Dimerisation constant, K_D, of EtMeO(5)[Co(II)TrNPc]$_2$ in DCB at 20°C[a]

$C_T \times 10^5$ (M)	L	OD_{obs} (674 nm)	OD_M	$C_M \times 10^5$ (M)	$C_D \times 10^5$ (M)	$K_D \times 10^{-3}$ (M^{-1})
9.08	0.1	0.664	0.607	6.47	1.31	3.13
7.26	0.1	0.547	0.500	5.33	0.965	3.40
5.81	0.1	0.448	0.419	4.47	0.672	3.36
4.65	0.5	1.854	1.749	3.73	0.460	3.31
2.79	0.5	1.176	1.125	2.40	0.196	3.40
1.67	0.5	0.743	0.717	1.53	0.071	3.02

[a]L = cell pathlength; OD_{obs} = observed optical density; OD_M = corrected optical density of the monomeric species. $C_D = (C_T - C_M)/2$; $K_D = C_D/C_M^2$.

TABLE 4. Dimerisation constant, K_D of C(2)[Co(II)TrNPc]$_2$ in DCB at 20°C[a]

$C_T \times 10^5$ (M)	OD_{obs} (682 nm)	OD_M	$C_M \times 10^5$ (M)	$C_D \times 10^5$ (M)	$K_D \times 10^{-3}$ (M^{-1})
8.28	0.603	0.550	5.34	1.47	5.12
6.62	0.502	0.464	4.51	1.05	5.15
5.30	0.417	0.401	3.90	0.697	4.58
4.24	0.354	0.336	3.26	0.486	4.56
3.39	0.283	0.273	2.65	0.367	5.22
2.71	0.237	0.230	2.23	0.234	4.70

[a]Cell pathlength = 0.1 cm; OD_{obs} = observed optical density; OD_M = corrected optical density of the monomeric species. $C_D = (C_T - C_M)/2$; $K_D = C_D/C_M^2$.

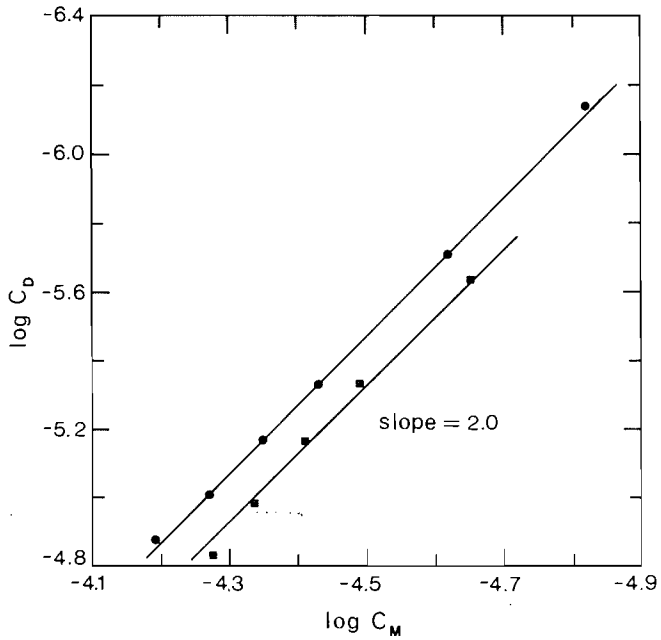

FIG. 3. Plots of log C_M versus log C_D for EtMeO(5)[Co(II)TrNPc]$_2$ (●) and C(2)[Co(II)TrNPc]$_2$ (■) in DCB solution. The solid lines are drawn with the theoretical slope of 2. The statistical R coefficient exceeds 0.99 for both plots.

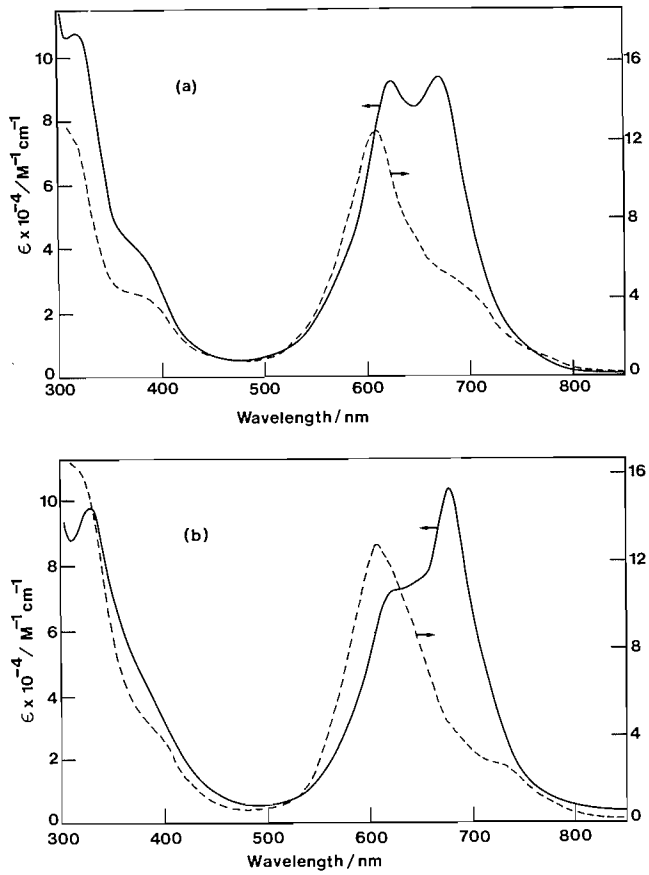

FIG. 4. Electronic absorption spectra of monomeric (—) and calculated aggregate dimer spectra, in DCB, of (*a*) EtMeO(5)[Co(II)TrNPc]$_2$ (ϵ_D(max)(610 nm) = $12.5 \times 10^4 M^{-1}$ cm^{-1}), and (*b*) C(2)[Co(II)TrNPc]$_2$ (ϵ_D(max) (605 nm) = $12.8 \times 10^4 M^{-1}$ cm^{-1}).

between a monomeric form and a dimer coupled via both rings of each binuclear molecule. Average values of K_D were calculated to be 3.3 ($\pm$0.2) $\times 10^3$ and 4.9 ($\pm$0.3) $\times 10^3$ M^{-1}, for EtMeO(5)[CoTrNPc]$_2$ and C(2)[CoTrNPc]$_2$, respectively.

The spectroscopic data can be used to derive the electronic spectra for the pure aggregate dimeric species following the method of West and Pearce (6, 7, 20). These spectra are shown in Figs. 2*b* and 4 and show the blue shifting to be anticipated as a consequence of the exciton coupling (11).

The values of K_D measured for these cobalt neopentoxy complexes in DCB are 2–3 orders of magnitude smaller than for CoTsPc in aqueous solution (1–4, 7). This is consistent with the 3–4 order of magnitude difference between K_D of $CuPcX_4$ in benzene (13, 14) and CuTsPc in water (3, 4, 6). In contrast, the K_D values of Zn and VO phthalocyanines are approximately of the same order for $MPcX_4$ in benzene (13, 14) and MTsPc in water (3–5).

Although the dimerisation constants of the cobalt neopentoxy phthalocyanine complexes are of the same order of magnitude, small differences are seen which may be related to the structural conformations of the molecules. Thus, the "open" conformation C(2) binuclear species appears to aggregate more readily than

Can. J. Chem. Downloaded from www.nrcresearchpress.com by 78.46.186.204 on 09/07/12
For personal use only.

the EtMeO(5) binuclear species, which can form a "closed clamshell" conformation in solution, an effect which may inhibit inter-molecular aggregation.

A tetranuclear cobalt(II) phthalocyanine (18) has an unexpectedly high aggregation constant in DCB, some two orders greater than the binuclear species reported here. It is tentatively proposed that the geometry of the tetranuclear species permits two clamshell halves to inter-penetrate to form a quadruple stack. Presumably such an inter-penetrated quadruple stack is not geometrically permissible for the EtMeO(5) species.

Acknowledgements

The authors are indebted to the Natural Sciences and Engineering Research Council of Canada (Ottawa), and the Office of Naval Research (Washington) for financial support.

1. Z. A. SCHELLY, R. D. FARINA, and E. M. EYRING. J. Phys. Chem. **74**, 617 (1970).
2. Y. C. YANG, J. R. WARD, and R. P. SEIDERS. Inorg. Chem. **24**, 1765 (1985).
3. H. SIGEL, P. WALDMEIER, and B. PRIJS. Inorg. Nucl. Chem. Lett. **7**, 161 (1971).
4. K. BERNAUER, and S. FALLAB. Helv. Chim. Acta, **44**, 1287 (1961).
5. R. D. FARINA, D. J. HALKO, and J. H. SWINEHART. J. Phys. Chem. **76**, 2343 (1972).
6. R. J. BLAGROVE and L. C. GRUEN. Aust. J. Chem. **25**, 2553 (1972).
7. E. W. ABEL, J. M. PRATT, and R. WHELAN. J. Chem. Soc. Dalton Trans. 509 (1976).
8. J. H. WEBER and D. H. BUSCH. Inorg. Chem. **4**, 469 (1965); **4**, 472 (1965).
9. B. SIMIC-GLAVASKI, Z. ZECEVIC, and E. YEAGER. Proceedings Electrochem. Soc. Meeting, OH. 1984. Abstract No. 414.
10. W. A. NEVIN, W. LIU, M. MELNIK, and A. B. P. LEVER. J. Electroanal. Chem. **213**, 217 (1986).
11. E. S. DODSWORTH, A. B. P. LEVER, P. SEYMOUR, and C. C. LEZNOFF. J. Phys. Chem. **89**, 5698 (1985).
12. A. R. MONAHAN, J. A. BRADO, and A. F. DELUCA. J. Phys. Chem. **76**, 446 (1972).
13. A. R. MONAHAN, J. A. BRADO, and A. F. DELUCA. J. Phys. Chem. **76**, 1994 (1972).
14. M. ABKOWITZ and A. R. MONAHAN. J. Chem. Phys. **58**, 2281 (1973).
15. C. C. LEZNOFF, S. GREENBERG, S. M. MARCUCCIO, P. C. MINOR, P. SEYMOUR, A. B. P. LEVER, and K. B. TOMER. Inorg. Chim. Acta, **89**, L35 (1984).
16. C. C. LEZNOFF, S. M. MARCUCCIO, S. GREENBERG, A. B. P. LEVER, and K. B. TOMER. Can. J. Chem. **63**, 623 (1985); S. M. MARCUCCIO, P. I. SVIRSKAYA, S. GREENBERG, A. B. P. LEVER, C. C. LEZNOFF, and K. B. TOMER. Can. J. Chem. **63**, 3057 (1985).
17. S. GREENBERG, S. M. MARCUCCIO, and C. C. LEZNOFF. Synthesis, 406 (1986).
18. W. A. NEVIN, W. LIU, S. GREENBERG, M. R. HEMPSTEAD, S. M. MARCUCCIO, M. MELNIK, C. C. LEZNOFF, and A. B. P. LEVER. Inorg. Chem. In press.
19. R. C. WEAST (*Editor*). Handbook of chemistry and physics. 57th ed. CRC Press, Cleveland. 1977; C. K. MANN. *In* Electroanalytical chemistry. Vol. 3. *Edited by* A. J. Bard. Marcel Dekker, New York. 1969.
20. W. WEST and S. PEARCE. J. Phys. Chem. **69**, 1894 (1965).

Can. J. Chem. Downloaded from www.nrcresearchpress.com by 78.46.186.204 on 09/07/12
For personal use only.

Chimie des radioprotecteurs : synthèse d'alkylamino-2 éthanethiols encombrés sur l'atome d'azote

JOELLE LADURANTY, FRANCIS BARBOT ET LÉONE MIGINIAC[1]

Laboratoire de synthèse organique, Unité Associée 574 Centre national de la recherche scientifique, Université de Poitiers, 40, avenue du Recteur Pineau, 86022 Poitiers, France

Reçu le 30 juillet 1986

JOELLE LADURANTY, FRANCIS BARBOT et LÉONE MIGINIAC. Can. J. Chem. **65**, 859 (1987).

La mise au point de la synthèse d'alkylamino-2 éthanethiols portant un groupe tertiaire sur l'atome d'azote a été réalisée. L'action de magnésiens allyliques sur les thiazolidines, les alkyl-2 thiazolines et les thiométhyl-2 thiazolines s'est révélée une méthode de choix pour obtenir ces composés avec un groupe tertiaire comportant respectivement un, deux et trois motifs allyliques.

JOELLE LADURANTY, FRANCIS BARBOT, and LÉONE MIGINIAC. Can. J. Chem. **65**, 859 (1987).

Synthesis of 2-alkylaminoethanethiols with a tertiary group fixed to the nitrogen atom has been achieved. A very convenient method of access to such 2-alkylaminoethanethiols with one, two, and three allyl substituents is the reaction between allylic organomagnesium compounds and thiazolidines, 2-alkylthiazolines, and 2-methylthiothiazolines respectively.

Can. J. Chem. Downloaded from www.nrcresearchpress.com by 78.46.186.204 on 09/07/12
For personal use only.

Introduction

Au cours de ces dix dernières années, l'emploi des radioprotecteurs chimiques a pris un essor considérable. En effet, de tels composés sont d'une utilité potentielle dans le traitement du cancer : en radiothérapie, ils possèdent la propriété de protéger les cellules saines et, en chimiothérapie, ont également un effet bénéfique spécifique en «saturant» ces mêmes cellules et en minimisant ainsi la toxicité des antimitotiques utilisés (1, 2).

Ces travaux ont en particulier mis en évidence l'intérêt de la cystéamine **I** et de ses dérivés aliphatiques (1–8), ainsi que le rôle déterminant du vecteur. Cependant la cystéamine présente une certaine toxicité : certaines transformations, par exemple la formation de thiazolidines (9–12) ou bien celle de ponts disulfure (13, 14), permettent de la diminuer; le passage de la cystéamine à sa forme *S*-phosphorylée **II** (15–18) ou encore sa transformation en acides *S*-[(aminopropyl-3)aminoéthyl-2] et *S*-[(*N*-méthylaminopropyl-3)aminoéthyl-2] phosphorothioïques **III** et **IV** (15–17, 19) conduit également à des radioprotecteurs très intéressants :

$H_2N—CH_2—CH_2—SH$ **I**

$H_2N—CH_2—CH_2—S—PO_3HNa$ **II**

$H_2N—(CH_2)_3—NH—CH_2—CH_2—SPO_3H_2$ **III**

$CH_3—NH—(CH_2)_3—NH—CH_2—CH_2—SPO_3H_2$ **IV**

La substitution d'un hydrogène de la fonction amine de la cystéamine par un groupe alkyle saturé, insaturé et (ou) fonctionnel, d'encombrement stérique notable, étant susceptible de jouer un rôle important sur les propriétés radioprotectrices (libération retardée de la cystéamine par déalkylation sélective par métabolisme) et sur la toxicité de la cystéamine, nous nous sommes proposés de mettre au point des méthodes simples et générales d'accès aux dérivés de type :

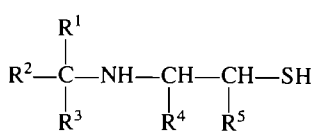

R_1, R_2, R_3 = alkyle, allyle, propargyle, alkyle fonctionnel
R_4, R_5 = H alkyle

1. Auteur à qui adresser toute correspondance.

I. Accès aux alkylamino-2 éthanethiols par action d'une amine primaire sur le mercaptoéthyl-2 carbonate d'éthyle

L'ouverture par une amine primaire (selon réfs. 21, 22) du thioépoxyde (produit peu stable) conduisant à des résultats décevants ou difficilement reproductibles, nous avons préféré utiliser le schéma réactionnel suivant :

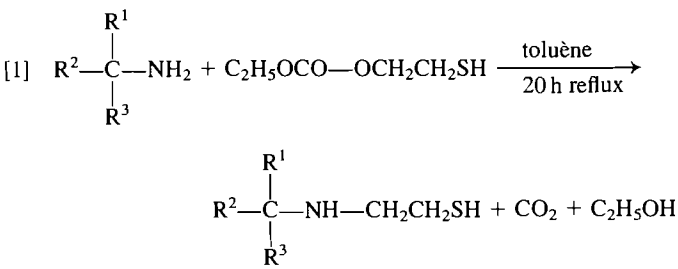

En présence d'une base, le mercaptoéthyl-2 carbonate d'éthyle se décompose en thioépoxyde selon le mécanisme réactionnel proposé dans la réf 20.

Nos essais ont été réalisés avec l'amino-1 tétraméthyl-1,1,3,3 butane et l'amino-2 méthyl-2 propanol, ainsi qu'avec trois autres amines primaires à groupe tertiaire, préparées selon les réfs. 23–25, pour lesquelles R^1, R^2, R^3 = cycloalkyle, allyle, éthynyle, vinyle ou alkyle fonctionnel; nous avons également considéré le cas particulier d'une diamine primaire de type néopentylique, le diméthyl-2,2 diamino-1,3 propane.

Les résultats du tableau 1 montrent que la réaction a lieu dans tous les cas et conduit avec des rendements de 30–68% à l'aminothiol attendu; la réaction n'a lieu qu'une seule fois avec la diamine, malgré l'utilisation d'une quantité double de réactif. Enfin, signalons la cyclisation partielle *in situ* de l'aminothiol à fonction acétylénique en sulfure vinylique (26) :

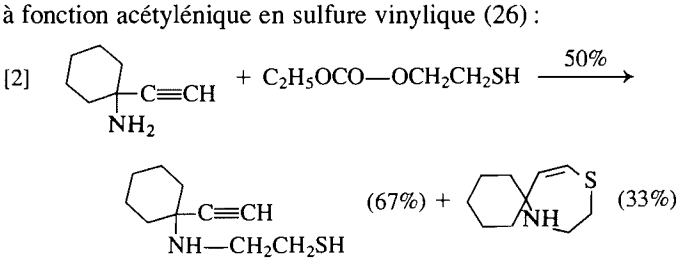

Cette méthode permet donc d'atteindre des aminothiols secondaires à groupe alkyle encombré, lorsque l'amine primaire nécessaire est commerciale ou facile à préparer; cependant,

Can. J. Chem. Downloaded from www.nrcresearchpress.com by 78.46.186.204 on 09/07/12
For personal use only.

TABLEAU 1. Préparation d'amino-2 thiols par action d'amines primaires sur le mercaptoéthyl-2 carbonate d'éthyle

Amine	Produit obtenu		Rdt (%)
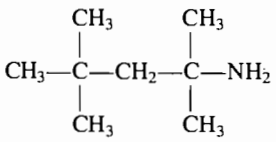	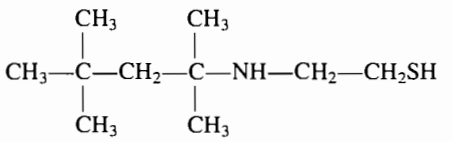	**1**	58
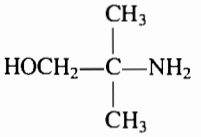	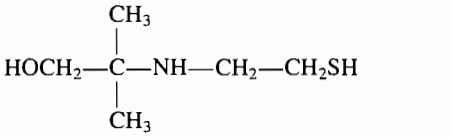	**2**	30
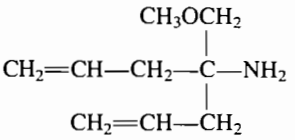	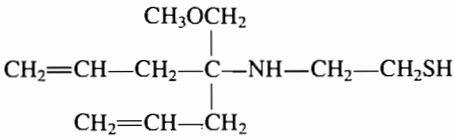	**3**	50
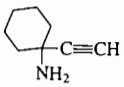	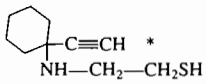	**4**	50
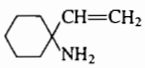	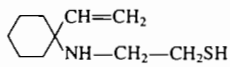	**5**	68
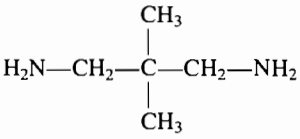	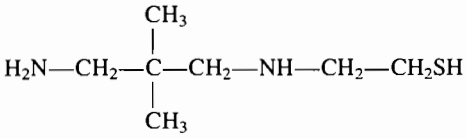	**6**	38

*Dans ce cas, l'amino-2 thiol attendu est accompagné du sulfure vinylique spirannique isomère **4'** (26).

cette dernière condition diminue beaucoup les possibilités d'application de cette méthode.

II. Accès aux alkylamino-2 éthanethiols par action d'un organomagnésien dérivant d'un halogénure α-insaturé sur une thiazolidine

Il a été montré qu'un *gem*-aminothioéther donne facilement une réaction avec les organométalliques, en particulier avec les organométalliques α-insaturés (27, 28), pour conduire à une amine et à un thiol :

[3] $R'S{-}CH_2{-}N(R'')_2 \xrightarrow[(2)\ H_2O]{(1)\ RM} R'SH + RCH_2N(R'')_2$

Une telle réaction, appliquée à un *gem*-aminothioéther cyclique tel qu'une thiazolidine, devait nous permettre d'atteindre des aminothiols à groupe tertiaire.

A notre connaissance, seule l'action sur quelques thiazolidines de divers hydrures tels que $NaBH_4$ a été envisagée (31, 32) et a permis dans certains cas d'obtenir le produit résultant de l'ouverture du cycle.

Nous avons donc préparé par des méthodes usuelles (12, 29, 30) plusieurs thiazolidines et étudié leur réaction avec les magnésiens dérivant d'halogénures allyliques ou propargyliques :

[4] 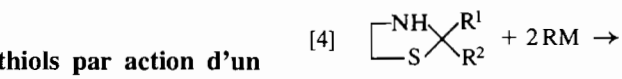

Les résultats du tableau 2 montrent que cette réaction a lieu dans tous les cas étudiés, le carbone C2 de la thiazolidine pouvant comporter des groupes saturés, insaturés ou fonctionnels. Les rendements (40–72%) en aminothiols isolés dépendent beaucoup des précautions prises lors de l'isolement (voir partie expérimentale); en effet, en opérant sans précautions particulières, il se forme par oxydation une quantité importante du disulfure correspondant :

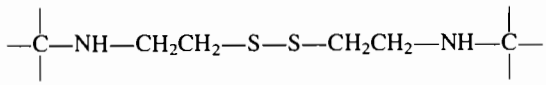

Dans un seul cas, le rendement s'est révélé faible, sans doute par suite d'une décomposition lors de la distillation : il se forme vraisemblablement une cétimine β-éthylénique par élimination de butène-1 (pour une décomposition analogue, voir réfs. 33, 34), laquelle peut par exemple se cycliser en thiazolidine ou s'isomériser :

[5] 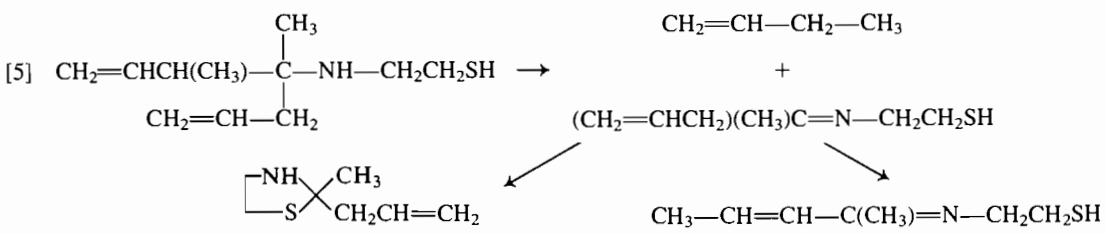

Can. J. Chem. Downloaded from www.nrcresearchpress.com by 78.46.186.204 on 09/07/12
For personal use only.

TABLEAU 2. Préparation d'amino-2 thiols par action de magnésiens α-insaturés sur les thiazolidines

Thiazolidine	RMgX	Produit obtenu		Rdt (%)
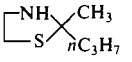	$CH_2{=}CHCH_2MgBr$	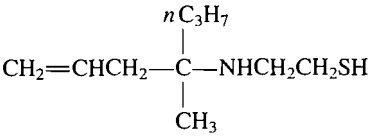	**7**	40
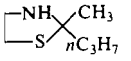	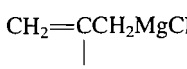	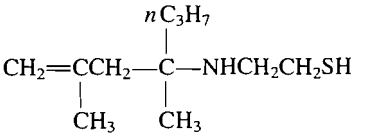	**8**	65
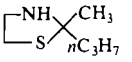	$CH_2{=}C{=}CHMgBr$	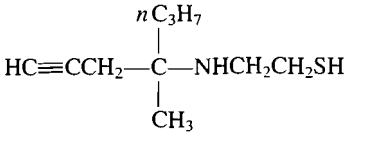	**9**	43
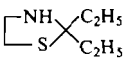	$CH_2{=}CHCH_2MgBr$	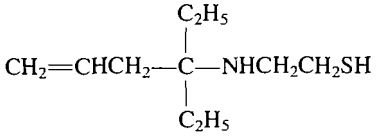	**10**	60
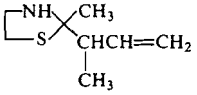	$CH_2{=}CHCH_2MgBr$	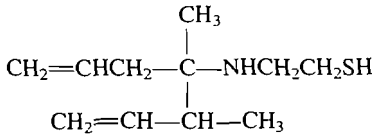	**11**	18*
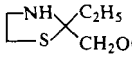	$CH_2{=}CHCH_2MgBr$	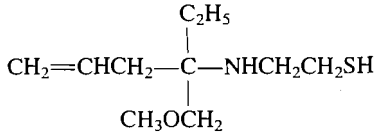	**12**	65
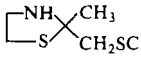	$CH_2{=}CHCH_2MgBr$	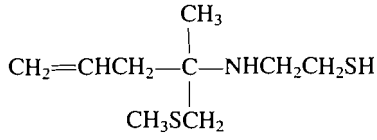	**13**	44
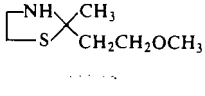	$CH_2{=}CHCH_2MgBr$	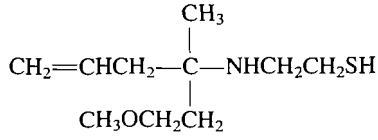	**14**	72
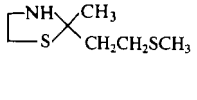	$CH_2{=}CHCH_2MgBr$	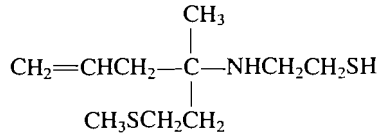	**15**	60

*Résidus abondants.

En résumé, cette réaction constitue donc une très bonne méthode de préparation d'alkylamino-2 éthanethiols secondaires à groupe tertiaire.

III. Accès aux alkylamino-2 éthanethiols par action d'un organomagnésien α-insaturé sur une thiazoline

Compte tenu des résultats précédents, il était intéressant d'essayer, à partir d'un substrat adéquat, d'introduire par voie organométallique deux, puis trois groupements allyles sur le groupe carboné rattaché à l'azote.

Nous avons donc envisagé de partir de thiazolines et d'étudier leur comportement vis à vis d'organomagnésiens allyliques; cette réaction peut se dérouler de la manière suivante en impliquant vraisemblablement d'ailleurs le passage à une thiazolidine *N*-métallée analogue à celles intervenant dans le paragraphe précédent :

[6] 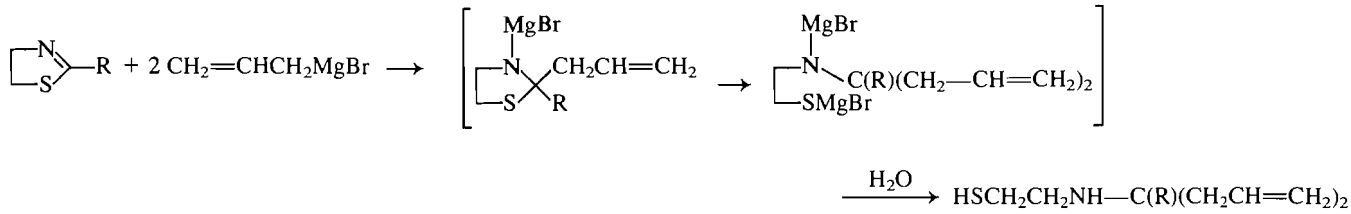

De même :

[7] 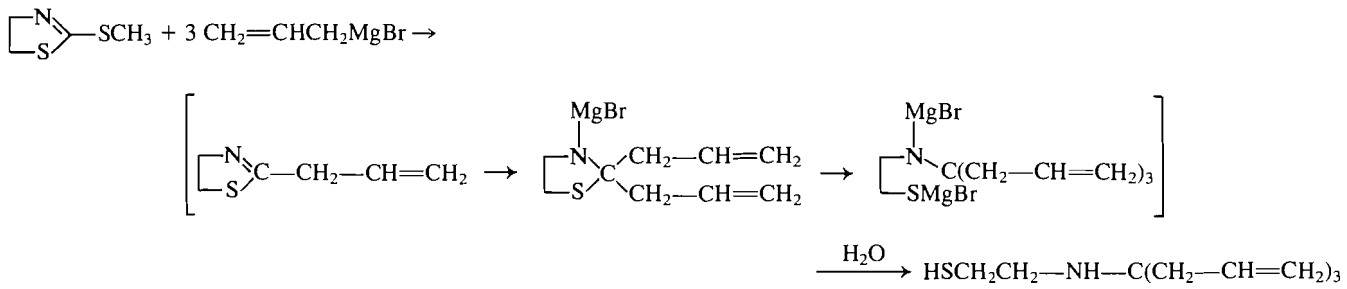

À notre connaissance, l'action des magnésiens allyliques sur des thiazolines simples n'a pas été envisagée; signalons cependant les travaux récents relatifs à l'action de divers magnésiens sur les benzothiazoles (35–38).

Alors que les magnésiens saturés réalisent généralement une réaction de métallation au niveau du groupe R (36), les magnésiens allyliques conduisent généralement à une ouverture de cycle (35, 37), les auteurs n'isolant pas l'aminothiol résultant, mais directement le disulfure :

[8] 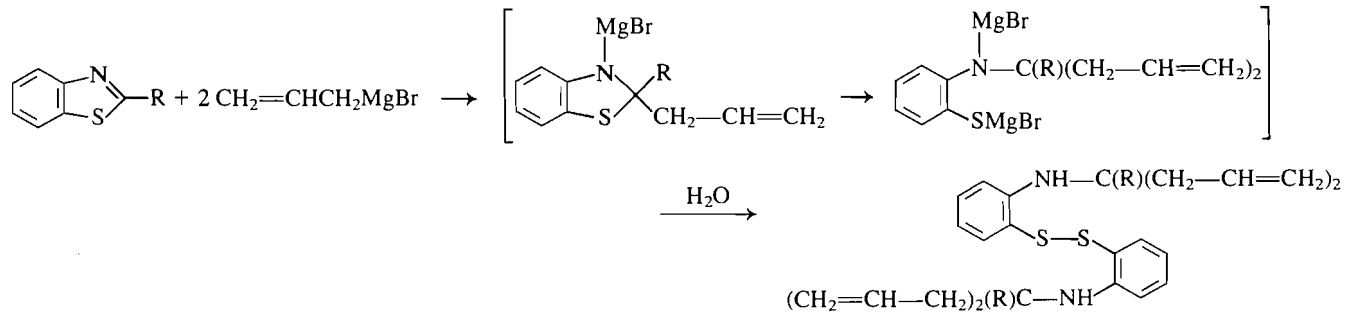

En outre, les auteurs signalent l'arrêt possible à la benzothiazoline, en utilisant le dichlorométhane au lieu de l'éther (38).

Nous avons préparé par des méthodes usuelles plusieurs alkyl-2 thiazolines diversement substituées (39–41; voir également la réf. 56) ainsi que deux thiométhyl-2 thiazolines (42–44), et étudié leur comportement vis à vis des magnésiens allyliques.

Les résultats obtenus dans cette étude figurent dans le tableau 3 et permettent de faire les remarques suivantes :

(*a*) La réaction a lieu dans tous les cas et permet d'atteindre les aminothiols attendus avec des rendements moyens (30–50%) avec une thiazoline non substituée sur la chaîne carbonée, et avec des rendements un peu plus faibles (20–40%) avec une thiazoline substituée. Le rendement est aussi plus faible lors de l'action du chlorure de méthallylmagnésium sur une thiazoline simple, la structure étant plus encombrée que dans le cas du groupe allyle. Là encore, les rendements en aminothiols isolés dépendent beaucoup des précautions prises lors de l'isolement (voir partie expérimentale).

À noter que contrairement à la réf. 38, l'action sur une thiazoline du bromure d'allylmagnésium, au sein de l'éther ou du dichlorométhane, conduit toujours au produit d'ouverture.

(*b*) La réaction permet également d'atteindre, à partir de la thiazoline non substituée en C2, des aminothiols à groupe secondaire. Ce résultat est intéressant, car il se forme le même dérivé que celui qui résulterait de l'action d'un hydrure sur la thiazolidine :

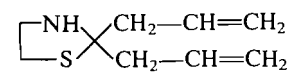

d'accès très difficile, puisqu'impliquant l'emploi d'une cétone β,β′-diéthylénique.

L'action des magnésiens allyliques sur les thiazolines permet donc de préparer aisément des aminothiols à groupe tertiaire comportant deux ou trois substituants allyliques.

Conclusion

Nous avons pu réaliser, dans des cas structuraux variés, la synthèse d'alkylamino-2 éthanethiols possédant un groupe tertiaire sur l'atome d'azote.

Nos résultats montrent également que la voie de synthèse

Can. J. Chem. Downloaded from www.nrcresearchpress.com by 78.46.186.204 on 09/07/12
For personal use only.

TABLEAU 3. Préparation d'amino-2 thiols par action de magnésiens α-insaturés sur les thiazolines

Thiazoline	RMgX	Produit obtenu		Rdt (%)
	$CH_2{=}CHCH_2MgBr$	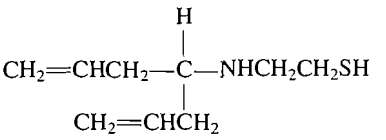	**16**	38
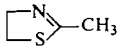	$CH_2{=}CHCH_2MgBr$	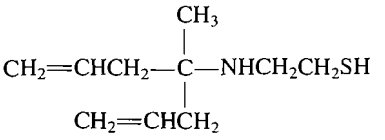	**17**	50
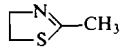	$CH_2{=}CCH_2MgCl$	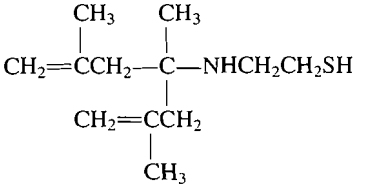	**18**	20
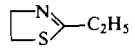	$CH_2{=}CHCH_2MgBr$	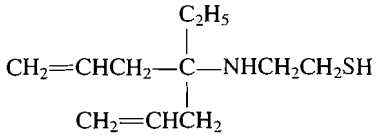	**19**	39
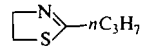	$CH_2{=}CHCH_2MgBr$	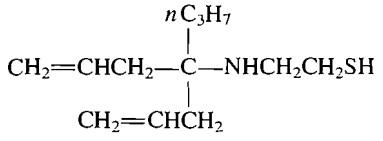	**20**	38
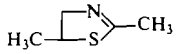	$CH_2{=}CHCH_2MgBr$	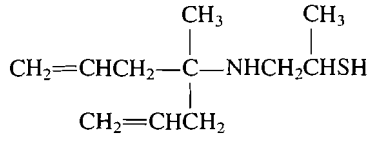	**21**	40
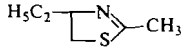	$CH_2{=}CHCH_2MgBr$	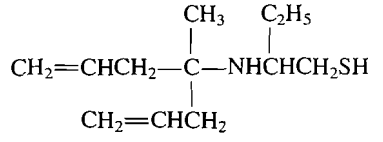	**22**	35
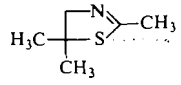	$CH_2{=}CHCH_2MgBr$	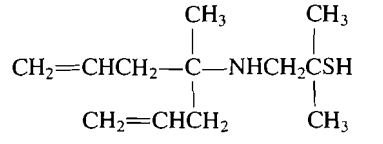	**23**	28
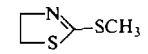	$CH_2{=}CHCH_2MgBr$	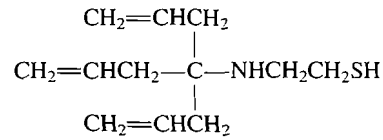	**24**	30
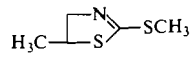	$CH_2{=}CHCH_2MgBr$	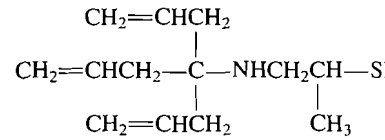	**25**	25

Can. J. Chem. Downloaded from www.nrcresearchpress.com by 78.46.186.204 on 09/07/12
For personal use only.

organométallique impliquant l'action d'organomagnésiens allyliques sur les thiazolidines, les alkyl-2 thiazolines et les thiométhyl-2 thiazolines est une méthode très intéressante, car générale et facile à mettre en oeuvre.

Partie expérimentale

Introduction

Les chromatographies en phase gazeuse ont été effectuées avec un appareil Intersmat IGC 12 M (détecteur à conductibilité thermique) équipé de colonnes analytiques de 2 m (diamètre : 0,63 cm), remplissage soit 20% SE 30, soit 20% Carbowax 20 M sur Chromosorb W.

Les spectres infrarouges ont été enregistrés sur les produits à l'état pur entre lames de chlorure de sodium avec un appareil IR 4240 Beckman. Intensités des bandes : F, forte; m, moyenne; f, faible; tf, très faible.

Les spectres rmn ont été enregistrés en solution dans CCl_4 à 60 MHz sur un appareil Perkin–Elmer R 24 A. Les déplacements chimiques sont exprimés en ppm par rapport au tétraméthylsilane utilisé comme référence.

Les analyses élémentaires ont été effectuées par le service central d'analyse du CNRS.

L'éther et le tétrahydrofuranne utilisés ont été préalablement desséchés et désoxygénés par distillation sur benzophénone/sodium, sous courant d'azote sec.

Préparation des magnésiens

Les bromures d'allylmagnésium, chlorure de méthallylmagnésium et bromure d'allénylmagnésium ont été préparés au sein de l'éther (45, 46).

Préparation des matières premières

(1) Amines primaires à groupe tertiaire

Les tétraméthyl-1,1,3,3 butylamine, diméthyl-1,1 hydroxy-2 éthylamine et diméthyl-2,2 diamino-1,3 propane sont des produits commerciaux utilisés après redistillation. Les amino-4 méthoxyméthyl-4 heptadiène-1,6 (23), amino-1 éthynyl-1 cyclohexane (24, 25, 47) et amino-1 vinyl-1 cyclohexane (25) ont été obtenus selon des méthodes usuelles.

(2) Thiazolidines

Elles sont obtenues selon les réfs. 29 et 30. Les cétones employées dans cette réaction sont des produits commerciaux (pentanone-2 et pentanone-3) ou ont été préparées selon des techniques usuelles : méthoxy-1 butanone-2 (52), thiométhyl-1 propanone-2 (49, 53), méthoxy-1 butanone-3 (48) et thiométhyl-1 butanone-3 (49–51).

Les constantes physiques des thiazolidines figurent dans le tableau 4.

(3) Alkyl-2 thiazolines

Elles sont préparées selon les réfs. 39–41. Les aminoalcools impliqués dans cette réaction sont des produits commerciaux (utilisés après redistillation) ou sont préparés selon des méthodes usuelles (54, 59).

Les constantes physiques des alkyl-2 thiazolines figurent dans le tableau 5.

(4) Thiométhyl-2 thiazolines

Elles sont préparées selon les réfs. 42–44. Leurs constantes physiques figurent dans le tableau 5.

Modes opératoires

Première méthode

On opère sous atmosphère d'azote dans un ballon à trois tubulures de 250 mL équipé d'une ampoule, de deux réfrigérants ascendants (le premier à circulation d'eau, le second réfrigéré par un courant d'alcool refroidi à −30°C).

L'amine primaire (0,3 mol) en solution dans 50 mL de toluène anhydre est chauffée à reflux; 0,1 mol de mercaptoéthyl-2-carbonate d'éthyle est alors ajoutée par un goutte à goutte rapide et le milieu réactionnel est chauffé à reflux pendant 20 h environ. Après concentration du milieu réactionnel à l'évaporateur rotatif à l'aide d'un bain d'eau à 45°C environ, le résidu est distillé sous pression réduite la plus faible possible.

TABLEAU 4. Constantes physiques des thiazolidines

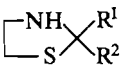

R^1	R^2	Réf. Litt.	Eb. (°C/Torr)	n_D^{20}	Rdt (%)
CH_3	nC_3H_7	29	87/16	1,5030	70
C_2H_5	C_2H_5	29	83/10	—	76
C_2H_5	CH_2OCH_3	—	63/0,07	1,5070	50
CH_3	CH_2SCH_3	—	78/0,05	1,5639	54
CH_3	$(CH_2)_2OCH_3$	—	55/0,05	1,5048	65
CH_3	$(CH_2)_2SCH_3$	—	103/0,5	1,5555	58

Deuxième méthode

(a) Cas d'un magnésien allylique. Dans un ballon à trois tubulures de 1000 mL préalablement séché à la flamme sous atmosphère d'azote, on place une solution de 0,06 mol de thiazolidine dans 220 mL d'éther. On introduit goutte à goutte, à t = 0–5°C, le magnésien, préalablement décanté, préparé selon la réf. 45 à partir de 13,0 g (0,535 mol) de Mg, 0,22 mol de bromure allylique et 190 mL d'éther.

À la fin de l'addition, le milieu réactionnel est chauffé à reflux pendant 2 h. Après retour à température ambiante, il est refroidi à t = 0–5°C et hydrolysé sous courant d'azote par addition lente d'une solution saturée de chlorure d'ammonium (420 mL).

Après décantation, extraction par 4 × 100 mL d'éther et séchage sur sulfate de magnésium, la phase organique est concentrée, puis l'aminothiol est distillé sous pression réduite la plus faible possible.

(b) Cas du bromure d'allénylmagnésium. À la solution du magnésien dérivant du bromure de propargyle, préparée à température inférieure à 18°C selon la réf. 46, à partir de 14,3 g (0,12 mol) de bromure de propargyle, 6,0 g de Mg broyé (0,247 mol) et de 85 mL d'éther, on additionne goutte à goutte une solution de 0,03 mol de thiazolidine dans 30 mL d'éther désoxygéné, en maintenant la température à 0–5°C. L'agitation est poursuivie pendant 2,5 h à une température inférieure ou égale à 18°C. Après l'hydrolyse *in situ* comme précédement et les traitements usuels, le résidu est distillé sous pression réduite la plus faible possible.

Troisième méthode

(a) Action du bromure d'allylmagnésium sur une alkyl-2 thiazoline. Une solution de bromure d'allylmagnésium (préparée sous azote, à 0–5°C, à partir de 19,4 g (0,16 mol) de bromure d'allyle, 10 g de Mg broyé (0,411 mol) et 140 mL d'éther est additionnée goutte à goutte (durée 2,5 h environ) à une solution de 0,04 mol d'alkyl-2 thiazoline dans 300 mL de dichlorométhane distillé, refroidie à 0–5°C. Après retour à température ambiante, le milieu est maintenu sous agitation pendant 2 h. Il est ensuite refroidi à 0°C et hydrolysé par addition lente d'une solution aqueuse saturée de chlorure d'ammonium (300 mL). Après les traitements usuels, le produit est distillé sous pression réduite la plus faible possible, en évitant les surchauffes. *N.B.* Dans le cas de l'action du chlorure de méthallylmagnésium sur une alkyl-2 thiazoline, on opère au sein de l'éther désoxygéné seul, la réaction risquant d'être incomplète au sein du mélange éther/dichlorométhane (38).

(b) Action du bromure d'allylmagnésium sur une thiométhyl-2 thiazoline. Une solution de bromure d'allylmagnésium (préparée sous azote à 0–5°C à partir de 24,2 g (0,2 mol) de bromure d'allyle, 12,6 g de Mg broyé (0,55 mol) et 170 mL d'éther) est ajoutée lentement sous azote, à 0–5°C, à une solution de 0,04 mol de la thiométhyl-2 thiazoline dans 170 mL de tétrahydrofuranne désoxygéné. Après retour à température ambiante, le milieu est chauffé à reflux pendant 2 h, puis laissé sous agitation pendant une nuit. Après refroidissement, une hydrolyse dans les mêmes conditions que précédemment est effectuée par addition d'une solution saturée de chlorure d'ammonium (400 mL). Après les traitements usuels, le produit brut est distillé sous pression réduite la plus faible possible.

Can. J. Chem. Downloaded from www.nrcresearchpress.com by 78.46.186.204 on 09/07/12
For personal use only.

TABLEAU 5. Constantes physiques des thiazolines

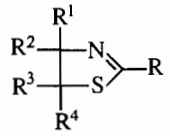

R	R^1	R^2	R^3	R^4	Réf. Litt.	Eb. (°C/Torr)	n_D^{20}	Rdt. (%)
H	H	H	H	H	41	64/57	1,5436	25
CH_3	H	H	H	H	41	45/16	1,5183	51
C_2H_5	H	H	H	H	41	57/10	1,5097	49
nC_3H_7	H	H	H	H	41	66/8	1,5031	47
CH_3	H	H	H	CH_3	55	39/8	1,4910	40
CH_3	H	H	CH_3	CH_3	40	65/30	1,4841	32
CH_3	C_2H_5	H	H	H	56	60/10	1,4936	53
SCH_3	H	H	H	H	57	87/8	1,5930	64
SCH_3	H	H	H	CH_3	58	101/13	1,5682	68

N-*Alkylamino-2 éthanethiols préparés selon la méthode 1*

N-*(Tétraméthyl-1,1,3,3 butyl)amino-2 éthanethiol* ***1***: Rdt = 58%; Eb 65°C/0,05 Torr (1 Torr = 133,3 Pa); n_D^{20} = 1,4737; ir (cm^{-1}) : 3300 tf (NH); 2560 tf (SH); rmn (CCl_4, δ ppm) : 2,3–2,9 (m, 4H, NCH_2CH_2S), 1,45 (s, 2H, CCH_2C), 1,05 (s apparent, 8H, $(CH_3)_2CNH$, SH), 0,95 (s, 9H, $(CH_3)_3C$). *Anal.* calc. pour $C_{10}H_{23}NS$: C 63,43, H 12,24, N 7,40, S 16,93; trouvée : C 63,48, H 12,21, N 7,43, S 16,88.

N-*(Diméthyl-1,1 hydroxy-2 éthyl)amino-2 éthanethiol* ***2***: Rdt = 30%; Eb. 74°C/0,06 Torr; *F* 90–91°C; ir (pastille KBr, cm^{-1}) : 3150 m (OH, NH chélatés); 2515 tf (SH chélaté) (60); rmn ($CDCl_3$, δ ppm) : 3,3 (s, 2H, CH_2O), 2,4–2,9 (m, 4H, NCH_2CH_2S), 2,1 (s élargi, 3H, NH, SH, OH), 1,05 (s, 6H, CH_3). *Anal.* calc. pour $C_6H_{15}NOS$: C 48,29, H 10,13, N 9,38, S 21,48; trouvée : C 48,34, H 10,09, N 9,32, S 21,53.

N-*[(Méthoxyméthyl-4 heptadiène-1,6 yl)-4]amino-2 éthanethiol* ***3***: Rdt = 50%; Eb. 76°C/0,04 Torr; n_D^{20} = 1,5001; ir (cm^{-1}) : 3330 tf (NH); 3080 m, 1640 m, 1000 m, 915 F (CH=CH_2); 2570 tf (SH); 1110 tF (C—O—C); rmn (CCl_4, δ ppm) : 5,35–6,15 (m, 2H, CH=), 4,65–5,2 (m, 4H, CH_2=), 3,20 (s, 3H, CH_3O), 3,05 (s, 2H, CCH_2O), 2,3–2,9 (m, 4H, NCH_2CH_2S), 2,1 (d, 4H, *J* = 7 Hz, CH_2C=), 1,35 (s élargi, 2H, NH, SH). *Anal.* calc. pour $C_{11}H_{21}NOS$: C 61,35, H 9,83, N 6,50, S 14,89; trouvée : C 61,30, H 9,86, N 6,46, S 14,93.

Ethynyl-1 (amino-2 éthanethiol-1)-1 cyclohexane ***4*** *+ aza-1 thia-5 spiro[5,6]dodécène-3,4* ***4'*** : Rdt = 50%; Eb. 77–78°C/0,03 Torr; ir (cm^{-1}) : 3320 tf (NH); 3300 m, 2120 tf (C≡CH); 2570 tf (SH); rmn (CCl_4, δ ppm) : 5,95 (d, SCH=, *J* = 11 Hz), 5,4 (d, CCH=, *J* = 11 Hz), 2,4–3,1 (m, NCH_2CH_2S), 2,25 (s, HC≡), 1,0–2,0 (m, C_6H_{10}, NH, SH). Les pourcentages (67/33) ont été déterminés par les rapports d'intégration entre les deux doublets centrés à 5,95 et 5,4 ppm d'une part, et le singulet à 2,25 ppm d'autre part.

Vinyl-1 (amino-2 éthanethiol-1)-1 cyclohexane ***5*** : Rdt = 68%; Eb. 70°C/0,05 Torr; n_D^{20} = 1,3960; ir (cm^{-1}) : 3310 tf (NH); 3080 m, 1635 m, 1000 m, 915 F (CH=CH_2); 2560 tf (SH); rmn (CCl_4, δ ppm) : 5,25–5,85 (m, 1H, CH=), 4,65–5,15 (m, 2H, CH_2=), 2,3–2,7 (m, 4H, NCH_2CH_2S), 0,9–1,7 (m, 10H, C_6H_{10}), 1,2 (s élargi, 2H, NH, SH). *Anal.* calc. pour $C_{10}H_{19}NS$: C 64,81, H 10,33, N 7,56, S 17,30; trouvée : C 64,75, H 10,30, N 7,60, S 17,34.

N-*(Amino-3 diméthyl-2,2 propyl)amino-2 éthanethiol* ***6*** : Rdt = 38%; Eb. 62°C/0,05 Torr; n_D^{20} = 1,4991; ir (cm^{-1}) : 3380 f, 3310 m, 3200 tf (NH_2, NH); 2555 tf (SH); rmn (DMSO-d_6, δ ppm) : 2,5–2,95 (m, 4H, NCH_2CH_2S), 2,3 et 2,4 (2s, 4H, CCH_2N), 1,65 (s élargi, 4H, NH_2, NH, SH), 0,85 (s, 6H, CH_3). *Anal.* calc. pour $C_7H_{18}N_2S$: C 51,81, H 11,18, N 17,26, S 19,75; trouvée : C 51,79, H 11,20, N 17,29, S 19,71.

N-*Alkylamino-2 éthanethiols préparés selon la méthode 2*

N-*[(Méthyl-4 heptène-1 yl)-4]amino-2 éthanethiol* ***7***: Rdt = 40%; Eb. 65°C/0,05 Torr; n_D^{20} = 1,4868; ir (cm^{-1}) : 3320 f (NH); 3080 f, 1640 f, 995 f, 910 m (CH=CH_2); 2560 f (SH); rmn (CCl_4, δ ppm) : 5,4–6,1 (m, 1H, CH=), 4,7–5,2 (m, 2H, CH_2=), 2,3–2,8 (m, 4H, NCH_2CH_2S), 2,05 (d, 2H, *J* = 7 Hz, CH_2C=), 1,1–1,5 (m, 6H, CH_2CH_2, NH, SH), 0,7–1,1 (m, 6H, CH_3). *Anal.* calc. pour $C_{10}H_{21}NS$: C 64,11, H 11,30, N 7,48, S 17,11; trouvée : C 64,17, H 11,24, N 7,45, S 17,16.

N-*[(Diméthyl-2,4 heptène-1 yl)-4]amino-2 éthanethiol* ***8*** : Rdt = 65%; Eb. 76°C/0,05 Torr; n_D^{20} = 1,4870; ir (cm^{-1}) : 3320 tf (NH); 3075 f, 1640 f, 885 m (CH_2=C); 2560 tf (SH); rmn (CCl_4, δ ppm) : 4,45–4,9 (m, 2H, CH_2=), 2,3–2,95 (m, 4H, NCH_2CH_2S), 2,0 (s, 2H, CH_2C=), 1,75 (s, 3H, CH_3C=), 1,05–2,55 (m, 6H, CCH_2CH_2C, NH, SH), 0,65–1,05 (m, 6H, CH_3). *Anal.* calc. pour $C_{11}H_{23}NS$: C 65,61, H 11,51, N 6,96, S 15,92; trouvée : C 65,68, H 11,55, N 6,94, S 15,90.

N-*[(Méthyl-4 heptyne-1 yl)-4]amino-2 éthanethiol* ***9*** : Rdt = 43%; Eb. 66°C/0,05 Torr; n_D^{20} = 1,4925; ir (cm^{-1}) : 3320 tf (NH); 3300 m, 2120 tf (C≡CH); 2560 tf (SH); rmn (CCl_4, δ ppm) : 2,4–2,9 (m, 4H, NCH_2CH_2S), 2,15 (d, 2H, *J* = 2 Hz, CH_2C≡), 1,95 (t, 1H, *J* = 2 Hz, HC≡), 1,15–1,65 (m, 6H, CCH_2CH_2C, NH, SH), 0,7–1,15 (m, 6H, CH_3). *Anal.* calc. pour $C_{10}H_{19}NS$: C 64,81, H 10,33, N 7,56, S 17,30; trouvée : C 64,85, H 10,36, N 7,53, S 17,27.

N-*[(Éthyl-4 hexène-1 yl)-4]amino-2 éthanethiol* ***10***: Rdt = 60%; Eb. 71°C/0,06 Torr; n_D^{20} = 1,4908; ir (cm^{-1}) : 3320 f (NH); 3075 f, 1640 f, 995 f, 910 m (CH=CH_2); 2560 f (SH); rmn (CCl_4, δ ppm) : 5,3–6,1 (m, 1H, CH=), 4,7–5,2 (m, 2H, CH_2=), 2,4–2,7 (m, 4H, NCH_2CH_2S), 2,0 (d, 2H, *J* = 7 Hz, CH_2C=), 1,0–1,5 (m, 6H, CH_2CH_3, NH, SH), 0,75 (t, 6H, *J* = 7 Hz, CH_3). *Anal.* calc. pour $C_{10}H_{21}NS$: C 64,11, H 11,30, N 7,48, S 17,11; trouvée : C 64,14, H 11,27, N 7,51, S 17,13.

N-*[(Diméthyl-3,4 heptadiène-1,6 yl)-4]amino-2 éthanethiol* ***11*** : Rdt = 18%; Eb. 72°C/0,03 Torr; n_D^{20} = 1,5103; ir (cm^{-1}) : 3320 tf (NH); 3075 m, 1640 m, 995 m, 910 F (CH=CH_2); 2570 tf (SH); rmn (CCl_4, δ ppm) : 5,2–6,1 (m, 2H, CH=), 4,7–5,2 (m, 4H, CH_2=), 2,2–2,7 (m, 4H, NCH_2CH_2S, deux diastéréoisomères), 1,8–2,2 (m, 3H, CH_2C=, CHC=), 1,0–1,7 (m, 5H, CH_3C, NH, SH), 0,6–1,0 (m, 3H, CH_3CH). *Anal.* calc. pour $C_{11}H_{21}NS$: C 66,27, H 10,62, N 7,03, S 16,08; trouvée : C 66,23, H 10,65, N 7,01, S 16,02.

N-*[(Méthoxyméthyl-4 hexène-1 yl)-4]amino-2 éthanethiol* ***12*** : Rdt = 65%; Eb. 76°C/0,05 Torr; n_D^{20} = 1,4913; ir (cm^{-1}) : 3320 tf (NH); 3080 f, 1640 f, 995 f, 915 m (CH=CH_2); 2560 tf (SH); 1110 F (C—O—C); rmn (CCl_4, δ ppm) : 5,35–6,1 (m, 1H, CH=), 4,7–5,2 (m, 2H, CH_2=), 3,25 (s, 3H, CH_3O), 3,05 (s, 2H, CH_2O), 2,25–2,75

Can. J. Chem. Downloaded from www.nrcresearchpress.com by 78.46.186.204 on 09/07/12
For personal use only.

Can. J. Chem. Downloaded from www.nrcresearchpress.com by 78.46.186.204 on 09/07/12
For personal use only.

(m, 4H, NCH_2CH_2S), 2,05 (d, 2H, J = 7 Hz, CH_2C=), 1,1–1,7 (m, 4H, CCH_2C, NH, SH), 0,8 (t, 3H, J = 6 Hz, CH_3C). *Anal.* calc. pour $C_{10}H_{21}NOS$: C 59,07, H 10,41, N 6,89, S 15,76; trouvée : C 59,01, H 10,40, N 6,86, S 15,79.

N-*[(Méthylthio-1 méthyl-2 pentène-5 yl)-2]amino-2 éthanethiol* ***13*** : Rdt = 44%; Eb. 95°C/0,04 Torr; n_D^{20} = 1,5270; ir (cm^{-1}) : 3300 tf (NH); 3080 f, 1640 f, 995 f, 915 m (CH=CH_2); 2560 tf (SH); rmn (CCl_4, δ ppm) : 5,4–6,1 (m, 1H, CH=), 4,7–5,25 (m, 2H, CH_2=); 2,35–2,9 (m, 4H, NCH_2CH_2S), 2,5 (s, 2H, CCH_2S), 1,95–2,35 (m, 2H, CH_2C=), 2,05 (s, 3H, CH_3S), 1,6 (s élargi, 2H, NH, SH), 1,05 (s, 3H, CH_3).*Anal.* calc. pour $C_9H_{19}NS_2$: C 52,63, H 9,33, N 6,82, S 31,22; trouvée : C 52,59, H 9,36, N 6,80, S 31,26.

N-*[(Méthoxy-1 méthyl-3 hexène-5 yl)-3]amino-2 éthanethiol* ***14*** : Rdt = 72%; Eb. 85°C/0,05 Torr; n_D^{20} = 1,4891; ir (cm^{-1}) : 3325 tf (NH); 3070 f, 1635 f, 995 f, 910 m (CH=CH_2); 2550 tf (SH); 1105 F (C—O—C); rmn (CCl_4, δ ppm) : 5,35–6,15 (m, 1H, CH=), 4,7–5,2 (m, 2H, CH_2=), 3,35 (t, 2H, J = 7 Hz, CH_2O), 3,15 (s, 3H, CH_3O), 2,3–2,9 (m, 4H, NCH_2CH_2S), 2,1 (d, 2H, J = 7 Hz, CH_2C=), 1,55 (t, 2H, J = 7 Hz, CH_2C), 1,35 (s élargi, 2H, NH, SH), 1,0 (s, 3H, CH_3C). *Anal.* calc. pour $C_{10}H_{21}NOS$: C 59,07, H 10,41, N 6,89, S 15,76; trouvée : C 59,10, H 10,38, N 6,90, S 15,74.

N-*[(Méthylthio-1 méthyl-3 hexène-5 yl)-3]amino-2 éthanethiol* ***15*** : Rdt = 60%; Eb. 110°C/0,05 Torr; n_D^{20} = 1,5274; ir (cm^{-1}) : 3310 tf (NH); 3070 f, 1635 f, 995 m, 910 m (CH=CH_2); 2550 tf (SH); rmn (CCl_4, δ ppm) : 5,3–6,1 (m, 1H, CH=), 4,7–5,2 (m, 2H, CH_2=), 2,0–2,9 (m, 8H, NCH_2CH_2S, CH_2SCH_3, CH_2C=), 2,0 (s, 3H, CH_3S), 1,3–1,8 (m, 2H, CCH_2CH_2S), 1,25 (s élargi, 2H, NH, SH), 0,95 (s, 3H, CH_3C). *Anal.* calc. pour $C_{10}H_{21}NS_2$: C 54,74, H 9,65, N 6,38, S 29,23; trouvée : C 54,78, H 9,62, N 6,36, S 29,27.

N-*Alkylamino-2 éthanethiols préparés selon la méthode 3*

N-*[(Heptadiène-1,6 yl)-4]amino-2 éthanethiol* ***16*** : Rdt = 38%; Eb. 50°C/0,05 Torr; n_D^{20} = 1,5018; ir (cm^{-1}) : 3310 tf (NH), 3070 m, 1635 m, 990 m, 910 F (CH=CH_2); 2550 tf (SH); rmn (CCl_4, δ ppm) : 5,35–6,15 (m, 2H, CH=), 4,75–5,35 (m, 4H, CH_2=), 2,3–2,95 (m, 5H, NCH_2CH_2S, CH), 1,9–2,3 (m, 4H, CH_2C=), 1,35 (s élargi, 2H, NH, SH). *Anal.* calc. pour $C_9H_{17}NS$: C 63,11, H 10,00, N 8,18, S 18,71; trouvée : C 63,15, H 10,02, N 8,15, S 18,68.

N-*[(Méthyl-4 heptadiène-1,6 yl)-4]amino-2 éthanethiol* ***17*** : Rdt = 50%; Eb. 67°C/0,05 Torr; n_D^{20} = 1,5035; ir (cm^{-1}) : 3310 tf (NH); 3070 m, 1635 m, 990 m, 905 F (CH=CH_2); 2550 tf (SH); rmn (CCl_4, δ ppm) : 5,4–6,1 (m, 2H, CH=), 4,7–5,2 (m, 4H, CH_2=), 2,3–2,8 (m, 4H, NCH_2CH_2S), 2,05 (d, 4H, J = 6 Hz, CH_2C=), 1,25 (s élargi, 2H, NH, SH), 0,95 (s, 3H, CH_3). *Anal.* calc. pour $C_{10}H_{19}NS$: C 64,81, H 10,33, N 7,56, S 17,30; trouvée : C 64,80, H 10,31, N 7,54, S 17,22.

N-*[(Triméthyl-2,4,6 heptadiène-1,6 yl)-4]amino-2 éthanethiol* ***18*** : Rdt = 20%; Eb. 78–80°C/0,05 Torr; pureté ≥ 90%; ir (cm^{-1}) : 3300 tf (NH); 3065 m, 1620 m, 885 F (CH_2=C); 2560 tf (SH); rmn (CCl_4, δ ppm) : 4,4–4,9 (m, 4H, CH_2=), 2,3–2,8 (m, 4H, NCH_2CH_2S), 2,0 (s, 4H, CH_2C=), 1,75 (s, 6H, CH_3C=), 1,25 (s, élargi, 2H, NH, SH), 1,0 (s, 3H, CH_3C).

N-*[(Éthyl-4 heptadiène-1,6 yl)-4]amino-2 éthanethiol* ***19*** : Rdt = 39%; Eb. 65°C/0,02 Torr; n_D^{20} = 1,5110; ir (cm^{-1}) : 3315 tf (NH); 3070 m, 1640 m, 995 m, 910 F (CH=CH_2); 2560 tf (SH); rmn (CCl_4, δ ppm) : 5,3–6,1 (m, 2H, CH=), 4,7–5,2 (m, 4H, CH_2=), 2,2–2,8 (m, 4H, NCH_2CH_2S), 2,0 (d, 4H, J = 8 Hz, CH_2C=), 1,05–1,6 (m, 4H, CH_2CH_3, NH, SH), 0,8 (t, 3H, J = 6 Hz, CH_3). *Anal.* calc. pour $C_{11}H_{21}NS$: C 66,27, H 10,62, N 7,03, S 16,08; trouvée : C 66,30, H 10,65, N 7,06, S 16,05.

N-*[(Propyl-4 heptadiène-1,6 yl)-4]amino-2 éthanethiol* ***20*** : Rdt = 38%; Eb. 74°C/0,03 Torr; n_D^{20} = 1,5001; ir (cm^{-1}) : 3310 tf (NH); 3070 m, 1635 m, 990 m, 905 F (CH=CH_2); 2555 tf (SH); rmn (CCl_4, δ ppm) : 5,3–6,1 (m, 2H, CH=), 4,7–5,2 (m, 4H, CH_2=), 2,3–2,8 (m, 4H, NCH_2CH_2S), 2,0 (d, 4H, J = 7 Hz, CH_2C=), 1,05–1,6 (m, 6H, CCH_2CH_2C, NH, SH), 0,85 (t, 3H, J = 5 Hz, CH_3). *Anal.* calc. pour $C_{12}H_{23}NS$: C 67,55, H 10,86, N 6,56, S 15,03; trouvée : C 67,52, H 10,85, N 6,54, S 15,07.

N-*[(Méthyl-4 heptadiène-1,6 yl)-4]amino-2 méthyl-1 éthanethiol* ***21*** : Rdt = 40%; Eb. 66°C/0,05 Torr; n_D^{20} = 1,4910; ir (cm^{-1}) : 3310 tf (NH); 3070 m, 1640 m, 995 m, 910 F (CH=CH_2); 2550 tf (SH); rmn (CCl_4, δ ppm) : 5,3–6,1 (m, 2H, CH=), 4,7–5,2 (m, 4H, CH_2=), 2,3–3,0 (m, 3H, NCH_2CHS), 2,05 (d, 4H, J = 7 Hz, CH_2C=), 1,2–1,5 (m, 2H, NH, SH), 1,25 (d, 3H, J = 6 Hz, CH_3CH), 0,9 (s, 3H, CH_3C). *Anal.* calc. pour $C_{11}H_{21}NS$: C 66,27, H 10,62, N 7,03, S 16,08; trouvée : C 66,29, H 10,60, N 7,00, S 16,11.

N-*[(Méthyl-4 heptadiène-1,6 yl)-4]amino-2 éthyl-2 éthanethiol* ***22*** : Rdt = 35%; Eb. 65°C/0,01 Torr; n_D^{20} = 1,5011; ir (cm^{-1}) : 3340 tf (NH); 3080 m, 1640 m, 995 m, 910 F (CH=CH_2); 2550 tf (SH); rmn (CCl_4, δ ppm) : 5,35–6,2 (m, 2H, CH=), 4,7–5,25 (m, 4H, CH_2=), 2,3–2,95 (m, 3H, $NCHCH_2S$), 2,05 (d, 4H, J = 7 Hz, CH_2C=), 1,1–1,8 (m, 4H, CH_2CH, NH, SH), 1,0 (s, 3H, CH_3C), 0,85 (t, 3H, J = 7 Hz, CH_3CH_2). *Anal.* calc. pour $C_{12}H_{23}NS$: C 67,55, H 10,86, N 6,56, S 15,03; trouvée : C 67,50, H 10,83, N 6,59, S 15,00.

N-*[(Méthyl-4 heptadiène-1,6 yl)-4]amino-2 diméthyl-1,1 éthanethiol* ***23*** : Rdt = 28%; Eb. 65°C/0,05 Torr; n_D^{20} = 1,4842; ir (cm^{-1}) : 3330 tf (NH); 3070 m, 1635 m, 995 m, 910 F (CH=CH_2); 2550 tf (SH); rmn (CCl_4, δ ppm) : 5,25–6,15 (m, 2H, CH=), 4,7–5,2 (m, 4H, CH_2=), 2,45 (s, 2H, CH_2N), 2,1 (d, 4H, J = 6 Hz, CH_2C=), 1,15–1,85 (m, 2H, NH, SH), 1,25 (s, 6H, $(CH_3)_2C$), 0,95 (s, 3H, CH_3). *Anal.* calc. pour $C_{12}H_{23}NS$: C 67,55, H 10,86, N 6,56, S 15,03; trouvée : C 67,59, H 10,88, N 6,60, S 15,08.

N-*[(Allyl-4 heptadiène-1,6 yl)-4]amino-2 éthanethiol* ***24*** : Rdt = 30%; Eb. 79°C/0,05 Torr; n_D^{20} = 1,5250; ir (cm^{-1}) : 3320 tf (NH); 3080 m, 1640 m, 995 m, 910 F (CH=CH_2); 2570 tf (SH); rmn (CCl_4, δ ppm) : 5,3–6,2 (m, 3H, CH=), 4,65–5,2 (m, 6H, CH_2=), 2,2–2,9 (m 4H, NCH_2CH_2S), 2,05 (d, 6H, J = 7 Hz, CH_2C=), 1,3 (s élargi, 2H, NH, SH). *Anal.* calc. pour $C_{12}H_{21}NS$: C 68,19, H 10,01, N 6,63, S 15,17; trouvée : C 68,25, H 10,04, N 6,60, S 15,18.

N-*[(Allyl-4 heptadiène-1,6 yl)-4]amino-2 méthyl-1 éthanethiol* ***25*** : Rdt = 25%; Eb. 114–116°C/0,05 Torr; pureté ≥ 90%; ir (cm^{-1}) : 3300 tf (NH); 3080 m, 1640 m, 995 m, 910 F (CH=CH_2); 2550 tf (SH); rmn (CCl_4, δ ppm) : 5,3–6,2 (m, 3H, CH=), 4,7–5,3 (m, 6H, CH_2=), 2,3–3,2 (m, 3H, NCH_2CHS), 2,05 (d, 6H, J = 7 Hz, CH_2C=), 1,5–1,9 (s élargi, 2H, NH, SH), 1,0–1,5 (m, 3H, CH_3C).

Remerciements

Cette étude a été réalisée dans le cadre d'une collaboration avec la Direction des recherches, études et techniques, Division Chimie–Pharmacologie, que nous remercions vivement pour son aide matérielle.

1. J. M. YUHAS. *Dans* Radiation–drug interactions in the treatment of cancer. *Éditeurs* : G. H. Sokol and R. P. Maickel. J. Wiley, New York. 1979. p. 113; J. M. YUHAS, J. M. SPELLMAN et F. CULO. *Dans* Radiation sensitizers. (Proc. Conf. 1979), *Éditeur* : L. W. Brady. Masson, New York. 1980. p. 303; J. M. YUHAS, J. M. SPELLMAN, S. M. JORDAN, M. C. PARDINI, S. M. J. AFZAL et F. CULO. Br. J. Cancer, **41**, 832 (1980); **42**, 574 (1980); J. M. YUHAS. J. Radiat. Oncol. Biol. Phys. **8**, 513 (1982); **8**, 519 (1982); **8**, 571 (1982); **8**, 575 (1982).
2. T. L. PHILLIPS. Br. J. Cancer, **39**, 987 (1977); P. R. TWENTYMAN. Br. J. Cancer, **43**, 745 (1981); **47**, 57 (1983); A. ROJAS, F. A. STEWART et J. DENEKAMP. J. Radiat. Oncol. Biol. Phys. **8**, 527 (1982); **9**, 507 (1983); Br. J. Cancer, **47**, 65 (1983).
3. H. M. PATT, E. B. TYREE, R. L. STRAUBE et D. E. SMITH. Science, **110**, 213 (1949).
4. Z. M. BACQ, A. HERVE, J. LECOMPTE, P. FISHER, J. BLAVIER, G. DECHAMPS, H. LE BIHAN et P. RAYET. Arch. Int. Physiol. **59**, 442 (1951).
5. D. G. DOHERTY, W. T. BURNETT et R. SHAPIRA. Radiat. Res. **7**, 13 (1957).
6. B. HANSEN et B. SORBO. Acta Radiol. **56**, 141 (1961).
7. D. L. KLAYMAN, M. M. GRENAN et D. P. JACOBUS. J. Med. Chem. **12**, 510 (1969).
8. YA. L. KOSTYUKOVSKII, V. G. VLADIMIROV, Y. E. STREL'NIKOF et N. M. SLAVACHEVSKAYA. Radiobiologiya, **11**, 141 (1971).
9. R. GRANGER, H. ORZALESI, Y. ROBBE, J. P. CHAPAT, M. RANDON, J. BITOUN et F. SIMON. Chim. Ther. **6**, 439 (1971).

10. M. FATOME, P. POUTRAIN, R. GRANGER, H. ORZALESI, Y. ROBBE et M. RANDON. Chim. Ther. **5**, 312 (1970).
11. A. TEROL, J. P. FERNANDEZ, Y. ROBBE, J. P. CHAPAT, R. GRANGER, M. FATOME, L. ANDRIEU et H. SENTENAC-ROUMANOU. Eur. J. Med. Chem. **13**, 149 (1978); **13**, 153 (1978).
12. D. MESNARD, L. MIGINIAC, M. FATOME, J. D. LAVAL, H. SENTENAC-ROUMANOU et C. LION. Eur. J. Med. Chem. **15**, 247 (1980).
13. Z. M. BACQ et P. ALEXANDER. Fundamentals of radiobiology. Pergamon Press, Oxford. 1965. p. 460 et références incluses.
14. V. S. YUSIPOV, P. G. ZHEREBCHENKO et N. M. SLAVACHEVSKAYA. Radiobiologiya, **9**, 850 (1969).
15. J. R. PIPER, C. R. STRINGFELLOW, R. D. ELLIOT et T. P. JOHNSTON. J. Med. Chem. **12**, 236 (1969); **12**, 244 (1969); **18**, 803 (1975).
16. J. R. PIPER et T. P. JOHNSTON. J. Org. Chem. **33**, 636 (1968).
17. J. R. PIPER et T. P. JOHNSTON. U.S. Patent No. 3,892,824. July 1, 1975; Chem. Abstr. **83**, 163631j (1975).
18. S. AKERFELD. Acta Chem. Scand. **13**, 1479 (1959).
19. J. LADURANTY, C. LION, D. MESNARD et L. MIGINIAC. Bull. Soc. Chim. Belg. **93**, 903 (1984).
20. D. D. REYNOLDS, D. L. FIELDS et D. L. JOHNSON. J. Org. Chem. **26**, 5119 (1961); **26**, 5125 (1961).
21. H. R. SNYDER, J. M. STEWART et J. B. ZIEGLER. J. Am. Chem. Soc. **69**, 2672 (1947).
22. G. I. BRAZ. Chem. Abstr. **45**, 9473g (1951).
23. B. B. ALLEN et H. R. HENZE. J. Am. Chem. Soc. **61**, 1790 (1939).
24. F. BERNADOU. Thèse de Docteur-Ingénieur. Université de Poitiers, 1976. AO CNRS 12334.
25. L. BRANDSMA et H. D. VERKRUIJSSE. Synthesis of acetylenes, allenes and cumulenes. Elsevier Publishing Company, Amsterdam. 1981. p. 230; G. F. HENNION et C. V. DIGIOVANNA. J. Org. Chem. **30**, 2645 (1965).
26. J. M. SURZUR, C. DUPUY, M. P. CROZET et N. AIMAR. C.R. Acad. Sci. Paris Ser. C, **269**, 849 (1969).
27. B. MAUZE et L. MIGINIAC. Bull. Soc. Chim. Fr. 2544 (1968); 3832 (1968).
28. I. E. POLLAK, A. D. TRIFUNAC et G. F. GRILLOT. J. Org. Chem. **32**, 272 (1967); **32**, 2892 (1967).
29. R. TONDEUR, R. SION et E. DERAY. Bull. Soc. Chim. Fr. 2493 (1964).
30. I. R. SCHMOLKA et P. E. SPOERRI. J. Am. Chem. Soc. **79**, 4716 (1957).
31. E. L. ELIEL, E. W. DELLA et M. M. ROGIC. J. Org. Chem. **27**, 4712 (1962).
32. G. LISO, G. TRAPANI, A. REHO et A. LATROFA. Synthesis, 288 (1985).
33. W. G. YOUNG et J. D. ROBERTS. J. Am. Chem. Soc. **68**, 1472 (1946).
34. R. C. ELDERFIELD et E. C. MCCLENACHAN. J. Am. Chem. Soc. **82**, 1982 (1960).
35. F. BABUDRI, G. BARTOLI, F. CIMINALE, S. FLORIO et G. INGROSSO. Tetrahedron Lett. **25**, 2047 (1984).
36. F. BABUDRI, F. CIMINALE et S. FLORIO. Tetrahedron Lett. **25**, 2051 (1984).
37. S. FLORIO, E. EPIFANI et G. INGROSSO. Tetrahedron, **40**, 4527 (1984).
38. F. BABUDRI, S. FLORIO et G. INGUSCIO. Synthesis, 522 (1985).
39. J. ROGGERO. Thèse de Doctorat ès-Sciences Physiques, Université d'Aix-Marseille. 1964.
40. J. L. LARICE, J. ROGGERO et J. METZGER. Bull. Soc. Chim. Fr. 3637 (1967).
41. H. WENKER. J. Am. Chem. Soc. **57**, 1079 (1935).
42. C. S. DEWEY et R. A. BAFFORD. J. Org. Chem. **30**, 491 (1965).
43. R. A. BAFFORD, F. CHANON, M. CHANON et J. METZGER. Bull. Soc. Chim. Fr. 971 (1973).
44. T. A. FOGLIA, L. M. GREGORY, G. MAERKER et S. F. OSMAN. J. Org. Chem. **36**, 1068 (1971).
45. R. H. DEWOLFE et W. G. YOUNG. Chem. Rev. **56**, 753 (1956) et références incluses.
46. M. GAUDEMAR. Ann. Chim. France, **1**[13], 161 (1956).
47. G. F. HENNION et E. G. TEACH. J. Am. Chem. Soc. **75**, 1653 (1953).
48. R. C. ELDERFIELD, B. M. PITT et I. WEMPEN. J. Am. Chem. Soc. **72**, 1334 (1950).
49. P. R. SHILDNECK et W. WINDUS. Org. Synth. Coll. Vol. IV. J. Wiley, New York. 1963. pp. 345 et 411.
50. D. B. REISNER. J. Am. Chem. Soc. **78**, 2132 (1956).
51. J. R. CATCH, A. H. COOK, A. R. GRAHAM et I. HEILBRON. J. Chem. Soc. 1609 (1947).
52. H. R. HENZE et N. E. RIGLER. J. Am. Chem. Soc. **56**, 1350 (1934).
53. C. K. BRADSHER, F. C. BROWN et R. J. GRANTHAM. J. Am. Chem. Soc. **76**, 114 (1954).
54. S. P. MCMANNUS, C. A. LARSON et R. A. HEARN. Synth. Commun. **3**, 177 (1973).
55. J. D. LOUDON. *Dans* Chemistry of carbon compounds. Vol. IV. *Éditeur* : E. H. Rodd. Elsevier Publishing Company, Amsterdam. Part A. 1957. p. 404.
56. G. R. HANDRICK, E. R. ATKINSON, F. E. GRANCHELLI et R. J. BRUNI. J. Med. Chem. **8**, 762 (1965).
57. S. GABRIEL. Chem. Ber. **22**, 1139 (1889).
58. P. HIRSCH. Chem. Ber. **23**, 964 (1890).
59. Dictionary of Organic Compounds. Eyre and Spottiswoode Publishers, London. 1965.
60. L. J. BELLAMY. The infrared spectra of complex molecules. J. Wiley, New York. 1964. p. 96.

Can. J. Chem. Downloaded from www.nrcresearchpress.com by 78.46.186.204 on 09/07/12
For personal use only.

Stereochemical assignment of 2-amino-1,2,3,4-tetrahydro-1-naphthalenols via oxazolidin-2-one derivatives

ANTONIO DELGADO, DAVID MAULEON,[1] AND CRISTINA MINGUILLON
Departament de Química Orgànica i Farmacèutica, Facultat de Farmàcia, Universitat de Barcelona, Av. Diagonal, 08028 Barcelona, Spain

AND

MIGUEL FELIZ, MIQUEL A. PERICAS,[1] AND ANTONI RIERA
Departament de Química Orgànica, Facultat de Química, Universitat de Barcelona, Martí i Franqués 1, 08028 Barcelona, Spain

Received September 29, 1986

ANTONIO DELGADO, DAVID MAULEON, CRISTINA MINGUILLON, MIGUEL FELIZ, MIQUEL A. PERICAS, and ANTONI RIERA. Can. J. Chem. **65**, 868 (1987).

The stereochemical assignment of *cis*- and *trans*-2-amino-1,2,3,4-tetrahydro-1-naphthalenols (**1**) can be performed by means of their conformationally restrained tricyclic tetrahydronaphtho[2,1-*d*]oxazol-2-one derivatives **2**–**6**. Thus, ^1H and ^{13}C nuclear magnetic resonance data of compounds **2**–**6** reveal differences between the *cis* and *trans* stereoisomers that are independent of the nature and number of the aromatic substituents. Conformational analysis of compounds **2**–**6** has been performed from the LAOCOON/3 analysis of their nuclear magnetic resonance spectra and MNDO theoretical results, through the use of the Karplus–Altona equation. Whereas the *trans* compounds exist in a rigid half-chair conformation, a 1:1 equilibrium of two interconverting half-chair conformers is found for the *cis* derivatives.

ANTONIO DELGADO, DAVID MAULEON, CRISTINA MINGUILLON, MIGUEL FELIZ, MIQUEL A. PERICAS et ANTONI RIERA. Can. J. Chem. **65**, 868 (1987).

On peut attribuer les configurations des amino-2 tétrahydro-1,2,3,4 naphtalénols-1-*cis* et -*trans* (**1**) en se basant sur leurs dérivés tricycliques, tétrahydronaphto[2,1-*d*]oxazolones-2 (**2**–**6**), qui sont restreints d'un point de vue conformationnel. Ainsi, les spectres rmn du ^1H et du ^{13}C des composés **2**–**6** présentent des différences, entre les isomères *cis* et *trans*, qui sont indépendantes de la nature et du nombre de substituants présents sur le cycle aromatique. En se basant sur une analyse à l'aide du programme LAOCOON/3 de leurs spectres rmn ainsi que sur des résultats théoriques analysés à l'aide de l'équation de Karplus–Altona, on a effectué une analyse conformationnelle des composés **2**–**6**. Alors que l'isomère *trans* existe sous une conformation rigide demi-chaise, les dérivés *cis* existent sous la forme d'un équilibre 1:1 de deux conformères demi-chaises qui se convertissent rapidement l'une dans l'autre.

[Traduit par la revue]

Introduction

In the course of studies of the adrenergic properties of conformationally restricted arylethanolamines, several isomeric pairs of substituted *cis*- and *trans*-2-amino-1,2,3,4-tetrahydro-1-naphthalenols **1** (see Fig. 1) have been described in the literature (1). Assignment of their stereochemistry is of major importance from a pharmacological standpoint and it has usually been carried out by ^1H nmr spectroscopy, on the basis of the H1 chemical shift[2] and the magnitude of the H1–H2 coupling constant (2). In the *trans* isomers H1 appears at 4–5 ppm as a doublet (J(H1–H2) = 8–10 Hz); in *cis* isomers this proton resonates at slightly lower field than in the *trans* compounds ($\Delta\delta$ = 0.2–0.3 ppm) and shows a H1–H2 coupling constant of about 3–5 Hz. However, the aforementioned criterion is not of general applicability. For instance, in a pair of *cis*-and *trans*-2-aminotetrahydro-1-naphthalenols prepared in our laboratories (**1**, $R^1 = R^4 = OCH_3$, $R^2 = R^3 = H$), we observed that the H1–H2 coupling constant was 4–5 Hz in each isomer, which did not allow an unambiguous stereochemical assignment. In fact, the observed values for J(H1–H2) depend on the position of the conformational equilibrium of the saturated ring. Only when this equilibrium in the *trans* isomer is shifted towards the di-pseudoequatorial conformer, will the J(H1–H2) values in the *cis* and *trans* derivatives be clearly different. Thus, we have considered of interest the development of a more reliable method for the stereochemical assignment of aminoalcohols **1**. In this context, we thought of the possibility of converting the aminoalcohols **1** into conformationally constrained tricyclic derivatives, so that the amino and hydroxyl groups in the parent compounds were forced to a fixed arrangement. The tetrahydronaphtho[2,1-*d*]oxazol-2-one derivatives **2**–**6** appeared quite suitable for this purpose since they can be easily obtained from aminoalcohols **1** under conditions where the stereochemistry of the starting material is preserved, and they possess the required rigidity.

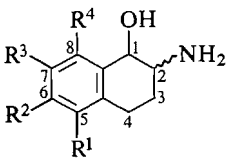

1

FIG. 1. General structure of 2-amino-1,2,3,4-tetrahydro-1-naphthalenols (**1**). The *cis* and *trans* stereochemistry refers to the hetero functions on C1 and C2.

Although there is one example in the literature in which a pair of stereoisomeric 2-aminotetrahydro-1-naphthalenols of known stereochemistry have been converted into the corresponding tetrahydronaphtho[2,1-*d*]oxazol-2-ones by treatment with phosgene (3), the usefulness of such tricyclic derivatives to confirm the stereochemistry of the starting aminoalcohols has not been explored. In this paper we report the synthesis of the

[1]Author to whom correspondence may be addressed.

[2]In this paper hydrogen atoms are designated by means of the numbering of the carbon atoms to which they are attached. When there is a choice, their stereochemistry is indicated by α or β, as pertinent.

Can. J. Chem. Downloaded from www.nrcresearchpress.com by 78.46.186.204 on 09/07/12
For personal use only.

TABLE 1. ^{1}H nuclear magnetic resonance data (200 MHz) of compounds **2–6** (in $CDCl_3$)

Compound	R	δH9b	δH3a	J_{9b-3a} (Hz)	ΔδH9b*	ΔδH3a*	ΔJ†
cis-**2**	H	5.60	4.22	8.0	0.52	0.62	−3.2
trans-**2**	H	5.02	3.66	11.2			
cis-**3**	6-OCH_3	5.53	4.16	8.3	0.45	0.49	−2.9
trans-**3**	6-OCH_3	5.08	3.67	11.2			
cis-**4**	8-OBzl	5.56	4.28	8.5	0.54	0.66	−2.9
trans-**4**	8-OBzl	5.02	3.62	11.4			
trans-**5**	6-OBzl	5.07	3.67	11.5	—	—	—
cis-**6**	6,9-$(OCH_3)_2$	5.90	4.26	8.2	0.76	0.46	−2.2
trans-**6**	6,9-$(OCH_3)_2$	5.14	3.80	10.4			

*Δδ is calculated as $\delta_{cis} - \delta_{trans}$.
†$\Delta J = J_{cis} - J_{trans}$.

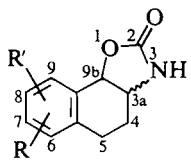

	R	R′	Stereochemistry
2	H	H	*cis* and *trans*
3	6-OCH_3	H	*cis* and *trans*
4	8-OBzl	H	*cis* and *trans*
5	6-OBzl	H	*trans*
6	6-OCH_3	9-OCH_3	*cis* and *trans*

SCHEME 1

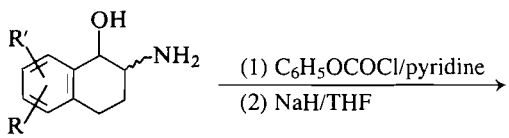

1 (*cis* or *trans*)

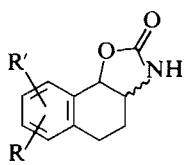

2–6 (*cis* or *trans*)

SCHEME 2

3a,4,5,9b-tetrahydronaphtho[2,1-*d*]oxazol-2-one derivatives **2–6**, their spectroscopic study by nmr techniques, and the corresponding conformational analysis using the obtained coupling constants and the results of MNDO semiempirical SCF MO calculations on compound **2**.

Results and discussion

Synthesis

Synthesis of compounds **2–6** has been accomplished in each case from the corresponding *cis* or *trans* aminoalcohol according to the reaction sequence outlined in Scheme 2.

Thus, reaction of the starting aminoalcohol with phenyl chloroformate in pyridine afforded an intermediate urethane, which was converted to the requisite naphtho[2,1-*d*]oxazol-2-one by treatment with excess sodium hydride in tetrahydrofuran. Since both of these transformations are carried out in alkaline media, we do not expect any stereochemical changes and therefore the product will have the same stereochemistry as the starting aminoalcohol.

Spectroscopic studies

Chemical shifts of the H3a and H9b protons as well as the coupling constants between them are summarized in Table 1. As it can be observed, the *cis* or *trans* stereochemistry can be unambiguously established for each compound from the above data. Thus, two different sets of chemical shifts/coupling constant values can be observed, both being almost completely independent of the nature, position, and number of substituents on the aromatic ring. In *trans* derivatives **2–6**, the H9b chemical shift ranges in the interval of 5.08 ± 0.04 ppm whereas the H3a proton resonates at 3.68 ± 0.06 ppm and the mean H9b–H3a coupling constant is 11.14 ± 0.38 Hz. Similarly, *cis* derivatives show narrow chemical shift intervals of 5.64 ± 0.15 ppm for the H9b proton and 4.24 ± 0.05 ppm for the H3a proton, as well as an average H9b–H3a coupling constant of 8.25 ± 0.18 Hz.

The ^{13}C nmr spectra of compounds **2–6** have been recorded in $CDCl_3/CD_3OD$ solution (Table 2). Signals have been assigned on the basis of their multiplicity, chemical shifts, additivity effects due to the introduction of substituents upon the aromatic ring, and, in the case of C4 and C5 carbon atoms of the model compounds **2**, by means of $^{13}C-^1H$ heterocorrelation experiments. The ^{13}C nmr spectra confirm that the chemical shift of the cycloaliphatic carbon atoms in each diastereomeric series is independent of the nature of the substituents on the aromatic ring. Thus, empirical increments between carbon atoms of the same position in each diastereomeric pair can be obtained (Table 3). For example, C9b and C3a carbon atoms are deshielded at least 5.9 ppm in *trans* derivatives with respect to *cis* ones. This effect can be rationalized on the basis of the higher deshielding effect exerted by equatorial O and N groups upon the corresponding α and ipso carbon atoms, in comparison to the lower deshielding effect exerted upon the same carbon atoms when one of those groups adopts an axial disposition (4), which is the case for both possible conformations of the *cis* derivatives (see below).

In the light of the significant differences observed in the ^{1}H and ^{13}C nmr spectra of *cis*- and *trans*-naphtho[2,1-*d*]oxazol-2-ones, we can conclude that conversion of 2-aminotetrahydro-1-naphthalenols into their corresponding cyclic carbonyl derivatives is a good procedure for stereochemical assignment. These differences are independent of the nature of the aromatic

Can. J. Chem. Downloaded from www.nrcresearchpress.com by 78.46.186.204 on 09/07/12
For personal use only.

TABLE 2. ^{13}C nuclear magnetic resonance data of compounds **2–6** (in $CDCl_3$ + CD_3OD)

Compound	R	C2	C3a	C4†	C5†	C5a	C6	C7	C8	C9	C9a	C9b
cis-**2**	H	159.7	51.6	28.2	24.9	138.3	126.9	128.9*	128.4*	130.5	131.1	75.7
trans-**2**	H	161.0	58.2	24.5	26.4	133.5	127.9	128.8	126.3	122.5	134.1	81.7
cis-**3**	6-OCH_3	159.7	51.6	27.2	17.8	127.2	156.4	110.3	127.3	122.5	132.2	75.5
trans-**3**	6-OCH_3	161.4	57.8	24.2	21.2	121.8	157.6	109.3	127.0	114.2	134.8	81.9
cis-**4**	8-OBzl	159.6	51.6	28.3	24.2	130.5	129.4	116.5	157.7	115.8	132.0	75.7
trans-**4**	8-OBzl	161.3	58.0	24.3	25.5	125.4	129.7	114.9	157.0	108.2	134.9	81.6
trans-**5**	6-OBzl	161.4	57.6	24.0	21.3	122.0	155.9	110.5	127.7	114.2	134.8	81.6
cis-**6**	6,9-$(OCH_3)_2$	171.6	51.3	26.9	17.8	129.3	150.7§	111.9*	109.0*	153.4§	121.2	71.9
trans-**6**	6,9-$(OCH_3)_2$	161.4	58.6	24.4	22.8	123.4	150.1§	110.1*	110.5*	151.6§	124.9	81.3

* and § denote that the values may be interchanged.
†In compounds *cis*- and *trans*-**2**, C4 and C5 chemical shifts have been assigned by heteronuclear chemical shift correlation ^1H–^{13}C.

TABLE 3. ^{13}C nuclear magnetic resonance empirical increments ($\Delta\delta = \delta_{trans} - \delta_{cis}$)

Diastereomeric pair	ΔδC3a	ΔδC4	ΔδC5	ΔδC5a	ΔδC9a	ΔδC9b
2	+6.6	−3.7	+1.5	−4.8	+3.0	+6.0
3	+6.2	−3.0	+3.4	−5.4	+2.6	+6.4
4	+6.4	−4.0	+1.3	−5.1	+2.9	+5.9
6	+7.3	−2.5	+5.0	−5.9	+3.7	+9.4
Mean (±SD)	+6.6±0.41	−3.3±0.59	+2.8±1.51	−5.3±0.41	+3.1±0.40	+6.9±1.44

TABLE 4. Chemical shifts (δ) and coupling constants (J) for *cis*- and *trans*-**2** obtained from the LAOCOON/3 analysis*

Protons	*cis*-**2**	*trans*-**2**
δ H3a	4.28	3.61
δ H4α	1.87	1.87
δ H4β	1.94	2.26
δ H5α	2.57	2.90
δ H5β	2.84	2.97
J(H3a–H4β)	4.4	4.3
J(H3a–H4α)	6.0	11.9
J(H4β–H5β)	4.4	8.4
J(H4β–H5α)	7.2	2.1
J(H4α–H5β)	7.2	8.7
J(H4α–H5α)	4.2	9.2

*In both cases, intensity threshold was 0.05. The total number of transitions above the intensity threshold were 80 and the number of transitions used in the fitting were 64 for *trans*-**2** and 62 for *cis*-**2**.

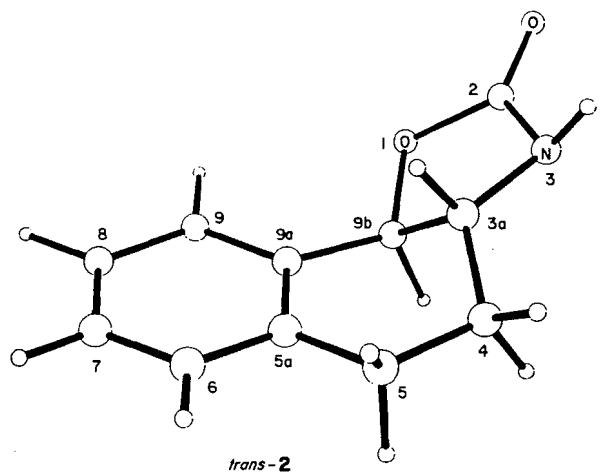

FIG. 2. Computer-generated drawing of the MNDO optimized geometry of compound *trans*-**2**.

substituents and thus they can be useful for the assignment even in those aminotetralols which are conformationally distorted and not directly assignable by nmr, as was the case for **1** ($R^1 = R^4 = OCH_3$, $R^2 = R^3 = H$).

Conformational analysis

Compounds *trans*-**2–5** showed a great similarity in the ^1H nmr coupling patterns of the cycloaliphatic protons, and the same is true within the *cis* series **2–4**. Compounds *cis*-**2** and *trans*-**2** were taken as standards for simulation of the cycloaliphatic region of the high-resolution ^1H nmr spectra by means of the LAOCOON/3 program (5). After full optimization, their simulated spectra were superimposable with the experimental ones (RMS error was in both cases less than 0.2 Hz). The observed coupling constants and chemical shifts from the LAOCOON/3 analysis appear in Table 4.

To obtain information on these molecules, we decided to perform a theoretical study by using the semiempirical SCF MO method MNDO (6). For compound *trans*-**2**, only one stationary point could be located (Fig. 2). This is completely in accord with that observed by simple inspection of a Dreiding molecular model of *trans*-**2**, in which only one rigid half-chair conformer could be found.

On the other hand, MNDO predicts the existence of two different minima for *cis*-**2**, corresponding to the two half-chair conformers (Fig. 3). These are also observed by direct inspection of its Dreiding molecular model. The greater strain in *trans*-**2** is reflected in the MNDO results. Thus, *cis*-**2** ($\Delta H_f = -60.9$ kcal/mol) is predicted to be 10.5 kcal/mol more stable than the *trans* isomer ($\Delta H_f = -50.4$ kcal/mol). On the

Can. J. Chem. Downloaded from www.nrcresearchpress.com by 78.46.186.204 on 09/07/12
For personal use only.

Can. J. Chem. Downloaded from www.nrcresearchpress.com by 78.46.186.204 on 09/07/12
For personal use only.

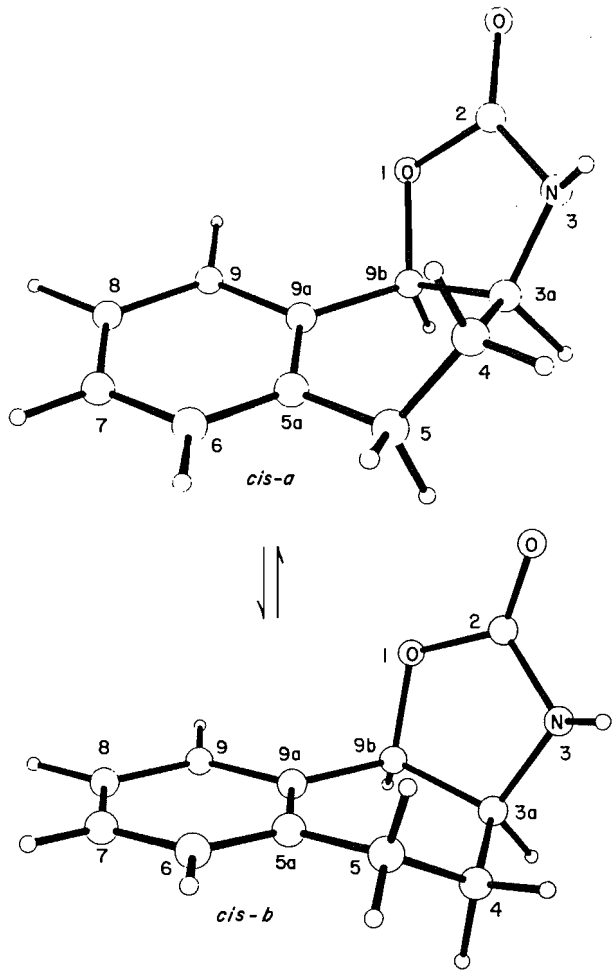

FIG. 3. Computer-generated drawing of the MNDO optimized geometries of the half-chair conformers of *cis*-**2**.

TABLE 5. Coupling constants (J) and dihedral angles (θ) between protons in the C(4)–C(5) fragment of compound *cis*-**2**

	Conformer *a*		Conformer *b*		Average
Protons	θ†	J_{calc}*	θ†	J_{calc}*	J_{calc}
H4β–H5β	−49.9	4.6	50.2	4.6	4.6
H4β–H5α	164.9	11.7	64.6	2.8	7.2
H4α–H5β	65.1	2.1	164.7	12.1	7.1
H4α–H5α	49.8	4.9	49.8	4.9	4.9

*From MNDO calculations through the use of the Karplus–Altona equation.
†From MNDO calculations.

other hand, both possible conformers of *cis*-**2** are predicted to have very similar energy contents.

The Karplus–Altona equation (7) opens a way for perfoming a conformational analysis of *cis*-**2**. From the MNDO optimized geometries of both conformers of the *cis* stereoisomer we obtained the dihedral angles between vicinal protons on C-4 and C-5, and the corresponding coupling constants were then calculated by the Karplus–Altona equation. The results compare very well with the set of experimental coupling constants (RMS error = 0.36 Hz) and are summarized in Table 5. The selected set of coupling constants is the most reliable one that can be obtained by using the Karplus–Altona equation, since the C4—C5 part of the molecule is strain free and the substituents on these carbon atoms are well parametrized in the equation. On the other hand, a simple inspection of the computer-generated drawings of conformers *a* and *b* of *cis*-**2** (Fig. 3) showed that J(H4α–H5β) and J(H4β–H5α) were the coupling constants most sensitive to the conformational equilibrium. A population analysis was subsequently performed on the basis of these coupling constants and the results indicate in both cases a 1:1 equilibrium (estimated errors are below ±5%). It is noteworthy that these analyses afford an identical value within the margins of experimental error. On the other hand, the very small energetic difference between the calculated heats of formation (0.05 kcal/mol) of the conformers of *cis*-**2** also predicts an essentially equal population of both species.[3]

Finally, it has to be mentioned that neither *cis*-**6** nor *trans*-**6** showed ^{1}H nmr coupling patterns comparable to those of the corresponding *cis* and *trans* analogues **2**–**5**, and that the nmr spectrum of the cycloaliphatic protons in these compounds could not be successfully simulated by means of the LAOCOON/3 program. These results can be rationalized on the basis of the *peri* effect exerted by the C9-methoxyl group, which can sensibly modify the structural features of such compounds. However, as has been stated, this limitation does not preclude the use of naphtho[2,1-*d*]oxazol-2-one derivatives to confirm the stereochemistry of the corresponding 2-aminotetrahydro-1-naphthalenols.

Experimental

Melting points were determined in a capillary tube on a Buchi apparatus and are uncorrected. Infrared spectra were recorded on a Perkin–Elmer 1430 spectrophotometer. Proton magnetic resonance spectra were measured at 200 MHz with an FT Varian XL-200 spectrometer. Signal positions are reported in ppm downfield from tetramethylsilane (δ scale) as an internal standard, with $CDCl_3$ as solvent. The number of protons, multiplicity, coupling constants, and proton assignments are indicated in parentheses. The ^{13}C nmr spectra were measured at 50.3 MHz in the same spectrometer, with internal tetramethylsilane as a reference. Multiplicity of the signals was determined by the ADEPT program (8) (automatic distortionless enhancement by polarization transfer). Heteronuclear chemical shift correlation ^{13}C–^{1}H was determined by the HETCOR program (9). The calculations were performed by the standard MNDO semiempircal SCF MO method (6) as implemented in the MOPAC program (10). Microanalyses were performed by the Departamento de Química Orgánica Biológica, C.S.I.C., Barcelona.

*General procedure for the synthesis of substituted 3a,4,5,9b-tetrahydro-3*H*-naphtho[2,1-*d*]oxazol-2-one derivatives* **2**–**6**

To an ice-cooled solution of 1.50 mmol of the starting aminoalcohol **1**[4] in 8.5 mL of dry pyridine under a nitrogen atmosphere, 235 mg (1.50 mmol) of phenyl chloroformate was added dropwise. After stirring for 2 hours at 20°C, the reaction mixture was poured into water, acidified with 2 *N* hydrochloric acid, and extracted with 3 × 50 mL of dichloromethane. The organic layer was washed successively with 2 *N* sodium hydroxide solution, 2 *N* hydrochloric acid, and water. Evaporation of the solvent afforded an oil, which was dissolved in 20 mL of dry tetrahydrofuran and added dropwise over a suspension of 430 mg of sodium hydride dispersion (50–60% in oil) in 20 mL of dry tetrahydrofuran. After stirring for 12 h at room temperature, the

[3]Tables of Cartesian coordinates (MNDO calculation) and heats of formation, dipole moments, and relevant bond distances for *cis*-**2***a*, *cis*-**2***b*, and *trans*-**2** may be purchased from the Depository of Unpublished Data, CISTI, National Research Council of Canada, Ottawa, Ont., Canada K1A 0S2.

[4]Syntheses of aminoalcohols **1** will be reported elsewhere. For related structures see ref. 1.

TABLE 6. Analytical data of compounds **2–6**

Compound (Formula)	Elution system	Melting point (°C)	Found % (calculated) C	H	N
cis-**2** ($C_{11}H_{11}NO_2$)	Benzene–chloroform (1:1)	121–123	69.9 (69.8)	5.7 (5.9)	7.7 (7.4)
trans-**2** ($C_{11}H_{11}NO_2$)	Benzene–chloroform (6:4)	145–147	70.0 (69.8)	6.0 (5.9)	7.1 (7.4)
cis-**3** ($C_{12}H_{13}NO_3$)	Benzene–chloroform (1:1)	133–136	66.0 (65.7)	6.1 (6.0)	6.5 (6.4)
trans-**3** ($C_{12}H_{13}NO_3$)	Benzene–chloroform (6:4)	118–120	65.6 (65.7)	5.8 (6.0)	6.5 (6.4)
cis-**4** ($C_{18}H_{17}NO_3$)	Chloroform	137–139	73.4 (73.2)	6.0 (5.8)	4.9 (4.7)
trans-**4** ($C_{18}H_{17}NO_3$)	Benzene–chloroform (1:1)	142–143	73.3 (73.2)	5.9 (5.8)	4.9 (4.7)
trans-**5** ($C_{18}H_{17}NO_3$)	Benzene–chloroform (1:1)	200–202	73.4 (73.2)	6.0 (5.8)	5.0 (4.7)
cis-**6** ($C_{13}H_{15}NO_4$)	Chloroform	183–185	62.5 (62.6)	6.2 (6.1)	5.8 (5.6)
trans-**6** ($C_{13}H_{15}NO_4$)	Benzene–chloroform (7:3)	176–178	62.5 (62.6)	6.3 (6.1)	5.3 (5.6)

reaction mixture was poured into water and the organic solvent was evaporated at reduced pressure. The aqueous layer was extracted with 3 × 50 mL of dichloromethane and the organic extracts were dried and evaporated to afford the naphtho[2,1-*d*]oxazol-2-one derivatives **2–6**. Silica gel column chromatography afforded pure compounds in an overall yield of 30–35% in all cases. The elution system and analytical data for each compound are listed in Table 6.

cis-**2**: ν_{max} (KBr): 3260 (NH), 1730–1700 (NH—CO—O) cm^{-1}; ^1H nmr (see also Table 1) δ: 1.92 (m, 2H, C(4)H_2), 2.64 (m, 1H, C(5)H), 2.82 (m, 1H, C(5)H′), 7.30 (m, 4H, aromatic); ^{13}C nmr: Table 2.

trans-**2**: ν_{max} (KBr): 3220 (NH), 1750 (NH—CO—O) cm^{-1}; ^1H nmr (see also Table 1) δ: 1.96 (m, 1H, C(4)Hα), 2.32 (m, 1H, C(4)Hβ), 3.06 (m, 2H, C(5)H_2), 7.26 (m, 4H, aromatic); ^{13}C nmr: Table 2.

cis-**3**: ν_{max} (KBr): 3290 (NH), 1750 (NH—CO—O) cm^{-1}; ^1H nmr (see also Table 1) δ: 1.84 (m, 2H, C(4)H_2); 2.58 (m, 1H, C(5)H), 2.80 (m, 1H, C(5)H′), 3.84 (s, 3H, OCH_3), 6.44 (br s, 1H, NH), 6.82 (dd, 1H, C(7)H), 7.04 (dd, 1H, C(9)H), 7.22 (dd, 1H, C(8)H); ^{13}C nmr: Table 2.

trans-**3**: ν_{max} (KBr): 3300 (NH), 1760–1730 (NH—CO—O) cm^{-1}; ^1H nmr (see also Table 1) δ: 1.92 (m, 1H, C(4)Hα), 2.38 (m, 1H, C(4)Hβ), 2.90 (m, 2H, C(5)H_2), 3.82 (s, 3H, OCH_3), 6.82 (dd, 1H, C(7)H), 7.02 (dd, 1H, C(9)H), 7.24 (dd, 1H, C(8)H); ^{13}C nmr: Table 2.

cis-**4**: ν_{max} (KBr): 3250 (NH), 1730–1700 (NH—CO—O) cm^{-1}; ^1H nmr (see also Table 1) δ: 1.95 (m, 2H, C(4)H_2), 2.58 (m, 1H, C(5)H), 2.87 (m, 1H, C(5)H′), 5.08 (s, 2H, ArCH_2O), 6.9–7.4 (m, 8H, aromatic); ^{13}C nmr: Table 2.

trans-**4**: ν_{max} (KBr): 3300 (NH), 1740–1710 (NH—CO—O) cm^{-1}; ^1H nmr (see also Table 1) δ: 1.88 (m, 1H, C(4)Hα), 2.26 (m, 1H, C(4)Hβ), 2.92 (m, 2H, C(5)H_2), 5.03 (s, 2H, ArCH_2O), 6.16 (br s, 1H, NH), 6.76–7.44 (m, 8H, aromatic); ^{13}C nmr: Table 2.

trans-**5**: ν_{max} (KBr): 3280 (NH), 1760–1730 (NH—CO—O) cm^{-1}; ^1H nmr (see also Table 1) δ: 1.92 (m, 1H, C(4)Hα), 2.36 (m, 1H, C(4)Hβ), 2.96 (m, 2H, C(5)H_2), 5.08 (s, 2H, ArCH_2O), 6.80–7.46 (m, 8H, aromatic); ^{13}C nmr: Table 2.

cis-**6**: ν_{max} (KBr): 3300 (NH), 1740 (NH—CO—O) cm^{-1}; ^1H nmr (see also Table 1) δ: 1.86 (m, 2H, C(4)H_2), 2.72 (m, 2H, C(5)H_2), 3.80 (s, 3H, OCH_3), 3.82 (s, 3H, OCH_3), 6.82 (dd, 2H, aromatic); ^{13}C nmr: Table 2.

trans-**6**: ν_{max} (KBr): 3220 (NH), 1740 (NH—CO—O) cm^{-1}; ^1H nmr (see also Table 1) δ: 1.86 (m, 1H, C(4)Hα), 2.32 (m, 1H, C(4)Hβ), 2.86 (m, 2H, C(5)H_2), 3.78 (s, 3H, OCH_3), 3.82 (s, 3H, OCH_3), 6.76 (s, 2H, aromatic); ^{13}C nmr: Table 2.

1. (*a*) T. CHIEMPRASERT, H. J. RIMEK, and F. ZYMALKOWSKI. Ann. Chem. **685**, 141 (1965); (*b*) R. I. THRIFT. J. Chem. Soc. C, 288 (1967); (*c*) K. ITOH, A. MIYAKE, N. TADA, M. HIRATA, and Y. OKA. Chem. Pharm. Bull. **32**, 130 (1984).
2. M. MOTOHASHI, E. MIZUTA, and M. NISHIKAWA. Chem. Pharm. Bull. **29**, 1501 (1981).
3. H. SUGIHARA, K. UKAWA, H. KURIKI, M. NISHIKAWA, and Y. SANNO. Chem. Pharm. Bull. **25**, 2988 (1977).
4. E. BREITMAIER and W. VOELTER. *In* ^{13}C nmr spectroscopy. Methods and applications in organic chemistry. 2nd ed. Verlag Chemie, Weinheim – New York. 1978.
5. D. F. DETAR. *In* Computer programs for chemistry. Vol. 1. W. A. Benjamin Inc., New York. 1968. p. 10.
6. M. J. S. DEWAR and W. THIEL. J. Am. Chem. Soc. **99**, 4899 (1977).
7. C. A. G. HASNOOT, F. A. A. M. DE LEEUW, and C. ALTONA. Tetrahedron. **36**, 2783 (1980).
8. (*a*) R. RICHARG, V. AMMAN, and T. WIRTHLIN. Varian Application Note 2-15. Zug. August 1982; (*b*) D. M. DODDELL, D. T. PEGG, and M. R. BENDALL. Org. Magn. Reson. **8**, 323 (1982).
9. A. BAX and G. MORRIS. J. Magn. Reson. **42**, 501 (1981).
10. S. OLIVELLA. IBM/CMS Version: Q.C.P.E. **4**, 109, number 486 (1984).

Can. J. Chem. Downloaded from www.nrcresearchpress.com by 78.46.186.204 on 09/07/12
For personal use only.

^{1}H nuclear magnetic resonance and molecular orbital studies of the structure and internal rotations in ethylbenzene

TED SCHAEFER, GLENN H. PENNER, AND RUDY SEBASTIAN
Department of Chemistry, University of Manitoba, Winnipeg, Man., Canada R3T 2N2

Received August 12, 1986

TED SCHAEFER, GLENN H. PENNER, and RUDY SEBASTIAN. Can. J. Chem. **65**, 873 (1987).

Rather extensive geometry-optimized computations at the STO-3G, 4-21G, 4-31G, and 6-31G levels of *ab initio* molecular orbital theory suggest that the fourfold component of the barrier to internal rotation about the C_{sp^2}—C_{sp^3} bond in ethylbenzene amounts to about 20% of the twofold component. The ^{1}H nuclear magnetic resonance spectral parameters, extracted by complete analyses of the spectra arising from the ten protons, are reported for ethylbenzene in acetone-d_6, CCl_4, CS_2, and perfluoromethylcyclohexane solutions. The long-range proton–proton spin–spin coupling constants demonstrate that the internal barrier is insensitive to the polarity of the solvent, in contrast to polar solute molecules such as benzyl fluoride. The coupling constants do not support a dependence of the internal barrier on the internal pressure of the solvent.

TED SCHAEFER, GLENN H. PENNER et RUDY SEBASTIAN. Can. J. Chem. **65**, 873 (1987).

Des calculs *ab initio* d'orbitales moléculaires ont été effectués d'une façon relativement approfondie aux niveaux STO-3G, 4-21C, 4-31G et 6-31G et on les a optimisés par rapport à la géométrie; les résultats suggèrent que la barrière à la rotation interne autour de la liaison C_{sp^2}—C_{sp^3} de l'éthylbenzène comporte une composante quadruple qui correspond à 20% de la composante binaire. On a déterminé les spectres rmn ^{1}H de l'éthylbenzène en solutions dans l'acétone-d_6, dans le CCl_4, dans le CS_2 et dans le perfluorométhylcyclohexane et on a déterminé les paramètres spectraux en procédant à des analyses complètes des spectres provenant des dix protons. Les constantes de couplage spin–spin, proton–proton à longue distance démontrent que la barrière interne n'est pas sensible à la polarité du solvant; ce résultat est en opposition avec ce qui est observé avec des molécules polaires comme le fluorure de benzyle. Les constantes de couplage ne présentent pas de relation entre la barrière interne et la pression interne du solvant.

[Traduit par la revue]

Introduction

Solvent perturbations of molecular conformational equilibria have been studied extensively (1–5). A well-known example is the *gauche–trans* equilibrium in *n*-butane. It was argued (6) that in the disordered liquid phase the intramolecular potential averages to that in the isolated molecule. Experimental data for the energy difference between the *trans* and *gauche* forms overlap for the liquid and gaseous states (1). Monte Carlo and molecular dynamics simulations and the so-called RISM calculations differ as to the effect of condensation or solvents on the equilibrium (2–4).

Because the *gauche* form of *n*-butane has a smaller volume (more globular) than the *trans* form, increased external or internal pressure (7, 8) should increase its population. At an external pressure of 3000 atm (1 atm = 101.3 kPa), Raman data are consistent with this idea (9), but do not prove it, whereas Monte Carlo simulations (10) suggest that pressures as high as 15 000 atm are needed to cause a significant change in population. From another viewpoint, the internal pressure of the liquid could cause a conformational shift. Internal pressures of common solvents range from about 2000 to 5000 atm and, if the volume difference between conformers is as large as 3 cm^3/mol, could then lead to an energy change of about 1 kJ/mol (7, 11). For *n*-butane in nonpolar solvents, the Raman (12) and neutron scattering (13) data suggest no change in the *gauche–trans* energy differences.

Turning to polar molecules, the general rule that a conformer with the greater dipole moment is favored in polar solvents (5) is confirmed by statistical mechanical calculations (1, 4). For example, the *gauche* conformer of 1,2-dichloroethane becomes about 4 kJ/mol more stable on condensation, both experimentally and theoretically (4).

Of course, as the barrier to interconversion between the conformers diminishes, the discussion in terms of energy differences between conformers becomes less meaningful. For example, in benzyl fluoride, conformer **1** (X = F) is ≤ 1 kJ/mol more stable than **2** in CS_2 solution (14), so that at ambient temperature a sensible discussion involves not an equilibrium between **1** and **2**, but the internal rotational potential, $V(\theta)$,

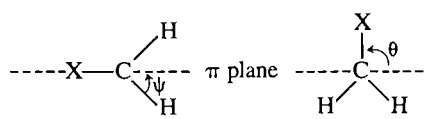

$\theta = 0°, \psi = 60°$ **1** $\theta = 90°, \psi = 30°$ **2**

defining rotation about the C_{sp^2}—C_{sp^3} bond. In fact, the use of $^nJ(^{13}C, ^{19}F)$, n = 2–5, $^nJ(^1H, ^1H)$, n = 4, 5, 6, and $^nJ(^1H, ^{19}F)$, n = 4, 5, 6, the long-range nuclear spin–spin coupling constants over n formal bonds between side-chain and ring nuclei, demonstrated that the twofold potential, V_2, governing this rotation, changes by 2 kJ/mol in passing from the nonpolar solvent CS_2 to the polar solvents acetone-d_6 or DMSO-d_6 (14). Conformer **2** becomes more stable than **1** in polar solvents. Qualitatively, this result is reasonable because **2** has a higher dipole moment than **1**.

Now, ethylbenzene is much less polar than benzyl fluoride and the dipole moments of **1** and **2** (X = CH_3) must differ by only a small amount. Hence any solvent effects on the internal rotational potential are expected to arise more from packing forces (internal pressure) than from electrostatic interactions. In consequence it is expected that $V(\theta)$ in ethylbenzene will be much the same in CS_2 and acetone solutions, which have very similar internal pressures (8) but quite different polarities. In a solvent such as perfluoromethylcyclohexane (PFMC), whose internal pressure is less than half that of CS_2, $V(\theta)$ might be altered if the volumes of **1** and **2** differ. The former conformer is expected to have a lower volume than that of **2**, which is analogous to the *trans* form of *n*-butane. Because $^6J(H, CH_2)$ is very precisely measurable at 300 MHz and because (15) it is

Can. J. Chem. Downloaded from www.nrcresearchpress.com by 80.58.250.72 on 09/07/12
For personal use only.

Can. J. Chem. Downloaded from www.nrcresearchpress.com by 80.58.250.72 on 09/07/12
For personal use only.

related to $V(\theta)$, this coupling constant can be taken as an indicator of such presumed changes in $V(\theta)$.

This paper reports precise analyses of the ^1H nmr spectra of ethylbenzene in CCl_4, CS_2, acetone-d_6, and PFMC solutions, covering a range of internal pressures and encompassing solvents of widely different polarity. Extensive molecular orbital calculations on $V(\theta)$ are also reported. Among other uses, the latter provide estimates of the intramolecular energies needed in statistical mechanical computations (1) of condensed phase perturbations. The barriers indicated by the long-range coupling constants are compared with theory.

Barrier computations by molecular orbital methods

The main purpose of these calculations was to establish the foldedness of the barrier to rotation about the exocyclic C_{sp^2}—C_{sp^3} bond in ethylbenzene. If, for example, the barrier is purely twofold, then $\langle \sin^2\theta \rangle$, as derived from $^6J(H,CH_2)$, is easily related via a hindered rotor model to the barrier, V_2. If a fourfold component also exists, then a given $\langle \sin^2\theta \rangle$ is compatible with a number of combinations of V_2 and V_4. A theoretical barrier can then suggest which of these combinations is the most probable.

Evidence exists for the usefulness of *ab initio* molecular orbital calculations of internal barriers for hydrocarbons containing the phenyl group. For example, STO-3G MO methods agree with experiment that the sixfold internal barrier in toluene is tiny (16). For styrene, experiment (17) has established a fourfold component amounting to 3.3 kJ/mol, about 25% of the magnitude of the twofold component of 12.8 ± 0.1 kJ/mol. STO-3G MO computations agree well with the magnitude of V_4 but overestimate V_2 by 3.5 kJ/mol (18). The 6-31G basis set yields an internal potential (19) effectively equal to that from experiment (17). Such computations demand rather full geometry optimization procedures.

In the present calculations for ethylbenzene, all bond angles and lengths were allowed to vary, with the constraint that the carbon and hydrogen atoms of the phenyl group remain in a plane. The angle θ was varied in 15° steps between 0° and 90°, except that at the 6-31G level only 0°, 45°, and 90° were used. The energies could be fit to potentials containing V_2 and V_4 terms, as in eq. [1].

$$[1] \quad V(\theta) = -V_2 \sin^2\theta + V_4 \sin^2 2\theta$$

	$-V_2$/kJ mol^{-1}	V_4	$-E_{90}$/a.u.
STO-3G	6.58(11)	0.78(12)	305.055 713
4-21G	7.70(11)	1.73(11)	308.134 706
4-31G	6.90(11)	1.45(11)	308.335 989
6-31G	6.04	1.19	308.664 033

The errors in parentheses are given at the 95% confidence level. These errors could be somewhat reduced by inclusion of a term in V_6. For example, for the 4-21G basis, such a fit gave V_2, V_4, V_6 as −7.85(5), 1.58(5), 0.37(5) kJ/mol, respectively. The present experimental data cannot distinguish between these numbers and those for a potential containing only V_2 and V_4. However, it is probable that the barrier is not purely twofold, containing a V_4 whose magnitude is about 20% of that of V_2.

Conformation **2** (X = CH_3) is clearly of lowest energy, in agreement with low-resolution microwave spectra (20). The computed structure **2** at the 6-31G level is given in Fig. 1 and will be of interest to microwave spectroscopists and other structural scientists.

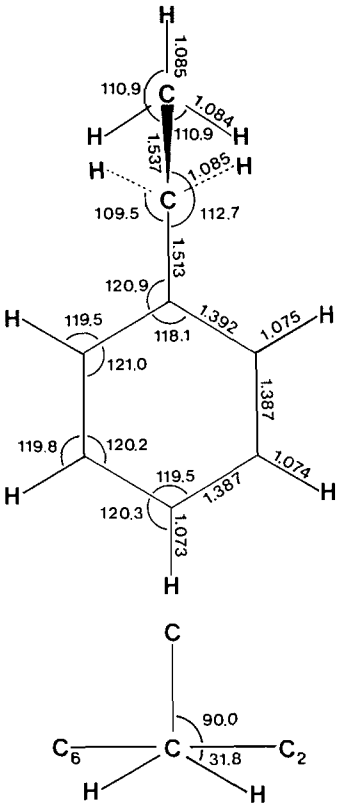

FIG. 1. The 6-31G structure of ethylbenzene in the conformation of lowest energy is displayed. The computed bond angles within the ring are remarkably close to those predicted (46, 47) from angular substituent parameters as given for a methyl substituent and determined mainly from X-ray crystallography. At the 6-31G level (48) these angular distortions from 120° in toluene are reproduced to within experimental error. The angle between the C(1)—C(4) vector and the C(1)—C(sp^2) bond is 1.6° in the sense that the methyl group moves away from the ring. The carbon atom of the methyl group lies in a plane perpendicular to the phenyl plane.

It is natural to assume that the barrier in ethylbenzene is steric in origin. In an attempt to discover how V_4 varies with various computed V_2 values, geometry optimized computations were carried out at the STO-3G level for various C_{sp^2}—C_{sp^3} bond lengths, the latter being changed in 10-pm steps between 105 and 185 pm. It was found that V_2 varied roughly as an inverse exponential function of bond length, decreasing as r increased, and that V_4 was linearly related to V_2. In fact, for 9 pairs of values, V_2/kJ mol^{-1} = −9.80 V_4 + 1.08 (r = 0.999), perhaps implying that when, in the high-energy conformation **1** (X = CH_3), the distance between the *ortho* C—H bond and the methyl group is large enough, the *ortho* C—H bond "sees" the methyl group as an "atomic entity" and no longer distinguishes among its individual C—H bonds.[1]

That the *ortho* C—H bond distinguishes between the C—H bonds of the methyl group in **1** (X = CH_3) is quite clear from the STO-3G values for rotation about the C_{sp^2}—C_{sp^3} bond. These rotational barriers are computed as 26.27(2) and −0.77(3) kJ/mol for V_3 and V_6, respectively, in **1** and as 15.05(7) and −0.01(8) kJ/mol in **2**. In ethane, V_3 and V_6 are 12.06(4) and 0.08(4) kJ/mol, respectively (22). Heat capacity data for ethylbenzene are consistent with 17.2 kJ/mol for V_3 (23), presumably corresponding to an ensemble average.

[1]The computed potential function for benzyl chloride is twofold (21), in line with the above interpretation.

TABLE 1. ^{1}H nuclear magnetic resonance spectral parameters for ethylbenzene at 300 K and 300.135 MHz

Parameter	$C_6F_{11}CF_3$[a]	CCl_4[b]	CS_2[b]	$(CD_3)C{=}O$[d]
ν_{CH_3}	364.164(2)[e]	362.277(2)[e]	362.277(2)[e]	359.732(2)[e]
ν_{CH_2}	781.453(1)	784.538(1)	775.312(1)	786.141(1)
$\nu_2 = \nu_6$	2132.878(1)	2125.572(1)	2114.212(1)	2160.189(1)
$\nu_3 = \nu_5$	2148.085(1)	2149.365(1)	2137.700(1)	2177.623(1)
ν_6	2115.924(1)	2118.106(1)	2106.668(1)	2144.767(1)
$^3J(CH_2,CH_3)$	7.644(1)	7.612(1)	7.598(1)	7.627(1)
$^3J_{23}$	7.721(2)	7.687(1)	7.670(2)	7.690(1)
$^3J_{34}$	7.477(2)	7.440(1)	7.426(2)	7.441(1)
$^4J_{26}$	1.938(2)	1.934(2)	1.932(2)	1.951(2)
$^4J_{24}$	1.243(1)	1.261(1)	1.259(1)	1.259(1)
$^4J_{35}$	1.439(2)	1.463(2)	1.461(2)	1.457(2)
$^5J_{25}$	0.604(1)	0.594(1)	0.587(1)	0.604(1)
$^4J(H,CH_2)$	−0.631(1)	−0.626(1)	−0.649(1)	−0.623(1)
$^5J(H,CH_2)$	0.288(1)	0.290(1)	0.291(1)	0.293(1)
$^6J(H,CH_2)$	−0.441(2)	−0.454(1)	−0.455(1)	−0.451(1)
$^5J(H,CH_3)$[f]	±0.04(2)	±0.04(2)	±0.04(2)	±0.04(2)
$^6J(H,CH_3)$[f]	±0.02(2)	±0.02(2)	±0.02(2)	±0.02(2)
$^7J(H,CH_3)$[f]	0.00(2)	0.00(2)	0.00(2)	0.00(2)
Calculated transitions	2544	2424	2424	2416
Assigned transitions[g]	639	1323	731	744
Peaks	169	189	230	201
Largest difference	0.036	0.044	0.033	0.037
Root mean square deviation[h]	0.015	0.014	0.014	0.014

[a]2.8 mol% in perfluoromethylcyclohexane, containing also 10 mol% C_6D_{12} and 0.5 mol% TMS.
[b]2.5 mol% in CCl_4 and C_6D_{12} and TMS as above.
[c]2.5 mol% in CS_2 and C_6D_{12}/TMS as above.
[d]2.5 mol% in acetone-d_6 and 0.5 mol% TMS.
[e]In Hz to high frequency of internal TMS. Numbers in parentheses are standard deviations in the last significant figure.
[f]Not iterated upon but estimated via decoupling experiments and simulations with various couplings and linewidths.
[g]Note that all peaks were assigned and that, of course, there are many degeneracies (ethyl group protons).
[h]There were no striking correlations involving the long-range couplings between side-chain and ring protons, except for one of 0.182 between $^4J(H,CH_2)$ and $\nu_2 = \nu_6$ for the $C_6F_{11}CF_3$ solution and one of −0.132 between $^4J(H,CH_2)$ and ν_{CH} in CS_2 solution.

Returning to the internal barrier about the C_{sp^2}—C_{sp^3} bond, it is not ascertainable at present which of the theoretical barriers is the most reliable. At 300 K, these potentials imply a $\langle\theta\rangle$ between 66 and 70° for a classical averaging procedure, which may be compared with a best fit value of 70° from electron diffraction patterns (24, 25).

Barriers derived from $^6J(H,CH_2)$ in solution

For toluene, $^6J(H,CH_2)$ has been written (26) as $^6J/\text{Hz} = {}^6J_{90}\sin^2\psi$, where $^6J_{90}$ is the magnitude of ^6J at $\psi = 90°$ and has a value of −1.204(4) Hz. In CS_2 solution (Table 1), ^6J is −0.455(1) Hz, so that the expectation value, $\langle\sin^2\psi\rangle$, is 0.378 if the methyl group does not alter the magnitude of $^6J_{90}$. From a hindered rotor model (15) relating the twofold potential to $\langle\sin^2\theta\rangle$, V_2 would then follow as 5.7 kJ/mol with **2** as the conformation of lowest energy. However, the magnitude of $^6J_{90}$ is reduced by electronegative substituents (14, 15, 21). On a scale on which the electronegativity of fluorine is 3.92 and that of hydrogen is 1.78 (27–29), $^6J_{90}$ is −0.95 Hz for fluorine (14). The electronegativity of the methyl group has been estimated by various methods (30–33). On the basis of the available data, it is here taken as 2.2 on the above scale. The assumption of a linear dependence of $^6J_{90}$ on electronegativity yields $^6J_{90}$ as −1.16 Hz. Then $\langle\sin^2\theta\rangle$ follows as 0.389 and the apparent V_2 as 5.0 kJ/mol. If the internal barrier about the C_{sp^2}—C_{sp^3} bond were purely twofold, then ^6J in CS_2 solution would imply its magnitude as $5.3_5 \pm 0.3_5$ kJ/mol.

However, the MO computations on the free molecule suggest substantial fourfold components. For the values quoted above, $\langle\sin^2\psi\rangle$, as obtained by a classical averaging procedure, is 0.355, 0.332, 0.345, and 0.360, respectively, for the STO-3G, 4-21G, 4-31G, and 6-31G basis sets. All these values are significantly lower than that obtained from ^6J (note that $\langle\sin^2\psi\rangle$ is 0.5 for a zero barrier and approaches 0.25 for a very large barrier).

One possible reason for the differences is that the barrier in solution is indeed lower than in the vapour phase. Consider the molecular volumes of **1** and **2**. Although these are not at all easy to calculate reliably (34), intuitively that of **1** is smaller than that of **2**. For *n*-hexane the molecular volume of the *trans* (extended) conformer has been estimated as 3.5 cm^3 less than that of the *gauche* conformer (34). If the difference between the conformers **1** and **2** of ethylbenzene is taken as 3 cm^3, an internal pressure of 4000 atm in CS_2 solution (8) will favor **1**, that is, will lower the internal barrier by about 1 kJ/mol.

A second possible reason is that the most flexible basis set employed above still overestimates the barrier magnitude, although it should be remembered that such a basis agrees very

Can. J. Chem. Downloaded from www.nrcresearchpress.com by 80.58.250.72 on 09/07/12
For personal use only.

Can. J. Chem. Downloaded from www.nrcresearchpress.com by 80.58.250.72 on 09/07/12
For personal use only.

well with the experimental barrier for another hydrocarbon, styrene. On the other hand, heat capacity measurements are consistent with an assumed V_2 of 4.85 kJ/mol (23) in the vapor. Gas phase electron diffraction data (24) give an internal barrier of 7 kJ/mol, assumed to be twofold, and, upon reconsideration, 9.2 kJ/mol (25). The charged core potential energy method relies on the calculation of one *ab initio* wave function, followed by electrostatic energy computations, and gives the barrier as 5.01 kJ/mol (35). In that work the GAUSSIAN 76 barrier was found to be 9.9 kJ/mol, presumably based on an STO-3G calculation.

In solution, ^{13}C spin-lattice relaxation times for 1,3-diethylpyridinium bromide in CD_3OD solution yield 5.9 ± 0.8 kJ/mol as the enthalpy of activation for rotation about the C_{sp^2}—C_{sp^3} bond (36), similar to the value of 5.9 ± 0.8 kJ/mol obtained by the same approach to 4-ethylaniline in $CDCl_3$ solution (37). Within experimental error these numbers agree with the apparent V_2 obtained from ^6J for ethylbenzene. However, the molecular polarizability studies for ethylbenzene in CCl_4 solution give V_2 as 9.6 kJ/mol (38). Yet the ^6J for ethylbenzene in this solvent (Table 1) is the same as in CS_2 and acetone-d_6 solutions (assuming an error of twice the standard deviations). In fact, the range of ^6J in the four solvents is only 0.014(3) Hz, implying no significant solvent effect on the barrier.

For toluene $^5J(H,CH_2)$ has been written (26) as the sum of a $\sigma-\pi$ component, proportional to $\langle\sin^2\theta\rangle$, and a σ component, proportional to $\langle\sin^2(\psi/2)\rangle$. For a twofold or fourfold barrier, the latter expectation value is 0.5, as for toluene itself. Hence any solvent dependence of ^5J should occur via changes in $\langle\sin^2\psi\rangle$. However, the $\sigma-\pi$ component of ^5J is only about one-third as large as that of ^6J in toluene. The observed changes in ^5J in Table 1 are consistent with the behaviour of ^6J.

$^4J(H,CH_2)$ in $C_6F_{11}CF_3$ and CS_2 solutions correlates significantly with other spectral parameters (footnotes in Table 1). Therefore, although ^4J appears to have a smaller magnitude in the former solution and is expected to have a predominant dependence (39) on $\langle\sin^2\psi\rangle$, it cannot be said that this appearance indicates a solvent dependence of the internal barrier.

Similar remarks apply to the coupling constants between protons situated on the phenyl group. For example, $^4J_{35}$ and $^5J_{25}$ are significantly correlated in $C_6F_{11}CF_3$ and CS_2 solutions. Consequently their sums are more reliable parameters and are indeed 2.043(3) and 2.048(3) Hz in the two solutions, so that an intrinsic solvent dependence of the two couplings is not established. In fact, $^5J_{25}$ has significant correlations with certain shift parameters in all the solutions in Table 1.

Derivatives of ethylbenzene

It is suggested that the barrier in ethylbenzene is influenced both by steric and hyperconjugative interactions (40), with C—C being larger than C—H hyperconjugation. In that event, **2** is stabilized by such an interaction. In 4-fluoroethylbenzene in acetone-d_6 solution (41), $^6J(CH_2,F)$ is 0.812(3) Hz, while $^6J(CH_3,F)$ is 1.149(3) Hz in 4-fluorotoluene in the same solvent (42). $^6J(CH_3,F)$ is predominantly a $\sigma-\pi$ coupling (42), implying that $\langle\sin^2\psi\rangle$ in 4-fluoroethylbenzene is 0.812(3)/2.298(6) or 0.353(3) if $^6J_{90}(CH_2,F)$ is not altered by the methyl group. An apparent V_2 of 7.5(3) kJ/mol is deduced. However, $^6J_{90}$ should probably be reduced by a factor of 1.16/1.20 (see discussion above), leading to an apparent V_2 of 6.5(3) kJ/mol. Both values are higher than for ethylbenzene in acetone-d_6, suggesting that C—C is a weaker hyperconjugative donor than C—H. This follows because the fluorine substituent is an π electron donor and would stabilize conformer **2**, in which the weaker of the two side-chain donors has a maximum interaction with the π electron system.

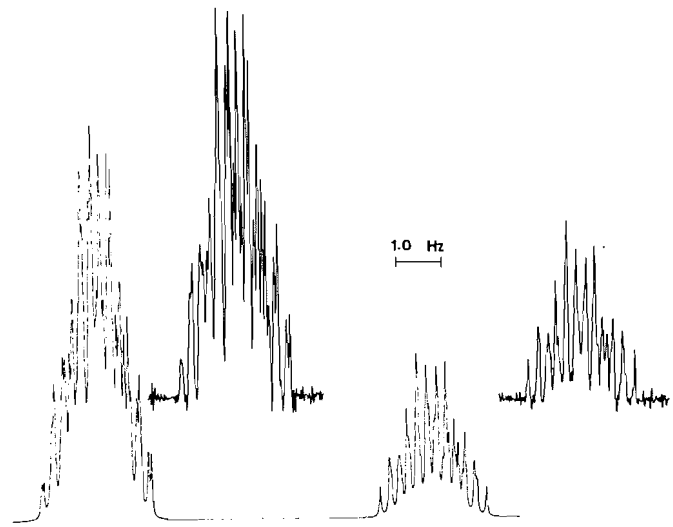

FIG. 2. Half of the observed and computed ^1H nmr spectrum of the methylene protons of ethylbenzene is displayed. The observed peaks arise from hundreds of transitions and the linewidth at half-height is about 0.06 Hz. The nmr sample contained 2.5 mol% ethylbenzene, 10 mol% C_6D_{12}, and 0.5 mol% TMS dissolved in CS_2. The probe temperature was 300 K and the carrier frequency was 300.135 MHz on the Bruker AM300 spectrometer.

Some support for a hyperconjugative contribution to the barrier in ethylbenzene comes from recent electron diffraction data on 4-ethylbenzaldehyde (43), from which the internal barrier is deduced as 1 kJ/mol *lower* than in ethylbenzene. In conformer **1**, the C—H bonds hyperconjugate more effectively than in **2**. Because the formyl group accepts π electron density from the ring, the reduction in barrier is expected if the C—H bonds are better donors than the C—C bond.

However, the apparent V_2 deduced from $^6J(CH_2,F)$ in 4-fluoroethylbenzene must be treated with circumspection because this coupling may contain a small contribution from other than a $\sigma-\pi$ mechanism (15). Indeed, the tenuousness of the barrier deduced from $^6J(CH_2,F)$ is indicated by the $^5J(H,CH_2)$ of 0.302(3) Hz for this compound. For 4-fluorotoluene, $^5J(H,CH_3)$ is 0.343(3) Hz and its increased magnitude relative to the 0.329(1) Hz in toluene (26) is attributable to an increased σ component (44). To within experimental error the ratios, $^5J(H,CH_2)/^5J(H,CH_3)$, are identical for the two types of compounds, implying the same barrier in ethylbenzene and its 4-fluoro derivative. Furthermore, to obtain 0.320(3) Hz in the 4-fluoroethylbenzene requires a $\langle\sin^2\psi\rangle$ of 0.378 and an apparent V_2 of 5.7 kJ/mol, the same as for ethylbenzene to within experimental error. A $^6J_{90}(CH_2,F)$ of 2.15 Hz follows from such a computation and is a reasonable number in view of the possible presence of a small non-$\sigma-\pi$ component.

Similar arguments can be made about $^4J(H,CH_2)$, and are complicated by considerations concerning the magnitude of the σ component in the presence of the methyl group (39). The observed value of −0.618(3) Hz in 4-fluoroethylbenzene (41) does not, in fact, support an increased barrier relative to the parent compound. In summary, the long-range coupling

constants do not establish a perturbation of the internal barrier in ethylbenzene by a 4-fluoro substituent.

Turning to 3,5-dibromoethylbenzene, $^6J(H,CH_2)$ is $-0.477(3)$ Hz for a solution in C_3D_6 (45) and is $-0.480(3)$ in CS_2 solution. In 3,5-dibromotoluene, as a 2.5 mol% solution in the CS_2/C_6D_{12}/TMS mixture, $^6J(H,CH_3)$ is $-0.613(2)$ Hz. In this molecule, therefore, $^6J_{90}$ is $-1.226(4)$ Hz. According to the previous discussion, $^6J_{90}$ in 3,5-dibromoethylbenzene then lies between -1.19 and -1.23 Hz, corresponding to a $\langle \sin^2 \psi \rangle$ of 0.395(10). Hence the apparent V_2 is 4.5(4) kJ/mol. This result indicates, at most, a very slight lowering of the barrier, it being $5.3_5 \pm 0.3_5$ kJ/mol for ethylbenzene in CS_2 solution. Rather more dramatic decreases in V_2 have been observed for the 3,5-dichloro derivatives of benzyl fluoride (14) and benzyl chloride (21).

Experimental

The spectral analytical procedures were identical to those described recently (26) and the footnotes in Table 1 give the relevant concentrations and temperatures. Figure 2 displays half of the observed and computed ^{1}H nmr spectrum of the methylene protons of ethylbenzene in CS_2 solution.

The molecular orbital concentrations used the program GAUSSIAN 82 (49) on an Amdahl 470/V7 system.

Conclusions

The long-range proton–proton coupling constants for ethylbenzene imply that the internal barrier to rotation about the C_{sp^2}—C_{sp^3} bond is independent of the polarity or internal pressure of the solvent. The barrier indicated by the coupling constants is slightly lower than that obtained from *ab initio* molecular orbital computations, which also suggest a significant fourfold, in addition to the dominant twofold, component.

Acknowledgments

This research was supported by the Natural Sciences and Engineering Research Council of Canada. We are also grateful to the University of Manitoba for significant allocations of computing time and to the referees for cogent criticism.

1. W. L. Jorgensen. J. Phys. Chem. **87**, 5304 (1983).
2. W. L. Jorgensen, J. D. Madura, and C. J. Swenson. J. Am. Chem. Soc. **106**, 6638 (1984).
3. A. Banon, F. Serrano Adan, and J. Santamaria. J. Chem. Phys. **83**, 297 (1985).
4. D. A. Zichi and P. J. Rossky. J. Chem. Phys. **84**, 1712 (1986).
5. R. J. Abraham and E. Bretschneider. *In* Internal rotation in molecules. *Edited by* W. J. Orville-Thomas. Wiley, London. 1974. Chap. 13.
6. P. J. Flory. Science, **188**, 1268 (1965).
7. R. J. Ouellette and S. H. Williams. J. Am. Chem. Soc. **93**, 466 (1971).
8. M. R. J. Dack. Chem. Soc. Rev. (London), **4**, 211 (1975).
9. J. Devaure and J. Lascombe. Nouv. J. Chim. **3**, 579 (1979).
10. W. L. Jorgensen. J. Am. Chem. Soc. **103**, 4721 (1981).
11. M. M. Folkendt, B. E. Weizz-Lopez, J. P. Chauvel, and N. S. True. J. Phys. Chem. **89**, 3347 (1985).
12. L. Rosenthal, J. F. Rabolt, and J. F. Hummel. J. Phys. Chem. **76**, 817 (1982).
13. E. W. Fischer, G. R. Strohl, M. Dettenmaier, M. Stamm, and N. Steidle. Discuss. Faraday Soc. **68**, 26 (1979).
14. T. Schaefer, J. Peeling, and R. Sebastian. Can. J. Chem. **63**, 3219 (1985).
15. W. J. E. Parr and T. Schaefer. Acc. Chem. Res. **13**, 400 (1980).
16. F. Pang, J. E. Boggs, P. Pulay, and G. Fogarasi. J. Mol. Struct. **66**, 281 (1980).
17. J. M. Hollas, H. Musa, T. Ridley, P. H. Turner, K. H. Weisenberger, and V. Fawcett. J. Mol. Spectrosc. **94**, 437 (1982).
18. T. Schaefer and G. H. Penner. Chem. Phys. Lett. **114**, 526 (1985).
19. C. W. Bock, M. Trachtman, and P. George. Chem. Phys. **93**, 431 (1985).
20. M. S. Farag. Diss. Abstr. Int. B: **35**, 1594 (1974).
21. T. Schaefer, R. Sebastian, and G. H. Penner. Can. J. Chem. **64**, 1372 (1986).
22. E. Hirota, Y. Endo, S. Saito, and J. L. Duncan. J. Mol. Spectrosc. **89**, 285 (1981).
23. A. Miller and D. W. Scott. J. Chem. Phys. **68**, 1317 (1978).
24. P. Scharfenberg, B. Rozsondai, and I. Hargittai. Z. Naturforsch. Part A, **35**, 431 (1980).
25. P. Scharfenberg. J. Chem. Phys. **77**, 4791 (1982).
26. T. Schaefer, R. Sebastian, and G. H. Penner. Can. J. Chem. **63**, 2597 (1985).
27. B. P. Dailey and J. N. Shoolery. J. Am. Chem. Soc. **77**, 3977 (1956).
28. J. R. Cavanaugh and B. P. Dailey. J. Chem. Phys. **34**, 1099 (1961).
29. M. L. Huggins. J. Am. Chem. Soc. **75**, 4123 (1953).
30. J. Mullay. J. Am. Chem. Soc. **107**, 7271 (1985).
31. N. Inamoto and S. Masuda. Chem. Lett. 1003 (1982).
32. S. G. Bratsch. J. Chem. Educ. **62**, 101 (1985).
33. J. E. Huheey. J. Phys. Chem. **69**, 3284 (1965).
34. T. Bleha, J. Gajdos, and I. Ivaroska. J. Mol. Struct. **68**, 189 (1980).
35. V. Sackwild and W. G. Richards. J. Mol. Struct. Theochem. **89**, 269 (1982).
36. D. Ghesquiere and C. Chachaty. Org. Magn. Reson. **9**, 392 (1977).
37. C. Chachaty, A. Forchioni, and J. C. Ronfard-Haret. Mol. Phys. **31**, 325 (1976).
38. M. Camail, A. Proutiere, and H. Bodot. J. Phys. Chem. **79**, 1966 (1975).
39. M. Barfield, C. J. Fallick, K. Hata, S. Sternhell, and P. W. Westerman. J. Am. Chem. Soc. **105**, 2178 (1983).
40. W. J. Hehre, L. Radom, and J. A. Pople. J. Am. Chem. Soc. **94**, 1496 (1972).
41. T. Schaefer, J. Peeling, G. H. Penner, A. Lemire, and R. Sebastian. Can. J. Chem. **63**, 24 (1985).
42. R. Wasylishen and T. Schaefer. Can. J. Chem. **49**, 94 (1971).
43. J. Brunvoll, M. Kolonits, R. K. Bohn, and I. Hargittai. J. Mol. Struct. **131**, 177 (1985).
44. T. Schaefer and R. Laatikainen. Can. J. Chem. **61**, 2785 (1983).
45. T. Schaefer, L. Kruczynski, and W. Niemczura. Chem. Phys. Lett. **38**, 498 (1976).
46. A. Domenicano and P. Murray-Rust. Tetrahedron Lett. 2283 (1979).
47. R. Norrestam and L. Schepper. Acta Chem. Scand. Part A, **35**, 91 (1981).
48. C. W. Bock, M. Trachtman, and P. George. J. Mol. Struct. Theochem. **122**, 155 (1985).
49. J. S. Binkley, M. J. Frisch, D. J. DeFrees, K. Rahgavachari, R. A. Whiteside, H. B. Schlegel, E. M. Fluder, and J. A. Pople. Department of Chemistry, Carnegie–Mellon University, Pittsburgh, PA.

Can. J. Chem. Downloaded from www.nrcresearchpress.com by 80.58.250.72 on 09/07/12
For personal use only.

Bis((*S*)-5,5-dimethylthiazolidine-4-carboxylic acid) protium chloride hydrate $[(C_6H_{11}NO_2S)_2H]Cl.H_2O$, a salt containing a hemi-protonated zwitterion

H. E. HOWARD-LOCK,[1] C. J. L. LOCK,[1] M. L. MARTINS, R. FAGGIANI, AND M. DUARTE

Laboratories for Inorganic Medicine, Institute for Materials Research, McMaster University, Hamilton, Ont., Canada L8S 4M1

Received August 18, 1986

H. E. HOWARD-LOCK, C. J. L. LOCK, M. L. MARTINS, R. FAGGIANI, and M. DUARTE. Can. J. Chem. **65**, 878 (1987).

The X-ray crystal structure of bis((*S*)-5,5-dimethylthiazolidine-4-carboxylic acid) protium chloride hydrate, **I**, has been determined. Crystals are orthorhombic, $P2_12_12_1$, with cell dimensions $a = 6.463(2)$, $b = 11.832(3)$, $c = 23.966(6)$ Å, and $Z = 4$. The structure was solved by standard methods and refined to $R = 0.073$, $R_w = 0.064$ for 2969 independent reflections. Compound **I** is composed of two zwitterion molecules bridged through a proton which causes a very short hydrogen bond, $O\ldots O' = 2.450(5)$ Å. The proton is located roughly halfway between the two carboxylate oxygen atoms, but is not on a special crystallographic position. Characteristic features of the infrared and Raman spectra, mass spectra, and ^1H and ^{13}C nmr spectra are discussed.

H. E. HOWARD-LOCK, C. J. L. LOCK, M. L. MARTINS, R. FAGGIANI et M. DUARTE. Can. J. Chem. **65**, 878 (1987).

Faisant appel à la diffraction des rayons-X, on a déterminé la structure cristalline de l'hydrate du chlorhydrate de l'acide bis((*S*)-diméthyl-5,5 thiazolidinecarboxylique-4) (**I**). Les cristaux sont orthorhombiques, $P2_12_12_1$, avec $a = 6{,}463(2)$, $b = 11{,}832(3)$ et $c = 23{,}966(6)$ Å et $Z = 4$. On a résolu la structure par les méthodes standards et on l'a affinée jusqu'à des valeurs de $R = 0{,}073$ et $R_w = 0{,}064$ pour 2969 réflexions indépendantes. Le composé **I** est formé de deux molécules zwitterioniques qui sont pontées par un proton qui provoque une liaison hydrogène très courte, $O\ldots O' = 2{,}450(5)$ Å. Le proton est situé approximativement au milieu des deux atomes d'oxygènes des carboxylates; toutefois, il ne se trouve pas dans une position cristallographique spéciale. On discute des caractéristiques principales des spectres infrarouge et Raman, des spectres de masse et des spectres rmn du ^1H et du ^{13}C.

[Traduit par la revue]

Introduction

We have been studying various derivatives of D-penicillamine and have reported that 2,2,5,5-tetramethylthiazolidine-4-carboxylic acid is an amino acid in the solid state rather than the zwitterion, and that even in aqueous solution about 5% exists as the amino-acid form (1). In contrast, thiazolidine-4-carboxylic acid is a zwitterion in the solid state and no amino-acid form is detectable in solution. We prepared and characterized a number of substituted thiazolidine-4-carboxylic acids in order to study the amino-acid–zwitterion equilibrium (2).

When attempting to prepare the sulfur-protected product of D-penicillamine with *N*-hydroxymethylacetamide, we were unsuccessful and instead isolated the title compound, **I**, bis((*S*)-5,5-dimethylthiazolodine-4-carboxylic acid) protium chloride hydrate, $[(C_6H_{10}NO_2S)_2H]Cl.H_2O$. Because the new compound fitted into our studies, we investigated compound **I** structurally and spectroscopically. We found that **I** is a salt containing a hemiprotonated zwitterion dimer, and that it contains a very strong hydrogen bond between two hemiprotonated zwitterion molecules. The hydrogen bond is very short and spectroscopic evidence suggests the hydrogen bond is symmetric, in which case it is one of the rare instances where a symmetrical hydrogen bond does not have the proton lying on a crystallographic symmetry element (3). We report this work here.

Experimental section

The D-(−)-penicillamine (free base) was of reagent grade, as supplied by Sigma Chemical Co., St. Louis, MI. *N*-Hydroxymethylacetamide was supplied by Alfa Products, Danvers, MA. The melting point of **I** was determined on a Gallenkamp capillary melting point apparatus and was not corrected. Chemical analyses were performed by the Guelph Chemical Laboratories, Ltd., Guelph, Ont. The pK's were obtained by titration of an aqueous solution of the salt against 0.01 *N* NaOH and 0.01 *N* HCl. The pH's were measured with a Corning Model 130 pH meter which was standardized with Scientific Products potassium hydrogen phthalate pH 4.00 buffer, BDH pH 7.00 buffer and Scientific Products boric acid/potassium hydroxide buffer, pH 10.00.

Preparation of bis(5,5-dimethylthiazolidine-4-carboxylic acid)protium chloride hydrate

N-Hydroxymethylacetamide, 0.6 g (0.005 mol) was added to 0.8 g (0.005 mol) D-penicillamine in 5 mL water. Dilute HCl was added to acidify the solution to pH < 2. The solution was stirred under nitrogen for 30 min, then the flask was stoppered and allowed to stand at room temperature. Following evaporation of the solution, a colourless oil was left. Upon standing overnight some separation of white solid from the oil was observed. Ethanol was added to dissolve the oil and the solid was filtered out. To the ethanol solution anhydrous diethyl ether was added and the mixture was left in the refrigerator. A white precipitate covered by a colourless oil was recovered. The oil dissolved in water readily, and the white precipitate was less soluble. The yield of white solid was 0.6 g (70%), mp 181–182°C (dec.).

Anal. calcd. C 38.2, H 6.7, N 7.4, O 21.2, S 17.0, Cl 9.4; found: C 37.2, H 6.9, N 7.8, O 20.3, S 18.4, Cl 9.4.

Long prismatic crystals for X-ray structure determination were obtained by slow crystallization from the reaction mixture over a period of one week.

Spectral measurements

Infrared spectra were recorded on both Nicolet 7199 FT-IR and Perkin-Elmer Model 283 spectrophotometers. The samples were ground with KBr at a concentration of approximately 1% by weight and then pressed into pellets. Spectra were calibrated with polystyrene. Raman spectra were excited by means of the $\lambda = 5145$ Å radiation from a Spectra-Physics Model 164-02 argon ion laser and recorded on a Spex 14018 double monochromator. Solid samples were contained in glass melting point tubes, and solutions in nmr tubes. The spectrometer was calibrated regularly against an indene standard and had previously been calibrated with a neon lamp; the wavelength readout scale was found not to change (± 1–2 cm^{-1}).

Solutions for nmr studies were prepared in D_2O and concentrations

[1]Authors to whom correspondence may be addressed.

Can. J. Chem. Downloaded from www.nrcresearchpress.com by 80.58.250.72 on 09/07/12
For personal use only.

TABLE 1. Crystal data

Compound	$[(C_6H_{11}NO_2S)_2H]Cl.H_2O$, $C_{12}H_{25}ClN_2O_5S_2$
f.w.	376.9
Crystal shape	Parallelepiped
size (mm)	0.23 × 0.33 × 0.50
Systematic absences	$h00, h = 2n + 1, 0k0, k = 2n + 1, 00l, l = 2n + 1$
Space group	$P2_12_12_1$ (No. 19)
Unit cell (Å)	$a = 6.463(2)$, $b = 11.832(3)$, $c = 23.966(6)$
Volume (Å^3)	1832.7(8)
Z	4
ρ_{calc}, ρ_{obs} (g cm^{-3})	1.365, 1.357(4)
Temperature (°C)	20
Linear absorption coeff. (cm^{-1})	4.52
Standard reflctns. (esd)	0 2 −8 (0.011); 2 4 −6 (0.011)
reflctns. meas. max, 2θ	$h, \pm k, \pm l$, 50°
No. of reflctns. meas.	6056
R merg.	0.028
No. of independent reflectns.	3068
No. with $I > 0$, used	2969
Final R, R_w[a]	0.073, 0.064
Secondary extinction, x	−0.00036
Final (shift/error) max., ave.	0.023, 0.006
Final difference e/Å^3, max., min.	0.61, −0.65
Weighting scheme	$w = (\sigma_F^2 + 0.000715F_0^2)^{-1}$
Error in an obs. of unit wt.	$S = 1.24$

[a] $R = \Sigma||F_o| - |F_c||/\Sigma|F_o|$; $R_w = \{\Sigma w(|F_o| - |F_c|)^2/\Sigma wF_o^2\}^{1/2}$.

were about 100 mg (solid) mL^{-1} of solvent. External tetramethylsilane was used as the reference. Proton nmr spectra were recorded on a Varian T60 spectrometer, and ^{13}C nmr spectra were recorded on a Bruker WP-80 spectrometer operating at 20.115 MHz.

Mass spectra were recorded on a VG Micromass 7070F mass spectrometer, with electron impact as the method of ionization.

Collection of the X-ray data and solution of the structure

A colourless, parallelepiped single crystal was sealed in a Lindemann capillary for the X-ray studies because we were worried about possible dehydration of the crystal. Precession photographs showed that crystals of **I** were orthorhombic. Unit cell parameters were obtained from least squares fit of χ, φ, and 2θ for 15 reflections in the range of $15.3° < 2\theta < 25.8°$ measured on a Syntex $P2_1$ diffractometer having graphite-monochromated MoKα_1 radiation ($\lambda = 0.70926$ Å at 22°C). Crystal data and other numbers related to data collection are summarized in Table 1. Intensities were also measured with use of the Syntex $P2_1$ diffractometer and a coupled θ(crystal)–2θ(counter) scan. The methods of determining scan rates and initial data treatment have been described (4, 5). Corrections were made for Lorentz and polarization effects but not for absorption. This will make a maximum error in F_o of <2.5%.

The structure was solved by direct methods with use of 85 reflections with $|E| > 1.68$ and 12 sets of starting phases. The chloride ion, and the rings were located in the subsequent E map. Full-matrix least-squares refinement followed by electron density difference syntheses revealed all the remaining atoms. The absolute configuration found, happened to be that expected on the basis of the known configuration of the starting product. No attempt was made to test the alternate configuration. At this stage the temperature factors of non-hydrogen atoms were made anisotropic and further full-matrix least-squares refinement, which minimized $\Sigma w(|F_o| - |F_c|)^2$ was terminated when the maximum (shift/error) fell below 0.1. Hydrogen atoms were included at the positions located in the difference maps but their positional parameters and temperature factors were not refined. Attempts to refine the hydrogen atoms were unsuccessful. Corrections were made for secondary extinction by the method of SHELX (6). Scattering curves were taken from ref. 7 and anomalous dispersion corrections from ref. 8 were applied to the curves for S and Cl. The atom parameters are listed in Table 2.[2]

TABLE 2. Atomic positional parameters (× 10^4) and temperature factors (Å^2 × 10^3)

Atom	x	y	z	U_{eq}*
S	722(2)	2193(1)	9055(1)	52.6(9)
C2	1499(9)	2554(4)	8363(2)	50(3)
N	2812(6)	1587(4)	8149(2)	36(2)
C4	3161(7)	697(4)	8584(2)	32(3)
C5	2962(7)	1273(4)	9156(2)	38(3)
C1	5246(7)	116(4)	8473(2)	38(3)
O1	6402(5)	499(3)	8116(1)	45(2)
O2	5527(5)	−745(3)	8781(2)	51(3)
C51	2375(11)	414(5)	9611(2)	66(5)
C52	4909(10)	1967(6)	9300(3)	65(4)
S′	13879(2)	−4587(1)	8895(1)	55(1)
C2′	14358(7)	−4018(4)	8204(2)	41(3)
N′	12464(6)	−3404(3)	8059(2)	32(2)
C4′	11694(7)	−3796(4)	8550(2)	32(3)
C5′	11646(7)	−3658(4)	9045(2)	36(3)
C1′	9602(7)	−2252(4)	8428(2)	36(3)
O1′	8684(5)	−2511(3)	8001(1)	46(2)
O2′	9011(6)	−1561(3)	8801(2)	59(2)
C51′	11900(11)	−3067(6)	9612(3)	53(4)
C52′	9680(8)	−4388(5)	9033(2)	74(5)
Cl	6472(2)	3397(1)	7812(1)	49(1)
O	−59(6)	5096(3)	7450(1)	43(2)

* $U_{eq} = \frac{1}{3}(U_{11} + U_{22} + U_{33})$.

[2]Tables of anisotropic temperature factors, hydrogen atom positions, bond lengths and angles involving hydrogen atoms, torsional angles, the moduli of F_o and F_c, and mass spectral fragmentation patterns (21 pages) have been deposited and may be purchased from the Depository of Unpublished Data, CISTI, National Research Council of Canada, Ottawa, Ont., Canada K1A 0S2.

Can. J. Chem. Downloaded from www.nrcresearchpress.com by 80.58.250.72 on 09/07/12
For personal use only.

TABLE 3. Selected interatomic distances (Å) and angles (deg)

Bond	Distance A*	Distance B	Bond	Distance A	Distance B	Bond	Distance A	Distance B
S—C2	1.784(5)	1.816(5)	C2—N	1.514(6)	1.465(6)	N—C4	1.500(6)	1.467(6)
C4—C5	1.537(6)	1.555(6)	C5—S	1.828(5)	1.847(5)	C4—C1	1.536(7)	1.526(6)
C1—O1	1.223(6)	1.222(5)	C1—O2	1.272(6)	1.270(6)	C5—C51	1.537(7)	1.548(7)
C5—C52	1.542(5)	1.536(7)						
Hydrogen bonds								
N′...O	2.818(5)		N′...Cl	3.062(4)		N...O	2.886(5)	
N...Cl	3.291(4)		O...Cl	3.133(4)		O...O1	2.766(5)	
O2...O2′	2.450(5)							

Bonds	Angle A*	Angle B	Bonds	Angle A	Angle B	Bonds	Angle A	Angle B
C5—S—C2	92.4(2)	94.8(2)	S—C2—N	107.0(3)	104.9(3)	C2—N—C4	112.2(3)	109.7(3)
N—C4—C5	107.3(4)	106.9(3)	C4—C5—S	102.3(3)	103.5(3)	N—C4—C1	109.0(4)	110.7(4)
C5—C4—C1	115.2(4)	113.8(4)	C4—C1—O1	119.4(5)	119.0(4)	C4—C1—O2	112.5(4)	113.7(4)
O1—C1—O2	128.0(5)	127.2(5)	C4—C5—C51	111.1(4)	111.7(4)	C4—C5—C52	111.6(4)	112.2(4)
S—C5—C51	107.0(4)	110.6(3)	S—C5—C52	111.0(3)	108.0(4)	C51—C5—C52	113.2(5)	110.5(4)

*B and A represent molecules with and without prime affixes.

Results and discussion

The reaction of *N*-hydroxymethylacetamide with cysteine produces a derivative with the sulfur protected by the acetamidomethyl group (9). When, in this work, a similar reaction was attempted with D-penicillamine, instead of the *S*-protected product, a protonated dimer of 5,5-dimethylthiazolidine-4-carboxylic acid, held together by a very short hydrogen bond, was separated from the reaction mixture. According to Veber *et al.* (9), only under extremely anhydrous conditions (in anhydrous HF at 0°C) is the yield of thiazolidine-4-carboxylic acid minimized. In the acidic solution, the *N*-hydroxymethylacetamide reagent must have broken down to generate formaldehyde (and acetamide); the reaction of the formaldehyde, so generated, with D-penicillamine in the acid solution gave **I**.

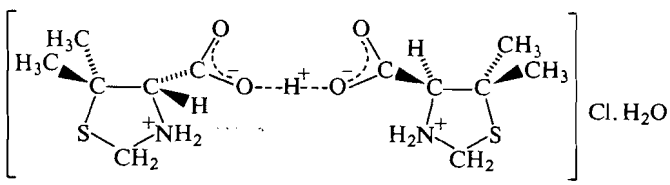

I

As expected, the dimer decomposes in aqueous (D_2O) solution and the ^1H nmr of the dimer is nearly identical to that of 5,5-dimethylthiazolidine-4-carboxylic acid prepared from formaldehyde (2), with a downfield shift of only 0.1 ppm for the C4-H peak at 3.95 ppm, presumably caused by a pH shift. Similar effects are seen in the carbon-13 spectrum where there is a downfield shift of 0.4 ppm of the C4 peak and a very small shift of the COOH carbon.

The hydrogen-bonded dimeric molecular cation is shown in Fig. 1. Each half of the cation is the hemi-protonated zwitterion form of (*S*)-5,5-dimethylthiazolidine-4-carboxylic acid. There are significant, but minor, differences in comparable bond

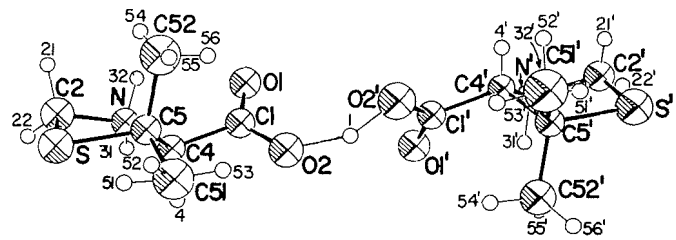

FIG. 1. The molecular cation bis((*S*)-5,5-dimethylthiazolidine-4-carboxylic acid)protium showing the atom numbering.

lengths and angles associated with the S—C2—N—C4 portion of the two rings, although others, particularly those in exocyclic fragments, do not differ significantly. The C5—S, C5′—S′ distances (1.828(5), 1.847(5) Å) are longer than the S—C2, S′—C2′ distances (1.784(5), 1.816(5) Å) presumably because of the greater repulsions of the methyl groups. In general, distances and angles are similar to those found in 2,2,5,5-tetramethylthiazolidine-4-carboxylic acid (1). Associated with the differences noted above there is a distinct difference in the conformation of the rings, as shown in Fig. 1. The unprimed ring has an envelope structure with C4 out of the plane, whereas the primed ring has a pseudo-C2, or $^4{}_3T$, structure. As can also be seen, the corresponding exocyclic torsional angles are very similar. N is nearly eclipsed with O1 and N′ with O1′, and these features have been invoked in the past as evidence of intramolecular hydrogen bonding (10). There is no evidence of this in the compound described here.

The two parts of the cation are joined by a very strong hydrogen bond (O2...O2′, 2.450(5) Å). This is in the range expected for symmetrical hydrogen bonds, although close to the upper limit. The hydrogen atom, H1, lies close to half-way between the two oxygen atoms O2 and O2′ but the errors in bond lengths and angles do not allow us to say with certainty that the bond is symmetric. The similarity of the C1—O1, C1—O2,

Can. J. Chem. Downloaded from www.nrcresearchpress.com by 80.58.250.72 on 09/07/12
For personal use only.

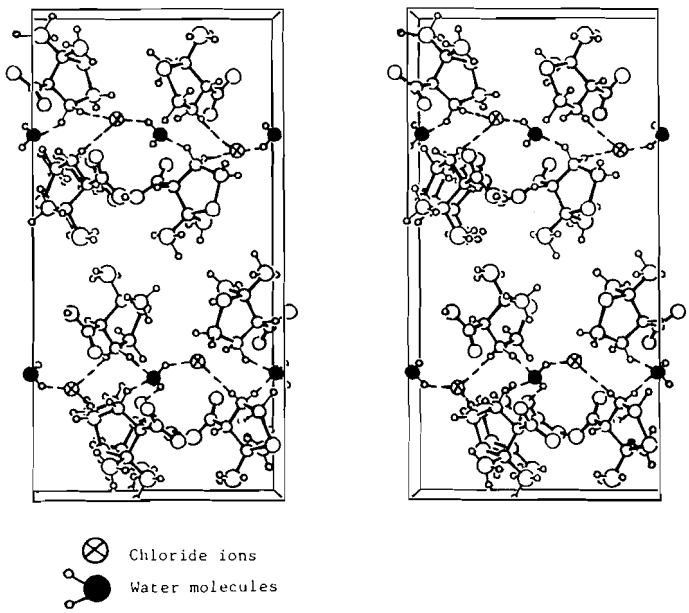

FIG. 2. The packing of the title compound in the unit cell. The hydrogen bonding network is shown by dotted lines. ***a*** and ***c*** are parallel to the bottom and sides of the page and the view is down ***b***.

and C1′—O1′ and C1′—O2′ distances, however, is consistent with a symmetric hydrogen bond. A similar strong (2.586(4) Å) but definitely asymmetric bond, found in (*R*)-2,2-dimethylthiazolidine-4-carboxylic acid caused considerable differences in the C—O lengths in the two carboxylate groups (11). The cation described here is one of the rare cases where the hydrogen atom in a very short hydrogen bond is not on, or disordered about, a crystallographic symmetry element, and thus the similarities in the two halves, noted above, are not artifacts of the space group.

The infrared and Raman spectral bands of **I** and its derivative obtained by D_2O exchange, **II**, are listed in Table 4. Many of the bands are assigned by comparison with the spectra determined recently for methyl-substituted thiazolidine-4-carboxylic acids (2) and for (*S*)2,2,5,5-tetramethylthiazolidine-4-carboxylic acid and its deuterated derivatives (1). A broad band at 3360 cm^{-1} (infrared) is typical of a weak hydrogen bond (O...O = 2.77 Å) and is assigned to hydrogen-bonded lattice water. The broad wing, 3100–2600 cm^{-1}, with multiple peaks on the low frequency side, is typical of these secondary amino acid compounds having zwitterion form (2), and includes absorption from ν_a and ν_s of the NH_2^+ group which is hydrogen bonded to the lattice water molecule, superimposed on the ν_a, ν_s bands of the CH_3, and CH_2 groups. The 2700–2300 cm^{-1} bands are combination bands. The NH...O bond lengths of 2.89 and 2.82 Å correlate with absorption frequencies of about 3100 cm^{-1} and new bands in **II** at 2240, 1990 cm^{-1} show H/D ratios of 1.36 and 1.42, which are reasonable for weak NH...O bonds (12). The carboxylate bands of the hemi-protonated groups are intermediate between those of carboxylate and carboxylic acid structures.

The most unusual feature of the spectra for **I** occurs in the infrared in the region below 1100 cm^{-1}; there is a very broad band, 1100–500 cm^{-1}, centred at ~800 cm^{-1}, with other peaks and windows superimposed on it. The general character of this band is not changed on D_2O exchange, but its maximum shifts to ~580 cm^{-1}. (νOH/νOD ratio = 1.38). This feature was not present in the 5,5-dimethylthiazolidine-4-carboxylic acid made with formaldehyde, nor indeed in any of our other substituted thiazolidines (2). We assign this band to antisymmetric stretching frequency (νOH) of the very strong hydrogen bond, O2...O2′ = 2.450(5) Å, linking the dimer through the carboxylate groups. We could not identify δ or γ for OHO(ODO), although this is expected to be one of the rare cases where ν is lower than both δ and γ (13). The Raman band at 302 cm^{-1}, which does not shift on deuteration, is assigned to the symmetric stretching frequency of this hydrogen bond; ν_s O...D...O is expected to have the same frequency as ν_s O...H...O because the proton (or deuteron) does not move in this mode.

In general, νOH frequencies are more difficult to assign for very strong O...H...O bonds than for weak or medium ones, because as the O...H...O distance becomes shorter, the OH band in the infrared spectrum becomes less prominent — lower in frequency, weaker in intensity, and ill-defined in shape. However, plots of νOH vs. O...O distance show good correlation for weak hydrogen bonds and a reasonably good one for strong hydrogen bonds. For a number of compounds containing strong hydrogen bonds, νOH is in the range 1800–700 cm^{-1}. In particular, the centred hydrogen bonds of acid salts of carboxylic acids have νOH below 1000 cm^{-1} (13). Thus there are precedents for our unusual assignment.

Moreover, our data for **I** and **II** show a parallel with data for sodium hydrogen diacetate and its deuterated derivatives, discussed by Novak (13) as an example of the special case of a symmetric, single-minimum potential for a short hydrogen bond. For that compound, the frequencies 720 (510), 1540 (1150), and 1285 (960) cm^{-1} were assigned to νOH (OD), δOH(OD), and γOH (OD) with H/D ratios of 1.41, 1.34, and 1.34, respectively. In addition, the ν_s O...H...O band was observed in the Raman spectrum at 320 cm^{-1}. (The ν_s O...D...O band was not mentioned, although it would be expected to have the same frequency, as we noted above.) The νOH/νOD isotopic ratio of 1.41 is much higher than that for strong O...H...O bonds of the double minimum type, and also higher than that for a free molecule (1.355). Thus deuterium substitution makes the O...O bond stronger, or at least does not weaken it, exactly as predicted for a single minimum potential (13).

The combination of the spectroscopic evidence with the crystallographic evidence, summarized above, indicates a very strong symmetric hydrogen bond. As we have noted, errors do not allow us to say that the bond is symmetric on the basis of the hydrogen atom position. We conclude that the title compound contains a strong single potential symmetric hydrogen bond which does not have crystallographic symmetry.

The packing within the unit cell is shown in Fig. 2. The dimeric cations lie roughly parallel to the [10$\bar{1}$] direction and are arranged in bilayers at $z = 1/4, 3/4$ with the halves of the bilayer at roughly $z = 1/8, 3/8$ and $z = 5/8, 7/8$. In the centre of the bilayers lie the chloride ions and the water molecules, and these are involved in an extensive and fairly strong hydrogen bonding network between both sides of the bilayer and in both the ***a*** and ***c*** directions. All the hydrogen atoms of the amine group are involved and there is one bond from the water molecule to O1. Between the bilayers, at roughly $z = 0, 1/2$, there are only van der Waals interactions involving methyl groups and sulfur atoms.

The mass spectra were measured of both the title compound and the corresponding partially deuterated species used for vibrational spectroscopy studies. The mass spectra are consis-

Can. J. Chem. Downloaded from www.nrcresearchpress.com by 80.58.250.72 on 09/07/12
For personal use only.

TABLE 4. Vibrational spectra of bis((*S*)-5,5-dimethylthiazolidine-4-carboxylic acid)protium chloride hydrate, **I**, and its derivative **II**, obtained by D_2O exchange

I		II		
Infrared[a]	Raman[b]	Infrared	Raman	Assignment[c]
3360, 70, 200		3300, 70, 200		OH···O bonding, weak, lattice water
3017, 95	3012, 40	3010, 95	3012, 40	maximum of wing (3100–2700) ν_a, ν_s NH_2^+ and NH···O bonding
	2992, 50		2992, 50	ν_a CH_3
	2980, 100		2980, 100	
2973, 100	2950, 40	2970, 100	2950, 40	ν_a CH_3, CH_2
	2940, 50		2940, 50	ν_s CH_3, CH_2
2920, 90	2910, 40		2910, 40	ν CH
	2868, sh		2868, sh	
2840, 80, br				NH···O bonding
	2735, 10		2735, 10	
2700, 80		2700, 60		
2605, sh		2600, sh		
2568, 80	2570, vw, br	2570, 68		Combination bands
2530, sh		2530, sh		
2490, 70		2490, 55		
2400, 45		2400, 15		
2320, 20		2320, 20		
		2240 2240 } 10, 100		ND···O bonding
		2040 1990 } 50, 120		ND···O bonding
		1860, w		
1727, 90 1692, 100 } 110		1730, sh 1692, 100 } 110		ν_a C=O
	1690, w, br		1690, br, w	ν_s C=O
1598, 40		1598, 18, w		δ NH_2^+
1454, 35	1468, 40	1454, 35	1468, 40	δ_a CH_3
	1440, 25		1438, 35	
1385, 45, shp	1395, 6	1383, 45, shp	1400, 6	δ_s CH_3, out-of-phase
1368, 50, shp	1372, w	1370, 48, shp		δ_s CH_3, in-phase
	1335, 10		1325, 5, br	
1305, 35, 60	1295, w	1305, 35, 60	1300, 5, br	ν C—O
1250, 20		1250, vw		τ NH_2^+
	1216, 6		1218, 15	
	1201, 20			
			1170, 20	δ ND_2^+, ρ = 1.37
1152, 20	1155, 15	1152, 5		$r$$NH_2^+$, + ν CCN, weaker D_2O
1125, 25	1130, 18	1125, 25	1130, 25	ν CCN
1030*	1040, 8	*	1020	* infrared, 1100–500 cm^{-1} v. broad band, max. intensity ~ 70 at 800 cm^{-1} in **I** and 580 cm^{-1} in **II**, other peaks superimposed; ν_a OH···O, OD···O strong hydrogen bond, O···O = 2.45 Å
1000	1005, 18			
	982, 15			
	951, 16 942, sh }		945	
	930, 15			
	918, w			
910			918 900	
	825, 12			
	808, 10			
	771, 20		770, 20	$r$$CH_3$, CH_2
765	760, 10	765	750, 25	
	738, 27		700, 20	
658	670, 15, br	658	660, 25, br	$r$$ND_2^+$
	612, 55 598, 40 } 35		605, 90 602, 95 } 15	ν C—S
*		580, br*		
	505, 22		500, 20	ν C—S
470, 20		470, 20		
	443, w		440, vw	
	385, 10		380, sh	

Can. J. Chem. Downloaded from www.nrcresearchpress.com by 80.58.250.72 on 09/07/12
For personal use only.

TABLE 4. (*Concluded*)

I		II		
Infrared[a]	Raman[b]	Infrared	Raman	Assignment[c]
373, s	369, 20	372, s	368, 30	δ CNC
337, m	337, 10	338, m	335, vw	δ $(CH_3)_2$ CS
320, m		320, m		δ CCS
306, m	305, 18, db	306, m	300, 15, br	ν_s O··H··O, O··D··O
296, m		296, m		
273, ms, br	275, w	272, ms, br	272, s	δ NCS
240, w		240, m		Stronger in **II**
	230, 18		222, 10	
207, s		207, s		δ CSC
	195, w			
189				
175				
168				
165				
	150, br, w		150, br, w	

[a]Infrared data ν, I, Δ: bands in cm^{-1}, intensity relative to strongest band = 100, half width at half maximum in cm^{-1}.
[b]Raman data ΔV, I, Δ: Raman shift in cm^{-1}, intensity relative to strongest band = 100, half width at half maximum in cm^{-1}.
[c]ν = stretch, a = antisymmetric, s = symmetric, δ = deformation, τ = twist, r = rock, ρ = isotopic ratio H/D.
Notations: s = strong, m = medium, w = weak, br = broad, v = very, sh = shoulder, shp = sharp.

tent with deuteration of the exchangeable hydrogen atoms of the cation to 30–40%. Major peaks were observed in the mass spectrum at M/z = 161, 128, 116, 114, 100, 87, 82, 75, 69. The peak at 161 is caused by the 5,5-dimethylthiazolidine-4-carboxylic acid moiety, which is half the protonated cation. The peak at M/z = 128 is caused by loss of H_2O + CH_3, and that at M/z = 116 by loss of —CO_2H.

Practically all the other peaks can be explained by 1,4 or 2,5 cleavages, which are established pathways for thiazolidine fragmentation (1, 14). The small peak at M/z = 100 is caused by loss of N from the M/z = 114 fragment. Further loss of H_2O gives a peak at 82. No change in the 82:83 ratio is seen in the deuterated compound, confirming the fragment contains no NH(D) or OH(D) groups. Peaks at M/z = 87 and 75 correspond to the primary fragments of the 2,5 cleavage, although the $(CH_3)_2{}^+C$—SH has acquired a hydrogen atom by transfer. The peak at M/z = 69 is derived from M/z = 87 by loss of H_2O.

Acknowledgements

We acknowledge, with thanks, financial support of this work from the Natural Sciences and Engineering Research Council of Canada, the Medical Research Council of Canada, Atomic Energy of Canada Ltd., and McMaster University Science and Engineering Research Board.

1. H. E. HOWARD-LOCK, C. J. L. LOCK, and P. S. SMALLEY. Can. J. Chem. **63**, 2411 (1985).
2. H. E. HOWARD-LOCK, C. J. L. LOCK, M. L. MARTINS, P. S. SMALLEY, and R. A. BELL. Can. J. Chem. **64**, 1215 (1986).
3. M. CATTI and G. FERRARIS. Acta Crystallogr. **832**, 2754 (1976).
4. B. LIPPERT, C. J. L. LOCK, B. ROSENBERG, and M. ZVAGULIS. Inorg. Chem. **16**, 1525 (1977).
5. R. P. HUGHES, N. KRISHNAMACHARI, C. J. L. LOCK, J. POWELL, and G. TURNER. Inorg. Chem. **16**, 314 (1977).
6. G. M. SHELDRICK. Program for crystal structure solution and refinement. Cambridge University, England. 1976.
7. D. T. CROMER and J. T. WABER. *In* International tables for X-ray crystallography. Vol. IV. *Edited by* J. A. Ibers and W. C. Hamilton. Kynoch Press, Birmingham, England. 1974. Table 2.2B, 99.
8. D. T. CROMER. *In* International tables for X-ray crystallography. Vol. IV. *Edited by* J. A. Ibers and W. C. Hamilton. Tables 2.3.1, pp. 149, 150.
9. D. F. VEBER, J. D. MILKOWSKI, S. L. VARGA, R. G. DENKEWLATER, and R. HIRSCHMANN. J. Am. Chem. Soc. **94**, 5456 (1972).
10. J. LOSCALZO, R. G. KALLEN, and D. VOET. Arch. Biochem. Biophys. **157**, 426 (1973).
11. R. FAGGIANI, H. E. HOWARD-LOCK, C. J. L. LOCK, and M. L. MARTINS. To be published.
12. W. C. HAMILTON and J. A. IBERS. Hydrogen bonding in solids. W. A. Benjamin, Inc., New York, NY. 1968.
13. A. NOVAK. Struct. Bonding, **18**, 177 (1974).
14. M. M. VESTLING and R. L. OGREN. J. Heterocycl. Chem. **12**, 243 (1975).

Can. J. Chem. Downloaded from www.nrcresearchpress.com by 80.58.250.72 on 09/07/12
For personal use only.

Extraction and transport of alkali metal salts by crown ethers and cryptands: estimation of extraction constants and their relationship to transport flux

THOMAS MURRAY FYLES
Department of Chemistry, University of Victoria, Victoria, B.C., Canada V8W 2Y2

Received August 27, 1986

THOMAS MURRAY FYLES. Can. J. Chem. **65**, 884 (1987).

A method is described for the estimation of two phase extraction constants from stability constants for complexation of alkali metal cations by crown ethers and cryptands. The total free energy change for extraction of alkali metal salts from water to a non-polar organic solvent is evaluated as a sum of free energy terms for complexation, transfers of cation, anion, and complex between solvents, and ion pairing in the non-polar solvent. The method gives satisfactory agreement with a variety of published extraction constants and can be used predictively. As an example, the influence of extraction constant on transport flux was examined using calculated extraction constants and the rate data of Lamb *et al.* (J. Am. Chem. Soc. **102**, 6820 (1980)); rates are adequately modelled by a simple analysis of diffusion.

THOMAS MURRAY FYLES. Can. J. Chem. **65**, 884 (1987).

On décrit une méthode permettant d'évaluer constantes d'extraction à partir des constantes de stabilité des complexations des cations des métaux alcalins par des éthers couronnes et par des cryptands. On évalue le changement total d'énergie libre pour l'extraction des cations des métaux alcalins de l'eau vers un solvant organique non-polaire en faisant la somme des termes d'énergie libre pour la complexation, pour les transferts de cation, d'anion et de complexe entre les solvants et pour l'arrangement par paire des ions dans le solvant non-polaire. La méthode donne un bon accord avec un grand nombre de constantes d'extraction publiées et on peut l'utiliser pour faire des prédictions. Par exemple, utilisant les constantes d'extraction calculées et les vitesses rapportées par Lamb et ses collaborateurs (J. Am. Chem. Soc. **102**, 6820 (1980)), on a évalué l'influence de la constante d'extraction sur le taux de transport; on peut faire un modèle adéquat des vitesses en faisant à une analyse simple de diffusion.
[Traduit par la revue]

The transport of cations across artificial membranes using synthetic ionophores such as crown ethers or cryptands has received considerable attention over the past decade (1, 2). The focus of such studies varies from the assessment of the complexation selectivity of new ligands to the development of specific separation processes (1–3). The actual mechanism of the transport has received somewhat less attention but it is widely assumed that the transport is controlled by diffusion processes in the unstirred boundary layers adjacent to the organic/water interfaces. A recent report summarized the predictions of a simple diffusion model and concluded that the narrow range of reported rates was consistent with a diffusion mechanism (4). Our interest in this area has centred on crown ether carboxylic acids which can exhibit cation–proton counter-transport across artificial membranes (5, 6). This system has been examined in detail and it is clear that under the usual conditions of stirring the transport is *not* controlled by diffusion (5–7). We have identified the rate-limiting processes as adsorption and desorption of the carrier at the interface and have shown, as one consequence, how the transport selectivity depends on the interfacial surface charge (8).

In search of other systems which might be controlled by interfacial processes, we set out to compare the literature data with the predictions of the simple diffusion model (4). This search is immediately hampered by the paucity of data on two phase extraction constants. The use of extractions, particularly of metal picrates, to assess cation binding and selectivity has a long tradition in crown ether chemistry (9–11). However, such tests are often used qualitatively (% extraction) and, moreover, the extraction "constant" can depend on the experimental conditions (10, 12, 13). Whatever its value, the extraction constant (K_{ex}) plays a central role in artificial membrane transport. For a diffusion limited process, the rate should increase with K_{ex}, reach a maximum at a critical value of K_{ex} ($= K_{ex}(\max)$) and then *decrease* as K_{ex} increases further (4). The value of K_{ex} for optimal transport depends on the system examined (co- or counter-transport) and upon experimental conditions (initial concentrations, extent of transport). The selectivity of transport depends on the relationship of the extraction constants of the two substrates to $K_{ex}(\max)$, hence the "selectivity" is also a function of experimental conditions (4).

The phenomenon of maximum transport flux at a critical value of K_{ex} has been only rarely demonstrated (14, 15). More typically, transport flux is noted to be maximal at a critical value of *stability constant for complexation* in homogeneous solution (K_s) (1, 16, 17). These are not the same, if only for the trivial reason that the units of K_{ex} and K_s differ (M^{-2} vs. M^{-1} for 1:1 electrolytes). The oft quoted maxim of maximal transport rate at $\log K_s \sim 5$–6 (methanol) is more indicative of a restricted range of initial conditions than of a fundamental relationship (4). Nevertheless, there does appear to be some roughly linear relationship between K_{ex} and K_s. If the form of this relationship were known precisely, then the large compilations of data on K_s for a diverse assortment of ligands (18) would provide an equally large and diverse compilation of K_{ex} values. Direct experimental values would still be lacking but the survey problem discussed above would be greatly simplified.

Significantly, this problem of the relationship between K_{ex} and K_s, arose within the context of the report of Lamb *et al.* (17), on the relationship betwen K_s and transport rate. In their kinetic analysis, they incorporate additional diffusion distances at the organic/water interfaces for diffusion of uncomplexed ion pairs (1, 17). These distances are equivalent to the "relaxation" distances of Friedlander and Keller (19), which may be shown to be the formal equivalent of slow interfacial processes (20). These "relaxation" distances are essential to the kinetic model described by Lamb and co-workers (1, 17) and vary depending on the cation considered. Is this therefore another example of transport controlled by an interfacial process? Or are these relaxation distances merely adjustable parameters which render K_{ex} a linear function of K_s?

Can. J. Chem. Downloaded from www.nrcresearchpress.com by 78.46.186.204 on 09/07/12
For personal use only.

Can. J. Chem. Downloaded from www.nrcresearchpress.com by 78.46.186.204 on 09/07/12
For personal use only.

We approach this problem in a stepwise fashion. We first examine the relationship of K_s in a reference solvent to K_{ex} for extraction between water and a non-polar organic solvent. The free energy changes of the constituent equilibria are evaluated using a simple model of ionic solvation (21, 22) and an equally simple model of ion pairing (23). This permits the calculation of K_{ex} from a knowledge of K_s in the reference solvent. Having compared calculated with experimental values of K_{ex} in a number of cases, we calculate the values required for the transport system of Lamb *et al.* (17). These values, with the experimental transport fluxes, can then be directly compared with a simple diffusion model (4) and with the more complex model including relaxation distances (1, 17).

Results and discussion

The two equilibria we wish to relate are

[1] $L_s + M_s^+ \rightleftharpoons LM_s^+$

and

[2] $\overline{L} + M_w^+ + X_w^- \rightleftharpoons \overline{LMX}$

Reaction [1] defines K_s, the association constant for complex formation between a ligand L (crown ether, cryptand) and a cation M^+ (alkali metal) in some solvent (subscript s, reference solvent). This discussion is restricted to 1:1 electrolytes since many of the subsequent terms discussed are only valid for univalent ions; in principal further generalization is possible. The reference solvent will usually be methanol as the majority of ligands have reported values of K_s in this solvent (18). Reaction [2] defines the extraction constant K_{ex} where the cation M^+ and the anion X^- are in the aqueous phase (subscript w) and the ligand L and complex LMX are in the organic phase (overlined). Typically, the organic phase has a low dielectric constant (CH_2Cl_2, $CHCl_3$, benzene) so electrostatic ion pairing is assumed to occur to a large extent (13).

In order to relate [1] and [2], the following additional processes must be considered. We start from methanol as the reference solvent, reaction [3] below:

[3] $L_m + M_m^+ \rightleftharpoons LM_m^+ \qquad K_m$

(*i*) The cation must be transferred from methanol to water [4]

[4] $M_w^+ \rightleftharpoons M_m^+ \qquad K_{tr}^+$

(*ii*) The anion must be transferred from water to the organic solvent [5]

[5] $X_w^- \rightleftharpoons \overline{X^-} \qquad K_{tr}^-$

(*iii*) The ligand L and the complex LM^+ must be transferred between methanol and the organic solvent. As written, reaction [6] is not an elementary process but results in convenient cancellations (below).

[6] $LM_m^+ + \overline{L} \rightleftharpoons \overline{LM^+} + L_m \qquad K_{tr}^{cplx}$

(*iv*) The complex and anion must associate in the organic solvent [7].

[7] $\overline{LM^+} + \overline{X^-} \rightleftharpoons \overline{LMX} \qquad K_{ip}$

Summation of [3]–[7] produces [2]. In terms of evaluation of K_{ex} it is somewhat more convenient to deal with the corresponding free energy changes. The two forms are given as [8] and [9]

[8] $K_{ex} = K_m \times K_{tr}^+ \times K_{tr}^- \times K_{tr}^{cplx} \times K_{ip}$

or

[9] $\Delta G_{ex} = \Delta G_{cplx} + \Delta G_{tr}^+ + \Delta G_{tr}^- + \Delta G_{tr}^{cplx} + \Delta G_{ip}$

The first term, ΔG_{cplx} is available from the experimental values of $\log K_m$ (or in general $\log K_s$) (18). The second term, ΔG_{tr}^+, the free energy of transfer of the cation from water to methanol (or in general the solvent s), is also available from "experiment". The single ion value chosen requires an extra thermodynamic assumption, hence the numerical value will vary somewhat, depending on the nature of the assumption (21, 22, 24, 25). For consistency, we utilize the values of Abraham and Liszi (21, 22) (see Appendix I).

The free energy of transfer of the anion from water to the non-polar solvent, ΔG_{tr}^-, is calculated by the method of Abraham and Liszi (21, 22). The solvation energy of an ion is divided into an electrostatic term (ΔG_{el}) and a neutral term (ΔG_n). The free energy of transfer of the ion from water to the organic solvent is thus

[10] $\Delta G_{tr} = \Delta G_{el} + \Delta G_n - \Delta G_h^0$

where ΔG_h^0 is the hydration free energy of the ion. The ion, of radius a, is assumed to be covered with a first layer of solvent molecules to a radius b where $b - a$ is the radius of the solvent as calculated from the molar volume. The dielectric constant of the first layer is taken to be ϵ_1. This solvated ion is then immersed in the bulk solvent with the bulk dielectric constant ϵ_0. Thus, ΔG_{el} is given by [11]

[11] $$\Delta G_{el} = \frac{z^2}{2}\left[\left(\frac{1}{\epsilon} - 1\right)\left(\frac{1}{a} - \frac{1}{b}\right) + \left(\frac{1}{\epsilon_0} - 1\right)\frac{1}{b}\right]$$

where z is the ionic charge. For univalent ions, the radii a and b in Å and $\epsilon_1 = 2$ (21, 22) [11] gives [12] in kcal mol^{-1}.

[12] $$\Delta G_{el} = 166.2\left[\left(\frac{1}{\epsilon_0} - 1\right)\frac{1}{b} - \frac{1}{2}\left(\frac{1}{a} - \frac{1}{b}\right)\right]$$

The neutral term ΔG_n, is evaluated using [13]

[13] $\Delta G_n = ma + c$

where m and c are empirical solvent parameters derived from solvation energies of neutrals (21, 22). Values of the various parameters utilized are given in Appendix I and are those of Abraham and Liszi (21, 22). The ΔG_{tr}^- term can thus be evaluated from [10]. An additional correction for change of standard state from unit mole fraction $\Delta G_{tr}(\chi)$ to unit molar concentration $\Delta G_{tr}([\,])$ is required. Thus

[14] $$\Delta G_{tr}(\chi) - \Delta G_{tr}([\,]) = -RT \ln\left(\frac{M_1\rho_2}{M_2\rho_1}\right)$$

for a transfer from a solvent having molecular weight M_1 and density ρ_1 to a solvent having molecular weight M_2 and density ρ_2 (21, 25).

To evaluate the term ΔG_{tr}^{cplx}, the free energy change of equation [6], we proceed in the spirit of the Abraham and Liszi model. To a first approximation the ligand acts as the first solvation layer of the cation which remains approximately constant from solvent to solvent. The solvation energy of the complex ion is again composed of an electrostatic and a neutral term. If L and LM^+ are the same shape and size, then $\Delta G_n(LM^+) \sim \Delta G_n(L)$ in each solvent and in the summation will cancel. Of course, $\Delta G_{el}(L) = 0$ thus to this first approximation,

[15] $\Delta G_{tr}^{cplx}(S_1 \rightarrow S_2) = \Delta G_{el}^{cplx}(S_2) - \Delta G_{el}^{cplx}(S_1)$

Can. J. Chem. Downloaded from www.nrcresearchpress.com by 78.46.186.204 on 09/07/12
For personal use only.

If the ligand is indeed the first solvation layer, ΔG_{el}^{cplx} will be given by [11] where b is the radius of the complex and ϵ_1 is the ligand dielectric constant. The actual value chosen for ϵ_1 is immaterial since [15] will result in cancellation of terms including ϵ_1. The complex radius, b, is potentially a more complex problem. Crystal structures are available for all the ligands considered in the subsequent comparisons, but we ignore this flurry of precise detail in favour of an approximate method proposed by Lehn (26). The approximate method has the advantage that it can be used for any ligand, whether crystalline or not, and gives an average value of the ligand thickness. Indeed averaging of some sort would be required from crystallographic data as most ligands have regions of different thickness. The method assumes that the ligand volume covers the cation in a spherical shell. The ligand volume (V_L) is derived as the sum of contributions for the volumes of various atoms and subgroups (V_w) in the ligand i.e. [16]

$$[16] \quad V_L = \sum^{n} V_w$$

where $V_w = 11.0$ Å^3 for O, $= 14.0$ Å^3 for N, $= 33.5$ Å^3 for CH_2 or CH_3, $= 125$ Å^3 for a benzene ring (26).

Thus, by simple geometry, the complex radius b is

$$[17] \quad b = \left(a^3 + \frac{3V_L}{4\pi}\right)^{1/3}$$

where a is the cation radius as used in [11]–[13].

This approximate method has both strengths and weaknesses. It is clearly a poorer picture for crown ethers than for cryptands and even cryptands do not completely cover the cation in a uniform spherical fashion. However, the method is simple, predictive and consistent with our view of the ligand as the first solvation sphere. Also the method gives a rough estimate, not readily available from crystal data, of the approximate size of an assembly of ligand, cation and the odd solvent molecule which fills the cracks in the first solvation shell. Clearly, we need only include those parts of the ligand adjacent to the binding site. Providing that a judicious choice of the parts of the ligand can be made, V_L may be calculated by [16] to give b via [17]. Equation [12] then gives ΔG_{el}^{cplx} for any solvent and the required term ΔG_{tr}^{cplx} can be calculated from [15], with the correction of [14] being applied here as well.

Turning finally to the ion pairing term ΔG_{ip}, we again begin from the assumption that the ligand covers the cation to produce a spherical ion of radius b as given by [17]. The association constant for electrostatic ion pairing with a spherical anion of radius c is then given by [18] (27).

$$[18] \quad K_{ip} = \frac{4\pi N d^3}{3000} \exp\left(\frac{e^2}{d\epsilon kT}\right)$$

where $d = b + c$, N is Avogadro's number, e is the electronic charge, ϵ the solvent dielectric constant, k is Boltzmann's constant, and T is the temperature. At 25°C and d in Å, K_{ip} is given by [19].

$$[19] \quad K_{ip} = 2.524 \times 10^{-3}\, d^3 \exp(560/\epsilon d)$$

to give

$$\Delta G_{ip} = -RT \ln K_{ip}$$

The assumptions made above will be most acceptable for cations which are well buried in the ligand, for non-coordinating anions such as picrate, perchlorate, or nitrate and for solvents with a sufficiently high dielectric constant so that ΔG_{ip} does not vastly outstrip the other terms in eq. [9]. Conversely, these assumptions will be less acceptable in a large number of real cases: large cations in small crown ethers and low dielectric solvents such as benzene. Additional corrections to [18] and [19] will thus be required. We can compare ΔG_{ip} for the "real" ligand with two other values: ΔG_{ip}^{ion} for the "naked" cation in the same solvent and ΔG_{ip}^{cplx} for a hypothetical complex in which the ligand completely covers the cation. The "real" value must lie between these two extremes as the real ligand is neither perfect, nor is the cation completely exposed to the anion. Real ligands therefore differ from ideal ligands to the extent to which they fail to provide complete coverage.

Consider a nearly ideal pair: cryptand 2.2.2/K^+. The ligand volume, V_L, is 700 Å^3 ([16]) with a ligand thickness ($b - a$) of 4.2 Å. A less ideal pair is 18-crown-6/K^+ with $V_L = 470$ Å^3 or only 67% (470/700) of the K^+ covered to a 4.2 Å depth. Viewed another way, the ΔG_{ip} of 18-crown-6/K^+ is about one third of the way from the ΔG_{ip}^{cplx} of a covered ion (at 4.2 Å thickness) to the ΔG_{ip}^{ion} of the naked cation. This then defines the approach to estimating ΔG_{ip} for cases where the simpler assumption becomes untenable.

Coverage of each cation with a 4.2 Å thick layer defines an optimum ligand volume for each cation

$$[20] \quad V_{opt} = \frac{4\pi}{3}\left(a + 4.2\right)^3$$

The value of ΔG_{ip} is then given by [21]

$$[21] \quad \Delta G_{ip} = \Delta G_{ip}^{cplx} + \left(1 - \frac{V_L}{V_{opt}}\right)\left(\Delta G_{ip}^{ion} - \Delta G_{ip}^{cplx}\right)$$

where ΔG_{ip}^{cplx} is given using [19] with $d = b + c$ and ΔG_{ip}^{ion} is given using [19] where $d = a + c$. The term V_L/V_{opt} can of course exceed 1; in these cases the ligand is assumed to be perfect and $\Delta G_{ip} = \Delta G_{ip}^{cplx}$.

There are thus two ways to estimate ΔG_{ip}. The first assumes a perfect, spherical ligand and [21] is ignored. This will be appropriate for solvents with $\epsilon > 4$ and picrate, perchlorate, and nitrate as counteranions. The second approach uses [21] and will be appropriate for solvents with $\epsilon < 4$ and coordinating anions. Examples of both approaches are given.

A referee has pointed out the inconsistency between the use of a one-layer model of solvation (eqs. [10]–[13]) with a contact model of ion pairing; should not the solvent layer around the anion be included as additional distance in the calculation of ΔG_{ip}? In principle, contributions from such solvent separated ion pairs should indeed be included. In addition, their importance will increase as the solvent dielectric constant increases. As discussed in the next section, the effect of this correction is minor (0.6 kcal) for the most polar of the solvents considered (CH_2Cl_2, $\epsilon = 8.93$). In view of the other adjustments to be made in the calculation of ΔG_{ip}, this particular correction is ignored.

Comparison of calculated and experimental values

The reliability of the methods outlined above can be readily seen by inspection of Tables 1 and 2. Table 1 unites data for extractions of metal picrates into CH_2Cl_2 and $CHCl_3$ with crown ethers and cryptands (12, 28, 29, 38) while Table 2 does the same for extractions into benzene and hexane (13, 29). In the former case the corrections of [21] are ignored. The results are quite satisfactory with an average value of ΔG_{ex}(calc) − ΔG_{ex}(expt) $= -0.28$ kcal/mol($\bar{x}$) and a standard deviation of $\sigma = 1.35$ kcal/mol. This corresponds to an average value of log K_{ex}(calc) − log K_{ex}(expt) of $\bar{x} = +0.21$ and $\sigma = -1.0$, i.e., K_{ex} is estimated to within an order of magnitude with a

TABLE 1. Sample calculations of ΔG_{ex} and comparison with experimental values[a]

Ligand	Salt	ΔG_{cplx}	ΔG_{tr}^{+}	ΔG_{tr}^{-}	ΔG_{tr}^{cplx}	ΔG_{ip}	ΔG_{ex}(calc)	ΔG_{ex}(expt)	δ[b]
DB18C6	NaPic	−5.9	−1.1	4.2	6.3	−8.9	−5.4	−4.1[c]	−1.3
DB18C6	KPic	−6.9	−1.4	4.2	6.3	−8.9	−6.7	−8.2[c]	1.5
DB18C6	KPic	−6.9	−1.4	0.6	2.8	−4.8	−9.7	−9.3[d]	−0.4
DB18C6[e]	NaPic	−5.7	−1.1	0.6	2.7	−4.6	−8.1	−5.7[d]	−2.4
DB18C6[e]	KPic	−8.1	−1.4	0.6	2.7	−4.6	−10.8	−8.6[d]	−2.2
DB18C6[f]	KPic	−8.2	−1.4	0.6	2.7	−4.6	−10.9	−9.0[d]	−1.9
DB18C6[g]	KPic	−7.3	−1.4	0.6	2.7	−4.6	−10.0	−8.2[d]	−1.8
2.2.NMe	NaPic	−5.0	−1.1	4.2	6.3	−8.9	−4.5	−6.9[h]	2.4
2.2.NMe	KPic	−7.2	−1.4	4.2	6.3	−8.9	−7.0	−7.4[h]	0.4
18.6	NaPic	−5.9	−1.1	4.2	6.5	−9.1	−5.4	−4.7[i]	−0.7
18.6	KPic	−8.3	−1.4	4.2	6.5	−9.1	−8.1	−8.3[i]	0.2
18.6	RbPic	−7.3	−1.5	4.2	6.5	−9.1	−7.2	−7.7[i]	0.5
18.6	CsPic	−6.4	−1.3	4.2	6.5	−9.1	−6.1	−6.3[i]	0.2
2.2.1	KPic	−11.6	−1.4	4.2	6.0	−8.9	−11.7	−10.9[c]	−0.8
2.2.2	KPic	−14.6	−1.4	4.2	5.8	−8.6	−14.6	−14.3[c]	−0.3
2.2.2	CsPic	−6.0	−1.3	4.2	5.8	−8.6	−5.9	−5.8[c]	−0.1
2.2.C_8	NaPic	−4.8	−1.1	4.2	5.7	−8.5	−4.5	−5.0[c]	0.5
2.2.C_8	KPic	−7.1	−1.4	4.2	5.7	−8.5	−7.1	−7.5[c]	0.4
2.2.C_8	CsPic	−3.7	−1.3	4.2	5.7	−8.5	−3.6	−3.1[c]	−0.5
3.2.2	KPic	−9.5	−1.4	4.2	5.6	−8.4	−9.5	−10.1[c]	0.6

[a]In kcal/mol for extractions at 25°C from water into CH_2Cl_2 or $CHCl_3$ as noted in footnotes *c*, *d*, and *h*.
[b]$\delta = \Delta G_{ex}(\text{calc}) - \Delta G_{ex}(\text{expt})$.
[c]$CHCl_3/H_2O$, data of ref. 28.
[d]CH_2Cl_2/H_2O, data of ref. 10.
[e]"Mixed isomers".
[f]*cis–syn–cis* isomer.
[g]*cis–anti–cis* isomer.
[h]$CHCl_3/H_2O$, data of ref. 12.
[i]CH_2Cl_2/H_2O, data of ref. 38.

TABLE 2. Comparison of calculated and experimental values of ΔG_{ex}[a]

Ligand	Salt	Expt ΔG_{ex}	Calc. using [19] ΔG_{ex}	δ[b]	Calc. using [21] ΔG_{ip}	δ[b]
15C5	NaPic	−5.3	0.6	5.9	−5.1	0.2
15C5	KPic	−3.5	0.2	3.7	−5.6	−2.1
15C5	CsPic	−2.6	1.3	3.9	−4.5	−1.9
B15C5	NaPic	−4.5	1.1	5.6	−3.8	0.7
B15C5	KPic	−2.6	0.9	3.5	−4.3	−1.7
B15C5	CsPic	−1.5	2.1	3.6	−3.3	−1.8
18C6	NaPic	−4.6	−1.1	3.5	−4.9	−0.3
18C6	KPic	−8.1	−3.8	4.3	−8.5	−0.4
18C6	RbPic	−7.4	−2.9	4.5	−7.7	−0.3
18C6	CsPic	−5.9	−1.8	4.1	−6.9	−1.0
DB18C6	NaPic	−2.9	−1.2	1.7	−2.4	0.5
DB18C6	KPic	−6.2	−2.4	3.8	−5.3	0.9
DB18C6[c]	KPic[c]	−4.9[c]	−2.5	2.4	−6.0	−1.1
DB18C6	RbPic	−5.2	−1.5	3.7	−4.8	0.4
DB18C6	CsPic	−4.1	−0.3	3.8	−4.3	−0.2

[a]In kcal/mol for extractions into benzene at 25°C unless otherwise noted. Data of ref. 13.
[b]$\delta = \Delta G_{ex}(\text{calc}) - \Delta G(\text{expt})$.
[c]Hexane–water. Data of ref. 10.

slight tendency to over estimate. Not unexpectedly the cryptands have a smaller average displacement ($\bar{x} = -0.03$ kcal/mol) and standard deviation ($\sigma = 0.54$ kcal/mol) than do the crown ethers ($\bar{x} = -0.42$ kcal/mol, $\sigma = 1.62$ kcal/mol). Inclusion of corrections to ΔG_{ip} via [21] results in a minor shift of the average difference (to $\bar{x} = -0.54$ kcal/mol) but does not alter the standard deviation. This is a result of two effects: (*i*) $V_L \sim V_{opt}$ for many of the ligands on Table 1 and (*ii*) $\Delta G_{ip}^{ion} - \Delta G_{ip}^{cplx}$ is small (2–5 kcal). As a result, the corrections to ΔG_{ip} are modest.

In contrast the results in Table 2 clearly show that some correction to ΔG_{ip} via [21] is required. Ignoring [21] gives an average difference $\Delta G_{ex}(\text{calc}) - \Delta G_{ex}(\text{expt})$ of $\bar{x} = 3.8$ kcal/mol ($\sigma = 1.04$ kcal/mol). Including [21] gives $\bar{x} = -0.54$ kcal/mol ($\sigma = 1.00$ kcal/mol). The solvents of Table 2 were chosen to ensure very strong ion pairing effects (13) and the ligands in general are less bulky than those of Table 1. In addition $\Delta G_{ip}^{ion} - \Delta G_{ip}^{cplx}$ is large (~20 kcal/mol). The net result is corrections to ΔG_{ip} of 2–5 kcal/mol for the cases in Table 2. This is sufficient to shift $\bar{x}$ to a value similar to that of Table 1 while preserving the relatively narrow standard deviation.

On the basis of these results, it is reasonable to assume that the method as described in the preceding section can be used to predict K_{ex} to within an order of magnitude from stability constants in methanol. But *caution is essential* as can be readily demonstrated in several ways. Consider first the choice of the reference solvent. Methanol is convenient choice but in principle any solvent could serve and equations [3] to [7] should apply equally well. An exhaustive comparison for a variety of solvents of all the cases of Tables 1 and 2 is not essential; the results in Table 3 are sufficient to show that other reference solvents produce a divergent set of results even for three well behaved cases. Of the six reference solvents, only methanol gives acceptable results. All other reference solvents show systematic errors and increased scatter from the experimental values. This may be due to a variety of factors: (*i*) the method of Abraham and Liszi gives poorer estimates of ionic solvation energies for DMF and DMSO than for the other solvents (21).

Can. J. Chem. Downloaded from www.nrcresearchpress.com by 78.46.186.204 on 09/07/12
For personal use only.

TABLE 3. Comparison of experimental and calculated values of ΔG_{ex} for difference "reference" solvents[a]

Reference solvent ΔG_{ex}(calc)	Ligand/salt 2.2.1 KPic	2.2.2 KPic	2.2.2 CsPic
H_2O	−2.3	−5.1	−0.3
MeOH	−11.7	−14.6	−5.9
PC	−12.4	−14.2	−4.7
DMF	−9.6	−11.4	−3.4
DMSO	−7.1	−8.9	−1.2
AN	−15.2	−17.9	−7.9
ΔG_{ex}(expt)	−10.9	−14.3	−5.8

[a]In kcal/mol at 25°C for extractions between $CHCl_3$ and H_2O. Experimental data of ref. 28.

As a result ΔG_{tr}^{cplx} will be more greatly in error in these cases. (*ii*) The entire set depends on the values of ΔG_{tr}^{+} utilized and the final values shift dramatically when values from different single ion scales are employed (21, 24, 25). (*iii*) The experimental values of stability constants may be more reliable in some solvents than in others. Systematic errors would only show in an inter-solvent comparison of this type. Whatever the reason, it is clear that the method outlined above may involve some convenient error cancellations for methanol which do not occur for other reference solvents.

The nature of these fortuitous cancellations can be partially uncovered by comparison of calculated and experimental values of ΔG_{ip} and ΔG_{tr}^{cplx}. Unfortunately, no completely comparable set of values is available from experiment so the two will have to be examined independently. Experimental values of ΔG_{ip} can be calculated from the data of Frensdorff for the extraction of Na^+ and K^+ picrates into CH_2Cl_2 (29). These values are 1.5–2.5 kcal more negative than those calculated by [21]. This might indicate acceptable agreement were it not for the fact that these cases already estimate ΔG_{ex} to be too negative by ca. 2 kcal/mol. Had experimental, rather than calculated values of ΔG_{ip} been used, the calculated value of ΔG_{ex} would have been ca. 4 kcal/mol more negative than the experimental value. Since ΔG_{ip} is too negative, this may be due to overestimating the importance of contact ion pairs compared to solvent separated ion pairs. As noted previously, the solvent layer around the anion should strictly be included in the calculation. This can only be part of the problem however as this correction amounts to only 0.3 and 0.6 kcal for the case of Na^+ and K^+ picrates in CH_2Cl_2 (29). Clearly the simple contact model, even including solvent, is inadequate.

Experimental values of ΔG_{tr}^{cplx} can be calculated for pairs of solvents from the stability constants for complexation in the two solvents and the ΔG_{tr}^{+} term for the cation complexed. Consider [22]–[25].

$$[22] \quad L(S_1) + M^+(S_1) \rightleftharpoons LM^+(S_1)$$

$$[23] \quad LM^+(S_2) \rightleftharpoons L(S_2) + M^+(S_2)$$

$$[24] \quad M^+(S_2) \rightleftharpoons M^+(S_1)$$

$$[25] \quad L(S_1) + LM^+(S_2) \rightleftharpoons LM^+(S_1) + L(S_2)$$

Reaction [22] and the reverse of [23] define the stability constants for complexation of M^+ by L in solvents S_1 and S_2. The summation of [22] and [23] with the transfer equilibrium [24] gives [25] which is identical to [6] where S_1 is the overline (organic) solvent.

Thus,

$$[26] \quad \Delta G_{tr}^{cplx} = \Delta G_{cplx}(S_1) - \Delta G_{cplx}(S_2) + \Delta G_{tr}^{-}(S_2 \rightarrow S_1)$$

The required transfer term ΔG_{tr}^{+} ($S_2 \rightarrow S_1$) can be evaluated from a cycle involving transfers to and from water hence "experimental" values of ΔG_{tr}^{cplx} can be determined from [26] (and corrected as previously using [14]). These "experimental" values depend on the single ion transfer values chosen as discussed above. As previously, we utilize the values of Abraham and Liszi (21) and combine these with the available data for the ligands of Tables 1 and 2 (18, 30) and the solvents water, methanol, DMF, DMSO, and acetonitrile. In each case methanol is chosen as S_1 (reference solvent). For 76 cases, the average value of ΔG_{tr}^{cplx} (calc by [12] and [13]) − ΔG_{tr}^{cplx} ("expt" by [26]) is $\bar{x} = 2.4$ kcal/mol ($\sigma = 1.15$ kcal/mol). It is therefore clear that eqs. [12] and [13] consistently provide values which are ca. 2 kcal/mol in error *on the positive side*. Although there is no solvent for which the summation of experimental values of ΔG_{tr}^{cplx} and ΔG_{ip} can be made, it is likely that the systematic errors uncovered in the analysis above persist and the summation results in a cancellation.

The calculation of ΔG_{tr}^{cplx} by [26] is similar to calculations by Abraham and Ling (31) and by Cox, Firman, Garcia-Rosas, and Schreider (32). The intent of these previous calculations was to examine the assumption that the ligand L provides a constant binding site in a range of solvents i.e., the point of departure for the calculation of ΔG_{tr}^{cplx} (above). To the extent that there are *consistent* errors in the calculated value of ΔG_{tr}^{cplx} and that the standard deviation is modest (1.15 kcal/mol) over such a large number of cases, the assumption seems to be reasonably well founded. Certainly the cation is exposed to the solvent (32, 33), certainly the exposure is greater for crown ethers than for cryptands (31, 32), certainly there are specific ligand–cation effects which are ignored in this analysis (30) and certainly there are also ligand–solvent effects which are also ignored (34, 35). Nonetheless, on average over a range of ligands and solvents, the assumption is tenable even if eqs. [12] and [13] fail to estimate the magnitude of ΔG_{tr}^{cplx} correctly.

In the final analysis, the method used to estimate ΔG_{ex} in Tables 1 and 2 is seen to be based on cancellations of errors but the values are internally consistent for methanol as a reference solvent. The systematic error in ΔG_{ip} due to [21] is apparently approximately cancelled by a systematic error in ΔG_{tr}^{cplx} [12] and [13]. Note however that the fundamental basis (eq. [8]) is exact and the errors arise only in the approaches used to calculate the contributing terms. More sophisticated models of ionic solvation, ligand structure, and ionic association could yield better results without alteration in the substance of the procedure.

Membrane transport and cation extraction

Turning finally to the basic rationale for the calculations outlined above, we wish to examine the system of Lamb *et al.* (1, 17) to discover if the kinetic parameters in the form of "relaxation distances" are essential for the analysis of the transport flux. The basic equation for the transport of M^+X^- from concentrated (in) to dilute (out) solution by crown ethers and cryptands across bulk liquid membranes, is given by Behr, Kirch, and Lehn (4) as:

Can. J. Chem. Downloaded from www.nrcresearchpress.com by 78.46.186.204 on 09/07/12
For personal use only.

$$[27] \quad J = \frac{DL_0}{2l} K_{ex} \frac{S_{in}^2 - S_{out}^2}{(1 + K_{ex}S_{in}^2)(1 + K_{ex}S_{out}^2)}$$

where J is the flux of transported cation in moles per time per unit area, D is a general diffusion coefficient of the species $\overline{L}$ and $\overline{LMX}$ across the unstirred boundary layers of thickness l, K_{ex} is the extraction constant as defined by [2] and S_{in} and S_{out} are the concentration of the 1:1 salt MX on the two sides of the membrane. The flux will be maximal (J_{max}) when $J = DL_0/2l$ (4). Equation [27] strictly applies when the areas of the two interfaces and the volumes of the two phases are equal. Neither of these conditions apply with the cells utilized (17, 36) but corrections for area and volume ratios are readily incorporated (Appendix II). More critical is the correction for extent of transport; Behr, Kirch, and Lehn give an analysis in terms of a fixed fraction of transport (f) (4) whereas the experiment actually performed dealt in terms of a fixed lapse of time (24 h) (17). The fraction transported therefore depends on J up to the maximum fraction which could be transported (f_{max}) at the maximum rate (J_{max}). Thus f will vary as J/J_{max} between 0 and f_{max}.

The fluxes in ref. 17 were examined to determine J_{max}. The experimental data for alkaline earth cations cannot be treated, so these flux data were ignored. Of the remaining data, J_{max} (reported) is 550×10^{-7} mol/24 h/area of cell for 2.2.1/$RbNO_3$. This value is subject to some question as it lies about 40% higher than the next highest flux. For conditions of high source phase salt concentration and low carrier concentration, such as occur in this experiment, the maximum flux is expected to occur over a broad range of values of the extraction constant (4). The 2.2.1/$RbNO_3$ value thus appears to be anomalously high.

The next highest flux gives J_{max} (reported) $= 340 \times 10^{-7}$ mol/24 h/area of cell for DC18C6/KNO_3; a number of other fluxes lie near to this value as expected for a broad maximum. If this is indeed J_{max} then $f_{max} = 0.0425$, i.e., at J_{max} 4.25% of the initial amount of KNO_3 is transported in 24 h. Using this value, with the area and volume ratios (1, 17, 36) permits a theoretical curve of J/J_{max} as a function of log K_{ex} to be constructed (Appendix II). The theoretical curve is sketched in Fig. 1. The experimental points, taken from ref. 17, can be readily compared; the calculated values of K_{ex} are given in Table 4 for those cases where $J > 0.1\ J_{max}$ and the points J/J_{max}(expt), log K_{ex}(calc)) are plotted on Fig. 1 (circles). The calculated value of log $K_{ex} = 0.9$ for the system DB18C6/KNO_3 can be compared with an "experimental" value of log $K_{ex} = 0.4$ derived from the data of ref. 37 using a Michaelis–Menton analysis of the variation in rate as a function of substrate concentration (5, 8).

As is apparent from [5], K_{ex} depends on the anion chosen. This is the origin of the anion effect on transport rate (37). Roughly comparable data can be corrected for different carrier concentrations and interfacial areas and added to the set of values from ref. 17. The three triangles on Fig. 1 are the KBr, KNO_3, and KI values for the carrier DB18C6. This in effect is a duplicate determination of the KNO_3 flux and the two values are well within experimental error of one another.

It is evident that the theoretical curve and the calculated points are in rough agreement. Only the two points marked with full circles are outside experimental error in the transport rate and the estimated error of ± 1 log unit in K_{ex}. More significantly, if the error is assumed to lie entirely on the log K_{ex} axis, the average deviation between "experimental" and "theoretical" values is -0.10 kcal/mol with a standard deviation of 0.90 kcal/mol. This lies well within the errors expected for the calculation of K_{ex}. It is important to note that transport flux errors of $\pm 10\%$ are not insignificant. An example is provided for only the one point with error bars but the other points are all subject to the same uncertainty. As a consequence there is little point in examining the question of whether the model with relaxation distances provides a "better" fit.

The calculation of the theoretical curve assumes that the ligand remains entirely in the organic phase (L_0 = constant = 1×10^{-3} mol L^{-1} for this experiment (17)). However, a number

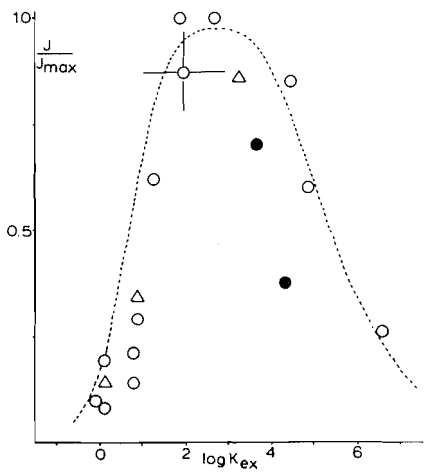

FIG. 1. Transport flux (J/J_{max}) as a function of log K_{ex}(calc). Circles – data of reference 17, triangles – data of reference 37. Error bars on one point apply to all points. The full circles lie outside of the errors in both J/J_{max} and log K_{ex}. Dashed line is the theoretical curve based on [27].

TABLE 4. Calculated extraction constants and transport rate data[a]

Ligand	Salt	log K_{ex} (calc)	J^b	J/J_{max}	δ^c (kcal/mol)
18C6	KNO_3	2.0	280	0.82	−0.6
18C6	$RbNO_3$	1.3	210	0.62	−0.5
18C6	$CsNO_3$	0.5	34	0.10	−1.1
21C7	KNO_3	0.1	67	0.19	−0.3
21C7	$RbNO_3$	0.8	72	0.21	−0.9
21C7	$CsNO_3$	0.8	48	0.14	−1.2
DB18C6	KBr	0.1	48[d]	0.14	−0.3
DB18C6	KNO_3	0.9	101	0.29	−0.7
DB18C6	KNO_3	0.9	116[d]	0.34	−0.7
DB18C6	KI	3.3	290[d]	0.86	1.1
DC18C6	KNO_3	1.9	340	1.0	1.2
DC18C6	$CsNO_3$	−0.1	34	0.10	−0.2
2.2.1	$NaNO_3$	4.3	130	0.38	2.0
2.2.1	KNO_3	4.5	290	0.85	−0.4
2.2.1	$RbNO_3$	2.7	340[e]	1.0[e]	−0.1
2.2.1	$CsNO_3$	0.1	28	0.08	−0.7
2.2.2	$NaNO_3$	3.7	240	0.70	1.4
2.2.2	KNO_3	6.6	88	0.26	−0.2
2.2.2	$RbNO_3$	4.9	205	0.60	0.3

[a]At 25°C for $CHCl_3/H_2O$ extractions. Calculations of ΔG_{ip} by [19].
[b]Transport flux in mol/24 h/cell area $\times 10^7$, data of ref. 17.
[c]$\delta = \Delta G_{ex}$(calc) − ΔG_{ex} (predicted by [27]).
[d]Calculated from ref. 37 as described in text.
[e]Experimental value questioned in text. Set to J_{max} arbitrarily.

Can. J. Chem. Downloaded from www.nrcresearchpress.com by 78.46.186.204 on 09/07/12
For personal use only.

Can. J. Chem. Downloaded from www.nrcresearchpress.com by 78.46.186.204 on 09/07/12
For personal use only.

of the carriers utilized, notably 18C6 and 2.2.1, are significantly partitioned to the aqueous phase (28, 38). This acts to diminish L_0 and thus to diminish the flux. From available data on partition coefficients and stability constants for complex formation in water (18, 28, 38) one can estimate that up to 30% of the total amount of ligand is in the aqueous phase ($18C6/K^+$ and $2.2.1/Na^+$ as typical worst cases). Recalculation of the theoretical curve with $L_0 = 7 \times 10^{-4}$ mol L^{-1} results in only minor shifts in the curve shape and maximum. Since J_{max} is a linear function of L_0 however, the new curve must be below that of Fig. 1 with its maximum near 0.7. Stated another way, carriers which are partitioned to the aqueous phase will give points which lie below the calculated curve. Consistent with this analysis, the majority of the points lie below the curve with the most pronounced deviations occurring for $2.2.1/KNO_3$ and $2.2.1/NaNO_3$ (solid circles).

Is there a kinetic component to the transport in this system? Within the limits of the calculations and transport fluxes the answer is clearly "no". It is likely that the relaxation distances proposed previously (17) are simply artifacts of the linearization of K_m and K_{ex}. This conclusion is in general agreement with experiments in other cells (7) in which the transport of KNO_3 by DB18-6 is dependent upon stirring, and therefore primarily due to diffusion control. We continue the search for systems in which interfacial processes are slower than diffusion.

Acknowledgements

This work was supported by the Natural Sciences and Engineering Research Council of Canada. The hospitality and stimulating environment of the laboratory of Professor J. M. Lehn is also gratefully acknowledged.

1. D. W. McBride, R. M. Izatt, J. D. Lamb, and J. J. Christensen. *In* Inclusion compounds. Vol. 3. *Edited by* J. L. Atwood, J. E. D. Davies, and D. D. McNicol. Academic Press, London. 1984. p. 571.
2. M. Okahara and Y. Nakatsuji. Top. Curr. Chem. **128**, 37 (1985).
3. Z. Qi and E. L. Cussler. J. Membr. Sci. **19**, 259 (1984).
4. J. P. Behr, M. Kirch, and J. M. Lehn. J. Am. Chem. Soc. **107**, 241 (1985).
5. T. M. Fyles, V. A. Malik-Diemer, C. A. McGavin, and D. M. Whitfield. Can. J. Chem. **60**, 2259 (1982).
6. L. M. Dulyea, T. M. Fyles, and D. M. Whitfield. Can. J. Chem. **62**, 498 (1984).
7. T. M. Fyles. J. Membr. Sci. **24**, 229 (1985).
8. T. M. Fyles. J. Chem. Soc. Faraday I, **82**, 617 (1986).
9. C. J. Pederson. J. Am. Chem. Soc. **92**, 391 (1970).
10. H. K. Frensdorff. J. Am. Chem. Soc. **93**, 4004 (1971).
11. D. J. Cram and J. M. Cram. Acc. Chem. Res. **11**, 8 (1978).
12. P. Gramain and Y. Frère. Nouv. J. Chim. **3**, 53 (1979).
13. Y. Takeda. Top. Curr. Chem. **121**, 1 (1984).
14. J. M. Lehn, A. Moradpur, and J. P. Behr. J. Am. Chem. Soc. **97**, 2532 (1975).
15. J. M. Lehn. *In* Physical chemistry of transmembrane ion motions. *Edited by* G. Spach. Elsevier, Amsterdam. 1983. p. 181.
16. M. Kirch and J. M. Lehn. Angew. Chem. Intl. Edn. Engl. **14**, 555 (1975).
17. J. D. Lamb, J. J. Christensen, J. L. Oscarson, B. L. Nielsen, B. W. Asay, and R. M. Izatt. J. Am. Chem. Soc. **102**, 6820 (1980).
18. R. M. Izatt, J. S. Bradshaw, S. A. Nielsen, J. D. Lamb, J. J. Christensen, and D. Sen. Chem. Rev. **85**, 271 (1985).
19. S. K. Friedlander and K. H. Keller. Chem. Eng. Sci. **20**, 121 (1965).
20. R. Blumenthal and A. Katchalsky. Biochem. Biophys. Acta, **173**, 357 (1969).
21. M. H. Abraham and J. Liszi. J. Chem. Soc. Faraday I, **74**, 1604 (1978).
22. M. H. Abraham and J. Liszi. J. Inorg. Nucl. Chem. **43**, 143 (1981).
23. R. M. Fuoss. J. Am. Chem. Soc. **80**, 5059 (1958).
24. B. G. Cox. Ann. Rep. Prog. Chem. A, **70**, 249 (1973).
25. B. G. Cox, G. R. Hedwig, A. J. Parker, and D. W. Watts. Aust. J. Chem. **27**, 477 (1974).
26. J. M. Lehn. Struct. Bonding, **16**, 1 (1973).
27. R. M. Fuoss. J. Am. Chem. Soc. **80**, 5059 (1958).
28. M. Kirch. Thèse, Université Louis Pasteur, Strasbourg. 1984.
29. H. K. Frensdorff. J. Am. Chem. Soc. **93**, 4684 (1971).
30. B. G. Cox, J. Garcias-Rosas, and H. Schneider. J. Am. Chem. Soc. **103**, 1384 (1981).
31. M. H. Abraham and H. C. Ling. Tetrahedron Lett. **23**, 469 (1982).
32. B. G. Cox, P. Firman, J. Garcia-Rosas, and H. Schneider. Tetrahedron Lett. **23**, 3777 (1982).
33. I. M. Kolthoff and M. K. Chantooni. Anal. Chem. **52**, 1039 (1980).
34. P. A. Mosier-Boss and A. I. Popov. J. Am. Chem. Soc. **107**, 6168 (1985).
35. B. O. Strasser and A. I. Popov. J. Am. Chem. Soc. **107**, 7921 (1985).
36. J. D. Lamb, R. M. Izatt, D. G. Garrick, J. S. Bradshaw, and J. J. Christensen. J. Membr. Sci. **9**, 83 (1981).
37. J. D. Lamb, J. J. Christensen, S. R. Izatt, K. Bedke, M. S. Astin, and R. M. Izatt. J. Am. Chem. Soc. **102**, 3399 (1980).
38. Y. Takeda and A. Tanaka. Bull. Chem. Soc. Jpn. **59**, 733 (1986).

Appendix I

As noted in the text, the methods are parameter dependent. The solvent properties are given in Table 5 and ionic properties in Table 6. Abbreviations: PC, propylene carbonate; DMF, *N,N*-dimethylformamide; DMSO, dimethylsulfoxide; AN, acetonitrile; Pic, picrate. The compounds considered (abbreviation, radius in Å, volume in $Å^3$): 15-crown-5 (15C5, 4.55, 390); benzo-15-crown-5 (B15C5, 4.72, 440); 18-crown-6 (18C6, 4.86, 470); dibenzo-18-crown-6 (DB18C6, 5.14, 560); *N,N'*-dimethyl-1,10-diaza-18-crown-6 (2.2 NMe, 5.10, 540) dicyclohexano-18-crown-6 (DC18-6, 5.56, 710); 21-crown-7 (21C7, 5.12, 550); cryptand [2.2.1] (2.2.1, 5.30, 620); cryptand [2.2.2] (2.2.2, 5.53, 700); cryptand [3.2.2] (3.2.2, 5.73, 780); cryptand [2.2.C_8] (2.2.C_8, 5.63, 740).

None of the calculations are difficult but the tedium was relieved by the use of a programmable calculator.

Appendix II

The form of eq. [27] including volume and area corrections is [28] (4).

$$[28] \quad J = J_{max} K_{ex} \frac{S_{in}^2 - S_{i,out}^2}{(1 + K_{ex} S_{in}^2)(1 + K_{ex} S_{i,out}^2)}$$

where

$$J_{max} = DL_0/[l(1 + A_{in}/A_{out})]$$

A_{in}/A_{out} = ratio of the interfacial areas

$$S_{i,out} = frS_0 + \frac{L_0}{(1 + A_{in}/A_{out})} \frac{J}{J_{max}}$$

TABLE 5. Solvent properties utilized[a]

Solvent	M (g/mol)	Density (g/cm^3)	Solvent radius (Å)	Dielectric constant	m^b	c^b
H_2O	18.02	0.9971	1.553	78.36	−2.0514	9.7426
MeOH	32.04	0.7866	2.037	32.64	−2.4854	8.9465
PC	102.09	1.198	2.605	64.4		
DMF	73.10	0.9443	2.524	36.71		
DMSO	78.13	1.9058	2.456	46.68	−2.6786	9.7119
AN	41.05	0.7768	2.222	36.02		
CH_2Cl_2	84.93	1.3266	2.375	8.93	−3.3070	9.9616
$CHCl_3$	119.38	1.4832	2.558	4.72	−3.3070	9.9616
Benzene	78.12	0.8786	2.648	2.27	−3.2503	9.8205
Hexane	86.18	0.6603	3.01	1.90	−2.9718	8.7347

[a]United from refs. 21, 22 and 24.
[b]Coefficients of eq. [13].

TABLE 6. Properties of the ions considered[a]
(*a*) Cations

Ion	Radius (Å)	$\Delta G_{tr}(H_2O \rightarrow$ solv) in kcal/mol MeOH	DMF	DMSO[b]	AN
Na	1.05	1.1			
K	1.33	1.4	2.1	1.1	3.9
Rb	1.43	1.5			
Cs	1.66	1.3	2.1	1.0	3.1

(*b*) Anions

Ion	Radius (Å)	ΔG_h^0 (kcal/mol)	$\Delta G_{tr}(H_2O \rightarrow$ solv) in kcal/mol[c] CH_2Cl_2	$CHCl_3$	Benzene	Hexane
Picrate	3.0	−39.5	0.6	4.2	11.2	13.5
NO_3	1.95	−60.05		10.7		
Br	1.95	−61.5		11.8		
I	2.20	−52.6		7.4		

[a]United from refs. 21 and 22.
[b]When required, these values were also used for PC (Table 3).
[c]Calculated as described in text.

$S_{in} = (1 - f)S_0$

S_0 = total cation concentration on the "in" side at time = 0

r = ratio of the phase volumes = Vol_{in}/Vol_{out}

f = fraction of transport ($0 \leq f \leq 1/2$)

Setting $y = J/J_{max}$ and noting that $f = y \times f_{max}$ as described in the text gives [28] as a quadratic equation in K_{ex} (4) i.e.,

[29] $AK_{ex}^2 + BK_{ex} + C = 0$

where

$A = S_{in}^2 S_{i,out}^2 y$

$B = yS_{in} + yS_{i,out}^2 - S_{in}^2 + S_{i,out}^2$

$C = y$

The given set of input constants; $L_0 = 0.001\ M$, $S_0 = 0.46\ M$ (activity of 1.0 M KNO_3), $r = 0.16$ (17), $A_{in}/A_{out} = 0.25$ (17), $f_{max} = 0.0425$, defines the problem. Equation [29] was repeatedly solved for K_{ex} with an increment of 0.05 in y. The roots were plotted and interpolated as a smooth curve by hand. At the crest of the curve additional roots with a 0.01 increment in y were computed. Calculations were done with a programmable calculator.

Can. J. Chem. Downloaded from www.nrcresearchpress.com by 78.46.186.204 on 09/07/12
For personal use only.

Effect of protonation on the ground state properties of retinal analogs: an *ab-initio* study

RAYMOND A. POIRIER, ARPITA YADAV, AND PÉTER R. SURJÁN[1]

Department of Chemistry, Memorial University of Newfoundland, St. John's, Nfld., Canada A1B 3X7

Received August 18, 1986

RAYMOND A. POIRIER, ARPITA YADAV, and PÉTER R. SURJÁN. Can. J. Chem. **65**, 892 (1987).

The ground state properties (bond lengths, bond orders, net atomic charge distribution) of various *cis* and *trans* isomers of retinal analogs have been studied at *ab initio* SCF and correlated levels. The effect of protonation on the properties of the retinal Schiff base analogs has also been studied. Convergence in various properties has been observed with increasing chain length justifying the use of smaller analogs mimicking retinal. Convergence is, however, slower for the protonated retinal Schiff base analogs. The protonated retinal Schiff base analogs show an increased conjugation reflected in the bond orders, bond lengths, and in the decrease in the HOMO–LUMO gap. The nodal characteristics of the HOMO of the protonated retinal Schiff base analog also indicate a strong conjugation in the vicinity of the protonated nitrogen. Based on the results of calculations at the correlated level, the sudden polarization charge transfer mechanism is shown to be an artifact of HF-based methods used in the calculations.

RAYMOND A. POIRIER, ARPITA YADAV et PÉTER R. SURJÁN. Can. J. Chem. **65**, 892 (1987).

Utilisant des méthodes *ab initio* en champ auto-cohérent et à des niveaux permettant d'établir une corrélation, on a étudié les propriétés à l'état fondamental (longueurs des liaisons, ordres des liaisons, distributions des charges atomiques nettes) des divers isomères *cis* et *trans* d'analogues du rétinal. On a aussi étudié l'effet de la protonation sur les propriétés d'analogues des bases de Schiff du rétinal. On a observé une convergence des diverses propriétés avec une augmentation de la longueur de la chaîne et cette observation justifie l'utilisation d'analogues plus petits qui reproduisent les propriétés du rétinal; toutefois, la convergence est plus lente pour les analogues protonés des bases de Schiff du rétinal. Les analogues protonés des bases de Schiff du rétinal présentent une plus grande conjugaison qui se réflète dans les ordres et les longueurs des liaisons et par une diminution de la différence entre la haute occupée et la basse vacante. Les caractéristiques nodales de la haute occupée de l'analogue protoné de la base de Schiff du rétinal suggèrent qu'il existe une forte conjugaison au voisinage de l'azote protoné. En se basant sur les résultats de ces calculs aux niveaux où l'on peut établir une corrélation, on démontre que la polarisation soudaine dans le mécanisme de transfert de charge n'a pas de signification physique et qu'elle est inhérente aux méthodes basées sur HF qui sont utilisées dans les calculs.

[Traduit par la revue]

I. Introduction

Recently a great deal of experimental (1–14, 18, 21) as well as theoretical (15–21) work has been done to understand the process initiated by the impinging of light on a visual pigment resulting in vision. It is well known that in both vertebrates and invertebrates, the protonated Schiff base (PSB) of 11-*cis* retinal is the chromophore group in the visual pigment rhodopsin (1). During this process the geometry of this retinal is changed from 11-*cis* to the all-*trans* form and in vertebrates the chromophore–opsin linkage is broken (2). In invertebrates the photocycle does not lead to rupture of the chromophore–opsin bond (13, 21). *In vivo* the photoreaction is followed by enzymatic processes regenerating the original 11-*cis* pigment. The impinging of light on retinal (that is, the primary event of the process) can be illustrated as follows:

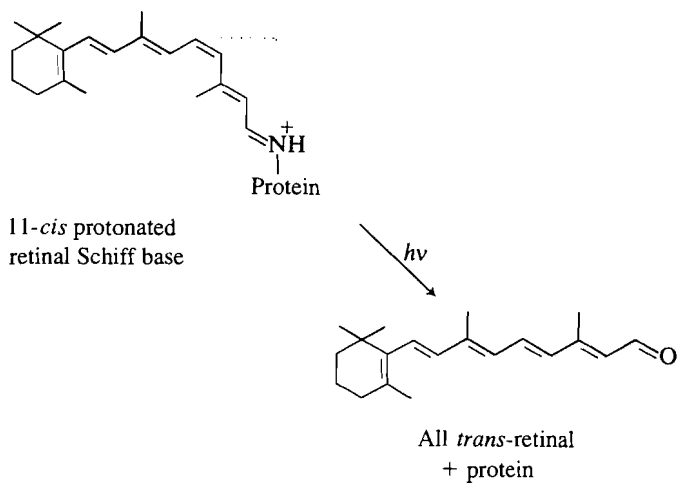

This leads to a general statement that vision is initiated by photoisomerization of the retinal and occurs during the primary event (9). It has, however, even fairly recently been proposed that proton-transfer could be a fast competing process (3, 7, 8).

This photochemical reaction is not only important for the visual process, but has also been shown to be used for bioenergetics (14, 21). When grown under anaerobic conditions *Halobacterium halobium* develops a purple protein pigment, bacteriorhodopsin, whose role is to convert light energy directly into a gradient of hydrogen ions across the membrane which subsequently leads to the synthesis of ATP. Thus, very similar chromophoric systems are responsible in different organisms for different roles. There are, however, some basic structural differences between the systems. For the visual process the chromophore is the 11-*cis* retinal, whereas in bacteriorhodopsin, the chromophore is the all-*trans* retinal (10). For bacteriorhodopsin, the primary event is believed to be an all-*trans* to 13-*cis* isomerization and like invertebrates, the chromophore does not detach from the opsin during the photocycle.

Attempts to utilize computational chemistry for understanding this process in the past have been limited mainly to methods such as Hückel and Pariser–Parr–Pople (PPP) π-electron methods on simple polyenes (17, 18). Honig *et al.* (19) calculated the torsional potential of the cyclohexene ring for rotation around the C_6—C_7 and C_{12}—C_{13} bonds utilizing a LCAO—MO–CI semi-empirical method of PPP type corrected for the nearest neighbour overlap. Formerly, *ab-initio* calcula-

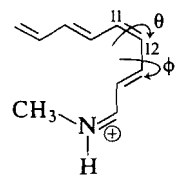

[1]On leave from CHINOIN Research Centre, H-1325 Budapest, Hungary.

Can. J. Chem. Downloaded from www.nrcresearchpress.com by 78.46.186.204 on 09/07/12
For personal use only.

Can. J. Chem. Downloaded from www.nrcresearchpress.com by 78.46.186.204 on 09/07/12
For personal use only.

tions have been performed on a nonatetraenylidene methyliminium molecule using a minimal basis set (15).

Salem and Bruckmann (15) suggested a specific hypothesis that the lowest singlet excited state obtained by a $\pi-\pi^*$ excitation of the chromophore creates a sudden polarization within the molecule that triggers a sudden short-lived electrical signal, causing charge transfer from one end of the molecule to the other. However, this hypothesis is in contradiction with many experimental data (18). To our knowledge, geometry optimizations were not performed for any of these calculations.

Recent INDO-CISD (16) and MNDOC (20) calculations show that the retinal Schiff base ground state properties depend sensitively on protonation and on the charge environment. (All essential geometrical parameters were allowed to relax in the latter.) Ground state MNDOC calculations have shown that a protein, by protonating the retinal Schiff base and by providing one or two negative ions in the environment, can reduce double-bond isomerization barriers and can increase single bond barriers. The excited state INDO-CISD calculations predict a barrierless first excited singlet state potential surface for *cis–trans* isomerization of the retinal PSB chromophore.

As a first step it is important to understand the properties of retinal in its ground electronic state. In this paper we report *ab-initio* results on the ground state properties of various *cis* and *trans* isomers of retinal analogs. The geometries of the studied models have been fully optimized in all the cases. The effect of protonating the Schiff base on the ground state properties is studied. The use of smaller analogs mimicking retinal is justified by studying convergence in properties with increasing chain length.

II. Computational details

Closed Shell Hartree-Fock SCF calculations were performed using the MONSTERGAUSS program (22). A minimal STO-3G basis-set (23) was used throughout. In all cases the geometry optimizations were performed using the optimally conditioned method of Davidon and Nazareth (24) (the gradient length was required to be less than 5.0×10^{-4}). Bond orders (B_{ab}) were calculated according to the definition of Mayer (25). Correlational effects were taken into account in some cases within the same basis set by a simple model of strictly localized geminals (SLG) (26–28). This approach corresponds to a first order many-body perturbation theory with a correlated, but fully localized reference state. The latter is obtained by solving the two-electron Schrodinger equation exactly for each chemical bond, lone pair, etc., within a limited subspace of basis orbitals (hybrids) assigned to that bond. As a consequence, delocalization and dispersion interactions between different bonds are neglected by this model, but some interbond interactions like electrostatic inductive effects are accounted for. Obviously, the SLG method cannot describe any conjugational effect, thus its error can be considered as a measure of the conjugation.

III. Results and discussion[2]

In this study a series of the retinal chromophore analogs were investigated, starting with the smallest analog and then gradually increasing the chain length up to and including the double bond of the cyclohexene ring (excluding the methyl substituents). In each case full geometry optimizations were performed (no constraints) in order to determine the convergence as a function of chain length in some properties of the retinal analogs, such as, the bond lengths, bond orders, and charge distribution. Similarly, analogs of the retinal Schiff base (retinal SB) as well as the protonated retinal Schiff base (retinal PSB) were also studied.

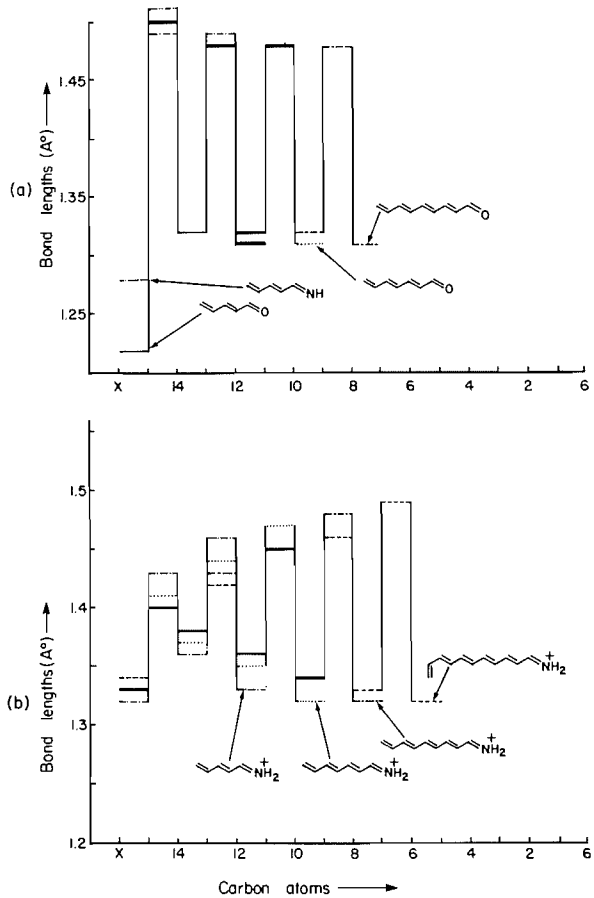

FIG. 1. Variation in the SCF optimized C—C bond lengths for the retinal, retinal SB (*a*) and retinal PSB (*b*) analogs. X = O or N. The numbering of carbon atoms is as defined in structure **I**. The different analogs are identified with different (dashed, dotted etc) horizontal lines, for each bond; the vertical lines are just visual guidelines. Thick horizontal solid lines indicate coincidence.

III.1 Bond lengths and bond orders

The C—C bond lengths for different analogs of retinal, retinal SB, and retinal PSB are shown in Fig. 1, and the C—C bond orders for the same analogs are given in Fig. 2. The numbering of carbon atoms has been kept the same as in retinal and is consistent throughout this paper. The numbering for the full retinal is as follows:

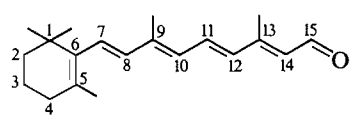

1

It is evident from Figs. 1 and 2, that there is a remarkable difference in the behaviour of the retinal SB analogs and that of retinal PSB analogs. Namely, in case of the former, bond length (r_{ab}) and bond orders (B_{ab}) are fairly independent of the chain length, that is, they show a *convergence* with increasing chain length. In turn, the same quantities in case of the retinal PSB show a slower convergence, that is, slightly more variation in

[2]Tables including the optimized geometries for the *cis* and *trans* isomers of retinal, retinal Schiff base, and protonated retinal Schiff base analogs may be purchased from the Depository of Unpublished Data, CISTI, National Research Council of Canada, Ottawa, Ont., Canada K1A 0S2.

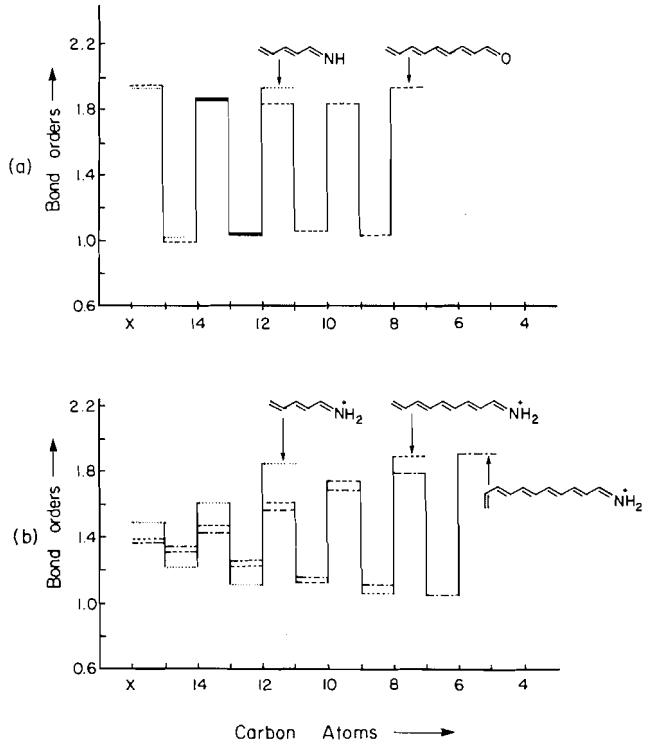

FIG. 2. Variation in the SCF optimized C—C bond orders for the retinal, retinal SB (*a*) and retinal PSB (*b*) analogs. For other notations, see Fig. 1.

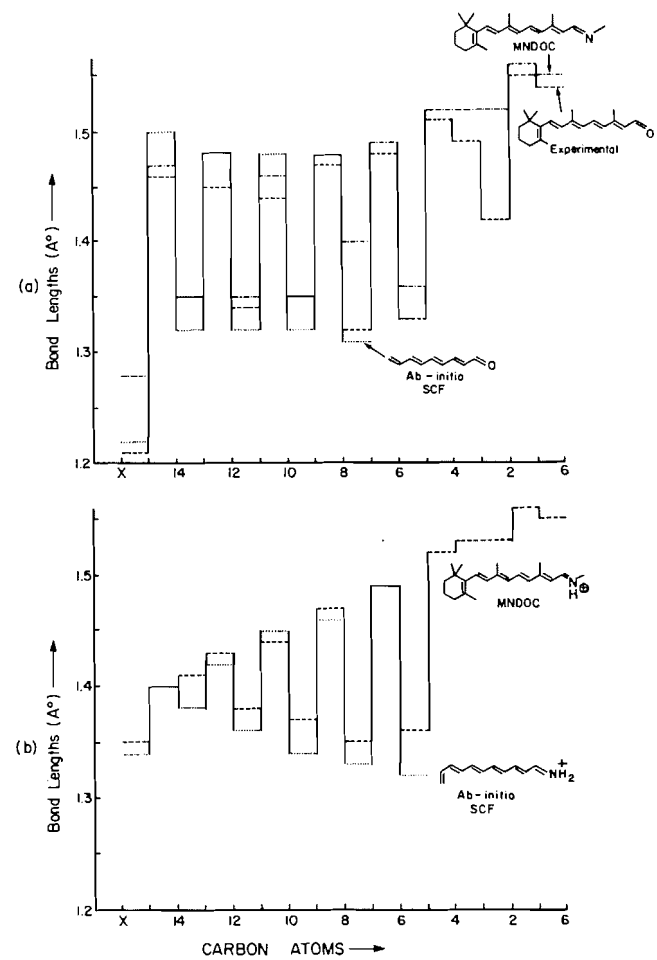

FIG. 3. Variation in the SCF and MNDOC optimized C—C bond lengths for different analogs of retinal, retinal SB (*a*) and retinal PSB (*b*). Experimental bond lengths (29) for retinal are also shown. For other notations, see Fig. 1.

r_{ab} and B_{ab}. As a consequence, the smallest analogs (up to three double bonds) do not give a good estimation for the corresponding properties of the larger retinal PSB analogs.

From Figs. 1 and 2 one can see that r_{ab} and B_{ab} values for the retinal SB analog are very similar to those for the retinal analogs, while the corresponding quantities for retinal PSB are rather different. In the case of the former two, the single and double bonds are easily identified indicating a limited conjugation along the whole chain. In other terms, the C—C bond lengths of the retinal and retinal SB show a strong regular alternation. On the other hand, the retinal PSB analogs show an increased conjugation around the NH_2^+ group manifested in a decreased alternation of bond lengths and bond orders. The conjugation subsequently dies off on moving towards the cyclohexene ring end of the molecule. Experimental results (29) show an increase in the frequency of the C_{14}—C_{15} stretch on protonation of the Schiff base, which is in agreement with the above results. The bond order of the C_{11}—C_{12} double bond is reduced considerably on protonation of the Schiff base thereby facilitating the rotation of the C_{11}—C_{12} double bond or in other words facilitates the *cis–trans* isomerization (c.f. Fig. 2).

In Fig. 3 the optimized geometries for the retinal and the retinal PSB analogs are compared with the experimental and the theoretical data available from semiempirical calculations. The bond lengths for the retinal analog are very close to the experimental geometry for retinal obtained by X-ray crystallography (30). The MNDOC results (20) for the retinal SB predict a very long bond length for the C_7—C_8 double bond and therefore predict the dihedral angle between the plane of the ring and the chain to be 83° which is larger than the experimentally observed angle of 62° (30). Also, MNDOC does not assign enough torsional stability to the C_6—C_7 π single bond to compete with the steric interaction between the methyl groups at C_1 and C_5 and the hydrogens at C_7 and C_8. The present *ab initio* results for the retinal PSB analog are in general agreement with the MNDOC results (c.f. Fig. 3), though the latter seems to overestimate most of the bond lengths.

III.2 Charge distribution

The net atomic charges for the different analogs of retinal, retinal SB, and retinal PSB are often studied because of their importance in understanding the energetics of the interaction between the chromophore and protein residual charges in simple electrostatic terms. The atomic charge distribution is also useful in monitoring the changes in the electronic structure of different analogs. We have determined the atomic charges by means of Mulliken's population analysis, which is expected to give reasonable relative values in the minimal basis set used throughout.

In Fig. 4 net atomic charges are plotted for various analogs of different chain lengths. An alternation pattern of the atomic charges can be observed in each case. The heteroatom is always strongly negative, C_{15} is positive, and the charge alternation on remaining carbon atoms decreases subsequently. However, similar to the cases of bond lengths and bond orders, the retinal and retinal SB analogs show a rather different behaviour as compared to retinal PSB. In the former case (Fig. 4*a*), the charges after C_{15} are all negative with a minor alternation,

Can. J. Chem. Downloaded from www.nrcresearchpress.com by 78.46.186.204 on 09/07/12
For personal use only.

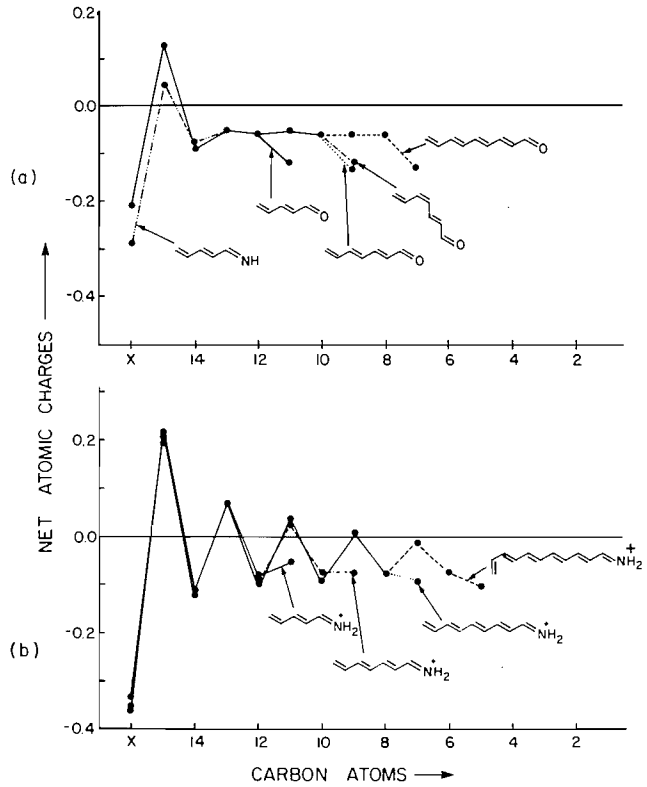

FIG. 4. Variation in the SCF net atomic charges on the C, N, or O atoms for different analogs of retinal, retinal SB (*a*) and retinal PSB (*b*). X = O or N. This numbering of carbon atoms is as defined in structure **I**.

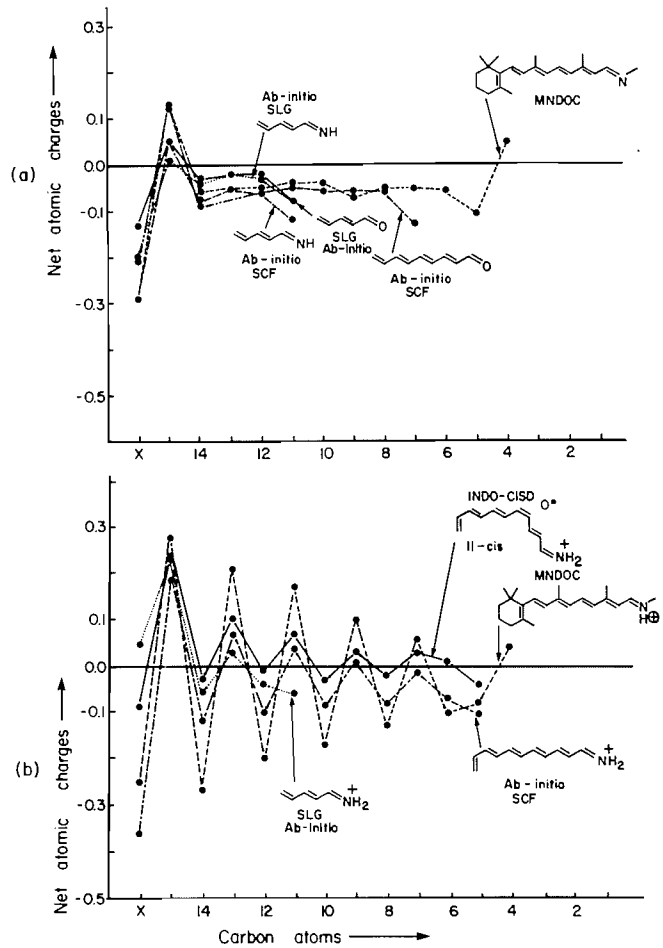

FIG. 5. Variation in net atomic charges on the C, N, and O atoms for retinal, retinal SB (*a*), and retinal PSB (*b*) analogs as obtained by *ab initio* SCF and SLG methods and semi-empirical MNDOC and INDO-CISD calculations. X = O or N, the numbering of carbons is as defined in structure **I**.

while in Fig. 4*b* for retinal PSB analogs we see a much larger alternation which keeps the odd-numbered carbon atoms slightly positive. The charge alternation according to our calculations is almost the same for *cis* and *trans* isomers.

The alternation of atomic charges along a chain introduced by a heteroatom as an "impurity" is well known; it can be understood by simple topological Huckel-type models (31) or, alternatively, on the basis of the induction of local dipoles. The reason of the remarkable difference between 4*a* and *b* is less obvious, though it has been studied formerly in several cases. In Fig. 5 we have collected some previous INDO-CISD and MNDOC results from the literature (16, 20). The charges obtained by the SLG wave function (cf. Section II) are also plotted. It turns out that all methods agree in the overall pattern of the charges though the MNDOC results seem to overestimate the actual values. The significance of the SLG method is important in this respect, because it does not take into account any delocalization or conjugation effects, and still shows a similar charge distribution. This implies that the essential difference between the charge distribution of retinal PSB and the retinal and retinal SB analogs reflected by Fig. 4 is not to be attributed to the increased conjugation of the former. The increased charge alternation in retinal PSB should be a consequence of the extra positive charge on N which induces larger local dipoles in the bonds over the whole molecule — an effect which is properly accounted for by the simple SLG wave function where the bonds are electrostatically coupled.

An interesting difference in the charge alternation pattern has been observed upon rotating the chromophore around the C_{11}—C_{12} "double bond" in excited state (16). The INDO-CISD calculations for the excited state predict an extra polarization at 90° of rotation around the C_{11}—C_{12} bond. However, the charges obtained by the properly correlated SLG wave function do not show the spurious extra polarization at 90° reported in refs. 15 and 16. The extra polarization is therefore most likely an artifact of the calculations. It should be emphasized that the HF-based methods are incapable of describing rotations around double bonds and do lead to charge polarization. Therefore, based on these results the sudden polarization charge transfer hypothesis can be eliminated as a possible mechanism in this process.

III.3 MO diagrams

Figure 6 shows the π molecular orbitals (MO's) for the analogs of retinal, retinal SB, and retinal PSB, in a simple diagrammatic representation. It clearly indicates that the π MO's in the retinal SB analog and the retinal analog have the same nodal characteristics. However, the nodal character of the HOMO changes in going from retinal SB to retinal PSB. The nodes in the HOMO of the retinal SB analog are located at the C_{14}—C_{15} and C_{12}—C_{13} bonds whereas in the case of retinal PSB analog the nodes are located at the C_{15}—N and C_{12}—C_{13} bonds. The strong conjugational effect on protonation near the NH_2^+ group end of the molecule is reflected by the nodal characteristics of the HOMO of the retinal PSB analog. The HOMO of the retinal PSB analog clearly shows conjugation

Can. J. Chem. Downloaded from www.nrcresearchpress.com by 78.46.186.204 on 09/07/12
For personal use only.

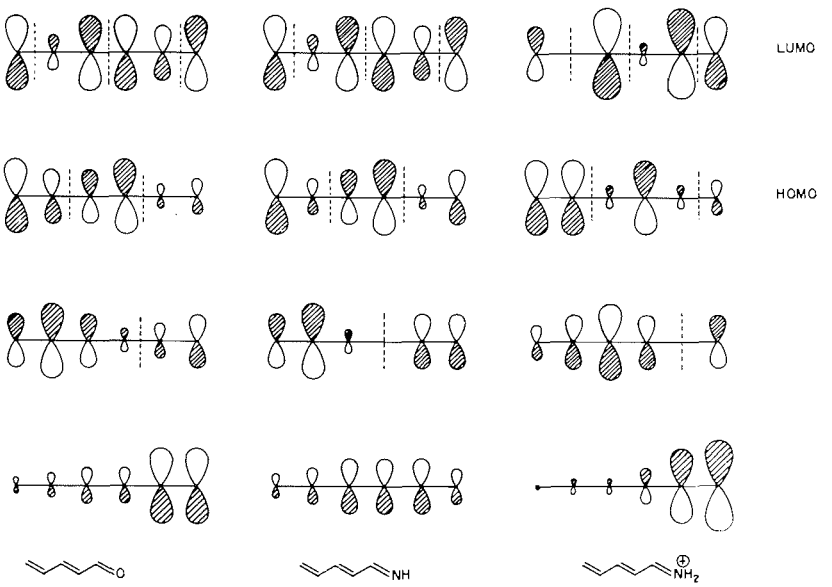

FIG. 6. Schematic representation of π-type MO's of retinal, retinal SB and retinal PSB analogs. The orbitals are drawn in order of ascending energy, the LUMO being at the top of the Figure.

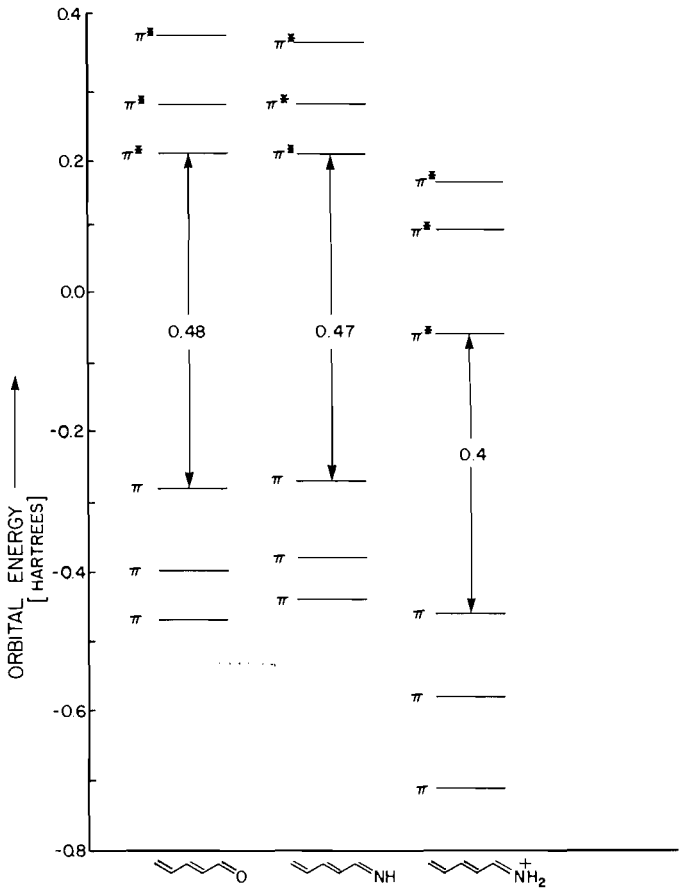

FIG. 7. π orbital energy diagram for retinal, retinal SB, and retinal PSB analogs.

between C_{13}—C_{14} and C_{14}—C_{15} bonds. Figure 7 shows the energy level diagram for the π MO's for the analogs containing three double bonds. In the retinal PSB analog the energy separation between the two highest filled π orbitals and two lowest antibonding π orbitals increases thereby reducing the gap between the HOMO and the LUMO. In other words, a red-shift in the π–π^* excitation energy is observed when the retinal Schiff base is protonated. The reason for this red shift is given by the increased conjugation of retinal PSB resulting in an equalization of "single" and "double" C—C bond lengths indicated by Fig. 1. We note that the larger analogs show the same trend (red shift upon protonation) with all the π–π^* orbital energy differences decreased due to the increased chain length.

IV. Conclusions

The results of the present paper are based on *ab-initio* STO-3G calculations, which reasonably describe the ground state properties of retinal. The conclusions can be summarized as follows:

(*1*) For the case of the retinal Schiff base and retinal analogs, convergence in bond lengths, bond orders, and atomic charges have been observed with increase in chain length showing that it is possible to mimic some properties of retinal with a smaller analog. This holds for protonated retinal Schiff base analogs only to a lesser extent.

(*2*) Protonation of the Schiff base causes more conjugational effects (i.e. elongation of double bonds and shortening of single bonds) in the vicinity of the NH_2^+ group which slowly dies off on moving towards the cyclohexene ring end of the molecule. This is reflected by the bond lengths and bond orders.

(*3*) Atomic charges alternate along the chain. This alternation is a result of induced local dipoles and is considerably stronger for protonated retinal Schiff base analogs.

(*4*) Regarding the studied properties various *cis* isomers show the same properties as the *trans* molecules.

(*5*) The change in nodal properties of the HOMO in the unprotonated retinal Schiff base and the protonated case is consistent with the conjugational effects and the difference in charge-distribution in the two cases.

(*6*) The protonated retinal Schiff base analog shows a red shift in π–π^* orbital energy difference, indicating a red shift in the corresponding excitation energy.

(*7*) The charge distribution of the studied models changes significantly at the SCF level when rotating around a double bond. This sudden charge polarization was shown to be an

Can. J. Chem. Downloaded from www.nrcresearchpress.com by 78.46.186.204 on 09/07/12
For personal use only.

artifact of the closed shell HF calculations, which disappears if the properly correlated SLG wavefunction is used.

The systematic study of the various properties presented in this paper shows the analogy between retinal and retinal Schiff base, and the differences introduced on protonation. This is reflected by all the properties studied in this work.

Acknowledgements

The continued financial support of the Natural Sciences and Engineering Research Council of Canada (NSERC) is gratefully acknowledged.

The authors would like to thank the Newfoundland and Labrador Computer Services (NLCS) and Memorial University of Newfoundland Computing Services for their generous allocation of computer time.

1. G. WALD and P. K. BROWN. Proc. Natl. Acad. Sci. U.S.A., **38**, 84 (1950).
2. T. YOSHIWAZA and S. HORIUCHI. Biochemistry and physiology of visual pigments. *Edited by* H. Langer. Springer-Verlag, Berlin. 1973. pp. 69–81.
3. A. KROPF. Nature (London), **264**, 92 (1976).
4. R. CALLENDER and B. HONIG. Ann. Rev. Biophys. Bioeng. **6**, 33 (1977).
5. S. KAWAMURA, T. JOSHI, K. HORIUCHI, M. ITO, A. KODAMA, and K. TSUKIDA. Biochim. Biophys. Acta, **518**, 147 (1979).
6. H. AKITA, S. P. TANIS, M. ADAMS, V. BALOGH-NAIR, and K. NAKANISHI. J. Am. Chem. Soc. **102**, 6370 (1980).
7. M. H. ABDEL-KADER. Photochemistry and Photobiology: Proceedings of the International Conference. Vol. 2. 1983. p. 1397.
8. C. SANDORFY. Int. J. Quantum Chem. **26**, 907 (1984).
9. A. G. DOUKAS, M. R. JUNNARKAR, R. R. ALFANO, R. H. CALLENDER, and V. BALOGH-NAIR. Biophys. J. **47**, 795 (1985).
10. C. H. CHANG, R. GOVINDJEE, T. EBREY, K. A. BAGLEY, G. DOLLINGER, L. EISENSTEIN, J. MARQUE, H. RODER, J. VITTITOW, J. M. FANG, and K. NAKANISHI. Biophys. J. **47**, 509 (1985).
11. R. S. BECKER and K. FREEDMAN. J. Am. Chem. Soc. **107**, 1477 (1985).
12. H. J. POLLAND, M. A. FRANZ, W. ZINTH, W. KAISER, E. ROLLING, and D. OESTERHELT. Biophys. J. **49**, 651 (1986).
13. E. W. ABRAHAMSON and R. S. FAGER. Curr. Top. Bioenerg. **5**, 125 (1973).
14. R. R. BIRGE and T. M. COOPER. Biophys. J. **42**, 61 (1983).
15. L. SALEM and P. BRUCKMANN. Nature (London), **258**, 526 (1975).
16. R. R. BIRGE and L. M. HUBBARD. J. Am. Chem. Soc. **102**, 2195 (1980).
17. A. WARSHEL and A. LAPPICIRELLA. J. Am. Chem. Soc. **103**, 4664 (1981).
18. A. WARSHEL and N. BARBOY. J. Am. Chem. Soc. **104**, 1469 (1982).
19. B. HONIG, A. WARSHEL, and M. KARPLUS. Acc. Chem. Res. **8**, 92 (1975).
20. P. TAVAN, K. SCHULTEN, and D. OESTERHELT. Biophys. J. **47**, 415 (1985).
21. M. OTTOLENGHI. Adv. Photochem. **12**, 99 (1980).
22. M. R. PETERSON and R. A. POIRIER. MONSTERGAUSS, Dept. of Chem., Univ. of Toronto, Toronto, Ont., Canada and Dept. of Chem., Memorial Univ. of Newfoundland, St. John's, Nfld., Canada.
23. W. J. HEHRE, R. F. STEWART, and J. A. POPLE. J. Chem. Phys. **51**, 2657 (1969).
24. (*a*) W. C. DAVIDON and L. NAZARETH. Technical Memos 303 and 306. 1977. Applied Mathematics Division Argonne National Laboratories, Argonne, IL. (*b*) W. C. DAVIDON. Math. Prog. **9**, 1 (1975).
25. I. MAYER. Chem. Phys. Lett., **97**, 270 (1983).
26. P. R. SURJÁN. Phys. Rev. A, **30**, 43 (1984).
27. P. R. SURJÁN. Croatica Chem. Acta, **57**, 833 (1984).
28. P. R. SURJÁN, I. MAYER, and I. LUKOVITS. Phys. Rev. A, **32**, 748 (1985).
29. S. O. SMITH, A. B. MYERS, R. A. MATHIES, J. A. PARDOEN, C. WINKEL, E. M. M. VAN DEN BERG, and J. LUGTENBURG. Biophys. J. **47**, 653 (1985).
30. T. HAMANAKA, T. MITSUI, T. ASHIDA, and M. KAKUDO. Acta Crystallogr. B., **28**, 214 (1972).
31. I. GUTMAN. Theoret. Chim. Acta, **50**, 287 (1979).

Can. J. Chem. Downloaded from www.nrcresearchpress.com by 78.46.186.204 on 09/07/12
For personal use only.

The synthesis, crystal and molecular structures of triphenyl(phenylthio)silane, Ph_3SiSPh, and of bis(μ-thiophenolato)bis[tetracarbonyltungsten(I)], $[W(CO)_4(SPh)]_2$[1]

C. Robert Lucas and Michael J. Newlands
Department of Chemistry, Memorial University of Newfoundland, St. John's, Nfld., Canada A1B 3X7

and

Eric J. Gabe and Florence L. Lee
Division of Chemistry, National Research Council of Canada, Ottawa, Ont., Canada K1A 0R9

Received July 8, 1986

C. Robert Lucas, Michael J. Newlands, Eric J. Gabe, and Florence L. Lee. Can. J. Chem. **65**, 898 (1987).

Preparations and X-ray structure determinations are described for Ph_3SiSPh and $[W(CO)_4(\mu\text{-}SPh)]_2$. The compound Ph_3SiSPh crystallizes in space group *Pcab* with $a = 15.260$ Å, $b = 15.968$ Å, $c = 16.757$ Å, $Z = 8$, $d_{calc} = 1.20$ g cm^{-3} (MoKα1, λ = 0.70930 Å). The structure was solved with MULTAN and refined to the final $R = 0.050$ for 1933 significant reflections. The molecule has an unusual C—S—Si angle of 99.5° and a short Si—S bond length of 2.156 Å. The compound $[W(CO)_4(\mu\text{-}SPh)]_2$ crystallizes in the space group $P2_1/c$ with $a = 9.164$ Å, $b = 12.054$ Å, $c = 11.163$ Å, β = 111.63°, $Z = 2$, $d_{calc} = 2.35$ g cm^{-3} (MoKα1, λ = 0.70930 Å). The structure was solved with MULTAN and refined to the final $R = 0.062$ for 2748 significant reflections. The molecule is a dimer with a crystallographic center of symmetry. There is a short W—W distance (2.972 Å), a wide S—W—S′ angle (106.3°), a compressed W—S—W′ angle (73.67°) and there is distortion of a CO on each W due to the close approach of an *ortho*-H in a phenyl ring.

C. Robert Lucas, Michael J. Newlands, Eric J. Gabe et Florence L. Lee. Can. J. Chem. **65**, 898 (1987).

On décrit les préparations et les déterminations de structure par diffraction des rayons-X du Ph_3SiSPh et $[W(CO)_4(\mu\text{-}SPh)]_2$. Le composé Ph_3SiSPh cristallise dans le groupe d'espace *Pcab*, avec $a = 15{,}260$, $b = 15{,}968$ et $c = 16{,}757$ Å, $Z = 8$ et $d_{calc} = 1{,}20$ g cm^{-3} (MoKα1, λ = 0,70930 Å). On a résolu la structure à l'aide du programme MULTAN et on l'a affinée jusqu'à une valeur finale de $R = 0{,}050$ pour 1933 réflexions indépendantes. La molécule comporte une angle C—S—Si qui est inhabituel à 99,5° et une liaison Si—S relativement courte à 2,156 Å. Le composé $[W(CO)_4(\mu\text{-}SPh)]_2$ cristallise dans le groupe d'espace $P2_1/c$, avec $a = 9{,}164$, $b = 12{,}054$ et $c = 11{,}163$ Å, β = 111,63°, $Z = 2$ et $d_{calc} = 2{,}35$ g cm^{-3} (MoKα1, λ = 0,70930 Å). On a résolu la structure à l'aide du programme MULTAN et on l'a affinée jusqu'à une valeur finale de $R = 0{,}062$ pour 2748 réflexions indépendantes. La molécule est un dimère comportant une centre de symétrie cristallographique. On observe une distance W—W qui est courte à 2,972 Å, un angle S—W—S′ qui est grand à 106,3°, un angle W—S—W′ qui est comprimé à 73,67° et une distortion d'un CO de chacun des W qui est due à une approche d'un H en ortho d'une groupement phényle.

[Traduit par la revue]

Introduction

Recently, one of us has described the synthesis of a series of organometallic thioethers R_3MSR' (M = C, Si, Ge, or Sn) and their metal complexes with $W(CO)_6$ (1, 2). During studies of these compounds, it became apparent that structural evidence for p_π—d_π S → M π-bonding was probably accessible via an X-ray study of the ligands in which M = Si. It was also observed that decomposition of many of the complexes, $W(CO)_5(R_3MSR')$, to *cis*-disubstituted W(I) derivatives, $[W(CO)_4(SR')]_2$, was possible under appropriate conditions. This paper reports preparations and structures of the ligand Ph_3SiSPh and of $[W(CO)_4SPh]_2$, a W(I) decomposition product of the 1:1 complex between $W(CO)_6$ and Ph_3SiSPh.

Experimental

Reagents were obtained from the Aldrich Chemical Co. Inc., and were used without further purification. Spectroscopic data were obtained using the following instruments: ir, Perkin Elmer Model 283; nmr, Varian EM-360 or Bruker WP80 Fourier transform; mass spectra, VG Micromass 7070HS. X-ray diffraction data were collected using a Picker FACS-I four circle diffractometer with local (NRC) automation. Standard Schlenk techniques were used throughout and unless noted, procedures were carried out under an atmosphere of dry nitrogen. Analyses were performed by Canadian Microanalytical Service Ltd.

[1]NRCC No. 27026.

Preparative

(a) DABCO·HSPh

DABCO, (1,4-diazabicyclo[2.2.2]octane) (2.2 g, 20 mmol), was dissolved in dry toluene (15 mL) (freshly distilled from sodium) and thiophenol (2.1 mL, 20 mmol) was added portionwise. The precipitate of DABCO·HSPh which began to form after a few seconds was stirred for 2 h under a $CaCl_2$ drying tube. The suspension was filtered, transferred without washing to a Schlenk tube, covered with a glass wool plug, and placed under vacuum. After continuous pumping for 2 h at an oil pump, the solid was dry. Yield 3.1 g (70%), mp 95–97°C (lit. 97–98°C) (3).

(b) Ph_3SiSPh

DABCO·HSPh (3.1 g, 14 mmol) and Ph_3SiCl (4.1 g, 14 mmol) were suspended in dry benzene (42 mL) and stirred under a $CaCl_2$ drying tube for 2 days. The suspension was filtered and volatiles were removed from the filtrate under vacuum to leave a nearly colourless oil which crystallized upon standing. Crystals from hexane have mp 97–98°C (lit. 95–96°C) (3). Mass spectrum has major peaks at m/e = 368 $(Ph_3SiSPh)^+$, 259 $(Ph_3Si)^+$. Nuclear magnetic resonance in CCl_4 consists of a complex multiplet centered at 7.3 ppm from internal TMS.

(c) $[W(CO)_4SPh]_2$

Tungsten hexacarbonyl (5.3 g, 15 mmol) was dissolved in dry tetrahydrofuran (200 mL) in a Pyrex flask fitted with a double surface condenser, a magnetic stirrer, and a gas dispersion inlet tube. The top of the condenser was connected to an oil bubbler and the solution was irradiated for 4 h with a 100 W uv lamp while stirring and passing a stream of nitrogen bubbles through the solution. The lamp was switched off, Ph_3SiSPh (5.5 g, 15 mmol) was added, and the solution

Can. J. Chem. Downloaded from www.nrcresearchpress.com by 78.46.186.204 on 09/07/12
For personal use only.

Can. J. Chem. Downloaded from www.nrcresearchpress.com by 78.46.186.204 on 09/07/12
For personal use only.

was stirred for half an hour at which time water (1.0 mL, 55 mmol) was added. The solution was stirred a further half hour, volatiles were removed in vacuum on a warm water bath leaving a sticky residue and benzene (200 mL) was added. The mixture was stirred and refluxed overnight. The green solution was filtered, the off-white residue of $Ph_3SiOSiPh_3$ discarded and the filtrate taken to dryness in vacuum at 50°C. The residue was extracted several times with hexane, the extracts combined and concentrated and then chromatographed on Florisil using hexane as the eluant. The first green material to be eluted was discarded. The remaining green eluate was taken to dryness and placed in a sublimer at 40°C and 0.1 mm Hg to remove $W(CO)_6$. The residue was recrystallized from hexane. Yield 2.0 g (33%), mp 93°C (dec.). The mass spectrum shows a molecular ion peak at $m/e = 810$ and other peaks corresponding to sequential loss of all eight carbonyls. Nuclear magnetic resonance: ($CDCl_3$) multiplet 7.7 ppm from internal TMS. Infrared: (hexane) 2038 (s), 1979 (m), 1973 (m), 1964 (vs). *Anal.* calcd. for $C_{20}H_{10}O_8S_2W_2$: C 29.65, H 1.24, W 45.39; found: C 29.72, H 1.96, W 45.50.

X-ray studies

(a) Ph_3SiSPh

The compound crystallizes in the space group *Pcab* with a = 15.260(3) Å,[2] b = 15.968(2) Å, c = 16.757(2) Å, $Z = 8$ and d_{calc} = 1.20 g cm^{-3}. The space group was uniquely determined by the occurrence of systematic absences. The diffraction intensities of an approximately 0.25 × 0.35 × 1.0 mm crystal mounted in silicone grease inside an evacuated Lindemann capillary were collected at 295 K with graphite monochromatized MoKα radiation using the $\theta/2\theta$ scan technique with profile analysis (4) to $2\theta_{max} = 50°$ at a scan speed of 4°/min. A total of 3610 unique reflections were measured of which 1933 were considered significant with $I_{net} > 2.5\sigma(I_{net})$. Three standards were measured after every 100 reflections and no significant crystal decay was detected. Lorentz and polarization factors were applied but no absorption corrections were applied (μ = 2.13 cm^{-1}). Altogether, 440 systematic absences were measured, only three of which had significant intensities. No evidence for extinction was observed. The cell parameters were obtained by least-squares refinement of the setting angles of 90 reflections with $2\theta > 40°$ (MoKα1, λ = 0.70930 Å).

The structure was solved with MULTAN (5) plus a difference Fourier map, and refined by full-matrix least-squares with counting statistics weights. H-atom positions were calculated but their parameters were not refined. All heavier atoms were refined anisotropically. The final residuals are $R_F = 0.050$ and $R_W = 0.036$ for the significant data (R_F = 0.115 and R_W = 0.036 for all data). All calculations were performed with the NRCVAX system of programs (6). Scattering factors were taken from the International tables for X-ray crystallography (7).

The final atomic positional parameters and the equivalent isotropic temperature factors are listed in Table 1 while distances and angles are in Table 2. Anisotropic thermal parameters and final structure factors are available as supplementary data.[3] Figure 1 shows the molecule with the atomic numbering scheme.

(b) $[W(CO)_4SPh]_2$

The compound crystallizes in the space group $P2_1/c$ with a = 9.164(3) Å, b = 12.054(2) Å, c = 11.163(2) Å, β = 111.63(2)°, $Z = 2$ and d_{calc} = 2.35 g cm^{-3}. The space group was uniquely determined by the systematic absences. The diffraction intensities of an approximately 0.35 × 0.25 × 0.25 mm crystal glued to a glass fibre inside an evacuated Lindemann capillary were collected at 300 K with graphite monochromatized MoKα radiation using the $\theta/2\theta$ scan technique with profile analysis (4) to $2\theta_{max} = 60°$ at a scan speed of 4°/min. A total of 3356 unique reflections were measured of which 2748 were considered significant with $I_{net} > 2.5\sigma(I_{net})$. Three standards were measured after every 100 reflections and no significant crystal decay was detected. Lorentz and polarization factors were applied. It was not possible to calculate absorption corrections (μ = 10.5 mm^{-1}) because the mounting of the crystal made it impossible to measure the faces. No evidence for extinction was observed. Cell parameters were obtained by least-squares refinement of the setting angles of 58 reflections with $2\theta > 55°$ (MoKα1, λ = 0.70930 Å).

The structure was solved with MULTAN (5) and refined by full-matrix least-squares with counting statistics weights. H-atom positions were calculated and fixed in the refinement. The final residuals are $R_F = 0.062$ and $R_W = 0.062$ for the significant data (R_F = 0.072 and R_W = 0.062 for all data). All calculations were performed with the

TABLE 1. Positional and thermal parameters for Ph_3SiSPh

Atom	X	Y	Z	B_{eq}[a]
SI	0.45508(7)	0.29817(8)	0.48572(7)	4.37(6)
S	0.34075(7)	0.37272(8)	0.51153(7)	5.59(6)
C1	0.2907 (3)	0.3724 (3)	0.4156 (3)	4.48(24)
C2	0.2325 (3)	0.3095 (3)	0.3938 (3)	6.2 (3)
C3	0.1931 (3)	0.3133 (4)	0.3201 (4)	7.1 (3)
C4	0.2110 (3)	0.3769 (4)	0.2677 (3)	6.6 (3)
C5	0.2700 (3)	0.4386 (3)	0.2890 (3)	6.9 (3)
C6	0.3094 (3)	0.4363 (3)	0.3629 (3)	5.6 (3)
C7	0.5126 (3)	0.3408 (3)	0.39669(24)	3.70(20)
C8	5.5870 (3)	0.3897 (3)	0.4052 (3)	4.70(24)
C9	0.6296 (3)	0.4235 (3)	0.339 (3)	6.3 (3)
C10	0.5998 (3)	0.4059 (3)	0.2641 (3)	5.8 (3)
C11	0.5273 (3)	0.3569 (3)	0.25360(25)	4.92(24)
C12	0.48470(24)	0.3238 (3)	0.3191 (3)	4.65(24)
C13	0.4225 (3)	0.1869 (3)	0.4706 (3)	4.94(25)
C14	0.4670 (3)	0.1333 (3)	0.4202 (3)	6.0 (3)
C15	0.4435 (5)	0.0485 (4)	0.4129 (3)	8.6 (4)
C16	0.3762 (5)	0.0174 (4)	0.4559 (5)	9.5 (5)
C17	0.3307 (4)	0.0700 (5)	0.5058 (5)	10.9 (5)
C18	0.3542 (3)	0.1513 (3)	0.5148 (3)	7.8 (3)
C19	0.5257 (3)	0.3110 (3)	0.57573(25)	4.6 (3)
C20	0.5967 (4)	0.2578 (3)	0.5849 (3)	5.7 (3)
C21	0.6540 (4)	0.2663 (4)	0.6490 (4)	7.2 (3)
C22	0.6408 (4)	0.3290 (5)	0.7038 (4)	8.1 (4)
C23	0.5700 (4)	0.3798 (3)	0.6965 (3)	7.0 (3)
C24	0.5132 (3)	0.3724 (3)	0.6320 (3)	5.5 (3)
H2	0.2178	0.2605	0.4342	7.5
H3	0.1489	0.2650	0.3023	8.1
H4	0.1799	0.3780	0.2120	7.7
H5	0.2842	0.4853	0.2463	8.2
H6	0.3533	0.4851	0.3786	7.0
H8	0.6103	0.4013	0.4634	5.9
H9	0.6849	0.4606	0.3478	6.8
H10	0.6345	0.4293	0.2141	6.5
H11	0.5024	0.3459	0.1962	5.8
H12	0.4298	0.2845	0.3112	5.4
H14	0.5210	0.1550	0.3857	7.4
H15	0.4774	0.0066	0.3754	9.5
H16	0.3535	−0.0426	0.4514	9.6
H17	0.2774	0.0477	0.5412	11.9
H18	0.3196	0.1898	0.5555	8.9
H20	0.6073	0.2092	0.5441	6.8
H21	0.7086	0.2258	0.6541	8.0
H22	0.6854	0.3383	0.7494	8.6
H23	0.5571	0.4256	0.7412	7.7
H24	0.4596	0.4132	0.6265	6.4

[a] B_{eq} is the mean of the principal axes of the thermal ellipsoid.

[2] Throughout this work, esd's are in parentheses and refer to the last digit printed.

[3] A complete set of data may be purchased from the Depository of Unpublished Data, CISTI, National Research Council of Canada, Ottawa, Ont., Canada K1A 0S2.

TABLE 2. Selected distances (Å) and angles (deg) in Ph_3SiSPh

Bond	Distances	Bonds	Angle
S—C(1)	1.779(5)	Si—S—C(1)	99.5(1)
S—Si	2.156(2)	S—Si—C(19)	104.2(2)
Si—C(7)	1.860(4)	S—Si—C(13)	109.7(2)
Si—C(13)	1.863(5)	S—Si—C(7)	109.9(1)
Si—C(19)	1.865(4)	C(13)—Si—C(19)	111.7(2)
C(1)—C(2)	1.389(8)	C(7)—Si—C(13)	111.5(2)
C(2)—C(3)	1.376(9)	C(7)—Si—C(19)	109.6(2)
C(10)—C(11)	1.367(7)	C(1)—S—Si—C(7) (dihedral)	51.5(1)
C(15)—C(16)	1.349(11)	$Ph_{(S)}$—$Ph_{(Si)}$ (inter-plane)	27.4(1)
C(22)—C(23)	1.357(10)		
C(1)—C(7)	3.438(4)		
C(2)—C(12)	4.054(2)		
C(3)—C(12)	4.453(3)		
C(4)—C(12)	4.348(1)		
C(5)—C(12)	3.787(3)		
C(6)—C(12)	3.304(2)		

NRCVAX system of programs (6). The final difference map showed two peaks with electron density equivalent to 5 e/Å^{-3} on the W—S and W—C(3) bonds about 0.9 Å from W which may be due to the lack of absorption correction. Scattering factors were taken from the International tables for X-ray crystallography (7). The final atomic positional parameters and the temperature factors are listed in Table 3 while distances and angles are in Table 4. Anisotropic thermal parameters and final structure factors are available as supplementary data.[3] Figure 2 shows the molecule with the atomic numbering scheme.

Results and discussion

Preparative

(a) Ph_3SiSPh

Although we have had difficulty with the preparation of Ph_3SiSPh described in ref. 3, the modified method (use of stoichiometric amounts of reagents and careful exclusion of moisture) reported herein works reproducibly in our hands and the properties of the substance obtained by this method agree with those of the material reported previously.

(b) $[W(CO)_4SPh]_2$

Preparations of bridged W(I) dimers $[M(CO)_4X]_2$ (X = PR_2 (8), I (9), SH (10), and SR (11); M = Mo or W) including $[W(CO)_4SPh]_2$ (12) have been reported previously and some of these W(I) compounds have been the subject of X-ray crystallographic structure determinations (9, 13). Generally, however, W(I) is less common than other oxidation states of tungsten and therefore all aspects of the formation, bonding, reactivity, and structure of its compounds are of interest. Isolation of $[W(CO)_4SPh]_2$ from solutions containing $W(CO)_5(Ph_3SiSPh)$ may seem surprising but in fact a series of steps, all previously demonstrated, could give rise to green $[W(CO)_4SPh]_2$.

[1] $W(CO)_6 + Ph_3SiSPh \rightarrow W(CO)_5(Ph_3SiSPh)$

[2] $2W(CO)_5(Ph_3SiSPh) + H_2O \rightarrow 2W(CO)_5(HSPh) + Ph_3SiOSiPh_3$

[3] $W(CO)_5(HSPh) \rightarrow W(CO)_5SPh + (1/2)H_2$

[4] $2W(CO)_5SPh \rightarrow [W(CO)_4SPh]_2 + 2CO$

Reaction [1] is a normal carbonyl substitution and requires no further comment whereas [2] involves hydrolytic cleavage of a Si—S bond analogous to that reported many years ago for uncomplexed R_3SiSR' (14). More recently, the latter process has also been observed by Vahrenkamp (15) during formation of $W(CO)_5SH_2$ from $W(CO)_5S(SiMe_3)_2$ by hydrolysis. During workup of our reaction, a white solid was obtained with mass and ir spectra corresponding to $Ph_3SiOSiPh_3$.[4]

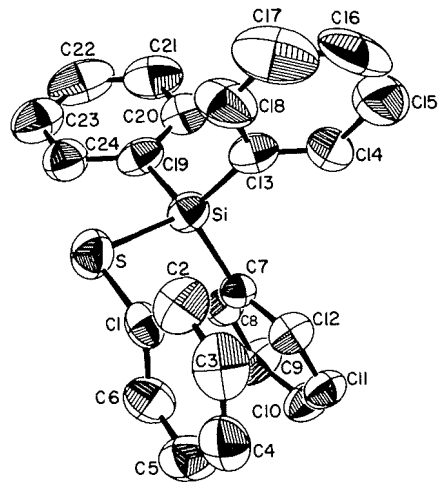

FIG. 1. ORTEP drawing of Ph_3SiSPh.

Reaction [3] represents a spontaneous process observed for ruthenium complexes of H_2S and EtSH (17) and for $W(CO)_5SH_2$ (10) while [4] is the equivalent of the dimerization of $W(CO)_5SH$ to $[W(CO)_4SH]_2$ reported by Vahrenkamp (10) which presumably involves a *cis*-labilizing effect in the monomer due to the lone pairs on sulfur (18).

Structural

(a) Ph_3SiSPh

The structure of Ph_3SiSPh (Fig. 1) is unremarkable except for the bond angle at S (99.5°) and the Si—S bond length (2.156 Å). Bond angles at sulfur in thioethers and organometallic thioethers are typically 105–109° (19, 20) and there are no close interactions between molecules in the unit cell of Ph_3SiSPh which would account for the significant closing of its C—S—Si angle. There is, however, a close approach of the phenyl ring on sulfur to one of those on silicon (Table 2). Van der Waal's forces of attraction between these two phenyl rings

[4]Mass spectrometry: molecular ion, M^+_{calc} = 534; M^+_{found} = 534. Infrared: corresponds to literature (16), in particular a strong, broad band at 1058 cm^{-1} due to Si—O stretching.

Can. J. Chem. Downloaded from www.nrcresearchpress.com by 78.46.186.204 on 09/07/12
For personal use only.

TABLE 3. Positional and thermal parameters for $[W(CO)_4SPh]_2$

Atom	X	Y	Z	B_{iso}[a]
W	0.42011(6)	0.03508(4)	0.08794(5)	2.512(23)
S	0.3387 (4)	0.0792 (3)	−0.1442 (3)	2.80 (15)
O1	0.0882 (14)	0.1224 (11)	0.0660 (12)	6.4 (7)
O2	0.5422 (14)	0.2839 (8)	0.1199 (11)	5.6 (6)
O3	0.5051 (15)	0.0591 (10)	0.3838 (11)	5.9 (7)
O4	0.2580 (13)	−0.2026 (9)	0.0612 (12)	5.6 (7)
C1	0.2090 (18)	0.0910 (13)	0.0719 (14)	3.9 (7)
C2	0.5078 (15)	0.1936 (12)	0.1079 (14)	3.2 (7)
C3	0.4774 (16)	0.0453 (12)	0.2708 (18)	4.3 (8)
C4	0.3154 (14)	−0.1183 (13)	0.0693 (13)	3.2 (7)
C11	0.1550 (16)	0.0163 (11)	−0.2434 (12)	2.9 (6)
C12	0.1407 (18)	−0.0866 (12)	−0.2922 (15)	4.1 (7)
C13	−0.0038 (19)	−0.1246 (13)	−0.3733 (16)	4.9 (8)
C14	−0.1329 (18)	−0.0590 (14)	−0.4045 (15)	4.5 (8)
C15	−0.1175 (18)	0.0448 (16)	−0.3547 (17)	5.6 (9)
C16	0.0277 (19)	0.0844 (13)	−0.2773 (15)	4.7 (8)
H12	0.244	−0.141	−0.267	4.6
H13	−0.016	−0.211	−0.405	5.4
H14	−0.247	−0.088	−0.470	5.1
H15	−0.223	0.098	−0.371	6.1
H16	0.041	0.169	−0.237	4.8

[a] B_{iso} is the mean of the principal axes of the thermal ellipsoid.

TABLE 4. Selected distances (Å) and angles (deg) in $[W(CO)_4SPh]_2$

Bond	Distances (Å)	Bonds	Angle (deg)
W—S	2.476(4)	S—W—S′	106.3(1)
W—S′	2.481(4)	S—W—C(1)	85.7(5)
W—C(1)	1.99(2)	S—W—C(2)	82.4(4)
W—C(2)	2.05(1)	S—W—C(3)	163.8(4)
W—C(3)	1.91(2)	S—W—C(4)	97.9(4)
W—C(4)	2.06(1)	S′—W—C(1)	162.8(5)
S—C(11)	1.81(1)	S′—W—C(2)	102.3(4)
O(1)—C(1)	1.15(2)	S′—W—C(3)	84.1(4)
O(2)—C(2)	1.13(2)	S′—W—C(4)	82.3(4)
O(3)—C(3)	1.20(2)	C(1)—W—C(2)	91.3(6)
O(4)—C(4)	1.13(2)	C(1)—W—C(3)	87.1(6)
C(11)—C(12)	1.34(2)	C(1)—W—C(4)	83.9(6)
C(11)—C(16)	1.36(2)	C(2)—W—C(3)	83.2(6)
C(12)—C(13)	1.38(2)	C(2)—W—C(4)	175.2(6)
C(13)—C(14)	1.36(2)	C(3)—W—C(4)	95.8(6)
C(14)—C(15)	1.35(3)	W—S—C(11)	113.9(5)
C(15)—C(16)	1.38(2)	W′—S—C(11)	117.7(5)
W—W′	2.972(1)	W—C(1)—O(1)	178(1)
H(12)—O(2′)	2.670(1)	W—C(2)—O(2)	174(1)
		W—C(3)—O(3)	175(1)
		W—C(4)—O(4)	179(1)
		S—C(11)—C(12)	125(1)
		S—C(11)—C(16)	115(1)
		C(12)—C(11)—C(16)	120(1)
		C(11)—C(12)—C(13)	120(1)
		C(12)—C(13)—C(14)	121(1)
		C(13)—C(14)—C(15)	119(1)
		C(14)—C(15)—C(16)	121(1)
		C(11)—C(16)—C(15)	120(1)

may therefore be the cause of the sharp angle at sulfur since the minimum distances between carbon atoms on the adjacent rings are about the same as the sum of the van der Waal's radii for carbon (2 × 1.70 Å) (21) (Table 2).

In our earlier spectroscopic studies (1, 2), evidence was presented for the presence of S → M p_π—d_π bonding in R_3MSR' (M = Si, Ge, Sn). Furthermore, the evidence suggested that this bonding was weak and unlikely to cause observable shortening of the M—S bond except perhaps when M = Si. This expectation has now been supported by experiment because when M = Ge or Sn, M—S bonds are usually found to be nearly the same (±0.01 Å) as those predicted by addition of covalent radii (20). In contrast, we find that when M = Si, shortening of 0.05 Å is observed (Table 2).

(b) $[W(CO)_4SPh]_2$

The molecule is a dimer with a crystallographic center of symmetry as shown in Fig. 2. Each W atom is six-coordinated to four CO groups and two S atoms which form a distorted octahedron. A phenyl ring is attached to each S atom which in turn coordinates to the two symmetry-related distorted octahedra with an S—W—S′ angle of 106.3(1)° and an S—W—C(3) angle of 163.8(4)° indicating maximum deviations of 16.3° from a right angle between the two coordinated sulfurs and 16.2° from a linear arrangement of S—W—CO. The distance between the planes of the two phenyl rings is 1.97(1) Å.

The compound contains formal W(I) which should be paramagnetic. The fact that a normal unshifted and unbroadened nmr spectrum is obtained suggests, however, that the substance is diamagnetic. Formation of a W—W bond would give such a diamagnetic compound in which each tungsten atom has achieved 18 valence electrons. Consistent with this hypothesis, the bond angles at W and S in the W_2S_2 ring are obtuse and acute, respectively, and the W—W distance is 2.972(1) Å which may be compared to the W—W distance of 3.222 Å in $[(\eta^5\text{-}C_5H_5)W(CO)_3]_2$ (22). The average W—S distance of 2.48 Å is substantially shorter than the distance of 2.59 Å found in the singly bridged W(O) ion $[W(CO)_5(\mu\text{-}SC_6Cl_5)W(CO)_5]^-$ (23). The *trans* influence relative to CO of the sulfur ligand is seen from the difference between the average length of the metal–carbonyl bonds *trans* to sulfur (1.95 Å) and that of the *cis* bonds (2.05 Å).

Can. J. Chem. Downloaded from www.nrcresearchpress.com by 78.46.186.204 on 09/07/12
For personal use only.

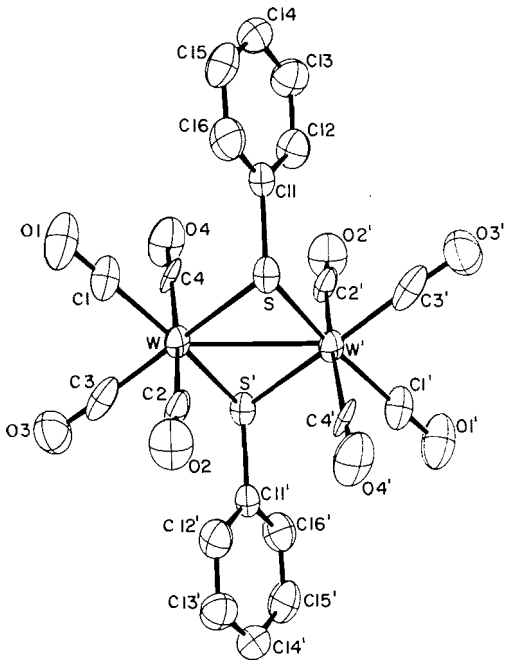

FIG. 2. ORTEP drawing of $W_2(CO)_8(SPh)_2$.

The tendency for binuclear tungsten carbonyl complexes with single sulfur bridges to distort to relieve CO repulsions between the two halves of the molecule has been noted for $[W(CO)_5(\mu\text{-}SH)W(CO)_5]^-$ (24) and it may be that distortion of two of the carbonyls that are *cis* to both sulfurs in $[W(CO)_4SPh]_2$ is due to the fact that the double sulfur bridges hold the two halves of the molecule in a nearly eclipsed conformation (OC(2)—W—W′—C(4′)O torsion angle 2.67°). It is more likely, however, that the distortion of just one of those carbonyls in each half of the molecule is due to close contact between the O of the distorted carbonyl and one of the *ortho*-H's of the phenyl ring (H(12)—O(2′) = 2.670 Å); sum of van der Waal's radii 2.70 Å (21). The very wide S—W—S′ angle (106.3°) has little effect on the rest of the octahedron but is matched by a correspondingly small W—S—W′ angle (73.67°), consistent with the presence of a W—W bond. The W—W distance (2.972 Å), W—S average (2.478 Å), W—C_{eq} average (1.954 Å) and W—C_{ax} average (2.056 Å) are very similar to the corresponding distances in the Mo(I) compound $[Mo(CO)_4\text{-}\mu\text{-}SBu']_2$ (Mo—Mo 2.984 Å; Mo—S 2.48 Å; Mo—C_{eq} 2.01 Å; Mo—C_{ax} 2.05 Å) (25) and to those in $[W(CO)_4\text{-}\mu\text{-}SMe]_2$ (W—W 2.97 Å; W—S 2.47 Å; W—C_{CO} 1.98–2.03 Å) (13). Comparable distances in $[\eta^5\text{-}(C_5H_5)M(CO)_3]_2$ (M = Mo or W) are Mo—Mo 3.235 Å; W—W 3.222 Å; W—CO 1.975, 1.956, 1.996 Å; Mo—CO 1.984, 1.964, 1.983 Å (22).

Acknowledgements

This work was supported by the Department of Chemistry, Memorial University of Newfoundland, and by the Division of Chemistry, NRC, Ottawa. The assistance of Miss M. Baggs and Dr. B. Gregory with mass spectra and of Dr. L. K. Thompson with aspects of the structural studies is gratefully acknowledged.

1. C. R. LUCAS. Can. J. Chem. **61**, 1096 (1983).
2. C. R. LUCAS. Can. J. Chem. **64**, 1758 (1986).
3. D. BRANDES. J. Organomet. Chem. **136**, 25 (1977).
4. D. F. GRANT and E. J. GABE. J. Appl. Crystallogr. **11**, 114 (1978).
5. G. GERMAIN, P. MAIN, and M. M. WOOLFSON. Acta Crystallogr. A**27**, 368 (1971).
6. E. J. GABE, F. L. LEE, and Y. LEPAGE. *In* Crystallographic computing 3. *Edited by* G. Sheldrick, C. Kruger, and R. Goddard. Clarendon Press, Oxford. 1985. p. 167.
7. International tables for X-ray crystallography. Vol. IV. Kynoch Press, Birmingham, England. 1974. p. 99, Table 2.2B.
8. A. TRENKLE and H. VAHRENKAMP. Chem. Ber. **114**, 1366 (1981).
9. G. SCHMID and R. BOESE. Ber. **109**, 2148 (1976).
10. M. HERBERHOLD and G. SUSS. J. Chem. Res. M2720 (1977).
11. B. ZHUANG, S. W. MCDONALD, F. A. SCHULTZ, and W. E. NEWTON. Inorg. Chim. Acta, **99**, L29 (1985).
12. W. SCHULZE and M. L. Ziegler. Z. Anorg. Allg. Chem. **481**, 78 (1981).
13. A. WINTER, O. SCHEIDSTEGER, and G. HUTTNER. Z. Naturforsch. **38**B, 1525 (1983).
14. E. W. ABEL. J. Chem. Soc. 4406 (1960).
15. H. VAHRENKAMP. *In* Sulfur, its significance for chemistry, for the geo-, bio- and cosmosphere and technology. *Edited by* A. Muller and B. Krebs. Elsevier, Amsterdam. 1984. p. 125.
16. H. KRIEGSMAN and K. H. SCHOWTKA. Z. Phys. Chem. Leipzig, **209**, 261 (1958).
17. C. G. KUEHN and H. TAUBE. J. Am. Chem. Soc. **98**, 689 (1976).
18. D. L. LICHTENBERG and T. L. BROWN. J. Am. Chem. Soc. **100**, 366 (1978).
19. J. C. J. BART and J. J. DALY. J. Chem. Soc. Dalton Trans. 2063 (1975).
20. J. PICKARDT, H. SCHUMANN, C. F. CAMPANA, and L. F. DAHL. J. Organomet. Chem. **216**, 245 (1981).
21. A. BONDI. J. Phys. Chem. **68**, 441 (1964).
22. R. D. ADAMS, D. M. COLLINS, and F. A. COTTON. Inorg. Chem. **13**, 1086 (1974).
23. M. K. COOPER, P. A. DUCKWORTH, M. SAPORTA, and M. MCPARTLIN. J. Chem. Soc., Dalton Trans. 570 (1980).
24. M. K. COOPER, P. A. DUCKWORTH, K. HENRICK, and M. MCPARTLIN. J. Chem. Soc. Dalton Trans. 2357 (1981).
25. M. KAMATA, T. YOSHIDA, and S. OTSUKA. J. Am. Chem. Soc. **103**, 3572 (1981).

Can. J. Chem. Downloaded from www.nrcresearchpress.com by 78.46.186.204 on 09/07/12
For personal use only.

Detection of the isotopes of lithium using the Faraday effect

SHI-LIAN JING AND ROGER STEPHENS[1]

Department of Chemistry, Dalhousie University, Halifax, N.S., Canada B3H 4J3

Received September 11, 1986

This paper is dedicated to Professor Douglas E. Ryan on the occasion of his 65th birthday

SHI-LIAN JING and ROGER STEPHENS. Can. J. Chem. **65**, 903 (1987).

Lithium is atomised in an air–acetylene flame within a longitudinal magnetic field. Birefringent and dichroic signals are separately measured using a pulsed hollow cathode source. The arrangement is found to give isotopic selectivity and is useable down to concentrations of about 10 μg/mL. The signal ratio of birefringence: dichroism is found to be approximately independent of sample concentration at the high and low extremes of the calibration curve. However, severe distortions occur at intermediate concentrations. In addition, a reversal of signal magnitudes is observed between ^{6}Li and ^{7}Li. This effect is attributed primarily to a distortion of the source profile as a result of self-absorption.

SHI-LIAN JING et ROGER STEPHENS. Can. J. Chem. **65**, 903 (1987).

Le lithium est atomisé dans une flamme air/acétylène comportant un champ magnétique longitudinal. On peut faire des mesures séparées des signaux biréfringent et dichroïque en utilisant une source à cathode creuse et pulsée. On a trouvé que cet arrangement donne une bonne sélectivité isotopique et qu'on peut l'utiliser jusqu'à des concentrations aussi faibles que 10 μg/mL. On a trouvé que, aux limites extrèmement élevée ou basse de la courbe de calibration, le rapport des signaux de biréfringence/dichroïsme est pratiquement indépendant de la concentration de l'échantillon. Toutefois, il se produits d'importantes distortions aux concentrations intermédiaires. De plus, on observe un renversement des amplitudes des signaux entre le ^{6}Li et le ^{7}Li. On attribue principalement cet effet à une distortion du profil de la source qui provient d'une auto-absorption.

[Traduit par la revue]

Introduction

Magneto-optic rotation (MOR) has been used for the selective detection of the isotopes of lead (*1*). The technique employed the ratio of birefringence to dichroism in a Voigt optical configuration as a measurement parameter. The particular advantage of this approach is an ability to identify the different isotopes with an apparatus which uses a conventional, commercially available light source and atomiser: the method can tolerate the overlap of the hyperfine components of the atomic spectra without recourse to the use of isotopically pure sources and low pressure atomisers in order to optimise spectroscopic resolution.

The ratio parameter is isotopically sensitive because the shape of an atomic line profile changes as the isotopic composition of the atomic vapor is altered. Since birefringence and dichroism show a different functional dependence on the form of the profile their ratio is automatically responsive to such variations. The ratio parameter is otherwise robust, being largely independent of source intensity and of background absorption by non-atomic species, and with a reasonable tolerance towards limited changes in the sample concentration.

One disadvantage of the original apparatus proved to be a need for high sample concentrations in order to obtain adequate signal-to-noise (S/N) ratios. Subsequently this problem became even more apparent during an attempt to extend the technique to lithium. In spite of the known suitability of the isotopes ^{6}Li, ^{7}Li for selective detection by conventional spectroscopic methods (*2–4*), which implies that the differences between their respective response functions should be unusually large, the S/N ratio of the MOR apparatus remained poor. The present work examines the origin of this problem, and describes an instrumental modification which improves the sensitivity of the technique by one to two orders of magnitude.

Theory

Three main reasons are responsible for the poor S/N ratio observed in earlier experiments. The first lies in the use of a flame atomiser of short path length. The flame offers a convenient way to obtain a stable, continuous signal, but does not represent the most efficient way to atomise a sample. This point will not be expanded on here. The second reason arises from the optical configuration employed in the original apparatus, which lacked the flexibility to allow the S/N ratio to be optimised for any particular combination of atomiser background emission, source intensity, optical bandwidth etc. which might be encountered in a given experiment. Finally, attention must be given to the effect of magnetic field strength. In any MOR apparatus the field strength controls the S/N ratio of the birefringent and dichroic signals. In an isotopic system it also influences the degree of discrimination between the different isotopic responses. These are independent requirements which tend to place conflicting demands on the value of the field strength to be used. For instance, a field which gives the best selectivity may be so low that the individual birefringent and dichroic signals are too weak to give a satisfactory S/N ratio unless high sample concentrations are available (a situation previously encountered with ^{206}Pb (*1*)).

The sensitivity losses caused by the last two factors can be offset by use of a Faraday optical configuration. At low field strengths the signals from the Faraday effect are stronger than from the Voigt, for reasons given elsewhere (*5*). The need to compromise between the requirements of selectivity and sensitivity is correspondingly less severe. The converse is also true: if the best selectivity is obtained at a field strength exceeding that for optimum sensitivity then the Voigt configuration becomes preferable (it should be noted that the field strengths which give the best selectivity are unlikely to be identical in the two configurations).

The ability of the Faraday configuration to allow for an optimisation of the birefringent and dichroic signals to suit any particular experimental situation is shown by the following argument. Consider the optical system which is shown schematically in Fig. 1. The Jones matrix, $\mathbf{J}$, of this system is given by:

$$[1] \quad \mathbf{J} = \mathbf{P}_y\mathbf{R}(\theta)\mathbf{r}\mathbf{U}^{-1}\mathbf{F}\mathbf{U}\mathbf{P}_x$$

where $\mathbf{P}_x$, $\mathbf{P}_y$, $\mathbf{F}$, $\mathbf{r}$ are respectively the Jones matrices of

[1]To whom all correspondence should be addressed.

Can. J. Chem. Downloaded from www.nrcresearchpress.com by 78.46.186.204 on 09/07/12
For personal use only.

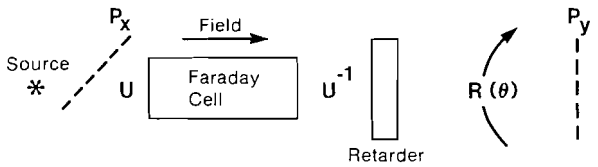

FIG. 1. Schematic MOR apparatus. $\mathbf{P}_x$, $\mathbf{P}_y$: polariser and analyser. $\mathbf{U}, \mathbf{U}^{-1}, \mathbf{R}(\theta)$ show the locations of the transformation matrices relative to the positions of the optical components.

polarisers P_x and P_y, of the Faraday cell, F, and of the retarder, r; $\mathbf{R}(\theta)$ is the rotation matrix which describes the displacement of P_y by some angle θ from an orthogonal position relative to P_x; and $\mathbf{U}, \mathbf{U}^{-1}$ are the similarity transform matrices between linear and circular basis vectors.

Writing the complex refractive index of the vapor in the Faraday cell as $\tilde{n} = n' + in''$ gives

$$\mathbf{F} = \begin{pmatrix} e^{i\tilde{n}_+ l} & 0 \\ 0 & e^{i\tilde{n}_- l} \end{pmatrix}$$

where l is the path length, and the subscripts +, − specify right and left handed circular components. Hence

$$[2] \quad \mathbf{F} = e^{i(\tilde{n}_+ + \tilde{n}_-)l/2} \begin{pmatrix} e^{i\Delta\tilde{n}l/2} & 0 \\ 0 & e^{i\Delta\tilde{n}l/2} \end{pmatrix}$$

where $\Delta\tilde{n} = \tilde{n}_+ - \tilde{n}_-$. Similarly, if 2δ is the retardance of r then

$$[3] \quad \mathbf{r} = \begin{pmatrix} e^{i\delta} & 0 \\ 0 & e^{-i\delta} \end{pmatrix}$$

Substitution of eqs. [2] and [3] into [1] allows eq. [1] to be evaluated as:

$$[4] \quad I = (1/4)I_0 e^{-(n''_+ + n''_-)l} \times [(\cosh \Delta n''l + \sin 2\delta \sin 2\theta \sinh \Delta n''l) - (\cos \Delta n'l \cos 2\theta + \cos 2\delta \sin 2\theta \sin \Delta n'l)]$$

where I is the transmitted intensity and I_0 is the unpolarised source intensity. The two terms in the inner brackets are the contributions from dichroism ($\Delta n''$) and birefringence ($\Delta n'$), respectively.

If r is a sinusoidal modulator with a peak retardance of $2\delta_0$ and circular frequency ω then $\delta = \delta_0 \sin \omega t$. The first and second harmonics contained in eq. [4] are then given by:

$$[5] \quad \begin{aligned} I_\omega &= (1/2)I_0 e^{-(n''_+ + n''_-)l} \sin 2\theta \, J_1(2\delta_0) \sinh \Delta n''l \sin \omega t \\ I_{2\omega} &= (1/2)I_0 e^{-(n''_+ + n''_-)l} \sin 2\theta \, J_2(2\delta_0) \sin \Delta n'l \cos 2\omega t \end{aligned}$$

where $J_1(2\delta_0)$, $J_2(2\delta_0)$ are the Bessel functions of order 1,2.

As $\tilde{n} \rightarrow$ unity then $\Delta\tilde{n} \rightarrow 0$, and the background transmission of eq. [4] becomes

$$[6] \quad I_B = (1/2)I_0 \sin^2 \theta$$

This result illustrates a significant advantage of the type of optical system shown in Fig. 1, namely that it produces a selective modulation of the signal of interest. Thus its use makes it relatively easy to reach a S/N ratio which is limited by shot noise rather than flicker, since it is technically feasible to employ a value of ω which is high enough for the flicker carried by I_B in eq. [6] to lie below shot noise. At the same time flicker noise caused by instability of the modulator (i.e. of δ_0) falls as the signal of interest falls, since the modulated terms in eq. [5] are all connected to $\Delta\tilde{n}$. The S/N behavior of this type of optical configuration is discussed at greater length elsewhere (6).

In practice additional terms are present in eq. [6]. These originate with the background emission from the atomiser or from non-resonance emission from the source (for example, if a wide aperture optical system of low resolving power is used). Given this extra input of stray light then optimisation of the S/N ratio is achieved by increasing θ. Equation [5] shows that the dichroic and birefringent signals increase simultaneously. Thus their S/N ratios both increase with θ until the background intensity contribution of eq. [6] becomes comparable to that of the other background sources, after which the S/N ratio becomes approximately constant (7). Thus the experimental adjustment of θ provides the means to simultaneously optimise the S/N ratios of both of the signals in eq. [5] for any particular conditions of background illumination. An application of the results of earlier work on optical linearisation shows that this use of θ as a linearising factor to improve the S/N ratio is almost ideal provided that θ is small (8). In other words one can probably find other types of (passive) optical system which will allow a comparable performance to be attained. However, the only way to achieve a significant improvement over the S/N ratios given by eqs. [5] and [6] is by a manipulation of the value of $\Delta\tilde{n}$, through some change in the way in which the optical anisotropy is introduced.

Finally it will be noted that a complete optimisation of the birefringent and dichroic signals in eq. [5] cannot be achieved simultaneously. This conclusion is quite general (8); it arises in the particular system considered here through the occurrence of the Bessel functions $J_1(2\delta_0)$, $J_2(2\delta_0)$ in the coefficients of the modulated birefringent and dichroic term. No single value of δ_0 exists which will allow $J_1(2\delta_0)$, $J_2(2\delta_0)$ to be maximised at the same time.

Experimental

The apparatus used here is shown in Fig. 2. The offset angle, θ, was applied to the analyser. The magnetic field was produced by a pair of air-cored coils driven by single half-cycles of the ac mains. The hollow cathode source (IL) was synchronised with the field coil to produce an emission pulse of 500 μs duration at the peak of the field. The pulse current was fixed at 80 mA. Observations were made over the duration of the emission pulse by gating the phototube pre-amplifier to the lamp supply. Details of this type of arrangement have been given (9). The field coils accommodated an air–acetylene burner with a 2.6 cm path length. In the Faraday configuration the peak field available was 0.2 Tessla.

The variable retarder shown in Fig. 2 was a PEM 80 photoelastic modulator (Hinds International, Portland, OR), ω = 50 kHz. Thus the birefringent and dichroic signals of eq. [5] appeared at frequencies of 100 kHz and 50 kHz, respectively. The value of δ_0 for the PEM was set empirically to give equal values of $J_1(2\delta_0)$, $J_2(2\delta_0)$ by inserting known static dichroic and birefringent optical elements in place of the burner head in the manner described previously (1).

Lamp emission at 670.8 nm was isolated by a 1/4 m monochromator (Oriel #7240, reciprocal dispersion = 6.4 nm/mm, slitwidth = 3 mm) and detected by an IP 28 photomultiplier. Electrical signals were taken through the gated pre-amplifier to 50 kHz and 100 kHz synchronous detectors which were phase-locked to the PEM. These circuits were built in the laboratory.

The isotopes ^{6}Li, ^{7}Li were supplied as their hydroxides by Stohler Isotope Chemicals, Montreal. Solutions were prepared in dilute HCl (Fisher; ACS reagent grade).

Results

The dependence of the S/N ratios of the birefringent and dichroic signals on the linearisation angle θ are shown in Fig. 3. The responses are quite normal, showing an initial,

Can. J. Chem. Downloaded from www.nrcresearchpress.com by 78.46.186.204 on 09/07/12
For personal use only.

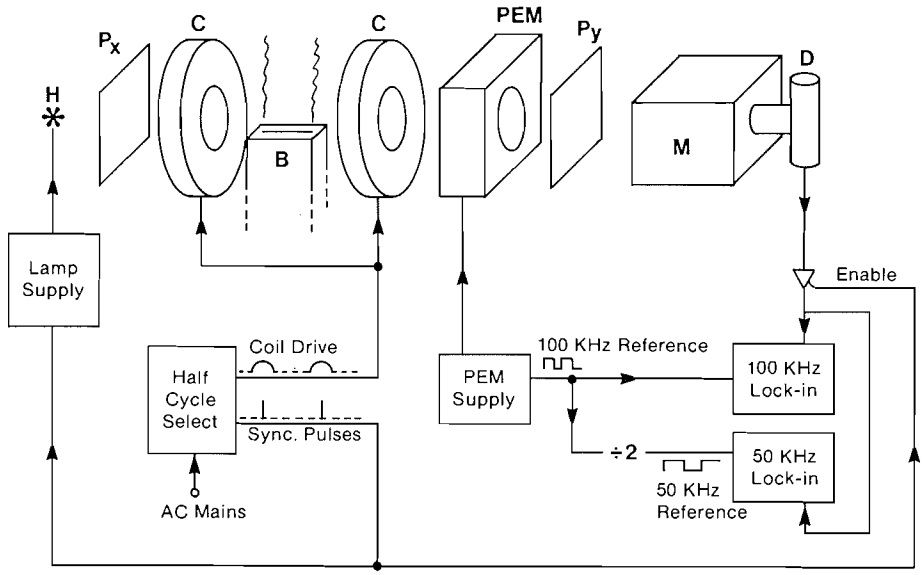

FIG. 2. Apparatus: B, air-acetylene burner; C, air-cored field coils; D, detector; H, hollow cathode source; M, monochromator; P_x, P_y, polariser, analyser.

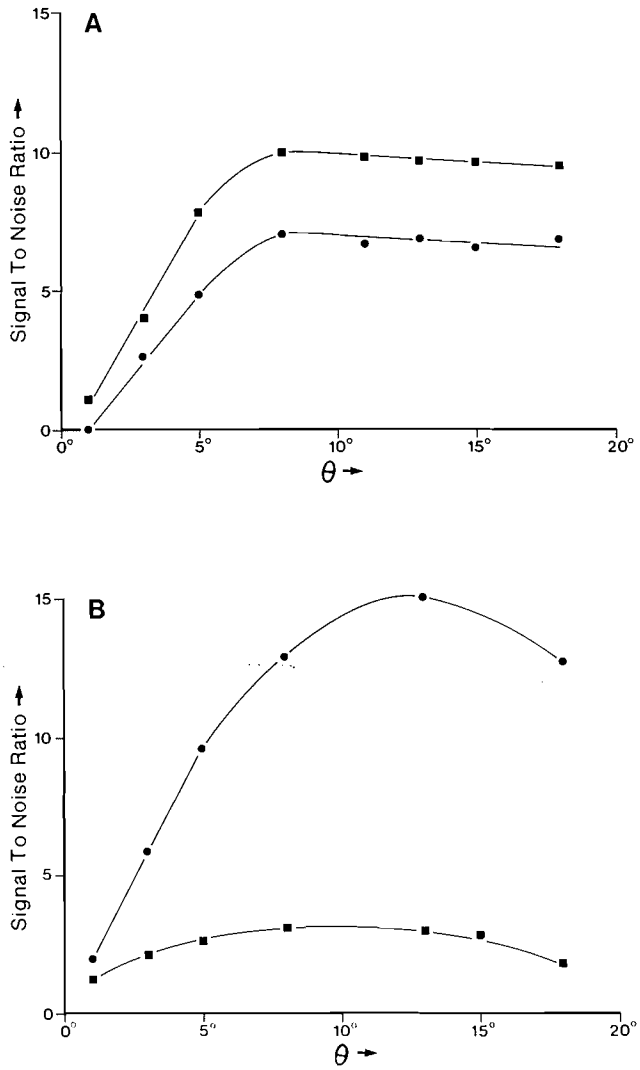

FIG. 3. 50 kHz dichroic signals ■ and 100 kHz birefringent signals ● observed for increasing values of the offset angle θ. A, ^{6}Li; B, ^{7}Li.

approximately linear increase followed by a slow reduction. The shapes of the response curves and the relatively large value of the optimum angle are characteristic of a shot noise limited measurement at a high background light level (7). A shot noise limited response of some form is to be expected: flicker in this type of modulation system can be detected using a laser source (6), but the flux from a hollow cathode lamp is normally insufficient for flicker to become significant relative to shot noise. The high level of stray light apparent from these data is the direct result of the use of a flame atomiser. All subsequent measurements in the Faraday configuration were made at a fixed offset angle of 10°.

The signal dependence on magnetic field strength, given in Fig. 4, shows that no particular selectivity advantage is obtained by working below the maximum available field strength. It is of interest to note that the results show dichroism to be stronger than birefringence for ^{6}Li, and *vice versa* for ^{7}Li. This observation demonstrates the isotopic selectivity of the measurement. However it also represents an exact reversal of the expected form of the response, since the lamp cathode (natural Li) would be expected to emit essentially the spectrum of ^{7}Li. The reason for the reversal lies partly in the frequency shift of the pressure broadened flame line, and partly in the use of a pulsed measurement by the present apparatus. The high pulse current through the source produces self-absorption of the lamp emission profile, which leads to a broadening and splitting of the emission lines. The quantitative explanation of the mechanism by which self-absorption reverses the response functions of the two isotopes will be given in more detail elsewhere.

The enhanced sensitivity of the present apparatus relative to the system based on the Voigt configuration is illustrated by their respective signals, shown in Fig. 5. It is clear that a considerable improvement in performance is obtained. This improvement allows a corresponding extension to be obtained at the low concentration end of the calibration curves. The results (Fig. 6) show that the ratio parameter is approximately independent of sample concentration at the high and low ends of the concentration range, in agreement with earlier results (1), and therefore allows isotopic composition to be determined

Can. J. Chem. Downloaded from www.nrcresearchpress.com by 78.46.186.204 on 09/07/12
For personal use only.

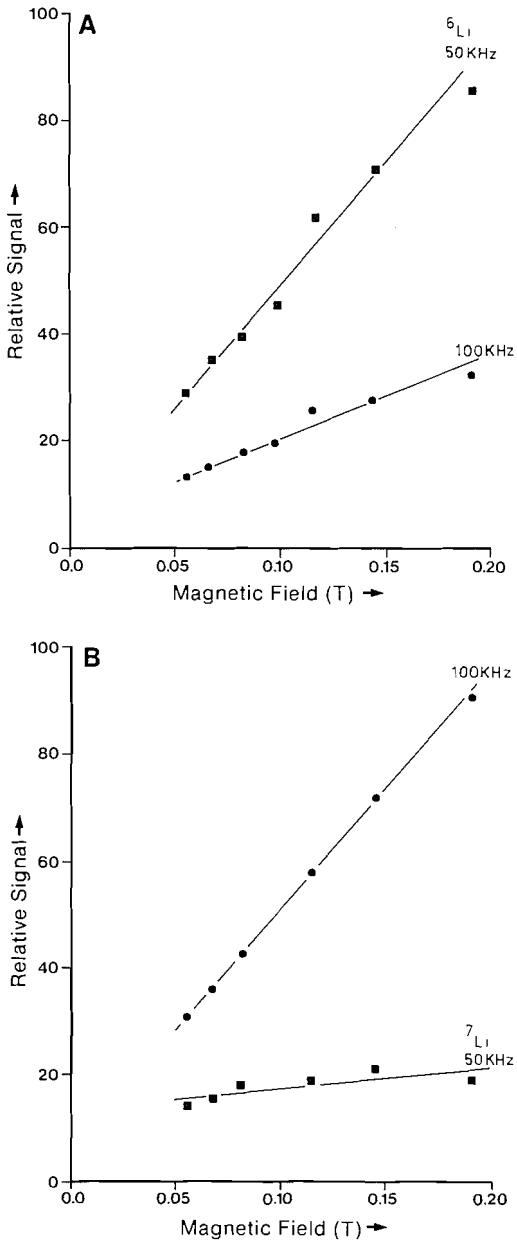

FIG. 4. 50 kHz ■ and 100 kHz ● signals observed with increasing magnetic field strength (Tessla). A, ^{6}Li; B, ^{7}Li.

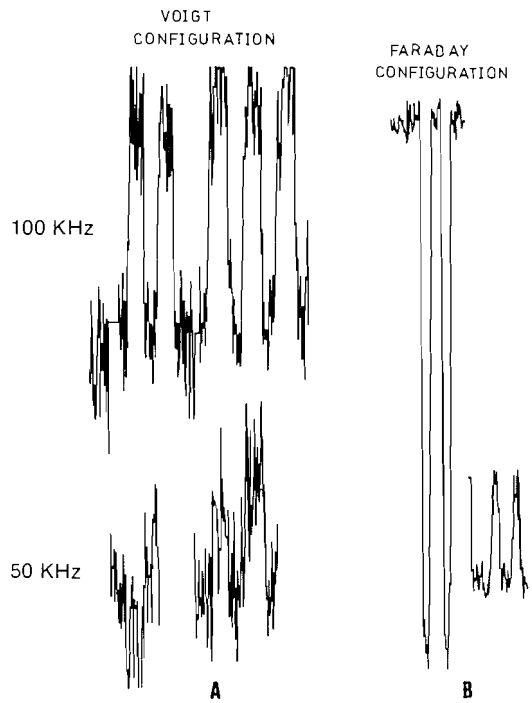

FIG. 5. 50 kHz and 100 kHz signals. (*A*) Voigt configuration at 0.4 Tessla (100 μg/mL); (*B*) Faraday configuration at 0.2 Tessla (30 μg/mL). Results were observed for natural Li.

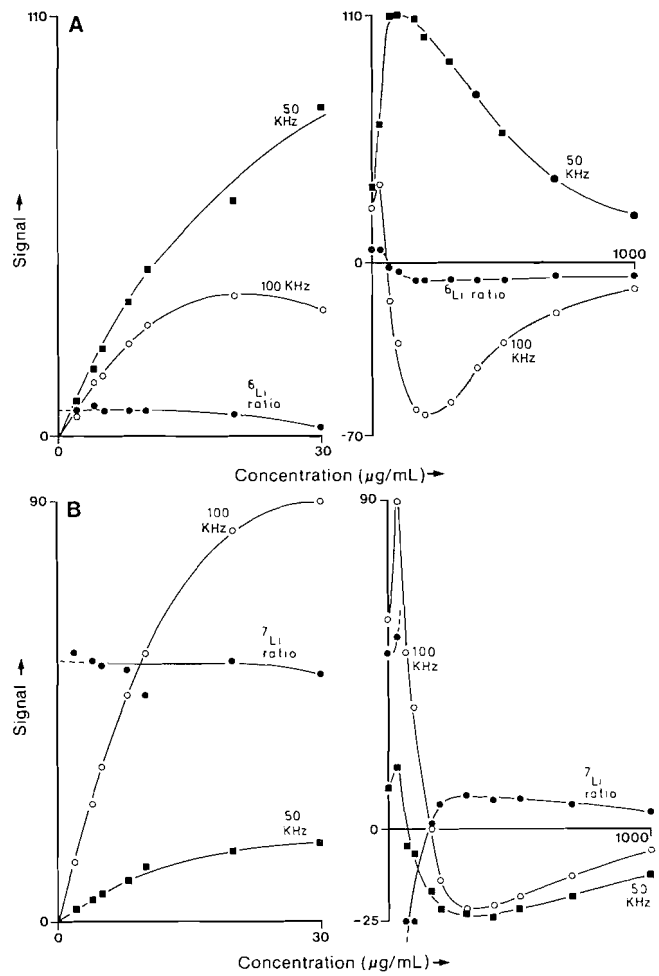

FIG. 6. Calibration curves, 0–30 and 0–1000 μg/mL. Symbols: ■ = 50 kHz; ○ = 100 kHz; ● = ratio of birefringence to dichroism; *A* and *B* give results for ^{6}Li and ^{7}Li, respectively.

without an exact knowledge of the sample concentration. However, the numerical values of the calibration constants at the two extremes do not coincide. Furthermore the fluctuations within the transition range are potentially quite drastic. Thus the stability of the ratio parameter towards variations in sample concentration is of only limited extent. Measurements can be made at one or other end of the concentration range but they cannot be mixed, while measurements in the transition range should be avoided altogether unless the sample concentration is known accurately.

The dependence of the signal ratio (birefringence:dichroism) on isotopic composition is shown in Fig. 7. Measurements were made at a fixed concentration of 2.3 m*M* (~15 μg/mL). This value lies approximately in the centre of the low concentration range data of Fig. 6, where the ratio parameter is relatively insensitive to concentration changes. The results suggest that the technique can be expected to distinguish variations in the proportion of ^{7}Li by perhaps ±5% relative to natural Li.

Can. J. Chem. Downloaded from www.nrcresearchpress.com by 78.46.186.204 on 09/07/12
For personal use only.

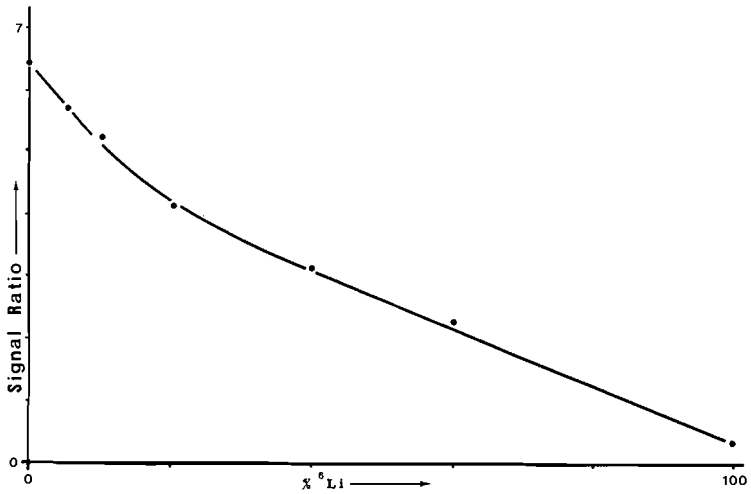

FIG. 7. Ratio of birefringence to dichroism for varying isotopic composition. Total concentration of Li fixed at 2.3 m*M*.

Conclusions

The present experiments have shown that the problem of poor sensitivity in the determination of isotopic composition by MOR can be largely overcome. The use of a Faraday optical configuration, linearised response functions, and the selective high frequency modulation of both birefringent and dichroic signals comprise the main features of the design. The system is built around standard, commercially available optical components, and the simplicity of the original system remains largely unchanged.

Two problems are evident as a result of the present work. The most serious of these is the limited range over which the response parameter remains independent of sample concentration. This increases the difficulties in developing a technique which will operate without the use of calibration standards. The second problem is the extent of the sensitivity of the measurement to self-absorption in the source, which suggests in general that calibration constants will be influenced by changes in the shape of the source profile. This behaviour is unsurprising and, given the excellent stability of modern hollow cathode sources, it seems likely that if the problem cannot be overcome it can at least be controlled simply by accurate regulation of the lamp supply. The trends observed in Fig. 6 imply that the sensitivity to the shape of the source profile may be less apparent at high concentrations.

Finally, it will be noted that the optical design described here is close to optimal, for the reasons outlined in the derivation of eq. [5]. Therefore it is concluded that the solution concentrations required to obtain the present results are approaching the lower limit to be expected for an apparatus which separately measures birefringence and dichroism by optical rotation in a flame atomiser. Small gains can be anticipated by, for example, increasing the field strength or improving the duty cycle of the source. Large improvements in performance appear likely to require more extensive adaptation, for instance through the use of non-flame atomisation.

Acknowledgement

The authors are indebted to the Natural Sciences and Engineering Research Council of Canada for support of this work.

1. R. STEPHENS. Spectrochim. Acta, **40B**, 1259 (1985).
2. D. C. MANNING and W. SLAVIN. At. Abs. Newlett. **8**, 1 (1962).
3. J. A. GOLEB and Y. YOKOYAMA. Anal. Chim. Acta, **30**, 213 (1964).
4. J. A. WHEAT. Appl. Spectrosc. **25**, 328 (1971).
5. J. J. KANKARE and R. STEPHENS. Appl. Spectrosc. **34**, 590 (1980).
6. J. J. KANKARE and R. STEPHENS. Talanta, **33**, 571 (1986).
7. J. J. KANKARE and R. STEPHENS. Spectrochim. Acta, **38B**, 1301 (1983).
8. R. STEPHENS. Spectrochim. Acta, **38**, 1077 (1983).
9. T. Z. GUO and R. STEPHENS. Anal. Chem. **57**, 424 (1985).

Can. J. Chem. Downloaded from www.nrcresearchpress.com by 78.46.186.204 on 09/07/12
For personal use only.

Concerning lone-pair stereospecificity of intramolecular OH hydrogen bonds to oxygen and sulfur in solution

TED SCHAEFER, DAVID M. MCKINNON, RUDY SEBASTIAN, JAMES PEELING,[1] GLENN H. PENNER, AND RICHARD P. VEREGIN

Department of Chemistry, University of Manitoba, Winnipeg, Man., Canada R3T 2N2

Received July 23, 1986

This paper is dedicated to Professor Douglas E. Ryan on the occasion of his 65th birthday

TED SCHAEFER, DAVID M. MCKINNON, RUDY SEBASTIAN, JAMES PEELING, GLENN H. PENNER, and RICHARD P. VEREGIN. Can. J. Chem. **65**, 908 (1987).

The ^{1}H nuclear magnetic resonance spectra for CCl_4 solutions are analyzed for 2-(thiocthyl)phenol, 2,3-dimethoxyphenol, and 8-hydroxythiochroman. The chemical shifts of the hydroxyl protons in these compounds, in 2,3-dihydroxyanisole, and 2-hydroxybenzyl methyl ether are discussed in terms of stereospecific intramolecular OH hydrogen bonds to lone-pair electrons on oxygen and sulfur. The O—H...O hydrogen bonds can be adequately discussed in terms of equivalent lone pairs on oxygen. There is very little difference between the hydrogen bond energies for 2,3-dihydroxyanisole and 2,3-dimethoxyphenol. In the latter the central hydrogen bonded methoxy group lies nearly perpendicular to the ring plane. The O—H...S hydrogen bonds are best described in terms of nonequivalent, 3*s* and 3*p*, lone pairs on sulfur. It is estimated that an O—H...3*s* hydrogen bond is at least 8 kJ/mol weaker than an O—H...3*p* hydrogen bond. The former is predominant in the thiochroman derivative and the latter in the thioethylphenol, in which the thioethyl group prefers a plane perpendicular to the benzene ring. The long-range benzylic coupling constants in the thiochroman derivative indicate inversion of the saturated ring between distorted half-chair conformations. The boat conformation can be ruled out.

TED SCHAEFER, DAVID M. MCKINNON, RUDY SEBASTIAN, JAMES PEELING, GLENN H. PENNER et RICHARD P. VEREGIN. Can. J. Chem. **65**, 908 (1987).

On a analysé les spectres de résonance magnétique nucléaire du ^{1}H, déterminés en solution dans le CCl_4, du thioéthyl-2 phénol, du diméthoxy-2,3 phénol et de l'hydroxy-8 chromane. On discute des déplacements chimiques des protons hydroxyles de ces composés ainsi que ceux du dihydroxy-2,3 anisole et de l'hydroxy-2 benzyl méthyl éther en fonction des liaisons hydrogènes OH intramoléculaires stéréospécifiques vers les paires d'électrons libres de l'oxygène et du soufre. On peut discuter d'une façon adéquate des liaisons hydrogènes O—H...O en fonction des paires équivalentes d'électrons libres sur l'oxygène. Il y a peu de différences entre les énergies des liaisons hydrogènes du dihydroxy-2,3 anisole et du diméthoxy-2,3 phénol. Dans ce dernier cas, le groupement méthoxyle central, qui est impliqué dans le liaison hydrogène, est pratiquement perpendiculaire au plan du cycle. La meilleur façon de décrire les liaisons hydrogènes O—H...S implique l'utilisation des paires libres non-équivalentes, 3*s* et 3*p*, du soufre. On évalue qu'une liaison hydrogène O—H...3*s* est plus faible que la liaison hydrogène O—H...3*p* et que la différence d'énergie est d'au moins 8 kJ/mol. Le premier type prédomine dans le dérivé thiochromane et le dernier type prédomine dans le thioéthylphénol, dans lequel le groupement thioéthyle se retrouve préférentiellement dans un plan perpendiculaire au plan du noyau benzénique. Les constantes de couplage benzylique à longue distance dans le dérivé thiochromane indiquent qu'il se produit une inversion du cycle saturé entre des conformations demi-chaises déformées. On peut exclure la présence de la conformation bateau.

[Traduit par la revue]

Introduction

An interesting aspect of hydrogen bonds concerns their formation along lone-pair directions (1–4). For example, intermolecular O—H...O bonds in the solid state, sampled over many such bonds, do not display a preference for the tetrahedral[2] lone-pair directions when the acceptor atom is divalent, but do prefer the plane of such lone pairs (1, 3). This observation is consistent with MO computations (5), which indicate that the proton donor molecule can move in this plane without a large loss in energy of interaction, and with experimental electron density maps of the lone-pair region of an epoxide (2). In the gas phase, F—H...O bonds display a (weak) preference for the lone-pair directions (6, 7). For N—H...O=C bonds in solids, formation along the direction of the sp^2 lone pairs is apparent (3). According to Taylor and Kennard (1), the directionality of sp^2 lone pairs may well be more marked than for sp^3 lone pairs.[3] In solution, the directionality of intermolecular X—H...Y bonds is less easily measured and has not been described.

However, *intramolecular* hydrogen bonding to a specific lone pair is known for O—H...S bonds in molecules in solution (10, 11). In benzenethiol the stable conformation is the one in which the S—H bond lies in the benzene plane and the barrier to internal rotation about the C—S bond is 3.4 kJ/mol (12), reflecting some $3p...\pi$ conjugational stabilization of the planar form. However, for 2-hydroxybenzenethiol, **1** (R = H), long-

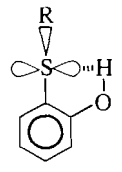

1

range spin–spin coupling constants in CCl_4 solution demonstrate that the S—H bond prefers a plane perpendicular to

[1]University of Petroleum and Minerals, Dhahran, Saudi Arabia.

[2]Canonical molecular orbitals for divalent oxygen compounds distinguish between a mainly 2*s* lone pair and a mainly 2*p* lone pair perpendicular to the R—O—R plane. The tetrahedral localized lone pairs can be derived from the canonical orbitals by unitary transformations.

[3]Some theoretical approaches consider the deformation of the lone pair caused by formation of the hydrogen bond (8, 9).

Can. J. Chem. Downloaded from www.nrcresearchpress.com by 78.46.186.204 on 09/07/12
For personal use only.

Can. J. Chem. Downloaded from www.nrcresearchpress.com by 78.46.186.204 on 09/07/12
For personal use only.

the benzene ring (10). This result is most simply interpreted as a consequence of a stereospecific hydrogen bond to the directional $3p$ lone pair on sulfur. The barrier to rotation about the C—O bond is much larger than about the C—S bond (stronger conjugation), so that it is energetically favorable to twist the $3p$ lone pair into the benzene plane to yield the O—H...S bond (10). Such a bond also has marked conformational consequences for **1** (R = CH_3, C_6H_5, and S—C_6H_5) (11).

In the gas phase the geometry of the complexes, H_2S,HCl and H_2S,HF, can be interpreted in an entirely analogous fashion, the X—H...S direction being very nearly perpendicular to the H_2S plane (13, 14). This model is consistent with the observation that electrophiles approach sulfur atoms along the hypothesized $3p$ lone-pair directions, whereas nucleophiles do so in the plane perpendicular to this lone pair (15).

It appears, therefore, that the stereospecificity observed for O—H hydrogen bonds to oxygen can be interpreted in terms of equivalent lone pairs, while those to divalent sulfur are best discussed in terms of nonequivalent lone pairs. A reason for this distinction may lie in the relative extensions of the orbitals in oxygen and sulfur atoms. Detailed computations (16) show that the $2s$ and $2p$ valence electrons in first row atoms occupy more or less the same region of space (the $2p$ lobes do not extend much beyond the $2s$ sphere while, of course, retaining their directionality). In atoms of higher rows (sulfur) the p valence orbitals extend[4] significantly beyond the s valence orbitals. Consequently, their preferred electrostatic interactions with the X—H donor rationalize the structures discussed above for gaseous intermolecular and (solution) intramolecular hydrogen bonds to sulfur.

Returning to divalent oxygen, the actual angle between the (approximately) tetrahedral lone-pair directions may well vary from molecule to molecule. Thus, in the complex formed by oxirane and H—F, the angle between the lone pairs, as probed by the H—F direction, is 144°, instead of 109° for an sp^3 lone pair (17). In fact, the indicated angle is midway between those expected for a $2s$–$2p$ model and an sp^3 model. Furthermore, for phenol it is usual to invoke something very close to a $2s$–$2p$ model, the $2p$ orbital in the planar molecule being available for conjugation with the π system of the ring. Naturally, if the angle between the equivalent orbitals is very large (as large, say, as in oxirane), then conjugation is still substantial ($\sin^2\theta$ is then 0.9) in the planar form of phenol and is 0.1 for the perpendicular form, θ being the angle by which a lone pair twists away from the plane of the ring).

The ambiguity introduced by these considerations may have its origins in the very similar extensions of the $2s$ and $2p$ orbitals in the oxygen atom. One experimental fact, that the methyl group prefers to lie near the double bond, as in vinyl ether, or near that ring C—C bond with the larger mobile bond character, as in anisoles (18–20), is consistent with the equivalent lone-pair model if it is assumed that the two lone pairs are repelled by the π electrons in a C=C bond (proximity). However, an alternative interpretation (21, 22) has it that the lower energy arises from a structure that completes an aromatic sextet.

An attempt at discrimination between the two models might proceed as follows. If O—H...O intramolecular hydrogen bonds were as strongly directional as O—H...S bonds, then in 2-hydroxyphenol they would favor a conformational analogous to **2**. Of course, the rotation about the C—O bond is more strongly hindered than about a C—S bond in such compounds, so that the preferred directionality of an O—H...O bond might be masked. Alternatively, if, say, the central methoxy group in 2,3-dimethoxyphenol lay perpendicular to the benzene plane, then the hydrogen bond might be stronger than in 2,3-dihydroxyanisole because the p-type lone pair on oxygen-2 would now penetrate a region favoring its interaction with the O—H bond.

There is evidence (23, 24*a*,*b*) that the ^{1}H nmr chemical shift, δ(OH), measures the strength of an intramolecular O—H...X hydrogen bond in *ortho*-substituted phenols. The shift to high frequency on hydrogen bond formation is caused by the depletion of charge at hydrogen (25). In the measurements below, δ(OH) values for selected derivatives of phenol are examined from the viewpoint of intramolecular hydrogen bonding to specific lone pairs on oxygen and sulfur.

Results and discussion

Divalent oxygen

In 2,3-dihydroxyanisole, **2**, in CCl_4 solution, δ_2(OH)/ppm is 5.20 and δ_3(OH) is 5.06. This molecule has the indicated conformation at 300 K in CCl_4 solution (see Experimental) and is chosen for comparison with **3**. The latter, forming part of a

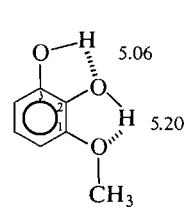

2

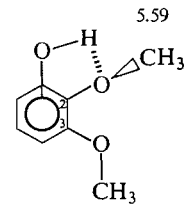

3

larger molecule in the solid state (26), displays an out-of-plane orientation of the methoxy group attached to C(2). The C(1)—C(2)—O—C(H_3) torsion angle is 107(2)°, showing a 17(2)° deviation from a plane perpendicular to the benzene plane, whereas the other methoxy group lies in the benzene plane. Such a conformation is consistent with the ^{1}H nmr spectral parameters of **3** in CCl_4 solution and δ(OH) is 5.59 ppm at 300 K. In a number of 1,2,3-trimethoxy aromatic compounds, the 2-methoxy group has a perpendicular conformation (27, 28).

The empirical relationship (23), $\Delta\delta(OH) = -0.4 \pm 0.2 + E/\text{kcal mol}^{-1}$, relates $\Delta\delta$(OH), measured relative to δ(OH) of phenol, to the strength of the intramolecular O—H...X bond in phenol derivatives.[5] Therefore the intramolecular hydrogen bond in **3** is 1.9 ± 0.8 kJ/mol stronger than in **2**. If the ether oxygen atoms in **2** and **3** are considered to possess equivalent lone pairs, then in **2** the O—H...O bond is bifurcated, the O—H bond lying in a plane bisecting the angle between the lone pairs (but recall the remarks above concerning sp^3 pairs). For the near-perpendicular orientation of the 2-methoxy substituent, one of the lone pairs is proximate to the O—H bond. In this model, the slightly stronger hydrogen bond in **3** arises from the latter situation and is consistent with the remarks in the introduction concerning weak stereospecificity for sp^3 lone

[4]The sulfur atom is much more polarizable than the oxygen atom, so that it is conceivable that the approaching O—H dipole distorts the higher-energy $3p$ orbital more than the $3s$ orbital, leading to the conformational effects discussed above.

[5]In this paper, $\Delta\delta$(OH) need only measure relative strengths within O—H...O and within O—H...S bonds. See Appendix.

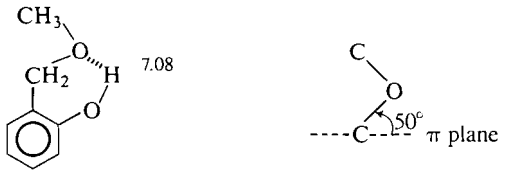

4

pairs. A dihedral angle of 90° instead of the observed value of 107° would have favored the $2s$–$2p$ model.

In **2** and **3**, the hydrogen bond completes a five-membered ring and the distance between the oxygen atoms is about 2.7 Å. In **4**, the known conformation (29) also has 2.7–2.8 Å for this distance, considered as a rigid conformation. However, this geometry is much more favorable to formation of a "linear" hydrogen bond. According to the δ(OH) of 7.08 ppm, the hydrogen bond is 6.2 ± 0.8 kJ/mol stronger than in **3**. Because the internal barrier to rotation about the C_{sp^2}—C_{sp^3} bond in benzyl alcohol in solution is only 1.3 ± 0.8 kJ/mol (30, 31) and is very similar in benzylmethyl ether,[6] the ether moiety can easily accommodate itself to formation of an optimum hydrogen-bonding interaction with the phenolic hydroxyl group. Examination of models in which the methyl group points away from the ring indicates that the hydrogen bond involves only one of the equivalent lone pairs (all bonds and lone pairs staggered, with the usual parallel 1:3 arrangements (22) of C—H bonds in the ether linkage). Furthermore, the empirical relationship above implies 11.7 ± 0.8 kJ/mol as the energy of the hydrogen bond (δ(OH) is 4.3 ppm for phenol). The combined molecular mechanics and nmr approach (32) agrees with this energy, as does an STO 3G MO computation (32), which, however, has θ as 33°.

One further comparison seems apt. In **4** and in salicylaldehyde the H...O distances (33–36) are deducible as 1.70–1.75 Å, but the energy of the hydrogen bond in salicylaldehyde is at least 15 kJ/mol greater (from δ(OH) and MO calculations) than in **4** (36, 37). This result is consistent with the higher stereospecificity found for hydrogen bonds to sp^2 lone pairs in the solid state (1, 3). In **2** the H...O distance is closer to 2.2 Å, helping to account for its relatively weak hydrogen bond.

In summary, the chemical shifts of the hydroxyl protons in **2**–**5** are consistent with the hypothesis of weak stereospecificity of intramolecular O—H...O bonds to ether oxygen atoms relative to those involving carbonyl groups, entirely analogous to observations on intermolecular O—H...O bonds in the solid.

O—H...S bonds for divalent sulfur

As noted above, the model involving nonequivalent lone pairs on divalent sulfur, the $3p$ orbital being more extended than the $3s$ orbital, provides an easy rationalization of the conformation of **1** and of the geometry of intermolecularly hydrogen bonded complexes of H_2S. In **5**, chosen to mimic the electronic environment of the sulfur atom in **6**, δ(OH) is 6.58.

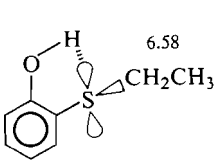

5

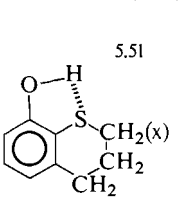

6

[6]Unpublished work in this laboratory.

In **6** the $3p$ orbital on sulfur is probably not strictly perpendicular to the aromatic plane. The ^{1}H nmr spectrum (see Experimental) suggests an inverting saturated ring on the nmr time scale, which does not mean, of course, that the $3p$ orbital is necessarily perpendicular on average. In an analogous oxygen compound, θ (see **7**) is perhaps as large as 20° (38). Accordingly, the

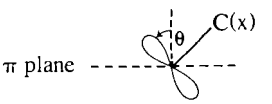

7

O—H...S bond in **6** will not be pure O—H...$3s$ in nature. In **6**, δ(OH) is 5.49, certainly implying a weaker hydrogen bond than in **5**. In the latter, formation of the hydrogen bond twists the C_{sp^2}—S bond into a plane perpendicular to the benzene plane. δ(OH) does not measure the energy of twisting (loss of $3p...\pi$ conjugation), which may be estimated as at least 4 kJ/mol (see Experimental), the barrier to internal rotation in phenyl methyl sulfide being over 5 kJ/mol (39). The empirical relationship above yields 4.6 ± 0.8 kJ/mol as the difference in the hydrogen bond strengths between **5** and **6**. Addition of 4 kJ/mol, and remembering that θ is not zero in **6**, **7**, suggests a *minimum* of 8 kJ/mol as the difference in energy between O—H...$3p$ and O—H...$3s$ hydrogen bonds for divalent sulfur[7] in which they complete a five-membered ring. In summary, intramolecular hydrogen bonding to sulfur, as well as the intermolecular geometries previously mentioned, are best discussed in terms of a $3s...3p$ model, unlike the bonds to oxygen, where equivalent lone pairs appear adequate as a model.

STO 3G MO computations

STO 3G MO calculations on planar and perpendicular (**1**) conformations of the thiomethyl group in 2-hydroxythioanisole, allowing all bond angles and lengths to vary but constraining the benzene ring to be planar, gave the perpendicular form as 8.4 kJ/mol lower in energy. For thioanisole itself such computations agree with experiment about the energy difference between the stable planar and the perpendicular conformations (39). The present result happens to agree with the difference in the O—H...$3s$ and O—H...$3p$ hydrogen bond energies estimated on the basis of δ(OH) in **5** and **6** above. Another calculation kept the perpendicular conformation of the thiomethyl group but turned the hydroxyl group away from the former. This conformation was 9.2 kJ/mol higher in energy than the hydrogen bonded form.

For 2-hydroxyanisole, the planar hydrogen bonded conformer is computed as 8.6 kJ/mol more stable than the perpendicular conformer. Unfortunately the internal barrier to rotation about the C_{sp^2}—O bond in anisole itself is uncertain (41*a*).

Experimental

Compounds

Both 2,3-dihydroxyanisole, **2**, and 2,3-dimethoxyphenol, **3**, came from Aldrich, while 2-(ethylthio)phenol, **5**, was a gift from Ethyl Corporation (41*b*). The 8-hydroxythiochroman, **6**, was made by the following procedure. Cyclization of 3-(2-nitrophenylthio)propanoic acid, prepared from 2-nitrophenylthiocyanate, gave 8-nitrothiochroman-4-one by cyclization in polyphosphoric acid, which was the most effective of many reagents tried. The nitroketone was converted directly under Clemmensen-type conditions to 8-aminothiochroman,

[7]The δ(OH) values suggest that O—H...S bonds are stronger than O—H...O bonds for divalent atoms, as is also deduced from Schroeder–Lippincott potential functions (40).

Can. J. Chem. Downloaded from www.nrcresearchpress.com by 78.46.186.204 on 09/07/12
For personal use only.

Can. J. Chem. Downloaded from www.nrcresearchpress.com by 78.46.186.204 on 09/07/12
For personal use only.

both carbonyl and nitro functions being reduced. The amine was converted to the phenol by diazotization. Yields were low (14%), probably because of reaction of the diazonium group with the sulfide function. The phenol is a colorless oil and gave a satisfactory ^{1}H nmr spectrum.

Nuclear magnetic resonance samples and spectra

All ^{1}H nmr spectra were measured in CCl_4 as a solvent. Compound **2** was prepared as a 0.9 mol% solution, containing some tetramethylsilane (TMS) to provide an internal lock on an HA100 nmr spectrometer. Compound **4** was measured as a 0.5 v% solution in CCl_4, containing some C_6D_{12} as an internal lock material for a WH90 nmr spectrometer (29). The concentrations of **3**, **5**, and **6** are given in the tables below. All solutions were transferred to 5 mm od nmr sample tubes, were degassed by several freeze–pump–thaw cycles, and were then flame-sealed.

For **2**, the ^{1}H nmr spectrum was calibrated at 100 MHz by continuous wave techniques at a probe temperature of 305 K by a procedure described in detail previously (42). The ^{1}H nmr spectra of **3**, **5**, and **6** were accumulated at 300 K on an AM300 nmr spectrometer. Wide sweepwidth survey spectra were obtained in order to reference the spectra with respect to TMS. Each spectral region was then examined in detail, with sweepwidth and data region adjusted to give acquisition times of about 40 s. As many as 16 scans were acquired. Before transforming the FIDs, using a small amount of gaussian multiplication, zero-filling to twice the original data region was done. Peak widths at half-height were typically well below 0.1 Hz. Figure 1 gives the ^{1}H nmr spectrum of the 3-methoxy protons in **3**. The smaller splitting is 0.09 Hz in magnitude.

Spectral analyses

The programs PANIC, provided as part of the software on the AM300, and NUMARIT (43) were used in the analyses of the ^{1}H nmr spectra. That for **2** was not highly precise and the spectral parameters are therefore not recorded here. The hydroxyl proton chemical shifts are given above in the structural formula for **2**. The chemical shift assignments followed from the characteristic through-space coupling constant (44) of −0.25(2) Hz between the methyl protons and the proton placed *ortho* to the methoxy group, having this magnitude for a preferred orientation of the latter as indicated in **2**. The assignment of the other two ring protons was then straightforward and that of the two hydroxyl protons followed from their stereospecific couplings over five bonds (45, 46) to these two ring protons for the conformation depicted in **2**. An alternative conformation, in which the central hydroxyl proton is hydrogen bonded to its neighbouring hydroxyl group, was excluded because no coupling was observable from it to the proton *ortho* to the methoxy group. Confirmation of this conclusion was found in the typical (47) aromatic-solvent-induced-shifts (ASIS) found at sites near a methoxy substituent (0.5 mol% in C_6D_6).

Tables 1, 2, and 3 contain the ^{1}H nmr spectral parameters for **3**, **5**, and **6**. Those for **4** are available elsewhere (29). The assignments for **3** in Table 1 followed from the characteristic coupling constants for the 3-methoxy (44) and the hydroxyl protons (45), the stereospecificities of which imply the conformation displayed in **3**. Again, the spectral data for 2-(thioethyl)phenol in Table 2 leave little doubt that the conformation is that shown in structure **5**. Thus, the virtual absence of through-space coupling between the methylene protons and the ring proton placed *ortho* to the ethyl group is consistent (11, 48) with a perpendicular conformer. The ring proton chemical shifts of **5** and of 2-hydroxythioanisole, **1** (R = CH_3), differ by only 0.02 ppm on average (11), as expected if their conformations are analogous (11, 49). See ref. 11 for a detailed approach to the proof that the thioanisole derivative has conformation **1**. It may also be noted that the mean difference of the coupling constants in **5** and **1** (R = CH_3) is less than 0.008 Hz, certainly consistent with similar conformations for the two molecules.

Turning to 8-hydroxythiochroman, **6**, the spectral parameters in Table 3 show that the peaks arising from the methylene protons were not fully analyzed. Two methylene groups gave rise to bands interpretable as roughly 1:2:1 triplets, each of whose components consisted of many peaks. The triplet components were spaced by approximately 6.5 Hz, arising from fluxionally averaged vicinal proton–proton coupling constants. The shift assignments followed from the known long-range coupling constants of benzylic (50) and thioanisole (51) protons. Unfortunately, the intermolecular exchange of the hydroxyl proton was too fast (an acidic or basic impurity was presumably present, but the amount of **6** was too small to encourage further purification procedures) to observe the characteristic coupling constant to H-6 over five bonds. However, the chemical shift of 5.49 ppm is characteristic of a hydrogen bond and is treated as such above.

The long-range coupling constants between the benzylic and aromatic protons allow a decision as to the conformation of the saturated part of the molecule. As noted above, the coarse features of

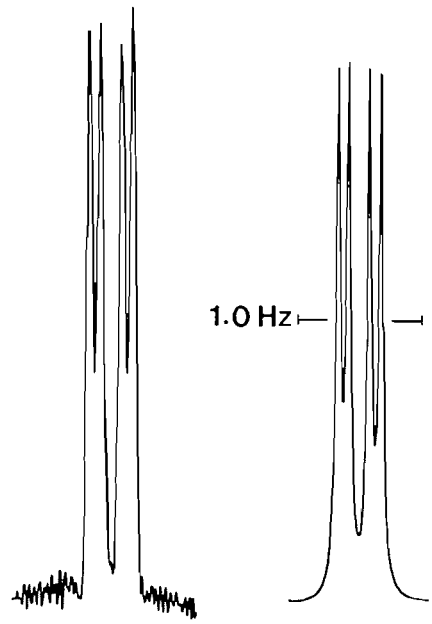

FIG. 1. The experimental and computed ^{1}H nmr spectra of the 3-methoxy protons for 1.6 mol% solution of 2,3-dimethoxyphenol in CCl_4 at 300 K and 300.135 MHz. They illustrate a linewidth of 0.04 Hz, a coupling to H-4 of 0.267(1) Hz, and one of 0.091(1) Hz to H-5. These coupling magnitudes show that the 3-methoxy group is lying in the benzene plane (19). The ^{1}H nmr spectrum of the 2-methoxy group is a singlet with a linewidth of 0.04 Hz.

TABLE 1. The ^{1}H nmr spectral parameters for 2,3-dimethoxyphenol, **3**, as a 1.6 mol% solution in CCl_4/C_6D_{12}/TMS[a] at 300 K and 300.135 MHz

Parameter	Value	Parameter	Value
ν(OH)[b]	1677.886(1)[c]	$^3J_{56}$	8.241(1)
ν(OCH_3)	1154.589[e]	$^4J_{46}$	1.393(1)
ν(OCH_3)	1142.708(1)	^4J(OH,H-6H)	−0.149(1)[f]
ν_4	1898.218(1)	^5J(OH,H-5)	0.404(1)
ν_5	2033.581(1)	^5J(CH_3,H-4)	−0.267(1)[d]
ν_6	1942.879(1)	^6J(CH_3,H-5)	0.091(1)[d]
$^3J_{45}$	8.348(1)	Root mean square deviation	0.004

[a]Composition as in Table 2.
[b]In Hz to high frequency of internal TMS.
[c]Numbers of parentheses are probable errors as given by PANIC.
[d]The signs of these coupling constants are assumed to follow the patterns previously determined (57, 58).
[e]Assigned to the 2-methoxy group, which displays no couplings to other protons.
[f]Shown to be of opposite sign to $^3J_{56}$ by tickling (59) experiments.

TABLE 2. The ^{1}H nmr spectral parameters for 2-hydroxyphenylethyl sulfide, **5**, as a 2.0 mol% solution in CCl_4 at 300 K and 300.135 MHz

Parameter	Value	Parameter	Value
$\nu(CH_3)^a$	367.111(4)[b]	$^3J_{56}$	7.691(2)
$\nu(CH_2)$	801.203(3)	$^4J_{35}$	1.341(2)
ν(OH)	1974.015(1)	$^4J_{46}$	1.688(2)
ν_3	2070.726(1)	^4J(OH,H-3)	−0.109(2)
ν_4	2154.887(1)	$^5J_{36}$	0.392(2)
ν_5	2032.018(1)	^5J(OH,H-4)	0.451(2)
ν_6	2213.205(1)	$^6J(CH_2,H\text{-}3)$	±0.040(2)
$^3J(CH_2,CH_3)$	7.351(3)	Calculated transitions	80[c]
$^3J_{34}$	8.180(2)	Assigned transitions	78[c]
$^3J_{45}$	7.363(2)	Root mean square deviation	0.005

[a]In Hz at 300.135 MHz to high frequency of internal TMS present as 0.5 mol%, together with 10 mol% C_6D_{12}.
[b]Numbers in parentheses are standard deviations in the last significant figure (NUMARIT analysis).
[c]The ethyl proton region, containing 16 observed peaks, was analyzed separately and 24 transitions were assigned to these peaks, giving an rms deviation of 0.011 Hz.

TABLE 3. The ^{1}H nmr parameters of 8-hydroxythiochroman, **6**, in CCl_4 solution[a] at 300.135 MHz and 300 K

Parameter	Value	Parameter	Value
ν(OH)	1648.25[b]	$^5J(H,CH_2\text{-}4)$	0.285(1)
$\nu(CH_2\text{-}4)$	830.66	$^6J_p(H,CH_2\text{-}4)$	−0.594(1)
$\nu(CH_2\text{-}3)$	619.60	^6J(H-7,CH_2-S)	0.133(1)
$\nu(CH_2\text{-S})$	888.88	^6J(H-5,CH_2-S)	0.064(1)
ν_5	1996.518(1)[c]	^7J(H-6,CH_2-S)	−0.054(1)
ν_6	2056.613(1)	Calculated transitions	768[d]
ν_7	1977.575(1)	Assigned transitions	643
$^3J_{67}$	8.056(1)	Peaks observed	101
$^3J_{56}$	7.539(1)	Largest difference	0.026
$^4J_{57}$	1.274(1)	Root mean square deviations	0.0087
$^4J_0(H,CH_2\text{-}4)$	−0.861(1)		

[a]Composition of solvent mixture as in Table 2, for a very dilute solution, <0.5 mol%, of **6**.
[b]In Hz to high frequency of internal TMS.
[c]Standard deviations in the last significant figure are given in parentheses.
[d]For the aromatic protons.

the ^{1}H nmr spectra of the methylene protons indicate a conformational averaging process at 300 K. From models it may be concluded that the saturated ring is inverting between pure boat, distorted half-chair, or undistorted half-chair forms. Now assume that the barrier to inversion is rather larger than kT, as seems reasonable (52), so that the benzylic coupling constants can be discussed in terms of a two-site model. Define ϕ as the angle by which the benzylic C—H bond twists out of the aromatic plane. In toluene, eqs. [1]–[3] describe (50, 53) the

$$[1]\quad {}^6J/\text{Hz} = -1.20\langle\sin^2\phi\rangle$$

$$[2]\quad {}^5J/\text{Hz} = 0.336\langle\sin^2\phi\rangle + 0.322\langle\sin^2(\phi/2)\rangle$$

$$[3]\quad {}^4J/\text{Hz} = -1.08\langle\sin^2\phi\rangle - 0.32\langle\cos^2\phi\rangle$$

ϕ dependence of $^{4,5,6}J(H,CH_3)$, in which angular brackets indicate average values.

^6J is discussed first. From Dreiding models it appears that ϕ is very near 15° and 75° for the two benzylic C—H bonds in the distorted half-chair form. Then $\langle\sin^2\phi\rangle$ is very near 0.5. Accordingly, ^6J is calculated as −0.60 Hz from eq. [1], rather close to the observed value of −0.594(1) Hz. For an undistorted half-chair form, ϕ values are 30° and 90°, yielding $\langle\sin^2\phi\rangle$ as 0.625, implying ^6J as −0.75 Hz. Finally, in a pure boat form, the ϕ values are 5° and 65° or perhaps 0° and 60°, with the consequence that $\langle\sin^2\phi\rangle$ is 0.414 or 0.375; hence ^6J should lie between −0.45 and −0.50 Hz. The choice among the three forms seems clear.

Turning to ^5J, it must be noted that ϕ is defined as 0° when the C—H bond of the sidechain and the *meta* C—H bond in the ring point towards the same side of the ring and as 180° when the bonds point away from each other (50). For the distorted half-chair conformation, ϕ becomes 15° and 105°. Hence $\langle\sin^2(\phi/2)\rangle$ is 0.323 and eq. [2] yields ^5J as 0.27 Hz. The observed value is 0.285(1) Hz. The pure boat and undistorted half-chair conformations imply ^5J as <0.25 Hz and 0.30 Hz, respectively. The choice of the correct conformation is less unequivocal here but the distorted half-chair, given by ^6J, is at least as compatible with ^5J as the undistorted form. It might be noted that eq. [1] is better established (50) than eq. [2].

Finally, eq. [3] is probably the least reliable as a conformational indicator for **6**. The coefficient of $\langle\sin^2\phi\rangle$ depends on the mutual atom–atom polarizability (53) and in **6** will surely differ from its value in toluene. Although eq. [3] reproduces ^4J in toluene exactly (5), it is clear that ^4J in a variety of *ortho* substituted toluene derivatives is generally about 10% higher in magnitude (54–56) than would be expected from eq. [3]. Yet it is unclear how such an increase should be divided between the two terms in eq. [3]. Furthermore, a resonance structure that contributes to marked double-bond character of the intervening aromatic C—C bond can cause a dramatic increase in the magnitude of ^4J. Thus, in 2-nitro-4-methylphenol, ^4J(H-3,CH_3) is −1.00 Hz (53) and is attributed to the importance of structure **8**, while ^4J(H-5,CH_3) is −0.62 Hz. A similar structure for **6** involving a hydrogen bond to sulfur can also be conceived, but it is impossible to deduce a priori how much it would contribute to an increase in the magnitude of ^4J. However, if the distorted half-chair is taken as the

Can. J. Chem. Downloaded from www.nrcresearchpress.com by 78.46.186.204 on 09/07/12
For personal use only.

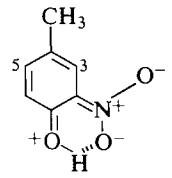

8

correct conformation of **6**, so strongly indicated by ^6J (whose value in toluene derivatives is remarkably insensitive to substituents), then the coefficient of $\langle \sin^2 \phi \rangle$ in eq. [3] becomes -1.40 Hz. This result assumes that the coefficient of $\langle \sin^2 \phi \rangle$, the σ-electron contribution, is unchanged from its value in toluene. A similar approach to **8** yields the coefficient of $\langle \sin^2 \phi \rangle$ as -1.7 Hz, the larger magnitude being expected for this rather more strongly hydrogen-bonded molecule. These considerations then imply a ^4J of -1.0 Hz for an undistorted half-chair, and -0.62 Hz for a pure boat conformation of **6**. The latter can be discarded on the basis of all three coupling constants. On the basis of our extensive experience with such long-range coupling constants, it seems clear that **6** exists as rapidly inverting, distorted half-chair conformations at 300 K in CCl_4 solution. These conformations agree with structure **7** and are similar to the solid state structure of the analogous compound containing oxygen in place of sulfur.

In view of the long-range coupling constants of the methyl protons in thioanisole (51), those involving the corresponding methylene protons in **6** and given in Table 3 will contribute to the eventual elucidation of the coupling mechanisms for these poorly understood parameters.

Acknowledgments

We thank the Natural Sciences and Engineering Research Council of Canada for financial support and Paul F. Rankin of the Ethyl Corporation for the sample of 2-(ethylthio)phenol.

1. R. Taylor and O. Kennard. Acc. Chem. Res. **17**, 320 (1984).
2. P. Murray-Rust and J. P. Glusker. J. Am. Chem. Soc. **106**, 1018 (1984).
3. R. Taylor, O. Kennard, and W. Versichel. J. Am. Chem. Soc. **105**, 5761 (1983).
4. F. H. Allen, O. Kennard, and R. Taylor. Acc. Chem. Res. **16**, 146 (1983).
5. P. Schuster. *In* The hydrogen bond. *Edited by* P. Schuster, G. Zundel, and C. Sandorfy. North-Holland, Amsterdam. 1976. p. 130.
6. A. C. Legon and D. J. Millen. Faraday Disc. Chem. Soc. **73**, 71 (1982).
7. M. M. Szczesniak, S. Scheiner, and Y. Bouteiller. J. Chem. Phys. **81**, 5024 (1984).
8. M. S. Gordon, D. E. Tallman, C. Monroe, M. Steinbach, and J. Armbrust. J. Am. Chem. Soc. **97**, 1326 (1975).
9. S. Scheiner and V. M. Kolb. Proc. Natl. Acad. Sci. U.S.A. **77**, 5602 (1980).
10. T. Schaefer, T. A. Wildman, and S. R. Salman. J. Am. Chem. Soc. **102**, 107 (1980).
11. T. Schaefer, S. R. Salman, T. A. Wildman, and P. D. Clark. Can. J. Chem. **60**, 342 (1982).
12. N. W. Larsen and F. M. Nicolaisen. J. Mol. Struct. **29**, 29 (1974).
13. R. Viswanathan and T. R. Dyke. J. Chem. Phys. **77**, 1166 (1982).
14. E. J. Goodman and A. C. Legon. J. Chem. Soc. Faraday Trans. 2, **80**, 51 (1984).
15. T. N. Guirow and R. Parthasarathy. J. Am. Chem. Soc. **103**, 477 (1981).
16. W. Kutzelnigg. Angew. Chem. Int. Ed. Engl. **23**, 272 (1984).
17. A. S. Georgiou, A. C. Legon, and D. J. Millen. Proc. R. Soc. Lond. Part A, **373**, 511 (1981).
18. L. I. Kruse, C. W. DeBrosse, and C. H. Kruse. J. Am. Chem. Soc. **107**, 5435 (1985).
19. T. Schaefer, T. A. Wildman, and J. Peeling. J. Magn. Reson. **56**, 144 (1984).
20. R. H. Contreras, D. G. DeKowalewski, and J. C. Facelli. J. Mol. Struct. **81**, 147 (1982).
21. D. A. Forsyth, V. M. Osterman, and J. R. DeMember. J. Am. Chem. Soc. **107**, 818 (1985).
22. N. D. Epiotis, W. R. Cherry, S. Chaik, R. Yates, and F. Bernardi. Top. Curr. Chem. **70**, 1 (1977).
23. T. Schaefer. J. Phys. Chem. **79**, 1888 (1975).
24. (*a*) M. Takasuka and Y. Matsui. J. Chem. Soc. Perkin 2, 1743 (1979); (*b*) J. Reuben. J. Am. Chem. Soc. **108**, 1735 (1986).
25. J. W. Clymer, N. Goldstein, J. L. Ragle, and E. L. Reed. J. Chem. Phys. **76**, 4535 (1982).
26. J. M. Arrieta, E. Dominiguez, E. Lete, M. J. Villa, and G. Germain. Acta Crystallogr. Part C, **40**, 859 (1984).
27. G. W. Burton and K. U. Ingold. J. Am. Chem. Soc. **103**, 6472 (1981).
28. G. W. Burton, Y. LePage, E. J. Gabe, and K. U. Ingold. J. Am. Chem. Soc. **102**, 7792 (1980).
29. R. Laatikainen. Magn. Reson. Chem. **24**, 588 (1986).
30. R. J. Abraham and J. M. Bakke. Tetrahedron, **34**, 2947 (1978).
31. T. Schaefer, W. Danchura, W. Niemczura, and W. J. E. Parr. Can. J. Chem. **56**, 1721 (1978).
32. R. Laatikainen and K. Tuppurainen. Magn. Reson. Chem. **24**, 595 (1986).
33. H. Jones and R. F. Curl. J. Mol. Spectrosc. **42**, 65 (1972).
34. M. J. Hunt and A. L. Mackay. J. Magn. Reson. **15**, 402 (1974).
35. L. M. Jackman, J. C. Trewella, and R. C. Haddon. J. Am. Chem. Soc. **102**, 2519 (1980).
36. T. Schaefer, R. Sebastian, R. Laatikainen, and S. R. Salman. Can. J. Chem. **62**, 326 (1984).
37. P. George, C. W. Bock, and M. Trachtman. J. Mol. Struct. **133**, 11 (1985).
38. T. Doba, G. W. Burton, and K. U. Ingold. J. Am. Chem. Soc. **105**, 6505 (1983).
39. T. Schaefer and J. D. Baleja. Can. J. Chem. **64**, 1376 (1986).
40. W. R. Snyder, H. D. Schreiber, and J. N. Spencer. Spectrochim. Acta, Part A, **29**, 1225 (1973).
41. (*a*) T. Schaefer, R. Laatikainen, T. A. Wildman, J. Peeling, G. H. Penner, J. Baleja, and K. Marat. Can. J. Chem. **62**, 1592 (1984); (*b*) P. F. Rankin and B. G. McKinnie. Synthesis, 117 (1984).
42. T. Schaefer and R. Sebastian. J. Magn. Reson. **41**, 395 (1980).
43. A. R. Quirt and J. S. Martin. J. Magn. Reson. **5**, 318 (1971); J. S. Martin, A. R. Quirt, and K. E. Worvill. The NMR program library. Daresbury Laboratory, Daresbury, U.K.
44. T. Schaefer, S. R. Salman, T. A. Wildman, and G. H. Penner. Can. J. Chem. **63**, 782 (1985).
45. J. B. Bowbotham and T. Schaefer. Can. J. Chem. **52**, 3037 (1974).
46. S. Forsén and B. Åkermark. Acta. Chem. Scand. **17**, 1712 (1963).
47. R. Wasylishen, T. Schaefer, and R. Schwenk. Can. J. Chem. **48**, 2885 (1970).
48. T. Schaefer, G. H. Penner, K. J. Davie, and R. Sebastian. Can. J. Chem. **63**, 777 (1985).
49. L. B. Krivdin, G. A. Kalabin, and B. A. Trofimov. Izv. Akad. Nauk SSSR, Ser. Khim. 565 (1982).
50. T. Schaefer, R. Sebastian, and G. H. Penner. Can. J. Chem. **63**, 2597 (1985).
51. T. Schaefer and J. D. Baleja. J. Magn. Reson. **60**, 131 (1984).
52. M. Ōki. Applications of dynamic nmr spectroscopy to organic chemistry. VCH Publishers, Deerfield Beach, Florida.
53. M. Barfield, C. J. Fallick, M. Hata, S. Sternhell, and P. W. Westerman. J. Am. Chem. Soc. **105**, 2178 (1983).
54. T. Schaefer and K. Chum. Can. J. Chem. **56**, 1788 (1978).
55. T. Schaefer, R. Sebastian, R. P. Veregin, and R. Laatikainen. Can. J. Chem. **61**, 29 (1983).
56. T. Schaefer, T. A. Wildman, and R. Sebastian. Can. J. Chem. **63**, 773 (1985).

Can. J. Chem. Downloaded from www.nrcresearchpress.com by 78.46.186.204 on 09/07/12
For personal use only.

57. H. A. GAUER, J. VRIEND, and W. G. B. HUYSMANS. Tetrahedron Lett. 1999 (1969).
58. T. SCHAEFER and R. LAATIKAINEN. Can. J. Chem. **61**, 224 (1983).
59. R. FREEMAN and W. A. ANDERSON. J. Chem. Phys. **37**, 2053 (1962).
60. J.-P. SEGUIN, F. GUILLAUME-VILPORT, R. UZAN, and J.-P. DOUCET. J. Chem. Soc. Perkin Trans. 2, 773 (1986).
61. G. A. JEFFREY and Y. YEON. Acta Crystallogr. Part B, **42**, 410 (1986).
62. R. M. BADGER and S. H. BAUER. J. Chem. Phys. **5**, 839 (1937).
63. H. RATAJCZAK, W. J. ORVILLE-THOMAS, and C. N. R. RAO. Chem. Phys. **17**, 197 (1976).

Appendix

A referee suggests that the empirical relationship between the energy of the hydrogen bonds and the chemical shift is rather tenuous and that therefore the quoted energies should be expressed more tentatively. While we cannot state the real accuracy of the derived energies, we believe that the order of the energies is reliable and that it is consistent with the arguments presented. In this connection it is interesting that a recent (60) study demonstrates a linear dependence of $\Delta\delta$(OH) on the computed charges for the atoms in the hydroxyl groups of a large variety of phenol derivatives. There also appears to be a direct proportionality between δ(OH) and the stretching frequency of the O—H bond, the latter being linearly related to the computed O—H bond length (60). It is also interesting that a linear relationship (61) exists between the (isotropic) chemical shift of the hydroxyl proton and the H...O distance in the O—H...O bond in crystals containing a large variety of such bonds. It is therefore noteworthy that the Badger and Bauer rule (62), relating the enthalpy of formation of intermolecular hydrogen bonds to the infrared frequency shifts, holds well for *closely related* compounds (63).

Can. J. Chem. Downloaded from www.nrcresearchpress.com by 78.46.186.204 on 09/07/12
For personal use only.

Speciation of soluble manganese in lakewater with Chelex-100 and polyacrylate resin, XAD-7

ALFIO CORSINI, GWEN WADE, CHI-CHUNG WAN, AND SHAREEN PRASAD
Department of Chemistry, McMaster University, Hamilton, Ont., Canada L8S 4M1

Received August 30, 1986

This paper is dedicated to Professor Douglas E. Ryan on the occasion of his 65th birthday

ALFIO CORSINI, GWEN WADE, CHI-CHUNG WAN, and SHAREEN PRASAD. Can. J. Chem. **65**, 915 (1987).

Two fractions of (soluble) manganese in Lake Ontario water have been detected and measured with the aid of sequential preconcentration on the polyacrylic ester resin, XAD-7, and Chelex-100. One fraction, consisting of free Mn(II), was retained on the XAD-7 column; the second fraction, consisting of one or more unidentified forms, was retained on Chelex-100. After elution from the columns, the concentration of manganese in each fraction in the lakewater was determined by graphite-furnace AAS. Because both fractions are retained by Chelex-100, the second fraction could also be determined by difference on passage of two separate aliquots through Chelex-100 and XAD-7. Analysis of samples from three locations in the western basin of Lake Ontario showed that about 12–22% of total (soluble) manganese was present as free Mn(II).

ALFIO CORSINI, GWEN WADE, CHI-CHUNG WAN et SHAREEN PRASAD. Can. J. Chem. **65**, 915 (1987).

Faisant appel à la préconcentration en série sur de la résine polyacrylique XAD-7 et sur du Chelex-100, on a détecté et mesuré deux fractions de manganèse (soluble) dans l'eau du lac Ontario. Une fraction, comportant le Mn(II) à l'état libre, est retenue sur la colonne de XAD-7; la deuxième fraction, contenant une ou plusieurs formes qui n'ont pas été identifiées, est retenue par le Chelex-100. Après l'élution des colonnes, la concentration du manganèse, dans chacune des fractions d'eau du lac, a été déterminée par spectroscopie AA dans une fournaise de graphite. Les deux fractions étant retenues par le Chelex-100, on peut aussi déterminer la deuxième fraction par différence, lors du passage de deux aliquots séparés à travers des colonnes de Chelex-100 et de XAD-7. Des analyses effectuées sur des échantillons provenant de trois endroits différents dans le bassin ouest du lac Ontario démontrent que de 12 à 22% du manganèse soluble total est présent sous la forme de Mn(II).

[Traduit par la revue]

Introduction

Because the bioavailability and toxicity of trace metals in natural waters is strongly dependent on chemical form, speciation of trace metals has become an area of increasing significance. Manganese is an essential trace element for plant and animal life and its distribution in natural waters has received considerable attention (1–5). It is found in soluble and suspended particulate forms and in sediments. The fraction that passes through a 0.45 μm filter is operationally considered as "soluble" manganese and that retained on the filter as particulate manganese (2). In ocean and fresh waters, manganese is found as free and bound Mn(II) and as Mn(IV) dioxide. In oxic waters Mn(II) is readily oxidized, particularly above pH 6, to colloidal MnO_2 so that much of the manganese is in the particulate phase. MnO_2 is also produced by the catalytic action of oxidizing bacteria (6); colloidal forms of Mn(III) may also exist. In anoxic waters the proportion of soluble manganese as Mn(II) is increased (4). In seawater, small amounts of Mn(II) chloride complexes may exist and in fresh water, Mn(II) maybe present as sulfate and organic complexes and may also remain adsorbed onto colloidal iron and manganese oxides. Computational methods suggest that in both seawater and fresh waters, the predominant form of soluble Mn(II) is the free hydrated ion (7) although the action of bacteria and algae on Mn(II) were not taken into account in these studies.

In an earlier report (8), a procedure involving two columns of the polymethylmethacrylate resin, XAD-7, was described for the preconcentration of trace metals in natural waters. In this procedure, the sample was acidified to pH 1–2 and passed through the first column to remove organic complexing species such as humic substances. The effluent was then adjusted to pH 8 and passed through the second (analytical) column to concentrate the trace metals. These were subsequently eluted with a small volume of dilute HNO_3 and determined by graphite-furnace AAS. Two methods of calibration were used, external standard-curve and standard additions calibration. It was noted in this work that samples of Lake Ontario water contained at least two forms of (soluble) manganese. This conclusion was indicated by the fact that the two-column procedure utilizing standard-curve calibration returned a much lower value for total soluble manganese than the two-column procedure utilizing standard additions. Although breakthrough of manganese from the analytical column occurred in both procedures, rapid equilibration of the low-level Mn(II) spikes in the standard additions procedure negated the effect on recovered manganese. Indeed, the result for total soluble manganese by this procedure was in good agreement with results obtained by two independent methods; i.e., direct injection of the sample into the furnace, and preconcentration on Chelex-100, prior to measurement. Identification of the species was not made. In the present report, more detailed evidence is presented to show that the combination of XAD-7 and Chelex-100 columns can differentiate soluble fractions of manganese in natural waters. For Lake Ontario samples tested, one fraction was retained by both XAD-7 and Chelex-100 and was identified as free Mn(II). A second fraction, consisting of one or perhaps more forms of soluble manganese, was retained by only Chelex-100; it was polarographically inactive and was not identified.

Experimental

Reagents and solutions

Distilled-deionized water (DDW) was used throughout. All other common reagents were reagent grade or better (e.g., Baker Instra-analyzed HNO_3 and NH_3). Mn(II) stock solutions (5 μg/L to 1 mg/L) were prepared by appropriate dilution of 1000-mg/L standard solutions (Fisher Scientific). A solution of Mn(III) (~30 μg/L) was prepared by dissolving 150 μg of Mn(III) acetate in 1 L of DDW at pH 8. A solution of colloidal MnO_2 was made by shaking a mixture of precipitated MnO_2 and DDW at pH 8, filtering to remove the excess solid,

Can. J. Chem. Downloaded from www.nrcresearchpress.com by 78.46.186.204 on 09/07/12
For personal use only.

Can. J. Chem. Downloaded from www.nrcresearchpress.com by 78.46.186.204 on 09/07/12
For personal use only.

and passing the filtrate through a 0.45 μm membrane filter. NH_4Cl solutions were purified before use by passage through a Chelex-100 column to remove any trace amounts of manganese present.

The Lake Ontario samples (from Stations 3, 14, and 302, western basin) were supplied by Canada Centre for Inland Waters (CCIW), Burlington, Ontario. Aliquots were centrifuged to remove visible suspended particles and also filtered through 0.45 μm membrane filters prior to use. Portions of these aliquots were acidified to pH 1.7 to preserve the integrity of the trace metal content on storage.

Apparatus

All glass and polypropylene laboratory ware was cleaned as described previously (8). Atomic absorption measurements were made with a Perkin-Elmer Model 373 instrument equipped with a HGA-2200 graphite furnace. The wavelength (279.5 nm), slit width (0.2 nm), and lamp current (20 mA) were those recommended in the application manual. The drying temperature was 100°C for 20 s, charring temperature 1000°C for 20 s, and atomization temperature 2600°C for 7 s. During atomization, the Ar gas "interrupt mode" was used because of the very low concentrations involved. Sample volumes (20 μL) were manually injected with an Eppendorf micropipette. Concentrations of Mn in the samples were obtained from standard external calibration curves and by standard additions.

Ultraviolet irradiation to destroy organic material in the lakewater samples was carried out with a Rayonet Photochemical Reactor equipped with a 0.5 kW Hg lamp. Sample aliquots (100 mL in quartz cells) were exposed to intense 254 nm radiation for 8 h.

Differential pulse polarograms were obtained with a Metrohm Model E506 Polarecord instrument equipped with an E505 polarography stand which included the dropping-mercury and AgCl/Ag reference electrodes. The differential pulse mode (50 mV pulse), was used. Other settings were drop time, 1.2 s; sensitivity 2.5×10^{-10} A/mm.

Millipore membrane filters (MF) with pore sizes 0.45, 0.22, and 0.025 μm were used for filtration of samples. Filtration of a 100-mL aliquot through the 0.025 μm filter required about 20 h, under vacuum.

Column preparation

XAD-7, supplied as 20–50 mesh (Rohm and Haas), was ground and sieved to 80–100 mesh. The resin was cleaned and borosilicate columns (1 × 20 cm, Bio-Rad) were packed to a 3-cm height (0.5 g resin) and conditioned exactly as described by Wan *et al.* (8). Retained Mn(II) was eluted with 5 mL of 1% v/v HNO_3. After elution, the column was rinsed with dilute ammonia and DDW for future use. Chelex-100 resin (Rohm and Haas) was slurry-packed in borosilicate columns (1 × 4 cm bed height, 200–400 mesh, 0.5 g resin). The columns were conditioned with 50 mL of pH 8.0 buffer prior to percolation of samples or test solutions and were eluted with 25 mL of 14% v/v HNO_3.

Mn concentration

The total soluble manganese content of the Station 3, 14, and 302 samples was determined by several different methods: by direct injection of the sample (without preconcentration) into the graphite furnace; by preconcentration on a Chelex-100 column using external calibration; and by the two-column XAD-7 preconcentration method using both external and standard additions calibration. These methods have been used previously (8).

Breakthrough curves

Separate aliquots (100 mL) of lakewater samples were percolated through the XAD-7 and Chelex-100 columns at a flow rate of 1 mL/min. After passage of these samples, a 100-mL aliquot of a Mn(II) test solution (100 μg/L) was percolated through each column. The solutions and columns were at pH 8.0. A 0.5-mL increment of the effluent was taken at regular intervals and analyzed by GFAAS, to give data for construction of breakthrough curves. A breakthrough curve was also obtained for an aliquot of Station 3 lakewater which had been irradiated in the Rayonet apparatus. The sample was percolated sequentially through the XAD-7 and Chelex-100 columns.

DP polarography

Solutions were adjusted to pH 8.0 with dilute ammonia. They were made 0.01 *M* in NH_4Cl (supporting electrolyte) and Triton X-100 (10 drops/100 mL of solution) was added. Dissolved oxygen was removed by displacement with nitrogen and a nitrogen atmosphere was maintained during measurement. Solutions measured were as follows: test solutions of Mn(II) up to 150 μg/L; a solution of colloidal MnO_2 and a solution containing about 150 μg/L of Mn(III) acetate; test solutions containing soil humic acid and Mn(II); lakewater samples, some spiked with Mn(II) up to 100 μg/L; and the effluents of spiked lakewater samples that had been passed through the XAD-7 and Chelex-100 columns.

Filtration

Aliquots (100 mL) of Station 3 water (pH 7.9) were centrifuged to remove visible particulate matter and then filtered under vacuum through 0.45, 0.22, and 0.025 μm membrane filters. Afterwards, the 0.22 and 0.025 μm filters were soaked in 5 mL of 1% HNO_3 to dissolve any trapped manganese-bearing species (other than MnO_2, which is insoluble in 1% HNO_3) and the manganese was determined by GFAAS. Corresponding blank solutions were prepared by soaking unused filters in the same manner. The manganese in the blanks was <0.1 μg/L. The manganese content in the filtrate from the 0.025 μm filtration was also measured, after preconcentration at pH 8 on a XAD-7 column.

Results and discussion

For the preconcentration of trace metal ions, XAD-7 functions as a weak-acid ion-exchange resin of low capacity, about 30 μmol/g of 80–100 mesh dry resin (8). This capacity is more than adequate for the concentration of trace metals found in most natural waters.

The total soluble concentration of manganese in water from three locations in Lake Ontario was determined by three methods and is given in columns 2, 3, and 4 of Table 1. In the two-column XAD-7 procedure by both calibration methods, early breakthrough of manganese occurred through the analytical column (pH 8.0) when applied to the Station 14 and 302 samples; however, only the results by the calibration curve method are significantly low in comparison to those by the direct and Chelex-100 procedures. A typical breakthrough curve for the analytical column and Station 14 sample is shown in Fig. 1. To prove that the breakthrough was not due to insufficient capacity of the XAD-7 column, 100 mL of a standard solution containing 10 μg/L of Mn(II) (about eight times the total manganese concentration in the Station 14 lakewater) was percolated through the XAD-7 column after passage of 100 mL of lakewater. No breakthrough was observed. Therefore, the capacity was sufficient and the breakthrough species was not free Mn(II). Furthermore, when either a separate Station 14 sample or the effluent from the analytical XAD-7 column or the standard Mn(II) solution was passed through the Chelex-100 column, there was no breakthrough of manganese species (Fig. 1). This experiment demonstrates conclusively that soluble manganese in lakewater can be (operationally) speciated into two fractions, one which is retained by both XAD-7 and Chelex-100, and one which is retained by Chelex-100 but not XAD-7. Furthermore, it is reasonable to conclude that neither form involves colloidal MnO_2 in significant amounts. This conclusion is based on the following observations: (*a*) colloidal MnO_2 is inactive to Chelex-100, and (*b*) the results in Table 1 show that the soluble manganese content determined by the Chelex-100 method is only slightly lower than (or, in view of experimental error, arguably about the same as) the content yielded by direct GFAA measurement without column inter-

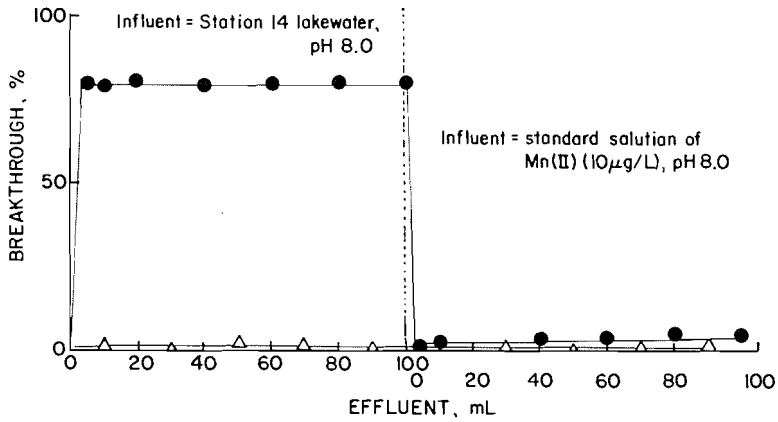

FIG. 1. Breakthrough curves for Mn in Lake Ontario water on a 1 × 3-cm XAD-7 analytical column (0.5 g, 80–100 mesh) (●), and a 1 × 4-cm Chelex-100 column (0.5 g, 200–400 mesh) (△). Flow rate = 1 mL/min.

TABLE 1. Soluble Mn in Lake Ontario waters, western basin[a]

Location	Direct analysis (μg/L)	Chelex-100 calib. curve (μg/L)	XAD-7 stand. add (μg/L)	Two-Column calib. curve (μg/L)
Station 3	0.50 ± 0.08	0.50 ± 0.05	Not done	0.11 ± 0.01[b]
Station 14	1.26 ± 0.14	1.13 ± 0.03	1.07 ± 0.02	0.15 ± 0.03
Station 302[c]	0.89 ± 0.08	0.72 ± 0.04	0.80 ± 0.02	0.12 ± 0.01

[a]Results are at least in duplicate; precision measure is one standard deviaton; all samples were previously filtered through 0.45 μm filters.
[b]Station 3 sample at natural pH (7.9) passed through one XAD-7 column only.
[c]Data from ref. 8.

cession. If MnO_2 is present in the samples, the bulk of it must have been removed by the 0.45 μm filter so that little or none is present in soluble form.

The two-column procedure requires acidification of the sample to about pH 1.7 and passage through a precolumn of XAD-7 to remove potentially complexing organic ligands such as humic substances (8). When the breakthrough experiments were repeated with unacidified samples passed through only the XAD-7 analytical column, the observations were essentially the same as for acidified samples (Station 3 sample, Table 1). In summary, 12–22% of total (soluble) manganese is retained on the XAD-7 column. This species is likely free Mn(II). It is a common form of manganese in lakewater; also, XAD-7 has been shown to retain free Mn(II) in standard solutions at pH 8, but not Mn(II) complexed to organic ligands such as humic material or colloidal forms of manganese (8).

Differential pulse polarography provided further evidence that the species retained by XAD-7 is free Mn(II). In Fig. 2, curves (*a*) and (*b*) represent, respectively, Station 3 water adjusted to pH 8.0 and the same sample spiked to 100 μg/L with Mn(II). In curve (*b*), the peak at −1.44 V is at the same potential as that for a standard solution of Mn(II) in DDW at pH 8.0 and, significantly, is only about 20% in height. About 80% of the spike has been converted to a polarographically non-labile form or forms. This conversion, of course, is why the standard addition two-column XAD-7 method returns a quantitative result for total soluble manganese. In curve (*a*), the natural concentration of Mn(II) (~0.1 μg/L) is simply too low for observation.

After passage of the spiked sample through the analytical

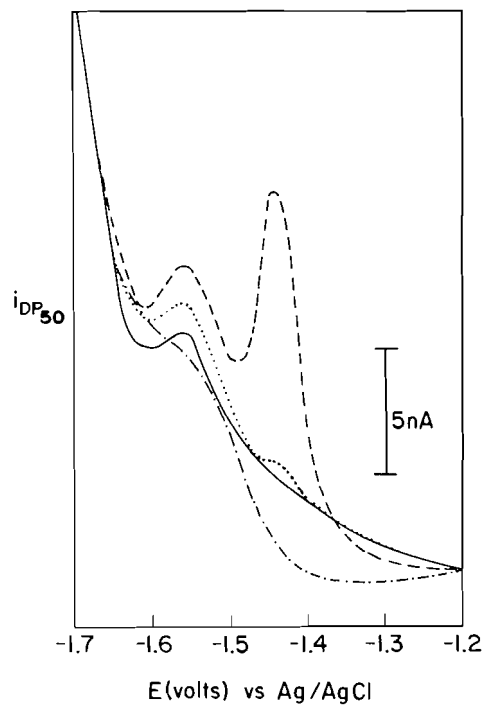

FIG. 2. Differential pulse polarograms of (*a*) Station 3 lakewater (—); (*b*) Station 3 sample spiked to 100 ppb with Mn(II) (---); (*c*) Sample in (*b*) after passage through XAD-7 column (····); (*d*) effluent from XAD-7 column in (*c*) passed through Chelex-100 column (-·-·-). Pulse = 50 mV; sensitivity = 2.5 × 10^{10} A/mm; droptime = 1.2 s; pH = 8.0, T = 21 ± 2°C.

Can. J. Chem. Downloaded from www.nrcresearchpress.com by 78.46.186.204 on 09/07/12
For personal use only.

XAD-7 column, only a residual peak at −1.44 V was observed (curve (*c*)), which was completely eliminated when the XAD-7 effluent was passed through Chelex-100 for the primary purpose of removing the second species (curve (*d*)). The peak at −1.56 V in curves (*a*), (*b*), (*c*) was diminished to a broad shoulder after passage of the XAD-7 effluent through Chelex-100. It is tempting to attribute the removed peak to the second species; however, this attribution cannot be made since the 80% conversion of the 100 ppm Mn(II) spike should have resulted in a far more intense peak at −1.56 V in curves (*b*) and (*c*) than in curve (*a*), for which the peak height would represent 0.4 μg/L of the second species. No firm polarographic evidence was found over the potential range −0.2 to −1.7 V for the manganese species inert to XAD-7. Of interest, the peak at −1.56 V was not observed in the solutions of humic acid, colloidal MnO_2 or Mn(III) acetate, although the last solution did yield a small Mn(II) peak at −1.44 V due to disproportionation of Mn(III) to Mn(II) and Mn(IV). The peak at −1.56 V remains unidentified.

The possibility that the unidentified manganese fraction consists of organic complexes of Mn(II) was considered. Organic complexes of trace metals break through the XAD-7 column (8). This possibility is not likely here, however, because the first column in the two-column procedure removes the bulk of organic substances. Also, Fe(III) and Cu(II) form more stable complexes but these ions did not break through the analytical XAD-7 column in the two-column procedure (see last column, Table III, ref. 8). Moreover, after intense uv irradiation of a separate sample to destroy organic matter, the breakthrough of manganese on XAD-7 and Chelex-100 was essentially as shown in Fig. 1. Another possibility is that the second fraction is colloidal Mn(III) produced by oxidation of Mn(II) at the surface of algae cells; however, in view of the rapid equilibration of Mn(II) spikes in the lakewater samples, this seems unlikely. More likely, the fraction consists of Mn(II) adsorbed on colloidal particles of iron oxides which, in view of the high concentration of iron in the western basin (8), would most certainly be present. Knox and Turner have made a similar suggestion regarding colloidally-bound manganese for an estuary water (9). Such colloidally-associated manganese was found to be polarographically inactive. Some evidence for colloidally-bound manganese was obtained by filtration of 100-mL aliquots of Station 3 water through a 0.025 μm membrane filter. Substantial amounts of manganese were retained on the filter, corresponding to 0.7 μg/L, but the precision on three replicates was inexplicably poor (±0.5 μg/L). Dissolution of the entrapped manganese species by 1% HNO_3 converted it to free Mn(II) and so it was inappropriate to test the activity of the species towards Chelex-100 and XAD-7. Presumably, if the species is colloidally-bound Mn(II), it would be kinetically labile to Chelex-100 but not to the low-capacity XAD-7 column. The concentration of manganese in the filtrate was 0.21 ± 0.02 μg/L, corresponding reasonably well, considering the low levels, to the concentration trapped on the XAD-7 column (0.11 μg/L, Table 1). This species is active to both XAD-7 and Chelex-100 and is therefore indicated as Mn(II). No significant amount of manganese was recovered from the 0.22 μm filter.

In summary, the combined use of XAD-7 and Chelex-100 columns for preconcentration provides a useful approach for the detection and quantitative estimation of free Mn(II) and a second fraction of soluble manganese species in lakewater. The manganese in this fraction may be colloidally adsorbed Mn(II).

Acknowledgements

We are indebted to the National Research Council of Canada and to the Natural Sciences and Engineering Research Council of Canada for support of this work. We are also indebted to one of the referees for helpful suggestions.

1. T. M. Florence. Talanta, **29**, 345 (1982).
2. A. Balikungeri, D. Robin, and W. Haerdi. Intern. J. Environ. Anal. Chem. **19**, 227 (1985).
3. M. P. Columbini and R. Fuoco. Talanta, **30**, 901 (1983).
4. N. Burns and J. O. Nriagu. J. Fish. Res. Board Can. **33**, 463 (1976).
5. K. Lum and J. K. Leslie. Sci. Total Environ. **30**, 99 (1983).
6. S. D. Chapnick, W. S. Moore, and K. H. Nealson. Limol. Oceanogr. **27**, 1004 (1982).
7. E. A. Jenne (*Editor*). Chemical modeling in aqueous systems. Am. Chem. Soc. Symp. Ser. No. 93. American Chemical Society, Washington, D.C. 1979. p. 857.
8. C. C. Wan, S. Chiang, and A. Corsini. Anal. Chem. **57**, 719 (1985).
9. S. Knox and D. R. Turner. Estuar. Coast. Mar. Sci. **10**, 317 (1980).

Can. J. Chem. Downloaded from www.nrcresearchpress.com by 78.46.186.204 on 09/07/12
For personal use only.

Versatile thin layer spectroelectrochemical cell employing specular reflectance

A. Scott Hinman and Brad J. Pavelich
Department of Chemistry, University of Calgary, Calgary, Alta., Canada T2N 1N4

Received June 26, 1986

This paper is dedicated to Professor Douglas E. Ryan on the occasion of his 65th birthday

A. Scott Hinman and Brad J. Pavelich. Can. J. Chem. **65**, 919 (1987).

A versatile thin layer spectroelectrochemical cell employing specular reflection of the incident light beam from the electrode surface is described. Its application to in-situ uv–vis and FTIR characterization of the products of electrochemical reactions and to thin layer voltammetry and coulometry as well as conventional cyclic voltammetry is demonstrated for the oxidation of tetraphenylporphinatozinc in dichloroethane/tetrabutylammonium perchlorate solution. The advantages and disadvantages of this type of cell as compared to more conventional sandwich type optically transparent thin layer electrodes are discussed.

A. Scott Hinman et Brad J. Pavelich. Can. J. Chem. **65**, 919 (1987).

On décrit une cellule spectroélectrochimique en couche mince qui est versatile et qui utilise la réflexion spéculaire d'un faisceau de lumière incidente provenant de la surface de l'électrode. Utilisant l'oxydation du tétraphénylporphinatozinc dans une solution de dichloroéthane/perchlorate de tétrabutylammonium, on a démontré l'application de cette cellule à la caractérisation par uv–vis et FTIR in-situ des produits des réactions électrochimiques, à la voltamétrie et à la coulométrie en couche mince ainsi qu'à la voltamétrie cyclique conventionnelle. On compare les avantages et les désavantages de ce type de cellule avec ceux des électrodes en couches minces plus conventionnelles, de type sandwiches et optiquement transparentes.
[Traduit par la revue]

Introduction

Recent literature shows a continuing interest in the design of thin layer electrochemical cells, especially those applicable to simultaneous spectrophotometric measurements (1–10). Particular emphasis has been placed on minimizing the resistance-induced potential distribution in the thin layer cavity, and on increasing the effective pathlength to improve spectral sensitivity. While the applicability of specular reflectance to thin layer spectroelectrochemical studies was reported as early as 1970 (11), the great majority of cells used for this purpose employ optically transparent electrodes, most often a gold minigrid, in a sandwich configuration of the general type described by DeAngelis and Heineman (12). Thin layer cells adapted for simultaneous specular reflectance measurements have more recently received attention as a result of their use for determining the infrared spectra of molecules within the thin layer cavity (13). Such cells can also be used in uv–visible studies and promise several advantages in this regard. In this paper we report on the design of a thin layer spectroelectrochemical cell employing reflectance of the light beam from the electrode surface, and demonstrate its utility for uv–visible and infrared spectral measurements as well as both conventional and thin layer voltammetric studies. The relative merits of this type of cell as compared to those employing optically transparent thin layer electrodes (OTTLE's) are discussed.

Cell design

The basic cell configuration is similar to that developed by Pons and co-workers for in-situ FTIR spectroelectrochemistry (13). The reader is referred to ref. 13 for optical considerations involved in in-situ infrared spectroelectrochemistry and references to the original literature. The important modifications to the basic Pons design included in our cell entail the provision for reproducible thin layer cavity thickness and greatly reduced sample volume requirement (5 mL). Also, the optical window seals directly to the cell body and does not require the use of epoxy cement or other sealing compound.

Figure 1 illustrates cross-section and front views of the cell and electrode assemblies. The cell body is constructed from a solid Teflon cylinder 50 mm in diameter and 50 mm in length.

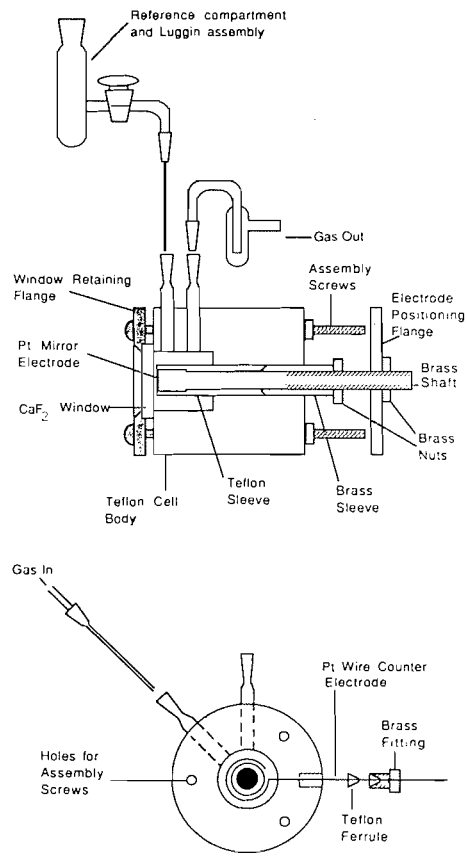

FIG. 1. Cross section of assembled cell and electrode assembly (upper drawing) and front view of cell with window and retaining flange removed (lower drawing).

A hollow concentric cylinder 20 mm × 20 mm is machined into it to form the sample compartment. A second cylindrical hole 11 mm in diameter is drilled concentrically through the remaining length of the cell body to accept the working electrode. Three holes are drilled radially into the sample compartment and ground glass joints (5/30 standard taper) are press fitted into these to accept Luggin capillary and degassing

Can. J. Chem. Downloaded from www.nrcresearchpress.com by 78.46.186.204 on 09/07/12
For personal use only.

Can. J. Chem. Downloaded from www.nrcresearchpress.com by 78.46.186.204 on 09/07/12
For personal use only.

accessories. A fourth hole provides for the Pt wire counter electrode. This is bent into a circle through which the working electrode can pass. The counter electrode is sealed by means of a Teflon ferrule and brass fitting which threads into the side of the cell body.

A 25 mm × 4 mm cylindrical calcium flouride window has been employed in this work. Although a variety of window materials may be used, CaF_2 has the advantages of being mechanically strong, resistant to scratching, stable to most aqueous and nonaqueous solvents, and transparent from approximately 1000 cm^{-1} in the infrared through to the near-uv region of the electromagnetic spectrum. The window is positioned in a machined brass flange and fastened to the cell by means of three bolts running the length of the cell assembly. The window seals directly against the front surface of the Teflon cell on tightening the fastening bolts.

The electrode is constructed from a brass shaft 80 mm in length. This is machined to a diameter of 6 mm except for a 1 cm length at one end which has a 7 mm diameter. A Pt disk cut from 0.5 mm thick Pt foil is silver soldered to this larger diameter end of the brass shaft while the other end is threaded for a length of 30 mm. The Pt disk is machined to a diameter 0.002 inches in excess of that of the shaft. This excess provides a leak-free seal to a Teflon sleeve 30 mm in length with an outside diameter of 11 mm. The inner diameter of the Teflon sleeve is machined to provide a press fit to the brass shaft. The difference between the 6 and 7 mm diameter sections of the brass shaft and a similar difference in the inside diameter of the Teflon sleeve prevent the sleeve from sliding forward on the electrode assembly. The Teflon sleeve is machined flush to the surface of the Pt disk after pressing it on. The Pt is then polished to a mirror finish on 0.3 μm alumina polishing powder. The end of the Teflon sleeve away from the electrode surface is chamfered inward at an angle of 45°. When the electrode assembly is inserted into the cell assembly a similarly chamfered brass sleeve 11 mm o.d. and 30 mm in length spreads the edges of the Teflon sleeve outward against the cell body to provide a leak-free seal. Pressure on the brass sleeve is provided by means of a nut threaded on to the electrode assembly and butting up against the back of sleeve. This is adjusted so that the electrode assembly may be easily slid forward and backwards in the cell assembly while still maintaining the seal. The maximum forward position of the electrode within the cell assembly is fixed by means of a lock nut and brass flange threaded on to the back of the electrode. The flange butts up against the cell assembly fastening bolts which provide a fixed reference position with respect to the cell window. Once the lock nut and flange have been adjusted to a suitable position, the thin layer of solution between the electrode surface and the window may be replenished by simply pulling the electrode back and pushing it forward again. This operation can be done while maintaining reproducible thin layer cavity thickness, as discussed below.

Experimental

A Cary model 16 uv–vis double beam scanning spectrometer was employed for spectroscopic studies in the visible region. A 25 mm hole was drilled into the side of the sample compartment along with three smaller holes to accept the cell assembly fastening bolts. The cell was then bolted directly to the side of the sample compartment. The sample beam was diverted with the aid of two 90° prisms, as illustrated in Fig. 2*a*. Absorbance spectra of the solution in the thin layer cavity were then recorded in double beam mode with an air reference. The reference beam was attenuated with the aid of an adjustable iris diaphragm to bring the absorbance on scale.

In-situ FTIR studies were performed with a Nicolet 5DX FTIR spectrometer employing the standard detector supplied with the instrument. The cell was placed in the sample compartment along with two planar front surfaced gold mirrors. The mirrors served to deflect the infrared beam onto the electrode and back to the detector, as illustrated in Fig. 2*b*. The cell was filled with the solution of interest and the thin layer thickness was adjusted to the desired value. (We have most often obtained best results with the electrode pushed ahead until it is in direct contact with the window. This serves to minimize solvent absorbance and increase the signal-to-noise ratio. The thin layer thickness in this case is determined by the accuracy with which the cell is machined.) A number of background energy spectra of the light reflected from the electrode surface were collected and signal averaged with the potential controlled at a value where no reaction occurs. The same number of spectra were then signal-averaged with the potential controlled at a value facilitating the reaction of interest. These were then ratioed against the background spectrum to give the normal %T versus wavenumber display. In this mode of operation, ir bands due to the reactant appear with greater than 100% T values, while bands due to the products of the electrochemical reaction have values less than 100%. (Solvent and supporting electrolyte bands are normally ratioed out, but can appear if they change their concentration in the double layer region or adsorb onto the electrode surface (13).)

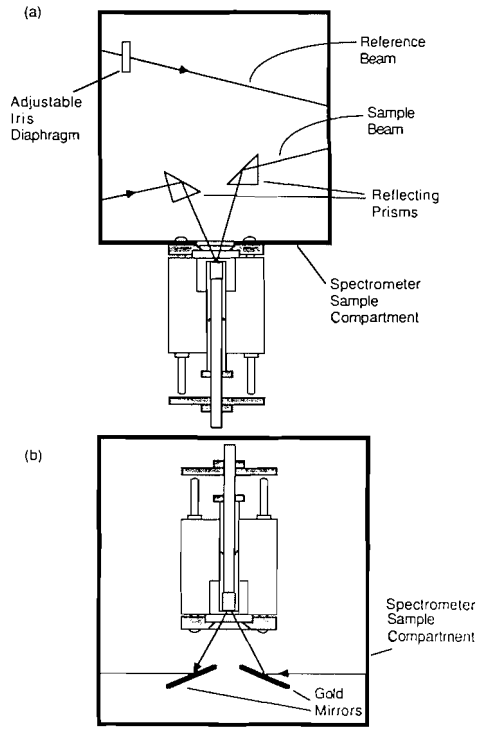

FIG. 2. Cell assembly and optical layout used for (*a*) Cary model 16 uv–vis spectrometer and (*b*) Nicolet 5DX FTIR spectrometer.

All solutions, reagents, and electrochemical equipment were used as described previously (2). The gas inlet tube illustrated in Fig. 1 extends directly into the solution in the sample cavity of the cell. Solutions were degassed by bubbling argon into the solution for approximately 2 min with the electrode pulled back. The bulb in the gas outlet port was filled with solvent, preventing diffusion of oxygen back into the cell when the argon flow was shut off. When operating in a thin layer configuration, a slow stream of argon could be maintained, as the resulting turbulence in the bulk solution had no effect on the voltammetry associated with the thin layer cavity. No pretreatment of the polished working electrode was performed other than rinsing with the solvent in use prior to the experiments.

Results and discussion

Figure 3 illustrates thin layer and conventional cyclic voltammetry obtained for 5,10,15,20-tetraphenylporphinatozinc(II) (TPPZn) in 1,2-dichloroethane containing 0.2 *M* tetra-*n*-butyl-

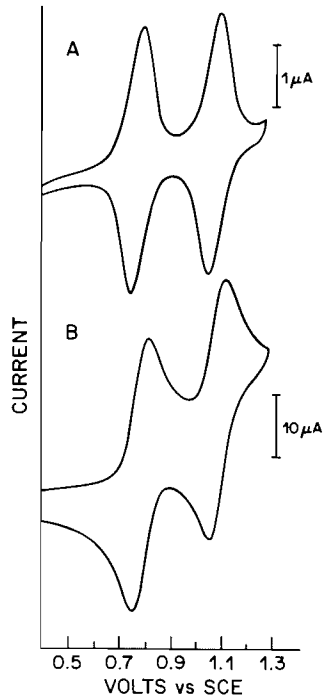

FIG. 3. Thin layer (*a*) and diffusion controlled (*b*) cyclic voltammograms for 0.48 m*M* TPPZn in $C_2H_4Cl_2$/0.2 *M* TBAP. Scan rates are (*a*) 2 mV/s and (*b*) 20 mV/s. The potential scale is vs. aqueous SCE.

ammonium perchlorate (TBAP). The two faradaic processes evident are well known and correspond to successive reversible formation of the porphyrin π-cation radical and π-dication (14). In the thin layer voltammogram the forward and reverse peaks are separated by 60 mV as compared to an ideal value of 0 (15), and the peak widths at half-height are 105 mV, as compared to a 90 mV theoretical value (1). The discrepancy between the theoretical and observed values results from resistance-induced potential distribution across the electrode surface (1). Although the resistance effects in this cell are fairly severe, the resolution between successive redox processes is still excellent even though their half-wave potentials are only separated by 300 mV. Also, the performance of this cell is still far superior to that obtained for TPPZn in the same media by us (2) and others (16) with more conventional cells employing minigrid electrodes in a sandwich configuration. It should be noted that near ideal thin layer voltammetric behaviour in this highly resistive solvent media has been reported by us (2) employing a 1 mm diameter thin layer electrode in a configuration similar to that described in this paper, and by Kadish and co-workers (3, 4) using a thin minigrid strip with two counter electrodes placed parallel and on either side of the strip. Theoretically, small reductions in the diameter of the electrode would lead to significantly improved performance (1). The relatively large 7 mm diameter employed in the present case is desirable, however, because it provides a larger area on which to focus the incident light beam, and thus simplifies the optics required. The beam diameter of the Nicolet 5DX FTIR spectrometer at its focal length is 8 mm, and a reduction of the electrode diameter below the 7 mm value we have used would probably require the inclusion of a beam condenser in the optical system to maintain the signal-to-noise ratio.

One problem encountered in designing thin layer cells is the provision of a means with which to change the solution in the thin layer cavity. With most conventional OTTLE cells, this requires careful and tedious rinsing of the thin layer cavity. With the present cell, changing the solution in the thin layer is readily accomplished by simply pulling the electrode assembly back and pushing it forward again until the electrode positioning flange butts up against the cell assembly bolts. To test the reproducibility of the thin layer thickness, five successive determinations of the charge required for complete 1-electron oxidation of a 1.0 m*M* TPPZn solution were carried out using thin layer chronocoulometry (2), pulling the electrode back and pushing it forward again between each run. The charges observed on successive runs all agreed within 2% of each other. This precision is readily obtainable by inexperienced workers employing thin layer thicknesses of ca. 50 μm. (The thin layer thickness is readily calculated from knowledge of the geometric area of the electrode and the quantity of charge required to bring about complete electrolysis of a solution of known concentration contained in the thin layer cavity.) At smaller thin layer thicknesses, this degree of precision is more difficult to obtain, and requires some practise. In particular, care must be taken not to rotate the electrode as it is pulled back and pushed forward again. We have been using the cell routinely for a year now, and an accuracy of 5% is readily obtainable in coulometric analyses when the thin layer volume is first calibrated with a solution containing a known concentration of electroactive species. While this is probably not as good as may be obtainable with cells employing fixed thin layer thicknesses, it is more than adequate for determining *n* values, the purpose for which thin layer coulometry is most often employed.

Figure 3*b* illustrates conventional cyclic voltammetry for TPPZn in the same solution as that used to obtain the thin layer voltammogram in Fig. 3*a*. These were obtained with the electrode pulled back to the rear of the cell sample compartment. Also, in the thin layer voltammogram, the luggin capillary reference probe was placed in the ground glass port closest to the window, while the port closest to the back of the cell was used in conventional cyclic voltammetric experiments. This allowed closer proximity of the luggin probe to the electrode. (The plane of the circular wire counter electrode lies between the two ground glass ports on top of the cell assembly. Hence the luggin probe may always be positioned to lie between the counter and working electrodes.) Although the peak currents were found to vary linearly with the square root of sweep rate throughout the range studied (10 to 200 mV s^{-1}) in accordance with theory, the peak separation varied between 68 and 92 mV, exceeding the 59 mV theoretical value for reversible charge transfer, even though electronic positive feedback compensation was employed to the fullest extent possible while maintaining potentiostat stability. In previous work (17) employing ac methods, one of us determined the standard heterogeneous rate constant for the first oxidation of TPPZn at Pt in the same solvent system to be $k^0 = 5.4 \times 10^{-2}$ cm s^{-1} with an associated diffusion coefficient of $D = 3.4 \times 10^{-6}$ cm^2 s^{-1}. Using this same diffusion coefficient, the cyclic voltammetric peak separations (18) lead to values of $k^0 = (6.0 \text{ to } 6.8) \times 10^{-3}$ cm s^{-1}, nearly an order of magnitude less than expected. The larger than expected peak separations probably result as much from uneven potential distribution at the electrode surface as uncompensated solution resistance, since all points on the planar working electrode are not equidistant from the circular wire counter electrode. Still, the agreement with theory is adequate for most purposes, and it is usually not possible to do conventional cyclic voltammetry at all in cells employing a fixed thin layer cavity thickness.

Figure 4 illustrates visible absorption spectra obtained at varying potentials throughout the first one-electron oxidation of

Can. J. Chem. Downloaded from www.nrcresearchpress.com by 78.46.186.204 on 09/07/12
For personal use only.

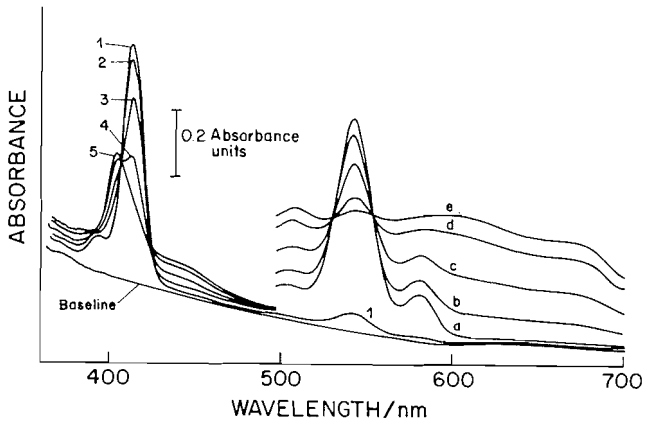

FIG. 4. Visible spectral changes observed for step-wise one electron oxidation of 1.14 mM TPPZn in $C_2H_4Cl_2$/0.2 M TBAP. Applied potentials vs. aqueous SCE are 650 mV, *1*, *a*; 740 mV, *2*, *b*; 780 mV, *3*, *c*; 820 mV, *4*, *d*; 860 mV, *5*, *e*. Spectra *a* through *e* were obtained after pulling the electrode back slightly to increase the absorbance, and utilized the same spectrometer sensitivity as *1* through *5*.

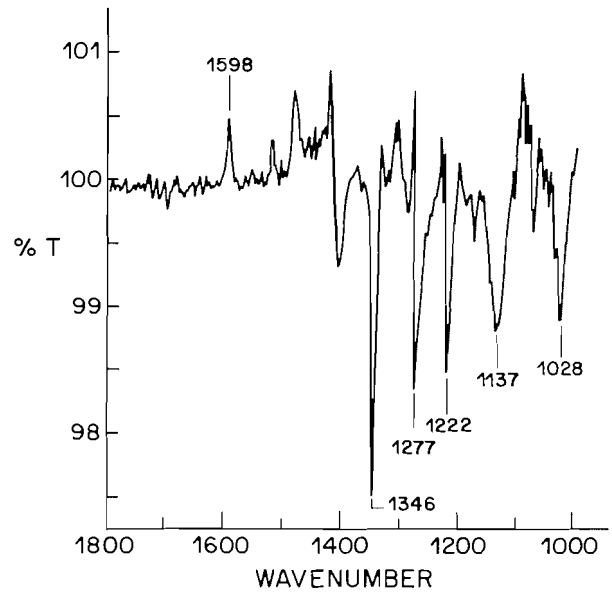

FIG. 5. In-situ FTIR spectra observed for one electron oxidation of 2.0 mM TPPZn in $C_2H_4Cl_2$/0.2 M TBAP. The base potential at which the reference spectrum was collected was 500 mV. The sample spectrum was collected after complete oxidation at 900 mV vs. aqueous SCE.

TPPZn. Spectra *a* through *e* were obtained at the same potentials and spectrometer sensitivity as *1* through *5*, respectively, after pulling the electrode back slightly to increase the thin layer thickness until adequate absorbance in the 500 to 700 nm range was observed. A comparison of the absorbance of the bands at 547 and 585 nm in spectrum *1* with the same bands in *a* demonstrates the dramatic variation in spectral sensitivity possible using thin layer cells employing specular reflectance. In OTTLE cells with fixed path length, generation of the spectra in Fig. 4 would have required the use of two solutions of different concentration.

The optical pathlength is given by eq. [1], as readily derived from geometric considerations (19).

$$[1] \quad l = 2d/\cos\theta$$

Here, d is the thickness of the thin layer cavity, and θ is the angle of incidence defined with respect to a perpendicular from the electrode surface. The molar absorptivity for TPPZn in dichloroethane/0.2 M TBAP was determined in a conventional uv–vis cell to be $2.25 \times 10^4\ M^{-1}\ cm^{-1}$ at 547 nm. From this value the optical pathlength l was determined to be 22 μm for spectra *1* through *5* in Fig. 4, and 240 μm for spectra *a* through *e*. From eq. [1], the thin layer thicknesses were less than 11 and 120 μm for these spectra. (A more precise calculation of d from eq. [1] requires knowledge of the angle of incidence, and subsequently the refractive index of the solution.) Kuwana and co-workers (9) have discussed a cell employing a gold minigrid which can be used in either a thin layer configuration or a semi-infinite linear diffusion configuration. It should be pointed out that cells employing their basic design might also have some applicability to obtaining thin layer spectra with varying optical pathlength, although this was not demonstrated. The degree to which the pathlength can be varied in a reflectance type cell cannot be realized utilizing optically transparent electrodes, however, as the light beam passes through the thin layer solution only once. Also, the use of a minigrid electrode limits the smallest obtainable pathlength to the thickness of the minigrid itself.

Although the greater sensitivity inherent in cells employing specular reflectance facilitates their use where variable optical sensitivity is desirable, precise knowledge of the optical pathlength is less readily available than in cells employing a fixed pathlength. Since there must always be a certain degree of variability in d, and since an exact knowledge of θ requires that the refractive index of the solution be known, the pathlength must be calibrated each time the cell is used if accurate determination of the molar absorptivities of the products of the electrochemical reaction is desired. In the case where the reactant has significant absorbance in the spectral region observed, this poses little problem, as the absorbance prior to the application of any potential to the electrode may be used for the calibration. The problem is more serious where the reactants do not absorb, in which case the pathlength must most often be deduced from the absorbance of a separate solution of known absorbance. Because the variability in pathlength is a factor $2/\cos\theta$ times the variability in the thin layer thickness, the resulting imprecision in the determination of molar absorptivities is a more serious problem than that in determining coulometric n values.

Figure 5 illustrates in-situ FTIR spectra associated with the first one-electron oxidation of TPPZn. The electrode was pushed into contact with the cell window to minimize solvent absorbance as discussed previously. The background spectrum was obtained at a potential of 0.5 V vs. SCE, while the sample spectrum ratioed against it was obtained after complete oxidation at 0.90 V. Each spectrum was the result of signal averaging 128 scans. (Each scan requires approximately 1 s.) Of particular interest is the strong absorbance at 1277 cm^{-1} observed for the TPPZn cation-radical. Absorbance bands very close to this value have been observed (20) for cation radicals of a number of metal–TPP complexes and have emerged as an important criterion for distinguishing between metal-centered as opposed to ring-centered oxidation of these complexes. Previous observation of this band, however, has required isolation of the oxidized species and determination of its solid-state vibrational spectrum. This, of course, is less convenient than in-situ characterization, and may not be possible in cases where the products have limited lifetime. It is noteworthy that this band is readily observable even though the solvent absorbs quite extensively in this region.

Can. J. Chem. Downloaded from www.nrcresearchpress.com by 78.46.186.204 on 09/07/12
For personal use only.

Also of note in Fig. 5 is the relatively strong absorbance at 1137 cm^{-1}. This band is not observed in spectral ratios recorded at the same potential in solutions of solvent and supporting electrolyte alone. It lies within the region anticipated for coordinated perchlorate (21) and thus suggests coordination of perchlorate anion to the zinc–porphyrin cation radical. Coordination of perchlorate to $TPP^{+\cdot}Zn$ has been observed in the X-ray crystal structure of the isolated cation radical (22), but its coordination in solution was not directly inferred.

Conclusions

The utilization of specular reflectance in thin layer electrochemical cell design can lead to a number of important advantages with respect to the use of optically transparent electrodes. Firstly, the pathlength is greater by a factor of $2/\cos\theta$, for cells with the same thin layer thickness, leading to an inherently greater sensitivity. Secondly, the pathlength is variable, making the cell applicable to studies in solutions of a wider range of concentrations. Thirdly, and perhaps most importantly, is the great versatility of this type of cell design. Hence, both conventional and thin layer voltammetric studies can be carried out, and the cell design is amenable to studies in the ir as well as uv–vis spectral regions. The availability of relatively inexpensive bench-top FTIR spectrometers designed for routine analysis, such as that used in the present study, should lead to more common use of this type of cell.

In fairness, the disadvantages of this type of cell design must also be pointed out. These are primarily that the precision affordable in coulometric studies and determination of molar absorptivities, while probably adequate for most purposes, may not be as good as that attainable with fixed thickness thin layer cells. Also, the construction of the cell requires more precise machining and probably more cost than most conventional OTTLE cells. It should be kept in mind that the reflectivity of Pt, and a variety of other metals, decreases sharply in the uv (note the sloping baseline in Fig. 4), and the resulting lower optical throughput can limit the applicability of reflectance type cells in this spectral region (11). We feel, however, that for most applications these disadvantages are outweighed by the advantages.

Acknowledgement

The authors gratefully acknowledge financial support from the Natural Sciences and Engineering Research Council of Canada.

1. A. S. Hinman, S. Pons, and J. Cassidy. Electrochim. Acta, **30**, 89 (1985).
2. A. S. Hinman, S. Pons, and J. Cassidy. Electrochim. Acta, **30**, 95 (1985).
3. X. Q. Lin and K. M. Kadish. Anal. Chem. **57**, 1498 (1985).
4. X. Q. Lin and K. M. Kadish. Anal. Chem. **58**, 1493 (1986).
5. R. K. Rhodes and K. M. Kadish. Anal. Chem. **53**, 1539 (1981).
6. J. Zak, M. D. Porter, and T. Kuwana. Anal. Chem. **55**, 2219 (1983).
7. M. D. Porter and T. Kuwana. Anal. Chem. **56**, 529 (1984).
8. D. A. Scherson, S. Sarangapi, and F. L. Urbach. Anal. Chem. **57**, 1501 (1985).
9. M. D. Porter, S. Dong, Y.-P. Gui, and T. Kuwana. Anal. Chem. **56**, 2263 (1984).
10. M. J. Simone, W. R. Heineman, and G. P. Kreishman. Anal. Chem. **54**, 2382 (1982).
11. P. T. Kissinger and C. N. Reilly. Anal. Chem. **42**, 12 (1970).
12. T. P. DeAngelis and W. R. Heineman. J. Chem. Ed. **53**, 529 (1976).
13. J. K. Foley and S. Pons. Anal. Chem. **57**, 945A (1985).
14. D. Dolphin, D. J. Halko, E. C. Johnson, and K. Rousseau. *In* Porphyrin chemistry advances. *Edited by* F. R. Longo. Ann Arbor Science, Ann Arbor. 1979. p. 335.
15. A. T. Hubbard and F. C. Anson. *In* Electroanalytical Chemistry. Vol. 4. *Edited by* A. J. Bard. Marcel Dekker, NY. 1970. p. 129.
16. K. M. Kadish, L. R. Shiue, R. K. Rhodes, and L. R. Bottomley. Inorg. Chem. **20**, 1274 (1981).
17. A. S. Hinman. Ph.D. Thesis. University of Alberta, Edmonton, Alta. 1983.
18. R. S. Nicholson. Anal. Chem. **37**, 1351 (1965).
19. R. L. McCreery, R. Pruiksma, and P. Fagan. Anal. Chem. **51**, 749 (1979).
20. E. T. Shimomura, M. A. Phillipi, H. M. Goff, W. F. Scholz, and C. A. Reed. J. Am. Chem. Soc. **103**, 6778 (1979).
21. K. Nakamoto. Infrared and Raman spectra of inorganic and coordination compounds. 4th ed. Wiley, NY. 1978. p. 242.
22. L. D. Spauling, P. G. Eller, J. A. Bertrand, and R. H. Felton. J. Am. Chem. Soc. **96**, 982 (1974).

Can. J. Chem. Downloaded from www.nrcresearchpress.com by 78.46.186.204 on 09/07/12
For personal use only.

Spectroscopic evidence for surface hydronium (H_3O^+) ions on hydrated single crystals

SIMONA BĂDILESCU AND CAMILLE SANDORFY
Département de Chimie, Université de Montréal, Montréal (Qué.), Canada H3C 3J7

Received August 21, 1986

This paper is dedicated to Professor Douglas E. Ryan on the occasion of his 65th birthday

SIMONA BĂDILESCU and CAMILLE SANDORFY. Can. J. Chem. **65**, 924 (1987).

Evidence has been obtained by attenuated total reflection Fourier transform infrared spectroscopy (ATR-FTIR) for the existence of hydronium ions on the surfaces of hydrated single crystals. The band near 1740 cm^{-1} due to the ν_4 (e) bending vibration of the hydronium ion has been identified on silicon, germanium, thallium bromide iodide (KRS-5), and zinc selenide single crystals. The protonating capability of these hydronium ions was demonstrated with pyridine derivatives.

SIMONA BĂDILESCU et CAMILLE SANDORFY. Can. J. Chem. **65**, 924 (1987).

Nous avons mis en évidence la présence d'ions hydronium sur les surfaces de monocristaux hydratés par des mesures de spectroscopie infrarouge par transformée de Fourier utilisant la technique de la réflexion totale atténuée. La bande ν_4 (e), vers 1740 cm^{-1} due à une vibration de déformation de l'ion hydronium a été retrouvée sur des surfaces de monocristaux de silicium, germanium, bromure-iodure de thallium et séléniure de zinc. Les spectres montrent que ces ions hydronium peuvent protoner les dérivés de la pyridine.

Can. J. Chem. Downloaded from www.nrcresearchpress.com by 78.46.186.204 on 09/07/12
For personal use only.

Introduction

The existence of the hydronium ion as a discrete chemical species in strong acid hydrates was established long ago (1). The equivalence of the three protons in the crystalline monohydrates of several inorganic acids was confirmed by nmr spectroscopy (2) and the precise molecular geometry of the H_3O^+ ion has been determined later by X-ray and neutron diffraction studies (3, 4).

The fundamental vibrations of H_3O^+ were identified (5–11) in various mineral acid solutions and assigned on the basis of a pyramidal structure by analogy with the isoelectronic NH_3 molecule. Normal coordinate treatment of the hydronium ion was accomplished by Basile *et al.* (12, 13) using the neutron diffraction data on solid *p*-toluenesulfonic acid monohydrate. In spite of the strong polarity of the ion, the vibrational spectrum of hydronium perchlorate could be obtained from the Raman spectra too. The infrared spectra of hydrogen halide solutions were examined by Taylor and Vidale (14) and Giguère and Turrell (15) who emphasized the role of the ionic charge in the strong hydrogen bonding nature of H_3O^+. For a detailed discussion of the spectroscopic aspects we refer to Williams (16) and Giguère (17).

Recently, we have examined the capability of the thallium bromide iodide (KRS-5) crystal to adsorb water, and we have identified some diagnostic bands (18) by FT-IR-ATR spectroscopy. The hydrated crystal surface was used as a substrate for hydration studies on mononucleotides and a methodology to maintain a constant and precisely controlled hydration degree on the surface was developed (19). Subsequently, we have examined the proton-donor ability of the adsorbed water (20). The influence of the lack of smoothness of the crystal surface on the dissociation of the adsorbed water has been noted.

Using ATR spectroscopy, Chabal and co-workers (21, 22) showed that water adsorption on silicon surfaces is dissociative and that hydride formation occurs upon molecular chemisorption of water on annealed surfaces. These results were in agreement with those of Ibach *et al.* (23) obtained by electron energy loss spectroscopy. Binding structures that may result from the dissociation of water molecules on silicon surfaces were discussed (24).

Our previous results indicated the possibility of the existence of the hydronium ion (H_3O^+) as a distinct chemical entity on the surface of the hydrated KRS-5 single crystal. The narrow band located at 1744 cm^{-1} in the ATR spectra of the hydrated thallium bromide iodide single crystal can be assigned to the asymmetrical bending mode ν_4 (e) of the surface hydronium ions. This band, appearing in a "window" of the strong water absorption in the transmission spectrum, is much more obvious in the ATR spectrum. In the OH stretching region a strong, broad band centered around 3760 cm^{-1} was observed.

In order to ascertain the assignment of these bands we have extended our studies to different internal reflection elements during various proton-acceptor systems. We were also interested in the study of hydrogen bonding interactions of the surface hydronium ion. This study reports a preliminary spectroscopic surface study (FT-IR-ATR) of some hydrated ATR single crystals, both with and without proton-acceptor compounds.

Experimental

Spectra were recorded on a Nicolet 5DXB FT-IR spectrometer equipped with a DTGS detector. Collection times for the spectra (100 co-added interferograms) were less than 2 min. The instrument was flushed with dry nitrogen during all measurements. Background spectra of the internal reflection elements (ATR single crystals) were recorded on a Perkin–Elmer Model 783 double beam grating spectrophotometer as well. Wide slit programs (resolution 3.2 cm^{-1}) and noise filter were used to reduce the noise level. The spectra were recorded with base line adjustment, without scale expansion.

The Model 300 ATR attachment (Barnes Analytical) was used. Commercially available (Barnes Analytical and Harrick Scientific Corp.) new KRS-5, ZnSe, Ge, and Si ATR plates (50 × 10 × 3 mm) were used to record the background spectra. Measurements were made over angles of incidence ranging from 30 to 55°. KRS-5 crystals were hydrated by keeping them for a day in an atmosphere of constant relative humidity.

Pyridine, 2,4,6-trimethylpyridine, and dioxan were used. Dioxan was deposited onto the crystal from aqueous solutions ($\sim 10^{-3}$) using a Hamilton microsyringe. Due to its higher volatility under vacuum, pyridine was deposited from a concentrated solution and the procedure was repeated three times for each side of the crystal. Water was removed under vacuum. Trimethylpyridine was deposited from a dilute chloroform-*d* solution. Crystals were cleaned with the proper solvent and distilled water. In some experiments cleaned crystals were heated up to 80°C in a vacuum oven. The cleanliness of the crystal was checked by the background spectrum.

TABLE 1. Frequencies of the ν_4 (e) bending vibration of the hydronium ion (H_3O^+) on the surfaces of ATR single crystals*

Crystal	Background spectra	Sample spectra			
		Py	2,4,6-Py	Oxonium of dioxan	Pyrimidinium (18)
Ge	1739	1738	1728	1740 1725	
Si	1722	1730	1728		
ZnSe	1737	1735	1727	1740 1725	
KRS-5	1740	1735	1728		1740

*Py = pyridinium, 2,4,6-Py = 2,4,6-trimethylpyridinium.

Results and discussion

Figure 1 shows the ATR spectrum of the silicon single crystal recorded on a Perkin-Elmer 783 double beam spectrophotometer. The most important feature of the spectrum is the narrow band located at 1720 cm^{-1} which stands out much clearer than in our previous spectra taken with the KRS-5 crystal. The silicon crystal is thinner than the others (2 mm compared to 3 mm) allowing a higher number of reflections and therefore an increased sensitivity. No shift or distortion of the band with changes in the angle of incidence was detected. The absorption bands of the silicon crystal (lattice bands) were recorded in order to show the relative intensities. In the water stretching and bending regions it is difficult to make precise assignments for the silicon crystal.

Background spectra of the germanium and zinc selenide crystals (25 × 10 × 3 mm) were recorded with the FT-IR instrument. The spectra show weak narrow bands at 1739 and 1737 cm^{-1}, respectively. Table 1 shows the band frequencies corresponding to the four single crystals (for the KRS-5 single crystal spectrum, see Fig. 1 in ref. 18). As already mentioned, the intensity of this band in the KRS-5 crystal depends strongly on the roughness of the surface. Generally, in the presence of defects on the surface, the 1740 and 3760 cm^{-1} bands are stronger than on a new crystal. In all cases (excepting the silicon crystal) the background spectra indicate the presence of the broad ν_2 water band accompanying the narrow high-frequency band, but the hydronium band is more intense.

The narrow band at 1720–1740 cm^{-1} has the right frequency to be assigned to the asymmetrical bending vibration ν_4 (e) of H_3O^+. It is in the same range as for crystals and for acid solutions (see above). The hydronium ions must result from the dissociation of some of the water molecules on the surface according to $2H_2O = H_3O^+ + OH^-$. The ions would then be adsorbed on the surface and further stabilized by hydrogen bonding with water molecules.

In order to examine this band further we added different compounds having proton acceptor capabilities. The results are presented in Figs. 2, 3, 4, and in Table 1. The general pattern of the spectra corresponds to the pyridinium ion and not to the molecule (25, 26). For the assignment of the bands of the pyridine molecule adsorbed on acidic solid surfaces we used the data of Parry (27) and Kirina *et al.* (28, 29). In this part of the work, however, we were interested more in the behaviour of the hydronium bands than in the acceptor's bands.

The first observation concerns the intensity of the ν_4 hydronium band. In all systems the relative intensity of the bands of the hydronium ion and of the acceptor molecules are of comparable intensity. The spectra were obtained by comparing the sample data with the corresponding background spectra. What we observe is an increase in the intensity of the band in the presence of the acceptor molecule. This is an important argument for the assignment of the band. Therefore any assignment involving crystal bands (overtones, impurities) is ruled out. The band centered around 1640 cm^{-1} (Fig. 2) receives contributions from the pyridinium ion (ν(C=NH$^+$)

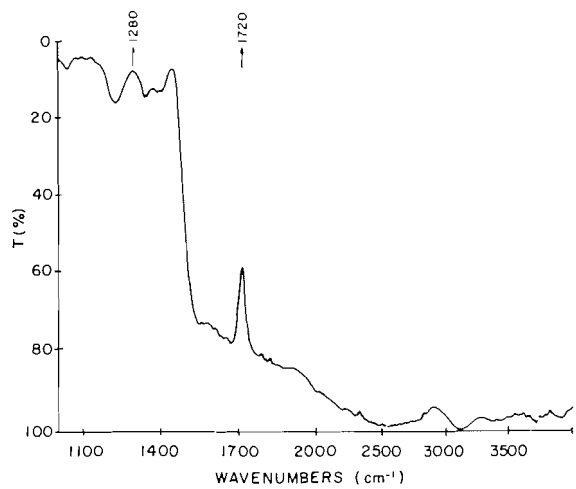

FIG. 1. ATR spectrum of the silicon (50 × 10 × 2 mm) single crystal (Perkin-Elmer 783, attenuated reference beam).

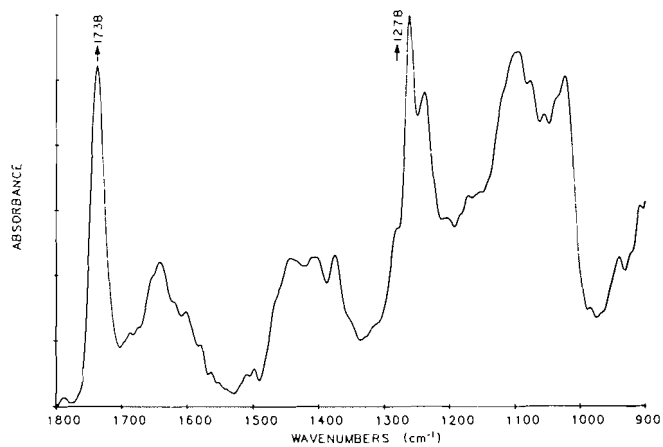

FIG. 2. ATR spectrum of pyridine adsorbed on a germanium crystal (from an aqueous solution).

Can. J. Chem. Downloaded from www.nrcresearchpress.com by 78.46.186.204 on 09/07/12
For personal use only.

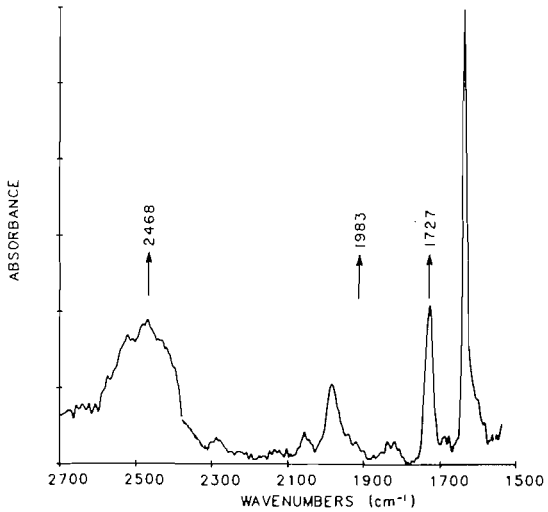

FIG. 3. ATR spectrum of 2,4,6-trimethylpyridine adsorbed on a silicon crystal (from $CDCl_3$ solution).

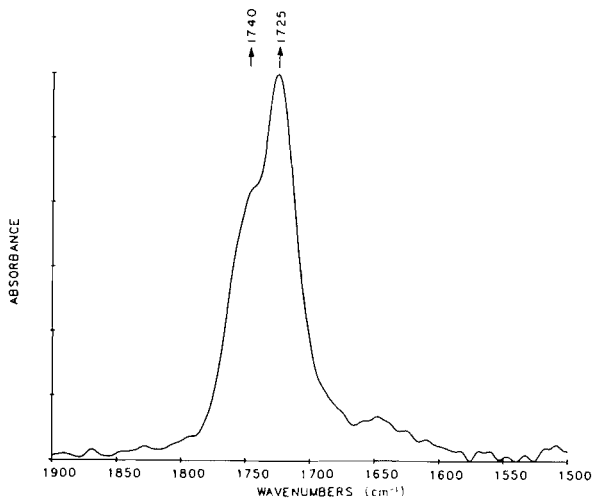

FIG. 4. ATR spectrum of dioxan adsorbed on a zinc selenide crystal.

and ν(C=C)) and also from the bending vibration of water. Similar results were obtained using the zinc selenide crystal under the same conditions. However, it is interesting to observe the different ratios of the bands at about 1735 and 1630 cm^{-1} corresponding to the hydronium and pyridinium ions, respectively, on the germanium and zinc selenide surfaces. On the germanium surface the 1735 band is much stronger while on the zinc selenide surface the relative intensities of the 1735 and 1630 bands are very nearly the same, indicating a higher degree of protonation of pyridine than on the germanium crystal (Fig. 2). We have already observed the decrease of the intensity of the hydronium band with the degree of protonation for Schiff bases (30). It is interesting to note that the heating of the crystal (pyridine adsorbed on zinc selenide) to 50°C during 2 h leaves the intensity of the pyridinium band unchanged. The results are supported by those obtained with a stronger base.

2,4,6-Trimethylpyridine. Figure 3 shows a strong band at 1636 cm^{-1} corresponding to the pyridinium ring and a weaker hydronium band at 1727 cm^{-1}. Figure 3 also shows some interesting features in the region corresponding to the stretching bands. An intense and broad band is present at about 2470 cm^{-1}. This is likely to correspond to the stretching vibration of an OH bond of the hydronium ion involved in a strong hydrogen bond. The N^+—H vibration may also contribute to it. The weaker band at 1983 cm^{-1} could be tentatively assigned to a combination involving the symmetrical bending vibration and a libration. The former can be assigned to a pronounced shoulder which is seen at about 1280 cm^{-1} in all our spectra. Figure 4 shows the 1900–1500 cm^{-1} region of the spectrum corresponding to dioxan adsorbed on a hydrated zinc selenide crystal. In this system the hydronium band is a double band with frequencies at 1740 and 1725 cm^{-1}. Table 1 shows that the ν_4 frequency of the hydronium ion depends more on the proton-acceptor molecule than on the crystal material; with the exception of the silicon crystal, the frequency of the hydronium ion is decreasing (compared to the free crystal) in the presence of the acceptor molecule. A lower frequency corresponds to a weaker hydrogen bond in the system.

The water environment of the hydronium ion on the crystal surface stabilizes the ion. It was established by diffraction studies that each of the three hydrogen atoms is strongly bonded to a water molecule; therefore the real structure of the ion corresponds to the formula $H_3O^+.3H_2O$ (17).

The counterion in these systems can be only the OH^- ion coordinated by the oxygen atom to the metal atom of the crystal. The hydronium ion in the crystal force field, stabilized by the water environment, is a stable, well-defined entity. The proton-acceptor molecules act as proton "sponges" displacing the dissociation equilibrium. The resulting protons are divided between the two possible acceptor sites — water and pyridine, for example.

Conclusion

The presence of the hydronium ion on the surface of some single crystals has been revealed by FT-IR-ATR spectroscopy. The bending vibration ν_4 (e) of the hydronium ion on different crystal surfaces has been assigned and the possible pattern of associations has been discussed. The hydronium ion protonates certain proton-acceptor molecules like pyridine derivatives.

Acknowledgements

Financial assistance from the Natural Sciences and Engineering Research Council of Canada and from le Ministère de l'Education du Québec is acknowledged.

1. M. VOLMER. Ann. Chem. **40**, 200 (1924).
2. R. E. RICHARDS and J. A. S. SMITH. Trans. Faraday Soc. **47**, 1261 (1951).
3. J. O. LUNDGREN and J. M. WILLIAMS. J. Chem. Phys. **58**, 788 (1973).
4. R. TRIOLO and A. H. NARTEN. J. Chem. Phys. **63**, 3624 (1975).
5. C. C. FERRISO and D. F. HORNIG. J. Chem. Phys. **23**, 1464 (1955).
6. M. FALK and P. A. GIGUÈRE. Can. J. Chem. **35**, 1195 (1957).
7. R. SAVOIE and P. A. GIGUÈRE. J. Chem. Phys. **41**, 2698 (1964).
8. P. A. GIGUÈRE and J. G. GUILLOT. J. Phys. Chem. **86**, 3231 (1982).
9. P. A. GIGUÈRE and C. MADEC. Chem. Phys. Lett. **37**, 569 (1976).
10. H. D. DOWNING and D. WILLIAMS. J. Phys. Chem. **80**, 1640 (1976).
11. P. A. GIGUÈRE, C. MARTEL, and S. TURRELL. Chem. Phys. Lett. **56**, 231 (1978).
12. L. J. BASILE, P. LABONVILLE, J. R. FERRARO, and J. M. WILLIAMS. J. Chem. Phys. **60**, 1981 (1974).
13. J. R. FERRARO, J. M. WILLIAMS, and P. LABONVILLE. Appl. Spectrosc. **28**, 379 (1974).

Can. J. Chem. Downloaded from www.nrcresearchpress.com by 78.46.186.204 on 09/07/12
For personal use only.

14. R. C. TAYLOR and G. L. VIDALE. J. Am. Chem. Soc. **78**, 5999 (1956).
15. P. A. GIGUÈRE and S. TURRELL. Can. J. Chem. **54**, 3477 (1976).
16. J. M. WILLIAMS. *In* The hydrogen bond. *Edited by* P. Schuster, G. Zundel, and C. Sandorfy. Vol. 2. North-Holland Publishing Co. Amsterdam. 1976. Chapt. 14. p. 657.
17. P. A. GIGUÈRE. J. Chem. Educ. **56**, 571 (1979).
18. S. BADILESCU and C. SANDORFY. Appl. Spectrosc. **40**, 1236 (1986).
19. S. BADILESCU and C. SANDORFY. Appl. Spectrosc. **41**, 10 (1987).
20. S. BADILESCU and C. SANDORFY. Can. J. Chem. **64**, 2404 (1986).
21. Y. J. CHABAL. Phys. Rev. B**29**, 3677 (1984).
22. Y. J. CHABAL and S. B. CHRISTMAN. Phys. Rev. B**29**, 6979 (1984).
23. H. IBACH, H. WAGNER, and D. BRUCHMANN. Solid State Commun. **72**, 457 (1982).
24. S. CIRACI and H. WAGNER. Phys. Rev. B**27**, 5180 (1983).
25. A. T. BALABAN, S. BADILESCU, and I. I. BADILESCU. *In* Physical methods in heterocyclic chemistry. *Edited by* R. R. Gupta. J. Wiley and Sons. 1984. Chapt. 1. p. 1.
26. J. H. S. GREEN and D. J. HARRISON. Spectrochim. Acta, **29**A, 293 (1973).
27. E. P. PARRY. J. Catal. **2**, 371 (1963).
28. T. V. ANTIPINA, G. D. CHUKIN, and O. F. KIRINA. Russ. J. Phys. Chem. **46**, 1663 (1972).
29. O. F. KIRINA, T. V. ANTIPINA, and G. D. CHUKIN. Russ. J. Phys. Chem. **47**, 248 (1973).
30. S. BADILESCU and C. SANDORFY. To be published.

Can. J. Chem. Downloaded from www.nrcresearchpress.com by 78.46.186.204 on 09/07/12
For personal use only.

The direct electrochemical synthesis of dialkyldithiocarbamate and diethyldithiophosphate complexes of main group and transition metals

CORRADO GELOSO, RAJESH KUMAR, JAIME ROMERO LOPEZ-GRADO,[1] AND DENNIS G. TUCK[2]

Department of Chemistry and Biochemistry, University of Windsor, Windsor, Ont., Canada N9B 3P4

Received September 18, 1986

This paper is dedicated to Professor Douglas E. Ryan on the occasion of his 65th birthday

CORRADO GELOSO, RAJESH KUMAR, JAIME ROMERO LOPEZ-GRADO, and DENNIS G. TUCK. Can. J. Chem. **65**, 928 (1987).

Dialkyldithiocarbamate derivatives $(R_2NCS_2)_nM$ of a number of metals (M = Fe, Co, Ni, Cu, Ag, Zn, Cd, In, Tl) have been synthesised in good yield by electrochemical oxidation of appropriate sacrificial anodes in non-aqueous solutions of either the corresponding tetraalkylthiuram disulphide $(R_2NCS_2)_2$ (R = Me, Et) or a mixture of carbon disulphide plus the secondary amine R_2NH (R = Et, *i*-Pr; R_2NH = piperidine). Similar experiments with solutions of $(EtO)_2P(S)SH$ (= HL) gave ML_n derivatives (M = Fe, Co, Ni, Cu, Ag, Au, Zn, Cd, Hg, Ga, In, Tl) while in the presence of HL + 1,10-phenanthroline, ML_n.phen derivatives were obtained for M = V, Mn, Fe, Co, Zn, and Ga.

CORRADO GELOSO, RAJESH KUMAR, JAIME ROMERO LOPEZ-GRADO et DENNIS G. TUCK. Can. J. Chem. **65**, 928 (1987).

On a synthétisé avec de bons rendements les dérivés dialkyldithiocarbamates $(R_2NCS_2)_nM$ d'un certain nombre de métau (M = Fe, Co, Ni, Cu, Ag, Zn, Cd, In, Tl) en mettant en jeu l'oxydation électrochimique d'anodes sacrifiées appropriées dans des solutions non-aqueuses soit des disulfures de tétraalkylthiurames correspondants $(R_2NCS_2)_2$ (R = Me, Et) soit d'un mélange de disulfure de carbone plus l'amine secondaire R_2NH (R = Et, *i*-Pr; R_2NH = pipéridine). Des expériences semblables avec des solutions de $(EtO)_2P(S)SH$ (= HL) conduisent aux dérivés ML_n (M = Fe, Co, Ni, Cu, Ag, Au, Zn, Cd, Hg, Ga, In, Tl) alors que, en présence de HL + phénanthroline-1,10, on obtient des dérivés ML_n.phen (M = V, Mn, Fe, Co, Zn et Ga).

[Traduit par la revue]

Introduction

The chemistry of metal complexes involving bidentate sulphur donor ligands continues to be of considerable importance in analytical chemistry, and in the preparative and the structural aspects of coordination chemistry. Alkyl dithiocarbamates, $R_2NCS_2^-$, are among the more important examples of such ligands, and some authors have reviewed these and related metal complexes (1, 2). The present work represents a continuation of studies in this laboratory of the preparation of metal salts of weak acids by electrochemical oxidation of a sacrificial anode in non-aqueous media. Earlier examples of such direct syntheses have lead to neutral and anionic thiolates (3–5), thiocyanates (6), phenylacetylene copper(I) (7), β-diketonates (8, 9), and carboxylates (10). We have now shown that the anodic oxidation of typical transition or Main Group metals into solutions of a tetraalkylthiuram disulphide $(R_2NCS_2)_2$, or a mixture of a secondary amine R_2NH with carbon disulphide, gives the $(R_2NCS_2)_nM$ derivatives in almost quantitative yield.

Dialkyldithiophosphate complexes represent another group of derivatives of bidentate sulphur donor ligands which are themselves the anions of weak acids (11). The present paper also reports the efficient direct electrochemical synthesis of a series of transition and Main Group metal complexes of diethyldithiophosphate from the parent acid.

Experimental

Materials

Solvents were dried by refluxing over calcium hydride (acetonitrile) or anhydrous magnesium sulphate (acetone). Carbon disulphide was dried over phosphorus pentoxide. All other organic reagents were used as supplied, as were metals used as anodes.

Analysis and spectroscopy

The metal content of the products was determined by atomic absorption spectrophotometry, and microanalysis on selected compounds was performed by Guelph Chemical Laboratories Ltd.

Infrared spectra were recorded on Perkin-Elmer IR 180 or Nicolet 5DX instruments; ^1H nmr spectra were obtained with a Perkin-Elmer EM 360 spectrometer at 60 MHz, and ^{31}P spectra on a Bruker CXP instrument.

Electrochemical synthesis

Dialkyldithiocarbamate complexes

Two different methods were used in the synthesis of $M(S_2CNR_2)_n$ complexes, but in each case, and in the preparation of diethyldithiophosphate derivatives described below, the cell was a 100-mL tall-form beaker fitted with a rubber bung through which the electrical leads entered the cell. The anode consisted of a rod or foil, as supplied, with the foils suspended on a platinum wire. The cathode was a platinum foil (12). Gallium anodes were prepared by the method described earlier, which in essence is melting the metal in a glass tube around a platinum wire (13). A stream of dry nitrogen served to stir the solution phase during electrolysis.

The two cells used can be summarized as:

(*i*) $Pt_{(-)}/CH_3CN$ (or acetone) + $(R_2NCS_2)_2/M_+$

(*ii*) $Pt_{(-)}/CH_3CN + R_2NCS_2H/M_{(+)}$

In case (*i*), the solutions of tetraalkylthiuram disulphide (R = Me, Et) were prepared immediately prior to electrolysis, the conditions of which are reported in Table 1. For (*ii*), solutions of $R_2NC(S)SH$ were prepared *in situ* by dropwise addition of excess CS_2 to a stirred solution of R_2NH (R = Et, *i*-Pr, or R_2NH = piperidine). The conditions for these experiments are set out in Table 2.

Isolation of dialkyldithiocarbamate complexes

The formation of an insoluble product at the anode was generally visible within a few minutes, although in some cases longer periods were required. Hydrogen gas evolved at the cathode when solutions of $R_2NC(S)SH$ were used. At the end of the electrolysis, the solid product was collected, washed several times with acetonitrile and then petroleum ether, and dried *in vacuo*.

Problems were encountered with anodes of gallium and thallium in

[1]Permanent address: Departmento de Quimica Inorganica, Facultad de Farmacia, Universidad de Santiago de Compostela, Spain.

[2]To whom correspondence should be addressed.

Can. J. Chem. Downloaded from www.nrcresearchpress.com by 78.46.186.204 on 09/07/12
For personal use only.

TABLE 1. Experimental conditions for the electrochemical synthesis of $M(S_2CNR_2)_n$ complexes from dialkylthiuram disulphide

Metal	Solvent[a]	Vol (mL)	L_2[b] (g)	Initial voltage (V)[c]	Time of electrolysis (h)	Metal dissolved (mg)
R = Me						
Fe	Acetone	50	0.25	25	2	44
Co	Acetone	50	0.20	20	4	90
Ni	Acetone	50	0.20	25	2	50
Cu	CH_3CN	70	0.30	30	1	53
Ag	CH_3CN	50	0.13	20	1	83
Zn	CH_3CN	70	0.76	10	4	117
Cd	CH_3CN	70	0.63	15	4	160
Ga	CH_3CN	60	0.30	20	3	[d]
In	CH_3CN	50	0.42	20	1.5	155
Tl	CH_3CN	50	0.40	20	1.5	262
R = Et						
Fe	Acetone	50	0.30	25	2	43
Co	Acetone	50	0.30	30	4.3	109
Ni	Acetone	50	0.30	30	1.3	32
Cu	CH_3CN	70	0.16	20	1	58
Ag	CH_3CN	50	0.13	20	1	82
Au	CH_3CN	30	0.20	20	18	130
Zn	CH_3CN	70	0.69	10	4	125
Cd	CH_3CN	70	0.76	18	4	176
Ga	CH_3CN	60	0.20	20	5	[d]
In	CH_3CN	50	0.44	25	1	89
Tl	CH_3CN	50	0.50	20	1	174

[a]Plus 25 mg Et_4NClO_4.
[b]$L_2 = (R_2NCS_2)_2$.
[c]Voltage to produce a current of 20 mA.
[d]See text.

TABLE 2. Experimental conditions for the electrochemical synthesis of $M(S_2CNR_2)_n$ complexes from $R_2NH + CS_2$

Metal	Solution composition[a]			Initial voltage[b] (V)	Time of electrolysis (h)	Metal dissolved (mg)
	R_2NH	(mL)	CS_2 (mL)			
Cu	Et_2NH	2	2	10	1	53
	i-Pr_2NH	1	1.5	15	1	
	Piperidine	0.2	0.12	20	1	50
Cd	Et_2NH	3	5	15	2.3	111
	Piperidine	0.2	0.12	10	2	80
Tl	Et_2NH	3	4	20	1	174

[a]In 60 mL CH_3CN, plus 20 mg Et_4NClO_4.
[b]Voltage to produce a current of 20 mA.

the isolation of products, and these cases are discussed below. No reaction was observed with anodes of mercury.

Diethyldithiophosphate complexes

The cells here were of the form $Pt_{(-)}/CH_3CN + (EtO)_2PS_2H/M_{(+)}$, but in all other respects, the experiments followed those described above for dialkyldithiocarbamate complexes. The details of cell composition, etc. are shown in the top section of Table 3 while in the bottom section we report the conditions for preparing various ML_n.phen adducts by anodic oxidation using acetone solutions of $(EtO)_2PS_2H$ + 1,10-phenanthroline.

Isolation of diethyldithiophosphate derivatives

The $M[S_2P(OEt)_2]_n$ compounds precipitated as the electrolysis proceeded, and these solids were collected, washed with acetonitrile and then diethyl ether, and dried *in vacuo*. Similar procedures gave a number of ML_n.phen adducts, which were washed with acetone and then *n*-pentane before drying *in vacuo*. Certain specific observations are noted below.

Results and discussion

Dialkyldithiocarbamate compounds

The studies reported above show that the preparation of $M(S_2CNR_2)_n$ compounds of both transition and Main Group elements by direct electrochemical synthesis from the metal can be satisfactorily achieved by two related routes. The first of

Can. J. Chem. Downloaded from www.nrcresearchpress.com by 78.46.186.204 on 09/07/12
For personal use only.

Can. J. Chem. Downloaded from www.nrcresearchpress.com by 78.46.186.204 on 09/07/12
For personal use only.

TABLE 3. Experimental conditions for the electrochemical synthesis of $M[S_2P(OEt)_2]_n$ complexes

Metal	Solvent	Vol[a] (mL)	Initial voltage (V)[b]	Time of electrolysis (h)	Metal dissolved (mg)
Fe	CH_3CN	30	14	7	121
Co	CH_3CN	30	24	7	131
Ni	CH_3CN	30	18	6.5	145
Cu	CH_3CN	50	45	3	152
Ag	CH_3CN	80	33	2	167
Au	CH_3CN	50	26	3	105
Zn	CH_3CN	50	32	3	89
Cd	CH_3CN	50	26	2	97
Hg	CH_3CN	65	40	2.5	[c]
Ga	CH_3CN	30	43	2	137
In	CH_3CN	30	23	1.2	117
Tl	CH_3CN	30	24	2.5	423

Metal	phen[d] (g)	Initial voltage (V)[b]	Time of electrolysis (h)	Metal dissolved (mg)
V	0.35	8	7	47
Mn	0.26	8	3.8	[c]
Fe	0.38	10	2.5	39
Co	0.51	6	2	33
Zn	0.46	6	3	83
Ga	0.47	6	2.5	[c]

[a]Containing 0.8 ± 0.2 mL $(EtO)_2PS_2H$ and ca. 25 mg Et_4NClO_4.
[b]Voltage to produce current of 20 mA.
[c]Not recorded.
[d]In 50 mL acetone, plus 0.8 ± 0.2 mL $(EtO)_2PS_2H$ and ca. 25 mg Et_4NClO_4.

these uses the appropriate tetraalkylthiuram disulphide as the source of the ligand, which has the advantage of employing a stable (and in some cases commercially available) starting material. The products, listed in Table 4, are generally those of the metals concerned in conventional oxidation states, and many of these compounds have been previously prepared by other workers (see ref. 1 and references therein). As noted earlier, the yields were essentially quantitative, based on the quantity of metal dissolved from the sacrificial anode; in most cases, the product is insoluble in the solution phase of the cell, making recovery a simple operation. The conditions described in Table 1 suggest that fairly wide variations in solvent and solute concentration have little or no effect on the synthesis, and given these variations, it seems reasonable to suggest that the method is a general one. The present experiments were carried on a small scale, but the yield is easily increased by using larger cells and/or using a number of cells in series.

In keeping with our previous practice, we have measured the electrochemical yield defined as the quantity of metal dissolved per Faraday of electricity (E_F, mol F^{-1}). For Fe, Co, Ni, Zn, and Cd, the E_F values were 0.5 ± 0.05 mol F^{-1}, corresponding to the processes

$$\text{cathode: } (R_2NCS_2)_2 + 2e \rightarrow 2R_2NCS_2^-$$

$$\text{anode: } 2R_2NCS_2^- + M \rightarrow M(S_2CNR_2)_2 + 2e$$

and for all but one of these metals (i.e., iron), the products are indeed the ML_2 species. With Cu, Ag, In, and Tl, E_F values of 1.0 ± 0.1 mol F^{-1} imply analogous reactions to form ML, although Table 4 shows that only with silver is this the only product identified. For the remaining elements one can reasonably postulate that the formation of ML at the anode is followed by the oxidative addition reactions

$$CuL + (1/2)L_2 \rightarrow CuL_2$$

$$ML + L_2 \rightarrow ML_3 \qquad (M = In, Tl)$$

and an analogous process presumably explains why FeL_3 is isolated despite an E_F value which indicates the formation of FeL_2 at the anode. Such oxidation steps have been observed in other electrochemical syntheses (cf. refs. 4, 9).

The reactions of anodic gallium, indium, and thallium require discussion in this context. Gallium electrodes were prepared by the method described elsewhere (13), and in view of the low melting point of the metal, electrolysis (see Table 1) was carried out with the cell cooled in ice. Under these conditions a white solid deposited on the anode as electrolysis proceeded, and this in turn caused a decrease in current. No significant quantities of solid deposited in the cell and the product could only be collected by scraping the anode subsequent to electrolysis; this material contained the $R_2NCS_2^-$ ligand (as shown by the infrared spectrum) but elemental analysis on the Ga/$Me_2NCS_2^-$ product (C 7.14, H 2.2, N 3.3) showed that this is highly contaminated, probably with gallium metal from the anode. Under these circumstances, the electrochemical synthesis offers no advantages over the standard methods. With indium, the products are the conventional ML_3 species, formed via the unstable InL^I (see above), but with thallium the detailed behaviour depends on the $R_2NCS_2^-$ ligand being used. With R = Me, the solution gradually became yellow–orange as electrolysis proceeded, and eventually coloured crystals of $Tl(S_2CNMe_2)_3$ deposited (see Table 4). When R = Et, the same yellow–orange colour developed in the solution phase, but a white solid also deposited after about 10 min; this solid is the thallium(I) compound $Tl(S_2CNEt_2)$. Concentration of the filtrate at the end of the electrolysis yielded yellow–orange crystals of $Tl(S_2CNEt_2)_3$. These results confirm the oxidative mechanism proposed above, requiring the formation of In^I or TL^I species at the anode, followed by oxidation in the solution phase. Similar reactions have been observed recently in a number of systems involving the electrochemical synthesis of complexes of Group III elements with sulphur donor ligands.[3]

The synthesis of $M(S_2CNR_2)$ compounds can also be simply achieved by mixing solvent with R_2NH and CS_2, cooling to dissipate the heat generated in the formation of $R_2NC(S)SH$, and then proceeding with the synthesis. The electrochemical behaviour of these systems (see Table 2) differs only in that hydrogen is evolved at the cathode, as in other HL systems, so that the sequence of reactions is

$$\text{cathode: } nR_2NCS_2H + ne \rightarrow \left(\frac{n}{2}\right)H_2(g) + nR_2CNS_2^-$$

$$\text{anode: } nR_2NCS_2^- + M \rightarrow M(S_2CNR_2)_n + ne$$

The products of these syntheses were characterised by elemental analysis, comparison of melting points with literature values, and infrared spectroscopy which established the presence of the ligand (cf. ref. 1).

Diethyldithiophosphate compounds

As with dialkyldithiocarbamates, we have investigated the electrochemical oxidation of transition and Main Group metals in the presence of $(EtO)_2PS_2H$. With some exceptions, the compounds produced (Table 5) are analogous to the dithio-

[3]R. Kumar, H. Mabrouk, and D. G. Tuck. Unpublished results.

TABLE 4. Analytical and related results for dithiocarbamate complexes

Compound	Colour	Melting point[a] (°C)	Metal	
			Found	Calcd
$Fe(S_2CNMe_2)_3$	Black	>300 (>300)	12.8	13.4
$Fe(S_2CNEt_2)_3$	Black	255 (252–255)	11.8	11.2
$Co(S_2CNMe_2)_2$	Green	>300	13.7	14.0
$Co(S_2CNEt_2)_2$[b]	Green	268 (263–264)	11.8	11.7
$Ni(S_2CNMe_2)_2$	Green	>300	18.8	19.6
$Ni(S_2CNEt_2)_2$	Green	238 (236)	16.1	16.5
$Cu(S_2CNMe_2)_2$[c]	Brown	265, dec. (260, dec.)	20.3	20.9
$Cu(S_2CNEt_2)_2$[d]	Brown	203 (191)	18.1	17.7
$Cu(S_2CNPr^i_2)_2$	Brown	>300	15.2	15.5
$Cu(S_2CNPip)_2$	Brown	271	17.0	16.6
$Ag(S_2CNMe_2)$	Pale yellow	255, dec. (260)	47.8	47.3
$Ag(S_2CNEt_2)$	Yellow	97	41.8	42.1
$Au(S_2CNEt_2)$[e]	Yellow	[f]		
$Zn(S_2CNMe_2)_2$	Pale yellow	257	21.1	21.4
$Zn(S_2CNEt_2)_2$	Pale yellow	184	17.8	18.1
$Cd(S_2CNMe_2)_2$	White	>300	32.5	31.8
$Cd(S_2CNEt_2)_2$	White	255	27.7	27.5
$Cd(S_2CNPip)_2$	White	266	26.7	26.0
$In(S_2CNMe_2)_3$	White	207	23.5	24.1
$In(S_2CNEt_2)_3$[g]	White	262 (250)	20.9	20.5
$Tl(S_2CNMe_2)_3$	Yellow	228	35.6	36.1
$Tl(S_2CNEt_2)$	White	117 (118)	57.9	57.9
$Tl(S_2CNEt_2)_3$	Yellow	203 (201)	31.5	31.5

[a]Literature values in parentheses (ref. 1*a*).
[b]*Anal.* calcd. for $Co(S_2CNEt_2)_2$: C 35.7, H 5.9, N 8.4; found: C 35.4, H 6.0, N 10.3.
[c]*Anal.* calcd. for $Cu(S_2CNMe_2)_2$: C 23.7, H 4.0, N 9.2; found: C 24.0, H 4.1, N 8.1.
[d]*Anal.* calcd. for $Cu(S_2CNEt_2)_2$: C 33.4, H 5.6, N 7.8; found: C 33.5, H 5.8, N 7.9.
[e]*Anal.* calcd. for $Au(S_2CNEt_2)$: C 17.3, H 2.9, N 4.1; found: C 16.3, H 3.1, N 5.9.
[f]Not recorded.
[g]*Anal.* calcd. for $In(S_2CNEt_2)_3$: C 22.7, H 3.8, N 8.8; found: C 22.4, H 4.0, N 9.1.

TABLE 5. Analytical and related results for diethyldithiophosphate complexes

Compound	Colour	Melting point (°C)	Metal		$\delta^{31}P$, ppm[a]
			Found	Calcd	
FeL_2	Black	114	13.2	13.1	83.75
CoL_2	Blue	235 (dec.)	14.4	13.7	[b]
CoL_3	Black	125	10.1	9.6	85.14
NiL_2[c]	Purple	83[d]	13.0	13.7	91.84
CuL	White	203 (dec.)	24.7	25.5	99.52
AgL	White	204 (dec.)	36.5	36.8	107.2
ZnL_2[e]	White	>300[f]	16.2	15.0	112.2[g]
CdL_2	White	158	22.7	23.3	107.77[g]
HgL_2	White	129[h]	35.8	35.1	97.56
InL_3	White	123	17.0	17.1	99.11
TlL	White	100	51.8	52.5	97.72
VL_2.phen[i]	Green	144			[b]
MnL_2.phen	Yellow	224	9.7	9.1	[b]
FeL_2.$phen_2$	Red	186	7.1	7.1	112.92[g]
CoL_3.phen	Orange	200	7.2	7.4	110.96
ZnL_2.phen	Orange	205	9.7	10.6	112.18
GaL.phen[j]	Yellow	159	[j]		113.00

[a]In CH_2Cl_2 solution; shifts relative to external 85% H_3PO_4.
[b]No ^{31}P resonance observed.
[c]*Anal.* calcd. for NiL_2: C 22.4, H 4.7; found: C 22.2, H 4.9.
[d]Lit. mp 105°C (14).
[e]*Anal.* calcd. for ZnL_2: C 22.2, H 4.2; found: C 20.7, H 4.3.
[f]Lit. mp 77°C (15).
[g]In Me_2SO solution.
[h]Lit. mp 124°C (16).
[i]*Anal.* calcd. for VL_2.phen: C 39.9, H 4.7, N 4.7; found: C 39.9, H 5.3, N 4.6.
[j]*Anal.* calcd. for GaL.phen: C 44.2, H 4.2, N 6.4; found: C 44.2, H 5.0, N 6.7.

Can. J. Chem. Downloaded from www.nrcresearchpress.com by 78.46.186.204 on 09/07/12
For personal use only.

carbamate species, and the E_F values are also similar, with $E_F = 0.5 \pm 0.05$ mol F^{-1} for iron, cobalt, nickel, zinc, and cadmium, and $E_F = 1.04 \pm 0.05$ mol F^{-1} for copper, silver, indium, and thallium. As noted earlier, the compounds were characterised analytically and spectroscopically; the infrared spectra demonstrated the presence of the $(EtO)_2PS_2$-ligand with the characteristic ν(P—S) modes in the 530–650 cm^{-1} region (cf. ref. 11). The proton nmr spectra of the diamagnetic complexes, in d_6-DMSO solution, showed a splitting of the CH_2 resonance, which is at ca. 4 ppm from Me_4Si; the CH_3 resonance at ca. 1.5 ppm was the conventional triplet. In the case of InL_3, which was studied in detail, we observed two quartets ($J = 7$ Hz) separated by 10.5 Hz (J(P—H)). The ^{31}P spectra (Table 5) show significant shifts from neat $(EtO)_2PS_2H$ for which the resonance is at 82.5 ppm. The resonance frequencies are in general close to those reported for these or similar complexes (17, 18), given the different solvents used, and confirm the bidentate coordination of ligand to metal.

The following points may be noted about the preparative work. With vanadium, electrolysis gave rise to a green solution, which eventually threw down a black solid which we were not able to characterise. Similarly, with chromium, substantial quantities of metal were dissolved, but an intractable black solid deposited from the dark yellow solution, while with manganese a colourless solution formed and a black deposit formed on the cathode. With iron, the product is a Fe^{II} derivative, rather than the Fe^{III} dithiocarbamate, perhaps reflecting the absence of an oxidising L_2 unit in solution. No product was isolated when gold was the anode. Thallium yielded only TlL (cf. comments on iron above).

When 1,10-phenanthroline was present in the electrolyte solution adducts were obtained (Table 5); some of these compounds have been reported previously (11). No doubt many other adducts of this and other donor ligands could be prepared by this simple and direct method.

Acknowledgement

This work was supported in part by Operating Grants to (D.G.T.) from the Natural Sciences and Engineering Research Council of Canada.

1. D. Coucouvanis. Prog. Inorg. Chem. (*a*) **11**, 233 (1970); (*b*) **22**, 301 (1979).
2. R. Eisenberg. Prog. Inorg. Chem. **12**, 295 (1970).
3. F. F. Said and D. G. Tuck. Inorg. Chim. Acta, **59**, 1 (1982).
4. J. L. Hencher, M. A. Khan, F. F. Said, R. Sieler, and D. G. Tuck. Inorg. Chem. **21**, 2787 (1982).
5. J. L. Hencher, M. A. Khan, F. F. Said, and D. G. Tuck. Polyhedron, **4**, 1263 (1985).
6. C. Oldham, M. J. Taylor, and D. G. Tuck. Inorg. Chim. Acta, **100**, L9 (1985).
7. R. Kumar and D. G. Tuck. J. Organomet. Chem. **281**, C47 (1985).
8. J. J. Habeeb, D. G. Tuck, and F. H. Walters. J. Coord. Chem. **8**, 27 (1978).
9. L. Matassa, N. Kumar, and D. G. Tuck. Inorg. Chim. Acta, **109**, 19 (1985).
10. N. Kumar, D. G. Tuck, and K. D. Watson. Can. J. Chem. **65**, 740 (1987).
11. J. R. Wasson, G. M. Woltermann, and H. J. Stoklosa. Fortschr. Chem. Forsch. **35**, 65 (1973).
12. C. Oldham and D. G. Tuck. J. Chem. Educ. **59**, 420 (1982).
13. M. J. Taylor and D. G. Tuck. Inorg. Synth. **22**, 135 (1983).
14. J. F. McConnell and Kastalsky. Acta Crystallogr. **22**, 853 (1967).
15. D. R. Dakternieks and G. P. Graddon. Austr. J. Chem. **23**, 1989 (1970); **23**, 2521 (1970).
16. P. F. Chen and W. Cheng. Sci. Sinica, **6**, 661 (1957).
17. C. Glidewell. Inorg. Chim. Acta, **25**, 159 (1977).
18. J. A. McCleverty, R. S. Z. Kowalski, N. A. Bailey, R. Mulvaney, and D. A. O'Cleirigh. J. Chem. Soc. Dalton Trans. 627 (1983).

Can. J. Chem. Downloaded from www.nrcresearchpress.com by 78.46.186.204 on 09/07/12
For personal use only.

Solvolytic rearrangement studies with (*E*)- and (*Z*)-2-anisyl-1,2-ditolyl[2-^{13}C]vinyl bromides

CHOI CHUCK LEE AND DAVE WANIGASEKERA
Department of Chemistry, University of Saskatchewan, Saskatoon, Sask., Canada S7N 0W0

Received October 1, 1986

This paper is dedicated to Professor Douglas E. Ryan on the occasion of his 65th birthday

CHOI CHUCK LEE and DAVE WANIGASEKERA. Can. J. Chem. **65**, 933 (1987).

Reaction of (*E*,*Z*)- or (*E*)-2-anisyl-1,2-ditolyl[2-^{13}C]vinyl bromides ((*E*,*Z*)- or (*E*)-**6**-Br-2-^{13}C) with HOAc–AgOAc gave a 1:1 mixture of (*E*)- and (*Z*)-2-anisyl-1,2-ditolyl[1,2-^{13}C]vinyl acetates ((*E*,*Z*)-**6**-OAc-1,2-^{13}C), with about 37.4% scrambling of the label from C-2 to C-1 arising from degenerate 1,2-anisyl shifts in the 2-anisyl-1,2-ditolyl[2-^{13}C]vinyl cation (**6**-2-^{13}C). No detectable amount of 1-anisyl-2,2-ditolylvinyl acetate was formed, indicating no nondegenerate 1,2-tolyl shift in cation **6** to give the more stable 1-anisyl-2,2-ditolylvinyl cation (**10**) in the reaction with HOAc–AgOAc. Reaction of (*E*)-**6**-Br-2-^{13}C with 2,2,2-trifluoroethanol (TFE) in the presence of 2,6-lutidine gave as major product 1-anisyl-2,2-ditolyl[1,2-^{13}C]vinyl 2,2,2-trifluoroethyl ether (**10**-OTFE-1,2-^{13}C) and a 1:1 mixture of (*E*)- and (*Z*)-2-anisyl-1,2-ditolyl[1,2-^{13}C]vinyl 2,2,2-trifluoroethyl ethers ((*E*,*Z*)-**6**-OTFE-1,2-^{13}C) as minor products, the ratio of **10**-OTFE to (*E*,*Z*)-**6**-OTFE being about 80:20. Scrambling on the ^{13}C label in the major product, **10**-OTFE-1,2-^{13}C, was 48.8 ± 0.9% and scrambling in the minor products, (*E*,*Z*)-**6**-OTFE-1,2-^{13}C, was 47.2 ± 1.4%. The present work with cation **6** completes the series of nine possible triarylvinyl cations, with various combinations of phenyl (Ph), *p*-tolyl (Tol), and (or) *p*-anisyl (An) as the three aryl groups, that can give rise to degenerate 1,2-aryl shifts across the double bond, and the present results are discussed in conjunction with data from previous work on the other eight triarylvinyl cationic systems.

CHOI CHUCK LEE et DAVE WANIGASEKERA. Can. J. Chem. **65**, 933 (1987).

La réaction des bromures d'anisyl-2 ditolyl-1,2 [^{13}C-2] vinyles-(*E*,*Z*) ou -(*E*) (**6**-Br ^{13}C-2-(*E*,*Z*) ou -(*E*)) avec HOAc–AgOAc conduit à un mélange 1:1 des acétates d'anisyl-2 ditolyl-1,2 [^{13}C-1,2] vinyles-(*E*) et -(*Z*) (**6**-OAc ^{13}C-1,2-(*E*,*Z*)) comportant 37,4% de répartition au hasard du marqueur de la position C-2 vers C-1; cette distribution proviendrait de migrations-1,2 dégénérées des groupements anisyles qui conduisent au cation anisyl-2 ditolyl-1,2 [^{13}C-2] vinyle (**6** ^{13}C-2). On n'a pas pu mettre en évidence la présence de quantités détectables d'acétate d'anisyl-1 ditolyl-2,2 vinyle; ce résultat indique que, dans la réaction avec le HOAc–AgOAc, il ne se produit pas de migration-1,2 non-dégénérée du tolyle du cation **6** qui conduirait au cation plus stable anisyl-1 ditolyl-2,2 vinyle (**10**). La réaction du **6**-Br ^{13}C-2-(*E*) avec le trifluoro-2,2,2 éthanol (TFE), en présence de lutidine-2,6, conduit à l'éther trifluoro-2,2,2 éthylique de l'anisyl-1 ditolyl-2,2 [^{13}C-1,2] vinyle (**10**-OTFE ^{13}C-1,2) comme produit principal et à un mélange 1:1 des éthers trifluoroéthyliques des anisyl-2 ditolyl-1,2 [^{13}C-1,2] vinyles-(*E*) et -(*Z*) (**6**-OTFE ^{13}C-1,2-(*E*,*Z*)) comme produits mineurs; le rapport des produits **10**-OTFE/**6**-OTFR-(*E*,*Z*) est d'environ 80:20. La répartition au hasard du marqueur ^{13}C dans le produit majeur, **10**-OTFE ^{13}C-1,2, est d'environ 48,8 ± 0,9% alors que dans les produits mineurs, **6**-OTFE ^{13}C-1,2-(*E*,*Z*), cette valeur est d'environ 47,2 ± 1,4%. Le présent travail avec le cation **6** complète la série de travaux entrepris sur les neuf cations triarylvinyles possibles avec les diverses combinaisons de phényle (Ph), *p*-tolyle (Tol) et (ou) *p*-anisyle (An) comme les trois groupements aryles et qui peuvent donner lieu à des migrations-1,2 dégénérées de groupements aryles à travers la double liaison. On discute des résultats obtenus dans le présent travail de concert avec les données obtenues dans les travaux antérieurs avec les huit autres systèmes cationiques triarylvinyles.

[Traduit par la revue]

Introduction

The early literature on vinyl cations, including rearrangements in these cations, has been reviewed (1, 2), and more specifically, work on degenerate rearrangements in triarylvinyl cations arising from 1,2-aryl shifts across the double bond, detected with use of isotopic labels as typified by eqs. [1] and [2], has been summarized in 1980 (3).

[1] $(Ar)_2C^*{=}\overset{+}{C}Ar \rightleftarrows Ar\overset{+}{C}^*{=}C(Ar)_2$

[2] $Ar(Ar')C^*{=}\overset{+}{C}Ar \rightleftarrows Ar\overset{+}{C}^*{=}C(Ar')Ar$

In the case of eq. [2], a nondegenerate rearrangement from a less stable to a more stable vinyl cation, which may occur before and after the degenerate rearrangement, as illustrated in eq. [3], is also possible.

[3] $Ar(Ar')C^*{=}\overset{+}{C}Ar \rightleftarrows Ar\overset{+}{C}^*{=}C(Ar')Ar$

$\downarrow$ $\downarrow$

$Ar'\overset{+}{C}^*{=}C(Ar)_2$ $(Ar)_2C^*{=}\overset{+}{C}Ar'$

With various combinations of phenyl (Ph), *p*-tolyl (Tol), and (or) *p*-anisyl (An) as the three aryl groups, nine triarylvinyl cationic systems, represented by structures **1** to **9**, are capable of giving rise to degenerate 1,2-aryl shifts across the double bond. In addition, cations **2**, **3**, and **6** should also be able to give a nondegenerate 1,2-phenyl or 1,2-tolyl shift to a more stable

$(Ph)_2C{=}\overset{+}{C}Ph$	$Ph(Tol)C{=}\overset{+}{C}Ph$	$Ph(An)C{=}\overset{+}{C}Ph$
1	**2**	**3**
$Tol(Ph)C{=}\overset{+}{C}Tol$	$(Tol)_2C{=}\overset{+}{C}Tol$	$Tol(An)C{=}\overset{+}{C}Tol$
4	**5**	**6**
$An(Ph)C{=}\overset{+}{C}An$	$An(Tol)C{=}\overset{+}{C}An$	$(An)_2C{=}\overset{+}{C}An$
7	**8**	**9**

cation as shown in eq. [3], while with cations **4**, **7**, and **8**, only the degenerate rearrangement as given in eq. [2] should occur because a 1,2-tolyl or 1,2-anisyl shift in these latter systems would not give a more stable cation. Up to the present, some work has been done on eight of these nine triarylvinyl cationic systems (3–5). The one exception is that no degenerate or

Can. J. Chem. Downloaded from www.nrcresearchpress.com by 78.46.186.204 on 09/07/12
For personal use only.

nondegenerate rearrangement studies have been made so far on the 2-anisyl-1,2-ditolylvinyl cation (**6**). In the present work, we have investigated the reaction of (*E*)- and (*Z*)-2-anisyl-1,2-ditolyl[2-^{13}C]vinyl bromides ((*E*)- and (*Z*)-**6**-Br-2-^{13}C) with HOAc–AgOAc or with 2,2,2-trifluoroethanol (TFE) in the presence of 2,6-lutidine, determined the extents of rearrangements in cation **6** generated from these reactions, and compared the results with those previously reported for other triarylvinyl cationic systems.

Results and discussion

A mixture of (*E*)- and (*Z*)-2-anisyl-1,2-ditolyl[2-^{13}C]vinyl bromides ((*E*)- and (*Z*)-**6**-Br-2-^{13}C) was prepared via a series of reactions analogous to those described for the preparation of (*E*)- and (*Z*)-2-phenyl-1,2-ditolyl[2-^{13}C]vinyl bromides ((*E*)- and (*Z*)-**4**-Br-2-^{13}C) (6). Reaction of 1,2-ditolyl[1-^{13}C]ethanone (6) with AnMgBr gave 1-anisyl-1,2-ditolyl[1-^{13}C]ethanol, which, in turn, was treated with Br_2 in HOAc to give an approximately 4:1 mixture of (*E*)- and (*Z*)-**6**-Br-2-^{13}C. After separation by fractional crystallization from absolute ethanol, the higher melting isomer was tentatively assigned the (*E*) or *trans* configuration (4, 7) and this major product, (*E*)-**6**-Br-2-^{13}C, was utilized in most of the subsequent solvolytic reactions.

An old criterion for differentiating between geometrical isomers is based on the assumption of a higher melting point for the more symmetrical isomer (7). For triarylvinyl derivatives with two identical aryl groups, the *trans* isomer would have a higher melting point. From observations of the chemical shifts in the ^{1}H nmr spectra of *cis* and *trans* pairs of triarylvinyl derivatives, it was suggested that for the lower melting *cis* isomer, the methoxy protons of an anisyl group should appear at higher field and the methyl protons of a tolyl group should appear at lower field than those for the corresponding *trans* isomer (4, 8, 9). For (*E*)- and (*Z*)-1,2-dianisyl-2-tolylvinyl bromides ((*E*,*Z*)-**8**-Br), a crystallographic study did show that the lower melting isomer with methoxy absorptions at higher fields and a methyl absorption at lower field was indeed the (*E*) or *cis* isomer (4). In the trifluoroethanolysis of (*E*)- and (*Z*)-1,2-diphenyl-2-tolylvinyl bromides ((*E*,*Z*)-**2**-Br) (5), the product with a methyl absorption at lower field was found by crystallographic study to be the expected (*Z*)- or *cis*-1,2-diphenyl-2-tolylvinyl 2,2,2-trifluoroethyl ether ((*Z*)-**2**-OTFE) (10). However, the crystal structures of *cis*- or (*Z*)- and *trans*- or (*E*)-**2**-Br showed that the lower melting isomer with methyl absorption at lower field was the *trans* isomer, opposite to predictions based on melting point and nmr (11). The present assignment of the higher melting major product with methyl absorption at higher field as *trans*- or (*E*)-**6**-Br is, therefore, only tentative. Even if this assignment were incorrect and the major product was the (*Z*) isomer, conclusions drawn from data derived from subsequent solvolytic studies should still be valid since both (*E*)- and (*Z*)-**6**-Br would give rise to the same vinyl cation **6**.

The reaction of a 4:1 mixture of (*E*)- and (*Z*)-**6**-Br-2-^{13}C or pure (*E*)-**6**-Br-2-^{13}C with HOAc in the presence of AgOAc gave an essentially 1:1 mixture of (*E*)- and (*Z*)-2-anisyl-1,2-ditolyl[1,2-^{13}C]vinyl acetates ((*E*,*Z*)-**6**-OAc-1,2-^{13}C). Some scrambling of the ^{13}C label from C-2 to C-1 was observed and this arose from 1,2-anisyl shifts in cation **6**, giving rise to (*E*,*Z*)-**6**-OAc-2-^{13}C and (*E*,*Z*)-**6**-OAc-1-^{13}C. No 1-anisyl-2,2-ditolylvinyl acetate (**10**-OAc) was formed, indicating no nondegenerate 1,2-tolyl shift in cation **6** under the acetolysis conditions. The same observation has been made previously

Tol(An)C*=C(Br)Tol
(*E*,*Z*)-**6**-Br-2-^{13}C

Tol(An)C*=C(OAc)Tol
(*E*,*Z*)-**6**-OAc-2-^{13}C

Tol(AcO)C*=C(An)Tol
(*E*,*Z*)-**6**-OAc-1-^{13}C

that, in reactions with HOAc–AgOAc, no nondegenerate rearrangement took place for (*E*)- or (*Z*)-1,2-diphenyl-2-tolylvinyl bromide ((*E*)- or (*Z*)-**2**-Br) (5) or (*E*)-2-anisyl-1,2-diphenylvinyl bromide ((*E*)-**3**-Br) (12).

Each sample of (*E*,*Z*)-**6**-OAc-1,2-^{13}C derived from the acetolysis reactions was treated twice successively (13) with $LiAlH_4$ to give a mixture of *erythro*- and *threo*-2-anisyl-1,2-ditolyl[1,2-^{13}C]ethanol (**11**-1,2-^{13}C), which was analyzed by

$(Tol)_2C{=}C(OAc)An$
10-OAc

Tol(An)C*HC*H(OH)Tol
11-1,2-^{13}C

^{13}C nmr to give the extent of scrambling of the ^{13}C label from C-2 to C-1, using the intensity ratio method with the methoxy absorption containing ^{13}C in its natural abundance as an internal standard (13). The results, as summarized in Table 1, show a remarkably reproducible extent of 37.4–37.5% scrambling for the reaction of (*E*,*Z*)- or (*E*)-**6**-Br-2-^{13}C in HOAc–AgOAc, the scrambling being the result of 1,2-anisyl shifts in cation **6**. The formation of a 1:1 mixture of (*E*)- and (*Z*)-**6**-OAc-1,2-^{13}C with the same extent of scrambling from reaction of either (*E*,*Z*)-**6**-Br-2-^{13}C or (*E*)-**6**-Br-2-^{13}C would indicate the formation of the dissociated, linear 2-anisyl-1,2-ditolylvinyl cation **6** as intermediate in these reactions, a conclusion that is in agreement with those drawn previously in support of dissociated, linear triarylvinyl cations (3–5).

In preliminary work with unlabeled material, the reaction of (*E*,*Z*)- or (*E*)-**6**-Br with 2,2,2-trifluoroethanol (TFE) in the presence of 1.2 equivalents of 2,6-lutidine gave, according to ^{1}H nmr, 1-anisyl-2,2-ditolylvinyl 2,2,2-trifluoroethyl ether (**10**-OTFE) as the major product and a 1:1 mixture of (*E*)- and (*Z*)-2-anisyl-1,2-ditolylvinyl 2,2,2-trifluoroethyl ethers ((*E*,*Z*)-**6**-OTFE) as minor products, the ratio of **10**-OTFE to (*E*,*Z*)-**6**-OTFE being about 80:20. The formation of **10**-OTFE is attributable to a nondegenerate 1,2-tolyl shift in cation **6** to give the more stable 1-anisyl-2,2-ditolylvinyl cation (**10**) analogous to the general processes illustrated in eq. [3]. This behavior is also similar to that observed previously for the trifluoroethanolysis of (*E*,*Z*)-**2**-Br (5) or (*E*)-**3**-Br (12) in which the major product was derived from a nondegenerate 1,2-phenyl shift in cation **2** or **3**.

The reaction of (*E*)-**6**-Br-2-^{13}C with TFE–2,6-lutidine gave rise to **10**-OTFE-1,2-^{13}C and (*E*,*Z*)-**6**-OTFE-1,2-^{13}C, some scrambling of the isotopic label between C-2 and C-1 being observed in both major and minor products. This mixture of products was degraded by ozonolysis to give a mixture of labeled and unlabeled ditolyl and anisyl tolyl ketones and these ketones were then analyzed by gc–ms to give the extents of scrambling of the ^{13}C label from C-2 to C-1 in both **10**-OTFE-1,2-^{13}C and (*E*,*Z*)-**6**-OTFE-1,2-^{13}C, using procedures as previously described for the determination of the extents of scrambling in the trifluoroethanolysis of (*E*,*Z*)-**2**-Br-2-^{13}C (5).

Given in Scheme 1 are the processes involved in the trifluoroethanolysis of (*E*)-**6**-Br-2-^{13}C, the ozonolysis of the solvolysis products, and the m/z values for the molecular ions and base peaks of the ketones derived from the degradation. From the gc–ms analysis, the mass spectral data in the regions

Can. J. Chem. Downloaded from www.nrcresearchpress.com by 78.46.186.204 on 09/07/12
For personal use only.

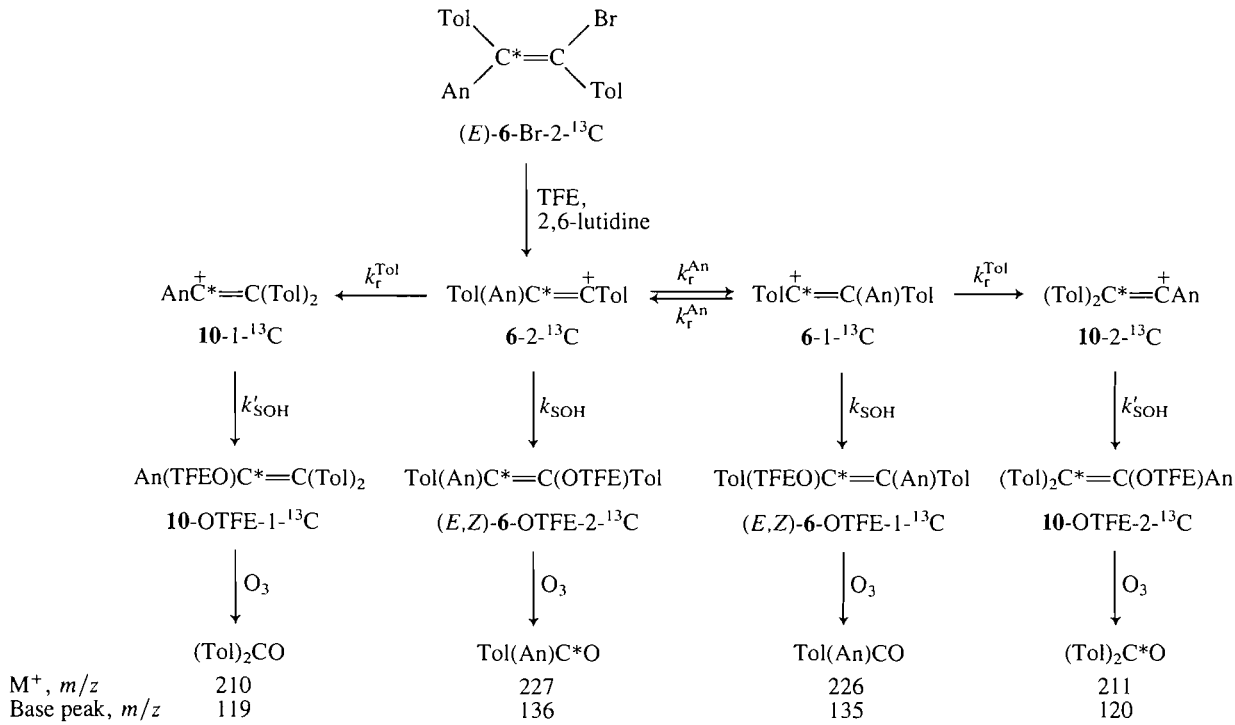

SCHEME 1

TABLE 1. Isotopic scrambling data from ^{13}C nmr spectra of 2-anisyl-1,2-ditolyl[1,2-^{13}C]ethanol (**11**-1,2-^{13}C) derived from reaction of (*E*,*Z*)- or (*E*)-**6**-Br-2-^{13}C with HOAc–AgOAc

Substrate	Intensity ratio[a]		^{13}C enrichment (%)[b]		Scrambling from C-2 to C-1 (%)
	I_1/I_s	I_2/I_s	I_1^*	I_2^*	
Unlabeled **6**-Br	1.05	0.997	—	—	—
(*E*,*Z*)-**6**-Br-2-^{13}C	13.08	20.12	12.6	21.1	37.4
(*E*)-**6**-Br-2-^{13}C	12.89	19.76	12.4	20.7	37.5
(*E*)-**6**-Br-2-^{13}C	13.56	20.86	13.1	21.9	37.4

[a] I_1, I_2, and I_s are the integrated intensities of the ^{13}C nmr absorptions for C-1, C-2, and CH_3O of the anisyl group at 76.5, 59.1, and 54.1 ppm, respectively. [b] I_1^* and I_2^* are the ^{13}C enrichments at C-1 and C-2, respectively, calculated from the intensity ratios; for an illustration of the calculations, see ref. 13.

of the molecular ions and base peaks for the unlabeled and labeled anisyl tolyl ketones and ditolyl ketones are summarized in Tables 2 and 3. After correcting for $[M + 1]^+$ absorptions and for the fact that the ^{13}C enrichment in the original reactant, (*E*)-**6**-Br-2-^{13}C, was 90%, an illustration of the calculations for these corrections having been given previously (5), the relative intensities for the unlabeled anisyl tolyl ketone at *m/z* 226 and 135 gave the extent of scrambling of the ^{13}C label from C-2 to C-1 in the minor products, (*E*,*Z*)-**6**-OTFE-1,2-^{13}C, and the relative intensities for the labeled ditolyl [^{13}C]ketone at *m/z* 211 and 120 gave the extent of scrambling of the label from C-1 to C-2 in the major product, **10**-OTFE-1,2-^{13}C. It is seen that the scrambling from C-2 to C-1 in (*E*,*Z*)-**6**-OTFE-1,2-^{13}C arising from degenerate 1,2-anisyl shifts in cation **6** was 47.2 ± 1.4% (Table 2), and the scrambling in **10**-OTFE-1,2-^{13}C arising from nondegenerate 1,2-tolyl shifts that took place before and after the degenerate rearrangement was 48.8 ± 0.9% (Table 3).

The rearrangement processes in Scheme 1 are shown again in Scheme 2 with the mean % scramblings ± standard deviations given in parentheses. Since the ratio of **10**-OTFE-1,2-^{13}C to (*E*,*Z*)-**6**-OTFE-1,2-^{13}C was 80:20, in the product mixture, the relative distribution of the unrearranged **10**-OTFE-1-^{13}C and the rearranged **10**-OTFE-2-^{13}C would be 0.80(51.2 ± 0.9) = 41.0 ± 0.7% and 0.80(48.8 ± 0.9) = 39.0 ± 0.7%, respectively. Similarly, the relative distribution of the unrearranged (*E*,*Z*)-**6**-OTFE-2-^{13}C and the rearranged (*E*,*Z*)-**6**-OTFE-1-^{13}C would be 0.20(52.8 ± 1.4) = 10.6 ± 0.3% and 0.20(47.2 ± 1.4) = 9.4 ± 0.3%, respectively. These distributions are also given in Scheme 2. It is of interest to note that the ratios of **10**-OTFE-1-^{13}C/(*E*,*Z*)-**6**-OTFE-2-^{13}C, or (41.0 ± 0.7)/(10.6 ± 0.3) = 3.9 ± 0.2, and **10**-OTFE-2-^{13}C/(*E*,*Z*)-**6**-OTFE-1-^{13}C, or (39.0 ± 0.7)/(9.4 ± 0.3) = 4.1 ± 0.2, are the same within experimental error, and this finding would indicate that the extents of nondegenerate 1,2-tolyl shifts from cation **6** to the more stable cation **10** are essentially the same before and after the degenerate 1,2-anisyl shifts in cation **6**. A similar conclusion was also obtained from the data derived from the trifluoroethanolysis of (*E*,*Z*)-**2**-Br-2-^{13}C (5). Again similar to the results obtained with (*E*,*Z*)-**2**-Br-2-^{13}C (5), the formation of **10**-OTFE-2-^{13}C as observed in the present work constitutes another demonstration of the occurrence of successive 1,2-aryl shifts, since this product was derived from a 1,2-anisyl shift in cation **6**-2-^{13}C to **6**-1-^{13}C followed by a 1,2-tolyl shift to **10**-2-^{13}C. Previously, using doubly labeled substrates (14, 15), successive 1,2-aryl shifts in triarylvinyl cations have also been demonstrated.

With the present work on cation **6**, isotopic scramblings arising from degenerate 1,2-aryl shifts have been determined for all of cations **1**–**9** generated in HOAc–AgOAc. Scrambling data from reactions in TFE–2,6-lutidine are also known for most of these nine cations. These results are summarized in Table 4. In the cases for which reactions with TFE–2,6-lutidine

Can. J. Chem. Downloaded from www.nrcresearchpress.com by 78.46.186.204 on 09/07/12
For personal use only.

TABLE 2. Data from the mass spectra of Tol(An)CO and Tol(AN)^{13}CO

	Observed intensity		Corrected for $[M + 1]^{+}$ [b]		Corrected for 90% ^{13}C enrichment[b]		% Distribution[c]	
m/z[a]	Run 1	Run 2	Run 1	Run 2	Run 1	Run 2	Run 1	Run 2
225	0.43	2.26						
226	37.47	39.60	37.44	39.31	30.04	31.79	45.1	47.0
227	39.33	40.95	36.51	35.88	36.51	35.88	54.9	53.0
228	2.96	5.23						
134	—	1.50						
135	100.00	100.00	100.00	99.88	81.20	81.34	48.0	48.8
136	93.47	93.27	88.02	85.50	88.02	85.50	52.0	51.2
137	5.09	7.25						

[a]Molecular ions for $[Tol(An)CO]^{+}$ and $[Tol(An)^{13}CO]$ at m/z 226 and 227, respectively; the base peak is $[AnCO]^{+}$ at m/z 135.
[b]For an illustration of the calculations, see ref. 5.
[c]Percentages for m/z 226 ($[Tol(An)CO]^{+}$) and for m/z 135 ($[AnCO]^{+}$) correspond to % scrambling from C-2 to C-1 in (*E*,*Z*)-**6**-OTFE-1,2-^{13}C (Scheme 2); mean value = (45.1 + 47.0 + 48.0 + 48.8)/4 = 47.2 ± 1.4%.

TABLE 3. Data from the mass spectra of $(Tol)_2CO$ and $(Tol)_2{}^{13}CO$

	Observed intensity		Corrected for $[M + 1]^{+}$ [b]		Corrected for 90% ^{13}C enrichment[b]		% Distribution[c]	
m/z[a]	Run 1	Run 2	Run 1	Run 2	Run 1	Run 2	Run 1	Run 2
209	1.79	2.48						
210	31.28	31.46	31.05	31.12	25.42	25.50	50.2	50.4
211	29.22	29.42	25.22	25.08	25.22	25.08	49.8	49.6
212	3.75	4.06						
118	0.72	0.15						
119	100.00	100.00	99.95	99.99	82.33	82.50	51.9	52.4
120	83.57	82.45	76.26	74.86	76.26	74.86	48.1	47.6
121	6.11	6.26						

[a]Molecular ions for $[(Tol)_2CO]^{+}$ and $[(Tol)_2{}^{13}CO]^{+}$ at m/z 210 and 211, respectively; the base peak is $[TolCO]^{+}$ at m/z 119.
[b]For an illustration of the calculations, see ref. 5.
[c]Percentages for m/z 211 ($[(Tol)_2{}^{13}CO]^{+}$) and for m/z 120 ($[(Tol{}^{13}CO]^{+}$) correspond to % scrambling from C-1 to C-2 in **10**-OTFE-1,2-^{13}C (Scheme 2); mean value = (49.8 + 49.6 + 48.1 + 47.6)/4 = 48.8 ± 0.9%.

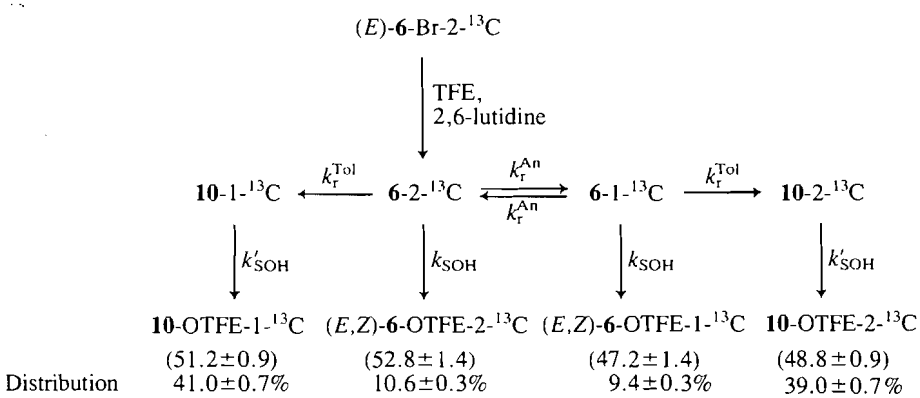

SCHEME 2

Can. J. Chem. Downloaded from www.nrcresearchpress.com by 78.46.186.204 on 09/07/12
For personal use only.

TABLE 4. Isotopic scrambling data from degenerate 1,2-aryl shifts in labeled triarylvinyl cations

Reactant[a]	Cation	Reaction with HOAc–AgOAc			Reaction with TFE–2,6-lutidine		
		% Scrambling[b]	k_{SOH}/k_r[c]	Ref.	% Scrambling[b]	k_{SOH}/k_r[c]	Ref.
$(Ph)_2C^*{=}C(Br)Ph$	**1**	6.8	25	16	44.1	0.54	17
$Ph(Tol)C^*{=}C(Br)Ph$	**2**	18.3	3.5	5	44.6		5
$Ph^*(An)C{=}C(Br)Ph$	**3**	46.4	0.16	12	50		12
$Tol(Ph)C^*{=}C(Br)Tol$	**4**	1.7	57	6	34.7[d]	0.88	6
$(Tol)_2C^*{=}C(Br)Tol$	**5**	13.5	11	18	46.5[d]	0.30	18
$Tol(An)C^*{=}C(Br)Tol$	**6**	37.4[e]	0.16		47.2[e]		
$An^*(Ph)C{=}C(Br)An$	**7**	0[f]		19	26.5[g]		19
$An(Ph)C^*{=}C(Br)An$	**7**	0		20	2.4[h]	40	
$An(Tol)C^*{=}C(Br)An$	**8**	0.5	2×10^2	4	25.5	1.9	4
$An^*(An)C{=}C(Br)An$	**9**	18[f,i]		19	50[j]		19
$(An)_2C^*{=}C(Br)An$	**9**	19.8	6.1	13	50[d]		13

[a] $C^* = {}^{13}C$ or ${}^{14}C$; $Ph^* = C_6D_5$; $An^* = CD_3OC_6H_4$.
[b] Mean value after complete reaction, the maximum extent of scrambling between C-2 and C-1 being 50%.
[c] Calculated from eq. [4] or [5], using the mean % scrambling values.
[d] From reaction with CF_3COOH–CF_3COOAg.
[e] From the present work.
[f] From reaction with HOAc–NaOAc.
[g] This value is probably too high (4) since it would suggest a greater extent of 1,2-phenyl shift in cation **7** than the analogous 1,2-tolyl shift in cation **8**; difficulties may be due to overlapping of peaks in the analysis by ^1H nmr (19).
[h] Unpublished work of David Tsui carried out in this laboratory using ^{13}C labelling; a much lower extent of scrambling was observed than the 26.5% in the preceding entry.
[i] Reported as 35 ± 2% rearrangement (19), with 100% rearrangement corresponding to 33.3% scrambling of the labeled An* from C-2 to C-1; the 35 ± 2% rearrangement would be equivalent to about 18% scrambling, assuming the maximum scrambling between C-2 and C-1 is 50%.
[j] Reported as 100% rearrangement (19) with 33.3% scrambling of the labeled An* from C-2 to C-1, and this would be equivalent to about 50% scrambling between C-2 and C-1.

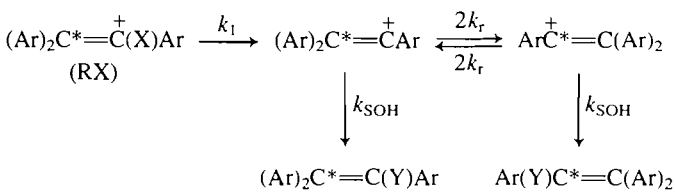

SCHEME 3

$$[4] \quad [RY]/[R_rY] = 1 + (k_{SOH}/2k_r)$$

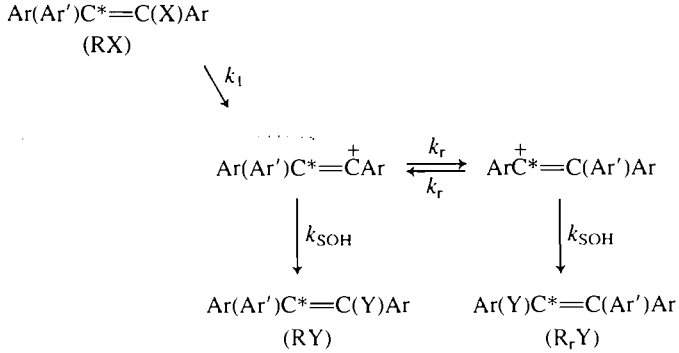

SCHEME 4

$$[5] \quad [RY]/[R_rY] = 1 + (k_{SOH}/k_r)$$

have not been carried out, scramblings observed in reactions with CF_3COOH–CF_3COOAg are included in Table 4 as illustrations of the extents of scrambling from solvolyses in a medium of low nucleophilic character. For the scrambling processes as depicted in Scheme 3 or 4, at complete reaction, eq. [4] or [5], respectively, would apply (21). Some values of k_{SOH}/k_r, calculated from eq. [4] or [5], are included in Table 4 for those cations for which eq. [4] or [5] holds.

Some generalizations may be made from the data summarized in Table 4. First of all, it is seen that the extent of scrambling for a given cation generated from reaction in TFE–2,6-lutidine or CF_3COOH–CF_3COOAg is much greater than the corresponding scrambling for the same cation generated from reaction in HOAc–AgOAc. This is not surprising since in solvents of low nucleophilic character, such as TFE or trifluoroacetic acid (TFA) (22), the cation would have a longer lifetime, thus allowing for more 1,2-shifts and giving rise to a greater amount of scrambling. For a given set of cations that differ only in the migrating aryl group, with the aryl groups at the migration origin and migration terminus remaining the same, such as cations **1**, **2**, and **3**, **4**, **5**, and **6**, or **7**, **8**, and **9**, an increasing extent of scrambling follows the order of increasing migratory aptitude, i.e., the order in the extent of scrambling is **3** > **2** > **1**, **6** > **5** > **4**, and **9** > **8** > **7**, in accord with the expected order of migratory aptitude of An > Tol > Ph.

A more quantitative evaluation of migratory aptitudes may be made utilizing the k_{SOH}/k_r values given in Table 4 (21). For cations **1** and **2** from reactions with HOAc–AgOAc, for example, k_{SOH}/k_r may be more specifically designated as k_{SOH}/k_r^{Ph} and k'_{SOH}/k_r^{Tol}. If one were to assume that the rate constants for the capture of cations **1** and **2**, k_{SOH} and k'_{SOH}, were the same in the HOAc–AgOAc medium, then $(k_{SOH}/k_r^{Ph})/(k'_{SOH}/k_r^{Tol}) = k_r^{Tol}/k_r^{Ph} = 25/3.5 = 7.1$. Similarly, for cations **1** and **3**, $k_r^{An}/k_r^{Ph} = 25/0.16 = 156$, giving rise to relative migratory aptitudes for Ph:Tol:An of 1:7.1:156. For cations **4**, **5**, and **6**, again generated from reactions with

Can. J. Chem. Downloaded from www.nrcresearchpress.com by 78.46.186.204 on 09/07/12
For personal use only.

Can. J. Chem. Downloaded from www.nrcresearchpress.com by 78.46.186.204 on 09/07/12
For personal use only.

HOAc–AgOAc, $k_r^{Tol}/k_r^{Ph} = 57/11 = 5.2$, and $k_r^{An}/k_r^{Ph} = 57/0.67 = 85$, giving relative migratory aptitudes for Ph:Tol:An of 1:5.2:85. While these two sets of values do show some variations, on an energy scale, the differences are only minor. Moreover, since the calculations were based on the assumption that k_{SOH} for different cations was identical, and since the k_{SOH}/k_r values were calculated from the mean % scramblings, which may show considerable deviations, the results for the two sets of migratory aptitudes may be regarded as showing reasonable agreement.

Another comparison of the scrambling data in Table 4 may be made by keeping the migrating group the same while varying the aryl groups at the migration origin and migration terminus. From reactions with HOAc–AgOAc for which data from all nine cations are available, for cations **1**, **4**, and **7** with the same migrating Ph group, and with Ph, Tol, and An, respectively, as the α-aryl substituent, the extents of scrambling follow the order of **1** > **4** > **7**. Similarly, for cations **2**, **5**, and **8** with the same migrating Tol group, and cations **3**, **6**, and **9** with the same migrating An group, the extents of scrambling again follow the order of **2** > **5** > **8** and **3** > **6** > **9**. In each of these sets of cations, the one that gives the most or the least extent of scrambling, respectively, has an α-phenyl or an α-anisyl substituent, indicating that, other factors being equal, the more stable triarylvinyl cation gives rise to a lesser extent of scrambling. This generalization may be explained by assuming that the more stable the initial triarylvinyl cation (**12**), the lower is its energy and the higher would be the activation energy in going from **12** to transition state **13**, thus giving rise to a lesser extent of scrambling. Such an explanation has also been discussed previously (6).

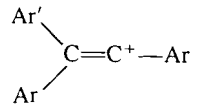

12

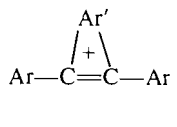

13

Finally, let us consider cations **2**, **3**, and **6**, all of which are capable of giving rise to both degenerate and nondegenerate rearrangements as depicted by eq. [3]. Summarized in Table 5 are the relative yields obtained under different conditions for the structurally unrearranged product from capture of the cation that may have undergone degenerate 1,2-aryl shifts, and the structurally rearranged product that resulted from a nondegenerate 1,2-aryl shift from a less stable to a more stable cation. It is seen from Table 5 that the relative yields of products are highly dependent on the reaction media. For all three cations, **2**, **3**, and **6**, no nondegenerate rearrangement to the more stable cation was observed for reactions in HOAc–AgOAc, while for reactions in TFE–2,6-lutidine, the major product was derived from the more stable cation resulting from a nondegenerate 1,2-aryl shift. With cation **6**, for example, the anisyl-bridged transition state **14** for the degenerate 1,2-shift may be of lower energy than the tolyl-bridged transition state **15** for the

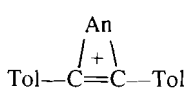

14

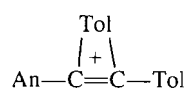

15

nondegenerate 1,2-shift; thus the degenerate 1,2-shift may be a faster process than the nondegenerate 1,2-shift to give a more stable cation. However, since the nondegenerate rearrangement, such as from cation **6** to the more stable cation **10** (Scheme 1), is not likely to be readily reversible, the possibility of the nondegenerate 1,2-shift as under equilibrium control and the degenerate 1,2-shift as under kinetic control may not apply.

As suggested in our studies on cation **2** (5, 23), the nucleophilic character of the reaction medium and the lifetime of the cation in that medium may play an important role in determining whether nondegenerate 1,2-shifts would take place. In HOAc–AgOAc, the lifetime of a cation is short and only the faster degenerate 1,2-shifts could occur, while in TFE-2,6-lutidine, a medium of low nucleophilic character, the cationic lifetime is long, thus allowing a major part of the cation to proceed via slower nondegenerate 1,2-shifts to give a more stable cation. In solvents such as HOAc–H_2O and EtOH–H_2O (Table 5), the lifetime of a cation would be intermediate between the lifetimes in HOAc–AgOAc and TFE–2,6-lutidine, and only a small extent of nondegenerate 1,2-shifts could take place, resulting in the formation of only a minor amount of product derived from the more stable cation.

Experimental

1-Anisyl-1,2-ditolyl[1-^{13}C]ethanol

To a Grignard solution prepared from 9.0 g (48 mmol) of *p*-bromoanisole and 1.5 g (62 mmol) of Mg in 300 mL of dry tetrahydrofuran (THF), and cooled in an ice bath, was added dropwise and with stirring over a period of 1 h a solution of 5.4 g (24 mmol) of 1,2-ditolyl[1-^{13}C]ethanone, prepared from 90% enriched [^{13}C]$BaCO_3$ (6), in 75 mL of dry THF. The resulting material was stirred at room temperature for 1 h, heated under reflux for 2 h, and then poured into 200 mL of H_2O containing 25 g of NH_4Cl and 5 mL of concentrated NH_4OH. The organic layer was washed with H_2O (3 × 25 mL) and, after drying over $MgSO_4$, the solvent was removed under reduced pressure to give 5.2 g (77%) of 1-anisyl-1,2-ditolyl[1-^{13}C]ethanol, which was crystallized from methanol, mp 101–102°C. A similar preparation with nonlabeled material gave 1-anisyl-1,2-ditolylethanol, which also melted at 101–102°C; ^{1}H nmr δ($CDCl_3$): 2.23 (shoulder, OH), 2.23, 2.29 (6H, 2s, $2CH_3$), 3.48 (2H, s, CH_2), 3.69 (3H, s, CH_3O), 6.56–7.28 (12H, m, Ar). *Anal.* calcd. for $C_{23}H_{24}O_2$: C 83.10, H 7.28; found: C 83.59, H 7.19.

(E)- and (Z)-2-anisyl-1,2-ditolyl[2-^{13}C]vinyl bromides ((E,Z)-6-Br-2-^{13}C)

To a solution of 5.0 g (18 mmol) of 1-anisyl-1,2-ditolyl[1-^{13}C]ethanol in 50 mL of HOAc was added dropwise and with stirring 4.0 g (25 mmol) of Br_2 in 20 mL of HOAc over a period of 0.5 h. During this time, the reaction mixture was maintained below 50°C by periodic cooling in a water bath, and any HBr that was produced was flushed out with N_2. The resulting mixture was stirred overnight at room temperature and the yellow solid product that was formed was collected by filtration, then washed with 10% $Na_2S_2O_3$ solution and with H_2O. The yield of the dried product was 5.5 g (78%), consisting of an approximately 4:1 mixture of (*E*)- and (*Z*)-**6**-Br-2-^{13}C according to ^{1}H nmr. Fractional crystallization from absolute ethanol gave the pure (*E*) isomer, which was used in most of the solvolytic reactions.

The similarly prepared unlabeled (*E*,*Z*)-**6**-Br were separated by fractional crystallization from absolute ethanol to give the major product, tentatively assigned the (*E*) structure, with a higher mp of 116–117°C, and the minor product, (*Z*)-**6**-Br, mp 104–105°C. For (*E*)-**6**-Br, ^{1}H nmr δ($CDCl_3$): 2.17, 2.23 (6H, 2s, $2CH_3$), 3.75 (3H, s, CH_3O), 6.72–7.30 (12H, m, Ar). *Anal.* calcd. for $C_{23}H_{21}OBr$: C 70.23, H 5.38; found: C 70.78, H 5.49. For (*Z*)-**6**-Br, ^{1}H nmr δ($CDCl_3$): 2.25, 2.35 (6H, 2s, $2CH_3$), 3.75 (3H, s, CH_3O), 6.40–7.20 (12H, m, Ar). *Anal.* calcd. for $C_{23}H_{21}OBr$: C 70.23, H 5.38; found: C 70.79, H 5.36.

Reaction with HOAc–AgOAc

In a typical experiment, 900 mg (2.3 mmol) of (*E*)-**6**-Br-2-^{13}C and

TABLE 5. Relative yields of structurally unrearranged product, Ar(Ar′)C=C(Y)Ar, and structurally rearranged product, Ar′(Y)C=C(Ar)$_2$, from cations **2**, **3**, and **6**, Ar(Ar′)C=$\overset{+}{C}$Ar

Cation[a]	Medium	Ref.	Relative yield (%) Ar(Ar′)C=C(Y)Ar	Ar′(Y)C=C(Ar)$_2$
2	HOAc–AgOAc	5	100	0
2	70% HOAc – 30% H_2O	23	85	15
2	TFE–2,6-lutidine	5	38	62
3	HOAc–AgOAc	12	100	0
3	60% EtOH – 40% H_2O	12	99.5	0.5
3	80% EtOH – 20% H_2O	12	94	6
3	TFE–2,6-lutidine	12	15	85
6	HOAc–AgOAc[b]		100	0
6	TFE–2,6-lutidine[b]		20	80

[a]For **2**, Ar = Ph, Ar′ = Tol; for **3**, Ar = Ph, Ar′ = An; for **6**, Ar = Tol, Ar′ = An.
[b]From the present work.

420 mg (2.5 mmol) of AgOAc in 25 mL of HOAc containing about 5% Ac_2O were heated under reflux for 24 h. The resulting mixture was filtered and the filtrate was evaporated to dryness under reduced pressure by a rotary evaporator. The residue was redissolved in 100 mL of ether, washed with H_2O (2 × 20 mL), 5% $NaHCO_3$ (2 × 20 mL), and again with H_2O (1 × 10 mL). After drying over $MgSO_4$, the ether was removed, giving 650 mg (74%) of product the ^{1}H nmr spectrum of which showed it to be an approximately 1:1 mixture of (*E*)- and (*Z*)-**6**-OAc-1,2-^{13}C.

From a larger scale experiment with unlabeled (*E*,*Z*)-**6**-Br, fractional crystallization of the product mixture, with methanol as solvent, gave only one pure product, tentatively assumed to be (*Z*)-**6**-OAc, mp 168–169°C; ^{1}H nmr δ($CDCl_3$): 1.99 (3H, s, AcO), 2.77, 2.34 (6H, 2s, $2CH_3$), 3.75 (3H, s, CH_3O), 6.60–7.30 (12H, m, Ar). *Anal.* calcd. for $C_{25}H_{24}O_3$: C 80.61, H 6.50; found: C 80.96, H 6.48. From the ^{1}H nmr spectrum of the original product mixture, data for the other isomer, (*E*)-**6**-OAc, were deduced; δ($CDCl_3$): 2.00 (3H, s, AcO), 2.27 (6H, s, $2CH_3$), 3.79 (3H, s, CH_3O), 6.60–7.30 (12H, m, Ar). No other acetoxy or methoxy absorption was presented in the product mixture, indicating no formation of 1-anisyl-2,2-ditolylvinyl acetate (**10**-OAc).

Erythro- *and* threo-*2-anisyl-1,2-ditolyl[1,2-^{13}C]ethanol (**11**-1,2-^{13}C)*

Each sample of (*E*,*Z*)-**6**-OAc-1,2-^{13}C obtained from a reaction in HOAc–AgOAc was diluted with some unlabeled (*E*,*Z*)-**6**-OAc as carrier and then reduced twice successively with $LiAlH_4$ as previously described (13) to give **11**-1,2-^{13}C for analysis of the extent of scrambling with ^{13}C nmr (13). A second treatment with $LiAlH_4$ was necessary to ensure complete reduction of any 2-anisyl-1,2-ditolylethanone that may be present after the first $LiAlH_4$ treatment (13). Typically, from 900 mg (2.4 mmol) of (*E*,*Z*)-**6**-OAc-1,2-^{13}C, 450 mg (58%) of *erythro*- and *threo*-2-anisyl-1,2-ditolylethanol-1,2-^{13}C (**11**-1,2-^{13}C) was obtained, mp 124–126°C; ^{1}H nmr δ($CDCl_3$): 2.17 (1H, s, OH), 2.25, 2.33, 2.37 (6H, 3s, $2CH_3$, *erythro* and *threo*, 2.33 overlapping), 3.72, 3.82 (3H, 2s, CH_3O, *erythro* and *threo*), 4.26 (1H, d, J = 7.8 Hz, CH at C-2), 5.30 (1H, d, J = 7.8 Hz, CH at C-1), 6.57–7.35 (12H, m, Ar). According to the relative intensities of the CH_3O absorption at 3.72 and 3.82 ppm, the *erythro* to *threo* ratio was about 2:1, the major component being assumed to be *erythro* since this diastereomer has the An and OH as well as the two Tol groups at the *anti* orientation in the most stable conformation. Analysis of the *erythro* and *threo* mixture gave the following results: *Anal.* calcd. for $C_{23}H_{24}O_2$: C 83.10, H 7.28; found: C 83.28, H 7.24.

Reaction in TFE–2,6-lutidine

Typically, 900 mg (2.3 mmol) of (*E*)-**6**-Br-2-^{13}C in 15 mL of TFE containing 300 mg (2.8 mmol) of 2,6-lutidine in a sealed glass ampule was heated in an oil bath at 120 ± 2°C for 4 days. After cooling, the content was transferred to a round bottom flask and the excess solvent was removed by distillation under reduced pressure. The residual yellow oil was redissolved in 100 mL of ether and the solution was washed successively with H_2O (3 × 15 mL), 1 *M* HCl (1 × 10 mL), and H_2O (1 × 10 mL). After drying over $MgSO_4$, the ether was removed under reduced pressure to give 580 mg (61%) of a mixture of **10**-OTFE-1,2-^{13}C and (*E*,*Z*)-**6**-OTFE-1,2-^{13}C as an oil. Ozonolysis of this product mixture gave a mixture of labeled and unlabeled ditolyl and anisyl tolyl ketones, which was analyzed to give the isotopic scramblings by gc–ms as previously described (5).

In a larger scale experiment using unlabeled (*E*,*Z*)-**6**-Br, the ^{1}H nmr spectrum of the product mixture gave three methoxy absorptions with a major peak at δ 3.77 ppm, assigned to **10**-OTFE, and two other smaller peaks of equal intensity at 3.71 and 3.81 ppm, assigned to (*E*,*Z*)-**6**-OTFE, the ratio of **10**-OTFE to (*E*,*Z*)-**6**-OTFE being about 80:20. From fractional crystallization of the product mixture using methanol as solvent, only the major product, **10**-OTFE, was isolated as colorless crystals, mp 103–104°C; ^{1}H nmr δ($CDCl_3$): 2.25, 2.36 (6H, 2s, $2CH_3$), 3.77 (3H, s, CH_3O), 3.90 (2H, q, J = 8.4 Hz, CH_2), 6.65–7.30 (12H, m, Ar). *Anal.* calcd. for $C_{25}H_{23}O_2F_3$: C 72.80, H 5.62; found: C 72.79, H 6.65.

Acknowledgment

The financial support given by the Natural Sciences and Engineering Research Council of Canada is sincerely acknowledged.

1. P. J. STANG, Z. RAPPOPORT, M. HANACK, and L. R. SUBRAMANIAN. Vinyl cations. Academic Press, New York. 1979.
2. A. A. SHCHEGALEV and M. KANISHCHEV. Russ. Chem. Rev. **50**, 553 (1981).
3. C. C. LEE. *In* Isotopes in organic chemistry. Vol. 5. Isotopes in cationic reactions. *Edited by* E. Buncel and C. C. Lee. Elsevier, Amsterdam. 1980. pp. 1–44.
4. D. WANIGASEKERA, C. C. LEE, Y. HOUMINER, M. AVIV, and Z. RAPPOPORT. J. Org. Chem. **49**, 4367 (1984).
5. C. C. LEE and D. WANIGASEKERA. Can. J. Chem. **64**, 1228 (1986).
6. C. C. LEE, A. J. PAINE, and E. C. F. KO. J. Am. Chem. Soc. **99**, 7267 (1977).
7. E. L. ELIEL. Stereochemistry of carbon compounds. McGraw–Hill, New York. 1962. pp. 326–327.
8. Z. RAPPOPORT and Y. APELOIG. J. Am. Chem. Soc. **91**, 6734 (1969).
9. Z. RAPPOPORT and Y. HOUMINER. J. Chem. Soc. Perkin Trans. 2, 1506 (1973).
10. Y. LUO, R. J. BARTON, B. E. ROBERTSON, C. C. LEE, and D. WANIGASEKERA. Acta Crystallogr. Sect. C: Cryst. Struct. Commun. **42**, 1220 (1986).

Can. J. Chem. Downloaded from www.nrcresearchpress.com by 78.46.186.204 on 09/07/12
For personal use only.

11. Y. LUO, R. J. BARTON, B. E. ROBERTSON, C. C. LEE, and D. WANIGASEKERA. Acta Crystallogr. Sect. C: Cryst. Struct. Commun. In press.
12. Z. RAPPOPORT, E. NOY, and Y. HOUMINER. J. Am. Chem. Soc. **98**, 2238 (1976).
13. M. OKA and C. C. LEE. Can. J. Chem. **53**, 320 (1975).
14. C. C. LEE, C. Y. FIAKPUI, and K. K. MIDHA. J. Org. Chem. **48**, 1025 (1983).
15. Z. RAPPOPORT, C. Y. FIAKPUI, X.-D. YU, and C. C. LEE. J. Org. Chem. **49**, 570 (1984).
16. F. H. A. RUMMENS, R. D. GREEN, A. J. CESSNA, M. OKA, and C. C. LEE. Can. J. Chem. **53**, 314 (1975).
17. C. C. LEE and E. C. F. KO. Can. J. Chem. **56**, 2459 (1978).
18. C. C. LEE, A. J. PAINE, and E. C. F. KO. Can. J. Chem. **55**, 2310 (1977).
19. Y. HOUMINER, E. NOY, and Z. RAPPOPORT. J. Am. Chem. Soc. **98**, 5632 (1976).
20. C. C. LEE and M. OKA. Can. J. Chem. **54**, 604 (1976).
21. C. C. LEE, E. C. F. KO, and Z. RAPPOPORT. Can. J. Chem. **58**, 884 (1980).
22. F. L. SCHADT, T. W. BENTLEY, and P. v. R. SCHLEYER. J. Am. Chem. Soc. **98**, 7667 (1976).
23. C. C. LEE, D. WANIGASEKERA, and C. Y. FIAKPUI. Can. J. Chem. **64**, 1235 (1986).

Can. J. Chem. Downloaded from www.nrcresearchpress.com by 78.46.186.204 on 09/07/12
For personal use only.

A ^{13}C and ^{15}N nuclear magnetic resonance study of solid ammonium thiocyanate

ROSS M. DICKSON, MICHAEL S. MCKINNON, JAMES F. BRITTEN, AND RODERICK E. WASYLISHEN[1]
Department of Chemistry, Dalhousie University, Halifax, N.S., Canada B3H 4J3

Received October 6, 1986

This paper is dedicated to Professor Douglas E. Ryan on the occasion of his 65th birthday

ROSS M. DICKSON, MICHAEL S. MCKINNON, JAMES F. BRITTEN, and RODERICK E. WASYLISHEN. Can. J. Chem. **65**, 941 (1987).

The static ^{13}C nmr powder pattern for solid ammonium thiocyanate is analyzed to obtain the ^{13}C chemical shielding anisotropy, 321 ± 7 ppm, and the $^{13}C-^{14}N$ dipolar splitting, 1295 ± 25 Hz. Slow magic angle spinning ^{15}N nmr experiments are analyzed to obtain a nitrogen chemical shielding anisotropy of 415 ± 15 ppm. The $^{13}C-^{14}N$ dipolar splitting leads to an effective C—N bond length of 1.19 ± 0.01 Å, in good agreement with the value of 1.176 Å reported from accurate X-ray and neutron crystallographic studies. In solid NH_4NCS absolute values of the average shielding constants $\sigma(N\underline{C}S)$ and $\sigma(\underline{N}CS)$ are 52 and 34 ppm, respectively. Comparison of calculated and observed $\sigma_{\parallel}{}^{d}$ values indicates that intermolecular interactions decrease the ^{13}C and ^{15}N shielding constants by approximately 10 and 30 ppm, respectively.

ROSS M. DICKSON, MICHAEL S. MCKINNON, JAMES F. BRITTEN et RODERICK E. WASYLISHEN. Can. J. Chem. **65**, 941 (1987).

Dans le but de déterminer l'anisotropie du blindage chimique du ^{13}C, 321 ± 7 ppm, ainsi que le couplage dipolaire $^{13}C-^{14}N$, 1295 ± 25 Hz, on a analysé le patron de poudre de la rmn ^{13}C statique du thiocyanate d'ammonium. On a aussi analysé des expériences des tournoiement lent de l'angle magique en rmn du ^{15}N pour obtenir l'anisotropie de blindage chimique de l'azote, 415 ± 15 ppm. Le couplage dipolaire $^{13}C-^{14}N$ conduit à une longueur réelle de la liaison C—N de 1,19 ± 0,01 Å; cette valeur est en bon accord avec la valeur de 1,176 Å qui a été obtenue par des études précises faites par diffraction des rayons-X et des neutrons. À l'état solide, les valeurs absolues des constantes moyennes de blindage $\sigma(N\underline{C}S)$ et $\sigma(\underline{N}CS)$ sont respectivement 52 et 34 ppm. Une comparaison des valeurs calculées et observées pour $\sigma_{\parallel}{}^{d}$ indique que les interactions intermoléculaires diminuent les constantes de blindage ^{13}C et ^{15}N par des valeurs respectives de 10 et 30 ppm.

[Traduit par la revue]

Introduction

Static powder lineshapes contain, in theory, information on all solid-state carbon-13 nmr interactions: chemical shielding anisotropy (CSA), dipole–dipole couplings (DD), and indirect couplings (J) (1–3). The principal challenge in powder nmr is to extract these observables from a powder spectrum or to devise ingenious experiments that allow one to separate these interactions so that they can be observed individually (1–10).

In this study we present a simple analysis of the static spin-1/2 powder pattern that results when the spin-1/2 nucleus has an axially symmetric CSA and is dipolar coupled to a quadrupolar nucleus (I = 1). The analysis is applied to the ^{1}H decoupled ^{13}C nmr powder spectrum of solid ammonium thiocyanate, NH_4NCS (Fig. 1). The ^{13}C chemical shielding anisotropy for this simple ion has not been previously reported. Also, the C—N bond length that we calculate from the observed dipolar coupling can be compared with values obtained from accurate X-ray and neutron diffraction measurements (11). Previously, Kaplan *et al.* (12) carried out a similar analysis for the cyano carbon of solid acetonitrile at 83 K; however, to our knowledge details of the analysis have not been presented. Carbon-13 nmr spectra of the cyano group in a single crystal of $K_2Pt(CN)_4Br_{0.3}\cdot 3H_2O$ have been presented by Stoll *et al.* (13). As well, Ripmeester *et al.* (14) have used ^{13}C nmr to study a single crystal of the acetonitrile–hydroquinone clathrate.

In the present study we have also obtained natural abundance ^{13}C and ^{15}N nmr spectra of NH_4NCS by magic angle spinning (MAS) and cross-polarization (CP) techniques (1–3). The observed ^{13}C nmr spectrum was an asymmetric doublet and was analyzed using known procedures (14–19). The spinning sidebands observed in the ^{15}N nmr spectra of NH_4NCS obtained with slow MAS were analyzed to obtain the ^{15}N CSA using the graphical procedure of Herzfeld and Berger (20). The values of σ (^{13}C and ^{15}N) obtained here for the thiocyanate ion are compared to the corresponding values observed for other linear molecules with a C_∞ axis (21, 22). The importance of these shielding constants in defining an absolute shielding scale is discussed. On an absolute shielding scale the bare nucleus has a shielding constant of zero.

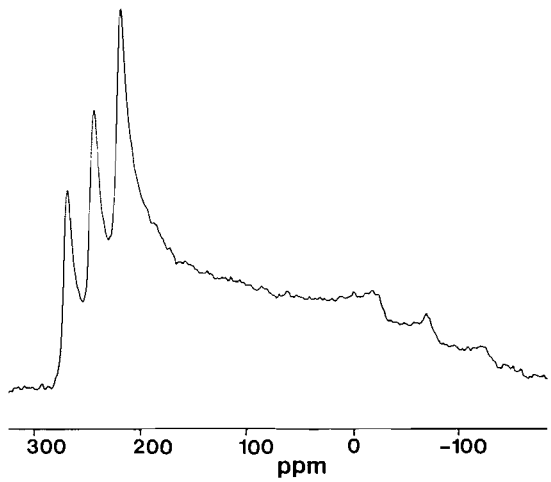

FIG. 1. Static carbon-13 powder spectrum of solid NH_4NCS obtained with high-powered proton decoupling and cross-polarization.

Experimental

Natural abundance ^{13}C and ^{15}N nmr spectra of NH_4NCS were obtained at 50.323 and 20.300 MHz, respectively, using a Bruker MSL-200 spectrometer (B_0 = 4.70 T). Powder samples (≈0.5 g) were packed into aluminum oxide rotors and all spectra were recorded at 20°C with high-power proton decoupling and cross-polarization using the Hartmann–Hahn match. Proton and ^{13}C 90° pulse widths were

[1]Author to whom all correspondence may be addressed.

Can. J. Chem. Downloaded from www.nrcresearchpress.com by 78.46.186.204 on 09/07/12
For personal use only.

4 μs. The static ^{13}C spectrum in Fig. 1 was obtained with 48 K scans using a contact time of 10 ms and a recycle time of 5 s. The acquisition time was 0.041 s and a sensitivity enhancement corresponding to 100-Hz line broadening was applied before Fourier transformation. Carbon-13 chemical shifts were referenced with respect to external adamantane, which has shifts of 38.56 ppm ($\underline{C}H_2$) and 29.50 ppm ($\underline{C}H$) with respect to TMS (23).

Carbon-13 MAS spectra were obtained with acquisition times of 0.205 s and recycle times of 4 s. Similarly the ^{15}N MAS spectra were acquired with 10 ms contact time and 5 s recycle delay. Proton ^{15}N 90° pulse widths were 5 μs. All spectra were obtained at ambient temperature.

Spectral simulations were done with FORTRAN 5 computer programs run on a CDC Cyber 170/730 operating under NOS 2.2. The program used to simulate the carbon–nitrogen dipolar splitting in the CP-MAS ^{13}C nmr spectrum was adapted from ref. 17*c*.

Results and discussion

(a) The static ^{13}C nuclear magnetic resonance spectrum

Here we briefly outline the theory necessary to analyze the ^{13}C nmr spectrum shown in Fig. 1. For the ^{13}C spin of the thiocyanate ion, three basic interactions must be considered: the Zeeman interaction, the chemical shielding anisotropy, and the ^{13}C–^{14}N dipolar interaction. The carbon (I) spin Hamiltonian is given in eq. [1] (24):

$$[1]\quad h^{-1}\hat{H}_C = -\nu_C[1 - \sigma_{iso} + \Delta\sigma(1/3 - \cos^2\theta)]\hat{I}_z + R[(1 - 3\cos^2\theta)\hat{I}_z\hat{S}_z - (3\sin\theta\cos\theta)\hat{I}_z\hat{S}_x]$$

with

$$\nu_C = (\gamma_C/2\pi)B_0, \qquad R = \frac{\gamma_C\gamma_N\hbar}{2\pi}\left\langle\frac{1}{r^3}\right\rangle\left(\frac{\mu_0}{4\pi}\right)$$

and θ being the angle between the C—N bond (ion symmetry axis) and the static magnetic field B_0. Here r is the C—N bond length, γ_C and γ_N are the magnetogyric ratios of carbon and nitrogen respectively, $\Delta\sigma = \sigma_\parallel - \sigma_\perp$ is the chemical shielding anisotropy, and $\sigma_{iso} = (2\sigma_\perp + \sigma_\parallel)/3$. All other symbols have their usual meanings. Note that in Fig. 1, the ^{13}C nmr spectrum of NH_4NCS appears on a chemical shift axis, δ, where by definition δ = 0 ppm is the isotropic chemical shift of TMS.

If we use the Zeeman states for the nitrogen spins (S), then we obtain three carbon transitions, one corresponding to each nitrogen state:

$$\nu_{+1} = \nu_C(1 - \sigma_{iso}) + (\nu_C\Delta\sigma/3 - R)(1 - 3\cos^2\theta)$$

$$[2]\quad \nu_0 = \nu_C(1 - \sigma_{iso})$$

$$\nu_{-1} = \nu_C(1 - \sigma_{iso}) + (\nu_C\Delta\sigma/3 + R)(1 - 3\cos^2\theta)$$

This gives rise to a powder pattern that is simply a sum of three axially symmetric CSA powder patterns, which may be individually simulated as described by Mehring (1). When $\Delta\sigma \geq 3R$, it appears as in Fig. 2. If we define the zero of frequency to be $\nu_C(1 - \sigma_{iso})$, the extrema of each powder pattern are at

$$\nu_{+1}: \nu_C\Delta\sigma/3 - R \quad \text{and} \quad -2\nu_C\Delta\sigma/3 + 2R$$

$$[3]\quad \nu_0 : \nu_C\Delta\sigma/3 \quad \text{and} \quad -2\nu_C\Delta\sigma/3$$

$$\nu_{-1}: \nu_C\Delta\sigma/3 + R \quad \text{and} \quad -2\nu_C\Delta\sigma/3 - 2R$$

corresponding to θ = 90° and θ = 0°, respectively. As illustrated in Fig. 2, this would allow one to read $\Delta\sigma$ and R directly from the powder pattern.

The assumption in this analysis that Zeeman spin functions describe the nitrogen spin states is not necessarily valid. If the

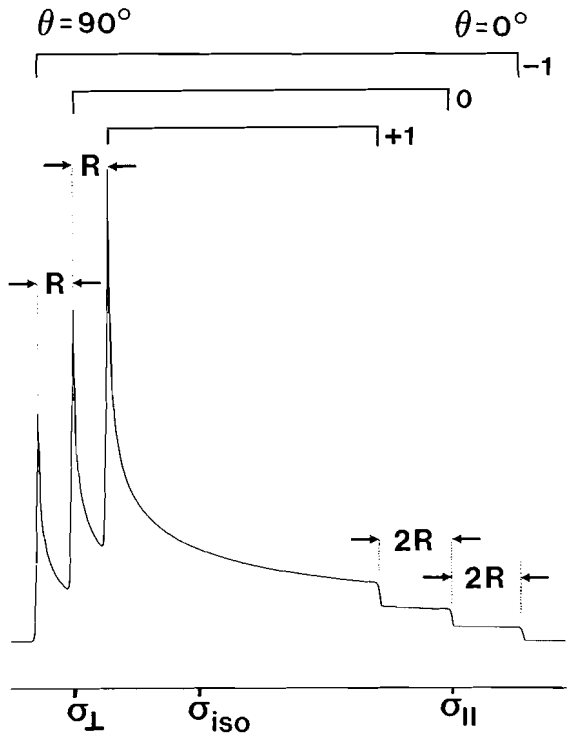

FIG. 2. Simulated NH_4NCS carbon-13 static powder pattern. The extrema of the three components arising from the three nitrogen-14 spin states (−1, 0, +1) are indicated. The nitrogen quadrupolar perturbation on the carbon dipolar Hamiltonian has not been considered in this simulation.

^{14}N quadrupole coupling constant is not negligible compared to the ^{14}N Larmor frequency, then linear combinations of Zeeman spin functions must be used, and the expectation value for $\hat{S}_z$ depends on the orientation of the nitrogen electric field gradient in the static magnetic field. This expectation value can be calculated from the eigenvectors of the ^{14}N Hamiltonian matrix, which is constructed from eq. [4] using a basis set of Zeeman spin functions (14).

$$[4]\quad \hat{H}_N = -\gamma_N\hbar B_0\hat{S}_z + (3/4)e^2qQ\{[\hat{S}_z^2 - (1/4)[\hat{S}_+\hat{S}_- + \hat{S}_-\hat{S}_+]](\cos^2\theta - 1/3) + (1/4)[\hat{S}_+^2 + \hat{S}_-^2]\sin^2\theta + (1/4)[\hat{S}_+\hat{S}_z + \hat{S}_z\hat{S}_+ + \hat{S}_-\hat{S}_z + \hat{S}_z\hat{S}_-]\sin(2\theta)\}$$

This equation assumes axial symmetry of the electric field gradient at the nitrogen nucleus, a reasonable approximation since the measured asymmetry of the ^{14}N quadrupole coupling is 0.0296 (25). For the singularity at θ = 0°, we find the Zeeman states are unmixed since the electric field gradient tensor is aligned with the Zeeman interaction, and so the shoulders of the powder pattern (Fig. 2) are separated by $2R$ irrespective of the nitrogen quadrupole coupling. For the singularity at θ = 90°, the expectation value of $\hat{S}_z$ varies with the ratio, Z/A, the magnitude of the Zeeman interaction to the quadrupole interaction, as shown in Fig. 3: $Z = \gamma_N B_0/2\pi$ and $A = e^2qQ/h$. This expectation value directly scales the splitting of the 90° peaks in the ^{13}C powder pattern in Fig. 2. Thus we can see that when $Z \geq 2A$, this splitting is very nearly R. In the present experimental case, $Z/A = 6.3$, hence the expectation value of $\hat{S}_z$ is greater than 0.998, and so the 90° splitting is $\geq 0.998R$.

From Fig. 1 we find the ^{13}C chemical shielding anisotropy

Can. J. Chem. Downloaded from www.nrcresearchpress.com by 78.46.186.204 on 09/07/12
For personal use only.

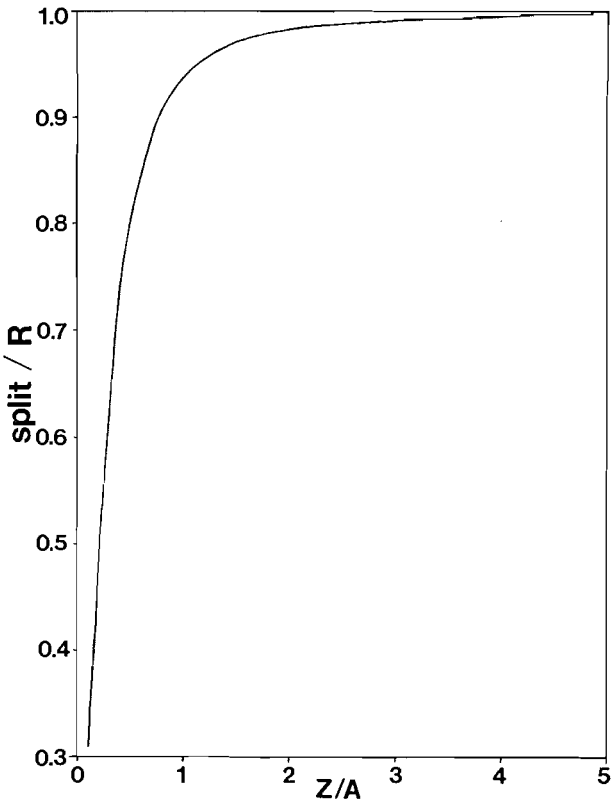

FIG. 3. Apparent dipolar splitting in the singularities corresponding to $\theta = 90°$ in the powder pattern in Fig. 2 as a function of the relative sizes of the nitrogen-14 Zeeman and quadrupole interactions.

in NH_4SCN is 321 ± 7 ppm and the isotropic chemical shift, $\delta_{iso} = 133$ ppm. This value of $\Delta\sigma$ is comparable to the results of Beeler *et al.* (21) on linear neutral molecules. The isoelectronic OCS has $\Delta\sigma = 365$ ppm. Moreover, for NH_4NCS, $\delta_{\parallel} = 133$ ppm − (2/3)321 ppm = −81 ± 5 ppm is quite close to the −90 ppm value reported by Beeler *et al.* for $\delta_{\parallel}$ in six linear molecules. See part (*c*) below for further discussion.

The apparent dipolar coupling constant $R = 1295 \pm 25$ Hz allows the calculation of an effective C—N bond length, $r_{CN} = 1.190 \pm 0.008$ Å. The lower limit on the bond length determined in the present study, 1.182 Å, is only 0.006 Å longer than the value of 1.176 ± 0.001 Å determined by neutron diffraction (11). There are several factors that could account for the small discrepancy noted here and these will be discussed below.

1. Since the neutron diffraction measurements were carried out at 81 K (11) and the nmr powder pattern was obtained at 293 K, the dipolar splitting should be corrected for librational motion (26–29). Motion of the linear thiocyanate ion at 293 K will partly average the dipolar interaction and reduce the dipolar splitting by a factor of approximately $(3\cos^2\delta - 1)/2 \simeq (2 - 3\delta^2)/2$ where δ^2 is the mean-square libration angle (14). The reduction in R leads to an apparent internuclear separation that is too large. One can estimate δ^2 from the known temperature dependence of the principal components of the ^{14}N quadrupolar coupling tensor (25). Using the procedure of Barten (30*a*), we estimate $\delta_x^2 = \delta_y^2 \simeq 5 \times 10^{-3}$ rad^2, which results in a corrected value for R of 1305 Hz ($r = 1.187 \pm 0.008$ Å).

2. A second source of error in the nmr method is the neglect of indirect nuclear spin–spin coupling in the above analysis. The indirect nuclear spin–spin interaction arises through a polarization mechanism involving the electrons; it is anisotropic and expressed by a second rank tensor (1, 31). In the case of a linear molecule or ion, the splitting between the $m = 0$ and $m = \pm 1$ peaks (Fig. 2) becomes $\pm(2R - J_{\parallel})$ for $\theta = 0°$ and approximately $\pm(R + J_{\perp})$ for $\theta = 90°$ (14). If $J_{\perp}(^{14}N,^{13}C) = -40$ Hz then the corrected value of R would be 1345 ± 25 Hz; hence $r = 1.176 \pm 0.008$ Å. In general, the average value of one-bond $^{14}N,^{13}C$ indirect spin–spin couplings rarely exceeds ±20 Hz (32–35); however, it is possible that the magnitude of the principal components of the J tensor could be substantially larger. For example, in the case of the acetonitrile–hydroquinone clathrate Ripmeester *et al.* (14) have suggested that $J_{\parallel}(^{14}N,^{13}C) = 301 \pm 20$ Hz and $J_{\perp}(^{14}N,^{13}C) = -130 \pm 11$ Hz. Studies of acetonitrile in partially oriented systems indicate anisotropies in $^1J(^{14}N,^{13}C)$, $\Delta J = J_{\parallel} - J_{\perp}$, of 144 ± 78 Hz (36). Molecular orbital calculations suggest that $\Delta J(^{14}N,^{13}C)$ in acetonitrile is less than 40 Hz (36, 37). In summary, it is very difficult to obtain reliable values of indirect coupling constant anisotropies (38, 39); this is clearly illustrated in a recent study by Jokisaari *et al.* (39).

3. Finally, it is important to note that diffraction studies and nmr measure two different averages. The diffraction measurements measure $\langle r \rangle$ while the dipolar coupling depends on $\langle r^{-3} \rangle^{-1/3}$ (29, 40).

Clearly the small discrepancy in r determined by neutron diffraction and ^{13}C nmr can readily be accounted for by correcting the observed dipolar splitting for librational motion of the thiocyanate ion, and by considering the possible influence of indirect spin–spin coupling.

Concerning the motion of the thiocyanate ion, it has been reported that in solid KSCN the SCN^- ion is undergoing rapid overall reorientation at room temperature (41). This suggestion was based on the observation of a relatively sharp, ≃10 ppm, ^{13}C nmr spectrum obtained from a static sample. We have been unable to reproduce this observation and propose that the line narrowing resulted from water-solvated NCS^- ions on the surface of KSCN, which is very hygroscopic. The earlier suggestion of rapid reorientation of the thiocyanate ion in solid KSCN is also incompatible with the structure determined by X-ray diffraction (42).

(b) Magic angle spinning experiments

(i) ^{13}C nuclear magnetic resonance

The observed CP-MAS ^{13}C nmr spectrum of NH_4NCS is shown in Fig. 4*a*. The isotropic shift is 133.1 ± 1 ppm from TMS, very similar to the value in aqueous solution, 133.8 ppm (43). The observed doublet (splitting 199 ± 10 Hz) is caused by residual dipolar splitting arising from the large ^{14}N quadrupole interaction described above. Under conditions where the quadrupolar interaction may be treated as a perturbation of the Zeeman interaction, the magnitude of the splitting observed in the MAS spectrum is directly proportional to e^2qQ/h and R, but inversely proportional to the square of the strength of the applied field B_0. This phenomenon has been observed by numerous workers and is well understood (14–19).

The spectrum in Fig. 4*b* was calculated using the method of Hexem (17) with $B_0 = 4.70$ *T*, $e^2qQ/h = 2.284$ MHz, $\eta_Q = 0.0296$ (25). A splitting of 199 ± 10 Hz was calculated with $r_{CN} = 1.16 \pm 0.02$ Å. Although the calculated spectrum reproduces the gross features of the observed spectrum, the detailed line shape of the low frequency peak is not in good agreement with experiment. The calculated peak centred at approximately −100 Hz is actually a doublet when more

Can. J. Chem. Downloaded from www.nrcresearchpress.com by 78.46.186.204 on 09/07/12
For personal use only.

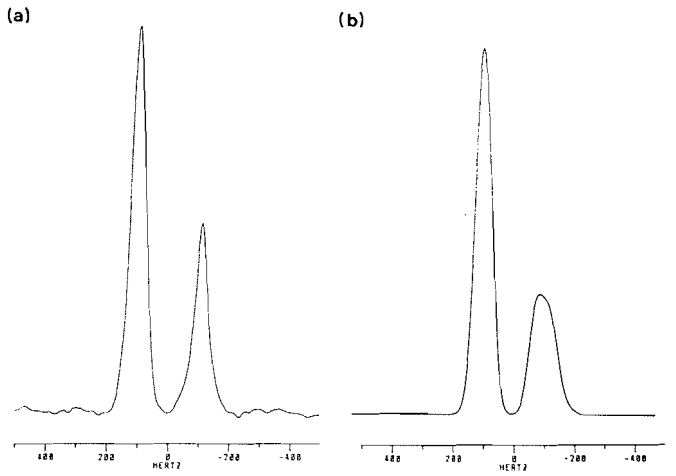

FIG. 4. (*a*) CP-MAS carbon-13 nmr spectrum of NH_4NCS, rotating at 3.6 kHz. (*b*) Simulated lineshape with 50-Hz Gaussian broadening.

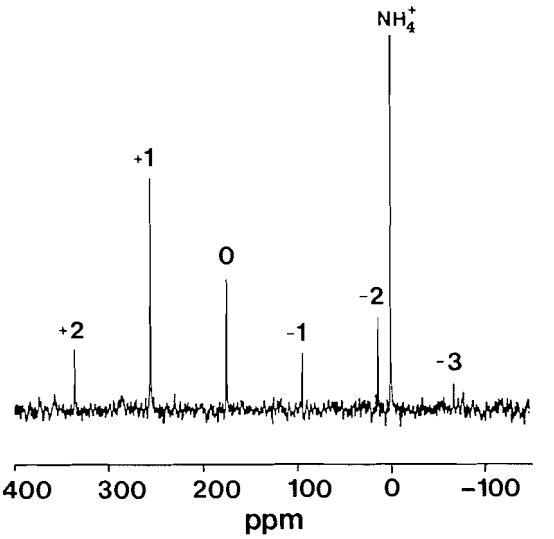

FIG. 5. CP-MAS nitrogen-15 nmr spectrum of NH_4NCS, rotating at 1.63 kHz.

realistic Gaussian line broadenings of 15–30 Hz are applied. Since our simulation program reproduces the calculated spectra of several other groups (for example, refs. 14, 16, 17) we are confident in the calculated spectrum. However, it is important to point out that the calculated spectrum does not take into account indirect spin–spin coupling. In the high field limit the MAS ^{13}C resonance will be a 1:1:1 triplet with splitting equal to $(J_{\parallel} + 2J_{\perp})/3$. Depending on the sign and magnitude of J it is possible that the low frequency portion of the spectrum might be influenced to a greater extent than the high frequency portion. This is the only explanation that we have for the sharp low frequency component observed in Fig. 4*a*. Initially we thought that the principal component of the nitrogen electric field gradient tensor might not be colinear with the C—N dipolar axis; however, this is inconsistent with the small observed asymmetry parameter, $\eta = 0.030$, obtained from nqr (25), and the nearly cylindrical symmetry of the electron density about the C—N bond (11). We did carry out line shape calculations varying the angle, β, between eq_{zz} and r_{CN}. The line shape is essentially independent of β for angles between 0° and 15°; the main effect of increasing β is to decrease the large splitting (see Fig. 6 of ref. 17*b*). Also, we found the ^{13}C MAS line shape to be very dependent on the angle between the spinning axis and B_0, as predicted by the calculations of Zumbulyadis *et al.* (16). The magic angle was adjusted by mixing KBr with NH_4NCS and using the ^{79}Br resonance of KBr as described by Frye and Maciel (44).

It is interesting to note that the observed splitting in the CP-MAS ^{13}C spectrum is directly proportional to e^2qQ/h, while the splittings in the static spectrum for $\theta = 0°$ and 90° are independent and almost independent, respectively, of e^2qQ/h. Therefore if one wishes to obtain an estimate of the ^{14}N quadrupole coupling constant from a ^{13}C spectrum it is desirable to have both the static and the MAS spectrum.

(ii) ^{15}N nuclear magnetic resonance

The CP-MAS ^{15}N spectrum of NH_4NCS, rotating at 1.63 kHz, is shown in Fig. 5. The ^{15}N resonance corresponding to the thiocyanate nitrogen is centered at 174.9 ppm to high frequency of that due to the ammonium ion in NH_4NCS. This difference in ^{15}N chemical shifts is in excellent agreement with the observations of Ratcliffe *et al.* (45). The large intensity of the spinning sidebands observed for the thiocyanate nitrogen indicates that the ^{15}N CSA (in Hz) is large compared to the rate of sample spinning. As described in Herzfeld and Berger (20), one can use the intensities of these sidebands to determine the ^{15}N CSA. Analyzing the intensities measured at 1.63 kHz and at 3.02 kHz we obtain $\Delta\sigma = \sigma_{\parallel} - \sigma_{\perp} = 415 \pm 15$ ppm. An independent estimate of the ^{15}N shielding anisotropy was also obtained from a static powder pattern. The singularity corresponding to $\sigma_{\perp}$ was 311 ± 10 ppm to high frequency of the ammonium ion resonance, or 136 ± 10 ppm from σ_{iso}, so $\Delta\sigma = 3(136 \pm 10 \text{ ppm}) = 408 \pm 30$ ppm. The poor signal-to-noise ratio precluded direct measurement of the low frequency singularity.

From the ^{15}N nmr powder pattern observed for the ammonium ion resonance we estimate $\Delta\sigma \leqslant 10$ ppm.

We have referenced the ^{15}N chemical shifts of solid NH_4NO_3 with respect to those of external NH_3 (liq.) at 298 K. The ammonium ion resonance in NH_4NO_3 is 23.8 ± 0.3 ppm to high frequency of that in liquid ammonia, thus $\delta_{iso}(\underline{N}H_4NCS) = 36.1$ ppm and $\delta_{iso}(NH_4\underline{N}CS) = 211.0$ ppm (45). Note $\delta_{iso}(NH_3(liq.)) = 0$ (33). In a saturated aqueous solution of KNCS, $\delta(\underline{N}CS) = 211.9$ ppm (34).

(c) ^{13}C and ^{15}N chemical shielding in molecules of C_{∞} symmetry

In Ramsey's theory (46), total chemical shielding at a nucleus may be expressed as a sum of diamagnetic and paramagnetic parts, eq. [5].

$$[5] \quad \sigma = \sigma^d + \sigma^p$$

The diamagnetic term depends on only the ground state electronic wavefunction and can be accurately calculated using molecular orbital theory or the approximate method devised by Gierke and Flygare (47). The paramagnetic term depends on both the ground and excited electronic states and consequently is much more difficult to calculate using molecular orbital theory. Fortunately, σ^p is closely related to the spin-rotation tensor, which can, in principle, be obtained from molecular beam measurements (48, 49).

Using the procedure outlined above, absolute chemical shielding scales have been derived for both carbon and nitrogen (50, 22). The carbon shielding scale is based on the absolute value derived for carbon monoxide, $\sigma_{iso}(CO) = 3.2 \pm 0.3$ ppm (50*c*,*d*). Using this shielding constant and the observed ^{13}C chemical shift of carbon monoxide with respect to TMS, the absolute value of $\sigma_{iso}(TMS)$ is 185.4 ppm (50*b*). Similarly, an

Can. J. Chem. Downloaded from www.nrcresearchpress.com by 78.46.186.204 on 09/07/12
For personal use only.

TABLE 1. Experimental and calculated carbon shielding constants in a series of linear triatomics

Molecule	Experimental[a]		Calculated	
	$\sigma_\perp$	$\sigma_\parallel$	$\sigma_\parallel{}^{d\,b}$	$\sigma_\parallel{}^{d\,c}$
OCO	−59.6	275.4	284.2	296.5
OCS	−89.6	275.4	286.7	298.9
SCS	−146.6	277.4	290.5	301.3
NCS^-	−55.0	266.0	—	296.7

[a]Reference 21, except for NCS^- (this study).
[b]Reference 53.
[c]Calculated using the method described in refs. 47–49; bond lengths used in the Flygare calculations: OCO: 1.163 Å; SCS: 1.553 Å; OCS: 1.157 Å; OCS: 1.560 Å; NCS$^-$: 1.176 Å; NCS$^-$: 1.649 Å.

absolute nitrogen shielding scale has been derived that leads to an absolute nitrogen shielding in liquid ammonia (300 K), σ_{iso} = 244.6 ppm (22).

It is interesting that for a nucleus in a linear molecule the paramagnetic contribution to shielding along the symmetry axis is zero (51, 52), i.e., $\sigma_\parallel{}^p = 0$; therefore the parallel component of the shielding anisotropy is given by $\sigma_\parallel{}^d$. If $\sigma_\parallel{}^d$ can be accurately calculated, an absolute shielding scale can also be derived from an experimental determination of $\Delta\sigma = \sigma_\parallel - \sigma_\perp$, via eq. [6].

$$[6] \quad \sigma_{iso} = (3\sigma_\parallel{}^d - 2\Delta\sigma)/3$$

In Table 1 we have compared absolute values of $\sigma_\perp$(C) and $\sigma_\parallel$(C) obtained here for NCS^- with those recently reported for several related linear molecules (21). Also in Table 1 calculated values of $\sigma_\parallel{}^d$ obtained from the *ab initio* calculations of Amos and Battaglia (53) are compared with those calculated using the method of Gierke and Flygare (47–49). Unfortunately, *ab initio* calculated values of σ^d for the NCS^- ion are unavailable in the literature. There are a number of features of Table 1 that deserve comment:

1. The observed values of $\sigma_\perp$ in these related molecules show considerable variation while the observed values of $\sigma_\parallel$ show little variation. The value of $\sigma_\parallel$ for the NCS^- ion is within 12 ppm of the corresponding values observed for other triatomics.

2. The observed values of $\sigma_\parallel{}^d$ are 9–13 ppm smaller than *ab initio* calculated values. This difference must arise in part from intermolecular interactions in the solid state (54, 55). The calculated values of course pertain to isolated molecules.

3. The approximate values of $\sigma_\parallel{}^d$ we calculate using the method of Gierke and Flygare are uniformly about 12 ppm larger than the *ab initio* values.

In the case of linear nitrogen-containing molecules one also finds a very small variation in *ab initio* calculated $\sigma_\parallel$ (N) values (56, 57). For N_2, HCN, and ONN the calculated values are 338.8, 336.9, and 342.0 ppm respectively (56). Similarly for N_2, HCN, ONN, and SCN^- the method of Gierke and Flygare (47–49) gives 349, 348, 349, and 350 ppm, respectively. Again the method of Gierke and Flygare consistently gives values which are 7–10 ppm too large. The value of $\sigma_\parallel$ that we observe for SCN^- in this study, $\sigma_{iso} + 2/3(\Delta\sigma) = 34 + 2/3\,(415) =$ 311 ppm, is about 30 ppm smaller than the value expected from *ab initio* calculations. As found above for the ^{13}C shielding constants, intermolecular interactions on the ^{15}N shielding constant are most likely responsible for this discrepancy.

If observed $\sigma_\parallel$(C) and $\sigma_\parallel$(N) values are to be used in establishing better absolute shielding scales, it would appear from this study that some effort must be made to account for the influence of intermolecular effects (50*a*, 51, 54, 55).

Acknowledgements

We wish to thank Dr. J. A. Ripmeester for his interest in this study, and the Natural Sciences and Engineering Research Council of Canada for financial support in the form of an undergraduate summer research scholarship (R.M.D.), a post-doctoral fellowship (M.S.M.), and operating and equipment grants (R.E.W.). J. F. Britten is the holder of a Killam Postdoctoral Fellowship.

1. M. MEHRING. Principles of high resolution NMR in solids. 2nd ed. Springer Verlag, New York. 1983.
2. C. A. FYFE. Solid state NMR for chemists. CFC Press, Guelph. 1983.
3. B. C. GERSTEIN and C. R. DYBOWSKI. Transient techniques in NMR of solids—An introduction to theory and practice. Academic Press, Inc., Orlando. 1985.
4. J. S. WAUGH. Proc. Natl. Acad. Sci. (USA), **73**, 1394 (1976).
5. S. J. OPELLA and J. S. WAUGH. J. Chem. Phys. **65**, 4919 (1977).
6. M. LINDER, A. HÖHENER, and R. R. ERNST. J. Chem. Phys. **73**, 4959 (1980).
7. A. NAITO, P. B. BARKER, and C. A. MCDOWELL. J. Chem. Phys. **81**, 1583 (1984).
8. E. T. OLEJNICZAK, S. VEGA, and R. G. GRIFFIN. J. Chem. Phys. **81**, 4804 (1984).
9. D. B. ZAX, A. BIELECKI, K. W. ZILM, A. PINES, and D. P. WEITEKAMP. J. Chem. Phys. **83**, 4877 (1985).
10. W. S. VEEMAN. Prog. Nucl. Magn. Reson. Spectrosc. **16**, 193 (1984).
11. J. W. BATS and P. COPPENS. Acta Crystallogr. Sect. B: Struct. Crystallogr. Cryst. Chem. **33**, 1542 (1977).
12. S. KAPLAN, A. PINES, R. G. GRIFFIN, and J. S. WAUGH. Chem. Phys. Lett. **25**, 78 (1974).
13. M. E. STOLL, R. W. VAUGHAN, R. B. SAILLANT, and T. COLE. J. Chem. Phys. **61**, 2896 (1974).
14. J. A. RIPMEESTER, J. S. TSE, and D. W. DAVIDSON. Chem. Phys. Lett. **86**, 428 (1982).
15. (*a*) A. NAITO, S. GANAPATHY, and C. A. MCDOWELL. J. Chem. Phys. **74**, 5393 (1981); (*b*) J. Magn. Reson. **48**, 367 (1982).
16. N. ZUMBULYADIS, P. M. HENRICHS, and R. H. YOUNG. J. Chem. Phys. **75**, 1603 (1981).
17. (*a*) J. G. HEXEM, M. H. FREY, and S. J. OPELLA. J. Am. Chem. Soc. **103**, 224 (1981); (*b*) J. Chem. Phys. **77**, 3847 (1982); (*c*) J. G. HEXEM. Ph.D. Thesis, University of Pennsylvania. 1982.
18. J. BÖHM, D. FENZKE, and H. PFEIFER. J. Magn. Reson. **55**, 197 (1983).
19. R. K. HARRIS, P. JONSEN, and K. J. PACKER. Magn. Reson. Chem. **23**, 565 (1985).
20. J. HERZFELD and A. E. BERGER. J. Chem. Phys. **73**, 6021 (1980).
21. A. J. BEELER, A. M. ORENDT, D. M. GRANT, P. W. CUTTS, J. MICHL, K. W. ZILM, J. W. DOWNING, J. C. FACELLI, M. S. SCHINDLER, and W. KUTZELNIGG. J. Am. Chem. Soc. **106**, 7672 (1984).
22. C. J. JAMESON, A. K. JAMESON, D. OPPUSUNGGU, S. WILLE, P. M. BURRELL, and J. MASON. J. Chem. Phys. **74**, 81 (1981).
23. W. L. EARL and D. L. VANDERHART. J. Magn. Reson. **48**, 35 (1982).
24. D. L. VANDERHART, H. S. GUTOWSKY, and T. C. FARRAR. J. Am. Chem. Soc. **89**, 5056 (1967); (*b*) D. L. VANDERHART and H. S. GUTOWSKY. J. Chem. Phys. **49**, 261 (1968).
25. T. ASAJI, R. IKEDA, and D. NAKAMURA. J. Magn. Reson. **31**, 437 (1978).
26. J. A. IBERS and D. P. STEVENSON. J. Chem. Phys. **28**, 929 (1958).

Can. J. Chem. Downloaded from www.nrcresearchpress.com by 78.46.186.204 on 09/07/12
For personal use only.

27. B. PEDERSEN. J. Chem. Phys. **41**, 122 (1964).
28. (*a*) R. SJÖBLUM. J. Magn. Reson. **22**, 411 (1976); (*b*) R. SJÖBLOM and J. TEGENFELDT. J. Magn. Reson. **27**, 405 (1977).
29. E. R. HENRY and A. SZABO. J. Chem. Phys. **82**, 4753 (1985).
30. (*a*) B. L. BARTON. J. Chem. Phys. **46**, 1553 (1967); (*b*) H. CHIHARA and N. NAKAMURA. Advances in nuclear quadrupole resonance. Vol. 4. *Edited by* J. A. S. Smith. Heyden, London. 1980. p. 1.
31. J. B. ROBERT and L. WIESENFELD. Phys. Rep. **86**, 363 (1982).
32. (*a*) R. E. WASYLISHEN. Annual reports on NMR spectroscopy. Vol. 7. *Edited by* G. A. Webb. Academic Press, New York. 1977. p. 245; (*b*) K. A. FRIESEN and R. E. WASYLISHEN. J. Magn. Reson. **48**, 152 (1982); (*c*) J. Magn. Reson. **41**, 189 (1980).
33. G. C. LEVY and R. L. LICHTER. Nitrogen-15 nuclear magnetic resonance spectroscopy. John Wiley and Sons, New York. 1979. p. 119.
34. (*a*) M. WITANOWSKI, L. STEFANIAK, and G. A. WEBB. Annual reports on NMR spectroscopy. Vol. 11B. *Edited by* G. A. Webb. Academic Press, New York. 1981. p. 117; (*b*) M. WITANOWSKI, L. STEFANIAK, S. SZYMANSKI, and H. JANUSZEWSKI. J. Magn. Reson. **28**, 217 (1977).
35. G. J. MARTIN, M. L. MARTIN, and J. P. GOUESNARD. NMR basic principles and progress. Vol. 18. *Edited by* P. Diehl, E. Fluck, and R. Kosfeld. Springer Verlag, New York. 1981.
36. P. DIEHL, J. JOKISAARI, J. AMREIN, T. VÄÄNÄNEN, and P. PYYKKÖ. J. Magn. Reson. **48**, 495 (1982).
37. J. C. FACELLI and M. BARFIELD. J. Magn. Reson. **59**, 452 (1984).
38. P. N. TUTUNJIAN and J. S. WAUGH. J. Chem. Phys. **76**, 1223 (1982).
39. J. JOKISAARI, Y. HILTUNEN, and J. LOUNILA. J. Chem. Phys. **85**, 3198 (1986).
40. N. C. PYPER. Mol. Phys. **75**, 441 (1982).
41. N. ZUMBULYADIS and H. J. GYSLING. J. Am. Chem. Soc. **104**, 3246 (1982).
42. C. AKERS, S. W. PETERSON, and R. D. WILLETT. Acta Crystallogr. Sect. B: Struct. Crystallogr. Cryst. Chem. **24**, 1125 (1968).
43. J. A. KARGOL, R. W. CRECELY, and J. L. BURMEISTER. Inorg. Chem. **18**, 2532 (1979).
44. J. S. FRYE and G. E. MACIEL. J. Magn. Reson. **48**, 125 (1982).
45. C. I. RATCLIFFE, J. A. RIPMEESTER, and J. S. TSE. Chem. Phys. Lett. **99**, 177 (1983).
46. N. F. RAMSEY. Phys. Rev. **28**, 699 (1950).
47. T. D. GIERKE and W. H. FLYGARE. J. Am. Chem. Soc. **94**, 7277 (1972).
48. W. H. FLYGARE. J. Chem. Phys. **41**, 793 (1964).
49. W. H. FLYGARE. Chem. Rev. **74**, 655 (1974).
50. (*a*) C. J. JAMESON. Nucl. Magn. Reson. **15**, 1 (1986); (*b*) J. MASON. J. Chem. Soc. Perkin Trans. 2, 1671 (1976); (*c*) D. B. NEUMANN and J. W. MOSKOWITZ. J. Chem. Phys. **50**, 2216 (1969); (*d*) I. OZIER, L. M. CRAPO, and N. F. RAMSEY. J. Chem. Phys. **49**, 2314 (1968); (*e*) W. L. MEERTS, F. H. DELEEUW, and A. DYMANUS. Chem. Phys. **22**, 319 (1977).
51. J. MASON. Adv. Inorg. Chem. Radiochem. **18**, 197 (1976).
52. A. D. BUCKINGHAM and S. M. MALM. Mol. Phys. **22**, 1127 (1971).
53. R. D. AMOS and M. R. BATTAGLIA. Mol. Phys. **36**, 1517 (1978).
54. C. J. JAMESON, A. K. JAMESON, and P. M. BURRELL. J. Chem. Phys. **73**, 6013 (1980).
55. C. J. JAMESON. Bull. Magn. Reson. **3**, 3 (1980).
56. M. SCHINDLER and W. KUTZELNIGG. Mol. Phys. **48**, 781 (1983).
57. M. BARFIELD and D. M. GRANT. J. Chem. Phys. **67**, 3322 (1977).

Can. J. Chem. Downloaded from www.nrcresearchpress.com by 78.46.186.204 on 09/07/12
For personal use only.

High performance liquid chromatography as an analytical tool for the determination of sulfate in coconut and caffeine in tea

RASIAH S. RAMAKRISHNA, M. DIAS, S. PALAMAKUMBURA, AND M. JEGANATHAN

Centre for Analytical Research and Development, Chemistry Department, University of Colombo, Colombo, 3 Sri Lanka

Received October 21, 1986

This paper is dedicated to Professor Douglas E. Ryan on the occasion of his 65th birthday

RASIAH S. RAMAKRISHNA, M. DIAS, S. PALAMAKUMBURA, and M. JEGANATHAN. Can. J. Chem. **65**, 947 (1987).

The need for a rapid method for detecting sulphate sulphur in coconut and caffeine in manufactured tea initiated a study to compare high performance liquid chromatography with classical methods. We compare the methods in their applicability in rapid and selective analysis of coconut water, plant tissues, and soil, as well as of caffeine in tea samples from different regions. We present a statistical correlation between the methods and discuss the significance of our results.

RASIAH S. RAMAKRISHNA, M. DIAS, S. PALAMAKUMBURA et M. JEGANATHAN. Can. J. Chem. **65**, 947 (1987).

La nécessité d'avoir une méthode rapide pour déterminer le soufre à l'état de sulfate dans la noix de coco et la caféine dans le thé manufacturé nous a amené à comparer la chromatographie liquide à haute performance (CLHP) et les méthodes classiques. On a comparé les méthodes pour leurs facilités relatives d'application dans des analyses rapides et sélectives de l'eau de coco, des tissus de plantes et des sols ainsi ainsi que de caféine dans des échantillons de thé provenant de diverses régions. On présente une corrélation statistique entre les méthodes et on discute de la signification des résultats obtenus.

[Traduit par la revue]

Introduction

The Centre for Analytical Research and Development, CARD, established in 1980, at the University of Colombo, Sri Lanka, resulted from a collaborative project with the Trace Analysis Research Centre, TARC, Dalhousie University, Canada. The primary objective of the project has been using analytical chemistry in research of relevance to development efforts in Sri Lanka. Projects of importance to agriculture, industry, mineral resources development, food, nutrition, and environmental studies have been carried out. This paper reports the development and use of high performance liquid chromatography (hplc) in the analysis of sulfate sulphur in coconut, and caffeine in tea, both of which are national export commodities.

The recent change from ammonium sulphate to urea as fertilizer for coconut in Sri Lanka required studies of the sulphur status in coconut, since sulphur deficiency in coconut plants manifests characteristic symptoms (1–3). Conventional methods, such as gravimetry, turbidimetry and titrimetry, are tedious and time consuming, and are subject to operator error. A high performance liquid chromatographic procedure was found to be rapid and selective for routine determinations of SO_4^{2-}, and to allow simultaneous determinations of Cl^- and NO_3^- ions, of significance to studies of nutrient status. Correlation between classical methods, hplc, and the use of hot water as an extractant were also investigated along with the inter-method variability.

Several classical and spectrophotometric methods have been used for the quantitative estimation of caffeine in "manufactured tea" (4–12). The use of liquid chromatography enables more rapid estimation. Excess polyphenolic compounds, as found in tea, cause "peak broadening" (13). Both polyphenolic compounds and caffeine absorb strongly at 270 nm (14), the optimum wave length for caffeine in the hplc detector.

The reproducibility of hplc analyses of caffeine is improved if the polyphenolic material is removed from the tea extract using polyvinylpyrrolidone (PVP) as an adsorbent. The analysis of caffeine using hplc on chloroform extracts of tea, hplc on water extracts of tea following PVP pre-column treatment to remove polyphenolic material, and the modified Smith Conacher Rees' (S.C.R.) spectrophotometric method (9) were investigated. Statistical inter-method comparisons were also discussed.

Experimental

Apparatus

Spectrophotometer: A "MSE spectroplus-D" incorporating a grating monochromator was used with 1-cm matched silica cells. A Waters hplc system with a model-450 variable wavelength detector was used, along with a model-6000 A isochromatographic pump (flow rate, 2 cm^3/min at 2000–2500 psi) and a solvent programmer with gradient elution. The sample injection system consisted of a model U-6K injector (100 μL injection volume). The columns consisted of two Vydex anion exchange columns for estimation of sulphate sulphur and a Waters C_{18}μ Bondapak reverse phase analytical column, together with a polyvinylpyrrolidone (PVP) pre-column (10 cm × 0.2 cm) containing 150 mg of washed PVP and pH adjusted to 3.5 for optimum performance for the estimation of caffeine.

The mobile phases consisted of (*i*) 10^{-2} *M* phthalic acid — sodium borate solution at pH 6 for the estimation of sulphate sulphur and (*ii*) 30% methanol and 70% deionised distilled water, adjusted to pH 3.5 with glacial acetic acid, filtered through Whatman-40 filter paper and degassed in an ultrasonic bath, for the estimation of caffeine.

The variable wavelength detector was set at 254 nm for the estimation of sulphate sulphur, and at 270 nm for caffeine.

Estimation of sulphate sulphur in coconut

Rain water

Rain water (200 cm^3) was reduced to 10 cm^3 in a silica dish on a sand bath, transferred to a 25-cm^3 volumetric flask and made up to the mark. The sulphate content was estimated both by hplc and turbidimetry.

Total sulphur in leaf and kernel samples of coconut

A 1:1 $HNO_3/HClO_4$ acid mixture (25 cm^3) was added to 1-g samples and digested until $HClO_4$ acid fumes were visible (an additional 25 cm^3 $HClO_4$ was required for the kernel samples to obtain a clear solution). (CAUTION. $HClO_4$ fumes should be vented through a water scrubber or in a hood designed for wash-down.) The solution was cooled, filtered into a 50-cm^3 volumetric flask, and made up to volume. Aliquots were used for the estimation of sulphur by hplc and turbidimetry.

Water extractable sulphur in leaf and kernel samples of coconut

Samples (1–2 g) were ashed overnight at 450°C, and then digested with 5 cm^3 distilled water for 1 h at either room temperature, 60°C, or 100°C on a water bath. The extracts were next mixed in a "test tube mixer", filtered into 50-cm^3 volumetric flasks and made up to volume. Aliquots were taken for analysis of sulphur by hplc and turbidimetry.

Coconut water

"Nut water" (25 cm^3) was evaporated to dryness, ashed at 450°C

Can. J. Chem. Downloaded from www.nrcresearchpress.com by 78.46.186.204 on 09/07/12
For personal use only.

TABLE 1. Correlation values for sulphate sulphur in 30 ashed coconut leaf samples using water extraction at different temperatures†

Method	Cold hplc	60°C Turb.	60°C hplc	100°C Turb.	100°C hplc
Cold, turb.	0.9118***	0.6245***	0.7426***	0.3493ns	0.5101**
Cold, hplc		0.5427**	0.7763***	0.2423ns	0.6825***
60°C, turb.			0.8381***	0.5795***	0.6769***
60°C, hplc				0.4807***	0.8219***
100°C, turb.					0.4496*
100°C, hplc					

†***, $p = 0.001$ ($r = 0.570$); **, $p = 0.01$ ($r = 0.463$); *, $p = 0.05$ ($r = 0.361$); cold, room temperature; Turb., turbidimetry; ns, not significant.

overnight, dissolved in water, filtered, and made up to 50 cm^3. Aliquots were used for estimation by turbidimetry and hplc.

Extractable sulphur in soil

Air-dried, sieved soil (20 g) was extracted with 50 cm^3 of extracting solution ("100 ppm P" solution) and 1 g activated charcoal for 30 min in a mechanical shaker. The samples were filtered, 25 cm^3 aliquots transferred to silica basins, 2 cm^3 of 3% H_2O_2 added, and the contents evaporated to dryness. The basins were then heated in an oven at 110°C for 1 h, the residue taken up in a 25 cm^3 volumetric flask in distilled water, and the sulphate determined by hplc and turbidimetry.

Standardisation of hplc for sulphur in coconut

Aliquots (100 μL) of separate solutions containing 10 to 50 μl g cm^{-3} each of SO_4^{2-}, Cl^-, and NO_3^- were injected to obtain calibration plots. Peak heights were found to be linearly dependent on anion concentrations.

Turbidimetry

An aliquot was treated with 5 cm^3 of 50% acetic acid, 5 cm^3 of 25% HNO_3, and 1 cm^3 of H_3PO_4 in a 50 cm^3 volumetric flask and diluted to about 45 cm^3 with distilled water and well mixed. $BaCl_2$-"Tween 80" reagent (5 cm^3) was added and the solution made up to volume and mixed. The solution was again mixed after 1 h and the turbidity measured against a reagent blank at 420 nm. A calibration plot was made using standard sulphate solutions prepared from 0.02 *M* $MgSO_4.7H_2O$.

Modified S.C.R. procedure (9)

Individual 1-g portions of tea and 2 cm^3 chloroform were wetted with 5 cm^3 ammonia in a separating funnel. The resulting mixture was extracted four times with 25 cm^3 portions of chloroform. The separated organic layers were each washed with 10 cm^3 portions of 1% KOH, dried over anhydrous Na_2SO_4, filtered into a 100-cm^3 volumetric flask, and made up to mark. Aliquots of this solution were diluted 1:10 and the absorbance measured at 272 nm. The caffeine content was read off a calibration plot prepared from standard caffeine solutions over the concentration range of 1 to 30 ppm.

High performance liquid chromatography using chloroform extraction

Individual 1-g portions of tea were extracted with 25 cm^3 portions of chloroform and the extract evaporated to dryness on a water bath. The residue was dissolved in distilled water, filtered, and together with washings made up to 100 cm^3; 100 μL of the resulting solution was injected into the hplc system.

High performance liquid chromatography using water extraction

Individual 1-g portions of tea were extracted with 80 cm^3 of boiling water for 4 min, filtered, and made up to 100 cm^3. A 2-cm^3 aliquot of this filtrate was passed through a 10 cm × 0.2 cm column containing about 150 mg of polyvinylpyrrolidone (PVP). The filtrate along with the distilled water washings was made up to 10 cm^3 in a volumetric flask; 100 μL of this solution was injected into the hplc system.

Standardisation of the hplc procedure for caffeine

Five standard solutions of caffeine with progressive increase in concentrations were prepared. For each solution 100-μL portions were injected into the hplc in duplicate.

Results and discussion

Sulphate determinations

The analyses of processed coconut water, leaf, kernel, and soil samples for sulphate sulphur are normally carried out by gravimetry, turbidimetry or titrimetry. Studies of the variability among these methods showed that whereas tetrimetry is subject to much operator error, turbidimetry is affected by the nature of stabilizing agents, as well as by other factors that influence dissolution of the barium sulphate precipitate (15). In addition, turbidimetry involves several experimental steps and suffers from interferences from other ions.

The hplc procedure was found to be rapid. A total of about 100 samples could be analysed per working day, whereas only about 20 samples could be so analysed using turbidimetry. In addition, hplc enables determination at 254 nm of Cl^- and NO_3^- in addition to sulfate; both are of importance to the nutritional status of coconut.

The detection limits for both turbidimetry and hplc were found to be about 1 ppm.

The hplc procedure gave higher values. The lower values observed with turbidimetry could be due to the interferences from other ions, as well as the possibility of the precipitate dissolving due to the introduction of various acids during the development of turbidity. Butters and Chenery (15) studied a number of factors that influence uniform precipitation of the solution, such as the quantity and size of the barium chloride crystals, type and concentration of acids, time and speed of stirring or inverting, time of standing, and the choice of optical filter. The manual method requires skill and considerable care, whilst automation requires standardisation of the procedure to obtain uniform sized particles.

Often a drift is found in the hplc base line due to adsorption of barium sulphate on the inner walls of the colorimetric flow cell. The higher values obtained with hplc could thus be an indication of the absolute values of the sulphur content.

Application of the hplc procedure to leaf samples required use of water extracts with ashed samples, since the normal acid digestion procedure introduces high Cl^- concentrations that mask both NO_3^- and SO_4^{2-}, thus making measurements difficult.

TABLE 2. Average leaf sulphur content, estimated by turbidimetry and hplc using different extractants

Extractant	Turbidimetry (μg cm^{-3})	% of value using $HNO_3/HClO_4$ digestion	hplc (μg cm^{-3})	% of value using HNO_3 digestion
Cold water	896 ± ($n = 30$)	57.7	982 ± ($n = 30$)	63.3
Hot water, 60°C	940 ± ($n = 30$)	60.5	1024 ± ($n = 30$)	65.9
Hot water, 100°C	950 ± ($n = 28$)	61.2	1104 ± ($n = 24$)	71.1

Can. J. Chem. Downloaded from www.nrcresearchpress.com by 78.46.186.204 on 09/07/12
For personal use only.

TABLE 3. Comparison of three methods on the recovery of 20 mg of pure caffeine, added to 1-g portions of decaffeinated tea

Method	Amount taken (mg/g)	Amount found (mg/g)	Recovery (%)
Modified S.C.R.	20.10	20.09	100.00
	20.30	20.10	98.01
	20.40	20.10	98.52
hplc, $CHCl_3$ extraction	20.00	20.01	100.05
	20.12	20.06	99.70
	20.06	20.01	99.75
hplc, water extraction with PVP pre-column	20.00	19.78	98.90
	20.00	19.97	99.85
	20.00	20.01	100.06

Correlation values using water extraction at different temperatures with 30 ashed leaf samples are given in Table 1. The correlation coefficient for turbidimetry with hplc was best for cold water extracts ($r = 0.9118$), and for water extracts at 60°C ($r = 0.8381$). However, use of water extraction at 100°C gave poor correlation ($r = 0.4496$).

Table 2 shows average leaf sulphur content using different extractants and the total sulphur content in %, as obtained by double acid digestion. Extraction at 60°C for estimation of sulphur requires careful temperature control. Extraction at 100°C is simple and convenient for large numbers of samples.

Several samples (n) of coconut leaf were extracted with boiling water and analysed in duplicate using both turbidimetry and hplc. A paired "t" test between the duplicate samples obtained by each of these methods showed no significant differences between them ($t = 1.54$, $n = 28$ and $t = 0.92$, $n = 24$ for turbidimetry and hplc, respectively). Further, significant intraclass correlations were found between duplicate samples by both turbidimetry ($r = 0.54$) and hplc ($r = 0.43$). These results support the reproducibility of boiling water extraction for the determination of the sulphur content in coconut leaves by both turbidimetric and hplc procedures.

A study of extraction conditions for soil for hplc and turbidimetry showed that the highest correlation ($r = 0.9947$) was found when boiling water was used as the extractant.

In summary, these results show that hplc is suitable for the estimation of sulphate in coconut water, as well as in boiling water extracts of coconut plant tissues and soil. The fact that water can be utilized as the extracting medium is of biological interest and is more economical for monitoring studies of the sulphur status of coconut.

Caffeine determinations

The spectrophotometric procedure, as well as the use of hplc, to determine caffeine in food and beverages normally involves prior extraction with chloroform (16, 17). Enhanced extraction of caffeine has been reported with an aqueous medium (7). However, the large quantities of polyphenolic compounds present in tea interfere in the determination of caffeine in aqueous extracts because both compounds absorb at 270 nm, the wavelength often used in uv detectors for hplc. Use of a pre-column of polyvinylpyrrolidone (PVP) to remove the polyphenolic compounds was found to give sharper hplc peaks, without interfering with determination of the caffeine present.

Known amounts of pure caffeine added to a decaffeinated solution of tea were quantitatively recovered after passage through a PVP column. Pure caffeine when added to a tea extract showed caffeine peak enhancement corresponding to the amount being added after passage through a PVP column.

Recovery studies carried out on pure samples of caffeine showed that PVP does not retain caffeine (Table 3). All three methods investigated were found to give a high degree of recovery on pure caffeine samples (Table 3). Eleven 1-g subsamples of Sri Lanka "up country" tea were analysed for caffeine by the three methods described. Statistical analysis of the results showed that all three methods were comparable at the 5% level of significance ($p = 0.05$). However, it was impossible to compare methods involving chloroform and water extracts for hplc (Table 4).

The correlation coefficient between the modified S.C.R. procedure and hplc using water extraction with a PVP pre-column ($r = 0.923$), was the most significant, whilst the correlation coefficient between the hplc procedure with chloroform and with water extraction was the least significant ($r = 0.816$).

The coefficient of variation, in %, for each of the methods using PVP pre-column, was: Modified S.C.R. procedure, 3.72; hplc using $CHCl_3$ extraction, 6.02; and hplc using water extraction, 3.21. For the hplc procedure with PVP pre-column the detector sensitivity at 270 nm was 0.15 absorption units at full scale (AUFS) for a 1 ppm solution of caffeine.

Mean levels of caffeine of several samples of manufactured tea from different regions in Sri Lanka and from other countries were each analysed in triplicate, to quantitatively estimate the percentage of caffeine present, using the three methods described. The results obtained are given in Table 5.

TABLE 4. Inter-method comparison of results obtained for the analysis of caffeine using 11 replicates of a sample of Sri Lanka "up country" tea

Methods	T value	Degrees of freedom	Significant limit, p	Significance at $p = 0.05$	Correlation coefficient
Modified S.C.R. vs. hplc using $CHCl_3$ extract	0.73	10	0.48	Not significant	0.86
Modified S.C.R. vs. hplc using water extraction with PVP pre-column	−1.63	10	0.12	Not significant	0.92
hplc using $CHCl_3$ extraction vs. hplc using water extraction with PVP pre-column	−2.81	10	0.01	Significant	0.82

Can. J. Chem. Downloaded from www.nrcresearchpress.com by 78.46.186.204 on 09/07/12
For personal use only.

TABLE 5. Percent of caffeine in nine different varieties of manufactured tea as determined by the three analytical methods investigated. Results are expressed as % of "dry" weight. The quantities denote the mean values obtained. All analyses were carried out in triplicate

Tea variety	Number of samples	% Caffeine		
		Modified S.C.R. method	hplc using $CHCl_3$ extraction	hplc using PVP with water extraction
Sri Lanka "up country"	12	2.17 ± 0.43	1.76 ± 0.41	2.88 ± 0.44
Sri Lanka "mid country"	12	1.35 ± 0.41	1.61 ± 0.41	2.02 ± 0.37
Sri Lanka "low country"	12	1.24 ± 0.37	1.56 ± 0.34	1.79 ± 0.34
India (Doorars)	6	2.30 ± 0.39	1.88 ± 0.40	2.26 ± 0.36
India (Assam)	6	0.99 ± 0.34	1.21 ± 0.40	1.23 ± 0.42
India (Darjeeling)	6	2.63 ± 0.46	1.72 ± 0.36	2.92 ± 0.44
Malawi	3	1.77 ± 0.21	1.69 ± 0.19	2.42 ± 0.29
Kenya	3	1.87 ± 0.19	1.72 ± 0.20	2.68 ± 0.26
China	4	0.65 ± 0.26	0.65 ± 0.21	1.34 ± 0.38

Acknowledgements

The authors are grateful for the facilities provided by the Canadian International Development Centre to set up a Centre for Analytical Research and Development (CARD) in Sri Lanka. The paper illustrates the use of analytical instrumentation for the study of specific agricultural problems in Sri Lanka — an objective of CARD, which has derived initiative and active collaboration from Professor D. E. Ryan. The authors are also thankful to Mr. D. T. Mather, Coconut Research Institute, Sri Lanka for advice and useful discussions on statistical analysis of the results.

1. J. R. FOSSEY, E. V. DEGUSMAN, and B. T. NARCADO. Philipp. Agric. Anal. Chem. **43**, 548 (1960).
2. P. J. SOUTHERN. Papua New Guinea. Agric. J. **19**, 18 (1967).
3. M. OLLAGNIER and R. OCHS. Oleagineaux, **27**, 193 (1972).
4. E. M. BAILEY. J. Assoc. Off. Agric. Chem. **5**, 288 (1921).
5. R. E. ANDREW. J. Assoc. Off. Agric. Chem. **6**, 107 (1922).
6. K. S. JAYARAMAN, S. RAMANUJAN, and P. K. VIJAYARAGHAVAN. Curr. Sci. **31**, 282 (1962).
7. R. F. SMITH and D. I. REES. Analyst, **88**, 310 (1963).
8. D. S. GROSSIER. Am. J. Clin. Nutr. **31**, 1727 (1978).
9. P. L. D. S. PERERA. M.Sc. dissertation, University of Colombo. 1979.
10. H. R. S. CONACHER and D. I. REES. Analyst, **89**, 806 (1964).
11. J. B. WILSON. J. Assoc. Off. Agric. Chem. **39**, 712 (1956).
12. J. LEVINE. J. Assoc. Off. Agric. Chem. **45**, 254 (1962).
13. R. A. ANDERSON and J. A. SOWERS. Phytochemistry, **7**, 293 (1968).
14. E. A. H. ROBERTS and D. M. WILLIAMS. J. Sci. Food Agric. **9**, 217 (1958).
15. B. BUTTERS and E. M. CHENERY. Analyst, **84**, 239 (1959).
16. D. S. SMYLY, B. B. WOODWARD, and E. C. CONRAD. J. Assoc. Off. Anal. Chem. **59**, 14 (1976).
17. W. R. KREISER and R. A. MARTIN. J. Assoc. Off. Anal. Chem. **61**, 1424 (1978).

Can. J. Chem. Downloaded from www.nrcresearchpress.com by 78.46.186.204 on 09/07/12
For personal use only.

A nuclear magnetic resonance study of aqueous solutions of several nitrate salts

A. Martin de P. Nicholas and Roderick E. Wasylishen[1]
Department of Chemistry, Dalhousie University, Halifax, N.S., Canada B3H 4J3

Received November 19, 1986

This paper is dedicated to Professor Douglas E. Ryan on the occasion of his 65th birthday

A. Martin de P. Nicholas and Roderick E. Wasylishen. Can. J. Chem. **65**, 951 (1987).

Rotational correlation times for the end-over-end rotation of the C_3 symmetry axis of the nitrate anion in the temperature range 3–80°C are studied by nuclear magnetic resonance spectroscopy for a variety of nitrate salts in aqueous solution. The counterion is found to retard the rotation of the anion in the following order: $Sc^{3+} > La^{3+} > Pb^{2+} > Ca^{2+}$, $Sr^{2+} > Al^{3+}$, K^+, Na^+, $(CH_3)_4N^+ > Zn^{2+}$, Mg^{2+}, Li^+, NH_4^+, H_3O^+. This relative order is discussed in terms of the association of the nitrate ion with the cation. Oxygen-17 nmr spin-lattice relaxation times in combination with ^{14}N nmr T_1 values are used to derive rotational diffusion constants for the in-plane rotations of the nitrate anion. In all cases the in-plane rotations are found to be slower than the corresponding end-over-end motion.

A. Martin de P. Nicholas et Roderick E. Wasylishen. Can. J. Chem. **65**, 951 (1987).

Opérant à des températures allant de 3 à 80°C et faisant appel à la spectroscopie rmn d'une variété de nitrates en solution aqueuse, on a déterminé les temps de corrélation rotationnelle pour la rotation d'un bout à l'autre de l'axe de rotation C_3 de l'anion nitrate. On a trouvé que le contre ion retarde la rotation de l'anion dans l'ordre suivant : $Sc^{3+} > La^{3+} > Pb^{2+} > Ca^{2+}$, $Sr^{2+} > Al^{3+}$, K^+, Na^+, $(CH_3)_4N^+ > Zn^{2+}$, Mg^{2+}, Li^+, NH_4^+, H_3O^+. On discute de cet ordre relatif en fonction de l'association de l'ion nitrate avec le cation. On a utilisé les temps de relaxation spin-réseau de la rmn du ^{17}O de concert avec les valeurs T_1 de la rmn du ^{14}N pour obtenir les valeurs des constantes de diffusion rotationnelle pour les rotations dans le plan de l'anion nitrate. Dans tous les cas, on a trouvé que les rotations dans le plan sont plus lentes que le mouvement correspondant d'un bout à l'autre.

[Traduit par la revue]

Introduction

Nuclear magnetic resonance spectroscopy is one of several techniques available for studying the rotations of ions in solution (1–4). The ease of application and sensitivity of this method make it an attractive choice, especially for studying more dilute solutions. Recently we have shown (5) the importance of using ^{14}N and ^{17}O nmr spin-lattice relaxation measurements to study the rotations of the nitrate and carbonate anions in aqueous solution in the presence of the sodium cation. We found rotations of the carbonate ion to be more hindered than those of the nitrate anion because of stronger cation–anion pairing and stronger anion–solvent interactions (hydrogen bonding). Some evidence for ion association was found for $NaNO_3$ at solute concentrations of 1 *M*; however, ion pairing is much more important for the divalent carbonate anion.

James and Frost (6–8) used Raman spectroscopy to derive rotational correlation times for the nitrate anion and to study ion–solvent interactions in a variety of nitrate salts at anion concentrations ≥ 1 *M*. However, it is important to study the anion rotations by several techniques because of the inherent limitations in the various approaches used (5, 9). As well, more dilute solutions, where viscosity effects are small, should be investigated. Here, nmr spectroscopy is used in a systematic study of the effects of monovalent (NH_4^+, Li^+, H_3O^+, K^+, and $(CH_3)_4N^+$), divalent (Pb^{2+}, Zn^{2+}, Ca^{2+}, Sr^{2+}, and Mg^{2+}), and trivalent (Sc^{3+}, La^{3+}, and Al^{3+}) cations on the end-over-end rotations of NO_3^- at anion concentrations of approximately 0.1 and 1.0 molar in aqueous solution. Our results are discussed in terms of ion pairing and compared with previous results obtained using Raman spectroscopy and Rayleigh scattering experiments. In some cases, for 1 *M* solutions, the temperature dependence of anion rotations is determined. Oxygen-17 relaxation data for solutions ≥ 1 *M* together with the ^{14}N data permitted measurement of both $D_\parallel$ and $D_\perp$ (**1**). Here $D_\parallel$ and $D_\perp$ represent rotational diffusion constants parallel and perpendicular to the ion plane. In-plane rotations have not been probed previously by other techniques, and hence our results should be of interest.

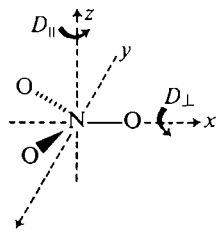

1

Theory

Under conditions of extreme narrowing the relaxation rate $(1/T_1)$ of a quadrupolar nucleus of spin I is given by (5, 10–15):

$$[1] \quad 1/T_1 = \frac{3\pi^2}{10}\frac{2I+3}{I^2(2I+1)}(e^2Qq_{xx}/h)^2\tau_{eff}$$

where (e^2Qq_{xx}/h) is the principal x component (in Hz) of the quadrupolar coupling tensor and τ_{eff} is an effective rotational correlation time, which includes a contribution from the asymmetry parameter, $\eta_q = (q_{yy} - q_{zz})/q_{xx}$ (11–13).

Assuming that the rotations of the nitrate anion can be described by small step rotational diffusion, the effective rotational correlation time obtained from ^{17}O spin-lattice relaxation data is given by eq. [2]:

$$[2] \quad \tau_{eff} = \{[4 + (\eta_q - 1)^2]D_\perp + (\eta_q + 1)^2 D_\parallel\}/4D_r$$

where

$$D_\perp = D_{xx} = D_{yy}$$
$$D_\parallel = D_{zz}$$
$$D_r = 3D_\perp(D_\perp + 2D_\parallel)$$

For the symmetrically bonded ^{14}N of the NO_3^- ion, the largest

[1]Author to whom correspondence may be addressed.

Can. J. Chem. Downloaded from www.nrcresearchpress.com by 78.46.186.204 on 09/07/12
For personal use only.

principal component of the electric field gradient tensor is perpendicular to the ion plane, $q_{xx} = q_{yy} = -(1/2)q_{zz}$, corresponding to $\eta_q = 3$; hence the relaxation rate is given by the more familiar equation (eq. [3]), which is a simplified form of eq. [1]:

$$[3] \quad 1/T_1(^{14}N) = 1.5\pi^2(e^2Qq_{zz}/h)^2\tau_{2R}$$

where e^2Qq_{zz}/h is the nuclear quadrupole coupling constant, QCC, (in Hz) and τ_{2R} is the rotational correlation time for rotations of the C_3 axis ($\tau_{2R} = \tau_\perp$). Oxygen-17 and nitrogen-14 quadrupolar coupling constants for the nitrate anion in the solid state are available from nuclear quadrupole resonance (16) and nmr experiments (17), respectively.

Experimental

The nmr measurements were performed on a Nicolet 360 NB (B_0 = 8.48 T) spectrometer using a broad-band variable-temperature 10-mm probe. All spin-lattice relaxation time measurements were made using the inversion recovery pulse sequence (IRCA), which uses compensating pulses (18) as previously described (5).

T_1's were calculated from peak heights obtained at twelve or more D_1 values, using a nonlinear three-parameter least-squares fitting procedure available on the Nicolet software (19).

Solutions of the nitrates were prepared by weighing out appropriate amounts of laboratory reagent grade chemicals and diluting volumetrically with distilled water. The solutions of $Al(NO_3)_3$ and $Sc(NO_3)_3$ were maintained at a pH of 2 to suppress hydrolysis (20).

Results and discussion

(a) Effect of cations on τ_{2R} of NO_3^- at ambient temperature

The effect of cations on the measured ^{14}N T_1 values and derived rotational correlation times, τ_{2R}, for the nitrate anion in aqueous solution at anion concentrations of 1 and 0.1 *M* is given in Table 1. The τ_{2R} values were calculated using eq. [3] taking QCC(^{14}N) = 745 kHz (21, 22), and are the same rotational correlation times measured by other spectroscopic methods (1, 9). A rotational correlation time, τ_{2R}, of 0.94 ps for a "free nitrate ion" in aqueous solution was calculated from the $T_1(^{14}N)$ of 130 ms obtained for a 0.01 *M* aqueous solution of ammonium nitrate. Identical results were obtained for a 0.01 *M* solution of sodium nitrate at the same temperature, 23 ± 2°C. For comparison, the effective rotational correlation time for water at 25°C has been estimated to be approximately 2.6 ps (23).

Table 1 shows that the end-over-end rotations of the nitrate anion are significantly affected by the cations Sc^{3+}, La^{3+}, Pb^{2+}, Sr^{2+}, and Ca^{2+} even in a dilute solution of concentration 0.1 *M* in nitrate. The influence of the cation on nitrate anion rotations varies from being very small for H_3O^+, NH_4^+, Li^+, Mg^{2+}, and Zn^{2+} to being very large for Sc^{3+}, La^{3+}, and Pb^{2+} where evidence for ion pairing was reported previously (24–28). These effects are a result of cation–anion and cation– and anion–solvent interactions, which retard rotations of the nitrate ion. At anion concentrations of 1 *M*, where the population of cation–anion associated species will be large relative to 0.1 *M*, the τ_{2R} values increase as expected.

The τ_{2R} values deduced in this work suggest the following order in the ability of the cations to coordinate with the nitrate anion and retard its end-over-end rotation: $Sc^{3+} > La^{3+} > Pb^{2+} > Ca^{2+}$, $Sr^{2+} > Al^{3+}$, K^+, Na^+, $(CH_3)_4N^+ > Zn^{2+}$, Mg^{2+}, Li^+, NH_4^+, H_3O^+. This order is in general agreement with previous studies of the extent of ion pairing of cations with the nitrate anion in aqueous solution (29, 30).

It should be pointed out that the observed T_1 values and hence the calculated τ_{2R} values in Table 1 represent an average value for all species present (see section (*c*) below). If the lifetime of a particular nitrate-associated species is long with respect to its rotational correlation time, then τ_{2R} for *that* species will be related to its hydrodynamic volume. The contribution that each species makes to any given τ_{2R} value in Table 1 will depend on the relative population of that species and its lifetime. Species with a lifetime on the order of 1 ps or less will have little effect on the observed T_1 values and resulting τ_{2R} value.

TABLE 1. The effect of the counter ion on the $T_1(^{14}N)$ and $\tau_{2R}(\tau_\perp)$ of the nitrate anion in aqueous solution[a]

	$T_1(^{14}N)$/ms		τ_{2R}/ps	
Cation	0.1 *M*[b]	1.0 *M*[c]	0.1 *M*	1.0 *M*
H_3O^+	127.3	116.5	0.96	1.04
NH_4^+	121.8	112.4	1.00	1.08
Mg^{2+}	122.2	103.2	1.00	1.18
Li^+	115.4[d]	105.7	1.05[d]	1.15
Zn^{2+}	121.9	96.3	1.00	1.26
K^+	119.4	89.7	1.02	1.36
Na^+	117.0	86.8	1.04	1.40
$(CH_3)_4N^+$	114.3	88.1	1.06	1.38
Al^{3+}	—	87.9	—	1.38
Ca^{2+}	91.8	46.1	1.33	2.64
Sr^{2+}	90.8	41.9	1.34	2.90
Pb^{2+}	71.0	34.1	1.71	3.57
La^{3+}	70.1	26.3	1.74	4.63
Sc^{3+}	48.8	22.3	2.49	5.46

[a]Unless stated otherwise, all measurements at 23 ± 2°C.
[b]Error of 7%.
[c]Error of 3%.
[d]At 20°C.

The $T_1(^{14}N)$ results in Table 1 indicate that the NH_4^+ does not associate with the nitrate anion. Previous work suggests this to be true even at high NH_4^+ concentration (6). The weak complexing power of NH_4^+ is apparently due to its tetrahedral shape, which enables it to fit into the hydrogen-bonded network without disrupting the water structure around the nitrate anion (31). Also, the structure-forming H_3O^+, Li^+, Mg^{2+}, and Zn^{2+} cations all possess a strong first hydration sphere and are not readily susceptible to attack by the nitrate anion, a well-known weak ligand. These cations are strongly hydrated because of their large charge to size ratio (32). Thus, the NH_4^+ ion and strongly hydrated cations are not susceptible to association with the nitrate anion, and hence do not significantly affect the rotation of this ion in solution at concentrations of less than 1 *M* NO_3^-.

For the nitrates of Na^+, K^+, and $N(CH_3)_4^+$ the τ_{2R} values increase slightly as the solute concentration increases from 0.1 *M* to 1 *M*. The implication is that the population of ion pairs must be small. The rate constant for dissociation of the $Na^+NO_3^-$ ion pair has been estimated to be 12×10^{10} s^{-1} (lifetime ≈ 7.7 ps) in 2 *M* sodium nitrate (33).

The behaviour of the nitrate ion for aqueous solutions of $Ca(NO_3)_2$ compared to those of $Mg(NO_3)_2$ is striking. For a 0.5 *M* $Ca(NO_3)_2$ solution the τ_{2R} value is 2.64 ps compared to 1.18 ps for a 0.5 *M* $Mg(NO_3)_2$ solution. Such a difference in these two salts was not evident in the Raman study of James and Frost (7); however, other work (27–30) has clearly indicated that the ion-pairing ability of Ca^{2+} should be considerably greater than that of Mg^{2+}, as implied in the present study. It is of interest to mention that from the analysis of depolarized

Can. J. Chem. Downloaded from www.nrcresearchpress.com by 78.46.186.204 on 09/07/12
For personal use only.

Can. J. Chem. Downloaded from www.nrcresearchpress.com by 78.46.186.204 on 09/07/12
For personal use only.

Rayleigh scattering line shapes of 0.9 *M* $Ca(NO_3)_2$, Whittle and Clarke (27) have found evidence for a slowly reorientating nitrate species ($\tau_{2R} \approx 50$ ps), which they tentatively assigned to a contact pair, $CaNO_3^+$. This species accounted for approximately 20% of the integrated intensity of the reorientational spectrum at a concentration of 0.9 *M*. If their analysis is valid, our results would indicate that the population of contact pairs is less than 10% at 0.5 *M* $Ca(NO_3)_2$. The data in Table 1 indicate very similar behaviour for the nitrate ion in $Sr(NO_3)_2$ and $Ca(NO_3)_2$.

The inability of Al^{3+} to significantly influence the rotational correlation time of the nitrate ion is in accord with previous nmr (34) and Raman (35) studies, which find no evidence for contact ion pairs.

The long τ_{2R} values observed here for the nitrates of lead, lanthanum, and scandium indicate significant concentrations of species such as $Pb(NO_3)^+$, $La(NO_3)^{2+}$, and $Sc(NO_3)^{2+}$. In fact recent ^{207}Pb nmr chemical shift data indicate that for a 0.5 *M* $Pb(NO_3)_2$ solution 25% of the nitrate ions are complexed with lead, $Pb(NO_3)^+$ (24). The longer τ_{2R} values observed for La^{3+} and Sc^{3+} imply a larger fraction of cation–nitrate associated species for aqueous solutions of these salts. The previously reported Raman value of τ_{2R} for the nitrate ions of 0.33 *M* $La(NO_3)_3$, 1.65 ps (8), is not in accordance with our results or with the known ion-pairing ability of La^{3+} (36). For aqueous solutions of $La(NO_3)_3$ at 25°C Irish and co-workers (36) have found the step stability constants $\beta_1 = 1.51$ and $\beta_2 = 0.14$. It is important to note that in aqueous solution the average coordination number of La^{3+} is 8; hence when the nitrate ion is associated with the lanthanum cation the overall ion rotation is expected to be impeded relative to a complex of coordination number 6. Previous ^{45}Sc nmr studies (37, 38) indicate extensive cation–anion association in the case of $Sc(NO_3)_3$, in agreement with our results.

The results in Table 1 indicate that ^{14}N nmr T_1's can be a useful probe to study ion pairing in solution. Clearly, the main advantage of the ^{14}N nmr technique over the Raman technique is its ability to measure τ_{2R} over a wide range of solute concentrations, from approximately 0.01 *M* to saturated solutions. Also, we believe that in studying cation – nitrate ion association ^{14}N nmr is generally more informative than nmr studies of the metal nuclide since the interpretation of metal nuclide relaxation data is difficult (e.g. ^{25}Mg nmr studies of $Mg(NO_3)_2$ (39, 40)).

The main assumption that we have made in calculating the τ_{2R} values in Table 1 is that the nitrogen-14 quadrupolar coupling constant in aqueous solution is the same as the value measured in the solid state. Calculations by Gourdji *et al.* (21, 22) indicate that the electric field gradient at the nitrogen nucleus in the nitrate ion is primarily intraionic in origin and that the contribution of neighbouring ions is 5% or less. Also, the excellent agreement in τ_{2R} values obtained for the nitrate ion in 1 *M* $NaNO_3$ by nmr (5) and by recent Raman fluctuation spectroscopic studies (41) indicates that the ^{14}N QCC in aqueous solution and in the solid state are very similar. Finally, we do not expect ion pairing to dramatically influence the value of the ^{14}N QCC used here because nqr studies of the nitrate ion in a variety of zinc imidazole complexes indicate that the factor QCC (^{14}N) $[(1 + (\eta^2/3)]^{1/2}$ is within 10–20% of the value found in solid $NaNO_3$ (42).

(b) Temperature dependence of ^{14}N T_1 (3–80°C)

The temperature dependence of the ^{14}N T_1 data is illustrated in Fig. 1 with a plot of log T_1 (^{14}N) against $1/T$, where T is the absolute temperature. Since the rate of nitrogen relaxation ($1/T_1$) is directly proportional to τ_{2R} (eq. [3]), the temperature dependence of T_1 is equivalent to that of τ_{2R}. For many molecules in solution the rotational correlation time shows an Arrhenius behaviour, and the temperature dependence of τ_{2R} is given by eq. [4]

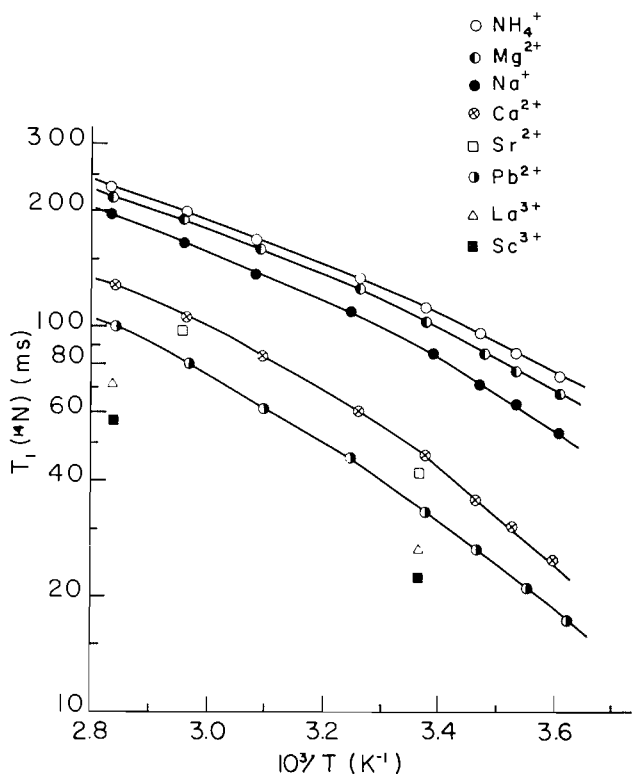

FIG. 1. Plots of log T_1(^{14}N) vs. $10^3/T$ for a variety of nitrate salts in aqueous solution at an anion concentration of 1.0 *M*.

[4] $\tau_2 = \tau_{2,0} \exp(E_a/RT)$

where E_a is an activation energy that should be related to the barrier to rotation (43). The relationship between E_a and the barrier to rotation has been discussed by a number of workers (43–47).

The results in Fig. 1 clearly indicate that log T_1 is not linearly related to the inverse of temperature; hence τ_{2R} is not simply related to temperature by a simple equation of the form of eq. [4] over the entire temperature range investigated. This type of behaviour is common for most transport properties of water (48, 49) and it has been found that two separate equations of the form of eq. [4] are often reasonably accurate over a low temperature range (0–25°C) and a high temperature range (35–80°C). We have arbitrarily separated our data in this way and the results are summarized in Table 2.

The nitrate counterions in Table 2 may be divided into three groups: those which do not associate with the nitrate ions or only very weakly so (NH_4^+, Li^+, Mg^{2+}, and Zn^{2+}), those which associate weakly ($(CH_3)_4N^+$ and Na^+), and finally those for which association is relatively strong (Ca^{2+} and Pb^{2+}). The average low temperature activation energies for each of these three groups of cations are 3.8, 4.45, and 5.55 kcal mol^{-1}, respectively. The corresponding average high temperature (30–80°C) E_a values are 2.55 kcal mol^{-1} (NH_4^+, Li^+, Mg^{2+}, Zn^{2+}), 2.85 kcal mol^{-1} ($(CH_3)_4N^+$, Na^+), and 3.75 kcal mol^{-1} (Ca^{2+}, Pb^{2+}). As expected, one finds that in any given

Can. J. Chem. Downloaded from www.nrcresearchpress.com by 78.46.186.204 on 09/07/12
For personal use only.

TABLE 2. Apparent activation energies for the rotation of the nitrate anion in aqueous solution[a,b]

	E_a/kcal mol^{-1}	
Counterion	0–25°C	30–80°C
NH_4^+	3.6	2.5
	3.7[c]	2.7[c]
Li^+	3.9	2.7
Mg^{2+}	3.7	2.6
Zn^{2+}	4.0	2.4
$(CH_3)_4N^+$	4.3	2.9
Na^+	4.6[d]	2.8[d]
Ca^{2+}	5.6	3.5
Pb^{2+}	5.5	4.0

[a]Estimated error of 15%.
[b]Unless stated otherwise, the concentration of NO_3^- is 1 *M*.
[c]Concentration of NO_3^- is 3 *M*.
[d]Reference 5.

TABLE 3. Concentration dependence of the reorientation of the nitrate anion in aqueous solution at 24 ± 2°C

Concentration	$T_1(^{14}N)$/ms	τ_{2R}/ps	τ_{2R}(Raman)/ps[a]
0.01 *M* NH_4NO_3	130[b]	0.94	—
0.1 *M*	122[c]	1.00	—
1 *M*	114	1.09	1.33
3 *M*	90	1.35	—
4 *M*	83	1.47	1.55
8 *M*	54	2.25	2.19
0.01 *M* $NaNO_3$	130[b]	0.94	—
0.1 *M*	121	1.01	—
0.4 *M*	106	1.15	—
1 *M*	87	1.40	1.44
2 *M*	66	1.84	1.60
4 *M*	41	2.97	1.90(3.5 *M*)

[a]Reference 53 (at 29°C).
[b]At 23°C.
[c]At 22°C.

temperature range the activation energies consistently increase as ion association increases. This is expected because, as ion association increases, the nitrate ion on average finds itself associated with a larger, less mobile entity, for example in a species such as $[(H_2O)_5PbNO_3]^+$.

Several explanations for the larger activation energies at low temperature relative to those at high temperatures have been advanced (45–47); however, we do not wish to speculate on this point here.

(c) Concentration dependence of ^{14}N T_1

The concentration dependence of the ^{14}N T_1 (and hence the rotational correlation times) for the nitrate anion in the presence of the counterions Na^+ and NH_4^+ is given in Table 3. The values of τ_{2R} increase with increasing concentration. While the variation in τ_{2R} is large for the Na^+ salt it is small for the NH_4^+ salt, where ion pairing is small even at very high concentrations as already discussed (31). In principle it should be possible to obtain an estimate of the equilibrium constant for the formation of an ion pair and the T_1 for this ion pair from the concentration dependence of T_1 (50).

In the presence of association the observed T_1 values is a composite of the T_1 values for the free and complexed nitrate anion. In the region of motional narrowing when the rate of chemical exchange ($M^{n+} + NO_3^- \rightleftharpoons (MNO_3)^{(n-1)+}$) is slow relative to the rates of molecular reorientation of the nitrate anion and the ion-pair complex, T_1 is given by (51):

$$[5] \quad 1/T_1 = (1/T_1)_{free}(1 - A) + (1/T_1)_{complexed}(A)$$

where A is the mole fraction of the complexed nitrate anion. When the rates of exchange are fast relative to the reorientation rates (51):

$$[6] \quad T_1 = (T_1)_{free}(1 - A) + (T_1)_{complexed}(A)$$

If we assume that $1/T_1$ varies linearly with the macroscopic viscosity at a given temperature, then the T_1 term in eqs. [5] and [6] must be replaced by $T_1\eta_{rel}$, where η_{rel} is the macroscopic viscosity of the solution relative to that of pure water.

In practice it is difficult to determine A and $T_{1\,complexed}$ from relaxation data alone. As already mentioned, the equilibrium constant for dissociation of $Pb(NO_3)^+$ is known from ^{207}Pb nmr (24), hence it is instructive to apply the above analysis to this system. The value of $(T_1)_{free}$ can be obtained by studying very dilute solutions. At 23°C we estimate $(T_1)_{free}$ = 130 ms, corresponding to a rotational correlation time of 0.94 ps. Using the ^{14}N T_1 data for 0.5 and 0.05 *M* $Pb(NO_3)_2$ at 23°C, and obtaining the A values from K_{assoc} = 1.233 (24), we find that eq. [5] fits the data better than eq. [6]. As expected, this indicates relatively slow exchange rates for the ion-pair equilibrium. It must be noted that the exchange rate is still fast in the nmr chemical-shift time scale. Using eq. [5], we estimate $(1/T_1)_{complexed}$ = 9 ± 4 ms. Assuming QCC($^{14}NO_3^-$) is not affected by association, we obtain τ_{2R} ($[PbNO_3]^+$) = 14 ± 6 ps. This is to be compared with a value of ca. 50 ps estimated for $\tau_{2R}([CaNO_3]^+)$ using Rayleigh scattering (27). If the stick boundary condition applied to the rotation of the $M(H_2O)_5NO_3^+$ complex, 50 ps would seem more reasonable! However, because of the assumptions and errors involved in calculating both of these values, we do not care to speculate on the interpretation of these values.

(d) Anisotropy of reorientation

In this section effective rotational correlation times derived from ^{17}O nmr T_1 data are used to extract information about the influence of temperature, nature of the cation, and the cation concentration on the anisotropy of reorientation of the nitrate anion. The results are summarized in Table 4. The τ_{eff} values were calculated by using eq. [1] and taking QCC(^{17}O) = 12.57 MHz (52). The ratios of $D_\parallel/D_\perp$ derived from the correlation times using eqs. [1]–[3] and $\eta_q = -0.747$ (52) are listed in column 6 of Table 4. We did not attempt ^{17}O T_1 measurements at temperatures where the line width exceeded ca. 200 Hz, because of the large experimental errors anticipated under these circumstances (5). It must be noted that errors of 10 and 5% in the ^{17}O T_1 values and the QCC (^{17}O), respectively, correspond to an error of ca. 30% in the $D_\parallel/D_\perp$ ratio. Nevertheless, the relative error in this ratio is probably much less, and study of its variation with temperature, the counterion, and counterion concentration is of interest because it is difficult to obtain $D_\parallel/D_\perp$ by any other technique. Our results may be summarized as follows:

1. For a 3 *M* aqueous solution of NH_4NO_3, variable temperature ^{14}N and ^{17}O nmr results (Fig. 2) indicate $D_\parallel/D_\perp \approx 0.51 \pm 0.06$, essentially independent of temperature.

TABLE 4. An analysis of the anisotropy of the reorientation of the nitrate anion in aqueous solution

Cation	Temperature/°C	$T_1(^{14}N)$/ms	$T_1(^{17}O)$/ms	τ_{eff}/ps	$D_\parallel/D_\perp$
3 *M* NH_4^+	4	57.3	1.82	3.67	0.53
	9	64.5	2.09	3.20	0.54
	15	72.7	2.42	2.76	0.57
	24	90.5	2.81	2.38	0.50
	34	105.8	3.28	2.04	0.50
	47	130.5	4.03	1.66	0.49
	61	154.2	4.61	1.45	0.46
	72	176.7	5.45	1.23	0.49
1 *M* H_3O^+	24	116.5	2.84	2.35	0.29
1 *M* NH_4^+	25	114.7	3.15	2.12	0.39
1 *M* Na^+	22	85.2	2.48	2.69	0.44
0.5 *M* Zn^{2+}	26	100.1	2.74	2.44	0.38
0.5 *M* Ca^{2+}	47	79.0	2.41	2.77	0.48
0.5 *M* Pb^{2+}	50	61.1	1.88	3.55	0.49
0.33 *M* La^{3+}	80	71.0	2.39	2.79	0.59
1 *M* NH_4^+	25	114.7	3.15	2.12	0.39
3 *M* NH_4^+	24	90.5	2.81	2.38	0.50
4 *M* NH_4^+	24	83.2	2.70	2.47	0.55
8 *M* NH_4^+	24	54.3	2.03	3.29	0.71
0.5 *M* Zn^{2+}	26	100.1	2.74	2.44	0.38
1.5 *M* Zn^{2+}	24	58.0	2.02	3.31	0.62

Previously, similar results were obtained for 1 *M* $NaNO_3$ where $D_\parallel/D_\perp \approx 0.45 \pm 0.03$ (5). As discussed in our earlier study (5), it is difficult to account for the observation that in-plane rotations are slower than end-over-end rotations. One naive explanation would be that three N—O...H—O hydrogen bonds must be broken for in-plane rotation (**2**) compared to two for an end-over-end rotation (**3**).

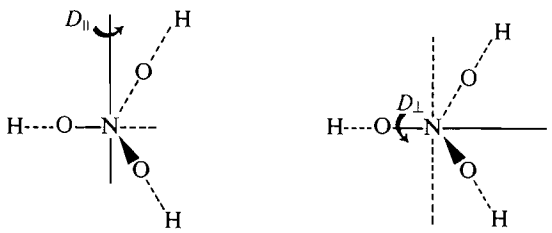

2. Assuming that $D_\parallel/D_\perp$ is approximately independent of temperature (see results for the ammonium ion), it appears that the anisotropy of the motion decreases (i.e., $D_\parallel/D_\perp \rightarrow 1$) as ion association increases. For example, comparing samples which are 1 *M* in nitrate for the following cations, in approximate order of their ability to associate with the nitrate anion, gives:

Cation:	H_3O^+	NH_4^+	Zn^{2+}	< Na^+	< Ca^{2+}	< Pb^{2+}	< La^{3+}
$D_\parallel/D_\perp$:	0.29	0.39	0.38	0.44	0.48	0.49	0.59

These results are precisely what one would expect. For the systems where ion association is relatively strong, there will be a significant population of complexes of the type $[(H_2O)_nMNO_3]^{x+}$. These large complexes are expected to be more spherical than an isolated nitrate ion; hence the rotations should be more isotropic, as observed.

3. For cations that only associate weakly with the nitrate ion the ratio $D_\parallel/D_\perp$ increases with solute concentration. For example, in the case of NH_4NO_3, $D_\parallel/D_\perp$ increases from approximately 0.4 to 0.7 as the concentration increases from 1 *M* to 8 *M*. Similarly for $Zn(NO_3)_2$, $D_\parallel/D_\perp$ increases from 0.38 to 0.62 when the nitrate ion concentration increases from 1 *M* to 3 *M*. An increase in the salt concentration corresponds to a decrease in the number of water molecules available to hydrate the nitrate anion. In fact, the ratio of the molar concentration of H_2O to that of NO_3^- decreases from a high of 53 for 1 *M* solution to ca. 4 for the 8 *M* solution. That is, the $D_\parallel/D_\perp$ ratio is sensitive to amount of water available in the medium and increases with decreasing water content. This is in accordance with the hypothesis that hydration of the nitrate anion is the major factor responsible for a $D_\parallel/D_\perp$ ratio of less than unity.

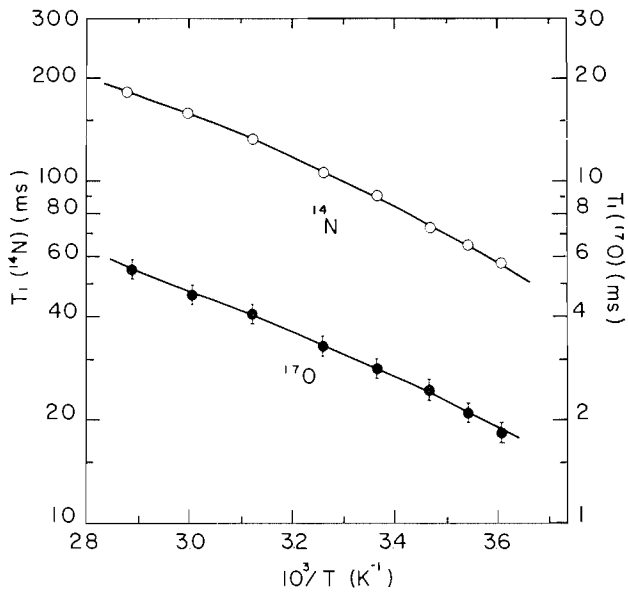

FIG. 2. Plots of log $T_1(^{14}N)$ and log $T_1(^{17}O)$ vs. $10^3/T$ for the nitrate anion in an aqueous solution of 3 *M* NH_4NO_3.

4. The nmr ^{14}N and ^{17}O T_1 values for the nitrate anion given in Table 4 are fairly well correlated (correlation coefficient $r = 0.96$) and their relationship is given by:

Can. J. Chem. Downloaded from www.nrcresearchpress.com by 78.46.186.204 on 09/07/12
For personal use only.

[7] $T_1(^{17}O) = 0.027T_1(^{14}N) + 0.36$

This relationship, which is valid for the nitrate ion, may be used to obtain *approximate* ^{17}O T_1 values from the corresponding ^{14}N values. These initial estimates are useful in setting up appropriate delay values (D_1) in the ^{17}O T_1 IRCA experiment. The T_1 values are in units of ms.

Conclusions

In this study we have demonstrated the utility of ^{14}N and ^{17}O nmr in characterizing rotations of the nitrate anion in aqueous solution. We believe the nmr technique complements the results obtained by other techniques and we encourage others to apply this technique. The ^{14}N T_1 measurements are relatively straightforward on almost any modern multinuclear nmr spectrometer; however, natural abundance ^{17}O relaxation measurements are less routine and require a substantial amount of spectrometer time. Oxygen-17 labelling of the nitrate ion would permit one to significantly extend the present study.

Acknowledgements

We wish to thank Marco Gruwel for several helpful discussions regarding anisotropic rotational diffusion. All nmr spectra were obtained at the Atlantic Regional NMR Centre, Dalhousie University. We are grateful to NSERC for financial support in helping establish and maintain this centre and for an operating grant (R.E.W.).

1. W. A. Steele. Adv. Chem. Phys. **34**, 1 (1976).
2. J. E. Griffiths. *In* Vibrational spectra and structure. Vol. 6. *Edited by* J. R. Durig. 1977. p 273.
3. W. G. Rothschild. Dynamics of molecular liquids. Wiley, New York. 1984.
4. B. Berne and R. Pecora. Dynamic light scattering. Wiley, New York. 1976.
5. A. M. de P. Nicholas and R. E. Wasylishen. J. Phys. Chem. **89**, 5446 (1985).
6. R. L. Frost, and D. W. James. J. Chem. Soc. Faraday Trans. 1, **78**, 3235 (1982).
7. D. W. James and R. L. Frost, Aust. J. Chem. **35**, 1793 (1982).
8. R. L. Frost and D. W. James. J. Chem. Soc. Faraday Trans. 1, **78**, 3263 (1982).
9. D. W. James. Prog. Inorg. Chem. **33**, 353 (1985).
10. A. Abragam. The principles of nuclear magnetism. Oxford University Press, New York. 1961.
11. W. T. Huntress. Adv. Magn. Reson. **4**, 1 (1970).
12. R. E. Stark, R. L. Vold, and R. R. Vold. Chem. Phys. **20**, 337 (1977).
13. E. J. Pedersen, R. R. Vold, and R. L. Vold. Mol. Phys. **35**, 997 (1978).
14. J. P. Kintzinger and J. M. Lehn. Mol. Phys. **22**, 273 (1971).
15. J. P. Kintzinger and J. M. Lehn. Mol. Phys. **27**, 491 (1974).
16. E. A. C. Lucken. *In* Nuclear quadrupole coupling constants. Academic Press, New York. 1969.
17. E. R. Henry and A. Szabo. J. Chem. Phys. **82**, 4753 (1985).
18. R. Freeman, S. P. Kempsell, and M. H. Levitt. J. Magn. Reson. **38**, 453 (1980).
19. G. C. Levy and I. R. Peat. J. Magn. Reson. **18**, 500 (1975).
20. J. E. Huheey. Inorganic chemistry. 3rd ed. Harper, New York. 1983. Chap. 7.
21. M. Gourdji and L. Guibé. C.R. Acad. Sci. Paris, **260**, 1131 (1965).
22. M. Gourdji, L. Guibé, and A. Peneau. J. Phys. (Les Ulis, Fr.) **35**, 497 (1974).
23. R. T. Boeré and R. G. Kidd. Annu. Rep. NMR Spectrosc. **13**, 319 (1982), and references therein.
24. P. G. Harrison, M. A. Healy, and A. T. Steel. J. Chem. Soc. Dalton Trans. 1845 (1983).
25. G. H. Nancollas. J. Chem. Soc. 1458 (1955).
26. H. M. Hershenson, M. E. Smith, and D. N. Hume. J. Am. Chem. Soc. **75**, 507 (1953).
27. M. Whittle and J. H. R. Clarke. Chem. Phys. Lett. **98**, 172 (1983).
28. R. E. Hester and R. A. Plane. J. Chem. Phys. **40**, 411 (1964).
29. D. E. Irish and M. H. Brooker. *In* Advances in infrared and Raman spectroscopy. Vol. 2. *Edited by* R. J. H. Clark and R. E. Hester. Heydon and Sons, London. 1976. p. 212.
30. (*a*) R. M. Smith and A. E. Martell. Critical stability constants. Vol. 4. Inorganic complexes. Plenum Press, New York. 1976. p. 48; (*b*) L. G. Sillen. Stability constants of metal–ion complexes. Spec. Publ. Chem. Soc. No. 17. 1964. p. 166.
31. D. W. James and R. F. Armishaw. J. Phys. Chem. **80**, 50 (1978).
32. T. G. Chang and D. E. Irish. J. Phys. Chem. **77**, 5 (1973).
33. H. Strehlow, I. Wagner, and P. Hildebrandt. Ber. Bunsenges. Phys. Chem. **85**, 516 (1983).
34. N. A. Matwiyoff, P. E. Darley, and W. G. Movius. Inorg. Chem. **7**, 2173 (1968).
35. D. E. Irish, G. Chang, and D. L. Nelson. Inorg. Chem. **9**, 425 (1970).
36. D. E. Irish. *In* Proc. 6th Int. Conf. Raman Spectrosc. Vol. 1. *Edited by* E. D. Schmid, R. S. Krishnan, and W. Kiefer. Heyden, London. 1978. p. 245.
37. A. Fratiello, V. M. Nishida, R. E. Lee, and R. E. Schuster. J. Chem. Phys. **50**, 3624 (1969).
38. A. Fratiello, R. E. Lee, and R. E. Schuster. Inorg. Chem. **9**, 391 (1970).
39. L. Simeral and G. E. Maciel. J. Phys. Chem. **80**, 552 (1976).
40. M. Holz, S. Günther, O. Lutz, A. Nolle, and P.-G. Schrade. Z. Naturforsch. A: Phys. Phys. Chem. Kosmophys. **34**, 944 (1979).
41. M. Perrot, F. Guillaume, and W. G. Rothschild. J. Phys. Chem. **87**, 5193 (1983).
42. C. I. H. Ashby, C. P. Cheng, and T. L. Brown. J. Am. Chem. Soc. **100**, 6057 (1978).
43. D. M. Doddrell, M. R. Bendall, A. J. O'Connor, and D. T. Pegg. Aust. J. Chem. **30**, 943 (1977).
44. A. M de P. Nicholas and R. E. Wasylishen. Can. J. Chem. **64**, 1839 (1986).
45. C. L. Perrin and A. K. Gipe. J. Am. Chem. Soc. **108**, 1088 (1986).
46. D. J. Wilbur and J. Jonas. J. Chem. Phys. **62**, 2800 (1975).
47. D. E. Irish and T. Jarv. Appl. Spectrosc. **37**, 50 (1980).
48. (*a*) L. Endom, H. G. Hertz, B. Thül, and M. D. Zeidler. Ber. Bunsenges. Phys. Chem. **71**, 1008 (1967); (*b*) O. Conde and J. Teixeria. Mol. Phys. **53**, 951 (1984).
49. D. Eisenberg and W. Kauzmann. The structure and properties of water. Oxford University Press, New York. 1969. Chap. 4.
50. W. Egan. J. Am. Chem. Soc. **98**, 4091 (1976).
51. J. E. Anderson and P. A. Fryer. J. Chem. Phys. **50**, 3784 (1969).
52. C. P. Cheng and T. L. Brown. J. Am. Chem. Soc. **102**, 6418 (1980).
53. T. Katō, J. Umemura, and T. Takenaka. Mol. Phys. **36**, 621 (1978).

Can. J. Chem. Downloaded from www.nrcresearchpress.com by 78.46.186.204 on 09/07/12
For personal use only.

The voltammetric determination of Mo in seawater after adsorptive accumulation of the Eriochrome Blue Black R complex[1]

S. N. WILLIE AND S. S. BERMAN
Chemistry Division, National Research Council of Canada, Ottawa, Ont., Canada K1A 0R9

AND

J. A. PAGE AND G. W. VANLOON
Department of Chemistry, Queen's University, Kingston, Ont., Canada K7L 3N6

Received November 3, 1986

This paper is dedicated to Professor Douglas E. Ryan on the occasion of his 65th birthday

S. N. WILLIE, S. S. BERMAN, J. A. PAGE, and G. W. VANLOON. Can. J. Chem. **65**, 957 (1987).

A method for direct determination of molybdenum in seawater has been developed, and uses linear sweep voltammetry after adsorptive accumulation of the Erichrome Blue Black R (EBBR) complex on a static mercury drop electrode. To an acidified (pH 1.6) seawater (SW) sample, 6.0×10^{-6} *M* EBBR is added and preconcentration by adsorption is carried out for 30 s at a potential of −0.05 V vs. the Ag/AgCl/SW reference electrode. The potential is then scanned in the negative direction, giving a current peak for the reduction of the Mo—EBBR complex at −0.17 V. Under these conditions the limit of detection is 0.50 ng/mL. Experimental results for Mo in seawater using this technique agree well with certified values for two reference seawater samples (NASS-1, CASS-1).

S. N. WILLIE, S. S. BERMAN, J. A. PAGE et G. W. VANLOON. Can. J. Chem. **65**, 957 (1987).

On a développé une méthode directe pour la détermination du molybdène dans l'eau de mer; cette méthode fait appel à la voltamétrie à balayage linéaire, après une accumulation par adsorption du complexe de l'Erichrome Bleu Noir R (EBNR) sur une électrode à goutte de mercure statique. A un échantillon acidifié (pH de 1,6) d'eau de mer (EM), on ajoute $6{,}0 \times 10^{-6}$ *M* de EBNR et on effectue une préconcentration par adsorption pendant 30 s, à un potentiel de −0,05 V vs l'électrode de référence Ag/AgCl/EM. On effectue un balayage du potentiel dans la direction négative qui donne un pic du courant pour la réduction du complexe Mo—EBNR à −0,17 V. Utilisant ces conditions, la limite de détection est 0,50 ng/mL. Les résultats obtenus pour le Mo dans l'eau de mer, en utilisant cette technique, sont en bon accord avec les valeurs certifiées pour deux échantillons d'eau de mer (NASS-1, CASS-1).

[Traduit par la revue]

Can. J. Chem. Downloaded from www.nrcresearchpress.com by 78.46.186.204 on 09/07/12
For personal use only.

Introduction

Anodic stripping voltammetry (ASV) is well suited for the determination of trace metals in seawater, but has been limited to the analysis of elements, most notably Zn, Cd, Pb, and Cu, which may be readily reduced and then reoxidized at the Hg electrode. However, a recent approach which significantly widens the scope of voltammetric analysis involves the use of adsorptive accumulation as a preconcentration technique. This technique requires the addition of reagent(s) to form a surface-active complex with the analyte species of interest; accumulation on the electrode surface then results due to adsorption under an applied potential.

Adsorptive accumulation voltammetry techniques have been reported for Ti (1) and Al (2) using solochrome violet RS, Mn (3) using eriochrome black T, and the lanthanides (4) using *o*-cresolphthalexon. The application of this technique to the determination of a number of trace elements in seawater has also been reported, Ni (5) using the dimethylglyoxime (DMG) complex, Cr (6) using diethylenetriaminepentaacetic acid (DTPA), and Fe, V, Cu, and U (7–10) using catechol to form chelates. A method for determining Mo in seawater has been described (11) which uses 8-hydroxyquinoline to form a complex.

The present work reports an alternate procedure for the analysis of Mo after formation of a complex with 3-hydroxy-4-[2-hydroxy-1-naphthylazo]-1-naphthalene sulphonic acid monosodium salt (Eriochrome Blue Black R or EBBR). EBBR is an *o,o'*-dihydroxyazo compound that has found extensive application as an indicator in EDTA titrations of a variety of metals (12). This dye and related compounds have also been recommended for the direct polarographic analysis of metals including Al, Fe, Ga, Mg, V, Zn, and the lanthanides (13).

In preliminary experiments (14) it was found that EBBR could be adsorbed onto a hanging Hg drop electrode in both its free state and also as metal complexes. By scanning the electrode potential in a negative direction, separate current peaks for the uncomplexed dye and metal complex could be observed. The latter peak height was found to be proportional to the concentration of metal ion in the solution.

This paper describes the analytical conditions required for the determination of Mo in seawater. The advantage of the present approach is that direct analysis is possible, without separate preconcentration such as co-precipitation (15, 16), ion exchange (17), or solvent extraction (18).

Experimental

Apparatus

An EG&G Princeton Applied Research Model 174A polarographic analyser was used in conjunction with a static mercury drop electrode Model 303 and a Model 305 stirrer. Voltammograms were recorded using a Hewlett Packard Model 7004B recorder. A Commodore Vic 20 computer was interfaced with the 174A to control the timing of the electrolysis cycle.

The borosilicate glass cell supplied with the unit was used and did not produce any observable contamination. Solutions were stirred with a Teflon-coated stirring bar (14 mm × 3 mm) at "slow" speed (500 Hz).

The auxilary electrode was a Pt wire and the reference electrode was an Ag/AgCl electrode immersed in acidified seawater (SW) (pH 1.6) and separated from the analyte solution by a Vycor plug. The potential of the Ag/AgCl/SW reference was −0.010 V vs. a conventional SCE at 25°C. All potentials quoted in this work are referenced to the Ag/AgCl/SW electrode.

[1]NRC No. 27138.

Can. J. Chem. Downloaded from www.nrcresearchpress.com by 78.46.186.204 on 09/07/12
For personal use only.

Reagents

Water used in dilutions was triply distilled to remove trace metals.

Eriochrome Blue Black R, EBBR (also known as Mordant Black 17, Calcon or Solochrome Dark Blue), C.I. 15705, was supplied by G. Fredrick Smith Chemical Co. and used directly without further purification.

Stock solutions of the EBBR reagent were prepared daily by dissolving 20 mg dye in dilute aqueous ammonia (50 μL aqueous NH_3 (28%) in 50 mL H_2O) and then acidifying with 0.5 mL of acetic acid to inhibit decomposition (19). Acetic acid was used since it was found that hydrochloric acid precipitated the EBBR. The final dye solution was then filtered through Whatman #30 filter paper.

The concentration of the dye solution was determined by completely dissolving an appropriate weighed amount of dye in ethanol to make a standard solution. A spectrophotometric calibration curve at 510 nm was prepared by dilution of the standard solution with ethanol and water, keeping the ethanol concentration constant in the final solutions. The stock dye solution was diluted with ethanolic solution so that its absorbance was within the calibration range. The ethanol/water concentration was kept the same as in the standards. It was found that approximately half of the dye had dissolved in the stock solution to give a EBBR concentration of 6.0×10^{-4} *M*. Using this value a Job Plot was constructed; this indicated a Mo:EBBR combining ratio of 1:1 in accordance with what has been previously reported (19).

A 1000 μg/mL Mo standard was prepared from $(NH_4)_6Mo_7O_{24}\cdot H_2O$ (BDH, reagent grade) after drying at 100°C. A working solution of 10.0 μg/mL Mo was prepared by dilution with distilled water.

A concentrated aqueous buffer system was prepared from high purity aqueous ammonia and acetic acid. The acetic acid was purified by sub-boiling distillation from a quartz still using reagent grade acid as a feed stock. Aqueous ammonia (28%) was prepared by isopiestic distillation in a closed system. Appropriate amounts of acetic acid and ammonia were then mixed to give a 4.5 *M* $CH_3COO^-NH_4^+$ aqueous buffer.

A National Research Council of Canada (NRCC) open ocean seawater sample, NASS-1 (20), was used as a reference material. The sample had not been filtered and had a salinity of 35.07‰. A NRCC coastal seawater reference material, CASS-1, was also analysed. This sample, which has a salinity of 31.8‰, was filtered through a 0.45 μm membrane filter. Both seawater reference materials had been acidified to pH 1.6 with high purity NHO_3, immediately after collection and were stored in precleaned polyethylene bottles.

Procedure

All voltammetric operations involving cell and solution manipulations were performed in a laminar flow clean hood to minimize contamination.

For analysis, a 10.0 ± 0.1 mL sample of seawater (pH 1.6) was deaerated for 8 min using purified N_2 gas. Using a micropipet 100 μL of the aqueous 6.0×10^{-4} *M* EBBR solution was then added to the cell. The solution was allowed to equilibrate, with stirring, for 1 min before a fresh mercury drop (size "M") was dispensed and the potential applied to initiate adsorptive accumulation. The accumulation period (τ) was restricted to 30 s at a potential of −0.050 V with stirring, after which a further 10 s equilibration without stirring was allowed. The voltammogram was then recorded at a scan rate of 50 mV/s from −0.050 V to −0.550 V with no filtering of the signal. A single peak corresponding to reduction of the adsorbed Mo complex occurred at −0.170 V. Calibration was achieved by the method of standard additions using peak height measurements to quantify the analytical signal. A fresh mercury drop was dispensed for each calibration measurement.

Blanks analysed in triply distilled water were below the limit of detection in this method.

Results and discussion

Free EBBR may be adsorbed onto a Hg electrode under conditions of applied potential (Fig. 1). After adsorptive accumulation, scanning the potential in the negative direction

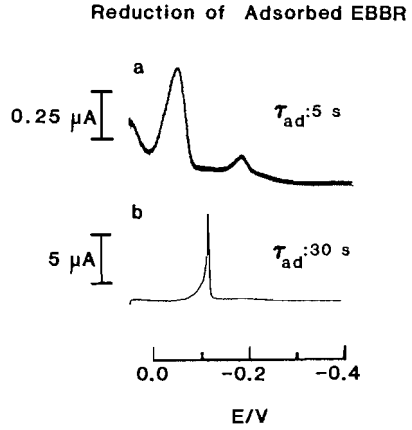

FIG. 1. Reduction peaks for EBBR in seawater at pH 1.6, [EBBR] = 6.0×10^{-6} *M*, ν 50 mV/s, E_{ad} +0.02 V. (*a*) τ_{ad} 5 s, (*b*) τ_{ad} 30 s.

results in a peak due to reduction of the adsorbed dye. A seawater sample with 6.0×10^{-6} *M* EBBR gave a reduction peak at −0.070 V after a few seconds of accumulation. Corresponding direct polarographic analysis of the same solution resulted in a wave with $E_{1/2}$ = −0.100 V for the EBBR.

The mechanism of reduction for the *o,o'*-dihydroxyazo dyes on a mercury electrode has been extensively studied by Florence and co-workers (21–23). Although this work pertains to solochrome violet RS and other aromatic azo compounds, it can be assumed that the same 4-electron reduction mechanism occurs for EBBR.

Figure 1 shows the reduction peak for the free dye after adsorption at a potential of +0.050. For Fig. 1*a*, the adsorption time was 5 s and a relatively broad, rounded peak occurred. Over a range of accumulation times from 0 to 20 s, the height of this peak varied directly with τ. However, for values of τ longer than 20 s, the character of the peak changed significantly to give a sharp spike with maximum peak current which was independent of the deposition time.

Laviron (24) observed similar behavior with the reduction of adsorbed *trans*-4',4"-pyridyl-1,2-ethylene. The phenomenon of narrow peaks was explained as the result of formation of a compact layer on the mercury surface, with attractive forces between the closely packed molecules. Due to the high density and strong intermolecular forces, reduction is difficult and occurs at more negative potentials. Once a fraction of the molecules are reduced, the intermolecular forces weaken, the reaction rate increases, and the rest of the molecules are reduced almost simultaneously, resulting in a large, narrow peak.

In the case of long adsorption times or large bulk concentrations (C_0*), the amount of adsorbed material is above the critical value required to form a compact layer. At low adsorption times a compact layer does not form; instead, the adsorbed material is spread out over the electrode surface with minimal interaction between molecules. The adsorbed species is then reduced over a broader potential range.

A current peak due to reduction of the Mo—EBBR complex was found after adsorptive accumulation. This reduction peak occurred at a potential approximately 0.07 V more negative than that for the adsorbed free dye and may be seen as a very small peak at about −0.17 V on Fig. 1*a*. To observe the voltammetry of the Mo complex without interference from the uncomplexed EBBR, an accumulation potential of −0.05 V was chosen. Under these conditions, reduction of the free dye was not observed on the voltammogram (Fig. 2).

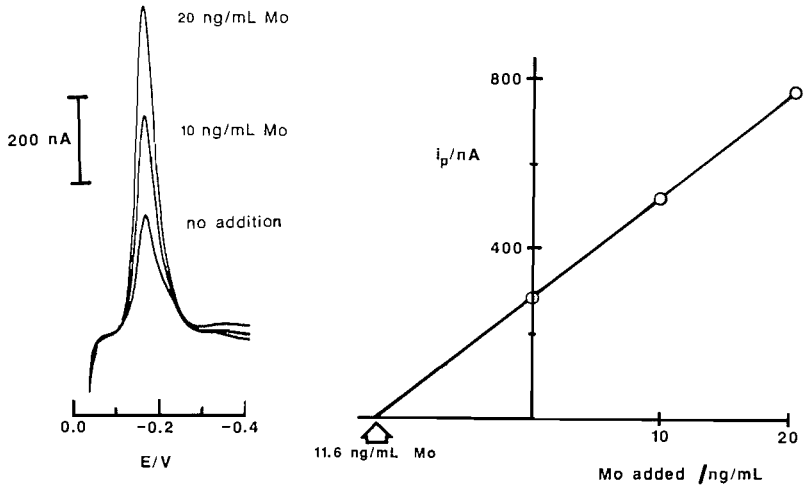

FIG. 2. Voltammograms and standard addition calibration for Mo in NASS-1, [EBBR] = 6.0×10^{-6} *M*, ν 50 mV/s, E_{ad} −0.05 V.

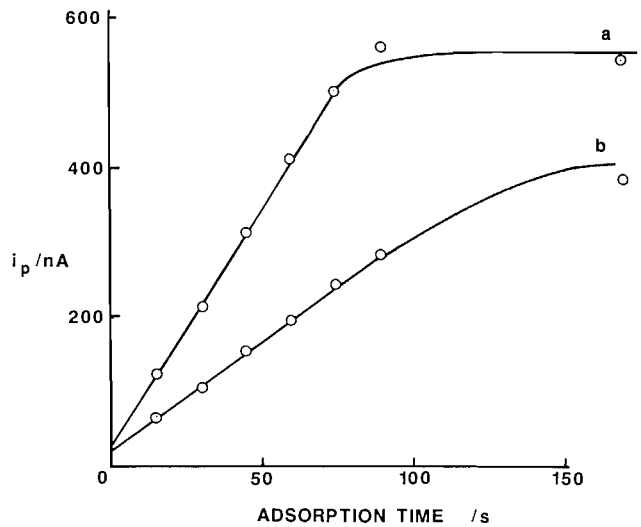

FIG. 3. Effect of adsorption time on peak height: seawater pH 1.6, [EBBR] = 6.0×10^{-6} *M*, E_{ad} −0.050 V, ν 50 mV/s. (*a*) 13 ng/mL Mo, (*b*) no Mo added.

Effect of pH

The peak potential for both the adsorbed dye and the Mo-complex became more negative with increasing pH. The reduction peak for the uncomplexed dye occurred over the pH range 1 to 6 without any decrease in height. However, the current peak for the reduction of the Mo complex decreased sharply at pH values greater than 3.

It is known that EBBR is insoluble in the presence of chloride at low pH (19), therefore, to avoid potential problems, a sample pH of 2.8 was initially chosen. However, no precipitation was observed in seawater at pH 1.6 unless the sample was allowed to stand overnight. Subsequent analyses were therefore performed at pH 1.6. This was convenient since the seawater had previously been acidified to this pH, and thus no addition of buffer was required prior to analysis.

Peak height vs. adsorption time

Figure 3 shows the effect of adsorption time on the measured peak current for Mo in seawater for a spiked (13 ng/mL) and an unspiked sample. The spiked sample reached a limiting current plateau at accumulation periods longer than 90 s. The current plateau for the peak may occur when there is complete surface coverage of the mercury drop with adsorbed species. As complete coverage of the electrode surface is to be avoided when performing standard addition calibrations, adsorption times were kept short (30–60 s).

Peak height vs. EBBR concentration

A seawater sample with 50 ng/mL Mo achieved a limiting current of 280 nA with a minimum of 6.0×10^{-6} *M* dye after 30 s accumulation time. A seawater sample with no Mo spike reached a limiting 40 nA with a minimum of 1.8×10^{-6} *M* EBBR after the same accumulation time.

The limiting current is reached when the EBBR is present in sufficient excess to quantitatively convert Mo in the sample to the dye complex. For analysis, a EBBR concentration of 6.0×10^{-6} M was used. This was sufficient to achieve the limiting maximum peak current for spikes with up to 50 ng/mL Mo(VI). Samples would normally not be expected to exceed this concentration value.

Peak height vs. scan rate

A linear relationship between peak current for the adsorbed Mo—EBBR complex and scan rate was obtained between 5 and 200 mV/s, when the other parameters were kept constant. This correlation agrees with theoretical predictions for redox reactions of an adsorbed species (24).

As scan rate increased, it became increasingly difficult to draw a baseline for measuring peak height. A scan rate of 50 mV/s was chosen as a compromise to give adequate response and precision.

Peak height vs. Mo concentration

Using the conditions described in the experimental section above, a linear relationship between peak height and concentration of added Mo was found (Fig. 2). The linear dynamic range was from 0 to 5×10^{-7} mol L^{-1} Mo and the sensitivity over this range was 15×10^{-3} A M^{-1} s^{-1}. When oxine was used as a complexing agent for adsorptive accumulation voltammetry of Mo (11), non-linear calibration curves were obtained if the solution was stirred during the accumulation step. An unstirred solution gave linear response curves up to 3×10^{-7} mol L^{-1} but the sensitivity was only 1.1×10^{-3} A M^{-1} s^{-1} under these analytical conditions.

Interferences

A number of metals gave reduction peaks at potentials near

Can. J. Chem. Downloaded from www.nrcresearchpress.com by 78.46.186.204 on 09/07/12
For personal use only.

TABLE 1. Metal-EBBR reduction peaks at pH 2.8*

Element	Sensitivity, A/M	E_p (V)	Concentration in seawater† (ng/mL)
Mo(VI)	65×10^{-3}	−0.28	9.6–12.
Ga(III)	4.0×10^{-3}	−0.35	0.2
Zr(IV)	3.7×10^{-3}	−0.44	0.01–0.03
Ti(IV)	2.0×10^{-3}	−0.38	1.0
V(V)	10×10^{-3}	−0.38	0.5–3.2

*Seawater: pH 2.8, τ_{ad} 30 s, E_{ad} −0.140, ν 50 mV/s, [EBBR] = 6.0×10^{-6} *M*.
†Reference 25.

those of Mo when analysis was done at pH 2.8 (other conditions as in Table 1). Some of these metal complexes formed only slowly at room temperature and therefore, in each case, solutions were heated to 60°C and then cooled prior to analysis. When the pH was reduced to 1.6, all of the peaks except that due to Mo disappeared. The ions Co(II), Cu(II), Cr(III), Cr(IV), Al(III), Sn(IV), Ni(II), Fe(III), Zn(II), Pb(II), Te(IV), In(III), W(VI), and U(VI) were tested at both pH values and gave no response, nor did they interfere with the Mo peak itself.

Limit of detection

The limit of detection, calculated as the concentration corresponding to three times the standard deviation of the *y*-intercept from the standard addition calibration curve, was determined to be 0.5 ng mL^{-1}. This could be reduced further by utilizing longer adsorption times, but since seawater Mo concentrations are typically near 10 ng mL^{-1}, there was no need to seek lower values. The detection limit in the oxine method was 0.3 ppb after a 1 min accumulation period.

Analysis of standard seawater samples

The Mo value in NASS-1, a reference seawater (20), has been determined by two independent analytical techniques — isotope dilution spark source mass spectrometry and graphite furnace atomic absorption spectroscopy (GFAAS). For NASS-1, the mean of six determinations by the present method was 11.6 ng/mL, std. dev. 1.2 ng/mL, which compares favorably with the reference value of 11.5 ± 1.9 ng/mL. For CASS-1, the mean of six values was 9.1 ng/mL, std. dev. 0.6 ng/mL, which again compares favorably with the reference value of 9.6 ± 0.5 ng/mL determined by GFAAS.

1. J. WANG and J. S. MAHMOUD. J. Electroanal. Chem. **208**, 383 (1986).
2. J. WANG, P. A. M. FARIAS, and J. S. MAHMOUD. Anal. Chim. Acta, **172**, 57 (1985).
3. J. WANG and J. S. MAHMOUD. Anal. Chim. Acta, **182**, 147 (1986).
4. J. WANG, P. A. M. FARIAS, and J. S. MAHMOUD. Anal. Chim. Acta, **171**, 215 (1985).
5. B. PIHLAR, P. VALENTA, and H. W. NÜRNBERG. Fres. Z. Anal. Chem. **307**, 337 (1981).
6. J. GOLIMOWSKI, P. VALENTA, and H. W. NÜRNBERG. Fres. Z. Anal. Chem. **322**, 315 (1985).
7. C. M. G. VAN DEN BERG and Z. Q. HUANG. J. Electroanal. Chem. **177**, 269 (1984).
8. C. M. G. VAN DEN BERG and Z. Q. HUANG. Anal. Chem. **56**, 2383 (1984).
9. C. M. G. VAN DEN BERG. Anal. Chim. Acta, **164**, 195 (1984).
10. C. M. G. VAN DEN BERG and Z. Q. HUANG. Anal. Chim. Acta, **164**, 209 (1984).
11. C. M. G. VAN DEN BERG. Anal. Chem. **57**, 1532 (1984).
12. G. P. HILDERBRAND and C. N. REILLEY. Anal. Chem. **29**, 258 (1957).
13. G. W. LATIMER. Talanta, **15**, 1 (1968).
14. S. N. WILLIE. M.Sc. Thesis, Queen's University, Kingston, Ont., Canada, 1983.
15. Y. S. KIM and H. ZEITLIN. Anal. Chim. Acta, **46**, 1 (1969).
16. A. KULATHILAKE and A. CHATT. Anal. Chem. **52**, 828 (1980).
17. M. TERNERO and I. GRACIA. Analyst, **108**, 310 (1983).
18. C. W. MCLEOD, A. OTSUKI, K. OKAMOTO, H. HARAGUCHI, and K. FUWA. Analyst, **106**, 419 (1981).
19. G. L. SILVER and R. C. BOWMAN. Talanta, **14**, 893 (1967).
20. S. S. BERMAN, R. E. STURGEON, J. A. H. DESAULNIERS, and A. P. MYKYTIUK. Marine Poll. Bull. **14**, 69 (1983).
21. T. M. FLORENCE. J. Electroanal. Chem. **52**, 115 (1974).
22. T. M. FLORENCE and G. H. AYLWARD. Aust. J. Chem. **15**, 65 (1962); **15**, 416 (1962).
23. T. M. FLORENCE and W. L. BELEW. J. Electroanal. Chem. **21**, 157 (1969).
24. E. LAVIRON. J. Electroanal. Chem. **52**, 355 (1974).
25. J. P. RILEY. *In* Chemical oceanography. Vol. 3. 2nd ed. *Edited by* J. P. Riley and G. Skirrow. Academic London. 1975. Chap. 19.

Can. J. Chem. Downloaded from www.nrcresearchpress.com by 78.46.186.204 on 09/07/12
For personal use only.

Determination of total tin in National Research Council of Canada marine reference materials[1]

R. E. STURGEON,[2] J. W. MCLAREN, S. N. WILLIE, D. BEAUCHEMIN, AND S. S. BERMAN
Division of Chemistry, National Research Council of Canada, Ottawa, Ont., Canada K1A 0R9

Received November 3, 1986

This paper is dedicated to Professor Douglas E. Ryan on the occasion of his 65th birthday

R. E. STURGEON, J. W. MCLAREN, S. N. WILLIE, D. BEAUCHEMIN, and S. S. BERMAN. Can. J. Chem. **65**, 961 (1987).

An intralaboratory determination of total Sn in three National Research Council of Canada reference materials, i.e., estuarine sediments BCSS-1 and MESS-1 and lobster hepatopancreas TORT-1 was undertaken. Samples were solubilized by acid mineralization and analyzed by stable isotope dilution inductively coupled plasma mass spectrometry, direct solution injection graphite furnace atomic absorption spectrometry (GFAAS), and hydride generation-GFAAS. The materials were homogeneous at the 500 mg subsample size. Good agreement was obtained amongst the results from the three instrumental methods of analysis. Certified values of total Sn in these materials are 1.85 ± 0.20 μg/g in BCSS-1, 3.98 ± 0.44 μg/g in MESS-1, and 139 ± 11 ng/g in TORT-1. The above uncertainties represent 95% tolerance limits for an individual (500 mg) subsample.

R. E. STURGEON, J. W. MCLAREN, S. N. WILLIE, D. BEAUCHEMIN et S. S. BERMAN. Can. J. Chem. **65**, 961 (1987).

Une détermination intralaboratoire du Sn total dans trois matériaux de référence du Conseil National de Recherches du Canada, soit les sédiments BCSS-1 et MESS-1 provenant d'estuaires, et l'hépatopancréas de homard TORT-1, fut entreprise. Des échantillons furent mis en solution par minéralisation acide et ensuite analysés par spectrométrie de masse à plasma à couplage inductif, au moyen de la dilution isotopique; par spectrométrie d'absorption atomique à four de graphite (SAAFG), avec injection directe des solutions; et par génération d'hydrure/SAAFG. Les matériaux sont homogènes au niveau de sous-échantillons de 500 mg. Un bon accord fut obtenu entre les résultats des trois méthodes instrumentales d'analyse. Les valeurs certifiées pour le Sn total dans ces matériaux sont 1,85 ± 0,20 μg/g dans BCSS-1; 3,98 ± 0,44 μg/g dans MESS-1; et 139 ± 11 ng/g dans TORT-1. Les incertitudes ci-dessus représentent des limites de tolérance de 95% pour un sous-échantillon individuel (500 mg).

Can. J. Chem. Downloaded from www.nrcresearchpress.com by 78.46.186.204 on 09/07/12
For personal use only.

Concentrations of total tin in many environmental samples vary from 100 μg/g (sediments) through low ng/g (biota) to the pg/g (aquatic) range (1). Growing concern over the accumulation of (toxic) anthropogenic alkyltin compounds and their degradation products in the environment (2, 3) has fostered development of sensitive analytical approaches for the determination of this element (1). Meaningful results (e.g. refs. 4–7) have been obtained only recently, however, due to the attention devoted to control of sample contamination.

Although the average crustal abundance of tin is only 3 μg/g (1), it is one of the most highly enriched metals in atmospheric particulate matter (7, 8). Additionally, tin is a ubiquitous contaminant in laboratory sampling vessels (including quartz and many plastics) and stringent control of airborne and reagent contamination as well as vessel surface cleanliness is imperative if accurate analyses are to be achieved.

Considering the difficulties associated with the accurate determination of tin at trace levels (1), and the paucity of international interest in this element in the past, it is not surprising that there are no biological or environmental materials presently available which are certified for their tin content (9). Systematic use of (certified) reference materials is the best way to evaluate measurement accuracy in such circumstances and a close correspondence between these materials and the test samples is desirable if valid inferences are to be made from comparative measurements.

This report summarizes work undertaken in our laboratory to determine the concentration of total Sn in three marine reference materials currently available from the National Research Council of Canada (NRCC), i.e., estuarine sediments BCSS-1 and MESS-1 and lobster hepatopancreas, TORT-1.

Use of several different analytical methods for this determination, wherein none of the methods would be expected to suffer identical interferences, should serve to minimize measurement error and provide a reliable estimate of the true value of the analyte concentration in the sample.

Experimental

Instrumentation

Determinations of total tin were made by graphite furnace atomic absorption and inductively coupled plasma mass spectrometry.

A Perkin-Elmer Model 5000 atomic absorption spectrometer was fitted with an HGA-500 graphite furnace and Zeeman effect background correction. Sample solutions were delivered to the furnace with a Perkin-Elmer AS-40 autosampler. Solid pyrolytic graphite (L'vov) platforms were used in conjunction with pyrolytic graphite coated grooved tubes. A Perkin-Elmer hollow cathode lamp served as the line source.

In addition to quantitation by direct injection of dissolved samples into the furnace, the volatile hydride of Sn was generated and trapped on a preheated graphite tube from which it was subsequently atomized. A conventional hydride generation cell was used and a quartz tube, leading from the outlet of the cell, served to transfer the hydride into the graphite tube (10).

A SCIEX ELAN 250 inductively coupled plasma mass spectrometer (Perkin-Elmer SCIEX Ltd., Thornhill, Ont.) was used for isotope ratio measurements in the analysis of dissolved samples using a stable isotope dilution technique. The only modifications to the instrument were the addition of a mass flow controller (Model 5850, Brooks Instrument Division, Emerson Electric, Hatfield, PA) to the nebulizer gas line and a Minipuls II peristaltic pump (Gilson, Middletown, WI) to the sample delivery tube.

Reagents

A 1000 mg/L stock solution of Sn, prepared by dissolution of high purity tin shot (Spex Industries, Metuchen, NY) in sub-boiling distilled nitric acid, served as the primary working standard.

Isotopically enriched (89.2%) ^{117}Sn was purchased from Oak Ridge

[1]NRC No. 27144.

[2]To whom all correspondence should be addressed.

Can. J. Chem. Downloaded from www.nrcresearchpress.com by 78.46.186.204 on 09/07/12
For personal use only.

National Laboratory in the form of SnO_2. A solution was prepared by fusion of 25 mg SnO_2 with 500 mg lithium tetraborate and 100 mg lithium carbonate in a platinum crucible placed in a muffle furnace at 900°C for 2 h. Overnight dissolution of the melt was effected in dilute nitric acid. The isotope abundances in this solution were checked against the values provided by Oak Ridge to assure that there was no significant contamination by the flux. The concentration of the ^{117}Sn solution was subsequently verified by a reverse spike isotope dilution analysis.

High purity mineral acids were prepared by sub-boiling distillation in quartz (HCl, HNO_3, $HClO_4$) and polypropylene stills (HF).

A 1% m/v sodium tetraborate(III) solution was prepared daily by dissolution of 0.25 g pellets of $NaBH_4$ (Alpha Inorganics) in deionized distilled water (DDW).

A 2000 mg/L solution of Pd (in HCl) was used as a matrix modifier for direct AAS determination of Sn, as suggested by Voth-Beach and Shrader (11).

Sample preparation

All sample preparations were conducted in a clean laboratory equipped with laminar-flow benches and fume cupboards providing a class 100 working environment.

Complete dissolution of the estuarine sediments can be obtained using closed vessel techniques without the danger of loss of any volatile analyte species. However, because of their limited sample capacity for organic materials, the Lorran vessels could not be used for the digestion of TORT-1. Dry ashing of this material is unsuitable due to potential losses of volatile organotin compounds as well as formation of insoluble SnO_2 in the sample residues. Wet ashing with mixed acids in clean quartzware was found to be unsatisfactory because of the resultant high blanks (up to 75 ng).

Sediment samples (BCSS-1 and MESS-1) were solubilized in LORRAN Teflon pressure decomposition vessels (H.K. Morrison and Sons Ltd., Mount Uniacke, N.S.). Nominal 0.5 g samples were mixed with 3 mL HNO_3, 3 mL HF, and 2 mL $HClO_4$ and the vessels submerged for 3 h in a water bath at 100°C. After cooling, the contents were quantitatively transferred to 50 mL Teflon PFA beakers and evaporated directly on a hot plate (with an ir lamp as an additional heat source) to incipient dryness. A further 1 mL HF and 1 mL $HClO_4$ were added and the samples again taken to near dryness. A final addition of 1 mL HCl and 1 mL HNO_3 followed by gentle warming and dilution to 50.0 mL with DDW resulted in complete solubilization of the sample. An initial white-colored sediment (presumably slightly soluble perchlorate salts) completely dissolved after the samples were permitted to stand for 12 h.

Duplicate samples were taken from each of four bottles of both sediments. Two blanks were run concurrently with each set of four sample decompositions.

The biological reference material TORT-1 was solubilized by addition of 20 mL HNO_3 to nominal 0.5 g samples in PFA beakers. The vessels were covered with Teflon watch covers and heated on a hot plate under reflux conditions for at least 4 h. The covers were then removed, 1 mL HF and 1 mL $HClO_4$ added to each, and the samples evaporated to near dryness. A further 5 mL HNO_3 and 1 mL $HClO_4$ were then added and the solutions again taken to near dryness. The surface temperature of the hot plate is approximately 190°C during these steps. Following a final 1 mL addition of $HClO_4$ with heating to near dryness, the residues were dissolved in 1 mL HCl and diluted to 25.0 mL with DDW.

Duplicate samples were taken from each of four different bottles of TORT-1. Two blanks were run concurrently with each set of four sample decompositions.

Isotopically spiked solutions of MESS-1, BCSS-1, and TORT-1 were prepared by adding an appropriate aliquot of the ^{117}Sn solution to the sample at the beginning of the acid digestion procedure. The mass of the ^{117}Sn spike was adjusted to make the $^{118}Sn/^{117}Sn$ ratio close to unity. Blank solutions were spiked with one-tenth the amount of ^{117}Sn added to the samples. Sets of four samples (along with two blanks) of each reference material were analyzed by the isotope dilution technique.

Procedure

The GFAAS furnace program and instrument conditions for direct injection analysis were as recommended by Slavin *et al.* (12) with the exception that 20 μg Pd was used as the matrix modifier (11). Calibration was by the method of additions using two incremental spikes of natural tin standard.

Volatile SnH_4 was produced by the addition of 2 mL 1% $NaBH_4$ to the hydride generation cell containing 20 mL 0.1 *M* HCl and 20 μL dissolved BCSS-1 or MESS-1 solution or 200 μL dissolved TORT-1 solution. The hydride was deposited at 800°C onto the tube wall of the graphite furnace and subsequently atomized at 2700°C. A detailed description of this technique has been presented by Sturgeon *et al.* (10, 13). Calibration was achieved against the response from simple aqueous standards treated in an identical manner.

The ELAN 250 ICP-MS was operated with a standard ICP-AES torch, with plasma, auxiliary and nebulizer gas flow rates of 14, 2.0, and 0.9 L min^{-1}, respectively. The torch box was positioned as close as possible to the sampler (i.e., 17 mm from sampler tip to top of RF load coil). The mass spectrometer was operated with low resolution and each ratio determination involved a total of 150 measurements of 0.1 s duration at m/z 118 and m/z 117. Fifty measurements were made at the assumed peak centers, while a further 100 were made at ±0.1 u. The use of the stable isotope dilution technique in ICP-MS has previously been described in applications to coastal seawater (14), river water (15), and marine sediment reference materials (16).

Prior to performing the isotope dilution analyses, $^{117}Sn/^{118}Sn$ isotope ratios were measured for a 100 μg/L natural abundance tin solution to check for mass discrimination and for several unspiked solutions of each of the samples to check for possible isobaric interferences from molecular species. The following values were obtained: 100 μg/L Sn standard, 0.317 ± 0.002; TORT-1 solution, 0.319 ± 0.005; MESS-1 solution, 0.314 ± 0.003. None of these differ significantly from the accepted value based on natural abundances (0.3171) not only confirming that mass discrimination is negligibly small, but also suggesting that there are no significant isobaric interferences on either of the Sn isotopes.

All sample weights were corrected for moisture content and results reported on a dry weight basis. A sample of TORT-1 reference material (not subsequently used for analysis due to possible contamination) was dried to constant weight by placing it in a vacuum oven at room temperature for 24 h. Similarly, samples of BCSS-1 and MESS-1 were dried to constant weight by heating overnight at 105°C.

Results and discussion

Maher (17) as well as Burns *et al.* (18) have reported that organotin compounds in biological materials and aqueous solutions can be quantitatively converted to Sn(IV) by acid digestion and that concentrated HNO_3 does not produce insoluble SnO_2 (17). The efficiency of recovery of total Sn from TORT-1 samples was verified by undertaking a $HNO_3/HClO_4$ digestion of 250 mg subsamples in closed 120 mL Savillex Teflon PFA vessels. Decomposition was effected by heating for 30 min at 60–70 psig (internal pressure in the vessel) using a MDS-81D microwave digestion system (CEM Corp. Indian Trail, NC). Analyses by ICP-MS using the isotope dilution technique (ID ICP-MS) produced results which were not significantly different from those obtained on samples digested in open PFA beakers.

Analytical blanks and methodological detection limits

Procedural blanks for ID ICP-MS were equivalent to 180 ± 30 ng/g for the sediments and 12 ± 4 ng/g for TORT-1. These blanks reflect the cumulative contamination from all

Can. J. Chem. Downloaded from www.nrcresearchpress.com by 78.46.186.204 on 09/07/12
For personal use only.

sources, including reagents, contact with vessels, and sample handling with the major amount arising from the nitric acid. No measurable blanks were obtained by direct GFAAS since the Sn concentrations in these solutions were below the detection limit for this technique. For hydride generation GFAAS, the primary source of the blank was the generation cell. No effort was made to clean up the $NaBH_4$ reagent. In this case the "cell blank" was determined to be 0.110 ± 0.024 ng, irrespective of the addition of 20 μL aliquots of sediment blank solution or 200 μL aliquots of TORT-1 blank solution.

Corresponding methodological detection limits (concentration corresponding to 3 × standard deviation of the blank) for Sn in sediments as determined by hydride generation GFAAS and ID ICP-MS are 0.36 μg/g (based on a 20 μL sample aliquot) and 0.09 μg/g, respectively. The detection limit for direct GFAAS, 0.9 μg/g, was estimated from the precision of determination of Sn in BCSS-1. Methodological detection limits for the determination of Sn in biological tissue (i.e., TORT-1) are 0.018 μg/g for hydride generation GFAAS (based on a 200 μL sample aliquot) and 0.012 μg/g for ID ICP-MS. Concentrations of Sn in dissolved TORT-1 were too low to permit accurate quantitation by direct GFAAS.

Detection limits may be further improved by decreasing the magnitude and variability of the procedural blank. Improvements in instrumental sensitivity by factors of 2 may be possible but will not significantly change the performance of the system. Complete sample decompositions in the Teflon pressure vessels in combination with microwave heating may serve to decrease dissolution blanks. Hydride generation GFAAS detection limits may be improved by cleaning up the $NaBH_4$ reagent through coprecipitation of Sn with added lanthanum or sodium hydroxide (e.g. ref. 19).

Analytical results

Results for the determination of Sn in BCSS-1, MESS-1, and TORT-1 are presented in Table 1 and are reported on a dry weight basis.

Of the eight test portions of MESS-1 and BCSS-1 taken for analysis by ID ICP-MS, one result was statistically rejected from each data set (by application of a simple *t*-test).

Of the eight test portions of MESS-1 and BCSS-1 taken for analysis by direct GFAAS and by HG-GFAAS, one was physically lost during preparation and one direct GFAAS result was statistically rejected.

No ID ICP-MS results for TORT-1 were rejected (only six test portions were initially taken for analysis). Of the eight test portions of this material taken for analyses by HG-GFAAS, one sample was physically lost during mineralization and one analytical result was statistically rejected. In general, good agreement is evident amongst the various techniques. The mean of results reported for the direct solution analysis of BCSS-1 by GFAAS is biased low. The reason for this is not clear, considering the acceptable results obtained on these same solutions by hydride generation GFAAS and the good performance of direct solution analysis of MESS-1 by GFAAS. The lower concentration of Sn in the solutions of BCSS-1 was not favorable in that the determination was being attempted at only 2-fold above the estimated detection limit for this technique. It is clear that hydride generation-GFAAS is the preferred optical spectroscopic method in this case (as well as for determinations in TORT-1 solutions).

Results from different bottles showed no significant differences compared to results from subsamples within bottles. The subsampling uncertainty (on 500 mg test portions) is thus equal to or less than the measurement uncertainty. Thus, heterogeneity of the materials does not contribute significantly to the overall analytical uncertainty when 500 mg test portions are used. It is probable that smaller subsamples may be utilized without the subsampling error exceeding the specified tolerance limits (20, 21).

TABLE 1. Analytical results for total tin, μg/g[a]

Technique	Sample		
	MESS-1	BCSS-1	TORT-1
GFAAS	3.9 ± 0.3 (8)	1.5 ± 0.3 (6)	ND[b]
HG-GFAAS	4.0 ± 0.2 (8)	1.9 ± 0.2 (7)	0.144 ± 0.016 (6)
ID ICP-MS	3.9 ± 0.2 (7)	1.78 ± 0.06 (7)	0.141 ± 0.006 (6)
Certified values[c]	3.98 ± 0.44	1.85 ± 0.20	0.139 ± 0.011

[a]Mean and standard deviation of (*n*) replicate determinations.
[b]Not determined.
[c]95% tolerance limit for an individual subsample.

Conclusions

With the exception of direct GFAAS results for BCSS-1, comparable data for total Sn concentrations were obtained by all three instrumental analytical techniques. Good agreement with certified values, i.e., 1.85 ± 0.20 μg/g in BCSS-1; 3.98 ± 0.44 μg/g in MESS-1, and 139 ± 11 ng/g in TORT-1 in the three reference materials was also demonstrated. The above uncertainties represent 95% tolerance limits for an individual subsample. That is, 95% of samples, 500 mg or greater, from any bottle would be expected to have concentrations within the specified range 95% of the time. It should be noted that certified values are based on the data presented here as well as on additional data not cited in this study.

Release of certified values for total Sn in these reference materials is significant in that they represent the first available environmental samples for which certified concentrations of this element (9) are given.

1. G. WEBER. Fres. Z. Anal. Chem. **321**, 217 (1985).
2. L. FRIDBERG. Mar. Pollut. Bull. **16**, 381 (1985).
3. A. R. D. STEBBING. Mar. Pollut. Bull. **16**, 383 (1985).
4. E. J. PARKS, W. R. BLAIR, and F. E. BRINCKMAN. Talanta, **32**, 633 (1985).
5. V. F. HODGE, S. L. SEIDEL, and E. D. GOLDBERG. Anal. Chem. **51**, 1256 (1979).
6. R. S. BRAMAN and M. A. TOMPKINS. **51**, 12 (1979).
7. J. T. BYRD and M. O. ANDREAE. Science, **218**, 565 (1982).
8. K. H. WEDEPOHL. Handbook of geochemistry. Springer Verlag, Berlin. 1969.
9. Y. MURAMATSU and R. M. PARR. Survey of currently available reference materials for use in connection with the determination of trace elements in biological and environmental materials. IAEA/RL/128, Vienna. 1985.
10. R. E. STURGEON, S. N. WILLIE, and S. S. BERMAN. Fres. Z. Anal. Chem. **323**, 788 (1986).
11. L. M. VOTH-BEACH and D. E. SHRADER. Spectroscopy, **1**, 49 (1986).
12. W. SLAVIN, D. C. MANNING, and G. R. CARNRICK. At. Spectrosc. **2**, 137 (1981).
13. R. E. STURGEON, S. N. WILLIE, and S. S. BERMAN. Anal. Chem. To be published.

14. J. W. McLAREN, A. P. MYKYTIUK, S. N. WILLIE, and S. S. BERMAN. Anal. Chem. **57**, 2907 (1985).
15. D. BEAUCHEMIN, J. W. McLAREN, A. P. MYKYTIUK, and S. S. BERMAN. Anal. Chem. In press.
16. J. W. McLAREN, D. BEAUCHEMIN, and S. S. BERMAN. Anal. Chem. In press.
17. W. MAHER. Anal. Chim. Acta, **138**, 365 (1982).
18. D. T. BURNS, F. GLOCKLING, and M. HARRIOTT. Analyst (London), **106**, 921 (1981).
19. M. O. ANDREAE and J. T. BYRD. Anal. Chim. Acta, **156**, 147 (1984).
20. B. KRATOCHVIL, R. S. THAPA, and N. MOTKOSKY. Can. J. Chem. **63**, 2679 (1985).
21. B. KRATOCHVIL, M. J. M. DUKE, and D. NG. Anal. Chem. **58**, 102 (1986).

Can. J. Chem. Downloaded from www.nrcresearchpress.com by 78.46.186.204 on 09/07/12
For personal use only.

Time-resolved quenched phosphorescence detection of chromate in water samples using paired-ion reversed phase high performance liquid chromatography

ROBERT A. BAUMANN, MARRY SCHREURS, CEES GOOIJER,[1] NEL H. VELTHORST, AND ROLAND W. FREI
Department of General and Analytical Chemistry, Free University, De Boelelaan 1083, 1081 HV Amsterdam, The Netherlands

Received September 17, 1986

This paper is dedicated to Professor Douglas E. Ryan on the occasion of his 65th birthday

ROBERT A. BAUMANN, MARRY SCHREURS, CEES GOOIJER, NEL H. VELTHORST, and ROLAND W. FREI. Can. J. Chem. **65**, 965 (1987).

The feasibility of time-resolved quenched phosphorescence as a detection method for chromate based on paired-ion reversed phase high performance liquid chromatography is shown. After separation detection is achieved by monitoring the time-resolved phosphorescence signal of biacetyl at 515 nm. Optimization of the time-resolution parameters of the luminescence detector results in a limit of detection of 1.4×10^{-7} *M* (2 ng on column) for chromate standard solutions. The linearity of the method is three orders of magnitude. Chromatograms of tapwater and surface water samples spiked with chromate show the potential applicability of the method for real samples.

ROBERT A. BAUMANN, MARRY SCHREURS, CEES GOOIJER, NEL H. VELTHORST et ROLAND W. FREI. Can. J. Chem. **65**, 965 (1987).

On démontre la possibilité d'utiliser la phosphorescence piégée et résolue en fonction du temps comme méthode de détection du chromate; la méthode est bassé sur la chromatographie liquide à haute performance en phase inversée sur des ions pairés. Après la séparation, la détection se fait en observant, à 515 nm, le signal de la phosphorescence, résolue en fonction du temps, du biacétyl. Une optimisation des paramètres de la résolution en fonction du temps permet d'atteindre une limite de détection de $1{,}4 \times 10^{-7}$ *M* (2 ng sur la colonne) de solutions standard de chromate. La linéarité de la méthode s'étend sur trois ordres de grandeur. Les chromatogrammes d'échantillons d'eaux d'aqueduc ou de surface dans lesquels on a ajouté du chromate permettent de démontrer le potentiel d'application de la méthode à des échantillons réels.

[Traduit par la revue]

Introduction

The speciation of metal ions with respect to their toxic properties is of great importance in clinical, toxicological, and environmental analysis. In the case of chromium, the trivalent cation Cr(III) is an essential trace element to man. It is present in natural waters at the ppb level and plays a role in biochemical processes of aquatic plants and animals (1). On the other hand, the chromate ion Cr(VI) is an enzymatic poison which leads to hepatic and renal damage by exposure (2). Furthermore, Cr(VI) is a suspected carcinogen. The maximum allowable concentration in drinking water established in 1963 by the World Health Organization is 50 ppb. Sources of chromium pollution are metallurgic, glass, ceramic, textile, and tannery industries. It is extensively used in electroplating, as a corrosion inhibitor and in chrome tanning liquors (3).

Most analytical methods used for the speciation of Cr(III) and Cr(VI) are based on an off-line separation and/or a preconcentration step by means of extraction or ion-exchange with subsequent detection of the different species by atomic absorption (4–7) or emission (8) spectrometry. Recently, separation by paired-ion reversed phase high performance liquid chromatography (hplc) of Cr(III) and Cr(VI) followed by inductively coupled plasma emission detection has also been published (9, 10). Additionally, reversed phase hplc separations of Cr(III)/Cr(VI) as dithiocarbamate complexes combined with uv (11, 12) or electrochemical (13) detection are known. Furthermore, a post column reaction detection method with a lead dioxide solid phase reactor has been reported (14).

In the present paper the selective determination of chromate after separation on a paired-ion reversed phase hplc system with the recently developed quenched phosphorescence detection method is described. With this detector Cr(III) gives almost no response. For the first time the possibility of time resolution is quantitatively examined by measuring the influence of the instrumental parameter settings of the commercially available detector on the sensitivity of the method. To show their influence theoretically the well-known Stern–Volmer equation for dynamic quenching has to be modified. Relevant analytical data obtained for chromate standard solutions are given. Chromatograms of spiked tapwater and spiked surface water samples clearly indicate the selectivity and sensitivity of the quenched phosphorescence detector for real samples.

Theoretical

Quenched room temperature phosphorescence in liquids (qrtpl) has been developed in our lab as a detection method in hplc (15, 16). It is based on the measurement of the phosphorescence of biacetyl (2,3-butanedione) present in the deoxygenated mobile phase. Analytes able to interact with biacetyl in the excited triplet state cause a decrease of the phosphorescence signal. In the past use was made of a luminescence detector with a continuum excitation source and the phosphorescence emission signal was monitored continuously. In absence of quenchers a constant phosphorescence signal with intensity I_0 is observed, corresponding to a triplet lifetime τ_0 of biacetyl. In presence of a dynamic quencher, τ_0 is decreased to τ and I_0 to I according to Stern-Volmer.

$$[1] \quad \frac{I_0}{I} = \frac{\tau_0}{\tau} = 1 + k_q \tau_0 [Q]$$

In eq. [1] k_q is the bimolecular rate constant of the quenching reaction ($M^{-1}\ s^{-1}$) and [Q] the quencher concentration (*M*).

Until recently, the possibility of time resolution on the microsecond time scale in quenched phosphorescence detection, to exclude scattering and background fluorescence, was not invoked. The Perkin–Elmer LS-2 luminescence detector applied in our experiments can be operated in a pulsed-source – time-resolved phosphorescence mode. The emission signal is gated, during a time interval t_g, after the source flash by a delay time t_d. Under these conditions the signal intensities in absence

[1]To whom all correspondence should be addressed.

Printed in Canada

Can. J. Chem. Downloaded from www.nrcresearchpress.com by 78.46.186.204 on 09/07/12
For personal use only.

and presence of quenchers I_0' and I' are given, respectively, by the time integrals

$$[2] \quad I_0' = \int_{t_d}^{t_d+t_g} B_0 \exp(-t/\tau_0)dt$$

and

$$[3] \quad I' = \int_{t_d}^{t_d+t_g} B_0 \exp(-t/\tau)dt$$

where $B_0\, e^{-t/\tau_0}$ and $B_0 e^{-t/\tau}$ are the phosphorescence decay curves. For biacetyl, B_0, the radiation flux, is the product of an instrumental constant, the rate of light absorption at the applied excitation wavelength, the efficiency of intersystem crossing, and the rate constant of the phosphorescence process (15). In our experiments t_g is about $5\tau_0$. Under these conditions more than 99% of I_0' falls within the upper integration limit $t_d + t_g$, of course the same holds for I' since $\tau < \tau_0$. This means that $t_d + t_g$ can be replaced by an integration to infinity so that eqs. [2] and [3] give

$$[4] \quad \frac{I_0'}{I'} = \frac{\tau_0}{\tau} \exp(-t_d/\tau_0 + t_d/\tau)$$

Combination of eqs. [1] and [4] leads to

$$[5] \quad \frac{I_0'}{I'} = (1 + \tau_0 k_q[Q]) \exp(t_d k_q[Q])$$

Thus in the time-resolved mode a modified Stern–Volmer expression is obtained; the intensity ratio is the product of a linear and an exponential term. The influence of the latter decreases when t_d is shortened. This is an important conclusion in view of the linearity of calibration curves, as can be seen in Fig. 3.

As noted before, if $t_d + t_g$ is much larger than τ_0 this sum can be replaced by infinity and I_0' from eq. [2] can be written as

$$[6] \quad I_0' = B_0\tau_0 \exp(-t_d/\tau_0)$$

so that

$$[7] \quad \ln I_0' = \ln(B_0\tau_0) - t_d/\tau_0$$

Experimental

Chemicals

All reagents used were analytical grade. K_2CrO_4, $NaH_2PO_4.H_2O$, and sodium hydroxide were purchased from Merck (Darmstadt, F.R.G.). Acetonitrile (hplc) grade was obtained from Baker (Deventer, The Netherlands); biacetyl from Aldrich (Beerse, Belgium), and tetrabutylammoniumchloride (TBACl) from Ventron (Karlsruhe, F.R.G.). Deionized water was distilled twice before use.

Instrumentation

Batch experiments were carried out as described previously (17). A description of the hplc system was published in ref. 18.

The Perkin–Elmer LS-2 luminescence detector was employed in the pulsed-source – time-resolved phosphorescence mode. For excitation of biacetyl a broad band filter with maximum transmission at 400 nm was used; the emission wavelength was 515 nm.

Results and discussion

Batch experiments

For most metal ions that occur in more than one oxidation state, as for instance platinum and tin, the ion in the lowest oxidation state has the highest quenching constant (16, 17). This can be readily conceived if the quenching of the biacetyl phosphorescence is caused by electron transfer. For chromium this is obviously not the case. Bimolecular quenching constants of chromate under various conditions, measured as described before (17), are given in Table 1. Rather unexpected, they are about one order of magnitude larger than the value found for Cr(III). The quenching mechanism for chromate could be based on energy transfer instead of electron transfer, which is only possible if chromate possesses an excited electronic state with a lower energy than the triplet state of biacetyl. Table 1 shows that the influence of the pH on k_q is small; with decreasing pH from 7 to 4, k_q increases slightly. In the pH-range 0.75–6.45 $HCrO_4^-$ is the dominating species, while above pH = 6.45 mainly CrO_4^{2-} is present in solution (19).

TABLE 1. k_q values of chromate under various conditions

	Solvent	k_q (M^{-1} s^{-1})
Chromate	Water/acetonitrile 50/50 (v/v)	8.5×10^8
	Water	7.5×10^8
	2×10^{-3} *M* phosphate buffer pH 7	3.5×10^8
	2×10^{-3} *M* phosphate buffer pH 6	5×10^8
	2×10^{-3} *M* phosphate buffer pH 5	8×10^8
	2×10^{-3} *M* phosphate buffer pH 4	8×10^8
Cr^{3+}	Water/acetonitrile 16.3/83.7 (v/v)	5.8×10^7 (17)

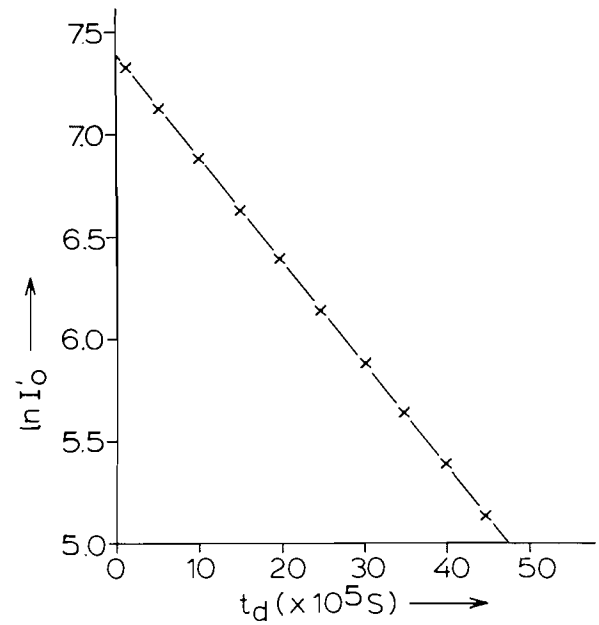

FIG. 1. ln I_0' vs. t_d for the determination of the phosphorescence lifetime τ_0 of biacetyl. t_g = 1.00 ms.

Time-resolved phosphorescence detection

In order to investigate the influence of the delay time t_d and the gating time t_g on the phosphorescence intensity measured in absence of quenching analyte we refer to the theoretical section.

Equation [7] predicts a straight line upon plotting ln I_0' versus t_d with intercept ln $B_0\tau_0$ and slope $-1/\tau_0$. Figure 1 shows such a plot obtained for a freshly prepared mobile phase after deoxygenation under flow conditions (t_g = 1.00 ms). The calculated lifetime of biacetyl τ_0 is 0.20 ms.

In Fig. 2 the influence of t_g on I_0' is visualized (measured at t_d = 0.01 ms, the minimum instrumental setting). When t_g becomes larger than 1.0 ms, corresponding to $t_g \approx 5\tau_0$, I_0' reaches a plateau; then the approximations of eqs. [2] and [3] apply.

Can. J. Chem. Downloaded from www.nrcresearchpress.com by 78.46.186.204 on 09/07/12
For personal use only.

Can. J. Chem. Downloaded from www.nrcresearchpress.com by 78.46.186.204 on 09/07/12
For personal use only.

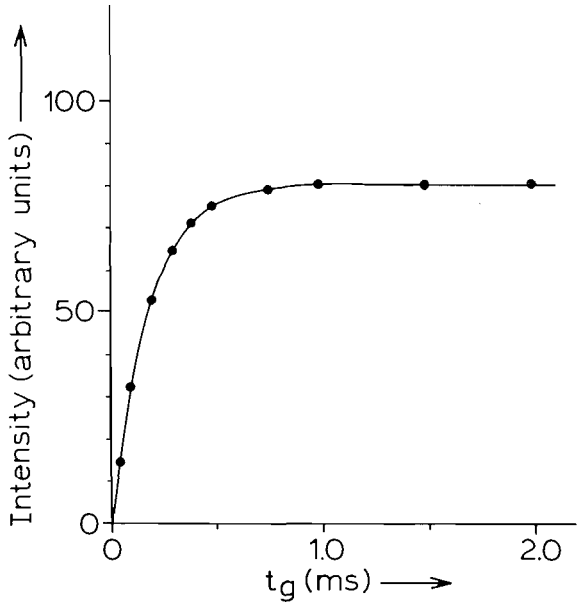

FIG. 2. I_0' vs. t_g; t_d = 0.01 ms.

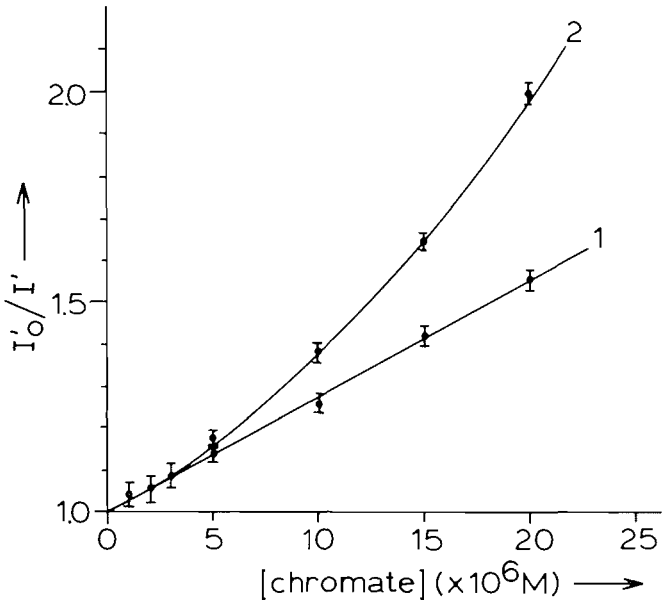

FIG. 3. I_0'/I' plotted against the chromate concentration. (*1*) t_d = 0.01 ms; (*2*) t_d = 0.25 ms. In both cases, t_g = 1.00 ms. The intensity ratios are calculated from actual chromatograms.

Equation [5] predicts a non-linear dependence of I_0'/I' and [Q] because of the presence of an exponential term in the Stern–Volmer equation for the time-resolved mode. The role of this term will depend on t_d. This is shown in Fig. 3. The deviation from linearity is negligible for t_d = 0.01 ms but is very strong if t_d is 25 times larger. The latter curve increases exponentially for higher chromate concentrations.

Of course the experimental settings t_d and t_g not only influence the signal but also the noise of the system. The optimum choice for t_g can be readily derived from Fig. 2: for t_g about 0.9–1.0 ms the signal-to-noise ratio (S/N) will be the most favourable. Further increase of t_g does not improve the signal but only implies a higher noise level. For the choice of t_d two points must be taken into account. If only shot noise is

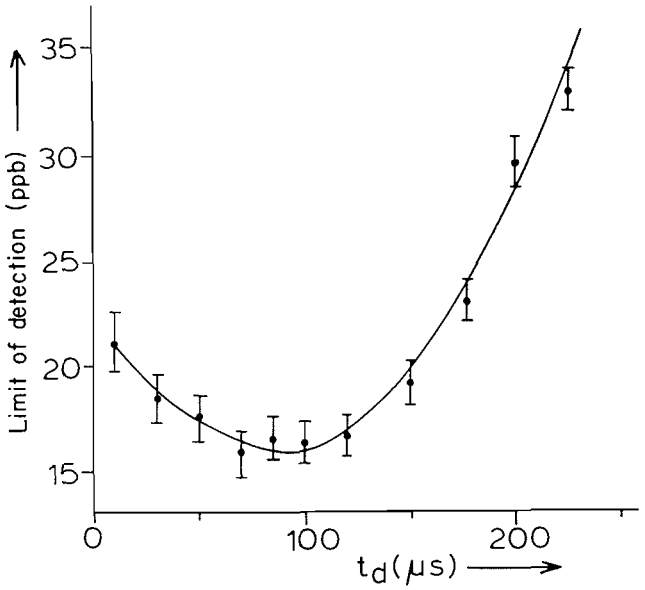

FIG. 4. Limit of detection (lod) of chromate vs. t_d to estimate the maximal signal-to-noise ratio. t_g = 1.00 ms. The injected chromate concentration is 100 ppb. Chromatographic conditions: column 12 cm × 4.6 mm inner diameter; 5 μm ODS. Spherisorb; mobile phase 95/5 (v/v) water/acetonitrile, 2×10^{-3} *M* phosphate buffer pH 7.1, 2×10^{-4} *M* TBACl and 5×10^{-3} *M* biacetyl. Injection volume 100 μL; flow rate 1.0 mL min^{-1}.

considered S/N is proportional to $(I_0')^{1/2}$; hence t_d must be chosen as short as possible because I_0' is proportional to $\exp(-t_d/\tau_0)$, see eq. [6]. On the other hand, an increase of t_d leads to a decrease of scattering and background fluorescence resulting in a lower noise level. Experiments have shown that the best value for t_d is 0.10 ms, which is in line with our earlier reported source pulse duration of the LS-2 instrument of about 0.08 ms (20). In Fig. 4 the limit of detection (lod) of chromate is depicted as a function of t_d (S/N = 3). The chromate concentration used was small (100 ppb) to assure working in the (quasi) linear range of the calibration curves. The gain in lod is about 30% when t_d is increased from 0.01 to 0.10 ms.

Summarizing we conclude that for routine analysis with the quenched biacetyl phosphorescence system a combination t_d = 0.01 and t_g = 1.00 ms can be used. To achieve the lowest limits of detection, t_d must be set equal to 0.1 ms.

Chromatographic experiments and application to real samples

The use of paired-ion, reversed phase hplc for the separation of Cr(III) and chromate has been described by several authors (9, 10, 14). When TBACl as ion pairing reagent is added to the mobile phase chromate is retained on a reversed phase type column while Cr(III) elutes in the solvent front. The mobile phase was buffered at pH 7.1 because of the favourable chromatographic properties of the divalent CrO_4^{2-} ion (21). At this pH chromate is almost quantitatively present as CrO_4^{2-} (20). In Fig. 5 a chromatogram is given for a 200 ppb (1.7×10^{-6} *M*) chromate standard solution. Peaks 1 and 2 are attributed to quenching impurities. The lod measured as a signal-to-noise ratio of 3 under optimal detector conditions (t_d/t_g resp. 0.10/1.00 ms) is 16 ppb (1.4×10^{-7} *M*), see also Fig. 4. For routine analysis, when a large linear range is required usually, t_d and t_g are set equal to 0.01 and 1.00 ms, respectively. In that case, the lod is 21 ppb. The calibration curve is linear over three orders of magnitude (r = 0.998, n = 7)

Can. J. Chem. Downloaded from www.nrcresearchpress.com by 78.46.186.204 on 09/07/12
For personal use only.

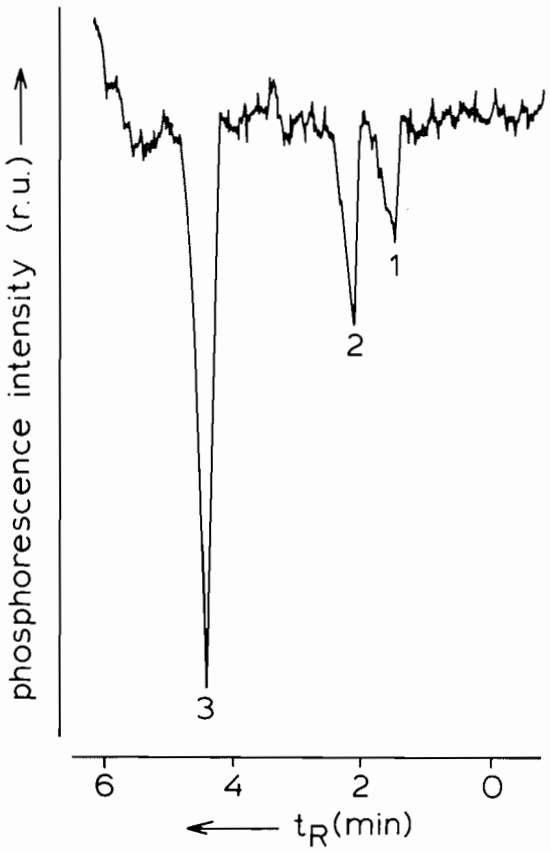

FIG. 5. Chromatogram of a 200 ppb (1.7×10^{-6} *M*) standard solution of chromate. (*1*) and (*2*) are quenching impurities, (*3*) is the chromate peak. Chromatographic conditions as in Fig. 4.

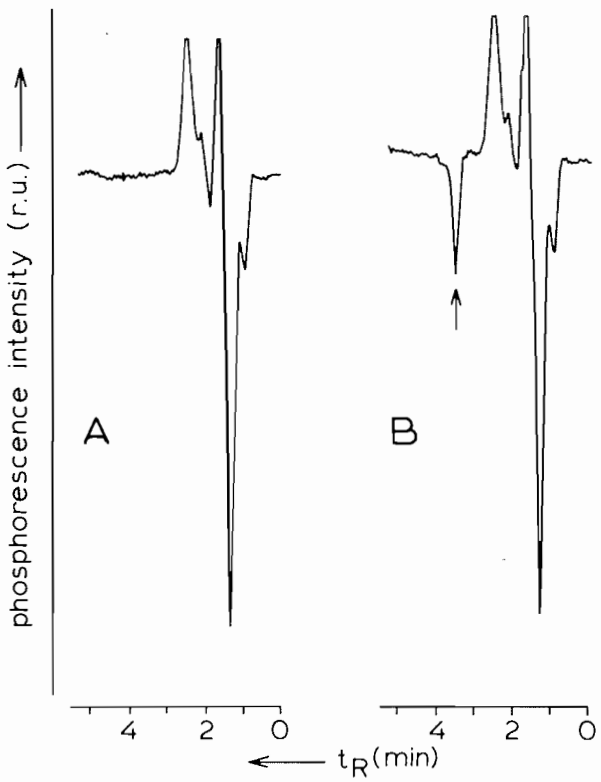

FIG. 6. Chromatogram of a blank tap water sample (*A*) and of a tap water sample spiked with 1×10^{-5} *M* chromate (B). The positive peaks in the chromatograms in Figs. 6 and 7 are attributed to impurities present in the samples exhibiting native fluorescence or sensitized phosphorescence of biacetyl. The negative peaks are caused by quenching compounds. Chromatographic conditions as in Fig. 4.

when I_0'/I' vs. [Q] is plotted. At the 50 ppb level the relative standard deviation is 4.2% and at the 500 ppb level 1.7%, both based on eight repetitive injections.

To show the potential applicability of the method to real samples tapwater and surface water samples were spiked with chromate, filtered over a 0.2 μm filter and after deoxygenation injected onto the column. In Fig. 6 chromatograms are given of a blank and a spiked tap water sample respectively. To improve the shape of the chromate peak, 3% acetonitrile was added to the spiked sample before injection. If this was not done, peak tailing was observed, caused probably by interaction of chromate with residual silanol groups on the silica matrix (22). Addition of a small amount of acetonitrile appeared to suppress this effect. The recovery of chromate was 60% at the 1×10^{-5} *M* level and 42% at the 5×10^{-6} *M* level. These low recoveries are probably due to reducing components present in tap water that react with chromate, or due to sorption onto or reaction with the filter used. Chromatograms of a blank and a spiked surface water sample are shown in Fig 7. In this case, the recovery of chromate was 85% at the 5×10^{-6} *M* level.

Figures 6 and 7 additionally indicate the selectivity of the detection method at hand. Both the chromatograms of the blanks for tap water and surface water are relatively clean; from this point of view sample preparation can be done quite easily.

The dependence of the recovery from the spiked amount of chromate makes it difficult to calculate a limit of detection for real samples. However, as the chromate peak is clearly separated from matrix interferences in all water samples, 20 ppb, corresponding to 2 ng absolute, seems a realistic value in view of the results of standard solutions. It is emphasized

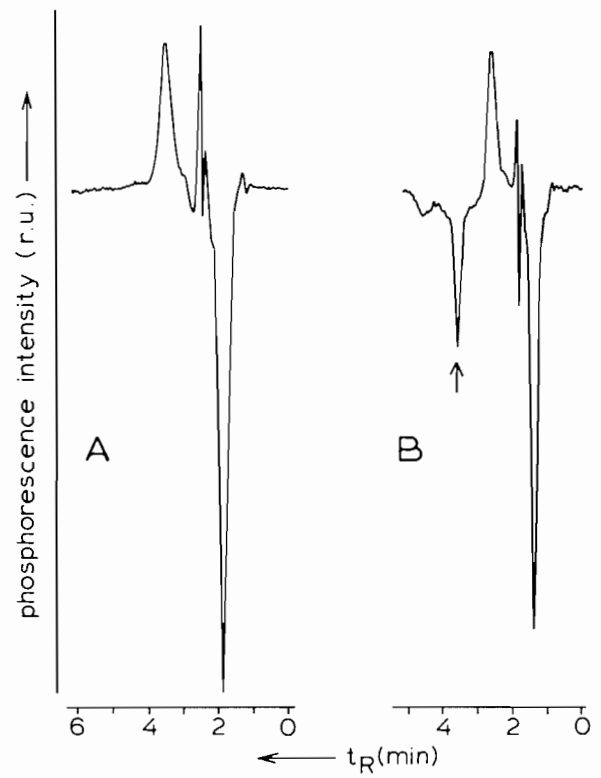

FIG. 7. Chromatogram of a blank surface water sample (*A*) and of a surface water sample spiked with 5×10^{-6} *M* chromate (*B*). Chromatographic conditions as in Fig. 4.

TABLE 2. Comparison of lod values for chromate obtained with different hplc methods

Detection method	Limit of detection (ng/mL)	Reference
Electrochemical (as diethyldithiocarbamate complex)	4	13
Colorimetric (as 1,5-diphenylcarbazide complex)	100	14
Direct current plasma (dcp) emission spectroscopy	7	10
Quenched rtpl	16	This work

that in originally chromate containing samples the concentration remains stable once an equilibrium situation has been reached.

In Table 2 a comparison in sensitivity is made between our method and other recently described hplc methods which deal with the separate detection of chromate; the lod's are essentially the same (4–17 ng) except for the colorimetric method (100 ng). Although the dcp (direct current plasma) detection method (10) claims a slightly lower lod than our method, a dcp emission spectrometer is not easily available in most laboratories. The electrochemical detection method as described by Bond and Wallace (13) has the disadvantage that the complex formation of chromate with diethyldithiocarbamate is extremely slow, resulting in a time-consuming sample pretreatment procedure.

Conclusions

The quenched phosphorescence detection method can be used in combination with paired-ion reversed phase hplc for the detection of chromate in water samples. The sensitivity of the method achievable with the commercially available Perkin–Elmer LS-2 detector should be sufficient for the control of drinking water quality (50 ppb limit) if time-resolution is applied and the instrumental parameters are chosen carefully.

1. A. J. RUBIN (*Editor*). Aqueous-environmental chemistry of metals. 1st ed. Ann Arbor Science Publishers Inc., Ann Arbor, MI, U.S.A. 1974. Chap. 2.
2. U. FÖRSTNER and G. MÜLLER. Schwermetalle in Flüssen und Seen, Springer-Verlag Berlin, Heidelberg, G.F.R. 1974. Chap. 3.
3. L. KLEIN. River pollution I. Chemical analysis. Butterworth and Co. Ltd., London, Great Britain. 1959. Chap. 8.
4. M. S. CRESSER and R. HARGITT. Anal. Chim. Acta, **81**, 196 (1976).
5. A. ISOZAKI, K. KUMAGAI, and S. UTSUMI. Anal. Chim. Acta, **153**, 15 (1983).
6. G. J. DE JONG and U. A. TH. BRINKMAN. Anal. Chim. Acta, **98**, 243 (1978).
7. D. NARANJIT, Y. THOMASSEN, and J. C. VAN LOON. Anal. Chim. Acta, **110**, 307 (1979).
8. A. MIYAZAKI and R. M. BARNES. Anal. Chem. **53**, 364 (1981).
9. I. S. KRULL, D. BUSHEE, R. N. SAVAGE, R. G. SCHLEICHER, and S. B. SMITH. Anal. Lett. **15**, (A3) 267 (1982).
10. I. S. KRULL, K. W. PANARO, and L. L. GERSHMAN. J. Chromatogr. Sci. **21**, 460 (1983).
11. T. TANDE, J. E. PETTERSEN, and T. TORGRIMSEN. Chromatographia, **103**, 607 (1980).
12. G. SCHWEDT. Fres. Z. Anal. Chem. **295**, 382 (1979).
13. A. M. BOND and G. G. WALLACE. Anal. Chem. **54**, 1706 (1982).
14. J. RÜTER, U. P. FISLAGE, and B. NEIDHART. Chromatographia, **19**, 62 (1985).
15. J. J. DONKERBROEK. Thesis, Free University, Amsterdam. 1983.
16. C. GOOIJER, A. C. VELTKAMP, R. A. BAUMANN, N. H. VELTHORST, R. W. FREI, and W. J. F. VAN DER VIJGH. J. Chromatogr. **312**, 337 (1984).
17. J. J. DONKERBROEK, A. C. VELTKAMP, C. GOOIJER, N. H. VELTHORST, and R. W. FREI. Anal. Chem. **55**, 1886 (1983).
18. J. J. DONKERBROEK, N. J. R. VAN EIKEMA HOMMES, C. GOOIJER, N. H. VELTHORST, and R. W. FREI. Chromatographia, **15**, 218 (1982).
19. M. POURBAIX. Atlas of electrochemical equilibria in aqueous solutions. Pergamon Press. London, Great Britain. 1966. Chap. 4.
20. R. A. BAUMANN, C. GOOIJER, N. H. VELTHORST, and R. W. FREI. Anal. Chem. **57**, 1815 (1985).
21. R. VESPALEC, J. NEČA, and M. VRCHLABSKÝ. J. Chromatogr. **286**, 171 (1984).

Can. J. Chem. Downloaded from www.nrcresearchpress.com by 78.46.186.204 on 09/07/12
For personal use only.

Prospectives of polymeric liquid crystal stationary phases for capillary column gas chromatographic separations

K. P. NAIKWADI, A. M. MCGOVERN, AND F. W. KARASEK
Department of Chemistry, Faculty of Science, University of Waterloo, Waterloo, Ont., Canada N2L 3G1

Received October 17, 1986

This paper is dedicated to Professor Douglas E. Ryan on the occasion of his 65th birthday

K. P. NAIKWADI, A. M. MCGOVERN, and F. W. KARASEK. Can. J. Chem. **65**, 970 (1987).

The liquid crystalline polysiloxane substrate offers unique selectivity when used in capillary column gas chromatography. The separation and identification of priority pollutants along with other compounds is very difficult but important. In particular, the separation of isomeric organic compounds having similar volatilities could not be obtained on capillary columns using conventional stationary phases. The complete separation of *ortho*, *meta*, and *para* isomers of certain disubstituted benzenes as well as polycyclic aromatic compounds was achieved on a capillary column using a liquid crystalline polysiloxane stationary phase. The complete separation of octachlorodibenzodioxin from octachlorodibenzofuran was also obtained on this column which is not possible on columns of identical lengths using conventional stationary phases. The separation of polycyclic aromatic compounds in a complex sample of airborne particulate matter extract on the liquid crystal column is demonstrated.

K. P. NAIKWADI, A. M. MCGOVERN et F. W. KARASEK. Can. J. Chem. **65**, 970 (1987).

Le polysiloxane à l'état de cristal liquide, utilisé comme substrat en chromatographie en phase gazeuse avec des colonnes, offre une sélectivité unique. La séparation et l'identification des polluants prioritaires de même que celle d'autres composés est difficile, mais importante. En particulier, la séparation de composés organiques isomères possédant des volatilités semblables ne peut être réalisée à l'aide de colonnes capillaires remplies de phases stationnaires conventionnelles. La séparation complète des isomères *ortho*, *méta* et *para* de certains dérivés benzéniques disubstitués, de même que celle de composés aromatiques polycycliques a pu être réalisée sur une colonne capillaire contenant du polysiloxane à l'état de cristal liquide comme phase stationnaire. Utilisant cette colonne, on a aussi réalisé la séparation complète de l'octachlorodibenzodioxine de l'octachlorodibenzofuranne; cette séparation ne peut toutefois pas être réalisée à l'aide de colonnes de longueurs semblables remplies de phases stationnaires conventionnelles. On démontre, à l'aide de la colonne à cristaux liquides, comment on peut séparer les composés aromatiques polycycliques contenues dans un échantillon complexe de substances extraites de matières solides transportées dans l'air.

[Traduit par la revue]

Can. J. Chem. Downloaded from www.nrcresearchpress.com by 78.46.186.204 on 09/07/12
For personal use only.

Introduction

Liquid crystalline compounds have been used as stationary phases in packed column gas chromatography (GC) for the last two decades. Their application for the separation of a variety of isomeric organic compounds has been reviewed several times (1–5). The continued research and interest in these phases resulted in the development of high temperature liquid crystals suitable for use in packed columns for separation of isomeric polycyclic aromatic compounds (PAC) (6–8). Capillary columns are highly efficient compared to packed columns and the separation of several hundred compounds can be carried out as reported previously (9). The use of high temperature monomeric liquid crystals in capillary columns presents several difficulties (10). Their use by blending with polymeric silicone phases in capillary columns resulted in moderate selectivities and higher efficiencies than packed columns (11, 12). The synthesis of new liquid crystalline compounds and separation of disubstituted benzene isomers (13), insect sex pheromones (14), and the effect of the chemical structure of liquid crystalline compounds on separation potential is reported in the literature (8). Recently, polymeric liquid crystals were developed for use in capillary columns (15–20). These phases can be coated in capillary columns by dynamic or static coating techniques. Their application in supercritical fluid chromatography has been reported previously (21).

In this paper, the application of a liquid crystalline polysiloxane stationary phase in a fused silica capillary column for the separation of various isomeric organic compounds will be shown. The novel application of this column for the separation of pac in airborne particulate matter will be demonstrated.

Materials and methods

A fused silica capillary column (20 m × 0.25 mm) coated with a liquid crystalline polysiloxane stationary phase (SB-Liquid Crystal) was obtained from Lee Scientific, Salt Lake City, Utah (U.S.A.). The column was coated by the static method (film thickness ca. 0.15 μm) and crosslinked using azo-*t*-butane. All the standard PAC were obtained from Aldrich Chemical Co. The halogenated standards were obtained from Ultra Scientific, Rhode Island (U.S.A.). The gas chromatograph was a Hewlett Packard model 5880 equipped with a flame ionization detector and cool on-column injector. The GC/MS system was a Hewlett Packard 5987A along with an HP 1000 data system. The data acquisition and storage system allows mass chromatograms to be reconstructed at any mass in the scan range. The library search system includes probability-based matching (PBM) based on 78 000 reference mass spectra. The airborne particulate matter extracts were separated into acidic, basic, and neutral groups of compounds by acid–base extraction.

The separation of neutrals into aliphatic, polycyclic aromatic, and polar compounds was achieved using a Varian 5000 Liquid Chromatograph with a Vista 401 data system. The data system has a capacity to recalculate and replot the stored data of a particular analysis. A semipreparative Spherisorb silica (10 μm) column (250 × 9.4 mm i.d., Tetrochem, Toronto, Canada) was employed with a 100 μL sample loop. The solvent gradient programme used consisted of 100% hexane for 30 min, programmed to 100% dichloromethane over 20 min, held for 10 min and programmed back to 100% hexane in 10 min. A constant flow rate, 2 mL/min was used. During this gradient programme four fractions were collected at elution times, start to

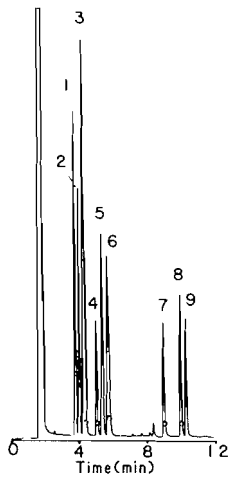

FIG. 1. Chromatogram of a mixture of disubstituted benzene isomers. Peaks: *1*, *m*-bromochlorobenzene; *2*, *o*-bromochlorobenzene; *3*, *p*-bromochlorobenzene; *4*, *m*-bibromobenzene; *5*, *o*-dibromobenzene; *6*, *p*-dibromobenzene; *7*, *o*-bromonitrobenzene; *8*, *m*-bromonitrobenzene; *9*, *p*-bromonitrobenzene. Temperature: 100°C for 1 min then programmed 3°C/min.

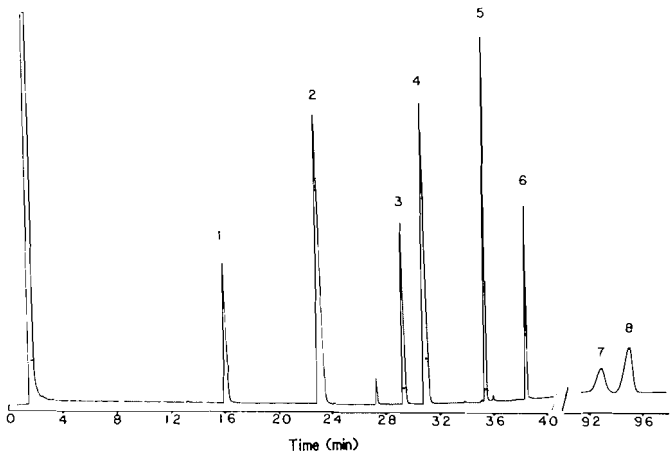

FIG. 2. Chromatogram of chlorinated compounds. Peaks: *1*, 2,2-dichlorobiphenyl; *2*, 2,2′,5,5′-tetrachlorobiphenyl; *3*, 2,3,4,5,6-pentachlorobiphenyl; *4*, 2,2′,4,4′,5,5′-hexachlorobiphenyl; *5*, 3,3′,4,4′-tetrachlorobiphenyl; *6*, 1,2,3,4-tetrachlorodibenzodioxin; *7*, octachlorodibenzodioxin; *8*, octachlorodibenzofuran. Temperature: 100°C for 1 min then programmed 3°C/min to 270°C.

14, 20, 35, and 80 min. First and last fractions consisted of nonpolar and highly polar compounds, respectively. Polycyclic compounds were collected between 14 to 20 and 20 to 35 min and designated as pac fraction I and pac fraction II, respectively. The separation and identification of pac's were carried out using a polymeric liquid crystal column in GC/MS.

Results and discussion

Disubstituted benzene isomers

The baseline separation of three isomers each of bromochloro, bromonitro, and dibromo disubstituted benzenes is shown in Fig. 1. The separation of these isomers using conventional packed or capillary columns is very difficult. The *ortho* isomer has a different volatility than the respective *meta* and *para* isomers, hence its separation is possible from the latter two isomers. However, *meta* and *para* isomers have identical volatilities resulting in their coelution on conventional columns. Based on the mechanism of separation on liquid crystal stationary phases it is possible to separate the *ortho*, *meta*, and *para* isomers using packed columns, but the *ortho* isomer may coelute with either the *meta* or *para* isomer. A capillary column coated with a polymeric liquid crystal stationary phase gives baseline separation of *ortho*, *meta*, and *para* isomers because of the high efficiency of the capillary column along with the traditional advantage of selectivity of the stationary phase.

TABLE 1. Retention times and molecular weights for PAC in a standard mixture (Fig. 3)

Peak no.	Compound	Retention time (min)	Mol. wt.
1	2,3-Dimethylnaphthalene	9.74	156
2	2,6-Dimethylnaphthalene	10.38	156
3	1,2-Dihydroacenaphthalene	11.17	154
4	9*H*-Fluorene	15.99	166
5	9,10-Dihydroanthracene	17.96	180
6	Phenanthrene	23.73	178
7	Anthracene	25.88	178
8	9-Methylanthracene	30.05	192
9	2-Methylanthracene	31.16	192
10	Pyrene	36.14	202
11	Unknown	42.46	217
12	Triphenylene	47.44	228
13	Chrysene	52.30	228
14	Aminopyrene	56.90	217
15	Benzo(*e*)pyrene	62.78	252
16	Unknown	65.05	278
17	Benzo(*a*)pyrene	68.48	252

Polychlorinated biphenyls, dioxins, and furans

The separation and identification of polychlorinated biphenyls (PCB), polychlorinated dibenzodioxins (PCDD), and polychlorinated dibenzofurans (PCDF) is very challenging. In particular, the separation of pentachlorobiphenyls from the tetrachlorodibenzodioxins (TCDD) has special importance because of the acute toxicity of the latter. The identification of TCDD is extremely difficult when there is a large number of pentachlorobiphenyl isomers because of strong interference that occurs even in the selected-ion-monitoring mode in mass spectrometry.

Hence, there is a need to develop a technique or column which can separate these isomers. We have attempted the separation of the 1,2,3,4-TCDD isomer from standard PCB isomers (Fig. 2). From the chromatogram it is clear that TCDD is retained longer than the tetra-, penta-, and hexachlorobiphenyls. However, it coelutes with the PCB isomers on the DB-5 column. Due to the lack of a large number of isomers of PCB and TCDD, it is difficult to predict the retention trends for all isomers on this liquid crystalline column.

Octachlorodibenzodioxin and octachlorodibenzofuran are also very difficult to separate. Their partial separation can be obtained using a 60 m conventional capillary column, while they can be separated completely on the 20 m capillary column using the polymeric liquid crystal stationary phase (Fig. 2).

Polycyclic aromatic compounds

Polycyclic aromatic compounds comprise the largest class of chemical carcinogens known to enter the environment through various sources. The separation of isomeric PAC's is

Can. J. Chem. Downloaded from www.nrcresearchpress.com by 78.46.186.204 on 09/07/12
For personal use only.

Can. J. Chem. Downloaded from www.nrcresearchpress.com by 78.46.186.204 on 09/07/12
For personal use only.

TABLE 2. Retention times and molecular weights of compounds in airborne particulate matter extracts, PAC fractions I and II

Peak no.	Compound	Retention time (min)	Mol. wt.	Identified by*	Peak no.	Compound	Retention time (min)	Mol. wt.	Identified by*
Fraction I									
1	Phenanthrene	23.73	178	a,b,c,d	14	Unknown	32.65	204	a
2	Anthracene	25.97	178	a,b,c,d	15	Unknown	32.99	204	a
3	Unknown	26.35	204	a	16	Fluoranthene	34.11	202	a,b,c,d
4	Methylphenanthrene/anthracene	26.82	192	a	17	Unknown	35.70	202	a
5	Methylphenanthrene/anthracene	27.45	192	a	18	Pyrene	36.02	202	a,b,c,d
6	4*H*-Cyclopenta(*def*)phenanthrene	27.72	190	a	19	Unknown	37.43	218	a
7	Methylphenanthrene/anthracene	28.55	192	a	20	1,2-Benzenedicarboxylic acid est.	39.02	—	a
8	Methylphenanthrene/anthracene	29.04	192	a	21	Methylpyrene	40.34	216	a
9	Methylphenanthrene/anthracene	29.44	192	a	22	Methylpyrene	41.40	216	a,c,d
10	2-Methylanthracene	31.28	192	a,b	23	Methylpyrene	41.71	216	a,c,d
11	2-Ethylphenanthrene	31.50	206	a,c	24	Unknown	42.32	215	a
12	Unknown	31.74	204	a	25	Unknown	45.86	226	a
13	4,5-Dihydropyrene	32.30	204	a					
Fraction II									
1	Phenanthrene	23.81	178	a,b,c,d,e	41	Benzo(*a*)fluorene	42.85	216	a,c,d
2	Methylphenanthrene/anthracene	26.74	192	a	42	Benzo(*a*)furan	43.15	216	a,c,d
3	Methylphenanthrene/anthracene	27.61	192	a	43	Unknown	43.64	228	a
4	4*H*-Cyclopenta(*def*)phenanthrene	27.69	190	a,e	44	Methylpyrene/fluoranthene	44.10	216	a
5	Unknown	28.23	190	a	45	Unknown	44.72	228	a
6	Methylphenanthrene/anthracene	28.46	192	a	46	Benzo(*ghi*)fluoranthene	45.76	226	a,b,c,d
7	Methylphenanthrene/anthracene	28.94	192	a	47	Unknown	46.11	230	a
8	Methylphenanthrene/anthracene	29.33	192	a	48	Unknown	46.79	226	a
9	Unknown	29.88	190	a	49	Unknown	47.29	228	a
10	Naphthalene,1,8-di-1-propynyl	30.55	204	a,c	50	Triphenylene	47.46	228	a,b,c,d
11	Unknown	31.24	202	a	51	Triphenylene,1-methyl	47.85	242	a
12	2-Ethylphenanthrene	31.41	206	a,c,e	52	Benz(*a*)anthracene	48.47	228	a,c,d
13	2-Ethylphenanthrene	31.84	206	a,c	53	Unknown	49.14	226	a
14	7*H*-Benz(*de*)anthracene-7-one	31.95	230	a	54	1,2′-Binaphthalene	49.74	254	a,c

Can. J. Chem. Downloaded from www.nrcresearchpress.com by 78.46.186.204 on 09/07/12
For personal use only.

TABLE 2. (*concluded*)

Peak no.	Compound	Retention time (min)	Mol. wt.	Identified by*	Peak no.	Compound	Retention time (min)	Mol. wt.	Identified by*
15	Naphthalene, 1-phenyl	32.11	204	a,c	55	Unknown	50.01	239	a
16	Naphthalene, 1-(phenylmethyl)	32.24	218	a,c	56	Unknown	50.27	228	a
17	Unknown	32.47	206	a	57	Unknown	50.65	242	a
18	Fluoranthene	34.11	202	a,b,c,e	58	Unknown	50.77	256	a
19	Dimethylphenanthrene	34.71	206	a	59	Benzo(*a*)anthracene, 12-methyl	50.96	242	a
20	Naphthalene, 2-phenyl	35.12	204	a,c	60	Unknown	51.46	240	a
21	Unknown	35.37	206	a	61	Methyltriphenylene/chrysene	51.68	242	a
22	Unknown	35.52	202	a	62	Chrysene	52.29	228	a,b,c,d
23	Pyrene	36.05	202	a,b,c	63	2,8-Bis(formyl)dibenzothiophene	52.82	240	a
24	Unknown	36.57	206	a	64	Methyltriphenylene/chrysene	53.12	242	a
25	Unknown	36.86	202	a	65	Unknown	53.40	242	a
26	Naphthalene, 2-(phenylmethyl)	37.30	218	a,c	66	Methyltriphenylene/chrysene	54.64	242	a
27	Methylpyrene	37.40	216	a	67	Methyltriphenylene/chrysene	55.64	242	a
28	Unknown	37.80	228	a	68	2-Propen-1-one, 1-(2-hydroxyphenyl)			
29	Benzo(*b*)fluorene	38.02	216	a		3-(4-hydroxy)phenyl	55.89	240	a
30	Methylpyrene/fluoranthene	38.54	216	a	69	Unknown	57.26	240	a
31	Methylpyrene/fluoranthene	39.17	216	a	70	Methyltriphenylene/chrysene	57.69	242	a
32	Methylpyrene/fluoranthene	39.39	216	a	71	Unknown	58.30	252	a
33	Methylpyrene/fluoranthene	39.91	216	a	72	Benzo(*b*)fluoranthene	60.26	252	a,c,d
34	Methylpyrene/fluoranthene	40.24	216	a	73	Benzo(*j*)fluoranthene	60.70	252	a,c,d
35	Methylpyrene/fluoranthene	40.60	216	a	74	Benzo(*a*)fluoranthene	61.12	252	a,c,d
36	Methylpyrene/fluoranthene	41.28	216	a	75	Benzo(*k*)fluoranthene	62.46	252	a,c,d
37	Methylpyrene/fluoranthene	41.59	216	a	76	Benzo(*e*)pyrene	62.81	252	a,b,c,d
38	1,1′:2′1″-Terphenyl	42.02	230	a	77	Unknown	65.03	252	a
39	Unknown	42.23	228	a	78	Perylene	65.70	252	a,b,c,d
40	Methylpyrene/fluoranthene	42.42	216	a	79	Benzo(*a*)pyrene	68.54	252	a,b,c,d
					80	Unknown	71.21	264	a

*a, Probability-based matching (PBM); b, matching of retention time with standard; c, retention trend on liquid crystal substrates; d, retention order reported (17, 19, 20); e, overlap from fraction I.

Can. J. Chem. Downloaded from www.nrcresearchpress.com by 78.46.186.204 on 09/07/12
For personal use only.

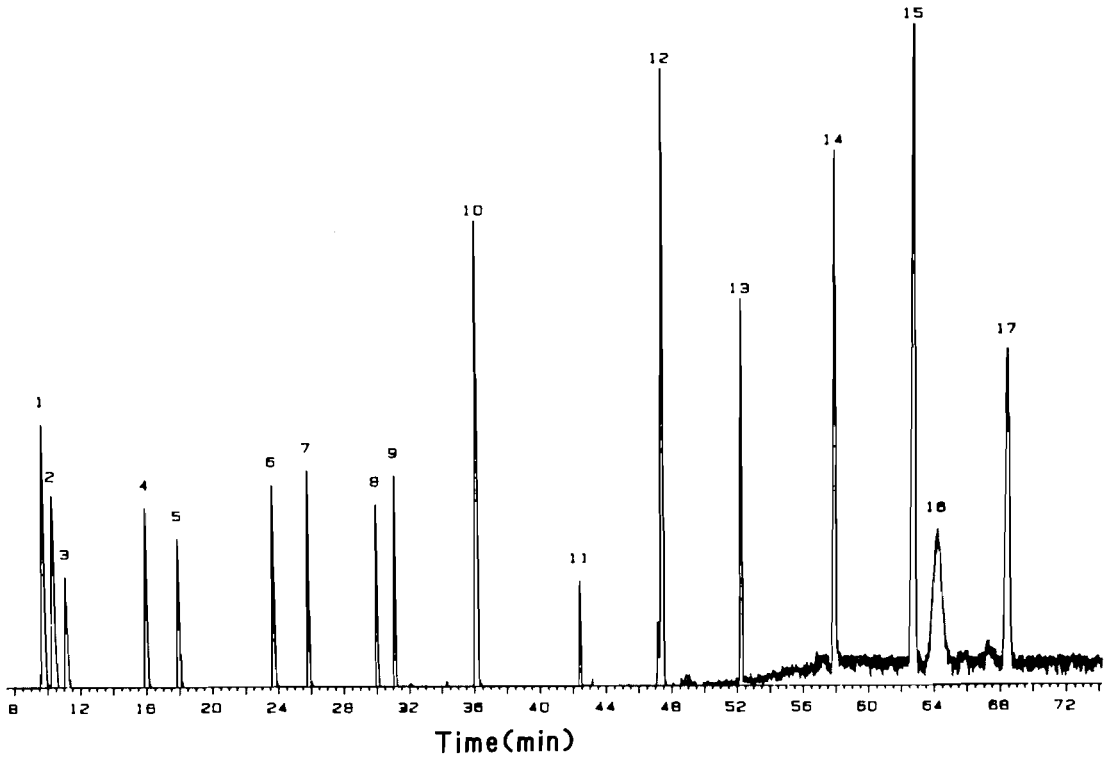

FIG. 3. Total ion current trace of mixture of standard PAC. Peaks: Table 1, other conditions as in Fig. 2.

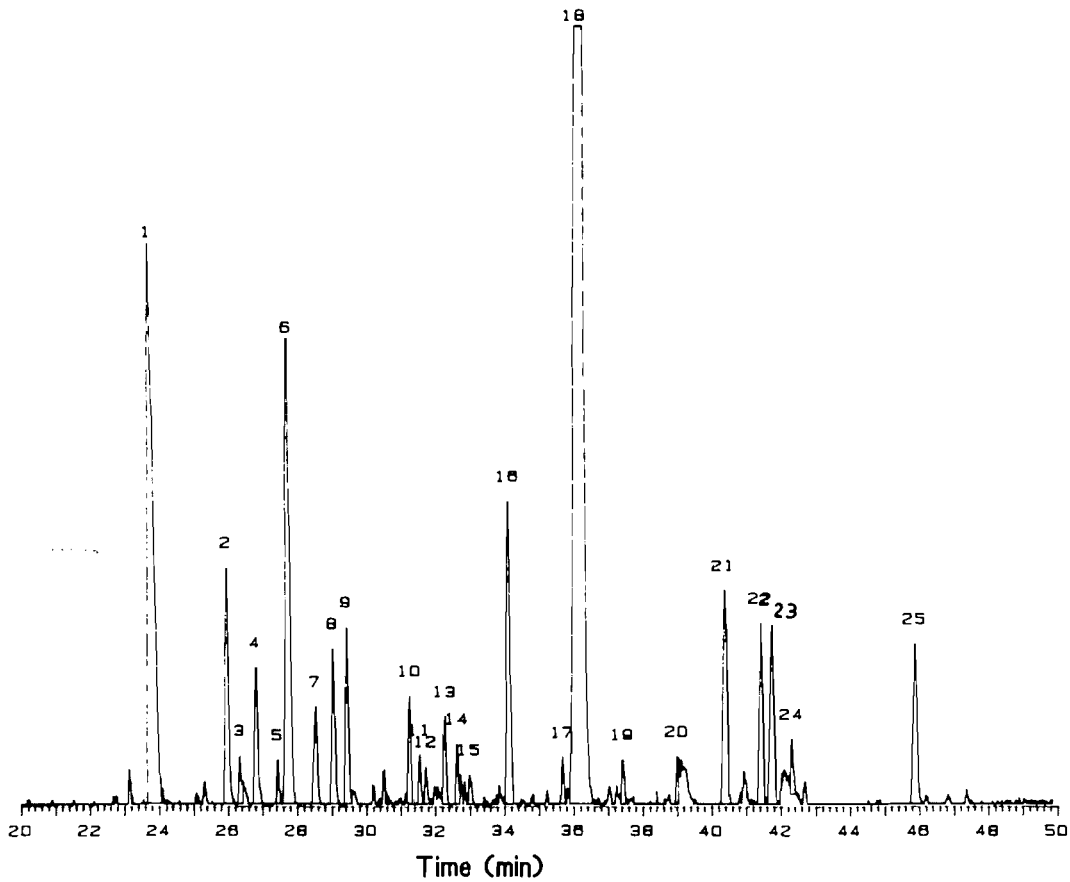

FIG. 4. Total ion current trace of PAC fraction I. Peaks as in Table 2, other conditions as in Fig. 2.

very difficult by gas chromatography using capillary columns coated by conventional stationary phases. The liquid crystalline stationary phases can separate isomeric PAC's based on their length-to-breadth ratio. The separation of a three-to-five ring standard pac mixture is shown in Fig. 3. The complete separation of phenanthrene/anthracene, triphenylene/chrysene and benzo(*e*)pyrene/benzo(*a*)pyrene was easily obtained. A list of the standard compounds separated is given in Table 1.

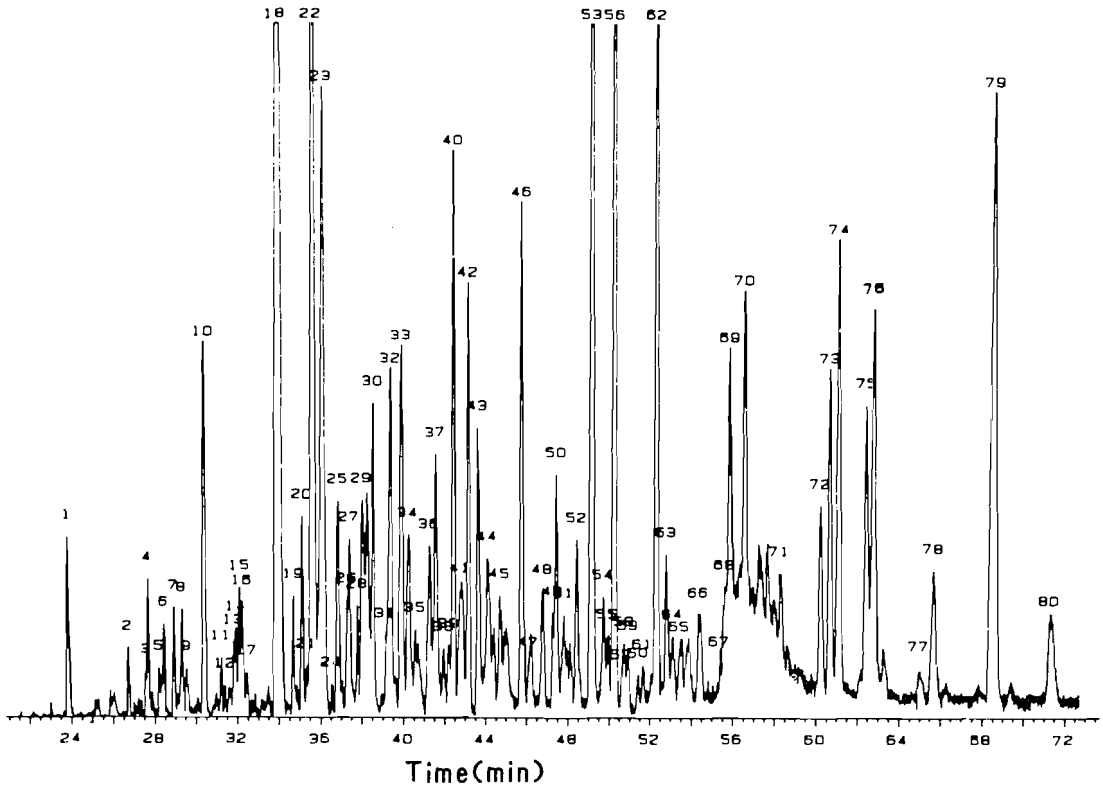

FIG. 5. Total ion current trace of PAC fraction II. Peaks as in Table 2, other conditions as in Fig. 2.

The retention time values and retention trends observed for standards were used for the identification of pac's present in airborne particulate matter along with the reference spectra obtained by pbm.

A normal phase, silica column in hplc was used to separate aliphatic compounds from aromatics. Reproducible separations were observed as compared to those obtained by open column chromatography. The separations achieved on silica column were based on the polarity of solutes, where increase in elution time was observed with increase in number of rings in the polycyclic aromatic compounds. A large number of three-ring PAC's were eluted in PAC fraction I, while PAC fraction II consisted of three-to-five-ring PAC's (Table 2). The total-ion-current (TIC) traces of these fractions are shown in Figs. 4 and 5.

It is very difficult to identify the pac isomers even using a pbm search. All identifications are based on the retention times of standard compounds injected at identical conditions, the mass spectral data of compounds in the sample compared with reference mass spectra, and the elution trend of various compounds on liquid crystal stationary phases in gas chromatography. A little work has been done regarding the application of liquid crystalline stationary phases for the separation of very complex mixtures (17, 19, 20). Our results show the practical application of capillary columns using a polymeric liquid crystal stationary phase for the separation of a large number of organic compounds in a complex environmental sample of airborne particulate matter.

1. J. M. JANINI. *In* Advances in chromatography. Vol. 17. *Edited by* J. C. Giddings, E. Grushka, J. Cazes, and P. R. Brown. Marcel Dekker Inc., New York. 1982. p. 231.
2. Z. WITKIEWICZ. J. Chromatogr. **251**, 311 (1982).
3. M. S. VIGDERGAUZ, R. V. VIGALOK, and G. V. DMITRIVA. Russ. Chem. Rev. **50**, 498 (1981).
4. J. P. SCHROEDER. *In* Liquid crystals and plastic crystals. Vol. 1. *Edited by* G. W. Gray and P. A. Winsor. Ellis Horwood, New York. 1974. p. 365.
5. H. KELKER and E. VON SCHIRIZHOFFEN. *In* Advances in chromatography. Vol. 6. *Edited by* J. C. Giddings and R. A. Keller. Marcel Dekker Inc., New York. 1968. p. 247.
6. J. M. JANINI, G. M. MUSCHIK, and W. L. ZIELINSKI, JR. Anal. Chem. **48**, 809 (1976).
7. J. M. JANINI, K. JOHNSTON, and W. L. ZIELINSKI, JR. Anal. Chem. **47**, 670 (1975).
8. A. ZIOLEK, A. WITKIEWICA, and R. DABROWSKI. J. Chromatogr. **299**, 159 (1984).
9. H. Y. TONG, D. L. SHORE, F. W. KARASEK, P. HELLAND, and E. JELLUM. J. Chromatogr. **285**, 423 (1984).
10. F. JANSSEN and T. KALIDIN. J. Chromatogr. **235**, 323 (1982).
11. R. J. LAUB, W. L. RUBERTS, and C. A. SMITH. HRC & CC, **3**, 355 (1980).
12. R. C. KONG, M. L. LEE, Y. TOMINAGA, R. PRATAP, M. IWAO, and R. N. CASTLE. J. Chromatogr. Sci. **20**, 502 (1982).
13. P. P. PAWAR, K. P. NAIKWADI, S. M. LIKHITE, B. V. BAPAT, and B. B. GHATGE. J. Chromatogr. **245**, 57 (1982).
14. K. P. NAIKWADI, S. ROKUSHIKA, H. HATANO, and M. OHSHIMA. J. Chromatogr. **331**, 69 (1985).
15. H. FINKELMANN, R. J. LAUB, W. L. ROBERTS, and C. A. SMITH. *In* Polynuclear aromatic hydrocarbons. *Edited by* M. Cooke, A. J. Dennis, and G. L. Fisher.
16. B. A. JONES, J. S. BRADSHAW, M. NISHIOKA, and M. L. LEE. J. Org. Chem. **49**, 4947 (1984).
17. M. A. APFEL, H. FINKELMANN, G. M. JANINI, R. J. LAUB, and B. A. SMITH. Anal. Chem. **57**, 651 (1985).
18. K. P. NAIKWADI, A. L. JADHAV, S. ROLUSHIKA, H. HATANO, and M. OSAHI. Macromol. Chem. **187**, 1407 (1986).
19. K. E. MARKIDES, M. NISHIOKA, B. J. TARBET, J. S. BRADSHAW, and M. L. LEE. Anal. Chem. **57**, 1296 (1985).
20. R. C. KONG, M. L. LEE, Y. TOMINAGA, R. PRATAP, M. IWAO, and R. N. CASTLE. Anal. Chem. **54**, 1802 (1982).
21. S. ROKUSHIKA, K. P. NAIKWADI, A. L. JADHAV, and H. HATANO. HRC & CC, **8**, 480 (1985).

Can. J. Chem. Downloaded from www.nrcresearchpress.com by 78.46.186.204 on 09/07/12
For personal use only.

Surface photochemistry: Semiconductor mediated reactions of some 1,2-diarylcyclopropanes[1]

PHILIP A. CARSON AND PAUL DE MAYO

Photochemistry Unit, Department of Chemistry, The University of Western Ontario, London, Ont., Canada N6A 5B7

Received October 6, 1986

This paper is dedicated to Professor Douglas E. Ryan on the occasion of his 65th birthday

PHILIP A. CARSON and PAUL DE MAYO. Can. J. Chem. **65**, 976 (1987).

1,2-Diphenylcyclopropane (**1**) was found to be oxidized on illuminated ZnO in the presence of air while 1-(*p*-methoxyphenyl)-2-phenylcyclopropane (**2**) and 1,2-bis(*p*-methoxyphenyl)cyclopropane (**3**) were found to be similarly oxidized on illuminated CdS. Compounds **2** and **3** were found, also, to undergo a rapid photochemical *cis–trans* isomerization on CdS whereas **1** did not undergo such isomerization. An electron transfer mechanism involving formation of the radical cations of the substrates is proposed.

PHILIP A. CARSON et PAUL DE MAYO. Can. J. Chem. **65**, 976 (1987).

On a trouvé que, en présence d'air, le diphényl-1,2 cyclopropane (**1**) peut être oxydé sur du ZnO illuminé; par ailleurs, on a trouvé que le (*p*-méthoxyphényl)-1 phényl-2 cyclopropane (**2**) et le bis(*p*-méthoxyphényl)-1,2 cyclopropane (**3**) peuvent aussi être oxydés sur du CdS illuminé. On a aussi trouvé que les composés **2** et **3** subissent une isomérisation *cis–trans* photochimique rapide sur le CdS; toutefois, le composé **1** ne subit pas de telle isomérisation. On propose que la réaction se produit par un mécanisme de transfert d'électron impliquant la formation de cations radicaux des substrats.

[Traduit par la revue]

Introduction

Photocatalysis on semiconductors has recently become an area of intensive investigation. In addition to the more extensively studied use of electron transfer reactions at semiconductors for inducing the photolysis of water as a means of solar energy storage, recent attention has been paid to the use of semiconductors for initiating electron transfer processes in organic media. Numerous reports of semiconductor catalyzed electron transfer photoreactions of organic molecules have been made, involving oxidative (both addition of O_2 and loss of hydrogen) and non-oxidative (e.g. isomerization) reactions. Among the more popular semiconductors are ZnO, TiO_2, and, because of its good spectral response in the visible region, CdS. Examples of non-oxidative reactions on CdS are, *inter alia*, the dimerization of phenyl vinyl ether (1), the *cis–trans* isomerization of styrene derivatives and other olefinic substances (2), and a [2 + 2] retrocycloaddition of a cage compound (3). We wish now to report the semiconductor-mediated reactions of some 1,2-diarylcyclopropanes.

1,2-Diarylcyclopropanes are known to undergo electron transfer reactions in homogeneous systems. Thus, 1,2-diphenylcyclopropane (**1**) is reportedly oxidized by addition of $^3O_2$ to its radical cation, which can be generated in CH_3CN solution by electron transfer to excited 9,10-dicyanoanthracene (DCA) (4); 1-(*p*-methoxyphenyl)-2-phenylcyclopropane (**2**) and 1,2-bis(*p*-methoxyphenyl)cyclopropane (**3**) have both been shown to isomerize and to undergo oxidation using similar conditions (4). The band gap of CdS is 2.4 eV, which corresponds to an adsorption maximum of 520 nm (5). The position of the valence band of CdS, determined in acetonitrile, is +1.55 V vs. SCE (5*a*) and this value has been taken as being close to the value in methylene chloride, the solvent used exclusively in the experiments reported here. Thus, *trans*-**1** and both the *cis* and *trans* isomers of **2** and **3**, having oxidation potentials (Table 1) less positive than the potential of the valence band of CdS, fulfil the electrochemical requirement for electron transfer to illuminated CdS.

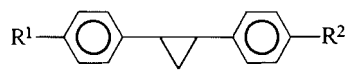

1: $R^1 = R^2 = H$
2: $R^1 = H$, $R^2 = OCH_3$
3: $R^1 = R^2 = OCH_3$

Several molecules, which have been shown to react by electron transfer using homogeneous sensitizers, have also been shown to react using semiconductor dispersions (refs. 3 and 7, 1 and 8, 3 and 9, 1 and 10). The latter have the advantage (to compensate for their frequent lesser photoefficiency) of not being involved in irrelevant chemistry themselves, as frequently happens with aromatic sensitizers. By virtue of these precedents, and because they meet the electrochemical requirements for electron transfer to CdS, cyclopropanes **1**, **2**, and **3** seemed excellent candidates for electron transfer studies at illuminated semiconductors.

Experimental

Samples were prepared using CH_2Cl as solvent (Baker or Fisher; spec. grade), which was used as received or after filtration through alumina. In the latter case (used in studies on **3**) 50 mL of Baker CH_2Cl_2 were percolated through 25 g alumina (Aluminum Oxide, Neutral, Baker, Brockman activity grade 1) in a 1 cm i.d. burette.

All reaction vessels and magnetic stirbars were washed by rinsing with concentrated HCl followed by washing 3× with water, 1× with acetone, 3× with water, 3× with 10% NH_4OH, 3× with distilled water, and 3× with acetone.

A solution of ca. 10.0 mg of cyclopropane in CH_2Cl_2 was added to a 5.00-mL volumetric flask (containing any additional compounds such as quenchers) and diluted to 5.00 mL with CH_2Cl_2. ([**1**] = 10.3×10^{-3} *M*; [**2**] = 8.9×10^{-3} *M*; [**3**] = 7.8×10^{-3} *M*.) This solution was then poured into a Pyrex reaction vessel containing ca. 30 mg of CdS and a magnetic stirbar. All samples were stoppered and wrapped in aluminum foil until irradiation. Samples containing **1** or **2** but not **3** were sonicated 5 min prior to irradiation or dark reaction.[2]

Irradiation was conducted using either a 1-kW Xe (PRA) lamp

[1]Publication No. 371 from the Photochemistry Unit, The University of Western Ontario.

[2]Sonication was a factor not easily monitored and might contribute to the difficulty found in obtaining reproducibility. Strict attention to detail was essential to achieve such reproducibility as was obtained.

Can. J. Chem. Downloaded from www.nrcresearchpress.com by 78.46.186.204 on 09/07/12
For personal use only.

Can. J. Chem. Downloaded from www.nrcresearchpress.com by 78.46.186.204 on 09/07/12
For personal use only.

TABLE 1. Oxidation potentials of 1,2-diarylcyclopropanes

Compound	E_{ox} vs. SCE (ref.)
t-**1**	1.5 (6)
c-**1**	1.7 (6)
t-**2**	1.2[a]
c-**2**	1.3[a]
t-**3**	0.85 (4*c*)
c-**3**	0.95 (4*c*)

[a]Courtesy of Mr. A. M. Draper.

operating at 840 W or a 150-W Xe lamp (PRA) operating at 140 W. Compressed air was used as a coolant and a water filter was employed to remove ir radiation. The output of both lamps was checked periodically with a Scientech 364 power energy meter and was found to remain satisfactorily constant. Corning cut-off filters were used such that no light was absorbed by the substrate. Samples were stirred magnetically during both irradiated and dark reactions. Unless degassed, samples containing **1** or **2** were open to the atmosphere through a condenser while samples containing **3** were stoppered and sealed with Teflon tape. For degassed samples, three freeze–thaw cycles were used before sealing to a residual pressure of $<2 \times 10^{-5}$ Torr (1 Torr = 133.3 Pa).

After irradiation the CdS was removed by filtration through Celite and cotton wool and the product analysed using a Varian 3700 gas chromatograph equipped with a flame ionization detector connected to a Hewlett Packard 3390A integrator. The mass balance was monitored by the use of calibrated internal standards (normal alkanes) added prior to irradiation. The CdS (usually Fisher) was used as received unless otherwise specified.

Because of difficulties with reproducibility, a more rigorous procedure was employed in reactions of **3**. To ensure homogeneity of **3**, *cis*-**3** was ground to a fine powder and mixed well. All samples were prepared, transported, and manipulated in the dark. Two filters were used in series, having cut-off wavelengths of 400 and 430 nm. The sample holder was a rigidly fixed aluminum block, and the lamp, the sample, and its holder, as well as the path of light between the lamp and the sample, were completely shielded to eliminate stray light. The stirring rate and stirrer position were optimized and kept constant and the lamp was run for 45 min prior to irradiation.

The products of oxidation were isolated by thin-layer chromatography and derivatives were prepared (ethanolic 2,4-dinitrophenylhydrazine). Potassium ferrioxalate actinometry was used (12). A Corning 558 filter and a Corning cut-off filter (430 nm) were used to allow only wavelengths between 430 and 480 nm to enter the sample cell. A wire mesh screen was used to reduce the light intensity where required. The *cis* → *trans* conversion was kept below 15% to minimize the reverse reaction. The approximate quantum yield for the photoisomerization of **3** (using Strem Luminescent CdS) was 3.3 ± 0.2, assuming all incident light was absorbed.

Cyclopropane preparation

The preparation of compounds **2** and **3** closely followed the method described by Overberger *et al.* (13*a*). Compound **1** was formed as a liquid (30% *cis*, 70% *trans*) and was chromatographed until it was transparent to 350 nm. Compound **2** was formed in 10% yield as a 95:5 mixture of the *trans* and *cis* isomers. Crystallization (methanol) resulted in the separation of >99% *trans*-**2**, mp 80.0–80.5°C. Direct irradiation of *trans*-**2** (Pyrex) resulted in a 50% conversion to *cis*-**2**. Purification by chromatography (CH_2Cl_2; silica gel) and crystallization (methanol) resulted in crystals (25% *cis*, 75% *trans*-**2**), used for experimentation. A sample of 95% pure *cis*-**2** isomer was prepared (oil) by preparative gas chromatography (10% OV-101 on Chromasorb W 80–200 mesh, 200°C).

Compound **3** was formed (57%, based on bis-(*p*-methoxy)chalcone) as a mixture of (14% *cis* and 86% *trans*) isomers. Greater than 99% isomerically pure *cis*-**3** and *trans*-**3** were separated by fractional crystallization from methanol; *trans*: mp 69.5–69.8°C (lit. (13) mp 70.5–71.0°C); *cis*: mp 57.5–58.0°C (lit. (13) mp 56.0–58.0°C).

TABLE 2. Dark reaction of **3** on Fisher CdS: Effect of washing and drying CdS

	% *trans*	
Conditions[a]	Initial	Final[b]
Untreated	3	47
Dried at 100°C	3	51
Washed 3 times, dried	3	12.6
Washed 8 times, dried	3	6.4
Wet only	3	54

[a]One-hour stirring of samples in foil wrapped vessels.
[b]Average of four samples.

TABLE 3. Effect of electron donors on the reaction of **3**

Quencher[a]	E_{ox} vs. SCE	[*Q*]	% Conversion[d]	
No quencher	—	—	12.8	13.2
DABCO	1.0[b]	8.9×10^{-4}	0.0	0.9
DIPA	1.3[b]	4.9×10^{-4}	0.0	0.0
TMB	1.1[c]	12×10^{-4}	3.1	3.1
QMB	0.81[c]	10×10^{-4}	3.5	2.9
QMB	0.81[c]	5×10^{-6}	6.3	

[a]DABCO = 1,4-diazobicyclooctane; DIPA = diisopropylamine; TMB = 1,2,4-trimethoxybenzene; QMB = 1,2,4,5-tetramethoxybenzene.
[b]See ref. 14*a*.
[c]See ref. 14*b*.
[d]Initially 0.0% *trans*; 15 min $h\nu$; [**3**] = 7.9×10^{-3} *M*; % conversion tabulates results of two separate irradiations.

Results

Compound *cis*-**3**, in the presence of CdS, isomerized rapidly (50% conversion in 15 min, 150-W lamp) to the *trans* isomer when irradiated at wavelengths longer than 430 nm. The ^{1}H nmr analysis confirmed the identity of the product. The mass balance for isomerization was over 95%. In the absence of CdS there was no reaction following irradiation, after the elimination of an acid catalysed isomerization by prior percolation of the solvent through alumina.

On Fisher CdS a fast dark reaction of **3** occurred (40% conversion in 1 h), which was quenched by addition of 1,2,4,5-tetramethoxybenzene (QMB). There was no dark reaction of **3** on CdS from other suppliers. Drying Fisher CdS under vacuum at 100°C or wetting it by storage in a highly humid environment had no significant effect on the dark reaction, while washing three times with distilled water and drying at 100°C in air for 24 h decreased but did not eliminate this process (Table 2). The residue obtained by evaporating the wash water weighed about 1% of the mass of the CdS sample and was found, by itself, to cause a dark reaction of **3**. Addition of Fe^{3+} in amounts equal to and 100 times greater than the supplier's assay of Fe^{3+} content in Fisher CdS (0.007%) to an inactive CdS sample (Strem Luminescent) was found not to induce a dark reaction.

The light-induced reaction of **3** on CdS could be entirely quenched by degassing or partially quenched by the addition of the electron donors (Table 3) (QMB), 1,2,4-trimethoxybenzene (TMB), 1,4-diazobicyclooctane (DABCO), and diisopropyl

Can. J. Chem. Downloaded from www.nrcresearchpress.com by 78.46.186.204 on 09/07/12
For personal use only.

amine (DIPA). Approached from both sides, the equilibrium composition for the photoisomerization of **3** on Strem Luminescent CdS was 95% *trans*, 5% *cis*.

Reproducibility of the reaction of **3** was a continuing problem. Using Fluka purissim, Aldrich Gold Label, or Strem Luminescent cadmium sulfide samples, photoreactions of **3**, conducted using a single stock solution and using the special procedure described for **3**, had an error of ± 10%, limiting the extent of any quantitative work. The acid sensitivity of **3** is known (15).

Compound **2** was found to isomerize on both illuminated Fisher CdS and in the dark on the same CdS. The reaction under irradiation was six times faster than in the dark. This dark reaction limited the scope of investigation using **2**. The light reaction of **2** was quenched by addition of QMB but the dark reaction remained. The equilibrium composition was found to be 95% *trans*, 5% *cis*. In contrast, no reaction of **1** occurred after 4 h of irradiation with a 1-kW lamp in the presence of Fisher CdS.

Irradiation of **1** in the presence of air and ZnO at $\lambda > 340$ nm resulted in the formation of three products. These were separated by tlc, and identified as benzaldehyde, acetophenone, and chalcone (1,3-diphenylpropenone). No reaction occurred in the absence of semiconductor. A freshly prepared product mixture was found to contain material that formed a red spot on a tlc plate when sprayed with acidic iron ammonium sulfate and ammonium thiocyanate, indicating the presence of a peroxide (11). This spot had a very much greater R_f than did either perbenzoic acid or hydrogen peroxide, which also turned red under this treatment.

Prolonged irradiation of **3** in the presence of CdS resulted in oxidation to form *p*-anisaldehyde, characterized as its 2:4 dinitrophenylhydrazone, and *p*-methoxyacetophenone, tentatively identified by its gc retention time and nmr spectrum. Prolonged irradiation of **2** also resulted in oxidation to form many unidentified products.

Discussion

All of the reactions induced by irradiation in the presence of semiconductor were quenched by the addition of electron donors. This is taken as evidence of electron transfer mechanisms involving formation of the radical cations of the cyclopropanes.

Cyclopropanes **2** and **3** but not **1** underwent rapid photoisomerization on CdS and were oxidized by prolonged irradiation. Compound **1**, on the other hand, was only efficiently oxidized on ZnO. This observation is not unexpected, since the oxidation potential of *cis*-**1** may be higher than the valence band of CdS in CH_2Cl_2, (i.e., electron transfer may be endergonic, hence slow (16)) and the oxidation potential of *trans*-**1** is very close. The actual position of the valence band of CdS in CH_2Cl_2 is not known.

On ZnO, which has a valence band potential (+2.4 V vs. SCE) (5*a*) higher than the oxidation potential of **1**, oxidation of **1** occurred, producing chalcone, benzaldehyde, and acetophenone: the same products were formed by homogeneous photocatalysis (4). It has been proposed that the DCA-sensitized oxidation of 1,2-diarylcyclopropanes proceeds via addition of either superoxide ($O_2^{\ddagger}$) or triplet oxygen to the cyclopropane radical cation to form a dioxolane (4). Prolonged irradiation or thermolysis of the dioxolane prepared from **3** was reported to yield 1,3-bis(4-methoxyphenyl)-1-hydroxypropan-3-one, *p*-anisaldehyde, and *p*-methoxyacetophenone (4*c*). An analogous route to the similar oxidation products from **1** and **3** using semiconductor catalysts is supported by the oxidation of **1** on ZnO, where there is evidence for the formation of a peroxide that was neither hydrogen peroxide nor perbenzoic acid, and which may be a dioxolane.

A mechanism can be proposed for the oxidation of **1**, **2**, and **3** on illuminated semiconductors. The radical cation is formed by electron transfer from the substrate to the photogenerated hole, while $O_2^{\ddagger}$ can be generated by electron transfer from the conduction band to oxygen.[3]

The *cis* and *trans* isomerization of compounds **2** and **3** on illuminated CdS occurred rapidly, while no isomerization of **1** was observed on either ZnO or CdS (4, 17). The radical cation of 1,2-diphenylcyclopropane **1** has been shown to maintain bonding between c_1 and c_2: CIDNP effects observed during photoinitiated electron transfer to chloranil or 9-cyanophenanthrene show that the radical cation of **1** is formed, but that it does not isomerize (17). In **1**, bearing no electron donating groups to stabilize the radical cation, there is a strong interaction in the benzylic π orbitals, resulting in the formation of a relatively strong one-electron, two-centre bond (17, 18). In cyclopropanes **2** and **3**, delocalization of the positive charge of the radical cation is provided by the electron donating groups, resulting in a weaker bond and a lower barrier to *cis–trans* isomerization.

The equilibrium compositions reached in the CdS catalysed isomerization of **2** and **3** are the same as that found in the homogeneous electron transfer reaction. This composition resembles that expected for a thermodynamic equilibrium between the *cis* and *trans* closed shell isomers. If every step of the radical cation route from one isomer to the other follows the principle of microscopic reversibility, then indeed these equilibria will be identical, but this has yet to be demonstrated. For comparison, acid catalyzed isomerization of **3** results in an equilibrium composed of 96% *trans*-**3** (15*a*). In contrast, triplet sensitization of **3**, where the principle does not hold, leads to a photostationary state containing ~70% *cis* isomer.[4]

The quantum yield for the photoisomerization of **3** on CdS was determined to be 3.3 ± 0.2 (at < 15% conversion), showing that the radical cation mediated reaction proceeds via a chain mechanism, propagated as follows:

[1] $\quad c^{\ddagger} \rightleftharpoons t^{\ddagger}$

$$t^{\ddagger} + c \rightleftharpoons t + c^{\ddagger}$$

The oxidation potential of *cis*-**3** is 0.95 V vs. SCE, while that of *trans*-**3** is 0.85 V vs. SCE. Even with slight endergonicity, chain propagation can, apparently, compete favourably with termination reactions (16) such as back electron transfer from the electron in the semiconductor conduction band.

Quenching by good electron donors is evidence supportive of an electron transfer mechanism for the reaction of **3**. Such quenching is more effective when the oxidation potential of the quencher is less than that of the substrate (1, 2, 19). This is interpreted as quenching by electron transfer to the radical cation of the substrate. It is therefore surprising that quenching by TMB, having an oxidation potential higher than that of **3**, is as efficient as quenching by QMB. This may be explained in at least two ways. The quenching may occur primarily by quenching of the valence band hole. Any electron donor with an oxidation potential low enough for electron transfer to CdS,

[3]This electron transfer is electrochemically allowed. E_{red} O_2 = −0.82 V vs. SCE (14*c*); conduction band = −0.85 V vs. SCE (5).

[4]Sensitization of **3** with benzophenone led to *cis–trans* isomerization. When approached from both sides, the equilibrium composition neared 70% *cis*. Other products were formed (~5%).

Can. J. Chem. Downloaded from www.nrcresearchpress.com by 78.46.186.204 on 09/07/12
For personal use only.

particularly one adsorbed strongly on the catalyst, may quench by this process, thus preventing initiation of the radical cation chain mechanism. Alternatively, quenching may still be occurring by less than diffusion controlled quenching of the radical cations themselves, thus terminating the chain reaction. Fifty per cent quenching by QMB was observed at concentrations as low as $5 \times 10^{-6} M$, which was less than 0.1% of the concentration of **3**, so it is unlikely that the quenching occurred by preferential occupation of all the active surface sites on CdS.

Some observations lend credence to the suggestion that it is the valence band hole which is quenched. Quenching by the amines 1,4-diazobicyclooctane and diisopropylamine, presumably by electron transfer, was more effective than quenching by the methoxybenzenes, and this was true for either electron donors with oxidation potentials above that of **3** (TMB, DIPA) or for donors with oxidation potentials below (QMB, DABCO). The amines may quench the reaction in part by occupying the more active sites on the catalyst, thus preventing adsorption and electron transfer by 3; the amine will, because of stronger adsorption on the CdS surface, be more effective in transferring an electron to the valence band hole than **3** or the methoxybenzenes. Quenching by the amines may not only be by electron transfer, but also by the neutralization of any acidic sites on the CdS surface: the reaction does not persist when the illumination ceases.

Quenching by termination of the radical cation chain requires that there be endergonic electron transfer from the quencher to **3**. This is not impossible, since the chain is itself propagated by an endergonic electron transfer, but is not likely in view of the expected reversibility of such electron transfer and the substantial quenching by QMB at concentrations 1000 times lower than that of the substrate. Further, endergonic quenching should be less efficient than exergonic: this was not observed either for the methoxybenzenes or amines. ΔG for the chain propagation steps and for this endergonic quenching is approximately 2–3 kcal/mol^{-1}. For such a change in free energy the rate constant for electron transfer in homogeneous systems might be expected to be near 10^8–10^9 L mol^{-1} s^{-1} (20) as against 10^{10} for an exergonic process.

Molecular oxygen probably plays a role in the stabilization of the electron-hole pair, possibly by prolonging the lifetime of the e^-/h^+ pair by accepting a photogenerated electron from the semiconductor conduction band to form adsorbed superoxide ($O_2^{\cdot-}$) (3, 21, 22, 23). Return of electrons trapped in chemisorbed oxygen to the conduction band is extremely slow at room temperature in the dark (26). An alternative rationalization of the effect of oxygen is that it may, as a strongly adsorbed electron acceptor, cause greater polarization in the charge depletion layer of CdS and in the layer of adsorbate than in its absence (22, 24, 25). The increased electric field would increase the band bending, accelerating the charge separation of the hole and electron and lowering the potentials of the conduction and valence bands.

In conclusion, it may be pointed out that one of the disadvantages of the use of homogeneous electron transfer photocatalysts is that they may react chemically with the substrate (for one example among many see ref. 27). In addition, back electron transfer from the sensitizer radical anion to the substrate radical cation may result in formation of an excited state of the substrate: this has been observed, for instance, for the 1,4-dicyanonaphthalene sensitized reaction of **1** (17). Both of these complications are avoided by the use of semiconductor catalysts, which act only to form the radical cation. Back transfer to give the substrate triplet plus two doublets on the semiconductor does not yet appear to have been observed. Disadvantages of heterogeneous systems can be low efficiency, especially if a chain is not involved, and a possible susceptibility to irrelevant surface-catalysed side reactions.

Acknowledgments

The authors are grateful to Mr. A. M. Draper for oxidation potential measurements and to the Natural Sciences and Engineering Research Council of Canada for financial support.

1. (*a*) A. M. Draper, M. Ilyas, P. de Mayo, and V. Ramamurthy. J. Am. Chem. Soc. **106**, 6222 (1984); (*b*) R. A. Barber, P. de Mayo, and K. Okada. J. Chem. Soc. Chem. Commun. 1073 (1982).
2. (*a*) H. Al-Ekabi and P. de Mayo. J. Phys. Chem. **89**, 5815 (1985); (*b*) T. Hasegawa and P. de Mayo. Langmuir, **2**, 362 (1986); S. Yanagida, K. Mizumoto, and C. Pac. J. Am. Chem. Soc. **108**, 647 (1986).
3. K. Okada, K. Hisamitsu, and T. Mukai. J. Chem. Soc. Chem. Commun. 941 (1980).
4. (*a*) K. Mizuno, N. Kamiyama, and Y. Otsuji. Chem. Lett. 477 (1983); (*b*) K. Mizuno and Y. Otsuji. Chem. Lett. 1059 (1983); (*c*) K. Mizuno, N. Kamiyamu, N. Ichinose, and Y. Otsuji. Tetrahedron, **41**, 2207 (1985).
5. (*a*) A. J. Bard and P. A. Kohl. J. Am. Chem. Soc. **99**, 7531 (1977); (*b*) J. J. Ramsden and M. Grätzel. J. Chem. Soc. Faraday Trans. 1, **80**, 919 (1984).
6. P. C. Wong and D. R. Arnold. Tetrahedron Lett. **23**, 2101 (1979).
7. T. Mukai, K. Sato, and Y. Yamashita. J. Am. Chem. Soc. **103**, 670 (1981).
8. K. Mizuno, J. Ogawa, M. Kamura, and Y. Otsuji. Chem. Lett. 731 (1979).
9. H. D. Roth and M. L. M. Schilling. J. Am. Chem. Soc. **101**, 1898 (1979).
10. S. Kuwata, Y. Shigemitsu, and Y. Odaira. J. Org. Chem. **21**, 3803 (1973).
11. J. C. Touchstone and M. F. Dobbins. Practice of thin layer chromatography. John Wiley and Sons, New York. 1978. p. 199.
12. J. C. Calvert and J. N. Pitts, Jr. Photochemistry. John Wiley and Sons, Inc., New York. 1969. pp. 783–786.
13. (*a*) C. G. Overberger, N. Weinshenker, and J. P. Anselme. J. Am. Chem. Soc. **87**, 4119 (1965); (*b*) S. G. Beach, J. H. Turnbull, and W. Wilson. J. Chem. Soc. 4686 (1952).
14. C. K. Mann and K. K. Barnes. Electrochemical reactions in non-aqueous systems. Marcel Dekker, New York. 1970. (*a*) p. 252; (*b*) p. 497; (*c*) p. 505.
15. (*a*) L. A. Flippin. Ph.D. Thesis, University of Colorado, Boulder (1980); (*b*) Y. S. Shabarov. Zh. Org. Khim. **9**, 521 (1973); Chem. Abstr. **79**, 41692b (1973); (*c*) L. A. Flippin and M. A. Dombroski. J. Am. Chem. Soc. **108**, 4661 (1986).
16. (*a*) S. Mattes and S. Farid. Organic photochemistry. Vol. 6. *Edited by* A. Padwa. Marcel Dekker, New York. 1973; (*b*) J. Kavarnos and N. J. Turro. Chem. Rev. **86**, 401 (1986).
17. H. D. Roth and M. L. M. Schilling. J. Am. Chem. Soc. **103**, 7210 (1981).
18. (*a*) D. R. Arnold and D. D. M. Wayner. Can. J. Chem. **64**, 100 (1986); (*b*) D. D. M. Wayner and D. R. Arnold. Can. J. Chem. **61**, 2301 (1983).
19. S. Yanagida, H. Kizumoto, Y. Ishimaru, C. Pac, and H. Sakurai. Chem. Lett. 141 (1985).
20. D. Rehm and A. Weller. Isr. J. Chem. **8**, 259 (1970).
21. M. A. Fox. Acc. Chem. Res. **16**, 314 (1983).
22. F. Steinbach. Fortschr. Chem. Forsch. **25**, 117 (1972).
23. J. R. Harbour. J. Phys. Chem. **81**, 1791 (1977).
24. A. J. Nozik. Ann. Rev. Phys. Chem. **29**, 189 (1978).
25. H. Gerisher and F. Willig. Top. Curr. Chem. **61**, 31 (1976).
26. A. Many. CRC Crit. Rev. Solid State Sci. **4**, 515 (1974).
27. A. Albini, E. Fasani, and M. Mella. J. Am. Chem. Soc. **108**, 4119 (1986).

First rotational analysis of the $A^2\Pi$–$X^2\Pi$ system of the $P^{35}Cl^+$ cation

JOHN A. COXON, STAVROS NAXAKIS,[1] AND UTPAL K. ROYCHOWDHURY[1]
Department of Chemistry, Dalhousie University, Halifax, N.S., Canada B3H 4J3

Received October 28, 1986

This paper is dedicated to Professor Douglas E. Ryan on the occasion of his 65th birthday

JOHN A. COXON, STAVROS NAXAKIS, and UTPAL K. ROYCHOWDHURY. Can. J. Chem. **65**, 980 (1987).

The visible $A^2\Pi \rightarrow X^2\Pi$ band system of PCl^+ has been recorded photoelectrically with a resolution of 0.006 nm. Fourteen $^2\Pi_{1/2}$–$^2\Pi_{1/2}$ and six $^2\Pi_{3/2}$–$^2\Pi_{3/2}$ sub-bands of $P^{35}Cl^+$ in the $v' = 0$ and 1 progressions with $10 \leq v'' \leq 20$ have been rotationally analysed. The measured positions of 1214 lines have been fitted directly by least squares to obtain a set of reliable constants for the two states that reproduce the entire data. These constants include the first estimated spin–orbit coupling constants for both states. The reliability of these estimates is discussed. The equilibrium internuclear separations are $r_e(X) = 0.1900$ and $r_e(A) = 0.2334$ nm.

JOHN A. COXON, STAVROS NAXAKIS et UTPAL K. ROYCHOWDHURY. Can. J. Chem. **65**, 980 (1987).

Opérant à une résolution de 0,006 nm, on a enregistré le spectre photoélectronique du système des bandes visibles $A^2\Pi \rightarrow X^2\Pi$ du PCl^+. On a analysé, d'un point de vue rotationnel, quatorze sous-bandes $^2\Pi_{1/2}$–$^2\Pi_{1/2}$ et six sous-bandes $^2\Pi_{3/2}$–$^2\Pi_{3/2}$ du $P^{35}Cl^+$, avec des progressions de $v' = 0$ et 1 et $10 \leq v'' \leq 20$. On a fait concorder directement les positions mesurées pour 1214 raies en faisant appel à la méthode des moindres carrés; on en a déduit un ensemble de constantes dignes de confiance pour les deux états et ces constantes permettent de reproduire l'ensemble des données. Ces constantes incluent la première évaluation de constantes de couplage spin–orbite des deux états. On discute de la fiabilité de ces évaluations. Les séparations internucléaires à l'équilibre sont $r_e(X) = 0{,}1900$ et $r_e(A) = 0{,}2334$ nm.

[Traduit par la revue]

Introduction

Spectroscopic information on diatomic Group 5 monohalide cations with 11 valence electrons (e.g. NF^+, PF^+, PCl^+) is rather limited, although the corresponding Group 6 diatomic cations such as O_2^+ (1), SO^+ (2–4), SeO^+ (5), and S_2^+ [2] are relatively well characterised. The ground electronic states of NF^+ (6) and PF^+ (unpublished results quoted in ref. 7) have been identified by photoelectron spectroscopy. A band system of PF^+ has been analyzed vibrationally by Douglas and Frackowiak (8). Very recently, work in this laboratory has led to the first spectroscopic observations of PCl^+ (9) and $AsCl^+$ (10) through vibrational analyses of their visible $A^2\Pi \rightarrow X^2\Pi$ band systems. Until now, the only analysis of a rotationally resolved spectrum for the Group 5 monohalide cations was limited to five red-degraded bands of PF^+ (8). The present paper reports the first rotational spectroscopic analysis of the $A^2\Pi$–$X^2\Pi$ system of PCl^+.

In our low resolution study of this system of PCl^+, excited by the reaction of discharged helium with PCl_3, an extensive band spectrum was observed over the range 400–700 nm. In view of the weakness of the source, it was necessary to limit the present work to a selected group of fourteen of the most intense bands of $P^{35}Cl^+$. No attempt was made to investigate any bands of the less abundant isotopic species $P^{37}Cl^+$, even though several heads had been readily identified in the low resolution spectrum. For all fourteen bands of $P^{35}Cl^+$, the recorded spectra were exceptionally clean and free of overlap from any other species. The bands studied belong to the $v' = 0$ and 1 progressions in the ranges $v'' = 11$–20 and $v'' = 10$, 12–14, respectively. The molecular constants of the Hamiltonians of the two electronic states were fitted directly to the measured line positions of individual bands. Multiple estimates of these constants, which include the first estimates of the spin–orbit coupling constants, were reduced by the method of merging (11, 12) to a reliable set of single-valued constants that reproduce the entire data.

Experimental

The experimental arrangement has been described in detail elsewhere (3). PCl_3 vapour from a side-arm reservoir was introduced into a fast flow system, 5 cm downstream of a helium discharge between two cylindrical tantalum foil electrodes. The flow of PCl_3 vapour was controlled by a Teflon needle valve to optimize the brightness of the visible conical flame. The flow system was pumped by a 160 $m^3\ h^{-1}$ rotary pump (Leybold-Heraeus E150), and the system pressure was maintained at about 500 Pa. A 1.26 m scanning monochromator (Spex 1269), equipped with a 2400 groove mm^{-1} grating blazed at 500 nm, was used for recording the spectra. The slit height and width were 10 mm and 20 μm, respectively. The data acquisition system was fully automated (13) under control of a PDP 11/23 computer (Digital MINC). A uranium hollow cathode lamp was used for wavelength calibration. In a typical calibration for an individual sub-band, 25 uranium lines were fitted with a standard deviation of about 0.0008 nm.

Data fitting

The $A \rightarrow X$ system of PCl^+ is an example of a Hund's case (*a*) → case (*a*) transition. The ground states of numerous other 11-valence electron diatomics are all regular with large spin–orbit coupling constants, in accord with the electron configurations. It is assumed by analogy that the $X^2\Pi$ state of PCl^+ is also regular. The spectrum at low resolution (9) shows well separated sub-bands for both $P^{35}Cl^+$ and $P^{37}Cl^+$ in accord with the selection rules $\Delta\Sigma = 0$ and $\Delta\Omega = 0$ for such transitions. With the assumption of a regular ground state, the present work identifies the sub-bands as $^2\Pi_{1/2}$–$^2\Pi_{1/2}$ and $^2\Pi_{3/2}$–$^2\Pi_{3/2}$, with the more intense $\Omega = 1/2$ sub-bands lying at shorter wavelengths.

The 0–16, 0–17, and 0–18 bands are overlapped by only very weak bands from $v' \geq 1$, and are well separated from corresponding $P^{37}Cl^+$ bands. Both sub-bands were recorded in each case, and showed well-resolved rotational structure even at low *J*-values. Accordingly, these three bands were selected for preliminary assignment by the method of combination

[1]Present address: Unisearch Associates, Inc., 222 Snidercroft Road, Concord, Ont., Canada L4K 1B5.

[2]K. Brabaharan and J. A. Coxon. In preparation.

Can. J. Chem. Downloaded from www.nrcresearchpress.com by 78.46.186.204 on 09/07/12
For personal use only.

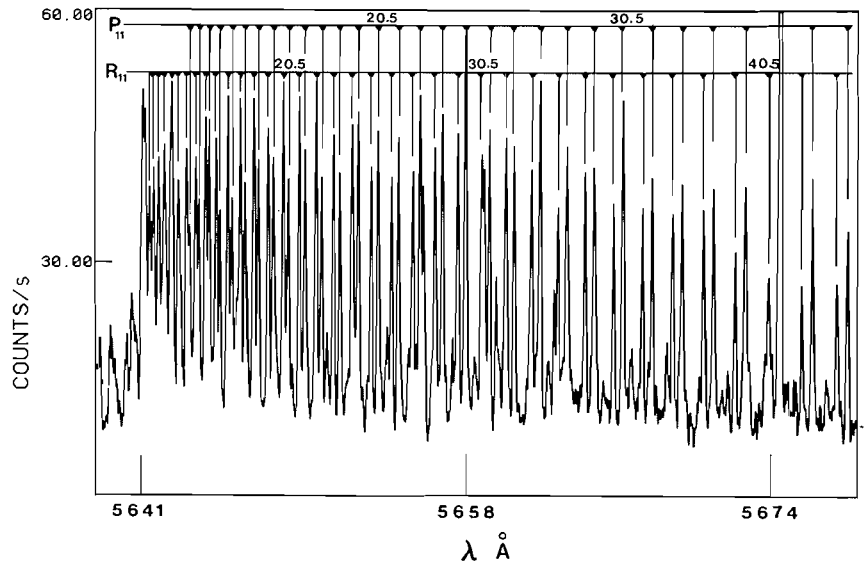

FIG. 1. The $A^2\Pi_{1/2}$–$X^2\Pi_{1/2}$ 0–17 sub-band of $P^{35}Cl^+$. The trace was recorded photoelectrically from the flame of the $He_2^+ + PCl_3$ reaction. The spectral resolution is about 0.006 nm.

differences. Trial sets of combination differences for the upper $v' = 0$ level were formed, leading to unequivocal identification of the P_1,R_1 and P_2,R_2 branch structures and relative J numbering. Absolute J numbering was readily established by the requirement for D_0' to be close to the theoretical value of $4B_e^3/\omega_e^2$. Even at the highest J values, there was no evidence with the spectral resolution (~0.006 nm) of the present work for any Λ-doubling.

Of the 14 bands analyzed, both sub-bands were recorded for only six of the strongest bands in the $v' = 0$ progression with $13 \leq v'' \leq 18$. For these bands, estimates of seven constants (ν_0, B', D', A', B'', D'', A'') could be obtained by fitting directly the measured line positions of both sub-bands. The calculated line positions were given as the differences of the eigenvalues of a standard $^2\Pi$ Hamiltonian (14, 15) containing different parameter values for the upper and lower states. The ability to determine A' and A'' directly in such fits is due to the significantly different values of $Y = A/B$ for the two states, leading to different J dependences of the spin–orbit splittings (16). For the remaining eight bands, only the P_1,R_1 structure of the stronger $^2\Pi_{1/2}$–$^2\Pi_{1/2}$ sub-bands has been assigned. For these bands, A' and A'' were constrained in the fits at approximate values given by preliminary fits of the other bands, and only five constants were adjusted (ν_0, B', D', B'', D''). Errors in the constrained A' and A'' will have negligible effect on the fitted rotational parameters, and are correlated strongly with the band origin estimates.

For several of the bands, the R(J) and P($J - n$) lines were blended over a range of lower J values ($n = 6$ for the 0–20 and 0–19 bands; $n = 5$ for the 0–15, 0–13, 0–12, 1–14, and 1–13 bands). For the 0–14 band, such blending of the R(J) and P($J - 5$) lines occurred for all J values. Although satisfactory fits for individual bands is often possible when the measured positions of such blends are included as data for both transitions, the fitted constants are generally in poor agreement with the constants obtained from bands with resolved structure. The non-linear fitting program used in the present work was modified so that blended line positions were adequately modelled. Calculated blend positions were obtained as intensity-weighted means of the individual R(J) and P($J - n$) positions, with weights taken as the squares of the relative intensities. The relative intensities were calculated from the line strengths and the experimental Boltzmann rotational temperature of 300 K.

Results

A portion of the $^2\Pi_{1/2}$–$^2\Pi_{1/2}$ sub-band of the 0–17 band is shown in Fig. 1. This is a fairly typical trace, and illustrates the quality of the spectra for all the sub-bands recorded in the present work. The two branches, P_{11} and R_{11}, are readily identified, and show little blending with overlapping weak structure of other bands. There is no indication for the presence of a Q branch. Blending of the two branches near the head occurs only at very low J values; such blending occurs over larger J ranges in some of the other $\Omega = 1/2$ and $\Omega = 3/2$ sub-bands. The 0–17, $\Omega = 1/2$ sub-band shown in Fig. 1 was assigned up to $P_{11}(56.5)$ and $R_{11}(61.5)$. At these highest values of J, there was no indication of any broadening of the lines from Λ-doubling.

Table 1 provides a summary of the bands investigated in the present work. The standard deviations ($\hat{\sigma}$) of the final least-squares fits for individual bands (or sub-bands) are tabulated along with the numbers of lines fitted. For the 0–13 to 0–18 bands, both sub-bands were analysed, and values of A' and A'' were estimated from the fits. For all other bands, only the stronger $\Omega = 1/2$ sub-bands were analysed, and A' and A'' were constrained at the values shown in Table 1. The standard deviations lie in the range 0.030 to 0.053 cm^{-1}, in accord with the estimated measurement precision. Fitted band origins are also listed in Table 1; as described in the following section, these estimates were obtained after merging the results for individual bands.

The individual band fits of Table 1 yielded 82 estimated constants, many of which are multiple estimates of the same constants. Single-valued estimates for all the constants were obtained by merging (11, 12) the individual band constants to a new set of 47 constants (Merge 1). Since the estimates of D_v'' in this output set showed no systematic change with v'', it was decided to reduce these 11 constants to a single vibrationally independent parameter D'' (Merge 2). This merge was very

Can. J. Chem. Downloaded from www.nrcresearchpress.com by 78.46.186.204 on 09/07/12
For personal use only.

Can. J. Chem. Downloaded from www.nrcresearchpress.com by 78.46.186.204 on 09/07/12
For personal use only.

TABLE 1. Least squares fits[a] for individual bands of the $A^2\Pi \rightarrow X^2\Pi$ system of $P^{35}Cl^+$

Band	ν_0	A'	A''	N	$\hat{\sigma}$	rms
0–11	21327.179(21)	[99.125]	[285.92]	54	0.0442	0.0442
0–12	20698.269(18)	[99.125]	[285.36]	57	0.0537	0.0709
0–13	20074.777(12)			97	0.0389	0.0381
0–14	19456.673(10)			73	0.0286	0.0282
0–15	18843.984(23)			123	0.0408	0.0471
0–16	18236.605(13)			131	0.0415	0.0413
0–17	17634.812(11)			129	0.0372	0.0372
0–18	17038.642(14)			116	0.0483	0.0491
0–19	16447.943(17)	[99.125]	[281.46]	69	0.0457	0.0476
0–20	15862.639(12)	[99.125]	[280.90]	68	0.0303	0.0297
1–10	22279.140(19)	[99.125]	[286.48]	74	0.0476	0.0496
1–12	21016.069(12)	[99.125]	[285.36]	84	0.0310	0.0304
1–13	20392.612(14)	[99.125]	[284.80]	71	0.0394	0.0387
1–14	19774.386(13)	[99.125]	[284.239]	68	0.0339	0.0351

[a]For each band, N is the number of fitted data, ν_0 is the fitted band origin from Merge 2, A' and A'' are constrained values of the spin–orbit coupling constants, $\hat{\sigma}$ is the standard deviation, rms is the root-mean square of the residuals between the observed and calculated line positions. All data are in cm^{-1} units. Values in parentheses are estimated standard errors in units of the last digit of the corresponding constant.

TABLE 2. Fitted constants[a] for the $A^2\Pi$ state of $P^{35}Cl^+$

v	B_v	$10^7 D_v$	A_v
0	0.187780(87)	2.33(27)	99.72(252)
1	0.186555(85)	2.52(26)	

[a]The results, in cm^{-1} units, are from Merge 2; see text. Values in parentheses are estimated standard errors, in units of the last digit of the corresponding constant.

TABLE 3. Fitted constants[a] for the $X^2\Pi$ state of $P^{35}Cl^+$

v	B_v	A_v
10	0.268684(88)	
11	0.267178(89)	
12	0.265589(87)	
13	0.264072(87)	285.40(251)
14	0.262499(86)	284.82(251)
15	0.260941(88)	284.28(250)
16	0.259367(87)	283.72(251)
17	0.257865(88)	283.38(251)
18	0.256255(87)	282.63(251)
19	0.254763(89)	
20	0.253044(87)	

[a]The results, in cm^{-1} units, are from Merge 2; see text. Values in parentheses are estimated standard errors, in units of the last digit of the corresponding constant. The fitted value $D'' = 1.68(28) \times 10^{-7}$ cm^{-1} was also obtained in this fit.

satisfactory; the variance of the equivalent single step merge to the 37 output parameters of Merge 2 is $\hat{\sigma}^2 = (1.837)^2$ with $f = 45$ degrees of freedom. The upper and lower state constants from this merge are listed in Tables 2 and 3, respectively; the band origins are listed in Table 1.

A third merge was performed in which the ground state rotational constants were represented by a polynomial expansion in $(v'' + 1/2)$. Three coefficients were estimated, B_e'', α_e', and γ_e''. However, this merge was not so satisfactory; the variance of the equivalent single step merge to the 29 output parameters, $\hat{\sigma}^2 = (2.762)^2$ with $f = 53$ degrees of freedom, is appreciably larger than that of Merge 2. There was no significant improvement when either the expansion of B_v'' was carried out to higher order or when the constraint of Merge 2 was not adopted. The result is indicative of small systematic error in some of the estimated B_v''. Nevertheless, the results of Merge 3 provide the best estimates of the equilibrium rotational parameters of the $X^2\Pi$ ground state of PCl^+; these are listed in Table 4, together with other fitted parameters given by Merge 3. Calculated line positions for all the bands analysed in this work have been obtained with the parameters of Merge 2. The calculations include lines that were not measured, and are listed[3] in Table 5 together with the corresponding residuals (observed − calculated positions). The root-mean squares of the residuals for individual bands have been listed in Table 1,

TABLE 4. Molecular parameters[a] for the $X^2\Pi$ and $A^2\Pi$ states of $P^{35}Cl^+$

$X^2\Pi$		$A^2\Pi$	
Parameter	Value	Parameter	Value
B_e	0.28437(21)	B_0	0.18773(13)
α_e	$1.471(21) \times 10^{-3}$	B_1	0.18650(13)
γ_e	$-2.84(66) \times 10^{-6}$		
r_e (nm)	0.1900(1)	r_e (nm)	0.2334(1)
D	1.45×10^{-7}	D_0	$2.12(41) \times 10^{-7}$
		D_1	$2.29(39) \times 10^{-7}$
A_{13}	282.3(35)	A_0	96.6(35)
A_{14}	281.7(35)		
A_{15}	281.2(35)		
A_{16}	280.6(35)		
A_{17}	280.3(35)		
A_{18}	279.5(35)		

[a]The results, in cm^{-1} units, are from Merge 3; see text. Values in parentheses are estimated standard errors, in units of the last digit of the corresponding constant.

[3]Table 5 is too extensive to reproduce here; copies may be purchased from the Depository of Unpublished Data, CISTI, National Research Council of Canada, Ottawa, Ont., Canada K1A 0S2.

and are generally very similar in magnitude to the corresponding standard deviations. This indicates that the parameters of Merge 2 reproduce the entire data very satisfactorily.

Discussion

It is apparent from Table 1 that for all four bands with $v' = 1$, only five fitted constants were obtained from the $\Omega = 1/2$ sub-bands. Not only are the corresponding $1-v''$, $\Omega = 3/2$ sub-bands considerably weaker, they are also overlapped by $0-v''$, $\Omega = 1/2$ sub-bands of the less abundant $P^{37}Cl^+$ ion. Despite this problem, it was possible to make tentative assignments of the P_{22} and R_{22} branches for one of the bands, 1–12. However, attempts to fit these data simultaneously with the $\Omega = 1/2$ transitions were not successful. It was concluded that the $^2\Pi_{1/2}$ and $^2\Pi_{3/2}$ components of $v' = 1$ were associated with different (effective) rotational constants. The possibility that incompatibility between the data for the two sub-bands was due to an unknown error in calibration of the 1–12, $^2\Pi_{3/2}$–$^2\Pi_{3/2}$ sub-band was ruled out since the separations of the R(J) and P($J - 5$) lines were also inconsistent with the B_1' value of the $^2\Pi_{1/2}$ component. A fit of the $^2\Pi_{3/2}$–$^2\Pi_{3/2}$ 1–12 sub-band alone was very satisfactory ($\hat{\sigma} = 0.039\ cm^{-1}$). This fit determined only ν_0 and B_1', with D_1', A_1', B_{12}'', D_{12}'', and A_{12}'' constrained at the values given by Merge 2. The results of this fit, which gave $\nu_0(^2\Pi_{3/2}) = 21013.97(1)$ and $B_1'(^2\Pi_{3/2}) = 0.18692(2)\ cm^{-1}$, are included in Table 5. It is apparent that not only is the fitted B_1' significantly different from that for $^2\Pi_{1/2}$, but also that the fitted origins for the two sub-bands differ by more than $2\ cm^{-1}$. This would imply that A_1' is about $2\ cm^{-1}$ less that A_0'. Since such a large vibrational dependence of a spin–orbit coupling constant would not be expected, the results suggest the existence of an unidentified perturbation of $v = 1$ in the $A^2\Pi_{3/2}$ state.

As shown in Table 4, the variation of A_v'' with v'' is well established with A'' decreasing by $\sim 0.56\ cm^{-1}$ per quantum with increasing v''. The value of A_{17}'' is somewhat out of line with this trend. These statements can be made confidently despite the $\sim 3.5\ cm^{-1}$ standard errors of the spin–orbit coupling constants, since the relative A_v'' values, as well as the differences, $A_v'' - A_0'$, are determined with much greater accuracy. It is possible, in fact, that the absolute values of A_v'' and A_0' are considerably less reliable than is suggested by the quoted standard errors. As mentioned earlier, the ability to discriminate between A'' and A' derives from the different J *dependences* of the spin–orbit splittings. However, the different J dependences for the upper and lower states of a $^2\Pi$–$^2\Pi$ transition may be due only in part to different Y (A/B) values. For a transition in which both Y values are large, the magnitudes of such J dependence become small, and comparable to higher order effects (centrifugal distortion of spin–orbit coupling and second order spin–rotation, which are strongly correlated (14)). As a consequence, the absolute magnitude of the fitted spin–orbit coupling constants obtained from a $^2\Pi$–$^2\Pi$ transition can depend significantly on the corresponding γ (or A_D) values. The precision of the present data did not afford determinations of γ_v for either state, so that to some extent, A' and A'' are effective parameters that absorb unknown spin–rotation/centrifugal distortion effects. Although data of better precision from a future study or from the photoelectron spectrum of PCl might resolve this problem, it is still interesting to comment on the values given in Table 4. The spin–orbit coupling constant in the ground $^2\Pi$ state of PF^+ is well determined (8) from a $^2\Sigma$–$X^2\Pi$ transition as $323.95\ cm^{-1}$. For the isoelectronic species SiF and SiCl, the ground state A'' values are 161.9 (17) and 207.2 (18) cm^{-1}, respectively. If a similar halogen dependence holds for PF^+ and PCl^+, A'' for PCl^+ would be $\sim 370\ cm^{-1}$, considerably larger than the effective value in Table 4. This topic thus merits further investigation.

Acknowledgements

Support from The Natural Sciences and Engineering Research Council of Canada through an Operating Grant and a Graduate Scholarship fo S.N. is gratefully acknowledged.

1. J. A. Coxon and M. P. Haley. J. Mol. Spectrosc. **108**, 119 (1984).
2. D. Cossart, H. Lavendy, and J. M. Robbe. J. Mol. Spectrosc. **99**, 366 (1983).
3. J. A. Coxon and S. C. Foster. J. Mol. Spectrosc. **103**, 281 (1984).
4. J. L. Hardwick, Y. Luo, D. H. Winicur, and J. A. Coxon. Can. J. Phys. **62**, 1792 (1984).
5. J. A. Coxon, S. Naxakis, and A. B. Yamashita. Chem. Phys. Lett. **117**, 235 (1985).
6. J. M. Dyke, N. Jonathan, A. E. Lewis, and A. Morris. J. Chem. Soc. Faraday Trans. II, **78**, 1445 (1982).
7. J. M. Dyke, N. Jonathan, and A. Morris. Int. Rev. Phys. Chem. **2**, 3 (1982).
8. A. E. Douglas and M. Frackowiak. Can. J. Phys. **40**, 832 (1962).
9. J. A. Coxon and S. Naxakis. Chem. Phys. Lett. **119**, 223 (1985).
10. J. A. Coxon, S. Naxakis, and A. B. Yamashita. Spectrochim. Acta A, **41**, 1409 (1985).
11. D. L. Albritton, A. L. Schmeltekopf, and R. N. Zare. J. Mol. Spectrosc. **67**, 132 (1977).
12. J. A. Coxon. J. Mol. Spectrosc. **72**, 252 (1978).
13. L. Ramaley, S. C. Foster, and J. A. Coxon. Chem. Biomed. Environ. Instr. **12**, 229 (1982–83).
14. J. A. Coxon. Can. J. Phys. **58**, 933 (1980).
15. J. M. Brown, E. A. Colbourn, J. K. G. Watson, and F. D. Wayne. J. Mol. Spectrosc. **74**, 294 (1979).
16. G. Herzberg. Spectra of diatomic molecules. 2nd ed. Van Nostrand, Princeton. 1950.
17. J. W. C. Johns and R. F. Barrow. Proc. Phys. Soc. (Lond.) **71**, 476 (1958).
18. R. D. Verma. Can. J. Phys. **42**, 2345 (1964).

Can. J. Chem. Downloaded from www.nrcresearchpress.com by 78.46.186.204 on 09/07/12
For personal use only.

Selective extraction of trace metals associated with hydrous aluminum oxides

JANECE SLAVEK AND WILLIAM FREDERICK PICKERING
Chemistry Department, University of Newcastle, N.S.W., 2308, Australia

Received September 29, 1986

This paper is dedicated to Professor Douglas E. Ryan on the occasion of his 65th birthday

JANECE SLAVEK and WILLIAM FREDERICK PICKERING. Can. J. Chem. **65**, 984 (1987).

In soil/sediment analysis, subdivision of trace metal content into different categories is usually based on selective extraction schemes. To assess the disposition of metal ions bound to aluminum hydrous oxides in such schemes, suspensions of $Al(OH)_3$ gel, gibbsite, or alumina were loaded with up to 5 μmol of Cu, Pb, Cd, or Zn ions prior to being extracted for 24 h with one of fifteen different chemical solutions. The percentage of sorbed ion retrieved varied along the reagent sequence: NaCl, $CaCl_2$ < $MgCl_2$, NH_4NO_3 < CH_3COONH_4, Na citrate, $Na_4P_2O_7$ < EDTA, DTPA < CH_3COOH, $H_2C_2O_4$, HCl, HNO_3. In each system, the recovery value varied with the initial surface loading (a function of sorption pH) and reflected changes in metal species form, e.g., bonded M^{2+}, (MOH^+), $M(OH)_2$. With low loading levels up to 40% was displaced by salt solutions; with 1 to 2 μmol sorbed, as little as 10% was displaced by acids or complex formers but this increased to ~90% with higher loadings. The relationship between sorption pH, amount sorbed, and extraction value was complex, and since in selective extraction schemes classification is based on recovery values, changes in initial retention parameters (e.g. system pH) lead to varying fractions of the different metal ions being classified as "ion exchangeable", "chemisorbed", and "incorporated in the lattice".

JANECE SLAVEK et WILLIAM FREDERICK PICKERING. Can. J. Chem. **65**, 984 (1987).

Lors de l'analyse des sols et des sédiments, la subdivision des échantillons en diverses catégories d'éléments contenus à l'état de trace est généralement basée sur des schémas d'extractions sélectives. Pour évaluer la disponibilité des ions métalliques liés à des oxydes hydratés d'aluminium dans de tels schémas, on a chargé des suspensions de $Al(OH)_3$, de gibbsite ou d'alumine avec des quantités allant jusqu'à 5 μmol d'ions Cu, Pb, Cd ou Zn avant de les extraire pendant 24 h avec l'une des solutions chimiques décrites plus loin. Les pourcentages d'ions adsorbés que l'on a pu récupérer varient selon la séquence suivante des réactifs : NaCl, $CaCl_2$ < $MgCl_2$, NH_4NO_3 < CH_3COONH_4, citrate de Na, $Na_4P_2O_7$ < EDTA, DTPA < CH_3COOH, $H_2C_2O_4$, HCl, HNO_3. Dans chacun des systèmes, la quantité de produit qui est récupérée varie avec le chargement initial de la surface (qui est une fonction du pH de l'adsorption) et elle est un reflet des changements dans la forme des espèces métalliques, comme M^{2+}, (MOH^+) ou $M(OH)_2$. Lorsque les quantités de métaux qui sont chargées sont faibles, des niveaux allant jusqu'à 40%, les métaux sont déplacés par les solutions de sels. Lorsqu'on fait adsorber de 1 à 2 μmol, il n'y a que 10% des métaux qui sont déplacés par les acides ou par les composés pouvant former des complexes; toutefois, cette quantité croit jusqu'à 90% avec des chargements plus élevés. La relation entre le pH d'adsorption, la quantité adsorbée et la valeur de récupération est complexe; puisque la classification des schémas d'extractions sélectives est basée sur les valeurs de récupération, des changements dans les paramètres de rétention initiale (comme le pH du système) conduisent à des fractions variables d'ions métalliques différents qui sont classifiés comme "échangeables", "chemisorbés" ou "incorporés au réseau".

[Traduit par la revue]

Introduction

Only a small fraction of the trace element content of soils and sediments is liable to be "biologically active". In recognition of this, analysts have developed a series of chemical extraction schemes which attempt to subdivide total contents into segments which bear labels such as "detrital (or residual)", "non-detrital", "ion exchangeable", "bound to carbonates", "organically bound", or "associated with hydrous oxides". In respect to the latter group, most of the extended "fractionation" procedures include steps which help identify the fraction of total element content associated with the Mn(IV) and/or Fe(III) oxide components (1, 2). None of the analytical methods, however, attempt to identify the amount associated with hydrous aluminum oxides, a soil/sediment component formed during weathering of alumino-silicate minerals or via hydrolysis of leached aluminum salts. The Al–hydroxy species can control the pH of acid soils (3) and can sorb both metal ions (4, 5) and anions (e.g. F^- (6)).

The omission of analytical procedures for identifying the Al-bound metal fraction could arise from the bland assumption that treatments which disrupt Fe(III) or Mn(IV) oxides should simultaneously release ions bound to Al oxides. Alternatively, it may arise from limited knowledge of sorbed metal ion behaviour.

The chemical and structural form of the Al species found in environmental samples depends on the source, and the conditions prevailing during the aging cycle. The hydrogel $[Al(OH)_3]$ formed by hydrolysis of Al(III) salts (pH 3 to 9) spontaneously loses water to form the polyhydroxide known as β-aluminum hydroxide. On aging, this gradually converts to boehmite (AlOOH) and gibbsite ($Al_2O_3 \cdot 3H_2O$) (7, 8). These transitions are accompanied by: (*i*) a change from amorphous to crystalline structural form. During the structural rearrangement, incorporation of favored ion (e.g. Mg, Ni, Zn) can occur, and it has been postulated (9) that this results in two types of cation adsorption, namely, specific and non-specific (i.e. displaceable by Ba^{2+}); (*ii*) a significant decrease in acid or base solubility; and (*iii*) a reduction in the adsorptive capacity for metal ions (e.g. freshly precipitated gel's capacity for Zn^{2+} (~160 mmol/kg) was found to be tenfold that of aged oxide, and corresponded to a tenfold difference in surface area (10)).

During the sorption of metal ions H^+ are displaced, and the specific sorption of divalent cations to fresh gel may involve coordination to two (or even three) surface —OH groups. Metal ion uptake tends to vary from very little to near total uptake over a narrow (1–2 unit) pH range, and if selectivity is defined in terms of the pH required for 50% retention (pH_{50}), then the sequence is Cu(4.8) > Pb(5.2) > Zn(5.6) > Ni(6.3) > Co(6.5) > Cd(6.6) > Mg(8.1) > Ca > Sr(9.2) > Ba (4.5).

On α-Al_2O_3, sorption of Zn, Mn, Co, or Ba from $<10^{-7}$ *M* solutions follows a log adsorption isotherm, with the pH required for 50% retention being virtually independent of

Printed in Canada

Can. J. Chem. Downloaded from www.nrcresearchpress.com by 78.46.186.204 on 09/07/12
For personal use only.

TABLE 1. Percentage of total Al in substrate dissolved by extracting agents

Sorbed Metal	Pb		Cu		Zn		Cd	
Substrate*	A	B	A	B	A	B	A	B
0.5 *M* HCl	75	—	81	6	72	6	68	5
1 *M* HNO_3	78	6	77	6	71	6	81	6
0.5 *M* CH_3COOH	82	2	80	2	80	2		2
0.25 *M* CH_3COOH/ 0.25 *M* CH_3COONH_4	62			2	58	2		2
0.5 *M* $(COOH)_2$	87	8	84	7	86	7	100	8
0.1 *M* $(COOH)_2$/ 0.18 *M* $(COONH_4)_2$	80		77	5		6		8
0.1 *M* $Na_4P_2O_7$	33	13	76	8	72	10	59	14
1.0 *M* Na_3 citrate	59	2	76	2	68	1.5	62	2
0.005 *M* EDTA	27	1	61	2	38	2	29	2
0.005 *M* DTPA	24	6	39	4	19	4	19	7
1 *M* CH_3COONH_4	3		<0.5	<0.5	<0.5	nd	2	nd
1 *M* NH_4NO_3	1	nd	2	<0.5	3	nd		0.5
1 *M* $MgCl_2$	2	<0.5	1	0.5	3	0.5	0.5	nd
0.05 *M* $CaCl_2$	1	0.5	2	nd	3	<0.5	2	<0.5
0.5 *M* NaCl	3	nd	3	<0.5	1	nd	1	<0.5

*Substrates: A, $Al(OH)_3$ gel, aged 24 h; B, α-Al_2O_3. With gibbsite, Al detected was extremely low; e.g. <1% with acid solutions.

concentration (e.g. for Zn, $pH_{50} \sim 6.8$) (11). With Cd sorption, the pH_{50} value shifts to lower regions (e.g. 8.0 to 6.7) when the α-Al_2O_3 suspension concentration is increased (e.g. from 2 to >20 g/L) (12).

γ-Al_2O_3 uptake behaviour is altered by the presence of nitrolotriacetate (NTA), yielding an affinity sequence such as Cu > Zn > Cd > Pb, Ni (13).

In the corundum-type structure of α-Al_2O_3 a layer of Al atoms lies between two layers of oxygen atoms; the γ modification has a spinel-type structure in which the O atoms have an approximate face-centred cubic order with Al atoms occupying half of the octahedral interstices.

It has been proposed (14) that synthetic Fe and Al hydrous oxides serve as useful models for some of the species found in the environment, and in view of the role that these materials can play in soil/sediment chemistry, improved understanding of metal ion desorption processes was deemed to be highly desirable. The results obtained in systematic examinations of the Fe and Mn systems have been published (15, 16). This paper outlines the extraction behaviour observed using hydrous Al oxides loaded with varying amounts of Cu, Pb, Cd, or Zn ions, and a selection of the reagents used in analytical speciation schemes.

Experimental

Adsorbents

A suspension of $Al(OH)_3$ was prepared (as required) by slowly adding NaOH solution to vigorously stirred M/60 $Al(NO_3)_3$ until the pH was ~7. The suspension was kept well stirred and aliquots taken for transfer to vials (~13 mg solid/10 cm^3).

A suspension of A.R. aluminum hydroxide powder (May and Baker, 36% H_2O) containing 2 g L^{-1} was prepared as required. XRD examination of the powder showed it to be predominantly gibbsite.

Suspensions of alumina (2 g L^{-1}) were prepared from chromatography grade Al_2O_3, supplied by May and Baker.

Extraction procedure

Aliquots (10 cm^3) of $Al(OH)_3$ gel or solid suspension (i.e. 13 mg $Al(OH)_3$ gel or 20 mg crystalline solids) were transferred to acid-washed glass vials. An appropriate volume of 0.01 *M* NaOH was then added to raise the system pH and ensure adsorption of a high proportion of the 5 μmol of M^{2+} subsequently added (as 10.0 cm^3 of 5×10^{-4} *M* $Me(NO_3)_2$ solution). With fresh gel and alumina there was a marked pH effect on uptake in the vicinity of pH_{50} and accordingly the amounts sorbed varied between individual vials. Each test solution was diluted to 25.0 cm^3 with demineralised water and the vial was capped before being mixed overnight in an end-over-end stirring unit. The pH of the systems stabilized after about 12 h of mixing.

After this equilibration period, the solid phase was collected on a 0.45 μm (25 mm diameter) membrane (using an Amicon Vacuum manifold unit) and washed with 5.0 cm^3 water. The pH of each aqueous phase was measured using a Philips® Meter, Model 9407, and the Pb, Cu, Zn, or Cd content was determined using a Varian® AA875 Atomic Absorption Spectrometer and appropriate C_2H_2, air flame conditions. (For Al determinations a C_2H_2–N_2O flame was utilised.)

Each filter membrane plus transferred solid was returned to the original vial, and 30.0 cm^3 of extracting solution (selected from the range listed on Table 1) was then added. Care was taken to ensure minimal loss of solid to the walls of the filter vessel. To compensate for random losses or experimental variations, each extraction study was replicated (i.e. more than six samples per reagent). To identify loading effects, most studies were repeated using different initial NaOH additions (i.e. system pH values), in order to vary the amount of M^{2+} sorbed by the substrates. As the pH required for onset of significant adsorption varied with substrate nature and the metal ion involved, suitable conditions had to be determined from trial runs.

The vials containing the solid, membrane, and extractant solution were equilibrated overnight at 25°C in the end-over-end mixer before being centrifuged (and filtered when necessary) to yield a clear aqueous phase which could be analysed for metal content. The AAS unit was calibrated by adding known amounts of metal ion to the same extractant solution as involved in the test study.

The percentage recovery of metal ion was calculated by comparing the μmol M^{2+} found in the extractant against the μmol sorbed in the uptake stage.

Determination of the Al content of extractant solutions provided an indication of the solubility of the substrate in the various reagents, and these results are summarized on Table 1.

Results

With $Al(OH)_3$ gel and Al_2O_3, the effect of pH on uptake followed the pattern reported by earlier workers, that is, uptake increased from low values to near total retention over a narrow

Can. J. Chem. Downloaded from www.nrcresearchpress.com by 78.46.186.204 on 09/07/12
For personal use only.

Can. J. Chem. Downloaded from www.nrcresearchpress.com by 78.46.186.204 on 09/07/12
For personal use only.

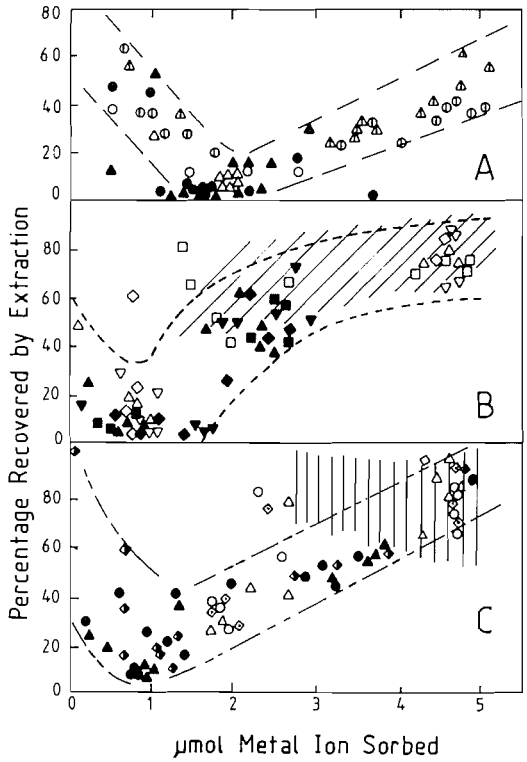

FIG. 1. Effect of amount of metal ion sorbed by substrates on the percentage recovered by 24 h extraction at 25°C. *A*, Cd displaced by NH_4NO_3 (●, ○, ⓘ) or CH_3COONH_4 (▲, △, ⧋). Symbol shading represents data using gibbsite, Al_2O_3 or $Al(OH)_3$ gel, respectively. *B*, Zn displaced using different acid solutions, e.g. HCl (■, □), HNO_3 (◆, ◇), CH_3COOH (▲, △), or $(COOH)_2$ (▼, ▽). The extraction values found using $Al(OH)_3$ gel as substrate fell within the zone defined by sloped shading. *C*, Cu displaced using different complex forming extractants e.g. EDTA (●, ○), DTPA (▲, △), or sodium citrate (◆, ◇). The recoveries obtained using the same reagents on $Al(OH)_3$-sorbed metal ion fell within the area outlined by vertical shading.

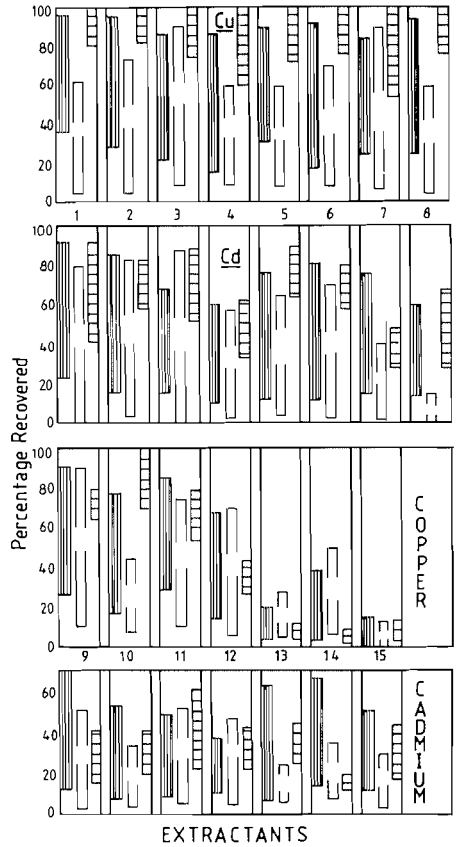

FIG. 2. Block diagram showing the effect of substrate and extractant type on the percentage of sorbed Cu or Cd recovered. Each rectangle indicates the spread of recovery values obtained (covers different amounts sorbed) and shading indicates the substrate: vertical (|||||), Al_2O_3; horizontal (≡≡≡), $Al(OH)_3$ gel; and open box, gibbsite. Reagent code: *1*, 0.5 *M* HCl; *2*, 1 *M* HNO_3; *3*, 0.5 *M* CH_3COOH; *4*, 0.25 *M* CH_3COOH/0.25 *M* CH_3COONH_4; *5*, 0.5 *M* $H_2C_2O_4$; *6*, 0.1 *M* $H_2C_2O_4$/0.18 *M* $(NH_4)_2C_2O_4$; *7*, 0.005 *M* EDTA; *8*, 0.005 *M* DTPA; *9*, 1 *M* sodium citrate; *10*, 0.1 *M* $Na_4P_2O_7$; *11*, 1 *M* CH_3COONH_4; *12*, 1 *M* NH_4NO_3; *13*, 1 *M* $MgCl_2$; *14*, 0.5 *M* NaCl; and *15*, 0.05 *M* $CaCl_2$.

pH range. However, in the presence of the aluminum substrates, metal ion hydrolysis continued overnight, as shown by a drop in pH which ranged from ~1 pH unit using gel to ~0.3 pH units with Al_2O_3 suspensions. These changes, plus aging effects caused the pH_{50} values to vary marginally from those quoted in the Introduction. With gibbsite, slow partial dissolution of the solid (possibly accompanied by secondary formation of gel) led to wide variations (e.g. 15%) in uptake at most pH values. Hence plots of amount sorbed versus pH yielded broad zones rather than steeply sloping curves.

Due to the significant effect of pH on metal ion uptake in all of the systems studied, each replicate tended to adsorb different amounts of metal ion, and this was found to lead to variations in the amount of sorbed metal ion recovered by extraction.

Figure 1 shows the effect of amount sorbed on the percentage recovered in three different systems, and highlights the distinct minimum in uptake values discerned in some of the extraction studies. This minima is considered to correspond to maximum uptake of a MOH^+ species. At higher loadings increasing amounts of $M(OH)_2$ should exist. With lead sorbed on $Al(OH)_3$, the minimum release zone was followed at higher coating levels by an abrupt increase in the percentage extracted. In many of the copper and zinc studies, the percentage of metal ion retrieved increased almost linearly as coating levels increased. By contrast, recovery values using the chloride salts of Na, Ca, or Mg, tended to continually decline as the amount of metal ion initially sorbed increased, that is, there was a gradual change from the maximum values shown on Figs. 1 and 2 (reagents *13* to *15*) to the lower limits indicated by the rectangles.

The trends were complex, and explanation difficult, hence detailed consideration of this aspect has been deferred to a later publication.

The loading effect contributed significantly to the range of recovery values reported in Figs. 2 and 3. On these diagrams the spread of values obtained is indicated by the length of the rectangular plots. Figure 2 highlights the effect (if any) of substrate nature on the extractability of sorbed copper and cadmium ions (Pb and Zn responses were generally similar to one or other of these two studies).

Figure 3 summarises the effect of metal ion on the amount recovered by different extractants using partially aged $Al(OH)_3$ as substrate.

Other factors, besides "loading effects", contributed to the broad spread of results. Perusal of the points shown on Fig. 1, shows that recoveries varied widely even when the amount sorbed by replicates varied little. Partly to blame are experi-

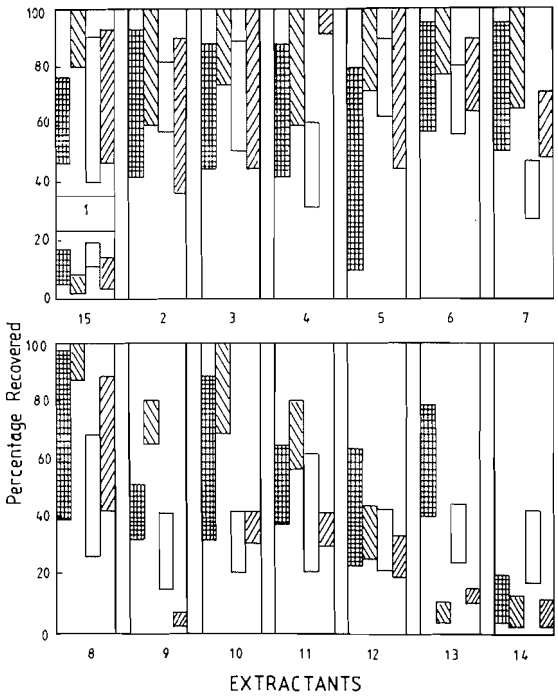

FIG. 3. Diagrams showing the ability of different extractants to retrieve metal ions sorbed on $Al(OH)_3$ gel. Metal ion code: Pb, ▦; Cu, ▧; Cd, □; and Zn, ▨. Reagent code, *1* to *15*, same as for Fig. 2.

mental design limitations (e.g. gel filtration problems, colloid loss during substrate isolation, aging effects, and calculations based on analysis differences). Similar problems were encountered in earlier studies using Fe(III) and Mn(IV) oxides (15, 16), but in these investigations precision was far better (e.g. ±5 to 10% deviation from a mean value).

The "solubility" of the substrate also contributed to system behaviour. As noted in the Introduction, changes in gel structure during aging reduces solubility. In our study, aging (~48 h total) plus chemical interaction with metal ions at the surface reduced gel solubility in acids by about 25% (cf. Table 1). The values quoted are the mean of 5 to 20 determinations, with reproducibility being around ±10%. Variations in matrix dissolution could have contributed to varying amounts of "occluded and/or chemi-sorbed metal ion" being retrieved.

The alumina solubility was quite low, and with gibbsite suspensions (which only slowly reach saturation values (17)), dissolved Al was close to the AAS detection limit. With these materials, metal ion recovery levels were often lower than observed with gel, but loading effects blurred any substrate based trends.

Discussion

Selective extraction of metal ions sorbed on aluminum hydrous oxides

A primary aim of this study was to elucidate the conditions required for release of any metal ion associated with aluminum oxide or hydroxide species in soils and/or sediments.

The diverse results obtained in this controlled study indicate, however, that sorbed metal ions are bonded by several different mechanisms, and the initial loading was only occasionally fully retrieved (cf. upper limits of rectangles drawn on Figs. 2 and 3).

The reagents used included strong acids and EDTA, systems recommended for distinguishing between detrital and non-detrital metal fractions.

The detrital fraction consists mainly of fragments of the original ground rock (in which metals are usually present in lattice structures); the non-detrital material contains weathering products of fine particle size with a high sorptive capacity for metal ions. The sorbed ions may be bound through electrostatic attraction (ion exchangeable), by less definable weak bonding or by compound formation (chemisorption). The reagents tested included many recommended for identifying ion exchangeable fractions, weakly sorbed material and bound to the hydrous oxides of Fe and Mn(IV).

In terms of extraction behaviour, the responses could be grouped under four major headings, namely, *acids*, *complex forming ligands*, *ammonium salts*, and *chloride salts*.

The last two groups embrace reagents used (by some) to evaluate the ion exchange capacity of soils or to estimate the amount of ion exchangeable metal ion present in sediments. A study of Figs. 2 and 3 show that up to 80% of sorbed Pb, Cu, or up to 60% of Cd was occasionally displaced by these reagents. The recovery value varied with the nature of the substrate (Fig. 2), element of interest (Fig. 3), the amount initially sorbed (Fig. 1) and the reagent selected. One ion in this group (Mg^{2+}) was very effective in displacing Pb^{2+}, a result that suggests that a high proportion of sorbed lead was non-specifically bonded.

The enhanced ability of ammonium salts to effectively displace sorbed metal ions may be due to preferential sorption of the small NH_4^+ ion (ionic radius ~ 2.5 Å), complemented by the tendency of Cu, Cd, and Zn to form ammine complexes (with H^+ transfer to surface hydroxyl groups). With acetate salts, formation of aceto-complexes may also contribute to recovery values.

The effective stability of any metal complexes formed, relative to substrate bonding strength, strongly influenced the amount recovered, as shown by the variable responses observed using chelating agents (e.g. EDTA, DTPA, citrate) and complex formers (e.g. oxalate, pyrophosphate). All these reagents form complexes whose structure, charge, and effective stability is a function of system pH and ligand concentration. Some products had limited solubility (e.g. Zn^{2+} with citrate, Pb^{2+}, and $(COOH)_2$). As shown in Table 1, these reagents also partially dissolved gel substrates.

If one accepts the oft assumed premise that complex-forming ligands release both displaceable and chemi-sorbed metal ions, while chloride salts release only the exchangeable fraction, then comparison of the recoveries listed on Figs. 2 and 3 indicates that up to half of the Cu, Pb, and Zn was chemi-sorbed; with Cd non-specific sorption appears to have predominated.

Acid reagents also had the potential to release both weakly held and chemi-sorbed ions, through a combination of substrate dissolution and preferential sorption of H^+ (aided by metal complex formation when using acetic and oxalic acid systems). The total recovery predicted was not achieved, however, due to part of the sorbed material becoming incorporated in a crystal lattice or converted into a sparingly soluble product. The fraction in this category was influenced by the amount of metal ion initially sorbed (cf. Fig. 1).

Specific sorption persists down to quite low initial metal ion concentrations, with at least three bonding modes still involved. In anodic voltammetry studies, using $\mu g\ L^{-1}$ levels of metal ion and acetate buffer solutions, it was found (18) that added $Al(OH)_3$ gel sorbed significant amounts of the nanomoles of metal ion present (even though it existed in solution primarily as aceto-complexes). Sorption by α-Al_2O_3 from $<10^{-7}$ *M*

Can. J. Chem. Downloaded from www.nrcresearchpress.com by 78.46.186.204 on 09/07/12
For personal use only.

Can. J. Chem. Downloaded from www.nrcresearchpress.com by 78.46.186.204 on 09/07/12
For personal use only.

solutions (11) and uptake by γ-Al_2O_3 in the presence of the chelating agent NTA (13) was noted earlier.

With metal ions sorbed on alumino-silicates (e.g. kaolin, illite, montmorillonite) extraction behaviour resembled that reported in this paper in many respects. Most of the sorbed metal ion was strongly held, with pH 3 ammonium oxalate being the most efficient releasing agent, followed by EDTA and acid solutions (19).

Analytical schemes

The absence of specific mention of aluminum-bound metal ion in any of the published selective extraction procedures (cf. refs. 1 and 2) is now understandable, since no single reagent appears to have the capacity to consistently achieve optimum release of this particular sub-category.

Treatment of sediments by any of the published sequential procedures would lead to Al associated material appearing in different segments of the scheme, e.g., a significant part could appear with the ion exchangeable fraction, some would be classified as weakly sorbed, part would be released with the Fe, Mn hydrous oxide sediment, and varying amounts would be detected in the "residual" sub-group.

At this point, it should also be noted that satisfactory procedures for differentiating between extractable forms of Al have yet to be developed. It has been reported, for example, that the approach used for extractable Fe (based on oxalate, dithionite, and pyrophosphate extractions) was less useful for distinguishing between the various forms of Al in soils (20). A more recent study demonstrated that a 4 h extraction with acidified (pH 3) ammonium oxalate was the most efficient single procedure for assessing the amount of translocated Al, Fe, and Si present as inorganic compounds in the non-crystalline weathering products found in podzol B horizon samples (21). A pyrophosphate extraction provided an estimate of the organic bound Al fraction. For evaluating the amount of poorly ordered alumina gels in samples, extraction with cold 5% Na_2CO_3 has been proposed (22).

As shown in our investigation, the precision of determinations based on "selective extraction" can be quite poor. With real samples, this variability may be matched by sampling errors or sample heterogeneity. In addition, only a small fraction of the trace element content may be bonded to Al species.

Bonding modes

Factors which contribute to the observed extraction behaviour include the different types of bonding sites at the surface of aluminium oxide/hydroxide substrates, variations in the chemical form of the sorbed metal ion, ion diffusion into gel structures, and surface charge. Freshly precipitated Al gel has a zero point charge value of around 9.4 (4) while the value quoted for α-Al_2O_3 is 8.8 (11) and since the system pH in the sorption studies was lower than these values the substrates should have maintained a net positive charge during the various sorption cycles.

As pH increases (and more metal ions are sorbed) chemisorption (involving bonding to Al—OH sites) becomes more pronounced. This is preceded or accompanied by proton loss from coordinated water molecules, yielding hydroxy species in which the average $OH^-:M^{2+}$ ratios vary from near zero to two (when all the initial M^{2+} has been sorbed or precipitated). To explain the minima in extraction values noted in some studies (cf. Fig. 1), the solubility of one of the intermediate species (e.g. $\overline{S}MOH$ where $\overline{S}$ is substrate surface) must be lower than that of other species.

In the presence of kaolinite, illite, or montmorillonite clay particles the term $pM + pOH$ remained virtually constant, up to the pH_{50} point (23). This suggested that the sorbed species was probably a polymer having the general formula $(MOH)_x$. When over half of the total metal content had been sorbed/precipitated the term $pM + 2pOH$ became constant, which implied that both sorbed metal ion and precipitated excess had the empirical formula $M(OH)_2$. The presence of particulate matter tends to lower the pH required for metal—hydroxide formation, and the pH associated with 50% precipitation (pH_{50}) varies with substrate composition (for example, using 10^{-4} *M* solutions Pb (or Cd) pH_{50} values range from 3.1 (or 5.8) on hydrous Fe oxide (5) to 5.9 (or 7.3) on clay minerals (19)).

Terminology in extraction studies

For quantitative recovery of sorbed metal ions, an extractant must have the capacity to dissolve aged metal hydroxy polymers, disrupt chemisorption bonds, release occluded material, and displace electrostatically attracted species.

Any reagent capable of performing some, of all, of these tasks in respect to aluminum bound species, will undoubtedly have the potential to displace the same element from other substrates, particularly clays and hydrous iron oxides. Accordingly selective extraction of the aluminum bound fraction appears to be an unattainable goal.

This conclusion highlights the inappropriateness of some of the terminology used in chemical extraction studies. Categories such as hydrous oxide bound, organic bound have limited significance (due to varied bonding modes) and it would be preferable to standardise on a reagent based system (e.g. acetate-buffer soluble; released by pH 3 ammonium oxalate; released by HNO_3, H_2O_2 attack; and so on).

For reasons outlined in review articles, it is equally important to closely specify experimental conditions, for example, reagent concentration, solid-to-liquid ratios, time of contact, and temperature.

Selective extraction procedures have useful applications, but their limitations have also to be recognised.

Acknowledgement

This investigation received financial support from the Australian Research Grants Scheme, and this assistance is acknowledged with thanks.

1. W. F. Pickering. CRC Crit. Rev. Anal. Chem. **12**, 233 (1981).
2. W. F. Pickering. Oregeo Rev. **1**, 83 (1986).
3. B. W. Bache. J. Soil Sci. **25**, 320 (1974).
4. D. G. Kinniburgh, J. K. Syers, and M. L. Jackson. Soil Sci. Soc. Am. Proc. **39**, 464 (1975).
5. D. G. Kinniburgh, M. L. Jackson, and J. K. Syers. Soil Sci. Soc. Am. J. **40**, 796 (1976).
6. C. A. Bower and J. J. Hatcher. Soil Sci. **103**, 151 (1967).
7. V. N. Tikhonov. Analytical chemistry of the elements — aluminium. J. Wiley and Sons, New York. 1973.
8. P. H. Hsu. Soil Sci. Soc. Am. Proc. **30**, 173 (1966).
9. M. Kalbasi, G. J. Racz, and L. A. Loewen-Rudgers. Soil Sci. **125**, 146 (1978).
10. L. M. Shuman. Soil Sci. Soc. Am. J. **41**, 703 (1977).
11. R. T. Lowson and J. V. Evans. Aust. J. Chem. **37**, 2165 (1984).
12. B. D. Honeyman and J. O. Leckie. NSF/CEE Report No. 81088, National Technical Information Services, U.S. Dept. of Commerce, Springfield. 1981.
13. H. A. Elliott and C. P. Huang. Water Sci. Technol. **17**, 1017 (1985).

14. B. D. MITCHELL, V. C. FARMER, and W. J. MCHARDY. Adv. Agron. **16**, 327 (1964).
15. J. SLAVEK and W. F. PICKERING. Water, Air, Soil Pollut. **28**, 151 (1986).
16. J. SLAVEK and W. F. PICKERING. Chem. Geol. **51**, 213 (1985).
17. H. M. MAY, P. A. HELMKE, and M. L. JACKSON. Geochim. Cosmochim. Acta, **43**, 861 (1979).
18. T. U. AUALIITIA and W. F. PICKERING. Water Air Soil Pollut. In press.
19. H. FARRAH and W. F. PICKERING. Water Air Soil Pollut. **9**, 491 (1978).
20. J. A. MCKEAGUE, J. E. BRYDON, and N. M. MILO. Soil Sci. Soc. Am. Proc. **35**, 33 (1971).
21. V. C. FARMER, J. D. RUSSELL, and B. F. L. SMITH. J. Soil Sci. **34**, 571 (1983).
22. V. C. FARMER, B. F. L. SMITH, and J. M. TAIT. Clay Miner. **12**, 195 (1977).
23. H. FARRAH and W. F. PICKERING. Chem. Geol. **25**, 317 (1979).

Can. J. Chem. Downloaded from www.nrcresearchpress.com by 78.46.186.204 on 09/07/12
For personal use only.

Heat capacities and volumes in aqueous polymer and polymer–surfactant solutions

GÉRALD PERRON
Institut National de la Recherche Scientifique, C.P. 7500, Ste-Foy (Qué.), Canada G1V 4C7

JOSÉE FRANCOEUR
Department of Chemistry, Université de Sherbrooke, Sherbrooke (Qué.), Canada J1K 2R1

JACQUES E. DESNOYERS
Institut National de la Recherche Scientifique, C.P. 7500, Ste-Foy (Qué.), Canada G1V 4C7

AND

JAN C. T. KWAK[1]
Department of Chemistry, Dalhousie University, Halifax, N.S., Canada B3H 4J3

Received October 9, 1986

This paper is dedicated to Professor Douglas E. Ryan on the occasion of his 65th birthday

GÉRALD PERRON, JOSÉE FRANCOEUR, JACQUES E. DESNOYERS, and JAN C. T. KWAK. Can. J. Chem. **65**, 990 (1987).

The apparent molar volumes and heat capacities of aqueous mixtures of neutral polymers and ionic surfactants were measured at 25°C. The polymers chosen were poly(vinylpyrrolidone) (PVP) and poly(ethyleneoxide) (PEO) and the surfactants were the C_8, C_{10}, and C_{12} homologs of sodium alkylsulfates and the C_{10}, C_{12}, and C_{16} homologs of alkyltrimethylammonium bromides. The polymer–surfactant interactions depend on the nature of both components and on the chain length of the surfactant. The thermodynamic properties of the cationic surfactants are essentially the same in the absence and presence of polymer indicating little surfactant–polymer interaction. On the other hand, the thermodynamic properties of anionic surfactants are shifted, upon the addition of polymers, in the direction of enhanced hydrophobic association. The effect increases with the surfactant chain length and with the polymer concentration. The effect is larger with PVP than with PEO.

GÉRALD PERRON, JOSÉE FRANCOEUR, JACQUES E. DESNOYERS et JAN C. T. KWAK. Can. J. Chem. **65**, 990 (1987).

Opérant à 25°C, on a mesuré les volumes molaires apparents et les capacités calorifiques de mélanges aqueux de polymères neutres et d'agents de surface ioniques. Les polymères choisis sont la poly(vinylpyrrolidone) (PVP) et poly(oxyde d'éthylène) (POE) alors que les agents de surface sont les homologues C_8, C_{10} et C_{12} des alkylsulfates de sodium et les homologues C_{10}, C_{12} et C_{16} des bromures d'alkyltriméthylammonium. Les interactions polymère/agent de surface dépendent de la nature de chacun de composants et sur la longueur de la chaîne de l'agent de surface. En présence ou en l'absence de polymères, les propriétés thermodynamiques des agents de surface cationiques sont essentiellement les mêmes; ces résultats indiquent qu'il y a peu d'interactions entre le polymère et les agents de surface. Par ailleurs, l'addition de polymères déplace les propriétés thermodynamiques des agents de surface anioniques dans la direction d'une augmentation de l'association hydrophobe. L'effet augmente avec la longueur de la chaîne de l'agent de surface et avec la concentration de polymère. L'effet est plus important avec la PVP qu'avec le POE.

[Traduit par la revue]

Introduction

The interaction of macromolecules and amphiphilic small molecules is of importance in a wide variety of biological systems and industrial processes. Polymer–surfactant systems are also of considerable interest for fundamental studies, because they combine the effects of ionic, dipolar, and hydrophobic interactions, and the aggregates formed provide a new microenvironment, for instance, for hydrophobic solutes. In recent years, polymer–surfactant solutions have been the topic of a large number of investigations, and the solution aspects of these mixtures have been reviewed extensively (1–4). Most of these studies are concerned with the determination of binding isotherms, using techniques such as dialysis equilibrium, surface tension, selective ion electrodes, etc. Generally, it is found that the binding of ionic surfactants by polyions of opposite charge starts at concentrations as much as two orders of magnitude lower than the critical micelle concentration (cmc) of the surfactant. On the other hand, in the case of non-ionic polymers, binding of ionic surfactants occurs close to the cmc. In both cases, hydrophobic interactions between the bound surfactant ion play an important role in the overall aggregation process, as is perhaps most clearly shown in the dependence of the binding constant on the alkyl chain length of the surfactant (5, 6).

In view of the extensive work on binding isotherms, it is perhaps surprising that the determination of thermodynamic parameters other than free energies or activities in these systems has been relatively neglected. Goddard's review (4) only mentions a few direct calorimetric measurements of enthalpies in neutral polymer – ionic surfactant solutions (5, 7). In aqueous electrolyte and non-electrolyte solutions and in micellar systems, the direct determination of thermodynamic quantities such as enthalpies, volumes, and heat capacities has been applied widely. In particular, partial molar volumes and partial molar heat capacities have been shown to be sensitive indicators of hydrophobic interactions in micellar aggregation and in microemulsions (8, 9). In the case of ternary systems such as those considered here, the relevant thermodynamic quantities are more easily expressed in terms of transfer functions (10).

In the present study, the apparent molar volumes and heat capacities of anionic and cationic surfactants have been measured in dilute solutions of two typical water-soluble polymers, poly(vinylpyrrolidone) (PVP) and poly(ethylene oxide) (PEO), and compared with the corresponding properties in water. Any interaction between the surfactant and the polymer should be reflected as a shift in the cmc of the surfactant

[1]To whom correspondence should be addressed.

Can. J. Chem. Downloaded from www.nrcresearchpress.com by 78.46.186.204 on 09/07/12
For personal use only.

TABLE 1. Apparent molar quantities for PEO and PVP in water*

Parameter	Value						
	PEO						
	Exp.	a	b	Exp.	a	b	c
$V_{2,0}$ ($cm^3\ mol^{-1}$)	36.3	36.7 ± 0.2[1] 36.9[3]	38.9	87.6	87.9 ± 0.5[2] 87.1[3]	94	103.5
$C_{p,2,0}$ ($JK^{-1}\ mol^{-1}$)	129	131[3]	133	257	257.2[3]	288	366.4

*Due to the experimental configuration, the volume data are at 24.6°C, heat capacities at 25.0°C. a: literature values; superscript 1, ref. 11 (average of five values); superscript 2, ref. 11 (average of eight values); superscript 3, ref. 17. b: From group additivity using scheme of Cabani *et al.* (17). c: Measured values for 1-*n*-vinyl-2-pyrrolidone (16).

and in the thermodynamic properties in the pre- or post-micellar region. These two non-ionic polymers have been chosen because they have been shown to interact with anionic surfactants, and their solution properties are well known (11). In addition, interactions between these polymers and the anionic surfactants (sodium octyl-, decyl-, and dodecyl sulfate) occur in sufficiently high concentrations to make the direct measurement of molar volume and heat capacity possible.

Experimental

The two techniques used for the measurement of the differences in densities (12) and of relative changes in heat capacities per unit volume (13–15) using a commercial SODEV densimeter (Model 01D) and flow microcalorimeter (Model CPC) have been well described in the literature. The apparent molar quantities of the component i, $V_{i,\phi}$ and $C_{p,i,\phi}$, are calculated from

$$[1] \quad V_{i,\phi} = M_i/d - 1000(d - d^*)/mdd^*$$

and

$$[2] \quad C_{p,i,\phi} = M_i c_p + 1000(c_p - c_p^*)/m$$

M_i is the molar mass of solute i, m the molality in moles per kg of (polymer) solution, and $d - d^*$ is the difference in densities, where the asterisk stands for the reference solvent (pure H_2O or H_2O–polymer solution). The difference in specific heat capacities, $c_p - c_p^*$, is calculated from the relative change in heat capacities per unit volume σ and the densities d (15).

Under the best conditions, differences in densities can be obtained to 3 ppm and relative changes in heat capacities per unit volume to 0.5%. This limits the precise measurements of apparent molar quantities to concentrations above 0.01 mol kg^{-1}.

Sodium octyl- and decylsulfate (NaC_xSO_4) (Eastman Kodak) and sodium dodecylsulfate (BDH, Specially Pure Biochemical) were recrystallized from absolute ethanol. Decyltrimethylammonium bromide ($C_{10}Me_3NBr$) (Eastman Kodak) and $C_{12}Me_3NBr$ and $C_{16}Me_3NBr$ (Sigma Chemicals) were recrystallized from spectrograde acetone. The purified surfactants were washed with diethylether and dried under vacuum at temperatures lower than 60°C to minimize possibilities of decomposition. They were then cooled and kept under vacuum over P_2O_5. Purity of surfactants was checked by surface tension. Note that for octyl- and decylsulfate molar volume in the dilute region, as measured here, is one of the best indicators of purity.

The polymers were used as received; PEO from Polyscience, sample 2L3811, approximate molecular weight 100 000 and PVP from GAF Corporation, sample Plasdone K-25 approximate molecular weight 35 000.

All solutions were prepared by mass using deionized distilled water. The majority of solutions were prepared from a stock solution of the ternary system and diluted with a polymer solution. All measurements were made on the ternary system (water + polymer + surfactant) relative to the binary solution (water + polymer). In the case of PEO, some stock solutions were heated at 55°C for half an hour before dilution to ensure complete dispersion of the polymer. Measurements with these samples were identical, within experimental uncertainty, to the samples that had not been heated.

Results and discussion

The original data for the densities and heat capacities and the derived apparent molar quantities for the surfactants in water and in the polymer solutions, as a function of the surfactant molality, are available from the Depository of Unpublished Data.[2] The microcalorimeter and densimeter were placed in series using the same temperature controller. As a consequence the densities were measured at 24.67°C and the heat capacities at a mean temperature of 25.00°C. The error introduced by this difference in temperature is negligible. Whenever possible, the data in water were compared with values previously measured in our laboratory and the agreement was inside the experimental uncertainty.

Polymers in water

From the data on the binary polymer solutions, it is possible to calculate the apparent molar quantities for the repeating unit of the two polymers. These values can then be compared with those of the literature and with those calculated by group additivity using data on related solutes in water. These results are compared in Table 1. In comparing our present data to those of Riedl (16) and the data collected by Molyneux (11), we note that our values both for $V_{2,\phi}$ and $C_{p,2,\phi}$ agree with those of Riedl within measurement error. Our value for $V_{2,\phi}$ for PVP agrees well with the average given by Molyneux, however in the case of PEO our value is slightly lower (equivalent to 0.824 $cm^3\ g^{-1}$ where Molyneux's average is 0.834). In part this may be due to the concentration difference (up to 0.4 wt% in this work, 2% for most of the data quoted by Molyneux). More importantly, we note that for PEO the measured values for $V_{2,\phi}$ and $C_{p,2,\phi}$ are close to the values calculated from Cabani's group additivity principle (17). This indicates that the polymer is extended and fully hydrated in water, the properties of the polymer in water being equal to the sum of those of the individual groups in water (given the high molecular weight, end effects can reasonably be neglected). The situation is less clear with PVP. The measured value for $C_{p,2,\phi}$ for this polymer is significantly below the group additivity value, and far below the measured value for 1-*n*-vinyl-2-pyrrolidone (17). Intramolecular hydrophobic interactions are known to result in lower molar heat capacity values, thus the lower than expected molar heat capacity for PVP in aqueous solution is an indication of such interactions in the aqueous polymer solution. On the other hand, such interactions

[2]Complete set of data may be purchased from the Depository of Unpublished Data, CISTI, National Research Council of Canada, Ottawa, Ont., Canada K1A 0S2.

Can. J. Chem. Downloaded from www.nrcresearchpress.com by 78.46.186.204 on 09/07/12
For personal use only.

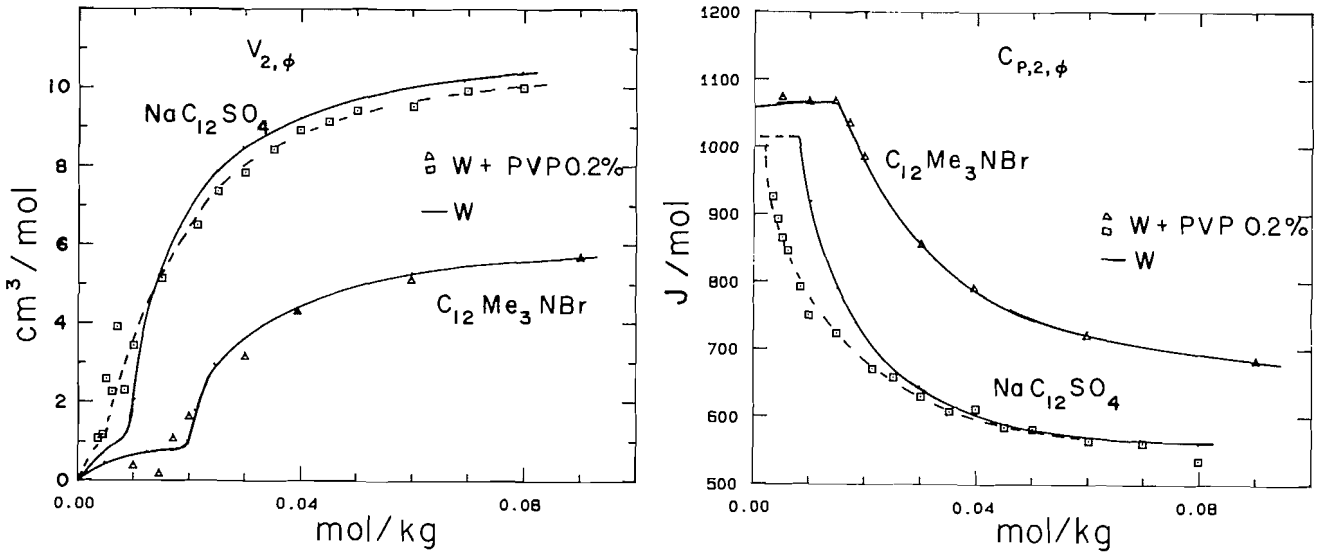

FIG. 1. Apparent molar volumes and heat capacities of typical anionic and cationic surfactants in water (full lines) and in 0.2% PVP (□,△).

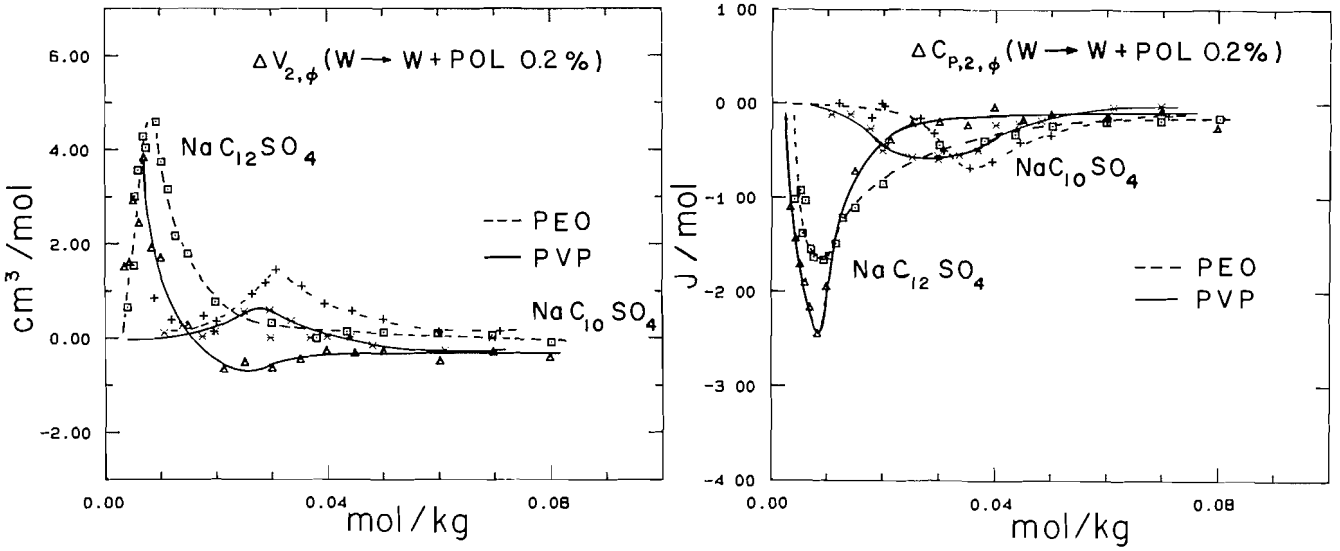

FIG. 2. Changes in apparent molar volumes and heat capacities of sodium alkylsulfates in 0.2% PVP and PEO relative to data in water.

should lead to higher molar volumes (8), contrary to what is observed. Molyneux (11) noted that the low molar volume of PVP in solution, compared to the molar volume of the bulk polymer, is an indication of the "compacting effect" of the polymer on the solvent. A more detailed study of volume changes associated with hydrophobic interactions in these systems would probably be worthwhile.

Polymer–surfactant interactions

Examples of trends of $V_{i,\phi}$ and $C_{i,i,\phi}$ as a function of m, for two types of surfactants in water and in water + polymer solution are shown in Fig. 1. With the cationic surfactants $C_{10}Me_3NBr$ and $C_{12}Me_3NBr$ the values with and without polymer coincide, indicating negligible polymer–surfactant interactions. This is in agreement with what is normally reported for interactions between neutral polymers and cationic surfactants with chloride or bromide counterions (2). Efforts to determine any binding in these systems using surfactant selective electrodes also gave negative results.[3]

[3]N. Ohno and J. C. T. Kwak. Unpublished results.

In the case of anionic surfactants large differences are observed when polymer is added, especially in the region of the cmc. In this region, the data in the polymer solution are more positive for the volumes and more negative for the heat capacities. These changes are as expected for enhanced micellization or hydrophobic interactions (8). As can be seen more clearly in Fig. 2, the deviations start at a definite free surfactant concentration, consistent with the notion of a "first critical concentration" (2, 4, 20, 21), go through a maximum and return close, but not always equal, to zero at high added surfactant concentrations. Unfortunately the calorimetric measurements in particular for SDS do not yield an accurate value for this point of first binding. On the other hand, binding isotherms determined by other methods in particular for SDeS are not very clear (18), making a comparison of the results for the first critical concentrations as obtained by calorimetry and by binding measurements difficult (4, 5, 7, 18–21).

Effect of surfactant chainlength

Differences between the properties of binary systems (water + surfactant) and ternary systems (water + polymer +

Can. J. Chem. Downloaded from www.nrcresearchpress.com by 78.46.186.204 on 09/07/12
For personal use only.

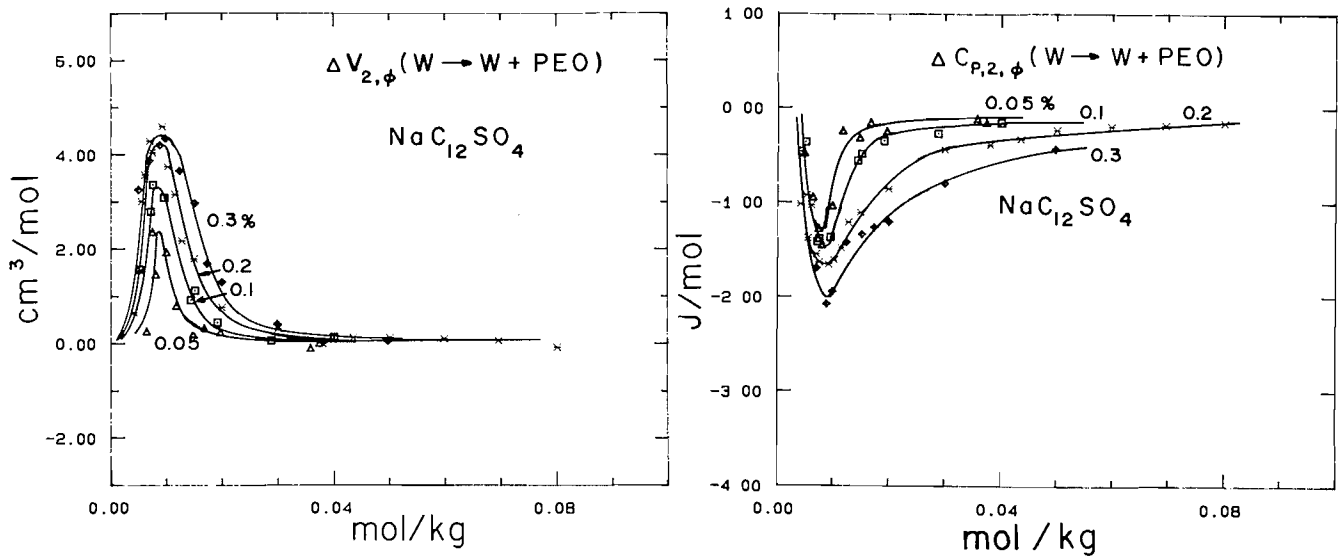

FIG. 3. Changes in apparent molar volumes and heat capacities of sodium dodecylsulfate in PEO of varying concentration relative to data in water.

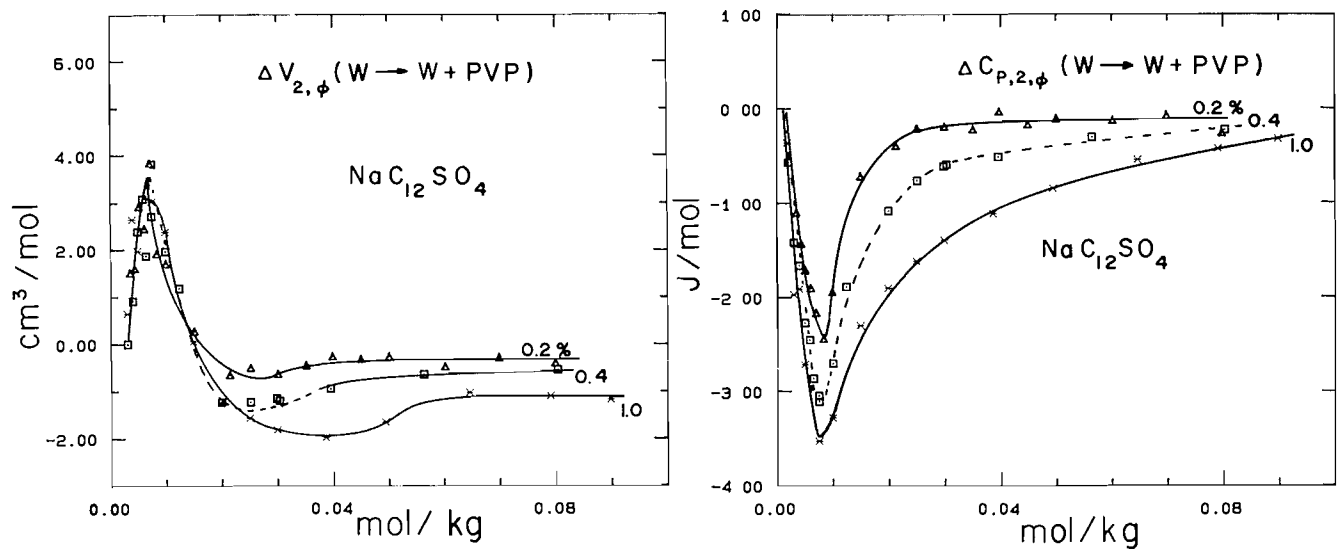

FIG. 4. Changes in apparent molar volumes and heat capacities of sodium dodecylsulfate in PVP of varying concentration relative to data in water.

surfactant) are more relevant than the actual values of those properties in understanding polymer–surfactant interactions. Transfer or difference functions can be defined as:

$$[3]\quad Y_i(\mathrm{W} \rightarrow \mathrm{W} + \text{polymer}) = Y_{i,\phi}(\mathrm{W} + \text{polymer}) - Y_{i,\phi}(\mathrm{W})$$

where W stands for the solvent water. Transfer functions for volume and heat capacity of the surfactant, as defined above, are plotted in Fig. 2 as a function of surfactant concentration, and for a fixed 0.2% (by weight) polymer concentration. In these and subsequent figures the data for sodium octylsulfate are omitted, because the effects are small compared to sodium decylsulfate since the ratio polymer to surfactant is too small (0.2% of polymer for a surfactant that has a cmc of 0.3 mol kg^{-1}). However, even for sodium octylsulfate the effects are measurable.[2] The surfactant chain length dependence is clear both in the magnitude of the effect and in the concentration of first binding. In comparing the results for PEO and PVP, we note that a 0.2 wt% solution corresponds to a 0.045 mol of repeating unit kg^{-1} for PEO and 0.018 mol kg^{-1} for PVP. This difference in concentration should not influence the concentration where binding first occurs but it will affect the overall stoichiometry and the magnitude of the deviation, as discussed in the next section. In general, we find that binding of the alkylsulfates starts at lower surfactant concentrations with PVP than with PEO and that the magnitude of the effect on $V_{2,\phi}$ and $C_{p,2,\phi}$ is larger with PVP.

Effect of polymer concentration

Figures 3 and 4 show the effect of polymer concentration on the volume and heat capacity transfer functions as defined by eq. [3] for sodium dodecylsulfate with PEO and PVP. The transfer functions show two effects: (*1*) The shift of the cmc. There is a definite lower critical binding concentration, this concentration is independent of polymer concentration, but lower for PVP than for PEO. (*2*) The effects above the cmc.

Can. J. Chem. Downloaded from www.nrcresearchpress.com by 78.46.186.204 on 09/07/12
For personal use only.

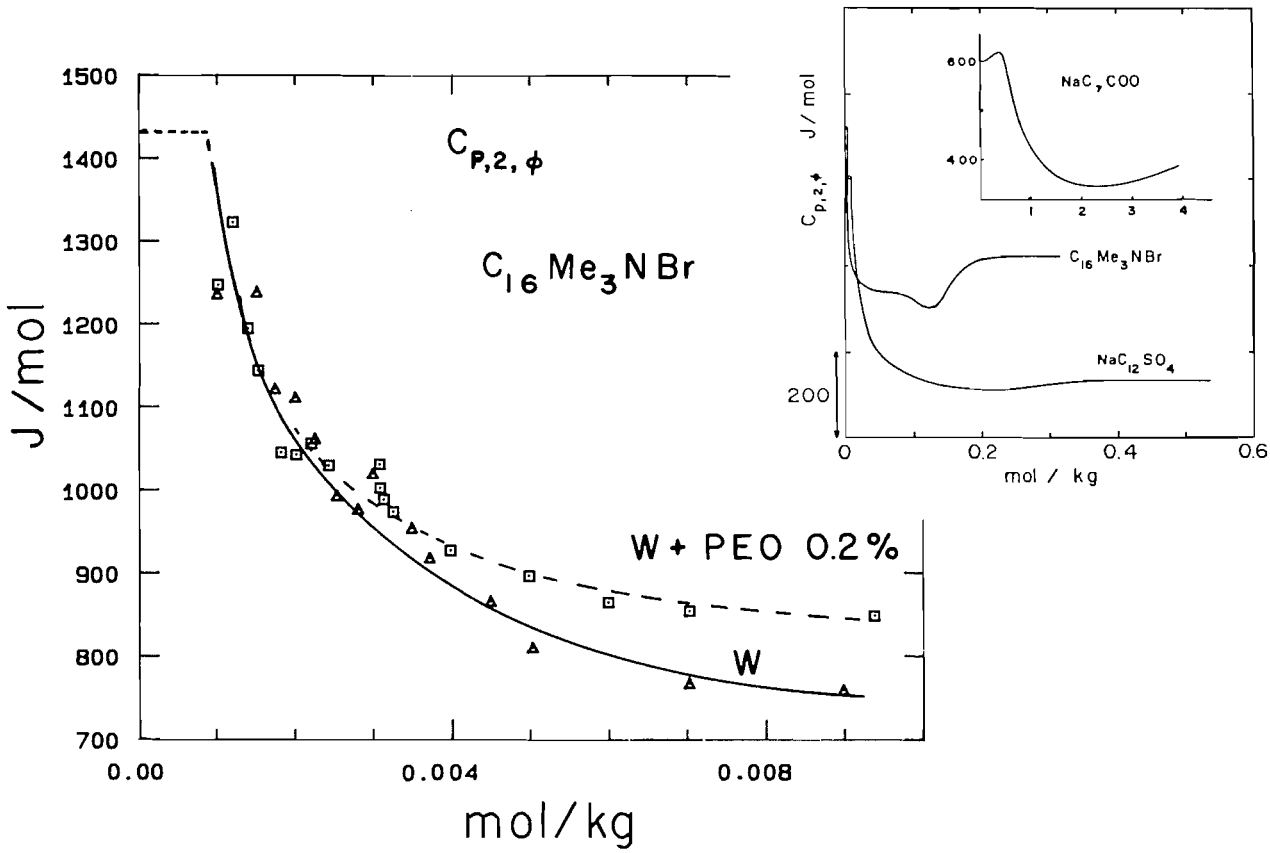

FIG. 5. Apparent molar heat capacities of cetyltrimethylammonium bromide in water and in 0.2% PEO. Insert from ref. 24.

The transfer volume in PEO solution returns to zero at high surfactant concentration. This is not the case for PVP, where negative transfer volumes are observed above the cmc. This effect increases with increasing PVP concentration.

In general, we conclude that the interactions are stronger with PVP than with PEO, as is clear in particular from the C_p data. This observation is supported by the lower critical binding concentration with PVP. In addition, the volume data at high surfactant concentration point at a micelle–polymer interaction for PVP but not for PEO. The negative sign of the transfer volume in this region would indicate lower hydrophobic interaction and may be related to the unusual molar volume of PVP itself.

The system $C_{16}(CH_3)_3NBr$(HTAB)–PEO

We have already seen that PVP and PEO do not shift the cmc of C_{10} and C_{12} cationic surfactants. In the case of a C_{16} alkyl chain length the cmc is too low to allow volume or heat capacity measurements. However, with this surfactant the region far above the cmc can be studied. We did not observe any change in the apparent molar volume of CTAB upon addition of PEO, although there is a small but significant effect on the heat capacity at surfactant concentrations above 0.003 mol kg^{-1} (Fig. 5). This effect was not observed for PVP. Note that there is considerable and unavoidable scatter in the data at the lowest concentrations. At higher concentrations, however, the data become much more accurate. Thus, we conclude that there is some interaction between PEO and CTAB micelles, an interaction which is not observed with PVP. Quirion and Desnoyers (24, 25) have shown that CTAB, like other surfactants such as sodium dodecylsulfate, undergoes a post-micellar transition at high concentration and that this transition is shifted to lower concentrations in the presence of additives such as alcohols. The increase in heat capacity of CTAB in the post-micellar region, in the presence of PEO, is most probably related to such a shift.

Conclusions

We have shown that thermodynamic measurements can be applied to the study of polymer–surfactant interactions in the same way as they have been applied to micellar systems. Direct apparent molar volume and molar heat capacity measurements give additional information to the more generally used binding measurements, and are particularly useful to show the effects of hydrophobic interactions. The binding of anionic alkylsulfate type surfactants by PVP and PEO can be demonstrated by this technique, and in general the results are in agreement with conclusions obtained from binding isotherms (2, 4, 5, 19, 21, 26). We did not observe any effects associated with binding or polymer–micelle interactions in systems containing C_{10} and C_{12} chain length cationic surfactants and PVP and PEO. Earlier negative results of direct binding studies[3] were attributed to differences in the micellar surface between alkylsulfate- and alkyltrimethylammonium surfactants (22, 23).

Acknowledgements

This research was supported by the Natural Sciences and Engineering Research Council of Canada through grants to J.E.D. and J.C.T.K.

1. M. M. BREUER and I. D. ROBB. Chem. Ind. 530 (1972).
2. I. D. ROBB. *In* Anionic surfactants, physical chemistry of surfactant action. *Edited by* E. H. Lucassen Reynders. Marcel

Can. J. Chem. Downloaded from www.nrcresearchpress.com by 78.46.186.204 on 09/07/12
For personal use only.

Dekker, New York, NY. 1981; Surfactant Science Series, Vol. 11, p. 109.
3. I. D. ROBB. *In* Chemistry and technology of water soluble polymers. *Edited by* C. A. Finch. Plenum Press, New York, NY. 1983. p. 193.
4. E. D. GODDARD. Colloids Surf. **19**, 255 (1986); **19**, 301 (1986).
5. K. SHIRAHAMA and N. IDE. J. Colloid Interface Sci. **54**, 450 (1976).
6. A. MALOVIKOVA, K. HAYAKAWA, and J. C. T. KWAK. J. Phys. Chem. **88**, 1930 (1984).
7. G. C. KRESHECK and W. A. HARGRAVES. J. Colloid Interface Sci. 283 (1982).
8. J. E. DESNOYERS. Pure Appl. Chem. **54**, 1469 (1982).
9. A. H. ROUX, D. HETU, G. PERRON, and J. E. DESNOYERS. J. Solution Chem. **13**, 1 (1984).
10. G. PERRON, R. DELISI, I. DAVIDSON, S. GENEREUX, and J. E. DESNOYERS. J. Colloid Interface Sci. **79**, 432 (1981).
11. P. MOLYNEUX. Water-soluble synthetic polymers: properties and behaviour. Vol. I, CRC Press, Boca Raton, FL. 1984.
12. P. PICKER, E. TREMBLAY, and C. JOLICOEUR. J. Solution Chem. **3**, 377 (1974).
13. P. PICKER, C. JOLICOEUR, and J. E. DESNOYERS. J. Chem. Thermodyn. **1**, 469 (1969).
14. P. PICKER. Can. Res. Develop. **7**(1), 11 (1974).
15. J. E. DESNOYERS, C. DE VISSER, G. PERRON, and P. PICKER. J. Solution Chem. **5**, 605 (1976).
16. B. RIEDL. Ph.D. Thesis, Université de Sherbrooke, Sherbrooke (Qué.), Canada J1K 2R1. 1985.
17. S. CABANI, P. GIANNI, V. MOLLICA, and L. LEPORI. J. Solution Chem. **10**, 563 (1981).
18. M. MURATA and H. ARAI. J. Colloid Interface Sci. **44**, 475 (1973).
19. B. CABANE and R. DUPLESSIX. J. Phys. **43**, 1529 (1982).
20. T. GILANYI and E. WOLFRAM. Colloids Surf. **3**, 181 (1981).
21. M. L. FISHMAN and F. R. EIRICH. J. Phys. Chem. **75**, 3135 (1971).
22. K. A. DILL, D. E. KOPPEL, R. S. CANTOR, J. D. DILL, D. BENDEDOUCH, and S.-H. CHEN. Nature, **309**, 42 (1984).
23. J. TABONY. Mol. Phys. **51**, 975 (1984).
24. F. QUIRION and J. E. DESNOYERS. J. Colloid Interf. Sci. In press.
25. J. E. DESNOYERS, G. PERRON, and A. H. ROUX. *In* Surfactant solutions: new methods of investigation. *Edited by* R. Zana. M. Dekker Inc., New York. 1986. p. 1.
26. G. C. KRESHECK and I. CONSTANTINIDIS. Anal. Chem. 56, 152 (1984).

Can. J. Chem. Downloaded from www.nrcresearchpress.com by 78.46.186.204 on 09/07/12
For personal use only.

Basicity of 1,8-bis(dimethylamino)naphthalene and 1,4-diazabicyclo[2.2.2]octane in water and dimethylsulfoxide

ROBERT L. BENOIT, DIANE LEFEBVRE, AND MONIQUE FRÉCHETTE

Département de Chimie, Université de Montréal, C.P. 6128, Succ. A, Montréal (Qué.), Canada H3C 3J7

Received October 31, 1986

This paper is dedicated to Professor Douglas E. Ryan on the occasion of his 65th birthday

ROBERT L. BENOIT, DIANE LEFEBVRE, and MONIQUE FRÉCHETTE. Can. J. Chem. **65**, 996 (1987).

The ionization constants of the conjugate acids BH_n^{n+} of two bases widely used in synthesis, 1,8-bis(dimethylamino)naphthalene (PS), and 1,4-diazabicyclo[2.2.2]octane (DABCO), have been obtained in Me_2SO and water. The partition coefficients of both bases B and their heats of solution and protonation have also been determined. The basicity of PS is dramatically reduced when passing from water to Me_2SO while the basicity of DABCO remains unchanged, thus making DABCO the stronger base in Me_2SO. The solvent effect on the base strength is analyzed in terms of free energy and enthalpy of transfer for B and H^+, and for BH^+, from water to Me_2SO. The entropy-controlled much stronger solvation of PS in Me_2SO is in line with that of aromatic compounds while the increased solvation of DABCO in water is due to H-bonding of its two nitrogens. PSH^+, like H^+, is better solvated by Me_2SO while $DABCOH^+$ does not show a definite preference for one solvent. The calculated enthalpy of solution of gaseous PSH^+ is abnormally low when compared to that of $DABCOH^+$ and of related BH^+ ions, thus indicating that the proton of PSH^+, in a strong intramolecular H-bond, does not normally H-bond to the solvent. Our results suggest that the proton sponge acid–base system could be used as a convenient reference to determine the free energy and enthalpy of transfer of H^+ between solvents.

ROBERT L. BENOIT, DIANE LEFEBVRE et MONIQUE FRÉCHETTE. Can. J. Chem. **65**, 996 (1987).

Les constantes d'ionisation des acides conjugués BH_n^{n+} du bis(diméthylamino)-1,8 naphtalène (PS) et du diaza-1,4 bicyclo[2.2.2]octane (DABCO), deux bases largement utilisées en synthèse, ont été obtenues dans le Me_2SO et l'eau. Les constantes de partage des deux bases B et leurs chaleurs de solution et protonation ont aussi été déterminées. On note une diminution remarquable de la basicité du PS lorsque l'on passe de l'eau au Me_2SO, alors que la basicité du DABCO n'est pas affectée, de telle sorte que le DABCO devient la base la plus forte dans le Me_2SO. On analyse l'effet du solvant sur la force des bases à partir des énergies libres et enthalpies de transfert de B et H^+, et de BH^+, de l'eau au Me_2SO. La solvatation plus forte du PS dans le Me_2SO, controlée par un terme entropique, est analogue à celle des composés aromatiques alors que la solvatation accrue du DABCO dans l'eau est due à des liaisons-H avec les deux azotes. PSH^+, comme H^+, est mieux solvaté par le Me_2SO tandis que $DABCOH^+$ n'a pas de préférence nette pour l'un des solvants. L'enthalpie de solution calculée pour l'ion gazeux PSH^+ est anormalement basse si on la compare à celle du $DABCOH^+$ et d'ions BH^+ voisins, ceci indique que le proton de PSH^+, engagé dans une liaison-H intramoléculaire forte, ne forme pas de liaison-H normale avec le solvant. Ces résultats nous suggèrent d'utiliser le système acide–base du PS comme référence simple pour déterminer l'énergie libre et l'enthalpie de transfert de H^+ entre les solvants.

Can. J. Chem. Downloaded from www.nrcresearchpress.com by 78.46.186.204 on 09/07/12
For personal use only.

Introduction

In aqueous solution 1,8-bis(dimethylamino)naphthalene (proton sponge) shows an unusually high basicity for an aromatic amine (1, 2). Since it was first proposed by Alder *et al.*, this high basicity has generally been attributed to steric strain in the neutral base which is effectively relieved in the conjugate acid where the proton is intramolecularly H-bonded to the two nitrogen atoms (3). Proton sponge (denoted PS) is of interest not only for its high basicity but also for its weak *nitrogen* nucleophilicity due to steric hindrance resulting from the vicinity of the two bulky dimethylamino groups (1). In fact with strong electrophiles PS reacts preferably as a *carbon* nucleophile (4). The unusual rates of proton transfer between PS, and related compounds, and their conjugate acids have also attracted wide interest (5).

As a continuation of our comparative thermodynamic study of the protonation of nitrogen bases in water and Me_2SO (6) we recently examined the behaviour of a series of aliphatic α,ω-diamines in both solvents (7) and searched for possible evidence in solution of the intramolecular H-bonded monoprotonated form observed in the gas phase. During this work we looked briefly at two other diamines, PS and DABCO (1,4-diazabicyclo[2.2.2]octane), and also at related quinuclidine. While we found that the basicity of DABCO is little changed when passing from water to Me_2SO, the pK_a of PSH^+ shows a dramatic decrease of some 4.5 units in Me_2SO so that

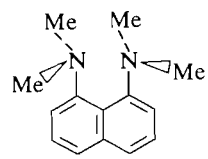

1,8-bis(dimethylamino)naphthalene
Proton sponge
PS

1,4-diazabicyclo[2.2.2]octane
DABCO

DABCO becomes a better base than PS in Me_2SO. Terrier and Hallé (8), during the course of recent preparative work, also observed the superior basicity of DABCO over PS in Me_2SO.

Because of the synthetic utility of PS and DABCO and the wide use of Me_2SO as reaction medium, we have further explored our preliminary findings and compared more fully the thermodynamics of protonation of PS and DABCO in water and Me_2SO. In addition, we evaluated the part played by solvent effects on PS and PSH^+ in modifying the intrinsic high basicity of PS and shed some light on the interactions between the intramolecular H-bonded proton in PSH^+ and both solvents.

Experimental

Materials

Proton sponge (Aldrich) was twice recrystallized in ethanol, washed with water, and dried under vacuum at room temperature. Purity of the compound as checked by titration with trifluoromethanesulfonic acid in Me_2SO was 101 ± 1%. DABCO (MCB) was purified by sublimation at

Can. J. Chem. Downloaded from www.nrcresearchpress.com by 78.46.186.204 on 09/07/12
For personal use only.

75°C then dried under vacuum at room temperature and kept in a desiccator over P_4O_{10}. Its purity was 99 ± 1% as determined by HCl titration. Tetraethylammonium perchlorate (Eastman Kodak) was recrystallized in a 4:1 water–ethanol mixture and dried under vacuum at room temperature. NaCl (McArthur), trifluoromethanesulfonic acid (Aldrich) and H_2SO_4 (Baker) were used as received. HCl (0.1 *M*) and NaOH (0.1 *M*) were from BDH. Buffer solutions were prepared from reagent grade chemicals. Finally, Me_2SO (BDH, analytical reagent) and *n*-heptane (A & C American Chemicals), were used without further purification. Me_2SO-d_6 was from Cambridge Isotope Laboratories.

pK_a determinations

Potentiometric titrations of Me_2SO solutions of PS and DABCO (5×10^{-3} to 1×10^{-2} *M*) with standardized 0.1 *M* HCF_3SO_3 in Me_2SO were carried out at 25.0 ± 0.1°C as previously described (6). The solutions were made initially 0.100 *M* in NEt_4ClO_4 to keep the ionic strength constant.

A spectrophotometric procedure was used to determine the pK_a value for PSH^+ in water. The spectrum of PSH^+ (pH < 9.0) shows an absorption band with a maximum at 285 nm, two small shoulders at 275 and 295 nm, and negligible absorption above 335 nm. When the pH is increased this band decreases in intensity and a new one appears at longer wavelengths (λ_{max} = 335 nm). Absorbance measurements were made at 335 nm on PS solutions containing 10^{-1}–10^{-3} *M* NaOH and 0.11 *M* NaCl. Because of the slow rate of dissolution and low solubility of PS in water, the PS aqueous solutions (10^{-4}–10^{-5} *M*) were obtained by dilution of 10^{-2}–10^{-3} *M* solutions in Me_2SO. Preparation of PS solutions by neutralization of PSH^+ solutions with NaOH, or extraction of *n*-heptane solutions of PS with NaOH proved unsatisfactory. The absorbances were measured with a PMQII Zeiss spectrophotometer using 2 cm thermostated cells. The values of K_b, the basicity constant, and of the molar absorptivity ε of PS were obtained at 25°C from the absorbances at 335 nm by the graphical procedure used by Hibbert (2). This ε value, 6500 ± 200 M^{-1} cm^{-1}, was used to calculate K_b at other temperatures from additional measurements made at 5-deg intervals up to 55°C. The solutions were less stable at higher temperatures and the absorbances increased on standing.

Solubility and partition coefficient determinations

The solubility of PS in water is very low ($\sim 1 \times 10^{-5}$ *M*) and is difficult to determine directly. On the other hand, the solubility of PS in Me_2SO is high (~0.8 *M*), while that of DABCO is high in both water and Me_2SO (>2 *M*), so that the saturated solutions of the bases in both solvents may not behave ideally. Thus, in order to avoid the problems inherent in determining the activities of both PS and DABCO in their saturated solutions in water and Me_2SO, we determined the partition coefficient of PS and DABCO between water and Me_2SO using *n*-heptane as the common immiscible reference solvent.

First, the partition coefficient of PS between *n*-heptane and Me_2SO, $P_{h/s}$, was obtained by determining potentiometrically the concentration of PS in the Me_2SO phase after equilibration of three 50 mL samples of 2.2×10^{-2} *M* PS solution in *n*-heptane with 50 mL Me_2SO, and also of two 50 mL *n*-heptane with 50 mL 0.7–1.0 $\times 10^{-2}$ *M* PS in Me_2SO. The equilibrium concentration of PS in *n*-heptane was calculated by difference. Since it was not practical to determine directly $P_{h/w}$, the partition coefficient of PS between *n*-heptane and water, $P_{h/w}$ was obtained indirectly from experimental values of the distribution coefficient $D = (PS)_h/[(PS) + (PSH^+)]$ at several pH and the relation

$$[1] \quad \log D = \log P_{h/w} - pK_a + pH$$

which is valid for pH ≪ pK_a. Then, 50 mL of 3.3–0.12 $\times 10^{-3}$ *M* PS solutions in *n*-heptane were equilibrated with 50 mL of five buffer solutions (pH 4.80, 5.74, 6.29, 6.86, 6.99). The equilibrium PS concentration in *n*-heptane was determined by spectrophotometry at 327 nm with ε = 9020 and that of PS (i.e. PSH^+) in water was calculated by difference.

The determination of the partition coefficients of DABCO, $P_{h/s}$, and $P_{h/w}$ did not present any difficulty. First, 20 mL samples of 0.172 *M* DABCO solution in Me_2SO were equilibrated with 20 mL of *n*-heptane, and the Me_2SO phase was analyzed potentiometrically with standard HCl after flooding with water. The equilibrium DABCO concentration in *n*-heptane was found by difference. Second, 2 mL portions of 1.51 *M* DABCO solutions in water were equilibrated with 25 mL of *n*-heptane; then 20 mL of this *n*-heptane solution was analyzed for DABCO by equilibrating with 20 mL water and titrating the aqueous phase with standard acid.

Calorimetric measurements

The heats of solution of PS in Me_2SO, and of DABCO in water and in Me_2SO were measured at 25.0°C with a LKB Model 8725-2 isoperibol calorimeter as previously described (6), the amount of base dissolved being known from the weights of the glass ampoules. For each base, three to five separate determinations were made at different concentrations by dissolving 3–10 $\times 10^{-4}$ mole of base in 100 mL of solvent. The heats of neutralization of the solid bases were determined similarly using an excess of 0.1 *M* HCF_3SO_3 in Me_2SO or 0.1 *M* HCl in water. For DABCO the heat of neutralization for the first protonation was subsequently determined by dissolving a known excess of DABCO in 2.4–5.2 $\times 10^{-3}$ *M* HCF_3SO_3 in Me_2SO. Some difficulties were experienced in determining the heat of neutralization of PS in aqueous 0.1 *M* HCl because the PS particles dissolve slowly and have a tendency to float. In order to improve the accuracy, 0.35 *M* HCl and H_2SO_4 solutions were also used. The heat of solution of PS in water could only be determined indirectly from its heat of neutralization, and from its heat of protonation which was, in turn, obtained from the variation of pK_a with temperature.

Nuclear magnetic resonance measurements

The second protonation of PS was studied by ^{13}C nmr. Spectra of 0.3 *M* solutions of PS were recorded rapidly between 10–18 *M* H_2SO_4 because some decomposition takes place on standing. The quaternary carbons were easily singled out and other carbons were identified from literature data on aniline and dimethylaniline (9). The ^{13}C spectra were acquired at 28°C on a Bruker WP-80 spectrometer operating at 20.2 MHz. Data acquisition and Fourier transformation were performed with 8 K data point. ^{13}C chemical shifts were measured relative to external dioxane in D_2O and converted to the Me_4Si scale with $\delta_{Me_4Si} = \delta_{dioxane} + 67.40$ ppm. ^{13}C spectra in Me_2SO were also taken on 0.2 *M* PS solutions to which HCF_3SO_3 was added to obtain molar ratios of acid-to-base equal to 0, 0.25, 0.50, 1.00, and 2.00. Similar molar ratio experiments were carried out on 0.1 *M* PS solutions in Me_2SO-d_6 for the recording of ^1H spectra. A Bruker WH-90 spectrometer operating at 90.0 MHz was used and ^1H chemical shifts were determined using Me_4Si as internal reference. The protonation of DABCO was also studied by ^{13}C nmr using the molar ratio method, first by adding HCF_3SO_3 to a 0.2 *M* DABCO solution in Me_2SO, then by adding $HClO_4$ to 0.1 *M* DABCO in water.

Results

pK_a and free energies of transfer

The ionization constants K_a of the protonated bases PSH^+, $DABCOH^+$, and $DABCOH_2^{2+}$ in Me_2SO were obtained from the potentiometric neutralization data by using a program described previously (6). Our pK_a values for BH_n^{n+} are given in Table 1 together with the very accurate values of Paoletti *et al.* (10) for $DABCOH^+$ and $DABCOH_2^{2+}$ in water. No corrections were made for the effect of ionic strength, which would be small for such reactions.

The basicity constant K_b and molar absorptivity of PS in water at 25°C were determined from absorbance measurements in 10^{-3}–10^{-1} *M* NaOH by using the graphical procedure of Hibbert (2). The corresponding pK_a value in Table 1 was then deduced from $pK_b = 1.8 \pm 0.1$ and the dissociation constant of water at 0.11 ionic strength. The pK_a for PSH_2^{2+} was obtained from the ^{13}C nmr data in 10–18 *M* H_2SO_4 by using the excess acidity method and the program developed by Cox as previously described (11).

TABLE 1. Ionization constants K_a of BH_n^{n+} ions at 25°C

BH_n^{n+}	pK_a		ΔpK_a
	Me_2SO	H_2O	
PSH^+	7.47 ± 0.04	12.0 ± 0.1	−4.5
PSH_2^{2+}		−9.0 ± 0.2	
ϕNMe_2H^+ [a]	2.5	5.2	−2.7
Me_3NH^+ [b]	8.4	9.8	−1.4
Quinuclidine H^+ [c]	9.8	11.0	−1.2
$DABCOH^+$	8.93 ± 0.05	8.82 ± 0.01 [d]	+0.1
$DABCOH_2^{2+}$	2.97 ± 0.05	2.97 ± 0.01 [d]	0

[a]Reference 18.
[b]Reference 21.
[c]M. Fréchette. Unpublished data.
[d]Reference 10.

The free energy of transfer ΔG_t^0 (hypothetical 1 *M* solution as standard state) from water to Me_2SO for both PS and DABCO was obtained from the partition coefficient $P_{s/w}$ calculated in turn from the partition coefficient between Me_2SO and *n*-heptane, $P_{h/s}$, and the partition coefficient, $P_{h/w}$, between water and *n*-heptane. For PS, we determined $P_{h/w}$ from the experimental relation between the distribution coefficient *D* and pH, $\log D = 6.8 \pm 0.1 + pH$ ($4.8 \leq pH \leq 7.0$). By comparison with eq. [1] and with $pK_a = 12.0 \pm 0.1$ we find $\log P_{h/w} = 5.2 \pm 0.2$. Since we obtained $P_{h/s} = 1.9 \pm 0.1$, we calculate $P_{s/w} = 10^{4.9 \pm 0.2}$ and $\Delta G_t^0(PS) = -28 \pm 1$ kJ mol^{-1}. For DABCO, we determined directly $P_{h/s} = 0.37 \pm 0.01$ and $P_{h/w} = 5.3 \pm 0.5 \times 10^{-4}$ so that $P_{s/w} = 10^{-2.82 \pm 0.05}$ and $\Delta G_t^0(DABCO) = +16.1 \pm 0.3$ kJ mol^{-1}.

The values of the free energies of transfer $\Delta G_t^0(BH^+)$ of the conjugate acids BH^+, from water to Me_2SO, are calculated by means of relation [2] derived from the thermodynamic cycle relating protonation processes in both solvents.

$$[2] \quad \Delta G_t^0(BH^+) = \Delta G_t^0(B) + \Delta G_t^0(H^+) + \Delta G_{ps}^0 - \Delta G_{pw}^0$$

where ΔG_{ps}^0 and ΔG_{pw}^0 are the free energies of protonation in both solvents calculated from the pK_a values in Table 1. The free energy of transfer of the proton, −19 kJ mol^{-1}, is based on an extrathermodynamic assumption (12).

The $\Delta G_t^0(BH^+)$ values are, respectively, −21 and −3 kJ mol^{-1} for PSH^+ and $DABCOH^+$; the errors are unknown, since they depend on the validity of the extrathermodynamic assumption. All of our free energies of transfer are listed in Table 2.

Protonation enthalpies and enthalpies of transfer

The plots of the heats of solution of DABCO in water and of both bases in Me_2SO and Me_2SO solutions of 0.1 *M* HCF_3SO_3 against the number of moles dissolved were linear and the least-squares slopes gave $\Delta H_s^0(B)$ or $\Delta H_w^0(B)$ [3] and $\Delta H_{ns}^0(B)$ or $\Delta H_{nw}^0(B)$ [4] according to

$$[3] \quad B(c) = B(s \text{ or } w)$$

$$[4] \quad B(c) + H^+(s \text{ or } w) = BH^+(s \text{ or } w)$$

$$[5] \quad DABCO(c) + 2H^+(s) = DABCOH_2^{2+}(s)$$

$$[6] \quad B(s \text{ or } w) + H^+(s \text{ or } w) = BH^+(s \text{ or } w)$$

ΔH_{ps}^0, the enthalpy for the first protonation of DABCO (eq. [6]) in Me_2SO was obtained by subtracting from Q_{ns}, the heat change found for dissolving n_b moles of DABCO in n_a moles of acid ($n_b \gg n_a$), $Q_s = n_b \times \Delta H_s^0(B)$, and by taking $\Delta H_{ps}^0 = (Q_{ns} - Q_s)/n_a$. The heat of neutralization of PS (reaction [4]) in water, ΔH_{nw}^0, is an average of values determined in 0.1–0.35 *M* HCl and H_2SO_4. The pK_b values for PS were determined at 5-deg intervals between 25 and 55°C from absorbance measurements at 335 nm on three series of solutions with 2.5, 5.0, and 10.0×10^{-3} *M* NaOH. The pK_b values were plotted against $1/T$ to give by a least-squares procedure the associated enthalpy value, -11 ± 4 kJ mol^{-1}, which, in turn, was combined with the enthalpy for the dissociation of water at 25°C and 0.11 ionic strength to give the enthalpy of protonation $\Delta H_{pw}^0 = -65 \pm 4$ kJ mol^{-1} according to [6].

Then ΔH_w^0 for PS was obtained from

$$[7] \quad \Delta H_w^0(B) = \Delta H_{nw}^0(B) - \Delta H_{pw}^0(B)$$

A similar equation was used to calculate this time ΔH_{ps}^0 for PS and DABCO in Me_2SO. The ΔH_{pw}^0 values used for DABCO were from Paoletti *et al.* (10). The values of the enthalpy of solution and protonation of PS and DABCO are listed in Table 3.

The values of the enthalpies of transfer of PS and DABCO, $\Delta H_t^0(B)$, were calculated from the enthalpies of solution of both bases in water and Me_2SO. $\Delta H_t^0(BH^+)$ was obtained from eq. [8] for $DABCOH^+$ and from eq. [9] for PSH^+ taking $\Delta H_t^0(H^+) = -25.5$ kJ mol^{-1} (12).

$$[8] \quad \Delta H_t^0(BH^+) = \Delta H_t^0(B) + \Delta H_t^0(H^+) + \Delta H_{ps}^0 - \Delta H_{pw}^0$$

$$[9] \quad \Delta H_t^0(BH^+) = \Delta H_t^0(H^+) + \Delta H_{ns}^0 - \Delta H_{nw}^0$$

The enthalpies of transfer are given in Table 4.

Enthalpies of transfer from the gas phase to Me_2SO and water

The enthalpies of protonation of both PS and DABCO in the gas phase ΔH_{pg}^0 according to

$$[10] \quad B(g) + H^+(g) = BH^+(g)$$

have been determined by several groups of workers (13–15). The values of ΔH_{pg}^0, i.e. minus the proton affinity, given in Table 3, are averages and based on PA = 207 kcal mol^{-1} for NH_3, 224 kcal mol^{-1} for pyridine, and 229 kcal mol^{-1} for trimethylamine. Thus, the ΔH_{pg}^0 values taken for PS and DABCO are respectively, 1030 and 970 kJ mol^{-1}, these values being rounded to the nearest 5 kJ mol^{-1}.

We can now obtain the valuable enthalpies of transfer of BH^+ ions from the gas phase to water, $\Delta H_{gw}^0(BH^+)$, and to Me_2SO, $\Delta H_{gs}^0(BH^+)$, by using relations derived from the thermodynamic cycles relating protonation processes in the gas phase and Me_2SO or water. For example, from eqs. [4] and [10], we derive

$$[11] \quad \Delta H_{gs}^0(BH^+) = \Delta H_{gc}^0(B) + \Delta H_{gs}^0(H^+) + \Delta H_{ns}^0 - \Delta H_{pg}^0$$

$\Delta H_{gs}^0(H^+)$ is taken as −1155 kJ mol^{-1} which is based on $\Delta H_t^0(H^+) = -25$ kJ mol^{-1} and $\Delta H_{gw}^0(H^+) = -1130$ kJ mol^{-1} (−270 kcal mol^{-1}) (12). ΔH_{gc}^0 is $-\Delta H_{sub}^0$, the enthalpy of sublimation. ΔH_{sub}^0 is calculated for DABCO as +65 kJ mol^{-1} from a literature value at 65°C (16) corrected to 25°C (17). ΔH_{sub}^0 for PS was estimated as follows. The enthalpy of fusion of PS ($t_f = 48$°C) was estimated as +20 kJ mol^{-1}, from a heat of solution in Me_2SO, +25 kJ mol^{-1}, minus a small enthalpy of solution of a non-associated liquid in Me_2SO taken as +5 kJ mol^{-1} (18). The enthalpy of vaporization ΔH_v^0 of liquid PS at 25°C, +70 kJ mol^{-1}, was obtained from a correlation line between ΔH_v^0 and normal boiling points t_b for tertiary amines (19) and an estimated $t_b \sim 320$°C. Finally, ΔH_{sub}^0 is obtained as +90 kJ mol^{-1} which is interestingly near the value for

Can. J. Chem. Downloaded from www.nrcresearchpress.com by 78.46.186.204 on 09/07/12
For personal use only.

TABLE 2. Free energies of transfer (kJ mol^{-1}) of B and BH$^+$ from water to Me_2SO at 25°C

B or BH$^+$	PS	PSH$^+$	DABCO	DABCOH$^+$	Me_3N[b]	Me_3NH^+[b]	H$^+$[c]
ΔG_t^0(B or BH$^+$)[a]	−28	−21	+16	−3	+5.3	−5.4	−19

[a]Standard state as hypothetical 1 *M* solution.
[b]Reference 21.
[c]Reference 12.

TABLE 3. Enthalpies of solution and enthalpies of protonation (kJ mol^{-1}) of PS and DABCO at 25°C

B	ΔH_s^0(B) Me_2SO	ΔH_w^0(B) H_2O	ΔH_{ps}^0 Me_2SO	ΔH_{pw}^0 H_2O	ΔH_{pg}^0 gas phase
PS	+24.3 ± 1.0	+30 ± 5	−48.5 ± 0.6	−65 ± 4	−1030[b]
DABCO	+19.4 ± 0.4	−24.6 ± 0.4	−53 ± 1	−30.54 ± 0.04[a]	−970[c]
DABCOH$^+$			−38 ± 2	−12.56 ± 0.06[a]	

[a]Reference 10.
[b]Reference 13.
[c]Reference 14, 15.

TABLE 4. Enthalpies of transfer (kJ mol^{-1}) of B and BH$^+$ from water to Me_2SO (ΔH_t^0) and from the gas phase to Me_2SO (ΔH_{gs}^0)

B	ΔH_t^0(B)	ΔH_t^0(BH$^+$)	ΔH_{gs}^0(BH$^+$)
PS	−6.	−15.	−239.
DABCO	+44.	−4.	−284.
Me_3N[a]	+33.	−15.	−277.
Py[b]	+11.	−22.	−285.
ϕNMe_2[b]		−14.	−276.

[a]Reference 21.
[b]Reference 18.

TABLE 5. ^{13}C shift values[a] (ppm) of PS, PSH$^+$, and PSH_2^{2+} in Me_2SO and water

	C-1	C-2	C-3	C-4	C-9	C-10	CH_3
PS (Me_2SO)	151.3	113.8	126.5	122.5	120.9	138.4	45.3
PSH$^+$ (Me_2SO)	145.6	122.8	128.0	130.0	120.0	135.9	46.9
PSH$^+$ (H_2O)	144.3	121.9	127.8	130.0	118.9	135.8	46.6
PSH_2^{2+} (H_2O)	135.4	124.4	128.2	135.4	116.9	138.3	51.5

[a]Standard deviation usually better than 0.1 ppm.

1,8-dimethylnaphthalene, +83 kJ mol^{-1} (20). Although our ΔH_{sub}^0 value is obviously a crude estimate, the error is not unlike that on PA values, 5–10 kJ mol^{-1}. Our calculated enthalpies of transfer from the gas phase are listed in Table 4.

Nuclear magnetic resonance data

The ^{13}C limit chemical shift values obtained for PSH$^+$ and PSH_2^{2+} from our data in 10–18 *M* H_2SO_4 are summarized in Table 5. The ^{13}C shift values for PS and PSH$^+$ in Me_2SO are also given. The spectra corresponding to Me_2SO solutions containing molar ratios of acid to PS between 0 and 1 showed signals for both PS and PSH$^+$. Apparently the exchange between the nonprotonated and protonated forms is too slow to be observed on the nmr time scale at room temperature. ^{1}H signals for both PS and PSH$^+$ were also observed in solutions with molar ratios of acid to PS between 0 and 1 and the proton of PSH$^+$ appeared at unusually low field, 18.36 ppm. Further addition of acid did not cause shift of the PSH$^+$ proton, so that the exchange between PSH$^+$ and protonated Me_2SO (HCF_3SO_3 is a strong acid in Me_2SO) is also slow. The PSH$^+$ spectrum shows a doublet signal for the methyl protons. The splitting (J = 2.4 Hz) is due to coupling with the PSH$^+$ proton.

In contrast, the study of the protonation of DABCO by ^{13}C nmr, using the molar ratio method, indicated exchange between DABCO and both protonated species both in water and in Me_2SO. The plots of the ^{13}C shifts against the molar ratio of acid-to-base consisted of three straight lines whose intersections corresponded to molar ratios 1.0 and 2.0. The C-1 shift values for DABCO, DABCOH$^+$, and $DABCOH_2^{2+}$, deduced from the graphs, are respectively 48.2, 45.3, 44.1 ppm in Me_2SO and 46.0, 44.9, and 44.4 ppm in water.

Discussion

Ionization constants and free energies of transfer

We will consider the ionization constants K_a of PSH$^+$ and DABCOH$^+$ first, since they are our initial raw data. We will then discuss the solvent effect on K_a in terms of free energy of transfer of B and BH$^+$.

The data in Table 1 show that on passing from water to Me_2SO the pK_a change is −4.5 for PSH$^+$ and +0.1 for DABCOH$^+$, thus confirming our preliminary findings that while in water PS is a much better base than DABCO, the reverse holds true in Me_2SO. Our previously determined ΔpK_a for dimethylaniline (−2.7) and for trimethylamine (−1.4) (18) listed in Table 1 for comparison, suggest that, at least in part, the pK_a changes for PSH$^+$ and DABCOH$^+$ in Me_2SO are in line with what is expected for related amines in the aromatic and aliphatic series. However, PS and DABCO must have some additional specific structural factors which would account for their ΔpK_a being larger than for the simple parent amines considered. For DABCO at least, it is clear that its diamine nature plays a part in explaining its ΔpK_a = +0.1 since its monoamine analog, quinuclidine, has a ΔpK_a = −1.2 (Table 1) very close to that of Me_3N, −1.4.

Can. J. Chem. Downloaded from www.nrcresearchpress.com by 78.46.186.204 on 09/07/12
For personal use only.

Can. J. Chem. Downloaded from www.nrcresearchpress.com by 78.46.186.204 on 09/07/12
For personal use only.

The very weak basicity of PSH^+ is noteworthy with a corresponding pK_a value of -9.0 ± 0.2 (half protonation in 15.2 *M* H_2SO_4, $m^* = 1.12 \pm 0.04$ (11)). The extraordinary stability of PSH^+ (1) with respect to protonation and deprotonation as shown by both its pK_a values, is totally different from what is observed both for $DABCOH^+$ (Table 1) and for BH^+ ions in the α,ω-diamines series where there is no "dicoordination" of the proton (7).

Turning now to the free energies of transfer of B and BH^+ in Table 2, we note first the highly contrasted ΔG_t^0 values for both bases, PS and DABCO. The high and negative $\Delta G_t^0 = -28$ kJ mol^{-1} for PS is typical of aromatics behaviour with their very low solubility in water and high solubility in Me_2SO. The situation is completely reversed for DABCO with $\Delta G_t^0 = +16$ kJ mol^{-1}, indicating that DABCO is more strongly solvated by water through H-bonding to both nitrogens. Looking next at the values of $\Delta G_t^0(BH^+)$, we find that PSH^+ exhibits a strong preference for Me_2SO while $DABCOH^+$ is only slightly better solvated by Me_2SO. To conclude this free energy analysis of the solvent effect on the base strength, the much reduced basicity of PS when passing from water to Me_2SO comes from three nearly equal contributions of some 23 kJ mol^{-1}, those on PS and H^+ being opposed by that on PSH^+. For DABCO, the absence of solvent effect on its basicity is due to nearly equal and opposite effects on the neutral base and H^+.

Enthalpies of transfer

Our values of the enthalpies of transfer ΔH_t^0 of PS, DABCO, PSH^+, and $DABCOH^+$ from water to Me_2SO (Table 4) present interesting results when compared with previous data (18, 21) for aliphatic and aromatic amines. First, the small ΔH_t^0 for PS is typical of what is observed for aromatics[1] (for C_6H_6, $\Delta H_t^0 = -0.3$ kJ mol^{-1}) so that, given the high negative value of ΔG_t^0, there must be a very large compensating positive entropy of transfer, as is common to aromatics, and which reflects the peculiarities of water as a solvent. For DABCO, ΔH_t^0 is large and positive indicating much stronger interactions with water, as was already clear with ΔG_t^0. Again the ΔH_t^0 value for DABCO is near that for the aliphatic amine Me_3N; the ΔS_t^0 values for both bases are also positive (21) and almost identical. The negative ΔH_t^0 values for all the BH^+ ions which are listed in Table 4 indicate some 15–20 kJ mol^{-1} stabilization in Me_2SO though much less for $DABCOH^+$.

Finally, if we turn our attention to the enthalpies of transfer of a series of BH^+ ions from the gas phase to Me_2SO in Table 4, we draw some highly valuable conclusions. We note first that the values of $\Delta H_{gs}^0(BH^+)$ for very different nitrogen bases, B = DABCO, Me_3N, Py, and ϕNMe_2 are all within -280 ± 5 kJ mol^{-1} while $\Delta H_{gs}^0(PSH^+)$ is some 40 kJ mol^{-1} less exothermic. We previously found (18, 21) that the exothermic heat of solution of substituted ammonium ions decreases with the number of N—H protons which can H-bond to Me_2SO, the size of the substituent being of lesser importance. The average decrease of the heat of solution of the gaseous ions per H-bond was about 35 kJ mol^{-1}. Then it is clear that while $DABCOH^+$, Me_3NH^+, PyH^+, and ϕNMe_2H^+ all form one H-bond with Me_2SO, PSH^+ does not normally H-bond to the solvent. If the solvation of the PSH^+ cation is non-specific, its heat of solution $\Delta H_{gs}^0 = -239$ kJ mol^{-1} should be near that of ions such as the tetraalkylammonium. Unfortunately, these latter values are not well established because they depend on some assumptions for the calculation of lattice enthalpies of related salts (22). Our comparisons of enthalpies of solution of BH^+ ions in Me_2SO (Table 4) could have been made with water as the solvent. The values of $\Delta H_{gs}^0(BH^+)$ are easily calculated from our data in Table 4 with $\Delta H_{gw}^0(BH^+) = \Delta H_{gs}^0(BH^+) - \Delta H_t^0(BH^+)$. For B = Me_3N, Py, and ϕNMe_2, we obtain an enthalpy of solution in water of -262 kJ mol^{-1} while for DABCO the value is more exothermic, -280 kJ mol^{-1}, largely because of H-bonding of the second nitrogen of this diamine to water (there was no such H-bonding with Me_2SO). For B = PS, $\Delta H_{gw}^0(PSH^+) = -224$ kJ mol^{-1} which is much less exothermic and is close to the rough estimate given by Taft (-210 kJ mol^{-1}) (23) for "limiting physical ion–dipole and ion – induced dipole solvation of univalent cations which do not involve specific cation–molecule chemical bonding". We, therefore, conclude that the proton of PSH^+ is involved in a strong intramolecular H-bond which precludes H-bonding to water, or even to more basic Me_2SO as we have seen. Further support of this point comes from the remarkable correlation of Taft *et al.* (23) which suggests that the solvation behaviour of PSH^+ in water is more like that of resonance-stabilized carbonium ions.

The exceptionally slow rate of proton transfer from PSH^+ to OH^- also implies that there is an unusually strong intramolecular H-bond in PSH^+ (2). The lack of exchange on the nmr time scale between PS, PSH^+, and acids in Me_2SO and other solvents (1, 24) is as well indicative of unusual properties of the proton in PSH^+ and the ^1H nmr spectra of PSH^+ in Me_2SO is compatible with the presence of a strong H-bond with H^+ in a bridge between the nitrogen atoms.

The proton sponge acid–base system as a reference

There is a most interesting consequence of the apparent lack of specific chemical interactions between PSH^+ and Me_2SO or water, and presumably between PSH^+ and other solvents. We propose to use the PSH^+/PS acid–base system as a reference system to obtain values of $\Delta G_t^0(H^+)$, the free energy of transfer of H^+ between solvents, and hence obtain values of ΔG_t^0 for other cations and anions. Equation [2] can be rearranged to give

$$[12] \quad \Delta G_t^0(H^+) = \Delta G_{p1}^0 - \Delta G_{p2}^0 + \Delta G_t^0(PSH^+) - \Delta G_t^0(PS)$$

where t stands for transfer from solvent 1 to solvent 2 and ΔG_{p1}^0 and ΔG_{p2}^0 are the free energies of protonation in solvents 1 and 2, respectively. Assuming

$$[13] \quad \Delta G_t^0(PSH^+) = \Delta G_t^0(PS)$$

we obtain

$$[14] \quad \Delta G_t^0(H^+) = \Delta G_{p1}^0 - \Delta G_{p2}^0$$

For example, with water and Me_2SO we calculate from our data in Table 1 $\Delta G_t^0(H^+) = -26$ kJ mol^{-1}. The extrathermodynamic assumption corresponding to eq. [13] is equivalent to supposing first that PS is an excellent neutral analog[2] of PSH^+ and second that the electrostatic contribution $\Delta G_t^{elec}(PSH^+)$ is negligible (12). The first assumption is the direct consequence of our finding that PSH^+ does not give any specific interaction with the solvent, and the second assumption is reasonable as long as the solvent dielectric constant is not too low. Although more data with other solvents are obviously needed to assess completely the validity of our proposed extrathermodynamic assumption, it is interesting to note that the corresponding $\Delta G_t^0(H^+)$ value for the transfer from water to Me_2SO, -26 kJ mol^{-1}, is in acceptable agreement with the $\Delta G_t^0(H^+)$

[1]For naphthalene, $\Delta H_t^0 = -11$ kJ mol^{-1}.

[2]Interactions between nitrogens of PS and water, or other H-bond donor solvents, are likely to be minimal.

value -19 kJ mol^{-1} deduced from the widely used TATB assumption, i.e. $\Delta G_t^0(As\phi_4^+) = \Delta G_t^0(B\phi_4^-)$, considering that the ferrocene assumption used by electrochemists gives a -32 kJ mol^{-1} value (12) and the Hammett type hypothesis $\Delta G_t^0(BH^+) = \Delta G_t^0(B)$ where B is a Hammett base) leads to -9 kJ mol^{-1} (12). One advantage of our proposed assumption is its directness: we only need the pK_a values of the PSH^+/PS system in both solvents to calculate $\Delta G_t^0(H^+)$ while the other assumptions usually require a large number of experimental determinations which lead to an increased margin of error. It is clear that the PSH^+/PS system can also be used as a reference to establish an enthalpy scale for the transfer of H^+ between solvents. By assuming

[15] $\Delta H_t^0(PS) = \Delta H_t^0(PSH^+)$

we calculate for $\Delta H_t^0(H^+)$ (eq. [8]) -16 kJ mol^{-1} for the water–Me_2SO transfer, a value which also is in reasonable agreement with -25 kJ mol^{-1} deduced from the TATB assumption. Here, again, our extrathermodynamic assumption leads to more directly accessible values of $\Delta H_t^0(H^+)$ than does the TATB assumption.

Acknowledgements

We wish to acknowledge a grant and a scholarship (D.L.) from the Natural Sciences and Engineering Research Council of Canada and financial assistance from the Ministère de l'Education. We also thank Professor F. Terrier and Dr. J. C. Hallé for their interest in this research.

1. R. W. Alder, P. S. Bowman, W. R. S. Steele, and D. R. Winterman. Chem. Commun. 723 (1968).
2. F. Hibbert. J. Chem. Soc. Perkin II, 1862 (1974).
3. R. Stewart. The proton: application to organic chemistry. Organic chemistry. Vol. 46. Academic Press, London. 1985.
4. F. Terrier, J. C. Hallé, M. J. Pouet, and M. P. Simonnin. J. Org. Chem. **51**, 409 (1986).
5. G. H. Barnett and F. Hibbert. J. Am. Chem. Soc. **106**, 2080 (1984).
6. R. L. Benoit, D. Boulet, L. Seguin, and M. Fréchette. Can. J. Chem. **63**, 1228 (1985).
7. M. Fréchette. M.Sc. Thesis, Université de Montréal, Montréal (Qué.). 1982.
8. F. Terrier and J. C. Hallé. Private communication.
9. (*a*) R. J. Abraham and P. Loftus. Proton and carbon-13 NMR spectroscopy. Heyden, London. 1980. p. 28; (*b*) J. L. Llinares, J. Elguero, and E. J. Vincent. Org. Magn. Reson. **14**, 20 (1980).
10. P. Paoletti, J. H. Stern, and A. Vacca. J. Phys. Chem. **69**, 3759 (1965).
11. R. L. Benoit and M. Fréchette. Can. J. Chem. **63**, 3050 (1985), and references therein.
12. R. L. Benoit and C. Louis. The chemistry of non-aqueous solvents, V. VA. *Edited by* J. J. Lagowski. Academic Press, New York. 1978, and references therein.
13. Y. K. Lau, P. P. S. Saluja, P. Kebarle, and R. W. Alder. J. Am. Chem. Soc. **100**, 7328 (1978).
14. R. H. Staley and J. L. Beauchamp. J. Am. Chem. Soc. **96**, 1604 (1974).
15. D. H. Aue, H. M. Webb, and M. T. Bowers. J. Am. Chem. Soc. **98**, 311 (1976).
16. T. Wada, E. Kishida, Y. Tomiie, H. Suga, S. Seki, and I. Nitta. Bull. Chem. Soc. Jpn. **33**, 1317 (1960).
17. P. M. Burkinshaw and C. T. Mortimer. J. Chem. Soc. Dalton, 75 (1984).
18. R. L. Benoit, M. J. Mackinnon, and L. Bergeron. Can. J. Chem. **59**, 1501 (1981).
19. I. Wadsö. Acta Chim. Scand. **23**, 2061 (1969).
20. M. Mansson. Acta Chim. Scand. **28**, 677 (1974).
21. A. Mucci, R. Domain, and R. L. Benoit. Can. J. Chem. **58**, 953 (1980).
22. H. F. Halliwell and S. C. Nyburg. J. Chem. Soc. 4603 (1960).
23. (*a*) J. F. Wolf, P. G. Harch, and R. W. Taft. J. Am. Chem. Soc. **97**, 2904 (1975); (*b*) R. W. Taft. Prog. Phys. Org. Chem. **14**, 247 (1983).
24. R. L. de Groot and D. J. Sikkema. Rec. Trav. Chim. **95**, 10 (1976).

Can. J. Chem. Downloaded from www.nrcresearchpress.com by 78.46.186.204 on 09/07/12
For personal use only.

The significance of the variability in analytical results for lead, copper, nickel, and zinc in street dust

JACK E. FERGUSSON
Department of Chemistry, University of Canterbury, Christchurch, New Zealand

Received October 17, 1986

This paper is dedicated to Professor Douglas E. Ryan on the occasion of his 65th birthday

JACK E. FERGUSSON. Can. J. Chem. **65**, 1002 (1987).

Street dust has frequently been used as a material for the monitoring of trace element pollution, and in particular for the metal lead. The value of the analytical data, as a measure of pollution, depends on understanding the spatial, temporal, and bulk characteristics of the dust. The influence of each of these factors on the variability of trace element analytical results has been investigated in order to determine whether or not the variations reflect differing pollution levels. The concentrations of the four metals Pb, Cu, Ni, and Zn have been measured in street dust collected from a variety of situations. Coefficients of variation >20% (particularly for lead) for a series of samples have been taken as a guide to real differences in lead levels between samples in the series. An important factor in the variability of heavy metal levels in dust is the distribution of particle size within a sample. Concentrations of the trace metals fall and then rise as the particle size decreases from 1000 μm down to silt sized particles.

JACK E. FERGUSSON. Can. J. Chem. **65**, 1002 (1987).

On utilise fréquemment la poussière des rues comme matériel permettant d'évaluer la pollution par les éléments à l'état de traces et, en particulier, par le plomb métallique. La valeur des données analytiques, comme mesure de la pollution, dépend de la compréhension des caractéristiques spaciales, temporales et globales de la poussière. Afin de déterminer si les variations sont réellement un reflet de différents niveaux de pollution, on a étudié l'influence de chacun de ces facteurs sur la variabilité des résultats analytiques des éléments à l'état de traces. On a mesuré les concentrations de quatre métaux (Pb, Cu, Ni et Zn) dans des échantillons de poussières recueillis dans diverses situations. On considère que les coefficients de variation >20%, observés pour une série d'échantillons et particulièrement pour le plomb, révélent la présence de différences dans les niveaux de plomb contenus dans divers échantillons de la série. Un facteur important dans la variabilité des niveaux des métaux lourds dans la poussière est la distribution des grosseurs des particules à l'intérieur d'un échantillon. Les concentrations des métaux présents à l'état de trace commencent par diminuer puis augmentent quand la grosseur des particules passe de 1000 μm à des particules de la grosseur des boues.

[Traduit par la revue]

Introduction

Street dust has frequently been used as a material for the monitoring of heavy metal pollution, and especially for the metal lead. A cursory glance at reported results indicates that a wide range of concentrations have been found for different elements in the dust (1–4). The question has been raised (5) as to whether the analytical results are reliable indicators of pollution, because of the variability of the levels over short distances and periods of time, and problems of sampling and analysis.

There are a number of factors that can influence the level of a trace element in street dust.

1. The method of taking the sample is important, and a number of these are reported. Samples are taken from pavements or gutters, with brushes or scoops or by suction, and from areas of different sizes such as 1 m^2 or 5 m^2 (4, 6–11).

2. The precision and accuracy of the analysis establishes the lower limit of variability between samples (12). The limit is the number, below which the variability must be attributed to analytical variation and not environmental or pollution factors.

3. The variability in the results will be influenced by spatial considerations, such as the distance of samples from each other, and the nature of the surrounding environment (6, 11, 13).

4. A temporal variability in trace element levels can be expected because of the effect of seasonal factors, such as wind and rain. In addition street cleaning and the duration of exposure is important (7, 11, 12).

5. The size of the particles in street dust vary from large (>1 mm) down to clay particle size. Owing to temporal changes and different sources of the dust (1, 11, 14, 15), some fractionation of the particles can occur influencing the variability of trace metal levels (1, 2).

6. Contamination of the street dust samples during collection and analysis may also influence the variability of the levels found. This is probably less of a problem when the levels of the trace elements are relatively high.

The analytical, spatial, source, temporal, and particle size aspects of street dust are considered in this present study in order to arrive at an estimate as to when variability reflects a real difference in trace element levels. For this purpose the coefficient of variation (expressed as a percent),

$$\text{cv} = (\text{standard deviation}/\text{mean}) \times 100\%$$

will be used as a measure of variability. The cv allows comparisons to be made irrespective of the level of concentration of an element in the dust, and it is also possible to compare different elements as it is independent of units. The elements Pb, Cu, Ni, and Zn are investigated in some samples, and Pb in all samples.

Experimental

Sampling

Street dust was sampled using a 3–5 cm brush and a plastic scoop. Each sample at each site was collected within a square metre, though not all the material within the 1 m^2 was taken. The samples were taken from pavements and gutters, being careful not to include soil, e.g. samples were not taken close to a grass berm. Care was taken not to discriminate on the basis of particle size when sampling. The samples were then transferred to clean plastic bags.

Treatment of samples

Each sample was oven dried at 110–120°C for 6–8 h, or at 60°C

Can. J. Chem. Downloaded from www.nrcresearchpress.com by 78.46.186.204 on 09/07/12
For personal use only.

TABLE 1. Analytical data on reference materials[a]

Element	Mean concentration	N	Standard deviation	Range	Coefficient variation	Recommended value
IAEA SD-N-1/2 (sediment)[b]						
Pb	121	16	5.9	113–135	4.9	120
Cu	71.1	21	4.2	64.4–77.0	5.9	75.9
Ni	31.5	17	2.6	27.2–36.8	8.3	30.6
Zn	423	11	14	405–448	3.4	434
Internal reference (street dust)[b]						
Pb	10862	23	291	10396–11410	2.7	
Cu	204	12	18	186–235	8.7	
Ni	22.5	22	2.5	18.7–28.5	11	
Zn	455	17	21	426–499	4.7	
Internal reference (street dust)[c]						
Pb	10409	12	125	10310–10510[d]	1.2	
Cu	209	12	13	199–219	6.2	
Ni	22.2	12	3.7	19.3–25.1	17	
Zn	477	12	13	468–487	2.7	
Internal reference (street dust)[c]						
Pb	828	10	45	739–865	5.4	
Internal reference (soil)[c]						
Pb	393	10	8	387–406	2.0	
Pb	663	9	13	643–687	2.0	

[a]Concentrations in $\mu g\ g^{-1}$.
[b]Each sample measured at different times over a period of 3 to 4 years.
[c]Samples all prepared and measured on the same day.
[d]99% confidence limits.

overnight. Samples were then sieved through 1 mm or 500 μm or 250 μm sieves as required. Around 1 g samples were digested for 30 min in 20 mL 4 *M* AR HNO_3 and then filtered through acid washed Whatman 40 or 540 filter papers. A few samples were re-digested a further time. In addition some samples were treated with a mixture of AR HF (7 mL) and AR $HClO_4$ (0.7 mL) in platinum crucibles after first igniting the dust in the crucibles to red-heat. The acid mixture was heated to 200–230°C until fuming had ceased (i.e. all the $HClO_4$ had gone) and the residue taken up in 4 *M* AR HNO_3 and filtered as before.

Atomic absorption analysis

The elements Pb, Cu, Ni, and Zn were determined using flame AAS (Varian Techtron AA1475) at wavelengths Pb, 217.0 nm; Cu, 324.7 nm; Ni, 352.4 nm; and Zn, 213.9 nm. Background correction was used for lead and zinc. Multielement standards were prepared in 0.4 *M* AR HNO_3.

Description of samples

Reference materials

No street dust reference material was availabe. An IAEA sediment sample SD-N-1/2 (16), recently used in an interlaboratory study, has been used as a primary reference material. The accepted levels are (overall mean, range of accepted laboratory means): Pb, 120, 93–154; Cu, 75.9, 53.4–92.0; Ni, 30.6, 21.0–45.0; Zn, 434, 342–549 $\mu g\ g^{-1}$. Our analytical results are given in Table 1. Internal reference samples of street dust were prepared by grinding a composite sample to a fine powder in a tungsten carbide mill. A soil sample was treated similarly. The analytical results for Pb, Cu, Ni, and Zn on these materials are given in Table 1.

Street dust samples

A number of street dust samples were collected at various times.

(*a*) A set of 10 samples were collected at the same time. The ten samples were taken 0.5 m apart over a length of 5 m. Two such sets were collected, one from the pavement and one from the gutter.

(*b*) Samples were taken from 20 sites around an intersection involving three T junctions, and controlled by traffic signals. Samples 1–14 were taken along the main thoroughfare, and samples 15–20 were taken from the side streets, two from each street. The 20 sites were sampled at monthly intervals for eight months.

(*c*) Street dust samples were taken from various sites around the city, corresponding to industrial, residential, commercial, and heavy-traffic carrying areas. Samples were also collected from different cities.

(*d*) Street dust samples after drying were fractionated into a range of sizes, being careful not to alter the size of the particles by the sieving. The nylon sieve sizes (measured under a calibrated microscope) were (mean ± standard deviation): 963 ± 38, 564 ± 14, 213 ± 14, 165 ± 13, 111 ± 11, 54 ± 7, 33 ± 8 μm. A study of the fraction <33 μm under the calibrated microscope, indicated that most of the particles were in the 10–20 μm range. Some samples were also separated on the basis of density, using tetrabromoethane (density = 2.67 $g\ mL^{-1}$).

Results and discussion

Reference materials

The results of the analysis of the IAEA material and internal reference materials are given in Table 1. The measurements were done on samples either at different times over a 3 to 4 year period, whenever the material was used as a control in a batch of analyses, or prepared and analysed on the same day.

For the IAEA standard the coefficient of variation, cv, is <10% for the four metals (<6% for Pb, Cu, and Zn), and except for Ni the cv's for the internal reference materials are (9% ≪ 6% for Pb and Zn).

A second extraction of the samples with HNO_3 removed very little more of the metals into solution. The mean and (standard deviation) for six samples indicate that of the extractable metal

Can. J. Chem. Downloaded from www.nrcresearchpress.com by 78.46.186.204 on 09/07/12
For personal use only.

TABLE 2. Spatial and temporal variations in trace element levels[a]

	Lead		Copper		Nickel		Zinc	
Site	A	B	A	B	A	B	A	B
1	5160[b]	4310	200	196	20.3	20.0	533	542
	300[c]	1210	45	39	4.2	3.7	140	131
	5.8[d]	28	23	20	21	19	27	24
2	5620	4630	190	193	24.2	22.6	584	501
	569	1400	29	30	3.8	3.7	112	139
	10	30	15	16	16	16	19	28
3	8890	7710	245	249	24.0	22.8	600	542
	840	1703	53	50	2.8	3.5	71	106
	9.4	22	22	20	12	15	12	20
4	10460	8830	238	233	24.1	22.6	509	447
	490	2370	24	22	1.8	2.9	69	73
	4.7	27	10	9.4	7.6	13	14	15
5	9150	7710	243	231	20.9	20.6	454	428
	720	1300	25	31	2.2	1.8	32	50
	7.9	30	10	13	10	8.7	7.1	12
6	8490	7830	210	224	20.0	19.7	476	438
	1660	1570	39	35	2.0	1.6	53	72
	20	20	19	16	9.8	8.1	11	16
7	7590	6040	202	206	20.2	18.9	501	432
	2740	3090	29	45	5.2	4.9	117	123
	36	51	14	22	26	26	23	28
8	6160	5780	215	214	17.9	17.5	432	433
	2640	2200	40	34	3.4	2.9	83	79
	43	38	19	16	19	17	19	18
9	9350	8390	213	215	25.3	22.9	589	495
	1050	1910	17	13	4.9	4.7	169	175
	11	23	8.1	6.1	19	21	29	35
10	9730	9080	197	203	20.7	22.5	627	519
	1230	1270	33	39	2.0	3.7	133	166
	13	14	17	19	9.6	16	21	32
11	11340	9630	205	221	19.8	18.6	408	391
	1900	4020	63	59	2.4	3.0	85	90
	17	42	31	27	12	16	21	23
12	7980	8330	152	152	18.2	17.5	355	366
	3070	2760	58	47	1.3	1.5	75	65
	38	33	38	31	7	8.6	22	18
13	10450	9060	204	206	21.9	20.2	384	366
	1310	2630	23	24	2.4	3.6	57	56
	13	29	11	12	11	18	15	15
14	11470	7980	299	241	26.7	23.7	516	442
	1150	3400	33	61	1.8	3.7	14	69
	10	43	11	25	6.6	16	2.7	16
15	3020	3020	131	140	19.2	18.2	679	656
	270	220	9	16	2.3	2.6	71	90
	9	7	6.9	11	12	14	11	14
16	2130	2270	147	140	22.3	20.8	546	520
	240	550	31	30	3.3	3.7	57	65
	11	24	21	21	15	18	10	13
17	5770	5380	192	186	18.8	17.7	529	503
	850	1020	58	45	2.9	2.7	101	116
	15	19	30	24	15	15	19	23
18	3800	3260	187	167	18.1	17.1	625	565
	560	1040	41	49	1.5	2.1	88	141
	15	30	22	29	8.2	12	14	25

Can. J. Chem. Downloaded from www.nrcresearchpress.com by 78.46.186.204 on 09/07/12
For personal use only.

TABLE 2. (*concluded*)

Site	Lead		Copper		Nickel		Zinc	
	A	B	A	B	A	B	A	B
19	6310	5700	126	119	16.9	16.4	619	601
	1150	1260	13	24	2.6	2.2	103	161
	18	22	10	20	15	13	17	27
20	2540	2650	116	128	18.7	19.4	358	400
	610	480	23	23	1.4	3.5	77	116
	24	18	19	18	7.6	18	21	29

[a]A, five months February–June with relatively uniform weather; B, eight months February–September with severe flooding after the 5th month; concentrations in $\mu g\ g^{-1}$.
[b]Mean.
[c]Standard deviation.
[d]Coefficient of variation %.

Can. J. Chem. Downloaded from www.nrcresearchpress.com by 78.46.186.204 on 09/07/12
For personal use only.

ions 99% (0.9) Pb, 99% (0.5) Cu, 97% (2.1) Ni, 99% (2.3) Zn (i.e. cv's < 2%) are removed by the first extraction. This does not mean that all the metal in the dust has been removed as a $HF/HClO_4$ digestion indicates that around 98% Pb, 89% Cu, 86% Ni, and 95% Zn is obtained by the nitric acid digestions. Therefore it appears that little of the variability in the analytical results arises from inconsistent extractions, particularly for hot, strong acid extractions.

A coefficient of variation < 10% may therefore be considered as encompassing experimental and extraction errors in analysis, and any inhomogeneity in the sample.

Spatial effect

Two sets of ten samples of dust, each set taken from a 5 m spread and samples 0.5 m apart have mean lead levels (in $\mu g\ g^{-1}$) of 2280, 3430, standard deviations 320, 270, ranges 1830–2680, 2800–3800, and coefficient of variation 14%, 7.9%, respectively. The results are similar to those reported by Day (12). The cv's calculated from his data are 14% and 5.8%. The variability is relatively low, and in two of the four cases close to the analytical variability. This suggests that the level of lead in a spot sample taken from the sites are reasonably representative of the level in the material at the site (over a 5 m distance). These results indicate that for lead a total variability of 20%, as measured by the coefficient of variability, includes the analytical and sample variability for a particular site.

The mean, standard deviation, and cv for 20 sampling sites around an intersection involving three T junctions are given in Table 2, one sample per month for eight months. The data for the first five months are given in the columns labelled A. During that time the weather conditions, in particular rainfall, were relatively uniform. It may be seen from the data that the cv's for lead at each site range from 4.7% to 43% with 16 of the sites having a cv < 20%. For Cu, Ni, and Zn the number of sites with cv < 20% are 13, 18, and 13, respectively. The results for Pb and Ni suggest a reasonable constancy in their levels for most sites over the five months, and a somewhat lesser constancy for Cu and Zn.

Source of trace elements

From previous studies of the sources of trace elements in dust, soil appears to be the major contributor, around 75–90% (1, 14, 17). Because of the high contribution of soil to street dust it could be expected that the variability of the levels of elements originating primarily from the soil is less than for pollution-type elements. This is found to be the situation. For the soil-based elements Mn, Ti, Al, Ce, La, and Sm, the cv range for 11 samples taken from five cities (1) is 22–54%, and for 12 samples from one city (17) 11–24%. For the three pollution based elements, Pb, Cu, and Zn, the cv ranges are 71–107% and 66–74%, respectively.

TABLE 3. Size distribution of particles in street dust

Size range μm	Mean[a] %	Standard deviation	cv%	Range
963–563	17.1	10.5	62	2.6–30.7
563–213	29.1	9.2	32	11.1–43.9
213–165	13.9	5.1	36	7.2–25.4
165–111	14.4	8.1	56	5.0–36.5
111–54	13.1	4.5	34	6.5–19.3
54–33	6.1	3.9	63	1.7–16.7
<33	6.2	4.6	74	0.5–13.6

[a]12 samples, mass of each sample: 702.4, 332.7, 172.4, 221.3, 203.9, 260.1, 258.7, 409.7, 211.2, 1227.8, 226.8, 65.7 g. Total mass for each size fraction: 590.7, 1099.6, 711.5, 591.1, 620.7, 366.2, 313.0 g.

Temporal effect

The data in columns B in Table 2 are the means, standard deviations, and cv's for the same 20 sites over eight months (the original 5 months + the next three). Severe flooding occurred between the fifth and sixth month sampling periods. A significant reduction occurred in the levels of some of the heavy metals, especially lead. The cv's < 20% for Pb, Cu, Ni, and Zn in this case are 5, 13, 18, and 10, respectively. There is a clear temporal effect for lead due to the rainfall (3, 7), and little overall change for the other metals.

Size effect

Street dust consists of a wide range of particle sizes, and the % size distribution within samples is not constant. Over 12 sites covering industrial, residential, heavy-traffic and commercial areas, the % mass distribution of dust in different size ranges are listed in Table 3. There is a large variability for each size fraction. In addition the amount of sample >963 μm is as variable. The different distributions would be of little consequence if the concentrations of the heavy metals did

Can. J. Chem. Downloaded from www.nrcresearchpress.com by 78.46.186.204 on 09/07/12
For personal use only.

TABLE 4. Level of trace elements in street dust in relation to dust particle size[a]

Size range (μm)	% Mass distribution	Concentration μg g^{-1} Pb	Cu	Ni	Zn
Sample 1					
963–563	8.0	18500	45.5	9.0	1426
563–213	27.3	6421	58.0	10.3	829
213–165	11.3	3301	46.1	7.2	654
165–111	17.3	4896	70.3	10.4	841
111–54	19.3	6420	162	15.0	1013
54–33	8.8	7451	165	20.0	1171
<33	7.6	11306	221	24.7	1742
Mean (W)		7663	96.6	12.5	1008
Mean (S)		8329	110	13.8	1097
sd		5122	71.4	6.4	381
cv		62	65	47	35
Sample 2					
963–563	13.3	1280	86.3	20.0	656
563–213	32.5	1210	82.5	14.2	541
213–165	12.6	924	62.5	11.4	384
165–111	14.2	1070	72.8	12.1	436
111–54	13.5	1850	174	15.0	642
54–33	6.3	1990	156	16.4	720
<33	7.5	1920	158	15.7	747
Mean (W)		1365	103	14.6	563
Mean (S)		1463	113	15.0	590
sd		443	47	2.9	139
cv		30	42	19	23
Sample 3					
963–563	2.7	474	36.0	10.3	174
563–213	12.2	407	17.4	7.1	109
213–165	25.4	260	6.2	4.4	84.3
165–111	12.7	156	10.6	5.0	68.6
111–54	19.1	311	23.7	8.4	128
54–33	16.7	556	30.9	10.2	213
<33	11.3	785	51.1	14.9	268
Mean (W)		389	21.5	7.9	138
Mean (S)		421	25.1	8.6	149
sd		209	15.6	3.6	72.5
cv		50	62	42	49

[a]Mean (W) = weighted mean, mean (S) = straight concentration mean, sd = standard deviation for mean (S), cv = coefficient of variation.

not vary with size, but this is not the case, as indicated by representative data for three of the sites given in Table 4. Each element displays the same size/concentration profile, i.e. a minimum in concentration around the 213–165 μm range. The profiles are of the same general form for the other nine samples, but less so for the samples taken from industrial areas. The form of the profile does not relate simply to the surface area of the particles.

The straight concentration means are greater than the weighted means, but surprisingly close. However, the cv's for the means generally show a wide variability. Therefore significant variability may occur between samples as a result of differences in the distribution of sizes within the samples. This could well be one of the factors which influences the actual level obtained (1, 2, 4, 7, 11, 15). Sampling methods, street cleaning, and rain and wind could all produce some fractionation of the dust in the street. The fall in lead levels after a flooding event suggests that some fractionation has occurred, removing a greater proportion of either the large size particles or smaller size particles, or both. The size fraction <33 μm was mainly made up of particles 10–20 μm. It appears that the finest particles in street dust (i.e. clay size) are not sampled by the method used, and probably by most methods reported in the literature.

The density of the dust particles may influence natural and man-made fractionation processes. From the twelve city-wide sites dense material (>2.67 g mL^{-1}) decreased regularly from 12% to 5% of the total sample, as the particle size decreased, whereas the light material (<2.67 g mL^{-1}) increased from 83% to 95%. There is proportionately more light material in the smaller-sized particles, and it could be that these particles are the ones preferentially lost during rain storms, reducing the lead content of the remaining dust. It is known that the lead levels in the dense dust fraction are significantly greater than in the light material (2, 7). This contributes to the higher levels of lead in the larger particles.

Concluding remarks

It appears that the factors that may influence the variability of levels of trace elements in street dust are spatial, temporal, source, particle size, and particle density. For any sample all these factors may contribute to the actual trace element levels, and their variability. However, provided the particle size is taken into account, and there is knowledge of the temporal and sampling factors that may have influenced the sample, and for a cv > 20% there is reason to be confident in the reliability of the trace element concentrations as a measure of pollution levels. Of the four metals studied this conclusion is only clearly applicable to lead, a widely dispersed pollution element.

Acknowledgements

The author acknowledges grants from the New Zealand Universities Grants Committee, for the purchase of equipment. The following people have contributed at different times to the analytical results; Bernard S. W. Dawson, Joanne M. Deely, Carol A. Hulse, Robyn J. Schroeder, Peter R. Simmonds, Carol Stewart, and Tan Seow Yong.

1. J. E. FERGUSSON and D. E. RYAN. The Sci. Total Environ. **34**, 101 (1984).
2. R. W. LINTON, D. F. S. NATUSH, R. L. SOLOMON, and C. A. EVANS. Environ. Sci. Techn. **14**, 159 (1980).
3. J. E. FERGUSSON and P. R. SIMMONDS. N. Z. J. Sci. **26**, 219 (1983).
4. A. ARCHER and R. S. BARRATT. The Sci. Total Environ. **6**, 275 (1976).
5. Royal Commission on Environmental Pollution. 9th Report. Lead in the Environment. HMSO. 1983.
6. M. J. DUGGAN. The Sci. Total Environ. **33**, 37 (1984).
7. J. E. FERGUSSON, R. W. HAYES, T. S. YONG, and S. H. THIEW. N. Z. J. Sci. **23**, 293 (1980).
8. R. M. HARRISON. The Sci. Total Environ. **11**, 89 (1979).
9. B. BRUNEKREEF, D. NOY, K. BIERSTEKER, and J. S. M. BOLEY. J. Air Pollut. Control Ass. **33**, 872 (1983).
10. R. S. HAMILTON, D. M. REVITT, and R. S. WARREN. The Sci. Total Environ. **33**, 59 (1984).
11. M. J. DUGGAN. Public Health Rev. **13**, 1 (1985).
12. J. P. DAY. N. Z. J. Sci. **20**, 395 (1977).
13. M. J. DUGGAN. Clean Air, **11**, 87 (1981).
14. P. K. HOPKE, R. E. LAMB, and D. F. S. NATUSCH. Environ. Sci. Techn. **14**, 164 (1980).
15. J. B. ELLIS and D. M. REVITT. Water, Air, Soil Pollut. **17**, 87 (1982).
16. International Atomic Energy Agency. Progress Report No. 22. 1984.
17. J. E. FERGUSSON, E. A. FORBES, R. J. SCHROEDER, and D. E. RYAN. The Sci. Total Environ. **50**, 217 (1986).

Kinetics and mechanisms of the reaction of 2,4,6-trinitrocumene and 2,4,6-trinitroethylbenzene with 1,1,3,3-tetramethylguanidine in *N*,*N*-dimethylformamide solvent

MIHIR K. BISWAS,[1] ARNOLD JARCZEWSKI,[2] AND KENNETH T. LEFFEK
Department of Chemistry, Dalhousie University, Halifax, N.S., Canada B3H 4H6

Received August 27, 1986

This paper is dedicated to Professor Douglas E. Ryan on the occasion of his 65th birthday

MIHIR K. BISWAS, ARNOLD JARCZEWSKI, and KENNETH T. LEFFEK. Can. J. Chem. **65**, 1007 (1987).

The reaction of tetramethylguanidine (TMG) with trinitrocumene (TNC) and trinitroethylbenzene (TNEB) in dimethylformamide solvent has been studied with respect to products and kinetics. For TNC only σ-complex formation with the benzene ring was observed, for which the equilibrium constant, rate constants, and activation parameters were measured. For TNEB, both σ-complex formation and proton transfer from the α-carbon atom of the ethyl group were observed. The equilibrium constants, rate constants, and activation parameters were separately determined for each reaction and a primary deuterium isotope effect, k_H/k_D = 13.6 (at 20°C), was found for the proton transfer. The reaction parameters are compared to those for proton transfer from TNT to tetramethylguanidine in DMF solvent.

MIHIR K. BISWAS, ARNOLD JARCZEWSKI et KENNETH T. LEFFEK. Can. J. Chem. **65**, 1007 (1987).

Dans le but de déterminer la cinétique et la nature des produits des réactions, on a étudié les réactions de la tétraméthylguanidine (TMG) avec le trinitrocumène (TNC) et avec le trinitroéthylbenzène (TNEB), dans le diméthylformamide. Dans le cas du TNC, on n'a observé que la formation du complexe σ avec le noyau benzénique dont on a mesuré la constante d'équilibre, les constantes de vitesses ainsi que les paramètres d'activation. Dans le cas du TNEB, on a observé la formation d'un complexe σ ainsi qu'une réaction de transfert de proton du carbone σ du groupement éthyle. Pour chacune de ces réactions, on a déterminé les constantes d'équilibre, les constantes de vitesse et les paramètres d'activation; de plus, on a trouvé que l'effet isotopique primaire du deutérium, k_H/k_D = 13,6 (à 20°C). On a comparé les paramètres réactionnels avec ceux observés antérieurement pour le transfert de proton du TNT à la tétraméthylguanidine dans le DMF.

[Traduit par la revue]

Can. J. Chem. Downloaded from www.nrcresearchpress.com by 78.46.186.204 on 09/07/12
For personal use only.

Introduction

The reaction of 1,1,3,3-tetramethylguanidine (TMG) with 2,4,6-trinitrotoluene (TNT) in dipolar aprotic solvents has been shown to be a proton transfer from the methyl group (1, 2), and a number of primary deuterium kinetic isotope effects have been measured for the proton transfer reaction with various bases and solvents (3–7). Nevertheless, it has also been noted (3, 6, 7) that nucleophilic attack by some bases could take place on the benzene ring to yield a σ-complex. The ring attack took place at the 3 position instead of the 1 position as originally observed by Meisenheimer (8).

In this work, the methyl group in TNT is replaced by ethyl and isopropyl to observe how enhanced steric hindrance and reduction of acidity alter the balance between the two possible reactions of the base, i.e., proton abstraction from the α-carbon of the side chain and nucleophilic attack on the benzene ring. By observing which hydrogen atoms in the substrate molecules are preferentially replaced by deuterium under basic conditions and by measuring equilibrium constants, rate constants, primary kinetic isotope effects, and activation parameters of the reactions, it should be possible to determine the factors that lead to one reaction dominating the other.

Results and discussion

The trinitrocumene reaction

Sym-trinitrocumene (TNC) reacts with 1,1,3,3-tetramethylguanidine (TMG) base in DMF solvent to give a coloured product with λ_{max} at 454 and 505 nm. An analogous reaction in the same solvent with sodium hydroxide or alkoxide ions gave a product with absorption maxima at 448 and 495 nm. However, the rates of these latter reactions are very much faster than that of TMG.

When TNC was treated with NaOD or TMG-*d* in DMF solvent, followed by DCl in D_2O, the product was TNC deuterated in the 3 and 5 positions of the benzene ring. This result and the similar λ_{max} of the products suggests that TMG, NaOH, and NaOAlk give rise to the same type of product, a σ-complex, as shown in eq. [1] for the TMG reaction.

The slowness of the TMG reaction compared to that of the alkoxides may result from several factors, e.g. the large degree

[1] 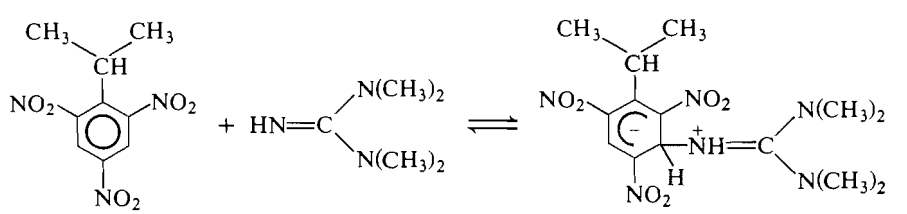

[1] Postdoctoral Fellow 1982–1983.
[2] Visiting Scientist 1985.

Can. J. Chem. Downloaded from www.nrcresearchpress.com by 78.46.186.204 on 09/07/12
For personal use only.

TABLE 1. The optical densities of the reaction of trinitrocumene* with tetramethylguanidine in DMF solvent at 25°C

10^2[TMG] (M)	1.53	2.04	2.55	3.06	3.57	4.60
OD at 450 nm	0.691	0.816	0.964	1.094	1.149	1.400

*Initial concentration of TNC = 5.16×10^{-4} M.

of steric hindrance of both the substrate and reagent molecules, the weak nucleophilicity of TMG, the weak basicity of TMG in DMF solvent due to the electron-donor character of DMF, and the reduced acidity of the proton on the α-carbon atom of the isopropyl group relative to that of the methyl protons in trinitrotoluene.

The equilibrium constant for the reaction was determined by the Hildebrand–Benesi method (9) from the optical densities shown in Table 1. These results fitted eq. [2]

$$[2] \quad [A]/OD = 1/K\varepsilon[B] + 1/\varepsilon$$

in which [A] is the concentration of TNC, [B] is the concentration of [TMG], OD is the optical density, K is the equilibrium constant, and ε is the molar absorptivity. The correlation coefficient was 0.996, with $K = 22.8 \pm 3.0$ dm^3 mol^{-1} and $\varepsilon = 5100$ dm^3 mol^{-1} cm^{-1} at 25°C. The reasonably good correlation coefficient suggests that there are no competing reactions.

Terrier[3] has suggested, by analogy with similar reaction systems (11), that the σ-complex in eq. [1] is deprotonated by a second molecule of TMG. Such a reaction probably does take place to some extent and is no doubt part of the mechanism for deuterium exchange of the ring hydrogen. However, the σ-complex should be rather a weak acid with high steric hindrance. The experimental fit of the optical density data to eq. [2], rather than to the equation derived from a reaction involving two TMG molecules, provides evidence that the deprotonation of the σ-complex proceeds only to a very limited extent.

The pseudo-first-order rate constants were measured at several temperatures by monitoring the optical density at 450 nm using an excess of TMG. The values of the k_{obs} were fitted to eq. [3] and the forward (k_f) and backward (k_b) rate

$$[3] \quad k_{obs} = k_f[TMG] + k_b$$

constants were calculated from a linear least-squares fit. The results are shown in Table 2. The k_f values yielded $\Delta H^{\ddagger} = 13.0 \pm 0.7$ kcal mol^{-1}, $\Delta S^{\ddagger} = -18.8 \pm 2.5$ cal mol^{-1} deg^{-1}. The equilibrium constant at 25°C calculated from k_f and k_b is 25.7 ± 2.4 dm^3 mol^{-1}, in good agreement with the above non-kinetic determination.

The trinitroethylbenzene reaction

The reaction of trinitroethylbenzene (TNEB) with sodium ethoxide in DMF gives a product with λ_{max} at 433 and 502 nm. This is similar to the reaction of sym-trinitroanisol with ethoxide in ethanol, which showed λ_{max} at 410 and 490 nm (12).

The reaction of TNEB with TMG is a fast reaction giving a product with λ_{max} at 447 and 508 nm, very similar to the reaction with trinitrocumene. This reaction, particularly for the deuterated substrate, is most clearly visible at lower TMG base concentrations, and the similarity of the absorption maxima of the products to those of the trinitrocumene reaction suggest σ-complex formation. At higher TMG base concentrations the initial orange colour from the above two absorptions changes slowly to a blue product. This product has three absorption maxima at λ_{max} 363, 514, and 785 nm. This absorption spectrum is similar to the product of the reaction of trinitrotoluene with TMG in acetonitrile (1) and in dimethylformamide (2), and is characteristic of a proton transfer reaction (4, 5).

In the case of the reaction of deuterated TNEB with TMG, the initial fast reaction is particularly clear since the subsequent deuteron transfer is very much slower.

The absorption peak at 363 nm does not overlap with the initial peak at 447 nm, so it is possible to measure the rate of the second reaction without interference by monitoring this peak with time. The nature of this reaction as a proton transfer was established by deuterating TNEB with TMG-*d* or diethylamine-*d*, the product of which exchange is TNEB deuterated 90% on the α-carbon atom of the ethyl group, although some deuteration also took place at the 3 and 5 positions of the ring.

The equilibrium constants for the proton and deuteron transfer reactions were calculated from the optical density measurements shown in Table 3, by the Hildebrand–Benesi method (9). The correlation coefficients for a fit to eq. [2] were 0.946 and 0.987 for the proton and deuteron reaction respectively. K_H^{25} was 540 ± 110 dm^3 mol^{-1} and K_D^{25} was 525 ± 45 dm^3 mol^{-1} with the molar absorptivity in the range of 5000–5500 dm^3 mol^{-1} cm^{-1}.

The first- and second-order rate constants were determined using excess TMG base by monitoring the optical density at 363 nm for both the normal and deuterated TNEB substrate. The observed pseudo-first-order rate constants, k_{obs}, were fitted to eq. [3] and the forward (k_f) and backward (k_b) rate constants for the proton transfer equilibrium were calculated by a linear least-squares fit.

The results are shown in Table 4, together with the isotope effects k_H/k_D. The activation parameters derived from the second-order rate constants are collated in Table 5.

An extra series of runs was carried out using deuterated TNEB substrate and deuterated TMG as the base at 30°C. This gave $k_f = 1.38 \pm 0.06 \times 10^{-3}$ mol^{-1} s^{-1}, and $k_b = 5.9 \pm 0.3 \times 10^{-5}$ s^{-1}, in satisfactory agreement with the rate constants for normal TMG, indicating no rapid isotopic scrambling in this reaction.

The initial fast reaction between TNEB and TMG was monitored at 447 nm for several base concentrations in large excess over that of TNEB. The results are collated in Table 6. The absorbance value at the end of these kinetic runs was used to calculate an approximate value for the equilibrium constant for this reaction, using eq. [2]. This calculation gave $K^{20} = 7.5 \pm 3.0$ dm^3 mol^{-1}, in good agreement with K^{20} calculated from k_f/k_b of 7.9 ± 1.6 dm^3 mol^{-1}.

The activation parameters derived from the second-order rate constants are $\Delta H^{\ddagger} = 5.2 \pm 0.7$ kcal mol^{-1}, $\Delta S^{\ddagger} = -31.4 \pm 2.5$ cal mol^{-1} deg^{-1}.

A summary of the reaction parameters that have been determined for the σ-complex and proton transfer reactions of trinitrocumene, trinitroethylbenzene, and trinitrotoluene (2) in DMF solvent are collected in Table 7.

The proton transfer reaction is not observed for trinitrocumene because the second-order rate constant for that reaction is probably at least 10^5 times slower than that for the σ-complex reaction. For trinitroethylbenzene, although the σ-complex reaction is kinetically favoured, the proton transfer reaction has a much larger equilibrium constant and, therefore, is observed at long reaction times. For trinitrotoluene, the equilibrium

[3]F. Terrier. Personal communication.

TABLE 2. Kinetics of the reaction of trinitrocumene with tetramethylguanidine in DMF

Temperature (°C)	10^2[TMG] (M)	k_{obs} (s^{-1})	$10^2 k_f$ ($dm^3 mol^{-1} s^{-1}$)	$10^3 k_b$ (s^{-1})
10.0	3.15–9.45	4.63–7.33	4.18±0.18	3.4±0.1
15.0	3.15–9.45	6.56–7.91	6.92±0.27	4.4±0.2
20.0	3.15–9.45	8.40–14.17	8.9±1.1	5.2±0.8
25.0	3.15–9.45	10.80–20.00	14.9±0.7	5.8±0.5
30.0	3.15–9.45	11.65–25.89	20.8±2.6	4.8±1.8

TABLE 3. The optical densities for the proton and deuteron transfer from trinitroethylbenzene* to tetramethylguanidine in DMF at 25°C

(a) Proton transfer					
10^2[TMG] (M)	0.33	0.83	1.67	3.33	8.33
OD at 363 nm	0.217	0.265	0.280	0.305	0.369
(b) Deuteron transfer					
10^2[TMG] (M)	0.40	1.00	2.00	4.00	6.00
OD at 363 nm	0.344	0.404	0.465	0.486	0.491

*Initial concentration of TNEB = 6.0×10^{-5} M; TNEB-d = 1.0×10^{-4} M.

constant for the σ-complex reaction will be quite small and thus that reaction is not observed in the presence of the proton transfer reaction, which is quite fast and has a large equilibrium constant.

Experimental

Materials

2,4,6-Trinitrocumene (TNC) was prepared by a double nitration of cumene, the first carried out by the procedure of Fittig *et al.* (13) using a 1:6 mixture of 90% HNO_3 and 98% H_2SO_4. The oily product of this reaction was extracted with dichloroethane and renitrated by the procedure of Kamlet *et al.* (14). The oily product (15 g) was dissolved in a mixture of 60 mL 90% HNO_3 and 300 mL 98% H_2SO_4 and the solution was stirred at 80°C when a vigorous reaction started. The temperature was raised slowly to 120–130°C, and the reaction allowed to proceed for 45 min. The reaction mixture was poured onto ice and the resulting white solid product was recrystallized from ethanol, mp 109–110°C; nmr δ: 8.53 (s, 2H), 1.36, 1.47 (d, 6H), 3.33 (h, 1H).

2,4,6-Trinitroethylbenzene (TNEB) was prepared by the procedure of Gay-Lussac and Ficheroulle (15). Ethylbenzene (20 g) was added dropwise to a mixture of 54 mL 100% HNO_3 and 250 mL 30% oleum at 20°C. After the addition, the mixture was warmed to 45°C for 2 h and then to 85°C for 5 h. After cooling to room temperature, the reaction mixture was poured onto ice. The crude trinitroethylbenzene was washed several times with cold $NaHCO_3$ solution and then with water. Recrystallization from ethanol gave yellow needles, mp 38.5°C; nmr δ: 8.76 (s, 2H), 2.98, 3.09 (g, 2H), 1.41 (t, 3H).

Tetramethylguanidine was dried over NaOH and fractionally distilled. The fraction distilling at 161°C was collected.

Dimethylformamide (DMF) was purified by the method of Zaugg and Schaefer (16). Reagent grade benzene (400 mL) was added to reagent grade DMF (2 L) and the mixture was distilled at atmospheric pressure until the boiling temperature reached 130°C. The undistilled liquid was transferred under nitrogen to storage bottles and 20–30 g P_2O_5 was added per litre of DMF. The bottles were shaken for 3–4 h, after which the DMF was transferred, under nitrogen, to fresh storage bottles containing 50 g BaO per litre of DMF. The bottles were shaken for a further 1–2 h. The DMF was then decanted and distilled under nitrogen at 20–25 Torr pressure (1 Torr = 133.3 Pa), using a capillary nitrogen bleed. The distillate was redistilled in the same manner and the middle cut of about 1 L was collected and stored under nitrogen.

Deuteration of 2,4,6-trinitrocumene

Trinitrocumene (0.25 g) was dissolved in dry freshly distilled DMF (25 mL), and D_2O (25 mL) was added. To this solution 0.1 M NaOD (7 mL) was added dropwise with stirring. After 2 h the reaction mixture was neutralized with a few drops of dilute DCl in D_2O and poured into excess D_2O. Very fine yellow crystals formed and this material was recrystallized from ethanol-d. This procedure was repeated 3 times, giving a product, mp 109.5–110°C. The nmr spectrum showed no

TABLE 4. Rate constants for the proton transfer reaction between trinitroethylbenzene and tetramethylguanidine in DMF solvent

Temperature (°C)	10^2[TMG] (M)	$10^5 k_{obs}$ (s^{-1})	$10^3 k_f$ ($dm^3 mol^{-1} s^{-1}$)	$10^5 k_b$ (s^{-1})	k_H/k_D
(*i*) Normal TNEB					
15	0.4–6.0	4.8–38.4	6.1±0.4	3.6±1.2	
20	0.4–6.0	6.1–57.0	8.9±0.1	3.6±0.6	
25	0.4–8.0	8.2–104.5	12.6±0.7	6.5±2.8	
30	0.4–6.0	14.0–123	19.6±0.6	7.7±1.9	
35	0.4–6.0	18.8–172	29.9±0.7	10.5±2.3	
40	0.4–6.0	27.8–247	39.3±1.2	15.6±4.1	
45	0.4–6.0	39.3–337	53.5±3.2	28±10	
(*ii*) Deuterated TNEB					
15	1.0–6.0	3.1–5.4	0.45±0.02	2.7±0.1	13.4±0.3
20	1.0–8.0	3.7–8.4	0.66±0.02	3.1±0.1	13.6±0.5
25	1.0–6.0	4.8–9.7	0.95±0.06	4.0±0.2	13.2±1.1
30	0.4–6.0	5.0–13.3	1.44±0.15	5.2±0.5	13.6±1.4
35	0.4–6.0	7.9–20.8	2.28±0.16	6.5±0.5	11.8±0.9
40	0.4–4.0	9.2–22.1	3.35±10.6	9.4±1.4	11.7±2.1
45	0.4–4.0	13.3–31.2	4.97±0.7	13.0±1.7	10.8±1.6

Can. J. Chem. Downloaded from www.nrcresearchpress.com by 78.46.186.204 on 09/07/12
For personal use only.

TABLE 5. Activation parameters from the proton and deuteron transfer reaction between trinitroethylbenzene and tetramethylguanidine in DMF solvent

Parameter	H-transfer	D-transfer
$\Delta H^{\neq}$ (kcal mol^{-1})	12.8 ± 0.2	14.1 ± 0.3
$\Delta S^{\neq}$ (cal mol^{-1} deg^{-1})	−24.3 ± 0.6	−24.9 ± 1.0
$(\Delta H_D^{\neq} - \Delta H_H^{\neq})$ (kcal mol^{-1})	1.3 ± 0.2	
$(\Delta S_D^{\neq} - \Delta S_H^{\neq})$ (cal mol^{-1} deg^{-1})	−0.6 ± 0.5	

signal at δ = 8.53 for the ring protons, whereas the aliphatic proton signals integrated in the ratio of 1:6 as for normal TNC.

TNC was also deuterated using TMG as base by a method similar to that used by Caldin and Mateo (10). After two exchanges the ring protons were about 50% replaced by deuterium, based on nmr signals.

Deuteration of 2,4,6-trinitroethylbenzene

The deuteration was carried out with both TMG-*d* and diethylamine-*d* as the base. 2,4,6-Trinitroethylbenzene (0.24 g) was dissolved in dry, freshly distilled DMF, and a base solution consisting of 1 mL of base in 5 mL DMF was added dropwise with stirring. After 3 h the reaction mixture was neutralized with a few drops of dilute DCl in D_2O. The solvent was removed under vacuum and then D_2O (20 mL) was added to dissolve the amine hydrochloride. The TNEB-*d* was extracted with chloroform and the extract washed several times before being evaporated to dryness, to yield an oil product of TNEB-*d*. This was washed several times with D_2O and then crystallized from ethanol-*d* at −7°C. All the operations were performed under dry, pure N_2.

The product obtained using diethylamine-*d* as the base gave nmr signals indicating more than 90% deuteration of the α-carbon atom of the ethyl group and about 50% deuteration of the benzene ring. The TMG-*d* base gave slightly less deuteration of the α-carbon of the ethyl group and about 80% deuteration of the ring. The diethylamine-*d* product was used in the kinetic runs.

Kinetic and equilibrium measurements

The kinetic runs and equilibrium measurements were carried out using a Cary 219 spectrophotometer with the cell block thermostat to ±0.1°C. The kinetic runs were completed under pseudo-first-order conditions with the base concentration in 50-fold to 400-fold excess. Pseudo-first-order rate constants were calculated from the traces of absorbance vs. time using the Guggenheim method and the second-order rate constants were calculated by a linear least-squares fit of the variation of k_{obs} with base concentration. The activation parameters were calculated by a linear least-squares fit of ln k/T vs. $1/T$.

TABLE 6. Kinetics of the initial reaction of trinitroethylbenzene* with tetramethylguanidine in DMF

Temperature (°C)	10^2[TMG] (M)	k_{obs} (s^{-1})	k_f (dm^3 mol^{-1} s^{-1})	k_b (s^{-1})
10.0	3.2–12.8	8.9–16.9	83 ± 23	5.0 ± 2.0
20.0	3.2–12.8	17.4–29.1	115 ± 18	14.5 ± 1.6
30.0	3.2–12.8	36.0–49.6	142 ± 6	32.0 ± 0.5
40.0	6.4–12.8	72.5–87.2	231 ± 44	58 ± 4

*Initial concentration 2.0×10^{-4} M.

TABLE 7. Summary of reaction parameters for the σ-complex and proton transfer reactions of trinitrocumene, trinitroethylbenzene, and trinitrotoluene with tetramethylguanidine in dimethylformamide solvent

TNC	α-complex with ring	
	$k_2^{20} = 8.9 \pm 1.1$ dm^3 mol^{-1} s^{-1}	
	$\Delta H^{\neq} = 13.0 \pm 0.7$ kcal mol^{-1}	
	$\Delta S^{\neq} = -18.8 \pm 2.5$ cal mol^{-1} deg^{-1}	
	$K^{25} = 22.8 \pm 3.0$ dm^3 mol^{-1}	
TNEB	σ-complex with ring	Proton transfer
	$k_2^{20} = 115 \pm 18$ dm^3 mol^{-1} s^{-1}	$k_2^{20} = 8.9 \pm 0.1 \times 10^{-3}$ mol^{-1} s^{-1}
	$\Delta H^{\neq} = 5.2 \pm 0.7$ kcal mol^{-1}	$\Delta H^{\neq} = 12.8 \pm 0.2$ kcal mol^{-1}
	$\Delta S^{\neq} = -31.4 \pm 2.5$ cal mol^{-1} deg^{-1}	$\Delta S^{\neq} = -24.3 \pm 0.6$ cal mol^{-1} deg^{-1}
	$K^{20} = 7.5 \pm 3.0$ dm^3 mol^{-1}	$k_H/k_D^{20} = 13.6 \pm 0.5$
		$\Delta H_D^{\neq} - \Delta H_H^{\neq} = 1.3 \pm 0.2$ kcal mol^{-1}
		$\Delta S_D^{\neq} - \Delta S_H^{\neq} = -0.6 \pm 0.5$ cal mol^{-1} deg^{-1}
		$K^{25} = 540 \pm 110$ dm^3 mol^{-1} at 363 nm
TNT		Proton transfer
		$k_2^{20} = 15.8 \pm 0.6$ dm^3 mol^{-1} s^{-1}
		$\Delta H^{\neq} = 9.8 \pm 0.3$ kcal mol^{-1}
		$\Delta S^{\neq} = -19.5 \pm 0.9$ cal mol^{-1} deg^{-1}
		$k_H/k_D^{20} = 16.9 \pm 0.4$
		$\Delta H_D^{\neq} - \Delta H_H^{\neq} = 2.6 \pm 0.4$ kcal mol^{-1}
		$\Delta S_D^{\neq} - \Delta S_H^{\neq} = 3.4 \pm 1.3$ cal mol^{-1} deg^{-1}
		$K^{25} = 1800$ dm^3 mol^{-1} at 377 nm

Can. J. Chem. Downloaded from www.nrcresearchpress.com by 78.46.186.204 on 09/07/12
For personal use only.

Acknowledgement

The authors are grateful for financial support by the Natural Sciences and Engineering Research Council of Canada.

1. A. JARCZEWSKI and P. PRUSZYNSKI. Ann. Soc. Chim. Pol. (Rocz. Chem.), **51**, 2171 (1977).
2. A. JARCZEWSKI, P. PRUSZYNSKI, and K. T. LEFFEK. Can. J. Chem. **57**, 669 (1979).
3. A. R. NORRIS. Can. J. Chem. **58**, 2178 (1980).
4. E. F. CALDIN and G. LONG. Proc. R. Soc. London, A: **228**, 263 (1955).
5. E. BUNCEL, A. R. NORRIS, K. E. RUSSELL, and R. TUCKER. J. Am. Chem. Soc. **94**, 1646 (1972).
6. E. BUNCEL, A. R. NORRIS, K. E. RUSSELL, P. SHERIDAN, and H. WILSON. Can. J. Chem. **52**, 1750 (1974).
7. E. BUNCEL, A. R. NORRIS, K. E. RUSSELL, and H. WILSON. Can. J. Chem. **52**, 2306 (1974).
8. J. MEISENHEIMER. Ann. **323**, 205 (1902).
9. H. BENESI and J. H. HILDEBRAND. J. Am. Chem. Soc. **71**, 2703 (1949).
10. E. F. CALDIN and S. MATEO. J. Chem. Soc. Faraday Trans. 1, **71**, 1876 (1975).
11. F. TERRIER. Chem. Rev. **82**, 77 (1982).
12. J. B. AINSCOUGH and E. F. CALDIN. J. Chem. Soc. 2528 (1956).
13. R. FITTIG, L. SCHAEFFER, and J. KONIG. Ann. **149**, 324 (1869).
14. M. J. KAMLET, J. T. HOFFSOMMER, and H. G. ADOLPH. J. Am. Chem. Soc. **84**, 3925 (1962).
15. A. GAY-LUSSAC and H. FICHEROULLE. Meml. Poudres, **36**, 71 (1954).
16. H. E. ZAUGG and A. D. SCHAEFER. Anal. Chem. **36**, 2121 (1964).

Can. J. Chem. Downloaded from www.nrcresearchpress.com by 78.46.186.204 on 09/07/12
For personal use only.

^{63}Ni β range and backscattering in confined geometries[1]

K. W. MICHAEL SIU[2] AND WALTER A. AUE[3]

Department of Chemistry, Dalhousie University, Halifax, N.S., Canada B3H 4J3

Received October 17, 1986

This paper is dedicated to Professor Douglas E. Ryan on the occasion of his 65th birthday

K. W. MICHAEL SIU and WALTER A. AUE. Can. J. Chem. **65**, 1012 (1987).

To know the spatial distribution of ion pairs resulting from ^{63}Ni β radiation in the gas phase is important for a variety of theoretical and practical reasons, in particular those concerning the electron capture detector. Literature estimates of this distribution vary by about one order of magnitude, yet this parameter is necessary for the modelling of this detector. The ^{63}Ni-induced, initial ion pair distribution was therefore measured in a variety of gases with two techniques: a conventional one based on the electrical saturation current at variable interelectrode distances, and an unconventional one based on luminescence from a plastic scintillator. The data are analyzed in terms of two ranges, d^{50} and d^{95}, that describe the distances from a planar radioactive foil within which 50% and 95% of the total gas-phase ionization occur. The data from the electrical measurement show unexpected evidence of strong β backscattering and secondary electron emission from the counter-electrode. Under these (non-exponential) conditions, d^{50} values in the common detector gases nitrogen and argon/methane vary from 0.5 to 1.0 mm, depending on the nature of the counter-electrode. Calculations based on the quasi-exponential range found at longer distances in electrical measurements yield values of about 2.5 mm (which are low because of geometric measurement bias). In contrast, the data from the luminescence measurement are almost completely exponential and d^{50} values for argon (+5% methane) and nitrogen are 2.8 and 3.8 mm, respectively. The d^{95} values vary from 12 to 16 mm for the luminescence, to 6 and 9 mm for the (less reliable) electrical measurement; all at ambient conditions. The luminescence data are considered closer to the "true" (unimpeded) charge distribution, while the ionization data may be closer to the initial charge topography inside an electron capture detector of confining geometry. All range data, however, are short enough to advise modelling the detector as a system with strongly heterogeneous charge distribution. No evidence was found for some of the very large range estimates found in the literature.

K. W. MICHAEL SIU et WALTER A. AUE. Can. J. Chem. **65**, 1012 (1987).

Connaître la distribution spaciale des paires d'ions provenant de la radiation β du ^{63}Ni est important pour diverses raisons théoriques et pratiques, en particulier celles concernant le détecteur à capture d'électrons. Les valeurs de la littérature, pour cette distribution, varient par environ un ordre de grandeur; pourtant ce paramètre est nécessaire à la réalisation d'un modèle de ce détecteur. La distribution initiale des paires d'ions, induite par le ^{63}Ni fut donc mesurée dans divers gaz au moyen de deux techniques : l'une conventionnelle, basée sur le courant de saturation électrique à des distances interélectrodes variables; et l'autre peu conventionnelle, basée sur la luminescence d'un scintillateur en plastique. Les données sont analysées en fonction de deux distances, d^{50} et d^{95}, qui décrivent les intervalles jusqu'à une feuille radioactive planaire, à l'intérieur desquels se produit 50% et 95% de l'ionisation totale en phase gazeuse. Les données provenant des mesures électriques montrent qu'il y a évidence inattendue de forte diffusion β rétrograde et d'émission secondaire d'électrons par la contre-électrode. Dans ces conditions (qui ne sont pas exponentielles), les valeurs de d^{50} dans l'azote et un mélange argon/méthane, des gaz usuels pour ce détecteur, varient de 0,5 à 1,0 mm, selon la nature de la contre-électrode. Des calculs basés sur le domaine quasi-exponentiel que l'on trouve à de plus grandes distances, lors des mesures électriques, donnent des valeurs d'environ 2,5 mm (qui sont basses à cause d'un biais associé aux mesures géométriques). Par contre, les données provenant des mesures de luminescence sont presque complètement exponentielles et les valeurs de d^{50} pour l'argon (5% de méthane) et l'azote sont respectivement 2,8 et 3,8 mm. Les valeurs de d^{95} varient de 12 à 16 mm pour la luminescence, à 6 et 9 mm pour les mesures électriques (moins fiables); le tout, aux conditions ambiantes. Les données provenant de la luminescence sont considérées plus proches de la valeur "vraie" (inaltérée) de la distribution de charge, tandis que les données provenant de l'ionisation sont possiblement plus proches de la topographie initiale de la charge à l'intérieur d'un détecteur à capture d'électrons de géométrie restreinte. Toutefois, toutes les données de distances sont suffisamment courtes pour indiquer que le modèle du détecteur devrait consister en un système ayant une distribution de charge nettement hétérogène. On n'a trouvé aucune évidence de quelques-unes des très grandes valeurs de distances trouvées dans la littérature.

Can. J. Chem. Downloaded from www.nrcresearchpress.com by 78.46.186.204 on 09/07/12
For personal use only.

Introduction

It is of basic interest to know the boundary and the density gradient of the plasma that surrounds a β emitter in the gas phase. It may also be of considerable practical importance.

Such is the case with the weak β emitter ^{63}Ni, the isotope of choice for the electron capture detector (ECD). The ECD is the most prominent of all selective detectors used in conjunction with gas chromatography, and it has played a role in the discovery and monitoring of almost every major area of environmental concern from DDT to Freons to PCB's.

Despite this prominence, the mechanism by which the ECD responds to electron-capturing analytes is not very well understood. As it turns out, one of the key impediments to understanding the mechanism of the ECD is the inadequately known range and distribution of ^{63}Ni β particles. Their energy spectrum has been reported (1), but literature estimates of their range in nitrogen or argon/methane — the typical carrier gases for electron capture detection — vary by roughly one order of magnitude. Experimental estimates are generally shorter than

[1]Work taken from Ph.D. thesis of first author (Dalhousie University, September 1981). Presented at the 65th CIC Conference, Toronto, Ont., June 1982.

[2]Present address: Division of Chemistry, National Research Council, Montreal Road, Ottawa, Ont., Canada K1A 0R6.

[3]To whom correspondence should be addressed.

Can. J. Chem. Downloaded from www.nrcresearchpress.com by 78.46.186.204 on 09/07/12
For personal use only.

theoretical ones, particularly in regard to the half range (the thickness of the zone in which the first 50% of ionization occur).

A brief selective review of some recent measurements and frequently cited literature values may illustrate this point. Ayala *et al.* assessed the maximum range as 7.9 cm, presented a β distribution plot and estimated "that ca. 30% of the distribution for Ni-63 is within 1.4 cm" (2). Grimsrud and Connolly measured the steady-state positive ion distribution of a Ni-63 disc at atmospheric pressure by mass spectrometry and showed approximately 50% of the ions occurring within 1 mm from the foil (3). Further, they developed an equation relating radiation intensity and distance. Their calculation showed the ion-pair production rate at the center of a cylindrical foil of 5 mm radius and 20 mm length to be 0.44 times that at 0.5 mm from the wall (in argon at 200°C). Popp *et al.* reported the extent of ionization in nitrogen as 15 mm (4). Pellizzari, in a widely quoted review article (5), spoke of a zone of electrons 6–8 mm thick. Simon and Rork measured the variation in saturation current in air between concentric spheres up to about 5 cm. From their data it appears that 50% of the ionization occurs within about 5 mm of the radioactive foil in concentric spherical and 3 mm in coaxial cylindrical geometries (6). (The latter should not be confused with typical coaxial cylindrical ECD's in which the foil is not the inner but the outer cylinder.) Our own group used impedance matching to locate the "centre of ionization", an estimated 1 mm away from a planar foil (7).

Even allowing for the fact of different conditions and criteria in the studies cited above, their results are too far apart to be used with confidence in certain considerations involving the ECD. The importance of usable data is particularly pronounced in the following contexts. First, certain physicochemical constants derived from the ECD depend on the volume in which the measured processes are assumed to occur. Second, any modelling of ion reactions and distributions inside the ECD must start with the initial ionization of the carrier gas. Third, the choice of dimensions in constructing new ECD models has to take into account the topography of the plasma. Fourth, the interpretation of certain experimental probes of the ECD's response mechanism depends in a crucial manner on the density distribution of its electrical charges.

The latter point is of particular interest to us. In an attempt to ascertain that an ECD could function (and function well) under conditions where it was impossible for analyte-derived anions to be neutralized by cations in the gas phase, we designed a detector in which the effluents from the gas chromatographic column could react with electrons close to the anode, but were not allowed near the radioactive cathode. Clearly, the choice of dimensions became crucial in this case. For instance, the radioactive foil in one of these constructions was located about 1.2 cm away from electron-capturing analytes (8). If it were indeed correct that "ca. 30% of the distribution for ^{63}Ni is within 1.4 cm" (2), i.e. if 70% of the β's reached *beyond* 1.4 cm, then our premise of no contact between cations and anions would no longer be valid and the recent criticism ((9) of our experiment would appear justified.

Furthermore, a clear definition of the extent and density distribution of the ECD plasma could help to distinguish between two currently held, opposing viewpoints: One considers the detector a bipolar, more or less homogeneous system where the plasma fills the entire detector volume (5, 10). Owing to this, the model is often referred to as a "stirred-reactor" model although, quite obviously, there is no physical stirring involved (11). The other viewpoint sees the ECD as containing both bipolar and unipolar regions — a limited plasma region near the radioactive cathode, and a plasma-free region populated only by electrons and (analyte-derived) anions near the anode (7). Speculation based on these two models leads to different mechanisms by which detector response arises. Obviously, a valuable first step toward attributing response to one or the other mechanism (or a mixture of the two) would be to define the spatial distribution of ionizing events caused by β radiation.

For these reasons it seemed appropriate to measure again the specific ionization produced by a typical ^{63}Ni foil, under conditions that would to some extent resemble those of electron capture detectors.

In addition, our initial choice of measurement technique was influenced by two considerations. First, we wanted to use a generally recognized approach. Our earlier work was based on impedance matching which, though convenient and appropriate for an ECD that relies on impedance for response, had no predecessor in the literature. Also, this measurement of choice was to be backed up by a second, different technique of probing the same radioactive source.

Second, the important measurements were to be those particularly relevant to the ECD. We would not measure the *maximum* range of the radiation, which is primarily of interest to nuclear physicists and best investigated by means other than those involving a gas phase. Rather, we wanted to know at which distances from the foil 50% and 95% of the ionization would take place. These distances, d^{50} and d^{95}, characterize in an immediately apparent way how rapidly the plasma density decreases with increasing distance from the foil, and how far the plasma extends for any practical purpose. In contrast, data for the last 5% of ionization carry large error limits and are of little consequence for the ECD.

Radioactive foils are shaped into cylinders, cups, or planes for use in the ECD. It was felt that a parallel-plane ECD configuration was the most facile and tractable one in terms of future use of plasma distribution data.

Two types of measurements were to be employed toward that goal: a direct and conventional one based on ionization, and an indirect and less conventional one based on luminescence. Similar to approaches taken by several other groups, the conventional electrical measurement would involve moving the radioactive foil toward the counter-electrode and observing, by saturation current, the decrease in gas-phase ionization events as more and more β particles struck the electrode. The less conventional, photoelectric measurement — for which we found no precedent in the ECD field — would consist of moving the radioactive foil toward a semitransparent scintillator disc and monitoring, from the disc's opposite side, its increase in luminescence. It was hoped that roughly comparable, hence confirmatory results would be produced by the two different approaches.

What results was one to expect? The discrepancies in the literature are far larger than appears justified for a relatively simple (but important) problem. This suggests that part of it may be conceptual: There are significant differences between the idealized concept of unimpeded β rays emanating from a pure ^{63}Ni monolayer, and the experimental situation of a conventional radioactive foil located inside an electron capture detector. Measuring the maximum range does not recognize these differences; measuring d^{50} and d^{95} values does.

Although fairly self-evident or even trivial, it may be appropriate to mention some factors that influence the density of initial ionization in the present context. Almost all of these tend

to compress the initial 50% or 95% of the plasma in comparison with an idealized setting. The factors are radioactive layer thickness, angular β distribution, energy dependence of the ion pair yield, scattering in the gas phase, and backscattering and secondary electron emission in solid phases (inside the foil, from materials surrounding the foil, and from the counter-electrode). These will be dealt with in turn.

Radioactive layer thickness

A typical (New England Nuclear) foil for ECD's has about 15 mCi ^{63}Ni deposited as a layer of 10 mCi/mg specific activity on a gold backing measuring 0.5 × 1.5 in. It is easy to calculate from these data that the radioactive layer, at 0.31 mg/cm^2, is on the average 3.5×10^{-4} mm thick. (Judged solely by density correlation, this would correspond to a 2.5 mm thick zone of nitrogen gas at STP.) This means that a significant portion of the β particles does not reach the foil surface and that the average (but not the maximum) β range is reduced. The thicker the layer, the shorter the half range d^{50} (this "half range", though like the radioactive "half life", the most descriptive parameter characterizing an exponential decay, is unfortunately not nearly as constant). Severe contamination of the foil in an ECD would obviously exert a similar effect.

Angular β distribution

β Emission occurs randomly in all directions. Those β particles that emerge at oblique angles to the foil, will on the average travel longer paths through the solid, and therefore shorter ones through the gas phase, than those that are emitted in a perpendicular direction. Again, this reduces the half range.

Ion pair yield

The number of ion pairs formed per unit pathlength — the specific ionization — is dependent on β energy. β Particles from ^{63}Ni, with a maximum energy of 67 keV, are among the weakest known. In the low-energy region, the specific ionization increases dramatically with decreasing energy. To illustrate, the literature data shown in Fig. 1 suggest that a β particle generates about 8 times as many ion pairs per mm at 6.7 keV than at 67 keV (12).

To express the above argument differently: since weaker β particles produce denser ionization but expend the same energy per ion pair created, they travel disproportionately shorter distances. This gas-phase effect is synergistic with the angular distribution effect mentioned earlier, in reducing the half range.

Scattering in the gas phase

β Rays are easily scattered. The more scattering occurs, the shorter is the half range.

Scattering and secondary electron emission in solid phases

Scattering is, of course, not restricted to the gas phase but will occur on any material that happens to bar the path of a β particle — for instance, the radioactive layer and its backing as well as (if they are situated close enough) the walls of the detector and the counter electrode. Backscattering inside the foil itself is sporadically mentioned in the ECD literature; backscattering (reflection) and secondary electron emission from the detector wall and the counter electrode has, to our knowledge, never before been considered in an ECD-related context.

Secondary electrons are the result of inelastic collisions between the primary electrons (β particles) and the solid material. Provided the primary is of high enough energy, more than one secondary electron may be produced per incident. The efficiency of the scattering and emission processes depends strongly on the atomic number of the solid and the angle of incidence: the heavier the material and the larger the angle of incidence, i.e. the more shallow the impact, the larger is the number of secondary electrons created (13–15). Gas-phase ionization resulting from such secondary electrons occurs very close to the surface.

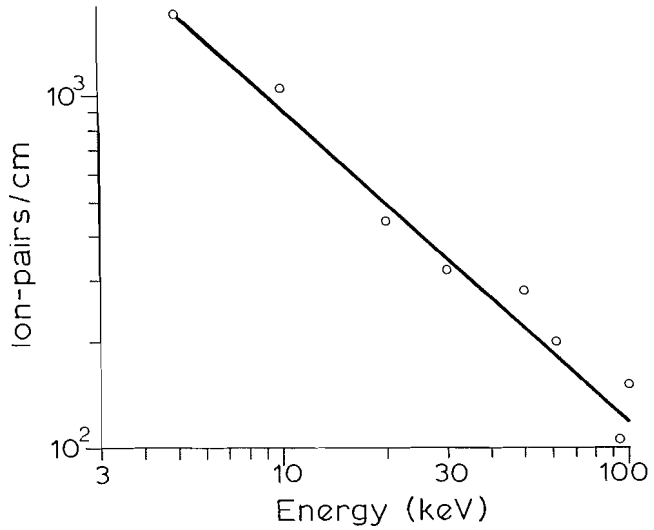

FIG. 1. Variation of specific ionization with actual β energy. Data taken from ref. 12.

All the scattering and secondary electron emission effects reduce the half range. Backscattering inside the foil, whether inside the ^{63}Ni layer or on the gold backing, leads to weaker β particles (of shorter range) emerging from the foil. If a counter electrode or constraining detector wall is situated close to the foil, scattering and secondary electron emission will produce more gas-phase ion pairs there than would have been present without the constraint.

Also, short distances can promote scattering to a disproportionately larger degree. Consider, for instance, a parallel-plate configuration in which the counter-electrode is being moved toward the foil. In the beginning, only β rays travelling roughly perpendicular to foil and electrode will be able to bridge the gap. As the gap decreases, increasingly more β particles leaving the foil and arriving at the electrode at *oblique* angles will enter the process. Thus, the average β impact will be not only more energetic but also more shallow, leading to increased scattering and secondary electron emission. If such an arrangement were to be used to determine half range, a counter-electrode with strong scattering ability would have to move closer to the foil to collect half of the maximum current than a (fictional) electrode simply absorbing the β particles.

Experimental

The ionization current measurement

The set-up used to measure the saturation current at different interelectrode distances is shown in Fig. 2. It is designed to represent a parallel-plate ECD free of confining walls. The design is similar to the one used earlier for impedance matching (7).

Two different ^{63}Ni foils were tested. These were rectangular plates measuring ca. 6 × 5 mm; one with a gold, the other with a nickel backing. Both originated from 0.5 × 1.5 in. conventional ECD foils of nominal 15 mCi activity (New England Nuclear). The radioactive plates were mounted on a stainless-steel disc of 8 mm diameter, which had been silver-soldered onto a threaded rod. By turning the rod through the compressed PTFE (polytetrafluoroethylene) ferrule, the

Can. J. Chem. Downloaded from www.nrcresearchpress.com by 78.46.186.204 on 09/07/12
For personal use only.

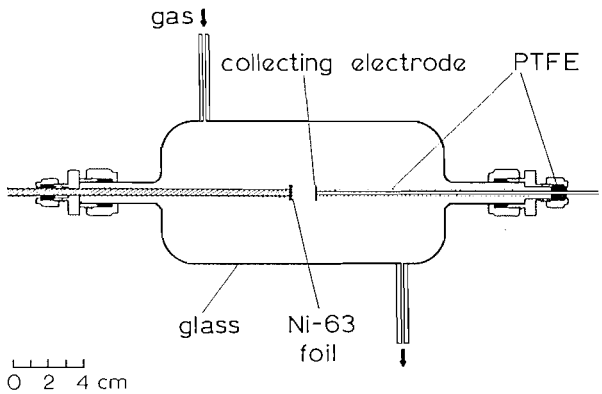

FIG. 2. Apparatus used for the ionization current measurement.

assembly could be easily moved toward, or away from, the stationary counter-electrode.

This counter-electrode was also a stainless-steel disc of 8 mm diameter, similarly soldered onto a rod. Electrodes of different scattering power were made by mounting a graphite disc, or a piece of lead foil, on the steel disc.

To permit measurements at elevated temperatures, the glass vessel was first covered with several layers of grounded aluminum foil (for electromagnetic shielding and improved heat distribution) and then tightly wrapped with two heating tapes in opposite directions. A small window was left open to allow the examination of electrode alignment. To improve reproducibility, the apparatus was routinely "baked" overnight prior to any measurement at temperatures higher than ambient.

Initially, the set-up was polarized, and the saturation current measured, in two configurations. These were expected to (and did) yield the same results in the initial series of experiments. In part for convenience, they were used interchangeably thereafter. In one configuration, the ^{63}Ni foil was polarized negative with respect to ground and the counter-electrode was connected directly to an electrometer. In the other configuration, the ^{63}Ni foil was at ground and the counter-electrode was biased to ca. +300 V by a battery box whose negative terminal provided the input to the electrometer. Measurements were made at least in duplicate, with triplicate and quadruplicate sampling being not infrequent.

The luminescence measurement

Figure 3 shows the set-up used to measure β-induced luminescence. The ^{63}Ni foil-and-rod assembly described above was re-used here, augmented by a PTFE "piston". This piston kept the foil parallel to the scintillator disc and prevented any contact between the two by virtue of a ca. 0.2 mm thick rim. The scintillator was of the conventional, transparent plastic type used in low-energy β counting.

The PMT (photomultiplier tube) was a Hamamatsu R268 unit polarized to −700 V. Two electrometers were used interchangeably. One was a conventional unit, the other a laboratory-made, inexpensive "electrometer substitute" (16).

β Ranges were studied in a variety of gases — some chosen for their common use in electron capture detection, others for their convenient molecular weight. These gases (minimum % purity or grade in parentheses) included nitrogen (99.998%), argon +5% methane ("high purity"), hydrogen (99.99%), helium (99.999%), methane (99.97%), sulfur hexafluoride (99.99%), difluorodichloromethane (99%), and butane (99.5%).

Results and discussion

While the current ECD debate calls for direct measurement of the ^{63}Ni β range — particularly the half range d^{50} — it also calls for an appreciation of the extent to which the data derived from such measurements can be affected by definitions and instrumental circumstances. Furthermore, it calls for consideration of factors that could conceivably account for significant

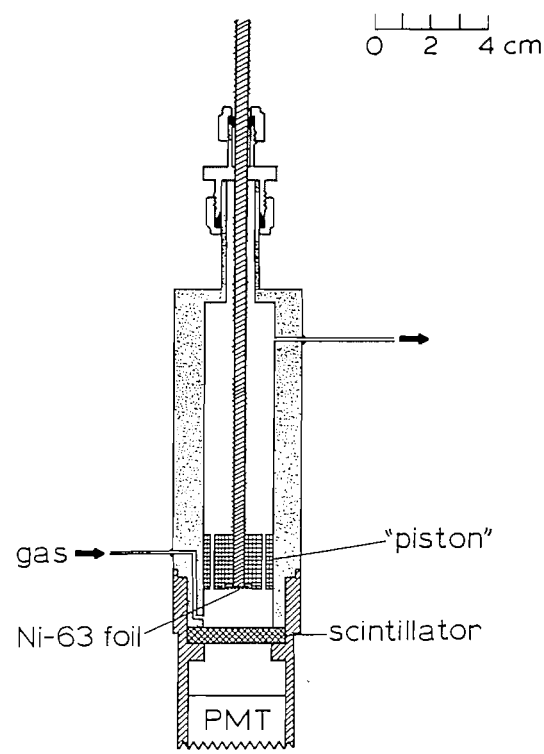

FIG. 3. Apparatus used for the luminescence measurement.

changes in half range when a foil is moved from a measurement device to an electron capture detector.

The 95% range is this study's expedient substitute for the true maximum range. Values for d^{95} — in contrast to the ideal d^{100} — can still be measured with some confidence. On the other hand, d^{50} values invite direct comparison with detector dimensions, i.e. they allow a crude but immediate assessment of a detector's likely charge heterogeneity.

The half range d^{50} will depend on the particulars of the ^{63}Ni source — i.e. whether it is a flat or cylindrical, a thinly or thickly coated, a large or small piece of foil — and the geometry and nature of materials that surround it in a detector. Even with a given source, however, and with the simplest and least obstructed geometry imaginable, the circumstances of the measurement set-up will have an influence on the results. Therefore we shall postpone reporting the data and first discuss implications of the way in which they were obtained.

Factors involved in the luminescence measurement

What was actually measured in this experiment was the photomultiplier current, originating from the combined luminescence in both the scintillator and the gas under investigation. Very little light was in general emitted by the gas, and its contribution was routinely subtracted from the total signal by baseline extrapolation. The validity of such linear extrapolation was confirmed by measurements with the scintillator disc removed from the apparatus. Since the luminescence was normally measured through — hence was attenuated by — the plastic scintillator, the two baselines differed by a small factor. It, however, was considered minute compared to other types of errors.

Another, entirely negligible error arose from the fact that, when the foil and the scintillator were close together, the β particles penetrated farther into the scintillator. Consequently photons were emitted more close to the PMT, resulting in a

Can. J. Chem. Downloaded from www.nrcresearchpress.com by 78.46.186.204 on 09/07/12
For personal use only.

Can. J. Chem. Downloaded from www.nrcresearchpress.com by 78.46.186.204 on 09/07/12
For personal use only.

higher light level. Considering the relative densities of a gas and a solid, this *axial* displacement factor must have been extremely small.

The *radial* displacement bias, however, was considered to be far from negligible. It is easy to see why. When the foil and the scintillator almost touched, the luminescing area seen by the PMT was little larger than the foil itself. However, as the two moved apart, the luminescence spread in the scintillator until it reached the confines of the disc (this, incidentally, can be easily seen with dark-adapted eyes). Any photons emitted from the peripheral regions — because of the longer distance, the more oblique angle to the photocathode, and the larger attenuation by the not perfectly transparent disc — contributed less than their share to the overall measurement. This effect decreased the half range (i.e. the observed half range was shorter than the true one).

Further, any β ray travelling beyond or outside the confines of the disc was completely lost to the light measurement. Since this occurred primarily when the foil and the scintillator were far apart, the effect decreased the 95%.range and, to a smaller extent, the half range as well.

Since intimate contact between the foil and the scintillator was to be avoided, the light output at zero distance was determined by extrapolation. As will be shown later, luminescence in the measurement of *light* gases did level off at very short distances. Thus it may have been erroneous to do so. However, the error — which would have decreased the half range — was considered to be extremely small.

More important at very close distances may have been the backscattering of β particles from the scintillator disc. The effect was not as large as backscattering from the counter-electrode in the ionization measurements — the average atomic number of the scintillator was only about 3 — but it was not negligible. Furthermore, surface charges on the electrically insulating scintillator could have had some repulsive effect. Both processes, since they occurred primarily at very short distances, increased the half range.

Perhaps the most basic question is one to which we cannot provide an answer: to what extent, and how far down in energy, can we assume a quantitative relationship between ionization and luminescence? The premise of using luminescence in the given context was, of course, that it accurately represented the ion pairs that *would have been* formed in the volume to which access was now barred by the scintillator. Aside from requiring a homogeneous, clean disc, this condition also required that the cross section for luminescence inside the disc had to represent precisely the cross section for ionization in the gas phase, and that this relationship had to be kept strictly intact throughout the available β energy range.

In a gas, the ionization cross section increases by about one order of magnitude at low — and, for ^{63}Ni, relevant — energies. Considering the importance of very weak β particles for the d^{50} measurement, one may need to be reassured of a strictly linear relationship between energy and luminescence — or, more precisely expressed, between the number of ion pairs created in the gas phase on one hand and the number of equivalent photons emitted in the plastic scintillator on the other.

It is well known, of course, that the energy expended in creating one ion pair in the gas phase is remarkably independent of the β energy (12). It is also known that the intensity of the light flash from a scintillator, for instance in γ ray spectrometry, is proportional to the energy of the incident γ photon (17). However, it is not entirely clear whether these general relationships can be extrapolated to the low-energy range while still satisfying the exact correlation demanded by this study. As will be seen later, the half ranges measured by luminescence differed considerably from those measured by ionization. Yet, it appears that this was not primarily due to a faulty correlation between ionization and luminescence, but that a variety of other effects were responsible for most of the discrepancy.

Factors involved in the ionization measurement

The same radioactive foils were used in the luminescence and ionization measurements. However, the target of the β particles — the plastic scintillator and the various counter-electrodes — differed not only in nature but also in size.

In designing the measurement set-up, dimensions were chosen similar to those that one might expect in a parallel-plate ECD, but any wall constraint was removed to avoid possible interference by a charged insulator surface. The design addressed possible multiple-purpose use in future experiments and took into account that an earlier study had shown the centre-of-ionization to be located only about one mm away from the foil (7).

This meant (judging mainly from hindsight) that some of the β particles, particularly those of greater energy and more oblique angles of emission as well as those emitted from the boundary regions of the foil, *did* have some chance to miss the target, i.e. travel beyond the plane of the counter-electrode without being intercepted. More gas phase ions would thus be created, leading to a decrease in d^{95} and, to a much smaller degree, in d^{50} values. How large this geometric effect was depended on conditions: at short distances and with heavy gases it was negligible, at long distances and with light gases it was significant.

A measurement of the distances at which 50% and 95% of the current were collected presumed knowledge of I_{max}, the maximum ionization current. I_{max} was taken to be the saturation current at distances considerably larger than d^{95}, i.e. the current that would remain constant during further increases in distance and voltage. Unfortunately, but not unexpectedly, this current was not perfectly independent of experimental circumstances. While this did not influence the half range to any significant degree, the d^{95} values were likely to carry some error because of it. Also, the I/d curve displayed a very gentle slope as it approached the I_{max} value, thus increasing the error in measuring d^{95}. One of the causes for small current fluctuations, which became particularly important at long interelectrode distances, could have been the presence of small amounts of electron-capturing substances. Even such trivial an influence as the magnetic field induced by a.c. resistance heating had to be reckoned with as a cause for variations in current. Although the described arrangement of crossed heating tapes largely eliminated the originally noticed aberration, a very small effect might have persisted.

On the other hand, it was the actual measurement of distance that introduced most of the error at *very close* range. Keeping the electrodes parallel and measuring a gap between them of a few tenth of a millimetre was difficult.

Summing up the paragraphs above, the various criticisms and caveats that have emerged from a closer consideration of the two experimental approaches should make it abundantly clear that the range data obtained were approximate ones. This will also become evident from the significant difference between the luminescence and the ionization sets of measurements. Yet, the uncertainty in the results needs to be viewed in the proper perspective.

First, as will be discussed later in more detail, the dimensions

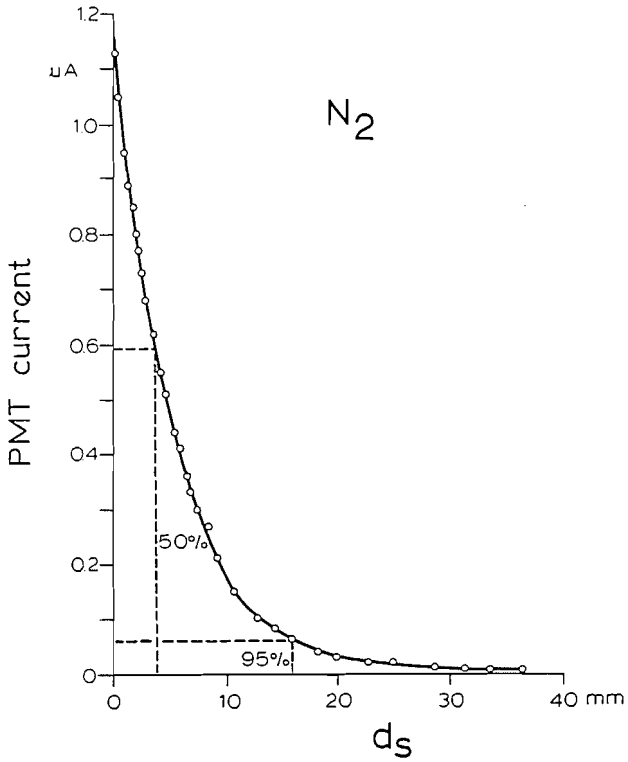

FIG. 4. Luminescence plot for nitrogen at ambient conditions.

and materials used in constructing an ECD are likely to produce changes in d^{50} and d^{95} values greater than the discrepancies between ionization and luminescence measurements reported here. Second, and more importantly, the literature of electron capture detection cites range values more than an order of magnitude apart — a much greater error than that arising from a comparison of the two techniques used in this study. Third, the use of *two* measurement techniques is likely to produce larger error limits and more reliable results.

Luminescence measurements

Figure 4 presents the result of a typical experiment, i.e., a plot of photomultiplier current versus the distance d_s ("s" for scintillator) between the foil and the disc. β Particles from the foil lose some of their energy by inelastic collision with gas (in this case nitrogen) molecules during their flight toward the disc. On entering the scintillator, a constant proportion — or so it is hoped — of their residual energy is converted to light and monitored. At 50% and 95% of the (extrapolated) maximum PMT current, the "directly measured" values of d_s^{50} and d_s^{95} are obtained. Table 1 lists these values for a series of gases ranging from the very light to the very dense, including the two common ECD carriers nitrogen and argon/methane.

The function displayed in Fig. 4 appears exponential in nature and it is therefore easy to calculate the number of ion pairs generated per second in any volume element ("slice") parallel to the foil. As shown in Appendix 1, the profile of the PMT current is identical in shape to that of the *initial* ion-pair distribution. In the particular case of Fig. 4, to convert the former to the latter, the ordinate covering the range from 0 to 1.2 μA PMT current can be replaced by one reading 0 to 3.1×10^9 ion pairs $s^{-1}\,mm^{-1}$. (Note that such a plot yields only the *number* of ion pairs created at a certain distance from a foil of particular activity and dimension; it does not provide immediate information on the ion pair *concentration*.)

Since this initial ion pair distribution does, however, provide a reasonable first step toward modelling the ECD, it may be appropriate to include here a few comments on the implications of such an approach.

TABLE 1. Ranges measured by luminescence

Gas	Molecular weight	Direct[a] d_s^{50}	Direct[a] d_s^{95}	Indirect[b] d_s^{50}	Indirect[b] d_s^{95}
H_2	2	10.2	38.0	8.0	34.3
He	4	10.6	44.6	9.7	41.9
CH_4	16	4.8	18.8	4.3	18.5
N_2	28	3.8	15.8	3.7	15.8
Ar–CH_4	~40	2.8	12.0	2.8	12.0
n-C_4H_{10}	58	2.0	7.4	1.7	7.4
CCl_2F_2	121	0.9	4.0	1.0	4.3
SF_6	146	1.0	5.0	1.1	4.8

[a]Direct measurement in mm, taken from PMT current plot.
[b]Indirect measurement in mm, calculated from semilogarithmic PMT current plot via linear regression analysis of slope.

To begin with, there are geometric effects to be considered. For instance, the initial ion pair density is constant at a constant distance from a planar foil only if that foil is infinitely large. In our set-up, ionization density in a particular parallel slice was highest in the middle — opposite the centre of the foil — and decreased toward its periphery, with profiles depending on the distance of the imagined slice from the foil.

Then there is recombination. Given a strictly second-order reaction with micro-homogeneity (no columnar effects interfering) and assuming that there is as yet no gas flow, no diffusion, no polarizing potential and, of course, no analyte, the distribution of charges would remain exponential — though the half range would double.

In the next step, however, the electrical potential imposed for operating the detector — for making any electrical measurement, in fact — must disturb the initial or steady-state distribution drastically. So must the introduction of analyte, with the concomitant generation of slow anions proportional to local electron concentrations. So must the neutralization reaction, reflecting the local concentrations of cations and anions. Furthermore, both charged and neutral species must be subject to diffusion and transport by the carrier gas, though to different extents. All of that, and more, will influence the charge distribution. (It is not surprising that the stirred-reactor concept of the ECD has proven so popular.)

Thus, knowing the initial ion-pair distribution represents only a simple (yet necessary) first step in the complex modelling sequence of the detector's charge topography. Still, the fact that the initial distribution is exponential should make the task easier.

Of course, this exponential relationship comes as no surprise. The absorption of β energy in metals — gases are generally less well characterized — is known to be largely exponential and conform to the relationship (18)

$$A = A_0 \exp(k_a l)$$

where A_0 is the activity (e.g. counts per second) measured without an absorber, A is the activity measured through an absorber of thickness l, and k_a is the absorption coefficient and an approximately linear function of the absorber's density. It may be added that this equation applies to β particles with their characteristic energy distribution; in contrast, monochromatic electrons will exhibit a linear rather than an exponential

Can. J. Chem. Downloaded from www.nrcresearchpress.com by 78.46.186.204 on 09/07/12
For personal use only.

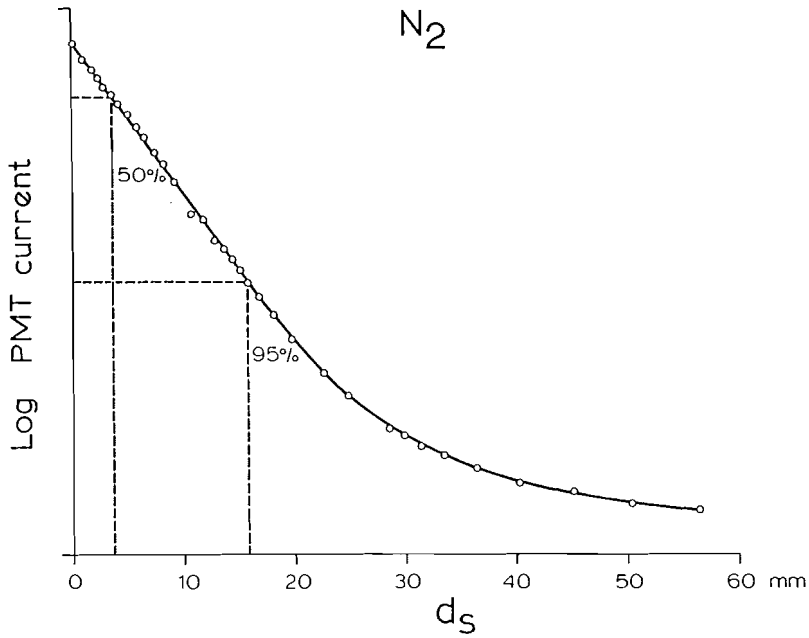

FIG. 5. Semilogarithmic luminescence plot for nitrogen at ambient conditions; data as in Figure 4.

dependence (14). In view of different energy distributions from different isotopes and the distinct upper limit in energy of any β radiation, clearly the above equation can only approximate the true distribution *within a certain range*. That becomes also obvious if one considers its mathematical equivalence to, *inter alia*, Beer's law and the integrated form of the first-order rate equation.

To find out how far this equation is obeyed by ^{63}Ni β particles moderated by a gas and monitored by their energy (as opposed to their numbers), the data of Fig. 4 were replotted in the semi-logarithmic format of Fig. 5. About 97% of the energy distribution fits the exponential pattern which, for the purpose of this study, can be rewritten as

$$\ln i = -kd + \ln i_{max}$$

where i is the photocurrent measured at the distance d between the foil and the scintillator disc, and i_{max} is the (extrapolated) photocurrent at distance 0. The slope k can be obtained directly from the plot or by linear regression analysis of its data points. The latter method has been used to arrive at "indirectly" measured ("calculated") values of d^{50} and d^{95}, some of which are shown in Table 1. (Note that $\ln 2/k$ equals d^{50}, $\ln 20/k$ yields d^{95}, and d^{95}/d^{50} is supposed to be 4.32.)

The "indirect" values thus calculated and the values obtained by "direct" measurement of the plot do differ, mainly because of deviations from the exponential relationship at the upper and lower ends.

The deviation at the upper end of the graph requires a low-density gas such as hydrogen or helium to show up clearly. (We do not know to what extent this can be attributed to backscattering from the scintillator.) The effect is demonstrated in Fig. 6. Incidentally, the plots for hydrogen and helium are almost identical, despite the fact that the two gases differ by a factor of two in density. A possible explanation is that the mean energy loss per unit path length, according to the Bethe-Bloch equation (12), is proportional to the ratio of atomic number over atomic weight. This ratio varies little amongst elements with the exception of hydrogen, for which it is about twice as large.

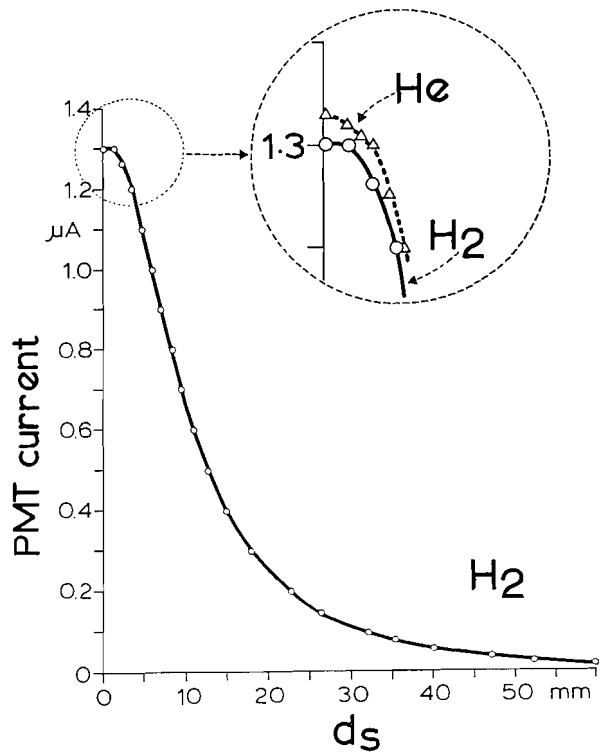

FIG. 6. Luminescence plots of hydrogen and helium at ambient conditions.

Hydrogen aside, the d_s^{50} and d_s^{95} values for different gases follow approximately the expected inverse proportionality with molecular weight, as shown in Figs. 7 and 8. The data are thus fairly consistent (though that does not, per se, establish their accuracy). Perhaps their greatest value in the present context is that they can be trusted to show how far the bulk of ^{63}Ni β particles can reach in the most favourable geometry. Hence we consider the luminescence data to be more characteristic of an "ideal" β range measurement — though not necessarily of a

Can. J. Chem. Downloaded from www.nrcresearchpress.com by 78.46.186.204 on 09/07/12
For personal use only.

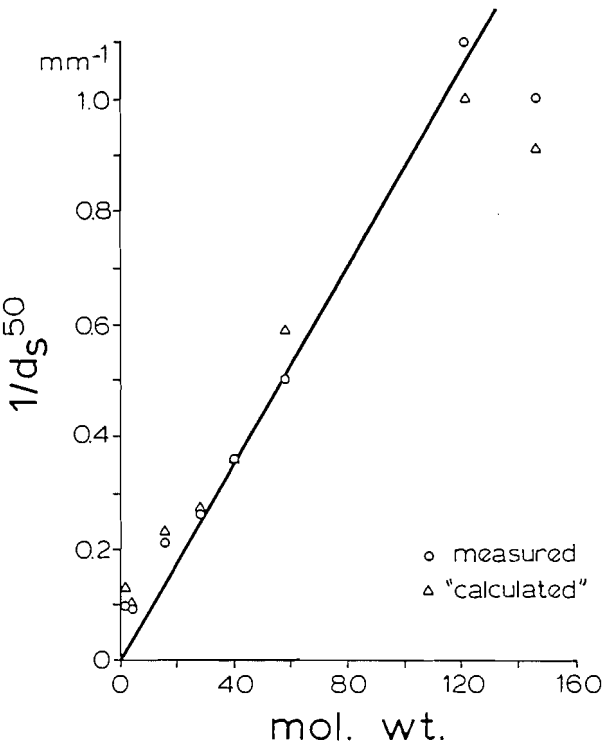

FIG. 7. Plot of $1/d_s^{50}$ versus molecular weight of different gases (listed in the experimental section) at ambient conditions. "Measured" data taken directly from i/d_s plot; "calculated" data derived from same plot via linear regression analysis.

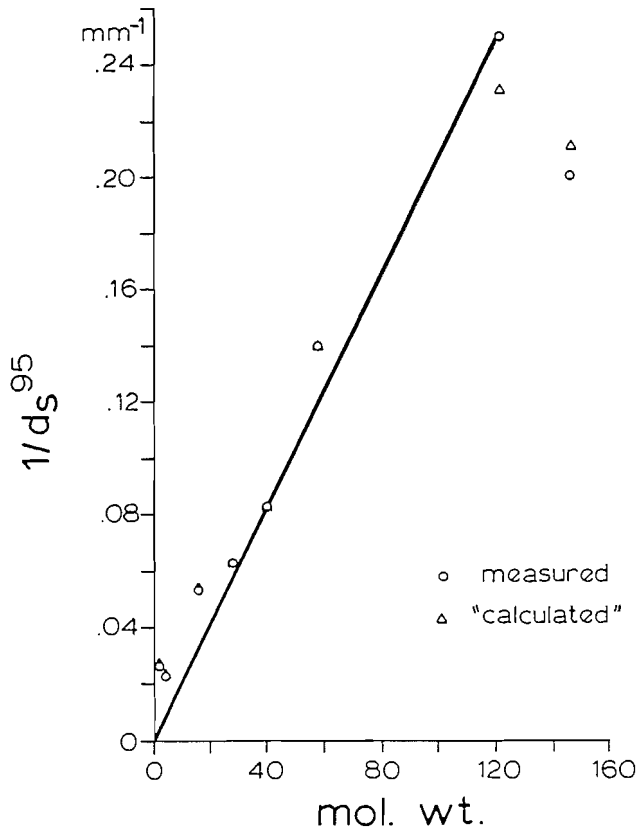

FIG. 8. Plot of $1/d_s^{95}$ versus molecular weight of different gases; similar to Fig. 7.

typical ECD arrangement — than the ionization data which are to follow.

Numerically, the luminescence data fall somewhere in the middle of the range estimates mentioned in the literature. Thus, in the common ECD carrier gases argon/methane and nitrogen at room temperature, approximately 95% of the total β energy from a planar foil is dissipated within 12 and 16 mm, and 50% is expended within 2.8 and 3.8 mm, respectively. We are not aware of any similar *luminescence* measurements in the ECD literature. However, as a formal comparison, our data are closest to ionization-based results obtained by Simon and Rork (6) in the context of smoke detectors. Estimated from the graphs in their paper, the d^{50} distances in air were approximately 5 mm for concentric-sphere and 3 mm for coaxial-cylinder geometry. (A parallel-plate configuration would be expected to yield a value somewhat less than 3 mm on geometric grounds.) Also close comes the statement of Popp *et al.* that all radiation from their foil was absorbed in nitrogen within 15 mm (4). There is no evidence for the claim of Ayala *et al.* (2) that 70% of β particles travel distances in excess of 1.4 cm.

In the context of this study, the luminescence data provided the *largest* range values even though these were still well within the requisites of the "space-charge" mechanism (7), and well within the premise for experiments using "separated" cation and anion chambers (8, 19). In the latter, the configuration most often used employed a cylindrical foil about 12 mm away from an aperture of 8 mm diameter leading to the anion chamber (8). We can now estimate that the β energy, which could have been transmitted through the aperture, was clearly below one percent, i.e. negligible — and that the recent criticism (9) of these experiments can therefore be safely dismissed.

While the luminescence measurements carry the appeal of an independent probe, the electron capture detector is, of course, based on the monitoring of charge, not light. If only for this reason, the following measurements of the ionization current could be considered more germane to the subject at hand.

Ionization measurements

When a large enough potential is maintained between a radioactive foil and an anode separated by a gas phase, and when that anode is located beyond the range of radiation, all accessible charges are collected from the gas phase, and the electrical current is the maximum one possible. (This statement accepts columnar recombination (20) as unavoidable but — given the very much larger voltages that would be necessary to diminish *that* reaction — remains correct for all practical purposes.)

However, when the anode is moved toward the radioactive foil and, as a consequence, starts intercepting β radiation, the ionization current from the gas phase decreases. Neglecting the extremely small contribution of the β particles' own charge, an arrangement of this sort can be used to map the unimpeded β energy distribution by current monitoring. This is the basis for most of the β range measurements in the literature. Their implicit premise is that the anode simply and totally absorbs any β particle that happens to hit it.

If, on the other hand, backscattering and secondary electron emission were to occur such that the gas phase would gain additional ion pairs, the measured current would have to be adjusted for this effect before it could be used to establish the ion pair distribution in an *uninterrupted* gas phase. To our knowledge, there is no reference in the ECD literature to elastic or inelastic scattering of β's on the anode or confines of the

Can. J. Chem. Downloaded from www.nrcresearchpress.com by 78.46.186.204 on 09/07/12
For personal use only.

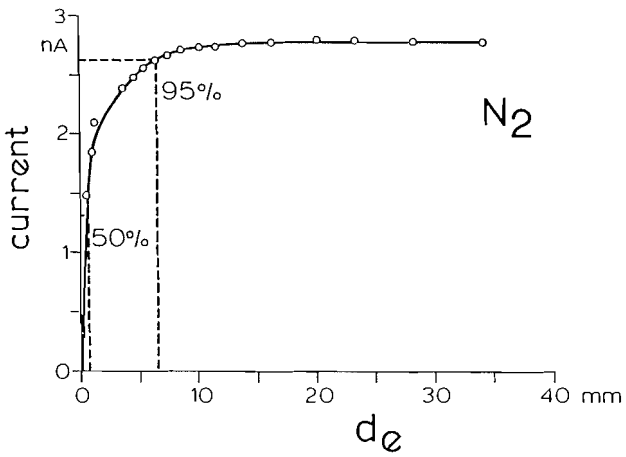

FIG. 9. Ionization current plot for nitrogen at ambient conditions; steel counter-electrode.

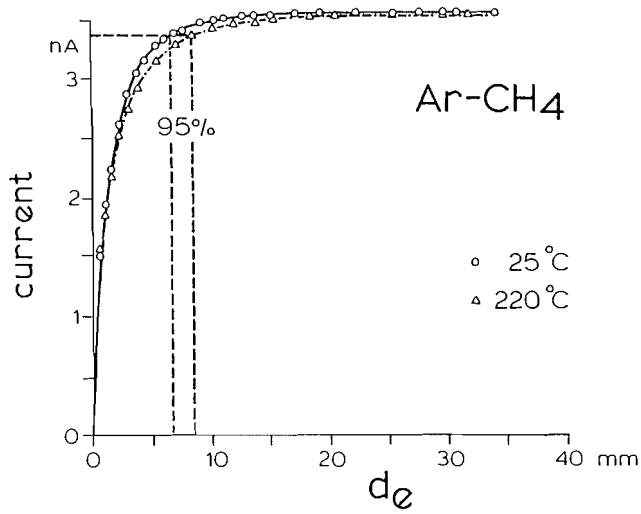

FIG. 10. Ionization current plot for argon/5% methane at two temperatures.

measurement apparatus nor, for that matter, on the anode or the walls of an electron capture detector. For the latter, the converse is true: data from an uninterrupted distribution would have to be adjusted for scattering effects, and estimates of ion pair distributions inside the ECD would have to take into account the nature and geometry of its relevant construction elements.

If scattering effects exist, they should be most easily observable in ionization measurements with heavy metal counter-electrodes located at very short distances from the foil and light gases in between — i.e. under conditions that produce the most shallow β impacts on the most heavy targets.

Figure 9 shows a typical run of ionization current versus distance between the foil and a stainless-steel counter-electrode in nitrogen at ambient temperature and pressure. Steel is not the heaviest of metals and nitrogen not the lightest of gases — though both are typical of the ECD — and yet there occur significant scattering effects.

Most evident is how close the counter-electrode has to approach the foil before the current drops to half its maximum value. The d_e^{50} value ("e" for electrode or electrical) is only 0.8 mm, compared with the d_s^{50} of 3.8 mm from the luminescence measurement. Furthermore, the d_e^{95}/d_e^{50} ratio jumps to 8.3 — indicating that the exponential function, which the luminescence data displayed, is not applicable to the ionization measurements. Similar behaviour is exhibited by a variety of test gases under a variety of circumstances: in every case, the saturation current decreases less than expected (from an exponential point of view) at short interelectrode distances.

Figure 10 shows two of these runs, carried out in argon/methane at two temperatures. Not only do the data fail to satisfy the exponential criterion $d^{95}/d^{50} = 4.32$, but they also deviate from the expected inverse proportionality with density. At 220°C, one expects the characteristic ranges to be about 1.6 times as large as those at room temperature. However, d_e^{95} increases only by a factor of about 1.3, and d_e^{50} hardly changes.

For the d_e^{95} measurements, the increased "fly-by" of β particles in a less dense medium — i.e. their crossing the plane of a counter-electrode which is too small to intercept them — contributes strongly to the discrepancy between 1.6 and 1.3. Furthermore, d_e^{95} values rely in a crucial manner on the I_{max} measurement and hence their error limits may be rather large. A variety of additional high-temperature runs were therefore done, using nitrogen or argon/methane as carrier gases, steel or graphite as counter-electrodes, and 220 or 298°C as temperatures. They suggest that some scattering is still present at longer distances but that the predominant reason for the discrepancy is indeed a geometric artifact of the measurement technique.

The d_e^{50} measurements, however, are *not* subject to the fly-by error to any significant extent — the interelectrode distance is too small compared to the electrode dimensions for that. Also, the measurements have been carefully repeated several times with essentially the same results.

We can see only one reasonable interpretation for these results: a considerable fraction of β energy hitting the counter-electrode must be turned back into the gas phase rather than being picked up by the solid phase, thus leading to a higher ionization yield between the two electrodes. That this yield increases disproportionately as the interelectrode distance decreases is to be expected. The yield of both elastic and inelastic processes, i.e. backscattering of electrons and secondary electron emission, is strongly angle-dependent, and the average angle of incidence on the counter-electrode increases as the interelectrode gap decreases. (We are using here the conventional angle-of-incidence definition (21): A zero degree angle means perpendicular impact, a 90 deg angle means grazing the surface.)

What is somewhat surprising, however, is the lack of such backscattering effects being mentioned in literature reports (including one from our own group (7)) of β range measurements. The clear premise there is that, once a β particle hits the counter-electrode, it is "lost" — i.e. it does not contribute any further to the observed current. While this does not introduce any errors in a maximum-range measurement, it will clearly do so the larger the angle of incidence and the shorter the interelectrode distance become.

Aside from its angular dependence, a characteristic feature of electron scattering and secondary electron emission is their increase with the atomic number of the scattering medium. This can, in fact, serve as an easy test for the presence of scattering. If several counter-electrodes of the same shape but different material are used, the electrodes with higher atomic numbers should be better able to scatter, elastically and inelastically, the β particles. Hence they should lead to shorter d_e values. (Analysts who electroplate the conducting inner surfaces of their ECD's with gold to reduce analyte decomposition may, if circumstances are right, wind up also with the benefits accruing from additional electrons and a shorter half range.)

Can. J. Chem. Downloaded from www.nrcresearchpress.com by 78.46.186.204 on 09/07/12
For personal use only.

TABLE 2. d_e^{50} values in mm with different gases and counterelectrodes[a]

Gas	Graphite [6]	Steel [26]	Lead [82]
H_2	2.3	0.6	
CH_4	1.6	0.6	
N_2	1.0	0.8	0.5
$Ar–CH_4$	1.0	0.9	0.5

[a]Atomic number in square brackets.

Indeed, counter-electrodes made of graphite (atomic number 6), steel (ca. 26), and lead (82) clearly demonstrate the expected effect. As shown in Table 2 for various gases (and as expected), the difference in scattering between materials of low and high atomic number shows up best in a light gas like hydrogen. (While graphite with its lower scattering power leads to half-range values that reflect the expected decrease with increase in gas density, steel does not. However, d_e^{95} values for steel — e.g. 17.4 mm for hydrogen, 10.4 mm for methane, and 6.6 mm for nitrogen — are less subject to scattering and do follow the expected trend.)

Though not as pronounced as in hydrogen, the effect of the atomic number of the counterelectrode material is still quite noticeable in the conventional carrier gas nitrogen, with d_e^{50} values of 1.0 mm for graphite, 0.8 mm for steel, and 0.5 mm for lead. It may be remembered at this point that the earlier measurement of the "centre-of-ionization" by (extrapolated) impedance matching was done with a similar steel arrangement and yielded a similar value, namely ca. 1 mm (7). This value is also in essential agreement with the (steady-state, we presume) measurement of a 1 mm half range in front of a mass spectrometer aperture by Grimsrud and Connolly (3). Using their data, Grimsrud and Connolly further calculated the ion pair generation rate and distribution in a cylindrical geometry. In view of β backscattering and other effects, it would be most interesting to obtain experimental verification of their results. Unfortunately, measurements of cylindrical geometries are inherently more difficult to carry out than those of parallel plates.

One may note that, at an interelectrode gap of 1 mm, border effects such as β particle fly-by are minimized and the system approaches the performance of an infinitely large parallel-plate geometry. It should be further noted that the atomic number of graphite used in the electrical measurement and the (average) atomic number of the scintillator plastic used in the luminescence measurement, differ only by a factor of two — yet the half ranges were measured as 1 mm and 3.7 mm, respectively. This strongly suggests that some backscattering must have occurred on the scintillator at short distances and that (though in part offset by errors in extrapolation to distance zero), the measured half range of 3.7 mm must have been too large.

At longer distances, border effects become increasingly important. Also, the average angle of incidence decreases and with it the scattered β particle fraction. Hence one would expect the d_e^{50} values to be more dependent on counter-electrode density than the d_e^{95} values. Figure 11 demonstrates that this is indeed so. Arguments can be made along similar lines in order to explain the somewhat smaller temperature dependence observed with denser electrodes as well as the fact that (as for instance shown in Fig. 10) the temperature dependence decreases with decreasing interelectrode gap.

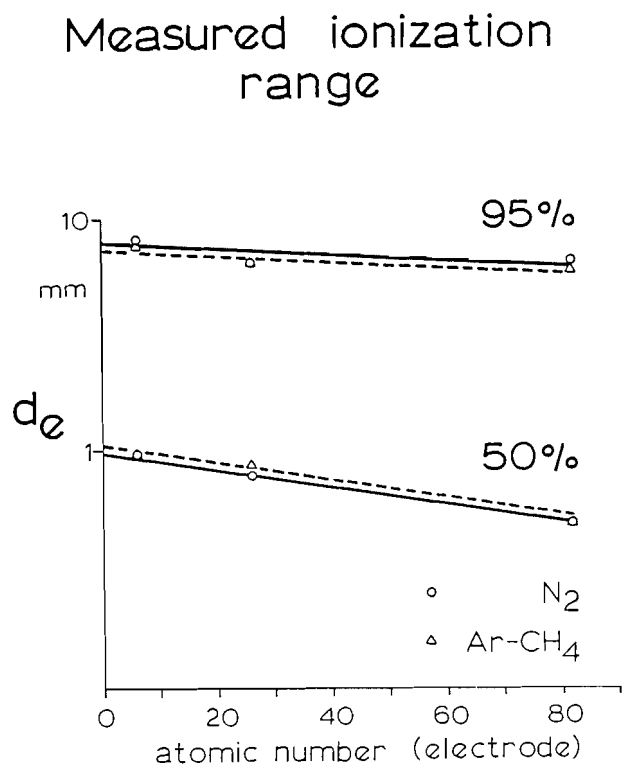

FIG. 11. Variation of d_e^{50} and d_e^{95} values with atomic number of graphite, steel, and lead counter-electrodes, for nitrogen and argon/5% methane at ambient conditions.

These scattering effects make for an interesting dilemma. Clearly, they represent an artifact of the measurement technique, and hence an annoying bias as far as the measurement of "true" β ranges is concerned. Yet, the important characteristic one wishes to establish for an ECD is the distribution of charges *within that particular detector*. Thus it may be that the present ionization measurement, however crude and fraught with dependence on geometry, is actually more relevant to conventional detector construction and function than a precise knowledge of unimpeded β topography.

Scattering could prove not only relevant but also helpful to the ECD. A case in point: ^{63}Ni is used in ECD's because of its superior thermal and chemical stability; yet some properties of the earlier favorite tritium — e.g. a shorter range allowing a smaller detector design — would still be useful to have. As a matter of speculation, then, one could perceive of, for example, a gold-plated screen or perforated plate that would be of slightly larger size than, and be located parallel to and about 1 mm away from, a ^{63}Ni foil. This screen would be designed to intercept most β particles but pass most secondary electrons (given a suitable potential). In effect, this arrangement could drastically reduce and unify the β range and allow, for instance, the construction of a relatively compact, *parallel-plate* ^{63}Ni-ECD. A *constant* β range, i.e. one essentially independent of carrier gas and temperature, could be used to advantage in a variety of scientific problems, not all of which need necessarily be related to the electron capture detector.

In retrospect, one may also note that scattering effects did most likely help the earlier "centre-of-ionization" measurement to succeed. As mentioned before, the matching of impedances — i.e. determining the interelectrode distance at which the impedances for regular and reversed electrical field became

Can. J. Chem. Downloaded from www.nrcresearchpress.com by 78.46.186.204 on 09/07/12
For personal use only.

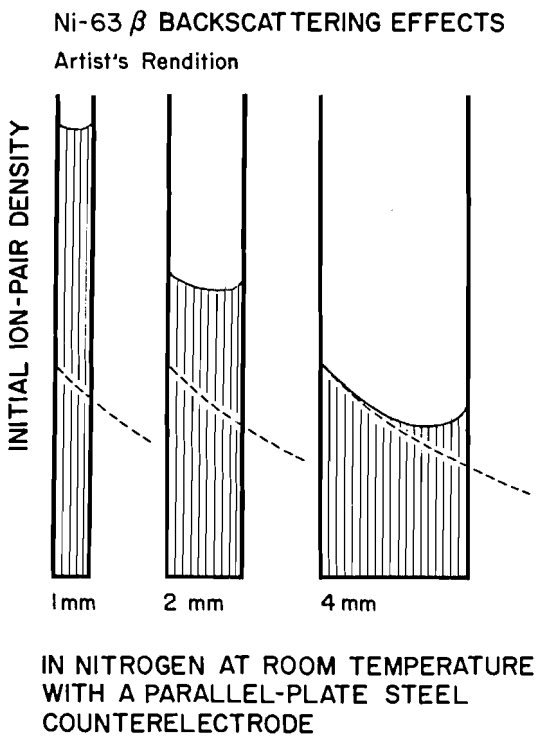

FIG. 12. Artist's rendition of β-induced ion-pair density under scattering conditions in a parallel-plate ECD with adjustable steel counter-electrode at three different interelectrode distances in nitrogen. Unimpeded ion-pair distribution indicated by dashed line. See text for explanation.

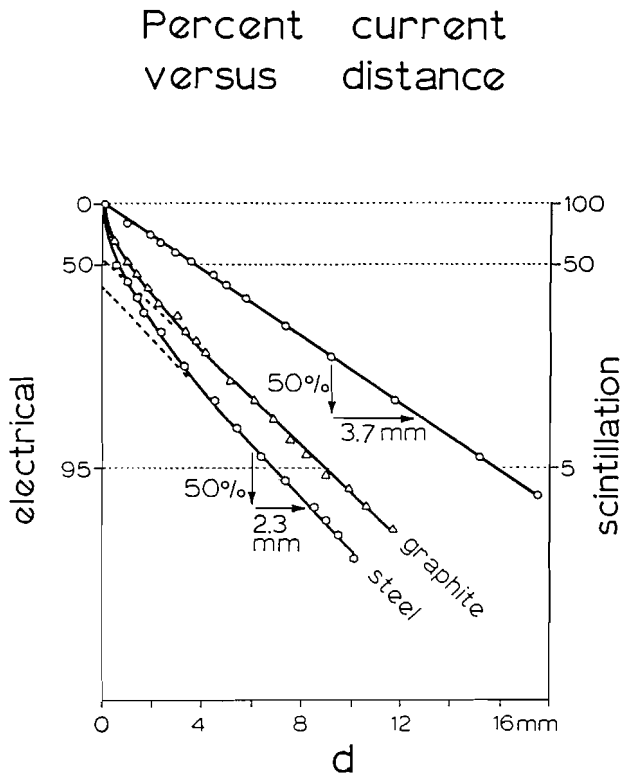

FIG. 13. Ionization current and photomultiplier current plots in semi-logarithmic format for nitrogen at ambient conditions. See text for explanation.

equal — did require some extrapolation. In fact, without scattering those two impedances could have never become quite the same: on the average, it would always be easier for the impedance-determining cations to drift to the foil than to the counter-electrode. However, backscattering from the latter does create additional cations (and electrons) in its immediate vicinity. When the electrodes are in close proximity to each other, one could visualize between them an almost homogeneous plasma (in the absence of an electric field). As a matter of ancillary interest, this is portrayed — with the help of data from ionization plots but still remaining highly speculative in its details — in the "artist's rendition" of Fig. 12.

Given the essential correctness of this rendition, it points to yet another use to which scattering effects can be put. With closely spaced electrodes, an ECD could indeed assume a fairly homogeneous initial ion-pair distribution. Such an ECD could approach, as closely as appears possible, the homogeneous (stirred-reactor) state preferred by kineticists. In addition, it would meet both conditions for ECD response according to the classical theory (5, 10): A high concentration of electrons for effective electron capture; and a high concentration of cations to allow — via the preferential neutralization of analyte-derived anions — the capture effect to be observed.

Comparison of luminescence and ionization results

The luminescence data follow an exponential relationship and can be used directly as an ion-pair density profile. The ionization data do not, but can be converted to the same format for the ease of comparison by plotting them as percent of maximum current. Figure 13 shows such a plot for nitrogen at room temperature, with two ionization profiles for graphite and steel counter-electrodes on the left and a luminescence profile on the right. (Additional ionization profiles for different gases and a steel counter-electrode are given in Fig. 14.)

The plots of Fig. 13 are normalized in the sense that all start from the same point at interelectrode distance zero: the ionization profiles with zero electrical current, the luminescence profile with (extrapolated) maximum photomultiplier current. Both ordinates list the respective currents as percent of maximum.

As discussed before and as expected, the ionization data show distinctive evidence of scattering while the luminescence data show little if any. (Note, however, the evidence of Fig. 6 where the low-density gases hydrogen and helium allow a closer inspection.) Scattering by the counter-electrode leads to a shorter half range, and scattering by the scintillator to a longer one. Thus, if one were to estimate the extent of scattering at small distances and deduct it from the data, the ionization profiles would become linear (as suggested by the dashed lines) and move up (by virtue of the normalization). The luminescence profile would, perhaps, show a slightly steeper slope — and the three plots would move closer together.

Even with all these adjustments made, however, the ionization and the luminescence curves are not likely to coincide. The primary reason for this is the difference in target areas between the plastic scintillator and the counter-electrodes. Secondary (and minor) reasons could be the differently dimensioned cells and the, perhaps, not exactly proportional ionization and luminescence yields.

The ionization profiles show a quasi-exponential (i.e. in Fig. 13, linear) region at longer distances from the foil. There,

Can. J. Chem. Downloaded from www.nrcresearchpress.com by 78.46.186.204 on 09/07/12
For personal use only.

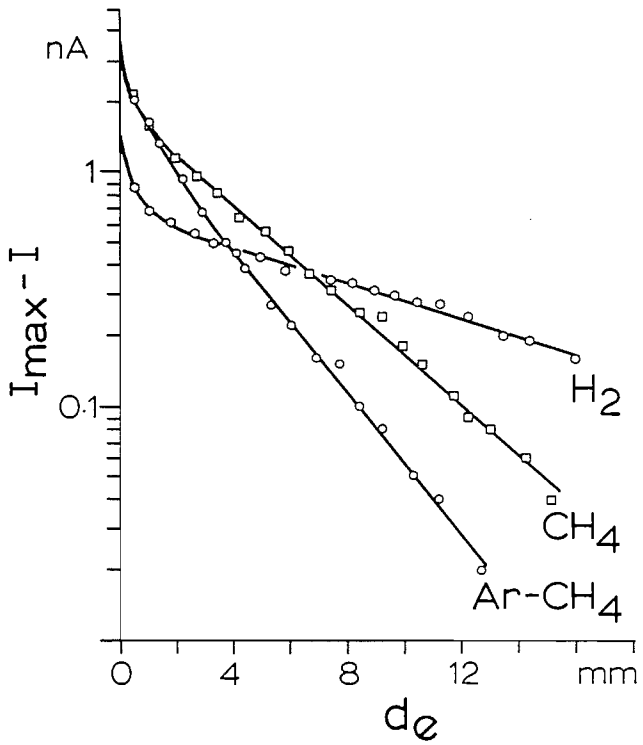

FIG. 14. Semilogarithmic plots of ($I_{max} - I$) versus d_e for three gases with steel counter-electrode under ambient conditions.

a 50% drop in current corresponds to ca. 2.2 mm for steel and 2.5 mm for graphite counter-electrodes. Taking scattering and geometric arguments into account, it seems reasonable to suggest that the "true", unimpeded β distribution would have a half range d^{50} between the 2.5 mm for ionization and the 3.8 mm for luminescence measurements, but would lie very close to the latter.

Further measurements that would eliminate much of the geometric bias and some of the scattering (but would move the apparatus farther away from resembling an ECD) could be made with an "infinite plate" counter-electrode — consisting, for instance, of a low-density, conductive plastic. However, as far as the ECD is concerned, this is not really necessary: the experimental numbers are already close enough to serve as a reasonable base for future calculations and simulations.

Yet, it bears stressing that a real-life ECD — depending on the shape of the foil and its surroundings — may have a very different (and non-exponential) initial ion-pair distribution. When scattering effects prevail, this distribution is likely to be steeper, i.e. the half range is likely to be shorter, than the one found with unimpeded β particles.

Acknowledgements

This work was supported by NSERC grant A-9604. The valuable "nuclear" discussions with A. Chatt, R. E. Jervis, and W. F. Meritt, and earlier correspondence with A. J. L. Collinson, are gratefully acknowledged. We thank E. P. Grimsrud for a prepublication copy of ECD-API-MS data (3) and his constructive critique as this paper's reviewer, and J. Mueller and R. Myatt for their technical expertise in constructing the measurement devices.

1. J. L. PREISS, R. W. FINK, and B. L. ROBINSON. J. Inorg. Nucl. Chem. **4**, 233 (1957).
2. J. A. AYALA, W. E. WENTWORTH, and E. C. M. CHEN. J. Chromatogr. **195**, 1 (1980).
3. E. P. GRIMSRUD and M. J. CONNOLLY. J. Chromatogr. **239**, 397 (1982).
4. P. POPP, J. LEONHARDT, and G. OPPERMANN. J. Chromatogr. **147**, 127 (1978).
5. E. D. PELLIZZARI. J. Chromatogr. **98**, 323 (1974).
6. F. N. SIMON and G. D. RORK. Rev. Sci. Instr. **47**, 74 (1976).
7. W. A. AUE and S. KAPILA. J. Chromatogr. **188**, 1 (1980).
8. K. W. M. SIU and W. A. AUE. Mikrochim. Acta, 419 (1983).
9. N. HERNANDEZ-GIL, W. E. WENTWORTH, T. LIMERO, and E. C. M. CHEN. J. Chromatogr. **312**, 31 (1984).
10. W. E. WENTWORTH and E. C. M. CHEN. *In* Electron capture. *Edited by* A. Zlatkis and C. F. Poole. Journal of Chromatography Library. Vol. 20. Elsevier, Amsterdam. 1981. Chap. 3.
11. J. E. LOVELOCK. J. Chromatogr. **99**, 3 (1974).
12. G. KNOP and W. PAUL. Interaction of electrons and alpha-particles with matter. *In* Alpha-, beta-, and gamma-ray spectroscopy. *Edited by* K. Siegbahn. North-Holland Publishing Co., Amsterdam. 1965. pp. 1–25.
13. A. J. DEKKER. Solid state physics. Prentice-Hall, NJ. 1962. pp. 419–445.
14. T. E. EVERHART. J. Appl. Phys. **31**, 1483 (1960).
15. E. W. MCDANIEL. Collision phenomena in ionized gases. John Wiley and Sons, Inc., New York. 1964. pp. 658–670.
16. K. W. M. SIU, J. R. HANCOCK, and W. A. AUE. Anal. Chem. **53**, 2383 (1981).
17. C. E. CROUTHAMEL, F. ADAMS, and R. DAMS. Applied gamma-ray spectrometry. 2nd ed. Pergamon Press, Oxford. 1970. p. 54.
18. W. J. MOORE. Physical chemistry. 4th ed. Longmans, London. 1963. p. 434.
19. W. A. AUE and K. W. M. SIU. J. Chromatogr. **203**, 237 (1981).
20. L. ONSAGER. Phys. Rev. **54**, 554 (1938).
21. J. H. BEYNON, D. CAMERON, and J. F. J. TODD. Anal. Chem. **54**, 679A (1982).

Appendix 1

If the photomultiplier current truly reflects the energy of the β particles entering the scintillator, the residual β energy E, arriving per second on the scintillator, can be represented as

[1] $E = E_0 \exp(-k' d_s)$

where E_0 is the maximum β energy available. Since the average energy spent in creating an ion pair is fairly independent (12) of the energy of the ionizing β particle, N^i, the number of ion pairs created per second in the gas volume between the foil and the scintillator (i.e. from $d_s = 0$ to d_s) is given by

[2] $N^i = w(E_0 - E)$

where w is a constant. Substituting [1] into [2] yields

[3] $N^i = wE_0[1 - \exp(-k' d_s)]$

The local ion-pair generation rate N (ion pairs created per second per unit length) at d_s can be found by differentiating N^i with respect to d_s

$$N = dN^i/d(d_s)$$

[4] $N = wE_0k' \exp(-k' d_s)$

[5] $N = N_0 \exp(-k' d_s)$

where $N_0 = wE_0k'$ is the ion-pair generation rate adjacent to the foil. Thus the initial ion-pair generation rate or, differently

Can. J. Chem. Downloaded from www.nrcresearchpress.com by 78.46.186.204 on 09/07/12
For personal use only.

expressed, the initial ion-pair distribution drops off exponentially with increasing distance from the foil.

Furthermore, from [4], the total number of ion pairs created per second, N_{inf} from $d_s = 0$ to d_s = infinite, can be calculated as

$$[6] \quad N_{inf} = \int_0^\infty dN^i = \int_0^\infty N d(d_s)$$

Substituting [5] into [6]

$$N_{inf} = N_0 \int_0^\infty \exp(-k' d_s) d(d_s)$$

$$[7] \quad N_{inf} = N_0/k'$$

However,

$$[8] \quad N_{inf} = I_{max} \times 6.023 \times 10^{23}/96500$$

where I_{max} is the maximum current available from the foil. Therefore, the initial ion-pair distribution is calculable if I_{max} and k', two measurable parameters, are known.

Can. J. Chem. Downloaded from www.nrcresearchpress.com by 78.46.186.204 on 09/07/12
For personal use only.

Cyclic single drop square wave polarography at spherical electrodes — the reversible case

LOUIS RAMALEY[1] AND WEE TEE TAN[2]

Trace Analysis Research Centre, Department of Chemistry, Dalhousie University, Halifax, N.S., Canada B3H 4J3

Received November 5, 1986

This paper is dedicated to Professor Douglas E. Ryan on the occasion of his 65th birthday

LOUIS RAMALEY and WEE TEE TAN. Can. J. Chem. **65**, 1025 (1987).

The influence of electrode sphericity and the results of sweep reversal are examined for square wave voltammetry and the square wave polarography in which an entire polarogram is obtained on a single drop. An expanding sphere treatment obtained by adding a spherical correction to expanding plane theory gives the best fit to the experimental data. Amalgam forming reactions fit the simple theory developed to a lesser extent than other reactions, especially on the reverse sweep. The shape of the differential polarogram is not significantly affected by sphericity and the reverse peak potential is approximately equal to the forward peak potential. Small differences in these potentials are due to the distortion of the square wave by the stairstep used for the sweep and the distortion of the polarogram due to drop growth. The ratio of the forward and reverse peak currents depends on the phasing of the square wave and stairstep in all cases and on other parameters for a growing drop.

LOUIS RAMALEY et WEE TEE TAN. Can. J. Chem. **65**, 1025 (1987).

On a examiné l'influence de la sphéricité de l'électrode et les résultats de l'inversion du balayage sur la voltamétrie à onde carrée et sur la polarographie à onde carrée dans lesquels le polarogramme complet est obtenu sur une goutte unique. Le meilleur accord avec les données expérimentales est obtenu en utilisant un traitement de sphère en expansion, qui est obtenu par l'addition d'une correction sphérique à la théorie du plan en expansion. Les réactions qui conduisent à un amalgame se produisent à un degré moindre que les autres réactions, principalement lorsqu'on renverse la balayage, et elles peuvent être expliquées par la théorie simple qui a été développée. La forme du polarogramme différentiel n'est pas affectée d'une façon importante par la sphéricité et le potentiel maximum de la réaction inverse est approximativement égal au potentiel maximum de la réaction normale. Les petites différences observées dans ces potentiels sont dues à la distortion de la vague carrée par les échelons utilisés pour le balayage ainsi qu'à la distortion du polarogramme qui est causée par la croissance de la goutte. Le rapport des courants maxima normaux et inverses dépend de la phase de la vague carrée et de l'échelon dans tous les cas et sur d'autres paramètres d'une goutte qui croît.

[Traduit par la revue]

Introduction

Until recently the ability to perform pulse electrochemical experiments at high sweep rates was limited to laboratories possessing rather specialized, lab-built equipment. The advent of new, commercial instrumentation (Bioanalytical Systems, Inc., and EG&G Princeton Applied Research) has altered this situation, leading Osteryoung and Osteryoung (1) to predict that square wave voltammetry (SWV) will become widely applied both for mechanistic studies and chemical analysis. In SWV a stationary test electrode is employed and the potential excitation waveform consists of a square wave of peak-to-peak amplitude ΔE and half-period τ superimposed on a staircase wave of step height E_s and length 2τ, as shown in Fig. 1. With the new instrumentation the step length can be in the low millisecond range, providing sweeps rapid enough to be carried out on a single drop at a dropping mercury electrode (dme). This latter experiment is referred to as single drop square wave polarography (SDSWP).

Drake *et al.* (2) have indicated that cyclic differential pulse voltammetry (DPV), where the sweep direction is reversed one or more times during the experiment, might be very useful in the study of electrode processes and in chemical analysis. Several experimental examples were presented. SWV may be looked upon as a special case of DPV in which the pulse waveform has a 50% duty cycle. Thus DPV and SWV will have many of the same characteristics. Gajda and Horák (3) applied a square wave superimposed on a linear sweep to a dme with a long drop time (100 s) and obtained low analytical detection limits. They reversed the sweep in some of their work but did not systematically study the effect of this reversal. Okamoto (4) first derived a theory for cyclic SDSWP assuming a small amplitude (<10 mV) square wave superimposed on a triangular sweep. The slow scan limit, an assumption that the linear sweep is too slow to distort the square wave, was implicit in his work. Theory and experiment agreed better on the forward than on the reverse sweep. All told, very little has been published on cyclic pulse voltammetry.

Recently interest has revived concerning the effect of electrode geometry on current–voltage curves. Some time ago a paper by Beigler and Laitinen (5) showed that the assumption of plane geometry for spherical electrodes led to errors under certain conditions when determining kinetic parameters from faradaic impedance measurements. This led to a series of papers by Smith and his group (6–10) on the effect of sphericity in first and second harmonic ac polarographic experiments. This has special relevance to reactions at mercury electrodes since these electrodes are almost always spherical. Somewhat later Bond *et al.* (11, 12) discussed the effect of electrode sphericity on the results of first and second harmonic ac voltammetry, considering the cases where the product of the reaction is soluble in solution and in the mercury electrode. More recently Bond and Oldham (13) have analyzed the behaviour of potential step experiments at spherical electrodes and concluded that distortions occur in the current–voltage curves (*vis-a-vis* those at planar electrodes) even for simple, reversible reactions. Myland and Oldham (14) and Tokuda *et al.* (15), and Myland *et al.* (16) came to the same conclusion in the cases of linear sweep voltammetry and cyclic voltammetry, respectively.

Using a perturbation approach involving the inverse of the electrode radius as the perturbation parameter, Goodisman (17) has formulated a general theory for spherical corrections in the voltammetry of nernstian systems. For the case of SWV, O'Dea

[1]To whom correspondence should be addressed.

[2]Present address: Department of Chemistry, Universiti Pertanian Malaysia, Serdang, Selangor, Malaysia.

Can. J. Chem. Downloaded from www.nrcresearchpress.com by 78.46.186.204 on 09/07/12
For personal use only.

Can. J. Chem. Downloaded from www.nrcresearchpress.com by 78.46.186.204 on 09/07/12
For personal use only.

et al. (18) and Whelan *et al.* (19) have noted that the shape of the voltammogram for differential or net current (the normal display) was unaffected by electrode radius for disk electrodes. Thus edge effects appeared to play little role in this regard. Finally Aoki *et al.* (20) have derived equations assuming the small amplitude limit ($n\Delta E < 10$ mV) for square wave voltammograms at electrodes of various geometries for reversible reactions. Their results indicate that the shape of the differential voltammogram should be independent of electrode geometry. This is in contrast to the current–voltage curves for normal pulse polarography (13) and linear sweep voltammetry (14–16).

In this paper we present a theoretical treatment for SWV and SDSWP at spherical electrodes which makes no assumption regarding either square wave amplitude or sweep rate. Results are given for both instantaneous and average current, the latter being the normal method of data measurement in chemical analysis. The treatment is extended to include sweep reversal. Theory and experiment are compared for systems in which the product is soluble both in solution and in the electrode, but the theory is strictly applicable only to the solution soluble case for reversible electrochemical reactions.

Theory

In the following it will be assumed that the elctrode reaction

[1] $\quad O + ne \rightarrow R$

is reversible, that diffusion is semi-infinite, that R is not present before the experiment, and that R is soluble in solution rather than in the electrode. Under these conditions the theory for the instantaneous current flowing to a stationary, planar electrode has been presented at various levels of sophistication (21–23). The method used by Rifkin and Evans (23) for pulse methods is quite general and provides results for any sequence of pulses with no restrictions on time symmetry or amplitude. Ramaley and Tan (24) have extended the treatment to include the expanding plane geometry and both average and instantaneous current. For the case of a stationary spherical electrode, presented in detail in the appendix, a general equation is developed for any pulse sequence. However, in the discussion to follow only the square wave pulse sequence will be examined because this waveform symmetry allows simpler nomenclature and because it is the most useful analytically (1).

For instantaneous current measurement, the measurement will be made at a constant fraction, β, of the square wave half-period, τ, where

[2] $\quad 0 \leq \beta \leq 1$

For average current measurement, which requires gated integration over a constant time period, integration will start at a fixed fraction, β_a, of τ and cease at a second fixed fraction, β_b, where

[3] $\quad 0 \leq \beta_a < \beta_b \leq 1$

The potential of the jth half-cycle of the pulse sequence is given by

[4] $\quad E_j = E_i + \text{Int}\,([j-1]/2)E_s + (-1)^j\Delta E/2$

where E_i is the potential applied before the pulse sequence begins and the term Int $([j-1]/2)$ represents the greatest integer not exceeding $[j-1]/2$.

In SWV and SDSWP the normal procedure is to establish the phase of the square wave such that at the time of the stairstep, the pulse potential changes in the same direction as the stairstep, as depicted in Fig. 1. The current that flows on the first half-cycle after the step is referred to as the forward current

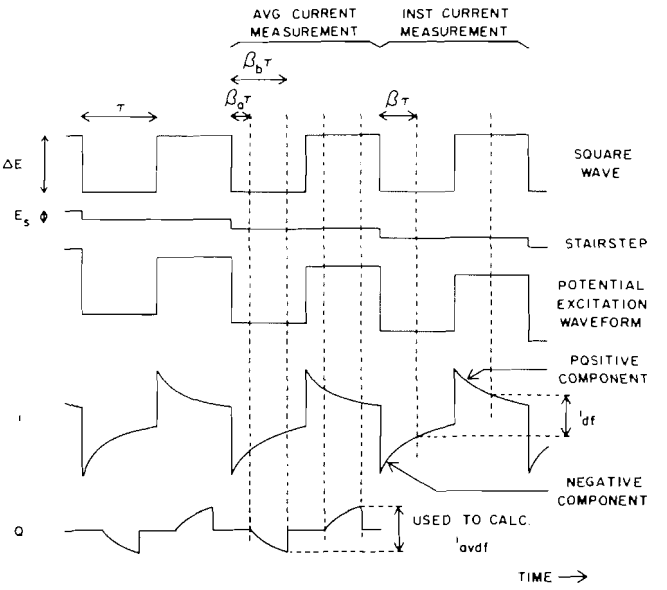

FIG. 1. Potential, current, and charge waveforms used and observed in SWV and SDSWP.

and that on the second as the reverse current. The difference between these two currents, the differential or net current, provides the current–voltage curve normally associated with these techniques. This paper will deal with sweep reversal in which it is customary to designate the current before reversal as the forward current and that after as the reverse current. Some confusion may arise due to the various meanings of forward and reverse current. Hereafter, forward current will signify that flowing on either half-cycle of the square wave before sweep reversal, the reverse current to that flowing after reversal. The negative current component will refer to the current flowing on the negative half-cycle of the square wave and the positive component to that flowing on the positive half-cycle, regardless of the manner of synchronizing the square wave and stairstep. The usual electrochemical convention that cathodic current is positive will be observed. The waveforms in Fig. 1, however, depict the current and charge as these are measured experimentally.

The differential current is obtained from the individual negative and positive current components using

[5] $\quad i_{df} = i_{j-1} - i_j \qquad$ with $j = 2, 4, 6, \ldots$

The following are useful in simplifying the equations for the various cases and geometries:

[6] $$Q_j = \frac{\exp\,[(E_j - E_{1/2})nF/RT]}{1 + \exp\,[(E_j - E_{1/2})nF/RT]}$$

[7] $\quad E_{1/2} = E^{0\prime} + (RT/2nF)\ln\,(D_R/D_O)$

where $E^{0\prime}$ is the formal potential for reaction [1], D_R and D_O are the diffusion coefficients of R and O, respectively, and the other symbols have their usual meanings,

[8] $\quad G = nFAD_O^{1/2}C^*/\pi^{1/2}\tau^{1/2}$

where A is the electrode area and C^* is the concentration of O in the bulk of solution, and

[9] $\quad H_k = (j - k + \beta)^{1/2}$

[10] $\quad H_k^a = (j - k + \beta_a)^{1/2}$

[11] $\quad H_k^b = (j - k + \beta_b)^{1/2}$

Can. J. Chem. Downloaded from www.nrcresearchpress.com by 78.46.186.204 on 09/07/12
For personal use only.

The equations for the currents flowing to a stationary, planar electrode on the jth half-cycle of the square wave are (21–24):

$$[12]\quad i_p = G\sum_{k=1}^{j}(Q_{k-1} - Q_k)/H_k \qquad \text{(inst. current)}$$

$$[13]\quad (i_p)_{av} = \frac{2G}{(\beta_b - \beta_a)}\sum_{k=1}^{j}(H_k^b - H_k^a)(Q_{k-1} - Q_k) \qquad \text{(avg. current)}$$

$$[14]\quad (i_p)_{df} = G\sum_{k=1}^{j}(Q_k - 2Q_{k-1} + Q_{k-2})/H_k \qquad \text{(diff. inst. current)}$$

$$[15]\quad (i_p)_{avdf} = \frac{2G}{(\beta_b - \beta_a)}\sum_{k=1}^{j}(H_k^b - H_k^a) \times (Q_k - 2Q_{k-1} + Q_{k-2}) \qquad \text{(diff. avg. current)}$$

and those for currents flowing to a stationary, spherical electrode are (see Appendix):

$$[16]\quad i_s = i_p + \frac{nFAD_OC^*}{r_0}(1 - Q_j) \qquad \text{(inst. current)}$$

$$[17]\quad (i_s)_{av} = (i_p)_{av} + \frac{nFAD_OC^*}{r_0}(1 - Q_j) \qquad \text{(avg. current)}$$

$$[18]\quad (i_s)_{df} = (i_p)_{df} + \frac{nFAD_OC^*}{r_0}(Q_{j-1} - Q_j) \qquad \text{(diff. inst. current)}$$

$$[19]\quad (i_s)_{avdf} = (i_p)_{avdf} + \frac{nFAD_OC^*}{r_0}(Q_{j-1} - Q_j) \qquad \text{(diff. avg. current)}$$

where r_0 is the radius of the electrode and Q_0 and Q_{-1} are both unity. Equations [12]–[19] may be applied to a dme with varying degrees of approximation by using the following substitution for the electrode area

$$[20]\quad A = (36\pi)^{1/3}(mt'/\rho)^{2/3}$$

where t' is the time from the beginning of drop life, m is the mass flow rate of mercury, and ρ is the density of mercury.

For comparison the equations for the expanding plane theory as applied to a dme (24) are shown below:

$$[21]\quad i_{xp} = (7/3)^{1/2}(36/\pi^{1/2})^{1/3}nF(m/\rho)^{2/3} \times [t_d + (j - 1 + \beta)\tau]^{4/3}D_O^{1/2}C^*\left\{\sum_{k=1}^{j}(Q_{k-1} - Q_k)\Big/ ([t_d + (j - 1 + \beta)\tau]^{7/3} - [t_d + (k - 1)\tau]^{7/3})^{1/2}\right\} \qquad \text{(inst. current)}$$

$$[22]\quad (i_{xp})_{av} = \frac{(12/7)^{1/2}(36/\pi^{1/2})^{1/3}nF(m/\rho)^{2/3}D_O^{1/2}C^*}{(\beta_b - \beta_a)\tau} \times \sum_{k=1}^{j}\{([t_d + (j - 1 + \beta_b)\tau]^{7/3} - [t_d + (k - 1)\tau]^{7/3})^{1/2} - ([t_d + (j - 1 + \beta_a)\tau]^{7/3} - [t_d + (k - 1)\tau]^{7/3})^{1/2}\} \times (Q_{k-1} - Q_k) \qquad \text{(avg. current)}$$

where t_d is the time between the beginning of drop life and the start of the experiment. The equations for the differential current do not simplify to any extent after appropriate substitution of [21] or [22] into [5] and so are not listed.

Experimental

A conventional three-electrode operational amplifier potentiostat interfaced to and controlled by a minicomputer was used to obtain data. A potentiostat almost identical to that employed has been described elsewhere (25, 26). The computer system, which was also used to perform the theoretical calculations, consisted of a Hewlett-Packard 21MX-M minicomputer with a magnetic tape operating system.

Unthermostated borosilicate glass cells of 20 mL capacity were employed. A conventional saturated calomel electrode (sce) was connected to the cell through a side arm filled with supporting electrolyte. The dme consisted of a 10 s capillary sealed above a 6 mm soft glass tube which was in turn drawn to a fine tip. Electrical contact was made through the soft glass tube below the capillary. This arrangement avoids the shielding and capillary resistance of the normal dme. No drop dislodging device was employed; the breaking of a light beam by the free falling drop signalled the beginning of a new drop and was used to synchronize the sweep electronics. All measurements were carried out between 23 and 25°C.

All chemicals were reagent grade and were used without additional purification except KCl which was crystallized once from distilled water. Cadmium(II) in a 1.00 *M* KCl medium was employed as an example of an amalgam forming system and Fe(III) in 0.500 *M* $K_2C_2O_4$ at pH 5.0 served as an example in which both halves of the redox couple are soluble in solution. Stock Fe(III) solutions were prepared by oxidation of the iron in $Fe(NH_4)_2(SO_4)_2\cdot 6H_2O$, taken as a primary standard, with concentrated nitric acid; Cd(II) solutions were prepared from $Cd(NO_3)_2\cdot 4H_2O$ and were standardized by EDTA titration. Laboratory distilled water was run through activated charcoal and distilled once more from an all-glass still before use.

Results and discussion

Results derived from theory

As seen from eqs. [16]–[19], the current flowing to a spherical electrode can be visualized as that flowing to a planar electrode plus an additional term or "correction" for sphericity. For the individual current components the spherical term is the same as that for a single pulse or step (13) and is the result predicted by the general voltammetric treatment of Goodisman (17). This term is a function only of the applied potential, E_j (through Q_j), and does not depend on time or any previously applied potentials. Since Q_j is unity when E_j is positive to $E_{1/2}$, the spherical term will be maximum at negative potentials and will disappear as the potential returns to its initial value in a cyclic experiment.

The magnitude of the spherical term relative to the planar term will depend on r_0, β or β_a and β_b, and τ (sweep rate), increasing with decreasing r_0 and increasing β and τ. The latter occurs because the spherical term is independent of β and τ and the planar term decreases with increasing β and τ. Sphericity will have a larger effect on average current measurements, again because the spherical term is unaffected by integration whereas the planar term usually decreases when integration is employed.

For differential or net current, the spherical term depends on $(Q_j - Q_{j-1})$ or ΔE. Thus if ΔE is small ($n\Delta E < 10$ mV), this term will be much smaller than that for the individual current components and may be considered negligible, as proposed by Aoki *et al.* (20). Since dQ/dE is maximum at $E_{1/2}$ and falls to zero on either side of $E_{1/2}$, the differential spherical correction will be maximum at and symmetrical about $E_{1/2}$. Even for large ΔE, the spherical term will be smaller for net current than for individual current and will distort the net current–voltage curve much less. This line of reasoning can be applied to any geometry (20) where the current can be represented as the sum of a planar term and a time independent geometrical "correction".

Typical values of the relative spherical correction for differential current are presented in Table 1. The insensitivity of the

TABLE 1. Relative spherical corrections in SWV*

ΔE (mV)	Sweep rate (V/s)	Correction (%)
10	2	0.2
10	0.0625	1.0
50	0.0625	1.1

*r_0 = 0.45 mm, E_s = −2 mV, n = 2, D_0 = 1 × 10^{-5} cm^2/s, T = 25°C, β_a = 0.5, β_b = 1.

correction to the magnitude of ΔE is explained by noting that an increase in ΔE causes increases in both the planar and spherical terms to approximately equal extents, leaving the relative correction almost unchanged.

The discussion above is strictly applicable only to the case where O and R share the same diffusion space and $D_O = D_R$. However, it should be a good approximation as long as $D_O \cong D_R$, the usual case experimentally. Brydon and Oldham (27) have shown that using a mean value for the diffusion coefficients when $D_O \cong D_R$ leads to the mathematical result that the surface concentrations of O and R are a function only of potential. This supports the soundness of the approximation. For amalgam forming reactions O and R do not share the same diffusion space and the approximation is much worse, regardless of the values of D_O and D_R.

Equations [12]–[19], [21], [22] assume a fixed time symmetry (50% duty cycle) but make no restrictions on pulse amplitude or direction. Thus the theory does not have to be extended to include sweep reversal. The reversal potential, E_λ, is given by

$$[23] \quad E_\lambda = E_i + \text{Int}([\lambda - 1]/2)E_s$$

where λ is the value of j, taken as even, at which reversal takes place. Prior to reversal eq. [4] is used to calculate E_j and after reversal the following may be used

$$[24] \quad E_j = E_\lambda - \text{Int}([j - \lambda + 1]/2)E_s + (-1)^j \Delta E/2$$

A cyclic square wave voltammogram for a reduction at a stationary spherical electrode is shown in Fig. 2. As expected, the forward and reverse peak potentials for the differential current appear to be the same; however, the reverse peak current is lower than the forward peak current. It was first pointed out by Ramaley and Krause (21) that the stairstep must distort the square wave on which it is superimposed. For example, a −2 mV stairstep synchronized with the positive pulse of a 10 mV square wave produces an 8 mV positive step and a 10 mV negative step, averaging 9 mV per step. Christie *et al.* (22) pointed out that sensitivity increased if the stairstep and square wave were synchronized such that both steps occurred in the same direction (as in Fig. 1). For the E_s and ΔE values above, a 10 mV positive and 12 mV negative step, averaging 11 mV, would result from this phasing. Although correct, this comment on phasing is somewhat academic since differences in phasing can be offset by changes in ΔE to produce exactly the same results (e.g. a 12 mV ΔE will produce the same current with the first phasing above as the 10 mV ΔE does with the second), indicating that synchronization is not important in achieving higher sensitivity.

The reverse current in Fig. 2 is lower than the forward current because the negative stairstep and negative pulse are synchronized together on the forward sweep, but on the reverse sweep the stairstep is positive, though still synchronized with

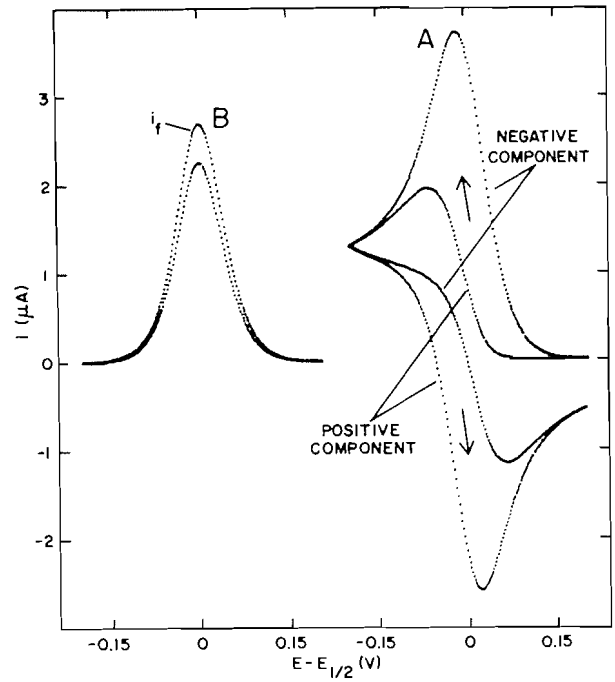

FIG. 2. Cyclic square wave voltammograms at a spherical electrode. Synchronization scheme [24], *A*, individual currents, *B*, differential current, E_s = −2 mV, ΔE = 10 mV, n = 1, r_0 = 0.5 mm, β_a = 0.5, β_b = 1, D_O = 1 × 10^{-5} cm^2/s, C^* = 1 × 10^{-4} M, sweep rate = 1 V/s, T = 25°C.

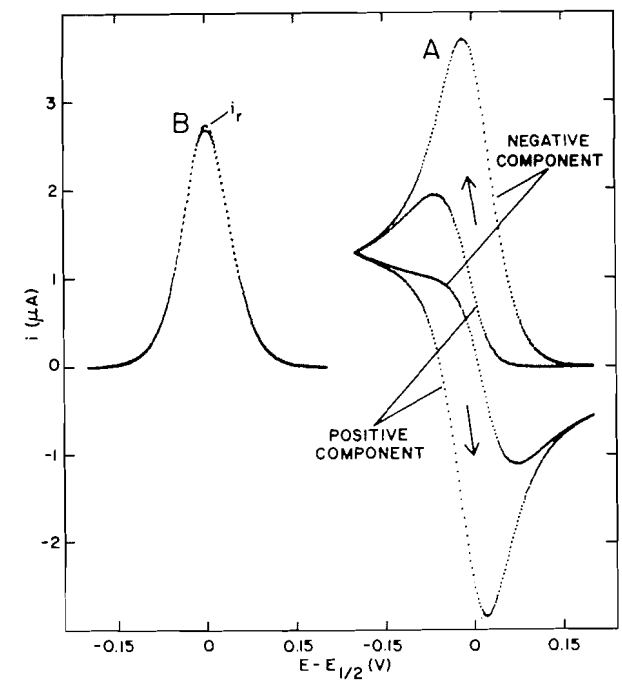

FIG. 3. Cyclic square wave voltammograms at a spherical electrode. Synchronization scheme [25], other conditions as in Fig. 2.

the negative pulse. This may be overcome by extending the stairstep at E_λ to a time equal to 3τ, synchronizing the positive stairstep with the positive pulse. For this case

$$[25] \quad E_j = E_\lambda - \text{Int}[j - \lambda]/2)E_s + (-1)^j \Delta E/2$$

after reversal. Figure 3 shows the voltammograms obtained for this synchronization. The reverse differential current is now

Can. J. Chem. Downloaded from www.nrcresearchpress.com by 78.46.186.204 on 09/07/12
For personal use only.

TABLE 2. Peak potentials (mV) in SWV*

E_s	ΔE	$(E_{pk})_f - E_{1/2}$	$(E_{pk})_r - E_{1/2}$ Equation [24]	$(E_{pk})_r - E_{1/2}$ Equation [25]
−2	10	−0.45	−0.17	0.88
−4	10	−1.04	−0.63	1.67
−6	10	−1.67	−1.29	2.46
−2	50	−0.15	0.19	1.19

*Same conditions as in Table 1, except sweep rate = 1 V/s.

slightly larger than the forward current. When this current is computed using eq. [25] with j even, the individual currents used in the calculation occur across a potential step of ΔE for the forward sweep and $(\Delta E + E_s)$ for the reverse sweep. This causes the calculated differential current in the reverse sweep to be slightly larger. For the same reason, the spherical correction will be slightly higher in the reverse direction. If the subtraction scheme after reversal is changed so that

[26] $i_{df} = i_j - i_{j-1}$ with j odd

the two values in the calculation always occur across a step of ΔE and the forward and reverse differential currents are equal.

Peak potentials were obtained from experimental data or data generated from eqs. [12]–[19], [21], [22] by regression analysis. This is most simply done by fitting a small number of data, e.g. nine points, centred on the peak to a parabola using linear regression analysis. The peak maximum is then obtained from the parameters calculated in the analysis. Since the shape of a reversible square wave polarogram closely approximates the first derivative of the dc polarogram, especially at small ΔE, a better fit is obtained using a function of the form of that derivative. Such a function is

[27] $i = \{(4i_{pk})\exp[K(E - E_{pk})]\}/\{\exp[K(E - E_{pk})] + 1\}^2$

The parameters i_{pk}, the peak current, E_{pk}, the peak potential, and K, a constant related to the peak half-width, must be evaluated by non-linear regression analysis (28). Both methods provide the same results at high resolution ($E_s \leqq 2$ mV) but the parabolic fit degrades at lower resolution.

For a stationary spherical electrode the peak potential on both the forward, $(E_{pk})_f$, and reverse, $(E_{pk})_r$, sweeps is very close to $E_{1/2}$ at high resolution. However, as E_s is increased, the values move away from $E_{1/2}$, $(E_{pk})_f$ moving toward negative values, and $(E_{pk})_r$ moving identically for the scheme of eq. [24] and toward positive values and to a greater extent for eq. [25], as shown in Table 2. This latter shift is more apparent than real and is mainly due to the method of data handling and plotting in our computer programs. It is convenient to use the potential of the stairstep for odd j as the average electrode potential for data analysis regardless of synchronization scheme. With the scheme of eq. [24] individual current measurements are made at potentials which average to this potential both before and after reversal. When the scheme of eq. [25] is used after reversal, the stairstep occurs between the two current measurements and the average potential is offset from the assumed potential by $E_s/2$. This is approximately the difference between the values of $(E_{pk})_r$ for the two schemes.

Increasing E_s also increases any difference between $(i_{pk})_f$ and $(i_{pk})_r$ in the different schemes. These problems are worst for small ΔE, where the distortion is largest. The use of small ΔE provides the narrowest and most ideal peak shapes; however, the best values for $E_{1/2}$ are obtained using large ($\geqq$50 mV) values of ΔE.

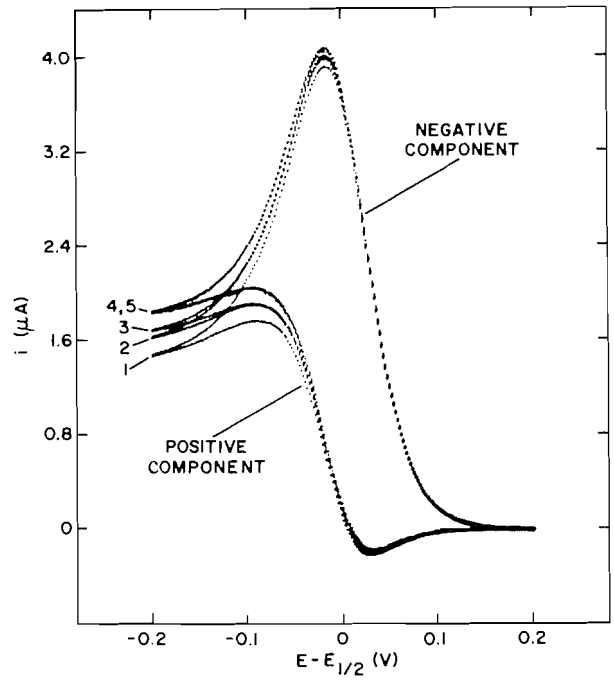

FIG. 4. Forward current components in SDSWP; *1*, planar theory; *2*, spherical theory; *3*, expanding plane theory; *4*, spherically corrected expanding plane theory; *5*, experiment; 4.00 × 10^{-4} *M* Fe(III); 0.500 *M* $K_2C_2O_4$; pH = 5.0; E_s = −2 mV, ΔE = 10 mV; sweep rate = 0.125 V/s, t_d = 0.992 s, β_a = 0.0625, β_b = 1, m = 0.001837 g/s, T = 23°C.

These phasing problems do not occur for a square wave superimposed on a linear sweep. However, the linear sweep produces a higher background due to the continuous flow of current needed to charge the double layer. This is especially evident at high sweep rates.

Experimental results with the Fe(III)/(II) system

All experimental work was done with a dme and most used the synchronizing scheme of eq. [24] after reversal. However, recently we have built an instrument (29) in which the potential excitation waveform is generated in software and the synchronizing scheme of eq. [25] can be employed. Experimental work with the two schemes agrees very well with predictions based on the theory presented above.

It has previously been shown (24) that both the planar (with the area calculated from eq. [20]) and expanding plane theories produce results which agree very well with experiment for the differential current. Differences appeared only when the individual current components were examined. This also holds true for spherical electrodes and for currents measured on the reverse sweep. All theories produce forward and reverse differential polarograms that are for all practical purposes identical to experiment. However, differences, which depend on the experimental parameters, are noted for the individual components. At high sweep rates ($\geqq$1 V/s), the electrode size changes little during the experiment and the expanding plane results are almost identical to the area corrected plane results. At large delay times, the drop is large and the spherical correction is small so that again the planar theories provide good agreement with experiment. The conditions used in obtaining the data shown in Figs. 4 and 5 were chosen such that both the drop

Can. J. Chem. Downloaded from www.nrcresearchpress.com by 78.46.186.204 on 09/07/12
For personal use only.

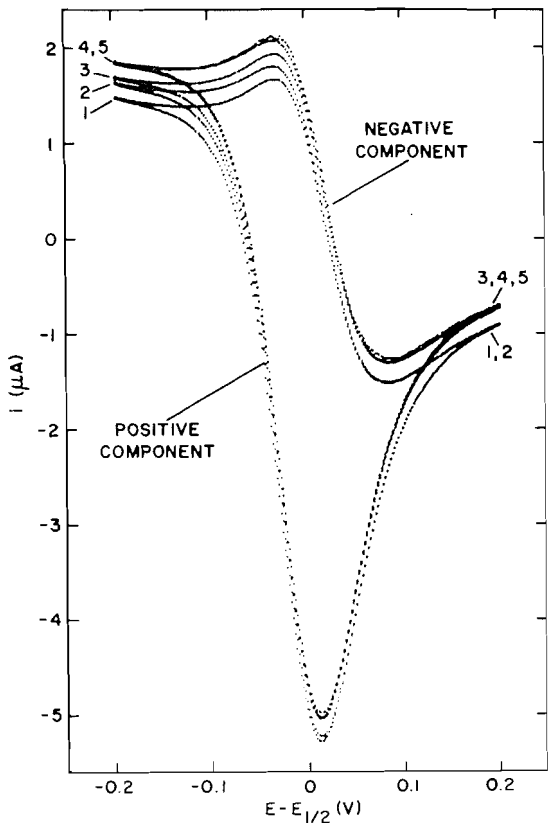

FIG. 5. Reverse current components in SDSWP. Same conditions and designations as in Fig. 4.

expansion and sphericity would cause deviations from simple area corrected planar theory.

In addition to the results of the planar, spherical, and expanding plane theories, those of a combination of expanding plane theory with a spherical correction are shown in these figures. This combination is obtained by the addition of the spherical correction term of eq. [17] to the right side of eq. [22]. Delmastro and Smith (6) noted that corrections for sphericity and expansion were almost independent of each other and that a reasonable treatment for an expanding sphere might be the combination of an expanding plane with a simple stationary spherical correction. McCord and Smith (10) later used this approach in obtaining data on quasireversible reactions using second harmonic ac polarography with good results.

A diffusion coefficient of 6.12×10^{-6} cm^2/s, which produced identical experimental and theoretical differential polarograms, was used to generate the theoretical curves of Figs. 4 and 5. This agrees well with the value of 6.31×10^{-6} cm^2/s obtained by Olmstead and Nicholson (30), but is somewhat higher than that of Myland *et al.* (31), 4.8×10^{-6} cm^2/s. This latter value was measured in 1.0 *M* $K_2C_2O_4$, whereas the concentration used in this work is 0.50 *M*.

As seen in the figures, area corrected planar theory gives the worst agreement and spherically corrected expanding plane theory the best, and quite satisfactory, agreement with experiment for both the forward and reverse sweeps. Expanding plane theory appears to be slightly superior to spherical theory, but this will depend on the experimental parameters chosen, holding only when the expansion "correction" is larger than the spherical correction. These results appear to substantiate the proposal of Delmastro and Smith (6) regarding the approximate

TABLE 3. ΔE_{pk} values in SDSWP*

Sweep rate (V/s)	$(E_{pk})_f - (E_{pk})_r$ (mV)	
	Theory	Experimental
0.0977	−4.0	−3.9
0.1953	−2.6	−2.4
0.3906	−1.5	−1.5
0.7813	−1.0	−0.6
1.563	−0.6	−0.4

*2.00×10^{-4} *M* Fe(III), 0.500 *M* $K_2C_2O_4$, m = 0.001325 g/s, peak time = 3.0 s, E_s = −2 mV, ΔE = 10 mV.

expanding sphere treatment. The reverse currents are larger than the forward currents mainly due to electrode expansion.

Variations in ΔE, E_λ, and the synchronizing scheme do not affect the agreement between theory and experiment. However, at higher sweep rates ($\geqq$1 V/s), even though the differential polarograms are still accurately predicted by theory, the agreement in the case of the individual components begins to degrade slightly. The cause of this is not presently known.

The positions of the peaks in and the shapes of the individual component polarograms depend on n, E_s, ΔE, and β(s) (24). However, the shapes of and the peak positions in differential polarograms depend very little on these parameters except that the peak shape is a strong function of n. Small variations in $(E_{pk})_f$ and $(E_{pk})_r$ as a function of E_s were discussed above. In addition a small difference in $(E_{pk})_f$ and $(E_{pk})_r$ was noted both for theory and experiment as a function of sweep rate, as shown in Table 3. This is unusual because (*a*) the greatest differences appear at the slowest sweep rates and (*b*) τ does not appear in the summations in eqs. [12]–[19] so that the peak potentials should not depend on τ. If the calculations are performed for stationary electrodes, the peak positions are independent of τ. Therefore the effect shown in Table 3 must be due to distortion of the polarograms by drop growth. As sweep rate increases, growth has a smaller effect on the polarogram and the effect decreases.

Much of the data taken in this study involved the averaging of the results from a number of drops, usually 16 or 25, to improve the signal-to-noise ratio. A depletion effect was sometimes noted when comparing single drop and multidrop results. The magnitude of this effect depended on the time the electrode potential was held negative to $E_{1/2}$ and was thus a function of sweep rate and reversal potential for cyclic work or final potential for linear sweep work. Decreases as large as 7% in peak current for multidrop experiments at sweep rates of 0.05 V/s were observed and thus caution should be used in sensitive experiments when averaging is employed.

Experimental results with the Cd(II)/Cd·Hg system

The data for the reduction of Cd(II) in experiments similar to those for Fe(III) are shown in Figs. 6 and 7. A value of 8.22×10^{-6} cm^2/s for D_O was needed to properly fit the data. A range of 6.8 to 7.7 $\times 10^{-6}$ cm^2/s has been reported for Cd(II) in 1.0 *M* nitrate and chloride media (13). Values of 7.3×10^{-6} cm^2/s (14) and 8.11×10^{-6} cm^2/s (15) have also recently been used for 1.0 *M* KCl electrolytes. Again the spherically corrected expanding plane approach provided the best fit to the experimental data. This fit, although not as good as with Fe(III), is satisfactory for the forward sweep. However, none of the models fit the data on the reverse sweep very

Can. J. Chem. Downloaded from www.nrcresearchpress.com by 78.46.186.204 on 09/07/12
For personal use only.

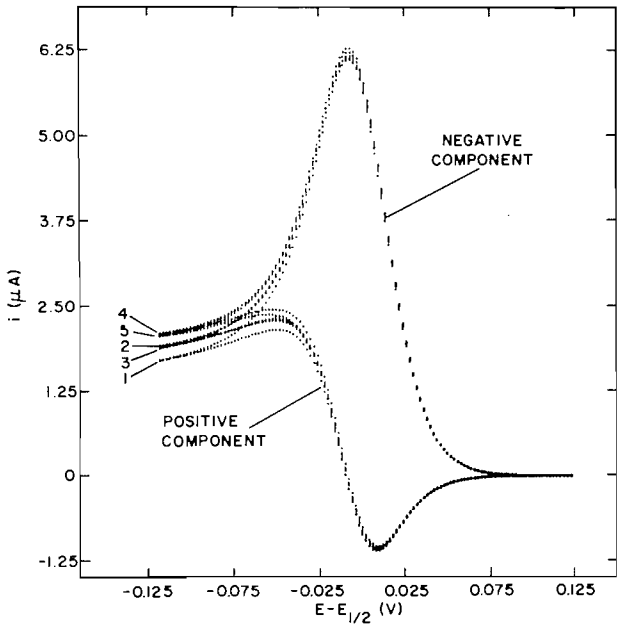

FIG. 6. Forward current components in SDSWP; 2.00×10^{-4} *M* Cd(II), 1.00 *M* KCl, other conditions and designations as in Fig. 4.

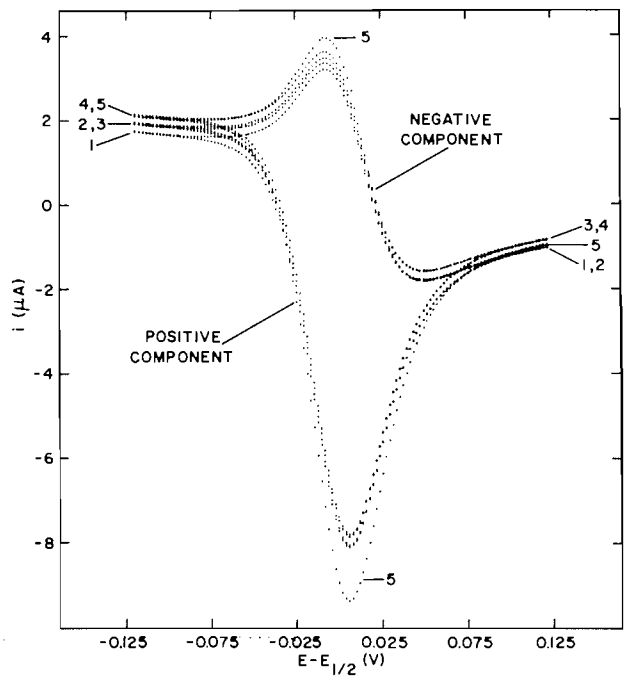

FIG. 7. Reverse current components in SDSWP. Same conditions as in Fig. 6.

well, either for individual or differential polarograms. The experimental current is invariably larger than that predicted by theory. The need for a diffusion coefficient larger than generally accepted and higher reverse currents are typical for systems involving diffusion into the mercury drop (6, 9, 12), when the theory for a solution soluble reduced species is applied.

The effect of changes in E_λ is shown in Fig. 8 for the synchronization scheme of eq. [24]. When reversal is carried out at or near $E_{1/2}$, the reverse current is smaller than the forward current as expected. However, reverse current can become considerably larger than forward current when E_λ is negative to $E_{1/2}$. For the data shown at $E_\lambda = -0.912$ V, the

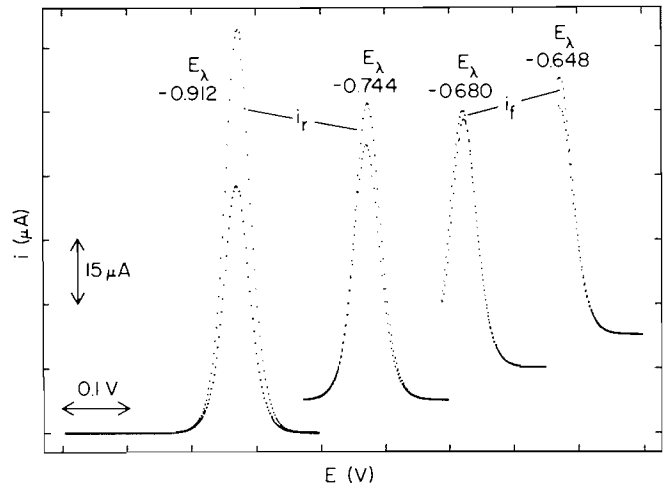

FIG. 8. Effect of reversal potential on differential polarograms. 1.00×10^{-3} *M* Cd(II), 1.00 *M* KCl, synchronization scheme [24], $E_s = -2$ mV, $\Delta E = 10$ mV, $E_{1/2} = -0.646$ V (sce), sweep rate = 0.0977 V/s, $t_d = 3.0$ s, $\beta_a = 0.125$, $\beta_b = 1$, $m = 0.00125$ g/s, $T = 23$°C.

reverse current is 63% higher than the forward current. This is due to a combination of drop growth and stripping from the spherical drop. For the reduction of Fe(III) under identical conditions where only drop growth is involved, the increase in reverse current over forward current is 33%. This phenomenon depends on sweep rate as well as reversal potential. As for ac polarography (9), amalgam formation does not affect the differential peak shape, with a half width of 90/n mV, or peak position on either the forward or reverse sweeps.

Acknowledgements

The authors thank the Faculty of Graduate Studies at Dalhousie University for financial support and Margaret-Anne Vaughan for obtaining some of the experimental data used. One of us (W.T.T.) wishes to thank the Universiti Pertanian Malaysia for granting study leave to pursue this research.

1. J. G. OSTERYOUNG and R. A. OSTERYOUNG. Anal. Chem. **57**, 101A (1985).
2. K. F. DRAKE, R. P. VANDUYNE, and A. M. BOND. J. Electroanal. Chem. **89**, 231 (1978).
3. V. GAJDA and K. HORÁK. Anal. Chim. Acta, **134**, 219 (1982).
4. K. OKAMOTO. Rev. Polarogr. Jpn. **12**, 40 (1964).
5. T. BIEGLER and H. A. LAITINEN. Anal. Chem. **37**, 572 (1965).
6. J. R. DELMASTRO and D. E. SMITH. Anal. Chem. **38**, 169 (1966).
7. D. E. SMITH. Anal. Chem. **38**, 347 (1966).
8. T. G. MCCORD, E. R. BROWN, and D. E. SMITH. Anal. Chem. **38**, 1615 (1966).
9. J. R. DELMASTRO and D. E. SMITH. Anal. Chem. **39**, 1050 (1967).
10. T. G. MCCORD and D. E. SMITH. Anal. Chem. **41**, 131 (1969).
11. A. M. BOND, R. J. O'HALLORAN, I. RUZIC, and D. E. SMITH. Anal. Chem. **48**, 872 (1976).
12. A. M. BOND, R. J. O'HALLORAN, I. RUZIC, and D. E. SMITH. Anal. Chem. **50**, 216 (1978).
13. A. M. BOND and K. B. OLDHAM. J. Electroanal. Chem. **158**, 193 (1983).
14. J. C. MYLAND and K. B. OLDHAM. J. Electroanal. Chem. **185**, 29 (1985).
15. K. TOKUDA, N. ENOMOTO, H. MATSUDA, and N. KOIZUMI. J. Electroanal. Chem. **159**, 23 (1983).
16. J. C. MYLAND, K. B. OLDHAM, and C. G. ZOSKI. J. Electroanal. Chem. **206**, 1 (1986).

Can. J. Chem. Downloaded from www.nrcresearchpress.com by 78.46.186.204 on 09/07/12
For personal use only.

17. J. GOODISMAN. J. Electroanal. Chem. **144**, 33 (1983).
18. J. O'DEA, M. WOJCIECHOUSKI, J. OSTERYOUNG, and K. AOKI. Anal. Chem. **57**, 954 (1985).
19. D. P. WHELAN, J. J. O'DEA, J. OSTERYOUNG, and K. AOKI. J. Electroanal. Chem. **202**, 23 (1986).
20. K. AOKI, K. TOKUDA, H. MATSUDA, and J. OSTERYOUNG. J. Electroanal. Chem. **207**, 25 (1986).
21. L. RAMALEY and M. S. KRAUSE, JR. Anal. Chem. **41**, 1362 (1969).
22. J. H. CHRISTIE, J. A. TURNER, and R. A. OSTERYOUNG. Anal. Chem. **49**, 1899 (1977).
23. S. C. RIFKIN and D. H. EVANS. Anal. Chem. **48**, 1616 (1976).
24. L. RAMALEY and W. T. TAN. Can. J. Chem. **59**, 3326 (1981).
25. L. RAMALEY. Chem. Instrum. **6**, 119 (1975).
26. L. RAMALEY and D. P. SURETTE. Chem. Instrum. **8**, 181 (1978).
27. G. A. BRYDON and K. B. OLDHAM. J. Electroanal. Chem. **122**, 353 (1981).
28. J. R. WOLBERG. Prediction analysis. D. VanNostrand Co. Inc., Princeton, NJ. 1967.
29. L. RAMALEY. Anal. Instrum. **15**, 101 (1986).
30. M. L. OLMSTEAD and R. S. NICHOLSON. Anal. Chem. **38**, 150 (1966).
31. J. C. MYLAND, K. B. OLDHAM, and C. G. ZOSKI. J. Electroanal. Chem. **193**, 3 (1985).
32. P. DELAHAY. New instrumental methods in electrochemistry. Interscience Publishers, New York. 1954.
33. R. DANIELSSON, P. BAECKLUND, and A. KÄLLSTRÖM. Anal. Chim. Acta, **158**, 305 (1984).

Can. J. Chem. Downloaded from www.nrcresearchpress.com by 78.46.186.204 on 09/07/12
For personal use only.

Appendix

For electrode reaction [1] Fick's second law of diffusion for spherical symmetry can be written (32)

$$[28] \quad \frac{\partial v(r,t)}{\partial t} = D_O \frac{\partial^2 v(r,t)}{\partial r^2}$$

where r is the radial distance from the centre of the electrode and

$$[29] \quad v = rC_O$$

where C_O is the concentration of the oxidized component.

The initial and boundary conditions that prevail are as follows:

$$[30] \quad C_O = C^* \qquad \text{for } t < 0$$

$$[31] \quad C_O \rightarrow C^* \qquad \text{as } r \rightarrow \infty \qquad \text{for } t \geqq 0$$

and at $r = r_0$,

$$C_O = C_1 \qquad 0 < t < t_1$$
$$C_O = C_2 \qquad t_1 < t < t_2$$
$$\vdots$$
$$C_O = C_j \qquad t_{j-1} < t$$

These can be reformulated as

$$[32] \quad C_O = \sum_{k=1}^{j} I_k C_k \qquad \text{at } r = r_0$$

where $I_1 = 1$ for $0 < t < t_1$, zero otherwise, $I_2 = 1$ for $t_1 < t < t_2$, zero otherwise, etc.

For use with the variable, v, [30], [31], and [32] become

$$[33] \quad v = v^* = rC^* \qquad \text{for } r \geqq r_0,\ t < 0$$

$$[34] \quad v \rightarrow v^* \qquad \text{as } r \rightarrow \infty \qquad \text{for } t \geqq 0$$

$$[35] \quad v = \sum_{k=1}^{j} I_k v_k \qquad \text{at } r = r_0$$

Solution is achieved by transforming [28], [33], [34], and [35] into Laplace space, where [28] becomes a simple differential equation. The resulting equation is solved for the transformed variable, $\bar{v}$, and then reverse transformed. After substitution of [29] the result is

$$[36] \quad C_O = C^* + \frac{r_0}{r}\sum_{k=1}^{j}(C_k - C_{k-1}) + \frac{r_0}{r}\sum_{k=1}^{j}(C_{k-1} - C_k)\,\text{erf}\left(\frac{r - r_0}{2D_O^{1/2}(t - t_{k-1})^{1/2}}\right)$$

where $C_{k=0}$ is C^* and $t_{k=0}$ is zero.

The Laplace transformations require the use of the unit finite impulse function or Heaviside unit function. Danielsson *et al.* (33) have questioned the use of this function (or the superposition principle) in the derivation of equations for use in pulse voltammetry. They conclude that its application is valid as long as the electrochemical system can be separated into a potential dependent part which may be non-linear and a linear part. These conditions prevail here. As usual, current is obtained from Fick's first law of diffusion

$$[37] \quad i = nFAD_O(\partial C_O/\partial r)_{r=r_0}$$

Application of [37] to [36] provides

$$[38] \quad i_j = \frac{nFAD_O^{1/2}}{\pi^{1/2}}\sum_{k=1}^{j}\frac{(C_{k-1} - C_k)}{(t - t_{k-1})^{1/2}} + \frac{nFAD_O(C^* - C_j)}{r_0}$$

As long as both halves of the redox couple are soluble in the solution, the electrode reaction is reversible, and $D_O = D_R$, the concentrations at the electrode surface are a function only of the applied potential (6) and are not influenced by prior potentials. Under these circumstances

$$[39] \quad C_k = \frac{C^*(\exp[(E_k - E_{1/2})nF/RT])}{1 + \exp[(E_k - E_{1/2})nF/RT]} = C^*Q_k$$

which leads to

$$[40] \quad i_j = \frac{nFAD_O^{1/2}C^*}{\pi^{1/2}}\sum_{k=1}^{j}\frac{Q_{k-1} - Q_k}{(t - t_{k-1})^{1/2}} + \frac{nFAD_OC^*(1 - Q_j)}{r_0}$$

Average current is obtained by applying the law of the mean to [40] resulting in

$$[41] \quad (i_j)_{av} = \frac{2nFAD_O^{1/2}C^*}{\pi^{1/2}(t_b - t_a)}\sum_{k=1}^{j}[(t_b - t_{k-1})^{1/2} - (t_a - t_{k-1})^{1/2}](Q_{k-1} - Q_k) + \frac{nFAD_OC^*(1 - Q_j)}{r_0}$$

Equations [40] and [41] are completely general in that any potential or time sequence may be applied without regard to symmetry in either sequence. When a pulse train, symmetric in time, is employed (this case includes SDSWP and SWV, among other techniques) the following equations apply:

$$[42] \quad t_{k-1} = (k - 1)\tau \qquad \text{for all cases}$$

$$[43] \quad t = (j - 1 + \beta)\tau \qquad \text{for instantaneous current}$$

$$[44] \quad t_a = (j - 1 + \beta_a)\tau \qquad \text{for average current}$$

$$[45] \quad t_b = (j - 1 + \beta_b)\tau \qquad \text{for average current}$$

On appropriate substitution of the above into [40] and [41], eqs. [16] and [17] result.

Analytical chemists and dinosaurs

R. R. BROOKS
Department of Chemistry and Biochemistry, Massey University, Palmerston North, New Zealand

Received September 28, 1986

This paper is dedicated to Professor Douglas E. Ryan on the occasion of his 65th birthday

R. R. BROOKS. Can. J. Chem. **65**, 1033 (1987).

The role of the analytical chemist in the development of the extraterrestrial impact theory for mass extinctions at the terminal Cretaceous Period is reviewed. High iridium concentrations in Cretaceous/Tertiary boundary clays have been linked to a terrestrial impact from an iridium-rich asteroid or large meteorite some 65 million years ago. Other evidence in favour of the occurrence of such an impact has been provided by the detection of shocked quartz grains originating from impact and of amorphous carbon particles similar to soot, derived presumably from wordwide wildfires at the terminal Cretaceous. Further evidence provided by the analytical chemist involves the determination of isotopic ratios such as $^{144}Nd/^{143}Nd$, $^{187}Os/^{186}Os$, and $^{87}Sr/^{86}Sr$. Countervailing arguments put forward by the gradualist school (mainly palaeontological) as opposed to the catastrophists (mainly chemists and geochemists) are also presented and discussed.

R. R. BROOKS. Can. J. Chem. **65**, 1033 (1987).

On présente une revue du rôle joué par les analystes dans le développement de la théorie des impacts extraterrestes sur les extinctions en masse qui se sont produites à la fin de la période crétacée. On a lié le fait que l'on retrouve des concentrations élevées d'iridium dans les argiles du limite entre les périodes crétacée et secondaire à une collision qui se serait produite il y a environ 65 millions d'années entre la terre et un astéroïde ou un gros météorite riche en iridium. D'autres indications en faveur d'une telle collision sont fournis par la détection de grains de quartz commotionnés provenant de cet impact ainsi que de particules amorphes de charbon, semblables à celles de la suie, qui pourraient provenir de feux grégeois qui se seraient produits au niveau mondial à la fin de la période crétacée. D'autres indications proviennent de résultats obtenus par les analystes lors de la détermination des rapports isotopiques $^{144}Nd/^{143}Nd$, $^{187}Os/^{186}Os$ et $^{87}Sr/^{86}Sr$. On présente et on discute aussi des arguments mis de l'avant par l'école gradualiste (principalement paléontologique) qui est en opposition à l'école des catastrophistes (principalement des chimistes et des géologues).

[Traduit par la revue]

Introduction

A famous benchmark paper by Alvarez *et al.* (1) in 1980 ushered in a new era of research (and controversy) concerning events which may have occurred on earth some 65 million years ago at the end of the Cretaceous period. One day in 1977 outside the town of Gubbio in the Italian Appennines, Walter Alvarez of the Berkeley campus of the University of California found a layer of clay that clearly marked the end of the fossil-rich Cretaceous limestone and the beginning of the fossil-poor Tertiary limestone that overlaid it. This layer corresponds to the Cretaceous–Tertiary (K–T) boundary and will be so designated in this review. Alvarez's father, the Nobel Laureate Luis Alvarez, had the clay analysed by analytical chemists Frank Asaro and Helen Michel at Berkeley, and found up to 8 ng/g (ppb) iridium in the sample (1): i.e. about 30 times the background level. Later, further iridium anomalies were detected in K–T boundary clays from Stevns Klint, Denmark, and from Woodside Creek, New Zealand (1).

Because iridium is abundant in meteorites (and in the earth's mantle), but rare in crustal rocks, it was proposed that the earth had been struck by a large (10 km diameter) chondritic (with character of stony meteorites) asteroid or meteorite. It was further suggested that this impact caused the ejection of a vast amount of dust that stayed in the atmosphere for about 6 months, resulting in the blotting out of the sun's rays with consequent cessation of photosynthesis, breakdown of food chains, and the extinction of 70% of all life forms on earth, including the dinosaurs.

It is probable that public interest in the subject has been stimulated precisely because such large and extravagant life forms such as dinosaurs had been involved. The ammonites were also rendered extinct but their demise has not captured the public imagination to any degree. It is also noteworthy that the

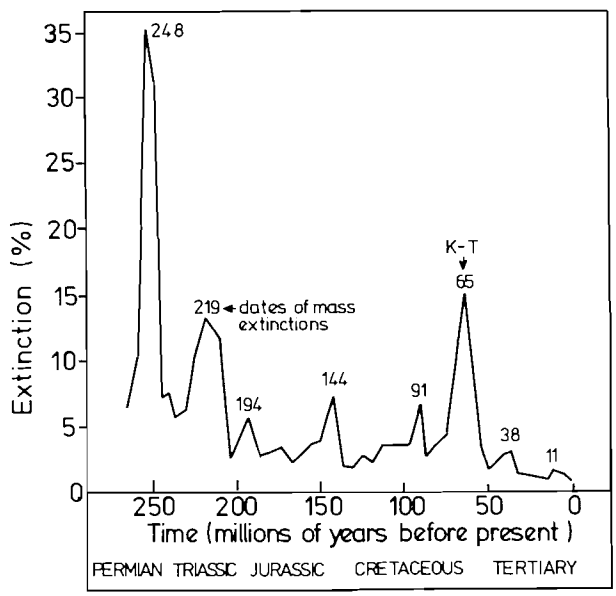

FIG. 1. Disappearance of families of marine animals from the fossil record (2). Copyright 1986 by the American Association for the Advancement of Science. Reprinted by permission.

K–T extinctions are by no means the greatest to have occurred. The Permian–Triassic (P–T) extinctions were far greater.

Some indication of the relative magnitude of past extinctions has been given by Raup and Sepkoski (2) who showed the existence of about eight of these events occurring in 26 million year (m.y.) cycles. These findings are shown in Fig. 1 but since they represent only marine families rather than individual taxa, the percentages are lower than would be obtained if the total of all biota were considered. For example, the 35% extinction

Printed in Canada

Can. J. Chem. Downloaded from www.nrcresearchpress.com by 78.46.186.204 on 09/07/12
For personal use only.

Can. J. Chem. Downloaded from www.nrcresearchpress.com by 78.46.186.204 on 09/07/12
For personal use only.

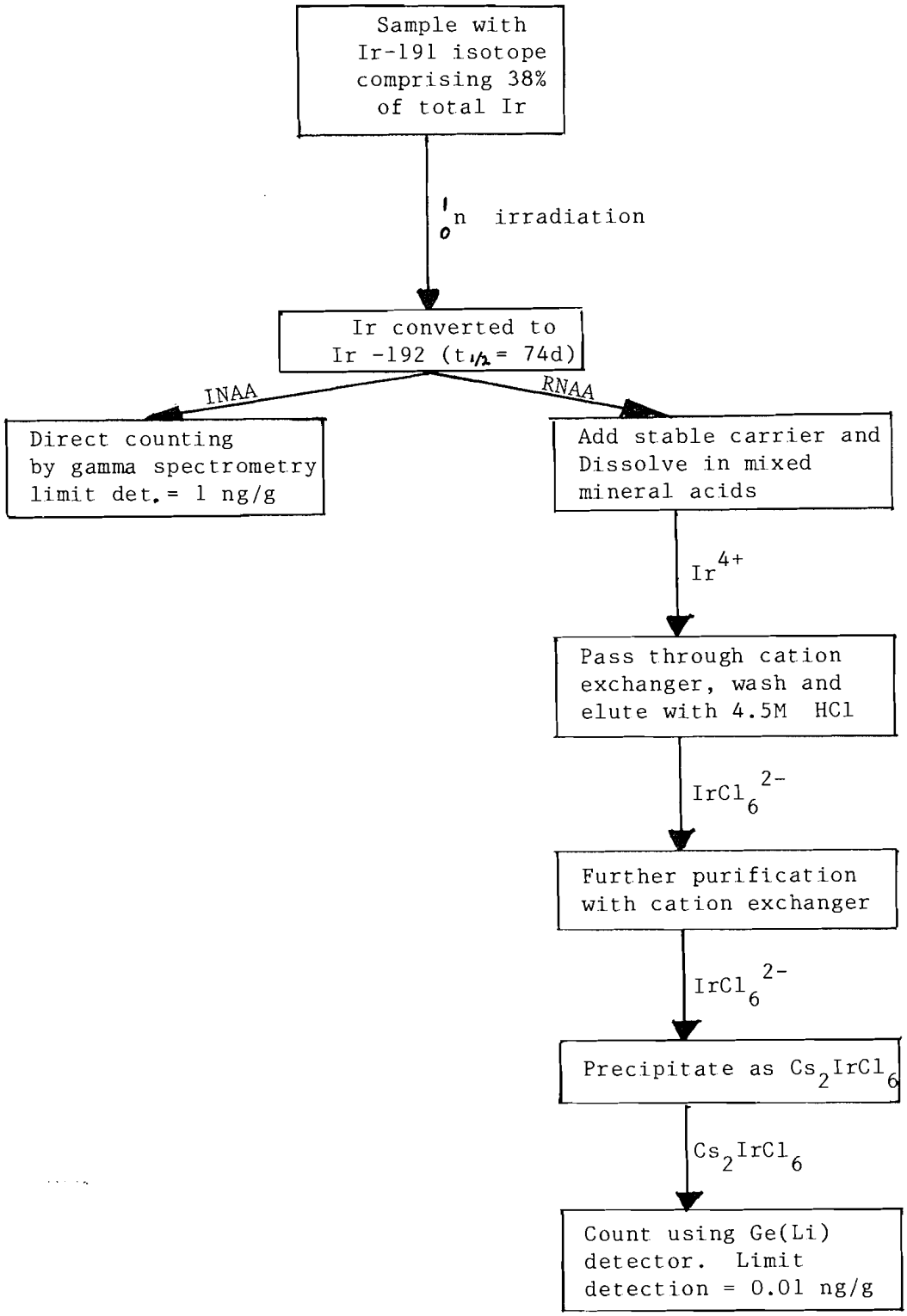

FIG. 2. Analytical scheme for determination of iridium by two types of neutron activation analysis.

of families at the P–T boundary represents 96% of all taxa involved. Using the data of Raup and Sepkoski, some scientists have proposed that the apparent periodicity of mass extinctions was caused by the sun having a dark companion ("Nemesis") with a 26 m.y. orbit. This star passing through the Oort cloud of comets every 26 m.y. would cause some to be dislodged from their regular orbits so that a shower of comets (rather than a single asteroid) would impact the earth at regular intervals. This theory will not be considered further since the chemical composition of cometary cores and asteroids are similar, and the nature of the bolide(s) is immaterial to the arguments which follow.

The original work of Alvarez *et al.* (1) has stimulated considerable research, discussion, and controversy worldwide, which in October 1981 resulted in a conference on the subject at Snowbird, Utah (3), in which perhaps as much heat as light was generated.

Some workers (4–6) have been strongly critical of the

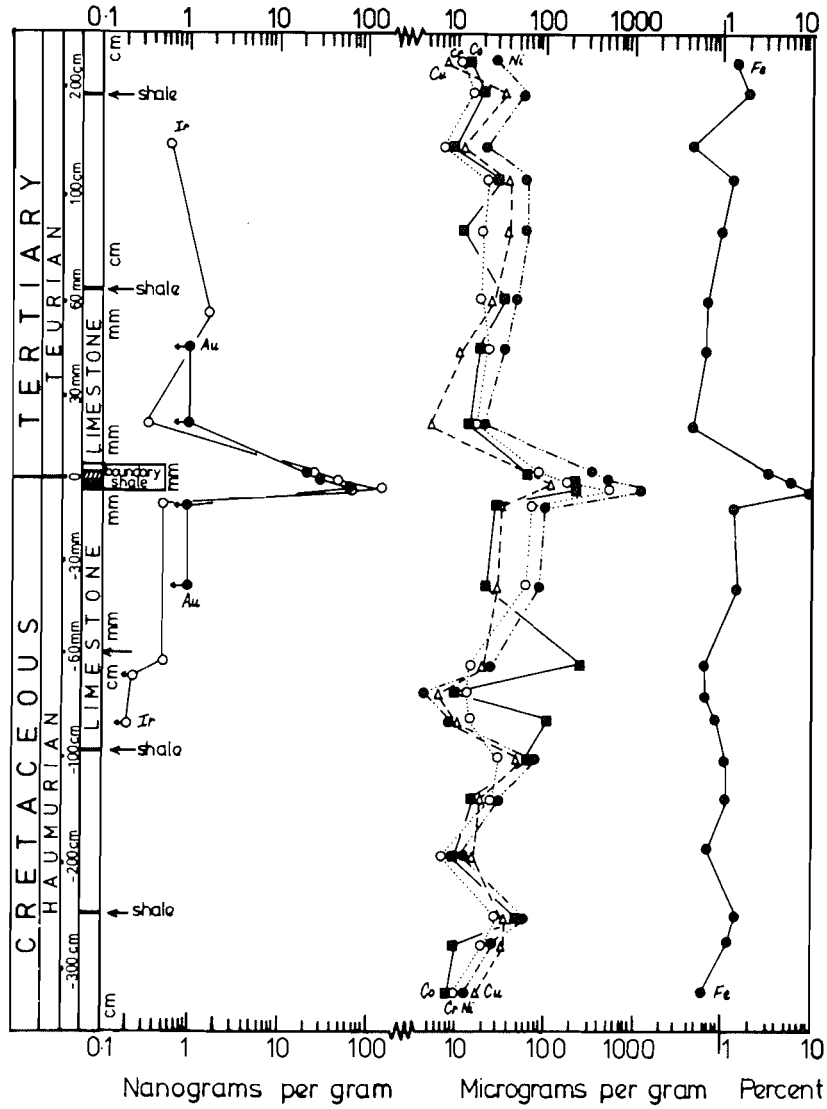

FIG. 3. Concentrations of siderophile elements (decalcified basis) in K–T boundary clays from Woodside Creek, New Zealand (7). Copyright 1984 by the American Association for the Advancement of Science. Reprinted by permission.

TABLE 1. Iridium abundances (ng/g) in various rock types

Rock type	Iridium content
K–T boundary clays	1–130
Crustal rocks	0.02–0.1
Upper mantle	1–8
Ocean floor basalts	0.001–0.1
Terrestrial impact melts	0.02–70
Lunar magmatic rocks	0.001–0.1
Lunar impact rocks	0.02–70
Chondrites (stony meteorites)	200–1000
Siderites (iron meteorites)	0.1–100 000 (0.01%)

Alvarez theory, but evidence is accumulating that an impact probably did occur on earth some 65 m.y. ago, though it may not have been partially or totally responsible for mass extinctions at this time. The evidence of such a collision having taken place has resulted mainly from the work of analytical chemists and it is therefore appropriate that the subject should be reviewed in this journal. It is also fitting that the review should appear in an issue in honour of D. E. Ryan since he himself has been involved in these studies.

Evidence for an impact at the terminal Cretaceous can be divided into four main categories of studies on K–T boundary clays. These are (*1*) the presence of anomalously-high iridium concentrations; (*2*) mineralogical studies showing the presence of shocked quartz grains and of extraterrestrial material; (*3*) the presence of amorphous carbon particles of similar morphology to soot; (*4*) the existence of isotopic ratios (such as $^{187}Os/^{186}Os$) indicating an extraterrestrial origin for some of the constituents of boundary clays. The following review will be concerned mainly with these four categories of evidence.

The iridium anomaly

The abundance of iridium in various rock types is summarised in Table 1. Clearly, concentrations of this element in meteorites are very much higher than in the earth's crust or even in its upper mantle.

Until recently, iridium was almost always determined by neutron activation analysis and this is still the most popular method, though it is being replaced to some extent by plasma source mass spectrometry (see below). An analytical scheme for neutron activation is given in Fig. 2. There are two main procedures which may be followed. The first of these is

Can. J. Chem. Downloaded from www.nrcresearchpress.com by 78.46.186.204 on 09/07/12
For personal use only.

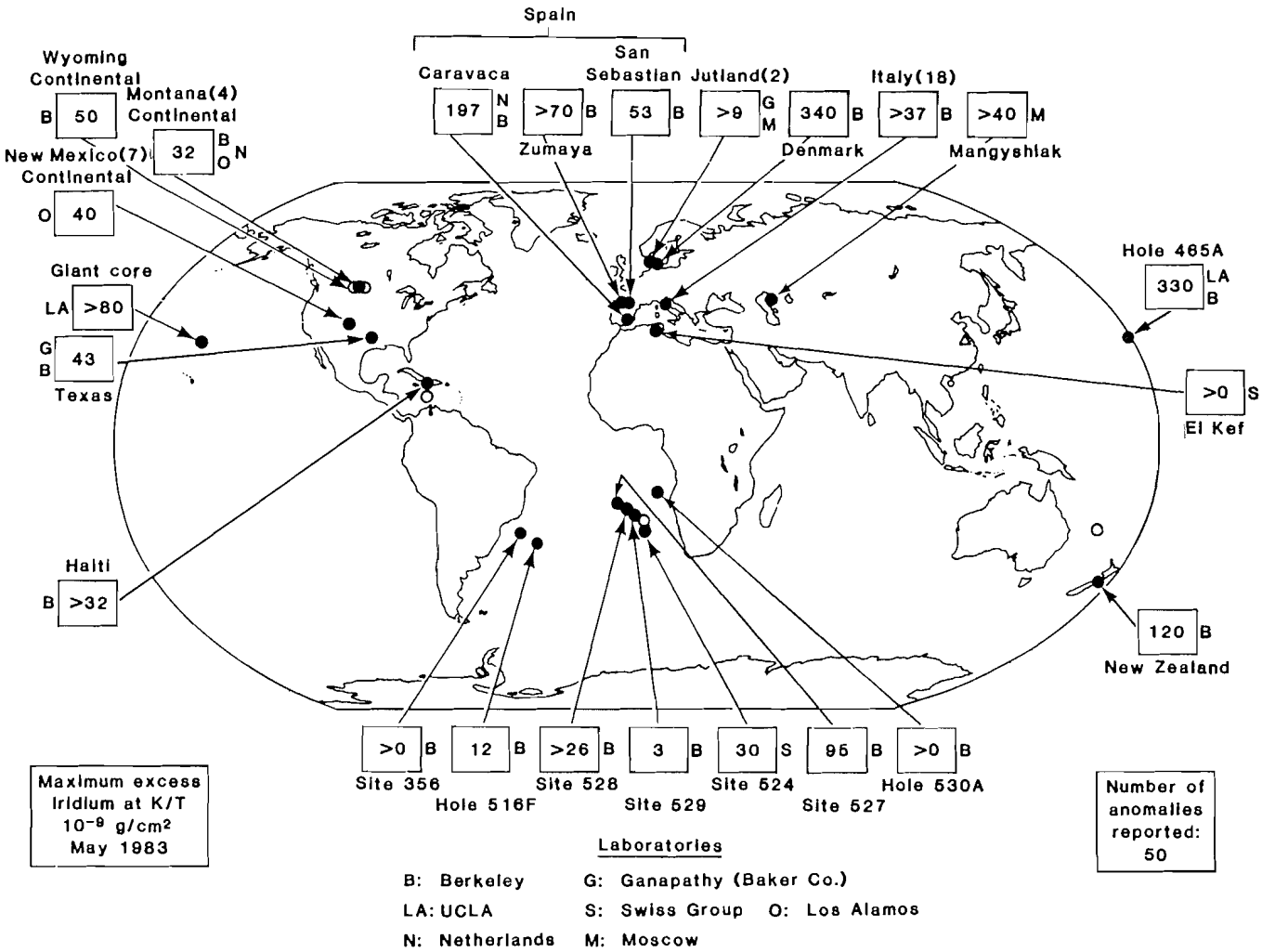

FIG. 4. Distribution of K–T boundary sites containing anomalously high iridium concentrations (8). Copyright 1984 by the American Association for the Advancement of Science. Reprinted by permission.

instrumental neutron activation (INAA) in which the sample is irradiated with neutrons to convert stable ^{191}Ir to radioactive ^{192}Ir (half life of 74 days). After an appropriate cooling period, the activity of the isotope is determined by γ spectrometry. The limit of detection is about 1 ng/g (ppb). For lower iridium concentrations, recourse has to be made to radiometric neutron activation (RNAA) in which the sample is first irradiated and then a stable carrier of ^{192}Ir is added. The sample plus carrier is then dissolved in a mixture of mineral acids ($HNO_3/HF/HClO_4$) so that the iridium is converted to the Ir^{4+} state. The solution is passed through a cation exchanger to absorb the iridium. After washing, the iridium is eluted with hydrochloric acid as the anionic $IrCl_6^{2-}$ complex. Following a further stage of purification in a second cation exchanger, the iridium is precipitated as Cs_2IrCl_6. The precipitate is filtered and dried and its activity measured. The detection limit is about 10 pg/g (ppt). It is clear that without the help of the analytical chemist, this work on iridium would have been impossible to carry out, as it is only in the past 10 years that neutron activation techniques have become sufficiently sensitive to determine iridium at the sub-ppb level. It should also be mentioned that the only reason that iridium was used as a marker for K–T impacts was because it is the most readily determined of all the platinum metals. The others are also present in K–T boundary clays with about the same abundance, but their limits of detection are higher than for iridium.

Apart from iridium, there are usually elevated concentrations of other siderophile (iron-loving) elements in K–T boundary clays. Examples of these are cobalt, chromium, and nickel. This is illustrated in Fig. 3 which gives abundance data for the Woodside Creek K–T sequence in New Zealand (7). It should be noted that it is customary to present data on a decalcified ($CaCO_3$-free) basis. This is to avoid criticisms that the elevated levels are merely due to subsequent dissolution of limestone after the initial deposition.

Since the original discovery of anomalous iridium levels in K–T boundary clays at Gubbio, Stevns Klint, and Woodside Creek, over 70 other such occurrences have been recorded worldwide including Alberta and Saskatchewan (37). The distribution of these anomalies, recorded worldwide (8), is shown in Fig. 4. It is particularly noteworthy that only one of these sites is on land in the Southern Hemisphere (Woodside Creek in New Zealand). Further investigations in New Zealand have resulted in the identification of four more K–T boundary sites with anomalously-high iridium levels (9, 10). It is usually more meaningful to express values as integrated mass of iridium per cm^2 of earth surface (ng/cm^2). This system has been used in Fig. 4. The most recent discovery of a K–T boundary in New Zealand (Flaxbourne River) gives an integrated iridium signature of nearly 150 ng/cm^2 (10). There is no apparent trend in the data of Fig. 4 which would indicate a specific location for the original impact. Since the oceans cover 70% of the earth's

Can. J. Chem. Downloaded from www.nrcresearchpress.com by 78.46.186.204 on 09/07/12
For personal use only.

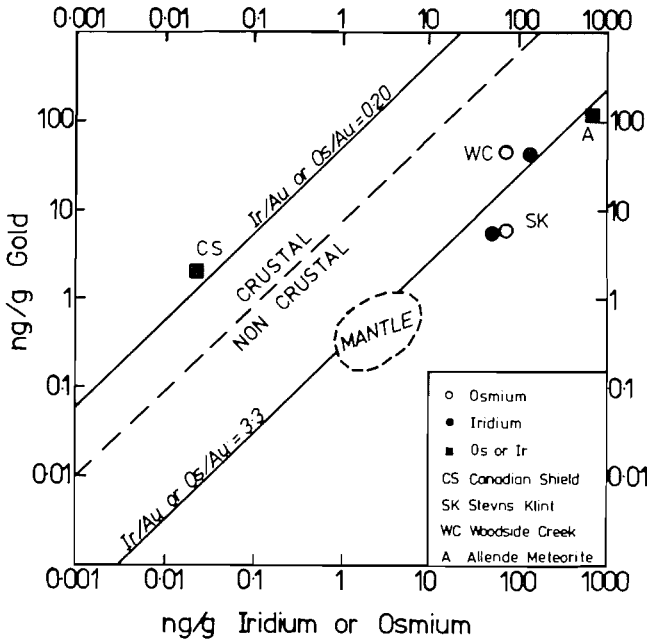

FIG. 5. Plots of gold vs. iridium or osmium in crustal, meteoritic, and K–T boundary material. CS = mean for Canadian Shield, SK = Stevns Klint, WC = Woodside Creek, A = Allende carbonaceous chondrite (25). Copyright 1986 by Macmillan Journals Ltd. Reprinted by permission from Nature, vol. 322, pp. 816, 817.

surface however, this impact is likely to have occurred in the sea and a crater would be hard to discover.

One of the earlier critics of the Alvarez theory (4) suggested that the iridium in the K–T boundary clays could have been derived from the water column itself during a period of unusual ocean chemistry. However, discoveries of iridium anomalies in a continental K–T section in New Mexico (11, 12) have answered this objection.

Because of the very low iridium levels in boundary clays, extreme care has to be taken to avoid contamination during the analytical procedures. For example, an iridium "anomaly" was once reported for samples handled by an analyst wearing a platinum ring with 10% iridium (8). We ourselves have noticed a distinct memory effect for osmium determinations after successive fusions in a zirconium crucible which appeared to be otherwise clean.

Despite vehement criticisms from some quarters, a broad concensus is emerging, at least among geochemists, that the elevated iridium levels found at most K–T boundary sites probably resulted from an impact (or impacts) with extraterrestrial material during the terminal Cretaceous. The possibility of the iridium having been derived from volcanic activity remains a distant option. The lava of deep-seated volcanoes does indeed contain iridium, but the levels are so low that vulcanism on an unimaginable scale would have had to have occurred to account for present levels of this element in boundary clays.

A useful geochemical "signature" in geological materials is the Ir/Au ratio. From Fig. 5 it will be noted that a ratio of 0.2 is typical of crustal rocks whereas extraterrestrial material clusters around a value of 3.3 The same is true of the Os/Au ratio.

Because of the great expense of neutron activation procedures, particularly RNAA, it is advisable for analysts to screen samples by first determining marker elements such as cobalt, chromium, and nickel which can be readily quantified by atomic absorption (AAS) or plasma emission (ICP) spectrometry. Only samples with anomalous concentrations of all or some of these elements will then need to be analysed for iridium.

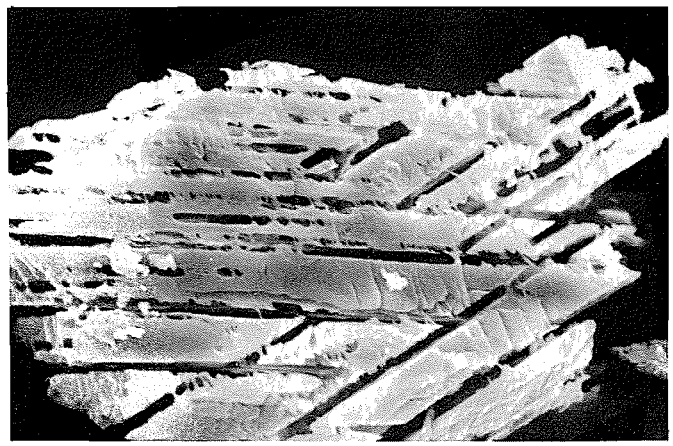

FIG. 6. Photograph of shocked quartz grain (30 μm × 20 μm) — courtesy of B. F. Bohor.

Shocked quartz and magnesioferrite

The second piece of evidence that an impact may have occurred on earth 65 m.y. ago has been provided by the discovery of shocked quartz grains in K–T boundary clays (13–16). Shocked quartz is usually associated worldwide with meteoritic impact craters. The grains have characteristic lamellar features as is shown in Fig. 6. The grains are isolated by removing the clay fraction by washing with water. The residual quartz is etched with hydrofluoric acid and examined under a scanning electron microscope (SEM). The worldwide abundance, maximum grain size, and distribution of shocked quartz has also been studied (15) and is shown in Fig. 7. The map shows the continents as they were at the terminal Cretaceous. There is a clear trend for maximum grain size and abundances to be greatest in North America and to show a steady decrease in a southeasterly direction with minimum values in New Zealand. This trend seems to indicate that the impact may have occurred in the vicinity of North America, since the larger grains should have deposited closest to the impact site. The ratio of shocked to unshocked quartz grains also shows a decrease along the southeast-trending direction.

The presence of extraterrestrial magnesioferrite at the K–T boundary at Caravaca in Spain and Umbria in Italy has also been demonstrated (17, 18). Material from the former site was washed to remove clay particles and the ferromagnetic material was removed with a magnetic separator. The composition of the separated material was similar to that of magnetic alloys injected into rocks in impact craters.

Soot particles in K–T boundary material

Further evidence favouring an asteroidal/meteoritic impact during the terminal Cretaceous has been provided by work at the University of Chicago (19, 20). Clay samples from three K–T boundary sites contained 0.36–0.58% graphitic carbon, morphologically similar to soot particles. It was proposed that the soot was derived from worldwide forest fires following the event. This amount of soot (0.021 g/cm^2) would have greatly enhanced the "winter" caused by dust particles in the atmosphere. A very good correlation between iridium levels and the abundance of soot paricles has also been demonstrated (20).

The findings of the Chicago group were hotly disputed by

Can. J. Chem. Downloaded from www.nrcresearchpress.com by 78.46.186.204 on 09/07/12
For personal use only.

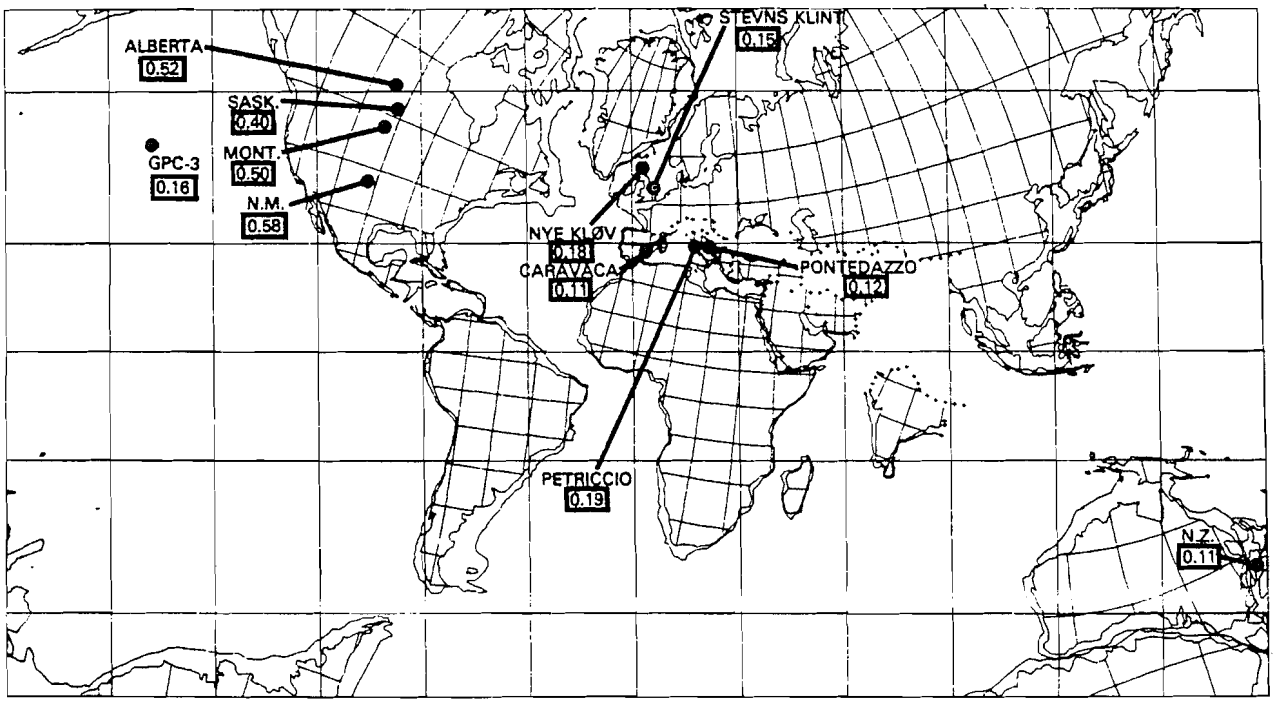

FIG. 7. Geographical distribution of shocked quartz grains in K–T boundary sites throughout the world. Values are maximum grain size and the continents are shown as they were at the K–T transition time (15).

some other scientists (21) who suggested that the high carbon content of the Stevns Klint material resulted from dissolution of the limestone (condensed section). The same mechanism would account for both the high carbon and iridium contents. In a rebuttal of these arguments (22), it was pointed out that redissolution of the carbonate layer would have required condensation of a 600 m thickness of rock to only 10 mm, and that the original limestone would have had to have contained 99.95% calcium carbonate.

Isotopic studies

Further compelling evidence for the past occurrence of an impact at the terminal Cretaceous has again been provided by the analytical chemist. The ratio $^{187}Os/^{186}Os$ is diagnostic of rock type. The ratio of these two isotopes in cosmic material 4.5×10^9 years BP (before present) is believed to have been 0.8:1.0. The ratio is now about 1.0:1.0 in material which has been cycled through the mantle due to production of ^{187}Os from decay of the long-lived isotope ^{187}Re. The earth's crust is, however, greatly enriched in rhenium compared with osmium so that the decay process has resulted in a much greater abundance of ^{187}Os in crustal rocks a ratio of about 26–30:1. Figure 8 shows the range of values which would have resulted within the limits of 2.0–3.8 billion years BP for the probable separation of the earth's crust from the mantle.

The original work on the osmium isotopes (23) was carried out by use of an ion probe mass spectrometer in which the sample surface is bombarded with a fast-moving ion beam which dislodges atoms and ions from the sample as gas phase species. The secondary ions then pass through a mass spectrometer. The technique is highly sensitive and permits analyses at the ng/g level. $^{187}Os/^{186}Os$ isotopic ratios of about 8 have been reported for oceanic manganese nodules (i.e. material derived from the sea water column) and 1.3 to 1.6 for K–T boundary clays (13).

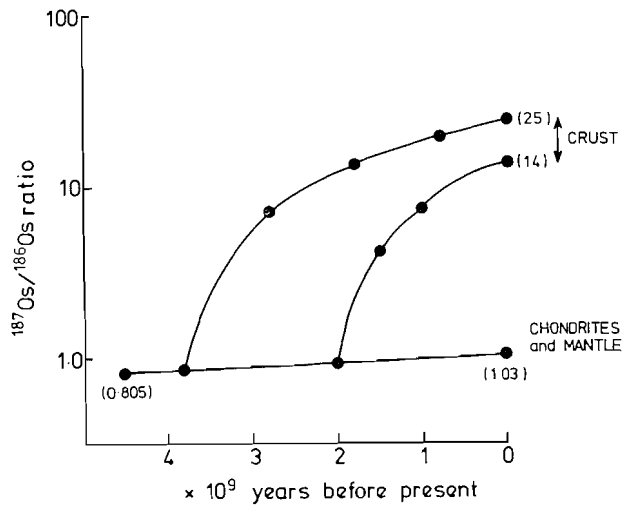

FIG. 8. $^{187}Os/^{186}Os$ ratios in chondritic meteorites, and the earth's mantle and crust expressed as a function of age — courtesy of R. D. Reeves.

A new analytical tool has been developed which offers great promise for determining isotopic ratios in geological materials. This is plasma source mass spectrometry (ICP-MS) in which an inductively-coupled plasma source is fed directly into a quadrupole mass spectrometer (24). Abundances of a large number of isotopes can be obtained very quickly and with very low detection limits (ca. 1 ng/mL). The technique has been used to determine the $^{187}Os/^{186}Os$ ratio in K–T boundary clay from New Zealand (25) for which a value of 1.12 was obtained. The same procedure was used to determine total osmium which is difficult to determine sensitively by IANA. As shown in Fig. 3, the Os/Au ratio afforded yet another means of determining extraterrestrial components of K–T boundary

Can. J. Chem. Downloaded from www.nrcresearchpress.com by 78.46.186.204 on 09/07/12
For personal use only.

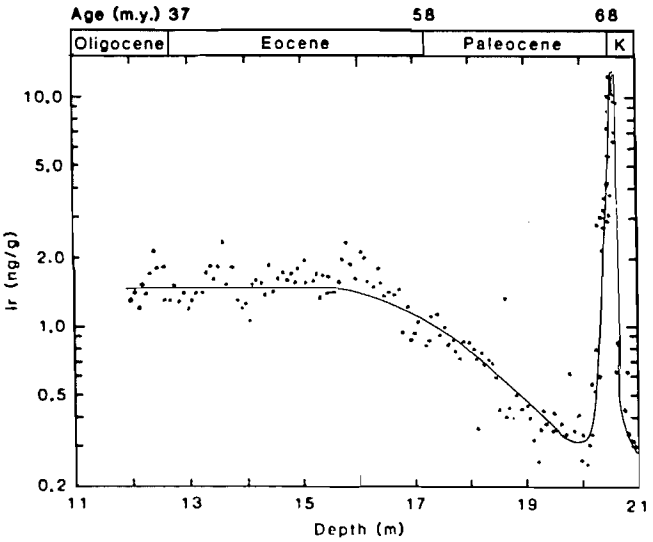

FIG. 9. Profile of iridium concentrations in a Pacific core. The only significant positive anomaly is at the K–T transition (34). Copyright 1986 by the American Society for the Advancement of Science. Reprinted by permission.

material. The ratio lies along the 3.3 isoratio line and the values are clustered close to those for the Allende carbonaceous meteorite. Though mantle rocks lies along the same line, values are clustered to the centre of the plot and do not overlap those for the K–T boundary clay.

The simplicity, cheapness, and very high sensitivity of the ICP-MS technique renders it a suitable alternative and competitor to neutron activation procedures for determining elements at very low abundances, though it does suffer from the disadvantage of requiring a solution rather than a solid.

Other isotopic ratios which may be used to establish the origin of material in K–T boundary clays are $^{143}Nd/^{144}Nd$ and $^{87}Sr/^{86}Sr$ (26). Recent isotopic studies at the Caravaca K–T marine sequence in Spain shows that the boundary clay was of terrestrial rather than of marine origin. This indicates fallout from dust ejected into the atmosphere.

Summary of evidence for an impact at the terminal Cretaceous

Because of the continuing discussion concerning the reality of an impact (or impacts) at the terminal Cretaceous (a paper by Alvarez (36) is a useful source for this), it will now be appropriate to first review the evidence in favour of such an event.

1. Iridium and other noble metals are enriched up to 1000-fold at the K–T boundary at more than 70 sites worldwide (8).

2. $^{187}Os/^{186}Os$ ratios, though not ruling out the possibility of a mantle source, indicate the probability of an extraterrestrial source for this element (25).

3. $^{144}Nd/^{143}Nd$ and $^{87}Sr/^{86}Sr$ ratios indicate a terrestrial origin for the clay found in K–T marine sections, thus pointing to aerial fallout as a source (26).

4. The presence of soot particles in K–T boundary material, which may have originated from worldwide fires after an impact (19).

5. Shocked quartz (13–16) and spherules resembling microtektites (27) have been found in K–T boundary clays.

The countervailing arguments by proponents of gradualism rather than catastrophism have been based on four main arguments:

1. Iridium in boundary clays was accumulated from the sea water column (4).

2. The iridium anomaly may have been derived from dissolution of limestone and in any case the iridium input may not have been constant over geological time (6).

3. Vulcanism may have been a source of iridium since it is known that this element can be found in lava and other volcanic emanations (28).

4. Shocked quartz is not necessarily always associated with impacts.

An answer to the first and second of these arguments has already been given above. As regards the third argument, vulcanism could indeed be a source of some of the iridium, but to have provided enough of this element to give the concentrations found uniformly worldwide in boundary clays, would have involved a degree of volcanic activity far beyond human comprehension. Even the basalts of the Deccan Traps in India, proposed by some to have been a source of such iridium, contain only 0.005 ng/g of this element.

As regards the final argument, a few shocked quartz grains have apparently been found in a volcanic formation (29). The discoverers do, however, admit that the abundance of these grains is very low and have ascribed this to annealing of shocked particles due to the high temperature involved. The same arguments must however also apply to shocked quartz associated with a K–T impact: i.e. if annealing does occur, the abundances of these grains at K–T sites would have been even greater than recorded, since the energy involved in the impact is many orders of magnitude greater than that of any volcanic event. It is always possible to find some support in favour of negation of any well-tried theory. For example, dinosaur bones have been reported from Hell Creek, Montana, in a stratum some 1.3 m above the putative K–T boundary (30). This has been advanced as proof that dinosaurs outlived the terminal Cretaceous. Other workers have, however, pointed out that the strata at Hell Creek are too muddled and reworked by ancient streams for any great credence to be placed on the observations. If the recent finding of shocked quartz in a volcanic environment is not to attract this same lack of credence, many more findings and observations will have to be made before current thinking on the origin of shocked quartz is to be seriously challenged.

Evidence for iridium anomalies at non-K–T boundaries

Since the original discovery of elevated iridium levels at the K–T boundary, there has been an active interest in finding such anomalies at other geological boundaries involving the transition from one period to another. The oldest boundary at which an anomaly has been found is at the junction of the Frasnian–Fammenian stages of the Devonian (365 m.y. BP). A value of 0.3 ng/g has been reported for material from this boundary (31). Though this is low, the iridium value is several times higher than local background. The iridium is, however, said to have been scavenged by a fossil cyanobacterium, *Frutexites* sp., and does not represent aerial contribution from an impact.

Mass extinctions at the Ordovician/Silurian (O–S) boundary (435 m.y. BP), when 22% of all marine families became extinct, are second in magnitude only to those of the Permian–Triassic (P–T) transition. In a thorough study of iridium and other elements in O–S boundary material from Anticosti Island, Quebec (32), anomalous iridium levels (60 pg/g) were indeed found. However, when expressed on a decalcified basis, the

Can. J. Chem. Downloaded from www.nrcresearchpress.com by 78.46.186.204 on 09/07/12
For personal use only.

Can. J. Chem. Downloaded from www.nrcresearchpress.com by 78.46.186.204 on 09/07/12
For personal use only.

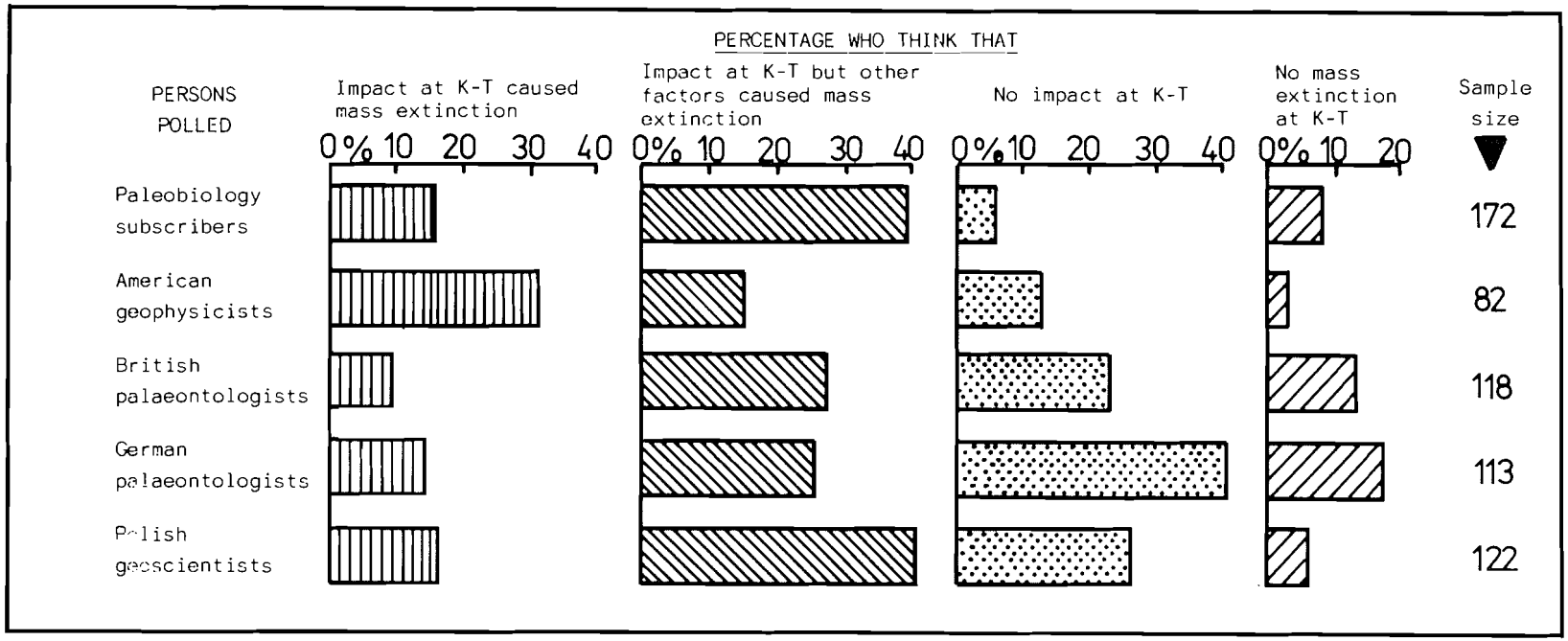

FIG. 10. Results of a poll of opinions among scientists carried out in 1984. Percentages do not add up to 100 because many respondents did not have an opinion (35). Reprinted by permission of Geology and the senior author.

levels were no longer anomalous. There is therefore no evidence for an impact to have occurred on earth at this time.

A claim by a Chinese group to have discovered 8 ng/g iridium at the P–T boundary (33) was apparently based on erroneous analytical techniques, though the work was reported in good faith. There are at present no reliable data supporting an iridium anomaly at this boundary.

Our knowledge of iridium levels in rocks whose ages span the period 33–67 m.y. BP: i.e. late Cretaceous and younger, has been enhanced by a recent paper (34) which presents data for iridium abundances in 149 samples from a continuous 9 m Pacific core of abyssal clay. The data are given in Fig. 9. Background iridium deposition fell to 0.3 ng/g in the Paleocene and rose to a maximum of 1.7 ng/g in the Eocene. A well-defined peak occurred only at the terminal Cretaceous. The annual global influx of meteoritic material is calculated at 78 000 tonnes. Superficially it seems that the K–T boundary represents the only significant impact event during this period, but it must be remembered that the samples were taken at average intervals of 6 cm, and much finer sampling would have been needed to detect smaller iridium anomalies.

Current status of the impact theory

As to whether or not there is general concensus among scientists about the reality of an asteroidal/meteoritic impact some 65 m.y. ago, depends on who is consulted. It will be very obvious that nearly all the evidence in favour of such an event having occurred is chemical. The analytical chemist is therefore ranged against some palaeontologists in a continuing controversy. This is illustrated (Fig. 10) by a recent survey (35) of opinions from scientists of different disciplines. Apparently 40% of subscribers to the palaeontological publication *Journal of Paleobiology* believed that an impact did indeed occur at the K–T transition, but only 15% believed that this impact was responsible for mass extinctions at that time. Initially many palaeontologists disbelieved in the reality of the impact itself, but were forced to change their views because of the compelling evidence put forward by chemists. Chemists will not, however, be able to prove beyond reasonable doubt that an impact caused mass extinctions. This is a matter for the palaeontologists to decide and is likely to remain controversial for many years to come. I feel, however, that we as chemists deserve some credit for having been able to read the message contained in iridium-rich boundary clays: a message that the Rosetta Stone of modern instrumentation has enabled up to decipher.

1. L. W. Alvarez, W. Alvarez, F. Asaro, and H. V. Michel. Science, **208**, 1095 (1980).
2. D. M. Raup and J. Sepkoski, Jr. Science, **231**, 833 (1986).
3. L. T. Silver and P. H. Schultz (*Editors*). Geol. Soc. Am. Spec. Pap. **190** (1982).
4. M. R. Rampino. Geol. Soc. Am. Spec. Pap. **190**, 455 (1982).
5. M. R. Rampino and R. C. Reynolds. Science, **219**, 495 (1983).
6. C. B. Officer and C. L. Drake. Science, **219**, 1383 (1983).
7. R. R. Brooks, R. D. Reeves, X. H. Yang, D. E. Ryan, J. Holzbecher, J. D. Collen, V. E. Neall, and J. Lee. Science, **226**, 539 (1984).
8. W. Alvarez, L. W. Alvarez, F. Asaro, and H. V. Michel. Science, **223**, 1183 (1984).
9. R. R. Brooks, C. P. Strong, J. Lee, C. J. Orth, and J. S. Gilmore. Geology, **14**, 727 (1986).
10. C. P. Strong, R. R. Brooks, S. M. Wilson, R. D. Reeves, C. J. Orth, L. R. Quintana, X. Y. Mao, and E. Anders. To be published.
11. C. J. Orth, J. S. Gilmore, J. D. Knight, C. L. Pillmore, R. H. Tschudy, and J. E. Fassett. Science, **214**, 1343 (1983).
12. C. J. Orth, J. S. Gilmore, J. D. Knight, C. L. Pillmore, R. H. Tschudy, and J. E. Fassett. Geol. Soc. Am. Spec. Pap. **190**, 423 (1982).
13. B. F. Bohor, E. E. Foord, P. J. Modreski, and D. M. Triplehorn. Lun. Planet. Sci. **XV**, 74 (1984).
14. B. F. Bohor, E. E. Foord, P. J. Modreski, and D. M. Triplehorn. Science, **224**, 867 (1984).
15. B. F. Bohor and G. A. Izett. Lun. Planet. Sci. **XVII**, 68 Pt. 1 (1986).
16. B. F. Bohor, P. J. Modreski, and E. E. Foord. Lun. Planet. Sci. **XVI**, 79 (1985).
17. B. F. Bohor, E. E. Foord, and P. J. Modreski. Lun. Planet. Sci. **XVI**, 77 (1985).
18. J. Smit and F. T. Kyte. Nature, **310**, 403 (1984).
19. W. S. Wolbach, R. S. Lewis, and E. Anders. Science, **230**, 167 (1985).
20. W. S. Wolbach. Abs. 38th Meteor. Soc. Mtg., Bordeaux, July 16–19, 1985.
21. C. B. Officer and A. A. Ekdale. Science, **234**, 262 (1986).
22. E. Anders, W. S. Wolbach, and R. S. Lewis. Science, **234**, 263 (1986).
23. J. M. Luck and K. K. Turekian. Science, **222**, 613 (1983).
24. A. R. Date and A. L. Gray. Analyst, **108**, 159 (1983).
25. F. E. Lichte, S. M. Wilson, R. R. Brooks, R. D. Reeves, J. Hozbecher, and D. E. Ryan. Nature, **322**, 816 (1986).
26. D. J. de Paulo, F. T. Kyte, B. D. Marshall, J. R. O'Neil, and J. Smit. Earth Planet. Sci. Lett. **64**, 356 (1983).
27. J. Smit and A. J. T. Romein. Earth Planet. Sci. Lett. **74**, 155 (1985).
28. W. H. Zoller, J. R. Parrington, and J. M. Phelan. Science, **222**, 1118 (1983).
29. N. L. Carter, C. B. Officer, C. A. Chesner, and W. I. Rose. Geology, **14**, 380 (1986).
30. R. E. Sloan, J. K. Rigby, Jr., L. M. Van Valen, and D. Gabriel. Science, **232**, 629 (1986).
31. P. E. Playford, D. J. McLaren, C. J. Orth, J. S. Gilmore, and W. D. Goodfellow. Science, **226**, 437 (1984).
32. C. J. Orth, J. S. Gilmore, L. R. Quintana, and P. M. Sheehan. Geology, **14**, 433 (1986).
33. Y. Y. Sun *et al.* Contr. 27th Int. Geol. Congr., Moscow, 235 (1984).
34. F. T. Kyte and J. T. Wasson. Science, **232**, 1225 (1986).
35. A. Hoffman and M. H. Nitecki. Geology, **13**, 884 (1985).
36. W. Alvarez. Eos, **67**, 649 (1986).
37. D. J. Nichols, D. M. Jarzen, C. J. Orth, and P. Q. Oliver. Science, **231**, 714 (1986).

Can. J. Chem. Downloaded from www.nrcresearchpress.com by 78.46.186.204 on 09/07/12
For personal use only.

Alkylammonium lead halides. Part 1. Isolated PbI_6^{4-} ions in $(CH_3NH_3)_4PbI_6 \cdot 2H_2O$

BEVERLY R. VINCENT,[1] KATHERINE N. ROBERTSON, T. STANLEY CAMERON, AND OSVALD KNOP
Department of Chemistry, Dalhousie University, Halifax, N.S., Canada B3H 4J3

Received October 14, 1986

This paper is dedicated to Professor Douglas E. Ryan on the occasion of his 65th birthday

BEVERLY R. VINCENT, KATHERINE N. ROBERTSON, T. STANLEY CAMERON, and OSVALD KNOP. Can. J. Chem. **65**, 1042 (1987).

The yellow $(CH_3NH_3)_4PbI_6 \cdot 2H_2O$ ($P2_1/n$, a = 10.421(3) Å, b = 11.334(2) Å, c = 10.668(2) Å, β = 91.73(2)°, Z = 2) contains isolated PbI_6^{4-} octahedra, $CH_3NH_3^+$ cations of two types and H_2O molecules. The cations and the water molecules are hydrogen-bonded to form *cat* 1···H_2O···*cat* 2 units arranged in centrosymmetric (*cat* 1···H_2O···*cat* 2)$_2^{4+}$ pairs; the centres of these composite units and the Pb atoms form a distorted NaCl-type lattice. The Pb—I bond lengths in the PbI_6^{4-} anions are compared with those in $[Pb(II)I_6]^{\epsilon}$ complexes containing shared I atoms and the effect of the sharing on the bond lengths is discussed. A scheme is proposed for the extensive three-dimensional hydrogen bonding in the structure.

BEVERLY R. VINCENT, KATHERINE N. ROBERTSON, T. STANLEY CAMERON et OSVALD KNOP. Can. J. Chem. **65**, 1042 (1987).

Le composé jaune, $(CH_3NH_3)_4PbI_6 \cdot 2H_2O$ ($P2_1/n$, a = 10,421(3), b = 11,334(2) et c = 10,668(2) Å, β = 91,73(2)° et Z = 2) contient un octaèdre isolé de PbI_6^{4-}, des cations $CH_3NH_3^+$ de deux types et des molécules de H_2O. Les cations et les molécules d'eau sont liés par des ponts hydrogènes qui forment des unités *cat* 1···H_2O···*cat* 2 qui sont arrangées en paires centrosymétriques (*cat* 1···H_2O···*cat* 2)$_2^{4+}$; les centres de ces unités composites et les atomes de Pb forment un réseau déformé du type NaCl. On compare les longueurs des liaisons Pb—I des anions PbI_6^{4-} avec celles observées dans les complexes $[Pb(II)I_6]^{\epsilon}$ contenant des atomes I partagés et on discute de l'effet du partage sur les longueurs des liaisons. On propose un schéma pour expliquer le réseau important de liaisons hydrogènes tridimensionnelles que l'on retrouve dans cette structure.

[Traduit par la revue]

Can. J. Chem. Downloaded from www.nrcresearchpress.com by 78.46.186.204 on 09/07/12
For personal use only.

Dropwise addition of a concentrated aqueous solution of $Pb(NO_3)_2$ to an aqueous solution containing CH_3NH_3I in 12-fold molar excess yields a black precipitate of $CH_3NH_3PbI_3$ when the addition is carried out above ca. 40°C. With the solutions below this temperature a pale yellow crystalline solid, originally believed to be hydrated $CH_3NH_3PbI_3$ (1), is obtained instead; it forms also by spontaneous conversion of the black $CH_3NH_3PbI_3$ precipitated above 40°C when the latter is cooled below this temperature in contact with the mother liquor. This yellow solid was of concern to us at first only as a potential contaminant of $CH_3NH_3PbI_3$ then under investigation (ref. 2 and to be published), but the suspicious closeness of the temperature limit given (1) for its formation to the upper transition temperature of solid $CH_3NH_3PbI_3$, ~54°C (to be published), eventually prompted us to investigate the yellow solid in some detail.

The ir spectrum of the yellow material indeed indicated the presence of water of hydration. With the preparation of larger quantities of the compound and further chemical characterization under way, we proceeded with the crystal-structure analysis, in the expectation that the composition could be established independently in this way.

The main features of the structure emerged almost immediately, owing to the presence of the heavy scatterers Pb and I. After several cycles of refinement it became clear that the compound was not a hydrate of $CH_3NH_3PbI_3$, but the hitherto unreported compound $(CH_3NH_3)_4PbI_6 \cdot 2H_2O$ (**1**) and, to our knowledge, the first compound shown to contain *isolated* Pb(II)I_6 octahedra (cf. Table 1).[2] The composition was subsequently confirmed by chemical analysis.

The structure of **1** consists of a distorted fcc array of PbI_6^{4-} ions interspersed with $CH_3NH_3^+$ cations of two types and water molecules of a single type (Fig. 1). Each water molecule is hydrogen-bonded to a cation 1 and a cation 2 to form *cat* 1···H_2O···*cat* 2 units (see below), which occur in centrosymmetric pairs. If the structure is regarded as an assembly of such (*cat* 1···H_2O···*cat* 2)$_2^{4+}$ dimers and PbI_6^{4-} octahedra, the centres of the ions are situated on a distorted NaCl-type lattice.

The centrosymmetric PbI_6 octahedron is quite regular (Table 2), testifying to the stereochemical inactivity of the lone pair on the Pb(II) atom. The Pb—I bond lengths range from 3.195 to 3.231 Å, with a mean of 3.217(16) Å (3.223(10) Å when corrected for thermal motion). This range, 0.036(2) Å, is relatively narrow compared to the variation of bond length in PbI_6 octahedra containing shared I atoms (Tables 1 and 3); in the extreme case of anhydrous and hydrated $APbI_3$ (**5**–**8**) the difference between the longest and the shortest Pb—I bond in the same PbI_6 octahedron is ~0.4 Å (see below).

The H atoms could not be found in difference Fourier maps and direct evidence of hydrogen bonding is thus lacking. However, the N···O distances of 2.90 Å almost certainly correspond to N—H···O bonds. The N(1)—O—N(2), C(1)—N(1)—O, and C(2)—N(2)—O angles are 112°, 102°, and 136°, respectively, and assuming that C—N—H = 109.5° and N—H = 1.02 Å, we have H_N···O ~ 1.90 Å, N—H—O ~ 168° for cation 1 and H_N···O ~ 2.04 Å, N—H—O ~ 141° for cation 2, values not exceptional for N—H···O bonds (9). Since the N—H···O bonds are stronger than O—H···I or N—H···I bonds, cation 1 and cation 2 may be regarded as hydrogen-bonded to the water molecule to form discrete cationic units $H_3N(1)$—H···OH_2···H—$N(2)H_3$, which in turn are linked by N—H···I and O—H···I bonds to the PbI_6 octahedra.

The shortest O···I separations in **1**, 3.63–3.65 Å (Table 4), are well within the range 3.59–3.67 Å reported for O···I^- distances in iodide hydrates (9). If the coordination of the O atom is assumed to be approximately tetrahedral, examination

[1]Holder of NSERC (1983–1987), Killam (1984–1987), and Sumner (1986–1987) graduate fellowships.

[2]The rhombohedral Cs_4PbI_6 (3, 4) is almost certain to be isostructural with K_4CdCl_6 (5) and therefore to contain isolated PbI_6^{4-} octahedra of C_{3i} symmetry. However, the structure of this iodide has not yet been reported.

TABLE 1. Connectivities of $[PbI_6]^e$ octahedra in complex Pb(II) iodides*

Complex	Symmetry	Occurs in	⟨Pb—I⟩ (Å)	IPbI range (deg)
1 $[PbI_{6/1}]^{4-}$	C_i	$(CH_3NH_3)_4PbI_6 \cdot 2H_2O$	3.217(16)	87.6–92.4
2 $[PbI_{4/2}{}^eI_{2/1}{}^a]^{2-}$	C_{2h}	Tl_4PbI_6 (6)	3.218(24)	87.4–92.6
3 $[PbI_{6/2}]^-$	O_h	$CH_3NH_3PbI_3$†	3.153	90
4 $[PbI_{4/2}{}^eI_{2/2}{}^a]^-$	C_{2h}	$TlPbI_3$ (6)	3.207(20)	87.3–92.7
5 $[PbI_{2/2}{}^eI_{2/3}{}^eI_{1/3}{}^aI_{1/1}{}^a]^-$	C_s	$RbPbI_3$ (7)‡	3.229(111)	84.1–93.5
6 ditto	C_s	$KPbI_3 \cdot 2H_2O$ (8)	3.239(137)	85.8–92.3
7 ditto	C_s	$NH_4PbI_3 \cdot 2H_2O$ (8)	3.244(140)	86.1–92.6
8 ditto	C_s	$RbPbI_3 \cdot 2H_2O$ (8)		
9 $[PbI_{6/3}]^0$	D_{3d}	PbI_2	3.22§	§

*e, equatorial; a, axial. For the notation $I_{p/q}$ see text. ⟨Pb—I⟩, mean of the six Pb—I distances in the complex, with the standard deviation in parentheses.

†Cubic high-temperature form isotypic with the room-temperature phases of the cubic perovskites $CH_3NH_3PbCl_3$ and $CH_3NH_3PbBr_3$; ⟨Pb—I⟩ = Pb—I (σ = 0.001 Å) refers to ~57°C (to be published).

‡$CsPbI_3$ is isostructural, ⟨Pb—I⟩ = 3.24(12) Å (3).

§Depends on the polytype.

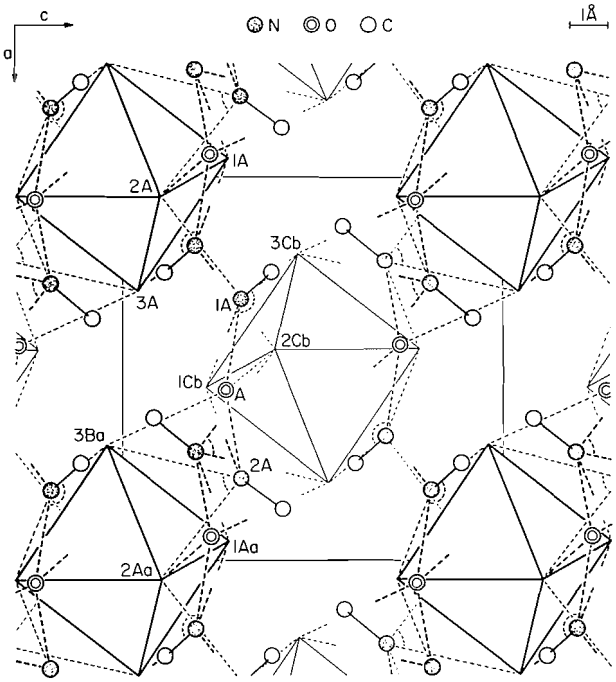

FIG. 1. $(CH_3NH_3)_4PbI_6 \cdot 2H_2O$: projection of the structure on (010) (the β angle of 91.7° is approximated by 90°). Broken arcs indicate N—H···I bonds presumed bifurcated. For symmetry code see Table 4.

of the N—O—I and I—O—I angles (Table 4) shows that a reasonable hydrogen-bonding scheme results when N(1) and N(2) are taken to be the donor and I(2C) and I(3B) the acceptor atoms of the hydrogen bonds (Fig. 2). Although the deviations of some of the N—O—I angles from tetrahedral are large, the OH_4 tetrahedron is likely to be closer to regular than these deviations might suggest, owing to the nonlinearity of the N—H···O (and probably also O—H···I) bonds.

In the absence of accurate knowledge of the positions of the H_N atoms bonded to the oxygen the description of the bonding engagement of the remaining H_N atoms can only be tentative. The shortest N···I distances, 3.54–3.72 Å (Table 4), are comparable to the N···I^- distance in Et_3NHI, 3.60(3) Å, which is reliably known and which corresponds to an N—H···I^- bond straight by symmetry (10). However, the two shortest N(1)···I distances, N(1)···I(3C) and N(1)···I(1C), correspond to

TABLE 2. $(CH_3NH_3)_4PbI_6 \cdot 2H_2O$: interatomic distances (Å) and bond angles (deg)*

Atoms	Distance	Atoms	Angle
Pb—I(1)	3.225(1)†	I(1A)—Pb—I(2B)	87.57(3)
Pb—I(2)	3.231(1)†	I(1A)—Pb—I(3B)	89.64(3)
Pb—I(3)	3.195(1)†	I(2A)—Pb—I(3A)	91.30(3)
Pb—I, mean	3.217(16)		
I(1A)···I(2A)	4.661(2)		
I(1A)···I(3A)	4.554(2)		
I(1A)···I(2B)	4.468(2)		
I(1A)···I(3B)	4.526(2)		
I(2A)···I(3A)	4.595(2)		
I(2A)···I(3B)	4.492(2)		
I···I, mean	4.549(65)		
N(1A)—C(1A)	1.476(3)		
N(2A)—C(2A)	1.498(3)		

*For symmetry code see Table 4.

†Corrections based on a rigid-body motion model add 0.005 Å to Pb—I(1) and 0.006 Å to Pb—I(2) and Pb—I(3). Corrections to the I—Pb—I angles do not exceed 0.02°.

C(1)—N(1)—I angles of 94° and 157°, respectively, indicating that if N—H···I bonds are involved here, they must be appreciably bent. Placing an H_N atom on a straight line defined by N(1) and the midpoint of I(1C) and I(3C) would result in a bifurcated N(1)—H···2I bond with the N(1)—H vector ca. 110° from the N(1)···O line and a C(1)—N(1)—H angle of 129°. While these values are not close to ideal, it is clear that the N(1)—H···I bond in the direction of the two nearest I atoms is either strongly bent or bifurcated.

Similar considerations of other short N···I distances and of plausible hydrogen-bonding geometries have produced the overall hydrogen-bonding scheme illustrated in Figs. 1 and 2. Although the proposed scheme is tentative in the specific assignment of the N—H···I bonds, it does indicate that (*1*) not all (and perhaps none) or the hydrogen bonds can be close to straight; (*2*) the two strongest hydrogen bonds are those linking the two cations to the water molecule to form identifiable *cat* 1···H_2O···*cat* 2 units; (*3*) the cations and the water molecules cross-link the PbI_6 octahedra to form a three-dimensional edifice; and (*4*) all the I atoms participate in hydrogen bonding. These conclusions would stand even if some re-positioning of the proposed N—H···I bonds was required

Can. J. Chem. Downloaded from www.nrcresearchpress.com by 78.46.186.204 on 09/07/12
For personal use only.

TABLE 3. Mean Pb(II)—I distances (Å) in octahedral $[PbI_6]^\epsilon$ complexes*

	ϵ			
q	0	1−	2−	4−
1		3.031(5)/3†	3.187(2)/1	3.217(16)/6
2		3.193(31)/6	3.234(2)/1	
3		3.318(86)/6‡		
4	3.22§			

*q = number of Pb—I bonds in which the I atom participates. The number of nonequivalent Pb—I distances included in the mean is indicated by the number after the oblique stroke. The number in parentheses is the standard deviation of the mean; where only one Pb—I distance is available, this number is the quoted esd for this distance.

†*trans* to I(q = 3).

‡*trans* to I(q = 1).

§PbI_2; the Pb—I distance depends somewhat on the polytype.

TABLE 4. $(CH_3NH_3)_4PbI_6 \cdot 2H_2O$: interatomic distances (Å) and bond angles (deg) possibly involved in hydrogen bonding*

Atoms		Distance†	Atoms	Angle
O(A)	N(1A)	2.903	N(1A)—O(A)—N(2A)	112(1)
	N(2A)	2.904	I(3Ba)	118.9(7)
	I(3Ba)	3.633	I(2Cb)	96.5(5)
	I(2Cb)	3.646	I(3A)	70.4(5)
	I(3A)	3.792	N(2A)—O(A)—I(3Ba)	77.5(5)
	I(1C)	4.106	I(2Cb)	133.1(7)
	I(2D)	4.131	I(3A)	147.9(7)
	I(1Aa)	4.342	I(2Cb)—O(A)—I(3Ba)	121.6(4)
			I(3A)	76.3(3)
			I(3Ba)—O(A)—I(3A)	74.5(3)
N(1A)	O(A)	2.903	C(1A)—N(1A)—O(A)	102(2)
	I(3C)	3.675	I(3C)	94(1)
	I(1C)	3.702	I(1C)	157(1)
	I(2A)	3.737	I(2A)	100(1)
	I(2D)	3.887	I(2D)	85(1)
	I(3A)	3.914	I(3A)	90(1)
N(2A)	O(A)	2.904	C(2A)—N(2A)—O(A)	136(2)
	I(1C)	3.539	I(1C)	118(2)
	I(1Aa)	3.670	I(1Aa)	89(2)
	I(2Aa)	3.716	I(2Aa)	90(1)
	I(2D)	4.017	I(2D)	76(1)
	I(3Ba)	4.091	I(3Ba)	154(2)

*Symmetry code: A, (x, y, z); B, ($-x$, $-y$, $-z$); C, ($\frac{1}{2} - x$, $\frac{1}{2} + y$, $\frac{1}{2} - z$); D, ($\frac{1}{2} + x$, $\frac{1}{2} - y$, $\frac{1}{2} + z$); a, $X + (1, 0, 0)$; b, $X + (0, -1, 0)$.

†The esd's are 0.003 Å for the N···O and 0.001 Å for the N···I distances.

as a result of an actual location of the H atoms by neutron diffraction or single-crystal nmr.

The engagement of every I atom in at least two N—H···I bonds tends to find support in the result of a TLS analysis on the PbI_6 octahedron. The rigid-body motion model accounts moderately well for the observed thermal parameters: $R(U_{ij})$ = 7.3%, and the rms discrepancy for U_{ij} is 0.0018 compared to the rms discrepancy for esd(U_{ij}) of 0.0005. The mean amplitudes about the principal axes of libration are small and quite similar, 1.9°, 2.5°, and 2.8°, which reflects a largely isotropic hindering potential to librational motion. The translational component of the motion is quite small and nearly isotropic.

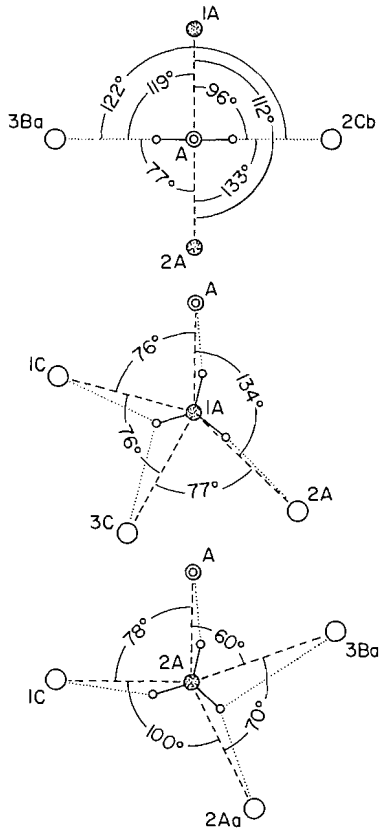

FIG. 2. Schematic representation of the hydrogen-bonding scheme proposed for $(CH_3NH_3)_4PbI_6 \cdot 2H_2O$. Symbols as in Fig. 1. Dashed lines, donor···acceptor distances; dotted lines, H···acceptor bonds. For symmetry code see Table 4.

Bond lengths in $[Pb(II)I_6]^\epsilon$ complexes

Since a $[Pb(II)I_6]^\epsilon$ octahedron in a crystal may be linked to another such octahedron or octahedra, its I atoms may participate in more than one Pb—I bond each. The connectivity of the octahedron can be represented by $[PbI_{p_1/q_1}I_{p_2/q_2}\cdots]^\epsilon$, $\Sigma(p_i/q_i) = 2 - \epsilon$, $\Sigma p_i = 6$, where q_i is the number of Pb atoms forming a bond to the ith I atom, p is the number of I atoms of the same type, and ϵ is the charge on the complex. The length of an individual Pb—I bond in the octahedron will then depend on p, q, and ϵ. This is illustrated in Table 3. The number of Pb—I bond lengths reported to date is too small for a detailed analysis, but it is clear that the bond length at constant q increases with increasing anionic charge $|\epsilon|$ and, at constant ϵ, with increasing q, as would be expected. However, the variation is not independent of the symmetry and connectivity of the octahedron: the configuration and the p/q values of the other Pb—I bonds also play a rôle. Thus in **5**–**7** the shortest (p/q = 1/1) and the longest (p/q = 1/3) bonds are both axial. They average 3.032(6) and 3.435(46) Å, respectively, but their *means* average 3.234(17) Å, i.e. they are close to the mean for the C_s complex (Table 1) and to the overall mean of the Pb—I distances in the $[PbI_6]^\epsilon$ complexes of Table 1, 3.216(78) Å. This "*trans*" effect reflects an extreme unbalance of the bond strength across the Pb atom in the infinite double chain of PbI_6 octahedra and renders the individual bond lengths involved untypical for the particular combination of q and ϵ. Similarly, the *means* of the *trans* bonds involving the $I_{2/2}$ and $I_{2/3}$ atoms in **5**–**7** average 3.239(4) Å, but here the two bond lengths *trans* to each other differ by much less.

Can. J. Chem. Downloaded from www.nrcresearchpress.com by 78.46.186.204 on 09/07/12
For personal use only.

Can. J. Chem. Downloaded from www.nrcresearchpress.com by 78.46.186.204 on 09/07/12
For personal use only.

The overall mean of the individual bond lengths in **1**–**7** and **9** is 3.216(78) Å (high–low spread, 3.153–3.462 Å), that of all the *trans*-pair means is 3.216(29) Å (high–low spread, 3.153–3.247 Å), and that of the ⟨Pb—I⟩ means for the eight octahedra is 3.216(26) Å (high–low spread, 3.153–3.239 Å). It would thus appear that the ⟨Pb—I⟩ values for different $[PbI_6]^{\epsilon}$ octahedra are quite similar and, furthermore, that the bond-length compensation is accomplished by pairwise averaging of Pb—I bonds *trans* to each other.

Table 1 details the geometries of the $[PbI_6]^{\epsilon}$ complexes of different types reported to date. This list of types is far from exhaustive, for in principle any geometrically permissible combination $[PbI_{p_1/q_1}I_{p_2/q_2}\cdots]^{\epsilon}$ can occur. In particular, $[PbI_{4/1}{}^{e}I_{2/2}{}^{a}]^{3-}$ would represent an infinite chain of octahedra linked by *trans* corners; however, an example of this or any other such trivalent anion is yet to be found.

Experimental

A quantity of **1** was prepared by hot precipitation of $CH_3NH_3PbI_3$ (as in ref. 1) and allowing the solution and the precipitate to cool slowly to room temperature. On standing overnight in contact with the mother liquor the black solid had converted completely to small pale yellow crystals of good quality. A batch of handpicked crystals constituted the sample used in this investigation.

The compound is difficult to obtain completely dry because of a risk of dehydration on prolonged drying in air and of decomposition when washing with organic liquids. The presence of residual accidental water rendered chemical analysis difficult. Nevertheless, determination of Pb as $PbCrO_4$ (in triplicate) gave 17.5(1) wt% Pb, in reasonable agreement with theory (18.3 wt% Pb).[3] The water content was determined from the weight loss on dehydrating a sample under mechanical-pump vacuum at the bp of acetone. The low weight percentage of H_2O in **1** necessitated a large sample (3.3 g) and only one determination was therefore made, resulting in 4.05 wt% H_2O (theory for $2H_2O$, 3.18 wt%). The low analytical figure for Pb corresponds to at most 2.8 extra H_2O molecules per formula unit, while the H_2O analysis corresponds to ca. 0.6 extra H_2O molecules. The discrepancy stems from the variable residual water content of the samples, crystal size playing a rôle in the removal of accidental water by rapid air drying. In spite of their shortcomings these analytical results clearly support the composition of **1** as determined by the crystal-structure analysis, in particular as regards the number of H_2O molecules of hydration, which cannot be less than two.

Water decomposes **1** immediately with the formation of PbI_2. Heating in air or pumping at room temperature dehydrates **1** to a black mixture of $CH_3NH_3PbI_3$ and CH_3NH_3I. Treating this dehydration product with acetone or MeCN yields dark yellow solutions, from which **1** is recovered by evaporation of the solvent (in large crystals when MeCN is used). Recombination of the dehydration product to **1** in nitromethane is limited by low solubility but otherwise proceeds as in acetone or MeCN. Treating **1** with nitromethane results in an initial slight blackening of the solid followed by reappearance of the yellow colour; evaporation of the colourless solution yields **1**. The starting compound is also recovered when **1** is treated with acetone or MeCN and the solvent evaporated, but in this case the solid first turns rapidly and completely black while the solution is yellow.

Crystal data

$C_4H_{28}I_6N_4O_2Pb$ fw = 1132.9

Monoclinic, $P2_1/n$ (no. 14) (systematic absences: $h0l$, $h + l = 2n + 1$; $h00$, $h = 2n + 1$; $0k0$, $k = 2n + 1$; $00l$, $l = 2n + 1$); $a = 10.421(3)$ Å, $b = 11.334(2)$ Å, $c = 10.668(2)$ Å, $\beta = 91.73(2)°$, $V = 1259.5(5)$ Å^3, $Z = 2$, $\rho_c = 2.987$ g/cm^3, $F(000) = 992$ e.

Structure determination

Radiation, Mo $K\alpha_1$, $\lambda = 0.70926$ Å (graphite monochromator); crystal, 0.1 mm radius sphere in sealed capillary; $\mu_{Mo} = 140.4$ cm^{-1}; limits of transmission, 0.27–0.54. Reflections (CAD-4 four-circle diffractometer): total counted, 2562; total unique, 1749; total used ($I_o \geq 3\sigma(I_o)$), 1425. Scattering factors for neutral atoms and corrections for anomalous scattering taken from ref. 11. Weighting schemes: SHELX, $w^{-1} = \sigma^2|F_o| + 0.00542F_o{}^2$; CRYSTALS, $w^{-1} = \sigma^2|F_o|$. Temperature factor, $T = \exp[-2\pi^2(U_{11}h^2a^{*2} + U_{22}k^2b^{*2} + U_{33}l^2c^{*2} + 2U_{23}klb^*c^* + 2U_{13}hla^*c^* + 2U_{12}hka^*b^*)]$.

The structure was solved and a preliminary refinement carried out using the SHELX system (12) and intensities not corrected for absorption. Absorption corrections were then applied and the refinement completed using CRYSTALS (13); the latter system was also used in the TLS analysis. The final R value (based on 1425 unique reflections corrected for absorption) was 4.29%, $R_w = 4.36\%$. The C, N, and O atoms could be clearly distinguished; the hydrogen atoms were not seen. The final difference maps were flat, without recognizable residual features.

The positional and thermal parameters are listed in Table 5, structure factors in Table 6,[4] and interatomic distances and bond angles in Tables 2 and 4.[5]

TABLE 5. $(CH_3NH_3)_4PbI_6\cdot 2H_2O$: positional and thermal parameters ($\times 10^4$)

Atom	x y z	U_{11} U_{22} U_{33}	U_{12} U_{13} U_{23}
Pb	0	318(4)	−14(3)
	0	296(5)	−20(3)
	0	264(4)	−4(3)
I(1)	−0537(1)	502(6)	−17(5)
	−0953(1)	405(6)	14(4)
	2784(1)	284(5)	10(4)
I(2)	0467(1)	488(6)	−24(5)
	2666(1)	335(6)	−16(5)
	0985(1)	402(6)	−70(5)
I(3)	2981(1)	307(5)	8(5)
	−0604(1)	560(7)	−25(5)
	0381(1)	467(7)	52(5)
N(1)	3220(11)	331(65)	−75(71)
	1731(13)	668(97)	37(57)
	3081(12)	514(73)	85(75)
C(1)	2543(20)	858(134)	−140(119)
	0923(17)	670(139)	14(109)
	3921(18)	594(113)	48(99)
N(2)	7848(13)	445(90)	125(86)
	1901(13)	669(120)	−13(83)
	3129(14)	760(112)	−134(99)
C(2)	8724(19)	622(133)	−64(135)
	2160(22)	1121(212)	61(104)
	4234(18)	519(120)	−289(132)
O	5584(11)	565(77)	92(73)
	0450(11)	676(97)	55(65)
	2676(11)	593(78)	−108(85)

[3]Duplicate determinations of Pb in dry $CH_3NH_3PbI_3$ by the same method gave 33.51(3) wt% Pb compared to the theoretical 33.42 wt%.

[4]A copy of this table may be purchased from the Depository of Unpublished Data, CISTI, National Research Council of Canada, Ottawa, Ont., Canada K1A 0S2.

[5]NOTE ADDED IN PROOF: The hexagonal Me_4NPbI_3 (14) contains infinite columns of $[PbI_{6/2}]^-$ ions of symmetry C_{3i}. The Pb—I distance, 3.223(1) Å, is at the upper limit of ⟨Pb—I⟩ for $q = 2$, $\epsilon = 1-$ (Table 3); IPbI range, 86.3–93.8°.

Acknowledgments

This work was supported by grants from the Natural Sciences and Engineering Research Council of Canada to T.S.C. and O.K.

1. D. WEBER. Z. Naturforsch. **33**b, 1443 (1978).
2. R. E. WASYLISHEN, O. KNOP, and J. B. MACDONALD. Solid State Commun. **56**, 581 (1985).
3. C. K. MØLLER. Mat.-fys. Medd. Danske Vid. Selsk. **32**, nos. 1, 2 (1960).
4. B. D. STEPIN, G. M. SEREBRENNIKOVA, G. P. CHICHERINA, V. K. TRUNOV, and YU. V. OBOZNENKO. Zh. Neorg. Khim. **21**, 3148 (1976).
5. G. BERGERHOFF and O. SCHMITZ-DUMONT. Z. Anorg. Allg. Chem. **284**, 10 (1956).
6. W. STOEGER. Z. Naturforsch. **32**b, 975 (1977).
7. H. J. HAUPT, F. HUBER, and H. PREUT. Z. Anorg. Allg. Chem. **408**, 209 (1974).
8. D. BEDLIVY and K. MEREITER. Acta Crystallogr. B, **36**, 782 (1980).
9. M. FALK and O. KNOP. *In* Water: a comprehensive treatise. Vol. 2. *Edited by* F. Franks. Plenum Press, New York. 1973. Chap. 2.
10. M. A. JAMES, T. S. CAMERON, O. KNOP, M. NEUMAN, and M. FALK. Can. J. Chem. **63**, 1750 (1985).
11. International tables for X-ray crystallography. Vol. IV. The Kynoch Press, Birmingham, England. 1974.
12. G. M. SHELDRICK. SHELX system report. University Chemical Laboratories, Lensfield Road, Cambridge, England. 1976.
13. J. R. CARRUTHERS and D. L. WATKINS. CRYSTALS, issue 5. Chemical Crystallography Laboratory, Oxford, England. 1981.
14. J. G. CONTRERAS, G. V. SEGUEL, B. UNGERER, W. F. MAIER, and F. J. HOLLANDER. J. Mol. Struct. **102**, 295 (1983).

Can. J. Chem. Downloaded from www.nrcresearchpress.com by 78.46.186.204 on 09/07/12
For personal use only.

Determination of trace aluminum concentration and homogeneity in biological reference material TORT-1 by instrumental neutron activation analysis and graphite furnace atomic absorption spectroscopy

BYRON KRATOCHVIL AND NORINE MOTKOSKY
Department of Chemistry, University of Alberta, Edmonton, Alta., Canada T6G 2G2

AND

M. JOHN M. DUKE AND DENNIS NG
SLOWPOKE II Nuclear Reactor Facility, University of Alberta, Edmonton, Alta., Canada T6G 2N8

Received October 20, 1986

This paper is dedicated to Professor Douglas E. Ryan on the occasion of his 65th birthday

BYRON KRATOCHVIL, NORINE MOTKOSKY, M. JOHN M. DUKE, and DENNIS NG. Can. J. Chem. **65**, 1047 (1987).

The biological reference material TORT-1, lobster hepatopancreas, was analyzed for aluminum by instrumental neutron activation analysis (INAA) and graphite furnace atomic absorption spectroscopy (GFAAS). After correction of the INAA results for interferences from ^{28}Al produced by $^{31}P(n,\alpha)^{28}Al$ and $^{28}Si(n,p)^{28}Al$ reactions, and use of HNO_3 plus HF for sample dissolution for the GFAAS analyses, the methods gave similar results of 43 ± 3 and 42 ± 2 μg/g respectively for 200 to 300-mg test portions. Analysis of six portions from each of six bottles of TORT-1 showed no statistical difference at the 95% confidence level for the between and within bottle variances. Therefore, the material can be considered homogeneous for aluminum if 200- to 300-mg test portions are taken. The variance was greater and the average lower when 30-mg test portions were analyzed for aluminum by GFAAS. The pattern of the results, together with the need for HF in the dissolution procedure, suggests the presence of aluminum-containing microparticulate mineral matter, perhaps silicate material, in the material.

BYRON KRATOCHVIL, NORINE MOTKOSKY, M. JOHN M. DUKE et DENNIS NG. Can. J. Chem. **65**, 1047 (1987).

Faisant appel à l'analyse instrumentale par activation neutronique (AIAN) et à la spectroscopie par absorption atomique avec fournaise de graphite (SAAFG), on a analysé l'aluminium contenu dans le produit biologique de référence TORT-1, un hépatopancréas de homard. Après correction des résultats de AIAN pour les interférences provenant du ^{28}Al qui est produit par les réactions de $^{31}P(n,\alpha)^{28}Al$ et $^{28}Si(n,p)^{28}Al$ et l'utilisation de HNO_3 plus HF pour dissoudre l'échantillon pour les analyses par SAAFG, les méthodes donnent des résultats semblables de 43 ± 3 et 42 ± 2 μg par gramme respectivement pour des essais sur des échantillons de 200 à 300 mg. Les analyses effectuées sur six échantillons provenant de chacune des six bouteilles de TORT-1 ne présentent pas de différences statistiques, au niveau de confiance de 95%, pour des variations entre bouteilles et à l'intérieur de la même bouteille. Si on utilise des échantillons de 200 à 300 mg pour faire les essais, on peut donc considérer que le matériel est homogène pour l'aluminium. Lorsqu'on a analysé l'aluminium sur des échantillons de 30 mg par la SAAFG, les variations étaient plus grandes et la moyenne plus basse. L'ensemble des résultats, couplé au fait qu'il est nécessaire d'utiliser du HF pour dissoudre l'échantillon, suggère qu'il contient probablement substances minérales porteuses d'aluminium, comme des silicates, à l'état de microparticules.

[Traduit par la revue]

Introduction

Accurate determination of trace aluminum in biological materials is difficult. Problems include contamination or loss during sample collection and preparation for measurement, and bias and scatter in the measurement steps. As a result, only two of the biological standard reference materials presently available from the U.S. National Bureau of Standards, Pine Needles SRM 1575 and Tomato Leaves SRM 1573, are certified for aluminum. For Bovine Liver SRM 1577a, a provisional value of 2 μg/g is given, but values ranging from 1.8 to 65 μg/g have been reported in the literature (1).

The marine biological reference material TORT-1 of the National Research Council of Canada, prepared from acetone-extracted lobster hepatopancreas, has been certified for 15 trace elements, but not for aluminum because of the poor reproducibility of results obtained by various methods in different laboratories. A study was therefore made of the homogeneity and concentration of Al in this material using two methods, instrumental neutron activation analysis (INAA) and graphite furnace atomic absorption spectroscopy (GFAAS). A third method, inductively coupled plasma emission spectroscopy, has also been used to determine Al in biological matrices (2), but was not studied here.

The determination of trace aluminum in biological and environmental materials is of increasing interest. Acid rain has been connected with elevated levels of aluminum in water; aluminum is reported to affect fish at concentrations as low as 100 μg/L (3). Also, concern about the neurotoxicity of aluminum is growing, and it has been implicated in the development of senility, and of Alzheimer's disease (4).

Experimental

GFAAS measurements

Apparatus

The atomic absorption measurements were made on a Perkin Elmer Model 5000 spectrophotometer with background correction, an HGA 2200 furnace, and an AS-1 autosampler. Pyrolytic graphite tubes with platforms (Perkin Elmer Part No. B012-1091) were used (5). Operating conditions are given in Table 1. The argon purge gas flow was continued during atomization at the normal (40 mL/min) setting for 7 s. Peak areas were recorded on a Perkin Elmer PRS-10 printer sequencer. Working curves were linear over the range 0 to 3.7×10^{-6} *M* aluminum (0 to 2 ng Al per 20 μL injection). A typical working curve had a slope of 0.215 ± 0.016 absorbance units per μg injected and an intercept of 0.08 ± 0.06 ng Al for two replicates each of 3 standards and a blank (uncertainties are one standard deviation). Blanks carried through the same procedure as the samples were run on the instrument after every few measurements and the absorbance for the appropriate blank subtracted from the sample

Can. J. Chem. Downloaded from www.nrcresearchpress.com by 78.46.186.204 on 09/07/12
For personal use only.

Can. J. Chem. Downloaded from www.nrcresearchpress.com by 78.46.186.204 on 09/07/12
For personal use only.

TABLE 1. Operating conditions for graphite furnace atomic absorption measurements of aluminum

Parameter	Value
Wavelength	308.2 nm
Integration time	6 s
Spectral slit width	0.7 nm
Drying temperature and time	110°C, 30 s
Ashing temperature and time	1400°C, 40 s
Atomization temperature and time	2550°C, 6 s
HCL current	25 mA

absorbances to correct for blank components including drift and furnace deterioration. Each injection of 20 μL was repeated two or three times.

Reagents

Distilled water was further purified by passage through a column of mixed strong acid and strong base ion exchange resins (Amberlite MB-3, Rohm and Haas Co.). The nitric acid for sample dissolution was double sub-boiling distilled in quartz (Seastar Chemicals, Sidney, B.C., Canada). All other chemicals were either analytical or reagent grade. A certified standard solution of aluminum (Spex Industries 1000 μg/mL) was used to prepare the calibration curves and for standard additions.

Sample preparation

Six bottles of TORT-1, obtained from the Marine Standards Analytical Program, Division of Chemistry, National Research Council, Ottawa, Canada, were tumbled end-over-end for 2 to 2½ h. Approximately 5-g portions were then removed from each bottle and dried in glass weighing bottles for 24 h at room temperature (23–24°C) in a vacuum oven (National Appliance Co., Model 5851-6) at approximately 0.06 mm Hg. The vacuum was produced with a pump (Welch Co.) separated from the oven by a dry ice – acetone cold trap. Previous studies have shown these drying conditions to be optimum (6). The dried samples were stored in closed weighing bottles in a desiccator over magnesium perchlorate.

To check the methods, U.S. National Bureau of Standards standard reference materials Oyster Tissue SRM 1566 and Pine Needles SRM 1575 were also analyzed. These materials were dried in the same way as TORT-1.

For the study of small samples approximately 35-mg portions of the biological materials were weighed to ±0.01 mg on a Mettler H-51 semimicro balance and transferred into Teflon thick-walled, screw-capped decomposition vessels of about 20-mL capacity (H. K. Morrison and Sons, Mt. Uniacke, N.S., Canada). About 3 mL of concentrated HNO_3 and 0.2 mL concentrated HF (1 mL HF for NBS SRM 1575 Pine Needles) were added to each vessel and the cover tightly secured. The vessels were placed in a boiling water bath for 3 h, then removed, wiped immediately, and allowed to cool to room temperature. After cooling, the contents of each vessel were transferred into a Teflon bottle containing a solution of 0.185 g H_3BO_3 (0.93 g for Pine Needles) in 5 mL of water. The amount of H_3BO_3 added is determined by the amount of HF used in the dissolution step, since its purpose is to remove excess HF as fluoroborate. The solutions were diluted to approximately 15 mL for TORT-1, 25 mL for Oyster Tissue and 100 mL for Pine Needles. The final volumes were determined by weighing the solutions and by determining their densities from the weights of 1-mL portions.

The standard-additions solutions were prepared by pipetting 1 mL of 0.0547 *M* $Mg(NO_3)_2$ and 2 mL of sample solution into four or five 30-mL Teflon bottles followed by 0 to 0.6 mL of standard Al solution (1 μg per mL). The Al standard was added with a variable micropipet (Socorex 60–100 μL). Three or four standard additions were made to each digested sample. The solutions were then diluted to about 10 mL and the final volume determined by weight as described above.

For large samples approximately 300-mg portions of TORT-1 were weighed into the Teflon decomposition vessels and 3 mL HNO_3 and 1 mL HF were added. After 6 h digestion in a boiling water bath the vessels were removed, wiped, and allowed to cool. The digestion mixture was added to a polypropylene 100-mL volumetric flask containing 0.93 g H_3BO_3 dissolved in about 20 mL of water. The solution was diluted to volume, transferred to a Teflon bottle, and 2-mL portions taken for preparation of the standard-additions solutions as described before. All solutions were run on the atomic absorption spectrophotometer immediately after preparation. Plots of absorbance against aluminum added were drawn and the *x*-axis intercept, obtained by least-squares calcuation, was used to calculate the aluminum present in the sample solution.

INAA measurements

Approximately 200-mg portions of biological reference material were weighed into nitric acid-washed 400-μL polyethylene micro-centrifuge tubes. The tubes were heat-sealed and then enclosed in second larger polyethylene vials for irradiation. Standards were prepared from commercial atomic absorption standard solutions (Alpha) by pipetting 5 to 100 μL of stock solution onto Whatman #1 filter paper that had been rolled and inserted into micro-centrifuge tubes.

Irradiation and counting

The irradiation and counting operations were carried out at the SLOWPOKE II reactor facility of the University of Alberta. Conditions used for the analysis were: 120-s irradiation at 1×10^{11} n cm^{-2} s^{-1}, 10-s delay, and 180-s count 6 cm from an unshielded detector.

Counting of the 1779 keV γ radiation of ^{28}Al (half-life 2.24 m) was carried out with an Ortec 86 cm^3 active volume Win-15 coaxial Ge(Li) detector coupled to a Nuclear Data (ND) 660 multichannel analyzer with an Ortec 572 amplifier and ND 575 ADC. The detector specifications include a relative efficiency of 18.5%, and a measured FWHM of 2.1 keV and peak-to-Compton ratio of 53:1, for the 1332 keV photopeak of ^{60}Co. Signals were assigned to one of 4096 channels and the spectral data were stored on floppy discs for later analysis.

The specific activity (counts/μg) for Al was determined for the irradiation-decay counting period described, and the mass of Al in the NBS standards and TORT-1 was determined via an adaptation of the comparator (semi-absolute) method for INAA (7), that is, by dividing the 1779-keV photopeak area of the unknowns by the specific activity of Al. Deadtime corrections (8) for the decay of short-lived radioisotopes were applied; in addition, a correction factor for random summing effects was calculated and applied following the procedure of Wyttenbach (9).

The measurement of aluminum using the 1779 keV photopeak of ^{28}Al produced via the reaction ^{27}Al(n,γ)^{28}Al suffers a nuclear interference from the fast neutron reaction ^{31}P(n,α)^{28}Al. The interference factor for this reaction, that is, the mass of phosphorus that would produce the equivalent activity of 1 μg aluminum irradiated and analyzed under identical conditions, was empirically determined by irradiating and counting P and Al standards (10). Potassium dihydrogen phosphate and aluminum AA standards were irradiated for 120 s in the SLOWPOKE reactor at a thermal flux of 2.5×10^{11} n cm^{-2} s^{-1}. After a decay period of 30 s each test portion was counted for 180 s live-time at 6-cm geometry using the Win-15 coaxial Ge(Li) detector. The potassium phosphate standard was also analyzed for aluminum by GFAAS. A concentration of 7 μg Al per g was found and a correction made for this amount when calculating the interference factor. Analysis of twelve standards gave a corrected phosphorus interference factor to aluminum of 668 ± 30 (1 std. dev.) μg/g. From the certified NRC phosphorus content of TORT-1, 0.879% ± 0.021% (95% tolerance limits), and this interference factor, the phosphorus is calculated to produce an activity equivalent to 13.2 ± 0.6 μg Al per g of TORT-1. This interference was subtracted from the total aluminum determined by INAA for all TORT-1 test portions.

A similar correction was made for the ^{28}Si(n,p)^{28}Al interference reaction. The interference, based on a measured silicon concentration

TABLE 2. Analytical results in μg/g for aluminum in TORT-1 by INAA and GFAAS[a]

Method	Sample size (mg)	Bottle Number 5	155	811	881	887	908	Average
INAA	200	41.4±2.9	44.8±2.5	42.5±1.8	45.5±2.5	39.5±2.1	47.2±4.2	43±3
GFAAS	300	40.1±7.1	41.5±6.9	41.8±5.1	41.4±4.2	40.4±3.6	44.8±4.7	42±2
GFAAS	30	42±11	32±10	29±6	35±8	30±6	36±8	34±5

[a]Each value is the average of measurements on six separate test portions from each bottle except for the GFAAS data for 300-mg portions for bottle 881 where five measurements were made. Uncertainties are one standard deviation.

TABLE 3. Analytical results in μg/g for aluminum in NBS SRM's by GFAAS and INAA

Reference material	This work GFAAS	This work INAA	NBS value	Literature values
SRM 1566 Oyster Tissue	231 ± 9 (n = 3)	240 ± 7 (n = 6)	NR[a]	291 ± 24(1)
SRM 1575 Pine Needles	541 ± 14 (n = 3)	553 ± 12 (n = 6)	545 ± 30[b]	417 ± 96(22), 495(18) 565 ± 44(23), 490(21) 734(20), 529 ± 6(27) 522 ± 45(19), 560 ± 10(24) 582 ± 47(26), 585(25)

[a]No value reported.
[b]Uncertainty as 95% tolerance level. All other uncertainties are one standard deviation.

Can. J. Chem. Downloaded from www.nrcresearchpress.com by 78.46.186.204 on 09/07/12
For personal use only.

of 231 ± 33 μg/g in TORT-1 by GFAAS and an interference factor of 192, is equivalent to 1.2 μg Al per g of TORT-1 (10). The aluminum results from the INAA measurements were corrected for the phosphorus and silicon interferences, therefore, by subtracting a total of 14.4 μg/g from all measured aluminum values. The additional uncertainty in the result for Al introduced by this correction is about 0.7 μg/g.

When phosphorus and silicon concentrations are not known from other measurements it is possible to determine these elements concurrently with aluminum by irradiating a second test portion with epithermal and fast neutrons. This allows the contribution of phosphorus and silicon to the ^{28}Al activity to be estimated. Procedures using this approach have been reported (11–14). It was not used here because the amount of phosphorus present was already known from the certificate data, and because the level of silicon was so small a GFAAS measurement was more convenient and precise.

All spectral analyses were performed off-line in batch mode using standard Nuclear Data software (with modifications made by personnel at the SLOWPOKE facility).

Results and discussion

The results of the analyses of TORT-1 for aluminum are summarized in Table 2, and of the NBS standard reference materials SRM 1566 Oyster Tissue and SRM 1575 Pine Needles in Table 3.

Initial results for aluminum in TORT-1, using the HNO_3 dissolution procedure that was successful for the determination of lead and cadmium (15), were not satisfactory. Values tended to be low and erratic on 300-mg portions. Reproducibility was achieved only after HNO_3 was replaced by a mixture of HNO_3 and HF, and magnesium nitrate was added to the solutions before measurement by GFAAS. The presence of magnesium has been reported previously to reduce early loss of aluminum during the sample charring stage (16–18). Scatter for 30-mg portions analyzed by GFAAS remained larger than expected on the basis of the 300-mg results, however, even with the addition of HF (Table 1). This variability may be caused by non-uniform distribution of aluminum in the material, but this has not been proven. The averages for 30-mg portions are significantly lower than for 200- to 300-mg portions, with occasional values higher than would be expected for a Gaussian distribution. Preliminary data on 30-mg portions by INAA indicate values of the same order as for the 300-mg portions. Work on this aspect of the problem is continuing. Figure 1 shows the distribution patterns for 200- to 300-mg test portions by the two methods and for the two test-portion sizes by GFAAS.

Data for aluminum in reference materials similar in composition to TORT-1 are rare. Table 2 shows results of a limited number of analyses of SRM 1566 Oyster Tissue and SRM 1575 Pine Needles. Results for aluminum in both materials agree reasonably well between the two methods; those for Pine Needles agree with the NBS certified value and with values reported in the literature. One literature value has been reported for Oyster Tissue; NBS does not give a certified value. The literature value is somewhat higher than ours.

A one-way analysis of variance of the results for the 200- and 300-mg test portions in Table 2 indicates that there is no difference in the between and within bottle variances for aluminum by either method at the 95% confidence level. Furthermore, no statistical difference is observed at the 95% confidence level between the average values obtained by the two analytical methods.

Although the average values for the 30-mg portions are much lower than for the larger sample sizes, the scatter is much higher. An F test indicates that the variances for the 30- and 300-mg analyses by GFAAS differ significantly at the 95% confidence level ($F = 6.25$, $F_{.95} = 5.05$ for $\upsilon_1 = \upsilon_2 = 5$ d.f.), so the 30-mg data set cannot be compared with the 300-mg set by analysis of variance. The same conclusion holds when variances of the 30- and 200-mg portions are compared.

In summary, our best estimate of the aluminum content of

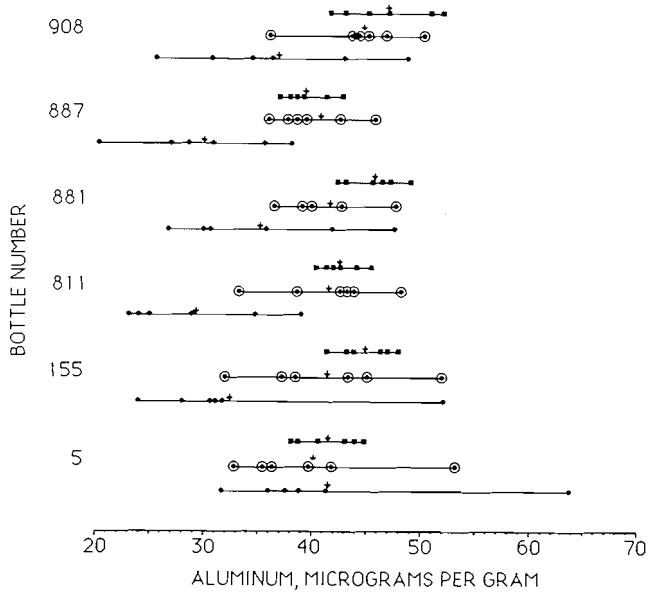

FIG. 1. Distribution of individual analytical results for Al in randomly selected bottles of TORT-1 certified reference material by graphite furnace atomic absorption spectroscopy (GFAAS) and by instrumental neutron activation analysis (INAA). The short vertical arrows above each data set identify the average value of that set. (■) INAA, 200-mg test portions; (○) GFAAS, 300-mg test portions; (●) GFAAS, 30-mg test portions.

TORT-1 is 43 ± 3 μg/g, where the ±3 denotes one standard deviation based on 72 analyses. The results indicate that TORT-1 is homogeneous for aluminum when 200 to 300 mg or larger test portions are taken, but that homogeneity is suspect at the 30-mg level. Also, dissolution in HNO_3 alone is not adequate to dissolve all the aluminum-containing material; addition of HF is necessary. This requirement differs from previous studies of lead and cadmium in TORT-1, where HNO_3 alone was shown to be sufficient to release both metals from the matrix (15).

Acknowledgements

This research was supported by the National Research Council of Canada under Contract OSC84-00580 for the Marine Analytical Chemistry Standards Program, by the University of Alberta, and by the Natural Sciences and Engineering Research Council of Canada through an infrastructure grant to the SLOWPOKE II reactor facility. Also, we thank S. Hrudey and W. George of the Department of Civil Engineering, University of Alberta, for the use of the atomic absorption spectrophotometer and furnace.

1. E. S. GLADNEY, C. E. BURNS, D. R. PERRIN, I. ROELANDTS, and T. E. GILLS. 1982 Compilation of elemental concentration data for NBS biological, geological, and environmental standard reference materials. NBS Spec. Publ. 260-88, U.S. Natl. Bur. Stand. Gaithersburg, MD. 1984.
2. F. E. LICHTE, S. HOPPER, and T. W. OSBORN. Anal. Chem. **52**, 120 (1980).
3. T. H. MAUGH. Science, **226**, 1408 (1984).
4. R. J. BOEGMAN and L. A. BATES. Can. J. Physiol. Pharmacol. **62**, 1011 (1984).
5. C. L. CHAKRABARTI, C. C. WAN, and W. C. LI. Spectrochim. Acta, **35B**, 547 (1980).
6. B. KRATOCHVIL. Evaluation of homogeneity of spray dried hepatopancreatic tissue from lobster for the National Research Council of Canada. DSS Contract No. OSC83-00225, DSS File No. 08SC.31028-3-3552, Ottawa, Ont., Canada. 1984.
7. L. ZIKOVSKY and J.-L. GALINIER. J. Radioanal. Chem. **67**, 193 (1981).
8. T. TAKEUCHI, S. UEHARA, and T. HAYASHI. J. Radioanal. Chem. **56**, 25 (1980).
9. A. WYTTENBACH. J. Radioanal. Chem. **8**, 335 (1971).
10. B. KRATOCHVIL, M. J. M. DUKE, and D. NG. Anal. Chem. **58**, 102 (1986).
11. W. GATSCHKE and D. GAWLIK. J. Radioanal. Chem. **56**, 203 (1980).
12. H. BEM and D. E. RYAN. Anal. Chim. Acta, **135**, 129 (1982).
13. Z. B. ALFASSI and N. LEVI. Analyst, **109**, 959 (1984).
14. A. CESANA and M. TERRANI. Int. J. Appl. Radiat. Isot. **35**, 405 (1984).
15. B. KRATOCHVIL, R. THAPA, and N. MOTKOSKY. Can. J. Chem. **63**, 2679 (1985).
16. D. C. MANNING, W. SLAVIN, and G. R. CARNRICK. Spectrochim. Acta, **37B**, 331 (1982).
17. F. Y. LEUNG and A. R. HENDERSON. At. Spectrosc. **4**, 1 (1983).
18. W. SLAVIN, G. N. CARNRICK, and D. C. MANNING. Anal. Chem. **54**, 621 (1982).
19. R. A. NADKARNI. Anal. Chem. **56**, 2233 (1984).
20. K. B. PIERSON and M. A. EVENSON. Anal. Chem. **58**, 1744 (1986).
21. H. C. KAUFMANN and J. STEENBLIK. Nucl. Inst. Methods Phys. Res. **B3**, 198 (1984).
22. E. S. GLADNEY. Anal. Chim. Acta, **118**, 385 (1980).
23. J. B. JONES, JR. J. Asso. Off. Anal. Chem. **58**, 764 (1975).
24. R. A. NADKARNI. Radiochem. Radioanal. Lett. **30**, 329 (1977).
25. P. SCHRAMEL. Spectrochim. Acta, **38B**, 199 (1983).
26. N. M. ARAFAT and W. A. GLOOSCHENKO. Analyst, **106**, 1174 (1981).
27. S. J. KIRCHNER, H. OONA, S. J. PERRON, Q. FERNANDO, J. J.-H. LEE, and H. ZEITLIN. Anal. Chem. **52**, 2195 (1980).

Can. J. Chem. Downloaded from www.nrcresearchpress.com by 78.46.186.204 on 09/07/12
For personal use only.

Pulse cyclic voltammetry. I. Static solutions

GORDON N. ECCLES AND WILLIAM C. PURDY
Department of Chemistry, McGill University, 801 Sherbrooke St. West, Montreal, P.Q., Canada H3A 2K6

Received September 28, 1986

This paper is dedicated to Professor Douglas E. Ryan on the occasion of his 65th birthday

GORDON N. ECCLES and WILLIAM C. PURDY. Can. J. Chem. **65**, 1051 (1987).

By using pulse cyclic voltammetry rather than cyclic voltammetry at a relatively high scan rate, an increase in sensitivity and a lowering of the detection limit by more than a factor of two are demonstrated for the ferricyanide–ferrocyanide couple at a carbon electrode. The test for reversibility based on peak shape or symmetry comparison is enhanced significantly with pulse cyclic voltammetry. Another reversibility test, by observing peak variations as a function of scan rate, was applied to pulse cyclic voltammetry and was found to be as diagnostically informative as the cyclic voltammetry test. These tests are illustrated by a study of the hydroquinone–quinone couple.

GORDON N. ECCLES et WILLIAM C. PURDY. Can. J. Chem. **65**, 1051 (1987).

Dans le cas du couple ferricyanure/ferrocyanure à une électrode de carbone, on démontre que l'utilisation de la voltamétrie cyclique pulsée plutôt que la voltamétrie cyclique à des taux de balayage relativement élevés augmente la sensibilité et diminue la limite de détection par un facteur qui est plus grand que deux. Avec la voltamétrie cyclique, on augmente considérablement le test pour la réversibilité qui est basé sur la forme du maximum ou sur une comparaison de la symétrie. On a aussi appliqué un autre test de réversibilité, basé sur les variations des maxima observés en fonction du taux de balayage, à la voltamétrie pulsée et on a trouvé que ce test permet un aussi bon diagnostique que le test de la voltamétrie cyclique. On illustre ces tests par une étude du coupe hydroquinone/quinone.

[Traduit par la revue]

Can. J. Chem. Downloaded from www.nrcresearchpress.com by 78.46.186.204 on 09/07/12
For personal use only.

Introduction

Cyclic voltammetry (CV) is a well documented electroanalytical technique offering a wealth of information for the study of redox couples, reaction kinetics, and the mechanism of many electrochemical reactions (1–4). Its use, however, has been restricted primarily to the gathering of qualitative information. Quantitative determinations are better made by other electroanalytical techniques such as differential-pulse (5, 6) and square-wave voltammetry (5, 7, 8). By comparison these latter techniques offer increased sensitivity over CV due to their ability to effectively separate charging current, which contributes largely to the background, from the faradaic current and interpretation of the peak readout is much simpler. In multicomponent analysis well-defined peaks are simpler to resolve as opposed to the semi-peak readout for CV. It would, therefore, be plausible to expect the same benefit when using CV with pulsed techniques. The present work was undertaken to confirm this model using the ferricyanide–ferrocyanide couple as the example.

When a new redox couple is studied with the aim of evaluating the reaction mechanism, cyclic voltammetry can provide critical information about the electrochemical reversibility of the electrode reaction. The usual procedure involves measuring either peak separations or peak height ratios for the anodic and cathodic peaks as a function of scan rate (3, 4). If a couple is reversible, the separation will equal $59/n$ mV, where n is the number of electrons involved in the electrode reaction, and the peak height ratio will be close to unity. A somewhat simpler method is to examine the symmetry or shape of the response curves obtained for each scan direction (1). If the couple is reversible, then the curves for the two scan directions will be superimposable. When a redox couple is slightly or quasi-reversible, the shapes of a cyclic voltammogram are not sufficiently different to determine reversibility at a glance. In contrast, pulse cyclic voltammetry (PCV) emphasizes peak symmetry differences. This effect will be illustrated with the data collected for the hydroquinone–quinone couple.

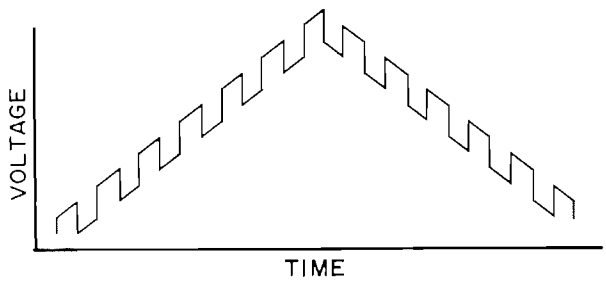

FIG. 1. Working electrode waveform.

Experimental

Electrochemical apparatus

The microprocessor-controlled potentiostat used to carry out CV and pulse cyclic voltammetry (PCV) has been described previously (9). The work described in that paper was based on the waveform shown in Fig. 1. A square wave is superimposed on a linear sweeping voltage and the data are obtained prior to each pulse transition. This type of waveform offers electrochemical information in two time domains. In addition to the conventional CV time scale, another short time scale is obtained from the negative and positive going pulses. During the lifetime of a pulse in this waveform the potential continues to ramp, introducing a charging current component. Additional equipment required includes an IBM PC with 640 kbytes of memory, an IBM colour monitor, a HP 7470 2-pen plotter, and a three-electrode cell consisting of an SCE reference, platinum wire auxiliary, and a low temperature isotropic carbon (LTIC) working electrode (1.57 cm^2, available from Carbomedics Inc., Austin, TX). This cell was fitted with a nitrogen gas purging system.

The software language used to operate the instrument and manipulate the data was written in TURBO Pascal-87. The program is menu-driven and communicates interactively with the operator for smooth operation.

Chemicals

Reagent grade chemicals were used in preparation of all solutions. A 2.00 m*M* stock solution of potassium ferricyanide was prepared by dissolving the salt in 1 *M* potassium nitrate. Solutions of 1.00, 0.400, 0.200, and 0.080 m*M* were subsequently prepared by diluting

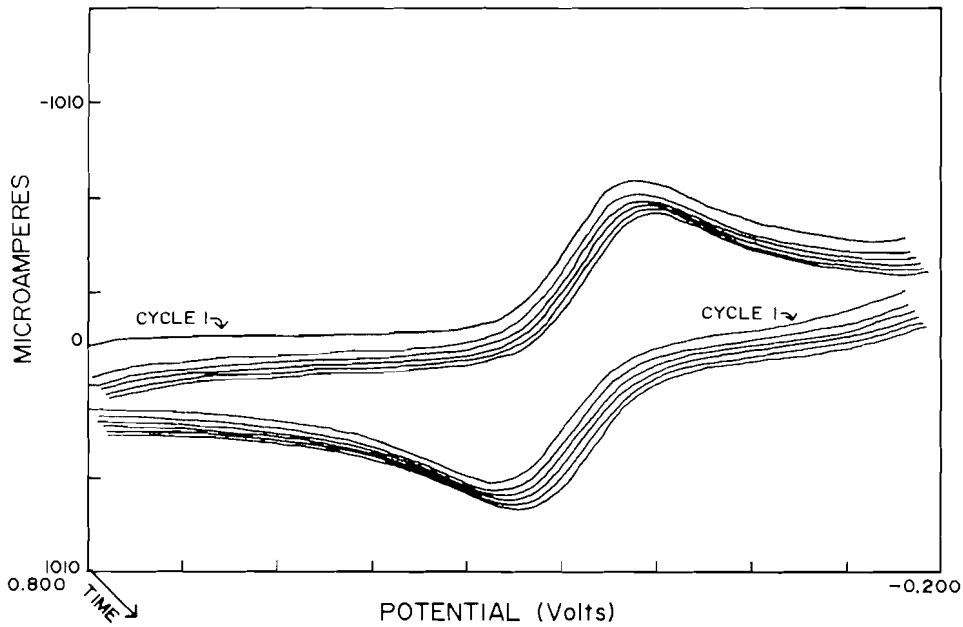

FIG. 2. Multiple scan cyclic voltammogram of 2 m*M* ferricyanide in 1 *M* potassium nitrate. Number of cycles = 6. Data acquisition frequency = 120 Hz. Voltage ramp = 1 V/s.

the appropriate volume of the stock solution in 1 *M* potassium nitrate. Solutions of quinone and hydroquinone, 1 m*M*, were prepared by dissolving the required weights in 1 *M* sulfuric acid.

Procedure

Cyclic and pulse cyclic voltammograms were obtained for various concentrations of ferricyanide in 1 *M* potassium nitrate. The sequence was to purge each solution with nitrogen gas for 15 min, hold the working electrode at 0.800 V for several minutes, and then apply the waveform. A total of two runs containing six consecutive cycles was obtained for each concentration in both modes of operation.

Cyclic and pulse cyclic voltammograms were obtained from 1 m*M* solutions of quinone and hydroquinone in 1 *M* sulfuric acid at various scan rates. The sequence was similar to the one described above except the holding potential for the quinone solution was −0.200 V. One run containing five consecutive cycles was obtained for each solution in both modes of operation.

All the data were stored on a hard disk in the computer and processed later by outputting the response current vs. potential curves to a plotter.

Results

CV and PCV as a quantitative tool

It is rare to continue the waveform in a CV experiment for more than two or three cycles (4). In fact, much of the diagnostic information available from a cyclic voltammogram can be obtained from the first cycle. In quantitative work using an LTIC electrode, however, it is best to use the data collected after completion of this cycle. This is illustrated by the results of a multiple scan CV of 2 m*M* potassium ferricyanide in 1 *M* potassium nitrate shown in Fig. 2. To reduce confusion from overlapping lines, the forward and reverse scan results are arbitrarily spaced apart on the response current axis. The residual current becomes reproducible after completion of the first cycle and as a consequence the analyte signal does as well. Therefore there is little advantage to continuing the scan beyond the third cycle.

A PCV experiment on the same redox couple is shown in Fig. 3. It is difficult to observe a background current difference between the first cycle and subsequent cycles and this would indicate that PCV can be used for quantitative work on the first cycle. It is appropriate here to discuss the format and information obtained in this plot. The data presented on the left half of the figure were acquired from the forward scans. These curves represent the current obtained by calculating the absolute difference between a point acquired during a forward pulse and another during the respective reverse pulse. In an identical manner, the data on the other side of the switching potential (right half of the figure) were obtained from the pulses applied during the reverse scan.

The peak currents for both CV and PCV experiments for various concentrations of potassium ferricyanide were plotted and are shown in Fig. 4. The two upper curves, acquired from PCV data, show the expected increase in sensitivity in comparison to CV data. The pulsed data show a drop in signal at 2 m*M* which is probably due to departure from the dynamic range of this technique at this scan rate. The linear regression equation for the forward-scan peak in PCV excluding the data for 2 m*M* ferricyanide (top curve) was $y = -16.37 + 493.34x$ with a correlation coefficient of 0.998. The equation obtained for the forward-scan peak in CV (second from the bottom) was $y = -10.06 + 327.36x$ with a correlation coefficient of 0.9997. The detection limits obtained were 0.4×10^{-5} *M* and 1×10^{-5} *M* for PCV and CV.

Comparison of CV and PCV response curve symmetry differences for the hydroquinone–quinone redox couple

Consistent with the above, a multiple CV scan of the hydroquinone–quinone couple shows reproducibility after the first cycle (Fig. 5). The shapes of the forward and reverse scan peaks obtained during these cycles do not appear sufficiently different to test reversibility of the couple and further information is needed using one or both of the measurement techniques described above.

An alternative method of presenting PCV data which is diagnostically more informative is to plot the raw data obtained during the forward and reverse pulses. This gives an insight in

Can. J. Chem. Downloaded from www.nrcresearchpress.com by 78.46.186.204 on 09/07/12
For personal use only.

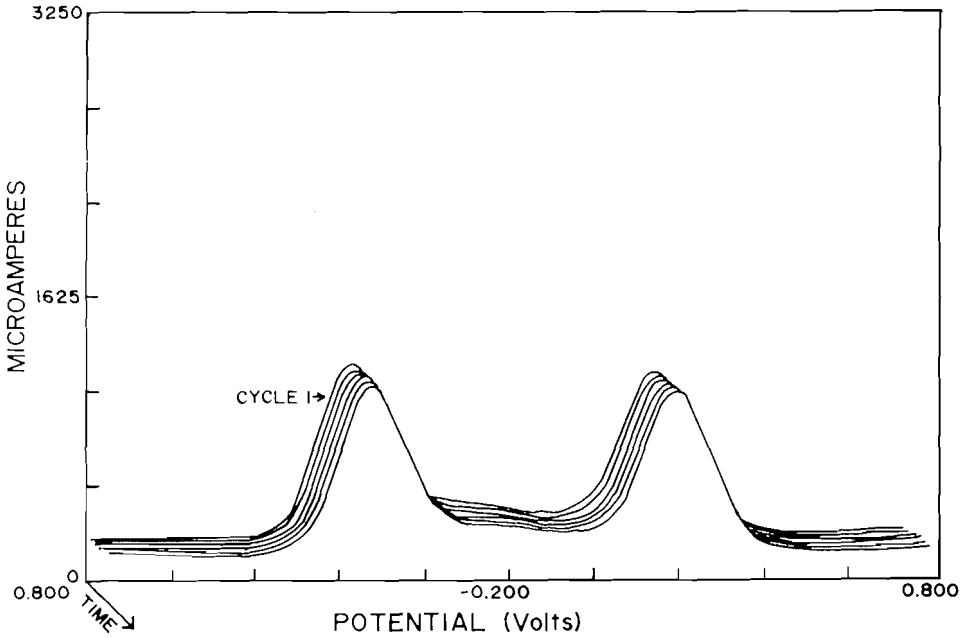

FIG. 3. Multiple scan pulse cyclic voltammogram of 2 m*M* ferricyanide in 1 *M* potassium nitrate. Number of cycles = 6. Data acquisition frequency = 130 Hz. Square wave frequency = 65 Hz. Square wave amplitude = 100 mV. Voltage ramp = 1 V/s.

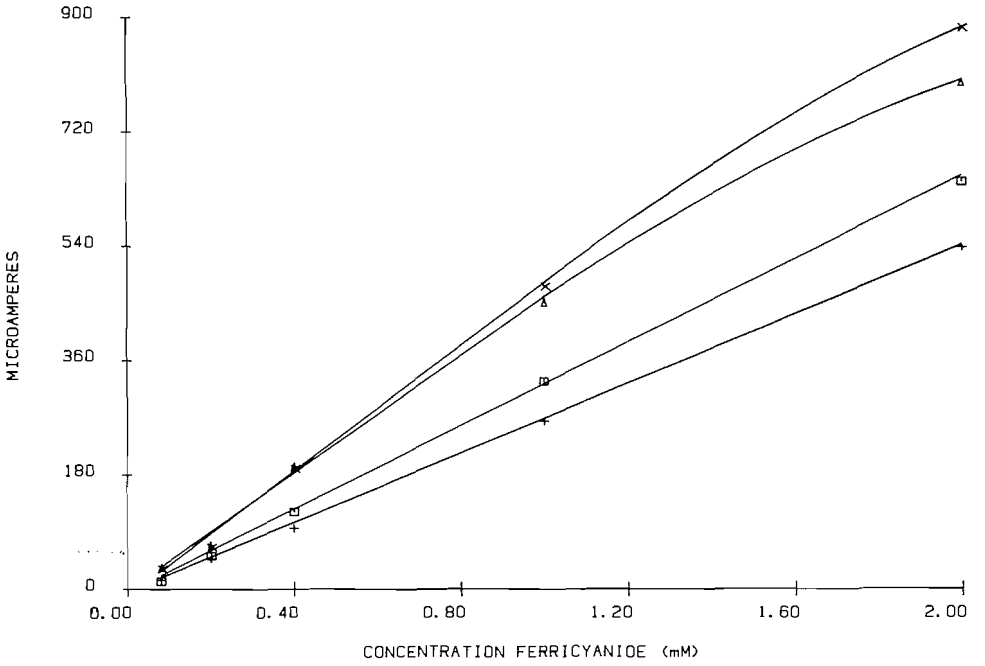

FIG. 4. Comparison of pulse cyclic and cyclic voltammetry calibration curves for various concentrations of ferricyanide: (●) PCV reduction, (△) PCV oxidation, (□) CV reduction, (×) CV oxidation.

two time domains (see Fig. 6). For clarity, in this and the following two figures the third run is plotted to give the pulsed cyclic voltammogram. The two peaks on the left-hand side of Fig. 6 (or to the left of the −0.200 V switching potential) describe what is occurring during the forward scan. The major peak (in the negative microampere region) represents the reduction current for the reduction of quinone to hydroquinone and is obtained from the upward pulses of the applied waveform. The minor peak represents the oxidation of the generated hydroquinone during the downward pulses (short time scale).

On the right-hand side of Fig. 6 the major peak (long time scale) is the oxidation current obtained from the downward pulses in the reverse scan. The poorly defined hump in the upper trace was the contribution of reduction current taken in the short time scale. It is clear from the difference plot of these data (Fig. 7), that the height of the reverse-scan peak exceeds that of

Can. J. Chem. Downloaded from www.nrcresearchpress.com by 78.46.186.204 on 09/07/12
For personal use only.

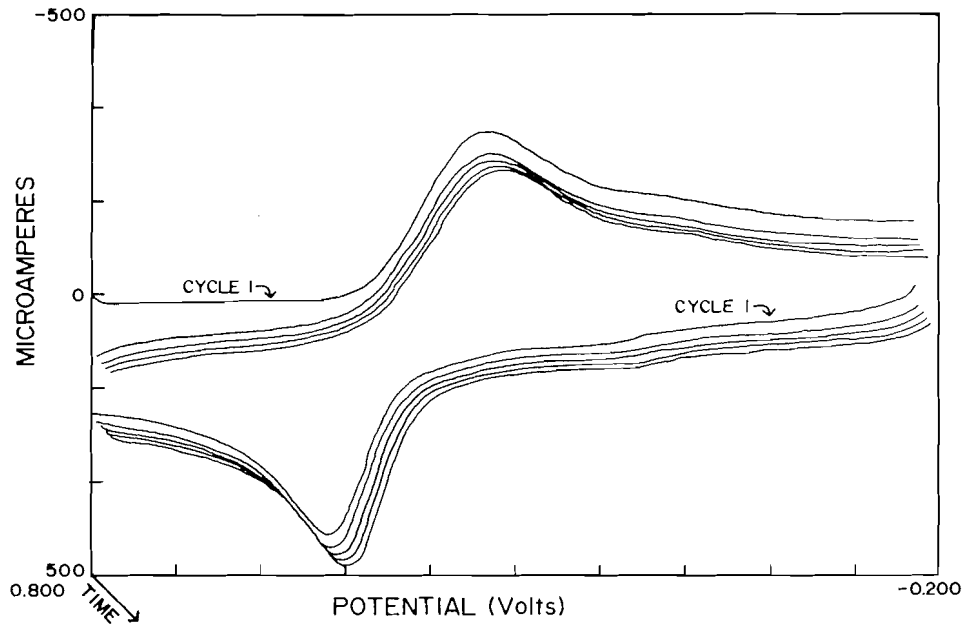

FIG. 5. Multiple scan cyclic voltammogram of 1 m*M* quinone in 1 *M* sulfuric acid. Number of cycles = 5. Data acquisition frequency = 120 Hz. Voltage ramp = 100 mV/s.

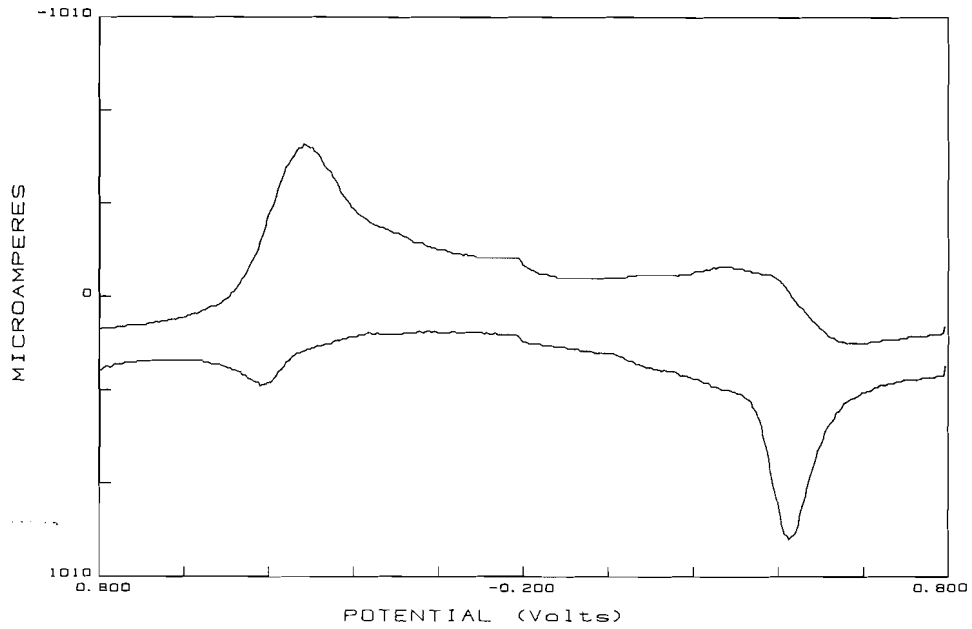

FIG. 6. Third cycle of a multiple scan pulse cyclic voltammogram of 1 m*M* quinone in 1 *M* sulfuric acid. Number of cycles = 5. Data acquisition frequency = 130 Hz. Square wave frequency = 65 Hz. Square wave amplitude = 100 mV. Voltage ramp = 100 mV/s.

the forward scan and that the shapes are different. This signifies that this redox couple is irreversible at the scan rate studied. Further tests are required to determine whether the couple is slightly or quasi-reversible. Nevertheless the plot does indicate at a glance that the couple is not reversible, a feature that the cyclic voltammogram of the same couple (Fig. 5) does not as convincingly provide. It follows then, that a difference current plot of a hydroquinone solution would likely show irreversibility as well. Figure 8 confirms this and also indicates that the forward-scan difference peak current is greater in magnitude than the peak in the reverse scan. This is exactly opposite to what was observed with the quinone solution.

The variation of peak positions as a function of scan rate for CV and PCV difference plots to determine reversibility were obtained for the solutions hydroquinone and quinone. The results tabulated in Table 1 indicate that peak separations

Can. J. Chem. Downloaded from www.nrcresearchpress.com by 78.46.186.204 on 09/07/12
For personal use only.

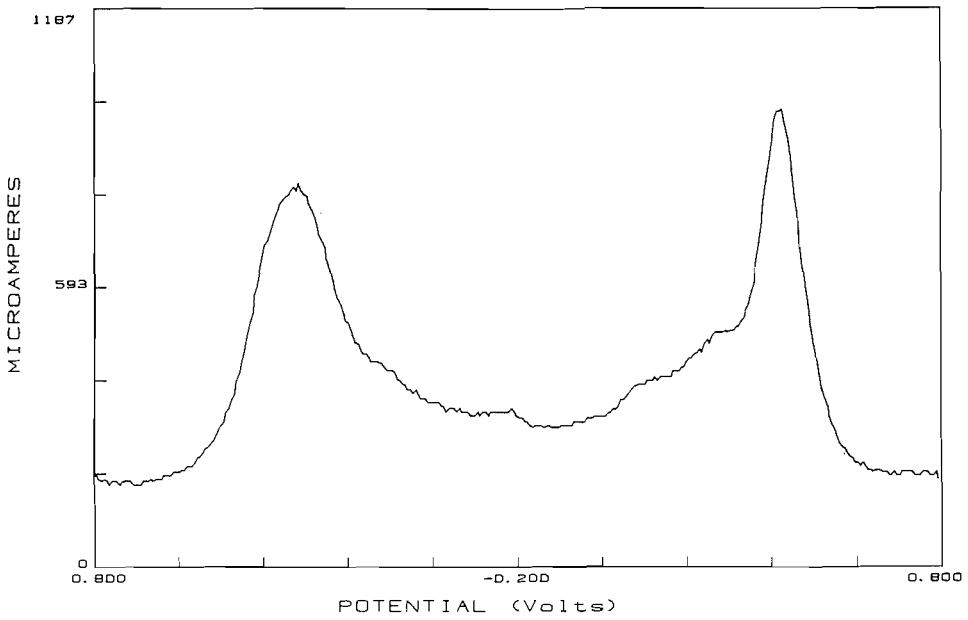

FIG. 7. Third cycle of a multiple scan difference pulse cyclic voltammogram of 1 m*M* quinone in 1 *M* sulfuric acid. Number of cycles = 5. Data acquisition frequency = 130 Hz. Square wave frequency = 65 Hz. Square wave amplitude = 100 mV. Voltage ramp = 100 mV/s.

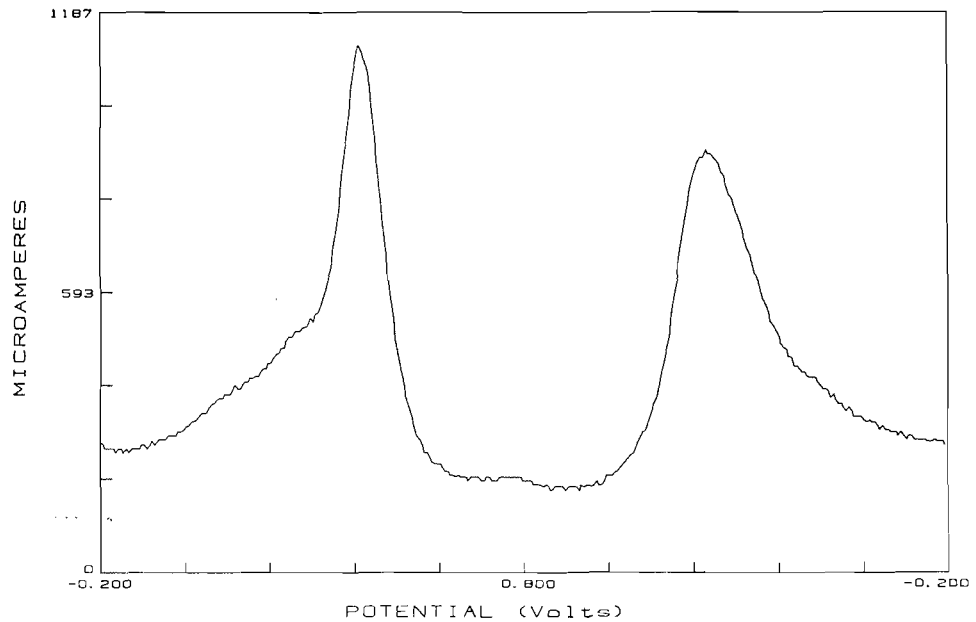

FIG. 8. Third cycle of a multiple scan difference pulse cyclic voltammogram of 1 m*M* hydroquinone in 1 *M* sulfuric acid. Number of cycles = 5. Data acquisition frequency = 130 Hz. Square wave frequency = 65 Hz. Square wave amplitude = 100 mV. Voltage ramp = 100 mV/s.

are narrower but do expand with increasing scan rate for the PCV data. This confirms that this test of reversibility is another useful diagnostic tool that PCV has to offer.

To investigate the use of PCV as a quantitative tool for a solution of hydroquinone, the calibration curve may be best obtained from the major peak during the forward scan in terms of sensitivity (Fig. 8). Linear sweep square-wave voltammetry would, as the forward scan, yield the same type of curve. In contrast, however, a pulse cyclic voltammogram of a quinone solution (Fig. 7) exhibits the major peak during the reverse scan, indicating an ability that the linear sweep technique lacks. A range of scan rates was applied to 1 m*M* solutions of quinone and hydroquinone using CV and PCV. The peak currents for both the forward and reverse scans for CV were plotted against the log of the scan rate. Included on each plot are four PCV curves; two forward and reverse difference current curves and

Can. J. Chem. Downloaded from www.nrcresearchpress.com by 78.46.186.204 on 09/07/12
For personal use only.

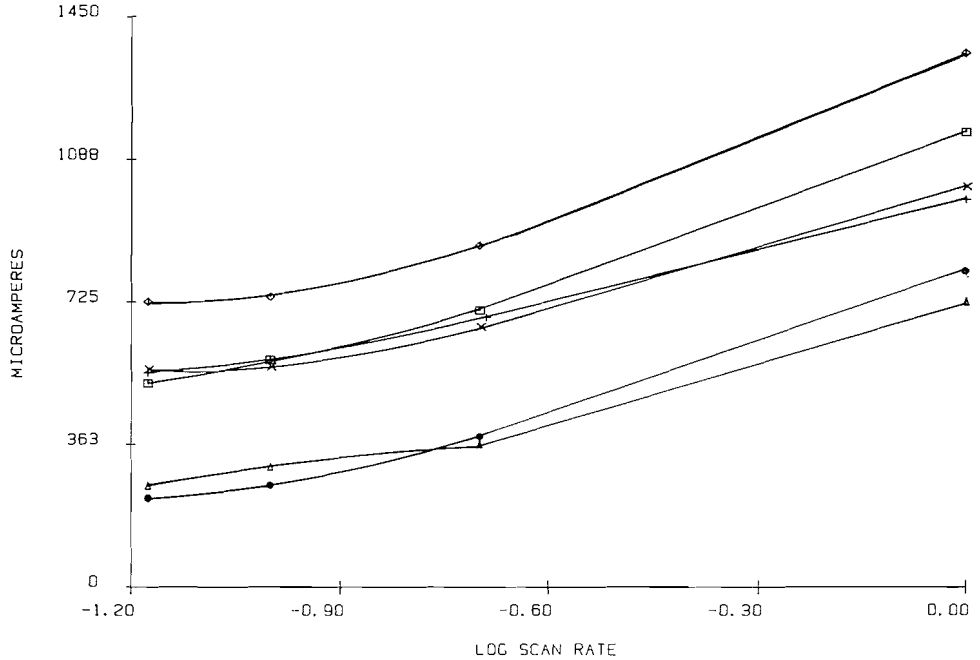

FIG. 9. Response vs. log scan rate for 1 m*M* quinone using cyclic and pulse cyclic voltammetry: (●) CV reduction, (△) CV oxidation, (□) PCV reduction, (+) PCV oxidation, (×) PCV difference reduction, (◇) PCV difference oxidation.

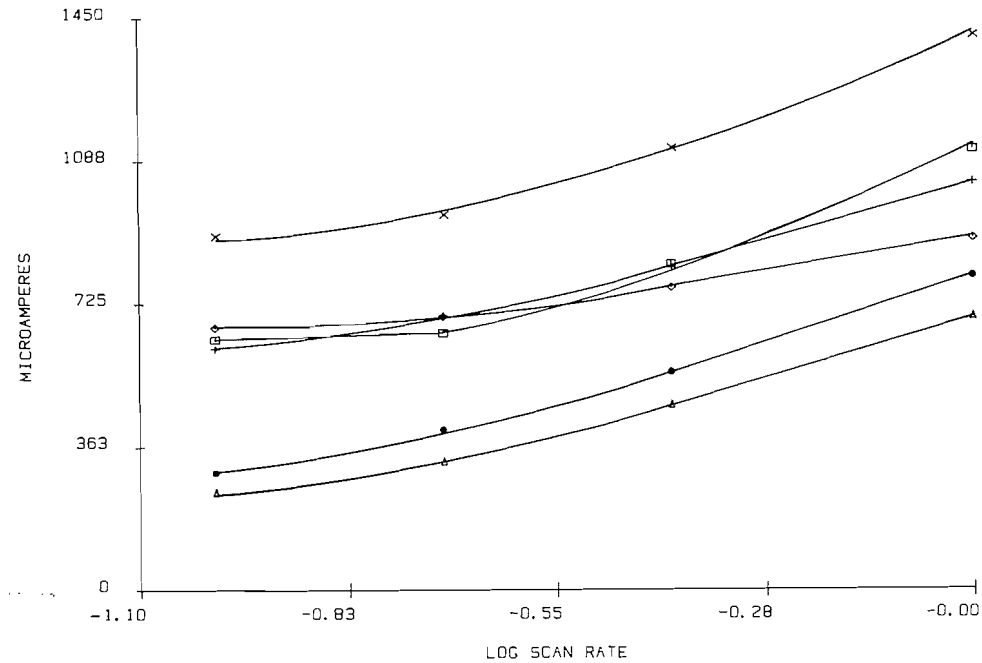

FIG. 10. Response vs. log scan rate for 1 m*M* hydroquinone using cyclic and pulse cyclic voltammetry: (●) CV reduction, (△) CV oxidation, (□) PCV reduction, (+) PCV oxidation, (×) PCV difference reduction, (◇) PCV difference oxidation.

the raw data curves plotted against log scan rate (Figs. 9 and 10). By examining both plots it can be concluded that at the scan rates studied, the PCV difference oxidation peak for either solution offers the greatest sensitivity for quantitative work and indeed CV offers the least.

Conclusions

PCV and CV offer quantitative information if the second or third cycle is used for data analysis as was shown using the ferri–ferrocyanide couple on an LTIC electrode. The detection limit of ferricyanide was found to be 0.4×10^{-5} *M* using PCV and 1×10^{-5} *M* using CV at a scan rate of 1 V/s. The relative sensitivity of these two techniques was shown to be greater for PCV experiments. Present work includes the use of signal averaging and fourier smoothing techniques to further increase the sensitivity.

PCV emphasizes shape or symmetry contrast as a test of reversibility for the quinone–hydroquinone redox couple

Can. J. Chem. Downloaded from www.nrcresearchpress.com by 78.46.186.204 on 09/07/12
For personal use only.

TABLE 1. Peak separation as function of scan rate for hydroquinone and quinone using CV and PCV data

Scan rate (V/s)	Peak separation (V)			
	Hydroquinone		Quinone	
	CV	PCV	CV	PCV
1.000	0.245	0.148	0.270	0.169
0.400	0.208	0.112	0.235	—
0.200	0.184	0.077	0.220	0.121
0.100	0.184	0.054	0.183	0.099
0.067	0.139	—	0.156	0.063

studied. The difference current plots obtained, provide a rapid conclusive test. In contrast, CV data for the same couple were not as informative. Another popular CV test of reversibility using peak separation as a function of scan rate was applied and ratified by PCV data obtained on the same redox couple. It was also shown that the major peak for either a solution of quinone or hydroquinone was due the oxidation of hydroquinone. In the case of the quinone solution the hydroquinone was generated during the forward-scan of the applied waveform.

Acknowledgement

The authors are indebted to the Natural Sciences and Engineering Research Council of Canada for financial support of this work.

1. R. N. ADAMS. Electrochemistry at solid electrodes. Marcel Dekker Inc., New York. 1969.
2. A. J. BARD and L. R. FAULKNER. Electrochemical methods. Wiley, New York. 1980.
3. P. T. KISSINGER and W. R. HEINEMAN. J. Chem. Ed. **60**, 9 (1983).
4. P. T. KISSINGER and W. R. HEINEMAN. Laboratory techniques in electroanalytical chemistry. Marcel Dekker Inc., New York and Basel. 1984.
5. G. C. BARKER. Anal. Chim. Acta, 18 (1958).
6. J. G. OSTERYOUNG and K. HASEBE. Rev. Polarogr. Jpn. **22**, 1 (1976).
7. J. M. CHRISTIE, J. A. TURNER, and R. A. OSTERYOUNG. Anal. Chem. **49**, 1899 (1977).
8. J. G. OSTERYOUNG and R. A. OSTERYOUNG. Anal. Chem. **57**, 101A (1985).
9. G. N. ECCLES and W. C. PURDY. Anal. Lett. **18**(A6), 657 (1985).

Can. J. Chem. Downloaded from www.nrcresearchpress.com by 78.46.186.204 on 09/07/12
For personal use only.

The X-ray photoelectron spectroscopy of ancient murals in the tombs at Beni Hasan, Egypt

K. M. WILSON-YANG AND GEORGE BURNS

Lash Miller Chemical Laboratories, University of Toronto, 80 St. George St., Toronto, Ont., Canada M5S 1A1

Received January 29, 1986[1]

This paper is dedicated to Professor Douglas E. Ryan on the occasion of his 65th birthday

K. M. WILSON-YANG and GEORGE BURNS. Can. J. Chem. **65**, 1058 (1987).

The once colourful mural paintings at the Beni Hasan tombs (ca. 2100 B.C.), an important Egyptian archaeological site, are covered with an obscuring grey deposit. Qualitative observations made over the past 150 years were assembled and correlated with each other by us. Cumulatively, they indicate that recently the development of this layer has accelerated. To study this surface degradation, X-ray photoelectron spectra of fragments from the painted walls have been collected. Empirical XPS sensitivity factors have been employed to treat the data semiquantitatively. Three types of surfaces were identified. The first surface consists of $CaCO_3$ and SiO_2 as major constituents, and was the only surface identified previously. Our XPS data indicate that it also contains Al_2O_3, NaCl, MgO, sulphates, and phosphates as minor and trace components. The second surface consists predominantly of aluminium silicates. The third surface consists mostly of calcium carbonate. A preliminary mechanism for opaque layer formation is proposed herein. It suggests that the principal physicochemical processes are adsorption of water in the presence of carbon dioxide, followed by dissolution of the substrate walls upon which the murals were painted. This mechanism is consistent with our finding that mural deterioration is recent; it also indicates that deterioration is progressive, continuous, and cumulative. Further experiments are designed to verify the proposed mechanism. Two mechanisms proposed earlier are found to be inconsistent with at least some of our findings. Relatively recent efforts in removing obtrusive surface layers with dilute HCl were found to be performed carefully; there was no evidence of excess chlorides on cleaned surfaces. However, this finding does not provide a guarantee that murals were undamaged by HCl below the surface. It does suggest that progressive damage due to the formation of hygroscopic $CaCl_2$ on the surface has been avoided.

K. M. WILSON-YANG et GEORGE BURNS. Can. J. Chem. **65**, 1058 (1987).

Les peintures murales très colorées des tombes de Beni Hasan (environ 2100 B.C.), un site archéologique égyptien important, sont couvertes par un dépot gris qui les rend moins claires. On a rassemblé et établi des corrélations entre les diverses observations qualitatives qui ont été faites au cours des 150 dernières années. Ces observations prises d'une manière cumulative indiquent que le développement de cette couche s'est récemment accéléré. Dans le but d'étudier cette dégradation de la surface, on a recueilli les spectres photoélectroniques par rayons-X de fragments provenant de la peinture des murs. Dans le but de faire un traitement semi-quantitatif des données, on a utilisé des facteurs empiriques pour la sensibilité des SPX. On a identifié trois types de surfaces. Les constituants principaux de la première sont le $CaCO_3$ et le SiO_2; il s'agit de la seule surface qui avait été identifiée antérieurement. Nos données de SPX indiquent qu'elle contient aussi du Al_2O_3, du NaCl, du MgO, des sulfates et des phosphates, comme constituants mineurs et à l'état de traces. La deuxième surface est formée principalement de silicates d'aluminium. La troisième surface consiste essentiellement en carbonate de calcium. On propose un mécanisme préliminaire pour la formation de la couche opaque. Ce mécanisme suggère que le principal processus physico-chimique est l'adsorption de l'eau, en présence de bioxyde de carbone, qui est suivie d'une dissolution des murs qui agissent comme substrats et sur lesquels les murales avaient été peintes. Ce mécanisme est en accord avec nos observations selon lesquelles la détérioration murale est récente; il indique aussi que la détérioration est progressive, continue et cumulative. Dans le but de vérifier le mécanisme proposé, on envisage d'autres expériences. On a trouvé que deux mécanismes proposés antérieurement ne sont pas en accord avec un certain nombre de nos observations. Des efforts ont été déployés récemment dans le but d'enlever les couches superficielles qui créent des obstructions et, pour ce faire, on procède à des lavages avec du HCl dilué; nos observations, à l'effet que l'on ne retrouve pas de résidus d'ions chlorures sur les surfaces nettoyées, démontrent que que cette opération peut être effectuée avec soins. Toutefois, ces observations ne fournissent aucune garanties relativement aux dommages que le HCl aurait pu faire subir aux murales en-dessous de la surface. Ces observations suggèrent toutefois que l'on a pu éviter les dommages progressifs qui auraient pu être causés par la formation de $CaCl_2$ hygroscopique sur la surface.

[Traduit par la revue]

Introduction

The tombs at Beni Hasan, near Minya in Middle Egypt, date from circa 2400 B.C. to 1700 B.C. (6th Dynasty, Old Kingdom, to 12th Dynasty, Middle Kingdom). They are cut in levels in cliffs on the east bank of the Nile, and number over 400. The tombs in the uppermost level, carved from a single stratum of polycrystalline calcite (nummulitic limestone) have attracted much interest (1, 2). Of the 39 upper level tombs, 12 have fine murals dating from circa 2180 B.C. to 1786 B.C. (First Intermediate Period to Middle Kingdom) and are not only important artistically but also constitute a significant record of ancient Egyptian life. The First Intermediate Period is the "dark age" of Egyptian history which immediately followed the earliest known breakdown of a major advanced civilization. Complete disintegrations of major civilizations, and the socio-economic chaos which follows them, are now known to have occurred a number of times in the past; there is much evidence and concern that they continue to occur even at present (3). Although these phases of history attract the considerable attention of scholars in a number of disciplines, they are still poorly understood, because historic evidence from the "Time of Troubles" (3) is often irretrievably lost. Predictably, historic sources from the First Intermediate Period are also scarce. Therefore, it is particularly important to preserve such historic monuments. Yet, ancient artifacts deteriorate with time and, in the case of Beni Hasan, even the basic physicochemical processes which are responsible for such deterioration, are still inadequately identified. No comprehensive conservation and restoration efforts can be undertaken unless these processes are precisely determined; otherwise preservation efforts may only

[1]Revision received January 20, 1987.

Can. J. Chem. Downloaded from www.nrcresearchpress.com by 78.46.186.204 on 09/07/12
For personal use only.

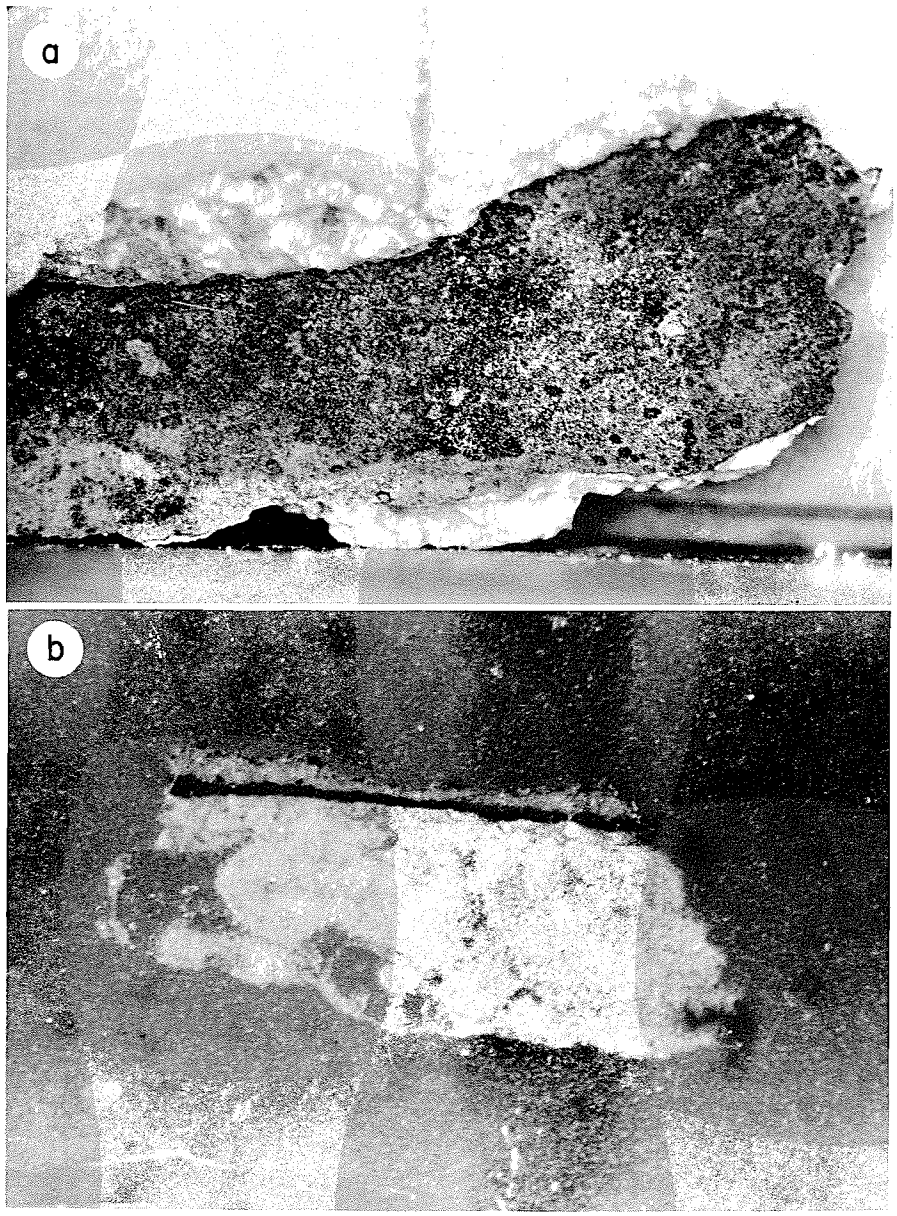

FIG. 1. (*a*) The surface of sample 4, indicating the appearance of the painted surface; the magnification is 2× on 35 mm negative. (*b*) Sample 4 in cross-section; the magnification is 63× on 35 mm negative. The dark layer seen is pigment; the upper layer is the obscuring surface deposit; 20–70 μm thick. The lower region is substrate.

Can. J. Chem. Downloaded from www.nrcresearchpress.com by 78.46.186.204 on 09/07/12
For personal use only.

further damage these ancient sources of information and destroy this great work of art.

A physicochemical investigation of this site was prompted by the presence of an ubiquitous, almost opaque layer on the wall surfaces. Figure 1 illustrates the general appearance of this layer and its cross-section. The earliest mechanism for opaque layer formation was suggested on the basis of visual assessments (4). It proposes that the formation of these layers was initiated by the percolation of water through rock; calcium carbonate and calcium sulphate are carried from any underlying plaster to the surface and deposited as the water evaporated. The idea that water flow could be involved, was novel because it was not obvious that moisture could play an important role in physicochemical processes in the arid regions of Egypt, and to that extent, the mechanism (4) had merit. Nonetheless, it is unlikely that water *percolation* was involved because there was no evidence of extensive water flow. There are no stalactites or stalagmites in these cave-like tombs. No irregularities or discontinuities associated with flow-lines or cracks are seen; on the contrary, the surface is disfigured in a continuous manner.

In a more recent study (5, 6), X-ray diffraction (XRD) analysis of the opaque surface layer showed that it was composed, not of sulphates, as was suggested in the first mechanism (4), but predominantly of $CaCO_3$, SiO_2, and feldspar. Isolated resistivity measurements made within the walls showed no water (5). On the basis of this information, a second, alternative, mechanism was suggested, in which CO_2-saturated, dew-point condensation on the wall surfaces dissolves calcium carbonate present in deposited dust (5, 6). Silica and other less soluble dust constituents are then sealed within a carbonate matrix formed as $CaCO_3$ precipitates. There is a considerable difference between the two mechanisms

TABLE 1. Sample description and provenance

Parameter	Value for sample					
	1	2	3	4	5	6
Size, mm × mm	4 × 4	2 × 2	2 × 5	5 × 10	4 × 4	3 × 10
Tomb	3	3	15	33	2	23
Distance from floor, m (approximate)	1.2	0.9	2.3	1.5	1.8	2.1

in ref. 4 and refs. 5, 6, especially because the first mechanism predicts disintegration of the substrate upon which the murals were painted while the second does not.

The time of formation of this surface layer was placed in the early part of the Christian era (5), because habitation of these tombs appears to have been commonplace at that time and therefore, the partial pressure of CO_2, P_{CO_2}, and relative humidity, RH, were high (5). Although this suggestion appeared reasonable, it was not based on experimental findings. However, a review of empirical and historical evidence (2) suggests an alternative explanation. In 1798, it was reported that the murals were well-conserved throughout (7). By 1890, deterioration was recognized and it was noted that many of the painted records were indecipherable (7). In the 1930's, copyists referred to a salty coating which made the assessment of colour difficult; however, it was noted that the pigmentation could be uncovered by lightly touching the coating with a brush (8). In 1981, it was reported that the disfiguring coating had coalesced and could no longer be brushed off (2). These findings do not preclude a possibility that at least some opaque layers had been formed in the early Christian era, as was earlier (5) suggested. However, the second mechanism (5, 6) does not account for the recent acceleration of opaque layer formation, and therefore, does not explain the existence of the bulk of it. It can be concluded that neither one of the existing mechanisms (4–6) explains the nature or the dynamic development of the opaque layer.

X-Ray photoelectron spectroscopy

To begin a systematic study of the degradation phenomena now occurring in the Beni Hasan tombs, X-ray photoelectron spectroscopy (XPS) was employed here. This technique makes it possible to examine the first few nanometers of surfaces and is therefore suitable for study of the growth of the obtrusive surface layer. A representative selection of six painted fragments from these tombs was so studied.

The use of the powerful XPS technique in the archaeometric studies of surfaces has been limited. However, this method of analysis has been employed to investigate oxidation states and compositions of unprepared surfaces with or without Ar^+ etching (9, 10).

The inherent heterogeneity of archaeological surfaces makes it difficult to secure representative and accurate data. It is possible, however, to treat data semiquantitatively. Simple intensity ratios (9) and ratios correlated with known weight percentages (11) have been used in pottery analyses. Inter-element comparisons of Egyptian pigments have been made from intensity ratios corrected using empirical sensitivity factors (10) or photoelectric cross-sections (12). In this paper, recent sensitivity factors (13), with a correction for detector efficiency, are used to reduce the data semiquantitatively.

Experimental

Red and yellow pigmented fragments of painted surfaces were cut from different areas of six of the thirty-nine upper level tombs at Beni Hasan using a clean, stainless-steel scalpel handled with disposable plastic gloves. The sample size was, on the average, approximately 3 mm × 1 mm × 0.5 mm. The samples were stored in pre-cleaned plastic screw-topped vials (Provial and Nalgene) packed with glass wool and sealed with strips of Parafilm. The number of collected samples was representative, but limited; the Beni Hasan tombs are considered an Egyptian National Treasure, and only limited but judicial intrusion on our part was justifiable.

Six samples were chosen from the total set for analysis by XPS (Table 1). These samples are representative of surface appearance, colour, and physical position. Samples 1 and 2 have yellow and red paint layers, respectively. Both samples appear irregular with some smooth, glaze-like patches. Sample 3, at one time painted red, is severely disfigured by a uniform white layer. Sample 4 has a black surface and originates from a heavily encrusted tomb which had evidence of severe smoke damage. Sample 5 is a fragment of red painted surface which had been cleaned on site with HCl about 10 years earlier (4). Sample 6 was originally yellow in colour and was taken from a portion of the wall which was slightly slanted in such a way as to prevent direct deposition of dust by gravity alone.

All Beni Hasan tombs face west and have access to the exterior by either open doors or windows. There is a noticeable decrease in disfigurement of the murals with height above the tomb floors. Therefore, all samples were taken from selected heights above floor level (Table 1).

To remove loose dirt and packing material, the surfaces were lightly vacuumed with a Pasteur pipette packed with glass wool attached through a control valve and trap to a mechanical pump.

XPS spectra were obtained on a McPherson ESCA-36 photoelectron spectrometer in the Surface Science Laboratory at the University of Western Ontario. An Mg X-ray anode operated at 200 W was used and data collection was under the control of a PDP-8E computer. Samples were mounted on the 8-place sample stage by Cu pins and secured thereon by a conducting Ag paste. Sample 4, due to its relatively large size (Table 1), was mounted by means of an Al mask. Typically, spectra were collected for 1 h over the full energy range of 0–1000 eV. Narrow energy range spectra, 10 eV in width, were obtained for Ca, N, S, P, and Si in sample 4 and for the carbon region in all samples except in sample 3. These latter spectra were collected for ten scans of the relevant energy region. Analysed areas were approximately 5 mm^2 maximum.

Results

Figure 2 provides the full energy range spectrum for sample 2. Energy resolution for this application of XPS has been assessed as 1.4 eV based on the fwhm of the Au($4f_{7/2}$) line[2] at 83.2 eV. However, when experimental fwhm from these heterogeneous surfaces are used, the resolution is approximately 2.3 eV. The accuracy of the spectra was found to be ±1 eV, based on the

[2]Dr. N. S. McIntyre, Surface Science Laboratory, University of Western Ontario, personal communication.

Can. J. Chem. Downloaded from www.nrcresearchpress.com by 78.46.186.204 on 09/07/12
For personal use only.

TABLE 2. Elements found by XPS: experimental and literature binding energies

Element and subshell assignment	Experimental binding energy, eV ± 1 eV *Narrow range spectra	Literature binding energy, eV	
Ca (2*p*)	348–350	349 Ca^0 $2p_{1/2}$[a]	349.5 $CaCO_3$[b]
	348.4*	345 Ca^0 $2p_{2/3}$	348.4 CaO[b]
(2*s*)	440		
(3*s*)	45		
C (1*s*)	(1) 284–286	284 C^0	
	(2) 289	284.1 graphite[c]	
		285 benzene	
		289 CO_3^{2-}[b]	
Si (2*p*)	102–204	100 Si^0	
	103.0*	103 SiO_2	
(2*s*)	155		
Al (2*s*)	120–122	117 Al^0	121 Al_2O_3[c]
(2*p*)	76		
N (1*s*)	401–403	399 N^0	
	401.0*	402 $(CH_3)_3NO$ i.e. organics	
		407 KNO_3[c]	
S (2*p*)	170–171	165 S^0	
	169.8*	164.2 S_8	
		168.9 Na_2SO_4	
P (2*p*)	134–137	130.5 P^0	132 Na_2PO_4
	132.7*	130 P^0, red	
(2*s*)	192		
Cl (2*p*)	199–202	203 Cl^0	
		201.4 NaCl	
Mg (2*s*)	90	88 Mg^0	91 MgO[c]
(2*p*)	50		
Na (2*s*)	65	62 Na^0	64 NaCl
KLL auger	265		
O (1*s*)	530	534 O^0	
(2*p*)	27		

[a]All values from ref. 16 unless otherwise noted.
[b]Personal communication with N. S. McIntyre, University of Western Ontario.
[c]Reference 23.

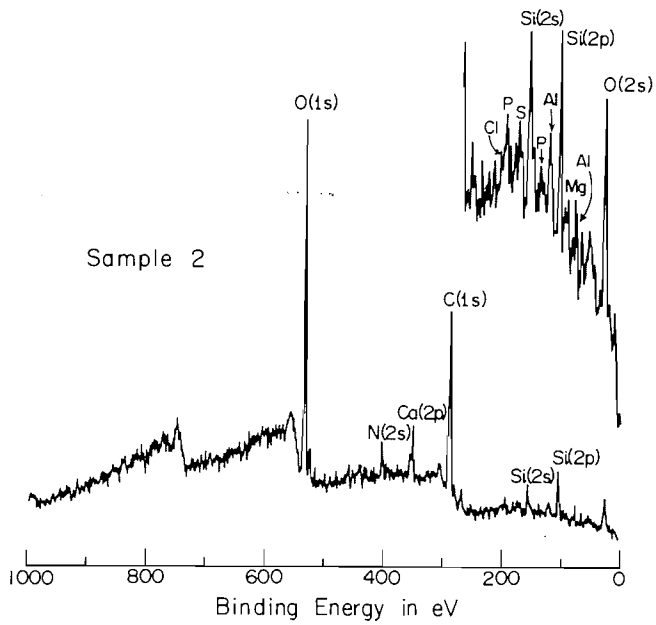

FIG. 2. X-ray photoelectron spectrum of sample 2. Arbitrary linear scale; inset is expanded vertically four times.

energies of the hydrocarbon C(1*s*) and the silica Si(2*p*) peaks at 285 eV and 103 eV, respectively. These peaks were found in each spectrum. The uncertainty of ±1 eV is predominantly due to charging differences between samples. Table 2 compares literature binding energies with experimental energies for the major peaks of each detected element and provides oxidation state assignments. The experimental energies of some confirming peaks are given also. No unusual difficulties were encountered in making assignments.

In order to obtain semiquantitative intensity comparisons, peak height ratios versus the O(1*s*) peak in each spectrum were taken. Peak heights rather than peak areas were used since it was found from short energy range spectra that the peak widths were constant at 2.3 eV fwhm. The ratios were further modified by a weighting factor. Each weighting factor is a product of improved empirical sensitivity factors (13) and a correction term which compensates for the energy dependence of the spectrometer detection efficiency. Mole ratios were found from the following expression:

$$[1] \quad \frac{n_i}{n_{O(1s)}} = \left(\frac{h_i}{h_{O(1s)}}\right)\left(\frac{S_{O(1s)}}{S_i}\right)\left(\frac{E_{O(1s)}}{E_i}\right)^2$$

For every element i, S_i is the empirical sensitivity factor (13),

Can. J. Chem. Downloaded from www.nrcresearchpress.com by 78.46.186.204 on 09/07/12
For personal use only.

TABLE 3. Mole ratios from XPS peak heights versus O(1*s*)

Element sample	Ca	C	Si	S	Mg	Na[a]	Cl	Al	P	N
1	0.03	2.4[b] 0.23	0.11	D[c]	0.11	D	0.04	0.09	D	D
O(1*s*)77[d]	8[d]	121 12	9		4		7	3		
2	0.04	0.75 0.23	0.13	N[c]	D	D	D	0.09	D	0.12
O(1*s*)120	19	61 19	16					7		13
3	0.07	0.31 0.41	0.09	0.02	0.02	D	D	0.04	0.01	0.02
O(1*s*)134	37	28 13	13	6	1			4	3	2
4	0.12	0.56 0.42	0.04	0.03	D	D	0.02	0.04	0.05	0.07
O(1*s*)117	50	44 33	5	7			7	6	3	7
5	N	3.3 N	0.10	N	N	N	D	0.07	N	0.06
O(1*s*)55		119 —	6					3		3
6	0.06	1.2 0.15	N	N	N	N	0.02	N	D	N
O(1*s*)130	30	104 36					5			

[a]Confirmed by the Na KLL Auger line at 265 eV.
[b]C as hydrocarbon; C as CO_3^{2-} second entry.
[c]D, detected i.e. peak height ≥ 2× average background peak height. N, not detected i.e. peak height < 2× average background peak height.
[d]Peak heights, mm from raw data. Maximum mole ratios versus O for pure compounds: Ca in $CaCO_3$, 0.33; Si in SiO_2, 0.50; S in SO_4^{2-}, 0.25; C in CO_3^{2-}, 0.33; Mg in MgO, 1; Al in Al_2O_3, 0.66; P in PO_4^{3-}, 0.25.

E_i is the kinetic energy of the emitted photoelectron from i, h_i is the peak height, and n_i is the number of moles. Results are presented in Table 3.

The sensitivity factor, S_i, reflects the influence of sample area and photoelectric cross-section on the measured intensity. It also contains contributions from the energy and the matrix dependence of the photoelectron mean-free path as well as the probability of detecting a photoelectron, i.e. the transmission factor. The transmission factor is a function of spectrometer design (14) and detector efficiency. Electron angular distributions and the competition of shake-off and shake-up events (15) are also included in the value of S_i. They are considered minor in this application (15).

The literature values S_i are valid only for flat, homogeneous solids without surface contamination, measured on the spectrometer type used in the literature (13). However, reliable use of the literature S_i values is possible through several compensating features of the data treatment procedure used here. The energy factor, $(E_{O(1s)}/E_i)^2$, removes the E^{-1} dependence (13, 14) of the spectrometer transmission factor of the retarding-voltage spectrometers used by Wagner (13) and replaces it with an E dependence (13, 14) for the double-focussing spherical-sector instrument (16) employed in this study. Roughness features are extremely varied on these surfaces and can be as great as 1000 times the X-ray mean-free path. Normalizing to the O(1*s*) peak decreases those intensity variations between samples which are due to irregularities in the surfaces. Variation in sample size is also compensated by this normalization process.

The literature values of $S_i/S_{O(1s)}$ (13) do not completely remove the variation in photoelectron mean-free paths due to heterogeneous matrices. However, it has been found that the ratio of the photoelectron mean-free paths is only slightly matrix dependent (13, 17).

We estimate 20% precision for the reported mole ratios based on a 10% precision for each S_i (12) and a 10% error in peak height measurements. As a gauge of accuracy, mole ratios versus oxygen were calculated from the pure compounds (Table 3): using these maximum values as criteria, the experimental mole ratios are correct within an order of magnitude.

Discussion

The oxidation state assignments (Table 2) and the semi-quantative mole ratios (Table 3) make it possible to differentiate between samples on the basis of surface composition. Surface hydrocarbon, an expected XPS artifact (18, 19), is prominent in all samples. The sources of this carbon peak cannot be elucidated from these spectra; carbon may arise from sample handling, the pre-analysis atmosphere and from hydrocarbon impurities in the surface deposit. Organic nitrogen is seen also and likewise may arise from varied sources. Iron, which is the principle pigment constituent, was not detected in any of the six samples studied. This finding indicates that the

Can. J. Chem. Downloaded from www.nrcresearchpress.com by 78.46.186.204 on 09/07/12
For personal use only.

surface deposit screens the pigment layer from analysis by XPS. The experimental limit of detection of Fe based on twice the average peak height of the background has been estimated as 0.09 Fe/O; this is the upper limit of the Fe versus O mole ratio in the surface layer.

Samples 1–4 have surfaces which consist of calcium carbonate and silica, i.e. essentially limestone and sand. The composition of these four samples is similar to those studied earlier (5, 6) using XRD. However, because the XPS technique is more sensitive than XRD, Al_2O_3, MgO, NaCl, sulphates, and phosphates are also detected by us.

The carbon-to-oxygen mole ratios for carbonate in samples 3 and 4 are comparable to that of pure carbonate (Table 3). The carbon-to-oxygen ratios of samples 3 and 4 are greater than the corresponding ratios for samples 1 and 2 based on the 20% precision estimate. Samples 3 and 4 have the most damaged surfaces of all the samples. However, they are visually dissimilar to each other. Sample 3 is white to the point of opacity whereas sample 4 is severely blackened because it originated from a tomb which had suffered smoke damage. The similarity in the XPS surface compositions of these two samples suggests that the layer formation process in these samples is the same and the deposit seen by XPS in sample 4 was formed after the wall surfaces were damaged by smoke. The latter point confirms previous conclusions based on descriptive evidence (2) for recent layer development and suggests that this aspect of the second mechanism proposed earlier (5, 6) is not supported by our experimental findings.

Sample 5 contains only SiO_2, Al_2O_3, and a just detectable amount of Cl on its surface, which is unlike the predominant composition of the previously mentioned four samples. The surface from which sample 5 was taken had been cleaned with HCl approximately 10 years ago to remove the disfiguring layer. This finding strongly suggests that the silica and alumina are recent deposits, again verifying earlier conclusions (2).

There has been considerable concern (5) that the use of HCl to clean the surfaces may damage the painted walls by dissolving the underlying rock:

$$CaCO_3(s) + 2HCl \rightarrow CaCl_2(s) + H_2O + CO_2$$

However, it can be seen (Table 3) that three of the five uncleaned samples have greater chloride contents than does sample 5. This suggests that damage associated with residual HCl and the formation of hygroscopic $CaCl_2$ is negligible in the sample studied.

Sample 6 represents another extreme in composition. Calcium and carbonate with minor amounts of phosphate and chloride make up the surface in this instance. The carbon-energy range spectra of samples 5 and 6 are shown in Fig. 3. Note the lack of a carbonate peak in sample 5.

No specific correlations were found between sample heights above the floor (Table 1) and composition. Since XPS provides information on the first few nanometers of a surface, it is planned to look for these correlations using bulk-analysis techniques.

Present results identify the mechanism of the surface-layer formation at Beni Hasan with a reasonable degree of certainty. Normally, the initial step of degradation is the deposition of dust or sand on the surface of murals; sample 5, which is the most recently exposed fresh surface, exemplifies this early stage of deterioration. The presence of deposited particles increases the amount of adsorbed water. Under these circumstances, diffusion processes are initiated at the liquid–solid interface

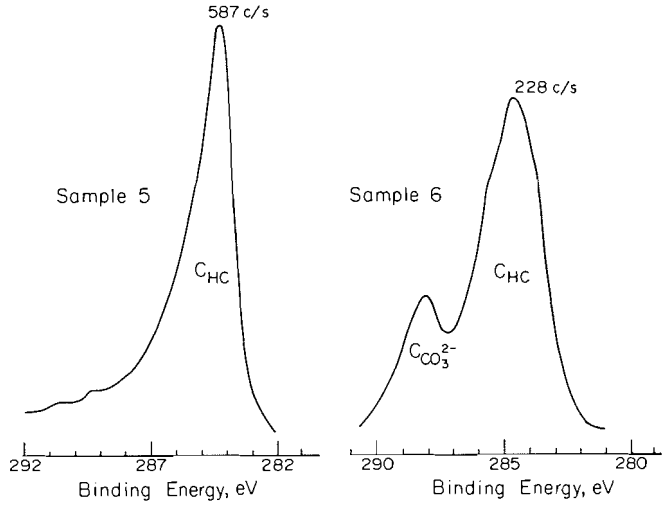

FIG. 3. Carbon energy region of samples 5 and 6 showing the absence of carbonate in sample 5.

along particle boundaries. These processes occur both above and at dew-point temperatures. Thus, at 50% RH, in the presence of particulates, capillary condensation may supply solvent (20). Subsequently, water diffuses through the murals to the limestone walls, a continuous and progressive process which dissolves $CaCO_3$. The presence of CO_2 from the air acidifies the adsorbed water and therefore accelerates deterioration. Daily fluctuations in temperature and humidity make it possible for Ca^{2+} to diffuse to the surface; this leads to the formation of the surface observed on our samples 1–4.

If wall surfaces are slanted so that direct particle deposition on the murals from the air is not favoured, water adsorption still may take place. This process should be less extensive and will involve a smaller effective surface area. In such cases, a third type of surface is formed in which the obtrusive layer consists predominately of calcium carbonate (sample 6).

This mechanism suggests that calcite walls, upon which murals were painted, deteriorate progressively and cumulatively. However, it should be pointed out that we lack *direct* evidence for such type of deterioration. Further investigations have been designed to elucidate this point and examine the nature of the surface deposit to a greater depth than is attainable by XPS.

The key difference between the mechanism proposed here and the earlier mechanism (5, 6) is that the latter attributes carbonate layer formation to dissolution and reprecipitation of $CaCO_3$ dust particles from the air, while the new mechanism predicts an accelerating disintegration of the substrate upon which murals were painted. In support of the new mechanism, our results (sample 5) indicate that there is no detectable carbonate deposit in recent dust deposits. The experimental limit of detection for carbonate has been calculated, based on twice the average background, as 0.004 carbon-to-oxygen ratio. Therefore, the recent deposits on sample 5 contain only an insignificant amount of carbonate. This implies that $CaCO_3$ is not necessary to initiate layer formation. However, this does not exclude the possibility that at least some of the $CaCO_3$ deposit was generated by dissolution of $CaCO_3$ dust from calcite and therefore some carbonate dust may be present. Nonetheless, the tombs are open to the natural elements for a considerable period of time, and Egyptian dust is a result of persistent winds from the Sahara, which carry with them often minute, all-pervasive

Can. J. Chem. Downloaded from www.nrcresearchpress.com by 78.46.186.204 on 09/07/12
For personal use only.

particles of sand. This sand is predominantly silica or silicates and contains practically no carbonates. The earliest mechanism (4) which involved water percolation leading to the subsurface removal of material, is, as noted in the introduction, inconsistent with observations (5). It was originally rejected (5) on the basis of isolated resistivity measurements and the absence of sulphates. Our mechanism supports the conclusion of earlier work (4) to the extent that both mechanisms predict dissolution of the substrate. However, the mechanism of ref. 4 and the present mechanism diverge at this point: we substitute diffusion of solvent water through the surface, a more pervasive and dangerous process, for percolation of water through the rock wall. The suggestion (4) that percolation brings out sulphate from the substrate to become a dominant component of the surface, is inconsistent with our measurements because only a negligible amount of sulphate (Table 3) is detected by us.

In the context of the current mechanism, the absence of sulphates in the opaque surface implies that gypsum-based plasters were not used in the Beni Hasan tombs studied by us. Gypsum plasters are known to have been used throughout Egypt in preceding and succeeding dynasties (21), however. The absence of these plasters could imply a deterioration of painting technology in the Beni Hasan area, at least in the "Time of Troubles" when the tombs presently investigated, were constructed. Additional experiments have been designed to investigate more extensively the apparent absence of sulphate plasters.

The rate of layer formation as prescribed by the present mechanism is strongly dependent on environmental and climatic factors. Since the ambient temperature defines the saturation water-vapour pressure, at low temperatures both capillary condensation and dew-point condensation are probable. Beni Hasan is situated in the coldest part of Egypt; it is too far north to be influenced by the equatorial climate and is not moderated by the Mediterranean Sea. Winter lows at Beni Hasan can reach near 0°C. The solubility of CO_2 also increases with decreasing temperature. Continuous monitoring of climatic conditions, such as relative humidity and temperature, would contribute towards a quantitative understanding of surface-deposit growth. Increases in dust and sand deposition, in P_{CO_2} (22), and in condensation should accelerate the growth of the opaque surface layers. All of these parameters increase as a result of extensive visitor access. Capillary condensation increases with relative humidity which is associated with the pronounced increases in irrigation in the Nile Valley that followed construction of the Aswan Dam in 1965. Therefore, the recent increase in the rate deterioration of the Beni Hasan murals (2) appears to be associated with increases in both irrigation and tourism.

Can. J. Chem. Downloaded from www.nrcresearchpress.com by 78.46.186.204 on 09/07/12
For personal use only.

Acknowledgements

The authors wish to thank the Egyptian Antiquities Organization for permission to take samples from the tombs at Beni Hasan. Special thanks are extended to Dr. Ali el Khouli, Mr. Mottawi Balboosh, Mr. Gamal Mustapha Amin, and Mr. Sobhi G. Bishay. Dr. Donald Spanel, Virginia Museum, Richmond, VA, advised us on Egyptological aspects of this study. Dr. N. S. McIntyre of the Surface Science Laboratory, University of Western Ontario, ran the XPS spectra. This work was supported in part by the Natural Sciences and Engineering Research Council and in part by the University of Toronto. We are also pleased to acknowledge the support of the Canadian Commission for Unesco/CIDA Assistance Programme for this project.

1. W. Stevenson Smith. The art and architecture of ancient Egypt. Pelican Books Ltd., Harmondsworth, Middlesex. 1981. p. 110.
2. K. M. Wilson-Yang and G. Burns. J. Am. Res. Cent. Egypt, **19**, 119 (1982) and references therein.
3. A. Toynbee. A study of history. Vol. 1. *Abridgement by* D. C. Somerville. Dell Publishing Co., Oxford University Press, London and New York. 1978. Chaps. 4 and 5, p. 287.
4. A. Stoppelaere. Ann. Serv. Antiquities l'Egypte, **40**, 941 (1940).
5. H. J. Plenderlith, P. Mora, G. Torraca, and G. de Guichen. Conservation problems in Egypt. UNESCO Consultant Report, Contract No. 33.591. 1970.
6. G. Torraca. Deterioration process of mural paintings. Application of science in examination of works of art. *Edited by* Wm. Young. Museum Fine Art, Boston. 1970. pp. 170–175.
7. P. E. Newberry. Beni Hasan. Vols. 1, 2. Egypt Exploration Fund, London. 1894 and references therein.
8. N. M. Davies. Ancient Egyptian paintings. The Oriental Institute of the University of Chicago, Oxford. 1936. p. 18, p. xxiii.
9. J. B. Lambert and D. C. McLaughlin. Archaeometry, **18**, 169 (1976).
10. E. T. Levanthal and M. Thompson. J. Inter. Inst. Conservation – Canadian Group, **3**, 16 (1978).
11. J. B. Lambert, D. C. McLaughlin, and A. Leonard, Jr. Archaeometry, **20**, 107 (1978).
12. K. J. S. Gilles and D. S. Urch. Archaeometry, **25**, 29 (1983).
13. C. D. Wagner, L. E. Davies, M. V. Zeller, J. A. Taylor, R. H. Raymond, and L. H. Gale. Surf. Interfac. Anal. **3**, 211 (1981).
14. M. P. Seah. Surf. Interfac. Anal. **2**, 222 (1980).
15. T. A. Carlson. Surf. Interfac. Anal. **4**, 125 (1982).
16. T. A. Carlson. Photoelectron and auger spectroscopy. Plenum, New York. 1975. Appendix 3.
17. K. Yabe and T. Yamashina. Appl. Surf. Sci. **8**, 387 (1981).
18. P. Swift. Surf. Interfac. Anal. **4**, 47 (1982).
19. E. S. Brandt, D. F. Unterrecker, C. N. Reilly, and R. W. Murray. J. Electron Spectrosc. **14**, 113 (1978).
20. A. D. Zimon. The adhesion of dust and powders. 2nd ed. Consultants Bureau, New York. 1982. pp. 109–119.
21. A. Lucas and J. R. Harris. Ancient Egyptian materials and industries. 4th ed. J. R. Harris and Edward Arnold, London. 1962.
22. E. M. Winkler. Stone: properties, durability in man's environment. 2nd ed. Springer-Verlag, New York. 1975. p. 140.
23. K. Siegbahn, D. A. Allison, and J. H. Allison. ESCA photoelectron spectroscopy. Handbook of spectroscopy. Vol. 1. *Edited by* J. W. Robinson. CRC Press, Cleveland. 1974. pp. 517–752.

Syntheses of 3-deoxy-3-substituted-D-glucose derivatives. Part I. Improvements in preparation of and nucleophilic additions to 1,6:2,3-dianhydro-4-*O*-benzyl-β-D-allopyranose

T. Bruce Grindley, Gerry J. Reimer, and Jaroslav Kralovec
Department of Chemistry, Dalhousie University, Halifax, N.S., Canada B3H 4J3

Robert G. Brown
Department of Biology, Dalhousie University, Halifax, N.S., Canada B3H 4J1

and

Max Anderson
Agriculture Canada, Kentville, N.S., Canada B4N 1J5

Received October 28, 1986

This paper is dedicated to Professor Douglas E. Ryan on the occasion of his 65th birthday

T. Bruce Grindley, Gerry J. Reimer, Jaroslav Kralovec, Robert G. Brown, and Max Anderson. Can. J. Chem. **65**, 1065 (1987).

The yield of the five-step preparation of 1,6:2,3-dianhydro-4-*O*-benzyl-β-D-allopyranose from 1,6-anhydro-β-D-glucopyranose has been raised to 33% from 12% by modifying conditions or methods for four of the steps. It has been demonstrated that nucleophilic addition to the former compound provides a general route to 1,6-anhydro-3-deoxy-3-substituted-β-D-glucopyranose derivatives, although reactions with large nucleophiles proceed either slowly or not at all. A number of nucleophiles, including chloride, fluoride, cyanide, alkylsulfide, and dimethylamine, gave this type of product in good yield (73–87%). The conditions used to introduce a chloro group, a catalytic amount of tetraethylammonium chloride in 1,1,2,2-tetrachloroethane at reflux, had not previously been used for carbohydrate epoxides. The methyl substituted product was obtained in highest yield with dimethyl magnesium. By-products from this reaction included the products of a Witting rearrangement and of an elimination. All addition products were present in the $^1C_4$ conformation.

T. Bruce Grindley, Gerry J. Reimer, Jaroslav Kralovec, Robert G. Brown et Max Anderson. Can. J. Chem. **65**, 1065 (1987).

En modifiant les méthodes ou les conditions expérimentales de quatre des étapes, on a pu augmenter de 12 à 33% le rendement global de la synthèse en cinq étapes du dianhydro-1,6:2,3 *O*-benzyl-4 β-D-allopyrannose à partir de l'anhydro-1,6 β-D-glucopyrannose. On a démontré que l'addition de nucléophiles sur le premier composé fournit une méthode générale d'accès aux dérivés de l'anhydro-1,6 déoxy-3 β-D-glucopyrannoses substitués en position 3, même si les réactions des nucléophiles volumineux se produisent lentement ou pas du tout. Avec un certain nombre de nucléophiles comprenant les ions chlorure, fluorure et cyanure ainsi que la diméthylamine et les sulfures d'alkyles, on a pu obtenir ce type de produit avec un bon rendement (73–87%). Les conditions utilisées pour introduire le groupement chloro, une quantité catalytique de chlorure de tétraéthylammonium dans du tétrachloro-1,1,2,2 éthane, n'avaient jamais été utilisées jusqu'à maintenant pour ouvrir des époxydes de carbohydrates. Pour obtenir le meilleur rendement du produit substitué par un groupement méthyle, il faut utiliser le diméthylmagnésium. Parmi les sous-produits de cette réaction, on retrouve des produits provenant d'une transposition de Wittig ainsi que d'une élimination. Tous les produits d'addition existent dans la conformation $^1C_4$.

[Traduit par la revue]

Introduction

There has been considerable interest in 3-deoxy-3-substituted-D-glucose derivatives over a period of time. 3-Amino-3-deoxy-D-glucose (kanosamine), a component of the antibiotics kanamycin (1), nebramycin (2), and hikizimycin (3) has been synthesized by a number of groups (4–6). 3-Fluoro-3-deoxy-D-glucose has been an attractive synthetic target because of the continuing interest in deoxyfluoro-D-glucose derivatives for positron emission tomography (7). Pougny and Sinay prepared 3-deoxy-3-*C*-methyl-D-glucose by a different route during the synthesis of a pheromone (8).

Our interest in 3-substituted-D-glucose derivatives was sparked by observations by one of us that 3-*O*-methyl-D-glucose affected the amino acid uptakes and rates of growth of certain yeasts and fungi (9). We wanted to obtain a variety of other 3-substituted-D-glucose derivatives for study and thus required a general synthetic route. The most commonly used synthetic approach to 3-deoxy-3-substituted-D-glucose derivatives has involved nucleophilic displacement of sulfonate derivatives of 1,2:5,6-di-*O*-isopropylidene-D-allofuranose. This reaction works well for good nucleophiles (5, 7) but has not been reported for carbon-based nucleophiles.

An attractive approach to the synthesis of substituted deoxy sugars is the addition of nucleophiles to epoxides (10). These reactions occur under milder conditions than those used for displacements of secondary sulfonates and hence allow use of a greater variety of nucleophiles. The regiochemistry and stereochemistry of the product from an epoxide fused to a pyranose sugar is fixed by the favoured *trans*-diaxial opening (11). To prepare 3-deoxy-3-substituted-D-glucose derivatives, the pyranose ring must be in the less stable $^1C_4$ conformation. 1,6-Anhydro derivatives provide a convenient source of pyranose sugars fixed in this conformation (12). Additions to a blocked derivative of either 1,6:3,4- or 1,6:2,3-dianhydro-β-D-allopyranose would be appropriate. However, a convenient synthetic route to the 4-*O*-benzyl derivative (**6**) of the latter compound has been published (13) and a few reactions with nucleophiles have been tried, with it and with its unblocked precursor.

Two types of results were obtained from these reactions.

Can. J. Chem. Downloaded from www.nrcresearchpress.com by 78.46.186.204 on 09/07/12
For personal use only.

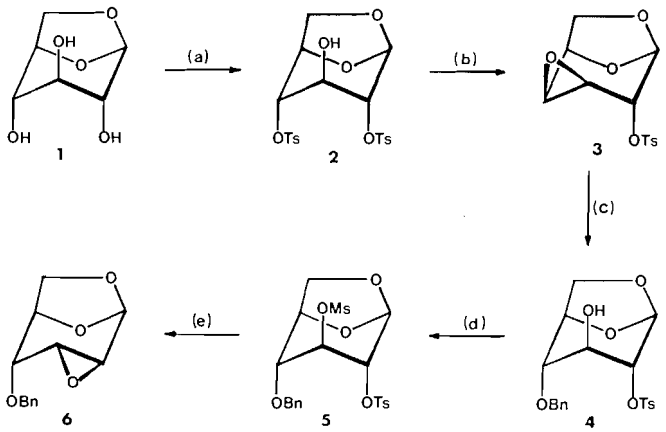

SCHEME 1. Conversion of **1** to **6**: (a) TsCl/pyridine; (b) NaOMe/MeOH; (c) BnOH, $BF_3 \cdot Et_2O$, benzene, 50°C; (d) MsCl/pyridine; (e) NaOMe/MeOH, −18°C.

The parent compound, 1,6:2,3-dianhydro-β-D-allopyranose gave only decomposition on reaction with a potassium hydroxide solution, in contrast to the addition reactions observed with 1,6:2,3-anhydrohexoses having different stereochemistry (14). The decomposition reaction may have proceeded by a retroaldol reaction (14). Compound **6** formed an alkene on reaction with potassium *tert*-butoxide (14), as did the closely related 1,6:2,3-dianhydro-4-deoxy-β-DL-*ribo*-hexopyranose with *n*-butyl lithium (15). More promisingly, compound **6** gave the product of nucleophilic addition with sodium azide in 2-ethoxyethanol (16) and with sodium methoxide in methanol (17).

The original five-step preparation of 1,6:2,3-dianhydro-4-*O*-benzyl-β-D-allopyranose from 1,6-anhydro-β-D-glucopyranose (**1**) (readily available by pyrolysis of starch) had an overall yield of 12% (13). In this publication, we report improvements to the synthesis of **6** and also demonstrate that a wide variety of nucleophiles add to **6**.

Results and discussion

Improvements in the synthesis of 1,6:2,3-dianhydro-4-O-benzyl-β-D-allopyranose

The five-step sequence proceeding from 1,6-anhydro-β-D-glucopyranose (**1**) to 1,6:2,3-dianhydro-4-*O*-benzyl-β-D-allopyranose (**6**) is shown in Scheme 1. Some improvements to this scheme have appeared since it was initially published (13). In particular, the yield of the first step was raised to 79% by using toluenesulfonyl anhydride as the sulfonating reagent (18).

The yield of step two was raised to 82% here, from 55% reported initially (19), by adding the sodium methoxide solution very slowly. The third step, opening the 3,4-epoxide ring, was originally performed with benzyl alcohol and *p*-toluenesulfonic acid as an acid catalyst in 62% yield (20). A number of methods were investigated for improving this step. Use of a Lewis acid catalyst, boron trifluoride etherate, gave the best yield (78%). Other Lewis acid catalysts, including the highly recommended phosphorotungstic acid (21), were less effective, as were base-catalysed conditions.

The yield of step four was increased to a slight extent (from 76 to 81%) by conducting the reaction at a lower temperature under nitrogen. The yield of the last step was significantly improved (from 61 to 80%) by adding the sodium methoxide slowly and performing the reaction at −20°C. An alternative improvement consisted of changing the reaction medium (16). These changes in the last four steps raised the overall yield for the five-step process to 33% from 12%.

Nucleophilic additions to 1,6:2,3-4-O-benzyl-β-D-allopyranose

The preferred site for attack by nucleophiles on 1,6:2,3-dianhydro-4-*O*-benzyl-β-D-allopyranose (**6**) is expected to be at carbon-3 since oxiranes open to give diaxially substituted six-membered rings preferentially (11). Because diequatorial products have been obtained with other 1,6:2,3-dianhydrohexopyranoses using the soft nucleophile, sodium benzyl sulfide (22), caution was observed in product identification. All products obtained here by nucleophilic addition to **6** were characterized by high-field ^1H and ^{13}C nmr spectroscopy. The spectral results are shown in Tables 1–3. Most ^1H nmr signals were assigned by means of extensive decoupling experiments. The H-3 signal was assigned by consideration of substituent chemical shift effects. The signals for H-2 and H-4 were distinguished in some spectra by D_2O exchange of the coupled OH-2 signal. The ^{13}C nmr signals were assigned by analogy with literature assignments of other 1,6-anhydro-β-D-glucopyranose derivatives (23) and by consideration of chemical shift changes as substituents change. In some cases, the chemical shifts of the de-*O*-benzylated derivatives were considered.[1]

A product with the *gluco* stereochemisty has the skeletal protons, H-1 to H-5, in equatorial orientations if the compound adopts the $^1C_4$ conformation observed for **1** (25). As a result,

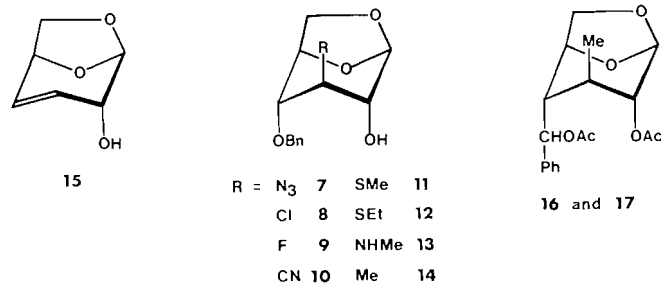

these protons gave rise to narrow signals with multiple small (<2.5 Hz) splittings due to vicinal and long-range couplings. Sometimes these splittings were resolved either in the original or in the decoupled spectra; often they were not. In general, the magnitudes of the coupling constants matched those reported by Cerny and co-workers (25) for **1**, although in certain compounds the magnitudes of some long-range couplings were somewhat different. The product of a diequatorial opening would be evident through the observation of a large $J_{2,3}$ value in its ^1H nmr spectrum. Similarly, products with the *gluco* configuration that adopted a conformation different than **1** would give spectra with coupling constants of different magnitudes. All compounds obtained here by nucleophilic additions to **6** gave similar patterns of coupling constants (see Table 2).

Approach to the epoxide ring of **6** by a nucleophile is likely to be hindered by the axial CH_2 group of the 1,6-anhydro bridge, particularly if the attacking nucleophile is large. Cerny *et al.* (16) have reported that **6** did not react with methanolic ammonia whereas other 1,6:2,3-dianhydrohexopyranoses did.

Compound **6** reacted with sodium azide in ethanol at reflux

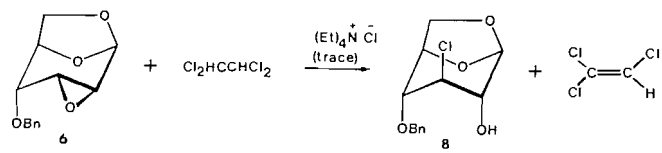

[1]J. Kralovec, G. Reimer, T. B. Grindley, R. G. Brown, and M. Anderson. In preparation.

Can. J. Chem. Downloaded from www.nrcresearchpress.com by 78.46.186.204 on 09/07/12
For personal use only.

TABLE 1. ^{1}H nuclear magnetic resonance chemical shifts (ppm[a])

Compound	Frequency (MHz)	H-1	H-2	H-3	H-4	H-5	H-6$_{en}$	H-6$_{ex}$	CH_2Ph	Phenyl	Other
2	361	5.31	4.28	3.96	4.43	5.22	4.12	3.63		7.2–8.5	TsMe 2.36, 2.35
3	60	5.17	4.40	3.13	3.53	4.83	3.93	3.53		7.3–7.9	TsMe 2.47
4	60	5.30	4.23	3.30	4.01	4.53	3.87	3.57	4.63	7.3–7.9	TsMe 2.40 OH 2.87
5	60	5.33	4.90	4.43	3.60	4.57	3.97	3.63	4.69, 4.71	7.3–7.8	TsMe 2.43 MsMe 3.10
6	361	5.65	3.09	3.31	3.45	4.50	3.62	3.89	4.74, 4.87	7.36	
7	361	5.43	3.82	3.31	3.57	4.57	4.02	3.73	4.64, 4.67	7.2–7.5	OH-2 4.76
8	361	5.47	3.76	4.08	3.61	4.59	4.25	3.77	4.62, 4.72	7.3–7.6	OH-2 2.90
9	361	5.46	3.66	4.65	3.51	4.61	4.00	3.78	4.67, 4.70	7.3–7.4	OH-2 2.56
10	361	5.46	3.83	3.12	3.69	4.64	4.25	3.84	4.64, 4.65	7.3–7.4	OH-2 3.05
11	361	5.43	3.70	2.90	3.51	4.61	4.35	3.73	4.62, 4.65	7.3–7.4	OH-2 2.89 SMe 2.10
12	361	5.43	3.71	2.98	3.54	4.61	4.36	3.73	4.64	7.3–7.4	OH-2 2.91 SCH_2 2.51 Me 1.24
13	361	5.45	3.44	2.77	3.39	4.60	4.06	3.72	4.64	7.3–7.4	N-Me 2.43
14	361	5.38	3.25	2.08	3.10	4.56	3.72	3.66	4.56	7.2–7.4	Me 1.15
15	60	5.53	3.63	5.82	6.18	4.69	3.69				
16	361	5.42	4.38	1.42	1.87	4.77	3.91	3.81		7.32	H-4′ 5.95 Me 1.08 Ac 2.05, 2.15
17	361	5.43	4.45	2.03	1.77	3.99	3.85	3.60		7.2–7.5	H-4′ 6.03 Me 1.36 Ac 2.03, 2.12

[a]Downfield from internal tetramethylsilane in chloroform-*d* solutions.

TABLE 2. ^{1}H nuclear magnetic resonance coupling constants (Hz)

Compound	$J_{1,2}$	$J_{1,3}$	$J_{1,4}$	$J_{2,3}$	$J_{2,4}$	$J_{3,4}$	$J_{3,5}$	$J_{4,5}$	$J_{5,6en}$	$J_{5,6ex}$	$J_{6en,6ex}$	Others
2[a]										5.7	−7.6	
3[a]						4.0	4.8			4.8	−6.6	
4[a]				3.5						5.5	−7.6	
5	1.2	1.2		2.0		1.4		1.5	1.2	5.6	−7.8	
6	0.9			4.1		4.6	2.0		2.0	7.0	−8.0	
7	1.8	0.8	1.3	1.0	0.8	1.8	1.8			5.5	−7.4	
8	1.8	1.8	0.5	1.6	1.5	1.5	1.5	1.6	0.6	5.7	−7.8	
9[b]	1.3	1.8	0.6	1.5	1.3	1.7	1.8	1.5	0.9	5.9	−7.7	$J_{2,OH}$ 12.2
10[a]	2.1									5.5	−8.4	$J_{2,OH}$ 12.5
11[a]										5.4	−7.6	$J_{2,OH}$ 11.8
12[a]										5.5	−7.7	$J_{2,OH}$ 11.6 $J_{CH_2,Me}$ 7.4
13	1.6	1.6		1.6	1.5	1.6	1.6	1.2	0.7	5.5	−7.5	
14[a]	2.4									5.4	−7.8	$J_{3,Me}$ 8.0
15	1.2	2.0		4.0		9.8		4.6		[c]	[c]	
16[a]						0.9				4.9	−7.2	$J_{4,4'}$ 10.2 $J_{3,Me}$ 7.8
17[a]										5.2	−7.4	$J_{4,4'}$ 10.6 $J_{3,Me}$ 7.9

[a]Numerous small couplings not resolved.
[b]*J* values to F in experimental.
[c]Not first order.

to give 1,6-anhydro-3-azido-3-deoxy-β-D-glucopyranose (**7**) in somewhat higher yield (86%) than obtained at reflux in 2-ethoxyethanol (16).

Addition of chloride ion directly to epoxides is difficult because Cl^- is inherently much more stable than an alkoxide ion (26). Successful reagents supply an electrophile to neutralize the oxyanion. Those used to add chloride to carbohydrate epoxides include HCl in acetone (27), which is known to hydrolyze 1,6-anhydro rings, and (chloromethylene)dimethyliminium chloride (28), which yields chloro *O*-formyl derivatives. The reagent employed here was 1,1,2,2-tetrachloroethane containing a catalytic amount of tetraethylammonium chloride. Buddrus has shown in reactions with simple epoxides that the alkoxide intermediate formed from the addition of chloride abstracts a proton from 1,1,2,2-tetrachloroethane (26). Loss of chloride gives 1,1,2-trichloroethene. This method was found here to be a good one for the addition of chloride to **6** (recrystallized yield 73%) and would presumably work for other complex epoxides.

Fluoride was added to **6** in excellent yield (87%, recrystallized) using a standard reagent (29), potassium hydrogen fluoride in ethylene glycol. Cesium fluoride was less effective. Since both this reaction and subsequent deblocking steps can be performed rapidly,[1] this reaction is another potential method for obtaining ^{18}F labelled sugars for positron emission tomography.

Cyanide was added to **6** using diethylaluminum cyanide, a reagent previously used for addition to several epoxides (30), including carbohydrate ones (31). This reagent gave a 5:1 mixture of diaxial and diequatorial adducts with methyl 3,4-

Can. J. Chem. Downloaded from www.nrcresearchpress.com by 78.46.186.204 on 09/07/12
For personal use only.

TABLE 3. ^{13}C nuclear magnetic resonance chemical shifts[a]

Compound	C-1	C-2	C-3	C-4	C-5	C-6	CH_2Ph	Phenyl	Other
2	99.8	77.4	68.8	78.8	74.6	65.7		124.1, 127.9, 130.0, 133.3, 133.5, 136.7, 145.2, 149.3	TsMe 21.6
3	98.1	72.0	47.6	52.9	71.6	64.8		128.1, 130.3, 132.9, 145.7	TsMe 21.7
4	100.0	79.3	70.3	78.5	75.3	66.4	71.8	128.0, 128.6, 130.0, 133.3, 145.2	TsMe 21.7
5	98.7	75.3	73.8	74.5	74.9	65.4	71.6	132.8, 137.1, 145.7	TsMe 21.7
6	97.2	47.9	47.6	72.6	75.6	65.5	70.8	128.0, 128.6, 137.5	
7	103.4	69.6	61.6	77.1	75.5	66.6	73.0	130.4, 130.8, 131.1, 139.4	
8	101.6	71.3	54.3	77.9	74.7	65.5	71.8	127.9, 128.3, 128.7, 136.8	
9	101.3	67.5	88.4	74.3	73.6	65.0	71.6	127.9, 128.3, 128.7, 136.9	
10	101.2	67.7	32.2	73.4	74.1	65.4	71.7	127.9, 128.6, 128.8, 136.2	CN 118.5
11	102.0	70.9	48.1	76.6	75.1	65.9	71.3	128.0, 128.2, 128.5, 138.0	SMe 17.5
12	101.8	71.3	45.4	77.4	74.6	65.5	71.0	127.8, 128.0, 128.5, 137.2	SEt 27.7, 14.4
13	102.4	69.2	62.2	76.3	74.6	65.4	71.1	127.8, 128.0, 128.6, 137.7	N-Me 35.4
14	102.8	71.0	37.7	78.5	74.6	65.2	70.6	127.6, 127.8, 128.4, 137.7	Me 18.9
15	102.8	66.0	126.2	130.8	70.7	69.0			
16	100.2	71.9	30.0	46.8	75.9	67.8		127.7, 128.4, 128.6, 138.8	C-4′ 73.9 CO 169.7, 170.1 Me 21.2, 21.3
17	100.6	72.4	31.0	47.6	77.1	67.6		127.6, 128.5, 128.8, 139.1	C-4′ 72.4 CO 170.0, 170.6 Me 21.2, 21.7

[a]In ppm from internal tetramethylsilane in chloroform-*d* solutions.

anhydro-2,6-di-*O*-benzyl-α-D-galactopyranoside, a substrate which is strongly biased conformationally but which has an axial methoxyl group in a 1,3-diaxial relationship to the incoming cyanide group (31). A second product was not detected here.

The sulfur-containing nucleophiles, sodium thiomethoxide and sodium thioethoxide, similarly added to **6** at C-3. High-field ^1H nmr spectra of the crude products did not contain any signals attributable to the product of diequatorial addition. This outcome is in contrast to results obtained in the reaction of sodium benzyl sulfide with different 1,6:2,3-dianhydrohexopyranosides (22). A methylamino group was introduced in excellent yield (80%) by reaction of **6** with aqueous methylamine under pressure at 150°C.

The reactions of a number of reagents used to add methyl groups to epoxides have been investigated. However, the results of reaction of **6** with nucleophilic methyl groups were consistent with the suggestion that the epoxide group of compound **6** is relatively hindered. The best yield (32%, isolated by chromatography) of 1,6-anhydro-4-*O*-benzyl-3-deoxy-3-*C*-methyl-β-D-glucopyranose (**14**) was obtained by reaction with dimethyl magnesium in dioxane at reflux for 14 h. This yield is in contrast to the excellent yield obtained in the reaction of dimethyl magnesium with the unhindered epoxide ring in 1,6:2,3-dianhydro-4-*O*-benzyl-β-D-mannopyranose (32). This product was accompanied by benzyl alcohol (14%) and three interesting by-products, 1,6-anhydro-3,4-dideoxy-β-D-*erythro*-hex-3-enopyranose (**15**) (3%) and, following acetylation, an approximately 1:1 mixture of the two diastereomers of 2-*O*-acetyl-1,6-anhydro-3,4-dideoxy-4-*C*-acetoxyphenylmethyl-3-*C*-methyl-β-D-glucopyranose (**16** and **17**) (7%). A reaction conducted at 20°C gave lower yields of **14** (19%) and higher yields of benzyl alcohol (22%) and **15**. The benzyl alcohol probably arises from a process that results in sugar decomposition, since the overall product yields were low.

The structure of compound **15** was derived from the analytical and spectral data. The ^{13}C nmr chemical shifts indicated that an alkene was present and the ^1H nmr coupling constants

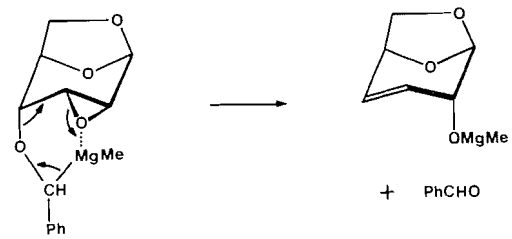

SCHEME 2. Possible mechanism for the formation of **15**.

showed that the double bond was between carbons 3 and 4. The ^1H nmr spectral data were very similar to those reported from 100-MHz ^1H nmr spectra of the racemic modification of **15** (15). A probable mechanism for the formation of **15** is shown in Scheme 2. This mechanism would result in the release of benzaldehyde, which would be methylated under the reaction conditions. The ^1H nmr spectrum of the crude chromatographic fraction containing benzyl alcohol showed methyl and methine signals at the same chemical shifts as those of 1-phenylethanol (33), having one-fifth the intensity of those of benzyl alcohol.

The two remaining products came from a Wittig rearrangement (34) of the initial adduct (**14**). Compounds **16** and **17** were obtained by acetylation followed by chromatographic separation. Their structures followed from the spectral (see Tables 1–3) and analytical data. The ^{13}C nmr spectra established that **16** and **17** each contained two secondary aliphatic deoxy carbons. Observation of quartets at 1.42 and 2.03 ppm and doublets at 1.87 and 1.77 ppm, each attributable to one hydrogen in the ^1H nmr spectra of **16** and **17**, respectively, was in agreement with this conclusion. The absence of observable coupling constants between H-1, H-2, H-3, H-4, and H-5 indicated that the configurations at the corresponding carbons were the same as in compounds **7**–**14**. The configurations at the new chiral centre (C-4′) could be established tentatively from the chemical shift of H-5. The chemical shift of H-5 was relatively constant in all of the products of nucleophilic addition to **6** (**7**–**14**), 4.57–4.64 ppm. In the ^1H nmr spectra of **16** and **17**, the signals of H-5 appeared at 4.77 and 3.99 ppm, respectively.

Can. J. Chem. Downloaded from www.nrcresearchpress.com by 78.46.186.204 on 09/07/12
For personal use only.

Can. J. Chem. Downloaded from www.nrcresearchpress.com by 78.46.186.204 on 09/07/12
For personal use only.

The magnitudes of $J_{4,4'}$ were 10.2 and 10.6 Hz in the spectra of **16** and **17**, respectively, indicating that the predominant conformation about the C-4—C-4′ bond had H-4 and H-4′ *anti* in both compounds. As a result, the phenyl group is *anti* to C-5 in one compound and *gauche* in the other. The most likely explanation for the marked upfield shift for H-5 in the ^{1}H nmr spectrum of **17** is that the phenyl group is *gauche* to C-5 and shields H-5. On this basis, **17** is (4′*R*)-2-*O*-acetyl-1,6-anhydro-3,4-dideoxy-4-*C*-acetoxyphenylmethyl-3-*C*-methyl-β-D-glucopyranose and **16** is the 4′*S* isomer. In contrast to the current result, Schollkopf found that the chiral centre in lithiobenzyl *sec*-butyl ether mostly racemized during the Wittig rearrangement in tetrahydrofuran at −60°C (34).

Reaction with lithium dimethyl cuprate gave lower yields of the *C*-methyl product than did reaction with dimethylmagnesium, while a higher order cuprate, $Me_2Cu(CN)Li_2$ (35), did not react with **6**.

Product conformations

All of the 1,6-anhydro-4-*O*-benzyl-3-deoxy-3-substituted-β-D-glucopyranose derivatives prepared here exist predominantly in the $^1C_4$ conformation in solution, as does the parent compound **1**. In contrast, 3-amino-1,6-anhydro-3-deoxy-β-D-glucopyranose (**18**) is present in solution as an approximately 1:1 mixture of the $^1C_4$ and $B_{O,3}$ conformations (16), and its hydrochloride and other cationic derivatives exist predominantly in the latter conformation. Both compounds are present in the chair conformation in the solid state (36, 37). One explanation considered for the unusual conformation of **18** was that the NH_2 group was larger than an OH group (16). Compound **14**, which contains the still larger methyl group, was observed to adopt the chair conformation in solution. Thus, the size of the 3-substituent does not appear to have a particularly important influence on the conformations of these derivatives.

An interesting phenomenon observed in the ^{1}H nmr spectra of several of these derivatives (**9**, **10**, **11**, and **12**) measured in chloroform-*d* solutions was that the OH group on C-2 was coupled to H-2. The coupling constants ranged from 11.6 to 12.5 Hz. A Karplus type relationship has been reported for H—C—O—H fragments and similarly large values of coupling constants have been observed in situations where hydrogen bonding causes the H—C—O—H conformation to be close to *anti* (38). In crystals of **1**, OH-2 adopted an *anti* orientation to H-2, perhaps as a result of weak intramolecular hydrogen bonds to both O-4 and O-5 (39).

Experimental

General methods

Most general methods were as in ref. 40. Accurate masses were obtained on VG-7070 or Dupont CEC 21-110B mass spectrometers.

*1,6:3,4-Dianhydro-2-*O*-p-toluenesulfonyl-β-D-galactopyranose (3)*

A solution of sodium methoxide in methanol (1.15 L of 0.60 *M* solution, 0.7 *M*) was added dropwise over 1.4 h to a stirred solution of the 1,6-anhydro-2,4-di-*O*-*p*-toluenesulfonyl-β-D-glucopyranose–pyridine (1:1) complex (**2**) (19) (85.5 g, 0.155 *M*) in dry methanol (1.76 L). After being stirred 11 h, the reaction mixture was neutralized to pH 7 (pH meter) by adding 5% aqueous hydrochloric acid dropwise. Removal of methanol left an aqueous mixture, which was extracted with chloroform (2 × 500 mL). The combined chloroform extracts were washed with water (100 mL), dried ($MgSO_4$), and concentrated to about 200 mL. Methanol (500 mL) was added and the solution kept at 5°C for 12 h. The white crystals of the title compound (**3**) were filtered, washed with methanol, and dried under vacuum (0.1 Torr; 1 Torr = 133.3 Pa) at 56°C; mp 148°C (lit. (19) mp 148–150°C); $[\alpha]_D^{22}$ −41° (*c* 2.70, chloroform) (lit. (19) $[\alpha]_D$ −40°). An average yield of 77% was obtained from six reactions (lit. (19) 55%, (41) 70%).

*1,6-Anhydro-4-*O*-benzyl-2-*O*-p-toluenesulfonyl-β-D-glucopyranose (4)*

Compound **3** (326.4 g, 1.09 *M*), benzyl alcohol (350 mL, 3.38 *M*), and freshly distilled boron trifluoride etherate (21 mL, 0.17 *M*) were stirred under nitrogen in benzene at 50°C for 24 h. The cooled solution was washed with sodium bicarbonate solutions (1 *M*, 2 × 400 mL) and water (200 mL), then dried ($MgSO_4$) and evaporated. The solid produced was separated from unreacted benzyl alcohol by filtration, washed with ether, and dried (56°C, 0.1 Torr, 12 h). The combined filtrate and washings were concentrated to dryness at 100°C and 1 Torr. The remaining solution was diluted with an equal amount of ether, then kept 12 h at 5°C and filtered, total yield 348.9 g, 78% (lit. (20) 62%); mp 124–125°C (lit. (20) mp 126–127°C); $[\alpha]_D^{22}$ −19° (*c* 2.09, chloroform) (lit. (20) $[\alpha]_D$ −18°).

*1,6:2,3-Dianhydro-4-*O*-benzyl-β-D-allopyranose (6)*

A solution of sodium methoxide in methanol (3.4 L of 1.32 *M*) was added dropwise over 5 h to a solution of 1,6-anhydro-4-*O*-benzyl-3-*O*-methanesulfonyl-2-*O*-toluenesulfonyl-β-D-glucopyranose (**5**) (335.5 g, 0.692 *M*) in dry chloroform (1 L), cooled to −18°C, and stirred under nitrogen. The reaction mixture was stirred a further 11 h at 25°C, then neutralized with an aqueous 10% HCl solution (pH meter), and concentrated. The residue was extracted with hot chloroform (1.5 L and 2 × 0.5 L). The combined extracts were washed with water, dried ($MgSO_4$), and concentrated. The resulting syrup was diluted with ethyl acetate (0.4 L) and petroleum ether (30–60°C) (0.5 L). The colorless crystalline product was removed by filtration and washed with pentane; yield 130.2 g, 80%; mp 75–79°C (lit. (12) mp 74–76°C); $[\alpha]_D^{24}$ +119° (*c* 3.00, chloroform) (lit. (12) $[\alpha]_D$ +127°, (42) +121°).

*1,6-Anhydro-3-deoxy-3-azido-4-*O*-benzyl-β-D-glucopyranose (7)*

Compound **6** (20.22 g, 86.3 mmol), ammonium chloride (35.6 g, 0.67 *M*), and sodium azide (35.8 g, 0.55 *M*) were mixed with ethanol (95%, 400 mL) and water (100 mL), then heated under reflux for 30 h. The cooled reaction mixture was filtered and the precipitate washed with ethanol. The combined filtrate and washings were concentrated to an orange solid, which was taken up in chloroform (100 mL). The chloroform solution was washed with water (2 × 100 mL), dried ($MgSO_4$), and concentrated to a light yellow syrup. The syrup was diluted with ethyl acetate (30 mL) and pentane (50 mL), then kept at 5°C for 12 h. The large colorless prisms of compound **6** were collected and washed with pentane, yield 20.47 g, 86%; mp 76–77°C (lit. (16) mp 74–76.5°C); $[\alpha]_D^{20}$ −12.1° (*c* 8.50, chloroform) (lit. (16) $[\alpha]_D$ −13°).

*1,6-Anhydro-4-*O*-benzyl-3-chloro-3-deoxy-β-D-glucopyranose (8)*

1,6:2,3-Dianhydro-4-*O*-benzyl-β-D-allopyranose (**6**) (2.34 g, 10 mmol) and tetraethylammonium chloride (0.25 g, 1.5 mmol) were mixed in dry 1,1,2,2-tetrachloroethane (25 mL), then stirred at 110°C for 12 h. The solvent was removed by steam distillation. An ethereal solution of the residue (25 mL) was washed with water (3 × 10 mL), dried ($MgSO_4$), decolorized with charcoal, and concentrated to 10 mL. The crystalline product was recrystallized from ether to give the title compound (**8**), 1.98 g, 73%; mp 75–78°C; $[\alpha]_D^{26}$ −51.1° (*c* 1.25, acetone); M − Cl, calcd. for $C_{13}H_{15}O_4$: 235.097; found: 235.097; M − HCl, calcd. for $C_{13}H_{14}O_4$: 234.089; found: 234.091.

*1,6-Anhydro-4-*O*-benzyl-3-deoxy-3-fluoro-β-D-glucopyranose (9)*

Compound **6** (2.34 g, 10 mmol) and potassium hydrogen fluoride (4.70 g, 7 mmol) were refluxed in ethylene glycol for 5 h. The cooled mixture was poured into an aqueous solution of potassium carbonate (5%, 200 mL), which was stirred 5 min, then extracted with chloroform (5 × 20 mL). The combined extracts were washed with water (3 × 10 mL), dried ($MgSO_4$), and concentrated. Crystallization and then recrystallization from ether gave the title compound (**9**) as colorless crystals, 2.21 g, 87%; mp 106–108°C; $[\alpha]_D^{26}$ −67.5° (*c* 1.31, acetone); H,F coupling constants, to H-2, -3, -4, -6_{endo}, and -6_{exo}: 12.3, 42.4, 13.1, 0.9, and 2.1 Hz, respectively; C,F coupling constants, to C-2, -3, and -4: 22.6, 181.6, and 26.3 Hz, respectively.

Can. J. Chem. Downloaded from www.nrcresearchpress.com by 78.46.186.204 on 09/07/12
For personal use only.

For other spectral data, see Tables 1–3. *Anal.* calcd. for $C_{13}H_{15}FO_4$: C 61.41, H 5.95, F 7.47; found: C 61.30, H 5.94, F 7.06.

*1,6-Anhydro-4-O-benzyl-3-cyano-3-deoxy-β-D-glucopyranose (**10**)*

A solution of diethyl aluminium cyanide (25 mL, 1.0 *M* in toluene, 25 mmol) was added to a solution of epoxide **6** (2.34 g, 10 mmol) in dry benzene (50 mL) and the solution was stirred under nitrogen at reflux for 2 h. The cooled reaction mixture was poured onto an ice-cold HCl solution (0.1 *M*, 250 mL) with stirring. The organic layer was washed with brine, dried ($MgSO_4$), decolorized with charcoal, and concentrated. The crude product was recrystallized from chloroform to give colorless crystals of the title compound (**10**); 2.12 g, 81%; mp 134–136°C; $[\alpha]_D^{26}$ −85.3° (*c* 1.08, acetone). *Anal.* calcd. for $C_{14}H_{15}NO_4$: C 64.36, H 5.79, N 5.36; found: C 64.37, H 5.56, N 5.35.

*1,6-Anhydro-4-O-benzyl-3-deoxy-3-methylthio-β-D-glucopyranose (**11**)*

A mixture of epoxide **6** (240 mg, 1 mmol) and sodium thiomethoxide (140 mg, 2 mmol) in tetrahydrofuran (5 mL) was refluxed 6 h. The product mixture was poured into water (150 mL) with stirring and the aqueous solution was extracted with ether (5 × 20 mL). The combined extracts were washed with water (3 × 10 mL), dried ($MgSO_4$), and concentrated. The syrupy product (**11**) was purified by chromatography on silica using chloroform as eluent; yield: 229 mg, 81%; $[\alpha]_D^{25}$ −38.7° (*c* 1.06, chloroform). *Anal.* calcd. for $C_{14}H_{18}O_4S$: C 59.55, H 6.43; found: C 59.76, H 6.49.

*1,6-Anhydro-4-O-benzyl-3-deoxy-3-ethylthio-β-D-glucopyranose (**12**)*

A suspension of sodium (100 mg, 4 mmol) in a solution of ethanethiol (1.25 g, 20 mmol) in tetrahydrofuran (4 mL) was stirred under reflux until all the sodium had reacted (3 h). A solution of epoxide **6** (240 mg, 1 mmol) in tetrahydrofuran (3 mL) was added and the solution was refluxed 4 h. The product mixture was cooled and water (5 mL) was added. The organic layer was separated and the aqueous solution extracted with ether (3 × 10 mL). The combined organic layers were washed with water (3 × 5 mL), dried ($MgSO_4$), and concentrated. The syrupy product (**12**) was purified by chromatography on silica using chloroform as eluent; yield, 249 mg, 84%; $[\alpha]_D^{25}$ −30° (*c* 2.33, chloroform). *Anal.* calcd. for $C_{15}H_{20}O_4S$: C 60.79, H 6.80; found: C 60.93, H 6.89.

*1,6-Anhydro-4-O-benzyl-3-deoxy-3-methylamino-β-D-glucopyranose (**13**)*

A solution of epoxide **6** (240 mg, 1 mmol) in 40% aqueous methylamine (20 mL) was kept at 150°C in a sealed tube for 24 h. The product mixture was extracted with chloroform (3 × 20 mL). The combined extracts were washed with water (3 × 5 mL), dried ($MgSO_4$), and concentrated. The residue was purified by column chromatography on silica gel using chloroform as eluent. The solid obtained was recrystallized from ethanol to give colourless crystals of **13**; yield: 201 mg, 76%; mp 61–62°C; $[\alpha]_D^{25}$ −34.3° (*c* 0.97, chloroform). *Anal.* calcd. for $C_{14}H_{19}NO_4$: C 63.38, H 7.22, N 5.28; found: C 63.20, H 7.09, N 5.30.

*Reaction of 1,6:2,3-dianhydro-4-O-benzyl-β-D-glucopyranose (**6**) with dimethyl magnesium*

A fresh solution of dimethyl magnesium (43) (0.5 *M* (24)) in ether (1 L) (containing very little chloride ion, 0.01 *M*) was added to a solution of compound **6** (7.97 g, 34 mmol) in dry dioxane (500 mL) under nitrogen. The ether was distilled until the distillation head temperature reached 70°C, then the reaction was heated under reflux for 13.6 h. The stirred reaction mixture was cooled in an ice bath and saturated aqueous ammonium chloride (75 mL) was added. The reaction mixture was filtered and the filtrate concentrated to a volume of 50 mL. The residue was diluted with chloroform (30 mL) and the solution washed with saturated sodium bicarbonate solutions (2 × 40 mL), dried ($MgSO_4$), and concentrated to a brown oil (7.21 g). The oil was separated into two fractions by column chromatography on silica gel (266 g) using ethyl acetate – petroleum ether (30–60°C) 1:1 as eluant.

The first fraction (R_f 0.43 using the same eluant) was a syrup, 1,6-anhydro-4-*O*-benzyl-3-deoxy-3-*C*-methyl-β-D-glucopyranose (**14**); 2.73 g, 32%; $[\alpha]_D^{20}$ −59° (*c* 5.10, chloroform); *m/z*: 250 (0.6%), 192 (1.1%), 147 (12%), 146 (7%), 143 (3%), 141 (4%), 118 (6%), 113 (8%), 91 (100%). *Exact Mass* calcd. for $C_{14}H_{18}O_4$: 250.1205; found: 250.1202.

The second fraction (0.89 g) was a mixture, which was separated into two fractions by column chromatography on silica gel (40 g) using hexanes – 2-propanol 3:2 as eluant. The slower moving fraction, a solid (R_f 0.55 using pentane – 2-propanol 3:2 as eluant), was recrystallized from ethanol–water to give colorless needles of 1,6-anhydro-3,4-dideoxy-β-D-*erythro*-hex-3-enopyranose (**15**); mp 50–52°C; $[\alpha]_D^{22}$ −238° (*c* 2.70, chloroform); ir (solution in chloroform): 3595, 3470 (OH stretch), 3057 (CH stretch of alkene) cm^{-1}. *Anal.* calcd. for $C_6H_8O_3$: C 56.25, H 6.29; found: C 56.33, H 6.24.

The faster moving fraction (0.57 g), a mixture, was kept with acetic anhydride (1 mL) and pyridine (1.5 mL) for 24 h. Normal work-up gave a slightly yellow oil, 0.45 g. The two components were separated by column chromatography on silica gel (37 g) using ethyl acetate – hexanes 3:7 as eluant.

The faster moving component (R_f 0.44) (110 mg) was a syrup, one diastereomer of 2-*O*-acetyl-4-*C*-(acetoxyphenylmethyl)-1,6-anhydro-3,4-dideoxy-β-D-glucopyranose (**16**); $[\alpha]_D^{25}$ −36.5° (*c* 1.13, chloroform).

The slower moving component (R_f 0.32) (120 mg) was a solid, which was recrystallized from 95% ethanol to give long needles of the other diastereomer of 2-*O*-acetyl-4-*C*-(acetoxyphenylmethyl)-1,6-anhydro-3,4-dideoxy-β-D-glucopyranose (**17**); mp 152–154°C; $[\alpha]_D^{25}$ −80.8° (*c* 1.36, chloroform). *Anal.* calcd. for $C_{18}H_{22}O_4$: C 64.66, H 6.63; found: C 64.52, H 6.72.

Acknowledgements

This work was supported by Agriculture Canada under the Agri-Food Development Agreement and by an NSERC grant to T.B.G. We thank Drs. L. Ramaley and B. Gregory for accurate mass measurements. High field ^1H and ^{13}C nmr spectra were recorded at the Atlantic Region Magnetic Resonance Center.

1. M. Murase. J. Antibiot. Ser. A, **14**, 367 (1961).
2. K. F. Koch and J. A. Rhoades. Antimicrob. Agents Chemother. 309 (1970).
3. B. C. Das, J. Defaye, and K. Uchida. Carbohydr. Res. **22**, 293 (1972).
4. R. Kuhn and G. Baschang. Ann. Chem. **628**, 206 (1959); H. H. Baer. J. Am. Chem. Soc. **83**, 1882 (1961); S. Umezewa, K. Umino, S. Shibahara, M. Hamada, and S. Omoto. J. Antibiot. Ser. A, **20**, 355 (1967).
5. D. T. Williams and J. K. N. Jones. Can. J. Chem. **45**, 7 (1967); J. S. Brimacombe, J. G. H. Bryan, A. Hussain, M. Stacey, and M. S. Tolley. Carbohydr. Res. **3**, 318 (1967); M. W. zu Reckendorf. Chem. Ber. **101**, 3802 (1968); I. Jezo. Chem. Zvesti, **27**, 681 (1973).
6. T. Trnka, M. Cerny, M. Budesinsky, and J. Pacak. Collect. Czech. Chem. Commun. **40**, 3038 (1975).
7. P. J. Card. J. Carbohydr. Chem. **4**, 451 (1985), and references therein; T. J. Tewson and M. J. Welch. J. Org. Chem. **43**, 1090 (1978).
8. J.-R. Pougny and P. Sinay. J. Chem. Res. (M), 186 (1982).
9. P. Bhanot and R. G. Brown. Can. J. Microbiol. **26**, 1289 (1980); R. G. Brown and J. M. Embil. Can. J. Microbiol. **31**, 514 (1985).
10. J. G. Smith. Synthesis, 629 (1984).
11. N. R. Williams. Adv. Carbohydr. Chem. Biochem. **25**, 109 (1970).
12. M. Cerny and J. Stanek, Jr. Adv. Carbohydr. Chem. **34**, 23 (1977).
13. M. Cerny, T. Trnka, P. Beran, and J. Pacak. Collect. Czech. Chem. Commun. **34**, 3377 (1969).
14. T. Trnka and M. Cerny. Collect. Czech. Chem. Commun. **36**, 2216 (1971).

15. U. P. SINGH and R. K. BROWN. Can. J. Chem. **48**, 1791 (1970); **49**, 3342 (1971).
16. M. CERNY, T. ELBERT, and J. PACAK. Collect. Czech. Chem. Commun. **39**, 1752 (1974).
17. P. A. SEIB. J. Chem. Soc. (C), 2552 (1969).
18. J. M. MACLEOD, L. R. SCHROEDER, and P. A. SEIB. Carbohydr. Res. **30**, 337 (1973).
19. M. CERNY, V. GUT, and J. PACAK. Collect. Czech. Chem. Commun. **26**, 2542 (1961).
20. M. CERNY, L. KALVODA, and J. PACAK. Collect. Czech. Chem. Commun. **33**, 1143 (1968).
21. Y. IZUMI and K. HAYASHI. Chem. Lett. 787 (1980).
22. L. VEGH and E. HARDEGGER. Helv. Chim. Acta, **56**, 1961 (1973).
23. R. G. S. RITCHIE, N. CYR, and A. S. PERLIN. Can. J. Chem. **54**, 2301 (1976); H. PAULSEN, V. SINNWELL, and W. GREVE. Carbohydr. Res. **49**, 27 (1976); T. TRNKA and M. CERNY. Carbohydr. Res. **76**, 39 (1979).
24. L. F. FIESER and M. FIESER. Reagents for organic synthesis. Vol. 1. (1967); H. GILMAN, E. A. ZOELLNER, and J. B. DICKEY. J. Am. Chem. Soc. **51**, 1576 (1929).
25. M. BUDESINSKY, T. TRNKA, and M. CERNY. Collect. Czech. Chem. Commun. **44**, 1949 (1979).
26. J. BUDDRUS. Angew. Chem. Int. Ed. Engl. **11**, 1041 (1972).
27. J. E. G. BARNETT. Adv. Carbohydr. Chem. **22**, 177 (1967).
28. S. HANESSIAN and N. R. PLESSAS. J. Org. Chem. **34**, 2163 (1969).
29. J. PACAK, P. DRASAR, J. NERUDOVA, and M. CERNY. Collect. Czech. Chem. Commun. **37**, 4120 (1972).
30. W. NAGATA, M. OSHIOKA, and T. Okumura. J. Chem. Soc. C, 2365 (1970).
31. A. MUBARAK and B. FRASER-REID. J. Org. Chem. **47**, 4265 (1982).
32. N. K. KOCHETKOV, A. F. SVIRIDOV, and M. S. ERMOLENKO. Tetrahedron Lett. **22**, 4315 (1981); A. F. SVIRIDOV, M. S. ERMOLENKO, and N. K. KOCHETKOV. Izv. Akad. Nauk SSSR, Ser. Khim. 2557 (1982).
33. C. J. POUCHER. The Aldrich library of NMR spectra. Vol. I. 2nd ed. Aldrich Chemical Co. Inc., Milwaukee, WI. 1983. p. 921.
34. U. SCHOLLKOPF. Angew. Chem. Int. Ed. Engl. **9**, 763 (1970).
35. B. H. LIPSHUTZ, R. S. WILHELM, J. A. KOZLOWSKI, and D. PARKER. J. Org. Chem. **49**, 3928 (1984).
36. J. H. NOORDIK and G. A. JEFFREY. Acta Crystallogr. Sect. B: Struct. Crystallogr. Cryst. Chem. **33**, 403 (1977).
37. M. MALUSZYNSKA, S. TAGAKI, and G. A. JEFFREY. Acta Crystallogr. Sect. B: Struct. Crystallogr. Cryst. Chem. **33**, 1792 (1977).
38. R. R. FRASER, M. KAUFMAN, P. MORAND, and G. GOVIL. Can. J. Chem. **47**, 403 (1969); P. DAIS and A. S. PERLIN. Carbohydr. Res. **146**, 177 (1986).
39. Y. A. PARK, H. S. KIM, and G. A. JEFFREY. Acta Crystallogr. Sect. B: Struct. Crystallogr. Cryst. Chem. **27**, 220 (1971); K. B. LINDBERG. Acta Chem. Scand. Ser. A, **28**, 1181 (1974).
40. T. B. GRINDLEY, S. KUSUMA, and T. S. CAMERON. Can. J. Chem. **64**, 2388 (1986).
41. R. W. JEANLOZ and A. M. C. RAPIN. J. Org. Chem. **28**, 2978 (1963).
42. N. M. MERLIS, E. A. ANDRIEVSKAYA, L. I. KOSTELIAN, and O. P. GOLOVA. Izv. Akad. Nauk SSSR, Ser. Khim. 139 (1975).
43. B. G. CHRISTENSON, R. G. STRACHAN, N. R. TRENNER, B. H. ARISON, R. HIRSCHMANN, and J. M. CHEMERDA. J. Am. Chem. Soc. **82**, 3995 (1960).

Can. J. Chem. Downloaded from www.nrcresearchpress.com by 78.46.186.204 on 09/07/12
For personal use only.

Preparation of integrated chemical sensors using commercial VLSI technology

PAUL G. GLAVINA AND D. JED HARRISON[1]

Department of Chemistry, University of Alberta, Edmonton, Alta., Canada T6G 2G2

Received October 31, 1986

This paper is dedicated to Professor Douglas E. Ryan on the occasion of his 65th birthday

PAUL G. GLAVINA and D. JED HARRISON. Can. J. Chem. **65**, 1072 (1987).

The fabrication of ion sensitive field effect transistors (ISFET) and microelectrode arrays for use as chemical sensors using a commercial CMOS fabrication process is described. The commercial technology is readily available through the Canadian Microelectronics Corporation; however, several of the recommended design rules must be ignored in preparing chemical sensors using this process. The ISFET devices show near theoretical response to K^+ in aqueous solution (55 mV slope) when coated with a K^+ sensitive membrane. An extended gate ion sensitive device is presented which offers advantages in encapsulation of ISFET sensors. The source-drain current of both devices show a linear response to log a_{K^+} in contrast to ISFETs previously reported that have high internal lead resistances. Al and poly-Si microelectrode arrays are fabricated commercially and then Pt is electrodeposited on the microelectrodes. The resulting arrays show good cyclic voltammetric response to $Fe(CN)_6^{4-}$ and $Ru(NH_3)_6^{3+}$ and are relatively durable.

PAUL G. GLAVINA et D. JED HARRISON. Can. J. Chem. **65**, 1072 (1987).

On décrit la fabrication, à l'aide du processus de fabrication commercial CMOS, de transistors à effet de champ sensibles aux ions (TECSI) et de revêtements de microélectrodes qui peuvent être utilisées comme sondes chimiques. La technologie commerciale est facilement disponible par le biais de la Corporation canadienne de microélectronique; toutefois, plusieurs des règles recommandées doivent être ignorées lors de la préparation des sondes chimiques. Les TECSI qui sont recouverts d'une membrane sensible aux ions K^+ présentent une réponse qui est pratiquement théorique pour le K^+ en solution aqueuse (pente de 55 mV). On propose un dispositif, sensible aux ions et offrant plus de possibilités, qui offre des avantages pour l'encapsulation des sondes TECSI. Le courant source-drain de chacun de ces dispositifs présente une réponse linéaire par rapport aux log a_{K^+} et ce résultat est en opposition avec ceux obtenus antérieurement avec d'autres TECSI qui avaient des résistances élevées du fil interne. On a fabriqué commercialement des revêtements de microélectrodes en Al et en poli-Si et on a procédé à l'électrodéposition du Pt sur des microélectrodes. Les revêtements qui en résultent présentent de bonnes réponses pour la voltammétrie cyclique du $Fe(CN)_6^{4-}$ et du $Ru(NH_3)_6^{3+}$ et ils sont relativement durables.

[Traduit par la revue]

There is an increasing interest in the design and fabrication of chemical sensors which may function as remote, implantable, or field portable transducers in the determination of biologically or environmentally important species (1, 2). One of the keys to development of advanced sensors is the determined exploitation of Si integrated circuit processing technology. Most of the devices that have been reported in the literature have been fabricated at research facilities which offer considerable flexibility in materials selection and processing steps (1, 2). However, the significant cost of establishing microlithographic capability limits the access of many researchers to this technology. It is important to develop means of using commercially available fabrication facilities to prepare integrated sensors, which may then require modest post-processing steps (3). In addition to increasing access to researchers, this is also an important step to the eventual commercialization of integrated chemical sensors, since it will significantly reduce the initial capital investment required to produce devices.

The Canadian Microelectronics Corporation (CMC), funded through the Natural Sciences and Engineering Research Council, has been established to encourage research in microelectronics and act as a liaison with Northern Telecom. Through the CMC the CMOS-1b (5 μm minimum feature dimension) and the CMOS-3 (3 μm dimension) Si fabrication processes of Northern Telecom are available to Canadian researchers. There are presently more than 25 Canadian universities equipped with design stations that submit projects to this facility. However, to our knowledge these projects have not involved chemical sensors. Utilization of a commercial facility for chemical sensor fabrication presents a number of difficulties. A significant feature of most chemical sensors is the need for access of the sensing element to the environment; this requires unique fabrication considerations since a standard CMOS process is designed to protect the device from the environment. Additionally, the most commonly used materials for interconnects and metallization are P-doped polycrystalline Si (poly-Si) and Al. Many electrochemical sensors utilize other materials as electrodes (1, 2), and poly-Si and Al are not compatible with many applications.

In this paper we present techniques we have used to design and fabricate ion sensitive field effect transistors (ISFETs) and microelectrode arrays using the Northern Telecom CMOS-1b process. Microelectrode arrays and interdigitated electrodes have been previously demonstrated to be integral components of a variety of chemical sensors (2) such as the chemical transistor (4) and chemiresistors (5). We have developed techniques for the fabrication of Al or poly-Si microelectrodes using the CMOS-1b process, followed by electrodeposition of Pt, resulting in microelectrode arrays that can be used in aqueous solution. In the fabrication of ISFETs the use of the Northern Telecom process introduces several features not usually found in ISFET design. These include the use of an overglass layer to protect and passivate the Al interconnects, and the consequent ability to use low impedance contacts to the transistor source and drain. These features lead to linear device output, which is important in simplifying the signal processing stage.

Experimental

Integrated devices were fabricated by Northern Telecom using the poly-Si gate CMOS-1b process. Access to this facility is provided through the VLSI Implementation Centre (VLSIIC) of the CMC. Mask layout was performed using the graphics editor program KIC (6)

[1]Author to whom correspondence should be addressed.

Can. J. Chem. Downloaded from www.nrcresearchpress.com by 78.46.186.204 on 09/07/12
For personal use only.

Can. J. Chem. Downloaded from www.nrcresearchpress.com by 78.46.186.204 on 09/07/12
For personal use only.

as a VLSI design tool, running on a VAX-11/780 using the UNIX operating system. Design stations consisting of DEC UT240 and AED graphics terminals provided by the CMC were used. The file in CIF format was transferred to VLSIIC using the CDN-net electronic mail network. Several of the designs were prepared on a different system using the CADDS 2/VLSI graphics editor operating on a Computervision Model 4001 mainframe computer. The output format was Calma GDS-II (Version 3) which was converted to CIF format using software written in the Department of Electrical Engineering, University of Alberta. The files were sent on magnetic tape to VLSIIC.

The semiconductor dies received from CMC were bonded in 40 pin dual in-line packages (DIP) by Northern Telecom. An HP 4145A Semiconductor Parameter Analyzer (on loan from the CMC) with a 16658A test fixture was used to test the characteristics of the reference FETs paired to each ISFET on the Si chip. To test devices in solution the bonding wires and contact pads were encapsulated with Epon 828 resin, hardened with Epon V-40 (1:1 ratio) (Miller Stephenson Co., Connecticut), and cured for 24 h. The DIP was then made into a "beaker" by attaching a 1 cm × 1.25 cm glass ring to the assembly with epoxy. Several drops of a polyvinylchloride, dioctyladipate, valinomycin, and $KB(C_6H_5)_4$ mixture in tetrahydrofuran (BDH, distilled), prepared according to Bond *et al.* (7), was evaporated on the surface of the chip to prepare K^+ sensitive ISFETs. Transistor and diode characteristics were obtained for the ISFETs using a Pine Instruments RDE-4 bipotentiostat and a Kipp and Zonen BD90 $x-y$ recorder. To obtain transistor characteristics, the reference and counter electrode terminals of the RDE-4 were connected to the device source/substrate contact. The device drain was connected to working electrode K1, and a saturated calomel reference electrode (SCE) was connected to working electrode K2. Sweeping the potential of K1 (500 mV/s) acts to vary V_{DS} (see Fig. 2), while the potential of K2 is varied in stepwise fashion to obtain a family of curves with different values of V_g. Diode characteristics (8) were obtained by connecting the ISFET as above, but the SCE was also connected to K1 (see Fig. 2*b*). K^+ test solutions were adjusted to constant ionic strength with 0.1 *M* NaCl.

Electrical response times of the K^+ sensitive ISFETs were evaluated using a square wave from a PAR 175 waveform generator, input into the Pine RDE-4 potentiostat, to modulate either V_g or V_{DS}. The current response, I_{DS}, was recorded with a Tektronix Model 2430 digital storage oscilloscope. The response time (to 100% of the final value) of the Pine potentiostat was determined to be ~30 μs; sufficient for this application. Chemical response time of the ISFETs to an increase in K^+ concentration was evaluated under conditions of fixed V_g and V_{DS}. A small volume (~0.3 mL) of 10^{-4} *M* KCl was first introduced into the "beaker" on the DIP, and then ~0.7 mL of 1 *M* KCl was vigorously injected from a pipette. The change in I_{DS} during this procedure was recorded on the Tektronix oscilloscope, and on an $x-y$ recorder.

Microelectrode arrays were encapsulated as described for ISFET devices. To electroplate Pt on interdigitated Al fingers, the Al was first etched with a 25% aqueous solution of 25:1 H_3PO_4:HNO_3 for 12 min and rinsed thoroughly with doubly distilled H_2O. The Al array was then briefly exposed to the air before exposing to the plating solution. For both Al and poly-Si surfaces, Pt was electrodeposited in 5 m*M* K_2PtCl_4 (Strem), 1 *M* $NaClO_4$ (G. F. Smith) at −0.8 V vs. SCE for about 7 min, and the devices were rinsed in doubly distilled H_2O. Reagent grade $K_4Fe(CN)_6$ (J. T. Baker), $Ru(NH_3)_6^{3+}$ (Strem), KCl and NaCl (GIC), were used as received.

A Cambridge S250 Scanning Electron Microscope equipped with a Kevex 7000 Energy Dispersive X-ray Analyzer was used to obtain electron micrographs. Samples were Au-coated to ~200 Å thickness. A Bausch and Lomb Microzoom microscope with a Wild MPS-12 camera adaptor and a Wild Mikrophot MPSO5 light meter was used to obtain optical micrographs.

Results

The ion sensitive field effect transistor and related devices have been the subject of intense research activity (1, 2*a*, 3, 8–10). We have used the Northern Telecom CMOS-1b process to fabricate two types of ISFET devices. Figure 1 shows a schematic representation of an ISFET (device 1) with an opened gate region on the left hand side which can be subsequently coated with an ion-sensitive material and exposed to solution. On the right hand side is a reference transistor which remains insulated from solution and shares a common drain with the ISFET; it can be used to characterize the transistor assembly.

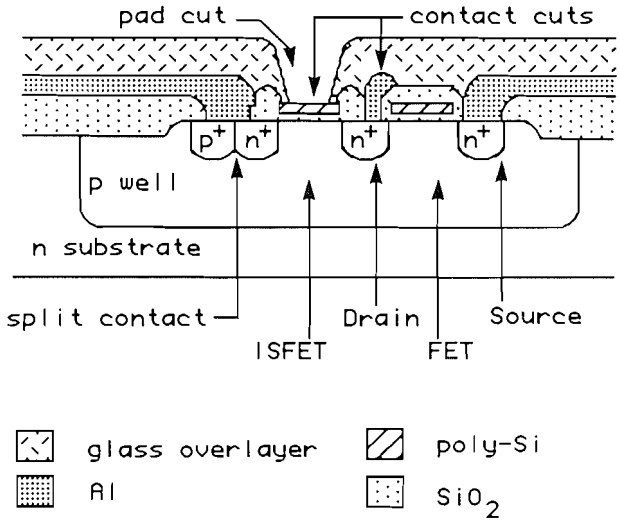

FIG. 1. Schematic of the opened gate ISFET (left) and a paired reference FET (right) prepared in the same p-Si device well (device 1) using the Northern Telecom CMOS-1b process. A split contact is made to the ISFET source and the p-well substrate to short these terminals together. The symbols p^+ and n^+ refer to heavily doped p and n type regions, respectively. The source contact for the FET is on the opposite side of the device, and both the FET and ISFET share a common drain. Contact cuts through the SiO_2 are made over the source and drain diffusions as well as over the ISFET gate. A pad cut is made over the ISFET gate down to the poly-Si layer through the overglass layer which protects and passivates the Si chip.

The transistors are designed with a split contact, Fig. 1, that shorts together the n^+ source diffusion and the p^+ substrate diffusion contacts as indicated in the circuit diagrams, Fig. 2. In the fabrication process SiO_2 is thermally grown over the entire wafer following definition of the source, drain, and gate. Contact cuts are etched through the oxide to regions that are subsequently metallized, allowing electrical contact to the transistor. To prepare an ISFET a contact cut is also made over the gate region of the transistor. This removes the SiO_2 layer over the poly-Si which defines the gate area. This step violates a CMOS-1b design rule (11) but is compatible with the actual fabrication process (11*a*). The wafer is then aluminum coated and the metal interconnect layer is patterned microlithographically. In this step Al is removed from the contact cut over the gate by not defining this region in the Al patterning mask. Although this violates another design rule (11*b*), X-ray fluorescence spectra indicate Al is successfully removed from the gate. The final step in the Northern Telecom CMOS-1b process involves chemical vapour deposition of a pyrox overglass from SiH_4, PH_3, and O_2. This layer serves to passivate the device and protect it from the environment. Bonding pads are formed by etching through to the metallized regions, and in this step a region of appropriate dimensions is etched out over the ISFET gate, down to the poly-Si layer. This step also breaks a design rule (11*c*).

An alternative device configuration (device 2) has also been

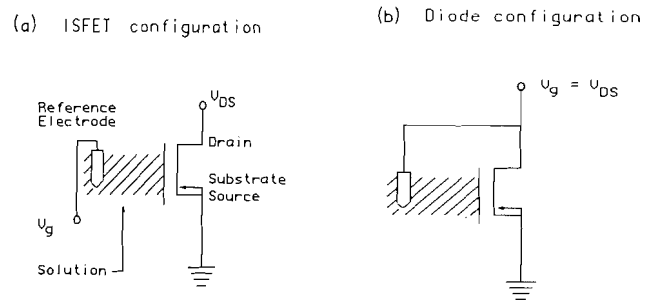

FIG. 2. (*a*) The configuration of an ISFET is shown. A solution replaces the metal contacts to the device gate. The potential of a reference electrode in solution is controlled by varying V_g with respect to the source and substrate potential. The drain-source voltage V_{DS} is set independently. (*b*) In the so-called diode configuration the reference electrode potential $V_g = V_{DS}$ relative to the source and substrate. In this configuration the square root of the drain-source current is proportional to V_g.

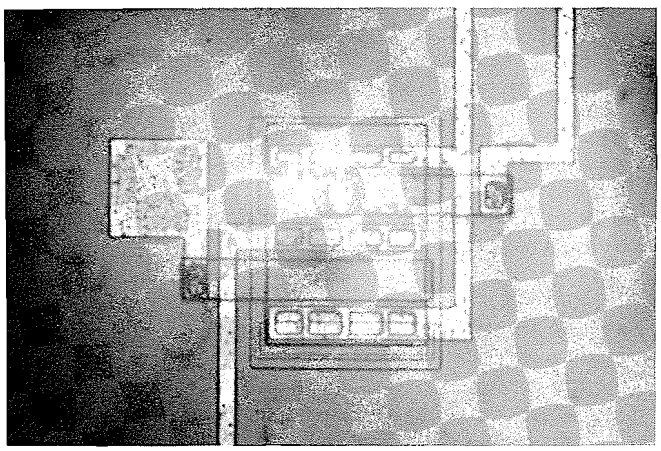

FIG. 3. Photomicrograph of the extended gate ISFET (device 2) with paired reference FET. The poly-Si lead of the ISFET gate is contacted to an exposed Al pad away from the sensitive gate region in contrast to the device configuration of Fig. 1.

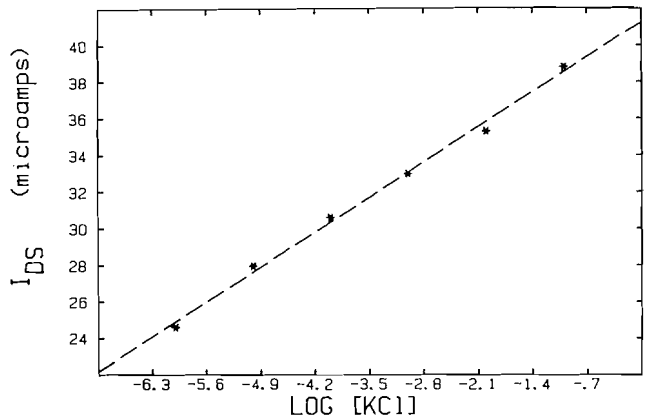

FIG. 4. Response of device 1 opened gate ISFET to log [KCl]. Drain source current, I_{DS}, was measured at constant $V_{DS} = 1.0$ V with 2.0 V applied as V_g. Ionic strength was adjusted to 0.1 *M* with NaCl.

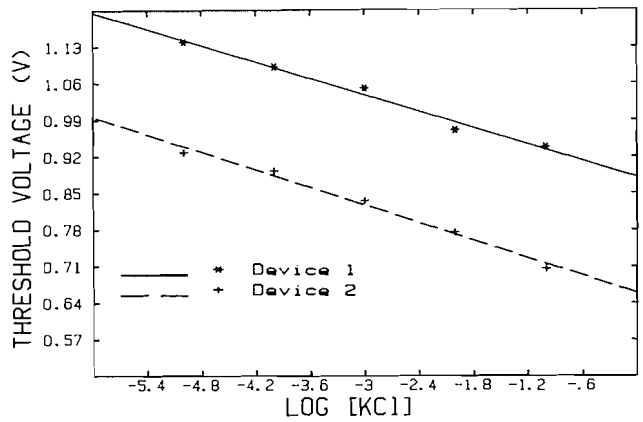

FIG. 5. Values of the threshold voltages, V_{Th}, as a function of log [KCl] for opened gate (device 1) and extended gate (device 2) configurations. V_{Th} with respect to an SCE was determined at each concentration from plots of $\sqrt{I_{DS}}$ versus V_g with the device operated in the diode configuration.

fabricated and is shown in Fig. 3. In this device the relatively fragile FET gate is not directly exposed to solution. Instead the poly-Si layer over the gate is extended beyond the device, and a contact cut is made to the poly-Si layer where a 50 μm × 50 μm Al pad is defined in the metallization step. Following device passivation with the pyrox overglass, the pad area is re-opened using the final lithographic step that also opens the bonding pads. In this design the chemically sensitive region can be located a considerable distance from the active Si device, and connected to the gate via poly-Si or Al leads producing an "extended" gate.

Devices 1 and 2 may be coated with organic ion sensitive membranes, which impart selectivity to a specific ion (2*a*). Coating the exposed transistors with a mixture of polyvinylchloride, dioctyladipate, and valinomycin (7) produces devices with good sensitivity and selectivity for K^+ in aqueous solution. Operating device 1 at a constant value of V_{DS} and apparent gate voltage V_g (see Fig. 2*a*) results in the drain-source current, I_{DS}, varying linearly with log [K^+], as shown in Fig. 4. This configuration results in a signal which is low impedance and provides immediate amplification of the response to K^+. The sensor may also be operated in the diode configuration (8), with the reference electrode shorted to the drain, Fig. 2*b*. In this configuration $\sqrt{I_{DS}}$ is proportional to V_g, for devices with no significant internal resistance, and a plot of $\sqrt{I_{DS}}$ versus V_g should be linear, with the threshold voltage, V_{Th}, given by the voltage axis intercept. The threshold voltage represents the value of V_g at which the conductivity in the channel under the gate becomes sufficient for the current, I_{DS}, to flow. It has been shown that V_{Th} measured with respect to a reference electrode is proportional to log (ion activity) (2*a*). For devices 1 and 2 coated with K^+ sensitive membrane, plots of $\sqrt{I_{DS}}$ vs. V_g are linear, and values of apparent V_{Th} vs. SCE as a function of [K^+] are readily attained. Figure 5 shows that for both device types V_{Th} varies linearly with log [K^+], and a slope of 55 mV is obtained, in reasonable agreement with the 59 mV slope predicted by the Nernst equation. The two devices show about 200 mV difference in the value of apparent V_{Th} at a given concentration. A similar variation in V_{Th} is observed for the reference transistors paired to each ISFET, and apparently represents normal variation between transistors for the CMOS-1b process, rather than a real difference between the design properties of devices 1 and 2.

The response of I_{DS} to a step function perturbation of either V_g or V_{DS} was evaluated for devices 1 and 2. Operating at

Can. J. Chem. Downloaded from www.nrcresearchpress.com by 78.46.186.204 on 09/07/12
For personal use only.

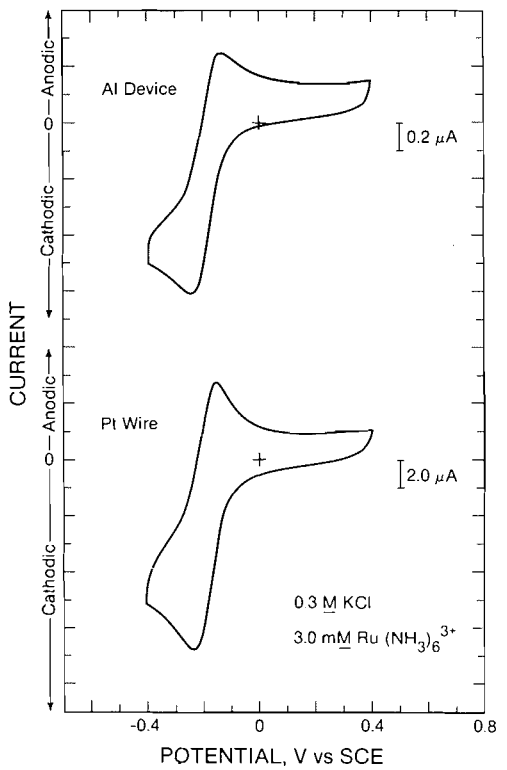

FIG. 6. Cyclic voltammetry at 50 mV/s of $Ru(NH_3)_6^{3+}$ at Pt electroplated Al microelectrodes, fabricated using the Northern Telecom CMOS-1b process, compared to that at a Pt wire electrode (0.01 cm^2).

constant V_{DS} a step in V_g from 1.8 to 2.2 V results in I_{DS} reaching 95% of the final value in 15 ms for device 1 and 10 ms for device 2. A step change in V_{DS}, with fixed V_g equal to 1.75 V, requires 3 ms and 4 ms for devices 1 and 2 to settle to 95% of the final value. The response times observed are shorter by a factor of two than those previously reported for ISFET devices with K^+ membranes (12). When bias voltages are held constant and the concentration of K^+ is stepped from 10^{-4} *M* to 0.7 *M* the final value of I_{DS} is attained in 90 ms. This represents an upper limit on the response time of the ISFET, since it is difficult to evaluate the time required for mixing of solutions with the procedure used.

Microlithographic patterning of conducting electrode arrays is an attractive route to developing a variety of electrochemical sensors (4, 5). The conducting interconnect layers in most commercial processes are Al or doped poly-Si, yet neither of these materials is overly satisfactory for electrochemical applications. We have used the CMOS-1b and CMOS-3 facilities to produce Al interdigitated fingers, and poly-Si microelectrode arrays, and have subsequently electrodeposited Pt on the electrodes to prepare them for electrochemical applications.

Immediately prior to electrodeposition of Pt on Al substrate arrays, an active Al surface is prepared by etching the array in an acid solution. This fresh Al surface is briefly exposed to air (~60 s) allowing formation of a thin oxide, and approximately 1 to 10 mmol/cm^2 of Pt is then electrodeposited from the plating solution, at a potential of −0.7 V vs. SCE. Figure 6 compares the cyclic voltammetry for $Ru(NH_3)_6^{3+}$ observed at a bulk Pt electrode and a platinized Al microelectrode array in 0.1 *M* KCl. The peak-to-peak separation is ~10 mV greater at the Pt-coated Al device, which is consistent with a voltage drop across the thin aluminum oxide layer formed during preparation

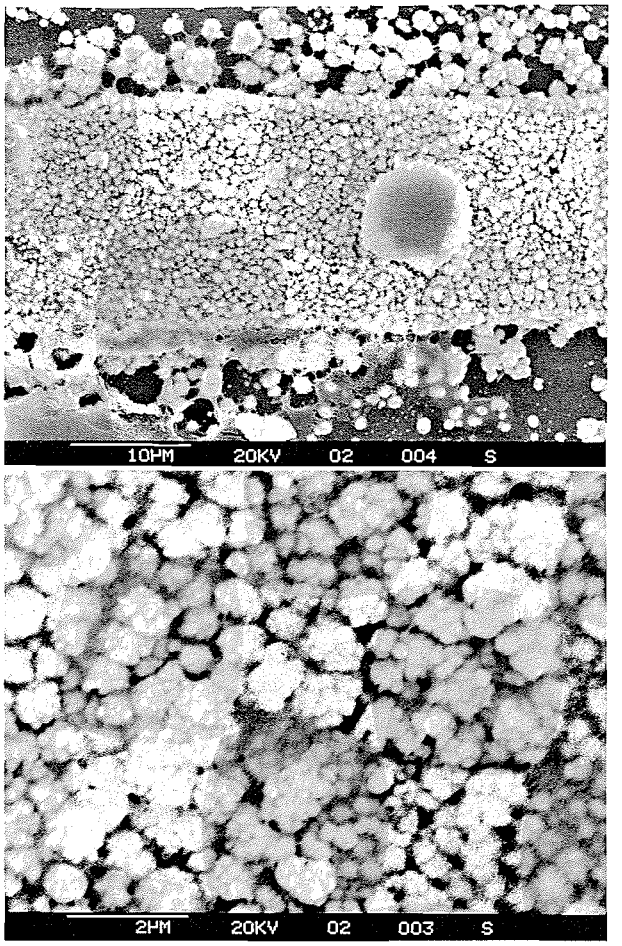

FIG. 7. Electron micrographs of Pt electrodeposit on the Al microelectrode substrate. The upper micrograph shows small Pt particles, identified by X-ray fluorescence (XRF), deposited over an Al lead, with larger Pt particles scattered nearby. A large featureless nodule is also observed on the electrode. XRF identifies Al and Cl as its constituents, indicating corrosion of the Al substrate. The lower micrograph shows a close-up of the Pt particles deposited on the Al leads.

of the surface for Pt electroplating. There is no significant background oxidation current for Al observed at the positive potential extreme, and the platinized electrodes can be cycled more than 50 times with no significant change in the electrochemistry. However, excursions to potentials at which H_2 or O_2 is evolved result in loss of Pt from the electrodes.

The nature of the Pt deposit on Al was examined by scanning electron microscopy (SEM). Figure 7 shows that Pt is deposited uniformly on the Al, and displays a microcrystalline structure. However, larger Pt nodules are observed deposited over the SiO_2 substrate between Al leads. Spreading of the Pt deposit beyond the electroactive area has been observed previously for Pt deposition at Au microelectrodes, and has been used to narrow the inter-electrode separation to as little as 0.2 μm (13). Unfortunately, there is a tendency for the separate fingers of the interdigitated Al leads to short together as Pt is deposited and we have not been able to isolate Al electrodes separated by less than ~40 μm. The other feature of concern is the large nodule in the centre of the Al lead, Fig. 7. Energy dispersive X-ray fluorescence under the SEM probe identifies Al and Cl as two of the major components. This structure clearly results from corrosion of the Al layer. While it is often not a problem,

Can. J. Chem. Downloaded from www.nrcresearchpress.com by 78.46.186.204 on 09/07/12
For personal use only.

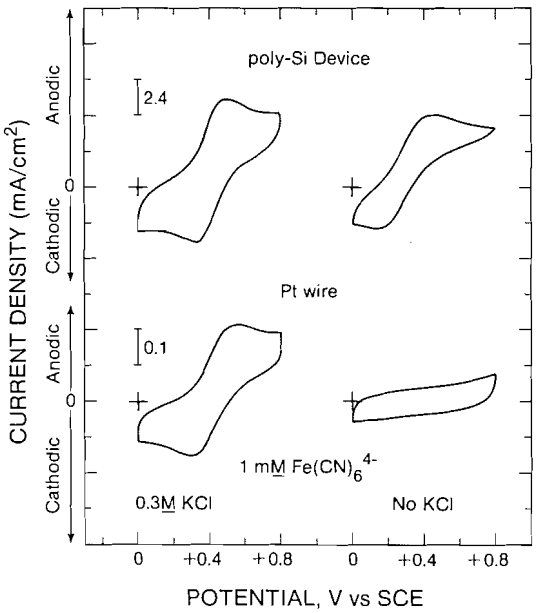

FIG. 8. Cyclic voltammetry at 50 mV/s of 1 m*M* $Fe(CN)_6^{4-}$ in 0.3 *M* KCl at Pt electroplated poly-Si microelectrodes compared to the response at a Pt electrode (0.01 cm^2). Also shown is the response to 1 m*M* $Fe(CN)_6^{4-}$ in the absence of supporting electrolyte. The Pt electrode response is severely distorted by *IR* drop in solution, while the Pt coated poly-Si electrodes show response typical of microelectrodes in high resistance media.

in some cases an entire electrode finger is destroyed by this corrosion process.

We have also prepared microelectrode arrays consisting of P-doped poly-Si electrodes 20 μm wide, 190 μm long, separated by 20 μm, and all connected to a common bus. The poly-Si layer was exposed using the contact cut and bonding pad steps in the CMOS-1b microlithographic process. Again these steps involve breaking of CMOS-1b design rules (11*b*, *c*). It proved possible to electrodeposit Pt on poly-Si without need for an etching step to activate the poly-Si. The cyclic voltammetric response to $Fe(CN)_6^{4-}$ of a Pt coated poly-Si electrode array is shown in Fig. 8, and compared to that at a bulk Pt electrode. There is no significant difference in peak-to-peak separation for the bulk and the electrodeposited Pt electrodes. The platinized electrode arrays can be cycled more than 50 times in $Fe(CN)_6^{4-}$ solution with no change in the cyclic voltammograms. The observed current densities at the electrodes are significantly different, based on the projected geometric areas of the bulk Pt electrode (1×10^{-2} cm^2) and the microelectrode array (4.2×10^{-4} cm^2). The projected area does not account for surface roughness factors, which are clearly important in evaluating the true area of the platinized array, Fig. 9. However, enhanced current density is expected due to cylindrical diffusion (14) to the electrodes in the array, as has been reported previously for microelectrodes of similar geometry (15). Evidence for microelectrode behaviour at the poly-Si device is shown by the response to $Fe(CN)_6^{4-}$ in absence of supporting electrolyte, for which a reasonably well defined cyclic voltammogram is observed, Fig. 8. This contrasts with the distorted response observed at a bulk Pt electrode of macroscopic dimensions in the same solution.

Electron micrographs of electrodeposited Pt on poly-Si arrays are shown in Fig. 9. The poly-Si electrodes are relatively uniformly covered, and there is much less deposition on

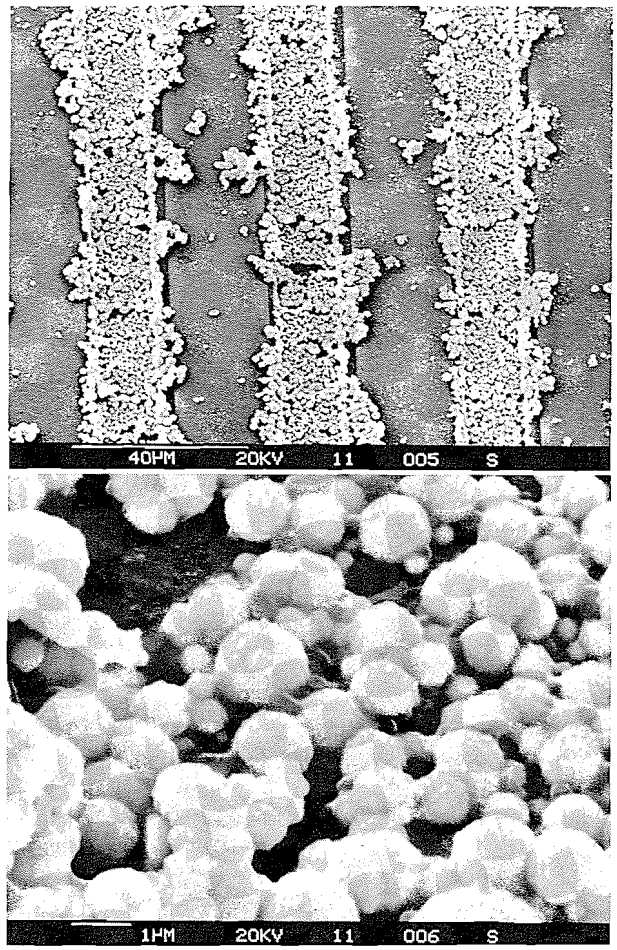

FIG. 9. Electron micrographs of Pt electrodeposited on poly-Si microelectrodes. Lower micrograph shows close-up of Pt deposit on the poly-Si lead indicating much less dense packing obtained on poly-Si relative to Al (Fig. 8).

the insulated region between electrodes than is found for Al electrode arrays. Some Pt growth between electrodes does occur, but it occurs much less frequently, and isolation of electrodes separated by 20 μm is readily achieved. A close up of the Pt deposit, Fig. 9, shows it is less uniform than on Al electrodes, and appears to have a different structure. The corrosion problems observed with Al electrodes are not observed on poly-Si, due to rapid passivation of Si arising from oxide growth at positive potentials.

Discussion

The commercial CMOS-1b fabrication process can be used successfully to produce a variety of sensor devices. In fabricating an ISFET using the CMOS-1b process the gate material exposed to solution is conducting poly-Si, in contrast to most ISFETs (2, 8–10) which have insulating SiO_2 or Si_3N_4 layers on the gate. The data in Figs. 4 and 5 for K^+ membrane coated devices demonstrate that the presence of poly-Si on the gate does not affect device performance. However, unlike Si_3N_4 coated ISFETs (2*a*), device 1 with poly-Si on the gate and no organic membrane coating does not exhibit Nernstian response to pH.

Protection of the Al interconnects using a pyrox overglass decreases problems associated with packaging of ISFETs. With pyrox passivation low resistance Al contact leads can be used to

Can. J. Chem. Downloaded from www.nrcresearchpress.com by 78.46.186.204 on 09/07/12
For personal use only.

directly contact the source and drain of the devices, as has been done for the devices presented here. This approach differs from that used with many ISFETs reported in the literature (2, 8–10, 16, 17) which have high internal source and drain resistances due to the use of n^+ diffusions as the contact leads for source and drain. The effect of the internal resistance is non-linearity in the response of I_{DS} to log a_{K^+} when a device is operated at constant V_g. Additionally, when such devices are operated in the diode configuration (Fig. 2*b*) $\sqrt{I_{DS}}$ varies in a non-linear fashion with V_g. Non-linearity of ISFET response due to the internal resistance of n^+ diffusion leads has led to considerable efforts (16–18) to design compensatory circuitry and feedback control to obtain a linear output. The devices presented here, using low resistance Al contacts and a passivating overglass, obviate the need for much of the additional complex circuitry and matching of transistors used for other devices, since I_{DS} is linear over the range of concentration for which the membrane responds in a Nernstian fashion, Fig. 4.

Figure 5 demonstrates that the extended gate configuration of device 2 is as satisfactory as the more common exposed gate configuration of device 1. One of the difficulties associated with preparing ISFETs is packaging of the device to prevent transistor failure. The standard ISFET configuration of device 1 presents a particularly severe challenge, since it is the gate oxide which is most sensitive to environmental damage. The configuration of device 2 separates the device and the active chemically responsive element on the Si die. This extended gate structure should be more easily packaged and more durable.

Microelectrode arrays have been used to prepare a number of types of chemical sensors (4, 5). It is clear that noble metal electrodes prepared by vapor deposition and subsequent microlithographic patterning are superior to the electrodeposited Pt electrodes presented here. However, the approach presented provides access to microelectrode arrays for many researchers who do not have independent microlithographic capabilities.

Despite deposition of a layer of Pt on the Al electrode substrate, corrosion of the Al layer remains a problem, particularly in the presence of Cl^-. While cyclic voltammetry, Fig. 6, indicates that Al corrosion is not rapid, the large Al and Cl containing nodules observed in electron micrographs, Fig. 7, provide evidence that corrosion occurs. This is expected unless the Pt coating is totally non-porous, due to galvanic effects. The deposition of multiple metal layers on Al has been shown (19) to produce smooth Ni films and a similar procedure to produce better Pt deposits is under examination. Overall, the anodic self-passivating nature of the Si/SiO_x system makes the poly-Si arrays the preferred substrate for Pt coated electrochemical arrays.

The porous nature of the Pt deposit and the deposition conditions used are the probable cause for loss of Pt coating from the arrays during H_2 and O_2 evolution. Formation of gas in pockets inside the Pt film could lead to mechanical disruption of the film. The Pt was plated at a potential at which H_2 is not evolved, to allow determination of the amount deposited coulometrically. This differs from many methods for Pt deposition during electroplating. One consequence of a high overvoltage is a mechanically more durable Pt film, as weakly adhered material is immediately lost due to mechanical disruption by the gas bubbles formed.

The peak separation observed in the cyclic voltammetry for $Ru(NH_3)_6^{3+}$ reduction at the Pt coated, Al substrate electrodes, Fig. 6, indicates a kinetic barrier to electron transfer. This most likely arises from the presence of a thin Al oxide at the Al/Pt interface, resulting in a resistive potential drop (*IR* drop) which causes increased peak separation. The Pt-plated, poly-Si substrate arrays show no increase in peak separation in cyclic voltammetric scans at 50 mV/s, compared to a bulk Pt electrode. However, at sufficiently high scan rates the native oxide, SiO_x, present on the poly-Si surface would be expected to introduce some resistive losses. The presence of an *IR* drop at the electrode substrate/Pt interface reduces the applicability of these arrays to kinetic studies, but is unlikely to interfere with most sensor applications, such as electrochemical detection in liquid chromatography. The arrays should also make suitable substrates for moderately thick coatings ($\gtrsim 10$ μm) used in the preparation of chemiresistors. However, the surface roughness probably makes the arrays unsuitable for use with thin films (< 1 μm).

There are presently more than 25 Canadian universities with the capability to design and submit integrated circuitry for fabrication through the CMC. The methods of preparation of chemical sensors we have developed are compatible with this commercial process. Not only will chemical sensor fabrication using the Northern Telecom CMOS-1b process open this field to a variety of researchers, but the development of means to utilize a commercial facility is an important step in furthering commercialization of integrated sensors.

Acknowledgements

We wish to acknowledge D. Fraser and R. F. B. Turner of the Department of Electrical Engineering, University of Alberta, for assistance in the early design stages, and R. F. B. Turner for providing the interdigitated Al electrodes. We thank the Electron Microscopy Lab, Department of Entomology, University of Alberta, for use of their facility. We thank NSERC of Canada for support of this research.

1. (*a*) H. WOHLTJEN. Anal. Chem. **56**, 87A (1984); (*b*) R. E. DESSY. Anal. Chem. **57**, 1188A (1985); (*c*) J. D. CZABAN. Anal. Chem. **57**, 345A (1985).
2. (*a*) J. JANATA and R. J. HUBER. (*Editors*). Solid state chemical sensors. Academic Press, Orlando, Fl. 1985; (*b*) W. H. KO, J. MUGICA, and A. RIPART. (*Editors*) Implantable sensors for closed-loop prosthetic systems. Futura Publishing, Mount Kisco, NY. 1985.
3. J. VAN DER SPIEGEL, I. LAUKS, P. CHAN, and D. BABIC. Sens. Actuat. **4**, 291 (1983).
4. (*a*) H. S. WHITE, G. P. KITTLESEN, and M. S. WRIGHTON. J. Am. Chem. Soc. **106**, 5375 (1984); (*b*) J. W. THACKERAY, H. S. WHITE, and M. S. WRIGHTON. J. Phys. Chem. **89**, 5133 (1985).
5. H. WOHLTJEN, W. R. BARGER, A. W. SNOW, and N. L. JARVIS. IEEE Trans. Elec. Dev. **ED-32**, 1170 (1985).
6. G. BILLINGSLEY and K. KELLER. KIC: a graphics editor for integrated circuits. University of California, Berkeley, CA. 1984.
7. D. M. BOND, J. KRATOCHVIL, and T. TREASURE. Proc. Physiol. Soc. **265**, 5P (1976).
8. P. W. CHEUNG, W. H. KO, D. J. FUNG, and S. H. WONG. *In* Theory, design, and biomedical applications of solid state chemical sensors. *Edited by* P. W. Cheung, M. R. Neuman, D. G. Fleming, and W. H. Ko. CRC Press, West Palm Beach, FL. 1978.
9. P. BERGVELD. Sens. Actuat. **1**, 17 (1981).
10. (*a*) Y. OHTA, S. SHOJI, M. ESAHI, and T. MATSUO. Sens. Actuat. **2**, 387 (1982); (*b*) Y. SANADA, T. AKIYAMA, Y. UJIHIRA, and E. NIKI. Fres. Z. Anal. Chem. **312**, 526 (1982).
11. (*a*) Guide to the Integrated Circuit Implementation Services of the Canadian Microelectronics Corporation, Version 2.0, Section C.1.3, available from the CMC, Queen's University, Kingston,

Can. J. Chem. Downloaded from www.nrcresearchpress.com by 78.46.186.204 on 09/07/12
For personal use only.

Ontario; Minimum Separations Rule D.7; (*b*) Enclosure Rule C.5. (*c*) Pad Rule F.2, F.5.
12. R. L. SMITH and J. JANATA. J. Electrochem. Soc. **127**, 1599 (1980).
13. G. P. KITTLESEN, H. S. WHITE, and M. S. WRIGHTON. J. Am. Chem. Soc. **107**, 7373 (1985).
14. P. M. KOVACH, W. L. CAUDILL, and R. M. WIGHTMAN. J. Electroanal. Chem. **185**, 285 (1985).
15. K. R. WEHMEYER, M. R. DEAKEN, and R. M. WIGHTMAN. Anal. Chem. **57**, 1913 (1985).
16. A. SIBBALD, P. D. WHALLEY, and A. K. COVINGTON. Anal. Chim. Acta, **159**, 47 (1984).
17. A. SIBBALD. Sens. Actuat. **7**, 23 (1985).
18. P. BERGVELD. Sens. Actuat. **5**, 13 (1984).
19. W. G. ZELLEY. *In* Modern electroplating. *Edited by* F. A. Lowenheim. John Wiley and Sons, New York. 1953. Chap. 24.

Can. J. Chem. Downloaded from www.nrcresearchpress.com by 78.46.186.204 on 09/07/12
For personal use only.

Atomization efficiency of a graphite furnace in atomic absorption spectrometry at high heating rates

C. L. CHAKRABARTI,[1] D. FERRAROTTO, S. J. CATHUM, AND C. J. RADEMEYER[2]
Department of Chemistry, Carleton University, Ottawa, Ont., Canada K1S 5B6

FOR ERRATA SEE 65(11)1987 P. 2685

Received November 21, 1986

This paper is dedicated to Professor Douglas E. Ryan on the occasion of his 65th birthday

C. L. CHAKRABARTI, D. FERRAROTTO, S. J. CATHUM, and C. J. RADEMEYER. Can. J. Chem. **65**, 1079 (1987).

The efficiency of an HGA-400 for production and containment of atomic vapour was determined for several elements using relatively high heating rates. Two different atomization efficiencies β_1 and β_2 were experimentally determined by two variations of a method. Assuming that atomization in the HGA-400 can be described by consecutive, first-order reactions $D \xrightarrow{k_1} B \xrightarrow{k_2} C$, the method consisted of making the absorbance signal profile (at least the decay part of it) appear at constant tube wall (at the centre) temperature and determining first-order rate constants for atom formation and atom loss, k_1 and k_2, respectively. Two atomization efficiencies were calculated: β_1 and β_2, which gave the fraction of analyte which was present as atomic vapour at the peak of the absorbance signal profile. Experimental atomization efficiencies reported for Al, Cu, Co, Fe, Ag, and Ga average: β_1 0.42 and β_2 0.30, with a range from 0.30 to 0.50 for β_1 and from 0.18 to 0.43 for β_2. Significance of the results and limitations of the two variations of the method in terms of validity of their underlying assumptions have been brought out in a critical assessment of the atomization efficiencies measured by the two variations of the method. In both the variations of the method, the heating rates used were much higher than those used by some other authors, with the result that in agreement with the prediction of the theory, the atomization efficiencies measured in this work were considerably higher than those reported by those authors.

C. L. CHAKRABARTI, D. FERRAROTTO, S. J. CATHUM et C. J. RADEMEYER. Can. J. Chem. **65**, 1079 (1987).

On a déterminé l'efficacité d'un HGA-400 pour produire et contenir la vapeur atomique de plusieurs éléments à des taux élevés de chauffage. Utilisant deux variations d'une même méthode, on a déterminé expérimentalement deux efficacités différentes d'atomisation, β_1 et β_2. Faisant l'hypothèse que l'atomisation dans un HGA-400 peut être décrite par les réactions consécutives, du premier ordre $D \xrightarrow{k_1} B \xrightarrow{k_2} C$, la méthode consiste à faire apparaître le profil du signal d'absorption (au moins sa portion de dégénérescence) à température constante de la paroi du tube (au centre) et à déterminer les constantes de vitesse du premier ordre pour la formation des atomes et pour la perte des atomes, soit respectivement k_1 et k_2. On a calculé les deux efficacités d'atomisation β_1 et β_2 qui donne la fraction de l'analyte qui est présente sous la forme de vapeur atomique au maximum du profil du signal d'absorption. La moyenne des efficacités expérimentales d'atomisation rapportées pour Al, Cu, Co, Fe, Ag et Ga sont $\beta_1 = 0{,}42$ et $\beta_2 = 0{,}30$ et les valeurs de β_1 varient de 0,30 à 0,50 alors que celles de β_2 varient de 0,18 à 0,43. La signification de ces résultats et les limitations des deux variations de la méthode en fonction de la validité des hypothèses sousjacentes ont été déterminées grâce à une évaluation critique des efficacités d'atomisation qui ont été mesurées par les deux variations de la méthode. Dans chacune des variations de la méthode, les taux de chauffage utilisés étaient beaucoup plus élevés que ceux utilisés par d'autres auteurs; il en résulte, en accord avec les prédictions de la théorie, que les efficacités d'atomisation mesurées dans ce travail sont beaucoup plus élevées que celles rapportées par d'autres auteurs.

[Traduit par la revue]

Introduction

Atomization efficiencies of some commercial graphite furnaces have been studied by several authors (1–4). However, the differences in the published results of different authors indicate that the problem of atomization efficiency still remains unresolved. Probably, part of the problem lies in the definition of atomization efficiency of graphite furnaces. Sturgeon and Berman (1) measured the absolute atomization efficiencies of the HGA-2200 for nine elements by determining electron concentrations using microwave attenuation techniques. Relative values of atomization efficiencies subsequently calculated by the authors (1) for several elements were, however, subject to uncertainties in the *gf* values (from the literature) used in the calculation (5). van den Broek and de Galan (2) calculated the overall atomization efficiencies of two graphite furnaces (CRA-63 and HGA-72) for the atomization of Ag, Pb, Mn, and Cd. They concluded that, under common operating conditions, atomization efficiencies averaged less than 10% for the above elements. Smets (3) in his study of atom formation in and dissipation from an open strip atomizer made the following estimate of the atomization efficiency (taking into account the relative oscillator strengths of the atomic resonance lines): 1 for Au, Ag, Cu, Fe, Mn, and Mg, and less than 0.1 for Al. Kitagawa *et al.* (4) spectroscopically determined the atomization efficiency of a glassy carbon tube atomizer for Cu and calculated relative atomization efficiencies for Cr and Ag based on the absolute value established for Cu.

The objective of the present work was to determine atomization efficiencies of an HGA-400 for several elements using relatively high heating rates and to make a critical assessment of the atomization efficiencies.

Theory

For simplicity, we shall confine our analysis to the passage of an atomic vapour through the analysis volume, without considering all other chemical reactions and physical processes that lead to formation of atomic vapour in and loss of atomic vapour from the graphite furnace. We shall also ignore any complicating processes that may accompany the transport of the material through the analysis volume and shall further assume that all of the element we are determining is in the atomic state while inside the analysis volume. The above assumptions are

[1]To whom all correspondence should be addressed.

[2]On leave of absence from Technikon Pretoria, 420 Church Street, Pretoria 0002, South Africa.

Can. J. Chem. Downloaded from www.nrcresearchpress.com by 78.46.186.204 on 09/07/12
For personal use only.

admittedly valid only for a limited number of elements which are completely atomized in graphite furnace and the ionization of which can be ignored at the atomization temperature used. These simplifying assumptions allow considerable simplification of the mathematical formulation of the model.

Assuming that consecutive, first-order reactions that occur during atom formation in and atom loss from the HGA-400 can be described by the following model (6):

$$[D] \xrightarrow{k_1} [B] \xrightarrow{k_2} [C]$$

where [D] represents the concentration of the pre-atomization analyte species; [B] represents the concentration of the absorbing analyte atomic vapour formed; [C] represents the concentration of the analyte atomic vapour that is lost from the analysis volume; k_1 and k_2 are then identified as the first-order rate constants for analyte atom formation and loss, respectively. At all times the concentrations are related by:

$$[1] \quad [D]_t + [B]_t + [C]_t = [D]_0$$

where the subscript t and 0 represent the time and the initial concentration (at time $t = 0$), respectively. The above model yields the differential eqs. [2] and [4].

$$[2] \quad \frac{d[D]}{dt} = -k_1[D]$$

By solving eq. [2] one gets eq. [3]:

$$[3] \quad [D] = [D]_0 \exp(-k_1 t)$$

$$[4] \quad \frac{d[B]}{dt} = k_1[D] - k_2[B]$$

In the limit, [D] tends to zero, which is identified with the exhaustion of the supply of the pre-atomization species D. At this point, eq. [4] simplifies to:

$$[5] \quad \frac{d[B]}{dt} = -k_2[B]$$

Since absorbance is proportional to the concentration of the absorbing species, B, the rate constant for the atom loss, k_2, can be determined from this part of the absorbance signal profile. A plot of the logarithm of absorbance vs. time should be linear, yielding the rate constant k_2 from the slope.

Extrapolation of this straight line plot to zero time (i.e., t_0) will give the concentration of B (resulting from complete conversion of $[D]_0$ into [B]) necessary to produce the decay of the signal by diffusion process alone. However, eq. [4] shows that the rate of formation of B is equal to the difference between the rate of conversion of species D into species B and the rate of loss of species B by concentration diffusion. The difference between the extrapolated absorbance and the experimental absorbance at any time t is equal to the concentration of the pre-atomization species D. Equation [2] suggests that a plot of the natural logarithm of this difference vs. time should be linear, with a slope equal to the rate constant for atom formation k_1.

If the kinetic parameters are evaluated, the shape of the absorbance signal profile may then be determined by solving eq. [4]. The use of the solution of eq. [2] with the initial concentration of the species D and $[D]_0$ and with no B present initially, gives the following solution of eq. [4]:

$$[6] \quad [B]_t = \frac{[D]_0 k_1}{k_1 - k_2}[\exp(-k_2 t) - \exp(-k_1 t)]$$

where $[B]_t$ represents [B] at time t. The concentration of B, which is initially zero, at first increases and reaches a maximum when $d[B]/dt$ is zero; the system is then said to have reached a stationary state.

$[B]_t$ can be related to the measured absorbance by using a pre-exponential factor p:

$$[7] \quad \text{Absorbance} = \frac{p[D]_0 k_1}{k_1 - k_2}[\exp(-k_2 t) - \exp(-k_1 t)]$$

where p is a function of the oscillator strength (a constant) of the analysis line and the efficiency of formation of analyte atoms. The p is therefore directly related to atomization efficiency. The atomization efficiency, which can be increased by forming analyte species that is readily vaporized and atomized, and by increasing the heating rate which increases k_1 and shifts the absorbance signal profile (at least the decay part) into the isothermal region of the tube wall temperature curve, thereby making the analyte atom loss by concentration diffusion only, which makes k_2 relatively small and constant at constant temperature.

The time t_{max} is identified with the time required to attain the absorbance maximum. Use of high heating rates coupled with moderately high atomization temperatures should yield $k_1 \gg k_2$. The resulting low t_{max} value (0.1–0.2 s) should yield $k_1 t_{max} \gg k_2 t_{max}$. Equation [7] is then reduced to:

$$[8] \quad \text{Absorbance} \simeq p[D]_0$$

yielding high atomization efficiency.

On differentiating eq. [6] we obtain the following expression for the time t_{max} required for the attainment of the stationary state:

$$[9] \quad k_1 \exp(-k_1 t_{max}) = k_2 \exp(-k_2 t_{max})$$

or

$$[10] \quad t_{max} = \frac{1}{k_1 - k_2} \ln \frac{k_1}{k_2}$$

The maximum concentration of B is seen to be:

$$[11] \quad [B]_{t=t_{max}} = [D]_0 \exp(-k_2 t_{max})$$

where $[D]_0$ is the initial concentration of D. The efficiency of atomization, β_1, is defined here as the fraction of analyte present as atomic vapour at t_{max} (the time when this fraction is a maximum) and is given by

$$[12] \quad \beta_1 = \frac{[B]_{t=t_{max}}}{[D]_0} = \exp(-k_2 t_{max})$$

It is important to note that this definition of atomization efficiency does not take into account those atoms that are lost by the process:

$$[B] \xrightarrow{k_2} [C]$$

in going from time $t = 0$ to $t = t_{max}$. It is a measure of those atoms that are present at t_{max}.

An alternative method of calculating the atomization efficiency can be derived from the above definition of β_1. This atomization efficiency (to be called β_2) is defined as the number of atoms, N_{max}, present as atomic vapour at t_{max} over the total number of atoms present in the injected sample, N_0 (i.e., at time = t_0).

$$[13] \quad \beta_2 = \frac{N_{max}}{N_0}$$

Can. J. Chem. Downloaded from www.nrcresearchpress.com by 78.46.186.204 on 09/07/12
For personal use only.

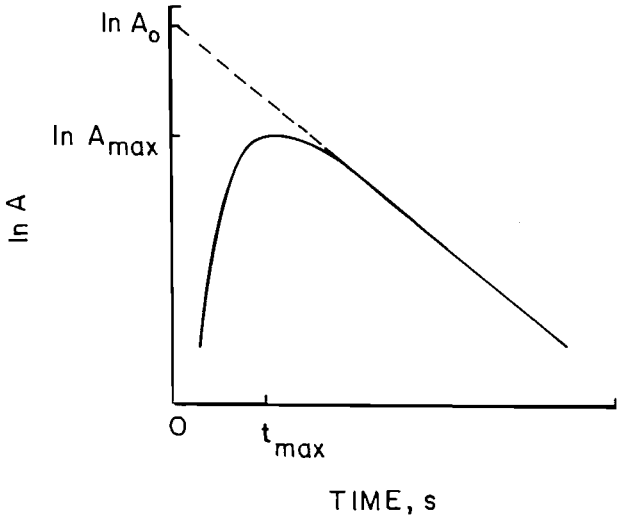

FIG. 1. Plot of natural logarithm of absorbance vs. time (linear scale). A_{max} and A_0 are absorbance at time $t = t_{max}$ and t_0, respectively.

However,

$$[14] \quad p = \frac{A_{max}}{N_{max}}$$

where A_{max} is the absorbance at time $t = t_{max}$.

As stated earlier, extrapolation of the straight line plot to zero time (i.e., t_0) will give the concentration of B necessary to produce the decay of the absorbance signal by diffusion process alone. Therefore,

$$[15] \quad p = \frac{A_0}{N_0}$$

where A_0 is the absorbance at time $t = t_0$. A_{max} and A_0 are defined in Fig. 1.

The final result is that the atomization efficiency, β_2, can be obtained readily from the equation:

$$[16] \quad \beta_2 = \frac{A_{max}}{A_0}$$

Theoretically, having been derived from the same definition, β_1 should be equal to β_2.

Because k_2 is weakly dependent on temperature, it is important for the calculation of β_1 that the descending part of the absorbance signal profile be located in the isothermal region of the tube wall (at the centre) temperature vs. time curve. The k_2 values are calculated from the data points from the tail end of the experimental trace.

It can be seen from eq. [12] that $\beta_1 \simeq 1$ when $k_2 t_{max} \ll 1$. Hence, for the highest atomization efficiency, both k_2 and t_{max} must be made as small as possible. The time t_{max} is sensitive to heating rate; generally, relatively high heating rates yield small t_{max} values. However, the rate constant k_2 for atom loss by concentration diffusion increases with increasing temperature, although k_2 is less sensitive to higher temperatures than k_1 (7). This method employs relatively high heating rates coupled with moderately high atomization temperatures to keep both k_2 and t_{max} values small so as to approach the condition $k_2 t_{max} \ll 1$. As can be seen later, with the maximum heating rate available with the modified HGA-400 (about 7 K ms^{-1}), this attempt has been only partly successful.

TABLE 1. Experimental and analytical parameters*

Element	Wavelength (nm)	Mass of elements (pg)	Charring temperature (K)
Cu	324.8	50	1470
Co	240.7	100	1670
Fe	248.3	50	1670
Al	309.3	100	1970
Ag	328.1	40	920
Ga	287.4	1000	1070

*Spectral band width = 0.7 nm; test solution injected = 10 μL; Ar gas in gas-stop mode of operation during the atomization cycle.

Experimental

Apparatus

A modified Perkin-Elmer atomic absorption spectrometer, model 503, equipped with a Deuterium-Arc Background Corrector and an HGA-400 atomizer was used. The atomizer was fitted with a laboratory-made power supply capable of supplying variable heating rates up to about 7 K ms^{-1}, with independent control of the heating rates and temperatures. The details of the modified instrument have been published earlier (8). High temperatures of the graphite tube were measured with an Ircon 1100 series automatic optical pyrometer (Ircon Inc. Skokie, IL). Low temperatures were measured with an Ircon series 300 pyrometer (Ircon Inc.). Perkin-Elmer pyrolytically coated graphite tubes (part no. 091504) were used. Graphite tubes were replaced with new tubes after about 12 firings. Argon gas was used in the gas-stop mode of operation at the atomization step. Absorbance and temperature profiles were recorded with a four-channel, Nicolet digital oscilloscope, series 4094, with two plug-in units, model 4562 (Nicolet Instrument Co. Madison, WI).

Hollow-cathode lamps of cobalt (Perkin-Elmer), aluminium (EEL), and copper, silver, iron, and gallium (the last four by Westinghouse) were operated at the lamp current recommended by the manufactures.

Reagents

Chemically pure metals or their salts were used to prepare standard solutions. Stock solutions of cobalt and iron were prepared separately by dissolving an appropriate mass of the metal in nitric acid (ULTREX, J. T. Baker Chemical Co.) and diluting the solution to 1000 μg mL^{-1} with ultrapure water. The stock solution for silver was prepared by dissolving an appropriate mass of silver nitrate in ultrapure water. Stock solutions for gallium and copper were prepared separately by dissolving the metals in concentrated nitric acid (ULTREX) and 50% (v/v) nitric acid, respectively, with heating. The final solutions were made by dilution to 1000 μg mL^{-1} with ultrapure water. The stock solution for aluminium was prepared by dissolving the metal in 20% HCl (ULTREX) with heating. The final solution was made by dilution to 1000 μg mL^{-1} with ultrapure water. All stock solutions were made 1% (v/v) in HNO_3.

All test solutions were prepared by diluting the stock solutions to desired concentrations with ultrapure water immediately prior to use. They contained 1% (v/v) HNO_3 (ULTREX). Ultrapure water of resistivity 18.3 megohm-cm was obtained direct from a Milli-Q2 water purification system (Millipore Corporation).

Procedure

Sample solutions were injected into the atomizer using a 10 μL Eppendorf pipet fitted with disposable plastic tips. High heating rates and moderately high atomization temperatures were used in order to shift the atomic absorbance signal profile (at least the decay part) into the isothermal region of the tube wall (at the centre) temperature vs. time curve so that the assumption of consecutive, first-order reactions was valid. The absorbance values were corrected for blanks.

Experimental and analytical parameters

Table 1 summarizes the experimental and analytical parameters used.

Can. J. Chem. Downloaded from www.nrcresearchpress.com by 78.46.186.204 on 09/07/12
For personal use only.

Can. J. Chem. Downloaded from www.nrcresearchpress.com by 78.46.186.204 on 09/07/12
For personal use only.

TABLE 2. Atomization efficiency values obtained in this work

Element	Atomization temperature (K)	Appearance temperature (K)	Heating rate at the appearance temperature (K ms^{-1})	% of the absorbance signal under isothermal region	β_1	β_2
Al	2800	2420	3.5	75	0.36	0.22
	2840			74	0.33	0.20
	2910		4.3	67	0.35	0.24
				Mean =	0.35	0.22
Cu	2560	2040	5.2	72	0.50	0.44
	2470			76	0.49	0.43
	2420			82	0.50	0.43
				Mean =	0.50	0.43
Co	2840	2420	5.6	92	0.50	0.40
	2710			94	0.48	0.30
	2640			95	0.48	0.36
				Mean =	0.49	0.35
Fe	2680	2130	6.2	72	0.44	0.30
	2710			67	0.45	0.26
	2880			72	0.49	0.35
				Mean =	0.46	0.30
Ag	2220	1670	6.0	56	0.44	0.31
	2190			56	0.41	0.28
	2150			62	0.46	0.33
				Mean =	0.44	0.31
Ga	2900	2280	6.6	58	0.23	0.17
	2760			62	0.35	0.20
	2620			75	0.33	0.17
				Mean =	0.30	0.18

Results and discussion

Table 2 summarizes the atomization efficiency values of a selected group of elements at various heating rates and atomization temperatures. The heating rates listed were calculated from the tube wall temperature curve (such as the one shown in Fig. 2) using its nearly-straight-line segment which encompasses the appearance temperature of the element. For example, in Fig. 2, the appearance temperature of Al was 2420 K and the heating rate was calculated as follows.

$$\text{Heating rate} = \frac{(2560 - 2420)\text{K}}{(200 - 160)\text{ms}} = 3.5\ \text{K ms}^{-1}$$

The reason for using the above segment of the tube wall temperature curve was that the heating rate so calculated was what the analyte actually experienced at the appearance time of the signal and at times immediately following the appearance time. The above heating rate was greater than the average heating rate over the entire period of rise in the tube wall temperature shown in Fig. 2. The heating rate is one of the important factors that determine the rate of atom formation during the rising part of the atomic absorption signal profile (9–11), and hence, affects atomization efficiency strongly. The gas temperature, which like the tube wall temperature, was time- and space-dependent, roughly followed the tube wall temperature in the immediate vicinity of the spot on the tube wall surface where the test solution was placed (12, 13) — the tube wall temperature of that spot and the gas temperature in its immediate vicinity determined the rate of atom formation at the appearance time and at times immediately following the appearance time.

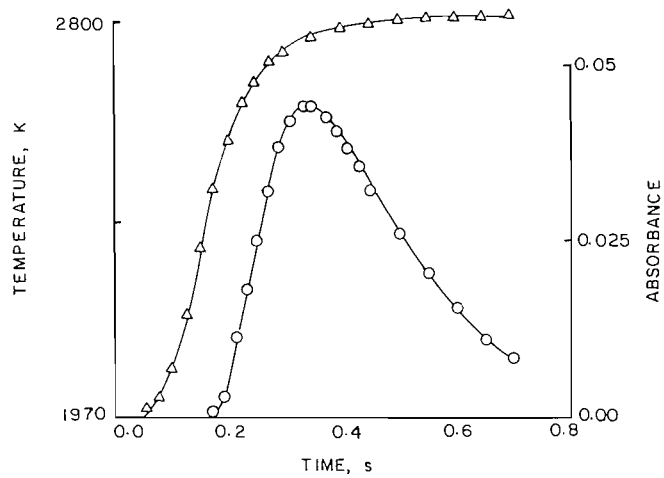

FIG. 2. Absorbance profile of aluminium and the corresponding temperature profile of the graphite furnace. △: tube wall temperature measured with the automatic optical pyrometer. ○: 0.1 ng of Al in 1% (v/v) HNO_3 aqueous solution. Atomization temperature = 2800 K. Heating rate = 3.5 K ms^{-1}.

Most of the absorbance profiles were located more than 70% within the isothermal region of the tube wall temperature vs. time curves. This was achieved by using the highest possible heating rates and moderately high atomization temperatures.

Figure 3 shows the absorbance signal profile of aluminium vs. the time drawn using a logarithmic scale for the ordinate. The rate constant for aluminium atom loss, k_2, was obtained from the slope of line B, which was drawn from the experimental data points at the tail of the absorbance signal profile.

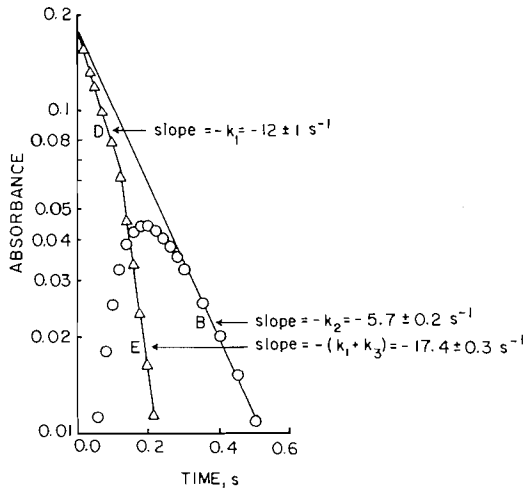

FIG. 3. Plot of absorbance (logarithmic scale) vs. time (linear scale) for aluminium shown in Fig. 2. Curve B: Loss of $Al_{(g)}$: $Al_{(g)} \xrightarrow{k_2} C$. Curve D: Formation of $Al_{(g)}$: $AlO_{(g)} \xrightarrow{k_1} Al_{(g)} + (1/2)O_{2(g)}$. Curve E: Formation of $Al_{(g)}$ by dissociation of $AlO_{(g)}$, and loss of the latter:

$$\begin{array}{l} AlO_{(g)} \xrightarrow{k_1} Al_{(g)} + (1/2)O_{2(g)} \\ \downarrow k_3 \\ C' \end{array}$$

Atomization temperature = 2800 K. Heating rate = 3.5 K ms^{-1}.

The value of the slope of line B was calculated by least-square linear regression involving the last few data points on the decay part of the absorbance signal profile. The points of line D represent the "concentration" of the species D. The curve D has been plotted using the difference between the extrapolated absorbance and the experimental absorbance vs. time, plotted on the same axes, and shows two intersecting straight lines of different slope. These intersecting straight lines correspond to two different modes of loss of the species D. The straight line, D, corresponding to the earlier times and having the lower absolute slope, gives the value of the rate constant, k_1, for the reaction $D \xrightarrow{k_1} B$. The straight line, E, corresponding to later times and having a slightly steeper slope yields the sum of the rate constants ($k_1 + k_3$) for the two modes of loss of the species D, as shown below:

$$[17] \qquad \begin{array}{l} D \xrightarrow{k_1} B \xrightarrow{k_2} C \\ \downarrow k_3 \\ C' \end{array}$$

where C′ is the product of the other loss process of species D. Any D taking the path indicated by the arrow marked k_3 will not yield an atomic absorption signal. The mathematical treatment adopted above is admittedly a simplified treatment of a more complex process, but has the merit of showing the correct temperature dependence of the rate constants. However, where two straight-line segments are observed (as for aluminium) a more rigorous mathematical treatment is necessary if the mechanism is as shown above; the slower must be treated like B above, then the faster extracted from the differences.

Following the treatment described in ref. 6 the following mechanism for aluminium atomization involving three first-order rate processes is proposed.

$$\begin{array}{lll} AlO_{(g)} & \xrightarrow{k_1} & Al_{(g)} + (1/2)O_{2(g)} \\ \downarrow k_3 & & \downarrow k_2 \\ C' & & C \end{array}$$

The above mechanism shows that a part of the $AlO_{(g)}$ is lost as $AlO_{(g)}$ (with a rate constant k_3), a part is dissociated to $Al_{(g)}$ (with a rate constant k_1), and the $Al_{(g)}$ is then lost (with a rate constant k_2). This mechanism is in agreement with what has been observed in another study from this laboratory (14). Smets (3) has also reported that the mechanism of aluminium atomization is by dissociation of $AlO_{(g)}$.

The β_1 and β_2 values in Table 2 are internally consistent; the β_1 values are consistently larger than the β_2 values. Probably, the large extrapolations involved in obtaining the A_0 values result in their over-estimation and in lower β_2 values from eq. [16].

Table 3 shows the values of k_1, k_2, and measured t_{max} at various final, steady-state atomization temperatures. Precision values of the rate constants are not shown since values of precision from least-square regression calculations depend on the number of points included, whereas the value of the rate constant itself does not. However, the precision of any rate constant value can be no better than 5% relative standard deviation, as the absorbance values used in the calculation of rate constants have this order of relative precision.

The t_{max} values used in calculating the β_1 values in Table 3 were measured graphically from Fig. 1 since the measured t_{max} values had a smaller uncertainty than the t_{max} value calculated from eq. [10]. The uncertainty in the measured t_{max} arose

TABLE 3. First-order rate constants for atom formation and atom loss

Element	Atomization temperature (K)	Rate constants (s^{-1}) k_1	k_2	Measured t_{max} (s)
Al	2800	12	5.7	0.180
	2840	12	6.7	0.166
	2910	13	6.4	0.164
Cu	2420	13	3.0	0.229
	2470	11	3.1	0.229
	2560	13	3.5	0.196
Co	2640	10	3.0	0.245
	2710	10	3.2	0.228
	2840	11	3.6	0.195
Fe	2680	11	4.2	0.195
	2710	11	4.0	0.197
	2880	15	4.8	0.148
Ag	2220	24	8.3	0.100
	2190	21	8.0	0.111
	2150	24	6.8	0.115
Ga	2620	16	7.3	0.151
	2760	16	7.8	0.135
	2900	18	8.8	0.169

Can. J. Chem. Downloaded from www.nrcresearchpress.com by 78.46.186.204 on 09/07/12
For personal use only.

from manually locating the appearance time and the time corresponding to A_{max} (Fig. 1); the digital oscilloscope calculated the difference (t_{max}) in the above times. If t_{max} values were calculated from eq. [10], it would have required use of the k_1 and k_2 values, each of which had an uncertainty of at least 5% relative standard deviation. The k_1 values were also subject to unknown systematic error as they were calculated from the absorbance values from the rising part of the absorbance signal profile which was located in the non-isothermal region of the tube wall temperature curve (Fig. 2). Also, there are further complications in determining k_1 values in the case of an element such as Al in which there is an additional, first-order loss process (identified as C′ in mechanism 17 given earlier) having a rate constant k_3. In such a case, eq. [10] must be modified as shown below (6).

$$[18] \quad t_{max} = \frac{\ln (k_1 + k_3) - \ln k_2}{k_1 + k_3 - k_2}$$

The measurement of t_{max} with the digital oscilloscope was preferred because it avoided the complications that would arise in the above mathematical formulation of t_{max} in terms of the two rate constants involved in the loss of species D, and thereby simplified the task considerably. This was in addition to lower uncertainty in measuring t_{max} graphically from Fig. 1 than that in calculating t_{max} from eqs. [10] or [18]. However, by using still higher heating rates as used in ref. 6, the location of the entire absorbance signal profile can be shifted to the isothermal region of the tube wall temperature curve; in that case, t_{max} can be readily evaluated also from eq. [10] or [18] since the uncertainty and error in measuring k_1 from the absorbance signal profile would then be comparable to those in measuring k_2 and t_{max} from the same absorbance signal profile.

Comparison with the atomization efficiency values reported by other authors

Sturgeon and Berman (1) used an HGA-2200 and van den Broek and de Galan (2) used an HGA-72 and a CRA-63, whereas this work was done with an HGA-400. Also, before comparison can be made, it must be noted that the efficiency values determined in this study were for the HGA-400, and were only applicable under the specific experimental conditions, especially the heating rates used in this work. The most important difference between this work and those of the above authors was that the heating rates used in this work were much higher (Table 2) than those used by the above authors (1, 2). Regardless of whether atomization was isothermal or non-isothermal, higher heating rates increased k_1 values much more than k_2 values, and hence decreased t_{max} values by eq. [10]. Equation [12], which shows $\beta_1 = \exp(-k_2 t_{max})$, holds good as long as the decay of analyte atom is by a first-order rate process with a rate constant k_2. Fulfillment of the above condition required only that the tail end of the absorbance signal from which the experimental data points for evaluating k_2 values were taken must be located in the constant-temperature region of the temperature vs. time curve. As Table 2 shows, this condition was certainly fulfilled by all the elements in this work. It can be predicted from eq. [12] that much higher heating rates used in this work should produce higher β_1 values than those reported by the other workers (1, 2) who used much lower heating rates. The β_1 values reported in this work confirm the above prediction.

Sturgeon and Berman (1) defined the absolute atomization efficiency of the HGA-2200 for a particular point in time (conveniently at the time of maximum signal) as the ratio of the sum of the number of neutral and ionized analyte atoms to the number of analyte atoms initially introduced into the furnace. Since all of the elements in this work have ionization energies of about 6 eV or higher, loss of neutral atoms by ionization in the HGA-400 at the atomization temperatures used can be considered negligible. Table 4 shows that most of the atomization efficiencies reported by Sturgeon and Berman (1) are of the same order of magnitude as those of this work.

TABLE 4. Comparison of mean atomization efficiency values of this work with those reported by the other authors (1, 2)

Element	This work* β_1	This work* β_2	Sturgeon and Berman† (1) β	van den Broek and de Galan§ (2) β_{theor}	van den Broek and de Galan§ (2) β_{expt}
Al	0.35	0.22	0.10	—	—
Cu	0.50	0.43	0.19	—	—
Co	0.49	0.35	—	—	—
Fe	0.46	0.30	—	—	—
Ag	0.44	0.31	0.35	0.45	0.20
Ga	0.30	0.18	0.06	—	—

*Used HGA-400.
†Used HGA-2200.
§Used HGA-72. β = Atomization efficiency.

van den Broek and de Galan (2) reported that atomization efficiency of the HGA-72 for Ag — a theoretical value of 0.45 and experimental value of 0.20. These authors (2) defined the atomization efficiency as N_{max}/N_0 — the ratio of the maximum number of atoms, N_{max} (obtained from the measured peak absorbance), and the amount of analyte injected into the furnace, N_0. Table 4 shows that the atomization efficiencies reported by van den Broek and de Galan (2) are similar to those in this work.

It should be noted that not only were the atomizers of the above authors (1, 2) different from the HGA-400 used in this work, but also the experimental and analytical parameters, especially the heating rates used, were different.

Critical appraisal of the atomization efficiency values, β_1 and β_2

The atomization efficiency values, β_1 and β_2, were obtained from the same theory and were subject to the assumptions made in developing the theory. However, as stated earlier, the two methods that were used to obtain β_1 and β_2 values had different sources of uncertainties and errors. The β_1 values were affected by uncertainties in k_2 (Fig. 3) and in t_{max} values (Fig. 1) used in solving eq. [12]. The β_2 values were affected by uncertainties in measuring A_{max} and A_0 used in solving eq. [16].

Since all k_2 values were obtained from the last few experimental data points at the tail end of the absorbance signal which was located in the isothermal region of the tube wall temperature curve, and since these experimental data points related to the time when atom loss by concentration diffusion was the only process occurring, it can be concluded that the k_2 values listed in Table 3 are fairly good. The line from which k_2 was calculated (Fig. 3) was reasonably straight, especially at the last few data points at the tail end of the absorbance signal. However, as explained earlier, k_2 values had an uncertainty of about 5% relative standard deviation, which, added to the uncertainty in manually locating t_{max}, was transmitted to β_1 values. The uncertainty in β_2 was mainly due to the measurement of A_0 values since large extrapolation from the tail end of the

Can. J. Chem. Downloaded from www.nrcresearchpress.com by 78.46.186.204 on 09/07/12
For personal use only.

absorbance signal were required for the determination of A_0 (Fig. 1). As can be seen from Table 2, β_2 is usually very close in magnitude to β_1, but in each case β_2 is less than β_1. As explained in the theory, it is reasonable to expect the β_1 and β_2 values to have approximately the same magnitude. The above difference was probably due to the sources of uncertainty mentioned above. Since the uncertainty in measuring k_2 and t_{max} was not nearly as large as that due to large extrapolations in calculating A_0, the β_1 values seem to be a more reliable estimate of the fraction of analyte present as atomic vapour at t_{max} than the β_2 values.

The β_1 values were obtained by solving eq. [12], i.e., by using the k_2 and t_{max} values, and were therefore not affected by uncertainty in the k_1 values. The k_1 values were, however, subject to larger uncertainty and errors than the k_2 values because the k_1 values were obtained from the experimental data points (Fig. 3) lying in the non-isothermal region of the tube wall temperature curve (Fig. 2). In contrast, the k_2 values were obtained from the last few experimental data points at the tail end of the absorbance signal (Fig. 3) in order to make sure that the only process occurring at those times was loss of analyte atoms by concentration diffusion at constant temperature. In view of the above, the β_1 values are more reliable than the β_2 values. It is to be noted that the k_1 values were not used in calculating β_1 and β_2 values. However, from the k_1 and k_2 values in Table 3 and from eq. [7], one finds that under the experimental and analytical parameters used in this work, elements such as Cu, Co, Fe, and Ag for which the condition $k_1 \gg k_2$ is more closely approached than elements such as Al, and Ga, yield greater β_1 values than the latter group of elements.

Conclusions

1. Kinetic parameters can be used to determine atomization efficiencies of graphite furnaces.
2. As expected from the theory, significantly higher heating rates than what are usually provided for in commercial graphite furnaces yield significantly higher atomization efficiencies than those reported for some commercial graphite furnaces.

Acknowledgements

The authors are grateful to the Natural Sciences and Engineering Research Council of Canada for financial support of this research project. One of the authors (S.J.C.) is also grateful to the Government of Iraq for a postgraduate scholarship.

1. R. E. STURGEON and S. S. BERMAN. Anal. Chem. **55**, 190 (1983).
2. W. M. G. T. VAN DEN BROEK and L. DE GALAN. Anal. Chem. **49**, 2176 (1977).
3. B. SMETS. Spectrochim. Acta, **35**B, 33 (1980).
4. K. KITAGAWA, Y. IDE, and T. TAKEUCHI. Anal. Chim. Acta, **113**, 21 (1980).
5. C. T. H. J. ALKEMADE and R. HERRMANN. Fundamentals of analytical flame spectroscopy. Hilger, London. 1979.
6. C. L. CHAKRABARTI, C. C. WAN, R. J. TESKEY, S. B. CHANG, H. A. HAMED, and P. C. BERTELS. Spectrochim. Acta, **36**B, 427 (1981).
7. B. V. L'VOV. Atomic absorption spectrochemical analysis. Adam Hilger Ltd., London. 1970. p. 287.
8. C. L. CHAKRABARTI, S. WU, and P. C. BERTELS. Spectrochim. Acta, **38**B, 1041 (1983).
9. C. L. CHAKRABARTI, H. A. HAMED, C. C. WAN, W. C. LI, P. C. BERTELS, D. C. GREGOIRE, and S. LEE. Anal. Chem. **52**, 167 (1980).
10. N. G. ZHOU, W. FRECH, and L. DE GALAN. Spectrochim. Acta, **39**B, 225 (1984).
11. C. L. CHAKRABARTI, S. B. CHANG, S. R. LAWSON, and S. M. WONG. Spectrochim. Acta, **38**B, 1287 (1983).
12. C. L. CHAKRABARTI, S. WU, R. KARWOWSKA, J. T. ROGERS, and R. DICK. Spectrochim. Acta, **40**B, 1663 (1985).
13. S. WU, C. L. CHAKRABARTI, and J. T. ROGERS. Prog. Anal. Spectrosc. **10**, 110 (1987).
14. C. L. CHAKRABARTI, S. J. CATHUM, and C. J. RADEMEYER. Unpublished results.

Can. J. Chem. Downloaded from www.nrcresearchpress.com by 78.46.186.204 on 09/07/12
For personal use only.

Recent advances in ultratrace analysis of dioxins and related halogenated hydrocarbons

B. K. Afghan and J. Carron
National Water Quality Laboratory, Canada Centre for Inland Waters, 867 Lakeshore Road, Burlington, Ont., Canada L7R 4A6

P. D. Goulden and J. Lawrence
National Water Research Institute, Canada Centre for Inland Waters, 867 Lakeshore Road, Burlington, Ont., Canada L7R 4A6

D. Leger
National Water Quality Laboratory, Canada Centre for Inland Waters, 867 Lakeshore Road, Burlington, Ont., Canada L7R 4A6

and

F. Onuska, J. Sherry, and R. Wilkinson
National Water Research Institute, Canada Centre for Inland Waters, 867 Lakeshore Road, Burlington, Ont., Canada L7R 4A6

Received October 24, 1986

This paper is dedicated to Professor Douglas E. Ryan on the occasion of his 65th birthday

B. K. Afghan, J. Carron, P. D. Goulden, J. Lawrence, D. Leger, F. Onuska, J. Sherry, and R. Wilkinson. Can. J. Chem. **65**, 1086 (1987).

Analytical methodology for polychlorinated dioxins and furans (PCDDs and PCDFs) in environmental samples is not standardized. Many variations exist for the extraction, cleanup, quantitation, and confirmation of these compounds and reported detection limits and recoveries vary over several orders of magnitude. This paper describes research carried out at the Canada Centre for Inland Waters over the past seven or eight years to develop reliable methodology at ultratrace levels (10^{-12}–10^{-15} g/g) applicable to a wide range of environmental samples. Extraction techniques are described for biological tissue (fish, clams, leaches, eggs), fly ash, sediments, and water. Detailed cleanup procedures for the various matrices consist of most or all of the following: gel permeation chromatography liquid/liquid extraction with Na_3PO_4, liquid/liquid extraction with H_2SO_4, basic alumina chromatography, and carbon fibre chromatography. Preliminary screening of the cleaned extracts is achieved by gas chromatography equipped with a mass selective detector and positive identification by gas chromatography/mass spectrometry operated in electron impact and chemical ionization modes and with full scan and multiple ion detection. Custom software permitting the analysis of a wide range of compounds in a single run by gc/ms is reported. The presence of specific isomers of PCDDs and PCDFs is confirmed by high resolution gas chromatography/mass spectrometry. A radioimmunoassay screening procedure for PCDDs in environmental samples is also described.

B. K. Afghan, J. Carron, P. D. Goulden, J. Lawrence, D. Leger, F. Onuska, J. Sherry et R. Wilkinson. Can. J. Chem. **65**, 1086 (1987).

Les méthodes d'analyse des dioxinnes et des furannes polychlorés (DPC et FPC) ne sont pas standardisées. Plusieurs variations existent pour l'extraction, le nettoyage, la quantification et la confirmation de la présence de ces composés; de plus, les limites de détection ainsi que les taux de récupération rapportés varient par plusieurs ordres de grandeur. Dans ce travail, on décrit les études effectuées au cours des 7 à 8 dernières années au centre canadien des eaux intérieures dans le but de développer une méthodologie applicable à des niveaux d'ultratraces (10^{-12} à 10^{-15} g/g) et à un grand éventail d'échantillons prélevés dans l'environnement. On décrit des techniques d'extraction pour des tissus biologiques (poissons, moules, eaux de lessivage et oeufs), des suies, des sédiments et des échantillons d'eau. Les diverses méthodes détaillées proposées pour le nettoyage de diverses matrices comportent la plupart ou toutes les techniques suivantes: chromatographie par perméation de gel; extraction liquide/liquide avec du Na_3PO_4; extraction liquide/liquide avec du H_2SO_4; chromatographie standards sur de l'alumine ou des fibres de charbon. On a effectué des essais préliminaires sur des extraits lavés en faisant appel à la chromatographie en phase gazeuse couplée à un détecteur sélectif de masses; on a procédé à l'identification positive par chromatographie en phase gazeuse couplée à la spectrométrie de masse, opérée soit dans le mode d'impact électronique ou d'ionisation chimique et avec un balayage complet et une détecteur ionique multiple. On rapporte le développement de logiciels faits sur mesure pour permettre l'analyse d'un grand nombre de composés dans une seule expérience de cg/sm. On peut confirmer la présence d'isomères spécifiques des DPC ou des FPC en procédant à la chromatographie en phase gazeuse couplée à la spectrométrie de masse opérée à haute résolution. On décrit aussi une méthode radioimmunologique permettant de vérifier la présence des DPC dans des échantillons provenant de l'environnement.

[Traduit par la revue]

Introduction

The presence of polychlorinated dioxins and furans (PCDDs and PCDFs) in the environment is cause for concern to public, government, and municipalities in industrialized societies. This is mainly due to the pronounced toxicity of the 2,3,7,8-tetrachlorodibenzo-*p*-dioxin (2,3,7,8-TCDD) isomer to certain biological species (1). Many agencies have established guidelines for these compounds and recently the Ontario Ministry of Environment has recommended a maximum daily human intake for 2,3,7,8-TCDD or its toxic equivalent of PCDDs and PCDFs of less than 10 pg/km of body weight (2).

Methods for determining PCDDs and PCDFs in various types of samples have been well documented (2, 3). A recent worldwide survey conducted by the Ontario Ministry of the Environment has shown a proliferation of extraction, cleanup, quantitation, and confirmation techniques for analysis of these compounds (4). The reported range of detection limits and recoveries obtained for various types of samples are shown in Table 1 (4). The large range of reported detection limits and recoveries can be attributed to variations in the size of samples, complexity of samples, the amount of determinand in relation to the amount of interfering substances in samples together with

Can. J. Chem. Downloaded from www.nrcresearchpress.com by 78.46.186.204 on 09/07/12
For personal use only.

TABLE 1. Reported limits of detection (lod) and range of percent recovery for PCDDs by laboratories responding to worldwide survey (4) (all values in parts per trillion: 10^{-12} g/g)

Sample type	Compound	Range of lod	Range of % recovery
Soil	2,3,7,8-TCDD	0.1–1000	10–179
	OCDD	1.0–500	0–184
Fish	2,3,7,8-TCDD	0.1–1000	6–150
	OCDD	1.0–100	10–110
Water	2,3,7,8-TCDD	0.0005–300	40–110
	OCDD	0.0001–50	40–116
Fly ash	2,3,7,8-TCDD	0.1–300	10–118
	OCDD	1.0–100	37–122

variations in the procedures used for cleanup and quantitation of the PCDDs and PCDFs.

Work at the Canada Centre for Inland Waters for the past seven or eight years has been directed at systematic development of analytical capability to detect and determine hazardous substances including PCDDs and PCDFs down to 10^{-12} g/g with a high degree of reliability and confidence. Developed methodologies had to be applicable to a wide range of environmental samples. This initially involved designing and constructing a special laboratory facility to (*a*) minimize errors due to cross contamination of samples during cleanup and pretreatment and (*b*) provide maximum safety to personnel when handling hazardous chemicals such as 2,3,7,8-TCDD during method development and/or sample analysis (5). Several methods for extraction, cleanup, quantitation, and confirmation of PCDDs and PCDFs at parts-per-trillion (ppt) and parts-per-quadrillion (ppq) levels have been developed to analyze chlorophenol formulations, fish tissues, sediments, and fly ash (6, 7). The methodologies were also applied to a study of the formation and fate of PCDDs and PCDFs during chlorophenol combustion (8).

This paper presents the recent work carried out by the authors in areas of large volume extraction of contaminants at ultratrace levels (10^{-12} to 10^{-15} g/g) from water, the application of radioimmunoassay as a screening technique for PCDDs, improvements in the cleanup of environmental samples and the use of hydrogen negative ion chemical ionization mass spectrometry to obtain improved precision and increased reliability for PCDDs analysis.

Experimental

Apparatus and equipment

(a) Glassware

Consists of Erlenmeyer flasks, separating funnels, Allihn filters, round bottom flasks, micro syringes, centrifuge tubes, disposable glass pipettes, and chromatographic columns.

(b) Extraction and concentration and filtering apparatus

Consists of rotary evaporators, vortex evaporator, homogenizers, soxhlet apparatus, centrifugation apparatus capable of accommodating 250 mL centrifuge cups and 4500–5000 rpm, gas tight syringes capable of accepting disposable filter units (25 mm diameter × 0.2 μm porocity).

(c) Gel permeation liquid chromatographic system

Assembled using suitable injection valve, 5 mL sample loop, 60°A Styragel column, uv detector with 254 nm filter, and a solvent delivery system capable of constant flow with medium and low back pressure.

(d) Alumina column cleanup apparatus

Consists of 2 cm id × 35 cm glass column with Teflon stopcock with a glass wool plug. A 30 g alumina column (Brockman activity 1, 80–200 mesh, activated at 550°C for 6 h and deactivated with 1%-w:w distilled–deionized water) is used. A 2 cm layer of sodium sulfate was added to cover the alumina in order to maintain its activity. The column must be prepared just prior to use.

(e) Carbon–fibre system

This system consists of a solvent delivery system capable of constant flow at low back pressure, solvent selector value allowing selection of five or six solvents, fraction collector, and controller, and a 6-port switching valve equipped with 1 mL sample loop. The carbon–fibre column consists of 4 mm id × 7.2 cm annealed glass and fitted with zero dead volume fittings and 2 μm stainless steel frits. The column packing is prepared as described below:

Glass fibre filter paper (0.6 g) (type GA200, Toyo Roshi Co. Ltd.) is weighed in a suitable size beaker, 0.05 g of activated carbon (PX-21, Amoco Research Corp) is added along with 100 mL methylene chloride. The mixture is shredded and mixed with a Polytron, so that the fibres are of a size capable of retaining the carbon particles. This slurry of carbon fibres is then packed, using an aspirator, into a 7.2 cm, 6 mm od, annealed glass tube, equipped with zero dead volume fittings and 2μ frits.

(f) Gas chromatography – mass spectrometry apparatus

Preliminary screening and subsequent positive identification, confirmation, and quantitative analysis are carried out using a wide variety of instruments and columns. The details of specific instruments and the operating conditions are described in the analytical protocols section of this paper.

(g) Continuous-flow extractors

A variety of continuous extractors have been developed to cover the various sampling procedures that may be required. They are designed primarily as portable units for use in the field, however, they can also be setup on board ship or in the laboratory. All the extractors are basically mixer–settlers in which the incoming water is passed through a chamber where it is mixed with solvent.

The extractors were produced in two sizes, "large" to extract up to 1 L/min and "small" to extract up to 0.5 L/min. The water can be sampled as "whole water", i.e. with no separation of particulates or as "clarified water" by extracting the effluent of a continuous flow centrifuge. The suspended solids can also be collected and analyzed at the same time. The flow rate through the extractor and total sampling time can be adjusted so that there is sufficient material for analysis of corresponding suspended sediment and clarified water. For long sampling times (one week) the solvent can be stripped from the extractor effluent water and recirculated so that no solvent make up is required.

(h) Apparatus for radioimmunoassay

Incubator, refrigerator, freezer, γ counter, and refrigerated centrifuge are essential to carry out the assay.

(i) Reagents and materials for radioimmunoassay

Antiserum to TCDD, raised in rabbits as described by Albro *et al.* (9), antiserum to rabbit γ-globulin raised in goats, ^{125}I-labelled 1-*N*-(5-iodovaleramido)-3,7,8-trichlorodibenzo-*p*-dioxin, detergent solution, bovine γ-globulin, rabbit γ-globulin, phosphate buffer saline, antibody diluent, and second antibody reagent.

(j) Internal (spiking) standard

A mixture of ^{13}C-labelled dioxins consisted of 50 pg/μL of 2,3,7,8-^{13}C TCDD, and 100 pg/μL each of 1,2,3,7,8-^{13}C-PCDD, 1,2,3,4,6,7,8-^{13}C-HpCDD, and ^{13}C-OCDD in toluene. The ^{13}C hexa isomer was not available at our laboratory.

Sample extraction techniques

(a) Tissue extraction (fish, clams, leeches, and eggs)

Homogenized tissue (10 g) is subsampled into a 500 mL Erlenmeyer flask and spiked with 25 μL internal standard. After the addition of 100 mL 1 *N* HCl the contents of the flask are mixed by swirling and allowed to stand for 30 min. A 100 mL aliquot of toluene is added and

Can. J. Chem. Downloaded from www.nrcresearchpress.com by 78.46.186.204 on 09/07/12
For personal use only.

Can. J. Chem. Downloaded from www.nrcresearchpress.com by 78.46.186.204 on 09/07/12
For personal use only.

the flask is placed on the wrist shaker overnight. The density of the resulting emulsion will determine the next analytical step. Light to medium emulsions that show some separation are transferred to a separatory funnel and allowed to separate. The lower aqueous layer, solids and emulsion remnants are then placed into stainless steel centrifuge cups and homogenized with an additional 100 mL of toluene, followed by centrifugation to break emulsions. Dense or persistent emulsions may be directly transferred to the centrifuge cups and centrifuged at 4000–4500 rpm for 10–15 min prior to decantation into a separatory funnel and subsequent separation. This separation, homogenation centrifugation scheme is repeated twice with 100 mL of toluene and the extracts are combined for further cleanup steps.

(b) Fly ash and sediments

An appropriate size sample (1–10 g) is spiked with 25 μL internal standard, treated with 100 mL 1 *N* HCl and allowed to stand 1 h. The mixture is then filtered and washed with 100 mL of distilled deionized water. The filtrate is extracted three times with 50 mL portions of toluene. The solids are mixed with sodium sulfate to obtain a free flowing mixture and soxhlet extracted for 6 h with 300 mL of toluene. The toluene extracts are combined for further cleanup.

(c) Water

A 50–200 L sample size, depending upon the concentration factor required, is extracted with 300 mL of dichloromethane using a continuous-flow extractor. The extraction is carried out by passing the sample through the extraction chamber where it is mixed with dichloromethane. The water phase is separated and passed to waste through a small packed column, the solvent is recirculated back into the mixing chamber. The effluent water contains dissolved solvent (about 1.5% by volume) which is replenished by adding solvent to the top of the small packed column through which the effluent water is passing, thus giving a counter-current extraction with clean solvent. The packing is "Teflon" Raschig rings which also serve, by virtue of the solvent wetability of "Teflon", to break any emulsions and coalesce small solvent drops.

In all extractions a metering pump is used to meter surrogate standard solution into the water sample flow as it enters the extractor. In this way for every sample extracted the recovery of the surrogate standards gives an immediate measure of the material balance obtained in the extraction–analytical process. The surrogate standards are chosen so that they have similar extraction characteristics to the analytes of interest and are compatible with the chromatographic procedure and detection system used. For example, when analyzing for PCDDs, where a mass detector is used, isotopically labelled dioxins such as ^{13}C are ideal surrogates.

Extraction of small volumes of water (1–4 L size) is carried out using the separatory funnel technique. A sample is spiked with 25 μL of internal standard solution. The spiked sample is then extracted with dichloromethane. The extract is concentrated and exchanged to hexane or chloroform depending upon the type of cleanup required to eliminate interferences that may be encountered.

Cleanup procedures

(a) Liquid /liquid extraction using trisodium phosphate

The sample extracts are treated with 100 mL of 0.05 *M* trisodium phosphate ($Na_3PO_4 \cdot 12H_2O$) for 2 min followed by a wash with 100 mL deionized water.

(b) Liquid/liquid extraction using sulphuric acid

The sample extracts are treated with 100 mL of 1 *N* sulphuric acid (H_2SO_4) for 2 min followed by a wash with 100 mL deionized water.

(c) Mercury treatment

Approximately 0.5 mL triple-distilled mercury is added to the concentrated organic extract (5 mL) and vigorously shaken until formation of a black precipitate ceases. The chloroform extract is filtered using a 0.2 μm nylon filter and a 5 mL gas-tight syringe. Additional chloroform is used to wash the mercury until a volume of 12 mL is reached.

(d) Gel permeation chromatography (gpc)

The sample extract is evaporated to dryness, and the residue, reconstituted in small volumes of chloroform, is filtered through a 0.2 μm nylon filter until a volume of 12 mL is reached. Aliquots (4.5 mL) are injected into the gpc system operated at 5 mL/min using chloroform as a mobile phase. The previously calibrated fraction containing the PCDDs and PCDFs is collected. This procedure is repeated for the entire sample volume and the fractions are combined for further cleanup.

(e) Alumina chromatography

The extract from each sample is evaporated to dryness and the residue is dissolved in 1 mL of 1% methylene chloride in hexane. The residue is transferred to the basic alumina column with solvent washings. The column is eluted with a total of 200 mL 1% (v:v) methylene chloride:hexane (fraction 1) and subsequently with 150 mL 50% (v:v) methylene chloride hexane (fraction 2). Fraction 2, containing PCDDs and PCDFs, is evaporated and the residue redissolved in 0.9 mL 50% (v:v) methylene chloride:cyclohexane.

(f) Carbon–fibre chromatography

The concentrated extract from the alumina cleanup is injected into the carbon–fibre cleanup system and eluted at 4 mL/min in succession as follows: 20 mL 50% (v:v) methylene chloride:cyclohexane, 30 mL ethyl acetate, 20 mL 4% benzene in ethyl acetate, 20 mL 20% benzene in ethyl acetate, and 30 mL 50% benzene in ethyl acetate. The carbon fibre is then back eluted with 30 mL toluene. The toluene fraction containing the PCDDs and PCDFs is concentrated to dryness and reconstituted with 25 μL ^{37}Cl-labelled 2,3,7,8-TCDD in toluene for high resolution gas chromatography/low resolution mass spectrometry analysis.

Isolation of dioxins from environmental samples

Isolation procedures vary with type, nature, and concentration of interfering substances in the environmental sample. The detailed sequence of the sample pretreatment, extraction, and cleanup procedures is determined by the sample type. Figure 1 illustrates the schematic, depending upon the matrix, employed for isolation of dioxin and related compounds prior to analysis.

Analytical protocols

Preliminary screening using gas chromatography with mass selective detector

The system employing an HP5880A gas chromatograph fitted with a 30 m × 0.25 mm id SPB-5 capillary column and HP5970 mass selective detector is used on a routine basis.

The end of the column is inserted directly into the source of an HP 5970 mass selective detector (msd) used in the electron impact (EI) mode at 70 eV. The electron multiplier is set at 2200 V and the dwell times at 200 ms.

Screening of the samples for the presence of dioxins is done in the single ion monitoring (sim) mode by monitoring the three most intense ions in the molecular cluster and the (M − COCl) ion for each congener group over pre-determined time windows (Table 2). These chromatographic windows are determined by running a mixture of all available dioxin isomers and by monitoring simultaneously the most intense ion for each congener group. The detection of the four specified ions in the correct ratios and at the right retention times provides confirmation of the presence of a particular dioxin isomer in the sample which is then subjected to the quantitation procedure.

The quantitative analysis protocol described here is similar to that reported by Norstrom *et al.* (10). It involves quantitation by monitoring, for the correct congener group and over its specified time window, the most intense ion in the molecular cluster of the unlabelled and ^{13}C-labelled (internal standard) dioxin (Table 3). Use is made of the quantitation and reporting software provided with the HP 59970 data acquisition system. The quantitation is based on the ^{13}C internal standards which automatically correct for losses of material during the clean up and for chromatographic variations between injections. A mixture consisting of equal concentrations of unlabelled and ^{13}C-labelled dioxins is first run in order to calibrate the system. The amount of each labelled dioxin is the same as that initially spiked in the sample. After integration of each ion peak, the system automatically updates the calibration table and creates a response ratio (unlabelled/labelled) versus concentration ratio calibration curve for

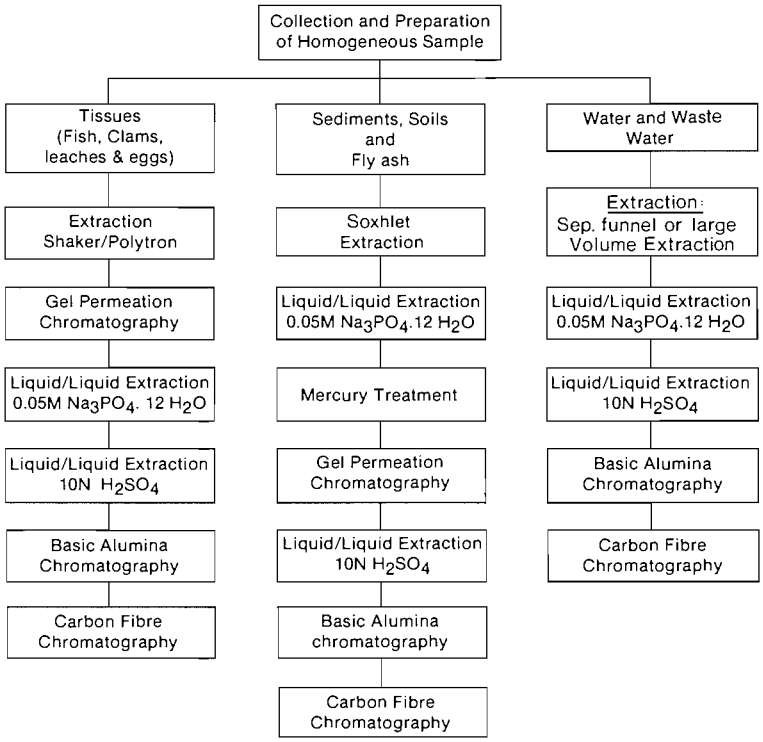

FIG. 1. Sample extraction schematic.

TABLE 2. Nominal masses of the three most intense ions in the molecular cluster of unlabelled dioxins and of the corresponding COCl loss

Congener	Time window (min)	Nominal masses of monitored molecular ions			M-COCl
Tetra	13.0–17.0	319.9	321.9*	323.9	258.9*
Penta	17.0–20.0	353.9	355.9*	357.8	292.9*
Hexa	20.0–23.0	387.8	389.8*	391.8	326.8*
Hepta	23.0–27.5	423.8*	425.8	427.8	360.8*
Octa	27.5–32.0	457.7	459.7*	461.7	396.8*

*Most intense ion in cluster.

TABLE 3. Nominal masses of the three most intense ions in the molecular cluster of ^{13}C-labelled dioxins

^{13}C Dioxin	Three most intense ions in molecular cluster		
Tetra	331.9	333.9*	335.9
Penta	365.9	367.9*	369.9
Hexa	399.9	401.9*	403.8
Hepta	435.8*	437.8	439.8
Octa	469.8	471.8*	473.8

*Most intense ion in cluster.

each isomer specified in the table. The ratios found for the sample are then compared with the curves and the concentration of each specified dioxin determined. Recoveries are determined by running an external standard.

(b) Positive identification

A Finnigan 4500 gas chromatograph/mass spectrometer is used for routine confirmation. The cleaned sample extracts are injected into the system using a standard H.P. injector in the splitless mode at 260°C. The gas chromatographic separations are performed using a 60 m × 0.32 mm id fused silica column coated with SP2331 to a film thickness of 0.2 μm. To achieve maximum sensitivity, the exit end of the capillary column is inserted directly into the ion source while maintaining the transfer line area at 250°C. Mass spectra are acquired in various modes such as full scan (fs) and multiple ion detection (MID) using both electron impact and negative ion chemical ionization. The following gas chromatographic and mass spectrometric conditions are used during the preliminary identification of PCDDs.

Gas chromatography conditions	
Carrier gas	Hydrogen at 14 psi head pressure
Initial temperature	80°C
Initial time	2 min
Program at 15°C/min to	200°C
Program at 4°C/min to	250°C
Final holding time	40 min

Mass spectrometry conditions		
Parameter	Electron impact	Chemical ionization
Ion source temperature	150°C	50°C
Manifold assembly temperature	100°C	100°C
Reagent gas	—	Hydrogen
Ion source pressure	—	0.7 to 1.0 Torr
Emission current	0.36 mA	0.36 mA
Electron voltage	70 eV	70 eV
Electron multiplier set at	1100 V, 3 kV on the dynodes for both modes	
Electron multiplier gain		$\times 10^{-7}$ A/V

The acquired data are processed using a Finnigan SUPER INCOS data system. A supplementary data system, developed under contract

Can. J. Chem. Downloaded from www.nrcresearchpress.com by 78.46.186.204 on 09/07/12
For personal use only.

Can. J. Chem. Downloaded from www.nrcresearchpress.com by 78.46.186.204 on 09/07/12
For personal use only.

for use in our laboratory, is also employed to carry out quantitation using multiple peak scanning mode. The latter system utilizes customized software to enable sufficient sensitivity and selectivity to be obtained for PCDDs through use of an integrated selected ion signal.

(c) Custom software

Custom software permitting the analysis of a wide range of compounds in a single run was developed under contract for use in our laboratory (11). The data system operates on a Zenith Z-100 computer controlling the Finnigan 4500 gc/ms system. The data system is highly automated and yet allows for operator interaction for optimization of sensitivity and selectivity and for verification of results. The sensitivity of the custom software falls between single ion monitoring and full scan mode of operation. It targets in on specific compounds in relationship to an internal standard rather than general time window in the chromatogram. Quantitation is achieved using the response factor of a single characteristic ion (base peak) relative to an internal standard. The identity of the compound is verified by monitoring up to six confirming ions. The system also includes a quality assurance protocol to monitor long-term performance of the gc/ms system and continuously updates the detection limits of individual compounds.

(d) Isomer specific confirmation

A Varian MAT 311A mass spectrometer directly coupled to a Carlo Erba Model 4160 gas chromatograph is utilized for confirmation. The gc is equipped with a 60 m × 0.25 mm id open tubular column (otc) coated with Silar 10C. The carrier gas is helium with a linear velocity of 27 cm/s. The ms is equipped with a combination electron impact (EI) and chemical ionization (CI) source but operated only in the electron impact mode. Each four channels of the hardware multiple ion detection device can be individually controlled for selection of acceleration voltage, range output, signal bandwidth, background baseline level, and integration rate. The intensities of the selected masses are monitored on a four-channel recorder. The adjustable integration rate can accurately reproduce open tubular column peaks of less than 2 s width at half peak height.

The high voltage unit is monitored using a KEITHLEY Model 191 digital multimeter to calculate the exact acceleration voltage required for the specific masses to be monitored. The magnet is set at perfluorokerosene (PFK) peak at m/z 318.9793 and the resolution is adjusted to between 5 500 and 7 000 mass resolution. The high voltage unit is monitored and used for calculating the exact acceleration voltages for the masses and ions given below.

Ion	Mass (m/z)
$C_{12}H_4O_2{}^{35}Cl_4$	319.8965
$C_{12}H_4O_2{}^{35}Cl_3{}^{37}Cl$	321.8936
$C_{12}H_4O_2{}^{37}Cl_4$	327.8847
$^{13}C_{12}H_4O_2{}^{35}Cl_4$	333.9337

The calculated values are introduced into sim channels.

Using the Silar 10C column, we are able to resolve 18 baseline separated peaks from a mixture of 22 tetrachlorodebenzo-*p*-dioxin isomers. The column is also suitable for isomer specific confirmation of 2,3,7,8-TCDD.

(e) Radioimmunoassay procedure

A procedure recommended by Albro *et al.* (9) is employed. The organic extract is passed through appropriate cleanup steps to reduce interferences and concentrated to 10 μL or less per sample. The residue is solubilized by sonication in a detergent–buffer mixture and incubated with a previously optimized dilution of antiserum from rabbits. A threefold excess of a radiolabelled derivative of trichlorodibenzo-*p*-dioxin over what can be bound by the amount of antiserum used is added and incubation is continued until equilibrium binding occurs. An optimum amount of antiserum to rabbit γ-globulin prepared in goats is then added to precipitate the bound radiolabel. After precipitation is complete, the sample is centrifuged. The supernate is drained off and the pellets radioassayed to a γ counter. The presence of chlorinated dibenzo-*p*-dioxins in the sample extract results in decreased radioactivity being precipitated relative to procedural blanks, and the decrease is a measure of the amount of analyte present.

Results and discussion

Comparison and choice of extraction techniques

Considerable work has been reported on the concentration and/or extraction of dioxin and related compounds at ultratrace levels (ng to pg/L, ng/kg) from a wide variety of environmental samples. Adsorption, solvent extraction, homogenization, and sonication have been used with numerous combinations of different solvents. In spite of the above, a wide variation in extraction efficiency and inability of certain techniques to quantitatively extract dioxins is universally recognized. Therefore, work was initiated to critically evaluate various techniques and select a narrow range of extraction techniques for different types of matrices. The choice of extraction technique was found to depend upon the type of sample and relative concentration of interferences in the samples. Improved recoveries of PCDDs in fish tissue and sediments have been obtained when samples were pretreated with hydrochloric acid and extracted with toluene using mechanical agitation or soxhlet respectively. Sediments with high sand or gravel content can be satisfactorily extracted using sonication with organic solvents such as methylene chloride or toluene. Air particulates and fly ash must be soxhlet extracted after pretreatment with hydrochloric acid and filtration. Our work confirms the earlier findings of Hutzinger *et al.* (1) who have critically evaluated various extraction techniques in a wide variety of environmental samples.

Cleanup procedures

The cleanup scheme utilized for PCDD analysis of environmental samples has evolved from the methodology previously developed for the analysis of 2,3,7,8-TCDD in fish tissue samples (6). Certain fish species and sediment samples require a more comprehensive and exhaustive clean-up scheme to remove interfering compounds. The removal of sulphur compounds prior to gel permeation chromatography is necessary to prevent their deposition within the system and a resulting deterioration of efficiency. Phenolic compounds are one of the most prolific groups of chemical compounds found in nature, and their removal from sediment extracts greatly enhances the stability and resolution of the gpc step. Previously, a micro alumina column employing neutral alumina had been used to separate aliphatics from aromatics (6, 7), however, it was found that certain fish extracts were contaminated with polychlorinated biphenyls at a level sufficiently high to result in a break-through of material which in turn led to failure of the carbon fibre isolation procedure. A higher capacity aluminia column similar to that employed by Norstrom *et al.* (10), was incorporated into the cleanup process for a more reliable removal of PCBs. It was also found that a more stable elution pattern resulted if a six-solvent elution scheme similar to that established by Stalling *et al.* (12, 13) was employed with the carbon fibre system.

The detailed sequence of the cleanup procedure is determined by the nature of the sample and the type of its extract (Fig. 1). The choice and the order of cleanup steps, to eliminate interfering substances, is determined by the nature of samples, extraction technique employed and the relative concentration of interfering substances in the extract. Sediment samples, dumpsite samples containing organic matter, sludges, and fly ash required the most extensive cleanup. However, other types

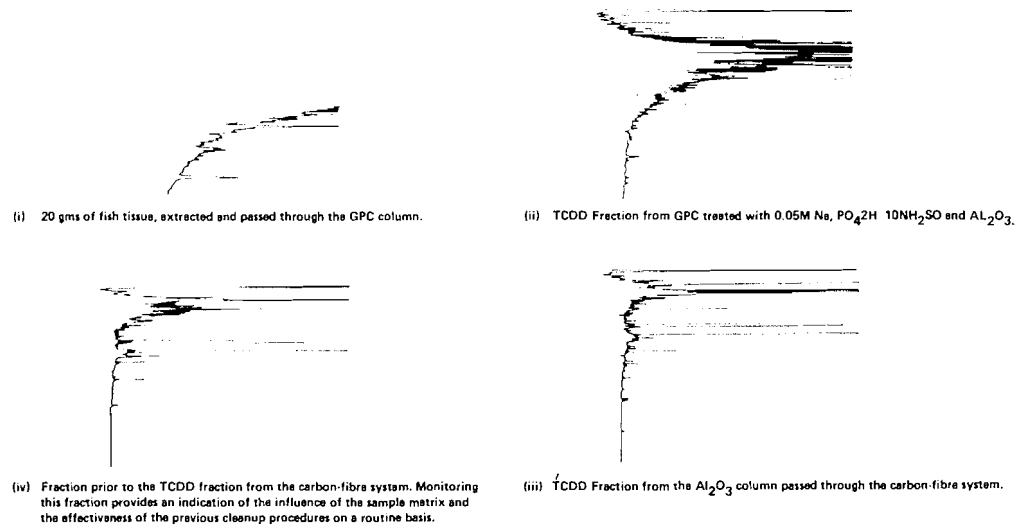

FIG. 2. Chromatograms showing effect of sequential cleanup steps.

of samples can be analyzed by eliminating some of the cleanup steps described in the experimental part of this paper. Figure 1 illustrates the recommended cleanup steps for various types of samples.

The effectiveness of individual cleanup steps to eliminate interferences is shown in Fig. 2. In this example, 25 g of fish tissue extract was carried through the cleanup procedure illustrated in Fig. 1. After each major step an aliquot was taken, corresponding to approximately 0.8 g of fish tissue, and injected into a capillary gas chromatograph. It can be seen that each step significantly reduces the background interferences and thus enables more accurate quantitative analysis of PCDD.

Radioimmunoassay technique for dioxins

Conventional methods for the analysis of PCDDs, which combine gas chromatography with mass spectrometry following extensive extraction and cleanup procedures, are excessively time consuming and expensive when used for routine environmental monitoring. A gas chromatography – mass spectrometry laboratory with two operators, could be realistically expected to process a maximum of 10 samples a day; with an individual analysis, including isomer confirmation, costing between $500 and $1000. These are serious limitations when considered from the perspective of an environmental surveillance or monitoring program. In the event of an environmental accident involving the release of PCDDs into the environment, a requirement would exist for the short-term analysis of large numbers of environmental and biological samples, to be followed in all probability by an intensive monitoring program. Such demands would severely stress existing PCDD analytical facilities.

The inclusion of an effective screening test in the analytical protocol for PCDDs could resolve some of the foregoing problems by eliminating those samples that are free of PCDD from further time consuming conventional analyses. A screening method for PCDDs need not be isomer specific. Rather, positive samples from the screening step could be subsequently analyzed for specific PCDD isomers, using conventional techniques. Three screening methods have been proposed for the detection of PCDDs: radioimmunoassay (9), aryl hydrocarbon hydroxylase (AHH) induction assay (14), and cytosol receptor assay (15). For reasons that have been adequately described by Albro *et al.* (9), radioimmunoassay was considered to offer the best potential for eventual incorporation into an analytical protocol for the routine analysis of PCDDs.

Based on the classical antigen-antibody reaction, radioimmunoassay is a relatively simple, powerful, and adaptable technique for the rapid determination of trace levels of organic compounds. Originally developed for the micro-determination of proteinaceous substances, radioimmunoassay is also extensively used in the detection and determination of steroidal hormones and other low molecular weight organic molecules. Immunoassays have been proposed for the detection of several environmentally important compounds in addition to PCDDs (9): PCBs (16), dieldrin and aldrin (17), atrazin (18), benomyl and methyl 2-benzimidazolecarbamate (19), diclofop-methyl (20), 2,3,7,8-tetrachlorodibenzofuran (21), and 2,4-D and 2,4,5-T (22). Recently, the International Union of Pure and Applied Chemistry, reporting on improved cost effective approaches to pesticide residues analysis, concluded that immunochemical methods, while being traditionally unfamiliar to the residue chemist, offer exciting possibilities for newer, cost effective approaches (23).

Developed by Albro and co-workers (9), the radioimmunoassay for PCDDs is a double antibody procedure with a reported detection limit of approximately 25 pg of 2,3,7,8-TCDD, and a reliable sensitivity in human fat of 100 pg ($P < 0.05$) (24). The precision of the radioimmunoassay for PCDDs remains to be determined for other sample types. The assay uses detergent micelles to solubilize the highly insoluble PCDD molecules which are then incubated, in a competitive binding reaction, with an ^{125}I-labelled dioxin derivative and antibodies raised in rabbits against 2,3,7,8-TCDD. When equilibrium binding has been reached, bound and free labelled hapten are separated, and the bound radioactivity is quantified. A decrease in bound radioactivity, relative to the control tubes, is proportional to the amount of PCDD present. Concentrations of unknowns are interpolated from a standard curve.

A preliminary evaluation of the radioimmunoassay for PCDDs was undertaken in order to confirm that the procedure has potential for the detection of PCDDs in fish extracts, a matrix routinely analyzed for PCDDs at CCIW. A set of fish samples (Table 4) consisting of a variety of tissue homogenates that had been previously extracted and prepared for TCDD

Can. J. Chem. Downloaded from www.nrcresearchpress.com by 78.46.186.204 on 09/07/12
For personal use only.

TABLE 4. Analysis of fish samples for 2,3,7,8-TCDD using RIA and GC–MS

Sample	Lipid (%)	Fraction	GC–MS (ng)	RIA (ng)
Lake trout #1	18.5	D*	ND‡	>20
Lake trout #1	18.5	F†	ND	0
Ocean haddock	0.4	D	ND	12.0
Ocean haddock	0.4	F	ND	0.3
Lake trout #2	24.7	D	3.4	>20
Lake trout #2	24.7	F	—	>20
Rainbow trout	19.8	D	3.7	>20
Rainbow trout	19.8	F	ND	0.6
Lake trout #7§	35.6	E	0.8	0
Lake trout #7§	35.6	F	ND	0.19
Lake trout #7§	35.6	E+F	ND	0
Lake trout #7	35.6	E	4.0	>20
Lake trout #7	35.6	F	ND	0.16
Fish sample #10	ND	E+F	ND	0.5
Fish sample #13	ND	E+F	ND	0.5
2,3,7,8-TCDD	—	‖	10.0	>20

*15% ethyl acetate fraction, passed through Al_2O_3 on 40% $MeCl_2$/hexane.
†25% ethyl acetate fraction, passed through Al_2O_3 on 40% $MeCl_2$/hexane.
‡ND: none detected.
§Hexane extraction of HCl digested fish.
‖Standard run through gpc column, fraction 30–40 min at a flow rate of 5 μL/min, collected.

analysis using a deactivated florisil cleanup procedure (R. Thomson, personal communication) was analyzed using radioimmunoassay and gc–ms. The radioimmunoassay analyses were undertaken by Dr. C. Mituma, SRI International, Menlo Park, CA, USA.

Three of the fish extracts (lake trout #2 fraction D, rainbow trout fraction D, and lake trout #7 fraction E) had high TCDD contents, observations that were confirmed by the radioimmunoassay analyses. Overloading of the low capacity florisil probably caused carryover of TCDD from the D fraction, where it would be expected to elute from the column, to the F fraction where it was detected using radioimmunoassay in the lake trout #2 sample. The discrepancies between the TCDD levels detected in the extracts using gc–ms and radioimmunoassay are unimportant, since radioimmunoassay is proposed as a pre-screening method rather than for quantitative determination. Furthermore, radioimmunoassay is responsive to PCDD isomers other than 2,3,7,8-TCDD (9) and to some PCDF isomers (9).

Several contradictions are apparent between the gc–ms and radioimmunoassay results. No TCDD was detected in the lake trout #1 fraction D, and ocean haddock fraction D samples using gc–ms, whereas >20 and 12 ng respectively were detected using radioimmunoassay. The presence of positive interferences, PCDDs other than 2,3,7,8-TCDD, or cross-reacting PCDFs in the sample extract, or the failure to detect TCDD using the gc–ms protocol in use at that time could cause such an effect. Fraction E of the acid-digested lake trout #7 sample, was the only sample tested that gave a false negative result using radioimmunoassay. The remainder of the samples, in which no TCDD was detected using gc–ms, yielded zero or low readings using radioimmunoassay.

These preliminary data demonstrate that radioimmunoassay can detect TCDD in fish samples. However, the problem of low level false positive results obtained using radioimmunoassay requires investigation to clarify whether it is due to positive interferences, assay variability, or the presence of PCDDs other than 2,3,7,8-TCDD. Selection and optimization of an appropriate simplified cleanup procedure would help to eliminate positive interferences from sample extracts. The use of matrix blanks and control samples covering a range of analyte concentrations would further reduce the effect of low level positive interferences and assay variability and instability in the radioimmunoassay for PCDDs. The detection of PCDDs other than 2,3,7,8-TCDD, or of PCDFs, is not a problem, since the presence of such compounds in environmental samples is also cause for concern. Samples containing such interferences should be further analyzed using gc/ms.

Efforts to date have focussed on evaluating the potential of radioimmunoassay for the detection of PCDDs in samples from aquatic environments, interfacing the radioimmunoassay procedure with appropriate cleanup procedures and evaluating its performance when so interfaced, and investigating various means of improving the responsiveness, and precision of the radioimmunoassay. Some basic changes to the original radioimmunoassay procedure have resulted. The modified assay, which uses dimethylsulfoxide (DMSO) as the solubilization agent, will be described in a later publication.

Confirmatory techniques using gc/ms

Standard electron impact ionization at 70 eV is the most widely used form of ionization in conventional mass spectrometry. The majority of gc/ms operators use this mode for the confirmation of PCDDs and PCDFs.

Recently, several other modes of mass spectrometry involving chemical ionization with reagent gases such as methane, oxygen-doped methane, and isobutane have been used to improve sensitivity and in some cases isomer specificity (25–27).

All PCDDs available in our laboratory were analysed using full scan (FS) and also multiple ion scanning (MID) modes of detection. Preliminary data acquired using electron impact and pulsed positive ion negative ion chemical ionization (PPINICI) indicated that TCDDs were most sensitive using the electron impact – multiple ion detection mode, while the H_2 negative ion chemical ionization/multiple ion detection mode provided enhanced sensitivity for the other PCDDs ranging from penta to octa chlorinated isomers.

In the past, the use of negative ion chemical ionization with hydrogen as reagent gas has not been exploited. Presumably this is because it is not as good a reagent gas as methane or isobutane and in the presence of water molecules the H_3O^+ ions formed would compete for sample molecules and result in poor reproducibility of the chemical ionization spectra (28). In addition, hydrogen is a difficult gas to pump from the mass spectrometer system.

In our laboratory, we initially used methane as reagent gas with helium as the gc carrier gas. The use of negative ion chemical ionization gave rise to a significant enhancement, compared to the more conventional electron impact mode, of mass spectrometry for the penta to octa substituted isomers of PCDDs. Because methane contaminates the ion source, the instrument sensitivity declines throughout the decay. Substituting hydrogen for methane gives results that are about 70% as sensitive as for methane but additional benefits accrue which more than make up for this decrease in sensitivity. These advantages are: (*a*) the use of hydrogen allows the He gc carrier gas to be replaced resulting in improved gas chromatography peformance; (*b*) the ion source does not become contaminated with the reagent gas and does not show a loss in sensitivity with time. Time-consuming source cleanups are eliminated.

Can. J. Chem. Downloaded from www.nrcresearchpress.com by 78.46.186.204 on 09/07/12
For personal use only.

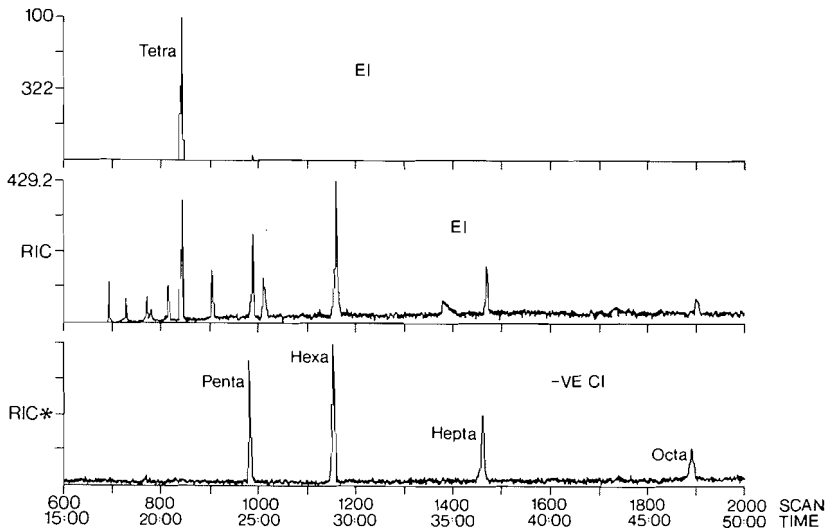

FIG. 3. Ion chromatogram with H_2 NICI scanning from 240 to 480 amu for dioxin standard mixture. Tetra shown at mass 322 for top mass chromatogram.

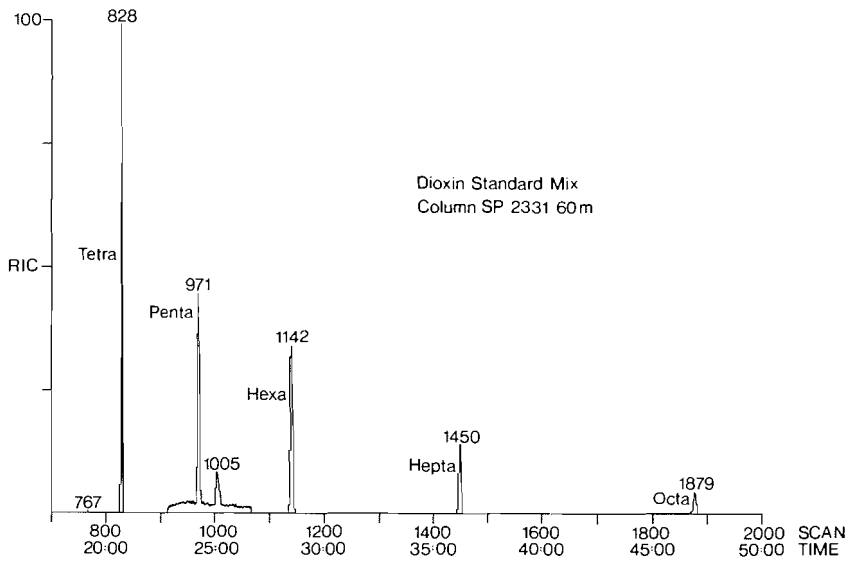

FIG. 4. Ion chromatogram with electron impact multiple ion scan for dioxin standard mixture.

Changing ion volumes, alternate and negative ion chemical ionization electron impact modes of operation can be used with no apparent loss of sensitivity; (*c*) analysis of sample extracts produce significantly lower background noise using H_2 negative ion chemical ionization mass spectrometry compared to the electron impact mode. However, similar background noise is observed when standard solutions of PCDDs are run in both modes; (*d*) the spectra for PCDDs using electron impact and H_2 negative ion chemical ionization are similar in fragmentation of the M and M–Cl clusters. Because of this it is possible to use a common multiple ion detection descriptor(s) with the data system and later reconstruct a dual display for both modes of operation, thereby enabling a direct comparison of spectra for peaks within ± 1% retention time of each other; (*e*) the use of multiple ion detection both electron impact and H_2 negative ion chemical ionization provides an additional confirmatory step to increase the confidence of PCDD identification.

All PCDDs available in our laboratories are analyzed using full scan as well as multiple ion detection modes. Data acquired for electron impact, positive ion chemical ionization and negative ion chemical ionization indicates that 2,3,7,8-TCDD is more sensitive using the electron impact – multiple ion detection mode, while H_2 negative ion chemical ionization mode provides enhanced sensitivity for the penta–octa chlorinated PCDDs. Figures 3–5 and Table 5 present data for a selected isomer mix run under different mass spectrometric conditions. These results indicate that the combination of HP OV-1 and H_2 negative ion chemical ionization in multiple ion scanning mode provide maximum sensitivity for the majority of the higher chlorinated PCDDs. However, the HP OV-1 column does not resolve as many dioxin isomers as the SP2331 column under the conditions described in the experimental section.

With the current protocol, qualitative and confirmatory analysis of PCDDs consist of running the sample extract several times using gc–ecd, gc–msd, hrgc–lrms with various modes of ionization followed by a final reconfirmation of results using magnetic sector hrgc/ms.

Analysis of environmental matrices

Our earlier work was aimed at developing a reliable analytical

Can. J. Chem. Downloaded from www.nrcresearchpress.com by 78.46.186.204 on 09/07/12
For personal use only.

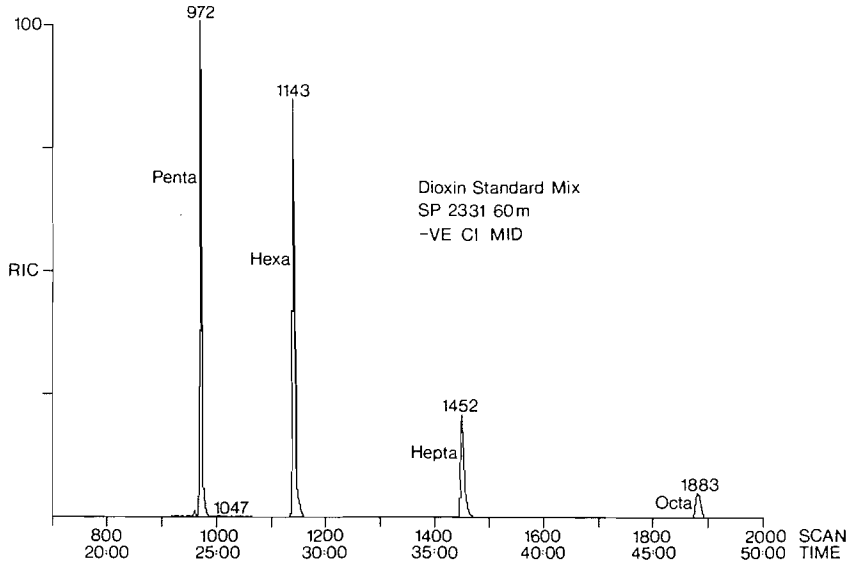

FIG. 5. Ion chromatogram with H_2 NICI multiple ion scan for dioxin standard mixture. Note – no response for tetra.

TABLE 5. Response ratios for selected PCDDs using various capillary columns and modes of mass spectrometry

No. of Cl/ abbreviation	Ions monitored	GS columns H_2NICI-FS	Full scan	Multiple ion detection	H_2NICI
		OV-1/SP2331	H_2NICI/EI	H_2NICI/EI	MID/FS
4/TCDD	257,† 259,† 320, 322*, 328,‡ 332§	ND‖	0.14	<0.01	ND
5/PnCDD	354, 356*, 358, 368§	2.00	9.70	5.40	30
6/HxCDD	388, 390*, 392, 402§	2.70	4.00	5.70	25
7/HpCDD	422, 424*, 426, 436§	3.25	4.80	3.30	22
8/OCDD	456, 458, 460*, 472§	2.25	5.80	1.56	15

*Ion used for quantitation.
†COCl loss in EI mode.
‡Ion for ^{37}C-labelled isomer.
§Ion for ^{13}C-labelled isomer.
‖ND = not detected.

TABLE 6. Percent recovery of labeled dioxins in different matrices

Sample	Amount spiked/recovery observed (ng) (%)			
	T_4CDD	P_5CDD	H_7CDD	O_8CDD
Tap water (410 L)	1.25/105	2.50/106	2.50/119	2.50/124
Suspended sediment (10 g)	1.25/96	2.50/119	2.50/113	2.50/92
Bottom sediment (10 g)	1.25/69	2.50/96	2.50/92	2.50/93
Leeches (13.5 g)	1.25/76	2.50/87	2.50/115	2.50/117
Landfill (10 g)	1.25/112	2.50/114	2.50/112	2.50/146

method, using mild cleanup steps with least derivatization potential, for TCDDs in environmental samples. The application of this procedure to the analysis of other homologues and complex matrices such as polluted sediments, fly ash and samples from dumpsites indicated that certain samples could not be analyzed, as indicated by low recoveries of spiked labelled isomers (6, 7).

The modifications reported in this paper enabled us to analyze the above samples with increased accuracy and precision. The modifications which enabled improved recoveries included changes in alumina chromatography, addition of mercury cleanup step and change in the order of cleanup procedures. Table 6 and Figs. 6 and 7 illustrate the type of recoveries and mass-chromatograms obtained by the proposed method using highly contaminated samples. Furthermore, the modified procedure was also found to be satisfactory for analysis of a wide variety of tissue samples (e.g. herring gull eggs, clams, leachates, and fish with high lipid content). The results of replicate analysis of herring gull egg pool samples are shown in Table 7 which illustrates the concentration in ng/kg, of native dioxins found in each replicate. The mean values with standard deviation are also given for each isomer. It should be noted that the native dioxins are reported as the 2,3,7,8-TCDD, 1,2,3,7,8-PCDD, and 1,2,3,4,6,7,8-H7CDD isomers. There is only one OCDD. Table 8 lists the recoveries of the method spike and of the samples internal standard. No recoveries are reported for ^{13}C hexa since we do not have that labeled isomer.

A few comments can be made about the analysis. The ms chromatograms were very "clean" with no interference presence except in the case of samples #1 and #2. An interference was

Can. J. Chem. Downloaded from www.nrcresearchpress.com by 78.46.186.204 on 09/07/12
For personal use only.

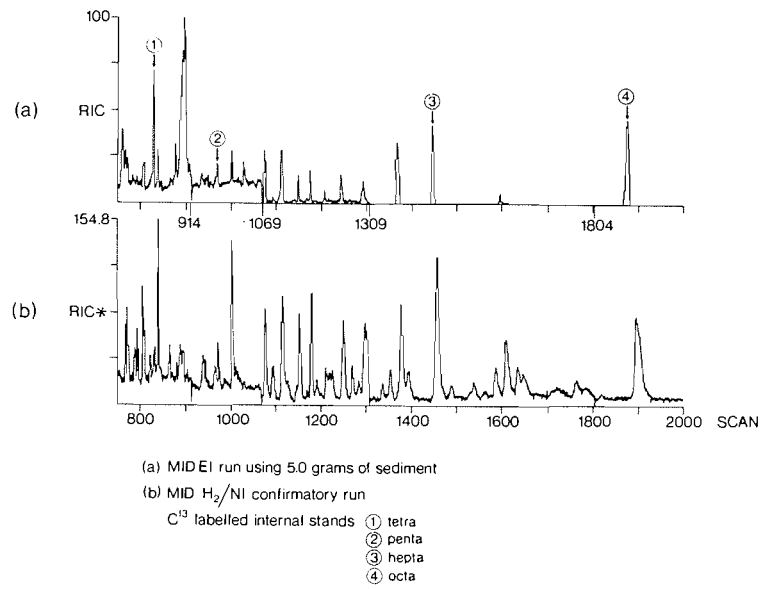

FIG. 6. Electron impact (EI) versus chemical ionization (CI) reconstructed ion chromatogram of contaminated sediment sample. (*a*) MID EI run using 5.0 g of sediment, (*b*) MID H_2/NI confirmatory run ^{13}C-labelled internal stands ① tetra, ② penta, ③ hepta, ④ octa.

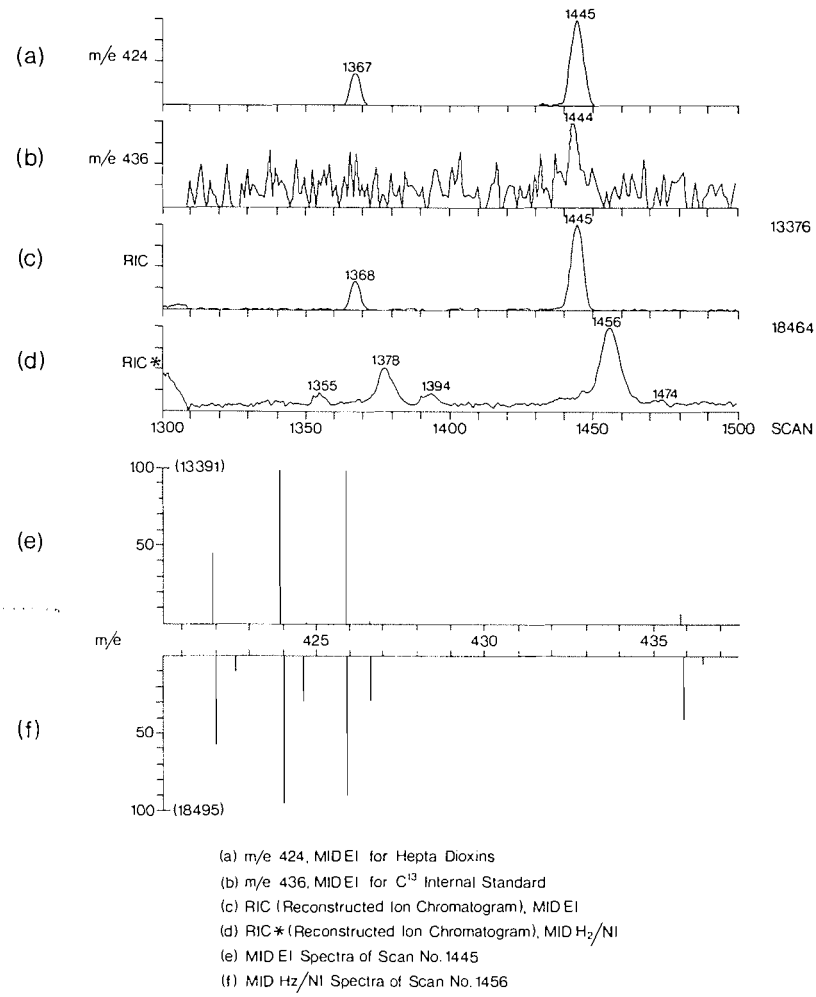

FIG. 7. Blow up of the hepta dioxin region of the mass chromatograph shown in Fig. 6. (*a*) *m/e* 424, MID EI for hepta dioxins, (*b*) *m/e* 436, MID EI for ^{13}C internal standard, (*c*) RIC (reconstructed ion chromatogram), MID EI, (*d*) RIC* (reconstructed ion chromatogram), MID H_2/NI, (*e*) MID EI spectra of Scan No. 1445, (*f*) MID Hz/NI spectra of Scan No. 1456.

Can. J. Chem. Downloaded from www.nrcresearchpress.com by 78.46.186.204 on 09/07/12
For personal use only.

TABLE 7. Levels of dioxins found in Herring Gull egg samples

	Blank*	Herring Gull egg, replicate no.					
		#1	#2	#3	#4	$\bar{x}$	$\sigma\bar{x}$
Sample weight	—	25.30 g	25.30 g	25.30 g	28.75 g	—	—
Tetra (ng/kg)	ND	53.5	55.0	47.5	52.7	52.2	3.3
Penta (ng/kg)	ND	10.6	9.3	9.5	9.4	9.7	0.6
Hexa (ng/kg)	ND	13.2	11.6	11.7	12.0	12.1	0.7
Hepta (ng/kg)	ND	1.9	2.0	1.4	2.1	1.9	0.3
Octa (ng/kg)	ND	23.2	19.5	18.1	19.7	20.1	2.2

*ND = not detected.

TABLE 8. Recoveries of method spike and samples internal spike

	Method spike	% Recoveries egg replicate no.			
		#1	#2	#3	#4
C13 tetra	107	92	100	99	99
C13 penta	87	60	78	84	91
C13 hepta	85	52	61	65	62
C13 octa	70	40	46	47	47

masking the octa M − COCl confirmation ion in those samples. But this was not the case for samples #3 and #4 in which the confirmation ion was clearly detectable thus allowing confirmation of octa in the samples.

Very low levels of native hepta were found in all the samples, typically 1.9 ng/kg, which correspond to a signal-to-noise ratio of about 10. Accordingly, the M − COCl confirmation ion could not be detected and confirmation was based on the three most intense ions in the molecular cluster and the retention time of the peak. Traces of the other hepta isomer also appeared to be present in all the samples but its presence was not confirmed.

The lower recoveries for the higher chlorinated dioxins were linked to a loose frit in the carbon fibre column. This resulted in small carbon particles finding their way into the collection flask and sticking to the wall along with minute quantities of dioxins. Since the highest chlorinated dioxins, especially octa, adsorb strongly to carbon, they could not be recovered completely by the toluene washings. To confirm the above, the loose frit in the carbon fibre system was repaired and the performance of the system was tested using the internal (spiking) standard. A 1 mL aliquot of 50% (v:v) methylene chloride:cyclohexane, containing 25 μL of the internal (spiking) solution, was injected into the carbon fibre cleanup system and the toluene fraction containing PCDDs and PCDFs was analyzed using gas chromatography with mass selective detector. The repaired system afforded recoveries of over 95% for all the spiked dioxin isomers.

Overall, because of the very good efficiency of the cleanup and of the use of an internal standard, the results were considered quite reliable. Our laboratory also participated in an interlaboratory comparison study which demonstrated that the results obtained, using a herring gull egg pool, were comparable to the reference values for the sample.

Further work is in progress to validate the above methodology which will include: (*a*) estimation of practical detection limits for each type of matrix at 95% confidence level, (*b*) determination of the mean recoveries of a series of representative samples from each matrix using three levels of labeled dioxin isomers and varying sample size, (*c*) determining the scope of the methods by analyzing samples across Canada and determining the success rate for the procedure, and (*d*) by "blind" analysis of blanks, reference samples, and fortified replicate samples covering the range of matrices described in this paper.

Acknowledgements

The authors acknowledge the assistance provided by Dr. P. Albro and his associates and Dr. F. Bishia during the establishment of the radioimmunoassay facility within CCIW.

1. O. HUTZINGER, R. W. FRIE, E. MERIAN, and F. POCCHIARI (*Editors*). Chlorinated dioxins and related compounds — Impact on the environment. Pergamon Press, Oxford. 1982.
2. National Research Council. Polychlorinated dibenzo-*p*-dioxins: limitations to the current analytical techniques. NRCC Publication No. 18576. 1981.
3. Ontario Ministry of the Environment. Polychlorinated dibenzo-*p*-dioxins and polychlorinated dibenzofurans — scientific criteria document for standard development. No. 4-84. 1985.
4. R. E. CLEMENT and S. A. LENNOX. Worldwide survey on chlorinated dibenzo-*p*-dioxin and dibenzofuran analysis capabilities. Unpublished Report, Ontario Ministry of Environment, Rexdale, Ont., Canada. August 1986.
5. B. K. AFGHAN and J. LAWRENCE. Can. Res. November/December (1981).
6. B. K. AFGHAN. Can. Res. 36, November, 1983.
7. J. LAWRENCE, F. ONUSKA, R. WILKINSON, and B. K. AFGHAN. Chemosphere, **15**, 1085 (1986).
8. T. BRIDLE *et al.* Proceedings of 77th Annual Meeting of the Air Pollution Control Association. 1984. pp. 1–15.
9. P. W. ALBRO, M. I. LUSTER, K. CHAE, S. K. CHAUDHARY, G. CLARK, L. D. LAWSON, J. T. CORBETT, and J. D. MCKINNEY. Toxicol. Appl. Pharmacol. **50**, 137 (1979).
10. R. J. NORSTROM, M. SIMON, and M. J. MULVIHILL. Intern. J. Environ. Anal. Chem. **23**, 267 (1986).
11. S. SHRADER. Shrader Analytical and Consulting Laboratories (Canada) Ltd., Mississauga, Ont., Canada. June 1985. Unpublished work.
12. L. M. SMITH, D. L. STALLING, and J. I. JOHNSON. Anal. Chem. **56**, 1830 (1984).
13. M. A. RIBICK, L. M. SMITH, G. R. DUBAY, and D. L. STALLING. Application and results of analytical methods used in monitoring environmental contaminants. ASTM Committee E35 on Aquatic Toxicity Symposium, Chicago, IL. 1979.
14. J. A. BRADLAW and J. A. CASERLINE. J. Asso. Off. Anal. Chem. **62**, 904 (1979).
15. A. POLAND, E. GLOVER, and A. S. KENDE. J. Biol. Chem. **251**, 4936 (1976).

Can. J. Chem. Downloaded from www.nrcresearchpress.com by 78.46.186.204 on 09/07/12
For personal use only.

16. W. H. NEWSOME and J. B. SHIELDS. Intern. J. Environ. Anal. Chem. **10**, 295 (1981).
17. J. J. LANGONE and H. VAN VUNAKIS. Res. Commun. Chem. Path. Pharm. **10**, 163 (1975).
18. S. J. HUBER. Chemosphere, **14**, 1795 (1985).
19. W. H. NEWSOME and J. B. SHIELDS. J. Agric. Food Chem. **29**, 220 (1981).
20. M. SCHWALBE, E. DORN, and K. BEYERMANN. J. Agric. Food Chem. **32**, 734 (1984).
21. M. I. LUSTER, P. W. ALBRO, K. CHAE, L. D. LAWSON, J. T. CORBETT, and J. D. MCKINNEY. Anal. Chem. **52**, 1497 (1980).
22. D. F. RINDER and J. R. FLECKER. Bull. Environ. Contam. Toxicol. **26**, 375 (1981).
23. R. J. HEMINGWAY. Pure Appl. Chem. **56**, 1131 (1984).
24. J. MCKINNEY, P. ALBRO, M. LUSTER, B. CORBETT, J. SCHROEDER, and L. LAWSON. *In* Chlorinated dioxins and related compounds: impact on the environment. *Edited by* O. Hutzinger. Pergamon Press. 1982. pp. 67–75.
25. J. R. HASS, M. D. FRIESEN, and M. K. HOFFMAN. Org. Mass Spectrom. **14**, 9 (1979).
26. R. K. MITCHUM, G. F. MOLER, and W. A. KORFMACHER. Anal. Chem. **52**, 2278 (1980).
27. R. K. MITCHUM, W. A. KORFMACHER, G. F. MOLER, and D. L. STALLING. Anal. Chem. **54**, 719 (1982).
28. G. W. A. MILNE and M. J. LACEY. Crit. Rev. Anal. Chem. **4**, 81 (1974).

Can. J. Chem. Downloaded from www.nrcresearchpress.com by 78.46.186.204 on 09/07/12
For personal use only.

Binding of isocyanides to five-coordinate, durene-capped hemes

SHANTHA DAVID, BRIAN R. JAMES, AND DAVID DOLPHIN
Department of Chemistry, University of British Columbia, Vancouver, B.C., Canada V6T 1Y6

Received November 14, 1986

This paper is dedicated to Professor Douglas E. Ryan on the occasion of his 65th birthday

SHANTHA DAVID, BRIAN R. JAMES, and DAVID DOLPHIN. Can. J. Chem. **65**, 1098 (1987).

Solution data at 20°C are presented for the binding of *t*-butylisocyanide and tosylmethylisocyanide (TMIC) to the five-coordinate hemes Fe(porp)(Cy_2Im), where Cy_2Im = 1,5-dicyclohexylimidazole and porp = the dianion of some durene-capped porphyrins with variable length linking methylene straps on either side of the durene moiety (4/4, 5/5, or 7/7 methylenes). The ^{t}BuNC and TMIC ligands are used to probe the steric nature of the distal binding site under the cap, in particular the respective "central" and "peripheral" effects as defined by Traylor *et al.* The binding constants range from $1.1 \times 10^9\ M^{-1}$ for the 7/7—TMIC system to immeasurably small for the 4/4—^{t}BuNC system, this range spanning data reported in the literature for related anthracene- and adamantane-capped systems.

SHANTHA DAVID, BRIAN R. JAMES et DAVID DOLPHIN. Can. J. Chem. **65**, 1098 (1987).

On rapporte des données relatives à la complexation des isocyanures de tert-butyle et de tosylméthyle (ICTM) avec des hèmes penta-coordonnées Fe(porp)(Cy_2Im) dans lesquels Cy_2Im = dicyclohexyl-1,5 imidazole et porp = le dianion de porphyrines «cappées» par un durène rattaché par des unités méthyléniques de longueurs variables (4/4, 5/5 ou 7/7 méthylènes). On a utilisé les ligands tert-BuNC et ICTS comme sondes pour la nature stérique du site de complexation «distal» et en particulier pour les effets respectifs «central» et «périphéral» définis par Traylor et ses collaborateurs. Les constantes de complexation vont de $1,1 \times 10^9\ M^{-1}$ pour le système 7/7—ICTM à un niveau tellement faible qu'il ne peut être mesuré pour le système 4/4—tert-BuNC; cet éventail de valeurs recouvre les données rapportées dans la littérature pour les systèmes «cappés» par de l'anthracène ou de l'adamantane.

[Traduit par la revue]

Introduction

Protein residues that surround the heme moiety in hemoproteins can play a crucial role in determining the nature of the axial coordinated ligand(s). Further, for example in reversible O_2-carrying hemoproteins, the protein environment around the distal binding pocket controls (via steric and electronic effects) the extent of O_2-coordination, both in absolute terms and relative to other ligands such as CO (1). Extensive studies (2–7) involving the ligation of various isocyanides (RNC), including bulky ones, have proven useful for gaining an overall appreciation of the structural nature of the binding pocket within protein systems. More recently, isocyanide ligation studies have been extended to model hemes, where Traylor *et al.* (1, 8) have compared the affinities of sterically hindered five-coordinate anthracene (**1**) and adamantane (**2**) model hemes toward ^{t}BuNC and tosylmethylisocyanide (TMIC, see Fig. 1), two structurally dissimilar isocyanides which differ with respect to their relative steric requirements on coordination to the iron(II) centre (Fig. 1). Low affinity of a hindered heme toward ^{t}BuNC, with branching in the third atom away from the iron, is considered to result from a "central steric effect" imposed by a crowded distal environment directly above the metal; in the case of TMIC, a reduced affinity is considered to result largely via a "peripheral steric effect" because the bulky tosyl moiety lies off the Fe—C≡N—C axis.

We decided to probe, using the isocyanides, the steric nature of the distal binding sites within the five-coordinate durene-capped hemes (**3**). The syntheses of the base porphyrins (9, 10), as well as the *in situ* generation of Fe(porp) and Fe(porp)B species from the isolated hemin (Fe^{III}) chlorides (11), have been described (porp = the dianion of the durene-capped porphyrin, and B = an imidazole base). The bulky 1,5-dicyclohexylimidazole, Cy_2Im, was chosen as axial base B because it is unable to coordinate under even the largest 7/7 cap (11). The affinities for the isocyanides are found to reflect decreasing

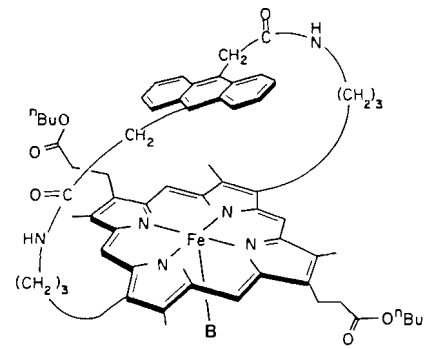

1: anthracene-capped 5-coordinate heme; B = imidazole base.

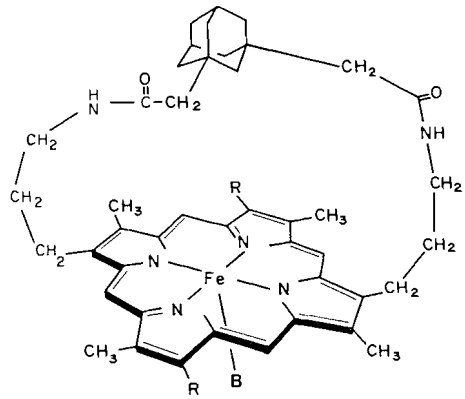

2: adamantane-capped 5-coordinate heme; B = imidazole base; R = $CH_2CH_2CO_2CH_2Ph$.

flexibilities of the durene cap in the trend 7/7 > 5/5 > 4/4, and indeed the 4/4 system binds neither ^{t}BuNC or TMIC. Preliminary binding constant data for some of the systems

Can. J. Chem. Downloaded from www.nrcresearchpress.com by 78.46.186.204 on 09/07/12
For personal use only.

TABLE 1. Binding of isocyanides to model hemes[a]

Complex	K^{TMIC}, M^{-1}	Peripheral reduction factor	K'^{BuNC}, M^{-1}	Central reduction factor
Chelated protoheme **4**	7.0×10^{9}	"1.0"	1.7×10^{8}	"1.0"
Fe(anthracene—7/7)(Cy_2Im)	7.0×10^{8}	10	8.0×10^{4}	2×10^{3}
Fe(anthracene—6/6)(MeIm)[b]	7.0×10^{5}	10^{4}	1.5×10^{2}	1×10^{6}
Fe(adamantane)(MeIm)	2.0×10^{5}	3×10^{4}	3.0×10^{4}	5×10^{3}
Fe(durene—7/7)(Cy_2Im)[c]	1.1×10^{9}	6.4	2.5×10^{5}	680
Fe(durene—5/5)(Cy_2Im)[c]	1.4×10^{7}	5×10^{2}	2.1×10^{3}	8.1×10^{4}
Fe(durene—4/4)(Cy_2Im)[c]	<1	$>7.0\times10^{8}$	<1	$>1.7\times10^{7}$

[a]Data at 20°C in toluene (for the present durene work), or in benzene or toluene for the other systems (1, 8).
[b]MeIm = *N*-methylimidazole; equilibrium constant for binding of CO to this complex = $6\times10^{5}\ M^{-1}$ at 20°C in toluene (1).
[c]Equilibrium constants for binding of CO to these complexes in toluene at 20°C are 6.6×10^{7}, 8.6×10^{7}, and $4.3\times10^{6}\ M^{-1}$ for the 7/7-, 5/5-, and 4/4-systems, respectively (13, 19).

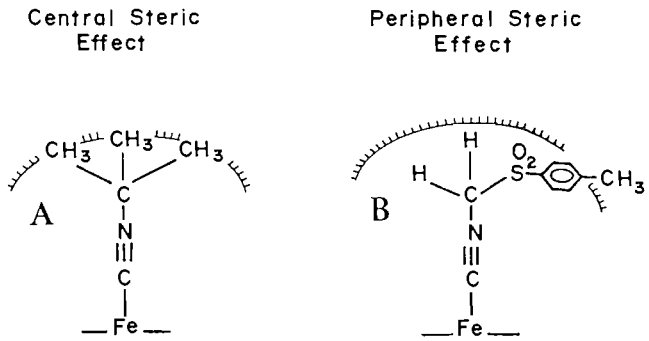

FIG. 1. Distal site steric effects resulting from coordination of bulky isocyanides within a heme binding pocket: **A**, *t*-butylisocyanide; **B**, tosylmethylisocyanide (via ref. 8).

described here were initially presented at recent conferences (12, 13).

Experimental

Toluene (reagent grade) was distilled over CaH_2 immediately prior to use. Cy_2Im was prepared according to a procedure described by Traylor *et al.* (1). ^{t}BuNC, TMIC, and ^{n}BuNC (Aldrich) were used as received. All spectrophotometric titrations were carried out under N_2, which had been passed through Ridox (Fisher) and molecular sieve columns to remove trace O_2 and H_2O.

The 5-coordinate ferrous complexes Fe(porp)(Cy_2Im) were prepared in toluene, and transferred directly into specially designed tonometers as described previously (11, 14); aliquots of the appropriate isocyanide in deoxygenated toluene were then added by a syringe via a septum plug in the tonometer and the heme solution was then equilibrated at 20°C in a Cary 17 spectrophotometer, the spectra being recorded in the 250–700 nm region.

Results

Durene—7/7 and —5/5 systems

Titration of toluene solutions of Fe(porp)(Cy_2Im), at about $3\times10^{-6}\ M$, with aliquots of the concentrated (1.0 *M*) ^{t}BuNC solutions to give [^{t}BuNC] $\geq 2\times10^{-5}\ M$, afforded directly the values for the isocyanide binding, K'^{BuNC}. A large excess of Cy_2Im (0.3 *M*) was maintained in solution to ensure that the equilibrium changes observed corresponded exclusively to the binding of ^{t}BuNC on the capped side of the heme, without complication caused by displacement of the Cy_2Im axial base: the binding constants of this imidazole to all three durene systems are in the range $(2.0–6.0)\times10^{3}\ M^{-1}$ at 23°C in toluene (11), and thus negligible amounts of the 4-coordinate hemes are present under the chosen conditions. Additions of ^{t}BuNC gave spectral changes with excellent isosbestics (and typical of a change in coordination from five to six (11)), and analyses of the data in the 420 nm region were made according to standard methods using Hill plots (15–17); the plots gave slopes of 1.00 ± 0.06, consistent with the binding of one ^{t}BuNC ligand, and the *K* values (±10%) listed in Table 1.

The two larger cap 5-coordinate hemes show an affinity for TMIC too high to be measured by direct titration with the isocyanide, at least at the heme concentration used ($\sim3\times10^{-6}\ M$); even at additions of TMIC as low as $5\times10^{-6}\ M$, formation of the 6-coordinate Fe(porp)(Cy_2Im)(TMIC) was essentially complete, implying $K^{TMIC} > 10^{6}\ M^{-1}$. The K^{TMIC} values were thus determined using competitive ligation methods using both TMIC and CO, analogous to the procedure described by Traylor *et al.* (1). From preliminary trial experiments, it became clear that binding of TMIC is comparable with, or stronger than, that of CO, and thus relative concentrations of TMIC and CO can be chosen to study the equilibrium *K'* for the overall displacement, reaction [1],

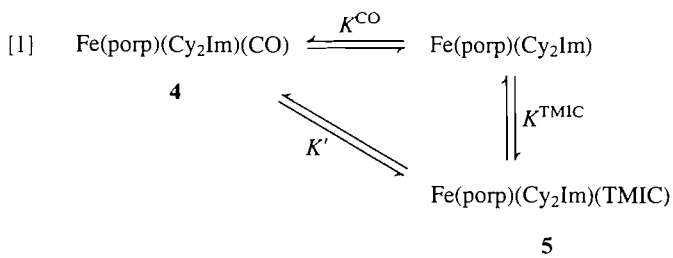

where $K' = K^{TMIC}/K^{CO}$.

The titrations are carried under a constant CO pressure (and concentration) which is chosen such that the carbonyl **4** is fully formed prior to the addition of the TMIC. Figure 2 illustrates the data for one such titration at a CO partial pressure of 24 Torr, which corresponds to a concentration of $2.4\times10^{-4}\ M$ (18). Again, a high [Cy_2Im] was maintained to ensure that neither TMIC nor CO displaced the axial imidazole base, and the isosbestic spectral changes observed both in the Soret (Fig. 2) and visible regions (500–600 nm) are entirely consistent with the equilibrium in which TMIC simply replaces CO under the cap.

The equilibrium expression for *K'* leads to eq. [2],

[2] $\log [\mathbf{5}]/[\mathbf{4}] = \log K' + \log [\text{TMIC}] - \log [\text{CO}]$

Can. J. Chem. Downloaded from www.nrcresearchpress.com by 78.46.186.204 on 09/07/12
For personal use only.

Can. J. Chem. Downloaded from www.nrcresearchpress.com by 78.46.186.204 on 09/07/12
For personal use only.

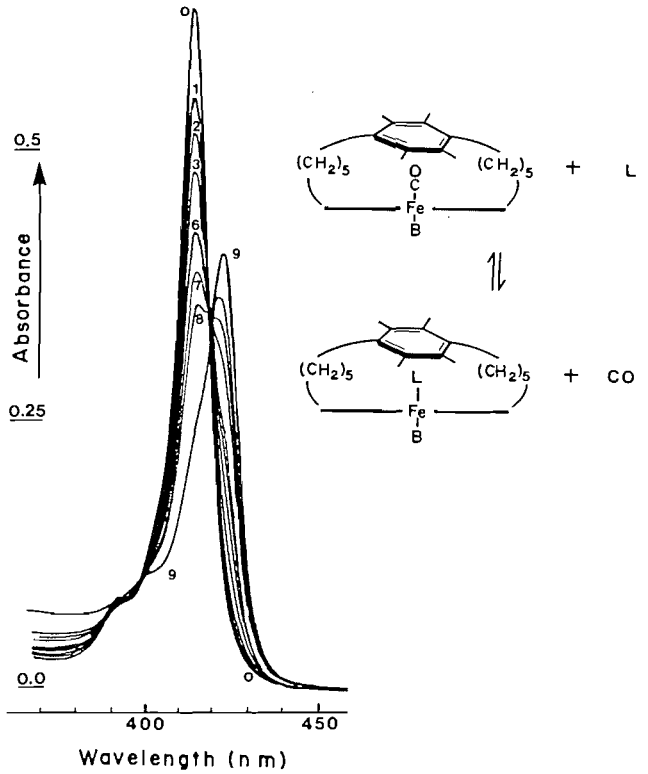

FIG. 2. Spectrophotometric titration (Soret region) of Fe(durene—5/5)(Cy_2Im)(CO) with TMIC at 20°C in toluene, under a CO pressure corresponding to [CO] = 2.4×10^{-4} *M*. Curves *0–9* (*4* and *5* are not shown) correspond to added [TMIC] = 0.0, 4.84, 6.92, 9.00, 11.10, 13.50, 16.90, 23.50, 33.59, and 200×10^{-4} *M*, respectively; B = Cy_2Im, L = TMIC.

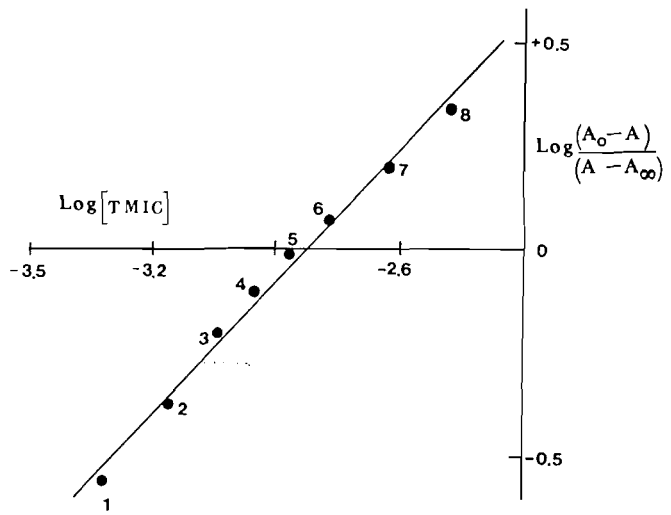

FIG. 3. Hill plot for the data of Fig. 2 at 415 nm (see text). The slope of the least-squares line drawn is 1.1, and the intercept on the *x* axis = log [CO] − log *K'*, which yields *K'* = 0.167; using $K^{CO} = 8.6 \times 10^7\ M^{-1}$ (Table 1) gives $K^{TMIC} = 1.4 \times 10^7\ M^{-1}$.

and a Hill plot of log [**5**]/[**4**] vs. log [TMIC] (Fig. 3) allows for an estimation of *K'*, and hence K^{TMIC} (±20%, Table 1). The [**5**]:[**4**] ratio is given simply by $(A_0 - A)/(A - A_\infty)$, where A_0 and A_∞ are the absorbances for pure **4** and pure **5**, respectively, and *A* is the absorbance of mixtures of **4** and **5** at any given [TMIC]; the slopes of the Hill plots were 1.0 ± 0.1.

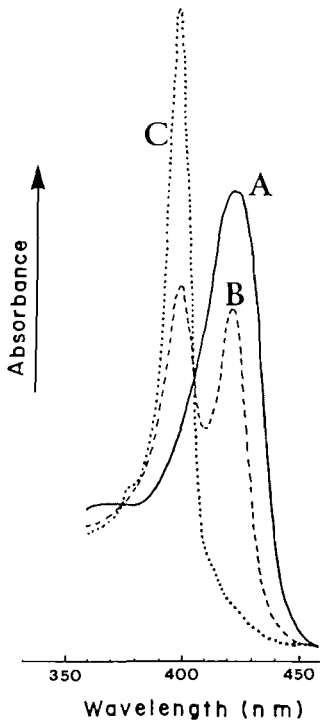

FIG. 4. Spectral trends for coordination of isocyanides to Fe(durene—4/4) species. **A** (—) is the spectrum of Fe(durene—4/4)(Cy_2Im); **B** (---) is the spectrum obtained on adding 0.02 *M* 'BuNC or TMIC to **A**; **C** (····) is the spectrum obtained on adding TMIC (at 10^{-3} *M*) to *in situ* Fe (durene—4/4), and is considered to be that of Fe(durene—4/4)(TMIC).

Durene—4/4 system

For the 5-coordinate Fe(durene—4/4)(Cy_2Im) species, a high [RNC] of ~0.02 *M* was necessary before any spectral change was observable at all, in contrast to the larger cap systems where binding was evidenced even for 'BuNC in the 10^{-5} *M* range. However, the blue shift to 400 nm observed for the 4/4-system (Fig. 4) is unlike the red shift changes seen for the coordination of isocyanides under the larger caps (ref. 11, and for example Fig. 2); indeed, the blue shift is similar to that obtained when TMIC is added to the 4-coordinate durene—4/4 heme in the absence of any other ligand (Fig. 4). Thus it seems certain that addition of 'BuNC or TMIC at sufficiently high concentration to Fe(durene—4/4)(Cy_2Im) results only in replacement of the imidazole by the isocyanide with no binding under the cap. Further support for this conclusion comes from qualitative binding studies with ^{n}BuNC, a sterically less

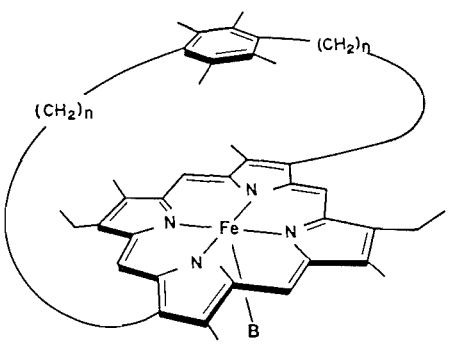

3: durene-capped 5-coordinate heme; B = imidazole base; *n* = 4, 5, 7, correspond to the durene—4/4, —5/5, and —7/7 species.

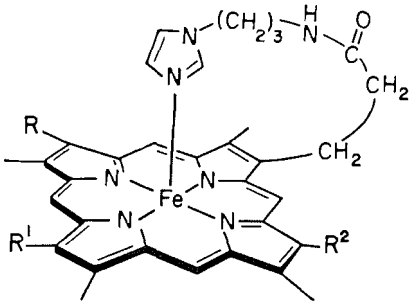

4: chelated protoheme; $R^1 = CH{=}CH_2$, $R^2 = CH_2CH_2CO_2CH_3$.

demanding isocyanide (1, 7); this readily binds to Fe(durene—4/4)(Cy_2Im) and gives the red-shifted spectral changes typically found for binding under the cap and formation of a 6-coordinate Fe(porp)(Cy_2Im)(RNC) (see above and ref. 11). The $K^{^nBuNC}$ value was about 50 M^{-1}.

Discussion

The data for the binding of the isocyanide probes TMIC and 'BuNC to the durene systems and anthracene and adamantane species, as well as to an unencumbered system (chelated protoheme, **4**), are summarized in Table 1. The chelated protoheme (1, 8), which encompasses a covalent attachment of the imidazole base to a side-chain of the porphyrin periphery, has an open, unhindered face for optimum binding of any isocyanide, and the terms "peripheral and central reduction factors" have been coined for other model hemes to indicate binding constants of TMIC and 'BuNC, respectively, relative to those for the chelated protoheme (1, 8). It is first noted that the data for the various durene systems reveal reduction factors of a very wide range that covers those reported for the anthracene and adamantane systems.

The data for the durene—7/7 and —5/5 systems are also shown in Scheme 1 which incorporates relative factors for these two systems. The most significant finding is the substantial reduction for the binding of 'BuNC relative to TMIC for both hemes (105- to 160-fold). According to Traylor's differentiation for the relative steric requirements of these isocyanides (1, 8), the results are readily interpreted in terms of a "central" steric effect imposed by the durene moiety in both heme systems. Examination of the consecutive reduction factors in the series: chelated protoheme → 7/7 → 5/5 reveals that the binding of 'BuNC is retarded 680-fold by the initial introduction of the central durene cap in the 7/7-complex, with a less pronounced reduction in affinity (120-fold) on shortening to the 5/5 strap. In the case of TMIC, however, peripheral steric interaction largely arises within the more enclosed environment of the 5/5-capped heme, 80-fold relative to an affinity reduction of 6.4-fold for the 7/7-complex.

Of interest, a further decrease in binding pocket size to the 4/4—durene capped heme severely retards coordination of either bulky isocyanide, where spectral changes characteristic of ligation under the cap are not observed. The less sterically demanding ^{n}BuNC can coordinate under the 4/4-cap.

It is interesting to note here a distinction between the durene—4/4 and anthracene—6/6 systems. Although the Fe(durene—4/4)(Cy_2Im) species shows a much reduced affinity for 'BuNC relative to that of Fe(anthracene—6/6)(MeIm), at least 150-fold, the durene heme shows about a 7-fold higher affinity for CO (Table 1). The pronounced porphyrin skeletal distortion inherent in the durene—4/4 heme complex presumably results in a "basket-shaped" 5-coordinate system where access to the iron is not obstructed significantly for a small diatomic (Fig. 5). In the case of the anthracene—6/6 system, the amide functions, which link the cap to the porphyrin periphery, probably add considerable rigidity to the distal hindrance provided by the cap, to the extent that accessibility to the metal is diminished even for diatomics. This suggestion is strongly supported by data that show a higher rate of CO association to the 5-coordinate durene—4/4 heme than to the anthracene system: $k = 3.0 \times 10^6\ M^{-1}\ s^{-1}$ (19) vs. $3.0 \times 10^4\ M^{-1}\ s^{-1}$ (1), both in toluene at 20°C. Nevertheless, the potential flexibility of the anthracene cap, having a larger number of adjoining atoms than the durene—4/4 heme, allows for coordination to some degree of even the bulkiest isocyanide, 'BuNC. The extremely restrictive distal cavity imposed by the tight cap in the durene—4/4 system does not allow for the required orientation for coordination of the bulky isocyanide.

These findings on the binding of the isocyanides to the durene-capped hemes will be invaluable in attempting to understand factors (steric and electronic) that govern the relative binding characteristics (kinetic and thermodynamic) of CO and O_2 to these hemes (19).

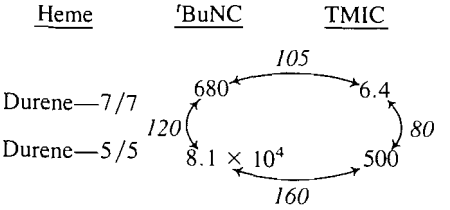

SCHEME 1. The relative factors (shown in *italics*) between the central and peripheral reduction factors for binding of 'BuNC and TMIC to the iron(II) durene—7/7 and —5/5 systems (shown in normal type).

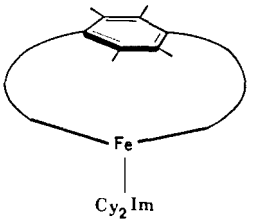

FIG. 5. Suggested "basket-shaped" conformation of distorted Fe(durene—4/4)(Cy_2Im) that could provide for greater accessibility of the Fe atom for incoming CO.

Acknowledgements

We thank the Natural Sciences and Engineering Research Council of Canada for support via an operating grant to B.R.J., and the National Institute of Health, U.S.A., for a grant (AM 17989) to D.D.

1. T. G. TAYLOR, S. TSUCHIYA, D. CAMPBELL, M. MITCHELL, D. STYNES, and N. KOGA. J. Am. Chem. Soc. **107**, 604 (1985), and references therein.
2. R. C. C. ST. GEORGE and L. PAULING. Science, **114**, 629 (1951).
3. S. AINSWORTH, Q. H. GIBSON, and F. J. W. ROUGHTON. Proc. R. Soc. London. Biol. Sci. **152**, 331 (1960).
4. M. BRUNORI, B. TALBOT, AL. COLOSIMO, E. ANTONINI, and J. WYMAN. J. Mol. Biol. **65**, 423 (1972).
5. F. STETZKOWSKI, R. CASSOLY, and R. BANERJEE. J. Biol. Chem. **254**, 11351 (1979).

Can. J. Chem. Downloaded from www.nrcresearchpress.com by 78.46.186.204 on 09/07/12
For personal use only.

6. P. I. REISBERG and J. S. OLSON. J. Biol. Chem. (*a*) **255**, 4144 (1980); (*b*) **255**, 4151 (1980); (*c*) **255**, 4159 (1980).
7. M. P. MIMS, A. G. PORRAS, J. S. OLSON, R. W. NOBLE, and J. A. PETERSON. J. Biol. Chem. **258**, 14219 (1983).
8. T. G. TRAYLOR, N. KOGA, L. A. DEARDURFF, P. N. SWEPSTON, and J. A. IBERS. J. Am. Chem. Soc. **106**, 5132 (1984).
9. S. DAVID, D. DOLPHIN, B. R. JAMES, J. B. PAINE, III, T. P. WIJESEKERA, F. W. B. EINSTEIN, and T. JONES. Can. J. Chem. **64**, 208 (1986).
10. S. DAVID, T. P. WIJESEKERA, J. B. PAINE, III, B. R. JAMES, and D. DOLPHIN. J. Org. Chem. To be published.
11. S. DAVID, B. R. JAMES, and D. DOLPHIN. J. Inorg. Biochem. In press.
12. (*a*) S. DAVID, B. R. JAMES, and D. DOLPHIN. Intern. Chem. Congr. Pacific Basin Socs. Honolulu, 1984. Abstract 10C25; (*b*) S. DAVID, T. P. WIJESEKERA, P. D. SMITH, D. DOLPHIN, and B. R. JAMES. 68th C.I.C. Meeting, Kingston, Ont. 1985. Abstract IN-C2-3.
13. S. DAVID, D. DOLPHIN, and B. R. JAMES. Frontiers in bioinorganic chemistry. *Edited by* A. V. Xavier. VCH, Weinheim. 1986. p. 163.
14. B. R. JAMES, K. J. REIMER, and T. C. T. WONG. J. Am. Chem. Soc. **99**, 4815 (1977).
15. D. V. STYNES, H. C. STYNES, B. R. JAMES, and J. A. IBERS. J. Am. Chem. Soc. **95**, 1796 (1973).
16. P. E. ELLIS, J. E. LINARD, T. SZYMANSKI, R. D. JONES, J. R. BUDGE, and F. BASOLO. J. Am. Chem. Soc. **102**, 1889 (1980).
17. T. HASHIMOTO, R. L. DYER, M. J. CROSSLEY, J. E. BALDWIN, and F. BASOLO. J. Am. Chem. Soc. **104**, 2101 (1982).
18. A. SEIDELL. Solubilities of inorganic and metal–organic compounds. Vol. 1, 3rd ed. Van Nostrand, New York, NY. 1970. p. 218.
19. S. DAVID. Ph.D. Dissertation. University of British Columbia. 1985; S. DAVID, B. R. JAMES, and D. DOLPHIN. To be published.

Can. J. Chem. Downloaded from www.nrcresearchpress.com by 78.46.186.204 on 09/07/12
For personal use only.

Extraction of alkali metal cations into polyester-based polyurethane foam using crown ether and picric acid

A. S. KHAN, W. G. BALDWIN, AND A. CHOW
Department of Chemistry, University of Manitoba, Winnipeg, Man., Canada R3T 2N2

Received October 17, 1986

This paper is dedicated to Professor Douglas E. Ryan on the occasion of his 65th birthday

A. S. KHAN, W. G. BALDWIN, and A. CHOW. Can. J. Chem. **65**, 1103 (1987).

The distribution of alkali metal picrates between water and polyester-based polyurethane foam in the presence of dicyclohexyl-18-crown-6 was studied. The order of extraction coefficients of the alkali metals is governed by the ratio of the cation size to that of the crown ether, although the degree of extraction may depend on the nature of the organic phase. The extraction of alkali metals by polyurethane foam from an aqueous solution in the presence of crown ether and a bulky anion can be considered as an ion pair extraction of MCrA by an organic solvent.

A. S. KHAN, W. G. BALDWIN et A. CHOW. Can. J. Chem. **65**, 1103 (1987).

On a étudié la distribution des picrates de métaux alcalins entre l'eau et des mousses de polyuréthanes contenant des polyesters, en présence de la dicyclohexyl 18-couronne-6. L'ordre des coefficients d'extraction des métaux alcalins est lié au rapport entre la taille du cation et celle de l'éther couronne, même si le degré d'extraction peut dépendre de la nature de la phase organique. On peut considérer que l'extraction des métaux alcalins, d'une solution aqueuse par de la mousse de polyuréthane, en présence d'un éther couronne et d'un anion volumineux, correspond à l'extraction d'une paire d'ions MCrA par un solvant organique.
[Traduit par la revue]

Can. J. Chem. Downloaded from www.nrcresearchpress.com by 78.46.186.204 on 09/07/12
For personal use only.

Due to their reluctance to form stable complexes with most complexing agents, the separation of alkali metals has been accomplished usually by ion exchange chromatography. Alternative precipitation procedures are not very selective and are generally not suitable for small quantities of alkali metals. Extractions of alkali metals reported before 1968 are almost all based on the ion association principle and used bulky anions (e.g. polyiodide (1), tetraphenyl borate (2), and phenols (3)). However, following the discovery of the complexing ability of macrocyclic polyethers (crown ethers), several studies on the solvent extraction of alkali metals by crown ethers have been reported.

The stability constants of various crown ether – cation complexes have been measured both in aqueous and in organic media by calorimetric titration techniques (4), by potentiometric measurements (5), and by spectrophotometric methods (6). On the basis of these studies, it has been concluded that the stability of the metal – crown ether complex is determined by the fit of the metal ion into the cavity of the ligand together with the charge of the cation and the nature of the solvent. Pedersen and Frensdorff (7) have reported that crown ethers containing five to ten oxygen atoms, each separated from the next by two carbon atoms, are the most effective complexing agents.

Jawid and Ingman (8) studied the extraction into dichloromethane of ion-pairs formed by alkali metal complexes of dicyclohexyl-18-crown-6 with a series of anions and concluded that the efficiency of extraction increases with large and highly polarizable anions. Frensdroff (9) has reported the extraction of sodium and potassium picrates from water into methylene chloride and into hexane using both isomer A and isomer B of dicyclohexyl-18-crown-6 (DCHC-6). He reported a higher value of K_{ex} for the potassium/picrate system containing isomer A than for that containing isomer B and also found that K_{ex} is one hundred times smaller in hexane than it is in methylene chloride. Jaber *et al.* (10) also have reported the extraction of alkali and alkaline earth metal picrates into methylene chloride using DCHC-6.

Sadakane *et al.* (11) studied the extraction of alkali metal picrates into benzene using dibenzo-18-crown-6 and found that the K_{ex} value increases, passes through a maximum at potassium, and then falls off as the size of the alkali metal cation increases further. They also noticed higher extraction of the cation in more polar solvents. Takeda and Goto (12) studied the extraction of monovalent metal picrates with 15-crown-5 and 18-crown-6 into benzene, and reported the following order for K_{ex} using 18-crown-6:

$$Tl^+ > K^+ > Rb^+ > Ag^+ > Cs^+ > Na^+ \gg Li^+$$

Although enhancement of extraction with increase in polarity of organic phase has been observed by most workers, Danesi *et al.* (13) have reported some interesting results from a study of the extraction of alkali metal picrates into different mixtures of nitrobenzene and toluene using dibenzo-18-crown-6. In 50:50 and 30:70 mixtures of nitrobenzene and toluene (dielectric constant, D = 15.6 and 10.6), K_{ex} was decreased with respect to pure nitrobenzene (D = 35). On the other hand, they observed an increase in the extraction for a 5:95 mixture of nitrobenzene and toluene (D = 3.4).

It is generally accepted that esters are more polar than ethers and it would be expected that this is also true for polyester versus polyether, although experimental values for the dielectric constants are not available. The use of polyester foam for the extraction of alkali metal cations was initiated because of the prospect of improving the degree of extraction over that obtained using polyether foam (14).

Experimental

Apparatus and reagents

Absorption measurements were made using a model 306 Perkin-Elmer atomic absorption spectrophotometer, analyzing for rubidium and cesium, or an Evans Electroselenium Ltd. flame photometer, analyzing for sodium and potassium. Measurements of pH were made using a Fisher Accumet model 520 digital pH meter.

Dicyclohexyl-18-crown-6 (DCHC-6) was obtained from Aldrich Chemical Co. and was used without further purification. No attempt was made to separate the two isomers, therefore the results are valid only for the isomeric mixture whose composition is not available from the supplier. Sodium chloride, potassium chloride, rubidium chloride, and cesium chloride salts were reagent grade. A 0.05 M solution of

picric acid was prepared from BDH reagent grade picric acid and standardized potentiometrically with sodium hydroxide. Water used was doubly distilled and deionized.

The polyester type polyurethane foam employed in this study is marketed as "Displo"$^{T.M.}$ foam plugs by Scientific Products, McGraw Park, IL, and was obtained locally from Canlab, Winnipeg.

Procedures

Polyurethane foam was cut into cubes weighing approximately 0.2 g each, soaked in 0.5 *M* HNO_3 for 12 h, washed several times with distilled water until free from acid, washed with acetone in a Soxhlet apparatus for 6 h, and finally air dried.

For each experiment, 40 mL of sample solution was equilibrated with a 0.2 g foam cube for 6 h at room temperature using the procedure described previously (14). The amount of metal extracted was determined by measuring the concentration before and after extraction with the foam, using atomic absorption or flame emission.

The distribution coefficient for metal ion is given by the ratio of the concentration of the metal ion on the foam to the concentration of the metal left in the solution at equilibrium and is equal to

$$[1]\quad D = \frac{\text{amount of metal on foam}}{\text{weight of foam}} \times \frac{\text{volume of solution}}{\text{amount of metal left in solution}}$$

Defined in this way, D has the units of volume per weight, i.e., of mL/g or L/kg.

The distribution coefficients between polyester-based polyurethane foam and water for crown ether, DCHC-6, and for picric acid were determined using the method previously reported (14). The average distribution coefficient for DCHC-6, (K'), was found to be 19 ± 7 L/kg while the value for picric acid, (D'), was determined to be 106 ± 19 L/kg.

Trial experiments showed little or no extraction of the metal ions if either the crown ether or picric acid was absent from the alkali metal solution.

Results and discussion

Extraction mechanism

Metal – picrate ion pairs have been extracted into both organic solvents like nitrobenzene (15) and into polyurethane foam (16). Similarly, the extraction of metal ions from aqueous solutions containing both picrate and crown ethers have been reported (14). Thus, the equilibria between an aqueous solution containing metal cation, M^+, the picrate anion, A^-, crown ether, Cr, and polyurethane foam can be written as:

$$M^+ + A^- \rightarrow MA_f \qquad K_{1ex} = [MA_f]/[M^+][A^-]$$

$$M^+ + Cr + A^- \rightarrow MCrA_f \qquad K_{2ex} = [MCrA_f]/[M^+][Cr][A^-]$$

where MA and MCrA denote the two ion pairs, the subscript f indicates the foam phase and the absence of subscript denotes the aqueous phase. The overall extraction equilibria can be analyzed in terms of the following equilibria:

(*i*) Ion-pair formation between metal ion and picrate ion

$$M^+ + A^- \rightarrow MA \qquad K_3$$

(*ii*) Extraction of the ion-pair between the two phases

$$MA \rightarrow MA_f \qquad K_{3ex}$$

(*iii*) Complexation of the metal ion with the crown ether

$$M^+ + Cr \rightarrow MCr^+ \qquad K_4$$

(*iv*) Ion-pair formation between the metal/crown ether complex and the picrate ion

$$MCr^+ + A^- \rightarrow MCrA \qquad K_5$$

(*v*) Distribution of the ion-pair between the two phases

$$MCrA \rightarrow MCrA_f \qquad K_{5ex}$$

(*vi*) Dissociation of the ion-pairs and the complexes in the organic phase

$$MCrA_f \rightarrow MCr^+{}_f + A^-{}_f \qquad K_{5d^*}$$

$$MCr^+{}_f \rightarrow M^+{}_f + Cr_f \qquad K_{4d^*}$$

$$MA_f \rightarrow M^+{}_f + A^-{}_f \qquad K_{3d^*}$$

The distribution relation is then:

$$D = \frac{\text{total metal on the foam per unit weight of foam}}{\text{total metal in solution per unit volume of solution}}$$

$$= \frac{[M^+{}_f] + [MA_f] + [MCr^+{}_f] + [MCrA_f]}{[M^+] + [MA] + [MCr^+] + [MCrA]}$$

Assuming equilibrium between crown ether in the aqueous solution and crown ether "dissolved" in the foam,

$$[Cr_f] = K'[Cr]$$

where [Cr] is the concentration of crown ether not complexed with the metal ion; $[Cr_f]$ is the "concentration" of crown ether in the foam. Similarly

$$[A_f] = D'[A]$$

Substituting,

$$[2]\quad D = \frac{K_{3d^*}K_{3ex}K_3/D' + K_{4d^*}K_{5d^*}K_{5ex}K_5K_4/D'K' + K_{5d^*}K_{5ex}K_5K_4[Cr]/D' + K_{3ex}K_3[A^-] + K_{5ex}K_5K_4[Cr][A^-]}{1 + K_3[A^-] + K_4[Cr] + K_5K_4[Cr][A^-]}$$

In deriving the above equation, the formation of only 1:1 complexes has been assumed. If complexes of higher stoichiometry are important, additional terms must be incorporated. In particular, if polynuclear complexes are important, one or more terms involving the metal ion concentration are required; that is, the distribution ratio, D, will vary with the concentration of the metal ion.

Extraction equilibrium constants

To test for polynuclear complexes, the extraction was studied as a function of crown ether concentration at three different total metal concentrations. In Fig. 1 it can be seen that the plots of log D as a function of the log of the initial crown ether concentration are coincident for the three different initial concentrations of potassium ion, indicating that the extraction is independent of metal ion concentration. This observation suggests that polynuclear species are not important in these solutions. This is consistent with the conclusions reached in the earlier study (14) of polyether-based polyurethane foam extraction.

To compare the extraction of alkali metal ion complexes by polyester-based polyurethane foam to the results obtained by the earlier study of polyether-based foams, the distribution coefficient, D, was studied as a function of initial crown ether concentration at constant metal ion and picric acid concentration (Fig. 2). The results show that the extraction of the cations

Can. J. Chem. Downloaded from www.nrcresearchpress.com by 78.46.186.204 on 09/07/12
For personal use only.

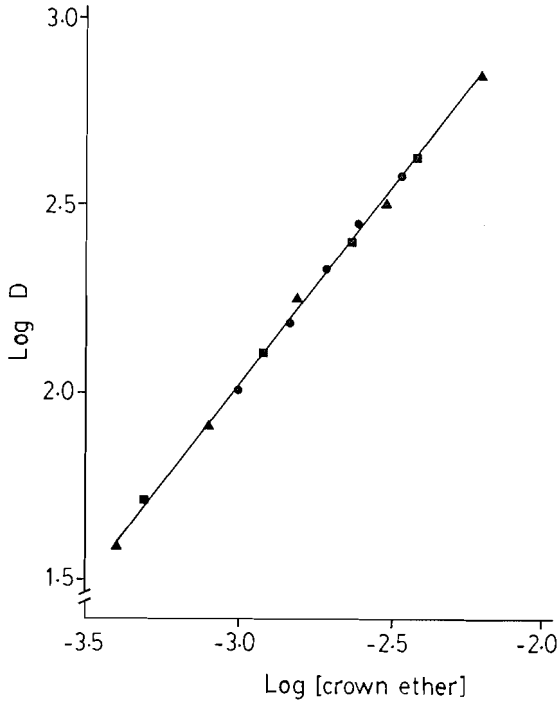

FIG. 1. Distribution ratio as a function of initial concentration of DCHC-6 at different concentrations of potassium: $K^+ = 0.25 \times 10^{-4}$ *M* (▲), 1×10^{-4} *M* (■), 2×10^{-4} *M* (●), [picric acid] = 4×10^{-3} *M*. Weight of foam 0.20 g, volume of solution 40 mL, temperature 25.00 ± 0.05°C; slope 1.045 ± 0.013; intercept 5.147 ± 0.036; correlation coefficient 0.999.

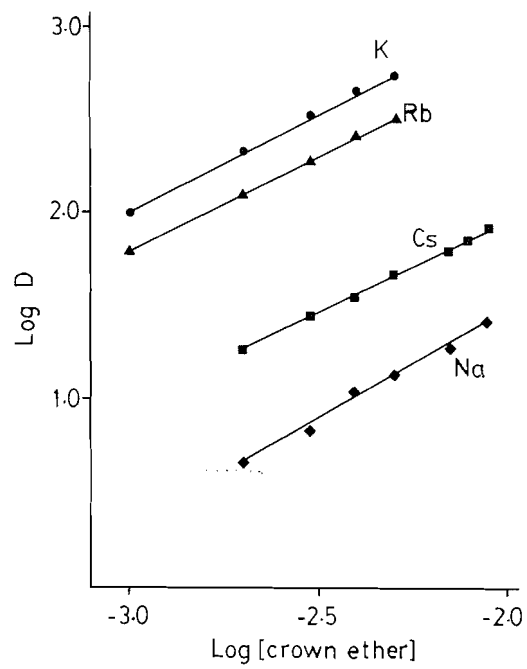

FIG. 2. Plots of log *D* vs. log [crown ether] for the distribution of alkali metal picrates between polyester foam and aqueous solution: Na^+ (◆), K^+ (●), Rb^+ (▲), Cs^+ (■), [cations] = 1×10^{-4} *M*, [picric acid] = 4×10^{-3} *M*. Weight of foam 0.20 g; volume of solution 40 mL; temperature 25.00 ± 0.05°C. K^+ slope 1.03 ± 0.04, intercept 5.10 ± 0.099, correlation coefficient 0.998; Rb^+ slope 1.03 ± 0.04, intercept 4.87 ± 0.101, correlation coefficient 0.998; Cs^+ slope 0.953 ± 0.032, intercept 3.832 ± 0.075, correlation coefficient 0.997; Na^+ slope 1.16 ± 0.06, intercept 3.780 ± 0.15, correlation coefficient 0.994.

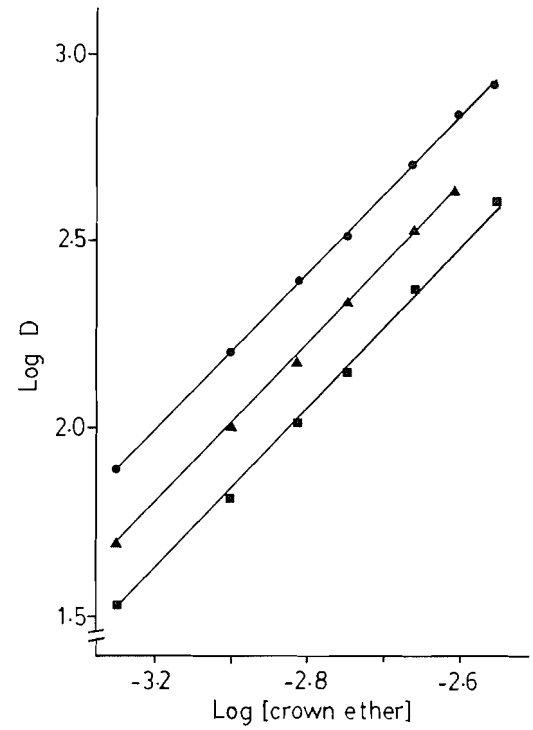

FIG. 3. Extraction of potassium as a function of initial concentration of crown ether at different initial concentrations of picric acid: [picric acid] = 2×10^{-3} *M* (■), 4×10^{-3} *M* (▲), 8×10^{-3} *M* (●); [potassium] = 1×10^{-4} *M*; volume of solution 40 mL; weight of foam 0.20 g; temperature 25.00 ± 0.05°C. 2×10^{-3} *M* slope 1.11 ± 0.03, intercept 5.162 ± 0.073, correlation coefficient 0.999; 4×10^{-3} *M* slope 1.05 ± 0.02, intercept 5.146 ± 0.067, correlation coefficient 0.999; 8×10^{-3} *M* slope 1.03 ± 0.01, intercept 5.298 ± 0.035, correlation coefficient 1.000.

studied increases with the increase in crown ether concentration and that the sequence of the extraction of alkali metal picrates using DCHC-6 is $K^+ > Rb^+ > Cs^+ > Na^+$. This same sequence was observed with polyether-based foam, but the magnitudes of extraction observed then were significantly lower, e.g., for K^+, $D = 536$ L/kg in polyester versus $D = 220$ L/kg in polyether foam for solutions both initially 4×10^{-3} *M* in picrate. The order of extraction can be attributed to the ability of DCHC-6 to complex these cations, whereas the higher magnitude of extraction is most likely due to the greater polarity of the polyester foam. This result is consistent with solvent extraction studies reported. Sadakane *et al.* (11) reported a higher extraction of potassium picrate using dibenzo-18-crown-6 in polar solvents such as isobutyl methyl ketone and nitrobenzene than in nonpolar benzene, while Frensdorff (9) reported that methylene chloride is a better solvent than benzene for the extraction of potassium picrate using dibenzo-18-crown-6.

The linear plots of approximately unit slope (Fig. 2) for the extraction of all alkali metal cations into polyester foam suggest a 1:1 crown ether:cation stoichiometry for the extracted complexes. Unit slope has been reported by several authors for the extraction of monovalent cations into various organic solvents using 18-crown-6 and its derivatives (11, 12, 17, 18). Takeda *et al.* (12, 17) studied the extraction of several monovalent metal picrates by 15-crown-5 and 18-crown-6 into benzene, and on the basis of slope analysis concluded that both crown ethers form 1:1 complexes with all metal cations studied.

Experiments were carried out under varied crown ether and

Can. J. Chem. Downloaded from www.nrcresearchpress.com by 78.46.186.204 on 09/07/12
For personal use only.

Can. J. Chem. Downloaded from www.nrcresearchpress.com by 78.46.186.204 on 09/07/12
For personal use only.

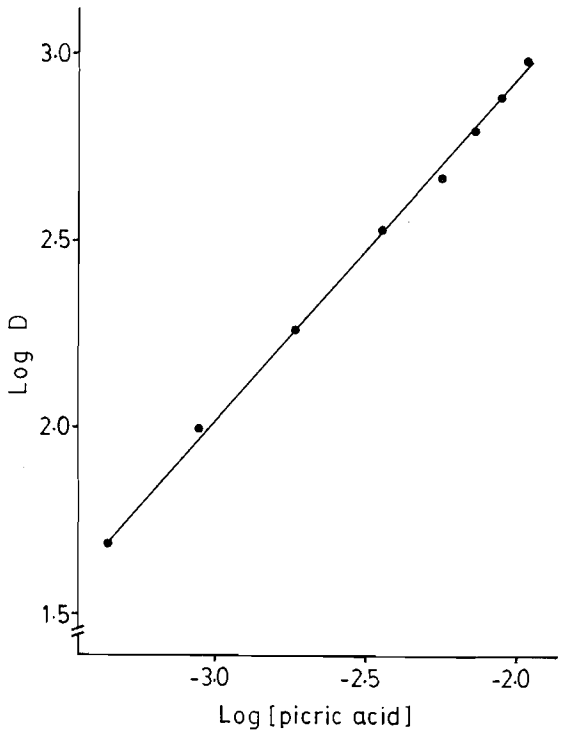

FIG. 4. Distribution ratio of potassium between polyester foam and aqueous picric acid solutions: $K^+ = 1 \times 10^{-4}$ *M*, DCHC-6 = 4×10^{-3} *M*; weight of foam 0.20 g; volume of solution 40 mL; temperature 25.00 ± 0.05°C; slope 0.912 ± 0.017; intercept 4.766 ± 0.043; correlation coefficient 0.999.

picrate concentrations to confirm the validity of 1:1 stoichiometry of complex formation between crown ether and metal cation over a wide range of picrate (anion) concentration. The extraction of potassium by DCHC-6 into polyester-based polyurethane foam was studied under three sets of experimental conditions differing in the initial concentration of picric acid. The results are shown in Fig. 3, where the logarithm of the distribution coefficient is plotted against the logarithm of the initial crown ether concentration. The linear plots of approximately unit slope further demonstrate that a 1:1 complex of crown ether and potassium is formed under these conditions of crown ether and picrate.

To verify the relationship between the metal ion and picrate ion, the extraction of potassium ion by DCHC-6 into polyester-based polyurethane foam was studied at constant potassium ion and at constant crown ether concentrations while varying the initial concentration of picric acid. The results of this experiment are shown in Fig. 4, where the logarithm of the distribution coefficient is plotted against that of the initial picric acid concentration. The linear plot of approximately unit slope suggests that the complex extracted has a stoichiometric ratio of picrate to metal ion of 1:1 under these conditions.

Evaluation of equilibrium constants

To evaluate the equilibrium constants using eq. [2], it is necessary to have an estimate of the concentrations of both the crown ether and the picrate which are in the aqueous solution and not bound to metal. Although these values can not be easily determined experimentally, the concentrations can be estimated. Yamane *et al.* (15) have reported values for the ion pair constants, K_3, and the extraction equilibrium constants, K_{3ex}, while Izatt *et al.* have given values for the metal – crown ether complex formation constants, K_4. The ion pair constants, K_5, have been estimated previously (14).

From the literature and the experimental results, the values of most of the constants needed can be obtained. However, there remains the difficulty of deciding the "free" (i.e. not bound to metal) concentrations of both picrate and crown ether in aqueous solution. These values have been estimated under five sets of assumptions: (*1*) The extraction of "free" or bound picrate and DCHC-6 is negligible with respect to the total concentrations. Therefore the "free" picrate and DCHC-6 concentrations are equal to the initial concentrations of these compounds. In the aqueous solution the amount of metal bound is also negligible. For this assumption $K_3[A^-]$, $K_4[Cr]$, and $K_5K_4[Cr][A^-] \ll 1$, $[A^-] = [A^-]_{initial}$, and $[Cr] = [Cr]_{initial}$. (*2*) Both the amount of bound metal and also the amounts of bound picrate and crown ether in the aqueous solution are negligible compared to the "free" concentrations. The "free" concentrations of picrate and DCHC-6 are corrected for the amount of these species extracted in the absence of metal ion. In this assumption, $K_3[A^-]$, $K_4[Cr]$, and $K_5K_4[Cr][A^-] \ll 1$, and $[Cr] = [Cr]_{initial}/(1 + K'w/v)$ and $[A^-] = [A^-]_{initial}/(1 + D'w/v)$, where w = weight of foam and v = volume of solution. (*3*) Similar assumptions as in *1* are made for "free" picrate and crown ether but consideration is given to the metal ion bound to only one of picrate or DCHC-6. For this assumption, $[A^-] = [A^-]_{initial}$, $[Cr] = [Cr]_{initial}$, and $K_5K_4[Cr][A^-] \ll 1$. (*4*) The same assumptions for "free" crown ether and picrate are made as in *2*, but also assumes that metal bound only to picrate or only to crown ether is important. Only $K_4K_4[Cr][A^-] \ll 1$. (*5*) A reduction in the concentrations of "free" picrate ion and DCHC-6 is made by accounting for the amount of each extracted in a 1:1:1 complex with the metal ion as well as that extracted in the absence of any metal. Further, it is assumed that $K_4[A^-]$ and $K_4[Cr]$ are not negligible compared to one. For this assumption, $K_5K_4[Cr][A^-] \ll 1$.

Table 1 shows representative data calculated using these assumptions with eq. [2]. Since in all cases, regardless of the set of assumptions used, the intercept is within one standard deviation of zero or is negative, it is reasonable to assume that there is negligible dissociation of the extracted complex in the foam and no significant extraction of the metal ion into the foam either on its own or bound only to picrate or only to crown ether. Therefore eq. [2] can be simplified to

$$D = \frac{K_{5ex}K_5K_4[Cr][A^-]}{1 + K_3[A^-] + K_4[Cr] + K_5K_4[Cr][A^-]}$$

Assumptions *1–4* effectively allow a plot of $D(1 + K_3[A^-] + K_4[Cr])$ versus the concentration of either initial crown ether or initial picrate, keeping the other constant. The slope is then the product of $K_{5ex}K_5K_4$ times the concentration of either DCHC-6 or picrate which was fixed for the calculation. With assumption *5*, it is necessary to plot $D(1 + K_3[A^-] + K_4[Cr])$ versus the product of the concentrations of both crown ether and picrate since these are varied simultaneously as the amount of metal extracted varies.

Despite the significant differences in the assumptions used it is interesting to note that the data in Table 1 gives values for the extraction coefficient K_{2ex} ($= K_{5ex}K_5K_4$) which are quite consistent (within a factor of three) for the individual metal ions.

The simplest assumption, *1*, overestimates the "free" concentrations and therefore leads to the lowest value for the

TABLE 1. Slope and intercept values from linear least-squares regression analysis of data from Fig. 2 (calculations done using the assumptions indicated in the text)

Ion	Assumption	Slope[a]	Intercept[a]	Correlation coefficient	$K_{5ex}K_5K_4$[a]
Na^+	1	$2.93 \pm 0.14 \times 10^3$	-1.49 ± 0.79	0.9952	$7.32 \pm 0.36 \times 10^5$
	2	3.21 ± 0.16	-1.49 ± 0.79	0.9952	12.3 ± 0.6
	3	3.70 ± 0.18	-2.77 ± 1.01	0.9951	9.25 ± 0.46
	4	3.90 ± 0.19	-2.63 ± 0.97	0.9951	14.9 ± 0.7
	5	$1.50 \pm 0.07 \times 10^6$	-2.65 ± 0.98	0.9951	15.0 ± 0.7
K^+	1	$1.052 \pm 0.045 \times 10^6$	4.37 ± 15.0	0.9972	$2.63 \pm 0.11 \times 10^7$
	2	1.151 ± 0.050	4.37 ± 15.0	0.9972	4.40 ± 0.19
	3	1.891 ± 0.053	-69.6 ± 17.7	0.9988	4.72 ± 0.14
	4	1.939 ± 0.054	-63.4 ± 16.3	0.9988	7.42 ± 0.20
	5	76.0 ± 2.1	-59.9 ± 16.0	0.9989	7.60 ± 0.21
Rb^+	1	$6.03 \pm 0.31 \times 10^4$	2.55 ± 10.13	0.9961	$1.51 \pm 0.08 \times 10^7$
	2	6.61 ± 0.34	2.55 ± 10.13	0.9961	2.53 ± 0.13
	3	9.32 ± 0.34	-10.6 ± 11.2	0.9980	2.34 ± 0.11
	4	9.34 ± 0.34	-9.70 ± 10.19	0.9980	3.57 ± 0.13
	5	$3.65 \pm 0.14 \times 10^7$	-9.11 ± 10.36	0.9979	3.65 ± 0.14
Cs^+	1	$8.41 \pm 0.36 \times 10^3$	1.27 ± 2.14	0.9954	$2.10 \pm 0.09 \times 10^6$
	2	9.21 ± 0.40	1.27 ± 2.14	0.9954	3.52 ± 0.16
	3	13.94 ± 0.63	-1.59 ± 3.74	0.9949	3.49 ± 0.15
	4	13.62 ± 0.62	-1.49 ± 3.34	0.9949	5.21 ± 0.24
	5	$5.26 \pm 0.24 \times 10^6$	-1.60 ± 3.37	0.9948	5.26 ± 0.24

[a] Value ± one standard deviation given.

TABLE 2. "Best" combinations of equilibrium constants, K, for alkali metal ion – crown ether – picrate extraction

Cation	K_3[a] / L mol^{-1}	K_{3ex}	K_4[b] / L mol^{-1}	K_5[c] / L mol^{-1}	$K_{5ex}K_5K_4$ / L^3 mol^{-2} kg^{-1}	Organic phase	Reference
Na^+	24	—	16	0.77	$1.5 \pm 0.4 \times 10^6$	Polyester	This work
Na^+			16	0.77	4.0×10^5	Polyether	14
Na^+	24	0.0028				Nitrobenzene	15
K^+	44	—	104	0.85	$7.9 \pm 2.1 \times 10^7$	Polyester	This work
K^+			104	0.85	9.6×10^6	Polyether	14
K^+	44	0.014				Nitrobenzene	15
Rb^+	87	—	34	0.88	$3.7 \pm 1.0 \times 10^7$	Polyester	This work
Rb^+			34	0.88	4.4×10^6	Polyether	14
Rb^+	87	0.022				Nitrobenzene	15
Cs^+	117	—	17	0.94	$5.3 \pm 1.4 \times 10^6$	Polyester	This work
Cs^+			17	0.94	8.8×10^5	Polyether	14
Cs^+	117	0.068				Nitrobenzene	15

[a] K_3 from ref. 15.
[b] K_4 from ref. 4.
[c] K_5 from ref. 14.

extraction coefficient. The extraction coefficient calculated using assumption *5* is the highest value and is most likely as it reflects a closer approximation to the actual concentrations of the species in the solution.

In Table 2, the "best" values (i.e. those resulting from assumption *5*) are listed. From several replicates done using potassium ion the uncertainty in its extraction coefficient can be estimated at about 25%. A similar uncertainty is assumed for the other ions in the listed values.

Conclusions

This study has demonstrated the ability of polyester-based polyurethane foam to extract alkali metal cations from aqueous solution using DCHC-6 in the presence of picrate ions. The ratios of the distribution coefficients for the alkali metals are about 1:3:21:40 for Na^+:Cs^+:Rb^+:K^+ from the data used for Fig. 2. This indicates that each of the ions should be separable from the others and that a column of polyester-based polyurethane foam could be used to separate all of these ions.

The efficiency of the extraction depends on the nature of the organic phase, with extraction into the more polar polyester foam being greater than into the less polar polyether foam. The same order of K_{ex} of alkali metals obtained for both polyester and polyether foams suggests that although the degree of extraction may depend on the nature of the organic phase, the order of extractability may be governed by the ratio of the cation size to that of the crown ether cavity. Similar results have been reported for ion pair extraction of metal – crown ether – picrate

Can. J. Chem. Downloaded from www.nrcresearchpress.com by 78.46.186.204 on 09/07/12
For personal use only.

in various organic solvents (7, 8, 11). This similarity suggests that the extraction of alkali metals from an aqueous solution by polyurethane foam in the presence of crown ether and a bulky anion, can be considered as an ion pair extraction of MCrA by an organic solvent. However, in contrast to previous reports (19) that polyether is a better extractor than is polyester foam, it is clear from the $K_{5ex}K_5K_4$ values (Table 2) that the opposite is true here. This study also reveals that there is no appreciable dissociation of the extracted complex in the polyester foam. It is hoped that these studies have led to a better understanding of the mechanism of extraction with the use of polyurethane foam.

Acknowledgement

This work was supported by the Natural Sciences and Engineering Research Council of Canada.

1. A. Ituku. Bull. Chem. Soc. Jpn. **39**, 465 (1966).
2. T. Sekine and D. Dyrssen. Anal. Chim. Acta, **45**, 433 (1969).
3. W. J. Ross and J. C. White. Anal. Chem. **36**, 1998 (1964).
4. R. M. Izzat, D. P. Nelson, J. R. Rything, B. L. Haymore, and T. J. Christensen. J. Am. Chem. Soc. **93**, 1619 (1971).
5. H. K. Frensdorff. J. Am. Chem. Soc. **93**, 600 (1971).
6. J. J. Christensen, J. D. Eatough, and R. M. Izzat. Chem. Rev. **74**, 351 (1974).
7. C. J. Pedersen and H. D. Frensdorff. Angew. Chem. Int. Ed. **11**, 16 (1972).
8. M. Jawaid and F. Ingman. Talanta, **25**, 91 (1978).
9. H. D. Frensdorff. J. Am. Chem. Soc. **93**, 4684 (1971).
10. A. M. Y. Jaber, G. J. Moody, and J. D. R. Thomas. J. Inorg. Nucl. Chem. **39**, 1689 (1977).
11. A. Sadakane, T. Iwachido, and K. Toei. Bull. Chem. Soc. Jpn. **48**, 60 (1975).
12. Y. Takeda and H. Goto. Bull. Chem. Soc. Jpn. **52**, 1920 (1979).
13. P. R. Danesi, H. M. Gorilan, R. Chiaizia, and G. Seibona. J. Inorg. Nucl. Chem. **37**, 1479 (1975).
14. A. S. Khan, W. G. Baldwin, and A. Chow. Can. J. Chem. **59**, 1490 (1981).
15. M. Yamane, T. Iwachido, and K. Toei. Bull. Chem. Soc. Jpn. **44**, 745 (1971).
16. A. S. Khan, W. G. Baldwin, and A. Chow. Anal. Chim. Acta, **146**, 201 (1983).
17. Y. Takeda and H. Kato. Bull. Chem. Soc. Jpn. **52**, 1027 (1979).
18. T. Iwachido, A. Sadakane, and K. Toei. Bull. Chem. Soc. Jpn. **51**, 629 (1978).
19. R. F. Hamon. Ph.D. Thesis, Chemistry Department, University of Manitoba. 1981.

Can. J. Chem. Downloaded from www.nrcresearchpress.com by 78.46.186.204 on 09/07/12
For personal use only.

How does the geometry of the tetrahedral $XF_{4-n}Cl_n^{\epsilon}$ (X = Al, Si, P) species depend on composition, or *ab initio si certum nescio*

S. C. Choi, Russell J. Boyd, and Osvald Knop
Department of Chemistry, Dalhousie University, Halifax, N.S., Canada B3H 4J3

Received November 2, 1986

This paper is dedicated to Professor Douglas E. Ryan on the occasion of his 65th birthday

S. C. Choi, Russell J. Boyd, and Osvald Knop. Can. J. Chem. **65**, 1109 (1987).

The molecular parameters of the isoelectronic tetrahedral species NaF_4^{3-}, MgF_4^{2-}, $AlF_{4-n}Cl_n^-$, $SiF_{4-n}Cl_n$, $PF_{4-n}Cl_n^+$, SF_4^{2+}, and ClF_4^{3+} have been investigated by *ab initio* calculations at the 6-31G* level. The bond lengths and the critical radii of X in XF_4^{ϵ} are found to decrease monotonically with the formal oxidation state m of X up to and including X = S but show an upturn at X = Cl. The relative position of the critical point in the X—F bond, $r_c(X)/(X—F)$, remains relatively constant for m = 1–3; for m = 4–6 the critical point moves gradually closer to X, but for m = 7 it shifts appreciably away from X. The increase in the electron density at the bond critical point of XF_4^{ϵ} (and probably also of XCl_4^{ϵ}) is represented reasonably closely by a power function am^b. The effect of progressive replacement of F in XF_4^{ϵ} (X = Al, Si, P) by Cl on the bond lengths and angles depends on the sign of ϵ. For $\epsilon = -1$, X—F and X—Cl decrease and FXF increases; for ϵ = 0 and 1, X—F and X—Cl increase and FXF decreases. These changes increase in magnitude, in their respective directions, with $|\epsilon|$. Relationships between the bond lengths and the bond angles are described. The excess total electronic energies $\Delta E = E(XF_{4-n}Cl_n^{\epsilon}) - \frac{1}{4}(4-n)E(XF_4^{\epsilon}) - \frac{1}{4}nE(XCl_4^{\epsilon})$ are negative for all three X; they are largest (and approximately symmetric with respect to n) for Al, smaller (and asymmetric) for P, and very small for Si. The amount of charge transferred from F or Cl to X varies in a complicated manner with m and n, and the rates of transfer of charge with n in an $XF_{4-n}Cl_n^{\epsilon}$ molecule are not the same for F and Cl. More than one unit of charge is transferred from a halogen atom to X in ClF_4^{3+} and PCl_4^+.

S. C. Choi, Russell J. Boyd et Osvald Knop. Can. J. Chem. **65**, 1109 (1987).

Utilisant des calculs *ab initio* au niveau 6-31G*, on a étudié les paramètres moléculaires des espèces tétraédriques isoélectroniques NaF_4^{3-}, MgF_4^{2-}, $AlF_{4-n}Cl_n^-$, $SiF_{4-n}Cl_n$, $PF_{4-n}Cl_n^+$, SF^{2+} et ClF_4^{3+}. On a trouvé que, dans XF_4^{ϵ}, les longueurs des liaisons ainsi que les rayons critiques de X diminuent d'une façon monotone avec l'état d'oxydation formel m de X, jusqu'à X = S; toutefois, ces valeurs augmentent lorsque X = Cl. La position relative du point critique de la liaison X—F, $r_c(X)/(X—F)$, demeure constante pour m = 1 à 3; toutefois, pour m = 4 à 6, le point critique se déplace graduellement vers X alors que pour m = 7, il s'éloigne considérablement de X. L'augmentation de la densité électronique au point critique de la liaison des composés XF_4^{ϵ} (et probablement aussi dans les composés XCl_4^{ϵ}) peut être représentée d'une façon assez raisonnable en faisant appel à une fonction du type am^b. Si on remplace progressivement des F par des Cl dans les composés XF_4^{ϵ} (X = Al, Si, P), l'effet qui se fait sentir sur les longueurs ainsi que sur les angles de liaison dépend du signe de ϵ. Pour $\epsilon = -1$, les liaisons X—F et X—Cl diminuent alors que FXF augmente; pour ϵ = 0 et 1, les longueurs X—F et X—Cl augmentent alors que FXF diminue. Ces changements augmentent en amplitude, dans leurs directions respectives, avec $|\epsilon|$. On décrit les relations qui existent entre les longueurs des liaisons et les angles de liaisons. Pour chacun des X, les énergies électroniques totales en excès, $\Delta E = E(XF_{4-n}Cl_n^{\epsilon} - \frac{1}{4}(4-n)E(XF_4^{\epsilon}) - \frac{1}{4}nE(XCl_4^{\epsilon})$ sont négatives; ces valeurs sont les plus grandes (et approximativement symétriques par rapport à n) pour les composés du Al, alors qu'elles sont plus petites (et asymétriques) pour les composés du P et qu'elles sont très faibles pour les composés du Si. La quantité de charge qui est transférée du F ou du Cl vers X varie d'une façon compliquée avec m et n; dans une molécule $XF_{4-n}C_n^{\epsilon}$, les variations des vitesses de transfert de charges avec n ne sont pas les mêmes avec F et avec Cl. Dans les cas des composés ClF_4^{3+} et PCl_4^+, il y a plus d'une unité de charge qui est transférée d'un atome d'halogène X.

[Traduit par la revue]

The purpose of this investigation is to discover, and subsequently predict, trends that may exist in the geometric and other molecular parameters in series of isoelectronic tetrahedral $XF_{4-n}Cl_n^{\epsilon}$ species. Experimentally determined values of bond lengths and bond angles for the mixed species are available only for X = C, Si, and Ge (refs. 1–15; Table 1). They are generally of insufficient accuracy and show a considerable scatter. However, they do suggest that the X—F and X—Cl bond lengths increase with n. The low accuracy makes comparisons of the FXF and ClXCl angles even more tentative, but it is thought (e.g. ref. 13) that in $CF_{4-n}Cl_n$ the FCF angle is always the smallest. It came therefore as a surprise when it turned out, in our recent investigation of $AlF_{4-n}Cl_n^-$ species by *ab initio* calculations, that the opposite is true in this case: the Al—F and Al—Cl bond lengths *decrease* with increasing n, and for the bond angles actually present the sequence, for a given n, is FAlF > FAlCl > ClAlCl. This finding demonstrated that it was desirable not only to verify, by calculation, the trends believed to exist for X = C, Si, and Ge, but also to extend the calculations for Al to at least X = P. We have now investigated the complete series for X = Al, Si, P and, in addition, the pure species NaF_4^{3-}, MgF_4^{2-}, SF_4^{2+}, and ClF_4^{3+}, with the results reported below. The corresponding systematic calculations for X = B, C, and N are contemplated for the near future; they are required for determining the importance of orbital size for the trends now established for elements of the second row.

Method

The main objective was to obtain an internally consistent systematic comparison of equilibrium molecular geometries that on a reasonable expectation would be closely similar. The 6-31G* basis set was thought well suited for the task in hand, as mean absolute differences between the experimental and theoretical bond lengths were expected, from previous experience, to be about 0.01–0.02 Å (23). This basis set, or more precisely, the 6-31G* set for fluorine (24) and 66-31G* for the second-row elements (23), was therefore used for all calculations. The validity of this choice is borne out by the good

Can. J. Chem. Downloaded from www.nrcresearchpress.com by 78.46.186.204 on 09/07/12
For personal use only.

TABLE 1. Literature values of bond lengths and bond angles in $XF_{4-n}Cl_n^{\epsilon}$ species[a]

Species	Method[b]	X—F	X—Cl	FXF	FXCl	ClXCl
AlF_4^-	xl[c]	⟨1.66⟩	—		—	—
$AlCl_4^-$	xl[d] (18)	—	⟨2.15(1)⟩	—	—	
SiF_4	ed (14)	1.554(4)	—	τ	—	—
	xl[e] (19)	1.56(1)	—		—	—
	STO-3G (16)	1.5845	—	τ	—	—
	3-21G (16)	1.5843	—	τ	—	—
SiF_3Cl	mw (3)	1.560(10)	1.989(25)	108.5[f]		—
$SiFCl_3$	mw (11)	1.520(5)	2.019(3)	—	109.55(50)	109.36(50)
$SiCl_4$	ed (12)	—	2.019(9)	—	—	τ
	STO-3G (16)	—	2.0708	—	—	τ
	3-21G (16)	—	2.1232	—	—	τ
PCl_4^+	xl[g] (20)	—	⟨1.944(6)⟩	—	—	
	xl[h] (21)	—	⟨1.93(4)⟩	—	—	
	pseudopot. (22)	—	2.001	—	—	τ

[a]Bond lengths in Å, bond angles in deg. Bond lengths in crystals will depend on the bond strengths of the Hal ligands and would have to be extrapolated to "free"-species values if they are to be compared with the calculated values.
[b]Abbreviations as follows: ed, electron diffraction; mw, microwave spectroscopy; xl, crystal structure.
[c]Estimated from AlO_4^{5-} (cf. ref. 17).
[d]Mean of Al—Cl distances in nine compounds, corrected for therml motion.
[e]At −145°C.
[f]Assumed.
[g]Mean of 12 values from three compounds, corrected for thermal motion.
[h]Uncorrected mean of P—Cl distances in $(PCl_4)VCl_5$.

TABLE 2. The energies E (au), bond lengths (Å), and bond angles (deg) of $XF_{4-n}Cl_n^{\epsilon}$ species[a]

		Bond length		Bond angle		
Species	E	X—F	X—Cl	FXF	FXCl	ClXCl
NaF_4^{3-}	−559.22471	2.4300	—	τ	—	—
MgF_4^{2-}	−597.47760	1.8742	—	τ	—	—
AlF_4^-	−640.03991	1.6769	—	τ	—	—
AlF_3Cl^-	−1000.09285	1.6678	2.2055	110.36	108.58	—
$AlF_2Cl_2^-$	−1360.14191	1.6624	2.1879	110.87	109.22	109.06
$AlFCl_3^-$	−1720.18767	1.6594	2.1765	—	109.54	109.40
$AlCl_4^-$	−2080.23052	—	2.1694	—	—	τ
SiF_4	−686.94982	1.5571	—	τ	—	—
SiF_3Cl	−1046.97445	1.5606	2.0066	108.77	110.16	—
SiF_2Cl_2	−1406.99884	1.5650	2.0130	108.06	109.22	111.88
$SiFCl_3$	−1767.02296	1.5704	2.0205	—	108.28	110.69
$SiCl_4$	−2127.04702	—	2.0289	—	—	τ
PF_4^+	−738.27238	1.4795	—	τ	—	—
PF_3Cl^+	−1098.30802	1.4925	1.8989	107.15	111.79	—
$PF_2Cl_2^+$	−1458.34090	1.5052	1.9164	105.13	109.23	114.79
$PFCl_3^+$	−1818.37287	1.5183	1.9341	—	106.94	112.00
PCl_4^+	−2178.40557	—	1.9520	—	—	τ
SF_4^{2+}	−794.10380	1.4391	—	τ	—	—
ClF_4^{3+}	−854.58542	1.4802	—	τ	—	—

[a]The symmetry is T_d for $n = 0$ and 4, C_{3v} for $n = 1$ and 3, and C_{2v} for $n = 2$; τ = 109.471°.

agreement between the observed and the calculated values of the bond lengths for X = Si (Tables 1 and 2; see below).

The calculations were carried out using the GAUSSIAN 80 set of programs (25) on a Perkin-Elmer 3230 computer. Net atomic charges were computed from standard Mulliken population analyses (26) and bond critical points were investigated using the AIMPAC series of programs (27). Complete geometry optimizations, subject to the symmetries listed in Table 2, were performed for all species.

The energies, bond lengths, and bond angles are listed in Table 2, critical radii, net charges, and electron densities at the critical points in Table 3.

Notation

The symbols used are defined as follows: f, number of degrees of freedom; m, oxidation state of X; p, number of data; ϵ, charge on the $XF_{4-n}Cl_n^{\epsilon}$ molecule; τ, the tetrahedral angle; E, total electronic energy (au); $\Delta E(n)$, excess energy (au), $\Delta E(n) = E[XF_{4-n}Cl_n^{\epsilon}] - [1 - (n/4)]E(XF_4^{\epsilon}) - (n/4)E(XCl_4^{\epsilon})$; $E_f(0)$, $E_f(4)$, energy of formation (au) of XF_4^{ϵ}

Can. J. Chem. Downloaded from www.nrcresearchpress.com by 78.46.186.204 on 09/07/12
For personal use only.

TABLE 3. Critical radii r_c (Å), net charges (e), and electron densities at the critical points $\rho(r_c)^F$ and $\rho(r_c)^{Cl}$ (au) for $XF_{4-n}Cl_n^{\epsilon}$ species[a]

Species	Critical radius		Net charge				
	$r_c(X)^F$	$r_c(X)^{Cl}$	$\epsilon(X)$	$\epsilon(F)$	$\epsilon(Cl)$	$\rho(r_c)^F$	$\rho(r_c)^{Cl}$
NaF_4^{3-}	1.0815	—	0.230	−0.808	—	0.01485	—
MgF_4^{2-}	0.8341	—	0.880	−0.720	—	0.05298	—
AlF_4^-	0.7239	—	1.535	−0.634	—	0.09287	—
AlF_3Cl^-	0.7205	0.8150	1.427	−0.615	−0.581	0.09557	0.05420
$AlF_2Cl_2^-$	0.7184	0.8091	1.274	−0.598	−0.539	0.09720	0.05722
$AlFCl_3^-$	0.7172	0.8051	1.090	−0.582	−0.503	0.09806	0.05932
$AlCl_4^-$	—	0.8026	0.882	—	−0.471	—	0.06071
SiF_4	0.6502	—	1.855	−0.464	—	0.14144	—
SiF_3Cl	0.6514	0.7144	1.641	−0.455	−0.275	0.13988	0.11053
SiF_2Cl_2	0.6528	0.7165	1.421	−0.446	−0.264	0.13800	0.10935
$SiFCl_3$	0.6545	0.7189	1.188	−0.436	−0.251	0.13575	0.10793
$SiCl_4$	—	0.7216	0.931	—	−0.233	—	0.10631
PF_4^+	0.5972	—	2.040	−0.260	—	0.20214	—
PF_3Cl^+	0.6014	0.6606	1.752	−0.279	0.086	0.19429	0.18428
$PF_2Cl_2^+$	0.6054	0.6678	1.448	−0.294	0.070	0.18720	0.17753
$PFCl_3^+$	0.6095	0.6758	1.097	−0.305	0.069	0.18058	0.17113
PCl_4^+	—	0.6848	0.662	—	0.084	—	0.16496
SF_4^{2+}	0.5625	—	2.218	−0.054	—	0.27586	—
ClF_4^{3+}	0.6709	—	2.456	0.136	—	0.34642	—

[a]Dipole moments have been obtained for $SiF_{4-n}Cl_n$: n = 1, 0.200 D; n = 2, 0.290 D; n = 3, 0.302 D.

Can. J. Chem. Downloaded from www.nrcresearchpress.com by 78.46.186.204 on 09/07/12
For personal use only.

and XCl_4^{ϵ}, respectively: $E_f(0) = E(XF_4^{\epsilon}) - E(X^{m+}) - 4E(F^-)$, $E_f(4) = E(XCl_4^{\epsilon}) - E(X^{m+}) - 4E(Cl^-)$; $\epsilon(X)_n$, $\epsilon(F)_n$, $\epsilon(Cl)_n$, net charges (e) on X, F, and Cl, respectively; $\epsilon(X)_n + (4 - n)\epsilon(F)_n + n\epsilon(Cl)_n = \epsilon = m - 4$; $r_c(X)_n^F$, $r_c(X)_n^{Cl}$, critical radius (Å) of X in an X—F and an X—Cl bond, respectively; $r_c(F)_n$, $r_c(Cl)_n$, critical radii of F and Cl, respectively; $r^{iv}(X^{m+})$, Shannon's (28) effective ionic radius (Å) of X^{m+} in 4-coordination; $\rho(r_c)_n^F$, $\rho(r_c)_n^{Cl}$, electron density (au) at the critical point in an X—F and an X—Cl bond, respectively; $\rho(r_c)_0$ for XF_4^{ϵ}, $\rho(r_c)_4$ for XCl_4^{ϵ}.

Validity of the results

Because of the paucity of experimental results for $XF_{4-n}Cl_n^{\epsilon}$ species we can assess the overall accuracy of our calculated values of the molecular parameters only with reference to Table 1. The experimental values of bond lengths listed there correlate linearly ($r^2 = 0.996$) with the calculated values to a σ of 0.016 Å. This must be regarded as a satisfactory agreement. The discrepancies originate mainly in the bond lengths in crystals, which are subject to a variety of constraints not considered in the calculations. It may be noted that the agreement of the observed and the calculated X—Hal distances, where the former are available, is significantly better than for previous theoretical calculations.

No estimate can be provided for the absolute accuracy of the $E(XF_{4-n}Cl_n^{\epsilon})$, but where values for the single atoms close to the Hartree–Fock limit are available (29, 30), the differences are not negligible (Table 4).

The 6-31G* energies $E(X^{m+})$ can be adequately represented by $E(X^{m+}) = -128.483722 - 31.158188m - 2.0027179m^2$ ($r^2 = 1.000$, $\sigma = 0.0075$ au ~ 4.7 kcal/mol $\sim 0.002\%$ of the m = 0–8 range). This representation is approximately of the form $-a(m + b)^2 \sim -2(m + 8)^2$. A significant reduction of σ is obtained by omitting Ne^0 (m = 0) from the regression ($\sigma = 0.0040$ au). A cubic regression including Ne^0 improves σ only marginally, but if Ne^0 is not included, a dramatic drop in σ results:

TABLE 4. Electronic energies (au) of selected atoms and ions

Atom	E(6-31G*)	E(~HF limit)[a]	Difference
Ne^0	−128.47441	−128.54705	0.07264
Na^0	−161.84144	−161.85890	0.01746
Na^+	−161.65929	−161.67692	0.01763
Mg^{2+}	−198.81210	(−198.83051)	(0.01841)
Al^{3+}	−239.97887	(−240.00001)	(0.02114)
Si^{4+}	−285.15631	(−285.18058)	(0.02427)
P^{5+}	−334.34116	(−334.36932)	(0.02816)
S^{6+}	−387.53159	(−387.56427)	(0.03268)
Cl^{7+}	−444.72581	(−444.76411)	(0.03830)
Ar^{8+}	−505.92316	(−505.96783)	(0.04467)
F^0	−99.36496	−99.40930	0.04434
F^-	−99.35048	−99.45937	0.10889
Cl^0	−459.44796	−459.48187	0.03391
Cl^-	−459.52600	−459.57670	0.05070

[a]These values are from ref. 29; those in parentheses (somewhat lower level of theory) are from ref. 30.

[1] $E(X^{m+}) = -128.52000 - 31.130826m - 2.0084983m^2 + 0.00036657m^3$

($r^2 = 1.000$, $\sigma = 0.0006$ au ~ 0.38 kcal/mol). Considering the magnitude of $E(X^{m+})$, this goodness of fit (and for that matter even that for the parabolic regression) must be regarded as remarkable. The reason for the $E(Ne^0)$ value not fitting satisfactorily into this regression is at present not understood.[1]

The ionization potential of Na calculated from the E values of Table 4 is within 4% of the experimental value, but the electron

[1]A cubic regression of the E(~HF limit) values of Table 4 on m gives a similar result: $r^2 = 1.000$, $\sigma = 0.0018$ au for m = 0–8, and $r^2 = 1.000$, $\sigma = 0.0008$ au for m = 1–8.

affinities calculated for F and Cl agree poorly with experiment even for E(~HF limit):

Parameter	Value		
	6-31G*	~HF limit	Expt.
Na (ionization potential), eV	4.957	4.952	5.139
F (electron affinity), eV	−0.394	1.363	3.448
Cl (electron affinity), eV	2.124	2.581	3.613

However, because of our particular choice of basis set, the deficiencies of the model used in the energy optimization, which manifest themselves with high visibility in the parameters deriving directly from the E values for single atoms, appear to be much less reflected in the values of the geometric parameters of the $XF_{4-n}Cl_n^{\epsilon}$ species. It should be noted that the smooth trends of the parameters described below emerge on assembling the results of calculations performed separately for each of the individual species. We therefore believe that these trends are real and that they are at least qualitatively correct. In the circumstances even qualitative knowledge is of value, for some of the $XF_{4-n}Cl_n^{\epsilon}$ species investigated here may be accessible experimentally only with difficulty or not at all, and a more extensive theoretical treatment at a higher SCF level or beyond does not appear to be imminent.

In the following the results of the 6-31G* level calculations are presented as statements of fact, but it is of course clear that the validity, in the absolute sense, of any of the assertions is restricted to the framework of the present study and is subject to the limitations of the basis set employed. The parameter sets are examined for trends and correlations both by graphical display and analytically. Where p is sufficiently large, an attempt is made to represent the visually identified trend by fitting the data set to a function which is compatible with the constraints imposed by the particular situation. Where the analytical representation has a high degree of fidelity (as judged by r^2 and σ), it is regarded as an adequate approximation to the (unknown) true correlation function and usable for numerical comparisons and for further phenomenological manipulation. Otherwise it merely serves to display the qualitative features of a trend. This is so *a fortiori* when $f = 0$; the function is then used only for convenience of interpolation. In yet other cases a surmised correlation is presented only graphically after free-hand smoothing.

Results and discussion

Total electronic energy

The availability of the E values, $E(0)$, for all the members of the XF_4^{ϵ} series permits an examination of the regularity of the variation of $E(0)$ with m. A cubic regression yields

$$[2]\quad E(0) = -525.12659 - 32.0264635m - 2.0506510m^2 - 0.01394827m^3$$

($r^2 = 1.000$, $\sigma = 0.0173$ au ~ 11 kcal/mol ~ 0.006% of the $E(0)$ range for $m = 1$–7). This approximation is useful in that it gives estimates of $E(0)$ for NeF_4^{4-} and ArF_4^{4+}, of importance in connection with the stability of these species (see Energy of formation).

Excess energy ΔE(n)

The excess energy measures the stability, in terms of the total electronic energy, of the mixed species relative to mixtures of XF_4^{ϵ} and XCl_4^{ϵ} of the appropriate molar ratios. Its variation with n, ϵ, and n,ϵ is shown in Fig. 1. The skewness of the $\Delta E(n)$ vs. n curves increases sharply from Al to P: γ_1(Al) = 0.05, γ_1(Si) = 0.15, γ_1(P) = 0.60. Since $\Delta E < 0$ for all three elements, the mixed species are always more stable. The stability increases, in magnitude, toward $n = 2$ with decreasing ϵ, and in composition, toward $n = 0$ with increasing ϵ. However, examination of the shape of the ΔE vs. n curve for $\epsilon = 1$ (and to a less certain extent, for $\epsilon = 0$) reveals that a sign inversion of ΔE may exist. If it does (and this cannot be established with certainty from the present results limited to $m = 3$–5), it would occur at $n \sim 3.8$ for $\epsilon = 1$; for $\epsilon = 2$ it could be expected at a significantly lower value of n, probably below $n = 3$. In that case $SFCl_3^{2+}$ would be unstable relative to $\frac{1}{4}SF_4^{2+} + \frac{3}{4}SCl_4^{2+}$. This interesting possible evolution will have to be verified by extending the calculations beyond $m = 5$.

As the position of ΔE_{min} in the ΔE vs. n,ϵ contour map shifts, with increasing ϵ, toward $n = 0$ and, with decreasing ϵ, quasi-asymptotically toward $n = 2$, the species most stable relative to $XF_4^{\epsilon} - XCl_4^{\epsilon}$ mixtures of the same molar ratio would seem to be SF_3Cl^{2+} for $\epsilon = 2$ and $MgF_2Cl_2^{2-}$ for $\epsilon = -2$.

The $|\Delta E|_{max}$ value is smallest for Si (~0.25 kcal/mol), about 1/16 that of $|\Delta E(Al)|_{max}$ and about 1/6 of $|\Delta E(P)|_{max}$, i.e. the SiF_4–$SiCl_4$ system is almost indifferent to formation of the mixed species. On the other hand, it is surprising that for P the preferential stability of the mixed species returns: $|\Delta E(P)|_{max} > |\Delta E(Si)|_{max} < |\Delta E(Al)|_{max}$.

Bond lengths

The Al—F and Al—Cl bond lengths decrease non-linearly with increasing n, while the Si—F, Si—Cl, P—F, and P—Cl bond lengths all increase, P—F and P—Cl linearly and Si—F and Si—Cl very nearly so (Fig. 2). The absolute value $|\Delta$(X—F)| of the percentage variation of X—F relative to XF_4^{ϵ} is largest for $n = 3$ and X = P, and that of X—Cl relative to XCl_4^{ϵ} is largest for $n = 1$ and X = P.

The differences $(X—F)_3 - (X—F)_0$ are, respectively, −0.018, 0.013, and 0.039 Å for Al, Si, and P, corresponding to −1.06, 0.85, and 2.62% of $(X—F)_0$; the $(X—Cl)_1 - (X—Cl)_4$ values are 0.036, −0.022, and −0.053 Å, corresponding to 1.66, −1.09, and −2.72% of $(X—Cl)_4$, respectively. The bond-length changes on progressive replacement of F in XF_4^{ϵ} by Cl are thus not insignificant. Their order of magnitude must be close to reality, as comparison with experiment for $SiF_{4-n}Cl_n$ (Table 1) shows that the available experimental Si—F and Si—Cl values all differ by less than three times their stated σ's from the calculated values. The exception is $SiFCl_3$, where the difference in Si—F is 0.051(5) Å.

Since XF_4^{ϵ} and XCl_4^{ϵ} are balanced configurations (T_d), the X—F and X—Cl bond lengths in them are not indicative of the "true" strength of the X—F and X—Cl bonds. The shortening of the Al—F bond with increasing n shows that this bond in AlF_4^- is capable of being strengthened (∂(Al—F)/$\partial n \rightarrow 0$ as $n \rightarrow \sim 4$), whereas the Si—F and P—F bonds in corresponding circumstances are weakened in proportion to the number of F atoms replaced by Cl.

These changes are associated with the net charge on the halogen atom. Quadratic regression of the difference $(X—F)_n - (X—F)_0$ on ϵ(F) yields a very high degree of correlation for Al and P; for Si, linear regression leads to an equally satisfactory result. In addition, a plot of $(X—F)_n - (X—F)_0$ vs. ϵ(F) (Fig. 3) shows that the points of equal n define parabolas ($f = 0$) intersecting at a crossover point at ϵ(F) ~ −0.506. Although

Can. J. Chem. Downloaded from www.nrcresearchpress.com by 78.46.186.204 on 09/07/12
For personal use only.

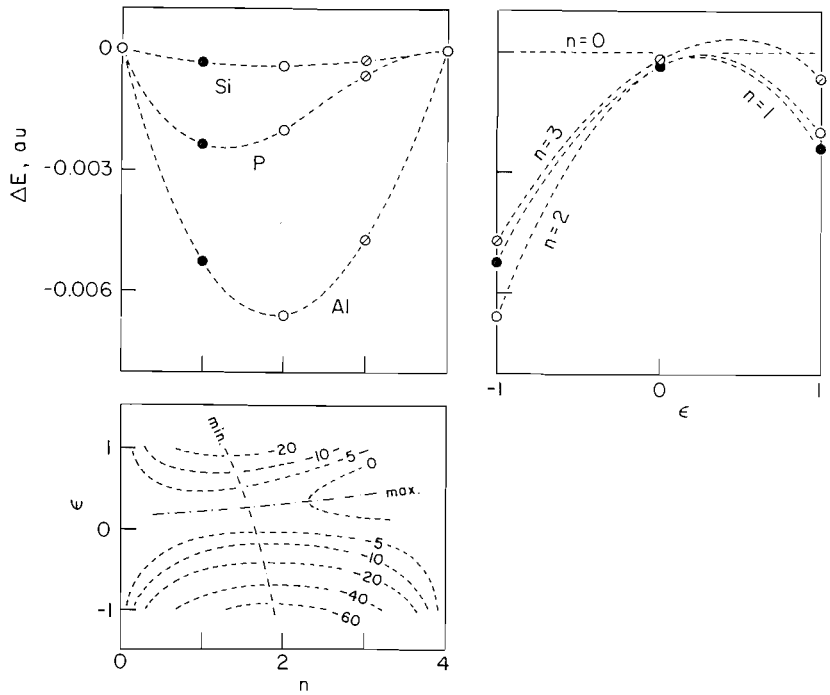

FIG. 1. Variation of the excess energy ΔE of $XF_{4-n}Cl_n^{\epsilon}$ (X = Al, Si, P) with n, ϵ, and ϵ, n. The ΔE contour values (au) have been multiplied by 10^4. The broken lines represent parabolic or visual fits.

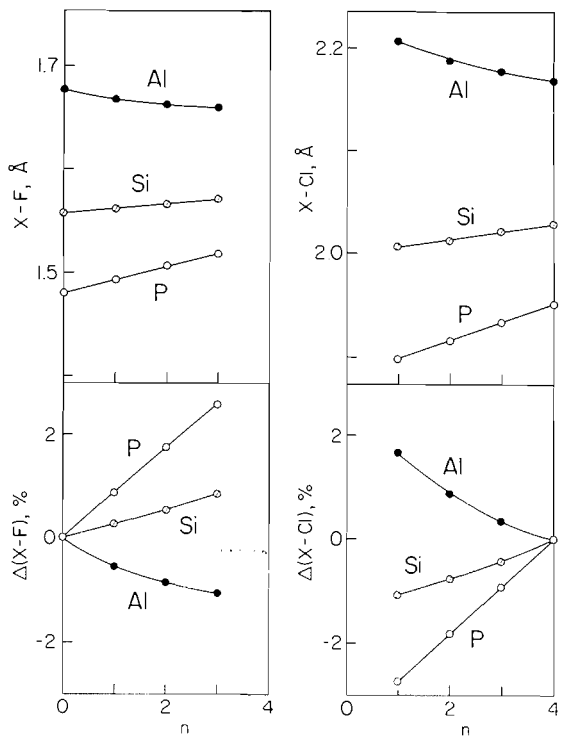

FIG. 2. Variation of the bond lengths and of the relative changes $\Delta(X—Hal)_n = 100[(X—Hal)_n - (X—Hal)_{0,4}]/(X—Hal)_{0,4}$ in $XF_{4-n}Cl_n^{\epsilon}$ with n.

there is no theoretical justification for a parabolic interpolation, the apparent existence of the crossover point is unlikely to be fortuitous, for an analogous behaviour is shown by the $(X—Cl)_n - (X—Cl)_4$ vs. $\epsilon(Cl)$ curves (Fig. 3), and similar points are present in other plots (see below). The crossover point for the X—Cl bonds lies at $\epsilon(Cl) \sim -0.408$.

For a more general idea of the dependence of the bond length on ϵ, the calculations were extended to include XF_4^{ϵ}, X = Na, Mg, S, and Cl (Tables 2 and 3). The $(X—F)_0$ values decrease with increasing m from Na to S, but unexpectedly at X = Cl there is a sudden upturn (Fig. 4). On the assumption that NeF_4^{4-} is unstable, i.e. $(X—F)_0 \rightarrow \infty$ as $m \rightarrow 0$, the $(X—F)_0$ vs. m variation for $m = 1$–5 can be represented with considerable fidelity ($\sigma = 0.002$ Å) by a power function, $(X—F)_0 = 2.01(m - 0.6)^{-0.2076}$, with the difference between the given and the fitted $(X—F)_0$ values increasing steadily as m approaches and then exceeds 5. This suggests that the variation for $m = 0$–7 can be represented as a sum of two power functions corresponding to opposing tendencies in the physical process of bond formation. To evaluate the contribution from the repulsive term adequately one needs to have an estimate of the bond length for the end member of the series, ArF_4^{4+}. However, numerous attempts to optimize the geometry of this species at the 6-31G* level failed to converge in the SCF procedure. Optimization using the minimal STO-3G basis set resulted in E values dropping steadily over the range $(Ar—F)_0 = 2$–4 Å, with no clear indication of a minimum beyond 4 Å. This was taken as evidence of instability of ArF_4^{4+}, i.e. $(Ar—F)_0 \rightarrow \infty$ as $m \rightarrow 8$. On this assumption the data points could be fitted to the composite power function $(X—F)_0 = 2.0073(m - 0.6)^{-0.2080} + 0.1145(8 - m)^{-2.4800}$, $\sigma = 0.0040$ Å $\sim 0.4\%$ of the $(X—F)_0$ range for $m = 1$–7.

Evaluation of the repulsive term is less certain than that of the attractive term, for a significant contribution to the former comes only from the $(X—F)_0$ values for $m = 5$–7, but it is clear that the repulsive term varies with m steeply as $m \rightarrow 8$ and in fact its rate of change begins to exceed, numerically, that of the attractive term at $m \sim 6.4$; the ratio (attractive term)/(repulsive term) from the above power function is 2645 for $m = 1$ but 11.9 for $m = 7$. If the assumption that $(Ar—F)_0 \rightarrow \infty$ as $m \rightarrow 8$ turns out not to be correct and $(Ar—F)_0$ is finite, the regression

Can. J. Chem. Downloaded from www.nrcresearchpress.com by 78.46.186.204 on 09/07/12
For personal use only.

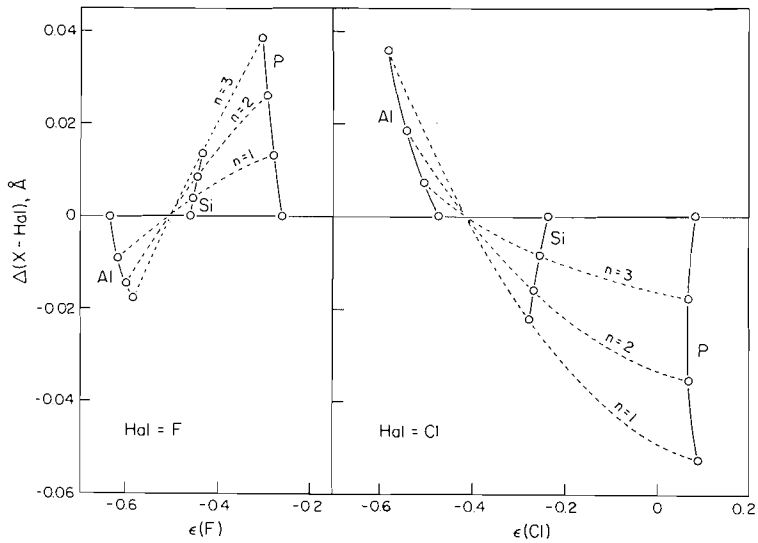

FIG. 3. Variation of the change in the bond length $\Delta(X—Hal)_n = (X—Hal)_n - (X—Hal)_{0,4}$ with ϵ(Hal).

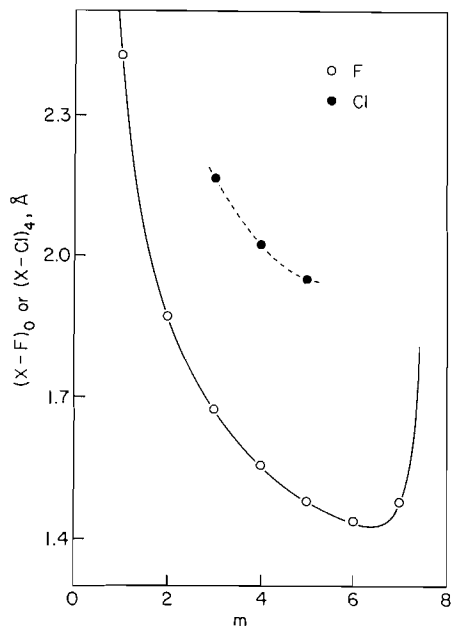

FIG. 4. Variation of the bond lengths $(X—F)_0$ and $(X—Cl)_4$ in $XF_{4-n}Cl_n^{\epsilon}$ with the oxidation state m of X. For the significance of the solid line see text. The broken line represents a visual fit.

function will have to be modified, but this will affect our analysis only numerically.

The three data points available for $(X—Cl)_4$ are insufficient for a similar treatment, but it would seem that the minimum in the $(X—Cl)_4$ vs. m curve occurs at a lower m than in the case of $(X—F)_0$ (Fig. 4); this would be consistent with the notion of lateral repulsion of the halogen atoms.

As would be expected, the bond length varies also with the critical radii of X and Hal (Fig. 5) and with ϵ(X) (Fig. 6). In the first case the decrease in X—Hal is monotonic and not far from linear from Na to S, with an upturn at X = Cl. The variation of X—Hal with ϵ(X) is, for XF_4^{ϵ}, also monotonic and decreasing from Na to S, though less regular, while for XCl_4^{ϵ} it is re-entrant, with the data points for the mixed species showing regular progressions both for n and X.

Bond angles

Analogous to the shortening of the bonds in $AlF_{4-n}Cl_n^-$ with increasing n and thus to increasing lateral repulsion of the halogen atoms, the bond angles also increase with n (Fig. 7). Conversely, in $SiF_{4-n}Cl_n$ and $PF_{4-n}Cl_n^+$ the angles decrease with increasing n. For X = Si and P the variation of FXF, FXCl, and ClXCl is linear or close to linear, while for Al it is non-linear and its rate decreases with increasing n. The ranges of FXF and ClXCl are quite substantial, about 105–111° and 109–115°, respectively; the ClXCl angle drops only slightly below τ for the m range considered here.

The variation with ϵ at constant n is, at least for the present m range, linear (Fig. 8). Assuming that the linearity persists, for $\epsilon < -1$ and $\epsilon > 1$, even more substantial departures from τ can be expected for $\epsilon < -1$ and $\epsilon > 1$. The estimated range for $-3 \leq \epsilon \leq 3$ is 98–116° for FXF and 104–122° for ClXCl.

For the molecular symmetries under consideration here, the bond angles are related by $(n-4)(n-3)(FXF)_n + 2n(4-n)(FXCl)_n + n(n-1)(ClXCl)_n = 12\tau$, so that, for $n = 1$ and 3, $\delta = (FXF)_n - \tau$ (or $(ClXCl)_n - \tau$) must be offset by $(FXCl)_n - \tau = -\delta$. For $n = 2$ the angles have an additional interesting property: $(ClXCl)_2 = 219.74(315) - 0.998(3)(FXF)_2$ ($r^2 = 1.000$, $\sigma = 0.02°$) (Fig. 9), i.e. $(ClXCl)_2 + (FXF)_2 \sim 219.7°$, and because of $\delta(FXCl)_2 = -\frac{1}{4}[(FXF)_2 + (ClXCl)_2 - 2\tau]$, $(FXCl)_2 = \tau - 0.200 - 0.0005(FXF)_2$, which explains the constancy of the $(FXCl)_2$ angle (Table 2).

Bond angle vs. bond length

An unexpected correlation results when the FXF angle is plotted against X—F and the ClXCl angle against X—Cl (Fig. 10). The bond length vs. bond angle variation for each X is linear, with the exception of Al—Cl vs. ClAlCl. The σ of the regressions of bond angle on bond length at constant X, with $(X—F)_\tau, \tau$ and $(X—Cl)_\tau, \tau$ as the respective pivot points, amount to only 2–3% of the observed $|FXF - \tau|$ and $|ClXCl - \tau|$ ranges; for Si/F the value is somewhat higher, ~7%, but in absolute terms still small.

The variation of X—F with FXF and of X—Cl with ClXCl at constant n is non-linear, except of course for $n = 0$ and 4. Parabolic fit to the data points ($f = 0$) yields a family of curves that intersect (or very nearly so) at a crossover point; this point

Can. J. Chem. Downloaded from www.nrcresearchpress.com by 78.46.186.204 on 09/07/12
For personal use only.

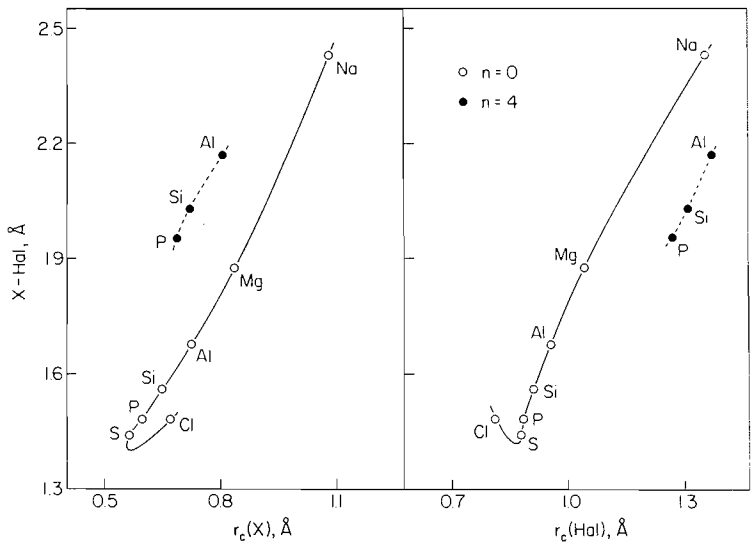

FIG. 5. Variation of $(X—Hal)_{0,4}$ in $XF_{4-n}Cl_n^{\epsilon}$ with the critical radii $r_c(X)_{0,4}$ and $r_c(Hal)_{0,4}$.

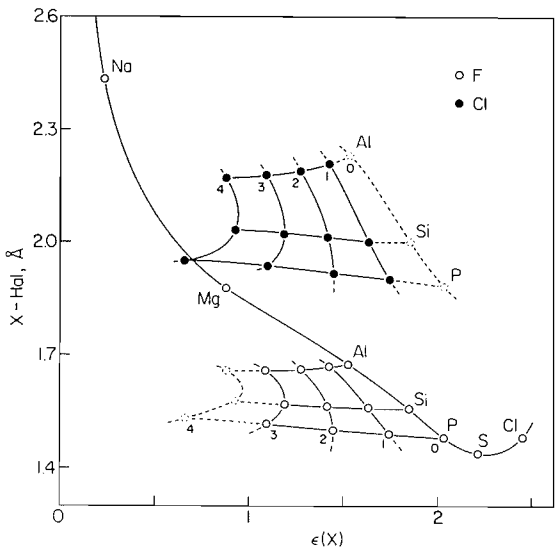

FIG. 6. Variation of $(X—Hal)_n$ in $XF_{4-n}Cl_n^{\epsilon}$ with $\epsilon(X)$.

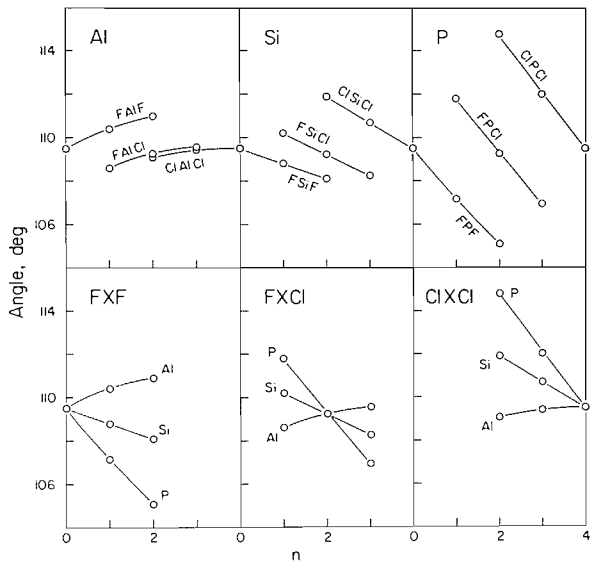

FIG. 7. Variation of the bond angles FXF, FXCl, and ClXCl in $XF_{4-n}Cl_n^{\epsilon}$ with n.

for ClXCl is much closer to Al than that for FXF. When the FXF vs. n and ClXCl vs. n curves on Fig. 7 are represented by parabolas ($f = 0$) passing through τ at $n = 0$ and 4, respectively, the fictitious extrapolated FXF angles for $n = 3$ and the corresponding ClXCl angles for $n = 1$ are such that the $|FXF_{extrapol} - \tau|$ values differ from the $|FXF_{calc} - \tau|$ values obtained from the linear FXF vs. X—F regressions by only 15% for Al, 14% for Si, and 7% for P. All these differences are less than 0.5°. For ClXCl the corresponding differences are 7% for both Si and P; for Al the extrapolation is less certain because of the pronounced curvature of the ClXCl vs. Al—Cl variation. When the three fictitious FXF,X—F points for $n = 3$ are represented by a parabola, the bond-length value at τ is ~1.61 Å, i.e. the curve again passes through the crossover point. Furthermore, when the constant-n curves are represented by exponential curves instead of parabolas, the respective positions of the crossover points for F and Cl remain practically unchanged. The FXF,X—F set thus shows a remarkable internal consistency.

The plot of Fig. 10 reveals at a glance the expectations for X not included in the present investigation. It would seem that significant non-linearity of the angle–distance correlation may develop for $|\epsilon| > 1$; for Mg/Cl and Na/Cl strong non-linearity may be taken for granted. Estimates, from consideration of Figs. 7–10, of the bond angle ranges for X = Na to Cl are 98–116° for FXF and 104–122° for ClXCl. The sensitivity of the bond angle to variation in bond length increases rapidly with $|\epsilon|$ on either side of the respective crossover point, although the magnitude of this rate of change is less easy to predict for $\epsilon < 0$ than for $\epsilon > 0$.

Whether by chance or for an unknown specific reason, the positions of the crossover points in Fig. 10 correspond quite closely to the positions of the points of intersection of the $(ClXCl)_2$ vs. $(FXF)_2$ straight line with the FXF = τ and ClXCl = τ lines (Fig. 9).

The correlation of the change in the bond length, $(X—F)_n - (X—F)_0$, with the change in the bond angle, FXF − τ, is displayed in yet another way in Fig. 11. This plot shows that

Can. J. Chem. Downloaded from www.nrcresearchpress.com by 78.46.186.204 on 09/07/12
For personal use only.

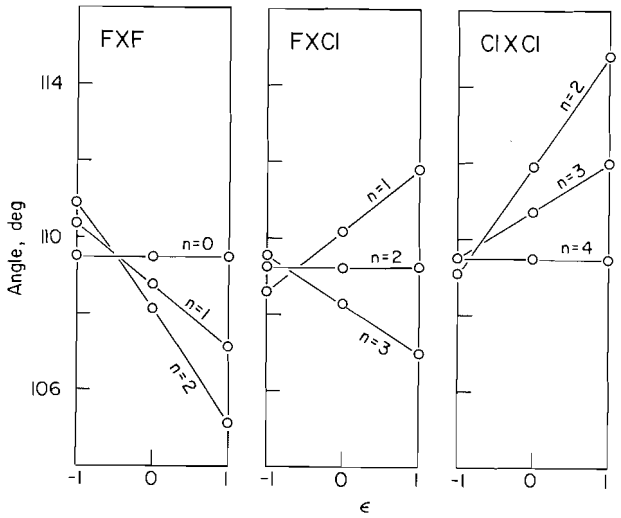

FIG. 8. Variation of the bond angles FXF, FXCl, and ClXCl in $XF_{4-n}Cl_n^{\epsilon}$ with ϵ.

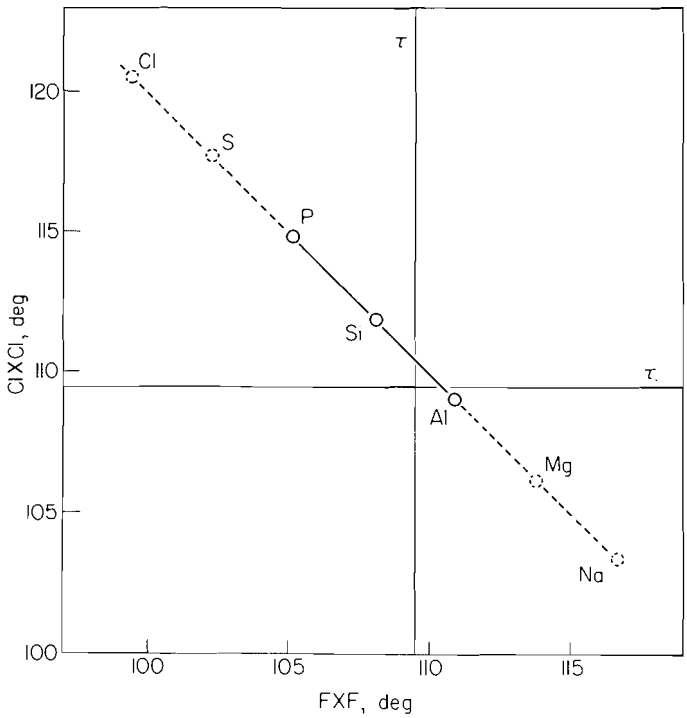

FIG. 9. Variation of the ClXCl with the FXF bond angle in $XF_2Cl_2^{\epsilon}$. Broken circles: data points obtained from extrapolations of FXF vs. ϵ and ClXCl vs. ϵ.

the variation is linear, but the rate of change is different for Al and for Si and P, −0.00590(6) and −0.0104(2) Å/deg, respectively. The correlation is thus decomposed into two branches, one for $\epsilon < 0$ and another for $\epsilon > 0$, intersecting at 0,0. Since the separate regressions for Si and P are statistically indistinguishable from the regression for Si and P combined, one may anticipate that the plot of Fig. 11 represents a correlation of $(X—F)_n - (X—F)_0$ and FXF − τ valid even for $-1 > \epsilon > 1$, with points for $\epsilon < -1$ falling on the Al branch and those for $\epsilon > 1$ on the Si,P branch. A similar behaviour is observed for $(X—Cl)_n - (X—Cl)_4$ vs. ClXCl − τ (Fig. 11), but here the Al branch is not linear. The slopes of the Si,P branches for F and Cl are −0.00590(6) and −0.00678(7) Å/deg,

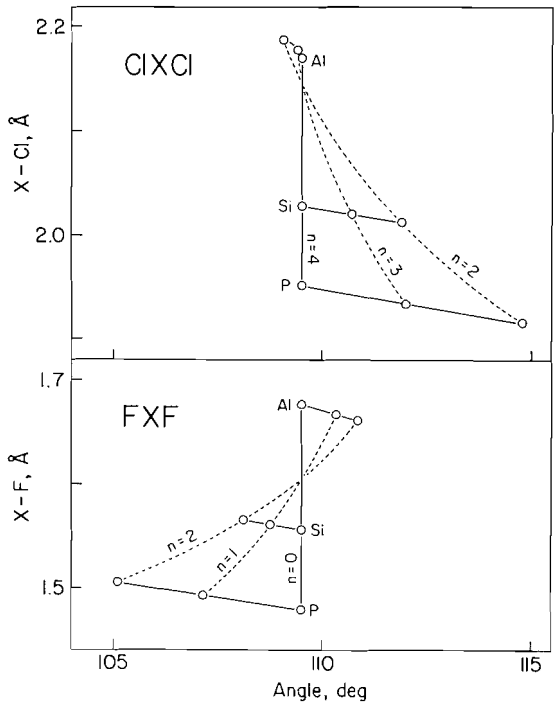

FIG. 10. Variation of the bond angle FXF with X—F and of ClXCl with X—Cl (parabolic interpolation for fixed n).

respectively. Statistical comparison of the two regressions shows that the difference between the two slopes is significant, i.e. the rate of change of the bond-length difference with the difference in the bond angle is ca. 15% larger for Cl.

Net charges $\epsilon(X)$, $\epsilon(F)$, and $\epsilon(Cl)$

Variation of $\epsilon(X)$

The charge on X in XF_4^{ϵ}, $\epsilon(X)_0$, is positive and increases monotonically though irregularly with m (Fig. 12). A polynomial probably of a degree at least four would be required to fit the curve, with the constraint $\epsilon(X)_0 \rightarrow 0$ as $m \rightarrow 0$. The $\epsilon(X)_0$ values, which range from 0.230 for X = Na to 2.456 for X = Cl, indicate that there is considerable transfer of electronic charge from F to X. In ClF_4^{3+} more than one unit of charge is transferred from F to Cl (Fig. 13). Beginning at $m = 3$ the amount of charge transferred from an F atom, $\frac{1}{4}[m - \epsilon(X)_0]$, increases at an almost constant rate.

In XCl_4^{ϵ}, on the other hand, $\epsilon(X)_4$ reaches a maximum at X = Si and then decreases, a change of sign for X = Cl being a distinct possibility (Fig. 12). For a given X the amount of charge transferred to X from a Cl atom in XCl_4^{ϵ} is significantly larger than from an F atom in XF_4^{ϵ} (Fig. 13), a little more than one unit of charge being transferred already at X = P. The greater readiness of Cl to give up charge is illustrated in Fig. 14*A*, where $\epsilon(Cl)_4$ is plotted against $\epsilon(F)_0$. The three available points can be accommodated on a straight line passing through $\epsilon(F)_0 = \epsilon(Cl)_4 = -1$ ($r^2 = 0.999$, see below), with $\partial\epsilon(Cl)_4/\partial\epsilon(F)_0 \sim 1.45$.

The $\epsilon(X)_n$ vs. m curves for the mixed species fall between those for $n = 0$ and $n = 4$ (Fig. 12). The shapes of these curves suggest the existence of $\epsilon(X)_n$ maxima at $m = 5$, $n = 2$ and at $m = 4$, $n = 3$; the direction of the continuation of the $n = 1$ curve beyond $m = 5$ is not self-evident.

The m,n combinations at which the net charge on X equals the charge on the complex are defined by the $\epsilon(X) = \epsilon$ line in Fig. 12. In the species located farthest to the left of this line the

Can. J. Chem. Downloaded from www.nrcresearchpress.com by 78.46.186.204 on 09/07/12
For personal use only.

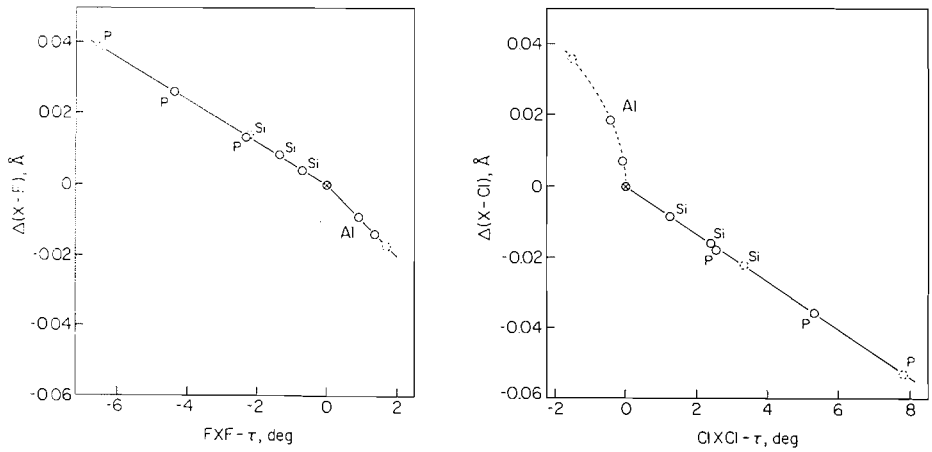

FIG. 11. *A* (*left*), variation of $\Delta(X—F)_n = (X—F)_n - (X—F)_0$ with the bond-angle difference FXF − τ. *B* (*right*), variation of $(X—Cl)_n - (X—Cl)_4$ with the bond-angle difference ClXCl − τ. Broken circles: values obtained by linear extrapolation of the X—F vs. FXF lines (Fig. 10) to $n = 3$, or of the X—Cl vs. ClXCl lines to $n = 1$.

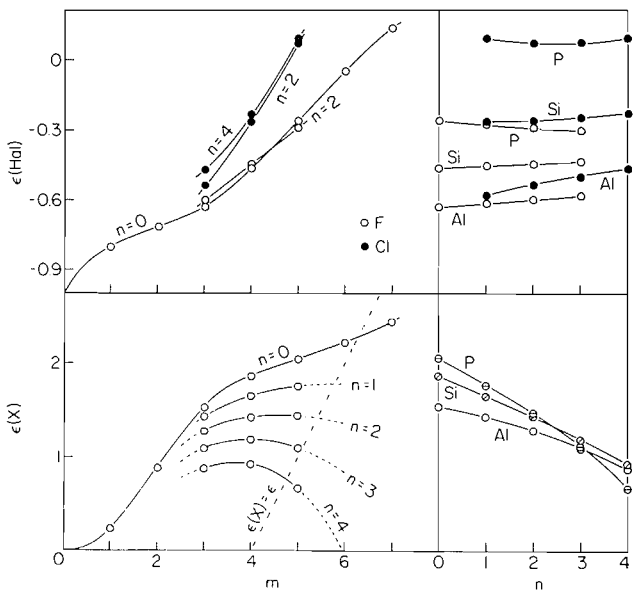

FIG. 12. Variation of ε(X) and ε(Hal) with *m* and *n*. The curves in the ε(X) and ε(Hal) vs. *m* plots represent visual fits, as the appropriate functional relationships are not known and the number of data points in general is insufficient to define the polynomials (of degree four or higher) that would be required for analytic representation.

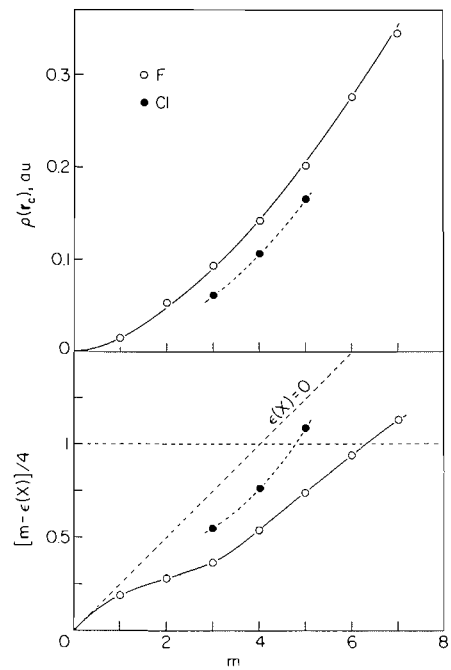

FIG. 13. Variation, with the oxidation state *m* of X, of the electron density at the critical point $\rho(r_c)$ (*A*, *top*) and of the amount of negative charge $\frac{1}{4}[m - \epsilon(X)]$ transferred from a F^- atom in XF_4^{ϵ}, or from a Cl^- atom in XCl_4^{ϵ}, to X (*B*, *bottom*). The points for $n = 1$–3 fall between the curves for $n = 0$ and 4.

total charge on the complex resides essentially on the halogens, whereas in the species to the right it resides essentially on X.[2] In SF_4^{2+}, where ε(F) is, numerically, about 40 times smaller than ε(S), the F atoms carry very little net charge and ε is located almost entirely on the S atom.

The steady variation of ε(X) with *n* is non-linear for all three elements studied, even though for X = Si the departure from linearity is slight (Fig. 12). In all three cases ε(X) decreases with increasing *n*, which again indicates that Cl loses charge to X more readily than does F. The rate of the decrease accelerates from Al to P; in $PF_{4-n}Cl_n^+$ it overtakes Al and Si at $n = 3$ and causes the order of ε(X) to change from P—Si—Al for $n = 0$ to Si—Al—P for $n = 4$.

Variation of ε(Hal)

In the balanced species, $4\epsilon(Hal) = \epsilon - \epsilon(X)$ and so the ε(Hal) vs. *m* curves for $n = 0$ and 4 of Fig. 12 are the same as the corresponding curves in Fig. 13 if allowance is made for $m = \epsilon + 4$. For $n = 2$ the $\epsilon(F)_2$ and $\epsilon(Cl)_2$ curves are quite close to those for $\epsilon(F)_0$ and $\epsilon(Cl)_4$, respectively. This is not surprising in view of the relatively small variation of $\epsilon(Hal)_n$ with *n* (Fig. 12). For F this variation is almost linear, but the slopes for Al and Si are positive while that for Si is negative. The curvatures for $\epsilon(Cl)_n$ are more pronounced, and the curve for P

[2]Removal of an electron from AlF_4^- produces relatively small changes in the net charges: for AlF_4^0 (6-31G*, D_{2d}; unpublished results), ε(Al) = 1.650, ε(F) = −0.412, ε(F) − ε(Cl) = −2.062 (−2.179 for AlF_4^-).

Can. J. Chem. Downloaded from www.nrcresearchpress.com by 78.46.186.204 on 09/07/12
For personal use only.

Can. J. Chem. Downloaded from www.nrcresearchpress.com by 78.46.186.204 on 09/07/12
For personal use only.

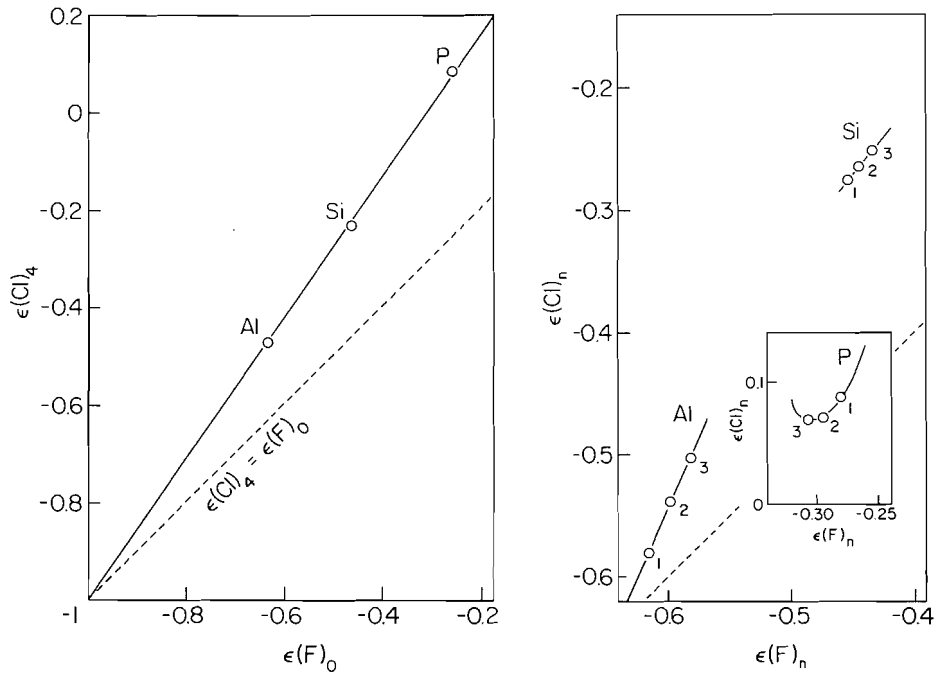

FIG. 14. *A* (*left*), variation of $\epsilon(Cl)_4$ with $\epsilon(F)_0$. *B* (*right*), variation of $\epsilon(Cl)_n$ with $\epsilon(F)_n$.

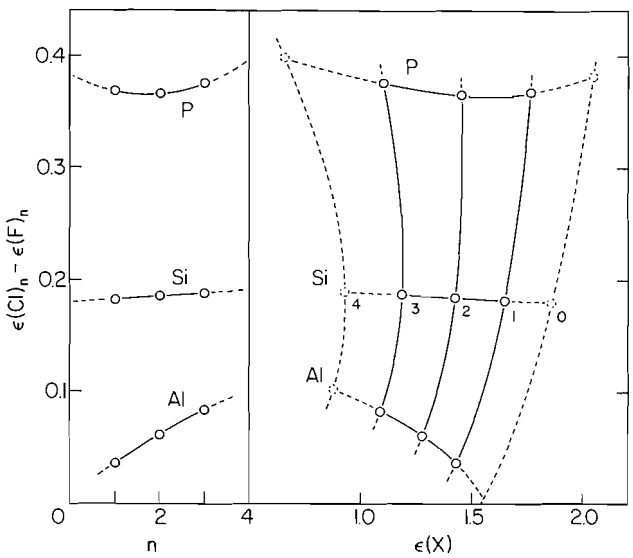

FIG. 15. Variation of the difference $\epsilon(Cl)_n - \epsilon(F)_n$ with n (*A*, *left*) and $\epsilon(X)$ (*B*, *right*). Broken circles: data points obtained by extrapolation.

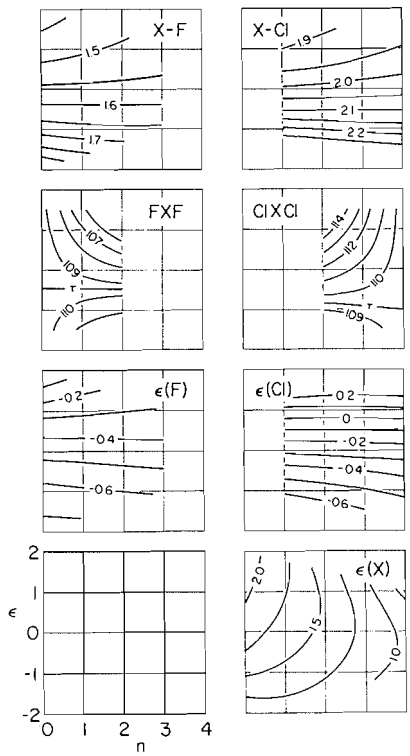

FIG. 16. Variation, with n and ϵ, of the bond lengths X—F and X—Cl, the bond angles FXF and ClXCl, and the net charges $\epsilon(X)$, $\epsilon(F)$, and $\epsilon(Cl)$ in $XF_{4-n}Cl_n^{\epsilon}$.

has an $\epsilon(Cl)_n$ minimum between $n = 2$ and 3, whereas that for Al is convex with respect to the n axis.

The rate at which electronic charge is transferred, with varying n, from a halogen atom to X depends on m and is not the same for F and Cl. The difference $\Delta = \epsilon(Cl)_n - \epsilon(F)_n = [\epsilon - \epsilon(X) - 4\epsilon(F)]/n$, which may be taken as a measure of the relative strength of the X—Hal bond, is quite small for Al and increases rapidly with n; for X = Si it is nearly constant and about double that for Al, and for X = P it is about four times that for Al and goes through a minimum (Fig. 15*A*). These features are preserved when Δ is plotted against $\epsilon(X)$ (Fig. 15*B*). The extent of the charge transfer from an F atom relative to that from a Cl atom thus depends both on m and, for a given X, on $\epsilon(X)$.

The trend in the variation of Δ (Fig. 15*A*) and visual extrapolation in Fig. 15*B* both suggest that with decreasing m the difference Δ eventually will become negative, i.e. the transfer of charge from the halogen atom to X becomes progressively easier for F than for Cl as the anionic charge on the complex increases. This is also evident in Fig. 14*B*, where the $\epsilon(Cl)_n, \epsilon(F)_n$ data points approach the $\epsilon(Cl)_n = \epsilon(F)_n$ line with decreasing m. Although this seemingly paradoxical result

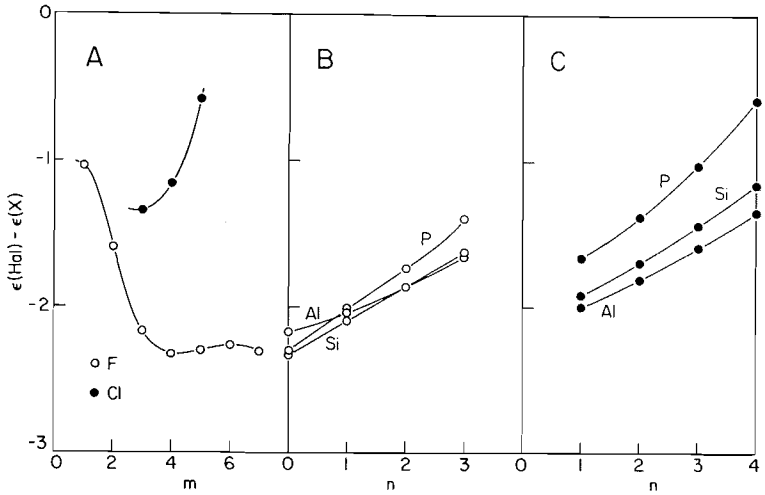

FIG. 17. Variation of the polarity of the X—Hal bond (as measured by $\epsilon(F)_0 - \epsilon(X)_0$ and $\epsilon(Cl)_4 - \epsilon(X)_4$, respectively) with m (*A*) and n (*B*, *C*).

may be an artefact of the 6-31G* chemistry, it is consistent with the experimental fact that the ionization potential of F^- (= the reverse of the electron affinity of F) is ca. 0.16 eV smaller than that of Cl^-, i.e. it is easier to remove an electron from a free F^- ion than from a free Cl^- ion. As the slopes of the lines for Al in Figs. 14*B* and 15*B* indicate, charge is withdrawn from Cl more rapidly with n than from F, and this would be expected to be even more the case for Mg and Na. The competition for charge is, however, reversed with increasing m, as shown by the n sequence for P in Fig. 14*B*.

The difference between F and Cl is displayed also by comparing $\epsilon(F)_0$ and $\epsilon(Cl)_4$ (Fig. 14*A*). Assuming that in $NeHal_4^{4-}$ $\epsilon(Hal)_{0,4} = -1$, the data points for X = Al, Si, and P can be accommodated quite well on the straight line $\epsilon(Cl)_4 = 0.4521 + 1.4521\epsilon(F)_0$ ($r^2 = 0.999$, $\sigma = 0.010$), i.e. the negative charge on Cl in XCl_4^ϵ decreases more rapidly with increasing m than the negative charge on F in XF_4^ϵ. To what extent this correlation is fortuitous will be determined when results for m = 1, 2, 6, and 7 have become available.

A conspectus of the simultaneous dependence of X—Hal, FXF, ClXCl, $\epsilon(X)$, $\epsilon(F)$, and $\epsilon(Cl)$ on n and ϵ is presented in Fig. 16.

Variation of $\epsilon(Hal) - \epsilon(X)$

This difference may be taken as an index of the polarity of the X—Hal bond. In XF_4^ϵ it varies steeply with m from Na to Al, after which it remains more or less constant, whereas in XCl_4^ϵ it rises appreciably from Al to P (Fig. 17*A*). In the mixed species it increases with n at comparable rates for all three X, the increase for X = P being somewhat steeper than for Al or Si (Figs. 17*B*,*C*).

Critical points, ionic radii, and deformation of the electron-density distribution

At a bond critical point r_c the electron density ρ satisfies $\nabla\rho(r_c) = 0$,[3] i.e. constitutes an electron-density minimum along the bond path between atoms A and B and a maximum with respect to a lateral displacement. The distance r_c^A from nucleus A to r_c and the distance r_c^B from nucleus B to r_c are the corresponding critical radii of A and B.

Critical radii of X^{m+}

The variation of $r_c(X)_0$ with m (Fig. 18*A*) strongly resembles

[3]These points are also known (31) as the (3, −1) critical points, since they are associated with three curvatures, one positive and two negative (+1 − 1 − 1 = −1).

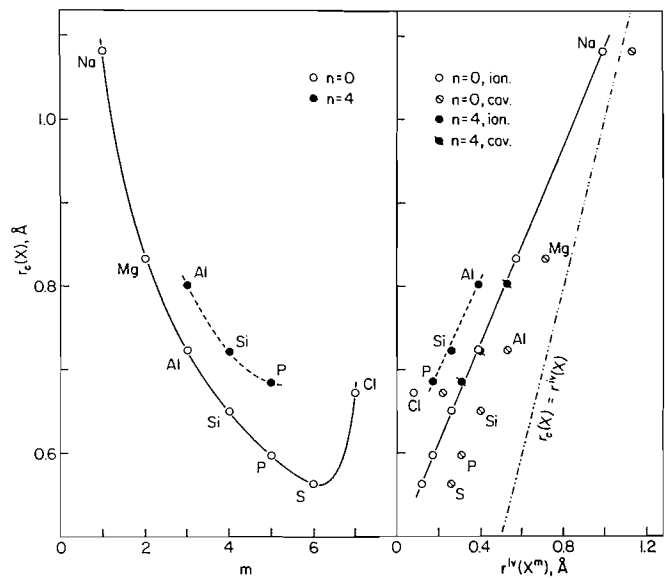

FIG. 18. *A* (*left*), variation of the critical radius $r_c(X)$ in XF_4^ϵ and XCl_4^ϵ with the oxidation state m of X. *B* (*right*), correlation of the critical radii $r_c(X)$ in XF_4^ϵ and XCl_4^ϵ with Shannon's effective ionic and covalent radii $r^{iv}(X^{m+})$ of X^{m+} in tetrahedral coordination.

that of X—Hal with m (Fig. 4). This would suggest that the variation of $r_c(X)_0$, too, could be resolved into an attractive and a repulsive component. The $r_c(X)_0$ values for m = 1–6 can be represented to a σ of 0.003 Å ($r^2 = 1.000$) by $r_c(X)_0 = 1.07923m^{-0.36554}$. This means that the effect of the repulsive forces does not become significant until m = 7, but after X = S the contribution of the repulsive component rises very steeply with m, similar to the X—Hal vs. m variation.

Since X—Hal = $r_c(X) + r_c(Hal)$, the $r_c(X)$ values may be expected to correlate with Shannon's effective ionic (or covalent) radii of X^{m+} in 4-coordination. Indeed, regressing $r^{iv}(X^{m+})$ on $r_c(X)_0$ for m = 1–6 yields $r^{iv}(X^{m+}$, ionic) = $-0.8314 + 1.6828r_c(X)_0$ ($r^2 = 1.000$, $\sigma = 0.003$ Å). The two radii would become equal only at ~1.22 Å, i.e. for $m < 1$ (Fig. 18*B*). Since Shannon's $r^{iv}(X^{m+}$, covalent) exceed his $r^{iv}(X^{m+}$, ionic) by the constant amount of 0.14 Å, $r^{iv}(X^{m+}$, covalent) would equal $r_c(X)_0$ at ~1.01 Å, i.e. roughly at m = 1.

For $r_c(X)_4$, the linear regression (three values only) yields $r^{iv}(X^{m+}$, ionic) = $-1.0689 + 1.8221r_c(X)_4$, $r^2 = 0.989$, σ =

Can. J. Chem. Downloaded from www.nrcresearchpress.com by 78.46.186.204 on 09/07/12
For personal use only.

Can. J. Chem. Downloaded from www.nrcresearchpress.com by 78.46.186.204 on 09/07/12
For personal use only.

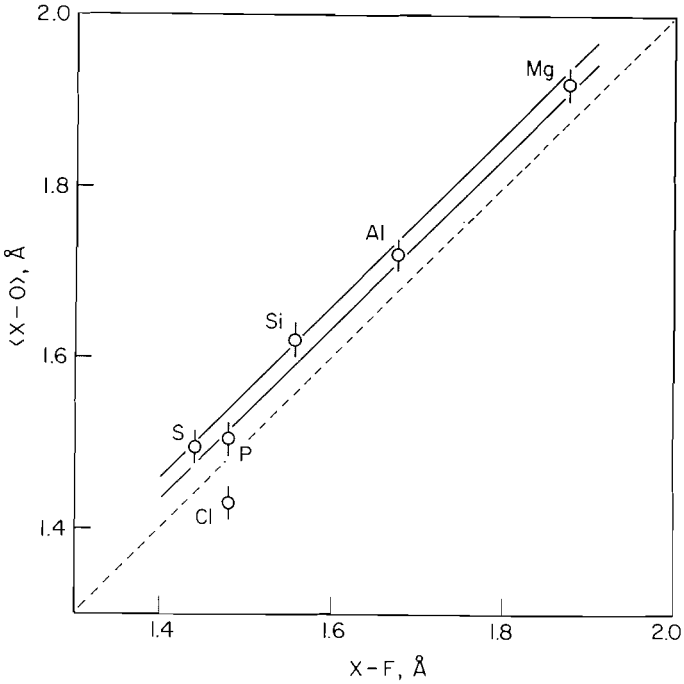

FIG. 19. Average X—O bond lengths in tetrahedral oxyanions $XO_4^{\epsilon-4}$ plotted against the calculated X—F distances in XF_4^{ϵ}. The width of the band is 2σ of the linear regression (excluding X = Cl). The estimated error bars on ⟨X—O⟩ represent ±0.02 Å.

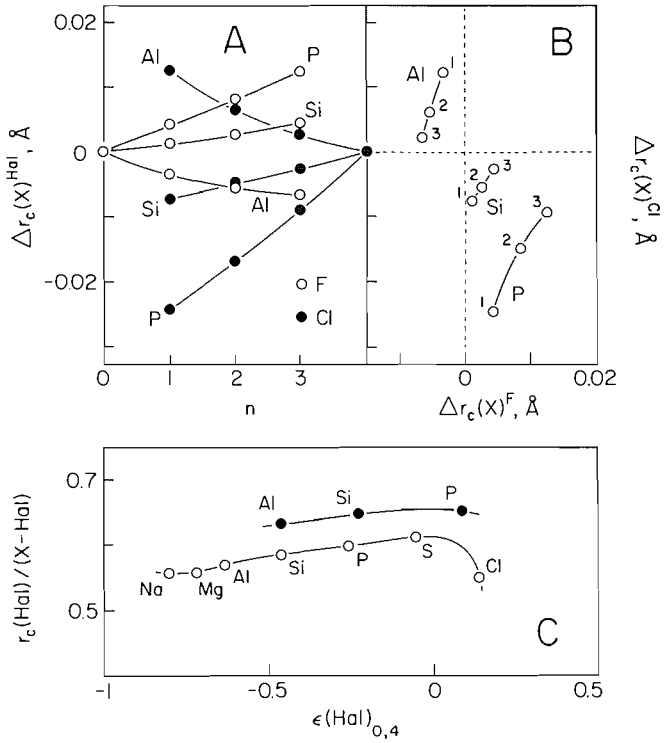

FIG. 20. (*A*) Variation of the critical radius of X with n; $\Delta r_c(X)^{Hal} = r_c(X)_n^{F} - r_c(X)_0$ or $r_c(X)_n^{Cl} - r_c(X)_4$. (*B*) Correlation of $r_c(X)_n^{Cl} - r_c(X)_4$ with $r_c(X)_n^{F} - r_c(X)_0$. (*C*) Variation of the relative position of the critical point in the X—Hal bond, $r_c(Hal)/(X—Hal)$, with $\epsilon(F)_0$ and $\epsilon(Cl)_4$.

0.012 Å. However, the line defined by $r^{iv}(X^{m+}$, covalent) = $0.14 - 1.0689 + 1.8221 r_c(X)_4$ practically coincides with the regression line for $r^{iv}(X^{m+}$, ionic) vs. $r_c(X)_0$, which would suggest that the $r^{iv}(X^{m+}$, covalent) set of radii is appropriate to the chlorides and the $r^{iv}(X^{m+}$, ionic) set to the fluorides. This is not unreasonable, considering that Shannon's set of ionic radii was devised primarily for use with oxides and to a lesser degree with fluorides. The breakdown of the $r^{iv}(X^{m+})$ vs. $r_c(X)_0$ correlation for X = Cl is thus not surprising, for the $r^{iv}(Cl^{7+})$ values have been derived exclusively from the experimental bond lengths in ClO_4^-. A plot of average experimental X—O bond lengths in the tetrahedral oxyanions $XO_4^{\epsilon-4}$ (ref. 17; Mg—O and Al—O from $MgAl_2O_4$) against the X—F in XF_4^{ϵ} (Fig. 19) in fact demonstrates that ClF_4^{3+} is a clear misfit in the X—O vs. X—F correlation for m = 2–6, ⟨X—O⟩ = 0.045(64) + 1.001(40)(X—F)$_0$ (r^2 = 0.995, σ = 0.014 Å), even when differences arising from experimental circumstances are taken into account, and that the parallellism of the two isoelectronic series does not extend beyond $m = 6$.[4]

The variation of $r_c(X)_n^{F}$ for m = 3–5 with n, relative to $r_c(X)_0$, does not exceed 0.015 Å, and that of $r_c(X)_n^{Cl}$ relative to $r_c(X)_4$ is within 0.025 Å (Fig. 20*A*), but here again the sign of the variation for Al is the opposite of that of Si and P, both for $r_c(X)_n^{F}$ and $r_c(X)_n^{Cl}$. The rate of change for $r_c(X)$ with n is highest for $r_c(P)_n^{Cl}$, ca. 0.008 Å/n. The differences $r_c(X)_n^{F} - r_c(X)_0$ and $r_c(X)_n^{Cl} - r_c(X)_4$ are correlated in Fig. 20*B*.

Critical radii of F and Cl

The variation of $r_c(F)_0$ and $r_c(Cl)_4$ with m is shown in Fig. 21*A*; the corresponding plots against $\epsilon(F)_0$ and $\epsilon(Cl)_4$, or against $m - \epsilon(X)_0$ and $m - \epsilon(X)_4$, have essentially the same features. Compared to $r_c(X)_0$ (Fig. 18*A*), the $r_c(F)_0$ values taper off more rapidly with m; unlike for $r_c(X)_0$, where $r_c(Cl)_0 > r_c(S)_0$, there is an additional sudden decrease in $r_c(F)_0$ on going from X = S to X = Cl. The range of $r_c(F)_0$ (m = 1–7), ~0.54 Å, is similar to the range of $r_c(X)_0$, ~0.52 Å; for $r_c(Cl)_4$ (m = 3–5) the ranges are ~0.10 and ~0.12 Å, respectively. The lengths of these intervals demonstrate the difficulty, in principle, of devising a "universal" effective radius of F^- or Cl^- even for a narrowly specified stereochemistry. However, the critical radius of F in NaF_4^{3-}, 1.35 Å, is close to Pauling's "crystal" radius of F^-, 1.36 Å, and to Shannon's $r^{iv}(F^-)$, 1.33 Å.

The effect of the polarity of the X—Hal bond is examined in Fig. 21*B*, where the $r_c(Hal)_{0,4}$ are plotted against $\epsilon(Hal) - \epsilon(X)$. While $r_c(F)_0$ is not a single-valued function of $\epsilon(F)_0 - \epsilon(X)_0$, similar values of this difference correspond to similar values of $r_c(F)_0$, the data point for X = Cl again being an exception. The corresponding curve for $r_c(Cl)_4$ (m = 3–5) is, to all appearances, analogous to the Si—P—S portion of the curve for $r_c(F)_0$.

Position of the critical point

The relative position of the critical point in the X—F bond, $r_c(F)_0/(X—F)_0$, in XF_4^{ϵ} is nearly the same for m = 1 and 2, after which the critical point begins to move gradually toward X only to shift again, appreciably, away from X at m = 7 (Fig. 20*C*). The variation in XCl_4^{ϵ} parallels that for XF_4^{ϵ} at least in the limited range m = 3–5.

In the mixed species the relative position of the critical point changes very slightly with n. The total change in $r_c(F)_n/(X—F)_n$ between n = 0 and n = 3 is 0.0005 for Al, −0.0008 for Si, and −0.0022 for P; the total change in $r_c(Cl)_n/(X—Cl)_n$ between n = 4 and n = 1 is −0.0005 for Al, 0.0003 for Si, and −0.0029 for P (note the change of sign).

[4]The compatibility but non-coincidence of an empirical set of radii with a corresponding set of critical radii is well known from simple ionic crystals, e.g. alkali halides (for a discussion of this problem see, for example, ref. 32).

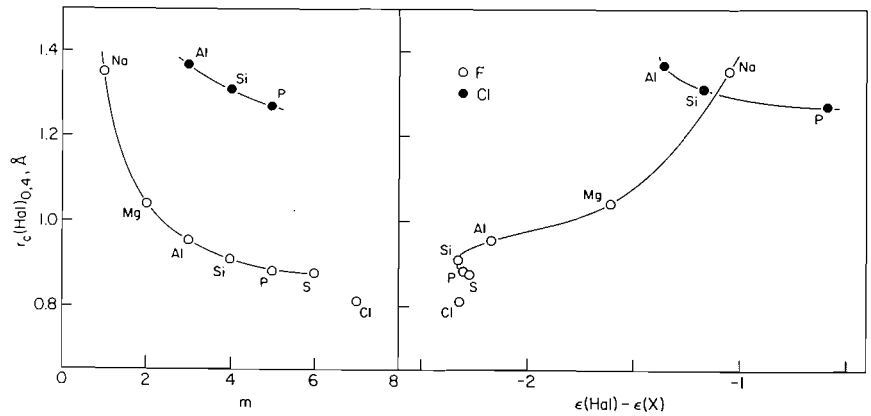

FIG. 21. *A* (*left*), variation of $r_c(F)_0$ and $r_c(Cl)_4$ with m. *B* (*right*), variation of $r_c(F)_0$ and $r_c(Cl)_4$ with the polarity of the X—Hal bond as measured by the difference $\epsilon(Hal) - \epsilon(X)$.

Electron density at the critical point

Assuming that $\rho(r_c) = 0$ for $m = 0$, the change in $\rho(r_c)_0$ with m can be approximated with reasonable accuracy by the power function $\rho(r_c) = 0.01584m^{1.59416}$ ($r^2 = 0.998$, $\sigma = 0.00423$ au $\sim 1.2\%$ of range) (Fig. 13*A*). The individual differences, which for $m = 1$ and 2 are $\sim 7\%$ and $\sim 10\%$, respectively, may be indicative of a weak fine structure in this variation. A power fit to the three points for $\rho(r_c)_4$ yields $0.007071m^{1.95638}$ ($r^2 = 1.000$, $\sigma = 0.00005$ au).

The increase in $\rho(r_c)$ with ϵ(Hal) is monotonic both for $\rho(r_c)_0$ and $\rho(r_c)_4$, for the latter at least for $m = 3$–5, but while the increase of $\rho(r_c)_0$ with $\epsilon(X)_0$ is monotonic and up to X = Al quasi-linear, the curve representing $\rho(r_c)_4$ vs. $\epsilon(X)_4$ is re-entrant (Fig. 22*A*). It appears possible, both for $\rho(r_c)_0$ vs. $\epsilon(F)_0$ and $\rho(r_c)_0$ vs. $\epsilon(X)_0$, to accommodate the point for X = Cl in a reasonable manner on a smooth extension of either curve. The course of such a continuation is, however, much less obvious for the variation of $\rho(r_c)_0$ with the critical radius of X or F (Fig. 22*B*), especially as the $\rho(r_c)_0$ vs. $r_c(X)_0$ curve can be approximated quite satisfactorily by a power function $\rho(r_c)_0 = 0.02195[r_c(X)_0]^{-4.38943}$ ($r^2 = 0.998$, $\sigma = 0.0054$ au $\sim 2\%$ of range) for $m = 1$–6, which renders the misfit of ClF_4^{3+} the more conspicuous.

The variation of $\rho(r_c)$ with n (Fig. 23*A*) again shows the difference between Al on the one hand and Si and P on the other. Because of its relative smallness this variation is better displayed as the difference $\Delta\rho(r_c)_n = \rho(r_c)_n - \rho(r_c)_{0,4}$. When $\Delta\rho(r_c)_n^{Cl}$ is plotted against $\Delta\rho(r_c)_n^{F}$ (Fig. 23*B*), interesting features reminiscent of Figs. 3 and 20*B* emerge, suggesting that the $\Delta\rho(r_c)_n$ points for Mg would fall in the Al quadrant and those for S in the Si,P quadrant. It remains to be seen whether the additional data points follow the tie-line relationships of Fig. 23*B*.

The $\rho(r_c)$ values being single numbers, the information they provide is valuable but limited. The electron-density contours (Fig. 24) give a more detailed insight into the deformation of the electron-density distribution in the X—F bond and a clearer understanding of what occurs when going from SF_4^{2+} to ClF_4^{3+}. Comparison of the shapes of the 0.2 au contour for the two species shows that the change which takes place here is qualitatively different from the progressive reduction of the separation of the individual electron-density distributions on the X and F atoms from X = Na to S. The bond in ClF_4^{3+} appears to be much more covalent, in spite of the lengthening of the internuclear X—F distance, and the change appears to affect even the 2 au contour.

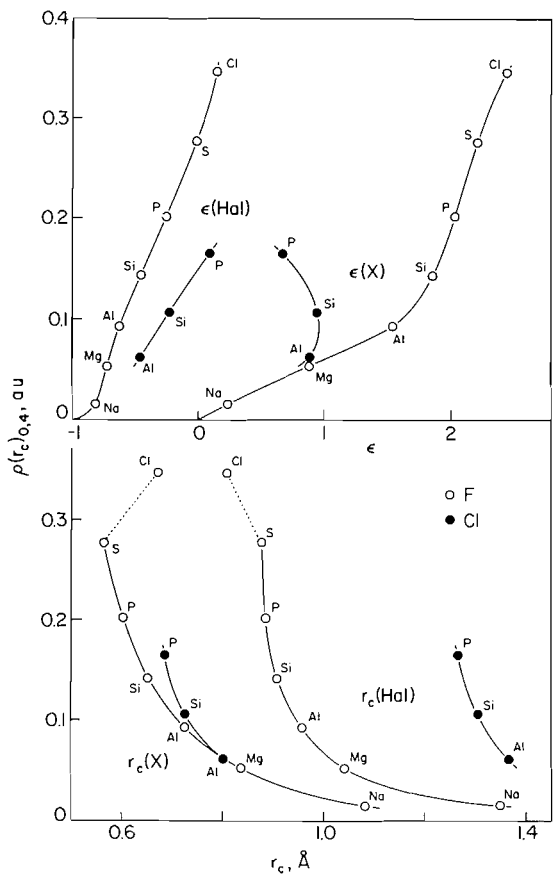

FIG. 22. Variation of the electron density at the critical point, $\rho(r_c)_{0,4}$, with ϵ(X) and ϵ(Hal) (*A*, *top*), and with r_c(X) and r_c(Hal) (*B*, *bottom*). Continuation of the visually fitted curves beyond X = S is uncertain. The label ϵ in *A* stands for ϵ(X) or ϵ(Hal).

Energy of formation

The energy of formation $E_f(0)$ of XF_4^{ϵ} decreases steadily from Na to Cl, and a similar trend is observed for $E_f(4)$ (Fig. 25). The functional form of the $E_f(0)$ vs. m variation is not known, but a cubic fit yields

$$[3] \quad E_f(0) = 0.79684 - 0.897527m - 0.04154661m^2 - 0.01436946m^3$$

($r^2 = 1.000$, $\sigma = 0.017$ au $\sim 0.14\%$ of the $m = 1$–7 range; zero at $m \sim 0.845$).

From the definition of $E_f(0)$, and using the analytical

Can. J. Chem. Downloaded from www.nrcresearchpress.com by 78.46.186.204 on 09/07/12
For personal use only.

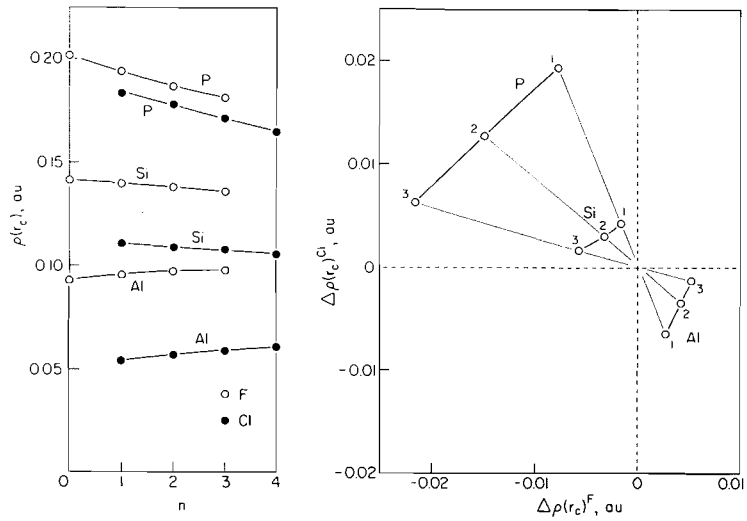

FIG. 23. *A* (*left*), variation of the electron density at the critical point, $\rho(\boldsymbol{r}_c)$, with n. *B* (*right*), correlation of $\Delta\rho(\boldsymbol{r}_c)^{Cl} = \rho(\boldsymbol{r}_c)_n{}^{Cl} - \rho(\boldsymbol{r}_c)_4$ with $\Delta\rho(\boldsymbol{r}_c)^{F} = \rho(\boldsymbol{r}_c)_n{}^{F} - \rho(\boldsymbol{r}_c)_0$.

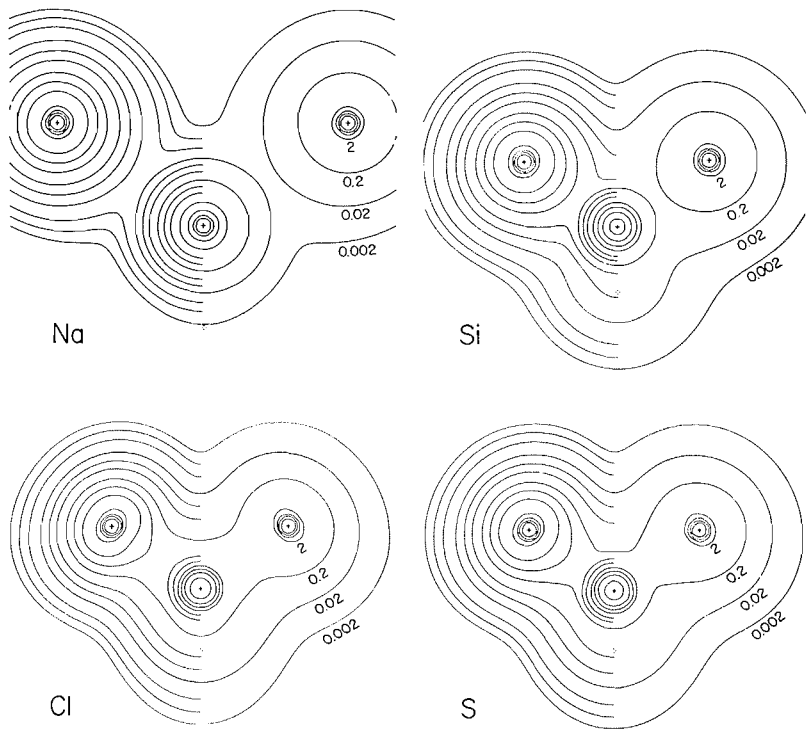

FIG. 24. Electron-density contours for NaF_4^{3-}, SiF_4, SF_4^{2+}, and ClF_4^{3+} in planes defined by the X and two of the F nuclei. The other two F nuclei project onto a position indicated by a small cross. The contours are in ten-multiples of 0.002, 0.004, and 0.008 au up to 8 au followed by 16 au.

representations of $E(0)$ (eq. [2]) and $E(X^{m+})$ (eq. [1]) together with $E(F^-)$, one obtains

$$[4]\quad E_f(0) = 0.79533 - 0.895638m - 0.0421527m^2 - 0.0143148m^3$$

($r^2 = 1.000$, $\sigma = 0.017$ au; zero at $m \sim 0.845$), from which $E_f(0)$ is 0.79533 for NeF_4^{4-} and -16.39674 au for ArF_4^{4+}. This confirms that for NeF_4^{4-} $E_f(0) > 0$, in accord with expectation. At the same time the large negative $E_f(0)$ calculated from eq. [4] for ArF_4^{4+} indicates that this species ought to be stable; the difference between $E(0)$ of ArF_4^{4+} calculated from eq. [2] and $E(Ar^{8+}) + 4E(F^-)$ is -16.39635 au, i.e. indistinguishable from the corresponding $E_f(0)$ value from eq. [3]. This conflicts with the result of the STO-3G optimization process (see above), which suggested instability of ArF_4^{4+}.

Conclusions[5]

1. Where verification is possible, the X—Hal bond lengths obtained from calculations at the 6-31G* level for the series of isoelectronic tetrahedral $XF_{4-n}Cl_n^{\epsilon}$ ($n = 0$, X = Na to Cl; $n =$ 1–4, X = Al, Si, P) species are in reasonable agreement with

[5]ADDED IN THE PROOF. The suggestion of one of the referees that we consider the results of Cremer and Kraka (33, 34) and S. Bachrach (to be published) in our discussion of the bond critical points came too late to be acted upon here. We intend to take it into account in a sequel to the present paper.

Can. J. Chem. Downloaded from www.nrcresearchpress.com by 78.46.186.204 on 09/07/12
For personal use only.

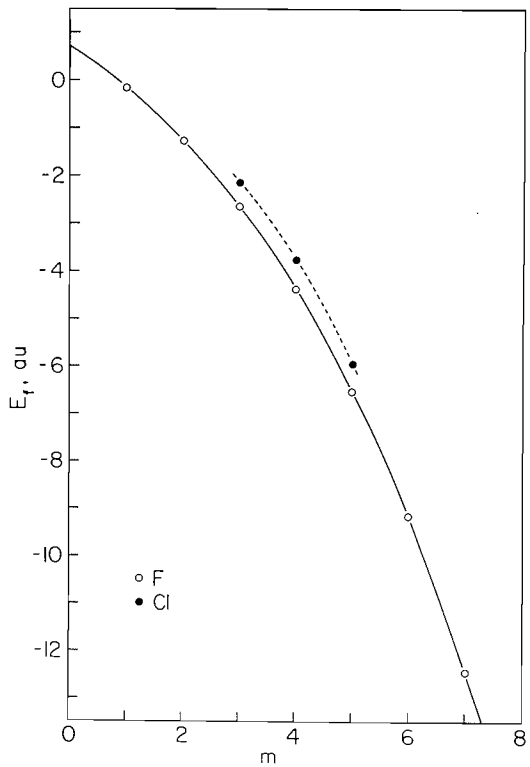

FIG. 25. Variation of the energy of formation E_f of XF_4^{ϵ} and XCl_4^{ϵ} with the oxidation state m of X.

experiment. This lends, at least qualitatively, credibility to the trends observed in the calculated molecular parameters.

2. The SCF procedure failed to converge for ArF_4^{4+}, even though the trend in the electronic energy of formation E_f suggests that this species should be more stable than any of the other XF_4^{ϵ} species in the series. On the other hand, the species SF_4^{2+} and ClF_4^{3+}, for which equilibrium geometries have been obtained, do not seem to have been reported to date, in spite of vigorous activity in fluorine chemistry in recent years. One cannot therefore conclude with certainty on the physical existence of a particular $XF_{4-n}Cl_n^{\epsilon}$ species from the result of an SCF calculation alone.

3. In general, correlations between the calculated molecular parameters for the series are not simple, but occasionally quasi-linear relationships between parameters or their changes emerge.

4. The direction in which the bond lengths, bond angles and other molecular parameters change on progressive replacement of F in XF_4^{ϵ} by Cl depends on the ionic charge ϵ. On existing indications the dividing line falls between $\epsilon < 0$ and $\epsilon > 0$.

A more detailed analysis of the results will be presented when the calculations for the mixed species $XF_{4-n}Cl_n^{\epsilon}$ (X = Na, Mg, S, Cl) and the corresponding calculations for elements of the first row (now in progress) have been completed. Comparison of the second-row with the first-row series cannot fail to be interesting, as effects of composition on the molecular parameters are always more pronounced for the first-row elements.

Acknowledgments

This investigation was supported by grants from the Natural Sciences and Engineering Research Council of Canada to R.J.B. and O.K.

1. Tables of interatomic distances and configuration in molecules and ions. Spec. Publ. No. 11. The Chemical Society, London. 1958.
2. Tables of interatomic distances and configuration in molecules and ions. Spec. Publ. No. 18. The Chemical Society, London. 1965.
3. J. SHERIDAN and W. GORDY. Phys. Rev. **77**, 719L (1950).
4. W. E. ANDERSON, J. SHERIDAN, and W. GORDY. Phys. Rev. **81**, 819 (1951).
5. P. W. ALLEN and L. E. SUTTON. Acta Crystallogr. **3**, 46 (1950).
6. R. L. LIVINGSTON and D. H. LYON. J. Chem. Phys. **24**, 1283 (1956).
7. Y. MORINO, Y. NAKAMURA, and T. IIJIMA. J. Chem. Phys. **32**, 643 (1960).
8. M. W. LONG, Q. WILLIAMS, and T. L. WEATHERLY. J. Chem. Phys. **33**, 508 (1960).
9. J. H. N. LOUBSTER. J. Chem. Phys. **36**, 2808 (1962).
10. Y. MORINO and Y. MURATA. Bull. Chem. Soc. Jpn. **38**, 104 (1965).
11. R. HOLM, M. MITZLAFF, and H. HARTMANN. Z. Naturforsch. **22**a, 1287 (1967).
12. R. R. RYAN and K. HEDBERG. J. Chem. Phys. **50**, 4986 (1969).
13. R. J. GILLESPIE. Molecular geometry. Van Nostrand Reinhold Company, London. 1972.
14. K. HAGEN and K. HEDBERG. J. Chem. Phys. **59**, 1549 (1973).
15. H. TAKEO and C. MATSUMURA. Bull. Chem. Soc. Jpn. **50**, 636 (1977).
16. R. A. WHITESIDE, M. J. FRISCH, J. S. BINKLEY, D. J. DEFREES, H. B. SCHLEGEL, KRISHNAN RAGHAVACHARI, and J. A. POPLE. Carnegie-Mellon Quantum Chemistry Archive. 2nd. ed. Carnegie-Mellon University, Pittsburgh, PA. 1981.
17. A. F. WELLS. Structural inorganic chemistry. 5th ed. Clarendon Press, Oxford. 1984.
18. O. KNOP, T. S. CAMERON, D. ADHIKESAVALU, B. R. VINCENT, and J. A. JENKINS. Can. J. Chem. To be published.
19. M. ATOJI and W. N. LIPSCOMB. Acta Crystallogr. **7**, 597 (1954).
20. T. J. KISTENMACHER and G. D. STUCKY. Inorg. Chem. **10**, 122 (1971).
21. M. L. ZIEGLER, B. NUBER, K. WEIDENHAMMER, and G. HOCH. Z. Naturforsch. **32**b, 18 (1977).
22. G. TRINQUIER, J.-P. DAUDEY, G. CARUANA, and Y. MADAULE. J. Am. Chem. Soc. **106**, 4794 (1984).
23. M. M. FRANCL, W. J. PIETRO, W. J. HEHRE, J. S. BINKLEY, M. S. GORDON, D. J. DEFREES, and J. A. POPLE. J. Chem. Phys. **77**, 3654 (1982).
24. P. C. HARIHARAN and J. A. POPLE. Theor. Chim. Acta, **28**, 213 (1973).
25. J. S. BINKLEY, R. A. WHITESIDE, R. KRISHNAN, R. SEEGER, D. J. DEFREES, H. B. SCHLEGEL, S. TOPIOL, L. R. KHAN, and J. A. POPLE. GAUSSIAN 80. Department of Chemistry, Carnegie-Mellon University, Pittsburgh, PA. 1980.
26. R. S. MULLIKEN. J. Chem. Phys. **23**, 1833; **23**, 1841 (1955).
27. R. F. W. BADER. AIMPAC series of programs. Department of Chemistry, McMaster University, Hamilton, Ont. 1983.
28. R. D. SHANNON. Acta Crystallogr. A, **32**, 751 (1976).
29. E. CLEMENTI and C. ROETTI. Atom. Data Nucl. Data Tables, **14**, 177 (1974).
30. E. CLEMENTI. IBM J. Res. Devel. **9**, 2 (1965).
31. R. F. W. BADER. Acc. Chem. Res. **18**, 9 (1985).
32. D. M. ADAMS. Inorganic solids. Wiley, London. 1974. pp. 35–40.
33. D. CREMER and E. KRAKA. Angew. Chem. Int. Ed. **23**, 627 (1984).
34. D. CREMER and E. KRAKA. Croat. Chem. Acta, **57**, 1259 (1984).

Can. J. Chem. Downloaded from www.nrcresearchpress.com by 78.46.186.204 on 09/07/12
For personal use only.

Extraction and spectrophotometric determination of molybdenum(VI) with *N*-phenylbenzohydroxamic acid and phenylfluorone

H. DASARATHA GUNAWARDHANA[1] AND S. AMARASIRI FERNANDO

Centre for Analytical Research and Development, Department of Chemistry, University of Colombo, P.O. Box 1490, Colombo-3, Sri Lanka

Received October 21, 1986

This paper is dedicated to Professor Douglas E. Ryan on the occasion of his 65th birthday

H. DASARATHA GUNAWARDHANA and S. AMARASIRI FERNANDO. Can. J. Chem. **65**, 1124 (1987).

N-Phenylbenzohydroxamic acid reacts with molybdenum(VI) in 3.5–6.0 *M* hydrochloric acid to give a complex that is extractable into chloroform. The chloroform extract of the molybdenum complex, on second extraction from a dilute hydrochloric acid medium (0.2–0.3 *M*) in the presence of phenylfluorone and ethanol, forms an intensely coloured complex possessing an absorption maximum at 518 nm. Job's method of continuous variation reveals that the complex is Mo(VI)—2NPBHA—PF. The molar absorptivity under optimum conditions is 7.4×10^4 dm^3 mol^{-1} cm^{-1}. The system obeys Beer's law up to 0.6 ppm of molybdenum(VI). Considerable amounts of many cations and anions can be tolerated. The interference from vanadium(IV) and vanadium(V) can be eliminated by the addition of sodium metabisulphite, whereas the interference from titanium(IV) is mitigated by oxalate ions. The method has been successfully applied for the determination of molybdenum in a standard steel sample.

H. DASARATHA GUNAWARDHANA et S. AMARASIRI FERNANDO. Can. J. Chem. **65**, 1124 (1987).

L'acide *N*-phénylbenzohydroxamique réagit avec le molybdène(VI), dans des solutions contenant de 3,5 à 6,0 *M* d'acide chlorhydrique, pour donner un complexe que l'on peut extraire par le chloroforme. La solution chloroformique du complexe de molybdène, soumise à une seconde extraction avec une solution diluée (0,2 à 0,3 *M*) d'acide chlorhydrique, en présence de phénylfluorone et d'éthanol, forme un complexe extrèmement coloré qui possède un maximum d'absorption à 518 nm. La méthode de Job de variation continue permet de mettre en évidence que le complexe est Mo(VI)—2 ANPBH—PF. L'absorption molaire, dans des conditions optimales, est égale à $7,4 \times 10^4$ dm^3 mol^{-1} cm^{-1}. Le système obéit à la loi de Lambert-Beer jusqu'à une concentration de 0,6 ppm de molybdène(VI). Des quantités considérables de plusieurs cations ou anions peuvent être tolérées. On peut éliminer les interférences dues au vanadium(IV) et (V) en additionnant du métabisulfite de sodium et l'on peut mitiger les interférences dues au titane(IV) en ajoutant des ions oxalates. On a appliqué la méthode avec succès à la détermination du molybdène dans un échantillon standard d'acier.

[Traduit par la revue]

Can. J. Chem. Downloaded from www.nrcresearchpress.com by 78.46.186.204 on 09/07/12
For personal use only.

Introduction

In the determination of molybdenum using atomic absorption spectrometry, it is difficult to obtain high sensitivity, owing to the formation of stable oxides in the flame and sometimes stable carbides in non-flame atomizers. Therefore, it is useful to develop highly sensitive and selective spectrophotometric methods for the determination of molybdenum.

Pilipenko and co-workers (1, 2) reported the use of phenylfluorone(9-phenyl-2,6,7-trihydroxy-3*H*-xanthen-3-one) (PF) and an alcohol in conjunction with *N*-phenylbenzohydroxamic acid (NPBHA) to achieve an enhanced intensity of colour in the determination of titanium. *N*-Phenylfurohydroxamic acid (3) and *N*-phenyllaurohydroxamic acid (4) have also been used in place of NPBHA. The method consists of first extraction of metal from a strong mineral acid medium into a chloroformic solution of NPBHA, followed by a second extraction of the resulting chloroform extract with an alcoholic solution of PF and very dilute hydrochloric acid. The first extraction provides a certain amount of selectivity for molydbenum and gives a colourless chloroform extract (5), and the second extraction imparts a coloured organic layer possessing a maximum absorption at 518 nm.

Experimental

Apparatus

A Cecil model 373 visible spectrophotometer was used for absorptiometric measurements. A Varian DMS 90 UV/Visible spectrophotometer was used for the spectra.

Reagents

Analytical grade reagents were used wherever possible. All solvents were purified and distilled prior to use. NPBHA was prepared using a procedure described by MAJUMDAR (5), and the purity of the recrystallised product was checked by melting point determination. Analytical reagent grade phenylfluorone (Eastman) was used without further purification.

A stock solution of molybdenum(VI) was prepared by dissolving ammonium molybdate in water. The final solution of approximately 1000 ppm was standardised by using a Jones reductor (6).

Recommended procedure for the spectrophotometric determination of molybdenum(VI)

First extraction

Transfer an aliquot of sample solution containing up to 6 μg of molybdenum(VI) into a separating funnel. Add 3.0 cm^3 of concentrated hydrochloric acid and dilute to 10 cm^3. Add 10 cm^3 of 0.005% m/V NPBHA in chloroform and equilibrate for 3–5 min.

Second extraction

Withdraw 5.0 cm^3 of the organic phase from the first extraction and transfer it into a separating funnel. Add 2.0 cm^3 of 0.025% m/V PF in ethanol. Then add 5.0 cm^3 of a solution which is 0.25 *M* with respect to hydrochloric acid and 0.64 *M* with respect to sodium chloride. Equilibrate for 1 min. After 20 min, measure the absorbance of the organic phase at 518 nm against a reagent blank.

The solution of PF in ethanol was prepared by mixing 1.0 cm^3 of 0.3% m/V PF in dimethylformamide with 10.0 cm^3 of ethanol. In this way, it is possible to achieve a greater solubility of PF in ethanol. This preparation was done daily.

Results and discussion

Absorption spectra and the composition of the extracted species Mo(VI)—NPBHA—PF

Molybdenum(VI) forms a colourless complex with NPBHA. This complex on the second extraction with phenylfluorone forms an intensely coloured complex possessing a prominent

Can. J. Chem. Downloaded from www.nrcresearchpress.com by 78.46.186.204 on 09/07/12
For personal use only.

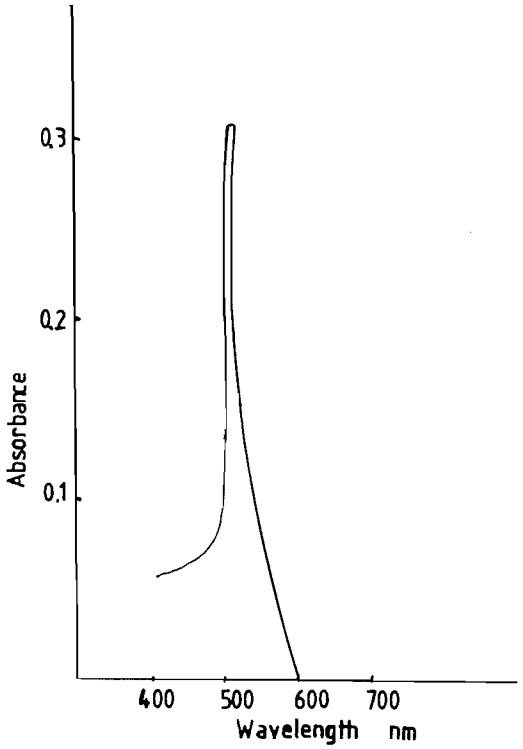

FIG. 1. Absorption spectra of Mo(VI)—NPBHA—PF complex in chloroform against a reagent blank. Mo(VI) = 0.5 ppm, NPBHA = 0.005% m/V in chloroform, PF = 0.025% m/V in ethanol.

absorption maximum at 518 nm against a reagent blank (Fig. 1). Job's method of continuous variation was applied to Mo(VI)—NPBHA by keeping the concentration of PF in excess. The Job's plot (Fig. 2(*A*)) obtained in this manner suggests the formation of a 1:2 complex between molybdenum(VI) and NPBHA. The second Job's plot (Fig. 2(*B*)) was obtained by keeping the stoichiometric ratio of molybdenum(VI) to NPBHA at 1:2, which reveals the stoichiometry of the complex Mo(VI):NPBHA:PF as 1:2:1. Greater curvature of graph *A* compared with graph *B* reveals a strong bonding between molybdenum(VI) and PF.

The absorbance at 518 nm increases with time and reaches a maximum about 20 min after the second extraction. This remains constant even 2 h after the second extraction if the organic phase is separated from the aqueous phase soon after the extraction.

Effect of concentration of hydrochloric acid and chloride ions

The concentration of hydrochloric acid in the first extraction was varied from 1.0 to 11.0 *M* and the concentration was determined by titrating with a standard solution of sodium carbonate (0.05 *M*) using methyl orange as the indicator. The optimum concentration of hydrochloric acid that could be used for the first extraction of molybdenum with NPBHA was found to be in the range 3.0–5.5 *M*.

In the second extraction, the concentration of hydrochloric acid was varied from 0.06 to 0.5 *M* maintaining the chloride ion concentration at 0.5 *M*. The results indicate that the optimum concentration of hydrochloric acid is 0.25 *M* (Table 1), which is equivalent to a calculated pH of 0.6. Variation of the concentration of chloride ions at optimum concentration of hydrochloric acid reveals (Table 2) that absorbance is highest at 0.64 *M* chloride ion concentration.

At low acidities (high pH) the Mo(VI)—NPBHA—PF complex breaks down due to hydrolysis of molybdenum(VI) and also due to the formation of an insoluble red complex of Mo(VI)—PF (Table 1). With increasing concentration of hydrochloric acid, beyond 0.25 *M*, the organic phase became more yellow in appearance, and was accompanied by a decrease in absorbance at 518 nm against a reagent blank. The protona-

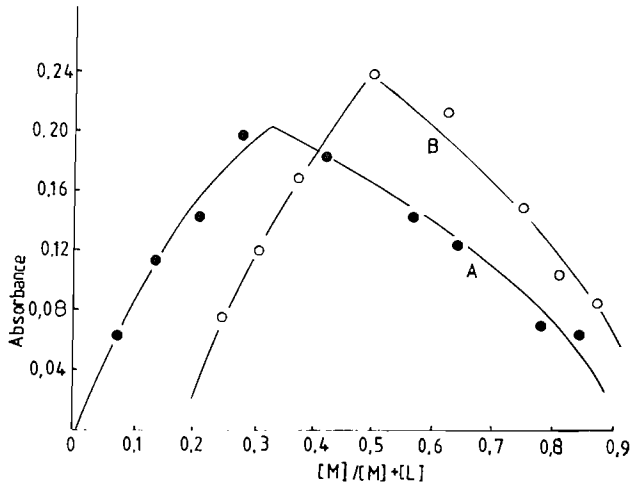

FIG. 2. Continuous variation plot of (*A*) Mo(VI)—NPBHA, (*B*) Mo(VI):2 NPBHA—PF.

TABLE 1. Effect of hydrogen ion concentration on the second extraction*

Hydrogen ion concentration (mol dm^{-3})	pH (calculated)	Absorbance at 518 nm
0.50	0.30	0.535
0.38	0.42	0.575
0.33	0.48	0.620
0.25	0.60	0.650
0.20	0.70	0.610
0.16	0.80	0.600
0.10	1.00	0.510

*Molybdenum(IV) = 1.00 ppm, HCl = 4.0 *M* (first extraction), NPBHA = 0.005% m/V in chloroform, PF = 0.025% m/V in ethanol.

TABLE 2. Effect of chloride ion concentration on the second extraction*

Chloride ion concentration (mol dm^{-3})	Absorbance at 518 nm
0.24	0.520
0.32	0.540
0.40	0.580
0.46	0.560
0.48	0.600
0.56	0.630
0.64	0.660
0.72	0.640
0.80	0.585
0.88	0.550
0.96	0.525

*Molybdenum(IV) = 1.0 ppm, HCl = 4.0 *M* (first extraction), NPBHA = 0.005% m/V in chloroform, PF = 0.025 m/V in ethanol.

TABLE 3. Effect of different alcohols on the absorbance*

Alcohol	Absorbance at 518 nm
Methanol	0.515
Ethanol	0.690
n-Butanol	0.635
iso-Butanol	0.625
Amyl alcohol	0.595

*Molybdenum(VI) = 1.0 ppm, HCl = 4 *M* (first extraction), NPBHA = 0.005% m/V in chloroform, PF = 0.025% in ethanol, HCl = 0.25 *M* (second extraction).

TABLE 4. Tolerance limits for diverse ions in the determination molybdenum(IV) by the proposed method

Foreign ion	Tolerance limit (ppm)	Molar ratio Mo(V):ion
Vanadium(V) and vanadium(IV)*	—	—
Titanium(IV)†	12.5	50
Zirconium(IV)	20.0	42
Fluoride	100.0	1010
Oxalate	800.0	1744
Phosphate	300.0	606

*In the presence of sodium metabisulphite.
†In the presence of 800 ppm of oxalate.

tion of PF at high acidities (low pH) may lead to a break down of the Mo(VI)—NPBHA—PF complex. The variation of the chloride ion concentration also reveals a somewhat similar effect (Table 2), indicating that chloride ions are involved in complex formation. However, concentrations of chloride ions above 0.64 *M* lead to a break down of the mixed ligand complex.

Effect of concentrations of the reagents (NPBHA and PF)

The absorbance of the Mo(VI)—NPBHA—PF complex at 518 nm increases with increasing concentration of NPBHA and reaches a maximum when the concentration of NPBHA in chloroform is maintained around 0.005% m/V. This corresponds to a 59-fold molar excess of NPBHA. The observed decrease in absorbance at low NPBHA concentrations may be due to incomplete extraction of molybdenum(VI). Higher NPBHA concentrations are undesirable, probably owing to increased interaction between NPBHA and PF, resulting in a decrease in interaction with molybdenum(VI), thus giving lower absorbance values.

The absorbance at 518 nm reaches a maximum when the concentration of PF is in 60-fold molar excess. A decrease in absorbance at lower and higher concentrations has been observed. At higher concentrations of PF, a practical difficulty arose as a result of precipitation. This can be accounted for by the formation of a Mo(VI)—PF complex, which in general is not soluble in the organic phase and also not extracted by the chloroform–ethanol organic phase (4).

Effect of different alcohols

Table 3 shows that ethanol gives the highest absorbance values among the five alcohols investigated. The results in the Table 3 were obtained while keeping the chloroform:alcohol ratio at 5:2 by volume.

Verification of Beer's law

The verification of Beer's law was carried out under optimum conditions. They were NPBHA = 0.005% m/V in chloroform, HCl = 4.0 *M* (first extraction), PF = 0.025% m/V in ethanol, HCl = 0.25 *M* (second extraction) and shaking time of 4 min. The system obeys Beer's law at 518 nm up to 0.6 ppm of molybdenum(VI). A negative deviation has been observed at higher concentrations. The molar absorptivity at 518 nm was $7.4 \times 10^4\ dm^3\ mol^{-1}\ cm^{-1}$. A plot of Beer's law gave a highly precise, reproducible straight line calibration graph that passed through the origin.

Effect of diverse ions

The system was found to tolerate a large excess of cobalt(II), chromium(III), copper(II), aluminium, manganese, zinc, nickel, iron, thorium, and lanthanum(III). The tolerance limit was considered as the amount of foreign ion causing a deviation of more than 0.02 absorbance. There is interference from titanium(IV), tungsten(VI), vanadium(V) and vanadium(IV). The interference from vanadium(V) and vanadium(IV) can be completely eliminated by the addition of sodium metabisulphite. As the system can tolerate a 1700-fold molar excess of oxalate (Table 4), the ability of titanium to form stable complexes with oxalate more readily than molybdenum was taken into consideration. It was observed that in the presence of a 1700-fold molar excess of oxalate (approximately 800 ppm) the system was capable of tolerating a 50-fold molar excess of titanium without affecting the overall sensitivity appreciably.

Application of the method

The proposed spectrophotometric method was applied to the determination of molybdenum in standard low alloy steel samples. Steel sample number 401 (B.C.S.), containing 1.03% molybdenum, was analysed and was found to contain 1.03% molybdenum. Similarly, sample 406 (B.C.S. certified value 0.53% molybdenum) was found to contain 0.52%. A sample containing an apatite matrix was also analysed for molybdenum using the proposed method. The results obtained were comparable to those obtained by inductively coupled plasma emission spectroscopy (ICP). The ICP analyses reported the following elements in the sample were molybdenum = 0.54 ppm, iron = 22.05 ppm, aluminium = 11.50 ppm, vanadium = 0.13 ppm, calcium = 214.00 ppm, manganese = 1.46 ppm, zinc = 0.13 ppm, cadmium = 0.01 ppm, copper = 0.11 ppm, and strontium = 2.16 ppm. The concentration of molybdenum in the sample obtained by the proposed method was 0.50 ± 0.016 ppm.

Highly sensitive and selective spectrophotometric methods of this nature will find many advantages in the determination of unbound or "free" concentrations of molybdenum (7), provided that the concentration of the bound species of molybdenum is unaffected by 3–5 *M* hydrochloric acid NPBHA in chloroform.

Acknowledgement

The authors record their gratitude to Professor D. E. Ryan for proposing this study. They are also grateful to the Canadian International Development Agency (CIDA) for providing funding to establish the Centre for Analytical Research and Development (CARD), University of Colombo, Sri Lanka. Dr. O. C. Wickremasinghe of Geological Survey Department, Sri Lanka, and Dr. Nimalasiri de Silva of National Research

Can. J. Chem. Downloaded from www.nrcresearchpress.com by 78.46.186.204 on 09/07/12
For personal use only.

Council, Canada, are gratefully acknowledged for providing standard steel samples and the ICP facilities, respectively.

1. A. T. PILIPENKO, E. A. SHPAK, and O. S. ZUL'FIGAROV. Zh. Anal. Khim. **29**, 1074 (1974).
2. A. T. PILIPENKO, E. A. SHPAK, and O. S. ZUL'FIGAROV. Zh. Anal. Khim. **30**, 1009 (1975).
3. A. T. PILIPENKO, E. A. SHPAK, and M. V. GREMENKO. Zh. Anal. Khim. **30**, 1535 (1975).
4. H. DASARATHA GUNAWARDHANA. Analyst, **108**, 952 (1983).
5. A. K. MAJUMDAR. *N*-benzoylphenylhydroxylamine and its analogues. Pergamon Press, Oxford. 1972.
6. A. I. VOGEL. Text book of quantitative inorganic analysis. 4th ed. Longman, London. 1978. p. 394.
7. R. FULTON and B. KRATOCHVIL. Anal. Chem. **52**, 546 (1980).

Can. J. Chem. Downloaded from www.nrcresearchpress.com by 78.46.186.204 on 09/07/12
For personal use only.

Identification of the photolysis products of nitrofurazone irradiated with laboratory illumination

MICHAEL A. QUILLIAM,[1] BRIAN E. MCCARRY, AND KEN H. HOO
Department of Chemistry, McMaster University, Hamilton, Ont., Canada L8S 4M1

AND

DENNIS R. MCCALLA AND SUSAN VAITEKUNAS
Department of Biochemistry, McMaster University, Hamilton, Ont., Canada L8N 3Z5

Received October 24, 1986

This paper is dedicated to Professor Douglas E. Ryan on the occasion of his 65th birthday

MICHAEL A. QUILLIAM, BRIAN E. MCCARRY, KEN H. HOO, DENNIS R. MCCALLA, and SUSAN VAITEKUNAS. Can. J. Chem. **65**, 1128 (1987).

Illumination of aqueous or organic solutions of nitrofurazone, **1**, with fluorescent or tungsten light caused the appearance of two new compounds, **2** and **3**. Compound **2**, which eluted just before nitrofurazone on a reverse phase hplc column, had a mass spectrum identical to that of **1** and converted back to **1** at a rate proportional to the temperature and the polarity of the solvent when allowed to sit in the dark. High resolution proton nmr spectroscopy provided conclusive evidence that compound **2** is the *syn* isomer of **1**. Compound **3** had a retention time, ultraviolet spectrum, and mass spectrum that were indistinguishable from those of synthetic 5-nitrofuraldehyde azine. The toxicity of **3** to *E. coli* was determined to be the same as **1** while its mutagenicity was over 10-fold lower. No detectable cross-links were formed in the DNA of *E. coli* in the presence of compound **3**. Thus, it is unlikely that the relatively small amounts of the azine **3** formed have much influence on the antibacterial potency or mutagenicity of nitrofurazone solutions. However, these results do confirm the desirability of conducting experiments with these agents in the dark or under yellow light. Photochemical formation of *syn* isomers was also observed with two other Schiff's base nitrofuran derivatives, nitrofurantoin and furazolidone.

MICHAEL A. QUILLIAM, BRIAN E. MCCARRY, KEN H. HOO, DENNIS R. MCCALLA et SUSAN VAITEKUNAS. Can. J. Chem. **65**, 1128 (1987).

L'irradiation de solutions aqueuses ou organiques de nitrofurazone (**1**) par de la lumière fluorescente ou au tungstène conduit à l'apparition des deux nouveaux composés, **2** et **3**. Le spectre de masse du composé **2**, qui est élué juste avant la nitrofurazone par clhp en phase inverse, est identique à celui du composé **1** et, lorsqu'on le laisse reposé dans un solvant à l'abri de la lumière, il se retransforme dans le composé **1** à une vitesse qui est proportionnelle à la température et à la polarité du solvant. La rmn ^1H à haute résolution a permis de démontrer sans ambiguïté que le composé **2** est l'isomère *syn* du composé **1**. Les temps de rétention et les spectres de masse et ultraviolet du composé **3** ne peuvent être différenciés de ceux de l'azine synthétique du nitro-5 furaldéhyde. On a déterminé que la toxicité du composé **3** pour l'*E. coli* est la même que celle du composé **1** et que sa mutagénicité est dix fois moindre. On n'a pas pu détecter de réticulation de l'ADN du *E. coli* en présence du composé **3**. Il semble donc peu probable que les petites quantités de l'azine **3** qui se forment puissent influencer le pouvoir antibactérien ou la mutagénicité de solutions de nitrofurazone. Toutefois, nos résultats confirment qu'il est désirable d'effectuer, avec ces agents, des expériences à l'abri de la lumière ou en présence de lumière jaune. On a aussi observé la formation photochimique des isomères *syn* avec deux autres bases de Schiff dérivées du nitrofuranne, soit la nitrofurantoïne et la furazolidone.

[Traduit par la revue]

Introduction

Nitrofurans are used as antibacterial agents in clinical and veterinary medicine and as additives to feed for livestock (see review in ref. 1). In the course of examining the bacterial metabolism of one of these agents, nitrofurazone, **1**, using reverse phase high performance liquid chromatography (hplc) we observed two new compounds which retained the strong absorption band near 370 nm. These compounds were not observed in the absence of nitrofurazone but were formed even in the absence of bacteria. Further analysis showed that both of these compounds are photoproducts formed from nitrofurazone by laboratory illumination. We show here that one of these compounds is the *syn* isomer of nitrofurazone, **2**, and that the other is the 5-nitro-2-furaldehyde azine, **3**. We also show that the azine is a considerably weaker mutagen than nitrofurazone and that it does not induce the formation of cross-links in DNA in *E. coli*.

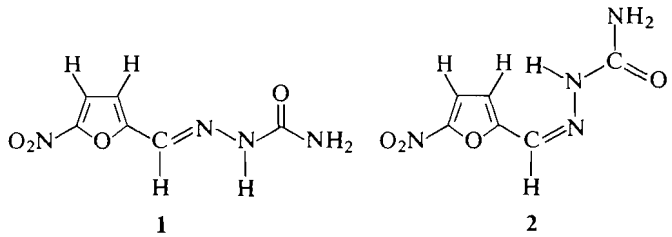

1

2

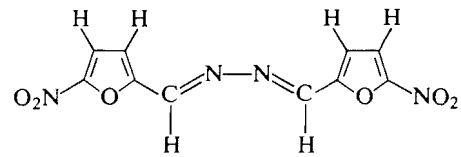

3

Experimental

Materials

Hydrazine hydrate, semicarbazine hydrochloride, and 5-nitro-2-furaldehyde diacetate were purchased from Aldrich Chemical. Nitrofurantoin and furazolidone were purchased from Sigma Chemical. HPLC-grade methanol and acetonitrile were purchased from Caledon Chemicals and HPLC-grade water was produced with a Millipore Milli-Q purification unit.

Synthesis

5-Nitro-2-furaldehyde, **4**, was prepared by hydrolysis of the

[1]Author to whom correspondence may be addressed.

Can. J. Chem. Downloaded from www.nrcresearchpress.com by 78.46.186.204 on 09/07/12
For personal use only.

5-nitro-2-furaldehyde diacetate (3). Nitrofurazone (**1**, 2-[[5-nitro-2-furanyl]methylene]-hydrazinecarboxamide) was prepared by condensing 5-nitro-2-furaldehyde, **4**, with semicarbazide (2) and was purified by recrystallization and silica gel column chromatography. The 5-nitro-2-furaldehyde azine, **3**, was prepared by condensation of 3.0 g (0.02 mol) of **4** with 0.5 g (0.01 mol) of hydrazine hydrate (4). The hydrazone of 5-nitro-2-furaldehyde, **5**, was prepared from 5-nitro-2-furaldehyde diacetate and hydrazine hydrate (5).

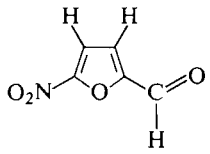

4

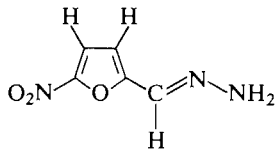

5

Photolysis by fluorescent illumination

Nitrofurazone (0.05 mg/mL) in 200 mL Davis Mingioli culture medium (6) was exposed for 1 h at 37°C to light from standard cool white fluorescent laboratory illumination or incubated under the same conditions in the dark. Aliquots of these solutions (10 mL) were extracted with equal volumes of ethyl acetate, the organic extracts were evaporated and the residues dissolved in 0.5 mL methanol for analysis. The samples were protected from light during these steps.

Photolysis by tungsten illumination

Solutions of nitrofurazone (0.1 mg/mL) in water, methanol, or tetrahydrofuran were illuminated for 5 min with a Sylvania tungsten photographic lamp (type ECT, 500 W) at a distance of 7 cm while immersed in an ice bath. Analyses were performed directly on these solutions before and after illumination.

A solution of nitrofurazone (1.0 mg/mL) in methanol-d_4 was similarly illuminated for 50 min. High performance liquid chromatographic and nmr analyses were performed on this solution before and after illumination.

Chromatography and ultraviolet spectroscopy

High performance liquid chromatographic analyses were performed using a Hewlett-Packard model HP1090 liquid chromatograph with detection and ultraviolet spectrum scanning provided by a built-in HP1040A photodiode array detector (set to scan 200 to 400 nm every 2 s). A Beckman reverse phase hplc column (5 μm Ultrasphere-ODS, 25 cm × 4.6 mm id) was operated with 1 mL/min flow rate and a gradient elution that started at 10% aqueous methanol and was programmed linearly first to 50% methanol in 13 min and then to 100% methanol in a further 3 min. Samples were injected with a 20 μL Rheodyne injector. Separated compounds were isolated for further analysis by collecting eluent at the detector outlet into glass tubes protected from light.

Mass spectrometry

Electron ionization mass spectra were acquired on a VG7070F mass spectrometer with an electron energy of 70 eV and a source temperature of 200°C. Samples were introduced either via the solid probe inlet or via the hplc and the VG moving belt lc/ms interface. Only 20% of the hplc eluent was taken to the lc/ms interface and an infrared evaporator was used to evaporate the solvent prior to the vacuum lock system.

Nuclear magnetic resonance spectroscopy

Proton nmr spectra were obtained at 500 MHz on a Brucker AM-500 spectrometer.

Mutagenicity assays

With *Escherichia coli* WP2 and WP2 *uvr A* the "treat and plate" protocol described by Green and Muriel (7) was followed. Assays with *Salmonella typhimurium* were carried out as described by Ames *et al.* (8). Bacteria were exposed to the azine, **3**, for 20 min before plating.

Crosslinking assay

E. coli B/r of WP2 *uvr A* (8×10^{10} bacteria in 200 mL) were exposed to 1 μg/mL mitomycin C and 1 or 5 μg/mL of **3** in a 37°C water bath for 60 min. DNA was isolated as described by Marmur (9).

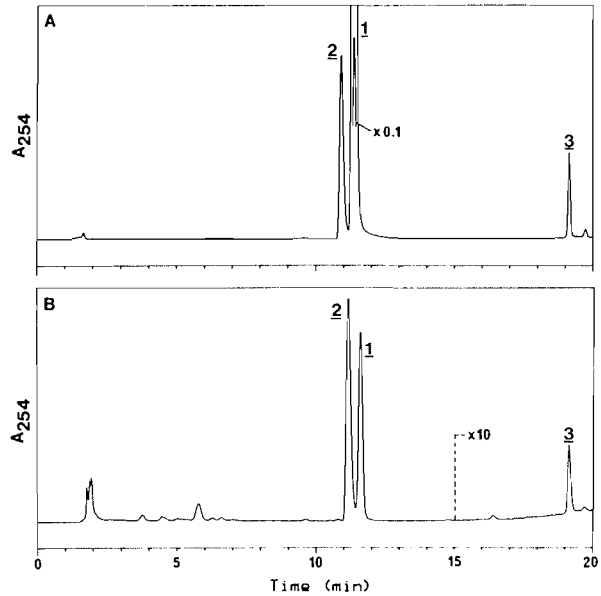

FIG. 1. Reverse phase hplc chromatograms with detection at 254 nm of: (*A*) nitrofurazone in Davis Mingioli culture medium exposed for 1 h to light from fluorescent laboratory illumination; (*B*) nitrofurazone in methanol exposed for 5 min to high intensity tungsten illumination.

The percentage reversibility of DNA denaturation was estimated using the general procedure described by Rutman *et al.* (10).

Results

Figure 1*a* shows the chromatogram resulting from the reverse phase hplc analysis of a solution of nitrofurazone in Davis Mingioli culture medium that had been incubated at 37°C and exposed to laboratory fluorescent illumination for 1 h. An identical solution that had been kept in the dark under the same conditions showed only nitrofurazone, **1**, to be present. Thus, compounds **2** and **3** are formed as a result of a photochemical reaction of nitrofurazone. High performance liquid chromatographic analysis of a methanolic solution of nitrofurazone that had been exposed to intense tungsten illumination for 10 min at 0°C gave the chromatogram shown in Fig. 1*b*. A maximum yield of **2**, approximately equal to that of **1**, was achieved within 5 min of exposure. In addition to a small amount of compound **3**, a number of polar products with short retention times were also observed. Through the use of a combination of hplc with a scanning photodiode array detector and with a mass spectrometer (equipped with a moving belt lc/ms interface), the ultraviolet and mass spectra were acquired for compounds **2** and **3** (see Figs. 2 to 4).

The mass spectrum of compound **2** (see Fig. 3) is identical to that of nitrofurazone, showing a molecular ion at m/z 198 and fragment ions due to loss of OH from the nitro group (m/z 181) and HNCO from the amide group (m/z 155). The facts that compounds **1** and **2** have the same molecular weight and very similar ultraviolet spectra (see Fig. 2) suggested that the two compounds are geometrical isomers. This was supported by the observation that, as the exposed solutions sat in the dark, the concentration of compound **2** decreased while that of **1** increased proportionately. The rate of the dark reaction was proportional to temperature, supporting a thermally induced *syn/anti* isomerization. When compound **2** was isolated by hplc and then re-chromatographed, both compounds **1** and **2** were again observed due to isomerization during the time between peak collection and re-injection.

Can. J. Chem. Downloaded from www.nrcresearchpress.com by 78.46.186.204 on 09/07/12
For personal use only.

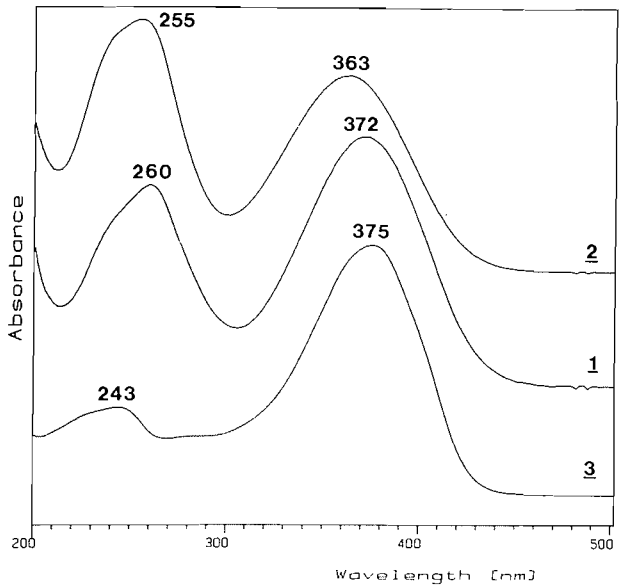

FIG. 2. Ultraviolet spectra for compounds **1** to **3**.

A nitrofurazone solution in methanol-d_4 was examined by high resolution proton nuclear magnetic resonance spectroscopy before and after exposure to tungsten illumination; the nmr spectra are shown in Fig. 5. Before irradiation nitrofurazone showed three resonances at 7.025 (doublet), 7.509 (doublet), and 7.777 (singlet) ppm; after irradiation, in addition to these resonances, three new ones appeared at 7.102 (doublet), 7.243 (singlet), and 7.578 (doublet) ppm. The greatest change in chemical shift was observed for the imino C—H proton which underwent an upfield shift of 0.534 ppm. Similar upfield shifts have been observed in the *syn* isomers of a wide range of hydrazones, oximes, and related compounds (11). Thus, the unstable product from irradiation of compound **1** is the *syn* isomer of nitrofurazone, compound **2**.

When different solvents were used for the photolysis experiments, it was observed that the rate of thermal isomerization of the *syn* to *anti* isomer depended on the polarity of the solvent. The $t_{1/2}$ values for water, methanol, and tetrahydrofuran were very roughly estimated to be in the order of 1 min, 1 h, and 10 h, respectively. Since the mobile phase used in the hplc experiments is aqueous methanol, we should expect some conversion of **2** to **1** during the time period of the chromatographic experiment. Evidence for this isomerization is apparent from the chromatograms in Fig. 1, where the peak for compound **2** is wider and more asymmetric than that for compound **1**. To provide further evidence for on-column isomerization, isocratic elutions were conducted at elevated column temperatures. Unfortunately, an increased column temperature resulted in a decreased separation factor. At 50°C the peaks were fused together so that any increased tailing could not be observed. Using acetonitrile in place of methanol gave poorer resolution of **1** and **2** at any temperature. The polarity of the solvent used in the photolysis did not appear to substantially affect the yield of **3**.

Chromatographic analysis of the illuminated solutions of two other Schiff's base nitrofuran derivatives, **6** (nitrofurantoin) and **7** (furazolidone), revealed in each case a new peak which eluted

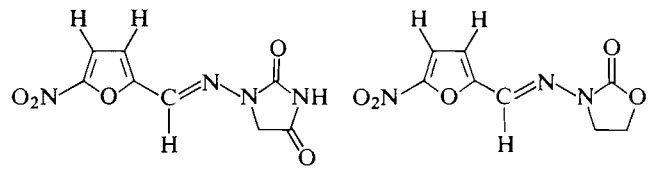

6 **7**

just before the original nitrofuran. Re-chromatography of these products gave the original as well as the more rapidly eluting material. Therefore, we conclude that these compounds also undergo a light induced *anti*/*syn* isomerization.

Compound **3** was much less polar than the nitrofurazone but retained the absorption maximum near 370 nm (see Fig. 2) suggesting that it contained one or more intact nitrofuran groups attached to a side chain having conjugated double bonds. The mass spectrum of **3** revealed a molecular weight of 278. The azine of 5-nitro-2-furaldehyde was synthesized and compared with the compound produced in the photolysis mixtures; the mass spectrum, ultraviolet spectrum and retention time of the synthetic azine were identical to compound **3**.

It was of interest to determine whether the azine would have an appreciable influence on the antibacterial potency or mutagenicity of nitrofurazone solutions. Tests with *E. coli* showed that the azine is toxic to the WP2 strain and its *uvr A* derivative and mutagenic to the *uvr A* strain. However, in comparison with nitrofurazone the azine was a rather weak mutagen giving 14-fold fewer mutations at 180 μM than nitrofurazone. Somewhat unusual results were obtained when the azine was tested with *S. typhimurium* TA98 in the standard plate assay. Without added S-9 extract, the azine gave a weakly positive result at 2.5 μg/plate. At higher concentrations the chemical precipitated out and no colonies were seen on the plates. However, in the presence of S-9 preparation from the livers of Arochlor-1254

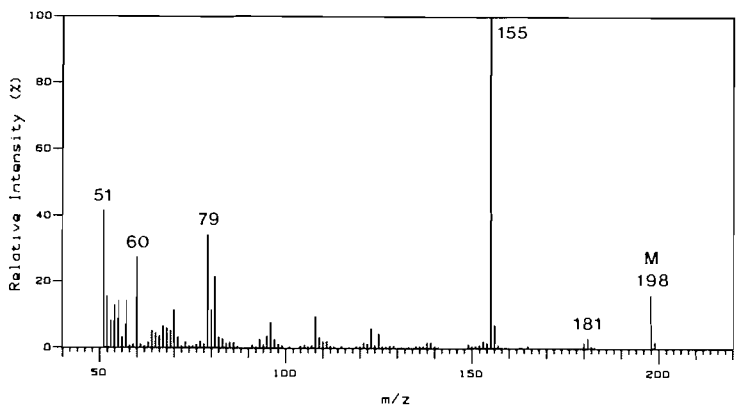

FIG. 3. The electron ionization mass spectrum of compound **2**. This spectrum is identical to that acquired for compound **1**.

Can. J. Chem. Downloaded from www.nrcresearchpress.com by 78.46.186.204 on 09/07/12
For personal use only.

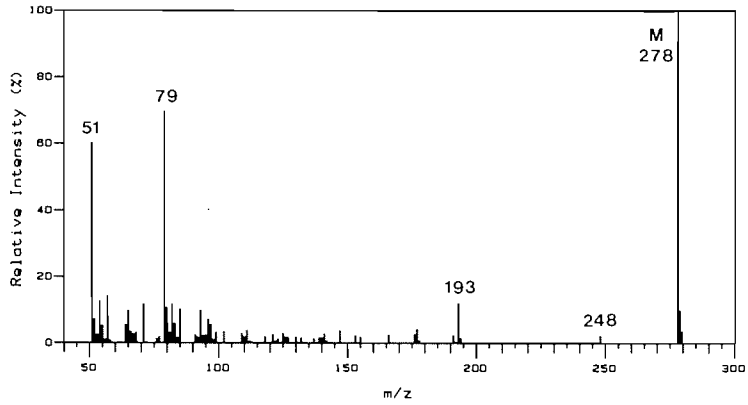

FIG. 4. The electron ionization mass spectrum of compound **3**. Authentic 5-nitro-2-furaldehyde azine gave an identical spectrum.

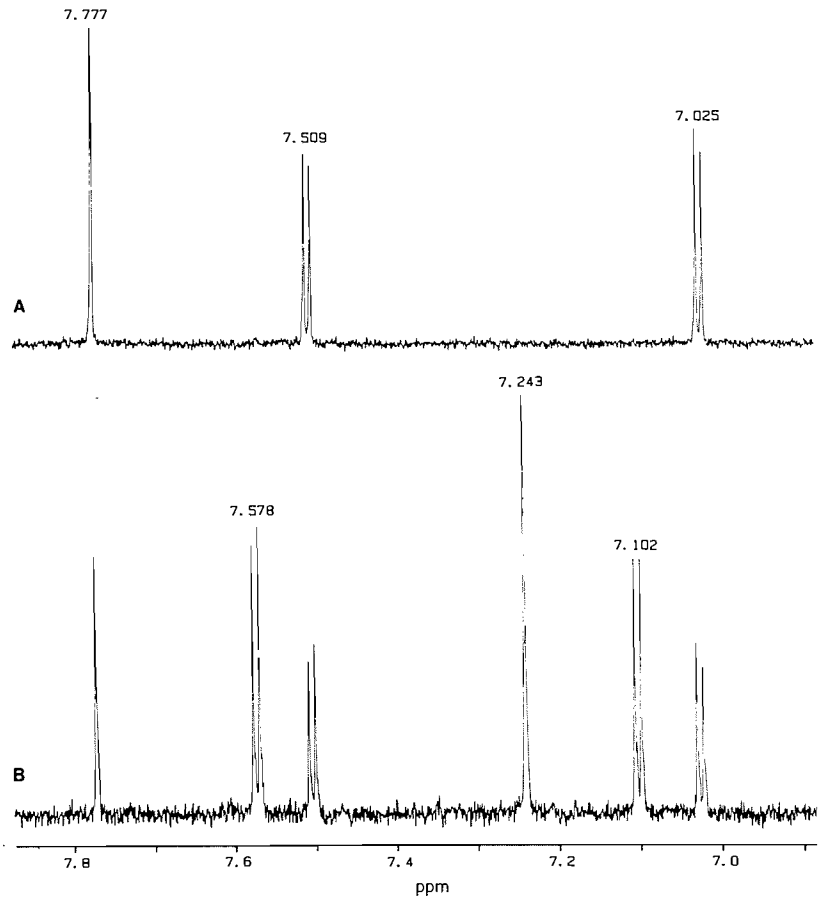

FIG. 5. The proton nmr spectra of a methanol-d_4 solution of nitrofurazone before (*A*) and after (*B*) exposure for 50 min to high intensity tungsten illumination.

induced rats (8) and using up to 25 μg/plate nitrofurazone, the initial precipitate dissolved and a substantial increase in revertants was observed.

Since the azine has two nitrofuryl groups, it could conceivably act as a bifunctional agent and cross-link DNA. This possibility was tested by isolating DNA from *E. coli* B/r and WPS *uvr A* exposed to 1 or 5 μg or azine per mL for 60 min, heating the DNA above its melting point and rapidly cooling the preparation. In a typical experiment, all of the DNA from the azine-treated cells remains denatured while 22% (B/r) and 45% (WP2 *uvr A*) of the DNA of bacteria treated with 1 μg/mL of mitomycin (a known cross-linking agent used as a positive control) renatured. These results show that the azine at concentrations up to 5 μg/mL did not induce detectable stable DNA cross-links in either of these strains.

Discussion

Our results provide dramatic confirmation of the photolability of nitrofuran derivatives and emphasize that experiments using these agents should be conducted in the dark or under yellow light. Interference from *anti/syn* isomerization due to accidental exposure to light can also be minimized by keeping

Can. J. Chem. Downloaded from www.nrcresearchpress.com by 78.46.186.204 on 09/07/12
For personal use only.

samples dissolved in aqueous solvents, since the thermal conversion of *syn* to *anti* is facilitated. A high column temperature and aqueous acetonitrile as a mobile phase can also be used to avoid the HPLC resolution of the isomer pair, although slightly different extinction coefficients would lead to slight quantitative errors.

The rapid conversion of *anti-* to *syn*-nitrofurazone and the corresponding isomerization of nitrofurantoin and furazolidone have not been reported previously. However, it has been suggested that the *anti/syn* isomerization might account for the lack of fluorescence or phosphorescence when nitrofurans are irradiated with ultraviolet light by providing a nonradiative path for reversion of excited molecules to the ground state (12). The photochemistry of the carbon-nitrogen double bond and the *anti/syn* isomerization of such compounds is, of course, a well known phenomenon (13). The photodecomposition of some nitrofurans in UV light has been investigated previously (14–17), but the only photoproducts reported were the corresponding aldehydes formed by hydrolysis of the azomethine bond. We did not observe any 5-nitro-2-furaldehyde, **4**, in our experiments.

Given the relatively small amount of the azine that is formed and the relatively weak mutagenicity of this compound, it seems unlikely that the reported actions of nitrofurazone can be due to azine generated by photolysis. Some commercial preparations contain appreciable concentrations of azine as a synthetic byproduct and quite lengthy analytical assays have been used in the past (4). The reverse phase hplc method reported here allows a very rapid and precise measurement of azine levels.

At this point we are unable to provide a plausible mechanism for the photochemical conversion of nitrofurazone to the azine. It appears that the hydrazone, **5**, is not intermediate in this process since we did not observe the hydrazone (it elutes just before compound **2**) and added hydrazone did not increase the amount of azine formed in either the light or the dark.

Acknowledgements

This work was supported by grants from the Natural Sciences and Engineering Research Council of Canada and from the National Cancer Institute of Canada. The authors wish to thank Marianne Gouin and Claudia Lu for technical assistance during the early part of this work.

1. D. R. McCalla. *In* Antibiotics V-1: mechanisms of action of antibacterial agents. *Edited by* F. E. Hahn. Springer-Verlag, New York. 1979. p. 176.
2. R. L. Shriner, R. C. Fuson, and D. Y. Curtin. The systematic identification of organic compounds. Wiley, New York. 1956. p. 218.
3. H. Gilman and G. W. Wright. J. Am. Chem. Soc. **53**, 1923 (1931).
4. R. F. Bird and S. G. E. Stevens. Analyst, **87**, 362 (1962).
5. E. Menachemoff and R. Haber. Patent. Chem. Abs. **57**, 3416a.
6. B. D. Davis and E. S. Mingioli. J. Bacteriol. **60**, 17 (1950).
7. M. H. L. Green and W. J. Muriel. Mutation Res. **38**, 3 (1976).
8. B. N. Ames, F. McCann, and E. Yamasaki. Mutation Res. **31**, 347 (1975).
9. J. Marmur. J. Mol. Biol. **3**, 208 (1961).
10. R. J. Rutman, E. H. L. Chun, and J. Jane. Biochem. Biophys. Acta, **174**, 663 (1969).
11. L. M. Jackman and S. Sternell. Nuclear magnetic resonance spectroscopy in organic chemistry. Pergamon Press, New York. 1969. p. 226.
12. W. Kemula and J. Zawadowska. Bull. Acad. Pol. Sci., Ser. Sci. Chim. **24**, 155 (1976).
13. A. Padwa. Chem. Rev. **77**, 37 (1977).
14. M. Shahjahan and R. P. Enever. J. Bangladesh Acad. Sci. **3**, 65 (1979).
15. M. Shahjahan. Bangladesh J. Biol. Sci. **8**, 55 (1979).
16. A. B. Narbutt-Mering and W. Weglowska. Acta Pol. Pharm. **37**, 301 (1980).
17. D. R. McCalla and A. Reuvers. J. Protozool. **17**, 127 (1970).

Can. J. Chem. Downloaded from www.nrcresearchpress.com by 78.46.186.204 on 09/07/12
For personal use only.

Nafion-coated mercury-coated glassy carbon electrodes for metals analysis and speciation

ROBERT D. GUY[1] AND SARATH NAMARATNE

Trace Analysis Research Centre, Department of Chemistry, Dalhousie University, Halifax, N.S., Canada B3H 4J1

Received November 5, 1986

This paper is dedicated to Professor Douglas E. Ryan on the occasion of his 65th birthday

ROBERT D. GUY and SARATH NAMARATNE. Can. J. Chem. **65**, 1133 (1987).

The properties of mercury-coated glassy carbon electrodes coated with a thin membrane of Nafion 117 were studied to evaluate the potential analytical applications in metal ion analysis. The Nafion membrane was found to contain two types of binding sites — a strong site that bound metal ions in a nonelectroactive form and cation exchange sites that were useful for preconcentrations prior to differential pulse voltammetry. The exchange constants for the weak sites ranged from 0.413 for copper to 12.5 for methyl viologen. The differential pulse currents were increased by a factor of 75 to 100 and a linear calibration curve was observed from about 25 n*M* to 1000 n*M* for copper, lead, cadmium, and zinc. The ion exchange reaction is very sensitive to ionic strength and significant enrichments occur only in solutions of ionic strength below 0.10. The Nafion-coated glassy carbon electrode in a flow cell can be used to determine the free copper ion concentration in samples by a combination of ion exchange and differential pulse voltammetry. The flow-through system required about 15 mL of sample solution and an analysis time of about 10 min. The ion exchange measurement gave a linear calibration from 40 n*M* to 10 μ*M* for free copper.

ROBERT D. GUY et SARATH NAMARATNE. Can. J. Chem. **65**, 1133 (1987).

Dans le but d'évaluer leurs applications analytiques potentielles dans l'analyse des ions métalliques, on a étudié les propriétés d'électrodes de charbon vitreux, recouvertes de mercure et recouvertes d'une fine membrane de Nafion 117. On a trouvé que la membrane de Nafion contient deux types de sites de liaison — un site fort qui lie les ions métalliques par une forme qui n'est pas électroactive et des sites d'échanges cationiques qui sont utiles pour les préconcentrations réalisées avant la voltamétrie différentielle pulsée. Les constantes d'échange des sites faibles varient de 0,413 pour le cuivre à 12,5 pour le viologène de méthyle. Les courants différentiels pulsés ont été augmentés par un facteur de 75 à 100 et on a observé une courbe de calibration linéaire d'environ 25 n*M* à 1000 n*M* pour le cuivre, le plomb, le cadmium et le zinc. La réaction d'échange ionique est très sensible à la force ionique et il ne se produit des enrichissements importants que dans des solutions de force ionique inférieure à 0,10. Si on fait appel à une combinaison de l'échange ionique et de la voltamétrie différentielle pulsée, on peut utiliser l'électrode de charbon vitreux recouverte de Nafion dans une cellule à flux pour déterminer la concentration d'ions cuivres libres. Le système à écoulement nécessite environ 15 mL de solution de l'échantillon et un temps d'analyse d'environ 10 min. Pour le cuivre libre, les mesures d'échanges ioniques donnent une calibration linéaire d'environ 40 n*M* à 10 μ*M*.

[Traduit par la revue]

Introduction

Voltammetric techniques provide a sensitive method for the detection and quantification of inorganic and organic species in aqueous and organic solutions. The modification of electrodes has recently provided methods to improve both the selectivity and sensitivity of voltammetric methods. Wang and co-workers (1, 2) have coated a mercury-coated glassy carbon electrode (MCGCE) or glassy carbon electrode with a cellulose acetate membrane. The membrane was hydrolyzed with base to form a porous structure. The membrane acts like a miniature dialysis membrane and reduced the adsorption interferences from organic substances. A second approach to altering the selectivity of voltammetric methods is to form a species that adsorbs onto the mercury surface. Wang and Mahmoud (3) have used adsorptive preconcentration to determine titanium in natural waters. A third approach is to form a permanent membrane on the electrode surface that chemically reacts with metal ions in solution. Polymer-coated electrodes with attached chelating groups have been shown (4) to selectively preconcentrate iron and copper.

A non-selective approach to sensitivity enhancement is to coat the electrode surface with a cation exchange membrane. A commonly used membrane is the Nafion series of polymers produced by Dupont. The membrane is perfluorinated hydrocarbon with sulphonate exchange sites and can be obtained commercially dissolved in low molecular weight alcohols. This solution can be easily used to coat glassy carbon or mercury-coated glassy carbon electrodes. Szentirmay and Martin (5) have studied the electrochemistry of methyl viologen and ruthenium complexes at the Nafion-coated glassy carbon electrode. They measured exchange constants on the order of 10^4 for the hydrophobic cations. These can be compared with values less than 10 for most inorganic cations (6). This paper describes two applications of the Nafion-coated electrode — preconcentration of copper, lead, cadmium, and zinc prior to differential pulse or anodic stripping voltammetry and a rapid ion exchange speciation procedure combined with electrochemical detection.

[1]Author to whom correspondence should be addressed.

Experimental

Chemicals

A 5% Nafion 117 solution in aliphatic alcohols was obtained from Aldrich. Nafion 117 has an equivalent weight of 1100 g and the solution has the polymer in the hydrogen form. Citric acid, acetate buffers, and sodium nitrate solutions were prepared from reagent grade chemicals and the stock solutions were passed through a short column of Chelex 100 in the sodium form to remove trace metal impurities. Methyl viologen was obtained from Aldrich and standardized by ion exchange (7).

Electrochemical measurements were made using a Princeton Applied Research Model 174A Polarographic Analyzer equipped with a Model 303 SMDE and a glassy carbon electrode was used for batch studies. A Bioanalytical Services Model TL-5 glassy carbon detector block was used for flow studies. All potential measurements are against a BAS Model RE-1 Ag/AgCl reference electrode. A Masterflex pump was used for the flow studies. Ion selective electrode measurements were made using an Orion Model 94-29A copper ion selective electrode and

Can. J. Chem. Downloaded from www.nrcresearchpress.com by 78.46.186.204 on 09/07/12
For personal use only.

Can. J. Chem. Downloaded from www.nrcresearchpress.com by 78.46.186.204 on 09/07/12
For personal use only.

a Fisher Accumet 144 pH meter. The copper ion selective electrode was calibrated using triethylenetetramine/copper metal ion buffers.

The glassy carbon electrodes were polished with alumina before use. A mercury film was formed on glassy carbon by plating a 1.0×10^{-4} *M* mercuric nitrate solution in 0.01 *M* acetate buffer at pH 4 at −1.00 V for 15 min. The potential was changed to +0.10 V for 30 s to remove trace metal impurities. The electrode was removed from the SMDE assembly, washed with distilled water and acetone, and dried with a stream of nitrogen. The dry electrode was coated with 5 μL of a 3% Nafion solution (prepared by dilution of the stock with 50% methanol) and dried for 15 min. After visual inspection to ensure uniform coating the electrode was immersed in 0.01 *M* acetate buffer (pH 5.0) overnight to allow the polymer to swell and convert the polymer to the sodium form.

The membrane exchange constants were determined by placing 300 μL of the 5% Nafion solution on clean, dry microscope slides and allowing the solvent to evaporate. The glass slides were placed in 25 mL of 10 μ*M* metal ion solution and 0.010 *M* sodium nitrate. The membrane and solution were allowed to equilibrate for 12 h and the equilibrium metal ion concentrations in solution were determined by flame atomic absorption. Methyl viologen measurements were done using differential pulse polarography. Preliminary studies indicated that the differential pulse voltammetry (DPV) calibration curves for the ions were linear over the range of 10 n*M* to 100 n*M*. A second set of exchange constants were determined at 0.10 μ*M* metal ion by comparing the DPV currents of solutions equilibrated twice with fresh membranes on the MCGCE — the second current measurement gave the equilibrium concentration of the ion remaining in solution from the first equilibration. The amount bound to the membrane was determined by difference.

Metal ion preconcentration experiments were done using the PAR glassy carbon electrode coated with mercury and a Nafion membrane. The electrochemical cell was filled with 15 mL of test solution, placed in contact with the Nafion-coated MCGCE, deoxygenated with nitrogen for 4 min, and stirred for an additional 1 min with a magnetic stirrer bar. The preconcentrations in differential pulse polarography were done open circuit. Differential pulse voltammograms were recorded using a negatively going scan at a rate of 5 mV/s, a pulse of 100 mV, and measurement time of 0.5 s. The DPASV measurements were done using 15 mL of test sample adjusted to pH 5 with 0.01 *M* acetic acid buffer. The sample was placed in contact with the Nafion-coated MCGCE, deoxygenated for 4 min with nitrogen, stirred for 1 min. The DPASV voltammograms were recorded using a 5 min plating time at −1.40 V and stripping at a rate of 5 mV/s, a pulse of 100 mV, and measurement time of 0.5 s.

The simple metal ion speciation studies were done using the BAS flow cell and the Masterflex pump. The glassy carbon (without a mercury film) was coated with 10 μL of the 5% Nafion solution. After drying, a visual inspection showed that the Nafion film covered the glassy carbon electrode and some of the surrounding polyethylene block. The cell was used with a second glassy carbon electrode as the counter electrode and was connected to the Masterflex pump using 0.8 mm id Teflon tubing. A 0.10 *M* sodium nitrate solution adjusted to pH 5.0 with acetic acid buffers was passed through the cell for 2 h to convert the membrane to the sodium form. The speciation solutions were made up in 0.10 *M* sodium nitrate solutions and the pH adjusted to 5.0 with 0.01 *M* acetic acid buffers. The differential pulse current of the detector cell was continuously monitored at the copper peak potential. The sample solutions were passed through the cell at 2 to 3 mL/min until the current attained a plateau.

Results and discussion

The measured exchange constants for calcium, copper, cadmium, lead, zinc, and methyl viologen are given in Table 1 for the reaction:

[1] $2NaR + M^{2+} = MR_2 + 2Na^+$

$$K = \frac{X_M a_{Na}^2}{X_{Na}^2 a_M}$$

TABLE 1. Exchange constants for Nafion 117*

Cation	K^M_{2Na} (10 μ*M*)	K^M_{2Na} (0.10 μ*M*)
Copper	0.413	430
Lead	0.745	657
Cadmium	0.516	37
Zinc	0.589	105
Calcium	3.68	nd
Methyl viologen	12.5	139

*Values are the average of three measurements. Typical uncertainties were ±0.005 at 10 μ*M* and ±5 at 0.10 μ*M*; nd = not detected.

where *a* represents the activity of the ions in the solution and *X* represents the equivalent ionic fractions of the metal ions in the membrane. The measured concentrations were converted to activities using the single ion activity coefficients given by Kielland (8). The values for the metal cations compare favorably with values reported by Steck and Yeager (6) for a Nafion 120 membrane. The value for methyl viologen, however, is three orders of magnitude lower than the value reported by Szentirmay and Martin (5) for Nafion films on glassy carbon electrodes. The methyl viologen work on the Nafion/glassy carbon electrode system was done at concentrations two to three orders of magnitude lower than those reported in this work. A possible reason for some of the discrepancy between this work and the earlier report is that at low cation concentrations a small percentage of strong adsorption sites may dominate the exchange reaction between the membrane and solution. Blaedel and Niemann (9) attributed some nonlinearities in the exchange reaction for Nafion XR-170 (at low metal concentrations) to carboxylate or olefinic impurities. A study of Nafion 811X in our laboratory showed that at pCu values above 7 that the adsorption isotherm changed slope and a strong site dominated the adsorption reaction. A comparison of exchange constants measured at cation concentrations of 0.10 and 10 μ*M* are shown in Table 1 and tend to support the hypothesis of strong and weak sites on the membrane. At low metal concentrations the exchange constant tends to increase by two orders of magnitude. This dependence of exchange constant on cation concentration means that the analytical usefulness of the Nafion-coated electrodes may be limited to linear calibrations over narrow concentration ranges.

Exchange constants of 0.4 to 3 may still provide useful preconcentrations for the metal cations. The Nafion coatings on the MCGCE used in these studies corresponded to 0.437 mg Nafion or 3.97×10^{-7} mol of sites (assuming an equivalent weight of 1100). Equilibrium calculations using 1.0×10^{-7} *M* copper, an ionic strength of 0.010, and an exchange constant of 0.413 indicate that X_{Cu} would be about 0.0004 which corresponds to 5% of the copper removed from 10 mL of solution. The density of the swelled sodium form of Nafion is 1.58 g/cm^3 so the "volume" of the membrane on the Nafion-coated electrode would be about 2.8×10^{-7} L. The copper concentration in the membrane would correspond to 0.29 m*M* or an enrichment factor of about 3000. One could expect, therefore, that currents should be enhanced significantly at the Nafion-covered mercury coated glassy carbon electrode. Figure 1 shows the differential pulse voltammogram for 50 n*M* copper, lead, cadmium, and zinc ions in 0.01 *M* sodium acetate buffer at pH 5.5. The voltammogram was obtained using a membrane formed from 5 μL of a 1% Nafion solution and a

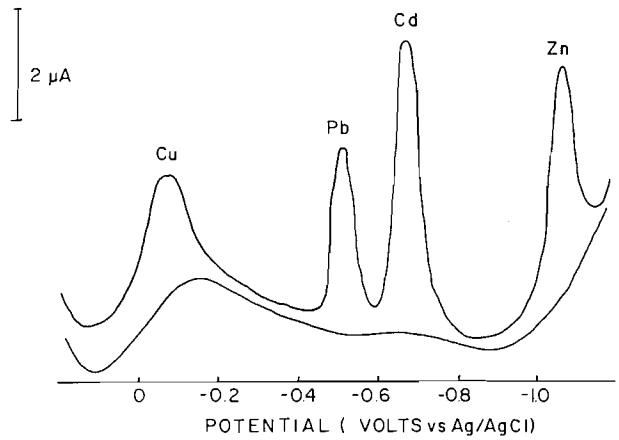

FIG. 1. Differential pulse voltammogram of copper, lead, cadmium, and zinc in 0.01 *M* acetic acid buffer at pH 5.5. A 10 min equilibration and a membrane formed from 5 μL of 1% Nafion were used in this experiment. The second curve is a blank equilibration with electrolyte.

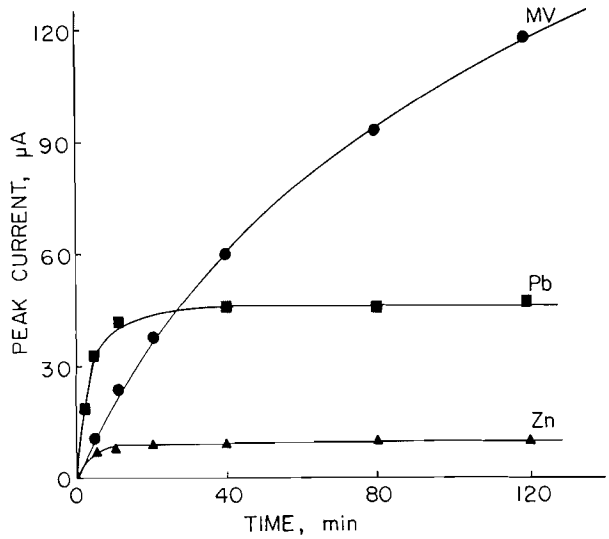

FIG. 2. Time study of the ion exchange equilibration for a membrane formed from 5 μL of a 3% Nafion solution.

10 min equilibration. The current enhancements observed for the four ions ranged from about 50 to 100 — considerably lower than the 3000 calculated above. The lower than expected current enhancement can be explained by considering the effects of diffusion and strong sites on the observed currents.

The usefulness of the Nafion-coated mercury coated glassy carbon electrode will depend on the kinetics of exchange, sensitivity of the exchange reaction to secondary ions and ionic strength, and the linearity of the calibration curve. The kinetics of equilibration for lead, methyl viologen, and zinc onto a Nafion membrane formed by adding 5 μL of the 3% stock solution to the mercury-coated electrode is given in Fig. 2. The lead and zinc equilibrate rapidly and attain the maximum response at 20 min but methyl viologen required greater than 120 min to attain equilibrium. The slow equilibration of methyl viologen was also noted by other workers (5) and was attributed to slow diffusion of the cation in the Nafion film. Diffusion coefficients in Nafion membranes have been reported (5) to range from $\sim 10^{-10}$ cm^2/s (for methyl viologen) to 9.44 × 10^{-7} cm^2/s for sodium. These diffusion constants are considerably smaller than diffusion constants noted for ions in solution.

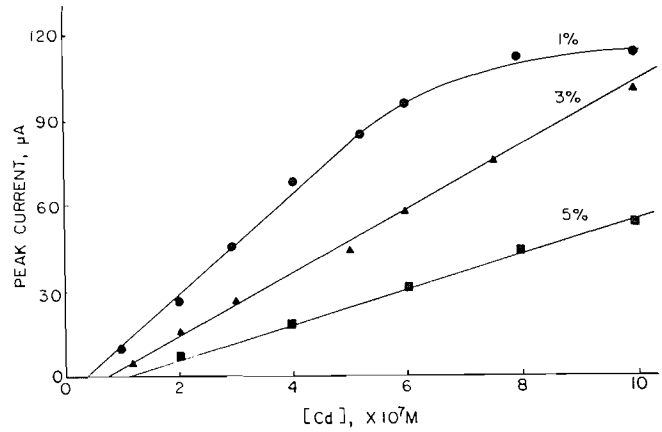

FIG. 3. Effect of membrane thickness on the calibration curves for cadmium. The membranes were formed by adding 5 μL of 1, 3, or 5% Nafion solutions and preconcentrations were done in 0.01 *M* acetic acid buffer at pH 5.5.

The slow diffusion of the ions in the Nafion membrane will affect the analysis of metal cations in two ways: the slow diffusion will increase the time necessary for equilibration of the membrane with the sample solution and the slow diffusion will affect the reduction currents at the mercury-coated glassy carbon electrode.

The effect of film thickness on the analytical response is given in Fig. 3. These calibration curves were obtained using a 5 min equilibration period. The decrease in slopes as one goes from a 1% membrane to a 5% membrane reflects the longer time necessary to reach equilibrium as one increases the thickness of the membrane. A longer time is required for the ions to diffuse through the thick membrane. Each of the calibration curves do not pass through the origin and it appears that one titrates a site before one obtains a measureable current. As one increases the thickness by using 1, 3, and 5% Nafion solutions the intercept changes from 2.5 to 7.5 to 10 × 10^{-8} *M*. This supports the earlier argument that the Nafion contains at least two types of sites: the first site binds metal ions strongly and the bound metal is not electroactive and a second, more numerous type of site that binds the metal in an electroactive form. A rough calculation suggests that about 1% of the exchange capacity is present in the strong sites. The presence of the strong sites will limit the analytical applications of the membrane to metal ion concentrations above about 20 to 50 n*M* if one uses the 3% membrane.

The ion exchange reaction given in eq. [1] indicates that the response will be very sensitive to the ionic strength of the solutions. Figures 4 and 5 illustrate the effect of sodium and calcium on the analytical response for several ions. The data in Fig. 4 indicate that the membrane will only give significant enhancements at ionic strengths below 0.10 but Fig. 5 indicates that at calcium levels typical of natural waters one can determine the four metal ions. The two diagrams do suggest that analytical measurements can be best done using a standard addition procedure to compensate for variations in ionic compositions of unknown solutions. It should be noted that over the concentration ranges of interest (50 n*M* to 1 μ*M*) there were no interferences between copper, zinc, cadmium, and lead and each calibration was linear. It should also be noted that the current enhancements will depend on the pH of the sample solution. At pH values lower than 2 the proton will start to compete for sites on the membrane and at pH values greater than

Can. J. Chem. Downloaded from www.nrcresearchpress.com by 78.46.186.204 on 09/07/12
For personal use only.

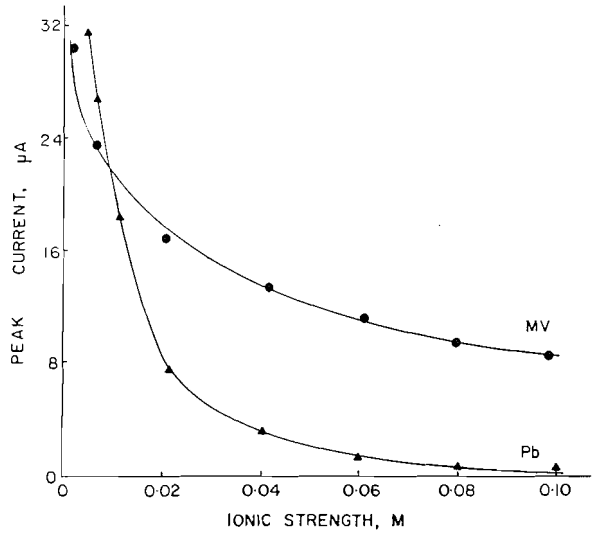

FIG. 4. Effect of sodium nitrate concentration on the differential pulse voltammetry current after a 10 min equilibration. The membrane was formed from 5 μL of a 3% Nafion solution.

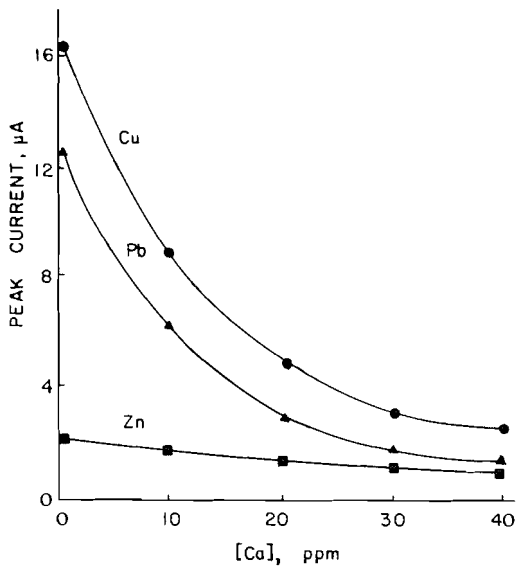

FIG. 5. The effect of calcium on the differential pulse voltammetry currents for a 5 μL of 3% Nafion membrane.

five formation of hydroxy species will lower the activity of the free ion.

The analytical usefulness of the Nafion-coated electrode is limited by the sensitivity of the ion exchange reaction to ionic strength variations and the presence of strong, non-electroactive sites on the membrane. One advantage of the membrane is that it may isolate the mercury surface from surfactants and organics in the sample solution. Wang and Hutchins-Kumar (1) have shown that a cellulose acetate membrane decreases adsorption effects at the mercury-coated glassy carbon electrode. Figure 6 shows that a Nafion-coated electrode, like the cellulose-acetate-coated electrode, also removes the interference of gelatin on the DPASV of copper. The slight decrease in stripping current as the concentration of gelatin increases is probably due to the binding of copper to sites on the gelatin. A similar decrease in copper currents was noted for DPASV at the cellulose-acetate-coated electrode. The removal of organic interferences and

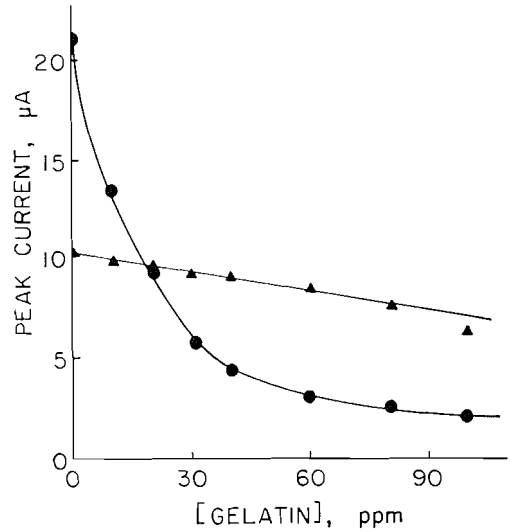

FIG. 6. The effect of gelatin on the DPASV of copper: ● MCGCE and ▲ Nafion-coated MCGCE (5 μL of 3% solution).

TABLE 2. Metal ion concentrations in water samples*

Ion	Concentration in Mineral water	Rain water	Lake water
Cu	2.6	7.8	nd
Pb	0.7	3.4	1.9
Cd	nd	nd	0.9
Zn	2.0	1.7	16.7

*All values are in ppb, the mean of 4 measurements made using pH 5.5 buffer, and using standard additions. The relative standard deviations for the values are 10%; nd = not detected.

slight current enhancements does permit the application of DPASV at the Nafion-coated glassy carbon electrode for the analysis of some simple solutions. The results for several types of water samples are given in Table 2. These measurements were done by adding acetate buffers to adjust the pH to 5.5 and the ionic strength to 0.01. The metals were quantified by a standard additions procedure. The lake water sample gives no copper and this is probably a result of the pH adjustment — the copper may be bound to organic colloids in water and not sufficiently labile to be detected in this experiment.

The Nafion-coated MCGCE improves the sensitivity of differential pulse polarography by a factor of about 75 but the sensitivity does not compare favorably with conventional differential pulse anodic stripping voltammetry. The Nafion-coated MCGCE effects the preconcentration by an ion exchange reaction and the membrane system is sensitive to ionic strength and pH variations in the samples. Conventional DPASV, however, is relatively insensitive to sample ionic strength and, for cadmium, copper, and lead, can be done at low pH values. A second limitation of the Nafion-coated MCGCE is the non-zero intercepts in the calibration curves noted for batch equilibrations. This limits the practical usefulness of the membranes to metal ion concentrations above 50 n*M* for DPV. The analytical usefulness of the ion exchange perconcentration may be more fully realized for cations that do not deposit electrolytically, for example, iron. Preliminary results suggest that iron preconcentrates on the membrane and is electrochemically active and this is under further investigation.

Can. J. Chem. Downloaded from www.nrcresearchpress.com by 78.46.186.204 on 09/07/12
For personal use only.

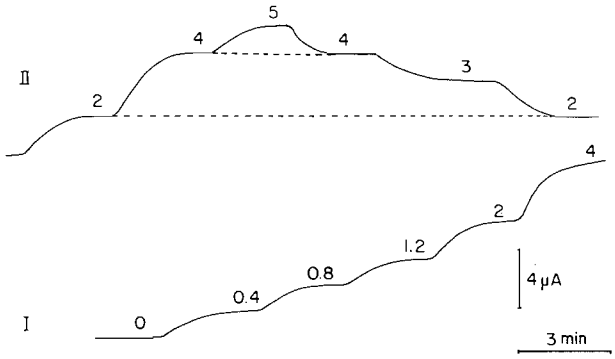

FIG. 7. Current traces for the ion exchange measurement of free copper in 0.10 *M* sodium nitrate at pH 5 (adjusted with 0.01 *M* acetate buffer). Trace I represents the calibration curve and Trace II is an extension that shows that the exchange process is reversible. The numbers written on the curves are the copper concentrations in μ*M* units. Measurements taken using the BAS flow cell.

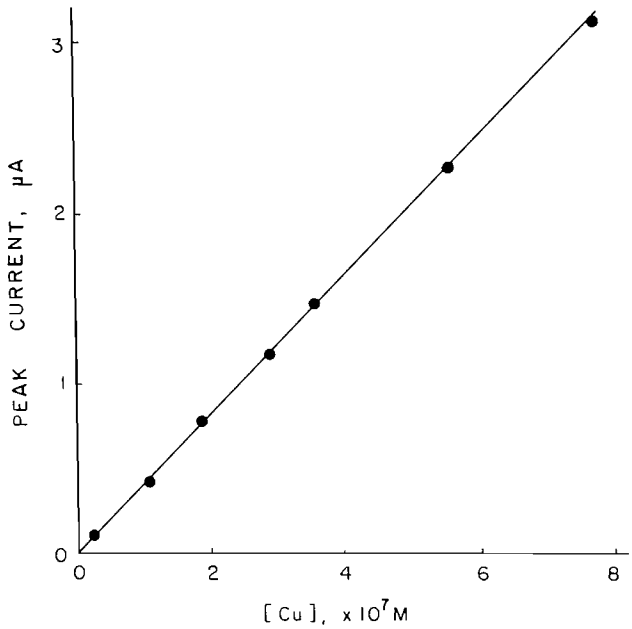

FIG. 8. Calibration curve for copper in citric acid metal ion buffers. The metal ion buffers were calibrated using a copper ion selective electrode calibrated with TRIEN metal ion buffers.

The Nafion-coated electrode can be used to measure the activity of the free metal ion by using an ion exchange reaction. Cantwell *et al.* (10, 11) have shown that short ion exchange columns can be used with atomic absorption analysis to determine the free copper and nickel ions in water samples. Zorkin *et al.* (12) have also shown that the ion exchange method gives a limited agreement with bioassay results. A glassy carbon electrode was coated with Nafion and placed in the BAS flow cell to permit a flow through equilibration of the membrane with the sample solution. The copper currents were monitored as a function of time and the results are given in Fig. 7 for copper ions in 0.10 *M* sodium nitrate. The lower curve in Fig. 7 shows the data used to obtain a calibration curve — it is evident that the equilibration is rapid and about 15 mL of solution are necessary to attain the plateau. The upper curve in Fig. 7 shows that the exchange membrane is reversible — it is possible to use the membrane continuously without washing the membranes between samples (note that these solutions were not metal ion buffers). Citric acid metal ion buffers were used to calibrate a membrane over an extended pCu range and the calibration from 40 n*M* to 800 n*M* is shown in Fig. 8. The calibration gives a linear response between free copper and current and, though not shown in Fig. 8, the linear range extended up to 10 μ*M* free copper. A second point that should be noted in the calibration curve is the zero intercept. The difference between the calibrations of Figs. 3 and 8 is that in the flow cell configuration the membrane equilibrates with fresh metal ion solution — in the flow cell the strong and weak sites can both equilibrate fully with the metal ion solution. A separate study using cadmium in 0.01 *M* sodium nitrate and the flow cell also showed a linear calibration with zero intercept. This suggests that the flow cell configuration may also be used in the preconcentration mode with zero intercepts and no interference from the strong membrane sites.

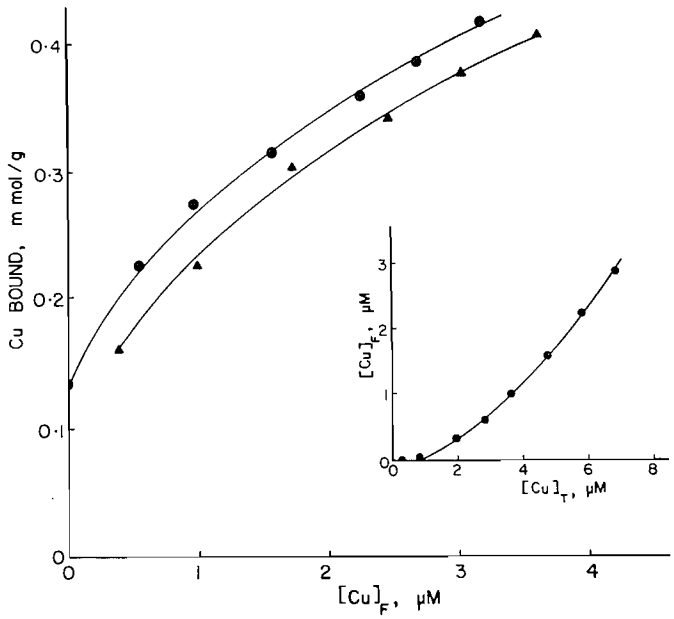

FIG. 9. Ion exchange measurements of free copper in a 10 ppm humic acid solution at pH 5.0. The inset shows the titration curve and the main figure shows the binding isotherm for copper onto humic acid. ▲, Potentiometric determination of free copper; ●, ion exchange determination of free copper.

One application of the metal speciation is to study the binding capacity of water samples and the binding of metal ions to soil organic matter. A preliminary study using a copper ion selective electrode and the Nafion membrane system indicated good agreement for EDTA solutions at the micromolar level. Figure 9 shows the copper titration and binding isotherm for a humic acid solution in 0.10 *M* sodium nitrate at pH 5.0. The isotherm obtained by potentiometric measurements with the copper ion selective electrode is also given in Fig. 9. The ion exchange method and the ion selective electrode do not give the same isotherm and the ion exchange method gives a lower measured free copper than the ion selective electrode (hence more copper binding). A similar result has been noted in our laboratory using the ion exchange column method described by Cantwell *et al.* (10). The ion selective electrode results may be in error because the electrode is sensitive to organic substances (13) and it has been reported in the literature that the presence of humic materials can interfere with the copper ion selective electrode (14).

The Nafion-coated glassy carbon electrode can be used for

Can. J. Chem. Downloaded from www.nrcresearchpress.com by 78.46.186.204 on 09/07/12
For personal use only.

current enhancements in analysis under well-defined sample conditions of fixed ionic strength, pH, and using a standard additions method. The more important application would be in measurement of pCu in complexing solutions of interest in bioassays.

Acknowledgement

This work was supported, in part, by the Natural Sciences and Engineering Research Council of Canada.

1. J. WANG and L. D. HUTCHINS-KUMAR. Anal. Chem. **58**, 402 (1986).
2. J. WANG and L. D. HUTCHINS. Anal. Chem. **57**, 1536 (1985).
3. J. WANG and J. S. MAHMOUD. J. Electroanal. Chem. **208**, 383 (1986).
4. A. R. GUADALUPE and H. D. ABRUNA. Anal. Chem. **57**, 142 (1985).
5. M. N. SZENTIRMAY and C. R. MARTIN. Anal. Chem. **56**, 1898 (1984).
6. A. STECK and H. L. YEAGER. Anal. Chem. **52**, 1215 (1980).
7. D. R. NARINE. Ph.D. thesis, Dalhousie University, Halifax, N.S. 1980.
8. J. KIELLAND. J. Am. Chem. Soc. **59**, 1675 (1937).
9. W. J. BLAEDEL and R. A. NEIMANN. Anal. Chem. **47**, 1455 (1975).
10. F. F. CANTWELL, J. S. NIELSEN, and S. E. HRUDEY. Anal. Chem. **54**, 1498 (1982).
11. J. TREIT, J. S. NIELSEN, B. KRATOCHVIL, and F. F. CANTWELL. Anal. Chem. **55**, 1650 (1983).
12. N. G. ZORKIN, E. V. GRILL, and A. G. LEWIS. Anal. Chim. Acta, **183**, 163 (1986).
13. G. J. M. HEIJNE and W. E. VAN DER LINDEN. Anal. Chim. Acta, **96**, 13 (1978).
14. I. SEKERKA and J. F. LECHNER. Anal. Lett. A**11**, 415 (1978).

Can. J. Chem. Downloaded from www.nrcresearchpress.com by 78.46.186.204 on 09/07/12
For personal use only.

The voltammetric determination of trace U(VI) in seawater — adsorptive preconcentration of the 2-(5-bromo-2-pyridylazo)-5-diethylaminophenol complex

JAMAL ELWERFALLI, JOHN A. PAGE,[1] AND GARY W. VANLOON
Department of Chemistry, Queen's University, Kingston, Ont., Canada K7L 3N6

Received October 22, 1986

This paper is dedicated to Professor Douglas E. Ryan on the occasion of his 65th birthday

JAMAL ELWERFALLI, JOHN A. PAGE, and GARY W. VANLOON. Can. J. Chem. **65**, 1139 (1987).

Trace U(VI) in seawater has been determined by voltammetry after preconcentration by adsorption of the U(VI)/Br—PADAP complex (Br—PADAP = 2-(5-bromo-2-pyridylazo)-5-diethylaminophenol).

The reagent and the metal complex are adsorbed at a Hg drop electrode polarized at −0.40 V vs. a Ag/AgCl reference from a seawater electrolyte containing 3×10^{-7} *M* added Br—PADAP and buffered at pH 7.8 by the addition of triethanolamine/$HClO_4$. The adsorption is at a mass transfer controlled rate. Voltammetry of the adsorbed electroactive material gave two peaks, one at −0.56 V for reduction of adsorbed Br—PADAP and one at −0.65 V for reduction of adsorbed U(VI)—PADAP complex. The height of the second peak was a sensitive measure of the concentration of U(VI) in the electrolyte. Analysis is carried out with preconcentration restricted to a low fractional electrode coverage with calibration by the method of standard additions. The method is subject to interference from organic surfactants but not from common metal ions. Interferences were minimized by the use of short adsorption times in the preconcentration step.

For a 60 s adsorption time, a scan rate of 0.050 V s^{-1} and peak current measurement, the sensitivity was 8.2 nA/($\mu g\ L^{-1}$ U(VI)). Values of 3.44 and 3.21 $\mu g\ L^{-1}$ U(VI) were determined for NASS-1 and CASS seawater reference standards.

JAMAL ELWERFALLI, JOHN A. PAGE et GARY W. VANLOON. Can. J. Chem. **65**, 1139 (1987).

Appliquant la voltamétrie à des échantillons préconcentrés par adsorption du complexe U(VI)/Br—PADAP (Br—PADAP = (bromo-5 pyridyl-2 azo)-2 diéthylamino-5 phénol), on a déterminé des traces de U(VI) dans de l'eau de mer.

Pour un électrolyte d'eau de mer contenant 3×10^{-7} *M* de Br—PADAP et tamponné à un pH de 7,8 par l'addition de triéthanolamine/$HClO_4$, le réactif et le complexe métallique sont adsorbés sur une électrode de goutte de mercure polarisée à −0,40 V par rapport à une référence Ag/AgCl. L'adsorption se produit à une vitesse qui est contrôlée par le transfert de masse. La voltamétrie du matériel électroactif adsorbé donne deux maxima, l'un à −0,56 V pour la réduction du Br—PADAP adsorbé et un à −0,65 V pour la réduction du complexe U(VI)—PADAP adsorbé. La hauteur de la deuxième vague est une mesure sensible de la concentration de U(VI) dans l'électrolyte. On a effectué l'analyse en procédant à une préconcentration restreinte impliquant une couverture fractionaire faible de l'électrode et une calibration par la méthode des additions standards. La méthode est sujette à des interférences de la part des agents de surface organiques; toutefois, il n'y a pas d'interférences de la part des ions des métaux usuels. On peut minimiser les interférences en n'utilisant que des temps d'adsorption courts dans l'étape de la préconcentration.

Pour un temps d'adsorption de 60 s, un taux de balayage de 0,050 V s^{-1} et une mesure au maximum du courant, la sensibilité de la méthode est 8,2 nA/($\mu g\ L^{-1}$ U(VI). On a pu déterminer des valeurs de 3,44 et 3,21 $\mu g\ L^{-1}$ U(VI) dans les échantillons de référence standards NASS-1 et CASS.

[Traduit par la revue]

Introduction

Uranium is normally present in seawater at the trace level as a U(VI) species. In aqueous non-complexing systems, U(VI) exists as a uranyl UO_2^{2+} species but U(VI) forms moderately stable complexes with chloride and very stable complexes with carbonate and these would be expected to dominate in natural sea water. A number of different techniques have been used to measure the concentration of the element and recent reports have given values of 2.6 $\mu g\ L^{-1}$ U in a coastal seawater by isotope dilution mass spectrometry after Chelex-100 preconcentration (1), 3.08 $\mu g\ L^{-1}$ U in a similar seawater by neutron activation analysis after preconcentration by adsorbing colloid flotation (2) and a value of 3.16 $\mu g\ L^{-1}$ U in Sea of Japan water by a spectrophotometric method using Arsenazo III reagent (3). The values reported presumably represent U(VI), but the specificity of these methods for the particular oxidation state of uranium is uncertain.

Electrochemical analysis is attractive but most methods are not sufficiently sensitive for the determination of uranium in sea water. Milner *et al.* (4) used a pulsed polarographic method but a complex separation and preconcentration step was required. Whitnack (5) attempted a direct polarographic analysis but was unable to detect uranium in seawater. A sensitive "catalytic" polarographic measurement involving nitrate ion is known but interferences prevent its use in seawater analysis (6). Attempts to determine uranium by anodic stripping voltammetry have failed because of the difficulty in depositing the element and the poor form of the stripping peaks (7).

A sensitive electrochemical method would appear dependent upon other forms of preconcentration of the uranium species from the electrolyte. It has been reported that U(VI) can be adsorbed on a mercury drop electrode and then determined voltammetrically by reduction of the adsorbed U(VI) (8). Preconcentration has also been achieved by the reaction of U(VI) with organophosphorus compounds adsorbed on a graphite electrode surface. Tripropyl- and tributyl-phosphate have been employed with the adsorbed U(VI) again determined by a voltammetry (9). Graphite electrodes modified by a surface coat of trioctylphosphine oxide have also been employed (10, 11). The U(VI) is effectively adsorbed from a chloride electrolyte at 0 V vs. a Ag/AgCl reference and determined by voltammetry. The method has been used to determine uranium in seawater, with the only pretreatment being removal of carbonate by boiling of an acidified sample before adjustment to pH 4 (3). A value of 3.14 $\mu g\ L^{-1}$ U(VI) was reported for Sea of Japan water, and this compared well with a value of 3.16 $\mu g\ L^{-1}$ U determined by a spectrophotometric procedure.

Catechol has also been employed for adsorptive accumula-

[1]Author to whom all correspondence may be addressed.

Can. J. Chem. Downloaded from www.nrcresearchpress.com by 78.46.186.204 on 09/07/12
For personal use only.

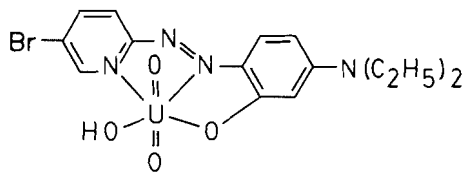

FIG. 1. Structure of the U(VI)/Br—PADAP complex with OH^- as auxiliary ligand.

tion of uranium. Lam *et al.* (12) adsorbed the U(VI) complex from a pH 4.7 electrolyte onto a mercury drop electrode at −0.10 V vs. a Ag/AgCl reference. The adsorbed species gave a reduction peak at −0.35 V. The direct determination of uranium in seawater was not possible but after preconcentration and ion exchange separation steps a value of 1.48 μg L^{-1} U, presumably U(VI), was reported for Atlantic seawater. Other techniques gave a value of 1.70 μg L^{-1} U for the sample. Van den Berg and Huang (13) also used the reagent for direct analysis of seawater buffered to pH 7. The U(VI) catechol complex was adsorbed at −0.40 V vs. a Ag/AgCl reference with a reduction peak for the electroactive material at −0.55 V. Values of 3.14 μg L^{-1} U(VI) in an Irish Sea sample and 3.21 μg L^{-1} U(VI) in an Atlantic seawater were reported. However, catechol is not a selective reagent and interferences were noted. It is known that adsorption processes involving catechol can enhance the voltammetric response of a number of ions including those of Cd(II), Cu(II), Fe(III), Pb(II), and Sn(IV) (14, 15) and these and other ions are potential interferences in the method.

While there are no specific guidelines for choosing reagents for such adsorptive preconcentration, candidates can be found in the analytical literature. A possibility exists with 2-(5-bromo-2-pyridylazo)-5-diethyl aminophenol (Br—PADAP) which has been recommended by Johnson and Florence as the most suitable spectrophotometric reagent for uranium (16). The reaction of the reagent with U(VI) is highly specific and it forms a stable 1:1 complex over the pH range 4.0–8.4. Incorporation of an auxiliary ligand such as OH^- gives a neutral chelate as shown in Fig. 1. For the complex, $\log \beta_1 = 5.1$ with OH^- as auxiliary ligand, while the incorporation of F^- is said to result in a more stable complex than with OH^-. The complex absorbs strongly with $\lambda_{max} = 578$ nm and $\epsilon = 74\,000\ cm^{-1}/(mol\ L^{-1})$.

The reagent itself is electroactive and can be reduced at a mercury electrode. Such aromatic azo dyes have been extensively studied by polarography and when present in excess with a metal exhibit two discreet polarographic reduction processes, one due to free reagent, the other due to the metal ligand complex. Under most conditions the reduction involves 4 Faradays per mole of ligand, leading to scission and formation of amine groups. Under some circumstances there can be a 2 Faraday per mole reduction leading to a dihydroazo compound (17).

The reagent and its metal complexes would also appear to be adsorbable species. The related pyridylazo-5-diethylamino-phenol reagent (PADAP) can be readily adsorbed on C-18 bonded glass beads and the immobilized reagent has been used for the concentration of trace metal ions such as Cd(II), Cu(II), Pb(II), and Zn(II). The metals can then be stripped from the substrate for determination by conventional anodic stripping voltammetry (18).

Experimental

The inverse voltammetric measurements were made using an E G and G Princeton Applied Research Corporation (PARC) Model 384 Analyzer. A PARC Model 303 Static Mercury Drop Electrode assembly was used with a Model 350 Stirrer Drive operating at 500 Hz. The three electrode system consisted of a Hg drop ("M" 0.017 cm^2), a Pt auxiliary electrode and a Ag/AgCl reference electrode. With the seawater electrolyte the reference had a potential of −0.010 V vs. a conventional SCE electrode at 25°C. The electrode capillaries were silanized according to the PARC instructions. A 15 mL quartz glass cell was used with a 1.0 cm diameter Teflon "SpinFin" for stirring. The voltammograms were stored in a digital form and subsequently plotted using a Houston Instruments HiPlot Plotter. For the polarographic and triangular wave experiments a PARC Model 174A Analyzer was used with the cell assembly but without electrolyte stirring. Voltammograms were recorded using a Hewlett Packard Model 7005 X–Y Recorder.

The N_2 gas used to deareate and blanket the electrolyte solutions was CANOX "oxygen-free" grade purified by passage over hot BASF catalyst. The sample and cell manipulations were carried out in a Canadian Cabinets Model HB-97-T laminar flow clean hood equipped with a high efficiency air filter. All glass and plastic ware was cleaned and conditioned by soaking in 3 *M* aq. nitric acid and thoroughly rinsed with good quality distilled water before use. While contamination of the cell and electrolyte was evident in some cases, it could be removed by rinsing and filling the cell with fresh sample electrolyte and continuing the process until satisfactory results were obtained.

The nitric acid used in this work was purified by sub-boiling distillation in a quartz still. The triethanolamine (TEA) buffer solution was prepared from 97% "BDH Assured" TEA and Analar Grade 70% "Aristar" perchloric acid supplied by BDH Chemicals. The stock buffer solution was 1.0 *M* in TEA and 0.5 *M* in added $HClO_4$ and had a pH of 8.0. Normally 500 μL of the stock buffer solution was added to each 0.010 L seawater sample to give a pH of 7.8. For experiments in which pH was a variable, additions of 1.0 *M* TEA or 0.5 *M* $HClO_4$ were made, as required, to the buffered system. The Br—PADAP reagent was of reagent grade quality supplied by the Aldrich Chemical Company, Inc. It was used without further purification. Dilute stock solutions, approximately 1×10^{-4} *M* in dissolved Br—PADAP, were accurately prepared by dissolving weighed amounts of reagent in a 1:1 H_2O/methanol solvent. The methanol was HPLC Grade supplied by the J. T. Baker Chemical Company. While the stock solution was evidently stable for periods exceeding 30 days, fresh solutions were prepared at 7 days intervals.

The stock U(VI) solution was prepared by dissolving 0.0214 g of uranyl acetate dihydrate in water, acidifying with 2.0 mL of nitric acid and making up to a volume of exactly 1 L. The uranyl acetate was an "Analar" reagent supplied by BDH Chemicals. The stock solution had a concentration of 12.1 μg mL^{-1} U(VI) and was diluted as needed for standard addition calibrations. The concentration was verified by a Zn(Hg) reduction of the U(VI), air oxidation to U(IV), and titration with an aq. $KMnO_4$ oxidant (19).

Direct voltammetry

Sampled current polarography gave a single well-defined but drawn out reduction wave with $E_{1/2}$ of −0.65 V for Br—PADAP in the buffered seawater electrolyte. The ratio of the limiting current to that for the reduction of an equal concentration of Cd(II) was 1.07:1, indicating a two electron mass transfer controlled reduction process for the Br—PADAP. The inequality in the limiting currents may be due to differences in the diffusion coefficients of the species involved, or there may be a small contribution from a four electron process for the reduction of the Br—PADAP. Triangular wave voltammograms are shown in Fig. 2. A fresh Hg drop was used for each voltammogram but the results were dependent upon the time of contact of the drop with the electrolyte. The Br—PADAP gave a cathodic peak at −0.58 V and an anodic peak at a corresponding potential on the reverse scan. The peak was nearly symmetrical in keeping with reduction of an adsorbed species and did not tail as might be expected for a mass transfer controlled contribution to the reduction process. The appearance

Can. J. Chem. Downloaded from www.nrcresearchpress.com by 78.46.186.204 on 09/07/12
For personal use only.

Can. J. Chem. Downloaded from www.nrcresearchpress.com by 78.46.186.204 on 09/07/12
For personal use only.

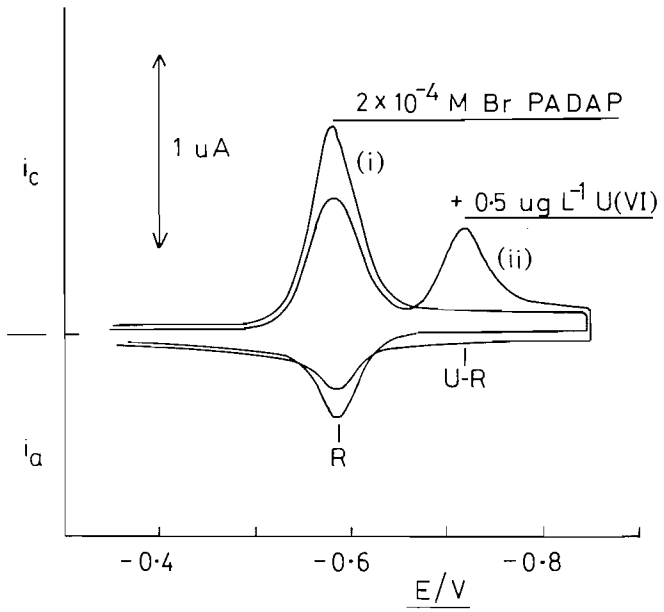

FIG. 2. Triangular wave voltammetry: seawater electrolyte, pH 7.8, 2×10^{-4} *M* Br—PADAP, scan rate 0.10 V s^{-1}; (*i*) no added U(VI), (*ii*) 0.5×10^{-6} g mL^{-1} added U(VI).

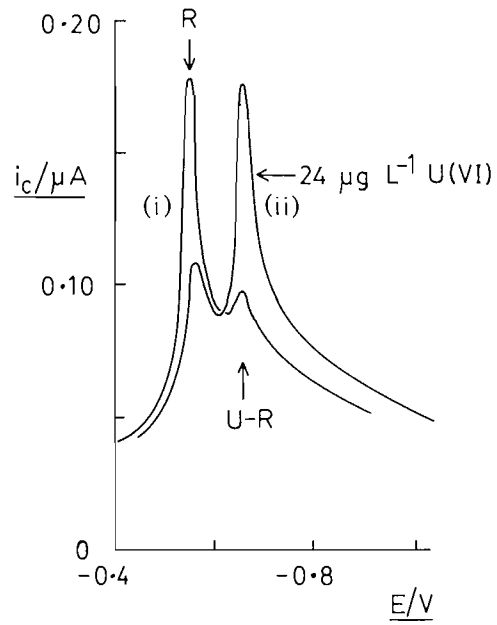

FIG. 3. Reduction of adsorbed reagent and U-complex species: seawater electrolyte, pH 7.8, 3×10^{-7} *M* Br—PADAP; 120 s adsorption at −0.40 V, scan rate 0.05 V s^{-1}; (*i*) no added U(VI); (*ii*) 24×10^{-6} g L^{-1} added U(VI).

of a symmetrical oxidation peak at the same potential on the reverse scan indicates that the reduction product was adsorbed on the electrode. Addition of trace substoichiometric amounts of U(VI) to the system produced a second symmetrical reduction peak at −0.72 V with no corresponding anodic peak. This would indicate a reduction step involving metal complex adsorbed on the electrode. The reduction is irreversible or desorption and loss of the reduced species from the electrode surface occurs. The height of the second peak was dependent upon the concentration of added U(VI).

Inverse voltammetry

(1) Adsorption/reduction

Inverse voltammograms obtained after adsorption of the electroactive species from the seawater electrolyte are shown in Fig. 3. Two cathodic current peaks are evident, at −0.55 V, corresponding to reduction of adsorbed Br—PADAP and at −0.66 V corresponding to reduction of adsorbed complex. The seawater shows a large peak for Br—PADAP and a small peak evident of trace U(VI). The sample with added U(VI) shows a small peak for uncomplexed reagent and a large peak for the metal complex. The peaks are relatively sharp, with a half-maximum width of 0.038 V, in keeping with reduction of a surface layer of electroactive material. The peak current for reduction of the complex was a linear function of scan rate over the range examined from 0.02–0.08 V s^{-1}.

Integration of the Br—PADAP peak (in the absence of added U(VI)) to a tangent baseline gave 4.4×10^{-8} C for reduction of the reagent. An equivalent Cd amalgam prepared by deposition at −0.90 V from a seawater electrolyte with 3×10^{-7} *M* added Cd(II) required 5.4×10^{-8} C for stripping. The near equality of the quantities of electricity indicates that equivalent amounts Br—PADAP and Cd are collected at the Hg drop electrode under comparable conditions. Adsorption of Br—PADAP, like deposition of Cd, appears to be a mass transfer controlled process.

Figure 4 shows the effects of added U(VI) on the voltammetric behaviour. Reproducible voltammograms were obtained within 10 min after addition of the metal, indicating a rapid

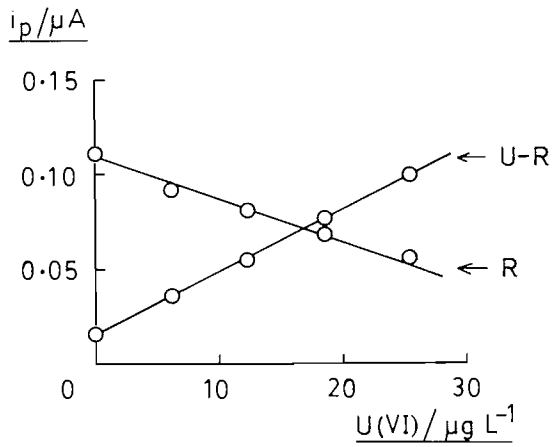

FIG. 4. Effect of added U(VI) on voltammetric response: seawater electrolyte, pH 7.8, 3×10^{-7} *M* Br—PADAP; 120 s adsorption at −0.40 V, scan rate 0.05 V s^{-1}.

reaction between the U(VI) and the Br—PADAP. The height of the peak at −0.65 V grew in a linear fashion with added U(VI), while that at −0.56 V decreased. The slopes of the plots were for Br—PADAP, −2.2 and for the U-complex, +3.2 nA/(μg mL^{-1} U(VI)). The larger sensitivity for the metal complex may indicate a coreduction of the ligand and the metal of the adsorbed complex or the diffusion coefficient of the complex may be significantly greater than that of the free ligand. Only one peak for reduction of adsorbed metal complex was apparent in the voltammograms.

If the height of the peak at −0.56 V is assumed proportional to the concentration of free Br—PADAP in the electrolyte, then the ratio: (amount Br—PADAP removed)/(amount added U(VI)) = 1.3. The result differs from the unit value expected for a 1:1 metal–ligand complex, but could be explained by errors in the estimation of the concentration of free Br—PADAP.

(2) Surface saturation

The effect of increased adsorption time on the response is

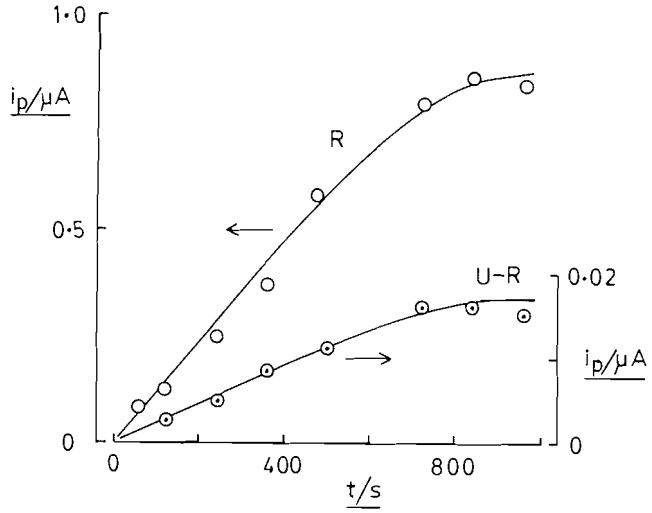

FIG. 5. Effect of adsorption time on voltammetric response: seawater electrolyte, pH 7.8, 3×10^{-7} *M* Br—PADAP; Adsorption at -0.40 V, scan rate 0.05 V s^{-1}.

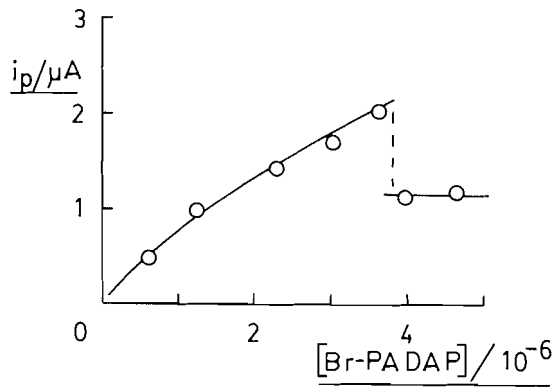

FIG. 6. Effect of Br—PADAP concentration on voltammetric response: seawater electrolyte, pH 7.8, 60 s adsorption at -0.40 V, scan rate 0.05 V s^{-1}.

shown in Fig. 5. Both the Br—PADAP and the metal complex peaks grew to a limiting value corresponding to saturation of the Hg drop surface with electroactive material. The reduction peak for the Br—PADAP broadened at high electrode coverage and shifted to more negative potentials. At low fractional coverage, the complex peak grew linearly with time despite the simultaneous adsorption of Br—PADAP. The adsorption of both the reagent and the complex would appear to be mass transfer controlled at low fractional electrode coverage. Integration of the peak for reduction of the Br—PADAP at saturation gave a cathodic process of 1.3×10^{-6} C. If the reduction is a two electron process, then a Faraday Law calculation gives 6.7×10^{-12} mol adsorbed reagent on a 0.017 cm^2 electrode corresponding to an area of $(0.65\ nm)^2$ per molecule. This value in keeping with dimensions previously reported for adsorbed molecules (13, 20). Figure 6 shows the effect of increased concentration of Br—PADAP on the response at a fixed adsorption time. The results are again in keeping with a saturation of the electrode surface with a degree of surface supersaturation evident at intermediate Br—PADAP concentrations.

(3) pH

The response was dependent upon the pH of the electrolyte. A reduction peak for adsorbed metal complex was apparent only above pH 7.4 but the response remained constant up to pH 8.8. The lack of a response at low pH may be due to an insignificant degree of formation of the complex or a low activity of OH^- as the auxiliary ligand required for an uncharged metal complex. The peak for reduction of adsorbed Br—PADAP was apparent over the whole range of pH examined. The reagent has two N atoms as protonation sites and one phenolic proton. For H_3L^{2+}, $pK_{a1} = 0.1$, $pK_{a2} = 2.02$, and $pK_{a3} = 11.30$ so that the reagent exists in an uncharged form over the pH range 3–10 (21). No significant shift in peak potential for either the reagent or the complex was observed over the range of pH examined.

(4) Adsorption potential

The response was sensitive to the adsorption potential. The metal complex was adsorbed over a range of potential from -0.20 to -0.50 V but the sensitivity was maximum at -0.40 V. Over this range, the Br—PADAP sensitivity decreased with increasingly negative values of potential, probably due to simultaneous adsorption and reduction of the reagent species. The metal complex peak remained well defined over the range of potentials.

Analysis

(1) Procedure

The analysis procedure was based on the optimal values of the experimental parameters. The adsorption time was kept short, despite a decreased sensitivity, to minimize electrode coverage and the adsorption of interfering species. The concentration of added Br—PADAP was chosen to give a minimum excess relative to the concentration of U(VI).

The normal procedure involved a 0.010 L sample of seawater, with addition of 500 μL of TEA stock buffer reagent and 50 μL of stock Br—PADAP reagent. The samples as provided were normally acidified to pH 1.8 with HNO_3 and the buffered system had a pH of 7.8. The precise volume of sample was determined from electrolyte weight at the end of an analysis/calibration sequence. For analysis, adsorptive preconcentration was carried out at -0.40 V for 60 s with stirring. The stirring was then shut down and after an additional 20 s at the initial potential the electrode potential was scanned at 0.05 V s^{-1} to more negative potentials to reduce the adsorbed electroactive material. The peak current for the reduction of adsorbed uranium complex at -0.66 V was measured relative to an estimated baseline. For the standard addition calibration, aliquots of a standard U(VI) solution were added to the electrolyte. A fresh Hg drop was used for each preconcentration/analysis step. Allowing for a two fold excess of Br—PADAP limits the U(VI) concentrations measurable to 60 μg L^{-1}.

(2) Interferences

The Br—PADAP is not completely specific for U(VI) and can form complexes with other metal species. A series of metal ions that would constitute possible interferences in the analysis were added to the buffered seawater electrolyte at concentrations of 50 μg L^{-1} in separate experiments. No response or interference was observed with added Al(III), Cd(II), Co(II), Cr(III), Cu(II), Mo(V), Ni(II), Pb(II), Zn(II), and V(V). A reduction peak was obtained with added Fe(III) evidently resulting from the reduction of an adsorbed Fe(III) complex. The peak appeared at -0.80 V and was well removed from the peak for reduction of the adsorbed U(VI) complex.

Non-electroactive surface active substances also constitute a potential interference in the analysis by preferential adsorption

Can. J. Chem. Downloaded from www.nrcresearchpress.com by 78.46.186.204 on 09/07/12
For personal use only.

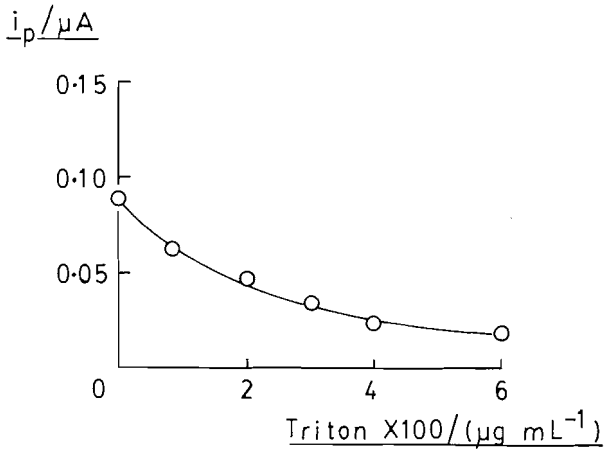

FIG. 7. Effect of added surfactant on voltammetric response: seawater electrolyte, pH 7.8, 3×10^{-7} *M* Br—PADAP. 120 s adsorption at −0.40 V, scan rate 0.05 V s^{-1}.

TABLE 1. Analysis of seawater for U(VI): standard addition analyses

NASS-1:	3.45, 3.44, 3.44, 3.43 μg L^{-1} U(VI)
	Mean, s.d.: 3.44 ± 0.05 μg L^{-1}
	Sensitivity: 8.8 ± 0.2 nA/(μg L^{-1})
CASS-1:	3.21, 3.16, 3.26, 3.24, 3.19, 3.21, 3.22 μg L^{-1} U(VI)
	Mean, s.d.: 3.21 ± 0.19 μg L^{-1}
	Sensitivity: 7.7 ± 0.3 nA/(μg L^{-1})

and blocking of the electrode surface. Triton X-100 was used as a model non-ionic surfactant and the effect of added surfactant on the metal complex peak is shown in Fig. 7. The added surfactant resulted in a decrease in sensitivity of the measurement but the effect was only significant at surfactant concentrations at the ppm level, rather greater than those normally present in seawater. Surfactants constitutes a serious potential interference in the method, and adsorption times should be kept short to minimize the effect. A compensation for the interference is provided by the standard addition calibration of the method.

(3) Calibration and analysis

NASS-1 and CASS-1 Reference Seawater Samples provided by the Marine Analytical Chemistry Standards Program of The National Research Council of Canada (22) were analyzed by the standard procedure with results from standard addition calibration as given in Table 1. While there are no certificate values for the element available for comparison purposes, the results obtained were in agreement with values of 2.6 μg L^{-1} (1) and 3.08 μg L^{-1} (2) recently reported for coastal seawaters. The method was found to be convenient to apply and required a minimum of handling and pretreatment of a sample. While other sorts of aqueous samples have yet to be examined, the procedure should be applicable, although experience has indicated that the presence of organic surfactants can constitute a serious interference in methods involving preconcentration by adsorption at an electrode.

Acknowledgements

Support from the Marine Analytical Standards Program of the National Research Council of Canada in the way of a contract and support from the Natural Sciences and Engineering Research Council of Canada in the way of an operating grant is gratefully acknowledged. Mr. Elwerfalli is a graduate student sponsored by the Libyan Government and their scholarship support is also gratefully acknowledged.

1. A. P. MYKYTIUK, D. S. RUSSELL, and R. E. STURGEON. Anal. Chem. **52**, 1281 (1980).
2. R. S. S. MURTHY and D. E. RYAN. Anal. Chem. **55**, 682 (1983).
3. K. IZUTSU, T. NAKAMURA, and T. ANDO. Anal. Chim. Acta, **152**, 285 (1983).
4. G. W. C. MILNER, J. D. WILSON, G. A. BARNETT, and A. A. SMALES. J. Electroanal. Chem. **2**, 25 (1961).
5. G. C. WHITNACK. Anal. Chem. **47**, 618 (1975).
6. R. KEIL. Fresenius Z. Anal. Chem. **292**, 13 (1978).
7. F. VDRYA, K. STULIK, and E. JULAKOVA. Electrochemical stripping analysis. Halsted Press. John Wiley and Sons. 1976. p. 253.
8. H. BERGE and H. RINGSTORFF. Anal. Chim. Acta, **55**, 201 (1971).
9. H. BERGE and H. RINGSTORFF. Anal. Chim. Acta, **55**, 193 (1971).
10. K. H. LUBERT, M. SCHNURRBUSCH, and A. THOMAS. Anal. Chim. Acta, **144**, 123 (1982).
11. K. IZUTSU, T. NAKAMURA, R. TAKIZAWA, and H. HANAWA. Anal. Chim. Acta, **149**, 147 (1983).
12. N. K. LAM, R. KALVODA, and M. KOPANICA. Anal. Chim. Acta, **154**, 79 (1983).
13. C. M. G. VAN DEN BERG and Z. Q. HUANG. Anal. Chim. Acta, **164**, 209 (1984).
14. C. M. G. VAN DEN BERG. Anal. Chim. Acta, **164**, 195 (1984).
15. C. MCCRORY-JOY and J. M. ROSAMILIA. Anal. Chim. Acta, **142**, 231 (1982).
16. D. A. JOHNSON and T. M. FLORENCE. Anal. Chim. Acta, **53**, 73 (1971).
17. T. M. FLORENCE, D. A. JOHNSON, and G. E. BATLEY. J. Electroanal. Chem. **50**, 113 (1974).
18. S. TAGUCHI, T. YAI, Y. SHIMADA, K. GOTO, and M. HARA. Talanta, **30**, 169 (1983).
19. G. E. F. LUNDELL and H. B. KNOWLES. J. Am. Chem. Soc. **47**, 2637 (1925).
20. W. WESTENBRINK. M.Sc. Thesis, Queen's University, Kingston, Ont. 1983.
21. D. A. JOHNSON and T. M. FLORENCE. Talanta, **22**, 253 (1975).
22. Marine Analytical Chemistry Standards Program, Division of Chemistry, National Research Council of Canada, Montreal Road, Ottawa, Canada K1A 0R9.

Can. J. Chem. Downloaded from www.nrcresearchpress.com by 78.46.186.204 on 09/07/12
For personal use only.

The preferred rotamer about the C_5—C_6 bond of D-galactopyranoses[1] and the stereochemistry of dehydrogenation by D-galactose oxidase

HIROSHI OHRUI,[2] YOSHIHIRO NISHIDA, HIROKO HIGUCHI, HIROSHI HORI, AND HIROSHI MEGURO
Department of Food Chemistry, Faculty of Agriculture, Tohoku University, Tsutsumidori-Amamiyamachi, Sendai 980, Japan

Received January 3, 1986[3]

HIROSHI OHRUI, YOSHIHIRO NISHIDA, HIROKO HIGUCHI, HIROSHI HORI, and HIROSHI MEGURO. Can. J. Chem. **65**, 1145 (1987).

^{1}H nuclear magnetic resonance studies on D-galactopyranoses with chirally deuterated hydroxymethyl groups revealed that the preferred rotamer about the C_5—C_6 bond of the D-galactopyranoses was not *tg* but *gt*. Studies on the stereochemistry of dehydrogenation of D-galactose oxidase from *Dactylium dendroides* with chirally pure deuterated methyl β-D-galactopyranosides showed that there were two mechanisms for the enzymatic reaction: an efficient *pro-S* hydrogen atom specific oxidation and a far less efficient non-specific or *pro-R* specific oxidation.

HIROSHI OHRUI, YOSHIHIRO NISHIDA, HIROKO HIGUCHI, HIROSHI HORI et HIROSHI MEGURO. Can. J. Chem. **65**, 1145 (1987).

Des études de résonance magnétique nucléaire du ^{1}H sur des D-galactopyrannoses portant des groupements hydroxyméthyles deutérés d'une façon chirale révèlent que le rotamère privilégié autour de la liaison C_5—C_6 des D-galactopyrannoses n'est pas *tg* mais plutôt *gt*. Des études sur la stéréochimie de la déshydrogénation, par l'oxydase du D-galactose provenant du *Dactylium dendroides*, de β-D-galactopyrannosides de méthyles deutérés et purs d'un point de vue chiral ont démontré qu'il existe deux mécanismes pour la réaction enzymatique; une oxydation spécifique de l'atome d'hydrogène *pro-S* qui est efficace et un oxydation non-spécifique ou spécifique *pro-R* qui est beaucoup moins efficace.

[Traduit par la revue]

Can. J. Chem. Downloaded from www.nrcresearchpress.com by 78.46.186.204 on 09/07/12
For personal use only.

Introduction

A complete understanding of the interaction between carbohydrates and proteins (enzymes, antibiotics, and lectins) is to a large extent dependent on the information available about the preferred conformation of the carbohydrate molecule in solution (1, 2). For example, the current stereochemical concept that D-galactose residues favor the *tg* rotamer as shown in Fig. 1 (3) in the binding sites of D-galactosyl binding proteins (1) has been based mainly on the conformational analyses of methyl β-D-galactopyranoside by Lemieux and co-workers (1, 4) and of acetylated D-galactoses by Hall *et al.* (5) and Perlin and co-workers (6). The assignment of the preferred rotamer about the C_5—C_6 bond of D-galactose and its derivatives has been a controversial problem. For example, Yamana (7), by a chiroptical method, reported that the preferred rotamer was *gg*. Hall, by an ^{1}H nmr study on D-galactopyranose peracetate (5), reported it to be *tg*. On the other hand, De Bruyn suggested it to be *tg* (8) and Lemieux first assigned it to be *gt*, based on both ^{1}H nmr and chiroptical studies (9), and later corrected it to be *tg*, based on a detailed ^{1}H nmr study on methyl β-D-galactopyranoside (4). Recently Lew and Nakanishi assigned the preferred rotamer of methyl D-galactopyranoside perbenzoates to be *tg* on the basis of their "dibenzoate chirality rule" (10). Therefore *tg* has been accepted as the preferred rotamer of both acylated and OH-free D-galactopyranoses. The difficulty in the conformational analysis of the C_5—C_6 bond of D-galactopyranose by ^{1}H nmr has been ascribed to the difficulty of differentiating unequivocally the two protons, H6*proR* and H6*proS*, and of obtaining the precise coupling constants, $J_{H5,H6proR}$ and $J_{H5,H6proS}$, which is the key information needed for the study. Our recent development of syntheses of sugars with chirally deuterated hydroxymethyl groups has enabled us to differentiate the two protons and obtain the coupling constants (11–14).[4] In this paper, we would like to describe the results of our conformational analyses and the stereochemistry of oxidation by D-galactose oxidase from *Dactylium dendroides* using the chirally deuterated D-galactopyranoses as substrates.

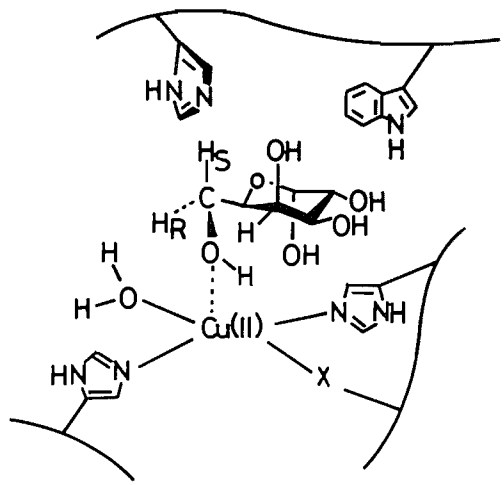

FIG. 1. The current concept of the active site of D-galactose oxidase.

Results and discussion

Previously we reported the synthesis of (6*R*)- and (6*S*)-(6-$^2H_1$)-D-galactoses through photobromination (15) of 1,6-anhydro-2,3,4-tri-*O*-benzoyl-D-galactopyranose **1** followed by

[1]Part of this study has been already reported in ref. 13.
[2]Author to whom correspondence may be addressed.
[3]Revision received October 15, 1986.

[4]The authors are very grateful to a referee for pointing out the errors in assigning the ^{1}H nmr spectrum of 1,6-anhydro-D-glucopyranose (11). The correction will be reported in another manuscript (see footnote 5).

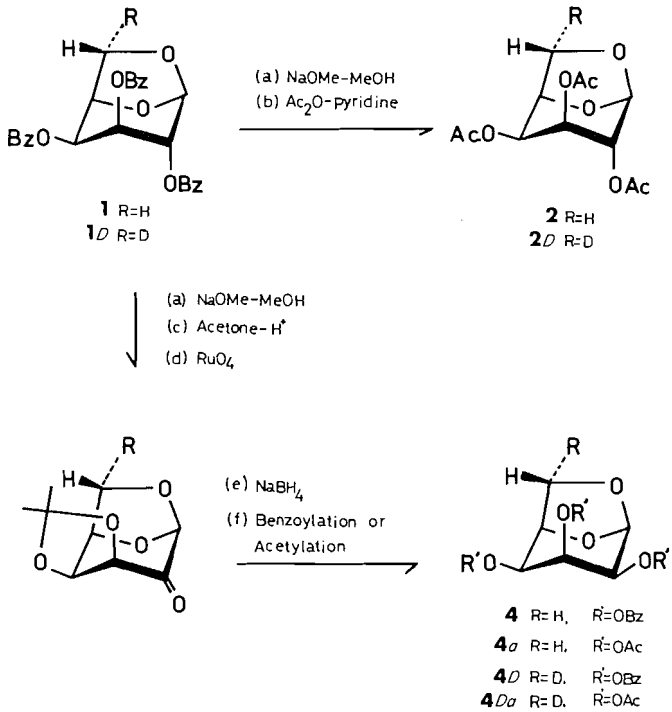

SCHEME 1

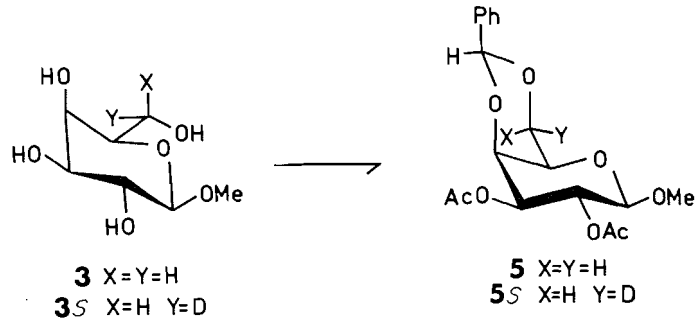

SCHEME 2

tri-*n*-butyltindeuteride reduction of the resulting *exo*-bromide (12). Our assignments of absolute configuration of the specifically deuterated galactose derivatives have been based on the "assumption" that protons at C-6 of 1,6-anhydrohexopyranose 2,3,4-tri-*O*-benzoates, which resonate at higher field and have larger coupling constants with H-5 than the other proton at C-6, could be assigned to H-6*exo* (12), because the same findings have been reported for 1,6-anhydro-D-hexopyranoses and for their 2,3,4-tri-*O*-acetate (16, 17).

In the present paper, several other pieces of evidence that confirm the correctness of our previous assignments are presented.

Compound **1***D*, which we had assigned to (6*S*) (12), was converted to the acetate **2***D* by a conventional method (sodium methoxide in MeOH and then acetylation) (Scheme 1). In the ^{1}H nmr spectra of **2***D* the signal at 3.72 ppm, which had been assigned to H-6*exo* of nondeuterated **2** by Černý (17), disappeared completely and the doublet at 4.347 ppm, which had been assigned to H-6*endo* (17), appeared at 4.326 ppm (0.021-ppm upfield shift by deuterium isotope effect (18, 19)) as a singlet. The result supports the correctness of our previous assignments.

Next, our methyl (6*R*)-(6-^{2}H$_1$)-β-D-galactopyranoside **3***R* and methyl (6*S*)-(6-^{2}H$_1$)-β-D-galactopyranoside **3***S* were converted to the corresponding acetates **3***Ra* and **3***Sa*, respectively. The partial ^{1}H nmr spectra of **3***Ra* and **3***Sa* and nondeuterated **3***a* are shown in Fig. 2. The assignments of H6*proR* and H6*proS* are consistent with those reported by Perlin and co-workers (6). This result also supports the validity of our previous assignments. The ^{1}H nmr spectra of both **3***Ra* and **3***Sa* show the presence of a very small amount of **3***a*. This amount depends on the quality of tin deuteride used. As is observed clearly in Fig. 2, deuteration causes a 0.015-ppm upfield shift of H6*proR*, a 0.017-ppm upfield shift of H*proS*, and a 0.004-ppm upfield shift of H-5; however, *deuteration has little effect on the coupling constants*. Similar deuterium isotope-induced chemical shifts of protons have been reported by Hall and Wong (18).

Another method of assignment of H-6*exo* in 1,6-anhydrohexopyranoses is measurement of the "W" arranged long-range coupling between H-6*exo* and H-4, since only H-6*exo* can enjoy the "W" type long-range coupling (17, 20). Irradiation at 5.74 ppm of **1** sharpened the quartet of broad signals at 3.85 ppm, which we assigned to H-6*exo* (12), indicating the presence of long-range coupling in the signal of H-6*exo*. However, the result does not give us an unequivocal assignment of H-6*exo* because the chemical shifts of H-1 and H-4 are almost the same at 5.74 ppm, and long-range coupling between H-1 and H-6*exo* has been reported (16).

Therefore, compound **1** was transformed to 1,6-anhydrotalopyranose-2,3,4-tri-*O*-benzoate **4** (mp 178°C, $[\alpha]_D^{21}$ −58° (*c* 0.1, $CHCl_3$)) and tri-*O*-acetate **4***a* by the established method (20) (Scheme 1). The "W" arranged long-range coupling between H-6*exo* and H-4 of **4***a* has already been reported by Horton and Jewell (20) and a "W" arranged long-range coupling is observed between H-6 (quartet of a small doublet at 3.993 ppm) and H-4 (triplet of small doublets at 5.608 ppm) of **4**. Therefore the H-6 signal at 3.993 ppm, which has a larger coupling with H-5 than the other H-6 signal at 4.78 ppm, is assigned to H-6*exo*. Compound **1***D* was also converted to **4***D* and **4***Da*. The ^{1}H nmr spectra of **4***D* and **4***Da* showed complete disappearance of the signals for H-6*exo* protons. Therefore **4***D* and **4***Da* are unequivocally assigned to be the (6*S*)-(6-^{2}H$_1$) derivatives of **4** and **4***a*, respectively. Since all reactions used for transformations proceed with retention of configuration at C-6, **1***D* is definitively assigned to be the (6*S*)-(6-^{2}H$_1$) derivative of **1**.

To confirm further the assignment of absolute configuration of these C-6 chirally deuterated galactoses, **3** and **3***S* were converted into methyl 2,3-di-*O*-acetyl-4,6-*O*-benzylidene-β-D-galactopyranosides **5** and **5***S*, respectively, with the *gg* fixed conformation (Scheme 2).

In the ^{1}H nmr spectrum of **5**, it is reasonable to assign the more deshielded H-6 proton to H6*proS* and the more shielded one to H6*proR* because H6*proS* and H6*proR* are in equatorial and axial dispositions, respectively, with respect to the 4,6-*O*-benzylidene ring structure. Thus, in the ^{1}H nmr spectrum of **5**, the H-6 proton signals at 4.34 ppm (dd, 1.7 and 12.4 Hz) and 4.07 ppm (dd, 1.7 and 12.4 Hz) are assigned to H6*proS* and H6*proR*, respectively. In the spectrum of **5***S*, the lower field signal in that of **5** disappeared and the other appeared as a doublet at 4.06 ppm (1.7 Hz). These results also confirm our previous assignments.

All these pieces of evidence strongly confirm the assignments

Can. J. Chem. Downloaded from www.nrcresearchpress.com by 78.46.186.204 on 09/07/12
For personal use only.

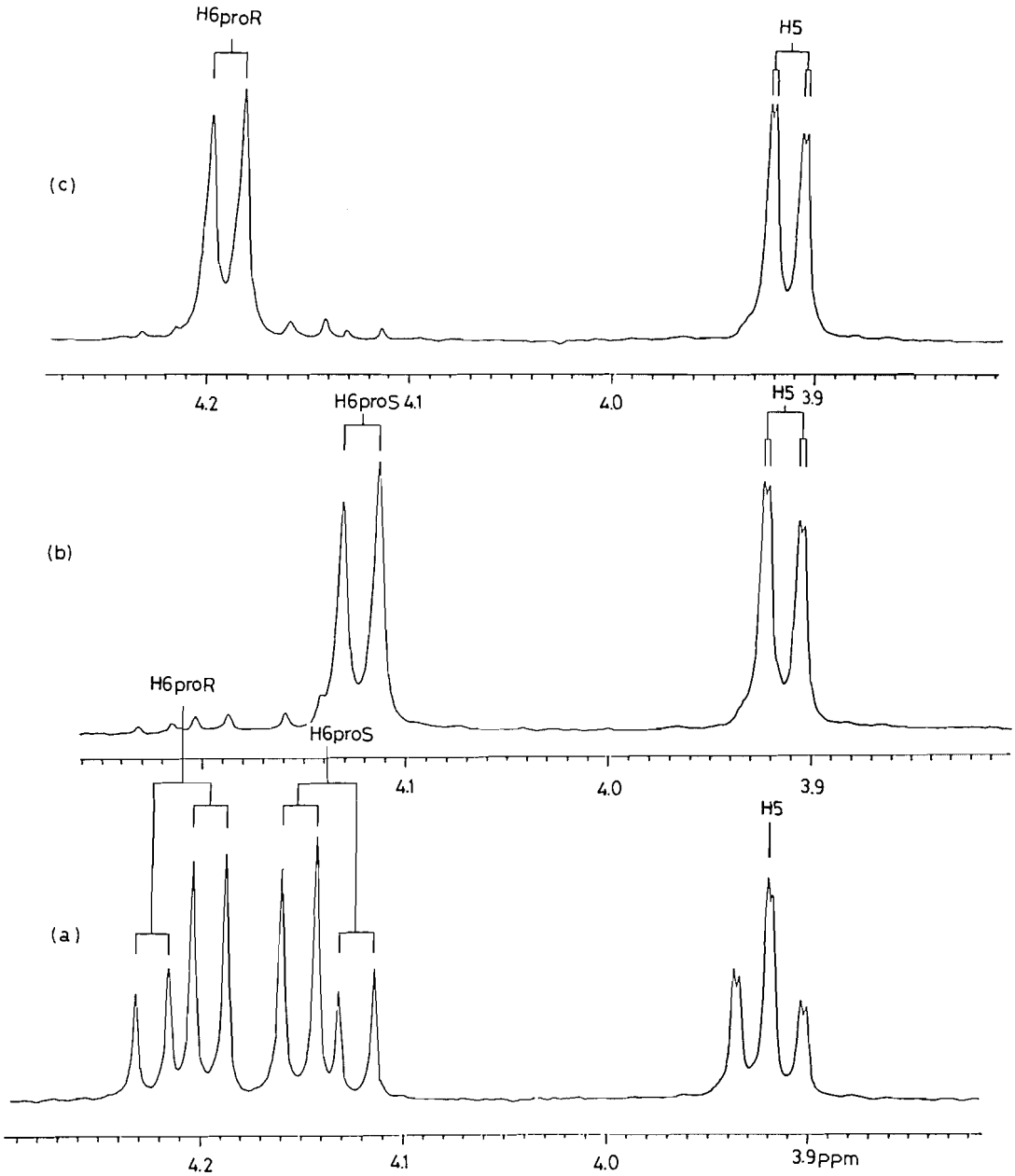

FIG. 2. The ^{1}H nmr spectra of (*a*) methyl tetra-*O*-acetyl-β-D-galactopyranoside **3***a*, (*b*) methyl (6*R*)-(6-$^2H_1$)-tetra-*O*-acetyl-β-D-galactopyranoside **3***Ra*, and (*c*) methyl (6*S*)-(6-$^2H_1$)-tetra-*O*-acetyl-β-D-galactopyranoside **3***Sa* at 400 MHz in $CDCl_3$.

of absolute configuration of the two specifically 6-deuterated galactoses made by us.[5]

The ^{1}H nmr spectra of methyl β-D-galactopyranoside **3**, methyl (6*R*)-(6-$^2H_1$)-β-D-galactopyranoside **3***R*, and methyl (6*S*)-(6-$^2H_1$)-β-D-galactopyranoside **3***S* are shown in Fig. 3 to demonstrate how the chirally deuterated sugars are useful for the study. The complex signals of H-5, H-6*proR*, H-6*proS* of **3** are dramatically simplified in the spectra of deuterated **3***R* and **3***S*. Therefore it is very easy to assign the signals and to measure $J_{H5,H6proR}$ and $J_{H5,H6proS}$. Deuterium-isotope induced upfield chemical shifts (18, 19) are also observed in these spectra. Therefore the chemical shifts of H6*proR* and H6*proS* of nondeuterated **3** should be about 0.015–0.02 ppm lower than those obtained with deuterated derivatives **3***R* and **3***S*.

So far as the data obtained by us is concerned, *a deuterium isotope effect on the coupling constants has not been observed*; therefore the coupling constants obtained with deuterated derivatives can be considered those of normal compounds.

The ^{1}H nmr parameters of **3**, **3***R*, **3***S* and their acetates **3***a*, **3***Ra*, **3***Sa*, together with those of **3** reported by Bock and Thøgersen (21) and De Bruyn (8), are listed in Table 1. Differences between our chemical shifts and theirs arise from differences in the conditions of measurement, for example the different internal standards. We used 3-(trimethylsilyl)propane-

[5]We are now very confident that the assignments of H-6 protons of 1,6-anhydrohexopyranoses can be made by the rule that the *exo* protons resonate at higher field and have larger coupling with H-5 than do the *endo* protons. This is discussed in a paper that has been submitted to the Journal of Carbohydrate Chemistry.

Can. J. Chem. Downloaded from www.nrcresearchpress.com by 78.46.186.204 on 09/07/12
For personal use only.

TABLE 1. Comparison of the ^1H nmr parameters of methyl β-D-galactopyranoside (**3**), its (6*R*)-(6-$^2H_1$) derivative (**3***R*), and (6*S*)-(6-$^2H_1$) derivative (**3***S*) with the reported data

Chemical shifts[a] (Coupling constant)	H1 ($J_{1,2}$)	H2 ($J_{2,3}$)	H3 ($J_{3,4}$)	H4 ($J_{4,5}$)	H5 ($J_{5,6R}$)	H6*proR* ($J_{6R,6S}$)	H6*proS* ($J_{5,6S}$)	OMe
De Bruyn and Anteunis (8)					3.70 (3.5)	3.76	3.83 (8.5)	
Bock and Thøgersen (21)	4.20 (8.0)	3.39 (10.0)	3.53 (3.8)	3.81 (0.8)	3.57 (7.6)	3.69 (11.2)	3.64 (4.4)	3.45
3[b]	4.3245 (8.0)	3.5081 (10.0)	3.6532 (3.5)	3.9291 (0.9)	[3.705 [(8.2)	3.802 (11.8)	3.763][d] (3.6)][d]	3.5820
3*S*[b]	4.3245 (8.0)	3.5082 (10.0)	3.6539 (3.5)	3.9292 (0.9)	3.702 (8.0)	3.784 —	— —	3.5826
3*R*[b]	4.3242 (8.0)	3.5079 (10.0)	3.6539 (3.5)	3.9278 (0.9)	3.702 —	— —	3.744 (4.4)	3.5820
Δ **3***S* − **3**	0	+0.0001	+0.0007	+0.0001	−0.003	−0.018	—	+0.0006
Δ **3***R* − **3**	−0.003	−0.0002	+0.0007	−0.0013	−0.003	—	−0.019	0
3*a*[c]	4.4061 (7.9)	5.2072 (10.5)	5.0210 (3.4)	5.3977 (1.0)	3.9189 (6.6)	4.207	4.140 (6.8)	3.5259
3*Sa*[c]	4.4046 (7.9)	5.2070 (10.5)	5.0202 (3.4)	5.3956 (1.0)	3.9149 (6.6)	4.192 —	— —	3.5259
3*Ra*[c]	4.4053 (7.9)	5.2076 (10.5)	5.0208 (3.4)	5.3969 (1.0)	3.9149 —	— —	4.123 (7.0)	3.5267
Δ **3***Sa* − **3***a*	−0.0015	−0.0002	−0.0008	−0.0021	−0.0040	−0.015	—	0
Δ **3***Ra* − **3***a*	−0.0008	+0.0004	−0.0002	−0.0008	−0.0040	—	−0.017	+0.0008

[a](ppm) ±0.0005, Hz ±0.2.
[b]Measured at 400 MHz in D_2O at 296 K relative to internal 3-(trimethylsilyl)propanesulfonic acid sodium salt (0.0000 ppm).
[c]Measured in $CDCl_3$ relative to internal TMS (0.0000 ppm).
[d]Values obtained through ABX analyses.

TABLE 2. The chemical shifts, coupling constants, and calculated populations of rotamers of stereospecifically deuterated D-galactose derivatives and of those reported in the literature (6, 21)

						Rotamers (%)[b]								
						Equation A			Equation B			Equation C		
	Solvents	H6*R* (ppm)	H6*S* (ppm)	$J_{5,6R}$ (Hz)[a]	$J_{5,6S}$ (Hz)[a]	*gg*	*gt*	*tg*	*gg*	*gt*	*tg*	*gg*	*gt*	*tg*
α-D-Galactopyranose	D_2O	3.71	3.71	7.9	4.6	21	54	25	17	63	20	20	60	20
(21)		3.72 – 3.62		6.4	6.4	25	30	45	18	38	44	21	36	43
β-D-Galactopyranose	D_2O	3.76	3.73	7.8	4.6	22	53	25	18	62	20	21	59	20
(21)		3.70 – 3.62		7.8	3.8	27	56	17	24	66	10	27	62	11
Methyl α-D-galactopyranoside	D_2O	3.76	3.75	8.3	4.0	21	61	18	13	70	17	20	67	13
(21)		3.67	3.61	8.2	4.6	19	57	24	14	66	20	17	62	21
Methyl β-D-galactopyranoside	D_2O	3.79	3.75	8.0	4.4	22	55	23	17	65	18	21	62	18
(21)		3.69	3.64	7.6	4.4	25	52	23	21	61	18	25	57	18
Methyl tetra-*O*-acetyl-β-D-galactopyranoside	$CDCl_3$	4.19	4.12	6.6	6.8	21	30	49	13	38	59	16	37	47
(6)				6.3	7.2	21	25	54	13	32	55	16	32	52
Penta-*O*-acetyl-α-D-galactopyranose	$CDCl_3$	4.07	4.12	6.6	7.1	19	29	52	11	36	53	14	36	50
Methyl tetra-*O*-benzoyl-α-D-galactopyranoside	$CDCl_3$	4.61	4.41	—[c]	8.8	—	— tg ≅ 80 —		—			—	—	
Methyl tetra-*O*-benzoyl-β-D-galactopyranoside	$CDCl_3$	4.69	4.45	6.3	6.6	24	29	47	18	36	46	21	35	44

[a]First-order analysis, $J_{5,6}$ ± 0.2 Hz.
[b]Errors by ±0.2 Hz are *gg* ± 3, *gt* ± 3, and *tg* ± 3.
[c]The values could not be obtained because of overlapping of signals.

Can. J. Chem. Downloaded from www.nrcresearchpress.com by 78.46.186.204 on 09/07/12
For personal use only.

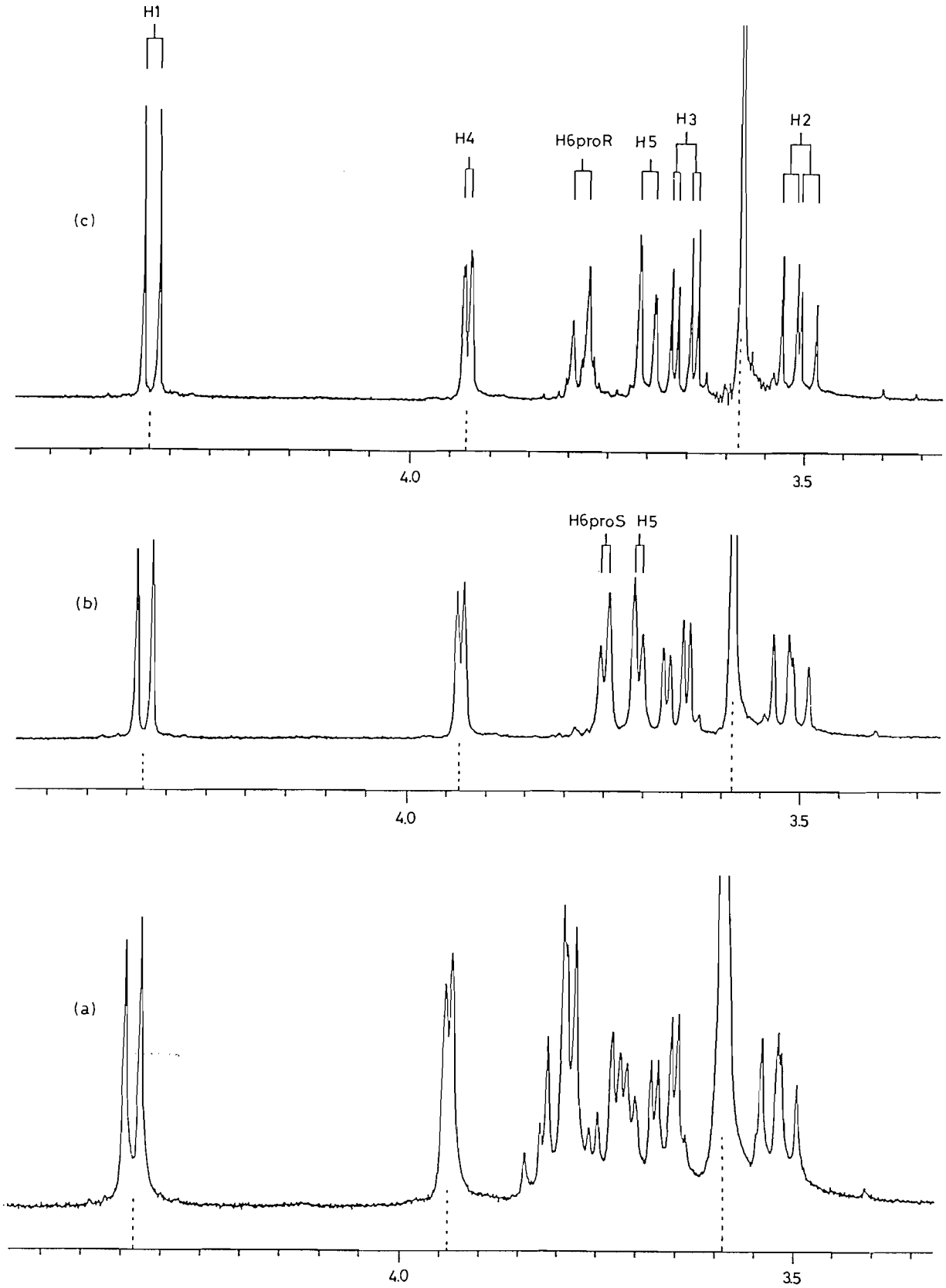

FIG. 3. The ^{1}H nmr spectra of (*a*) methyl β-D-galactopyranoside **3**, (*b*) methyl (6*R*)-(6-$^2H_1$)-β-D-galactopyranoside **3***R*, and (*c*) methyl (6*S*)-(6-$^2H_1$)-β-D-galactopyranoside **3***S* at 400 MHz in D_2O.

Can. J. Chem. Downloaded from www.nrcresearchpress.com by 78.46.186.204 on 09/07/12
For personal use only.

Can. J. Chem. Downloaded from www.nrcresearchpress.com by 78.46.186.204 on 09/07/12
For personal use only.

sulfonic acid sodium salt as 0.00 ppm and Bock and Thøgersen used acetone as 2.12 ppm.

The chemical shifts and the coupling constants by first-order analysis[6] of the stereospecifically deuterated D-galactose derivatives and those reported in the literature (6, 21), together with rough proportions of the populations of rotamers about the C_5—C_6 bond calculated by equations A devised by Rabczenko and co-workers (22), and B and C by Altona and co-workers (23, 24) are listed in Table 2. Although the two H-6 protons in the literature (21) have not been specifically assigned to H6*proR* and H6*proS*, they can be assigned unequivocally to H6*proR* and H6*proS*, respectively, by comparing their chemical shifts and coupling constants with those of the stereospecifically deuterated derivatives. Here, our value of $J_{H5,H6proS}$ of methyl β-D-galactopyranoside is revised from 6.0 (13) to 4.4 Hz, because the former value was obtained by comparing the first-order analysis of the two H-5 signals of nondeuterated compound **3** and of (6*S*)-(6-$^2H_1$) derivative **3***S* and the latter value was obtained directly from the (6*R*)-(6-$^2H_1$) derivative **3***R*.

The finding that $J_{H5,H6proS} > J_{H5,H6proR}$ in acylated derivatives and $J_{H5,HproR} > J_{H5,H6proS}$ in OH-free derivatives indicates (4, 8) that the preferred rotamer of acylated galactoses is *tg*, which is consistent with the reported results (5, 6, 10); however, the preferred rotamer of OH-free galactoses is not the previously predicted *tg* (1, 4, 6, 8), but *gt*. The same results were obtained by all three calculations except for the reported data of α-D-galactopyranose (4, 21). Although the populations of "unfavored" *gg* rotamers might be overestimated in our calculations, the not negligible contributions of *gg* will be partially rationalized in terms of the "*gauche* effect" (25).

As has been assumed (1, 2), if the conformation of the substrates in the binding sites of protein is the preferred conformation in solution, our results suggest that the *gt* rotamer should be the most plausible candidate for the galactosyl-binding protein.

The discrepancy between our result and the result previously suggested (4, 8), concerning the preferred rotamer of OH-free galactoses and chirally deuterated galactoses of high purity (99% deuterium content and no trace of diastereomer), prompted us to investigate the stereochemistry of the D-galactose oxidase reaction.

D-Galactose oxidase catalyzes the reaction:

[1] D-Galactose + O_2 → DL-galactohexodialdose + H_2O_2

The stereochemistry of D-galactose oxidase from *Polyporus circinatus* has been shown by Perlin and co-workers (6) to be a specific *pro-S* 6-hydrogen atom removal.

Methyl β-D-galactopyranoside **3**, methyl (6*R*)-(6-$^2H_1$)-β-D-galactopyranoside **3***R* (99% pure, 1% of **3**), methyl (6*S*)-(6-$^2H_1$)-β-D-galactopyranoside **3***S* (99% pure, containing 1% of **3**), and methyl (6,6-$^2H_2$)-β-D-galactopyranoside **3***DD* (99% pure, containing 1% of **3**) were used as the substrates of D-galactose oxidase (Fig. 4).

The galactose oxidase reactions were carried out under conditions similar to those reported by Perlin and co-workers (6). Acetylation and chromatographic purification (6) of the 6-aldehyde product of **3** gave three isolable products. One of

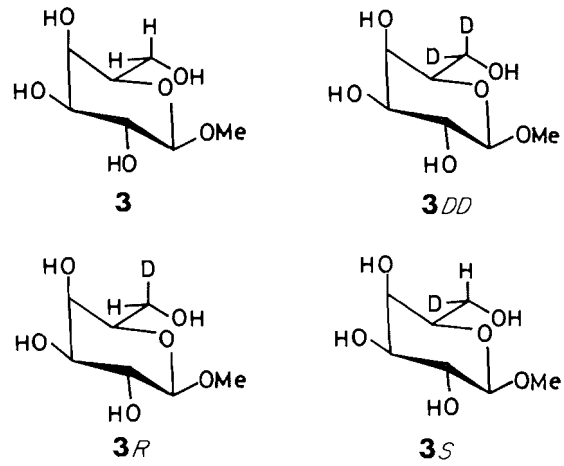

FIG. 4. Structures of substrates.

these was characterized as the known methyl 2,3-di-*O*-acetyl-L-*threo*-4-deoxyhex-4-eno-dialdopyranoside **6** (6, 26), and the others were acetylated dimers **7***a* and **7***b* of the 6-aldehyde (Fig. 5) on the basis of their ^1H nmr spectra (Table 3) and elemental analyses. The main dimer **7***a* was identified as the hexaacetate of dimeric methyl β-D-galactohexo-dialdo-1,5-pyranoside reported by Maradufu and Perlin (26).

The elemental analysis of the minor product **7***b* gave the same compositions of C, H, O as that of **7***a*. The ^1H nmr spectrum of **7***b* indicated that **7***b* had six acetyl groups and five signals that were almost the same as those of the ring protons (H_1', H_2', H_3', H_4', H_5') of the methyl D-galactopyranoside residue (ring B) of **7***a*. In **7***b*, H-4 resonates at 4.21 ppm, which is 0.19 ppm more shielded than H-4 of **7***a*; H-6′ resonates at 4.80 ppm, which is 0.21 ppm more shielded than H-6′ of **7***a* and, further, H-6 resonates at 5.91 ppm, which is 0.39 ppm more shielded than H-6 (6.22 ppm) of **7***a*. The chemical shifts of other protons of **7***b* showed little difference from those of **7***a* (in the order of −0.02 to 0.07 ppm).

All these results suggested that **7***b* has the same fundamental structure as that of **7***a*. The upfield shifts of H-4, H-6′, and H-6 indicate the change of configuration of the 6-OAc group from axial (6*R*) to equatorial (6*S*), since the change loses the 1,3-diaxial relationships between H-4, H-6′, and 6-OAc and converts H-6 from equatorial to axial configuration.

The chemical shift of H-5 of **7***b* is 3.66 ppm, which is 0.29 ppm more deshielded than that of **7***a*. Similar differences in the chemical shifts of the H-2 protons between α- and β-D-mannopyranose acetates are usually observed and reported for L-rhamnopyranose tetraacetate (27). Compound **7***a* is more dextrorotatory than **7***b*. The predominant formation of **7***a* may be rationalized in terms of the anomeric effect (26, 28). Therefore the structures of **7***a* and **7***b*, including the absolute configurations at C-6 and C-6′, are elucidated to be methyl (6*R*)-6-acetoxy-2,3-di-*O*-acetyl-4,6-*O*-[(6′*R*)-methyl-2′,3′,4′-tri-*O*-acetyl-6′-deoxy-β-D-galactopyranosid-6′-ylidene]-β-D-galactopyranoside and its (6*S*) isomer, respectively.

The ratio of the yields of **6** and **7** was a function of the enzymic reaction time, and prolonged reaction time caused the preponderant formation of the dimer **7**.

Since the structures of all isolable products were elucidated, and the H-6 signals of these products in their ^1H nmr spectra turned out to be diagnostically useful for our study, the galactose oxidase reaction with deuterated substrates was investigated.

[6]It is recognized that our coupling constants, obtained by first-order analysis, given in Table 2, and hence the rotamer populations in Table 2, are only approximately correct. The true coupling constants can only be obtained by full analysis including all spins involved.

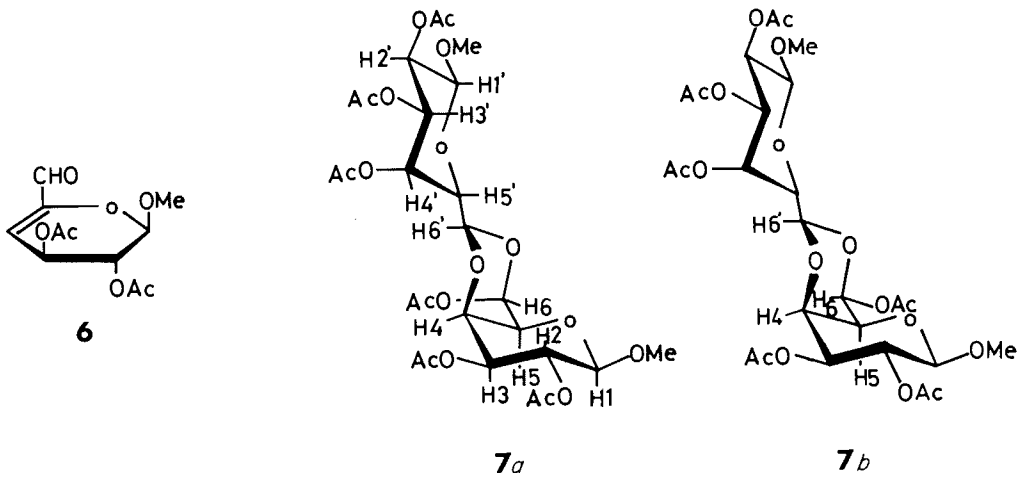

FIG. 5. Structures of the products.

TABLE 3. Proton chemical shifts of **7***a* and **7***b*

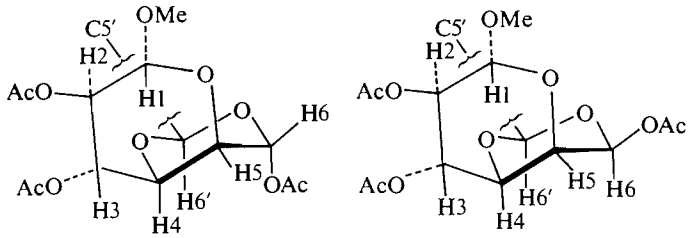

Proton	Shift (ppm)[a] 7*a*	7*b*	Δ 7*b* − 7*a*
H1	(4.39)[b]	4.36–4.37	−0.02 to −0.03
H2	5.05–5.25 (5.18)[b]	5.05–5.25	±0
H3	4.77	4.75	−0.02
H4	(4.40)[b]	4.21	−0.19
H5	3.37 (3.39)[b]	3.66	+0.29
H6	6.22 (6.22)[b]	5.91	−0.31
H1′	(4.37)[b]	4.37	±0
H2′	5.27	5.25	−0.02
H3′	5.05–5.25 (5.08)[b]	5.05–5.25	±0
H4′	5.54 (5.55)[b]	5.54	−0.01
H5′	3.78 (3.81)[b]	3.85	+0.07 to +0.04
H6′	5.03	4.80	−0.21
OAc	1.9–2.2 (six OAc)	1.9–2.2 (six OAc)	±0

[a]Measured at 100 MHz in $CDCl_3$ at 296 K relative to internal TMS (0.000 ppm).
[b]Values quoted from ref. 26.

The relative rates of oxidation of these four substrates were first examined. Although the detailed kinetics (6) were not examined, under the same conditions it took 1.5 h for **3***R*, 3.0 h for **3**, 4.5 h for **3***S*, and more than 30 h for **3***DD* to be completely oxidized, judged by the disappearance of the starting material on tlc. Here it is interesting to note that the most favorable substrate for the enzyme is not the normal galactoside **3** but the (6*R*)-(6-$^2H_1$)-galactoside **3***R*.

The products from (6,6-$^2H_2$)-galactoside **3***DD* completely retained a deuterium atom at C-6, which indicated no exchange of hydrogen atom with the reaction medium during the reactions. The products **6**, **7***a*, and **7***b* from **3***R* contained 1% of proton at C-6, judged by both ^1H nmr and mass spectra. The results indicated the complete stereospecific removal of the *pro-S* hydrogen atom from the substrate. The products from (6*S*)-(6-$^2H_1$)-galactoside **3***S* (99% pure) retained about 80% of one proton at C-6 (loss of about 20% proton). The result indicated that the *pro-S* stereospecificity of the enzyme was substantially retained for the substrate but some of the *pro-R* hydrogen atoms were removed.

The above results can be rationalized as follows: There are two mechanisms by which the enzyme can oxidize the substrate; one is a very efficient *pro-S* hydrogen specific removal mechanism and the second is a far less efficient non-specific or *pro-R* hydrogen specific removal mechanism, which does not work detectably for the *pro-R* deuterium because of its inefficiency (see isotope effect (6) and the reaction rates (*vide supra*)).

The difference between the stereospecificity of the galactose oxidase oxidations of Perlin (6) and ourselves might be attributed to the difference in the origins of the enzymes.

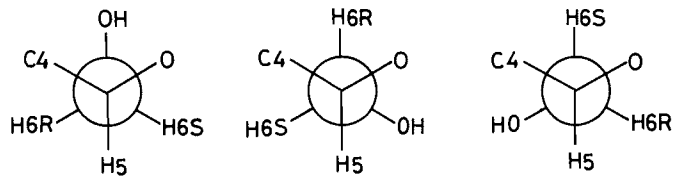

Here, the plausible conformation of D-galactose residues in the binding site of D-galactose oxidase should be discussed based on the above results. Although Fig. 1 explains the selective removal of the *pro-S* 6-hydrogen atom, the *tg* conformation is somewhat questionable because of the following: (1) The preferred rotamer of D-galactose is not *tg* but *gt*. (2) In the *tg* conformation, the more acidic hydrogen atom of 4-OH is accessible to the imidazole group, resulting in the deactivation of the imidazole group (Fig. 6). (3) Since the assignments of H6*proR* and H6*proS* have been mistaken (4, 8), the proton that has been assigned as axial by ^{13}C and ^{19}F nmr relaxation experiments (3) would not be H6*proS* but H6*proR*. If this is the case, these nmr experiments indicate also that the preferred rotamer of D-galactose is *gt*.

It has been known that 4-deoxy-D-galactose (4-deoxy-D-glucose) is a fairly good substrate for the enzyme, indicating

Can. J. Chem. Downloaded from www.nrcresearchpress.com by 78.46.186.204 on 09/07/12
For personal use only.

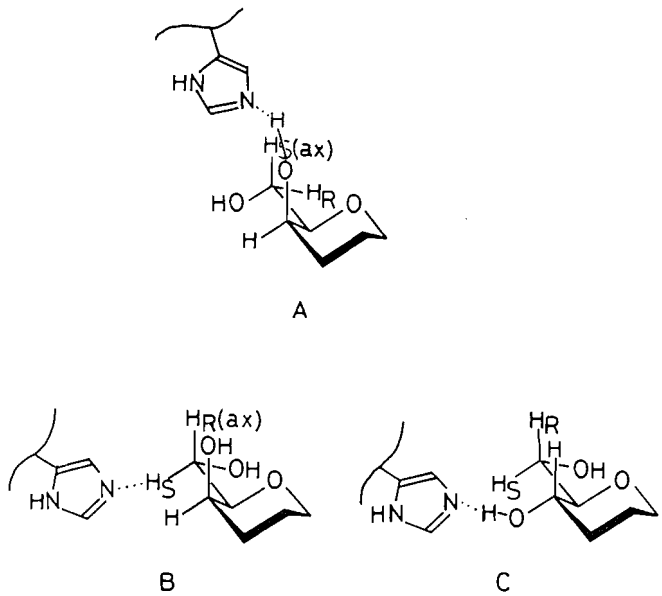

FIG. 6. Possible conformation of hexopyranose residues in the binding site of D-galactose oxidase; A, *tg* rotamer of D-galactose; B, *gt* rotamer of D-galactose; and C, *gt* rotamer of D-glucose.

that the 4-OH of D-galactose is not an important factor in the sugar being a substrate, but D-glucose is not a substrate at all, indicating that the 4-OH of D-glucose (equatorial 4-OH) should not be present if the sugar is to be the substrate of the enzyme (3). If the hydroxymethyl groups of the hexopyranoses are oxidized in the *gt* conformation as shown in Fig. 6, the above problems are solved, and the fact that D-glucose is not the substrate will be rationalized as follows (of course other steric factors have to be taken into account): In the *gt* conformation the more acidic hydrogen atom of the 4-OH of D-glucose, which is in 1,3-*syn*-diaxial relation with the *pro-S* 6-hydrogen, is accessible to the imidazole and reacts much faster than the *pro-S* 6-hydrogen, resulting in no oxidation of the hydroxymethyl group. Therefore, the *gt* conformation is recommended as a more plausible rotamer of D-galactose than *tg* in the binding sites of the enzyme.

Our results show that chirally pure deuterated sugars are very useful for both ^{1}H nmr studies of carbohydrates and stereochemical studies of enzymatic reactions. Studies along this line are being undertaken in our laboratory.

Experimental

Melting points were taken with a Yanako Model P hotplate apparatus and were uncorrected. The ^{1}H nmr spectra were recorded on JEOL JNM-FX 100 or JEOL FX 400 instruments with TMS as an internal standard in $CDCl_3$, or with 3-(trimethylsilyl)propanesulfonic acid sodium salt as an internal standard in D_2O. Direct mass spectra were recorded on a Hitachi M-52 spectrometer with the ionizing potential at 70 eV. Specific rotations were measured on a Jasco ORD/UV at 589 nm. Merck silica gel 60 (Art. 7734) was used for column chromatography and Merck silica gel 60 F_{254} (Art. 5548) was used for both preparative and analytical thin-layer chromatographies (tlc).

Materials

The substrates **3***R* and **3***S* were prepared from the corresponding (6*R*)-(6-$^2H_1$)- and (6*S*)-(6-$^2H_1$)-D-galactoses (12, 13), respectively, according to conventional methods (6). D-Galactose oxidase (EC 1.1.3.9.) Type V from *Dactylium dendroides* and catalase from bovine liver were purchased from Sigma Chemical Company.

*1,6-Anhydro-2,3,4-tri-O-benzoyl-D-talopyranose (**4**)*

To a solution of 1,6-anhydrotalopyranose (20) (1.7 g) in dry pyridine (50 mL) was added benzoyl chloride (10 g). After the mixture had been stirred for 12 h at room temperature, water (50 mL) was added to the reaction mixture and it was stirred for 2 h. The mixture was extracted with $CHCl_3$ (25 mL × 3) and the $CHCl_3$ layer was successively washed with water, saturated $NaHCO_3$, and water and then dried over $MgSO_4$. Evaporation of the solvent gave a syrup, which was crystallized from ethyl ether – hexane to give **4** (4.5 g, 90%); mp 178°C; $[\alpha]_D^{21}$ −58° (*c* 0.1, $CHCl_3$).

*Methyl 2,3-O-acetyl-4,6-O-benzylidene-β-D-galactopyranoside (**5**) and its (6S)-(6-$^2H_1$) derivative (**5S**)*

A solution of **3** (500 mg, 2.6 mmol), benzaldehyde dimethyl acetal (1 g, 6.6 mmol), and *p*-toluenesulfonic acid (5 mg) in *N*,*N*-dimethylformamide (20 mL) was stirred for 1 h at 55–60°C under reduced pressure (water pump) to remove methanol from the reaction mixture. To the stirred solution was added anhydrous sodium acetate (100 mg), pyridine (20 mL), and acetic anhydride (5 mL), and the suspension was stirred overnight at room temperature. The tlc analysis of the reaction mixture indicated the formation of two products (R_f 7.4, minor, and R_f 6.8, main; benzene/ethyl acetate 8:1, v/v). The mixture was evaporated *in vacuo* and the residue was chromatographed on a silica gel column with a mixture of benzene and ethyl acetate (50:1, v/v) to give methyl 2,3-di-*O*-acetyl-4,6-*O*-benzylidene-β-D-galactopyranoside **5** (480 mg, 50%), mp 148–150°C; $[\alpha]_D^{23}$ +65.2° (*c* 1.1, $CHCl_3$). ^{1}H nmr (δ(ppm, $CDCl_3$)): 4.44 (1H, d, 8.0 Hz, H-1), 5.39 (1H, dd, 8.0 and 10.4 Hz, H-2), 4.96 (1H, dd, 3.6 and 10.4 Hz, H-3), 4.38 (1H, br d, ≅3.6 Hz, H-4), 3.5 (1H, br s, H-5), 4.07 (1H, dd, 1.7 and 12.4 Hz, H6*proR*), 4.34 (1H, dd, 1.7 and 12.4 Hz, H6*proS*), 3.52 (3H, s, OMe), 5.51 (1H, s, Ph-CH), 2.07 (6H, s, OAc). *Anal.* calcd. for $C_{18}H_{23}O_8$: C 58.84, H 6.31; found: C 58.71, H 6.13. Also obtained was methyl 2,6-di-*O*-acetyl-3,4-*O*-benzylidene-β-D-galactopyranoside (70 mg, 7%), mp 132–143°C; $[\alpha]_D^{23}$ +16.8° (*c* 0.8, $CHCl_3$). ^{1}H nmr (δ(ppm, $CDCl_3$)): 4.35 (1H, d, 7.7 Hz, H-1), 5.11 (1H, dd, 5.5 and 7.7 Hz, H-2), 4.51 (1H, dd, 5.5 and 6.5 Hz, H-3), 4.22 (1H, dd, 2.0 and 6.5 Hz, H-4), 3.98 (1H, q, 2.0, 5.6 and 7.7 Hz, H-5), ≅4.4 (2H, H-6,6′). *Anal.* calcd. for $C_{18}H_{23}O_8$: C 58.84, H 6.31; found: C 59.10, H 6.22.

The (6*S*)-(6-$^2H_1$) derivative (**5***S*) of **5** was obtained by the same procedures as described for **5**. The physical data of **5***S* are essentially the same as those of **5** except for the chemical shifts of H6*proR* (δ 4.06) and H5 (δ 3.49).

Oxidation of methyl β-D-galactopyranosides with D-galactose oxidase

In a typical experiment, the substrate (40 mg) was dissolved in phosphate buffer (4 mL:0.1 *M*, pH 6.0) and incubated with D-galactose oxidase (5 mg, 350 units) and catalase (5 mg) at 28°C. The reaction was monitored by tlc (*n*-propanol:acetic acid:water 6:1:2, v/v). The reaction was stopped when the tlc showed the complete disappearance of the substrate (R_f 0.58) and the formation of main product (R_f 0.69) (it took 1.5 h for **3***R*, 3.0 h for **3**, 4.5 h for **3***S*, and more than 30 h, i.e., usually did not complete, for **3***DD*). A mixture of Amerlite IR-120 (H^+) and Dowex-1 (bicarbonate) was added to the digest with stirring, and it then was lyophilized. The product (40 mg) was treated with pyridine (1 mL) and acetic anhydride (0.5 mL) at room temperature overnight, the reaction mixture was concentrated, and the syrupy residue was chromatographed on a column of silica gel (5 g). Elution with a mixture of benzene and ethyl acetate (10:1, v/v) afforded methyl 2,3-di-*O*-acetyl-α-L-*threo*-4-deoxyhex-4-eno-dialdopyranoside **6** as a syrup (4 mg) (R_f 0.75, benzene:ethyl acetate 10:1, v/v). The subsequent elution with a mixture of benzene and ethyl acetate (3:1, v/v) afforded a mixture of **7***a* and **7***b* (18 mg). The mixture was separated by preparative tlc using a mixture of $CHCl_3$ and MeOH (70:1, v/v, three developments) to give a crystalline **7***a* (9 mg), mp 204–205°C, $[\alpha]_D^{22}$ +38.4° (*c* 0.07, EtOH) (lit. (26) mp 206–208°C; $[\alpha]_D^{22}$ +41.6° (*c* 2.1, $CHCl_3$)). *Anal.* calcd. for $C_{26}H_{36}O_8$: C 49.00, H 5.70; found: C 49.08, H 5.95; and **7***b* (3 mg), mp 130–131°C; $[\alpha]_D^{22}$ ±0° (*c* 0.04, EtOH). *Anal.* calcd. for $C_{26}H_{36}O_{18}$: C 49.00, H 5.70; found: C 49.25, H 6.00.

The (6,6′-$^2H_2$) derivative of **7***a*, obtained by oxidation of **3***DD*, had

Can. J. Chem. Downloaded from www.nrcresearchpress.com by 78.46.186.204 on 09/07/12
For personal use only.

mp 208–210°C; $[\alpha]_D^{22}$ +45.5° (*c* 0.05, EtOH) (lit. (26) mp 210–211°C; $[\alpha]_D^{22}$ +47° (*c* 0.4, $CHCl_3$)).

Oxidation of **3** R *and* **3** S

Oxidation of **3***R* gave the same products as with **3***DD*. Oxidation of **3***S* gave mixtures of **6** and the (6-$^2H_1$) derivative of **6**, and of **7***a* and the (6,6′-$^2H_2$) derivative of **7***a* in ratios ca. 80:20 judged by both ^{1}H nmr and mass spectroscopies.

Acknowledgements

The authors are most grateful to Dr. J. Uzawa of the Institute of Physical and Chemical Research for the 400-MHz ^{1}H nmr and to Mrs. Chieko Suzuki for the 100-MHz ^{1}H nmr spectra. This work was supported by a Grant-in-Aid for Scientific Research from the Ministry of Education, Science, and Culture of Japan.

1. C. Lough, O. Hindsgaul, and R. U. Lemieux. Carbohydr. Res. **120**, 43 (1983).
2. K. Bock. Pure Appl. Chem. **55**, 605 (1983).
3. M. J. Ettinger and D. J. Kosman. Met. Ions Biol. **3**, 219 (1981).
4. H. Thøgersen, R. U. Lemieux, K. Bock, and B. Meyer. Can. J. Chem. **60**, 44 (1982).
5. L. D. Hall, J. F. Manville, and N. S. Bhacca. Can. J. Chem. **47**, 1 (1969).
6. A. Maradufu, G. M. Cree, and A. S. Perlin. Can. J. Chem. **49**, 3429 (1971).
7. S. Yamana. Bull. Chem. Soc. Jpn. **31**, 558 (1958).
8. A. De Bruyn and M. Anteunis. Carbohydr. Res. **47**, 311 (1976).
9. R. U. Lemieux and J. C. Martin. Carbohydr. Res. **13**, 139 (1970).
10. H. W. Lew and K. Nakanishi. J. Am. Chem. Soc. **103**, 5591 (1981).
11. H. Ohrui, H. Kishi, H. Horiki, and H. Meguro. Agric. Biol. Chem. **47**, 1101 (1983).
12. H. Ohrui, Y. Nishida, and H. Meguro. Agric. Biol. Chem. **48**, 1049 (1984).
13. Y. Nishida, H. Ohrui, and H. Meguro. Tetrahedron Lett. **25**, 1575 (1984).
14. H. Ohrui, T. Misawa, and H. Meguro. Agric. Biol. Chem. **1**, 239 (1985).
15. R. J. Ferrier and R. H. Furneaux. Aust. J. Chem. **33**, 1025 (1980).
16. K. Heyns and J. Weyer. Liebigs Ann. Chem. **718**, 224 (1968).
17. M. Budesinsky, T. Trnka, and M. Černý. Collect. Czech. Chem. Commun. **44**, 1949 (1979).
18. L. D. Hall and K. F. Wong. J. Chem. Soc. Chem. Commun. 953 (1979).
19. G. V. O. Tiers. J. Chem. Phys. **29**, 963 (1958).
20. D. Horton and J. S. Jewell. Carbohydr. Res. **5**, 149 (1967).
21. K. Bock and H. Thøgersen. Annu. Rep. NMR Spectrosc. **13**, 1 (1983).
22. P. C. Manor, W. Saenger, D. B. Davies, K. Jankowski, and A. Rabczenko. Biochim. Biophys. Acta, **340**, 472 (1974).
23. (*a*) C. Altona and C. A. G. Haasnoot. Org. Magn. Res. **13**, 417 (1980); (*b*) C. A. G. Haasnoot, F. A. A. M. de Leeuw, and C. Altona. Tetrahedron, **36**, 2783 (1980).
24. C. A. G. Haasnoot, F. A. A. M. de Leeuw, and C. Altona. Bull. Soc. Chim. Belg. **89**, 125 (1980).
25. S. Wolfe. Acc. Chem. Res. **5**, 102 (1972).
26. A. Maradufu and A. S. Perlin. Carbohydr. Res. **32**, 127 (1974).
27. E. Hemmer and S. L. Jensen. Acta. Chem. Scand. **24**, 3019 (1970).
28. R. U. Lemieux, A. A. Pavia, J. C. Martin, and K. A. Watanabe. Can. J. Chem. **47**, 4427 (1969).

Can. J. Chem. Downloaded from www.nrcresearchpress.com by 78.46.186.204 on 09/07/12
For personal use only.

Structure of 5,5-dimethyl-2-phenylimino-Δ^3-1,3,4-thiadiazoline from oxidative cyclization of a thiosemicarbazone

R. FAGGIANI, M. KAMINSKI, C. J. L. LOCK,[1] AND J. WARKENTIN[1]

Department of Chemistry and Institute for Materials Research, McMaster University, Hamilton, Ont., Canada L8S 4M1

Received May 7, 1986[2]

R. FAGGIANI, M. KAMINSKI, C. J. L. LOCK, and J. WARKENTIN. Can. J. Chem. **65**, 1154 (1987).

The X-ray crystal structure of 5,5-dimethyl-2-phenylimino-Δ^3-1,3,4-thiadiazoline, $C_{10}H_{11}N_3S$, has been determined. The compound is monoclinic, $P2_1/c$ (No. 14), with $a = 13.200(5)$, $b = 6.340(4)$, and $c = 13.823(4)$ Å, $\beta = 113.50(4)°$, and $Z = 4$. The structure was determined by direct methods and refined to $R = 0.061$, $R_w = 0.067$ for 1277 unique reflections. The molecule has the *Z* configuration. The thiadiazoline ring is planar. C—N and N=N bond lengths are within the normal range. The C—S bond lengths are similar to those we have observed previously in thiazolidines. Angles differ markedly from an expected average 108°. The small C—S—C angle (90.6(2)°) is accompanied by larger C—N=N angles (114.9(3), 117.8(3)°). The phenyl ring is not coplanar with the thiadiazoline ring (dihedral angle 38.6(4)°) because of repulsive interaction of the phenyl *o*-hydrogen atom with the sulphur atom.

R. FAGGIANI, M. KAMINSKI, C. J. L. LOCK et J. WARKENTIN. Can. J. Chem. **65**, 1154 (1987).

On a déterminé la structure cristalline de la diméthyl-5,5 phénylimino-2 Δ^3-thiadiazoline-1,3,4, $C_{10}H_{11}N_3S$, par diffraction des rayons-X. Le composé est monoclinique, $P2_1/c$ (N° 14), avec $a = 13,200(5)$, $b = 6,340(4)$ et $c = 13,823(4)$ Å, $\beta = 113,50(4)°$ et $Z = 4$. On a déterminé la structure par des méthodes directes et on l'a affinée jusqu'à des valeurs de $R = 0,061$ et $R_w = 0,067$ pour 1277 réflexions indépendantes. La molécule possède une configuration *Z*. Le noyau thiadiazoline est plan et les longueurs des liaisons C—N et N=N sont dans les limites normales. Les longueurs des liaisons C—S sont semblables à celles qui ont été observées antérieurement dans les thiazolidines. Les angles divergent toutefois considérablement de la valeur moyenne prévue de 108°. L'angle C—S—C qui est petit (90,6(2)°) est accompagné d'angles C—N=N qui sont plus grands (114,9(3) et 117,8(3)°). Le noyau phényle n'est pas coplanaire avec le cycle thiaziazoline (angle dièdre de 38,6(4)°) à cause de l'interaction répulsive de l'atome d'hydrogène en *ortho* du phényle avec l'atome de soufre.

[Traduit par la revue]

Introduction

Oxidation of semicarbazones (1–3),[3] thiosemicarbazones (3, 4), guanylhydrazones (5), carbohydrazones (6), and thiocarbohydrazones (6) of ketones (**1**) affords heterocycles **2** and (or) **3**, eq. [1], depending on the reaction conditions. The structures of the products were inferred from analytical and spectroscopic data and, for the cases of **2***b* (Y = *p*-C_6H_4Br, $R^1 = R^2 = CH_3$), **2***h* (3), **3***b* (Y = C_6H_5, $R^1 = R^2 = CH_3$) (3), and **3***c* (Y = C_6H_5, $R^1 = R^2 = CH_3$) (3), these were confirmed by X-ray crystallography. Crystal structures are particularly important for elucidating the complete structures of **2**, which can have either the *E* or the *Z* configuration at the exocyclic nitrogen. In both cases (**2***b*, **2***h* above) the material obtained from oxidation of the appropriate semicarbazone with lead tetraacetate had the *Z* configuration (3, 7). For other members of the family **2**, namely, iminothiadiazolines **2***c*, **2***g* and iminotriazolines **2***e*, the configurations were still uncertain although the *Z* configurations might appear to be the more likely, assuming that similar mechanisms are involved in the oxidative cyclizations. However, for the iminothiadiazolines, the mechanistic analogy is weak because they are prepared (4) by oxidation on manganese dioxide, whereas the others are prepared by oxidation in homogeneous solution with lead tetraacetate.

We now report the crystal structure for one of the type **2***c* (Y = C_6H_5, $R^1 = R^2 = CH_3$), which we designate **A** and which not only confirms the *Z* configuration but also permits extension of the comparisons of **2** and **3**, particularly of the bond lengths and angles at C(2) of the ring, begun by Katritzky *et al.* (3). Moreover, the complete structure of **A** provides a basis for reducing the number of likely geometric isomers for some of Landquist's thiadiazolines (4*a*) from four to two.

Experimental

The compound 5,5-dimethyl-2-phenylimino-Δ^3-1,3,4-thiadiazoline, **A**, was prepared by the method of Landquist (4). Crystals

[1] $R^1R^2C{=}NNHCNHY \xrightarrow{\text{oxidation}}$ 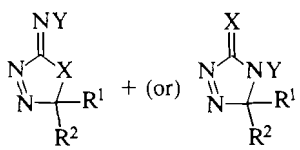 + (or)

2 **3**

a X = O, Y = $R^1 = R^2$ = alkyl; *b* X = O, Y = Ar, $R^1 = R^2$ = alkyl; *c* X = S, Y = Ar, $R^1 = R^2$ = alkyl;
d X = NH, Y = H, $R^1 = R^2$ = alkyl; *e* X = NC_6H_5, Y = C_6H_5, $R^1 = R^2$ = alkyl;
f X = O, Y = $NCAr_2$, $R^1 = R^2$ = alkyl; *g* X = S, Y = $NCAr_2$, $R^1 = R^2 = CH_3$;
h X = O, Y = $R^1 = R^2 = C_6H_5$

[1]Authors to whom correspondence may be addressed.
[2]Revision received January 13, 1987.
[3]L. M. Cabelkova-Taguchi and J. Warkentin. Unpublished observations.

Can. J. Chem. Downloaded from www.nrcresearchpress.com by 78.46.186.204 on 09/07/12
For personal use only.

Can. J. Chem. Downloaded from www.nrcresearchpress.com by 78.46.186.204 on 09/07/12
For personal use only.

TABLE 1. Crystal data

Compound	$C_{10}H_{13}N_3S$
Formula weight	205.28
Crystal shape, size (mm)	Acicular, 0.20 × 0.23 × 0.40
Systematic absences	$h0l$, $l = 2n + 1$, $0k0$, $k = 2n + 1$
Space group	$P2_1/c$ (No. 14)
Unit cell parameters (Å and deg)	a = 13.200(5), b = 6.340(4), c = 13.823(4) β = 113.50(4)
Volume (Å^3)	1060.9(3)
Z	4
ρ_{calc}, ρ_{obs} (g cm^{-3})	1.285, 1.15(2)
Temperature (°C)	22
Linear absorption coeff. (cm^{-1})	2.25
Standard reflections (e.s.d.)	−2 −1 2 (0.009) −3 −1 2 (0.009)
Reflections collected; max 2θ	h = 0–14, k = 0–6, l = −13–13; 45°
No. of reflections collected	1611
R_{merg}	0.0206
No. of unique reflections	1394
No. with $I > 0$ used	1277
x (extinction coefficient)	0.00291
Final R, R_w[a]	0.061, 0.067
Final shift/error (max, ave.)	<0.001, <0.001
Final difference map max, min (e Å^3)	0.29, −0.25
Weighting scheme	$w = (\sigma_F^2 + 0.001567F_o^2)^{-1}$
Error in an observation of unit wt.	1.138

[a] $R = \Sigma||F_o| - |F_c||/\Sigma|F_o|$; $R_w = \{\Sigma w(|F_o| - |F_c|)^2/\Sigma wF_o^2\}^{1/2}$.

TABLE 2. Atomic positional coordinates (× 10^4) and temperature factors (Å^2 × 10^3)

Atom	x	y	z	U_{eq}[a]
S(1)	2315(1)	6023(2)	9146(1)	46.9
C(2)	1949(3)	5869(6)	7787(3)	40
N(3)	1073(3)	7390(5)	7232(2)	47
N(4)	752(2)	8446(5)	7807(2)	45
C(5)	1287(3)	8090(5)	8951(2)	40
C(6)	1840(4)	10155(7)	9459(3)	60
C(6′)	407(3)	7397(7)	9344(3)	53
N(7)	2256(3)	4697(5)	7217(2)	47
C(8)	3072(3)	3115(6)	7631(3)	44
C(9)	2907(3)	1297(6)	7026(3)	52
C(10)	3667(4)	−305(7)	7362(4)	65
C(11)	4611(4)	−127(8)	8270(4)	69
C(12)	4786(3)	1690(8)	8867(3)	64
C(13)	4025(3)	3307(7)	8550(3)	53

[a] $U_{eq} = 1/3(U_{11} + U_{22} + U_{33} + 2U_{13}\cos\beta)$.

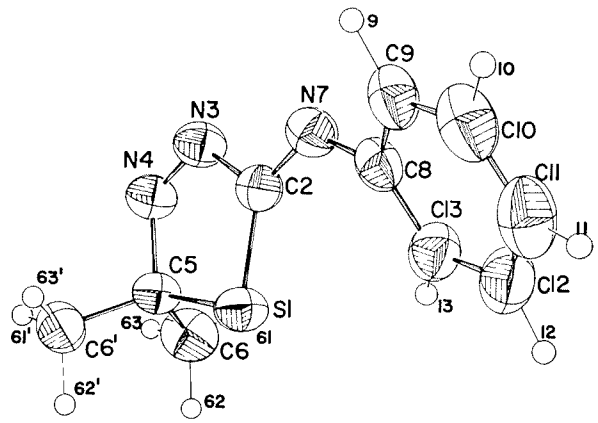

FIG. 1. The molecule of **A**, showing the atom numbering. Hydrogen atoms are shown by affixes only, in smaller numbers.

were prepared by crystallization from petroleum ether (60–80°). The crystals were pale yellow needles. Precession photographs of one, mounted along the long axis, revealed the monoclinic symmetry, and unit cell parameters were obtained from the least-squares fit of χ, φ, and 2θ for 15 reflections in the range 19° < 2θ < 30°, measured on a Nicolet P3 diffractometer with graphite monochromatized MoKα$_1$ radiation (λ = 0.70926 Å). Crystal data and other numbers related to data collection are summarized in Table 1. The density was obtained by flotation in aqueous zinc bromide solution. Intensities were also measured on the P3 diffractometer with use of a coupled θ(crystal) – 2θ(counter) scan. The methods of selection of scan rates and initial data treatment have been described (8, 9). Corrections were made for Lorentz and polarization effects but not for absorption. This will introduce a maximum error in F_o of <1.5%.

The phases were determined by direct methods with use of 50 reflections with $|E| > 1.255$ and 12 sets of starting phases. All non-hydrogen atoms were found in the subsequent E map. Subsequent refinement and electron density difference syntheses revealed the hydrogen atoms. At this stage, the temperature factors for all non-hydrogen atoms were made anisotropic. Further refinement with full-matrix least squares, which minimized $\Sigma w(|F_o| - |F_c|)^2$, was continued with four cycles varying all parameters except the hydrogen atom temperature factors, and was terminated after another two cycles in which only parameters for non-hydrogen atoms were varied and when the maximum shift/error had fallen below 0.03. Corrections were made for secondary extinction by the method of SHELX.[4] Scattering curves were taken from ref. 10, and anomalous dispersion

[4]All calculations were carried out on a CYBER 170-815 computer. Programs for initial data treatment were from the XRAY 76 package (ref. 22). The structure was solved with SHELX (ref. 23). Planes, and dihedral and torsional angles were calculated by using NRC-22 (ref. 24). Diagrams were prepared with ORTEP II (ref. 25).

TABLE 3. Selected interatomic distances and angles

Atoms	Distance (Å)	Atoms	Distance (Å)	Atoms	Distance (Å)
S1—C2	1.745(5)	C2—N3	1.465(4)	N3—N4	1.236(5)
N4—C5	1.469(4)	C5—S1	1.827(4)	C5—C6	1.527(5)
C5—C6′	1.531(6)	C2—N7	1.262(5)	N7—C8	1.415(5)
C8—C9	1.389(6)	C9—C10	1.372(6)	C10—C11	1.376(6)
C11—C12	1.381(7)	C12—C13	1.379(6)	C13—C8	1.392(4)

Atoms	Angle (deg)	Atoms	Angle (deg)	Atoms	Angle (deg)
C5—S1—C2	90.6(2)	S1—C2—N3	110.4(3)	C2—N3—N4	114.9(3)
N3—N4—C5	117.8(3)	N4—C5—S1	106.2(3)	N4—C5—C6	107.5(3)
N4—C5—C6′	108.6(3)	S1—C5—C6	110.9(3)	S1—C5—C6′	111.5(3)
C6—C5—C6′	112.0(4)	S1—C2—N7	133.2(3)	N3—C2—N7	116.3(3)
C2—N7—C8	123.2(3)	N7—C8—C9	115.7(3)	N7—C8—C13	124.9(3)
C13—C8—C9	119.3(4)	C8—C9—C10	119.5(3)	C9—C10—C11	121.5(4)
C10—C11—C12	119.2(4)	C11—C12—C13	120.2(4)	C12—C13—C8	120.2(4)

corrections from ref. 11 were applied to the curve for sulphur. The atom parameters are listed in Table 2.[5]

Discussion

The molecule is shown in Fig. 1 and bond lengths and angles are given in Table 3. The molecule has the *Z* configuration. In this configuration, H13 on the phenyl ring interacts repulsively with S1 (S1...H13 = 2.73(5) Å vs. van der Waals distance of 3.0 Å (12)) and the strain is relieved by rotating the plane of the phenyl ring with respect to the plane of the thiadiazoline ring (dihedral angle 38.6(4)°), by the large S1—C2—N7 angle (133.2(3)°), and by increasing the N7—C8—C13 angle (124.9(3)°) at the expense of the N7—C8—C9 angle (115.7(3)°) from the ideal 120°. A similar effect is found in 5,5-diphenyl-2-phenylimino-Δ^3-1,3,4-oxadiazoline, **B** (or **2***h*) (3). Katritzky *et al.* (3) have also examined the structures of similar compounds 3,3-dimethyl-4-phenyl-Δ^1-1,2,4-triazoline-5-one, **C**, and 3,3-dimethyl-4-phenyl-Δ^1-1,2,4-triazoline-5-thione, **D**.

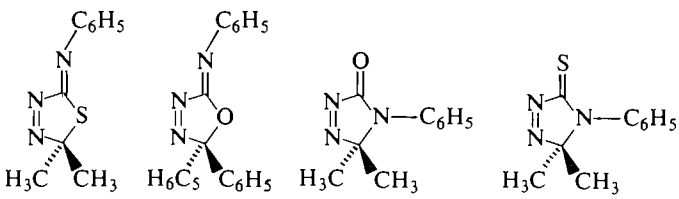

A **B** **C** **D**

The thiazolidine ring is planar, within the errors, although exocyclic N7 is significantly out of the plane of the ring (0.062(4) Å). C2—N3, C5—N4, and N3—N4 are within the normal range for C—N single and N=N double bonds (13). C2—S1 (1.745(5) Å) is significantly shorter than C5—S1 (1.827(4) Å), and the former distance lies outside the range we have observed in thiazolidine rings (1.784(5)–1.869(6) Å) (14, 15). The difference is in the expected direction since an sp^2 carbon atom is smaller than an sp^3 carbon atom (0.743 vs. 0.763 Å) (16). The difference is greater than expected, however, and the distances are respectively shorter and longer than the distances calculated from covalent radii (1.783, 1.803 Å) (13, 16). There may be some delocalization of the S1 nonbonding electrons into the C2—N7 bond and consequent further shortening of the S1—C2 bond. C2—N7 and N7—C8 are in the normal range (13), as are bond lengths or angles involving methyl or phenyl groups attached to the tetrahedral ring carbon in **A**–**D**. The deviation of the internal ring angles at this carbon atom (range 101.1(2)°–106.2(3)°) from the tetrahedral angle is compensated for by the larger C(exocyclic)—C(ring)—C(exocyclic) angle (range 112.0(4)°–116.8(6)°) for the exocyclic methyl or phenyl groups. The internal ring angle at sulphur in **A** (C2—S1—C5, 90.6(2)°) is much smaller than that observed at oxygen in **B** (107.3(5)°) or at nitrogen in **C** and **D** (110.6(2)°, 110.7(2)°). It is also marginally smaller than C—S—C angles we have observed in thiazolidine rings (range 92.4(2)°–95.4(3)°) (14, 15). Nevertheless, it lies well within the range of C—S—C angles observed in five-membered rings since the earliest X-ray studies (range 83°–95° (17–21). The small C—S—C angle is accompanied by an increase in the ring

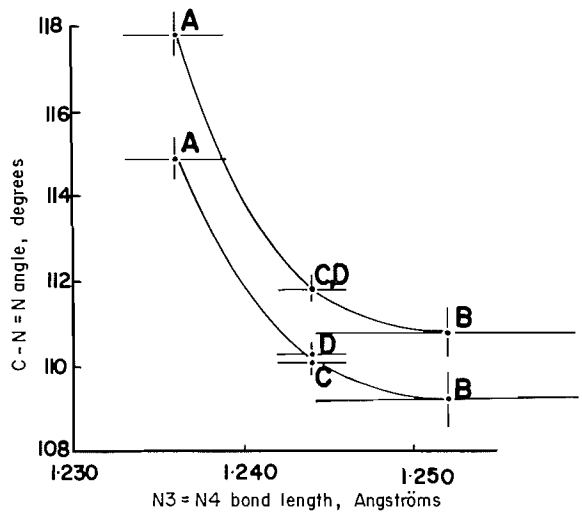

FIG. 2. The relationship between the N3=N4 bond and the C—N=N angles. The upper set represents the C5—N4=N3 angles and the lower set the C2—N3=N4 angles. The error bars are one e.s.d. Points **A**–**D** are for the molecules shown as **A**–**D** in the text.

[5]Lists of anisotropic temperature factors, hydrogen atom positional parameters, bond lengths and angles involving hydrogen atoms, best planes, dihedral and torsional angles, and a listing of the moduli of the observed and calculated structure factors may be purchased from the Depository of Unpublished Data, CISTI, National Research Council of Canada, Ottawa, Ont. Canada K1A 0S2.

Can. J. Chem. Downloaded from www.nrcresearchpress.com by 78.46.186.204 on 09/07/12
For personal use only.

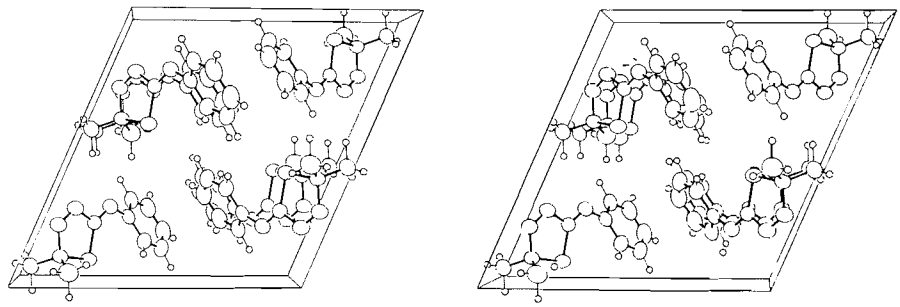

FIG. 3. The packing of **A** within the unit cell. **a** and **c*** are parallel to the bottom and sides of the page and the view is down **b**.

angles at the azo nitrogen atoms rather than at the carbon atoms (Δ = **A** minus **B**); (N3, $\Delta = +4.8°$, N4, $\Delta = +7.0°$) (C2, $\Delta = +0.5°$, C5, $\Delta = +3.5°$). In **C** and **D** the changes at carbon and nitrogen atoms are comparable. We postulate that the angular change occurs at the nitrogen atoms rather than at the carbon atoms because the strain in **B** is greater at these points. The relaxation of this strain in **A** causes a change which brings the C—N=N angles much closer to the expected 120°. One might expect that a relaxation of the angular strain at the nitrogen atoms will cause the N3—N4 bond to strengthen. This distance differs from **A** to **B** by 1.70σ ($\sigma = (\sigma_1^2 + \sigma_2^2)^{1/2}$), which is significant only at the 90% confidence level. Nevertheless, a plot of ring angles at the nitrogen atoms vs. N—N bond length suggests that such a relationship exists (Fig. 2).

The packing of the molecules in the unit cell is shown in Fig. 3. Surprisingly, there is no evidence of any $\pi-\pi$ interactions between the phenyl rings or the phenyl rings and the N=C—N=N system. The packing does not allow this and all interactions are van der Waals.

The *Z* configuration of **A**, expected on the basis of analogy to the oxadiazoline analogue, but not previously established, nicely explains Landquist's finding (4*a*) that only two isomeric 1,3,4-thiadiazolines are obtained by cyclization of 4-substituted thiosemicarbazones of ketones such as 2-methylcyclohexanone. Presumably those isomers are different in configuration at C5 of the thiadiazoline ring, as assumed by Landquist, and not *E*,*Z*-isomers at the exocyclic nitrogen.

Acknowledgements

We acknowledge, with thanks, financial support from the Natural Sciences and Engineering Research Council of Canada and from the McMaster University Science and Engineering Research Board.

1. S. L. LEE, G. B. GUBELT, A. M. CAMERON, and J. WARKENTIN. Chem. Commun. 1074 (1970).
2. P. KNITTEL, S. L. LEE, and J. WARKENTIN. Can. J. Chem. **50**, 3248 (1972).
3. A. R. KATRITZKY, H. M. FAID-ALLAH, H. AGHABOZORG, and G. J. PALENIK. Chem. Scr. **23**, 134 (1984).
4. (*a*) J. K. LANDQUIST. J. Chem. Soc. C, 63 (1970); (*b*) J. Chem. Soc. C, 323 (1970).
5. L. M. CABELKOVA-TAGUCHI and J. WARKENTIN. Can. J. Chem. **56**, 2194 (1978).
6. P. R. WEST and J. WARKENTIN. J. Org. Chem. **33**, 2089 (1978).
7. A. PRAKASH, C. CALVO, A. M. CAMERON, and J. WARKENTIN. J. Cryst. Mol. Struct. **3**, 71 (1973).
8. B. LIPPERT, C. J. L. LOCK, B. ROSENBERG, and M. ZVAGULIS. Inorg. Chem. **16**, 1525 (1977).
9. R. P. HUGHES, N. KRISHNAMACHARI, C. J. L. LOCK, J. POWELL, and G. TURNER. Inorg. Chem. **16**, 314 (1977).
10. D. T. CROMER and J. T. WABER. *In* International tables for X-ray crystallography. Vol. IV. *Edited by* J. A. Ibers and W. C. Hamilton. Kynoch Press, Birmingham, England. 1974. Table 2.2B. pp. 99–101.
11. D. T. CROMER. *In* International tables for X-ray crystallography. Vol. IV. *Edited by* J. A. Ibers and W. C. Hamilton. Kynoch Press, Birmingham, England. 1974. Table 2.3.1 pp. 149, 150.
12. A. BONDI. J. Phys. Chem. **68**, 441 (1964).
13. L. E. SUTTON, O. KENNARD, H. M. POWELL, and D. H. WHIFFEN (*Editors*). Tables of interatomic distances and configuration in molecules and ions. Supplement 1956–1959. Special publication No. 13. The Chemical Society, London. 1965.
14. H. E. HOWARD-LOCK, C. J. L. LOCK, M. L. MARTINS, and R. FAGGIANI. Can. J. Chem. In press.
15. H. E. HOWARD-LOCK, C. J. L. LOCK, and P. S. SMALLEY. Can. J. Chem. **63**, 2411 (1985).
16. L. N. FERGUSON. The modern structural theory of organic chemistry. Prentice–Hall Inc., New Jersey. 1963. p. 39.
17. B. BAK, D. CHRISTENSEN, J. RASTRUP-ANDERSEN, and E. TANNENBAUM. J. Chem. Phys. **25**, 892 (1956).
18. M. NARDELLI, G. FARA, and L. ARMELLINI. Ric. Sci. **28**, 383 (1958).
19. Y. TASHPULATOV, Z. V. ZVONKOVA, and G. S. ZHDANOV. Kristallografiya, **2**, 33 (1957).
20. E. G. COX, R. J. J. H. GILLOT, and G. A. JEFFERY. Acta Crystallogr. **2**, 356 (1949).
21. G. J. PITT. Acta Crystallogr. **5**, 770 (1952).
22. J. M. STEWART. Technical Report TR-446. University of Maryland, College Park, MD. 1976.
23. G. M. SHELDRICK. SHELX. Cambridge University, Cambridge, England. 1976.
24. F. A. AHMED and M. E. PIPPY. NRC-22. National Research Council of Canada, Ottawa, Ont., Canada. 1981.
25. C. K. JOHNSON. Report ORNL-5138. Oak Ridge National Laboratory, Oak Ridge, TN. 1976.

Can. J. Chem. Downloaded from www.nrcresearchpress.com by 78.46.186.204 on 09/07/12
For personal use only.

An improved synthesis of 1,3-dihydro-1-methyl-5-phenyl-2*H*-pyrido[3,4-*e*]-1,4-diazepin-2-one via *ortho*-directed lithiation of 3-*tert*-butyl and 3-*tert*-butoxycarbonylaminopyridine

CHARLES Y. FIAKPUI AND EDWARD E. KNAUS[1]

Faculty of Pharmacy and Pharmaceutical Sciences, University of Alberta, Edmonton, Alta., Canada T6G 2N8

Received July 8, 1986

CHARLES Y. FIAKPUI and EDWARD E. KNAUS. Can. J. Chem. **65**, 1158 (1987).

The *ortho*-directed lithiation of 3-*tert*-butyl- or 3-*tert*-butoxycarbonylaminopyridines (**3**) with alkyllithiums and reaction with *N*,*N*-diethylbenzamide followed by acid hydrolysis gave 3-amino-4-benzoylpyridine (**6**) in good yield. Reaction of BTBO with the glycine derivatives **7***a*, *b* and then reaction with **6** afforded 3-alkoxycarbonylaminomethylcarbonylamino-4-benzoylpyridines **8***a*, *b*. Acid-catalyzed hydrolysis and cyclization of **8***a*, *b* yielded **9**, which on methylation gave 1,3-dihydro-1-methyl-5-phenyl-2*H*-pyrido[3,4-*e*]-1,4-diazepin-2-one (**10**) in 36% overall yield from **3***a*.

CHARLES Y. FIAKPUI et EDWARD E. KNAUS. Can. J. Chem. **65**, 1158 (1987).

La lithiation en position *ortho* des *tert*-butyl- ou *tert*-butoxycarbonylamino-3 pyridines (**3**) par les alkyllithiens ou leur réaction avec du *N*,*N*-diéthylbenzamide, suivie d'une hydrolyse acide, conduisent à l'amino-3 benzoyl-4 pyridine (**6**) avec de bons rendements. La réaction du BTBO avec les dérivés **7***a*, *b* de la glycine, suivie d'une réaction avec le composé **6**, conduit aux alkoxycarbonylaminométhylcarbonylamino-3 benzoyl-4 pyridines (**8***a*, *b*). L'hydrolyse acido-catalysée des composés **8***a*, *b*, suivie d'une cyclisation, conduit au composé **9** qui, par méthylation, fournit la dihydro-1,3 méthyl-1 phényl-5 2*H*-pyrido[3,4-*e*] diazépine-1,4 one-2 (**10**), avec un rendement global de 36% à partir du composé **3***a*.

[Traduit par la revue]

Can. J. Chem. Downloaded from www.nrcresearchpress.com by 72.64.146.136 on 09/07/12
For personal use only.

Introduction

The 1,4-benzodiazepin-2-ones **1** are a clinically useful class of compounds that exhibit a wide spectrum of powerful effects on the central nervous system, including anxiolytic, sedative, hypnotic, anticonvulsant, and muscle relaxant properties (1). Although it is known that an electronegative X substituent at C-7 of **1** is required for high potency (1), very few electronically analogous pyrido-1,4-diazepin-2-ones **2** have been investigated. Methods for the synthesis of **2** are often laborious, of narrow applicability, require the relatively inaccessible aminopyridinecarboxylic acid precursors, and provide low overall yields (2). Although **2***c* has been reported, no experimental details were provided (2). An efficient synthesis of **2***c*

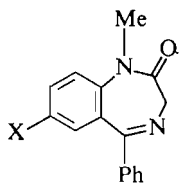

1

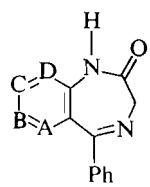

2

a, A = N; B, C, D = CH
b, B = N; A, C, D = CH
c, C = N; A, B, D = CH
d, D = N; A, B, C = CH

and the 4-benzoyl-3-aminopyridine derivatives **4**–**6** and **8** was required for the synthesis of bicyclic and monocyclic reduced pyridyl analogues for other studies in our drug design program. The regioselective *ortho*-directed metallation of 3-substituted pyridines possessing pivaloylamino (3), dialkylaminocarbonyl (4), O-carbamate (5), 4,4-dimethyl-2-oxazolinyl (6), and halogeno (7) substituents is a versatile method for the synthesis of 3,4-disubstituted pyridines. *Ortho*-lithiation of 2- and 4-*tert*-butoxycarbonylaminopyridine has been utilized for the synthesis of 3-substituted-2-aminopyridines (8) and 3-substituted-4-aminopyridines (9), respectively. We now report an improved synthesis of 1,3-dihydro-1-methyl-5-phenyl-2*H*-pyrido[3,4-*e*]-1,4-diazepin-2-one (**10**) using *ortho*-directed lithiation of 3-*tert*-butyl- or 3-*tert*-butoxycarbonylaminopyridine (**3**).

Results and discussion

Lithiation of 3-*tert*-butylcarbonylaminopyridine (**3***a*) in THF using *n*-butyllithium and reaction with *N*,*N*-diethylbenzamide yielded 3-*tert*-butylcarbonylamino-4-benzoylpyridine (**4***a*, 70% yield, Scheme 1). Recent reports have suggested that clean metallation of **3***a* is not possible with *n*-butyllithium in THF (3*b*, 10), that specific conditions (THF, Et_2O, TMEDA, 20°C) are required for optimum yields of 50–60% (3*b*), or that C-4 metallation was competitive with nucleophilic attack by the metallation reagent at C-4 (3*a*). Other metallating agents such as lithium diisopropylamide and methyllithium lead neither to *ortho*-lithiation nor nucleophilic addition to the nucleus (3*b*). Alternatively, **4***a* was prepared less efficiently by a multiple step reaction sequence, involving *ortho*-lithiation of **3***a* with *n*-butyllithium, reaction with benzaldehyde, and oxidation of **5***a* with pyridinium dichromate.[2] A similar *ortho*-lithiation of 3-*tert*-butoxycarbonylaminopyridine (**3***b*),[3] using *tert*-butyllithium or *n*-butyllithium, in THF followed by reaction with *N*,*N*-diethylbenzamide as described previously, afforded **4***b* in 65 and 63% yield, respectively. There was no evidence of metallation at any position other than C-4 nor of any nucleophilic addition of the metallating agent to the pyridine ring. The 3-*tert*-butoxycarbonylamino substituent of **3***b* is therefore an example of a single electron-donating substituent that is capable of inducing *ortho*-lithiation of **3***b* by a "coordination-only" mechanism (3*a*). In contrast, reaction of pyridines possessing such electron-attracting substituents as cyano, diethylaminocarbonyl, and oxazolinyl at C-3, with nucleophilic alkyllithium reagents, yielded 1,2-, 1,4-, and (or) 1,6-dihydropyridine products where proton abstraction was superseded by nucleophilic addition to the pyridine ring (6, 12).

[1]Author to whom correspondence may be addressed.

[2]The synthesis of **5***a* has been reported using different reagents and (or) reaction conditions (3*a*, *b*).

[3]1,2,2,2-Tetrachloroethyl *tert*-butyl carbonate has also been reported to be a simple and efficient reagent for the *tert*-butoxycarbonylation of amines and aminoacids, see ref. 11.

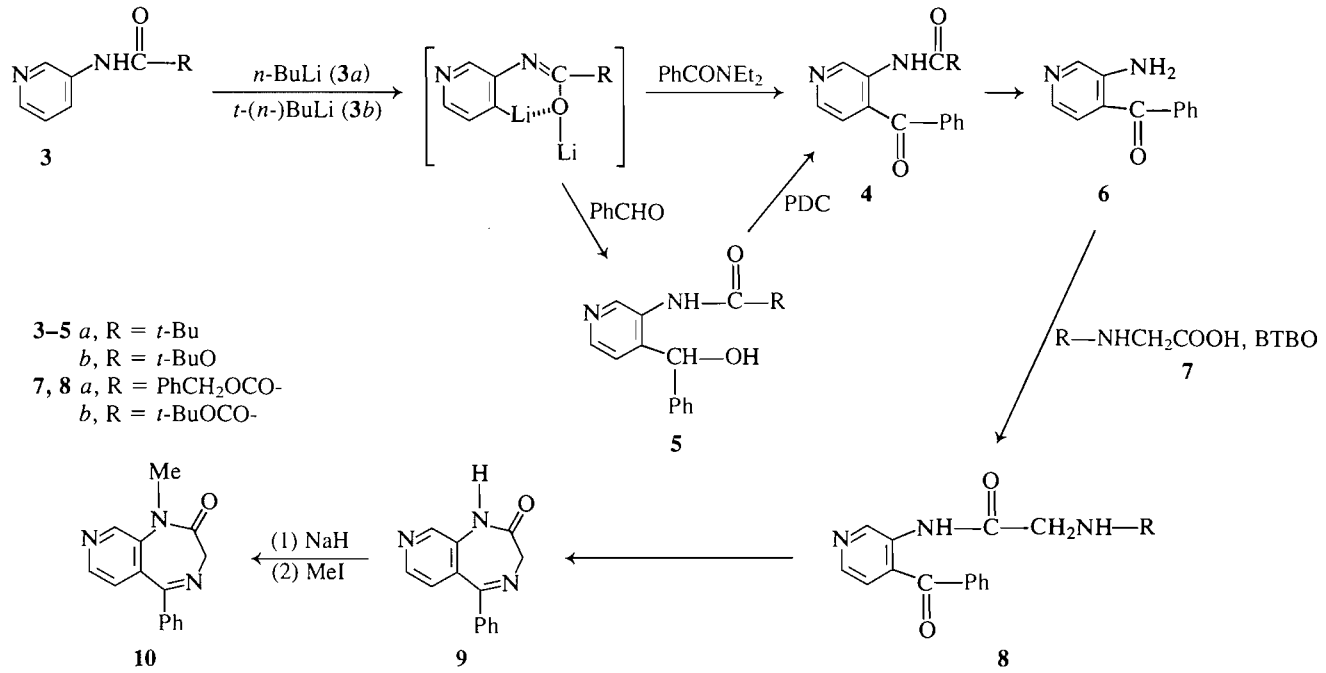

SCHEME 1

The reaction of **3***b* with *tert*-butyllithium or *n*-butyllithium, condensation with benzaldehyde to yield **5***b* (68 and 62% yield respectively), and oxidation of **5***b* with pyridinium dichromate also yielded **4***b* (89% yield). Hydrolysis of the 3-*tert*-butylcarbonylamino analog **4***a* using ethanol – hydrochloric acid at reflux afforded 3-amino-4-benzoylpyridine (**6**) in 94% yield, whereas hydrolysis of the 3-*tert*-butoxycarbonylamino derivative **4***b* with trifluoroacetic acid in 1,2-dichloroethane at 25°C yielded **6** in 97% yield. Although the overall yields of **6** prepared from **3***a* and **3***b* are quantitatively similar (**3***a* → **4***a* → **6**, 66% yield, and **3***b* → **4***b* → **6**, 63% yield), the *tert*-butoxycarbonylamino *ortho*-directing substituent may be advantageous for compounds possessing labile substituents or ring systems, due to its more facile conversion to a free amino group.[4]

Activation of *N*-benzyloxycarbonylglycine (**7***a*) with 1,1′-bis-[6-(trifluoromethyl)benzotriazolyl] oxalate (BTBO) (14), followed by condensation with **6**, afforded crystalline **8***a* in 90% yield. A similar reaction of BTBO with *tert*-butoxycarbonylglycine (**7***b*) followed by reaction with **6** yielded crystalline **8***b* in 83% yield.[5] Acid hydrolysis of **8***a* (HBr–CH_3COOH) and **8***b* (CF_3COOH) at 25°C gave the pyridodiazepinone **9** in 82 and 89% yield, respectively. Methylation of **9** using sodium hydride and iodomethane afforded the title compound 1,3-dihydro-1-methyl-5-phenyl-2*H*-pyrido[3,4-*e*]-1,4-diazepin-2-one (**10**) in 73% yield.

The synthesis of 3-amino-4-benzoylpyridine, using *ortho*-lithiation methodology, has provided a shorter, simpler, and more efficient method for the synthesis of the pyridodiazepinone **10**. This methodology will be applicable to the construction of structurally related bicyclic nitrogen heterocycles.

Experimental

Melting points were determined with a Büchi capillary apparatus and are uncorrected. Nuclear magnetic resonance spectra were determined for solutions of deuteriochloroform or deuteriodimethyl sulfoxide with a Bruker AM-300 spectrometer. Infrared spectra were recorded on a Nicolet 5DX FT spectrometer. Mass spectra were measured on a Hewlett Packard 5995A gas chromatograph – mass spectrometer using the direct insertion probe method. Kieselgel silica gel DSF-5 (Camag) was used for preparative thin-layer chromatography (tlc). Silica gel (Baker, 70–200 mesh) was used for column chromatography. Tetrahydrofuran and ether were distilled from sodium-benzophenone immediately before use. *n*-Butyllithium (2.6 *M* solution in hexanes) and *tert*-butyllithium (2.0 *M* solution in pentane) were obtained from the Aldrich Chemical Co. Elemental analyses were performed by the Microanalytical Laboratory, Department of Chemistry, University of Alberta. 3-*tert*-Butylcarbonylaminopyridine (**3***a*) was prepared by the literature procedures (**3***a*, *b*).

*3-*tert*-Butylcarbonylamino-4-benzoylpyridine (**4**a)*

Method 1

A solution of *n*-butyllithium (27 mL, 70 mmol) was added dropwise to a solution of **3***a* (5.12 g, 29 mmol) in 100 mL THF at −78°C with stirring under a nitrogen atmosphere. The temperature was maintained at −78°C for a further 15 min, and then at 0°C for 3 h. The reaction mixture was cooled to −78°C, a solution of *N*,*N*-diethylbenzamide (9.92 g, 52 mmol) in 20 mL THF was added dropwise, and the reaction mixture was allowed to stir at 25°C overnight. The reaction mixture was poured into a mixture of ice (100 g) and 5 *N* HCl (20 mL); this mixture was stirred for 10 min and neutralized with aqueous potassium carbonate prior to extraction with ethyl acetate. The organic extract was washed with brine, dried ($MgSO_4$), and the solvent removed *in vacuo*. Recrystallization from ethyl acetate – hexane (2:1 v/v) afforded **4***a* (5.71 g, 70%): mp 125–126°C; ir (KBr): 3337, 2968, 1688, 1680, 1647 cm^{-1}; ^1H nmr ($CDCl_3$) δ: 10.5 (br s, 1H, NH, exchanges with deuterium oxide), 9.98 (s, 1H, H-2), 8.52 (d, J = 5.8 Hz, 1H, H-6), 7.54–7.88 (m, 5H, phenyl hydrogens), 7.43 (d, J = 5.8 Hz, 1H, H-5), 1.35 (s, 9H, *tert*-butyl); ms, m/z: 282 (M^+). *Anal.*

[4]The *ortho*-functionalization of *N*-(*tert*-butoxycarbonyl)aniline and near quantitative hydrolysis of the *tert*-butoxycarbonylamino group to a free amino group has been reported (13).

[5]BTBO is a superior coupling reagent to dicyclohexylcarbodiimide (DCC) since reactions employing DCC yielded **8** as oils due to the difficulty in removing dicyclohexylurea and *N*-acylurea side products. Compound **8** has been reported as an oil (2*b*).

Can. J. Chem. Downloaded from www.nrcresearchpress.com by 72.64.146.136 on 09/07/12
For personal use only.

Can. J. Chem. Downloaded from www.nrcresearchpress.com by 72.64.146.136 on 09/07/12
For personal use only.

calcd. for $C_{17}H_{18}N_2O_2$: C 72.32, H 6.43, N 9.92; found: C 72.30, H 6.41, N 10.04.

Method 2

A solution of benzaldehyde (22.3 g, 210 mmol) in THF (35 mL) was added dropwise to a solution of 4-lithio-3-*tert*-butylcarbonylaminopyridine, prepared from reaction of **3***a* (25.1 g, 140 mmol) in 350 mL THF and *n*-butyllithium (135 mL, 351 mmol) as described under Method 1 at −78°C, and the reaction mixture was allowed to stir at 25°C overnight. The reaction mixture was poured into water (200 mL) and the THF fraction was separated. Removal of the solvent *in vacuo* gave a residue that was dissolved in chloroform and washed with water. The chloroform fraction was dried ($MgSO_4$), the solvent was removed *in vacuo*, and the residue was triturated with hexane to yield **5***a*, which was recrystallized from ethyl acetate – hexane (24.1 g, 60%): mp 208–209°C (lit. (3*b*) mp 200–202°C; lit. (3*a*) mp 206–209°C).

A solution of **5***a* (6.79 g, 24 mmol) in 40 mL DMF and pyridinium dichromate (12 g, 32 mmol) was stirred at 25°C for 2 h prior to pouring into water (300 mL). Extraction with ethyl acetate, drying ($MgSO_4$), and removal of the solvent *in vacuo* yielded the product **4***a*, which was purified by silica gel column chromatography using hexane – ethyl acetate (1:1 v/v) as eluant. The product **4***a* (5.6 g, 83%) was identical (mp, ^{1}H nmr) to that of **4***a* described under Method 1.

*3-*tert*-Butoxycarbonylaminopyridine (**3**b)*

A mixture of di-*tert*-butyldicarbonate (41 g, 188 mmol), 3-aminopyridine (17.3 g, 184 mmol), and *tert*-butyl alcohol (200 mL) was heated at 80°C for 2 h. The solvent was removed *in vacuo*, and the residue was dissolved in ethyl acetate and washed with 0.5 *M* citric acid (30 mL) and water. The ethyl acetate fraction was dried (Na_2SO_4) and the solvent removed *in vacuo*. The product was purified by silica gel column chromatography, using ethyl acetate – hexane (2:1 v/v) as eluate, and subsequent recrystallization from ethyl acetate – hexane (2:1 v/v) to yield **3***b* (27.1 g, 74%): mp 115–116°C; ir (KBr): 3238, 2976, 1729, 1598, 1548 cm^{-1}; ^{1}H nmr ($CDCl_3$) δ: 8.56 (d, J = 2.5 Hz, 1H, H-2), 8.35 (dd, J = 1.5 Hz, J = 5 Hz, 1H, H-6), 8.14 (dd, J = 8 Hz, J = 2.5 Hz, 1H, H-4), 7.75 (br s, 1H, NH, exchanges with deuterium oxide), 7.3 (dd, J = 8 Hz, J = 2.5 Hz, 1H, H-5), 1.55 (s, 9H, *tert*-butyl); ms, m/z: 194 (M^+). *Anal.* calcd. for $C_{10}H_{14}N_2O_2$: C 61.84, H 7.26, N 14.42; found: C 61.53, H 7.32, N 14.38.

*3-*tert*-Butoxycarbonylamino-4-benzoylpyridine (**4**b)*

Method 1

A solution of *tert*-butyllithium (24.6 mL, 40 mmol) was added dropwise, with stirring, to a solution of **3***b* (3.3 g, 17 mmol) in THF (30 mL) at −78°C under a nitrogen atmosphere. The temperature was maintained at −78°C for a further 15 min and then at −20°C for 3 h. The reaction mixture was cooled to −78°C and a solution of *N*,*N*-diethylbenzamide (5.79 g, 32.7 mmol) in THF (10 mL) was added dropwise. The reaction mixture was allowed to warm to 25°C, poured into a mixture of ice (100 g) and 5 *N* HCl (20 mL), stirred for 10 min, and neutralized with aqueous potassium carbonate. The THF layer was separated and the aqueous fraction was extracted with ethyl acetate. The combined organic fractions were washed with brine, dried (Na_2SO_4), and the solvent was removed *in vacuo*. The product was purified by silica gel column chromatography with hexane – ethyl acetate (1:1 v/v) as eluant prior to recrystallization from the same solvent mixture to yield **4***b* (3.3 g, 65%): mp 123–124°C; ir (KBr): 3353, 2984, 1729, 1655 cm^{-1}; ^{1}H nmr ($CDCl_3$) δ: 9.75 (s, 1H, H-2), 9.22 (br s, 1H, NH, exchanges with deuterium oxide), 8.44 (d, J = 5.8 Hz, 1H, H-6), 7.52–7.88 (m, 5H, phenyl hydrogens), 7.35 (d, J = 5.8 Hz, 1H, H-5), 1.56 (s, 9H, *tert*-butyl); ms, m/z: 298 (M^+). *Anal.* calcd. for $C_{17}H_{18}N_2O_3$: C 68.44, H 6.08, N 9.39; found: C 68.55, H 6.03, N 9.74.

Use of *n*-butyllithium, rather than *tert*-butyllithium as described above, afforded **4***b* in 63% yield.

Method 2

A solution of benzaldehyde (4.15 g, 39 mmol) in THF (10 mL) was added dropwise to a solution of 4-lithio-3-*tert*-butoxycarbonylaminopyridine, prepared from reaction of **3***b* (5.0 g, 26 mmol) in 40 mL THF and *tert*-butyllithium (38 mL, 75 mmol), as described above, at −78°C. The reaction mixture was allowed to warm to 25°C and water (25 mL) was added. Extraction with ethyl acetate, drying (Na_2SO_4), removal of the solvent *in vacuo*, and recrystallization from hexane – ethyl acetate yielded **5***b* (5.26 g, 68%): mp 134–135°C; ir (KBr): 3337 (br), 2976, 1606 cm^{-1}; ^{1}H nmr ($CDCl_3$) δ: 8.99 (s, 1H, H-2), 8.09 (br s, 1H, NH, exchanges with deuterium oxide), 8.0 (d, J = 5.8 Hz, 1H, H-6), 7.38 (m, 5H, phenyl hydrogens), 7.0 (d, J = 5.8 Hz, 1H, H-5), 6.3 (br s, 1H, OH, exchanges with deuterium oxide), 5.89 (s, 1H, -*CH*—OH), 1.57 (s, 9H, *tert*-butyl); ms, m/z: 300 (M^+). *Anal.* calcd. for $C_{17}H_{20}N_2O_3$: C 67.98, H 6.71, N 9.33; found: C 68.13, H 6.70, N 9.36.

Use of *n*-butyllithium, rather than *tert*-butyllithium as described above, afforded **5***b* in 62% yield.

A solution of **5***b* (2.3 g, 7.7 mmol) in DMF (15 mL) and pyridinium dichromate (3.6 g, 9.6 mmol) was stirred at 25°C for 2 h before pouring into water (150 mL). Isolation and purification of the product, as described for **4***a* under Method 2, afforded **4***b* in 89% yield.

*3-Amino-4-benzoylpyridine (**6**)*

Method 1

A solution of 95% ethyl alcohol (10 mL) and 5 *N* HCl (30 mL) was added to **4***a* (1.0 g, 3.5 mmol) and the mixture was heated at reflux for 6 h. After cooling to 0°C the reaction mixture was neutralized with aqueous ammonium hydroxide to yield **6** as yellow crystals (0.6 g, 94%): mp 127–129°C (lit. (2*a*) mp 126–128°C).

Method 2

A solution of trifluoroacetic acid-1,2-dichloroethane (1:12 v/v) (50 mL) was added to **4***b* (1.0 g, 3.4 mmol) and the mixture was stirred at 25°C for 3.5 h. The mixture was neutralized with aqueous potassium carbonate at 0°C, extracted with chloroform, washed with water, dried ($MgSO_4$), and the solvent removed *in vacuo*. Recrystallization from *n*-heptane–chloroform yielded **6** (0.645 g, 97%): mp 126–128°C.

*3-Benzyloxycarbonylaminomethylcarbonylamino-4-benzoylpyridine (**8**a)*

A suspension of BTBO (14) (1.03 g, 2.2 mmol) in acetonitrile (20 mL) was added to a mixture of **7***a* (0.455 g, 2.2 mmol) and pyridine (0.174 g, 2.2 mmol) in acetonitrile (20 mL) at 25°C. The reaction mixture became clear in a few seconds. The mixture was stirred for a further 2 h at 25°C, **6** (0.4 g, 2 mmol) in THF (20 mL) and triethylamine (0.215 g, 2 mmol) were added, and the mixture was allowed to stir at 25°C for an additional 6 h. Removal of the solvent *in vacuo*, dissolution in ethyl acetate (30 mL), and washing with 10% aqueous sodium carbonate and then brine were performed consecutively. The ethyl acetate fraction was dried (Na_2SO_4) and most of the solvent was removed *in vacuo*, at which time hexane was added to afford **8***a* (0.694 g, 90%): mp 88–90°C; ir (KBr): 3385, 3017, 2286, 1704, 1655, 1401 cm^{-1}; ^{1}H nmr ($CDCl_3$) δ: 10.56 (s, 1H, *NH*CO, exchanges with deuterium oxide), 9.86 (s, 1H, H-2), 8.62 (d, J = 5.8 Hz, 1H, H-6), 7.3–7.84 (m, 11H, phenyl hydrogens, H-5), 5.68 (br t, 1H, *NH*CH_2, exchanges with deuterium oxide), 5.17 (s, 2H, *CH_2*-Ph), 4.06 (d, J = 6.5 Hz, *CH_2*NH); ms, m/z: 389 (M^+). *Anal.* calcd. for $C_{22}H_{19}N_3O_4$: C 67.86, H 4.92, N 10.79; found: C 67.70, H 4.92, N 10.73.

*tert-Butoxycarbonylglycine (**7**b)*

Di-*tert*-butyldicarbonate (6.4 g, 29.3 mmol) in DMF (15 mL) was added to a mixture of glycine (2.03 g, 27 mmol) and triethylamine (4.04 g, 39.9 mmol) in water (15 mL) and the reaction was allowed to proceed with stirring at 25°C overnight. Water (200 mL) was added, the mixture was cooled to 0°C, and the pH of the solution was adjusted to 2 with 5 *N* HCl. Extraction with ethyl acetate, washing with brine, drying (Na_2SO_4), and removal of the solvent *in vacuo* gave the product **7***b*. Recrystallization from petroleum ether (bp 30–60°C) – ethyl acetate yielded **7***b* (4.05 g, 87%): mp 88–90°C (lit. (15) mp 87–90°C).[6]

*3-*tert*-Butoxycarbonylaminomethylcarbonylamino-4-benzoylpyridine (**8**b)*

Reaction of BTBO (28.52 g, 62 mmol) in acetonitrile (200 mL) with

[6]This synthesis of **7***b* provides a simple alternative to the preparation from *tert*-butyl *S*-4,6-dimethylpyrimidin-2-ylthiocarbonate and glycine reported in ref. 15.

7*b* (10.9 g, 62 mmol) and pyridine (4.9 g, 62 mmol) in acetonitrile (300 mL) followed by addition of **6** (12.3 g, 62 mmol) and triethylamine (6.27 g, 62 mmol) in THF (200 mL), and completion of the reaction as described for the synthesis of **8***a*, afforded **8***b* (18.4 g, 83%): mp 144–145°C; ir (KBr): 3353, 2976, 2935, 2853, 1704, 1655, 1598, 1565, 1516, 1401 cm^{-1}; ^1H nmr ($CDCl_3$) δ: 10.5 (s, 1H, *NH*CO, exchanges with deuterium oxide), 9.84 (s, 1H, H-2), 8.48 (d, J = 5.8 Hz, 1H, H-6), 7.34–7.84 (m, 6H, phenyl hydrogens, H-5), 5.38 (br t, 1H, *NH*CH_2, exchanges with deuterium oxide), 3.98 (d, J = 6 Hz, 2H, *CH_2*NH), 1.44 (s, 9H, *tert*-butyl); ms, m/z: 355 (M^+). *Anal.* calcd. for $C_{19}H_{21}N_3O_4$: C 64.21, H 5.96, N 11.82; found: C 64.01, H 5.88, N 11.83.

*1,3-Dihydro-5-phenyl-2*H*-pyrido[3,4-*e*]-1,4-diazepin-2-one (**9**)*

Method 1

A saturated solution of hydrogen bromide in acetic acid (40 mL) was added to **8***a* (2.15 g, 5.5 mmol) and the mixture was stirred at 25°C for 2 h. Ether (50 mL) and then 10% aqueous methanol (100 mL) were added. Neutralization with aqueous ammonium hydroxide at 0°C, extraction with chloroform, drying the chloroform extract (Na_2SO_4), and removal of the solvent *in vacuo* afforded a residue, which was heated at reflux in toluene (200 mL) and pyridine (2 mL) for 7 h. Removal of the solvent *in vacuo* and addition of hexane yielded **9** (1.31 g, 82%), which was recrystallized from benzene–methanol: mp 258–260°C (lit. (2*a*) mp 258–260°C).

Method 2

A 1 *N* solution of trifluoracetic acid in 1,2-dichloroethane (50 mL) was added to **8***b* (0.227 g, 0.64 mmol) and the resulting solution was stirred at 25°C for 6 h. The solvent was removed *in vacuo*, and the residue was dissolved in ethyl acetate (30 mL) and neutralized with aqueous potassium carbonate. The ethyl acetate fraction was washed with brine, dried (Na_2SO_4), and the solvent removed *in vacuo*. Toluene (20 mL) and pyridine (0.5 mL) were added to the residue and the solution was heated at reflux for 7 h. Removal of the solvent *in vacuo* and purification of the residue by preparative tlc, using plates 1.0 mm in thickness, with chloroform–ether–methanol (7:2:1 v/v/v) as development solvent afforded **9**, R_f 0.4 (0.135 g, 89%): mp 258–260°C.

*1,3-Dihydro-1-methyl-5-phenyl-2*H*-pyrido[3,4-*e*]-1,4-diazepin-2-one (**10**)*

Sodium hydride (50% dispersion in oil, 0.64 g, 13.2 mmol) was added in aliquots to a solution of **9** (2.95 g, 12.4 mmol) in DMF (20 mL) with stirring at 0°C. Stirring was continued for 25 min, at which time iodomethane (1.76 g, 12.4 mmol) in ether (1 mL) was added. The reaction mixture was stirred for an additional 30 min at 0°C. Addition of water (200 mL), extraction with ethyl acetate, drying ($MgSO_4$), and removal of the solvent *in vacuo* gave a residue. Purification by preparative tlc, using plates 1.0 mm in thickness, with dichloromethane–methanol (11:1 v/v) as development solvent gave **10** (2.28 g, 73%). Recrystallization from ethyl acetate – hexane afforded **10** as white needles: mp 126–127°C; ir (KBr): 3058, 3000, 2992, 1688, 1614 cm^{-1}; ^1H nmr ($CDCl_3$) δ: 8.84 (s, 1H, H-9), 8.52 (d, J = 5.8 Hz, 1H, H-7), 7.45–7.69 (m, 5H, phenyl hydrogens), 7.27 (d, J = 5.8 Hz, 1H, H-6), 4.97 (d, J_{gem} = 12 Hz, 1H, NCH′CO), 3.82 (d, J_{gem} = 12 Hz, 1H, NCH″CO), 3.52 (s, 3H, N-CH_3); ms, m/z: 251 (M^+). *Anal.* calcd. for $C_{15}H_{13}N_3O$: C 71.70, H 5.21, N 16.72; found: C 71.53, H 5.20, N 16.71.

Acknowledgments

We are grateful to the Medical Research Council of Canada (Grant MT-4888) for financial support of this work and to the Alberta Heritage Foundation for Medical Research for a fellowship awarded to one of us (C.Y.F.). The grant from the Alberta Heritage Foundation to purchase the Bruker AM-300 spectrometer is also gratefully acknowledged.

1. (*a*) L. H. Sternbach. J. Med. Chem. **22**, 1 (1979); (*b*) M. Williams. J. Med. Chem. **26**, 619 (1983); (*c*) S. J. Childress and M. I. Gluckman. J. Pharm. Sci. **53**, 577 (1964); (*d*) L. O. Randall, W. Schallek, L. H. Sternbach, and R. Y. Ning. *In* Psychopharmacological agents. *Edited by* M. Gordon. Academic Press, New York. 1974. p. 175.
2. (*a*) R. Littell and D. S. Allen. J. Med. Chem. **8**, 722 (1965); (*b*) R. Littell, D. S. Allen, and D. Ferry. U.S. Patent 3 314 941 (1967); (*c*) W. Von Bebenburg and H. Offermanns. U.S. Patent 4 008 223 (1977); Chem. Abstr. **86**, 190032h (1977); (*d*) N. Kanji, A. Nakagawa, S. Yamazaki, Y. Ishikura, T. Hachiya, H. Terumi, M. Hirano, and H. Ide. Japan Patent 76 80 899 (1976); Chem. Abstr. **86**, 43752q (1977).
3. (*a*) J. A. Turner. J. Org. Chem. **48**, 3401 (1983); (*b*) T. Gungor, F. Marsais, and G. Queguiner. Synthesis, 499 (1982); (*c*) Y. Tamura, L. C. Chen, M. Fujita, and Y. Kita. Chem. Pharm. Bull. **30**, 1257 (1982).
4. (*a*) J. Epsztajn, A. Bieniek, J. Z. Brzezinski, and A. Jozwiak. Tetrahedron Lett. **24**, 4735 (1983); (*b*) M. Iwao and T. Kuraishi. Tetrahedron Lett. **24**, 2649 (1983); (*c*) J. Epsztajn, Z. Berski, J. Z. Brzezinski, and A. Jozwiak. Tetrahedron Lett. **21**, 4739 (1980).
5. M. A. J. Miah and V. J. Snieckus. J. Org. Chem. **50**, 5438 (1985).
6. A. I. Meyers and R. A. Gabel. J. Org. Chem. **47**, 2633 (1982).
7. (*a*) G. W. Gribble and M. G. Saulnier. Tetrahedron Lett. **21**, 4137 (1980); (*b*) F. Marsais and G. Queguiner. Tetrahedron, **39**, 2009 (1983); (*c*) F. Marsais, P. Breant, A. Ginguene, and G. Queguiner. J. Organometal. Chem. **216**, 139 (1981); (*d*) M. Mallet and G. Queguiner. Tetrahedron, **38**, 3035 (1982); (*e*) E. J. Corey and S. G. Pyne. Tetrahedron Lett. **24**, 3291 (1983).
8. D. M. Roland and W. Macchia. 10th International Congress of Heterocyclic Chemistry, August 11–16, 1985, Waterloo, Canada. Abstract P1–10.
9. C. W. G. Fishwick, R. C. Storr, and P. W. Manley. J. Chem. Soc. Chem. Commun. 1304 (1984).
10. Y. Tamura, M. Fujita, L. C. Chen, M. Inoue, and Y. J. Kita. J. Org. Chem. **46**, 3564 (1981).
11. G. Barcelo, J. P. Senet, and G. Sennyey. J. Org. Chem. **50**, 3591 (1985).
12. (*a*) M. G. El Din, E. E. Knaus, and C. S. Giam. Can. J. Chem. **60**, 1821 (1982); (*b*) S. K. Dubey, E. E. Knaus, and C. S. Giam. Heterocycles, **22**, 1091 (1984); (*c*) A. E. Hauck and C. S. Giam. J. Chem. Soc. Perkin Trans. 1, 2227 (1984); (*d*) J. Chem. Soc. Perkin Trans. 1, 2070 (1980).
13. J. M. Muchowski and M. C. Venuti. J. Org. Chem. **45**, 4798 (1980).
14. K. Takeda, K. Tsuboyama, K. Yamaguchi, and H. Ogura. J. Org. Chem. **50**, 273 (1985).
15. T. Nagasawa, K. Kuroiwa, K. Narita, and Y. Isowa. Bull. Chem. Soc. Jpn. **46**, 1269 (1973).

Can. J. Chem. Downloaded from www.nrcresearchpress.com by 72.64.146.136 on 09/07/12
For personal use only.

The sonolysis of cytosine and thymine

TAIN-JEN YU, RONALD G. SUTHERLAND, AND RONALD E. VERRALL[1]
Department of Chemistry, University of Saskatchewan, Saskatoon, Sask., Canada S7N 0W0

Received July 25, 1986

TAIN-JEN YU, RONALD G. SUTHERLAND, and RONALD E. VERRALL. Can. J. Chem. **65**, 1162 (1987).

Sonolysis of cytosine has been studied at 630 kHz in the presence of air and nitrogen. The degradation products were identified by gas chromatographic – mass spectral analysis. Under aerated conditions the following products were found: urea, formyl urea, parabanic acid, isobarbituric acid, oxaluric acid, alloxan monohydrate, alloxantin, dialuric acid, and uracil glycols. Under nitrogen the degradation products were isobarbituric acid, alloxan monohydrate, and uracil glycols. The observed products have been used to develop a possible mechanism for the sonolytic degradation. There appears to be some similarity with the products reported from radiolysis studies of this compound. Sonolysis of thymine in the presence of air was reinvestigated and the gc–ms analysis shows that a previously reported, unidentified, product may be 5-hydroxy-5-methylbarbituric acid.

TAIN-JEN YU, RONALD G. SUTHERLAND et RONALD E. VERRALL. Can. J. Chem. **65**, 1162 (1987).

Opérant en présence d'air et d'azote, on a étudié la sonolyse de la cytosine à 630 kHz. On a identifié les produits de dégradation en faisant appel à la sm/cpg. Dans les produits obtenus par des réactions effectuées en présence d'air, on a retrouvé de l'urée, de la formyl-urée, de l'acide parabanique, de l'acide isobarbiturique, de l'acide oxalurique, du monohydrate d'alloxane, de l'alloxantine, de l'acide dialurique et des glycols d'uracile. Les produits obtenus au cours des réactions effectuées dans un atmosphère d'azote comprennent l'acide isobarbiturique, le monohydrate d'alloxane et des glycols d'uracile. On a utilisé les produits observés pour développer un mécanisme plausible pour la dégradation par sonolyse. Il semble qu'il existe une certaine similarité avec la nature des produits observés lors des études de radiolyse effectuées sur ce composé. La sonolyse de la thymine, en présence d'air, a été réétudiée; la sm/cpg démontre qu'un produit qui avait été observé antérieurement et qui n'avait pas été identifié, est l'acide hydroxy-5 méthyl-5 barbiturique.

[Traduit par la revue]

Introduction

Ultrasonically induced chemical reactions of biologically important molecules related to RNA and DNA have been reported previously (1–4).[2] In this paper we report the results of the sonolytic degradation of the pyrimidine bases cytosine and thymine. Results of such studies on thymine have been reported earlier (2); however, analyses of products were carried out using tlc techniques. This study reports an attempt to determine whether gc–ms techniques could reveal any additional compounds not observed in the previous work (2), and allows a direct comparison with the results obtained with cytosine.

The radiolysis of cytosine has been investigated in aerated aqueous solutions (5–9). Since the primary reactions in the sonolysis of aqueous solutions (10–14) are now known to be essentially similar to those produced in radiolytic reactions, the sonolysis and radiolysis are compared and contrasted.

Experimental

Ultrasonic irradiation and general analysis procedures

The ultrasound generator and power output, gc–ms equipment, and all other instruments and methods used in the experiment are as previously reported (3). The calculation of per cent degradation of a compound is based on the change in absorbance at λ_{max} of the sample before and after sonolysis. Cytosine absorbance was measured at 267 nm. Aqueous solutions of cytosine and thymine were saturated with the appropriate gas for at least 30 min prior to and during sonolysis. A Beckman Expandomatic SS-2 pH meter was used to measure pH values.

The sonolytic degradation products were identified using both CI and EI mass spectra. Whenever possible, final confirmation was made by comparison with authentic samples.

Materials

Cytosine, thymine (Aldrich Chemical Co.), and all authentic samples were used without further purification. The procedures and materials for converting degradation products to their trimethylsilyl derivatives for gc–ms analysis were as reported previously (3).

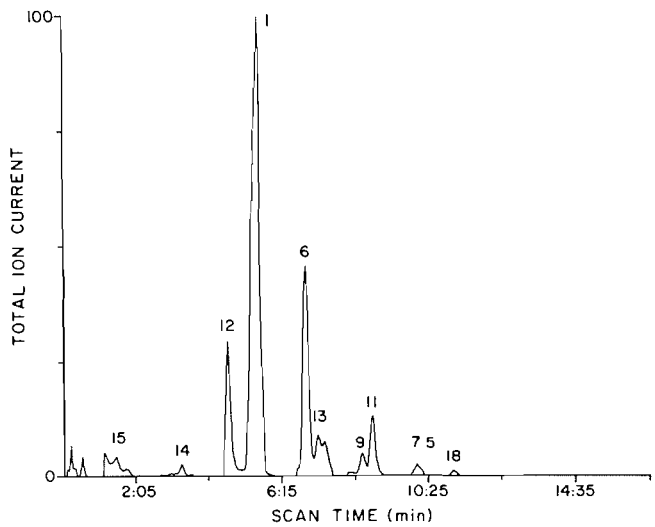

FIG. 1. Mass spectral reconstructed ion chromatogram of a 2 m*M* aqueous solution of cytosine insonated at 630 kHz in the presence of air.

Results and discussion

Figure 1 shows the gc spectrum of a 2 m*M* aqueous solution of cytosine sonicated at 630 kHz for 2 h in the presence of air. Absorbance measurements showed that the upper limit of the cytosine degradation was 67%. A pH decrease from 6.2 to 4.2 was observed during insonation. Ten compounds, including unreacted cytosine, are identified. They are urea (**15**), formyl urea (**14**), parabanic acid (**12**), cytosine (**1**), isobarbituric acid (**6**), oxaluric acid (**13**), alloxan monohydrate (**9**), alloxantin (**11**), dialuric acid (**7**), and uracil glycols (**5**).

A gc spectrum of a 2 m*M* aqueous solution of cytosine

[1]Author to whom correspondence may be addressed.

[2]A paper describing the sonolytic degradation of adenine is in the course of preparation.

Can. J. Chem. Downloaded from www.nrcresearchpress.com by 78.46.186.204 on 09/07/12
For personal use only.

Can. J. Chem. Downloaded from www.nrcresearchpress.com by 78.46.186.204 on 09/07/12
For personal use only.

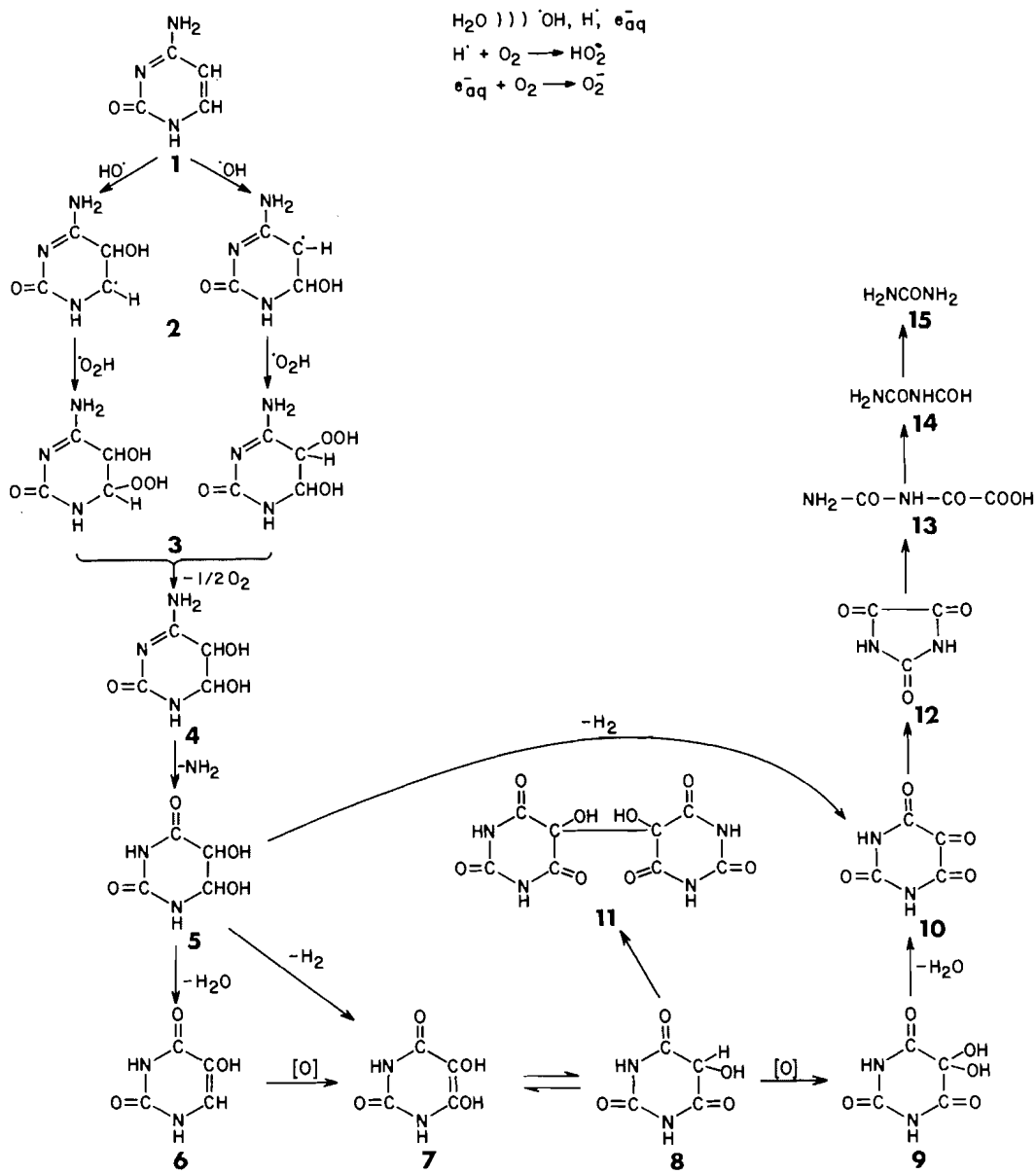

FIG. 2. Proposed sonolytic mechanism of degradation of aqueous cytosine solutions in aerated state.

sonicated at 630 kHz for 2 h in the presence of nitrogen revealed only three compounds in addition to cytosine. They are isobarbituric acid (**6**), alloxan monohydrate (**9**), and uracil glycols (**5**). The percent degradation of cytosine under these conditions decreased to 18% and the acidity of the solution remained constant at pH 6 during the sonication.

A mechanism for the sonolytic degradation of cytosine in the presence of air is summarized in Fig. 2 and is described briefly as follows. In the presence of air, $OH^{\bullet}$, $HO_2^{\bullet}$, and O_2^{-} are the primary species produced during the cavitation process induced by the high intensity ultrasonic waves (2, 3). Cytosine hydroxyhydroperoxides (**3**) may arise from the successive attacks of $OH^{\bullet}$ and $HO_2^{\bullet}$ across the 5,6 double bond of cytosine. Cytosine glycols (**4**) can arise from the peroxides through loss of oxygen (**2**) and can give rise to uracil glycols (**5**) by means of a deamination pathway. Isobarbituric acid (**6**) could be formed from uracil *cis*-glycol through loss of a water molecule. Dialuric acid (**7**) may be derived both by the dehydrogenation of uracil glycols (**5**) or by the oxidation of isobarbituric acid (**6**). Alloxan monohydrate (**9**) could be oxidized from isodialuric acid (**8**), the tautomer of dialuric acid (**7**). Alloxantin (**11**) may arise from isodialuric acid (**8**) and (or) from alloxan (**10**), the dehydrated product of alloxan monohydrate (**9**). Alloxan (**10**) can be produced also from uracil glycols (**5**) by dehydrogenation.

Parabanic acid (**12**) may be derived from the ring opening and rearrangement of alloxan (**10**). Further hydrolysis of parabanic acid would lead to open chain products like oxaluric acid (**13**), formyl urea (**14**), and urea (**15**).

Most of these degradation products have been observed in the sonolysis of uracil (3) and are similar to those observed in radiolysis studies of cytosine (6, 8) that give radiation products belonging to the deamination pathway. However, non-deamination pathway products such as 4-amino-isobarbituric acid, 1-carbamoyl-5-hydroxyhydrantoin, and 1-carbamyl-imidazolidone-4,5-diols also have been identified in radiolysis work (5, 7, 9). We did not detect any sonolysis products arising from ring cleavage.

Since oxygen is absent in the case of sonolysis under nitrogen

atmosphere, then hydroxyl radicals, hydrogen atoms, as well as the possibility of hydrated electrons must be considered (3) as the primary reactive species. In a manner similar to that proposed for the sonolysis of uracil, OH• attack of the 5,6 double bond of cytosine occurs, producing adducts. These adducts may undergo disproportionation reaction to produce cytosine and cytosine glycols. The uracil glycols (**5**) can be formed by the deamination of cytosine glycols (**4**). The remaining products may occur as follows: isobarbituric acid (**6**) derives from uracil *cis*-glycol by loss of a water molecule; alloxan monohydrate (**9**) may result from hydration of alloxan (**10**), which is derived from uracil glycols (**5**) by loss of H_2.

No degradation products have been identified that can be related to attack of hydrogen atoms or hydrated electrons. However, three gc peaks were observed in which the molecular weights of the trimethylsilyl derivatives were determined by mass spectral methods to be 371, 406, and 477 atomic mass units. The peak having a mass of 371 is found also in the sonolysis work in the presence of air and is labelled as compound **18**. Attempts to identify these compounds have not been successful and we report them simply for information.

Previous results of the sonolysis of of thymine (2) were analyzed using tlc methods and the following compounds were positively identified: *cis*- and *trans*-5,6-dihydroxy-5,6-dihydrothymine (thymine glycols), 5-hydroxymethyluracil, urea, and *N*-pyruvyl-*N'*-formyl urea. The concentration of organic peroxides was estimated indirectly (2).

In this work insonation at 630 kHz of an aqueous 2 m*M* solution of thymine in the presence of air for 2 h produced five products in addition to the unreacted thymine. These include *N*-pyruvyl-*N'*-formyl urea, 6-hydroxymethyluracil, *cis*- and *trans*-5,6-dihydroxydihydrothymine, and 5-hydroxy-5-methylbarbituric acid. It is to be noted that the last compound was not observed in previous sonolysis studies (2), although it is known to be a product arising from radiolysis work on thymine (15, 16). We could not identify urea in this study. However, since authentic samples of urea come off the column packing (8% SE-30 on AW-DMCS Chromosorb W, 80–100 mesh) very quickly, small amounts of urea may not be detectable using this separation technique. Previous work (2) has shown that a very small amount of urea is formed and that the amount produced decreases with increasing sonication time.

Organic peroxides observed in radiolysis studies on thymine (15, 16) were not detected in our analysis, although we cannot rule out that the derivatization procedure may be sufficiently harsh to induce their thermal decomposition.

In previous work one unidentified product was isolated using tlc methods. It would appear that 5-hydroxy-5-methylbarbituric acid could be this compound.

Finally, the energy output in previous work at 450 kHz (2) was not measured on the same quantitative basis as reported here and in other work (3). Consequently, it is still uncertain as to whether there is any ultrasonic frequency dependence of the product distribution. On balance, it would appear that the majority of products are the same and the gc–ms analysis procedure is more efficient in identifying products.

Acknowledgements

The authors wish to acknowledge the use of the gc–ms facility of the National Research Council of Canada Prairie Regional Laboratory and to thank Mr. L. Hogge for his technical assistance. One of us (T.J.Y.) acknowledges the award of a University of Saskatchewan Postdoctoral Fellowship. Financial support from the Natural Sciences and Engineering Research Council of Canada to R.G.S. and R.E.V. is gratefully acknowledged.

1. I. E. El'piner. Ultrasound, its physical, chemical and biological effects. Consultants Bureau, New York, NY. 1964.
2. E. L. Mead, R. G. Sutherland, and R. E. Verrall. Can. J. Chem. **53**, 2394 (1975).
3. T.-J. Yu, R. G. Sutherland, and R. E. Verrall. Can. J. Chem. **58**, 1909 (1980).
4. J. R. McKee, C. L. Christman, W. D. O'Brien, Jr., and S. Y. Wang. Biochemistry, **16**, 4651 (1977).
5. B. Ekert and R. Monier. Nature, **188**, 309 (1960).
6. R. Pletichia-Lansky and J. J. Weiss. Anal. Biochem. **16**, 510 (1966).
7. B. S. Hahn, S. Y. Wang, J. L. Flippen, and I. L. Karle. J. Am. Chem. Soc. **95**, 2711 (1973).
8. M. Polverelli and R. Teoule. Z. Naturforsch. C: Biosci. **29**, 12 (1974).
9. M. Polverelli and R. Teoule. Z. Naturforsch. B: Anorg. Chem. Org. Chem. **31**, 580 (1976).
10. A. Weissler. J. Am. Chem. Soc. **81**, 1977 (1959).
11. M. Anbar and I. Pecht. J. Phys. Chem. **68**, 352 (1964).
12. M. A. Margulis and A. N. Mal'tsev. Russ. J. Phys. Chem. **42**, 1412 (1968).
13. M. Anbar and I. Pecht. J. Phys. Chem. **68**, 1460 (1964).
14. C. Sehgal, R. P. Steer, R. G. Sutherland, and R. E. Verrall. J. Phys. Chem. **81**, 2618 (1977).
15. R. Teoule and J. Cadet. Bull. Soc. Chim. Fr. 927 (1970).
16. G. A. Infante, P. Jirathane, J. H. Fendler, and Z. J. Fendler. J. Chem. Soc. Faraday Trans. 1, **69**, 1586 (1973).

Can. J. Chem. Downloaded from www.nrcresearchpress.com by 78.46.186.204 on 09/07/12
For personal use only.

$Ba(OH)_2$ as the catalyst in organic reactions. Part XIV. Mechanism of Claisen–Schmidt condensation in solid–liquid conditions

A. AGUILERA, A. R. ALCANTARA, J. M. MARINAS, AND J. V. SINISTERRA[1]

Department of Organic Chemistry, Faculty of Sciences, Córdoba, Spain

Received August 15, 1986

A. AGUILERA, A. R. ALCANTARA, J. M. MARINAS, and J. V. SINISTERRA. Can. J. Chem. **65**, 1165 (1987).

The mechanism of the Claisen–Schmidt condensation, catalyzed by a series of activated barium hydroxide catalysts, is discussed. Two kinds of ketones are studied: R—CO—CH_3 (R = Me, Et, Pr^i, Bu^t) and acetophenone (R = Ph). The influence of the chemical and textural properties of the catalysts, as well as the nature of the solvent, are studied. The process is an interfacial solid–liquid reaction between the adsorbed carbanion and the benzaldehyde. The different structures of the adsorbed carbanion produced from Ph—CO—CH_3 and R—CO—CH_3 are analyzed by infrared spectroscopy, and could explain the different reactivities observed in the process. The kinetic runs are discussed.

A. AGUILERA, A. R. ALCANTARA, J. M. MARINAS et J. V. SINISTERRA. Can. J. Chem. **65**, 1165 (1987).

On discute du mécanisme de la condensation de Claisen–Schmidt, catalysée par une série de catalyseurs d'hydroxydes de baryum activés. On a étudié deux sortes de cétones : R—CO—CH_3 (R = Me, Et, i-Pr et *t*-Bu) et l'acétophénone (R = Ph). On a étudié l'influence des propriétés chimiques et texturales des catalyseurs ainsi que la nature du solvant. Le processus est une réaction interfaciale solide–liquide entre le carbanion qui est adsorbé et le benzaldéhyde. Faisant appel à la spectroscopie infrarouge, on a analysé les différentes structures des carbanions formés à partir des cétones Ph—CO—CH_3 et R—CO—CH_3. Ces structures peuvent expliquer les diverses réactivités observées dans ce processus. On discute des données cinétiques.

[Traduit par la revue]

Introduction

Aldol condensation type reactions catalyzed in the homogeneous phase have been studied extensively from a mechanistic point of view. In heterogeneous conditions, catalyzed by solids (1, 2), the mechanism is not well known, due to the presence of acidic as well as basic sites on the catalyst surface. Claisen–Schmidt condensation (3) is a process, related to aldol condensation, that leads to styril ketones and chalcones, very useful compounds in pharmaceutics (4). The mechanism of the process has been studied in the homogeneous phase (5, 6), but we cannot say the same about the processes in the heterogeneous phase (7). In this case, the reaction seems to be first order in benzaldehyde, with a Langmuir–Hinshelwood type kinetic equation, when the reaction is carried out using Al_2O_3 (7). The ketone is adsorbed on basic sites and reacts with the aldehyde (7, 8).

$$\underset{\mathbf{1}}{\text{Ph—CHO}} + \underset{\mathbf{2}}{\text{R—CO—CH}_3} \xrightarrow{\text{base}} \underset{\mathbf{3}}{\text{Ph—CH=CH—CO—R}} + \text{H}_2\text{O}$$

R = Me, Et, Pr^i, Bu^t, Ph

Earlier we described some new barium hydroxide catalysts (9), and studied their catalytic activity in interfacial solid–liquid processes, in some organic reactions, e.g., aldol condensation (10), Michael addition (11), Wittig–Horner reaction (12), and Claisen–Schmidt condensation (13), from a synthetic point of view. These catalysts are more active and selective than the commercial ones: K_2CO_3, KOH, etc., in similar experimental conditions (interfacial solid–liquid processes) (12, 13). In the present paper we discuss the mechanism of the process and the influence of the chemical and textural properties of the catalysts on the condensation mechanism.

Experimental

Catalysts

The activated barium hydroxide catalysts C-200 and C-300 were obtained by dehydration of commercial $Ba(OH)_2 \cdot 8H_2O$ Probus S.A. (C-0). The preparation of these catalysts has been previously described (10).

The surface area of the catalysts was determined by a Sortomatic Carlo–Erba. The values obtained were C-0, (1.4 ∓ 0.1) $m^2\ g^{-1}$; C-200, (1.9 ∓ 0.1) $m^2\ g^{-1}$; C-300, (1.4 ∓ 0.1) $m^2\ g^{-1}$.

The titration of basic sites was carried out by a spectrophotometric method previously described (14). Benzoic acid (BA) was used to titrate the total amount of basic sites. The values obtained were C-0, (0.68 ∓ 0.07) × 10^{-3} equiv./g catalyst; C-200, (0.91 ∓ 0.09) × 10^{-3} equiv./g catalyst; C-300, (0.85 ∓ 0.09) × 10^{-3} equiv./g catalyst.

TABLE 1. Ultraviolet spectrometric characteristics of the enones (Ph—CH=CH—CO—R)

R	λ_{max} (nm)[a]	ϵ ($cm^{-1}\ mol^{-1}\ L$) × 10^{-4}[b]
Me	310 ± 2	(1.86 ± 0.03)
Et	288 ± 2	(1.65 ± 0.02)
iPr	305 ± 2	(1.18 ± 0.02)
*t*Bu	310 ± 2	(2.10 ± 0.09)
Ph	314 ± 2	(2.31 ± 0.03)

[a] b = 1 cm.
[b] Solvent, EtOH (96%).

Claisen–Schmidt condensation

The kinetic runs of the condensation were carried out with 20 mL of ethanolic Ph—CHO and ketone solutions. The initial concentration was 0.1 *M* in both compounds. The conversion was determined by ultraviolet–visible measurements at λ_{max} of the enone (R—CH=CH—CO—Ph), using an ultraviolet–visible Varian model Cary 219 spectrometer.

Reactions with the supported polymeric reagent Ⓟ-CHO

The supported polymeric reagent Ⓟ-CHO was obtained according to a previously described method (15), using Merrifield's peptide resin (1% cross-linked; 200–400 mesh; 1 mequiv. Cl/g; Aldrich).

Fourteen grams of resin were mixed with 300 mL of DMSO and 19 g of $NaHCO_3$, and refluxed for 6 h. Afterwards the resin was filtered and washed with (2:1 v/v) 1,4-dioxane–water mixture and with acetone, and dried at 110°C. A 1695 cm^{-1} C=O band was detected in the ir spectrum of the polymer.

The reaction with the polymeric reagent (Ⓟ-CHO) was carried out

[1] Author to whom correspondence may be addressed.

Can. J. Chem. Downloaded from www.nrcresearchpress.com by 78.46.186.204 on 09/07/12
For personal use only.

with 0.0196 mol of R—CO—Me, 0.1 g of polymeric reagent Ⓟ-CHO (equivalent to 0.001 equiv. of —CHO/g polymer), and 10 mL of EtOH (96%).

The mixture was refluxed for 6 h. Then 1 *M* HCl was added to destroy the barium hydroxide catalyst (C-200). The resin was filtered and washed with EtOH, and dried to get the ir spectrum.

Adsorption experiments

The adsorption experiments with ketones (R—CO—Me; R = Ph, Me, Et, Pr^i, and Bu^t Merck p.a.) and benzaldehyde (Panreac S.A.) were carried out using 0.2 mL of carbonylic compound, 0.1 g of catalyst, and 10 mL of EtOH (96%). The mixture was refluxed for 15 min, and filtered. The ir spectra of the solid and liquid were obtained on an ir spectrometer (Perkin–Elmer model 599B) with a Perkin–Elmer Data Station model 2000. The PECDS program was used for accumulation and manipulation of the spectra of the adsorbed species.

Results and discussion

1. Catalysts

In a previous paper (14) we discussed the nature and number of active sites of our catalysts. We showed that acidic and oxidizing sites were not present in the catalysts, due to the nature of Ba(II). Only reducing sites versus 1,3-dinitrobenzene and basic sites versus benzoic aicd (BA) were detected (14). In the experimental part of this work, the total number of basic sites versus benzoic acid is shown. We can observe that the number of basic sites is very similar in the three catalysts:

$$\text{C-200} \gtrsim \text{C-300} > \text{C-0}$$

On the other hand, the surface area is similar and very small in all cases (1.9, 1.4, and 1.4 m^2/g respectively), and this fact is due to the microcrystalline structure of the solids. An X-ray study was carried out to learn more about that point. The results were

C-0

$Ba(OH)_2 \cdot 8H_2O$

Cell lattice: a_0 = 9.35 Å; b_0 = 9.38 Å; c_0 = 11.87 Å; $\alpha = \gamma = 90°$; $\beta = 99°$

C-200

Empirical formula from TGA (16) = $Ba(OH)_2 \cdot 0.8H_2O$; main compound: $Ba(OH)_2 \cdot H_2O$

Cell lattice: a_0 = 6.366 Å; b_0 = 6.955 Å; c_0 = 3.895 Å; $\alpha = \beta = \gamma = 90°$

Secondary product: $\beta\,Ba(OH)_2$

Cell lattice: a_0 = 9.40 Å; b_0 = 6.79 Å; c_0 = 3.95 Å; $\alpha = \gamma = 90°$; $\beta = 97.6°$

C-300

Empirical formula from TGA (16) = $Ba(OH)_2 \cdot 0.39H_2O$; main compound: $\alpha\,BA(OH)_2$

Cell lattice: a_0 = 11.03 Å; b_0 = 12.56 Å; c_0 = 7.11 Å ($\alpha = \beta = \gamma = 90°$)

Secondary product: $Ba(OH)_2 \cdot H_2O$

A more detailed study (17) of the equilibria between α and β barium hydroxide and the monohydrate leads us to deduce that the C-200 catalyst contains β $Ba(OH)_2$ in the bulk of the solid, and $Ba(OH)_2 \cdot H_2O$ on the surface. The monohydrate is produced from the original β $Ba(OH)_2$ by the adsorption of water during storage in the presence of anhydrous NaOH.

The equilibrium between β $Ba(OH)_2$ and the $Ba(OH)_2 \cdot H_2O$ is reached in 24 h of storage, and the product obtained presents an empirical formula of $Ba(OH)_2 \cdot 0.8H_2O$. This rehydration is very easy, because the cell lattice dimensions of both barium hydroxides are very similar. These structures are very similar to those described for the isotypic structures of $Sr(OH)_2 \cdot H_2O$ (18) and $Sr(OH)_2$ (18, 19). Thus we can postulate the structure pictured in Fig. 1 for the C-200 catalyst. The β $Ba(OH)_2$ stands inside the bulk and the $Ba(OH)_2 \cdot H_2O$ is on the surface.

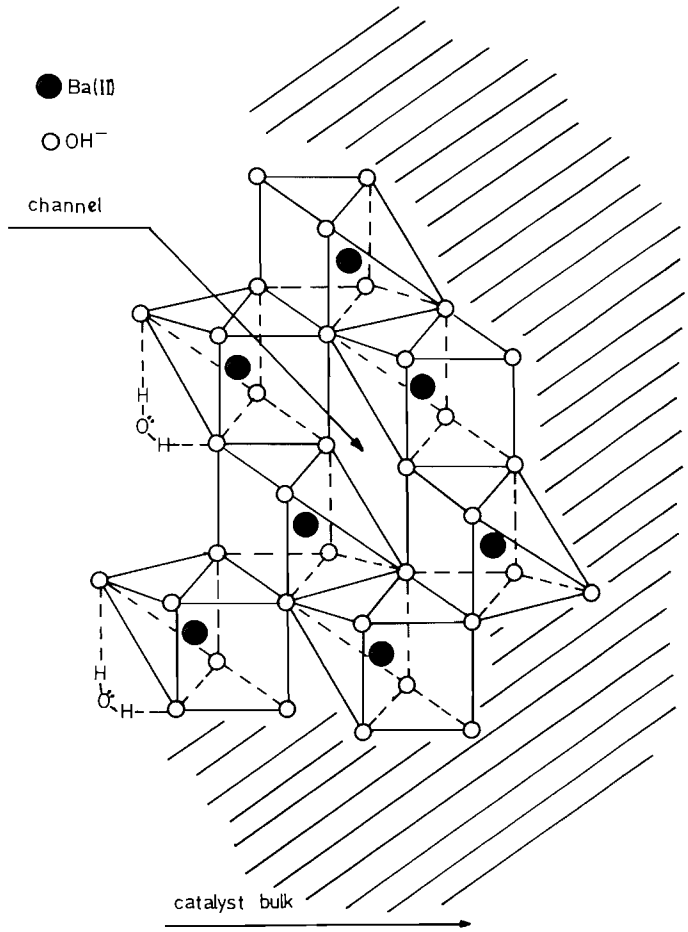

FIG. 1. Proposed structure for C-200 catalyst; average Ba(II)—OH^- = 2.6 Å; average OH^-—OH^- or OH^-—H_2O = 3.5 Å.

When the C—O is calcinated at 300°C, α $Ba(OH)_2$ (stable form at $T > 250°C$) (20) is produced. This solid is stored in a bottle in the presence of anhydrous NaOH. As in the case of C-200, the α $Ba(OH)_2$ is partially rehydrated to get the C-300 catalyst.

From X-ray analysis (17), we could deduce that the C-300 is a mixture of α $Ba(OH)_2$ and $Ba(OH)_2 \cdot H_2O$, with an empirical formula of $(Ba(OH)_2 \cdot 0.3H_2O)$. Rehydration is slower in this case, because of the quite different cell lattice dimensions of both compounds. Therefore we can say that C-300 consists of α $Ba(OH)_2$ in bulk and of $Ba(OH)_2 \cdot H_2O$ on the surface.

The structure of commercial barium hydroxide C-0 ($Ba(OH)_2 \cdot 8H_2O$) has been described in the literature (21) as an antiprism around the Ba(II) with an average distance Ba—OH^- = 3.63 Å.

2. Influence of the chemical and textural properties of the catalysts on the yield

The influence of the nature of the catalyst upon the yield of the process, with different ketones, was analyzed. The results are shown in Table 2.

From these results we can observe that the steric hindrance of the alkyl group in the ketone (R) diminishes the yield of **3** in all cases. This group will hinder the adsorption and generation of

Can. J. Chem. Downloaded from www.nrcresearchpress.com by 78.46.186.204 on 09/07/12
For personal use only.

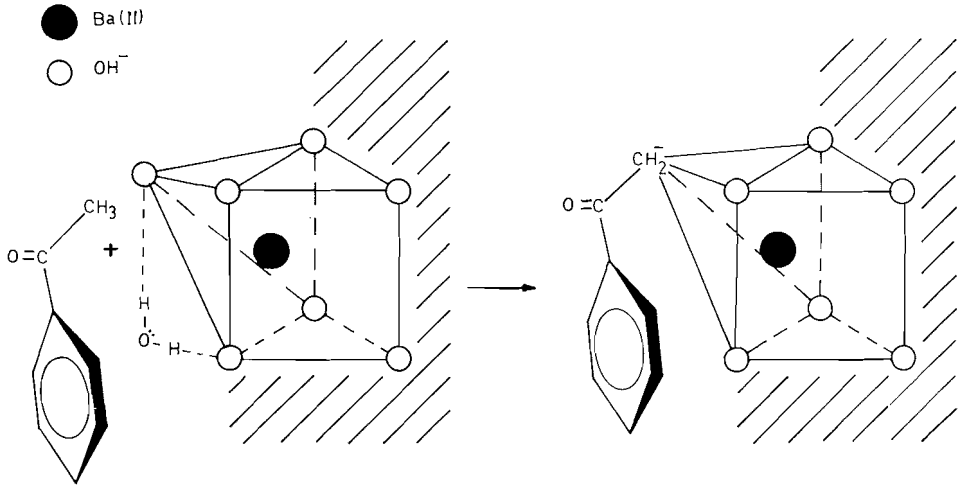

FIG. 2. Adsorbed carbanion from acetophenone on C-200 surface.

TABLE 2. The influence of the structure of the catalyst upon yield[a] in the Claisen–Schmidt reaction

R	Benzylidene derivative yield (% molar)[b] C-0	C-200	C-300
Me	33	54	40
Et	66	68	74
iPr	40	46	47
*t*Bu	11	9	8
Ph	100	98	88

[a]Moles of PhCHO = moles of ketone (R—CO—Me = 0.0196); 10 mL of EtOH (96%); 0.1 g of catalyst. Reaction time = 15 min. Temperature of reflux of EtOH.
[b]Error ±5%.

the carbanion from the ketone (see Sect. 4) so that the yield will be lower.

The high yields obtained with Ph—CO—CH_3 can be related to the different nature of adsorbed carbanion compared to that obtained from R—CO—CH_3 (see Sect. 4).

The catalytic activity of the three catalysts is similar with the same ketone. Therefore we can say that the reaction seems to be insensitive to the structure of the catalyst for this kind of ketone. This behaviour has only been observed in the hydrolysis of the salicylic esters (22). It can be related to a similar structure of the adsorbed carbanion produced from the R—CO—CH_3 ketones (see Sect. 4).

Nevertheless, in the case of Ph—CO—CH_3, the process actually seems to be sensitive to the structure of the catalyst:

$$C—O \approx C\text{-}200 > C\text{-}300$$

The structures of C-0 and the main component of C-200 ($Ba(OH)_2 \cdot H_2O$) present very similar distances Ba—OH^- (3.63 Å) and OH^-—H_2O (3.66 Å) (17, 21). These distances allow the unconjugated carbanion (Sect. 4) to be placed where the OH^- was in the lattice, and the aromatic ring will interact with the Ba(II) by means of a charge transfer complex, which will stabilize the intermediate.

In the case of C-300, the amount of $Ba(OH)_2 \cdot H_2O$ is lower than in C-200. Therefore the number of active sites is not as high as in the C-200 catalyst (14, 17), and the yield diminishes.

TABLE 3. Yields obtained in Ph—CH=CH—CO—R (% molar)[a]

% (v/v)	ε (mixture)	Yield[b] Ph	Me	Et	iPr	*t*Bu
1,4-Dioxane–EtOH (96%)						
100/0	2.2	0	2	6	0	0
70/30	14	29	30	10	10	2
50/50	20	39	45	12	26	3
30/70	25	44	48	39	36	7
0/100	31	98	54	68	36	9
Cyclohexane–EtOH (96%)						
100/0	1.89	0	2	1	0	0
70/30	13.7	55	34	3	26	3
50/50	21.7	51	45	14	33	6
30/70	29.6	72	48	36	32	6
0/100	31	98	54	68	36	9

[a]Moles of PhCHO = moles of ketone = 0.0196; 0.1 g of catalyst; 20 mL of solvent (EtOH 96%). Reaction time = 10 min; T = 60°C.
[b]Error ±5%.

3. Influence of the dielectric constant of the solvents

To learn more about the influence of the solvent in the process, we chose two low dielectric constant solvents, cyclohexane (ϵ = 1.89) and 1,4-dioxane (ϵ = 2.2). The latter could chelate the Ba(II), due to the pair of oxygen atoms, and could lead to an homogeneous catalysis by means of ionic pairs, as in the Michael addition (16). The mixtures chosen were cyclohexane/EtOH (96%) and 1,4-dioxane/EtOH (96%), and the ϵ of these mixtures was calculated as follows:

$$[1] \quad \epsilon = \Sigma_i x_i \epsilon_i$$

where: x_i = molar fraction of component "i" in the mixture of solvents and ϵ_i = dielectric constant of component "i." The experimental results are shown in Table 3.

From the results in Table 3, we can deduce that the process needs a high value of dielectric constant. This could be explained if we postulate an homogeneous catalytic process by ionic pairs (R—CO—CH_2^-) (Ba(II), OH^-), but we must reject this idea because those species have not been observed in solution (using ir or uv–visible spectroscopy) for these reaction

Can. J. Chem. Downloaded from www.nrcresearchpress.com by 78.46.186.204 on 09/07/12
For personal use only.

TABLE 4. Main infrared bands (cm^{-1}) of adsorbed species from Me—CO—R (R = Me, Et, iPr, *t*Bu) on C-200

R	R—CO—Me	Adsorbed species
Me	1715	—
		1590 C=O
		1545 $(CO)_2$[a]
		1320 C=C
Et	1730	—
		1590 C=O
		1545 (CO_2)[a]
		1320 C=C
iPr	1730	—
		1590 C=O
		1545 (CO_2)[a]
		1320 C=C
*t*Bu	1725	—
		1590 C=O
		1545 (CO_2)[a]
		1320 C=C

[a]From adsorbed CO_2.

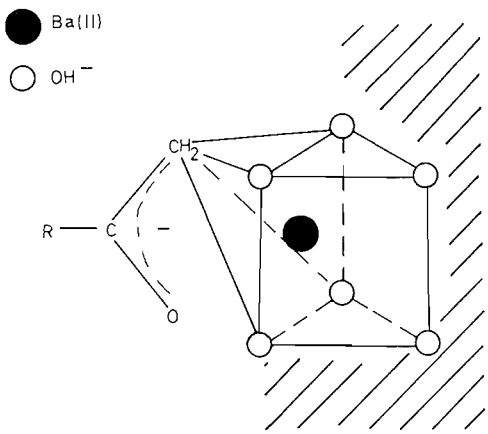

FIG. 3. Adsorbed carbanion from R—CO—CH_3 (R = Me, Et, iPr, and *t*Bu) on C-200 catalyst.

conditions (see Sect. 4). Another reason for rejecting the ionic pair process is that these pairs have not been trapped by the polymeric reagent (Ⓟ-CHO). Thus we can say that a high value of dielectric constant is necessary to relax the catalyst lattice, giving a more active OH^- on the catalytic surface.

On the other hand, the chelating power of 1,4-dioxane over the Ba(II) is not important in this process, because similar yields are obtained with the same amount of 1,4-dioxane and cyclohexane. Comparable results were obtained in the Michael addition (16).

The increase in the percentage of water (related to the percentage of commercial EtOH (96%) in the mixture) does not seem to affect the catalytic activity of C-200, because this basic solid may act in aqueous media (e.g., hydrolysis of esters (22)). This property makes this catalyst interesting from the synthetic point of view, because many basic catalysts are only active in anhydrous media.

4. Study of the reaction intermediates

The ir spectra of adsorbed species over the catalytic surface on the C-200 were carried out in open air (see Experimental).

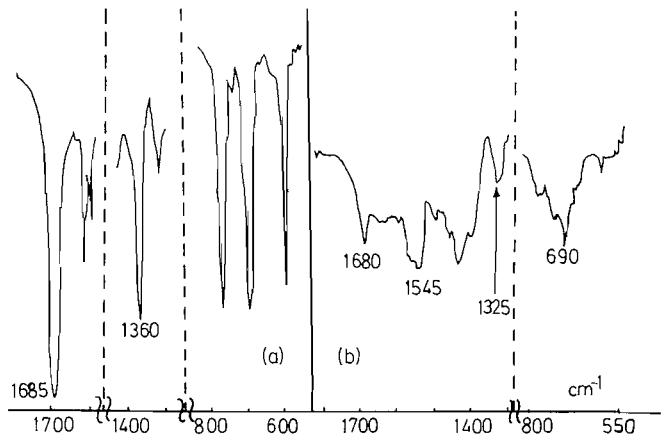

(a) acetophenone
(b) adsorbed species

FIG. 4. Infrared spectra: (*a*) acetophenone; (*b*) adsorbed species from acetophenone on C-200 catalyst.

Thus, an absorption at 1545 cm^{-1}, related to the adsorbed CO_2, was detected in all cases (20). The main bands of adsorbed species produced from CH_3—CO—R (R = Me, Et, Pr^i, and Bu^t) are shown in Table 4.

From the results in Table 4 we can deduce that the C=O bond is not present in the adsorbed species produced from ketones of type R—CO—CH_3 (there is no band at 1715–1730 cm^{-1}). The absorptions at 1590 and 1320 cm^{-1} can be related to the presence of C=O and C=C, according to the literature (23, 24), and to the ir spectra of sulfur ylids adsorbed on C-200 (25). Therefore we can postulate the generation of a carbanion (Fig. 3) from the ketone. Due to the low pK_a of the ketones, these species should be produced on the strong basic sites of the catalyst, titrated with BA as has been described in the Michael addition (26), and in the Corey–Chaykowsky reaction (25), because they are not trapped by the polymeric supported reagent Ⓟ-CHO. The ir bands of enone Ⓟ-CH=CH—CO—R were not detected in the resin after the reaction.

When the adsorption of acetophenone was carried out, a different ir spectrum (Fig. 4) was obtained.

The 1680 cm^{-1} band (quite close to the conjugated C=O of the acetophenone) was present in the spectrum. There is a clear band at 1325 cm^{-1}, besides the CO_2 adsorbed band (1545 cm^{-1}). The former can be related to the presence of a C=C bond in a $(O=C=CH_2)^-$ carbanion. On the other hand, there is no band at 1360 cm^{-1} related to CH_3—CO, and the aromatic zone is very altered (see Fig. 3). So we could postulate adsorbed species like **4** (Fig. 2), where the negative charge is practically unconjugated with C=O, and there is a π interaction between the aromatic ring and the $5d^0$ orbital of Ba(II).

The negative charge is thus greater in the "CH_2" of the carbanion from Ph—CO—CH_3 than in the case of R—CO—CH_3. Therefore the yield obtained with acetophenone will be greater than those with R—CO—CH_3, as has been observed (see Table 2). This could be explained by the different structure of the intermediate in each case: in the methyl alkyl ketones, a conjugated carbanion is produced (as has been proved by the ir spectrum); in the aromatic ketone, the intermediate could be pictured as **4**, because in this case the C=O band at 1680 cm^{-1} is present. The difference in behaviour could be explained by the geometry of the catalytic crystal, where the distance between C and O (2.5 Å) is smaller than 3.6 Å (in the lattice).

Can. J. Chem. Downloaded from www.nrcresearchpress.com by 78.46.186.204 on 09/07/12
For personal use only.

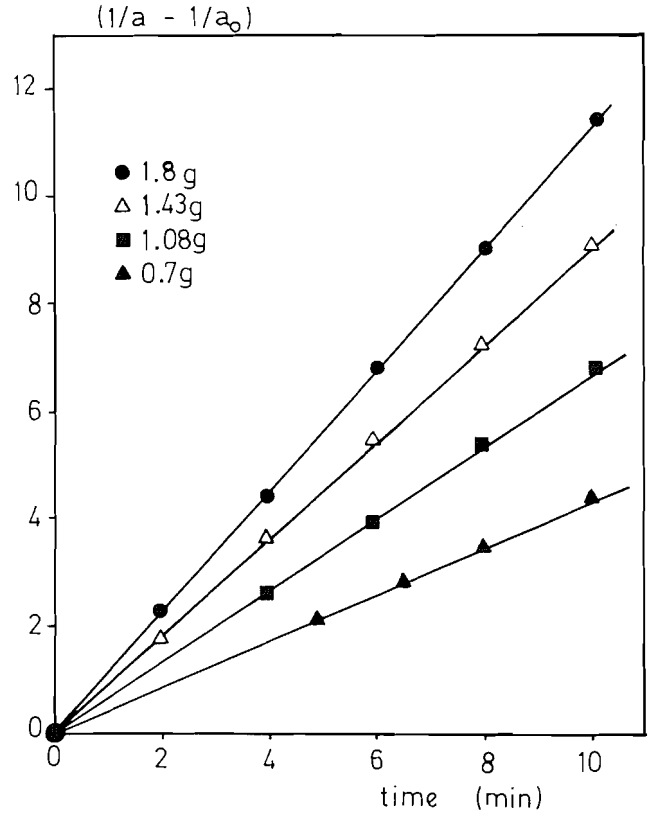

FIG. 5. Second-order kinetic plots: Ph—CH=CH—CO—Ph synthesis with C-200 catalyst.

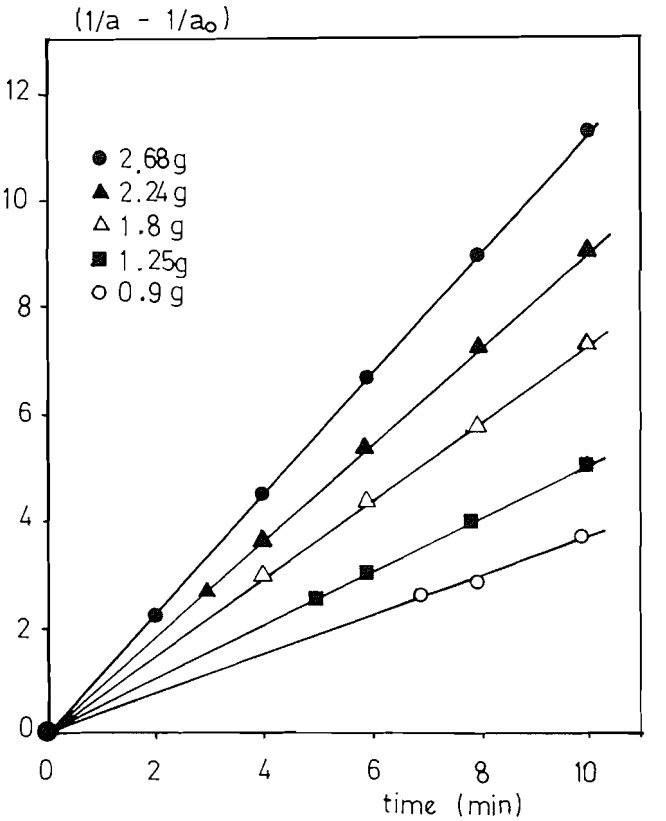

FIG. 6. Second-order kinetic plots: Ph—CH=CH—CO—Et synthesis with C-200 catalyst.

In the case of aliphatic ketones, the only possible adsorption state is that produced by the enolate, because the R group cannot interact with the Ba(II).

When the adsorption of benzaldehyde was carried out, no C=O band (1695 cm^{-1}) was observed, and there was a band at 1590 cm^{-1}. This band could be related to a $\pi^2_{C=O} \rightarrow 5d^0$ Ba(II) interaction, as has been shown in several substituted benzaldehydes (27).

On the other hand, ionic pairs such as ($R—CO—CH_2^-$, $Ba(OH)^+$) have not been detected by ir or uv–visible spectroscopy. This observation is consistent with the fact that these species were not trapped by the polymeric supported reagent Ⓟ-CHO.

Therefore we can say that the Claisen–Schmidt condensation catalyzed by C-200 is an interfacial solid–liquid process. The reaction takes place between an adsorbed carbanion (generated by reaction between the ketone and the basic site), and an adsorbed aldehyde molecule on a barium ion of the surface.

5. Kinetic runs

The kinetic runs of the Claisen–Schmidt reaction were carried out with Et—CO—CH_3 and Ph—CO—CH_3. These compounds were taken as models for the two kinds of adsorbed carbanions.

The kinetic runs were fitted to a second-order kinetic equation using [R—CO—Me] = [Ph—CHO] = 0.1 *M*. The experimental results obtained by several amounts of C-200 catalyst are shown in Figs. 5 and 6.

The van't Hoff plot gave a partial kinetic order in basicity (basicity = [(wt. cat. (g) · ((mequiv./g)/20 mL)] equal to one.

$$R = Ph;\ \ln r_0 = -2.041 + 1.02 \ln (\text{mequiv. base/L})$$

$$R = Et;\ \ln r_0 = -2.45 + 1.03 \ln (\text{mequiv. base/L})$$

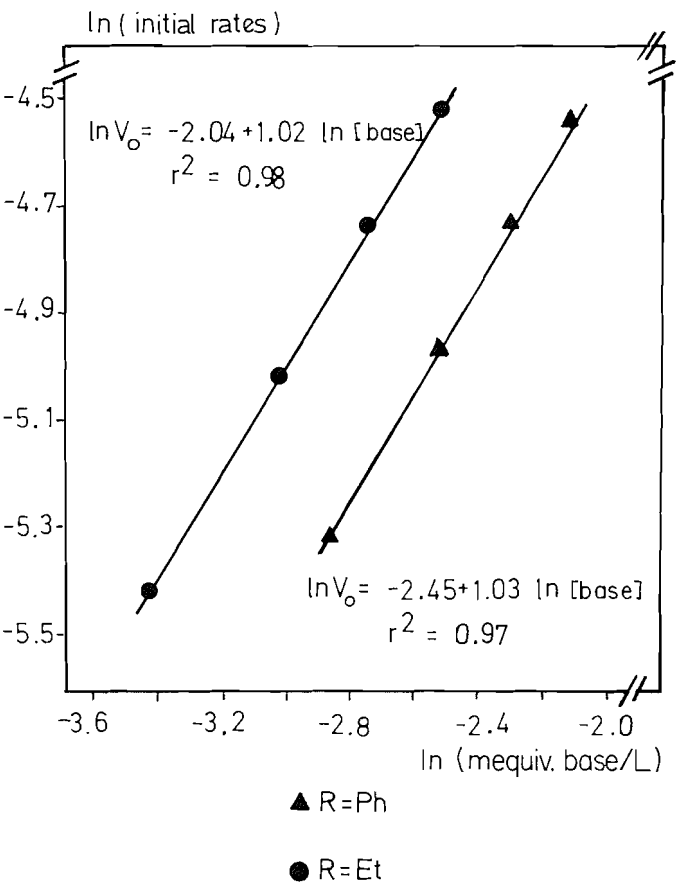

FIG. 7. van't Hoff plot for the catalyst kinetic order.

Can. J. Chem. Downloaded from www.nrcresearchpress.com by 78.46.186.204 on 09/07/12
For personal use only.

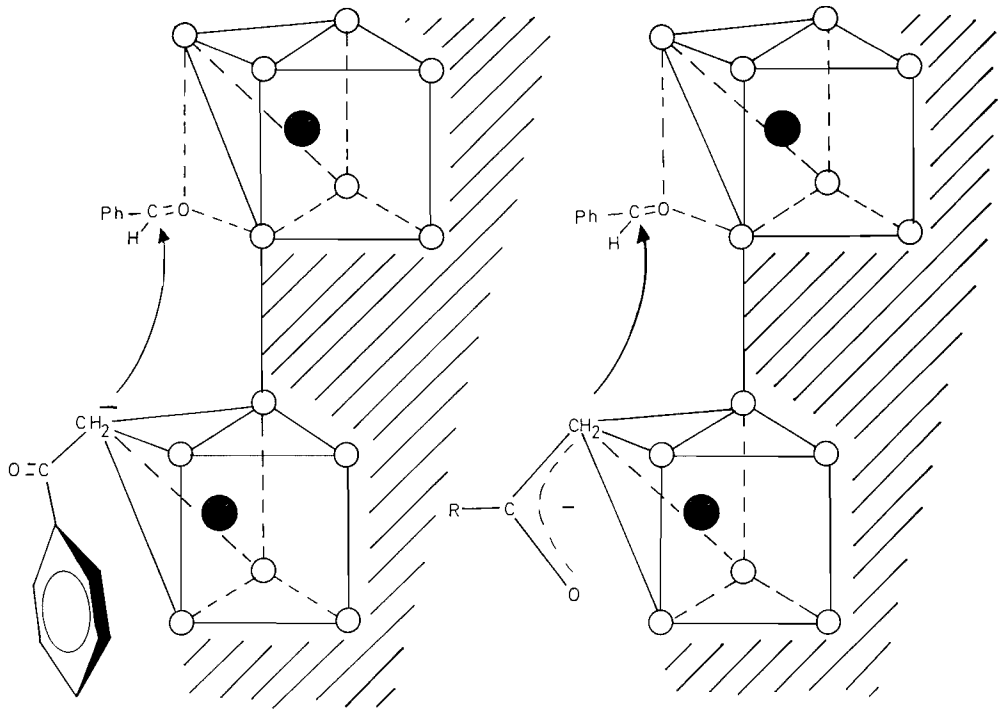

FIG. 8. Transition state for the Claisen–Schmidt condensation.

So we can say that the Claisen–Schmidt reaction catalyzed by C-200 has a rate governed by a rate law, eq. [2]

[2] $r = k$[R—CO—CH_3][Ph—CHO][equiv. base/L]

for both kinds of ketones, as in the homogeneous phase (28, 29).

This equation shows that only one active site of the catalyst acts in the rate controlling step. It agrees with a process in which the carbanion (produced from the reaction of ketone and the basic site) reacts with the adsorbed aldehyde, which is on a Ba(II) crystal. This structure can be pictured as in Fig. 8.

This interaction increases the electrophilicity of the carbon of the C=O bond, favouring the process.

If we represent the apparent kinetic constant of the second-order equation,

$$k_{ap} = k[\text{equiv. base/L}]$$

we obtain the straight line that appears in Fig. 9.

The slopes of these lines give us the true kinetic constant:

Ph—CO—CH_3 (50°C)

$$k = (13.8 \mp 0.2)\ \text{L}^2\ \text{equiv.}^{-2}\ \text{min}^{-1}$$

Et—CO—CH_3 (50°C)

$$k = (8.9 \mp 0.1)\ \text{L}^2\ \text{equiv.}^{-2}\ \text{min}^{-1}$$

The Arrhenius plot gives us the apparent activation energy:

Ph—CO—CH_3 $E_{ap} = (9 \mp 1)$ kcal/mol

$$PZ = (6.9 \mp 0.8)\ \text{L}^2\ \text{equiv.}^{-2}\ \text{min}^{-1}$$

Et—CO—CH_3 $E_{ap} = (12 \mp 1)$ kcal/mol

$$PZ = (8.3 \mp 0.8)\ \text{L}^2\ \text{equiv.}^{-2}\ \text{min}^{-1}$$

The higher value of k for Ph—CO—CH_3 than for Et—CO—CH_3, and the lower value of the apparent activation energy for Ph—CO—CH_3 than for Et—CO—CH_3 an be explained by the different nature of the adsorbed carbanion.

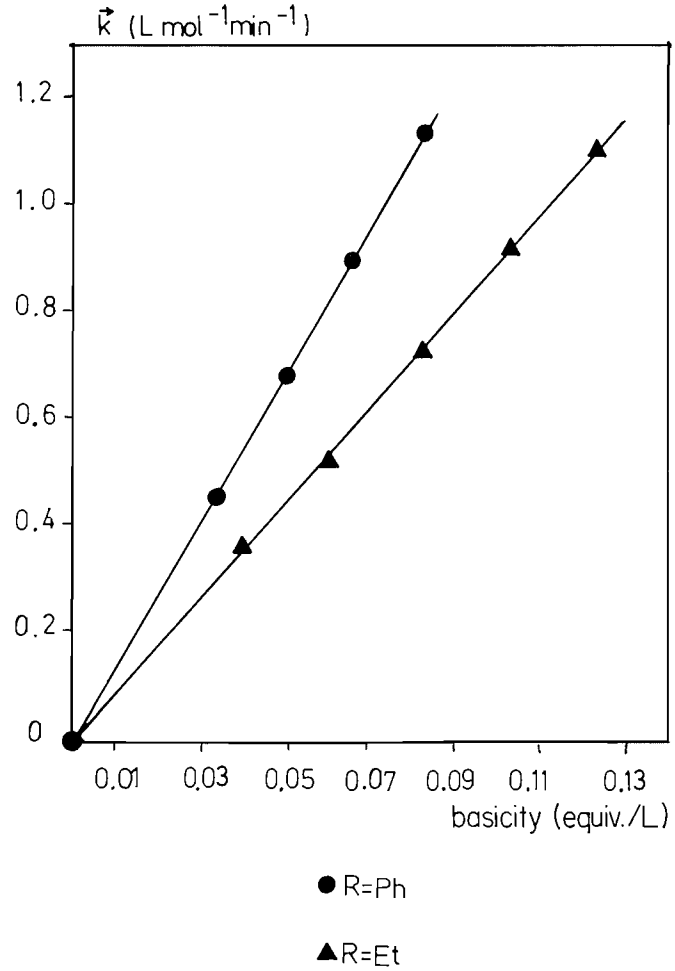

FIG. 9. Real kinetic constants in the synthesis of Ph—CH=CH—CO—R catalyzed by C-200.

Can. J. Chem. Downloaded from www.nrcresearchpress.com by 78.46.186.204 on 09/07/12
For personal use only.

In the case of Ph—CO—CH_3, we think there is a practically unconjugated carbanion (Ph—CO—CH_2^-), because the C=O band of the adsorbed species (1680 cm^{-1}) is very close to the C=O band of the original ketone (1685 cm^{-1}). In the case of the R—CO—CH_3 ketones, the carbanion is actually conjugated with the C=O bond (absorption at 1590 cm^{-1}, from a C=O bond). The more active carbanion of acetophenone reacts more quickly, and with lower activation energy, than the conjugated carbanion from Et—CO—CH_3. This assumption agrees with the experimental results.

Therefore, although the kinetic equation is the same for the two kinds of ketones, the mechanism is different, due to the nature of the adsorbed carbanions. This fact shows us the importance of the study of the adsorbed species in verifying the true mechanism of the interfacial solid–liquid reaction.

Acknowledgments

This work has been possible thanks to a grant-in-aid from the Comisión Asesora Científica y Técnica (C.A.I.C.Y.T.).

1. A. T. Nielsen and W. J. Houlikan. Org. React. **16**, 1 (1968).
2. L. Nondek and J. Malek. Org. React. **44**, 2384 (1979).
3. J. March. Advanced organic chemistry: Reactions, mechanism and structure. 3rd ed. McGraw–Hill, New York. 1985.
4. D. N. Dhar. The chemistry of chalcones and related compounds. John Wiley & Sons Inc., New York. 1981. pp. 213–232, and references cited therein.
5. J. D. Gettler and L. P. Hammet. J. Am. Chem. Soc. **65**, 1824 (1943).
6. D. S. Noyce and W. L. Reed. J. Am. Chem. Soc. **81**, 624 (1959).
7. L. Nondek and J. Malek. Collect. Czech. Chem. Commun. **45**, 1812 (1980).
8. M. Stiles, D. Wolf, and G. W. Hudson. J. Am. Chem. Soc. **81**, 628 (1959).
9. A. Garcia-Raso, J. V. Sinisterra, and J. M. Marinas. Pol. J. Chem. **56**, 1435 (1982).
10. A. Garcia-Raso, J. V. Sinisterra, and J. M. Marinas. React. Kinet. Catal. Lett. **18**, 33 (1981).
11. A. Garcia-Raso, J. A. Garcia-Raso, B. Campaner, R. Mestres, and J. V. Sinisterra. Synthesis, 1037 (1982).
12. J. V. Sinisterra, Z. Mouloungui, M. Delmas, and A. Gaset. Synthesis, 1097 (1985).
13. J. V. Sinisterra, A. Garcia-Raso, J. A. Cabello, and J. M. Marinas. Synthesis, 502 (1984).
14. J. V. Sinisterra, F. Garcia-Blanco, M. Iglesias, and J. M. Marinas. React. Kinet. Catal. Lett. **25**, 277 (1984).
15. J. M. Frechet and G. Pelle. Chem. Commun. 225 (1975).
16. M. Iglesias. Ph.D. thesis, University of Córdoba, December, 1985.
17. J. Barrios, J. M. Marinas, and J. V. Sinisterra. Bull. Soc. Chim. Belg. **95**, 107 (1986).
18. H. D. Lutz, W. Eckers, G. Schneider, and H. Haguseler. Spectrochim. Acta, Part A, **37**, 561 (1981).
19. H. Barnigausen. Z. Anorg. Allg. Chem. **342**, 233 (1966).
20. M. Michaud. C.R. Acad. Sci. Paris, **262**, 1143 (1966).
21. H. Mahonar and S. Ramasesnan. Current Sci. **32**, 248 (1963); Chem. Abstr. **69**, 8212a (1963).
22. A. Garcia-Raso, J. V. Sinisterra, and J. M. Marinas. Rev. Roum. Chim. **27**, 1047 (1982).
23. T. Bottin-Strzalko, J. Corset, F. Fromet, M. J. Pouet, J. Seyden-Penne, and M. P. Simonin. J. Org. Chem. **45**, 1270 (1980).
24. J. Seyden-Penne, G. Etemad-Moghadam, T. Bottin-Strzalko, and M. P. Simonin. Phosphorous Sulfur, **18**, 179 (1983).
25. J. V. Sinisterra, M. E. Borredon, Z. Mouloungui, M. Delmas, and A. Gaset. React. Kinet. Catal. Lett. **29**, 41 (1985).
26. J. V. Sinisterra, F. Garcia-Blanco, M. Iglesias, and J. M. Marinas. React. Kinet. Catal. Lett. **27**, 263 (1985).
27. A. R. Alcantara, J. M. Marinas, and J. V. Sinisterra. React. Kinet. Catal. Lett. In press.
28. E. Coombs and D. P. Evans. J. Chem. Soc. 1295 (1940).
29. D. S. Noyce, W. A. Pryor, and A. Bottini. J. Am. Chem. Soc. **77**, 1402 (1955).

Can. J. Chem. Downloaded from www.nrcresearchpress.com by 78.46.186.204 on 09/07/12
For personal use only.

The rates and products of addition of 4-chlorobenzenesulfenyl chloride to a series of trisubstituted alkenes

GEORGE H. SCHMID,[1] DENNIS G. GARRATT, AND COLEEN L. DEAN
Department of Chemistry, University of Toronto, Toronto, Ont., Canada M5S 1A1

Received August 22, 1986

GEORGE H. SCHMID, DENNIS G. GARRATT, and COLEEN L. DEAN. Can. J. Chem. **65**, 1172 (1987).

The rates and products of addition of 4-chlorobenzenesulfenyl chloride to *E*- and *Z*-3-methyl-2-pentene, *E*- and *Z*-3,4-dimethyl-2-pentene, *E*- and *Z*-3,4,4-trimethyl-2-pentene, and 2,4,4-trimethyl-2-pentene were studied to determine if the mechanism involved a tertiary β arylthio carbocation. It was found that the rates of addition are not as fast as one would predict based on the polar effects of the substituents on the rate of addition to mono- and disubstituted alkenes. The products are formed by *anti*-stereospecific addition as in the case of addition to 1,2-disubstituted alkenes. As a result it is concluded that the reaction occurs by means of the usual mechanism involving a bridged thiiranium ion.

GEORGE H. SCHMID, DENNIS G. GARRATT et COLEEN L. DEAN. Can. J. Chem. **65**, 1172 (1987).

Dans le but de déterminer si le mécanisme de la réaction implique un carbocation β-arylthio tertiaire, on a déterminé les vitesses de réaction ainsi que la nature des produits obtenus lors de l'addition du chlorure de chloro-4 benzènesulfènyle sur les méthyl-3 pentènes-2 (*E* ou *Z*), sur les diméthyl-3,4 pentènes-2 (*E* ou *Z*), sur les triméthyl-3,4,4 pentènes-2 (*E* ou *Z*) et sur le triméthyl-2,4,4 pentène. On a trouvé que les vitesses d'addition ne sont pas aussi rapides que celles que l'on pourrait prévoir en se basant sur les effets polaires des substituants sur les vitesses d'addition sur des alcènes mono- ou disubstitués. Les produits se forment par une addition stéréospécifique *anti*, comme dans les cas des additions sur des alcènes disubstitués en positions 1,2. Sur la base de ces résultats, on en conclut que la réaction se produit par le biais du mécanisme usuel impliquant un ion thiiranium ponté.

[Traduit par la revue]

The systematic study of the addition of arenesulfenyl chlorides to alkenes carried out in this laboratory has established many of the mechanistic features of this reaction (1). It is possible to conclude that in this addition reaction the rate-determining transition state is bridged and there is little charge on either carbon or sulfur (2). Furthermore, in the product-determining step, attack by chloride ion occurs at the least hindered carbon of the thiiranium ion (3). These results are in contrast to the reactions of stable thiiranium ions, which undergo reactions with nucleophiles at the most hindered carbon atom (4). A possible explanation (5) for this difference in product regiochemistry is that the addition reaction, carried out in relatively nonpolar solvents, occurs by means of a contact ion pair. The reaction of stable thiiranium ions, carried out in highly polar solvents, occurs by means of a dissociated ion.

The importance of ion pairs in the mechanism of many reactions in solution is well documented (6). Electrophilic additions are no exception. A number of people have proposed that the mechanism of an electrophilic addition reaction could involve ion-pair intermediates (7). Subsequent work by Rolston and Yates (8) and Garnier and Dubois (9) established the importance of ion pairs in the bromination of alkenes. In 1972, we provided evidence that the mechanism of the electrophilic addition of arenesulfenyl chlorides to alkenes and the mechanism of neighboring sulfur participation in the reaction of β-chloroalkyl aryl sulfides both involve the same series of thiiranium ions (10). The mechanism that we proposed is shown in Scheme 1 (ref. 1, p. 838).

The upper sequence of reactions in the scheme involving ion pairs **3** and **4** is the general solvolysis scheme proposed by Winstein (for a summary and complete references see ref. 13) and applied to the reactions of β-chloroalkyl aryl sulfides. Evidence for ion pairs **3** and **4** and ion **5** is provided by the fact that a special salt effect, common ion rate depression and radioactive chloride ion exchange, is observed in the solvolysis of 2-chlorocyclohexyl 4-chlorophenyl sulfide (10). The lower sequence of reactions is similar to that proposed by Poutsma and Kartch (7*c*). The increase in rearranged, solvent incorporated, and perchlorate products caused by added $LiClO_4$ in the addition of arenesulfenyl chlorides to alkenes has been cited as evidence for ion pairs **1** and **2** (12). Not included in the scheme are an episulfurane (**1***a*) and a charge transfer complex, because there is no evidence for either of these species. Ion pairs **1** and **3** are contact ion pairs and **2** and **4** are solvent-separated ion pairs that differ only in the location of the counterion. Our contribution to the mechanism was to link these two paths either directly between ion pairs **1**–**3** and **2**–**4** or by means of the dissociated ion **5**. We propose in the scheme that electrophilic addition of arenesulfenyl chlorides to alkenes, isomerization of the Markownikoff–*anti*-Markownikoff adducts, and solvolysis of β-chloroalkyl aryl sulfides all occur by means of a common mechanism (14).

There is an additional difference between the reactions of stable thiiranium ions and the ion formed in the addition reaction that is not explained by our original proposal. This difference can be illustrated by the following example. The addition of 4-chlorobenzenesulfenyl chloride to *Z*-1-phenylpropene in methylene chloride forms products by *anti*-stereospecific but nonregiospecific addition (15). Such a reaction involves a thiiranium ion as an intermediate. This same thiiranium ion, prepared by the addition of 4-chlorophenyl(bis-4-chlorophenyl)sulfonium hexachloroantimonate to *Z*-1-phenylpropene in methylene chloride at −70°C according to the method of Modena and co-workers (16), reacts with chloride ion to form products whose stereochemistry varies with time (17). Thus at short reaction times, the product is formed via a thiiranium ion, while at longer reaction times the thiiranium ion forms an open β arylthio carbocation, which is the precursor to the reaction products. Therefore this thiiranium ion, formed under stable conditions, has a pathway to products not available to the thiiranium ion formed in the addition of 4-chlorobenzenesulfenyl chloride to *Z*-1-phenylpropene. We have added this new path to form an open ion **6** in the scheme. The possibility of

[1]Author to whom correspondence may be addressed.

Can. J. Chem. Downloaded from www.nrcresearchpress.com by 72.64.146.136 on 09/07/12
For personal use only.

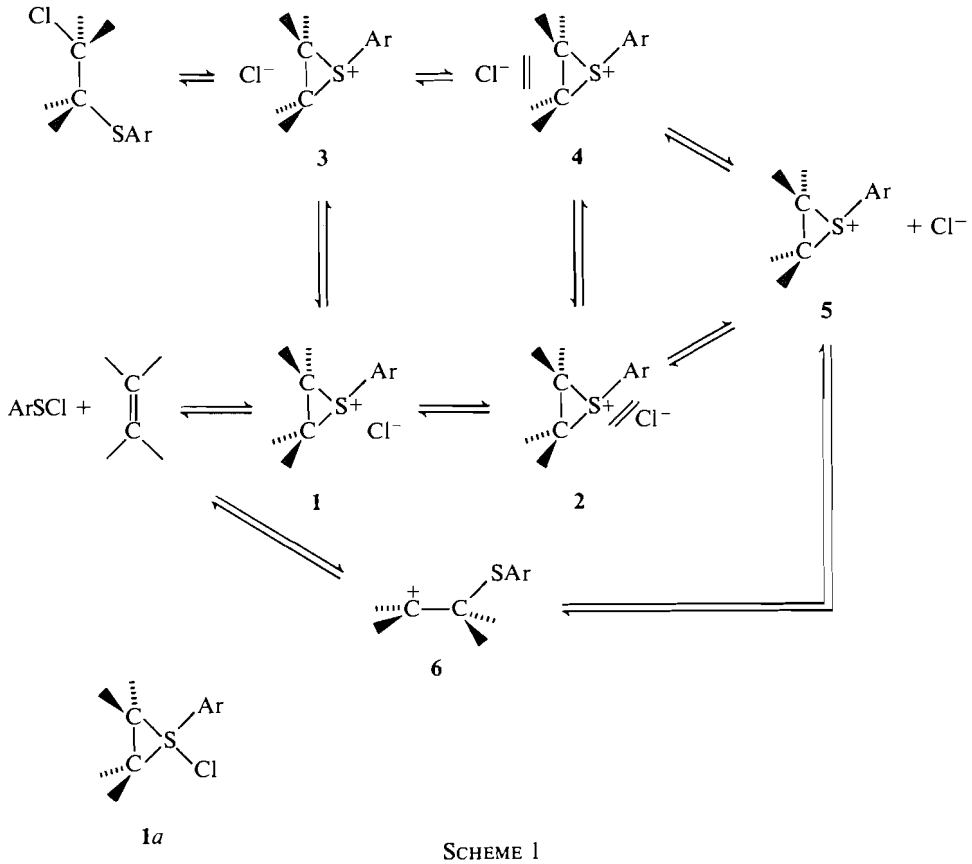

SCHEME 1

the intervention of open ions in the reactions of stable thiiranium has not previously been seriously considered.

These results suggest that in certain systems the energy difference may not be very great between an open β arylthio carbocation and a thiiranium ion. In the case of addition to *Z*-1-phenylpropene, the path leading to a thiiranium ion is still of lower energy than the one leading to an open ion. However, nonstereospecific addition of 2,4-dinitrobenzenesulfenyl chloride to *Z*-1-(4′-methoxyphenyl)propene is known (18). Thus an open ion is lower in energy in this system. It seems from all available data that addition of arenesulfenyl chlorides to styrene is close to the borderline between a bridged mechanism and one involving an open ion. This suggests that an alkene that would form an open β arylthio carbocation, which is slightly more stable than the analogous benzylic ion, might add arenesulfenyl chlorides in a nonstereospecific manner. Likely candidates include trisubstituted alkenes that can form a tertiary open β arylthio carbocation. Thus the open ion **7** may be of comparable energy to the thiiranium ion **8** particularly if the groups R^1, R^2, and R^3 are bulky, causing an increase in the intramolecular interactions in the transition state for the addition reaction.[2]

Surprisingly few studies of electrophilic additions to trisubstituted alkenes have been carried out. We have extended our structure–reactivity studies of arenesulfenyl chloride additions

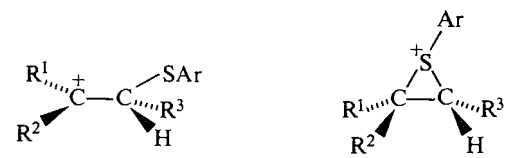

7 **8**

to trisubstituted alkenes to investigate whether it is possible that the mechanism of this reaction involves an open ion. For this purpose we have measured the rates and products of addition of 4-chlorobenzenesulfenyl chloride (**9**) to a series of *E*- and *Z*-trisubstituted alkenes. The data and the mechanistic conclusions reached from these data are reported in this paper.

Results

The rates of addition of **9** to the trisubstituted alkenes **10–16** were measured in 1,1,2,2-tetrachloroethane at 25°C by means of the stopped-flow technique using a Durrum–Gibson stopped-flow spectrophotometer.

TABLE 1. Second-order rate constants for the addition of 4-chlorobenzenesulfenyl chloride to trisubstituted alkenes in 1,1,2,2-tetrachloroethane at 25°C

Alkene	$k \times 10^3$, M^{-1} s^{-1}
E-3-methyl-2-pentene (**10**)	2.28 ± 0.09
Z-3-methyl-2-pentene (**11**)	4.84 ± 0.06
E-3,4-dimethyl-2-pentene (**12**)	1.06 ± 0.04
Z-3,4-dimethyl-2-pentene (**13**)	5.96 ± 0.07
E-3,4,4-trimethyl-2-pentene (**14**)	0.108 ± 0.005
Z-3,4,4-trimethyl-2-pentene (**15**)	0.523 ± 0.004
2,4,4-Trimethyl-2-pentene (**16**)	1.46 ± 0.05

[2]As has been the custom in previous publications in this series, the counterion is included in the structure only if its presence is important to the discussion at hand. For an example in which the counterion is specifically included see ref. 19. *The absence of the counterion in the structures in these publications does not imply, and should not be taken as any indication of, the presence or absence of ion pairs in the reaction mechanism.*

Can. J. Chem. Downloaded from www.nrcresearchpress.com by 72.64.146.136 on 09/07/12
For personal use only.

TABLE 2. Proton magnetic resonance parameters of 4-chlorobenzenesulfenyl chloride adducts[a]

Alkene	Group assignments 1	2	3	4	5	Chemical shift assignment[b] ($CDCl_3$), δ 1	2	3	4	5
10 M	CH_3CH_2CCl	CH_3CH_2CCl	CH_3CCl	CH_3CS	CHS	1.00t	1.8–1.9m	1.62s	1.43d	3.38q
aM	CH_3CH_2CS	CH_3CH_2S	CH_3CS	CH_3CCl	CHCl	0.96t	1.8–1.9m	1.50s	1.55d	3.89q
11 M	CH_3CH_2CCl	CH_3CH_2CCl	CH_3CCl	CH_3CS	CHS	1.03t	1.9–2.0m	1.58s	1.38d	3.48q
aM	CH_3CH_2CS	CH_3CH_2S	CH_3CS	CH_3CCl	CHCl	0.99t	1.9–2.0m	1.49s	1.52d	4.00q
12 M	$(CH_3)_2CHCl$	$(CH_3)_2CHCl$	CH_3CCl	CH_3CS	CHS	1.00d 1.03d	2.36sp	1.60s	1.50d	3.46q
aM	$(CH_3)_2CHS$	$(CH_3)_2CHS$	CH_3CS	CH_3CCl	CHCl	0.96d 0.90d	2.50sp	1.41s	1.70d	4.38q
13 M	$(CH_3)_2CHCl$	$(CH_3)_2CHCl$	CH_3CCl	CH_3CS	CHS	1.00d 1.10d	2.50sp	1.56s	1.42d	3.44q
aM	$(CH_3)_2CHS$	$(CH_3)_2CHS$	CH_3CS	CH_3CCl	CHCl	0.96d 1.06d	2.83sp	1.32s	1.72d	4.22q
14 M	$(CH_3)_3C$	CH_3CCl	CH_3CS	CHS	—	1.23s	1.70s	1.38d	3.63q	—
aM	$(CH_3)_3C$	CH_3CS	CH_3CCl	CHCl	—	1.12s	1.65s	1.55d	3.78q	—
15 M	$(CH_3)_3C$	CH_3CCl	CH_3CS	CHS	—	1.21s	1.72s	1.40d	3.66q	—
aM	$(CH_3)_3C$	CH_3CS	CH_3CCl	CHCl	—	1.10s	1.62s	1.59d	3.84q	—
16 M	$(CH_3)_2C$	$(CH_3)_3C$	CHS	—	—	1.90bs	1.03s	3.25s	—	—
aM	$(CH_3)_2C$	$(CH_3)_3C$	CHCl	—	—	1.81bs	1.10s	3.55s	—	—

[a]25°C.
[b]Abbreviations: s singlet, d doublet, t triplet, q quartet, sp septet, m multiplet, bs broad singlet.

The rate of disappearance of **9** was followed by measuring the decrease in its absorption at 392.5 nm. The addition was found

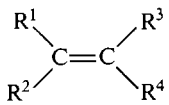

	R^1	R^2	R^3	R^4
10	C_2H_5	CH_3	H	CH_3
11	C_2H_5	CH_3	CH_3	H
12	i-Pr	CH_3	H	CH_3
13	i-Pr	CH_3	CH_3	H
14	*t*-Bu	CH_3	H	CH_3
15	*t*-Bu	CH_3	CH_3	H
16	*t*-Bu	H	CH_3	CH_3

to follow a normal second-order rate law, first order in both alkene and sulfenyl chloride to 80% completion of the reaction. The rate data are presented in Table 1.

The product compositions were determined by ^{1}Hmr spectroscopy. Additions to the *E*- and *Z*-isomeric alkenes formed the four possible regio- and stereo-isomers. Isomerization of the Markownikoff to the *anti*-Markownikoff isomer served to identify the peaks associated with each regioisomer. Their identification could be made based on the fact that the chemical shifts of protons α or β to chlorine are further downfield than the corresponding protons α or β to sulfur (20). The ^{1}Hmr data are given in Table 2. The product compositions, determined by integration of nonoverlapping ^{1}Hmr peaks, are given in Table 3.

Discussion

It is known that the first step in the addition of arenesulfenyl chlorides to alkenes is the rate-determining step (ref. 1, p. 836; ref. 21) and the reaction of the thiiranium ion intermediate is product determining. The data in Tables 1 and 3 allow us to compare the effect of substituents on the reactivity of alkenes **10–16** with the effect of the same substituents on the reactivity of mono- and disubstituted alkenes. First consider their effect on the rate-determining step.

The rate of addition of **9** to the alkenes **10–16** is not as fast as one would predict based on the polar effects of the substituents on the rate of addition to mono- and disubstituted alkenes. This rate-retarding effect can best be seen by comparing the effect of an alkyl group R on the reactivity of the trisubstituted alkenes to that of the same group R in the corresponding mono- and disubstituted alkenes. The reactivity ratio $I = k_2(R)/k_2(CH_3)$ has been proposed (22) and can be applied to the following series of compounds.

Series 1

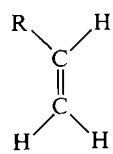

Series 2

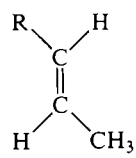

Series 3

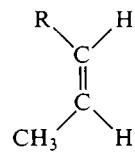

Series 4

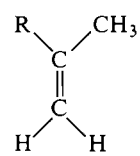

Series 5

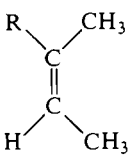

Series 6

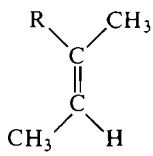

The specific compounds, their rates of addition, and the reactivity ratios are given in Table 4.

A consistent pattern emerges in the reactivity ratio for Series 1–4. Substituting a methyl group by an ethyl group causes a modest increase in the reactivity ratio while substituting an isopropyl group causes a decrease. Replacing the methyl group by a tertiary butyl group causes a further decrease in the ratio. In contrast, replacing one methyl group by any of the three substituents causes a decrease in the ratio in Series 5 and 6. From this we can conclude that the rate enhancement expected by increasing the number of substituents

Can. J. Chem. Downloaded from www.nrcresearchpress.com by 72.64.146.136 on 09/07/12
For personal use only.

TABLE 3. Product composition for the addition of 4-chlorobenzenesulfenyl chloride to trisubstituted alkenes in 1,1,2,2-tetrachloroethane at 25°C

Alkene	Initially observed product composition[a]		Thermodynamically controlled products	
	M	aM	M	aM
E-Et(CH_3)C=$CHCH_3$ (**10**)	82	18	100	—
Z-Et(CH_3)C=$CHCH_3$ (**11**)	86	14	100	—
E-iPr(CH_3)C=$CHCH_3$ (**12**)	95	5	100	—
Z-iPr(CH_3)C=$CHCH_3$ (**13**)	100	—	100	—
E-*t*Bu(CH_3)C=$CHCH_3$ (**14**)	60	40	[b]	[b]
Z-*t*Bu(CH_3)C=$CHCH_3$ (**15**)	100	—	[b]	[b]
*t*BuCH=$C(CH_3)_2$ (**16**)	78	22	[b]	[b]

[a]These percentages are not the kinetically controlled product composition. See text.
[b]Extensive decomposition.

TABLE 4. Reactivity ratios for the addition of 4-chlorobenzenesulfenyl chloride to a series of mono-, di-, and tri-substituted alkenes

Alkene	$k \times 10^3$, M^{-1} s^{-1}	*I*	Alkene	$k \times 10^3$, M^{-1} s^{-1}	*I*
Series 1			Series 2		
CH_3CH=CH_2	0.205[a]	1.0	*E*-CH_3CH=$CHCH_3$	0.434[a]	1.0
EtCH=CH_2	0.248[a]	1.21	*E*-EtCH=$CHCH_3$	0.568[a]	1.31
iPrCH=CH_2	0.140[a]	0.68	*E*-iPrCH=$CHCH_3$	0.325[a]	0.75
*t*BuCH=CH_2	0.095[a]	0.46	*E*-*t*BuCH=$CHCH_3$	0.162[a]	0.37
Series 3			Series 4		
Z-CH_3CH=$CHCH_3$	1.34[a]	1.0	$(CH_3)_2C$=CH_2	0.551[a]	1.0
Z-EtCH=$CHCH_3$	2.69[a]	2.0	Et(CH_3)C=CH_2	0.611[a]	1.11
Z-iPrCH=$CHCH_3$	2.62[a]	1.96	*i*Pr(CH_3)C=CH_2	0.420[a]	0.76
Z-*t*BuCH=$CHCH_3$	1.03[a]	0.77	*t*Bu(CH_3)C=CH_2	0.147[a]	0.27
Series 5			Series 6		
$(CH_3)_2C$=$CHCH_3$	7.70[a]	1.0	$(CH_3)_2C$=$CHCH_3$	7.70[c]	1.0
E-Et(CH_3)C=$CHCH_3$ (**10**)	2.28[b]	0.30	*Z*-Et(CH_3)C=$CHCH_3$ (**11**)	4.84[b]	0.63
E-iPr(CH_3)C=$CHCH_3$ (**12**)	1.06[b]	0.14	*Z*-iPr(CH_3)C=$CHCH_3$ (**13**)	5.96[b]	0.77
E-*t*Bu(CH_3)C=$CHCH_3$ (**14**)	0.108[b]	0.014	*Z*-*t*Bu(CH_3)C=$CHCH_3$ (**15**)	0.523[b]	0.067

[a]Value taken from ref. 3.
[b]This work.
[c]Value taken from ref. 11.

on the double bond is substantially lower than that expected from polar substituent effects estimated in less-substituted alkenes. Thus the effect on the rate of increasing the number of alkyl substituents on the double bond is noncumulative. Consequently the accumulation of alkyl substituents on the double bond results in an increasingly important contribution from steric effects on the reaction rate.

Similar substituent effects are found in the addition of bromine to trisubstituted alkenes (22). In bromination, substituting a methyl group by an ethyl group causes an increase in the reactivity ratio for all the series while, as before, substituting an isopropyl group causes a decrease. Such behavior is consistent with previous observations (1), from which it has been concluded that the rate-determining transition state for the addition of arenesulfenyl chlorides is more congested than that for bromination.

It is clear from the data in Table 2 that the addition of **9** to the trisubstituted alkenes **10**–**16** forms products in a stereospecific manner. The question is whether these adducts are formed by *syn* or *anti* addition. The large majority of products of the reaction of arenesulfenyl chlorides and alkenes are formed by *anti* stereospecific addition (1). Very few cases of nonstereospecific addition have been reported (18), while products of *syn* addition have never been observed. Therefore the only reasonable conclusion is that the addition of **9** to **10**–**16** is *anti* stereospecific. Further support for this conclusion is provided by the isomerization of the adducts. Both Markownikoff and *anti*-Markownikoff regioisomers are formed in the addition reaction to five of the seven alkenes. Such isomerization between Markownikoff and *anti*-Markownikoff regioisomers is known to occur stereospecifically by means of a thiiranium ion (1). Thus both addition and isomerization involve a thiiranium ion.

There is a difference in the relative proportions of Markownikoff to *anti*-Markownikoff regioisomers in Series 5 and 6 when compared to Series 1–4. The initially observed product composition is richer in the Markownikoff isomer than in the kinetically controlled product compositions found in the addition to mono- and disubstituted alkenes (3). But in the reactions studied here, the Markownikoff to *anti*-Markownikoff

Can. J. Chem. Downloaded from www.nrcresearchpress.com by 72.64.146.136 on 09/07/12
For personal use only.

TABLE 5. Analytical data for sulfenyl chloride adducts

Alkene	Analyses (%)					
	C		H		S	
	Calcd.	Found	Calcd.	Found	Calcd.	Found
E-3-methyl-2-pentene (**10**)	54.76	54.83	6.12	6.12	12.18	11.99
Z-3-methyl-2-pentene (**11**)	54.76	54.89	6.12	6.15	12.18	12.24
E-3,4-dimethyl-2-pentene (**12**)	56.32	56.09	6.54	6.36	11.56	11.73
Z-3,4-dimethyl-2-pentene (**13**)	56.32	56.30	6.54	6.59	11.56	11.68
E-3,4,4-trimethyl-2-pentene (**14**)	57.73	57.56	6.92	6.81	11.01	11.09
Z-3,4,4-trimethyl-2-pentene (**15**)	57.73	57.68	6.92	6.90	11.01	10.97
2,4,4-Trimethyl-2-pentene (**16**)	57.73	57.78	6.92	7.01	11.01	11.10

rearrangement occurs very rapidly. The rearrangement is complete within 15 minutes of adding **9** to the alkenes. Consequently the initially observed product composition is not the kinetically controlled product composition. Unfortunately, this means that we cannot determine which carbon atom of the thiiranium ion is attacked preferentially by the chloride ion in the product-determining step.

All of the data presented here are consistent with the addition of **9** to the trisubstituted alkenes occurring by means of the normal mechanism involving a thiiranium ion. Therefore we conclude that the path leading to a thiiranium ion is lower in energy than the one leading to an open ion in the addition of arenesulfenyl chlorides to trisubstituted alkenes in nonpolar solvents.

Experimental

Proton nmr spectra were obtained on a Varian T-60, HA-100, or HX-400 spectrometer. All spectra are referenced to tetramethylsilane as an internal standard.

Microanalyses were carried out by A. B. Gygli Microanalysis Laboratory, Toronto.

The alkenes were obtained commercially and their purity was verified by glc.

4-Chlorobenzenesulfenyl chloride was prepared as previously described (23). 1,1,2,2-Tetrachloroethane was purified as previously described (23).

Kinetics, product composition, and analytical samples were carried out or prepared as previously described (23). The elemental analyses for the adducts are given in Table 5.

Acknowledgements

Continued financial support from the Natural Sciences and Engineering Research Council of Canada is gratefully acknowledged.

1. G. H. SCHMID and D. G. GARRATT. *In* The chemistry of double bonded functional groups. *Edited by* S. Patai. Wiley, New York. 1977. Chap. 8.
2. G. H. SCHMID and D. G. GARRATT. Tetrahedron Lett. 5299 (1983).
3. G. H. SCHMID, D. G. GARRATT, and C. L. DEAN. Can. J. Chem. **54**, 1253 (1976).
4. (*a*) A. S. GYBIN, M. Z. KRIMER, W. A. SMIT, B. C. BOGDONOV, and E. V. VOROB'EVA. Izv. Akad. Nauk SSSR, Ser. Khim. 510 (1979); (*b*) J. B. BOLSTER and R. M. KELLOG. J. Chem. Soc. Chem. Commun. 630 (1978); (*c*) G. CAPOZZI, O. LUCCHINI, V. LUCCHINI, and G. MODENA. Tetrahedron Lett. 2603 (1975).
5. B. GIESE and C. DAUB. Chem. Ber. **110**, 1101 (1977).
6. J. E. GORDON. The organic chemistry of electrolyte solutions. Wiley, New York. 1975.
7. (*a*) P. B. D. DE LA MARE, N. V. KLASSEN, and R. KOENIGSBERGER. J. Chem. Soc. 5285 (1961); (*b*) M. C. CABALEIRO and M. D. JOHNSON. J. Chem. Soc. B, 565 (1967); (*c*) M. L. POUTSMA and J. L. KARTCH. J. Am. Chem. Soc. **89**, 6595 (1965).
8. J. H. ROLSTON and K. YATES. J. Am. Chem. Soc. **91**, 1477 (1969).
9. F. GARNIER and J. E. DUBOIS. Bull. Soc. Chim. Fr. 3797 (1968).
10. P. H. FITZGERALD. Ph.D. thesis, University of Toronto, 1973; Diss. Abstr. **34**, 4855 (1973).
11. G. H. SCHMID and D. G. GARRATT. Can. J. Chem. **51**, 2463 (1973).
12. V. R. KARTASHOV, I. V. BODRIIIKOV, E. V. SCOROBOGATOVA, and N. S. ZEFIROV. Zh. Org. Khim. **12**, 297 (1976).
13. P. D. BARTLETT. J. Am. Chem. Soc. **94**, 2161 (1972).
14. G. H. SCHMID. Top. Sulfur Chem. **3**, 103 (1977).
15. G. H. SCHMID and D. G. GARRATT. Can. J. Chem. **52**, 1807 (1974).
16. G. CAPOZZI, O. DE LUCCHI, V. LUCCHINI, and G. MODENA. Tetrahedron Lett. 2603 (1975).
17. G. H. SCHMID and D. I. MACDONALD. Tetrahedron Lett. 157 (1984).
18. G. H. SCHMID and V. J. NOWLAN. J. Org. Chem. **37**, 3086 (1972).
19. G. H. SCHMID and P. H. FITZGERALD. J. Am. Chem. Soc. **93**, 2547 (1971).
20. (*a*) J. R. CAVANAUGH and B. P. BAILEY. J. Chem. Phys. **34**, 1093 (1961); (*b*) B. P. BAILEY and J. N. SCHOOLERY. J. Am. Chem. Soc. **77**, 3977 (1955).
21. M. KANSKA and A. FRY. J. Am. Chem. Soc. **105**, 7666 (1983).
22. D. GROSJEAN, G. MOUVIER, and J. E. DUBOIS. J. Org. Chem. **41**, 3869 (1976).
23. G. H. SCHMID, V. M. CSIZMADIA, V. J. NOWLAN, and D. G. GARRATT. Can. J. Chem. **50**, 245 (1972).

Can. J. Chem. Downloaded from www.nrcresearchpress.com by 72.64.146.136 on 09/07/12
For personal use only.

Reactions of diazoalkanes with isocyanates. Synthesis of imidazolidine-2,4-diones, oxindoles, and oxazolidinones

JANET B. FULTON AND JOHN WARKENTIN[1]

Department of Chemistry, McMaster University, Hamilton, Ont., Canada L8S 4M1

Received September 15, 1986

JANET B. FULTON and JOHN WARKENTIN. Can. J. Chem. **65**, 1177 (1987).

Thermolysis of a 5,5-dialkyl-Δ^3-1,3,4-oxadiazolin-2-one in nitrobenzene containing an aryl isocyanate at 150°C affords a 1,3-diaryl-5,5-dialkyl imidazolidine-2,4-dione, an *N*-arylcarbamoyl-3,3-dialkyloxindole, and a 3-aryl-2-arylimino-5,5-dialkyl-1,3-oxazolidin-4-one. Those products arise from attack of a diazoalkane, generated *in situ* from the oxadiazolinone by thermal cycloreversion, on the isocyanate function. Two imidazolidine diones, three oxazolidinones, and 14 oxindoles were prepared.

JANET B. FULTON et JOHN WARKENTIN. Can. J. Chem. **65**, 1177 (1987).

La thermolyse d'une dialkyl-5,5 Δ^3-oxadiazoline-1,3,4 one-2, à 150°C et dans du nitrobenzène contenant un isocyanate d'aryle, conduit à une diaryl-1,3 dialkyl-5,5 imidazolidinedione-2,4, un *N*-arylcarbamoyl dialkyl-3,3 oxindole et une aryl-3 arylimino-2 dialkyl-5,5 oxazolidine-1,3 one-4. Ces produits proviennent d'une attaque d'un diazoalkane, généré *in situ* par une cycloréversion thermique de l'oxadiazolinone, sur la fonction isocyanate. Deux imidazolidinediones, trois oxazolidinones et 14 oxindoles ont été préparés.

[Traduit par la revue]

Can. J. Chem. Downloaded from www.nrcresearchpress.com by 72.64.146.136 on 09/07/12
For personal use only.

Introduction

Reactions of diazoalkanes with heterocumulenes have been known since Staudinger *et al.* first prepared a Δ^3-1,3,4-oxadiazoline by that approach (1), eq. [1]. Lipp and Köster (2)

[1] $Ph_2C{=}C{=}O + R^1R^2C{=}\overset{+}{N}{=}\overset{-}{N} \rightarrow Ph_2C$ (1,3,4-oxadiazoline ring: N=N, O, R^1, R^2)

obtained cyclobutanone (isolated as the semicarbazone derivative) from the 2:1 reaction of diazomethane with ketene (eq. [2])

[2] $2CH_2{=}\overset{+}{N}{=}\overset{-}{N} + CH_2{=}C{=}O \rightarrow$ (cyclobutanone, O) $+ 2N_2$

and Roberts and co-workers (3) demonstrated that cyclopropanone is a likely intermediate in that reaction. Hammond and Turro (4) isolated cyclopropanones by treating diazoalkanes with ketenes at low temperatures, and they postulated a dipolar intermediate as the precursor of a cyclopropanone, eq. [3].

[3] $RR'C{=}\overset{+}{N}{=}\overset{-}{N} + CH_2{=}C{=}O \rightarrow$

$CH_2{=}\overset{O^-}{\overset{|}{C}}{-}C(RR')\overset{+}{N}{\equiv}N \rightarrow$ (cyclopropanone, O, R, R^1) $+ N_2$

von Pechmann (5) and, later, Sheehan and Izzo (6), treated phenyl isocyanate with diazomethane to obtain a β-lactam, eq. [4]. Benzoyl isocyanate gave a 1:1 adduct, eq. [5]. Those

[4] $CH_2{=}\overset{+}{N}{=}\overset{-}{N} + PhN{=}C{=}O \rightarrow$

$[Ph{-}N{=}\overset{O^-}{\overset{|}{C}}{-}CH_2\overset{+}{N}_2] \xrightarrow{CH_2N_2}$ (β-lactam, Ph, N, O)

[5] $PhC(=O){-}N{=}C{=}O + CH_2{=}\overset{+}{N}{=}\overset{-}{N} \rightarrow$

$\left[Ph{-}C(O^-){=}N{-}C(CH_2\overset{+}{N}_2){=}O\right] \rightarrow$ (oxazolinone, Ph, O, N, O)

results were rationalized in terms of the dipolar intermediates written in the equations. A dipolar intermediate was postulated also in the process by which 3-oxo-1,2-diazetidinium hydroxide inner salts are formed from reaction of *N*-isocyanatoimines with diazoalkanes (7), eq. [6].

[6] $Ph_2C{=}N{-}N{=}C{=}O + Me_2CN_2 \xrightarrow{-N_2}$

$\left[Ph_2C{=}N{-}N{=}\overset{-O}{\overset{|}{C}}{-}\overset{+}{C}Me_2\right] \rightarrow$ ($Ph_2C{=}\overset{+}{N}{-}\overset{-}{N}$, Me, Me, O)

There are no publications, to the best of our knowledge, of reactions of dialkyl diazomethanes with aryl isocyanates. We now report the results of a study of such reactions.

Methods, results, and discussion

The thermal cycloreversion of a Δ^3-1,3,4-oxadiazolin-2-one (**1**) (eq. [7]) was used to generate a diazoalkane *in situ* (8) in the presence of an isocyanate. That fragmentation pathway has been shown to predominate over the competing fragmentation

[7] (oxadiazolinone, O, N, O, N, R^1, R^2) $\xrightarrow{a}$ $R^1R^2C{=}\overset{+}{N}{=}\overset{-}{N} + CO_2$

$\xrightarrow{b}$ $R^1R^2CO + N_2 + CO$

to R^1R^2CO, N_2, and CO in polar solvents (8). In neat aryl isocyanates the ratio of the fragmentation pathways (eq. [7]) was about a/b = 2. Although oxadiazolinones (8) are not very efficient as sources of diazoalkanes because of the competition between two fragmentation pathways, they are convenient alternatives to diazoalkanes prepared by oxidation of ketone hydrazones, partly because such hydrazones are generally contaminated with the corresponding azines unless special procedures are used (9) and also because diazoalkanes decompose readily (10), making their storage difficult.[2] Oxadiazolinones, on the other hand, are stable for many months in a freezer. Moreover, the alternative fragmentation (path b, eq. [7]) of

[1]Author to whom correspondence may be addressed.

[2]2-Diazopropane, for example, has a half-life of 3 h in solution at 0°C (10).

TABLE 1. 5,5-Dialkyl-Δ^3-1,3,4-oxadiazoline-2-ones,

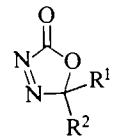

Compound	R^1	R^2	Infrared (cm^{-1})[a]	^1H nuclear magnetic resonance[b]
1*a*	CH_3	CH_3	1540, 1835	1.85 (s)
1*b*	CH_3	CH_2CH_3	1538, 1837	0.81 (t, 3H), 1.65 (s, 3H), 2.10 (q, 2H)
1*c*	CH_3	$(CH_2)_2CH_3$	1545, 1835	1.05 (m, 5H), 1.63 (s, 3H), 2.03 (m, 2H)
1*d*	CH_3	$CH(CH_3)_2$	1542, 1836	0.92 (d, 2H), 1.05 (d, 3H), 1.58 (s, 3H), 2.26 (m, 1H)
1*e*	CH_3	$CH_2CH(CH_3)_2$	1535, 1840	0.90 (m, 7H), 1.64 (s, 3H), 2.07 (m, 2H)
1*f*	CH_3	$C(CH_3)_3$	1540, 1838	1.03 (s, 9H), 1.60 (s, 3H)
1*g*		$(CH_2)_5$	1540, 1830	1.32–2.45 (m)
1*h*	CH_3	$CH_2C_6H_5$	1539, 1830	1.63 (s, 3H), 3.28 (s, 2H), 7.17 (m, 5H)
1*i*	$CH(CH_3)_2$	$CH(CH_3)_2$	1545, 1840	0.94 (d, 6H), 1.06 (d, 6H), 2.78 (m, 2H)

[a]CCl_4 solvent. The band near 1540 cm^{-1} is attributed tentatively to N=N stretching while that near 1835 cm^{-1} is attributed to C=O stretching.
[b]$CDCl_3$ solvent. The spectra were obtained at either 60 or 90 MHz.

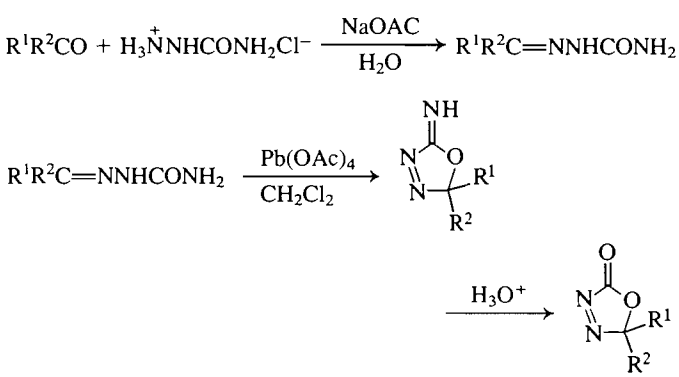

SCHEME 1. Synthesis of oxadiazolinones

oxadiazolinones, although undesirable because of inefficient production of diazoalkanes, leads to products that are innocuous and, in general, easily separated from desired final products. Finally, oxadiazolinones are relatively easy to prepare by the sequence of reactions in Scheme 1.

The oxadiazolinones prepared in connection with this study, and their diagnostic ir and ^1H nmr spectra, are listed in Table 1. Yields of recrystallized semicarbazones were generally near 70%. Their oxidation and hydrolysis (Scheme 1) afforded crude oxadiazolinones, in 55–65% yields, and pure oxadiazolinones, either by sublimination or bulb-to-bulb distillation at 40°C and 10^{-2} Torr (1 Torr = 133.3 Pa), in ca. 40% yields.

Thermolyses of oxadiazolinones were carried out in nitrobenzene solution of isocyanates at 150°C. Nitrobenzene was chosen for its high boiling point, its inertness toward isocyanates, and its polarity.

Characterization of reaction products

The major product from thermolysis of **1***a* in nitrobenzene containing phenylisocyanate (eq. [8]) was identified as 1-phenylcarbamoyl-3,3-dimethyloxindole (**2***a*) on the basis of microanalytical, spectroscopic, and chemical evidence. That evidence, applicable to other oxindoles of the family **2**, is summarized in Table 2 and is discussed below.

Both microanalyses and mass spectrometry indicated a 2:1 adduct of aryl isocyanate and diazoalkane, less N_2. The infrared spectra of compounds **2** showed a broad, intense band between 1700 and 1730 cm^{-1} that was partly resolved into two bands, suggesting two carbonyl groups. *N*-Methyl oxindoles exhibit a single intense ir absorption in the range 1700–1710 cm^{-1} (11). A weak to medium intensity band near 3240 cm^{-1} in the ir spectra of compounds **2** can be assigned to NH stretching.

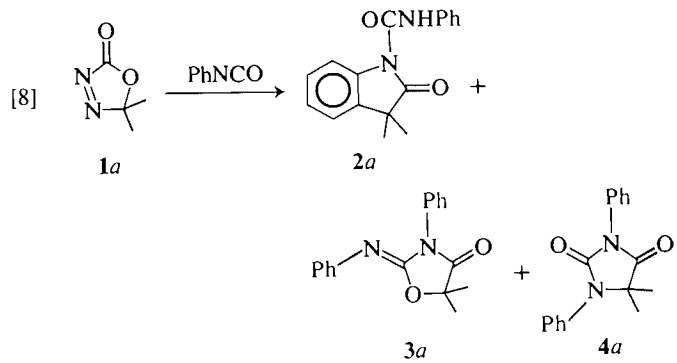

The ^1H nmr spectra of compounds **2** contained an interesting feature in the low field region. One aryl proton was significantly deshielded (δ ca. 8.2) compared to the rest. In spectra of products from *p*-substituted phenyl isocyanates, that low field signal was a doublet with ca. 8 Hz splitting. That unique 1-proton signal was assigned to H-7, on the basis of the spectra of the model compounds below (12).

The ^{13}C nmr spectra of the *N*-arylcarbamoyl oxindoles **2**

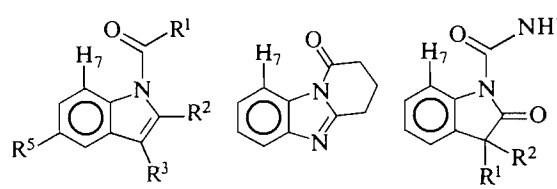

H-7, δ 8.4 H-7, δ 8.2 **2**(H-7, δ = 8.2)

(Table 3) were consistent with the assigned structure. In particular, the signal at δ 184.0 ± 1.0 could be assigned to the carbonyl carbon of the 5-membered ring and the signal at δ 149.5 ± 0.2 could be assigned to the second carbonyl carbon, modelled with *N*,*N*′-diphenylurea (δ 152.6). Signals from the

Can. J. Chem. Downloaded from www.nrcresearchpress.com by 72.64.146.136 on 09/07/12
For personal use only.

TABLE 2. 1-Arylcarbamoyl-3,3-dialkyl oxindoles,

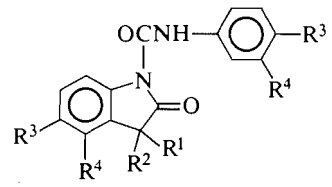

Compound	R^1	R^2	R^3	R^4	Yield (%)[a]	Melting point, °C	^{1}H nuclear magnetic resonance[b]
2*a*	CH_3	CH_3	H	H	36	74–76	1.38 (s, 6H), 7.46 (m, 8H), 8.38 (m, 1H), 10.79 (s, br, 1H)
2*b*	CH_3	CH_2CH_3	H	H	49	Oil	0.67 (t, 3H), 1.47 (s, 3H), 1.87 (m, 2H), 7.40 (m, 8H), 8.37 (m, 1H), 10.85 (s, br, 1H)
2*c*	CH_3	$CH_2CH_2CH_3$	H	H	[c]	Oil	0.90 (m, 5H), 1.46 (s, 3H), 1.90 (m, 2H), 7.43 (m, 8H), 8.46 (m, 1H), 10.93 (s, br, 1H)
2*d*	CH_3	$CH(CH_3)_2$	H	H	[c]	Oil	0.86 (d, 6H), 0.96 (d, 6H), 1.50 (s, 3H), 2.18 (m, 1H), 7.47 (m, 8H), 8.47 (m, 1H), 10.97 (s, br, 1H)
2*e*	CH_3	$CH_2CH(CH_3)_2$	H	H	24	Oil	0.70 (d of d, 6H), 0.97 (m, 1H), 1.43 (s, 3H), 1.94 (m, 2H), 7.35 (m, 8H), 8.34 (m, 1H), 10.77 (s, br, 1H)
2*f*	CH_3	$C(CH_3)_3$	H	H	46	Oil	1.00 (s, 9H), 1.43 (s, 3H), 7.40 (m, 8H), 8.44 (m, 1H), 10.94 (s, br, 1H)
2*g*	$(CH_2)_5$		H	H	39	101–103	1.82 (s, br, 10H), 7.36 (m, 8H), 8.34 (m, 1H), 10.78 (s, br, 1H)
2*h*	CH_3	$CH_2C_6H_5$	H	H	[c]	Oil	1.53 (s, 3H), 3.12 (s, 2H), 7.15 (m, 13H), 8.13 (m, 1H), 10.61 (s, br, 1H)
2*i*	$CH(CH_2)_2$	$CH(CH_3)_2$	H	H	[c]	Oil	0.87 (d, 6H), 0.96 (d, 6H), 2.43 (m, 2H), 7.47 (m, 8H), 8.28 (m, 1H), 10.99 (s, br, 1H)
2*j*	CH_3	CH_3	CH_3	H	36	125.5–126.5	1.42 (s, 6H), 2.33 (s, 6H), 7.15 (m, 6H), 8.10 (d, 1H), 10.56 (s, br, 1H)
2*k*	CH_3	CH_3	OCH_3	H	48	118.5–120	1.47 (s, 6H), 3.77 (s, 3H), 3.81 (s, 3H), 7.22 (m, 6H), 8.23 (d, 1H), 10.57 (s, br, 1H)
2*l*	CH_3	CH_3	Cl	H	33	170.5–171.5	1.44 (s, 6H), 7.42 (m, 6H), 8.28 (d, 1H), 10.72 (s, br, 1H)
2*m*	CH_3	CH_3	H	CH_3	[d]	77–80	1.54 (s, 6H), 2.38 (s, 3H), 2.42 (s, 3H), 7.17 (m, 6H), 8.25 (m, 1H), 10.79 (s, br, 1H)
2*n*	(Isomer of **2***m*)				[d]	Oil	1.44 (s, 6H), 2.36 (s, 3H), 2.40 (s, 3H), 7.22 (m, 6H), 8.16 (s, br, 1H), 10.68 (s, br, 1H)

[a]Yields of isolated product. Satisfactory analyses (C, H, N) were obtained for **2***a*, **2***e*, **2***g*, **2***i*, **2***j*, and **2***l*.
[b]$CDCl_3$ with internal TMS.
[c]Not determined.
[d]The isomers **2***m* and **2***n* were obtained in 1:1 ratio. The yield, estimated before separation of the isomers from each other and from minor impurities, was 44%.

ring atoms were assigned on the basis of empirical substituent shielding parameters (13). Agreement between calculated and observed chemical shifts was poor in cases where large *ortho* interactions (13) might be expected. Ultraviolet spectra of representative 1-arylcarbamoyl-3,3-dialkyloxindoles (250 nm, inflection, log ε 4.58; 244 nm, log ε = 4.45 for **2***a*) were similar to those of oxindole (11), 249 nm (log ε 3.97), 277 nm (inflection, log ε 3.26), and *N*-methyloxindole (14).

Finally, basic hydrolysis of **2***a* afforded the known 3,3-dimethyloxindole. Moreover, 3,3-dimethyloxindole reacted with phenyl isocyanate in nitrobenzene at 150°C to form **2***a*.

The minor products from the reaction (eq. [8]) were identified as 5,5-dimethyl-3-phenyl-2-phenylimino-4-oxazolidinone (**3***a*) and 5,5-dimethyl-1,3-diphenyl imidazolidine-2,4-dione (**4***a*) as described below.

Mass spectrometry showed that both minor products were isomers of **1***a*. Both gave a fragment ion (m/z = 161) suggestive of the loss of phenyl isocyanate from the parent ion. One of them also gave an intense signal (m/z = 194) attributable to *N*,*N*′-diphenyl carbodimide, and that isomer was therefore assigned structure **3***a*. The infrared spectrum of isomer **3***a* included a broad intense band between 1685 and 1710 cm^{-1}, which was partially resolved into two bands with maxima at 1690 and 1705 cm^{-1}. In addition, there was a sharp band of medium intensity at 1745 cm^{-1}. The broad, partially resolved band was attributed to stretching of both the carbonyl group and the exocyclic imine group. The model compounds below were used to support the assignment of structures **3** (14).

The infrared spectrum of **4***a* had bands at 1775 and 1710 cm^{-1},

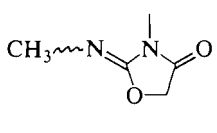

ν_{CO} = 1700 cm^{-1}

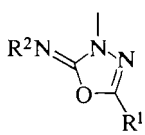

R^1	R^2	$\nu_{C=N}$(cm^{-1})
Ph	CH_3	1710
Ph	Ph	1600–1680
H	Ph	1675

Can. J. Chem. Downloaded from www.nrcresearchpress.com by 72.64.146.136 on 09/07/12
For personal use only.

Can. J. Chem. Downloaded from www.nrcresearchpress.com by 72.64.146.136 on 09/07/12
For personal use only.

TABLE 3. ^{13}C spectra of compounds **2**

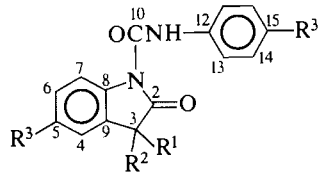

Oxindole, **2**	C-2	C-3	C-4	C-5	C-6	C-7	C-8	C-9	C-10	C-12	C-13	C-14	C-15	R^1	R^2	R^3
$R^1 = R^2 = CH_3$, $R^3 = H$	184.3	45.4	124.4	125.0	128.4	116.7	137.3	134.3	149.7	138.9	120.5	129.1	122.0	25.1	25.1	
$R^1 = R^2 = R^3 = CH_3$	184.3	45.4	122.6	134.8	128.8	116.4	134.6	134.3	149.7	136.6	120.5	129.6	133.9	25.1	25.1	20.8, 21.1
$R^1 = R^2 = CH_3$, $R^3 = OCH_3$	183.9	45.6	108.7	157.4	112.5	117.4	130.4	135.8	149.7	132.2	122.8	114.2	156.5	25.0	25.0	55.3, 55.5
$R^1 = R^2 = CH_3$, $R^3 = Cl$	183.7	45.6	122.5	130.7	129.2	117.9	136.1	135.7	149.3	137.2	121.7	129.7	128.5	25.0	25.0	
$R^1 = CH_3$, $R^2 = CH_2CH_3$, $R^3 = H$	183.9	50.2	124.4	125.0	128.4	116.6	137.4	132.5	149.5	139.9	120.5	129.1	122.2	24.0	32.4, 8.8	
$R^1 = CH_3$, $R^2 = n$Pr, $R^3 = H$	184.0	49.9	124.4	125.0	128.3	116.6	137.3	132.8	149.6	139.7	120.5	129.1	122.1	24.6	41.6, 17.9, 14.1	
$R^1 = CH_3$, $R^2 = i$Pr, $R^3 = H$	184.1	52.7	124.5	124.7	128.3	116.4	137.4	132.0	149.6	140.0	120.5	129.2	123.0	22.1	36.8, 17.4, 17.2	
$R^1 = CH_3$, $R^2 = i$Bu, $R^3 = H$	184.3	49.3	124.4	124.5	128.3	116.7	137.4	132.7	149.6	139.5	120.4	129.1	122.5	27.1	47.4, 25.6, 24.0, 23.0	
$R^1 = CH_3$, $R^2 = t$Bu, $R^3 = H$	183.6	54.7	124.4	124.5	128.2	116.1	137.4	132.2	149.5	140.1	120.5	129.1	124.0	29.7	37.3, 25.3, 18.1	
$R^1 = R^2 = i$Pr, $R^3 = H$	183.1	60.1	124.3	124.5	128.1	116.1	137.4	130.2	149.4	140.9	120.5	129.0	123.0		33.1, 17.0, 17.4	
$R^1R^2 = (CH_2)_5$, $R^3 = H$	183.3	48.0	124.2	124.5	128.0	116.5	137.4	134.1	149.6	139.0	120.4	129.0	122.9	33.8, 26.0, 20.8		
$R^1 = CH_3$, $R^2 = CH_2C_6H_5$, $R^3 = H$	183.2	51.2	124.4	124.6	128.5	116.5	137.3	131.7	149.3	139.6	120.5	129.1	122.9	23.6	45.3, 135.1, 129.7, 128.5, 127.1	

TABLE 4. ^{13}C chemical shifts of compounds **3** and **4**

Compound		^{13}C signals								
		C-2	C-4	C-5	C-6	C-7	C-8	C-1	C-1′	Other aromatic
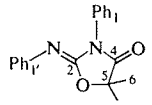	(**3***a*)	147.0	174.3	83.5	24.0	23.7		132.2	144.6	129.1, 128.7 128.5, 126.8 123.8
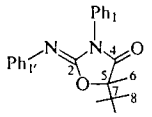	(**3***b*)	147.7	173.7	90.0	24.7	38.0	18.5	132.2	144.8	129.1, 128.6 128.1, 126.9 123.6, 123.5
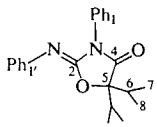	(**3***c*)	148.7	173.0	93.4	31.9	16.5	16.2	132.2	145.0	129.2, 128.7 127.0, 126.7 124.5, 123.5
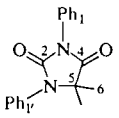	(**4***a*)	153.5	175.3	63.5	24.2			137.4	132.0	129.9, 129.6 129.1, 128.2 126.2
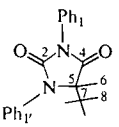	(**4***b*)	155.1	174.3	72.1	25.8	39.5	19.7	137.3	132.0	129.3, 129.0 128.8, 128.2 128.0, 126.4

in good agreement with the infrared spectrum of 1,3-diphenyl imidazolidine-2,4-dione (1780 and 1720 cm^{-1}) (15). Those bands are attributed to the symmetric and antisymmetric coupled stretching vibrations of the carbonyl groups of **4***a*.

^1H nuclear magnetic resonance spectroscopy supported the structural assignments in the following way. Isomer **3***a*, with phenyl groups in quite different environments, gave aryl proton signals spread over a width of 45 Hz at 60 MHz, whereas **4***a* gave more collimated aryl proton signals. The high field signals, on the other hand, were not useful for differentiating between **3***a* and **4***a*.

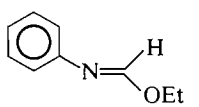

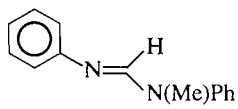

The ^{13}C nmr spectra, although not definitive, were consistent with the assignments of the isomeric minor products, **3***a* and **4***a*. Thus, the imino-carbon signal of **3***a* at δ 147.0 is similar to that of imino ethers (δ 154.2) and of aryl amidines (δ 149.8), the compounds that are illustrated below (16). Moreover, the ^{13}C-signal of **4***a* (δ 153.5), assigned to the ureide carbon, is very close to those of 1,3-diphenyl imidazolidine-2,4-dione (δ 153.1) and *N,N′*-diphenylurea (δ 152.6). Thus, all the evidence, taken together, leaves no room for doubt about the assignments of structures **3***a* and **4***a*. The fact that only one ^{13}C signal was observed near δ 147 in the spectrum of **3***a* indicates that only one of the two possible configurations about the imino group was represented. Although it was not possible to make a choice on the basis of the spectroscopic evidence, the *Z*-configuration (eq. [8]) is the more likely from considerations of steric interactions.

The structures of other members of the families **3** and **4** were assigned on the basis of analogy (Table 4).

Mechanism

A concerted 1,3-cycloaddition between a diazoalkane and phenyl isocyanate, to form cycloadduct **5** (Scheme 2), is a potential first step. An alternative first step is nucleophilic addition of the diazoalkane to the isocyanate carbonyl carbon to form dipolar intermediate **6**. Theory suggests that the reactivity and regioselectivity of dipolarophile–dipole reactions are controlled by the interaction between the dipole's HOMO and the dipolarophile's LOMO (17). Isocyanates have a low-lying in-plane LUMO and a vacant π MO only slightly above it in energy (18). The latter interacts well with an aryl substituent, affording stabilization for a dipolar intermediate. That feature, together with the fact that out-of-plane approach to the isocyanate carbon cannot be accompanied by the $[\pi^2s + \pi^2a]$ interaction (18), has led to the prediction that only nonconcerted cycloadditions to aryl isocyanates are to be expected. We assume, therefore, that the initial species formed from attack of a diazoalkane on phenyl isocyanate is **6**. The subsequent steps must account for the apparent difference between diazomethane (which leads to β-lactams, see Introduction) and disubstituted diazomethanes, which afford **2**, **3**, and **4** but not β-lactams. We propose that the intermediate **6**, which may be in equilibrium with **5** at high temperature, loses N_2 to form **7** and (or) **8** and **9**, in steps reminiscent of the Favorskii reaction. Ring closure to **8** or **9** would be most likely to occur directly from **6** in the case of the diazomethane-derived intermediate ($R^1 = R^2 = H$), but via **7** in cases where R^1 and R^2 are alkyl groups. From thermochemical considerations, the α-lactam intermediate **9** is more likely than the imino oxirane **8**. We postulate that the point of diversion, between the chemistry of diazomethane and its dialkyl derivatives, comes at the α-lactam stage. In the case where $R^1 = R^2 = H$, **8** and **9** are relatively long lived and **9** (the major isomer) reacts with diazomethane in a ring-expansion sense (eq. [9]) reminiscent of the ring expansion of cyclic

Can. J. Chem. Downloaded from www.nrcresearchpress.com by 72.64.146.136 on 09/07/12
For personal use only.

Can. J. Chem. Downloaded from www.nrcresearchpress.com by 72.64.146.136 on 09/07/12
For personal use only.

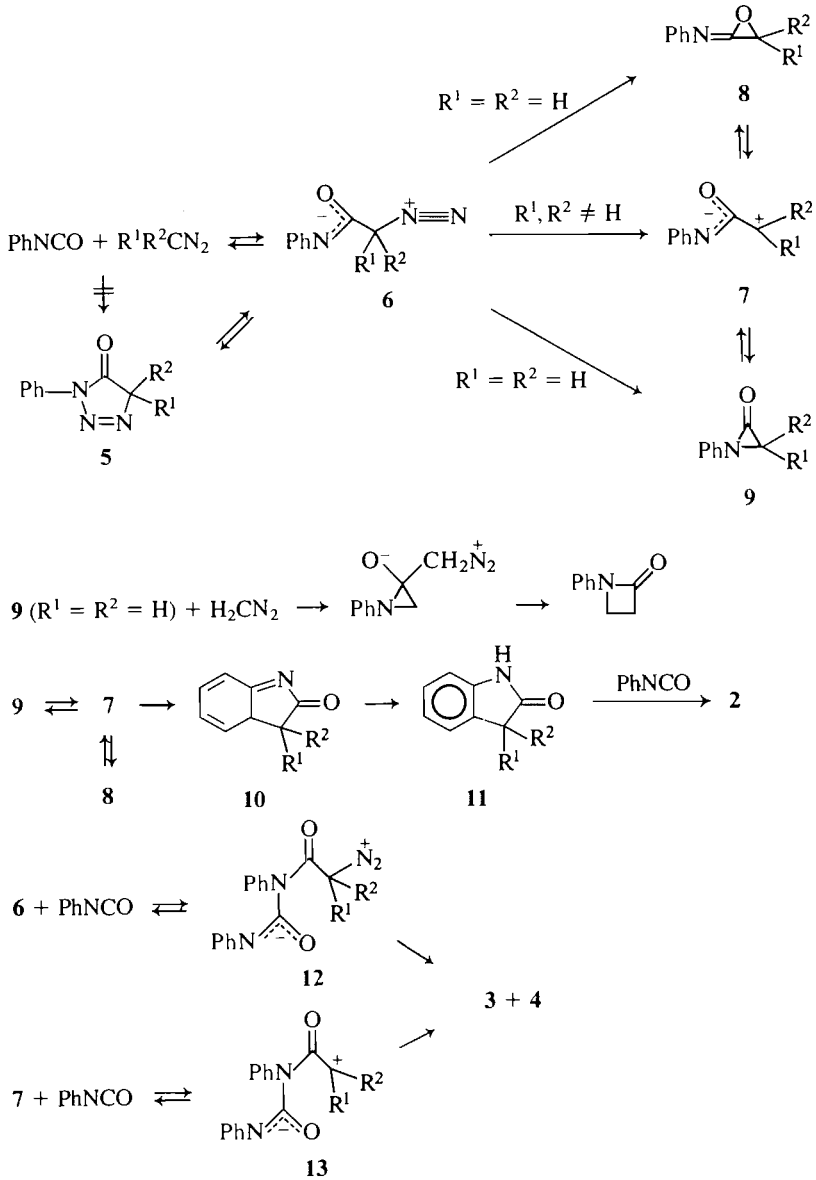

SCHEME 2

[9] $PhN{-}CH_2 + CH_2N_2 \rightarrow PhN{-}CH_2 \rightarrow PhN{-} + N_2$

ketones with diazomethane. In cases where $R^1 = R^2$ = alkyl and where the steady state concentration of $R^1R^2CN_2$ is low (as in the present experiments), the reaction of **9** with diazoalkane is very slow and **7**, in equilibrium with **8** and **9**, is consumed by intramolecular electrocyclic ring closure to **10** (Scheme 2). That closure can be viewed as the first step of an electrophilic aromatic substitution on a highly activated phenoxide-like aromatic system. Tautomerization of **10** to **11**, followed by its attack on excess aryl isocyanate, affords **2**. Intermediates **6** and **7** can also be intercepted by aryl isocyanate to form new dipolar intermediates (**12** and **13**), which undergo ring closure through both O and N of the anionic moiety to form **3** and **4**, respectively. The above steps, illustrated in Scheme 2 for the case of phenyl isocyanate, form a mechanistic hypothesis for the formation of **2**, **3**, and **4**. It is based in part on analogy (see Introduction) and in part on the evidence discussed below.

2-Diazopropane, prepared by oxidation of acetone hydrazone with mercuric oxide, was obtained as an ethereal solution containing water and ethanol (10). A portion of that solution, upon treatment with excess phenylisocyanate at room temperature, afforded α-hydroxy isobutyranilide and α-ethoxy isobutyranilide (as well as *N,N'*-diphenylurea) but not **2***a*, **3***a*, or **4***a*. Another portion of the diazopropane solution, dried before treatment with phenyl isocyanate, gave mostly α-ethoxy isobutyranilide and a trace of the hydroxy compound. Since **5**, from a concerted cycloaddition, is expected to be kinetically stable at room temperature (**14** and **15** are very stable) (19) the

14 **15**

above observations point to an acyclic intermediate (e.g., **6** or **7**, $R^1 = R^2 = CH_3$) formed from phenyl isocyanate and diazopropane, which can be intercepted efficiently by water and

TABLE 4. Effects of concentration and temperature on the product distribution from **1***a* and PhNCO[a]

		Relative yields[c]		
T, °C	[PhNCO], *M*[b]	**2***a*	**3***a*	**4***a*
149	2.2	4.8	1	1
149	6.3	2.4	1	1
112	2.2	2.7	1	1.2
112	6.3	1.2	1.6	1
65	2.2	1.1	1.6	1
68	6.3	1.0	1.7	2

[a]These experiments were conducted under conditions that might be used by synthetic chemists. They are not strictly comparable because of differences in the way in which the reactant concentrations and the medium were changed. See Experimental.

[b]Calculated final concentration, excluding isocyanate consumed.

[c]Determined by ^{1}H nmr spectrometry of the mixture of products and subject to errors of ca. 10%.

by ethanol. Similarly, the fact that the relative yields of **3** and **4** rose with increasing concentration of phenyl isocyanate, while that of **2** fell, requires a competition such as that between unimolecular cyclization of **7** and its bimolecular reaction with PhNCO.

Although **6** is included in Scheme 2 as a species that can react with PhNCO, we have not included **6** as a direct source of **10**. The preferred route for forming **10**, from **7** instead of from **6**, is based on the assumption that steric hindrance to direct closure of **6** to **10** would be excessive, at least in the reactions leading to **2***f* and **2***i*. The fact that *m*-tolyl isocyanate afforded oxindoles **2***m* and **2***n* in 1:1 ratio is also more easily accommodated in terms of cyclization of a species like **7** rather than **6**.

The effects of isocyanate concentration and of the reaction temperature on the distribution are predictable from Scheme 2. The yield of a given **2** should fall, and the sum of the yields of the corresponding **3** and **4** should rise, with increasing isocyanate concentration. At a given isocyanate concentration, the yield of **2** should fall with increasing temperature while the sum of the yields **3** and **4** should rise because bimolecular reactions normally have more negative entropies of activation than unimolecular reactions. Those expectations were borne out for the case of **2***a*, **3***a*, and **4***a*, from **1** and phenyl isocyanate (Table 5) and they can probably be extrapolated with confidence to the other members to design favourable conditions for a given synthetic objective. We have not attempted to optimize conditions for the formation of a given product in this work, although our conditions were chosen, in general, to favour oxindoles. For that reason, and also because the separation of **2**, **3**, and **4** from mixtures containing all three was difficult in some cases, only a few members of the families **3** and **4** were characterized.

Experimental

Synthesis of ketone semicarbazones

Ketone semicarbazones were prepared by the method described by Vogel (20). They are listed below in the format: starting ketone, % yield of purified semicarbazone, mp, mp (lit.), ^{1}H nmr spectrum ($CDCl_3$, 90 MHz). Propanone, 75%, 187–188°C, 190°C (21), δ: 1.90 (s, 3H), 1.98 (s, 3H), 5.62 (s, br, 2H), 8.09 (s, br, 1H); 2-butanone, 65%, 143–144°C, 146°C (21), δ: 1.08 (t, 3H), 1.83 (s, 3H), 2.28 (q, 2H), 5.83 (s, br, 2H), 8.56 (s, br, 1H); 2-pentanone, 60%, 107–108°C, 106°C (21), δ: 0.94 (t, 3H), 1.52 (m, 2H), 1.83 (s, 3H), 2.22 (m, 2H), 5.99 (s, br, 2H), 8.82 (s, br, 1H); 3-methyl-2-butanone, 45%, 113–114°C, 113°C (21), δ: 1.06 (d, 6H), 1.77 (s, 3H), 2.46 (sept, 1H), 6.03 (s, br, 2H), 8.78 (s, br, 1H); 4-methyl-2-pentanone, 75%, 129–131°C, 132°C (21), δ: 0.94 (m, 7H), 1.81 (s, 3H), 2.10 (m, 2H), 5.79 (s, br, 2H), 8.48 (s, br, 1H); 3,3-dimethyl-2-butanone, 60%, 156.5–157°C, 155°C (22), δ: 1.12 (s, 9H), 1.83 (s, 3H), 6.07 (s, br, 2H), 8.85 (s, br, 1H); cyclohexanone, 70%, 165–166°C, 166°C (21), δ: 1.37–2.52 (m, 10H), 5.89 (s, br, 2H), 9.71 (s, br, 1H); 1-phenyl-2-propanone, 70%, 196–198°C, 198°C (20), δ (DMSO-d_6): 1.40 (s, 3H), 3.17 (s, 2H), 5.95 (s, br, 2H), 6.98 (s, 5H), 8.78 (s, br, 1H); 2,4-dimethyl-3-pentanone, 60%, 161°C, 160°C (21), δ: 1.09 (d, 12H), 2.74 (sept, 2H), 6.03 (s, br, 2H), 8.69 (s, br, 1H).

*5,5-Disubstituted-Δ^3-1,3,4-oxadiazolin-2-ones (**1**)*

To the semicarbazone (0.030 mol) in well-stirred, ice-cooled methylene chloride (200 mL) under dry N_2 was added lead tetraacetate (0.035 mol). After the initially pale yellow colour was discharged (ca. 30 min), ice water (100 mL) was added followed by hydrochloric acid (2.4 *M*, 20 mL). The reaction mixture, still cooled with ice, was stirred for 30 min more before it was filtered through a bed of Celite to remove insoluble inorganic material. The separated organic layer was washed in succession with ice water (200 mL), saturated sodium bicarbonate solution (200 mL), and ice water (200 mL) before it was dried over anhydrous magnesium sulfate. Filtration and evaporation of the solvent with a rotary evaporator afforded the crude product as an oil or as a solid. Oils were purified by bulb-to-bulb distillation at 10^{-2} Torr, with the pot at 40°C and the receiver at −78°C. Solids were sublimed at ambient temperature and 10^{-2} Torr. Yields of crude oxadiazolinones ranged from 65 to 55% and yields of purified compounds were ca. 40%. The infrared spectra of the oxadiazolinones showed a strong band between 1835 and 1840 cm^{-1} characteristic of carbonyl group stretching for that ring system (23). Proton nmr spectra for compounds **1** are included in Table 1.

Thermolysis of an oxadiazolinone in the presence of an aryl isocyanate

The following is a typical procedure for the preparation and separation of products **2**, **3**, and **4**. A solution of the oxadiazolinone (4.0 mmol) in nitrobenzene (25 mL, fractionally distilled after ordinary distillation from P_2O_5) was added dropwise, with stirring during one hour, to a solution of freshly distilled phenyl isocyanate (80 mmol) in nitrobenzene (10 mL), at 150°C and under nitrogen (L-grade). After addition was complete, the solution was kept at 150°C for 2 hours before the solvent and the excess phenyl isocyanate were largely removed by vacuum distillation. The crude residue was taken up in a small volume of chloroform for column chromatography on neutral alumina (100 g, Brockman activity II, 80–200 mesh), using a solution of light petroleum ether (bp 30–45°C, 5 parts) and ether (2 parts) for elution. Separated fractions were either recrystallized or rechromatographed on preparative tlc plates (20 × 20 cm, neutral alumina with fluorescent indicator, uv-254) using ether in light petroleum ether, in ratios between 1:15 and 1:5, for plate development. Some liquid fractions had to be chromatographed four times on tlc plates before a product of satisfactory purity could be obtained.

Concentration and temperature dependence of product ratios

A typical run in which the isocyanate concentration changed from an initial value of ca. 4.6 *M* to a final value of 2.2 *M* is described first.

A solution of **1***a* (0.52 g, 4.5 mmol) in nitrobenzene (20 mL) was added dropwise during 1 hour, with stirring and under N_2, to a solution of phenyl isocyanate (9 mL, 0.083 mol) in nitrobenzene (9 mL) at 150°C. Heating and stirring were continued for 2 hours after addition was complete. Removal of nitrobenzene and excess phenyl isocyanate under reduced pressure left a residue that was analyzed qualitatively by tlc and quantitatively by ^{1}H nmr spectroscopy. The average of the ratios **2***a*:**3***a*:**4***a* from three separate runs was 4.8:1.0:1.0.

A typical run in which the isocyanate concentration changed from an initial value of ca. 9.2 *M* (neat phenyl isocyanate) to a final concentration near 6.3 *M* follows.

A solution of **1***a* (0.49 g, 4.3 mmol) in nitrobenzene (10 mL) was added as described above to phenyl isocyanate (22 mL, 0.20 mol).

Can. J. Chem. Downloaded from www.nrcresearchpress.com by 72.64.146.136 on 09/07/12
For personal use only.

Quantitative analysis of the product ratio, as described above, gave **2***a*:**3***a*:**4***a* = 2.4:1.0:1.0.

Thermolyses at lower temperatures followed procedures already described for the appropriate final isocyanate concentration, with the following exception. For the 65°C and 68°C runs (Table 5) the oxadiazolinone solution was added all at once and the heating period was extended to 48 h.

Reaction of 2-diazopropane with phenylisocyanate

2-Diazopropane, prepared by the method of Whiting and co-workers (10) was obtained as a pink ethereal solution containing unknown quantities of ethanol and water. The initial solution was redistilled quickly and dried briefly over sodium sulfate.

The partially dried ethereal solution, containing ca. 0.11 mol of 2-diazopropane, was dropped during 1 hour into a stirring solution of phenyl isocyanate (13.1 g, 0.11 mol) in ether (50 mL) at room temperature. Two hours after addition was complete, the pink colour had disappeared and the solution was concentrated with a rotary evaporator. Addition of petroleum ether to the crude residue resulted in precipitation of α-hydroxyisobutyranilide, which was recrystallized from a chloroform – petroleum ether solvent: mp 133–134°C (lit. (24) mp 135°C); ir: 3400 and 1695 cm^{-1}; ^1H nmr ($CDCl_3$), δ: 1.54 (s, 6H), 2.95 (s, br, 1H), 7.29 (m, 5H), 9.00 (s, br, 1H); ms (low resolution) *m/z*: 179.

The mother liquor from the precipitation was concentrated and the residue was chromatographed on a column (Florisil, 60–100 mesh, 200 g) using light petroleum for elution. α-Ethoxyisobutyranilide was obtained as a colourless liquid: ir: 3395, 1730, and 1690 cm^{-1}; ^1H nmr ($CDCl_3$), δ: 1.32 (t, 3H), 1.52 (s, 6H), 3.43 (q, 2H), 7.26 (m, 5H), 8.43 (s, br, 1H); ms (low resolution) *m/z*: 206.

A similar reaction, in which the ethereal diazopropane solution was first dried briefly over KOH pellets, gave largely α-ethoxyisobutyranilide.

Hydrolysis of 1-phenylcarbamoyl-3,3-dimethyloxindole

1-Phenylcarbamoyl-3,3-dimethyloxindole (0.25 g, 0.89 mmol) in a solution made from 10% KOH (15 mL) and methanol (15 mL) was refluxed for 1 h. The resulting solution was neutralized with aqueous HCl and extracted with ether (3 × 50 mL). The ether extract was washed with saturated sodium bicarbonate solution, dried, and concentrated. Crystallization of the residue from methanol afforded 3,3-dimethyl oxindole (0.11 g, 79%) as colourless prisms: mp 152–154°C (lit. (25) mp 150°C); ir: 3450 and 1720 cm^{-1}; ^1H nmr, δ: 1.40 (s, 6H), 7.06 (m, 4H), 9.37 (s, br, 1H); ms (low resolution) *m/z*: 161.

Reaction of 3,3-dimethyloxindole with phenyl isocyanate

3,3-Dimethyloxindole (0.15 g, 0.93 mmol), dissolved in a solution made from phenyl isocyanate (1 mL) and nitrobenzene (8 mL), was heated at 150°C for 2 h. Concentration of the resulting solution by vacuum distillation afforded a residual viscous oil, which crystallized from aqueous ethanol to afford colourless needles (0.20 g, 80%) of 1-phenylcarbamoyl-3,3-dimethyloxindole, mp 73–75°C, with spectra matching those of **2***a* obtained from oxadiazolinone **1***a* and phenyl isocyanate.

Acknowledgements

The authors are grateful to Dr. A. J. Paine, who provided samples of two of the oxadiazolinones, and to Ms. Irene Tse-Sheepy, who purified one of the oxindoles for analysis. Financial support from the Natural Sciences and Engineering Research Council of Canada is gratefully acknowledged.

1. (*a*) H. Staudinger, E. Anthes, and F. Pfenninger. Chem. Ber. **49**, 1939 (1916); (*b*) H. Staudinger and A. Gaule. Chem. Ber. **49**, 1959 (1916); (*c*) H. Staudinger and Th. Reber. Helv. Chim. Acta, **4**, 3 (1921).
2. P. Lipp and R. Köster. Chem. Ber. **64**, 2823 (1931).
3. D. A. Semenow, E. F. Cox, and J. D. Roberts. J. Am. Chem. Soc. **78**, 3221 (1956).
4. (*a*) W. B. Hammond and N. J. Turro. J. Am. Chem. Soc. **88**, 2880 (1966); (*b*) N. J. Turro and W. B. Hammond. J. Am. Chem. Soc. **88**, 3672 (1966); (*c*) N. J. Turro and W. B. Hammond. Tetrahedron, **24**, 6017 (1968).
5. H. v. Pechmann. Chem. Ber. **28**, 861 (1895).
6. (*a*) J. C. Sheehan and P. T. Izzo. J. Am. Chem. Soc. **70**, 1985 (1948); (*b*) J. Am. Chem. Soc. **71**, 4059 (1949).
7. (*a*) P. C. Ip, K. Ramakrishnan, and J. Warkentin. Can. J. Chem. **52**, 3671 (1974); (*b*) K. Ramakrishnan, J. B. Fulton, and J. Warkentin. Tetrahedron, **32**, 2685 (1976).
8. (*a*) S. L. Lee, A. M. Cameron, and J. Warkentin. Can. J. Chem. **50**, 2326 (1972); (*b*) A. J. Paine and J. Warkentin. Can. J. Chem. **57**, 2681 (1979); (*c*) A. J. Paine and J. Warkentin. Can. J. Chem. **59**, 491 (1981).
9. A. C. Day and M. C. Whiting. Org. Synth. **50**, 3 (1970).
10. S. D. Andrews, A. C. Day, P. Raymond, and M. C. Whiting. Org. Synth. **50**, 27 (1970).
11. A. H. Beckett, R. W. Daisley, and J. Walker. Tetrahedron, **24**, 6093 (1968).
12. J. Elguero, C. Marzin, and M. E. Peek. Org. Magn. Reson. **6**, 445 (1975).
13. J. B. Stothers. Carbon-13 NMR spectroscopy. Academic Press, Inc., New York, NY. 1972.
14. (*a*) H. Najer, J. Menin, and R. Guidicelli. C. R. Hebd. Seances Acad. Sci. **258**, 4579 (1964); (*b*) C. R. Hebd. Seances Acad. Sci. **259**, 2868 (1964); (*c*) R. Guidicelli, J. Menin, and H. Najer. C. R. Hebd. Seances Acad. Sci. **260**, 4538 (1965).
15. The Sadtler Standard Spectra. Vol. 25. Sadtler Research Laboratories, Philadelphia, PA. No. 25298.
16. N. Naulet, M. L. Filleux, G. J. Martin, and J. Pornet. Org. Magn. Reson. **7**, 326 (1975).
17. (*a*) K. N. Houk. J. Am. Chem. Soc. **94**, 8953 (1972); (*b*) K. N. Houk, J. Sims, R. E. Duke, Jr., R. W. Strozier, and J. K. George. J. Am. Chem. Soc. **95**, 7287 (1973); (*c*) K. N. Houk, J. Sims, C. R. Watts, and L. J. Luskus. J. Am. Chem. Soc. **95**, 7301 (1973).
18. K. N. Houk, R. W. Strozier, and J. A. Hall. Tetrahedron Lett. 897 (1974).
19. (*a*) N. J. Turro and W. B. Hammond. Tetrahedron, **24**, 6017 (1968); (*b*) L. M. Cabelkova-Taguchi and J. Warkentin. Can. J. Chem. **59**, 100 (1981).
20. A. I. Vogel. Elementary practical organic chemistry. Part II. Qualitative organic analysis. Longmans, Green and Co., Ltd., London. 1957.
21. F. S. Mann and B. C. Saunders. Practical organic chemistry. Longmans, Green and Co., Ltd., London. 1962.
22. Y. P. Kitaev, G. K. Budnikov, and I. M. Skrebkova. Izv. Akad. Nauk SSSR, Ser. Khim. 224 (1962); Chem. Abstr. **57**, 7014e (1962).
23. P. Knittel, S. L. Lee, and J. Warkentin. Can. J. Chem. **50**, 3248 (1972).
24. R. F. Rekker and W. Th. Nauta. Recl. Trav. Chim. Pays-Bas, **70**, 241 (1951).
25. E. Wenkert, B. S. Bernstein, and J. H. Udelhofen. J. Am. Chem. Soc. **80**, 4899 (1958).

Can. J. Chem. Downloaded from www.nrcresearchpress.com by 72.64.146.136 on 09/07/12
For personal use only.

Polarized absorption spectra of radical ions of some azanaphthalenes and biphenyls in stretched polymer films

HIROSHI HIRATSUKA

Department of Chemistry, Tokyo Institute of Technology, Ohokayama, Meguro-ku, Tokyo 152, Japan and Radiation Laboratory, University of Notre Dame, Notre Dame, IN 46556, USA

AND

KEN'ICHI SEKIGUCHI, YOSHIHIKO HATANO, YOSHIE TANIZAKI,[1] AND YUJI MORI

Department of Chemistry, Tokyo Institute of Technology, Ohokayama, Meguro-ku, Tokyo 152, Japan

Received September 11, 1986

HIROSHI HIRATSUKA, KEN'ICHI SEKIGUCHI, YOSHIHIKO HATANO, YOSHIE TANIZAKI, and YUJI MORI. Can. J. Chem. **65**, 1185 (1987).

The stretched polymer film technique combined with γ-irradiation has been employed to measure the polarized absorption (linear dichroism) spectra of radical anions of quinoline, isoquinoline, quinoxaline, phthalazine, phenylpyridine, 4,4′-bipyridyl, and 2,2′-bipyridyl. Profiles of polarized absorption spectra of all the radical anions are similar to those of the parent naphthalene or biphenyl radical anions. Those of radical cations of isoquinoline and 2,2′-bipyridyl are also similar to those of radical cations of their parent molecules. Quinoxaline radical cations, however, show quite a different spectrum from that of naphthalene radical cations; a long vibrational structure with ca. 550 cm^{-1} intervals was observed and peaks of these vibrational bands were polarized parallel to the molecular short-axis or normal to the molecular plane.

HIROSHI HIRATSUKA, KEN'ICHI SEKIGUCHI, YOSHIHIKO HATANO, YOSHIE TANIZAKI et YUJI MORI. Can. J. Chem. **65**, 1185 (1987).

On a utilisé la technique du film de polymère étiré, combinée avec l'irradiation-γ, pour mesurer les spectres d'absorption polarisée (dichroïsme linéaire) des anions radicaux de la quinoléine, de l'isoquinoléine, de la quinoxaline, de la phtalazine, de la phénylpyridine, des bipyridyles-4,4′ et 2,2′. Tous les spectres d'absorption polarisée de ces anions radicaux sont semblables à ceux des anions radicaux du naphtalène ou du biphényle parent. Les spectres des anions radicaux de l'isoquinoléine et du bipyridyle-2,2′ sont aussi semblables à ceux des cations radicaux de leurs molécules parentes. Toutefois, le spectre des cations radicaux de la quinoxaline est très différent de celui des cations radicaux du naphtalène; on a observé une longue structure vibrationnelle ayant des intervalles d'environ 550 cm^{-1} et les maxima de ces bandes de vibration sont polarisés d'une manière parallèle à l'axe court de la molécule ou normale au plan de la molécule.

[Traduit par la revue]

Introduction

Extensive studies have been carried out on absorption spectra of aromatic radical ions which are one of the important intermediates in electrochemical, photochemical, and radiation chemical reactions. Polarization measurements on electronic spectra were carried out by Hoytink *et al.* for radical anions of aromatic hydrocarbon molecules (1). Absorption spectra of radical ions of aza-aromatic molecules were also extensively studied (2–7) but, to the best of our knowledge, there has been no report on polarization measurements of electronic spectra for these aza-aromatic radicals.

In previous papers we have shown that the stretched polymer film technique combined with γ-irradiation is available for polarization measurements (linear dichroism) on radicals and radical ions, such as aromatic hydrocarbons and their derivatives (8, 9). We have also measured the polarization spectra of radical ions of acridine and phenazine (aza-anthracenes) prepared in polyethylene or poly(vinyl chloride) films (10). In this paper we present the results of polarization measurements on the radical ions of some derivatives of aza-naphthalene and -biphenyl in comparison with those of the parent hydrocarbon radical ions.

Experimental

Ultra pure grade naphthalene and biphenyl, guaranteed grade quinoline, quinoxaline, 4,4′-bipyridyl, and 2,2′-bipyridyl, extra pure grade isoquinoline (Tokyo Kasei Co.), and phthalazine and 4-phenylpyridine (Aldrich Chem. Co. Inc.) were used as received. Poly(fluorinated ethylene-propylene) (PFEP) films, ca. 0.2 mm thick, were obtained from Mitsui Fluorochemical Co. Freon 113 (1,1,2-trichloro-1,2,2-trifluoroethane), *s*-butylamine, and *s*-butylchloride (Tokyo Kasei Co.) were used without further purification.

In the same way as before (10), radical anions were prepared at 77 K by γ-irradiation of the polyethylene (PE) films containing the sample and solvent *s*-butylamine. Radical cations were prepared by use of poly(vinyl chloride) (PVC) films containing the sample and *s*-butylchloride. To prepare radical cations of quinoxaline, PEEP films and solvent Freon 113 were used. Films containing sample molecules were stretched to three times their original length and then irradiated by ^{60}Co γ-rays for 5 h at 77 K with a dose rate of 1.0×10^6 rads/h. Polarized absorption spectra were measured in the range from 300 to 850 nm on a JASCO SS-50 spectrophotometer equipped with a Rochon polarizer. Absorption base lines for sample films were recorded before γ-irradiation and then absorption spectra of irradiated films were recorded. The spectra observed are shown in Figs. 1 and 3–6 in the region where the absorption band due to the parent molecule does not overlap with that of radical ions or is negligibly small. In the case of PFEP films, photobleaching of the film was carried out for 10 min after γ-irradiation, using a high pressure mercury lamp combined with a uv light cut-off filter in order to remove the absorption due to the positive holes and/or charge-transferred species (5). The difference in absorbance before and after irradiation was ascribed to the absorption of the produced species. Dichroic ratio, R_d, is defined as the absorbance ratio $A_\parallel / A_\perp$, where $A_\parallel$ and $A_\perp$ denote the absorbances when the electric vectors of the incident light are parallel and perpendicular to the stretching direction of the film, respectively. Error in R_d value is less than 5%. In order to analyze polarized absorption spectra qualitatively, this R_d value is employed in reference to the results of MO calculations in a π-electron approximation (10*a*).

[1]Present address: The Department of Materials Science and Technology, Technological University of Nagaoka, Niigata 949-54, Japan.

Printed in Canada / Imprimé au Canada

Can. J. Chem. Downloaded from www.nrcresearchpress.com by 78.46.186.204 on 09/07/12
For personal use only.

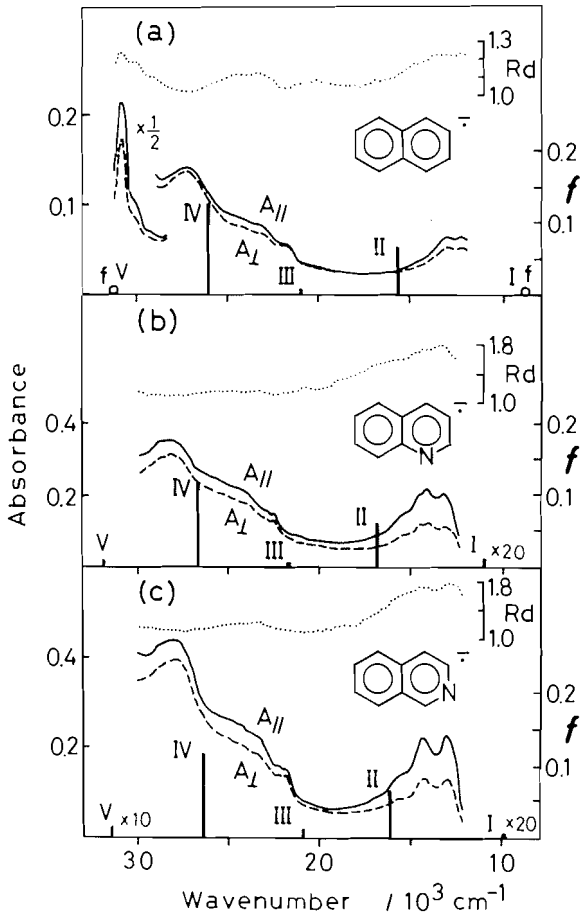

FIG. 1. Polarized absorption spectra of radical anions of naphthalene (*a*) in the γ-irradiated PVA film, quinoline (*b*), and isoquinoline (*c*) in the γ-irradiated PE films. $A_{\parallel}$ and $A_{\perp}$ are the absorbances when the electric vectors of the incident light are parallel and perpendicular, respectively, to the stretching direction of the films. R_d is $A_{\parallel}/A_{\perp}$. Calculated results are shown as the vertical lines and open circles. Roman figures represent the transition number and f (open circle) is the forbidden transition.

When polarization directions of electronic transitions of radical ions are limited to the directions parallel to the molecular long- and short-axis, a quantitative analysis can be easily carried out by use of R_d values; "polarization" resolved spectra can be determined by reducing the absorption spectrum (A) according to eqs. [1] and [2] given below as shown in previous papers (8, 9).

$$[1]\quad A_l = \frac{R_d - R_d^s}{R_d^l - R_d^s}\frac{R_d^l + 2}{R_d + 2}A$$

$$[2]\quad A_s = \frac{R_d^l - R_d}{R_d^l - R_d^s}\frac{R_d^s + 2}{R_d + 2}A$$

where A_l and A_s are absorption components whose transition moments are polarized parallel to the molecular long- and short-axis, respectively. R_d^l and R_d^s are extreme R_d values of the "purely" long- and short-axis polarized bands. These equations are identical with those derived by Margulies and Yogev (11). This analysis was applied to the aromatic radicals of hydrocarbon molecules and their derivatives which belong to C_{2v} symmetry or higher (8, 9, 10*b*).

Results and discussion

Absorption spectra of the γ-irradiated non-stretched films containing sample molecules are similar to those reported previously for the corresponding radical ions of aza-naphthalenes and -biphenyls (2–5, 7). Polarized absorption spectra observed for aza-naphthalenes and -biphenyls in γ-irradiated stretched films are shown in Figs. 1 and 3–6. Results of MO calculations for the corresponding radical ions are also shown in the figures by vertical lines.

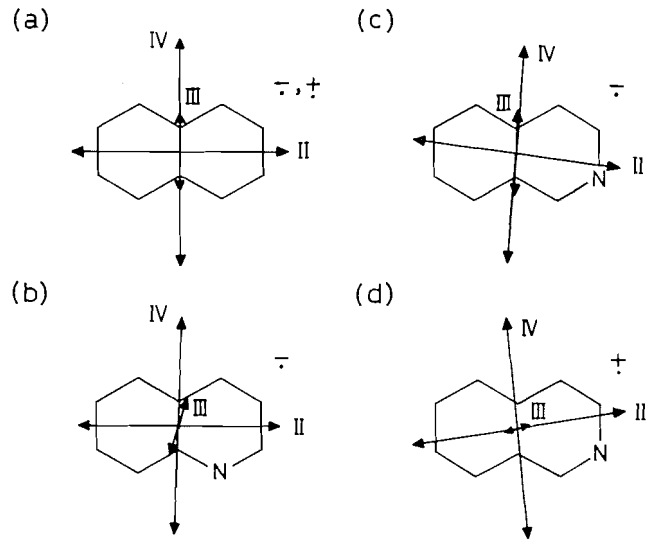

FIG. 2. Direction of transition moments of some electronic transitions of *N*-aza-substituted naphthalene radical ions.

Polarized absorption spectra can be analyzed qualitatively by examining the R_d curve based on the assumption that the molecular long-axis inclines preferentially along the stretched direction of films. The validity of this assumption has been confirmed for some radical ions (8–10). If the molecular long-axis inclines along the stretched direction of the film, an electronic transition polarized parallel to the molecular long-axis should give greater R_d values than those of the other transitions, while a transition parallel to the short-axis a smaller R_d value than the others. Therefore we can qualitatively determine the polarization direction of absorption bands by analyzing the profile of the R_d curve.

Figure 1*a* shows the polarized absorption spectra of radical anions of naphthalene in a poly(vinyl alcohol) film. For the radical anions of naphthalene resolved spectra were determined and reported elsewhere (8), but here we show the results as an example for a qualitative analysis of R_d profile. R_d values are greater in the region below 15×10^3 cm^{-1} and in the intense band of $(30–31) \times 10^3$ cm^{-1} than those of the others, while R_d values are relatively small at the absorption bands of $(21–28) \times 10^3$ cm^{-1}. These results indicate that transition moments of the absorption bands appearing below 15×10^3 cm^{-1} and in the $(30–31) \times 10^3$ cm^{-1} region are polarized parallel to the molecular long-axis, and the bands in the region $(21–28) \times 10^3$ cm^{-1} are to the short axis. The long-axis polarized absorption bands are respectively assigned to the second (below 15×10^3 cm^{-1}) and the seventh ($(30–31) \times 10^3$ cm^{-1} band) transitions, where the seventh transition is calculated to appear at 40.03×10^3 cm^{-1} with an oscillator strength 0.412 (8) but it is not shown in this figure. The short-axis polarized ones in the region of $(21–28) \times 10^3$ cm^{-1} are attributed to the third and fourth electronic transitions.

Figures 1*b* and *c* show the polarized absorption spectra of radical anions of quinoline and isoquinoline, respectively. These spectra are similar to those of naphthalene radical anions. R_d profile is also similar to that of naphthalene radical anions,

Can. J. Chem. Downloaded from www.nrcresearchpress.com by 78.46.186.204 on 09/07/12
For personal use only.

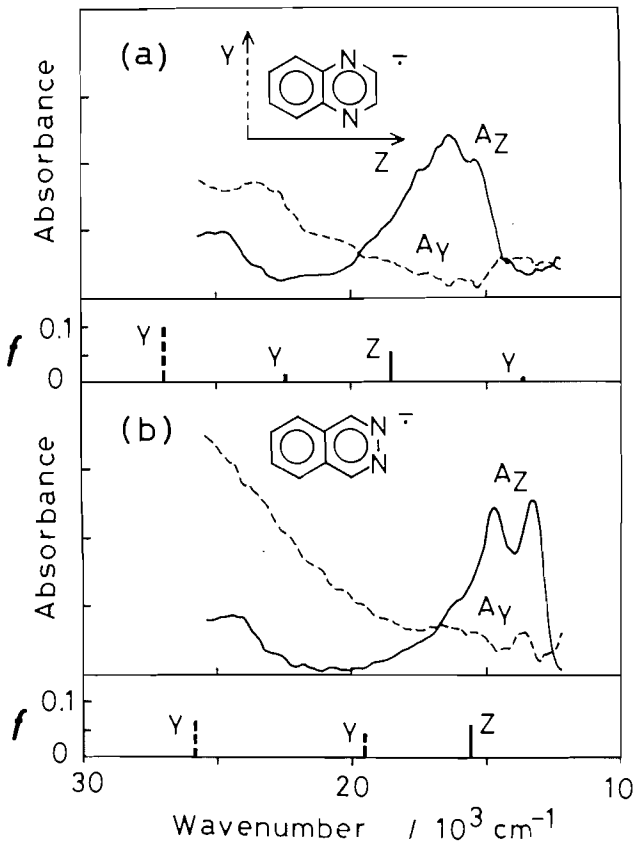

FIG. 3. Resolved spectra of the radical anions of quinoxaline (*a*) and phthalazine (*b*). Extreme R_d values used are as follows; $R_d^l = 1.60$ and $R_d^s = 0.99$ for quinoxaline and $R_d^l = 1.40$ and $R_d^s = 0.98$ for phthalazine. Calculated results for these radicals are also shown in the bottom. *Z* and *Y* mean that the transition moments are polarized parallel to the molecular long- and short-axis, respectively.

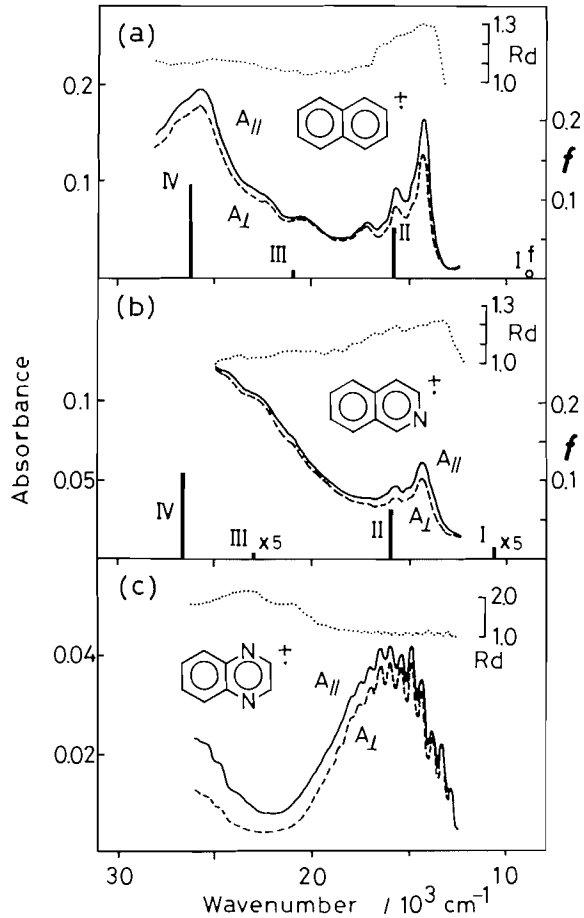

FIG. 4. Polarized absorption spectra of radical cations of naphthalene (*a*), isoquinoline (*b*) in the γ-irradiated PVC films and quinoxaline (*c*) in the γ-irradiated PFEP film. See the footnotes of Fig. 1.

R_d values in the region below 16 × 10^3 cm^{-1} are greater than those of other regions. This indicates that the polarization direction of absorption bands in (12–16) × 10^3 cm^{-1} is rather close to the molecular long-axis compared to those of the other bands. As shown in Fig. 2, directions of transition moments of the second, third, and fourth transition are not varied so much by *N*-aza-substitution in the naphthalene radical anion. Thus, as in the case of naphthalene, it is reasonable to assign the absorption band at (12–16) × 10^3 cm^{-1} to the second transition, while the weak band at (21–26) × 10^3 cm^{-1} and the intense one at (26–29) × 10^3 cm^{-1} can be assigned to the third and fourth transitions, respectively.

Figures 3*a* and *b* show the "polarization"-resolved spectra of radical anions of quinoxaline and phthalazine. These spectra have been obtained by resolving the absorption spectra by use of eqs. [1] and [2]. Extreme R_d values (R_d^l and R_d^s) used are shown in the figure caption. The long-axis polarized band (A_z absorption) appears at low wavenumbers of the spectrum and is assigned to the second transition. As shown in Figs. 1*b* and *c*, only a very small shift is observed for this long-axis polarized band between isoquinoline and quinoline, while a rather large blue shift (ca. 2 × 10^3 cm^{-1}) is observed from phthalazine to quinoxaline as can be seen in Fig. 3, in agreement with MO calculations.

Figure 4 shows the polarized absorption spectra of isoquinoline, and quinoxaline radical cations. For comparison those of naphthalene radical cations are also shown in Fig. 4. Naphthalene (Fig. 4*a*) and isoquinoline radical cations (Fig. 4*b*) were prepared in PVC films by γ-irradiation, while the absorption spectra of quinoxaline radical cations (Fig. 4*c*) was observed in PFEP films. The absorption spectrum of quinoxaline cation radicals was not observed in γ-irradiated PVC films containing quinoxaline. This difference in the radical cation formation between isoquinoline and quinoxaline in PVC films can be attributed to the difference in ionization potentials of isoquinoline (8.5 eV) and quinoline (9.0 eV) (12).

Profiles of R_d curves in Figs. 4*a* and *b* are similar to each other; the absorption band around 15 × 10^3 cm^{-1} shows relatively greater R_d values than those of the other bands. This indicates that the directions of transition moments of the second and the fourth electronic transitions are not affected so much by *N*-aza-substitution at the β-position in naphthalene radical cation. This is rationalized by the results of MO calculations on these radicals as shown in Figs. 2*a* and *d*.

The absorption spectra of quinoxaline radical cations, however, are quite different from those of naphthalene radical cations. A long vibrational structure extends from 13 × 10^3 cm^{-1} to 18 × 10^3 cm^{-1} with approximately constant intervals of 550 cm^{-1} and with the maximum around 15 × 10^3 cm^{-1}. This long progression can be related to the a_1 vibration (526 cm^{-1}) observed for the n–π* absorption band of quinoxaline in durene (13). The R_d curve shows minima at each absorption peak of the vibrational structure. This indicates that the transition moment is polarized parallel to the molecular

Can. J. Chem. Downloaded from www.nrcresearchpress.com by 78.46.186.204 on 09/07/12
For personal use only.

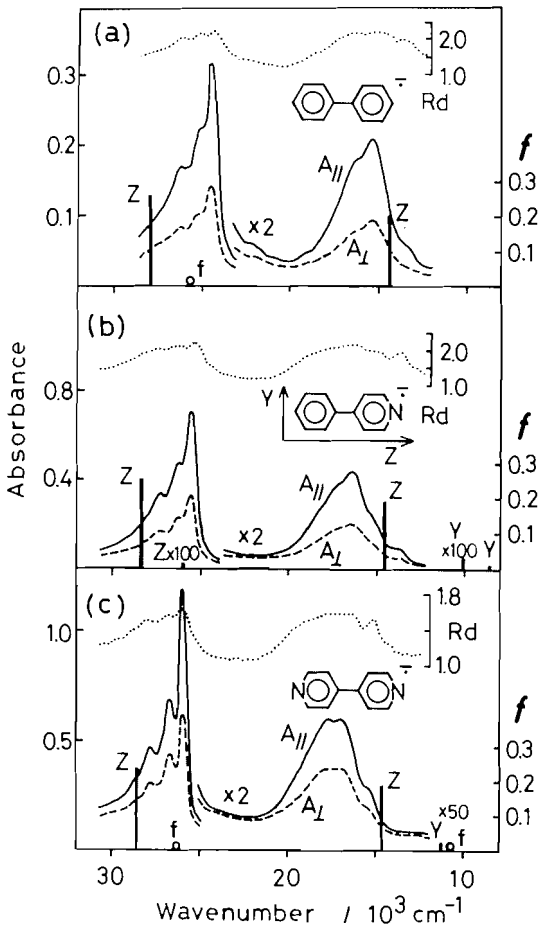

FIG. 5. Polarized absorption spectra of radical anions of biphenyl (*a*), phenylpyridine (*b*), and 4,4′-bipyridyl in the γ-irradiated PE films. See the footnotes in Figs. 1 and 3.

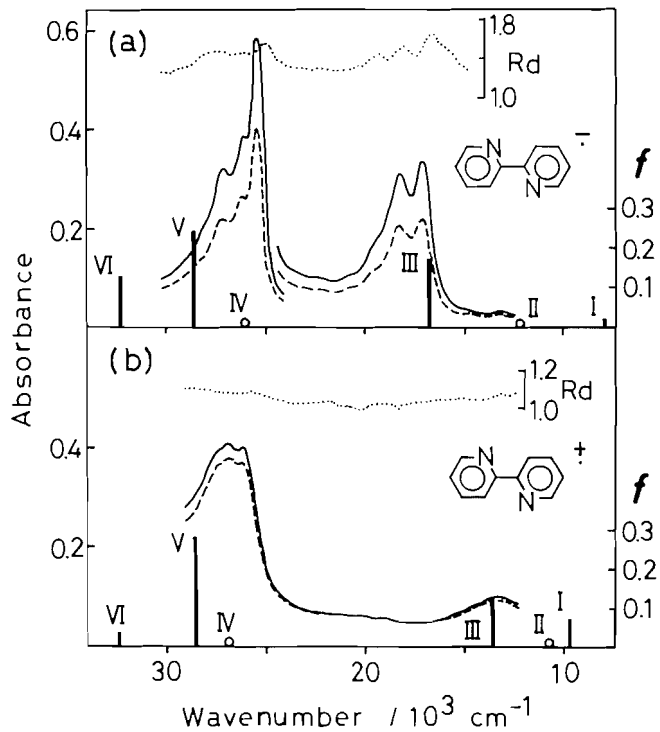

FIG. 6. Polarized absorption spectra of 2,2′-bipyridyl radical anions (*a*), in the γ-irradiated PE film and cations (*b*) in PVC films. See the footnotes of Fig. 1.

short axis or normal to the molecular plane. Therefore the absorption band can be attributed to a $\pi-n_+$ or $n_+-\pi^*$ transition with the polarization normal to the molecular plane, or an n_+-n_- transition with the short-axis polarization, where $n_+ = (n_1 + n_2)/\sqrt{2}$ and $n_- = (n_1 - n_2)/\sqrt{2}$, and n_1 and n_2 are the two non-bonding orbitals of nitrogen atoms.

Katoh and Shida observed the absorption spectrum of quinoxaline radical cations in a Freon mixture at 77 K (5). They studied esr and optical absorption spectra, and concluded that the cation is an "n cation"; the spin density is localized mostly on the in-plane lone-pair orbitals on nitrogen atoms. In comparison with the photoelectron spectrum of quinoxaline, the singly occupied lone-pair orbital has been assigned to the n_+ orbital. They assigned this band to the transition between n_+ and n_- orbitals by taking into account the spectral resemblance in esr and optical absorption spectra to those of pyrazine radical cations. Our results of polarization measurement on quinoxaline cation radicals are consistent with their assignment. However, the possibility that this structured absorption band is due to $n_+-\pi^*$ or $\pi-n_+$ transition is still not excluded because a long progression is also observed for the $n-\pi^*$ band of parent quinoxaline in durene (13).

Figure 5 shows the polarized absorption spectra of biphenyl (Fig. 5*a*), phenylpyridine (Fig. 5*b*), and 4,4′-bipyridyl (Fig. 5*c*) in PE films at 77 K. These spectra are similar in profile to each other but slight blue shifts are observed for the intense absorption bands by *N*-aza-substitution. R_d curves for these absorption spectra are also similar to each other in profile. R_d values around the intense bands are great, indicating these bands are polarized parallel to the molecular long-axis. No distinct short-axis polarized band is observed (8). These characteristics in absorption spectra are consistent with the calculated results.

Figure 6 shows the polarized absorption spectra of the 2,2′-bipyridyl radical anion in a PE film (*a*) and the radical cation in a PVC film (*b*). The spectra in Fig. 6*a* are similar to those of Fig. 5 but the visible absorption band and the R_d curve of 2,2′-bipyridyl radical anion show more resolved structure than those of biphenyl. The wavenumbers at the R_d curve maxima do not coincide with those of the absorption peaks but are slightly shifted to red. Maximum R_d values in the intense bands in the visible region are almost equal to those in the near-uv region for biphenyl, phenylpyridine, and 4,4′-bipyridyl radical anions, while the maximum R_d value in the visible region of 2,2′-bipyridyl is clearly greater than that of the near-uv region. These observations seem to indicate that 2,2′-bipyridyl radical anions in PE film do not have C_{2v} symmetry; the absorption spectra in Fig. 6*a* cannot be attributed to the *cis*-form.

The absorption spectra shown in Fig. 6*b* are similar to those of the biphenyl radical cation and explained by MO calculations (vertical lines). The R_d value is nearly constant but relatively great R_d values are obtained in the vicinity of the intense absorption band.

Concluding remarks

Polarized absorption (linear dichroism) spectra of the radical anions of quinoline, isoquinoline, quinoxaline, phthalazine, phenylpyridine, 4,4′-bipyridyl, and 2,2′-bipyridyl have been measured in stretched polymer films and analyzed for the first

Can. J. Chem. Downloaded from www.nrcresearchpress.com by 78.46.186.204 on 09/07/12
For personal use only.

time. Those of the radical cations of isoquinoline, quinoxaline, and 2,2′-bipyridyl were also measured and discussed.

Acknowledgments

We are greatly indebted to Professor Shida of Kyoto University and Dr. Das of the University of Notre Dame for their valuable suggestions on this work. This work was partially supported by a Grant-in-Aid for Scientific Research from the Ministry of Education, Science and Culture of Japan, and also by funds from the United States Department of Energy (H.H.). This is Document No. NDRL-2900 from the Radiation Laboratory.

1. (*a*) G. J. HOYTINK and P. J. ZANDSTRA. Mol. Phys. **3**, 371 (1960); (*b*) K. H. J. BUSCHOW, J. DIELEMAN, and G. J. HOYTINK. Mol. Phys. **7**, 1 (1964).
2. J. CHAUDHURI, S. KUME, J. JANGUR-GRODZINSKI, and M. SZWARC. J. Am. Chem. Soc. **90**, 6421 (1968).
3. J. WENDENBERG and H. MOCKEL. Z. Naturforsch. **236**, 1171 (1968).
4. C. DAVID, P. JANSSEN, and G. GEUSKENS. Spectrochim. Acta, **27**A, 367 (1971).
5. T. KATOH and T. SHIDA. J. Am. Chem. Soc. **101**, 6869 (1979).
6. K. EZUMI, T. KUBOTA, H. MIYAZAKI, and M. YAMAKAWA. J. Phys. Chem. **80**, 980 (1976).
7. Y. TORII, Y. YAZAKI, Y. KAIZU, S. MURASATO, and H. KOBAYASKI. Bull. Chem. Soc. Jpn. **42**, 2264 (1969).
8. H. HIRATSUKA, Y. HATANO, Y. TANIZAKI, and Y. MORI. J. Chem. Soc. Faraday Trans. 2, **81**, 1653 (1985).
9. H. HIRATSUKA, H. NAKAMURA, Y. TANIZAKI, and K. NAKAJIMA. Bull. Chem. Soc. Jpn. **55**, 3407 (1982).
10. (*a*) K. SEKIGUCHI, H. HIRATSUKA, Y. HATANO, and Y. TANIZAKI. J. Phys. Chem. **84**, 452 (1980); (*b*) H. HIRATSUKA, K. SEKIGUCHI, Y. HATANO, Y. TANIZAKI, and Y. MORI. J. Chem. Soc. Faraday Trans. 2, **82**, 795 (1986).
11. L. MARGULIES and A. YOGEV. Chem. Phys. **27**, 89 (1978).
12. F. BROGLI, E. HEILBRONNER, and T. KOBAYASHI. Helv. Chim. Acta, **55**, 274 (1972).
13. A. D. JORDAN, G. FISCHER, K. ROKOS, and I. G. ROSS. J. Mol. Spectrosc. **45**, 173 (1973).

Can. J. Chem. Downloaded from www.nrcresearchpress.com by 78.46.186.204 on 09/07/12
For personal use only.

The preparation and characterization of polysulfanotungsten[1] complexes of the type $(\eta^5\text{-}C_5H_5)W(CO)_3S_xR$, where $x = 2$, 3 and $(\eta^5\text{-}C_5H_5)W(CO)_3SS(O)R$, where $R = CH_2C_6H_5$, $p\text{-}C_6H_4CH_3$

ALAN SHAVER AND JUDY HARTGERINK

Department of Chemistry, McGill University, 801 Sherbrooke St. W., Montreal, P.Q., Canada H3A 2K6

Received August 27, 1986

ALAN SHAVER and JUDY HARTGERINK. Can. J. Chem. **65**, 1190 (1987).

The polysulfano complexes $(\eta^5\text{-}C_5H_5)W(CO)_3Q$, where Q = SSR, SSSR, SS(O)R, and R = $CH_2C_6H_5$ and $p\text{-}C_6H_4CH_3$ have been prepared via treatment of $(\eta^5\text{-}C_5H_5)W(CO)_3SH$ with RSphth, RSSphth, and RS(O)phth, respectively, at −20°C, where phth = *N*-phthalimido. The complexes where Q = SSR and SSSR lost sulfur spontaneously in solution to give the thiolato complexes $(\eta^5\text{-}C_5H_5)W(CO)_3SR$ and the disulfano complexes, respectively. The presence of PPh_3 accelerated this reaction for Q = SSR. Treatment of $(\eta^5\text{-}C_5H_5)W(CO)_3SSR$ with *m*-chloroperbenzoic acid gave a mixture of complexes for which Q = SR, SO_2R, SS(O)R, and higher oxidized sulfur ligands. $As(C_6H_5)_4[W(CO)_5SH]$ reacted with $p\text{-}CH_3C_6H_4Sphth$ to give an unstable first product, tentatively identified as $As(C_6H_5)_4[W(CO)_5SS\text{-}p\text{-}C_6H_4CH_3]$, the isolated product being $As(C_6H_5)_4[W(CO)_5S\text{-}p\text{-}C_6H_4CH_3]$.

ALAN SHAVER et JUDY HARTGERINK. Can. J. Chem. **65**, 1190 (1987).

On a préparé les complexes polysulfurés $(\eta^5\text{-}C_5H_5)W(CO)_3Q$, dans lesquels Q = SSR, SSSR et SS(O)R et R = $CH_2C_6H_5$ et $p\text{-}C_6H_4CH_3$, en faisant réagir respectivement les composés RSphth, RSSphth et RS(O)phth avec le $(\eta\text{-}C_5H_5)W(CO)_3SH$, à −20°C. En solution, les complexes dans lesquels Q = SSR et SSSR perdent spontanément du soufre pour donner respectivement les complexes thiolato $(\eta^5\text{-}C_5H_5)W(CO)_3SR$ et disulfano. La présence de PPh_3 accélère cette réaction lorsque Q = SSR. La réaction du $(\eta^5\text{-}C_5H_5)W(CO)_3SSR$ avec l'acide *m*-chloroperbenzoïque conduit à un mélange de complexes contenant des groupements Q = SR, SO_2R, SS(O)R et d'autres ligands sulfurés plus oxydés. Le composé $As(C_6H_5)_4[W(CO)_5SH]$ réagit avec le $p\text{-}CH_3C_6H_4Sphth$ pour donner un produit préliminaire instable, temporairement identifié comme étant le $As(C_6H_5)_4[W(CO)_5\text{-}SS\text{-}p\text{-}C_6H_4CH_3]$; le produit isolé est le $As(C_6H_5)_4[W(CO)_5S\text{-}p\text{-}C_6H_4CH_3]$.

[Traduit par la revue]

Can. J. Chem. Downloaded from www.nrcresearchpress.com by 78.46.186.204 on 09/07/12
For personal use only.

Catenated polycarbon systems are the basis for σ and π type ligands in organometallic chemistry. Sulfur, an excellent catenator (1), might also be expected to form similar classes of ligands. However, while metal thiolates (MSR) form a very large and important class of molecules (2), metal disulfanes (MSSR) and trisulfanes (MSSSR) are quite rare (3). In view of the importance of metal–sulfur chemistry in biology and industry, it seems appropriate to investigate the chemistry of simple catenated polysulfano ligands.

The preparation of unsymmetrical organic di- and trisulfanes can be accomplished (4) via the application of sulfur-transfer reagents of the type RS_xphth, where phth = *N*-phthalimido and $x = 1, 2$ (5). Treatment of such reagents with a thiol gives the desired products (reaction [1]).

[1] $RS_x\text{phth} + R'SH \rightarrow RS_xSR' + \text{Hphth}$

Accordingly, the metal thiolo complexes $AsPh_4[W(CO)_5SH]$ (6) and $CpW(CO)_3SH$ (7), where Cp = $(\eta^5\text{-}C_5H_5)$, were chosen for treatment with the sulfur-transfer reagents. The results of these reactions, which give novel polysulfanotungsten species, are reported below. Some of this work has appeared as part of a preliminary communication (8).

Results and discussion

The preparation of $CpW(CO)_3SH$, **1**, from $CpW(CO)_3I$ and NaSH is a viable alternative to that reported (*7a*) which was unsuccessful in our hands. **1** decomposes upon heating but reacts smoothly with sulfur transfer reagents (reaction [2]).

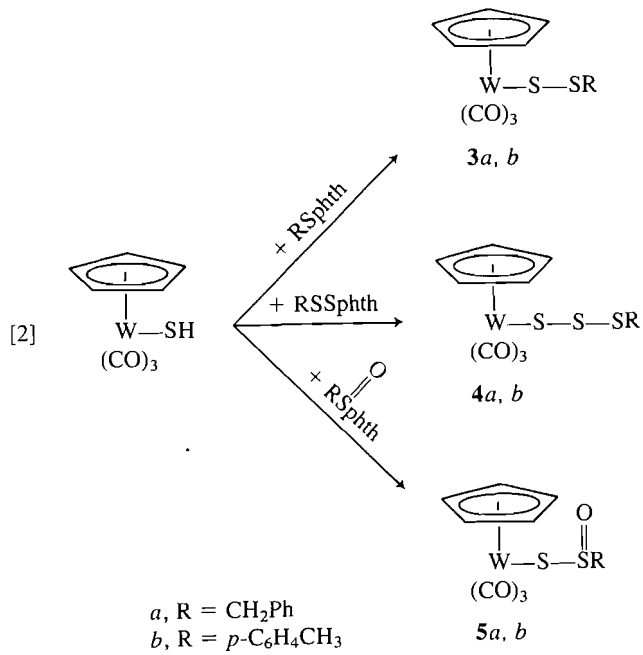

a, R = CH_2Ph
b, R = $p\text{-}C_6H_4CH_3$

At room temperature, the mono-sulfur transfer reagents, RSphth, gave a mixture of the thiolates, $CpW(CO)_3SR$, **2**, and the disulfanes, $CpW(CO)_3SSR$, **3**, in the ratio 1:4, where R = CH_2Ph (**2***a*, **3***a*) and $p\text{-}C_6H_4CH_3$ (**2***b*, **3***b*). The presence of **2** was determined by comparison of the nmr spectra of the crude products to that of authentic samples. Lowering the reaction temperature to −20°C reduced the contamination by **2** to 5%. The disulfanes could not be isolated by chromatography since

[1]The IUPAC convention for linear polysulfur compounds is that they be named polysulfanes (33).

TABLE 1. ν(CO) band positions (cm^{-1}) for $(\eta^5\text{-}C_5H_5)W(CO)_3Q$[a]

Q	Compound number	Bands		
SH	**1**	2028 (m)	1961 (sh)	1949 (s)
SCH_2Ph	**2***a*	2024 (m)	1948 (s)	1938 (s)
S-*p*-$C_6H_4CH_3$	**2***b*	2020 (m)	1935 (s)	
$SSCH_2Ph$	**3***a*	2022 (m)	1947 (sh)	1942 (s)
SS-*p*-$C_6H_4CH_3$	**3***b*	2028 (m)	1956 (s)	1943 (s)
$SS(O)CH_2Ph$	**3***a*	2036 (m)	1960 (s)	1950 (s)
SS(O)-*p*-$C_6H_4CH_3$	**3***b*	2034 (m)	1958 (s)	1949 (s)

[a]In cyclohexane solvent.

they desulfurize to the thiolates on the column. Recrystallization at −40°C gave good yields (70%) of **3***a*,*b*. Treatment of **1** with the disulfur transfer reagents, RSSphth, at −20°C, gave a mixture of two complexes also in the ratio 1:4 as determined by the relative heights of the peaks due to the Cp groups in the nmr spectra. The minor products were identified as **3***a*,*b* on the basis of their nmr spectra. The major products were assigned to be the trisulfane complexes $CpW(CO)_3SSSR$, (**4***a*,*b*), on the basis of their infrared and nmr spectra in solution since pure samples could not be isolated due to contamination by **3** and **2**. Treatment of **1** with the sulfinyl phthalimides, RS(O)phth at −20°C gave the novel oxodisulfanes $CpW(CO)_3SS(O)R$ (**5***a*,*b*) as the only products.

Elemental analyses consistent with their formulation were obtained for all of the above complexes, except **4***a*,*b*. The X-ray structure of **3***b* has been determined (8) and confirms the disulfane linkage.

The infrared spectra in the metal carbonyl stretching region and the nmr spectra of the complexes are summarized in Tables 1 and 2, respectively. The carbonyl stretching frequencies are fairly insensitive to the length of the sulfur chain. The spectra of crude **4** were superimposable on those of pure **3**. The bands observed for **5** exhibit a 5–10 cm^{-1} shift to higher wave numbers consistent with a slight reduction of electron density at the metal due to the presence of the SS(O) functionality. The latter complexes also gave bands (1073(m), 1049(m) cm^{-1}, **5***a*; and 1075(m), 1052(m) cm^{-1}, **5***b*) which do not appear in the spectra of **3**. These are assigned to S=O stretching modes (9); the presence of two bands possibly indicating conformational isomerism in **5** (10).

The ^{1}H nmr spectra of **2**–**5** are qualitatively very similar, as expected. Comparing **2***a*, **3***a*, and **4***a*, the peaks are shifted to lower field as the sulfur chain increases. This is consistent with the nmr spectra of organic polysulfides (11). A similar shift is observed for **2***b*, **3***b*, and **4***b* except that the band due to the Cp protons in **3***b* is upfield of that of **2***b*. The spectra of **5** are shifted slightly downfield from those **2**, **3**, and **4**, again consistent with the chemical shift observed (12) for organic thiosulfinates relative to organic disulfides. The resonance for the methylene protons of **5***a* is a doublet due to the presence of the oxygen on the sulfur atom which makes the latter chiral, thus rendering the methylene protons of **5***a* diastereotopic. Similar splitting is observed by this moiety in $PhCH_2S(O)$phth (13).

Complexes **3** and **4** spontaneously desulfurized in solution at room temperature to give **2** as the final products. The process was more rapid in benzene than in acetone. Thiolate formation from **3** was generally detected after 3 to 4 h in solution. For example, **3***b* showed 15% conversion after 5 h in deuteroacetone as shown by monitoring the nmr spectrum. The trisulfanes desulfurized more rapidly in solution than **3**. Complex **4***a* desulfurized to **3***a* upon attempted crystallization from CH_2Cl_2/hexanes; whereas **3***a* was isolated as a crystalline product under similar conditions. The nmr spectra of fresh crude **4** always indicated the presence of significant amounts of **3** but minimal formation of the final thiolates. The preparations of **3** and **4** were performed in THF which should be similar in its solvent effects to acetone. However, in the room temperature preparation of **3**, 20% of the thiolate was detected in the crude product after a reaction time of only 30 min. Thus desulfurization occurs to a greater extent during the preparation of the disulfanes than would be expected. This implies that thiolate formation during the preparation does not arise solely from desulfurization of the disulfane products. The observation of a significant amount of disulfane, but very little thiolate, in the crude product mixture of the trisulfanes is further indication that loss of sulfur may occur during the reactions.

Triphenylphosphine greatly enhanced the rate of desulfurization of **3** in C_6D_6. In the absence of PPh_3, 25% conversion to **2** had occurred after 4 h as shown by nmr while in the presence of PPh_3 conversion was complete. Desulfurization is a characteristic reaction of organic polysulfanes both thermally (14) and induced by trivalent phosphorus compounds (15). Normally, however, thermal desulfurization is slow at room temperature for organic trisulfanes and very slow for disulfanes; in addition, PPh_3 will not desulfurize most disulfanes. Thus, these metal polysulfanes are much more prone to desulfurization than their organic analogues. However, the greater lability of **4** compared to **3** is consistent with the relative ease of desulfurization of organic trisulfanes and disulfanes. Complexes **5** seemed to decompose more readily than the disulfanes **4** to give intractable mixtures. This behaviour is consistent with the behaviour of organic thiolsulfinates, RSS(O)R′, which are very unstable and disproportionate readily to disulfanes and thiolsulfonate esters, $RS(O)_2SR$, under mild conditions (16). However, the presence of an organometallic substituent appears to inhibit decomposition somewhat.

Oxidation of **3** with metachloroperbenzoic acid, under conditions similar to those used in the oxidation of organic sulfur compounds (13), led to the detection of several compounds in the ^{1}H-nmr spectra of the crude products. The cyclopentadienyl peaks were particularly diagnostic of the number of products formed (Table 3). In addition to **3**, significant amounts of **2**, and the oxodisulfanes, **5**, were identified in the ^{1}H-nmr spectra of the product mixtures. The cyclopentadienyl resonance of the known sulfinate complex $CpW(CO)_3SO_2CH_2Ph$, **6***a*, appears at 5.75 ppm (17) which corresponds to a peak in the spectrum of oxidized **3***a*. Peroxidation of **2***b* under similar condition gives a product, **6***b*, whose cyclopentadienyl resonance appears at 5.91 which corresponds to one of the products of oxidized **3***b*. The infrared spectra of the mixtures obtained upon oxidation of **3** displayed bands consistent with the presence of —S(O)— and $—SO_2—$ moieties (1050–1100 cm^{-1}, S=O stretch (9); 1100–1200 cm^{-1}, SO^2 asymmetric stretch (17)).

The peracid oxidation of unsymmetrical organic disulfanes (18) initially results in the preferential formation of a specific thiosulfinate, RS(O)SR′ or RSS(O)R′, depending on the nature of R and R′. Further oxidation occurs at the sulfur atom already oxidized to give a $—SO_2—$ moiety. However, due to the instability of organic thiosulfinates, complex mixtures are

Can. J. Chem. Downloaded from www.nrcresearchpress.com by 78.46.186.204 on 09/07/12
For personal use only.

Can. J. Chem. Downloaded from www.nrcresearchpress.com by 78.46.186.204 on 09/07/12
For personal use only.

TABLE 2. ^{1}H-nmr data for $(\eta^5\text{-}C_5H_5)W(CO)_3Q$ and $AsPh_4[W(CO)_5Q]$[a]

Q	Compound number	$\delta(C_5H_5)$	CH_2Ph $\delta(CH_2)$	CH_2Ph $\delta(C_6H_5)$	$CH_3C_6H_4$ $\delta(CH_3)$	$CH_3C_6H_4$ $\delta(C_6H_4)$[b]
$CpW(CO)_3Q$						
SH[c]	**1**	5.66				
SCH_2Ph	**2***a*	5.34	3.60	7.30		
$SSCH_2Ph$	**3***a*	5.66	3.95	7.30		
$SSSCH_2Ph$	**4***a*	5.80	4.09	7.33		
$SS(O)CH_2Ph$	**5***a*	5.78	4.34[d]	7.35		
S-*p*-$C_6H_4CH_3$	**2***b*	5.71			2.29	7.12
SS-*p*-$C_6H_4CH_3$	**3***b*	5.54			2.33	7.29
SSS-*p*-$C_6H_4CH_3$	**4***b*	5.71			2.35	7.35
SS(O)-*p*-$C_6H_4CH_3$	**5***b*	5.89			2.39	7.44
$AsPh_4[W(CO)_5Q]$[e,f]						
S-*p*-$C_6H_4CH_3$	**8**				2.14	7.05
SS-*p*-$C_6H_4CH_3$	**9**				2.23	7.21

[a]In $CDCl_3$.
[b]Quartet J(H—H) = 8 Hz.
[c]δ(SH) = −2.55.
[d]Doublet, J = 3 Hz.
[e]$\delta(As(C_6H_5)_4)$ = 7.7–7.8.
[f]$AsPh_4[(W(CO)_5)_2SC_6H_4CH_3]$ $\delta(CH_3)$ = 2.27, $\delta(C_6H_4)$ = 7.19.

TABLE 3. The ^{1}H-nmr spectra in the cyclopentadienyl region of the products of oxidation of $CpW(CO)_3SSCH_2Ph$ and $CpW(CO)_3SS$-*p*-$C_6H_4CH_3$

$CpW(CO)_3SSR$	Ratio of reagents 1:1	Ratio of reagents 1:25	Assignment
R = CH_2Ph	6.42 (1.0)[a]	[b]	
	5.78 (2.0)	5.78 (4.7)	**5***a*
	5.75 (1.0)	5.75 (2.3)	**6***a*
	5.66 (3.6)	5.66 (1.7)	**3***a*
	5.34 (1.7)	5.35 (1.0)	**2***a*
R = *p*-$C_6H_4CH_3$	[b]	6.24 (1.0)	
	6.17 (1.0)	6.17 (1.1)	
	5.92 (1.1)	5.91 (3.7)	**6***b*
	5.90 (1.4)	5.90 (2.0)	**5***b*
	5.85 (2.5)	[b]	
	5.71 (3.9)	5.71 (7.6)	**2***b*
	5.54 (6.6)	5.54 (1.9)	**3***b*

[a]Relative intensities given withint parentheses.
[b]Not observed.

isolated. At least eight products can be envisioned from the oxidation of **3** and the detection of **2** indicates that their oxidized forms must be considered.

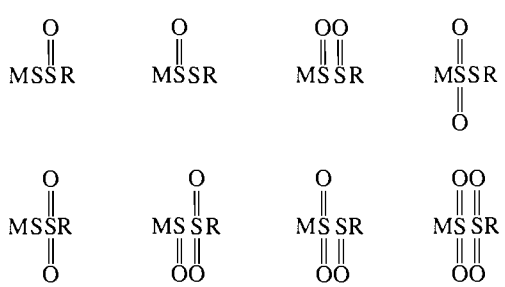

The disappearance of certain cyclopentadienyl peaks upon addition of excess peracid implies the further oxidation of products such as **5**. The appearance of the new Cp peaks to low field of those of **3** and **5** is also consistent with increased oxygenation of the ligands. The —SO_2SO_2— linkage has been observed in $[CpFe(CO)_2]_2S_2O_4$ (19) and $[Cp^*M(CO)_3]_2S_2O_4$, where Cp* = C_5Me_5 and M = Mo and W (20).

The tungsten thiol $AsPh_4[W(CO)_5SH]$, **7**, reacts with $CH_3C_6H_4Sphth$ to give, after recrystallization, the thiolate $AsPh_4[W(CO)_5S$-*p*-$C_6H_4CH_3]$, **8**. The nmr spectrum of fresh crude product from this reaction (Table 2) indicated that the first product was not **8** but another species tentatively assigned as the disulfane $AsPh_4[W(CO)_5SS$-*p*-$C_6H_4CH_3]$, **9**. After 24 h the spectrum indicated the presence of **8** at the expense of **9**. The results are consistent with formation of the disulfane during the reaction and its subsequent desulfurization upon work up.

The tendency of **3**, **4**, and **8** to lose sulfur easily contrasts with the complexes *cis*-$(PPh_3)_2Pt(phth)SSR$ which are quite stable (8, 21) and with complexes containing the biscyclopentadienyltitanium moiety which tend to incorporate sulfur into long chains (3*c*, 22). The factors which determine the length of the sulfur chain in a catenated polysulfano ligand are not well understood; however, an inverse correlation between the electron density at the metal center and sulfur chain length has been proposed (22). Thus, the lability observed for these tungsten systems is consistent with the relatively high electron density at the metal, particularly in the case of **8**.

Experimental

Apparatus and general procedures

All reactions and manipulations were carried out under nitrogen atmosphere, using the appropriate-sized three-necked round bottom flask, one neck of which was always equipped with a gas inlet. Standard inert atmosphere techniques were used (23). Chromatography was performed on activated alumina (Anachemia) (80–200 mesh). Irradiations were performed in a water-cooled Pyrex apparatus using an

Can. J. Chem. Downloaded from www.nrcresearchpress.com by 78.46.186.204 on 09/07/12
For personal use only.

immersion lamp (Hanovia, Hg vapour, 100 W). Infrared spectra were obtained on a Perkin–Elmer 297 spectrophotometer using 0.1 mm pathlength sodium chloride solution cells or pressed potassium bromide pellets containing the sample. The instrument was calibrated with the 1601.4 cm^{-1} band of polystyrene. ^{1}H-nmr spectra were measured on a Varian XL-200 spectrometer and all data are reported in ppm relative to an internal standard, TMS. Mass spectra were measured on an LKB 9000 mass spectrometer at the McGill University Mass Spectrometry Unit, with ionizing potentials of 15 or 70 eV. All mass ions are reported only for the lowest isotope (24) of tungsten (i.e. 182) as this simplified interpretation of overlapping fragmentation patterns. Elemental analyses were carried out by Midwest Microlab Ltd., Indianapolis, IN, and Guelph Chemical Laboratories Ltd., Guelph, Ont. Melting points were measured with a Thomas Hoover capillary melting point apparatus, and are uncorrected.

Tetrahydrofuran (THF), toluene, and dimethoxyethane were refluxed over sodium metal and benzophenone and collected by distillation under nitrogen. Spectrograde chloroform was passed through activated alumina and collected under nitrogen. Ethanol was refluxed over calcium hydride and distilled under nitrogen. The solvents used for recrystallizations and chromatography were spectrograde quality and, with the exception of ethanol and acetone, were stored over type 3A molecular sieves and purged with nitrogen prior to use. The following reagents were prepared as reported: *N*-(phenylmethyl)thiophthalimide, ($PhCH_2$Sphth) (25), *N*-(phenylmethyl)bisthiophthalimide ($PhCH_2$SSphth) (26), *N*-(phenylmethyl)sulfinylphthalimide ($PhCH_2$S(O)phth) (13), *N*-(4-methylbenzene)thiosuccinimide (*p*-$CH_3C_6H_4$Ssucc) (25), *N*-(4-methylbenzene)thiophthalimide (*p*-$CH_3C_6H_4$Sphth) (27), *N*-(4-methylbenzene)bisthiophthalimide (*p*-$CH_3C_6H_4$SSphth) (26), *N*-(4-methylbenzene)sulfinylphthalimide (*p*-$CH_3C_6H_4$S(O)phth) (13), sodium hydrogen sulfide (28), $AsPh_4$[W(CO)$_5$SH] (6*b*,*c*). The thiolato complexes $AsPh_4$[W(CO)$_5$S-*p*-$C_6H_4CH_3$] and $AsPh_4$[W(CO)$_5$)$_2$S-*p*-$C_6H_4CH_3$] (29) were prepared by an analogous route (6*b*,*c*) from W(CO)$_5$THF (30) and sodium 4-methylbenzenethiolate, both prepared *in situ*, in the appropriate ratio (1:4 and 1:1, respectively). Cp$_3$W(CO)$_3$I was prepared by the method reported (31) for the analogous molybdenum complex (^{1}H-nmr ($CDCl_3$): 5.65 ppm; infrared (cyclohexane) ν(CO): 2030 (w), 1961 (m), 1948 (m) cm^{-1}. This complex was treated with the appropriate sodium thiolate to give Cp$_3$W(CO)$_3$SCH_2Ph and Cp$_3$W(CO)$_3$S-*p*-$C_6H_4CH_3$ (32).

*Cyclopentadienyltricarbonylthiolotungsten(II), Cp$_3$W(CO)$_3$SH, **1***

A solution of (C_5H_5)W(CO)$_3$I (3.33 g, 7.29 mmol) in 100 mL of tetrahydrofuran was added dropwise over 0.5 h to a solution of NaSH (22 mmol, 3 equiv.) prepared *in situ* in 40 mL of ethanol. The resultant mixture was stirred for 12 h at room temperature, followed by removal of the solvent under reduced pressure (water aspirator). Sublimation of the crude material, under vacuum at 70°C, gave 0.99 g (39%) of the title compound as orange needles (mp 105°C, lit. (7) 106°C; infrared (cyclohexane) ν(CO): 2028 (w), 1961 (sh), 1949 (s) cm^{-1}. Mass spectrum: *m*/*e* 364 (M^+), 336 (M^+ − CO), 308 (M^+ − 2CO), 303 (M^+ − CO − SH), 280 (M^+ − 3CO), 275 (M^+ − 2CO − SH), 247 (M^+ − 3CO − SH), 252–259 (unassigned peaks). *Anal.* calcd. for $C_8H_6O_3SW$: C 26.2, H 1.64, S 8.75; found: C 26.3, H 1.71, S 8.82.

*Cyclopentadienyltricarbonylphenylmethyldisulfanotungsten(II), Cp$_3$W(CO)$_3$SSCH_2Ph, **3**a*

This preparation is typical of the general methods employed and is described in detail. A solution of $PhCH_2$Sphth (0.221 g, 0.82 mmol), in 20 mL of THF was added dropwise over 15 min to Cp$_3$W(CO)$_3$SH (0.300 g, 0.82 mmol) in 300 mL of THF, at −20°C. The resulting red solution was stirred, at −20°C, for an additional 15 min, and reduced to dryness under vacuum at 0°C. The residue was extracted twice with carbon disulfide (25 mL total). The combined extracts were filtered through celite and evaporated to dryness under vacuum. The crude product was dissolved in a minimum of methylene chloride (5–10 mL) and 20–40 mL of hexane was added so as to form a layer on top of this solution. Cooling at −40°C overnight gave the complex as red crystals. The mother liquors were removed with a syringe and the crystals were washed with pentane and dried *in vacuo* for 6 h (0.28 g, 70%, mp 89°C). Infrared (cyclohexane) ν(CO): 2022 (w), 1947 (sh), 1942 (m) cm^{-1}. Mass spectrum *m*/*e*$^+$ 458 (M^+ − CO), 426 (M^+ − CO − S), 402 (M^+ − 3CO), 398 (M^+ − S − 2CO), 370 (M^+ − S − 3CO), 367 (M^+ − CO − $CH_2C_6H_5$), 338 (M^+ − 3CO − 2S), 335 (M^+ − CO − S$CH_2C_6H_5$), 307 (M^+ − 2CO − S$CH_2C_6H_5$), 279 ((C_5H_5)WS$^+$), 275 ((C_5H_5)W(CO)$^+$), 247 ((C_5H_5)W$^+$). *Anal.* calcd. for $C_{15}H_{12}O_3S_2W$: C 36.9, H 2.46, S 13.1; found: C 36.8, H 2.57, S 12.8.

*Cyclopentadienyltricarbonyl-4-methylbenzenedisulfanotungsten(II), Cp$_3$W(CO)$_3$SS-p-$C_6H_4CH_3$, **3**b*

As above, *p*-$CH_3C_6H_4$Sphth (0.081 g, 0.30 mmol) in THF (20 mL) was stirred, at −20°C, with Cp$_3$W(CO)$_3$SH (0.110 g, 0.30 mmol) in THF (20 mL) for 0.5 h. Recrystallization gave orange crystals (0.125 g, 70%, mp 89°C). Infrared (cyclohexane) ν(CO): 2028 (w), 1956 (m), 1943 (m) cm^{-1}. Mass spectrum: *m*/*e*$^+$ 458 (M^+ − CO), 454 (M^+ − S), 430 (M^+ − 2CO), 426 (M^+ − CO − S), 402 (M^+ − 3CO), 398 (M^+ − S − 2CO), 370 (M^+ − S − 3CO), 367 (M^+ − CO − $C_6H_4CH_3$), 335 (M^+ − CO − S$C_6H_4CH_3$), 307 (M^+ − 2CO − S$C_6H_4CH_3$), 279 ((C_5H_5)WS$^+$), 279 ((C_5H_5)WS$^+$), 247 ((C_5H_5)W$^+$). *Anal.* calcd. for $C_{15}H_{12}O_3S_2W$: C 36.9, H 2.46, S 13.1; found: C 37.3, H 2.50, S 13.0.

*Cyclopentadienyltricarbonylphenylmethyltrisulfanotungsten(II), Cp$_3$W(CO)$_3$SSSCH_2Ph, **4**a*

Cp$_3$W(CO)$_3$SH (0.096 g, 0.26 mmol) in THF (10 mL) was stirred for 30 min with $PhCH_2$SSphth (0.080 g, 0.27 mmol) in THF (10 mL) at −20°C. The ^{1}H-nmr spectrum ($CDCl_3$) showed that the crude product was contaminated by Cp$_3$W(CO)$_3$SSCH_2Ph present in about 25% with respect to the title complex. Attempts to isolate the trisulfano complex were unsuccessful leading instead to the production of more of the disulfano contaminant or to decomposition. The infrared spectrum of the crude product in cyclohexane gave three bands in the carbonyl region, at 2028 (w), 1959 (m), and 1944 (m) cm^{-1}.

*Cyclopentadienyltricarbonyl-4-methylbenzenetrisulfanotungsten(II), Cp$_3$W(CO)$_3$SSS-p-$C_6H_4CH_3$, **4**b*

Cp$_3$W(CO)$_3$SH (0.046 g, 0.126 mmol) in THF (10 mL) was stirred for 30 min with $CH_3C_6H_4$SSphth (0.038 g, 0.126 mmol) in THF (10 mL) at −20°C. The ^{1}H-nmr spectrum ($CDCl_3$) showed that the crude product contained Cp$_3$W(CO)$_3$SS$C_6H_4CH_3$ present in about 25% with respect to the title complex. Repeated recrystallizations from methylene chloride/hexane gave solids which exhibited spectra identical to the crude material. The infrared spectrum in cyclohexane gave bands at 2026 (w), 1956 (m), and 1945 (m) cm^{-1}.

*Cyclopentadienyltricarbonylphenylmethyl-2-oxodisulfanotungsten(II), Cp$_3$W(CO)$_3$SS(O)CH_2Ph, **5**a*

$PhCH_2$S(O)phth (0.075 g, 0.27 mmol) in THF (10 mL) was added to Cp$_3$W(CO)$_3$SH (0.088 g, 0.25 mmol) in THF (10 mL) at −20°C and stirred for 30 min. The product was obtained as orange–red microcrystals (0.075 g, 61%, mp 97°C). Infrared (cyclohexane) ν(CO): 2036 (w), 1960 (m), 1950 (m). Mass spectrum: *m*/*e*$^+$ 458 (M^+ − CO − O), 430 (M^+ − 2CO − O), 418 (M^+ − 3CO), 402 (M^+ − 3CO − O), 370 (M^+ − 3CO − S − O), 335 (M^+ − CO − S(O)$CH_2C_6H_5$), 307 (M^+ − 2CO − S(O)$CH_2C_6H_5$), 247 ((C_5H_5)W$^+$). *Anal.* calcd. for $C_{15}H_{12}O_4S_2W$: C 35.7, H 2.38, S 12.7; found: C 35.6, H 2.46, S 12.9.

*Cyclopentadienyltricarbonyl-4-methybenzene-2-oxodisulfanotungsten(II), Cp$_3$W(CO)$_3$SS(O)-p-$C_6H_4CH_3$, **5**b*

p-$CH_3C_6H_4$S(O)phth (0.114 g, 0.40 mmol) in THF (15 mL) was added, at 0°C, to Cp$_3$W(CO)$_3$SH (0.146 g, 0.40 mmol) in THF (15 mL) and the solution stirred for 30 min. The complex is orange–red in colour (0.086 g, 41%, mp 96°C). Infrared (cyclohexane) ν(CO): 2034 (w), 1958 (m), 1949 (m) cm^{-1}. Mass spectrum: *m*/*e*$^+$ 430 (M^+ − 2CO − O), 418 (M^+ − 3CO), 402 (M^+ − 3CO − O), 370 (M^+ − 3CO − S(O)), 366 (M^+ − 2CO − SS(O)), 279 ((C_5H_5)WS$^+$), 247 ((C_5H_5)W$^+$). *Anal.* calcd. for $C_{15}H_{12}O_4S_2W$: C 35.7, H 2.38, S 12.7; found: C 35.4, H 2.53, S 12.7.

Desulfurization of $CpW(CO)_3SSCH_2Ph$ and $CpW(CO)_3SS$-p-$C_6H_4CH_3$

Two nmr samples in C_6D_6 were prepared for each complex: one, A, contained only the complex while the other, B, contained equimolar amounts of complex and triphenylphosphine. The peaks due to the starting complexes gradually decreased in intensity while those due to the thiolates concommitantly appeared and increased in intensity in all samples. For **3***a*, the ratio of starting complex to thiolate after 5 h was 5:2 in sample A while in sample B signals due to starting complex were not detected. For **3***b*, the corresponding ratio after 4 h was 4:1 in sample A and no signal was observed for the disulfano complex in sample B. The dried residue from the B samples exhibited ir bands characteristic of triphenylphosphinesulfide superimposed on those due to the thiolate complexes.

Oxidation of $CpW(CO)_3SSCH_2Ph$ and $CpW(CO)_3SS$-p-$C_6H_4CH_3$ with m-chloroperbenzoic acid

Each complex was treated with a stoichiometric amount of oxidant and, in a second reaction, with 2.5 equiv. *m*-Chloroperbenzoic acid in $CHCl_3$ (10 mL) was added dropwise over 15 min to the complex in $CHCl_3$ (10 mL) at 0°C. After stirring for an additional 15 min, the solution was rapidly transferred to a separatory funnel and washed with 5% aqueous sodium bicarbonate (3 × 15 mL) and with 15 mL of distilled water, purging the chloroform layer with nitrogen after each washing. The solution was dried (under nitrogen) with anhydrous sodium sulfate and filtered. The solvent was vacuum evaporated and the residue dried under vacuum for 12 h. These residues were characterized by their ^{1}H-nmr spectra in $CDCl_3$ (Table 3).

*Attempted synthesis of tetraphenylarsonium pentacarbonyl-4-methylbenzenedisulfanotungstate(0), $AsPH_4[W(CO)_5SS$-p-$C_6H_4CH_3]$, **9***

p-$CH_3C_6H_4S$succinimido (0.111 g, 0.50 mmol) in THF (15 mL) was added dropwise to $AsPh_4[W(CO)_5SH]$ (0.346 g, 0.49 mmol) in THF (50 mL) and the mixture was stirred for 90 min. Then it was filtered and evaporated under vacuum to a yellow oil. This was dissolved in a minimum of 1:1 ethanol/methanol and treated with 2 volumes of hexane. Cooling at −40°C gave a yellow crystalline solid in low yield, identified as $AsPh_4[W(CO)_5S$-*p*-$C_6H_4CH_3]$, **8**, on the basis of its ^{1}H-nmr and ir spectra and elemental analysis. Repeating the preparation using *p*-$CH_3C_6H_4$Sphth gave the same result. However, in one experiment the latter reaction was conducted at −20°C for 15 min and rapidly vacuum dried at 0°C. The ^{1}H-nmr spectrum of the residue in acetone-d_6 gave peaks at 7.21 (q, 4H, C_6H_4, J(H—H) = 8 Hz) and 2.23 (s, 3H, CH_3) in addition to peaks due to *p*-$CH_3C_6H_4$Sphth and phthalimide. After 24 h peaks due to **8** had appeared at the expense of those originally observed.

Acknowledgements

This research was supported by grants from the Natural Sciences and Engineering Research Council of Canada (NSERCC) and the Quebec Department of Education. A NSERCC postgraduate scholarship award to J.H. is gratefully acknowledged.

1. (*a*) P. C. Jocelyn. Biochemistry of the SH group. Academic Press, London. 1972; (*b*) A. B. Roy and P. A. Trudinger. The biochemistry of inorganic compounds of sulfur. Cambridge University Press, Cambridge, U.K. 1970; (*c*) E. E. Ried. Organic chemistry of bivalent sulfur. Vol. 3. Chemical Publishing Co., New York. 1960. p. 362.
2. (*a*) E. W. Abel and B. C. Crosse. Organomet. Chem. Rev. **2**, 443 (1967); (*b*) S. E. Livingstone. Q. Rev. **19**, 386 (1965).
3. (*a*) S. N. Bhattacharyya, C. V. Senoff, and F. S. Walker. Inorg. Chim. Acta, **44**, L273 (1980); (*b*) D. M. Giolando and T. B. Rauchfuss. J. Am. Chem. Soc. **3**, 487 (1984); (*c*) A. Shaver, J. M. McCall, P. H. Bird, and N. Ansari. Organometallics, **2**, 1894 (1983).
4. F. Field. *In* Organic chemistry of sulfur. *Edited by* S. Oae. Plenum Press, New York. 1977. p. 303.
5. (*a*) D. N. Harpp, D. K. Ash, T. G. Back, J. G. Gleason, B. A. Orwig, W. F. van Horn, and J. P. Snyder. Tetrahedron Lett. 3551 (1970); (*b*) K. S. Boustany and A. B. Sullivan. Tetrahedron Lett. 3547 (1970); (*c*) D. N. Harpp and D. K. Ash. Int. J. Sulfur Chem. A, **1**, 211 (1971).
6. (*a*) R. G. W. Gingerich and R. J. Angelici. J. Am. Chem. Soc. **101**, 5604 (1979); (*b*) H. Hausmann, M. Höfter, T. Kruck, and H. W. Zimmermann. Chem. Ber. **114**, 975 (1981); (*c*) M. K. Cooper, P. A. Duckworth, K. Henrick, and M. McPartlin. J. Organomet. Chem. **212**, C10 (1981).
7. (*a*) W. Beck, W. Danzer, and G. Thiel. Angew. Chem. Int. Ed. **12**, 582 (1973); (*b*) W. Danzer, W. P. Fehlhammer, A. T. Liu, G. Thiel, and W. Beck. Chem. Ber. **115**, 1682 (1982).
8. A. Shaver, J. Hartgerink, R. D. Lai, P. Bird, and N. Ansari. Organometallics, **2**, 938 (1983).
9. (*a*) S. J. Markham, Y. L. Chung, G. D. Branum, and D. M. Blake. J. Organomet. Chem. **107**, 121 (1976); (*b*) S. Ghersetti and G. Modena. Spectrochim. Acta, **19**, 1809 (1963).
10. A. Shaver. Can. J. Chem. **56**, 2281 (1978).
11. J. R. Van Wazer and D. Grant. J. Am. Chem. Soc. **86**, 1450 (1964).
12. T. Takata, Y. H. Kim, and S. Oae. Tetrahedron Lett. 4303 (1978).
13. D. N. Harpp and T. G. Back. J. Org. Chem. **38**, 4328 (1973).
14. E. Bock. Q. Rep. Sulfur Chem. **4**, 237 (1969).
15. (*a*) A. Schönberg and M. Z. Barakat. J. Chem. Soc. 892 (1949); (*b*) A. A. Watson. J. Chem. Soc. 2100 (1964); (*c*) C. G. Moore and B. R. Trego. Tetrahedron, **18**, 205 (1962).
16. (*a*) E. Block. J. Am. Chem. Soc. **95**, 5046 (1973); (*b*) D. Barnard. J. Chem. Soc. 4675 (1957); (*c*) W. E. Savige and A. Fava. J. Chem. Soc. Chem. Commun. 417 (1965).
17. J. O. Kroll and A. Wojcicki. J. Organomet. Chem. **66**, 95 (1974).
18. (*a*) P. Allen and J. W. Brook. J. Org. Chem. **27**, 1019 (1962); (*b*) E. E. Ried. Organic chemistry of bivalent sulfur. Vol. 1. Chemical Publishing Co., New York. 1958. p. 330; (*c*) L. Field, H. Härle, T. C. Owen, and A. Ferette. J. Org. Chem. **29**, 1632 (1964).
19. C. A. Poffenberger, N. H. Tennent, and A. Wojcicki. J. Organomet. Chem. **181**, 107 (1980).
20. G. J. Kubas, H. J. Wasserman, and R. R. Ryan. Organometallics, **4**, 2012 (1985).
21. R. D. Lai. Ph.D. Thesis, McGill University, Montreal. 1981.
22. A. Shaver and J. M. McCall. Organometallics, **3**, 1823 (1984).
23. D. F. Shriver. The manipulation of air-sensitive compounds. McGraw Hill, New York. 1969. p. 141.
24. C. M. Lederer, J. M. Hollander, and I. Perlman. Table of isotopes. 6th ed. Wiley and Sons, New York. 1968. p. 108.
25. M. Behforouz and J. E. Kerwood. J. Org. Chem. **34**, 51 (1969).
26. D. N. Harpp and D. K. Ash. Int. J. Sulfur Chem. **1**, 57 (1971).
27. Y. Abe, T. Nakabayashi, and J. Tsurugi. Bull. Chem. Soc. Jpn. **46**, 1898 (1973).
28. R. E. Eibeck. Inorg. Synth. **7**, 128 (1963).
29. J. K. Ruff and R. B. King. Inorg. Chem. **8**, 180 (1969).
30. D. W. Strohmeier. Angew. Chem. Int. Ed. **3**, 730 (1964).
31. T. S. Piper and G. Wilkinson. J. Inorg. Nucl. Chem. **3**, 104 (1956).
32. D. D. Watkins and T. A. George. J. Organomet. Chem. **102**, 71 (1975).
33. K. L. Leoning. *In* Sulfur in organic and inorganic chemistry. Vol. 3. *Edited by* A. Senning. Marcel Dekker, New York. 1972. pp. 339–354.

Can. J. Chem. Downloaded from www.nrcresearchpress.com by 78.46.186.204 on 09/07/12
For personal use only.

Preparation, properties, and characterization of methanesulfonato complexes of arsenic(III), antimony(III), and bismuth(III)

RAMESH KAPOOR, POONAM WADHAWAN, AND PRATIBHA KAPOOR
Department of Chemistry, Panjab University, Chandigarh-160014, India

Received July 25, 1986[1]

RAMESH KAPOOR, POONAM WADHAWAN, and PRATIBHA KAPOOR. Can. J. Chem. **65**, 1195 (1987).

Arsenic(III), antimony(III), and bismuth(III) oxides, sodium arsenite and bismuthate react with methanesulfonic anhydride, $(CH_3)_2S_2O_5$, to yield $M(SO_3CH_3)_3$ (M = As(III), Sb(III), and Bi(III)), $Na[AsO(SO_3CH_3)_2]$, and $Na[Bi(SO_3CH_3)_4]$, respectively, in quantitative yield. Reaction of arsenic(III) oxide with pure methanesulfonic acid yields oxo(methanesulfonato)arsenic(III), $AsO(SO_3CH_3)$, which behaves as a non-electrolyte in 100% methanesulfonic acid. The compounds have been characterized by elemental analysis, conductance, infrared, ^1H nmr and thermal measurements. Their properties have been studied by ligand substitution and complex formation reactions. The $M(SO_3CH_3)_3$ (M = As(III), Sb(III), and Bi(III)) compounds are capable of functioning both as Lewis acids and bases. These compounds exhibit basic behaviour in 100% methanesulfonic acid. The synthesis of complex mathanesulfonates $Cs[M(SO_3CH_3)_4]$ (M = As(III), Sb(III), and Bi(III)) is also described.

RAMESH KAPOOR, POONAM WADHAWAN et PRATIBHA KAPOOR. Can. J. Chem. **65**, 1195 (1987).

Les oxydes d'arsenic(III), d'antimoine(III) et de bismuth(III) ainsi que l'arsénite et le bismuthate de sodium réagissent avec l'anhydride de l'acide méthanesulfonique, $(CH_3)_2S_2O_5$, pour conduire respectivement et quantitativement aux sels $M(SO_3CH_3)_3$ (M = As(III), Sb(III) et Bi(III)), $Na[AsO(SO_3CH_3)_2]$ et $Na[Bi(SO_3CH_3)_4]$. La réaction de l'oxyde d'arsenic(III) avec l'acide méthanesulfonique pur conduit à l'oxo(méthanesulfonato)arsenic(III), $As(O(SO_3CH_3)$, qui se comporte comme un non-électrolyte dans l'acide méthanesulfonique à 100%. On a caractérisé les composés en se basant sur les analyses élémentaires, sur les conductivités, sur les spectres infrarouges et rmn du ^1H ainsi que sur des mesures thermiques. On a étudié les propriétés chimiques en procédant à des réactions de substitution de ligands et de formation de complexes. Les composés $M(SO_3CH_3)_3$ (M = As(III), Sb(III) et Bi(III)) peuvent aussi bien fonctionner comme acides que comme bases de Lewis. Dans l'acide méthanesulfonique à 100%, ces composés agissent comme bases. On décrit aussi la synthèse des méthanesulfonates complexes $Cs[M(SO_3CH_3)_4]$ (M = As(III), Sb(III) et Bi(III)).

[Traduit par la revue]

Introduction

Methanesulfonates of only a few elements have been prepared in the past mainly using solvolytic reactions in methanesulfonic acid (1–12). This paper describes the synthesis and characterization of compounds $M(SO_3CH_3)_3$ (M = As(III), Sb(III), and Bi(III)), $[NaAsO(SO_3CH_3)_2]$, and $Na[Bi(SO_3CH_3)_4]$ by reaction of methanesulfonic anhydride with suitable oxides or oxosalts. The corresponding $M(SO_3X)_3$ salts (M = Sb(III) and Bi(III), and X = F and CF_3) have been reported in the literature (13–15) and are compared here with the methanesulfonates.

Experimental

All reagents (As_2O_3, Sb_2O_3, Bi_2O_3, As_2O_5, Sb_2O_5, $NaAsO_2$, $NaBiO_3$, $(CH_3)_4N^+Br^-$, NH_4SCN) were dried by heating them under vacuum at about 110°C for several hours. Methanesulfonic acid (BDH, 98%) was made anhydrous by equilibrating it with methanesulfonic anhydride for about 4 to 6 h at ≅70°C and then distilling it under reduced pressure (bp 165°C at 2 mm Hg). Acid having a minimum conductivity of ca. 4.8×10^{-4} ohm^{-1} cm^{-1} was used (5). Methanesulfonic anhydride was prepared by mixing methanesulfonic acid (60 g) and P_4O_{10} (20 g) and heating the mixture to ≅100°C for about 2 h to complete the dehydration of the acid. The equilibrated mixture was then distilled under reduced pressure and methanesulfonic anhydride was obtained as a white crystalline solid, mp 68–70°C. 1,2-Dimethyoxyethane was refluxed over sodium metal for 8 h and then distilled. The distilled product was kept over sodium wire. Dimethylformamide was dried over molecular sieves and distilled at reduced pressure. Pyridine was distilled after keeping it over KOH pellets for 24 h. Acetonitrile was distilled over P_4O_{10} and kept over molecular sieves. Cesium methanesulfonate was prepared by dissolving cesium carbonate in aqueous methanesulfonic acid and evaporating to dryness. It was recrystallized from water and dried for several hours at 110°C.

[1]Revision received December 29, 1986.

Instrumentation

Conductance measurements were performed with a Toshniwal C1 01/01 type conductivity bridge at 25°C using conductivity cell having a cell constant of 51.98 cm^{-1}. Infrared spectra were recorded on a Perkin-Elmer 621 double beam grating spectrophotometer as Nujol and hexachlorobutadiene mulls between NaCl and polyethylene plates. Potassium bromide plates could not be used as the compounds react with them to liberate bromine. Thermal analysis was carried out on MOM Budapest Derivatograph, type Paulik, Paulik, Erdey. ^1H nmr spectra were recorded in formamide solutions on Varian EM 390 with reference to TMS as internal standard. Mass spectra were recorded on VG Micromass mm 70/70.

Synthesis

All the compounds discussed here are air-sensitive and required handling in dry nitrogen atmosphere, dry box, or *in vacuo*.

Tris(methanesulfonates) of arsenic, antimony, and bismuth, M-$(SO_3CH_3)_3$: These comounds were prepared by heating metal oxide (10 mmol) and methanesulfonic anhydride (40 mmol) to approximately 140°C for 24 h. The time taken for completion of the reaction decreased with increasing basicity of the oxide, i.e., reaction of Bi_2O_3 with $(CH_3)_2S_2O_5$ was over only in 2 to 3 h. The contents were then stirred with 40–50 mL of freshly distilled diethylether. The white-to-grey solid products were removed by vacuum filtration and then washed with several portions of diethylether. The final products were obtained by drying them under vacuum for several hours.

Ammonium methanesulfonatotris(isothiocyanato)arsenate(III)/antimonate(III)/bismuthate(III), $NH_4[M(SO_3CH_3)(NCS)_3]$ (M = As, Sb or Bi): To a solution of 0.20 g (0.5 mmol) of $As(SO_3CH_3)_3$ in 1,2-dimethyloxyethane (15 mL) was added a clear solution of 0.16 g (2.1 mmol) of NH_4CNS in 20 mL of the same solvent. A white precipitate immediately appeared which was stirred for about an hour. The product was filtered and dried under vacuum. The compound is highly air-sensitive. To 0.34 g (0.8 mmol) of $Sb(SO_3CH_3)_3$ was added a solution of 0.26 g (3.4 mmol) NH_4CNS in 30 mL of dimethoxyethane. The suspension immediately gave a white precipitate which

Can. J. Chem. Downloaded from www.nrcresearchpress.com by 78.46.186.204 on 09/07/12
For personal use only.

TABLE 2. Pertinent infrared spectral bands (cm^{-1}) of some methanesulfonates

Assignments C_{3v}	Compounds					
	$As(SO_3CH_3)_3$	$Sb(SO_3CH_3)_3$	$Bi(SO_3CH_3)_3$	$Na[AsO(SO_3CH_3)_2]$	$Na[Bi(SO_3CH_3)_4]$	$AsO(SO_3CH_3)$
SO_3 asym. str.	1260m, 1200s, br	1260m, 1200s, br	1260m, 1200s, br	1255w, 1190–1170s, br	1260m, 1200m, 1170m	1260m, 1200s, 1175w, 1140m
SO_3 sym. str.	1065m, 1055m	1080m 1065m	1075m, 1065m	1075m, 1060m 980m, 910m?	1060m 1015w?	1070m 980m, 910m?
S—CH_3 str.	795m	790m, 720m	790m, 720m	780m	780m, 725w	805m, 795m, 645m
SO_3 asym. bend	560m	565m	565m	555m	565sh	560m
SO_3 sym. bend.	540m, 515m	540m, 525m	538m, 510m	530m, 500m	545m, 505m	535m, 525m
SO_3 rock	350m, 330m	370m, 330m	380m, 340m	— 350m, br	360m, 335m	365m, 320m

was filtered and dried *in vacuo*. The procedure used for bismuth complex was identical with that for the antimony complex. However, the product was a pale-yellow compound which was quite stable to moist air.

Tetramethylammonium tetrabromoantimonate(III)/bismuthate(III), $[(CH_3)_4N]^+[MBr_4]^-$ (M = Sb and Bi): To about 0.4–0.5 g (≅1 mmol) of $Sb(SO_3CH_3)_3$ or $Bi(SO_3CH_3)_3$ was added a solution of about 0.9 to 1.0 g (≅6 mmol) of $(CH_3)_4NBr$ in 20 mL of anhydrous methanol. The resulting suspension immediately turned into a thick creamy white precipitate. It was stirred for 4 to 6 h and then filtered. The precipitates were washed with methanol and dried *in vacuo*. The products are air-stable. Reaction of $As(SO_3CH_3)_3$ with $(CH_3)_4NBr$ did not yield any precipitate. On addition of diethylether to the solution, the original compound $As(SO_3CH_3)_3$ separated out.

Pyridine and dimethylformamide complexes: All the complexes were prepared in the same general manner. In a typical experiment, excess amount of pyridine or DMF was added to the suspension of metal(III) methanesulfonate (4:1) in light petroleum ether at about −10°C. The contents were stirred for about 4 to 6 h. The products were vacuum filtered, washed several times with fresh samples of light petroleum ether, and finally dried *in vacuo*.

Boron tribromide complexes, $M(SO_3CH_3)_3 \cdot BBr_3$ (M = As, Sb, or Bi): In a typical experiment, $As(SO_3CH_3)_3$ (0.47 g, 1.3 mmol) was taken in $CHCl_3$ (10 mL) and a solution of BBr_3 (0.33 g, 1.3 mmol) in $CHCl_3$ (5 mL) was added. An exothermic reaction occurred immediately and the mixture was allowed to stir for 2 h at −10°C. The contents were vacuum filtered and dried under vacuum. Complexes of BBr_3 with $Sb(SO_3CH_3)_3$ and $Bi(SO_3CH_3)_3$ were prepared in a similar fashion. The pale-yellow adducts were unstable and highly sensitive to moist air.

Cesium tetrakis(methanesulfonato)arsenate(III)/antimonate(III)/bismuthate(III), $Cs[M(SO_3CH_3)_4]$ (M = As, Sb or Bi): Equimolar solutions of cesium methanesulfonate and tris(methanesulfonate) arsenic(III)/antimony(III)/bismuth(III) in pure methanesulfonic acid were heated for about 12 h around 140°C. The complexes were recovered as greyish-white precipitates by adding a large excess of dry diethylether to the solution. The complexes were vacuum filtered and dried *in vacuo*.

Sodium oxobis(methanesulfonato)arsenate(III), $Na[AsO(SO_3CH_3)_2]$: Sodium arsenite, $NaAsO_2$ (1.3 g, 10 mmol), was stirred with methanesulfonic anhydride (3.8 g, 22 mmol) in diethylether at room temperature for 2–4 h. The fluffy white precipitate was vacuum filtered, washed with several lots of freshly distiled diethylether, and dried *in vacuo*.

Sodium tetrakis(methanesulfonato)bismuthate(III), $Na[Bi(SO_3CH_3)_4]$: Sodium bismuthate, $NaBiO_3$ (1.4 g, 5 mmol), was stirred with methanesulfonic anhydride (2.6 g, 15 mmol) in diethylether for about 4 h at room temperature. The rest of the procedure was the same as followed above.

Oxo(methanesulfonato)arsenic(III), $AsO(SO_3CH_3)$: Saturated solution of As_2O_3 in pure methanesulfonic acid at room temperature gave a white precipitate which was filtered, washed with diethylether, and dried *in vacuo*. Its adduct with pyridine was obtained by stirring $AsO(SO_3CH_3)$ with excess of pyridine in light petroleum ether at room temperature for 6 to 8 h. The product was filtered, washed with light petroleum ether, and dried *in vacuo*.

Arsenic and antimony in these compounds were estimated volumetrically by titrating with standard potassium iodate. Bismuth was estimated gravimetrically as oxyiodide, BiOI. Sulfur and bromine were estimated gravimetrically as $BaSO_4$ and AgBr, respectively. Carbon, hydrogen, and nitrogen were estimated microanalytically. Table 1 summarizes the analytical data of the complexes prepared above.[2]

Results and discussion

Arsenic(III), antimony(III), and bismuth(III) methanesulfonates have been prepared in quantitative yield by the reaction of methanesulfonic anhydride with the respective metal oxides.

$$M_2O_3 + 3(CH_3)_2S_2O_5 \rightarrow 2M(SO_3CH_3)_3$$

M = As(III), Sb(III), and Bi(III)

This reaction is a very convenient preparative route to the synthesis of methanesulfonate derivatives. Reactions of methane and trifluoromethanesulfonic acids with metal halides/acetates or oxides even at elevated temperatures often do not yield desired products in pure form due to contamination with side products.

These compounds are highly sensitive to moisture. They do not melt up to 240°C. They are insoluble in common organic solvents such as $C_6H_5NO_2$, CH_3NO_2, and CH_3CN. They are, however, soluble in basic organic solvents such as MeOH, DMF, NMF, DMSO. Λ_M values of their millimolar solutions in DMF (81 to 98 ohm^{-1} cm^2 mol^{-1}) and DMSO (66 to 73 ohm^{-1} cm^2 mol^{-1}) suggest that the compounds behave as 1:1 electrolytes (16):

$$[1] \quad M(SO_3CH_3)_3 \xrightarrow{DMF} [M(SO_3CH_3)_2(DMF)_2]^+ + CH_3SO_3^-$$

[2]Table 1 may be purchased from the Depository of Unpublished Data, CISTI, National Research Council of Canada, Ottawa, Ont., Canada K1A 0S2.

Can. J. Chem. Downloaded from www.nrcresearchpress.com by 78.46.186.204 on 09/07/12
For personal use only.

Can. J. Chem. Downloaded from www.nrcresearchpress.com by 78.46.186.204 on 09/07/12
For personal use only.

Possibly, the basic solvent molecules (DMF or DMSO) displace the weakly coordinating $CH_3SO_3^-$ group.

Methanesulfonate anion, $CH_3SO_3^-$, has the potential to bond to metal ions as bidentate or tridentate bridging ligand with the consequent formation of highly polymeric materials. In view of this it is essential to visualize the changes in the vibrational spectrum of the CH_3SO_3 group in different stereochemical environments. (*i*) The symmetry of an isolated CH_3SO_3 group (CSO_3 moiety) is C_{3v} which is responsible for six fundamentals, three *E* ($\nu_{as}(SO_3)$, $\delta_{as}(SO_3)$, and $\rho_r(SO_3)$) and three *A* ($\nu_s(SO_3)$, ν(S—CH_3), and $\delta_s(SO_3)$) modes of ir-active vibrations. (*ii*) A tridentate methanesulfonate group has C_{3v} symmetry which suggests that it will have the vibrational spectrum quite similar to that of the free ion. This mode of coordination has been observed in some bivalent transition metal methanesulfonates (10). (*iii*) If CH_3SO_3 group enters into monodentate type of coordination, its symmetry is lowered from C_{3v} to C_s. With this lowering of symmetry the three *E* modes are split to give a total of six bands (7), and a total of nine ir-active bands are expected.

The ir spectra of $M(SO_3CH_3)_3$ (M = As, Sb, and Bi) were recorded in the region 4000–200 cm^{-1} (Table 2). Similarities in their infrared spectra suggest structural similarities in these compounds. Band assignments have been made by comparison with the spectra of ionic $K^+CH_3SO_3^-$ (17) and trivalent metal methanesulfonates (10, 12). The doubly degenerate SO_3 asymmetric stretching, and SO_3 asymmetric bending modes, show very significant splitting which suggests reduction of the CSO_3 symmetry below C_{3v}. This is consistent with six coordinate arsenic(III), antimony(III), and bismuth(III) since the stoichiometry requires that for MO_6 chromophores each methanesulfonate ion must utilize only two of its oxygen atoms for bonding. The ^1H nmr spectra of $M(SO_3CH_3)_3$ (M = As, Sb, and Bi) in formamide at 90 MHz show only a single peak at 2.80 to 2.85 ppm. The methyl protons are deshielded relative to those in methanesulfonic anhydride which exhibit a single peak at 2.45 ppm.

TG/DTG studies of $M(SO_3CH_3)_3$ (M = As, Sb, and Bi) compounds show that they all begin to decompose when heated above 45–50°C. These compounds decompose to their oxo-salts with the loss of methanesulfonic anhydride. The thermal decomposition schemes for these compounds are given below:

[1] $As(SO_3CH_3)_3 \xrightarrow{A} AsO(SO_3CH_3) \xrightarrow{B}$ No residue

[II] $Sb(SO_3CH_3)_3 \xrightarrow{A} SbO(SO_3CH_3) \xrightarrow{B} \underbrace{\tfrac{1}{3}[Sb + Sb_2(SO_4)_3]}_{C}$

$\tfrac{1}{6}Sb_2O_4 \xleftarrow{D} \tfrac{1}{6}Sb_2O_3$

[III] $Bi(SO_3CH_3)_3 \xrightarrow{A} BiO(SO_3CH_3) \xrightarrow{B} \underbrace{\tfrac{1}{3}[Bi + Bi_2(SO_4)_3]}_{C}$

$\tfrac{1}{6}Bi_2O_3$

The observed weight loss (or gain) values for the different steps agree closely with the theoretically required values (Table 3). In reaction [1], no residue was obtained in the ceramic crucible. Possibly, As_2O_3 which may have been formed on heating above 350°C sublimes at this temperature (18) and the crucible was completely empty by the time the temperature had reached 600°C when the run was stopped. The residue in [II] and [III] was qualitatively checked for the presence of SO_4^{2-} ions. Methanesulfonic anhydride was distilled when each of these compounds was heated separately under vacuum in the line.

TABLE 3. Thermal analysis data of tris(methanesulfonates) of arsenic, antimony, and bismuth

Compound	Step	Temperature range (°C)	Wt. loss (or gain) (−) (+) % found (calcd.)
$As(SO_3CH_3)_3$	*A*	45–350	−47.4 (48.3)
$Sb(SO_3CH_3)_3$	*A*	60–370	−42.6 (42.8)
	B	370–430	−47.2 (46.5)
	C	430–500	+2.0 (2.0)
	D	500–620	+2.6 (2.6)
$Bi(SO_3CH_3)_3$	*A*	70–360	−35.4 (35.2)
	B	360–420	−39.4 (38.3)
	C	420–540	+1.7 (1.6)

Solutions in 100% methanesulfonic acid: These compounds should also be suitable solutes for solution studies in CH_3SO_3H and simple ionization should lead to solvated $[M(SO_3CH_3)_2]^+$ cations. Solubility of $M(SO_3CH_3)_3$ (M = As, Sb, and Bi) compounds decreases in going from arsenic to the bismuth compound. The specific conductivities of $As(SO_3CH_3)_3$ and $Sb(SO_3CH_3)_3$ in 100% methanesulfonic acid are shown in Fig. 1. Tris(methanesulfonato)bismuth(III) is only very sparingly soluble in methanesulfonic acid and it was not possible to study the conductivity of its solutions. The specific conductivities of $As(SO_3CH_3)_3$ and $Sb(SO_3CH_3)_3$ are compared with solutions of pyridine in CH_3SO_3H in which it is known to behave as a fully ionized base (19). Both $As(SO_3CH_3)_3$ and $Sb(SO_3CH_3)_3$ behave as weak electrolytes. In order to ascertain whether $As(SO_3CH_3)_3$ ionized as an acid or a base, the conductivities of solutions obtained by adding small amounts of pyridine to $As(SO_3CH_3)_3$ solutions were measured. The conductivity increased immediately and no minimum conductivity was observed even at very low pyridine concentrations, suggesting that $As(SO_3CH_3)_3$ behaves as a base:

[2] $As(SO_3CH_3)_3 \overset{CH_3SO_3H}{\rightleftharpoons} [As(SO_3CH_3)_2]^+_{solv.} + CH_3SO_3^-$

This mode of ionization of $As(SO_3CH_3)_3$ was also confirmed when a decrease in conductivity of its solution was observed on addition of small amounts of antimony(V) chloride; the latter has been shown to behave as a strong acid in methanesulfonic acid (20). Surprisingly, this behaviour of $As(SO_3CH_3)_3$ in methanesulfonic acid is different from that observed for $As(HSO_4)_3$ which ionizes as an acid in 100% sulfuric acid (21).

[3] $As(HSO_4)_3 + 2H_2SO_4 \rightleftharpoons H_3SO_4^+ + As(HSO_4)_4^-$

Tris(methanesulfonato)antimonate(III) which behaves as a very weak electrolyte in 100% CH_3SO_3H was also shown to behave as a base.

Thiocyanato complexes from $M(SO_3CH_3)_3$ (M = As, Sb, and Bi): Ammonium thiocyanate reacts rapidly with tris(methanesulfonates) of arsenic, antimony, and bismuth to form mixed-ligand complexes of the general formula, $NH_4[M(SO_3CH_3)(NCS)_3]$. The infrared spectra of these complexes indicate N bonding for the thiocyanate ligands. The presence of bands at about 2080 (C—N stretch), 790 (C—S stretch), and 470 cm^{-1} (N—C—S bending mode) are consistent with some known complexes having N-bonded thiocyanate ligand (22). The methanesulfonate group may be considered to be very weakly coordinated. The S—O asymmetric and symmetric stretching vibrations are observed at 1246 and 1050 cm^{-1}, respectively, as would be

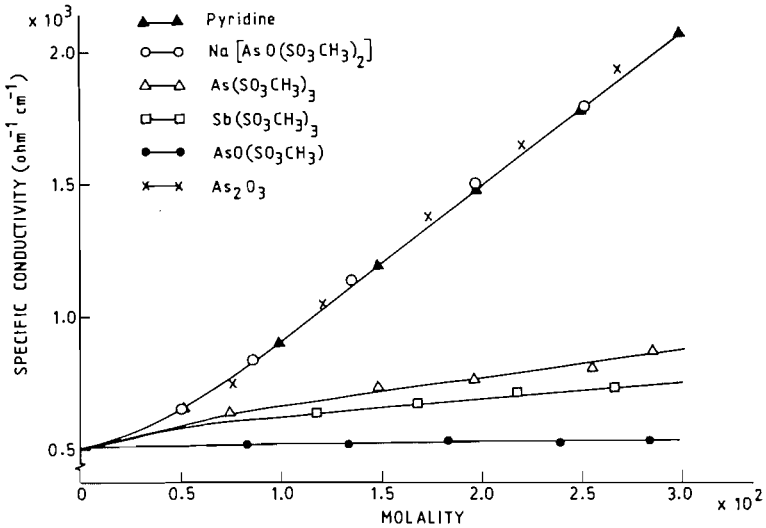

FIG. 1. Plot of specific conductivities in methanesulfonic acid at 25°C.

expected on coordination of the CH_3SO_3 group. However, the other two asymmetric modes observed at about 540 and 330 cm^{-1} are not split.

Bromide complexes from $M(SO_3CH_3)_3$ (M = Sb and Bi): Tetramethylammonium bromide reacts instantly with tris(methanesulfonates) of antimony and bismuth to form complexes of the formula, $(CH_3)_4N^+[MBr_4]^-$ in which all the three methanesulfonate groups have been replaced. Their ir spectra are quite similar above 400 cm^{-1} and contain no bands due to the $CH_3SO_3^-$ group.

Complexes of $M(SO_3CH_3)_3$ with DMF and pyridine (M = As, Sb, and Bi): The Lewis acid character of MCl_3 (M = As, Sb, and Bi) compounds is well known (23). It is also possible that two monodentate ligands could displace a methanesulfonate ligand. In order to distinguish between these two possibilities, we have investigated the reactions of $M(SO_3CH_3)_3$ compounds with DMF and pyridine (Table 1). As would be expected the adducts are considerably less moisture-sensitive than the parent compounds. Comparison of their infrared spectra with those of the original compounds suggest the following: (*1*) Bands due to S—O stretching modes are observed in these compounds. Their frequencies are very close to those observed in the parent compounds. Some additional bands assignable to ionic methanesulfonate S—O stretches (1190, 1050, 780, 550, 530, and 350 cm^{-1}) are also observed in their spectra. (*2*) The amide I band observed in DMF at 1680 cm^{-1} is shifted to a lower value around 1630–1640 cm^{-1} in these compounds which is suggestive of coordination via the carbonyl oxygen (24). (*3*) The C—C and C—N stretching modes which are usually observed between 1450 and 1615 cm^{-1} show definite positive shift indicating coordination through nitrogen (25).

Two bidentate methanesulfonate ligands, two monodentate ligands, and an ionic methanesulfonate group suggest the formulation $[M(SO_3CH_3)_2L_2]^+CH_3SO_3^-$ for these compounds.

Complexes of $M(SO_3CH_3)_3$ (M = As, Sb, and Bi) with BBr_3: Like MCl_3 compounds which are known to function as Lewis acids and Lewis bases (23), $M(SO_3CH_3)_3$ (M = As, Sb, and Bi) compounds also appear capable of functioning in both these capacities. It was not possible to characterize these adducts by infrared largely because of their instability at room temperature and extreme moisture sensitivity.

Complexes of $M(SO_3CH_3)_3$ (M = As, Sb, and Bi) with $CsSO_3CH_3$: An investigation was made of the ability of the methanesulfonato derivatives to form complexes with further methanesulfonate ions. It was found that cesium methanesulfonate gave cesium tetrakis(methanesulfonato)arsenate(III)/antimonate(III)/bismuthate(III) by reaction with the appropriate trismethanesulfonate. These compounds are highly sensitive to moisture. They are not soluble in $C_6H_5NO_2$, CH_3NO_2, and CH_3CN but dissolve in basic organic solvents like formamide and DMF. As expected Λ_M of $Cs[Bi(SO_3CH_3)_4]$ in DMF (200 $ohm^{-1}\,cm^2\,mol^{-1}$) corresponds to 2:2 electrolyte (16).

$$[4]\quad Cs[Bi(SO_3CH_3)_4] \overset{DMF}{\rightleftharpoons} Cs^+ + [Bi(SO_3CH_3)_2(DMF)_2]^+ + 2CH_3SO_3^-$$

Sodium oxobis(methanesulfonato)arsenate(III) and sodium tetrakis(methanesulfonato)bismuthate(III): Sodium arsenite, $NaAsO_2$, and sodium bismuthate, $NaBiO_3$, react with methanesulfonic anhydride at room temperature to yield $Na[AsO(SO_3CH_3)_2]$ and $Na[Bi(SO_3CH_3)_4]$, respectively. Both these compounds are insoluble in common organic solvents. Conductometric studies on $Na[AsO(SO_3CH_3)_2]$ in 100% CH_3SO_3H (Fig. 1) show that it ionizes as follows:

$$[5]\quad Na[AsO(SO_3CH_3)_2] \overset{CH_3SO_3H}{\rightleftharpoons} Na^+ + AsO(SO_3CH_3) + CH_3SO_3^-$$

The conductivity of the solution corresponds to the formation of only one mole of conducting $CH_3SO_3^-$ ions per mole of the solute, thereby suggesting that $AsO(SO_3CH_3)$ was behaving as a non-electrolyte. The bismuth double salt was insoluble in pure methanesulfonic acid. Infrared spectra (Table 2) show that the S—O region is quite complex and may be interpreted in terms of the presence of bridging bidentate methanesulfonato groups. The *E* modes ($\nu_{as}(SO_3)$ and $\delta_{as}(SO_3)$) show wide splitting while the lower *E* mode $\rho_r(SO_3)$ does not exhibit any splitting. This observation suggests the presence of bridging CH_3SO_3 groups in these compounds (26).

Solutions of M_2O_3 (M = As, Sb, and Bi) in 100% CH_3SO_3H: Cryoscopic and conductometric studies in 100% sulfuric acid have shown that As_2O_3 in 100% sulfuric acid forms arsonyl(III) hydrogensulfate, $AsO\cdot HSO_4$ which is partly ionized to give the

Can. J. Chem. Downloaded from www.nrcresearchpress.com by 78.46.186.204 on 09/07/12
For personal use only.

AsO^+ cation (21). The present investigations are concerned with the possible formation of AsO^+ species in methanesulfonic acid. The conductometric behaviour of solutions of As_2O_3 in 100% methanesulfonic acid is shown in Fig. 1. As As_2O_3 is only slightly soluble in methanesulfonic acid it was not possible to study solutions more concentrated than 0.04 m. The number of moles of methanesulfonate ions, $CH_3SO_3^-$, formed by the ionization of 1 mol of As_2O_3 was found by the comparison of the concentrations of As_2O_3 and of C_5H_5N having the same specific conductance. Possible modes of ionization including some which are not consistent with the experimental results, are given below:

[6] $As_2O_3 + 3CH_3SO_3H = 2AsO^+ + H_3O^+ + 3CH_3SO_3^-$

[7] $As_2O_3 + 3CH_3SO_3H = 2AsO(SO_3CH_3) + H_3O^+ + CH_3SO_3^-$

[8] $As_2O_3 + 6CH_3SO_3H = 2As(SO_3CH_3)_3 + 3H_3O^+ + 3CH_3SO_3^-$

[9] $As_2O_2 + 9CH_3SO_3H = 2As(SO_3CH_3)_4^- + 3H_3O^+ + CH_3SO_3^-$

[10] $As_2O_3 + 6CH_3SO_3H = [As(SO_3CH_3)_2]_2O + 2H_3O^+ + 2CH_3SO_3^-$

The observed results (number of $CH_3SO_3^-$ ions = 1) easily rule out reactions [6], [8], and [10]. Reaction [9] can be ruled out as it has been shown earlier (reaction [2]) that the conductivity of $As(SO_3CH_3)_3$ in methanesulfonic acid is due to its basic ionization. The experimental results are consistent with reaction [7] in which it is assumed that $AsO(SO_3CH_3)$ is unionized in pure methanesulfonic acid. This observation gets further support from the isolation of a white precipitate formed slowly in the more concentrated solutions of As_2O_3 in methanesulfonic acid. Analysis of the precipitate showed that it had a composition corresponding to $AsO(SO_3CH_3)$ (Table 1). It behaves as a non-electrolyte in nitrobenzene ($\Lambda_M = 2.0$ ohm^{-1} cm^2 mol^{-1}) (16) and in pure CH_3SO_3H. Its infrared spectrum (Table 2) showed bands which may be attributed to the presence of bridging bidentate methanesulfonato group. The sulfur–oxygen stretching modes are split beyond what is anticipated for reduced C_s symmetry upon coordination of CH_3SO_3 group. The additional bands may be attributed to the splitting of S—O modes by the local crystal symmetry or to the binding of the free oxygen atom of one complex to the arsenic atom of the adjacent complex. Its mass spectrum shows the molecular ion with highest intensity (100%, 70 eV) at m/e 372 $[As_2O_2(SO_3CH_3)_2]^+$. The spectrum shows prominent fragments at 292 $[M - SO_3]^+$ (54%), 182 $[M - SO(CH_3)_2]^+$ (4%), and 91 $[M - AsO(SO_3CH_3)_2]^+$ (35%). Oxo(methanesulfonato)arsenic(III) reacts with pyridine to give 1:1 adduct, $AsO(SO_3CH_3)\cdot NC_5H_5$ (Table 1).

Antimony(III) and bismuth(III) oxides have very limited solubility in 100% CH_3SO_3H and therefore conductivity data on their solutions in the pure acid could not be obtained. These oxides, on stirring for a few hours, yield white precipitates which on analyses were found to be the fully solvolysed products, $Sb(SO_3CH_3)_3$ and $Bi(SO_3CH_3)_3$. Because of the increasing basicity of the oxides in going from arsenic to bismuth, we observe this change in the nature of the reaction products.

Attempted reactions of As_2O_5 and Sb_2O_5 with $(CH_3)_2S_2O_5$: Reaction between As_2O_5 and Sb_2O_5 with methanesulfonic anhydride do not yield methanesulfonate derivatives and the oxides are recovered unchanged even when the contents are refluxed at $\simeq$ 160°C for several days. This lack of reactivity of the pentoxides may be attributed to their increased acidity vis-à-vis the trioxides.

1. R. Feld. J. Chem. Soc. 3963 (1964).
2. P. A. Yeats, J. R. Sams, and F. Aubke. Inorg. Chem. **10**, 1877 (1971).
3. R. C. Paul, V. P. Kapila, and S. K. Sharma. Indian J. Chem. **12**, 651 (1974).
4. R. C. Paul, V. P. Kapila, Miss N. Palta, and S. K. Sharma. Indian J. Chem. **12**, 825 (1974).
5. R. C. Paul, V. P. Kapila, and S. K. Sharma. J. Inorg. Nucl. Chem. **36**, 1933 (1974).
6. A. L. Arduini, M. Garnett, R. C. Thompson, and C. T. C. Wong. Can. J. Chem. **53**, 3812 (1975).
7. N. C. Johnson, J. T. Turk, W. E. Bull, and H. G. Mayfield, Jr. Inorg. Chim. Acta, **25**, 235 (1977).
8. E. Hochberg and E. H. Abbott. Inorg. Chem. **17**, 506 (1978).
9. R. C. Paul, V. P. Kapila, R. Kumar, and S. K. Sharma. J. Inorg. Nucl. Chem. **42**, 281 (1980).
10. J. S. Haynes, J. R. Sams, and R. C. Thompson. Can. J. Chem. **59**, 669 (1981).
11. J. E. Drake, L. N. Khassou, and A. Majid. J. Inorg. Nucl. Chem. **43**, 1473 (1981).
12. S. K. Sharma, R. K. Mahajan, B. Kapila, and V. P. Kapila. Polyhedron, **2**, 973 (1983).
13. E. L. Mutterties and D. D. Coffman. J. Am. Chem. Soc. **80**, 5914 (1958).
14. R. C. Paul, S. Singh, R. C. Kumar, R. D. Sharma, and R. D. Verma. Indian J. Chem. **17**A, 273 (1979).
15. S. Singh, Amita, and R. D. Verma. Indian J. Chem. **22**A, 814 (1983).
16. W. J. Geary. Coord. Chem. Rev. **7**, 81 (1971).
17. R. J. Gillespie and E. A. Robinson. Can. J. Chem. **40**, 644 (1962).
18. C. Duval. *In* Inorganic thermogravimetric analysis. Elsevier, New York. 1963. p. 425.
19. R. C. Paul, V. P. Kapila, R. Kumar, S. K. Gupta, and S. K. Sharma. Z. anorg. allg. Chem. **203**, 471 (1980).
20. S. K. Sharma. Ph.D. Thesis. Panjab University, Chandigarh, India. 1976.
21. R. J. Gillespie and E. A. Robinson. Can. J. Chem. **41**, 450 (1963).
22. R. A. Bailey, S. L. Kozak, T. W. Michelsen, and W. N. Mills. Coord. Chem. Rev. **6**, 407 (1971).
23. R. C. Paul and G. Singh. *In* The chemistry of nonaqueous solvents. Vol. VB. *Edited by* J. J. Lagowskii. Academic Press, Inc., New York. 1978.
24. J. Arehambault and R. Rivest. Can. J. Chem. **38**, 1331 (1960).
25. N. N. Greenwood and K. Wade. J. Chem. Soc. 1130 (1960).
26. S. Kumar, R. K. Mahajan, and V. P. Kapila. Indian J. Chem. **22**A, 490 (1983).

Can. J. Chem. Downloaded from www.nrcresearchpress.com by 78.46.186.204 on 09/07/12
For personal use only.

Reactions of 4-*tert*-butyl-5-methylene-3,3-dimethyl-Δ^1-1,2,4-triazoline with dimethyl acetylenedicarboxylate[1]

FOR ERRATA SEE 66(5) 1988 P.1342

ADRIAN L. SCHWAN AND JOHN WARKENTIN[2]
Department of Chemistry, McMaster University, Hamilton, Ont., Canada L8S 4M1

Received September 12, 1986

ADRIAN L. SCHWAN and JOHN WARKENTIN. Can. J. Chem. **65**, 1200 (1987).

4-*tert*-Butyl-5-methylene-3,3-dimethyl-Δ^1-1,2,4-triazoline (**1**) reacts rapidly with dimethyl acetylenedicarboxylate (**2**) to afford dienamines **3** and **4** from Michael addition and enamine **5** by extensive skeletal rearrangement. Assignments of their structures and probable mechanisms of their formation are discussed.

ADRIAN L. SCHWAN et JOHN WARKENTIN. Can. J. Chem. **65**, 1200 (1987).

La *tert*-butyl-4 méthylène-5 diméthyl-3,3 Δ^1-triazoline-1,2,4 (**1**) réagit rapidement avec l'acétylènedicarboxylate de diméthyle (**2**) pour conduire aux dièmamines **3** et **4**, par addition de Michael, et à l'ènamine **5**, par une transposition importante du squelette. On discute des attributions de structure et des mécanismes qui sont probablement impliqués dans la formation de ces composés.

[Traduit par la revue]

Introduction

The literature concerning reactions of nitrogen compounds with dimethyl acetylenedicarboxylate (**2**, EC≡CE, E = CO_2CH_3) and with other substituted acetylenes is very extensive (1–4). Principal nitrogenous nucleophiles that react with **2** (or with analogues of **2**) are amines (5–8), pyridines (9, 10), and enamines (11–21). Typical reactions are illustrated with eqs. [1] (6), [2] (7), and [3] (12), in which E = CO_2CH_3.

[1] $\rangle NH + \mathbf{2} \longrightarrow \rangle NC(E)=CHE$ (both isomers)

[2] $PhCOCH_2NHPh + \mathbf{2} \longrightarrow$ (*Z*)-$PhCOCH_2N(Ph)C(E)=CH(E)$

[3] 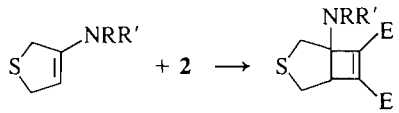

In many cases where more than one product is obtained, the product ratio is sensitive to the reaction temperature and to the polarity of the solvent.

The potential for interesting chemical reactions between **1** and **2** seemed to us to be particularly high because of the presence of the azo functional group. That feature held promise for formation of an azomethine ylide following quaternization of C-5 of **1** by overall cycloaddition of **2**, eq. [4]. Moreover, there was the interesting possibility for cyclization of dipolar intermediate **6**, if it were on the reaction coordinate, not only in the 4-*exo* sense, to form **7**, but also in the 5-*exo* sense to form **9** and **10**, eq. [5].

[4] 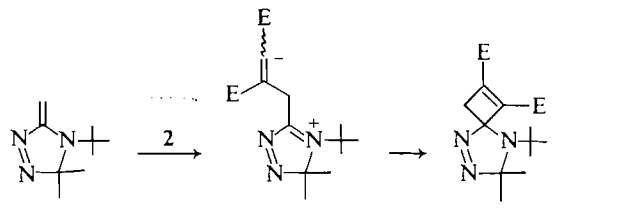

1 **6** **7** **8**

[5] 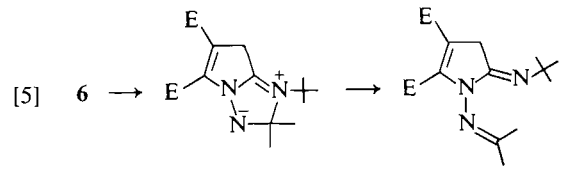

9 **10**

We now report our findings concerning the reactions of **1** with **2**.

Results and discussion

Synthesis of 1

Triazoline **1** was prepared by the sequence of reactions below (22), Scheme 1.

$$CH_3CN + (CH_3)_3CCl \xrightarrow{FeCl_3} CH_3C{\equiv}\overset{+}{N}C(CH_3)_3FeCl_4^-$$

$$\xrightarrow{(CH_3)_2C=NNHLi} CH_3C(=NC(CH_3)_3)NHN=C(CH_3)_2$$

$$\xrightarrow[C_6H_6,\ K_2CO_3]{Pb(OAc)_4} \mathbf{1}$$

SCHEME 1

Identification of products

Compounds **3** (*Z*,*E*) and **4** (*Z*,*Z*) were identified as geometric isomers from Michael addition of **1** to **2** on the basis of their ^1H nmr, ^{13}C nmr, uv, ir, and mass spectra (Table 1). The *Z* configuration about the double bond exocyclic to the triazoline ring was assigned for each on the basis of nuclear Overhauser effect (nOe) enhancement of the intensity of the vinyl proton signal as a result of irradiating at the absorption frequency of the *tert*-butyl group (Table 1). The *Z* configurations about that double bond are not surprising, in view of the larger steric interactions that would exist in the *E* isomers. Configurations about the double bonds bearing carbomethoxy groups were assigned on the basis of the following observations. The isomer assigned structure **4** eluted more slowly than **3** from a silica-packed hplc column and it had the smaller R_f value on alumina-coated tlc plates (Experimental). Those differences between maleates and fumarates, in chromatographic retention

[1]Presented in part at the Fourth Annual Graduate Student Symposium, SUNY (State University of New York) at Buffalo, Buffalo, NY, May, 1986.

[2]Author to whom correspondence may be addressed.

Can. J. Chem. Downloaded from www.nrcresearchpress.com by 78.46.186.204 on 09/07/12
For personal use only.

TABLE 1. Spectral data for **1**, **3**, **4**, and **5**

Compound (mp, °C)	Infrared (CCl_4)[a]	Ultraviolet (nm, CH_3OH) log E	^1H nmr ($CDCl_3$)[b]	^{13}C nmr ($CDCl_3$)[c]	Mass spectra (ei, m/z)
1 (oil)	1636[d] 1511[d]	216, 3.68; 364, 3.49	1.41 (s, 9H), 1.58 (s, 6H), 4.16 (d, J = 2.2 Hz, 1H), 4.76 (d, J = 2.2 Hz, 1H),	83.70, 163.13 52.82, 28.12 104.23, 26.02	167.1427[e] 139.1354[f]
3 (115–116)	1741 1705 1611 1568 1432	216, 3.87; 268, 3.60; 318, 3.87; 420, 4.13	2.55 (s, 9H), 2.66 (s, 3H), 3.70 (s, 3H), 3.81 (s, 3H), 5.52 (s, 1H)[g], 7.01 (s, 1H)[h]	52.71, 51.28 170.67, 167.62 110.56, 93.37 158.57, 148.16 106.09, 25.45 54.56, 28.44	309 (25%) 294, 238 234, 197 166, 57 (100%) 309.1686[i]
4 (oil)	1734 1713 1671 1615 1565 1439	200–275, 3.27–3.33 (no max); 308, 3.67; 414, 3.55	1.42 (s, 9H), 1.58 (s, 6H), 3.68 (s, 3H), 3.86 (s, 3H), 5.30 (s, 1H),[j] 5.67 (s, 1H)[k]		281 (8%) 205, 166, 139, 108, 57 (100%) 281.1609[l]
5 (90–91)	1736 1690 (br)	206, 4.58; 310, 4.18	1.28 (s, 9H), 1.52 (s, 3H), 1.94 (m, 1H), 2.14 (m, 1H), 2.46 (m, 1H), 2.79 (m, 1H), 3.58 (s, 3H), 3.65 (s, 3H) 7.56 (s, 1H)	172.67, 166.43 51.91, 50.38 59.78, 55.65 34.93, 26.61 73.97, 151.34 101.70, 31.09 22.14	281 (8%) 280 (24%) 253, 250 221, 193 165 (100%) 134, 107 57 281.1603[m]

[a]Select bands only.
[b]At 90 MHz except for **5** (250 MHz).
[c]Relative to $CDCl_3$, δ 77.2. The ^{13}C chemical shifts are listed in numerical order by row according to the arbitrary numbering schemes depicted below.

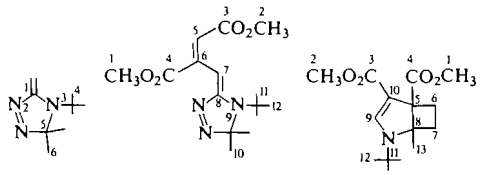

1 **3** **5**

[d]Neat.
[e]High resolution; calcd. for $C_9H_{17}N_3$, m/z 167.1432.
[f]Calculated for $C_9H_{17}N$ ($M^+ - N_2$), m/z 139.1347.
[g]H-5. No nOe enhancement of this signal.
[h]H-7, numbering as in footnote *c*. The nOe enhancement of this signal, from irradiation at the frequency of the *tert*-butyl signal, was 35%.
[i]High resolution; calcd. for $C_{15}H_{23}N_3O_4$, m/z 309.1689.
[j]H-7, numbering as in **3**. The nOe enhancement of this signal was 46%.
[k]H-5. The nOe enhancement of this signal was 9%.
[l]High resolution; calcd. for $C_{15}H_{23}NO_4$ (M1 − N_2), m/z 281.1627.
[m]High resolution; calcd. for $C_{15}H_{23}NO_4$, m/z 281.1627.

times, are normally observed and are a consequence of the larger dipole moments of maleates compared with those of fumarates (23, 5). The faster eluting isomer (**3**) had λ_{max} = 420 nm (log ε = 4.13) in the uv spectrum compared to λ_{max} = 414 nm (log ε = 3.55) for the isomer that was eluted more slowly (**4**). These observations too are characteristic of simpler fumarates and maleates, the higher transition energy and the lower transition probability of the maleates being ascribed to out-of-plane twisting of the Z-ester functions because of nonbonded interactions between them (24). Finally, nOe measurements (irradiation at the frequency of the *tert*-butyl signal) showed a significant enhancement (ca. 9%) of the intensity of the terminal vinyl proton signal of **4** and no enhancement of the corresponding signal of **3**. Thus, all of the evidence from physical properties and from spectroscopy is consistent with the *Z,E* configuration for **3** and the *Z,Z* configuration for **4**. Structure **5** was determined by single crystal X-ray crystallography.[3] The ^1H and ^{13}C nmr spectra of **5** are included in Table 1.

Mechanisms

The dependence of product yields on the solvent is given in Table 2. In methanol solvent the isomeric Michael adducts (**3** and **4**) predominate, but in dichloromethane the azabicycloheptene (**5**) is the major product. Those results can be rationalized in terms of the mechanisms of Scheme 2. Formation of zwitterionic intermediate **11** is postulated as the first step, in accord with some precedents from the literature (25, 26). Reinhoudt *et al.*, however, have proposed recently that cycloadditions between enamines and **2** to form aminocyclobutenes are concerted and that a dipolar species, analogous to **11**, can

[3]We thank Professor C. J. L. Lock and Mr. R. Faggiani for determining the crystal structure of **5**. The crystallographic data will be published elsewhere.

Can. J. Chem. Downloaded from www.nrcresearchpress.com by 78.46.186.204 on 09/07/12
For personal use only.

TABLE 2. Solvent dependence of yields (25°C)

Solvent	Yields (%) 3	4	5
CH_3OH	72	4	19
CH_2Cl_2	17	5	56

be formed by ring opening of first-formed aminocyclobutenes, analogous to **13**, in polar solvents (14). We postulate a stepwise mechanism[4] for formation of **13**, primarily because **3** and **4** are obtained from reactions carried out in CH_2Cl_2, albeit in lower yields than in CH_3OH. It seems unlikely to us that **13** would undergo ring opening to **11** in CH_2Cl_2 at room temperature although that reaction may occur to a limited extent in CH_3OH.

Protonation of **11** is probably faster at oxygen than at carbon, by analogy to the protonation of enolates, forming **12** initially, and **12** can give rise to **3** and **4** by a series of proton transfers. Deprotonation from the methylene group followed by protonation at the allenic carbon and deprotonation from oxygen would lead to **3** and **4**. The large preference for formation of **3** in CH_3OH may be the result of internal hydrogen bonding at the transition state for protonation at carbon, as illustrated with **19**.

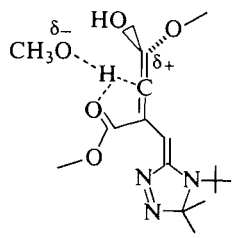

19

Proton transfers involving CH_3OH were confirmed by showing that **3** and **4**, isolated from a reaction carried out in CH_3OD, were fully deuterated at the terminal vinyl position.

Mechanisms by which **3** and **4** could be formed in CH_2Cl_2 include proton transfers between **11** (or **12**) and **1**, or between **12** and the conjugate base of **11**, for example. Adventitious impurities, including moisture as well as reaction products not shown in Scheme 2, may also be involved.

A 1,3-sigmatropic rearrangement of **11** to **3** and (or) **4** in the absence of protic solvent molecules need not be considered seriously because it would have to be antarafacial (27) and therefore very slow.

Equilibration or partial equilibration of **3** and **4** after their formation could be ruled out when it was found that **4** was not isomerized to **3** and **3** was not isomerized to **4** in CH_3OH containing either **1** or **2**.

No isomers of **3** and **4**, with the *E* configuration about the exocyclic double bond, could be detected among the products obtained in either solvent. Although the *Z* configurations are undoubtedly the preferred ones, because of steric congestion in the *E* isomers, the possibility that there is equilibration of a kinetically formed mixture of those isomers cannot be ruled out at this stage.

[4]Since our aminocyclobutene intermediates are spiro compounds, whereas those of Reinhoudt *et al.* are not, and because the substituents are different, it is possible that the mechanisms by which they are formed are different also.

Cyclobutenes analogous to **13** have been isolated in a few cases (12, 14, 28) but, in general, they undergo electrocyclic ring opening rapidly, in the sense **13** → **14** (11, 13, 26, 29). We were unable to isolate any **14**. Ring opening of **13** to **14** is presumably suppressed because loss of N_2 from **13**, to generate **15**, is faster. Azomethine ylide **15** isomerizes to **16** by H-atom transfers analogous to those that convert some carbonyl ylides to enol ethers (30). In CH_2Cl_2 those transfers may be intramolecular but in CH_3OH there is a stepwise process, probably involving protonation at the cyclobutyl carbon followed by deprotonation from the isopropylidene function. That mechanism was indicated by the finding that **5**, generated in CH_3OD, was deuterium labelled at the vinyl position. Incorporation of the label during the steps by which **15** is converted to **16** is in keeping with the known high reactivity of ylides toward alcohols (31).

Conrotatory electrocyclic ring opening of aminocyclobutene **16**, already mentioned above in connection with the minor process **13** → **14**, would generate trienamine **17** and its geometric isomer (not shown in Scheme 2), with the alternative configuration about the nonterminal enamine double bond. Those isomers must be interconvertible, because the yield of **5** in CH_2Cl_2 could not be as high as 56% if more than half of the **17** formed were unable to close to **18**. Cyclization of **17** to **18** is a conrotatory electrocyclic reaction analogous to that of octatetraenes (32), and conversion of **18** to **5** presumably occurs by disrotatory electrocyclic ring closure. As precedent for the steps that lead from **16** to **5** (Scheme 2) we site the example reported by Acheson and Procter (33), eq. [6].

[6] 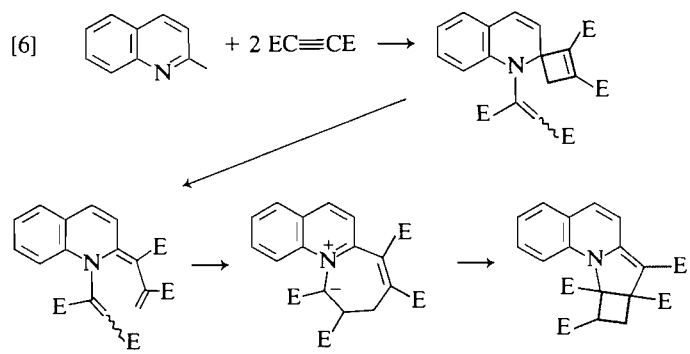

Although the various steps of Scheme 2 are based largely on precedents and on deuterium incorporation from methanol-OD, there is direct evidence for the formation of unstable intermediates. Monitoring of the progress of the reaction by ^1H nmr spectroscopy revealed the growth and decay, with time, of several vinyl signals not present in either the reactants or the final products. However, the spectra were too complex to permit assignments of those signals to likely intermediates (**16**, **17**, **18**) or to permit a kinetic description of the reactions of **1** with **2**.

Experimental

General

Melting points were determined on a Thomas Hoover capillary melting point apparatus and are uncorrected. Proton nuclear magnetic resonance (^1H nmr) spectra were recorded on a Bruker WM-250 or a Varian EM-390 spectrometer using either TMS or the residual $CHCl_3$ in $CDCl_3$ as the internal standard. Carbon-13 nuclear magnetic resonance (^{13}C nmr) spectra were obtained with a Bruker WM-250 or a Bruker WP-80/90 machine. Infrared (ir) spectra, obtained with a Perkin–Elmer model 283 instrument, are reported in wavenumbers calibrated against the 1601.4 cm^{-1} band of polystyrene. Ultraviolet (uv) spectra were obtained with a Hewlett–Packard model 8451A

Can. J. Chem. Downloaded from www.nrcresearchpress.com by 78.46.186.204 on 09/07/12
For personal use only.

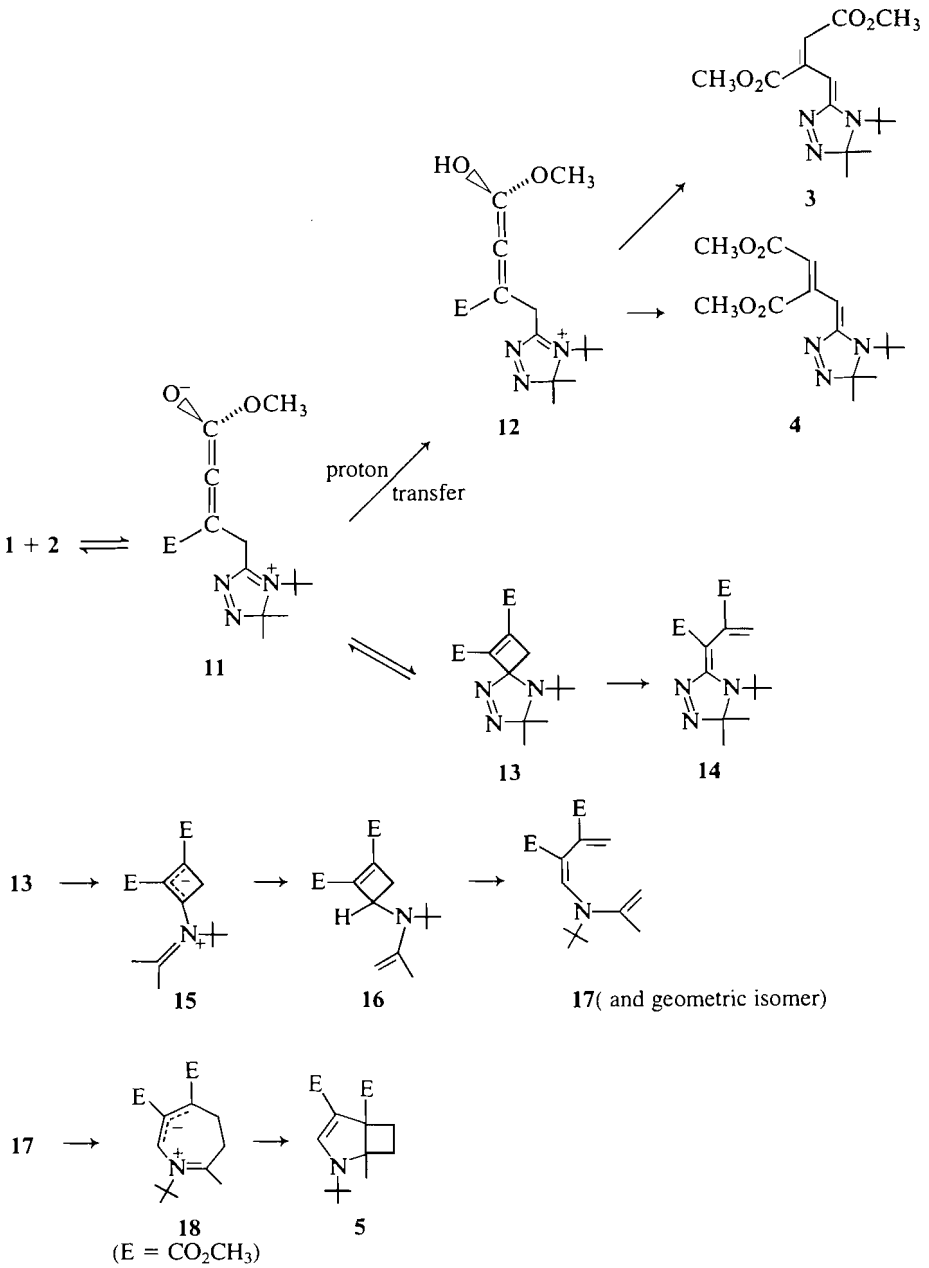

SCHEME 2

diode array spectrometer. Mass spectra (ms) were recorded on a VG 70-70F double focussing spectrometer.

Analyses by high performance liquid chromatography (hplc) were carried out with a Varian 5000 instrument equipped with a Varian Vista 402 processor and with a uv detector set at 310 nm. A Varian SI-5 silica column (4 × 150 mm) was used with the following elution program: 0–10 min (10% CH_2Cl_2 in hexane changing to 9% CH_2Cl_2, 1% isopropyl alcohol in hexane); 10–35 min (no change); 35–40 min (return to initial composition). With that program and a pumping rate of 1 mL min^{-1}, the retention times were 19 min (**3**), 23 min (**5**), and 27 min (**4**).

Dimethyl acetylenedicarboxylate, from Aldrich Chemical Co., was distilled under vacuum before use. Dichloromethane (Caledon) was dried over molecular sieves (4Å) before use. Methanol (Baker Analyzed) and methanol-OD (Aldrich) were used as received.

Nuclear Overhauser enhancement (nOe) measurements

The substrate (10–20 mg) in ca. 0.4 mL of $CDCl_3$ containing a trace of CH_2Cl_2 was sealed into a medium-walled nmr tube after three cycles of freeze–pump–thaw degassing at 0.03 Torr (1 Torr = 133.3 Pa). Eight normal scans on the WH-250 spectrometer were followed by eight scans taken during irradiation at the frequency of the substrate's *tert*-butyl signal. Each spectrum was integrated against the signal from internal CH_2Cl_2. No correction was made for enhancement, if any, of the reference signal during double irradiation.

N^1-*Isopropylidene*-N^3-tert-*butylacetamidrazone* (*$((CH_3)_2C{=}NNHC(CH_3){=}NC(CH_3)_3$*, ***19***)

The procedure for preparation of **19** is based on that of Fuks (34). A two-necked flask, fitted with an efficient mechanical stirrer and a pressure equalizing dropping funnel, was charged with anhydrous ferric chloride (30 g, 0.18 mol). During constant stirring and cooling with ice were added, dropwise and in succession, anhydrous ether (40 mL), anhydrous acetonitrile (7.6 g, 0.19 mol) in ether (10 mL), and *tert*-butyl chloride (17.1 g, 0.18 mol) in 20 mL of dry ether. The mixture was stirred for 30 min at ice temperature, during which time an orange-red suspension was formed. The suspension was added quickly, at −78°C, to a solution of the lithium salt of acetone

Can. J. Chem. Downloaded from www.nrcresearchpress.com by 78.46.186.204 on 09/07/12
For personal use only.

hydrazone, prepared as follows. Methyllithium in hexane (0.31 mol of MeLi) was added to 400 mL of ether at −78°C. Acetone hydrazone (20.4 g, 0.28 mol) in ether (80 mL) was then added, dropwise with stirring, to the cold solution.

When addition of the suspension was complete the resulting mixture was allowed to reach 0°C, approximately, during 1 h of stirring, after which aqueous sodium hydroxide solution (0.64 mol of NaOH in 50 mL) was added. The subsequent work-up according to the procedure of Fuks (34) gave crude amidrazone, which was distilled. After an initial fraction of acetone azine, **19** and *N-tert*-butyl acetamide distilled together at 80–85°C (1.5 Torr). That fraction was chromatographed on Al_2O_3(II) to afford **19** (14.2 g, 47% based on acetonitrile) as a low-melting solid. A sample of **19** collected by preparative gc had mp 49–50.5°C.

4-tert-Butyl-3,3-dimethyl-5-methylene-Δ^1-1,2,4-triazoline, 1 (22)

In a typical oxidation, amidrazone **19** (1.0 g, 5.9 mmol) in 10 mL of benzene was added all at once to lead tetraacetate (2.9 g, 6.5 mmol) in 30 mL of benzene over 16 g of anhydrous potassium carbonate. The reaction mixture was stirred and cooled with ice-water during the addition and for 45 min after. Aqueous sodium bicarbonate solution (5%) was then added, the mixture was filtered through Celite, and the organic phase was separated. It was washed with brine and dried over magnesium sulfate. The dried benzene solution was concentrated and the residue was chromatographed on Al_2O_3(II) using ether (10%) in light petroleum for elution. After pure **1** had been collected, the solvent was changed to 50% ether in petroleum to elute unreacted **19**. Addition of solid NaOH to the aqueous phase (above), extraction with dichloromethane, washing the organic phase with brine, drying over $MgSO_4$, and evaporation of the dichloromethane afforded additional **19** (25–35% total recovery) of the same quality, after distillation, as that initially used for oxidation. The yield of **1**, based on **19** consumed, was 45%. It is an oil at room temperature but it freezes during storage at ca. −20°C. The spectral data are in Table 1.

Reaction of 1 with 2

A solution of **1** (200 mg, 1.2 mmol) and **2** (200 mg, 1.4 mmol) in 20 mL of solvent (methanol or dichloromethane, see text) was stirred at room temperature for 12 h. The solution was concentrated with a rotary evaporator and the residue was chromatographed on Al_2O_3(II). The column was developed initially with 10% ether in light petroleum and the polarity was increased gradually after each component was eluted. The component to be eluted first was **3** (R_f 0.65 on 0.20-mm alumina tlc plates, ether), which was recrystallized from petroleum to mp 115–116°C. Compound **5** (R_f 0.50) was obtained second, mp 90–91°C (from petroleum) and **4** (R_f 0.36) was eluted last. Spectral data are in Table 1.

Acknowledgments

This work was financed from a grant provided by the Natural Sciences and Engineering Research Council of Canada. We are grateful to Mr. J. Kapron and Mr. F. A. Ramelan for mass spectra and to Mr. B. G. Sayer for the nOe work and for other assistance with nmr spectroscopy.

1. M. V. George, S. K. Khetan, and R. K. Gupta. Adv. Heterocycl. Chem. **19**, 279 (1976).
2. R. M. Acheson. Lectures in heterocyclic chemistry. Vol. 6. *Edited by* R. N. Castle and T. Kappe. HeteroCorporation, Tampa, FL. 1982. p. S-159.
3. R. M. Acheson. Adv. Heterocycl. Chem. **1**, 125 (1963).
4. R. M. Acheson and N. F. Elmore. Adv. Heterocycl. Chem. **23**, 263 (1978).
5. R. Huisgen, K. Herbig, A. Siegel, and H. Huber. Chem. Ber. **99**, 2526 (1966).
6. J. E. Dolfini. J. Org. Chem. **30**, 1298 (1965).
7. S. K. Khetan, J. G. Hiriyakkamavar, and M. V. George. Tetrahedron, **24**, 1567 (1968).
8. R. J. Alaimo and D. G. Farnum. Can. J. Chem. **43**, 700 (1965).
9. R. M. Acheson and A. O. Plunkett. J. Chem. Soc. 2676 (1964).
10. R. L. Letsinger and R. Lasco. J. Org. Chem. **21**, 764 (1956).
11. A. G. Cook. Enamines. Marcel Dekker, New York. 1969. p. 211.
12. D. N. Reinhoudt and C. G. Kouwenhoven. Recl. Trav. Chim. Pays-Bas, **92**, 865 (1973).
13. W. Eberbach and J. C. Carré. Tetrahedron Lett. **21**, 1145 (1980).
14. D. N. Reinhoudt, W. Verboom, G. W. Visser, W. P. Trompenaars, S. Harkema, and G. J. van Hummel. J. Am. Chem. Soc. **106**, 1341 (1984).
15. D. N. Reinhoudt, J. Geevers, W. P. Trompenaars, S. Harkema, and G. J. van Hummel. J. Org. Chem. **46**, 424 (1981).
16. R. M. Letcher, M. C. K. Choi, and R. M. Acheson. J. Chem. Res. (M), 1634 (1984).
17. R. M. Letcher, M. C. K. Choi, and R. M. Acheson. J. Chem. Soc. Perkin Trans. 1, 515 (1983).
18. R. M. Acheson, J. N. Bridson, and T. S. Cameron. J. Chem. Soc. Perkin Trans. 1, 1569 (1972).
19. C. Vicillescazes, S. Coen, B. Ragonnet, and J.-P. Roggero. Heterocycles, **23**, 927 (1985).
20. G. J. M. Vos, D. N. Reinhoudt, P. H. Benders, S. Harkema, and G. J. van Hummel. Chem. Commun. 661 (1985).
21. W. Verboom, G. W. Visser, W. P. Trompenaars, D. N. Reinhoudt, S. Harkema, and G. J. van Hummel. Tetrahedron, **37**, 3525 (1981).
22. A. L. Schwan and J. Warkentin. Chem. Commun. 1721 (1986).
23. C. G. LeFévre, R. J. W. LeFévre, and W. T. Oh. Aust. J. Chem. **10**, 218 (1957).
24. The Sadtler Standard Spectra. UV spectra. Sadtler Research Laboratories, Philadelphia. Vol. 1. #300; Vol. 2. #458.
25. W. K. Gibson and D. Leaver. J. Chem. Soc. (C), 324 (1966).
26. C. Hubschwerlen, J. P. Fleury, and H. Fritz. Tetrahedron, **32**, 3031 (1976).
27. I. Fleming. Frontier orbitals and organic chemical reactions. Wiley–Interscience, London. 1976. p. 99.
28. K. C. Brannock, R. D. Burpitt, V. W. Goodlett, and J. G. Thweatt. J. Org. Chem. **28**, 1464 (1963).
29. F. Fried, J. F. Taylor, and R. Westwood. Chem. Commun. 1226 (1971).
30. M. Bekhazi and J. Warkentin. J. Org. Chem. **47**, 4870 (1982).
31. (*a*) N. Shimizu and P. D. Bartlett. J. Am. Chem. Soc. **100**, 4260 (1978); (*b*) S. N. Ege, J. E. Gess, A. Thomas, P. Umrigar, G. W. Griffin, P. K. Das, A. M. Trozzolo, and T. M. Leslie. Chem. Commun. 1263 (1980); (*c*) M. Békhazi and J. Warkentin. J. Am. Chem. Soc. **103**, 2473 (1981).
32. (*a*) R. Huisgen, A. Dahmen, and H. Huber. J. Am. Chem. Soc. **89**, 7130 (1967); (*b*) E. N. Marvell and J. Seubert. J. Am. Chem. Soc. **89**, 3377 (1967).
33. R. M. Acheson and G. Procter. J. Chem. Soc. Perkin Trans. 1, 2171 (1979).
34. R. Fuks. Tetrahedron, **29**, 2147 (1973).

Can. J. Chem. Downloaded from www.nrcresearchpress.com by 78.46.186.204 on 09/07/12
For personal use only.

New positive mixed alkali and mixed anion effects on fast Na^+ ion conductivity in Na_2SO_4[1,2]

U. M. GUNDUSHARMA AND E. A. SECCO[3]

Chemistry Department, St. Francis Xavier University, Antigonish, N.S., Canada B2G 1CO

Received September 2, 1986

U. M. GUNDUSHARMA and E. A. SECCO. Can. J. Chem. **65**, 1205 (1987).

The ac conductivity data for the binary alkali sulfate Rb^+:Na_2SO_4 reveal a new positive mixed alkali effect in contrast to the so-called mixed alkali effect observed in β-aluminas. The binary alkali sulfate Rb^+:Li_2SO_4 exhibits conductivity behavior intermediate between the two mixed alkali effects. A new positive mixed anion effect is also reported for the MoO_4^{2-}:Na_2SO_4 system. The higher Na^+ conductivity in the Rb^+:Na_2SO_4 and MoO_4^{2-}:Na_2SO_4 solid solutions is attributed to lattice expansion in a hexagonal structure effected by the larger radius isovalent guest ion and is interpreted in terms of a percolation type of transport mechanism.

U. M. GUNDUSHARMA et E. A. SECCO. Can. J. Chem. **65**, 1205 (1987).

Des données relatives à la conductivité c.a. du sulfate alcalin binaire Rb^+:Na_2SO_4 révèle la présence d'un nouvel effet positif des métaux alcalins mixtes; ces données sont en opposition avec l'effet des métaux alcalins mixtes observé dans les β-alumines. Le comportement de la conductivité du sulfate alcalin binaire Rb^+:Li_2SO_4 est intermédiaire entre celui des deux effets alcalins mixtes. On rapporte aussi un nouvel effet positif de l'anion mixte dans le système MoO_4^{2-}:Na_2SO_4. On attribue la conductivité plus élevée du Na^+ dans les solutions solides de Rb^+:Na_2SO_4 et de MoO_4^{2-}:Na_2SO_4 à une expansion du réseau vers une structure hexagonale qui est affectée par un rayon plus grand de l'ion hôte isovalent et on l'interprète en fonction d'un mécanisme de transport du type percolation.

[Traduit par la revue]

Introduction

Solid state fast ion conductors are characterized by very high ionic conductivity, either anionic or cationic relative to the ionic conductivity of most crystalline solids. This relatively small group of solids, also known as solid electrolytes, has a specific ion which is not confined to specific lattice sites but is essentially free to move throughout the three-dimensional structure.

Recent attention has been focused on Na_2SO_4 which exhibited a sharp jump by a factor of 10 in electrical conductivity (1) as it transforms from Na_2SO_4(III) → Na_2SO_4(I) accompanied by a volume expansion of 4%. The structure of Na_2SO_4(I) is hexagonal, space group $P6_3/mmc$, characterized by orientational disorder of the SO_4 tetrahedra in the SO_4 sublattice (2). The ionic conductivity in Na_2SO_4(I) is increased appreciably by the presence of low concentrations of isovalent cations or anions (3–5). The consistent result of higher Na^+ conductivity in Na_2SO_4 when a larger radius isovalent guest ion is present in minor concentration supports the dominant role of "free" or "unoccupied" volume in facilitating intersite mobility within structural limits. Furthermore, the higher conductivity with 10 mol% Rb^+ in Na_2SO_4 suggested that the Na^+ mobility might attain higher values at higher concentrations of Rb^+ in Na_2SO_4. This result runs contrary to the so-called mixed alkali effect observed for Li/Na and Li/Rb disilicate glasses of composition $0.33A_2O{:}0.67SiO_2$ where A_2O is the alkali oxide component (6, 7) and for Na/K β-aluminas and Na/K gallate (8). This paper presents ac electrical conductivity results of a study designed to test the hypothesis that higher conductivity will result over the complete composition range in mixed alkali, Li/Rb and Na/Rb, sulfate and mixed anion, Na_2SO_4–MoO_4, compositions where the guest ions are of larger ionic radius.

Experimental procedure

All chemicals used were the Alfa Products with the specified grade cited: $Li_2SO_4 \cdot H_2O$ and Na_2SO_4 ultrapure, Rb_2SO_4 99.9%, $Na_2MoO_4 \cdot 2H_2O$ 99.5%. All studied samples were prepared by fusing in air the requisite composition mixture of the respective dehydrated compounds, previously well ground manually, at 50–75 K above its melting point (11, 12) in a platinum crucible. There was no discernible weight loss after fusion. The fused product in each case was a solid solution as evidenced by its DTA peak temperature which was within ±5 K of temperatures reported in the phase diagrams (11, 12) and the effect of temperature lowering associated with solid solution formation.

Electrical conductivity measurements were made on compressed, a force of 1.2×10^4 kg, polycrystalline specimen in a stainless steel conductivity cell. The experimental procedure for these measurements as described earlier (9), maintained the sample by a spring-loaded support between stainless steel leads using two polished Pt discs as electrodes. The two surfaces of the sample were touched with graphite (DAG #54 Acheson) to ensure proper contact. Each sample was installed and allowed to stand in the cell ca. 15 h at ~150°C under reduced pressure (~10^{-3} Torr) prior to measurement. The conductivity was measured under reduced pressure at 0.1 kHz, 1 kHz, and 10 kHz as a function of temperature using a GR 1608-A impedance bridge; the heating rate was 60 deg h^{-1}. The specific conductivity σ values were within experimental limits for 0.1–1 kHz frequencies with higher values at 10 kHz; this behavior is consistent with the reported impedance dependence on frequency in Na_2SO_4 (10). Most samples were discs of ~1 mm thickness and 100 mm^2 surface area; other samples were ~1 mm thick and ~70 mm^2 surface area which was the crack-free portion recovered from the compressed disc. Temperature was monitored within ±1 K by standardized chromel–alumel thermocouples with a Keithley digital multimeter.

Results and discussion

The ionic conductivity σ in a condensed phase is a composite quantity $\sigma = nqu$ where n is the number of carriers of charge, q per unit volume, and u is the mobility of these charged carriers. The dependence of the ionic conductivity on temperature usually follows an Arrhenius-type expression.

$$[1] \quad \sigma T = \sigma_0 \exp(-Q_c/RT) = n^2q^2\lambda^2\nu/k \exp(-Q_c/RT)$$

the result of combining the Nernst–Einstein relation $\sigma/D =$

[1]Preliminary results of this study, Paper no. LB-125, presented at World Congress on High Tech Ceramics, Milan, Italy, June 23–28, 1986, are to be published in High Technology Ceramics, *edited by* P. Vincenzini, Elsevier Science Publishers B.V., Amsterdam.

[2]This study received partial support from the Natural Sciences and Engineering Research Council of Canada.

[3]To whom correspondence should be addressed.

Can. J. Chem. Downloaded from www.nrcresearchpress.com by 78.46.186.204 on 09/07/12
For personal use only.

Can. J. Chem. Downloaded from www.nrcresearchpress.com by 78.46.186.204 on 09/07/12
For personal use only.

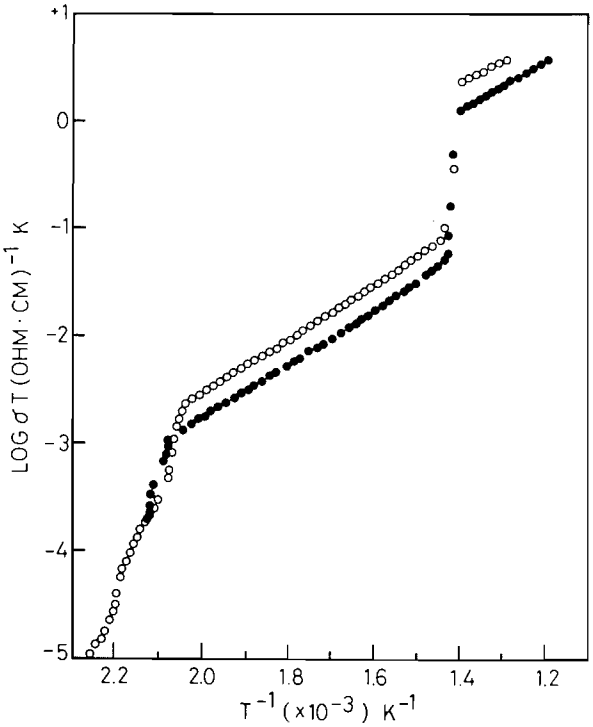

FIG. 1. Plots of log σT versus $T(\mathrm{K})^{-1}$ of Na_2SO_4–Rb_2SO_4 in mole ratios 1:2 (●) and 2:1 (○).

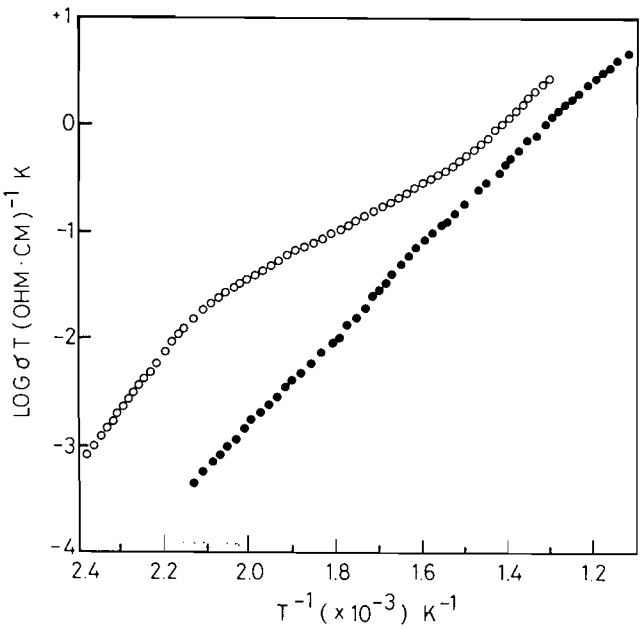

FIG. 2. Plots of log σT versus $T(\mathrm{K})^{-1}$ of Na_2SO_4–Na_2MoO_4 in mole ratios 1:1 (●) and 4:1 (○).

nq^2/kT and the diffusion equation $D = D_0 \exp(-Q_c/RT)$. In this equation ν is the vibration frequency, λ the inter-atomic distance, and Q_c the apparent activation energy for mobility of the specific ion, k and R are fundamental constants.

On the basis of eq. [1] for temperature dependence of ionic conductivity typical cool mode plots of log σT at 1 kHz versus $T(\mathrm{K})^{-1}$ are given in Fig. 1 for Rb^+:Na_2SO_4 compositions and in Fig. 2 for MoO_4^{2-}:Na_2SO_4 compositions. The solid–solid phase transition temperatures observed in the conductivity measurements are within ±5 K of the peak temperatures

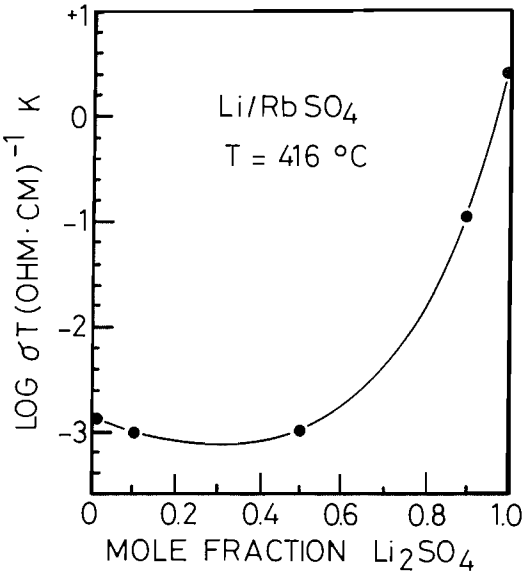

FIG. 3. Plot of log σT versus mole fraction Li_2SO_4 of binary alkali sulfate system Li_2SO_4–Rb_2SO_4 at T = 416°C (reproduced by permission of North Holland Physics Publishing).

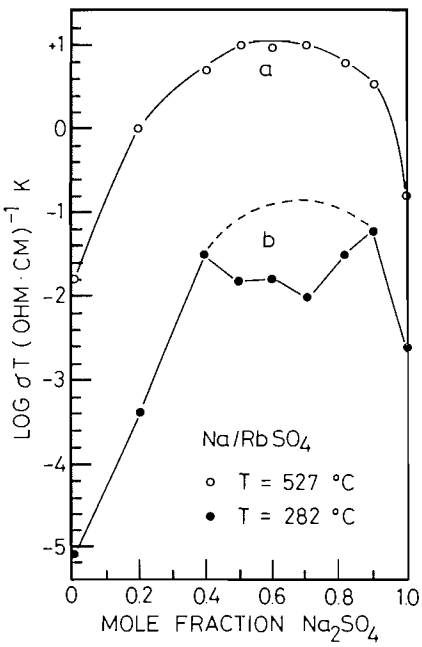

FIG. 4. Plots of log σT versus mole fraction Na_2SO_4 of binary alkali sulfate system Na_2SO_4–Rb_2SO_4 at T = 527°C (a) and T = 282°C (b); --- in (b) represents the expected behavior paralleling (a). The points are linked for guidance.

obtained in our DTA and DSC traces for these transitions. Similar plots of log σT versus $T(\mathrm{K})^{-1}$ for $Li/RbSO_4$ compositions, not shown, exhibit a monotonic behavior with no evidence of phase transition in the temperature interval 200–500°C.

The log σT (1 kHz) values at a constant temperature as a function of alkali composition are plotted in Figs. 3 and 4 for Rb^+:Li_2SO_4 and Rb^+:Na_2SO_4 systems, respectively, and for the MoO_4^{2-}:Na_2SO_4 system in Fig. 5. The temperature 416°C was chosen for the Rb^+:Li_2SO_4 system because no phase transition is evident over the complete Rb^+:Li_2SO_4 composition according to its phase diagram (11) and our DTA traces. Above 518°C a phase transition occurs on the Li_2SO_4-rich side of the

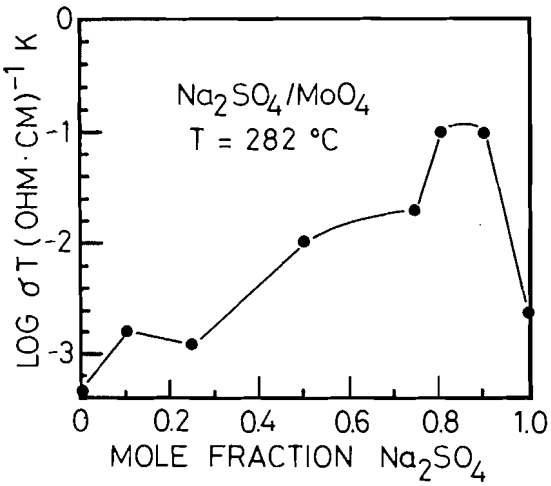

FIG. 5. Plot of log σT versus mole fraction Na_2SO_4 of binary system Na_2SO_4–Na_2MoO_4 at T = 282°C. The points are linked for guidance.

1:1 compound identified with $RbLi_5(SO_4)_3$. The temperatures 282°C and 527°C were chosen for the Rb^+:Na_2SO_4 system because these represented in each case a stable state of the system over the complete Rb^+:Na_2SO_4 composition range according to its phase diagram (12) and our DTA traces. The state of the Rb^+:Na_2SO_4 system at 282°C is taken as hexagonal Na_2SO_4(I) phase incorporating Rb_2SO_4 whereas at 527°C a solid solution exists with structures or phases dominated by the high temperature hexagonal phase of Rb_2SO_4 and identified as α, β, γ. Again the state of the MoO_4^{2-}:Na_2SO_4 system at 282°C is taken to be the hexagonal Na_2SO_4(I) phase incorporating Na_2MoO_4.

Tables 1 and 2 give the activation energy values for the Rb^+:Na_2SO_4 and MoO_4^{2-}:Na_2SO_4 systems, respectively, for the two phases. The Q_c values for the Na_2SO_4-rich compositions remain essentially constant for the Na_2SO_4(I) phase at 282°C in both Rb^+:Na_2SO_4 and MoO_4^{2-}:Na_2SO_4 systems.

The conductivity–alkali composition behavior for the Rb^+:Li_2SO_4 system shown in Fig. 3 is to be expected to a first approximation where a decrease in the fraction of highly mobile carrier Li^+ ion, with all other factors remaining constant, effects a decrease in the overall conductivity. The structure of Li_2SO_4 is monoclinic and that of Rb_2SO_4 is orthorhombic below 580°C. Such an interpretation suggests that the number of mobile Li^+ ions depends on the number of Li^+ ions per unit volume which is not unexpected. The hypothesis that the large Rb^+ ions provide more "free" volume to enhance the mobility of the smaller Li^+ is not confirmed. Since Li_2SO_4 and Rb_2SO_4 structures differ significantly this result suggests that the hypothesis of large guest ion-free volume contribution is only valid for isomorphous structure systems.

The positive conductivity–alkali composition effect for the Rb^+:Na_2SO_4 system in two structural states is obvious in Fig. 4. Only solid solutions are present and no compound formation is evident in this system. Since one can assume that the fraction of mobile charge carriers Na^+ decreases with mole fraction of Na_2SO_4 in the binary alkali sulfate then it would appear that the compositional structure is conducive to higher mobility of the Na^+ ions. That is, the decrease in the number of carriers is more than compensated by the facility of Na^+ mobility provided by the structural factor, especially over the Na_2SO_4 mole fraction inverval 0.4–0.9.

TABLE 1. Ionic conductivity activation energy Q_c for Na/$RbSO_4$ mixed alkali effect

Additive Rb_2SO_4 (mol%)	Q_c (kJ/mol) 282°C	Q_c (kJ/mol) 527°C
0	55±5	55±5
10	44±3	57±5
18.5	48±3	67±5
30	46±4	72±4
40	50±3	36±3
50	46±4	52±5
60	46±4	90±6(?)
67	50±3	42±3
75	70±4	65±4
100	150±8	120±5

TABLE 2. Ionic conductivity activation energy Q_c for Na_2SO_4/MoO_4 mixed anion effect

Additive Na_2MoO_4 (mol %)	Q_c (kJ/mol) 282°C
0	55±5
10	44±3
20	44±3
25	52±4
50	72±5
75	86±6
90	86±6

Again the positive conductivity–anion composition effect for the MoO_4^{2-}:Na_2SO_4 system is evident in Fig. 5. Since the mole fraction of Na^+ remains constant one can assume that the fraction of mobile Na^+ also remains effectively constant. The fact that Na_2MoO_4 is isomorphous with Na_2SO_4(I), $P6_3/mmc$, in this temperature range suggests ease of substitution in their respective anion sublattices. The presence of MoO_4^{2-} in the SO_4^{2-} sublattice would effect lattice expansion, $R_{Mo—O}$ = 1.77 Å versus $R_{S—O}$ = 1.44 Å (13), providing more "free" volume to allow greater facility for Na^+ mobility leading to higher conductivity.

The conductivity results presented herein are in strong contrast to the mixed alkali effect observed in disilicate glasses (6, 7), β-aluminas and β-gallate (8), where a dramatic decrease in conductivity occurs when one alkali ion is in the presence of another alkali ion. It is obvious that the weak electrolyte model or the "quasiliquid" conduction model proposed to interpret the mixed alkali effect cannot be used in the case of mixed alkali sulfate and sodium mixed anion systems.

The central questions in the theory of conductivity in fast ion conductors revolve on n and Q_c in eq. [1]. The activation energy for ionic conductivity Q_c involving defects is a composite quantity consisting mainly of two terms (*i*) the enthalpy of defect formation h_s and (*ii*) the enthalpy of migration Δh_c (14). At low temperatures ~200°C, Q_c is identified with Δh_c where the fractional molar concentration of mobile Na^+ in the Na_2SO_4-rich compositions can be taken as effectively constant at 1×10^{-3} as calculated earlier (5). The minimum Q_c values correlate with the maximum σT values excepting the 90 kJ/mol at 527°C for 60 mol% Rb^+, for mixed alkali and mixed anion

Can. J. Chem. Downloaded from www.nrcresearchpress.com by 78.46.186.204 on 09/07/12
For personal use only.

effects. The same σT values, within experimental limits, for the same Rb^+ and MoO_4^{2-} concentrations strongly support the straightforward physical or lattice expansion basis for the enhanced ionic conductivity. Recent results from the experimental test for the anion-rotatory motion or paddle-wheel mechanism which showed convincingly that the anion-rotation mechanism does not contribute to the enhanced cationic conductivity in Na_2SO_4 (4) is further confirmed by the MoO_4^{2-} results. A contribution to ionic conductivity and Q_c can originate with the lower vibrational amplitude of the heavier guest ion (Rb^+, MoO_4^{2-}) giving a more rigid cation or anion sublattice network which would reduce the scattering of the mobile Na^+ ions.

Our cationic conductivity data for the Li_2SO_4–Rb_2SO_4, Na_2SO_4–Rb_2SO_4, and Na_2SO_4–Na_2MoO_4 systems can be explained in terms of a percolation type of transport mechanism in a lattice structure with an increased degree of "free" volume or openness (15). We visualize the existence of percolation paths through a network of interconnected, irregularly positioned sites with Li^+ or Na^+ occupancy. In pure Li_2SO_4 or Na_2SO_4 a minimum of interconnected sites, that is, a restricted number of complete pathways, exist in the low temperature ordered phase. But in the transformation to the high temperature disordered phase, the lattice expands (3% increase in molar volume in Li_2SO_4, 4% increase in molar volume in Na_2SO_4) so the number of accessible interconnected sites involving lower Q_c increases resulting in higher ionic conductivity. In the Li_2SO_4–Rb_2SO_4 system the results are for the low temperature ordered structure prior to any phase transition, monoclinic for Li_2SO_4 and orthorhombic for Rb_2SO_4, with no volume increase and no change in the accessibility of interconnected sites. On the other hand, the Rb^+:Na_2SO_4 system transforms from the ordered phase to the disordered hexagonal phase of Na_2SO_4(I) above 200°C as does the MoO_4^{2-}:Na_2SO_4 system. The Rb^+:Na_2SO_4 system undergoes a further phase transition to a more open or larger "free" volume structure characteristic of Rb^+:Na_2SO_4 solid solution above 460°C. The solid solution phase above 460°C dominated by the high temperature phase of Rb_2SO_4 is speculated to be hexagonal, paralleling the orthorhombic–hexagonal transition of its analogs, e.g. Rb_2WO_4 (16). The higher conductivity in the Rb^+:Na_2SO_4 and MoO_4:Na_2SO_4 systems is attributed to lattice expansion in a hexagonal structure effected by the presence of the larger radius guest ions, Rb^+ and MoO_4^{2-}. However, the conductivity versus composition profiles of Figs. 4 and 5 prompt some fundamental questions relating to (*i*) the effectiveness of guest ion in the cation sublattice versus the guest ion in the anion sublattice, (*ii*) the effect of cation–cation interaction versus the mixed anion pair presence, and (*iii*) the effect of the reduced vibrational amplitude of heavier guest ion on the reduced scattering of mobile ions. These questions will be explored in our laboratory in the future.

1. R. MacL. Murray and E. A. Secco. Can. J. Chem. **56**, 2616 (1978).
2. W. Eysel, H. H. Hofer, K. L. Keester, and Th. Hahn. Acta Crystallogr. B**41**, 5 (1985).
3. M. S. Kumari and E. A. Secco. Can. J. Chem. **61**, 2804 (1983).
4. E. A. Secco. Phys. Status Solidi (*a*), **88**, K75 (1985).
5. M. D. Leblanc, V. M. Gundusharma, and E. A. Secco. Solid State Ionics, **20**, 61 (1986).
6. J. O. Isard. J. Non-Cryst. Solids, **1**, 235 (1969).
7. D. E. Day, J. Non-Cryst. Solids, **21**, 343 (1976).
8. M. D. Ingram and C. T. Moynihan. Solid State Ionics, **6**, 303 (1982).
9. M. Natarajan and E. A. Secco. Can. J. Chem. **52**, 712 (1974).
10. Y. Saito, T. Maruyama, and K. Kobayashi. Solid State Ionics, **14**, 265 (1984).
11. I. S. Rassonskaya and N. K. Semendyaeva. Zh. Neorgan. Khim. **11**, 1134 (1966); Russ. J. Inorg. Chem. (Engl. Transl.) 608 (1966).
12. V. E. Plyushchev, R. G. Samuseva, and I. F. Poletaeiv. Zh. Neorgan. Khim. **7**, 860 (1962); Russ. J. Inorg. Chem. (Engl. Transl.) 445 (1962).
13. S. C. Abrahams and J. M. Reddy. J. Chem. Phys. **43**, 2533 (1965).
14. L. W. Barr and A. B. Lidiard. *In* Physical chemistry, an advanced treatise. *Edited by* H. Eyring, D. Henderson, and W. Jost. Academic, New York. 1970. p. 151.
15. J. M. Ziman. Models of disorder. Cambridge University, Cambridge. 1979. Chap. 9.
16. A. J. van den Berg, F. Tuinstra, and J. Warczewski. Acta Crystallogr. B**29**, 586 (1973).

Can. J. Chem. Downloaded from www.nrcresearchpress.com by 78.46.186.204 on 09/07/12
For personal use only.

A theoretical study of the structures and stabilities of $C_2H_3S^+$ ions

CHRISTOPHER F. RODRIQUEZ AND ALAN C. HOPKINSON
Department of Chemistry, York University, Downsview, Ont., Canada M3J 1P3

Received August 12, 1986

CHRISTOPHER F. RODRIQUEZ and ALAN C. HOPKINSON. Can. J. Chem. **65**, 1209 (1987).

Ab initio molecular orbital calculations at the 6-31G* level have been used to locate eight minima and five saddle points on the $C_2H_3S^+$ hypersurface. The thioacetyl ion, H_3CCS^+ (**1**), is the global minimum and the 1-thiovinyl cation (**4**), 106 kJ mol^{-1} higher, is the next lowest. Interconversion of **1** and **4** has the highest barrier calculated for this surface (250 kJ mol^{-1} above **4**) but all transition structures to intramolecular rearrangement are lower than the energies of the dissociation products. These results are consistent with the experimental observation that there is only one dissociation channel for ions $C_2H_3S^+$, regardless of the structure of organosulphur compound from which $C_2H_3S^+$ was produced. Comparisons are made with the $C_2H_3O^+$ hypersurface.

CHRISTOPHER F. RODRIQUEZ et ALAN C. HOPKINSON. Can. J. Chem. **65**, 1209 (1987).

On a utilisé des calculs d'orbitales moléculaires au niveau 6-31G* pour déterminer la position de huit minima et de cinq cols sur l'hypersurface du $C_2H_3S^+$. L'ion thioacétyl, H_3CCS^+ (**1**), correspond au minimum global et le cation thio-1 vinyle (**4**), dont l'énergie est 106 kJ mol^{-1} plus élevée, est le minimum suivant. La barrière à l'interconversion des ions **1** et **4** est la plus élevée de cette surface (250 kJ mol^{-1} au-dessus de **4**); toutefois, toutes les structures de transition de la transposition intramoléculaire possèdent des énergies qui sont plus basses que celles des produits de dissociation. Ces résultats sont en accord avec les données expérimentales selon lesquelles, quelle que soit la structure du composé organosulfuré à partir duquel l'ion $C_2H_3S^+$ est produit, il n'existe qu'une seule voie de dissociation pour la dissociation de ces ions. On fait des comparaisons avec l'hypersurface de l'ion $C_2H_3O^+$.

[Traduit par la revue]

Can. J. Chem. Downloaded from www.nrcresearchpress.com by 72.64.146.136 on 09/07/12
For personal use only.

The relative energies and structures of gaseous ions $C_2H_3O^+$ have been examined in considerable detail both by *ab initio* molecular orbital theory (1–3) and by experiment (4–10). Two isomers, the acetyl and 1-hydroxyvinyl cations, have been identified as long-lived species in the gas phase (5, 8) and the existence of a third isomer, the oxiranyl cation, has been indicated by collisional activation studies (9). High level *ab initio* molecular orbital calculations (3) have shown these three ions to be at minima on the $C_2H_3O^+$ hypersurface and two other structures, $H_3C—O^+{=}C$: and $HC{\equiv}C—OH_2^+$, have low energies and high barriers to rearrangement, making them potentially detectable in the gas phase.

For $C_2H_3S^+$ the hypersurface is less well understood. $C_2H_3S^+$ is produced in the mass spectrum of organosulphur compounds of widely differing structure but collisionally activated decomposition mass-analysed kinetic energy spectroscopy of these $C_2H_3S^+$ ions shows almost identical fragmentation patterns regardless of the structure of the precursor organosulphur compound (11). These results have been interpreted as evidence for a single common ion and the question arises as to what structure any such ion might have. By analogy with the $C_2H_3O^+$ surface the common ion is expected to be the thioacetyl ion (structure **1**, Fig. 1), but decomposition of the observed $C_2H_3S^+$ ion produces very little CH_3^+ and this has been taken as evidence that the common ion does not have structure **1**.

We have been studying carbenium ions containing heteroatoms from the second and third rows (12, 13) of the periodic table and, in an attempt to resolve the problem posed by the experimental results, we now present our molecular orbital results on isomers on the $C_2H_3S^+$ hypersurface. The eight structures, all minima, which we have examined are labelled **1** → **8** and are given in Fig. 1. *Ab initio* molecular orbital calculations, at lower levels of theory, have been previously reported for four of these structures (**2**, **3**, **4**, and **5**) (14, 15).

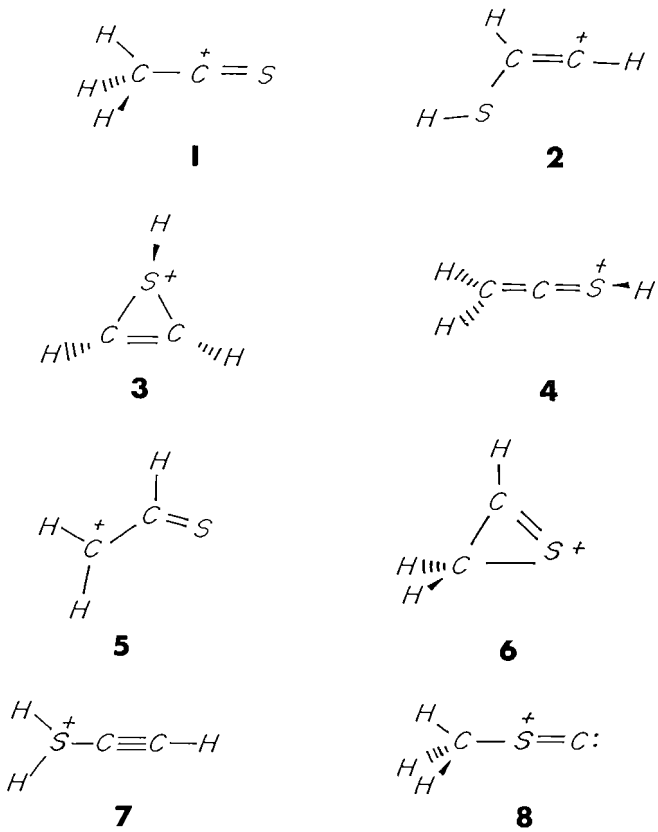

FIG. 1. Possible structures for ion $C_2H_3S^+$.

Method

Standard closed shell *ab initio* molecular orbital calculations were carried out using the Monstergauss program (16). Minima were located using the optimally conditioned (OC) method (17) and transition structures using the VA05AD technique (18). All structures were optimised initially at the STO-3G level (19) and then subsequently at the 6-31G* level (20).

Results and discussion

1. Structures and energies

The structures for the ions, as optimised at the 6-31G* level,

TABLE 1. Total energies (hartrees) and relative energies (kJ mol^{-1}) of $C_2H_3S^+$ species

Species	STO-3G//STO-3G		6-31G*//6-31G*	
	Total	Relative	Total	Relative
H_3CCS^+ (**1**)	−469.48327	0	−474.68974	0
$HCCHSH^+$ (**2**)	−469.37000	297	−474.59507	249
$HCCHSH^+$ (**3***b*)	−469.40006	219	−474.62478	171
H_2CCSH^+ (**4**)	−469.42660	149	−474.64907	106
H_2CCHS^+ (**5**)	−469.40329	210	−474.62111	180
$HC—CH_2S^+$ (**6**)	−469.42477	154	−474.64903	128
H_2SCCH^+ (**7**)	−469.33115	399	−474.55226	361
$H_3C—S=C^+$ (**8**)	−469.32137	425	—	—
TS **9**, **2** → **3**	−469.36454	312	−474.59257	254
TS **10**, **5** → **6**	−469.38813	250	−474.61883	186
TS **11**, **5** → **1**	—	—	−474.59015	261
TS **12**, **5** → **4**	−469.33693	384	−474.55385	357
TS **13**, **2** → **4**	−469.34932	352	−474.58789	267
$CH_3^+ + CS$	—	—	−474.53496	406
$CH_2 + HCS^+$	—	—	−474.48271	544
$CH_2 + HSC^+$	—	—	−474.30499	1010
$H_2C=C=S + H^+$	—	—	−474.35534	878

are given in Fig. 2 and the energies at both the STO-3G and 6-31G* levels are given in Table 1.

(a) Thioacetyl cation (1)

Ion **1** has the lowest energy on the hypersurface. The C—S bond length of **1** (1.468 Å) is shorter than that of CS (1.520 Å at 6-31G*) and the sulphur atom carries the majority of the positive charge (+0.521) indicating that valence bond structure **1***b* is an important contributor. The methyl group functions

$$H_3C—\overset{+}{C}=S \longleftrightarrow H_3C—C\equiv S^+$$

1*a* **1***b*

as a donor, mainly through hyperconjugation (charge on CH_3 is +0.318) and the carbon–carbon bond is intermediate between a single and a double bond. Curiously the geometry of the H_3C—C fragment is identical to that calculated for H_3CCO^+ at the 4-31G level (3).

(b) 2-Thiovinyl cation (2)

The *anti* conformer of the 2-thiovinyl cation (shown in Fig. 1) is lower in energy than the *syn* conformer by only 2 kJ mol^{-1} at the STO-3G level and by 1 kJ mol^{-1} at the 6-31G* level. By comparison for the 2-hydroxyvinly cation at the 4-31G level the *anti* conformer is lower than the *syn* by 11 kJ mol^{-1}. On the $C_2H_3S^+$ surface both conformers are higher in energy than the thiirenium ion, **3***b*, and are relatively unimportant as the barriers to collapse into **3***b* are very low. Extension of the calculations beyond the Hartree–Fock level is expected to improve the cyclic ion relative to the open (3) and it is questionable whether **2** will be at a minimum when correlation energy is included.

(c) Thiirenium ion (3)

The thiirenium ion has carbon–sulphur bonds which are slightly longer than a normal single bond and the carbon–carbon distance is intermediate between a double and a triple bond and is almost identical to that in the oxiranyl cation (3). The bonds within the ring are a little shorter than those calculated for thiirene at the 6-311G* level (21), consistent with a tightening of bonds resulting from the positive charge on the ring.

The SH bond is 77.9° out of the plane defined by the heavy atoms and the inversion barrier, calculated as the difference between the planar (**3***a*) and pyramidal (**3***b*) thiirenium ions, is 369 kJ mol^{-1}. This high barrier has been attributed to σ interactions with a relatively small contribution from four-electron – two-orbital interaction in the π system of the planar ion (14).

(d) 1-Thiovinyl cation (4)

The 1-thiovinyl cation is isoelectronic with allene (neglecting inner shells) and adopts the same twisted conformation for the terminal groups. The ∠CCS is 174.9° (ethynylthiol has ∠CCS of 176.7° (21) and the two hydrogens of the methylene group are very slightly bent away from the sulphur atom. The bond lengths between heavy atoms are both a bit shorter than double bonds. This structure has the second lowest energy on the hypersurface.

(e) Thioformylmethyl cation (5)

The carbon–carbon bond length is shorter than a single bond and the carbon–sulphur is longer than a double bond, indicating considerable donation to the cationic carbon from C=S. The π density on C^+ is 0.338 e and on S is 0.630 e. Sulphur also acts as a σ donor and has a net charge of +0.476. Isomer **5** is of little physical significance as rotation about the carbon–carbon bond has a low barrier and results in formation of the thiiranyl cation, **6**.

(f) Thiiranyl cation (6)

The HC—S bond length in **6** is shorter than a carbon–sulphur double bond and the calculated net charge on S is +0.505, indicating that resonance structure **6***a*, where most of the positive charge is located on sulphur rather than on carbon, is the best description. The π populations of the carbon of CH and of sulphur are 0.572 e and 1.406 e, respectively (excluding the inner shell electrons of π symmetry on sulphur). Hence structure **6***b* is not insignificant.

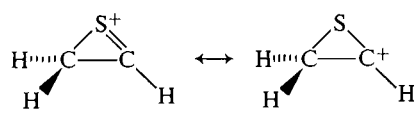

6*a* **6***b*

Can. J. Chem. Downloaded from www.nrcresearchpress.com by 72.64.146.136 on 09/07/12
For personal use only.

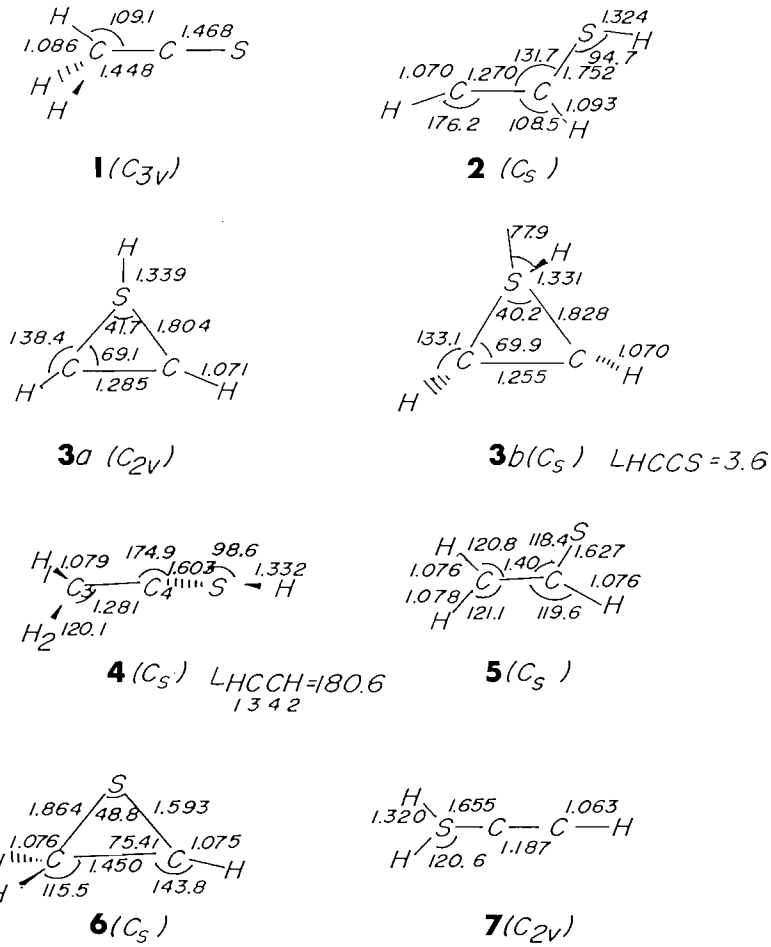

FIG. 2. Structural parameters for $C_2H_3S^+$ as obtained from optimisation at 6-31G* level. Bond lengths in Å and bond angles in deg.

(g) Structures 7 and 8

Isomer **7** is formed by protonation of ethynylthiol on sulphur and both the C—S and C—C bonds are shorter than those in the base. This structure has considerably higher energy than isomers **1** → **6** and consequently was not considered as a likely candidate for the common ion observed in mass spectrometry. Structure **4**, which is generated by protonation of ethynylthiol at the carbon, has much lower energy and it is interesting to note that for ethynylthiol the relative proton affinities are β-carbon > α-carbon > sulphur.

Structure **8**, by analogy with the $C_2H_3O^+$ surface, was expected to be low in energy, but in preliminary calculations at the STO-3G level it had higher energy than the other isomers and we did not consider this structure at the 6-31G* level.

2. Interconversion of open and cyclic ions

Sulphur is a large polarisable atom and in ions where the sulphur is in the β position relative to the carbon formally carrying the positive charge then bridging by sulphur is likely. We therefore examined the profiles for formation of cyclic ions from structures **2** and **5**.

(a) 2-Thiovinyl cation (2) → thiirenium ion (3b)

Ions **3***b* and **2** are models for the intermediates formed in the initial slow step in the electrophilic addition of arene and alkanesulphenyl halides to alkynes (for a review, see ref. 22). The structures of **3***b* and **2** and the profile to their interconversion have been previously studied by *ab initio* molecular orbital calculations in a comprehensive study of electrophilic addition to acetylene (refs. 14, 15, for a review, see ref. 23).

The transition structures for conversion of the *anti* conformer (**2**) and the *syn* conformer into **3***b* have activation energies of 5 kJ mol^{-1} and 11 kJ mol^{-1}, respectively, above the 2-thiovinyl cations. These energies are slightly smaller than the barrier to rotation previously calculated for conversion of the *syn* isomer into the *anti* (13.8 kJ mol^{-1} (14)) and both would collapse into the cyclic isomer in preference to interconverting.

The transition structure (**9**) for conversion of the *anti* conformer into **3***b* has similar geometric parameters to **2** with the major changes being a decrease in ∠SCC (to 118.7° from 131.7°), an increase in C—S (to 1.789 Å from 1.752 Å) and rotation about the C—S bond (by 28°). A small distortion of **2** then leads to transition structure **9** and the low energy barrier to formation of **3***b* seems to make observation of **2** by experiment to be very unlikely. We were unable to locate a transition structure for conversion of **3***b* into **6**, and conversion of **3***b* into other lower energy isomers appears to require formation of **2** as an intermediate. The direct observation of the stable trimethylthiirenium ion (24) supports this conclusion (Fig. 3).

(b) Thioformylmethyl cation (5) → thiiranyl cation (6)

The thiiranyl cation is lower in energy than the thioformylmethyl cation at both the STO-3G and 6-31G* levels and inclusion of correlation energy is expected to further favour the thiiranyl cation. Transition structure **10** for the collapse

Can. J. Chem. Downloaded from www.nrcresearchpress.com by 72.64.146.136 on 09/07/12
For personal use only.

Can. J. Chem. Downloaded from www.nrcresearchpress.com by 72.64.146.136 on 09/07/12
For personal use only.

of **5** into **6** is only 6 kJ mol^{-1} at the 6-31G* level and under experimental conditions **5** will not be observable. Transition structure **10** is similar in geometry to **5** with rotation of the methylene group and bending of ∠CCS being the major changes.

3. Intramolecular rearrangements leading to formation of 1 and 4

Ions **1** and **4** have the lowest energies on the $C_2H_3S^+$ hypersurface and if there is one common ion in the gas phase then it is likely to have one of these structures. Accordingly we have calculated transition structures for the formation of **1** and **4** from the other ions.

(a) Thioformylmethyl cation (5) → thioacetyl cation (1)

The thioformylmethyl cation is converted into the thioacetyl cation by a 1,2-shift of a hydrogen. The transition structure, **11**, for this rearrangement is 81 kJ mol^{-1} above **5**. **11** essentially has C_s symmetry and the major differences from structure **5** are increases in ∠CCS and the C_1—H distance, and decreases in $\angle C_1C_2H_3$ and the C—S distance. All these parameters are intermediate between the values for **5** and **1**.

As discussed earlier, structure **5** collapses into **6** with a very small barrier and at the 6-31G* level then conversion of **6** into **1** can be considered to pass through **5** as an intermediate and the activation energy for the reaction **6** → **1** by this mechanism has a barrier 143 kJ mol^{-1} above **6**.

(b) Thioformylmethyl cation (5) → 1-thiovinyl cation (4)

A 1,2-shift of a hydrogen from carbon to sulphur converts **5** into **4** via transition structure **12**. This is a high energy process although the calculated activation energy of 177 kJ mol^{-1} above **5** is probably an overestimate. Inclusion of correlation energy generally results in a lowering of barrier heights and for the analogous reaction on the $C_2H_3O^+$ energy hypersurface (3) the barrier at the HF/6-31G** level is 247 kJ mol^{-1} while at the MP2/6-31G** level it is reduced to 113 kJ mol^{-1}.

(c) Thiirenium ion (3b) → 1-thiovinyl cation (4)

Attempts at finding transition structures for the conversion of thiirenyl cation **3***b* into **4** by a 1,2-shift accompanied by ring opening was unsuccessful. One possible route for this reaction to occur is via **2** as an intermediate. Structure **9** is only 5 kJ mol^{-1} above **2** and for the second step the transition

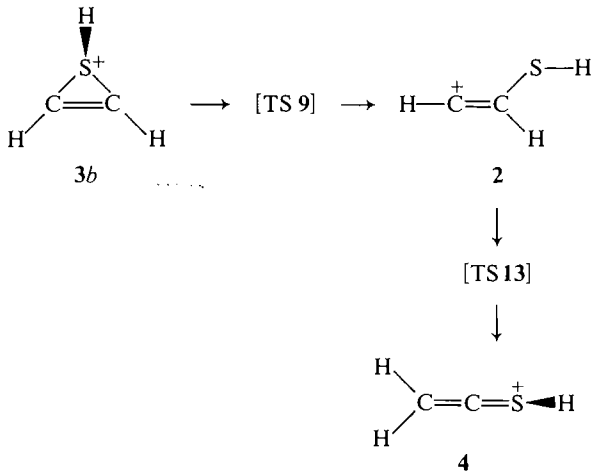

structure **13** is 18 kJ mol^{-1} above **2**. For the overall process **3***b* → **4** by this pathway the activation energy is 96 kJ mol^{-1} above **3***b*.

(d) 1-Thiovinyl cation (4) → thioacylium ion (1)

In general 1,3-hydrogen shifts along a linear molecule have high barriers (25, 26) and we have been unable to locate a transition structure for the 1,3-shift of a hydrogen required to convert **4** into **1**. Similar difficulties were encountered for the analogous isomers on the $C_2H_3O^+$ hypersurface (3).

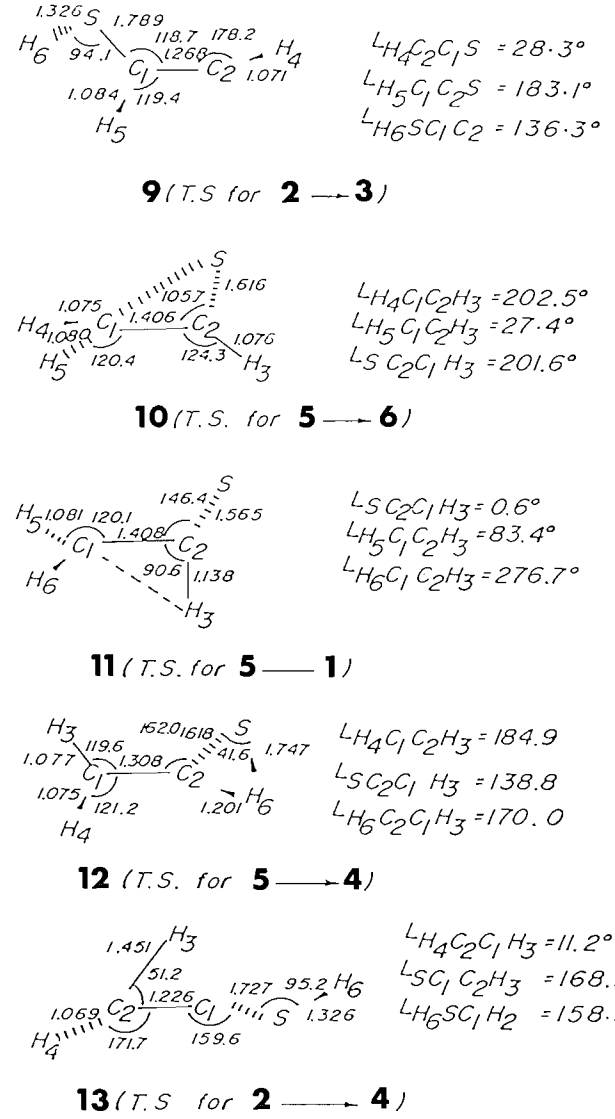

FIG. 3. Transition structures from optimisation at 6-31G* level. Bond lengths in Å and bond angles in deg.

One mechanism for achieving the 1,3-shift is to have a sequence of 1,2-shifts involving **4** → **5** → **1**.

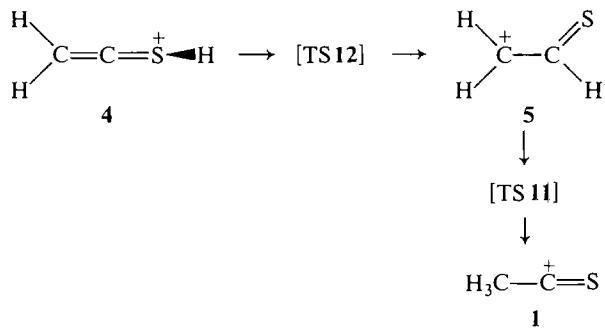

For this pathway transition structure **12** has the highest energy and conversion of **4** into **1** then has a barrier of 251 kJ mol^{-1} above **4**.

4. Protonation of thioketene

The experimental proton affinity of $H_2C{=}C{=}O$ is 842 kJ

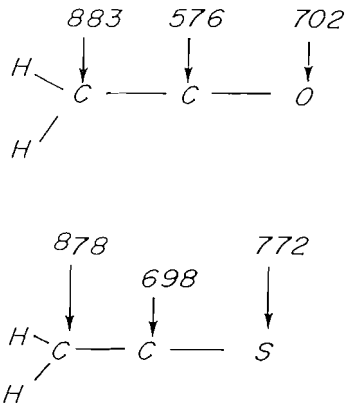

FIG. 4. $-\Delta E$ (kJ mol^{-1}) for protonation at each heavy atom in ketene (at 6-31G**) and in thioketene (at 6-31G* level).

mol^{-1} and Nobes *et al.* (3) have calculated values ranging from 848–883 kJ mol^{-1} at various levels of theory, with their highest level calculation giving 849 kJ mol^{-1}. At the 6-31G** SCF level the calculated proton affinity for ketene is 883 kJ mol^{-1}; this is almost identical to our 6-31G* level proton affinity for thioketene (878 kJ mol^{-1}). Clearly then the methylene carbon has almost the same basicity regardless of the heteroatom.

Protonation on the sulphur of thioketene occurs more easily than on the oxygen of ketene (Fig. 4). Protonation on the central carbon atom has the highest energy for both molecules but thioketene has the higher basicity.

5. Comparison of the $C_2H_3O^+$ and $C_2H_3S^+$ hypersurfaces

The relative energies of the isomers at 6-31G*//6-31G* is **1** < **4** < **6** < **3***b* < **5** < **2** < **7** and this order is also followed at the STO-3G level with **3***b* and **5** being interchanged. Structure H_3CS^+=C:, **8**, which, by analogy with the $C_2H_3O^+$ surface, was expected to be of low energy, had the highest energy of all species studied at the STO-3G level and was not considered at the higher level. There are, however, many similarities between the $C_2H_3O^+$ and $C_2H_3S^+$ surfaces. On the oxygen surface at the 6-31G** level, the order of the isomers is **1** < **8** < **4** < **6** < **5** < **2** < **7** < **3***b* and the energy differences are one and a half to two times larger than on the $C_2H_3S^+$ surface. The only major difference other than the low energy of **8** is that on the $C_2H_3O^+$ surface at the SCF level, protonated oxirene is high in energy and is the transition state for the 1,2-shift of a hydroxyl group in the degenerate hydroxyl shift in the 2-hydroxyvinyl cation. On the $C_2H_3S^+$ surface the bridging ability of sulphur results in **3***b* being at a minimum and the transition state for conversion of **2** into **3***b* is sufficiently low (5.5 kJ/mol) that **2** will not be observable under experimental gas phase conditions.

Conclusions

The thioacetyl ion (**1**) has the lowest energy of all $C_2H_3S^+$ isomers and if there is one common ion in the gas phase it is expected to have this structure. Ion **4** has the second lowest energy and conversion of this ion into **1** via the intermediate **5** has a high barrier, 250 kJ mol^{-1} above **4**. For the other ions considered here at the HF/6-31G* level relatively little energy is required to convert **5** and **6** into **1**, and to convert **2** and **3** into **4** and inclusion of correlation energy should further decrease these barriers. The high barrier for reaction **4** → **1** (via **5**) then determines whether all the ions interconvert. The transition structure for this reaction, **12**, is lower in energy (by 49 kJ mol^{-1}) than the dissociation products of lowest energy (CH_3^+ plus CS). Clearly then ions from all precursors will isomerise prior to dissociation and the existence of a common dissociation pathway is not surprising.

Of the possible dissociation products listed in Table 1 the combination of CH_3^+ and CS has the lowest energy and by comparison with the $C_2H_3O^+$ hypersurface it is probable that there is zero reverse activation energy for dissociation of H_3CCS^+. One of the observed major products, HCS^+, if accompanied by singlet methylene, requires 138 kJ mol^{-1} more energy to form and we are therefore at a loss to explain why dissociation into CH_3^+ and CS does not occur.

Acknowledgements

We thank the Natural Sciences and Engineering Research Council of Canada for financial support and the York University Computer Centre for generous allotments of computer time.

1. A. C. HOPKINSON. J. Chem. Soc. Perkin Trans. II, 795 (1973).
2. D. R. YARKONY and H. F. SCHAEFER. J. Chem. Phys. **63**, 4317 (1975).
3. R. H. NOBES, W. J. BOUMA, and L. RADOM. J. Am. Chem. Soc. **105**, 310 (1983).
4. D. G. KINGSTON and H. P. TANNENBAUM. Org. Mass. Spectrom. **10**, 263 (1975).
5. J. VOGT, A. D. WILLIAMSON, and J. L. BEAUCHAMP. J. Am. Chem. Soc. **100**, 3478 (1978).
6. P. AUSLOOS and S. G. LIAS. Chem. Phys. Lett. **51**, 53 (1977).
7. R. WEBER and K. LEVSEN. Org. Mass. Spectrom. **15**, 138 (1980).
8. J. K. TERLOUW, W. HEERMA, and G. DIJKSTRA. Org. Mass Spectrom. **15**, 660 (1980).
9. J. K. TERLOUW, W. HEERMA, and J. L. HOLMES. Org. Mass Spectrom. **16**, 306 (1981).
10. G. D. DEBROU, J. E. FULFORD, E. G. LEWARS, and R. E. MARCH. Int. J. Mass Spectrom. Ion Phys. **26**, 345 (1978).
11. C. PARADISI, G. SCORRANO, S. DAOLIO, and P. TRALDI. Org. Mass Spectrom. **19**, 198 (1984).
12. C. F. RODRIQUEZ. M.Sc. Thesis, York University, Downsview, Ont. 1985.
13. C. F. RODRIQUEZ and A. C. HOPKINSON. Org. Mass Spectrom. **20**, 691 (1985).
14. I. CSIZMADIA, F. BERNARDI, V. LUCCHINI, and G. MODENA. J. Chem. Soc. Perkin II, 542 (1977).
15. P. KOLLMAN, S. NELSON, and S. ROTHENBERG. J. Phys. Chem. **82**, 1403 (1978).
16. M. R. PETERSON and R. A. POIRIER. Monstergauss Program. Department of Chemistry, University of Toronto, Toronto, Ont. 1980.
17. W. C. DAVIDON and L. NAZARETH. Argonne National Laboratories Technical Memos 303 and 306, Argonne, IL. 60439; W. C. DAVIDON. Math. Programming, **9**, 1 (1975).
18. M. J. D. POWELL. Subroutine VA05AD, AERE Subroutine Library, Harwell, Didcot, Berkshire, U.K.
19. W. J. HEHRE, R. F. STEWART, and J. A. POPLE. J. Chem. Phys. **51**, 2657 (1969).
20. P. C. HARIHARAN and J. A. POPLE. Theoret. Chim. Acta, **28**, 213 (1978).
21. R. GOSAVI and O. P. STRAUSZ. Can. J. Chem. **61**, 2596 (1983).
22. G. H. SCHMID. *In* Topics in sulphur chemistry. Vol. 3. *Edited by* A. Senning and P. S. Magee. Georg Thieme Publishers, Stuttgart. 1977.
23. V. LUCCHINI and G. MODENA. Prog. Theoret. Org. Chem. Vol. 2. *Edited by* I. G. Csizmadia. Elsevier. 1977.
24. G. CAPOZZI, O. DELUCCHI, V. LUCCHINI and G. MODENA. J. Chem. Soc. Perkin Trans. II, 1722 (1975).
25. W. J. BOUMA, R. H. NOBES, L. RADOM, and C. E. WOODWARD. J. Org. Chem. **47**, 1869 (1982).
26. A. C. HOPKINSON. Prog. Theoret. Org. Chem. Vol. 2. *Edited by* I. G. Csizmadia. Elsevier. 1977.

Can. J. Chem. Downloaded from www.nrcresearchpress.com by 72.64.146.136 on 09/07/12
For personal use only.

^{17}O nuclear magnetic resonance spectroscopic study of substituted phthalic anhydrides and phthalides

DAVID W. BOYKIN[1] AND ALFONS L. BAUMSTARK
Department of Chemistry, Georgia State University, Atlanta, GA 30303-3083 U.S.A.

AND

MARGARET M. KAYSER[1,2] AND CHANTAL M. SOUCY
Department of Chemistry, Mount Allison University, Sackville, N.B., Canada E0A 3C0

Received July 16, 1986

DAVID W. BOYKIN, ALFONS L. BAUMSTARK, MARGARET M. KAYSER, and CHANTAL M. SOUCY. Can. J. Chem. **65**, 1214 (1987).

^{17}O chemical shift data (natural abundance) for 3-substituted phthalic anhydrides and 4- and 7-substituted phthalides in acetonitrile at 75°C are reported. Steric interactions of substituents *ortho* to the carbonyl groups result in deshielding effects (9–22 ppm) relative to parent compounds regardless of the electronic character of the substituents. Factors contributing to the deshielding effects are discussed. The relationship between ^{17}O chemical shifts and regiochemistry of the phthalic anhydrides is discussed.

DAVID W. BOYKIN, ALFONS L. BAUMSTARK, MARGARET M. KAYSER, et CHANTAL M. SOUCY. Can. J. Chem. **65**, 1214 (1987).

Les rmn ^{17}O (abondance naturelle) pour une serie d'anhydrides phtaliques substitués en position-3 et de phtalides isomères correspondants ont été étudiés dans une solution d'acétonitrile à 75°C. Les interactions stériques, entre le groupement carbonyle et les substituants de la position *ortho*, provoquent un déblindage de 9 à 22 ppm par rapport aux composés non-substitués. Le déblindage est indépendant du caractère électronique des substituants. Les effets contribuants au déblindage sont évalués. La relation entre le déplacement chimique ^{17}O et la régiochimie des anhydrides phtaliques est discutée.

Introduction

The differential reactivity of the two carbonyl groups of unsymmetrically substituted phthalic anhydrides has been extensively studied (1–9); however, clear understanding of the factors that control the selectivity has yet to be achieved. The utility of ^{17}O nmr spectroscopy has been rapidly increasing (10–12), and it has been successfully used to estimate electronic characteristics (13–15) and local environment changes arising from steric interactions for a number of functional groups (16–21), including carbonyl groups (18–21). For example, it has been recently demonstrated that large bulky groups (e.g., *tert*-butyl) cause considerable in-plane distortion of the molecular structure of phthalic anhydride when placed at the 3 position (22). The steric interactions were reflected in the ^{17}O chemical shift data of these compounds. In an effort to gain insight into the influence of substituents of varying electronic character on the properties and reactivities of the two carbonyl functions of 3-substituted phthalic anhydrides, we have studied the ^{17}O chemical shifts of a series of phthalic anhydrides (**1**) and related phthalides (**2** and **3**).

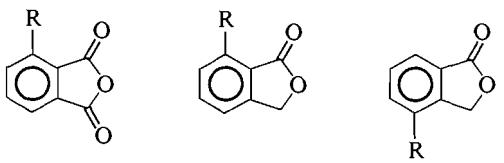

1 **2** **3**

Results and discussion

^{17}O chemical shift data for the 3-substituted phthalic anhydrides (**1**), 7-substituted phthalides (**2**), and 4-substituted phthalides (**3**) in acetonitrile at 75°C, measured at natural abundance, are given in Tables 1 and 2. The substituted anhydrides show two carbonyl signals in the 370–395 ppm region and one signal near 265 ppm (Fig. 1). The single bonded oxygen signal for all 3-substituted anhydrides is insensitive to substituents, with all chemical shift values at 263 ± 1 ppm with the exception of the value for 4-nitrophthalic anhydride. The carbonyl group *meta* to the substituent is relatively insensitive to the 3-substituent, ranging in value from 367 to 377 ppm. The chemical shift of the carbonyl *ortho* to the substituent for the 3-methoxy compound **1***b* is deshielded relative to the parent **1***e* by 9 ppm, and the shift data for the 3-nitro compound **1** is deshielded by 22 ppm relative to the parent. The carbonyl group *ortho* to the 3-substituent is deshielded relative to the parent compound by all substituents regardless of their electronic character.

The chemical shift data for the carbonyl group of the 7-substituted phthalides (**2**) are all deshielded by 10–26 ppm compared to that of the parent molecule **2***d*, which exhibits a carbonyl signal at 320 ppm. In series **2**, electron donating or electron withdrawing substituents result in deshielding, an effect also observed in series **1**. The resonances for the anhydride (dicoordinate) oxygens of **2** are essentially invariant, all appearing at 170 ± 2 ppm. The chemical shift values for the carbonyl oxygen for **3** are only slightly affected by the substituent, appearing at 323 ± 4 ppm, as are those of the single bonded oxygen, which appear at 171 ± 3 ppm.

The assignment of the two carbonyl signals for the anhydrides **1** is made possible by using the results from the corresponding phthalides **2** and **3** (Table 2). It is clear from the data for the phthalides **2** and **3** that the effect of a substituent *ortho* to the planar carbonyl is deshielding, regardless of the electronic character of the substituent. Consequently, the assignments for the two carbonyl signals of the anhydrides shown in Table 1 are made by analogy with the corresponding phthalides. With the exception of the 3-*tert*-butyl and the 3-nitro compounds in series

[1]Authors to whom correspondence may be addressed.
[2]Current address: Division of Sciences, University of New Brunswick, P.O. Box 5050, Saint John, N.B., Canada E2L 4L5.

Printed in Canada / Imprimé au Canada

Can. J. Chem. Downloaded from www.nrcresearchpress.com by 72.64.146.136 on 09/07/12
For personal use only.

TABLE 1. ^{17}O nuclear magnetic resonance data[a] for substituted phthalic anhydrides **1** in CH_3CN at 75°C

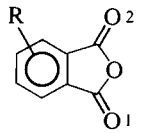

1

Compound	R	δ(C=O)$_1$	1/2ν	δ(C=O)$_2$	1/2ν	δ(—O—)	1/2ν	δ(R)	1/2ν
1*a*	3-C_2H_5O	370	145	384	256	264	160	91	325
1*b*	3-CH_3O	371	128	383	159	264	116	65	208
1*c*	3-CH_3[b]	372	120	383	120	264	140		
1*d*	3-$(CH_3)_3C$[b]	367	140	396	130	262	150		
1*e*	3-H[b]	374	146	374	146	263	98		
1*f*	3-F	376	90	385	70	264	95		
1*g*	3-Cl	375	115	386	140	264	110		
1*h*	3-Br	374	130	385	170	264	125		
1*i*	3-I	373	205	382	269	263	220		
1*j*	3-NO_2	377	170	395	190	262	140	613	256
1*k*	4-NO_2	381[c]	[c]	384[c]	[c]	268	170	586	450

[a]Chemical shift ± 1 ppm; 1/2ν in hertz.
[b]Previously reported in ref. 22.
[c]Tentative assignment; 1/2 height width for the combined signals was 354 Hz.

1, the effect of substituents is a uniform deshielding value of 9 ± 1 ppm. This, in part, is presumably a result of repulsive van der Waals interactions (23). It is of interest to note that there is no appreciable difference in the data for the compounds **1***f*–**1***i* even though the substituents (halogen) are quite different sterically. Molecular mechanics calculations (MM2) were carried out on this series (**1***f*–**1***i*). In-plane distortions were found to be similar to that calculated for **1***c* (22). Apparently the increase in halogen size is offset by the lengthening halogen–carbon bond distance, resulting in the effective steric interactions remaining roughly constant. A possible explanation for the relatively invariant deshielding effects noted for ^{17}O chemical shifts for the anhydrides is that the repulsive van der Waals interactions between substituents and the *ortho* carbonyl group are roughly constant. The two substituents that lead to large downfield shifts, 3-*tert*-butyl **1***d* (22 ppm) and 3-nitro **1***j* (21 ppm), exhibit opposite electronic effects, the former a moderate electron donor, the latter strongly electron withdrawing. In the case of **1***d* the large effective size causes larger in-plane distortions and presumably gives rise to increased repulsive van der Waals interactions (22). The large downfield shift for **1***j* is a composite of the electronic deshielding effect of the nitro group as well as the influence of repulsive van der Waals forces.

Due to steric congestion, the nitro group of 3-nitrophthalic anhydride **1***j* is forced to rotate from the plane and a reciprocal effect from this interaction is noted on the nitro group ^{17}O signal. This is in contrast to the steric effect on the carbonyls which are only in-plane distortions. On comparing the ^{17}O shift of the nitro signal for 3- and 4-nitrophthalic anhydride, some information regarding torsion angle rotation for the 3-nitro group can be deduced. Note that the nitro groups of both isomers are electronically equivalent; the 3-nitro isomer has one carbonyl *ortho* and the other *meta* to it whereas the 4-nitro isomer has one carbonyl *para* and the other *meta* to it. Therefore, it is reasonable to assume that the difference in chemical shifts (NO_2 group) for the two isomers (27 ppm) can be attributed to torsion angle rotation, which minimizes the lone pair repulsion of the carbonyl oxygen and the oxygens of the nitro group. Using the slope (0.76 δ/° angle) of the line for the nitro group ^{17}O chemical shift – torsion angle relationship previously reported (17, 20), it is estimated that the 3-nitro group is rotated 35° from the plane of the aromatic ring. It is of interest that this torsion angle rotation is roughly equivalent to that of placing a methyl group *ortho* to a nitro group (17).

The effect of substituents on the ^{17}O chemical shifts for the 3-substituted phthalic anhydrides **1** and 7-substituted phthalides **2** is similar, both experiencing a comparable magnitude of deshielding in relation to the respective parent molecules. The magnitude of the deshielding effect is surprisingly constant for all the groups except the large *tert*-butyl group and, to a lesser extent, the nitro group. The relative consistency in chemical shift for the substituents of varying size and electronic effects is explained in terms of competition between simple electronic effects and van der Waals interactions (in-plane). Series **3** has a *meta* relationship between the carbonyl group and the substituent. The small ^{17}O chemical shift differences can be explained by normal electronic effects. An interesting conclusion to be made from the results for all the 3-substituted compounds listed in Table 1 is that the ^{17}O chemical shift values suggest that reactivity difference 1–9 for the two carbonyl groups of these compounds cannot be explained by simple electronic effects alone.

Experimental

The phthalic anhydrides were either commercially available or prepared by literature methods (24). The phthalides were prepared by a variety of reductive methods from the corresponding anhydrides (24). The isomeric lactones were purified by chromatographic and physical methods (24). The ^{17}O spectra were obtained on a JEOL GX-270 spectrometer equipped with a 10-mm broad-band probe operating at 36.5 MHz. The spectra were acquired at natural abundance on 0.5 *M* solutions in acetonitrile (anhydrous, packed under nitrogen, Aldrich) at 75°C. Chemical shift data were referenced to external water at 75°C (1.0% butan-2-one added as internal standard, 558 ± 1 ppm). The instrument settings were 25 kHz spectral width, 2 K data points, 90° pulse angle (28 μs pulse width), 0.3 ms acquisition delay, and

Can. J. Chem. Downloaded from www.nrcresearchpress.com by 72.64.146.136 on 09/07/12
For personal use only.

Can. J. Chem. Downloaded from www.nrcresearchpress.com by 72.64.146.136 on 09/07/12
For personal use only.

TABLE 2. ^{17}O nuclear magnetic resonance data[a] for 7- and 4-substituted phthalides (**2**, **3**) in CH_3CN at 75°C

2

3

R	Compound	δ(C=O)	$1/2\nu$	δ(—O—)	$1/2\nu$	δ(R)	$1/2\nu$	Compound	δ(C=O)	$1/2\nu$	δ(—O—)	$1/2\nu$	δ(R)	$1/2\nu$
CH_3O	**2***a*	333	153	168	155	59	84	**3***a*	323	100	170	150	49	160
CH_3[b]	**2***b*	332	175	170	130									
*t*Bu[b]	**2***c*	346	130	168	150			**3***b*	319	130	173	160		
H[a]	**2***d*	320	160	170	130			**3***c*	320	160	170	130		
F	**2***e*	334	158	171	147			**3***d*	325	135	169	150		
Cl	**2***f*	335	120	170	150			**3***e*	327	110	170	140		
Br	**2***g*	334	145	170	180			**3***f*	327	135	171	155		
I	**2***h*	330	225	171	190			**3***g*	327	219	171	240		
NO_2	**2***i*	337	152	172	293	616	244	**3***h*	325	232	174	256	582	386

[a]Chemical shift ±1 ppm; $1/2\nu$ in hertz.
[b]Previously reported in ref. 22.

FIG. 1. The ^{17}O nmr spectra of 3-methoxyphthalic anhydride (**1***b*) and 7- and 4-methoxyphthalides (**2***a*, **3***a*) in acetonitrile at 75°C (2-butanone 558 ± 1, internal standard).

41 ms acquisition time. The spectra were recorded with sample spinning and without lock. The signal-to-noise ratio (S/N) was improved by applying a 25-Hz exponential broadening factor to the free induction decay prior to Fourier transformation. Data point resolution was improved to ±0.2 ppm by zero filling to 8 K data points. Generally, spectra with S/N of ca. 10:1 were obtained from ca. 10^5 scans.

Acknowledgments

Acknowledgment is made to the Donors of the Petroleum Research Fund, administered by the American Chemical Society, for partial support of this research and to the Georgia State University Research Fund. A.L.B. is a fellow of the Camille and Henry Dreyfus Foundation, 1981–1986. Financial support from the Mount Allison University Research Fund is gratefully acknowledged.

1. M. M. KAYSER and P. MORAND. Can. J. Chem. **58**, 2485 (1980).
2. M. M. KAYSER and O. EISENSTEIN. Can. J. Chem. **59**, 2457 (1981).
3. A. ALLAHDAD and D. W. KNIGHT. J. Chem. Soc. Perkin Trans. 1, 1855 (1982).
4. M. S. NEWMAN and P. E. SCHEURER. J. Am. Chem. Soc. **78**, 5004 (1956).
5. M. A. MAKHLOUF and B. RICKBORN. J. Org. Chem. **46**, 4810 (1981).
6. J. S. SWENTON, D. K. JACKSON, M. J. MANNING, and P. W. RAYNOLDS. J. Am. Chem. Soc. **100**, 6182 (1978).
7. A. J. MCALEES, R. MCCRINDLE, and D. W. SNEDDON. J. Chem. Soc. Perkin Trans. 1, 2037 (1977).
8. M. BRAUN. Angew. Chem. Int. Ed. Engl. **17**, 945 (1978); M. BRAUN. Tetrahedron Lett. 2885 (1979); Tetrahedron Lett. **21**, 3871 (1980).
9. P. CANONNE, G. LEMAY, and D. BELANGER. Tetrahedron Lett. **21**, 4167 (1980).
10. J.-P. KINTZINGER. *In* NMR-17. Oxygen-17 and silicon-29. *Edited by* P. Diehl, E. Fluck, and R. Kosfeld. Springer Verlag, New York. 1981 pp. 1–64.
11. W. G. KLEMPERER. *In* The multinuclear approach to NMR spectroscopy. *Edited by* J. B. Lambert and F. G. Riddell. D. Riedel, Dordrecht. 1983 pp. 245–260.
12. J. P. KINTZINGER. *In* NMR of newly accessible nuclei. Vol. 2. *Edited by* P. Laszlo. Academic Press, New York. 1983. pp. 79–104.
13. P. BALAKRISHNAN, A. L. BAUMSTARK, and D. W. BOYKIN. Org. Magn. Reson. **22**, 753 (1984).
14. T. E. ST. AMOUR, M. I. BURGAR, B. VALENTINE, and D. FIAT. J. Am. Chem. Soc. **103**, 1128 (1981).
15. R. R. FRASER, A. J. RAGAUSKAS, and J. B. STOTHERS. J. Am. Chem. Soc. **104**, 6475 (1982).
16. R. T. C. BROWNLEE, M. SADEK, and D. J. CRAIK. Org. Magn. Reson. **21**, 616 (1983).
17. P. BALAKRISHNAN and D. W. BOYKIN. J. Org. Chem. **50**, 3661 (1985).
18. D. J. SARDELLA and J. B. STOTHERS. Can. J. Chem. **47**, 3089 (1969).
19. M. G. OAKLEY and D. W. BOYKIN. J. Chem. Soc. Chem. Commun. 439 (1986).
20. A. L. BAUMSTARK, P. BALAKRISHNAN, M. DOTRONG, C. J. MCCLOSKEY, M. G. OAKLEY, and D. W. BOYKIN. J. Am. Chem. Soc. **109**, 1059 (1987).
21. P. C. VASQUEZ, D. W. BOYKIN, and A. L. BAUMSTARK. Magn. Reson. Chem. **24**, 409 (1986).
22. A. L. BAUMSTARK, P. BALAKRISHNAN, and D. W. BOYKIN. Tetrahedron Lett. 3079 (1986).
23. (*a*) S. LI and D. B. CHESNUT. Magn. Reson. Chem. **24**, 96 (1986); (*b*) Magn. Reson. Chem. **23**, 625 (1985).
24. M. M. KAYSER and C. M. SOUCY. Submitted.

Can. J. Chem. Downloaded from www.nrcresearchpress.com by 72.64.146.136 on 09/07/12
For personal use only.

Enthalpy of solution of tris(2,4-pentanedionato)cobalt(III) in aqueous mixed solvents of 1,4-dioxane and 2-methyl-2-propanol

YASUKI YOSHIMURA

Laboratory of Chemistry, College of Humanities and Social Sciences, Iwate University, Ueda, Morioka, 020 Japan

Received October 9, 1986

YASUKI YOSHIMURA. Can. J. Chem. **65**, 1218 (1987).

The solubilities X_s of tris(2,4-pentanedionato)cobalt(III) ($Co(acac)_3$) in water – 1,4-dioxane (D) and water – 2-methyl-2-propanol (TBA) mixtures were determined over the temperature range of 15–60°C and 20–43°C, respectively. These data were fitted to $\ln X_s = A(1/T) + B\sqrt{T} + C$ and the enthalpy of solution $\Delta\bar{H}_s$ of $Co(acac)_3$ was estimated by differentiating the equation. For the water–D system, a linear correlation was found between the excess enthalpy of solution $\delta\Delta\bar{H}_s$ of $Co(acac)_3$ and the excess internal pressure δP_i of the mixtures. $\Delta\bar{H}_s$ of $Co(acac)_3$ in the water–TBA mixtures showed complicated composition dependence due to microheterogeneity in the mixtures. The enthalpy of hydrophobic hydration $\Delta\bar{H}_h$ of $Co(acac)_3$ in the water–D mixtures was also estimated from the solubility curves and it was found that $\Delta\bar{H}_h$ decreased exponentially with decreasing mole fraction of water.

YASUKI YOSHIMURA. Can. J. Chem. **65**, 1218 (1987).

On a déterminé les solubilités X_s du tris(pentanedione-2,4 ato) cobalt(III) ($Co(acac)_3$) dans des mélanges eau/dioxanne-1,4 (D) et eau/méthyl-2 propanol-2 (ATB) à des intervalles de températures respectifs de 15 à 60°C et de 20 à 43°C. On a ajusté ces données à l'équation $\ln X_s = A(1/T) + B\sqrt{T} + C$ et on a évalué l'enthalpie de solution $\Delta\bar{H}_s$ du $Co(acac)_3$ en procédant à la différenciation de l'équation. Pour le système eau/D, on a trouvé une corrélation linéaire entre l'excès d'enthalpie de solution, $\delta\Delta\bar{H}_s$ du $Co(acac)_3$ et l'excès de pression interne δP_i des mélanges. On a démontré que le $\Delta\bar{H}_s$ du $Co(acac)_3$, dans les mélanges eau/ATB, présente une relation compliquée avec la composition qui est due à une microhétérogénéité des mélanges. On a aussi déterminé l'enthalpie d'hydratation hydrophobe $\Delta\bar{H}_h$ du $Co(acac)_3$ dans les mélanges eau/D à partir des courbes de solubilité et on a trouvé que le $\Delta\bar{H}_h$ diminue d'une façon exponentielle avec une diminution de la fraction molaire de l'eau dans les mélanges.

[Traduit par la revue]

Introduction

In analysis of metal ions in aqueous solutions, the technique of solvent extraction of metal chelates has been extensively applied. In the previous investigation, as an approach to clarify a behavior of metal chelates in aqueous solutions, the enthalpy of solution $\Delta\bar{H}_s$ of tris(2,4-pentanedionato)cobalt(III) ($Co(acac)_3$) in the mixtures of water and dimethyl sulfoxide (DMSO) has been examined and it has been found that the composition dependence of $\Delta\bar{H}_s$ can be satisfactorily related to the composition dependence of the internal pressure P_i of the water–DMSO mixtures (1).

Various properties of many aqueous organic mixtures have been very widely examined in connection with the effect of these organic solvents on the structure of water (2). Among these solvents, 1,4-dioxane (D) and 2-methyl-2-propanol (TBA) seem to be interesting from the following aspects: (*i*) in highly dilute aqueous solutions, TBA exhibits remarkable structure-making effect (3–6), while different explanations have been given to the effect of D on the structure of water, that is, structure-making (7–11) or structure-breaking effect (3, 12–16); (*ii*) microheterogeneity or pseudophase separation is brought about in the water-rich regions of the water–TBA mixtures (17–19) but not in the water–D mixtures (18, 19).

It would be of interest to determine whether the previous conclusion for $\Delta\bar{H}_s$ of $Co(acac)_3$ in the water–DMSO mixtures is valid for other aqueous organic mixtures or not. Furthermore, it would also be of interest to examine the behavior of dissolution of a third solute in the microheterogeneous water–TBA mixtures. The behavior may be characterized by comparison with that in the water–D mixtures.

Thus, in this study, the temperature dependence of the solubilities of $Co(acac)_3$ in both the water–D mixtures and the water–TBA mixtures is determined. From these data $\Delta\bar{H}_s$ of $Co(acac)_3$ is estimated and its composition dependence is discussed. The enthalpy of hydrophobic hydration $\Delta\bar{H}_h$ of $Co(acac)_3$ in the dilute aqueous D solution is also estimated.

Experimental

The purification of $Co(acac)_3$ was described previously (1). Commercial D (spectrophotometric grade reagent, Dojin Chemical Laboratories Ltd.) was passed through a column of activated alumina, refluxed over calcium hydride for a day under an atmosphere of nitrogen gas dried by passing through concentrated sulfuric acid and a column of sodium hydroxide, and then distilled. TBA (reagent grade, Wako Chemical Industries Ltd.) was refluxed over calcium hydride for a day and distilled. The water contents in the purified D and TBA, measured by Karl Fischer titration, were less than 0.02% and 0.04% by weight, respectively. These purified solvents were stored over molecular sieves (type 4A) in a dry box. The mixed solvents were prepared by the same method as described previously (1).

In order to minimize the influence of the evaporation of volatile TBA during the solubility measurement, the apparatus used for saturating the desired sample solutions with $Co(acac)_3$ was modified as shown in Fig. 1. The main modification was to reduce the volume of the apparatus. By this modification, the deviations of 95% confidence levels from the mean values of the solubilities in the water–TBA mixtures could be reduced to about half of those found by the use of the apparatus described previously (1). The procedure used for the solubility measurement was identical with that described previously (1), except that the saturated solution was passed through a cotton filter by injecting dry nitrogen gas.

Results

Solubility of $Co(acac)_3$ in water–D and water–TBA mixtures

The solubilities of $Co(acac)_3$ in molality (mol kg^{-1}), S_m in the water–D and water–TBA mixtures are listed in Tables 1 and 2, respectively. For the water–TBA mixtures, the solubilities were determined in the narrow temperature region 20–43°C because of the high melting point (about 25°C) and low boiling point (about 82°C) of TBA. The deviations of the 95% confidence levels from the mean values were less than 2% for the water–D system and less than 4% for the water–TBA system. It has been confirmed in the previous work that $Co(acac)_3$ is not decomposed in the course of the equilibration (1). The solubility data at 25°C were reproducible within

Printed in Canada / Imprimé au Canada

Can. J. Chem. Downloaded from www.nrcresearchpress.com by 78.46.186.204 on 09/07/12
For personal use only.

TABLE 1. Solubilities of $Co(acac)_3$ in water–D mixtures

	$S_m \times 10^2$/mol kg^{-1}* when X_D =					
T/°C	0.0153	0.0237	0.0570	0.0940	0.1379	0.1937
15	0.550±0.007	0.535±0.006	0.642±0.005	0.842±0.004	1.21±0.01	1.91±0.01
20	0.508±0.005	0.506±0.003	0.654±0.004	0.905±0.005	1.34±0.01	2.17±0.03
25	0.485±0.008	0.486±0.001	0.678±0.007	0.984±0.003	1.49±0.01	2.44±0.05
30	0.457±0.001	0.475±0.004	0.705±0.003	1.07±0.01	1.65±0.01	2.76±0.01
35	0.441±0.001	0.471±0.004	0.737±0.007	1.16±0.01	1.86±0.01	3.11±0.02
40	0.426±0.005	0.475±0.001	0.778±0.001	1.29±0.01	2.07±0.03	3.53±0.03
45	0.422±0.004	0.482±0.005	0.829±0.015	1.41±0.01	2.33±0.02	4.00±0.08
50	0.423±0.001	0.494±0.004	0.881±0.008	1.56±0.01	2.56±0.01	4.63±0.06
55	0.432±0.004	0.510±0.004	0.940±0.013	1.73±0.01	2.85±0.03	5.26±0.09
60	0.442±0.012	0.530±0.005				

	$S_m \times 10^2$/mol kg^{-1} when X_D =					
T/°C	0.2645	0.3192	0.4986	0.6840	0.7882	1.0000
15	3.18±0.01	4.41±0.01	8.60±0.04	12.6±0.2	13.5±0.1	12.7±0.1
20	3.65±0.03	5.03±0.03	9.71±0.17	13.8±0.1	15.0±0.1	14.2±0.2
25	4.14±0.03	5.73±0.06	10.9±0.1	15.5±0.2	16.7±0.1	15.9±0.3
30	4.74±0.06	6.59±0.03	12.3±0.1	17.4±0.2	18.8±0.1	17.6±0.4
35	5.40±0.03	7.51±0.02	14.2±0.2	19.7±0.1	21.1±0.1	19.5±0.2
40	6.20±0.08	8.60±0.06	16.4±0.1	22.5±0.2	23.8±0.1	21.5±0.3
45	7.18±0.06	9.93±0.16	18.6±0.1	25.8±0.5	26.6±0.4	24.0±0.3
50	8.29±0.05	11.4±0.1	21.3±0.4	29.4±0.4	30.1±0.2	26.5±0.5
55	9.51±0.22	13.2±0.3	24.4±0.4	32.8±0.6	33.9±0.6	29.3±0.3

*Errors denote 95% confidence levels.

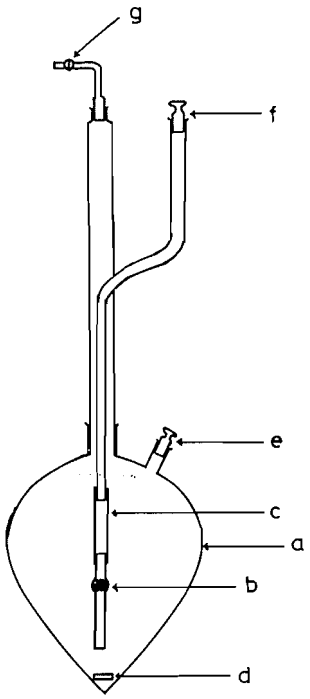

FIG. 1. Apparatus for solubility measurement: *a*, flask with a volume of 100 cm^3; *b*, filter filled with absorbent cotton; *c*, teflon tube; *d*, magnetic stirring bar; *e*, stopper for transferring water–D or water–TBA mixture and $Co(acac)_3$ to the flask; *f*, stopper for pipetting off saturated solution; *g*, stop-cock for injecting dry nitrogen gas.

experimental error when the solutions at the end of experiment at the highest temperature were allowed to attain equilibrium at 25°C. This finding shows that the evaporation of components during the equilibration produces no detectable effect.

The S_m values were converted to solubilities in mole fraction X_s and $\ln X_s$ was plotted against $1/T$. Typical plots are shown for the water–D and water–TBA mixtures in Figs. 2 and 3, respectively. The solubility curve in water passed through a minimum at about 55°C (1). The minima of the solubility curves in the aqueous D and TBA mixtures were shifted to lower temperatures with increases in the mole fraction of D or TBA, X_D or X_{TBA} (45°C for $X_D = 0.0153$, 35°C for $X_D = 0.0237$, about 45°C for $X_{TBA} = 0.0143$, 30°C for $X_{TBA} = 0.0234$). In the mixtures with a composition $X_D \geq 0.0570$ or $X_{TBA} \geq 0.0401$, the minimum was no longer distinct over the temperature range studied.

$\Delta\bar{H}_s$ of $Co(acac)_3$ in water–D and water–TBA mixtures

For representing the solubility curves, the experimental values were fitted to

$$[1] \quad \ln X_s = A(1/T) + B\sqrt{T} + C$$

where A, B, and C are fitting parameters.[1] Equation [1] could reproduce the X_s values within the errors of ±1.5% for the water–D mixtures and of ±1.8% for the water–TBA mixtures.

The $\Delta\bar{H}_s$ values at 25°C in the water–D and water–TBA

[1]In a previous work, experimental values were fitted to $\ln X_s = A(1/T) + B \ln T + C$. When the present values were fitted to this equation, standard deviations of fit were slightly higher than those obtained by using [1]. For the water–D system the values of $\Delta\bar{H}_s$ estimated by using the above equation were identical with those estimated from [1], while for the water–TBA system the two methods gave slightly different $\Delta\bar{H}_s$ values probably because of the narrow temperature range of the solubility measurement. Therefore, in the present work eq. [1] was adopted since it provided a better fit to the data.

Can. J. Chem. Downloaded from www.nrcresearchpress.com by 78.46.186.204 on 09/07/12
For personal use only.

TABLE 2. Solubilities of $Co(acac)_3$ in water–TBA mixtures

	$S_m \times 10^2$/mol kg^{-1}* when X_{TBA} =					
T/°C	0.0143	0.0234	0.0401	0.0621	0.0893	0.1099
20	0.456±0.007	0.448±0.003	0.454±0.007	0.547±0.009	0.703±0.009	0.903±0.017
25	0.431±0.002	0.444±0.003	0.480±0.003	0.618±0.012	0.836±0.015	1.07±0.02
30	0.416±0.002	0.442±0.002	0.514±0.007	0.688±0.006	0.958±0.022	1.25±0.01
35	0.406±0.001	0.447±0.002	0.549±0.009	0.760±0.009	1.11±0.03	1.36±0.05
40	0.400±0.001	0.456±0.005	0.578±0.019	0.832±0.004	1.24±0.03	1.55±0.05
45	0.398±0.003	0.464±0.010				
	$S_m \times 10^2$/mol kg^{-1} when X_{TBA} =					
T/°C	0.1356	0.1930	0.2698	0.3220	0.4424	0.5479
20	0.973±0.020	1.17±0.02	1.23±0.03	1.23±0.01	1.19±0.02	1.24±0.03
25	1.13±0.03	1.31±0.03	1.40±0.02	1.45±0.04	1.43±0.04	1.40±0.01
30	1.26±0.01	1.54±0.04	1.64±0.04	1.75±0.01	1.73±0.02	1.66±0.06
35	1.46±0.02	1.79±0.05	1.96±0.07	2.14±0.04	2.09±0.05	1.99±0.04
40	1.70±0.03	2.15±0.05	2.46±0.11	2.68±0.01	2.59±0.04	2.38±0.03
43		2.40±0.07	2.82±0.07	3.01±0.06	2.98±0.06	2.71±0.06
	$S_m \times 10^2$/mol kg^{-1} when X_{TBA} =					
T/°C	0.6746	0.7984	0.8501	0.9000	0.9470	1.0000
25	1.13±0.01	0.956±0.016	0.881±0.022	0.712±0.022		0.576±0.005†
30	1.31±0.04	1.11±0.03	1.05±0.04	0.855±0.005	0.753±0.006	0.639±0.008
35	1.47±0.02	1.26±0.04	1.21±0.02	1.04±0.03	0.906±0.019	0.752±0.013
40	1.76±0.06	1.47±0.02	1.44±0.01	1.23±0.03	1.08±0.02	0.889±0.019
43	1.91±0.07	1.57±0.04	1.59±0.02		1.19±0.02	
45					1.26±0.05	1.03±0.01
50						1.20±0.02

*Errors denote 95% confidence levels.
†Value at 27.5°C.

Can. J. Chem. Downloaded from www.nrcresearchpress.com by 78.46.186.204 on 09/07/12
For personal use only.

mixtures were estimated by

[2] $\Delta\bar{H}_s = R(-A + B/2 \times T^{3/2})$

where R is the gas constant 8.314×10^{-3} kJ mol^{-1} K^{-1} and are listed in Tables 3[2] and 4, respectively. The errors in these Tables were estimated from the 95% confidence levels of the parameters in [1]. The errors in the water–TBA system became large as indicated by the large 95% confidence levels of the parameters which were caused by the narrow temperature range of the solubility measurement.

Discussion

Composition dependence of $\Delta\bar{H}_s$ of $Co(acac)_3$ in water–D and water–TBA mixtures

The composition profile of $\Delta\bar{H}_s$ of $Co(acac)_3$ in the water–D and water–TBA mixtures is shown in Fig. 4. $\Delta\bar{H}_s$ in the water–D mixtures increased rapidly up to $X_D = 0.2$, passed through a small maximum at $X_D = 0.3$, and then decreased nearly linearly to $\Delta\bar{H}_s$ in pure D. A similar maximum or minimum has been found for various properties in the water–D mixtures such as the enthalpy (10, 20–22) and volume (21, 23) of mixing, ultrasonic absorption (9, 24), and compression (14, 25). $\Delta\bar{H}_s$ in the water–TBA mixtures showed a complicated composition profile with three maxima at $X_{TBA} = 0.1$, 0.4–0.5, and 0.95. It has been extensively reported that several properties in the water–TBA mixtures exhibit a maximum or a minimum at a lower concentration than $X_{TBA} = 0.1$ (3–6, 17, 18). Nakanishi and Ozasa have found a sharp maximum at $X_{TBA} = 0.05$ and broad one at about $X_{TBA} = 0.6$ in the composition profile of diffusion of iodine in the water–TBA mixtures (26). To the author's knowledge there are no literature references to a maximum or a minimum in the TBA-rich region of $X_{TBA} = 0.95$.

In the previous work (1), it has been found that the excess enthalpy of solution $\delta\Delta\bar{H}_s$ of $Co(acac)_3$ in the water–DMSO mixtures can be explained in terms of the excess enthalpy of cavity formation $\delta\bar{H}_c$ by

[3] $\delta\Delta\bar{H}_s = \delta\bar{H}_c = (\bar{V}_c - a^3N\pi/6)(R/82.05)\delta P_i$

where $\bar{V}_c$, a, and N are the partial molar volume of cavity formation, the hard-sphere diameter of the solute, and Avogadro's number, respectively. $\delta\Delta\bar{H}_s$ and δP_i are defined by

[4] $\delta Y = Y - \{(1 - X_W)Y(0) + X_W Y(W)\}$

where the symbol Y stands for $\Delta\bar{H}_s$ or P_i, X_W is the mole fraction of water, and $Y(0)$ and $Y(W)$ are the values of Y in pure D or TBA and in water, respectively.

In Fig. 5, $\delta\Delta\bar{H}_s$ of $Co(acac)_3$ is plotted against δP_i for the water–D and water–TBA systems. Values of δP_i were calculated from values found in the literature of P_i in the water–D (27) and water–TBA mixtures (28). For the water–D system, the plot showed the linear relationship expected from [3] between $\delta\Delta\bar{H}_s$ and δP_i similar to the finding in the water–DMSO system (1). On the other hand, for the water–TBA

[2] $\Delta\bar{H}'_s$ and $\Delta\bar{H}_h$ in Table 3 will be discussed in the last section.

Can. J. Chem. Downloaded from www.nrcresearchpress.com by 78.46.186.204 on 09/07/12
For personal use only.

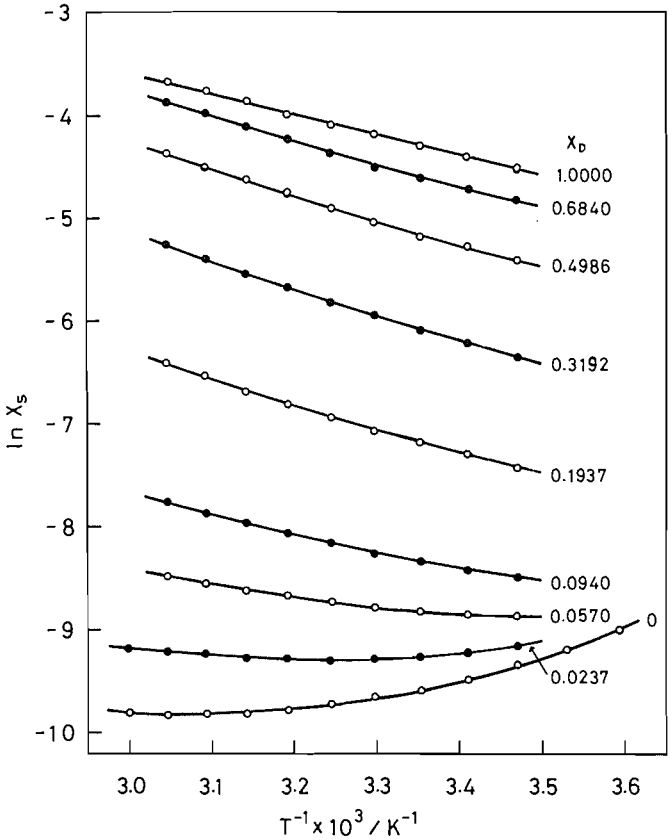

FIG. 2. Typical plot of ln X_s vs. $1/T$ for $Co(acac)_3$ in water–D mixtures: solid lines are solubility curves calculated by [1].

TABLE 3. Enthalpy of solution $\Delta\bar{H}_s$, enthalpy of solution without hydrophobic hydration $\Delta\bar{H}_s'$, and enthalpy of hydrophobic hydration $\Delta\bar{H}_h$ for $Co(acac)_3$ at 25°C in water–D mixtures given in kJ mol^{-1} *

X_D	$\Delta\bar{H}_s$†	$\Delta\bar{H}_s'$‡	$\Delta\bar{H}_h$§
0.0153	−8.4 ± 0.7	3.8 ± 1.1 (50–60°C)	−12.2
0.0237	−4.3 ± 0.5	5.6 ± 1.8 (45–60°C)	−9.9
0.0570	5.4 ± 0.5	10.2 ± 0.9 (35–55°C)	−4.8
0.0940	12.2 ± 0.5	15.3 ± 1.1 (25–55°C)	−3.1
0.1379	15.9 ± 0.5	16.9 ± 0.7 (15–55°C)	
0.1937	17.9 ± 0.6	19.8 ± 1.1 (15–55°C)	
0.2645	19.6 ± 0.5	21.5 ± 1.1 (15–55°C)	
0.3192	19.7 ± 0.4	21.4 ± 1.0 (15–55°C)	
0.4986	18.5 ± 0.7	20.5 ± 1.2 (15–55°C)	
0.6840	17.0 ± 1.0	19.1 ± 1.3 (15–55°C)	
0.7882	16.4 ± 0.3	17.9 ± 0.8 (15–55°C)	
1.0000	15.6 ± 0.2	16.1 ± 0.3 (15–55°C)	

*Errors were estimated from 95% confidence levels of the parameters in [1] or [6].

†Values were estimated from slopes at 25°C of the solubility curves obtained by fitting the solubility data to [1].

‡Values were estimated from slopes of the straight lines obtained by fitting the solubility data in the temperature regions shown in parentheses to [6].

§$\Delta\bar{H}_h = \Delta\bar{H}_s - \Delta\bar{H}_s'$.

system, the linear correlation between $\delta\Delta\bar{H}_s$ and δP_i could not be confirmed, which was anticipated from the unique composition profile of $\Delta\bar{H}_s$ in the water–TBA mixtures.

The water–TBA mixtures with higher concentrations than about $X_{TBA} = 0.05$ have been considered to become micro-heterogeneous, consisting of water-rich and TBA-rich domains

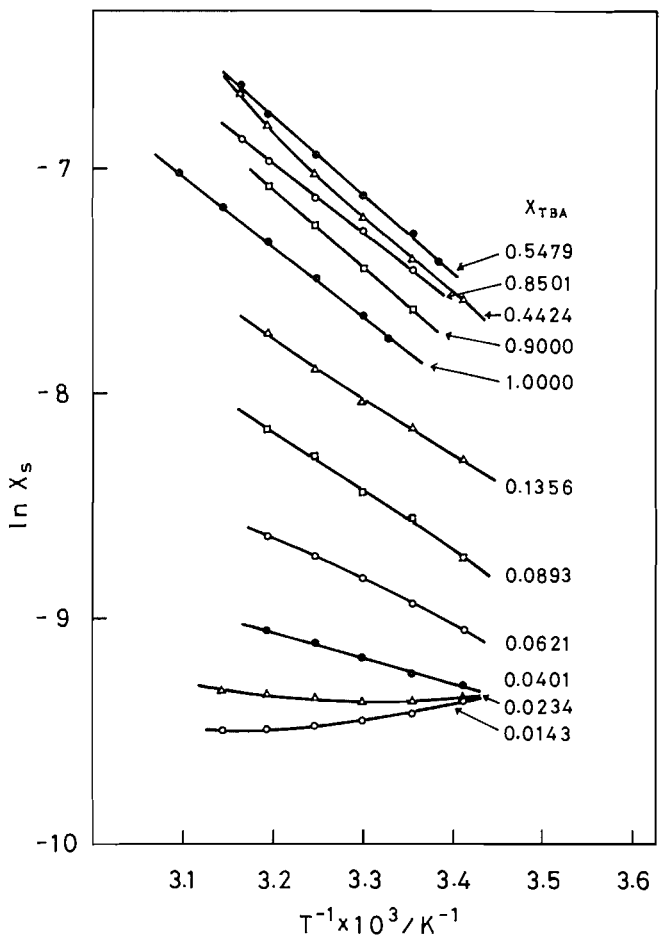

FIG. 3. Typical plot of ln X_s vs. $1/T$ for $Co(acac)_3$ in water–TBA mixtures: solid lines are solubility curves calculated by [1].

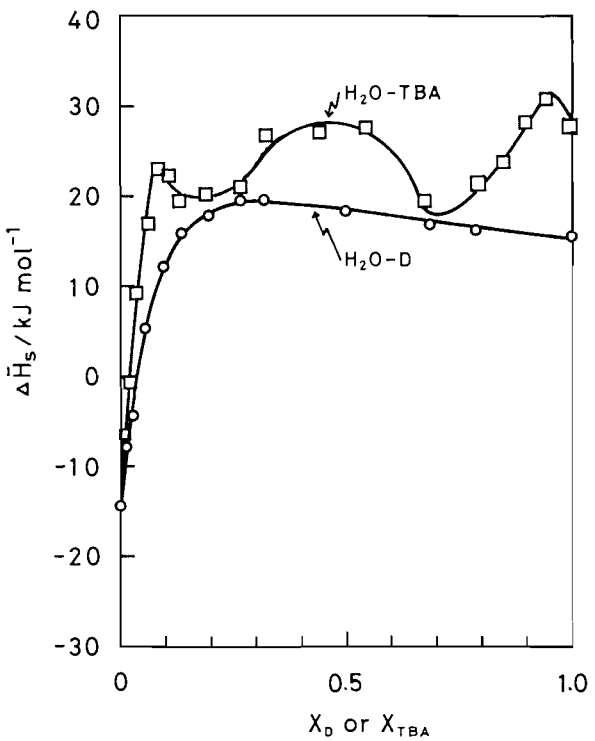

FIG. 4. Composition profiles of $\Delta\bar{H}_s$ of $Co(acac)_3$ at 25°C in water–D and water–TBA mixtures: ○, water–D mixtures; □, water–TBA mixtures.

Can. J. Chem. Downloaded from www.nrcresearchpress.com by 78.46.186.204 on 09/07/12
For personal use only.

TABLE 4. Enthalpy of solution $\Delta\bar{H}_s$ of $Co(acac)_3$ at 25°C in water–TBA mixtures given in kJ mol^{-1}

X_{TBA}	$\Delta\bar{H}_s$*	X_{TBA}	$\Delta\bar{H}_s$*
0.0143	−6.5±1.1	0.3220	26.8±2.2
0.0234	−0.7±1.0	0.4424	27.2±2.0
0.0401	9.3±2.1	0.5479	27.7±5.3
0.0621	16.9±0.7	0.6746	19.5±12.2
0.0893	23.1±2.5	0.7984	21.6±8.6
0.1099	22.3±6.3	0.8501	24.0±7.0
0.1356	19.5±4.2	0.9000	28.4±18.5
0.1930	20.2±2.3	0.9470	30.8±7.6
0.2698	21.1±2.7	1.0000	27.7±3.5

*$\Delta\bar{H}_s$ values and errors were estimated from slopes at 25°C of the solubility curves obtained by fitting the solubility data to [1] and from 95% confidence levels of the parameters in [1], respectively.

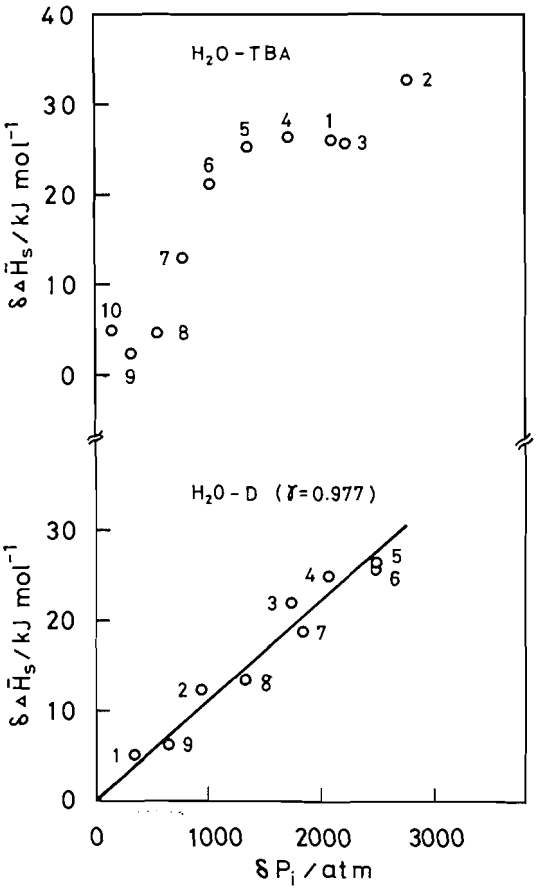

FIG. 5. Correlation between excess enthalpy of solution $\delta\Delta\bar{H}_s$ of $Co(acac)_3$ and excess internal pressure δP_i for water–D and water–TBA systems. For water–D system X_D is as follows: *1*, 0.0122; *2*, 0.0345; *3*, 0.0780; *4*, 0.1039; *5*, 0.1650; *6*, 0.2787; *7*, 0.4787; *8*, 0.6125; *9*, 0.8097. For water–TBA system X_{TBA} is as follows: *1*, 0.05; *2*, 0.1; *3*, 0.2; *4*, 0.3; *5*, 0.4; *6*, 0.5; *7*, 0.6; *8*, 0.7; *9*, 0.8; *10*, 0.9. Value of γ is correlation coefficient.

(6, 17–19). In studies of the heat capacities of such microheterogeneous mixtures, it has been found that composition profiles of the apparent molar heat capacities or the partial molar heat capacities of organic components show maxima (5, 8, 17, 29–31).

In order to make clearer the unique behavior of the dissolution

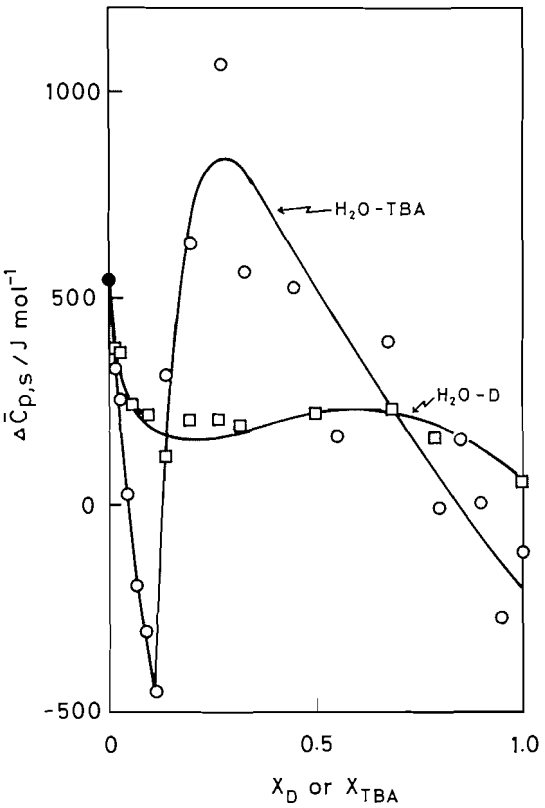

FIG. 6. Composition dependence of heat capacity of solution $\Delta\bar{C}_{p,s}$ of $Co(acac)_3$ in water–D and water–TBA mixtures: □, water–D mixtures; ○, water–TBA mixtures.

of $Co(acac)_3$ in the water–TBA mixtures, the heat capacities of solution $\Delta\bar{C}_{p,s}$ of $Co(acac)_3$ at 25°C in the water–D and water–TBA mixtures were estimated by [5] obtained by differentiating eq. [2]

$$[5]\quad \Delta\bar{C}_{p,s} = (3/4)BR\sqrt{T}$$

and are plotted against X_D or X_{TBA} in Fig. 6. In the water–D mixtures which are not microheterogeneous (18, 19), $\Delta\bar{C}_{p,s}$ decreased slightly up to $X_D = 0.14$ and then was nearly constant. When $\Delta\bar{C}_{p,s}$ estimated from the previous data in the water–DMSO mixtures (1) was plotted, a similar trend was found. In the water–TBA mixtures, $\Delta\bar{C}_{p,s}$ decreased markedly up to $X_{TBA} = 0.1$, increased discontinuously in the X_{TBA} region 0.1–0.25, and then decreased to $\Delta\bar{C}_{p,s}$ in pure TBA.

Though the values of $\Delta\bar{C}_{p,s}$ derived from the second derivative of [1] lack accuracy, a feature characteristic of the dissolution of $Co(acac)_3$ in the water–TBA mixtures can be recognized satisfactorily in Fig. 6.

The present results suggest that, in general, the composition dependence of $\Delta\bar{H}_s$ of a nonelectrolyte in aqueous organic mixtures except for microheterogeneous mixtures depends primarily on the enthalpy of cavity formation. The finding that $\delta\Delta\bar{H}_s$ can be linearly correlated to δP_i is practical from the viewpoint that the composition dependence of $\Delta\bar{H}_s$ can be explained in terms of P_i which is measurable.

Enthalpy of hydrophobic hydration of $Co(acac)_3$

In the previous study, a method to estimate approximate values of $\Delta\bar{H}_h$ of $Co(acac)_3$ in the water–DMSO mixtures was presented (1). The method is based on the assumption that the curvature of the solubility curves in Figs. 2 and 3 results from the hydrophobic hydration of $Co(acac)_3$ and a disappearance

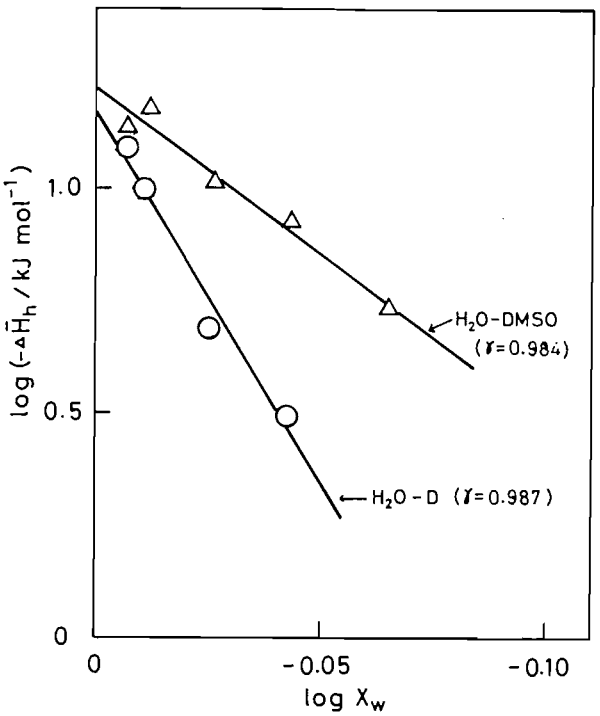

FIG. 7. Correlation between log $(-\Delta\bar{H}_h)$ for $Co(acac)_3$ and log X_w in water–D and water–DMSO mixtures. The values of log $(-\Delta\bar{H}_h)$ in water–DMSO mixtures were taken from ref. 1. Values of γ are correlation coefficients.

of the hydrophobic hydration results in straightening of the solubility curves (32).

For the water–D system, the solubility data in the temperature regions given in the parentheses in Table 3 were also fitted to

[6] $$\ln X_s = a(1/T) + b$$

and the enthalpy of solution without the hydrophobic hydration $\Delta\bar{H}_s'$ for $Co(acac)_3$ was calculated from the slope of [6].

Table 3 shows that in the concentration region $X_D \geq 0.14$, $\Delta\bar{H}_s$ and $\Delta\bar{H}_s'$ agree with each other within the experimental errors and suggests that the hydrophobic hydration disappears practically in the concentration region. As significant differences between $\Delta\bar{H}_s$ and $\Delta\bar{H}_s'$ were found in the concentration region $X_D \leq 0.094$, the values of $\Delta\bar{H}_h$ were obtained by subtracting $\Delta\bar{H}_s'$ from $\Delta\bar{H}_s$.

When log $(-\Delta\bar{H}_h)$ was plotted against log X_W, satisfactory linear relationship was recognized as shown in Fig. 7. This result shows that the following empirical equation settled in the previous work (1) is also valid for the water–D system.

[7] $$\Delta\bar{H}_h = \Delta\bar{H}_h(W)X_W^n$$

Thus, the enthalpy of hydrophobic hydration of $Co(acac)_3$ in water $\Delta\bar{H}_h(W)$ may be estimated to be -14.7 ± 1.6 kJ mol^{-1} from the intercept of the straight line for the water–D system in Fig. 7. This value agrees fairly well with the value of -16.7 ± 1.2 kJ mol^{-1} obtained in the water–DMSO system (1).

The estimation of $\Delta\bar{H}_h(W)$ is strictly tentative since validity of the above assumption to estimate $\Delta\bar{H}_h$ in these mixtures has not been established. The author intends to examine an experiment to establish this assumption.

1. Y. YOSHIMURA, N. SATO, and M. KIKUCHI. Bull. Chem. Soc. Jpn. **59**, 2135 (1986).
2. T. S. SARMA and J. C. AHLUWALIA. Chem. Soc. Rev. **2**, 203 (1973).
3. R. K. MOHANTY, T. S. SARMA, S. SUBRAMANIAN, and J. C. AHLUWALIA. Trans. Faraday Soc. **67**, 305 (1971).
4. B. KINGSTON and M. C. R. SYMONS. J. Chem. Soc. Faraday Trans. II, **69**, 978 (1973).
5. L. AVEDIKIAN, G. PERRON, and J. E. DESNOYERS. J. Solution Chem. **4**, 331 (1975).
6. T. M. BENDER and R. PECORA. J. Phys. Chem. **90**, 1700 (1986).
7. C. J. CLEMETT. J. Chem. Soc. A, **455**, 761 (1969).
8. O. KIYOHARA, G. PERRON, and J. E. DESNOYERS. Can. J. Chem. **53**, 2591 (1975).
9. G. ATKINSON, S. RAJAGOPALAN, and B. L. ATKINSON. J. Chem. Phys. **72**, 3511 (1980).
10. A. INGLESE, I. FERINO, B. MARONGIU, V. SOLINAS, and S. TORRAZZA. Thermochim. Acta, **65**, 169 (1983).
11. J. D. PANDEY, A. K. PURI, and K. MISRA. Thermochim. Acta, **74**, 313 (1984).
12. A. BEN-NAIM and G. MORAN. Trans. Faraday Soc. **61**, 27 (1965).
13. J. KORPELA and J. KOSKIKALLIO. Suom. Kemistil. B, **39**, 165 (1966).
14. P. J. PEARCE and W. STRAUSS. Aust. J. Chem. **21**, 1213 (1968).
15. F. FRANKS, M. A. J. QUICKENDEN, D. S. REID, and B. WATSON. Trans. Faraday Soc. **66**, 582 (1970).
16. D. S. NEWMAN, E. BLINN, and B. L. CARLSON. J. Phys. Chem. **83**, 676 (1979).
17. C. DE VISSER, G. PERRON, and J. E. DESNOYERS. Can. J. Chem. **55**, 856 (1977).
18. N. MULLER. J. Magn. Reson. **28**, 203 (1977); J. Phys. Chem. **83**, 2041 (1979).
19. K. IWASAKI and T. FUJIYAMA. J. Phys. Chem. **81**, 1908 (1977); **83**, 463 (1979).
20. J. R. GOATES and R. J. SULLIVAN. J. Phys. Chem. **62**, 188 (1958).
21. K. W. MORCOM and R. W. SMITH. Trans. Faraday Soc. **66**, 1073 (1970).
22. H. NAKAYAMA and K. SHINODA. J. Chem. Thermodyn. **3**, 401 (1971).
23. F. HOVORKA, R. A. SCHAEFER, and D. DREISBACH. J. Am. Chem. Soc. **58**, 2264 (1936).
24. K. ARAKAWA and N. TAKENAKA. Bull. Chem. Soc. Jpn. **42**, 5 (1969).
25. M. NAKAGAWA, Y. MIYAMOTO, and T. MORIYOSHI. J. Chem. Thermodyn. **15**, 15 (1983).
26. K. NAKANISHI and T. OZASA. J. Phys. Chem. **74**, 2956 (1970).
27. D. P. SINGH and S. S. BHATTI. Acoust. Lett. **8**, 84 (1984).
28. D. D. MACDONALD and J. B. HYNE. Can. J. Chem. **49**, 2636 (1971).
29. G. ROUX, G. PERRON, and J. E. DESNOYERS. J. Phys. Chem. **82**, 966 (1978); J. Solution Chem. **7**, 639 (1978).
30. C. JOLICOEUR, L.-L. LEMELIN, and R. LAPALME. J. Phys. Chem. **83**, 2806 (1979).
31. G. ROUX, D. ROBERT, G. PERRON, and J. E. DESNOYERS. J. Solution Chem. **9**, 629 (1980).
32. K. SHINODA. J. Phys. Chem. **81**, 1300 (1977).

Can. J. Chem. Downloaded from www.nrcresearchpress.com by 78.46.186.204 on 09/07/12
For personal use only.

Diisopropylethylamine eliminates dipeptide formation during the acylation of amino acids using benzoyl chloride and some alkyl chloroformates

FRANCIS M. F. CHEN AND N. LEO BENOITON
Department of Biochemistry, University of Ottawa, Ottawa, Ont., Canada K1H 8M5

Received August 22, 1986

FRANCIS M. F. CHEN and N. LEO BENOITON. Can. J. Chem. **65**, 1224 (1987).

Acylation of amino acids using benzoyl chloride in aqueous alkali leads to benzoylamino acids containing one percent of benzoyldipeptide. Use of diisopropylethylamine instead of sodium hydroxide as base eliminates the side reaction responsible for the contaminant. Ethoxycarbonylamino acids are advantageously prepared in the same manner using ethyl chloroformate or diethyl dicarbonate. The latter gives rise to some *N*-substituted dipeptide when used in aqueous alkali. The method is unsatisfactory for the benzyloxycarbonylation of amino acids. Use of 9-fluorenylmethyl chloroformate and diisopropylethylamine gives the pure derivative of leucine in moderate yield.

FRANCIS M. F. CHEN et N. LEO BENOITON. Can. J. Chem. **65**, 1224 (1987).

L'acylation des acides aminés par le chlorure de benzoyle en solution aqueuse alcaline conduit à des acides benzoylaminés qui contiennent un pourcent de benzoyldipeptide. L'utilisation de la diisopropyléthylamine à la place de l'hydroxyde de sodium permet d'éliminer la réaction secondaire qui est responsable du contaminant. Faisant appel à la même méthode, on peut préparer avantageusement les acides éthoxycarbonylaminés en utilisant le chloroformate d'éthyle ou le dicarbonate de diéthyle. Lorsqu'on utilise des solutions aqueuses alcalines, ce dernier composé donne lieu à la formation de dipeptides *N*-substitués. La méthode n'est pas satisfaisante pour la benzyloxycarbonylation d'acides aminés. L'utilisation du chloroformate de fluorènyl-9 méthyle et de la diisopropyléthylamine conduit, avec un rendement raisonnable, à un dérivé de la leucine qui est pur.
[Traduit par la revue]

Can. J. Chem. Downloaded from www.nrcresearchpress.com by 78.46.186.204 on 09/07/12
For personal use only.

It is now recognized that a small amount of *N*-substituted dipeptide **5***a* is formed as side product when 9-fluorenylmethyl chloroformate (**1***b*) (1–5) or benzyl chloroformate (**1***c*) (4, 5) is used as reagent for the acylation of amino acids in aqueous alkali. It is also generally agreed that the source of peptide **5***a* is aminolysis of mixed anhydride **4***a*, which is generated during acylation by reaction of *N*-alkoxycarbonylamino acid anion product **3***a* with reagent **1***a* (1–6). The corresponding side product **5***d* has also been detected in some cases when the acylating agent was di-*tert*-butyl dicarbonate (**6***d*) (4, 5). Use of alternative reagents that disallow formation of anhydride **4***a* has been recommended, 9-fluorenylmethyl succinimidyl carbonate first suggested by Paquet (6) being the most favoured for the synthesis of Fmc-amino acids[1] (**3***b*) (2, 3).

In the course of studies on the side reaction of urethane formation associated with the use of anhydrides **4***a* for the synthesis of peptides (7), it was found that the amount of urethane produced depended significantly on the nature of the tertiary amine used to generate the anhydride from **1***a* and **3***a*. In fact, when DIEA was used as base in a mixed anhydride coupling of Boc-Ile with Lys(Z)-OMe in dichloromethane, no peptide at all was formed.[2] The product isolated was the urethane, ROCO-Lys(Z)-OMe, in 90% yield. The conclusion was that the mixed anhydride had not been generated, and that the amino acid ester had reacted with the unconsumed chloroformate. That the mixed anhydride is generated much more slowly when DIEA instead of *N*-methylmorpholine or *N*-methylpiperidine is used as base was established by isolating the anhydrides from reaction mixtures at various times (8). The reluctance of mixed anhydrides to form in the presence of DIEA suggested to us that if the mixed anhydride indeed were responsible for the dimerization side reaction, eqs. [2] and [3], the use of DIEA instead of NaOH for acylation reactions, eq. [1], might eliminate the side reaction. Our studies on the use of DIEA to try to eliminate the dimerization side reaction associated with the acylation of amino acids are the subject of this communication. The study includes the acylation of amino acids with benzoyl chloride (**1***f*) since it is in the preparation of these derivatives **3***f* that the dimerization reaction was first encountered many years ago (9, 10).

[1]Abbreviations: Bz, benzoyl; Boc, *tert*-butoxycarbonyl; Eoc, ethoxycarbonyl; Fmc, 9-fluorenylmethoxycarbonyl; Moc, methoxycarbonyl; Z, benzyloxycarbonyl; DIEA, diisopropylethylamine; DMF, dimethylformamide; hplc, high-performance liquid chromatography. The amino acid symbols have no configurational implication. For convenience, derivatives of acids are indicated without the terminal OH; e.g. Bz-Ala instead of Bz-Ala-OH.

[2]Couplings of Boc-Ile, Boc-Leu, and Boc-Pro with Lys(Z)-OMe using EtOCOCl in the presence of DIEA in tetrahydrofuran also gave no peptide (unpublished).

Results and discussion

A method by which a reference mixture of the two pertinent products **3***a* and **5***a* (acid form) is prepared and analyzed was devised and has been published (5). It involves reaction of the symmetrical anhydride **7***a* (11, 12) of the protected amino acid **3***a* with the corresponding amino acid anion **2** in aqueous DMF. The proportions of the two compounds in the mixture are determined by ^{1}H nmr spectroscopy. The components are separated and the relative absorbances of the two are established by reversed-phase hplc on a C_{18} column with uv absorbance monitoring. The same analytical method was used for determining the benzoylation products **3***f* and **5***f* (acid form). However, the reference mixtures could not be prepared in the same manner since the symmetrical anhydride **7***f* of an acylamino acid, in contrast to that of the alkoxycarbonylamino acid, does not exist (13). The reference benzoyldipeptides **5***f* were nevertheless prepared in an analogous manner by reaction of the 2-alkyl-5(4*H*)-oxazolone **8***f* (14) with the amino acid anion **2** in aqueous DMF, except for the lysyl derivative. This acylation reaction with oxazolone **8**, R^1 = alkyl, in partially aqueous solutions is novel and will be discussed further in detail elsewhere.

Amino acids were benzoylated in aqueous solution according to the conventional procedure using NaOH as base (15), and with DIEA instead of NaOH. It was found that some amino acids remained insoluble in the presence of DIEA. Therefore

TABLE 1. Data on the preparation of *N*-substituted acids **3**

Acid **3**	Reagent	NaOH or Na_2CO_3[a] Yield (%)	NaOH or Na_2CO_3[a] Dipeptide **5** (molar %)	DIEA[a] Yield (%)	DIEA[a] Dipeptide **5** (molar %)
Bz-Gly	**1***f*	70	0.14	70	<0.05
Bz-Ala	**1***f*	60	1.20	72	<0.05
Bz-Leu	**1***f*	81	1.18	77	<0.05
Bz-Phe	**1***f*	97	0.9	99	<0.05
Bz-Lys(Z)	**1***f*	88	1.1	79	0.4
Z-Asp	**1***c*		0.22[b]		0.07
Z-Val	**1***c*	60	1.0	53	1.12
	1*c*	47	0.2		
Boc-Gly[c]	**6***d*	80	<0.10	70	<0.10
Boc-Leu[c]	**6***d*	87	<0.10	97	<0.10
Boc-Val[c]	**6***d*	82	0.34[b]	90	0.73
Boc-Phe(Cl)[c]	**6***d*	86	0.18[b]	95	<0.10
Eoc-Phe	**1***e*		0.17	70	<0.02
Eoc-Val	**1***e*		0.05	70–80	<0.02
	6*e*		3.9	78	<0.02
	6*e*[c]		0.5		
	6*e*[d]		4.3		
Fmc-Gly	**1***b*		14–20[e]	62	0.48[f]
Fmc-Leu	**1***b*	77	1.8[c]	65	<0.02[f]
				75	1.0[e]

[a]See Experimental.
[b]Data from ref. 5.
[c]Tetrahydrofuran–water used as solvent.
[d]*tert*-Butanol–water (2:1) used as solvent.
[e]Data from ref. 3.
[f]DMF–water used as solvent.

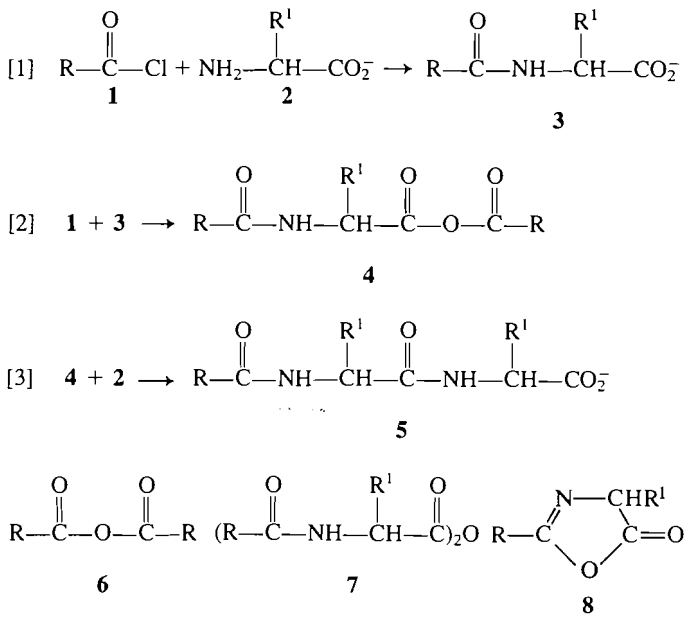

a: R = alkoxy
b: R = 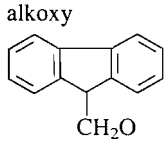
c: R = $PhCH_2O$
d: R = $(CH_3)_3CO$
e: R = C_2H_5O
f: R = Ph

the procedure adopted in all cases was to dissolve the amino acid by the addition of 1 equiv. of NaOH, and the DIEA was used only to neutralize the acid generated during the acylation. Acidic products were isolated by extraction of the mixture at acidic pH with ethyl acetate. Contaminating benzoic acid was removed by extracting solid product mixtures with hot carbon tetrachloride (15). It was noticeable with leucine in particular that the product, Bz-L-Leu, mp 105–106°C, obtained using DIEA, crystallized readily, while that with mp 103–105°C, obtained using NaOH, crystallized with difficulty. The results of the analyses of the products appear in Table 1. It is seen that the four benzoylamino acids **3***f* prepared using DIEA contained no *N*-acyl dimer **5***f*, while the three products with $R^1 \neq H$ prepared using NaOH contained about 1% of **5***f*. Only in the case of the side-chain substituted derivative H-L-Lys(Z)-OH, which is notoriously insoluble in water, was the dimerization side reaction not completely eliminated but only suppressed, the amount of contaminant being reduced by two-thirds. The yields obtained by the two methods were comparable. Thus, the acylation of amino acids with benzoyl chloride in the presence of NaOH invariably leads to the production of a significant amount of benzoyldipeptide. The contaminant is not readily removed by crystallization of the benzoylamino acid. Use of DIEA instead of NaOH eliminates the formation of the side product during the benzoylation of amino acids. The method may find application in the acylation of amino acids, also with ring-substituted benzoyl chlorides. The results substantiate the proposition that the mixed anhydride **4***f* is not generated when the counterion to the benzoylamino acid anion is $DIEAH^+$. The phenomenon which obtains for *N*-benzoylamino acids in aqueous solution is thus the same as that which obtains

Can. J. Chem. Downloaded from www.nrcresearchpress.com by 78.46.186.204 on 09/07/12
For personal use only.

Can. J. Chem. Downloaded from www.nrcresearchpress.com by 78.46.186.204 on 09/07/12
For personal use only.

for *N*-alkoxycarbonylamino acids in dichloromethane (7). The validity of the original hypothesis also substantiates the notion that generation of mixed anhydride **4** is responsible for the formation of *N*-substituted dipeptide **5**. Generation of anhydride **4** by reaction of **3***a* with benzoyl chloride was the basis for the development of the mixed anhydride method of coupling in peptide synthesis (10).

Alkoxycarbonylation of amino acids in the presence of DIEA proved to be less straightforward than benzoylation. Varying success was achieved depending on the nature of R. Representative results appear in Table 1. Fmc-Leu was obtained free of Fmc-dipeptide when the solvent was aqueous DMF, but not when it was aqueous tetrahydrofuran. Fmc-Gly contained much less contaminant than when prepared by the conventional procedure (3), but still a significant amount. No general pattern could be discerned for the benzyloxycarbonylation reaction, other than that the yields were poor. *Z*-Asp was obtained purer using DIEA, but in other cases the organic base increased the amount of dimer. A similar situation obtained in the synthesis of Boc-amino acids using di-*tert*-butyl dicarbonate (**6***d*) for acylation, except that the yields were high. The amount of dimer was increased by DIEA for Boc-Val but reduced for Boc-Phe(Cl). However, the use of DIEA proved satisfactory for the preparation of Eoc- and Moc-amino acids. Dimer was completely absent in Eoc-Val and Eoc-Phe (16), and Moc-Val, Moc-Leu, and Moc-Phe (17, 18) prepared on frequent occasions, and the products were enantiomerically pure. Eoc-L-Val was obtained in crystalline form for the first time by this procedure. With respect to generation of dimer **5***e*, an unexpected observation is that in the presence of NaOH much more was generated when diethyl dicarbonate (**6***e*) was the acylating agent than when it was EtOCOCl. This is surprising but not inconsistent with the observation that **6***e* reacted more readily than **6***d* with anion **3***a* in dichloromethane (8). No dimer was generated when **6***e* was used in the presence of DIEA.

The present study emerged from the observation that no anhydride was formed from **1***a* and **3***a* in dichloromethane in the presence of DIEA (7). It was uncertain if the same phenomenon would obtain in other solvents. The results indicate that the course of events depends both on the nature of the acylating agent and the side chain of the amino acid in question. The initial observation seems to hold in aqueous solution for the reagents benzoyl chloride and ethyl chloroformate. Attempts to get consistent behaviour from Z-Cl by effecting the reactions in aqueous DMF or tetrahydrofuran proved unsuccessful. In addition, the yields of product **3***c* were poor, we suspect, because of destruction of the Z-Cl by the tertiary amine. Z-Cl is quickly decomposed in pyridine (personal observation). Fmc-Cl may undergo the same fate, but at a slower rate. Despite the moderate yield of Fmc-Leu obtained, its successful synthesis using Fmc-Cl with DIEA indicates that the method might be a viable alternative to the use of 9-fluorenyl succinimidyl carbonate (2, 3, 6) in some cases.

Experimental

Reference mixtures of **3***a* and **5***a* were prepared by reaction of **7***a* (11, 12) with **2** in aqueous DMF (5). Separation and quantitation were done by hplc (C_{18}-μBondapak column, isocratic elution, uv absorbance monitoring at 208 nm, or 215 nm for aromatics) as previously described (5). Analyses of products **3***f* and **5***f* were carried out in identical manner using hplc. Reference compounds **5***f* (50–70% yields) were prepared by reaction of **8***f* (14) with **2** in aqueous DMF, with the same work-up as described (5). Bz-Lys(Z)-Lys(Z)-OH could not be obtained this way because of the slight solubility of H-L-Lys(Z)-OH. It was obtained by saponification of Bz-Lys(Z)-Lys(Z)-OMe, which had been prepared by reaction of the oxazolone with H-Lys(Z)-OMe in dichloromethane. All products **5***f* (solids) were epimeric mixtures resulting from the use of racemic **8***f* or racemization of **8***f* during aminolysis. As example of purity, Bz-Leu-Leu contained 0.8% of Bz-Leu. The hplc data not appearing in ref. 5 are as follows (solvent; k' = capacity factor = $(t - t_0)/t_0$; R_s = resolution = $2(t_2 - t_1)/(w_1 + w_2)$): 11% CH_3CN, Bz-Gly 1.40, Bz-Gly-Gly 0.99, R_s 1.06; 17% CH_3CN, Bz-Ala 1.57, Bz-Ala-Ala 1.39, R_s 0.85; 50% CH_3CN, Bz-Leu 0.82, Bz-Leu-Leu 1.39, R_s 1.52; 50% CH_3CN, Bz-Phe 0.77, Bz-Phe-Phe 1.47, R_s 1.79; 50% CH_3CN, Bz-Lys(*Z*) 1.16, Bz-Lys(*Z*)-Lys(*Z*) 2.76; R_s 4.58; 40% CH_3OH, Eoc-Val 1.81, Eoc-Val-Val 2.83, R_s 3.07; 50% CH_3OH, Eoc-Phe 2.62, Eoc-Phe-Phe 6.20, R_s 7.0. Emergence from the column of **5***f* before **3***f*, for glycine and alanine, is consistent with the chromatographic behaviour of **5***a* and **3***a* (5).

N-Benzoyl- and N-ethoxycarbonyl-amino acids

To a vigorously stirred solution containing amino acid (10 mmol) and NaOH (10 mmol) in 30 mL of water at 0°C was added alternately in small portions during 30 min benzoyl chloride or ethyl chloroformate (11 mmol) and DIEA or 1 *N* NaOH (11 mmol). The cooling bath was removed, the mixture was stirred an additional 30 min, then cooled again and acidified to Congo red with 6 *N* HCl. The oil that separated was extracted into ethyl acetate, the extract was washed with 1 *N* HCl, dried ($MgSO_4$), and the solvent was removed with a rotary evaporator. For Bz-amino acids, the residue was triturated in boiling carbon tetrachloride (20 mL), the mixture was cooled to 23°C, and the Bz-amino acid was collected by filtration. Products were analyzed for dimer **5** content before any recrystallization. Eoc-amino acids were then recrystallized from ethyl acetate – light petroleum. Eoc-DL-Phe, mp 78–79°C; Eoc-L-Phe, mp 86–87°C, $[\alpha]_D^{22}$ +23.4° (*c* 2.0, ethanol); Eoc-L-Val, mp 37°C, $[\alpha]_D^{22}$ +1.8° (*c* 2.0, ethanol), lit. (12) oil.

Fmc- and Boc-amino acids

These were prepared as described above except that the inorganic base was Na_2CO_3, the solvent was 20 mL of tetrahydrofuran–water (1:1), or DMF–water (1:1), the acylating reagent was dissolved in 10 mL of the organic solvent, the mixture was stirred 1 h after removal of the ice bath, and 10% aqueous citric acid was used to acidify solutions of Boc-amino acids.

Acknowledgements

This research was financially supported by the Medical Research Council of Canada of which N.L.B. is a Career Investigator. We thank Michele Chouinard, holder of a Natural Sciences and Engineering Research Council Summer Studentship, for carrying out some of the experiments.

1. M. Tessier, F. Albericio, E. Pedroso, A. Grandas, R. Eritja, E. Giralt, C. Granier, and J. van Rietschoten. Int. J. Pept. Protein Res. **22**, 125 (1983).
2. L. Lapatsanis, G. Milias, K. Froussios, and M. Kolovos. Synthesis, 671 (1983).
3. G. F. Sigler, W. D. Fuller, N. C. Chaturvedi, M. Goodman, and M. Verlander. Biopolymers, **22**, 2157 (1983).
4. E. Wünsch. *In* Peptides, structure and function. *Edited by* V. J. Hruby and D. R. Rich. Pierce Chemical Co., Rockford, IL. 1984. p. 55.
5. N. L. Benoiton, F. M. F. Chen, R. Steinauer, and M. Chouinard. Int. J. Pept. Protein Res. **27**, 28 (1986).
6. A. Paquet. Can. J. Chem. **60**, 976 (1982).
7. F. M. F. Chen, Y. Lee, R. Steinauer, and N. L. Benoiton. Can. J. Chem. **65**, 613 (1987).
8. F. M. F. Chen and N. L. Benoiton. Can. J. Chem. **65**, 619 (1987).
9. T. Curtius. J. Prakt. Chem. **24**, 239 (1881); **26**, 145 (1882).
10. T. Wieland and R. Sehring. Ann. Chem. **569**, 122 (1950).

11. F. M. F. CHEN, K. KURODA, and N. L. BENOITON. Synthesis, 928 (1978); 232 (1979).
12. A. PAQUET, F. M. F. CHEN, and N. L. BENOITON. Can. J. Chem. **62**, 1335 (1984).
13. N. L. BENOITON and F. M. F. CHEN. *In* Peptides 1982. *Edited by* K. Blaha and P. Malon. Walter de Gruyter & Co., Berlin. 1983. p. 167.
14. F. M. F. CHEN, K. KURODA, and N. L. BENOITON. Synthesis, 230 (1979).
15. J. P. GREENSTEIN and M. WINITZ. *In* Chemistry of the amino acids. Vol. 2. John Wiley & Sons, New York. 1962. p. 1266.
16. N. L. BENOITON, R. STEINAUER, Y. LEE, and F. M. F. CHEN. 13th Int. Congr. Biochem. Amsterdam, Abstract TU-195, 1985.
17. F. R. AHMED, F. M. F. CHEN, and N. L. BENOITON. Can. J. Chem. **64**, 1396 (1986).
18. F. M. F. CHEN and N. L. BENOITON. Can. J. Chem. **65**, 1228 (1987).

Can. J. Chem. Downloaded from www.nrcresearchpress.com by 78.46.186.204 on 09/07/12
For personal use only.

N,N-Dialkoxycarbonylamino acid formation from a mixed anhydride through intramolecular urethane acylation

FRANCIS M. F. CHEN AND N. LEO BENOITON

Department of Biochemistry, University of Ottawa, Ottawa, Ont., Canada K1H 8M5

Received August 22, 1986

FRANCIS M. F. CHEN and N. LEO BENOITON. Can. J. Chem. **65**, 1228 (1987).

Methoxycarbonylation at the urethane nitrogen of *N*-benzyloxycarbonyl- and *N*-methoxycarbonylvaline has been identified as a side reaction accompanying the aminolysis of the mixed anhydride formed from the acid and methyl chloroformate when the anhydride is coupled in aqueous dimethylformamide and the nucleophile is an amino acid anion. The side reaction occurs to a lesser but still significant extent when the activated residue is leucyl.

FRANCIS M. F. CHEN et N. LEO BENOITON. Can. J. Chem. **65**, 1228 (1987).

On a identifié la méthoxycarbonylation de l'azote de l'uréthane de la *N*-benzyloxycarbonyl- et de la *N*-méthoxycarbonylvaline comme une réaction secondaire accompagnant l'aminolyse de l'anhydride mixte qui se forme à partir de l'acide et du chloroformate de méthyle lorsqu'on effectue un couplage dans le diméthylformamide aqueux et que le nucléophile est un anion d'acide aminé. La réaction secondaire se produit aussi à des degrés qui ne sont pas négligeables, même si son importance est moindre, lorsque le résidu activé est la leucine.

[Traduit par la revue]

Can. J. Chem. Downloaded from www.nrcresearchpress.com by 72.64.146.136 on 09/07/12
For personal use only.

Previous papers have reported the use of symmetrical anhydrides of *N*-alkoxycarbonyl amino acids **1** as reagents for preparing reference mixtures of monomer **1** and the *N*-alkoxycarbonyldipeptide (1) and for converting amino acid enantiomers into epimeric *N*-substituted dipeptides for the analysis of enantiomeric mixtures (2). The products are generated by reaction of the anhydride with the amino acid anion in aqueous dimethylformamide. Accompanying this peptide bond forming reaction, however, is a side reaction involving rearrangement of the symmetrical anhydride to give the *N,N'*-bisalkoxycarbonyldipeptide (3, 4). Our interest in mixed carboxylic acid – carbonic acid anhydrides **3** (5, 6) and their availability in pure form (7) prompted us to examine the reaction of **3** with the same nucleophile under identical conditions. To simplify the interpretation of nmr spectra, anhydride **3***a* with R^1 and R^2 = methyl was used at the start of the investigation. The identify of the side product emanating from the symmetrical anhydride was not known to us at the time. A completely novel rearrangement of the mixed anhydride was identified, and this reaction forms the subject of the present communication. The different but related side reaction of urethane acylation accompanying mixed anhydride couplings of *N*-protected glycine derivatives has been described (8–11).

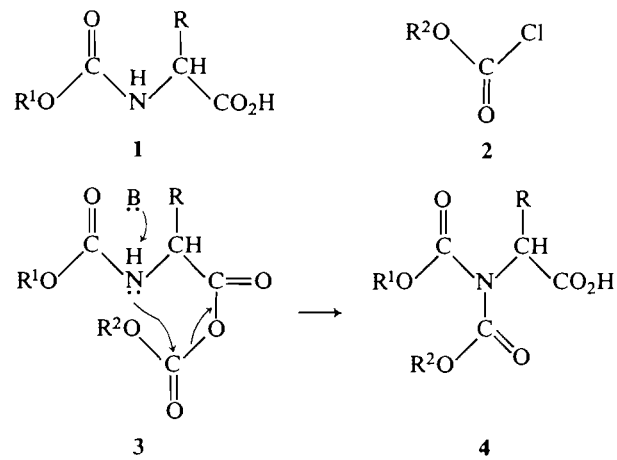

	R	R^1	R^2
a:	$(CH_3)_2CH$	CH_3	CH_3
b:	$(CH_3)_2CH$	$PhCH_2$	CH_3
c:	$(CH_3)_2CH$	$(CH_3)_3C$	CH_3

Results and discussion

Moc-Val-O-COOMe[1] (**3***a*), prepared by the standard procedure in dichloromethane from Moc-Val-OH (**1***a*) and MeOCOCl (**2***a*) followed by aqueous washes (7), was left at room temperature in aqueous DMF containing $NaHCO_3$. Acidification of the mixture followed by extraction with ethyl acetate and removal of solvent gave a mixture of starting material **1***a* and a second product that was stable to aqueous acid and $NaHCO_3$. Removal of **1***a* by its crystallization led to a mixture containing only a small amount of **1***a*. The nmr curve of the mixture showed a major methoxy singlet peak at δ = 3.80 ppm compared with 3.69 ppm for the singlet of **1***a*. The ratio of methyl to isopropyl groups was close to 2. Mass spectrometric analysis indicated a molecular ion of 233 corresponding to the molecular weight of *N,N*-dimethoxycarbonylvaline (**4***a*). The amount isolated corresponded to a yield of 20%. It was apparent that the mixed anhydride underwent the same initial deprotonation of the urethane nitrogen as the symmetrical anhydride (4) followed by nucleophilic attack at the carbon atom of the carbonate moiety, i.e. **3** → **4**. Confirmatory evidence for this was obtained by using Z-Val-O-COOMe (**3***b*) as the starting anhydride. Catalytic hydrogenation of the acid fraction isolated after acidification of the reaction mixture gave a 13% yield of crystalline Moc-Val-OH. There is one report in the literature on the existence of *N,N*-dialkoxycarbonylamino acids, namely $(Boc)_2$-Gly-OCH_2Ph obtained by the reaction of Boc-Gly-OCH_2Ph with $(Boc)_2O$ in the presence of 4-dimethylaminopyridine (14).

The proton nmr spectrum of **4***a* is characterized by a sharp α-proton doublet indicating the absence of the N-H proton, and two well-separated doublets of the isopropyl methyl groups indicating a rigid molecule. The pattern is similar to that seen in the nmr curves of the 2-alkyl and 2-alkoxy-4-isopropyl-5(4*H*)-oxazolones derived from derivatives of valine (7, 12, 13), except that the integration of the peak corresponding to the 2-substituent is twice that of the peaks of the 4-substituent.

[1]Abbreviations: Boc, *tert*-butoxycarbonyl; Moc, methoxycarbonyl; Z, benzyloxycarbonyl. The symbols for the amino acid residues represent the L isomers.

Can. J. Chem. Downloaded from www.nrcresearchpress.com by 72.64.146.136 on 09/07/12
For personal use only.

The methoxy protons appeared as a singlet with a chemical shift (δ = 3.80 ppm) close to that observed for the protons of the methoxy group of —CO—N(OCOCH$_3$)—CHR— of *N*,*N*′-bismethoxycarbonylvalylvaline (3), both compounds being *N*,*N*-diacylamines. The same chemical shift was observed for the methoxy protons in *N*-Z,*N*-Moc-Val-OH (**4***b*) (not obtained pure), the PhCH$_2$O protons at δ = 5.22 ppm showing a similar downfield displacement compared with those at 5.08 ppm in Z-Val-OH (**1***b*).

Initial attempts to gain further insight into the reaction involved studies on the reaction of Z-Val-O-COOMe and Boc-Val-O-COOMe (**3***c*) with the sodium salt of valine under various conditions. Deprotection of the products led to unusually high yields (15–20%) of Moc-Val-OH, but it was realized that aminolysis at the carbonate moiety of the anhydride (7) could account for some of the product. Meaningful results were then obtained using a different nucleophile. Z-Val-O-COOMe was reacted at 23°C with an equivalent of phenylalanine in DMF–H$_2$O (3:1) containing an equivalent of NaHCO$_3$. Hydrogenolysis of the acidic fraction gave a mixture of Moc-Val-OH (6%) originating from rearrangement of the anhydride, and Moc-Phe-OH (12%) originating from aminolysis at the carbonate moiety of the anhydride. The same experiment in tetrahydrofuran gave no Moc-Val-OH and 18% of Moc-Phe-OH, while an experiment using Na$_2$CO$_3$ instead of NaHCO$_3$ gave 2% of Moc-Val-OH and 22% of Moc-Phe-OH. A similar experiment with Z-Leu-O-COOMe in DMF (NaHCO$_3$) gave 0.5% of Moc-Leu-OH and 6% of Moc-Phe-OH. Experiments with Boc-Val-O-COOMe, Z-Val-O-COOEt, and Z-Val-O-COOiBu with appropriate deprotection of the products yielded only traces of the corresponding R^{1}OCO-Val-OH derivatives with R^1 = Me, Et, iBu respectively. Reaction of Z-Val-O-COOMe with H-Phe-OCH$_2$Ph in DMF at 23°C followed by acidification and hydrogenation of the ethyl acetate-soluble fraction gave no Moc-Val-OH (<0.5%) and 5% of Moc-Phe-OH. Finally, coupling of Z-Val-OH with H-Phe-OCH$_2$Ph by the conventional mixed-anhydride procedure, using MeOCOCl and *N*-methylpiperidine in tetrahydrofuran at −5°C followed by the same work-up, gave no detectable amount of Moc-Val-OH. We conclude that the side reaction of rearrangement of anhydride **3** to *N*,*N*-dialkoxycarbonylamino acid **4** occurs only in aqueous DMF when R^2 is methyl and R^1 is benzyl or methyl (R^1 = ethyl was not examined), and furthermore only when the nucleophile is the amino acid anion. The reaction does not occur when R^1 = *tert*-butyl and R^2 = ethyl or isobutyl. Ten times as much side product is formed when R = isopropyl (of valine) than when R = isobutyl (of leucine). On this basis, amongst the other amino acids, only when R = *sec*-butyl (of isoleucine) is a significant amount of the side product to be expected.

With respect to the formation of side product by aminolysis at the carbonate moiety of a mixed anhydride, it is possible to conclude that the amounts are greater when the reation is carried out in aqueous solvents with the amino acid anion as the nucleophile (12% of Moc-Phe-OH from **3***a* and H-Phe-O$^-$) than when the reaction is carried out in anhydrous solvents with the amino acid ester as the nucleophile (5% of Moc-Phe-OH from **3***a* and H-Phe-OCH$_2$Ph).

Experimental

The source of reagents and the general methods of operation were as previously described (7). Proton nmr spectra were determined in deuterochloroform using a Varian EM-360 60-MHz instrument. Chemical shifts are given in ppm relative to Me$_4$Si as internal standard. Mixed anhydrides **3** were obtained as described (7), and used immediately. Moc-Val-OH, mp 109–110°C, $[\alpha]_D^{22}$ +0.6° (*c* 2.0, ethanol), was prepared by a modified Schotten–Baumann procedure using MeOCOCl and diisopropylethylamine (15).

*Preparation of (Moc)$_2$-Val-OH (**4**a)*

A solution of Moc-Val-O-COOMe (309 mg; 1 mmol) in 6 mL of DMF was added to 2 mL of water containing NaHCO$_3$ (1 mmol) and the mixture was stirred at 23°C for 30 min. The solution was acidified with 1 *N* HCl and extracted with ethyl acetate (10 mL × 2), the extract was dried (MgSO$_4$), and the solvent was removed with a rotary evaporator. The residue contained (nmr) **4***a* and Moc-Val-OH (**1***a*) in ratio of 1:3. The mixture was dissolved in ethyl acetate to which was added light petroleum. The crystals of Moc-Val-OH were removed by filtration, and the crystallization was repeated three times. The residue (oil) remaining after removal of the solvent contained **4***a* contaminated with 5% of **1***a*; nmr of **4***a* (δ, ppm): 0.87 (3H, d, *J* = 7 Hz), 1.17 (3H, d, *J* = 7 Hz), 2.50 (1H, m), 3.80 (6H, s), 4.63 (1H, d, *J* = 9 Hz); ms *m*/*e*: 233 (M$^+$).

Aminolysis reactions

Z-Val-O-COOMe (**3***b*) (1 mmol) in 9 mL of DMF was added to a solution containing phenylalanine (1 mmol) and NaHCO$_3$ (1 mmol) in 3 mL of water and the mixture was stirred at 23°C for 1 h. The solution was acidified and extracted with ethyl acetate (10 mL × 2), the extract was dried, and the solvent was removed by evaporation. The residue was dissolved in 15 mL of 95% ethanol containing 1 mL of acetic acid and the mixture was hydrogenated over 10% palladium-on-charcoal for 16 h. The mixture was filtered, the filtrate was concentrated to a small volume, dichloromethane (20 mL) was added, and the solution was extracted with 10 mL of 1 *N* HCl. The organic layer was dried, the solvent was removed, and the residue was weighed and examined by nmr spectroscopy to determine the ratio of Moc-Val-OH to Moc-Phe-OH.

Acknowledgement

This research was financially supported by the Medical Research Council of Canada of which N.L.B. is a Career Investigator.

1. N. L. Benoiton, F. M. F. Chen, R. Steinauer, and M. Chouinard. Int. J. Pept. Protein Res. **27**, 28 (1986).
2. N. L. Benoiton, R. Steinauer, Y. Lee, and F. M. F. Chen. 13th Int. Congr. Biochem. Amsterdam, Abstract TU-195, 1985.
3. F. R. Ahmed, F. M. F. Chen, and N. L. Benoiton. Can. J. Chem. **64**, 1396 (1986).
4. N. L. Benoiton and F. M. F. Chen. *In* Peptides 1986. *Edited by* D. Theodoropoulos. Walter de Gruyter & Co. Berlin. 1986. In press.
5. F. M. F. Chen, R. Steinauer, and N. L. Benoiton. J. Org. Chem. **48**, 2939 (1983).
6. F. M. F. Chen, Y. Lee, R. Steinauer, and N. L. Benoiton. Can. J. Chem. **65**, 613 (1987).
7. F. M. F. Chen and N. L. Benoiton. Can. J. Chem. **65**, 619 (1987).
8. T. Wieland and B. Heinke. Ann. Chem. **599**, 70 (1956).
9. K. D. Kopple and R. J. Renick. J. Org. Chem. **23**, 1565 (1958).
10. P. Schellenberg and J. Ullrich. Chem. Ber. **92**, 1276 (1959).
11. R. B. Merrifield, A. R. Mitchell, and J. E. Clarke. J. Org. Chem. **39**, 660 (1974).
12. F. M. F. Chen, K. Kuroda, and N. L. Benoiton. Synthesis, 230 (1979).
13. N. L. Benoiton and F. M. F. Chen. Can. J. Chem. **59**, 384 (1981).
14. L. Grehn and U. Ragnarsson. Angew. Chem. Int. Ed. Engl. **24**, 510 (1985).
15. F. M. F. Chen and N. L. Benoiton. Can. J. Chem. **65**, 1224 (1987).

Evidence for an intermediate phosphaborene

CLAUDE COURET AND JEAN ESCUDIE
Laboratoire de chimie des organominéraux, U.A. du C.N.R.S. n° 477, Université Paul Sabatier, 31062 Toulouse CEDEX, France

BERNARD GARRIGUES
Laboratoire de synthèse, structure et réactivité de molécules phosphorées, U.A. du C.N.R.S. n° 454, Université Paul Sabatier, 31062 Toulouse CEDEX, France

AND

MOHAMED LAZRAQ AND JACQUES SATGE
Laboratoire de chimie des organominéraux, U.A. du C.N.R.S. n° 477, Université Paul Sabatier, 31062 Toulouse CEDEX, France

Received October 15, 1986

CLAUDE COURET, JEAN ESCUDIE, BERNARD GARRIGUES, MOHAMED LAZRAQ, and JACQUES SATGE. Can. J. Chem. **65**, 1230 (1987).

Addition of *tert*-butyllithium to chloroborylphosphine **2** to give **3** and **4** provides evidence for the phosphaborene **1**, a compound with dicoordinated double-bonded boron and phosphorus.

CLAUDE COURET, JEAN ESCUDIE, BERNARD GARRIGUES, MOHAMED LAZRAQ et JACQUES SATGE. Can. J. Chem. **65**, 1230 (1987).

L'addition de *tert*-butyllithium à la chloroborylphosphine **2**, qui conduit à **3** et **4**, a permis de mettre en évidence le phosphaborène **1**, composé possédant des atomes de bore et de phosphore dicoordonnés doublement liés.

Can. J. Chem. Downloaded from www.nrcresearchpress.com by 72.64.146.136 on 09/07/12
For personal use only.

Introduction

There is now a great deal of interest in the field of low coordinated species of groups 13, 14, and 15 (1). Some doubly-bonded molecules of silicon, germanium, and tin have been recently prepared, but many more doubly-bonded phosphorus compounds are known. Among doubly-bonded boron compounds are those with nitrogen (2), carbon (3), and oxygen (4), though the last ones have been identified only by trapping reactions.

Simultaneous with us, Cowley's group has characterized by mass spectroscopy the phosphaborene **1** formed by thermolysis of diphosphadiboretane **3** at 250°C (5).

We present here a chemical characterization of phosphaborene **1** by trapping reactions on lithio compounds.

Experimental

Syntheses were performed under an atmosphere of dry nitrogen using standard Schlenk and high-vacuum line techniques. Solvents were dried by distillation from sodium benzophenone ketyl immediately prior to use. ^{1}H nmr spectra (reference TMS) were recorded on a Varian EM 360 A at 60 MHz. ^{11}B (reference $BF_3 \cdot OEt_2$) and ^{31}P (reference 85% H_3PO_4) nmr spectra were recorded on a Bruker WH 90, respectively, at 28.88 and 36.44 MHz. Nuclear magnetic resonance spectra were measured on samples in C_6D_6 solution. Infrared spectra were recorded on a Perkin Elmer 457 grating spectrometer. Mass spectra were measured on a Varian MAT 311 A spectrometer (EI). Experimental molecular peak patterns were assigned after comparison with theoretical peak patterns calculated on a Tektronics 4051. Melting points were determined on a Reichert apparatus and are uncorrected. Elemental analyses were done by the "Service de Microanalyse de l'ENSCT" Toulouse.

Synthesis of chloroborylphosphine 2

Equimolar quantities of dichloro-2,2,6,6-tetramethylpiperidinoborane $RBCl_2$ (5.20 g, 0.023 mol) and 2,4,6-tri-*tert*-butylphenyllithiophosphide ArP(H)Li (prepared from 6.39 g (0.023 mol) of $ArPH_2$ and 14.4 mL (0.023 mol) of a solution of *n*-butyllithium in hexane (1.6 *N*)), were allowed to react in Et_2O (50 mL) at 0°C for half an hour before warming to 25°C. After the mixture was stirred for an hour at room temperature, solvents were removed *in vacuo* and crude **2** was recrystallized from pentane as white crystals (7.67 g, yield: 72%, mp 155–156°C). nmr: ^{1}H: 1.25 (s, 12H, CH_3(R)), 1.50–1.60 (m, 6H, CH_2), 1.66 (s, 9H, *p*-*t*Bu), 1.83 (s, 18H, *o*-*t*Bu), 4.23 (d, $^1J_{P-H}$ = 229 Hz, 1H, PH), 7.70 (d, $^4J_{P-H}$ = 2.0 Hz, 2H, arom H). ^{11}B: +47.6, ^{31}P: −98.7, $^1J_{P-H}$ = 229 Hz. Mass spectrometry (EI) *m/e*: 463 (M^+).

Addition of tert-*butyllithium to 2 (reaction* a*)*

To a solution of **2** (5.09 g, 0.011 mol) in THF (30 mL) cooled at −78°C was slowly added via syringe a solution of *tert*-butyllithium in pentane (1.7 *N*, 12.9 mL, 0.022 mol). A red coloration appeared immediately. The reaction mixture was allowed to warm to room temperature; ^{31}P nmr analysis showed the formation of **3** and **4** in the ratio 30/70. After elimination of solvents *in vacuo*, a selective recrystallization from pentane afforded 0.99 g (yield: 21%) of yellow–green crystals of **3** (mp: 164–165°C) ^{31}P nmr −92.8. Mass spectrometry (EI) *m/e*: 854 (M^+, 5%); 740 ($(M - 2tBu)^+$, 15%); 427 ($M^+/2$, 70%); 370 ($(M/2 - tBu)^+$, 100%). *Anal.* calcd. for $C_{54}H_{94}B_2N_2P_2$: C 75.86, H 11.08, N 3.28; found: C 75.80, H 10.81, N 3.54.

Addition of 2 to tert-*butyllithium (reaction* a′*)*

To a solution of *tert*-butyllithium in pentane (1.7 *N*, 6.5 mL, 0.011 mol) and THF (30 mL) at −78°C was added a solution of **2** (2.54 g, 0.0055 mol) in THF (20 mL). ^{31}P nmr analysis (see Results and discussion) after warming to room temperature showed the nearly quantitative formation of **4**.

Synthesis of 5 and 6 from 4

In a typical experiment, to a solution of **4** (0.005 mol) prepared according to reaction *a′*, was added a solution of equimolar quantities of methanol, methyl iodide, or trimethylchlorosilane, respectively, in THF at room temperature. After removal of lithio salts and solvents **5**, **6***a*, and **6***b* were crystallized from pentane.

5: yellow–green crystals, mp 102–103°C, 2.06 g, yield: 85%; nmr: ^{1}H: 0.83 (broad s, 9H, *t*BuB), 1.33 (s, 9H, *p*-*t*Bu), 1.37–1.57 (m, 18H, CH_3(R), and CH_2), 1.67 (s, 18H, *o*-*t*Bu), 5.37 (d, $^1J_{P-H}$: 320 Hz, 1H, PH), 7.50 (d, $^4J_{P-H}$: 2.2 Hz, 2H, arom H). ^{11}B: +46.2,

^{31}P: −51.1 ($^{1}J_{PH}$ = 320 Hz), ir (KBr disc) ν(PH): 2407 cm^{-1}. Mass spectrometry (EI) m/e: 485 (M^+). *Anal.* calcd. for $C_{31}H_{57}BNP$: C 76.67, H 11.83, N 2.88; found: C 76.16, H 11.46, N 3.05.

6*a*: yellow–green crystals, mp 147–148°C, 2.02 g, yield: 81%; nmr: ^{1}H: 0.83 (d, $^{4}J_{P-H}$ = 1.2 Hz, 9H, *t*BuB), 1.33 (s, 9H, *p*-*t*Bu), 1.13–1.53 (m, 6H, CH_2), 1.47 (s, 12H, CH_3(R)), 1.67 (s, 18H, *o*-*t*Bu), 2.17 (d, $^{2}J_{P-H}$ = 12.0 Hz, 3H, CH_3—P), 7.57 (d, $^{4}J_{P-H}$ = 2.3 Hz, 2H, arom, H). ^{11}B: +58; ^{31}P: −14.6; mass spectrometry (EI) m/e: 499 (M^+). *Anal.* calcd. for $C_{32}H_{59}BNP$: C 76.92, H 11.90, N 2.80; found: C 76.68, H 12.01, N 3.04.

6*b*: yellow–green crystals, mp 152–153°C, 2.17 g, yield: 78%; nmr: ^{1}H: 0.53 (d, $^{3}J_{P-H}$ = 6.0 Hz, 9H, CH_3Si), 1.10 (d, $^{4}J_{P-H}$: 1.0 Hz, 9H, *t*BuB), 1.33 (s, 9H, *p*-*t*Bu), 1.20–1.66 (m, 6H, CH_2), 1.53 (s, 6H, CH_3(R)), 1.60 (s, 6H, CH_3(R)), 1.83 (s, 18H, *o*-*t*Bu), 7.67 (d, $^{4}J_{P-H}$ = 2.6 Hz, 2H, arom H). ^{11}B: +62; ^{31}P: −23.9; mass spectrometry (EI) m/e: 557 (M^+). *Anal.* calcd. for $C_{34}H_{65}BNPSi$: C 73.21, H 11.75, N 2.51; found: C 72.98, H 11.60, N 2.67.

Results and discussion

Chloroborylphosphine **2**,[1] the precursor of **1**, was synthesized (reaction [1]) by the reaction of dichloro-2,2,6,6-tetramethylpiperidinoborane with 2,4,6-tri-*tert*-butylphenyllithiophosphide in pentane or diethylether:

[1] $RBCl_2 + ArP(H)Li \xrightarrow[-LiCl]{} R—B(Cl)—P(H)—Ar$ **2**

R = 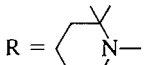

Ar = 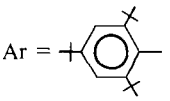

Addition of *tert*-butyllithium[2] to **2** at −78°C in THF (reaction [2], path *a*) resulted in an immediate red coloration; room temperature ^{31}P nmr measurements showed the formation of **3** and **4** in the ratio 30/70. The last two products probably result from the phosphaborene intermediate **1** which either dimerizes to give **3**, or reacts with *tert*-butyllithium to afford **4**. The formation of phosphaborene **1** seems to be confirmed by the "reverse" reaction *a'* in which **2** is added to an excess of *tert*-butyllithium, this producing compound **4** exclusively. Here **1** is quantitatively trapped by *tert*-butyllithium prior to dimerization:

[2] 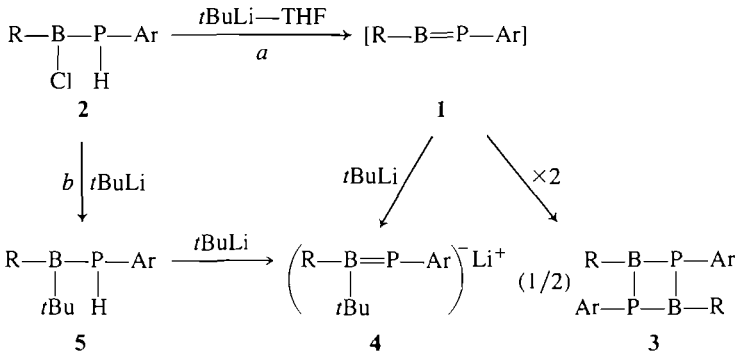

The formation of **4** could also be explained by an alkylation of **5** (route *b*). However, the complete absence of **5** in reaction *a* and of **3** in the "reverse" reaction *a'* (**3** does not react with *t*BuLi) support route *a*. It should be noted that Cowley's group has reacted **2** with *t*BuLi in Et_2O at 25°C but obtained exclusively **4**. In this case, due to the absence of **3**, the intermediate formation of **1** was not evidenced in this reaction.

In mass spectral measurements of **3** at 200°C, we also observed an intense peak at 427, attributable to the phosphaborene **1**. Heterocycles such as 2,4-diphospha-1,3-diboretane **3**, are rare (6).

Compound **4** is extremely air-sensitive and is characterized by ^{31}P nmr and its chemical reactivity. The ^{31}P spectrum immediately after the reaction generates two signals at +84 (90%) and +82 ppm (10%), indicating deshielded phosphorus atoms. Chemical shifts of lithiophosphides are generally at high field, e.g. at −109 ppm for ArP(H)Li and at −151 ppm for $ArP(SiMe_3)Li$ in THF (7) and so we postulate that one electron pair on phosphorus is involved in multiple bonding to boron in **4**. From our data, further support for this is the presence of two ^{31}P signals, that result probably from the existence of the two geometric isomers:

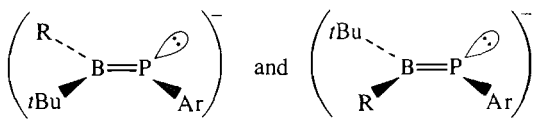

At about the same time as we did our experiments, Power's group obtained, from the reaction between *tert*-butyllithium and $Mes_2BP(H)R$ (R = Ph, C_6H_{11}, mesityl) in Et_2O, the derivatives $Mes_2BP(R)Li(Et_2O)_2$ (8); as demonstrated by X-ray studies of these compounds, bond distances are consistent with a high degree of BP double bond character.

Compound **4** reacts very easily with protic reagents such as water, and methanol, to afford **5**,[3] and with alkyl halides such as methyl iodide or trimethylchlorosilane to give quantitatively **6**:

[1]Compound **2** has been prepared by Cowley's group but only ^{31}P nmr and mass spectroscopy data are given (5).

[2]An attempt to remove HCl from **2** with other basic reagents such as Et_3N failed.

[3]Compound **5** was mentioned in the recent communication from Cowley's group but the physico-chemical data were not presented (5).

Can. J. Chem. Downloaded from www.nrcresearchpress.com by 72.64.146.136 on 09/07/12
For personal use only.

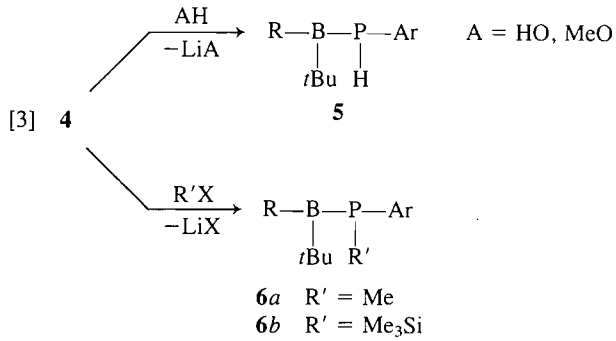

Further studies are now being directed towards the synthesis of more stable phosphaborenes.

1. A. H. COWLEY. Polyhedron, **3** (4), 389 (1984); Acc. Chem. Res. **17**, 386 (1984).
2. (*a*) P. PAETZOLD, A. RICHTER, T. THIJSSEN, and S. WURTENBERG. Chem. Ber. **112**, 3811 (1979); (*b*) H. NOTH and S. WEBER. Z. Naturforsch. **38**b, 1460 (1983); (*c*) P. PAETZOLD, C. VON PLOTHO, G. SCHMID, R. BOESE, B. SCHRADER, D. BOUGEARD, U. PFEIFFER, R. GLEITER, and W. SCHAFER. Chem. Ber. **117**, 1089 (1984); (*d*) M. HAASE and U. KLINGEBIEL. Angew. Chem. Int. Ed. **24**, 324 (1985); (*e*) M. HAASE, U. KLINGEBIEL, R. BOESE, and M. POLK. Chem. Ber. **119**, 1117 (1986).
3. H. KLUSIK and A. BERNDT. Angew. Chem. Int. Ed. **22**, 877 (1983); B. GLASER and H. NOTH. Angew. Chem. Int. Ed. **24**, 416 (1985).
4. B. PACHALY and R. WEST. J. Am. Chem. Soc. **107**, 2987 (1985).
5. A. M. ARIF, J. E. BOGGS, A. H. COWLEY, J. G. LEE, M. PAKULSKI, and J. M. POWER. J. Am. Chem. Soc. **108**, 6083 (1986).
6. (*a*) G. E. COATES and J. E. LIVINGSTONE. J. Chem. Soc. 5053 (1961); (*b*) G. FRITZ and W. HOLDERICH. Z. Anorg. Allg. Chem. **431**, 61 (1977); (*c*) A. M. ARIF, A. H. COWLEY, M. PAKULSKI, and J. M. POWER. J. Chem. Soc. Chem. Commun. 889 (1986); (*d*) P. KOLLE, H. NOTH, and R. T. PAINE. Chem. Ber. **119**, 2681 (1986).
7. M. YOSHIFUJI, K. TOYOTA, K. SHIBAYAMA, and N. INAMOTO. Chem. Lett. 1653 (1983).
8. R. A. BARTLETT, X. FENG, and P. P. POWER. J. Am. Chem. Soc. **108**, 6817 (1986).

Can. J. Chem. Downloaded from www.nrcresearchpress.com by 72.64.146.136 on 09/07/12
For personal use only.

ipso Nitration. XXIX.[1] Nitration of substituted 4-methylanisoles and phenols

ALFRED FISCHER,[2] GEORGE N. HENDERSON, AND SUMIT RAYMAHASAY
Department of Chemistry, University of Victoria, Victoria, B.C., Canada V8W 2Y2

Received November 11, 1986

ALFRED FISCHER, GEORGE N. HENDERSON, and SUMIT RAYMAHASAY. Can. J. Chem. **65**, 1233 (1987).

Nitration of 2-chloro-4-methylanisole (**1***a*) in acetic anhydride gives (*Z*)-4-chloro-3-methoxy-6-methyl-6-nitrocyclohexa-2,4-dienyl acetate (**2***a*), 2-chloro-4-methyl-4-nitrocyclohexa-2,5-dienone (**3***a*), and 2-chloro-4-methyl-6-nitroanisole (**4***a*). Similarly 2-bromo-4-methylanisole (**1***b*) gives (*Z*)-4-bromo-3-methoxy-6-methyl-6-nitrocyclohexa-2,4-dienyl acetate (**2***b*), 2-bromo-4-methyl-4-nitrocyclohexa-2,5-dienone (**3***b*), and 2-bromo-4-methyl-6-nitroanisole (**4***b*), whereas 4-methyl-2-nitroanisole (**1***c*) gives (*Z*)-3-methoxy-6-methyl-4,6-dinitrocyclohexa-2,4-dienyl acetate (**2***c*), (*Z*)-3-methoxy-6-methyl-2,6-dinitrocyclohexa-2,4-dienyl acetate (**7**), and 4-methyl-2,6-dinitroanisole (**4***c*). Nitration of 3-chloro-4-methylanisole (**9***a*) gives 3-chloro-4-methyl-4-nitrocyclohexa-2,5-dienone (**10***a*), 3-chloro-4-methyl-2-nitro anisole (**11***a*), and 5-chloro-4-methyl-2-nitroanisole (**12***a*), and 4-methyl-3-nitroanisole (**9***c*) gives (*Z*)-3-methoxy-6-methyl-5,6-dinitrocyclohexa-2,4-dienyl acetate (**13**), 4-methyl-2,3-dinitroanisole (**11***c*), and 4-methyl-2,5-dinitroanisole (**12***c*). Nitration of 2-chloro-4-methylphenol (**14**) in chloroform gives **3***a* and 2-chloro-4-methyl-6-nitrophenol (**5***a*), and 3-chloro-4-methylphenol (**15**) gives dienone **10***a*, 3-chloro-4-methyl-2-nitrophenol (**16**), and 5-chloro-4-methyl-2-nitrophenol (**17**).

ALFRED FISCHER, GEORGE N. HENDERSON et SUMIT RAYMAHASAY. Can. J. Chem. **65**, 1233 (1987).

La nitration du chloro-2 méthyl-4 anisole (**1***a*), dans l'anhydride acétique, conduit à l'acétate du chloro-4 méthoxy-3 méthyl-6 nitro-6 cyclohexadiène-2,4 yle-(*Z*) (**2***a*), à la chloro-2 méthyl-4 nitro-4 cyclohexadiène-2,5 one (**3***a*) et au chloro-2 méthyl-4 nitro-6 anisole (**4***a*). De la même manière, le bromo-2 méthyl-4 anisole (**1***b*) conduit à l'acétate du bromo-4 méthoxy-3 méthyl-6 nitro-6 cyclohexadiène-2,4 yle-(*Z*) (**2***b*), à la bromo-2 méthyl-4 nitro-4 cyclohexadiène-2,5 one (**3***b*) et au bromo-2 méthyl-4 nitro-6 anisole (**4***b*) alors que le méthyl-4 nitro-2 anisole (**1***c*) conduit à l'acétate du méthoxy-3 méthyl-6 dinitro-4,6 cyclohexadiène-2,4 yle-(*Z*) (**2***c*), à l'acétate du méthoxy-3 méthyl-6 dinitro-2,6 cyclohexadiène-2,4 yle-(*Z*) (**7**) et au méthyl-4 dinitro-2,6 anisole (**4***c*). La nitration du chloro-3 méthyl-4 anisole (**9***a*) fournit la chloro-3 méthyl-4 nitro-4 cyclohexadiène-2,5 one (**10***a*), le chloro-3 méthyl-4 nitro-2 anisole (**11***a*) et le chloro-5 méthyl-4 nitro-2 anisole (**12***a*) et celle du méthyl-4 nitro-3 anisole (**9***c*) fournit l'acétate du méthoxy-3 méthyl-6 dinitro-5,6 cyclohexadiène-2,4 yle-(*Z*) (**13**), le méthyl-4 dinitro-2,3 anisole (**11***c*) et le méthyl-4 dinitro-2,5 anisole (**12***c*). La nitration du chloro-2 méthyl-4 phénol (**14**), dans le chloroforme, conduit au composé **3***a* accompagné de chloro-2 méthyl-4 nitro-6 phénol (**5***a*) alors que celle du chloro-3 méthyl-4 phénol (**15**) conduit à la dienone **10***a* accompagnée de chloro-3 méthyl-4 nitro-2 phénol (**16**) et de chloro-5 méthyl-4 nitro-2 phénol (**17**).

[Traduit par la revue]

Can. J. Chem. Downloaded from www.nrcresearchpress.com by 72.64.146.136 on 09/07/12
For personal use only.

The nitration of 4-acetamido-, 4-bromo-, 4-chloro-, and 4-methoxy-toluene in acetic anhydride gives in each case, in addition to the nitro substitution product(s), a *cis* 1,2 nitronium acetate adduct (1, 2). Nitration of 4-fluorotoluene and of 4-*tert*-butyltoluene gives, in both cases, a pair of diastereomeric 1,4 nitronium acetate adducts and the *cis* 1,2 adduct (1, 3), whereas the nitration of other 4-alkyltoluenes gives, in addition to the nitro substitution products, only the diastereoisomeric 1,4 adducts (4–6). The extent of *ipso* nitration is explicable in terms of the relative activation of *ipso* and unsubstituted positions towards the electrophile (7). The factors that determine the addition of acetate to the *ortho* versus the *para* position of the *ipso*-nitrocyclohexadienyl cation are yet to be elucidated. The present study of nitration of substituted 4-methoxytoluenes represents an attempt to determine how the additional substituent affects the preferred position of addition of acetic acid to the *ipso* cation. We have also investigated the nitration of some related substituted 4-hydroxytoluenes.

Results and discussion

For each substrate, conditions were employed which led to the optimum yield(s) of adduct(s) and which were determined by carrying out preliminary reactions on a 0.5-mmol scale and following the reactions by nuclear magnetic resonance spectroscopy (^{1}H nmr). Products and their yields are shown in Scheme 1. Generally, the products consisted of dienes and (or) dienones formed by addition of nitronium ion *ipso* to the methyl group together with the nitro substitution derivative(s) of the substrates. Some secondary products were obtained in the course of work-up of the reaction mixtures and these are described below.

2-Chloro-4-methylanisole (**1***a*) was nitrated at −40°C. The ^{1}H nmr spectrum of the reaction mixture indicated the presence of (*Z*)-4-chloro-3-methoxy-6-methyl-6-nitrocyclohexa-2,4-dienyl acetate (**2***a*), 2-chloro-4-methyl-4-nitrocyclohexa-2,5-dienone (**3***a*), and 2-chloro-4-methyl-6-nitroanisole (**4***a*). After low temperature work-up, diene **2***a* separated out as a solid during evaporation of the solvent. The ^{1}H nmr spectrum of the remaining mixture indicated that dienone **3***a* had disappeared and that 2-chloro-4-methyl-6-nitrophenol (**5***a*) and 2-chloro-4-methyl-4-nitrocyclohexa-2,5-dienone dimethyl ketal (**6***a*) had been formed.

A mixture of (*Z*)-4-bromo-3-methoxy-6-methyl-6-nitrocyclohexa-2,4-dienyl acetate (**2***b*), 2-bromo-4-methyl-4-nitrocyclohexa-2,5-dienone (**3***b*), and 2-bromo-4-methyl-6-nitroanisole (**4***b*) was obtained on nitration of 2-bromo-4-methylanisole (**1***b*) at −40°C. The dienone rearranged during the low temperature work-up with ammonium hydroxide and the 2-bromo-4-methyl-6-nitrophenol (**5***b*) thus formed was partially removed in the basic solution. Pure diene **2***b* was obtained by crystallization.

(*Z*)-3-Methoxy-6-methyl-4,6-dinitrocyclohexa-2,4-dienyl acetate (**2***c*), (*Z*)-3-methoxy-6-methyl-2,6-dinitrocyclohexa-2,4-dienyl acetate (**7**), and 4-methyl-2,6-dinitroanisole (**4***c*) were formed on nitration of 4-methyl-2-nitroanisole (**1***c*) in acetic anhydride at 0°C. Diene **7** was precipitated by pouring the reaction mixture into ether at −78°C. After neutralization of the filtrate with ammonium hydroxide, diene **2***c* crystallized from the ethereal solution. When the nitration was carried out in mixtures of acetic anhydride and trifluoroacetic anhydride,

[1]For Part XXVIII, see ref. 1.

[2]Author to whom correspondence may be addressed.

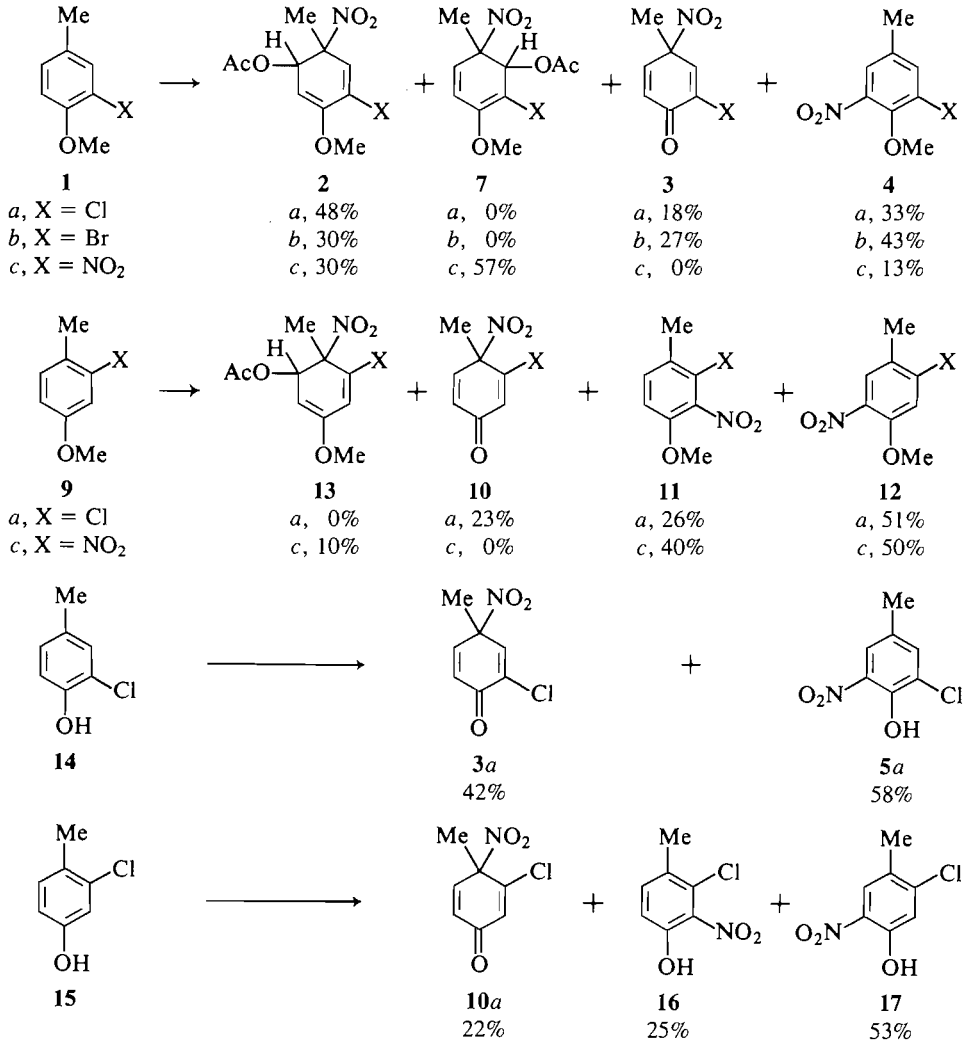

SCHEME 1

minor amounts of (*E*)-3-methoxy-6-methyl-2,6-dinitrocyclohexa-2,4-dienyl acetate ((*E*)-**7**) and 1-methoxy-4-methyl-2,4,6-trinitrocyclohex-2-enyl-1,5-diacetate (**8**) were formed in addition to the other products, and were isolated. 4-Methyl-2,4-dinitrocyclohexa-2,5-dienone dimethyl ketal (**6***c*), which was not present in the original mixture, was also obtained after chromatography.

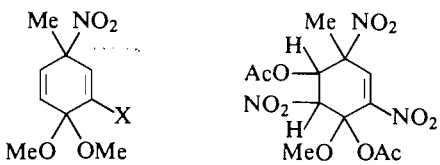

6
a, X = Cl
c, X = NO_2

8

Nitration of 3-chloro-4-methylanisole (**9***a*) at temperatures ranging from −60 to −40°C, with varying molar proportions of nitric acid and acetic anhydride, gave mixtures containing 3-chloro-4-methyl-4-nitrocyclohexa-2,5-dienone(**10***a*),3-chloro-4-methyl-2-nitroanisole (**11***a*), and 5-chloro-4-methyl-2-nitroanisole (**12***a*). Formation of diene was not detected.

Heterogeneous mixtures were invariably obtained on addition of 4-methyl-3-nitroanisole (**9***c*) to nitrating solutions and it was difficult to obtain homogeneous solutions for ^{1}H nmr, even after further dilution with acetic anhydride. (*Z*)-3-Methoxy-6-methyl-5,6-dinitrocyclohexa-2,4-dienyl acetate (**13**), 4-methyl-2,3-dinitroanisole (**11***c*), and 4-methyl-2,5-dinitroanisole (**12***c*) were present in the reaction mixture, although diene **13** could not be detected after low temperature work-up with ammonium hydroxide. Diene **13** evidently decomposed to 3,4-dinitro-4-methylcyclohexa-2,5-dienone (**10***c*) since some of this compound could be detected by ^{1}H nmr after work-up.

Nitration of 2-chloro-4-methylphenol (**14**) in acetic anhydride at −45°C gave dienone **3***a* and nitrocresol **5***a*. On work-up with ammonium hydroxide, followed by filtration of the ether solution of the product through basic alumina at −78°C, and removal of the solvent at −50°C, pure **3***a* was obtained. A solution of **3***a* in chloroform rearranged to **5***a*, with a half-life of 20 min at 0°C and 5 min at ambient temperature.

Nitration of 3-chloro-4-methylphenol (**15**) in chloroform at −60°C gave dienone **10***a*, 3-chloro-4-methyl-2-nitrophenol (**16**), and 5-chloro-4-methyl-2-nitrophenol (**17**). Pure **10***a* was separated by chromatography on alumina at −78°C. In chloroform-*d*, at 0°C, dienone **10***a* rearranged to an equimolar mixture of **16** and **17**, with a half-life of 10 min.

Structure and spectra of the adducts

The infrared spectrum of diene **2***a* exhibits characteristic peaks of nitro (1540 cm^{-1}) and acetate (1735 cm^{-1}) groups. The elemental analysis corresponds to the empirical formula of

Can. J. Chem. Downloaded from www.nrcresearchpress.com by 72.64.146.136 on 09/07/12
For personal use only.

TABLE 1. The ^{1}H nmr spectra of X-3-methoxy-6-methyl-6-nitrocyclohexa-2,4-dienyl acetates

		Chemical shifts/ppm							Coupling constants/Hz		
Compound	X	6-CH_3	OAc	OCH_3	1-H	2-H	4-H	5-H	1,2	1,5	4,5
2*a*	4-Cl	1.80	1.97	3.68	5.60	5.12	—	6.73	6.45	1.85	—
2*b*	4-Br	1.80	1.98	3.67	5.59	5.09	—	6.99	6.62	1.91	—
2*c*	4-NO_2	1.88	1.99	3.71	5.64	5.27	—	7.29	6.70	2.02	—
2*d*[a]	H[b]	1.77	1.95	3.60	5.62	4.97	5.93	6.56	6.57	1.52	10.20
(*Z*)-**7**	2-NO_2	1.88	1.97	4.03	6.57	—	6.47	7.09	—	2.06	10.60
(*E*)-**7**	2-NO_2	1.79	2.10	4.04	7.04	—	6.71	6.36	—	1.60	10.20

[a]From ref. 1.
[b]$J_{2,4}$ = 1.75 Hz.

TABLE 2. The ^{13}C nmr spectra of X-3-methoxy-6-methyl-6-nitrocyclohexa-2,4-dienyl acetates

		Chemical shifts/ppm									
Compound	X	6-CH_3	OAc	OCH_3	C-1	C-2	C-3	C-4	C-5	C-6	CO
2*a*	4-Cl	23.5	20.7	55.8	71.2	91.1	152.4	127.6	126.2	88.7	169.6
2*b*	4-Br	23.2	20.7	55.8	71.1	90.5	152.5	117.3	130.4	89.3	169.6
2*c*	4-NO_2	22.5	20.6	56.1	70.7	93.5	149.3	145.4	127.3	87.5	169.4
2*d*[a]	H	22.6	19.6	53.8	70.8	87.8	155.2	122.7	128.4	87.3	168.6
(*Z*)-**7**	2-NO_2	22.8	20.4	58.0	70.4	123.7	155.9	117.2	138.3	88.9	168.4
(*E*)-**7**	2-NO_2	21.8	20.5	58.1	68.2	124.3	156.5	122.4	135.6	86.3	169.2

[a]From ref. 1.

the adduct of **1***a* and acetyl nitrate. The close similarity between the nmr spectra, both ^{1}H (Table 1) and ^{13}C (Table 2), of (*Z*)-3-methoxy-6-methyl-6-nitrocyclohexa-2,4-dienyl acetate (**2***d*) and **2***a*, with the expected differences resulting from the presence of the 4-chloro substituent in **2***a*, allows the assignment of the structure of the latter. In particular, the 71.2-ppm peak in the ^{13}C nmr spectrum characteristic of the sp^3 carbon $CMeNO_2$ is within 0.5 ppm of the similar peak in **2***d*. The high field vinyl carbon (91.1 ppm) has an attached hydrogen and must be adjacent to the methoxyl-substituted carbon (152.4 ppm). The chlorine substituent must be attached to the carbon at 127.6 ppm, since this carbon shows no strong coupling to hydrogen in the gated spectrum. In the proton spectrum the methine hydrogen is at 5.6 ppm, as in **2***d*. The hydrogen vinylic to the methoxy substituent is at the expected high field (5.12 ppm in **2***a*, cf. 4.97 ppm in **2***d*) and shows the appropriate 6.5-Hz splitting with the methine proton. The chlorine must be attached to the 4,5 double bond since the 10-Hz splitting present in **2***d* is absent in **2***a*. The 1.85-Hz splitting of the methine proton must reflect a 1,5 coupling and this confirms that chlorine is at the 4 position. Parallel arguments can be made to assign the 4-bromo-3-methoxy-6-methyl-6-nitrocyclohexa-2,4-dienyl acetate structure (**2***b*) to the diene obtained on nitration of **1***b*.

The empirical formula of the two major dienes, **2***c* and **7**, and the minor diene, obtained from anisole **1***c*, is, in each case, $C_{10}H_{12}N_2O_7$, accounted for by the addition of one acetyl nitrate molecule. The ir spectra of these dienes confirmed the presence of acetate and nitro groups. The ^{1}H and ^{13}C nmr spectra of **2***c* are closely similar to those of dienes **2***a* and **2***b* with an essentially identical splitting pattern. In the assigned structure the 4-halo substituent of **2***a* and **2***b* is replaced by nitro, explaining the spectral similarity. The largest difference between the ^{13}C spectra of **2***a* and **2***c* is the 18-ppm downfield shift of C-4 in the latter. This is accounted for by the greater substituent shift effect of the nitro (attached to C-4) than that of chlorine (8). In the ^{1}H nmr spectra the 5-H is 0.6 ppm further downfield in **2***c* than in **2***a* and this is explained by the β-substituent effect of the nitro group attached at the other end of the 4,5 double bond. The general similarity of the ^{13}C nmr spectra of **2***c* and its isomers suggests that the structures are closely related. The most striking difference between the spectra is that the very high field vinyl carbon absorption, which appears close to 90 ppm in **2***d* and its 4-chloro, 4-bromo, and 4-nitro derivatives **2***a*, **2***b*, and **2***c*, respectively, and which is assigned to C-2, is absent in the isomers, for which the highest field sp^2 carbon (in the major isomer) is at 117 ppm. This implies that the nitro group in **7** is at C-2 and this is confirmed by the ^{1}H spectra, which show the 10-Hz splitting of adjacent vinyl protons (4-H and 5-H), also present in **2***d* but not present in the 4-substituted derivatives. Thus, there are no substituents on C-4 and C-5 in **7**, consistent with the location of the nitro group at C-2. Further confirmation is provided by the downfield shift of the adjacent methine proton (1-H). In the series of compounds in which C-2 is not substituted, this proton is consistently close to 5.6 ppm. Hence **7** has the 3-methoxy-6-methyl-2,6-dinitrocyclohexa-2,4-dienyl acetate structure. The ring protons of **7** are readily assigned since the 10-Hz coupling identifies the 4,5-vinylic pair and the 2-Hz splitting present in 1-H is also present in 5-H. In the ^{13}C nmr spectrum of the major isomer, C-1 (70.4 ppm), C-3 (155.9 ppm), and C-6 (88.9 ppm) have the chemical shifts and presence or absence of proton coupling appropriate for their substitution patterns. The C-2 signal (123.7 ppm) is readily identified as the remaining substituted vinyl carbon. The signals of the unsubstituted vinyl carbons C-4 (117.2 ppm) and C-5 (138.3 ppm) are assigned on the basis that the C-5 carbon is downfield, as in **2***d*. The nitro group conjugated with the diene system results in an additional downfield shift (9 ppm) of C-5,

Can. J. Chem. Downloaded from www.nrcresearchpress.com by 72.64.146.136 on 09/07/12
For personal use only.

whereas C-4 is moved upfield (5 ppm). The minor isomer has ^1H and ^{13}C nmr spectra that are closely similar to those of the major isomer: they are diastereomers. *Syn* 1,2 addition of acetyl nitrate appears to be preferred over *anti* addition (1,2) and thus the major isomer (the only isomer obtained in acetic anhydride) is assigned as the (*Z*) isomer and the minor isomer is (*E*)-**7**. The dienes **2***a*, **2***b*, and **2***c*, of which only one diastereoisomer was obtained, are assigned the (*Z*) configuration.

Diene **13** was characterized on the basis of its ^1H nmr spectrum. The cyclohexadienyl cation formed by attack by nitronium ion *ipso* to the methyl group can lead to three possible regioisomeric adducts **13***x*, **13***y*, and **13***z*. Structures 13*x* and

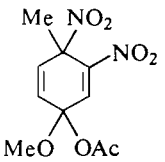

13*x*

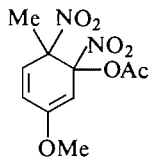

13*y*

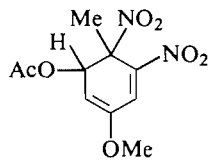

13*z*

13*y* have adjacent vinylic protons and their ^1H spectrum would exhibit a 10-Hz coupling that is not present in the spectrum of **13**. Thus **13** has the structure **13***z*. The 6.5-Hz coupling between protons at 5.32 and 5.58 ppm indicates that these are protons 2 and 1 with the 5.32-ppm assignment being confirmed as 2-H by the 1.5-Hz 2,4-coupling. The 1-H signal is at the 5.6-ppm position, characteristic of the 1-protons in dienes **2***a*, **2***b*, **2***c*, and **2***d*, which have the identical substitution pattern at each of C-2, C-3, and C-6. The 4-H is shifted downfield, as compared with the 4-H proton of **2***d*, by the vinylic nitro substituent.

Dienone **3***a* was characterized by its ^1H nmr and ^{13}C nmr spectra. The spectra of 4-methyl-4-nitrocyclohexa-2,5-dienone are known (9, 10) and the changes in the spectra of **3***a* are those that would be predicted from the introduction of the 2-chloro substituent. In the ^1H nmr spectrum there are three well-separated signals in the low field vinylic region, two below 7 ppm and one at 6.5 ppm. The lowest field signal (d, J = 2.8 Hz) is assigned to 3-H and the multiplicity can be explained by a four-bond coupling with 5-H at 7.20 ppm. The latter proton is a doublet of a doublet (J = 10.1 and 2.8 Hz) and the larger coupling constant is due to coupling with 6-H at 6.52 ppm. Similarly, in the ^{13}C spectrum, there are two unsubstituted vinyl carbons at ~140 ppm and one at ~130 ppm. Dienone **3***b*, observed by ^1H nmr in the reaction mixture obtained on the nitration of **1***b*, is evidently the bromo analog of **3***a*, as confirmed by its ^1H nmr spectrum.

The nmr spectra of dienone **10***a* exhibit the differences from those of **3***a* appropriate to **10***a* being the 3-chloro derivative of 4-methyl-4-nitrocyclohexa-2,5-dienone. In the ^1H nmr there is just one proton at ~7 ppm and two at ~6.5 ppm (all with the appropriate couplings) and in the ^{13}C nmr there is one unsubstituted carbon at 140 ppm and two at 130 ppm.

It is evident from the empirical formula ($C_{12}H_{15}N_3O_{11}$) of compound **8**, obtained from nitration of **1***c* in the trifluoroacetic anhydride mixtures, that it was formed by the addition of two acetyl nitrate molecules to the substituted anisole. In the ir spectrum there are two strong absorptions (1790 and 1755 cm^{-1}) due to acetate groups. The ^1H and ^{13}C nmr spectra also indicate the presence of the two acetate groups. The peaks at 68.0 and 87.3 ppm in the ^{13}C spectrum have the shifts and proton couplings appropriate to the ring carbons of the CHOAc and $CMeNO_2$ groups, respectively, and are so assigned. These must be the 1- and 6-carbon atoms (following the enumeration of **2***d*).

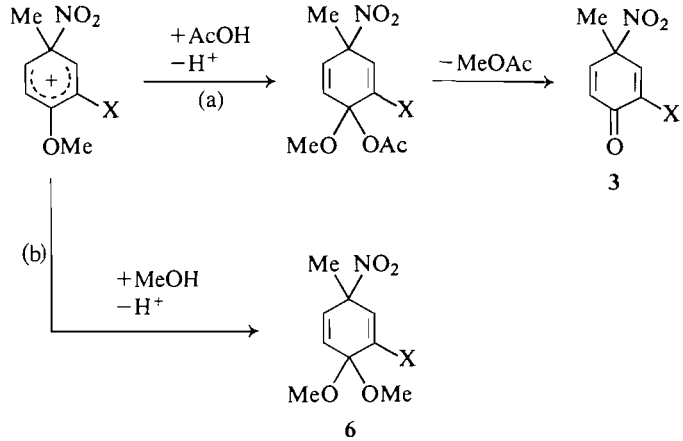

SCHEME 2

The single double bond is substituted at one end. It cannot terminate at C-3 because that carbon has a methoxyl substituent that would send the adjacent unsubstituted vinylic carbon to very high field (90 ppm), whereas the vinylic carbon is at 130 ppm. Thus the double bond must be between C-4 and C-5 and must have the original nitro substituent at C-4, and the second molecule of acetyl nitrate must have been added across the C-2, C-3 positions. The chemical shift of C-2 (87.6 ppm), as well as the directing effect of methoxyl on the addition of nitronium ion, indicates that the C-2 substituent is nitro and the second C-3 substituent is acetate. Thus the compound **8** has the structure 3-acetoxy-3-methoxy-6-methyl-2,4,6-trinitrocyclohexa-4,5-dienyl acetate. The ^1H nmr (experimental section) is readily assigned. The 11.8-Hz coupling identifies the methine protons, and the highest field signal of these is assigned to the proton attached to the same carbon as the nitro group.

Substituent effects

As described above, nitration of **1***a* and **1***b* gave the 1,2 adduct and dienone as well as the nitro substitution product. In the case of **9***a* only dienone and nitro substitution products were obtained. The formation of the dienone likely involves the addition of acetate (as acetic acid) to the 4-position of the *ipso* cation followed by loss of elements of methyl acetate, as shown in path (a) of Scheme 2. Thus the amount of the dienone is indicative of the extent of reaction of the *ipso* cation at the 4 position in competition with reaction at the 2 (or 6) position leading to the 1,2 adduct. Dienone formation also occurred in the course of work-up of some of the reaction mixtures. In such cases this secondary formation of dienone likely involves the re-formation of the *ipso* cation from adduct by protonation at acetate and loss of acetic acid, followed by capture of acetic acid or water at the 4 position. Nitrodienones are labile and readily rearrange to the corresponding *o*-nitrophenols (11), as was explicitly demonstrated in the cases of dienones **3***a* and **10***a*. This reaction accounts for the presence of nitrophenol, after work-up, in several of the product mixtures. The dimethyl ketal of the dienone was also observed in reaction mixtures after work-up. The formation of dimethyl ketal (e.g. **6***a*) presumably involves the capture of *ipso* cation by methanol, as shown in path (b), Scheme 2. The methanol would have been liberated on the formation of the dienone.

Moodie, Schofield, and co-workers have studied the nitration of **1***a* in aqueous sulphuric acid solutions (12). They obtained **4***a* and **5***a*, and detected dienone **3***a* as an intermediate, but did not observe the adduct analogous to **2***a*. Adduct formation may well

Can. J. Chem. Downloaded from www.nrcresearchpress.com by 72.64.146.136 on 09/07/12
For personal use only.

TABLE 3. Product distributions from the nitration of X-4-methoxytoluenes in acetic anhydride: amount of product/mol% with the nitro group at the indicated position

		Observed					Calculated[a]				
Substrate	X	1	2	3	5	6	1	2	3	5	6
1*a*	3-Cl	67	0	—	33	0	46	0	—	54	0
1*b*	3-Br	57	0	—	43	0	46	0	—	54	0
1*c*	3-NO_2	87	0	—	13	0	46	0	—	54	0
9*a*	2-Cl	23	—	26	51	0	13	—	15	72	0
9*c*	2-NO_2	10	—	40	50	0	34	—	40	26	0

[a]Calculated product distributions are based on isomer distributions for nitration of 4-methoxytoluene and the relevant monosubstituted benzenes.[3]

have occurred but, in the strongly acidic solutions, the adduct would rapidly re-form the *ipso* cation and eventually the dienone.

The effect of the third substituent on the position of attack of the nitronium ion on the substituted 4-methoxytoluene is shown by the data listed in Table 3. In 4-methoxytoluene the directing effect of the methoxyl substituent is dominant and substitution occurs only *ortho* and *para* (*ipso* to methyl) to methoxyl. Introduction of a third substituent at the 3 position (enumeration here and in the following discussion is as for toluene) should have no differential electronic effect at the 1 and 5 positions since both of these are *meta* to the 3 position. It is evident from the observation that no attack occurs at the 2 and 6 positions and, in accord with expectation, that the directing effect of the 3-halo substituents is overwhelmed by that of methoxyl. The directing effect of the 3-nitro substituent reinforces that of the methoxyl group. Since the introduction of a 3 substituent should not change the ratio of attack of nitronium ion at the 1 and 5 positions, it follows that this ratio should be the same as in 4-methoxytoluene. In fact, the ratio is increased from 46:54 (4-methoxytoluene) to 57:43 (**1***b*), or 67:33 (**1***a*), or 87:13 (**1***c*). Clearly, factor(s) other than additive electronic effects are involved, such as additional steric hindrance to substitution at the 5 position caused by the buttressing effect of the 3 substituent on the methoxyl group.

In the cases of the substrates that contain the 2-chloro or 2-nitro substituents (**9***a* and **9***c*), the chloro substituent reinforces the directing effect of the methoxyl and, while the directing effect of the nitro is in opposition to that of the methoxyl, it does not result in any attack at the 6 position, *meta* to methoxyl. Calculated and observed ratios of attack by nitronium ion are shown in Table 3.[3] As predicted, the chloro substituent reduces the extent of *ipso* attack, although not to the extent calculated. However, the nitro substituent, which should slightly increase the extent of *ipso* attack, actually leads to a significant reduction. Here again a steric effect may be involved, with steric hindrance at the substituted position being greater than at the unsubstituted 3 position. Directive effects in the substitutions of the chlorocresols **14** and **15** are completely dominated by the hydroxyl group, with attack by nitronium ion limited to positions *ortho* and *para* to hydroxyl. In the hydroxy-substituted *ipso* cation, addition of a nucleophile cannot compete with the facile deprotonation to dienone and no adduct is therefore obtained.

[3]The calculations involve the application of the relative partial rate factors for halo (13) and nitro (14) substituents to the observed ratios of attack in 4-methoxytoluene (1).

TABLE 4. Addition of acetate to X-4-methoxy-1-methyl-1-nitrocyclohexadienyl cations: amount of cation/mol% which undergoes addition of acetate at the indicated position

			Distribution of addition		
Substrate	X	Cation yield[a]	2	4	6
1*a*	3-Cl	67	0	27	73
1*b*	3-Br	57	0	47	53
1*c*	3-NO_2	87	66	0	34
9*a*	2-Cl	23	—	100	0
9*c*	2-NO_2	10	—	0	100

[a]Yield of X-4-methoxy-1-methyl-1-nitrocyclohexadienyl cation = yield of products from this cation.

In the earlier study of the nitration of **1***a*, yields of nitrocresol **5***a* (indicative of the extent of *ipso* attack) approaching 80% were obtained (12). This is somewhat larger than the extent of *ipso* attack observed in acetic anhydride (Table 3). The difference, in so far as it is significant, might arise from a greater selectivity of the nitronium ion for the *ipso* position in the aqueous acid, or from greater trapping efficiency of the carbocation by water than by acetic acid.

Table 4 shows the relative amount of capture of the relevant 4-methoxy *ipso* cation at the 2, 4, and 6 positions. In the cases of the 3 substituted cations (from **1***a*, **1***b*, and **1***c*), capture at the 2 or 6 position dominates over capture at the 4 position. In the parent cation (from 4-methoxytoluene), no capture occurs at the 4 position. No capture occurs at the 4 position in the 3-nitro cation and here again it appears that the extent of 2/6 versus 4 capture is not related in any simple way to the electronic effects of the substituent groups. A striking feature of the results is that selectivity between the 2 and 6 positions as to capture is completely in favour of 6 for the 3-halo substituted cations whereas it is largely in favour of 2 for the 3-nitro cation. Addition of acetic acid at the 2 position would be hindered by the adjacent 3 substituent. This would account for the observations in the cases of the 3-halo derivatives. In the case of the 3-nitro derivative, addition of the acetic acid to the 2 position would lead to a product and a prior transition state in which there is a strongly stabilizing resonance interaction between the methoxy and nitro groups through the 3,4 double bond. This interaction is absent when addition occurs at the 6 position and this factor may be sufficient to override the steric effect.

The minor amount of (*E*)-**7**, which was formed when nitration of **1***c* was carried out in the presence of trifluoroacetic anhydride, presumably arose from epimerization of (*Z*)-**7** by protonation at acetate and reversible dissociation of acetic acid in these, more acidic, conditions. Adduct **8** was likely formed from **2***c* by addition of nitronium acetate across the 3,4 double bond (diene enumeration). The addition of nitronium ion to the 4 position would occur readily since the bond is activated by the methoxyl group at 3.

Experimental

General experimental methods have been described previously (1, 2).

2-Bromo-4-methylphenol, 4-methyl-2-nitrophenol, and 4-methyl-3-nitrophenol were from Aldrich. 2-Chloro-4-methylphenol was prepared by chlorination of *p*-cresol with sulphuryl chloride. 3-Chloro-4-

Can. J. Chem. Downloaded from www.nrcresearchpress.com by 72.64.146.136 on 09/07/12
For personal use only.

Can. J. Chem. Downloaded from www.nrcresearchpress.com by 72.64.146.136 on 09/07/12
For personal use only.

methylphenol was prepared by the rearrangement of 4-chloro-4-methylcyclohexa-2,5-dienone in trifluoromethanesulphonic acid (15). 2-Bromo-4-methyl-6-nitrophenol (**5***b*) was prepared by nitrating 2-bromo-4-methylphenol with nitric acid in methylene chloride and had mp 69°C (lit. (16) mp 69°C); ^{1}H nmr (250 MHz, $CDCl_3$) δ: 2.35 (d, 3, J = 0.78 Hz, CH_3), 7.70 (d, 1, J = 1.00 Hz, 3-*H*), 7.89 (dd, 1, J = 1.00 and 0.78 Hz, 5-*H*), 10.97 (br s, 1, O*H*) ppm; ^{13}C nmr (62.9 MHz, $CDCl_3$) δ_C: 20.0 (*C*H_3), 112.8 (*C*-2), 124.0 (*C*-5), 130.6 (*C*-4), 133.8 (*C*-6), 141.7 (*C*-3), 150.0 (*C*-1) ppm.

Substituted anisoles were prepared by heating under reflux, for 3 h, an aqueous sodium hydroxide solution of the corresponding phenol with dimethyl sulphate. The crude product was purified by distillation. 2-Chloro-4-methylanisole (**1***a*) was obtained in 94% yield and had bp 214–218°C (lit. (17*a*) bp 215–218°C); ir (film): 1255 and 1062 (ArOCH_3) cm^{-1}; ^{1}H nmr (250 MHz, $CDCl_3$) δ: 2.20 (s, 3, CH_3), 3.79 (s, 3, OCH_3), 6.74 (d, 1, J = 8.40 Hz, 6-*H*), 6.95 (dd, 1, J = 8.40 and 2.30 Hz, 5-*H*), 7.11 (d, 1, J = 2.30 Hz, 3-*H*) ppm; ^{13}C nmr (62.9 MHz, $CDCl_3$) δ_C: 20.3 (*C*H_3), 56.3 (O*C*H_3), 112.3 (*C*-6), 122.2 (*C*-2), 128.3 (*C*-5), 130.9 (*C*-3), 131.1 (*C*-4), 153.1 (*C*-1) ppm.

3-Chloro-4-methylanisole (**9***a*) was obtained in 95% yield and had bp 210–213°C (lit. (17*a*) bp 212°C); ir (film): 1240 and 1045 (ArOCH_3) cm^{-1}; ^{1}H nmr (250 MHz, $CDCl_3$) δ: 2.29 (s, 3, CH_3), 3.76 (s, 3, OCH_3), 6.70 (dd, 1, J = 2.50 and 8.40 Hz, 6-*H*), 6.90 (d, 1, J = 2.50 Hz, 2-*H*), 7.99 (d, 1, J = 8.40 Hz, 5-*H*) ppm; ^{13}C nmr (62.9 MHz, $CDCl_3$) δ_C: 18.9 (*C*H_3), 55.5 (O*C*H_3), 112.8 (*C*-6), 114.6 (*C*-2), 127.9 (*C*-4), 131.2 (*C*-5), 134.3 (*C*-3), 158.4 (*C*-1) ppm.

2-Bromo-4-methylanisole (**1***b*) was obtained in 85% yield and had bp 125–126°C, 3 kPa (lit. (18) bp 126–127°C, 3 kPa); ir (film): 1255 and 1050 (ArOCH_3) cm^{-1}; ^{1}H nmr (250 MHz, $CDCl_3$) δ: 2.20 (s, 3, CH_3), 3.79 (s, 3, OCH_3), 6.72 (d, 1, J = 8.30 Hz, 6-*H*), 6.98 (dd, 1, J = 8.30 and 1.50 Hz, 5-*H*), 7.29 (d, 1, J = 1.50 Hz, 3-*H*) ppm; ^{13}C nmr (62.9 MHz, $CDCl_3$) δ_C: 19.9 (*C*H_3), 56.1 (O*C*H_3), 111.1 (*C*-2), 111.7 (*C*-6), 128.7 (*C*-5), 131.2 (*C*-4), 133.5 (*C*-3), 153.6 (*C*-1) ppm.

4-Methyl-2-nitro anisole (**1***c*) was obtained in 76% yield and had bp 272–274°C (lit. (17*b*) bp 274°C); ir (film): 1530 and 1350 (NO_2), 1260 and 1020 (ArOCH_3) cm^{-1}; ^{1}H nmr (250 MHz, $CDCl_3$) δ: 2.33 (s, 3, CH_3), 3.92 (s, 3, OCH_3), 6.98 (d, 1, J = 8.55 Hz, 6-*H*), 7.34 (dd, 1, J = 8.55 and 2.10 Hz, 5-*H*), 7.64 (d, 1, J = 2.10 Hz, 3-*H*) ppm; ^{13}C nmr (62.9 MHz, $CDCl_3$) δ_C: 19.8 (*C*H_3), 56.3 (O*C*H_3), 113.3 (*C*-6), 125.4 (*C*-3), 129.9 (*C*-4), 134.6 (*C*-5), 139.0 (*C*-2), 150.7 (*C*-1) ppm.

4-Methyl-3-nitroanisole (**9***c*) was obtained in 76% yield and had bp 263–269°C (lit. (17*b*) bp 266–267°C); ir (film): 1527 and 1345 (NO_2), 1250 and 1035 (ArOCH_3) cm^{-1}; ^{1}H nmr (250 MHz, $CDCl_3$) δ: 2.21 (s, 3, CH_3), 3.79 (s, 3, OCH_3), 6.72 (d, 1, J = 8.35 Hz, 5-*H*), 6.98 (dd, J = 8.35 and 1.40 Hz, 6-*H*), 7.30 (d, 1, J = 1.40 Hz, 2-*H*) ppm; ^{13}C nmr (62.9 MHz, $CDCl_3$) δ_C: 19.3 (*C*H_3), 55.5 (O*C*H_3), 108.9 (*C*-2), 119.6 (*C*-6), 125.2 (*C*-4), 133.2 (*C*-5), 149.2 (*C*-3), 157.9 (*C*-1) ppm.

2-Bromo-4-methyl-6-nitroanisole (**4***b*) was obtained in 87% yield and had mp 45°C; ^{1}H nmr (250 MHz, $CDCl_3$) δ: 2.37 (d, 3, J = 0.54 Hz, CH_3), 3.98 (s, 3, OCH_3), 7.52 (dd, 1, J = 0.55 and 2.05 Hz, 3-*H*, or 5-*H*), 7.60 (d, 1, J = 2.05 Hz, 5-*H* or 3-*H*) ppm; ^{13}C nmr (62.9 MHz, $CDCl_3$) δ_C: 20.3 (*C*H_3), 62.5 (O*C*H_3), 119.2 (*C*-2), 124.5 (*C*-5), 135.6 (*C*-4), 138.1 (*C*-3), 144.9 (*C*-6), 148.5 (*C*-1) ppm.

*Nitration of 2-chloro-4-methylanisole (1*a*)*

Anisole **1***a* (7.8 g, 0.05 mol) was added, over 2 min, to a nitrating mixture prepared from nitric acid (6.3 g, 0.1 mol) and acetic anhydride (25.5 g, 0.25 mol) at −40°C. The nitrating solution had been mixed at −78°C and warmed to 0°C before being brought to −40°C. After stirring the reaction mixture for 1 h at −40°C it was cooled to −78°C. At this stage the ^{1}H nmr spectrum showed that the composition was diene **2***a* (49%), dienone **3***a* (18%), and 2-chloro-4-methyl-6-nitroanisole (**4***a*) (33%). The mixture was poured into ether (500 cm^3) at −78°C. Ammonium hydroxide (75 cm^3, 1.1 mol) was slowly added to this mixture and stirring was continued for 1 h. The ether layer was separated and the residue was dissolved in water (200 cm^3) and extracted with ether (2 × 100 cm^3). The combined ether solution was washed with water (4 × 150 cm^3), dried, and concentrated on the rotovapor at 15°C to yield a heterogeneous mixture. Crude **2***a* (5.2 g) was obtained on filtration. Removal of ether from the filtrate gave a yellow oil (6 g). The ^{1}H nmr spectrum of this oil indicated the presence of unreacted **1***a* (10.5%), **2***a* (4%), **4***a* (56.5%), 2-chloro-4-methyl-6-nitrophenol (**5***a*) (22.5%), and 2-chloro-4-methyl-6-nitrocyclohexadienone dimethyl ketal (**6***a*) (5.5%). Pure diene **2***a* was obtained as white crystals after recrystallization from ether – petroleum ether mixture at −20°C. It had mp 82°C; ir (KBr): 1735 and 1230 (O$COCH_3$), 1540 and 1360 (NO_2), 1235 (OCH_3), 665 (C-Cl) cm^{-1}; uv (CH_2Cl_2): 275.6 nm (ε = 124 m^2 mol^{-1}); ^{1}H nmr (250 MHz, $CDCl_3$): Table 1; ^{13}C nmr ($CDCl_3$, 62.9 MHz): Table 2. *Anal.* calcd. for $C_{10}H_{12}NO_5Cl$: C 45.90, H 4.62, N 5.35; found: C 45.70, H 4.55, N 5.22. The nitroanisole **4***a* and nitrocresol **5***a* were isolated from further reactions of diene **2***a* (19) and had ^{1}H nmr identical with literature values (12). Ketal **6***a* was also isolated from further reactions of **2***a* and characterized (19).

*Nitration of 2-bromo-4-methylanisole (1*b*)*

Anisole **1***b* (8 g, 0.05 mol) was added over 2 min to a nitrating mixture prepared from nitric acid (7.56 g, 0.12 mol) and acetic anhydride (20.4 g, 0.2 mol) at −40°C. The ^{1}H nmr spectrum of the reaction mixture indicated the presence of diene **2***b* (30%), dienone **3***b* (27%), and **4***b* (43%). The mixture was stirred for 40 min, cooled to −78°C, and poured into ether (450 cm^3) at −78°C. The ^{1}H nmr spectrum of the crude mixture (8.6 g) after low temperature work-up with NH_4OH showed **2***b* (38%), **4***b* (46%), and 2-bromo-4-methyl-6-nitrophenol (**5***b*) (16%). Crystallization of the mixture from ether – petroleum ether mixture yielded pure **2***b* (1.05 g) as pale yellow crystals, mp 85°C; ir (KBr): 1749 (O$COCH_3$), 1550 and 1320 (NO_2) cm^{-1}; uv (CH_2Cl_2): 280.5 nm (ε = 232 m^2 mol^{-1}), 235.6 nm (ε = 288 m^2 mol^{-1}); ^{1}H nmr (250 MHz, $CDCl_3$): Table 1; ^{13}C nmr ($CDCl_3$, 62.9 MHz): Table 2. *Anal.* calcd. for $C_{10}H_{12}NO_5Br$: C 39.23, H 3.95, N 4.57; found: C 39.20, H 3.70, N 4.69. Dienone **3***b* was not isolated but it was readily identified by comparison of its ^{1}H nmr spectrum with that of **3***a*, its chloro analog. The identities of **4***b* and **5***b* were confirmed by comparison of their ^{1}H nmr spectra with the spectra of the authentic compounds (above).

*Nitration of 4-methyl-2-nitroanisole (1*c*)*

Anisole **1***c* (8.35 g, 0.05 mol) was added dropwise over 2 min to a nitrating mixture prepared from nitric acid (9.45 g, 0.15 mol) and acetic anhydride (51 g, 0.5 mol), at −40°C. The reaction mixture was warmed to 0°C in an ice bath and stirred for 1 h. After this time the reaction was complete and **2***c* (30%), **7** (57%), and **4***c* (13%) had been formed. The mixture was poured into cold ether (500 cm^3) at −78°C and the precipitate that formed was filtered off in a jacketed filtering funnel (−78°C). The residue was dissolved in CH_2Cl_2 (500 cm^3) and washed with 10% aqueous $NaHCO_3$ (3 × 150 cm^3). This solution was dried and evaporated to dryness. The residue, on crystallization from ether – petroleum ether mixture at −20°C, yielded pure diene **7** (3.5 g), mp 112–114°C; uv (CH_2Cl_2): 335.6 nm (ε = 812 m^2 mol^{-1}), 238.9 nm (ε = 239 m^2 mol^{-1}); ir (KBr): 1755 (O$COCH_3$), 1586 and 1565 (NO_2), 1210 (OCH_3) cm^{-1}; ^{1}H nmr (250 MHz, $CDCl_3$): Table 1; ^{13}C nmr ($CDCl_3$, 62.9 MHz): Table 2. *Anal.* calcd. for $C_{10}H_{12}N_2O_7$: C 44.12, H 4.44, N 10.29; found: C 44.11, H 4.10, N 10.02.

The original filtrate was placed in a 2-dm^3 three-necked round bottom flask, fitted with a mechanical stirrer and cooled to −78°C. Ammonium hydroxide (200 cm^3, 3 mol) was slowly added and the mixture was stirred for 2 h. The organic layer was decanted, washed with water (3 × 250 cm^3), dried, and evaporated to dryness to yield a yellow residue (2.05 g). The ^{1}H nmr spectrum of this mixture indicated the presence of diene **2***c* (75%) and anisole **4***c* (25%). Crystallization from ether – petroleum ether mixture gave pure **2***c* (550 mg), mp 99–100°C; uv (CH_2Cl_2): 248.9 nm (ε = 204 m^2 mol^{-1}); ir (KBr): 1745 and 1010 (O$COCH_3$), 1545 and 1360 (NO_2), 1060 (OCH_3) cm^{-1}; ^{1}H nmr (250 MHz, $CDCl_3$): Table 1; ^{13}C nmr ($CDCl_3$, 62.9 MHz): Table 2. *Anal.* calcd. for $C_{10}H_{12}N_2O_7$: C 44.12, H 4.44, N 10.29; found: C 44.02, H 4.29, N 10.18.

Can. J. Chem. Downloaded from www.nrcresearchpress.com by 72.64.146.136 on 09/07/12
For personal use only.

The ammonia solution, after separation of the organic layer, was diluted with water (250 cm^3) and extracted with ether (2 × 250 cm^3). The ether layer was washed with saturated brine (2 × 200 cm^3), dried, and evaporated to dryness to yield a brown residue (3 g). The ^1H nmr spectrum of this mixture showed **4***c* (75%) and **2***c* (25%). Anisole **4***c* was obtained after chromatography on silica and recrystallization, mp 122°C (lit. (17*c*) mp 122°C); ^1H nmr (250 MHz, $CDCl_3$) δ: 2.48 (s, 3, CH_3), 4.04 (s, 3, OCH_3), 7.85 (s, 2, 3-*H* and 5-*H*) ppm; ^{13}C nmr (62.9 MHz, $CDCl_3$) δ_C: 20.3 (CH_3), 64.5 (OCH_3), 129.2 (*C*-3 and *C*-5), 134.9 (*C*-4), 144.8 (*C*-2 and *C*-6), 145.1 (*C*-1) ppm.

Nitration of **1***c* was also carried out in the presence of trifluoroacetic anhydride. A mixture of **1***c* (4.4 g, 0.026 mol) and acetic anhydride (7 g, 0.068 mol) was added to a nitrating mixture prepared from nitric acid (8.8 g, 0.14 mol), acetic anhydride (35 g, 0.34 mol), and trifluoroacetic anhydride (5.88 g, 0.028 mol), at −20°C. The mixture was stirred for 30 min, cooled to −78°C, and poured into a mixture of aqueous sodium bicarbonate (160 g, 2 mol, in 750 cm^3) and ether (1 dm^3). The mixture was stirred for 2 h and the ether layer was separated. The aqueous layer was extracted with ether (2 × 500 cm^3). The combined ether solution was washed with saturated brine (4 × 500 cm^3), dried, and then evaporated to dryness on the rotovapor, at ambient temperature. The ^1H nmr of the yellow residue (5.5 g) was closely similar to that of the reaction mixture prior to work-up and indicated the formation of **2***c* (25%), (*Z*)-**7** (53%), (*E*)-**7** (5%), 1-methoxy-4-methyl-2,4,6-trinitrocyclohex-2-enyl-1,5-diacetate (**8**) (5%), and **4***c* (12%). The residue was triturated with ether (250 cm^3) and the residue (1.1 g) then obtained on filtration contained (*Z*)-**7** (80%) and (*E*)-**7** (20%). Fractional crystallization from CH_2Cl_2 at −20°C gave (*E*)-**7** (88 mg) as the first crop, a mixture of (*E*)-**7** and (*Z*)-**7** (18:82, respectively) in the second crop (200 mg), and pure (*Z*)-**7** (200 mg) in the third crop.

Crystallization from the filtrate of the trituration gave pure (*Z*)-**7** (500 mg). On further crystallization from the mother liquor only mixtures were obtained, and the residue after the separation of (*Z*)-**7** was therefore chromatographed on a silica gel column (125 g) at −40°C, using ether – petroleum ether mixtures as eluents. 1-Methoxy-4-methyl-2,4,6-trinitrocyclohex-2-enyl-1,5-diacetate (**8**) was obtained in the 10% ether fraction, **4***c* was obtained in the 20 and 25% ether fractions, and **2***c* was obtained in the 30% ether fractions. Later fractions contained mainly mixtures of **4***c* and 4-methyl-2,4-dinitrocyclohexa-2,5-dienone dimethyl ketal (**6***c*), which could not be separated.

All dienes were purified by recrystallization from ether – petroleum ether mixtures at −20°C. Diene (*E*)-**7** had mp 138°C; ir (KBr): 1755 ($OCOCH_3$), 1586 and 1565 (NO_2), 1210 (OCH_3) cm^{-1}; uv (CH_2Cl_2): 336.4 nm (ε = 800 m^2 mol^{-1}); ^1H nmr (250 MHz, $CDCl_3$): Table 1; ^{13}C nmr ($CDCl_3$, 62.9 MHz): Table 2. *Anal.* calcd. for $C_{10}H_{12}N_2O_7$: C 44.12, H 4.44, N 10.29; found: C 43.93, H 4.23, N 10.09. Compound **8** had mp 134°C; uv (CH_2Cl_2): 244.3 nm (ε = 257 m^2 mol^{-1}); ir (KBr): 1790 and 1755 ($OCOCH_3$), 1545 and 1560 (NO_2), 1190 (OCH_3) cm^{-1}; ^1H nmr (250 MHz, $CDCl_3$) δ: 1.88 (s, 3, CH_3), 2.07 (s, 3, 5-$OCOCH_3$), 2.21 (s, 3, 1-$OCOCH_3$), 3.66 (s, 3, OCH_3), 5.72 (d, 1, *J* = 11.8 Hz, 6-*H*), 6.33 (d, 1, *J* = 11.8 Hz, 5-*H*), 6.96 (s, 1, 3-*H*) ppm; ^{13}C nmr (62.9 MHz, $CDCl_3$) δ_C: 20.1 ($OCOCH_3$), 20.9 ($OCOCH_3$), 22.2 (CH_3), 53.4 (OCH_3), 68.0 (*C*-5), 87.3 (*C*-4), 87.6 (*C*-6), 95.1 (*C*-1), 130.1 (*C*-3), 148.5 (*C*-2), 168.1 ($OCOCH_3$), 168.7 ($OCOCH_3$) ppm. *Anal.* calcd. for $C_{12}H_{15}N_3O_{11}$: C 38.20, H 4.00, N 11.10; found: C 37.95, H 3.87, N 10.70.

*Nitration of 3-chloro-4-methylanisole (**9**a)*

Anisole **9***a* (78 mg, 0.5 mmol) was added to a nitrating mixture prepared from nitric acid (63 mg, 1 mmol) and acetic anhydride (510 mg, 5 mmol), at −45°C. After 3 min at −45°C an ^1H nmr sample was withdrawn and the reaction was followed by ^1H nmr while the sample remained in the probe at −40°C. After 35 min the reaction was complete and there was present **10***a* (23%), **11***a* (δ: 6.96 (d, *J* = 9 Hz) and 7.30 (d, *J* = 9 Hz) ppm) (26%), and **12***a* (δ: 7.14 (s) and 7.68 (s) ppm) (51%). Similar product mixtures were obtained from other nitrating solutions prepared from (*a*) a 1.5 mol proportion of nitric acid and a 10 mol proportion of acetic anhydride at −40°C and (*b*) a 2 mol proportion of nitric acid, a 10 mol proportion of acetic anhydride, together with a 1 mol proportion of trifluoroacetic anhydride at −60°C.

*Nitration of 4-methyl-3-nitroanisole (**9**c)*

Anisole **9***c* (1.17 g, 7 mmol) was added to a nitrating mixture prepared from nitric acid (2.21 g, 35 mmol), acetic anhydride (7 g, 70 mmol), and trifluoroacetic anhydride (2.94 g, 14 mmol), at −40°C. The resulting slurry was stirred for 30 min at −40°C and then poured into ether at −78°C. The ^1H nmr spectrum of the red solid residue (1.38 g) obtained after work-up with aqueous ammonia showed the presence of **11***c* (71%) and **12***c* (29%). Crystallization of the residue from ether – petroleum ether gave **11***c* (300 mg), which on recrystallization had mp 132°C (lit. (20) mp 132–133°C); ^1H nmr (250 MHz, $CDCl_3$) δ: 2.40 (s, 3, CH_3), 3.97 (s, 3, OCH_3), 7.18 (d, 1, *J* = 8.8 Hz, 6-*H*), 7.43 (d, 1, *J* = 8.8 Hz, 5-*H*) ppm; ^{13}C nmr (62.9 MHz, $CDCl_3$) δ_C: 17.2 (CH_3), 57.1 (OCH_3), 115.9 (*C*-6), 122.6 (*C*-4), 134.5 (*C*-5 and *C*-2), 143.3 (*C*-3), 150.0 (*C*-1) ppm.

The remaining residue was separated by chromatography on silica. Anisole **11***c* was eluted with 10% ether – 90% petroleum ether, and **12***c* with 60% ether – 40% petroleum ether. After crystallization **12***c* was obtained as pale yellow flakes, mp 122°C (lit. (20) mp 123–124°C); ^1H nmr (250 MHz, $CDCl_3$) δ: 2.58 (s, 3, CH_3), 4.03 (s, 3, OCH_3), 7.68 (s, 1, 6-*H*), 7.79 (s, 1, 3-*H*) ppm; ^{13}C nmr (62.9 MHz, $CDCl_3$) δ_C: 19.4 (CH_3), 57.3 (OCH_3), 110.2 (*C*-6), 125.8 (*C*-4), 129.3 (*C*-3), 141.7 (*C*-2), 151.2 (*C*-1), 161.3 (*C*-5) ppm.

Attempts were made to isolate the small amount of 3-methoxy-6-methyl-5,6-dinitrocyclohexa-2,4-dienyl acetate (**13**), which was also formed on nitration of **9***c*, in addition to **11***c* and **12***c*, and which could be detected by nmr in the reaction mixture before work-up. When the reaction mixture was poured into cold 50% ether – petroleum ether and the precipitated product filtered at −78°C the ^1H nmr spectrum of the precipitate indicated the presence of aromatic products only. The ^1H nmr spectrum of the residue, obtained after removing the solvent from the filtrate at −40°C, showed that it was a mixture of **11***c* and **12***c*, together with **13** (10%) and some 4-methyl-3,4-dinitrocyclohexa-2,5-dienone (**10***c*). The peaks corresponding to the **13** and **10***c* disappeared on raising the temperature of the probe to −30°C. Several attempts to isolate the diene after low temperature work-up of the filtrate with aqueous ammonia were not successful.

Diene **13** had ^1H nmr (90 MHz, Ac_2O, lock 2.15 ppm, −45°C) δ: 5.32 (dd, 1, 2-*H*), 5.58 (d, 1, 1-*H*), 7.13 (d, 1, 4-*H*) ppm, $J_{1,2}$ = 6 Hz, $J_{2,4}$ = 1.5 Hz. Dienone **10***c* had nmr (90 MHz, Ac_2O, lock 2.15 ppm, −45°C) δ: 6.50 (dd, 1, 6-*H*), 7.07 (d, 1, 5-*H*), 7.42 (d, 1, 2-*H*) ppm, $J_{2,6}$ = 2 Hz, $J_{5,6}$ = 10 Hz.

*Nitration of 2-chloro-4-methylphenol (**14**)*

Cresol **14** (1.42 g, 0.01 mol) was added to a nitrating mixture prepared from nitric acid (1.89 g, 0.03 mol) and acetic anhydride, at −45°C. The solution was stirred for 10 min, then cooled to −78°C. The ^1H nmr spectrum at this stage indicated the presence of **3***a* (42%) and **5***a* (δ: 7.50 (d, *J* = 2 Hz) and 7.76 (d, *J* = 2 Hz) ppm) (58%). The solution was poured into ether (200 cm^3) at −78°C and neutralized with excess aqueous ammonia (35 cm^3, 0.5 mol). After stirring the mixture for 1 h at −78°C, the ether layer was separated and the residue was diluted with water (100 cm^3) and extracted with cold ether (2 × 50 cm^3). The combined ether solution was washed with water (4 × 75 cm^3), dried, and filtered through a jacketed filtering funnel cooled to −78°C. The ether was removed from the filtrate at −40°C. The ^1H nmr spectrum of the remaining residue indicated the presence of **3***a* (88%) and **5***a* (12%). The mixture was dissolved in 80% ether – petroleum ether (30:60) (250 cm^3) and filtered through basic alumina (150 g) contained in a jacketed filtering funnel cooled to −78°C. The alumina was washed with 80% ether – petroleum ether (250 cm^3) and then with ether (250 cm^3). After evaporation of the solvent at −50°C from the filtrate and the washings, pure **3***a* was obtained. It had ^1H nmr (250 MHz, $CDCl_3$, −40°C) δ: 2.04 (s, 3, CH_3), 6.52 (d, 1, *J* = 10.12 Hz, 6-*H*), 7.20 (dd, 1, *J* = 10.12 and 2.80 Hz, 5-*H*), 7.34 (d, 1, *J* = 2.80 Hz, 3-*H*) ppm; ^{13}C nmr (62.9 MHz, $CDCl_3$, −40°C) δ_C:

25.1 (CH_3), 84.6 (C-4), 128.4 (C-6), 137.5 (C-3), 142.0 (C-5), 142.2 (C-2), 198.5 (C-1) ppm.

*Nitration of 3-chloro-4-methylphenol (**15**)*

Cresol **15** (490 mg, 3.4 mmol) was added dropwise over a period of 5 min to a mixture of nitric acid (270 mg, 4.28 mmol) and $CHCl_3$ (4 cm^3) at −60°C. The mixture was stirred for 30 min, during which time the temperature was allowed to rise to −40°C. The ^1H nmr spectrum of the mixture at this stage indicated the composition as **10***a* (22%), **16** (25%), and **17** (53%). The solution was cooled to −78°C and transferred onto a column of basic alumina (30 g), cooled to −78°C, and kept under argon. The column was eluted with ether (50 cm^3) followed by CH_2Cl_2 (200 cm^3). The eluents were collected in a receiving flask cooled to −78°C, and evaporated at −50°C to yield pure **10***a* (70 mg) as a colourless liquid; ^1H nmr (250 MHz, $CDCl_3$, −50°C) δ: 2.01 (s, 1, CH_3), 6.50 (dd, 1, J = 9.95 and 1.47 Hz, 6-*H*), 6.69 (d, 1, J = 1.47 Hz, 2-*H*), 6.95 (d, 1, J = 9.95 Hz, 5-*H*) ppm; ^{13}C nmr (62.9 MHz, $CDCl_3$, −50°C) δ_C: 22.3 (CH_3), 87.4 (C-4), 129.1 (C-2), 130.0 (C-6), 141.4 (C-5), 148.0 (C-3), 181.7 (C-1) ppm. The dienone decomposed to an equimolar mixture of cresols **16** and **17** at 0°C, over a period of 10 min. The alumina, after isolation of the dienone, was stirred with concentrated HCl in methanol (1:9 v/v, 200 cm^3). The filtrate was evaporated to dryness to yield a mixture of **15**, **16**, and **17**. The mixture was separated by chromatography on silica (80 g) using ether – petroleum ether mixtures as eluents. The fractions eluted with 5–10% ether solutions contained pure **17**. Mixtures of **17** and **15** were obtained on elution with 20% ether solutions. Pure **15** was eluted in the later 20% ether fractions. Elution with 40–80% ether solutions gave pure **16**. Cresol **17** crystallized from ether – petroleum ether mixtures as yellow flakes, mp 69–70°C; ir (KBr): 3500 (OH), 1569 and 1320 (NO_2) cm^{-1}; uv (CH_2Cl_2): 361 nm (ε = 580 m^2 mol^{-1}), 291 nm (ε = 1167 m^2 mol^{-1}); ^1H (250 MHz, $CDCl_3$) δ: 2.35 (s, 3, CH_3), 7.18 (s, 1, 6-*H*), 7.97 (s, 1, 3-*H*), 10.43 (s, 1, exchanges with D_2O, O*H*) ppm; ^{13}C nmr (62.9 MHz, $CDCl_3$) δ_C: 19.1 (CH_3), 120.1 (C-6), 120.4 (C-4), 126.0 (C-3), 128.8 (C-2), 144.2 (C-5), 153.4 (C-1) ppm; ms (70 eV, EI), *m/e* (relative intensity): 189 (16), 187.003 (48, $M_r(C_7H_6NO_3Cl)$ = 187.003), 157 (20), 129 (23), 90 (16), 77 (100). Cresol **16** was obtained as brown crystals, mp 68.5°C; ir (KBr): 3360 (OH), 1530 and 1390 (NO_2); uv (CH_2Cl_2): 365 nm (ε = 219 m^2 mol^{-1}), 286 nm (ε = 403 m^2 mol^{-1}); ^1H nmr (250 MHz, $CDCl_3$) δ: 2.37 (s, 3, CH_3), 6.97 (d, 1, J = 8.70 Hz, 6-*H*), 7.33 (d, 1, J = 8.70 Hz, 5-*H*), 8.80 (bs 1, O*H*) ppm; ^{13}C nmr (62.9 MHz, $CDCl_3$) δ_C: 18.9 (CH_3), 116.1 (C-6), 126.7 (C-3), 129.5 (C-4), 134.7 (C-2 and C-5), 151.0 (C-1) ppm; ms (70 eV), *m/e* (relative intensity): 189 (14), 187.003 (41, $M_r(C_7H_6NO_3Cl)$ = 187.003), 157 (17), 105 (13), 93 (10), 77 (100). The composition of the reaction mixture prior to chromatography was determined from a separate reaction using cresol **15** (71 mg, 0.5 mmol) and nitric acid (47.5 mg, 0.75 mmol) in $CDCl_3$ (0.5 cm^3). The ^1H nmr spectrum of the reaction mixture indicated the presence of dienone **10***a* (39%), cresol **16** (32%), and cresol **17** (29%).

Acknowledgements

We thank the Natural Sciences and Engineering Research Council of Canada for financial support, and the University of Victoria for the award of a Fellowship (to S.R.M.).

1. A. Fischer, D. L. Fyles, G. N. Henderson, and S. Ray-Mahasay. Can. J. Chem. **64**, 1764 (1986).
2. G. W. Bushnell, A. Fischer, G. N. Henderson, and S. Ray-Mahasay. Can. J. Chem. **64**, 2382 (1986).
3. A. Fischer and R. Roderer. Can. J. Chem. **54**, 3978 (1976).
4. D. J. Blackstock, J. R. Cretney, A. Fischer, M. P. Hartshorn, K. E. Richards, J. Vaughan, and G. J. Wright. Tetrahedron Lett. 2793 (1970).
5. A. Fischer and R. Roderer. Can. J. Chem. **54**, 423 (1976).
6. A. Fischer, G. N. Henderson, and R. J. Thompson. Aust. J. Chem. **31**, 1241 (1978).
7. A. Fischer and G. J. Wright. Aust. J. Chem. **27**, 217 (1974).
8. D. W. Brown. J. Chem. Educ. **62**, 209 (1985).
9. C. E. Barnes, K. S. Feldman, M. W. Johnson, H. W. H. Lee, and P. C. Myhre. J. Org. Chem. **44**, 3925 (1979).
10. S. Sankararaman. Ph.D. Dissertation, University of Victoria, Victoria, B.C., 1985.
11. C. E. Barnes and P. C. Myhre. J. Am. Chem. Soc. **100**, 973 (1978).
12. C. Bloomfield, A. K. Manglik, R. B. Moodie, K. Schofield, and G. D. Tobin. J. Chem. Soc. Perkin Trans. 2, 75 (1983).
13. J. D. Roberts, J. K. Sanford, F. L. J. Sixma, H. Cerfontain, and R. Zagt. J. Am. Chem. Soc. **76**, 4525 (1954).
14. A. D. Mesure and J. G. Tillett. J. Chem. Soc. (B), 669 (1966).
15. A. Fischer and G. N. Henderson. J. Chem. Soc. Chem. Commun. 279 (1979).
16. L. C. Raiford. J. Am. Chem. Soc. **41**, 2072 (1919).
17. J. Buckingham (*Editor*). Dictionary of organic compounds. 5th ed. Chapman and Hall, London, 1982. (*a*) Vol. 1. p. 1150; (*b*) Vol. 4. p. 3951; (*c*) Vol. 4. p. 3832.
18. H. E. Ungnade and E. F. Orwoll. J. Am. Chem. Soc. **65**, 1736 (1943).
19. S. RayMahasay. Ph.D. Dissertation, University of Victoria, Victoria, B.C., 1984.
20. H. E. Dadswell and J. Kenner. J. Chem. Soc. 580 (1927).

Can. J. Chem. Downloaded from www.nrcresearchpress.com by 72.64.146.136 on 09/07/12
For personal use only.

Chelated compounds and derivative of β-alkoxycarbonylalkyltin chlorides — 5-arylazo-8-quinolinolates, alizarinates, and thiocyanate: preparation and spectroscopic studies

BARUN KANTI DEB AND AMIYA KANTI GHOSH[1]

Department of Chemistry, University of North Bengal, Darjeeling – 734 430, India

Received August 29, 1986

BARUN KANTI DEB and AMIYA KANTI GHOSH. Can. J. Chem. **65**, 1241 (1987).

Complex formation with chelating ligands like 5-phenylazo-8-quinolinol, 5-(2[I]-carboxyphenylazo)-8-quinolinol, 1,2-dihydroxyanthraquinone (i.e., alizarin), and 1-nitroso-2-naphthol is due to nucleophilic attack on tin of the β-alkoxycarbonylalkyltin chlorides (a unique class of PVC stabilizer intermediates) with the subsequent elimination of hydrogen chloride. A number of complexes of the types R_2SnL_2, $RSnL_2Cl$, R_2SnLCl, $R_2Sn(L^IH^I)_2$, R_2SnL^{II}, and $RSnL^{II}Cl$ (where R = $CH_3OCOCH_2CH_2$—, $C_4H_9OCOCH_2CH_2$—, and $CH_3OCOCH(CH_3)CH_2$—; LH = 5-phenylazo-8-quinolinol, 1-nitroso-2-naphthol; L^IHH^I = 5-(2[I]-carboxyphenylazo)-8-quinolinol; and $L^{II}H_2$ = 1,2-dihydroxyanthraquinone) and a thiocyanate derivative viz. $(CH_3OCOCH_2CH_2)_2Sn(SCN)_2$ have been prepared. 5-Arylazo-8-quinolinols exhibit azo–hydrazone tautomeric equilibria but their complexes exist only in the azo form. β-Alkoxycarbonylethyltin alizarinates are somewhat different from other complexes. In these complexes two hydroxyl groups of alizarin have been utilised in complex formation, moreover, one of the two carbonyl groups of alizarin also remains involved in coordination to tin. In $(CH_3OCOCH_2CH_2)_2Sn(SCN)_2$, the thiocyanate group is possibly linked to tin atom through nitrogen. All the complexes and the thiocyanate derivative have been characterised by elemental analyses, electronic, ir, and ^1H nmr spectra. Possible structural features of the compounds are discussed.

BARUN KANTI DEB et AMIYA KANTI GHOSH. Can. J. Chem. **65**, 1241 (1987).

Les chlorures d'alkoxy-3 alkyl étain (une classe unique d'intermédiaires dans la préparation de stabilisants du PVC) forment des complexes avec les ligands chélatants comme le phénylazo-5 quinolinol-8, le (carboxy-2[I] phénylazo)-5 quinolinol-8, la dihydroxy-1,2 anthraquinone (c'est à dire l'alizarine) et le nitroso-1 naphtol-2; cette réaction implique une attaque nucléophile sur l'étain qui est suivie d'une élimination de chlorure d'hydrogène. On a préparé un certain nombre de complexes des types R_2SnL_2, $RSnL_2Cl$, R_2SnLCl, $R_2Sn(L^IH^I)_2$, R_2SnL^{II} et $RSnL^{II}Cl$ (dans lesquels R = $CH_3OCOCH_2CH_2$—, $C_4H_9OCOCH_2CH_2$— et $CH_3OCOCH(CH_3)CH_2$—; LH = phénylazo-5 quinolinol-8, nitroso-1 naphtol-2; L^IHH^I = (carboxy-2[I] phénylazo)-5 quinolinol et $L^{II}H_2$ = dihydroxy-1,2 anthraquinone) ainsi qu'un dérivé thiocyanate, soit le $(CH_3OCOCH_2CH_2)_2Sn(SCN)_2$. Alors que les arylazo-5 quinolinols-8 sont sujets à l'équilibre tautomère azo/hydrazone, leurs complexes n'existent que sous la forme azo. Les alizarinates d'alkoxycarbonyl-3 éthyl étains diffèrent un peu des autres complexes. Dans ces complexes, les deux groupements hydroxyles de l'alizarine sont utilisés dans la formation du complexe; de plus, l'un des deux groupements carbonyles de l'alizarine demeure impliqué dans la coordination avec l'étain. Dans le $(CH_3OCOCH_2CH_2)_2Sn(SCN)_2$, il est possible que le groupement thiocyanate soit lié à l'atome d'étain par le biais de l'azote. On a caractérisé tous les complexes ainsi que le dérivé thiocyanate par les analyses élémentaires, les spectres électroniques, ir et rmn ^1H. On discute des diverses caractéristiques possibles de ces composés.

[Traduit par la revue]

Introduction

β-Alkoxycarbonylalkyltin chlorides, a class of excellent PVC stabilizer intermediates (1), have aroused considerable interest because of their simple and relatively inexpensive methods of preparations (2–4). The existence of intramolecular carbonyl coordination to tin through their carbonyl functions (2, 5, 6) and the Lewis acidity of these compounds (7–11) have also been reported. Moreover, it has also been established that the reduction of Lewis acidity of the organotin chloride improves the efficiency of a stabilizer viz., the ketopentyl tin compounds, where the keto groups would be free, are more effective in stabilization than the corresponding dialkyl tin derivatives (12).

Although known for a long time as analytical reagents (13–15), literature contains very few reports of isolation and characterisation of organometallic complexes of 5-arylazo-8-quinolinols. Studies on this group of compounds deal with the azo–hydrazone tautomeric equilibria (16–18) and bacteriocidal properties (19, 20). Some of these compounds, especially 5-(2[I]-carboxyphenylazo)-8-quinolinol, are very suitable ligands for the preparation of some unique types of complexes in which the available coordination sites may be bonded to two different ions or groups. Moreover, organotin-5-(2[I]-carboxyphenylazo)-8-quinolinolates can be made water soluble through conversion to their sodium salts by reaction with $NaHCO_3$.

All the above findings have encouraged us to pursue the preparation and characterization of β-alkoxycarbonylalkyltin chelates with 5-phenylazo-8-quinolinol, 5-(2[I]-carboxyphenylazo)-8-quinolinol, 1,2-dihydroxyanthraquinone (i.e., alizarin) or 1-nitroso-2-naphthol as ligands. This paper describes the results of preliminary investigations in this area.

Experimental

All chemicals were of reagent grade and were used without further purification. Solvents used were dried by reflux over appropriate reagents and were distilled before use.

1. Preparation of β-alkoxycarbonylalkyltin chlorides

The compounds used were of the types R_2SnCl_2 and $RSnCl_3$, where R = $CH_3OCOCH_2CH_2$—, $C_4H_9OCOCH_2CH_2$—, and $CH_3OCOCH(CH_3)CH_2$. All these compounds were prepared by reported methods (2–4).

2. Preparation of 5-phenylazo-8-quinolinol (LH) and 5-(2[I]-carboxyphenylazo)-8-quinolinol (LHH^I; where H and H^I refer to the hydroxyl and carboxyl protons, respectively)

The ligands LH and LHH^I were synthesized by literature methods (14).

3. General method of preparation of complexes

All complexes, except the thiocyanate derivative, were prepared

[1]Author to whom correspondence is to be addressed.

Can. J. Chem. Downloaded from www.nrcresearchpress.com by 72.64.146.136 on 09/07/12
For personal use only.

Can. J. Chem. Downloaded from www.nrcresearchpress.com by 72.64.146.136 on 09/07/12
For personal use only.

by reacting stoichiometric quantities of β-alkoxycarbonylalkyltin chlorides and the ligands in appropriate molar ratios. The hydrochloric acid liberated was neutralised with ammonia solution (17 *N*) and the precipitated ammonium chloride was removed by filtration. The filtrate was refluxed, concentrated, and the resulting complexes were isolated and purified by fractional crystallisation (21).

4. Some typical preparations of complexes

(a) $(CH_3OCOCH_2CH_2)_2SnL_2$ (where LH = 5-phenylazo-8-quinolinol)

A mixture of $(CH_3OCOCH_2CH_2)_2SnCl_2$ (1.09 g, 2.99 mmol) and 5-phenylazo-8-quinolinol (1.50 g, 6.02 mmol) in benzene (200 mL) was heated on a water bath for 10 min. A few drops of ammonia solution were added and a sharp change in colour was observed. The resulting ammonium chloride was then filtered. The filtrate was refluxed for 2 h, concentrated, cooled, and petroleum ether (bp 60–80°C) added. The orange solid separated was recrystallised from benzene/petroleum ether (bp 60–80°C) mixture.

(b) $(CH_3OCOCH_2CH_2)_2Sn(L^IH^I)_2$ (where LHH^I = 5-(2^I-carboxyphenylazo)-8-quinolinol)

5-(2^I-Carboxyphenylazo)-8-quinolinol (1.17 g, 3.99 mmol) was soxhlet-extracted in tetrahydrofuran (THF) and then a hot solution of $(CH_3OCOCH_2CH_2)_2SnCl_2$ (0.73 g, 2.01 mmol) in THF and a few drops of ammonia solution were added. The resulting mixture was refluxed for 1 h, filtered, and the filtrate was evaporated to dryness. The residue was then extracted with hot benzene and the benzene extract was concentrated, cooled, and petroleum ether was added. A bright orange solid appeared and was recrystallised from benzene/petroleum ether.

(c) $(CH_3OCOCH_2CH_2)_2SnL^{II}$ (where $L^{II}H_2$ = alizarin)

A solution of alizarin (0.75 g, 3.00 mmol) in hot methanol was added to a stirred solution of $(CH_3OCOCH_2CH_2)_2SnCl_2$ (1.09 g, 2.99 mmol) in hot methanol. The resulting mixture was heated on a water bath, a few drops of ammonia solution were added and then filtered. The filtrate was refluxed for 1 h, concentrated, and cooled. Greenish black fluorescent crystals appeared and were recrystallised from chloroform/methanol.

(d) $(CH_3OCOCH_2CH_2)_2Sn(SCN)_2$

A suspension of potassium thiocyanate (0.60 g, 6.20 mmol) in hot ethanol was added slowly to a stirred solution of $(CH_3OCOCH_2CH_2)_2SnCl_2$ (1.09 g, 2.99 mmol) in hot ethanol. The resulting suspension was stirred for 1 h, filtered, and the filtrate was evaporated to dryness. The resulting white residue was extracted with chloroform and the chloroform extract was concentrated to a minimum volume. The white solid that crystallized overnight was filtered and dried *in vacuo*. The product was recrystallized from methanol.

5. Preparation of Ph_2ShL^{II} (where Ph = C_6H_5, $L^{II}H_2$ = alizarin)

A mixture of triphenyltin hydroxide (prepared from triphenyltin chloride and NaOH in ether/water mixture; 3.53 g, 9.61 mmol) and alizarin (2.35 g, 9.79 mmol) in 400 mL methanol was refluxed for 6 h, cooled, and the resulting solid was filtered off. The solid was treated with hot benzene and the benzene soluble fraction yielded tetraphenyltin (mp 224°C). The filtrate was evaporated to dryness and the residue was extracted with benzene. The benzene extract was concentrated and cooled. The red needles separated were recrystallised from benzene.

6. Reaction of triphenyltin hydroxide and quinalizarin (1,2,5,8-tetrahydroxy anthraquinone)

A solution of triphenyltin hydroxide (3.00 g, 8.17 mmol) and quinalizarin (2.25 g, 8.27 mmol) in 400 mL methanol was refluxed for 6 h and then reduced to dryness under vacuum. The solid obtained was dried *in vacuo* and found to weigh less (4.48 g) than the total weight of the reactants indicating the formation of volatile product due to reaction. The volatile product was identified as benzene by spectrophotometric technique. The solid was washed thoroughly with benzene and the benzene insoluble fraction was crystallized several times with THF/petroleum ether mixture to yield a violet compound which appeared to be polymeric in nature and was infusible up to 360°C. Dearylation of this compound with mercuric chloride showed that it contained two phenyl groups per molecule. Thus the compound yielded stepwise two equivalents of phenylmercuric chloride when refluxed first with one equivalent and then with excess of mercuric chloride. Analytical data of this compound (Table 1) support the composition to be $C_{54}H_{25}O_{18}Sn_2$.

The electronic spectra were recorded on a Beckman DU-2 or a Pye-Unicam SP-300 spectrophotometer using methanol (Uvasol – E. Merck) as the solvent. The ir spectra (KBr pellets) were recorded as Nujol mulls on a Beckman IR-20 spectrophotometer. The ^{1}H nmr spectra were recorded as solutions in $CDCl_3$ on a Varian EM-390 or a Zeol-Japan FT NMR or a Varian A-60 spectrophotometer.

Results and discussion

The analytical and physical data of the complexes are listed in Table 1. The electronic/ir and ^{1}H nmr spectral data are shown in Tables 2 and 3, respectively.

Electronic spectra

In azobenzene and related compounds the band at the longest wavelength is ascribed to an n–π* transition and the other bands are ascribed to π–π* transitions. Substituents like —OH, —COOH, —NH_2, —NMe_2 etc. may produce large bathochromic shift of the π–π* transitions (by extending conjugation) to such an extent that the characteristic n–π* absorption is masked by this strong absorption (22). In the electronic spectrum of 5-phenylazo-8-quinolinol (Table 2), an absorption band at 380 nm and an inflexion at 450 nm indicate the azo–hydrazone tautomerism well known is such systems (23, 24) and also the existence of intramolecular hydrogen bonding in the azo form (structure **I***a*). The band at 380 nm is due to the π–π* transition of the azo form and the inflexion at 450 nm is due to the hydrazone from (structure **I***b*). In the

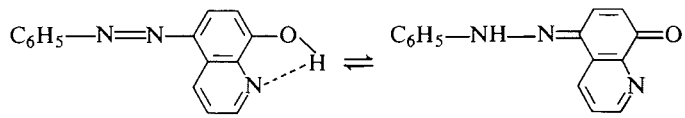

I*a* **I***b*

electronic spectra of all the β-alkoxycarbonylalkyltin 5-phenylazo-8-quinolinolates (Table 2) the 450 nm band of the free ligand is completely absent since the hydrazone form is not relevant for chelate formation. The 380 nm band of the free ligand suffers a red shift to ~400–430 nm in the complexes and is assigned to the π–π* transition of the azo form. Therefore, all the 5-phenylazo-8-quinolinol complexes exist only in the azo form. In these compounds the oxygen atom is expected to have a large negative charge because of the high polarity of the tin–oxygen bonds ($Sn^{\delta+}$ — $O^{\delta-}$) and the π–π* transition energy is expected to be further lowered (25). The bathochromic shift of the free ligand band from 380 nm to ~400–430 nm in all the compounds therefore results due to the chelation of the ligand (7, 8). The band at ~320–340 nm in these complexes is possibly associated with the ligand band as also observed in other metal oxinates or substituted oxinates (7). β-Alkoxycarbonylalkyltin 5-phenylazo-8-quinolinolates are thus structurally quite similar (structure **II**) to other organotin oxinates (7, 8, 26–29).

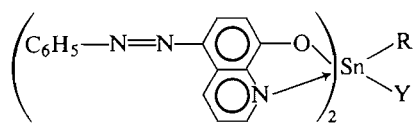

(R = $CH_3OCOCH_2CH_2$—, $C_4H_9OCOCH_2CH_2$—, $CH_3OCOCH(CH_3)CH_2$—; Y = R or Cl)

II

TABLE 1. Analytical and physical data of β-alkoxycarbonylethyltin complexes and others*

Compound	MP(°C); reflux reflux period (h); yield (%)	Analyses found (calculated) %			
		C	H	N	Sn
1. $R^{I}_{2}SnL_{2}$[a,f]	192;[k] 2; 79	57.99 (57.79)	3.68 (4.31)	10.86 (10.65)	14.98 (15.08)
2. $R^{I}SnL_{2}Cl$[a,f]	184;[k] 2; 76	54.60 (55.32)	3.69 (3.66)	11.27 (11.39)	15.98 (16.14)
3. $R^{II}_{2}SnL_{2}$[a,f]	135;[k] 2; 74	59.91 (60.48)	5.67 (5.27)	10.07 (9.62)	13.52 (13.63)
4. $R^{II}SnL_{2}Cl$[a,f]	162;[k] 2; 75	56.86 (56.96)	4.35 (4.23)	11.09 (10.78)	15.12 (15.27)
5. $R^{III}SnL_{2}Cl$[a,f]	184;[k] 2; 78	55.58 (55.89)	4.02 (3.86)	11.32 (11.18)	15.72 (15.83)
6. $R^{I}_{2}Sn(L^{I}H^{I})_{2}$[b,f]	174;[k] 1; 48	54.60 (54.73)	3.94 (3.88)	9.26 (9.58)	13.21 (13.57)
7. $R^{I}_{2}SnL^{II}$[c,g]	242; ½; 78	50.00 (49.72)	3.99 (3.77)	—	22.36 (22.41)
8. $R^{I}SnL^{II}Cl$[c,h]	210; 3; 56	44.80 (45.05)	2.60 (2.71)	—	24.52 (24.82)
9. $R^{II}_{2}SnL^{II}$[c,g]	215;[k] 3; 71	54.40 (54.63)	4.81 (5.20)	—	19.21 (19.35)
10. $R^{II}SnL^{II}Cl$[c,g]	180;[k] 2; 52	47.65 (48.32)	3.45 (3.64)	—	22.65 (22.82)
11. $R^{I}_{2}SnL^{III}Cl$[d,i]	120; 4; 42	43.80 (43.16)	3.80 (3.99)	2.79 (2.79)	33.69 (23.78)
12. $R^{I}_{2}Sn(SCN)_{2}$[e,h]	109; 1;[l] 58	29.80 (29.34)	3.52 (3.42)	7.08 (6.85)	29.00 (29.09)
13. $Ph_{2}SnL^{II}$[c,j]	232; 6; —	60.78 (61.05)	3.32 (3.13)	—	22.90 (23.28)
14. Product of reaction *6*	360; 6; —	53.81 (54.05)	2.30 (2.32)	—	19.72 (19.84)

*LH = 5-phenylazo-8-quinolinol; $L^{I}HH^{I}$ = 5-(2[I]-carboxyphenylazo)-8-quinolinol, where H and H^{I} refer to hydroxyl and carboxyl protons, respectively; $L^{II}H_{2}$ = alizarin; $L^{III}H$ = 1-nitroso-2-naphthol; Ph = phenyl group. R^{I} = $CH_{3}OCOCH_{2}CH_{2}$—, R^{II} = $C_{4}H_{9}OCOCH_{2}CH_{2}$—, and R^{III} = $CH_{3}OCOCH(CH_{3})CH_{2}$—. Supercripts *a*, *b*, *c*, *d*, and *e* refer to reaction medium as benzene, tetrahydrofuran, methanol, chloroform and ethanol, respectively. Superscripts *f*, *g*, *h*, *i*, and *j* refer to solvent for crystallisation as benzene – petroleum ether, chloroform–methanol, methanol, methanol–ether, and benzene, respectively; superscript *k* refers to decomposition point; superscript *l* stands for stirred instead of reflux.

TABLE 2. Characteristic electronic (in methanol) and infrared absorption bands (Nujol mulls, cm^{-1}) of β-alkoxycarbonylethyltin complexes and other compounds*

Compound	Electronic		Infrared			
	λ_{max} (nm)	log ϵ_{max}	$\nu_{C=O}$	for ν_{C-O} / C—O—Sn	ν_{Sn-O}	Other
1. $R^{I}_{2}SnL_{2}$	320 430	4.26 4.49	1725	1100	510	1250 (C_8—O); 1580 ($\nu_{C=N}$)
2. $R^{I}SnL_{2}Cl$	340 400	4.37 4.49	1720	1100	510	1250 (C_8—O); 1580 ($\nu_{C=N}$)
3. $R^{II}_{2}SnL_{2}$	325 430	4.37 4.55	1720	1100	520	1250 (C_8—O); 1580 ($\nu_{C=N}$)
4. $R^{II}SnL_{2}Cl$	340 400	3.94 4.11	1720	1100	520	1250 (C_8—O); 1580 ($\nu_{C=N}$)
5. $R^{III}SnL_{2}Cl$	325 410	4.55 4.99	1715	1095	510	1240 (C_8—O); 1575 ($\nu_{C=N}$)
6. $R^{I}_{2}Sn(L^{I}N^{I})_{2}$	 380[a] 420	 4.13 4.21	1725 1670 1650	1100	510	1570 ($\nu_{C=N}$); 3460 ($\nu_{OH-carboxylic}$)
7. $R^{I}_{2}SnL^{II}$	475	3.95	1730, 1675 1610–1650, 1510			
8. $R^{I}SnL^{II}Cl$	470	3.82	1705 1610–1650, 1510			
9. $R^{II}_{2}SnL^{II}$	480	3.82	1725, 1670 1610–1650, 1520			
10. $R^{II}_{2}SnL^{III}Cl$	480	3.70	1710 1610–1650, 1510			
11. $R^{I}_{2}SnL^{III}Cl$	580	3.57	1720			1510–1565 ($\nu_{N=O}$ coupled with ring breathing)
12. $R^{I}_{2}Sn(SCN)_{2}$			1650			2060 ($\nu_{C\equiv N}$), 860 (ν_{C-S})
13. $Ph_{2}SnL^{II}$			1610–1650 1530			
14. Product of reaction *6*			1530			

*R^{I} = $CH_{3}OCOCH_{2}CH_{2}$—, R^{II} = $C_{4}H_{9}OCOCH_{2}CH_{2}$—, R^{III} = $CH_{3}OCOCH(CH_{3})CH_{2}$—. $\nu_{C=O}$ of $R^{I}_{2}SnCl_{2}$ at 1677 cm^{-1}, $R^{I}SnCl_{3}$ at 1660 cm^{-1}, $R^{II}_{2}SnCl_{2}$ at 1675 cm^{-1}, $R^{II}SnCl_{3}$ at 1640 cm^{-1}, and $R^{III}SnCl_{3}$ at 1640 cm^{-1}. LH = 5-phenylazo-8-quinolinol (λ_{max} at 380 nm, 450 nm (inflexion)); $L^{I}HH^{I}$ = 5-(2[I]-carboxyphenylazo)-8-quinolinol (λ_{max} at 350 nm (inflexion), 475 nm; ν_{as}(OCO) at 1630 cm^{-1}, ν_{OH} at 3480 (carboxylic) and 3360 (phenolic) cm^{-1}); $L^{II}H_{2}$ = alizarin (λ_{max} at 430 nm; $\nu_{C=O}$ at 1655 and 1630 cm^{-1}, ν_{OH} at 3400 cm^{-1}); $L^{III}H$ = 1-nitroso-2-naphthol (λ_{max} at 370 nm, ν_{OH} at 3400 cm^{-1}, $\nu_{N=O}$ at 1610 cm^{-1}). Superscript *a* refers to inflexion.

Can. J. Chem. Downloaded from www.nrcresearchpress.com by 72.64.146.136 on 09/07/12
For personal use only.

TABLE 3. ^{1}H nmr spectral data of β-alkoxycarbonylethyltin complexes and others (in $CDCl_3$); chemical shifts (δ ppm, downfield from TMS)*

Compound	Aliphatic protons				Aromatic protons
	α-CH_2 [H_α]	β-CH_2 [H_β]	—OCH_3/OCH_2 [H_c]	Other	
1. R^ISnL_2Cl	1.66 (t, 2H)*	2.70 (t, 2H)	3.50 (S, 3H)		7.45 (d, 10H), 7.86 (N, 4H), 8.22 (d, 2H), 8.59 (N, 2H), and 9.36 (d, 2H)
2. $R^{II}_2SnL_2$	1.98 (t, 4H)	2.98 (t, 4H)	3.39 (S, 4N)	1.27 (d, 6H) (—CH_3) 1.08 (c, 8H) (—CH_2—CH_2)	6.90–7.38 (c, 12H), 7.53 (t, 4H), 8.17 (t, 2H), and 8.55 (N, 2H)
3. $R^{II}SnL_2Cl$	1.72 (t, 2H)	2.65 (t, 2H)	3.90 (t, 2H)	0.84 (t, 3H) (—CH_3) 1.20–1.58 (c, 4H) (—CH_2—CH_2)	7.43 (d, 10H), 7.87 (N, 4H), 8.26 (d, 2H), 8.60 (N, 2H), and 9.35 (d, 2H)
4. $R^{III}SnL_2Cl$	1.78 (N, 2H)	3.00 (N, 1H) (—CH)	3.43 (S, 3H)	1.33 (t, 3H) (—CH_3)	7.43 (d, 10H), 7.86 (N, 4H), 8.20 (d, 2H), 8.65 (S, 2H), and 9.35 (d, 2H)
5. $R^I_2Sn(L^IH^I)_2$	1.44 (t, 4H) 1.90	2.45 (t, 4H) 2.72	3.57 (S, 6H) 3.65		7.07–7.68 (c, 8H), 7.78 (d, 2H), 8.16 (d, 2H), 8.59 (d, 2H), 8.97 (N, 2H), and 9.30 (d, 2H)
6. $R^I_2SnL^{II}$	1.69 (t, 4H)	2.70 (t, 4H)	3.70 (S, 6H)		6.90 (d, 1H), 7.65 (c, 2H), 7.84 (d, 2H), and 8.23 (d, 1H)
7. $R^{II}_2SnL^{II}$	1.65 (t, 4H)	2.66 (t, 4H)	4.13 (Q, 4H)	0.84 (d, 6H) (—CH_3) 1.00–1.48 (c, 8H) (—CH_2—CH_2)	6.87 (d, 1H), 7.60 (c, 2H), 7.80 (d, 2H), and 8.19 (d, 1H)
8. $R^I_2SnL^{III}Cl$	1.74 (t, 4H)	2.82 (t, 4H)	3.76 (S, 6H)		6.58 (d, 1H), 6.96 (t, 1H), 7.36–7.72 (c, 2H), 7.84 (d, 1H), and 8.34 (d, 1H)
9. $R^I_2Sn(SCN)_2$	1.57 (t, 4H) 1.21 (t, 4H)	2.73 (N, 4H) 1.98 (N, 4H)	3.73 (S, 6H) 3.30 (S, 6H)		

*Multiplicity (S = Singlet, d = doublet, t = triplet, Q = quartet, c = complex pattern, and N = not resolved properly) and proton count in parentheses. R^I = $CH_3OCOCH_2CH_2$—, R^{II} = $C_4H_9OCOCH_2CH_2$—, and R^{III} = $CH_3OCOCH(CH_3)CH_2$—. LH = 5-phenylazo-8-quinolinol, L^IHH^I = 5-(2^ICarboxyphenylazo)-8-quinolinol, where H and H^I refer to hydroxyl and carboxyl protons respectively, $L^{II}H_2$ = alizarin, and $L^{III}H$ = 1-nitroso-2-naphthol. Chemical shifts (δ ppm) of (*i*) $R^I_2SnCl_2$ at 1.92 (H_α), 2.93 (H_β), and 3.82 (H_c), (*ii*) R^ISnCl_3 at 2.27 (H_α), 2.99 (H_β), and 3.97 (H_c), (*iii*) $R^{II}_2SnCl_2$ at 1.90 (H_α), 2.92 (H_β), and 4.24 (H_c), (*iv*) $R^{II}SnCl_3$ at 2.24 (H_α), 2.98 (H_β), 4.37 (H_c), 1.08 (—CH_3), and 1.11–2.02 (—CH_2—CH_2), and (*v*) $R^{III}SnCl_3$ at 2.25 (H_α), 3.30 (H_β i.e., —CH), 4.41 (H_c), and 1.56 (—CH_3).

The compound $(CH_3OCOCH_2CH_2)_2Sn(L^IH^I)_2$ absorbs predominantly at 420 nm in the donor solvent methanol (Table 2). Since, only donor solvents (capable of forming strong hydrogen bonds) give rise to a blue shift, the structure **III** may be

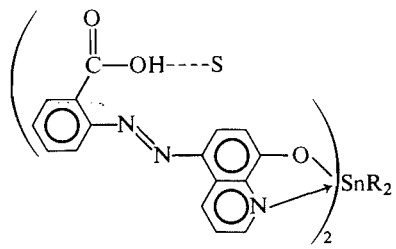

(S = donor solvent, R = $CH_3OCOCH_2CH_2$—)

III

suggested for this complex. Moreover, any interaction with azo-nitrogen atoms through intramolecular hydrogen bonding, as in 5-(2^I-carboxyphenylazo)-8-quinolinol, is expected to lead to a bathochromic shift. Since the hydrogen atom is not directly involved in the π-system (as shown in structure **III**), such systems will have little influence on the π–π* transition and consequently the absorption spectrum of this complex closely resembles those of the corresponding 5-phenylazo-8-quinolinol complexes.

In all the alizarin complexes (Table 2), the bands in the region ~460–480 nm, and in $(CH_3OCOCH_2CH_2)_2SnL^{III}Cl$ (where $L^{III}H$ = 1-nitroso-2-naphthol) the band at 580 nm, are also due to the bathochromic shift of the ligand band which indicates strong chelation.

Infrared spectra

In β-alkoxycarbonylethyltin chlorides the carbonyl coordinations to tin are intramolecular in origin (structure **IV**) and ν_{CO} appears in the region ~1640–1680 cm^{-1} (2, 3, 30).

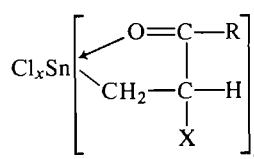

(R = OCH_3, OC_4H_9, CH_3; X = H or CH_3; n = 1 or 2; x = 4 − n)

IV

The ir spectra of β-alkoxycarbonylethyltin 5-phenylazo-8-quinolinolates (Table 2) show that the ν_{CO} appear at higher wave numbers (~1715–1725 cm^{-1}) and the intramolecular carbonyl coordinations (structure **V**) are thus cleaved (structure **VI**) on complex formation (7, 8).

Can. J. Chem. Downloaded from www.nrcresearchpress.com by 72.64.146.136 on 09/07/12
For personal use only.

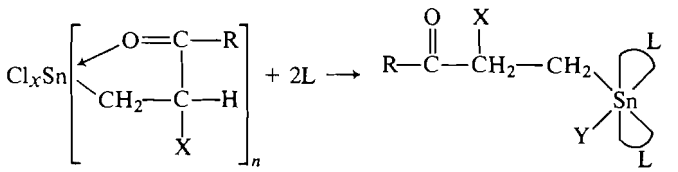

V VI

+ 2HCl

(R = OCH_3, OC_4H_9, CH_3; X = H or CH_3; L = ligand;
Y = $ROCH(X)CH_2$— or Cl; n = 1 or 2; $x = 4 - n$)

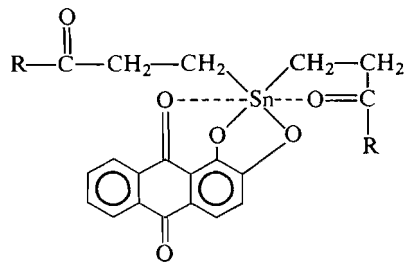

(R = OCH_3, OC_4H_9)

VII

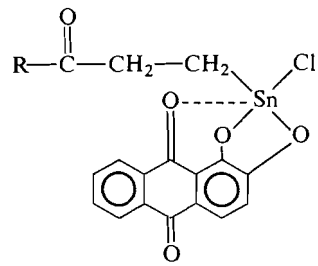

(R = OCH_3, OC_4H_9)

VIII

The ν_{OH} of 5-phenylazo-8-quinolinol disappeared in the complexes. Moreover, in these complexes the Sn—O stretch at ~510–520 cm^{-1} (9, 31, 32), the characteristic C—O stretching of =C—O—Sn site at ~1100 cm^{-1} (33) and the C=N stretching frequency (somewhat coupled with the pyridine ring vibration) at 1580 cm^{-1} (34) clearly indicate the chelating nature of the ligand. The upward shift of $\nu_{C_{(aryl)}—O}$ (i.e., C_8—O stretch of quinoline ring) in the complexes is expected, because the large polarity of —O—Sn= bond (35) increases the conjugative interaction of oxygen atoms with the π-ring resulting in an increase of the C—O bond order. The $\nu_{(N=N)}$ in the complexes is likely to be very weak (36).

In the ir spectrum of $(CH_3OCOCH_2CH_2)_2Sn(L^IH^I)_2$, hydrogen bonded ν_{OH} (phenolic) of the ligand at ~3360 cm^{-1} (shoulder) is absent whereas the bands at ~3460 cm^{-1} (broad) and 1650 cm^{-1} are due to the ν_{OH} (hydrogen bonded) and ν_{as} (OCO) of the carboxyl group respectively. Other characteristic ir bands (Table 2) of this complex are similar to those of the 5-phenylazo-8-quinolinol complexes. The bands at 1725 cm^{-1} and 1690 cm^{-1} in this complex may indicate that one of the two intramolecular coordinations by the estercarbonyl groups is cleaved while the other is still dominating.

The complete absence of ν_{OH} in the ir spectra of β-alkoxycarbonylethyltin alizarinates signifies that both the hydroxyl groups of alizarin are involved in complex formation. Moreover, in $(CH_3OCOCH_2CH_2)_2SnL^{II}$ the appearance of ν_{CO} at 1730 and 1675 cm^{-1} indicates that on complex formation one of the two intramolecular carbonyl coordinations in $(CH_3OCOCH_2CH_2)_2SnCl_2$ (at 1677 cm^{-1}) is cleaved while the other is still dominating. This is also observed in the case of $(C_4H_9OCOCH_2CH_2)_2SnL^{II}$. However, in $CH_3OCOCH_2CH_2$-$SnL^{II}Cl$ and $C_4H_9OCOCH_2CH_2SnL^{II}Cl$ the lone intramolecular carbonyl coordinations of the alkyl tin chlorides are cleaved and thus shifted to longer wave lengths (~1705–1710 cm^{-1}). In all the alizarinate complexes the carbonyl frequencies of alizarin appear at ~1610–1650 cm^{-1} along with a new band at ~1510–1520 cm^{-1} which is due to the coordination of one of the two carbonyl groups of alizarin to tin. Although it requires further detailed studies, on the basis of ir and ^1H nmr spectra, two types of bonding as shown in **VII** and **VIII** may be suggested which indicate that bis(β-alkoxycarbonylethyl)tin alizarinates are hexacoordinated whereas β-alkoxycarbonylethylchlorotin alizarinates are pentacoordinated around tin. The ir spectrum of diphenyltin alizarinate also shows similar behaviour. In the organotin quinalizarinate complex (product of reaction *6*) the complete absence of ν_{OH} and the appearance of ν_{CO} only at 1530 cm^{-1} indicate that all the hydroxyl and carbonyl groups of quinalizarin have participated in bonding.

In the nitrosonaphthol complex the shift of the N=O group frequency of the ligand (at 1610 cm^{-1}) (37) to lower wave number at ~1510–1565 cm^{-1} (somewhat coupled with the ring breathing mode), the appearance of ν_{CO} of estercarbonyl at higher wave number, and the absence of any ν_{OH}, also suggest chelation.

The appearance of two new bands at 2060 cm^{-1} and 860 cm^{-1} in $(CH_3OCOCH_2CH_2)_2Sn(SCN)_2$ are assigned to $\nu_{C\equiv N}$ and $\nu_{C—S}$ vibrations. Therefore, in this compound the SCN group is linked to tin through nitrogen (38). ν_{NCS} could not be assigned because the parent organotin chloride also exhibits a band at ~490 cm^{-1}. The shift of ν_{CO} in this compound to lower wave number is consistent with the more electronegative character of SCN group in comparison to chloride.

^1H nmr spectra

In the ^1H nmr spectra of all complexes the ratios of different protons are found to be consistent with their compositions. All types of protons in β-alkoxycarbonylethyl groups, with H_α, H_β, and H_c defined as:

$CH_3OCOCH_2CH_2$—; (H_c) (H_β)(H_α)

$CH_3CH_2CH_2CH_2OCOCH_2CH_2$—; ($H_c$) ($H_\beta$)($H_\alpha$)

$CH_3OCOCH(CH_3)CH_2$— (H_c) (H_β) (H_α)

on tin in 5-phenylazo-8-quinolinol and 5-(2^I-carboxyphenylazo)-8-quinolinol complexes (Table 3) exhibit shielding and thereby resonate at higher magnetic field which is in agreement with the increased electron density on the tin via ligand donation. From the chemical shift values it can be seen that both the β-methylenic and methyl protons in the complexes revert to positions characteristic of the free ester group which is again in support of the fact that the intramolecular estercarbonyl coordinations in β-alkoxycarbonylethyltin chlorides are cleaved in the complexes. In all these complexes the α-methylenic proton is shielded most, except in $R^{III}SnL_2Cl$ (Table 3) where the methyl proton is shielded most like its similar oxinate and dibromooxinate complexes (7). The aromatic protons at 2- and 4-positions in all the 5-phenylazo-8-quinolinolates are affected most and appear downfield as in oxine and substituted oxine complexes. The spectrum of $(CH_3OCOCH_2CH_2)_2Sn(L^IH^I)_2$ possibly indicates the presence of mixture of isomers.

In $(CH_3OCOCH_2CH_2)_2SnL^{II}$ and $(C_4H_9OCOCH_2CH_2)_2SnL^{II}$ also, the H_α, H_β, and H_c protons are shielded and the H_α proton is shielded most. In the nitrosonaphthol compound,

Can. J. Chem. Downloaded from www.nrcresearchpress.com by 72.64.146.136 on 09/07/12
For personal use only.

complex formation is indicated by the appearance of alkyl protons upfield where the H_α proton is shielded most.

The ^1H nmr spectrum of $(CH_3OCOCH_2CH_2)_2Sn(SCN)_2$ also indicates the existence of mixture of geometrical isomers and it requires further studies for confirmation. However, in this compound the alkyl protons appear upfield compared to those in $(CH_3OCOCH_2CH_2)_2SnCl_2$ which is quite consistent with the less electronegative character of the thiocyanate group.

Acknowledgements

One of the authors (B.K.D.) thanks the University of North Bengal for the award of a J.R.F. The authors gratefully acknowledge Dr. R. E. Hutton (AKZO Chemie, U.K. Ltd.) for the gift of a few estertin chlorides. The authors acknowledge the service of Central Drug Research Institute, Lucknow, for the analytical, electronic, and ^1H nmr spectral data. Thanks are also due to Dr. A. Roy, who investigated the reaction of triphenyltin hydroxide and alizarin or quinalizarin in this laboratory.

1. D. LANIGAN and E. L. WEINBERG. *In* Organotin compounds: new chemistry and applications. *Edited by* J. J. Zuckerman. Advances in Chemistry, Series 157. Am. Chem. Soc., Washington, D.C. 1976. Chap. 9.
2. R. E. HUTTON, J. W. BURLEY, and V. OAKES. J. Organomet. Chem. **156**, 369 (1978).
3. J. W. BURLEY, P. HOPE, R. E. HUTTON, and C. J. GROENENBOOM. J. Organomet. Chem. **170**, 21 (1979).
4. R. E. HUTTON and V. OAKES. *In* Organotin compounds: new chemistry and applications. *Edited by* J. J. Zuckerman. Advances in Chemistry Series 157. Am. Chem. Soc., Washington, D.C. 1976. Chap. 8.
5. R. M. HAIGH, A. G. DAVIES, and M. W. TSE. J. Organomet. Chem. **174**, 163 (1979).
6. P. G. HARRISON, T. J. KING, and M. A. HEALY. J. Organomet. Chem. **182**, 17 (1979).
7. B. K. DEB and A. K. GHOSH. Polyhedron, **5** (3), 863 (1986).
8. B. K. DEB and A. K. GHOSH. Z. Anorg. Allg. Chem. In press.
9. V. G. KUMAR DAS, N. S. WENG, and P. J. SMITH. Inorg. Chim. Acta, **49**, 149 (1981).
10. M. V. GARAD, S. GOPINATHAN, and C. GOPINATHAN. Z. Anorg. Allg. Chem. **465**, 204 (1980).
11. D. MAUGHAN, J. L. WARDELL, and J. W. BURLEY. J. Organomet. Chem. **212**, 59 (1981).
12. R. C. POLLER. *In* Organotin compounds: new chemistry and applications. *Edited by* J. J. Zuckerman. Advances in Chemistry, Series 157. Am. Chem. Soc. Washington, D.C. 1976. ch. 12.
13. J. MATHEUS. Ber. **21**, 1644 (1888).
14. F. J. WELCHER. Organic analytical reagents. Vol. 1. Nostrand, London. 1947.
15. V. M. IVANOV and T. F. RUDOMETKINA. Zh. Anal. Khim. **33**, 2426 (1978).
16. Y. MATSUNAGA. Bull. Chem. Soc. Jpn. **44**, 878 (1971).
17. G. M. BADGER and R. G. BUTTERY. J. Chem. Soc. 614 (1956).
18. E. SAWICKI. J. Chem. Soc. 743 (1956).
19. R. N. SHREVE and R. BENNETT. J. Am. Chem. Soc. **65**, 2243 (1943).
20. T. MATSUO, A. MUSASHI, and Y. NAITO. J. Pharm. Soc. Jpn. **72**, 1456 (1952).
21. B. K. DEB. Ph.D. Thesis. North Bengal University, India. 1983.
22. B. MAJEE and S. K. CHAKRAVARTI. Z. Phys. Chem. **57**, 89 (1968).
23. J. GRIFFITHS. Colour and constitution of organic molecules. Academic Press, New York. 1976.
24. J. A. POPLE and G. A. SEGAL. J. Chem. Phys. **44**, 3289 (1966).
25. B. MAJEE and T. K. CHATTOPADHYAY. J. Indian Chem. Soc. **59**(2), 219 (1982).
26. T. TANAKA, M. KOWURA, Y. KAWASIKI, and R. OKAWARA. J. Organomet. Chem. **1**, 484 (1964).
27. K. KAWAKAMI and R. OKAWARA. J. Organomet. Chem. **6**, 249 (1966).
28. K. KAWAKAMI, Y. KAWASAKI, and R. OKAWARA. Bull. Chem. Soc. Jpn. **40**, 2693 (1967).
29. W. KITCHING. J. Organomet. Chem. **6**, 586 (1966).
30. I. OMAE. Review of silicon, germanium, tin and lead compounds. Vol. 1. 1972. p. 59.
31. R. C. POLLER. The chemistry of organotin compounds. Logos. 1970, Chaps. 11 and 13; J. Organomet. Chem. **24**, 341 (1970).
32. R. OKAWARA and M. OHARA. *In* Organotin compounds. Vol. 2. *Edited by* A. K. Sawyer. Marcel Dekker. 1973. p. 253.
33. R. G. CHARLES, H. FREISER, R. FRIEDEL, L. E. HILLIARD, and W. D. JOHNSTON. Spectrochim. Acta, **8**, 11 (1956).
34. R. J. MAGEE and L. GORDON. Talanta, **10**, 851 (1963).
35. L. PAULING. The nature of chemical bond. 3rd ed. Cornell University, Ithaca, NY. 1960.
36. R. K. MILLER. *In* Analytical chemistry and synthetic dyes. *Edited by* K. Venkataraman. John Wiley and Sons. 1977. p. 208.
37. L. J. BELLAMY. The infrared spectra of complex molecules. Chapman and Hall Ltd., London. 1975.
38. A. SABATINI and I. BERTINI. Inorg. Chem. **4**, 959 (1965).

Can. J. Chem. Downloaded from www.nrcresearchpress.com by 72.64.146.136 on 09/07/12
For personal use only.

The reaction of 2,1-benzisothiazoline-3-thiones with acetylenic reagents

DAVID M. MCKINNON, ANTHONY S. SECCO, AND K. ANN DUNCAN
Department of Chemistry, University of Manitoba, Winnipeg, Man., Canada R3T 2N2

Received October 8, 1986

DAVID M. MCKINNON, ANTHONY S. SECCO, and K. ANN DUNCAN. Can. J. Chem. **65**, 1247 (1987).

N-Methyl-2,1-benzisothiazoline-3-thione reacts with acetylene esters to form *o*-iminobenzoquinone methides which either form diazocines **2** by head-to-tail dimerisation, or react further with the acetylenic ester forming diadducts. With phenylacetylene a 1,2-dithiolo[2,3-*b*]2,1-benzisothiazole structure is obtained by rearrangement of an initial adduct. Related thiones and acetylenes react similarly but in poorer yields. The crystal and molecular structures of the diazocine were determined by single crystal X-ray diffractometry techniques. The compound crystallizes in space group $P\bar{1}$ with unit cell dimensions a = 7.9465(10), b = 13.6421(14), c = 13.9183(18) Å, α = 82.38(1), β = 83.67(1), γ = 85.77(1) deg, and Z = 2. The structure was solved by direct methods and refined to an R value of 0.056 for 3037 observed reflections. The structure consists of molecules of **2***a* which have an approximate C_2 axis passing through the center of the eight-membered ring. Deviations from true symmetry result from internal ring strain, lone pair–lone pair repulsions, and packing effects.

DAVID M. MCKINNON, ANTHONY S. SECCO et K. ANN DUNCAN. Can. J. Chem. **65**, 1247 (1987).

La *N*-méthyl 2,1-benzisothiazolinethione-3 réagit avec les esters acétyléniques pour former des méthylures d'*o*-imino-benzoquinones qui conduisent soit à des diazocines **2**, par une dimérisation tête à queue, soit à des diadduits provenant d'une réaction subséquente avec l'ester acétylénique. Avec le phénylacétylène, on obtient une structure dithiolo-1,2[2,3-*b*] 2,1-benziothiazole qui provient d'une transposition de l'adduit initial. Des thiones et des acétylènes apparentés réagissent d'une façon semblable; les rendements sont toutefois moins bons. On a déterminé les structures cristalline et moléculaire de la diazocine en faisant appel à la diffraction des rayons-X sur un cristal unique. Le composé cristallise dans le groupe d'espace $P\bar{1}$, avec a = 7,9465(10), b = 13,6421(14) et c = 13,9183(18) Å, α = 82,38(1), β = 83,67 et γ = 85,77(1)° et Z = 2. On a résolu la structure par des méthodes directes et on l'a affinée jusqu'à une valeur de R de 0,056 pour 3037 réflexions observées. La structure comporte des molécules de **2***a* qui possèdent un axe approximativement C_2 qui traverse le centre du cycle à huit chaînons. Les déviations par rapport à la vraie symétrie proviennent d'une tension interne de cycle, de répulsions entre des paires libres et d'effets de remplissage.

[Traduit par la revue]

Can. J. Chem. Downloaded from www.nrcresearchpress.com by 78.46.186.204 on 09/07/12
For personal use only.

Introduction

While the reactions of monocyclic isothiazoline-3- and 5-thiones with various acetylenic reagents to form mono- and diadducts have been studied (1), surprisingly no data are reported on the reactions of their benzo- derivatives. It was of interest then to investigate these reactions to determine to what extent they paralleled the reactions of the monocyclic systems, or the structurally related benzo-1,2-dithiole-3-thiones which are reported to give diadducts (2).

Results and discussion

N-Methyl-2,1-benzisothiazoline-3-thione (**1***a*) treated with 1 equiv. of dimethyl acetylenedicarboxylate in benzene gave an immediate deep violet colour, which faded to yellow after several hours at room temperature or more quickly on heating.

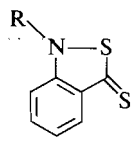

1
a, R = Me
b, R = Ph

When the reaction was performed in a more polar solvent, e.g. dioxane or tetrahydrofuran, the violet colour faded in a few minutes. Work-up of the yellow solution gave pale yellow prisms, whose nmr and mass spectral properties were consistent with a 1:1 adduct. However, an X-ray crystallographic structure determination indicated that this was in fact the dimer (**2***a*) of a 1:1 adduct (**3***a*) formed by a head-to-tail coupling. This molecule has a folded conformation, with the planes of the two aromatic rings at approximately 120° to each other.

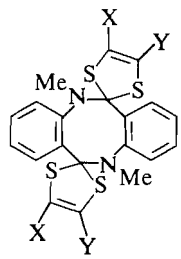

2
a, X = Y = CO_2Me
b, X = H, Y = CO_2Me

The two methoxycarbonyl groups on the spiro-1,3-dithiole rings thereby become non-equivalent, and indeed the nmr spectrum of **2***a* showed two types of O-methyl protons. Surprisingly, the nmr spectrum showed virtually no change on heating (by 30°), indicating some steric resistance to inversion of the diazocine ring, and an examination of a space filling model of **2***a* demonstrated great steric crowding and resistance to inversion. Other less substituted dibenzodiazocines have inversion energy barriers of approximately 20 kcal mol[1] (3).

The nature of the initially formed violet material is not known. It may be a charge transfer complex between the reactants,

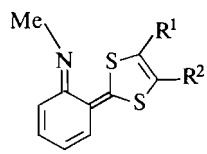

3
a, R_1 = R_2 = CO_2Me
b, R_2 = H, R_1 = CO_2Et
c, R_2 = CO_2Et, R_1 = H

Can. J. Chem. Downloaded from www.nrcresearchpress.com by 78.46.186.204 on 09/07/12
For personal use only.

or possibly the initially formed *o*-quinonoid 1:1 adduct (**3***a*). In this reaction the thione **1***a* parallels the reaction of benzo-1,2-dithiole-3-thione with dimethyl acetylenedicarboxylate (2), but there the monoadduct rapidly reacted with more acetylenic ester to form a diadduct. No such monoadduct dimers are reported from the reaction of the structurally related benzo- or naphtho-1,2-dithiole-3-thiones with acetylenic reagents, but the photo-reaction with alkenes produces adducts which are in equilibrium with dimers (4, 5). It is also reported that *o*-xylylenes may undergo dimerisation (6) but a more closely related imino-*o*-quinomethide only shows a [2 + 4] type addition (7). Polar factors induced by the 1,3-dithiole ring in **3***a* may be significant in this dimerisation. Since an adduct of type **3***a* should also react with more dimethyl acetylenedicarboxylate to give a diadduct, the thione was allowed to react with 2 mol of the ester. However, only the monoadduct dimer was isolated. In fact, only when the thione was warmed with a large excess of the ester was the diadduct **4***a* obtained.

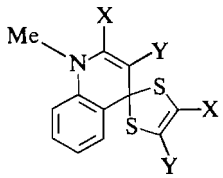

4

a, X = Y = CO_2Me
b, X = H, Y = CO_2Me
c, X = CO_2Et, Y = H

The reaction of the thione **1***a* with ethyl propiolate was complex. An initially produced dark red color faded after one hour and subsequent chromatography revealed a slow running yellow band, and faster running red and colorless bands. The red band could not be purified and indeed may have been converting into the colorless band. Isolation of the yellow band gave pale yellow needles, which were the only product when the thione was treated with excess ethyl propiolate. The properties of these were consistent with the diadduct **4***b*. This structure rather than the isomeric **4***c* is favored as the initial adduct **3***b* would be expected to have contributions from a polar structure **5**. If this has a bias towards addition in a conjugate fashion to the acetylenic ester, the adduct **4***b* should be obtained.

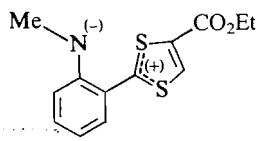

5

The colorless band on work-up gave a pale yellow oil which could not be crystallized. Its ^1H and ^{13}C nmr spectra indicated the presence of four different *N*-methyl and ester functions. We consider these to represent the signals of the three geometrical isomers of the monoadduct dimer **2***b* (plus enantiomers). As with the diazocine **2***a*, **2***b* should also resist inversion and therefore a dimerisation of an initially formed mono adduct by an "*exo*" approach, which has a similar transition state, should be unlikely. The most favoured approach is therefore "*endo*". The initial adduct of **1***a* and ethyl propiolate could exist as two geometrical isomers **3***b* or **3***c*, with **3***b* being favored if polar factors are significant in the reaction. The combination of two molecules of **3***b* would give the dimer **2***bi* (Fig. 1), i.e. with the ester functions in an "up–up" arrangement. Likewise

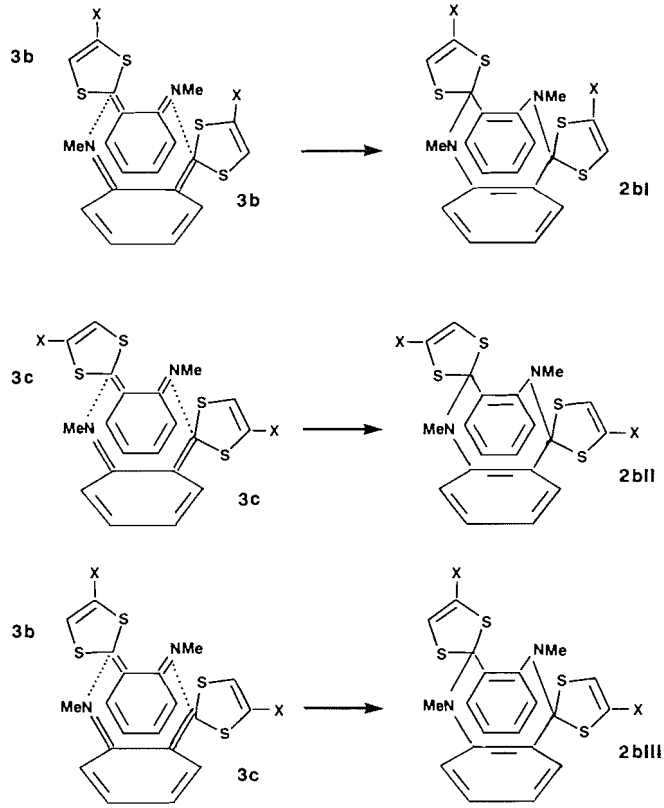

FIG. 1. Dimerisations of **3***b*, **3***c*.

dimerisation of **3***c* would give a "down–down" arrangement, i.e. **2***bii* and a **3***b*–**3***c* combination would give the compound **2***biii* with an "up–down" arrangement. Both **2***bi* and **2***bii* have axes of symmetry, therefore each possesses only one type of *N*-methyl group and one type of ester function, whereas **2***biii* lacks such an axis and possesses two *N*-methyl groups and two ester functions. Thus the nmr spectra are consistent with a **2***bi*–*iii* mixture.

To try to obtain another compound of related type, benzo-1,2-dithiole-3-thione was treated with ethyl propiolate. Since only a diadduct **6** was isolated these results are consistent with earlier studies (2).

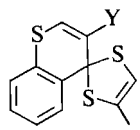

6

Y = CO_2Me

Reaction of the thione **1***a* with dibenzoylacetylene was also complex. An initial dark red color faded after 3 h at reflux in toluene and examination by chromatography showed many ill-defined bands. However, two products isolated in low yields had mass spectra corresponding to a 1:1 adduct and a 1:1 adduct less one atom of sulfur. The former then may have a structure analogous to compounds **2**.

Reaction of **1***a* with phenylacetylene was much slower than for the esters and no deep color was initially formed. Continued reflux gave a dark red solution which on work-up gave a dark red crystalline product, identical to the hypervalent sulfur system **7***a* prepared earlier by another method (8). This reaction is therefore related to the formation of 1,6,6*a*λ^4-trithiapentalenes from 1,2-dithiole-3-thiones by reaction with acetylenes (9–11).

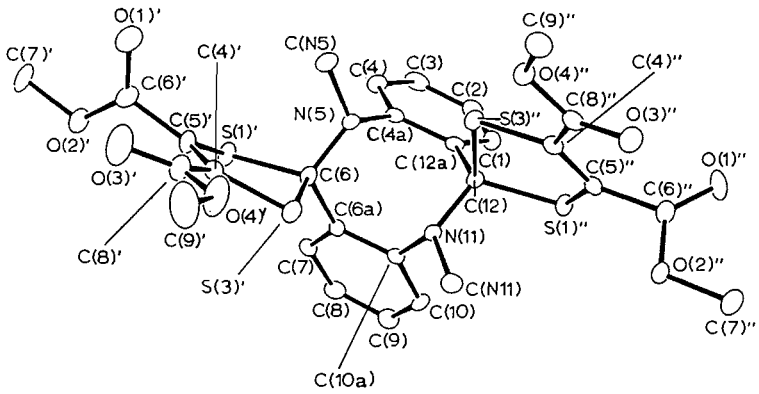

FIG. 2. ORTEP plot of the diazocine derivative, **2***a*, with boundary ellipses for atoms displayed at the 50% probability level.

N-Benzyl-2,1-benzisothiazoline-3-thione **1***c* reacted similarly to form **7***b*.

No products of type **2** or **4** were observed hence if any monoadduct of type **2** is formed it must be rearranging entirely to the system **7**, possibly by a reaction catalysed by sulfur

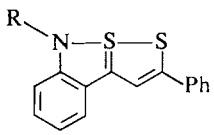

7

similar to that proposed or perhaps the compound **7** is formed from the reaction of the thione with an α-thiocarbene (12).

N-Phenyl-2,1-benzisothiazoline-3-thione **1***b* reacted rapidly with dimethyl acetylenedicarboxylate. A complex deep-colored mixture was obtained from which no definite product could be isolated, and *N*-benzyl-2,1-benzisothiazoline-3-thione **1***c* also gave a mixture of products which could not be purified satisfactorily, but on the basis of the nmr spectrum appears to contain a diadduct, possibly of type **4***a*.

With one example of an isomeric system, i.e. *N*-methyl-1,2-benzisothiazoline-3-thione, dimethyl acetylenedicarboxylate gave a yellow material, whose properties were consistent with the diadduct **8**.

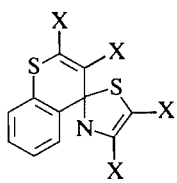

8

X = CO_2Me

With the exception of the ester moieties branching from C(5)′ and C(5)″, molecules of the *bis*-dithiolotetrahydrodibenzodiazocine, (**2***a*), (Fig. 2) have an approximate C_2 axis passing through the center of the eight-membered ring. The twofold molecular symmetry is preserved in all bond lengths (Table 1) and angles (Table 2) within experimental error. However, the deviation from true C_2 symmetry is manifested in the torsion angles involving the non-hydrogen atoms with differences averaging 5.7°. While the major deviations occur between torsion angles along the bonds joining esters to the dithiole rings at C(3)′ and C(3)″, smaller but significant differences exist between torsion angles involving bonds within the dithiole rings themselves.

The tetrahydrodibenzodiazocine ring system, including methyls

TABLE 1. Bond lengths (Å) with estimated standard deviations in parentheses

Bond	Length (Å)	Bond	Length (Å)
S(1)′—C(6)	1.886(5)	N(11)—C(12)	1.417(7)
S(1)′—C(5)′	1.736(6)	N(11)—C(10a)	1.432(7)
S(3)′—C(6)	1.864(5)	N(11)—C(N11)	1.456(7)
S(3)′—C(4)′	1.749(5)	C(5)′—C(4)′	1.342(8)
S(1)″—C(12)	1.906(5)	C(5)′—C(6)′	1.493(8)
S(1)″—C(5)″	1.727(5)	C(4)′—C(8)′	1.469(8)
S(3)″—C(12)	1.867(5)	C(4)″—C(8)″	1.479(7)
S(3)″—C(4)″	1.751(5)	C(5)″—C(4)″	1.339(7)
O(1)′—C(6)′	1.209(8)	C(5)″—C(6)″	1.508(7)
O(2)′—C(6)′	1.280(8)	C(1)—C(2)	1.378(8)
O(2)′—C(7)′	1.447(8)	C(2)—C(3)	1.360(10)
O(3)′—C(8)′	1.211(8)	C(3)—C(4)	1.371(9)
O(4)′—C(8)′	1.274(8)	C(4)—C(4a)	1.392(7)
O(4)′—C(9)′	1.455(9)	C(6)—C(6a)	1.520(7)
O(1)″—C(6)″	1.181(6)	C(6a)—C(7)	1.399(8)
O(2)″—C(6)″	1.318(7)	C(6a)—C(10a)	1.403(7)
O(2)″—C(7)″	1.454(7)	C(7)—C(8)	1.356(9)
O(3)″—C(8)″	1.202(6)	C(8)—C(9)	1.367(9)
O(4)″—C(8)″	1.320(6)	C(9)—C(10)	1.372(9)
O(4)″—C(9)″	1.446(7)	C(10)—C(10a)	1.390(8)
N(5)—C(4a)	1.435(7)	C(12a)—C(1)	1.384(7)
N(5)—C(6)	1.429(7)	C(12a)—C(4a)	1.383(7)
N(5)—C(N5)	1.459(7)	C(12)—C(12a)	1.541(7)

C(N5) and C(N11), shows perfect C_2 symmetry with the eight-membered ring adopting a slightly twisted boat conformation. The extent of the twist, given by the angle formed by projecting bond N(5)—C(6) onto bond C(12)—N(11), is 11.4(3)°. Whereas the twist in the boat conformation in the tetrahydrodiazocine ring is probably due to intramolecular steric effects and internal ring strain (*vide infra*), distortion from a symmetrical disposition of the dithioles and their extended ester substituents is a result of packing considerations. This is evident from the intermolecular steric crowding which would result between ester substituents on adjacent molecules translated on *b* if either of the ester groups attached to C(5)′ and C(5)″ were rotated approximately 180° about the C(5)′–C(6)′ or C(5)″—C(6)″ bonds, respectively (Fig. 3). Furthermore, the fact that the torsion angle S(3)″—C(4)″—C(8)″—O(3)″ (176.6(4)°) shows the largest deviation from its approximately twofold related counterpart S(3)′—C(4)′—C(8)′—O(3)′ (−171.4(6)°) is consistent with the relatively short contact distance of 3.035(8) Å between O(3)″ and C(N11) (2 − *x*, 1 − *y*, 2 − *z*). Normal

Can. J. Chem. Downloaded from www.nrcresearchpress.com by 78.46.186.204 on 09/07/12
For personal use only.

TABLE 2. Bond angles (deg) with estimated standard deviations in parentheses

Bonds	Angle (deg)	Bonds	Angle (deg)
C(6)—S(1)′—C(5)′	96.3(2)	C(12a)—C(1)—C(2)	120.8(6)
C(6)—S(3)′—C(4)′	96.9(2)	C(1)—C(2)—C(3)	120.2(6)
C(12)—S(1)″—C(5)″	97.0(2)	C(2)—C(3)—C(4)	120.4(6)
C(12)—S(3)″—C(4)″	97.6(2)	C(3)—C(4)—C(4a)	119.8(6)
C(6)′—O(2)′—C(7)′	117.6(5)	N(5)—C(4a)—C(12a)	118.8(4)
C(8)′—O(4)′—C(9)′	117.7(6)	N(5)—C(4a)—C(4)	120.9(5)
C(6)″—O(2)″—C(7)″	115.3(5)	C(12a)—C(4a)—C(4)	120.3(5)
C(8)″—O(4)″—C(9)″	115.9(4)	S(1)′—C(6)—S(3)′	104.1(3)
C(4a)—N(5)—C(6)	117.3(4)	S(1)′—C(6)—N(5)	112.4(3)
C(4a)—N(5)—C(N5)	116.7(5)	S(1)′—C(6)—C(6a)	109.6(4)
C(6)—N(5)—C(N5)	118.7(5)	S(3)′—C(6)—N(5)	110.3(3)
C(12)—N(11)—C(10a)	117.7(4)	S(3)′—C(6)—C(6a)	108.7(3)
C(12)—N(11)—C(N11)	118.8(5)	N(5)—C(6)—C(6a)	111.4(4)
C(10a)—N(11)—C(N11)	116.6(5)	C(6)—C(6a)—C(7)	123.5(5)
S(3)′—C(4)′—C(5)′	117.6(4)	C(6)—C(6a)—C(10a)	119.3(4)
S(3)′—C(4)′—C(8)′	119.5(4)	C(7)—C(6a)—C(10a)	117.1(5)
C(5)′—C(4)′—C(8)′	122.9(5)	C(6a)—C(7)—C(8)	121.8(6)
S(1)′—C(5)′—C(4)′	117.5(4)	C(7)—C(8)—C(9)	120.6(6)
S(1)′—C(5)′—C(6)′	116.2(4)	C(8)—C(9)—C(10)	119.7(6)
C(4)′—C(5)′—C(6)′	126.1(5)	C(9)—C(10)—C(10a)	120.5(6)
O(1)′—C(6)′—O(2)′	123.4(6)	N(11)—C(10a)—C(6a)	118.4(4)
O(1)′—C(6)′—C(5)′	122.7(6)	N(11)—C(10a)—C(10)	121.5(5)
O(2)′—C(6)′—C(5)′	113.5(6)	C(6a)—C(10a)—C(10)	120.0(5)
O(3)′—C(8)′—O(4)′	123.4(6)	S(1)″—C(12)—S(3)″	104.2(2)
O(3)′—C(8)′—C(4)	122.1(6)	S(1)″—C(12)—N(11)	112.5(3)
O(4)′—C(8)′—C(4)′	114.2(5)	S(1)″—C(12)—C(12a)	108.9(3)
S(3)″—C(4)″—C(5)″	117.7(4)	S(3)″—C(12)—N(11)	109.9(3)
S(3)″—C(4)″—C(8)″	119.3(4)	S(3)″—C(12)—C(12a)	108.8(3)
C(5)″—C(4)″—C(8)″	123.0(5)	N(11)—C(12)—C(12a)	112.2(4)
S(1)″—C(5)″—C(4)″	118.5(4)	C(12)—C(12a)—C(1)	123.8(5)
S(1)″—C(5)″—C(6)″	117.6(4)	C(12)—C(12a)—C(4a)	117.7(4)
C(4)″—C(5)″—C(6)″	123.9(5)	C(1)—C(12a)—C(4a)	118.5(5)
O(1)″—C(6)″—O(2)″	125.5(5)		
O(1)″—C(6)″—C(5)″	123.4(5)		
O(2)″—C(6)″—C(5)″	111.0(5)		
O(3)″—C(8)″—O(4)″	125.3(5)		
O(3)″—C(8)″—C(4)″	122.6(5)		
O(4)″—C(8)″—C(4)″	112.0(5)		

van der Waals intermolecular contacts are observed in the remainder of the structure.

Many crystal structures containing dithiole rings have been reported in the literature, invariably as a tetrathiafulvalene (TTF) derivative or addition complex. However, the present study appears to be the first crystal structure of a compound containing dithiole rings with the apical carbons being sp^3-hybridized. The rings are characterized by bends at the sulfurs giving two planar moieties, S(1)′, C(6)′, S(3)′ and S(1)′, C(4)′, C(5)′, S(3)′ in one ring, and S(1)″, C(6)″, S(3)″ and S(1)″, C(4)″, C(5)″, S(3)″ in the other with dihedral angles of 23.1° and 28.1°, respectively. These differ markedly from dithioles with sp^2-hybridized carbons at the apex, such as TTF (13) where the bend is only 2.1°. Molecular models show no intramolecular factors contributing to the large interplanar angles observed in the present structure. This suggests that packing forces accommodating the ester groups on carbons 4 and 5 of the dithioles dictate the pronounced ring bend.

The twist from the boat conformation in the tetrahydrodiazocine ring does not appear to be due to packing effects, but more likely originates from intramolecular effects such as internal ring strain. Hendrickson's tabulation of strain energies of various cycloalkanes (14) indicates that the boat conformation (the highest energy conformer) in cyclooctane is 10.3 kcal/mol greater in internal strain energy than the lowest energy conformer, the boat–chair suggesting that any degree of twist away from the boat conformation would be favored. In the present structure an additional tendency to twist from the boat conformation stems from a lone pair–lone pair repulsion between S(3)′...S(3)″. A pure boat conformation would place these lone pairs in close proximity to each other directly over the tetrahydrodiazocine ring, whereas a boat–boat conformation which maximizes the distance between the sulfur lone pairs would have the nitrogen-bound methyls overlapping. Hence, the twist from the pure boat conformation in the present structure represents a compromise between these two limiting interactions.

Bond angles around the nitrogens tend toward values of 120° indicating some degree of conjugation with the aromatic rings. However, the nitrogens cannot be considered pure sp^2-hybridized as they remain significantly distant (0.2 Å) from the planes defined by their three adjoining atoms. All other bond

Can. J. Chem. Downloaded from www.nrcresearchpress.com by 78.46.186.204 on 09/07/12
For personal use only.

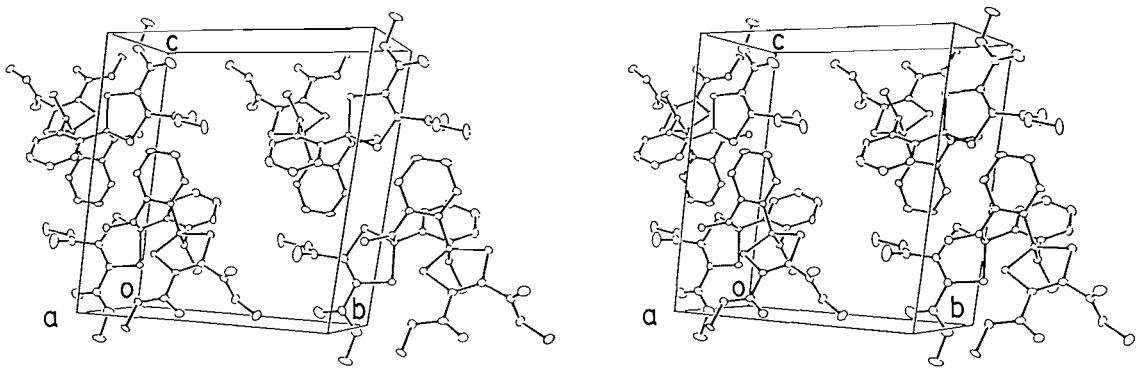

FIG. 3. Stereoview of the unit cell contents.

Can. J. Chem. Downloaded from www.nrcresearchpress.com by 78.46.186.204 on 09/07/12
For personal use only.

angles and lengths appear to have typical values with the exception of the dithiole rings for which there are no apparent crystallographic data with which to compare.

Experimental

The ^1H nmr and ^{13}C spectra were obtained in deuterochloroform solution using tetramethylsilane as an internal standard on Varian model EM360 and Bruker WH90 spectrometers, respectively. Mass spectra were obtained on a Finnigan model 1015 spectrometer, and thick-layer chromatography was performed on "Merck" silica gel type Kieselgel PF-254. Acetylenic reagents were distilled before use.

Reaction of N-*methyl-2,1-benzisothiazoline-3-thione (**1**a) with dimethyl acetylenedicarboxylate*

(*a*) Using equimolar proportions. The thione (**1***a*, 0.181 g, 1 mmol) and the ester (0.142 g, 1 mmol) were mixed in benzene (10 mL). An immediate purple color faded on standing or evaporation. The pale yellow oil from evaporation crystallized on trituration with ethanol and was recrystallized from a toluene/hexane 1:1 mixture or ethanol giving **2***a* as pale yellow prisms mp 195–196°C (93%).

(*b*) Using a 2:1 ratio of ester to thione. This gave substantially the same results as above.

(*c*) Using excess ester. To the thione (**1***a*, 0.181 g, 0.1 mmol) was added the ester (1 g, 0.704 mmol) and warmed gently until the purple color disappeared. The excess ester was removed *in vacuo* at 100°C and the residue chromatographed on silica gel with a benzene/chloroform 3:1 mixture. Two main bands were obtained. The faster running was the monoadduct dimer **2***a*, and the slower was the spiro diadduct **4***a*. The latter was eluted to give a pale yellow oil that crystallized from ethanol as pale yellow prisms mp 164–165°C (41%).

The nmr spectrum of **2***a*, δ, 3.23 (two 3H, s, N—CH_3); 3.82, 3.87 (four 3H, s, O—CH_3); 6.96–7.61 (two 5H bands, the aromatic protons). At 29 and 59°C the nmr spectra were identical. The mass spectrum, parent ion 323. $M^+/2 = 323$. *Anal.* calcd. for $C_{28}H_{26}N_2O_8S_4$: C 52.01, H 4.02, N 4.33, S 19.81; found: C 52.35, H 4.01, N 4.26, S 19.97.

The nmr spectrum of **4***a*, δ, 3.28 (3H, s, N—CH_3), 3.83 (two 3H, s, O—CH_3 on dithiole ring); 3.87, 3.90 (two 3H, s, O—CH_3 on the quinoline ring). *Anal.* calcd. for $C_{20}H_{19}NS_2O_8$: C 51.61, H 4.09, N 3.01, S 13.76; found: C 51.49, H 4.11, N 3.25, S 13.62.

Reaction of N-*methyl-2,1-benzisothiazoline-3-thione (**1**a) with ethyl propiolate*

(*a*) Using equimolar proportions. The thione (**1***a*, 0.362 g, 2 mmol) and ethyl propiolate (0.196 g, 2 mmol) in tetrahydrofuran (10 mL) were refluxed 1 h. The mixture became dark immediately but after 1 h was reddish. Evaporation gave a red oil which was chromatographed using a benzene:chloroform 3:1 mixture. A faster running colorless band overlaid by a red band and a slower running yellow band were evident. Removal of the faster band gave a reddish oil which on rechromatography could not be separated. However, the red material was labile and eventually a pale yellow oil was obtained. This was the monoadduct dimer **2***b* (65%). Removal of the slower running yellow band gave **4***b* as a crystalline solid which was recrystallized from ethanol as pale yellow needles mp 181–183°C (22%).

(*b*) Using 2 equiv. of ethyl propiolate. The thione (**1***a*, 0.085 g, 0.5 mmol) and ethyl propiolate (0.098 g, 1.00 mmol) in benzene (5 mL) were warmed gently. The solution rapidly became dark, then pale yellow. The solvent was removed under reduced pressure and the residue, a pale yellow semicrystalline material, was triturated with ethanol. The solid was collected and recrystallization from ethanol gave **4***b* as pale yellow needles (81%). The mother liquor on examination by tlc showed a complex mixture.

The mass spectrum of **2***b*, parent ion 279, $M^+/2 = 279$. The nmr spectrum, complex bands δ, 1.3, 4.3 (CH_3—CH_2—O—) 3.1–3.2 (N—CH_3), 6.9–7.6 (aromatic and vinyl). The ^{13}C spectrum likewise showed a mixture but at δ 160.8–161.2 (four carbonyl peaks) and 38.0–38.3 (four N—CH_3). *Anal.* calcd. for $C_{26}H_{26}N_2O_4S_4$: C 55.90, H 4.66, N 5.02, S 22.94; found: C 56.04, H 4.55, N 5.19, S 22.81.

The mass spectrum of **4***b*, 377, M^+ calcd. 377. The nmr spectrum. δ, 1.28 (two 3H, t, the ethyl CH_3), 4.15, 4.27 (two 2H, q, the CH_2—), 3.38 (3H, s, the N—CH_3), 6.97, 7.37 (two 1H, s, the vinyl protons); 6.65–8.50 (4H bands, the aromatic protons). *Anal.* calcd. for $C_{18}H_{19}NS_2O_4$: C 57.29, H 5.04, N 3.71, S 16.98; found: C 57.46, H 5.35, N 3.65, S 16.76.

Reaction of N-*methyl-2,1-benzisothiazoline-3-thione (**1**a) with dibenzoylacetylene*

The thione (**1***a*, 0.362 g, 2.0 mmol) and dibenzoylacetylene (0.468 g, 2.0 mmol) were mixed in toluene (10 mL). An immediate dark red color was produced. The solution was refluxed 3 h and evaporated. The dark red tar was examined by tlc, using 1% methanol in chloroform as an eluent. Four main bands were evident: yellow, orange, red, and orange in order of elution. The two middle bands were collected and evaporated to give oils which slowly deposited crystals under toluene. The red band gave small red crystals, mp 270–290°C, and the orange band gave orange prisms, mp 265–267°C. The mass spectrum of the red material, M 415, M^+ calcd. for a 1:1 adduct was 415. The mass spectrum of the orange prisms, M 383, M^+ calcd. for a 1:1 adduct − S, 383. Owing to the small quantities these were not examined further.

Reaction of N-*methyl-2,1-benzisothiazoline-3-thione (**1**a) with phenylacetylene to form* 7a

The thione (**1***a*, 0.362 g, 2.0 mmol) and phenyl acetylene (1 mL) were refluxed in toluene (10 mL) for 24 h. The mixture was separated by tlc and the intense red band collected. Evaporation and crystallization from a petroleum ether/benzene 1:1 mixture gave **7***a* as dark red needles mp 155°C lit (8) 155°C mixture mp 155°C (45%).

Reaction of N-*benzyl-2,1-benzisothiazoline-3-thione (**1**a) with phenylacetylene to form* 7b

The thione (**1***a*, 0.257 g, 1.0 mmol) and phenylacetylene (0.5 mL) in

Can. J. Chem. Downloaded from www.nrcresearchpress.com by 78.46.186.204 on 09/07/12
For personal use only.

toluene (10 mL) were refluxed for 24 h. The mixture was examined by tlc and many colored bands were evident, but the main dark red band contained most material. Extraction gave a dark red oil which crystallized partly under cyclohexane. The dark red material was collected. Recrystallization from cyclohexane gave **7***b* as dark red prisms mp 150–152°C (16%). The mother liquor contained another material but it could not be satisfactorily purified.

The nmr spectrum of **7***b* δ, 5.16 (2H, s, the benzylic protons), 7.02–8.24 (14H, bands, the aromatic protons), 8.57 (1H, s, the heterocyclic proton). The mass spectrum 359, M^+ calcd. 359. *Anal.* calcd. for $C_{22}H_{17}NH_2$: C 73.54, H 4.74, N 3.90, S 17.83; found: C 73.61, H 4.05, N 3.83, S 18.01.

Reaction of N*-methyl-1,2-benzisothiazoline-3-thione with dimethyl acetylenedicarboxylate to form* **4**d

The thione (0.181 g, 1.0 mmol) and dimethyl acetylenedicarboxylate (0.142 g, 1.0 mmol) in benzene (10 mL) were refluxed 24 h. Evaporation gave a yellow oil which on examination by tlc gave two main yellow bands. The first contained starting thione and the second on elution gave a yellow oil which crystallized under ethanol. Recrystallization from methanol gave **4***d* as yellow needles mp 126–127°C (42%).

When the reaction was performed with a 1:2 molar ratio of reactant, the yield was 63%.

The nmr spectrum of **4***d*, δ, 2.97 (3H, s, N—CH_3), 3.66, 3.85, 3.92, 3.96 (four 3H, s, O—CH_3), 7.22–7.93 (4H, bands, the aromatic protons). The mass spectrum, 465 M^+ calcd. 465. *Anal.* calcd. for $C_{20}H_{19}NS_2O_8$: C 51.61, H 4.09, N 3.01, S 13.76; found: C 51.47, H 4.21, N 3.16, S 13.85.

Reaction of N*-phenyl-2,1-benzisothiazoline-3-thione (***1***b) with dimethyl acetylenedicarboxylate*

Equimolar quantities of the two materials were allowed to react in benzene. A dark violet color was produced immediately. The solution was refluxed 1 h and examination by tlc showed a complex mixture which could not be separated.

Reaction of N*-benzyl-2,1-benzisothiazoline-3-thione (***1***c) with dimethyl acetylenedicarboxylate*

The thione (**1***c*, 0.257 g, 1.0 mmol) and the ester (0.142 g, 1.0 mmol) in benzene (10 mL) were refluxed 1 h. Work-up gave a yellow oil which was complex. This was chromatographed (benzene/chloroform, 1:1) and a strongly adsorbed yellow band removed. A yellow oil was obtained which was still a mixture, but appeared to be substantially a 1:2 adduct. This was not further examined.

Reaction of benzo-1,2-dithiole-3-thione with ethyl propiolate

The thione (0.92 g, 5 mmol) and the ester (0.49 g, 5 mmol) in benzene (10 mL) were heated 1 h at reflux. The red solution rapidly became dark yellow, then lightened somewhat. Evaporation gave an oil which was separated by chromatography (benzene/chloroform, 1:1) into starting thione and a yellow oil which crystallized on standing under methanol. This was crystallized from methanol giving **6** as yellow prisms mp 72°C (86%, based on the amount of ester). When the reaction was performed with a 2:1 molar ratio of ester to thione, only the compound **6** was isolated.

The nmr spectrum of **6**, δ, 1.13–1.43 (two superimposed 3H, t, C—CH_3), 4.03–4.53 (two superimposed 2H, q, —CH_2—), 6.97, 7.65 (two 1H, s, vinyl protons), 6.95–8.50 (4H bands, aromatic protons). The mass spectrum 380 M^+ calcd. 380. *Anal.* calcd. for $C_{17}H_{16}S_3O_4$: C 53.68, H 4.21, S 25.26; found: C 53.81, H 4.22, S 25.51.

Crystallographic analysis of **2**a

Crystals of **2***a* were grown from an ethanol solution at room temperature. The well-defined faces made the crystals readily indentifiable as belonging to the pinacoidal class. The one chosen for data collection measured 0.18 mm × 0.26 mm × 0.40 mm and was mounted in a general orientation on a Nicolet *R3m* diffractometer. The unit cell and an orientation matrix were derived from the setting angles of 25 centered reflections with $31° < 2\theta < 44°$. Data were collected with graphite-monochromatized MoKα radiation. An ω–2θ scan type was employed with scan widths determined by $2.00 + (2\theta_{K\alpha_2} - 2\theta_{K\alpha_1})°$. During each scan, peak and peak backgrounds were counted for equal times. Virtually no decrease in intensity of any of the three standard reflections was observed throughout the exposure period of 39.7 h. Data processing, which included corrections for Lorentz and polarization effects, indicated that 78% of the 3910 measured reflections with $3° \leq 2\theta \leq 45°$ were considered observed with $I \geq 1.5\sigma(I)$, where $\sigma(I) = R[S + B_L + B_R]^{1/2}$; R is the scan rate; S, the total scan count; and B_L, B_R, the left and right background counts, respectively.

The structure was solved by direct methods using the MULTAN system of programs (15) which indicated the positions of 39 out of a total of 42 non-hydrogen atoms in the asymmetric unit. Subsequent cycles of full-matrix least-squares refinement and difference Fourier

TABLE 3. Final positional parameters (fractional × 10^4) and isotropic thermal parameters ($Å^2$ × 10^3) with estimated standard deviations in parentheses

Atom	*x*	*y*	*z*	U_{eq}†
S(1)′	58233(22)	1341(11)	35806(11)	54
S(3)′	65651(21)	15427(10)	18035(10)	48
S(1)″	90703(19)	48916(10)	30815(10)	45
S(3)″	104738(18)	30367(10)	23045(9)	40
O(1)′	8180(8)	−1858(4)	2582(5)	110
O(2)′	5416(6)	−1932(3)	2779(4)	79
O(3)′	7043(10)	−897(5)	579(4)	118
O(4)′	7398(8)	661(4)	32(3)	94
O(1)″	12015(6)	6457(3)	1896(3)	70
O(2)″	10015(5)	6378(3)	916(3)	54
O(3)″	12900(5)	4924(3)	370(3)	56
O(4)″	12971(5)	3268(3)	668(3)	48
N(5)	8284(6)	1500(3)	3390(3)	40
N(11)	7099(5)	3450(3)	2632(3)	38
C(4)′	6712(7)	278(4)	1686(4)	47
C(5)′	6449(8)	−360(4)	2501(4)	51
C(6)′	6770(9)	−1459(5)	2585(5)	61
C(7)′	5600(10)	−3002(5)	2931(6)	80
C(8)′	7115(9)	−43(5)	716(5)	60
C(9)′	7676(15)	415(9)	−962(6)	115
C(4)″	11177(7)	4168(4)	1709(4)	40
C(5)″	10505(7)	4997(4)	2052(4)	41
C(6)″	10970(7)	6025(4)	1615(4)	43
C(7)″	10391(10)	7360(5)	431(6)	66
C(8)″	12424(7)	4173(4)	837(4)	41
C(9)″	14162(8)	3198(5)	−188(4)	58
C(1)	8623(7)	3469(5)	4922(4)	47
C(2)	8604(8)	2934(6)	5835(4)	55
C(3)	8531(8)	1932(6)	5945(4)	58
C(4)	8448(8)	1447(5)	5151(4)	51
C(4a)	8453(6)	1982(4)	4227(4)	38
C(6)	6605(7)	1407(4)	3152(3)	39
C(6a)	5362(7)	2184(4)	3563(4)	39
C(7)	3968(7)	1955(5)	4241(4)	46
C(8)	2893(8)	2669(5)	4597(5)	56
C(9)	3104(8)	3647(5)	4274(5)	61
C(10)	4463(8)	3911(5)	3617(5)	52
C(10a)	5615(6)	3191(4)	3269(4)	38
C(12)	8607(6)	3544(3)	3060(3)	35
C(12a)	8569(6)	2999(4)	4105(3)	35
C(N11)	6825(10)	4048(5)	1709(5)	51
C(N5)	9598(9)	738(5)	3157(5)	54

†U_{eq} is equal to one third the trace of the diagonalized anisotropic temperature-factor matrix.

maps[1] revealed the remaining non-hydrogen atoms, as well as 17 of the 26 hydrogens; the other 9 hydrogen atoms were placed at calculated positions and not refined. In the final cycles of refinement, all non-H atoms were assigned anisotropic temperature factors while the thermal motion of H atoms was assumed to be isotropic. The refinement of 448 parameters converged for the 3037 observed data at $R = 0.056$, $R_w = 0.075$ and $S = 1.209$ where $R = \Sigma||F_o| - k|F_c||/\Sigma|F_o|$ and $R_w = [\Sigma w(|F_o| - k|F_c|)^2/\Sigma w|F_o|^2]^{1/2}$. For all data $R = 0.076$ and $R_w = 0.075$. The function $\Sigma w\Delta^2$, where Δ^2 is $(|F_o| - k|F_c|)^2$ was minimized throughout the refinement with the weights, w, for observed reflections derived from the expression $w = [1 + ((|F_o| - a)/b)^2]^{-1}$. For this structure, $a = 11.6$ and $b = 20.0$ were found to be suitable constants in the above expression. Data classified as unobserved were assigned zero weights during refinement. Δ/σ (max) in the final cycle was 0.910 and the final difference map showed random fluctuations in the range -0.315–0.477 e Å^{-3}. X-ray atomic scattering factors were taken from Cromer and Mann (16) for non-H atoms, and from Stewart, Davidson, and Simpson (17) for H atoms. Final atomic positional parameters for non-H atoms are listed in Table 3.[2]

Crystal data are as follows:

$C_{28}H_{26}S_4O_8N_2$ fw = 646.784

Triclinic, $P\bar{1}$, $a = 7.9465(10)$, $b = 13.6421(14)$, $c = 13.9183(18)$ Å, $\alpha = 82.38(1)$, $\beta = 83.67(1)$, $\gamma = 85.77(1)$ deg, $F(000) = 672$, $V = 1483.8$ Å^3, $Z = 2$, $\rho_c = 1.448$, $\rho_o = 1.436$ g cm^{-3}, $\mu = 3.57$ cm^{-1} (21°C; MoKα, $\lambda = 0.71073$ Å).

[1]Computation was carried out on the University of Manitoba Computer Services Department's Amdahl 580/5850 mainframe computer using locally written programs and SHELXTL (version 4) for processing, and modified versions of the following programs for structure refinement and calculations. ORFLS: W. R. Busing; K. O. Martin; H. A. Levy. Report ORNL-TM-305, 1962; Oak Ridge National Laboratory, Oak Ridge, TN. FORDAP: A. Zalkin. ORFFE: W. R. Busing; K. O. Martin; H. A. Levy Report ORNL-TM-306, 1964; Oak Ridge, National Laboratory, Oak Ridge, TN. ORTEP II: C. K. Johnson Report ORNL-TM-306-5138, 1976; Oak Ridge National Laboratory, Oak Ridge, TN.

[2]Tables of hydrogen positional and thermal parameters, anisotropic thermal parameters, bond lengths and angles involving hydrogens, torsion angles, and observed and calculated structure factor amplitudes may be purchased from the Depository of Unpublished Data, CISTI, National Research Council of Canada, Ottawa, Ont., Canada K1A 0S2.

Acknowledgements

We wish to thank the Natural Sciences and Engineering Council of Canada for financial support of this work. We also wish to thank Mr. K. Marat for the preparation of nmr spectra, and Mr. W. Buchannon for the preparation of mass spectra. We also thank the University of Manitoba Geological Sciences Department for use of the X-ray diffraction facilities and the Computer Services Department for assistance.

1. M. S. CHAUHAN, M. E. HASSAN, and D. M. McKINNON. Can. J. Chem. **52**, 1738 (1974).
2. D. B. J. EASTON, D. LEAVER, and T. J. RAWLINGS. J. Chem. Soc. Perkin Trans. I, 41 (1972).
3. R. CROSSLEY, A. P. DOWNING, M. NOGRADI, A. BRAGGA DE OLIVIERA, W. D. OLLIS, and I. O. SUTHERLAND. J. Chem. Soc. Perkin Trans. I, 205 (1973).
4. P. DE MAYO and H. Y. NG. Can. J. Chem. **55**, 3763 (1977).
5. R. OKAZAKI, K. SUNAGAWA, M. KOTERA, and N. INAMOTO. TETRAHEDRON LETT. 3815 (1976).
6. A. PADWA, D. DEHM, T. OINE, and G. A. LEE. J. Am. Chem. Soc. **97**, 1837 (1975).
7. M. FISCHER and F. WAGNER. Chem. Ber. **102**, 3486 (1969).
8. D. M. McKINNON, K. A. DUNCAN, and L. M. MILLAR. Can. J. Chem. **60**, 440 (1982).
9. H. DAVY, M. DEMUYNCK, D. PAQUER, A. ROUESSAC, and T. VIALLE. Bull. Soc. Chim. Fr. 1150 (1966).
10. H. BEHRINGER, D. BENDER, J. FALKENBURG, and R. WIEDENMANN. Chem. Ber. **101**, 1428 (1968).
11. D. PAUER and R. POU. Bull. Soc. Chim. Fr. 120 (1976).
12. S. DAVIDSON and D. LEAVER. J. Chem. Soc. Chem. Commun. 540 (1972).
13. W. F. COOPER, N. C. KENNY, J. W. EDMONS, A. NAGEL, F. WUDL, and P. COPPENS. J. Chem. Soc. Chem. Commun. **889** (1971).
14. J. B. HENDRICKSON. J. Am. Chem. Soc. **89**, 7036 (1967).
15. P. MAIN, S. J. FISKE, S. E. HULL, L. LESSINGER, G. GERMAIN, J.-P. DECLERCQ, and M. M. WOOLFSON. MULTAN 80. A system of computer programs for the automatic solution of crystal structures from X-ray diffraction data. Universities of York, England, and Louvain, Belgium. 1980.
16. D. T. CROMER and J. B. MANN. Acta Crystallogr. Sect. A, **24**, 321 (1968).
17. R. F. STEWART, E. R. DAVIDSON, and W. T. SIMPSON. J. Chem. Phys. **42**, 3175 (1965).

Can. J. Chem. Downloaded from www.nrcresearchpress.com by 78.46.186.204 on 09/07/12
For personal use only.

Étude du comportement d'un alliage Cu–Ni 70:30 dans une solution de NaCl à 3% par la détermination de sa résistance de polarisation

YVAN MASSIANI, SYLVIE PETETIN, GUY NGO NGOC ET JEAN-PIERRE CROUSIER[1]

Laboratoire de chime des matériaux—corrosion, Université de Provence, 13331 Marseille CEDEX 3 France

Reçu le 19 septembre 1986

YVAN MASSIANI, SYLVIE PETETIN, GUY NGO NGOC et JEAN-PIERRE CROUSIER. Can. J. Chem. **65**, 1254 (1987).

L'utilisation d'une méthode galvanostatique permet de suivre l'évolution de la résistance de polarisation d'un alliage cuivre–nickel 70:30, en fonction du temps, malgré la présence d'une couche de produits de corrosion formée à la surface de l'échantillon au bout de plusieurs jours d'immersion. La résistance de polarisation de l'alliage qui est, au début de l'immersion, comparable à celle du cuivre, se rapproche, aprés plusieurs jours de celle du nickel pur.

YVAN MASSIANI, SYLVIE PETETIN, GUY NGO NGOC, and JEAN-PIERRE CROUSIER. Can. J. Chem. **65**, 1254 (1987).

A galvanostatic method can be used to measure the evolution of the polarization resistance of a 70:30 copper–nickel alloy with time, in spite of the presence of a layer of corrosion products formed on the surface of the sample after a few days of immersion. At the beginning, the polarization resistance of the alloy is similar to that of copper; after many days, it evolves toward that of pure nickel.

[Journal translation]

Can. J. Chem. Downloaded from www.nrcresearchpress.com by 72.64.146.136 on 09/07/12
For personal use only.

Introduction

Malgré un grand nombre de travaux, le mécanisme de dissolution des alliages Cu–Ni 70:30 n'est pas totalement élucidé. Si la plupart des auteurs concluent, comme dans le cas des alliages Cu–Zn, Cu–Mn, à la dissolution de l'élément allié au cuivre (1–3), d'autres envisagent la possibilité d'une décuprisation (4–6). Dans le cas des laitons, la dézincification est visible au microscope sur une coupe transversale (1). Dans le cas des alliages Cu–Ni, la dénickélisation ou la décuprisation n'a pas la même profondeur et ne peut être mise en évidence par observation au microscope. Les méthodes électrochimiques, qui concernent les atomes en surface, permettent d'observer des variations de composition superficielle.

Certains auteurs (2, 7–10) ont montré que la dissolution d'un alliage est différente en corrosion libre et sous polarisation anodique ou même cathodique. Selon le potentiel, l'alliage passe de la dissolution sélective de l'un des éléments à la dissolution simultanée de chacun d'eux.

Pour détecter une éventuelle modification de la composition à la surface de l'alliage, il faut suivre l'évolution du courant de corrosion en fonction de la durée de l'immersion. Cela est possible en utilisant une méthode qui permet d'effectuer des mesures à différents intervalles de temps, sans interrompre l'immersion de l'échantillon, tout en évitant de fortes surtensions éloignant trop l'électrode de l'équilibre.

Les mesures de résistance de polarisation R_p répondent à ces exigences. Elles présentent plusieurs avantages : (*i*) elles sont effectuées *in situ*; (*ii*) elles sont non destructives, permettant ainsi des études ultérieures du même échantillon; (*iii*) elles sont en général très rapides à effectuer; (*iv*) dans le cas d'expériences comparatives, elles constituent un test d'évolution du comportement du matériau.

Si on utilise l'approximation de l'équation de Butler–Volmer appliquable, pour une faible surtension, autour de E_{cor} ($\eta = \mp 10$ mV), i est une fonction linéaire du potentiel d'électrode.

Dans ces conditions, R_p et i_{cor} sont reliées par la relation de Stern et Geary :

$$R_p = \frac{1}{2{,}3\, i_{cor}} \cdot \frac{\beta_a \cdot \beta_c}{\beta_a + \beta_c}$$

avec

$$\left[\frac{d\eta}{di}\right]_{\eta \to 0} = R_p$$

η étant la surtension.

Puisque la résistance de polarisation est inversement proportionnelle à l'intensité du courant de corrosion, son évolution au cours du temps permet de suivre l'évolution du courant de corrosion, si on admet que β_a et β_c sont constantes.

Mais cette hypothèse est mise en défaut si, au cours du même temps il y a recouvrement de la surface comme dans le cas de la formation d'une couche de produit de corrosion. C'est la situation que nous avons rencontrée au cours de l'étude du comportement des alliages Cu–Ni dans des solutions de NaCl à 3%.

Dans ce cas, d'une part la pente anodique β_a varie et augmente avec le temps d'immersion, d'autre part la partie cathodique de la courbe de polarisation ne permet pas de tracer une droite de Tafel à cause de la «bosse cathodique» déjà signalée sur le cuivre pur (11). Il est donc difficile de passer de R_p à i_{cor}. Néanmoins une étude de l'évolution de la R_p en fonction du temps d'immersion peut donner des indications sur une modification de la composition en surface. Efird (12) a étudié aussi les alliages Cu–Ni 70:30 et 90:10 et montré que si dans les premières minutes leur résistance de polarisation est différente, celle du 90:10 étant la plus faible, après quelques heures d'immersion leur valeur est la même. Ce résultat peut s'expliquer par un enrichissement en nickel de la surface.

Nous avons repris cette méthode sur l'alliage Cu–Ni 70:30 mais aussi sur le cuivre et le nickel purs dont la modification en surface n'est pas le résultat d'une dissolution sélective comme dans le cas d'un alliage.

Mesures des résistances de polarisation

Très souvent, la méthode par balayage de potentiels autour du potentiel de corrosion est utilisée. C'est un test très rapide. Cependant, on n'est pas sûr avec un tel protocole d'être dans un état quasi stationnaire; de plus avec les méthodes à potentiel contrôlé, dans le cas où E_{cor} varie avec le temps, la tension appliquée peut ne plus correspondre à la zone de linéarité entre E et i.

Par contre, si on impose le courant, quelle que soit l'évolution

1. Auteur à qui adresser toute correspondance.

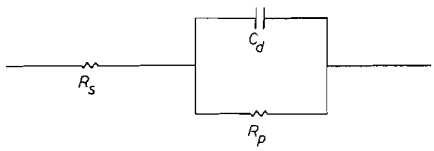

FIG. 1. Schéma équivalent de l'interface électrode–solution.

de E_{cor}, en choisissant convenablement l'échelon d'intensité, on peut ne perturber que très faiblement le système. C'est ce qui nous conduit à utiliser une méthode à intensité contrôlée. Plusieurs méthodes galvaniques sont utilisées :

Certains auteurs (13) appliquent un courant constant dont l'intensité crée une surtension très inférieure à 10 mV. Puis des incréments d'intensité sont ajoutés successivement, jusqu'à obtention d'une surtension de l'ordre de 10–15 mV. Le temps d'application du courant est le même, quelle que soit l'intensité choisie.

On obtient ainsi des couples de points (E,i) pendant la polarisation galvanostatique, dont le graphe est une droite de pente $\Delta E/\Delta i = R(\Omega)$. Si i est exprimé en A cm^{-2} et E en volts, on obtient R_p (Ω cm^2).

Cependant, cette technique est peu adaptée dans deux cas : (i) quand la résistance de l'électrolyte, R_s, est grande : on introduit alors un facteur IR_s qui est très important et qui conduit à une erreur importante sur la mesure des potentiels; et (ii) quand il y a modification des conditions à la surface, par exemple par formation d'une couche de produits de corrosion.

Utilisation d'une méthode galvanostatique alternative

Récemment, une méthode galvanostatique a été utilisée pour déterminer des résistances de polarisation dans des sols (9). Il s'agit d'appliquer un signal rectangulaire alternatif, d'intensité constante en valeur absolue, choisi pour provoquer une surtension de l'éléctrode de travail qui n'excède pas les limites de linéarité de E–i, c'est-à-dire $\eta = \mp 10$ mV.

Dans ces conditions, certains inconvénients des différentes autres méthodes sont supprimés : le potentiel obtenu par application du courant suit les éventuelles fluctuations du potentiel de repos, l'état quasi stationnaire est atteint rapidement, et la présence d'une couche de produit de corrosion n'est pas un obstacle à la mesure.

Cette méthode a été adaptée pour déterminer la résistance de polarisation du cuivre, nickel et du Cu–Ni 70:30.

Principe de la méthode

Lorsqu'on applique un échelon de courant I à un système représenté par le schéma équivalent (Fig. 1), la surtension $\eta = E - E_{cor}$ de l'électrode de travail peut s'exprimer par :

$$I = C_d \frac{d\eta}{dt} + I_{cor}\left[\exp\left(\frac{2{,}3\eta}{\beta_a}\right) - \exp\left(\frac{-2{,}3\eta}{\beta_c}\right)\right]$$

Si η est petit ($\eta = \pm 20$ mV), cette équation se réduit à :

$$I = C_d \cdot \frac{d\eta}{dt} + \frac{\eta}{R_p}$$

avec C_d la capacité de double couche (cf. équation de Stern et Geary).

Si l'impulsion de courant est alternative, carrée et appliquée à la fréquence f, l'équation précédente devient (14) :

$$E(f) = IR_s + IR_p \tanh\left(\frac{1}{4R_pC_d} \cdot \frac{1}{f}\right)$$

Quand la fréquence f est infiniment grande, cette équation

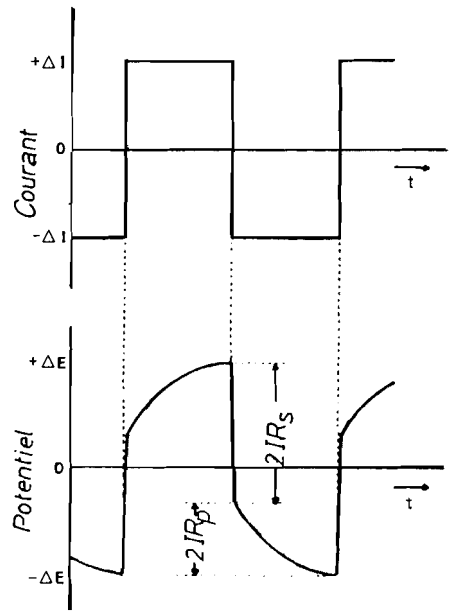

FIG. 2. Schéma du signal appliqué et du signal recueilli sur l'échantillon.

tend vers une valeur limite telle que :

$$E(f) = IR_s$$

mais quand $f \to 0$, $E(f) = IR_s + IR_p$. Par différence, on trouve donc la valeur de R_p.

Schématiquement, la figure 2 représente le signal appliqué, et la forme du signal réponse.

On peut par suite tracer le graphe R en fonction de la fréquence de balayage des impulsions galvanostatiques (fig. 3). Sur celui-ci, on repère directement les paliers permettant d'atteindre la valeur de R_s, et de $R_s + R_p$ donc de R_p.

Partie expérimentale

Les mesures ont été réalisées avec des échantillons de 1 cm^2 de surface préparés à partir d'un alliage Niclal 30 préparé par le Comptoir Lyon Alemand Louyot (Paris). Ces échantillons étaient polis sur papier abrasif 600 sous courant d'eau puis rincés plusieurs fois dans un bac à ultra-sons.

Tous les essais sont effectués dans une solution de NaCl à 3% en aération naturelle et non agitée. Ils nécessitent : un générateur de courant; un générateur de signaux rapides Tacussel type GSTP 3, celui-ci permet de choisir la forme du signal et sa fréquence entre 4×10^{-5} et 5000 Hz; un millivoltmètre à forte impédance d'entrée pour suivre la différence de potentiel entre l'éléctrode de travail et l'électrode de référence; une table traçante JJ Instruments PL3; un oscilloscope à deux voies permettant de visualiser le signal obtenu par application de courant à haute fréquence, en même temps que le signal appliqué. L'oscilloscope utilisé est un Hameg type HM 705; et un amplificateur différentiel assurant un double fonction : l'amplification (jusqu'à 1000 fois) du signal choisi, et un rôle de filtre, éliminant les phénomènes de «retour» jusqu'à l'oscilloscope. La limite d'amplification est de l'ordre de 10 V.

Le montage ainsi réalisé permet d'appliquer un courant de 0,5 μA. Ce courant de très faible intensité ne provoque qu'une faible surtension qu'il faut considérablement amplifier pour pouvoir la mesurer. C'est cette très faible surtension qui nous permet de toujours nous placer dans la zone où la relation entre E et i est linéaire.

Dans le cas du cupronickel 70:30, dans une solution de NaCl à 3%, le potentiel de corrosion est égal à -210 mV/ecs; lorsque l'on applique un courant alternatif carré de 0,5 μA, la surtension de l'électrode est très faible et la réponse en tension est apparemment identique à celle

Can. J. Chem. Downloaded from www.nrcresearchpress.com by 72.64.146.136 on 09/07/12
For personal use only.

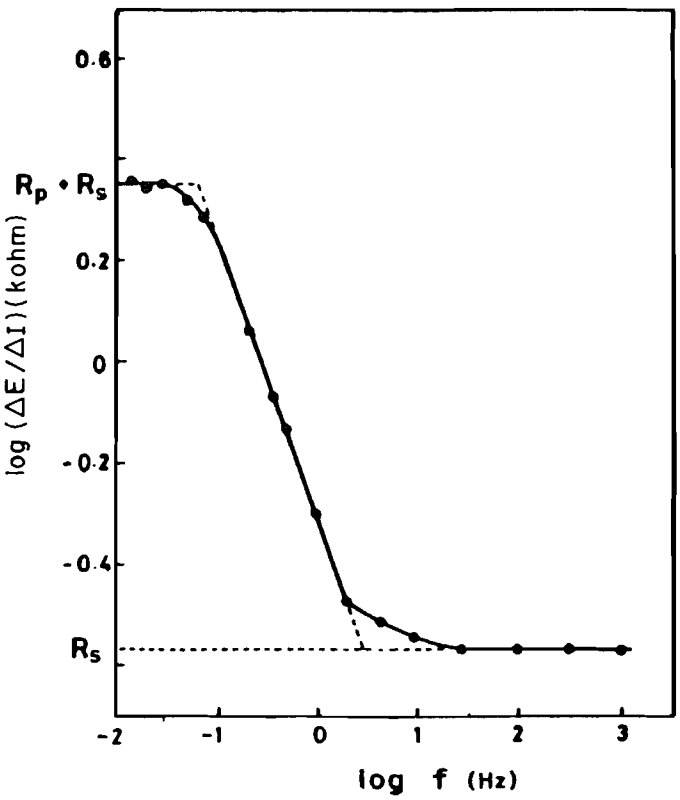

FIG. 3. Résistance de l'interface en fonction de la fréquence du signal appliqué (9).

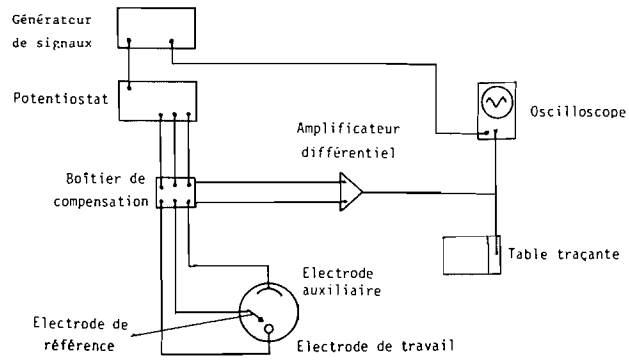

FIG. 4. Montage expérimental. La résistance extérieure, permettant de transformer la rampe de tension en rampe d'intensité, a été intégrée au boitier de compensation.

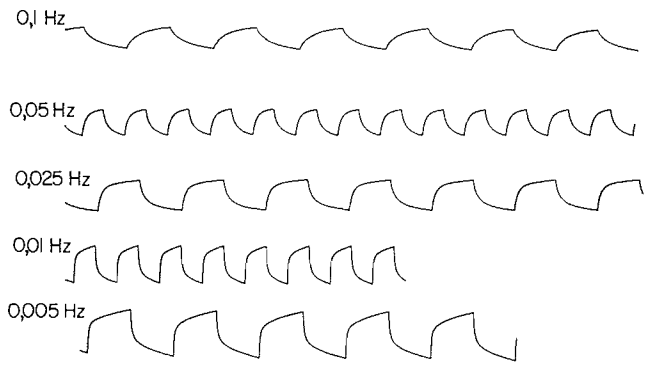

FIG. 5. Signal $E = f(t)$ sur Cu–Ni après 64 jours d'immersion.

obtenue sans surimposer de signal carré, c'est-à-dire identique à la tension délivrée par l'électrode au repos. Il faut donc amplifier ce signal. C'est le rôle de l'amplificateur différentiel. Mais ce dernier amplifie tout le signal : la tension de l'électrode au repos plus la surtension due au courant appliqué. On est, de ce fait, très vite limité dans l'amplification, par le maximum de l'appareil fixé à 10 V, soit environ 50 fois notre signal. Nous avons dû décaler le signal de la valeur du potentiel de corrosion, afin de n'amplifier que le signal provoqué par l'application du courant. Un système de compensation propre à notre montage a été mis au point.

Deux potentiomètres permettent d'opérer soit un réglage grossier, soit un réglage fin de la ligne de base. Pour un gain maximum de l'amplificateur différentiel et une bonne sensibilité de l'oscilloscope, celle-ci doit être centrée sur le zéro de l'écran.

Le montage définitif est représenté sur la figure 4.

Par cette technique nous avons mesuré la résistance de polarisation du cuivre, du nickel, du cupronickel 70:30 sans immersion préalable, et du cupronickel 70:30 après un temps d'immersion allant de quelques heures à 73 jours.

Une fois le potentiel de corrosion stabilise (pour les mesures faites après 15 min d'immersion), celui-ci est repéré sur l'oscilloscope. On branche alors le système de compensation, et par combinaison de celui-ci et de l'amplificateur différentiel, on décale la ligne de base sur le zéro de l'écran, jusqu'à obtention du gain optimum. Ce réglage effectué, on applique le courant alternatif carré d'intensité égale à 0,5 μA, en commençant par les fréquences élevées. En effet, celles-ci ne risquent pas d'endommager l'interface des échantillons. Nous reviendrons ultérieurement sur ce dernier point. On effectue un balayage en fréquence entre 5 kHz et 10^{-3} Hz, parfois 10^{-4} Hz. Pour chaque fréquence, on relève l'amplitude crête à crête du signal du potentiel de corrosion de l'électrode de travail. Grâce à la rémanence de son écran, l'oscilloscope permet de mesurer des signaux d'assez basse fréquence : 2,5–3 Hz. En deçà, les signaux sont enregistrés sur une table traçante.

Résultats

Chacun des échantillons de cuivre, nickel et cupronickel 70:30 a fait l'objet d'une étude de la résistance de polarisation en fonction de la fréquence du courant alternatif appliqué. L'allure générale des enregistrements sur table traçante ne diffère pas avec la nature de l'échantillon. Nous donnons l'exemple d'enregistrement pour Cu/Ni 70:30 (fig. 5). Les valeurs des résistances ainsi mesurées sont ensuite reportées sur un graphe $R = f(\log f)$ (fig. 6).

Le palier obtenu à basse fréquence représente la somme de la résistance de la solution, R_s, et de la résistance de polarisation, R_p. Le palier obtenu à haute fréquence donne la résistance de l'électrolyte R_s seule.

Nous avons obtenu après 15 min d'immersion des résistances de polarisation pour le cuivre et le nickel purs, égales à :

$$R_p(\text{Cu}) = 9\,000\,\Omega\ \text{cm}^2$$

$$R_p(\text{Ni}) = 115\,000\,\Omega\ \text{cm}^2$$

Ces mesures ont été effectuées un grand nombre de fois, donnant des valeurs très reproductibles pour le cuivre et pour le nickel.

Les valeurs de R_p et R_s obtenues pour le cupronickel 70:30 après différents temps d'immersion sont reportés dans le tableau 1.

La valeur trop grande de R_s pour des solutions aussi conductrice que NaCl 3% pourrait provenir de la limitation, avec notre appareillage, du balayage aux fréquences très élevées.

La valeur de la résistance de polarisation du cupronickel 70:30 après 15 min d'immersion est elle aussi très reproduc-

Can. J. Chem. Downloaded from www.nrcresearchpress.com by 72.64.146.136 on 09/07/12
For personal use only.

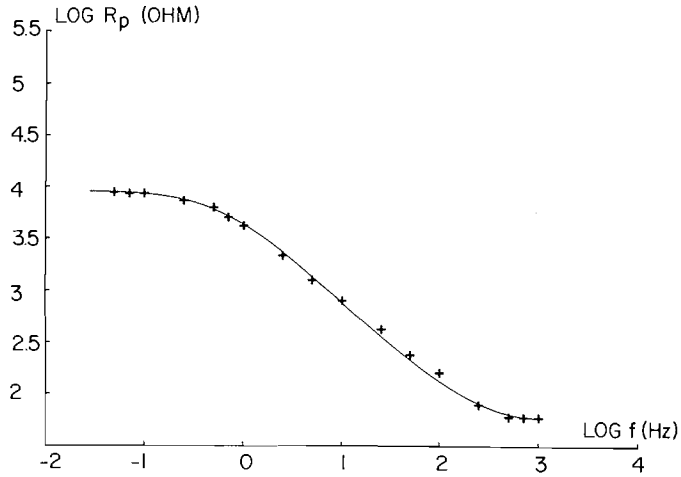

FIG. 6. Résistance de l'interface d'un Cu–Ni en fonction de la fréquence du signal.

TABLEAU 1. Evolution de la résistance de polarisation de l'alliage cuivre–nickel 70:30 en fonction du temps d'immersion

Temps d'immersion	R_p (Ω cm^2)	R_s(Ω)
15 min	8 950	50
5 h	11 040	60
1,5 d	37 000	40
2 d	31 600	40
4 d	43 300	40
5 d	41 000	40
68 d	59 220	30
71 d	95 000	90
73 d	100 000	120

tible, elle est pratiquement égale à celle du cuivre pur et vaut 8950 Ω cm^2.

Après environ 48 h, une couche de produits de corrosion se forme à la surface du cupronickel. Cette couche ne gêne en rien la mesure de résistance (fig. 5), alors qu'elle la perturbait grandement dans les méthodes classiques.

Conclusion

Cette méthode a permis de suivre l'évolution de la résistance de polarisation d'un alliage Cu–Ni 70:30 en fonction du temps d'immersion dans une solution de NaCl, malgré la formation d'une couche de produit de corrosion. Sa valeur, qui est proche de celle du cuivre pur au début de l'immersion, se rapproche, après plusieurs jours, de celle du nickel pur. Ceci indique une diminution de la vitesse de corrosion de l'alliage lorsque le temps d'immersion augmente; la vitesse de dissolution ne change pas avec le temps d'immersion dans le cas du cuivre ou du nickel pur et elle peut donc être reliée à une décuprisation de la surface de l'échantillon.

1. H. W. PICKERING et P. J. BYRNE. J. Electrochem. Soc. **116**, 1492 (1969).
2. M. J. PRYOR et K. S. KAR. J. Electrochem. Soc. **129**, 2157 (1982).
3. D. S. KEIR et M. J. PRYOR. J. Electrochem. Soc. **127**, 2138 (1980).
4. E. MOR, V. SCOTTO et A. TREVIS. Corros. Trait. Prot. Finition, **18**, 7 (1970).
5. H. P. DHAR, R. E. WHITE, G. BURNELL, L. R. CORNWELL et R. B. GRIFFIN. Corrosion (Houston), **41**, 317 (1985).
6. S. PETETIN, J. CROUSIER et J.-P. CROUSIER. Mater. Chem. Phys. **10**, 317 (1984).
7. R. G. BLUNDY et M. J. PRYOR. Corros. Sci. **12**, 65 (1972).
8. H. W. PICKERING. Corros. Sci. **23**, 1107 (1983).
9. H. W. PICKERING et P. J. BYRNE. J. Electrochem. Soc. **118**, 209 (1971).
10. YA. M. KOLOTYRKIN. Electrochem. Acta, **25**, 89 (1980).
11. A. L. BACARELLA et J. C. GRIESS. J. Electrochem. Soc. **120**, 459 (1973).
12. K. D. EFIRD. Corrosion (Houston), **31**, 77 (1975).
13. D. A. JONES. Corrosion (Houston), **39**, 444 (1985).
14. K. KASAHARA et F. KAJIYAMA. Corrosion (Houston), **39**, 475 (1983).

Can. J. Chem. Downloaded from www.nrcresearchpress.com by 72.64.146.136 on 09/07/12
For personal use only.

Relationship between gas-phase proton affinities of conjugate bases B's and free energies of hydration of conjugate acid ions BH^+'s for B = alkyl-substituted H_2O and NH_3

KENZO HIRAOKA
Faculty of Engineering, Yamanashi University, Takeda-4, Kofu 400, Japan

Received July 16, 1986[1]

KENZO HIRAOKA. Can. J. Chem. **65**, 1258 (1987).

An approximate linear relationship between the proton affinities of conjugate bases (B's) and the free energies of hydration of conjugate acid ions (BH^+'s) is found for B = alkyl-substituted H_2O and NH_3. With increase in proton affinities, the free energies of hydration increase linearly with a slope of about 1 for analogous compounds. The charge delocalization in the protonated bases and the structure-making effect induced by the hydrophobic groups in the alkyl-substituted H_3O^+ and NH_4^+ are crucial factors in the determination of the free energies of hydration.

KENZO HIRAOKA. Can. J. Chem. **65**, 1258 (1987).

Dans les cas des produits où B = du H_2O ou du NH_3 substitué par des groupements alkyles, on a trouvé qu'il existe une relation approximativement linéaire entre les affinités protoniques des bases conjuguées (B) et les énergies libres d'hydratation des ions de l'acide conjugué (BH^+). Lorsque les affinités protoniques augmentent, les énergies libres d'hydratation augmentent d'une façon linéaire; la pente est d'environ 1 pour les composés d'une même série d'analogues. La délocalisation de la charge dans les bases protonées et l'effet d'établissement de structure induit par les groupements hydrophobes des H_3O^+ et NH_4^+ substitués par des groupements alkyles sont des facteurs cruciaux dans la détermination des énergies libres d'hydratation.

[Traduit par la revue]

Introduction

The present work is part of a continuing effort from our laboratory to provide additional insights in ion solvation by means of intrinsic molecular properties such as basicities, acidities, and binding energies between ions and molecules measured in the gas phase (1, 2).

The study of ion/molecule reactions in the gas phase has led in recent years to precise determinations of intrinsic protic acid–base behavior. The proton affinity of a molecule B is defined as the negative enthalpy change of reaction [1]:

[1] $B + H^+ \rightarrow BH^+$

The determination of proton affinities is based on the measurements of the equilibrium constants of gas-phase proton transfer reactions:

[2] $BH^+ + A \rightleftarrows AH^+ + B$

where

[3] $-RT \ln K_{eq} = \Delta G = \Delta H^0 - T\Delta S^0$

and the equilibrium constants for reaction [2] is obtained from a mass spectrometric observation of the relative abundances of equilibrated ions, BH^+ and AH^+ in a mixture of known composition of compounds A and B. Recently, Lias *et al.* (3) have compiled a complete and internally-consistent set of proton affinities based mainly on the vast body of data generated by equilibrium constant measurements.

The hydrogen-bonded dimer cations BH^+---A have been investigated in the gas phase. A general trend relating ionic hydrogen bond strength of BH^+---A to the proton affinity difference $\Delta PA = PA(B) - PA(A)$ was observed by Kebarle (4–7). The dissociation energy of the ionic hydrogen bond decreases with the proton affinity difference, ΔPA. A qualitative interpretation of this trend is given by viewing the formation of the BH^+---A bond as partial proton transfer from BH^+ to A in the complex. The trend was further demonstrated in a series of ammonium ion hydrates (8), and also in hydrates of pyridinium ions $X_{py}H^+ \cdot OH_2$ and substituted anilinium ions $XC_6H_4NH_3^+ \cdot OH_2$ (7, 9). More recently, Meot-Ner and co-workers found a linear correlation between the bond dissociation energy of BH^+---A and the difference between the proton affinities for proton donor B and that for proton acceptor A (10–12). We found a similar trend for symmetric proton-held dimer cations $H^+(B)_2$ that the bond energies of the complexes decrease as the proton affinity of base B increases (13). It was indicated that the positive charge on the protic hydrogen atom in the protonated molecule BH^+ plays a most important role for the determination of the bond energies of $H^+(B)_2$.

Arnett and Taft have examined the gas and aqueous basicities of a majority of bases (14, 15). By means of Born-type cycles involving the gas phase and the aqueous proton transfer reactions as well as associated thermochemical data, these authors were able to obtain the relative hydration energies of protonated bases BH^+'s (14). The substituent and solvent effects on proton transfer equilibria were fully discussed (15). They found that when the alkyl-substituted amines have higher gas-phase basicities, their conjugate acid ions have smaller free energies of hydration (14). In our previous paper (2), we also found similar trends for H_2O and alcohols. This indicates that there is some correlation between gas-phase basicities and free energies of hydration. In the present work, the relationship between proton affinities of conjugate bases B's and free energies of hydration of conjugate acid ions BH^+'s for B = alkyl-substituted H_2O and NH_3 is studied in detail.

Discussion

Figure 1 shows the reproduced thermodynamic data for the dissolution of hydrocarbons in H_2O (17). As the number of carbon atoms in *n*-alkanes increases, both ΔH^0 and $T\Delta S^0$ decrease. However, the variation in ΔG^0 with solute size is very small compared to that in ΔH^0 and $T\Delta S^0$. The first detailed explanation for such an effect was provided by Frank and Evans and was based on the unique hydrogen-bonding properties of liquid water (16). The solvent H_2O molecules in the vicinity of hydrophobic groups were assumed to organize cooperatively, forming microscopic "ice-like patches". This causes reductions in both enthalpy and entropy. Since the changes in ΔH^0 and $-T\Delta S^0$ compensate each other, the ΔG^0 values stay almost

[1]Revision received January 6, 1987.

Can. J. Chem. Downloaded from www.nrcresearchpress.com by 72.64.146.136 on 09/07/12
For personal use only.

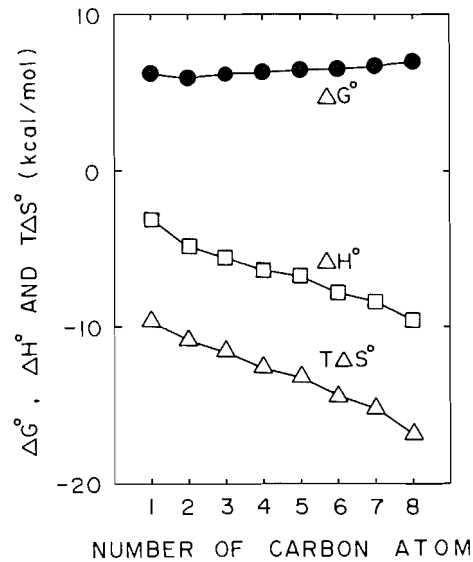

FIG. 1. Thermodynamic properties for the dissolution of aliphatic hydrocarbons (nC_1–nC_8) in water. ●: Standard free energy of hydration $\Delta G(G \rightarrow S)$. □: Standard enthalpy of hydration $\Delta H^0(G \rightarrow S)$. △: Standard entropy of hydration $T\Delta S^0(G \rightarrow S)$.

constant as shown in Fig. 1. When the solutes are ions, the following effects should also be taken into account (18): (*1*) The remnant of the central electric field, beyond the shielding caused by the first coordination sphere, still has an orienting influence on the outer molecules around it. The water molecules in the first coordination sphere exert their own orienting effect on the outer water molecules (1, 18). (2) The tetrahedral structure of bulk water will tend to orient the water molecules in conformity with the geometry favorable for the three dimensional hydrogen-bonded network (16). This effect will extend as close to the ion as the competition with other effects permits. If the ion contains nonpolar hydrophobic parts, these may shield the region near the ion from disruption of the tetrahedral structure by the thermal motion of free water molecules.

These two effects compete with each other in the orientation of water molecules beyond the first hydration shell. The incompatibility of the structures generated by these effects will cause a certain region around the ion to consist of disoriented water molecules, a thawed region (1, 2, 18).

1. Relationship between gas-phase proton affinities and enthalpies of hydration

Figure 2 shows the relationship between the gas-phase proton affinities (PA's) of the conjugate bases B and the enthalpies of hydration (ΔH_s^0's) of conjugate acid ions BH^+ for B = alkyl-substituted H_2O and NH_3. With an increase of PA, a general increase in the values of ΔH_s^0 is observed. The PA values increase with the increase in number and size of the hydrophobic groups, as shown in Fig. 2. With an increase of PA, the positive charge in the protonated base BH^+ gets more dispersed. This will lead to a decrease in the exothermicity for the hydration of protic hydrogens of BH^+ due to the smaller positive charges on the protic hydrogens of BH^+. On the contrary, the increase in the number and size of the hydrophobic groups promote the formation of ice-like patches around them, leading to a more exothermic contribution on the values of ΔH_s^0 (see Fig. 1). The observed rapid increase of ΔH_s^0 values with PA in Fig. 2 indicates that the former effect is much more prominent than the latter. It may thus be concluded that the proton affinity of the base B is the crucial factor in the determination of the enthalpy of hydration of the conjugate acid ion BH^+.

As shown in Fig. 2, the increases in ΔH_s^0 values for ammonia → primary amines → secondary amines → tertiary amines are large, while those for the compounds of the same analogues are small with increasing PA. It is well known (7, 14, 15) that the decrease in positive charge density on the ammonium group is rapid when direct substitution occurs, e.g. $MeNH_3^+$, $Me_2NH_2^+$, Me_3NH^+, compared with that for $MeNH_3$, $EtNH_3^+$, n-$PrNH_3^+$, n-$BuNH_3^+$, etc. Thus, both decrease in H-bonding hydrogens and decrease in positive charge density in the first series occurs and lead to less effective hydration of the onium ions. A similar trend is also observed for alkyl-substituted H_2O, that is, the increase of ΔH_s^0 (MeOH → EtOH) is less than that for ΔH_s^0 (MeOH → Me_2O).

It was found that (14, 19–22) the heats of hydration of amines become increasingly exothermic, as the carbon content is increased, and are apparently much more dependent on hydrophobic structure-making effect than on hydrogen bonding to or from the amino group. As shown in Fig. 2, the ΔH_s^0 values are about the same for primary amines, $MeNH_2$, $EtNH_2$, n-$PrNH_2$, and n-$BuNH_2$. The ΔH_s^0 value for n-$BuNH_2$ is even smaller than that for n-$PrNH_2$. This may be due to the fact that the aliphatic chain in aqueous solution acts as a structure maker and this leads to the negative contribution to the value of ΔH_s^0. This effect attenuates the increase of the values ΔH_s^0's to some extent with an increase of PA.

2. Relationship between the proton affinities and free energies of hydration

In Fig. 2 is also shown the relationship between the gas-phase proton affinities of bases B's and free energies of hydration (ΔG_s^0's) of conjugate acid ions BH^+'s. As shown in Fig. 2, it appears that there are approximate linear relationships between ΔG_s^0 and PA with a slope of about 1 for compounds of the same analogues:

$$[4] \quad \Delta G_s^0 = PA + \text{constant}$$

It is rather surprising that there is such a simple relationship between the PA value which represents the intrinsic molecular property and the ΔG_s^0 value which is determined by so many factors such as size and shape of the ion, charge and its density of the ion, size and structure of the hydrophobic group in the ion, number of protic hydrogen atoms in the ion, structure of the solvation shells, and so on. In any case, such a simple relationship would be very useful since the free energies of transfer of conjugate acid ions from the gas phase to the dilute aqueous solutions can be readily estimated from the available gas-phase proton affinities of conjugate bases (3).

While an approximately linear relationship is observed between ΔG_s^0 and PA, there is the scatter in the line, i.e., the ΔG_s^0 for the series of NH_4^+ → $MeNH_3^+$ → $Me_2NH_2^+$ → Me_3NH^+ increases faster than linearly. In fact, this faster increase is very important and leads to the famous "amine anomaly" of aqueous basicities with methyl substitution (NH_3 < $MeNH_2$ < Me_2NH > Me_3N). The relative aqueous basicities may be described as (14) $\delta\Delta G_i^0(w) = \delta\Delta G_i^0(g) + \delta\Delta G_s^0(B) - \delta\Delta G_s^0(BH^+)$ where $\Delta G_i^0(w)$ is the free energy of ionization $BH^+ = B + H^+$ in aqueous solution (i.e. the scale of basicity in solution), $\Delta G_i^0(g)$ is the free energy of ionization $BH^+ = B + H^+$ in the gas phase, $\Delta G_s^0(B)$ is the free energy of hydration of B, and $\Delta G_s^0(BH^+)$ is the free energy of hydration of BH^+. The $\Delta G_s^0(B)$ values for $MeNH_2$, Me_2NH, and Me_3N relative to

Can. J. Chem. Downloaded from www.nrcresearchpress.com by 72.64.146.136 on 09/07/12
For personal use only.

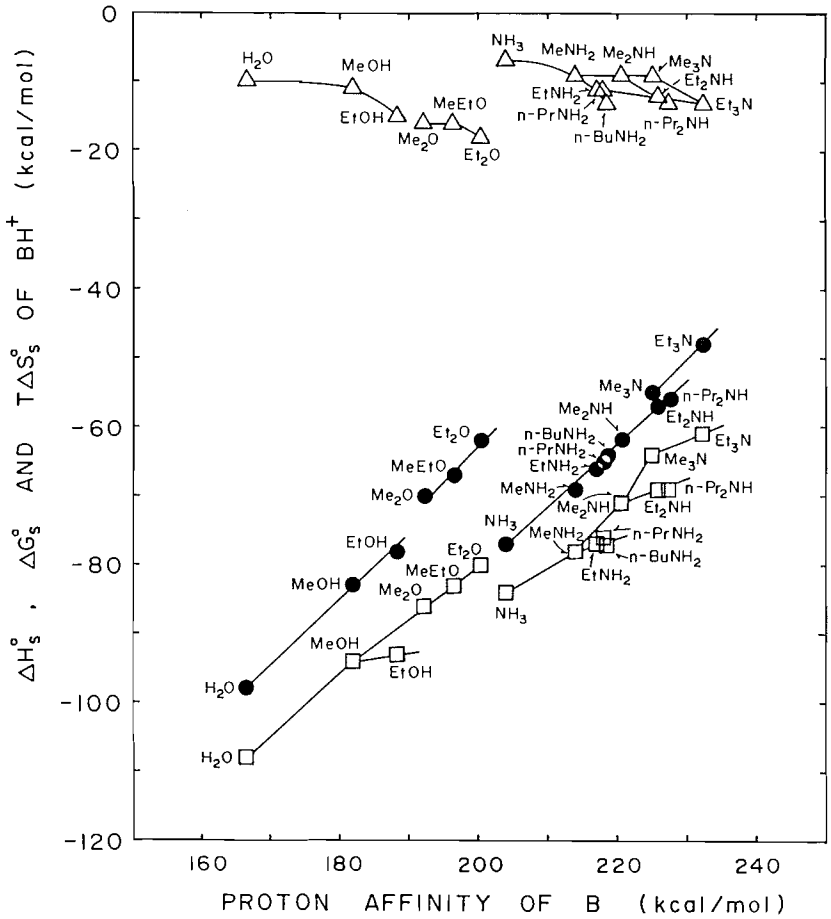

FIG. 2. □: The relationship between the proton affinity (PA) of the conjugate base measured in the gas phase and the enthalpy of hydration (ΔH_s^0) for the conjugate acid ion. ●: The relationship between the proton affinity (PA) of the conjugate base and the free energy of hydration (ΔG_s^0) for conjugate acid ion. △: The relationship between the gas-phase proton affinity of the conjugate base B and the entropy of hydration ($T\Delta S_s^0$) of conjugate acid ion BH^+. The $T\Delta S_s^0$ values are calculated from the ΔG_s^0 and ΔH_s^0 values reported by Taft (ref. 4).

NH_3 are small ($\lesssim$1 kcal/mol) (14) due to the compensation of enthalpy and entropy of hydration of B's (19, 20). Thus, relative basicities in aqueous solution $\delta\Delta G_i^0(w)$ are mainly determined by the values $\delta\Delta G_i^0(g) - \delta\Delta G_s^0(BH^+)$. Since $\delta\Delta G_i^0(g)$ are about the same with δPA (3), the approximate expression $\delta\Delta G_i^0(w) \approx \delta PA - \delta\Delta G_s^0(BH^+)$ may be derived. This relationship implies that the relative aqueous basicities $\delta\Delta G_i^0(w)$ may be roughly predicted by inspection of the inclination of the line in Fig. 2. For example, when the slope is unity, the aqueous basicities of BH^+'s falling on the line are predicted to be about the same. In Fig. 2, two straight lines with a slope of about 1 can be drawn on which NH_3 and Me_3N, and $MeNH_2$ and Me_2NH locate, respectively. This suggests that $\delta\Delta G_i^0(w)_{NH_3} \approx \delta\Delta G_i^0(w)_{Me_3N}$ and $\delta\Delta G_i^0(w)_{MeNH_2} \approx \delta\Delta G_i^0(w)_{Me_2NH}$, and the basicities for NH_3 and Me_3N are weaker than those for $MeNH_2$ and Me_2NH. This qualitatively predicts the quantitatively determined (14) $\delta\Delta G_i^0(w) = 0.00$, 1.92, 2.09, and 0.75 for NH_3, $MeNH_2$, Me_2NH, and Me_3N relative to NH_3. The most effective factors which determine the aqueous basicities are gas-phase basicities (PA) of B's and free energies of hydration of BH^+'s.

Close inspection of Fig. 2 indicates that the slopes of the linear relationships between ΔG_s^0 vs. PA are steeper than those between ΔH_s^0 vs PA for the analogous compounds, e.g., MeOH → EtOH, Me_2O → MeEtO → Et_2O, $MeNH_2$ → $EtNH_2$ → *n*-$PrNH_2$ → *n*-$BuNH_2$, Me_2NH → Et_2NH → *n*-Pr_2NH, and Me_3N → Et_3N. This is likely to be due to the more positive entropic contribution to the ΔG_s^0 values with an increase in the number and size of the structure-making hydrophobic groups (see Fig. 1).

The increase in the number and size of the aliphatic chains of alkyl-substituted H_3O^+ and NH_4^+ leads to an increase in PA due to the delocalization of positive charges in BH^+. The hydration energy of the protic hydrogens of BH^+ will decrease with an increase in PA. This may result in an *increase* in the entropy of hydration due to the formation of less tight hydration shells around the protic hydrogens. On the other hand, the ice-patch formation around the hydrophobic groups will be promoted with an increase in the number and size of the structure-making hydrophobic groups and this will *decrease* the entropy of hydration with an increase of PA. Figure 2 also shows the relationship between the gas-phase proton affinities of bases B's and entropies of hydration ($T\Delta S_s^0$) of conjugate acid ions BH^+'s which are calculated from the ΔH_s^0 and ΔG_s^0 values reported by Taft (15). Generally, the entropy of hydration $T\Delta S_s^0$ decreases with an increase of PA. This suggests that the contribution of the negative entropy change due to the hydration of hydrophobic groups is greater than that of the positive entropy change due to the hydration of protic hydrogen atoms of BH^+.

In Fig. 2, the change of $T\Delta S_s^0$'s values for NH_3 → $MeNH_2$ → Me_2NH → Me_3N is rather small. On the contrary, rapid

Can. J. Chem. Downloaded from www.nrcresearchpress.com by 72.64.146.136 on 09/07/12
For personal use only.

decreases in $T\Delta S_s^0$'s are observed for $MeNH_2 \rightarrow EtNH_2$(*n*-$PrNH_2$) $\rightarrow$ *n*-$BuNH_2$. As already pointed out, direct methyl substitution of NH_3 decreases the exothermicity of hydration of the conjugate acid ions and this reduces structure of the hydrates directly solvating the onium ends, i.e. an increase in ΔS_s^0. This compensates for the ΔS_s^0 decrease due to hydrophobic water structure-making for these alkyl groups. The same compensation is not available for the *n*-alkyl NH_2 because the gas-phase basicity changes for these compounds are small, i.e. the ΔS_s^0's due to onium ion hydration are approximately constant.

Concluding remarks

The relationships between ΔH_s^0, ΔG_s^0, $T\Delta S_s^0$ and the gas-phase PA are studied. Generally, the $T\Delta S_s^0$ and ΔH_s^0 values decrease and increase, respectively, with an increase in PA. The values of ΔG_s^0 ($= \Delta H_s^0 - T\Delta S_s^0$) are found to increase almost linearly with a slope of about 1 with an increase of PA for analogous compounds. Such a simple relationship would be very useful for the estimating free energies of transfer of protonated acid ions from the gas phase to the dilute aqueous solution using the available gas-phase PA.

The $-\Delta G_s^0$ values correspond to the energies required for the extraction of hydrated ions in aqueous solutions to the gas phase. The evaporation of ions from the condensed phases to the gas phase is a very important process in many fields such as the thermospray technique for the liquid chromatograph – mass spectrometer interface (23), electrohydrodynamic ionization (electrostatic spray) (24), field ionization, field-induced ion evaporation from liquid surface (25), etc. From the results presented here, one may draw a zeroth order principle that the protic acid ions whose conjugate bases have higher proton affinities are easier to be extracted from the aqueous solution to the gas phase.

Acknowledgement

The author thanks Professor P. Kebarle of the University of Alberta for stimulating discussions.

1. K. Hiraoka. Bull. Chem. Soc. Jpn. **59**, 2571 (1986).
2. K. Hiraoka, H. Takimoto, and K. Morise. J. Am. Chem. Soc. **108**, 5683 (1986).
3. S. G. Lias, J. F. Liebman, and R. D. Levin. J. Phys. Chem. Ref. Data, **13**, 695 (1984).
4. J. D. Payzant, R. Yamdagni, and P. Kebarle. Can. J. Chem. **49**, 3308 (1971).
5. R. Yamdagni and P. Kebarle. J. Am. Chem. Soc. **93**, 7139 (1971).
6. R. Yamdagni and P. Kebarle. J. Am. Chem. Soc. **95**, 3504 (1973).
7. W. R. Davidson, J. Sunner, and P. Kebarle. J. Am. Chem. Soc. **101**, 1675 (1979).
8. Y. K. Lau and P. Kebarle. Can. J. Chem. **59**, 151 (1981).
9. Y. K. Lau, K. Nishizawa, A. Tse, R. S. Brown, and P. Kebarle. J. Am. Chem. Soc. **103**, 6291 (1981).
10. M. Meot-Ner. J. Am. Chem. Soc. **106**, 1257 (1984).
11. C. V. Speller and M. Meot-Ner. J. Phys. Chem. **89**, 5217 (1985).
12. M. Meot-Ner and L. W. Sieck. J. Phys. Chem. **89**, 5222 (1985).
13. K. Hiraoka, H. Takimoto, and S. Yamabe. J. Phys. Chem. **90**, 5910 (1986).
14. E. M. Arnett, F. M. Jones, III, M. Taagepera, W. G. Henderson, J. L. Beauchamp, D. Holtz, and R. W. Taft. J. Am. Chem. Soc. **94**, 4724 (1972).
15. R. W. Taft. Prog. Phys. Org. Chem. **14**, 247 (1983).
16. H. S. Frank and M. W. Evans. J. Chem. Phys. **13**, 507 (1945).
17. J.-Y. Huot and C. Jolicoeur. *In* The chemical physics of solvation. Part A. Theory of solvation. *Edited by* R. R. Dogonadze, E. Kalman, A. A. Kornyshev, and J. Ulstrup. Elsevier, Amsterdam. 1985. Chap. II.
18. Y. Marcus. Ion solvation. John Wiley and Sons, Chichester. 1985. Chap. 5.
19. M. C. Cox, D. H. Everett, D. A. Landiman, and R. J. Munn. J. Chem. Soc. B, 1373 (1968).
20. E. M. Arnett and D. R. McKelvey. Solvent–solute interactions. *Edited by* J. F. Coetzee and C. D. Ritchie. Marcel Dekker, New York, NY. 1969.
21. C. V. Krishnan and H. L. Friedman. J. Phys. Chem. **75**, 3598 (1971).
22. F. E. Condon. J. Am. Chem. Soc. **87**, 4481 (1965); **87**, 4485 (1965); **87**, 4494 (1965).
23. C. R. Blakley and M. L. Vestal. Anal. Chem. **55**, 750 (1983).
24. M. Yamashita and J. B. Fenn. J. Phys. Chem. **88**, 4451 (1984).
25. B. A. Thomson and J. V. Iribarne. J. Chem. Phys. **71**, 4451 (1979).

Can. J. Chem. Downloaded from www.nrcresearchpress.com by 72.64.146.136 on 09/07/12
For personal use only.

Diels–Alder reactions of 4,4-dimethyl-2-cyclohexenones. A direct route to the 4,4-dimethyl-1-decalones[1]

HSING-JANG LIU AND ERIC N. C. BROWNE[2]
Department of Chemistry, The University of Alberta, Edmonton, Alta., Canada T6G 2G2

Received October 2, 1986

HSING-JANG LIU and ERIC N. C. BROWNE. Can. J. Chem. **65**, 1262 (1987).

Diels–Alder additions to enones **1** and **2**, synthetic equivalents of the synthon **3**, were studied using a variety of hydrocarbon dienes. The two enones have been shown to be effective and synthetically useful dienophiles. Spectroscopic (especially ^1H and ^{13}C magnetic resonance) and chemical techniques were used to define unambiguously the full structures of the adducts. The structures of the various reaction products were used to draw qualitative conclusions about the nature of the transition states involved and the various electronic and steric effects that play a role in the mechanistic course of the Diels–Alder reaction.

HSING-JANG LIU et ERIC N. C. BROWNE. Can. J. Chem. **65**, 1262 (1987).

Utilisant une grande variété d'hydrocarbures diéniques, on a étudié les réactions d'additions de Diels–Alder sur les cétones **1** et **2**, les équivalents de synthèse du synthon **3**. On a démontré que les énones sont des diénophiles efficaces et utiles d'un point de vue de synthèse. On a utilisé la spectroscopie (principalement la résonance magnétique nucléaire du ^1H et du ^{13}C) ainsi que des techniques chimiques pour définir sans ambiguïtés les structures complètes des adduits. On a utilisé les structures des divers produits réactionnels pour tirer des conclusions qualitatives sur la nature des états de transition impliqués et sur les divers effets électroniques et stériques qui jouent un rôle dans l'orientation des réactions de Diels–Alder.

[Traduit par la revue]

Can. J. Chem. Downloaded from www.nrcresearchpress.com by 72.64.146.136 on 09/07/12
For personal use only.

Introduction

Since the cycloaddition of dienes with olefins to give cyclohexenes was correctly formulated and seen to be a general process by Diels and Alder (1), it has proven to be one of the most versatile and powerful synthetic tools available to the organic chemist.[3] At the same time, mechanistic studies of the process have only lately begun to account successfully for the various effects upon the course of the reaction (3, 4). The early development of a series of empirical rules for predicting the structural outcome of the reaction facilitated its use in organic synthesis. The *cis* principle predicts that addition to the diene in the required cisoid conformation occurs from the same side at each end of the diene moiety and also that attack at both ends of the dienophilic double bond occurs from the same face of the dienophile. It further predicts that the relative configurations of the substituents in the transition state are preserved in the products. The *endo* rule, originally formulated (3, 5) for additions of cyclic dienes and dienophiles, has been explained (6) by a stabilization of the transition state in which secondary orbital overlap (6) can occur between the π system of the diene and a π system in conjugation with the dienophilic double bond. Using this requirement, it is evident that even in acyclic cases the term "*endo*" is correctly used when the addition proceeds by a transition state in which secondary orbital overlap occurs, while "*exo*" refers to additions via transition states in which no secondary orbital overlap occurs.

A group of orientation rules that predict the regiochemistry of additions between unsymmetrical dienes and dienophiles has also been developed. The *ortho* rule predicts that a substituent at C-1 of the diene promotes addition to give an adduct in which the substituent from the diene component is adjacent (*ortho*) to the substituent from the dienophile. In the case of 2-substituted dienes the *para* rule predicts formation of a product having the two substituents in a *para* relationship. More recently, using frontier orbital theory, Houk and Strozier predicted (7, 8) that, where substituents of both diene and dienophile are electron donating, the favoured product should be that with the *meta* orientation of the substituents.[4] This "*meta* rule" has since been observed experimentally by Fleming *et al.* (10).

Empirically determined priorities have been used to determine which of many possible substituent types and rule systems take precedence over others in any combination of experimental situations. The empirical rules can be broadened to a model of the controlling features of the reaction through the visualization of the reaction as an essentially electronically governed process, as highlighted by the rules of Woodward and Hoffmann (6) and by the many and various frontier orbital treatments that have been applied since that time (4, 6–8, 11). However, any model is necessarily a simplification of the actual process that occurs during a chemical reaction. Variation of actual results from those predicted by the model serves only to illustrate that the model lacks sufficient detail to cover all eventualities.

In theory the application of the Diels–Alder reaction (12, 13) to the synthesis of *cis*-1-octalones requires only a straightforward addition of a cyclohexenone to an appropriately substituted diene. The method has the potential for rapid assembly of the decalin skeleton of a number of natural products such as those of the eudesmane, drimane, and cadinane classes. As well, the unique stereo- and regioselectivity of the reaction promises that the required adducts could be obtained efficiently. Unfortunately, the thermal cycloaddition of dienes to cyclohexenone and its substituted analogs has been the least successful of the simple applications of the reaction. Early reports (14–16) of low yields and drastic conditions for the addition to cyclohexenones appear to have discouraged continued investigation on the direct generation of their adducts.

The observation that Lewis acid catalysis produces very large increases in the rates of the Diels–Alder additions of α,β-unsaturated carbonyl compounds (17–19) has made available

[1]Taken in part from the Ph.D. thesis of E.N.C. Browne, The University of Alberta, 1980.

[2]Present address: DeVoe–Holbein Canada Inc., 175 Bouchard Blvd., Dorval, Que., Canada H9S 1A9.

[3]The comments of Wenkert and co-workers (2) serve to highlight some of the very few limitations to this statement.

[4]This is also predicted by the heterolytic mechanism, which, however, incorrectly predicts the same outcome when both substituents are electron withdrawing (9).

Can. J. Chem. Downloaded from www.nrcresearchpress.com by 72.64.146.136 on 09/07/12
For personal use only.

many adducts that had previously been obtained only with difficulty. Furthermore, it has been observed that such catalysis also has a marked effect on the regio- and stereoselectivity of the reaction so that the *ortho* (20) and *para* selectivity (21, 22) of the addition as well as the *endo* selectivity (23) are markedly increased. The application of Lewis acid catalysis to acyclic α,β-unsaturated carbonyl containing dienophiles has received fairly rapid recognition but it was not until recently that investigations (2, 24–32) have shown that the practice is equally applicable to cyclohexenones.

In connection with synthetic studies on himachalenes (33) and other terpenoids, we investigated the Diels–Alder reaction of 4,4-dimethylcyclohexenones as a direct route to the 4,4-dimethyl-1-decalone ring system common to a wide variety of natural products (34). We have previously reported (33, 35, 36) briefly on the dienophilic character of the two enones **1** and **2** and we wish now to elaborate on the full scope of our work in this area and to comment on the mechanistic and spectroscopic aspects of the results.

Results and discussion

I. Diels–Alder reactions of 4,4-dimethyl-2-cyclohexenone (3)

The Diels–Alder reaction of the parent enone **3** (37) with isoprene and 1,3-butadiene[5] was first studied using boron trifluoride etherate or aluminum chloride as a catalyst[6] in a variety of solvents and at a wide range of temperatures (20–110°C). In virtually all cases, the dimeric compounds **4** and **5** were obtained as the major products and in no instance

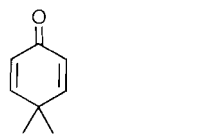

1

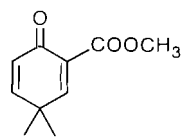

2

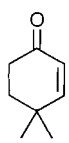

3

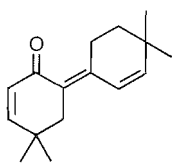

4

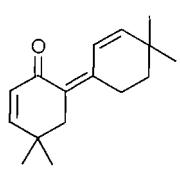

5

was a Diels–Alder adduct produced in a significant quantity (<14% yield). The Diels–Alder reactions were also examined under thermal conditions. The results were, however, equally disappointing; whereas enone **3** remained unchanged at lower temperatures, reaction with isoprene at 250°C in mesitylene in a sealed tube gave a complex mixture from which the desired adduct was absent. These findings indicated to us that enone **3** is a rather poor dienophile. Although Wenkert and co-workers have subsequently achieved cycloaddition of **3** in synthetically useful yield (2) by aluminum chloride catalysis, it was more promising in our context to investigate addition of dienes to a modified dienophile system.

II. Diels–Alder reactions of 4,4-dimethyl-2,5-cyclohexadienone (1)

Effective addition of the enone **3** synthon to dienes appears to require both increased dienophilicity and protection of the molecule against side reactions such as aldol condensation. The introduction of a second double bond into the ring of enone **3** offers the dual advantage of preventing the troublesome aldol condensation experienced with **3** as well as enhancing the desired reactivity of the molecule both by increasing the number of dienophilic double bonds and by increasing the planarity of the molecule. With this in mind we examined the Diels–Alder reactivity of dienone **1** (38, 39).

It was found that in ether solution at room temperature with boron trifluoride etherate as the catalyst and using a large excess of diene, adducts were obtained in moderate yield over rather extended reaction times. The results of this study are summarized in Table 1. The adducts were found to be those predicted on the basis of the normal rules governing the orientation and the stereochemistry of Diels–Alder addition (12), with one exception. The addition of isoprene to **1** (Entry 1) proceeded exclusively to give the adduct **6** formed in violation of the *para* rule.[7]

TABLE 1. Diels–Alder additions to dienone **1**

Entry	Diene (equiv.)	Time (days)	Yield (%)	Adduct
1	(40)	22	61[a]	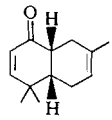 (36) **6**
2	(excess)	22	26	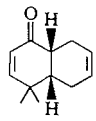 **7**
3	(30)	8	69	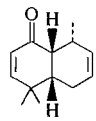 (36) **8**
4	(10)	7	20[b]	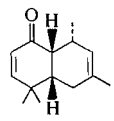 **9**
5	(4)	5	67	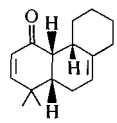 **10**

[a]This product was contaminated with ~5% of the *trans* isomer **11**.

[b]This reaction also produced an equal yield of a side product not observed for any other example in this series. On the basis of the spectral data, the structure of this product was assigned as phenol **12**, which may have been formed via Lewis acid induced dienone–phenol rearrangement (40) of **1**, followed by Friedel–Crafts alkylation with the diene.

[5]The amount of diene used ranged from 4 to 20 equivalents.

[6]0.1 to 0.5 equivalents of Lewis acid was used.

[7]The structural identification of adduct **6** and theoretical considerations of the abnormal orientation have been discussed in conjunction with its application to the synthesis of ionene (36).

TABLE 2. Aromatization and epimerization of Diels–Alder adducts **6–10**

Adduct	Aromatization Time (h)	Aromatization Product (% yield)[a]	Epimerization Time (h)	Epimerization *trans* Product	Epimerization *cis*/*trans* (% yield)
6	0.75	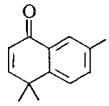 (38)[b]	1	**11**	30/70 (87)[b]
		13			
7	—	—	26	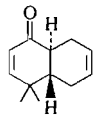	33/67 (72)
				18	
8	0.5	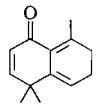 (12)[b]	20	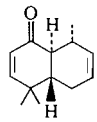	0/100 (64)[c]
		14		**19**	
9	1	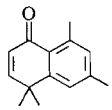 (17)	20	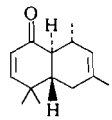	0/100 (44)[c]
		15		**20**	
10	1	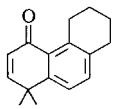 (30)	24	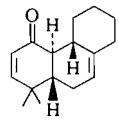	0/100 (49)[c]
		16		**21**	

[a]The balance of the material consisted of bromo derivatives of the starting material and the product as shown by ^{1}Hmr and mass spectra.

[b]See ref. 36.

[c]The corresponding 3-methoxy ketone (**22**, **23**, or **24**) arising from conjugate addition of methanol was also obtained in ~20% yield.

Structural assignments

Several aspects of the structural assignments of adducts **6–10** should be discussed. The regiochemistry of the Diels–Alder additions of unsymmetrical dienes (Table 1, Entries 1 and 3–5) was conclusively demonstrated by conversion of the enones to aryl-ketone derivatives by treatment with *N*-bromosuccinimide (36, 41) in refluxing carbon tetrachloride, as summarized in Table 2. The structures of the resulting ketones were unambiguously established by their ^{1}Hmr spectra, which showed, in each case, the absence of a *peri* proton and a profound *peri* effect (42) of the carbonyl on the substituent at C-8, which is held in the deshielding zone of the carbonyl group, causing the signal of that substituent to be shifted downfield significantly. For example, the ^{1}Hmr spectrum of **14** displayed an aryl methyl group as a singlet at δ 2.70 and three aromatic protons at δ 7.30 (2H) and 7.05. The absence of any signals at lower field[8] as well as the appearance of an aryl methyl group at a field considerably lower than normal (~δ 2.3) were in agreement only with the assigned structure.

The ring junction stereochemistry of all the adducts could be readily assigned on the basis of the *cis* principle (12), for which no violations have been observed. This was confirmed by conversion of each adduct with sodium hydroxide in aqueous methanol at room temperature to the thermodynamically more stable *trans* isomers **18–21**, as summarized in Table 2.

The relative stereochemistries of B-ring substituents in **8–10** were assigned as indicated on the basis of their ^{1}Hmr spectra presented and discussed below.

Nuclear magnetic resonance assignments

Nuclear magnetic resonance spectral data for adducts of **1** and their epimerization products are summarized in Tables 3 and 4. Spectra were readily assigned, based on first-order analysis. The chemical shifts of several protons and carbons on enones of this series are significantly different in the *cis*- and *trans*-enones and these nmr signals were used routinely in assigning the stereochemistry of the substituted enones obtained in this work. For instance, the readily distinguishable C-3 proton invariably appears at ~0.3–0.4 ppm higher field in the *cis* isomers than in

[8]In the ^{1}Hmr spectrum of the known ketone **17** (43), the *peri* proton appeared as a doublet with a coupling constant of 7 Hz at δ 8.25. Similarly, the ^{1}Hmr spectrum of ketone **13** (36) showed a narrowly split multiplet (<1 Hz) at δ 7.90, assigned to the *peri* proton.

Can. J. Chem. Downloaded from www.nrcresearchpress.com by 72.64.146.136 on 09/07/12
For personal use only.

TABLE 3. The ^{13}Cmr spectra (δ) of some 4,4-dimethyl-4a,5,8,8a-tetrahydro-1(4*H*)-naphthalenones

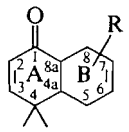

Carbon	Enone 3	*cis*-Fused enones 6[a]	8[a]	9	10	*trans*-Fused enones 11	19[a]	21
1	198.4	199.6	200.9	201.0	201.1	[b]	202.5	201.7
2	126.8	126.4	124.0[c]	127.1[c]	127.2	126.3	123.6[c]	126.5
3	159.3	155.7	153.4	153.4	152.9	160.7	160.5	159.5
4	32.7	36.5	37.0	36.9	36.7	36.0	35.9	35.7
4a	36.2	43.1	47.0	47.5[d]	47.1[c]	43.4	49.4	48.6
5	—	24.5	25.0	30.0	25.0	26.1	25.4	25.2
6	—	119.5	127.0[c]	131.0	117.4	119.4	126.4[c]	116.5
7	—	132.5	132.0	126.5[c]	138.1	132.7	132.9	140.5
8	—	28.8	34.2	34.3	40.7	27.8	31.4	38.4
8a	34.4	42.4	47.8	47.1[d]	46.9[c]	42.3	44.2	43.5
gem CH_3[e]	27.7	26.9	26.7	26.8	26.7	26.1	28.1	28.2
	27.7	26.2	26.0	26.0	26.0	21.0	20.6	20.6
R	—	23.3	19.0	23.3	34.1	23.2	23.2	37.0
				19.2	28.9			36.0
					26.5			28.4
					26.2			26.5

[a]Compare to shifts reported by Wenkert and co-workers (44).
[b]The signal for this carbon was not clearly defined in the spectrum.
[c,d]The specific assignment of these pairs of signals is uncertain.
[e]These signals were useful for distinguishing *cis* from *trans* enones.

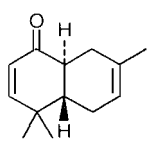

11

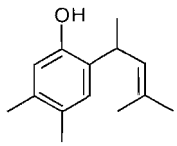

12

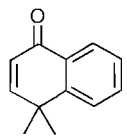

17

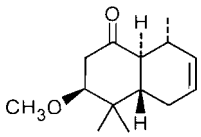

22

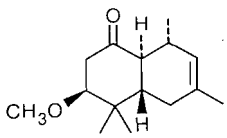

23

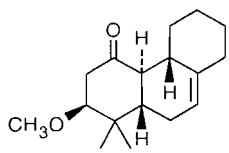

24

the corresponding *trans* isomers. Likewise the sharp singlets due to the *gem*-dimethyl group are consistently separated by ~0.1 ppm in the *trans* isomers and by ~0.2 ppm in the *cis* isomers. In the ^{13}Cmr spectrum, shifts for C-3 routinely differ by 5 ppm between *cis* and *trans* isomers, with the former at higher field, while the geminal methyl carbons differ from each other by less than 1 ppm for *cis* versus more than 5 ppm for *trans* isomers.

A detailed discussion of the ^{1}Hmr spectrum of **7** is warranted in order to introduce several features that apply to other adducts in this series. The ^{1}Hmr spectrum of **7** showed that the two protons at C-8 had quite different chemical shifts. The assignment of the signal at δ 2.83 to the α proton and the signal at δ 1.94 to the β proton was made after selection of conformation **7***a* as the more stable conformation of the molecule. In this conformation, the α proton is held in the deshielding zone of the carbonyl group and thus the signal appears at considerably lower field (δ 2.83) than a normal allylic proton (δ 2.0) (42). The β proton is out of the plane of the carbonyl and further from it than the α proton and so experiences virtually no deshielding by the carbonyl. This argument was demonstrated conclusively by proton decoupling experiments on adduct **6**. Successful extrapolation of these arguments to analysis of the other C-8 substituted *cis*-hexalones summarized in Table 4 clearly reflects the utility of this effect and its action on C-8 protons and substituents on the α face of the molecule. The epimeric products **39** and **40** as well as **43** and **44** obtained later by alternative routes (see Table 6) exhibited the spectral characteristics expected on the basis of the preceding arguments.

Most of the *cis* isomers also exhibited a particularly distinct coupling arrangement, which confirms the ring junction stereochemistry and preferred conformation. For instance, in the case of adduct **8**, a long range W-type coupling of 1.5 Hz was observed in the signal at δ 6.15, which was attributed to coupling of the proton at C-3 with the proton at C-4a. A W configuration of these two protons is possible only in the *cis*-enone **8** in which the proton at C-4a could assume a quasi-equatorial position relative to ring A in the preferred conformation **8***a*. Such a configuration cannot be achieved in the *trans* isomer.

Can. J. Chem. Downloaded from www.nrcresearchpress.com by 72.64.146.136 on 09/07/12
For personal use only.

Can. J. Chem. Downloaded from www.nrcresearchpress.com by 72.64.146.136 on 09/07/12
For personal use only.

TABLE 4. The ^{1}Hmr spectra (δ) of substituted 4,4-dimethyl-4a,5,8,8a-tetrahydro-1(4*H*)-naphthalenones

	cis-Fused enones							*trans*-Fused enones						
Protons	6	7[a]	8	9	10	26	39	43	11	18	19[a]	20	21	40	41	44
C-2 H	5.68	5.72	5.58	5.53	5.57	5.68	5.70	5.67	5.69	5.82	5.72	5.60	5.68	5.77	5.72	5.73
C-3 H[b]	6.28[c]	6.31[c]	6.15[c]	6.13[c]	6.12	6.29[c]	6.27[c]	6.25[c]	6.55	6.58	6.49	6.45	6.45	6.60	6.56	6.57
C-6,7 H	5.18	5.55	5.51/5.37	5.19	5.08	5.33	5.7–5.4	5.38	5.31	5.62	5.58/5.41	5.13	5.28	5.7–5.4	5.33	5.23
C-8α H	2.64	2.83	—	—	—	*d*	3.06	2.97	*d*	*d*	—	—	—	2.83	*d*	2.77
C-8β H	1.87	1.94	2.34	2.24	<2.5[d]	*d*	—	—	*d*	*d*	2.44	2.38	*d*	—	*d*	—
C-8a H[b]	2.89	2.92	2.86	2.77	2.86	2.82	2.55	2.46	*d*	*d*	*d*	*d*	*d*	*d*	*d*	*d*
C-8 CH_3	—	—	1.38	1.33	—	—	1.04	0.97	—	—	1.19	1.17	—	0.81	—	0.75
C-6,7 CH_3	1.66	—	—	1.57	—	1.58	—	1.56	1.67	—	—	1.66	—	—	1.66	1.64
gem CH_3[b]	1.30	1.31	1.33	1.31	1.28	1.30	1.30	1.28	1.13	1.13	1.14	1.14	1.10	1.17	1.14	1.16
	1.09	1.10	1.10	1.09	1.04	1.10	1.12	1.11	1.03	1.04	1.06	1.07	1.02	1.04	1.04	1.02

[a]Compare to shifts reported by Wenkert and co-workers (44).
[b]The signals for these protons were particularly useful for distinguishing the *cis* from the *trans* enones.
[c]This signal showed a long range W-type coupling to the proton at C-4a.
[d]The signal for this proton(s) was not clearly defined in the spectrum.

In confirming the stereochemistry at C-8[9] of adduct **10**, the only two ^{1}Hmr signals that might be attributable to the deshielded C-8 proton of the alternative epimer **25** were easily assignable to other protons. However, the α proton on the methylene carbon attached to C-8 lies in the deshielding zone of the carbonyl group and would be expected to be shifted downfield from its normal region (45) of δ 1.4. The predicted couplings for this proton fit well with the observed couplings of the signal at δ 2.50. No other proton in enone **10** would be expected to exhibit such a shift and coupling pattern, nor would any proton in structure **25**. This and the absence of any other signal in the region δ 2.5–5.0 would appear to rule out structure **25** and confirm structure **10** as the identity of the adduct.

Mechanistic discussion

The preceding results show that dienone **1** is a useful though moderately weak dienophile. Addition to simple hydrocarbon dienes proceeds smoothly to give acceptable yields of adducts. The most important item of note is the total violation of the *para* rule in the case of addition to isoprene. The normal addition of 1-substituted dienes leads to the conclusion that the cause of the abnormal addition of isoprene is a steric one; in the normal addition leading to the expected adduct **26**, the substituent at C-2 of the diene interacts with a substituent at C-4 of the dienophile as shown in the transition state **26A**.[10] If the steric effect were sufficiently strong, the electronically favoured *para* addition would be excluded and the otherwise less favourable *anti-para*[11] addition would predominate.

Comparison of the various dienes is interesting in this context. *trans*-Piperylene would not be expected to encounter any steric barrier to normal *ortho* addition and the *ortho*-addition product **8** is the only one observed. Similarly, only the expected product **10** is obtained from 1-vinylcyclohexene.

The addition of *trans*-2-methyl-1,3-pentadiene, however, raises an important point since the steric effect would act in opposition to the combined directing influence of the *ortho* and *para* rules. This offers the opportunity to determine the influence of the steric effect relative to the combined electronic effects. Total steric control would produce only enone **27** whereas electronic control would result only in formation of **9**. As we have seen, enone **9** is the only Diels–Alder addition product, indicating that a stronger electronic directing effect might be used to counteract the steric effect.

Clearly, this effect is tied to the influence of secondary orbital overlap (*endo*-rule addition) in the course of the reaction. The results of 2-substituted diene addition indicate that the influence of *endo* addition holds a higher level priority in this type of system than the steric effect and that indeed the *endo-anti-para* transition state **6A** is preferred to the extent of virtually complete exclusion over *endo-para* transition state **26A** and *exo-para* transition state **26B**.

One possible method to increase the influence of the electronic directing effect of **1** might be the use of a stronger, and therefore more electron-withdrawing, Lewis acid as the catalyst. The larger induced polarization of the dienophilic double bond should act to promote *para* addition. But the use of boron tribromide (benzene, room temperature, 11 days) did not

[9]The numbering scheme used in this discussion for phenanthrene ring systems and illustrated for structure **25** is applied only to be consistent with other compounds in this series.

[10]A similar explanation has been offered to account for the relatively poor dienophilicity of cyclohexenones (46).

[11]See ref. 36, footnote 5.

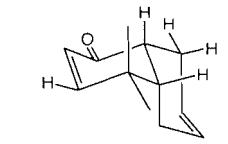

7a

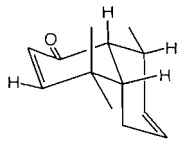

8a

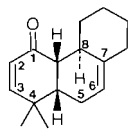

25

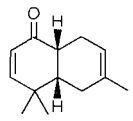

26

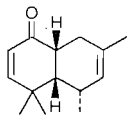

27

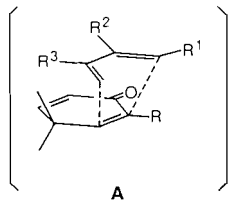

A

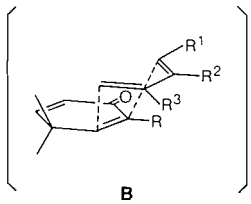

B

6A	R=R¹=R³=H, R²=CH_3	**26B**	R=R¹=R²=H, R³=CH_3
26A	R=R¹=R²=H, R³=CH_3	**35B**	R=$COOCH_3$, R¹=R²=H, R³=CH_3
34A	R=$COOCH_3$, R¹=R³=H, R²=CH_3	**38B**	R=$COOCH_3$, R¹=R³=CH_3, R²=H
35A	R=$COOCH_3$, R¹=R²=H, R³=CH_3		
37A	R=$COOCH_3$, R¹=R³=CH_3, R²=H		

produce any detectable trace of adducts of **1** with isoprene. Two other catalysts were also examined. Stannic chloride (ether, room temperature, 11 days) gave no detectable trace of Diels–Alder adduct, and ferric chloride (ether, room temperature, 7 days) produced an adduct in 3% yield, which ^{1}Hmr analysis showed to be almost exclusively enone **6**.[12] And, subsequently, Wenkert's work (44) using aluminum chloride provided only *anti-para* product **6** (and its *trans* isomer **11**).

III. Diels–Alder reactions of 2-carbomethoxy-4,4-dimethyl-2,5-cyclohexadienone (2)

Although Diels–Alder additions of dienone **1** produce acceptable yields of useful adducts, the long reaction times might tend to lessen its general utility. Furthermore, in the case of *para*-rule directed additions, the total violation of the electronic directing effect renders such *para*-substituted adducts inaccessible. On the basis of the Alder rule,[13] one method of increasing the reaction rate would be to place an additional electron-withdrawing substituent on the dienophilic double bond, increasing the polarization of that bond and the strength of the electronic *para*-directing effect on 2-substituted dienes, as well as the reaction rate. Appropriate choice of substituent could overcome the steric effect that promotes the observed *anti-para* addition.

In an effort to test these assumptions the dienone ester **2** was examined. The choice of a carbomethoxyl group as an activating substituent offers several advantages. It can be easily removed from the resulting β-keto-esters by decarboxylation, and it offered a level of functionalization that might be used effectively in synthetic schemes (for example see refs. 33 and 47).

On the basis of the Alder rule, the unsubstituted enone system of **2** is expected to be relatively less reactive and addition to the trisubstituted double bond would be preferred. In cases where the *endo* rule comes into effect, addition could occur with secondary orbital overlap either with the ketone or ester carbonyl system (transition states of type **A** or **B**). The factor determining which system would dominate the reaction pathway is expected to be a function of the stabilization of the transition state by secondary orbital overlap with the diene. However, in the case of addition of 2-substituted butadienes, it is apparent that preferential interaction with the ester carbonyl would totally eliminate the steric effect between the substituent and the methyl groups of the dienophile that might be experienced by overlap with the ketone carbonyl. This could contribute to the production of the electronically favoured product in the addition of 2-substituted dienes.

Dienone ester **2** was easily prepared from enone **3** by procedures published previously (33, 35). It was found to add rapidly to dienes in ether solution and, under boron trifluoride etherate catalysis, to give 1:1 adducts in good yield, as summarized in Table 5.

The adducts produced were, in general, consistent with those forecast by the usual rules. Addition occurred almost exclusively at the more highly activated site and orientational rules were maintained. *Endo*-rule addition by secondary orbital overlap with the ketone carbonyl predominated in simple cases where this could be observed (Entries 3, 4, and 7) uncomplicated by other factors. Again the notable exception to predicted behavior was the addition of isoprene (Entry 6), which proceeded under boron trifluoride etherate catalysis to give a 70:30 mixture of the *anti-para* and *para* addition products **34** and **35**.[14]

Structural assignments

The structural assignments of the various adducts deserve some explanation. In general, the keto-ester adducts were converted by decarboxylation with lithium iodide dihydrate in refluxing 2,4,6-collidine (48) to the corresponding hexalones, as summarized by the specific examples in Table 6. Those hexalones were identified by comparison with similar or identical compounds obtained directly from Diels–Alder additions to **1** (Table 2) on the basis of their ^{1}Hmr and ^{13}Cmr spectral (Tables 3 and 4) methods described previously (*vide supra*). As was the case with adducts of **1**, the regiochemistry of addition was conclusively demonstrated by aromatization of the decarboxylation products by treatment with *N*-bromosuccinimide (36, 41) and observation of the "*peri*" deshielding effect (42) of the carbonyl double bond on the C-8 substituent. The *cis* stereochemistry of the ring junction of the adducts of **2** was assigned based on the ^{1}Hmr evidence exemplified as follows for the case of adduct **28**. Firstly, it should be noted that *no exceptions* to the *cis* principle are known (46). Secondly, the ^{1}Hmr spectrum of the adduct (Table 7) showed a doublet of doublets (J = 6 Hz, J = 4 Hz) at δ 2.75. This signal showed no evidence of a geminal coupling and therefore was assigned to the methine proton at C-4a. The normal chemical shift of a proton β to a ketone is δ 1.95 (45). It was possible that the

[12]This was confirmed by comparison (gc, ^{1}Hmr) with authentic enones **6** (36) and **26** (33).

[13]The Alder rule predicts that substitution of an electron-withdrawing substituent on the dienophilic double bond increases the reactivity of that bond and that substitution of electron-donating substituents on the diene increases the reactivity of the diene (3).

[14]The structural identification of **34** and **35** and certain limited aspects of the effect of different catalysts on the product ratio have been discussed in connection with the application of this reaction to the synthesis of himachalenes (33).

Can. J. Chem. Downloaded from www.nrcresearchpress.com by 72.64.146.136 on 09/07/12
For personal use only.

Can. J. Chem. Downloaded from www.nrcresearchpress.com by 72.64.146.136 on 09/07/12
For personal use only.

TABLE 5. Diels–Alder additions to dienone ester **2**

Entry	Diene (equiv.)	Time (h)	Yield (%)	Product(s)	
1	(excess)	6	70	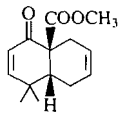 **28**	(35)
2	(20)	96	63	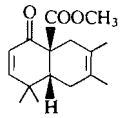 **29**	(35)
3	(20)	3	70	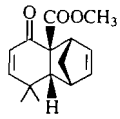 **30**	(35)
4	(10)	43	83[a,b]	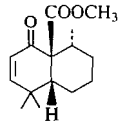 **31**	[c]
5	(10)	1.5[d]	74[e]	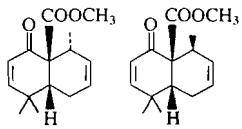 **31** (1:1) **33**	
6	(20)	72	73	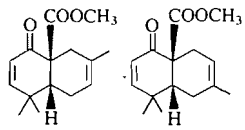 **34** (7:3) **35**	(33)
7	(20)	60	87	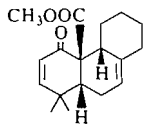 **36**	
8	(10)	2	83	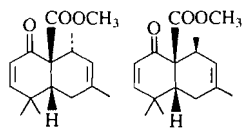 **37** (1:1) **38**	

[a]A small amount (~7% yield) of keto-ester **32** was observed in the unrecrystallized product.
[b]A small amount (<5% yield) of compound **33** was also obtained.
[c]An unambiguous confirmation of the structural assignment of this compound was made by X-ray analysis (J. Scheffer, personal communication).
[d]Ferric chloride was used as the catalyst.
[e]The formation of a pair of epimeric adducts **31** and **33** from addition of *cis*-piperylene probably stems from the presence of *trans*-piperylene (~3%) as an impurity in the commercial *cis*-piperylene used. *trans*-Piperylene is a much more reactive diene than the *cis* isomer and could compete effectively for the dienophile. The tenfold molar excess of diene used would provide sufficient *trans*-piperylene for conversion of up to 30% of the dienophile to **31**.

TABLE 6. Derivatization of adducts of **2** with unsymmetrical dienes

Adduct	Decarboxylation product (yield)	Aromatization product (yield)
31	**8** (66%)[a]	**14** (12%)[a,b]
33	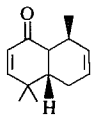 **39** + **40** (64%)	**14** (38)[b]
34	**6** + **11** (97%)[c]	**13** (37%)[a,b]
35	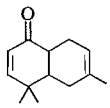 **26** + **41** (97%)[c]	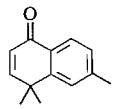 **42** (43%)[b,c]
36	**10** + **21** (61%)	**16** (20%)[b]
37	**9** + **20** (35%)	**15** (17%)[b,d]
38	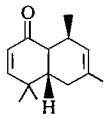 **43** + **44** (83%)	**15** (31%)[b]

[a]See ref. 36.
[b]The remaining product material consisted of brominated derivatives of the starting hexalone(s) and product aryl-ketone as shown by ^{1}Hmr and mass spectra.
[c]See ref. 33.
[d]Pure **9** was aromatized.

proton at C-4a was strongly deshielded by the ester carbonyl group and this was taken as evidence that the ester and the C-4a proton were on the same face of the molecule. Although this evidence for a *cis*-ring fusion is not absolutely conclusive in this particular case, several examples of this series (Entries 3, 4, and 8) give additional ^{1}Hmr evidence. These adducts show a long range W-coupling between the C-3 and C-4a protons in the ^{1}Hmr, which has been described previously for adducts of **1** and which can only be achieved by the *cis* isomer. We believe that, when coupled with the generality of the *cis* principle, the evidence is sufficient to warrant extrapolation of the stereochemical assignment to the whole series.

The relative stereochemistry of the B-ring substituents in **31**, **33**, **36**, **37**, and **38** was assigned as indicated on the basis of the ^{1}Hmr and ^{13}Cmr spectra (Tables 7 and 8) and also on the basis of identity of decarboxylation products with those obtained directly from addition to **1**.

Nuclear magnetic resonance spectral assignments

The nmr spectra for adducts of **2** are summarized in Tables 7 and 8, while nmr spectra of their decarboxylated derivatives are shown in Tables 3 and 4. Several points are noteworthy. Firstly, the previously mentioned downfield shift of the C-4a proton in the ^{1}Hmr spectrum from a normal value of δ 1.95 (45) to a range of δ 2.49–2.75, which is considered diagnostic for the *cis*-ring junction, is clearly evident. Secondly, the deshielding effect of the ketone carbonyl double bond on the C-8 α proton, which is diagnostic in the case of the adducts of **1**, must be treated more carefully in the case of adducts of **2**. While the effect is as predicted in the case of C-8 unsubstituted adducts, the C-8 substituted adducts generated in this sequence show an unexpected reversal. The signal due to the C-8 β proton of **31**, **36**, and **37** is deshielded by ~0.5 ppm relative to the corresponding proton in adducts of **1** (due to the ring junction carboxylate group), while the signals due to the C-8 α proton of **33** and **38**, rather than being unchanged relative to those in **39** and **43**, are in fact shielded by ~0.5 ppm.

In the ^{13}Cmr spectra, signals for C-3, C-4, C-4a, C-8, and the *gem*-dimethyl groups are all shifted significantly in the C-8 α-substituted group (**31** and **37**) relative to the C-8 β-substituted group (**33** and **38**).

The ^{1}Hmr spectrum was essential in assigning the bridge stereochemistry of **30**. In **30**, the conformation is a "sandwich-like" structure **30*a*** in which the isolated double bond is held above the carbon–carbon double bond of the enone system. As a result, the proton of C-2 would be shielded by the isolated double bond and the proton at C-6 would be shielded by the enone double bond. On the other hand, in **45** one of the C-9 protons would be shielded by the enone double bond.

On close examination of the ^{1}Hmr spectrum of the adduct, it was evident that neither of the C-9 protons (δ 1.60 and 1.41) was particularly shielded relative to the bridge protons of the model compound norbornene (δ 1.32 and 1.07 (42)). Comparison of the chemical shift of the proton at C-2 (δ 5.60) with other compounds in this series (δ 5.69–5.87) showed that it was experiencing a shielding effect. Furthermore, one of the olefinic protons (δ 5.75) was shifted upfield from the normal value of δ 5.95 for norbornene (42). These data supported the assignment of structure **30**.

In view of the unexpected shifts described previously for the C-8 substituted adducts of **2**, their C-8 stereochemistries are most reliably determined by ^{1}Hmr analysis of their decarboxylation products, the rationalization of whose spectra has been presented in the earlier discussion of Table 4. For example, conclusive evidence of the C-8 stereochemistry of keto-ester **38** was determined by analysis of the ^{1}Hmr spectrum of its decarboxylation products **43** and **44**. As was predicted in the discussion of Entry 4, Table 1, the C-8 proton of *cis*-enone **43** was deshielded by the ketone carbonyl and appeared at δ 2.97 while the C-8 methyl substituent appeared at the normal shift of δ 0.97. Such an effect is only possible if the C-8 stereochemistry is as depicted in **43**.

Mechanistic discussion

From the preceding results it can be seen that dienone ester **2** is a much more reactive dienophile than dienone **1** and reacts even with relatively unreactive dienes (Table 5, Entry 2) to give adducts in good yields. Furthermore, the dienophilicity (with one minor exception, Entry 4) is entirely restricted to the more substituted double bond. As expected, the *ortho* rule is followed when applicable (Entries 4, 5, 7, and 8). However, the anticipated promotion of *para* addition of 2-substituted dienes under boron trifluoride ethereate catalysis was disappointingly small (Entry 6). The *endo* selectivity of additions to dienone ester **2** appears to be with a dominant preference for secondary overlap (6) with the ketone carbonyl group (transition states of type **A**) rather than with the ester group (transition states of type **B**) (Entries 3–5 and 7). However, the formation of the two C-8 epimeric adducts **37** and **38** by addition of *trans*-2-methyl-1,3-pentadiene (Entry 8) clearly results from addition via two quite different transition states. Keto-ester **37** would be the result of addition via transition state **37A**, whereas keto-ester **38** would be the result of addition via transition state **38B**. The

Can. J. Chem. Downloaded from www.nrcresearchpress.com by 72.64.146.136 on 09/07/12
For personal use only.

TABLE 7. The ^{1}Hmr shifts (δ) for adducts of dienone ester **2**

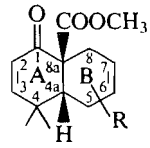

Adduct	**28**[a]	**29**	**30**	**31**	**33**	**34**	**35**	**36**	**37**	**38**
C-2 H	5.87	5.75	5.60	5.72	5.74	5.75	5.75	5.76	5.69	5.81
C-3 H	6.57	6.46	6.31[b]	6.11[b]	6.40	6.43	6.41	6.20	6.09[b]	6.40
C-4a H	2.75	2.63	2.49	2.56	2.63	2.62	2.71	2.56	2.53	2.63
C-5 H	2.11	1.92	3.00	2.10	2.02	2.08	1.91	2.03	Complex	1.89
C-6 H	5.66	—	5.05	5.50	5.48	5.29	—	5.16	—	—
C-7 H	5.66	—	5.75	5.35	5.48	—	5.34	—	5.17	5.20
C-8α H	2.70	2.47	3.45	—	2.52	2.47	2.62	—	—	2.52
C-8β H	2.25	2.09	—	2.70	—	2.08	2.14	2.70	2.65	—
gem CH_3	1.18	1.13	1.27	1.14	1.18	1.16	1.19	1.16	1.10	1.16
	1.07	0.94	1.17	1.10	1.06	1.00	1.02	1.10	1.10	1.02
R	—	1.58	1.60	1.20	1.10	1.66	1.67	Complex	1.57	1.64
		1.58	1.41						1.13	1.07

[a]This spectrum was determined in deuteriochloroform.
[b]Long range W-type coupling to C-4a proton.

competition of these two transition states is attributed to the now familiar destabilization of transition state **37A** by steric interaction between the C-2 methyl group of the diene and a C-4 methyl group of the dienophile in a manner analogous to that encountered in the addition of isoprene to dienone **1** (Table 1, Entry 1). The combined *ortho*- and *para*-directing electronic effects are sufficient to counteract the steric destabilization of transition state **37A** and no abnormal addition product **46** is observed. However, the steric destabilization in transition state **37A** can be alleviated without violation of the *ortho* and *para* rules in this case by addition via transition state **38B**. The experimental results confirm that reaction through this transition state does in fact compete effectively with **37A**.

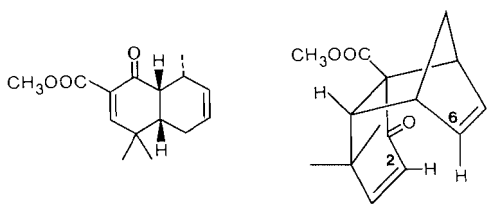

32 **30a**

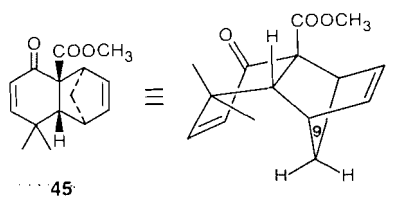

45

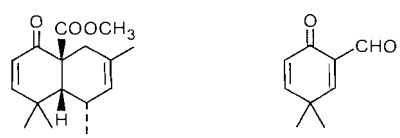

46 **47**

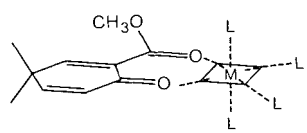

L=ligand : Cl^-, R_2CO and/or R_2O

48 M=Sn
49 M=Fe

The competition of the two different transition states **37A** and **38B** for addition of *trans*-2-methyl-1,3-pentadiene suggests that a similar effect might operate for addition of isoprene. A portion of the material would proceed via the *para*-rule guided transition state **35B**, in which there is no steric interaction between the methyl groups, to give only keto-ester **35**. The remainder would proceed via transition state **34A/35A** through which the ratio of products **34** and **35** would be governed by the relative strengths of the steric and electronic directing effects, and the ratio of the two competing pathways would thus be reflected in the product ratio.

Catalyst studies

In view of the preceding discussion, two possible methods are available for further enhancement of the *para* selectivity of addition of isoprene to dienophiles of this type. Increasing the polarization of the dienophilic double bond should lead to increased *para* selectivity regardless of which transition state type (**A** or **B**) is in effect. And secondly, any change in the reaction conditions that would favour a transition state of type **B** relative to one of type **A** should also increase the *para* selectivity, since only *para* addition of isoprene is expected via transition states of type **B**. The former requirement might be achieved either by the use of a stronger (and therefore more electron-withdrawing) Lewis acid catalyst or by substitution of the carbomethoxy group of **2** with a more electron-withdrawing substituent. Thus the ratio of *para:anti-para* addition products could well be a function of the relative Lewis acidity of the catalyst. However, both the addition of other activating groups and change of catalyst could have a less clearly defined influence on the course of the reaction.[15] *Endo* selectivity is

[15]Liotta *et al.* (49) have subsequently examined the Diels–Alder reaction of formyl substituted dienone **47** with piperylene and observed preference for a transition state of type **A**.

Can. J. Chem. Downloaded from www.nrcresearchpress.com by 72.64.146.136 on 09/07/12
For personal use only.

TABLE 8. The ^{13}Cmr shifts (δ) for some adducts of dienone ester **2**

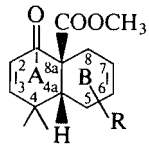

Adduct	**28**	**31**	**33**	**34**	**35**	**36**	**37**	**38**
C-1	197.3	196.3	197.0	197.4	197.7	197.6	196.7	197.4
C-2	124.3[a]	123.4	124.2[a]	124.0	123.9	126.9	125.2[a]	124.5[a]
C-3	157.8	152.5	157.5	158.0	157.9	155.0	152.6	157.3
C-4	36.2	38.0[a]	36.3	36.0	36.2	36.5	37.7	36.4
C-4a	40.8	47.1	42.2	40.4	41.3	43.7	47.4	42.8
C-5	23.9	27.2	24.3	24.2	29.0[a]	24.8	32.0	29.1
C-6	124.0[a]	127.1	124.5[a]	119.3	132.2	116.5	130.3	131.1
C-7	125.5[a]	130.5	131.2	131.1	118.5	137.0	127.3[a]	125.6[a]
C-8	28.6	37.7[a]	32.0	33.1	28.7[a]	41.5	38.4	32.5
C-8a	56.9	59.3	60.9	57.5	56.6	60.1	59.3	60.6
gem CH_3	30.4	28.4	31.3	30.4	30.4	30.5	28.5	31.3
	23.8	27.4	23.8	23.6[a]	23.5[b]	25.7	27.3	23.7
$-CO_2-$	172.9	174.6	171.6	173.0	173.0	174.3	174.8	171.6
$-O-CH_3$	52.5	52.1	51.9	52.4	52.4	52.4	52.1	51.9
R	—	16.8	16.0	23.4[b]	23.4[b]	35.3	23.9	23.1
						27.8	17.1	16.2
						26.8		
						26.4		

[a,b]The precise assignment of these pairs of signals is uncertain.

TABLE 9. Effect of catalysts on addition of isoprene to dienone ester **2**

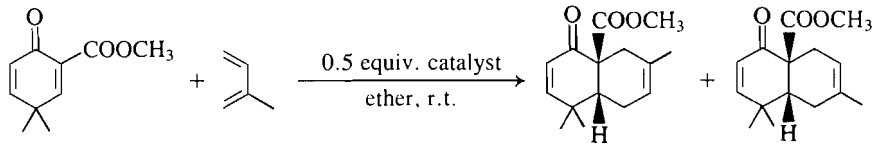

2 20 equiv. **34** **35**

Catalyst	Time for completion (h)	Yield (%)	**35**:**34**
$BF_3 \cdot Et_2O$	72	73	30:70
Toluene, 125°C	[a]		40:60
Mesitylene, 250°C	[a]		47:53
$TiCl_4$	14		48:52
$ZnCl_2$	48		48:52
$FeCl_3$	0.3		50:50
$SnBr_4$ (ref. 50)	168		51:49
$AlCl_3$	4		53:47
$AlBr_3$	265	64	56:44
$SbCl_5$	4		66:34
$SnCl_4$	44	99	82:18

[a]Reaction was not run to completion.

increased under the influence of Lewis acid catalysis (8, 23). Thus one might predict that appropriate choice of a Lewis acid that would, in the ideal case, complex *only* with the ester carbonyl would promote preferential secondary overlap with the ester group (as in type **B**) rather than with the ketone carbonyl (as in type **A**).

To study these possibilities, we examined a variety of Lewis acids as catalysts for the addition of isoprene to dienone ester **2** in ether solution and also briefly examined the reaction under thermal conditions. The results are summarized in Table 9. The table shows that the increase in the proportion of *para*-addition product obtained by varying the catalyst does not strictly parallel the general order of Lewis acidity (51): $BX_3 > AlX_3 > FeX_3 > SbX_5 > SnX_4 > ZnX_2$. It appears that the results are complicated by other factors, most probably the effect of the relative hardness or softness (52) of the Lewis acids and the effect of the Lewis acid on the relative stabilities of type **A** and type **B** transition states mentioned previously.

Can. J. Chem. Downloaded from www.nrcresearchpress.com by 72.64.146.136 on 09/07/12
For personal use only.

Can. J. Chem. Downloaded from www.nrcresearchpress.com by 72.64.146.136 on 09/07/12
For personal use only.

Several examples are particularly noteworthy. Firstly, the catalytic effect of boron trifluoride actually acts to decrease the *para* selectivity of the reaction relative to the thermal cases. This would appear to be due to the effect of preferential coordination of the relatively hard Lewis acid boron trifluoride with the ketone carbonyl group. The result is promotion of a type **A** transition state in which the electron-withdrawing effect on the dienophilic double bond promoting *para*-rule guided addition is insufficient to counteract the steric directing effect which promotes *anti-para* addition. Thus the predominant product is **34** rather than **35**.

In the case of stannic chloride, the Lewis acid is capable of forming 1:2 complexes with certain Lewis bases such as aldehydes, ketones, esters, and ethers (53). This could result in the formation of a complex such as **48** between the Lewis acid and the bidentate ligand dienone ester **2**. The electron-withdrawing effect of the Lewis acid exerted on the dienophilic double bond through the two carbonyl groups at once, together with the expected increase in contribution to the reaction from transition state **35B**,[16] could account for the surprisingly high **35**:**34** product ratio. Regardless of the reason for this effect, the ability to select the predominant product of addition (**34** or **35**) solely by the choice of the Lewis acid catalyst (boron trifluoride etherate or stannic chloride) constitutes a prime example[17] of the concept of "guidance by catalysis," which has been conceived and demonstrated by Valenta and co-workers (55, 56). The realization of this capability for product selection constitutes a powerful tool in the design of synthetic schemes.

The case of ferric chloride is also noteworthy. The remarkable increase in reaction rate brought about by this catalyst has made possible the addition to **2** of the relatively unreactive diene *cis*-piperylene (Table 5, Entry 5) to give keto-ester **33**, and has also allowed the rapid generation of adduct **36** in good yield with efficient use of the rather costly diene.[18]

The reasons for this effect could stem from the ability of Fe(III) to form hexacoordinate complexes (58) with β-dicarbonyl compounds, so that the bidentate ligand keto-ester **2** could form a complex such as **49**, as was suggested for stannic chloride. The electron-withdrawing effect of the Lewis acid acting through both carbonyls could lead to a particularly strong polarization of the double bond. Since ferric chloride is expected (51) to be a stronger Lewis acid than stannic chloride, the slower rate for stannic chloride is not considered unusual. Clearly the differing ligand field energies and bond lengths and angles introduced by the different size and electronic character of the two transition metals in these complexes also play a definitive role in this effect that is not yet clearly definable.

[16]This increase is expected for two reasons. Firstly, Lewis acid complexation of the ester carbonyl to any extent would be expected to promote secondary overlap with the ester group (8, 23) at the expense of secondary overlap with the ketone. And secondly, since the experimental evidence suggests that the hard Lewis acid boron trifluoride complexes preferentially with the ketone carbonyl, it is possible that the very soft Lewis acid stannic chloride might exhibit a preference for closer association with the ester carbonyl in complex **48**. This would further promote secondary overlap with the ester relative to the ketone and lead to an increased contribution to the reaction from **35B**.

[17]For another example, see ref. 54.

[18]Yield of 72% after 45 min using 2 equiv. of 1-vinylcyclohexene (57).

Conclusions

Demonstration of the scope of dienone **1** and dienone ester **2** as dienophiles makes available two useful new intermediates for the synthetic chemist. In particular, dienone ester **2** offers a reactive dienophile that can add efficiently even to relatively unreactive dienes. Furthermore, the activating substituent (carbomethoxyl) of **2** can either be removed or used as reactive site for further elaboration of the adducts.

Experimental

General

Melting points were determined on a Kofler hot stage apparatus and are uncorrected. Elemental analyses were performed by the microanalytical laboratory of this department. Infrared (ir) spectra were recorded on a Perkin–Elmer model 457 or Nicolet 7-199 FT-IR spectrophotometer and, except where otherwise stated, were obtained on solutions in chloroform. The ^{1}Hmr spectra were recorded on a Varian HA-100, HA-100/Digilab, or Bruker WH-200 spectrometer and, except where otherwise stated, were obtained on solutions in carbon tetrachloride with tetramethylsilane as internal reference. The ^{13}Cmr spectra were recorded on a Bruker WP-60/Nicolet BNC-12 system or a Bruker HFX-90/Nicolet 1085 system and were obtained on solutions in deuteriochloroform using tetramethylsilane as internal reference. Mass spectra (ms) were recorded using A.E.I. model MS9, MS12, or MS50 mass spectrometers. Gas chromatography (gc) was performed on a Hewlett Packard 5750 research chromatograph using stainless steel columns (8 ft × 1/8 in.) packed with either 10% diethylene glycol succinate (Column A) or 15% SE-30 (Column B) on 80–100 mesh Chromosorb W, acid washed and treated with dimethylchlorosilane. Unless stated otherwise, anhydrous magnesium sulfate was used for drying organic solutions.

Materials

Benzene was distilled over lithium aluminum hydride or sodium wire. Pyridine was distilled over barium oxide and stored over potassium hydroxide pellets. 2,4,6-Collidine was distilled over potassium hydroxide pellets. Isoprene was distilled prior to use. Boron trifluoride etherate was distilled over calcium hydride according to the procedure of Brown (59, 60). Nitrogen was passed through a purification train of Fieser's solution (60), saturated aqueous lead acetate, concentrated sulfuric acid, and potassium hydroxide pellets. 4,4-Dimethyl-2,5-cyclohexadienone (**1**) was prepared from 4,4-dimethyl-2-cyclohexenone (**3**) by the method of Zimmerman *et al.* (39). 4,4-Dimethyl-2-cyclohexenone was prepared from methyl vinyl ketone and *N*-(1-isobutenyl)-piperidine by the method of Djerassi and co-workers (37). *N*-(1-Isobutenyl)-piperidine was prepared by the method of Benzing (61). 1-Vinylcyclohexene was prepared according to the established procedure (62) or by a more efficient method described herein. Cyclopentadiene was prepared by thermal cracking of dicyclopentadiene and was stored at −30°C prior to use. *cis*-Piperylene (≥97% *cis*) was obtained from Fluka A.G.

*4,4-Dimethyl-4aβ,5,8,8aβ-tetrahydro-1(4*H*)-naphthalenone (7)*[19]

Dienone **1** (306 mg, 2.51 mmol) was dissolved in ether (20 mL) under an atmosphere of nitrogen. Boron trifluoride etherate (179 mg, 1.26 mmol) was added to the stirred solution and after 15 min dry butadiene gas[20] (passed through a drying tube of anhydrous calcium chloride) was bubbled into the solution. Additional butadiene gas was introduced for 15 min each day for 22 days. Then saturated aqueous

[19]The stereochemical designations used in this section denote *relative* stereochemistry. All compounds employed and obtained were racemic.

[20]A more convenient method of introducing butadiene to a reaction at atmospheric pressure and room temperature is to introduce a saturated solution of butadiene in benzene (~20% v/v in butadiene) to the ethereal solution of the dienophile (63).

Can. J. Chem. Downloaded from www.nrcresearchpress.com by 72.64.146.136 on 09/07/12
For personal use only.

sodium bicarbonate (3 mL) was added and the reaction mixture was extracted with methylene chloride. The extracts were washed with water, dried, filtered, and concentrated. Column chromatography of the residue on silica gel, eluting with 2% ether in petroleum ether, gave enone **7** (78 mg, 26% yield based on consumed starting material), which crystallized on standing. Further elution with 10% ether in petroleum ether gave recovered dienone **1** (99 mg, 31% recovery). Molecular distillation of chromatographically pure enone **7** in a Kugelrohr apparatus gave pure crystals of enone **7**; mp 69.5–70.5°C; ir (CCl_4): 1675 (C=O), 1383, and 1371 (CH_3) cm^{-1}; ^{1}Hmr δ: 6.31 (dd, 1H, J = 10, J' = 2 Hz, -C*H*=CH—CO-), 5.72 (d, 1H, J = 10 Hz, -CH=C*H*—CO-), 5.55 (m, 2H, -CH=CH-), 2.92 (m, 1H, —CH—CO—), 2.83 (dm, 1H, J = 18 Hz, C-8α H), 1.99 (m, 3H, C-4a H and C-5 -CH_2-), 1.94 (dm, 1H, J = 18 Hz, C-8β H), 1.31 (s, 3H, CH_3), and 1.10 (s, 3H, CH_3); ms M^+: 176.1202 (calcd. for $C_{12}H_{16}O$: 176.1202). *Anal.* calcd. for $C_{12}H_{16}O$: C 81.77, H 9.15; found: C 81.83, H 9.29.

*4,4,6,8β-Tetramethyl-4aβ,5,8,8aβ-tetrahydro-1(4*H*)-naphthalenone (**9**) and 2-(1,4-dimethyl-3-butenyl)-4,5-dimethylphenol (**12**)*

Dienone **1** (292 mg, 2.32 mmol) was dissolved in anhydrous ether (10 mL) and boron trifluoride etherate (104 mg, 1.16 mmol) was added followed by *trans*-2-methyl-1,3-pentadiene (1.90 g, 23.1 mmol). After stirring for 7 days, saturated aqueous sodium bicarbonate (1 mL) was added and the resulting mixture was extracted with methylene chloride. The extracts were washed with water, dried, filtered, and concentrated. Column chromatography of the residue on silica gel, eluting with 2–5% ether in petroleum ether, gave a mixture (236 mg) of enone **9** and phenol **12**. Further elution with 10–50% ether in petroleum ether gave recovered dienone **1** (33 mg, 12% recovery). Flash chromatography (64) of the mixture of enone **9** and phenol **12** on silica gel, eluting with 5% ethyl acetate in petroleum ether, gave pure enone **9** (84 mg, 20% yield based on consumed starting material); ir: 1687 (C=O), 1396, 1374, 1365 (CH_3), and 815 (C=CH) cm^{-1}; ^{1}Hmr δ: 6.13 (dd, 1H, J = 10, J' = 2 Hz, -C*H*=CH—CO-), 5.53 (d, 1H, J = 10 Hz, -CH=C*H*—CO-), 5.19 (br s, 1H, =CH—), 2.77 (dd, 1H, J = 4, J' = 3 Hz, C-8a H), 2.24 (m, 1H, —C*H*—CH_3), 1.57 (s, 3H, =C—CH_3), 1.33 (d, 3H, J = 7 Hz, —CH—CH_3), 1.31 (s, 3H, CH_3), and 1.09 (s, 3H, CH_3); ms M^+: 204.1510 (calcd. for $C_{14}H_{20}O$: 204.1514). Continued elution gave a mixture (20 mg) of ketone **9** and phenol **12** (~50:50 by ^{1}Hmr integration). Final elution gave pure phenol **12** (53 mg, 13% yield based on consumed starting dienone **1**); ir: 3438 (OH), 1668 (C=C), 1619, 1510 (aromatic C=C), and 1376 (CH_3) cm^{-1}; ^{1}Hmr δ: 6.73 (s, 1H, C-3 Ar-H), 6.38 (s, 1H, C-6 Ar-H), 5.18 (dm, 1H, J = 9, J' = 1 Hz, =CH—), 4.91 (br s, 1H, -OH), 3.70 (dq, 1H, J = 9, J' = 7 Hz, —C*H*—CH_3), 2.14 (s, 6H, 2 × Ar-CH_3), 1.70, 1.66 (both d, 6H total, each J = 1 Hz, =C(CH_3)$_2$), and 1.24 (d, 3H, J = 7 Hz, —CH—CH_3); ms M^+: 204.1508 (calcd. for $C_{14}H_{20}O$: 204.1514).

1-Vinylcyclohexanol

A 1.40 *N* solution of vinyllithium in tetrahydrofuran (300 mL, 0.42 mol of vinyllithium) was added to anhydrous ether (700 mL) by forced siphon (65) at 0°C under an atmosphere of nitrogen. A solution of cyclohexanone (39.3 g, 0.40 mol) in anhydrous ether (300 mL) was added to the stirred solution dropwise over 90 min. After stirring for 30 min the reaction mixture was poured into ice-cold saturated aqueous ammonium chloride with vigorous stirring. The resulting mixture was extracted with ether and the extracts were washed with water, dried (sodium sulfate), filtered, and concentrated. Distillation of the residue gave the pure alcohol (44.35 g, 78% yield) as a colourless oil: bp 67–69°C/16 Torr (1 Torr = 133.3 Pa); ir (neat): 3600 (OH, free), 3390 (OH, H-bonded), 3080 (-CH=CH_2), 1640 (C=C), 995 and 970 (-CH=CH_2) cm^{-1}; ^{1}Hmr δ: 5.87 (dd, 1H, J = 18, J' = 11 Hz, -C*H*=CH_2), 5.14 (dd, 1H, J = 18, J' = 2 Hz, -CH=CH—*H* (*Z*)), 4.90 (d, 1H, J = 11, J' = 2 Hz, -CH=CH—*H* (*E*)), 1.64 (s, 1H, -OH), and 1.47 (br s, 10H, 5 × -CH_2-).

1-(p-Toluenesulfonylcarbamoyl)-1-vinylcyclohexane

1-Vinylcyclohexanol (1.22 g, 9.71 mmol) was dissolved in benzene (10 mL) and a solution of *p*-toluenesulfonylisocyanate (2.11 g, 10.6 mmol) in benzene (5.0 mL) was added with stirring. After 1 h, a small amount of water (~100 μL) was added to destroy excess isocyanate and the solution was diluted with ether (~5 mL), dried, filtered, and concentrated under vacuum at room temperature. The crude carbamate (3.95 g, 126% yield) thus obtained as powdery crystals[21] was contaminated with *p*-toluenesulfonamide. Column chromatography of a portion (495 mg) of this crude product on silica gel, eluting with 25–50% ether in petroleum ether, gave the pure carbamate (230 mg, 59% yield from 1-vinylcyclohexanol) as a colourless viscous oil; ir (neat): 1780 (C=O), 1588, 1483 (C=C, aromatic), 1335 (-SO_2—N—), and 1145 (-SO_2-) cm^{-1}; ^{1}Hmr δ: 8.30 (s, 1H, -NH-), 7.83 (d, 2H, J = 8 Hz, 2 × -SO_2—C=CH-), 7.24 (d, 2H, J = 8 Hz, 2 × CH_3—C=C*H*—), 5.83 (dd, 1H, J = 18, J' = 11 Hz, -C*H*=CH_2), 4.96 (d, 1H, J = 11 Hz, -CH=CH—*H* (*E*)), 4.91 (d, 1H, J = 18 Hz, -CH=CH—*H* (*Z*)), 2.43 (s, 3H, -CH_3), 2.10 (br s, 2H, 2 × -O—C—CH—*H*), and 1.50 (br s, 8H, 3 × -CH_2- and 2 × -O—C—CH—*H*); ms (NH_3 chemical ionization) parent peak: 341 (M + NH_4^+). *Anal.* calcd. for $C_{16}H_{21}NO_4S$: C 59.42, H 6.54, N 4.33, S 9.91; found: C 59.21, H 6.83, N 3.96, S 9.55.

1-Vinylcyclohexene[22]

The crude carbamate (3.38 g, ~10.4 mmol) obtained from the preceding experiment was heated in a Kugelrohr apparatus to ~150°C and the distillate was collected in a water-cooled outer trap for 1 h. The distillate was found to be pure 1-vinylcyclohexene (790 mg, 87% from 1-vinylcyclohexanol) as a colourless liquid; ir (neat): 3090 (-CH=CH_2), 3030 (-CH=CH_2), 1645 (C=C), 995 and 905 cm^{-1} (-CH=CH_2); ^{1}Hmr δ: 6.21 (dd, 1H, J = 18, J' = 10 Hz, -C*H*=CH_2), 5.65 (br s, 1H, -C=CH—), 4.93 (d, 1H, J = 18 Hz, -CH=CH—*H* (*Z*)), 4.80 (d, 1H, J = 10 Hz, -CH=CH—*H* (*E*)), 2.02 (m, 4H, -CH_2—C=CH—CH_2-), and 1.64 (m, 4H, -CH_2—CH_2-).

*4,4-Dimethyl-4aβ,5,7,8,9,10,10aβ,10bβ-*octahydro-1(4H)*-phenanthrenone (**10**)*

Dienone **1** (160 mg, 1.31 mmol) was dissolved in anhydrous ether (10 mL). Boron trifluoride etherate (93 mg, 0.66 mmol) was added with stirring followed by 1-vinylcyclohexene (450 mg, 2.50 mmol). After 3 days, a solution of 1-vinylcyclohexene (450 mg, 2.50 mmol) in ether (2.0 mL) was added. The mixture was stirred for an additional 2 days and then saturated aqueous sodium bicarbonate (1 mL) was added. The mixture was extracted with methylene chloride. The extracts were washed with water, dried, filtered, and concentrated. Column chromatography of the residue on silica gel, eluting with

[21] One crystallization of the crude carbamate (900 mg) from ether gave colourless crystals (mp 48–59°C, 350 mg), which were identified as the mono-etherate complex of the carbamate by their ^{1}Hmr spectrum. In addition to signals due to the carbamate, two signals due to diethyl ether were observed at δ 3.35 (q, 4H, J = 7 Hz, 2 × -OCH_2-), and δ 1.12 (t, 6H, J = 7 Hz, 2 × -CH_3).

[22] This approach to 1-vinylcyclohexene was suggested to us by Dr. Z. Valenta as a reliable procedure which uses the 1-vinylcyclohexanol precursor more efficiently.

3–5% ether in petroleum ether, gave pure enone **10** (201 mg, 67% yield), which crystallized on standing; mp 43–47°C; ir: 1686 (C=O), 1392, 1373, and 1362 (CH_3) cm^{-1}; ^{1}Hmr δ: 6.12 (d, 1H, J = 10 Hz, -C*H*=CH—CO-), 5.57 (d, 1H, J = 10 Hz, -CH=C*H*—CO-), 5.08 (br s, 1H, =CH—), 2.86 (m, 1H, -CO—C*H*—), 2.50 (dddd, 1H, $J = J' = J'' = 12$, $J''' = 4$ Hz, C-10α H), 1.28 (s, 3H, CH_3), and 1.04 (s, 3H, CH_3); ^{1}Hmr (200 MHz, $CDCl_3$) δ: 6.23 (d, 1H, J = 10 Hz, -C*H*=CH—CO—), 5.71 (d, 1H, J = 10 Hz, -CH=C*H*—CO-), 5.21 (s, 1H, =CH—), 3.00 (dddd, 1H, $J = J' = J'' = 12$, $J''' = 4$ Hz, C-10α H), 1.28 (s, 3H, CH_3), and 1.04 (s, 3H, CH_3); ms M^+: 230.1666 (calcd. for $C_{16}H_{22}O$: 230.1670). *Anal.* calcd. for $C_{16}H_{22}O$: C 83.43, H 9.63; found: C 83.38, H 9.62.

*4,4,6,8-Tetramethyl-1(4*H*)-naphthalenone (**15**)*

Enone **9** (35 mg, 0.172 mmol) was dissolved in carbon tetrachloride (5 mL) and *N*-bromosuccinimide (61 mg, 0.343 mmol) was added, followed by benzoyl peroxide (3 mg, 0.012 mmol). The mixture was heated at reflux with vigorous stirring for 1 h, then cooled to room temperature, filtered, and concentrated. Column chromatography of the residue on silica gel, eluting with 1% ether in petroleum ether, gave pure aryl-ketone **15** (6 mg, 17% yield); ir: 1665 (C=O), 1604 (aromatic C=C), 1395, 1375, and 1363 (CH_3) cm^{-1}; ^{1}Hmr δ: 7.06 (br s, 1H, C-7 Ar-H), 6.86 (br s, 1H, C-5 Ar-H), 6.59 (d, 1H, J = 10 Hz, -C*H*=CH—CO-), 6.09 (d, 1H, J = 10 Hz, -CH=C*H*—CO-), 2.64 (s, 3H, C-8 Ar-CH_3), 2.34 (s, 3H, C-6 Ar-CH_3), and 1.43 (s, 6H, 2 × -CH_3); ms M^+: 200.1199 (calcd. for $C_{14}H_{16}O$: 200.1201).

*4,4-Dimethyl-7,8,9,10-tetrahydro-1(4*H*)-phenanthrenone (**16**)*

trans-Enone **21** (77 mg, 0.33 mmol) was dissolved in carbon tetrachloride (10 mL), and *N*-bromosuccinimide (119 mg, 0.67 mmol) and benzoyl peroxide (5 mg, 0.021 mmol) were added. The mixture was heated at reflux with stirring for 1 h, then cooled to room temperature, filtered, and concentrated. Column chromatography of the residue on silica gel, eluting with 2–3% ether in petroleum ether, gave aryl-ketone **16** (26 mg, 30% yield), which crystallized on standing. One recrystallization from petroleum ether gave yellowish crystals of aryl-ketone **16**; mp 102–110°C; ir: 1657 (C=O), 1631 (C=C), 1597 (aromatic C=C), 1375 and 1360 (CH_3) cm^{-1}; ^{1}Hmr δ: 7.17 (d, 1H, J = 4 Hz, C-6 H), 7.13 (d, 1H, J = 4 Hz, C-5 H), 6.59 (d, 1H, J = 10 Hz, -C*H*=CH—CO-), 6.12 (d, 1H, J = 10 Hz, -CH=C*H*—CO-), 3.24 (m, 2H, C-10 -CH_2-), 2.76 (m, 2H, C-7 -CH_2-), 1.76 (m, 4H, C-8 and C-9 -CH_2-), and 1.42 (s, 6H, 2 × -CH_3); ms M^+: 226.1358 (calcd. for $C_{16}H_{18}O$: 226.1358).

*Equilibrium of 4,4-dimethyl-4aβ,5,8,8aβ-tetrahydro-1(4*H*)-naphthalenone (**7**) and 4,4-dimethyl-4aβ,5,8,8aα-tetrahydro-1(4*H*)-naphthalenone (**18**)*

A mixture of *cis*- and *trans*-enones **7** and **18**[23] (43:57 by ^{1}Hmr integration, 202 mg, 1.15 mmol) was dissolved in methanol (10 mL) and 1 *N* aqueous sodium hydroxide (10 mL) was added. After stirring for 26 h, the mixture was extracted with methylene chloride. The extracts were washed with water, dried, filtered, and concentrated. Column chromatography of the residue on silica gel, eluting with 2% ether in petroleum ether, gave a mixture of *cis*- and *trans*-enones **7** and **18** (145 mg, 72% yield) in a 33:67 ratio as determined by gc analysis (Column B). The ^{1}Hmr analysis of this mixture showed two distinct sets of signals. The minor set was identical with the spectrum of pure *cis*-enone **7** while the major set was attributable to *trans*-enone **18**; ^{1}Hmr δ: 6.58 (d, 1H, J = 10 Hz, -C*H*=CH—CO-), 5.82 (d, 1H, J = 10 Hz, -CH=C*H*—CO-), 5.62 (m, 2H, -CH=CH-), 1.13 (s, 3H, CH_3), and 1.04 (s, 3H, CH_3). The following data were recorded for the mixture: ir (neat): 1680 (C=O), 1381, 1369 (CH_3), 670 (HC=CH, *cis*) cm^{-1}; ms M^+: 176.1202 (calcd. for $C_{12}H_{16}O$: 176.1201).

[23]This mixture was obtained in 78% yield by decarboxylation of keto-ester **28** under conditions similar to those used for decarboxylation of keto-esters **31** through **38** (*vide infra*).

*4,4,8α-Trimethyl-4aβ,5,8,8aα-tetrahydro-1(4*H*)-naphthalenone (**19**) and 3β-methoxy-4,4,8-trimethyl-3,4,4aβ,5,8,8aα-hexahydro-1(2*H*)-naphthalenone (**22**)*

Enone **8** (36) (108 mg, 0.57 mmol) was dissolved in methanol (5 mL) and an aqueous 1 *N* solution of sodium hydroxide (1 mL) was added with stirring. After 20 h, the reaction mixture was extracted with methylene chloride and the extracts were washed with water, dried, filtered, and concentrated. Column chromatography of the residue on silica gel eluting with 2–3% ether in petroleum ether gave pure *trans*-enone **19** (69 mg, 64% yield) as an oil; ir: 1677 (C=O), 1660 (C=C), 1374, 1360 (CH_3), and 690 (*cis* CH=CH) cm^{-1}; ^{1}Hmr δ: 6.49 (d, 1H, J = 10 Hz, -C*H*=CH—CO-), 5.72 (d, 1H, J = 10 Hz, -CH=C*H*—CO-), 5.58, 5.41 (each dm, total 2H, each J = 12 Hz, -CH=CH-), 2.44 (m, 1H, —CC*H*—CH_3), 1.19 (d, 3H, J = 6 Hz, —CH—CH_3), 1.14 (s, 3H, CH_3), and 1.06 (s, 3H, CH_3); ms M^+: 190.1360 (calcd. for $C_{13}H_{18}O$: 190.1358). *Anal.* calcd. for $C_{13}H_{18}O$: C 82.06, H 9.54; found: C 82.16, H 9.78. Further elution with 2–3% ether in petroleum ether gave methoxy ketone **22** (32 mg, 26% yield); ir: 1714 (C=O), 1383, 1360 (CH_3), and 683 (HC=CH) cm^{-1}; ^{1}Hmr δ: 5.51, 5.33 (each dm, total 2H, each J = 10 Hz, -HC=CH-), 3.26 (s, 3H, -OCH_3), 3.18 (dd, 1H, $J = J'$ = 3 Hz, —C*H*—OCH_3), 2.55 (d, 2H, J = 3 Hz, -CH_2—CO-), 1.07 (s, 3H, CH_3), 1.03 (s, 3H, CH_3), and 0.97 (d, 3H, J = 6 Hz, —CH—CH_3); ms M^+: 222.

*4,4,6,8α-Tetramethyl-4aβ,5,8,8aα-tetrahydro-1(4*H*)-naphthalenone (**20**) and 3β-methoxy-4,4,6,8α-hexahydro-1(2*H*)-naphthalenone (**23**)*

Enone **9** (18 mg, 0.088 mmol) was dissolved in methanol (5 mL) and aqueous 1 *N* sodium hydroxide (1 mL) was added. The mixture was stirred for 20 h, then extracted with methylene chloride. The extracts were washed with water, dried, filtered, and concentrated. Column chromatography of the residue on silica gel, eluting with 1% ether in petroleum ether, gave *trans*-enone **20** (8 mg, 44% yield); ir (neat): 1673 (C=O), 1379, and 1366 (CH_3) cm^{-1}; ^{1}Hmr δ: 6.45 (d, 1H, J = 10 Hz, -C*H*=CH—CO-), 5.60 (d, 1H, J = 10 Hz, -CH=C*H*—CO), 5.13 (br s, 1H, =CH-), 2.38 (m, 1H, —C*H*—CH_3), 1.66 (br s, 3H, =C—CH_3), and 1.07 (s, 3H, -CH_3); ms M^+: 204.1505 (calcd. for $C_{14}H_{20}O$: 204.1514). Further elution with 1–2% ether gave a mixture of enone **20** and methoxy-ketone **23** (5 mg, 75:25 by ^{1}Hmr integration). Final elution with 2% ether in petroleum ether gave pure methoxy-ketone **23** (5 mg, 24% yield); ir: 1713 (C=O), 1390, 1377, 1367 (CH_3), and 799 (C=CH) cm^{-1}; ^{1}Hmr δ: 5.05 (br s, 1H, =CH—), 3.22 (s, 3H, -OCH_3), 3.16 (dd, 1H, $J = J'$ = 3 Hz, —CH—O—), 2.53 (d, 2H, J = 3 Hz, —CH_2—CO—), 1.61 (s, 3H, =C—CH_3), 1.08 (s, 3H, -CH_3), 1.04 (s, 3H, -CH_3), and 0.93 (d, 3H, J = 7 Hz, —CH—CH_3).

*4,4-Dimethyl-4aβ,5,7,8,9,10,10aβ,10bα-octahydro-1(4*H*)-phenanthrenone (**21**) and 3β-methoxy-4,4-dimethyl-3,4,4aβ,5,7,8,9,-10,10aβ,10bα-*tetrahydro-1(2*H*)-phenanthrenone (**24**)*

Enone **10** (194 mg, 0.843 mmol) was dissolved in methanol (10 mL) and a 1 *N* aqueous solution of sodium hydroxide (2 mL) was added. The mixture was stirred for 24 h and then extracted with methylene chloride. The extracts were washed with water, dried, filtered, and concentrated. Column chromatography of the residue on silica gel, eluting with 3% ether in petroleum ether, gave enone **21** (92 mg, 49% yield), which crystallized on standing. One recrystallization from petroleum ether gave white crystals of *trans*-enone **21**; mp 36–45°C, ir: 1673 (C=O), 1395, 1377, 1365 (CH_3), and 799 (C=CH) cm^{-1}; ^{1}Hmr δ: 6.45 (d, 1H, J = 10 Hz, -C*H*=CH—CO-), 5.68 (d, 1H, J = 10 Hz, -CH=C*H*—CO-), 5.28 (br s, 1H, =CH—), 1.11 (s, 3H,

Can. J. Chem. Downloaded from www.nrcresearchpress.com by 72.64.146.136 on 09/07/12
For personal use only.

Can. J. Chem. Downloaded from www.nrcresearchpress.com by 72.64.146.136 on 09/07/12
For personal use only.

$-CH_3$), and 1.02 (s, 3H, $-CH_3$); ms M^+: 230.1667 (calcd. for $C_{16}H_{22}O$: 230.1670). *Anal.* calcd. for $C_{16}H_{22}O$: C 83.43, H 9.63; found: C 83.70, H 9.44. Continued elution gave a mixture (14 mg) of enone **21** and methoxy-ketone **24**. Further elution with 3–5% ether in petroleum ether gave pure methoxy-ketone **24** (20 mg, 9% yield); ir: 1712 (C=O), 1389, 1367 (CH_3) and 807 (C=CH) cm^{-1}; ^{1}Hmr δ: 5.28 (br s, 1H, =CH—), 3.27 (s, 3H, $-OCH_3$), 3.18 (dd, 1H, $J = J' =$ 3 Hz, —O—CH—), 2.55 (d, 2H, $J = 3$ Hz, $-CH_2$—CO-), 1.05 (s, 3H, $-CH_3$), and 1.02 (s, 3H, $-CH_3$); ms M^+: 262.

*8aβ-Carbomethoxy-4,4-dimethyl-4aβ,5,8,8a-tetrahydro-1(4H)-naphthalenone (**28**)*

Dienone ester **2** (311 mg, 1.73 mmol) was dissolved in ether (20 mL) under an atmosphere of nitrogen. Boron trifluoride etherate (106 μL, 122 mg, 0.86 mmol) was added and, after stirring for 15 min, dry butadiene gas (passed through calcium sulfate) was bubbled into the solution. After 6 h, saturated aqueous sodium bicarbonate (2 mL) was added and the resulting mixture was extracted with chloroform. The extracts were washed with water, dried, filtered, and concentrated. Column chromatography of the residue on silica gel, eluting with 10% ether in Skelly B, gave pure keto-ester **28** (286 mg, 70% yield); ir (KBr disk): 1730 (ester C=O), 1663 (enone C=O), 1619 (C=C), 1384, 1373, and 1361 (CH_3) cm^{-1}; ^{1}Hmr ($CDCl_3$) δ: 6.57 (d, 1H, $J =$ 10 Hz, -C*H*=CH—CO-), 5.87 (d, 1H, $J = 10$ Hz, -CH=C*H*—CO-), 5.66 (m, 2H, -CH=CH-), 3.70 (s, 3H, -O—CH_3), 2.75 (dd, 1H, $J =$ 6, $J' = 4$ Hz, C-4a H), 2.70 (dm, 1H, $J = 18$ Hz, C-8α H), 2.25 (dm, 1H, $J = 18$ Hz, C-8β H), 2.11 (m, 2H, C-5 $-CH_2$-), 1.18 (s, 3H, $-CH_3$), and 1.07 (s, 3H, $-CH_3$); ms M^+: 234.1258 (calcd. for $C_{14}H_{18}O_3$: 234.1256). *Anal.* calcd. for $C_{14}H_{18}O_3$: C 71.77, H 7.74; found: C 72.01, H 7.80.

*8aβ-Carbomethoxy-4,4,6,7-tetramethyl-4aβ,5,8,8a-tetrahydro-1(4H)-naphthalenone (**29**)*

Dienone ester **2** (343 mg, 1.91 mmol) was dissolved in ether (20 mL) under an atmosphere of nitrogen. Boron trifluoride etherate (118 μL, 136 mg, 0.96 mmol) was added and, after 15 min, 2,3-dimethyl-1,3-butadiene (4.34 mL, 3.15 g, 38.2 mmol) was added. After stirring for 4 days, saturated aqueous sodium bicarbonate (3 mL) was added and the resulting mixture was extracted with methylene chloride. The extracts were washed with water, dried, filtered, and concentrated. Column chromatography of the residue on silica gel, eluting with 10% ether in Skelly B, gave pure keto-ester **29** (316 mg, 63% yield). An analytical sample was prepared by molecular distillation in a Kugelrohr apparatus (60°C at 1 Torr) and this sample crystallized on standing; mp 77.5–78.5°C; ir (neat): 1746 (ester C=O), 1676 (enone C=O), 1383 and 1370 (CH_3) cm^{-1}; ^{1}Hmr δ: 6.46 (d, 1H, $J = 10$ Hz, -C*H*=CH—CO-), 5.75 (d, 1H, $J = 10$ Hz, -CH=C*H*—CO-), 3.61 (s, 3H, -O—CH_3), 2.63 (dd, 1H, $J = 6$, $J' = 4$ Hz, C-4a H), 2.47 (d, 1H, $J = 18$ Hz, C-8α H), 2.09 (d, 1H, $J = 18$ Hz, C-8β H), 1.92 (br s, 2H, C-5 $-CH_2$-), 1.58 (s, 6H, 2 × =C-CH_3), 1.13 (s, 3H, $-CH_3$), and 0.94 (s, 3H, $-CH_3$); ms M^+: 262.1568 (calcd. for $C_{16}H_{22}O_3$: 262.1569). *Anal.* calcd. for $C_{16}H_{22}O_3$: C 73.25, H 8.45; found: C 73.06, H 8.51.

*8aβ-Carbomethoxy-4,4-dimethyl-5,8β-methano-4aβ,5,8,8a-tetrahydro-1(4H)-naphthalenone (**30**)*

Dienone ester **2** (297 mg, 1.65 mmol) was dissolved in ether (20 mL) under an atmosphere of nitrogen. Boron trifluoride etherate (100 μL, 116 mg, 0.82 mmol) was added and, after stirring for 20 min, a solution of cyclopentadiene (2.71 mL, 2.17 g, 33 mmol) in dry ether (5 mL) was added. After stirring for 3 h, saturated aqueous sodium bicarbonate (2 mL) was added and the resulting mixture was extracted with methylene chloride. The extracts were washed with water, dried, filtered, and concentrated. Column chromatography of the residue on silica gel, eluting with 10% ether in Skelly B, gave pure keto-ester **30** (284 mg, 70% yield), which crystallized on standing. An analytical sample was prepared by molecular distillation in a Kugelrohr apparatus (60°C at 10 Torr); mp 57–59°C; ir (neat): 1738 (ester C=O), 1662 (enone C=O), 1379, 1366 (CH_3), and 720 (C=CH) cm^{-1}; ^{1}Hmr δ: 6.31 (dd, 1H, $J = 10$, $J' = 1.5$ Hz, -C*H*=CH—CO-), 6.05, 5.75 (each dd, each 1H, each $J = 6$, $J' = 2.5$ Hz, -CH=CH-), 5.60 (d, 1H, $J = 10$ Hz, -CH=C*H*—CO-), 3.65 (s, 3H, -O—CH_3), 3.45 (m, 1H, C-8 H), 3.00 (m, 1H, C-5 H), 2.49 (dd, 1H, $J = 2.5$, $J' = 1.5$ Hz, C-4a H), 1.60 (d, 1H, $J = 9$ Hz, bridge -CH*H*-), 1.41 (ddd, 1H, $J = 9$, $J' = J'' = 2$ Hz, bridge -CH*H*-), 1.27 (s, 3H, $-CH_3$), and 1.17 (s, 3H, $-CH_3$); ms M^+: 246.1253 (calcd. for $C_{15}H_{18}O_3$: 246.1256). *Anal.* calcd. for $C_{15}H_{18}O_3$: C 73.15, H 7.37; found: C 72.88, H 7.42.

*8aβ-Carbomethoxy-4,4,8α-trimethyl-4aβ,5,8,8a-tetrahydro-1(4H)-naphthalenone (**31**) and 2-carbomethoxy-4,4,8α-trimethyl-4aβ,5,8,8aβ-tetrahydro-1(4H)-naphthalenone (**32**)*

Dienone ester **2** (287 mg, 1.59 mmol) was dissolved in ether (20 mL) under an atmosphere of nitrogen. Boron trifluoride etherate (98 μL, 114 mg, 0.80 mmol) was added and, after 15 min, *trans*-piperylene (1.59 mL, 15.9 mmol) was added. After stirring for 43 h, saturated aqueous sodium bicarbonate (2 mL) was added and the resulting mixture was extracted with methylene chloride. The extracts were washed with water, dried, filtered, and concentrated. Column chromatography of the residue on silica gel, eluting with 7–8% ether in petroleum ether, gave keto-ester **31** (329 mg, 83% yield), which crystallized on standing. One recrystallization from ether gave white crystals of pure keto ester **31**; mp 66–68°C; ir (neat): 3010 (HC=CH), 1725 (ester C=O), 1685 (enone C=O), and 1375 (CH_3) cm^{-1}; ^{1}Hmr δ: 6.11 (dd, 1H, $J = 10$, $J' = 2$ Hz, -C*H*=CH—CO-), 5.72 (d, 1H, $J = 10$ Hz, -CH=C*H*—CO-), 5.50, 5.35 (each dm, 2H, each $J = 12$ Hz, -CH=CH-), 3.67 (s, 3H, -O—CH_3), 2.70 (m, 1H, —C*H*—CH_3), 2.56 (ddd, 1H, $J = 11$, $J' = 6$, $J'' = 6$, $J'' = 2$ Hz, C-4a H), 2.10 (m, 2H, C-4 $-CH_2$-), 1.20 (d, 3H, $J = 8$ Hz, —CH—C*H*$_3$), 1.14 (s, 3H, $-CH_3$), and 1.10 (s, 3H, $-CH_3$); ms M^+: 248.1413 (calcd. for $C_{15}H_{20}O$: 248.1414). *Anal.* calcd. for $C_{15}H_{20}O$: C 72.55, H 8.12; found: C 72.52, H 8.13. Further elution with 8–20% ether in petroleum ether gave keto-ester **32** (22 mg, 6% yield); ^{1}Hmr δ: 6.78 (d, 1H, $J = 2$ Hz, -CH=C—CO-), 5.45 (complex, 2H, -HC=CH-), 3.73 (s, 3H, -O—CH_3), 2.96 (dd, 1H, $J = J' = 4$ Hz, -CO—CH—), 2.33 (m, 1H, —C*H*—CH_3), 1.39 (s, 3H, $-CH_3$), 1.36 (d, 3H, $J = 8$ Hz, —CH—CH_3), and 1.18 (s, 3H, $-CH_3$); ms M^+: 248.

Lithium iodide dihydrate/collidine reagent

Finely divided anhydrous lithium iodide (514 mg, 3.84 mmol) was suspended in 2,4,6-collidine (3.05 mL) with vigorous stirring. Water (138 μL, 138 mg, 7.68 mmol) was added and the suspension rapidly dissolved. The resulting pale yellow solution had a calculated concentration of 1.28 *N* in lithium iodide dihydrate.

*4,4,8α-Trimethyl-4aβ,5,8α,8aβ-tetrahydro-1(4H)-naphthalenone (**8**) from keto-ester (**31**)*

Keto-ester **31** (315 mg, 1.27 mmol) was dissolved in lithium iodide hydrate/collidine reagent (2.04 mL, 2.61 mmol) and heated at reflux with stirring. After 1 h, the mixture was cooled to room temperature, poured into cold 5% aqueous hydrochloric acid, and extracted with ether. The extracts were washed with 5% aqueous hydrochloric acid and water, dried, filtered, and concentrated. Column chromatography of the residue on silica gel, eluting with 2% ether in petroleum ether, gave pure *cis*-enone **8** (104 mg, 45% yield based on consumed starting material), which was identical in its ^{1}Hmr and ir spectra with *cis*-enone **8** previously reported (36). Further elution with 4–10% ether in petroleum ether gave keto-ester **31** (86 mg, 27% recovery).

*8aβ-Carbomethoxy-4,4,8α-trimethyl-4aβ,5,8,8a-tetrahydro-1(4H)-naphthalenone (**31**) and 8aβ-carbomethoxy-4,4,8β-trimethyl-4aβ,5,8,8a-tetrahydro-1(4H)-naphthalenone (**33**)*

Dienone ester **2** (360 mg, 2.0 mmol) was dissolved in anhydrous ether (10 mL) and ferric chloride (162 mg, 1.0 mmol) was added, followed quickly by *cis*-piperylene (1.97 mL, 1.36 g, 20 mmol). After

Can. J. Chem. Downloaded from www.nrcresearchpress.com by 72.64.146.136 on 09/07/12
For personal use only.

stirring for 90 min, saturated aqueous sodium bicarbonate (2 mL) was added and the resulting mixture was extracted with methylene chloride. The extracts were washed with water, dried, filtered, and concentrated. Column chromatography of the residue on silica gel, eluting with 10–20% ether in petroleum ether, gave a mixture of keto-esters **31** and **33** (223 mg, 45% yield, 74% based on consumption of 61% of the starting dienone ester **2**, 50:50 mixture by ^{1}Hmr integration). One recrystallization from ether gave white crystals of keto-ester **33** (58 mg); mp 110–112°C; ir: 1741 (ester C=O), 1668 (enone C=O), 1382, 1376 (CH_3), and 702 (HC=CH) cm^{-1}; ^{1}Hmr δ: 6.40 (d, 1H, J = 10 Hz, -C*H*=CH—CO-), 5.74 (d, 1H, J = 10 Hz, -CH=C*H*—CO-), 5.48 (s, 2H, -CH=CH-), 3.60 (s, 3H, -O—CH_3), 2.63 (dd, 1H, $J = J'$ = 5 Hz, C-4a H), 2.52 (dq, 1H, J = 7, J' = 4 Hz, —C*H*—CH_3), 2.02 (m, 2H, C-5 -CH_2-), 1.18 (s, 3H, -CH_3), 1.10 (d, 3H, J = 7 Hz, —CH—C*H*$_3$), and 1.06 (s, 3H, -CH_3); ms M$^+$: 248.1414 (calcd. for $C_{15}H_{20}O_3$: 248.1412). *Anal.* calcd. for $C_{15}H_{20}O_3$: C 72.55, H 8.21; found: C 72.65, H 8.02. One recrystallization of the mother liquor gave additional colourless crystals of keto-ester **33** (37 mg). Further elution with ether gave dienone ester **2** (142 mg, 39% recovery).

*4,4,8β-Trimethyl-4aβ,5,8,8aβ-tetrahydro-1(4*H*)-naphthalenone (**39**) and 4,4,8β-trimethyl-4aβ,5,8,8aα-tetrahydro-1(4*H*)-naphthalenone (**40**)*

Keto-ester **33**[24] (67 mg, 0.27 mmol) was dissolved in 2,4,6-collidine (2 mL) under an argon atmosphere. Anhydrous lithium iodide (224 mg, 1.67 mmol) was added, followed by water (58 μL, 58 mg, 3.24 mmol). The mixture was heated at reflux with vigorous stirring for 90 min, then cooled to room temperature, poured into cold aqueous 5% hydrochloric acid, and extracted with ether. The extracts were washed with aqueous 5% hydrochloric acid and water, dried, filtered, and concentrated. Column chromatography of the residue on silica gel, eluting with 3–5% ether in petroleum ether, gave a 32:68 mixture of *cis*- and *trans*-enones **39** and **40** (33 mg, 64% yield). The ^{1}Hmr spectrum showed two sets of signals; one assignable to *cis*-ketone **39**, δ: 6.27 (dd, 1/3H, J = 10, J' = 2 Hz, -C*H*=CH—CO-), 5.70 (d, 1/3H, J = 10 Hz, -CH=*CH*—CO-), 5.70–5.40 (complex, 2 × 1/3H, -HC=CH-), 3.06[25] (m, 1/3H, —C*H*—CH_3), 2.55 (m, 1/3H, —C—H—CO-), 1.30 (s, 3 × 1/3H, -CH_3), 1.12 (s, 3 × 1/3H, -CH_3), and 1.04 (d, 3 × 1/3H, J = 7 Hz, —CH—C*H*$_3$); the other assignable to the *trans*-enone **40**, δ: 6.60 (d, 2/3H, J = 10 Hz, -C*H*=CH—CO-), 5.77 (d, 2/3H, J = 10 Hz, -CH=C*H*—CO-), 5.70–5.40 (complex, 2 × 2/3H, -HC=CH-), 2.83 (ddq, 2/3H, J = 7, $J' = J''$ = 5 Hz, —C*H*—CH_3), 1.17 (s, 3 × 2/3H, CH_3), and 1.04 (s, 3 × 2/3H, CH_3). The following data were recorded on the mixture of **39** and **40**: ir: 1671 (C=O), 1655 (C=C), 1396, 1378, 1367 (CH_3), and 714 (HC=CH) cm^{-1}; ms M$^+$: 190.1356 (calcd. for $C_{13}H_{18}O$: 190.1357).

*4,4,8-Trimethyl-1(4*H*)-naphthalenone (**14**) from enones **39** and **40***

A mixture of *cis*- and *trans*-enones **39** and **40** (32:68, 24 mg, 0.13 mmol) was dissolved in carbon tetrachloride (5 mL), and *N*-bromosuccinimide (45 mg, 0.25 mmol) and benzoyl peroxide (2 mg, 0.008 mmol) were added. The mixture was heated at reflux for 1 h, then cooled to room temperature, filtered, and concentrated. Column chromatography of the residue on silica gel, eluting with 0.5% ether in petroleum ether, gave aryl-ketone **14** (9 mg, 38% yield) identical with an authentic sample prepared from **8** (36).

*10bβ-Carbomethoxy-4,4-dimethyl-4aβ,5,7,8,9,10,10aβ,10b-octahydro-1(4*H*)-phenanthrenone (**36**)*

Dienone ester **2** (360 mg, 2.0 mmol) was dissolved in anhydrous ether (20 mL) under an atmosphere of nitrogen. Boron trifluoride etherate (126 μL, 142 mg, 1.0 mmol) was added and, after 15 min, a solution of 1-vinylcyclohexene (2.53 mL, 2.16 g, 20 mmol) in anhydrous ether (20 mL) was also added. After stirring for 60 h, saturated aqueous sodium bicarbonate (10 mL) was added and the resulting mixture was extracted with ether. The extracts were washed with water, dried, filtered, and concentrated. Column chromatography of the residue on silica gel, eluting with 10–12% ether in petroleum ether, gave keto-ester **36** (501 mg, 87% yield), which crystallized on standing. One recrystallization from ether – petroleum ether gave white crystals of pure keto ester **36**; mp 75.5–77°C; ir: 1728 (ester C=O), 1689 (enone C=O), 1370 (CH_3), and 835 (C=CH) cm^{-1}; ^{1}Hmr δ: 6.20 (d, 1H, J = 10 Hz, -C*H*=CH—CO-), 5.76 (d, 1H, J = 10 Hz, -CH=C*H*—CO-), 5.16 (br s, 1H, =CH—), 3.66 (s, 3H, -O—CH_3), 2.70 (m, 1H, C-10a H), 2.56 (dd, 1H, $J = J'$ = 6 Hz, C-4a H), 2.28 (dm, 1H, J = 14 Hz, C-7α H), 2.03 (br s, 3H, C-5 -CH_2- and C-7β H), 1.30 (m, 4H, C-8 and C-9 -CH_2-), 1.16 (s, 3H, -CH_3), and 1.10 (s, 3H, -CH_3); ms M$^+$: 288.1725 (calcd. for $C_{18}H_{24}O_3$: 288.1725). *Anal.* calcd. for $C_{18}H_{24}O_3$: C 74.97, H 8.39; found: C 74.79, H 8.32.

*4,4-Dimethyl-4aβ-5,7,8,9,10,10aβ,10bβ-octahydro-1(4*H*)-phenanthrenone (**10**) and 4,4-dimethyl-4aβ,5,7,8,9,10,10aβ,10bα-octahydro-1(4*H*)-phenanthrenone (**21**) from keto-ester **36***

Keto-ester **36** (170 mg, 0.59 mmol) was dissolved in lithium iodide dihydrate/collidine reagent (1.26 mL, 1.62 mmol). The mixture was heated at reflux with stirring for 1 h, then cooled to room temperature, poured into cold aqueous 5% hydrochloric acid, and extracted with ether. The extracts were washed with cold 5% aqueous hydrochloric acid and water, dried, filtered, and concentrated. Column chromatography of the residue on silica gel, eluting with 2% ether in petroleum ether, gave a mixture of *cis*- and *trans*-enones **10** and **21** (47:53 by ^{1}Hmr integration, 83 mg, 61% yield). The ^{1}Hmr spectrum of this mixture showed two sets of signals identical with those already reported for *cis*-enone **10** and *trans*-enone **21** (*vide supra*).

*4,4-Dimethyl-7,8,9,10-tetrahydro-1(4*H*)-phenanthrenone (**16**) from keto-ester **36***

A mixture of *cis*- and *trans*-enones **10** and **21** (47:53 by ^{1}Hmr integration, 81 mg, 0.35 mmol) obtained by decarboxylation of keto-ester **36** was dissolved in carbon tetrachloride (10 mL), and *N*-bromosuccinimide (125 mg, 0.70 mmol) was added. The mixture was heated at reflux with stirring for 1 h, then cooled to room temperature, filtered, and concentrated. Column chromatography of the residue on silica gel, eluting with 1.5% ether in petroleum ether, gave aryl-ketone **16** (16 mg, 20% yield), which showed an ^{1}Hmr spectrum identical with that already reported for aryl-ketone **16** (*vide supra*).

*8aβ-Carbomethoxy-4,4,6,8α-tetramethyl-4aβ,5,8,8a-tetrahydro-1(4*H*)-naphthalenone (**37**) and 8aβ-carbomethoxy-4,4,6,8β-tetramethyl-4aβ,5,8,8a-tetrahydro-1(4*H*)-naphthalenone (**38**)*

Dienone ester **2** (329 mg, 1.83 mmol) was dissolved in anhydrous ether (10 mL) and boron trifluoride etherate (112 μL, 130 mg, 0.95 mmol) was added. After stirring for 10 min, *trans*-2-methyl-1,3-pentadiene (2.08 mL, 1.50 g, 18.3 mmol) was added. The mixture was stirred for 2 h and saturated aqueous sodium bicarbonate (2 mL) was added. The resulting mixture was extracted with methylene chloride and the extracts were washed with water, dried, filtered, and concentrated. Column chromatography of the residue on silica gel, eluting with 5–20% ether in petroleum ether, gave a mixture of keto-esters **37** and **38** (396 mg, 83% yield, 50:50 by ^{1}Hmr integration). One recrystallization from ether gave white crystals of keto-ester **38** (72 mg); mp 112–116°C; ir: 1739 (ester C=O), 1672 (enone C=O), 1382, 1377, and 1369 (CH_3) cm^{-1}; ^{1}Hmr δ: 6.40 (d, 1H, J = 10 Hz, -C*H*=CH—CO-), 5.73 (d, 1H, J = 10 Hz, -CH=C*H*—CO-), 5.20 (br s, 1H, =CH—), 3.60 (s, 3H, -O—CH_3), 2.63 (dd, 1H, J = 6,

[24]It should be noted that the mixtures **8** + **19** and **39** + **40** are chromatographically separable from each other so that the separation of the precursors **31** and **33** by fractional crystallization is unnecessary for preparative purposes.

[25]This assignment was confirmed by the observation of significant sharpening of the signal upon irradiation of the protons of the adjacent methyl group (δ 1.04).

Can. J. Chem. Downloaded from www.nrcresearchpress.com by 72.64.146.136 on 09/07/12
For personal use only.

J' = 4 Hz, C-4a H), 2.52 (m, 1H, —C*H*—CH_3), 1.89 (br s, 2H, C-5 -CH_2-), 1.65 (s, 3H, =C—CH_3), 1.16 (s, 3H, -CH_3), 1.07 (d, 3H, J = 8 Hz, —CH—C*H*$_3$), and 1.02 (s, 3H, -CH_3); ms M^+: 262.1574 (calcd. for $C_{16}H_{22}O_3$: 262.1569). *Anal.* calcd. for $C_{16}H_{22}O_3$: C 73.25, H 8.45; found: C 73.21, H 8.38. One recrystallization from the mother liquor gave white crystals of keto-ester **37** (28 mg); mp 97–104°C; ir: 1728 (ester C=O), 1689 (enone C=O), 1374 (CH_3), and 729 (C=CH) cm^{-1}; ^{1}Hmr δ: 6.09 (dd, 1H, J = 10, J' = 2 Hz, -C*H*=CH—CO-), 5.69 (d, 1H, J = 10 Hz, -CH=C*H*—CO-), 5.17 (m, 1H, =CH—), 3.64 (s, 3H, -O—CH_3), 2.65 (m, 1H, —C*H*—CH_3), 2.53 (ddd, 1H, J = 10, J' = 6, J'' = 2 Hz, C-4a H), 1.57 (br s, 3H, =C—CH_3), 1.13 (d, 3H, J = 7 Hz, —CH—C*H*$_3$), and 1.10 (s, 6H, 2 × -CH_3); ms M^+: 262.1567 (calcd. for $C_{16}H_{22}O_3$: 262.1569). *Anal.* calcd. for $C_{16}H_{22}O_3$: C 73.25, H 8.45; found: C 72.91, H 8.61.

*4,4,6,8α-Tetramethyl-4aβ,5,8,8aβ-tetrahydro-1(4*H*)-naphthalenone (**9**) and 4,4,6,8a-tetramethyl-4aβ,5,8,8aα-tetrahydro-1(4*H*)-naphthalenone (**20**) from keto-ester **37***

Keto-ester **37**[26] (62 mg, 0.24 mmol) was dissolved in 2,4,6-collidine (2 mL) under an atmosphere of argon. Anhydrous lithium iodide (192 mg, 1.43 mmol) and water (51 μL, 51 mg, 2.85 mmol) were added and the mixture was heated at reflux for 90 min. The reaction mixture was then cooled to room temperature, poured into cold aqueous 5% hydrochloric acid, and extracted with ether. The extracts were washed with aqueous 5% hydrochloric acid and water, dried, filtered, and concentrated. Column chromatography on silica gel, eluting with 2–5% ether in petroleum ether, gave a 65:35 mixture of *cis*- and *trans*-enones **9** and **20** (16 mg, 35% yield).

*4,4,6,8β-Tetramethyl-4aβ,5,8,8aβ-tetrahydro-1(4*H*)-naphthalenone (**43**) and 4,4,6,8β-tetramethyl-4aβ,5,8,8aα-tetrahydro-1(4*H*)-naphthalenone (**44**)*

Keto-ester **38**[26] (112 mg, 0.43 mmol) was dissolved in 2,4,6-collidine (2 mL) under an atmosphere of argon. Anhydrous lithium iodide (343 mg, 2.56 mmol) and water (92 μL, 92 mg, 5.12 mmol) were added and the mixture was heated at reflux with vigorous stirring. After 2 h, the mixture was cooled to room temperature, poured into cold aqueous 5% hydrochloric acid, and extracted with ether. The extracts were washed with aqueous 5% hydrochloric acid and water, dried, filtered, and concentrated. Column chromatography of the residue on silica gel, eluting with 2–5% ether in petroleum ether, gave a 55:45 mixture of *cis*- and *trans*-enones **43** and **44** (73 mg, 83% yield). The ^{1}Hmr spectrum showed two sets of signals; one assignable to *cis*-enone **43**, δ: 6.25 (dd, ~1/2H, J = 10, J' = 2 Hz, -C*H*=CH—CO-), 5.67 (d, ~1/2H, J = 10 Hz, -CH=C*H*—CO-), 5.38 (d, ~1/2H, J = 5 Hz, =CH—), 2.97[27] (qm, ~1/2H, J = 7 Hz, —C*H*—CH_3), 2.46 (d, ~1/2H, J = 4 Hz, —CH—CO-), 1.56 (br s, 3 × ~1/2H, =C—CH_3), 1.28 (s, 3 × ~1/2H, -CH_3), 1.11 (s, 3 × ~1/2H, -CH_3), and 0.97 (d, 3 × ~1/2H, J = 7 Hz, —CH—C*H*$_3$); the other assignable to the *trans*-enone **44**, δ: 6.57 (d, ~1/2H, J = 10 Hz, -C*H*=CH—CO-), 5.73 (d, ~1/2H, J = 10 Hz, -CH=C*H*—CO-), 5.23 (m, ~1/2H, =CH—), 2.77 (qm, ~1/2H, J = 7 Hz, —C*H*—CH_3), 1.64 (br s, 3 × ~1/2H, =C—CH_3), 1.16 (s, 3 × ~1/2H, -CH_3), 1.02 (s, 3 × ~1/2H, -CH_3), and 0.75 (d, 3 × ~1/2H, J = 7 Hz, —CH—C*H*$_3$). The following data were recorded on the mixture of **43** and **44**: ir: 1681, 1670 (C=O), 1395, 1377, 1366 (CH_3), and 840 (C=CH) cm^{-1}; ms M^+: 204.1518 (calcd. for $C_{14}H_{20}O$: 204.1514).

[26]It should be noted that the mixtures **9** + **20** and **43** + **44** are chromatographically separable from each other so that the separation of **37** and **38** by fractional crystallization is unnecessary for preparative purposes.

[27]This assignment was confirmed by a decoupling experiment irradiating the methyl doublet at δ 0.97.

*4,4,6,8-Tetramethyl-1(4*H*)-naphthalenone (**15**) from keto-ester **38***

A 55:45 mixture of *cis*- and *trans*-enones **43** and **44** (72 mg, 0.35 mmol) was dissolved in carbon tetrachloride (10 mL), and *N*-bromosuccinimide (125 mg, 0.71 mmol) and benzoyl peroxide (5 mg, 0.02 mmol) were added. The mixture was heated at reflux for 1 h, then cooled to room temperature, filtered, and concentrated. Column chromatography of the residue on silica gel, eluting with 0.5% ether in petroleum ether, gave aryl-ketone **15** (22 mg, 31% yield).

*General conditions for Lewis acid catalyzed reaction of dienone ester **2** with isoprene*

Dienone ester **2** (95 mg, 0.52 mmol) was dissolved in anhydrous ether (5 mL). The Lewis acid catalyst (0.26 mmol) was added and, after 5–10 min, isoprene (1.04 mL, 10.4 mmol) was added. The progress of the reaction was followed by tlc and gc (Column A). After completion of the reaction, saturated aqueous sodium bicarbonate (~2 mL) was added and the mixture extracted with ether. The extracts were washed with water, dried, filtered, and concentrated. In several cases (see Table 9), the residue was purified by column chromatography on silica gel, eluting with 8–20% ether in petroleum ether. The crude residues or purified products were analyzed by gc (Column A) and the product ratios (**34**:**35**, Table 9) were determined by integration of the gc peaks. In the case of the boron trifluoride etherate and stannic chloride catalyzed reactions, the principal products (**34** and **35** respectively) were easily obtained pure by fractional crystallization from the product mixtures.

Acknowledgements

We are grateful to the Natural Sciences and Engineering Research Council of Canada and the University of Alberta for financial support and to Professor J. Scheffer for informing us of the X-ray results on compound **31**.

1. O. Diels and K. Alder. Ann. **460**, 98 (1928).
2. F. Fringuelli, F. Pizzo, A. Taticchi, T. D. J. Halls, and E. Wenkert. J. Org. Chem. **47**, 5056 (1982).
3. J. Sauer. Angew. Chem. Int. Ed. Engl. **6**, 16 (1967).
4. K. N. Houk. Acc. Chem. Res. **8**, 361 (1975).
5. K. Alder and G. Stein. Angew. Chem. **50**, 510 (1937).
6. R. B. Woodward and R. Hoffmann. Angew. Chem. Int. Ed. Engl. **8**, 781 (1969).
7. K. N. Houk. J. Am. Chem. Soc. **95**, 4092 (1973).
8. K. N. Houk and R. W. Strozier. J. Am. Chem. Soc. **95**, 4094 (1973).
9. Yu. A. Titov. Russ. Chem. Rev. **31**, 267 (1962).
10. I. Fleming, F. L. Gianni, and T. Mah. Tetrahedron Lett. 881 (1976).
11. M. J. S. Dewar, A. C. Griffin, and S. Kirschner. J. Am. Chem. Soc. **96**, 6220 (1974).
12. A. S. Onishchenko. Diene synthesis. Israel Program for Scientific Translation, Jerusalem. 1964.
13. J. Sauer. Angew. Chem. Int. Ed. Engl. **5**, 211 (1966).
14. P. D. Bartlett and G. F. Woods. J. Am. Chem. Soc. **62**, 2933 (1940).
15. M. D. Soffer, G. E. Günnay, O. Korman, and M. B. Adams. Tetrahedron Lett. 389 (1963).
16. M. D. Soffer and G. E. Günay. Tetrahedron Lett. 1355 (1965).
17. P. Yates and P. Eaton. J. Am. Chem. Soc. **82**, 4436 (1960).
18. G. I. Fray and R. Robinson. J. Am. Chem. Soc. **83**, 249 (1961).
19. T. Inukai and M. Kasai. J. Org. Chem. **30**, 3567 (1965).

20. T. INUKAI and T. KOJIMA. J. Org. Chem. **32**, 869 (1967).
21. E. F. LUTZ and G. M. BAILEY. J. Am. Chem. Soc. **86**, 3899 (1964).
22. T. INUKAI and T. KOJIMA. J. Org. Chem. **31**, 1121 (1966).
23. T. INUKAI and T. KOJIMA. J. Org. Chem. **31**, 2032 (1966).
24. F. FRINGUELLI, F. PIZZO, A. TATICCHI, and E. WENKERT. Synth. Commun. **9**, 391 (1979).
25. I. NAGAKURA, H. OGATA, M. UENO, and Y. KITAHARA. Bull. Chem. Soc. Jpn. **48**, 2995 (1975).
26. T. HARAYAMA, H. CHO, and Y. INUBUSHI. Tetrahedron Lett. 2693 (1975).
27. T. HARAYAMA, H. CHO, M. OHTANI, and Y. INUBUSHI. Chem. Pharm. Bull. Jpn. **22**, 2784 (1974).
28. P. A. GRIECO, S. FERRIÑO, and G. VIDARI. J. Am. Chem. Soc. **102**, 7586 (1980).
29. W. G. DAUBEN and D. M. MICHNO. J. Am. Chem. Soc. **103**, 2284 (1981).
30. J. DAS, M. KAKUSHIMA, Z. VALENTA, K. JANKOWSKI, and R. LUCE. Can. J. Chem. **62**, 411 (1984).
31. J. DAS, Z. VALENTA, H. J. LIU, and T. K. NGOOI. Can. J. Chem. **62**, 481 (1984).
32. H. J. LIU and T. K. NGOOI. Can. J. Chem. **62**, 2676 (1984).
33. H. J. LIU and E. N. C. BROWNE. Can. J. Chem. **59**, 601 (1981).
34. T. K. DEVON and A. I. SCOTT. Handbook of naturally occurring compounds. Vol. II. Academic Press, New York. 1972.
35. H. J. LIU and E. N. C. BROWNE. Tetrahedron Lett. 2919 (1977).
36. H. J. LIU and E. N. C. BROWNE. Can. J. Chem. **57**, 377 (1979).
37. R. L. N. HARRIS, F. KOMITSKY, and C. DJERASSI. J. Am. Chem. Soc. **89**, 4765 (1967).
38. J. N. MARX and L. R. NORMAN. Tetrahedron Lett. 2867 (1973).
39. H. E. ZIMMERMAN, P. HACKETT, D. F. JONES, J. M. MCCALL, and B. SCHRODER. J. Am. Chem. Soc. **93**, 3653 (1971).
40. M. J. S. DEWAR. Molecular rearrangements. Part 1. *Edited by* P. de Mayo. Wiley, New York. 1963. p. 295.
41. R. A. BARNES. J. Am. Chem. Soc. **70**, 145 (1948).
42. L. M. JACKMAN and S. STERNHELL. Applications of nuclear magnetic resonance spectroscopy in organic chemistry. 2nd ed. Pergamon, Oxford. 1969.
43. R. B. CARLIN and K. P. SIVARAMAKRISHNA. J. Org. Chem. **35**, 3368 (1970).
44. F. FRINGUELLI, L. MINUTI, F. PIZZO, A. TATICCHI, T. D. J. HALLS, and E. WENKERT. J. Org. Chem. **48**, 1810 (1983).
45. R. M. SILVERSTEIN and G. C. BASSLER. Spectrometric identification of organic compounds. 2nd ed. Wiley, New York. 1967.
46. J. G. MARTIN and R. K. HILL. Chem. Rev. **61**, 537 (1961).
47. H. J. LIU and E. N. C. BROWNE. Can. J. Chem. **65**, 182 (1987).
48. F. ELSINGER. Org. Synth. **45**, 7 (1965).
49. D. LIOTTA, M. SAINDANE, and C. BARNUM. J. Am. Chem. Soc. **103**, 3224 (1981).
50. P. M. DRUCE, M. F. LAPPERT, and P. N. K. RILEY. Chem. Commun. 486 (1967).
51. D. P. N. SATCHELL and R. S. SATCHELL. Chem. Rev. **69**, 251 (1969).
52. R. G. PEARSON and J. SONGSTAD. J. Am. Chem. Soc. **89**, 1827 (1967).
53. J. J. MYHER and K. E. RUSSEL. Can. J. Chem. **42**, 1555 (1964).
54. J. S. TOU and W. REUSCH. J. Org. Chem. **45**, 5012 (1980).
55. Z. STROJANAC, R. A. DICKINSON, N. STROJANAC, R. J. WOZNOW, and Z. VALENTA. Can. J. Chem. **53**, 616 (1975).
56. M. KAKUSHIMA, J. ESPINOSA, and Z. VALENTA. Can. J. Chem. **54**, 3305 (1976).
57. E. N. C. BROWNE. Ph.D. thesis. The University of Alberta, 1980.
58. F. A. COTTON and G. WILKINSON. Advanced inorganic chemistry. 2nd ed. Wiley, New York. 1966.
59. G. ZWEIFEL and H. C. BROWN. Org. React. **13**, 28 (1963).
60. L. F. FIESER and M. FIESER. Reagents for organic synthesis. Vol. 1. Wiley, New York. 1967.
61. E. BENZING. Angew. Chem. **71**, 521 (1959).
62. P. A. ROBINS and J. WALKER. J. Chem. Soc. 642 (1952).
63. H. J. LIU and E. N. C. BROWNE. Can. J. Chem. **96**, 306 (1978).
64. W. C. STILL, M. KAHN, and A. MITRA. J. Org. Chem. **43**, 2923 (1978).
65. C. F. LANE and G. W. KRAMER. Aldrichimica Acta, **10**, 11 (1977).

Can. J. Chem. Downloaded from www.nrcresearchpress.com by 72.64.146.136 on 09/07/12
For personal use only.

Associations of ajmaline and homatropine with bromocresol green and bromophenol blue in dichloromethane: thermodynamic and kinetic parameters

ALBERTO HERNÁNDEZ GAÍNZA

Departamento de Química Física, Facultad de Farmacia, Universidad de Granada, 18001 Granada, España

Received September 3, 1986

ALBERTO HERNÁNDEZ GAÍNZA. Can. J. Chem. **65**, 1279 (1987).

Ajmaline (AJ) and homatropine (HM) react with bromocresol green (BCG) and bromophenol blue (BPB) in dichloromethane forming 1:1 and 1:2 ion pairs clearly in a chemical equilibrium. Thermodynamic parameters ΔG^0, ΔH^0, and ΔS^0 are calculated using the Van't Hoff equation. In a large excess of HM a product P is formed from the 1:2 ion pair in a pseudo-first order kinetic process which fits Arrhenius' equation. The P product has been identified as a type of charge transfer complex. The thermodynamic parameters corresponding to the formation of the ion pairs BPB—$(AJ)_2$, BCG—$(AJ)_2$, BPB—$(HM)_2$, and BCG—$(HM)_2$ are, respectively: ΔG^0 at 294 K, −26, −21, −26, and −19 kJ/mol; ΔH^0, −63, −39, −63, and −61 kJ/mol; ΔS^0, −125, −62, −125, and −138 J/K mol (ΔH^0 and ΔS^0 determined in a 288 to 313 K range). The values of the activation energy, E_a, for the reaction of HM (in large excess) with BCG and BPB are 58 and 91 kJ/mol.

ALBERTO HERNÁNDEZ GAÍNZA. Can. J. Chem. **65**, 1279 (1987).

L'ajmaline (AJ) et l'homotropine (HM) réactionnent avec le vert de bromocresol et le bleu de bromophenol dans le chlorure de méthylène en formant des paires d'ions de stéchiométrie 1:1 et 1:2 (colorant:amine). On a démontré l'existence d'un équilibre chimique entre les complexes 1:1 et 1:2 et on a calculé les paramètres thermodynamiques, ΔG^0, ΔH^0 et ΔS^0 de la réaction. Pour des concentrations élevées de HM on met en évidence la formation d'un produit après un processus de pseudopremière ordre et on a demontré que les constantes de vitesse vérifient la relation d'Arrhenius. Le produit, P, est un complexe de transfert de charge. Les paramètres thermodynamiques correspondants à la formation des paires d'ions BPB—$(AJ)_2$, BCG—$(AJ)_2$, BPB—$(HM)_2$ et BCG—$(HM)_2$ sont respectivement : ΔG^0 à 294 K, −26, −21, −26 et −19 kJ/mol; ΔH^0, −63, −39, −63 et −61 kJ/mol; ΔS^0, −125, −62, −125 et −138 J/K mol (ΔH^0 et ΔS^0 determinés dans un intervale de 288–313 K). Les valeurs de l'énergie d'activation, E_a, pour la réaction des concentrations élevées d'HM avec BCG et BPB sont 58 et 91 kJ/mol.

Introduction

The two phase photometric titration of amines with sulphonphthaleinic dyes is an important method for the analysis of pharmacologically active substances.

The most widely proposed dye is bromothymol blue (BTB) because of its high hydrophobicity and exclusive extraction as 1:1 associates in the complete pH range (1–6).

The reaction, however, is unspecific. This is a disadvantage and a number of studies have been dedicated to this aspect (7, 8). More recently, Sakai (9, 10) has proposed a method of selective extraction for a number of quaternary ammonium ions using the 1:2 associates of bromocresol green (BCG) and bromophenol blue (BPB) and quinine as a favourable substance for quantitative extraction of the complex. The stoichiometry assigned to the complex is 1:1:1 (quinine:dye:ammonium ion) and it is the quinine which is responsible for the specificity of the extraction of the quaternary ammonium ion. The dye is extracted as divalent anion, X^{2-}, associated at the same time with protonated quinine, QH^+, and the quaternary ammonium compound, B^+.

In this study the formation of ion pairs of the divalent anion, X^{2-}, of BCG and BPB with the alkaloids ajmaline (AJ) and homatropine (HM) is investigated. The changes in the visible–ultraviolet absorption spectra of mixed solutions of BCG and BPB with variable quantities of AJ and HM in dichloromethane are elucidated. The formation of 1:1 and 1:2 ion pairs in a clear chemical equilibrium is established and the variations in the thermodynamic variables, ΔG^0, ΔH^0, and ΔS^0 are calculated from the spectrophotometric measurements.

With a large excess of HM there appear new changes in the visible absorption spectrum of BCG and BPB; changes which cannot be attributed to the formation of ion pairs. The formation of a third product, P, in a pseudo-first order kinetic process is established, and the kinetic parameters are calculated from the spectrophotometric measurements.

This study also provides conductivity measurements in the dichloromethane solutions of the dye:amine associates to complement the spectrophotometric interpretation.

Experimental procedure and results

Apparatus

Perkin Elmer Lambda 5 Spectrophotometer with a B. Braun Melsungen AG model Frigomix 1.495 and thermomix 1.441 (±0.2°C) thermostation system; quartz cells of 1 cm path length; Hewlett-Packard 9825A microcomputer; Model CDM 83 radiometer; conductometer.

Chemicals and reagents

The analytical grade amines supplied by Boerhinger–Ingelheim S.A. were used without prior purification and were kept in a desiccator with phosphorus pentoxide and under low pressure. The amines used were as follows:

α-Hydroxybenzeneacetic acid, 8-methyl-8-azabiciclo[3,2,1]oct-3-yl ester (homatropine base); ajmalan-17, -21 (diol) (Ajmaline base).

Analytical grade dyes from Merck were used without prior purification. The dyes used were bromocresol green and bromophenol blue. Carlo Erba analytical grade dichloromethane was used without prior purification.

Visible–ultraviolet spectrophotometry of dye–amine associates in dichloromethane

Bromocresol green (BCG) and bromophenol blue (BPB) in dichloromethane solution do not show any absorption in the visible spectrum range. On the other hand, upon mixing either of the dyes with ajmaline (AJ) or homatropine base (HM) in dichloromethane, intense absorption bands are seen in the visible spectrum range. The absorption spectra of BCG, BPB, AJ, and HM in dichloromethane and their corresponding mixtures BCG—AJ, BCG—HM, BPB—AJ and BPB—HM when the molar ratio is 1:1 (dye:amine) are shown in Fig. 1. In all cases the mixed solutions show a new band with a maximum at 410 nm. The absorption values at 410 nm of solutions with variable concentrations of each amine and an excess of BCG or BPB are presented at Table 1. As an example in Fig. 2, absorption spectra which correspond to mixed solutions of BCG—HM with variable concentrations of amine and

Can. J. Chem. Downloaded from www.nrcresearchpress.com by 78.46.186.204 on 09/07/12
For personal use only.

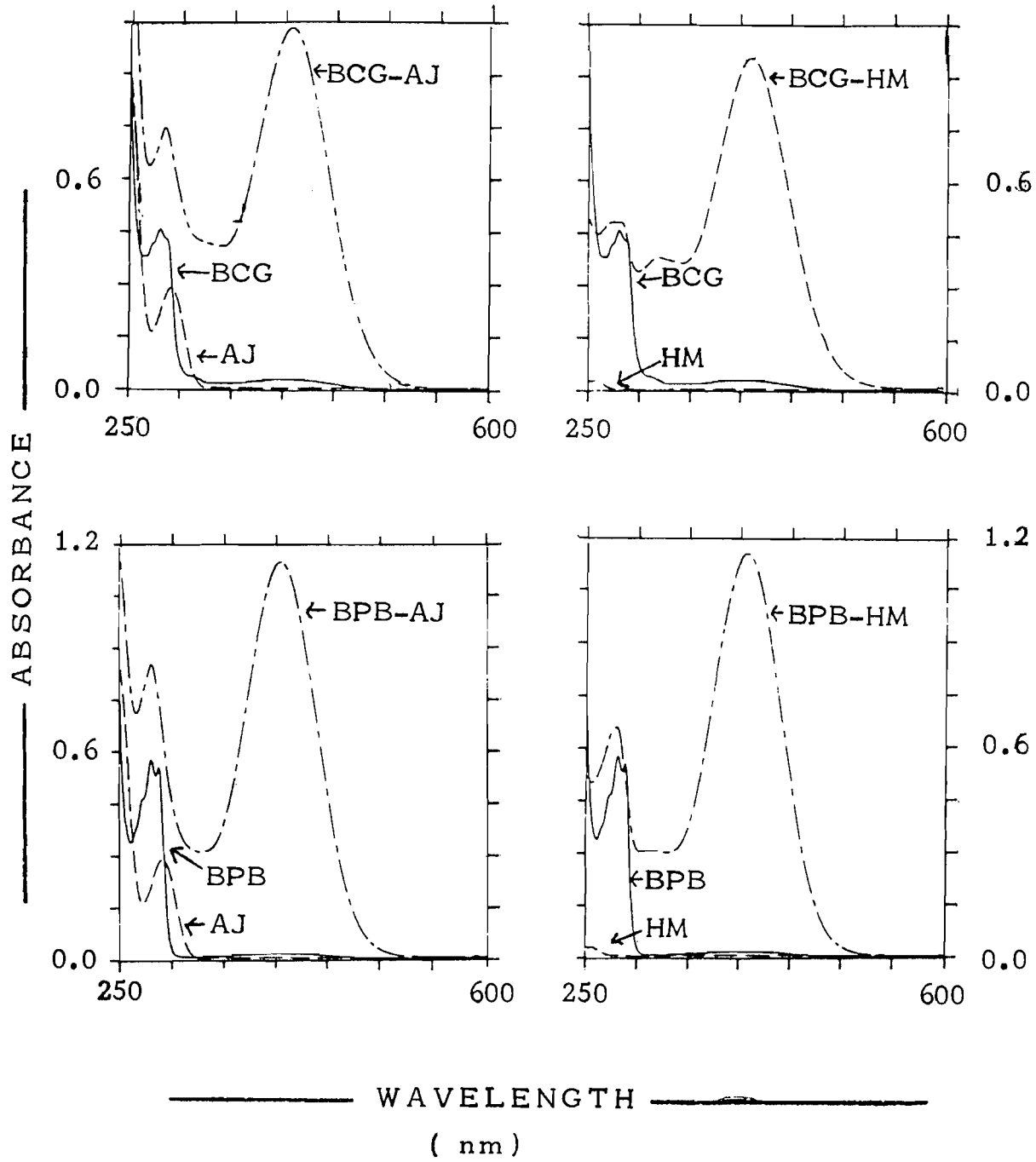

FIG. 1. Visible–ultraviolet spectra of solutions of dye 10^{-4} *M*, amine 10^{-4} *M*, and of dye–amine mixture 5×10^{-5} *M* in dichloromethane; $T = 293.16$ K.

excess of dye have been presented over the whole visible spectrum range.

When the dye–amine mixture is carried out with a slight excess of amine a second absorption band appears in the 560–580 nm region of the spectrum, the exact location of the maximum depending upon the dye:amine system being considered. This new absorption zone determines an isosbestic point which is seen beginning from an equimolar solution of dye–amine mixture and later addition of amine base in increasing concentrations. As an example of the obtained isosbestic points for BPB—AJ and BCG—HM mixtures in dichloromethane the v–uv spectra are presented in the upper part of Fig. 3.

In the lower part of Fig. 3 the v–uv spectra corresponding to the two mixtures BPB—AJ and BCG—HM with a slight excess of amine at different temperatures between 283.16 and 333.16 K are presented. Also from the spectra isosbestic points analogous to those seen in the upper part of Fig. 3 can be determined.

When BCG or BPB reacts with highly concentrated HM (if the HM dichloromethane solution is freshly prepared), a third new absorption zone is seen in the visible spectrum range with a maximum of 630 nm for BCG—HM and 600 nm for BPB—HM. The intensity increases with time until it reaches a maximum according to the temperature of the experiment. As an example the spectra of a solution of BCG in large excess of HM are presented in Fig. 4.

Mixtures of BCG—HM and BPB—HM in a large excess of HM and variable concentrations of BCG and BPB were also prepared, and their absorption spectra after 48 h recorded. Maximum absorption values (630 nm for BCG—HM and 600 nm for BPB—HM) were measured to see if BCG or BPB follows (lack of reagent) Beer's law. These

Can. J. Chem. Downloaded from www.nrcresearchpress.com by 78.46.186.204 on 09/07/12
For personal use only.

TABLE 1. Absorbancy values at 410 nm, A_{410}, of solutions of variable concentrations of amine, C_B^0, and excess concentrations of dye, C_{BCG}^0 or C_{BPB}^0, at $T = 293.16$ K

$C_{BCG}^0\ 10^4$	$C_B^0\ 10^5$	A_{410} (AJ)	A_{410} (HM)
5.0	1.67	0.335	0.330
5.0	2.50	0.490	0.440
5.0	3.33	0.700	0.670
5.0	4.17	0.800	0.790
5.0	5.00	0.960	0.980
$C_{BPB}^0\ 10^4$	$C_B^0\ 10^5$	A_{410} (AJ)	A_{410} (HM)
5.0	0.83	0.195	0.205
5.0	1.67	0.395	0.418
5.0	2.50	0.590	0.615
5.0	3.33	0.780	0.840
5.0	4.16	0.970	1.004

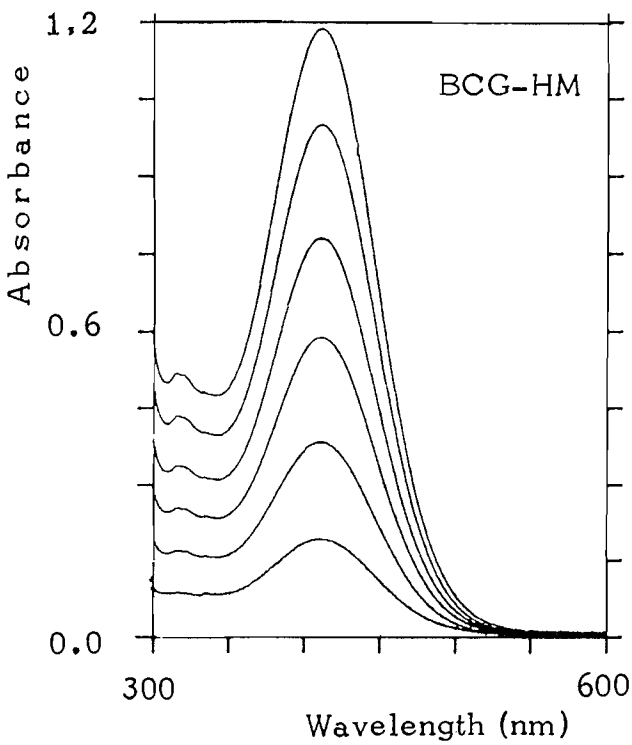

FIG. 2. Visible–ultraviolet spectra of solutions of BCG, 5×10^{-4} M and HM, 0.98, 1.97, 3.03, 3.94, 5.05, and 5.98×10^{-5} M in dichloromethane; $T = 293.16$ K.

experiments were carried out at 293.16 K. The absorption values for BCG—HM and BPB—HM mixtures at 630 and 600 nm, respectively, in a large excess of amine at longer times (48 h) are presented in Table 2. If the solution of HM in dichloromethane is prepared 36 h before being mixed with another solution of dye then the v–uv absorption spectrum immediately shows the bands of maximum intensity at 630 and 600 nm, respectively, and no variation is shown in the v–uv spectrum with the transition of time.

Analogous experiments were carried out in a large excess of AJ (including finally saturation of dichloromethane with ajmaline base) and for both BCG and BPB and no difference was observed in the spectrum compared to that seen using a slight excess of AJ. Thus with AJ the new third absorption band was not observed.

All absorption measurements and graphic recordings were carried out against pure dichloromethane.

Stoichiometry of the dye:amine compounds

The calculation of the stoichiometry of the reaction corresponding to each new absorption band was done using Job's (11) method of continuous variations. Dye–amine solutions of different molar ratios between 1:5 and 5:1 were prepared and their absorptions were measured at 410 nm and 560 nm for BCG—AJ, 564 nm for BPB—AJ, 577 nm for BCG—HM, and 573 nm for BPB—HM mixtures. Dichloromethane was used as the blank. The absorption values for each mixture are shown in Table 3. An example of Job's representation is drawn in Fig. 5.

The influence of temperature and time on the reactions

The absorption spectra of the mixtures of BCG and BPB with AJ and HM remain constant for at least 48 h, except if the reaction is carried out with a large excess of HM and, only if this latter solution is recently prepared.

The temperature does not significantly affect the spectrum of the amine–dye mixtures if they are equimolar, have an excess of dye, or a large excess of HM after reaching the maximum intensity of the third absorption range (after a longer time). The small variations in the spectra in these cases is attributed to the dilatation of the solvent.

On the other hand, in the dye:amine mixtures with a slight excess of amine, the absorption spectrum changes with the temperature owing to the presence of a chemical equilibrium, as can be seen in the lower part of Fig. 3.

It can also be seen that for dye–HM mixtures with a large excess of HM in freshly prepared solutions, intensification of the third absorption range changes markedly with the increase in temperature.

Determination of the number of absorbance species using Coleman's method

The study of the reactions using the changes in the absorption spectra is facilitated by applying Coleman's matrix procedure (12) for the assignment of species that cause the absorption. Coleman's method is the first step in a systematic spectrophotometric study and allows for the rigorous determination of the number of absorption species beginning from the absorbance values of a group of solutions at different wavelengths. This group of data is represented by the matrix $||A_{ij}||$ where A_{ij} is the absorbance of a particular solution, j, at wavelength i. Given that the observed changes in the v–uv absorption spectrum of dye–amine mixtures basically affect the visible spectrum range, the Coleman test is generally restricted to this range.

Firstly in order to apply Coleman's method, A_{ij} matrix corresponding to Figs. 2, 3, and 4 has been formed by spectrophotometric measurement of the absorption values at different wavelengths. From the A_{ij} matrix the matrices, $||A_{ij}/A_{nj}||$ and $||A_{ij} - A_{ij'}||$, have been formed. The graphic resolution of these three matrices gives rise to three Coleman tests for one, two, and two absorbance species whose sum of concentrations is always constant. The matrices obtained from Figs. 2, 3, and 4, together with other details about the application of Coleman's method, have been deposited.[1]

The graphic resolution of the matrix corresponding to Fig. 2 is shown in Fig. 6 for the BCG—HM system. In Fig. 6 it is suggested that the range of $||A_{ij}||$ is one, and, thus, in an excess of dye there only exists one absorbing species in the visible spectrum range. The selection of row A_{420j} for abcissa values is because they are the maximum values of the A_{ij} matrix elements. The same reasoning has been followed for all the dye–amine mixtures in an excess of dye. The matrices' range corresponding to Fig. 3*B*, which belongs to the BCG—HM reaction with a constant concentration of BCG and a slight and variable excess of HM, is deduced from the observation in Fig. 7 (upper graphics). In the upper part of Fig. 7 the Coleman tests are shown for two species (left hand side graphs) and two species whose sum of concentrations is

[1]Complete set of data may be purchased from the Depository of Unpublished Data, CISTI, National Research Council of Canada, Ottawa, Ont., Canada K1A 0S2.

Can. J. Chem. Downloaded from www.nrcresearchpress.com by 78.46.186.204 on 09/07/12
For personal use only.

Can. J. Chem. Downloaded from www.nrcresearchpress.com by 78.46.186.204 on 09/07/12
For personal use only.

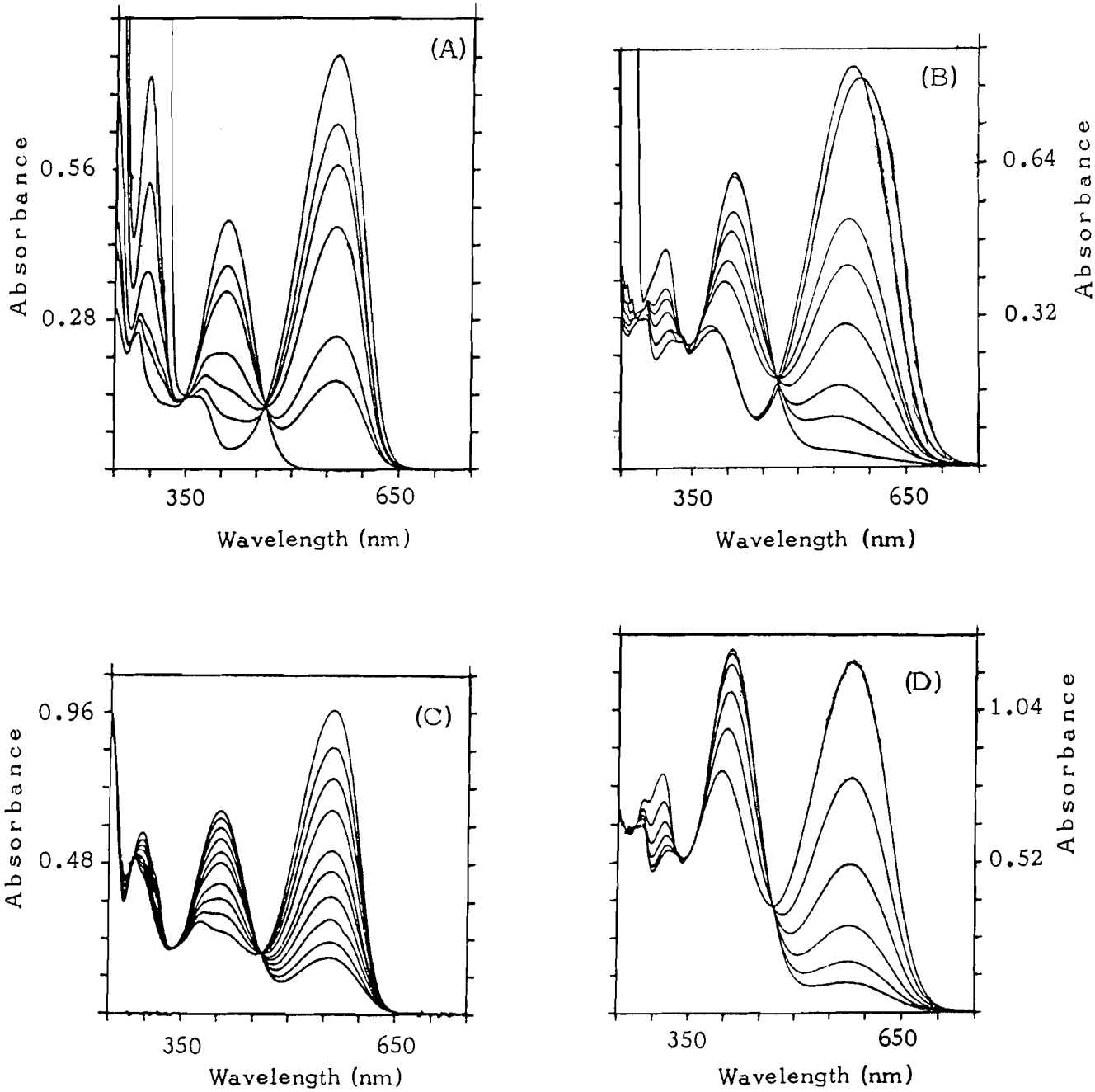

FIG. 3. (*A*) Visible–ultraviolet spectra of solutions of BPB 2×10^{-5} *M* and AJ, 2.0, 2.9, 3.5, 5.6, 8.2, 10.9, and 37.5×10^{-5} *M* in dichloromethane; $T = 293.16$ K. (*B*) Visible–ultraviolet spectra of solutions of BCG 3.2×10^{-5} *M* and HM 4.2, 6.9, 9.6, 16.1, 22.5, 34.6, 722.4, and 9000×10^{-5} *M* in dichloromethane; $T = 293.16$ K. (*C*) Visible–ultraviolet spectra of BPB 3.4×10^{-5} *M* and AJ 4.7×10^{-5} *M* at 283.16, 288.16, 293.16, 298.16, 303.16, 308.16, 313.16, 318.16, 323.16, and 328.16 K in dichloromethane. (*D*) Visible–ultraviolet spectra of BCG 6.3×10^{-5} *M* and HM 10.3×10^{-5} *M* at 283.16, 293.16, 303.16, 313.16, 323.16, and 333.16 K in dichloromethane.

constant (right hand side graphs) and which are positive for the visible spectrum range. In these tests 570 nm has been selected as corresponding to the maximum absorption of the BCG—HM mixture and a wavelength of 490 nm as an arbitrary but fixed wavelength. This result has been repeated for all the dye–amine mixtures with constant concentrations of dye and variable concentrations of amine (in slight excess), for the visible spectrum range. The test at Fig. 7 (lower left) corresponding to the BPB—AJ mixtures from Fig. 3*A* indicates two absorption species whose sum of concentration is a constant. On the other hand, the broken curves indicate that in the ultraviolet spectrum there are no two absorption species, this also being a general result given the overall character of the experimental conditions and of each dye–amine system tested in this study (three species exist because in the uv range the excess amine is absorbent). With a large excess of HM, in systems of BCG or BPB, the new changes in the absorption spectrum (Fig. 4) are also interpreted with the help of Coleman's method. Coleman's graphic resolution for the A_{ij} values in Fig. 4 for the BCG—HM system, with a large excess of HM, indicates two absorption species whose sum of concentrations is constant over time. An identical result has been demonstrated for the BPB—HM mixture under the same conditions.

However, when applying Coleman's test to BCG—HM or BPB—HM absorption spectra at longer times (48 h), just one absorption species is shown.[1]

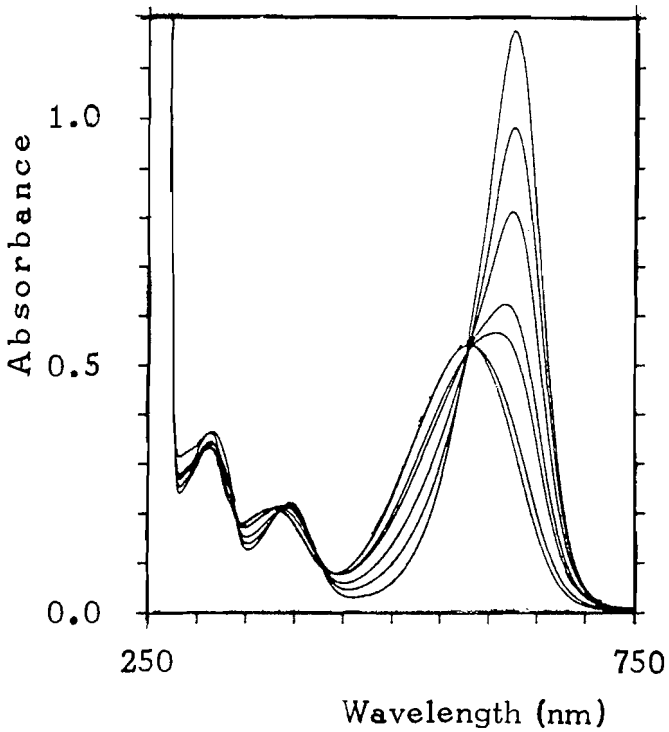

FIG. 4. Visible–ultraviolet spectra of a solution of bromocresol green 1.9×10^{-5} *M* and homatropine 0.091 *M* at 0, 9, 38, 55, 110, 194, and 2880 minutes; $T = 293.16$ K.

TABLE 2. Absorbancy values for solutions with variable concentrations of dye, $C^0_{XH_2}$, and an excess of homatropine (0.1 *M* for BCG and 0.05 *M* for BPB) at longer times (48 h), $T = 293.16$ K

$C^0_{BCG}\ 10^6$	A^{BCG}_{630}	$C^0_{BPB}\ 10^6$	A^{BPB}_{600}
2.0	0.150	2.4	0.186
4.0	0.268	4.8	0.515
6.0	0.380	7.2	0.780
8.0	0.500	9.6	1.031
10.0	0.670	12.0	1.221

TABLE 3. Absorbancy values calculated using Job's method for solutions of dye–amine in dichloromethane; the sum of the concentrations of dye and amine is constant ($C^0_{XH_2} + C^0_B = 10^{-4}$ *M*), $T = 293.16$ K

		Absorbance for each molar relation					
Amine	Dye	5:1	2:1	1:1	1:2	1:5	*i* (nm)
AJ	BCG	0.335	0.700	0.960	0.600	0.300	410
HM	BCG	0.330	0.670	0.980	0.660	0.320	410
AJ	BPB	0.395	0.780	1.180	0.390	0.115	410
HM	BPB	0.418	0.840	1.209	0.405	0.120	410
		Absorbance for each molar relation					
Amine	Dye	5:1	2:1	1:1	1:2	1:5	*i* (nm)
AJ	BCG	0.010	0.005	0.003	0.140	0.126	562
HM	BCG	0.008	0.004	0.004	0.090	0.086	577
AJ	BPB	0.002	0.003	0.005	0.645	0.500	564
HM	BPB	0.009	0.008	0.001	0.715	0.550	573

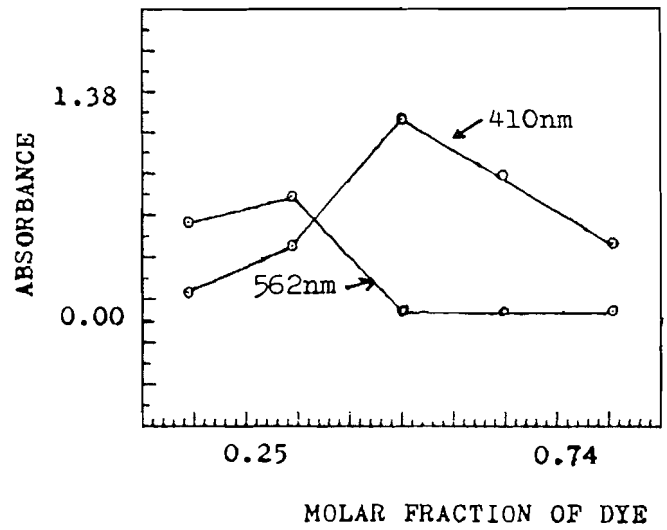

FIG. 5. Job's representation for the BCG—AJ complex from the data in Table 3.

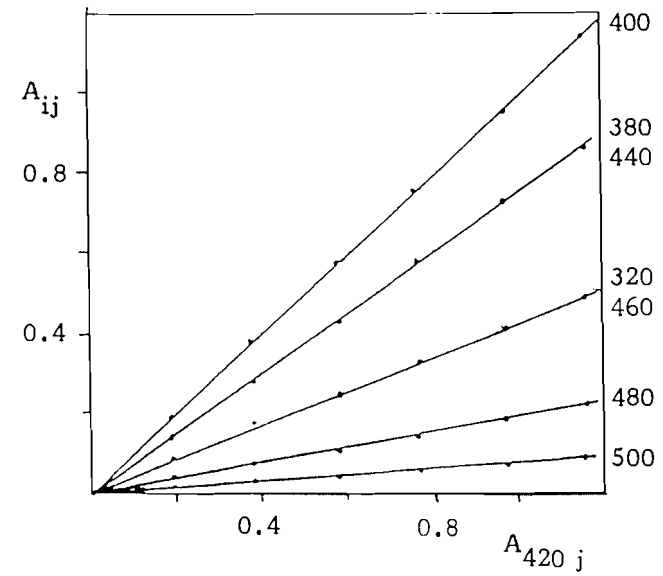

FIG. 6. Coleman's method for a species taken from the data in Fig. 2. The numbers correspond to the wavelength, *i*, of the row of the matrix $||A_{ij}||$ (see footnote 1).

Determination of the formation constants and molar extinction coefficients for 1:2 (dye:amine) ion pairs

The isosbestic points in Fig. 3 and the Coleman tests of Fig. 7 indicate a chemical equilibrium when a dye solution is mixed with another which contains a slight excess of amine. For this reason a series of experiments was carried out to determine the equilibrium constants, *K*, the molar extinction coefficients, ϵ, and the thermodynamic parameters of the reaction.

A series of solutions which contained dye–amine mixtures of different concentrations, always with a slight excess of the amine, were prepared in dichloromethane. In all the experiments the molar ratio of dye:amine was held constant to facilitate the experimental method and later treatment of the data using a computer program. The photometric measurement of the solutions was made at different temperatures between 287.16 and 313.16 K using pure dichloromethane as blank.

The dye–amine solutions, under these experimental conditions (slight excess of amine), presented two absorption maxima, the first at 410 nm (corresponding to a 1:1 ion pair) and the second in the 560–580 nm region (corresponding to a 1:2 ion pair), the exact location

Can. J. Chem. Downloaded from www.nrcresearchpress.com by 78.46.186.204 on 09/07/12
For personal use only.

Can. J. Chem. Downloaded from www.nrcresearchpress.com by 78.46.186.204 on 09/07/12
For personal use only.

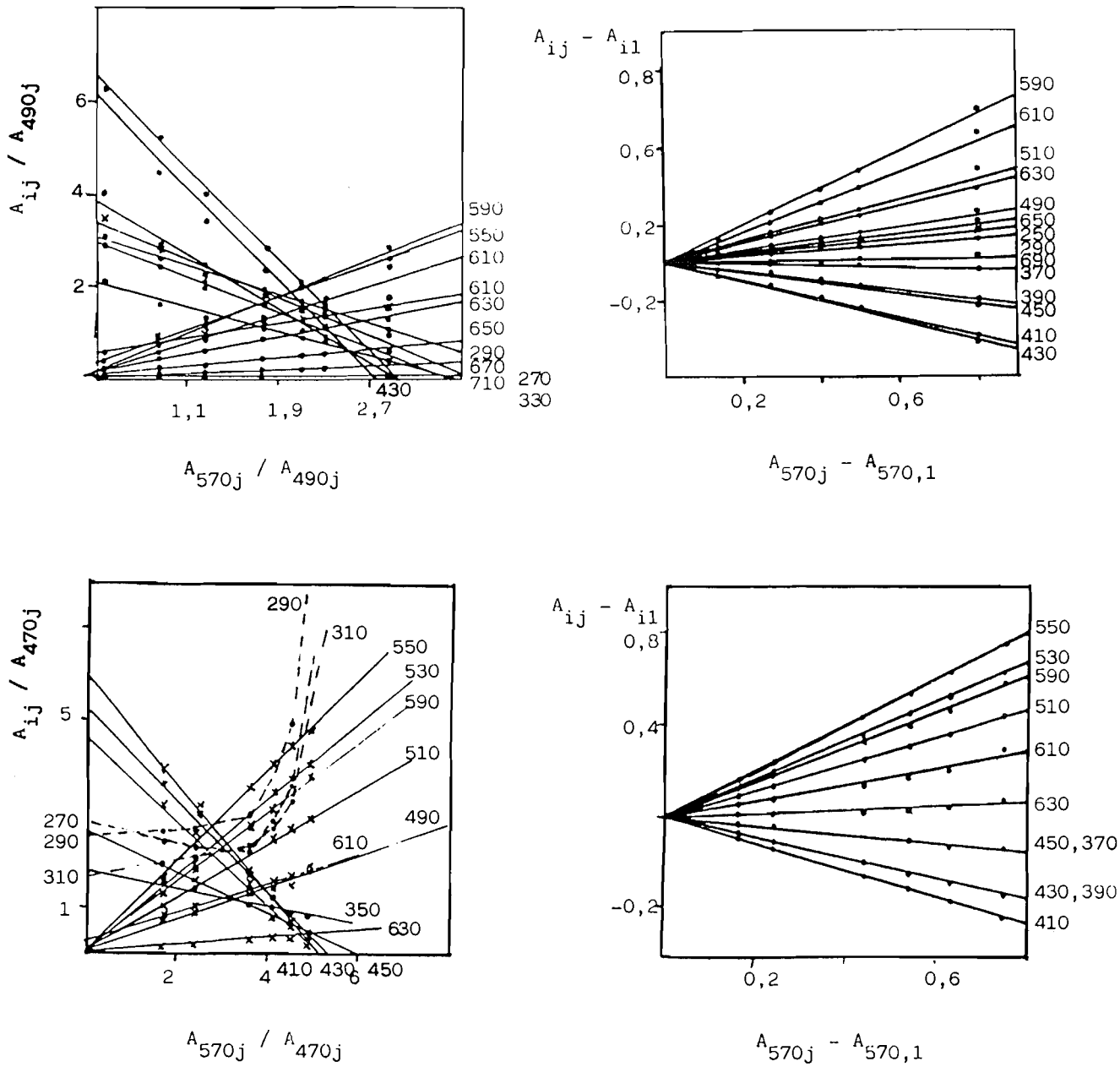

FIG. 7. Coleman's method for two species and for two species whose sum of concentrations is constant — (left and right upper figures) corresponding to the BCG—HM system taken from the data in Fig. 3*B*. The same tests in the lower zone for the BPB—AJ system taken from Fig. 3*A*. The numbers correspond to the wavelength, *i*, of the row of matrix which has been resolved graphically according to Coleman (see footnote 1).

of the maximum being dependent on the dye–amine system under consideration. The experimental absorption measures were carried out at the absorption maximum in the 560–580 nm region, corresponding to a 1:2 ion pair, since at this wavelength the 1:1 ion pair shows no absorption. The experimental data and other details are available from the Depository of Unpublished Data.[1]

Determination of the reaction constants

The v–uv absorption spectrum changes of the BCG and BPB dyes in dichloromethane on being mixed with solutions of HM in large excess suggest a kinetic process.

To determine the order of the reaction and the rate constants, a solution of dye–homatropine was prepared with a large excess of HM and the absorption of the mixture was measured at different times, against pure dichloromethane. The wavelengths for measurement were 630 nm for BCG—HM and 600 nm for BPB—HM. The experiments were done at different temperatures to see if Arrhenius' equation was followed. The homatropine solution was used immediately after its preparation. The experimental absorption measurements were carried out up to a maximum of 48 h, time enough for the reaction to complete. The experimental data and other details are available from the Depository of Unpublished Data.

Conductivity measures of the dye–amine solutions in dichloromethane

The specific conductivity, χ, of solutions of dye, amine, and a mixture of both in dichloromethane was measured. The amines HM and AJ, and the dyes BCG and BPB, show a specific conductivity close to zero, while on the other hand the dye–amine mixture shows a small but appreciable specific conductivity. The conductivity measurements were made at 293.16 K and are shown in Tables 4 to 7.

TABLE 4. Specific conductivity values, χ (μS cm^{-1}), for different concentrations of BCG and AJ in dichloromethane and concentrations of the BPB—AJ ionic pair, $C_{1:1}$, and of BCG—$(AJ)_2$, $C_{1:2}$, at $T = 293.16$ K

$C^0_{BCG}\ 10^3$	$C^0_{AJ}\ 10^3$	χ	$C_{1:1}$	$C_{1:2}$
2.00	0.00	0.037	0.00	0
1.97	0.62	0.097	0.62	0
1.95	1.22	0.119	1.22	0
1.93	1.81	0.137	1.81	0
1.90	2.38	0.197	1.46×10^{-3}	4.35×10^{-4}
1.88	2.94	0.281	9.63×10^{-4}	9.17×10^{-4}
1.86	3.49	0.340	5.70×10^{-4}	1.28×10^{-3}
1.84	4.02	0.373	3.35×10^{-4}	1.50×10^{-3}
1.82	4.54	0.397	2.16×10^{-4}	1.60×10^{-3}
1.78	5.55	0.420	1.18×10^{-4}	1.66×10^{-3}
1.74	6.52	0.430	8.01×10^{-5}	1.66×10^{-3}
1.70	7.44	0.439	6.02×10^{-5}	1.64×10^{-3}
1.67	8.33	0.444	4.85×10^{-5}	1.62×10^{-3}
1.62	9.18	0.450	4.02×10^{-5}	1.58×10^{-3}
1.60	10.00	0.454	3.44×10^{-5}	1.56×10^{-3}

TABLE 5. Specific conductivity values, χ (μS cm^{-1}), for different concentrations of BPB and AJ in dichloromethane and concentrations of the BPP—AJ ionic pair, $C_{1:1}$, and of BPB—$(AJ)_2$, $C_{1:2}$, at $T = 293.16$ K

$C^0_{BPB}\ 10^3$	$C^0_{AJ}\ 10^3$	χ	$C_{1:1}$	$C_{1:2}$
2.00	0.00	0.021	0	0
1.97	0.62	0.049	0.62×10^{-3}	0
1.95	1.22	0.075	1.22×10^{-3}	0
1.93	1.81	0.099	1.81×10^{-3}	0
1.90	2.38	0.200	1.43×10^{-3}	4.73×10^{-4}
1.88	2.94	0.382	8.44×10^{-4}	1.03×10^{-3}
1.86	3.49	0.568	3.23×10^{-4}	1.54×10^{-3}
1.84	4.02	0.690	8.24×10^{-5}	1.76×10^{-3}
1.82	4.54	0.718	3.76×10^{-5}	1.78×10^{-3}
1.79	5.06	0.730	2.32×10^{-5}	1.77×10^{-3}
1.78	5.55	0.738	1.74×10^{-5}	1.76×10^{-3}

TABLE 6. Specific conductivity values, χ (μS cm^{-1}), for different concentrations of BCG and HM in dichloromethane and concentrations of the BCG—HM ionic pair, $C_{1:1}$, and of BCG—$(HM)_2$, $C_{1:2}$, at $T = 293.16$ K

$C^0_{BCG}\ 10^3$	$C^0_{HM}\ 10^3$	χ	$C_{1:1}$	$C_{1:2}$
2.00	0	0.054	0	0
1.97	0.77	0.129	0.77	0
1.94	1.55	0.168	1.55	0
1.91	2.24	0.315	1.63×10^{-3}	2.80×10^{-4}
1.88	2.94	0.405	1.05×10^{-3}	8.30×10^{-4}
1.83	4.28	0.431	4.04×10^{-4}	1.42×10^{-3}
1.78	5.55	0.426	2.08×10^{-4}	1.57×10^{-3}

Discussion

Interpretation and assignment of the absorption bands

The new absorption bands that are shown by the solutions of dye–amine mixture are attributed to the formation of new compounds in the solution. In an excess of dye there is always a new band in the visible region with a maximum of 410 nm, as can be seen in Table 1 and in Figs. 1 and 2.

TABLE 7. Specific conductivity values, χ (μS cm^{-1}), for different concentrations of BPB and HM in dichloromethane are shown: concentrations of the BPB—HM ionic pair, $C_{1:1}$, and BPB—$(HM)_2$, $C_{1:2}$, at $T = 293.16$ K

$C^0_{BPB}\ 10^3$	$C^0_{HM}\ 10^3$	χ	$C_{1:1}$	$C_{1:2}$
2.00	0.00	0.030	0	0
1.97	0.77	0.115	0.77×10^{-3}	0
1.94	1.55	0.172	1.55×10^{-3}	0
1.91	2.24	0.316	1.58×10^{-3}	3.26×10^{-4}
1.88	2.94	0.580	8.42×10^{-4}	1.04×10^{-3}
1.83	4.28	0.753	4.72×10^{-5}	1.78×10^{-3}
1.78	5.55	0.750	1.55×10^{-5}	1.76×10^{-3}

TABLE 8. Molar absorptivity at 410 nm, ϵ_{410}, for dye:amine compound and confidence intervals to a probability of 0.95 for Student "t" test: intercept value, b, slope, m, and determination coefficients, r^2, obtained by least squares method; results obtained from Table 1; $T = 293.16$ K

Dye—amine	m (ϵ_{410})	b	r^2
BCG—AJ	18724 ± 3344	0.032	0.990
BCG—HM	19806 ± 3652	−0.028	0.990
BPB—AJ	23258 ± 380	0.005	1.000
BPB—HM	24280 ± 1897	0.009	0.998

This absorption complies with Beer's law for each amine, as is shown in Table 8 and indicates that the absorption corresponds to only one new compound, a result confirmed by the application of Coleman's (12) matrix method for the whole visible spectrum, and may be deduced from observations in Fig. 6.

In an excess of amine two new bands appear, one at 410 nm and the other at 580–600 nm. These are cut by an experimental isosbestic point as can be seen in Fig. 3. The isosbestic point allows us to suggest the existence of two new compounds in equilibrium, a conclusion which is again reinforced by Coleman's method. In this case the two absorption species satisfy the condition that the sum of their concentrations is constant. Figure 7 confirms this result, meaning the two new compounds which absorb in the visible spectrum range are in equilibrium.

In a large excess of homatropine (Fig. 4) the absorption in the region of 575 nm increases in intensity with the passage of time, and the maximum wavelength is displaced from 577 to 630 nm for BCG and from 573 nm to 600 nm for BPB. The elucidation of the two species assigned to this new change is also resolved by Coleman's method. The application of the test to the data of Fig. 4 for BCG—HM indicates two absorption species whose sum of concentration is constant,[1] one, already described, having a maximum at 577 nm and a new one at 630 nm. As the absorption intensity increases with the passage of time, different solutions with a large excess of HM and variable concentrations of BCG (always much less) were prepared and measured after 48 h at 293.16 K.[1] The application of Coleman's method again suggests only one absorption species at longer time,[1] which satisfies Beer's law as indicated in Table 16. Thus, at shorter times there are two species and at longer times there is only one, a finding to suggest that the new spectral change is a kinetic process.

The prior discussion indicates three new absorption species in the visible spectrum region as a result of the changes in the

Can. J. Chem. Downloaded from www.nrcresearchpress.com by 78.46.186.204 on 09/07/12
For personal use only.

absorption spectrum. The identification of these species can be facilitated by comparison with the absorption spectra of BCG and BPB in an aqueous medium at different pH values (13, 14). In effect, at pH 1 both dyes in water show a maximum at approximately 430 nm and at higher pH from 3 to 7, a second maximum appears in the region of 590 nm, both being cut by an isosbestic point. Both types of ions exist in an aqueous medium, namely, the monovalent anion, XH^-, and the divalent X^{2-} of the dye. By analogy with the dissociation in aqueous medium it is possible to assign it to a similar effect in an organic medium in which the amine in the form of a base neutralizes the protons of the dye. Given the low dielectric constant of the organic solvent, the stabilization of the dye with the amines is produced by formation of 1:1 and 1:2 ion pairs, that is to say $\{XH^-, BH^+\}$ and $\{X^{2-},(BH^+)_2\}$. The reactions in a non-polar medium could be the following:

$$[1] \quad XH_2 + B \rightarrow \{XH^-, BH^+\}$$

$$[2] \quad \{XH^-, BH^+\} + B \rightleftharpoons \{X^{2-}, (BH^+)_2\}$$

where XH_2 is the free dye, B, the amine in base state, $\{XH^-, BH^-\}$, the 1:1 ion pair, and $\{X^{2-}, (BH^+)_2\}$, the 1:2 ion pair. The formation of $\{XH^-, BH^+\}$ is quantitative from the spectrophotometric point of view while that of the 1:2 ion pair is clearly a chemical equilibrium which is displaced towards the formation of this last compound with an increase in the concentration of the alkaloid base or a decrease in temperature.

The first reaction is produced with excess or with equal concentrations of dye and the second in an excess of amine. This stoichiometry is confirmed by the application of Job's method, as indicated in Fig. 5 and suggests stoichiometry 1:1 for the maximum at 410 nm and stoichiometry 1:2 for that at 560–580 nm. From the absorption values in Table 2 it can be concluded that in an excess of dye or at equal concentrations of dye and amine (experiments with molar ratio 1:1, 2:1, and 5:1) the reaction is totally displaced to the right. Its formation constant is so high that it cannot be evaluated from the data using Job's method, unlike the reaction of bromothymol blue in which the formation constant can be found using Job's method (15, 16). Reaction [2] is clearly a chemical equilibrium whose formation constant is dependent on the temperature (Fig. 3). The fact that reaction [1] is quantitative and reaction [2] is an chemical equilibrium correlates with the fact that the first proton of the sulphonphthaleins is extremely acidic and the second proton is much less acidic.

The spectral change originating from a large excess of homatropine can be attributed, according to the points already discussed, to the formation of a third product originating from the 1:2 complex when it reacts again with HM.

This third interaction does not constitute a chemical equilibrium since at longer times, as previously discussed, there is only one absorption species. Apparently the 1:2 ion pair in a large excess of HM is transformed into another compound by a pseudo-first order kinetic process, as we will see subsequently. For small differences in amine–dye concentrations the changes in the absorption spectrum of BCG and BPB have been attributed to the formation of ion pairs but with a large excess of homatropine the displacement to higher wavelengths and the intensification of the bands cannot be interpreted in this way. The saturation of the central carbon of sulphonphthaleine is not possible since the colour then disappears and thus the visible absorption. The saturation of the central carbon has been described in the case of a strongly alkaline aqueous medium giving rise to carbinol which is colourless (17, 18).

The interaction with a large excess of homatropine can be written as

$$[3] \quad \{X^{2+},(HMH^+)_2\} + HM \rightarrow P$$

where P is the obtained product. The nature of P will be discussed subsequently. It is important to note that when bromhydrate of homatropine (analytical grade) is used none of the described associated reactions are produced whereas they are produced with homatropine in base state. It is therefore deduced that the nitrogen is the reactive element in amine, in agreement with the previous interpretation, since it is the nitrogen which contributes to the basic character of the amine. Obviously the bromhydrate of homatropine forms a more stable ion pair than those corresponding BCG—HM or BPB—HM associates.

Formation constants and thermodynamic parameters corresponding to the 1:2 ion pair

The formation constants, K, of the 1:2 ion pair are given by the following expression

$$[4] \quad K = \frac{[\{X^{2-},(BH^+)_2\}]}{[\{XH^-, BH^+\}][B]}$$

where B is the concentration of free amine.

The formation constants, K, have been determined from the spectrophotometric data using methods of specific calculation, since the molar extinction coefficient, ϵ, for the 1:2 ion pair is unknown and cannot be found directly. This is due to the fact that the equilibrium of reaction [2] cannot be displaced to the right to give a complete reaction, because of the weak character of the 1:2 associate. Moreover, with a large excess of homatropine the product, P, would be formed (reaction [3]).

The general equation that combines the concentrations of the chemical equilibrium of the reaction, e.g. [2], K, and ϵ is

$$[5] \quad \frac{C^0_{XH_2}(C^0_B - C^0_{XH_2})}{A} = -\frac{A}{\epsilon^2} + \frac{1}{K\epsilon} + \frac{C^0_{XH_2} + (C^0_B - C^0_{XH_2})}{\epsilon} + E$$

where A is the measured experimental absorption value at the absorption maximum for the 1:2 ion pair and E is a correction factor for experimental error. Equation [5] is the Rose–Drago expression (19, 20) applied to reaction [2]; seeing that $C^0_{XH_2} = C^0_{\{XH^-,BH^+\}}$ and the initial concentration of amine in reaction [2] is $C^0_B - C^0_{XH_2}$, as a result of the quantitative nature of reaction [1].

Spectrophotometric methods are known for the simultaneous calculation of K and ϵ (21–27). It is more frequent to solve eq. [5] using approximations disregarding the error, E, and it is perhaps the Benesi–Hildebrand (28, 29) treatment which is most known although it has the disadvantage of requiring a large excess of one of the reagents. Another approach is the linear approximation, which underestimates $1/\epsilon^2$ in eq. [5] but leads to error if K is large (30). Another proposed approximation is the modified Rose–Drago method (25) based on a linear approximation. This poses no restriction in the required concentration ranges but carries with it the Benesi–Hildebrand (B–H) approximation.

Both methods of approximation give a value of the linear determination coefficient, r^2, obtained by the least squares method and is an indication of the validity of the equations applied. The modified Rose–Drago method (MRD) has been used in this study as an approximation for the simultaneous

Can. J. Chem. Downloaded from www.nrcresearchpress.com by 78.46.186.204 on 09/07/12
For personal use only.

TABLE 9. Parameters K^{-1} (the inverse of the formation constant, K) and ϵ (molar absorptivity at 577 nm) for the bromocresol green — (homatropine)$_2$ ionic pair; confidence intervals at the 0.95 level, root-mean-squared deviations (r.m.s.d.) and values of r^2 for the approximation of Modified Rose–Drago

T (K)	$K^{-1} \times 10^4$ (mol/L)	ϵ (L/mol cm)	r.m.s.d.	r^2
289.16	1.6033 ± 0.46349	26767 ± 2245	0.010	0.997
295.16	2.9112 ± 0.92837	28535 ± 3716	0.010	0.991
301.16	4.0204 ± 1.67213	26396 ± 5245	0.011	0.972
304.16	5.8880 ± 3.22987	28730 ± 8872	0.012	0.955
309.16	8.5461 ± 6.95310	27398 ± 14337	0.012	0.851

TABLE 10. Parameters K^{-1} (the inverse of the formation constant, K) and ϵ (molar absorptivity at 573 nm) for the bromophenol blue — (homatropine)$_2$ ionic pair; confidence intervals at the 0.95 level, root-mean-squared deviations (r.m.s.d.) and values of r^2 for the approximation of Modified Rose–Drago

T (K)	$K^{-1} \times 10^5$ (mol/L)	ϵ (L/mol cm)	r.m.s.d.	r^2
288.16	1.2510 ± 0.63540	45736 ± 2325	0.009	0.999
294.16	1.7736 ± 0.74577	43752 ± 2428	0.008	0.999
301.16	4.8185 ± 1.35318	46708 ± 3533	0.007	0.998
306.16	6.9942 ± 1.35045	46031 ± 3005	0.004	0.999
313.16	8.5625 ± 7.77722	42569 ± 14225	0.018	0.974

TABLE 11. Parameters K (the formation constant) and ϵ (molar absorptivity at 562 nm) for the bromocresol green — (ajmaline)$_2$ ionic pair: confidence intervals at the 0.95 level, root-mean-squared deviations (r.m.s.d.), and values of r^2 for the approximation of Benesi–Hildebrand

T (K)	K (L/mol)	ϵ (L/mol cm)	r.m.s.d.	r^2
288.16	8118 ± 346	22163 ± 188	0.002	0.992
293.16	6642 ± 761	20963 ± 568	0.005	0.993
298.16	4633 ± 966	20735 ± 1317	0.009	0.990
303.16	4113 ± 1561	19857 ± 2650	0.015	0.988
308.16	2989 ± 353	18547 ± 860	0.004	0.995
313.16	2133 ± 454	18657 ± 1845	0.006	0.990

TABLE 12. Parameters K (the formation constant) and ϵ (molar absorptivity at 564 nm) for the bromophenol blue — (ajmaline)$_2$ ionic pair: confidence intervals at the 0.95 level, average squared deviations (r.m.s.d.), and values of r^2 for the approximation of Modified Rose–Drago

T (K)	K (L/mol)	ϵ (L/mol cm)	r.m.s.d.	r^2
289.16	82205 ± 32551	41353 ± 4471	0.014	0.993
294.16	50512 ± 12684	41487 ± 3411	0.009	0.996
300.16	28153 ± 7131	41129 ± 4548	0.006	0.986
305.66	20556 ± 6659	39730 ± 6191	0.007	0.988
311.66	11609 ± 2993	39044 ± 5280	0.007	0.985

calculation of K and ϵ in the reactions of BCG—HM and BPB—HM because with a large excess of HM, P is produced. For reactions of BCG—AJ and BPB—AJ, both approximation methods (the MRD and B–H) are possible as P is not produced at high concentrations of AJ. Both methods have been used, the MRD for the BPB—AJ reaction and the B–H method for the BCG—AJ reaction, since in the latter the concentration of AJ was 10 times higher than that of BCG.[1] The Benesi–Hildebrand and, likewise, the Modified Rose–Drago methods yield a value of K and ϵ and a linear determination coefficient, r^2, obtained from the least squares method.

As a means of calculation the Rosseinsky (31) iterative method is proposed. This method requires a first-approximate value for K and ϵ, obtained from the MRD and B–H approximations and has the advantage of estimating other indices of great experimental and statistical importance, such as the root-mean-squared deviation of the experimental absorption measures, r.m.s.d., and an estimation of the objective errors of K and ϵ.

Both methods (of approximation and calculation) imply (*a*) the addition reaction is 1:1, (*b*) the reagents do not absorb at the maximum absorption of the addition compound, and (*c*) the addition compound follows Beer's law.

Reaction [2] satisfies these prerequisites as will be shown.

The parameters selected for the Rosseinsky method were K^{-1}, $\alpha_{K^{-1}}$, ϵ, and α_ϵ, defined as the inverse of the formation constant, K, with the estimation of its standard deviation, $\alpha_{K^{-1}}$ and ϵ with its standard deviation, α_ϵ, respectively. In order to obtain K and ϵ, and their respective confidence intervals the Tchebicheff (32) inequalities have been used. The results are shown in Tables 9–12. The parameters selected for Rosseinsky's iterative procedure were obtained when in two consecutive iterations $\Delta\epsilon < 10^{-3}$ and $\Delta K^{-1} < 10^{-8}$, respectively. The root-mean-squared deviation (r.m.s.d.) values in Tables 9–12 indicate that the error in the absorption measures is of the order of 0.01, a result which is sufficiently precise to allow the acceptance of the validity, from a quantitative point of view, of the supposed equilibrium in eq. [2]. The values of r^2, which appear in Tables 9–12, are those which correspond to the last iteration of the modified Rose–Drago approximation, ($\Delta\epsilon < 10^{-3}$ is required) or the Benesi–Hildebrand approximation, which is an indication of the validity of the assumed equilibrium in reaction [2] and likewise of all other assumptions. Another important result in these tables is that the values of ϵ have the same degree of constancy at different temperatures for the 1:2 complex of homatropine or ajmaline.

Gupta (15) has suggested that the moderately high values for the formation constants can mean a complex character for the 1:1 addition products of bromothymol blue (but not one of salts) although the reaction has an acid–base character. By analogy the magnitude of the obtained constants reveals a complex character for the 1:2 compound given that the value of K is not high and oscillates in a wide range with temperature. However, the reaction is apparently an acid–base process in which the order of magnitude of the equilibrium constants depends as much on the basic properties of the amine as on the dye employed.

The calculation of the variation in the thermodynamic magnitudes ΔG^0, ΔH^0, and ΔS^0 was carried out using the expressions (34)

$$[6] \quad \ln K = \frac{\Delta S^0}{R} - \frac{\Delta H^0}{RT}$$

$$[7] \quad \Delta G^0 = -RT \ln K$$

The calculated constants justify, within their respective confidence intervals, the linear regression of eq. [6] as can be seen in Fig. 8. In Table 13 values of ΔG^0, ΔH^0, and ΔS^0 and their confidence intervals are given for each one of the dye–amine complexes following the Student "t"-test (33) for 95% proba-

Can. J. Chem. Downloaded from www.nrcresearchpress.com by 78.46.186.204 on 09/07/12
For personal use only.

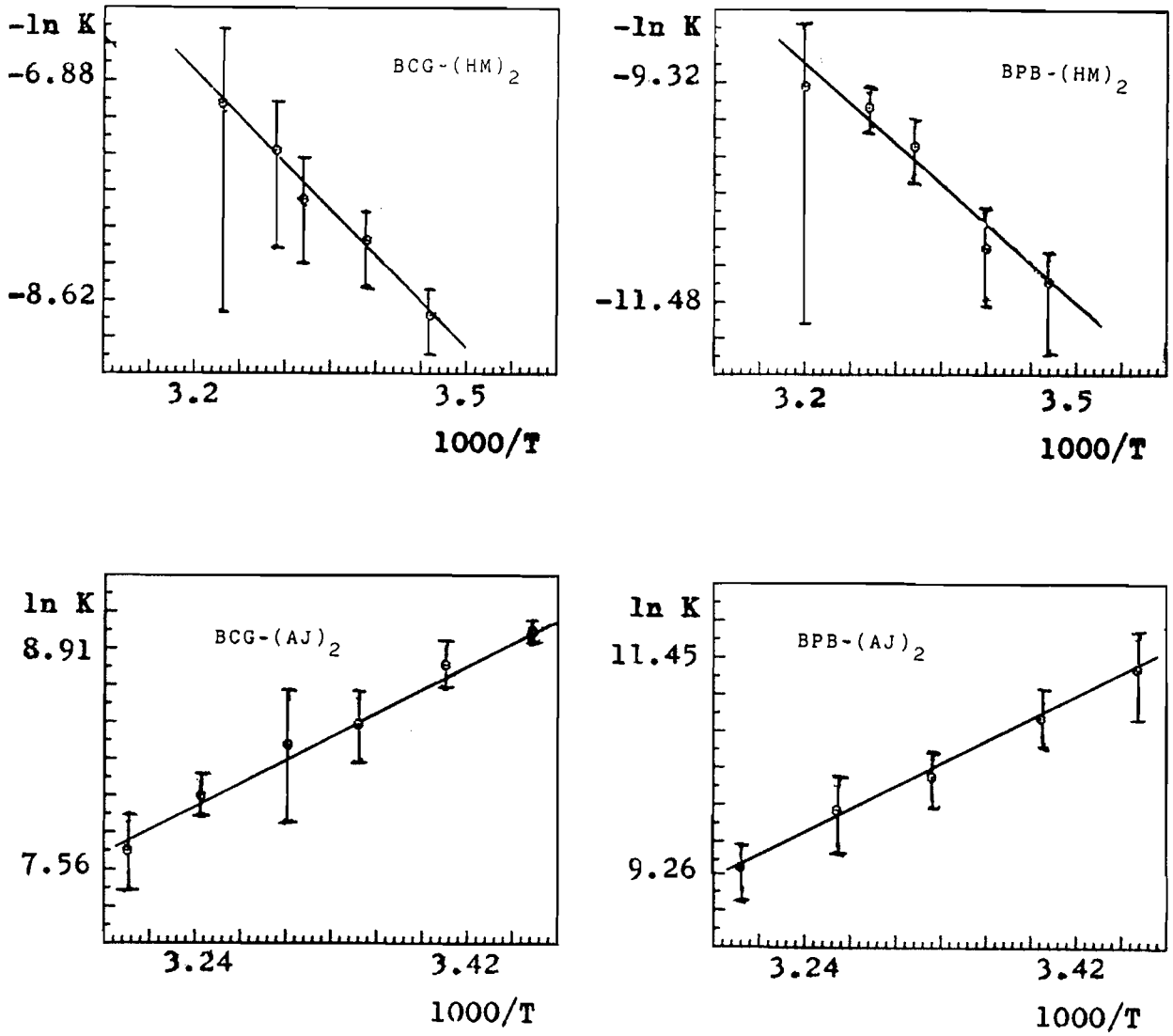

FIG. 8. The Van't Hoff representation for each dye–amine compound. The formation constants, K, or those of dissociation, K^{-1}, appear with their confidence intervals.

bility. The values of the determination coefficients obtained by least squares are 0.995 for BPB—$(AJ)_2$, 0.984 for BCG—$(AJ)_2$, 0.952 for BPB—$(HM)_2$, and 0.990 for BCG—$(HM)_2$ which indicates in general an acceptable fit of Van't Hoff's equation in the temperature ranges studied. The value of ΔG^0 is obtained from eq. [7] and its confidence interval from that of K.

The values of ΔH^0 are negative, indicating that the formation of the 1:2 ion pair is an exothermic process. The variation of entropy ΔS^0 is negative which suggests a greater ordering of the 1:2 complex and ΔG^0 is negative because of the spontaneous process.

Rate constants and kinetic parameters

As has been previously discussed, with a large excess of homatropine the absorption spectrum for the dye:(homatropine)$_2$ ion pair is displaced towards higher wavelengths and intensified by the transition of time, if the homatropine solution is recently prepared.

The experimental absorption values have been adjusted by the equation

$$[8] \quad \ln (A_\infty - A_t) = \ln (A_\infty - A_0) - k't$$

where ln is the Naperian logarithm, A_∞, the absorption at longer time, A_t the absorption at time t, in minutes, and k' the apparent constant of velocity for the pseudo-first order reaction. The rate constant of the process, k, is obtained from the quotient $k'/[HM]$ where HM is the homatropine which is always in excess. In Fig. 9*A* the absorption values at different times can be seen, and they suggest a first order process with respect to the dye. Quantitatively all the experimental results are adjusted by eq. [8] as can be seen in Fig. 9*B*. The values of the ordinate at the origin, ln $(A_\infty - A_0)$, the rate constant, k, and the determination coefficients, r^2, obtained by the least squares method for the reactions of HM with BCG and BPB are shown in Table 14.

The high value of r^2 suggests an exact fit of eq. [8] for all the experimental data at the temperatures studied. The rate constants are presented in Table 14 with a confidence interval for a 95% probability obtained by the Student "t"-test method (33).

The calculated rate constants also satisfy Arrhenius' equation

$$[9] \quad \ln k = \ln A - \frac{E_a}{RT}$$

Can. J. Chem. Downloaded from www.nrcresearchpress.com by 78.46.186.204 on 09/07/12
For personal use only.

TABLE 13. Thermodynamic parameters, ΔH^0, ΔS^0, and ΔG^0, confidence intervals at the 0.95 level, and linear determination coefficients, r^2, from the Van't Hoff representation for the reaction of the formation of the 1:2 (dye:amine) ionic pairs

(*a*) BPB—$(AJ)_2$ ion pair

T (K)	ΔH^0 (kJ/mol)	ΔS^0 (J/K mol)	ΔG^0 (kJ/mol)	r^2
289.16	−63.831 ± 8.293	−125 ± 29	−27.204 ± 1.213	0.995
294.16	−63.831 ± 8.293	−125 ± 29	−26.485 ± 0.707	0.995
300.16	−63.831 ± 8.293	−125 ± 29	−25.564 ± 0.707	0.995
305.66	−63.831 ± 8.293	−125 ± 29	−25.234 ± 0.996	0.995
311.66	−63.831 ± 8.293	−125 ± 29	−24.250 ± 0.774	0.995

(*b*) BCG—$(AJ)_2$ ion pair

T (K)	ΔH^0 (kJ/mol)	ΔS^0 (J/K mol)	ΔG^0 (kJ/mol)	r^2
288.16	−39.367 ± 6.908	−62 ± 25	−21.564 ± 0.105	0.984
293.16	−39.367 ± 6.908	−62 ± 25	−21.451 ± 0.297	0.984
298.16	−39.367 ± 6.908	−62 ± 25	−20.924 ± 0.577	0.984
303.16	−39.367 ± 6.908	−62 ± 25	−20.974 ± 1.201	0.984
308.16	−39.367 ± 6.908	−62 ± 25	−20.502 ± 0.322	0.984
313.16	−39.367 ± 6.908	−62 ± 25	−19.958 ± 0.623	0.984

(*c*) BPB—$(HM)_2$ ion pair

T (K)	ΔH^0 (kJ/mol)	ΔS^0 (J/K mol)	ΔG^0 (kJ/mol)	r^2
288.16	−63.371 ± 26.275	−125 ± 88	−27.041 ± 1.694	0.952
294.16	−63.371 ± 26.275	−125 ± 88	−26.752 ± 1.335	0.952
301.16	−63.371 ± 26.275	−125 ± 88	−24.486 ± 0.824	0.952
306.16	−63.371 ± 26.275	−125 ± 88	−24.351 ± 0.544	0.952
313.16	−63.371 ± 26.275	−125 ± 88	−24.380 ± 6.217	0.952

(*d*) BCG—$(HM)_2$ ion pair

T (K)	ΔH^0 (kJ/mol)	ΔS^0 (J/K mol)	ΔG^0 (kJ/mol)	r^2
289.16	−61.036 ± 16.464	−138 ± 54	−21.008 ± 0.820	0.990
295.16	−61.036 ± 16.464	−138 ± 54	−19.979 ± 0.941	0.990
301.16	−61.036 ± 16.464	−138 ± 54	−19.577 ± 1.343	0.990
304.16	−61.036 ± 16.464	−138 ± 54	−18.807 ± 2.012	0.990
309.16	−61.036 ± 16.464	−138 ± 54	−18.158 ± 1.531	0.990

TABLE 14. Rate constants k of the dye–homatropine reaction and confidence intervals to a probability of 0.95 for different temperatures; intercept values, $\ln (A_\infty - A_0)$, and determination coefficients, r^2, obtained by least squares method

Dye	T (K)	$\ln (A_\infty - A_0)$	k (min^{-1})	r^2
BCG	293.16	−0.356	0.084 ± 0.002	0.999
	303.16	−0.508	0.155 ± 0.006	0.998
	311.16	−0.428	0.356 ± 0.011	0.994
	321.16	−0.498	0.648 ± 0.017	0.999
BPB	293.16	−0.141	0.064 ± 0.001	0.999
	303.16	−0.326	0.259 ± 0.008	0.999
	313.16	−0.297	0.651 ± 0.038	0.996
	323.16	−0.596	2.271 ± 0.076	0.999

TABLE 15. Activation energy, E_a, frequency factor, $\ln A$, confidence intervals to a probability of 0.95 and determination coefficients, r^2, obtained by least squares method

Dye	E_a (kJ mol^{-1})	$\ln A$ (min^{-1})	r^2
BCG	58.859 ± 12.883	21.6 ± 5.1	0.988
BPB	91.337 ± 18.848	34.8 ± 7.4	0.995

where A is the frequency factor and E_a the activation energy. In Figs. 9*C* and *D* the straight lines obtained for the homatropine–bromocresol green, and homatropine – bromophenol blue reactions are drawn and in Table 15 the ordinate values at the origin, $\ln A$, the activation energy, E_a, and the determination coefficients, r^2, for the corresponding lines are presented.

The confidence intervals for $\ln A$ and E_a were obtained by the Student's "t"-test (33) for a probability of 0.95. The values of r^2 in Table 15 are very close to unity indicating that the described kinetic reactions satisfy the Arrhenius equation in the temperature ranges studied.

The reaction of homatropine with BCG or BPB can be shown schematically:

Can. J. Chem. Downloaded from www.nrcresearchpress.com by 78.46.186.204 on 09/07/12
For personal use only.

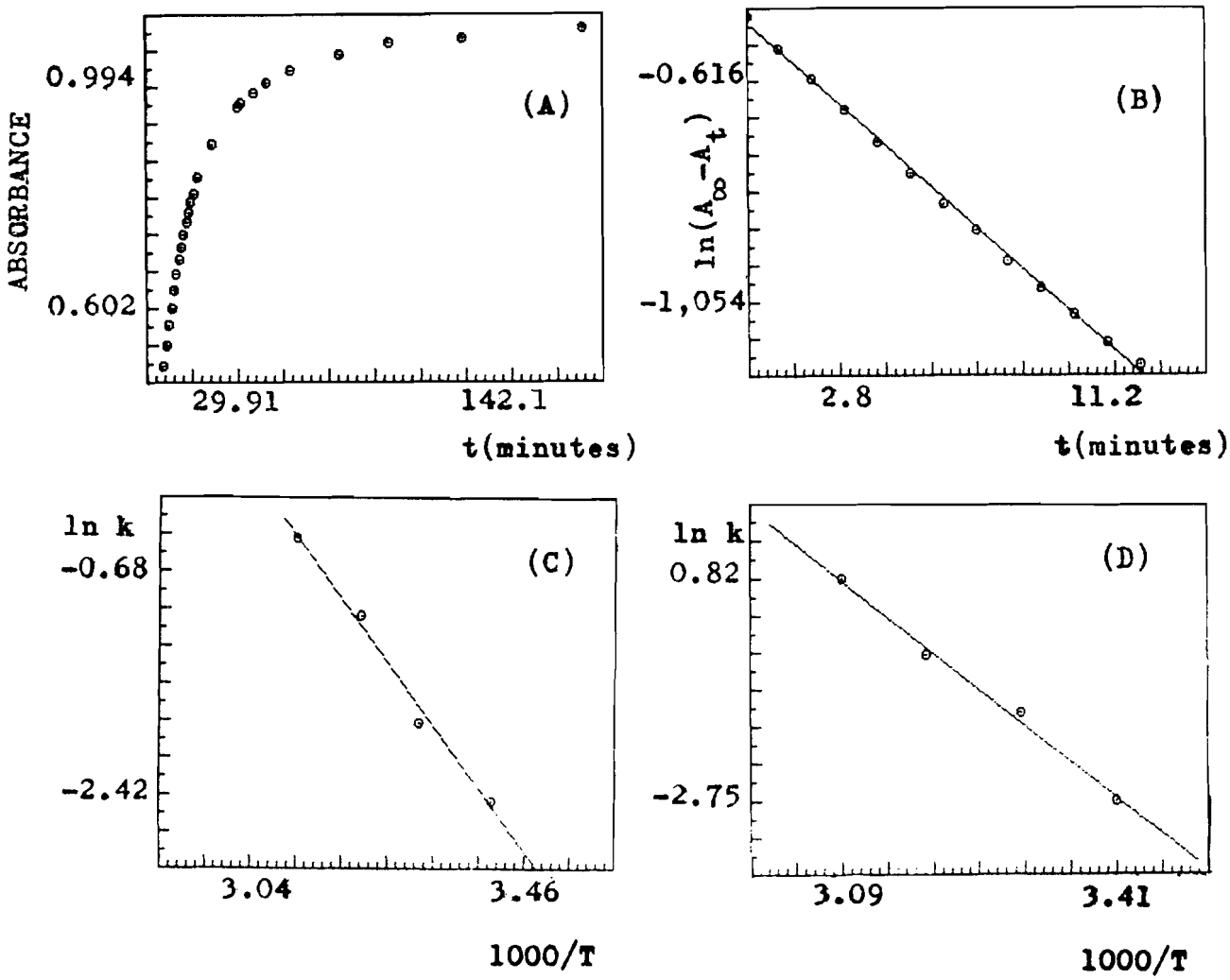

FIG. 9. (*A*) Representation of the absorption at 630 nm of a solution of BCG 1.82×10^{-5} *M* and of HM 0.091 *M* for different times (in minutes); $T = 321.16$ K. (*B*) Representation of ln $(A_\infty - A_t)$ against time, *t*, of a solution of BCG 1.82×10^{-5} *M* and of HM 0.091 *M*; $T = 321.16$ K. (*C*) Arrhenius' representation for the product, P, corresponding to the reaction BCG—HM. (*D*) Arrhenius' representation for the product, P, corresponding to the reaction BPB—HM.

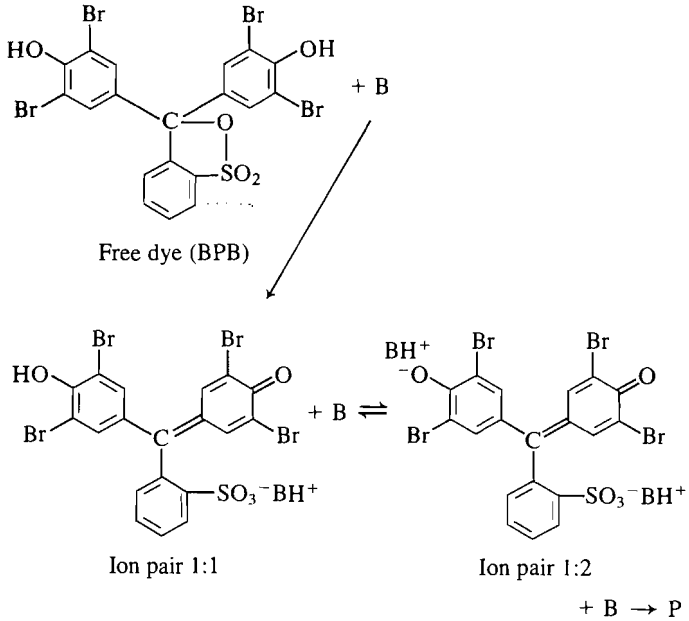

In the first two reactions B can be either HM or AJ but the formation of the product P is only possible with HM. The binding sites of the amine with sulphonphthaleine are not necessarily those shown in the diagram, since the dye (BCG or BPB) is an extensively conjugated molecule (14) and can show resonance.

Each P product obtained in the two reactions studied satisfies Beer's law. The intercept values, *b*, the slope, ϵ_P, and the linear determination coefficient, r^2, obtained by least squares are presented in Table 16. The confidence intervals for ϵ_P were obtained by the Student's "*t*"-test (33) for a probability of 0.95.

The calculated extinction coefficients are of the order of 10^5 L/mol cm, practically double that calculated for the molar extinction coefficients of the 1:2 ion pair (dye:homatropine).

The molar extinction coefficients of the 1:1 and 1:2 ion pairs and P are approximately in the order $\epsilon_{1:1} = \epsilon_{1:2}/2 = \epsilon_P/4$. The fact that $\epsilon_{1:2}$ is double $\epsilon_{1:1}$ could be due to the presence of two alternative quinonoid rings for the 1:2 ion pair. The intensification of the band with a maximum at 600 nm does not allow acceptance of the saturation of the central carbon which would break the chromophore group (17, 18).

The kinetic aspect of reaction [3] is only seen if the dye–amine mixture is carried out with a recently prepared solution of homatropine. If the solution of the tropane compound was prepared 36 h before mixing the P product is immediately formed. From this it is interpreted that the tropane alkaloid reacts slowly with the solvent in the first phase and later with the dye.

Can. J. Chem. Downloaded from www.nrcresearchpress.com by 78.46.186.204 on 09/07/12
For personal use only.

TABLE 16. Molar absorptivity of P product, ϵ_P, intercepts, b, and determination coefficients, r^2, obtained by least squares method; confidence intervals to a probability of 0.95 from Student "t" Test, $T = 293.16$ K

Compound	ϵ_P (L/mol cm)	b	r^2
BCG—HM	63600 ± 10007	0.014	0.994
BPB—HM	107750 ± 18679	−0.030	0.991

The data in Table 14 suggest that the order of magnitude of the calculated rate constants is the same as that of the acid strength of the dye used (BCG or BPB). In a previous paper (35) evidence has been presented that the rate constants of the reaction of the tropane derivative with bromophenol blue increase with the basicity of the tropane alkaloid considered (hyoscyamine and tropine base pK_a = 9.99 and 10.73, respectively).

The preceding discussion indicates that reaction [3] is a complex process in which the solvent plays an important role. Dichloromethane has a capacity to form hydrogen bridges with the tropane alkaloid at high concentrations. Probably in an excess of homatropine an electron is transfered to the 1:2 ion pair across such a bridge. As a result, P is probably a charge transfer complex type of compound. The fact that ajmaline does not form the P product, although its basic character is similar to homatropine (see the respective values of K), could be due to steric factors which make the transition of the electron from the ajmaline to the 1:2 ion pair dye—(ajmaline)$_2$ difficult.

Conductivity of dye–amine solutions in dichloromethane

The data in Tables 4–7 indicate that neither the amines nor the dyes conduct electric current in dichloromethane. On the other hand, mixtures of both do conduct electricity in dichloromethane. This result suggests an ionic nature for the associate species. The weak values of specific conductivity corroborate the conclusion that the associate species are ionic pairs, a conclusion which agrees with the spectrophotometric interpretation. In Tables 4–7 the specific conductivity values are given for the different concentrations of dye–amine ion pair obtained from the equilibrium constants, K, by spectrophotometric methods (Tables 9–12). The specific conductivity increases with an increase in the concentration of the ion pair, be it 1:1 or 1:2, probably because of the presence of a larger number of free ions. However, in the case of the BCG—AJ and BPB—AJ mixtures, after a certain excess concentration of AJ (the limiting AJ concentration is given in Tables 4 and 5) the specific conductivity does not have a stable value, decreasing as time passes. On the other hand, for the BCG—HM and BPB—HM mixtures, if the HM concentration increases sharply, the specific conductivity increases with time.

The interpretation of the spectrophotometric data is in agreement with the conductometric results since in a large excess of AJ the reaction is complete, making the ionization of the ion pair more difficult. On the other hand, in a large excess of HM the formation of product P may make its ionization easier. However, even after waiting 18 h, the specific conductivity did not exceed 2 μs/cm. Thus, the ionization in the solvent is practically negligible and it seems justified not to take it into account in the spectrophotometric study.

Conclusions

Ajmaline and homatropine react in dichloromethane with sulphonphthaleins in acid–base reactions, forming ion pairs of stoichiometry 1:1 and 1:2 in proportion with the increase in the amount of alkaloid base. The formation of the 1:1 ion pair is quantitative and shows evidence of a clear chemical equilibrium between 1:1 and 1:2 ion pairs. The thermodynamic parameters indicate that the formation of the 1:2 ion pair is spontaneous and exothermic, giving rise to a greater ordering. With a large excess of homatropine a new associate, P, is formed in a pseudo-first order kinetic process when the alkaloid base reacts once again with the 1:2 ion pair (dye:homatropine). The P product has been identified as being a kind of charge-transfer complex.

1. G. SCHILL and M. MARSCH. Sven. Pharm. Tidskr. **67**, 385 (1963).
2. G. SCHILL. Acta Pharm. Suec. **2**, 13 (1965).
3. A. HERNÁNDEZ, P. GUTIERREZ, and J. THOMAS. Cienc. Ind. Farm. **3**, 134 (1984).
4. V. D. GUPTA and H. B. GERMAN. Pharm. Sci. **62**, 311 (1973).
5. A. HERNÁNDEZ, P. GUTIERREZ, and J. THOMAS. An. Real. Acad. Farm. **50**, 115 (1984).
6. L. G. CHATTEN and K. O. OKAMURA. J. Pharm. Sci. **62**, 1318 (1973).
7. R. MODIN and G. SCHILL. Talanta, **22**, 1017 (1975).
8. F. MATSUI and W. N. FRENCH. J. Pharm. Sci. **60**, 287 (1971).
9. T. SAKAI. Analyst, **108**, 608 (1983).
10. T. SAKAI. Anal. Chim. Acta, **147**, 337 (1983).
11. P. JOB. Ann. Chem. **9**, 113 (1928).
12. J. S. COLEMAN, L. P. VARGA, and S. H. MASTIN. Inorg. Chem. **9**, 1015 (1970).
13. W. R. BRODE. J. Am. Chem. Soc. **46**, 581 (1924).
14. E. BÁNYAI. *In* Indicator. International Series of Monographs in Analytical Chemistry. Vol. 51. *Edited by* Edmund Bishop. Pergamon Press, Oxford. 1972.
15. V. D. GUPTA. Pharm. Sci. **60**, 1585 (1971).
16. A. HERNÁNDEZ, P. GUTIERREZ, and J. THOMAS. An. Real. Acad. Farm. **49**, 483 (1983).
17. S. HOCHBERG and V. K. LANER. J. Am. Chem. Soc. **63**, 3110 (1941).
18. E. E. SAGER, A. A. MARYOTT, and M. R. SCHOOLEY. J. Am. Chem. Soc. **70**, 732 (1948).
19. N. J. ROSE and R. S. DRAGO. J. Am. Chem. Soc. **81**, 6138 (1959).
20. R. S. DRAGO and N. J. ROSE. J. Am. Chem. Soc. **88**, 6141 (1959).
21. B. B. BHOWMIK. Spectrochim. Acta, **27**A, 321 (1971).
22. B. B. BHOWMIK and P. K. SRIMANI. Spectrochim. Acta, **29**A, 935 (1973).
23. R. L. SCOTT. J. Phys. Chem. **75**, 25 (1971).
24. C. CAZE and C. LOUCHEUX. J. Macromol. Sci. Chem. A7(4), 991 (1973).
25. M. C. CABEZA, J. M. ALVAREZ, and J. THOMAS. An. Quim. **79**, 348 (1983).
26. M. L. SMITH and J. L. MCHALE. J. Phys. Chem. **89**, 4002 (1985).
27. M. L. GRIBAUDO, F. J. KNORR, and J. L. MCHALE. Spectrochim. Acta, **41**A, 419 (1985).
28. H. A. BENESI and J. H. HILDEBRAND. J. Am. Chem. Soc. **70**, 2832 (1948).
29. H. A. BENESI and J. H. HILDEBRAND. J. Am. Chem. Soc. **71**, 2703 (1949).
30. R. A. LABUDDE and M. TAMRES. J. Phys. Chem. **74**, 4009 (1970).
31. D. R. ROSSEINSKY and H. KELLAWI. J. Chem. Soc. (A) 1207 (1969).
32. V. K. ROATGI. An introduction to probability theory and mathematical statistics. John Wiley and Sons. 1976. Chap. 12, pp. 506–519.
33. V. K. ROATGI. An introduction to probability theory and mathematical statistics. John Wiley and Sons. 1976. Chap. 2, p. 100.
34. W. E. WENTWORTH, W. HIRSCH, and E. CHEN. J. Phys. Chem. **71**, 218 (1967).
35. A. HERNÁNDEZ and J. M. ALVAREZ. To be published.

Can. J. Chem. Downloaded from www.nrcresearchpress.com by 78.46.186.204 on 09/07/12
For personal use only.

Cyclopentadienyl complexes with transition metal – main group metal bonds. VII.[1] ^{207}Pb and ^{95}Mo nuclear magnetic resonance studies on molybdenum and tungsten complexes $[(\eta^5\text{-}C_5H_5)(CO)_3M]_nPbR_{4-n}$ (n = 1, R = Me, Et, Ph; n = 2, R = Ph)

MAREK M. KUBICKI, JEAN-YVES LE GALL, RENÉ KERGOAT, AND LUIZ C. GOMES DE LIMA

Unité associée au Centre national de la recherche scientifique n° 322 «chimie, électrochimie et photochimie moléculaires», Équipe de chimie inorganique moléculaire, Université de Bretagne Occidentale, 29287 Brest, France

Received October 2, 1986

MAREK M. KUBICKI, JEAN-YVES LE GALL, RENÉ KERGOAT, and LUIZ C. GOMES DE LIMA. Can. J. Chem. **65**, 1292 (1987).

Nuclear magnetic resonance measurements of metallic nuclei (δ ^{207}Pb, δ ^{95}Mo, and ^1J(W–Pb)) have been carried out on dimetallic $Cp(CO)_3MPbR_3$ (M = Mo, W; R = Me, Et, Ph) and trimetallic $[Cp(CO)_3M]_2PbPh_2$ (M = Mo, W) complexes. ^{207}Pb chemical shifts increase in the sequence $PbEt_3 < PbMe_3 < PbPh_3$ and are observed at higher fields in the tungsten compounds than in the molybdenum ones. It is suggested that both paramagnetic and diamagnetic contributions determine the overall shielding of lead, and that the higher field resonances of ^{207}Pb in the case of W–Pb compounds are due to an efficacious operation of the Z/r dependent diamagnetic term (higher atomic number Z of tungsten and roughly the same Mo–Pb and W–Pb distances resulting from the $4f$ level induced lanthanide contraction). ^{95}Mo chemical shifts (−1838 to −2007 ppm) lie in the region typical of the molybdenum – main group metal bonded complexes but at lower fields than in the corresponding Mo–Sn compounds. It is concluded from this observation that the Z/r dependent diamagnetic contribution does not operate efficaciously for ^{95}Mo shieldings, which are hence primarily dominated by the paramagnetic term. The nature of metal–metal interactions is discussed.

MAREK M. KUBICKI, JEAN-YVES LE GALL, RENÉ KERGOAT et LUIZ C. GOMES DE LIMA. Can. J. Chem. **65**, 1292 (1987).

Des mesures de résonance magnétique nucléaire de noyaux métalliques (δ ^{207}Pb, δ ^{95}Mo et ^1J(W–Pb)) ont été réalisées sur des complexes dimétalliques $Cp(CO)_3MPbR_3$ (M = Mo, W; R = Me, Et, Ph) et trimétalliques $[Cp(CO)_3M]_2PbPh_2$ (M = Mo, W). Les déplacements chimiques δ ^{207}Pb augmentent selon $PbEt_3 < PbMe_3 < PbPh_3$ et se situent à des champs plus élevés dans les composés du tungstène que dans ceux du molybdène. On suggère qu'à la fois les contributions paramagnétique et diamagnétique déterminent le blindage global du noyau ^{207}Pb, et que les résonances du noyau ^{207}Pb à champs plus forts dans le cas des composés à liaison W–Pb sont dues à une intervention efficace du terme diamagnétique dépendant de Z/r (nombre atomique Z plus grand pour le tungstène et à peu près les mêmes distances Mo–Pb et W–Pb résultant de la contraction lanthanidique induite par la présence de la couche $4f$). Les déplacements chimiques δ ^{95}Mo (−1838 à −2007 ppm) se situent dans la région typique des complexes à liaison molybdène–métal (autre qu'un métal de transition) mais à des champs plus faibles que dans des composés correspondants à liaison Mo–Sn. On en conclue que la contribution diamagnétique dépendant de Z/r n'opère pas de manière efficace pour le blindage du molybdène ^{95}Mo dans lequel le terme paramagnétique entre de manière prépondérante. La nature des interactions métal–métal est discutée.

Can. J. Chem. Downloaded from www.nrcresearchpress.com by 78.46.186.204 on 09/07/12
For personal use only.

Introduction

For some years we have been interested in the scope of nmr studies of metallic nuclei and especially of ^{95}Mo in cyclopentadienyl (Cp) complexes. Our object consists of studies on the utility of this technique for chemical applications related to the nature of the transition metal – main group metal bonds.

Heteronuclear metal$^{(a)}$–metal$^{(b)}$ bonds in cyclopentadienyl complexes involving metal$^{(a)}$ of the chromium triad have been known for several years. However, very little has been done on the measurements of metallic nmr parameters of these complexes although they are of interest in light of the continuing discussion of the factors influencing variations in metal shieldings and the nature of metal–metal bonds. To our knowledge there are only three reports on this subject concerning monocyclopentadienyl complexes of the type $Cp(CO)_3M^a$–$[M^b]$ (containing formally M^a(II)), including the resonances of M^b = ^{119}Sn (1), ^{199}Hg (2), and our earlier paper on both M^a = ^{95}Mo and M^b = ^{199}Hg resonances (3). In the class of biscyclopentadienyl complexes of the type $Cp_2M^aX[M^b]$ or $Cp_2M^a[M^b]_2$ (containing formally M^a(IV)), the chemical shifts of ^{119}Sn (1) and of ^{199}Hg (4) have been measured. Our attempts to record the ^{95}Mo spectra in $Cp_2Mo\diagup$ compounds failed, except for that of Cp_2MoH_2 (δ ^{95}Mo = −2497 ± 30 ppm) (4). Recently, Grieves and Mason (5) published the ^{95}Mo data for Cp_2MoH_2 and $(Cp_2MoH_3)Cl$. The molybdenum is formally Mo(VI) in the cation of the latter. A compilation of ^{95}Mo studies covering all fields of molybdenum chemistry has recently been published (6). The overall range of the ^{95}Mo resonances in its monocyclopentadienyl complexes covers about 2000 ppm, but is restricted to about 300 ppm (in the high field part of the overall range) for the compounds with molybdenum – main group metal (Hg, Sn) bonds.

In our continuing interest in the application of nmr studies of metallic nuclei to the problem of chemical bonding, we recorded the ^{207}Pb resonances in monocyclopentadienyl complexes $Cp(CO)_3MPbR_3$ (M = Mo and W) together with the ^{95}Mo resonances for M = Mo, as well as in some trimetallic compounds $[Cp(CO)_3M]_2PbR_2$. The choice of lead derivatives was suggested by the fact that contrary to the complexes with $[M^a]$–Sn bonds, which were extensively studied, only a few publications report on the compounds with $[M^a]$–Pb bonds. These are the nmr studies of M^a = ^{59}Co (7), ^{55}Mn (8), ^{93}Nb (9), and ^{51}V (10). Both metallic nuclei (M^a and ^{207}Pb) were studied only in platinum–lead bonded compounds (11, 12).

Experimental

The complexes were synthesized as previously described (13, 14). Samples for nmr measurements were prepared under a nitrogen atmosphere by using dried and degassed CH_2Cl_2 and C_6D_6 as internal lock. Solutions close to saturation were sealed in 10-mm tubes.

The nmr spectra were recorded on a JEOL FX 100 spectrometer at ambient temperature. A 10-mm multinuclear probe model NM 3980 operating at 20.80 MHz for ^{207}Pb and at 6.44 MHz for ^{95}Mo measurements was used. The 90° pulse was found to be 40 μs for ^{207}Pb and 80 μs for ^{95}Mo. The routine acquisition parameters used in this

[1]Part VI of this series: ref. 35.

TABLE 1. δ ^{207}Pb and δ ^{95}Mo chemical shifts and ^1J(W–Pb) coupling constants for $[Cp(CO)_3M]_nPbR_{4-n}$ complexes

Complex	δ ^{207}Pb (ppm)	$\Delta\nu_{1/2}$ (Hz)	δ ^{95}Mo (ppm)	$\Delta\nu_{1/2}$ (Hz)	^1J(W–Pb) (Hz)
$Cp(CO)_3MoPbEt_3$	+301	8	−2007	120	
$Cp(CO)_3MoPbMe_3$	+229	8	−1989	80	
$Cp(CO)_3MoPbPh_3$	+125	8	−1927	180	
$[Cp(CO)_3Mo]_2PbPh_2$	+421	9	−1838	170	
$Cp(CO)_3WPbEt_3$	+25	8			115
$Cp(CO)_3WPbMe_3$	−87	6			170
$Cp(CO)_3WPbPh_3$	−217	6			390
$[Cp(CO)_3W]_2PbEt_2$[a]	−128	7			135
$[Cp(CO)_3W]_2PbPh_2$	−375	7			270

[a]This complex has not been synthesized; its formulation has been attributed for an extra peak observed during the recording of the ^{207}Pb resonance for $Cp(CO)_3WPbEt_3$; see text.

Can. J. Chem. Downloaded from www.nrcresearchpress.com by 78.46.186.204 on 09/07/12
For personal use only.

study were as follows: pulse width 40 μs (^{95}Mo) and 10 μs (^{207}Pb); acquisition time 5×10^{-2} s with the repetition time of $7–9 \times 10^{-2}$ s for ^{95}Mo and 0.4 s and 1 s, respectively, for ^{207}Pb (acquisition times for ^{95}Mo are shorter than for ^{207}Pb because of its quadrupole moment); spectral width 20 kHz; data points 2K (^{95}Mo) and 16K (^{207}Pb); number of scans $5 \times 10^4 – 6 \times 10^5$ (^{95}Mo) and $10^3–10^5$ (^{207}Pb) depending on the solubility of compounds. Na_2MoO_4 (2 *M*) at pH 11 (^{95}Mo) and neat $PbMe_4$ (^{207}Pb) were used as external references.

The ^{207}Pb and ^{95}Mo chemical shifts together with the line widths at half-height and the coupling constants W–Pb are given in Table 1.

Results and discussion

Before a discussion of the ^{95}Mo and ^{207}Pb nmr data, we indulge in a brief recall of the parameters determining the nuclear screening. These are usually discussed in the terminology developed by Ramsey (15), introducing the "diamagnetic" (σ_d) and "paramagnetic" (σ_p) components of the overall shielding (σ) (eq. [1]),

$$[1] \quad \sigma = \sigma_d + \sigma_p$$

where σ_d involves the free rotation of the electrons about the nucleus in question and σ_p describes the hindrance to this rotation caused by other electrons and nuclei in the molecule. The σ_d term for a nucleus A can be expressed by eq. [2].

$$[2] \quad \sigma_d^A = \text{const} \sum_\mu P_{\mu\mu} \langle \mu | r_{A\mu}^{-1} | \mu \rangle$$

where $P_{\mu\mu}$ is the charge density of the atomic orbital μ, which is at an average distance of $r_{A\mu}$ from nucleus A. An approximation to the paramagnetic term σ_p can be given by eq. [3] of Jameson and Gutowsky (16),

$$[3] \quad \sigma_p = -\text{const}\, \overline{\Delta E^{-1}} (\langle r_{np}^{-3} \rangle Q_p + \langle r_{nd}^{-3} \rangle Q_d)$$

where $\overline{\Delta E}$ is the mean energy of electronic excitation from the ground state to excited states, which can be mixed in by the magnetic field and interpreted often as HOMO–LUMO separation, $\langle r_{np} \rangle$ and $\langle r_{nd} \rangle$ are the radial expansion terms for the valence *p* and *d* electrons, and Q_p and Q_d represent the degree of ground-state electron imbalance in the bonds associated with the *p* and *d* components of the hydridized orbitals.

In another approach, the MO theory developed by Pople (17) within the framework of an independent electron model expresses the nuclear screening as the sum of local, non-local, and interatomic diamagnetic and paramagnetic contributions (eq. [4]),

$$[4] \quad \sigma = \sigma_d^{loc} + \sigma_d^{non\text{-}loc} + \sigma_d^{inter} + \sigma_p^{loc} + \sigma_p^{non\text{-}loc} + \sigma_p^{inter}$$

where the various σ_d and σ_p terms are not directly comparable with the expressions bearing these names in Ramsey's equations. In Pople's approach the local terms arise from electronic currents localized on the atom containing the nucleus of interest, both non-local contributions are derived from currents on neighboring atoms, and the interatomic contributions are due to the currents not localized on any atom in the molecule, e.g. ring currents. The interatomic contributions in eq. [4] are small, so the overall shielding may be considered as depending on the local and non-local σ_p and σ_d terms.

A chemist is particularly interested in the electronic structure of atoms forming the different kinds of bonds and therefore in the nature of their valence shell, which depends on the structure of their own electrons, local symmetry, and on the nature and symmetry of the orbitals associated with the neighboring atoms. The Ramsey paramagnetic term approximated by eq. [3] seems to respond well to the above chemical problems because the parameters determining the nature of the bonds are included therein. As the influence of the neighbors is thus involved, eq. [3] results from both local and non-local contributions.

Flygare and Goodisman (18) have proposed an atom–dipole model for estimating the diamagnetic contribution, in which the electronic eigenfunctions are not explicitly involved as in the case of eq. [2] (eq. [5]),

$$[5] \quad \sigma_d^A = \sigma_d^A \text{ (free atom)} + \frac{\mu_0 e^2}{12\pi m} \sum_{B \neq A} \frac{Z_B}{r_{AB}}$$

where Z_B is the atomic number of the atoms other than A present in the molecule and r_{AB} is the separation between nucleus A and its neighbors B. The values calculated by Dickinson may be taken as σ_d^A (free atom) (19). In this light, eq. [5] gives a σ_d^A contribution related to that defined by Ramsey. Using eq. [5] with the summation over only the atom in question and those bonded directly to it, Mason obtained the σ_d^{loc} values useful for interpretation of nitrogen (20) and carbon (21) chemical shifts. The increment in σ_d^A arises from the final, non-local, term in eq. [5] and thus, perhaps not wholly accurately from the theoretical point of view, the diamagnetic term may be separated into the local and non-local contributions as in Pople's approach. Such an artificial division is attractive for a chemist, especially when the chemical shifts are compared for the series of structurally similar compounds. Thus in this paper we shall use the term "local" for the nucleus studies and "non-local" for the influence of its neighbors (eq. [6]),

$$[6] \quad \sigma = \sigma_p + \sigma_d^{loc} + \sigma_d^{non\text{-}loc}$$

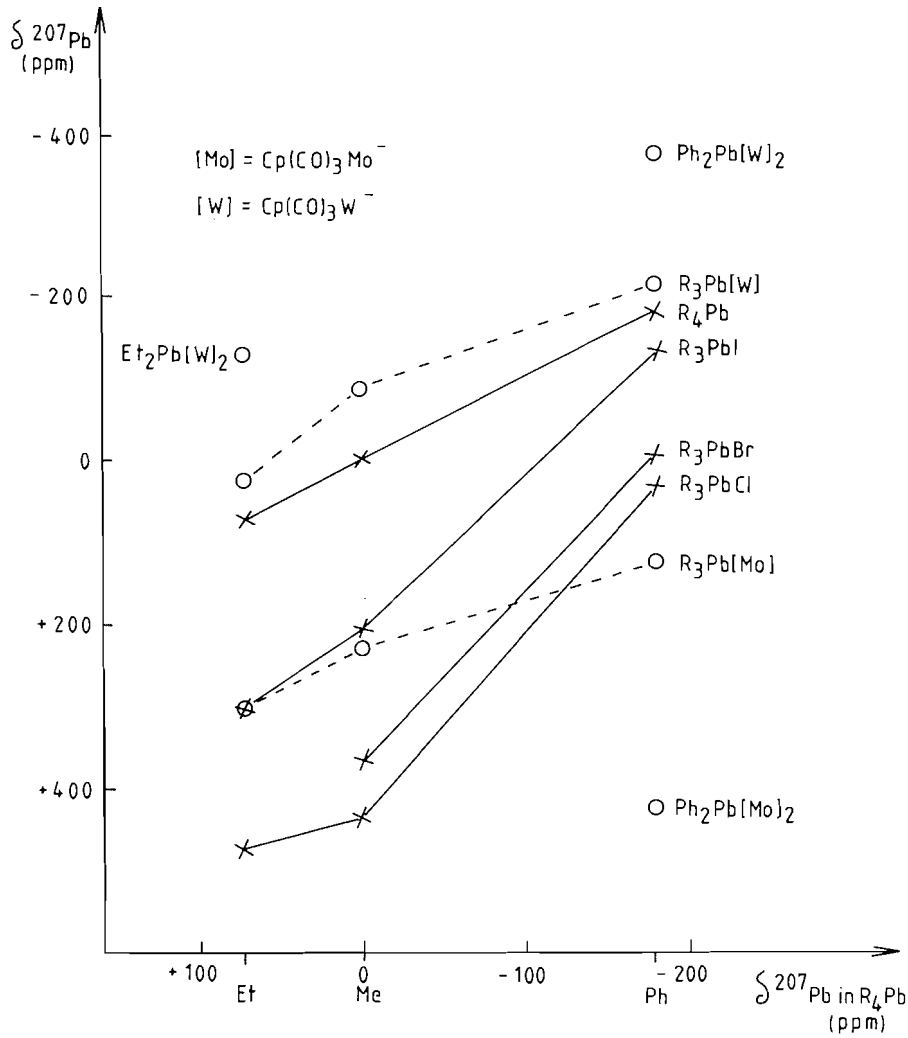

FIG. 1. ^{207}Pb chemical shifts in R_3PbY (×: Y = Cl, Br, I and R; ○: Y = $Cp(CO)_3Mo$ and $Cp(CO)_3W$) and $R_2Pb[M(CO)_3Cp]_2$ complexes as a function of δ (^{207}Pb) in R_4Pb.

^{207}Pb chemical shifts and coupling constants

Inspection of Table 1 shows that the shielding of the lead nucleus in $Cp(CO)_3MPbR_3$ complexes increases in the sequence $PbEt_3 < PbMe_3 < PbPh_3$, and is the same as that observed in triorgano- (R_3PbX, R = Et, Me, Ph; X = Cl, Br, I) and tetraorgano-lead (R_4Pb) compounds (22). In the analogous tin derivatives R_3SnCl and R_4Sn, the corresponding sequence of ^{119}Sn shieldings is inverted for R = Me and Et, although there exists a general linear relationship between the chemical shifts of ^{119}Sn and ^{207}Pb (23, 24). However, the differences of shielding in M^bMe_3 and M^bEt_3 are small compared to the much higher shieldings of tin and lead in phenyl derivatives. Thus it is possible that these weak differences (Me vs. Et), which have no chemical consequences, are due to a higher polarizability of lead, thus modifying the electron movements responsible for the shieldings of M^b.

Shielding variations of ^{207}Pb nuclei in the compounds $YPbR_3$, where Y is a halide (X), R, or $Cp(CO)_3M^a$, are graphically presented in Fig. 1 as a function of chemical shifts of ^{207}Pb measured for R_4Pb. One observes an important increase of shielding from R = Me and Et to R = Ph in the compounds R_3PbX but a moderate one in dimetallic complexes R_3Pb–$[M^a]$. This suggests clearly a different nature of R_3Pb—X and R_3Pb—M^a bonds with repercussions on, or as the consequence of, the Pb–Ph magnetic interactions.

Magnetic anisotropy of the phenyl ring, which generally leads to higher field resonances of neighboring nuclei, may operate more easily in Ph_3PbX than in Ph_3PbM^a compounds. In these latter complexes the higher covalency of Pb—M^a bonds and the presence or participation of metal (M^a) *d* orbitals in bonding can modify the nature of the valence electrons on lead. The differences (Δ) of the chemical shifts of ^{207}Pb in the compounds Me_3PbY and Ph_3PbY are given in Table 2. These data show a clear distinction between the halides (Y = X), R, and [M^a]. Because there is no doubt that, among the compounds involved, the Pb—Cl bond has the most pronounced ionic nature, the values of Δ reflect the covalency of Pb—Y bonds. Thus the Pb—M^a bonds are highly covalent and the covalency of the Pb—Mo bonds seems to be higher than that of the Pb—W bonds. This last statement may be confused with the problem of d_π–d_π interactions, which appear to be less important for heavier transition metals (25).

With the exception of tungsten complexes, the ^{207}Pb resonances in the compounds R_3PbY are observed, for a given R, at lower fields than in the corresponding tetraorganoleads (Fig. 1). This can be easily deduced from the paramagnetic contribution to the overall shielding (eq. [3]). For four-coordinate lead compounds, the *d*-electron term may be ignored if there is no π-bonding. In R_4Pb compounds Q_p is equal to 0, but the 6*p* electron imbalance increases in the compounds R_3PbY. More-

Can. J. Chem. Downloaded from www.nrcresearchpress.com by 78.46.186.204 on 09/07/12
For personal use only.

TABLE 2. δ ^{207}Pb chemical shifts (in ppm) and their differences Δ in R_3PbY compounds

	Y					
R	Cl	Br	I	R	$Cp(CO)_3Mo$	$Cp(CO)_3W$
Me, δ	+432[a]	+367[a]	+204[a]	0	+229	−87
Ph, δ	+33[b]	−3[b]	−131[b]	−179[b]	+125	−217
Δ (Me − Ph)	399	370	335	179	104	130

[a]Reference 23.
[b]Reference 22.

Can. J. Chem. Downloaded from www.nrcresearchpress.com by 78.46.186.204 on 09/07/12
For personal use only.

over, a change of symmetry from idealized T_d to C_{3v} decreases the $\overline{\Delta E}$ value. Both these parameters increase the value of the paramagnetic term σ_p and consequently decrease the overall shielding of ^{207}Pb.

The chemical shifts of lead in tungsten complexes are observed at higher fields than in R_4Pb, apparently in contradiction to the above symmetry related discussion of the paramagnetic term σ_p. However, the same phenomenon has been observed in group-VII transition metal complexes of tin: δ ^{119}Sn in $(CO)_5ReSnMe_3$ is −89 ppm (ref. $SnMe_4$), but the expected shielding (+63 ppm) appears in $(CO)_5MnSnMe_3$ (1). It has been suggested that the diamagnetic contribution due to the nearest neighbors (eq. [5]) may explain the high field resonances when heavier atoms are present in the coordination sphere of the nucleus studied (1) ($\sigma_d^{\text{non-loc}}$ term in eq. [6]). Similar trends in δ ^{119}Sn were observed in the complexes of Ru vs. Os and Rh vs. Ir (26). Such an influence of heavier nuclei on the nucleus studied is known as the "heavy atom effect" or "Z dependence" but its cause has not yet been satisfactorily stated. It appears that such a dependence should mainly affect the diamagnetic contribution (eq. [5]), but the strain reasoning fails when examples of "inverse halogen dependence" are encountered (6, 27, 28). Similar "anomalies" are also found when considering the influence of metallic nuclei. If Z dependence is apparently exhibited by the δ ^{119}Sn values in complexes of the type $Cp(CO)_3MSnMe_3$: M = Cr + 161, Mo + 121, W + 42 ppm (1), and by ^{199}Hg values in $Cp(CO)_3MHgCl$: M = Cr − 542, Mo − 617, W − 997 ppm (ref. $HgMe_2$) (2), it fails in trimetallic organomercurials $[Cp(CO)_3M]_2Hg$: M = Cr − 80, Mo + 115, W − 348 ppm (2). Other examples may be found with other nuclei, e.g. ^{1}H in the anions $HM(CN)_5^{3-}$: M = Co − 47.2, Rh − 45.4, Ir − 49.0 ppm (ref. bare proton) (29) or ^{13}C in $M(Me)_4$: M = Sn − 202.1, Pb − 196.2 ppm (ref. CS_2) and $M(Me)_2$: M = Zn − 197.0, Cd − 191.8, Hg − 169.3 (ref. CS_2) (30). Some cases involving transition metal [M[a]] resonances bonded to tin and lead will be cited below in the discussion of ^{95}Mo data. One can conclude from the examples cited above that, in the case of the influence of *transition metals*, the chemical shifts of the nucleus studied may or may not obey the Z dependence (eqs. [5] and [6]) if the metal belongs to the 3*d* or 4*d* blocks, but that in the presence of 5*d*-block metals the highest shieldings are observed. Thus it seems clear that the presence of the 4*f* level in 5*d* transition metals, leading to the well-known lanthanide contraction, may explain the high shieldings of the nuclei bonded to them. The σ_d term should vary more widely than does the σ_p term. The parameters determining the extent of σ_d domination should therefore be, aside from the atomic number Z, the covalent or ionic radii of the atoms and, hence, the interatomic distances r_{AB}. These increase on going down from 3*d* to 4*d* metals, but they are the same or even smaller for 5*d* than for 4*d* metals. It can be assumed that when "inverse Z dependence" for 3*d* vs. 4*d* metals in a similar structural environment is observed, the interatomic distances increase rapidly and the changes in paramagnetic contribution σ_p may overlap the increase in σ_d. The σ_p term is much more sensitive to variations in expansion of the orbitals involved (r^{-3} dependent, eq. [3], which depends on the bond distances) than is the σ_d term (r_{AB}^{-1}) dependent, eqs. [2] and [5]).

In trimetallic complexes $[Cp(CO)_3M]_2PbR_2$, the lead resonances are observed at higher fields for M = W (R = Et and Ph) but at lower field for M = Mo (R = Ph) than in the corresponding dimetallic complexes $Cp(CO)_3MPbR_3$ (Table 1, Fig. 1). The case of molybdenum may have been expected on the grounds of the increased value of the σ_p term. Replacement of a single R group in PbR_4 by a second-row transition metal entity gives a shift to low field, and multiple substitution does nothing to reverse the trend as it was still observed for ^{119}Sn resonances in the carbonyl complexes of the first-row transition metals $[(CO)_xM]_nSnMe_{4-n}$ (M = Co, x = 4; M = Mn, x = 5) (1). It is possible that d_π–d_π interactions in the trimetallic Mo complexes are stronger than in the dimetallic complexes and that this leads to an increased σ_p contribution as a consequence of electron delocalization reducing the $\overline{\Delta E}$ parameter in eq. [2]. An earlier study of $[\{(CO)_4Co\}_nSnMe_{4-n}]$ by ^{59}Co nuclear quadrupole resonance indicated such an increase in d_π–d_π Co–Sn interactions with increasing value of n (31). In complexes of tungsten the non-local diamagnetic contribution of two third-row transition metal nuclei and the lower extent (or absence) of d_π–d_π interactions (higher $\overline{\Delta E}$, lower σ_p) may be responsible for the high field resonances observed. A similar dependence of ^{119}Sn chemical shifts on multiple substitution has been observed in manganese and rhenium complexes (1). This is graphically shown in Fig. 2.

In Table 1 we reported the values of ^1J(W–Pb) coupling constants. These values increase with the increasing field of ^{207}Pb resonances in dimetallic complexes $Cp(CO)_3WPbR_3$, which agrees with the assumption that the coupling constants are primarily dominated by the Fermi contact term (32):

$$[7]\quad {}^1K(M^a\text{–}M^b) = \text{const.}\ \overline{\Delta E}\,\psi^2_{M^a}(0)\,\psi^2_{M^b}(0)\,\alpha^2_{M^a}\alpha^2_{M^b}$$

This term is related to the paramagnetic contribution σ_p to the overall shielding because its magnitude depends on the mean electron excitation energy ($\overline{\Delta E}$). Other parameters influencing this term are the valence-electron density (ψ^2) and the s character of the hybridized orbital of bonded nuclei. This correlation (higher δ ^{207}Pb, higher ^1J(W–Pb)) is less clear for trimetallic complexes $[Cp(CO)_3W]_2PbR_2$. Here the relation is verified by δ and J values for both complexes, R = Et and Ph (Table 1). However, for a given R, the W–Pb coupling constant is greater in the trimetallic complex $[Cp(CO)_3W]_2PbEt_2$ than in the dimetallic one $Cp(CO)_3WPbEt_3$, as expected from the δ ^{207}Pb values, but the tendency is inverted in the case of phenyl derivatives (higher δ, lower J).

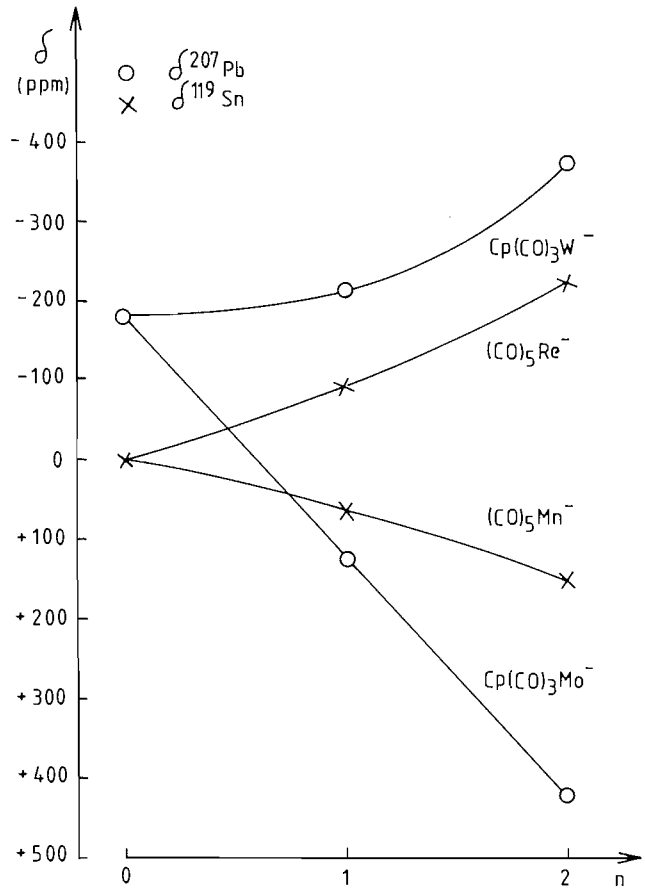

FIG. 2. δ (^{207}Pb) in $[Cp(CO)_3M]_nPbPh_{4-n}$ (ref. $PbMe_4$) and δ (^{119}Sn) in $[(CO)_5M]_nSnMe_{4-n}$ as a function of n.

^{95}Mo chemical shifts

Chemical shift values of ^{95}Mo (Table 1) lie well within the region observed for other compounds with molybdenum – heavy metal bonds: −1795 to −1939 ppm for $Cp(CO)_3MoHgX$(3) and −2072 ppm for $Cp(CO)_3MoSnMe_3$ (33). It is of interest to note that the ^{95}Mo resonances in the Mo–Pb complexes studied here are observed at lower fields than in the corresponding Mo–Sn derivatives (δ ^{95}Mo in [Mo] − $PbMe_3$ = −1989 ppm). The same trends have been observed for the chemical shifts of other transition metals, e.g. ^{55}Mn(8), ^{93}Nb(9), and ^{51}V(10), which were found at lower fields for M^a–PbR_3 than for M^a–SnR_3 compounds. However, one would expect that the shielding of transition metals bonded to lead should be higher than in the analogous tin complexes because of the influence of the $\sigma_d^{non\text{-}loc}$ (eq. [6]) term and the presence of the 4*f* level in the lead atom[2] (*vide supra*, discussion of the ^{207}Pb shielding). However, the lead is not a transition metal, so the lanthanide contraction does not operate effectively therein. It is evidenced by, for example, the ionic radii, Sn(IV) 0.69 and Pb(IV) 0.78 Å (34). Thus the diamagnetic contribution and especially the *Z* dependence become less efficacious as a consequence of longer M^a–Pb bonds, as compared with the M^a–Sn bonds. In this light, the higher shielding of ^{207}Pb nuclei in the tungsten than in the molybdenum compounds may be understood, because the W—Pb and Mo—Pb bond lengths are roughly the same in the structurally analogous complexes.

The above discussion indicates clearly that the non-local diamagnetic contribution (terminology of eq. [6]) to the overall shielding of transition metals bonded to tin and lead is overlapped by the paramagnetic term. With the statement that σ_p determines the overall shielding of ^{95}Mo, one can further ask which is the most important component of this contribution (eq. [3]). In the paramagnetic term, there are two main effects governing its value; (*i*) influences via ΔE, i.e., increase in σ_p and decrease in σ with decreasing ligand strength, and (*ii*) influences via $\langle r^{-3} \rangle Q$ factor that represents nephelauxetic and covalency effects and should give rise to a decrease in σ_p and an increase in σ as the polarizability of the ligating function increases and its electronegativity decreases. Because the ligand strength decreases and the polarizability increases down to a given group of the periodic table, it appears that ΔE is the most important factor determining the shieldings when the group 14 (lead and tin) atoms are present as ligands.

Inspection of Table 1 shows that in the bimetallic complexes $Cp(CO)_3MoPbR_3$, shielding of the lead nuclei is accompanied by deshielding of the molybdenum nuclei. A similar trend has been observed in complexes with a molybdenum–mercury bond (3) and one can suppose that the chemical shifts of ^{95}Mo and ^{207}Pb together reflect the polarization of electron density over the Mo—Pb bonds. Thus it seems that no d_π–d_π interaction is necessary to explain the trends of the shielding in dimetallic complexes. However, in the trimetallic complex $[Cp(CO)_3Mo]_2PbPh_2$, both ^{95}Mo and ^{207}Pb resonances are observed at lower fields than in the dimetallic $Cp(CO)_3MoPbPh_3$. In this case, the presence of d_π–d_π interactions, leading to a decrease of ΔE in eq. [2], as well as an involved electron imbalance increase the σ_p term and decrease the overall shielding σ.

As a final remark, we note that during the recording of the ^{207}Pb resonances for $Cp(CO)_3MoPbEt_3$ and $Cp(CO)_3WPbEt_3$ low intensity secondary peaks appeared on the spectra. In the case of the molybdenum complex a ghost peak centered at +73 ppm was identified as $PbEt_4$, resulting from degradation of the starting product. The extra peak detected for the tungsten compound was centered at −140 ppm with ^1J(W–Pb) equal to 135 Hz. A reasonable explanation of its appearance is the transformation of the parent dimetallic complex into the trimetallic one. Such a thermal transformation has been observed for Pannell and Kapoor (14).

[2]This point has been underlined in the report of one of the referees.

1. D. H. HARRIS, M. F. LAPPERT, J. S. POLAND, and W. MCFARLANE. J. Chem. Soc. Dalton Trans. 311 (1975).
2. M. J. ALBRIGHT and J. P. OLIVER. J. Organometal. Chem. **172**, 99 (1979).
3. M. M. KUBICKI, R. KERGOAT, J. Y. LE GALL, J. E. GUERCHAIS, J. DOUGLADE, and R. MERCIER. Aust. J. Chem. **35**, 1543 (1982).
4. M. M. KUBICKI, R. KERGOAT, J. E. GUERCHAIS, I. BKOUCHE-WAKSMAN, C. BOIS, and P. L'HARIDON. J. Organometal. Chem. **219**, 329 (1981).
5. R. A. GRIEVES and J. MASON. Polyhedron, **5**, 415 (1986).
6. M. MINELLI, J. H. ENEMARK, R. T. C. BROWNLEE, M. J. O'CONNOR, and A. G. WEDD. Coord. Chem. Rev. **68**, 169 (1985).
7. H. W. SPIESS and R. K. SHELINE. J. Chem. Phys. **53**, 3036 (1970).
8. G. M. BANCROFT, H. C. CLARK, R. G. KIDD, A. T. RAKE, and H. G. SPINNEY. Inorg. Chem. **12**, 728 (1973).
9. I. PFORR, F. NAÜMANN, and D. REHDER. J. Organometal. Chem. **258**, 189 (1983).
10. R. TALAY and D. REHDER. J. Organometal. Chem. **262**, 25 (1984).

Can. J. Chem. Downloaded from www.nrcresearchpress.com by 78.46.186.204 on 09/07/12
For personal use only.

11. S. CARR, R. COLTON, and D. DAKTERNIEKS. J. Magn. Reson. **47**, 156 (1982).
12. S. CARR, R. COLTON, and D. DAKTERNIEKS. J. Organometal. Chem. **240**, 143 (1982).
13. H. R. H. PATIL and W. A. G. GRAHAM. Inorg. Chem. **5**, 1401 (1966).
14. K. H. PANNELL and R. N. KAPOOR. J. Organometal. Chem. **214**, 47 (1981).
15. N. F. RAMSEY. Phys. Rev. **78**, 689 (1950).
16. C. J. JAMESON and H. S. GUTOWSKY. J. Chem. Phys. **40**, 1914 (1964).
17. J. A. POPLE. Mol. Phys. **7**, 301 (1964), and references cited therein.
18. W. H. FLYGARE and J. GOODISMAN. J. Chem. Phys. **49**, 3122 (1968).
19. W. C. DICKINSON. Phys. Rev. **80**, 563 (1950).
20. R. GRINTER and J. MASON. J. Chem. Soc. (A), 2196 (1970).
21. J. MASON. J. Chem. Soc. (A), 1038 (1971).
22. T. N. MITCHELL, J. GMEHLING, and F. HUBER. J. Chem. Soc. Dalton Trans. 960 (1978).
23. J. D. KENNEDY, W. MCFARLANE, and G. S. PYNE. J. Chem. Soc. Dalton Trans. 2332 (1977).
24. T. N. MITCHELL. J. Organometal. Chem. **255**, 279 (1983).
25. G. T. ANDREWS, I. J. COLQUHOUN, W. MCFARLANE, and S. O. GRIM. J. Chem. Soc. Dalton Trans. 2353 (1982).
26. H. MORIYAMA, P. S. PREGOSIN, Y. SAITO, and T. YAMAKAWA. J. Chem. Soc. Dalton Trans. 2329 (1984).
27. R. G. KIDD. Annu. Rep. NMR Spectrosc. **10**A, 19 (1979).
28. YU. A. BUSLAEV, V. D. KOPANEV, and V. P. TARASOV. Chem. Commun. 1175 (1971); R. G. KIDD, R. W. MATTHEWS, and H. G. SPINNEY. J. Am. Chem. Soc. **94**, 6686 (1972); B. G. SAYER, N. HAO, G. DÉNÈS, D. G. BICKLEY, and M. J. MCGLINCHEY. Inorg. Chim. Acta, **48**, 53 (1981).
29. L. L. LOHR, JR. and W. N. LIPSCOMB. Inorg. Chem. **3**, 22 (1964).
30. F. J. WEIGERT, M. WINOKUR, and J. D. ROBERTS. J. Am. Chem. Soc. **90**, 1566 (1968).
31. D. D. SPENCER, J. L. KIRSCH, and T. L. BROWN. Inorg. Chem. **9**, 235 (1970).
32. J. A. POPLE and D. P. SANTRY. Mol. Phys. **8**, 1 (1964).
33. J. Y. LE GALL, M. M. KUBICKI, and F. PETILLON. J. Organometal. Chem. **221**, 287 (1981).
34. J. E. HUHEEY. Inorganic chemistry: Principles of structure and reactivity. Harper & Row, London. 1975. p. 75.
35. M. M. KUBICKI, R. KERGOAT, J. Y. DE VANSAY, J. Y. LE GALL, and J. E. GUERCHAIS. Polyhedron, **3**, 365 (1984).

Can. J. Chem. Downloaded from www.nrcresearchpress.com by 78.46.186.204 on 09/07/12
For personal use only.

A simple and direct method of cyclization for the synthesis of 10-membered rings

PIERRE DESLONGCHAMPS, SERGE LAMOTHE,[1] AND HO-SHEN LIN

Laboratoire de synthèse organique, Département de chimie, Faculté des sciences, Université de Sherbrooke, Sherbrooke (Qué.), Canada J1K 2R1

Received December 4, 1986

PIERRE DESLONGCHAMPS, SERGE LAMOTHE, and HO-SHEN LIN. Can. J. Chem. **65**, 1298 (1987).

Ten-membered rings containing two unsaturations are produced without the use of high dilution techniques by the intramolecular malonate anion displacement of an allylic chloride.

PIERRE DESLONGCHAMPS, SERGE LAMOTHE et HO-SHEN LIN. Can. J. Chem. **65**, 1298 (1987).

La synthèse de cycles à 10 membres contenant deux insaturations est réalisée sans utiliser les techniques de haute dilution par déplacement intramoléculaire d'un chlorure allylique par l'anion malonate.

[Traduit par la revue]

Can. J. Chem. Downloaded from www.nrcresearchpress.com by 78.46.186.204 on 09/07/12
For personal use only.

The last decade has seen organic chemists gain interest in the synthesis of medium and large rings (1–8). The growing activity in this area was triggered by the sophistication of already existing techniques along with discovery of new ones for structure determination of organic molecules. Many naturally occurring compounds contain medium and large rings but few reliable methods for the preparation of such systems by direct cyclization involving carbon–carbon bond formation are known to this day (1–8). Moreover, most published methods require the use of high dilution techniques (either high dilution or slow additions of the substrate) to avoid polymerization. The 10-membered ring is known to be one of the most difficult rings to prepare; it combines strong enthalpy effects (Baeyer, Pitzer, and transannular strains) with a disfavorable entropy effect that keeps terminal carbon atoms from approaching within reacting distance (9).

An efficient way to overcome the problems associated with medium ring closure is to replace sp^3 carbon atoms in the chain by sp^2 or *sp* carbons. This has the effect of lowering the number of degrees of freedom of the molecule, thereby statistically favoring encounters between the ends of the chain (10). Moreover, the proper disposition of those unsaturated carbon atoms can substantially reduce transannular interactions.

With this in mind, we chose to prepare precursors **1***a* in all possible combinations (A–A, C–A, T–A, T–C, T–T, C–C) (Scheme 1) in order to obtain monomers **2***a* and cyclic dimers **3***a* (C = *cis* olefin, T = *trans* olefin, and A = acetylene).

The preparation of the different precursors **1***a* is described in Scheme 2. We chose commercial diol **4** as our starting material since it could readily be converted into all precursors but one **1***a*. Mono protection (11) followed by formation of the allylic chloride using Meyers's procedure (12) afforded olefin **6**. Three sequential alkylations were then carried out starting with dimethyl malonate to give **7**, which was coupled with 1,4-dichloro-2-butyne. The resulting chloride **8** was reacted with another equivalent of dimethyl malonate affording tetraester **9**. Simple deprotection (13) and chlorination of the resulting allylic alcohol **10** afforded precursor **1***a* [C–A].

Alkylation of **6** with tetraester **11** (obtained in 2 steps from 1,4-dibromo-2-butyne) afforded precursor **1***a* [C–C] after the usual deprotection and chlorination sequence.

For the *trans* series we needed to prepare chloride **16**, which was easily obtained by reduction and chlorination (14) of the known aldehyde **14** (previously prepared by Corey and Suggs (15)). Again, coupling with tetraester **11** gave **17**, which was readily transformed into precursor **1***a* [T–C] through alcohol **18**.

Introduction of a malonate moiety on chloride **16** gave **19**, which could be alkylated by either *trans*-1,4-dichloro-2-butene, affording precursor **1***a* [T–T], by the usual sequence or by 1,4-dichloro-2-butyne to give **23**, which was then converted to precursor **1***a* [T–A].

The last possible precursor was the one containing two triple bonds. 2-Butyne-1,4-diol was chosen as the starting material and afforded, after monochlorination (16) and alcohol protection, acetylene **28**. Three subsequent alkylations transformed **28** into tetraester **31**, which was readily converted to precursor **1***a* [A–A].[2]

The cyclization runs were carried out in a mixture of *N*,*N*-dimethylformamide and tetrahydrofuran with excess potassium carbonate at either 2×10^{-2} or 2×10^{-3} molar concentrations and without the use of high dilution techniques. The results are listed in Table 1. Monomer yields vary from 10 to 84% depending on the nature and geometry of the unsaturations, and the effect of concentration is important in most cases. Interestingly, yields as high as 42% were observed in the formation of cyclic dimers, showing that 20-membered ring cyclization is an important secondary process that can be even more important than polymerization, in some cases.

Molecular model examination of the cyclization process shows that one of the carbomethoxy groups in the middle of the chain must take an orientation (e.g. pseudo-axial in the case of [A–A]) generating unfavorable steric interactions that could be stronger than the favorable *gem*-dimethyl effect (17).[3] This could be demonstrated by comparing cyclization results for decarbomethoxylated precursors **1***b* (Scheme 1) with those obtained for tetraesters **1***a*.

The preparation of precursors **1***b* is detailed in Scheme 3. The previously prepared malonate **29** was alkylated with chloride **33** affording **34**, which after selective deprotection was decarbomethoxylated using Krapcho's procedure (18) at a relatively low temperature. The resulting propargylic alcohol **36** was readily converted to **1***b* [A–A] following the usual sequence.

Decarbomethoxylation prior to alkylation of malonate **7** provided a shorter route to precursors **1***b*. 1,4-Dibromo-2-

[1]NSERCC and FCAR predoctoral fellowships, 1983–1987.

[2]For preparation of a similar compound see ref. 7.

[3]Although the *gem*-dimethyl effect is known (17) to be small in saturated 10-membered ring formation, we believed that it could be stronger in the case of unsaturated substrates because of a larger degree of conformational restriction.

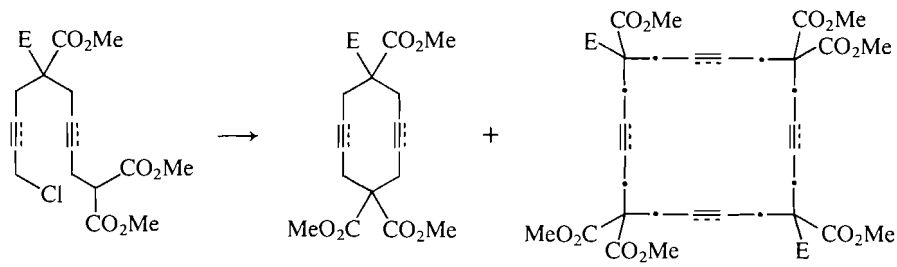

1*a* E = CO_2Me **2***a* E = CO_2Me **3***a* E = CO_2Me
1*b* E = H **2***b* E = H **3***b* E = H

≡ Represents double bond [*cis* (C) or *trans* (T)] or acetylene (A)

SCHEME 1

butyne was used to alkylate monoester **40** affording bromide **41**, which was converted in 3 steps to precursor **1***b* [C–A].

The same sequence using *trans* malonate **19** afforded *trans*-acetylene precursor **1***b* [T–A]. Alkylation of monoester **44** with *trans*-1,4-dibromo-2-butene afforded allylic bromide **50**, which was readily transformed into precursor **1***b* [T–T]. Finally, partial hydrogenation of intermediate **46** with Lindlar catalyst provided direct access to precursor **1***b* [T–C].

Triesters **1***b* were submitted to the same reaction conditions as tetraesters **1***a* (Table 2). The results clearly indicate that within experimental error most cyclization processes are not influenced by the removal of one carbomethoxy group. Two isolated cases (entries 2 and 10) give respectively much more monomer and dimer than the corresponding tetraesters but we found no consistent explanation to rationalize these facts. However, detailed molecular model studies could perhaps provide an explanation.

The 10-membered ring is one of the most difficult to synthesize by way of direct cyclization (9, 17). The above results show that suitably functionalized precursors can provide respectable yields of cyclic monomers even without the use of high dilution techniques. It has already been proven in our laboratory that this method can be extended to the preparation of large rings (1*a*,*b*). Progress is now being made in the synthesis of polycyclic molecules from macrocyclic precursors available by the above cyclization method.

TABLE 1. Cyclization results for tetraesters **1***a*

Entry	Compound	Time (h)	*M*	% Monomer **2***a*	% Dimer **3***a*
1	[A–A]	12	2×10^{-2}	26	40
2			2×10^{-3}	39	12
3	[C–A]	24	2×10^{-2}	60	17
4			2×10^{-3}	73	9
5	[T–A]	26	2×10^{-2}	17	35
6			2×10^{-3}	57	15
7	[T–C]	32	2×10^{-2}	44	25
8	[T–T]	26	2×10^{-2}	10	42
9			2×10^{-3}	43	13
10	[C–C]*	96	2×10^{-2}	84	—

*K_2CO_3/acetone, reflux.

TABLE 2. Cyclization results for triesters **1***b*

Entry	Compound	Time (h)	*M*	% Monomer	% Dimer*
1	[A–A]	16	2×10^{-2}	26	42
2			2×10^{-3}	70	13
3	[C–A]	24	2×10^{-2}	53	27
4			2×10^{-3}	80	9
5	[T–A]	24	2×10^{-2}	29	48
6			2×10^{-3}	68	28
7	[T–C]	38	2×10^{-2}	29	42
8			2×10^{-3}	69	9
9	[T–T]	24	2×10^{-2}	12	41
10			2×10^{-3}	41	42

**Cis–trans* mixture.

Experimental

All reactions were carried out under an argon atmosphere. The infrared spectra (ir) were taken on a Perkin–Elmer 681 spectrophotometer. Proton nmr spectra were recorded on a Varian EM-360, Bruker WP-60, Bruker WP-80 SY, or Bruker WP-250 instrument. Carbon nmr spectra were recorded on a Bruker WP-80SY instrument. Mass spectral assays (ms *m*/*e*) and peak matching were obtained using a VG Micromass ZAB-1F spectrometer. Chromatographic separations were made using Merck Kieselgel 60 (230–400 mesh ASTM). Chemical shifts are reported in δ values relative to tetramethylsilane. Abbreviations used are m: multiplet, s: singlet, t: triplet, d: doublet, dt: double triplets, app: apparent, br: broad, qc: quaternary carbon. No attempts were made to optimize the yields of most reactions.

Mono-protected diol **5**

To an ice-cooled solution of diol **4** (9.9 g; 114 mmol) and dihydropyran (9.6 g, 114 mmol) in 100 mL of methylene chloride and 250 mL of tetrahydrofuran was added *p*-toluenesulfonic acid (1.5 g) with vigorous stirring. After 90 min the mixture was allowed to warm up to room temperature and stirred an additional 90 min. Aqueous sodium bicarbonate (50 mL) was added to the mixture, and the water layer was separated and extracted with ether (2 × 75 mL). The combined organic layers were dried over sodium sulfate, filtered, and concentrated to give an oily residue that was purified by column chromatography (3% acetone in dichloromethane) to afford mono-protected diol **5** (10.4 g, 53%); ir (neat): 3400, 2945, 1120, 1030 cm^{-1}; nmr ($CDCl_3$) δ: 6.20–5.50 (2H, m, —CH=CH—), 4.90–4.60 (1H, m, O—CH—O), 4.60–3.30 (6H, m, —CH_2—CH_2—O and =C—CH_2—O), 2.75 (1H, s, -OH), 2.10–1.10 (6H, m, —$(CH_2)_3$—CH_2O); ms *m*/*e* (CI, CH_4): 173 (M^+ + 1).

Chloride **6** (Procedure A)

A stirred mixture of alcohol **5** (6.88 g, 40 mmol), *syn*-collidine (5.33 g, 44 mmol), and lithium chloride (1.70 g, 40 mmol) was dissolved in 60 mL of *N*,*N*-dimethylformamide. On cooling to 0°C, a suspension was formed, which was treated dropwise with methanesulfonyl chloride (3.41 mL, 44 mmol). Stirring was continued at 0°C for 15 min, then at room temperature for 1 h. The yellow reaction mixture was poured over ice-water (300 mL) and extracted with

Can. J. Chem. Downloaded from www.nrcresearchpress.com by 78.46.186.204 on 09/07/12
For personal use only.

Can. J. Chem. Downloaded from www.nrcresearchpress.com by 78.46.186.204 on 09/07/12
For personal use only.

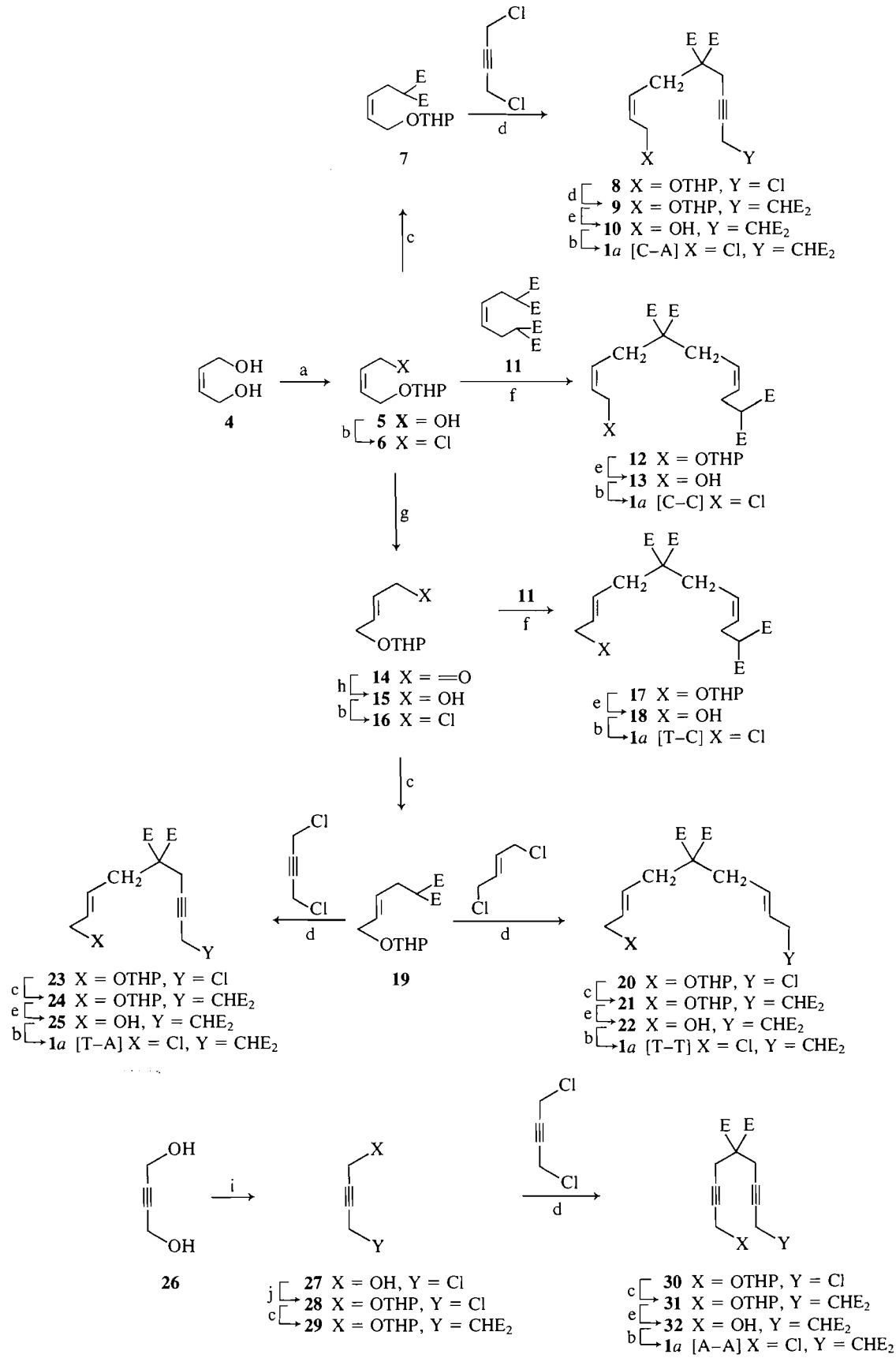

(a) DHP, PTSA, CH_2Cl_2–THF; (b) LiCl, MsCl, collidine, DMF; (c) $CH_2(CO_2Me)_2$, K_2CO_3, DMF–THF; (d) K_2CO_3, DMF–THF; (e) PPTS, MeOH; (f) sodium *tert*-amylate, benzene; (g) PCC, ACONa, CH_2Cl_2, molecular sieves 4Å; (h) DIBA-H, CH_2Cl_2; (i) $SOCl_2$, Py, benzene; (j) DHP, CF_3CO_2H, CH_2Cl_2

SCHEME 2

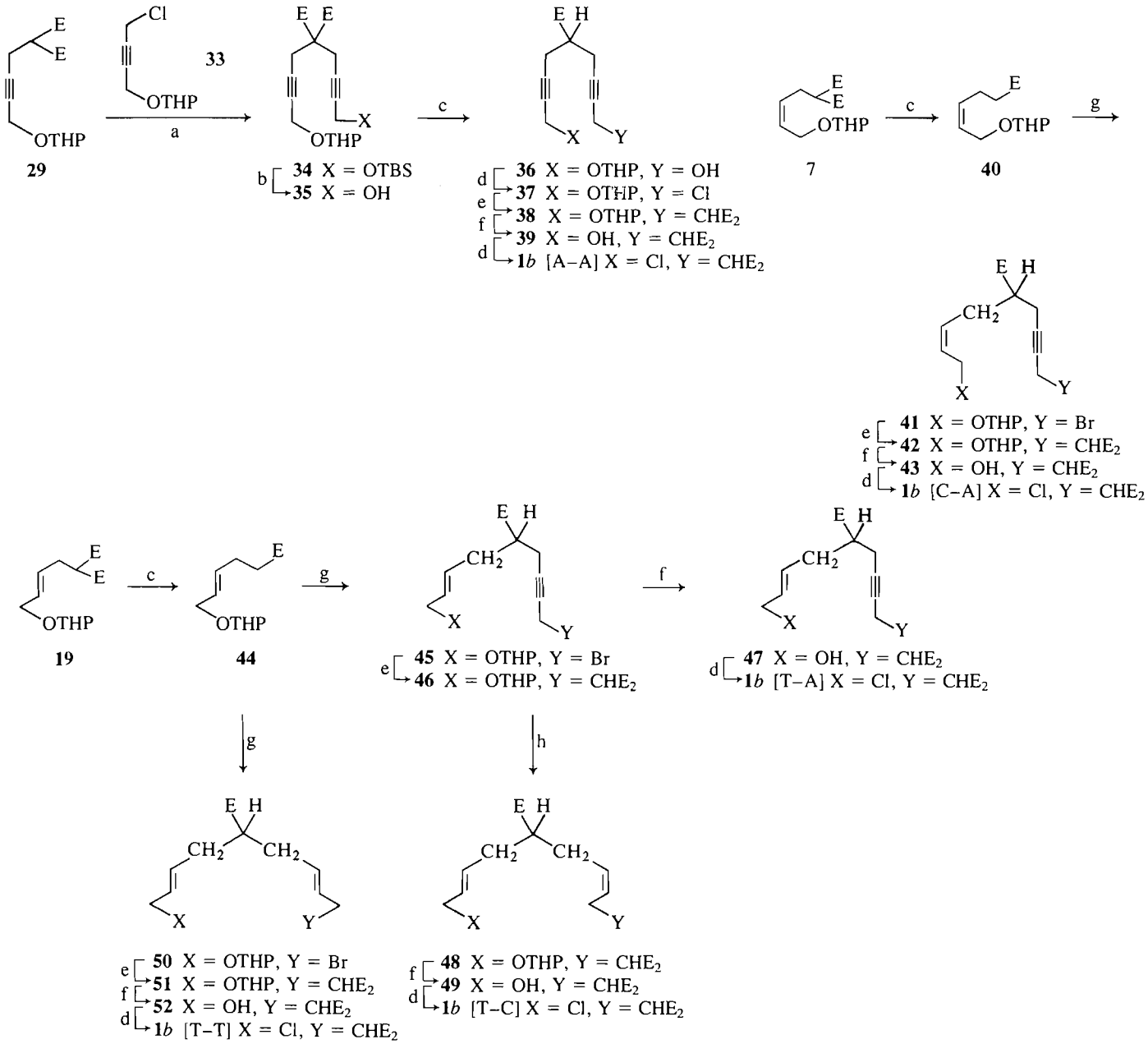

(a) K_2CO_3, DMF–THF; (b) *n*-Bu_4NF, THF; (c) NaCN, DMSO, H_2O; (d) LiCl, MsCl, collidine, DMF; (e) $CH_2(CO_2Me)_2$, K_2CO_3, DMF–THF; (f) PPTS, MeOH; (g) *i*: LDA, THF; *ii*: 1,4-dibromobutyne or 1,4-dibromobutene

SCHEME 3

ether–*n*-hexane (1:1, 2 × 300 mL). The combined extracts were washed successively with saturated aqueous copper nitrate solution to remove excess collidine, then with brine, and finally dried over sodium sulfate. Concentration followed by vacuum distillation (105–108°C/1 Torr; 1 Torr = 133.3 Pa) afforded chloride **6** (6.35 g, 83%) as a colorless oil; ir (neat): 2940, 1134, 1120, 1070, and 1030 cm^{-1}; nmr ($CDCl_3$) δ: 6.30–5.70 (2H, m, —CH=CH—), 5.10–4.65 (1H, m, O—CH—O), 4.65–3.30 (6H, m, CH_2—CH_2—O, =C—CH_2O, and =C—CH_2—Cl), 2.20–1.20 (6H, m, —$(CH_2)_3$—CH_2O); ms *m/e* (CI, CH_4): 191 (M^+(^{35}Cl) + 1), 193 (M^+(^{37}Cl) + 1), relative intensity 3:1.

Malonate 7 (Procedure B)

To a stirred solution of chloride **6** (3.36 g, 17.7 mmol) and dimethylmalonate (11.7 g, 88.2 mmol) in 60 mL of a 1:1 mixture of *N,N*-dimethylformamide and tetrahydrofuran was added dry potassium carbonate (12.2 g, 88.2 mmol). The resulting mixture was heated to reflux (oil bath temperature ≈90°C) for 13 h. The cooled reaction mixture was filtered through a short pad of Celite and the filtrate was concentrated at room temperature to ≈2 mL of volume. The residue was dissolved in 50 mL of dichloromethane, washed with water, and dried over sodium sulfate, giving, after concentration, a crude oil that was purified by column chromatography (2% acetone in dichloromethane) to afford malonate **7** (4.51 g, 89%); ir (neat): 2955, 1757, 1740, 1275–1120, 1028 cm^{-1}; nmr ($CDCl_3$) δ: 5.99–5.15 (2H, m, —CH=CH—), 4.40–4.80 (1H, m, —OCHO—), 4.17 (2H, app t, *J* = 4.5 Hz, =C—CH_2—O), 3.71 (6H, s, -CO_2Me), 4.02–3.24 (3H, m, -CH($CO_2Me)_2$ and CH_2—CH_2—O), 2.68 (2H, app t, *J* = 7.2 Hz, —CH_2—C($CO_2Me)_2$), 1.95–1.26 (6H, m, —$(CH_2)_3$—CH_2O); ms *m/e* (70 eV): 286 (M^+).

Chloride 8

Using procedure B, malonate **7** (2.86 g, 10 mmol) afforded, after column chromatography (1% acetone in dichloromethane), chloride **8** (2.05 g, 70%, based on 22% starting material recovered); ir (neat): 2955, 1740, 1440, 1210, 1028 cm^{-1}; nmr ($CDCl_3$) δ: 6.06–4.91 (2H,

Can. J. Chem. Downloaded from www.nrcresearchpress.com by 78.46.186.204 on 09/07/12
For personal use only.

Can. J. Chem. Downloaded from www.nrcresearchpress.com by 78.46.186.204 on 09/07/12
For personal use only.

m, —CH=CH—), 4.73–4.44 (1H, m, O—CH—O), 4.09 (2H, t, J = 2.3 Hz, —CH_2—Cl), 3.74 (6H, s, -CO_2Me), 4.44–3.31 (4H, m, CH_2—CH_2—O and =C—CH_2—O), 2.84 (2H, t, J = 2.3 Hz, ≡C—CH_2—), 2.97–2.59 (2H, m, =C—CH_2—C), 2.08–1.19 (6H, m, —$(CH_2)_3$—CH_2O); ms m/e (CI, CH_4): 373 (M^+(^{35}Cl) + 1), 375 (M^+)^{37}Cl) + 1), ratio 3:1.

Tetraester ***9***

Using procedure B, chloride **8** (1.94 g, 5.2 mmol) afforded, after column chromatography (2% acetone in dichloromethane), tetraester **9** (2.08 g, 85%); ir (neat): 2950, 1760–1730, 1440, 1205, 1028 cm^{-1}; nmr ($CDCl_3$) δ: 6.07–5.04 (2H, m, —CH=CH—), 4.75–4.45 (1H, m, O—CH—O), 4.21 (2H, app dt, J = 4.0 and 1.1 Hz, =C—CH_2—O), 3.76 (6H, s, $R_2C(CO_2Me)_2$), 3.72 (6H, s, -$CH(CO_2Me)_2$), 3.53 (1H, t, J = 7.0 Hz, -$CH(CO_2Me)_2$), 4.04–3.24 (2H, m, =C—CH_2—O), 3.04–2.48 (6H, m, =C—CH_2— and —CH_2—C≡C—CH_2—), 1.99–1.17 (6H, m, —$(CH_2)_3$—CH_2O); ms m/e (70 eV): 468 (M^+).

Alcohol ***10*** (Procedure C)

To a stirred solution of tetraester **9** (1.90 g, 4.1 mmol) in 75 mL of methanol was added pyridinium tosylate (102 mg, 0.41 mmol). The resulting mixture was stirred at room temperature for 24 h and then concentrated. The residue was subjected to column chromatography (2–10% acetone in dichloromethane) to afford alcohol **10** (1.43 g, 91%); ir (neat): 3500, 2960, 1760–1730, 1440, 1210, 1025 cm^{-1}; nmr ($CDCl_3$) δ: 6.18–4.91 (2H, m, —CH=CH—), 4.21 (2H, t, J = 6.0 Hz, —CH_2—OH), 3.77 (6H, s, $R_2C(CO_2Me)_2$), 3.73 (6H, s, -$CH(CO_2Me)_2$), 3.54 (1H, t, J = 7.0 Hz, -$CH(CO_2Me)_2$), 3.07–2.60 (6H, m, =C—CH_2—C and —CH_2—C≡$CH(CO_2Me)_2$), 1.82 (1H, t, J = 6.0 Hz, -OH); ms m/e (20 eV): 385 (M^+ + 1), 384 (M^+), 383 (M^+ − 1).

Precursor ***1****a* [C–A]

Following procedure A, alcohol **10** (1.40 g, 3.6 mmol) gave, after column chromatography (1% acetone in dichloromethane), pure chloride ***1a*** [C–A] (1.39 g, 95%); ir (neat): 2955, 1763–1730, 1440, 755 cm^{-1}; nmr ($CDCl_3$) δ: 6.05–5.10 (2H, m, —CH=CH—), 4.12 (2H, d, J = 7.4 Hz, —CH_2—Cl), 3.76 (6H, s, $R_2C(CO_2Me)_2$), 3.73 (6H, s, -$CH(CO_2Me)_2$), 3.52 (1H, t, J = 6.9 Hz, -$CH(CO_2Me)_2$), 2.95–2.34 (6H, m, =C—CH_2—C and —CH_2—C≡C—CH_2—); ms m/e (CI, CH_4): 403 (M^+(^{35}Cl) + 1), 405 (M^+(^{37}Cl) + 1) ratio 3:1.

Tetraester ***11***

1,1,6,6-Tetracarbomethoxy-3-hexyne, prepared following Johnson's method (16*a*) (2.75 g, 8.8 mmol), was dissolved in 20 mL of benzene. Quinoline (0.2 mL) and 5% Pd/$BaSO_4$ (550 mg) were added and the reaction mixture was stirred under hydrogen atmosphere until about 200 mL of hydrogen had been consumed. The reaction mixture was filtered on a short pad of Celite and concentrated to give tetraester **11** (2.75 g, 99%); ir (neat): 2955, 1750, 1730, 1440, 1240, 1160, 1030 cm^{-1}; nmr ($CDCl_3$) δ: 5.80–5.20 (2H, m, —CH=CH—), 3.80 (12H, s, -CO_2Me), 3.45 (2H, t, J = 7.5 Hz, -$CH(CO_2Me)_2$), 3.10–2.35 (4H, m, —CH_2—); ms m/e (70 eV): 316 (M^+).

Tetraester ***12*** (Procedure D)

To a stirred solution of sodium *tert*-amylate (5.0 mg, 5.4 mmol) in 5 mL of benzene was added tetraester **11** (1.27 g, 4.0 mmol) in 10 mL of benzene, followed by chloride **6** (768 mg, 4.0 mmol) in 10 mL of benzene. The resulting mixture was heated to reflux for 4.5 h. On cooling down, 20 mL of ether and 10 mL of a saturated aqueous NH_4Cl solution were poured into the reaction mixture. The organic layer was washed with brine, dried over sodium sulfate, and evaporated to give an oily residue that was purified by column chromatography (1% acetone in dichloromethane) to give tetraester **12** (588 mg, 31%); ir (neat): 2950, 1750, 1740, 1730, 1440, 1290–1120, 1030 cm^{-1}; nmr ($CDCl_3$) δ: 6.10–5.00 (4H, m, —CH=CH—), 4.84–4.54 (1H, m, O—CH—O), 3.80 (12H, s, -CO_2Me), 4.40–3.14 (5H, m, CH_2—CH_2—O, =C—CH_2—O, and -$CH(CO_2Me)_2$), 3.14–2.27 (6H, m, =C—CH_2—C), 2.07–1.10 (6H, m, —$(CH_2)_3$—CH_2O); ms m/e (CI, CH_4): 470 (M^+ + 1).

Alcohol ***13***

Following procedure C, tetraester **12** (550 mg, 1.2 mmol) gave, after column chromatography, alcohol **13** (433 mg, 96%); ir (neat): 3540, 1735, 1440, 1290–1208–1160 cm^{-1}; nmr ($CDCl_3$) δ: 6.10–4.90 (4H, m, —CH=CH—), 4.20 (2H, d, J = 6.0 Hz, —CH_2—OH), 3.80 (12H, s, -CO_2Me), 3.45 (1H, t, J = 7.0 Hz, -$CH(CO_2Me)_2$), 2.90–2.20 (7H, m, =C—CH_2—C and -OH); ms m/e (70 eV): 386 (M^+).

Precursor ***1****a* [C–C]

Following procedure A, alcohol **13** (386 mg, 1.0 mmol) afforded, after column chromatography (2% acetone in dichloromethane), pure ***1a*** [C–C] (403 mg, 100%); ir (neat): 2950, 1760–1720, 1440, 1300–1150, 750 cm^{-1}; nmr ($CDCl_3$) δ: 6.20–5.20 (4H, m, —CH=CH—), 4.20 (2H, d, J = 7.0 Hz, —CH_2—Cl), 3.82 (12H, s, -CO_2Me), 3.50 (1H, t, J = 7.5 Hz, -$CH(CO_2Me)_2$), 3.03–2.45 (6H, m, =C—CH_2—C); ms m/e (CI, CH_4): 405 (M^+(^{35}Cl) + 1), 407 (M^+(^{37}Cl) + 1), ratio 3:1.

Alcohol ***15***

Aldehyde **14** (1.1 g, 6.5 mmol), prepared according to Corey's procedure (15), was dissolved in 15 mL of methylene chloride at −78°C. DIBAH (7.1 mmol, 1 *M* in cyclohexane) was added dropwise and the mixture was stirred for 40 min after which it was quenched with 5 mL of aqueous saturated NH_4Cl solution, allowed to warm up to room temperature, and stirred for 40 min. After diluting with 50 mL of ether, the mixture was filtered through Celite and the water layer was extracted with ether (2 × 20 mL). The combined organic layers were washed with brine, dried over sodium sulfate, and concentrated to give an oily residue that was passed through a short column of silica gel (10% acetone in dichloromethane) to afford alcohol **15** (994 mg, 89%); ir (neat): 3610, 3440, 3010, 2950, 2870, 1020 cm^{-1}; nmr ($CDCl_3$) δ: 6.1–5.6 (2H, m, —CH=CH—), 5.0–3.0 (7H, m, CH_2—CH_2—O, —CH_2—OH, —CH_2—OTHP, and —OCHO—), 2.55 (1H, s, -OH), 2.70–0.70 (6H, m, —$(CH_2)_3$—CH_2O).

Chloride ***16***

Using procedure A, alcohol **15** (1.79 g, 10.4 mmol) gave, after column chromatography (1% acetone in dichloromethane), chloride **16** (1.98 g, 100%); ir (neat): 2940, 1135, 1125, 1078, 1040, 1025, 965 cm^{-1}; nmr ($CDCl_3$) δ: 6.40–5.60 (2H, m, —CH=CH—), 4.95–4.60 (1H, m, O—CH—O), 4.60–3.30 (6H, m, CH_2—CH_2—O, =C—CH_2—O, and —CH_2—Cl), 2.45–0.80 (6H, m, —$(CH_2)_3$—CH_2O); ms m/e (CI, CH_4): 191 (M^+(^{35}Cl) + 1), 193 (M^+(^{37}Cl) + 1), ratio 3:1.

Tetraester ***17***

Following procedure D, tetraester **11** (2.25 g, 7.1 mmol) and chloride **16** (686 mg, 3.6 mmol) afforded, after column chromatography (2% acetone in dichloromethane), tetraester **17** (638 mg, 38%); ir (neat): 2950, 1740, 1440, 1290–1205–1120, 1040, 1028 cm^{-1}; nmr ($CDCl_3$) δ: 6.00–5.30 (4H, m, —CH=CH—), 4.95–4.55 (1H, m, O—CH—O), 3.85 (6H, s, $R_2C(CO_2Me)_2$), 3.82 (6H, s, -$CH(CO_2Me)_2$), 3.48 (1H, t, J = 7.0 Hz, -$CH(CO_2Me)_2$), 4.55–3.20 (4H, m, CH_2—CH_2—O and =C—CH_2—O), 3.00–2.45 (6H, m, =C—CH_2—C), 2.05–1.10 (6H, m, —$(CH_2)_3$—CH_2O); ms m/e (CI, CH_4): 471 (M^+ + 1).

Alcohol ***18***

Following procedure C, tetraester **17** (630 mg, 1.3 mmol) gave, after chromatographic separation (10% acetone in dichloromethane), pure alcohol **18** (490 mg, 95%); ir (neat): 3500, 2955, 1735, 1440, 1340, 1280–1210–1180, 975 cm^{-1}; nmr ($CDCl_3$) δ: 6.00–5.28 (4H, m, —(CH=CH—), 4.20 (2H, d, J = 4.0 Hz, —CH_2—OH), 3.83 (12H, s, -CO_2Me), 3.50 (1H, t, J = 7.0 Hz, -$CH(CO_2Me)_2$), 3.10–2.48 (6H, m, =C—CH_2—C), 2.02 (1H, s, -OH); ms m/e (CI, CH_4): 387 (M^+ + 1), 386 (M^+), 385 (M^+ − 1).

Precursor ***1****a* [T–C]

Using procedure A, alcohol **18** (480 mg, 1.2 mmol) afforded, after column chromatography (1% acetone in dichloromethane), pure chloride ***1a*** [T–C] (450 mg, 90%); ir (neat): 2960, 1760–1730, 1440, 1345, 1285–1210–1160, 974 cm^{-1}; nmr ($CDCl_3$) δ: 6.10–5.30 (4H, m, —CH=CH—), 4.13 (2H, d, J = 5.5 Hz, —CH_2—Cl), 3.85 (12H, s, -CO_2Me), 3.52 (1H, t, J = 8.0 Hz, -$CH(CO_2Me)_2$),

Can. J. Chem. Downloaded from www.nrcresearchpress.com by 78.46.186.204 on 09/07/12
For personal use only.

3.10–2.38 (6H, m, =C—CH_2—C); ms *m/e* (CI, CH_4): 405 ($M^+(^{35}Cl)$ + 1), 407 ($M^+(^{37}Cl)$ + 1), ratio 3:1.

Malonate ***19***

Using procedure B, chloride **16** (800 mg, 4.2 mmol) and dimethyl malonate (2.77 g, 21.0 mmol) afforded, after column chromatography (2% acetone in dichloromethane), malonate **19** (1.08 g, 90%); ir (neat): 2950, 1755, 1740, 1440, 1155, 1025 cm^{-1}; nmr ($CDCl_3$) δ: 6.00–5.66 (2H, m, —CH=CH—), 4.93–4.56 (1H, m, O—CH—O), 3.83 (6H, s, -CO_2Me), 3.58 (1H, t, *J* = 7.5 Hz, -CH($CO_2Me)_2$), 4.56–3.33 (4H, m, CH_2—CH_2—O and =C—CH_2—O), 2.93–2.53 (2H, m, —CH_2—$C(CO_2Me)_2$), 2.03–1.23 (6H, m, —$(CH_2)_3$—CH_2O): ms *m/e* (CI, CH_4): 287 (M^+ + 1).

Chloride ***20***

Malonate **19** (4.0 g, 14.0 mmol) and *trans*-1,4-dichlorobut-2-ene (98% *trans*, 5.25 g, 42.0 mmol) were treated according to procedure B, yielding, after column chromatography (2% acetone in dichloromethane), chloride **20** (2.50 g, 45%) along with 50% recovered malonate **19**; ir (neat): 2950, 1740, 1732, 1440, 1205, 1025 cm^{-1}; nmr ($CDCl_3$) δ: 6.25–5.35 (4H, m, —CH=CH—), 4.90–4.55 (1H, m, O—CH—O), 3.82 (6H, s, -CO_2Me), 4.55–3.30 (6H, m, CH_2—CH_2—O, —CH_2—Cl, and —CH_2—OTHP), 2.90–2.50 (4H, m, —CH_2—$C(CO_2Me)_2$), 2.00–1.30 (6H, m, —$(CH_2)_3$—CH_2O); ms *m/e* (CI, CH_4): 375 ($M^+(^{35}Cl)$ + 1), 377 ($M^+(^{37}Cl)$ + 1), ratio 3:1.

Alcohol ***22***

Following procedure B, chloride **20** (1.80 g, 4.8 mmol) and dimethyl malonate (2.64 g, 20.0 mmol) gave, after work-up, crude malonate **21** (2.1 g), which was treated according to procedure C to afford, after column chromatography (5–20% acetone in dichloromethane), alcohol **22** (1.5 g, 81% overall); ir (neat): 3500, 2955, 1755–1725, 1440, 1280–1160, 975 cm^{-1}; nmr ($CDCl_3$) δ: 5.82–5.27 (4H, m, —CH=CH—), 4.07 (2H, t, *J* = 4.7 Hz, —CH_2—OH), 3.74 (6H, s, $R_2C(CO_2Me)_2$), 3.71 (6H, s, -CH($CO_2Me)_2$), 3.40 (1H, t, *J* = 7.2 Hz, -CH($CO_2Me)_2$), 2.80–2.40 (6H, m, =CH_2—C), 1.72–1.16 (1H, br s, -OH); ms *m/e* (70 eV): 386 (M^+).

Precursor ***1***a [T–T]

Following procedure A, alcohol **22** (1.0 g, 2.6 mmol) afforded, after column chromatography (1% acetone in dichloromethane), precursor **1***a* [T–T] (1.0 g, 94%); ir (neat): 2950, 1755–1727, 1438, 1340, 1275–1160, 972 cm^{-1}; nmr ($CDCl_3$) δ: 5.99–5.16 (4H, m, —CH=CH—), 3.98 (2H, app d, *J* = 6.1 Hz, —CH_2—Cl), 3.74 (6H, s, $R_2C(CO_2Me)_2$), 3.72 (6H, s, -CH($CO_2Me)_2$), 3.39 (1H, t, *J* = 7.5 Hz, -CH($CO_2Me)_2$), 3.03–2.21 (6H, m, =C—CH_2—C): ms *m/e* (20 eV): 405 ($M^+(^{35}Cl)$ + 1), 407 ($M^+(^{37}Cl)$ + 1), ratio 3:1.

Chloride ***23***

Using procedure B, malonate **19** (970 mg, 3.4 mmol) and 1,4-dichloro-2-butyne (2.1 g, 17.0 mmol) gave, after column chromatography (2% acetone in dichloromethane), chloride **23** (927 mg, 73%); ir (neat): 1740, 1210, 1200, 1023 cm^{-1}; nmr ($CDCl_3$) δ: 6.00–5.20 (2H, m, —CH=CH—), 4.84–4.45 (1H, m, O—CH—O), 4.09 (2H, t, *J* = 2.3 Hz, —CH_2—Cl), 3.75 (6H, s, -CO_2Me), 4.39–3.41 (4H, m, CH_2—CH_2—O and =C—CH_2—O—), 3.12–2.57 (4H, m, —CH_2—$C(CO_2Me)_2$), 2.20–1.20 (6H, m, —$(CH_2)_3$—CH_2O); ms *m/e* (70 eV): 373 ($M^+(^{35}Cl)$ + 1), 375 ($M^+(^{37}Cl)$ + 1), ratio 3:1.

Malonate ***24***

Chloride **23** (896 mg, 2.4 mmol) was treated according to procedure B, affording, after column chromatography (2% acetone in dichloromethane), malonate **24** (1.1 g, 94%); ir (neat): 2955, 1760–1730, 1438, 1280–1116, 1038, 1032, 1024 cm^{-1}; nmr ($CDCl_3$) δ: 5.94–5.14 (2H, m, —CH=CH—), 4.91–4.41 (1H, m, O—CH—O), 3.99 (2H, t, *J* = 5.2 Hz, —CH_2—Cl), 3.73 (6H, s, $R_2C(CO_2Me)_2$), 3.68 (6H, s, -CH($CO_2Me)_2$), 4.36–3.22 (5H, m, CH_2—CH_2—O, -CH($CO_2Me)_2$), and —CH_2—OTHP), 3.07–2.32 (6H, m, —CH_2—$C(CO_2Me)_2$)—CH_2— and —CH_2—CH), 2.04–0.81 (6H, m, —$(CH_2)_3$—CH_2O); ms *m/e* (70 eV): 468 (M^+).

Alcohol ***25***

Following procedure C, malonate **24** (1.02 g, 2.2 mmol) gave, after column chromatography (5–10% acetone in dichloromethane), alcohol **25** (783 mg, 94%); ir (neat): 3500, 1758–1730, 1440, 1338, 1280–1150 cm^{-1}; nmr ($CDCl_3$) δ: 6.03–5.18 (2H, m, —CH=CH—), 4.34–3.92 (2H, m, —CH_2—OH), 3.76 (6H, s, $R_2C(CO_2Me)_2$), 3.71 (6H, s, -CH($CO_2Me)_2$), 3.51 (1H, t, *J* = 7.2 Hz, -CH($CO_2Me)_2$), 2.99–2.41 (6H, m, C—CH_2—C), 2.09–1.39 (1H, br s, -OH); ms *m/e* (70 eV): 384 (M^+).

Precursor ***1***a [T–A]

Treatment of alcohol **25** (780 mg, 2.0 mmol) according to procedure A afforded, after column chromatography (2% acetone in dichloromethane), precursor **1***a* [T–A] (780 mg, 95%); ir (neat): 2960, 1760–1732, 1440, 1343, 1287–1152 cm^{-1}; nmr ($CDCl_3$) δ: 6.04–5.29 (2H, m, —CH=CH—), 3.99 (2H, d, *J* = 5.7 Hz, —CH_2—Cl), 3.77 (6H, s, $R_2C(CO_2Me)_2$), 3.72 (6H, s, -CH($CO_2Me)_2$), 3.53 (1H, t, *J* = 7.3 Hz, -CH($CO_2Me)_2$), 2.88–2.54 (6H, m, C—CH_2—C); ms *m/e* (CI, CH_4): 403 ($M^+(^{35}Cl)$ + 1) and 405 ($M^+(^{37}Cl)$ + 1), ratio 3:1.

Chloride ***28***

Known alcohol **27** (16*b*) (18.3 g, 175 mmol) and dihydropyran (16.2 g, 192 mmol) were dissolved in 400 mL of dichloromethane at 0°C. Trifluoroacetic acid (200 μL) was added to the mixture, which was stirred overnight at room temperature and concentrated to afford chloride **28** (31.6 g, 95%); ir (neat): 2943, 1264, 1120, 1025 cm^{-1}; nmr ($CDCl_3$) δ: 4.77 (1H, br s, O—CH—O), 4.29 (2H, t, *J* = 2.0 Hz, —CH_2—OTHP), 4.17 (2H, t, *J* = 2.0 Hz, —CH_2—Cl), 4.08–3.26 (2H, m, CH_2—CH_2—O), 2.68–0.69 (6H, m, —$(CH_2)_3$—CH_2O); ms *m/e* (70 eV): 187 ($M^+(^{35}Cl)$ − 1) 189 ($M^+(^{37}Cl)$ − 1), ratio 3:1.

Malonate ***29***

Crude chloride **28** (3.05 g, 16.2 mmol) and dimethyl malonate (10.69 g, 81.0 mmol) were treated according to procedure B to afford, after column chromatography (1–2% acetone in dichloromethane), malonate **29** (4.18 g, 91%); ir (neat): 2955, 1757, 1748, 1740, 1440, 1024 cm^{-1}; nmr ($CDCl_3$) δ: 4.71 (1H, br s, O—CH—O), 4.15 (2H, t, *J* = 2.1 Hz, —CH_2—OTHP), 3.71 (6H, s, $(CO_2Me)_2$), 3.92–3.24 (3H, m, -CH($CO_2Me)_2$ and CH_2—CH_2—O), 2.76 (2H, dt, *J* = 7.8 and 2.1 Hz, -CH_2—$CH(CO_2Me)_2$), 1.93–1.29 (6H, m, —$(CH_2)_3$—CH_2O); ms *m/e* (70 eV): 285 (M^+ + 1), 284 (M^+), 283 (M^+ − 1).

Chloride ***30***

Reaction of malonate **29** (3.0 g, 10.6 mmol) and 1,4-dichloro-2-butyne (6.50 g, 52.8 mmol) using procedure B gave, after column chromatography (1% acetone in dichloromethane), chloride **30** (2.33 g, 60%); ir (neat): 2950, 1742, 1435, 1205, 1024 cm^{-1}; nmr ($CDCl_3$) δ: 4.77 (1H, br s, O—CH—O), 4.21 (2H, t, *J* = 2.2 Hz, —CH_2—OTHP), 4.08 (2H, t, *J* = 2.2 Hz, —CH_2—Cl), 3.76 (6H, s, —$(CO_2Me)_2$), 4.04–3.39 (2H, m, CH_2—CH_2—O), 3.22–2.87 (4H, m, —CH_2—$C(CO_2Me)_2$—CH_2—), 2.04–1.27 (6H, m, —$(CH_2)_3$—CH_2O); ms *m/e* (10 eV): 371 ($M^+(^{35}Cl)$ + 1), 373 ($M^+(^{37}Cl)$ + 1), ratio 3:1.

Tetraester ***31***

Following procedure B, chloride **30** (2.10 g, 5.7 mmol) and dimethyl malonate (3.74 g, 28.4 mmol) afforded, after column chromatography (1% acetone in dichloromethane), tetraester **31** (2.45 g, 93%); ir (neat): 2953, 1762, 1733, 1438, 1021 cm^{-1}; nmr ($CDCl_3$) δ: 4.75 (1H, br s, O—CH—O), 4.20 (2H, t, *J* = 2.2 Hz, —CH_2—OTHP), 3.77 (6H, s, $R_2C(CO_2Me)_2$), 3.74 (6H, s, -CH($CO_2Me)_2$), 3.91–3.20 (3H, m, -CH($CO_2Me)_2$ and CH_2—CH_2—O), 3.06–2.53 (6H, m, ≡C—CH_2—C), 1.94–1.19 (6H, m, —$(CH_2)_3$—CH_2O); ms *m/e* (70 eV): 466 (M^+), 465 (M^+ − 1).

Alcohol ***32***

Using procedure C, tetraester **31** (2.36 g, 5.1 mmol) gave, after column chromatography (2–5% acetone in dichloromethane), alcohol **32** (1.83 g, 94%); ir (neat): 3500, 1745, 1440, 1345–1150 cm^{-1}; nmr ($CDCl_3$) δ: 4.20 (2H, dt, *J* = 6.1 and 2.1 Hz, -CH_2—OH), 3.77 and 3.74 (12H, both s, -CO_2Me), 3.53 (1H, t, *J* = 7.5 Hz, -CH($CO_2Me)_2$), 3.10–2.60 (6H, m, ≡C—CH_2—C), 1.92 (1H, t, *J* = 6.1 Hz, -OH); ms *m/e* (70 eV): 382 (M^+), 381 (M^+ − 1).

Precursor ***1***a *[A–A]*

Treatment of alcohol **32** (1.80 g, 4.7 mmol) according to procedure

Can. J. Chem. Downloaded from www.nrcresearchpress.com by 78.46.186.204 on 09/07/12
For personal use only.

A afforded, after column chromatography (1% acetone in dichloromethane), precursor **1***a* [A–A] (1.74 g, 92%); ir (neat): 2960, 1740, 1440, 1210 cm^{-1}; nmr ($CDCl_3$) δ: 4.06 (2H, t, J = 2.2 Hz, —CH_2—Cl), 3.75 and 3.73 (12H, both s, -CO_2Me), 3.51 (1H, t, J = 7.4 Hz, -$CH(CO_2Me)_2$), 3.23–2.44 (6H, m≡C—CH_2—C); ms m/e (70 eV): 401 (M^+(^{35}Cl) + 1) and 403 (M^+(^{37}Cl) + 1), ratio 3:1.

Chloride 33

To a stirred solution of alcohol **27** (16.4 g, 155 mmol) and triethylamine (17.2 g, 170 mmol) in 500 mL of dichloromethane at 0°C was added chloro-*tert*-butyl dimethylsilane (26.3 g, 170 mmol). The mixture was warmed to room temperature and stirred for 24 h. Water (600 mL) and ether (800 mL) were added and, after separation, the water layer was washed with 2 × 600 cm^3 ether. The combined organic layers were dried over sodium sulfate and concentrated to give an oily residue that was subjected to column chromatography (1% acetone in dichloromethane) to afford chloride **33** (23.2 g, 84%); ir ($CHCl_3$): 2960, 2930, 2860, 1260, 1145, 1080, 835 cm^{-1}; nmr ($CDCl_3$) δ: 4.4 and 4.0 (4H, both t, J = 2.0 Hz, —CH_2—), 0.91 (9H, s, *t*-Bu), 0.12 (6H, s, -CH_3).

Alcohol 35

Following procedure B, malonate **29** (18.2 g, 63 mmol) and chloride **33** (13.3 g, 69.7 mmol) gave, after work-up, crude adduct **34**, which was dissolved in tetrahydrofuran (500 mL) at 0°C. To that solution was added tetra-*n*-butylammonium fluoride (60 mmol) and the resulting mixture was stirred at room temperature for 2 h. Evaporation of the solvent gave a crude oil, which was purified by column chromatography (10% acetone in dichloromethane) to afford alcohol **35** (11 g, 58% overall); ir (neat): 3610, 3700–3100, 1740 cm^{-1}; nmr ($CDCl_3$) δ: 4.78 (1H, m, O—CH—O), 4.21 (4H, app t, J = 2 Hz, —CH_2—O), 3.76 (6H, s, -CO_2Me), 3.90–3.25 (2H, m, CH_2—CH_2—O), 3.00 (4H, t, J = 2 Hz, ≡C—CH_2—C), 1.90–1.25 (6H, m, —$(CH_2)_3$—CH_2O).

Chloride 37

A solution containing diester **35** (3.12 g, 8.9 mmol) and sodium cyanide (830 mg, 17.7 mmol) in 100 mL of dimethylsulfoxide was stirred at 100°C for 1.75 h. The cooled reaction mixture was then diluted with 400 mL of water and extracted with a mixture of ether, hexane, and methylene chloride 4:4:1 (4 × 200 cm^3). The combined organic layers were washed with water (2 × 50 cm^3) and dried over sodium sulfate. The residue was purified by column chromatography (10% acetone in dichloromethane) to afford ester **36** (58%), which was treated according to procedure A, giving, after column chromatography (1% acetone in dichloromethane), chloride **37** (1.42 g, 84%); ir (neat): 2950, 1740, 1025 cm^{-1}; nmr ($CDCl_3$) δ: 4.79 (1H, m, O—CH—O), 4.23 (2H, m, —CH_2—OTHP), 4.11 (2H, m, —CH_2—Cl), 3.73 (3H, s, -CO_2Me), 3.80–3.25 (2H, m, CH_2—CH_2—O), 3.00–2.25 (5H, m, —CH_2—$CH(CO_2Me)$—CH_2—), 1.90–1.25 (6H, m, —$(CH_2)_3$—CH_2O).

Alcohol 39

Using procedure B, chloride **37** (1.40 g, 4.5 mmol) and dimethyl malonate (2.96 g, 22.4 mmol) afforded, after work-up, crude malonate **38** (1.75 g), which was treated according to procedure C to give, after column chromatography (4–10% acetone in dichloromethane), alcohol **39** (1.16 g, 82% overall); ir (neat): 3520, 2960, 1735, 1435, 1030 cm^{-1}; nmr ($CDCl_3$) δ: 4.20 (2H, app d, J = 6.0 Hz, —CH_2—OH), 3.78 (6H, s, -$(CO_2Me)_2$), 3.72 (3H, s, -CO_2Me), 3.54 (1H, m, -$CH(CO_2Me)_2$), 2.90–2.25 (7H, m, —CH_2—$CH(CO_2Me)$—CH_2— and —CH_2—$C(CO_2Me)_2$), 1.90 (1H, app t, J = 6.0 Hz, -OH).

*Precursor 1*b [A–A]

Following procedure A, alcohol **39** (524 mg, 1.6 mmol) afforded, after column chromatography (2% acetone in dichloromethane), precursor **1***b* [A–A] (524 mg, 95%); ir (neat): 2960, 1740, 1440, 1030 cm^{-1}; nmr ($CDCl_3$) δ: 4.11 (2H, m, —CH_2—Cl), 3.77 (6H, s, -$(CO_2Me)_2$), 3.72 (3H, s, -$CH(CO_2Me)_2$), 3.55 (1H, t, J = 7.4 Hz, -$CH(CO_2Me)_2$), 2.90–2.50 (7H, m, —CH_2—$CH(CO_2Me)$—CH_2 and —CH_2—$C(CO_2Me)_2$).

Ester 40 (Procedure E)

To a solution containing malonate **7** (5.0 g, 17.5 mmol) in 35 mL of dimethyl sulfoxide was added sodium cyanide (1.7 g, 35 mmol) and water (315 mg, 17.5 mmol). The mixture was then stirred at 140–145°C for 5 h, poured over 500 mL of water, and extracted with ether–hexane (1:1) (3 × 200 mL). The combined organic layers were washed with water (2 × 75 mL) and saturated aqueous bicarbonate solution (1 × 75 mL), and dried over sodium sulfate. Column chromatography purification of the residue (2% acetone in dichloromethane) afforded ester **40** (2.1 g, 53%); ir ($CHCl_3$): 2950, 1740, 1025 cm^{-1}; nmr ($CDCl_3$) δ: 5.60 (2H, m, —CH=CH—), 4.62 (1H, m, O—CH—O), 4.18 (2H, m, —CH_2—OTHP), 3.67 (3H, s, -CO_2Me), 4.00–3.20 (2H, m, CH_2—CH_2—O), 2.40 (4H, m, —CH_2—CH_2—CO_2Me), 1.75–1.00 (6H, m, —$(CH_2)_3$—CH_2O).

Bromide 41 (Procedure F)

To a stirred solution of diisopropylamine (107 mg, 1.1 mmol) in 0.8 mL of tetrahydrofuran at 0°C was added *n*-butyllithium (1.0 mmol). After 30 min, the temperature was lowered to −78°C, ester **40** (200 mg, 0.9 mmol) was added, and the mixture was allowed to react for 20 min after which 1,4-dibromo-2-butyne (373 mg, 1.8 mmol) was added rapidly. The resulting mixture was stirred at −78°C for 1.5 h and quenched with saturated aqueous ammonium chloride. Water was added and the mixture was extracted with ether (3 × 20 mL). The combined organic layers were washed with bicarbonate (10 mL) and water (10 mL), dried over magnesium sulfate, and concentrated to give a crude oil that was subjected to column chromatography (1–2% acetone in dichloromethane) to afford bromide **41** (180 mg, 57%); ir ($CHCl_3$): 3005, 2945, 1735, 1020 cm^{-1}; nmr ($CDCl_3$) δ: 5.9–5.4 (2H, m, —CH=CH—), 4.61 (1H, m, O—CH—O), 3.70 (3H, s, -CO_2Me), 4.30–3.20 (6H, m, —CH_2—OTHP, CH_2—CH_2—O and —CH_2—Br), 2.80–2.30 (5H, m, —CH_2—$CH(CO_2Me)$—CH_2—), 1.60 (6H, m, —$(CH_2)_3$—CH_2O).

Malonate 42

Bromide **41** (1.40 g, 3.9 mmol) and dimethyl malonate (1.90 g, 4.4 mmol) were treated according to procedure B (except for temperature, which was kept at 35°C) affording, after column chromatography (2% acetone in dichloromethane), malonate **42** (1.50 g, 94%); ir ($CHCl_3$): 3020, 2950, 1740, 1440, 1025 cm^{-1}; nmr ($CDCl_3$) δ: 5.90–5.40 (2H, m, —CH=CH—), 4.60 (1H, m, O—CH—O), 3.75 (6H, s, -$(CO_2Me)_2$), 3.69 (3H, s, CO_2Me), 4.30–3.35 (5H, m, —CH_2—OTHP, CH_2—CH_2—O, and -$CH(CO_2Me)_2$), 2.90–2.25 (7H, m, —CH_2—$CH(CO_2Me)$—CH_2— and —CH_2—$C(CO_2Me)_2$), 1.60 (6H, m, —$(CH_2)_3$—CH_2O).

Alcohol 43

Using procedure C, malonate **42** (1.50 g, 3.7 mmol) afforded, after column chromatography (4–10% acetone in dichloromethane), alcohol **43** (1.03 g, 87%); ir ($CHCl_3$): 3620, 3530, 3020, 2960, 1735 cm^{-1}; nmr ($CDCl_3$) δ: 6.00–5.30 (2H, m, —CH=CH—), 4.30–4.00 (2H, m, —CH_2—OH), 3.75 (6H, s, -$(CO_2Me)_2$), 3.68 (3H, s, -CO_2Me), 3.54 (1H, app t, J = 7 Hz, -$CH(CO_2Me)_2$), 2.90–2.20 (7H, m, —CH_2—$CH(CO_2Me)$—CH_2— and —CH_2—$C(CO_2Me)_2$), 1.90–1.60 (1H, m, -OH).

*Precursor 1*b [C–A]

Following procedure A, alcohol **43** (1.0 g, 3.1 mmol) afforded, after column chromatography (1% acetone in dichloromethane), chloride **1***b* [C–A] (956 mg, 90%); ir ($CHCl_3$): 3030, 2960, 1740, 1440 cm^{-1}; nmr ($CDCl_3$) δ: 5.80–5.40 (2H, m, —CH=CH—), 4.10 (2H, m, —CH_2—Cl), 3.75 (6H, s, -$(CO_2Me)_2$), 3.68 (3H, s, -CO_2Me), 3.54 (1H, t, J = 7.7 Hz, -$CH(CO_2Me)_2$), 2.74 (2H, dt, J = 7.7 and 2.3 Hz, ≡C—CH_2—$C(CO_2Me)_2$), 2.65–2.30 (5H, m, —CH_2—$CH(CO_2Me)$—CH_2—).

Ester 44

Malonate **19** (12 g, 42 mmol) was treated according to procedure E to afford ester **44** (4.6 g, 48%); ir (neat): 2940, 1740, 1025 cm^{-1}; nmr ($CDCl_3$) δ: 5.90–5.50 (2H, m, —CH=CH—), 4.60 (1H, m, O—CH—O), 3.66 (3H, s, -CO_2Me), 4.30–3.20 (4H, m,

Can. J. Chem. Downloaded from www.nrcresearchpress.com by 78.46.186.204 on 09/07/12
For personal use only.

—CH_2—OTHP and CH_2—CH_2—O), 2.40 (4H, br s, —CH_2—CH_2—CO_2Me), 1.60 (6H, m, —$(CH_2)_3$—CH_2O).

Bromide ***45***

Following procedure F, ester **44** (2.0 g, 8.8 mmol) and 1,4-dibromo-2-butyne (3.7 g, 17.5 mmol) gave, after column chromatography (1% acetone in dichloromethane), bromide **45** (2.7 g, 86%) as a diastereoisomeric mixture; ir ($CHCl_3$): 3000, 2950, 1735 cm^{-1}; nmr ($CDCl_3$) δ: 5.64 (2H, m, —CH=CH—), 4.60 (1H, m, O—CH—O), 3.69 (3H, s, -CO_2Me), 4.35–3.30 (6H, m, —CH_2—OTHP, CH_2—CH_2—O, and -CH_2Br), 2.80–2.20 (5H, m, —CH_2—$CH(CO_2Me)$—CH_2—), 1.60 (6H, m, —$(CH_2)_3$—CH_2O).

Malonate ***46***

Treatment of bromide **45** (2.30 g, 6.5 mmol) and dimethyl malonate (2.90 g, 22.3 mmol) according to procedure B afforded, after column chromatography (2% acetone in dichloromethane), malonate **46** (2.30 g, 88%) as a diastereoisomeric mixture; ir (neat): 2950, 1740 cm^{-1}; nmr ($CDCl_3$) δ: 5.62 (2H, m, -CH=CH-), 4.60 (1H, m, O—CH—O), 3.75 (6H, s, -$(CO_2Me)_2$), 3.68 (3H, s, -CO_2Me), 4.30–3.20 (5H, m, —CH_2—OTHP, CH_2—CH_2—O, and -$CH(CO_2Me)_2$), 2.90–2.10 (7H, m, —CH_2—$CH(CO_2Me)$—CH_2— and —CH_2—$C(CO_2Me)_2$), 1.62 (6H, m, —$(CH_2)_3$—CH_2O).

Alcohol ***47***

Following procedure C, malonate **46** (800 mg, 1.9 mmol) afforded, after column chromatography (10% acetone in dichloromethane), alcohol **47** (584 mg, 92%); ir (neat): 3700–3100 (br), 2950, 1740 (br) cm^{-1}; nmr ($CDCl_3$) δ: 5.66 (2H, m, —CH=CH—), 4.06 (2H, m, —CH_2—OH), 3.74 (6H, s, -$(CO_2Me)_2$), 3.68 (3H, s, -CO_2Me), 3.54 (1H, app t, J = 7.5 Hz, -$CH(CO_2Me)_2$), 2.90–2.20 (7H, m, —CH_2—$CH(CO_2Me)$—CH_2— and —CH_2—$C(CO_2Me)_2$, 1.53 (1H, m, -OH).

Precursor ***1****b* [T–A]

Alcohol **47** (600 mg, 1.8 mmol) was treated according to procedure A to give, after column chromatography (25% AcOEt in hexane), chloride ***1b*** [T–A] (587 mg, 92%); ir (neat): 2950, 1740 cm^{-1}; nmr ($CDCl_3$) δ: 5.68 (2H, m, —CH=CH—), 4.00 (2H, m, —CH_2—Cl), 3.75 (6H, s, -$(CO_2Me)_2$), 3.69 (3H, s, -CO_2Me), 3.54 (1H, t, J = 7.7 Hz, -$CH(CO_2Me)_2$), 2.74 (2H, dt, J = 7.7 and 2.3 Hz, —CH_2—$C(CO_2Me)_2$), 2.65–2.25 (5H, m, —CH_2—$CH(CO_2Me)$—CH_2—); ms *m/e* (CI, CH_4): 347 (M^+ + 1). *Exact Mass* calcd.: 347.1261 (M^+ + 1); found: 347.1266 (M^+ + 1).

Alcohol ***49***

To a suspension of Lindlar catalyst (250 mg) in 20 mL of cyclohexane was added acetylene **46** (1.1 g, 2.7 mmol) dissolved in 5 mL of ethyl acetate and 5 mL of cyclohexane. The mixture was mechanically stirred under a hydrogen atmosphere for 5 h at room temperature. The catalyst was filtered off and the solvent evaporated to give an oil that was submitted to the conditions of procedure C to afford, after column chromatography (50% AcOEt in hexane), alcohol **49** (624 mg, 70% overall); ir (neat): 3650–3200 (br), 3000, 2950, 1740 (br) cm^{-1}; nmr ($CDCl_3$) δ: 5.68 (2H, m, —$\overset{H}{C}$=$\underset{H}{C}$—), 5.40 (2H, m, —$\overset{H}{C}$=$\overset{H}{C}$—), 4.10 (2H, m, —CH_2—OH), 3.73 (6H, s, -$(CO_2Me)_2$), 3.67 (3H, s, -CO_2Me), 3.39 (1H, app t, J = 7.5 Hz, -$CH(CO_2Me)_2$), 2.80–2.00 (7H, m, —CH_2—$CH(CO_2Me)$—CH_2— and —CH_2—$C(CO_2Me)_2$), 1.50–1.20 (1H, m, -OH).

Precursor ***1****b* [T–C]

Using procedure A, alcohol **49** (410 mg, 1.2 mmol) gave, after column chromatography (1% acetone in dichloromethane), precursor ***1b*** [T–C] (403 mg, 93%); ir (neat): 3000–2950, 1740 (br) cm^{-1}; nmr ($CDCl_3$) δ: 5.68 (2H, m, —CH=CH—CH_2Cl), 5.40 (2H, m, —CH=CH—CH_2—$C(CO_2Me)_2$), 4.00 (2H, m, —CH_2—Cl), 3.73 (6H, s, -$(CO_2Me)_2$), 3.66 (3H, s, -CO_2Me), 3.39 (1H, t, J = 7.6 Hz, —$CH(CO_2Me)_2$), 2.70–2.20 (7H, m, —CH_2—$CH(CO_2Me)$—CH_2— and —CH_2—$C(CO_2Me)_2$); ms *m/e* (70 eV): 347 (M^+ + 1), 315 (M − OMe), 311 (M − Cl). *Exact Mass* calcd.: 347.1261 (M^+ + 1); found: 347.1253 (M^+ + 1).

Bromide ***50***

Following procedure F, ester **44** (1.1 g, 4.8 mmol) and *trans*-1,4-dibromo-but-2-ene (1.5 g, 7.0 mmol) afforded, after column chromatography (1% acetone in dichloromethane), bromide **50** (1.1 g, 62%) as a diastereoisomeric mixture along with 8% starting material recovered; ir ($CHCl_3$): 3010, 2950, 1735 cm^{-1}; nmr ($CDCl_3$) δ: 5.80–5.50 (4H, m, —CH=CH—), 4.61 (1H, m, O—CH—O), 3.68 (3H, s, -CO_2Me), 4.20–3.30 (6H, m, —CH_2—OTHP, CH_2—CH_2—O, and —CH_2—Br), 2.60–2.10 (5H, m, —CH_2—$CH(CO_2Me)$—CH_2—), 1.63 (6H, m, —$(CH_2)_3$—CH_2O).

Malonate ***51***

Using procedure B, bromide **50** (1.05 g, 2.9 mmol) and dimethyl malonate (1.54 g, 11.7 mmol) afforded, after column chromatography (1–2% acetone in dichloromethane), malonate **51** (1.05 g, 88%) as a diastereoisomeric mixture; ir ($CHCl_3$): 3010, 2950, 1735 (br) cm^{-1}; nmr ($CDCl_3$) δ: 5.63 and 5.43 (4H, both m, —CH=CH—), 4.60 (1H, m, O—CH—O), 4.25–3.35 (4H, m, —CH_2—OTHP and CH_2—CH_2—O—), 3.72 (6H, s, -$(CO_2Me)_2$), 3.64 (3H, s, -CO_2Me), 3.39 (1H, t, J = 7.6 Hz, -$CH(CO_2Me)_2$), 2.57 (2H, app dd, J = 5.4 and 7.6 Hz, =C—CH_2—$C(CO_2Me)_2$), 2.55–2.10 (5H, m, —CH_2—$CH(CO_2Me)$—CH_2—), 1.90–1.45 (6H, m, —$(CH_2)_3$—CH_2O).

Alcohol ***52***

Treatment of malonate **51** (997 mg, 2.4 mmol) according to procedure C gave, after column chromatography (10% acetone in dichloromethane), alcohol **52** (741 mg, 96%); ir ($CHCl_3$): 3620, 3020, 2950, 1730 (br) cm^{-1}; nmr ($CDCl_3$) δ: 5.75–5.35 (4H, m, —CH=CH—), 4.08 (2H, app t, J = 5.2 Hz, =C—CH_2—OH), 3.73 (6H, s, -$(CO_2Me)_2$), 3.66 (3H, s, -CO_2Me), 3.40 (1H, t, J = 7.6 Hz, -$CH(CO_2Me)_2$), 2.58 (2H, m, —CH_2—$C(CO_2Me)_2$), 2.50–2.10 (5H, m, —CH_2—$CH(CO_2Me)$—CH_2—), 1.32 (1H, app t, J = 5 Hz, -OH).

Precursor ***1****b* [T–T]

Following procedure A, alcohol **52** (400 mg, 1.2 mmol) afforded, after column chromatography (1% acetone in dichloromethane), chloride ***1b*** [T–T] (418 mg, 99%); ir ($CHCl_3$): 3020, 2950, 1750–1720 (br) cm^{-1}; nmr ($CDCl_3$) δ: 5.65 and 5.42 (4H, both m, —CH=CH—), 3.99 (2H, m, —CH_2—Cl), 3.72 (6H, s, -$(CO_2Me)_2$), 3.65 (3H, s, -CO_2Me), 3.39 (1H, t, J = 7.5 Hz, -$CH(CO_2Me)_2$), 2.57 (2H, m, —CH_2—$C(CO_2Me)_2$), 2.50–2.10 (5H, m, —CH_2—$CH(CO_2Me)$—CH_2—); ms *m/e* (70 eV): 347 (M^+ + 1(^{35}Cl)), 349 (M^+ + 1(^{37}Cl)), ratio 3:1; ^{13}C nmr ($CDCl_3$) δ: 174.6 and 169.0 (CO_2Me), 131.9, 129.7, 128.3 and 128.1 (—CH=CH—), 52.2, 51.5, 51.2, 44.6, 44.5, 34.1, 33.5, and 31.5.

Monomer ***2****a* [C–C]

To a stirred solution of chloride ***1a*** [C–C] (84 mg, 0.21 mmol) in 5 mL of dry acetone was added dry potassium carbonate (287 mg, 2.1 mmol). The resulting mixture was refluxed with vigorous stirring for 4 days and neutralized with 30 mL of 0.1 *N* HCl solution. Crystalline cyclized product was filtered, washed with 15 mL of a 3:1 water–acetone mixture, and dried under vacuum to afford monomer ***2a*** [C–C] (64 mg, 84%); mp 221.5–222°C; ir ($CHCl_3$): 3030, 3020, 2955, 1735, 1285 cm^{-1}; nmr ($CDCl_3$) δ: 5.33–5.15 (4H, m, —CH=CH—), 3.75 (12H, s, -CO_2Me), 2.86–2.61 and 2.50–2.39 (8H, both m, —CH_2—); ms *m/e* (70 eV): 368 (M^+). *Exact Mass* calcd.: 368.1471; found: 368.1471; ^{13}C nmr ($CDCl_3$) δ: 171.2 (CO_2Me), 127.7 (C=C), 56.7 (qc), 52.7 (O—CH_3), 30.0 (CH_2).

Monomer ***2****a* [C–T] *and dimer* ***3****a* [C–T] (Procedure G)

To a stirred solution of precursor ***1a*** [C–T] (237 mg, 0.58 mmol) in 30 mL of dry DMF–THF (1:1) was added dry potassium carbonate (798 mg, 5.8 mmol). The resulting mixture was heated to reflux (oil bath temperature ≃90°C) for 32 h. The mixture was then filtered through a short pad of Celite at room temperature and the filtrate was concentrated under reduced pressure at room temperature to ≃2 mL of volume. The residue was dissolved in 50 mL of dichloromethane, washed with water, dried, filtered, and concentrated to afford a residue

Can. J. Chem. Downloaded from www.nrcresearchpress.com by 78.46.186.204 on 09/07/12
For personal use only.

that was purified by column chromatography (2% acetone in dichloromethane) yielding monomer **2***a* [C–T] (92.8 mg, 44%; crystallized from hexane–ether); mp 119–121°C; ir ($CHCl_3$): 3030, 2960, 1735, 1440, 1270–1200 (br), 1180 cm^{-1}; nmr ($CDCl_3$) δ: 5.57–5.07 (4H, m, —CH=CH—), 3.76, 3.75, 3.73 and 3.72 (12H, all s, -CO_2Me), 3.15–2.05 (8H, m including app d (3.10), J = 12.0 Hz and app t (2.14), J = 12.0 Hz, —CH_2—); ^{13}C nmr ($CDCl_3$) δ: 172.4, 171.7 and 170.8 (CO_2Me), 132.9, 128.9, 125.0 and 124.1 (C=C), 56.7, 56.9 (qc), 52.7, 52.4 (-OCH_3), 40.1, 36.3, 32.0 and 30.7 (-CH_2-); ms *m/e* (70 eV): 368 (M^+). *Exact Mass* calcd.: 368.1471; found: 368.1471; and dimer **3***a* [C–T] (52.8 mg, 25%) (crystallized from hexane–ether); mp: 155–156°C; ir ($CHCl_3$): 3030, 2960, 1733, 1200, 1180 cm^{-1}; nmr ($CDCl_3$) δ: 5.39–5.18 (8H, m, —CH=CH—), 3.72 (24H, s, -CO_2Me), 2.73–2.48 (16H, m, —CH_2—); ^{13}C nmr ($CDCl_3$) δ: 171.1 (CO_2Me), 128.7 and 126.5 (C=C), 57.1 (qc), 52.5 (-OCH_3), 29.9 and 35.5 (—CH_2—); ms *m/e* (70 eV): 736 (M^+). *Exact Mass* calcd.: 736.2942; found: 736.2929.

Monomer **2**a [C–A] *and dimer* **3**a [C–A]

Following procedure G, chloride **1***a* [C–A] (297 mg, 0.74 mmol) afforded, after column chromatography (2% acetone in dichloromethane), monomer **2***a* [C–A] (162 mg, 60%) (recrystallized from hexane–ether); mp 98.5–99.5°C; ir ($CHCl_3$): 3030, 2960, 1735, 1440, 1285–1220–1182, 1068, 1053 cm^{-1}; nmr ($CDCl_3$) δ: 5.55–5.35 (2H, m, —CH=CH—), 3.73 (12H, s, -CO_2Me), 3.25–2.40 (8H, m, —CH_2—); ^{13}C nmr ($CDCl_3$) δ: 170.7 (CO_2Me), 127.7 (C=C), 79.8 (C≡C), 55.1 (qc), 52.6 (-OCH_3), 31.4 (CH_2—C=), 24.5 (CH_2—C≡); ms *m/e* (CI, CH_4): 367 (M^+ + 1). *Exact Mass* calcd.: 366.1315; found: 366.1315; along with dimer **3***a* [C–A] (46.7 mg, 17%) (recrystallized from hexane–ether); mp 163.5–165.0°C; ir ($CHCl_3$): 3040, 2960, 1735, 1440, 1295, 1202 cm^{-1}; nmr ($CDCl_3$) δ: 5.52–5.21 (4H, m, —CH=CH—), 3.74 (24H, s, -CO_2Me), 2.78 (8H, s, —CH_2—C≡), 2.97–2.77 (8H, m, —CH_2—C=), ^{13}C nmr ($CDCl_3$) δ: 170.3 (CO_2Me), 127.7 (C=C), 78.1 (C≡C), 57.1 (qc), 52.7 (-OCH_3), 30.5 (CH_2—C=), 23.5 (CH_2—C≡); ms *m/e* (70 eV): 732 (M^+). *Exact Mass* calcd.: 732.2629; found: 732.2629.

Monomer **2**a [T–T] *and dimer* **3**a [T–T]

Using procedure G, chloride **1***a* [T–T] (400 mg, 0.99 mmol) afforded, after column chromatography (2% acetone in dichloromethane), monomer **2***a* [T–T] (37 mg, 10%) contaminated with a small amount (less 10%: gc) of **2***a* [C–T]; ir ($CHCl_3$): 3020, 2960, 1735, 1440, 1230, 1175 cm^{-1}; nmr ($CDCl_3$) δ: 5.26 (4H, m, —CH=CH—), 3.79 and 3.70 (12H, both s, -CO_2Me), 3.05 and 2.75 (8H, app d, J = 13.2 Hz and m, —CH_2—); ^{13}C nmr ($CDCl_3$) δ: 172.1 and 170.9 (CO_2Me), 132.3 (C=C), 54.0 (qc), 52.8 and 52.5 (-OCH_3), 39.5 (—CH_2—); ms *m/e* (70 eV): 368 (M^+). *Exact Mass* calcd.: 368.1471; found: 368.1471; along with dimer **3***a* ([T–T] (154 mg, 42%); ir ($CHCl_3$): 3030, 2960, 1735, 1440, 1200, 1170 cm^{-1}; nmr ($CDCl_3$) δ: 5.42–5.20 (8H, app t, J = 4.2 Hz, —CH=CH—), 3.69 (24H, s, -CO_2Me), 2.67–2.49 (16H, app d, J = 5.6 Hz, —CH_2—); ^{13}C nmr ($CDCl_3$) δ: 170.9 (CO_2Me), 128.3 (C=C), 57.1 (qc), 52.3 (-OCH_3), 35.0 (—CH_2—); ms *m/e* (70 eV): 736 (M^+). *Exact mass* calcd.: 736.2942; found: 736.2937.

Monomer **2**a [T–A] *and dimer* **3**a [T–A]

Precursor **1***a* [T–A] (376 mg, 0.934 mmol) was treated according to procedure G giving, after column chromatography (2% acetone in dichloromethane), monomer **2***a* [T–A] (59.2 mg, 17%) (recrystallized from hexane–ether); mp 101–102°C; ir ($CHCl_3$): 3035, 3025, 2960, 1732, 1440, 1250 cm^{-1}; nmr ($CDCl_3$) δ: 5.89–5.72 (2H, m, —CH=CH—), 3.79 and 3.69 (12H, both s, -CO_2Me), 2.98 (2H, app d, J = 12.7 Hz, —CH_2—), 2.88–2.66 (4H, m, —CH_2—), 2.59–2.45 (2H, m, —CH_2—); ^{13}C nmr ($CDCl_3$) δ: 171.3 and 169.8 (-CO_2Me), 130.1 (C=C), 84.1 (C=C), 55.1 (qc), 52.9 and 52.6 (OCH_3), 39.2 (CH_2—C=), 25.2 (CH_2—C≡); ms *m/e* (70 eV): 366 (M^+). *Exact Mass* calcd.: 366.1315; found: 366.1315; along with dimer **3***a* [T–A] (120 mg, 35%) (recrystallized hexane–ether–dichloromethane); mp 196.5–197.0°C; ir ($CHCl_3$): 3030, 2960, 1735, 1200 cm^{-1}; nmr ($CDCl_3$) δ: 5.55–5.35 (4H, m, —CH=CH—), 3.71 (24H, s, -CO_2Me), 2.80–2.64 (16H, m, —CH_2—); ^{13}C nmr ($CDCl_3$) δ: 170.2 (CO_2Me), 128.7 (—C=C—), 78.0 (C≡C), 56.7 (qc), 52.6 (OCH_3), 35.7 (CH_2—C=), 22.7 (CH_2—C≡); ms *m/e* (70 eV): 732 (M^+). *Exact Mass* calcd.: 732.2629; found: 732.2634.

Monomer **2**a [A–A] *and dimer* **3**a [A–A]

Following procedure G, chloride **1***a* [A–A] (383 mg, 0.96 mmol) afforded, after column chromatography (1% acetone in dichloromethane), monomer **2***a* [A–A] (89 mg, 26%) (recrystallized from benzene–hexane); mp 144.5–145.5°C); ir ($CHCl_3$): 3040, 3020, 2960, 1740, 1440, 1255 cm^{-1}; nmr ($CDCl_3$) δ: 3.77 (12H, s, -CO_2Me), 2.81 (8H, s, —CH_2—); ^{13}C nmr ($CDCl_3$) δ: 169.5 (CO_2Me), 80.4 (C≡C), 54.8 (qc), 53.0 (OCH_3), 25.6 (—CH_2—); ms *m/e* (70 eV): 364 (M^+). *Exact Mass* calcd.: 364.1158; found: 364.1158; along with dimer **3***a* [A–A] (138 mg, 40%) (recrystallized from benzene–hexane); mp 244.5–246.0°C; ir ($CHCl_3$): 3030, 2960, 1740, 1440, 1291 cm^{-1}; nmr ($CDCl_3$) δ: 3.72 (24H, s, -CO_2Me), 2.99 (16H, s, —CH_2—); ^{13}C nmr ($CDCl_3$) δ: 169.6 (CO_2Me), 78.0 (C≡C), 56.0 (qc), 52.9 (OCH_3), 23.3 (—CH_2—); ms *m/e* (70 eV): 728 (M^+). *Exact Mass* calcd.: 728.2316; found: 728.2326.

Monomer **2** b [A–A] *and dimer* **3** b [A–A]

Reaction of precursor **1***b* [A–A] (159 mg, 0.46 mmol) in the conditions of procedure G afforded, after column chromatography (4% acetone in dichloromethane), monomer **2***b* [A–A] (38 mg, 27%) (recrystallized from ether–hexane); mp 102.0–102.5°C; ir ($CHCl_3$): 3030, 3010, 2955, 1735, 1440, 1255 cm^{-1}; nmr ($CDCl_3$) δ: 3.78, 3.77, and 3.71 (9H, all s, -CO_2CH_3), 2.95–2.60 (5H, m, —CH_2—$C(CO_2Me)_2$—CH_2 and —CH—), 2.60–2.50 (4H, m, —CH_2—$C(CO_2Me)$—CH_2—); ^{13}C nmr ($CDCl_3$) δ: 173.1, 169.7, and 169.4 (CO_2Me), 82.0, 79.7 (C≡C), 54.6 (qc), 52.8, 52.9 (OCH_3), 40.8 (CH), 25.5, 22.1 (—CH_2—); ms *m/e* (70 eV): 306 (M^+). *Exact Mass* calcd.: 306.1103; found: 306.1103; along with an unseparable mixture of *cis* and *trans* dimers (54 mg, 38%) (recrystallized from ether–hexane); mp 143–148°C; ir ($CHCl_3$): 3020, 2955, 1735, 1438, 1200 cm^{-1}; nmr ($CDCl_3$) δ: 3.72 (12H, s, $(CO_2Me)_2$), 3.69 and 3.68 (6H, both s, -CO_2Me), 2.98 (4H, br s, —CH_2—), 2.63 (5H, br s, —CH_2— and —CH—); ^{13}C nmr ($CDCl_3$) δ: 1734, 169.8 (CO_2Me), 80.1, 76.8 (C≡C), 56.3 (qc), 53.0, 52.1 (OCH_3), 42.8, 42.6 (—CH—), 23.4, 20.2 (—CH_2—); ms *m/e* (70 eV): 612 (M^+). *Exact Mass* calcd.: 612.2207; found: 612.2216.

Monomer **2** b [C–A] *and dimer* **3** b [C–A]

Precursor **1***b* [C–A] (148 mg, 0.43 mmol) was treated under the conditions of procedure G to give, after column chromatography (2% acetone in dichloromethane), monomer **2***b* [C–A] (recrystallized from ether–pentane); mp 62–63°C; ir ($CHCl_3$): 3020, 2955, 1733, 1440 cm^{-1}; nmr ($CDCl_3$) δ: 5.70–5.30 (2H, m, —CH=CH—), 3.76 and 3.75 (6H, both s, -$(CO_2Me)_2$), 3.69 (3H, s, -CO_2Me), 3.25–3.05 and 2.85–2.35 (9H, both m, —CH_2— and —CH—); ^{13}C nmr ($CDCl_3$) δ: 174.8, 171.1 (-CO_2Me), 132.6, 124.3 (C=C), 81.7, 79.6 (C≡C), 55.6 (qc), 52.8, 51.9 (OCH_3), 42.1 (—CH—), 31.0, 29.7, 23.6, 22.0 (—CH_2—); ms *m/e* (70 eV): 309 (M^+ + 1). *Exact Mass* calcd.: 309.1337 (M^+ + 1); found: 309.1330 (M^+ + 1); along with dimer **3***b* [C–A] (35 mg, 27%) as an unseparable *cis–trans* mixture; ir ($CHCl_3$): 3030, 3015, 1733, 1438, 1200 cm^{-1}; nmr ($CDCl_3$) δ: 5.55–5.35 and 5.26–5.10 (4H, both m, —CH=CH—), 3.74, 3.72, 3.71, 3.70 (18H, all s, -CO_2Me), 3.00–2.35 (18H, m, —CH_2— and —CH—); ^{13}C nmr ($CDCl_3$) δ: 174.1, 170.4 (CO_2Me), 130.7, 130.5, 125.6, 125.5 (C=C), 80.0, 79.9 (C≡C), 57.0 (qc), 52.7, 51.8 (OCH_3), 44.1, 43.7 (-CH-), 30.2, 88.6, 28.1, 23.1, 23.0, 21.0, 20.7 (-CH_2-); ms *m/e* (70 eV): (M^+ + 1). *Exact Mass* calcd.: 616.2520; found: 616.2520.

Monomer **2** b [T–A] *and dimer* **3** b [T–A]

Using procedure G, chloride **1***b* [T–A] (159 mg, 0.46 mmol) gave, after column chromatography (2% acetone in dichloromethane), monomer **2***b* [T–A] (41 mg, 29%) assumed to be a mixture of conformers (4:1); ir ($CHCl_3$): 3020, 2955, 1735, 1140 cm^{-1}; nmr ($CDCl_3$) δ: 5.90–5.60 (2H, m, —CH=CH— minor conf.), 5.75–5.65 (2H, m, —CH=CH— major conf.), 3.80, 3.73, 3.70 (9H, all s,

$-CO_2Me$ minor conf.), 3.81, 3.70, 3.65 (9H, all s, $-CO_2Me$ major conf.), 3.05–2.20 (9H, m, $—CH_2—$ and —CH— both conf.); ^{13}C nmr ($CDCl_3$) δ: 174.8, 171.5, 169.9 ($-CO_2Me$), 132.9, 131.3 (C=C), 85.7, 83.4 (C≡C), 55.0 (qc), 52.9, 52.7, 51.9 ($-OCH_3$), 41.4, 39.2, 37.4, 25.3, 22.2 ($—CH_2—$ and —CH—); ms *m/e* (70 eV): 308 (M^+). *Exact Mass* calcd.: 308.1260; found: 308.1260; along with dimer **3***b* [T–A] (68 mg, 48%) as a *cis–trans* mixture; ir ($CHCl_3$): 3030, 2950, 1735, 1440 cm^{-1}; nmr ($CDCl_3$) δ: 5.65–5.25 (4H, m, —CH=CH—), 3.71 (12H, s, $-(CO_2Me)_2$), 3.67 (6H, s, $-CO_2Me$), 2.77 and 2.74 (4H, both br s, $CH_2—C≡$), 2.60–2.30 (5H, m, $—CH_2—CH—CH_2—$); ^{13}C nmr ($CDCl_3$) δ: 174.1, 170.4 (CO_2Me), 131.6, 131.4, 126.6, 126.4 (C=C), 80.4, 76.7 (C≡C), 65.8, 56.9, 56.8, 52.6, 51.7, 43.9, 43.6, 35.5, 33.4, 33.2, 22.7, 20.2, 19.9, 15.2; ms *m/e* (70 eV): 617 ($M^+ + 1$).

Monomer **2** b [T–C] *and dimer* **3** b [T–C]

Following procedure G, precursor **1***b* [T–C] (151 mg, 0.43 mmol) afforded, after column chromatography (2% acetone in dichloromethane), monomer **2***b* [T–C] (39.7 mg, 29%) assumed to exist as a mixture of conformers: ir ($CHCl_3$): 3030, 2955, 1730, 1440 cm^{-1}; nmr ($CDCl_3$) δ: (major conf.) 5.55–5.05 (4H, m, —CH=CH—), 3.76, 3.74 and 3.69 (9H, all s, $-CO_2Me$), 3.05–2.05 (9H, m, $—CH_2—$ and —CH—); ms *m/e* (70 eV): 310 (M^+). *Exact Mass* calcd.: 310.1416; found: 310.1424; along with dimer **3***b* [T–C] (56 mg, 42%) as a *cis–trans* mixture; nmr ($CDCl_3$) δ: 5.55–5.10 (8H, m, —CH=CH—), 3.71, 3.69 and 3.67 (18H, all s, $-CO_2Me$), 2.75–2.15 (18H, m, $—CH_2—$ and —CH—); ms *m/e* (70 eV): 620 (M^+). *Exact Mass* calcd.: 620.2832; found: 620.2828.

Monomer **2** b [T–T] *and dimer* **3** b [T–T]

Treatment of precursor **1***b* [T–T] (150 mg, 0.43 mmol) according to procedure G gave, after column chromatography (2% acetone in dichloromethane), monomer **2***b* [T–T] (13 mg, 10%) as a mixture of conformers (6:1 (nmr)); ir ($CHCl_3$): 3020, 2950, 1730, 1435, 1180 cm^{-1}; nmr ($CDCl_3$) δ: 5.40–5.10 (4H, m, —CH=CH—), 3.80, 3.72, 3.67 (9H, all s, $-CO_2Me$ (major conf.)), 3.79, 3.73, 3.71 (9H, all s, $-CO_2Me$ (minor conf.)), 3.15–3.00 and 2.90–2.40 (9H, both m, $—CH_2—$ and —CH—); ^{13}C nmr ($CDCl_3$) δ (major conf.): 175.7, 172.3 (CO_2Me), 135.0, 130.7 (C=C), 54.2 (qc), 52.8, 52.5, 51.8 ($-OCH_3$), 40.9 (—CH—), 29.6, 37.2 ($—CH_2—$); ms *m/e* (70 eV): 310 (M^+). *Exact Mass* calcd.: 310.1416; found: 310.1422; along with dimer **3***b* [T–T] (56 mg, 42%) as a *cis–trans* mixture; ir ($CHCl_3$): 3020, 2950, 1730, 1195 cm^{-1}; nmr ($CDCl_3$) δ: 5.55–5.38 and 5.35–5.18 (8H, both m, —CH=CH—), 3.71, 3.67 (18H, s, $-CO_2Me$), 2.60 (8H, app d, J = 7.2 Hz, $-CH_2C(CO_2Me)_2—CH_2—$), 2.50–2.15 (10H, m, $—CH_2—CH(CO_2Me)—CH_2—$); ms *m/e* (70 eV): 620 (M^+). *Exact Mass* calcd.: 620.2833; found: 620.2833.

1. (*a*) D. Brillon and P. Deslongchamps. Can. J. Chem. **65**, 43 (1987); **65**, 56 (1987); (*b*) D. Brillon and P. Deslongchamps. Tetrahedron Lett. **27**, 1131 (1986); (*c*) P. Deslongchamps, S. Lamothe, and H.-S. Lin. Can. J. Chem. **62**, 2395 (1984); (*d*) P. Deslongchamps. Bull. Soc. Chim. Fr. II, **9–10**, 349 (1984); (*e*) P. Deslongchamps. Aldrichimica Acta, **17**, 59 (1984).
2. (*a*) M. Kodama, S.-I. Yokoo, H. Yamada, and S. Itô. Tetrahedron, **34**, 3121 (1978); (*b*) M. Kodama, Y. Matsuki, and S. Itô. Tetrahedron Lett. 3065 (1975); 1121 (1976).
3. (*a*) T. Takahashi, T. Nagashima, and T. Tsuji. Tetrahedron Lett. **22**, 1359 (1981); (*b*) T. Takahashi, H. Nemoto, and J. Tsuji. Tetrahedron Lett. **24**, 2005 (1983); **24**, 3485 (1983).
4. (*a*) W. C. Still. J. Am. Chem. Soc. **99**, 4186 (1977); (*b*) J. Am. Chem. Soc. **101**, 2493 (1979); (*c*) W. C. Still, S. Murata, G. Revial, and K. Yoshihara. J. Am. Chem. Soc. **105**, 625 (1983); (*d*) W. C. Still and I. Galynker. Tetrahedron, **37**, 3981 (1981); (*e*) W. C. Still and D. Mobilio. J. Org. Chem. **48**, 4786 (1983); (*f*) J. A. Marshall and D. G. Cleary. J. Org. Chem. **51**, 858 (1986).
5. T. Kitahara and K. Mori. J. Org. Chem. **49**, 3281 (1984).
6. M. S. Frazza and B. W. Roberts. Tetrahedron Lett. **42**, 4193 (1981).
7. A. Etournaud and H. Wyler. Helv. Chim. Acta, **56**, 625 (1973).
8. (*a*) E. J. Corey and E. Hamanata. J. Am. Chem. Soc. **89**, 2758 (1976); (*b*) Y. Kitayama, A. Itoh, S. Hashimoto, H. Yamamoto, and H. Nozaki. J. Am. Chem. Soc. **99**, 3864 (1977); (*c*) B. M. Trost and R. W. Warner. J. Am. Chem. Soc. **104**, 6112 (1982); (*d*) B. M. Trost and T. Sato. J. Am. Chem. Soc. **107**, 719 (1985); (*e*) J. E. McMurry and P. Kocovsky. Tetrahedron Lett. **26**, 2171 (1985), and references cited therein.
9. J. Sicher. Prog. Stereochem. **3**, 202 (1962).
10. W. Baker, J. F. McOmie, and W. D. Ollis. J. Chem. Soc. 200 (1951).
11. K. F. Bernady, M. B. Floyd, J. F. Poletto, and M. J. Weiss. J. Org. Chem. **44**, 1438 (1979).
12. E. W. Collington and A. I. Meyers. J. Org. Chem. **36**, 3044 (1971).
13. M. Miyashita, A. Yoshikoshi, and P. A. Grieco. J. Org. Chem. **42**, 3772 (1977).
14. K. E. Wilson, R. T. Seider, and S. Masamune. Chem. Commun. 213 (1970).
15. E. J. Corey and J. W. Suggs. Tetrahedron Lett. **31**, 2647 (1975).
16. (*a*) A. W. Johnson. J. Chem. Soc. 1009 (1946); (*b*) W. J. Bailey and E. Fujiwara. J. Am. Chem. Soc. **77**, 165 (1955).
17. G. Illuminati and L. Mandolini. Acc. Chem. Res. **14**, 95 (1981).
18. A. P. Krapcho, G. A. Glynn, and B. J. Grenon. Tetrahedron Lett. **3**, 215 (1967).

Can. J. Chem. Downloaded from www.nrcresearchpress.com by 78.46.186.204 on 09/07/12
For personal use only.

Étude conformationnelle de cétopipérazines : (I) 3*R*-méthyl-6-carbéthoxy-2 oxopipérazine, (II) 3*R*-[*p*-hydroxybenzyl]-6-carbéthoxy-2 oxopipérazine : I, II en solution et structure cristalline de II

ANDRÉ MICHEL[1]

Laboratoire de chimie structurale, Université de Sherbrooke, Sherbrooke (Québec), Canada J1K 2R1

ET

GUY EVRARD ET B. NORBERG

Laboratoire de chimie moléculaire structurale, Facultés Universitaires Notre-Dame de la Paix, Rue de Bruxelles, 61, B-5000 Namur, Belgium

Reçu le 28 juillet 1986

ANDRÉ G. MICHEL, GUY EVRARD et B. NORBERG. Can. J. Chem. **65**, 1308 (1987).

La synthèse des composés indiqués dans le titre a été décrite récemment. Le mode de synthèse laissait croire à l'obtention de diastéréoisomères. Cependant, un seul isomère fut obtenu. Par le présent travail, nous montrons comment les propriétés conformationnelles justifient ces observations. La détermination de structure, par diffraction des rayons-X, du composé (*p*-hydroxybenzyl)-3*R* carbéthoxy-6 oxo-2 pipérazine montre que la molécule adopte une conformation repliée et que la configuration absolue au niveau du carbone C6 est [*R*]. L'étude en solution par la résonance magnétique nucléaire du ^{1}H montre l'existence de trois conformères et on discute des populations relatives. Ces travaux apportent également certains éléments quant à l'activité de tels composés au niveau du récepteur opiacé.

ANDRÉ G. MICHEL, GUY EVRARD, and B. NORBERG. Can. J. Chem. **65**, 1308 (1987).

The synthesis of the title compounds has been described recently. It was anticipated that the product would be a diastereomeric mixture. Surprisingly, only one isomer was obtained. The present work is an attempt to find the conformationnal properties accounting for those observations. X-ray structure determination of 3*R*-[*p*-hydroxybenzyl]-6-carbethoxy-2-oxopiperazine shows that the molecule adopts a folded conformation and that the absolute configuration at C6 is [*R*]. Investigation in solution using ^{1}H nuclear magnetic resonance shows the existence of three conformers and discusses the relative populations. Those findings are also relevant in terms of the activity of such compounds at the opiate receptor level.

Introduction

L'étude conformationnelle des cétopipérazines s'inscrit dans le cadre de nos recherches sur les propriétés géométriques des peptides andogènes et de leurs analogues. Les composés dont cette étude fait l'objet, sont à la base de la synthèse d'analogues rigidifiés de l'enképhaline (1). L'objectif final est de rechercher la conformation que ces dérivés doivent adopter au moment de l'association avec le site actif du récepteur opiacé. La présente étude a pour but de décrire les propriétés conformationnelles caractéristiques des composés indiqués dans le titre. Elle vise à mettre en évidence le comportement conformationnel du cycle phénolique, faisant partie du groupe tyramine, dont le rôle en tant que pharmacophore est essentiel dans l'activité morphinomimétique de tels dérivés (1).

Les dérivés faisant l'objet de cette étude sont présentés ci-dessous.

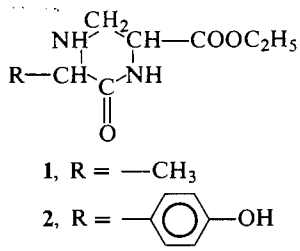

1, R = $-CH_3$

2, R =

Formule chimique

Les composés **I** et **II** ont fait l'objet d'une étude conformationnelle en solution grâce à la résonance magnétique nucléaire du proton à différentes températures.

Une étude cristallographique du composé **II** a permis de déterminer la chiralité du carbone C6. Cette détermination est basée sur la connaissance de la chiralité du carbone C3, correspondant à la chiralité «*S*» du produit de départ, la L-tyrosine, utilisée dans la synthèse. Il n'était donc pas nécessaire de l'établir expérimentalement.

La conformation de ces composés est alors comparée à celles qu'on observe pour les dioxopipérazines (8, 9).

Partie expérimentale

*Structure cristalline du composé **II***

Des cristaux incolores, de forme prismatique du composé **II** ont été obtenus par évaporation lente d'un mélange eau–méthanol dans un rapport 1:1. La solution a été maintenue dans un bain réfrigérant et conservé à 5°C jusqu'à obtention des cristaux. Les dimensions de la maille et les intensités ont été mesurées sur un diffractomètre Enraf–Nonius CAD-4. Les principales données concernant le cristal sont données au tableau 1. Aucune correction d'absorption n'a été appliquée, tenant de la faible valeur de ce terme. Le tableau 2 donne les conditions expérimentales de prise des données. La mesure de l'intensité de la réflexion standard a été réalisée après chaque groupe de 50 réflexions. Seule la correction de polarisation Lorentz a été effectuée au cours de la réduction des données. Les facteurs de diffusion atomiques ont été utilisés tels que générés dans le système SHELX (3); ceux-ci sont décrits à la référence 11.

La structure a été déterminée par méthodes directes, en utilisant le programme MULTAN (2), et affinée par la technique des moindres carrés (3). Tous les atomes, hydrogènes exceptés, ont été localisés dans la carte de Fourier calculée à partir des 180 valeurs les plus élevées des facteurs de structures normalisés. Les atomes d'hydrogène ont été tous positionnés grâce à une série de différence de Fourier.

En assignant des facteurs thermiques anisotropes à tous les atomes sauf les hydrogènes et des facteurs isotropes fixes pour ceux-ci, le dernier cycle d'affinement a donné un indice $R = 0.035$ pour toutes les réflexions observées. Le tableau 1 contient les données particulières à l'affinement. Les coordonnées finales sont données au tableau 3.

1. Auteur à qui toute correspondance doit être adressée.

Can. J. Chem. Downloaded from www.nrcresearchpress.com by 78.46.186.204 on 09/07/12
For personal use only.

Can. J. Chem. Downloaded from www.nrcresearchpress.com by 78.46.186.204 on 09/07/12
For personal use only.

TABLEAU 1. Données essentielles concernant le cristal de **II** utilisé pour la prise des données

Formule moléculaire	$C_{14}H_{19}N_2O_3$
Poids moléculaire	263,121
$F(000)$	564
Maille	Orthorhombique
a (Å)	13,563(1)
b	18,119(2)
c	5,728(2)
V(Å^3)	1407,6
d_{calc}/g cm^{-3})	1,233
Z	4
Groupe spatial	$P2_12_12_1$
Radiation Kα (Å)	Cu : 1,54178
T(K)	293
Dimension du cristal (mm)	0,2 × 0,1 × 0,15

TABLEAU 2. Conditions expérimentales pour l'acquisition des données et l'affinement

2θ maximum (deg)	140
Largeur de balayage (deg)	0,6 + 0,3 tg θ
Ouverture de la fente du détecteur (mm)	2,5 + 0,5 tg θ
Variation maximum de la réflexion standard (%)	1,0
Nombre de réflexions indépendantes	1420
Nombre de réflexions mesurées	751
Critère de discrimination : $I \geq a\sigma(I)$, a =	2,5
$R = \Sigma\|\Delta F\|/\Sigma\|F_o\|$	0,035
$R_w = [\Sigma w\Delta F^2/\Sigma F_o^2]^{1/2}$	0,041
$S = [\Sigma w\Delta F^2/(m-n)]^{1/2}$	1,42
$(\text{Variation}/\sigma)_{max}$	0,3
$(\text{Variation}/\sigma)_{moyen}$	0,03
Extrêmes de variation de la densité électronique (e Å^{-3})	−0,2, 0,2

La figure 1 présente la numérotation des atomes ainsi que les distances et angles de valence.

Les coordonnées des atoms d'hydrogène, ainsi que la liste des facteurs de structure calculés et observés font partie du matériel déposé.[2]

Étude en solution par rmn H des composés I et II

Les spectres rmn H ont été enregistrés sur un spectromètre Varian XL 200 à des concentration de 0,05 *M* dans D_2O. Les systèmes de spin étudiés sont présentés à la figure 2.

Ces systèmes ont été examinés simultanément afin d'élucider la conformation en solution : (*i*) le premier est constitué par les 3 protons, α, β^r, β^s du groupe *p*-hydroxybenzyl (composé **II**); (*ii*) le second est constitué par les 3 protons, α′, β'_1, β'_2 du cycle oxopiperazine (composés **I** et **II**).

Nous les avons considérés l'un et l'autre comme des systèmes de type ABX. Les paramètres rmn, déterminés à partir des mesures effectuées à différentes températures, sont repris dans le tableau 4.

Résultats et discussion

De l'étude par diffraction des rayons-X, il ressort que la caractéristique la plus surprenante est la forme repliée qu'adopte la molécule. La figure 3 illustre la conformation moléculaire. En effet, les groupes hydroxybenzyl et carbéthoxy sont tous les deux en position pseudo-axiale. Le quasi parallélisme entre les

2. On peut acheter la série complète de données des tableaux en s'adressant au Dépôt des données non publiées, ICIST, Conseil national de recherches du Canada, Ottawa (Ontario), Canada K1A 0S2.

TABLEAU 3. Coordonnées finales et facteurs de températures (× 10^4) avec les écarts-types entre parenthèses U_{eq} (Å^2 × 10^4) = $(U_{11}\cdot U_{22}\cdot U_{33})^{1/3}$

	x/a	y/b	z/c	U_{eq}
C (01)	6775 (5)	4189 (3)	9386 (11)	317
O (02)	7533 (3)	3984 (2)	8374 (8)	369
C (03)	6710 (4)	4123 (3)	12055 (10)	256
N (04)	5786 (4)	4400 (3)	13068 (9)	330
C (05)	5370 (4)	5023 (3)	11785 (12)	358
C (06)	5138 (4)	4808 (3)	9266 (12)	321
N (07)	6006 (4)	4473 (3)	8232 (9)	328
C (08)	6886 (5)	3318 (3)	12833 (11)	327
C (09)	6147 (4)	2768 (3)	11877 (11)	321
C (10)	6318 (5)	2419 (4)	9732 (12)	392
C (11)	5651 (5)	1915 (3)	8848 (11)	383
C (12)	4791 (5)	1747 (3)	10056 (11)	341
O (13)	4182 (3)	1240 (3)	9099 (9)	439
C (14)	4621 (5)	2083 (4)	12187 (12)	388
C (15)	5292 (5)	2590 (3)	13042 (12)	354
C (16)	4263 (5)	4285 (4)	9160 (13)	411
O (17)	3755 (4)	4108 (4)	10775 (10)	802
O (18)	4096 (4)	4051 (3)	7028 (10)	750
C (19)	3233 (8)	3564 (6)	6624 (19)	846
C (20)	2346 (6)	4034 (6)	6282 (18)	912

TABLEAU 4. Paramètres rmn pour les systèmes ABX : $-\alpha'\beta'_1\beta'_2$ pour les composés **I** et **II** $-\alpha\beta^r\beta^s$ pour le composé **I**

		Déplacements (ppm par rapport au TMS)			Couplages (Hz)		
Composé	T (°C)	α′	β'_1	β'_2	$\alpha'\beta'_1$	$\alpha'\beta'_2$	$\beta'_1\beta'_2$
I	10	4,63	3,77	3,93	4,3	5,5	−13,8
	20	4,63	3,77	3,92	4,2	5,6	−13,6
	40	4,62	3,77	3,90	4,5	5,6	−13,6
	70	4,61	3,76	3,86	4,6	5,6	−13,7
II	10	4,52	3,58	3,71	3,0	6,2	−13,5
	20	4,52	3,58	3,70	3,4	5,5	−13,6
	40	4,49	3,54	3,63	3,2	5,3	−13,6
	70	4,48	3,48	3,56	3,2	5,2	−14,1
		α	β^r	β^s	$\alpha\beta^r$	$\alpha\beta^s$	$\beta^r\beta^s$
I	10	4,41	3,24	3,47	3,9	9,8	−15,0
	20	4,41	3,26	3,46	4,9	8,6	−15,0
	40	4,40	3,27	3,33	5,6	7,3	−15,2
	70	—	3,25	3,25	6,0	6,0	—

plans moyens du phényl (C9—C10—C11—C12—C14—C15) et du groupe carboxylique (C6—C16—O17—O18—O19) (angle dièdre entre les deux plans : 20°) et les courtes distances entre les atomes de ces deux plans (entre 3,6 et 4,4 Å) conduisent à penser à une interaction stabilisant cette conformation. La nature de cette interaction est cependant difficile à caractériser. Elle a été également observée dans le cas des dipeptides cycliques en phase solide, pour des composés semblables, où une chaîne latérale aromatique fait face à un cycle dioxopipérazine (9).

À l'exception de l'atome C5, tous les atomes du cycle oxopipérazine sont coplanaires. La stéréochimie de la molécule est fixée sans ambiguïté. On sait en effet, que la configuration

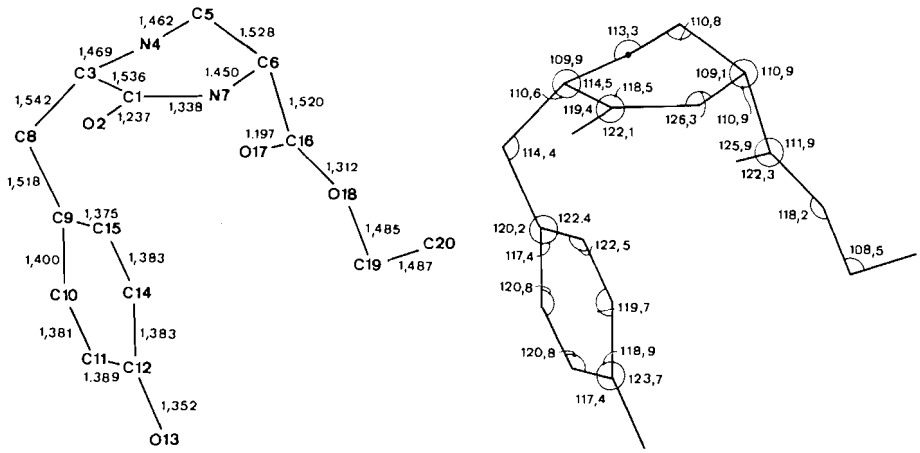

FIG. 1. Numérotation des atomes, longueurs des liaisons (Å) et angles (°), pour le composé **II**. Les déviations standards sont inférieures à 0,014 Å et 0,6° respectivement.

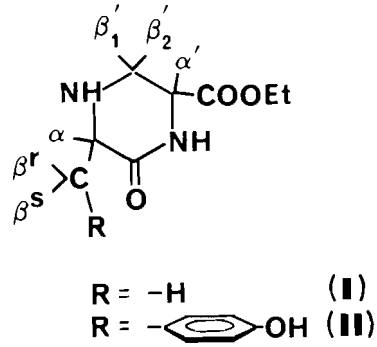

FIG. 2. Systèmes de spin utilisés pour interpréter les spectres en rmn H.

absolue du carbone C3 de la L-tyrosine utilisée dans la synthèse est «*S*»; l'atome de carbone C6 est donc de configuration «*R*».

L'empilement moléculaire à l'intérieur du cristal est présenté à la figure 4. Une première liaison hydrogène intermoléculaire (A) présente une longueur de 2.694 Å; elle est allongée selon *b* et formée entre le groupe —OH (*p*-hydroxybenzyl) et le groupe C=O (oxopipérazine). La deuxième liaison hydrogène assure la cohésion suivant l'axe *c*; elle relie les atomes d'azote N7 et N4 (N7—H...N4), l'un étant d'hybridation sp^2 et l'autre sp^3.

En ce qui concerne l'étude en solution par résonance magnétique nucléaire, nous avons examiné les déplacements chimiques et les constantes de couplage du système ABX formé des protons $\alpha'\beta'_1\beta'_2$, afin de déterminer l'orientation préférentielle du groupe carbéthoxy par rapport au cycle oxopipérazine. Les composés **I** et **II** présentent des signaux assez semblables et le système de spin ne se modifie pas dans le domaine de température étudié. L'examen des déplacements chimiques montre un effet de glissement simultané vers les fréquences plus basses ($-0,1$ ppm pour β'_1 et $-0,15$ ppm pour α' et β'_2) pour les protons et en fonction de la température. On peut corréler cet effet à une modification de l'orientation du groupe *p*-hydroxybenzyl du composé **II**; en effet ce phénomène n'est plus observé pour le composé **I**.

Les valeurs des constantes de couplage entre les protons $\alpha'\beta'_1$ et $\alpha'\beta'_2$ ont été utilisées pour estimer l'orientation préférentielle du groupe carbéthoxy. Les valeurs des angles de torsions obtenues en utilisant la relation de Karplus (4) sont données au tableau 4. On voit que le proton α' est dans une orientation bissectrice de l'angle β', β'_2, c'est-à-dire qu'il adopte une position pseudo-équatoriale par rapport au cycle oxopipérazine. En conséquence, le groupe carbéthoxy s'oriente de manière pseudo-axiale par rapport à l'hétérocycle.

Grâce au système ABX constitué par les protons $\alpha\beta^r\beta^s$, nous avons ensuite déterminé les populations relatives des différents rotamères du groupe *p*-hydroxybenzyl selon la méthode de Pachler (5). Les résultats sont indiqués au tableau 5.

Les conformations décrites correspondent à celles qui ont été observées pour les dipeptides cycliques contenant un acide aminé aromatique, tels que Deslauriers *et al.* (6) et Anteunis (7) le décrivent. Il est important d'observer que l'orientation pseudo-axiale du groupement carbéthoxy en position 6 n'empêche pas le rotamère *c* d'avoir un temps de résidence relativement important. Dans le cas plus particulier des dipeptides, il semble que le conformère *c* soit également prédominant.

En vue de comprendre quelles sont les forces intramoléculaires stabilisant ce conformère replié, des calculs d'énergie conformationnelle par méthode semi-empirique MO CNDO/2 ont été entrepris (9), sans cependant pouvoir reproduire les résultats expérimentaux que nous présentons. Ceux-ci sont cependant confirmés dans le cas des dipeptides cycliques (7). Kopple et Marr (10), qui les premiers avaient mis en évidence ce phénomène dans le cas de dioxopipérazines, proposent une stabilisation préférentielle de 15 kJ/mol en faveur du composé replié, ce qui rejoint assez bien nos résultats obtenus pour les dicétopipérazines.

Ils proposèrent alors une stabilisation par interaction dipole–dipole induit (μ–μ'), particulièrement dans le cas de solutions polaires, telles que nous les avons utilisées, tant pour l'étude rmn que pour la cristallisation. Cependant, Anteunis, quant à lui (7) considérait plutôt l'intervention prédominante de forces de dispersion. Revenant au problème posé au départ, la structure repliée fournit l'explication quant à la stéréospécificité observée au cours de la synthèse. La conformation adoptée (fig. 1) provoque un encombrement stérique important pour une des faces du cycle oxopipérazine et oriente ainsi l'attaque de l'agent catalyseur ou donneur ionique. Il en résulte une réduction stéréospécifique de la double liaison initiale C5=C6. Cette conformation justifie qu'au cours de la synthèse de ces composés (1) un seul des diastéréoisomères ait été obtenu, correspondant à la configuration «*R*» pour l'atome de carbone C6.

Can. J. Chem. Downloaded from www.nrcresearchpress.com by 78.46.186.204 on 09/07/12
For personal use only.

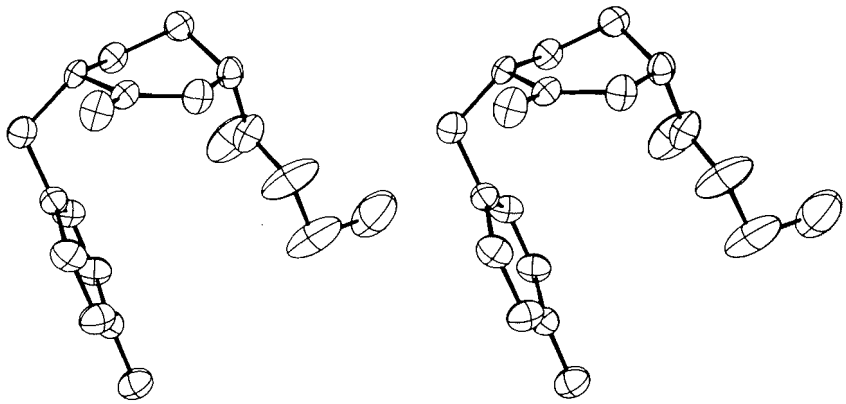

FIG. 3. Conformation moléculaire du composé **II** représentée grâce aux ellipsoïdes de vibration thermique (ORTEP).

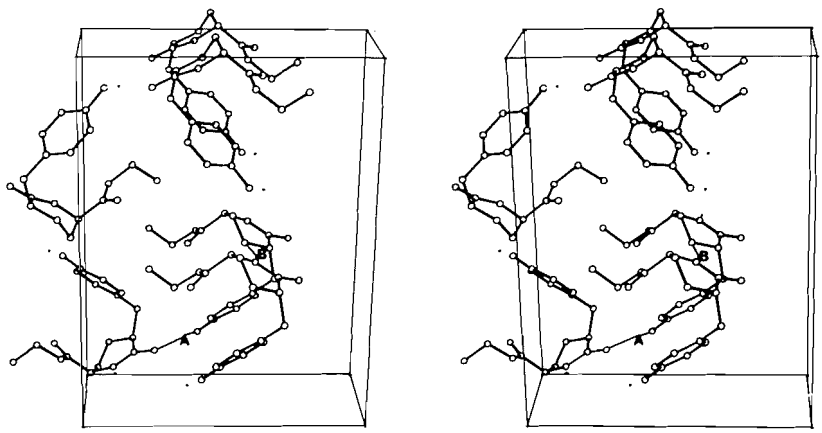

FIG. 4. Vue stéréographique de la maille cristalline; les liaisons H sont indiquées : A = 2,694(6) Å (—OH---O=C—); B = 2,976(7) Å (NH---N).

TABLEAU 5. Temps de résidence relatifs pour les isomères de rotation du groupe *p*-hydroxybenzyl calculés par la méthode de Pachler (5) à partir des valeurs J^g = 2,6 Hz et J^t = 13,6 Hz. La déviation standard estimée à partir de l'erreur expérimentale sur J, est de 8% sur les temps de résidence relatifs

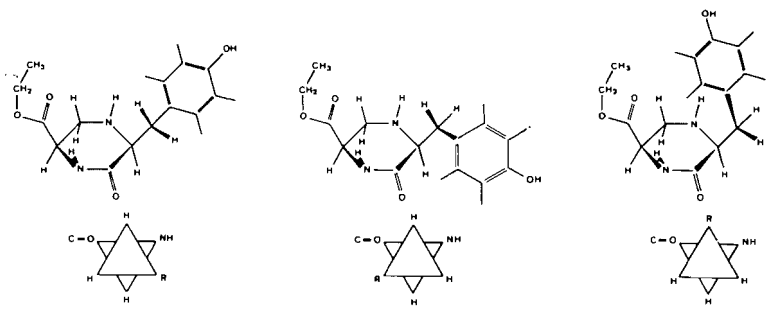

T(°C)	a	b	c
10	0,53	0,10	0,37
20	0,44	0,17	0,39
40	0,35	0,22	0,43
70	0,25	0,25	0,50

Can. J. Chem. Downloaded from www.nrcresearchpress.com by 78.46.186.204 on 09/07/12
For personal use only.

1. J. DiMaio. Synthesis and pharmacology of conformationally restricted analogues of enkephalin and the nitrogen lone pair effect in opiates. Ph.D. thesis, McGill University, Montréal, Canada. 1980.
2. P. Main, S. J. Fiske, S. E. Hull, L. Lessinger, G. Germain, J. P. Declercq et M. M. Woolfson. MULTAN 80, a system of computer programs for the automatic resolution of crystal structures from X-ray diffraction data. University of York, England, et Louvain-La-Neuve, Belgium. 1980.
3. G. Sheldrick. SHELX 76, a system of computing programs. Cambridge University, England. 1976.
4. S. Karplus et S. Lifson. Biopolymers, **10**, 1973 (1971).
5. K. G. R. Pachler. Spectrochim. Acta, **20**, 581 (1964).
6. R. Deslauriers, Z. Grzonka, K. Schaumburg, T. Shiba et R. Walter. J. Am. Chem. Soc. **97**, 5093 (1975).
7. M. J. O. Anteunis. Bull. Soc. Chim. Belg. **87**, 627 (1978).
8. A. Kilodziejczyk et J. Ciarkowski. Biopolymers, **25**, 771 (1986).
9. R. Ramani, K. Ventakesan et R. E. Marsh. J. Am. Chem. Soc. **100**, 949 (1978).
10. K. D. Kopple et D. H. Marr. J. Am. Chem. Soc. **89**, 6193 (1967).
11. International tables for X-ray crystallography. Tome 4. Reidel Publishing Company, London. 1973. pp. 99, 149.

Can. J. Chem. Downloaded from www.nrcresearchpress.com by 78.46.186.204 on 09/07/12
For personal use only.

Microanalytical determination of calcium, phosphate, and arsenate including kinetics of formation of molybdenum blue from reduction of molybdoarsenic acid by ferrous ammonium sulphate

U. S. RAI AND T. S. B. NARASARAJU[1]

Department of Chemistry, Banaras Hindu University, Varanasi-221 005, India

Received October 27, 1986

U. S. RAI and T. S. B. NARASARAJU. Can. J. Chem. **65**, 1313 (1987).

A method for the microdetermination of calcium, phosphate, and arsenate in mixtures of the three has been developed. In an aliquot of the mixture calcium was determined complexometrically using EDTA. Phosphate and arsenate were determined in second and third aliquots, respectively, using spectrophotometric methods. The interference of arsenate in the determination of phosphate was avoided by masking arsenate with thiosulphate. The kinetics of formation of molybdenum blue from molybdoarsenic acid by reduction with ferrous ammonium sulphate was also studied. The rate-determining step was found to be the reduction of molybdoarsenic acid with iron(II); the reaction was first order in iron(II) and arsenate over the concentration ranges studied. Values found for the enthalpy, entropy, and free energy of activation were 22, 0.05, and 7.5 kcal, respectively.

U. S. RAI et T. S. B. NARASARAJU. Can. J. Chem. **65**, 1313 (1987).

On a mis au point une méthode pour la microdétermination du calcium, du phosphate et de l'arsenate dans des mélanges de ces trois ions. Faisant appel à la complexométrie à l'aide de l'EDTA, on peut déterminer le calcium sur un aliquot du mélange. Utilisant des méthodes spectrophotométriques, on peut déterminer le phosphate et l'arsenate sur deux autres aliquots. On a éliminé le problème de l'interférence de l'arsenate dans la détermination du phosphate en masquant l'arsenate par du thiosulfate. On a aussi étudié la cinétique de la formation du bleu de molybdène à partir de l'acide moblydoarsenique par réduction avec du sulfate d'ammonium ferreux. On a trouvé que l'étape déterminante est la réduction de l'acide molybdoarsenique par le fer(II); pour toutes les concentrations étudiées, la réaction est du premier ordre en fer(II) ainsi qu'en arsenate. Les valeurs de l'enthalpie, de l'entropie et de l'énergie libre d'activation sont respectivement 22, 0,05 et 7,5 kcal.

[Traduit par la revue]

Can. J. Chem. Downloaded from www.nrcresearchpress.com by 72.64.146.136 on 09/07/12
For personal use only.

Introduction

A microanalytical determination of calcium, phosphate, and arsenate was needed in the course of some physicochemical investigations on the synthetic solid solutions of calcium hydroxylapatite, $Ca_{10}(PO_4)_6(OH)_2$, the principal inorganic constituent (1) of human bones and teeth, and the isomorph containing arsenic. Quantitative separation of the pairs: calcium, phosphate; calcium, arsenate; and phosphate, arsenate have been reported earlier (2–4). However, complications arise when all three ions are present simultaneously in microquantities. While microanalytical determinations of calcium and phosphate have been discussed earlier (5–8), that of arsenate needs further investigation. The estimation of microquantities of arsenate is based (7) on the reduction of molybdoarsenic acid by ferrous ammonium sulphate and subsequent spectrophotometric determination of the molybdenum blue formed. These investigations necessitated a study of the kinetics of formation of molybdenum blue from molybdoarsenic acid by reduction with ferrous ammonium sulphate. The present investigations into the microdetermination of calcium, phosphate, and arsenate were undertaken with a view to studying the solubility (9) of solid solutions of hydroxylapatites containing phosphorus and arsenic.

In the procedure developed here calcium in an aliquot of a solution containing calcium, phosphate, and arsenate was determined complexometrically (2, 6). Next, phosphate was determined spectrophotometrically in a second aliquot in the presence of calcium and arsenate. Calcium does not interfere, but arsenate does. The interference of arsenate was avoided by masking (10) with thiosulphate. In a third aliquot molybdenum blue was formed in the usual way. From knowledge of the contribution of phosphorus to this absorbance, obtained separately from a calibration curve relating the amount of phosphorus to absorbance under identical conditions, the contribution of arsenic was calculated. The kinetics of formation of molybdenum blue was studied spectrophotometrically at different temperatures, and a mechanism is suggested in light of the effect of change of concentrations of Fe^{2+} ion, acid, and arsenate ion on the reduction kinetics.

Experimental

Stock solutions were prepared by dissolving 0.25 g $CaCO_3$; 0.4393 g KH_2PO_4, and 0.4163 g $Na_2HAsO_4.7H_2O$, each in 1 L distilled water so that the resulting solutions contained 100 μg each of calcium, phosphorus, or arsenic per mL. A calibration curve representing the relationship between the amount of phosphorus and the absorbance was obtained by preparing ten solutions (Set No. 1) within the concentration range 25 to 200 μg per 100 mL. For each solution, an appropriate volume of the stock solution of phosphate was treated successively with 10 mL of 7.5 *N* sulphuric acid, 20 mL of 0.001 *N* sodium thiosulphate, and 10 mL each of 6.6% ammonium molybdate and 15% ferrous ammonium sulphate, and the resulting solution made up to 100 mL. The absorbance was recorded against a blank at 750 nm using a Beckman DB Spectrophotometer, the quartz cell width being 1.0 cm. A calibration curve representing the relationship between the amount of arsenic and the absorbance was obtained by preparing a set of solutions (Set No. 2) identical with Set No. 1, but without thiosulphate solution, which masks the arsenic. Each of these solutions was transferred to a 250-mL polyethylene beaker, heated on a water bath for about 15 min, cooled, transferred to a standard 100-mL volumetric flask, and made up to the mark. The absorbance was measured as for the phosphorus. To know the contribution of phosphorus to the absorbance after subjecting the solutions to heating, solutions of Set No. 1 were prepared once again (Set No. 3); the absorbance this time was measured by bringing about the colour reaction at 100°C as in the case of the arsenic system. A calibration curve was plotted of amount of phosphorus against absorbance after heating the solutions for about 15 min.

Having obtained these calibration curves, known and convenient volumes of calcium, phosphate, and arsenate solutions were mixed and

[1]Present address: School of Physical Sciences, North-Eastern Hill University, Shillong, India.

TABLE 1. Rate data for reduction of molybdoarsenic acid to molybdenum blue by ferrous ammonium sulphate

S. No.	Temperature (°C)	As in μg/100 mL	Ammonium molybdate per 100 mL (g)	Normality of H_2SO_4	Ferrous ammonium sulphate per 100 mL (g)	Rate constant k (min^{-1})
1	2	3	4	5	6	7
1	34	200	6.6	0.75	15	0.034
2	37	200	6.6	0.75	15	0.048
3	40	200	6.6	0.75	15	0.059
4	45	200	6.6	0.75	15	0.129
5	37	100	6.6	0.75	15	0.045
6	37	200	6.6	0.75	15	0.043
7	37	300	6.6	0.75	15	0.043
8	37	400	6.6	0.75	15	0.043
9	37	200	6.6	0.75	10	0.033
10	37	200	6.6	0.75	15	0.045
11	37	200	6.6	0.75	20	0.055
12	37	200	6.6	0.75	25	0.064

the resulting solution was made up to a known volume. Calcium was first estimated in an aliquot by titrating it against EDTA solution using Eriochrome black-T as an indicator (2). In a second aliquot, the amount of phosphorus was determined from the calibration curve obtained for Set No. 1. In a third aliquot, colour was produced without sodium thiosulphate as in Set No. 1 and the absorbance was measured against a blank. This absorbance is the sum of the absorbances due to phosphate and arsenate ions after heating. From knowledge of the amount of phosphate in the second aliquot, its corresponding absorbance after heating was calculated using the third calibration curve, and upon subtraction of this value from the absorbance obtained in the third aliquot, the contribution of arsenic to the absorbance could be determined. The amount of arsenic was determined from the second calibration curve.

Kinetic studies were carried out with a standard solution of sodium arsenate containing 100 μg arsenic per mL. Standard solutions of ammonium molybdate (66 g per L), 7.5 *N* sulphuric acid and ferrous ammonium sulphate (150 g per L) were prepared. All chemicals were of AR (BDH) or E Merck grade. To avoid possible interference of silica from glassware, all solutions were preserved in polyethylene containers and the experiments were carried out in polyethylene beakers. A convenient amount of arsenate solution was taken in a 100-mL volumetric flask and treated with 10 mL of 6.6% ammonium molybdate and 7.5 *N* sulphuric acid. Ferrous ammonium sulphate solution (10 mL) was then added and when the pipette was half empty the stop watch was started. The resulting solution was made up to 100 mL and transferred to a polyethylene beaker. About 3 mL of this solution was transferred to a spectrophotometer cell and the absorbance measured immediately, providing a zero time reading. At a convenient time interval, a fresh solution was placed in the cell and the absorbance was noted. To find the infinity reading, a separate system was prepared as above and the reaction was carried to completion by heating the solution in boiling water for about 15 min and measuring the final absorbance. The absorbance taken at different time intervals, when subtracted from the infinity reading, corresponds to the unreacted arsenic in the system. These data were found to obey the first order rate equation. To determine the slow step, a system was prepared as above without ferrous ammonium sulphate. The solutions were heated for about 15 min in a boiling water bath to complete the reaction, cooled, treated with the reducing agent, and the absorbance was measured as before. The results were found to obey the first order rate equation. To determine the effect of arsenic concentration, experiments were carried out at different concentrations of arsenate. The effect of temperature was studied by carrying out the experiment over the temperature range 34 to 45°C using a Colora thermostat. The dependence of the rate of the reaction on ferrous ammonium sulphate concentration was studied over a concentration range of 10 to 25%. To study the effect of acid concentrations on the reaction kinetics, experiments were carried out over the acid concentration range of 0.1 to 1.0 *N*. In the concentration range 0.1 to 0.6 *N* an instantaneous blue colour was obtained. The kinetics were not affected in the concentration range 0.7 to 1.0 *N* of sulphuric acid. The reaction was also carried out separately in the presence of 0.165 *N* NaCl and 0.01 *M* $CaCl_2$ and was found to be independent of their presence.

Results and discussion

Results of the kinetics of formation of molybdenum blue through reduction of molybdoarsenic acid by ferrous ammonium sulphate are given in Table 1. Rate constants, obtained by substituting the experimental data in the first order rate equation, are given in column 7 of the table. It is evident from the table that as temperature increases the rate constant also increases. A graph of log k vs. $1/T$ yields a straight line, from which the energy of activation is calculated to be 23 kcal. The enthalpy of activation, entropy of activation, and free energy of activation, were also calculated (11) and were found to be 22, 0.05, and 7.5 kcal, respectively. The increase in rate constant as a function of temperature is in accordance with the well known Arrhenius equation. When experiments were carried out with different concentrations of arsenic the rate constant was found to be unchanged, while the rate of the reaction was found to increase with the arsenic content of the reaction mixture, in agreement with theoretical considerations. It was also observed from Table 1 that the rate constant increases with increasing concentration of ferrous ammonium sulphate solution. This indicates that ferrous ammonium sulphate takes an active part in the reaction and its concentration alters as a result of the chemical change. The concentration of ferrous ammonium sulphate is very high and does not alter the order of the reaction, indicating a pseudo monomolecular reaction in the present investigation. It was observed that the rate of reaction increases with the concentration of ferrous ammonium sulphate; at a concentration of 25% the reaction is complete within 5 min. It is well known (12) that the formation of molybdenum blue from arsenate is a two-step reaction. Molybdoarsenic acid forms in the first step and is subsequently reduced in the second step. To determine the

Can. J. Chem. Downloaded from www.nrcresearchpress.com by 72.64.146.136 on 09/07/12
For personal use only.

TABLE 2. Microanalytical determinations of calcium, phosphorus, and arsenic when present together. Assessment of attainable accuracy

	Calcium wt. (mg)			Phosphorus wt. (mg)			Arsenic wt. (mg)		
S. No.	Theo.	Exptl.	% Error	Theo.	Exptl.	% Error	Theo.	Exptl.	% Error
1	2	3	4	5	6	7	8	9	10
1	4.00	4.00	0.0	1.60	1.62	+0.6	0.40	0.41	+2.5
2	3.80	3.78	−0.5	1.20	1.18	−1.3	0.80	0.79	−1.3
3	3.50	3.52	+0.6	0.80	0.79	−1.3	1.20	1.18	−1.7
4	3.30	3.28	−0.6	0.40	0.40	0.0	1.60	1.63	+1.9

rate-determining step, the first step of the reaction was allowed to proceed to completion, the reducing agent was added, and the kinetics were again studied. The reaction was found to follow the same reaction kinetics, indicating that the second step is the rate-determining step. In light of these results the following reaction scheme may be proposed:

[1] Arsenate + ammonium molybdate $\xrightarrow[\text{fast}]{k_1\ (\text{acid})}$ molybdoarsenic acid (MA)

[2] $\text{MA} + \text{Fe}^{2+} \xrightarrow[k_2]{\text{slow}} \text{molybdenum blue (MB)} + \text{Fe}^{3+}$

The velocity (v) of the overall reaction is given by

$$[3] \quad v = \frac{\text{d(MB)}}{\text{d}t} = k_2[\text{MA}][\text{Fe}^{2+}]$$

Since eq. [1] is instantaneous, the MA formed will be dependent on the amount of arsenate taken to start the reaction. Thus,

[4] [MA] = [arsenate]

The quantities given in square brackets represent molar concentrations. From eqs. [3] and [4],

$$[5] \quad v = \frac{\text{d(MB)}}{\text{d}t} = k_2[\text{arsenate}][\text{Fe}^{2+}]$$

The rate of reaction will depend on the concentration of arsenate as well as Fe^{2+}. Thus, Fe^{2+} takes an active part in the reaction and its concentration changes, even though it is present in excess and does not affect the order of the reaction. The intense blue colour obtained for acid concentrations below 0.6 N may be because of formation of molybdenum blue from molybdic acid. At higher acid concentrations molybdoarsenic acid reduction is independent of acid concentration. To obtain rapid quantitative conversion of arsenate into molybdoarsenic acid a very high concentration of ammonium molybdate was chosen in all the reactions. The intensity of the molybdenum blue obtained for the infinity reading was found to be independent of time for at least 50 h, indicating that the reaction is complete after heating for 15 min.

In light of the fact that both phosphorus and arsenic undergo an identical set of chemical reactions in the presence of molybdic acid and a reducing agent, the determination of the individual amounts of the two elements in a mixture is complicated. An expeditious formation of molybdenum blue in the presence of arsenate occurs only at about 100°C (9) while ordinary temperatures are suitable for the reaction in the case of phosphate (7). In addition, the occurrence of the reaction with arsenate can be prevented by the presence of $S_2O_3^{2-}$ ions (10); thiosulphate does not affect the reaction with phosphate. Based on these considerations a procedure has been developed for the determination of microquantities of phosphorus and arsenic in a mixture of the two.

The accuracy and precision of the method employed for the individual determination of calcium, phosphate, and arsenate when present together was assessed by applying it to sample solutions containing known amounts of these ions. The results, given in Table 2, suggest the maximum percent error to be of the order of ±2.5. The method is rapid and simple once the required calibration curves have been acquired.

Acknowledgements

The authors thank Professor S. M. Verma, Head, Department of Chemistry, Banaras Hindu University, for providing the necessary facilities. Financial assistance given to U.S.R. by U.G.C. (India) is also gratefully acknowledged.

1. A. S. POSNER. *In* Phosphorus and its compounds. Vol. II. *Edited by* J. R. Van Wazer. Interscience Publisher, Inc., New York. 1961. p. 1429.
2. R. P. SINGH, N. S. CHIKERUR, and T. S. B. NARASARAJU. Z. Anal. Chem. **237**, 117 (1968).
3. T. S. B. NARASARAJU, K. K. RAO, U. S. RAI, and B. K. KAPOOR. Indian J. Chem. **15**A, 1014 (1977).
4. T. S. B. NARASARAJU, U. S. RAI, and K. K. RAO. J. Sci. Res. **XXV**(1–2), 49 (1974–75).
5. T. S. B. NARASARAJU, M. LAL, and U. S. RAI. J. Sci. Res. **XXII**, 205 (1971–72).
6. T. S. B. NARASARAJU and V. L. N. RAO. Z. Anal. Chem. **258**, 365 (1972).
7. T. S. B. NARASARAJU, R. P. SINGH, and V. L. N. RAO. Z. Anal. Chem. **251**, 300 (1970).
8. S. R. CROUCH and H. V. MALMSTADT. Anal. Chem. **39**, 1084 (1967).
9. T. S. B. NARASARAJU and U. S. RAI. Can. J. Chem. **57**, 2662 (1979).
10. P. D. GOULDEN and P. BROOKSBANK. LIMOL. OCEANOGR. **19**(4), 705 (1974).
11. K. J. LAIDLER. Chemical kinetics. Tata McGraw Hill Publishing Co. Ltd., New Delhi. 1973. p. 89.
12. E. B. SANDELL. Colourimetric determination of traces of metals. Interscience Publishers Inc., New York. 1959. p. 282.

Can. J. Chem. Downloaded from www.nrcresearchpress.com by 72.64.146.136 on 09/07/12
For personal use only.

Determination of substituent effects by factor analysis and multiple linear regression for the carbon-13 nuclear magnetic resonance chemical shifts in 4-substituted phenols and 2-nitrophenols

HAROLD M. HUTTON,[1] KENNETH R. KUNZ,[2] JOHN D. BOZEK,[2] AND BARRY J. BLACKBURN[1]
Chemistry Department, University of Winnipeg, Winnipeg, Man., Canada R3B 2E9

Received August 1, 1986

HAROLD M. HUTTON, KENNETH R. KUNZ, JOHN D. BOZEK, and BARRY J. BLACKBURN. Can. J. Chem. **65**, 1316 (1987).

Carbon-13 nuclear magnetic resonance chemical shifts are reported for a series of 4-substituted phenols and 2-nitrophenols in dimethyl sulfoxide solution. For chemical shift correlations, it was found by factor analysis and iterative multiple linear regression that the *para* chemical shifts require two substituent factors whereas the *ipso*, *ortho*, and *meta* chemical shifts require three factors. Regression analyses were performed using the field and resonance parameters (σ_F, σ_R^0) and the appropriate *ipso*, *ortho*, and *meta* parameters (**I**, **O**, **M**) determined by Reynolds. Good correlations were obtained except for the three *meta* carbon analyses, where the correlation coefficients range from 0.877 to 0.963.

HAROLD M. HUTTON, KENNETH R. KUNZ, JOHN D. BOZEK et BARRY J. BLACKBURN. Can. J. Chem. **65**, 1316 (1987).

On a déterminé les déplacements chimiques, en rmn ^{13}C, d'une série de phénols substitués en position 4 ainsi que de nitro-2 phénols en solution dans le diméthylsulfoxyde. Pour les corrélations des déplacements chimiques, on a trouvé par des analyses factorielles et par des régressions linéaires multiples itératives que les déplacements chimiques des positions *para* requièrent deux facteurs de substituants alors que les déplacements chimiques des positions *ipso*, *ortho* et *méta* requièrent trois facteurs. On a effectué des analyses de régression en utilisant les paramètres de champ et de résonance (σ_F, σ_R^0) ainsi que les paramètres *ipso*, *ortho* et *méta* appropriés (**I**, **O** et **M**) déterminés par Reynolds. On a obtenu de bonnes corrélations, excepté pour trois analyses de carbones *méta* pour lesquelles on a obtenu des coefficients de corrélation allant de 0,877 à 0,963.

[Traduit par la revue]

Introduction

There has been considerable interest in the determination of electronic properties of aromatic compounds from the correlation of ^{13}C chemical shifts with various substituent parameters (1). A number of different procedures have been attempted, including the Swain–Lupton approach (2) and the Hammett analysis (3) using either a single substituent parameter (SSP) or dual substituent parameter (DSP) procedure (4, 5). The relative merits of the SSP and DSP scales have been discussed in detail (6–9). The DSP method, using the correlation of δ with the field/inductive and resonance substituent constants σ_F and σ_R^0, has been found to be effective in the determination of the relative contribution from the field and resonance effects (10–13). Since Reynolds has recently shown that the inductive parameter, I, is more accurately described as a field parameter, F (13), this convention will be used throughout this paper. For 1,4-disubstituted benzenes with one fixed substituent, Bromilow and co-workers (14, 15) have shown that the effect of substituents on *para* carbon chemical shifts is dependent on the electron demand exerted by the common group and can be analyzed with a dual substituent parameter nonlinear resonance effect (DSP–NLR) equation. The lack of statistical support (for example an F-test of the variance (14)) when applying a particular linear free-energy relationship has caused some concern (16, 17).

The use of factor analysis and principal component analysis has only recently been used to explore the effect of substituents on ^{13}C chemical shifts (17–21). Reynolds *et al.* (22) have used factor analysis on their extensive 3- and 4-substituted styrene data to show that the DSP procedure is necessary to fit the *para* chemical shifts, and that a third parameter is required for each of the *ortho*, *meta*, and *ipso* carbons in the styrene derivatives.

The purpose of this paper is to report the analysis of the substituent effects on the ^{13}C chemical shifts for a series of 4-substituted phenols and 2-nitrophenols and to determine if Reynolds parameters (22) apply to these aromatic systems.

Prior to this work there has not been a comprehensive study of the ^{13}C chemical shifts of phenols or 2-nitrophenols using a minimum substituent set. Lauterbur (23) has studied the ^{13}C chemical shifts of methylphenols, and Ilczyszyn *et al.* (24) reported the influence of substituents on the ^{13}C chemical shifts for a series of chloro and nitro substituted phenols. Smith and Proulx (25) examined the dependence of the ^{13}C chemical shifts of 2-substituted phenols with the Swain and Lupton parameters and the semiempirical factor Q (26).

The association that occurs in phenols has been well established. In nonpolar solvents, phenol (27) and many phenol derivatives (28) generally exist as a monomer–trimer equilibrium. In dimethyl sulfoxide (DMSO) solution, Ouellette has shown from ^1H nmr studies that these aggregates are eliminated as the phenolic hydrogen preferentially interacts with solvent molecules (29).

2-Nitrophenol is one of the exceptions where no association is found (28), due to the strong intramolecular hydrogen bond between the OH and NO_2 substituents. Evidence for the existence of this hydrogen bond has been provided by uv spectroscopy (30), ^1H nmr (31, 32), and the torsional frequency of the hydroxyl group (33). Although the energy of this hydrogen bond has not been measured directly, it has been estimated by Schaefer (34) to be about 6.6 kcal mol^{-1}. In 2,4-dinitrophenol de Kowalewski and co-workers (35) have shown that, even under conditions of fast exchange with the solvent, the OH group maintains its preferential *cis* conformation with the NO_2 group.

Experimental

Compounds

Phenol, the 4-substituted phenols, 2-nitrophenol, and some of the 4-substituted 2-nitrophenols, namely, the amino, chloro, nitro, and methyl derivatives, were obtained commercially and used with-

[1]Authors to whom correspondence should be addressed.
[2]Holder of an NSERC Student Research Award.

Can. J. Chem. Downloaded from www.nrcresearchpress.com by 78.46.186.204 on 09/07/12
For personal use only.

TABLE 1. ^{13}C chemical shifts of 4-substituted phenols and 2-nitrophenols in ppm from internal TMS[a]

	Phenol				2-Nitrophenol					
Substituent	C-1	C-2 C-6	C-3 C-5	C-4	C-1	C-2	C-3	C-4	C-5	C-6
H	157.6	115.5	129.6	119.1	152.6	136.6	125.2	119.5	135.6	119.4
NH_2	148.4	115.5*	115.8*	140.7	144.5	135.6	107.4	141.9	124.3	120.2
OCH_3	151.4	116.0*	114.8*	152.4	146.9	135.8	107.7	151.7	123.7	120.4
CH_3	155.2	115.2	129.8	127.3	150.4	136.0	124.6	128.8	136.4	119.2
F	153.8	116.3	115.8	155.7	148.9	136.2	111.5	153.9	122.8	120.6
Cl	156.4	117.1	129.2	122.6	151.2	137.2	124.5	122.5	134.9	120.9
Br	156.8	117.6	132.1	110.1	151.4	137.7	127.2	109.3	137.5	121.3
$COCH_3$	162.1	115.3	130.8	128.8	155.8	136.8	126.0	128.2	134.4	119.2
CHO	163.5	116.1	132.3	128.7	157.1	137.2	128.3	128.0	134.6	120.0
COOH	162.1	115.7	132.2	121.9	156.0	136.6	127.2	122.1	135.9	119.6
$COOCH_3$	162.1	115.5	131.6	120.5	156.2	136.5	126.9	120.6	135.4	119.6
CN	161.8	116.6	134.3	101.3	155.6	137.5	130.2	101.5	137.9	120.3
NO_2	164.1	115.9	126.2	139.8	157.6	136.4	122.0	138.5	129.5	119.9
$C(CH_3)_3$	155.2	114.9	126.0	141.0	150.3	135.9	120.9	142.1	133.0	119.1
I	157.4	118.3	138.0	80.8	151.8	138.2	132.8	79.9	143.2	121.5
COC_6H_5	162.2	115.4	132.7	128.1	155.9	136.9	127.8	127.8	136.1	119.4
$NHCOCH_3$	153.4	115.3	121.3	131.2	148.5	135.4	114.8	131.5	127.3	119.7
C_6H_5	157.3	115.9	127.8	131.1	151.6	137.3	122.7	131.5	133.5	119.8

[a]Chemical shifts were referenced to TMS using the DMSO resonance at 40.5 ppm.
*Assignments may be reversed.

Can. J. Chem. Downloaded from www.nrcresearchpress.com by 78.46.186.204 on 09/07/12
For personal use only.

out further purification. The following 4-substituted 2-nitrophenols were synthesized: 4-acetamido- (36*a*), 4-acetyl- (36*b*), 4-benzoyl- (36*c*), 4-bromo- (36*d*), 4-*tert*-butyl- (36*e*), 4-carbomethoxy- (36*f*), 4-carboxy- (36*g*), 4-cyano- (36*h*, *i*), 4-formyl- (36*j*), 4-fluoro- (36*k*), 4-iodo- (36*g*), 4-methoxy- (36*l*), and 4-phenyl-2-nitrophenol (36*m*). All compounds used were free of extraneous peaks in their ^{13}C nmr spectra.

Nuclear magnetic resonance

The carbon-13 nmr spectra were recorded on a Varian CFT-20 spectrometer at a temperature of 30°C. The compounds were run as 1.0 *M* solution in DMSO, using a coaxial tube with D_2O as external lock; chemical shifts were referenced to TMS by setting the DMSO resonance at 40.5 ppm (37).

Calculations

Factor analyses with the program FACTANAL (38) and the multiple linear regression analyses were performed on the Amdahl 470 computer at the University of Manitoba.

Results and discussion

Spectral assignment

The assignments for the 4-substituted phenols in Table 1 were primarily based on substituent-induced chemical shifts (SCS) (39), with C-2, C-6 usually to high field of C-3, C-5 and, similarly, C-4 to high field of C-1. The chemical shift difference between these pairs of resonances is sufficiently large to allow an unambiguous assignment, except for the amino and possibly the methoxy derivatives. With the substituted 2-nitrophenols in Table 1 the assignments were more straightforward since coupled spectra can be used to distinguish all carbon resonances except C-3 and C-5. However, the large chemical shift difference of these permits easy assignment on the basis of the *ortho* SCS values, with C-3 always to high field of C-5 as in 2-nitrophenol.

Factor analysis of the chemical shifts

The relationship between chemical shift data and substituent constants can either be expressed directly

$$[1] \quad \delta_x = \delta_0 + \Sigma\rho_n\sigma_n$$

or with the SCS relative to the parent compound

$$[2] \quad \Delta\delta_x = \Sigma\rho_n\sigma_n$$

The factor analysis of the data using eq. [1] should give one additional factor, the intercept, but the same number of substituent factors obtained by eq. [2], as has been shown by Reynolds *et al.* (22*a*). To determine the number of factors required to fit the data within the experimental accuracy, a number of tests can be applied (40). We have used the same indicators as Reynolds *et al.* (22*a*). In our analyses we estimate the overall average error to be 0.15 ppm for the chemical shifts and 0.2 ppm for the SCS values. To obtain the correct number of factors, (*a*) the residual standard deviation (RSD) for the data matrix should be approximately equal to the experimental uncertainty, (*b*) no individual value should have a deviation that is more than three times the experimental uncertainty (3σ), and (*c*) the empirical indicator function IND, where IND = RSD/($x - n$), should reach a minimum. In the definition of IND, x is the number of rows or columns (whichever is the lesser) in the data matrix and n is the number of factors.

The data used in the factor analysis of the substituted phenols and 2-nitrophenols is represented by a 18 × 10 matrix but the number of columns is reduced to the number of chemical shifts for a particular analysis. For example, there are only three different *ortho* chemical shifts in the two systems and thus 3 columns. Since there is some uncertainty in determining the correct number of factors with a limited data set, both the chemical shifts and the SCS were analyzed to serve as a check on the number of substituent factors. The results are given in Table 2. Four sets of analyses were used to determine the number of factors required for the short-range substituent effects. Using both compounds as one series, each of the *ortho* (C-3, C-5), *meta* (C-2, C-6), and *ipso* (C-4) chemical shifts was analyzed in combination with the long-range *para* (C-1) values.

TABLE 2. Results of the factor analysis of substituent effects in phenols and 2-nitrophenols

	C-1, C-3, C-5						C-1, C-2, C-6					
	δ^a			$\Delta\delta^b$			δ			$\Delta\delta$		
Factors	RSD[c]	3σ[d]	IND[e]	RSD	3σ	IND	RSD	3σ	IND	RSD	3σ	IND
1	2.95	81.2	0.18	2.05	64.7	0.13	2.04	86.6	0.13	0.76	22.4	0.05
2	1.08	44.5	0.12	0.54	16.5	0.06	0.27	3.3	0.03	0.32	2.4	0.04
3	0.29	4.4	0.07	0.35	3.5	0.09	0.21	1.1	0.05	0.16	0.0	0.04
4[f]	0.11	0.0	0.11	0.15	0.0	0.15	0.13	0.0	0.13	0.08	0.0	0.08

	C-1, C-2, C-3, C-4, C-5, C-6						C-1, C-4		
	δ			$\Delta\delta$			δ		
Factors	RSD	3σ	IND	RSD	3σ	IND	RSD	3σ	IND
1	7.22	95.6	0.09	2.60	73.5	0.03	2.93	66.2	0.33
2	1.81	79.4	0.03	1.14	52.9	0.02	0.37	10.3	0.13
3	0.94	46.7	0.02	0.60	21.7	0.01	0.14	0.0	0.29
4	0.36	10.6	0.01	0.34	5.3	0.009			
5	0.23	1.1	0.009	0.24	1.0	0.009			
6	0.19	0.0	0.009	0.16	0.0	0.01			
7	0.17	0.0	0.01	0.13	0.0	0.01			

[a]Factor analysis using chemical shifts with eq. [1].
[b]Factor analysis using chemical shifts, relative to parent compound, with eq. [2].
[c]Residual standard deviation.
[d]Percentage of points with errors more than 3 times the experimental uncertainty.
[e]Empirical indicator function (see text).
[f]Optimum number of factors as indicated by the tests (see text) is underlined. Note that the δ set requires an extra factor for the intercept.

Can. J. Chem. Downloaded from www.nrcresearchpress.com by 78.46.186.204 on 09/07/12
For personal use only.

Factor analysis could not be applied to the individual *ortho*, *meta*, *para* values because of the limited data set. For the same reason, the C-1, C-4 combination could only be determined with SCS values.

For the factor analysis of each of the *meta* and *ipso* chemical shifts with that of C-4, the RSD and 3σ tests indicate that three substituent parameters are required to fit the data; the RSD drops to about the value of the experimental uncertainty and the number of points with a deviation larger than 3σ drops to zero at the same time. However, IND does not give consistent results, possibly because of the limited data available. The results in Table 2 indicate an ambiguity with the factor analysis of the *ortho* chemical shifts. The analysis of δ values suggests three substituent factors (plus an intercept), whereas using $\Delta\delta$ values there is still 3.5% (3 points) of the data outside the 3σ limit with three factors. The *ortho*, *meta*, and *ipso* results are confirmed with the analysis of all ring carbons simultaneously since both the δ and $\Delta\delta$ results indicate that five substituent factors are required. As has been found by Reynolds *et al.* for substituted styrenes (22), the factor analysis shows that correlations should be possible with substituent parameters such as σ_F, σ_R^0, plus one additional factor for each of the *ortho*, *meta*, and *ipso* carbons.

Multiple linear regression of chemical shifts

(i) Long-range substituent effects

The values of the coefficients ρ_F and ρ_R determined from the multiple linear regression of the ^{13}C chemical shifts of the phenols and 2-nitrophenols using eq. [3] are given in Table 3.

$$[3] \quad \delta = \delta_0 + \rho_F\rho_F + \rho_R\rho_R^0$$

The data were analyzed using the σ_F (previously labelled as σ_I), σ_R^0 substituent constants given by Taft and co-workers (5). For the *para* carbon C-1, the substituent constants recently published by Reynolds (22) were also used in the analysis and the results given in Table 3. However, the number of data points is decreased since only 13 substituents (H, NH_2, OCH_3, CH_3, F, Cl, Br, I, $COCH_3$, CN, CO_2CH_3, NO_2, $C(CH_3)_3$) are common to those available from Reynolds (22). If Taft's values of σ_F, σ_R^0 are used, and the analyses restricted to these 13 substituents, the substituent coefficients do not differ significantly from those given in Table 3 using Reynolds' data; for phenol the correlation coefficient and F-test of the variance are 0.9974 and 949, respectively, while for the 2-nitrophenol they are 0.9978 and 1131. There is some improvement of the regression analysis for the phenol system, but for the 2-nitrophenols the results are virtually identical.

The values of the correlation coefficient and the F-test in Table 3 indicate an excellent correlation for the long-range substituent effects at C-1 for both the phenols and 2-nitrophenols. The goodness of the fit appears to be similar for both series, indicating that the nitro group does not significantly affect the chemical shift correlation.

The field and resonance contributions for C-1 can be examined in terms of λ, defined as ρ_R/ρ_F, the ratio of the resonance and field effects. From the results in Table 3 (Taft values) for C-1, λ is 4.42 for phenol and 5.05 for the 2-nitrophenol derivatives, in the range expected for these systems in DMSO. For monosubstituted benzenes in DMSO Bromilow *et al.* (11) found $\rho_F = 5.48$ and $\rho_R = 22.21$, with $\lambda = 4.05$. Comparing these results with the values given in

TABLE 3. Results of multiple linear regression analysis of substituent effects using eq. [3][a] with σ_F and σ_R^0

Compound	Carbon	δ_H[b]	δ_0[c]	ρ_F[c]	ρ_R[c]	r[d]	$F(2,15)$[e]	SD[f]
Phenol	C-1	157.6	158.14±0.22	4.50±0.65	19.38±0.57	0.9941	628	0.521
	C-1[f]	157.6	157.78±0.15	4.85±0.39	19.75±0.40	0.9983	1501	0.529
	C-2,C-6	115.5	115.19±0.31	2.85±0.92	−0.68±0.81	0.6304	5.0	0.743
	C-3,C-5	129.6	129.68±2.06	−0.58±6.05	22.08±5.31	0.7323	8.7	4.87
	C-4	119.1	127.78±7.48	−11.02±21.96	−24.25±19.28	0.3387	1.0	17.68
2-Nitrophenol	C-1	152.6	152.73±0.15	3.32±0.43	16.36±0.38	0.9962	983	0.349
	C-1[g]	152.6	152.58±0.15	3.39±0.37	16.79±0.38	0.9978	1161	0.373
	C-2	136.6	136.40±0.28	1.29±0.84	1.41±0.73	0.5518	3.3	0.673
	C-3	125.2	124.44±2.15	0.89±6.30	25.78±5.53	0.7708	11	5.07
	C-4	119.5	128.54±7.40	−14.29±21.73	−24.61±19.08	0.3604	1.1	17.49
	C-5	135.6	135.00±1.98	−2.79±5.83	14.55±5.11	0.5934	4.1	4.69
	C-6	119.4	119.22±0.20	2.45±0.60	−1.43±0.53	0.7749	11	0.483

[a] σ_F, σ_R^0 values taken from ref. 5, except as noted.
[b] Chemical shift of parent compound.
[c] Calculated values given with standard error.
[d] Multiple correlation coefficient.
[e] F-test of the variance, with the degrees of freedom due to regression, error indicated.
[f] Standard deviation.
[g] σ_F, σ_R^0 values taken from ref. 22*b*, with analysis restricted to 13 substituents (see text).

Table 3, the resonance effect at C-1 decreases with the common OH substituent, and a further decrease is obtained with the inclusion of the NO_2 substituent. The field effect decreases in the same manner but to a larger extent.

The influence of the 2-nitro group on the C-1 chemical shift of the phenol derivatives can be shown from the plots of the shifts of the phenol and 2-nitrophenol with respect to the shift of the corresponding benzene derivative (11). In Fig. 1, the chemical shift plot of phenol versus benzene derivatives in DMSO shows an approximately bilinear relationship. For the π-acceptor substituents the slope is 0.97 and for the π acceptors it is 0.76. For the common OH group, which is a π donor, these results are consistent with donor–acceptor conjugation for the π acceptors and π-repulsive saturation interactions (15, 41) for the π donors. The plot for the 2-nitrophenol and benzene shifts in Fig. 1 is a roughly linear relationship (the slopes are 0.69 for the π donors and 0.72 for the π acceptors, which is the same within the experimental uncertainty). This indicates that with the nitro group there is no longer any π saturation interaction. It is possible that the NO_2 group acts as an electron sink, by virtue of its $-R$ effect, to reduce the π-donor ability of the OH group, and that this is further enhanced by the stabilization that occurs with the O—H--O_2N hydrogen bond.

Both the linear regression analysis and the chemical shift plots indicate that the common groups are only weakly interacting with the substituents. For a strongly interacting common substituent, a nonlinear resonance effect equation (14, 15) would have been required to allow for the electron demand of the common group.

(ii) Short-range substituent effects

DSP correlations were also attempted with the ^{13}C chemical shifts for the *ortho*, *meta*, and *ipso* carbons in phenol and 2-nitrophenol. The results given in Table 3 indicate a rather poor set of correlations, as would be expected from the factor analysis data. Reynolds *et al.* (22*b*) have recently derived a set of short-range factors, which can be used with σ_F, σ_R^0:

$$[4] \quad \delta = \delta_0 + \rho_F\sigma_F + \rho_R\sigma_R^0 + \rho_X{}^X$$

In eq. [4] X represents the appropriate short-range factor and ρ_X is its weighting constant. These factors are **O**, **M**, and **I**, the *ortho*, *meta*, and *ipso* parameters, respectively. Using his extensive styrene chemical shift data, Reynolds has determined values of these short-range substituent constants. He has shown that it is reasonable to assume that these parameters represent an orthogonal nonelectronic component of the substituent effect and that σ_F and σ_R^0 still give reasonable field and resonance contributions after the nonelectronic effects are

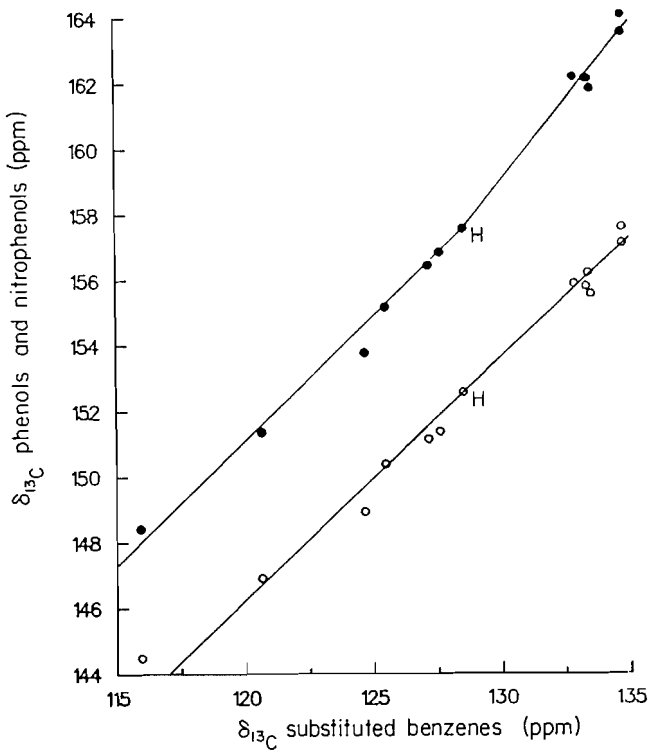

FIG. 1. A plot of the ^{13}C chemical shift for C-1 of 4-substituted phenols (●) and 4-substituted 2-nitrophenols (○) with respect to the corresponding chemical shift for substituted benzenes. The positions for the compounds with the hydrogen substituent are indicated on the plot.

Can. J. Chem. Downloaded from www.nrcresearchpress.com by 78.46.186.204 on 09/07/12
For personal use only.

Can. J. Chem. Downloaded from www.nrcresearchpress.com by 78.46.186.204 on 09/07/12
For personal use only.

TABLE 4. Results of multiple linear regression analysis of substituent effects using eq. [4] with σ_F, σ_R^0, and short-range parameters[a]

Compound	Carbon	Parameter X	δ_H[b]	δ_0[c]	ρ_F[c]	ρ_R[c]	ρ_X[c]	r[d]	$F(3,9)$[e]	SD[f]
Phenol	C-2,C-6	**M**	115.5	115.73±0.25	1.27±0.65	0.26±0.63	2.10±0.38	0.9378	22	0.410
	C-3,C-5	**O**	129.6	129.71±0.22	−2.69±0.56	25.60±0.57	0.94±0.02	0.9988	1281	0.413
	C-4	**I**	119.1	118.23±0.74	13.92±1.88	−43.18±1.85	1.08±0.02	0.9984	978	1.332
2-Nitrophenol	C-2	**M**	136.6	136.77±0.27	0.22±0.70	2.22±0.67	1.62±0.41	0.8774	10	0.440
	C-3	**O**	125.2	124.62±0.31	−1.52±0.79	29.75±0.81	0.97±0.03	0.9981	786	0.584
	C-4	**I**	119.5	119.21±0.83	10.32±2.11	−42.88±2.08	1.07±0.03	0.9981	776	1.492
	C-5	**O**	135.6	135.41±0.24	−5.16±0.61	18.03±0.62	0.90±0.02	0.9980	753	0.448
	C-6	**M**	119.4	119.50±0.16	1.51±0.40	−1.17±0.38	1.31±0.23	0.9634	39	0.251

[a] σ_F, σ_R^0, and short-range parameter X taken from ref. 22*b*.
[b] Chemical shift of parent compound.
[c] Calculated values given with standard error.
[d] Multiple correlation coefficient.
[e] *F*-test of the variance, with the degrees of freedom due to the regression, error indicated.
[f] Standard deviation.

factored out (22*b*). There is some question about the reliability of the *ipso* factor **I**. These *ipso* values were derived from cyclohexane α ^{13}C chemical shifts as the initial target testing input vector. The *ipso* factor and σ_F (and possibly σ_R^0) are partially related to substituent group electronegativity, but since this partially related component is factored out in deriving **I**, it would appear in the values of ρ_F and ρ_R in a σ_F, σ_R^0, **I** correlation (12, 22*b*). Thus the field and resonance components would not be reliable, as Reynolds has suggested (22*b*).

The results of the regression analysis using eq. [4] are given in Table 4. Reynolds' values of σ_F and σ_R^0 and the short-range parameters (22*b*) were used for these analyses. Similar results were obtained with the σ_F and σ_R^0 values published by Taft (5) and the short-range parameters. The use of the *ortho* factor, **O** and the *ipso* factor, **I**, significantly improves the correlations. However, the inclusion of **M** improves the correlation, but not to the same extent; the least improvement is at C-2 for the 2-nitrophenol series, although C-2 for the phenol derivatives is not much better. When these *meta* correlations were examined further, it was found that the π-donor substituents gave very good correlations for both series of compounds (correlation coefficient for C-2 and C-6 carbons varied from 0.993 to 0.999) while poor correlations were observed for the π acceptors (correlation coefficient varied from 0.733 to 0.908). These results again emphasize the requirement of a well-balanced set of substituents (5) ranging from electron withdrawing to electron releasing for any correlation analysis.

The standard deviation is given for each correlation in Tables 3 and 4. The results confirm that the two-parameter linear regression fits the data within the experimental uncertainty for the *para* carbon chemical shifts and that the three-parameter analysis is required for each of the *meta*, *ortho*, and *ipso* carbons. With the inclusion of the *meta* factor the standard deviation is reduced to the estimated error in the data, and thus it is possible that the values obtained for the correlation coefficient and *F*-test of the variance could result from the small range of *meta* chemical shifts. The standard deviation of the *ipso* carbon analysis is still about three times the error in chemical shifts, a further indication of the difficulties associated with an *ipso* factor.

In the derivation of the short-range substituent parameters the coefficient ρ_X (eq. [4]) was defined to be unity (22*b*). For the substituted phenols and 2-nitrophenols it is uncertain why the ρ_X coefficients for the *ortho* and *ipso* carbon analyses are close to unity whereas those for the *meta* are larger. Since there is a slight solvent dependence in σ_F values (5), the additional *meta* factor may also be attempting to correct for the uncertainties in σ_F, in addition to any *meta* effect. More systems would have to be analyzed using Reynolds' approach to determine if this is to be expected.

Acknowledgements

We thank the University of Winnipeg for financial assistance, and a referee for suggesting additional correlation statistics to assist interpretation of the results.

1. (*a*) D. W. EWING. Org. Magn. Reson. **12**, 499 (1979); (*b*) D. F. EWING. *In* Correlation analysis in chemistry: Recent advances. *Edited by* J. Shorter and N. B. Chapman. Plenum Press, New York. 1978. Chap. 8; (*c*) J. SHORTER. *In* Correlation analysis in chemistry: Recent advances. *Edited by* J. Shorter and N. B. Chapman. Plenum Press, New York. 1978. Chap. 4.
2. C. G. SWAIN AND E. C. LUPTON. J. Am. Chem. Soc. **90**, 4328 (1968).

Can. J. Chem. Downloaded from www.nrcresearchpress.com by 78.46.186.204 on 09/07/12
For personal use only.

3. L. P. HAMMETT. Physical organic chemistry. McGraw–Hill, New York. 1970.
4. P. R. WELLS, S. EHRENSON, and R. W. TAFT. Prog. Phys. Org. Chem. **6**, 147 (1968).
5. S. EHRENSON, R. T. C. BROWNLEE, and R. W. TAFT. Prog. Phys. Org. Chem. **10**, 1 (1973).
6. A. CORNELIS, S. LAMBERT, P. LASZLO, and P. SCHAUS. J. Org. Chem. **46**, 2130 (1981).
7. U. EDLUND and S. WOLD. J. Magn. Reson. **37**, 183 (1980).
8. W. F. REYNOLDS, P. DAIS, and D. W. MACINTYRE. J. Magn. Reson. **43**, 81 (1981).
9. D. J. CRAIK, R. T. C. BROWNLEE, and M. SADEK. J. Org. Chem. **47**, 657 (1982).
10. W. J. HEHRE, R. W. TAFT, and R. D. TOPSON. Prog. Phys. Org. Chem. **12**, 159 (1976).
11. J. BROMILOW, R. T. C. BROWNLEE, V. O. LOPEZ, and R. W. TAFT. J. Org. Chem. **44**, 4766 (1979).
12. W. F. REYNOLDS. J. Chem. Soc. Perkin Trans. 2, 985 (1980).
13. W. F. REYNOLDS. Prog. Phys. Org. Chem. **14**, 165 (1983).
14. H. M. HÜGEL, D. P. KELLY, R. J. SPEAR, J. BROMILOW, R. T. C. BROWNLEE, and D. J. CRAIK. Aust. J. Chem. **32**, 1511 (1979).
15. J. BROMILOW, R. T. C. BROWNLEE, D. J. CRAIK, M. SADEK, and R. W. TAFT. J. Org. Chem. **45**, 2429 (1980).
16. S. EHRENSON. J. Org. Chem. **44**, 1793 (1979).
17. D. JOHNELS, U. EDLUND, H. GRAHN, S. HELLBERG, M. SJÖSTRÖM, S. WOLD, S. CLEMENTI, W. J. DUNN. J. Chem. Soc. Perkin Trans. 2, 863 (1983).
18. K. B. WIBERG, W. E. PRATT, and W. F. BAILEY. J. Org. Chem. **45**, 4936 (1980).
19. W. F. BAILEY, E. A. CIOFFI, and K. B. WIBERG. J. Org. Chem. **46**, 4219 (1981).
20. U. EDLUNG and S. WOLD. J. Magn. Reson. **37**, 183 (1980).
21. W. J. DUNN, C. LINS, G. KUMAR, T. MANIMARAN, S. GRIGORAS, U. EDLUND, and S. WOLD. Org. Magn. Reson. **21**, 450 (1983).
22. (*a*) W. F. REYNOLDS, A. GOMES, A. MARON, D. W. MACINTYRE, R. G. MAUNDER, A. TANIN, H. E. WONG, G. K. HAMER, and I. R. PEAT. Can. J. Chem. **61**, 2367 (1983); (*b*) W. F. REYNOLDS, A. GOMES, A. MARON, D. W. MACINTYRE, A. TANIN, G. K. HAMER, and I. R. PEAT. Can. J. Chem. **61**, 2376 (1983).
23. P. C. LAUTERBUR. J. Am. Chem. Soc. **83**, 1846 (1961).
24. M. ILCZYSZYN, Z. LATAJKA, and H. RATAJCZAK. Org. Magn. Reson. **13**, 132 (1980).
25. W. B. SMITH and T. W. PROULX. Org. Magn. Reson. **8**, 205 (1976).
26. F. HRUSKA, H. M. HUTTON, and T. SCHAEFER. Can. J. Chem. **43**, 2392 (1965).
27. M. SAUNDERS and J. B. HYNE. J. Chem. Phys. **29**, 1319 (1958).
28. V. S. GRIFFITHS and G. SOCRATES. J. Mol. Spectrosc. **21**, 302 (1966).
29. R. J. OULETTE. Can. J. Chem. **43**, 707 (1965).
30. J. C. DEARDEN and W. F. FORBES. Can. J. Chem. **38**, 1852 (1960).
31. L. W. REEVES, E. A. ALLAN, and K. O. STROMME. Can. J. Chem. **38**, 1249 (1960).
32. S. CASTELLANO and R. KOSTELNIK. Tetrahedon Lett. 5311 (1967).
33. W. G. FATELEY, G. L. CARLSON, and F. F. BENTLEY. J. Phys. Chem. **79**, 199 (1975).
34. T. SCHAEFER. J. Phys. Chem. **79**, 1888 (1975).
35. P. E. BALONGA, C. VÀSQUEZ, R. H. COUTRERAS, V. J. KOWALEWSKI, and D. G. DE KOWALEWSKI. J. Magn. Reson. **59**, 58 (1984).
36. (*a*) M. A. GIRARD. Bull. Soc. Chim. Fr. **35**, 772 (1924); (*b*) C. K. BANKS and C. S. HAMILTON. J. Am. Chem. Soc. **61**, 357 (1939); (*c*) W. BLAKEY, W. I. JONES, and H. A. SCARBOROUGH. J. Chem. Soc. 2865 (1927); (*d*) H. VAN ERP. Recl. Trav. Chim. Pays-Bas, **29**, 187 (1910); Chem. Abstr. **4**, 2449 (1910); (*e*) A. W. ANISH. Chem. Abstr. **42**, 618f (1948); U.S. Patent 2,429,178; Oct. 14, 1947; (*f*) G. W. K. CAVILL. J. Soc. Chem. Ind. **64**, 212 (1945); (*g*) K. C. ROBERTS, C. G. M. DE WORMS, and H. B. CLARK. J. Chem. Soc. 196 (1935); (*h*) C. H. ANDREWS, H. KING, and J. WALKER. Proc. R. Soc. London B: **133**, 20 (1946); (*i*) S. S. BERG and G. NEWBERY. J. Chem. Soc. 642 (1949); (*j*) J. B. FISHMAN. J. Am. Chem. Soc. **42**, 2297 (1920); (*k*) F. SWARTS. Bull. Cl. Sci. Acad. R. Belg. 241 (1913); Chem. Abstr. **8**, 680 (1914); (*l*) T. TAKAHASHI, N. HATTORI, and M. SUYEMATSU. J. Pharm. Soc. Jpn. **65**, 9 (1945); Chem. Abstr. **45**, 8530e (1951); (*m*) L. C. RAIFORD and J. C. COLBERT. J. Am. Chem. Soc. **47**, 1454 (1925).
37. G. C. LEVY and G. L. NELSON. Carbon-13 nuclear magnetic resonance for organic chemists. Wiley–Interscience, New York. 1972. p. 23.
38. E. R. MALINOWSKI, D. G. HOWERY, P. H. WEINER, J. R. SOROKA, P. T. FUNKE, R. S. SELZER, and A. LEVINSTONE. FACTANAL, Program 320, Quantum Chemistry Program Exchange, Indiana University, Bloomington, IN. 1976.
39. J. B. STOTHERS. Carbon-13 nmr spectroscopy. Academic Press, New York. 1972. Chap. 5.
40. E. R. MALINKOWSKI and D. G. HOWERY. Factor analysis in chemistry. Wiley–Interscience, New York. 1980.
41. A. J. HOEFNAGEL, M. A. HOEFNAGEL, and B. M. WEPSTER. J. Am. Chem. Soc. **98**, 6194 (1976).

Crystal and molecular structure of 9-(2,4,6-trinitroanilino)-carbazole, $C_{18}H_{11}N_5O_6$

HONG WANG, RICHARD J. BARTON, AND BEVERLY E. ROBERTSON[1]
Department of Chemistry, University of Regina, Regina, Sask., Canada S4S 0A2

AND

JOHN A. WEIL AND KEITH C. BROWN
Department of Chemistry, University of Saskatchewan, Saskatoon, Sask., Canada S7N 0W0

Received September 23, 1986

HONG WANG, RICHARD J. BARTON, BEVERLY E. ROBERTSON, JOHN A. WEIL, and KEITH C. BROWN. Can. J. Chem. **65**, 1322 (1987).

The crystal structure of 9-(2,4,6-trinitroanilino)-carbazole, $C_{18}H_{11}N_5O_6$, has been determined by X-ray diffraction. Crystals are monoclinic, space group $P2_1/c$, a = 14.686(11), b = 24.601(12), c = 10.047(5) Å, β = 107.76(5)° at 292 K, with Z = 8. The two nitrogen atoms in the central fragment have a staggered conformation with an N—N distance of 1.381(4) Å, which is considerably shorter than N—N distances in related *N*-picrylhydrazine molecules. The picryl moiety has a geometry similar to that of related *N*-picrylhydrazine molecules. The title compound contains an N—H···O intramolecular bond to one of the *ortho* nitro groups on the picryl ring. The carbazole plane of one molecule and the picryl plane of a neighboring molecule overlap to form an infinite linear chain of the form...DhA:DhA...where D represents the carbazole donor, h the linear chain linkage within the molecule, and A represents the picryl acceptor of one molecule. The two interplanar distances between D of one molecule and A of an adjacent molecule are 3.28(13) and 3.34(13) Å, indicating a strong π-molecular interaction.

HONG WANG, RICHARD J. BARTON, BEVERLY E. ROBERTSON, JOHN A. WEIL et KEITH C. BROWN. Can. J. Chem. **65**, 1322 (1987).

On a déterminé la structure cristalline du (trinitro-2,4,6 anilino)-9 carbazole, $C_{18}H_{11}N_5O_6$, par diffraction des rayons-X. Les cristaux sont monocliniques, groupe d'espace $P2_1/c$, a = 14,686(4), b = 24,601(12) et c = 10,047(5) Å, β = 107,76(6)° à 292 K et Z = 8. Les deux atomes d'azote du fragment central sont dans une conformation décalée et la distance N—N de 1,381(4) Å est beaucoup plus courte que les distances N—N observées dans les molécules de *N*-picrylhydrazines apparentées. La portion picryle possède une géométrie qui est semblable à celle des molécules de *N*-picrylhydrazines apparentées. Le composé mentionné dans le titre possède une liaison N—H...O intramoléculaireimpliquant un des groupements nitro en position ortho du cycle picryle. Le plan du carbazole d'une molécule et le plan du picryle d'une molécule voisine se recouvrent pour former une chaîne linéaire de la forme...DhA:DhA...dans laquelle D représente le donneur carbazole, h représente la liaison linéaire de la chaîne à l'intérieur de la molécule et A représente l'accepteur picryle d'une molécule. Les deux distances entre les plans du D d'une molécule et du A de la molécule adjacente sont de 3,28(13) et 3,34(13) Å; ceci indique qu'il existe une interaction moléculaire π qui est forte.

[Traduit par la revue]

Introduction

2,2-Diaryl-1-picrylhydrazine compounds and related hydrazyl and hydrazinate compounds have been studied extensively because of the importance of the stable free radicals as standards in epr spectroscopy and as chemical reagents. 2,2-Diphenyl-1-picrylhydrazyl itself adopts a variety of polymorphic forms, often involving co-crystallized solvent (1). The hydrazine and related hydrazinate compounds have been studied by ^{1}H nmr (2, 3). The free radicals have been studied by various epr techniques (4, 5). The present analysis is one of a series of studies of the structures of these compounds. The structure of a hydrazinate has also been reported (6).

Experimental

$C_{18}H_{11}N_5O_6$ mw = 393.31

Monoclinic, space group $P2_1/c$, a = 14.686(11), b = 24.601(12), c = 10.047(5) Å, β = 107.76(5)°, T = 292 K, V = 3457 Å^3, Z = 8, D_x = 1.511 g cm^{-3}, μ(Mo Kα) = 1.26 cm^{-1}, λ = 0.71069 Å, F(000) = 1616.

9-Nitrosocarbazole was prepared by reacting carbazole with sodium nitrite in a mixture of acetic acid and water below 10°C. 9-Aminocarbazole was prepared by reducing the 9-nitrosocarbazole with lithium aluminum hydride. Picryl chloride was prepared by reacting picric acid with pyridine in ethanol followed by treatment of the precipitate with phosphorus oxychloride in refluxing benzene. The 9-aminocarbazole was fused with the picryl chloride in chloroform at 62°C. 9-(2,4,6-Trinitroanilino)-carbazole was recrystallized from ethanol and then from benzene.

An orange crystal with dimensions 0.60 × 0.10 × 0.16 mm was selected for X-ray study. The space group was determined to be $P2_1/c$ from precession photographs. The lattice constants were obtained by least-squares refinement using 30 reflections with 36° < 2θ < 45°. Data collection was carried out on a modified Picker four-circle diffractometer with graphite-monochromated Mo Kα radiation. Three reflections were measured as reference reflections after every 47 reflections. A total of 5559 reflections were collected with 3° ≤ 2θ ≤ 48°, 3140 of which were considered to be observed with $I \geq 2\sigma(I)$ ($\sigma(I)$ is the standard deviation of the intensity derived both from the counting statistics of the individual reflection, and the machine instability factor).

Intensity data were corrected for Lorentz-polarization effects. No corrections were made for absorption, dispersion, or extinction effects. Direct methods were used to solve the structure. A total of 2001 Σ_2 relations were generated using 641 reflections with $E > 1.75$. The coordinates of 42 non-hydrogen atoms in the two molecules were determined from the best E-map. The positions of all remaining non-hydrogen atoms were identified in the electron density Fourier map. After initial refinement, all hydrogen atoms were assigned positions 1.0 Å from their attached atoms. The final structure was refined by full-matrix least-squares with anisotropic temperature factors for non-hydrogen atoms and isotropic temperature factors for hydrogen atoms using 3140 observed reflections. The number of least-squares variables was 611. The weights used in the least-squares refinement were $w = (\sigma_c^2 + \sigma_m^2)^{-1}$ where σ_c is derived from $\sigma(I)$ and σ_m is chosen to make the average value of $w\Delta^2(F)$ independent of $|F_o|$ and sin θ/λ (7). The final agreement factors were R = 0.048,

[1]To whom correspondence should be addressed.

Can. J. Chem. Downloaded from www.nrcresearchpress.com by 78.46.186.204 on 09/07/12
For personal use only.

TABLE 1. Atom coordinates and temperature factors $U_{eq} = \frac{1}{3}\Sigma_i\Sigma_j U_{ij} a_i^* a_j^* \mathbf{a}_i \cdot \mathbf{a}_j$

Atom	x	y	z	U/U_{eq} (Å^2)
C(1)	0.3209(2)	0.3465(1)	0.0608(3)	3.9(2)
C(2)	0.2802(2)	0.3158(1)	−0.0629(3)	3.8(2)
C(3)	0.1935(2)	0.2897(1)	−0.0894(3)	4.4(2)
C(4)	0.1449(2)	0.2927(1)	0.0058(3)	4.4(2)
C(5)	0.1784(2)	0.3232(1)	0.1257(3)	4.6(2)
C(6)	0.2628(2)	0.3498(1)	0.1491(3)	4.3(2)
N(1)	0.3278(2)	0.3100(1)	−0.1693(3)	5.2(2)
O(1)	0.4047(2)	0.3331(1)	−0.1541(2)	6.7(1)
O(2)	0.2903(2)	0.2822(1)	−0.2717(2)	7.2(1)
N(2)	0.0550(2)	0.2632(1)	−0.0172(3)	6.4(2)
O(3)	0.0186(2)	0.2430(1)	−0.1316(3)	10.1(2)
O(4)	0.0216(2)	0.2596(1)	0.0785(3)	9.0(2)
N(3)	0.2863(2)	0.3872(1)	0.2707(3)	6.5(2)
O(5)	0.2926(2)	0.4353(1)	0.2479(3)	8.5(2)
O(6)	0.2907(2)	0.3666(1)	0.3832(3)	10.5(2)
N(4)	0.4093(2)	0.3688(1)	0.0909(3)	5.1(2)
N(5)	0.4587(2)	0.3876(1)	0.2227(2)	4.7(1)
C(7)	0.4895(2)	0.4419(1)	0.2488(3)	4.2(2)
C(8)	0.4649(2)	0.4868(1)	0.1636(4)	5.1(2)
C(9)	0.5044(2)	0.5356(1)	0.2181(4)	5.7(2)
C(10)	0.5653(3)	0.5390(2)	0.3533(4)	5.4(2)
C(11)	0.5888(2)	0.4942(1)	0.4384(3)	4.7(2)
C(12)	0.5507(2)	0.4440(1)	0.3862(3)	3.8(2)
C(13)	0.5579(2)	0.3895(1)	0.4435(3)	4.0(2)
C(14)	0.6041(2)	0.3668(2)	0.5735(4)	5.8(2)
C(15)	0.5965(3)	0.3123(2)	0.5919(4)	7.5(3)
C(16)	0.5457(3)	0.2786(2)	0.4836(4)	7.5(3)
C(17)	0.4978(2)	0.3000(1)	0.3533(4)	5.8(2)
C(18)	0.5034(2)	0.3551(1)	0.3374(3)	4.2(2)
C(21)*	−0.1606(2)	0.1476(1)	0.0499(3)	4.3(2)
C(22)	−0.2121(2)	0.1880(1)	−0.0432(3)	4.0(2)
C(23)	−0.2682(2)	0.1755(1)	−0.1780(3)	4.4(2)
C(24)	−0.2731(2)	0.1234(1)	−0.2232(3)	4.4(2)
C(25)	−0.2268(2)	0.0819(1)	−0.1368(3)	4.9(2)
C(26)	−0.1749(2)	0.0946(1)	−0.0029(3)	4.6(2)
N(21)	−0.2126(2)	0.2447(1)	−0.0023(3)	5.2(2)
O(21)	−0.1764(2)	0.2571(1)	0.1207(2)	6.2(1)
O(22)	−0.2511(2)	0.2781(1)	−0.0907(3)	8.4(2)
N(22)	−0.3340(2)	0.1098(1)	−0.3645(3)	5.8(2)
O(23)	−0.3883(2)	0.1450(1)	−0.4314(2)	7.3(2)
O(24)	−0.3273(2)	0.0641(1)	−0.4070(2)	8.3(2)
N(23)	−0.1430(2)	0.0468(1)	0.0888(3)	7.2(2)
O(25)	−0.1792(2)	0.0410(1)	0.1822(3)	10.0(2)
O(26)	−0.0887(2)	0.0158(1)	0.0570(3)	12.0(2)
N(24)	−0.1012(2)	0.1607(1)	0.1787(3)	5.7(2)
N(25)	−0.0368(2)	0.1236(1)	0.2585(3)	4.8(2)
C(27)	−0.0381(2)	0.1069(1)	0.3895(3)	4.4(2)
C(28)	−0.1037(3)	0.1172(2)	0.4585(4)	7.0(3)
C(29)	−0.0846(4)	0.0963(2)	0.5916(5)	8.5(3)
C(30)	−0.0051(3)	0.0653(2)	0.6545(4)	7.4(3)
C(31)	0.0593(3)	0.0551(1)	0.5847(4)	5.5(2)
C(32)	0.0454(2)	0.0767(1)	0.4503(3)	4.4(2)
C(33)	0.0990(2)	0.0767(1)	0.3539(3)	4.3(2)
C(34)	0.1864(3)	0.0542(2)	0.3582(5)	6.1(2)
C(35)	0.2204(4)	0.0639(2)	0.2499(6)	7.9(3)
C(36)	0.1724(4)	0.0944(2)	0.1362(6)	8.4(3)
C(37)	0.0828(3)	0.1176(2)	0.1258(4)	6.6(3)
C(38)	0.0489(2)	0.1077(1)	0.2374(3)	4.6(2)

*Atoms numbered greater than 20 belong to molecule **II** and are chemically equivalent to atoms in molecule **I** numbered less by 20.

$\omega R = 0.030$. XTAL crystallographic system of programs (8) was used for all calculations.

Discussion

Molecular structure

The atomic parameters, with standard deviations in parentheses, for the two independent molecules, labeled molecule **I** and molecule **II**, are listed in Table 1.[2] The atom numbering and a view of one of the two independent molecules are given in Fig. 1. Selected bond lengths and bong angles are given in Table 2.

As indicated earlier, this structure was refined with modified weights. The procedure used differs from the normal practice of adding a term proportional to $|F^2|$ or $\sin\theta/\lambda$ to $\sigma^2(F)$ in the numerator of the expression for the weights only in that it is more precise. Based on a comparison of refinement procedures, we have concluded that structures refined with modified weights tend to be more accurate than those refined with purely $\sigma^2(F)$ weights, but that the estimated standard deviations should be treated as estimates of the lower limit of the true standard deviation (7). A comparison of the differences between equivalent bond lengths in Table 2 suggests that the true esd's are no greater than two times those given by the data analysis. There is no significant difference in the geometry of the two molecules. In what follows the first and second quantities refer to molecule **I** and molecule **II**, respectively.

The C(1)—N(4) and C(21)—N(24) bond lengths, 1.355(4) and 1.361(4) Å, are shorter than a C—N single bond length (1.479 Å) and very close to the C—N partial double bond length (1.352 Å), which suggests that the lone-pair electrons of N(4) and N(24) are delocalized over the picryl rings. The Newman projection along the N(4)—N(5) and N(24)—N(25) linkages are shown in Fig. 2. The arrangement of atoms around the N atoms shows an approximately staggered conformation, caused by the spatial repulsion between the carbazole plane and picryl plane. Both N atoms of a molecule are sp^2 hybridized and one of them is conjugated to the aromatic system of the picryl moiety and the other to the carbazole moiety. The N(4)—N(5) and N(24)—N(25) bond lengths, 1.381(3) and 1.380(4) Å, suggest that they are single bonds with some limited double bond character. This is consistent with the observation that the staggered conformation is only approximated, i.e., the angles in Fig. 3 are not exactly 90°.

The H atoms on N(4) and N(24) form an intramolecular hydrogen bond to O(1) and O(21), respectively. The N(4)···O(1) and N(24)···O(21) distances are 2.596(4) and 2.608(4) Å which indicates a strong hydrogen bond, consistent with the ^{1}H nmr findings (9).

The conformation of the picryl moiety in 9-(2,4,6-trinitroanilino)-carbazole is quite different from that of related picryl hydrazyl and hydrazinate compounds. Due to the intramolecular hydrogen-bonding in 9-(2,4,6-trinitroanilino)-carbazole, the *ortho* nitro group involved in the hydrogen bond is coplanar with the picryl ring. The other *ortho* nitro group is twisted from the phenyl plane with dihedral angles of 59.4(1) and 64.2(2)°, because of steric repulsion from the carbazole moiety. The *para* nitro group is approximately coplanar with the phenyl plane. Selected dihedral angles are listed in Table 3.

[2]Lists of structure factor amplitudes, anisotropic thermal parameters, H-atom coordinates. Least-squares planes, and bond distances and angles may be purchased from the Depository of Unpublished Data, CISTI, National Research Council of Canada, Ottawa, Ont., Canada K1A 0S2.

Can. J. Chem. Downloaded from www.nrcresearchpress.com by 78.46.186.204 on 09/07/12
For personal use only.

Can. J. Chem. Downloaded from www.nrcresearchpress.com by 78.46.186.204 on 09/07/12
For personal use only.

TABLE 2. Bond lengths (Å) and bond angles (deg)

Bond	Length	
	Molecule **I**	Molecule **II**
C(1)—C(2)	1.422(4)	1.414(4)
C(1)—C(6)	1.408(5)	1.400(4)
C(2)—C(3)	1.377(4)	1.388(4)
C(3)—C(4)	1.360(5)	1.354(5)
C(4)—C(5)	1.376(4)	1.378(4)
C(5)—C(6)	1.357(5)	1.365(4)
C(7)—C(8)	1.377(4)	1.371(6)
C(7)—C(12)	1.400(4)	1.406(4)
C(8)—C(9)	1.372(5)	1.378(6)
C(9)—C(10)	1.382(5)	1.376(6)
C(10)—C(11)	1.373(5)	1.363(7)
C(11)—C(12)	1.390(4)	1.407(5)
C(12)—C(13)	1.451(4)	1.421(5)
C(13)—C(14)	1.392(4)	1.388(5)
C(13)—C(18)	1.403(4)	1.403(4)
C(14)—C(15)	1.363(6)	1.348(8)
C(15)—C(16)	1.390(6)	1.370(7)
C(16)—C(17)	1.388(5)	1.407(7)
C(17)—C(18)	1.372(4)	1.379(6)
C(1)—N(4)	1.355(4)	1.361(4)
C(2)—N(1)	1.453(5)	1.456(4)
C(4)—N(2)	1.463(4)	1.467(4)
C(6)—N(3)	1.484(4)	1.479(4)
C(7)—N(5)	1.408(4)	1.384(4)
C(18)—N(5)	1.392(3)	1.396(4)
N(4)—N(5)	1.381(3)	1.380(4)
N(1)—O(1)	1.231(4)	1.226(4)
N(1)—O(2)	1.219(3)	1.216(3)
N(2)—O(3)	1.216(4)	1.229(4)
N(2)—O(4)	1.209(5)	1.218(4)
N(3)—O(5)	1.213(4)	1.220(5)
N(3)—O(6)	1.223(4)	1.215(5)
N(4)—H(4)	0.82 (3)	0.87 (3)

Bonds	Angle	
	Molecule **I**	Molecule **II**
C(2)—C(1)—C(6)	114.0(3)	114.5(2)
C(2)—C(1)—N(4)	121.9(3)	121.5(3)
C(6)—C(1)—N(4)	124.0(2)	124.0(2)
C(1)—C(2)—C(3)	122.3(3)	122.0(3)
C(1)—C(2)—N(1)	121.8(3)	122.2(2)
C(3)—C(2)—N(1)	115.9(2)	115.7(2)
C(2)—C(3)—C(4)	119.4(3)	119.4(3)
C(3)—C(4)—C(5)	121.5(3)	121.6(3)
C(3)—C(4)—N(2)	120.2(3)	119.7(2)
C(5)—C(4)—N(2)	118.3(3)	118.6(3)
C(4)—C(5)—C(6)	118.5(3)	118.1(3)
C(1)—C(6)—C(5)	124.1(3)	124.1(3)
C(1)—C(6)—N(3)	121.4(3)	121.5(2)
C(5)—C(6)—N(3)	114.3(3)	114.1(3)
C(8)—C(7)—C(12)	123.4(3)	122.2(3)
C(8)—C(7)—N(5)	129.6(2)	129.9(3)
C(12)—C(7)—N(5)	107.0(2)	107.9(3)
C(7)—C(8)—C(9)	117.1(3)	117.1(4)
C(8)—C(9)—C(10)	120.8(3)	123.0(5)
C(9)—C(10)—C(11)	121.9(3)	119.4(4)
C(10)—C(11)—C(12)	118.8(3)	120.3(3)
C(7)—C(12)—C(11)	118.0(3)	117.9(3)
C(7)—C(12)—C(13)	107.7(2)	107.1(3)
C(11)—C(12)—C(13)	134.3(2)	134.9(3)

TABLE 2. (*concluded*)

Bonds	Angle	
	Molecule **I**	Molecule **II**
C(12)—C(13)—C(14)	134.4(3)	132.6(3)
C(12)—C(13)—C(18)	107.4(2)	108.1(3)
C(14)—C(13)—C(18)	118.2(3)	119.2(3)
C(13)—C(14)—C(15)	119.0(3)	118.0(4)
C(14)—C(15)—C(16)	121.8(4)	123.2(5)
C(15)—C(16)—C(17)	120.6(4)	121.0(6)
C(16)—C(17)—C(18)	117.0(3)	115.4(4)
C(13)—C(18)—C(17)	123.2(3)	123.1(3)
N(5)—C(18)—C(13)	107.4(2)	107.0(3)
N(5)—C(18)—C(17)	129.4(2)	129.9(3)
C(2)—N(1)—O(1)	119.5(2)	119.1(2)
C(2)—N(1)—O(2)	118.8(3)	118.9(2)
O(1)—N(1)—O(2)	121.7(3)	122.0(2)
C(4)—N(2)—O(4)	118.4(3)	117.4(2)
C(4)—N(2)—O(3)	117.9(3)	118.0(3)
O(3)—N(2)—O(4)	123.7(3)	124.6(2)
C(6)—N(3)—O(5)	117.4(3)	116.2(3)
C(6)—N(3)—O(6)	115.9(3)	116.3(3)
O(5)—N(3)—O(6)	126.5(3)	127.3(3)
C(1)—N(4)—N(5)	122.5(3)	121.6(3)
C(7)—N(5)—N(4)	122.7(2)	122.9(3)
C(18)—N(5)—N(4)	125.3(2)	125.9(3)
C(7)—N(5)—C(18)	110.3(2)	109.7(2)

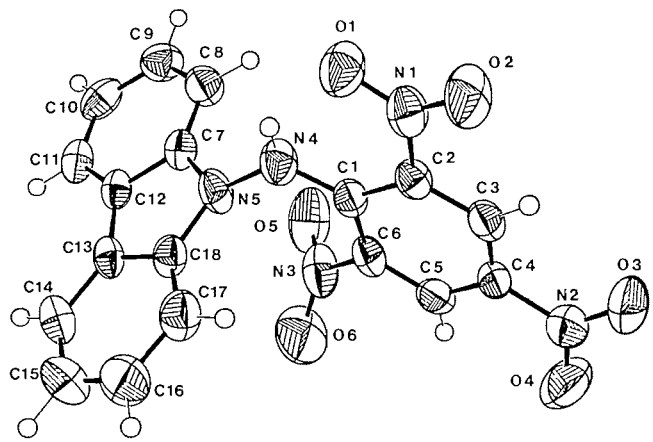

FIG. 1. The ORTEP view of molecule **I**, with numbering scheme. The ellipsoids correspond to 50% probability.

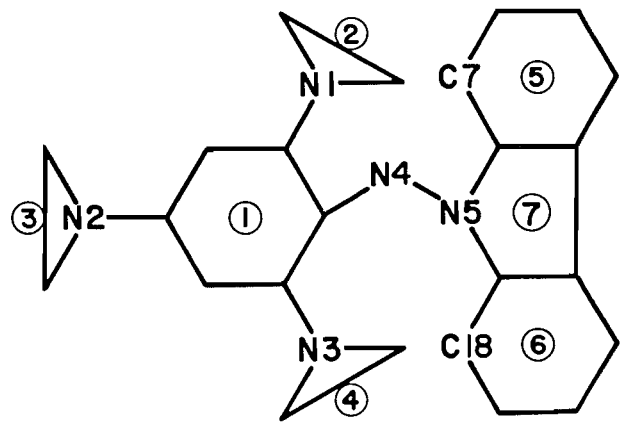

FIG. 2. Newman projection looking along the N—N linkage, with torsional angles.

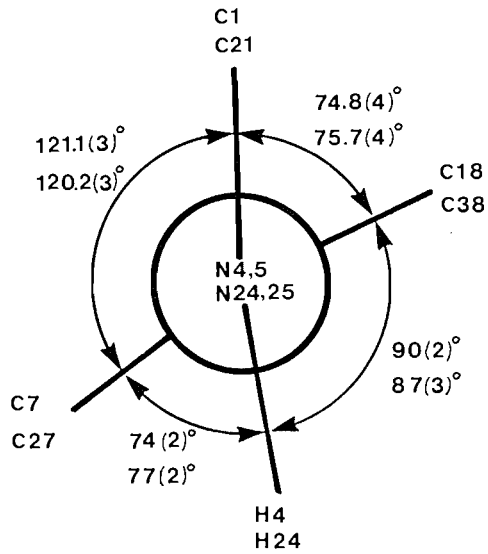

FIG. 3. Designation of the molecular planes.

TABLE 3. Selected dihedral angles between planes (°)

Planes*	Dihedral angle	
	Molecule **I**	Molecule **II**
1—2	1.1(3)	8.9(2)
1—3	11.9(2)	11.9(1)
1—4	59.4(1)	64.2(2)
1—5	72.9(1)	69.2(1)
1—6	72.5(1)	73.8(1)
1—7	73.1(1)	72.6(1)
5—6	2.9(1)	5.0(1)
5—7	0.4(1)	3.3(1)
6—7	3.3(1)	2.2(1)

*See Fig. 3.

Bearing in mind the aforementioned qualifications concerning the interpretation of the estimated standard deviations of the bond lengths and angles, the structure of the carbazole moiety is not significantly different from that of the carbazole molecule (10).

Molecular packing

The molecular packing diagram for a complete unit cell is shown in Fig. 4. The carbazole planes of one molecule overlap with the picryl planes of an adjacent molecule forming infinite chains. The two modes of overlap of one molecule with an adjacent molecule are shown in Fig. 5. The distance between the carbazole plane and the picryl plane is 3.28(13) Å in mode 1 and 3.34(13) Å in mode 2. The standard deviations in the interplanar spacings are $[\Sigma_i(l_i - \bar{l})^2/n - 1]^{1/2}$ where $\bar{l} = \Sigma_i l_i/n$ and l_i is the distance of the ith atom of the carbazole moiety from the plane of the six carbon atoms in the neighboring picryl moiety. This is similar to equivalent distances in related donor–acceptor (D:A) species of aromatic π-electron systems. In the D:A complex between carbazole and trinitrobenzene, the two independent interplanar distances are 3.37 and 3.38 Å (11).

This suggests that there is a strong π-molecular interaction between the picryl plane (A) of one molecule and carbazole plane (D) of an adjacent molecule. Therefore, 9-(2,4,6-trinitroanilino)-carbazole forms crystals containing single component donor–acceptor chains of the form ···DhA:DhA:DhA···, where

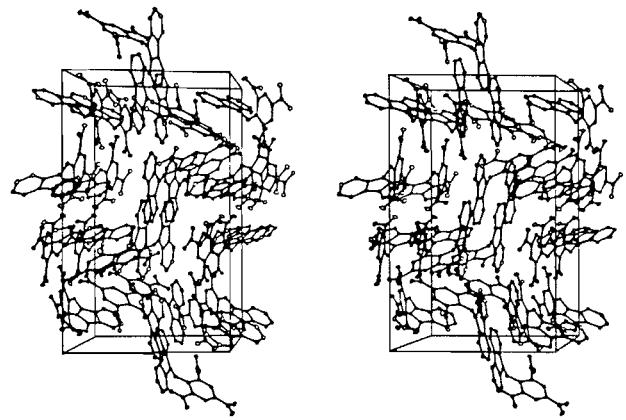

FIG. 4. ORTEP stereoscopic view of the unit cell, viewed along the *c* axis.

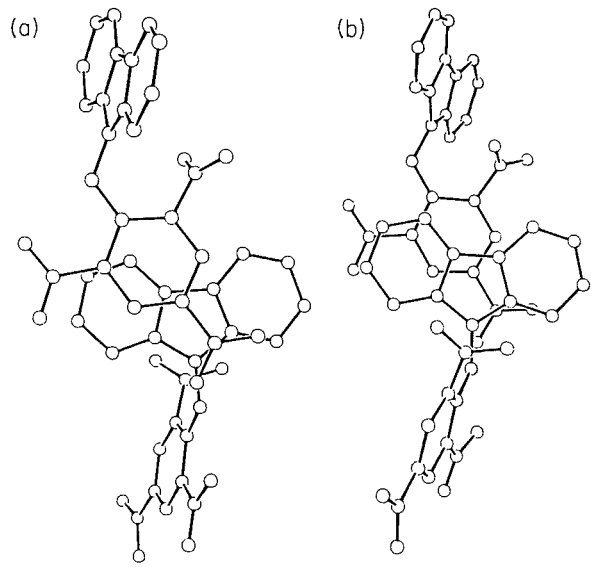

FIG. 5. The molecular overlap diagrams looking normal to the plane (*a*) mode 1; (*b*) mode 2.

the symbol h denotes the chain linkage between the donor and acceptor moieties within one molecule, which involves the hydrazine moiety. The internal degrees of freedom of one molecule do not permit the carbazole and picryl moieties to be coplanar. Therefore it is difficult to form an infinite linear chain with one independent molecule in the unit cell. The angles between the chain axis, [101], and the normals to the planes of the two picryl rings are 124.56(8)° and 58.40(4)°.

It has been suggested by Aviram and Ratner (12) that DσA molecules (σ representing a σ bond in the linkage between the donor and acceptor) might form a molecular crystal with the properties of a molecular rectifier. It would be necessary for the molecules to pack in the crystal with the donor and acceptor parts of one molecule in the same chain, and for the chains to all be of the same polarity. The structure reported here fulfils the first requirement but not the second. The lowest order bonds joining the donor and acceptor moieties of the molecule (N(4)—N(5) and N(24)—N(25)) are clearly not pure σ bonds, but they approximate σ bonds. It may be possible to modify 9-(2,4,6-trinitroanilino)-carbazole to force a more appropriate packing mode.

The unusual packing in this structure obviously owes its

Can. J. Chem. Downloaded from www.nrcresearchpress.com by 78.46.186.204 on 09/07/12
For personal use only.

existence to the C(12)—C(13) and C(32)—C(33) bonds, which force the two phenyl rings to be nearly co-planar, creating a flat three-ring aromatic donor moiety suitable for π-molecular donor–acceptor interaction with the picryl acceptor moiety.

Acknowledgements

The authors thank the Canadian International Development Agency for the support of H.W. and the Natural Sciences and Engineering Research Council for operating grants to R.J.B. and B.E.R. and to J.A.W.

1. C. TH. KIERS, J. L. DE BOER, R. OLTHOF, and A. L. SPEK. Acta Crystallogr. B**32**, 2297 (1976).
2. P. F. CURRIE, J. W. QUAIL, A. C. M. RUSK, and J. A. WEIL. Can. J. Chem. **61**, 1760 (1983).
3. J. A. WEIL and G. A. JANUSONIS. J. Org. Chem. **27**, 1248 (1962).
4. M. M. CHEN, K. V. SANE, R. I. WALTER, and J. A. WEIL. J. Phys. Chem. **65**, 713 (1961).
5. N. S. DALAL, D. E. KENNEDY, and C. A. MCDOWELL. Chem. Phys. Lett. **30**, 186 (1975).
6. R. GOPAL, B. E. ROBERTSON, and J. A. WEIL. Can. J. Chem. **61**, 2735 (1983).
7. H. WANG and B. E. ROBERTSON. Structure and statistics in crystallography. *Edited by* A. J. C. Wilson. 1985. pp. 125–136. Adenine Press.
8. J. M. STEWART and S. R. HALL. The XTAL system of crystallographic programs: user's manual. 2nd ed. TR-1364.1. Computer Science Center, University of Maryland, College Park, MD. 1985.
9. J. HEIDBERG, J. A. WEIL, G. A. JANUSONIS, and J. K. ANDERSON. J. Chem. Phys. **41**, 1033 (1964).
10. V. K. BEL'SKII. Sov. Phys. Crystallogr. **30**, 112 (1985).
11. F. BECHTEL, D. CHASSEAU, and J. GAULTIER. Cryst. Struct. Commun. **5**, 297 (1976).
12. A. AVIRAM and M. A. RATNER. Chem. Phys. Lett. **29**, 277 (1974).

Can. J. Chem. Downloaded from www.nrcresearchpress.com by 78.46.186.204 on 09/07/12
For personal use only.

Notes on the directed aldol synthesis and reduction of some compounds related to cycloheximide

DAVID M. PIATAK[1] AND PUI-FUN LOUISA TANG
Department of Chemistry, Northern Illinois University, DeKalb, IL 60115, U.S.A.

Received September 25, 1986

DAVID M. PIATAK and PUI-FUN LOUISA TANG. Can. J. Chem. **65**, 1327 (1987).

Several *N*-phenylcycloheximide analogues were prepared by $TiCl_4$-promoted aldol condensation between trimethylsilyl enol ethers of cyclic ketones and (*N*-phenylglutarimide)-β-acetaldehyde. Favored stereoisomers were isolated in several instances and identified from nuclear magnetic resonance data. Only for the analogue from 4-*tert*-butylcyclohexanone was it possible to obtain both *erythro* and *threo* isomers. Catalytic reduction of the β-hydroxyketone system over PtO_2 gave dihydrocycloheximide analogues possessing an axial ring hydroxyl group. Reduction in glacial HOAc was noted as promoting fission of the glutarimide ring with formation of lactone amides and, in several instances, concomitant reduction of the phenyl ring to a cyclohexyl group.

DAVID M. PIATAK et PUI-FUN LOUISA TANG. Can. J. Chem. **65**, 1327 (1987).

On a préparé plusieurs analogues de la *N*-phénylcycloheximide en procédant à la condensation aldolique, catalysée par le $TiCl_4$, d'éthers énoliques triméthylsilyles de cétones cycliques et de (*N*-phénylglutarimide)-β-acétaldéhyde. Dans plusieurs cas, on a isolé les stéréoisomères les plus favorisés et on les a caractérisés par la résonance magnétique nucléaire. L'analogue de la *tert*-butyl-4 cyclohexanone est le seul cas où l'on a pu isoler les isomères tant *érythro* que *thréo*. La réduction catalytique du système β-hydroxycétonique, à l'aide de PtO_2, conduit aux analogues dihydrocycloheximides possédant un groupement hydroxyle axial. On a noté que la réduction dans l'acide acétique glacial favorise une fission du noyau glutarimide qui conduit à la formation d'amides lactoniques et, dans plusieurs cas, à une réduction concomitante du noyau phényle en groupement cyclohexyle.

[Traduit par la revue]

Our prior work (1) with analogues of the antibiotic and DNA biosynthetic inhibitor cycloheximide **1***a* indicated that these compounds held some promise as potential anticonvulsants. A general synthetic procedure leading regio- and stereospecifically to the requisite β-hydroxyketone functionality was sought, since the previous methods we used were not as simple and direct as we had hoped. We began by examining the $TiCl_4$-promoted directed aldol condensation procedure, initially described by T. Mukaiyama *et al.* (2), to develop an efficient strategy for the synthesis of additional analogues whereby the cyclohexane ring substituents and (or) the imide ring portion of the molecule could be varied before introducing the β-hydroxyketone system. Recently, S. Kudo *et al.* (3, 4) used titanium and tin halide mediated methods to prepare optically active *trans*-cycloheximide isomers and chiral *cis*-cycloheximide isomers for antimicrobial activity studies. Thus, the method offered promise.

Our initial experience with the Mukaiyama procedure using the glutarimide-β-acetaldehyde (5) was unsatisfactory as we were unable to effect adequate protection of the imide group with benzyl chloride. Direct reaction of the imidealdehyde and 6-methyl-1-trimethylsiloxycyclohexene employing 2 equiv. of $TiCl_4$ to overcome its deactivation gave only a 3.3% yield of product **1***b*, isolated as the acetate.[2] The product was readily identified by its spectral data and contained an isomeric mixture as indicated by ^1H nmr doublets at δ 1.0 (J = 6.35) and 1.16 (J = 7.2) for the C-2 methyl group.

Studies were then continued with *N*-phenylglutarimide-β-acetaldehyde since the *N*-phenyl substituent should provide the necessary imide protection needed for the aldol condensation process. At the same time, this group should afford products containing a substituent that has been a feature of some biologically interesting glutarimides (6, 7). *N*-Phenylglutarimide-β-acetaldehyde was readily synthesized by starting with methanetriacetic acid (8) and one equivalent of aniline, converting the imideacid to the acid chloride, and then reducing the corresponding acid chloride by the Rosenmund procedure. The silylated enol ethers were available from the corresponding cyclohexanones and cyclopentanone by standard procedures (9), and their purity was established from nmr data.

The $TiCl_4$-promoted aldol condensation proceeded smoothly with the cyclohexanone enol ethers and the *N*-phenylglutarimide aldehyde at −78°C as described by Mukaiyama (2). The reaction mixtures crystallized upon standing and the products were recrystallized to afford purified materials (see Table 1). Although the quantity of recovered crystalline product was not high, overall yields averaged 60–70%, as tlc of the mother liquors often indicated only a single material with an R_f value identical to the recrystallized material. The products were generally characterized by three distinct ir carbonyl absorptions at about 1725, 1700, and 1680 cm^{-1} for the ketone and cyclic imide moieties as well as bands at 3555–3510 cm^{-1} for the hydroxy group. Also, two nmr multiplets at δ 7.1 and 7.4, equal to two and three protons in area, respectively, represented the aromatic ring protons as influenced by the proximity of the imide carbonyl groups. Further analysis of the nmr spectra of the crude products in many cases indicated the presence of isomers, as evidenced by two signals (about δ 4.2 and 3.85) for the carbinol proton and by more than one methyl doublet, for products originating from methylcyclohexanones. Attempts to effect a separation and isolation of individual isomers were not successful although recrystallization did result in the isolation of a single racemic isomer in some instances and in two separate *tert*-butyl analogue isomers **2***a*,*b*. The latter isomers nevertheless had tlc R_f values identical with one another and with the crude reaction product. This latter reaction also led to a small amount of an anhydro product **3**, which might be expected from dehydration of the aldol product.

The lack of high stereoselectivity was not surprising since

[1]Author to whom correspondence may be addressed.

[2]During this project we became aware of the work by S. Kudo *et al.* (refs. 3 and 4), in which they used the unprotected imidealdehyde with the *trans* and *cis* forms of 4,6-dimethyl-1-trimethylsiloxycyclohexene to achieve condensation yields of 18.3 and 10.8%, respectively.

Printed in Canada / Imprimé au Canada

Can. J. Chem. Downloaded from www.nrcresearchpress.com by 78.46.186.204 on 09/07/12
For personal use only.

TABLE 1. Data for the products from $TiCl_4$-promoted aldol condensations

Compound	Melting point (°C)	Yield[a] (%)	Formula	Analyses (C, H, N) Calcd.	Found	Infrared (cm^{-1})	^1H nuclear magnetic resonance (δ)
2-Methyl **2***c*	148–150	25[b]	$C_{20}H_{25}NO_4$	69.95 7.34 4.08	70.16 7.82 4.31	3520, 1725 1700, 1670 1590, 1490	7.39 (m, 3H), 7.13 (m, 2H), 3.85 (m, 1H), 3.1–1.3 (16H), 1.19 (d, J = 7.2), 1.03 (d, J = 5.9)
2-Methyl[c] **2***f*	138–141.5	6.6[d]	$C_{22}H_{27}NO_5$	68.55 7.06 3.64	68.56 7.17 3.64	1735, 1715 1680, 1235	7.4 (m, 3H), 7.1 (m, 2H), 5.35 (m, 1H), 3.2–1.3 (14H), 2.07 (s, 3H), 1.0 (d, 3H, J = 6.2); in C_6D_6 δ 5.42 (m, 1H)
4-Methyl **2***d*	152.5–154	20.6[d]	$C_{20}H_{25}NO_4$	69.95 7.34 4.08	69.67 7.53 4.54	3520, 1730 1705, 1665 1590, 1490	7.39 (m, 3H), 7.09 (m, 2H), 3.85 (br, 1H), 3.2–1.5 (16H), 1.19 (d, 3H, J = 6.7)
3,5-Dimethyl **2***e*	153–156	19.5[e]	$C_{21}H_{27}NO_4$	70.56 7.62 3.92	70.11 7.72 3.90	3510, 1725 1700, 1675 1590, 1490	7.4 (m, 3H), 7.08 (m, 2H), 3.9 + 3.8 (m, 1H), 3.2–1.5 (15H), 1.12 (d, 3H, J = 8.2), 1.04 (d, 3H, J = 4.8)
2,4-Dimethyl **2***g*	158.5–159.5	29.9[b]	$C_{21}H_{27}NO_4$	70.56 7.62	70.73 7.93	3525, 1720 1700, 1667 1590, 1490	7.39 (m, 3H), 7.09 (m, 2H), 3.15–1.5 (15H), 1.08 (d, 3H), J = 6), 1.0 (d, 3H, J = 5), 4.0 (m, 1H)
Normethyl **2***h*	149.5–151.5	28.7[b]	$C_{19}H_{23}NO_4$	69.28 7.04 4.25	68.97 7.27 4.01	3520, 1725 1705, 1678 1590, 1490	7.4 (m, 3H), 7.1 (m, 2H), 3.85 (br, 1H), 4.2 (d, 1H, J = 9), 3.3–1.2 (16H)

[a]No attempt was made to effect complete recovery of all isomers owing to similar tlc properties.
[b]From CH_2Cl_2–ether.
[c]Isolated only after extensive chromatography of the acetylated crude reaction mixture.
[d]From CH_2Cl_2.
[e]From acetone.

Mukaiyama *et al.* (2) and Heathcock *et al.* (10) have reported Lewis acid catalyzed aldol condensations to give poor diastereoselectivity. Nonetheless, the preferential formation of some isomers might ensue (2) when steric hindrance is encountered between the trimethylsiloxy group of the cyclohexene and a substituent at position 6. Kudo *et al.* (3, 4), for example, found a favored isomer to prevail in their work on 4,6-dimethyl-1-trimethylsiloxycyclohexenes.

Stereochemical identification of the isolated compounds was established through ^1H nmr data for the carbinol proton and for the cyclohexane ring methyl groups. For 1-methyl **2***c*, 4-methyl **2***d*, and 3,5-dimethyl **2***e* aldol products a multiplet at ca. δ 3.9 established a *threo* relationship between the glutarimide side chain attachment and the alcohol. Because of its bulk, the side chain was assumed to orient itself in the equatorial conformation on the cyclohexanone ring. Analysis of the methyl group signals for **2***c* revealed equatorial and axial epimers from two doublets at δ 1.03 and 1.19. Acetylation of crude product from the C-2 methyl reaction permitted the isolation of a *threo* product **2***f* with an equatorial methyl, albeit in poor yield. The C-4 methyl product **2***d* exhibited only one methyl doublet at δ 1.19 (J = 6.7) indicative of an axial configuration (the axial C-4 methyl of cycloheximide is found at δ 1.25 with J = 6.9), and, as expected, the 3,5-dimethyl analogue **2***e* had two separate doublets at δ 1.04 and 1.12 for various combinations of methyl group orientations.

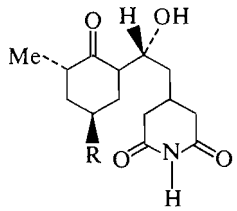

1*a* R = Me
b R = H

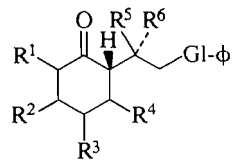

2*a* $R^1 = R^2 = R^4 = R^5 = H$; R^3 = eq CMe_3; R^6 = OH
b $R^1 = R^2 = R^4 = R^6 = H$; R^3 = eq CMe_3; R^5 = OH
c R^1 = ax/eq Me; $R^2 = R^3 = R^4 = R^6 = H$; R^5 = OH
d $R^1 = R^2 = R^4 = R^6 = H$; R^3 = ax Me; R^5 = OH
e $R^1 = R^3 = R^6 = H$; $R^2 = R^4$ = ax/eq Me; R^5 = OH
f R^1 = eq Me; $R^2 = R^3 = R^4 = R^6 = H$; R^5 = OAc
g $R^1 = R^3$ = eq Me; $R^2 = R^4 = H$; R^5/R^6 = H/OH
h $R^1 = R^2 = R^3 = R^4 = H$; R^5/R^6 = H/OH

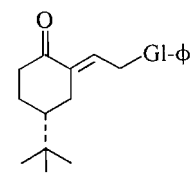

3

Can. J. Chem. Downloaded from www.nrcresearchpress.com by 78.46.186.204 on 09/07/12
For personal use only.

TABLE 2. Data for the *N*-phenyldihydroxycycloheximides

Compound	Melting point (°C)	Yield (%)	Formula	Analyses (C, H, N) Calcd.	Found	Infrared (cm^{-1})	^1H nuclear magnetic resonance (δ)
2-Methyl **7***a*	173–175	44.3	$C_{20}H_{27}NO_4$	69.54 7.88 4.05	69.53 7.92 3.95	3470, 1726 1665	7.4 (m, 3H), 7.1 (m, 2H), 4.1 (m, 1H), 3.8 (br, 1H), 3.3–1.2 (17H), 0.99 (d, 3H, J = 5)
4-Methyl **7***b*	155–158	51.8	$C_{20}H_{27}NO_4$	69.54 7.88 4.05	69.60 7.81 4.05	3535, 3400 1730, 1670	7.4 (m, 3H), 7.1 (m, 2H), 4.1 (m, 1H), 3.65 (m, 1H), 3.2–1.2 (17H), 1.01 (d, 3H, J = 7.2)
3,5-Dimethyl **7***c*	175–177.5	29.3[a]	$C_{21}H_{29}NO_4$	70.17 8.13 3.90	70.10 8.29 3.84	3500, 3380 1725, 1673	7.4 (m, 3H), 7.1 (m, 2H), 4.0 (d, 2H), 3.15–1.2 (16H), 1.0 (d, 3H, J = 8.5), 0.89 (d, 3H, J = 6.35)
Normethyl **7***e*	150–152	53.7	$C_{19}H_{25}NO_4$	68.86 7.61 4.23	68.75 7.75 4.35	3410, 3310 1720, 1660	7.4 (m, 3H), 7.1 (m, 2H), 4.3 (m, 1H), 3.7 (m, 1H), 3.2–1.1 (18H)
tert-Butyl (er) **7***f*	189–192	85.5	$C_{23}H_{33}NO_4$	71.29 8.58 3.61	71.43 8.56 3.62	3380, 1738 1665	7.4 (m, 3H), 7.1 (m, 2H), 4.0 (d, 1H), 4.1 (m, 1H), 3.2–1.1 (17H), 0.91 (s, 9H)
tert-Butyl (th) **7***g*	155–160	74.6	$C_{23}H_{33}NO_4$	71.29 8.58 3.61	71.01 8.19 3.55	3360, 1725 1675	7.4 (m, 3H), 7.1 (m, 2H), 4.3 (m, 1H), 3.7 (br, 1H), 3.2–1.1 (17H), 0.89 (s, 9H)

[a]This product was recrystallized from acetone, while EtOAc was used for all others.

Proton nmr data for the 2,4-dimethyl analogue **2***g* fit best with a *cis* dimethyl configuration (δ 1.0 and 1.08) for the cyclohexane ring methyls (4) and with an unassigned hydroxyl group orientation owing to a broad signal at δ 4.0. Without a methyl group on the cyclohexane ring to influence the course of the reaction as in the normethyl product **2***h*, stereospecificity should be lost and an equimolar mixture of isomers would be expected. The crystalline product, however, was a mixture of *threo* and *erythro* isomers in a 1:3 ratio, as determined from integration of the nmr multiplet at δ 3.85 for the *threo* isomer and the doublet at δ 4.2 for the *erythro* form.

In the case of the two separate *tert*-butyl analogue isomers, the *erythro* form **2***a* was readily ascertained by observation of a doublet at δ 4.25 for the proton on the carbinol carbon and the *threo* product **2***b* by a multiplet centered at δ 3.82. These assignments were supported by ^{13}C nmr spectra in which the hydroxyl carbon was at δ 66.77 for **2***a* and at δ 69.23 for **2***b*. Cycloheximide with its *erythro* configuration has this carbon atom absorption (11) at δ 66.5. In addition, ^1H nmr spectra of the corresponding acetates recorded first in $CDCl_3$, then C_6D_6, revealed an upfield shift from δ 5.35 to 5.29 for the *erythro* **2***a* acetate similar to the shift for cycloheximide acetate (δ 5.34 to 5.30), while a downfield shift from δ 5.39 to 5.41 was observed for the *threo* **2***b* acetate.

Use of cyclopentanone, the only non-cyclohexane type ketone employed, gave a crude product with a significant nmr signal at δ 6.5 indicative of a vinylic proton. Acetylation and tlc separation of the mixture led to three distinct compounds. The least mobile was identified as lactone amide **4**, primarily from ir bands at 3350 cm^{-1} for the NH, at 1680 and 1540 cm^{-1} for the amide I and II absorptions, and at 1725 cm^{-1} for the lactone carbonyl. Lactones of this type have been reported (12) to arise from glutarimide antibiotics under strongly acidic or basic conditions, and we encountered the same in our prior

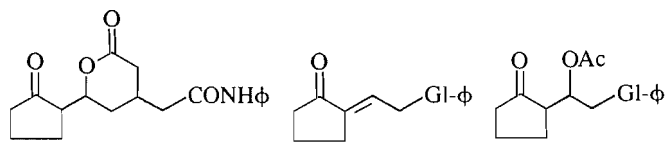

4 **5** **6**

work (1). The second compound was the unsaturated ketone **5**, characterized by ir peaks at 1730, 1710, 1689, and 1645 cm^{-1}, a uv maximum at 242 nm, and an nmr signal at δ 6.5 (m, 1H) for the vinylic proton. The most mobile compound on tlc was the anticipated product **6**. Major ir absorptions were evident at 1735, 1705, 1670, and 1250 cm^{-1} while nmr signals were seen at δ 5.96 (t, 1H) and 2.04 (s, 3H), supporting this assignment. The acetoxy moiety was found to eliminate readily, making isolation difficult.

To provide dihydrocycloheximide analogues, the aldol condensation products were reduced catalytically, essentially as before (1), except 5–10% HOAc–EtOAc was substituted for the glacial HOAc solvent to avoid appreciable glutarimide ring fission. The diols normally crystallized from the reaction mixture in an average yield of 60% and were characterized by their differences in the hydroxyl group region of the infrared, and by nmr signals at δ 4.0–4.3 for the proton on the ring hydroxyl carbon and at δ 3.4–3.8 for the proton on the side chain hydroxyl carbon (see Table 2). From the former nmr absorptions the ring hydroxyl group is considered to be axial, in agreement with previous stereochemical studies (13) on the reduction of cycloheximide and with our observations (1) on the reduction of dehydrocycloheximide compounds.

Analysis of the nmr signals for the methyl groups indicated that the 2-methyl diol **7***a* had an equatorial methyl, a result different from the parent compound in which both equatorial and axial methyl signals were observed. This orientation is

Can. J. Chem. Downloaded from www.nrcresearchpress.com by 78.46.186.204 on 09/07/12
For personal use only.

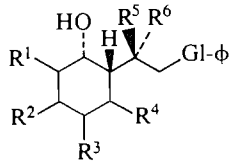

7*a* R^1 = ax/eq Me; $R^2 = R^3 = R^4 = R^6$ = H; R^5 = OH
b $R^1 = R^2 = R^4 = R^6$ = H; R^3 = ax Me; R^5 = OH
c $R^1 = R^3 = R^6$ = H; $R^2 = R^4$ = ax/eq Me; R^5 = OH
d $R^1 = R^3$ = eq Me; $R^2 = R^4$ = H; R^5/R^6 = H/OH
e $R^1 = R^2 = R^3 = R^4$ = H; R^5/R^6 = H/OH
f $R^1 = R^2 = R^4 = R^5$ = H; R^3 = eq CMe_3; R^6 = OH
g $R^1 = R^2 = R^4 = R^6$ = H; R^3 = eq CMe_3; R^5 = OH

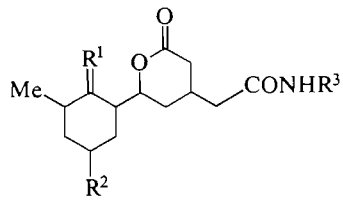

8*a* R^1 = H, OH; R^2 = Me; R^3 = phenyl
b R^1 = O; R^2 = Me; R^3 = phenyl
c R^1 = H, OAc; R^2 = Me; R^3 = C_6H_{11}
d R^1 = H, OH; R^2 = H; R^3 = C_6H_{11}
e R^1 = H, OAc; R^2 = H; R^3 = C_6H_{11}

9

probably a consequence of equilibration by an α-alkyl ketone in an acidic medium during a rather slow reduction. For the other diols the methyl group stereochemistry, as indicated by nmr, remained as observed in the aldol products, i.e., axial in the C-4 methyl diol **7***b*, a combination of both orientations in the 3,5-dimethyl analogue **7***c*, and diequatorial (*cis*) in the dihydrocycloheximide type compound **7***d*. For the *tert*-butyl analogues the reduction went smoothly and in good yield to afford the axial-*erythro* **7***f* and the axial-*threo* **7***g* diols with appropriate spectral characteristics.

Some unusual products, however, were obtained when the catalytic reductions were performed in glacial HOAc on material contained in the mother liquors, which were identical to crystalline material by tlc. These experiments prompted employment of a less acidic solvent for later reduction work. For example, the 2,4-methyl aldol product **2***g* mother liquors yielded the expected diol **7***d* but also hydroxy lactone **8***a* and keto lactone **8***b*. The acetoxy lactone **8***c*, characterized from the absence of aromatic proton signals in an nmr spectrum and correct C, H, N data, was not expected, however, since these hydrogenation conditions are not normally associated with reduction of an aromatic ring.

Hydrogenation of material from the 2-methyl aldol product **2***g* mother liquors under identical conditions, followed by acetylation to facilitate separation, also afforded similar aromatic ring reduced lactones **8***d* and **8***e*. Both were characterized from the absence of aromatic peaks in ir and nmr spectra and the presence of typical hydroxy, acetoxy, lactone, and amide ir bands, from analytical data, and from nmr proton integration. The acetoxy imide **9** was also isolated and was characterized from analytical and spectral data. This latter compound undoubtedly results from reduction of the α,β-unsaturated ketone (similar to **3**), which can be produced by acidic or basic dehydration of an aldol condensation product.

Experimental

Melting points were taken on a Fisher–Johns apparatus and are uncorrected. Infrared (ir) spectra were obtained with a Sargent–Welch 3-200 infrared spectrophotometer on solids incorporated into KBr wafers or on neat liquid samples. The nmr spectra were obtained on an IBM-NR 80 spectrometer on samples dissolved in $CDCl_3$ containing TMS as internal standard, unless otherwise noted. Ultraviolet spectra were recorded with a Varian 2290 spectrophotometer.

Precoated thin-layer chromatography (tlc) sheets of silica gel 60 F_{254} from EM Reagents were used for qualitative tlc, while preparative tlc was performed on 0.5-mm plates of silica gel PF_{254}.

N-*Phenyl-4-carboxymethyl-2,6-piperidinedione*

A solution of methanetriacetic acid (8) (8.87 g; 4.56 mmol), water (2 mL), and aniline (4.46 mL; 1 equiv.; distilled from zinc) was slowly heated to 180–200°C, then maintained at that tempeature for 1 h. The liquid materials were removed at 170°C/0.3 Torr (1 Torr = 133.3 Pa) and the residue was taken up in EtOAc and filtered. Concentration of the filtrate gave crystals, which were recrystallized to afford 8.54 g (81%); mp 200–201.5°C; ir: 3500–2600, 1730, 1670, 1600, 1490 cm^{-1}; nmr δ: 7.4 (m, 3H), 7.2 (m, 2H). *Anal.* calcd. for $C_{13}H_{13}NO_4$: C 63.15, H 5.30, N 5.66; found: C 63.24, H 5.31, N 5.82.

N-*Phenyl-4-carbonylmethyl-2,6-piperidinedione*

The *N*-phenylimidyl acid (5.92 g) and $SOCl_2$ (59 mL) were heated at reflux for 0.5 h until the solids dissolved, then the excess $SOCl_2$ was removed *in vacuo*. The resultant crystals were washed with dry benzene to afford 5.53 g (86.9%) of intermediate acid chloride; mp 115–117°C; ir: 1810, 1730, 1675 cm^{-1}.

The acid chloride, dry toluene (280 mL), and 5% $Pd/BaSO_4$ (2.24 g) were placed into a flask, hydrogen was introduced into the solution through a gas diffusion tube, and the mixture was heated to reflux. The excess H_2 and other gases were passed through a standardized NaOH solution until the evolution of HCl essentially stopped (5 h; 82.5% of theoretical). Removal of the catalyst and concentration of the filtrate yielded 4.01 g (83.2%) of crystals. Recrystallization from $CHCl_3$ gave colorless crystals (3.64 g; 75.7%) of the desired *N*-phenylimidyl aldehyde; mp 113–115°C; ir: 2850, 2745, 1730, 1710 cm^{-1}; nmr δ: 9.8 (s, 1H), 7.4 (m, 3H), 7.01 (m, 2H), 3.1–2.5 (7H). *Anal.* calcd. for $C_{13}H_{13}NO_3$: C 67.52, H 5.67, N 6.05; found: C 67.80, H 5.84, N 5.95.

Preparation of N-*phenylcycloheximide analogues*

In a typical experiment, a solution of the *N*-phenylimidyl aldehyde (1 g, 4.32 mmol) in CH_2Cl_2 (20 mL) at −78°C was treated with $TiCl_4$ (0.48 mL; 1 equiv.). The trimethylsilyl enol ether of 4-*tert*-butylcyclohexanone (1 equiv.) was added slowly, and the reaction was stirred at −78°C for 3 h, then at ambient temperature for 3 h. An ice–water mixture was used to quench the reaction, and the product was isolated by extraction with ether. Fractional recrystallization of the ether residue from acetone yielded first the *erythro tert*-butyl analogue **2***a* (310 mg; 18.7%); mp 184.5–187°C; ir: 3555, 1732, 1700, 1678, 1590, 1490 cm^{-1}; nmr δ: 7.4 (m, 3H), 7.1 (m, 2H), 4.25 (d, 1H, J = 10.9), 3.2–1.4 (16H), 0.95 (s, 9H); ^{13}C nmr δ: 66.77 (*C*HOH). *Anal.* calcd. for $C_{23}H_{31}NO_4$: C 71.66, H 8.11, N 3.63; found: C 71.52, H 8.15, N 3.85.

The *threo* analogue **2***b* was then isolated as colorless crystals (174 mg; 10.5%); mp 178–180.5°C; ir: 3540, 1730, 1700, 1680, 1590, 1490 cm^{-1}; ^1H nmr δ: 7.4 (m, 3H), 7.1 (m, 2H), 3.82 (br m, 1H), 3.2–1.3 (16H), 0.95 (s, 3H); ^{13}C nmr δ: 69.23 (*C*HOH). *Anal.* found: C 71.84, H 8.28, N 3.91.

Chromatography of the mother liquors by preparative tlc (50% EtOAc–hexane) gave 100 mg (6.0%) of anhydro compound **3**; mp 144–146°C; uv_{max}: 243 (ε 7680), sh 280–286 nm; ir: 1734, 1700, 1680, 1600 cm^{-1}; ^1H nmr δ: 7.4 (m, 3H), 7.1 (m, 2H), 6.58 (t, 1H),

Can. J. Chem. Downloaded from www.nrcresearchpress.com by 78.46.186.204 on 09/07/12
For personal use only.

3.1–1.25 (14H), 0.96 (s, 9H). *Anal.* calcd. for $C_{23}H_{29}NO_4$: C 75.17, H 7.95, N 3.81; found: C 74.86, H 8.11, N 3.78.

Each of the isomers was acetylated by acetic anhydride – pyridine to afford the corresponding acetate, which was recrystallized from EtOAc.

Erythro **2***a* acetate: mp 142.5–144°C; ir: 1740, 1710, 1678, 1240 cm^{-1}; ^1H nmr δ: 7.4 (m, 3H), 7.15 (m, 2H), 5.35 (m, 1H), 2.08 (s, 3H), 0.93 (s, 9H); ^1H nmr (C_6D_6) δ: 5.29 (m, 1H), 1.83 (s, 3H), 0.79 (s). *Anal.* calcd. for $C_{25}H_{33}NO_5$: N 3.28; found: N 2.95.

Threo **2***b* acetate: mp 131–132.5°C; ir: 1735, 1710, 1680, 1235 cm^{-1}; ^1H nmr δ: 7.4 (m, 3H), 7.1 (m, 2H), 5.39 (m, 1H), 2.09 (s, 3H), 0.95 (s, 9H); ^1H nmr (C_6D_6) δ: 5.41 (m, 1H), 1.8 (s, 3H), 0.78 (s). *Anal.* found: N 3.61.

Data for other aldol condensation products are in Table 1.

Directed aldol condensation with cyclopentanone enol ether

The *N*-phenylglutarimidyl aldehyde (0.76 g; 3.3 mmol) in CH_2Cl_2 (20 mL) at −78°C was treated with $TiCl_4$ (0.36 mL; 1 equiv.), then with 1-trimethylsilyloxycyclopentene (0.54 g; 1 equiv.). After the reaction mixture was stirred for 3 h, it was stirred at room temperature for another 3 h. Extraction with ether following ice–water quenching gave a crude oil (0.61 g), which was acetylated by acetic anhydride – pyridine and separated by preparative tlc (5% MeOH–$CHCl_3$) into three fractions.

The least mobile fraction (R_f 0.11) was determined to be amide lactone **4** (0.1 g); ir: 3350, 1725, 1715, 1680, 1545 cm^{-1}; nmr δ: 7.4, 7.1, 6.5, 5.3.

The next fraction (R_f 0.23) was recrystallized from ether–CH_2Cl_2 to yield pure unsaturated ketone **5** (0.12 g); mp 138–139°C; uv_{max}: 242 (ε 13 200), sh 275 nm; ir: 1730, 1710, 1689, 1645 cm^{-1}; nmr δ: 7.47 (m, 3H), 7.02 (m, 2H), 6.5 (m, 1H). *Anal.* calcd. for $C_{18}H_{19}NO_3$: C 72.71, H 6.44, N 4.71; found: C 72.58, H 6.44, N 4.99.

The most mobile material (R_f 0.38) was the acetylated aldol product **6**, which crystallized from ether to give 0.02 g; mp 108–109.5°C; ir: 1735, 1705, 1670, 1250 cm^{-1}; nmr δ: 7.4 (m, 3H), 7.1 (m, 2H), 5.96 (m, 1H), 2.04 (s, 3H). *Anal.* calcd. for $C_{20}H_{23}NO_5$: N 3.92; found: N 4.35. The product lost the acetate moiety readily.

Reduction of aldol condensation products

In a typical experiment a mixture of the 2,4-dimethyl analogue **2***g* (40 mg), PtO_2 (50 mg), and 10% HOAc–EtOAc (20 mL) was shaken under 50 psi (1 psi = 6.9 kPa) of H_2 for 26 h. Fresh catalyst was added (50 mg) and shaking was continued for 16 h. The catalyst was collected on Celite, and the filtrate was washed with dilute $NaHCO_3$, then with water, and dried. Removal of the EtOAc gave an oil (42 mg) that crystallized upon standing. Recrystallization from EtOAc yielded 19.1 mg (47.5%) of diol **7***d*; mp 130–135°C; ir: 3500, 3380, 1725, 1675 cm^{-1}; nmr δ: 7.4 (m, 3H), 7.1 (m, 2H), 4.18 (br m, 1H), 3.48 (br, 1H), 1.01 (d, 3H, J = 6.35), 0.84 (d, 3H, J = 6.4). *Anal.* calcd. for $C_{21}H_{29}NO_4$: C 70.17, H 8.13, N 3.90; found: C 69.81, H 8.47, N 3.73.

Data for other diols are given in Table 2.

Reduction of N*-phenyl-2,4-dimethyl analogue* **2***g mother liquors in HOAc*

A mixture of the mother liquor (0.41 g), (identical to crystalline material by tlc) from the condensation reaction leading to **2***g*, PtO_2 (55 mg), and glacial HOAc (15 mL) was stirred under H_2 (44 psi) for 22 h. The catalyst was removed and the filtrate was diluted with EtOAc, then washed with dilute $NaHCO_3$ and water. The crude product (0.42 g) was purified by flash chromatography into three fractions. The least polar fraction (9 mg) was determined to be diol **7***d* by comparative spectral data.

The second fraction was separated into two lactones by preparative tlc (40% EtOAc–hexane; two dips). The more polar fraction gave hydroxy lactone **8***a* as colorless crystals from $CHCl_3$ (13.7 mg); mp 165–167°C; ir: 3500, 3320, 1720, 1662, 1525 cm^{-1}; nmr δ: 7.4 (m, 3H), 7.1 (m, 2H), 4.37 (br, 1H), 3.73 (m, 1H), 0.96 (d, 3H, J = 2.8), 0.92 (d, 3H, J = 3.4). *Anal.* calcd. for $C_{21}H_{29}NO_4$: C 70.17, H 8.13, N 3.90; found: C 69.95, H 8.46, N 3.95.

The less polar lactone was keto lactone **8***b* (13.2 mg); mp 164–170°C; ir: 3300, 1720, 1700, 1655, 1535 cm^{-1}; nmr δ: 7.5 (m, 3H), 7.3 (m, 2H), 4.7 (br m, 1H), 3.35 (d, 1H), 3–1.4 (14H), 1.0 (d, 6H, J = 6.35). *Anal.* calcd. for $C_{21}H_{27}NO_4$: C 70.56, H 7.62, N 3.92; found: C 70.61, H 7.52, N 4.05.

A third column fraction furnished acetoxy lactone **8***c* (10 mg); mp 160.5–163°C; ir: 3280, 1730, 1710, 1675, 1630 cm^{-1}; nmr δ: 5.5 (br, 1H), 4.6 (br, 1H), 3.75 (br, 1H), 2.01 (s, 3H), 2.8–1.2 (28H), 1.0 (d, 6H, J = 4.1). *Anal.* calcd. for $C_{23}H_{37}NO_5$: C 67.78, H 9.15, N 3.44; found: C 67.55, H 9.45, N 3.95.

Reduction of 2-methyl analogue **2***c mother liquors in HOAc*

Mother liquors from preparation of 2-methylcycloheximide analogue **2***c* (0.67 g), which were identical by tlc to crystalline material, were reduced over PtO_2 (100 mg) in glacial HOAc (20 mL) as above. The crude product was acetylated by Ac_2O–pyridine as usual and then separated by preparative tlc (3% MeOH–$CHCl_3$; two dips) into five fractions. Three fractions crystallized and were identified.

The least mobile fraction gave hydroxy lactone **8***d* (11 mg); mp 167–169.5°C; ir: 3460, 3330, 1715, 1655, 1530 cm^{-1}; nmr δ: 5.4 (br, 1H, lost with D_2O), 4.45 (br, 1H), 3.74 (m, 1H), 2.8–1.2 (27H), 0.96 (d, 3H, J = 5.7). *Anal.* calcd. for $C_{20}H_{33}NO_4$: C 68.34, H 9.45, N 3.98; found: C 68.55, H 9.54, N 4.18.

The second fraction was identified as acetoxy lactone **8***e* (10 mg); mp 175–176°C; ir: 3330, 1725, 1645, 1530, 1245 cm^{-1}; nmr δ: 5.4 (m, 1H), 4.2 (m, 1H), 3.7 (m, 1H), 2.07 (s, 3H), 2.7–1.0 (29H), 0.85 (d, 3H, J = 6.1). *Anal.* calcd. for $C_{22}H_{35}NO_5$: C 67.14, H 8.97, N 3.56; found: C 67.08, H 9.11, N 3.56.

The most mobile fraction (82 mg) gave 12 mg of acetoxy imide **9** from EtOAc; mp 149–150°C; ir: 1725, 1680, 1250 cm^{-1}; nmr δ: 7.4 (m, 3H), 7.2 (m, 2H), 5.13 (m, 1H), 2.09 (s, 3H), 3.1–1.1 (17H), 0.85 (d, 3H, J = 5.4). *Anal.* calcd. for $C_{22}H_{29}NO_4$: C 71.13, H 7.87, N 3.77; found: C 71.16, H 8.18, N 3.88.

Acknowledgements

P. L. Tang thanks the Northern Illinois University Graduate School for a Doctoral Dissertation Fellowship.

1. D. M. Piatak and P. L. Tang. J. Med. Chem. **29**, 50 (1986).
2. T. Mukaiyama, K. Banno, and T. Narsaka. J. Am. Chem. Soc. **96**, 7503 (1974).
3. S. Kudo, T. Oritani, and K. Yamashita. Agric. Biol. Chem. **48**, 2315 (1984).
4. S. Kudo, T. Oritani, and K. Yamashita. Agric. Biol. Chem. **48**, 2739 (1984).
5. (*a*) T. Makaiyama, Y. Morita, J. Oya, and K. Wagatsuma. Japanese Patent 76 65 769, 1976; Chem. Abstr. **85**, P 177 260 (1976); (*b*) T. Makaiyama and K. Wagatsuma. Japanese Patents 77 83 70 and 77 83 571; Chem. Abstr. **88**, P 22635 and P 22638 (1978).
6. D. W. Cameron, J. G. Down, P. J. Kissane, G. M. Laycock, and A. Shulman. Aust. J. Chem. **30**, 1157 (1977).
7. A. U. De and A. K. Ghose. Indian J. Chem. Sect. B, **16**, 510 (1978).
8. E. P. Kohler and G. H. Reid. J. Am. Chem. Soc. **47**, 2803 (1925).
9. H. O. House, L. J. Czuba, M. Gall, and H. D. Olmstead. J. Org. Chem. **34**, 2324 (1969).
10. C. H. Heathcock, K. T. Hug, and L. A. Flippin. Tetrahedron Lett. **25**, 5973 (1984).
11. P. Jeffs and D. McWilliams. J. Am. Chem. Soc. **103**, 6185 (1981).
12. E. C. Kornfeld, R. G. Jones, and T. V. Parke. J. Am. Chem. Soc. **71**, 150 (1949).
13. F. Johnson, N. A. Starkovsky, A. C. Paton, and A. A. Carlson. J. Am. Chem. Soc. **88**, 149 (1966).

Can. J. Chem. Downloaded from www.nrcresearchpress.com by 78.46.186.204 on 09/07/12
For personal use only.

The ^{59}Co nuclear magnetic resonance spectra of polycrystalline complexes

DONALD R. EATON,[1] RICHARD J. BUIST, AND BRIAN G. SAYER
Department of Chemistry, McMaster University, Hamilton, Ont., Canada L8S 4M1

Received September 3, 1986

DONALD R. EATON, RICHARD J. BUIST, and BRIAN G. SAYER. Can. J. Chem. **65**, 1332 (1987).

The solid state ^{59}Co nmr spectra of a number of octahedral complexes are reported. In the case of sodium hexanitrocobaltate(III) the spectra have been obtained at several different field strengths and the results are analysed to give a quadrupole coupling constant of 9.4 MHz, an asymmetry parameter of zero and an axial chemical shift tensor with an anisotropy of 180 ppm. Several other complexes have been examined at high field (11.8T) to minimize the effects of quadrupole coupling and maximize the influence of chemical shift anisotropy. The results are, where possible, compared with single crystal X-ray and low field nmr data. It is concluded that high fields are necessary to obtain reliable chemical shift anisotropy values. The conditions necessary for obtaining reasonable quality spectra from polycrystalline samples containing quadrupolar nuclei are discussed.

DONALD R. EATON, RICHARD J. BUIST et BRIAN G. SAYER. Can. J. Chem. **65**, 1332 (1987).

On rapporte les spectres rmn ^{59}Co, à l'état solide, d'un certain nombre de complexes octaédraux. Dans le cas de l'hexanitrocobaltate(III) de sodium, on a déterminé les spectres à plusieurs forces de champs et on a analysé les résultats pour déterminer la constante de couplage quadrupolaire qui est égale à 9,4 MHz, le paramètre d'asymétrie qui égal à zéro et un tenseur de déplacement chimique axial comportant une anisotropie de 180 ppm. On a examiné les spectres de plusieurs autres complexes à champ élevé (11,8T) pour minimiser les effets des couplages quadrupolaires et pour maximiser l'influence de l'anisotropie du déplacement chimique. Lorsque cela est possible, on compare les résultats avec ceux obtenus par diffraction des rayons-x sur un cristal unique ainsi que par rmn à bas champs. On en conclut que les hauts champs sont nécessaires pour obtenir des valeurs fiables pour l'anisotropie du déplacement chimique. On discute des conditions nécessaires pour obtenir des spectres de qualité raisonnable à partir d'échantillons polycristallins contenant des noyaux quadrupolaires.

[Traduit par la revue]

Can. J. Chem. Downloaded from www.nrcresearchpress.com by 78.46.186.204 on 09/07/12
For personal use only.

Introduction

The introduction of cross polarization and magic angle spinning techniques (CPMAS) has lead to a large increase in interest in the nmr spectra of solid samples. The majority of these studies have been concerned with nuclei with $I = 1/2$ and particularly with ^{13}C. For nuclei with $I > 1/2$ there is the additional complication of quadrupole coupling and the CPMAS technique is no longer simply applicable. Modifications involving variable angle spinning (VASS) have been described (1–3) and have been applied to ^{17}O nmr spectroscopy. Some line narrowing results but the effects of chemical shift anisotropy cannot be completely eliminated.

The ^{59}Co nucleus has $I = 7/2$ and a rather large quadrupole moment. Compounds containing this nucleus have been extensively studied in solution but very little has been reported on their solid state ^{59}Co spectra. There are three possible motivations for obtaining such spectra:

(*a*) A comparison of the isotropic chemical shift in the solid state with that in solution may be informative. ^{59}Co chemical shifts are very sensitive to second sphere coordination effects and have been used to study this subject. The nature of the second coordination sphere in solution is always a topic for speculation whereas that in the solid is known if the crystal structure has been determined. Solid state spectra are therefore a logical starting point for second coordination sphere studies.

(*b*) In principle the chemical shift anisotropy, which is averaged out by molecular tumbling in solution, can be determined from solid state spectra. This is useful information since it can be easily and directly related to the kind of crystal field parameters obtained from optical and magnetic measurements.

(*c*) Quadrupole coupling constants can also be obtained from nmr powder spectra. However these parameters are not easy to interpret and for most cobalt complexes are more conveniently measured by nuclear quadrupole resonance.

Since ^{59}Co has $I = 7/2$ the selection rule $\delta m_i = +1$ predicts seven transitions in the nmr spectrum. Of these the central line, corresponding to the $+1/2$ to $-1/2$ transition, is only affected by the quadrupolar splitting to second order. If the quadrupole coupling is large, as it is for Co, this is likely to be the only transition observed in the nmr spectrum. The second order quadrupole interaction splits the line into a doublet. The splitting is proportional to the square of the quadrupole coupling constant and inversely proportional to the Zeeman term as measured by the spectrometer frequency. The effect of chemical shift anisotropy on the line shape is directly proportional to spectrometer frequency. It is anticipated therefore that at high magnetic fields chemical shift anisotropy effects will dominate and at low fields quadrupolar effects will be most important.

The calculation of the powder lineshape in the presence of quadrupolar and chemical shift anisotropy interactions has been considered by a number of authors (4–8). The problem becomes progressively more complex when both types of interaction are considered and when the molecule has non-axial symmetry. The most complete treatment is due to Baugher *et al.* (8) who give explicit formulae for the positions of the shoulders and singularities in terms of quadrupolar and chemical shift parameters. This treatment will be used to analyse the present data.

The amount of experimental data reported for Co complexes is quite small. All of the experiments have been carried out at low fields where quadrupolar effects dominate. Most studies have made use of single crystals. This leads to a more direct analysis of the data but, since rather large crystals are required, it is a time-consuming process which is impractical for an extended series of compounds. If the measurements are carried out at low field, as those reported in the literature have been, the effects of chemical shift anisotropy are small and the parameters correspondingly difficult to measure accurately. Saraswati and Vijayaraghavan (9) some years ago reported the ^{59}Co spectra of several polycrystalline complexes obtained at low field on a broad line instrument. The signal-to-noise ratio of the spectra

[1]Author to whom correspondence should be addressed.

obtained using this instrument was poor. This study did not provide chemical shift anisotropy information and subsequent single crystal studies did not in all cases agree with the quadrupole coupling constants reported.

In the present paper we report the ^{59}Co nmr spectra of several cobalt complexes in polycrystalline form. Our major interest is in the chemical shift tensor. Since the magnetic fields available at present are approximately one order of magnitude greater than those used by Saraswati and Vijayaraghaven the chances for obtaining useful chemical shift data are correspondingly enhanced. The increased sensitivity of high field instruments also results in much better quality spectra. One complex, the hexanitrocobaltate(III) (this ion is often called cobaltinitrite), has been examined at a number of different fields to check the feasibility of analysis using the formulae of Baugher *et al.* (8). The results for the remainder are reported at a single field which was the highest available since the quality of the spectra deteriorates rapidly at lower fields. The complexes chosen all have high molecular symmetry and most of their crystal structures have been reported, thus optimizing the chances for obtaining useful information. The quality of the spectra obtained with these compounds provides a basis for estimating the likely success of experiments with complexes of lower symmetry and with other quadrupolar metal nuclei.

Experimental

Samples of the cobalt complexes were purchased from Baker and were of analytical quality. They were used without further purification. Nuclear magnetic resonance spectra were obtained on Bruker WH90, CXP200, WM250, AM300, WM400, and AM500 instruments. Chemical shifts were measured relative to solutions of the corresponding complexes and were obtained by direct frequency calibration. The solvent used was water except in the case of the acetylacetonate which was dissolved in chloroform for reference purposes.

Results

Figure 1 shows the ^{59}Co nmr spectra of a polycrystalline sample of sodium cobaltinitrite obtained at several different field strengths. At low fields the appearance is that expected for a quadrupolar broadened resonance — a broad doublet. The spectra have been plotted on a uniform frequency scale and the inverse relationship between the doublet separation and field strength is readily apparent. At a field of 9.5T the quadrupolar splitting has been lost and at the highest field of 11.8T the pattern is typical of that expected from a molecule with axial chemical shift anisotropy. The observed isotropic chemical shifts and the measured peak separations at the lower fields are given in Table 1. Figure 1*B* shows a spectrum obtained at 4.7T but with MASS at 3.85 kHz. The peak separation has been reduced by a factor of 3.5. This reduction is in good agreement with the theoretical treatment of Ganapathy *et al.* (2). However, the quadrupolar splitting is not eliminated and the reduction is accompanied by the appearance of undesirable sidebands. There would seem to be no great advantage to magic angle spinning for samples such as these.

Figure 2 shows powder spectra obtained for five other Co(III) complexes. They were all obtained at 119.57 MHz using a Bruker AM500 spectrometer. Several types of behaviour are apparent. The trisethylene diamine complex gives a spectrum similar to that of the cobaltinitrite at the same spectrometer frequency. The effects of chemical shift anisotropy are dominant and the chemical shift tensor has axial symmetry. In this case though $\sigma_\perp$ is greater than $\sigma_\parallel$ rather than vice versa. The spectrum of the hexacyanocobaltate(III) ion also appears to

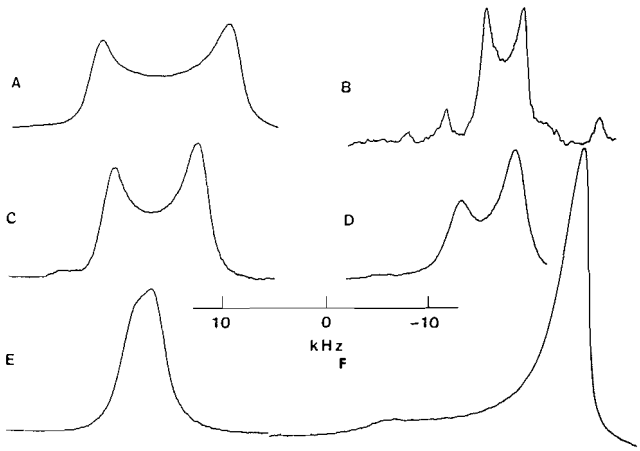

FIG. 1. ^{59}Co nmr spectra of polycrystalline sodium hexanitrocobaltate(III): (*A*) $B_0 = 4.7$T; (*B*) $B_0 = 4.7$T with MASS at 3.85 kHz; (*C*) $B_0 = 5.9$T; (*D*) $B_0 = 7.1$T; (*E*) $B_0 = 9.5$T; (*F*) $B_0 = 11.8$T.

TABLE 1. Spectra of polycrystalline $Na_3Co(NO_2)_6$

Resonance frequency (MHz)	Observed peak separation (kHz)	Calculated peak separation[a] (kHz)	Chemical shift[b]
21.52	35	35.4	7601
47.85	12.3	13.1	7604
59.80	8.0	9.0	7603
71.75	5.2	6.2	7598
95.66	—	2.6	7592
119.57	—	0.8	7594

[a]Calculated assuming $e^2qQ = 9.4$ MHz, asymmetry parameter = 0, $\sigma_\parallel - \sigma_\perp = 180$ ppm.
[b]In ppm relative to $K_3Co(CN)_6$ aqueous solution.

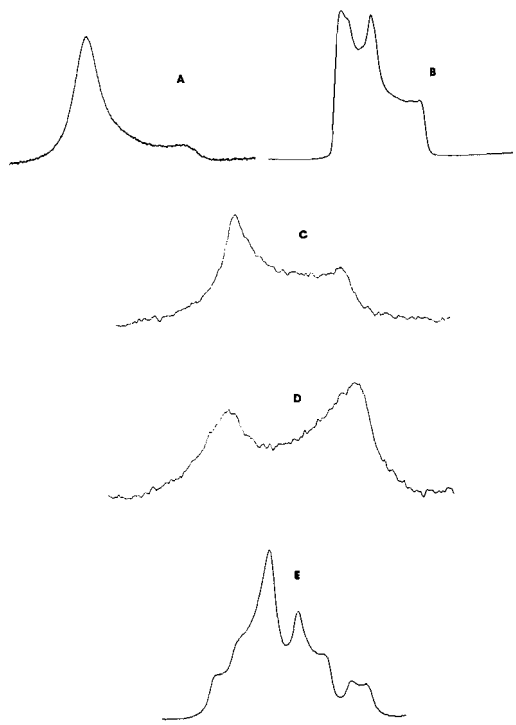

FIG. 2. ^{59}Co nmr spectra of polycrystalline samples of several Cobalt complexes obtained at 11.8T: (*A*) $Co(en)_3^{3+}$; (*B*) $Co(CN)_6^{3-}$; (*C*) $Co(acac)_3$; (*D*) $Co(C_2O_4)^{3-}$; (*E*) $Co(NH_3)_6^{3+}$.

Can. J. Chem. Downloaded from www.nrcresearchpress.com by 78.46.186.204 on 09/07/12
For personal use only.

TABLE 2. Chemical shifts of powdered samples[a]

Complex	Solution − solid (ppm)	$\sigma_{\parallel} - \sigma_{\perp}$ (ppm)
$Co(NO_2)_6^{3-}$	−129	180
$Co(CN)_6^{3-}$	+16	−110
$Co(acac)_3$	+344	—
$Co(C_2O_4)_3^{3-}$	+507	—
$Co(en)_3^{3+}$	−25	−255
$Co(NH_3)_6^{3+}$	~+250	—

[a]Positive chemical shifts are to low field.

be determined by chemical shift anisotropy effects but several chemically distinct sites are present. On the other hand, the appearance of the spectra obtained with the trisacetylacetonato and trisoxalato complexes are characteristic of quadrupolar splitting, or more probably a mixture of quadrupolar and chemical shift anisotropy effects, and are considerably broader than those in the two previous cases. Finally the spectrum of the hexammine complex is quite complicated and analysis has not been attempted. Chemical shift data are gathered together in Table 2.

Discussion

Baugher *et al.* (8) have calculated the powder nmr line shape for the $m = 1/2$ to $m = -1/2$ transition as a function of Zeeman frequency for the general case where both the quadrupole coupling tensor and the chemical shift tensor lack axial symmetry. They identified six locations for shoulders or singularities in the patterns and give explicit formulae for the frequencies of each of these positions. At low fields the prominent features of the spectrum are two maxima, the separation of which is primarily determined by the quadrupolar coupling. This is illustrated by the spectra in Fig. 1. If the effects of chemical shift anisotropy are neglected the separation of these maxima is inversely proportional to spectrometer frequency. If chemical shift anisotropy is included the separation is given by

$$[1] \quad \Delta\nu = A/\nu_0 + B\nu_0 + C\nu_0^3$$

where the constants A, B, and C represent the expressions

$$A = R/144(\eta^2 - 19\eta + 25)$$

$$B = \{\sigma_2 - [(5 - \eta)\sigma_3 + 2(2 - \eta)\sigma_1]\}$$

and

$$C = 4(\sigma_3 - \sigma_1)^2$$

where

$$R = \nu_Q^2[I(I + 1) - 3/4]$$

$$\nu_Q = 3e^2qQ/[2I(I + 1)h]$$

C depends upon the square of the chemical shift anisotropy and this term can be neglected if the field is not too high and if $\delta\sigma$ is no more than a few hundred parts per million as it is in the present case. A plot of $\nu_0\, d\nu$ versus ν_0^2 should therefore be linear. Such a plot is shown for the hexanitrocobaltate(III) data in Fig. 3. There are four unknows involved: two chemical shift parameters (the third chemical shift unknown is provided by the isotropic shift) and the quadrupole coupling constant and asymmetry parameter. In the present case the chemical shift information can be obtained directly from the high field spectra so that the slope and intercept of the line in Fig. 3 suffice to determine the quadrupole coupling constant and asymmetry. The high field spectra clearly show that the chemical shift tensor is axially symmetric and give an estimate of $\delta\sigma$. Fitting of the data to the formula of eq. [1] gives a best value of the quadrupole coupling constant of 9.4 MHz and of the asymmetry parameter of zero. The calculated splittings in Table 1 were obtained using these values together with a chemical shift anisotropy of 180 ppm. An asymmetry parameter as high as 0.1 is not ruled out but since the chemical shift tensor is axially symmetric it seems plausible that the quadrupole tensor will have similar symmetry although this is not mathematically required. This value is in reasonable agreement with the quadrupole coupling constant of 8.4 MHz reported by Saraswati and Vijayaraghavan (9) who were unable to obtain the assymmetry parameter independently but assumed it was zero.

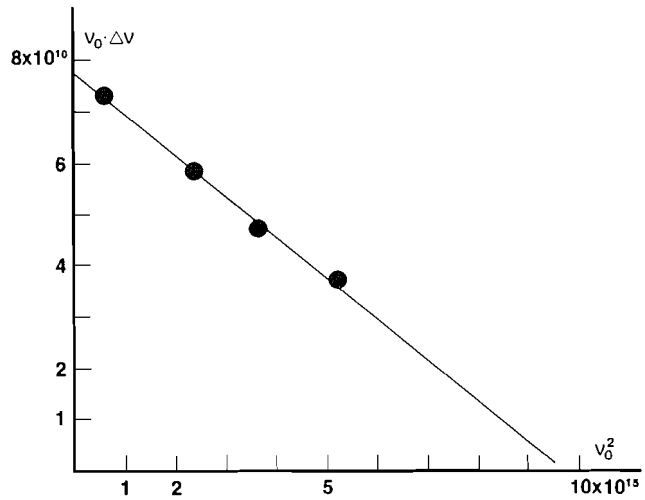

FIG. 3. Plot of $\nu_0\Delta\nu$ versus ν_0^2 for the sodium hexanitrocobaltate(III) data.

A crystal structure has been reported for the compound $K_2Na[Co(NO_2)_6]$ (10) but that of the simple sodium salt does not appear to have been determined. The structure reported shows cubic site symmetry for the Co atom so that neither quadrupole coupling nor chemical shift anisotropy would be anticipated. The observed axial symmetry implies either that the structure of the simple sodium salt is different or that effects beyond the second coordination sphere must be considered.

More relevant crystal structure data are available for the remaining compounds in Table 2. Thus Co(III) trisethylene diamine chloride shows only a single type of Co site with axially distorted octahedral symmetry (11). There is hydrogen bonding between the chloride anions and the ethylene diamine protons situated perpendicular to the three-fold axis. The nmr results are consistent with this structure. The trisacetylacetonato complex is structurally similar except that there are no strong hydrogen bonding possibilities. The nmr spectrum is consistent with a single type of Co site as expected from the reported crystal structure (12). The ^{59}Co nmr of a single crystal of this complex has been reported by Reynhardt (13). He measured a quadrupole coupling constant of 9.26 MHz, an asymmetry parameter of 0.9 and principal values of the chemical shift tensor of −510, −210, and +720 ppm. If these values are used to calculate the positions of the shoulders and singularities in the powder spectrum using the formulae of Baugher *et al.* (8) the calculated spectrum is broader than the observed spectrum by more than an order of magnitude.

Can. J. Chem. Downloaded from www.nrcresearchpress.com by 78.46.186.204 on 09/07/12
For personal use only.

The results for potassium cobalticyanide can also be compared with literature data (14–16). The single crystal nmr spectrum (16) of this compound shows three different chemically shifted types of cobalt which were associated with different polytypes resulting from the disordered stacking found in the X-ray crystallographic structure determination (17, 18). The quadrupole coupling constant measured by Lourens and Reynhardt (15) differed by a factor of more than two from that found by Saraswati *et al.* (9) from powder measurements. Three different principal chemical shift values were reported with separations of 155 and 178 ppm. These data may be used to calculate the powder spectrum at 119.5 MHz in the manner described above. In this case the observed spectrum is consistent with the three sites reported and the overall width is approximately correct (if only chemical shift anisotropy is included) but the line shape cannot be reconciled with the non-axially symmetric chemical shift tensor reported by Lourens and Reynhardt (16). There are also literature data on the X-ray structure and single crystal nmr spectrum of the hexammine complex (19, 20). This is a much more complicated case with four crystallographically distinct cobalt sites each with greatly differing quadrupole coupling constants and asymmetry parameters. The high field powder spectrum is clearly appropriately complex but we have not attempted any calculations leading to a quantitative comparison. There appears to be no relevant literature data on the oxalato complex.

Calculations have also been carried out on two less symmetric cobalt complexes for which Spiess *et al.* (21) have reported single crystal nmr studies. For the case of *trans*-$Co(en)_2(NO_2)_2$ (en = ethylene diamine) they report a quadrupole coupling constant of 13.217 MHz, an asymmetry parameter of 0.7272 and $\delta\sigma$'s of 300 and 400 ppm. These values lead to an overall width of the spectrum of some 600 ppm at 119.5 MHz which would probably be observable. On the other hand, calculations for the complex $Co(NH_3)_4CO_3^+$ which has a similar quadrupole coupling constant but a larger chemical shift anisotropy predict a width of some 1700 ppm which would make the spectrum difficult to observe.

From the above discussion it is apparent that although the expressions of Baugher *et al.* (8) will produce a good fit for the cobaltinitrite data at different fields, when these expressions are used to calculate high field powder spectra using low field single crystal data as input there are large discrepancies. We suspect that these discrepancies arise from two causes. At low fields the effects of chemical shift anisotropy are small compared with those due to quadrupolar coupling and the derived chemical shift anisotropy parameters are probably not accurate. Thus it seems very difficult to reconcile the high field powder spectrum of cobalticyanide with the non-axial chemical shift tensor reported. We also suspect that the theory breaks down when the chemical shift anisotropy is relatively large and the quadrupole coupling relatively small. In these circumstances at high fields the cross term involving both quadrupolar and chemical shift anisotropy, which is proportional to ν_0^3, becomes very large which does not seem plausible. It should also be noted that the second term in eq. [1] can be either positive or negative depending on the sign of the chemical shift anisotropy and that this is an important consideration in determining whether the spectrum will be reasonably narrow at high field. It seems likely therefore that high field powder nmr spectra of ^{59}Co and similar quadrupolar nuclei will prove useful in providing chemical shift anisotropy data for a fair number of complexes although complete line shape fitting by computer will probably be necessary to obtain reliable parameters. This information is of potential value to the understanding of both first and second sphere bonding in metal complexes.

Acknowledgements

We are indebted to the Natural Sciences and Engineering Research Council of Canada for financial support of this research and to the South West Ontario High Field NMR Centre at Guelph for use of the WM-400 and CXP-200 instruments.

1. A. Samosan, E. Kundla, and E. Lippma. J. Magn. Reson. **49**, 350 (1982).
2. S. Ganpathy, S. Schramm, and E. Oldfield. J. Chem. Phys. **77**, 4360 (1982).
3. S. Schramm, R. J. Kirkpatrick, and E. Oldfield. J. Am. Chem. Soc. **105**, 2483 (1983).
4. N. Bloembergen and T. J. Rowland. Acta Met. **1**, 731 (1953).
5. W. H. Jones, T. P. Graham, and R. G. Barnes. Phys. Rev. **132**, 1898 (1963).
6. P. A. Casabella. J. Chem. Phys. **40**, 149 (1964).
7. K. Narita, J. Umeda, and J. Kusumoto. J. Chem. Phys. **44**, 2719 (1966).
8. J. F. Baugher, P. C. Taylor, T. Oja, and P. J. Bray. J. Chem. Phys. **50**, 4914 (1969).
9. V. Saraswati and R. Vijayaraghavan. Proc. Ind. Acad. Sci. Sect. A, **66**, 253 (1967).
10. S. Ohba, K. Toriumi, S. Sato, and Y. Sato. Acta Crystallogr. B**34**, 3535 (1978).
11. P. A. Whuler, C. Brouty, and P. Herpin. Acta Crystallogr. B**31**, 2069 (1975).
12. G. J. Kruger and E. C. Reynhardt. Acta Crystallogr. B**30**, 822 (1974).
13. E. C. Reynhardt. J. Phys. C, **7**, 4135 (1974).
14. T. Sugawara. J. Phys. Soc. Jpn. **14**, 858 (1959).
15. J. A. J. Lourens and E. C. Reynhardt. J. Phys. Soc. Jpn. **30**, 898 (1971).
16. J. A. J. Lourens and E. C. Reynhardt. Phys. Stat. Sol. **11**, 739 (1972).
17. N.-G. Vannerberg. Acta Chem. Scand. **26**, 2863 (1972).
18. E. C. Reynhardt and J. C. A. Boeyens. Acta Crystallogr. B**28**, 524 (1972).
19. G. J. Kruger and E. C. Reynhardt. Acta Crystallogr. B**34**, 915 (1978).
20. E. C. Reynhardt. Can. J. Phys. **52**, 1398 (1974).
21. H. W. Spiess, H. Haas, and H. Hartmann. J. Chem. Phys. **50**, 3057 (1969).

Can. J. Chem. Downloaded from www.nrcresearchpress.com by 78.46.186.204 on 09/07/12
For personal use only.

The direct electrochemical synthesis of thiolato complexes of copper, silver, and gold; the molecular structure of $[Cu(SC_6H_4CH_3\text{-}o)(1,10\text{-phenanthroline})]_2.CH_3CN$

RAJ K. CHADHA, RAJESH KUMAR, AND DENNIS G. TUCK

Department of Chemistry and Biochemistry, University of Windsor, Windsor, Ontario N9B 3P4

Received October 3, 1986

RAJ K. CHADHA, RAJESH KUMAR, and DENNIS G. TUCK. Can. J. Chem. **65**, 1336 (1987).

The electrochemical oxidation of anodic copper or silver (= M) into non-aqueous solutions of RSH (R = alkyl, axyl) gives M^ISR as insoluble materials in high yield. In the presence of 1,10-phenanthroline (= L), the products are $M^ISR.phen$ for M = Cu, but not Ag. Gold resists oxidation under such conditions, and Au^ISR (R = n-C_4H_9, C_6H_5) was obtained in only poor yield. The crystal structure of the solvated dimeric adduct $[Cu(SC_6H_4CH_3\text{-}o).phen]_2.CH_3CN$ is triclinic, with a = 10.682(3) Å, b = 11.729(4) Å, c = 15.608(5) Å, α = 76.87(2)°, β = 76.35(2)°, γ = 68.07(2)°, V = 1742(1) Å^3, Z = 2 and space group $P\bar{1}$. The structure is based on a folded Cu_2S_2 ring with an unusually short Cu—Cu distance of 2.613(3) Å. Each copper atom has CuS_2N_2 pseudo-tetrahedral stereochemistry, with Cu—S = 2.337 Å(av) and Cu—N = 2.10 Å(av).

RAJ K. CHADHA, RAJESH KUMAR et DENNIS G. TUCK. Can. J. Chem. **65**, 1336 (1987).

L'oxydation électrochimique de l'argent ou du cuivre anodique (= M), dans des solutions non-aqueuses de RSH (R = alkyle, axyle), fournit, avec des rendements élevés, des M^ISR qui sont des produits insolubles. En présence de phénanthroline-1,10 (= L) et lorsque M = Cu, on obtient des composés du type $M^ISR.L$; ce n'est toutefois pas le cas lorsque M = Ag. Dans ces conditions, l'or ne s'oxyde que difficilement et les composés Au^ISR (R = n-C_4H_3 et C_6H_5) ne sont obtenus qu'avec de mauvais rendements. L'adduit dimère solvaté $[Cu(SC_4H_4CH_3\text{-}o).L]_2CH_3CN$ est triclinique et il cristallise dans le groupe d'espace $P\bar{1}$ avec a = 10,682(3), b = 11,729(4) et c = 15,608(5) Å, α = 76,87(2), β = 76,35(2) et γ = 68,07(2)°, V = 1742(1) Å^3 et Z = 2. La structure est basée sur un cycle Cu_2S_2 replié comportant une distance Cu—Cu qui est inhabituellement courte (2,613(3) Å). Chaque atome de cuivre possède une stéréochimie pseudo-tétraédrique CuS_2N_2 dans laquelle les distances moyennes Cu—S = 2,377 Å et Cu—N = 2,10 Å.

[Traduit par la revue]

Introduction

Previous papers from this laboratory have reported the direct electrochemical synthesis of metal thiolato complexes by the oxidation of a sacrificial anode in a non-aqueous solution of a thiol (RSH) or disulfide (R_2S_2). The metals successfully used in such experiments include zinc (1, 2), cadmium (1, 2), mercury (2), tin (3), lead (3), gallium (4), indium (4), thallium (4), nickel (4), and cobalt (4), to produce the neutral $M(SR)_n$ compounds, their adducts, or anionic complexes. We now report the use of these simple experimental techniques in the synthesis of thiolato derivatives of copper(I), silver(I), and gold(I), and a number of neutral adducts with the bidentate ligand 1,10-phenanthroline.

The structure of molecules containing copper–sulfur bonds has been the focus of considerable interest (see below), and the investigations therefore included the X-ray structural determination of the acetonitrile solvate of the dimeric adduct formed by *o*-tolylthiolatocopper(I) and 1,10-phenanthroline, $[Cu(SC_6H_4CH_3\text{-}o).C_{12}H_8N_2]_2.CH_3CN$, which involves a Cu_2S_2 ring and CuS_2N_2 coordination.

Experimental section

General techniques

Solvents were distilled from calcium hydride and stored over molecular sieves. Copper, silver, and gold foils were washed with concentrated aqueous nitric acid and then distilled water and dried immediately before use. Thiols, and 1,10-phenanthroline(phen), were used as supplied.

Copper analysis was by atomic absorption spectrophotometry; silver was determined gravimetrically. Microanalysis was performed by Guelph Chemical Laboratories Ltd. Infrared spectra were recorded on Perkin-Elmer PE 180 or Nicolet 5DX instruments; ^1H nmr spectra were obtained with Bruker WP-80 or Perkin-Elmer 20 spectrometers.

Electrochemical procedures

The electrochemical syntheses were carried out by the methods described in previous papers (e.g. refs. 5, 6). The anode was suspended in a solution of the appropriate composition (see Table 1) in a 100-mL tall-form beaker, with cells of the general form

$$Pt_{(-)}/CH_3CN + RSH\ (+ L)/M_{(+)}\ (M = Cu, Ag, Au)$$

The oxidations were carried out under an atmosphere of dry nitrogen which was bubbled through the solution and so also served to mix the contents of the cell. Details of isolation procedures are given below. Yields were generally better than 90%, based on the quantity of metal dissolved from the anode. Products were characterized by analysis (Table 2) and by infrared and ^1H nmr spectroscopy.

(i) Copper(I) thiolates. The electrolysis was carried out at room temperature (ca. 20°C). The product precipitated as the oxidation proceeded and was collected at the end of the reaction, washed with acetonitrile and then petroleum ether (30–65°C), and dried *in vacuo*. Diethyl ether could be substituted for petroleum ether without affecting the product. The compounds are amorphous powders, which are insoluble in hydrocarbon solvents, acetone, acetonitrile, and carbon disulfide, except that $CuSC(CH_3)_2CH_2CH_3$ and $CuSC_6HF_4$ are soluble in hot acetonitrile, and the former is soluble in CS_2. This compound is also photosensitive, changing color from yellow to orange on long exposure to light. Benzenethiolatocopper(I) could also be synthesized by oxidizing the metal in a solution of diphenyldisulfide in acetonitrile (see Table 1).

The electrochemical efficiency, defined as the quantity of metal (moles) dissolved per Faraday of charge, was found to be 1.0 ± 0.05 mol F^{-1} in all Cu/RSH systems studied, and the same value was found for Cu/Ph_2S_2.

(ii) 1,10-Phenanthroline adducts of copper(I) thiolates. Addition of 1,10-phenanthroline to the solution phase prior to electrolysis resulted in the direct electrochemical synthesis of CuSR.phen compounds. The color of the solution changed from light red–brown to deep red–brown as the electrolysis proceeded; no precipitation occurred, but slow cooling, or removing solvent slowly by bubbling nitrogen through the solution, lead to the formation of red–brown crystals which were collected, washed with acetonitrile and then diethyl ether, and finally dried *in vacuo*. In the case of $CuSC_6H_5$.phen, the same compound was obtained when either C_6H_5SH or $(C_6H_5)_2S_2$ was the source of the thiolate anion. No adduct was obtained from a solution containing

Can. J. Chem. Downloaded from www.nrcresearchpress.com by 78.46.186.204 on 09/07/12
For personal use only.

TABLE 1. Experimental conditions for the electrochemical synthesis of copper, silver, and gold thiolato compounds

Solute[a]	Quantity (mL)	Ligand	Quantity (g)	Voltage[b] (V)	Time of electrolysis (h)	Metal dissolved (mg)	Product
n-C_4H_9SH	1.5			10	1	50	CuSR
$C_5H_{11}SH$[c]	1			10	2.3	110	CuSR
C_6H_5SH	2			25	1	54	CuSR
o-$CH_3C_6H_4SH$	1.5			15	1	53	CuSR
m-$CH_3C_6H_4SH$	0.5			10	1	51	CuSR
p-$CH_3C_6H_4SH$	0.5			10	1	49	CuSR
2,3,5,6-C_6F_4HSH	0.3			20	1.6	94	CuSR
$C_{10}H_7SH$	0.37 g			20	1	50	CuSR
$(C_6H_5)_3CSH$	0.31 g			15	1	56	CuSR
$(C_6H_5)_2S_2$	0.41 g			20	1	72	CuSR
n-C_4H_9SH	1	phen	0.31	10	1	50	CuSR
$C_5H_{11}SH$[c]	1.5	phen	0.31	20	2	103	$(CuSR)_2L$
C_6H_5SH	2	phen	0.37	10	2	68	CuSR.L
o-$CH_3C_6H_4SH$	1.5	phen	0.31	20	2	70	$(CuSR.L)_2.CH_3CN$
m-$CH_3C_6H_4SH$	2	phen	0.6	10[d]	2.3	137	CuSR.L
p-$CH_3C_6H_4SH$	0.5	phen	0.7	5	5	152	CuSR.L
$C_{10}H_7SH$	0.39 g	phen	0.22	10	1	44	CuSR.L
$(C_6H_5)_3CSH$	0.32 g	phen	0.41	15	1	49	$(CuSR)_2.L$
$(C_6H_5)_2S_2$	0.33 g	phen	0.6	20[d]	1	69	CuSR.L
n-C_4H_9SH	0.5			25	1	83	AgSR
$C_5H_{11}SH$[c]	1.0			25	1	95	AgSR
C_6H_5SH	0.5			20	1	81	AgSR
o-$CH_3C_6H_4SH$	1			10	1	84	AgSR
m-$CH_3C_6H_4SH$	0.5			10	1	83	AgSR
p-$CH_3C_6H_4SH$	0.5			10	1	84	AgSR
$C_{10}H_7SH$	0.5 g	25	0.5	25	0.5	39	AgSR
$(n$-$C_4H_9S)_2$	1			25	5.1	40	AuSR
$(C_6H_5S)_2$	0.30 g			20	0.5	50	AuSR

[a]In 50 mL acetonitrile, plus ca. 25 mg Et_4NClO_4.
[b]Voltage required to produce an initial current of 20 mA.
[c]$C_5H_{11}SH$ = 2-methylbutane-2-thiol.
[d]Initial current 30 mA.

n-C_4H_9SH and phen, with $CuSC_4H_9$-n precipitating as the anode was consumed. The electrochemical efficiency for dissolution of copper remained at 1.0 ± 0.05 mol F^{-1} when phen was present in the cell, although this value fell if product adhered to the anode surface.

The phen adducts are soluble in acetonitrile, dimethylsulfoxide, and chlorinated hydrocarbons. The red solution formed on dissolving $CuSC_6H_5$.phen (0.3 g) in chloroform (30 mL) shows evidence of reaction, with a red–yellow solid precipitating at room temperature with stirring over 30–45 min. Chloride analysis of this solid gave Cl = 11.7% (cf. CuCl.phen, Cl calcd. 12.7). When stirring was continued for 3–4 h, a green precipitate was obtained (calcd. for $CuCl_2$.phen; Cl 22.5; found: Cl 20.3).

(iii) Silver(I) thiolates. A creamy white precipitate formed at the electrode within 5 min of beginning the electrolysis in each system studied. After 1 h, the solid which had accumulated in the bottom of the cell was collected, washed with acetonitrile and then n-pentane, and dried *in vacuo*. No adducts were obtained when phen was added to the cell; with C_6H_5SH + phen, the product was identified as $AgSC_6H_5$. The electrochemical efficiency for the dissolution of silver was found to be 1.00 ± 0.05 mol F^{-1}.

(iv) Gold(I) thiolates. When electrolysis was carried out with solutions of n-C_4H_9SH or C_6H_5SH in acetonitrile, the gold anode rapidly became covered with a heavy adherent deposit which effectively prevented any further reaction, and the current fell to almost zero. With solutions of the corresponding disulfide, a slow reaction occurred with AuSR precipitating as the reaction proceeded. The electrochemical efficiency for these systems was low for $(C_6H_5)_2S_2$ ($E_F \approx 0.6$), and very low for $(C_4H_9)_2S_2$ ($E_F \approx 0.05$ mol F^{-1}).

(v) Miscellaneous. Attempts to prepare pyridine or dimethylsulfoxide adducts of $CuSC_6H_5$ by electrolysis with an acetonitrile or acetone solution of these ligands were unsuccessful. We also found that acetone solutions of C_6H_5SH, or C_6H_5SH + phen, were unsatisfactory media for the electrochemical oxidation of copper; in each case, only 20–40 mg of metal dissolved over a period of 2–3 h, which implies an efficiency some 5–10 times lower than when acetonitrile was used.

Crystallographic analysis

Plate-like red–brown crystals of the acetonitrile solvate of $[Cu(SC_6H_4CH_3$-$o)(phen)]_2$, **1**, were obtained by electrochemical oxidation as described. The density was measured by flotation in CCl_4/benzene. A crystal was mounted along the largest dimension on a Syntex $P2_1$ diffractometer for X-ray data collection. Details on the data collection procedures have been given previously (7). Although the positions of the copper and sulphur atoms were obtained from MULTAN using 268 reflections with $|E_{min}| \geq 1.2$ and 2448 phase relationships, the quality of this data set was too poor to refine the structure using SHELX, because of one dimension being much smaller than the other two. Another crystal with maximum possible thickness was therefore chosen and the data were recollected (see Table 3 for dimensions and other relevant information). The intensity of three monitor reflections

Can. J. Chem. Downloaded from www.nrcresearchpress.com by 78.46.186.204 on 09/07/12
For personal use only.

Can. J. Chem. Downloaded from www.nrcresearchpress.com by 78.46.186.204 on 09/07/12
For personal use only.

TABLE 2. Analytical results for copper, silver, and gold thiolato compounds

Compound[a]	Found (%)				Calculated (%)			
	M	C	H	N	M	C	H	N
$CuSC_4H_9$-*n*	40.8				41.6			
$CuSC_5H_{11}$	38.8	37.2	6.54		38.1	36.0	6.65	
$CuSC_6H_5$	36.7				36.8			
$CuSC_6H_4CH_3$-*o*	34.5	45.1	3.59		34.0	45.0	3.78	
$CuSC_6H_4CH_3$-*m*	34.2				34.0			
$CuSC_6H_4CH_3$-*p*	33.9				34.0			
$CuSC_6F_4H$	25.8				26.0			
$CuSC_{10}H_7$	29.2				28.5			
$CuSC(C_6H_5)_3$	17.9				18.8			
$(CuSC_5H_{11})_2$phen	24.3	51.7	5.88	5.55	24.7	51.4	5.89	5.45
$CuSC_6H_5$·phen	17.8	62.3	3.98	7.94	18.0	61.3	3.71	7.94
$CuSC_6H_4CH_3$-*o*·phen)$_2$.CH_3CN	15.8	62.1	4.66	8.76	16.4	62.0	4.29	9.04
$CuSC_6H_4CH_3$-*m*·phen	16.9				17.3			
$CuSC_6H_4CH_3$-*p*·phen	18.1				17.3			
$CuSC_{10}H_7$·phen	15.2				15.8			
$[CuSC(C_6H_5)_3]_2$·phen	14.3				14.8			
$AgSC_4H_9$-*n*	54.3				54.8			
$AgSC_5H_{11}$	51.9				51.2			
$AgSC_6H_5$	49.0	33.0	2.00		49.7	33.2	2.32	
$AgSC_6H_4CH_3$-*o*	45.9				46.7			
$AgSC_6H_4CH_3$-*m*	46.5				46.7			
$AgSC_6H_4CH_3$-*p*	47.4				46.7			
$AgSC_{10}H_7$	41.2				40.4			
$AuSC_4H_9$-*n*		16.0	3.08			16.8	3.17	
$AuSC_6H_5$		23.9	1.80			23.5	1.63	

[a]phen = 1,10-phenanthroline; $C_5H_{11}S = CH_3CH_2C(CH_3)_2S$.

TABLE 3. Summary of crystal data, intensity collection, and structural refinement for $[Cu(SC_6H_4CH_3$-*o*$)(C_{12}H_8N_2)]_2.CH_3CN$

Cell constants	$a = 10.682(3)$, $b = 11.729(4)$, $c = 15.608(5)$ Å; $\alpha = 76.87(2)$, $\beta = 76.35(2)$, $\gamma = 68.07(2)°$
Cell volume (Å^3)	1742(1)
Crystal system	Triclinic
Space group	$P\bar{1}$
Mol. wt.	774.0
Z	2 (dimers)
Crystal dimensions (mm)	0.08 × 0.15 × 0.38
ρ_c (g cm^{-3})	1.48
ρ_o (g cm^{-3})	1.51
Absorption coefficient, μ(cm^{-1})	13.12
Minimum absorption correction	1.126
Maximum absorption correction	1.307
Radiation	MoKα, $\lambda = 0.71069$ Å
Monochromator	Highly oriented graphite
Temperature (°C)	21
2θ angle (°)	3.5–45
Scan type	Coupled θ (crystal)/2θ (counter)
Scan width	$K_{\alpha_1} - 1°$ to $K_{\alpha_2} + 1°$
Scan speed (deg min^{-1})	Variable, 2.02–4.88
Background time/scan time	0.5
Total reflections measured	4718 ($+h, \pm k, \pm l$) ($R = 0.0$)
Unique data used	3000 [$I > 3\sigma(I)$]
No. of parameters (NP)	341, blocked, see text
$R = (\Sigma\|\|F_o\| - \|F_c\|\|/\Sigma\|F_o\|)$	0.0967
$R_w = [\Sigma w(\|F_o\| - \|F_c\|)^2/\Sigma_w\|F_o\|^2]^{1/2}$	0.1029
$\Delta\rho_{max}$ (e Å^{-3})	0.3
Shift:error (max)	0.05

did not change significantly during data collection. The data were corrected for Lorentz and polarization effects and analytical absorption corrections were applied. Cell parameters were obtained from 15 strong reflections ($15 < 2\theta < 35°$). The space group $P\bar{1}$ was used and later assumed to be correct because of the successful refinement.

In the least-squares analysis, all atoms except the carbon atoms of one tolyl and one phenanthroline groups were refined anisotropically in blocks as follows: Cu(1) and Cu(2) every cycle; S(1), S(2), N(1)—N(4), C(1)—C(17) in alternate cycles with C(21)—C(62). The hydrogen atoms were fixed in ideal geometry (r(C—H) = 0.95 Å), and assigned thermal parameters whose values exceeded those for the appropriate carbon atoms by 0.01 U (Å^2). The anisotropic thermal parameters of a few atoms were too small along the x axis, the thinnest side of the crystal, due to the plate-like shape of the crystal. The refinement minimizing the function $\Sigma w(|F_o| - |F_c|)^2$ converged to $R = 0.0967$ and $R_w = 0.1029$. A weighting scheme of the form $w = 1/[\Sigma\sigma^2(F) + pF^2]$ was employed with a final p value of 0.0001. No evidence of secondary extinction correction was found. The final difference map showed no features of chemical significance. These high R values are a result of the difficulties encountered in choosing a suitable crystal, and of the relative dimensions of the crystal (see above). Computer programs, and sources of scattering factors, were those reported previously (3, 7). Positional and thermal parameters are given in Table 4 and interatomic distances and bond angles in Table 5. The molecular structure is shown in Fig. 1, and a view of the unit cell in Fig. 2. There are no intermolecular contacts of significance.

Tables of anisotropic thermal parameters, positional coordinates and thermal parameters for hydrogen atoms, and observed and calculated structure factors, are available as supplementary data.[1]

Results and discussion

Preparative

As with other electrochemical syntheses, the techniques described above provide an efficient one-step route to the M(SR) compounds of copper and silver and to adducts of copper thiolates with a typical bidentate nitrogen donor. As with other earlier work, the E_F values of 1.0 ± 0.05 mol F^{-1} for Cu and Ag correspond to the reactions

$$\text{Cathode: } RSH + e \rightarrow RS^- + (1/2)H_2(g)$$

$$\text{Anode: } RS^- + M \rightarrow MSR + e$$

for RSH, and

$$\text{Cathode: } R_2S_2 + 2e \rightarrow 2RS^-$$

$$\text{Anode: } 2RS^- + 2M \rightarrow 2MSR + 2e$$

for R_2S_2 systems.

The only experimental difficulty calling for comment is that gold resists attack, leading to low E_F values, and this is no doubt related to the chemical inertness of this metal. A more difficult point is that with RS^- generated from R_2S_2, the reaction with gold proceeds, albeit with low efficiency, whereas with the apparently identical anions from RSH a deposit forms on the cathode and inhibits further reaction. One possible explanation is that the AuSR which forms at the anode surface reacts with RSH to give an insoluble metal sulfide which is adherent, but that no such reaction occurs with R_2S_2, or that the product of such a reaction is soluble.

The spectroscopic properties of CuSR compounds (see below) suggest that these solids are sulfur bridged homo-polymers, as proposed for other d^{10}-metal thiolates (1, 8). Adduct formation then depends in part on the ligand–metal interaction being strong enough to overcome this metal–sulfur bridging, and the present evidence indicates that the typical bidentate donor phen satisfies this condition whereas monodentate donors do not for copper, except that with R = n-C_4H_9 the bridging prevails against the attempted formation of a phen adduct. Similar results have been recorded with alkylthiolate derivatives of

TABLE 4. Final fractional coordinates and isotropic thermal parameters for non-hydrogen atoms of $[Cu(SC_6H_4CH_3\text{-}o)(C_{12}H_8N_2)]_2 \cdot CH_3CN$ with standard deviations in parentheses

Atom	x	y	z	U_{eq}* (Å$^2 \times 10^3$)
Cu(1)	0.3239(2)	−0.0019(2)	0.2437(1)	36(1)
Cu(2)	0.0581(2)	0.0573(2)	0.2677(1)	39(1)
S(1)	0.1729(4)	0.1318(3)	0.3409(2)	35(2)
S(2)	0.2062(4)	−0.1320(3)	0.2301(3)	35(2)
N(1)	0.4677(13)	0.0416(11)	0.1384(8)	40(8)
N(2)	0.5067(12)	−0.1120(10)	0.2916(8)	38(7)
N(3)	−0.0502(11)	0.1709(11)	0.1675(7)	37(7)
N(4)	−0.1467(11)	0.0753(11)	0.3327(7)	42(7)
N	0.2216(21)	0.3535(23)	0.9197(14)	108(17)
C(1)	0.2092(21)	0.4140(24)	0.8533(16)	75(14)
C(2)	0.1863(19)	0.4979(18)	0.7732(14)	77(14)
C(11)	0.1594(13)	0.2877(14)	0.2914(10)	36(3)
C(12)	0.1790(14)	0.3190(15)	0.1988(11)	44(11)
C(13)	0.1729(16)	0.4376(17)	0.1604(12)	55(10)
C(14)	0.1518(18)	0.5289(15)	0.2088(15)	58(12)
C(15)	0.1351(16)	0.4971(16)	0.2978(15)	58(13)
C(16)	0.1370(14)	0.3792(15)	0.3432(12)	48(10)
C(17)	0.1222(18)	0.3480(17)	0.4420(11)	60(12)
C(21)	0.2424(14)	−0.2348(13)	0.3297(9)	30(1)
C(22)	0.1762(18)	−0.2080(15)	0.4119(10)	53(1)
C(23)	0.2077(21)	−0.2895(22)	0.4886(13)	73(2)
C(24)	0.3079(25)	−0.4034(21)	0.4856(17)	82(17)
C(25)	0.3774(22)	−0.4312(18)	0.4042(16)	67(14)
C(26)	0.3499(17)	−0.3538(15)	0.3258(11)	44(10)
C(27)	0.4339(19)	−0.3846(18)	0.2379(16)	87(16)
C(31)	0.4491(17)	0.1181(15)	0.0613(10)	50(4)
C(32)	0.5561(17)	0.1360(15)	0.0039(11)	52(4)
C(33)	0.6828(17)	0.0817(14)	0.0115(11)	49(4)
C(34)	0.7125(16)	0.0003(15)	0.0926(10)	46(4)
C(35)	0.6001(15)	0.0166(13)	0.1547(9)	36(4)
C(36)	0.6228(14)	−0.1002(13)	0.2376(9)	32(4)
C(37)	0.7522(16)	−0.1549(14)	0.2578(10)	42(4)
C(38)	0.7643(18)	−0.2302(15)	0.3369(11)	53(5)
C(39)	0.6561(17)	−0.2511(16)	0.3944(12)	57(5)
C(40)	0.5254(16)	−0.1891(14)	0.3662(10)	46(4)
C(41)	0.8470(16)	−0.0599(14)	0.1182(10)	43(4)
C(42)	0.8612(19)	−0.1313(16)	0.1951(12)	60(5)
C(51)	−0.0022(16)	0.2131(14)	0.0846(10)	42(4)
C(52)	−0.0861(16)	0.2878(14)	0.0231(11)	49(4)
C(53)	−0.2238(17)	0.3207(15)	0.0477(11)	52(5)
C(54)	−0.2787(17)	0.2760(15)	0.1340(11)	53(5)
C(55)	−0.1866(13)	0.1995(12)	0.1901(9)	25(3)
C(56)	−0.2411(15)	0.1520(13)	0.2785(9)	38(4)
C(57)	−0.3822(15)	0.1770(14)	0.3045(10)	40(4)
C(58)	−0.4225(20)	0.1200(17)	0.3934(12)	66(5)
C(59)	−0.3326(19)	0.0491(17)	0.4451(13)	67(5)
C(60)	−0.1942(16)	0.0279(14)	0.4126(10)	42(4)
C(61)	−0.4238(16)	0.3007(15)	0.1631(11)	49(4)
C(62)	−0.4701(17)	0.2526(14)	0.2449(10)	45(4)

*U_{eq} for the non-hydrogen atoms is calculated from the refined anisotropic thermal parameters ($U_{eq} = (1/3)\Sigma_i\Sigma_j U_{ij} a_i^* a_j^* \mathbf{a}_i \mathbf{a}_j$).

[1]Complete set of data may be purchased from the Depository of Unpublished Data, CISTI, National Research Council of Canada, Ottawa, Ont., Canada K1A 0S2.

Can. J. Chem. Downloaded from www.nrcresearchpress.com by 78.46.186.204 on 09/07/12
For personal use only.

TABLE 5. Bond distances (Å) and angles (deg) in $Cu(SC_6H_4CH_3\text{-}o)\text{-}(C_{12}H_8N_2)_2.CH_3CN$

Bond	Distance	Bonds	Angle
Cu(1)—Cu(2)	2.613(3)	S(1)—Cu(1)—S(2)	105.4(2)
Cu(1)—S(1)	2.324(4)	S(1)—Cu(1)—N(1)	125.6(4)
Cu(1)—S(2)	2.379(5)	S(2)—Cu(1)—N(1)	120.6(4)
Cu(1)—N(1)	2.08(1)	S(1)—Cu(1)—N(2)	112.7(4)
Cu(1)—N(2)	2.10(1)	S(2)—Cu(1)—N(2)	109.5(4)
Cu(2)—S(1)	2.341(6)	N(1)—Cu(1)—N(2)	79.1(4)
Cu(2)—S(2)	2.304(4)	S(1)—Cu(2)—S(2)	107.3(2)
Cu(2)—N(3)	2.08(1)	S(1)—Cu(2)—N(3)	121.4(4)
Cu(2)—N(4)	2.14(1)	S(2)—Cu(2)—N(3)	113.8(4)
S(1)—C(11)	1.78(2)	S(1)—Cu(2)—N(4)	113.5(4)
S(2)—C(21)	1.76(1)	S(2)—Cu(2)—N(4)	119.8(4)
N(1)—C(31)	1.34(2)	N(3)—Cu(2)—N(4)	79.5(4)
N(1)—C(35)	1.38(2)	Cu(1)—S(1)—Cu(2)	68.1(1)
N(2)—C(36)	1.36(2)	Cu(1)—S(1)—C(11)	108.9(5)
N(2)—C(40)	1.31(2)	Cu(2)—S(1)—C(11)	109.4(6)
N(3)—C(51)	1.33(2)	Cu(1)—S(2)—Cu(2)	67.8(1)
N(3)—C(55)	1.34(2)	Cu(1)—S(2)—C(21)	95.6(6)
N(4)—C(56)	1.39(2)	Cu(2)—S(2)—C(21)	107.9(5)
N(4)—C(60)	1.31(2)	Cu(1)—N(1)—C(35)	112.8(8)
N—C(1)	1.12(3)	C(31)—N(1)—C(35)	117.5(1)
C(1)—C(2)	1.41(3)	Cu(1)—N(2)—C(36)	115.2(8)
		Cu(1)—N(2)—C(40)	130(1)
		C(36)—N(2)—C(40)	115(1)
Ring C(11)—C(16):		Cu(2)—N(3)—C(51)	129(1)
Mean C—C	1.38(3)	Cu(2)—N(3)—C(55)	114.1(8)
Mean C—C—C	120(2)	C(51)—N(3)—C(55)	117(1)
C(16)—C(17)	1.49(2)	Cu(2)—N(4)—C(56)	111.5(8)
		Cu(2)—N(4)—C(60)	131(1)
Ring C(21)—C(26):		C(56)—N(4)—C(60)	117(1)
Mean C—C	1.37(3)	N—C(1)—C(2)	176(2)
Mean C—C—C	120(2)	S(1)—C(11)—C(12)	120(1)
C(26)—C(27)	1.49(3)	S(1)—C(11)—C(16)	122(1)
		C(11)—C(16)—C(17)	120(2)
		C(15)—C(16)—C(17)	122(2)
Rings C(31)—C(42):		S(2)—C(21)—C(22)	124(1)
Mean C—C	1.37(3)	S(2)—C(21)—C(26)	120(1)
Mean C—C—C	120(2)	C(21)—C(26)—C(27)	119(1)
		C(25)—C(26)—C(27)	122(2)
Rings C(51)—C(62):			
Mean C—C	1.38(3)		
Mean C—C—C	120(2)		

cadmium(II) and explained in terms of a strong polarized M—S bond (8). The experiments described did not yield adducts of silver, which may again be due to the increased strength of the polarized Ag—S bond, given that silver is a more electropositive element than gold.

The insolubility of the copper, silver, and gold thiolates prevented any study of the nmr spectra of these compounds. The phen adducts of CuSR are slightly soluble in d_6-*DMSO*, so that spectra could be recorded, but it was not possible to get reliable integration. The *p*-tolyl and triphenylmethyl thiolato compounds are insoluble in this solvent, but for the remainder multiplets in the 6.5–9.0 ppm region were assigned to phen, and to the aromatic thiolato ligand; the aliphatic protons of $n\text{-}C_5H_{11}S$ (0.43–1.55, m) were also observed.

Structure of $[Cu(SC_6H_4CH_3\text{-}o)phen]_2.CH_3CN$ (**1**)

Our X-ray studies establish that **1** is a dimeric molecule, with a molecule of acetonitrile present in the lattice but playing no role in the coordination of the metal. Each copper atom has quasi-tetrahedral stereochemistry (sum of all angles at Cu(1) = 652.9°, at Cu(2) = 655.3°), and is the centre of a CuS_2N_2 kernel. There is an unusually large number of reports of structures involving copper(I) derivatives and thiolate ligands, against which the present results can be compared. Two of these reports refer to the $Cu(SPh)_3^-$ anion (9, 10), in which the copper has approximately trigonal symmetry in the CuS_3 kernel, with Cu—S bond lengths 2.274(4)–2.335(4) Å in the Ph_4P^+ salt (9), and 2.239(2)–2.258(2) Å when the cation (10) is Et_4N^+. These values serve to establish the Cu—S bond distance in the absence of major ligand–ligand or bridging interactions, as well as the S—C(phenyl) distance of 1.75–1.76 Å.

Several of the structures are concerned with cages or clusters in which bridging by thiolate ligands plays an important role. Molecules containing three, four, five, and eight copper atoms have been structurally characterized, and the results up to 1980 have been reviewed elsewhere (9); more recent papers by Dance *et al.* have discussed the structural relationship involved (11, 12). The formation of six-membered rings in the boat conformation is apparently a common feature of such structures (cf. ref. 13), as is the extensive bridging by μ-SPh and

Can. J. Chem. Downloaded from www.nrcresearchpress.com by 78.46.186.204 on 09/07/12
For personal use only.

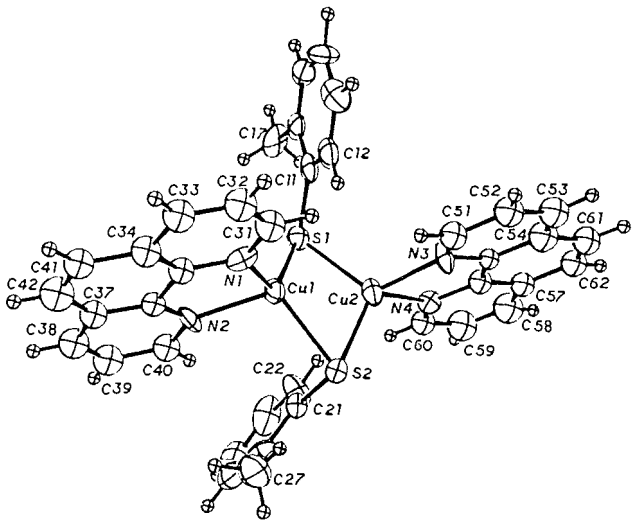

FIG. 1. Ortep diagram of $[Cu(SC_6H_4CH_3\text{-}o)(C_{12}H_8N_2)]_2.CH_3CN$; 50% probability for all atoms other than hydrogen.

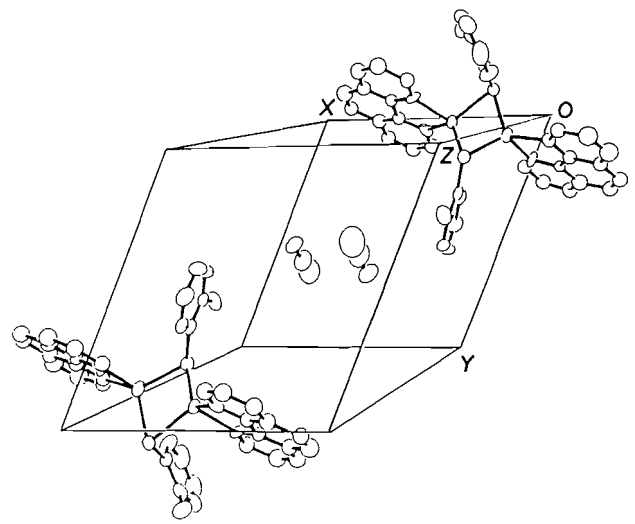

FIG. 2. Packing diagram.

μ_3-SPh groups. An examination of the bond distances and angles in these molecules serves to emphasize the effect of atomic environment on these parameters, especially in terms of the number of atoms being bridged, and of the other atoms bonded to copper, so that comparisons must be made with caution.

Two structures appear especially relevant to the present results. One is the dimeric $(CuSPh.2PPh_3)_2$ (14), or $(Ph_3P)_2Cu(\mu\text{-}SPh)_2Cu(Ph_3P)_2$ (**2**), and the other is $(CuSPh.PPh_3)_4$ (12), or $(\mu_3\text{-}SPh)_2(\mu\text{-}SPh)_2Cu_4.(PPh_3)_4$ (**3**). Both **1** and **2** are dimeric species, but with different neutral donor ligands supported on Cu_2S_2 rings. A striking feature of **2** is the planarity of this ring, with axially directed SPh ligands and approximately planar ligand stereochemistry at the sulfur atom. The steric interaction between the phenyl group of the thiolate and those of Ph_3P plays a major role in stabilizing this structure (14), but such factors are absent in **1**, so that arguably the shape observed in the present work is that which the $(RSCu)_2$ adopts in the absence of exterior constraints.

The relationship between **1** and **3** is also interesting, since the latter is a centrosymmetric molecule which can be described as two folded Cu_2S_2 units joined by Cu—S bonds which themselves produce a planar Cu_2S_2 rhombus. The folded units in **1** and **3** are rather similar, with $Cu_{tet\text{-}\mu_2\text{-}S}$ = 2.337 Å(av) in **1** and 2.327 Å in **3**, and Cu—μ-S—Cu angles of 68.0°(av) and 74.3°, respectively. Given the difference in the neutral donor ligands (see above), the different angles at Cu are not surprising (μ-S—Cu—μ-S = 106.3°(av) in **1**, μ-S—Cu_{tet}—μ_3-S = 99.2(1)°, 110.6(1)° in **3**). The fold angle, taken as the dihedral angle at the μ-S—μ-S diagonal, is 149.9° in **1** and 142.3° in **3**. The most significant difference lies in the Cu—Cu distance which is 2.782(1) Å in **3**, but significantly shorter at 2.613(3) in the present case, which represents a closeness of approach of these atoms comparable to that in copper metal (2.551 Å) (15). Similar close contacts have been reported for the dimeric copper(I) derivative of diazoaminobenzene (16) where the Cu—Cu distance is 2.45 Å, and for $[Cu(S_2CNEt_2)]_4$ (r(Cu—Cu) = 2.71 Å(av)) (17). Copper–copper bonding has been postulated for a number of dimeric copper(II) compounds, but the analogous copper(I) systems have not been investigated in detail, although Coucouvanis *et al.* (9) have discussed such effects in $Cu_8L_{12}^{4-}$ and $Cu_4L_6^{2-}$ structures, and Mehrotra and Hofmann (18) have analyzed the possible Cu—Cu bonding interactions in copper(I) cluster compounds. Since the present structure is one in which ligand–ligand steric interactions are apparently absent, in that there are no interligand distances below 2.3 Å, the folded Cu_2S_2 ring may be evidence for a significant Cu—Cu interaction in this system.

The remaining features of the stereochemistry call for little comment. The μ-S—C_{phenyl} distances (1.77 Å(av)) are close to those in the compounds discussed above, and the stereochemical features of the 1,10-phenanthroline ligand are also in agreement with previous results, as is the bite angle of 79.3°(av) at the copper atom.

Vibrational spectra

The infrared spectra of all the compounds prepared were routinely recorded over the range 4000–100 cm^{-1}, and these spectra served in part to demonstrate the presence of the appropriate alkyl or aryl thiolate, and of the neutral donor ligand. Results in the far infrared region should identify ν(M—S) modes, and there has been considerable discussion of the frequency range in which these are to be found in the case of copper, zinc, cadmium, and mercury thiolates (19–22). A major problem, and one which proved difficult in the present work, is that vibrations of the alkyl or aryl group, and of the neutral ligand, obscure much of the region of interest. Infrared absorptions in the region 323–74 cm^{-1} have been assigned as ν(S—M) modes in $(CH_3SCu)_n$ and $[Cu_2(SMe)_3]^-$, and we find bands at 304s and 238m in n-C_4H_9SCu, at 300s and 216m in n-C_4H_9SAg, and 280w, br cm^{-1} in n-C_4H_9SAu. These values are compatible with a polymeric structure (cf. ref. 21) with

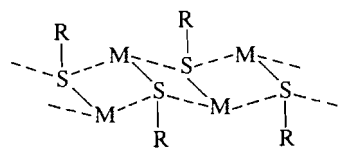

only a slight dependence of frequency on the metal. With 1,1-dimethylpropane-1-thiolates, the only vibrations which could be unambiguously identified were those at 195 and 130 (Cu) and 107 cm^{-1} (Ag). The dominant features in the spectra of derivatives of aryl thiols are due to vibrations of the phenyl group, and we cannot assign any ν(M—S) modes with

Can. J. Chem. Downloaded from www.nrcresearchpress.com by 78.46.186.204 on 09/07/12
For personal use only.

certainty, although metal-dependent absorptions were seen at 174 (Cu), 163 (Ag), and 110 cm^{-1} (Au).

Acknowledgement

This work was supported in part by Operating Grants (to D.G.T.) from the Natural Sciences and Engineering Research Council of Canada.

1. F. F. Said and D. G. Tuck. Inorg. Chim. Acta, **59**, 1 (1982).
2. J. L. Hencher, M. A. Khan, F. F. Said, and D. G. Tuck. Polyhedron, **4**, 1263 (1985).
3. J. L. Hencher, M. A. Khan, F. F. Said, R. Sieler, and D. G. Tuck. Inorg. Chem. **21**, 2787 (1982).
4. R. Kumar and D. G. Tuck. Unpublished results.
5. J. J. Habeeb and D. G. Tuck. Inorg. Synth. **19**, 257 (1979).
6. C. Oldham and D. G. Tuck. J. Chem. Ed. **59**, 420 (1982).
7. M. A. Khan, R. C. Steevensz, D. G. Tuck, J. G. Noltes, and P. W. R. Corfield. Inorg. Chem. **19**, 3407 (1980).
8. S. J. Amberson, F. W. B. Einstein, P. C. Hayes, R. Kumar, and D. G. Tuck. Inorg. Chem. **25**, 4181 (1986).
9. D. Coucouvanis, C. N. Murphy, and S. K. Kanodia. Inorg. Chem. **19**, 2993 (1980).
10. C. D. Garner, J. R. Nicholson, and W. Clegg. Inorg. Chem. **23**, 2148 (1984).
11. I. G. Dance, L. J. Fitzpatrick, and M. L. Scudder. J. Chem. Soc. Chem. Commun. 546 (1983).
12. I. G. Dance, M. L. Scudder, and L. J. Fitzpatrick. Inorg. Chem. **24**, 2547 (1985).
13. R. Chadha, R. Kumar, and D. G. Tuck. J. Chem. Soc. Chem. Commun. 188 (1986).
14. I. G. Dance, P. J. Guerney, A. D. Rae, and M. L. Scudder. Inorg. Chem. **22**, 2883 (1983).
15. A. F. Wells. Structural inorganic chemistry. 3rd ed. Oxford University Press. 1962. p. 985.
16. I. D. Brown and J. D. Dunitz. Acta Crystallogr. **14**, 480 (1961).
17. R. Hesse. Arkiv Kemi. **20**, 481 (1963).
18. P. K. Mehrotra and R. Hoffman. Inorg. Chem. **17**, 2187 (1978).
19. P. Biscarini, L. Fusina, and G. Nivellini. J. Chem. Soc. Dalton Trans. 2141 (1974).
20. N. Iwasaki, J. Tomooka, and K. Toyoda. Bull. Chem. Soc. Jpn. **47**, 1323 (1974).
21. A. J. Canty, R. Kishimoto, G. B. Deacon, and G. J. Farquharson. Inorg. Chim. Acta, **20**, 161 (1976).
22. G. A. Bowmaker and L.-C. Tan. Aust. J. Chem. **32**, 1443 (1979).

Can. J. Chem. Downloaded from www.nrcresearchpress.com by 78.46.186.204 on 09/07/12
For personal use only.

N-Allyloxycarbonyl derivatives of D-glucosamine as promotors of 1,2-*trans*-glucosylation in Koenigs–Knorr reactions and in Lewis acid catalyzed condensations

PAUL BOULLANGER,[1] JOSEPH BANOUB,[2] AND GÉRARD DESCOTES

Université Lyon I, École supérieure de chimie industrielle de Lyon, Unité associée 463, Centre national de la recherche scientifique, 43 Bd. du 11 Novembre 1918, 69622-Villeubranne CEDEX, France

Received November 7, 1986

PAUL BOULLANGER, JOSEPH BANOUB, and GÉRARD DESCOTES. Can. J. Chem. **65**, 1343 (1987).

The use of suitably blocked D-glucosamine derivatives possessing the *N*-allyloxycarbonyl protective group of the amino function represents potential new routes to 1,2-*trans*-glucosylations. Both 3,4,6-tri-*O*-acetyl-2-*N*-allyloxycarbonyl-2-amino-2-deoxy-α-D-glucopyranosyl bromide (**2**) and 1,3,4,6-tetra-*O*-acetyl-2-*N*-allyloxycarbonyl-2-amino-2-deoxy-β-D-glucopyranose (**3**) could be used in Koenigs–Knorr reactions or Lewis acid catalyzed condensations, respectively. Glucosides of simple alcohols and disaccharides were synthesized in good to excellent yields. The *N*-allyloxycarbonyl protective group was, moreover, easy to remove with Pd(0) complexes, thus affording, after acetylation, the corresponding *N*-acetyl-β-D-glucosamine glucosides under very smooth conditions.

PAUL BOULLANGER, JOSEPH BANOUB et GÉRARD DESCOTES. Can. J. Chem. **65**, 1343 (1987).

L'utilisation de dérivés de la D-glucosamine protégés sur la fonction amine par un groupement *N*-allyloxycarbonyle constitue une nouvelle voie d'accès potentielle aux glucosides 1,2-*trans*. Le bromure de tri-*O*-acétyl-3,4,6 *N*-allyloxycarbonyl-2-amino-2 désoxy-2 α-D-glucopyrannosyle (**2**) et le tétra-*O*-acétyl-1,3,4,6 *N*-allyloxycarbonyl-2 amino-2 désoxy-2 β-D-glucopyrannose (**3**) peuvent être utilisés respectivement dans les réactions de type Koenigs–Knorr ou dans les condensations catalysées par les acides de Lewis. Les glucosides d'alcools simples et les disaccharides ont été préparés avec des rendements de bons à excellents. Le groupe protecteur *N*-allyloxycarbonyle est, de plus, facile à cliver avec les complexes du Pd(0) et conduit, après acétylation, aux glucosides de la *N*-acétyl β-D-glucosamine dans des conditions très douces.

Introduction

The β-D-glucosides of *N*-acetyl glucosamine are widely distributed in living organisms where they constitute important building blocks of peptidoglycans, mucopolysaccharides (hyaluronic acids, keratan sulfate), glycoproteins (inner and outer core regions), oligosaccharides of human milk, and blood group determinants (1). They are also often encountered in bacterial antigens where they constitute part of the antigenic determinant (2). The teichoic acids of *Staphylococcus aureus* (3), for example, contain a β-D-GlcNAc-(1→4)-D-ribitol repeating unit, the synthesis of which was realized recently in our laboratory (4, 5).

The usual procedures for the 1,2-*trans*-glucosylation of D-glucosamine are mainly the so-called oxazoline method (6) and the phthalimido procedure (7). Despite their synthetic usefulness, these methods suffer some disadvantages. In the first method, the 2-methyl-(3,4,6-tri-*O*-acetyl-1,2-dideoxy-D-glucopyrano)[2,1-*d*]-2-oxazoline (6) or a synthetic precursor (8) is reacted with the alcohol (usually in refluxing nitromethane–toluene) in acidic medium. Yields are generally good with primary alcohols and still satisfactory with reactive secondary alcohols (9), affording the β-D-glucosides of *N*-acetylated glucosamine directly. Nevertheless, the rather drastic conditions do not allow the use of acid-sensitive protective groups in the glycosylating agent or the aglycon.

In the phthalimido method, the alcohol is reacted with 3,4,6-tri-*O*-acetyl-2-deoxy-2-phthalimido-D-glucopyranosyl bromide (usually at low temperature) in the presence of the silver triflate – collidine complex. The yields are generally excellent, even with weakly reactive alcohols, and this method is the most widely used for the preparation of complex oligosaccharides. The major disadvantage of the method is the need of further steps for deprotection and reacetylation of the amino function, requested for the synthesis of natural oligosaccharides. Despite some recent improvements (10), the phthalimido cleavage still remains a rather drastic procedure, which causes the removal of most alkaline-sensitive protective groups and which also often results in an important decrease of the overall yield.

The results described recently in the literature dealing with the versatile uses of the allyloxycarbonyl protective group (11, 12) prompted us to study its participating properties in 1,2-*trans*-glucosylation reactions. In a continuation of our studies on the glucosylation reactions (4, 5), we now report two different efficient methods for 1,2-*trans*-glucosylation of D-glucosamine. Both Koenigs–Knorr type reactions and condensations catalyzed by Lewis acids are depicted and compared.

Results and discussion

The carbamate approach for the synthesis of 1,2-*trans*-glucosides of D-glucosamine has already been mentioned in the literature. Using a benzyl carbamate derivative, K. Heyns *et al.* (13) did not succeed in obtaining the expected β-D-glucoside whereas J. Lessard *et al.* (14) were able to prepare such β-D-glucosides in moderate yields using reactive alcohols only. Most recently, S. Kusumoto *et al.* (15) described the synthesis of a disaccharide from a trichloroethyl carbamate derivative of D-glucosamine.

These rather divergent results induced us to undertake a systematic study on the glucosylation reactions of the *N*-allyloxycarbonyl derivatives of D-glucosamine.

As previously reported (16), the reaction of 3,4,6-tri-*O*-acetyl-2-*N*-allyloxycarbonyl-2-amino-2-deoxy-α-D-glucopyranosyl bromide (**2**) with alcohols promoted by mercury[II] or silver[I] salts afforded the expected β-D-glucosides (**4**), together with various amounts of oxazolidinone (**5**) as a by-product. This reaction has been extended to 1,2-*trans*-glucosylations promoted by Lewis acids (17) and both methods were compared with regard to the stability of the protective groups and the reactivity of the aglycons (Scheme 1).

[1]Author to whom correspondence may be addressed.

[2]On leave from Fisheries and Oceans Canada, Science Branch, P.O. Box 5667, St. John's, Nfld., Canada A1C 5X1.

Printed in Canada / Imprimé au Canada

Can. J. Chem. Downloaded from www.nrcresearchpress.com by 72.64.146.136 on 09/07/12
For personal use only.

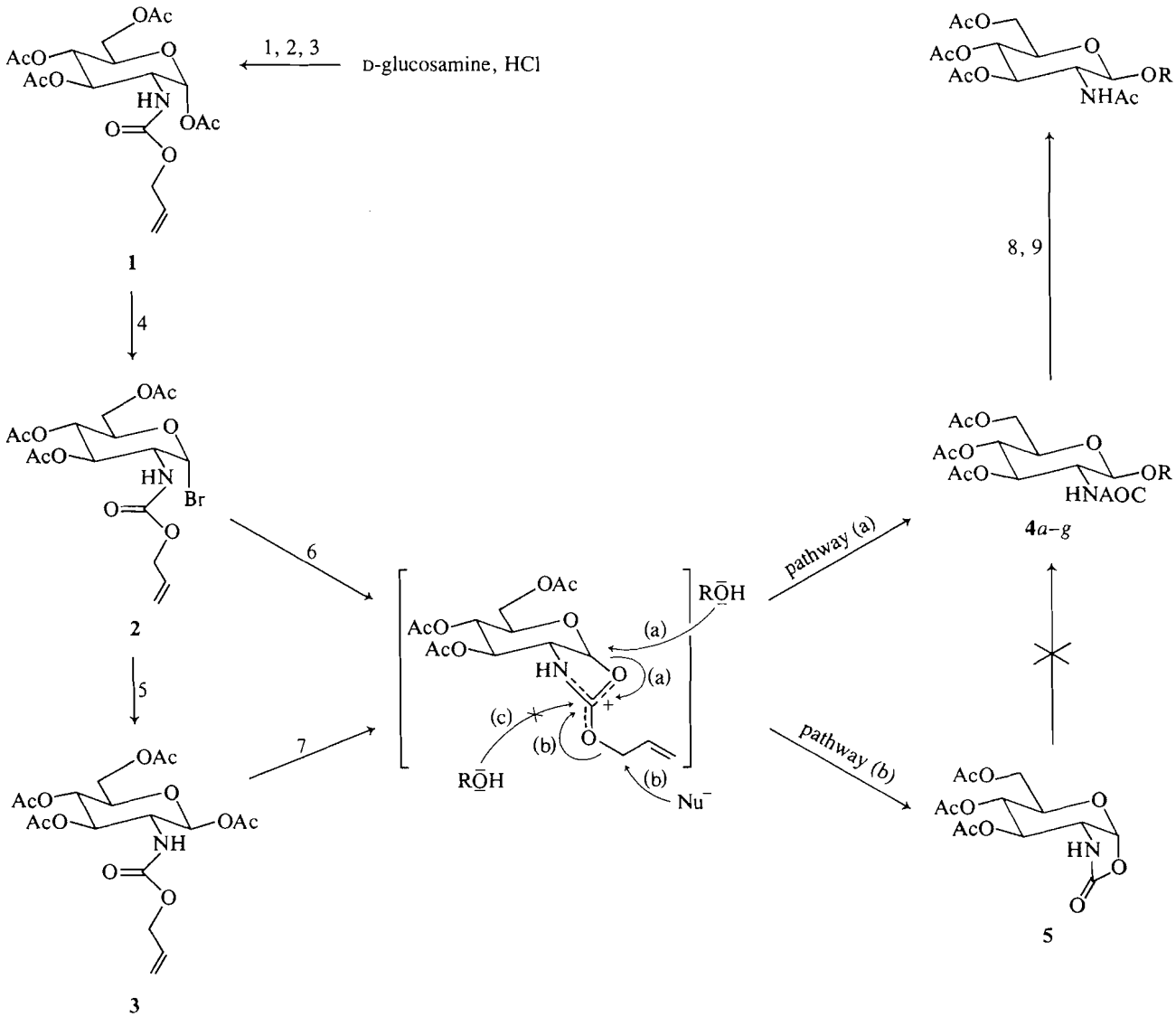

1. NaOMe, MeOH; 2. ClCOOAll, Et_3N; 3. Ac_2O, pyr.; 4. HBr, AcOH, CH_2Cl_2, 0°C; 5. $Hg(OAc)_2$, HOAc; 6, $Hg(CN)_2$, ROH; 7. TMS triflate, ROH; 8. $Pd(PPh_3)_4$, $CH_2(COOMe)_2$; 9. Ac_2O, pyr.

SCHEME 1

The glycosyl bromide (**2**) could be prepared with a 74% overall yield from D-glucosamine hydrochloride, via the intermediate 1,3,4,6-tetra-*O*-acetyl-2-*N*-allyloxycarbonyl-2-amino-2-deoxy-α-D-glucopyranose (**1**), as a stable crystalline material, contrary to its *N*-acetylated analog. This glucoside precursor was synthesized by a very classical pathway and could, in turn, be converted into another precursor, namely the corresponding β-acetate (**3**), by means of mercury[II] acetate in acetic acid, with an excellent yield. The preparation of compound **3** could be realized by shorter pathways, but the method described herein was the only one not requiring a chromatographic separation of α and β anomeric acetates at the final step of the synthesis.

The reaction of the glycosyl bromide (**2**) with one equivalent of alcohol and one equivalent of mercury[II] cyanide in dichloromethane at room temperature resulted in the complete consumption of the starting material in less than 24 h, depending on the aglycon. With reactive alcohols, the expected β-D-glucosides (**4***a–c* and **4***e–g*) were obtained in good yields, whereas with unreactive aglycons, such as 1,2:5,6-di-*O*-isopropylidene-α-D-glucofuranose, the glucoside (**4***d*) was accompanied by important amounts of the oxazolidinone (**5**), the formation of which was already reported by K. Heyns *et al.* (13).

The formation of both products (**4***a–g* and **5**) could be explained by the participation of the *N*-allyloxycarbonyl group giving rise to a strongly delocalized carbocationic species (Scheme 1). This intermediate could react following pathway (a) (leading to the β-D-glucosides **4**) or pathway (b) (forming the oxazolidinone **5**) but the possible pathway (c) resulting from an attack on the C-2 carbon atom of the oxazolidinium ion, was never observed. Pathway (a) was very preponderant with reactive alcohols (with regard to steric hindrance and (or) nucleophilicity) while pathway (b) gained in importance with less reactive alcohols (see entry **d** in Table 1). It was, moreover, observed that the oxazolidinone (**5**) was not reactive itself toward the alcohol under the experimental conditions, and therefore cannot constitute an intermediate in the formation of β-D-glucosides (**4**).

Can. J. Chem. Downloaded from www.nrcresearchpress.com by 72.64.146.136 on 09/07/12
For personal use only.

TABLE 1. Glucosylation of alcohols from 3,4,6-tri-*O*-acetyl-2-*N*-allyloxycarbonyl-2-amino-2-deoxy-α-D-glucopyranosyl bromide (**2**)[a] and 1,3,4,6-tetra-*O*-acetyl-2-*N*-allyloxycarbonyl-2-amino-2-deoxy-β-D-glucopyranose (**3**)[b]

			Glucosylations from compound **2**			Glucosylations from compound **3**	
	Alcohol	Glucoside	Glucoside yield (%)	Oxazolidinone(**5**) yield (%)	Reaction time (h)	Glucoside yield (%)	Reaction time (h)
a	Methanol	**4***a*	91	Traces	2	85	4
b	Isopropanol	**4***b*	76	~5	6	95	12
c	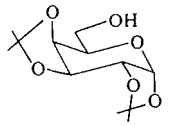	**4***c*	86	Traces	5	82	16
d	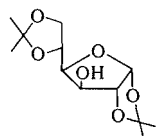	**4***d*[c]	12	~70	18	66	16
e	R = TBDMS	**4***e*	35[d]	~5	3	5[d]	16
f	R = All	**4***f*	81	Traces	12	83	16
g	R = AOC	**4***g*	63	~5	7	85	16

[a]Reactions performed with one equivalent of alcohol and one equivalent of mercury[II] cyanide with respect to **2**, at room temperature in dichloromethane.

[b]Reactions performed with one equivalent of alcohol and one equivalent of trimethylsilyl triflate with respect to **3**, at −35°C in dichloromethane.

[c](1→6)-β-D-glucoside resulting from a rearrangement of the isopropylidene protective group.

[d]The poor yield could be attributed to the cleavage of the tertiobutyldimethylsilyl protective group during the reaction and (or) extraction and purification of the disaccharide.

Several experimental observations allowed us to conclude that, contrary to Heyns' results, the nucleophile (Nu^-) involved in pathway (b) was not the alcohol but, probably, the bromide ion formed in the first step of the reaction, since no allylated alcohol (resulting from pathway (b) with Nu^- = ROH) was detected in any condensations and since the addition of one equivalent of tetraethylammonium bromide to the reaction medium resulted in an increase of oxazolidinone formation. The results obtained with this Koenigs–Knorr type reaction are summarized in Table 1.

The reaction of the β-D-acetate (**3**) with alcohols, on the other hand, could be conducted with various Lewis acids. Amongst those tested, the trimethylsilyl triflate gave the best results with regard to the yields of glucosides, ease of use, and lower amount of by-products. The reactions were conducted with one equivalent of the alcohol and one equivalent of the Lewis acid, with respect to the starting β-D-acetate at −35°C in dichloromethane. The β-D-glucosides were obtained in good yields, even with the unreactive aglycon previously mentioned, and the oxazolidinone resulting from pathway (b) (Scheme 1) was not observed in that case. The results obtained with the Lewis acid promoted glucosylations are reported in Table 1.

It should be noticed that the low yield of β-glucoside (**4***e*) obtained by both methods could be attributed to undesired cleavage of the tertiobutyldimethylsilyl protective group during the reaction and (or) the purification of the product, rather than to an important formation of oxazolidinone (**5**).

As already reported in the literature (18), the Koenigs–Knorr reaction carried out on 1,2:5,6-di-*O*-isopropylidene-α-D-glucofuranose resulted in an acetal migration from the 5,6 to the 3,5 position of the aglycon and therefore afforded a 1→6 glycoside (**4***d*) as attested mainly by ^{13}C nmr (the chemical shifts of the quaternary carbons of the acetal protective groups, 112.53 ppm and 101.36 ppm, correspond to those of dioxolane and dioxane rings, respectively). The isopropylidene migration had been observed in a glycosylation promoted by trimethylsilyl triflate (19).

The yields of glucosylations described in this paper can be compared favourably with those reported in the literature. The isopropyl glucoside, for example, was obtained in 85% yield only by the oxazoline method, using a 2–10 molar excess of the alcohol (20). The glucosides of 1,2:3,4-di-*O*-isopropylidene-α-D-galactopyranose (**c**) were obtained, under the best conditions, in 81% yield by the oxazoline method (21) and in 86% yield by both phthalimido (22) and *N*-allyloxycarbonyl procedures (Table 1). On the other hand, the glucosylations of the ribitol derivatives (**f** and **g**) were realized, in our laboratory, respectively in 71 (5) and 50% yields by the oxazoline method, in 79 and 71% yields by the phthalimido procedure, and in 83 and 85% yields by the *N*-allyloxycarbonyl procedure (Table 1).

As can be seen from Table 1, the yields are slightly better starting from the bromide **2** than from the β-acetate **3** with primary alcohols but lower with secondary and hindered alcohols. These two methods are quite complementary since the

Can. J. Chem. Downloaded from www.nrcresearchpress.com by 72.64.146.136 on 09/07/12
For personal use only.

Can. J. Chem. Downloaded from www.nrcresearchpress.com by 72.64.146.136 on 09/07/12
For personal use only.

lower reactivity of the bromide (**2**) is accompanied by a better selectivity towards primary alcohols and a better preservation of the acid-sensitive protective groups. The β-D-acetate (**3**), on the other hand, seems to be much more reactive; these two properties will be explored in the near future in the field of complex carbohydrate synthesis involving selectivity and (or) reactivity towards various alcohols.

The deprotection of the *N*-allyloxycarbonyl group could be realized by using the numerous methods reported in the literature; the reductive cleavage (23) and the deprotection promoted by nickel tetracarbonyl (24) have now been substituted by newer methods based on homogeneous palladium catalysis. These methods are promoted by Pd(0) complexes, usually tetrakis(triphenylphosphine) palladium, together with an allyl acceptor. Amongst these acceptors, the most widely used are dimedone (25), 2-ethylhexanoic acid (26), or tributyltin hydride (27); these acceptors give rise to by-products of low volatility, creating the need of further chromatographic purification to recover the free amine after deprotection. The Pd(0) catalyzed deprotection can also be realized by hydrogenolytic cleavage with formic acid (28) to afford the amine as a quaternary salt, requiring an ion exchange to remove the free amine. The results of these different techniques have been recently reviewed in the field of nucleotide synthesis (12).

To take advantage, in the field of carbohydrates, of the remarkable selectivity of Pd(0) complexes, and to avoid the above-mentioned inconveniences, we have used dimethyl malonate as allyl acceptor to obtain volatile by-products after allylation. After complete deprotection, the amino-free glycoside could be reacetylated to prepare natural oligosaccharide analogs (Scheme 1) or esterified with a fatty acid to obtain analogs of glycolipids (15).

This new strategy for the synthesis of β-D-glucosides of glucosamine should, in our opinion, complete the panel of well-known and classical methods of 1,2-*trans*-glucosylations. The *N*-allyloxycarbonyl approach is easy to use; the glucosylation conditions are very smooth, and compatible with most hydroxyl protective groups stable in slightly acidic medium. The choice between a glycosyl bromide and an anomeric β-D-acetate as glucosylation precursor will permit selective reactivities towards alcohols. The *N*-allyloxycarbonyl function is quite stable in most of the conditions encountered in saccharide chemistry and can survive the deprotection of many other groups; its cleavage is, moreover, perfectly selective and compatible with most *O*- and *N*-protective groups, which represents a real advantage over the classical methods used in that field.

Experimental

Melting points were determined on a Büchi apparatus and were uncorrected. Optical rotations were measured using a Perkin Elmer 241 polarimeter in 1-dm cells. The ^{1}H nmr spectra were recorded on Varian EM-360, Brucker W.P. 80 CW, or Brucker A.C. 200 instruments. The ^{13}C nmr spectra were recorded on a Varian XL-100A (25.3 MHz) spectrometer operating in the Fourier transform mode. Chemical shifts are relative to internal Me_4Si. In ^{13}C nmr spectra of the disaccharides, the primed carbon atom resonance signals are attributed to the carbohydrate moiety bound to β-D-glucosamine. The ^{13}C nmr spectra always contain additional signals corresponding to acetates and aromatics in the case of benzylated ribitol derivatives. Microanalyses were carried out by the Laboratoire Central d'Analyse du CNRS (Solaise, France) and acceptable values are reported to a ±0.4% tolerance. Chromatographic separations were performed on Merck silica gel (230–400 mesh). Dichloromethane was washed with water and dried on $CaCl_2$ before distillation over P_2O_5. Oxolane was treated with basic aluminium oxide (Alumina Woelm B) before distillation over $LiAlH_4$ and exhaustively flushed with argon just prior to use.

*1,3,4,6-Tetra-*O*-acetyl-2-*N*-allyloxycarbonyl-2-amino-2-deoxy-α-D-glucopyranose (**1**)*

D-Glucosamine hydrochloride (21.6 g, 0.1 mol) was added to a sodium methylate solution, obtained by reaction of methanol (100 mL) with sodium (2.3 g, 0.1 mol), and then shaken at room temperature for 10 min. After filtration, triethylamine (14 mL, 0.1 mol) and allyl-chloroformate (12.0 g, 0.104 mol) were added to the filtrate at a temperature maintained below 30°C. The reaction was completed after 3 h at room temperature and the solvent was evaporated to dryness, followed by acetylation overnight (acetic anhydride: 100 mL, pyridine: 200 mL). After the usual extraction procedure, the title compound (**1**) was recovered as a pink foamy material that could be used directly in the next step or recrystallized from ether (38.5 g, 89%): mp 119–121°C; $[\alpha]_D^{23}$ +27.6 (*c* 2.36, $CHCl_3$); 200-MHz ^{1}H nmr ($CDCl_3$) δ: 6.20 (d, 1H, *J* = 3.6 Hz, H-1), 5.96–5.70 (m, 1H, vinyl proton), 5.32–5.11 (m, 4H), 4.97 (d, 1H, *J* = 9.4 Hz, N*H*) 4.58–3.98 (m, 5H), 2.19, 2.12, 2.09, 2.04 (4s, 12H, 4OAc); ^{13}C nmr (CD_3COCD_3) δ: 156.37 (*C*O: allyloxycarbonyl), 133.87 (*C*H=CH_2), 117.11 (CH=*C*H_2), 90.96 (C-1), 71.33, 70.25 (C-5, C-3), 68.90 (C-4), 65.73 (*C*H_2—CH=CH_2), 62.24 (C-6), 53.48 (C-2). *Anal.* calcd. for $C_{18}H_{25}O_{11}N$ (Mol. Wt. 431.39): C 50.11, H 5.84, N 3.25; found: C 49.97, H 5.90, N 3.11.

*3,4,6-Tri-*O*-acetyl-2-*N*-allyloxycarbonyl-2-amino-2-deoxy-α-D-glucopyranosyl bromide (**2**)*

The above-mentioned derivative (**1**) (30 g, 0.07 mol) dissolved in dry dichloromethane (200 mL) was treated at 0°C with 33% hydrobromic acid in acetic acid (50 mL) for 0.5 h. The mixture was then poured into cold water and the aqueous layer extracted with chloroform. The mixed organic extracts were then neutralized with an aqueous solution of sodium carbonate, washed once with cold water, and dried over calcium chloride. After evaporation to dryness, compound **2** was recovered as a dark yellow foam. The pure derivative was recovered after two recrystallizations from ether (26 g, 82%): mp 93–94°C; $[\alpha]_D^{24}$ +147 (*c* 1.9, $CHCl_3$); 80-MHz ^{1}H nmr ($CDCl_3$) δ: 6.55 (d, 1H, *J* = 3.6 Hz, H-1); ^{13}C nmr (CD_3COCD_3) δ: 155.95 (*C*O: allyloxycarbonyl), 133.63 (*C*H=CH_2), 117.28 (CH=*C*H_2), 93.55 (C-1), 73.43, 71.17 (C-5, C-3), 68.10 (C-4), 65.96 (*C*H_2—CH=CH_2), 61.77 (C-6), 55.85 (C-2). *Anal.* calcd. for $C_{16}H_{22}O_9NBr$ (Mol. Wt. 452.25): C 42.49, H 4.90, N 3.10, Br 17.67; found: C 42.64, H 5.09, N 2.92, Br 17.48.

*1,3,4,6-Tetra-*O*-acetyl-2-*N*-allyloxycarbonyl-2-amino-2-deoxy-β-D-glucopyranose (**3**)*

The glycosyl bromide **2** (20 g, 0.044 mol) dissolved in acetic acid (100 mL), was treated for 45 min with mercury[II] acetate (16 g, 0.050 mol) at room temperature. After filtration on a bed of Celite, the filter cake was washed three times with chloroform and the mixed chloroformic extracts poured into cold water. After washing and neutralization with an aqueous solution of sodium carbonate, the organic extracts were dried over calcium chloride and evaporated, to leave crude compound **3** as a yellowish crystalline material. Recrystallization from ether afforded the pure derivative (16.5 g, 87%): mp 109–110°C; $[\alpha]_D^{23}$ +25.9 (*c* 2.14, $CHCl_3$); 200-MHz ^{1}H nmr ($CDCl_3$) δ: 5.87–5.76 (m, 1H, vinyl proton), 5.37–5.12 (m, 4H), 4.95 (m, 1H, N*H*), 4.58–3.81 (m, 6H), 2.15, 2.09, 2.08, 2.05 (4s, 12H, 4OAc); ^{13}C nmr (CD_3COCD_3) δ: 156.21 (*C*O: allyloxycarbonyl), 133.99 (*C*H=CH_2), 116.83 (CH=*C*H_2), 92.88 (C-1), 73.13, 72.98 (C-5, C-3), 69.08 (C-4), 65.54 (*C*H_2—CH=CH_2), 62.37 (C-6), 55.50 (C-2). *Anal.* calcd. for $C_{18}H_{25}O_{11}N$ (Mol. Wt. 431.39): C 50.11, H 5.84, N 3.25; found: C 50.35, H 5.91, N 3.20.

*General procedure for the Koenigs–Knorr glycosidations starting from compound **2***

The glycosyl bromide **2** (1.00 g, 2.21 mmol), the alcohol to be glucosylated (2.21 mmol), and dry mercury[II] cyanide (0.558 g, 2.21 mmol) were dissolved simultaneously in dry, alcohol-free dichloromethane (20 mL). The reaction, stirred at room tempeature, was monitored by tlc and stopped 1 h after completion (reaction times

Can. J. Chem. Downloaded from www.nrcresearchpress.com by 72.64.146.136 on 09/07/12
For personal use only.

in Table 1). The reaction mixture was filtered on Celite, the filter cake washed twice with chloroform, and the mixed chloroformic extracts washed once with water. After drying over calcium chloride and evaporation, the product was purified by column chromatography (eluent: ethyl acetate/hexane from 1:2 to 2:1 depending on the aglycon); yields are given in Table 1.

General procedure for the Lewis acid promoted glucosylations starting from compound **3**

The β-acetate **3** (1.00 g, 2.32 mmol), the alcohol to be glucosylated (2.32 mmol), and powered 5 Å molecular sieves (0.5 g) were added simultaneously in dry alcohol-free dichloromethane (50 mL). The reaction mixture was then flushed with argon while cooling to −35°C. Trimethylsilyl triflate (0.516 g, 2.32 mmol) was then introduced through a syringe and the argon flush maintained for 0.5 h; the external temperature was kept near −35 ± 5°C all during the processing. The reaction times indicated in Table 1 are purely indicative, since the reactions were not monitored to avoid hydrolysis during the withdrawal of aliquots. The reaction was stopped by addition of triethylamine (0.5 g, 4.94 mmol) at −35°C; the mixture was then allowed to reach 0°C, filtered on Celite, and the filtrate was collected into a cold, dilute aqueous solution of sodium carbonate. The same work-up and purification procedures as previously mentioned were then applied; yields are indicated in Table 1.

*Methyl 3,4,6-tri-*O*-acetyl-2-*N*-allyloxycarbonyl-2-amino-2-deoxy-β-*D*-glucopyranoside (***4***a)*

White crystalline material: mp 111–112°C (ether); $[\alpha]_D^{24}$ +10.2 (*c* 1.9, $CHCl_3$); 200-MHz ^{1}H nmr ($CDCl_3$) δ: 5.89 (m, 1H, vinyl C*H*), 5.33–5.15 (m, 3H, vinyl CH_2, H-3), 5.07 (t, 1H, *J* = 9.5 Hz, H-4), 4.92 (m, 1H, N*H*), 4.63–4.47 (m, 3H, allyl CH_2, H-1), 4.22 (m, 2H, $J_{6,6'}$ = 12.3 Hz, $J_{5,6}$ = 4.7 Hz, $J_{5,6'}$ = 2.4 Hz, H-6, H-6′), 3.70 (m, 1H, H-5), 3.60 (m, 1H, H-2), 3.52 (s, 3H, OCH_3), 2.09, 2.04, 2.03 (3s, 9H, 3OAc); ^{13}C nmr (CD_3COCD_3) δ: 156.19 (*C*O: allyloxycarbonyl), 133.84 (*C*H=CH$_2$), 116.74 (CH=*C*H$_2$), 102.30 (C-1), 73.40, 71.98 (C-5, C-3), 69.55 (C-4), 65.36 (*C*H$_2$—CH=CH$_2$), 62.60 (C-6), 56.68 (O*C*H$_3$), 56.33 (C-2). *Anal.* calcd. for $C_{17}H_{25}O_{10}N$ (Mol. Wt. 403.38): C 50.62, H 6.25, N 3.47; found: C 50.58, H 6.36, N 3.44.

*1-Methylethyl 3,4,6-tri-*O*-acetyl-2-*N*-allyloxycarbonyl-2-amino-2-deoxy-β-*D*-glucopyranoside (***4***b)*

White crystalline material: mp 148–149°C (ether); $[\alpha]_D^{24}$ +4.2 (*c* 1.0, $CHCl_3$); ^{13}C nmr (CD_3COCD_3) δ: 156.27 (*C*O: allyloxycarbonyl), 134.12 (*C*H=CH$_2$), 116.66 (CH=*C*H$_2$), 100.29 (C-1), 73.45, 72.53, 71.96 (C-5, C-3, *C*H: isopropyl), 69.84 (C-4), 65.27 (*C*H$_2$—CH=CH$_2$), 62.85 (C-6), 56.81 (C-2), 23.59, 22.17 (*C*H$_3$: isopropyl). *Anal.* calcd. for $C_{19}H_{29}O_{10}N$ (Mol. Wt. 431.44): C 52.89, H 6.78, N 3.25; found: C 52.85, H 6.75, N 3.21.

*6-O-(3,4,6-Tri-*O*-acetyl-2-*N*-allyloxycarbonyl-2-amino-2-deoxy-β-*D*-glucopyranosyl)-1,2:3,4-di-*O*-(1-methylethylidene)-α-*D*-galactopyranose (***4***c)*

The aglycon was prepared according to ref. 29. Compound **4***c* was obtained as a white crystalline material: mp 135–136°C (ether); $[\alpha]_D^{24}$ −41.3 (*c* 1.4, $CHCl_3$); 200-MHz ^{1}H nmr ($CDCl_3$) δ: 5.89 (m, 1H, vinyl C*H*), 5.52 (d, 1H, *J* = 5.2 Hz, H-1: galactose moiety), 5.53–5.18 (m, 3H, vinyl CH_2, H-3), 5.07 (t, 1H, *J* = 9.7 Hz, H-4), 4.92 (m, 1H, N*H*), 2.09, 2.02, 2.01 (3s, 9H, 3OAc), 1.51, 1.44, 1.32 (3s, 12H, 2 isopropylidene); ^{13}C nmr (CD_3COCD_3) δ: 156.19 (*C*O: allyloxycarbonyl), 134.20 (*C*H=CH$_2$), 116.74 (CH=*C*H$_2$), 109.29, 108.78 (quaternary *C*: isopropylidene), 102.15 (C-1), 96.79 (C′-1), 73.40, 72.18 (C-5, C-3), 71.56, 71.26, 71.11 (C′-2, C′-3, C′-5), 69.70 (C-4), 69.06 (C′-6), 67.70 (C′-4), 65.45 (*C*H$_2$—CH=CH$_2$), 62.94 (C-6), 56.88 (C-2), 26.30, 25.17, 24.53 (*C*H$_3$: isopropylidene). *Anal.* calcd. for $C_{28}H_{41}O_{15}N$ (Mol. Wt. 631.63): C 53.24, H 6.54, N 2.25; found: C 53.29, H 6.56, N 2.16.

*6-O-(3,4,6-Tri-*O*-acetyl-2-*N*-allyloxycarbonyl-2-amino-2-deoxy-β-*D*-glucopyranosyl)-1,2:3,5-di-*O*-(1-methylethylidene)-α-*D*-glucofuranose (***4***d)*

The aglycon was prepared according to ref. 29. Compound **4***d* was obtained as a white crystalline material: mp 109–111°C (ether/petroleum ether); $[\alpha]_D^{22}$ +15.5 (*c* 2.3, $CHCl_3$); ^{13}C nmr (CD_3COCD_3) δ: 156.56 (*C*O: allyloxycarbonyl), 134.54 (*C*H=CH$_2$), 117.03 (CH=*C*H$_2$), 112.53 (quaternary *C*: 1,2-isopropylidene), 106.90 (C′-1), 102.60 (C-1), 101.36 (quaternary *C*: 3,5-isopropylidene), 84.87 (C′-2), 79.73 (C′-4), 75.85 (C′-3), 73.76, 72.54, 72.45 (C-5, C-3, C′-5), 71.03 (C′-6), 70.04 (C-4), 65.62 (*C*H$_2$—CH=CH$_2$), 63.05 (C-6), 56.91 (C-2), 27.46, 26.83, 24.33 (*C*H$_3$: isopropylidene). *Anal.* calcd. for $C_{28}H_{41}O_{15}N$ (Mol. Wt. 631.63): C 53.24, H 6.54, N 2.22; found: C 53.29, H 6.75, N 2.21.

*2,3,5-Tri-*O*-benzyl-1-*O*-tertiobutyldimethylsilyl-*D*-ribitol (***e***)*

2,3,5-Tri-*O*-benzyl-D-ribitol (30) (2.55 g, 6.04 mmol), dissolved in dry DMF (20 mL), was treated for 36 h at room temperature with imidazole (1.0 g, 14.7 mmol) and tertiobutyldimethylsilyl chloride (1.21 g, 7.93 mmol). After concentration to 5 mL, the mixture was diluted with chloroform (20 mL) and washed with cold water. After drying ($CaCl_2$) and evaporation, a clear syrup was obtained (3.17 g, 98%). This compound (**e**), homogeneous in tlc, was purified by column chromatography for analytical purposes, but could be used directly for further steps: syrup; $[\alpha]_D^{23}$ +22.8 (*c* 7.0, $CHCl_3$); ^{13}C nmr (CD_3COCD_3) δ: 80.95, 80.04 (C-2, C-3), 73.75, 73.12, 72.55, 72.18 (C-5, 3CH_2: benzyl), 70.82 (C-4), 63.33 (C-1), 26.06 (*C*H$_3$: *tert*-butyl), 18.40 (quaternary *C*: *tert*-butyl), −5.27 (*C*H$_3$-Si). *Anal.* calcd. for $C_{32}H_{44}O_5Si$ (Mol. Wt. 536.79): C 71.60, H 8.26, Si 5.23; found: C 71.20, H 8.18, Si 5.27.

*4-O-(3,4,6-Tri-*O*-acetyl-2-*N*-allyloxycarbonyl-2-amino-2-deoxy-β-*D*-glucopyranosyl)-2,3,5-tri-*O*-benzyl-1-tertiobutyldimethylsilyl-*D*-ribitol (***4***e)*

Waxy material: $[\alpha]_D^{21}$ −3.3 (*c* 3.4, $CHCl_3$); ^{13}C nmr (CD_3COCD_3) δ: 156.43 (*C*O: allyloxycarbonyl), 134.23 (*C*H=CH$_2$), 116.97 (CH=*C*H$_2$), 101.54 (C-1), 80.76, 80.12 (C′-2, C′-3), 79.38 (C′-4), 74.40, 73.65, 72.98 (3CH_2: benzyl), 73.65, 72.32 (C-5, C-3), 71.23 (C′-5), 69.99 (C-4), 65.58 (*C*H$_2$—CH=CH$_2$), 63.87, 62.99 (C′-1, C-6), 57.26 (C-2), 26.46 (*C*H$_3$: *tert*-butyl), 18.89 (quaternary *C*: *tert*-butyl), −5.01 (*C*H$_3$-Si). *Anal.* calcd. for $C_{48}H_{65}O_{14}NSi$ (Mol. Wt. 908.13): C 63.49, H 7.21, N 1.54, Si 3.09; found: C 63.31, H 7.22, N 1.51, Si 3.13.

*4-O-(3,4,6-Tri-*O*-acetyl-2-*N*-allyloxycarbonyl-2-amino-2-deoxy-β-*D*-glucopyranosyl)-1-*O*-allyl-2,3,5-tri-*O*-benzyl-*D*-ribitol (***4***f)*

The aglycon was prepared according to ref. 5. Syrup; $[\alpha]_D^{24}$ −2.3 (*c* 2.8, $CHCl_3$); ^{13}C nmr (CD_3COCD_3) δ: 156.27 (*C*O: allyloxycarbonyl), 135.96 (*C*H=CH$_2$: allyl), 134.03 (*C*H=CH$_2$: allyloxycarbonyl), 116.76 (CH=*C*H$_2$: allyloxycarbonyl), 116.01 (CH=*C*H$_2$: allyl), 101.23 (C-1), 80.02, 79.03, 78.98 (C′-2, C′-3, C′-4), 74.18, 73.49, 72.56 (3CH_2: benzyl), 73.49, 72.29 (C-5, C-3), 72.10 (*C*H$_2$—CH=CH$_2$: allyl), 70.93, 70.72 (C′-1, C′-5), 69.76 (C-4), 65.39 (*C*H$_2$—CH=CH$_2$: allyloxycarbonyl), 62.81 (C-6), 57.03 (C-2). *Anal.* calcd. for $C_{45}H_{55}O_{14}N$ (Mol. Wt. 833.93): C 64.81, H 6.65, N 1.68; found: C 64.92, H 6.65, N 1.68.

*4-O-(3,4,6-Tri-*O*-acetyl-2-*N*-allyloxycarbonyl-2-amino-2-deoxy-β-*D*-glucopyranosyl)-1-*O*-allyloxycarbonyl-2,3,5-tri-*O*-benzyl-*D*-ribitol (***4***g)*

The aglycon was prepared according to ref. 31. Syrup; $[\alpha]_D^{22}$ −8.4 (*c* 4.4, $CHCl_3$); ^{13}C nmr (CD_3COCD_3) δ: 156.35 (*C*O, *N*-allyloxycarbonyl), 155.54 (*C*O: *O*-allyloxycarbonyl), 134.15 (*C*H=CH$_2$: *N*-allyloxycarbonyl), 132.95 (*C*H=CH$_2$: *O*-allyloxycarbonyl), 118.43 (CH=*C*H$_2$: *O*-allyloxycarbonyl), 116.94 (CH=*C*H$_2$: *N*-allyloxycarbonyl), 101.15 (C-1), 79.14, 78.39, 77.97 (C′-4, C′-3, C′-2), 74.39, 73.78, 72.64 (3CH_2: benzyl), 73.49, 72.26 (C-5, C-3), 70.77 (C′-5), 69.82 (C-4), 68.64 (C′-1), 67.52 (*C*H$_2$—CH=CH$_2$: *O*-allyloxycarbonyl), 65.55 (*C*H$_2$—CH=CH$_2$: *N*-allyloxycarbonyl), 62.94 (C-6), 57.08 (C-2). *Anal.* calcd. for $C_{45}H_{53}O_{16}N$ (Mol. Wt. 863.91): C 62.56, H 6.18, N 1.62; found: C 62.20, H 6.35, N 1.59.

General procedure for the cleavage of the N*-allyloxycarbonyl protective group*

Palladium bis(dibenzylidene acetone) (20 mg, 0.035 mmol) was reacted with triphenylphosphine (50 mg, 0.191 mmol) in dry, oxygen-

free oxolane (3.5 mL) at room temperature for 10 min. The *N*-allyloxycarbonyl-β-D-glucosaminide (**4***a–f*) (1.00 mmol) dissolved in oxygen-free oxolane (5 mL) and dimethyl malonate (0.6 mL, 7.0 mmol) was then added to the above solution and the mixture was stirred for 24 h at room temperature. After concentration to 1 mL, the mixture was applied at the top of a small silica gel column and eluted first with ethyl acetate, to remove the triphenylphosphine by-products, and then with methanol, to recover the expected amino-free derivative in almost quantitative yield.

Acknowledgements

The authors are indebted to C.N.R.S. for the postdoctoral position of one of us (J.B.), to Professor S. Czernecki for valuable discussions and suggestions, and to the French Société Nationale des Poudres et Explosifs (SNPE) for providing allyl-chloroformate.

1. N. SHARON. *In* Complex carbohydrates. Addisson–Wesley Publishing Company, Reading, MA. 1975.
2. K. JANN and B. JANN. Methods Enzymol. **50**, 251 (1978).
3. J. BADDILEY, J. G. BUCHANAN, U. L. RAJBHANDARY, and A. R. SANDERSON. Biochem. J. **82**, 432 (1962).
4. P. BOULLANGER, G. DESCOTES, J.-P. FLANDROIS, and D. MARMET. Carbohydr. Res. **110**, 153 (1982).
5. P. BOULLANGER, C. ANDRE, and G. DESCOTES. J. Carbohydr. Chem. **4**, 279 (1985).
6. S. E. ZURABYAN, T. P. VOLOSYUK, and Y. YA. KHORLIN. Carbohydr. Res. **9**, 215 (1969).
7. R. U. LEMIEUX, T. TAKEDA, and B. Y. CHUNG. Am. Chem. Soc. Symp. Ser. **39**, 90 (1976).
8. M. KISO and L. ANDERSON. Carbohydr. Res. **136**, 309 (1985).
9. H. PAULSEN. Angew. Chem. Int. Ed. Engl. **21**, 155 (1982).
10. H.-P. WESSEL, T. INVERSEN, and D. R. BUNDLE. Carbohydr. Res. **130**, 5 (1984).
11. M. KLOOSTERMAN, J. H. VAN BOOM, P. CHATELARD, P. BOULLANGER, and G. DESCOTES. Tetrahedron Lett. **26**, 5045 (1985).
12. Y. HAYAKAWA, H. KATO, M. UCHIYAMA, H. KAJINO, and R. NOYORI. J. Org. Chem. **51**, 2400 (1986).
13. K. HEYNS, R. HARRISON, and H. PAULSEN. Chem. Ber. **100**, 271 (1967).
14. J. LESSARD, H. DRIGUEZ, and J.-P. VERMES. Tetrahedron Lett. 4887 (1970).
15. S. KUSUMOTO, H. YOSHIMURA, M. IMOTO, T. SHIMAMOTO, and T. SHIBA. Tetrahedron Lett. **26**, 909 (1985).
16. P. BOULLANGER and G. DESCOTES. Tetrahedron Lett. **27**, 2599 (1986).
17. S. HANESSIAN and J. BANOUB. Carbohydr. Res. **59**, 261 (1977).
18. A. LIPTAK, P. NANASI, A. NESZMELYI, and H. WAGNER. Carbohydr. Res. **86**, 133 (1980).
19. H. PAULSEN and M. PAAL. Carbohydr. Res. **135**, 53 (1984).
20. M. KISO and L. ANDERSON. Carbohydr. Res. **72**, C12 (1979).
21. J.-C. JACQUINET, S. E. ZURABYAN, and Y. YA. KHORLIN. Carbohydr. Res. **32**, 137 (1974).
22. R. U. LEMIEUX, S. Z. ABBAS, and B. Y. CHUNG. Can. J. Chem. **60**, 58 (1982).
23. C. M. STEVENS and R. WATANABE. J. Am. Chem. Soc. **72**, 725 (1950).
24. E. J. COREY and J. W. SUGGS. J. Org. Chem. **38**, 3223 (1973).
25. H. KUNZ and C. UNERZAYT. Angew. Chem. Int. Ed. Engl. **23**, 436 (1984).
26. P. D. JEFFREY and S. W. MCCOMBIE. J. Org. Chem. **47**, 587 (1982).
27. F. GUIBE, O. DANGLES, and G. BALAVOINE. Tetrahedron Lett. **27**, 2365 (1986).
28. H. HEY and H. J. HARPE. Angew. Chem. Int. Ed. Engl. **12**, 928 (1973).
29. O. T. SCHMIDT. Methods Carbohydr. Chem. **2**, 318 (1963).
30. P. W. AUSTIN, F. E. HARDY, J. G. BUCHANAN, and J. BADDILEY. J. Chem. Soc. 2128 (1964).
31. P. BOULLANGER, P. CHATELARD, G. DESCOTES, M. KLOOSTERMAN, and J. H. VAN BOOM. J. Carbohydr. Chem. **5**, 541 (1986).

Can. J. Chem. Downloaded from www.nrcresearchpress.com by 72.64.146.136 on 09/07/12
For personal use only.

Synthesis and structural characterization of glycinatodimethylgallium, $(C_2H_4NO_2)Ga(CH_3)_2$

STEVEN J. RETTIG, ALAN STORR,[1] AND JAMES TROTTER[1]

Department of Chemistry, University of British Columbia, 2036 Main Mall, Vancouver, B.C., Canada V6T 1Y6

Received July 17, 1986

STEVEN J. RETTIG, ALAN STORR, and JAMES TROTTER. Can. J. Chem. **65**, 1349 (1987).

Details of the preparation and crystal structure of the title compound are given. Crystals of glycinatodimethylgallium are monoclinic, $a = 12.502(1)$, $b = 12.023(1)$, $c = 10.732(1)$ Å, $\beta = 110.05(1)°$, $Z = 8$, space group $P2_1/c$. The structure was solved by conventional heavy atom methods and was refined by full-matrix least-squares procedures to $R = 0.033$ and $R_w = 0.039$ for 1172 reflections with $I \geq 3\sigma(I)$. The structure consists of monomeric $(C_2H_4NO_2)GaMe_2$ molecules which are linked together by an extensive network of N—H···O hydrogen bonds. The Ga atoms have tetrahedral coordination geometry with bond lengths averaged over the two crystallographically independent molecules: Ga—O = 1.958(18), Ga—N = 2.031(5), and Ga—C = 1.937(7) Å.

STEVEN J. RETTIG, ALAN STORR et JAMES TROTTER. Can. J. Chem. **65**, 1349 (1987).

On décrit les détails de la préparation et de la structure cristalline du composé mentionné dans le titre. Les cristaux du glycinatodiméthylgallium sont monocliniques et ils cristallisent dans le groupe d'espace $P2_1/c$, avec $a = 12{,}502(1)$, $b = 12{,}023(1)$ et $c = 10{,}732(1)$ Å, $\beta = 110{,}05(1)°$ et $Z = 8$. On a résolu la structure par les méthodes conventionnelles aux atomes lourds et on l'a affinée par la méthode de moindres carrés (matrice entière) jusqu'à des valeurs de $R = 0{,}033$ et $R_w = 0{,}039$ pour 1172 réflexions avec $I \geq 3\sigma(I)$. La structure comporte des molécules monomères de $(C_2H_4NO_2)GaMe_2$ qui sont liées par un réseau important de liaisons hydrogènes N—H···O. Les atomes de Ga possèdent une géométrie de coordination tétraédrique et les longueurs des liaisons, déterminées en établissant une moyenne sur deux molécules qui sont indépendantes d'un point de vue cristallographique, sont les suivantes : Ga—O = 1,958(18), Ga—N = 2,031(5) et Ga—C = 1,937(7) Å.

[Traduit par la revue]

Introduction

The importance of α-amino acids as the principal constituents of protein and living matter is unquestionable. One such protein, transferrin (a glycoprotein of molecular weight ~ 80 000), is responsible for iron transport in mammalian systems and has been implicated in the transport of gallium in vivo (1, 2). Recently we have been interested in the area of gallium citrate chemistry (3), primarily since gallium citrate complexes are important clinical agents in medicinal chemistry (1) and definitive structural data on such complexes was entirely lacking. Our attention has also focussed on the coordination chemistry of gallium species with simple α-amino acids with a view to elucidating the binding of gallium by such compounds. The present paper details the preparation and structural characterization of the glycinatodimethylgallium complex.

Experimental

Air-sensitive materials were handled under oxygen-free dry nitrogen or on a high-vacuum line. Benzene was dried by refluxing over molten potassium followed by distillation under an atmosphere of nitrogen.

Starting materials

Trimethylgallium was synthesized from gallium metal and dimethylmercury as described previously (4). Glycine (Eastman Organic Chemicals) was used as supplied.

Synthesis of glycinatodimethylgallium

Me_3Ga (1.325 g, 11.55 mmol) was condensed onto glycine (0.866 g, 11.55 mmol) at −196°C. Alternate warming and cooling resulted in a vigorous reaction well below room temperature, with evolution of methane:

$$Me_3Ga + H_2NCH_2CO_2H \rightarrow H_2NCH_2CO_2GaMe_2 + CH_4$$

After cessation of methane evolution the product mixture was extracted with benzene and the mixture filtered. The resultant filtrate yielded crystals of the desired product on slow evaporation of the solvent. Yield 70%. *Anal.* calcd. for $(C_2H_4NO_2)GaMe_2$: C 27.60, H 5.76, N 8.06; found: C 27.69, H 5.83, N 7.93.

Mass spectrum

The mass spectrum displayed as its highest m/e signal one due to the monomer − Me^+ ion. In addition signals from ions arising from the expected fragmentation of the monomer species were also observed.

X-ray crystallographic analysis

Crystals were sealed under dry nitrogen in glass capillaries. A crystal bounded by the eight faces (followed by the distances in mm between parallel faces): {1 0 0}, 0.08, {1 1 0}, 0.18, {−1 0 1}, 0.31 was mounted in a general orientation. Unit-cell parameters were refined by least squares on 2 sin θ/λ values for 25 reflections (2θ = 30–36°) measured on a diffractometer with Mo-$K\alpha$ radiation ($\lambda(K\alpha_1) = 0.70930$, $\lambda(K\alpha_2) = 0.71359$ Å). Crystal data at 22°C are:

$C_4H_{10}GaNO_2$ fw = 173.85

Monoclinic, $a = 12.502(1)$, $b = 12.023(1)$, $c = 10.732(1)$ Å, $\beta = 110.05(1)°$, $V = 1515.4(5)$ Å^3, $Z = 8$, $\rho_c = 1.524$ Mg m^{-3}, $F(000) = 704$, μ(Mo-$K\alpha$) = 35.5 cm^{-1}. Absent reflections: $h0l$, l odd, and $0k0$, k odd, uniquely indicate the space group $P2_1/c$ (C_{2h}^5, No. 14).

Intensities were measured with graphite-monochromated Mo-$K\alpha$ radiation on an Enraf-Nonius CAD4-F diffractometer. An ω–2θ scan at 1.18–10.06° min^{-1} over a range of (0.75 + 0.35 tan θ) degrees in ω (extended by 25% on both sides for background measurement) was employed. Data were measured to 2θ = 50°. The intensities of three check reflections, measured every 3600 s throughout the data collection, decreased uniformly by 18.5%, the data being scaled accordingly. After data reduction,[2] an absorption correction was applied using the Gaussian integration method (5, 6). Transmission factors ranged from 0.474 to 0.782 for 180 integration points. Of the 2664 independent reflections measured, 1172 (44.0%) had intensities greater than or equal to $3\sigma(I)$ above background where $\sigma^2(I) =$

[1]Authors to whom correspondence should be addressed.

[2]The computer programs used include locally written programs for data processing and locally modified versions of the following: ORFLS, full-matrix least-squares, and ORFFE, function and errors, by W. R. Busing, K. O. Martin, and H. A. Levy; FORDAP, Patterson and Fourier syntheses, by A. Zalkin; ORTEP II, illustrations, by C. K. Johnson.

Can. J. Chem. Downloaded from www.nrcresearchpress.com by 72.64.146.136 on 09/07/12
For personal use only.

Can. J. Chem. Downloaded from www.nrcresearchpress.com by 72.64.146.136 on 09/07/12
For personal use only.

TABLE 1. Final positional (fractional × 10^4, Ga × 10^5) and isotropic thermal parameters ($U \times 10^3$ Å^2) with estimated standard deviations in parentheses

Atom	x	y	z	U_{eq}
Ga(1)	27657(7)	35971(6)	59739(7)	63
Ga(2)	83839(7)	23833(7)	63833(7)	73
O(1)	2772(4)	2606(3)	4506(4)	66
O(2)	3019(4)	880(4)	3966(4)	81
O(3)	7481(4)	2599(3)	4528(4)	61
O(4)	5735(4)	2524(4)	3089(5)	73
N(1)	3296(4)	2187(4)	7056(5)	58
N(2)	6984(5)	1547(4)	6426(5)	60
C(1)	1190(8)	3951(8)	5721(9)	116
C(2)	4043(8)	4582(6)	6238(8)	102
C(3)	9588(8)	1324(8)	6525(10)	141
C(4)	8417(10)	3828(7)	7213(9)	128
C(5)	2938(6)	1572(5)	4765(6)	56
C(6)	3032(6)	1234(5)	6154(6)	63
C(7)	6433(7)	2351(5)	4192(7)	53
C(8)	6039(6)	1841(5)	5244(6)	64

$S + 2B + (0.04(S - B))^2$ with S = scan count and B = normalized background count.

The structure was solved by conventional heavy atom methods, the coordinates of the two crystallographically independent Ga atoms being determined from the Patterson function and those of the remaining non-hydrogen atoms from a subsequent difference map. The non-hydrogen atoms were refined with anisotropic thermal parameters. In the final stages of refinement the hydrogen atoms were included as fixed contributors in idealized positions (N—H = 0.91, C—H = 0.98 Å, based on observed positions for methyl groups), recalculated after each least-squares cycle. The scattering factors of ref. 7 were used for non-hydrogen atoms and those of ref. 8 for hydrogen atoms. Anomalous scattering factors from ref. 9 were used for the Ga atoms. The weighting scheme $w = 1/\sigma^2(F)$, where $\sigma^2(F)$ is derived from the previously defined $\sigma^2(I)$, gave uniform average values of $w(|F_o| - |F_c|)^2$ over ranges of both $|F_o|$ and $\sin\theta/\lambda$ and was employed in the final stages of full-matrix refinement of 145 variables. Reflections with $I < 3\sigma(I)$ were not included in the refinement. Convergence was reached at $R = 0.033$ and $R_w = 0.039$ for 1172 reflections with $I \geq 3\sigma(I)$. For all 2664 reflections $R = 0.123$. The function minimized was $\Sigma w(|F_o| - |F_c|)^2$, $R = \Sigma||F_o| - |F_c||/\Sigma|F_o|$ and $R_w = (\Sigma w(|F_o| - |F_c|)^2/\Sigma w|F_o|^2)^{1/2}$.

On the final cycle of refinement the mean and maximum parameter shifts corresponded to 0.01 and 0.13σ, respectively. The mean error in an observation of unit weight was 1.492. A final difference map showed maximum fluctuations of −0.88 to +0.57 e A^{-3} near Ga and was featureless elsewhere. The final positional and thermal parameters appear in Tables 1 and 7,[3] respectively. Measured and calculated structure factors have been placed in the Depository of Unpublished Data.[3] Bond lengths, bond angles, intra-annular torsion angles, and details of the hydrogen bonding are given in Tables 2–5, respectively. Calculated hydrogen atom parameters (Table 6) and a complete listing of torsion angles (Table 8) are included as supplementary material.[3]

Results and discussion

The title compound, glycinatodimethylgallium, represents the second example of a simple α-amino acid coordinating a gallium atom. A previous study (10) reported the polymeric five-coordinate structure of (L-prolinato)dimethylgallium and more recently a structure with a Ga(III) ion octahedrally coordinated to the hexadentate ligand derived from the complex ethylenebis[(*o*-hydroxyphenyl)glycine] (EHPG) has been reported (11). The present structure consists of tetrahedrally coordinated Ga atoms in monomeric units (Fig. 1) which are linked together via extensive N—H···O hydrogen bonding (Fig. 2 and Table 5). The monomer units show no tendency to associate via formation of a $(Ga—O)_2$ four-membered ring system as was found previously in the solid-state structures of numerous five-coordinate gallium complexes (3, 12), or to form a polymeric chain via weak Ga—O bonding to the "uncoordi-

TABLE 2. Bond lengths (Å) with estimated standard deviations in parentheses

Bond	Length (Å)	Bond	Length (Å)
Ga(1)—O(1)	1.976(4)	Ga(2)—O(3)	1.940(4)
Ga(1)—N(1)	2.032(5)	Ga(2)—N(2)	2.030(5)
Ga(1)—C(1)	1.940(9)	Ga(2)—C(3)	1.936(9)
Ga(1)—C(2)	1.927(8)	Ga(2)—C(4)	1.943(8)
O(1)—C(5)	1.273(6)	O(3)—C(7)	1.268(8)
O(2)—C(5)	1.223(7)	O(4)—C(7)	1.224(7)
N(1)—C(6)	1.461(7)	N(2)—C(8)	1.449(8)
C(5)—C(6)	1.509(9)	C(7)—C(8)	1.507(8)

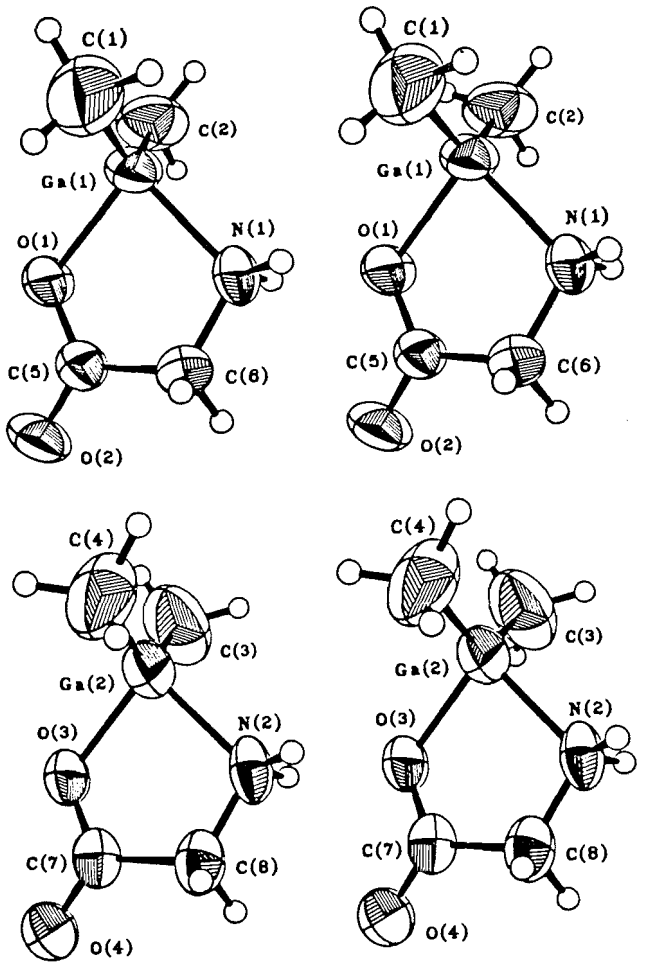

FIG. 1. Stereoscopic view of the two independent glycinatodimethylgallium molecules; 50% probability thermal ellipsoids are shown for the non-hydrogen atoms. Hydrogen atoms have been assigned arbitrary thermal parameters for the sake of clarity.

[3]The structure factor table, Table 7 (anisotropic thermal parameters), and other material mentioned in the text may be purchased from the Depository of Unpublished Data, CISTI, National Research Council of Canada, Ottawa, Ont., Canada K1A 0S2.

TABLE 3. Bond angles (deg) with estimated standard deviations in parentheses

Bonds	Angle (deg)	Bonds	Angle (deg)
O(1)—Ga(1)—N(1)	82.2(2)	O(3)—Ga(2)—N(2)	83.5(2)
O(1)—Ga(1)—C(1)	107.5(3)	O(3)—Ga(2)—C(3)	109.4(3)
O(1)—Ga(1)—C(2)	105.0(3)	O(3)—Ga(2)—C(4)	105.3(3)
N(1)—Ga(1)—C(1)	112.3(3)	N(2)—Ga(2)—C(3)	108.9(3)
N(1)—Ga(1)—C(2)	109.6(3)	N(2)—Ga(2)—C(4)	108.4(3)
C(1)—Ga(1)—C(2)	129.4(4)	C(3)—Ga(2)—C(4)	131.0(5)
Ga(1)—O(1)—C(5)	117.2(4)	Ga(2)—O(3)—C(7)	116.2(4)
Ga(1)—N(1)—C(6)	108.6(3)	Ga(2)—N(2)—C(8)	108.0(3)
O(1)—C(5)—O(2)	123.8(6)	O(3)—C(7)—O(4)	124.0(6)
O(1)—C(5)—C(6)	115.5(5)	O(3)—C(7)—C(8)	116.9(6)
O(2)—C(5)—C(6)	120.8(6)	O(4)—C(7)—C(8)	119.1(7)
N(1)—C(6)—C(5)	111.5(5)	N(2)—C(8)—C(7)	112.2(6)

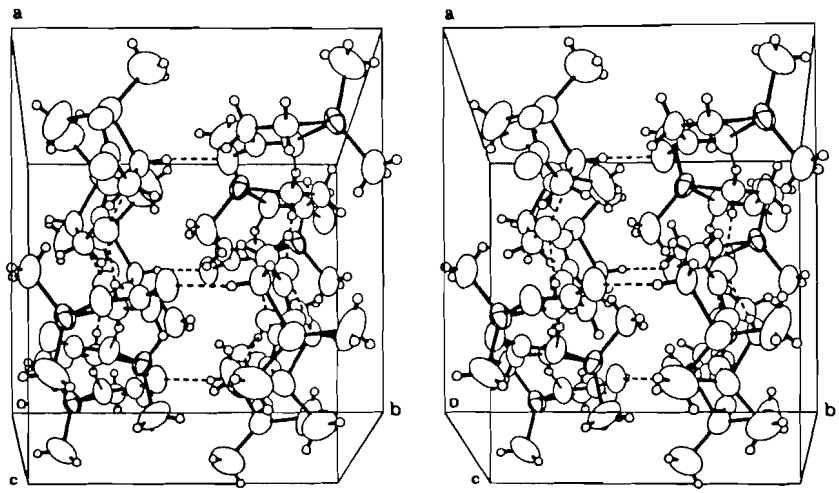

FIG. 2. Stereoscopic view of the packing arrangement of glycinatodimethylgallium; broken lines indicate hydrogen bonds.

nated" carboxylate oxygen atoms as in (L-prolinato)dimethylgallium (10). In this regard the complex is similar to the ethanolamine dimethylgallium complex, $H_2NCH_2CH_2O.GaMe_2$, which also exists in the solid state as discrete monomers linked by an extensive network of N—H···O hydrogen bonds (13). The five-coordinate dimeric structures of the methylated analogs $[Me_2NCH_2CH_2O.GaR_2]_2$ (R = Me, H) (14) support the contention that extensive hydrogen bonding involving ligand atoms in compounds of this type is energetically more favorable than the formation of oligomers involving weak Ga—O interactions.

The two crystallographically independent molecules of glycinatodimethylgallium are essentially identical, the most notable difference between the two being the shorter Ga—O bond in the molecule containing Ga(2) which probably results from differences in hydrogen bonding (see Table 5). The five-membered chelate rings in both molecules are non-planar, having conformations best described as *N*-envelopes. The mean Ga—O bond length of 1.958(18) Å is (as expected) shorter than the corresponding axial bond of 2.036(3) Å in the trigonal bipyramidal proline complex (10) and also shorter than the mean distance of 2.006(4) Å in octahedral $[Ga(EHPG)]^-$ (11). The mean Ga—N distance of 2.031(5) Å is similar to the equatorial bond of 2.027(3) Å in the proline complex and shorter than the mean of 2.090(12) Å in the EHPG complex. In the tetrahedral ethanolamine complex (13) a stronger Ga—O bond, mean 1.917(5) Å, is balanced by relatively weaker

TABLE 4. Intra-annular torsion angles (deg) standard deviations in parentheses

Atoms	Value (deg)
N(1)—Ga(1)—O(1)—C(5)	8.2(5)
Ga(1)—O(1)—C(5)—C(6)	3.8(7)
O(1)—C(5)—C(6)—N(1)	−19.2(8)
Ga(1)—N(1)—C(6)—C(5)	24.0(6)
O(1)—Ga(1)—N(1)—C(6)	−17.7(4)
N(2)—Ga(2)—O(3)—C(7)	11.9(4)
Ga(2)—O(3)—C(7)—C(8)	−4.5(7)
O(3)—C(7)—C(8)—N(2)	−9.7(7)
Ga(2)—N(2)—C(8)—C(7)	17.7(6)
O(3)—Ga(2)—N(2)—C(8)	−16.0(4)

TABLE 5. Hydrogen bond data*

D—H···A	H···A (Å)	D···A (Å)	∠DHA (deg)
N(1)—H(N1a)···O(4)^I	1.99	2.885(7)	167
N(1)—H(N1b)···O(1)^I	2.09	2.927(5)	152
N(2)—H(N2a)···O(2)^2	2.06	2.944(6)	164
N(2)—H(N2b)···O(4)^I	2.13	2.960(6)	151
N(2)—H(N2b)···O(3)^I	2.51	3.330(6)	150

*Superscripts refer to symmetry operations: (1) $x, \frac{1}{2} - y, \frac{1}{2} + z$; (2) $1 - x, -y, 1 - z$.

Can. J. Chem. Downloaded from www.nrcresearchpress.com by 72.64.146.136 on 09/07/12
For personal use only.

Ga—N and Ga—C bonds (means of 2.065(7) and 1.969(6) Å, respectively). In the related complex *N,N'*-ethylenebis(salicylideneiminato)bis(dimethylgallium) (15), which contains tetradedral gallium and six-membered chelate rings, the mean Ga—O, Ga—N, and Ga—C bond lengths are 1.872(3), 2.031(5), and 1.949(9) Å, respectively.

Acknowledgments

We thank the Natural Sciences and Engineering Research Council of Canada for financial support and the University of British Columbia Computing Centre for assistance. We also would like to thank Mr. P. Borda for the C, H, N analysis.

1. A. A. Noujaim. Int. J. Nucl. Med. Biol. **8**, 215 (1981).
2. M. A. Green, M. J. Welch, and J. C. Huffman. J. Am. Chem. Soc. **106**, 3689 (1984).
3. G. A. Banta, S. J. Rettig, A. Storr, and J. Trotter. Can. J. Chem. **63**, 2545 (1985).
4. A. Storr and B. S. Thomas. Can. J. Chem. **48**, 3667 (1970).
5. P. Coppens, L. Leiserowitz, and D. Rabinovich. Acta Crystallogr. **18**, 1035 (1965).
6. W. R. Busing and H. A. Levy. Acta Crystallogr. **22**, 457 (1967).
7. D. T. Cromer and J. B. Mann. Acta Crystallogr. Sect. A, **24**, 321 (1968).
8. R. F. Stewart, E. R. Davidson, and W. T. Simpson. J. Chem. Phys. **42**, 3175 (1965).
9. D. T. Cromer and D. Liberman. J. Chem. Phys. **53**, 1891 (1970).
10. K. R. Breakell, S. J. Rettig, A. Storr, and J. Trotter. Can. J. Chem. **55**, 4174 (1977).
11. P. E. Riley, V. L. Pecoraro, C. J. Carrano, and K. N. Raymond. Inorg. Chem. **22**, 3096 (1983).
12. S. J. Rettig, A. Storr, and J. Trotter. Can. J. Chem. **62**, 1705 (1984) (and references therein).
13. K. S. Chong, S. J. Rettig, A. Storr, and J. Trotter. Can. J. Chem. **57**, 586 (1979).
14. S. J. Rettig, A. Storr, and J. Trotter. Can. J. Chem. **53**, 58 (1975).
15. K. S. Chong, S. J. Rettig, A. Storr, and J. Trotter. Can. J. Chem. **55**, 2540 (1977).

Can. J. Chem. Downloaded from www.nrcresearchpress.com by 72.64.146.136 on 09/07/12
For personal use only.

Acidity level in concentrated mineral acid mixtures. Iso-acidic media

C. LOUIS, A. BEBBA, AND J. BESSIERE

Laboratoire de Chimie et Electrochimie Analytique, Faculté des Sciences. Université de Nancy 1, B.P. 239, 54506 Vandoeuvre Les Nancy Cedex, France

Received November 26, 1986

C. LOUIS, A. BEBBA, and J. BESSIERE. Can. J. Chem. **65**, 1353 (1987).

Assuming the relationship between the R_0(H) acidity function and the water activity in mineral acid concentrated solutions, iso-acidic solutions are prepared by mixing in all proportion two or three of the acids: H_3PO_4, HCl, $HClO_4$, H_2SO_4, H_2SiF_6. These solutions are characterized by an equal R_0(H) acidity level and different redox and complexing properties. Their R_0(H) acidity level is determined from potential measurements involving *o*-chloranil as an H^+ indicating system and ferricinium/ferrocene as a comparison system.

C. LOUIS, A. BEBBA et J. BESSIERE. Can. J. Chem. **65**, 1353 (1987).

En se basant sur la relation qui a été établie entre la fonction d'acidité R_0(H) et l'activité de l'eau dans des solutions concentrées d'acides minéraux, on a préparé des solutions iso-acides en procédant au mélange, dans toutes les proportions, de deux ou trois des acides suivants : H_3PO_4, HCl, $HClO_4$, H_2SO_4 et H_2SiF_6. Ces solutions sont caractérisées par le fait qu'elles ont des niveaux d'acidité R_0(H) qui sont égaux et par des propriétés redox et de complexation qui sont différentes. On a déterminé leurs niveaux d'acidité en se basant sur des mesures de potentiels impliquant l'*o*-chloranil comme système indicateur de H^+ et le couple ferricinium/ferrocène comme système de référence.

[Traduit par la revue]

Can. J. Chem. Downloaded from www.nrcresearchpress.com by 72.64.146.136 on 09/07/12
For personal use only.

Introduction

Concentrated mineral acid mixtures are very often used in surface processing: metal pickling, chemical polishing of crystal. The acidic treatment of phosphate ore with sulfuric, nitric, hydrochloric, or fluosilicic acids produces phosphoric acid concentrated solutions still containing a large proportion of the acid uses in the process (1). Any improvement of attack or solubilization processes requires a correct understanding of complexation and protonation phenomena in highly concentrated media.

From a fundamental point of view, the solvation properties of ionic or molecular species in concentrated acid solutions with various complexing or redox properties are significant: they allow one to foresee changes in solubilization and partition reactions when the nature of the acid changes or its concentration is modified (2, 3). The modification of the complexing properties of a concentrated acidic solution without any change of its acidity level is difficult to realize since most complexing compounds have basic properties.

We present in this paper means to prepare what we call "iso-acidic" solutions, that is solutions with the same R_0(H) acidity level and different complexing properties in the case of mixtures containing phosphoric acid and sulfuric, hydrochloric, or perchloric acids. Mixtures containing fluosilicic acid are also considered although its R_0(H) acidity function is not yet known.

Results and discussion

Bascombe and Bell (4) and Wyatt (5) brought evidence that the concentrated aqueous solutions of strong acids are characterized by the same H_0 acidity function value when they have the same water acidity value. This property has been experimentally verified in the case of HCl, $HClO_4$, H_2SO_4, and HNO_3 but not in the case of H_3PO_4 and HF which are not completely dissociated in concentrated media (5).

Recently, it has been shown by Louis and Bessiere (6) that the R_0(H) acidity function (Strehlow (7)) is the same for every acid solution having the same water activity. This relationship is also valid in the case of H_3PO_4 and HF. Owing to these two important results, the iso-acidity notion has been introduced in order to characterize acid mixtures. An iso-acidic solution is defined as the mixture in all proportion of two or several concentrated acid solutions, each of them having the same R_0(H) value. We assume that the mixture is characterized by a water activity value equal to those of each constituting solution. This assumption is related to those by Zdanovskii (8, 9) according to which mixtures of several strong electrolyte binary solutions, each of them with an equal water activity value, are characterized by the same water activity value provided that there is no chemical interaction between electrolyte species in the final mixture. Nevertheless, the solutions we are considering are not always completely dissociated and possibly contain molecular species.

The R_0(H) values are calculated from potential measurements involving an appropriate quinone/hydroquinone redox system (Q_s/QH_{2s}) by reference to the ferricinium/ferrocene (Fc^+/Fc) system in the various acidic media.

R_0(H) acidity function values have been experimentally determined in the case of iso-acidic solutions prepared in mixing 5.5 *M* or 11.5 *M* phosphoric acid solutions and the appropriate solutions of sulfuric, perchloric, or hydrochloric acids (Table 1).[1] They confirm that it is possible to prepare media with the same acidity level and different redox or complexing properties. For example, a 5.5 *M* phosphoric acid solution can be mixed in all proportion with a 3.25 *M* sulfuric acid solution, or a 3.4 *M*

[1] In all tables, the same abbreviations are used. Q_s/QH_{2s} represents the acidity indicating system: *o*-chloranil (3,4,5,6-tetrachloro-1,2-benzoquinone); $E^{w}_{Q} - E_0{}^{w}_{Fc} = +492$ mV represents the Q_s/QH_{2s} potential referred to the Fc^+/Fc normal potential at pH = 0 (phosphoric acid solution). E^{a}_{Q} represents the Q_s/QH_{2s} potential in the acidic mixture; $E_0{}^{a}_{Fc}$ represents the Fc^+/Fc normal potential in the acidic mixture. These potentials are referred to sce in 0.1 *M* H_3PO_4 separate compartment.

In Tables 1 and 4, the R_0(H) acidity function is calculated according to the relation:

$$R_0(H) = [(E^{w}_{Q} - E_0{}^{w}_{Fc}) - (E^{a}_{Q} - E_0{}^{a}_{Fc})]/0.058$$

In Tables 2 and 3, the R_0(H) acidity function is evaluated from the relation $R_0(H) = f(\log a_{H_2O})$.

Printed in Canada / Imprimé au Canada

TABLE 1. R_0(H) function in 5.5 *M* and 11.5 *M* H_3PO_4 iso-acidic solutions: (*1*) H_3PO_4–H_2SO_4; (*2*) H_3PO_4–$HClO_4$; (*3*) H_3PO_4–HCl

5.5 *M* H_3PO_4 (*1*) + *x*% (vol) 3.25 *M* H_2SO_4				11.5 *M* H_3PO_4 + *x*% (vol) 7.6 *M* H_2SO_4			
x % (vol)	$E_0{}^a{}_{Fc}$ (mV)	$E^a{}_Q$ (mV)	R_0(H)	*x* % (vol)	$E_0{}^a{}_{Fc}$ (mV)	$E^a{}_Q$ (mV)	R_0(H)
0	−40	562	−1.9	0	−250	579	−5.8
5	−36	567	−1.9	5	−242	578	−5.7
25	−36	564	−1.8	25	−242	574	−5.6
50	−44	566	−2.0	50	−254	576	−5.7
75	−36	566	−1.9	75	−250	575	−5.8
95	−40	560	−1.8	95	−252	579	−5.8
100	−40	566	−1.9	100	−252	575	−5.8
(*2*) + *x*% (vol) 3.4 *M* $HClO_4$				+ *x*% (vol) 7.1 *M* $HClO_4$			
x % (vol)	$E_0{}^a{}_{Fc}$ (mV)	$E^a{}_Q$ (mV)	R_0(H)	*x* % (vol)	$E_0{}^a{}_{Fc}$ (mV)	$E^a{}_Q$ (mV)	R_0(H)
0	−40	562	−1.9	0	−250	579	−5.8
5	—	—	—	5	—	—	—
25	−40	546	−1.7	25	−250	568	−5.7
50	−48	550	−1.8	50	−252	576	−5.8
75	−52	550	−1.9	75	−250	579	−5.8
95	—	—	—	95	—	—	—
100	−50	552	−1.9	100	−250	580	−5.8
(*3*) + *x*% (vol) 3.85 *M* HCl				+ *x*% (vol) 9.8 *M* HCl			
x % (vol)	$E_0{}^a{}_{Fc}$ (mV)	$E^a{}_Q$ (mV)	R_0(H)	*x* % (vol)	$E_0{}^a{}_{Fc}$ (mV)	$E^a{}_Q$ (mV)	R_0(H)
0	−40	562	−1.9	0	−250	579	−5.8
5	—	—	—	5	—	—	—
25	−32	568	−1.8	25	−246	581	−5.7
50	−30	567	−1.8	50	−250	578	−5.8
75	−36	569	−2.0	75	−253	580	−5.8
95	—	—	—	95	—	—	—
100	−36	568	−1.9	100	−255	583	−5.9

TABLE 2. H_0 and R_0(H) acidity functions in H_2O–H_2SiF_6 mixtures H_0 Hammett indicator: 4-chloro-2-nitroaniline

$[H_2SiF_6]$, *M*	H_0	$[H_2SO_4]$, *M*	$-\log a_{H_2O}$	R_0(H)
0.5	−0.52	1.5	0.030	−0.5
1.0	−0.75	2.0	0.044	−0.8
1.5	−1.05	2.5	0.062	−1.1
2.0	−1.34	3.0	0.085	−1.6
2.8	−2.01	4.5	0.179	−2.8

perchloric acid solution, or a 3.85 *M* hydrochloric acid solution giving binary mixtures characterized all by the same R_0(H) acidity function value: −1.9.

Binary or ternary mixtures containing H_2SiF_6 and iso-acidic of the 5.5 *M* phosphoric acid solution can be prepared only if the concentration for which its R_0(H) acidity level is the same as those of the phosphoric solution (that is −1.9) is known. It has been determined using the H_0 acidity function in sulfuric acid solutions as an intermediary. From the relations $H_0 = f$(acid concentration) for H_2SiF_6 solutions (Table 2) and H_2SO_4 solutions (10–12), the concentrations of solutions which have the same H_0 acidity level can be known. For example, 2.8 *M*

TABLE 3. H_0 and R_0(H) acidity functions in the iso-acidic solutions (binary mixtures): (*1*) H_2SO_4–H_2SiF_6, (*2*) H_3PO_4–H_2SiF_6

(*1*) 4.5 *M* H_2SO_4 + *x*% (vol) 2.8 *M* H_2SiF_6

x % (vol)	H_0	R_0(H)
0	−2.0	−2.8
25	−2.0	
50	−2.0	
75	−2.0	
100	−2.0	

(*2*) 5.5 *M* H_3PO_4 + *x*% (vol) 2.25 *M* H_2SiF_6

x % (vol)	H_0	R_0(H)
0	−0.73	−1.9
25	−0.96	
50	−1.27	
75	−1.45	
100	−1.58	

Can. J. Chem. Downloaded from www.nrcresearchpress.com by 72.64.146.136 on 09/07/12
For personal use only.

TABLE 4. R_0(H) function in 5.5 M H_3PO_4 iso-acidic solutions (ternary mixtures): H_3PO_4–H_2SO_4–H_2SiF_6 mixtures

x% (vol) 5.5 M H_3PO_4 + y% (vol) 3.25 M H_2SO_4 + z% (vol) 2.25 M H_2SiF_6

x–y–z % (vol)	E^a_{Fc} (mV)	E^a_Q (mV)	R_0(H)
50–40–10	−48	550	−1.8
60–20–20	−48	544	−1.7
50–10–40	−48	549	−1.8

H_2SiF_6 and 4.5 M H_2SO_4 are characterized by the same H_0 value: −2.01. The fact that it is also true for any mixture of the two acid solutions (Table 3) is in favour of the complete dissociation of H_2SiF_6 then an equal value of the term water activity in these solutions. From the relation $R_0(H) = f(\log a_{H_2O})$ it is then possible to determine that 2.25 M H_2SiF_6 and 5.5 M H_3PO_4 solutions are iso-acidic (Table 3).

It has also been shown (Table 4) that, whatever the ratio, ternary mixtures of 5.5 M H_3PO_4, 2.25 M H_2SiF_6, and 3.25 M H_2SO_4 solutions are characterized by the same R_0(H) acidity level.

Conclusion

Assuming the notion of iso-acidity, it is possible to modify in a continuous way the solvation, complexation, and oxidation –reduction properties of a concentrated acidic medium with no change of its acidity level. At the present time, these results are applied to the analysis of mineral species solution reactions in mixtures of mineral acids.

1. A. V. SLACK. Phosphoric acid. Vol. 1. Marcel Dekker Inc., New York. 1968. Parts 1, 2.
2. C. LOUIS. Thèse de Doctorat d'Etat, Nancy. 1983.
3. C. LOUIS and J. BESSIÈRE. Can. J. Chem. **64**, 608 (1986).
4. K. N. BASCOMBE and R. P. BELL. Faraday Discuss. Chem. Soc. **24**, 158 (1957).
5. P. A. H. WYATT. Faraday Discuss. Chem. Soc. **24**, 162 (1957).
6. C. LOUIS and J. BESSIÈRE. Can. J. Chem. **63**, 908 (1985).
7. H. STREHLOW. *In* The chemistry of non-aqueous solvents. Vol. 1. *Edited by* J. J. Lagowski. Academic Press, New York. 1966. Chap. 4, p. 129.
8. A. B. ZDANOVSKII. Trudy Solyanoi Laboratorii Akad. Nauk. SSSR. **6**, 1 (1936).
9. J. LY. Thèse de Doctorat d'Etat, Paris. 1984.
10. L. P. HAMMETT and A. J. DEYRUP. J. Am. Chem. Soc. **54**, 2721 (1932).
11. F. COUSSEMANT, M. HELLIN, and B. TORCK. Les fonctions d'acidité et leurs utilisations en catalyse acido-basique. Gordon and Breach, Paris, London, New York. 1969.
12. C. H. ROCHESTER. Acidity functions. Academic Press, London, New York. 1970.

Can. J. Chem. Downloaded from www.nrcresearchpress.com by 72.64.146.136 on 09/07/12
For personal use only.

Étude en résonance magnétique nucléaire du ^{13}C des F-méthyl-4 coumarines

RAPHAËL E. PASTOR, JOËLLE FABRON ET AIMÉ CAMBON

Laboratoire de chimie organique du fluor, Institut de mathématiques et sciences physiques, Université de Nice, Parc Valrose, 06034–Nice CEDEX, France

ET

YOU-CHUAN HU

Département de Chimie, Université de Xiamen, Chine Populaire

Reçu le 19 juin 1986[1]

RAPHAËL E. PASTOR, JOËLLE FABRON, AIMÉ CAMBON et YOU-CHUAN HU. Can. J. Chem. **65**, 1356 (1987).

Nous avons analysé les spectres de résonance magnétique nucléaire du ^{13}C de six F-méthyl-4 coumarines. La présence de ce substituant F-alkyle en 4 n'affecte que très peu les déplacements chimiques des divers atomes de carbone. Seuls les carbones C-10, C-4 et C-5 sont véritablement perturbés et apparaissent à champs plus forts. L'importance de ces effets a été évaluée et comparée avec ceux provoqués par un méthyle en 4. Le phénomène le plus important est l'apparition d'un couplage $^4J_{CF}$ (et $^5J_{CF}$ pour **6**). Nous montrons que ce couplage se transmet manifestement à travers l'espace et qu'il nécessite pour sa transmission la présence d'un troisième noyau intermédiaire couplé aux deux précédents.

RAPHAËL E. PASTOR, JOËLLE FABRON, AIMÉ CAMBON, and YOU-CHUAN HU. Can. J. Chem. **65**, 1356 (1987).

Analysis of ^{13}C nuclear magnetic resonance spectra of six 4-F-methyl coumarins are reported. This 4-F-alkyl substituent has a very slight effect on the chemical shifts of different carbon atoms. Only the C-10, C-4, and C-5 atoms are really affected and are shifted towards higher fields. The size of these effects was evaluated and compared with the corresponding effects of a 4-methyl substituent. The most important fact is the appearance of a $^4J_{CF}$ (and $^5J_{CF}$ for **6**) coupling constant. We have shown that this effect is a through-space coupling.

I. Introduction

Dans un travail précédent (1), nous présentions la synthèse de F-alkyl-4 coumarines.[2] L'étude rmn, proton et fluor, de ces composés nous a permis de mettre en évidence un couplage longue distance entre l'hydrogène en 5 et les fluors α de la chaine F-alkyle en 4.

Le squelette coumarine qui forme la structure de base de nombreux produits naturels a fait l'objet de nombreuses études tant en rmn du proton que du carbone 13 (2); l'influence de la substitution a été particulièrement étudiée afin d'établir des régles d'incrémentation permettant la prévision des déplacements chimiques des divers carbones cycliques et l'identification d'isomères de position.

À notre connaissance, aucun de ces travaux ne faisait mention de composé fluoré; aussi nous a-t-il paru intéressant d'étudier l'influence d'un substituant F-méthyle sur ce type de composés.

Dans ce travail, nous présentons l'étude rmn ^{13}C de six F-méthyl-4 coumarines : F-méthyl-4 ombelliférone (**1**), F-méthyl-4 daphnétine (**2**), F-méthyl-4 esculétine (**3**), F-méthyl-4 méthyl-8 ombelliférone (**4**), F-méthyl-4 nor-limettine (**5**) et F-méthyl-4 diméthyl-5,7 coumarine (**6**).

Composés étudiés

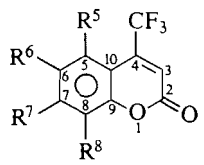

Composé	R^5	R^6	R^7	R^8
1	H	H	OH	H
2	H	H	OH	OH
3	H	OH	OH	H
4	H	H	OH	Me
5	OH	H	OH	H
6	Me	H	Me	H

II. Partie expérimentale

Les spectres rmn du ^{13}C ont été enregistrés à l'aide d'un appareil Bruker WH-90 à transformée de Fourier, opérant à la fréquence 22,63 MHz. Une fenêtre spectrale de 4000 Hz et une mémoire de 8 K ont été utilisées ce qui permet une résolution spectrale d'environ 0,5 Hz et une précision de 0,03 ppm. Une impulsion de 4 μs ($\alpha 90° = 11$ μs) et un délai de 0,3 s entre les acquisitions ont été les conditions de tous les enregistrements standards. L'irradiation des fluors a été réalisée à l'aide d'un découpleur Brucker de type BSV 3; leur fréquence a été déterminée à partir des spectres ^{19}F préalablement enregistrés.

Les solutions d'environ 0,4 mol L^{-1} étaient préparées en plaçant 0,3 g de composé dans 3 mL de $CDCl_3$ et en rajoutant si nécessaire une faible quantité (de quelques gouttes à 0,5 mL) de CD_3OD afin d'assurer une solubilisation totale. Dans ces conditions, de 50 000 à 100 000 acquisitions (une nuit) étaient nécessaires pour obtenir des spectres exploitables.

Les déplacements chimiques sont mesurés en ppm par rapport au TMS utilisé en référence interne.

Les diverses coumarines étudiées ont été préparées suivant les modes opératoires décrits précédemment (1).

III. Attribution des différents signaux et déplacements chimiques correspondants

A. Attribution des signaux

L'étude détaillée des spectres des composés les plus solubles (F-méthyl-4 ombelliférone (**1**) et F-méthyl-4 diméthyl-5,7 coumarine (**6**)) a constitué la base de toutes nos attributions. Pour ces deux composés, les multiplicités observées dans les spectres réalisés avec ou sans découplage, tant du fluor que du proton, et la comparaison des données de la littérature, concernant les déplacements chimiques (2–7), les couplages (2–7, 8–10) dans des composés homologues, nous ont permis d'effectuer les attributions sans ambiguïté (cf. tableau 1).

Par rapport à l'ombelliférone et à la méthyl-4 ombelliférone, la détermination des effets induits par un F-méthyle en 4 nous a permis d'établir une régle d'incrémentation qui complétée par les résultats de la littérature (2), nous a permis d'établir les attributions ultérieures de tous les composés. Celles-ci sont rassemblées dans le tableau 2.

B. Effets du substituant F-méthyle

Nous avons rassemblé dans le tableau 3 les différences

1. Révision reçue le 9 février 1987.

2. Nous conserverons le terme coumarine pour désigner le squelette 2,4-benzopyran-1 one-2 et le terme F-méthyle ou F-alkyle pour désigner un substituant perfluoré (Cf. réf. 19).

Printed in Canada / Imprimé au Canada

Can. J. Chem. Downloaded from www.nrcresearchpress.com by 78.46.186.204 on 09/07/12
For personal use only.

TABLEAU 1. Déplacements chimiques et constantes de couplage carbone–proton et carbone–fluor

Carbone	δ en ppm	$^1J_{CH}$	$^2J_{CH}$	$^3J_{CH}$	$^1J_{CF}$	$^2J_{CF}$	$^3J_{CF}$	$^4J_{CF}$	$^5J_{CF}$
C-2	160,5[a]		2,5 (H3)						
	158,4[b]		<1						
C-3	111,1	175					5,9		
	116,4	174					8,3		
C-4	142,2			2,5 (H5)		33,7			
	140,5					32,5			
C-5	126,7	164						3	
	135,4		6,5 (Me-5)						
C-6	114,4	167	2 (H5)	5 (H8)					
	130,8	161		5,5 (Me-5, Me-7, H8)					
C-7	162,3		4,5 (H6, H8)	11 (H5)					
	143,4		6,5 (Me-7)						
C-8	103,6	164		6 (H6)					
	116,1	156		4,5 (H6, Me-7)					
C-9	156,5		5 (H8)	10 (H5)					
	155,7		<2						
C-10	106,3	Massif non résolu, largeur à mi-hauteur 16 Hz							
	110,6								
CF_3	121,7			5 (H3)	275				
	121,6			7,5 (H3)	275				
Me-7	20,7	128		4,5 (H6, H8)					
Me-5	21,8	129		7,5 (H6)	275				8,33

[a]Ligne supérieure : F-méthyl-4 ombelliférone (**1**).
[b]Ligne inférieure : F-méthyl-4 diméthyl-5,7 coumarine (**6**).

des déplacements chimiques entre les hydroxycoumarines de référence et leurs homologues F-méthyl-4 substitués.

Malgré une certaine variation pouvant être attribuée à une non additivité déjà signalée dans le cas de dérivés di et tri substitués (2, 4), nous pouvons remarquer une certaine constance des effets du substituant F-méthyle sur les carbones voisins.

Effet α

Cet effet se manifeste sur le carbone C-4.

Notons qu'il est tout à fait inversé par rapport à ce que l'on pourrait attendre des données de la littérature. En effet, en série benzénique un substituant F-méthyle induit un déplacement vers les champs faibles d'environ +2,5 ppm (9, 11), alors que nous observons un déplacement vers les champs forts variant de −2 à −2,8 ppm.

Par contre, en série aliphatique, le remplacement d'un méthyle par un groupement F-méthyle ou F-alkyle provoque un déplacement vers les champs forts de −7 à −10 ppm (12). C'est bien ce que l'on observe en comparant avec les dérivés méthylés en 4.

Effets β

Deux carbones C-3 et C-10 sont à considérer. Ils subissent tous deux un déplacement vers les champs forts, voisin de −1 ppm pour le C-3 et de −6 ppm pour le C-10. Cet effet est bien en accord avec celui relevé en série benzénique (9, 11).[3]

Mais, c'est cette fois par rapport à la série coumarinique que l'on trouve une anomalie. En régle générale, dans le cas d'une substitution en 4 (méthyle, hydroxy), les signaux des carbones α sont déplacés vers les champs forts, mais le déplacement de carbone méthine (C-3) est toujours supérieur à ce qui est observé pour les carbones quaternaires C-10 (ou C-9).

Dans le cas d'un substituant F-méthyle, nous observons le phénomène inverse : le carbone C-10 est toujours le plus déplacé vers les champs forts.

Effets γ

Ils se manifestent sur les carbones C-2, C-9 et C-5.

Leurs valeurs relativement faibles sont de l'ordre de celles pouvant être produites par les variations de solvants et de concentration, mais ces effets sont tout de même significatifs (au moins pour les carbones C-2 et C-5).

Ces effets γ provoquent un déplacement vers les champs forts : ce déplacement est faible pour le C-2,[4] relativement important pour le C-5.

Cet effet *péri* en C-5 (−2,9 à −3,9 ppm) traduit un effet stérique diamagnétique bien connu, tout à fait comparable à ceux produits en série coumarinique par des substituants divers (méthyle, hydroxy ou méthoxy) qui vont de −3,2 à −5,3 ppm (2) et très voisins de celui observé (−3,4 ppm) dans le F-méthyl-1 naphtalène (11).

Effets longue distance

Nous ne discuterons pas des effets à plus longue distance qui nous paraissent vraiment négligeables.

Il eut par contre été beaucoup plus intéressant de discuter des effets provoqués par la proximité en *péri* des substituants hydroxy ou méthyle dans le cas des composés **5** et **6**. Malheureusement l'absence de tout élément de comparaison nous ôte cette possibilité. Malgré tout, nous pouvons noter qu'il n'y a aucune variation significative dans le déplacement chimique des CF_3 que le composé soit *péri* substitué ou non.

IV. Couplages fluor–carbone

Pour tous les composés étudiés, les différents couplages carbone–fluor sont bien distincts et aisément mesurables sur les

3. Il est probable qu'une erreur d'attribution entre carbones quaternaires C-9 et C-10 soit intervenue dans l'article de Doddrell *et al.* (11). La correction ainsi effectuée inverserait les déplacements chimiques de ces carbones et rendrait homogène les effets des CF_3.

4. L'effet sur le C-2 dans le composé **1** nous parait disproportionné et doit être ramené à une plus juste valeur en ajustant le déplacement chimique du C-2 de l'ombelliférone à 161 ppm, valeur moyenne de la littérature (2, 4, 6, 7).

Can. J. Chem. Downloaded from www.nrcresearchpress.com by 78.46.186.204 on 09/07/12
For personal use only.

Can. J. Chem. Downloaded from www.nrcresearchpress.com by 78.46.186.204 on 09/07/12
For personal use only.

TABLEAU 2. Déplacements chimiques dans les F-alkyl-4 coumarines

		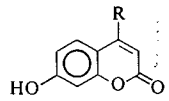	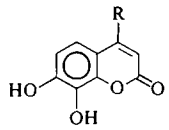	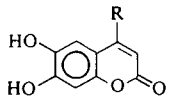	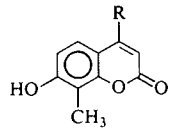	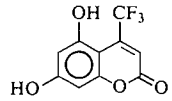	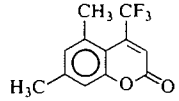
	R	**1**	**2**	**3**	**4**	**5**	**6**
C-2	CF_3	160,5	160,3	161,0	160,0	161,3	158,4
	H	163,19 (4)	161,1 (2,3)	161,4 (2,3)			
	CH_3	160,4 (2)	160,7 (2)	160,7 (2)	160,8 (2)		
C-3	CF_3	111,1 Q, J = 5,9	110,7 Q, J = 5,9	111,1 Q, J = 5,9	110,9 Q, J = 5,9	109,9 Q, J = 8,3	116,4 Q, J = 8,3
	H	111,7 (4)	111,7 (2,3)	112,0 (2,3)			
	CH_3	110,4 (2)	110,5 (2)	110,6 (2)	110,1 (2)		
C-4	CF_3	142,3 Q, J = 33,7	142,7 Q, J = 32,4	142,5 Q, J = 32,4	140,7 Q, J = 32,4	141,8 Q, J = 33,8	140,5 Q, J = 32,4
	H	145,14 (4)	145,4 (2,3)	144,5 (2,3)			
	CH_3	153,2 (2)	154,1 (2)	153,0 (2)	153,1 (2)		
C-5	CF_3	126,7 Q, J = 2,9	116,5 Q, J = 2,9	109,0 Q, J = 2,9	123,3 Q, J = 2,9	155,9 (singulet)	135,4 (singulet)
	H	129,64 (4)	119,4 (2,3)	112,9 (2,3)			
	CH_3	126,2 (2)	115,7 (2)	109,6 (2)	122,5 (2)		
C-6	CF_3	114,4	113,2	143,2	112,9	98,9	130,8
	H	114,09 (4)	113,0 (2,3)	143,2 (2,3)			
	CH_3	112,9 (2)	112,6 (2)	142,8 (2)	111,8 (2)		
C-7	CF_3	162,3	150,3	151,1	160,6	162,2	143,4
	H	162,05 (4)	150,0 (2,3)	150,6 (2,3)			
	CH_3	161,2 (2)	149,6 (2)	150,2 (2)	159,1 (2)		
C-8	CF_3	103,6	132,5	103,5	113,1	95,6	116,1
	H	103,17 (4)	132,6 (2,3)	103,2 (2,3)			
	CH_3	102,4 (2)	132,5 (2)	102,9 (2)	111,1 (2)		
C-9	CF_3	156,5	143,7	149,9	154,3	157,2	155,7
	H	156,2 (4)	144,2 (2,3)	149,1 (2,3)			
	CH_3	155,0 (2)	143,6 (2)	148,0 (2)	153,1 (2)		
C-10	CF_3	106,3	106,6	105,9	106,5	97,7	110,6
	H	112,19 (4)	112,7 (2,3)	111,4 (2,3)			
	CH_3	112,2 (2)	113,3 (2)	111,9 (2)	112,0 (2)		
CF_3		121,7 Q, J = 275,0	121,5 Q, J = 276,5	121,7 Q, J = 275,0	121,9 Q, J = 275,0	121,5 Q, J = 275,0	121,6 Q, J = 275,0
CH_3					8,0		CH_3-7 20,7 CH_3-5 21,8 Q, J = 8,33

Q : quadruplet.

TABLEAU 3. Effets comparés du remplacement d'un hydrogène ou d'un méthyle en 4 par un groupement CF_3

Position	Site		Composé 1	2	3	4	*a*	*b*
γ	C-2	H	−2,7 (−0,5)	−0,8	−0,4		−0,3	−1,7
		CH_3	+0,1	+0,4	+0,7	+0,8		
β	C-3	H	−0,6	−1,0	−0,9		−3,2	−1,2
		CH_3	+0,7	+0,2	+0,5	+0,8		
α	C-4	H	−2,8	−2,7	−2,0		+2,5	
		CH_3	−10,9	−11,4	−10,5	−12,4		
γ	C-5	H	−2,9	−2,9	−3,9		+0,3	−3,4
		CH_3	+0,5	+0,6	+0,6	+0,8		
	C-6	H	+0,3	+0,2	+0,0			+1,9
		CH_3	+1,5	+0,5	+0,4	+1,1		
	C-7	H	+0,2	+0,3	+0,5			+0,9
		CH_3	+1,1	+0,6	+0,9	+1,5		
	C-8	H	+0,4	−0,1	+0,3			+1,0
		CH_3	+1,2	−0,1	+0,6	+2,0		
γ	C-9	H	+0,3	−0,5	+0,8		+0,3	−4,2
		CH_3	+1,5	+0,1	+1,9	+1,2		
β	C-10	H	−5,9	−6,1	−5,5		−3,2	+0,7
		CH_3	−5,9	−5,7	−6,0	−5,5		

[a]Sur un noyau benzénique (9).
[b]Sur un noyau naphtalénique (11).

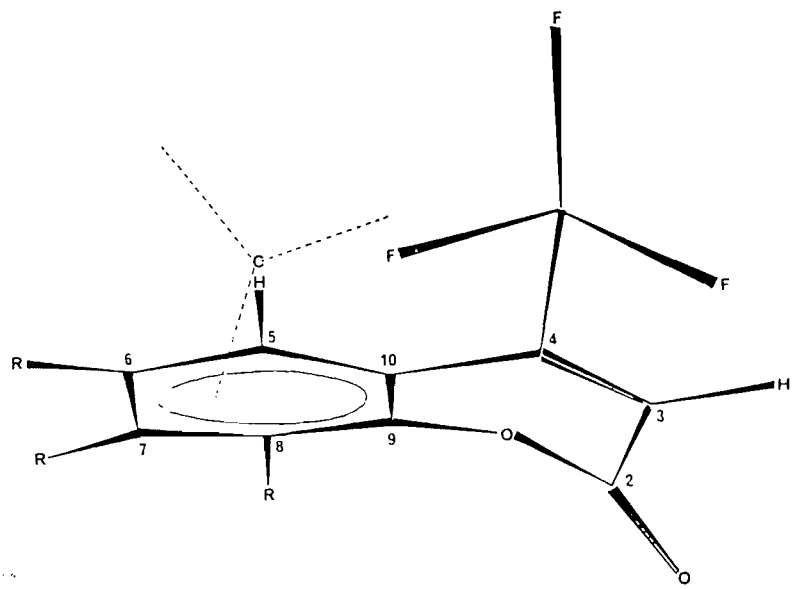

FIG. 1. Représentation perspective des F-méthyl-4 coumarines.

spectres : ils suivent l'ordre décroissant bien connu en série benzylique : $^2J_{CF} > {}^3J_{CF} > {}^5J_{CF} > {}^4J_{CF}$ (8–10).

Ce fait constitue d'ailleurs un critère d'attribution.

Un même type de couplage parait constant pour un même type de composé; c'est ainsi que l'on mesure $^1J_{CF}$ = 275 Hz, $^2J_{CF}$ = 32,4 et 33,8 Hz, $^3J_{CF}$ = 5,9 et 8,3 Hz, $^4J_{CF}$ = 2,9 Hz.

Plusieurs remarques s'imposent :

Si l'on peut mesurer un $^3J_{CF}$ de 5,9 ou 8,3 Hz sur les carbones C-3, les carbones C-10 similairement à 3 liaisons de distance des fluors ne manifestent aucun couplage.

Les carbones C-2 et C-9 ne présentent aucun couplage avec les atomes de fluor. Si ce fait n'est nullement surprenant (un $^4J_{CF}$ étant toujours très faible et souvent non observable), ce sont dés lors les couplages $^4J_{CF}$ apparaissant sur le C-5 qui deviennent exceptionnels par leur importance.

Enfin, dés que le composé est substitué en 5 (composés **5** et **6**), ce couplage $^4J_{CF}$ disparaît totalement. On peut alors observer un $^5J_{CF}$ particulièrement important (8,3 Hz) sur le méthyle en 5 du composé **6**. Or, dans notre travail précédent (1), nous faisions état d'un couplage proton–fluor longue distance entre les fluors α de la chaine F-alkyle et le proton en 5 (ou avec les protons méthyliques pour **6**). Nous avions attribué ces couplages exceptionnels à une transmission spatiale et à un phénomène de contact entre les deux noyaux couplés.

Can. J. Chem. Downloaded from www.nrcresearchpress.com by 78.46.186.204 on 09/07/12
For personal use only.

Toutes ces observations nous conduisent à formuler l'interprétation suivante concernant ces couplages $^4J_{C5-F}$ et $^5J_{C-Me-F}$.

Ces deux couplages procédent vraisemblablement du même processus :

—la transmission du couplage ne s'effectue pas à travers les liaisons du système carboné cyclique (absence de $^3J_{CF}$ en C-10, absence de $^4J_{CF}$ en C-5 pour **5** et **6**).

—la transmission du couplage s'effectue à travers l'espace, non par un phénomène de contact direct (absence de $^4J_{CF}$ en C-5 pour **5** et **6**), mais elle nécessite la présence d'un noyau intermédiaire lui-même couplé avec les fluors (hydrogènes en 5 ou hydrogènes du méthyle en 5). L'importance de ce couplage dés lors croît aussi corrélativement avec l'importance du couplage proton–fluor qui lui-même dépend de la distance entre les noyaux couplés.[5]

Nous relions ainsi les deux types de couplages carbone–fluor et fluor–hydrogène et donnons ainsi une explication globale à toutes les observations tant en rmn du proton et du fluor qu'en ^{13}C.

Les carbones C-10, C-2 et C-9 ne peuvent être couplés avec les fluors car ils ne peuvent prétendre à un tel processus.

La proximité entre les substituants en *péri*, n'a pas pour seul effet le couplage $^5J_{CF}$ avec le méthyle. Elle provoque aussi une variation du couplage $^3J_{C3-F}$ qui atteint ainsi 8,3 Hz (composés **5** et **6**).

Cette augmentation a probablement pour cause un rapprochement du site C-3 (hydrogène et carbone) soit par déformation de la géométrie du système, soit en privilégiant certaines conformations (17, 18) (cf. fig. 1). C'est le seul effet «*péri*» décelable.

Par contre, aucun effet direct ne se manisfeste sur la constante $^1J_{CF}$. Elle semble insensible à toute variation dépendant d'un effet *péri*.

5. Un tel phénomène était déjà signalé par Jerome et Servis (13) dans le cas du méthyl-4 fluoro-5 phénanthrène et a été dernièrement évoqué dans le cas de l'halogénure de fluoro-8 méthyl-1 quinolinium (14) et dans plusieurs travaux récents (15, 16).

Remerciements

Nous remercions Mr. Bernard Septe, Ingénieur C.N.R.S., pour la part active qu'il a apportée à la réalisation de ce travail, tant dans la partie technique que dans les interprétations.

1. V. Bayer, R. Pastor et A. Cambon. J. Fluorine Chem. **20**, 187 (1982).
2. H. Duddeck et M. Kaiser. Org. Magn. Reson. **20**, 55 (1982).
3. C. J. Chang, H. G. Floss et W. Steck. J. Org. Chem. **42**, 1337 (1977).
4. N. J. Cussans et T. N. Huckerby. Tetrahedron, **31**, 7719 (1975).
5. H. E. Gottlieb, R. Alves de Lima et F. Delle Monache. J. Chem. Soc. Perkin Trans. 2, 435 (1979).
6. S. A. Sojka. J. Org. Chem. **40**, 1175 (1975).
7. S. S. Sankar, R. D. Gilbert et R. E. Frones. Org. Magn. Reson. **19**, 222 (1982).
8. W. Adcock et A. N. Abeywickrema. Aust. J. Chem. **33**, 181 (1980).
9. R. A. Newmark et J. R. Hill. Org. Magn. Reson. **9**, 589 (1977).
10. T. Schaefer, K. Marat, J. Peeling et R. P. Veregin. Can. J. Chem. **61**, 2779 (1983).
11. D. Doddrell, M. Barfield, W. Adcock, M. Aurangzeb et D. Jordan. J. Chem. Soc. Perkin Trans. 2, 402 (1976).
12. M. Tordeux, J. Leroy et C. Wakselman. Org. Magn. Reson. **14**, 407 (1980).
13. F. R. Jerome et K. L. Servis. J. Am. Chem. Soc. **94**, 5896 (1972).
14. M. Barfield, S. R. Walter, K. A. Clark, G. W. Gribble, K. W. Haden, W. J. Kelly et C. S. Le Houllier. Org. Magn. Reson. **20**, 92 (1982).
15. G. W. Gribble et W. J. Kelly. Tetrahedron Lett. **26**, 3779 (1985).
16. J. R. Everett, J. S. Davies et J. W. Tyler. J. Chem. Soc. Perkin Trans. 2, 349 (1986).
17. T. Schaefer, R. Sebastian, R. P. Veregin et R. Laatikainen. Can. J. Chem. **61**, 29 (1983).
18. T. Schaefer, G. H. Penner, T. A. Wildman et J. Peeling. Can. J. Chem. **63**, 2256 (1985).
19. J. A. Young. J. Chem. Soc. **14**, 98 (1974); J. Fluorine Chem. **6**, 571 (1975).

Can. J. Chem. Downloaded from www.nrcresearchpress.com by 78.46.186.204 on 09/07/12
For personal use only.

Ternary charge transfer complexes. V.[1] Complexes with thiazyl salts[2]

SYDNEY BROWNSTEIN[3] AND BRENDA LOUIE
Division of Chemistry, National Research Council of Canada, Ottawa, Ont., Canada K1A 0R9

Received September 15, 1986

SYDNEY BROWNSTEIN and BRENDA LOUIE. Can. J. Chem. **65**, 1361 (1987).

Charge transfer complexes $NS^+MFn^-\cdot$arene, where M = B, n = 4; M = P, As, or Sb, n = 6; and arene is hexamethylbenzene, mesitylene, napthalene, or 9,10-dimethylanthracene, have been prepared and characterized. The reaction of $NS^+MF_6^-$ (M = As or Sb) with highly oriented pyrolytic graphite results in graphite intercalated only with the metal fluoride anions.

SYDNEY BROWNSTEIN and BRENDA LOUIE. Can. J. Chem. **65**, 1361 (1987).

On a préparé et caractérisé les complexes de transfert de charge $MS^+MFn^-\cdot$arène dans lesquels M = B, n = 4; M = P, As ou Sb, n = 6 et arène = hexaméthylbenzène, mésitylène, naphtalène ou diméthyl-9,10 anthracène. La réaction des composés $MS^+MF_6^-$ (M = As ou Sb) avec du graphite pyrolytique hautement orienté conduit à des graphites qui sont uniquement intercalés par des anions de fluorures métalliques.

[Traduit par la revue]

Introduction

Numerous charge transfer (CT) complexes of type $NO^-MXn^-\cdot$ arene have been previously reported, where M may be B, Al, Ga, Tl, P, As, Sb, Nb, Ta, Mo, W, U, or Fe; X may be F or Cl; n may be 4, 6, or 7; and arene may be benzene or a methyl substituted benzene (1–3). Some of these complexes exhibit appreciable conductivity in the solid state and have been structurally characterized. We have now prepared several analogs of this type of CT system incorporating the thiazyl cation, NS^+.

It has previously been reported that nitronium salts such as $NO_2^+SbF_6^-$ react with graphite to form highly conducting intercalation compounds. In CH_3NO_2 as solvent the simultaneous intercalation of solvent molecules and SbF_6^- occurs (4), and in one study a small amount of $NO_2^+SbF_6^-$ itself has been suggested as an additional intercalated species (5). In a related U.S. patent there is brief mention of intercalating numerous stable anions into graphite by exposing the carbon to a saturated solution of the nitrosyl salt of the anion (6). These reactions are related to the intercalation of AsF_6^- into graphite by the use of $O_2^+AsF_6^-$ (7). The cation of the salt is reduced to a neutral gas while the anion becomes the primary intercalated species in the oxidized graphite. Unlike NO, the isoelectronic NS does not exist as a stable entity. Therefore it was of interest to examine how thiazyl salts such as $NS^+SbF_6^-$ would behave when in contact with graphite.

Experimental

$F_2S{=}NCOF$ (8) was prepared by a literature method from $Si(OCN)_4$ (9) and SF_4. NSF was prepared by the decomposition of $F_2S{=}NCOF$ over CsF with the following modifications of the previously described method (10). $F_2S{=}NCOF$ (6 mmol) was heated with 2 g of dried CsF in a 20-mL Monel cylinder for 3 h at 126°C and then the reactor contents were fractionated through a series of U-tubes at −45, −78, and −196°C respectively. A small amount of $F_2S{=}NCOF$ was found in the −45°C U-tube, NSF was isolated from the −78°C U-tube, while the −196°C trap contained primarily COF_2. NSF was prepared only as needed since it polymerizes readily at room temperature.

For the reactions involving graphite, rectangular flakes (4 × 2 × 0.5 mm) of highly oriented pyrolytic graphite (HOPG) were heated to 280°C *in vacuo* for 8–10 h before use.

$(NSCl)_3$ was prepared by a standard method (7). Methylene chloride and 1,2-dichloroethane were purified (8), distilled from P_2O_5, and stored under vacuum. All other starting materials were used as purchased or purified as previously described (11–13).

$NS^+AsF_6^-\cdot$HMB (HMB = hexamethylbenzene)

HMB (0.4 mmol) was weighed accurately into a glass reactor equipped with a Teflon high vacuum stopcock and an nmr tube as a side arm. Approximately 2 mL of either CH_2Cl_2 or SO_2 was condensed into the reactor and the reactor reweighed. One equivalent each of AsF_5 and NSF were then condensed onto the reaction mixture, yielding an intense red-brown solution immediately upon thawing and mixing. The solution was mixed gently at room temperature for a few minutes and then all volatile materials were removed *in vacuo*. The resulting dark red-brown solid was dried *in vacuo* for a minimum of 2 h. *Anal.* calcd. for $C_{12}H_{18}NSF_6As$: C 36.28, H 4.57, N 3.53, S 8.07, As 18.86%; found: C 37.06, H 4.75, N 4.03, S 11.3, As 15.8%.

$NS^+AsF_6^-\cdot$HMB was also prepared by first isolating $NS^+AsF_6^-$ by the method of Mews (13), and subsequently adding one equivalent of HMB to the salt, followed by 2 mL of CH_2Cl_2 or SO_2. Evacuation of the solvent after gentle mixing for several minutes resulted in the same dark red-brown solid product. The complexes $NS^+MF_n^-\cdot$arene (M = B, n = 4; M = P, As, or Sb, n = 6; arene = HMB, mesitylene (mes), naphthalene (npth), or 9,10-dimethylanthracene (DMA)) were similarly prepared by the methods described above. *Anal.* calcd. for $C_{12}H_{18}NSF_6Sb$: C 32.46, H 4.09, N 3.15, S 7.22%; found: C 38.16, H 4.45, N 3.45, S 8.25%.

$NS^+MF_6^-$ (M = As or Sb) and HOPG

The graphite reactions were conducted in a glass U-tube closed on either end with a Teflon high vacuum stopcock. One side of the U-tube had an additional side arm, which could be isolated from the U-tube via another Teflon high vacuum stopcock. Graphite flakes were heated *in vacuo* in the side arm and then isolated from the U-tube. $NS^+SbF_6^-$ (13) was prepared by first condensing SbF_5 directly from the manufacturer's cylinder into the U-tube using a Dry Ice/acetone bath and a dynamic vacuum. SO_2 and NSF were subsequently introduced into the U-tube. The graphite flakes were tipped into this solution, containing an excess of $NS^+SbF_6^-$. After 8 days at room temperature the solution was tipped into the sidearm and the graphite was washed several times with recondensed SO_2. The graphite surfaces were steel blue in colour and the flakes had swollen to approximately 3 times their original thickness. The graphite was pumped *in vacuo* for several minutes to remove any residual SO_2. Infrared and ^{19}F resonance spectra of the graphite showed only the presence of intercalated SbF_6^- (14) and no evidence for intercalated NS^+. A similar procedure with AsF_5 showed only the hexafluoroarsenate anion, identified by its characteristic infrared and ^{19}F resonance spectra (15), intercalated in the HOPG.

[1]The preceding article in this series is ref. 3.
[2]Issued as NRCC No. 27477.
[3]Author to whom correspondence may be addressed.

Can. J. Chem. Downloaded from www.nrcresearchpress.com by 78.46.186.204 on 09/07/12
For personal use only.

TABLE 1. Spectral properties of some charge transfer complexes

Compound	Infrared (KBr pellet), cm^{-1} ν_{NS}	ν_{MF}	δ ^1H (CH_2Cl_2) −40°C CH_3	CH	δ ^{13}C (CH_2Cl_2) −40°C CH_3	CH	δ ^{19}F (CH_2Cl_2) −40°C	λ_{CT}, nm (CH_2Cl_2)
$NSBF_4$·HMB	1400	1087	2.40		16.8	147.0	−139.3	310
$NSPF_6$·HMB	1408	838	2.39				−69.8	361
		563					J = 710	
$NSAsF_6$·HMB	1400	702	2.40		17.1	147.2	−57.3	395
							J = 920	
$NSSbF_6$·HMB	1406	668	2.40		17.1	147.3	−113.5	406
$NSBF_4$·mes	1386	1085					−140.8	324
$NSPF_6$·mes	1400	840					−70.6	315
		560					J = 720	
$NSAsF_6$·mes	1384	700	2.56	7.30			−64.0	400
$NSSbF_6$·mes	1400	665	2.43	7.2			−120.8	310
$NSBF_4$·npth	1380	1089					−147.8	304
$NSPF_6$·npth	1400	834					−66.8	330
		561						
$NSAsF_6$·npth	1404	703					−63.1	325
$NSSbF_6$·npth	1401	667					−125	358
$NSBF_4$·DMA	1400	1089					−148	
$NSPF_6$·DMA	1389	850					−70.7	
		564					J = 700	
$NSAsF_6$·DMA	1383	705					−63.4	
$NSSbF_6$·DMA	1415	667						

Ultravilet–visible, infrared, and nmr spectra were obtained as previously described (13). Conductance measurements were performed on a pressed disc having a diameter and thickness of 19 and 0.2 mm respectively. In a nitrogen atmosphere the disc was mounted in a three-terminal, circular, parallel-plate, brass capacitor cell of an Andonion Associates, Inc. variable temperature cryogenic system (0–25/7M series). Conductance at a frequency of 10 kHz was measured with a Hewlett–Packard 4275A multi-frequency LCR meter and verified with a General Radio 1615-A capacitance bridge.

Results and discussion

$NS^+MF_n^-$·arene complexes have been prepared from NSF, MF_{n-1}, and the aromatic compound in CH_2Cl_2 or SO_2 as solvent. These intensely colored CT complexes have been identified by the physical properties listed in Table 1. All of these compounds are thermally unstable in solution at room temperature. Thus nmr spectra were recorded at −40°C, as solutions allowed to warm to ambient temperatures displayed decomposition via fluorination of the aromatic. All of the thiazyl complexes decompose fairly rapidly in air but can be stored in glass containers at room temperature in an inert atmosphere. As an added precaution the samples were routinely stored in the dark. Among the various hydrocarbons, the HMB adducts tend to be the most stable.

The N—S stretching vibration of the thiazyl cation, NS^+ (1437 cm^{-1}), is at a significantly higher frequency than that of NSF (1361 cm^{-1}) (16). We have found that the effect of an aromatic hydrocarbon on $NS^+MF_n^-$ salts is to consistently lower the N—S stretching frequency by about 40 cm^{-1}. A similar but much larger effect was observed for the NO^+ congeners (2), indicating that in these systems NO^+ is more effective in acquiring electron density from the arene than NS^+. The weaker charge transfer interaction present in the thiazyl compounds is manifested in the decreased stability of these species in solution or in the air as compared to their NO^+ analogs. As expected, the presence of the aromatic hydrocarbon has little effect on the frequencies observed for the M—F vibrations. This is consistent with π-electron donation from the arene into the π^* antibonding orbitals of the thiazyl cation. The close proximity of the cationic portion of the salt to the aromatic ring has been observed in the crystal structures of some of the NO^+ congeners (2, 3).

The ^1H and ^{13}C nmr spectra of the CT compounds further reflect the deshielding of the aromatic hydrocarbon by exhibiting resonances displaced downfield from those of the uncomplexed arene. In the ^{19}F nmr spectra the observed chemical shifts are those expected for BF_4^- or MF_6^- (M = P, As, Sb) anions.

The uv–visible spectra of the thiazyl CT compounds, where arene is HMB, mes, npth, display strong absorptions due to the aromatic hydrocarbon in the region of 250–300 nm. The CT band is present as a weaker absorption at slightly longer wavelength. In general the CT interaction broadens all of the peaks in the spectrum so that the CT band itself is not well defined, usually being partially obscured by the poorly resolved aromatic bands. For the HMB adducts the CT absorption shifts to longer wavelength as M is changed from B to P to As to Sb, a trend not previously observed for the NO^+ congeners (1, 2). For $NS^+MF_6^-$·HMB (M = As or Sb) the CT absorptions are sufficiently separated from the aromatic portion of the spectrum so that a definite band maximum can be observed. The spectra of HMB and $NS^+MF_n^-$·HMB (M = B, n = 4; M = As, n = 6) are shown in Fig. 1 as illustrative examples of typical uv spectra that were obtained. The CT peaks for the DMA derivatives were obscured by broadened bands due to the DMA and thus the positions of the maxima for the charge transfer peaks could not be measured. It is the long tail of these broad bands extending into the visible which causes the intense colour found for these solutions.

Any CT complexes initially formed between NO^+ salts and

Can. J. Chem. Downloaded from www.nrcresearchpress.com by 78.46.186.204 on 09/07/12
For personal use only.

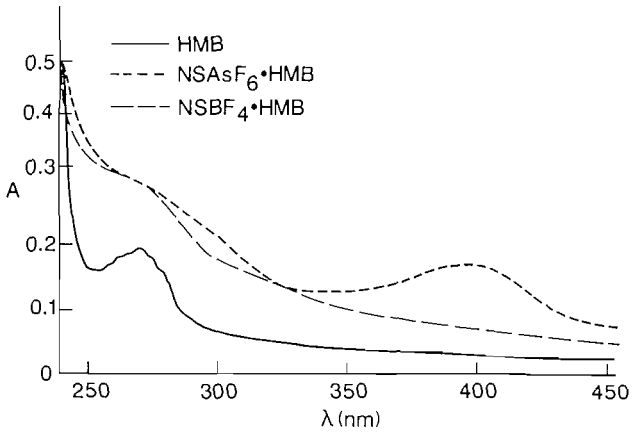

FIG. 1. The optical spectra of HMB, $NSAsF_6 \cdot HMB$, and $NSBF_4 \cdot HMB$.

npth or DMA underwent rapid oxygenation or halogenation of the aromatic portion (2). In contrast, the NS^+ CT complexes of these hydrocarbons can be isolated as solids although they are partially dissociated in solution. The increased dissociation of the polycyclic hydrocarbons relative to hexamethylbenzene has been reported for the tetracyanoethylene adducts (17). It was not possible to obtain meaningful magnetic resonance spectra of these complexes because of this dissociation.

From the limited crystal data previously reported for CT species containing the nitrosyl cation it appears that high conductivity ($>10^{-13}$ ohm^{-1} cm^{-1}) requires a long N—O bond (2, 3). We have so far been unable to obtain crystals of the NS^+ complexes suitable for X-ray diffraction. Routine conductance measurements on the thiazyl complexes presented difficulties due both to the quantity of material required to press an adequate pellet and the air sensitivity of the compounds. Nevertheless the conductivity of $NS^+AsF_6^- \cdot HMB$ at room temperature was measured to be 3.3×10^{-11} ohm^{-1} cm^{-1} at an operating frequency of 10 kHz. This is significantly smaller than the conductivity of 1.4×10^{-7} ohm^{-1} cm^{-1} reported for $NO^+AsF^- \cdot HMB$ (2) and may reflect the lesser extent of charge transfer in the NS^+ system.

We have observed that the thiazyl salts of AsF_6^- and SbF_6^- react with HOPG to yield a product in which the metal fluoride anions alone are intercalated into the graphite. This is a circuitous route to these materials, however, as the metal fluorides themselves lead to the same end products. With the thiazyl salts the cation NS^+ oxidizes the graphite, but does not itself intercalate.

The rather poor agreement of the elemental analyses with the theoretical values illustrates the difficulties in obtaining pure materials with these very reactive and thermally labile compounds.

The reaction of $(NSCl)_3$ and HMB with $AlCl_3$ or $FeCl_3$ in 1,2-dichloroethane yielded clear solutions with the dark red-brown colour characteristic of CT complex formation. However, removal of the solvent resulted only in tacky dark brown residues that would not solidify after prolonged pumping *in vacuo*. These residues were too unstable to obtain meaningful ir spectra, both samples being extremely hygroscopic. Because of their sensitivity to moisture these systems were not studied further.

Acknowledgements

We would like to thank Dr. A. Moore (Union Carbide) for the gift of HOPG and Dr. M. Desando for assistance with the electrical conductivity measurements.

1. S. BROWNSTEIN, A. MORRISON, and L. TAN. Can. J. Chem. **64**, 265 (1986).
2. S. BROWNSTEIN, E. GABE, F. LEE, and A. PIOTROWSKI. Can. J. Chem. **64**, 1661 (1986).
3. S. BROWNSTEIN, E. GABE, B. IRISH, F. LEE, B. LOUIE, and A. PIOTROWSKI. Can. J. Chem. **65**, 445 (1987).
4. D. BILLAUD, P. J. FLANDERS, A. PRON, and J. E. FISCHER. Mater. Science Eng. **54**, 31 (1982).
5. W. C. FORSMAN and M. MERTWAY. Synth. Met. **2**, 171 (1980).
6. F. L. VOGEL and W. C. FORSMAN. U.S. Patent 4, 461, 719; 24 July 1984.
7. T. E. THOMPSON, E. M. MCCARRON, and N. BARTLETT. Synth. Met. **3**, 255 (1981).
8. A. F. CLIFFORD and C. S. KOBAYASHI. Inorg. Chem. **4**, 571 (1965).
9. R. G. NEVILLE and J. J. MCGEE. Inorg. Synth. **8**, 23 (1966).
10. J. K. RUFF. Inorg. Chem. **5**, 1787 (1966).
11. W. L. JOLLY and K. D. MAGUIRE. Inorg. Synth. **9**, 102 (1967).
12. D. D. PERRIN, W. L. F. ARMAREGO, and D. R. PERRIN. Purification of laboratory chemicals. 2nd ed. Pergamon Press, Oxford. 1980.
13. R. MEWS. Angew. Chem. Int. Ed. Engl. **15**, 691 (1976).
14. G. R. MILLER, H. A. RESING, D. BRANT, M. J. MORAN, F. L. VOGEL, T. C. WU, D. BILLAUD, and A. PRON. Synth. Met. **2**, 237 (1980).
15. M. J. MORAN, G. R. MILLER, R. A. DEMARCO, and H. A. RESING. J. Phys. Chem. **88**, 1580 (1984).
16. O. GLEMSER and R. MEWS. Angew. Chem. Int. Ed. Engl. **19**, 883 (1980).
17. R. E. MERRIFIELD and W. D. PHILLIPS. J. Amer. Chem. Soc. **80**, 2778 (1958).

Can. J. Chem. Downloaded from www.nrcresearchpress.com by 78.46.186.204 on 09/07/12
For personal use only.

The reduction of specific disulfides with titanium(III) chloride

HUGH A. AKERS, MENG C. VANG,[1] AND TRACIE D. UPDIKE[2]
Department of Chemistry, Lamar University, Beaumont, TX 77710, U.S.A.

Received October 3, 1986

HUGH A. AKERS, MENG C. VANG, and TRACIE D. UPDIKE. Can. J. Chem. **65**, 1364 (1987).

The reaction between titanium(III) chloride and disulfides was investigated. Aryl and alkyl disulfides did not react while heterocyclic aromatic disulfides with a nitrogen α to the sulfur were reduced to the corresponding thiols. Products were identified and characterized by nuclear magnetic resonance and infrared spectra, and melting point comparisons with authentic compounds. The reductions occurred only in the presence of citrate and were found to require 2 moles of titanium(III) per mole of disulfide.

HUGH A. AKERS, MENG C. VANG et TRACIE D. UPDIKE. Can. J. Chem. **65**, 1364 (1987).

On a étudié la réaction du chlorure de titane (III) avec les disulfures. Les disulfures d'aryles ou d'alkyles ne réagissent pas alors que les disulfures d'hétérocycles aromatiques portant un azote en α du soufre sont réduits en thiols correspondants. On a identifié et caractérisé les produits grâce à des comparaisons de leurs spectres de résonance magnétique nucléaire et infra-rouge ainsi que de leurs points de fusion avec ceux de produits authentiques. Les réductions ne se produisent qu'en présence de citrate et on a trouvé qu'il faut deux moles de titane (III) par mole de disulfure.

[Traduit par la revue]

Interconversions between thiols and disulfide are important in a variety of chemical and biochemical situations. Numerous procedures have been presented for the oxidation of thiols or reduction of disulfides (1). Titanium(III) chloride has been reported as a mild reducing agent, most frequently for the reduction of nitrogen–oxygen bonds (2). A single often cited publication implicates titanium(III) in the reduction of disulfides (3); however, in this laboratory's continuing studies on the use of titanium(III) chloride for the reduction of substances of biochemical interest, it was observed that cystine (a disulfide) was not reduced. To resolve this problem, several model disulfides were exposed to titanium(III) chloride and the products of this exposure identified. In addition, the amounts of titanium(III) consumed during the exposure to these model disulfides were determined.

Experimental

Titanium(III) chloride as a 20% aqueous solution was from J. T. Baker Chemical Company or as a solid from Aldrich Chemical Company. The disulfides were obtained from Aldrich Chemical Co., Pfaltz and Bauer, Inc., Sigma Chemical Co., or were prepared by oxidation of the corresponding thiols with iodine (4). Thiols were purchased from the above suppliers or were prepared by reduction of the disulfide with zinc dust in acetic acid (5). 2-Thio-5-aminopyridine was prepared from 2,2′-dithio-bis(5-nitropyridine) by reduction with zinc dust and acetic acid (5). The free base of 2-thio-4(6)-methylpyrimidine was prepared (6) from the hydrochloride salt (Aldrich Chemical Co.).

Phenyl 2-pyridyl disulfide was synthesized from benzenesulfenyl chloride and the sodium salt of 2-thiopyridine (7). The resulting product gave an mp of 48–49°C (lit. (7) mp 49°C), a picrate salt with an mp of 127°C (lit. (7) mp 127°C), and upon gc/ms produced an M^+ ion of 219 m/e ($C_{11}H_9S_2N$ has a mol. wt. of 219).

All ir spectra (4000–600 cm^{-1}) were recorded on a Perkin–Elmer 710B infrared spectrophotometer. Samples were run on NaCl plates as mulls in Nujol or as the neat liquids. Melting points were determined with a Thomas Hoover Unimelt apparatus and were uncorrected. A Varian EM-390 nuclear magnetic resonance spectrometer was utilized to record 90-MHz proton spectra of the compounds and a Hewlett–Packard 5970B gc/ms was used for the analysis of phenyl 2-pyridyl disulfide. Chemical shifts were measured relative to an internal standard of tetramethylsilane for samples run in deuterochloroform and deuterated dimethylsulfoxide.

For exposure of disulfides to titanium(III) chloride, 0.11–2.0 g of disulfide was dissolved in 10–100 mL of acetic acid (8.7 or 17.4 *M*) and (or) ethanol, combined with 5–40 mL of 1.4 *M* aqueous sodium citrate, and aqueous titanium(III) chloride was added slowly until a faint purple color persisted. The solutions during reduction usually had a pH between 4.5 and 6.0. After a 3–24 h wait to allow any excess titanium(III) to oxidize with air to titanium(IV), the mixture was extracted with ether (often continuous) or $CHCl_3$. Solid products were usually crystallized by concentrating the extracting solvent, while liquids were recovered from the extraction solvent by distillation. Prior to extraction of 2-thio-5-aminopyridine the mixture was made alkaline (about pH 11) with NaOH.

Stoichiometric determinations were carried out by dissolving between 0.001 and 0.005 mol of the disulfide in 25 mL of ethanol, water, or acetic acid. Standard titanium(III) chloride (20 mL) and 10 mL of 1.7 *M* sodium citrate were added. After a measured period of time (usually 30 min), the excess titanium(III) chloride was titrated against standard ferric ammonium sulfate, using sodium thiocyanate as indicator (3, 8, 9). The titanium(III)/disulfide consumptive ratio was then calculated after applying a correction factor obtained from titration of a disulfide-free sample in the appropriate solvent. The values reported represent the average of at least 3 separate stoichiometric determinations.

Results

The effect of titanium(III) chloride on disulfides is presented in Table 1. Also recorded are the yield, melting (boiling) point, and mixture melting point of the product recovered. The ir and nmr were also determined (not shown) for each reactant and product. Products from exposure to titanium(III) chloride gave mp, nmr, and ir spectra that were identical to the original disulfides for substances **1** through **8** and to the corresponding thiol for substances **9**–**17**. Spectral comparisons were made with spectra from authentic compounds or published information (16). All disulfides failed to oxidize titanium(III) chloride in the absence of sodium citrate (data not shown). All products were found to burn without leaving an ash, and if soluble in water or ethanol did not produce a precipitate upon the addition of NaOH.

In addition to the substances listed in Table 1, the following

[1]Current address: Southwestern Medical School, University of Texas Health Center, Dallas, Texas 75235.

[2]Current address: Box 1608, Texaco Research Laboratory, Texaco, Inc., Port Arthur, Texas 77640.

Printed in Canada / Imprimé au Canada

Can. J. Chem. Downloaded from www.nrcresearchpress.com by 78.46.186.204 on 09/07/12
For personal use only.

TABLE 1. Exposure of disulfides to titanium(III) chloride in the presence of citrate[a]

	Substances	Stoichiometry[b]	Product recovered: Yield (%)	Product recovered: Melting point %°C)[c]	Product recovered: Mixture mp (°C)[d]	Literature mp[c,e]: Thiol	Literature mp[c,e]: Disulfide
1	*n*-Butyl disulfide	0.00	94	[88] 4 Torr	nd	[98–100]	[88–89] 4 Torr
2	*tert*-Butyl disulfide	0.00	96	[74–75] 10 Torr	nd	[63–64]	[73–75] 10 Torr
3	Benzyl disulfide	0.00	95	69–71	70–71[f]	[194–195]	71–72
4	Phenyl disulfide	0.00	99	58–60	60–61[f]	[169]	61
5	2-Aminophenyl disulfide	0.00	92	91–93	90–92[f]	26	93
6	4-Aminophenyl disulfide	0.00	31[g]	72–74	73–74[f]	46	74–76
7	DL-Cystine	0.00	86	258[h]	256–258[f,h]	178	260[h]
8	Phenyl 2-pyridyl disulfide	0.20[i]	75	48–49	nd	[169][j] 130(10)[k]	48–49(7)
9	2,2′-Dithiobis(pyridine-*N*-oxide)	5.87	38	127–128	128–129[l,k]	130(10)[k]	205
10	2,2′-Dipyridyl disulfide	1.87	40	128–129	127–129[l]	130(10)	58(10)
11	2,2′-Dithiobis(5-nitropyridine)	13.8	30	167–168	166–168[l,m]	170–171(10)[m]	150–151(10)
12	6,6′-Dithiobisnicotinic acid	1.84	30	268–270	271–272[l]	272(10)	247–249
13	2,2′-Dithiobisbenzothiazole	1.96	65	176–180	178–180[l]	177–181(11)	180–186(11)
14	2,2′-Dithiobisbenzimidazole	2.03	66	298–300	300–302[l]	301–305(10)	230(12)
15	2,2′-Dithiobisbenzoxazole	2.17	76	191–192	192–194[l]	193–194(13)	110(13)
16	2,2′-Dithiobisthiazoline	1.86	50	104–106	105–107[l]	106–107(4)	77–78(4)
17	2,2′-Dithiobis-(4-methylpyrimidine)	1.89	49	197–198	197–199[l]	200(14)	108(15)

[a]The substances listed were exposed to $TiCl_3$ and the products of this exposure were recovered.
[b]Moles of $TiCl_3$ consumed per mole of substance.
[c]Bracketed numbers are boiling points.
[d]nd, not determined.
[e]Unless references are noted (in parentheses), values are from handbooks. Thiol means the thiol form of the substance listed.
[f]Product recovered was mixed with authentic disulfide.
[g]Starting material was technical grade.
[h]With composition.
[i]Values ranged from 0.00 to 0.37 in 8 separate determinations.
[j]Thiolbenzene.
[k]2-Thiolpyridine.
[l]Product recovered was mixed with authentic thiol.
[m]5-Amino-2-thiolpyridine.

Can. J. Chem. Downloaded from www.nrcresearchpress.com by 78.46.186.204 on 09/07/12
For personal use only.

disulfides did not oxidize titanium(III) chloride in the presence or absence of sodium citrate: DL-6,8-thioctic acid (lipoic acid); DL-6,8-thioctic acid amide; *trans*-4,5-dithiane-4,5-diol; cystamine; oxidized glutathione (free acid); L-cystine dimethylester; and DL-homocystine. The original disulfides were not recovered following exposure to titanium(III) chloride; therefore the substances were not included in Table 1.

Discussion

The product of the exposure of disulfides to titanium(III) chloride in the presence of citrate is clearly the original disulfide for compounds **1** through **8** and the corresponding thiol for compounds **9** through **17**. From nmr observations it was determined that the carbon–hydrogen skeleton of the compounds was not altered by exposure to titanium(III). The determination of the thiol or disulfide nature of the product was determined primarily by ir (1). All thiols in Table 1 were found to have C=N stretching frequencies of 1600–1630 cm^{-1} while that of the disulfides was located at 1565–1585 cm^{-1}. The thione tautomer of all the thiols produced readily identifiable bands at 1100–1800 cm^{-1} (C=S stretching), 3110–3200 cm^{-1} (N—H stretching), and 1500–1590 cm^{-1} (N—H bending), which were absent in all spectra of the disulfides. Because all products burned without an ash and gave mps and ir spectra identical to titanium-free authentic compounds or reference spectra, the products were judged to be free of titanium.

The disulfides in Table 1 that were reduced by titanium(III) were observed to require 1.9 moles of titanium(III) per mole of disulfide, which is in agreement with the theoretical quantity of 2 moles of titanium(III) required per mole of disulfide. Substance **9** requires 6 moles of titanium(III) because the N-oxide portions are also reduced (requiring 2 moles of titanium(III) each). Each nitro group is reduced to an amino group with 6 moles of titanium(III); therefore, substance **11** required 14 moles of titanium(III). The stoichiometry observed for **16** suggests there may have been reduction in addition to the disulfide bond, possibly of the benzoxazole ring; however, no product in addition to the thiol was observed. Little systematic literature information exists on the reduction potentials of disulfides and titanium(III). However, diaryl disulfides and diheterocyclic disulfides (e.g., disulfide of 2-thiohistidine) are more readily reduced than dialkyl disulfides (17, 18). Titanium(IV) to titanium(III) is usually listed in handbooks with a reduction potential of −0.05 to −0.10 volts but the potential is quite pH dependent (19). In the presence of ligands or chelators, titanium(III) is known to be a stronger reducing agent (20) and has altered reactivities (2, 21).

The failure of disulfides **1** through **8** to be reduced by titan-

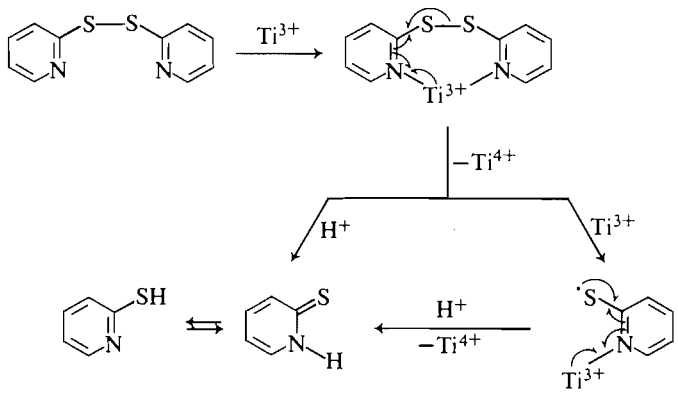

SCHEME 1. The proposed mechanism of reduction of heterocyclic aromatic disulfides by titanium(III) chloride.

ium(III) chloride suggests a reaction mechanism (Scheme 1) involving chelation of titanium(III) to both heteroaromatic nitrogens of **9** through **17**. The titanium(III) relinquishes an electron, the disulfide bond cleaves homolytically, titanium(IV) is released, and, following proton abstraction from the solvent, the thione tautomer of the thioamide and a free radical are produced. A second titanium(III) reduces the free radical to produce a second molecule of the thione (which then tautomerizes to the thiol). Support for this mechanism also comes from the fact that **10** is known to form seven-membered ring complexes with transition metal ions (22, 23). Also, because the disulfide bond of **10** is lengthened and the geometry was slightly altered by complex formation (23), it should become more susceptible to reduction.

The type of disulfide shown here to be reduced by titanium(III) is not the most common in nature; however, it could occur with such substances as 2-thiolhistidine (an ergot fungal product component) and the thiol tautomer of 4-thiouridine (a common tRNA component). Substances examined in Table 1 that were reduced include a common topical antifungal and antibacterial agent (substance **10**) and a compound used in the production of rubber (substance **13**). Compound **10** is also used extensively in thiol identification and quantification (24), and recently 3-(2-pyridyldithio)propanoyl derivatives have been used extensively by biochemists as covalent coupling tools (25). Because of the color change associated with the oxidation of titanium(III), this reaction makes a convenient spot test for the determination of the type of disulfide present in an unknown substance.

Acknowledgments

Support by the Lamar Research Council and the Robert A. Welch Foundation is acknowledged.

1. N. KHARASCH. Organic sulfur compounds. Vol. I, Pergamon Press, Oxford. 1961.
2. J. E. MCMURRY. Acc. Chem. Res. **7**, 281 (1974).
3. R. T. BROOKS and P. D. STERNGLANZ. Anal. Chem. **31**, 561 (1959).
4. A. G. M. BARRETT, D. H. R. BARTON, and R. COLLE. J. Chem. Soc. Perkin Trans. 1, 665 (1980).
5. D. S. TARBELL, D. A. BUCKLEY, P. P. BROWNLEE, R. THOMAS, and J. S. TODD. J. Org. Chem. **29**, 3314 (1964).
6. D. G. CROSBY, R. V. BERTHOLD, and H. E. JOHNSON. Org. Synth. **43**, 68 (1963).
7. F. RUNGE, A. JUMAR, and P. HELD. J. Prakt. Chem. **8**, 44 (1959).
8. H. A. AKERS, J. G. ABDO, and C. HAMILTON. Anal. Biochem. **154**, 559 (1986).
9. D. J. KUSHNER, T. A. LANDRY, M. C. TYRRELL, and H. A. AKERS. Anal. Biochem. **133**, 116 (1983).
10. A. BINZ, and C. RATH. Justus Liebigs Ann. Chem. **487**, 105 (1931).
11. L. B. SEBRELL and C. E. BOORD. J. Am. Chem. Soc. **45**, 2390 (1923).
12. K. MORI and J. KUNIHIRO. Japan Patent, Chem. Abstr. **72**, 43675 (1969).
13. S. CHELMICKI. J. Prakt. Chem. 440 (1890).
14. J. R. MARSHALL and J. WALKER. J. Chem. Soc. 1004 (1951).
15. D. R. GRASSETTI and F. J. MURRAY, JR. J. Med. Chem. **10**, 1170 (1967).
16. Sadtler infrared grating spectra and Sadtler nuclear magnetic resonance. Sadtler Research Laboratories, Philadelphia, pp. 1965–1982.
17. L. FIELD. *In* Organic chemistry of sulfur. *Edited by* S. Oae. Plenum Press, New York. 1977. p. 347.
18. P. A. LOACH. *In* Handbook of biochemistry. *Edited by* H. A. Sober. The Chemical Rubber Co., Cleveland. 1968. p. J-27.
19. J. A. DEAN (*Editor*). Lange Handbook of chemistry. 11th ed. McGraw–Hill, New York. 1973. pp. 6–15.
20. S. SIGGIA and J. G. HANNA. Quantitative organic analysis via functional groups. 4th ed. Wiley, New York. 1979. p. 788.
21. T. L. HO. Synthesis, 1 (1979).
22. M. E. BRIDSON and W. R. WALKER. Aust. J. Chem. **27**, 87 (1974).
23. M. M. KADOOKA, L. G. WARNER, and K. SEFF. Inorg. Chem. **15**, 812 (1976).
24. K. BROCKLEHURST and J. P. G. MALTHOUSE. Biochem. J. **193**, 819 (1981).
25. A. G. GITMAN, I. KAHANE, and A. LOYTER. Biochemistry, **24**, 2762 (1985).

Can. J. Chem. Downloaded from www.nrcresearchpress.com by 78.46.186.204 on 09/07/12
For personal use only.

Synthesis and characterization of transition metal complexes containing novel, unsymmetric tridentate organogallate ligands

EMMANUEL C. ONYIRIUKA AND ALAN STORR

Department of Chemistry, University of British Columbia, 2036 Main Mall, Vancouver, B.C., Canada V6T 1Y6

Received August 18, 1986

EMMANUEL C. ONYIRIUKA and ALAN STORR. Can. J. Chem. **65**, 1367 (1987).

Two novel unsymmetric tridentate anionic organogallate ligands have been synthesized and their coordinating properties toward a number of transition metal carbonyl species, and toward the "NINO" moiety, have been investigated. The ligand $[Me_2Ga(N_2C_3H_3)\cdot O(C_5H_3N)CH_2NMe_2]^-$, L_a, has shown unusual behaviour in that it produces both the *fac* and *mer* octahedral isomers, $L_aM(CO)_3$, (M = Mn or Re), on reaction with $Mn(CO)_5Br$ and $[Re(CO)_4Cl]_2$, respectively. In addition, this ligand gives a stable Rh(III) addition product, $L_aRh(Me)(I)CO$, on reaction of $L_aRh(CO)$ with MeI. The second ligand, $[Me_2Ga(N_2C_3H_3)\cdot O(C_9H_6N)]^-$, L_q, containing a quinolyl moiety in addition to a pyrazolyl group attached to dimethylgallium, displays more predictable behaviour in its coordinating properties.

EMMANUEL C. ONYIRIUKA et ALAN STORR. Can. J. Chem. **65**, 1367 (1987).

On a synthétisé deux nouveaux ligands organogallates anioniques, tridentates et qui ne sont pas symétriques et on a examiné leurs propriétés de coordination par rapport à un certain nombre d'espèces de métaux de transition carbonylés. Le ligand $[Me_2Ga(N_2C_3H_3)\cdot O(C_5H_3N)CH_2NMe_2]^-$, L_a, a un comportement inhabituel; par réaction respectivement avec le $Mn(CO)_5Br$ et le $[Re(CO)_4Cl]_2$, il conduit aux deux isomères octaédriques *fac* et *mer*. De plus, la réaction du produit $L_aRh(CO)$ avec le MeI conduit à un produit d'addition stable du Rh(III), soit le $L_aRh(Me)(I)CO$. Les propriétés de coordination du second ligand, $[Me_2Ga(N_2C_3H_3)\cdot O(C_9H_6N)]^-$, L_q, qui contient une portion quinoléyle en plus du groupement pyrazolyle attaché au diméthylgallium, sont plus prévisibles.

[Traduit par la revue]

Introduction

The first of a new class of unsymmetric tridentate chelating organogallate ligands was introduced some time ago (1). These ligand systems, containing a pyrazolyl group, together with a bifunctional donor moiety, both attached to a dimethylgallium unit, have been shown to coordinate facially in a variety of octahedral transition metal carbonyl compounds (2–4). In addition both the *fac* and *mer* isomers have been structurally characterized for the coordination compound $[Me_2Gapz(OCH_2CH_2NH_2)]_2Ni$ (pz = pyrazolyl, $N_2C_3H_3$) (5). The many novel aspects displayed by compounds incorporating this class of ligand prompted further investigation into the general area of unsymmetrical uninegative organogallate ligands to include the more sterically bulky amino-pyridyl moiety as well as a fused quinolyl "aromatic" unit in the ligand system to give L_a and L_q, respectively:

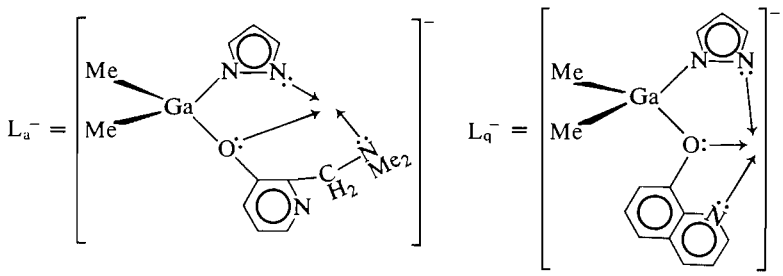

The present account details the reactivity of the above ligands toward a variety of transition metal halide species.

Experimental

Air-sensitive materials were handled in a glove box under an atmosphere of oxygen-free dry nitrogen, in a nitrogen-blanketed apparatus, or on a high-vacuum line. Tetrahydrofuran (THF) was dried by refluxing over Na/benzophenone and was used immediately following distillation. Benzene, CH_2Cl_2, and hexane were dried by refluxing over potassium, calcium hydride, and calcium sulphate respectively, followed by distillation. Sodium pyrazolide was prepared by reacting sodium hydride (Alfa) with pyrazole (K and K Laboratories) in THF. Trimethylgallium (6), Ni(NO)I (7), $Mn(CO)_5Br$ (8), $[Re(CO)_4Cl]_2$ (9), and $(MeCN)_2Mo(\eta^3\text{-}C_3H_5)(CO)_2Br$ (10) were prepared according to literature methods. $[Rh(CO)_2Cl]_2$ (Strem Chemicals), 2-(dimethylaminomethyl)-3-hydroxy pyridine (Aldrich), and 8-quinolinol (Eastman organic chemicals) were used as supplied.

Preparation of the ligands L_a^- and L_q^-

$$Me_3Ga + Na^+(N_2C_3H_3)^- \rightarrow Na^+[Me_3Ga(N_2C_3H_3)]^-$$

$$Na^+[Me_3Ga(N_2C_3H_3)]^- + HO(C_5H_3N)CH_2NMe_2 \rightarrow Na^+L_a^- + CH_4$$

Trimethylgallium (6.20 g, 54.0 mmol) in ~50 mL THF was added to sodium pyrazolide (4.86 g, 54.0 mmol) dissolved in ~50 mL THF. The reaction mixture was stirred for ~4 h. The solution was then diluted with THF to 500 mL in a volumetric flask. An 12.96 mmol aliquot of this standard $Na^+[Me_3Ga(N_2C_3H_3)]^-$ ligand solution was added to a stirred solution of 2-(dimethylaminomethyl)-3-hydroxy-

Can. J. Chem. Downloaded from www.nrcresearchpress.com by 78.46.186.204 on 09/07/12
For personal use only.

TABLE 1. Analytical and ir data for LMT complexes (L = L_a, L_q): L_a = $Me_2Gapz \cdot O(C_5H_3N)CH_2NMe_2$; L_q = $Me_2Gapz \cdot O(C_9H_6N)$*

L	M	T	Analysis: Calcd. C	Calcd. H	Calcd. N	Found C	Found H	Found N	ν_{CO}, ν_{NO} (cm^{-1}) C_6H_{12} (CH_2Cl_2)
L_a	Re†	$(CO)_3$	33.95	3.49	9.32	34.08	3.98	9.44	*A*2035s, 1920s, 1900s *B*2022w, 2015w, 1910s
L_a	Mn	$(CO)_3$	42.05	4.41	12.26	42.47	4.56	12.32	*A*2040s, 1943s, 1915s *B*2030w, 2020w, 1933s
L_a	Ni‡	(NO)	45.17	5.27	15.06	44.86	5.79	14.51	(1755)
L_a	Rh§	(CO)	40.23	5.17	11.73	40.32	5.07	11.52	1970s
L_q	Re	$(CO)_3$	36.36	2.69	7.07	36.21	2.93	7.06	2025s, 1927s, 1901s
L_q	Mn	$(CO)_3$	45.37	3.34	9.34	46.05	3.55	8.86	2040s, 1950s, 1920s
L_q	Mo	$(CO)_2(\eta^3\text{-}C_3H_5)$	45.27	3.97	8.34	46.03	3.91	8.33	1955s, 1863s
L_q	Rh‖	(CO)	43.62	3.64	8.98	43.22	3.63	9.34	1968s

*A, *fac* isomer; B, *mer* isomer; s = strong, w = weak.
†Contains $\frac{1}{6}C_6H_6$.
‡Contains $\frac{3}{4}C_6H_6$.
§Contains $\frac{1}{3}C_6H_{14}$.
‖Contains $\frac{1}{3}C_6H_6$.

pyridine (1.973 g, 12.96 mmol) in the same solvent. The reaction mixture was refluxed under N_2 until the evolution of methane gas had ceased completely (~2 days). The cooled solution was then diluted with THF to 250 mL in a volumetric flask. Aliquots of this standard $Na^+L_a^-$ ligand solution were used in subsequent reactions with transition metal halide species.

The ligand $Na^+L_q^-$ was prepared by an identical procedure to that described above, using 8-quinolinol, $HO(C_9H_6N)$, as the starting material. Aliquots of the resulting $Na^+L_q^-$ standard solution were used in subsequent reactions.

Preparation of $L_aM(CO)_3$ (M = Re, Mn)

A 40.0 mL aliquot of the ligand solution $Na^+L_a^-$ (0.64 mmol) was added slowly to $[Re(CO)_4Cl]_2$ (0.216 g, 0.324 mmol) dissolved in 30 mL THF. The reaction mixture turned cloudy almost immediately. The reaction mixture was refluxed for ~24 h during which time the cloudiness increased and the yellow coloration intensified. The solution was cooled to room temperature and the solvent removed under vacuum. The resulting residue was extracted with benzene and filtered. Evaporation of the benzene solvent containing the extracts afforded pale yellow crystalline needles of the product $L_aRe(CO)_3$ in approximately 80% yield.

The $L_aMn(CO)_3$ complex was prepared similarly using $Mn(CO)_5Br$ as the starting material. The orange solid product was collected in ~75% yield. Physical data for both complexes are compiled in Tables 1 and 2.

Preparation of $L_aNi(NO)$

To a stirred solution of Ni(NO)I (0.33 g, 1.5 mmol) in ~50 mL THF was added an equimolar amount of the $Na^+L_a^-$ (1.5 mmol) ligand solution in the same solvent. The resulting dark blue solution was stirred overnight and the solvent then removed under vacuum. The dark blue residue was extracted with benzene. The benzene filtrate was concentrated, and upon evaporation of the solvent, blue crystals of the product were recovered in ~60% yield. Analytical and spectroscopic data for the complex are collected in Tables 1 and 2.

Preparation of $L_aRh(CO)$

Two molar equivalents of the ligand $Na^+L_a^-$ were added to $[Rh(CO)_2Cl]_2$ (0.30 g, 0.77 mmol) dissolved in ~40 mL THF. The reaction mixture was refluxed under nitrogen until the disappearance of the $[Rh(CO)_2Cl]_2$ dimer (ν_{CO}: 2068, 1989 cm^{-1} THF) was indicated by ir measurements. At this juncture, three new brands had appeared in the ν_{CO} region of the spectrum at 2085, 2025, and 1970 cm^{-1}, respectively. The reaction mixture was cooled, and the solvent removed *in vacuo*. The residue was washed with hexane followed by extraction with benzene. Evaporation of the benzene solvent from the filtrate containing the extracts afforded orange crystals of the product in ~60% yield. The solid is moderately stable but its solutions decompose with time. Physical data for the complex are summarized in Tables 1 and 2.

Preparation of $L_qM(CO)_3$ (M = Re, Mn)

Two molar equivalents of $Na^+L_q^-$ ligand solution in THF were added to $[Re(CO)_4Cl]_2$ (0.18 g, 0.27 mmol) dissolved in 30 mL THF. The reaction mixture was refluxed overnight. The solvent was then removed under vacuum. The residue was extracted in benzene. Evaporation of the benzene from the filtrate resulted in a yellow cake. Recrystallization of the yellow cake from CH_2Cl_2/hexane (1:1) afforded yellow crystals of the $L_qRe(CO)_3$ product in ~80% yield.

The $L_qMn(CO)_3$ complex was prepared by an identical procedure using $Mn(CO)_5Br$ as starting material, and benzene as the crystallization solvent. The orange crystals of the product were collected in ~80% yield. Analytical, ir, and ^1H nmr data for both complexes are listed in Tables 1 and 2.

Preparation of $L_qMo(CO)_2(\eta^3\text{-}C_3H_5)$

Stoichiometric amounts of the $Na^+L_q^-$ ligand solution and $(MeCN)_2Mo(\eta^3\text{-}C_3H_5)(CO)_2Br$ were reacted in THF. After stirring the reaction mixture overnight, the solvent was removed *in vacuo*. The resulting residue was extracted with hexane and filtered. Evaporation of the hexane from the filtrate afforded red–orange crystals of the product in ~70% yield. Analytical, ir, and ^1H nmr data for this product are given in Tables 1 and 2.

Preparation of $L_qRh(CO)$

Preparation of the compound L_qRhCO was accomplished by a similar procedure to the one described above for $L_aRh(CO)$. New ν_{CO} bands at 2080, 2020, and 1965 cm^{-1} in THF were indicated by ir sampling of the reaction mixture prior to solvent removal *in vacuo*. After work-up, yellow orange crystals of the product were isolated in ~65% yield. Analytical, ir, and ^1H nmr data for the compound are collected in Tables 1 and 2.

Reaction of $L_aRh(CO)$ with MeI

$$L_aRhCO + MeI \rightarrow L_aRh(Me)(I)CO$$

A slight excess of methyl iodide in CH_2Cl_2 was added dropwise to a stirred solution of L_aRhCO (0.40 g, 0.70 mmol) in the same solvent. After stirring the reaction mixture at room temperature for about 18 h,

Can. J. Chem. Downloaded from www.nrcresearchpress.com by 78.46.186.204 on 09/07/12
For personal use only.

TABLE 2. ^{1}H nmr data for LMT (L = L_a, L_q): L_a = $Me_2Gapz{\cdot}O(C_5H_3N)CH_2NMe_2$; L_q = $Me_2Gapz{\cdot}O(C_9H_6N)$

L	M	T	GaMe[d]	NMe_2	CH_2	^{1}H nmr H^4	H^5	H^3	"η^3-C_3H_5"	
L_a	Re[b]	$(CO)_3$	**A** 10.53(s) 9.83(s)	8.21(s) 7.68(s)	obscured	4.19(t)	3.29(d)	2.41(d)		
			B 10.25(s)	8.39(s)	6.40(s)	3.96(t)	3.08(d)	2.21(d)		
L_a	Mn[b]	$(CO)_3$	**A** 10.65(s) 10.05(s)	7.58(s) 7.24(s)	6.73(br)	3.54(t)	3.00(d)	2.51(d)		
			B 10.31(s)	7.41(s)	6.00(s)	3.36(t)	2.85(d)	2.12(d)		
L_a	Ni[c]	(NO)	10.39(s)	7.63(s)	6.16(s)	4.13(t)	3.35(d)	2.66(d)		
L_a	Rh[a]	(CO)	10.27(s)	8.40(s)	6.41(s)	4.01(t)	2.76(d)	2.38(d)		
L_q	Re[a]	$(CO)_3$	10.33(s) 9.48(s)			4.05(t)	3.19(d)	2.23(d)		
L_q	Mn[a]	$(CO)_3$	10.35(s) 9.46(s)			3.86(t)	3.13(d)	2.14(d)		
L_q	Mo[a]	$(CO)_2(\eta^3\text{-}C_3H_5)$	10.28(s) 9.46(s)			3.85(t)	3.16(d)		8.41(d), (J = 9.0 Hz) 7.06(br)H_s 6.50(br)H_u	8.31(d)H_A
L_q	Rh[a]	(CO)	9.80(s)			3.84(t)	2.69(d)	2.28(d)		

[a] C_6D_6 solution, τC_6H_6 = 2.84 ppm.
[b] d_6-acetone solution, $\tau(CH_3)_2CO$ = 7.89 ppm.
[c] $CDCl_3$ solution, $\tau CHCl_3$ = 2.73 ppm.
[d] *A*, *fac* isomer; *B*, *mer* isomer; s, singlet; d, doublet; t, triplet; br, broad. $J_{HCCH} \approx 2$ Hz for pz protons.

the initial orange solution had turned deep red–orange. The ir spectrum of the solution at this stage revealed the presence of a new ν_{CO} band at ~2060 cm^{-1} and the complete disappearance of the ν_{CO} band at 1970 cm^{-1}, attributable to the L_aRhCO starting material. Removal of the solvent *in vacuo*, extraction of the residue in benzene, followed by recrystallization from CH_2Cl_2, afforded red crystals of the product in almost quantitative yield. This compound contained a trace of benzene solvate which remained after several days of pumping under vacuum.

Anal. calcd. for $[Me_2Gapz{\cdot}O(C_5H_3N)CH_2NMe_2]Rh(Me)(I)CO$ $0.5C_6H_6$: C 34.31, H 4.13, N 8.89; found: C 33.93, H 4.06, N 8.55. Infrared (CH_2Cl_2) ν_{CO}: 2060 cm^{-1}; ir (Nujol) ν_{CO}: 2055 cm^{-1}. ^{1}H nmr (270 MHz, $CDCl_3$) $\tau CHCl_3$ = 2.73 ppm, 10.34s, 10.12s (—$GaMe_2$); 8.85s, 7.63s (—NMe_2); 6.15s, (—CH_2); 3.71t (pz-H^4); 2.43d (pz-H^3); 2.98d (pz-H^5); 9.25s (Rh-Me) (J_{HCCH} = ~2 Hz for pz protons). Positive ion fast atom bombardment mass spectrometry (FABMS) in thioglycerol matrix: $[P + H]^+$, $[P - H]^+$, and $[P - Me]^+$ (P^+ = parent ion) ion signals were observed at 591, 589, and 575 mass units, respectively.

Reaction of L_qRh(CO) with MeI

$$L_qRhCO + MeI \rightarrow L_qRh(COMe)I$$

To a solution of L_qRhCO (0.40 g, 0.91 mmol) in ~35 mL CH_2Cl_2 was added one molar equivalent of MeI in the same solvent. The mixture was stirred for about 1½ h, at which stage ir evidence indicated the presence of two new bands in the ν_{CO} region of the spectrum at ~2070 and 1700 cm^{-1}, respectively; with no trace of the ν_{CO} band due to the L_qRhCO starting material. The solvent was then allowed to evaporate from the solution. The dark orange solid obtained was washed in hexane followed by benzene to give small dark orange crystals in low yield (~35%).

Anal. calcd. for $[Me_2GapzO(C_9H_6N)]Rh(COMe)I$: C 32.90, H 3.08, N 7.20; found: C 33.00, H 3.04, N 6.90, ir (CH_2Cl_2) ν_{CO}; 2070, 1700 cm^{-1}. Infrared (Nujol) ν_{CO}; 1710 cm^{-1}. ^{1}H nmr (270 MHz, $CDCl_3$) $\tau CHCl_3$ = 2.73 ppm, 10.08s, 9.89s (—$GaMe_2$); 7.58s (—CO*Me*); 3.71t (pz-H^4); 2.29d (pz-H^3); pz-H^5 obscured by the quinolyl ring proton resonances. Mass spectrum: P^+, $P - Me^+$, $P - Me - CO^+$, $P - Me - I^+$, and $P - 2Me - I^+$ (P^+ = parent ion) ion signals were observed.

Reaction of LRh(CO) (L = L_a; L_q) with I_2

$$LRhCO + I_2 \rightarrow LRh(I)_2(CO)$$

To a CH_2Cl_2 solution of LRhCO was added a slight excess of the dihalogen, I_2, in the same solvent. An immediate color change from orange to red was observed on mixing the reagents. After stirring the mixture for a few hours, an ir spectrum of the reaction solution indicated complete disappearance of the ν_{CO} band of the rhodium(I) monocarbonyl starting material, and the appearance of a new ν_{CO} band at ~2090 cm^{-1} (L = L_a), and ~2085 cm^{-1} (L = L_q). The single ν_{CO} band persisted in solution after stirring the reaction mixture overnight. Although the ir spectra of the reaction mixtures suggested the presence of six-coordinate Rh(III) monocarbonyl species in solution, analytically pure compounds of the expected diiodides, $LRh(I)_2(CO)$ could not be isolated from the black solid material obtained after removal of solvent.

Results and discussion

Metal derivatives of multi-dentate ligand systems incorporating both the pyrazolyl and pyridyl functional groups have been the subject of recent publications (4, 11, 12). It has been inferred that although pyrazole has stronger σ-donor properties than pyridine (1), the former has weaker π-acceptor capability (13). The present study extends our investigations in the area

Can. J. Chem. Downloaded from www.nrcresearchpress.com by 78.46.186.204 on 09/07/12
For personal use only.

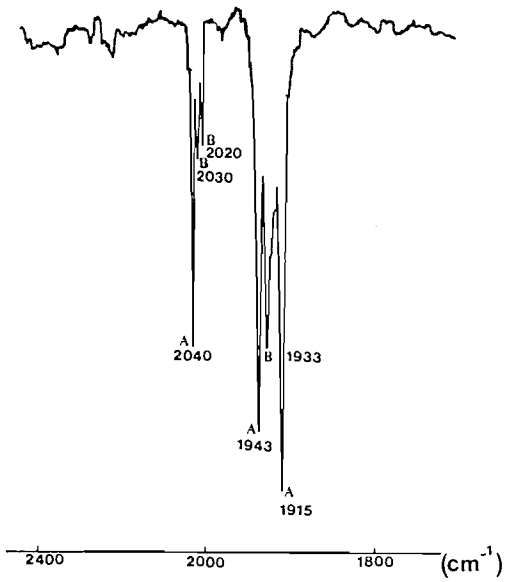

FIG. 1. Infrared spectrum of $[Me_2Gapz{\cdot}O(C_5H_3N)CH_2NMe_2]$-$Mn(CO)_3$ in C_6H_{12} solution: **A** *fac* isomer; **B** *mer* isomer.

of unsymmetrical tridentate organogallate ligands to include ligand systems incorporating both a pyrazolyl and (*i*) an amino pyridyl donor group and (*ii*) a quinolyl donor moiety. A variety of transition metal derivatives incorporating these ligands have been isolated and characterized by elemental analysis and ir, nmr, and mass spectral methods.

The first of this class of unsymmetrical tridentate ligands $[Me_2Ga(N_2C_3H_3)(OCH_2CH_2NR_2)]^-$ (R = H or Me), has been shown to be capable of either facial or meridional coordination in transition metal complexes (5). However, in all octahedral transition metal carbonyl compounds studied thus far, coordination of the unsymmetric tridentate organogallate ligand has been found to be exclusively facial (4, 14). The present manganese and rhenium tricarbonyl compounds incorporating the ligand $[Me_2Ga(N_2C_3H_3){\cdot}O(C_5H_3N)CH_2NMe_2]^-$ (L_a^-), therefore, represent the first and the only examples of such complexes featuring both the *fac* and *mer* isomers in solution. Evidence for the co-existence of both isomers in solution is provided by ir and ^1H nmr results. Infrared measurements in cyclohexane showed six bands (four strong, two weak) in the ν_{CO} region of the spectrum. A typical example of the spectra obtained for the $L_aM(CO)_3$ (M = Re, Mn) complexes is shown in Fig. 1 for the Mn compound. Three strong bands were assigned to the *fac* isomer, while one strong and two weak bands were assigned to the *mer* isomer. Thus, for octahedral transition metal tricarbonyl complexes, a *fac* arrangement of the unsymmetric tridentate ligand would give three strong ν_{CO} bands while for a *mer* arrangement one strong and two weak ν_{CO} bands would be observed (15, 16).

Additional evidence for the proposed *fac* and *mer* isomers in solution is provided by the room temperature ^1H nmr spectra of the $L_aM(CO)_3$ complexes. As a representative example, the room temperature ^1H nmr spectrum of the rhenium complex in C_6D_6 solution is shown in Fig. 2. In the spectrum, two sets of signals were displayed. In one set, the —Ga*Me*$_2$, —N*Me*$_2$, and the —CH_2 methylene group signals appeared as sharp singlets, consistent with a *mer* structure (**B**) (Fig. 3). The second set consists of two singlets each for the —$GaMe_2$ and NMe_2 moieties suggesting inequivalence of the methyl groups on gallium and the amino nitrogen as expected for a facially coordinated ligand (structure **A**, Fig. 3). The pyrazolyl proton resonances appeared as two sets again providing additional supporting evidence for the presence of both isomers in solution. The ir and ^1H nmr results discussed here, together with results for related compounds (4, 14), strongly support the presence of both *fac* and *mer* isomers in solution for the $L_aM(CO)_3$ complexes.

The room temperature ^1H nmr spectrum of the $L_aNi(CO)$ complex in $CDCl_3$ is interesting in that it displays sharp singlets for the —$GaMe_2$, —NMe_2, and —CH_2 groupings. This is suggestive of a square planar arrangement about the Ni center with a meridionally coordinated organogallate ligand. The "linear" NO group suggested by the ir result (ν_{CO} 1775 cm^{-1}), in conjunction with results from previous studies which have shown that square planar $\{MNO\}^{10}$ complexes should have an M—N—O bond angle of 120° (17–19), led us to suspect that a fluxional process must be occurring in solution at room temperature, in order to explain the observed ^1H nmr result. The closely related $[Me_2Ga(N_2C_5H_7)(OCH_2CH_2NMe_2)]NiNO$ has been shown to be stereochemically non-rigid at room temperature in solution and to possess a tetrahedral conformation about the Ni center in the solid state (20). Variable temperature ^1H nmr spectra in both d_6-acetone and toluene-d_8 did indeed reveal a fluxional process to be operative in solution for the present complex, $L_aNi(NO)$. In the experiment, the sharp —Ga*Me*$_2$ signal was monitored. As the solution was cooled, marked broadening of the —$GaMe_2$ signal was observed. At −85°C (the lowest temperature attainable), it was still not possible to collapse the original signal and observe new signals in this region. However, it is evident that at these lower temperatures, the fluxional process responsible for the average square-planar arrangement in solution at room temperature is beginning to slow down. Unfortunately, instrumental limitations precluded the attainment of temperatures low enough to observe splitting of the monitored signals. These results together with results for related compounds (4, 20), led us to the conclusion that the Ni atom in the L_aNiNO is probably facially coordinated by the L_a ligand, with the coordination geometry about Ni being tetrahedral. Possible mechanisms for the proposed fluxional process in solution at room temperature are shown in Fig. 4. Two possibilities may be envisaged. A trigonal planar intermediate (**A**) formed by breaking the Ni—N (amino) bond, followed by inversion at the pyramidal oxygen and reformation of the Ni—N (amino) bond; or a square planar intermediate (**B**) with inversion at the Ni center through the plane.

The ir spectral data for the octahedral $L_qM(CO)_3$ (M = Re, Mn) complexes compiled in Table 1, are consistent with a *fac* tridentate organogallate ligand in the two compounds. Thus, three strong ν_{CO} bands were observed for each complex, indicative of a facial arrangement of the tridentate ligand in the complexes (15, 16). The molybdenum dicarbonyl "allyl" complex $L_qMo(CO)_2(\eta^3\text{-}C_3H_5)$ showed two strong bands in the ν_{CO} region at the ir spectrum, indicative of a *cis* arrangement of the CO ligands.

Further confirmation of a facial tridentate organogallate ligand in the complexes incorporating the L_q ligand is provided by the ^1H nmr results. Of significance in the spectra of the $L_qM(CO)_3$ (M = Mn or Re) complexes is the gallium alkyl region (9–11τ), where two sharp singlets were observed for the "$GaMe_2$" moiety as expected for inequivalent methyl groups on gallium in a facial arrangement of the ligand. A meridionally

Can. J. Chem. Downloaded from www.nrcresearchpress.com by 78.46.186.204 on 09/07/12
For personal use only.

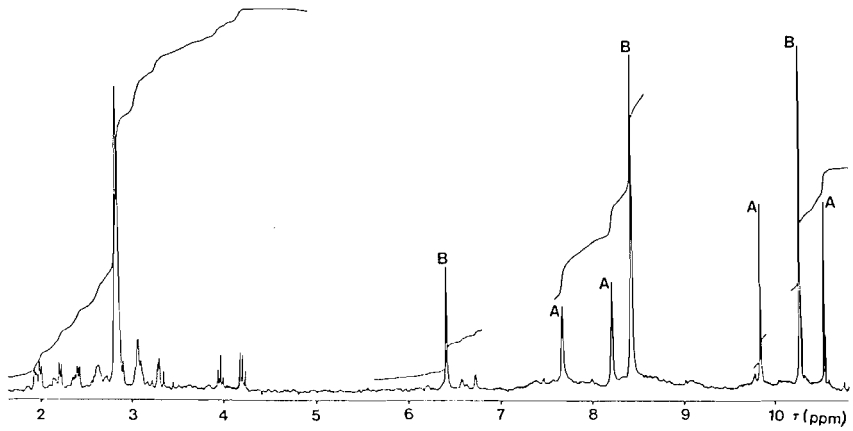

FIG. 2. Room temperature 80 MHz ^{1}H nmr spectrum of $[Me_2Gapz{\cdot}O(C_5H_3N)CH_2NMe_2]Re(CO)_3$ in C_6D_6 solution: **A** *fac* isomer; **B** *mer* isomer.

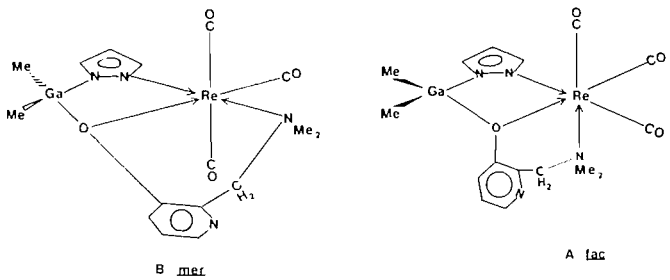

FIG. 3. *Fac* and *mer* isomers of $[Me_2Gapz{\cdot}O(C_5H_3N)CH_2NMe_2]$-$Re(CO)_3$.

coordinated ligand on the other hand, would lead to equivalent Ga–*Me* groups and therefore a singlet in this region of the spectrum.

The solution ^{1}H nmr spectrum of $L_qMo(CO)_2(\eta^2\text{-}C_3H_5)$ complex shown in Fig. 5 is again consistent with a facially coordinated ligand in the complex. Positional isomerism cannot be ruled out in this molybdenum allyl complex since interchange of the CO groups and the allyl group could potentially occur. It is clear, however, from the ^{1}H nmr spectrum, that only one positional isomer is produced in the reaction. Substitution of the allyl group in more than one position would lead to more than one set of Ga–*Me* signals in the spectrum, a feature which was not observed. Molecular models indicate that substitution opposite the "pyrazolyl" moiety is most favored sterically, a position confirmed by X-ray structural determination for the related complex $[Me_2Ga(N_2C_5H_7)(OCH_2CH_2NH_2)]Mo(CO)_2$-$(\eta^3\text{-}C_4H_7)$ (21). It is noteworthy, however, that in the related $[Me_2Ga(N_2C_5H_7)(OCH_2CH_2NH_2)]Mo(CO)_2(\eta^3\text{-}C_7H_7)$ (22) and $[Me_2Ga(N_2C_5H_7)(OCH_2CH_2SEt)]Mo(CO)_2(\eta^3\text{-}C_7H_7)$ (23), the η^3-C_7H_7 moiety occupies a position opposite the amino nitrogen and the alkyl sulfur donor atoms, respectively. This positional preference of the η^3-C_7H_7 and η^3-allyl ligands was rationalized using structural *trans* effect arguments. In addition molecular models show that an η^3-C_7H_7 group occupying a position *trans* to the pyrazolyl nitrogen would result in close contacts with the amino group or alkyl sulfido group in the latter complexes.

Mass spectral data obtained for the $L_aM(CO)_3$ and $L_qM(CO)_3$ (M = Re, Mn) compounds revealed some interesting differences dependent on the metal involved. For example, while the Re species displayed signals corresponding to the parent, P^+, and $P - Me^+$ ions prior to loss of the CO ligands, the highest mass fragment observed for the Mn species is attributable to the $P - 3CO^+$ ion. The reluctance to lose CO exhibited by the Re species reflects the comparatively stronger "M – CO" bonds in the Re complex than in the valence-isoelectronic Mn compound. This rationale is further supported by a comparison of the ν_{CO} values for the compounds. The ν_{CO} values for the Re compounds are consistently lower than those for the Mn compounds, indicating that the Re donates more electron density to the CO ligands. The increased M—CO back bonding in the Re compounds, as attested to by the lower ν_{CO} values, implies a stronger "M—CO" bond in the Re complexes (24).

The reaction of the sterically bulky L_a^- and L_q^- ligands with the $[Rh(CO)_2Cl]_2$ dimeric species afforded orange to dark orange crystals of Rh(I) monocarbonyl compounds via transient dicarbonyl species $LRh(CO)_2$, as evident from ir monitoring of the reaction mixture during the course of the reactions. It is interesting to compare similar Rh(I) carbonyl species. The cyclopentadienyl ligand, $C_5H_5^-$, and the comparable six-electron uninegative donor ligand $HB(3,5\text{-}Me_2pz)_3^-$ are known to react with $[Rh(CO)_2Cl]_2$ to give the $(\eta\text{-}C_5H_5)Rh(CO)_2$ (25) and $[HB(3,5\text{-}Me_2pz)_3]Rh(CO)_2$ (26, 27) dicarbonyl complexes, respectively. However, the introduction of the similar $HBpz_3^-$ and $MeGapz_3^-$ ligand systems led to the dinuclear rhodium species $[HBpz_3]_2Rh_2(\mu\text{-}CO)_3$ (28) and $[MeGapz_3]_2Rh_2(\mu\text{-}CO)_3$ (29). Recently, attempts at isolating rhodium dicarbonyl complexes incorporating the uninegative, unsymmetrical, tridentate $[Me_2Gapz(OCH_2CH_2NR_2)]^-$ (R = H, Me), and the $[Me_2GapzOCH_2(C_5H_4N)]^-$ ligand systems resulted in the isolation of stable, four-coordinate, square-planar Rh(I) monocarbonyl complexes. In the complexes, structurally characterized by X-ray crystallography as $[Me_2Gapz(OCH_2CH_2NH_2)]RhCO$ (30), and $[Me_2GapzOCH_2(C_5H_4N)]RhCO$ (31), the coordination mode of the tridentate organogallate ligands about the Rh(I) center was unequivocally demonstrated to be meridional. The ν_{CO} values obtained for the present complexes compare quite well with those reported for related Rh(I) monocarbonyl complexes (Table 3).

The ^{1}H nmr spectrum of the L_qRhCO complex in C_6D_6 solution clearly established the presence of a square planar Rh(I) species in solution for this complex. The sharp singlet observed for the —$GaMe_2$ group is consistent with a meridionally coordinated organogallate ligand in the complex. Similarly, with the L_aRhCO compound, sharp singlets were displayed for the "—$GaMe_2$," "—NMe_2," and "—CH_2—" moieties in conformity with a *mer* configuration of the ligand in this square-planar Rh(I) monocarbonyl compound.

Can. J. Chem. Downloaded from www.nrcresearchpress.com by 78.46.186.204 on 09/07/12
For personal use only.

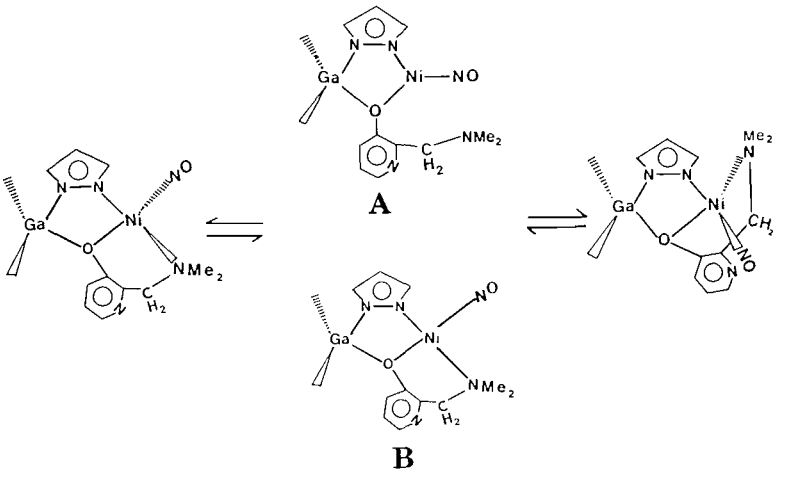

FIG. 4. Proposed mechanism for the fluxional process observed for $[Me_2Gapz{\cdot}O(C_5H_3N)CH_2NMe_2]Ni(NO)$ in d_8-toluene solution.

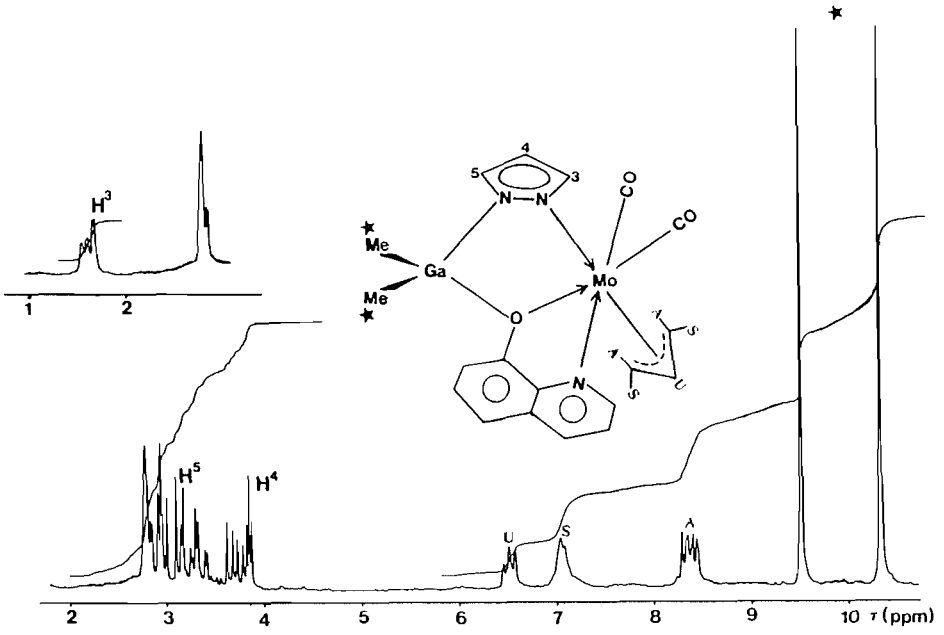

FIG. 5. Room temperature 80 MHz ^1H nmr spectrum of $[Me_2Gapz{\cdot}O(C_9H_6N)]Mo(CO)_2(\eta^3\text{-}C_3H_5)$ in C_6D_6 solution.

The mass spectrum of the L_aRhCO species showed trace signals (<0.5%) attributable to the $P - 3Me^+$ and $P - 2Me - CO^+$ ions. The parent (P^+) ion was not observed and the most intense signal in the spectrum was assigned to the $C_5H_4N^+$ ion fragments. In contrast, the mass spectrum of the L_qRhCO species displayed prominent signals due to the parent (P^+) ion, in addition to signals corresponding to the $P - Me^+$, $P - CO^+$, and $P - Me - CO^+$ ions, the latter being the most intense signal in the spectrum.

The reaction of L_qRhCO with methyl iodide, resulted in the isolation of a five-coordinate Rh(III) acetyl complex [MeGapz-$O(C_9H_6N)$]Rh(COMe)I, presumably via a six-coordinate Rh(III) oxidative–addition intermediate. Thus, the ν_{CO} band of the Rh(I) monocarbonyl starting material at 1968 cm^{-1} slowly disappeared upon addition of MeI, and was gradually replaced by two new bands at 2070 and 1700 cm^{-1} which intensified with time. Attempts at isolating the species responsible for the ν_{CO} band at 2070 cm^{-1} failed, and instead crystals of the Rh(III) acetyl complex, $L_qRh(COMe)I$, (ν_{CO}: 1710 cm^{-1}, Nujol mull) were obtained. A proposed reaction sequence for the formation of the Rh(III) acetyl species is shown in Fig. 6. It is postulated that the ν_{CO} band at 2070 cm^{-1}, observed in solution during the reaction, is probably due to the presence of a labile six-coordinate Rh(III) *trans*-addition product. Thus, alkyl halides are generally known to oxidatively add to square-planar d^8 Rh(I) and Ir(I) centers via this addition mode (32, 33). This six-coordinate Rh(III) intermediate subsequently undergoes a methyl migration or migratory insertion of CO to form the five-coordinate Rh(III) complex $L_qRh(COMe)I$, containing a terminal acetyl group. The solution ir spectrum of the Rh(III) acetyl product isolated is interesting in that it shows two bands at ~2070 cm^{-1} and 1700 cm^{-1} in CH_2Cl_2 but in Nujol mull, only one strong ν_{CO} band was observed at ~1710 cm^{-1}. This observation is suggestive of the presence of both the six-coordinate Rh(III) methyl carbonyl iodide species, and the five-coordinate Rh(III) acetyl iodide species in solution. A similar observation has been reported for the compound $[Ru(\eta^2\text{-}COMe)I(CO)(PMe_3)_2]$, an η^2-acyl complex which exists in equilibrium with

Can. J. Chem. Downloaded from www.nrcresearchpress.com by 78.46.186.204 on 09/07/12
For personal use only.

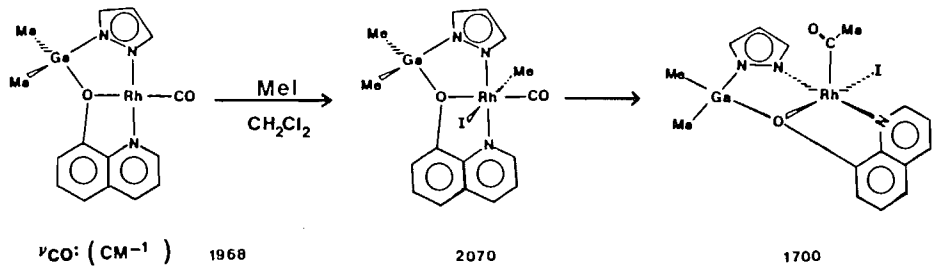

FIG. 6. Proposed reaction sequence for the formation of the $[Me_2Gapz \cdot O(C_9H_6N)]Rh(COMe)I$ complex.

TABLE 3. Comparison of ν_{CO} values in some L'RhCO complexes

L'	$\nu_{CO}(cm^{-1})$ in CH_2Cl_2	Reference
$[Me_2Gapz \cdot O(C_5H_3N)CH_2Me_2]$	1970	This work
$[Me_2Gapz \cdot O(C_9H_6N)]$	1968	This work
$[Me_2Gapz(OCH_2CH_2NR_2)]$	1957 (R = Me)	30
	1955 (R = H)	30
$[Me_2Gapz \cdot OCH_2(C_5H_4N)]$	1962	31
$[Me(Cl)Gapz \cdot OCH_2(C_5H_4N)]$	1968	31

TABLE 4. Comparison of ν_{CO} values in $L'RhI_2(CO)$ complexes

L'	$\nu_{CO}(cm^{-1})$ in CH_2Cl_2	Reference
$[Me_2Gapz \cdot O(C_5H_3N)CH_2NMe_2]$	2090	This work
$[Me_2Gapz \cdot O(C_9H_6N)]$	2085	This work
$[Me_2Gapz(OCH_2CH_2NR_2)]$ (R = H, Me)	2090	30
$[Me_2Gapz \cdot OCH_2(C_5H_4N)]$	2095	31
$[HB(3,5\text{-}Me_2pz)_3]$	2090	27
$[HBpz_3]$	2112	28
$[Bpz_4]$	2100	28
$[(\eta\text{-}C_5H_5)]$	2065 (Nujol)	37
$[(\eta\text{-}C_5Me_5)]$	2035	38

its carbonyl σ-alkyl isomer, $[Ru(CO)_2(Me)I(PMe_3)_2]$, in solution (34).

The ^1H nmr spectrum of the $L_qRh(COMe)I$ complex in $CDCl_3$ solution is consistent with a square pyramidal arrangement about the Rh center, since such a non-planar arrangement would render the methyl groups on gallium inequivalent and lead to two sharp singlets in the $GaMe_2$ region of the spectrum as observed. The position of the CO*Me* signal (7.58τ, $CDCl_3$), compares nicely with those reported for similar rhodium acetyl compounds (30, 31, 35) and the square pyramidal arrangement proposed for the present complex has been established by X-ray crystallography for the closely related $[Me_2Gapz(OCH_2CH_2NMe_2)]Rh(COMe)I$ (30) complex.

The mass spectrum of the $[Me_2GapzO(C_9H_6N)]Rh(COMe)I$ complex displayed signals corresponding to the parent, P^+, $P - Me^+$, $P - Me - I^+$, $P - 2Me - I^+$, and $P - Me - CO^+$ ions, but no $P - CO^+$ signals were observed. Signals arising from the latter ion are usually characteristic of transition metal carbonyl compounds containing terminally bound CO groups.

In contrast to the mode of reactivity discussed above for the L_qRhCO complex, the reaction of the L_aRhCO monocarbonyl complex with MeI proceeds directly to the formation of what is thought to be a six-coordinate Rh(III) oxidative *trans*-addition product $L_aRh(Me)(I)CO$. Quite interestingly, such six-coordinate addition products containing σ-bonded methyl groups have not been observed either as intermediates or as the net reaction products in the analogous reaction of the related cyclopentadienyl rhodium carbonyl compounds with MeI. For example, reaction of $(\eta\text{-}C_5Me_5)Rh(CO)_2$ with MeI proceeds directly to the $(\eta\text{-}C_5Me_5)Rh(CO)(COMe)I$ (36) acetyl complex at 50°C. Thus, the diagnostic ν_{CO} band at 2060 cm^{-1}, indicative of a terminal M—CO linkage, observed during the reaction of L_aRhCO with MeI provided strong evidence for the presence of a six-coordinate Rh(III) species in solution. The absence of a ν_{CO} band between 1600–1750 cm^{-1}, meanwhile, suggests that an acetyl derivative is not formed in this reaction.

The only crystalline product isolated from the reaction displayed a ν_{CO} band at 2060 cm^{-1} (CH_2Cl_2) and 2055 cm^{-1} (Nujol) which is consistent with the isolation of the six-coordinate Rh(III) species, $L_aRh(Me)(I)(CO)$. Such a formulation is consistent with the room temperature ^1H nmr data for the complex, which suggest a facial coordination mode for the tridentate ligand. Thus, two sharp singlets were observed for each of the —$GaMe_2$ and —NMe_2 groupings and a sharp singlet was observed for the Rh—Me resonance at ~9.3τ. It is noteworthy that no signal was seen in the —COMe region of the spectrum.

It is difficult to rationalize the difference in reactivity towards MeI observed for the L_aRhCO and L_qRhCO complexes. It is probable, however, that the Rh—Me bond is stronger in the $L_aRh(Me)(I)CO$ species compared to the $L_qRh(Me)(I)CO$ compound and hence methyl migration is discouraged in the former compound. Unfortunately, numerous attempts to grow crystals suitable for a definitive X-ray structural studies on the $L_aRh(Me)(I)CO$ complex have been unsuccessful.

Addition of molecular iodine to a CH_2Cl_2 solution of LRhCO (L = L_a, L_q), resulted in the immediate disappearance of the ν_{CO} band attributable to the appropriate Rh(I) monocarbonyl starting material with concomitant appearance of a new ν_{CO} band at 2090 cm^{-1} (L = L_a), or 2085 cm^{-1} (L = L_q). The new band suggests weakly-bound CO ligands in the products. Oxidation of the rhodium center (Rh(I)(d^8), Rh(III)(d^6)), would lead to a weaker backbonding contribution from the metal, a strengthening of the C—O bond and consequently an increased ν_{CO} value. Based on this observation, it does appear that six-coordinate Rh(III) diiodide species $LRhI_2(CO)$ had formed in solution, although analytically pure samples of the products could not be isolated. The ν_{CO} values of the present $LRhI_2(CO)$ species are in good agreement with those reported for some related Rh(III) diiodides (see Table 4).

It is interesting, however, that the ν_{CO} values for the pyrazolylgallate or borate-containing species are consistently higher than the values reported for the analogous cyclopentadienyl-containing rhodium diiodide species. This is rather unusual since these observations oppose the trend previously estab-

Can. J. Chem. Downloaded from www.nrcresearchpress.com by 78.46.186.204 on 09/07/12
For personal use only.

lished for complexes incorporating these ligands (39, 40). That is, pyrazolylgallate tridentate ligands, and the related isoelectronic tridentate pyrazolylborate ligands are generally stronger net electron donors compared to the tridentate cyclopentadienyl ligands and give rise to lower ν_{CO} values in analogous transition metal carbonyl complexes.

Acknowledgements

We thank the Natural Sciences and Engineering Research Council of Canada for financial support and Mr. P. Borda for elemental analyses.

1. K. S. CHONG, S. J. RETTIG, A. STORR, and J. TROTTER. Can. J. Chem. **55**, 4166 (1977).
2. K. S. CHONG and A. STORR. Can. J. Chem. **57**, 167 (1979).
3. K. S. CHONG and A. STORR. Can. J. Chem. **59**, 1331 (1981).
4. S. J. RETTIG, A. STORR, J. TROTTER, and K. UHRICH. Can. J. Chem. **62**, 2783 (1984).
5. K. S. CHONG, S. J. RETTIG, A. STORR, and J. TROTTER. Can. J. Chem. **56**, 1212 (1978).
6. A. STORR and B. S. THOMAS. Can. J. Chem. **48**, 3667 (1970).
7. B. HAYMORE and R. D. FELTHAM. Inorg. Synth. **14**, 81 (1973).
8. R. B. KING. Organometallic synthesis. Vol. 1. Academic Press, New York. 1965. p. 174.
9. G. DOLCETTI and G. R. NORTON. Inorg. Synth. **16**, 35 (1976).
10. R. G. HAYTER. J. Organomet. Chem. **13**, P1–P3 (1968).
11. A. J. CANTY and C. V. LEE. Organometallics, **1**, 1063 (1982).
12. P. J. STEEL, F. LAHOUSE, D. LERNER, and C. MARTIN. Inorg. Chem. **22**, 1488 (1983).
13. P. SULLIVAN, D. J. SALMON, T. J. MEYER, and J. PEEDIN. Inorg. Chem. **18**, 3369 (1979).
14. B. M. LOUIE, S. J. RETTIG, A. STORR, and J. TROTTER. Can. J. Chem. **63**, 2261 (1985).
15. D. M. ADAMS. Metal–ligand and related vibrations. Edward Arnold, London. 1971.
16. F. A. COTTON. Inorg. Chem. **3**, 702 (1964).
17. K. J. HALLER and J. H. ENEMARK. Inorg. Chem. **17**, 3552 (1978).
18. J. H. ENEMARK and R. D. FELTHAM. Coord. Chem. Rev. **13**, 339 (1974).
19. R. D. FELTHAM and J. H. ENEMARK. Topics in stereochemistry. Vol. 12. *Edited by* G. Geoffroy. John Wiley and Sons, New York. 1981. p. 155.
20. K. S. CHONG, S. J. RETTIG, A. STORR, and J. TROTTER. Can. J. Chem. **57**, 3107 (1979).
21. K. S. CHONG, S. J. RETTIG, A. STORR, and J. TROTTER. Can. J. Chem. **57**, 1335 (1979).
22. K. S. CHONG, S. R. RETTIG, A. STORR, and J. TROTTER. Can. J. Chem. **59**, 1665 (1981).
23. S. J. RETTIG, A. STORR, and J. TROTTER. Can. J. Chem. **59**, 2391 (1981).
24. F. A. COTTON and G. WILKINSON. Advanced inorganic chemistry. 4th ed. John Wiley and Sons Inc., New York. 1980.
25. E. O. FISCHER and K. BITTLER. Z. Naturforsch. **16B**, 225 (1961).
26. S. TROFIMENKO. Inorg. Chem. **10**, 1372 (1971).
27. S. MAY, P. REINSALU, and J. POWELL. Inorg. Chem. **19**, 1582 (1980).
28. M. COCIVERA, T. J. DESMOND, G. FERGUSON, B. KAITNER, F. J. LALOR, and D. J. O'SULLIVAN. Organometallics, **1**, 1125 (1982).
29. B. M. LOUIE, S. J. RETTIG, A. STORR, and J. TROTTER. Can. J. Chem. **62**, 633 (1984).
30. B. M. LOUIE, S. J. RETTIG, A. STORR, and J. TROTTER. Can. J. Chem. **63**, 3019 (1985).
31. D. A. COOPER, S. J. RETTIG, and A. STORR. Can. J. Chem. **64**, 566 (1986).
32. I. C. DOUCK and G. WILKINSON. J. Chem. Soc. A, 2605 (1965).
33. P. UGUAGLIATI, A. PALAZZI, G. DEGANELLO, and U. BELLUCO. Inorg. Chem. **9**, 724 (1970).
34. W. R. ROPER, G. E. TAYLOR, J. M. WATERS, and L. J. WRIGHT. J. Organomet. Chem. **182**, C46 (1979).
35. M. C. BAIRD, J. T. MAGUE, J. A. OSBORN, and G. WILKINSON. J. Chem. Soc. A, 1347 (1967).
36. J. W. KANG and P. M. MAITLIS. J. Organomet. Chem. **26**, 393 (1971).
37. R. B. KING. Inorg. Chem. **5**, 82 (1966).
38. J. W. KANG, K. MOSELEY, and P. M. MAITLIS. J. Am. Chem. Soc. **91**, 5972 (1969).
39. S. TROFIMENKO. J. Am. Chem. Soc. **91**, 588 (1969).
40. K. R. BREAKELL, S. J. RETTIG, D. L. SINGBELL, A. STORR, and J. TROTTER. Can. J. Chem. **56**, 2099 (1978).

Can. J. Chem. Downloaded from www.nrcresearchpress.com by 78.46.186.204 on 09/07/12
For personal use only.

The total synthesis of (±)-4-demethoxy-10-nordaunomycinone

C. M. WONG,[1] P. M. GORDON,[2] A. G. CHEN,[3] AND H. Y. P. LAM[4]

Department of Chemistry, University of Manitoba, Winnipeg, Man., Canada R3T 2N2

Received August 19, 1986

C. M. WONG, P. M. GORDON, A. G. CHEN, and H. Y. P. LAM. Can. J. Chem. **65**, 1375 (1987).

4-Demethoxy-10-nordaunomycinone (**4**) is synthesized starting with 4,7-dimethoxy-1-indanone (**8**). Nucleophilic addition of ethynyl magnesium bromide to **8** followed by mercuric acetate oxidation and iron pentacarbonyl – tri-*n*-butyltin hydride reduction gave 4,7-dimethoxy-1-acetylindane (**16**). Condensation of **16** with phthalic anhydride followed by methylation with dimethylsulfate and oxidation gave **22**, which was epimerized to **24** by 2,2-dimethoxypropane and trifluoroacetic acid. Demethylation of **24** with aluminum chloride gave the 4-demethoxy-10-nordaunomycinone (**4**).

C. M. WONG, P. M. GORDON, A. G. CHEN et H. Y. P. LAM. Can. J. Chem. **65**, 1375 (1987).

On a synthétisé la déméthoxy-4 nor-10 daunomycinone (**4**) à partir de la diméthoxy-4,7 indanone-1 (**8**). L'addition nucléophile du bromure d'éthynylmagnésium à la cétone **8**, suivie d'une oxydation par l'acétate mercurique et d'une réduction par l'hydrure de tri-*n*-butylétain/pentacarbonyle de fer, conduit au diméthoxy-4,7 acétyl-1 indane (**16**). La condensation de **16** avec l'anhydride phtalique, suivie d'une méthylation par le sulfate de méthyle et d'une oxydation, conduit au composé **22** que l'on a épimérisé en **24** par le diméthoxy-2,2 propane et l'acide trifluoroacétique. La déméthylation de **24** par le chlorure d'aluminium fournit la déméthoxy-4 nor-10 daunomycinone (**4**).

[Traduit par la revue]

Can. J. Chem. Downloaded from www.nrcresearchpress.com by 78.46.186.204 on 09/07/12
For personal use only.

Discovery of the antitumor properties of anthracyclines daunomycin (**1**) and adriamycin (**2**) and their subsequent successful clinical application raised interest in anthracycline research internationally (1–3). The study of the nature of their cardiotoxicity (4) and structure–activity relationship remains one of the most active areas of research into cancer chemotherapy. The challenge can be met, at least partially, by a new molecular structure, which exhibits stronger activity against a broader neoplastic syndrome and is much less toxic than daunomycin or adriamycin. Structure modification through partial or total synthesis or by mutant microorganism transformation has afforded a large number of new anthracycline derivatives, several of which have shown very encouraging results in terms of activity and toxicity (5–9). Of these numerous new anthracycline derivatives, no practical or biologically active example involving modification of the basic aglycone skeleton has been reported (3, 10), except the heteroanthracyclines, their aglycones (11–14), and the two recently reported syntheses of 4-demethoxy-8-nordaunomycinone (**4***a*) (16) and its dimethyl ether derivative. However, these elegantly designed syntheses were more laborious and meandering than anticipated and the juxtaposition of the C-7 and C-8 substitutions would eventually hinder the ensuing glycosidation process. All other syntheses involved functional group modification or substitution derivatives of daunomycin, adriamycin, aclacinomycins, and rhodomycins (3, 10, 15). In light of these considerations and of the fact that 4-demethoxydaunomycin is several times more potent than daunomycin and adriamycin (5), we would like to report the total synthesis of (±)-4-demethoxy-10-nordaunomycinone (**4**) and its C-7 epimer **25**.

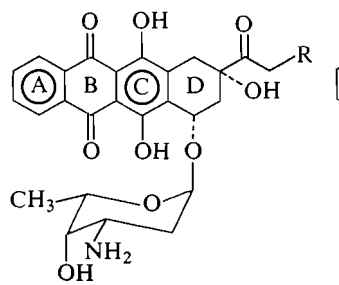

1 R = H
2 R = OH

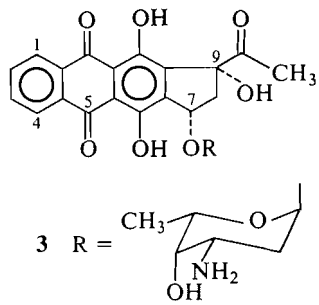

3 R =

4 R = H

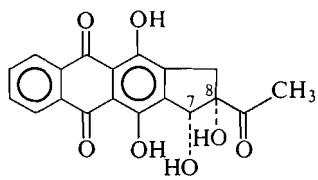

4*a*

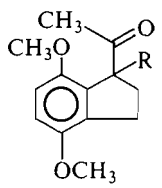

5 R = OH
6 R = OAc
16 R = H

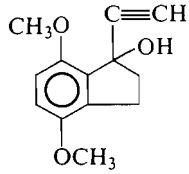

7

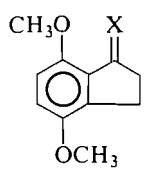

8 X = O
9 X = H_2

Results and discussion

A logical approach to the tetracyclic skeleton would be the Friedel–Crafts condensation of 4,7-dimethoxy-1-hydroxy-1-acetylindane (**5**) with phthalic anhydride, analogous to our early synthesis of 7-*O*-methyl-4-demethoxydaunomycinone (17). However, it was observed that **5** was not stable under acidic conditions. The compound decomposed in the presence of strong Lewis acids. Polymeric unidentifiable amorphous foam was the major product recovered from all reactions involving strong acids. Attempts to condense the corresponding acetoxy compound 4,7-dimethoxy-1-acetoxy-1-acetylindane (**6**) with phthalic anhydride were equally futile. The precursor, 4,7-dimethoxy-1-hydroxy-1-ethynyl-indane (**7**), was also very

[1]Author to whom correspondence may be addressed.

[2]Holder of The University of Manitoba Graduate Fellowship.

[3]Visiting scholar from The Chinese Academy of Sciences, People's Republic of China, 1981–1982.

[4]Manitoba Institute of Cell Biology, Department of Medicine, University of Manitoba.

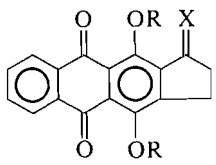

10 R = H, X = H_2
11 R = CH_3, X = H_2
12 R = CH_3, X = O
13 R = CH_3, X = OH, C≡CH

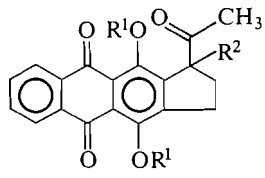

14 R^1 = CH_3, R^2 = OH
17 R^1 = R^2 = H
18 R^1 = CH_3, R^2 = H

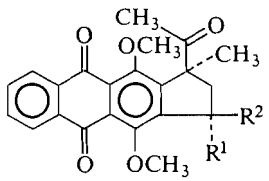

19 R^1 = R^2 = H
20 R^1 = OH, R^2 = H
21 R^1 = H, R^2 = OH

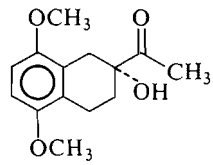

15

unstable in the presence of strong acids or bases. It regenerated the starting indanone **8**, which was inactive toward all Friedel–Crafts reactions. However, **9**, prepared by reduction of **8** by triethylsilane in trifluoroacetic acid solution, underwent the condensation with phthalic anhydride smoothly, forming the tetracyclic quinone **10** whose methyl ether **11** can be oxidized in good yield to **12** by chromium trioxide – acetic anhydride and converted to the fragile hydroxy acetylene **13** by excess lithium acetylide. Following the lithium acetylide nucleophilic addition process, it was observed that the quinone chromophore disappeared initially, and the D-ring carbonyl group remained practically unaffected until most of the quinone chromophore disappeared. Further reaction with excess lithium acetylide led to an unstable crude product, which displayed only very weak quinone absorption in the infrared spectrum and could not be characterized. But on standing, the quinone carbonyl group was regenerated at a rate faster than the regeneration of the D-ring carbonyl group. This allowed the isolation of **13**, albeit in poor yield. The acetylene group was converted to the acetyl group by mercuric acetate in aqueous acetic acid solution to form the stable intermediate **14**. The low yield of the acetylide addition necessitated a modification of our approach to this compound.

The disparate properties of **5** and its homologue **15** (17) very likely stemmed from the benzylic hydroxyl function, and its removal may facilitate the acylation process with phthalic anhydride. Dehydroxylation, however, proved to be more difficult than anticipated. The yield of **16** from either **5** or **6** under various conditions for dehydroxylation or deacetoxylation of α-hydroxy and α-acetoxyketones or benzylic alcohols was poor, and when reactions were carried out in acidic medium the product contained an unidentifiable polymeric solid as the major component. The small amount of **16** so accumulated did give excellent yield of **17** when it was allowed to react with phthalic anhydride in the presence of aluminium chloride. Thus allylic reduction by a free radical process in nonacidic medium is essential. Eventually, **16** was obtained in good yield when **6** was allowed to react with iron pentacarbonyl and tributylin hydride in xylene solution.

Attempts to methylate **17** by iodomethane under various basic conditions invariably gave **19** as the only methylated product. A 3H singlet at δ 1.55 showed unequivocally the presence of a methyl group, and oxidation of **19** by molecular oxygen in *tert*-butyl alcohol, potassium *tert*-butoxide, and dimethylformamide solution gave a mixture of two compounds whose ^{1}H nmr spectrum revealed the presence of two methyl singlets at δ 1.55 and 1.65 ppm, and four methoxy singlets at δ 3.87, 3.96, 4.05, and 4.08 ppm. Together with a molecular ion M^+ = 380 in the mass spectrum, it is very likely that the oxidation of **19** gave the two isomers **20** and **21**. This result ascertained that a one-step conversion of **18** to **22** and **4** is feasible.

Selective methylation of the phenolic groups of **17** was achieved following the HSAB principal. Thus, methylation of **17** in basic solution by dimethyl sulfate, whose conjugate anion and the phenolic anion were hard bases, gave exclusively the desired product **18**. Oxidation of **18** by molecular oxygen as before gave the *trans*-diol **22**. This convenient bishydroxlation process, reported independently by Swenton and co-workers (18*a*, *b*) and Wong *et al.* (18*c*), provided an easy route to the fully functionalized D-ring of the hetero- and noranthracyclinones. The monohydroxy compound **14** could be isolated as the major product if the reaction was quenched within 0.5 h by dilute acid.

The *trans*-diol **22** exhibits none of the general properties of daunomycinone and heteroanthracyclinone analogues, which gave a mixture of *cis*- and *trans*-diols under similar oxidation conditions, the *trans* isomers isomerizing to the *cis* isomers upon heating in trifluoroacetic acid; furthermore, the *trans* isomers exist in an equilibrium involving the C7-OH and the C9-acetyl groups (11–13) to form hemiacetals. The *trans*-diol **22** was recovered completely after being heated in trifluoroacetic acid for 72 h. Attempts to crystallize it also failed. The corresponding *trans*-diols in the heteroanthracyclinone and anthracyclinone series are also adverse to crystallization. The ^{1}H nmr spectrum of **22** (Fig. 1) shows no sign of an equilibrium between **22** and the hemiacetal **23**. It was thus easily mistaken for the *cis* isomer **24**. The epimerization to **24** was successfully carried out when **22** was heated in an acetone

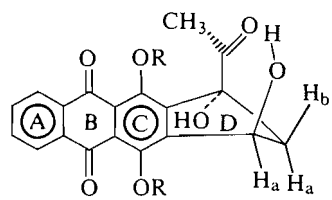

22 R = CH_3
25 R = H

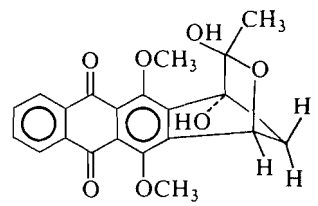

23

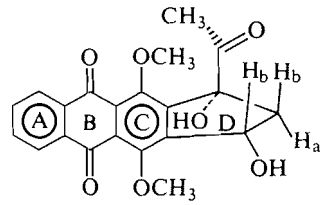

24

Can. J. Chem. Downloaded from www.nrcresearchpress.com by 78.46.186.204 on 09/07/12
For personal use only.

Can. J. Chem. Downloaded from www.nrcresearchpress.com by 78.46.186.204 on 09/07/12
For personal use only.

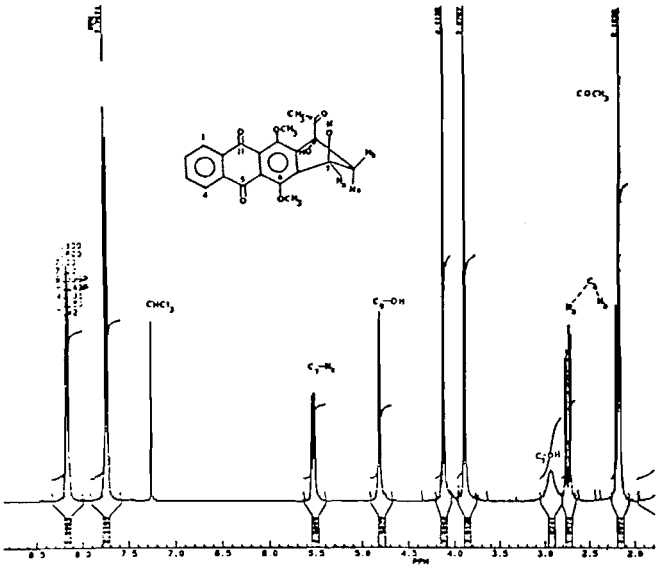

FIG. 1. The ^{1}H nmr spectrum of **22**.

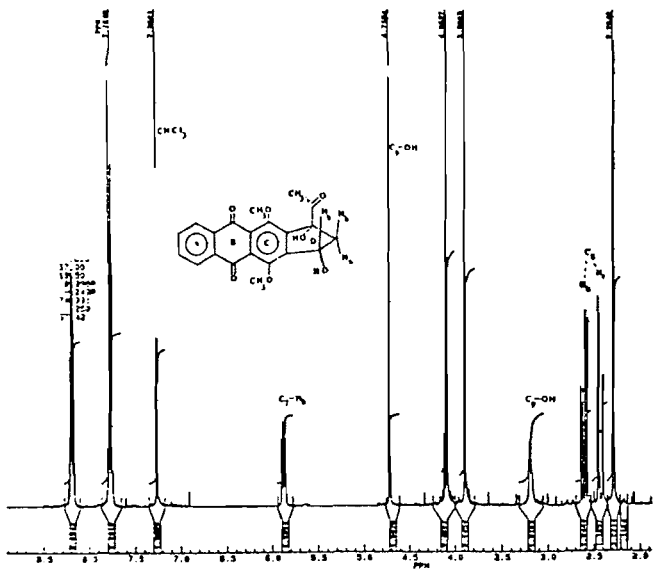

FIG. 2. The ^{1}H nmr spectrum of **24**.

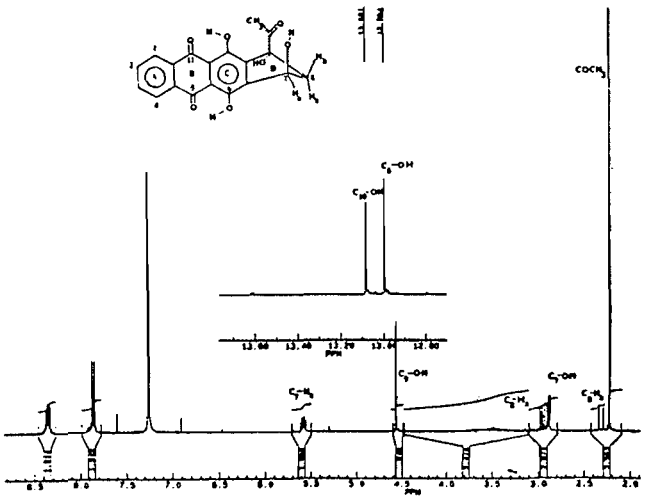

FIG. 3. The ^{1}H nmr spectrum of **25**.

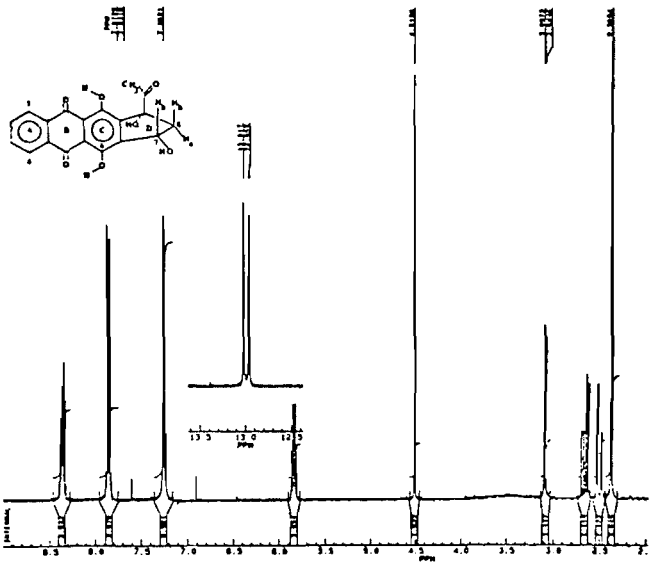

FIG. 4. The ^{1}H nmr spectrum of **4**.

solution of 2,2-dimethoxypropane and trifluoroacetic acid. The ^{1}H nmr spectra of **22** (Fig. 1) and **24** (Fig. 2) detail the structural features of these two isomers. Comparison of these two spectra reveals that the major differences are the chemical shifts and coupling constants of the C7-H_a, C7-H_b, and C8-H_a, H_b. For the *trans*-diol **22**, the free rotation of both C7-OH and C9-$COCH_3$ groups is impeded by the hydrogen bonding between these two groups, freezing the D-ring conformation to the extent that the acetyl methyl group experiences the diamagnetic anisotropic effect of the C-ring and thus appears at δ 2.163 ppm instead of δ 2.285 ppm for that of the *cis*-diol **24**. This conformation of the D-ring also places the C8-H_b of **22** at the fringe of the diamagnetic shielding zone of the acetyl carbonyl function, shifting it to a higher field of δ 2.174 ppm as compared to the C8-H_b of **24** at δ 2.428 ppm. The **22** value J_{7a8b} = 1.7 Hz versus the **24** J_{7b8a} = 5.1 Hz also reflects that the H8b—C8—H7a dihedral angle of **22** is close to 90° instead of 120° for the H7b—C7—C8—H8a dihedral angle of **24**. The H7b of **22** at δ 5.517 ppm, appearing as a broad doublet instead of an eight-line pattern of the X part of a ABMX spin system, is due to the small coupling of $J_{7a,8b}$ = 1.7 Hz and the spin–spin interaction with the fast exchanging C7-OH proton. Also in agreement with the structure is the H7b of **24** at δ 5.875 ppm appearing as a doublet of a doublet with J_{7b8b} = 7.2 Hz and J_{7b8a} = 5.1 Hz.

The demethylation of **22** and **24** to **25** and **4** by aluminum chloride was very easily achieved. Having observed the averseness of **22** to epimerize to **24**, it is surprising to note that **22** gave exclusively **25** and **24** gave exclusively **4**. No epimerization of **4** to **25** or vice versa was observed. The ^{1}H nmr spectra of **25** (Fig. 3) and **4** (Fig. 4) reveal explicitly the structural features of both **25** and **4** and are compatible with those of **22** (Fig. 1) and **24** (Fig. 2). Coupling of **4** to several amino sugars and their cytotoxic activities will be reported separately, together with the biological data of heteroanthracyclines.

Experimental

The ^{1}H nmr spectra were recorded on Bruker WH-90 or Bruker AM-300 spectrometers. Chemical shift is quoted in δ ppm downfield

Can. J. Chem. Downloaded from www.nrcresearchpress.com by 78.46.186.204 on 09/07/12
For personal use only.

from TMS using $CDCl_3$ as solvent, unless otherwise specified. The ir spectra were recorded on a Perkin–Elmer 710 Infracord or a Nicolet MX-1 FT spectrometer using CH_2Cl_2 as solvent, and transmittance is quoted in wave numbers (cm^{-1}). Mass spectra were recorded on a Finnigan 1015 spectrometer and high resolution mass spectra were recorded on a V.G. 7070 E HF spectrometer. Melting points were determined on a Fisher–Johns apparatus and are uncorrected.

Preparation of 4,7-dimethoxy-1-ethynyl-1-indanol (7)

To a 3-necked flask (2 L), equipped with a pressure equalized dropping funnel, condenser with drying tube, and a gas dispersion tube, and containing anhydrous tetrahydrufuran (750 mL) saturated with anhydrous acetylene, was added ethyl magnesium bromide in tetrahydrofuran solution (200 mL, 2 *M* solution) dropwise through the dropping funnel at room temperature. Acetylene was introduced continuously. The addition of the ethyl magnesium bromide – tetrahydrofuran solution was controlled at the rate of about 2 mL/min. The solution was then stirred for an additional 20 min and 4,7-dimethoxy-1-indanone (**8**) (30 g) (19) was added. Acetylene was introduced continuously for an additional 0.5 h. The solution was stirred for 2 h at room temperature under anhydrous conditions, poured into ice-cooled saturated ammonium chloride solution (100 mL) to decompose the excess ethynyl magnesium bromide, and then extracted by methylene chloride (3 × 700 mL), washed with water, dried over anhydrous $MgSO_4$, and evaporated to dryness to give the crude product (**7**) (26 g), a portion (1 g) of which was purified by fast chromatography over silica and recrystallized from ether–hexane; mp 77–79°C; ir: 3560 (OH), 3300 (C≡C—H), 1610 (aromatic); ^{1}H nmr: 2.38 (q, 1H, C2-H), 2.60 (s, 1H, —C≡C—H), 2.70 (dq, 1H, C2-H), 2.86 (q, 1H, C3-H), 2.97 (dq, 1H, C3-H), 3.74 (s, 1H, —OH), 3.79 (s, 3H, —OCH_3), 3.88 (s, 3H, —OCH_3), 6.72 (s, 2H, aromatic); ms: 218 (M^+), 203 ($M^+ - CH_3$), 201 ($M^+ - OH$), 185 ($M^+ - H_2O - CH_3$).

Preparation of 4,7-dimethoxy-1-acetoxy-1-acetylidane (6)

The crude indanol (**7**) from the previous preparation was dissolved in ethyl acetate (1.5 L) to which was added mercuric acetate (99.5 g) and the mixture was stirred for a period of 24 h at room temperature. Hydrogen sulfide was introduced into the solution until the formation of black precipitate ceased. The precipitate was removed by filtration and the solution was evaporated to dryness under reduced pressure giving the crude crystalline product (**6**) (52 g), which was further purified by recrystallization from methylene chloride – petroleum ether; mp 98–100°C; ir: 1730 (—O—$COCH_3$), 1715 (—$COCH_3$), 1605 (aromatic); ^{1}H nmr: 2.13 (s, 3H, —O—$COCH_3$), 2.25 (s, 3H, —$COCH_3$), 2.30–2.80 (m, 1H, C2-H), 2.85–3.20 (m, 3H, C2-H and C3-H), 3.78 (s, 3H, OCH_3), 4.0 (s, 3H, OCH_3), 6.72 (q, 2H, aromatic); ms: 278 (M^+), 235 ($M - COCH_3$), 192 ($M - 2 \times COCH_3$). *Exact Mass* (high resolution ms) calcd. for $C_{15}H_{18}O_5$: 278.1154; found: 278.1158. *Anal.* calcd.: C 64.72, H 6.52; found: C 64.8, H 6.57.

Preparation of 4,7-dimethoxy-1-acetylindane (16)

An *o*-xylene solution (250 mL) of iron pentacarbonyl (40 mL), tri-*n*-butyltin hydride (2 mL), and **6** (4.6 g) was heated in a 130°C oil bath under N_2 for 72 h. The solution was allowed to cool to room temperature and cupric chloride in acetone solution was added slowly until fizzing or carbon monoxide evolution ceased. The mixture was diluted with water and extracted with chloroform. The chloroform extract was washed with aqueous cupric chloride solution, dried, and evaporated to dryness, giving the crude product (**16**) (3.2 g), which was readily purified by column chromatography over silica and recrystallization from ether – petroleum ether; mp 56–58°C; ir: 1705 ($COCH_3$), 1610 (aromatic); ms: 220 (M^+), 177 ($M - COCH_3$); ^{1}H nmr: 2.144 (s, 3H, $COCH_3$), 2.223 (m, 1H, C2-H), 2.338 (m, 1H, C2-H), 2.78 and 3.03 (2 sym. m, 2H, C3-H3), 3.754 (s, 3H, OCH_3), 3.787 (s, 3H, OCH_3), 4.122 (dd, 1H, C1-H, J = 9 Hz, J = 5.4 Hz), 6.659 (1, 2H, aromatic, J = 9 Hz).

Preparation of 17

Pulverized phthalic anhydride (2.3 g), 4,7-dimethoxy-1-acetylindane (**16**) (2.2 g), NaCl (4 g), and pulverized freshly sublimed aluminum chloride (22 g) was mixed mechanically and heated in a 180°C oil bath for 10 min. The dark red syrupy mixture was allowed to cool, taken up in saturated oxalic acid solution, and stirred overnight at room temperature. The solution with red solid suspension was extracted exhaustively with chloroform and the chloroform extract was washed with saturated oxalic acid solution and water, dried, and evaporated to dryness. The red solid residue (2.7 g) was recrystallized from chloroform–ether; mp 188–192°C; ir: 3500–2700 (chelated OH), 1720 ($COCH_3$), 1625 (chelated quinone), 1595 (aromatic); ^{1}H nmr: 2.37 (s, 3H, $COCH_3$), 2.44 (m, 2H, C8-H2), 3.16 (m, 2H, C7-H2), 4.36 (dd, 1H, C9-H, J = 9 Hz, J = 5 Hz), 7.82 (m, 2H, C2-H, C3-H), 8.33 (m, 2H. C1-H, C4-H), 1304 (s, 1H, chelated OH), 13.15 (s, 1H, chelated OH); ms: 322 (M^+, 40%), 279 ($M - COCH_3$, 100%). *Exact Mass* (high resolution ms) calcd. for $C_{19}H_{14}O_5$: 322.0842; found: 322.0844. *Anal.* calcd.: C 70.78, H 4.38; found: C 70.81, H 4.42.

Preparation of 18 and 19

An acetone solution (100 mL) of dimethyl sulfate (5 mL), potassium carbonate (15 g), and **17** (1 g) was heated under reflux for 24 h. The acetone solution was cooled, filtered, and concentrated. The residue was taken up in methylene chloride, filtered, and evaporated to dryness under reduced pressure. The residue crystallized on standing and was recrystallized from methylene chloride – ether (910 mg); mp 135–137°C; ir: 1715 ($COCH_3$), 1675 (quinone), 1600–1585 (aromatic); ^{1}H nmr: 2.99 (s, 3H, $COCH_3$), 2.30 (m, 1H, C8-H), 2.43 (m, 1H, C8-H), 3.11 (m, 1H, C7-H), 3.25 (m, 1H, C7-H), 3.856 (s, 3H, OCH_3), 3.935 (s, 3H, OCH_3), 4.343 (dd, 1H, C9-H, J = 9.1 Hz, J = 5.7 Hz), 7.75 (m, 2H, C2-H, C3-H), 8.37 (m, 2H, C1-H, C4-H); ms: 350 (M^+, 90%), 307 ($M - COCH_3$, 100%). *Anal.* calcd. for $C_{21}H_{18}O_5$: C 72.0, H 5.14; found: C 72.1, H 5.1.

When dimethylsulfate was replaced by methyl iodide, **19** was isolated as the only product, mp 104–106°C; ir: 1710 ($COCH_3$), 1675 (quinone), 1600–1580 (aromatic); ^{1}H nmr: 1.55 (s, 3H, C9—CH_3), 2.01 (m, 1H, C8-H), 2.44 (m, 1H, C8-H), 3.18 (m, 2H, C7-H2), 3.86 (s, 3H, OCH_3), 3.97 (s, 3H, OCH_3), 7.75 (m, 2H, C2-H, C3-H), 8.19 (m, 2H, C1-H, C4-H); ms: 364 (M^+, 10%), 321 ($M - COCH_3$, 100%).

Preparation of 6,10-di-O-methyl-4-demethoxy-7-epi-10-nordaunomycinone (22) and 6,10-di-O-methyl-4-demethoxy-7-deoxy-10-nordaunomycinone (23)

To a solution of dry *N,N*-dimethylformamide (50 mL), *tert*-butyl alcohol (10 mL), and potassium *tert*-butoxide (2.2 g) was added **18** (700 mg). The solution was then cooled in a −30°C bath and dry O_2 was introduced for a period of 4 h. Trimethylphosphite (1 mL) was added, the solution was adjusted to pH 8–9 by dilute hydrochloric acid, stirred for 2 h, diluted with water, and extracted exhaustively with chloroform. The residue, obtained after routine work-up of the chloroform solution, was subjected to column chromatography on silica. Elution of the column by chloroform gave **23** (170 mg), recrystallized from methylene chloride – ether; mp 182–184°C; ir: 3450 (C9-OH), 1715 ($COCH_3$), 1675 (quinone), 1595, 1580 (aromatic); ^{1}H nmr: 2.21 (s, 3H, $COCH_3$), 2.22 (ddd, 1H, C8-H_b, J_{8b8a} = 14 Hz, J_{8b7b} = 8.2 Hz, J_{8b7a} = 3 Hz), 2.49 (ddd, 1H, C8-H_a, J_{8a8b} = 14 Hz, J_{8a7a} = 8.4 Hz, J_{8a7b} = 8.0 Hz), 3.23 (ddd, 1H, C7-H_a, J_{7a7b} = 17.5 Hz, J_{7a8a} = 8.5 Hz, J_{7a8b} = 3 Hz), 3.44 (ddd, 1H, C7-H_b, J_{7b7a} = 17.5 Hz, J_{7b8b} = 8.2 Hz, J_{7b8a} = 8.1 Hz), 3.88 (s, 3H, OCH_3), 4.01 (s, 3H, OCH_3), 4.75 (s, 1H, OH), 7.72–7.78 (m, 2H, C2-H, C3-H), 8.17–8.23 (m, 2H, C1-H, C4-H); ms: 366 (M^+, 1%), 323 ($M - COCH_3$, 100%). In a separate batch where **18** (70 mg) was oxidized under similar conditions for 0.5 h, only **23** (62 mg) was isolated. Further elution of the column by chloroform–acetone (10%) gave the product **22** (280 mg), which defied all attempts to induce crystallization; ir: 3550, (C7-OH), 3440 (C9-OH), 1715 ($COCH_3$), 1670 (quinone), 1600–1580 (aromatic); ^{1}H nmr: 2.163 (s, 3H, $COCH_3$), 2.173 (dd, 1H, C8-H_b, J_{8b8a} = 14.5 Hz, J_{8b7a} = 1.7 Hz), 2.730 (dd, 1H, C8-H_a, J_{8a8b} = 14.5 Hz, J_{8a7a} = 6.5 Hz), 2.920 (s, 1H, C7-OH), 3.877 (s, 3H, OCH_3), 4.113 (s, 3H, OCH_3), 4.80 (s, 1H, C9-OH), 5.517 (bd, 1H, C7-H, $J_{7,8a}$ = 5.9 Hz); ms: 382 (M^+, 1%), 339 ($M - COCH_3$, 100%).

Preparation of 6,11-di-O-methyl-4-demethoxy-10-nordaunomycinone (24)

An acetone solution (20 mL) of 2,2-dimethoxypropane (5 mL), trifluoroacetic acid (1/3 mL), and **22** (80 mg) was heated under reflux in a dry nitrogen atmosphere. The solution was concentrated under reduced pressure, diluted with CH_2Cl_2 (100 mL), and washed with water and sodium bicarbonate solution, then dried and evaporated to dryness. The residue, after separation by tlc on silica, afforded starting material **22** (12 mg) and the product **24** (42 mg), which was recrystallized from CH_2Cl_2–ether; mp 148–151°C; ir: 3560 (C7-OH), 3450 (C9-OH), 1715 ($COCH_3$), 1670 (quinone), 1600, 1580 (aromatic); ^{1}H nmr: 2.285 (s, 3H, $COCH_3$), 2.428 (dd, ^{1}H, C8-H_a, J = 14.4 Hz, J_{8a7b} = 5.1 Hz), 2.602 (dd, 1H, C8-H_b, J_{8b8a} = 14.4 Hz, J_{8b7b} = 7.2 Hz), 3.187 (s, H, C-OH), 3.889 (s, 3H, OCH_3), 4.093 (s, 3H, OCH_3) 4.718 (s, 1H, C9-OH), 5.874 (dd, 1H, C7-H_b, J_{7b8b} = 7.2 Hz, J_{7b8a} = 5.1 Hz), 7.785 (m, 2H, C2-H, C3-H), 8.178 (m, 2H, C1-H, C4-H).

Demethylation of 22 and 24

The *trans*-diol **22** (90 mg) was allowed to react with $AlCl_3$ (500 mg) in anhydrous chloroform solution (20 mL) for a period of 3 h at room temperature. Saturated oxalic acid solution (15 mL) was added and the solution was stirred for $1\frac{3}{4}$ h at room temperature. The aqueous phase was separated and extracted by chloroform, and the combined chloroform solutions, dried with anhydrous sodium sulfate and evaporated to dryness under reduced pressure, gave a red solid residue (50 mg), which was purified by precipitation from methylene chloride – ether; mp 225–228°C; ir: 3560 (C7-OH), 3450 (C9-OH), 3600–2600 (chelated phenols), 1720 ($COCH_3$), 1630 (chelated quinone), 1590 (aromatic); ^{1}H nmr: 2.222 (s, 3H, $COCH_3$), 2.307 (dd, 1H, C8-H_b, J_{8b8a} = 14.7 Hz, J_{8b7a} = 3.9 Hz), 2.881 (d, 1H, C7-OH, $J_{OH,7a}$ = 4.6 Hz), 2.943 (dd, 1H, C8-H_a, J_{8a8b} = 14 ***Hz,*** J_{8a7a} = 7.3 Hz), 4.561 (s, 1H, C9-OH), 5.583 (ddd, 1H, $J_{OH,7a}$ = 4.5 Hz, J_{7a8b} = 4.0 Hz, J_{7a8a} = 7.3 Hz), 7.849–7.878 (m, 2H, C2-H, C3-H), 8.235–8.370 (m, 2H, C1-H, C4-H), 12.994 (s, 1H, C6-OH), 13.081 (s, 1H, C10-OH); ms: 354 (M^+, 1%), 311 (M − $COCH_3$, 100%), 293 (M − $COCH_3$ − H_2O, 70%).

Demethylation of **24** to 4-demethoxy-10-nordaunomycinone (**4**) was carried out under identical condition with similar yield, and the crude product showed in tlc that **4** was the only demethylated product; mp 230–232°C; ir: 3560 (weak) (OH), 3430 (OH), 3560–2700 (chelated OH), 1715 ($COCH_3$), 1630 (chelated quinone), 1590 (aromatic); ^{1}H nmr (Fig. 4): 2.369 (s, 3H, $COCH_3$), 2.50 (dd, 1H, C8-H_a, J_{8a8b} = 10.75 Hz, J_{8a7b} = 3.96 Hz), 2.659 (dd, 1H, C8-H_b, J_{8b8a} = 10.74 Hz, J_{8a7b} = 7.4 Hz), 3.091 (d, 1H, C7-OH, $J_{OH,7b}$ = 3.8 Hz), 4.5 (s, 1H, C9-OH), 5.839 (ddd, 1H, C7-H_b, $J_{OH,7b}$ = 3.8 Hz, J_{7b8b} = 7.3 Hz, J_{7b8a} = 4.0 Hz), 7.842 (m, 2H, C2-H, C3-H), 7.872 (m, 2H, C1-H, C4-H), 12.956 (s, 1H, C6-OH), 13.017 (s, 1H, C10-OH).

Acknowledgements

Funding from NSERC of Canada and ABI Biotechnology Inc. is gratefully appreciated. The authors would like to thank Mr. Kirk Marat for nuclear magnetic resonance studies and Mr. Derek Wong for biological activities screening.

1. (*a*) H. Brockman. Fortschr. Chem. Org. Naturst. **21**, 121 (1963); (*b*) L. Ettinger, E. Gaumann, R. Hutter, W. Keller-Schierlein, F. Kradolfer, L. Neipp, V. Prelog, P. Reusser, and H. Zahner. Chem. Ber. **92**, 1867 (1959).
2. EORTC International Symposium. Adriamycin Review, Brussels. May, 1974. European Press Medikon. Ghent, Belgium. 1975.
3. F. Arcamone. Doxorubicin anticancer antibiotics. Medicinal Chemistry. Vol. 17. Academic Press, New York, 1981.
4. E. Hodgson, J. R. Bend, and R. M. Philpot. Rev. Biochem. Toxicol. **5**, 48 (1983).
5. F. Arcamone. Doxorubicin anticancer antibiotics. Medicinal Chemistry. Vol. 17. Academic Press, New York, 1981. Chap. 7. p. 261.
6. G. Cassinelli, F. DiMatteo, A. DiMarco, A. M. Casazza, C. Soranzo, and G. Pratesi. J. Antibiot. **33**, 1468 (1980).
7. F. Arcamone. Doxorubicin anticancer antibiotics. Medicinal Chemistry. Vol. 17. Academic Press, New York, 1981. Chap. 6. p. 209.
8. F. Arcamone. Doxorubicin anticancer antibiotics. Medicinal Chemistry. Vol. 17. Academic Press, New York, 1981. Chap. 6. p. 196.
9. E. M. Acton, G. L. Tong, C. W. Mosher, and R. L. Wolgemuth. J. Med. Chem. **27**, 638 (1984).
10. H. S. El Khadem. Anthracycline antibiotics. Academic Press, New York. 1982.
11. (*a*) C. M. Wong, W. Haque, H. Y. Lam, K. Marat, E. Bock, and A. Q. Mi. Can. J. Chem. **61**, 1788 (1983); (*b*) L. W. Lown and S. M. Sondhi. J. Org. Chem. **50**, 1413 (1985).
12. C. M. Wong, A. Q. Mi, J. Ren, W. Haque, H. Y. Lam, and K. Marat. Can. J. Chem. **62**, 1600 (1984).
13. C. M. Wong, A. Q. Mi, J. Ren, W. Haque, and K. Marat. Tetrahedron, **40**, 4789 (1984).
14. C. M. Wong. Cancer Chemotherapy Symposium, 69th Canadian Chemical Conference, Saskatoon. June, 1986.
15. F. Arcamone. Doxorubicin anticancer antibiotics. Medicinal Chemistry. Vol. 17. Academic Press, New York, 1981. Chap. 8.
16. (*a*) G. A. Flynn, M. J. Vaal, K. T. Stewart, D. L. Wenstrup, D. W. Beight, and E. H. Bohme. J. Org. Chem. **49**, 2252 (1984); (*b*) I. K. Khanna and L. A. Mitscher. Tetrahedron Lett. **26**, 691 (1985).
17. C. M. Wong, D. Popien, R. Schwenk, and J. TeRaa. Can. J. Chem. **49**, 2717 (1971).
18. (*a*) C. E. Coburn, D. K. Anderson, and J. S. Swenton. J. Chem. Soc. Chem. Commun. 987 (1982); (*b*) J. Org. Chem. **48**, 1455 (1983); (*c*) C. M. Wong, A. Q. Mi, H. Y. Lam, and K. Marat. Synth. Commun. **13**, 15 (1983).
19. R. T. Arnold and H. E. Zaugg. J. Am. Chem. Soc. **63**, 1317 (1941).

Can. J. Chem. Downloaded from www.nrcresearchpress.com by 78.46.186.204 on 09/07/12
For personal use only.

Target factor analysis of bond dissociation energies

DARRYL G. HOWERY[1] AND MATTHEW RUBENSTEIN
Department of Chemistry, The City University of New York, Brooklyn College, Brooklyn, NY 11210 U.S.A.

Received August 7, 1986

DARRYL G. HOWERY and MATTHEW RUBENSTEIN. Can. J. Chem. **65**, 1380 (1987).

Six data matrices of bond dissociation energies ranging from a 6 × 6 matrix involving only hydrocarbon radicals to a 14 × 14 matrix involving several types of radicals are target factor analyzed. The number of factors to reproduce the data near experimental error range from two to four for the six matrices. The hydrogen and fluorine radicals are shown to be the most unique radicals. Combination sets of vectors from the data matrices reproduce the data within experimental error, with the hydrogen, fluorine, and hydroxyl radicals being the most important ones. Using target testing, a few of the properties of the radicals are identified as basic factors.

DARRYL G. HOWERY et MATTHEW RUBENSTEIN. Can. J. Chem. **65**, 1380 (1987).

On a effectué une analyse par vecteurs spécifiques de six matrices de données d'énergies de dissociation de liaison qui vont d'une matrice 6 × 6 n'impliquant que des radicaux hydrocarbonés à une matrice 14 × 14 impliquant plusieurs types de radicaux. Pour les six matrices, il faut de deux à quatre facteurs pour reproduire lés données expérimentales en dedans des erreurs expérimentales. On démontre que les radicaux hydrogène et fluor sont les radicaux les plus typiques. Une combinaison d'ensembles de vecteurs des matrices de données permet de reproduire les données expérimentales en dedans des erreurs expérimentales; les radicaux hydrogène, fluor et hydroxyle sont les plus importants. Utilisant la méthode de la vérification des vecteurs spécifiques, on a identifié les propriétés des radicaux qui sont des facteurs de base.

[Traduit par la revue]

Can. J. Chem. Downloaded from www.nrcresearchpress.com by 78.46.186.204 on 09/07/12
For personal use only.

Introduction

The development of theoretical and empirical models for bond dissociation energies (BDE) is one of the most important objectives in modern chemistry (1). Though many correlations and theories for BDE have been proposed, general models which can account for observed BDE involving a diversity of radical types are not yet available. Factor analysis (FA) (2), a multivariate method for analyzing matrices of data, is particularly suited for correlating and modeling multifactor data such as BDE. A discussion of the methodology and applications of factor analysis in chemistry is given in Malinowski and Howery's monograph (2). Factor analysis can be applied to many kinds of chemical problems. For example, spectra of multicomponent solutions (3), properties of solvents (4), retention indices in gas–liquid chromatography (5), and solid-state nmr spectra (6) have been fruitfully studied using FA.

Factor analysis is particularly suited to studies of BDE. With FA, a bond dissociation energy can be characterized in terms of the properties of the two radicals resulting from the dissociation of the molecule. Specifically, a data matrix of BDE, [E], can be modeled via FA according to the equation:

$$[1] \quad [E] = [R_r][R_c]$$

where $[R_r]$ and $[R_c]$ are matrices involving the properties of the radicals associated with the rows and with the columns, respectively, of the data matrix. Abstract matrices which obey eq. [1] are calculated using principal-component analysis. Then, the number of fundamental factors responsible for the data can be determined by several methods. In addition, the abstract principal factors can be utilized to correlate the data by identifying groups of radicals which have similar behavior as well as individual radicals which have unique behavior. Finally, parameters of the radicals which represent the underlying factors influencing the BDE can be identified by a least-squares procedure called target testing. This last step of a factor analysis allows physical models for the BDE to be developed.

We report here some results from a factor analysis of bond dissociation energies involving 14 radicals of diverse properties. Using the various techniques of FA, we are able to correlate the data in several ways and to identify a few properties of the radicals which influence BDE.

Experimental section

Critically evaluated bond dissociation energies were furnished by Zavitsas.[2] A copy of the data matrix is available upon request. The values for the BDE which we used are in agreement with those reported by Egger and Cocks (7) usually within 1 kcal/mol, with our values generally being lower. Bonds involving all possible pairs of the 14 radicals listed in Table 1 were utilized to form a symmetrical 14 × 14 data matrix of BDE. In order to study the effects of the various groups of radicals, five symmetrical submatrices formed from the parent 14 × 14 matrix were also studied. The six problems studied with estimated experimental errors for each matrix are spelled out in the lower portion of Table 1.

A computer program in FORTRAN IV (8) was used to perform the factor analyses. All computations were conducted on an I.B.M. model 370/165 digital computer. The methodology employed is explained in detail in ref. 2, where particular emphasis is given to the techniques of an extended form of FA called target factor analysis.

Results and discussion

Number of factors

The number of factors to reproduce a data matrix near experimental error is a useful measure of the overall complexity of a problem. In the reproduction step of factor analysis, the complete set of least-squares principal-component factors is calculated and then, stepwise, reproduction is carried out using the first, most important, factor; the first and second factors together; the first three factors jointly; and so forth. For the correct, physically significant number of factors, the root-mean-square (rms) error for reproduction (calculated from a comparison of the original data with the FA reproduced data) is reasonably similar to the estimated experimental error.

Results for the six data matrices described in Table 1 are given in Table 2. The rms error for reproduction, the percentage of data points reproduced with errors exceeding the experi-

[1]To whom correspondence should be addressed.

[2]A. Zavitsas. Private communication.

TABLE 1. Radicals studied and description of problems

(*a*) Radicals

Symbol	Name	Symbol	Name
H	Hydrogen	F	Fluorine
Me	Methyl	Cl	Chlorine
Et	Ethyl	Br	Bromine
*i*Pr	Isopropyl	OH	Hydroxyl
*t*Bu	*tert*-Butyl	MeO	Methoxyl
Ph	Phenyl	MeCO	Acetyl
Bz	Benzyl	NH_2	Amine

(*b*) Problems

Designation[a]	Radicals involved	Estimated error (kcal/mol)
6 × 6	Me—Bz	2
7 × 7	H—Bz	2
9 × 9	Me—Br	2
10 × 10	H—Br	2
13 × 13	Me—NH_2	3
14 × 14	H—NH_2	3

[a]Indicates the dimensions of the data matrix.

mental error (listed in Table 1), and the magnitude of the largest error are all taken into account to arrive at the number of factors stated in the second column of Table 2. As the chemical complexity of a problem increases, the number of factors estimated from FA also increases. For example, the data for the 6 × 6 problem (hydrocarbon radicals only) reproduced well with only two factors, whereas the complete 14 × 14 matrix requires four factors. Adding a vector for the hydrogen radical to a matrix increases the rms error significantly, as seen, for example, by comparing the results for the 9 × 9 and the 10 × 10 problems. The group of four polar radicals, based on a comparison of results for the 10 × 10 and the 14 × 14 problems, also seem responsible for a major effect.

An approach based on a theory of error for abstract FA by Malinowski (9) can also be used to determine the number of factors. Malinowski found that a quantity called the factor indicator function usually has its minimum value at the correct number of factors. Further, for that number of factors, an estimate of the experimental error, called the real error, is predicted from the theory. In five of the six BDE problems, the indicator function exhibits a minimum value. The number of factors for which the indicator function has minimum values and the associated value for the real errors are given in the last two columns of Table 2. The number of factors indicated from the reproduction approach and from the theoretical approach are equivalent except for the 13 × 13 problem. In addition, the real errors from theory are reasonably close to the estimated experimental errors.

Combination of typical factors

A procedure called target combination is used to compress the information content of a data matrix into a much smaller matrix (3, 5). In the combination procedure, vectors from the data matrix, called typical vectors or typical factors, are tested in combination to determine which subsets of data columns best model the complete data matrix. The best model, which gives the smallest rms error in combination reproduction, is called the key combination set. For each of the six problems, all combinations of typical vectors, taken *n* at a time (where *n* for each problem is given in the second column of Table 2), were run to find the best model.

A summary of the results from the target combination procedure is shown in Table 3, in which are listed the rms errors and the radicals represented in each of the key sets. For each problem, the best model using typical factors has an rms error only slightly greater than the rms error calculated from reproduction using abstract, principal factors (column three of Table 2). The key combination sets are excellent models for the data. For instance, the rms error for the 14 × 14 problem using typical vectors is 1.41 kcal/mol, well within the estimated experimental error of 3 (from Table 1), and for practical purposes equivalent to the rms error of 1.33 (from Table 2) using the abstract factors. The methyl radical is incorporated in all but one of the five key combination sets, indicating that this radical best represents the group of hydrocarbon radicals in the overall model. Fluorine radical is the most important of the halogen radicals and the hydroxyl radical is the key radical in the group of four polar radicals, based on representations in the best combination models. Hydrogen radical is quite important in the 7 × 7 and 10 × 10 problems, being present in each of the five best combination sets for both problems. Fluorine radical occurs in nearly all of the five best models for the 9 × 9 through 14 × 14 problems. Finally, the key combination sets of typical factors for the 13 × 13 and 14 × 14 problems are chemically reasonable, consisting of a representative from each of the four types of radicals.

Target testing

Knowing the proper number of factors, we wish to transform the abstract, principal factors to factors having physical significance, called basic factors. A least-squares method called target testing is used to identify basic factors, one at a time. Parameters of the radicals are tested mathematically for possible identification with the fundamental influences on the BDE. A test vector representing the idea to be target tested is input and a predicted vector having the best least-squares fit to the target test vector is calculated. If the point-by-point agreement between the test vector and the predicted vector is satisfactory using chemical criteria, then the tested parameter is said to be a basic factor.

The uniqueness test is a simple, yet informative, target test designed to ascertain which radicals exhibit the most atypical behavior. A uniqueness test vector contains a "1" for the radical being tested for uniqueness and "0"'s for the remaining radicals on that test vector. A uniqueness test is run for each radical in each of the six problems. The radicals having the largest predicted uniqueness values are listed in Table 4. Predicted uniqueness values greater than say 0.75 are taken to indicate unique radicals. Thus, the fluorine radical, having by far the largest uniqueness value in the 14 × 14 problem, is a particularly important radical due to some property of a unique nature. Hydrogen radical in the 7 × 7 and 10 × 10 problems and the *t*-butyl radical in the 6 × 6 problem also exhibit unique behavior. Information from the uniqueness tests is reinforced by results from the target combination procedure. Invariably, the radicals which test as unique in Table 4 are identified as key radicals in Table 3.

Using target testing, the basic factors which control bond dissociation energies can be expressed in terms of the properties of the radicals forming the molecules. Nearly 50 candidates for basic factors, as well as the square, reciprocal and logarithm transforms of each test vector, were target tested one

Can. J. Chem. Downloaded from www.nrcresearchpress.com by 78.46.186.204 on 09/07/12
For personal use only.

TABLE 2. Number of factors based on the reproduction step and theoretical criteria

Problem[a]	Number of factors (reproduction)	rms error[b]	Percentage absolute errors > experimental error[a]	Largest error[b]	Number of factors (indicator function)	Real error[c]
6 × 6	2	0.66	0.0	1.78	[d]	0.81[b]
7 × 7	2	1.03	6.1	2.82	2	1.22
9 × 9	2	0.93	3.7	2.50	2	1.02
10 × 10	3	0.88	4.0	2.71	3	1.06
13 × 13	4	1.10	4.7	3.94	5	0.93
14 × 14	4	1.33	4.1	6.10	4	1.62

[a]See Table 1 for designations and experimental errors.
[b]Based on the number of factors indicated by reproduction (second column); kcal/mol.
[c]Based on the number of factors indicated by theory (sixth column); kcal/mol.
[d]Indicator function has no minimum.

TABLE 3. Key combination sets of typical factors

Problem[a]	rms error (kcal/mol)	Key radicals[a,b]
6 × 6	0.73	Me, *t*Bu
7 × 7	1.09	H, Et
9 × 9	0.99	Me, F
10 × 10	0.94	H, Me, F
13 × 13	1.17	Me, Ph, F, OH
14 × 14	1.41	Me, Ph, F, OH

[a]See Table 1 for designations.
[b]Radicals represented in best target-combination models.

TABLE 4. Summary of uniqueness tests

Problem[a]	Unique radicals (predicted uniqueness values)[a,b]
6 × 6	*t*Bu (0.76), Ph (0.44)
7 × 7	H (0.92)
9 × 9	F (0.77)
10 × 10	H (0.83), F (0.83)
13 × 13	F (0.90), OH (0.46)
14 × 14	F (0.87), OH (0.44)

[a]See Table 1 for designations.
[b]Only values greater than 0.40 are listed.

TABLE 5. Summary of selected target tests from the 14 × 14 problem using four factors

Property[a]	Example values[b] *i*Pr	Example values[b] MeCO	Points[c]	Fit[d]
Mass (R)	43	43	14	p
Group electronegativity (R)	2.39	1.93	14	f
Ionization potential (R)	7.90	8.08	14	g
Electron affinity (R)	1.0	ff	10	f
Unity	1.0	1.0	14	g
Carbon number (R)	3.0	2.0	14	p
Halogen uniqueness	0	0	14	p
Fluorine uniqueness	0	0	14	g
Number of electrons (A)[e]	13	14	12	f
Bond dissociation energy (RR)	77.7	67.2	14	f
Free energy of formation (RH)	−5.6	−32.0	14	p

[a]R = radical, A = atom of radical having unpaired electron, RR = molecule formed with same radical, RH = molecule formed with hydrogen radical. References 10 and 11 were particularly useful sources for physical-property data.
[b]Example values given for the two radicals: isopropyl (*i*Pr) and acetyl (MeCO). Missing value denoted by "ff" was free floated on the electron affinity vector for MeCO.
[c]Number of test values input on the test vector.
[d]Qualitative evaluation of the results of the target test: g = good agreement between the test and the predicted vectors, f = fair agreement (overall pattern predicted but a few points predicted poorly), p = poor agreement.
[e]Number of electrons on the atoms bonded to the atom having an unpaired electron.

at a time for the 13 × 13 and 14 × 14 problems. Parameters of the radicals which target test with fair or better fits between the test and predicted vectors are identified as basic factors. Some of the parameters tested are properties of the radicals, others are properties of the molecules formed from the radicals and a hydrogen radical (e.g., H_2 and CH_4), and still others are properties of the bonding atoms in the radicals (e.g., the oxygen atom in the hydroxyl radical).

Results for representative target tests from the 14 × 14 problem are summarized in Table 5. Shown for each parameter are the test values input on each test vector for the isopropyl and acetyl radicals, the number of points input on the test vector and a qualitative evaluation of the fit of the predicted vector with the test vector. Comparisons of the patterns and of the magnitudes for the test and predicted vectors led to the evaluation of fit given in the table. For example, a vector is considered to have a fair fit if the overall patterns in the test and predicted vectors are similar but one or a few test points are predicted with fairly large errors. Essentially all of the parameters which yielded good or fair fits are listed in the table. Since such a small number of the tested parameters appear to be basic factors, the detailed modeling of bond dissociation energies is indeed a difficult problem.

Details for four target tests from the 13 × 13 problem are shown in Table 6. The first and second tests, for ionization potential and group electronegativity to the 3/2 power, give acceptable fits between the test and predicted vectors. The two parameters of the radicals are basic factors. The power utilized for the group electronegativity vector was suggested by Zavitsas from empirical correlations.[2] Results for these two tests also illustrate that test vectors do not have to be complete. Some of the test points on a test vector can be left blank on the test vector, a procedure called free floating. For example, three test points (known values given in parentheses on the test vector) were deliberately free floated on both the ionization potential and the group electronegativity test in the table. Since the free floated points are predicted fairly accurately, the success of the two target tests is further validated. The third and

Can. J. Chem. Downloaded from www.nrcresearchpress.com by 78.46.186.204 on 09/07/12
For personal use only.

TABLE 6. Details of target tests for four properties in the 13 × 13 problem using four factors

Radical[a]	Ionization potential		GE$^{3/2}$[b]		Radical mass		Halogen uniqueness	
	Test[c]	Predicted	Test[c]	Predicted	Test	Predicted	Test	Predicted
Me	9.88	10.00	4.05	4.37	15	56.0	0.0	0.16
Et	(8.80)	9.50	3.88	4.05	29	53.5	0.0	0.14
*i*Pr	7.90	9.16	3.69	3.83	43	52.1	0.0	0.12
*t*Bu	7.42	8.39	3.58	3.44	57	49.0	0.0	0.06
Ph	9.90	10.29	(3.79)	4.28	77	57.1	0.0	−0.02
Bz	(7.78)	8.54	3.93	3.62	90	48.5	0.0	0.17
F	17.42	18.04	8.00	8.02	19	23.3	1.0	1.15
Cl	13.01	11.23	(5.43)	5.21	35	31.3	1.0	0.37
Br	11.84	8.87	4.64	4.19	80	31.6	1.0	0.20
OH	13.18	12.60	6.52	6.58	17	32.8	0.0	0.18
MeO	9.20	11.29	(6.27)	5.92	31	25.8	0.0	0.16
MeCO	8.08	7.26	2.68	2.62	43	51.2	0.0	−0.14
NH_2	(11.40)	11.26	5.07	5.15	16	24.3	0.0	0.21

[a]See Table 1 for designations.
[b]Group electronegativity of the radical.
[c]Known values in parentheses were free floated on the test.

fourth tests in the table, for the mass of the radical and for halogen-group uniqueness, do not show adequate agreement between the test and predicted vectors. These two parameters according to factor analysis are not basic factors.

Any property associated with the row-designee radicals in the data matrix (or with the column designees if the matrix were unsymmetrical) can be target tested. However, a vector involving a difference of properties, such as the difference of group electronegativities, cannot always be legitimately target tested. On the one hand, a test vector such as ($GE - GE_H$), which expresses the group electronegativity (GE) of the row-designee radicals relative to the constant value GE_H for the hydrogen radical, can be validly target tested. On the other hand, since factor analysis isolates the factors of the row designees from the factors of the column designees, any vector based on the difference between a property of the row designees and a property of a column designee cannot be validly tested. For example, a difference vector of the form ($GE_i - GE_j$) involving the ith row radical and the jth column radical of the data matrix, in which both GE's are varying along the test vector, should not be target tested.

Acknowledgments

A. Pollin and M. McAuliffe made useful contributions during the early phases of this research. We are grateful for partial support of this work from a PSC-BHE grant from the Faculty Research Award Program of the City University of New York and for the use of the facilities of the Computer Center of C.U.N.Y.

1. R. T. SANDERSON. Polar covalence. Academic Press, New York. 1983.
2. E. R. MALINOWSKI and D. G. HOWERY. Factor analysis in chemistry. John Wiley, New York. 1980.
3. E. R. MALINOWSKI, R. A. COX, and U. L. HALDNA. Anal. Chem. **56**, 778 (1984).
4. M. CHASTRETTE, M. RAJZMANN, M. CHANON, and K. F. PURCELL. J. Am. Chem. Soc. **107**, 1 (1985).
5. R. B. SELZER and D. G. HOWERY. J. Chromatogr. **115**, 139 (1975).
6. D. W. KORMOS and J. S. WAUGH. Anal. Chem. **55**, 633 (1983).
7. K. W. EGGER and A. T. COCKS. Helv. Chim. Acta, **56**, 1516 (1973).
8. E. R. MALINOWSKI, D. G. HOWERY, P. E. WEINER, J. M. SOROKA, P. T. FUNKE, R. B. SELZER, and A. LEVINSTONE. "FACTANAL", Program 320, Quant. Chem. Program Exchange, Indiana Univ., Bloomington, IN, U.S.A. 1976.
9. E. R. MALINOWSKI. Anal. Chem. **49**, 612 (1977).
10. V. I. VEDENEEV. Bond energies, ionization potentials and electron affinities. St. Martin's Press, New York. 1966.
11. R. C. WEAST (*Editor*). Handbook of chemistry and physics. 53rd ed., Chemical Rubber Co. Press, Cleveland, OH, U.S.A. 1972.

Can. J. Chem. Downloaded from www.nrcresearchpress.com by 78.46.186.204 on 09/07/12
For personal use only.

Major saponins from the starfish *Asterias forbesi*. Complete structures by nuclear magnetic resonance methods

JOHN A. FINDLAY AND MAHESH JASEJA
Department of Chemistry, University of New Brunswick, Fredericton, N.B., Canada E3B 6E2
D. JEAN BURNELL
Department of Chemistry, Memorial University of Newfoundland, St. John's, Nfld., Canada A1B 3X7
AND
JEAN-ROBERT BRISSON
Division of Biological Sciences, National Research Council of Canada, 100 Sussex Drive, Ottawa, Ont., Canada K1A 0R6

Received December 10, 1986

JOHN A. FINDLAY, MAHESH JASEJA, D. JEAN BURNELL, and JEAN-ROBERT BRISSON. Can. J. Chem. **65**, 1384 (1987).

The structures of the two major saponins isolated from the starfish *Asterias forbesi* have been deduced totally by nuclear magnetic resonance methods applied to the undegraded molecules. The structure of forbeside A, 6α-*O*-{β-D-galactopyranosyl-(1→3)-β-D-fucopyranosyl-(1→2)-β-D-galactopyranosyl-(1→4)-[β-D-quinovopyranosyl-(1→2)]-β-D-xylopyranosyl-(1→3)-β-D-quinovopyranosyl}-20-hydroxy-23-oxo-5α-cholest-9(11)-en-3β-yl sodium sulfate, was deduced principally from ^{1}H 2D-COSY, *J*-resolved, nuclear Overhauser enhancement and selected decoupling experiments. The structure of forbeside B, 6α-*O*-{β-D-quinovopyranosyl-(1→2)-β-D-galactopyranosyl-(1→4)-[β-D-quinovopyranosyl-(1→2)]-β-D-xylopyranosyl-(1→3)-β-D-quinovopyranosyl}-20-hydroxy-23-oxo-5α-cholest-9(11)-en-3β-yl sodium sulfate, was deduced principally from 2D-COSY, HCORR, RECSY, and NOESY experiments.

JOHN A. FINDLAY, MAHESH JASEJA, D. JEAN BURNELL et JEAN-ROBERT BRISSON. Can. J. Chem. **65**, 1384 (1987).

Faisant appel à des méthodes de résonance magnétique nucléaire appliquées à des molécules qui n'ont pas été dégradées, on a déterminé d'une façon complète les structures des deux saponines principales qui ont été isolées de l'étoile de mer *Asterias forbesi*. Pour la résolution de la structure de la forbeside A, le sulfate de sodium du *O*-{β-D-galactopyrannosyl-(1→3)-β-D-fucopyrannosyl-(1→2)-β-D-galactopyrannosyl-(1→4)-[β-D-quinovopyrannosyl-(1→2)]-β-D-xylopyrannosyl-(1→3)-β-D-quinovopyrannosyl}-6α hydroxy-20 oxo-23 5α-cholestène-9(11) yle-3β, on a principalement fait appel à des expériences de ^{1}H 2D-COSY, résolues pour *J*, d'effets Overhauser nucléaire et de découplages sélectifs. Pour déduire la structure de la forbeside B, le sulfate de sodium du *O*-{β-D-quinovopyrannosyl-(1→2)-β-D-galactopyrannosyl-(1→4)-[β-D-quinovopyrannosyl-(1→2)]-β-D-xylopyrannosyl-(1→3)-β-D-quinovopyrannosyl}-6α hydroxy-20 oxo-23 5α-cholestène-9(11) yle-3β, on a principalement fait appel à des expériences de 2D-COSY, HCORR, RECSY et de NOESY.

[Traduit par la revue]

In view of the widespread interest (1) in the biological functions, toxicity, and pharmacology of starfish saponins (asterosaponins), we recently embarked on structural studies on the asterosaponins of *Asterias forbesi*. This is a common species on the Atlantic seaboard and, in particular, in the Bay of Fundy.

Shimizu (2) reported antiviral activity in three glycosidic substances (probably asterosaponins) from *A. forbesi*, and Goldsmith and Carlson (3) demonstrated that analgesic, hypotensive, and anti-inflammatory properties were associated with asterosaponins from this species. An antimitotic substance from the ovaries of *A. forbesi* reported by Heilbrunn *et al.* (4) in 1954 was possibly an asterosaponin.

Previous chemical studies on *A. forbesi* have been limited to the structures of the steroidal products of hydrolysis of its asterosaponin mixture. Shimizu (5) isolated 3β,6α-dihydroxy-5α-pregn-9(11)-en-20-one (asterone) from the hydrolysate, and ApSimon *et al.* (6) reported asterone and the corresponding triol (asterogenol) from hydrolysed asterosaponin from the same organism.

A methanol extract of specimens collected in Passamaquoddy Bay (August 1984) was chromatographed on an Amberlite XAD2 column to yield a crude saponin-containing fraction, the chloroform/methanol (6:4) soluble portion of which was subjected to preparative layer chromatography (plc) on silica gel to provide three fractions, which, after further purification on reversed phase plc and high performance liquid chromatography (hplc), yielded four pure saponins that were designated forbesides A, B, C, and D (~2:3:1:1). This paper deals with the structures of A and B, which were deduced entirely by nuclear magnetic resonance methods.

One-dimensional nuclear magnetic resonance (nmr) methods have yielded limited information for the determination of complete structure and stereochemistry of complex saponins. No systematic method for complete structural analysis has resulted, largely because of the severe resolution problems encountered, since most oligosaccharide proton signals fall within a 2-ppm chemical shift range and substantial overlap of multiplets occurs.

In view of this, it has generally been necessary to resort to permethylation and hydrolysis experiments to determine the sugar sequence and the sites of interglycosidic linkage (7–11). The whole process is somewhat tedious and also consumes saponin, which is often very difficult to separate and purify and may be better employed in biological evaluation experiments.

These difficulties can be overcome by the use of modern high field 2D nmr experiments. The critical requirement is the unambiguous assignment of ^{1}H resonances, especially in the oligosaccharide portion. We have used two-dimensional (2D) nuclear proton correlation (COSY) (12), relayed correlation spectroscopy (RECSY) (13), *J*-resolved (12), nuclear Overhauser enhancement (NOESY) (14), and one-dimensional nuclear Overhauser enhancement experiments to determine the complete sugar sequence and the sites of interglycosidic linkage, thus obviating the need for hydrolysis reactions. In one case (forbeside B), we have utilized a hydrogen–carbon correlation (HCORR) (15) experiment to arrive at unambiguous assign-

Can. J. Chem. Downloaded from www.nrcresearchpress.com by 78.46.186.204 on 09/07/12
For personal use only.

TABLE 1. ^{1}H nuclear magnetic resonance assignments and nuclear Overhauser enhancement data for forbeside A oligosaccharide moiety (C_5D_5N/D_2O 5:1)

Carbon		δ (ppm)	J (Hz)	Signals irradiated/% enhancement					
				Q′1	X1	Q″1	G′1	F1	G″1
Q′	1	4.826	7.7	—					
	2	3.983[a]	7.7, 8.4	5.0	(8.7)[d]				
	3	3.885[a]	9.0, 8.4	11.7	22.0				
	4	3.558	9.0, 9.3	4.0	3.3				
	5	3.714	6.1, 9.3	14.3	3.6				
	6	1.594	6.1	3.7					
X	1	5.067	7.6		—				
	2	4.001	7.6, 8.6		(8.7)[d]	16.7			
	3	4.223[d]	8.9, 8.6		11.2	(3.2)[d]	(19.5)[d]		
	4	4.218[a]	8.9, 9.4, 4.9[b]		4.3	(3.2)[d]	(19.5)[d]		
	5	3.786	11.7, 9.4[b]		12.0		5.0		
	5	4.411	11.7, 4.9[b]		7.3				
Q″	1	5.163	7.3			—			
	2	4.061[a]	7.3, 9.6			(15.2)[d]			
	3	4.094[a]	8.6, 9.6			(15.2)[d]			
	4	3.951	8.6, 9.1						
	5	3.692	6.2, 9.1			16.0			
	6	1.831	6.2			3.6			
G′	1	4.921	7.6[b]				—		
	2	4.405	7.6, 9.5[b]				(16.7)[d]	20.8	
	3	4.118	2.9, 9.5[b]				13.2	3.1	
	4	4.436	2.9, 0.6[b]				(16.7)[d]		
	5	4.041	6.7, 0.6, 5.5[b]				13.6		
	6_A	4.401	6.7, 11.1[b]						
	6_B	4.282	5.5, 11.1[b]				2.6		
F	1	4.857	7.8[b]					—	
	2	4.514	7.8, 9.9[b]					5.0	
	3	4.073	2.9, 9.9[b]					8.2	4.5
	4	4.202	2.9, 0.4					4.7	(5.6)[d]
	5	3.570	6.3, 0.4					11.3	
	6	1.391	6.3					3.1	
G″	1	5.211	7.7						—
	2	4.518	7.7, 9.5						3.0
	3	4.171	3.2, 9.5						(5.6)[d]
	4	4.525	3.2, 0.4[c]						3.0
	5	4.114	6.7, 0.4[c], 5.6						4.2
	6_A	4.419[a]	6.7, 11.3						1.4
	6_B	4.376[a]	5.6, 11.3						

[a]Calculated values (2nd order).
[b]Connectivity corroborated by decoupling.
[c]Estimate (signal overlap).
[d]Signals coincident.

Can. J. Chem. Downloaded from www.nrcresearchpress.com by 78.46.186.204 on 09/07/12
For personal use only.

ment of ^{13}C chemical shifts. In the past the ^{13}C chemical shift assignments in the oligosaccharide moiety of saponins have been made mainly by comparisons with reference substances (10, 16).

2D nuclear magnetic resonance has enjoyed much success in the structural elucidation of a variety of natural products (16–20). In this paper we illustrate the utility of 2D techniques for the complete structural elucidation of marine saponins.

The 500-MHz ^{1}H nmr spectrum (pyridine-d_5/D_2O, 5:1) of forbeside A shows six anomeric proton doublets (see Table 1), while multiplets due to oligosaccharide ring protons appear in the region δ 3.5–4.6 ppm. In the upfield region are methyl doublets at δ 1.391 (6.3 Hz), 1.594 (6.1 Hz), and 1.831 (6.2 Hz) indicative of the presence of three 6-deoxy sugars, in addition to signals characteristic of the 18, 19, 21, 25, and 27 thornasterol A methyl groups (21).

Using 2D-COSY, *J*-resolved, nOe, and selected decoupling experiments, it has been possible to establish the connectivity of all proton resonances in the aglycone and the oligosaccharide side chain. A complete inventory of proton chemical shift assignments has thus been generated for the first time for this aglycone and is contained in Table 2. Table 1 shows the assignments for the oligosaccharide moiety. Thus the nature of the aglycone, the sugar units, their stereochemistry, and sequence have been deduced solely from ^{1}H nmr data. As an illustration, Fig. 1 shows the 2D-COSY spectrum from δ 3.30–5.30 ppm for forbeside A. The anomeric proton Q′1 at δ 4.826 is coupled to Q′2H at δ 3.983, which in turn is coupled

Can. J. Chem. Downloaded from www.nrcresearchpress.com by 78.46.186.204 on 09/07/12
For personal use only.

TABLE 2. Chemical shift data for aglycone moieties of forbesides A and B

	Forbeside A		Forbeside B	
C	$\delta^{H\,a}$	$\delta^{C\,b}$	$\delta^{C\,c}$	$\delta^{H\,c}$
1	1.38, 1.61	35.10	35.13	1.30, 1.58
2	2.80, 1.89	28.27	28.29	2.10, 1.37
3	4.94	75.26	75.27	3.85
4	3.40, 1.74	29.40	29.42	2.35, 1.00
5	1.49	48.37	48.40	1.04
6	3.81	78.01	78.08	3.42
7	1.27, 2.66	40.41	40.44	0.82, 2.21
8	2.09	34.52	34.56	1.97
9		145.02	145.11	
10		37.63	37.67	
11	5.20	115.81	115.90	5.23
12	2.08, 2.28	41.45	41.49	2.09, 1.92
13		40.62	40.66	
14	1.26	53.17	53.22	1.12
15	2.24, 1.79	22.19	22.23	1.85, 1.53
16	1.73, 1.59	24.31	24.34	1.63, 1.12
17	0.90	58.14	58.15	1.55
18	1.01	12.95	12.98	0.70
19	0.93	18.95	18.98	0.85
20		72.50	72.60	
21	1.62	26.17	26.22	1.20
22	2.86, 2.69	54.78	54.83	2.35, 2.52[d]
23		210.50	210.56	
24	2.49, 2.42	53.01	53.05	2.38, 2.32[d]
25	2.20	23.55	23.59	1.96
26	0.90	22.32	22.36	0.80
27	0.91	22.19	22.23	0.80

[a]In pyridine-d_5/D_2O (5:1) 13 mg/0.4 mL at 30°C.
[b]In dimethylsulfoxide-d_6 13 mg/0.4 mL at 30°C.
[c]In dimethylsulfoxide-d_6 30 mg/0.4 mL at 30°C.
[d]Tentative assignment.

to Q′3H at δ 3.885. The latter is coupled to Q′4H at δ 3.358, which is coupled to Q′5 at δ 3.714, which in turn is coupled to a methyl doublet at δ 1.594. From the coupling constant data (Table 1), it is evident that these signals must emanate from a quinovose (Q′) (6-deoxyglucose) moiety. That this unit is linked via a β-anomeric oxygen to C6 of the aglycone is revealed by nOe experiments. Figure 2 shows the δ 3.4–5.2 portion of the nOe difference spectra resulting from irradiation at the anomeric protons. Thus, upon irradiation of Q′1H (some irradiation at F1H is also occurring), substantial enhancement is noted for protons at Q′3 and Q′5 and lesser amounts at Q′2H, Q′4H, and Q′6H corroborating the stereochemistry deduced from coupling constant data. In addition, one notes the largest nOe is to a signal at δ 3.81 corresponding to 6βH of the aglycone while lesser but significant enhancements occur at signals for protons due to 4α, 4β, 5α, 7α, 7β, and 8β. Irradiation of the signal at δ 5.067, due to the xylose unit anomeric proton X1H, in addition to causing the anticipated enhancement at X2H, X3H, X4H, X5α, and X5β, gave a large enhancement (22%) of the signal for Q′3H and lesser enhancements for Q′2H, Q′4H, and Q′5H. Thus it is abundantly clear that the xylose unit X is connected via a β anomeric linkage to the Q′3 carbon. In like manner the nature and sequencing of the remaining sugars was determined, and their stereochemistry corroborated by nOe experiments. The structure **1**, 6α-*O*-{β-D-galactopyranosyl-(1→3)-β-D-fucopyranosyl-(1→2)-β-

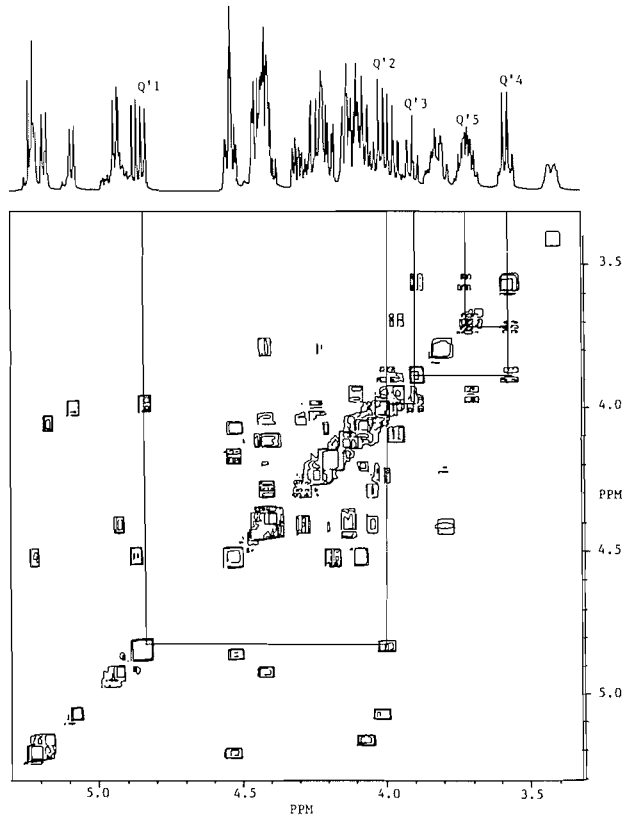

FIG. 1. 2D Nuclear proton correlation (COSY) spectrum (δ 3.30, 5.30 ppm) of forbeside A.

D-galactopyranosyl-(1→4)-[β-D-quinovopyranosyl-(1→2)]-β-D-xylopyranosyl-(1→3)-β-D-quinovopyranosy}-20-hydroxy-23-oxo-5α-cholest-9(11)en-3β-yl sodium sulfate, is assigned to forbeside A.

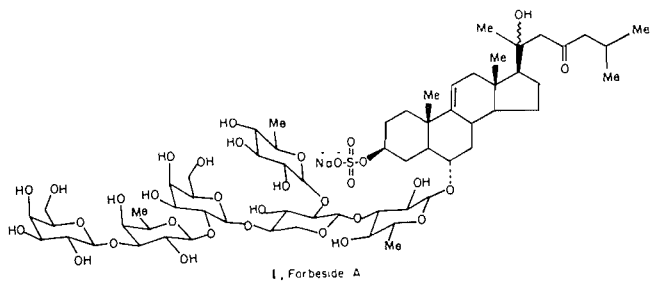

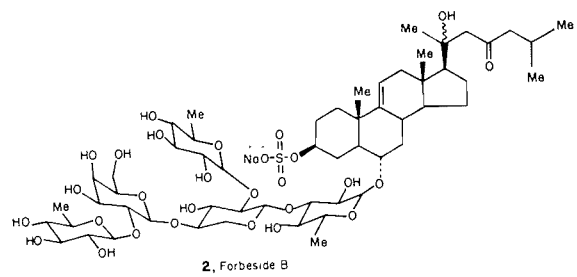

This structure is identical with that reported by Itakura *et al.* (10) for the saponin versicoside A isolated from *Asterias amurensis* and deduced chiefly from ^{13}C nmr, mass spectrometric data, and enzymatic hydrolyses experiments. Our ^{13}C nmr and FAB mass spectral data for forbeside A are in excellent agreement with those reported for versicoside A. The positive ion FAB mass spectrum of forbeside A shows pseudomolecular ion peaks at m/z 1429.4 (M + H) and 1451.6 (M + Na), which,

Can. J. Chem. Downloaded from www.nrcresearchpress.com by 78.46.186.204 on 09/07/12
For personal use only.

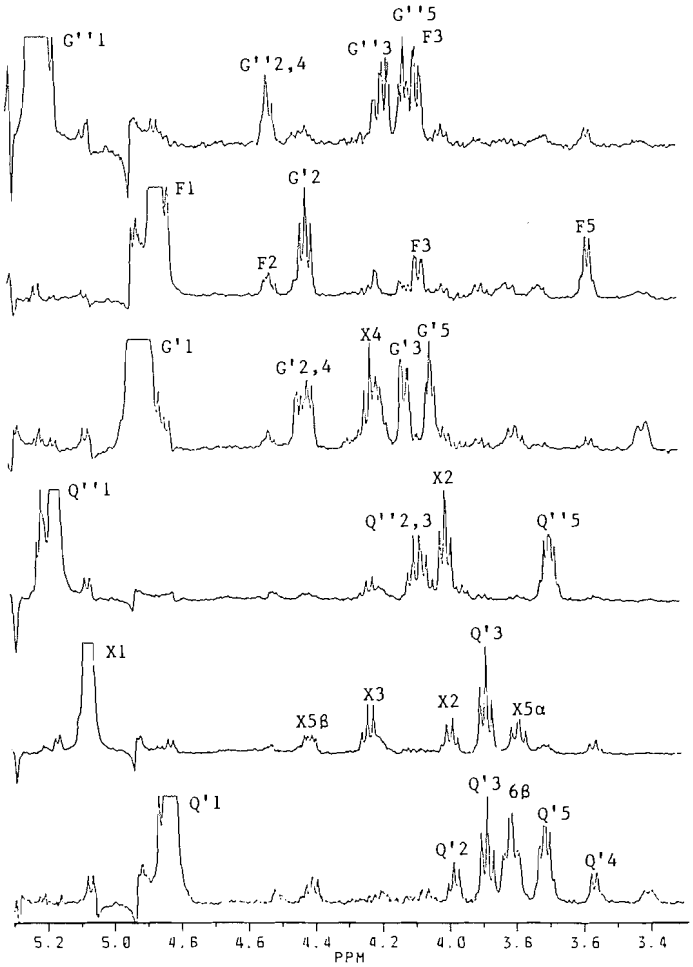

FIG. 2. Nuclear Overhauser enhancement difference spectra for forbeside A from successive irradiations of anomeric protons Q'1, X1, Q''2, G'1, F1, and G''1.

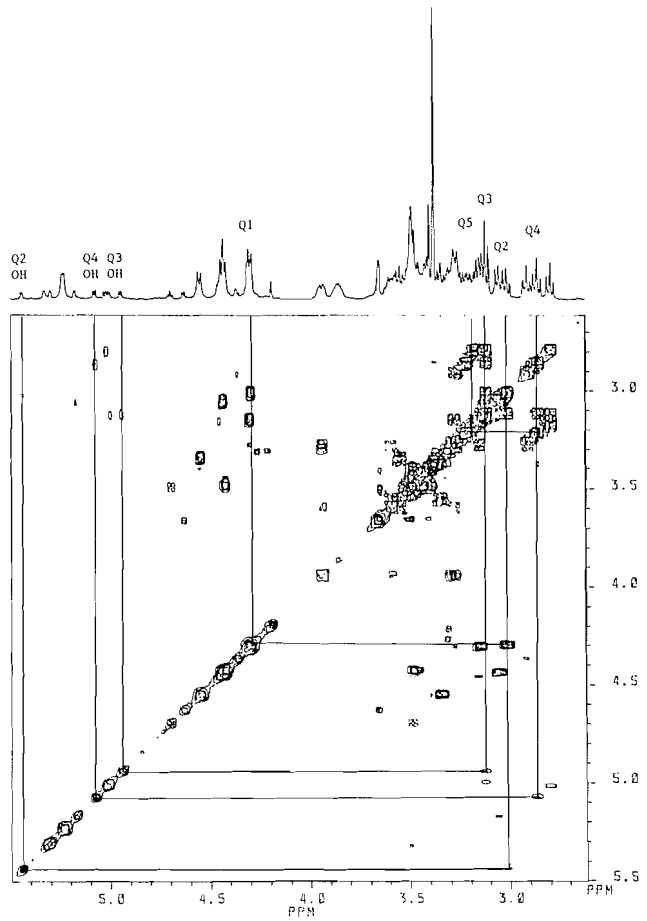

FIG. 3. 2D-COSY spectrum of forbeside B showing connectivity of protons in quinovose (Q''') unit.

in conjunction with ^{13}C data, confirm the molecular formula $C_{62}H_{101}O_{33}SNa$.

The structure of forbeside B, the second major saponin from *A. forbesi*, has been deduced also by nmr methods, employing 2D-COSY, HCORR, RECSY, and NOESY experiments.

Since forbeside B appeared to be sensitive to pyridine, prior to achieving final purification, most of the spectra were recorded in dimethyl sulfoxide-d_6. Table 2 contains a summary of chemical shift assignments for all carbon atoms and protons belonging to the aglycone of forbeside B derived from ^1H, ^{13}C, distortionless enhancement by polarization transfer (DEPT) analysis, and HCORR experiments. The virtually identical carbon chemical shifts for the aglycone moieties of forbesides A and B show they possess the same thornasterol A aglycone.

Table 3 contains the carbon and proton chemical shift assignments for the oligosaccharide moiety of forbeside B. The proton assignments for each sugar moiety were deduced from the 2D COSY experiment as in the case of forbeside A. For example, Fig. 3 shows the 2D COSY spectrum from δ 2.2 to 5.5 ppm. Starting from the anomeric proton signal Q'''1 at δ 4.29, one can trace out the complete *J* connectivity pathway to methyl signal Q'''6 establishing the chemical shifts of each proton in the sugar unit Q'''. The coupling constant values (Table 3), obtained from a 2D-*J* resolved experiment, show the deoxy hexose unit Q''' to be a quinovose unit.

The proton chemical shift assignments for the oligosaccharide chain were further corroborated by RECSY experiment. This assisted in establishing connectivities between remote nuclei belonging to the same ring spin system and thus provided an unambiguous chemical shift assignment of protons belonging to each saccharide unit. The contour plot shown in Fig. 4 illustrates the utility of this method. In it one can see peaks directly connecting resonances due to X1H, X2H, X3H, X4H, and X3H, X4H, X5Hα, X5Hβ, thus completing the connectivity pathway of protons in the xylose ring system.

From Table 4, which summarizes significant nOe effects as determined from a 2D-NOESY experiment, it is evident that sugar Q' is linked to the aglycone at C6 and that Q'3H and Q'5H are *cis* to Q'1H, while Q'2H and Q'4H are *trans* to Q'1H. Thus, in view of the coupling constant values (Table 3), it is evident that the first sugar directly attached to the aglycone is a quinovose unit. The nOe correlation between Q'3H and X1H shows sugar X is attached to the quinovose unit Q' at Q'3 position via an interglycosidic linkage. The stereochemistry and sequencing of the remaining sugars follow from a similar analysis of the remaining data.

To improve the quality of the nmr spectra of forbeside B, the sample was exchanged several times with D_2O prior to dissolution in DMSO-d_6. This resulted in an array of 12 partially exchanged hydroxyl doublets in the downfield region (δ 4.3–5.3 ppm), which from COSY and RECSY spectra could each be assigned without ambiguity to their respective secondary proton coupling partners (see Table 3) and provided an independent corroboration of the substitution pattern of the sugar units

TABLE 3. Nuclear magnetic resonance data for oligosaccharide moiety of forbeside B (in DMSO-d_6)

Sugar/carbon	No.	$\delta^{OH\,a}$ (ppm)	δ^{H} (ppm)	J_{XY} (Hz)[b]	$\delta^{C\,c}$ (ppm)
Q′	1		4.30	$J_{(1,2)} = 7.2$	104.7
(Quinovose)	2	4.45	3.15	$J_{(2,3)} = 8.9$	71.9
	3		3.28	$J_{(3,4)} = 9.1$	87.8
	4	4.37	2.90	$J_{(4,5)} = 9.1$	72.8
	5		3.25	$J_{(5,6)} = 6.0$	70.8
	6		1.14		17.8
X	1		4.54	$J_{(1,2)} = 7.3$	102.5
(Xylose)	2		3.33	$J_{(2,3)} = 9.3$	82.5
	3	5.28	3.54	$J_{(3,4)} = 9.1$	73.9
	4		3.59	$J_{(4,5)} = 4.8$	77.0
	5		α 3.29		63.0
			β 3.93		
Q″	1		4.43	$J_{(1,2)} = 7.2$	105.1
(Quinovose)	2	5.17	3.03	$J_{(2,3)} = 8.9$	74.7
	3	4.94	3.11	$J_{(3,4)} = 9.1$	75.6
	4	5.08	2.85	$J_{(4,5)} = 9.1$	74.5
	5		3.20	$J_{(5,6)} = 6.0$	72.4
	6		1.18		17.2
G	1		4.42	$J_{(1,2)} = 7.2$	104.6
(Galactose)	2		3.47	$J_{(2,3)} = 9.4$	81.4
	3	4.55	3.40	$J_{(3,4)} = 2.4$	75.1
	4	4.62	3.64		67.3
	5	4.30	3.51	$J_{(5,6A)} = 4.9$	72.9
	6		A 3.40	$J_{(6A,6B)} = 10.4$	60.1
			B 3.51		
Q‴	1		4.29	$J_{(1,2)} = 7.2$	102.8
(Quinovose)	2	5.45	3.00	$J_{(2,3)} = 8.9$	75.0
	3	4.99	3.11	$J_{(3,4)} = 9.1$	75.2
	4	5.05	2.80	$J_{(4,5)} = 9.3$	75.0
	5		3.17	$J_{(5,6)} = 6.2$	72.9
	6		1.10		17.9

[a]From COSY and RECSY data.
[b]Determined by 1D spectrum and 2D-*J* resolved experiments.
[c]Determined by ^1H, ^{13}C, 2D heterocorrelated experiments.

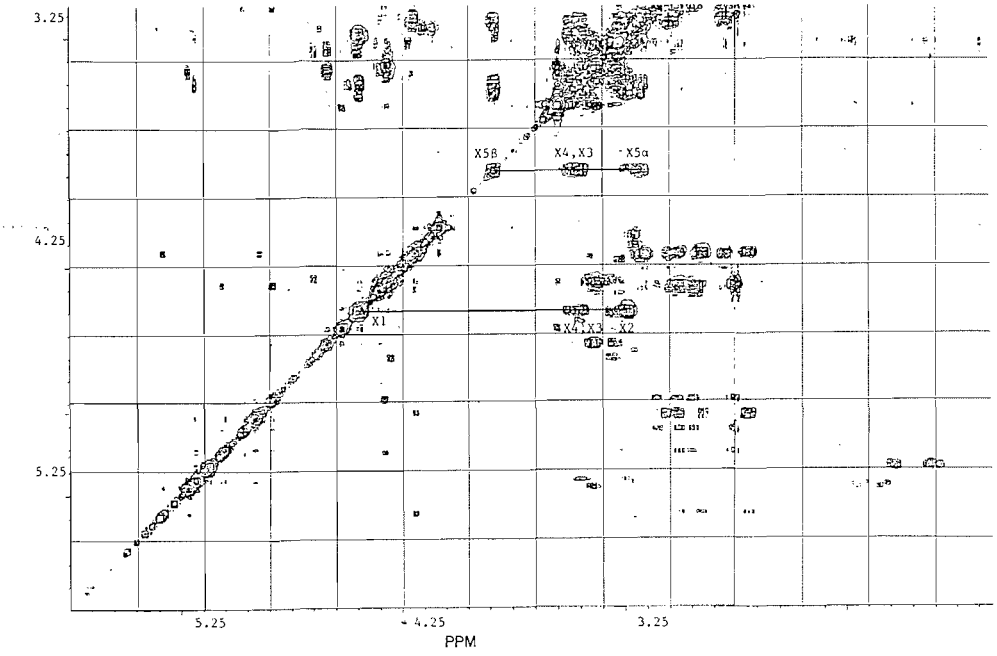

FIG. 4. Portion of relayed correlation (RECSY) spectrum of forbeside B showing connectivity of xylose unit protons.

Can. J. Chem. Downloaded from www.nrcresearchpress.com by 78.46.186.204 on 09/07/12
For personal use only.

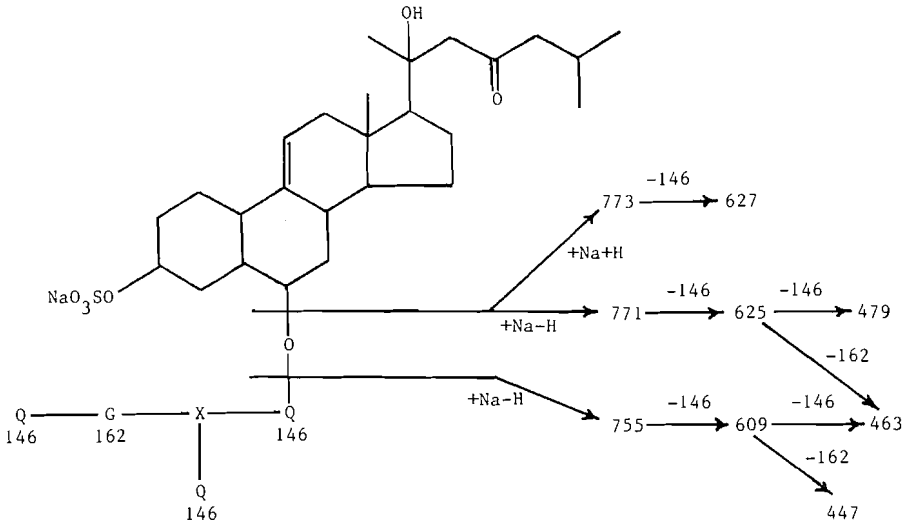

1289(100)	M + Na ($C_5H_{91}O_{28}SNa$)
1189(60)	M + Na − $C_6H_{10}O$ (aglycone sidechain)
1169(65)	M + Na − $NaSO_4H$
1143(18)	M + Na − $C_6H_{10}O_4$ (Q)
1069(75)	M + Na − $NaSO_4H$ − $C_6H_{10}O$
1023(26)	M + Na − $NaSO_4H$ − $C_6H_{10}O_4$ (Q)
981(18)	M + Na − $C_6H_{10}O_4$ (Q) − $C_6H_{10}O_5$ (G)
877(12)	M + Na − $NaSO_4H$ − 2 × $C_6H_{10}O_4$ (2Q)
861(18)	M + Na − $NaSO_4H$ − $C_6H_{10}O_4$ (Q) − $C_6H_{10}O_5$ (G)

Major significant ions from positive ion spectrum.

FIG. 5. FAB Mass spectral fragmentation of forbeside B.

and confirmed the sites of glycosidic linkages established by NOESY experiments.

We thus conclude that forbeside B possesses structure **2**, 6α-*O*-{β-D-quinovopyranosyl-(1→2)-β-D-galactopyranosyl-(1→4)-[β-D-quinovopyranosyl-(1→2)]-β-D-xylopyranosyl-(1→3)-β-D-quinovopyranosyl}-20-hydroxy-23-oxo-5α-cholest-9(11)en-3β-yl sodium sulfate. This is the same structure that has been assigned to glycoside B_2 from *A. amurensis* by Ikegami *et al.* (11) principally on the basis of hydrolysis products following permethylation experiments. No spectral data for the intact glycoside B_2 have appeared in the literature.

The FAB mass spectra of forbeside B provide corroboration for a number of its features in addition to its elemental composition $C_{56}H_{91}O_{28}SNa$ (Mol. Wt. 1266), which was revealed by the base peak at *m/z* 1289 (M + Na) in the +ve ion spectrum and by peaks at 1265 (M − H) and 1243 (M − Na) in the −ve ion spectrum. Significant ions at *m/z* 1023, 877, and 861 in the +ve ion spectrum (Fig. 5) are consistent with the presence of two terminal quinovose units, one of which is attached to a galactose moiety. The fragmentation patterns M + Na → 773 → 627, M + Na → 771 → 625 → 479, and M + Na → 755 → 609 → 463 are in full agreement with the sugar sequence deduced from nmr data. Other significant fragments correspond to dealdolization of the sidechain, loss of $NaSO_4H$, quinovose, and quinovose-galactose from the base peak. We have not noted distinctive fragments corresponding to these latter in the FAB mass spectrum of forbeside A, which is very similar to that published for versicoside A (10). Nor are they featured in the FAB mass spectral data reported for thornasteroside A (10). The latter differs from forbeside B only by the presence of a fucose (6-deoxygalactose) unit in place of Q‴ in structure **1**.

TABLE 4. Nuclear Overhauser enhancement data for oligosaccharide chain of forbeside B from NOESY experiments (DMSO-d_6)

Sugar		Chemical shift correlation through space coupling $\delta(y)_i$ (ppm)	$\delta(x)_j$ (ppm)
Q′	1[a]	4.30 (Q′1)	3.28 (Q′3)
(Quinovose)	2[b]	4.30 (Q′1)	3.25 (Q′5)
	3[c]	4.30 (Q′1)	3.42 (6H of aglycone)
X	1[a]	4.54 (X1)	3.54 (X3)
(Xylose)	2[b]	4.54 (X1)	3.29 (X5)
	3[c]	4.54 (X1)	3.28 (Q′3)
Q″	1[a]	4.43 (Q″1)	3.11 (Q″3)
(Quinovose)	2[b]	4.43 (Q″1)	3.20 (Q″5)
	2[c]	4.43 (Q″1)	3.33 (X2)
G	1[a]	4.42 (G1)	3.40 (G3)
(Galactose)	2[b]	4.42 (G1)	3.51 (G5)
	3[c]	4.42 (G1)	3.59 (X4)
Q‴	1[a]	4.29 (Q‴1)	3.11 (Q‴3)
(Quinovose)	2[b]	4.29 (Q‴1)	3.17 (Q‴5)
	3[c]	4.29 (Q‴1)	3.40 (G3)

[a]Intraresidual 1–3 axial–axial coupling.
[b]Intraresidual 1–5 axial–axial coupling.
[c]Interresidual coupling via glycosidic bond.

It is apparent from the foregoing that the complete structure and relative stereochemistry of starfish saponins can be obtained by appropriate combinations of 1D and 2D nmr experiments. It should be emphasized that this procedure is viable even when limited amounts of material are available; in the case of forbe-

Can. J. Chem. Downloaded from www.nrcresearchpress.com by 78.46.186.204 on 09/07/12
For personal use only.

side A only 13 mg of pure material was used for all nmr experiments. The minor saponins, forbesides C and D, are currently under investigation.

Experimental

Isolation of saponins

The starfish, *Asterias forbesi*, were collected on the shores of Passamaquoddy Bay, Bay of Fundy, in August 1984 and frozen prior to extraction. Frozen animals (20 kg wet wt) were defrosted, chopped into small pieces, and placed in vats containing methanol. After 24 h the solvent was decanted and replaced with fresh methanol. This was repeated three times and the total aqueous methanolic extract (8 L) was filtered and concentrated on a rotary evaporator at 30°C until all methanol was removed. The aqueous extract thus obtained was introduced onto an XAD-2 Amberlite resin (1 kg, mesh 30–50) column. After elution with water until halide ion was no longer detected, the column was eluted with a methanol/water gradient. The combined 80–100% methanol/water fractions contained saponins and were evaporated to dryness at 30°C on a rotary evaporator. The crude saponin residue was stirred for 1 h with chloroform/methanol (1 L, 3:2) and filtered. The filtrate was evaporated to dryness at 30°C and then dissolved in the minimum amount of water and lyophilized, giving the saponin mixture (8.1 g) as a yellow/beige powder.

A portion (3 g) of the saponin mixture thus obtained was chromatographed on precoated preparative tlc silica gel (F-254, 1 mm) plates (~90 mg/plate) using chloroform/methanol/water (66:44:5) as solvent. The following fractions were obtained:

Fraction (mg)	R_f
1 (200)	0.41–0.50
2 (175)	0.31–0.40
3 (186)	0.21–0.30
4 (126)	0.16–0.20

Fraction 1 proved to be an intractable mixture, while fractions 2 and 3 each had one major component, and fraction 4 displayed two major bands by tlc scrutiny. Fractions 2 and 3 were rechromatographed on precoated reverse phase (KC18F, 0.2 mm) plates (25–30 mg/plate) using methanol/water (62:38) to provide from each a pure saponin. Fraction 2 provided forbeside C (35 mg), while fraction 3 yielded forbeside B (76 mg).

Fraction 4 was rechromatographed on precoated reverse phase (KC18F, 0.2 mm) plates (~25 mg/plate) using methanol/aqueous NaCl 0.002 *M* (64:36) and provided forbeside D (18 mg) and forbeside A (52 mg).

The saponins were further purified by hplc using a semipreparative reverse phase column as below:

Saponin (mg)	Elution time (min)
Forbeside A (48)	11–12
B (70)	12.5–13.5
C (30)	12–13
D (15)	12–13

The hplc column (Whatman Partisil IUCCS/C8) was operated at 1800–2000 psi (1 psi = 6.9 kPa) using methanol/water (64:36) at a flow rate of 7.5 mL/min and a refractive index detector.

Forbeside A, a glassy foam, showed mp 200–203°C and $[\alpha]_D^{28}$ −1.5 (*c* 0.0067, H_2O).

Forbeside B, a glassy foam, showed mp 206–208°C and $[\alpha]_D^{28}$ −2.8 (*c* 0.009, H_2O).

Nuclear magnetic resonance experiments

^{13}C and ^1H nmr spectra were recorded on a Bruker AM-500 spectrometer at ambient temperature. Tetramethylsilane was used as the internal reference. Forbeside A was run in 0.4 mL of pyridine-d_5/D_2O (5:1) at a concentration of 13 mg/mL. Forbeside B was run in 0.4 mL of DMSO-d_6/D_2O (5:1) at a concentration of 30 mg/mL.

All one-dimensional and two-dimensional nmr experiments were performed using the standard pulse sequences provided by Bruker (DISNMRO).

The nOe difference experiments were performed as previously described (22). However, instead of irradiation at a single frequency of the whole multiplet, each line in the multiplet was sequentially irradiated for 100 ms for a total of 1 s/multiplet.

The proton homonuclear shift correlated 2-D nmr experiment on forbeside A was performed using the standard $90°-t_1-90°$ pulse sequence. Quadrature detection in both dimensions was used. The initial (t_1, t_2) matrix of 256 × 2048 data points over a sweep width of 10 ppm in both dimensions was zero-filled to 2048 × 4096 data points. Unshifted sine square bell functions were used for resolution enhancement. Magnitude calculations and symmetrization about the diagonal were used to represent the data.

Mass spectra

Low resolution FAB mass spectra were obtained on VG7070E and VGZAB-SE mass spectrometers employing xenon as an ionizing gas, accelerating voltages of 5 and 10 kV, respectively, and the DT's (a mixture of dithioerythritol, "magic bullet") (23) as a matrix.

Acknowledgements

The authors are grateful to Professor K. L. Rinehart, University of Illinois at Urbana–Champaign, for providing FAB mass spectra and to Larry Calhoun, Department of Chemistry, University of New Brunswick, for helpful discussions. Thanks are due to John R. Foster, Huntsman Marine Laboratory, St. Andrews, New Brunswick, for assistance in collecting material. This study was funded by grants from the Natural Sciences and Engineering Research Council of Canada.

1. D. J. BURNELL and J. W. APSIMON. *In* Marine natural products. Chemical and biological perspectives. Vol. V. *Edited by* P. J. Scheuer. Academic Press, New York. 1983. pp. 287–389; Y. HASHIMOTO. *In* Marine toxins and other bioactive marine metabolites. Japan Scientific Societies Press, Tokyo. 1979. pp. 280–288.
2. Y. SHIMIZU. Experientia, **27**, 1188 (1971).
3. L. A. GOLDSMITH and G. P. CARLSON. *In* Food–drugs from the sea. Proceedings 1974. *Edited by* H. H. Webber and G. D. Ruggieri. Marine Technology Society, Washington, DC. 1976. pp. 354–365.
4. L. V. HEILBRUNN, A. B. CHAET, A. DUNN, and W. L. WILSON. Biol. Bull. **106**, 158 (1954).
5. Y. SHIMIZU. J. Am. Chem. Soc. **94**, 4051 (1972).
6. J. W. APSIMON, J. A. BUCCINI, and S. BADRIPERSAUD. Can. J. Chem. **51**, 850 (1973); J. W. APSIMON, S. BADRIPERSAUD, J. A. BUCCINI, J. EENKHOORN, and M. W. GILGAN. Can. J. Chem. **58**, 2703 (1980).
7. R. RICCIO, O. SQUILLACE-GRECO, L. MINALE, J. PUSSET, and J. L. MENOU. J. Nat. Prod. **48**, 97 (1985).
8. R. RICCIO, C. PIZZA, O. SQUILLACE-GRECO, and L. MINALE. J. Chem. Soc. Perkin Trans. 1, 655 (1985).
9. L. MINALE, R. RICCIO, O. SQUILLACE-GRECO, J. PUSSET, and J. L. MENOU. Comp. Biochem. Physiol. B: Comp. Biochem. **80**, 113 (1985).
10. Y. ITAKURA, T. KOMORI, and T. KAWASAKI. Liebigs Ann. Chem. 2079 (1983).
11. S. IKEGAMI, K. OKANO, and H. MURAGAKI. Tetrahedron Lett. 1769 (1979).
12. W. P. AUE, E. BARTHOLDI, and R. R. ERNST. J. Chem. Phys. **64**, 2229 (1976); A. KUMAR, G. WAGNER, R. R. ERNST, and K. WUTHRICH. Biochem. Biophys. Res. Commun. **96**, 1156 (1980).
13. G. EICH, G. BODENHAUSEN, and R. R. ERNST. J. Am. Chem. Soc. **104**, 3731 (1982); S. W. HOMANS, R. A. DWEK, D. L.

Can. J. Chem. Downloaded from www.nrcresearchpress.com by 78.46.186.204 on 09/07/12
For personal use only.

FERNANDES, and T. W. RADEMACHER. Proc. Natl. Acad. Sci. U.S.A. **81**, 6286 (1984).
14. S. W. HOMANS, R. A. DWEK, D. L. FERNANDES, and T. W. RADEMACHER. FEBS Lett. **164**, 231 (1983).
15. R. LANZETTA, G. LAONIGRO, and M. PARRILLI. Can. J. Chem. **62**, 2874 (1984).
16. G. A. MORRIS and L. D. HALL. Can. J. Chem. **60**, 1431 (1982).
17. N. S. BHACCA, M. F. BALANDRIN, A. D. KINGHORN, T. A. FRIENKEL, R. FREEMAN, and G. A. MORRIS. J. Am. Chem. Soc. **105**, 2538 (1983).
18. J. C. BELOEIL, M. A. DELSUC, J. Y. LALLEMAND, G. DAUPHIN, and G. JEMINET. J. Org. Chem. **49**, 1797 (1984).
19. R. T. GAMPE, M. ALAM, A. J. WEINHEIMER, G. E. MARTIN, J. A. MATSON, M. R. WILCOTT III, R. R. INNERS, and R. E. HURD. J. Am. Chem. Soc. **106**, 1823 (1984).
20. G. A. MORRIS and M. S. RICHARDS. Magn. Reson. Chem. **23**, 676 (1985).
21. I. KITAGAWA, M. KOBAYASHI, and T. SUGAWARA. Chem. Pharm. Bull. (Tokyo), **26**, 1852 (1978); I. KITAGAWA and M. KOBAYASHI. Chem. Pharm. Bull. (Tokyo), **26**, 1864 (1978).
22. J.-R. BRISSON and J. P. CARVER. J. Biol. Chem. **258**, 1431 (1983).
23. J. L. WHITTEN, M. H. SCHAFFER, M. O'SHEA, J. C. COOK, M. E. HEMLING, and K. L. RINEHART, JR. Biochem. Biophys. Res. Commun. **124**, 350 (1984).

Can. J. Chem. Downloaded from www.nrcresearchpress.com by 78.46.186.204 on 09/07/12
For personal use only.

Synthesis and chemiluminescence of new derivatives of isoluminol

ALAIN BÉLANGER, PAUL BRASSARD, SYLVIE LAQUERRE, AND YVES MÉRAND

Department of Molecular Endocrinology, Le Centre Hospitalier de l'Université Laval, Ste-Foy, P.Q., Canada G1V 4G2 and Department of Chemistry, Université Laval, Ste-Foy, P.Q., Canada G1V 4G2

Received May 29, 1986[1]

ALAIN BÉLANGER, PAUL BRASSARD, SYLVIE LAQUERRE, and YVES MÉRAND. Can. J. Chem. **65**, 1392 (1987).

In an attempt to improve the sensitivity of luminescent immunoassays, we have prepared some new isoluminol, 7-(*N*,*N*-dialkylamino)-5-methyl-2,3-dihydrophthalazine-1,4-diones by means of a novel procedure involving the cycloaddition of dienamines to maleic acid derivatives. These compounds are characterized by the presence of a methyl group at C-5 and give quantum yields three to five times greater than those of the most efficient isoluminols in use at present.

ALAIN BÉLANGER, PAUL BRASSARD, SYLVIE LAQUERRE et YVES MÉRAND. Can. J. Chem. **65**, 1392 (1987).

Afin d'améliorer la sensibilité des dosages luminoimmunoétalonnages, nous avons préparé de nouveaux isoluminols: des *N*,*N*-dialkylamino-7 methyl-5 dihydro-2,3 phtalazinedione-1,4 par une synthèse originale qui implique la cycloaddition d'une diénamine à des dérivés de l'acide maléique. Ces produits caractérisés par un groupe methyle en position C-5 ont un rendement quantique de trois à cinq fois supérieur à celui du meilleur isoluminol actuellement utilisé.

Can. J. Chem. Downloaded from www.nrcresearchpress.com by 72.64.146.136 on 09/07/12
For personal use only.

Introduction

The chemiluminescence of cyclic hydrazides was first demonstrated by Albrecht in 1928 (1); since then the efficiency and mechanism of the process continue to raise wide interest. A considerable body of synthetic work has been carried out with the object of isolating the various factors that control light production (2–4). Several of these were early identified by Drew as substituent effects: thus, the unimpeded resonance of electron-donating groups with the system generally exerts a favorable influence as does mild steric hindrance of other substituents with adjacent carbonyls at C-1 and C-4. However, substitution of the heterocyclic moiety completely inhibits the process.

A major application of chemiluminescence to clinical analysis consists in using luminescent molecules as alternatives for radioactive and enzymatic labels in immunoassays. Indeed, luminescent immunoassay (LIA) procedures have recently been described for steroids (5–7), proteins (8, 9), and other biological compounds (10). In this respect, two factors play a major role in the sensitivity of the immunoassay: the affinity of antibodies for the tracer and the specific activity of the latter. In chemiluminescence, the quantum yield is the specific activity of the tracer and probably is the most important parameter affecting the sensitivity of LIA.

Although luminol provides a greater light yield than isoluminol, derivatives of the latter that can be coupled to proteins or steroids have been used extensively since by virtue of the foregoing rules they are more efficient than substituted luminols. Schroeder *et al.* (11) prepared several luminescent compounds and found that aminobutyl ethyl isoluminol in particular showed high efficiency. The use of such a derivative in the LIA of steroids has resulted in a procedure with a sensitivity comparable to that of radioimmunoassays (RIA) (5–7). In an attempt to further improve the sensitivity of LIA, we have prepared and characterized a series of new chemiluminescent derivatives of isoluminol. This novel synthesis involves the cycloaddition of dienamines to maleic acid derivatives and was designed to give compounds with a methyl group at the C-5 position, a feature expected to enhance the quantum efficiency.

Experimental

A. Synthesis (Fig.1)

All melting points were taken for samples in capillary tubes with a Thomas–Hoover Apparatus and are not corrected. The uv spectra were determined on a Hewlett-Packard 8450A spectrophotometer and the ir spectra on a Beckman Model IR 4250. Nuclear magnetic resonance spectra were recorded with Varian EM360 A and XL-200 spectrophotometers using tetramethylsilane as internal standard. Mass spectra were obtained with a Hewlett-Packard 5995 A spectrophotometer. Merck silica gel $60F_{254}$ for dry column chromatography and Woelm neutral aluminium oxide activity II were used throughout. Elementary analyses were carried out by Galbraith Laboratories Inc., Knoxville, TN. Exact masses were provided by the Laboratoire de spectrométrie de masse, Université de Sherbrooke, Sherbrooke, Canada.

*2-Alkylsiloxy-4-*N*-pyrrolidyl-2,4-pentadiene (**2**a or **2**a′)*

To a solution of lithium diisopropylamine (LDA) prepared in the usual way with *n*-butyllithium (*n*-BuLi) (10 mmol, 2.7 *M* in hexane), diisopropylamine (11 mmol) and tetramethylethylenediamine (TMEDA) (12) (10 mmol) in dry tetrahydrofuran (THF) (10 mL) at 0°C under nitrogen and cooled at −78°C, were added 4-*N*-pyrrolidyl-3-penten-2-one (**1***a*) (13) (10 mmol) in dry THF (15 mL) in 15 min, and then after 2 h, a solution of chlorotrimethylsilane (TMSCl) or *t*-butylchlorodimethylsilane (TBDMSCl) (11 mmol), in the same solvent (8 mL; 45 min). The reaction mixture was allowed to warm and kept for 90 min at room temperature, evaporated, diluted with dry petroleum ether (bp 30–60°C, 70 mL), filtered under nitrogen, and evaporated. These operations were repeated and finally the residue was stirred for 3 h under vacuum (0.2 Torr). The unstable dienamine **2***a* or **2***a′* was used without further purification.

2-Trimethylsiloxy-4-*N*-pyrrolidyl-2,4-pentadiene (**2***a*); nmr ($CDCl_3$) δ 5.00 (1H, s), 3.97 (1H, s), 3.57 (1H, s) 3.00 (4H, m), 1.78 (7H, m), and 0.13 (9H, s).

2-*t*-Butyldimethylsiloxy-4-*N*-pyrrolidyl-2,4-pentadiene (**2***a′*); nmr ($CDCl_3$) δ 5.06 (1H, s), 3.86 (1H, s), 3.6 (1H, s), 3.06 (4H, m), 1.86 (7H, m), 0.99 (9H, s), and 0.16 (6H, m).

*3-Methyl-5-*N*-pyrrolidylphthalic anhydride (**4**a)*

To a solution of bromomaleic anhydride (849 mg, 4.8 mmol) in dry benzene (20 mL) was added under nitrogen freshly prepared crude dienamine **2***a* (1.3 g, 5.8 mmol) in the same solvent (20 mL) in 30 min at 5–7°C. The dark reaction mixture was allowed to warm to room temperature and after 2 h, the solvent evaporated, the crude product dissolved in $CHCl_3$, and separated by chromatography on silica gel (50 g). Elution with $CHCl_3$ gives phthalic anhydride **4***a*, yellow needles (218 mg, 19.5%) mp 222–222.5°C; ir ν_{max} (KBr) 1823, 1753, 1620, 1578, and 865 cm^{-1}; uv λ_{max} (C_2H_5OH) 212, 267, 321, and 386 nm (log ε 4.23, 4.19, 4.05, and 3.89); nmr ($CDCl_3$) δ 6.83 (1H, d, J = 2.2 Hz), 6.55 (1H, d, J = 2.2 Hz) (this doublet is not well defined: coupling with the 3-methyl), 3.42 (4H, m) (s, with irradiation at δ 2.10), 2.59 (3H, s) and 2.10 (4H, m) (s, with irradiation at δ 3.42); mass spectrum: m/e 231 (M^+). *Anal.* calcd. for $C_{13}H_{13}O_3N$: C 67.52, H 5.66, N 6.06; found: C 67.65, H 5.62, N 6.02.

[1]Revision received February 11, 1987.

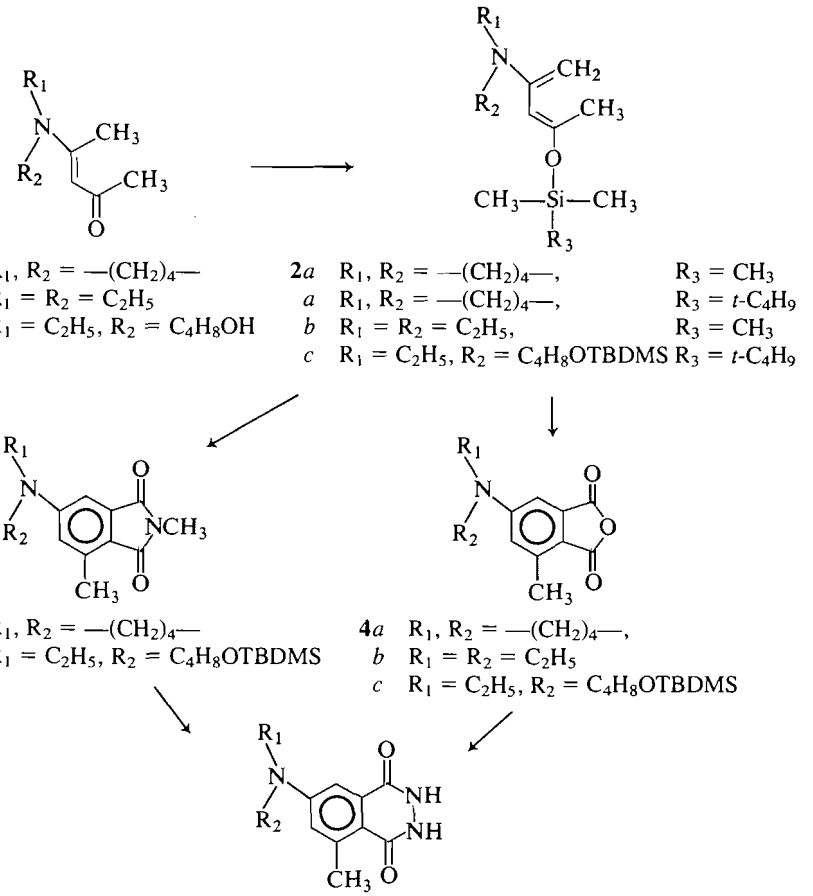

FIG. 1. Synthesis of chemiluminescent compounds.

*3-Methyl-5-*N*-pyrrolidyl-*N*-methylphthalimide (**3**a)*

To a solution of *N*-methylmaleimide (488 mg, 4.4 mmol) in dry benzene (10 mL) was added under nitrogen freshly prepared crude dienamine **2***a*′ (1.07 g, 4 mmol) in the same solvent (10 mL) in 30 min at 5–7°C. The reaction mixture was kept overnight at room temperature and then refluxed for 1 h. Palladium (10%) on activated charcoal (100 mg) was then added and refluxing continued for 3.5 h. After cooling, the catalyst was removed by filtration and the product isolated by chromatography on silica gel (100 g). Elution with CH_2Cl_2 gave methylphthalimide **3***a* (230 mg, 23.5%), yellow needles, mp 159.5–159.8°C (CH_2Cl_2, $(C_2H_5)_2O$); ir ν_{max} (KBr) 1748, 1685, 1610, 1575, and 855 cm^{-1}, uv λ_{max} (C_2H_5OH) 212, 268, 323, and 402 nm (log ϵ 4.46, 4.50, 3.93, and 3.92); nmr ($CDCl_3$) δ 6.83 (1H, d, J = 2.4 Hz), 6.38 (1H, d, J = 2.4 Hz) (this doublet is not well defined: coupling with 3-methyl), 3.39 (4H, m) (s with irradiation at δ 2.06), 3.10 (3H, s), 2.59 (3H, s), and 2.06 (4H, m) (s with irradiation at δ 3.39); $C_{14}H_{16}O_2N_2$ requires 244.1212; found 244.1206. *Anal.* calcd.: C 68.83, H 6.60, N 11.47; found: C 69.19, H 6.56, N 11.70.

*3-Methyl-5-*N,N*-dimethylaminophthalic anhydride (**4**b)*

In a similar reaction, 4-(*N*-dimethylamino)-3-penten-2-one (**1***b*) (13) (750 mg, 5 mmol) gave anhydride **4***b* (143 mg, 0.613 mmol, 12.3%), yellow needles, mp 128–128.5°C ($(C_2H_5)_2O$, petroleum ether); ir ν_{max} (KBr) 1823, 1750, 1615, 1570, and 840 cm^{-1}; uv λ_{max} (C_2H_5OH) 214, 268, 321, and 385 nm (log ϵ, 4.33, 4.31, 4.16 and 4.00); nmr ($CDCl_3$) δ 6.94 (1H, d, J = 2.2 Hz), 6.65 (1H, d of q, J = 2.2 and 0.6 Hz), 3.47 (4H, q, J = 7.3 Hz), 2.60 (3H, s), 1.24 (6H, t, J = 7.3 Hz); mass spectrum m/e 233 (M^+). *Anal.* calcd. for $C_{13}H_{15}O_3N$: C 66.93, H 6.48, N 6.00; found: C 66.89, H 6.21, N 5.91.

*7-(*N,N*-Dialkylamino)-5-methyl-2,3-dihydrophthalazine-1,4-dione (**5**a or **5**b)*

A solution of phthalic anhydride **4***a* or **4***b* (0.43 mmol) in acetic acid (4 mL) was refluxed with hydrazine hydrate (14) (85%) for 1 h under nitrogen and then poured, after cooling, into ice water. The resulting precipitate was filtered and dried: 5-methyl-7-*N*-pyrrolidyl-2,3-dihydrophthalazine-1,4-dione (**5***a*) (82 mg, 0.33 mmol, 77%), white crystals, mp 330–335°C dec. (CH_3OH, NH_4OH 10% in H_2O); ir ν_{max} (KBr) 1640, 1595, 1545, and 845 cm^{-1}, uv λ_{max} (0.1 *M* K_2CO_3) 226, 287, and 326 nm (log ϵ 4.34, 4.45, and 4.13); nmr [$(CD_3)_2SO$] δ 6.77 (1H, s), 6.75 (1H, s), 3.35 (4H, m) (under H_2O peak visible by addition of D_2O) (s with irradiation at δ 1.98), 2.72 (3H, s), 1.98 (4H, m) (s with irradiation at δ 3.35); mass spectrum m/e 245 (M^+). *Anal.* calcd. for $C_{13}H_{15}O_2N_3$: C 63.65, H 6.16, N 17.13, found: C 63.78, H 6.26, N 16.99.

This product (65 mg, 0.26 mmol, 63.4%) was also prepared under the same conditions (reflux time, 12 h) from *N*-methylphthalimide **3***a* (100 mg, 0.41 mmol).

5-Methyl-7-(*N*,*N*-dimethylamino)-2,3-dihydrophthalazine-1,4-dione (**5***b*) (93 mg, 0.37 mmol, 86%), white crystals, mp 290–292°C dec. (CH_3OH, NH_4OH 10% in H_2O); ir ν_{max} (KBr) 1635, 1595, 1540 and 845 cm^{-1}; uv λ_{max} (0.1 *M* K_2CO_3) 227, 288, and 326 nm (log ϵ 4.17, 4.43, and 4.11); nmr [$(CD_3)_2SO$] δ 6.89 (2H, s), 3.44 (4H, 1, J = 7.0 Hz), 2.72 (3H, s), 1.14 (6H, t, J = 7.0 Hz); mass spectrum m/e 247 (M^+). *Anal.* calcd. for $C_{13}H_{17}O_2N_3$: C 63.13, H 6.93, N 16.99; found: C 62.97, H 7.20, N 16.83.

*4-(*N*-ethyl-*N*-4′-hydroxybutylamino)-3-penten-2-one (**1**c)*

To 2,4-pentadione (20 g, 0.2 mol) in $CHCl_3$ (50 mL) was added

Can. J. Chem. Downloaded from www.nrcresearchpress.com by 72.64.146.136 on 09/07/12
For personal use only.

Can. J. Chem. Downloaded from www.nrcresearchpress.com by 72.64.146.136 on 09/07/12
For personal use only.

rapidly, redistilled oxalyl chloride (63 g, 0.5 mol) according to the procedure of Clark and Heathcock (15). The mixture was refluxed (45 min), evaporated, and upon distillation, the residue yielded 4-chloro-3-pentadien-2-one (15.8 g, 66%, bp 34°C/8 Torr, lit. (16) 44–45°C/23 Torr). This product (2.38 g, 20 mmol) in dry THF (10 mL) was added (5 min) to a solution of 4-(ethylamino)butanol (17, 18) (2.38 g, 20 mmol) and triethylamine (2.78 mL, 20 mmol) in the same solvent (10 mL). After 2 h at 50–55°C, an additional amount of this substance (1.19 g, 10 mmol) and triethylamine (1.4 mL) was added and the solution heated at 60°C for 1 h. After cooling, the precipitate was filtered, the solvent evaporated, and the oily residue purified by chromatography on aluminium oxide (150 g). Elution with CH_2Cl_2 and $CH_3CO_2C_2H_5$ yielded hydroxyenaminone **1***c* (2.4 g, 78%), white crystals, mp 41–41.5°C; ir ν_{max} (KBr) 3300, 1605, 1525, and 1043 cm^{-1}; uv λ_{max} (C_2H_5OH) 312 nm (log ϵ 4.38); nmr ($CDCl_3$) δ 5.09 (1H, s), 3.70 (2H, t, J = 6.0 Hz), 3.29 (5H, m), 2.52 (3H, s), 2.07 (3H, s), 1.7–1.5 (4H, m), and 1.17 (3H, t, J = 7 Hz); mass spectrum m/e 199 (M^+). *Anal.* calcd. for $C_{11}H_{21}O_2N$: C 66.29, H 10.62, N 7.03; found: C 66.02, H 10.85, N 6.93.

*2-(*t*-Butyldimethylsiloxy)-4-[*N*-4′-(*t*-butyldimethylsiloxy)butyl-*N*-ethylamino-2,4]-pentadiene (**2**c)*

To a solution of LDA prepared in the usual way from *n*-BuLi (8.8 mmol, 2.7 *M* in hexane), diisopropylamine (8.8 mmol), and TMEDA (12) (4.4 mmol) in dry THF (9 mL) at 0°C under nitrogen and then cooled to −78°C was added hydroxy enaminone **1***c* (800 mg, 4 mmol) in the same solvent (25 mL) during a period of 30 min. After 2 h, a solution of TBDMSCl (1.47 g, 9.6 mmol) in the same solvent (5 mL) was added over a period of 30 min. The reaction mixture was allowed to warm and kept for 90 min at room temperature, evaporated, diluted with dry petroleum ether (bp 30–60°C) (50 mL), filtered under nitrogen and evaporated. These operations were repeated and finally the residue was stirred for 3 h under vacuum (0.2 Torr). An nmr spectrum of the crude dienamine **2***c* (1.26 g, 2.9 mmol, 72%) was recorded, ($CDCl_3$, N_2) δ 1.9 (3H, m), 0.90 (18H, m) and 0.1 (12H, m); showing the disappearance of two singlets at δ 2.52 and 2.07. This very unstable dienamine **2***c* was used without further purification.

*5-N-4′-[t-Butyldimethylsiloxy)butyl-N-ethylamino]-3-methylphthalic anhydride (**4**c)*

To a solution of bromomaleic anhydride (684 mg, 3.87 mmol) in dry benzene (20 mL) was added in 30 min at 5–7°C under nitrogen freshly prepared crude dienamine **2***c* (700 mg, 1.6 mmol) from the preceding reaction in the same solvent (20 mL). The dark reaction mixture was allowed to warm to room temperature and after 15 h, the solvent was evaporated, the crude product dissolved in CH_2Cl_2, filtered, and separated by chromatography on silica gel (50 mg). Elution with CH_2Cl_2 gave phthalic anhydride **4***c*, yellow oil (28 mg, 0.072 mmol, 4.5%); ir ν_{max} (film) 1827, 1765, 1617, 1580, 1250, 1090, and 830 cm^{-1}; uv λ_{max} (C_2H_5OH) 214, 268, 322, and 387 nm (log ϵ 3.98, 3.97, 3.83, and 3.49); nmr ($CDCl_3$) δ 6.94 (1H, d, J = 1.9 Hz), 6.65 (1H, d, J = 1.9 Hz), (this doublet is not well defined: coupling with the 3-methyl), 3.67 (2H, t, J = 5.9 Hz), 3.46 (4H, m) (3.49, s and 3.42, m with irradiation at δ 1.23), 2.59 (3H, s) 1.8–1.5 (4H, m), 1.23 (3H, t, J = 7.2 Hz), 0.89 (9H, s), 0.06 (6H, s); $C_{21}H_{33}O_4NSi$ requires 391.2179; found 391.2181. *Anal.* calcd: C 64.41, H 8.49, N 3.57; found: C 64.98, H 8.56, N 3.34).

*5-[N-4′-(t-Butyldimethylsiloxy)butyl-N-ethylamino]-3-methyl-N-methylphthaleimide (**3**c)*

To a solution of *N*-methylmaleimide (286 mg, 2.58 mmol) in dry benzene (10 mL) was added in 30 min at 5–7°C under nitrogen freshly prepared crude dienamine **2***c* (1.1 g, 2.57 mmol) in the same solvent (10 mL). After 48 h at room temperature, the solvent was evaporated and palladium (10%) on activated charcoal (100 mg) with xylenes (10 mL) was added. The reaction mixture was refluxed (6 h), cooled, filtered, and then purified by chromatography on silica gel (100 g). Elution (CH_2Cl_2, $CH_3CO_2H_5$; 99:1) gave methylphthaleimide **3***c*, yellow oil (174 mg, 0.45 mmol, 17.5%), ir ν_{max} (film) 1755, 1695, 1612, 1585, 1245, 1090, and 830 cm^{-1}; uv λ_{max} (C_2H_5OH) 211, 270, 324, and 402 (log ϵ 4.06, 4.09, 3.51, and 3.51); nmr ($CDCl_3$) δ 6.88 (1H, d, J = 1.9 Hz), 6.44 (1H, d, J = 1.9 Hz) (this doublet is not well defined: coupling with the 3-methyl), 3.63 (2H, t, J = 5.8 Hz), 3.42 (2H, q, J = 7.1 Hz), 3.35 (2H, t, J = 7.6 Hz), 3.07 (3H, s), 2.55 (3H, s), 1.65–1.44 (4H, m), 1.17 (3H, t, J = 5.8 Hz), 0.86 (9H, s), 0.03 (6H, s); $C_{22}H_{36}O_3N_2Si$ requires 404.2495; found 404.2484.

*7-[N-4′-(t-Butyldimethylsiloxy)butyl-N-ethyl amino]-5-methyl-2,3-dihydrophthalazine-1,4-dione (**5**c)*

A solution of methylphthalimide **3***c* (47 mg, 0.12 mmol) in acetic acid (1 mL) was refluxed with hydrazine hydrate (14, 19) (85%) (2 mL) under nitrogen for 4 h. After cooling, precipitated dihydrophthalazinedione **5***c* (32 mg, 0.079 mmol, 66%) was isolated by filtration (this product (16 mg, 0.039 mmol, 64%) was also prepared from phthalic anhydride **4***c* (24 mg, 0.061 mmol)), white crystals, mp 107–108.5°C (CH_3COCH_3, hexanes); ir ν_{max} (KBr) 1650, 1592, 1250, 1100, and 830 cm^{-1}; uvλ_{max} (0.1 *M* K_2CO_3, C_2H_5OH 4:1) 224, 289, and 327 nm (log ϵ 4.24, 4.47, and 4.15); nmr ($CDCl_3$) δ 7.25 (1H, m), 6.86 (1H, m), 3.75 (2H, t, J = 6.0 Hz), 3.52–3.40 (4H, m), 2.87 (3H, s), 1.8–1.5 (4H, m), 1.24 (3H, t, J = 6.0 Hz), 0.9 (9H, s) and 0.065 (6H, s); $C_{21}H_{35}O_3N_3Si$ requires 405.2448; found 405.2444. *Anal.* calcd.: C 62.18, H 8.49, N 10.35; found: C 62.18, H 8.69, N 10.36.

*7-[N-Ethyl-N-4′-hydroxybutylamino]-5-methyl-2,3-dihydrophthalazine-1,4-dione (**5**d)*

Methylphthalimide **3***c* (56 mg, 0.144 mmol) was refluxed with hydrazine hydrate (19, 20) (85%, 1 mL) under nitrogen for 1 h. The solvent was evaporated, the product dried overnight under vacuum (0.2 Torr) over P_2O_5 and then dissolved in a dry THF (5 mL) solution of tetrabutylammonium fluoride (21) (0.432 mmol, 1 *M* in THF). The reaction mixture was stirred at room temperature (3 h), then evaporated; H_2O (10 mL) added and alcohol **5***d* isolated by filtration (17 mg, 0.058 mmol, 40.6%), light yellow crystals, mp 221–222°C (CH_3OH, CH_3COCH_3); ir ν_{max} (KBr) 3260, 1640, 1592, 1020, and 840 cm^{-1}; uv λ_{max} (0.1 *M* K_2CO_3) 227, 288, and 326 nm (log ϵ 4.18, 4.44, and 4.12); nmr [$(CD_3)_2SO$] δ 6.86 (2H, s), 4.45 (1H, broad, exchange with D_2O), 3.40 (6H, m) (under H_2O, visible by addition of D_2O), 2.69 (3H, s), 1.63–1.4 (4H, m) and 1.10 (3H, t, J = 6.7 Hz). *Anal.* calcd. for $C_{15}H_{21}O_3N_3$: C 61.83, H 7.27, N 14.42; found: C 61.82, H 7.38, N 14.42.

B. Chemiluminescence

Measurements of luminescence were made on a LKB-Wallac 1251 luminometer using the automatic mode for injection and reading of the decay portion of light from the 3rd second to the 12th. Aliquots of the luminescent compound in 100 μL of phosphate buffer (0.01 *M* phosphate-buffered saline, pH 7.4) were introduced into the cuvettes (Clinicon, polystyrene 2174-086) and volumes were completed with 200 μL of NaOH (0.03 *N* to 2.0 *N*) according to the desired pH. Fixed amounts of microperoxidase (MP-11) (42 μL, 0.4 n*M*) and hydrogen peroxide (33 μL, 0.6%) were then automatically injected and light emitted was recorded.

Results and discussion

A. Synthesis

Early work on cyclic hydrazides involved mainly the search for structure-efficiency relationships while more recent studies have concentrated on the mechanism of the luminescence reaction (2, 22, 23) and on applications of these molecules as potential tracers for biochemical analysis (5–10). Synthesis of luminescent compounds has been carried out starting with nitrophthalic acid derivatives (2, 3, 19, 20) but substituted luminols or isoluminols have only been obtained by tedious step-wise processes (10, 11). In the present approach, 5-alkyl isoluminols are formed by a simple and general procedure in which all substituents are introduced in a single step, the Diels–Alder addition of a 2-amino-4-siloxydiene to bromomaleic anhydride. The required diene **2** has been prepared from the corresponding tertiary enaminone **1** using the observation that silylation of enaminones though (24) easy in the case of primary ones, is more difficult with secondary and quite un-

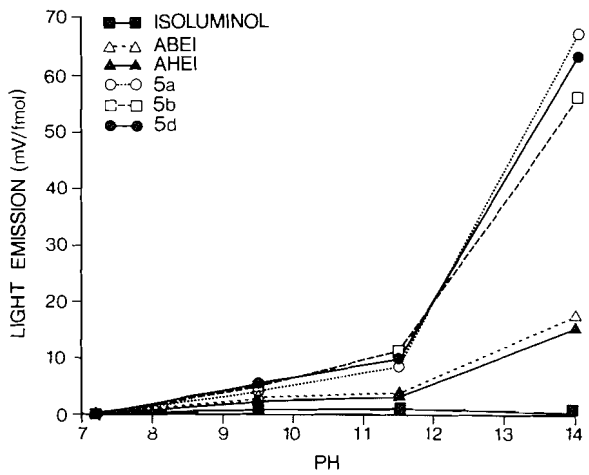

FIG. 2. Effect of pH on the decay portion (3rd to 12th second) light emission produced by isoluminol and its derivatives (ABEI, aminobutylethylisoluminol; AHEI, aminohexylethylisoluminol; **5***a*, **5***b*, and **5***c*, see Experimental).

known for tertiary examples. It was found (25) that strong base (LDA) was necessary for the regiospecific (and probably kinetic) removal of the hydrogen in the γ-position of enaminone **1** while the resulting enolate could readily be trapped as the enol silyl ether in the usual way (**1***a* and **1***b* are well described compounds; **1***c* can be prepared conveniently from 4-ethylaminobutanol (15, 17) and 4-chloro-3-pentene-2-one).

All of the dienes obtained are very labile particularly those containing a trimethylsilyl group; indeed hydroxyenaminone **1***c* does not give a detectable amount of the trimethylsiloxydiene. The crude dienol ethers were immediately added to bromomaleic anhydride or to *N*-methylmaleimide in benzene at 5–10°C. The corresponding 3-methylphthalic anhydrides were then obtained by rapid aromatization of the crude product on a column of silica gel. Use of the less reactive dienophiles *N*-methylmaleimide affords good yields of 3-methyl-*N*-methylphthaleimides **3** (especially in the case of the siloxy compound **3***c* where the yield improves by about 4-fold). In this approach, aromatization of the adduct requires an extra step involving dehydrogenation with 10% palladized charcoal and is followed by chromatography on silica gel. The pyridazine ring is formed by the well-documented action of hydrazine hydrate on anhydride **4** or *N*-methylimide **3**. In the instance of siloxyphthalazinedione **5***c* the *tert*-butyldimethylsiloxy group is best removed by fluoride ion at room temperature rather than by treatment with a refluxing mixture of acetic acid and water.

B. Chemiluminescence

With chemiluminescent substances of this type, it is a well-established fact that the pH of the medium plays an important role on the detection limit (5). Hence, we have first studied the effect of this parameter on the decay portion of the light produced by our new derivatives of isoluminol and have compared the results with those obtained for well known analogues. As in previous cases (5), the new derivatives show a clear dependency of light yield on pH (Fig. 1). This figure also indicates that the introduction of a methyl group at the C-5 position in derivatives **5***a*, **5***b*, and **5***d* also brings about a 3- to 5-fold increase on the efficiency of the chemiluminescent process.

These data extend and amplify previous observations by Brundrett *et al.* (2, 3) who had earlier shown that the presence of a methyl group at the C-5 position of luminol increases the efficiency of light production. Since the methyl groups show a weakly electron-donating character, the enhanced luminescence observed is probably accounted for by the *ortho* effect between it and the adjacent carbonyl (2, 3). Furthermore, the presence of terminal hydroxyl or amine groups seems to provide little or no influence on chemiluminescence since the three new derivatives all show approximately the same high yields.

TABLE 1. Luminescence reaction kinetics of isoluminol and its derivatives at pH 14

Compounds*	Percentage of light emitted between 0–2 s	3–12 s	13–60 s
Isoluminol	26	55	19
ABEI	21	55	24
AHEI	22	56	22
5*a*	25	60	15
5*b*	25	57	18
5*d*	22	56	22

*ABEI, aminobutylethylisoluminol; AHEI, aminohexylethylisoluminol.

Table 1 indicates the pattern of light emission of isoluminol and its derivatives. It can be seen that the increase of luminescence obtained with the new derivatives is not due to a change in the kinetics of the oxidation reaction since, as observed for the previous compounds, approximately 55% of light occurs between 3rd and 12th second at pH 14. These data confirm the high efficiency achieved when a methyl group is added.

Aminobutyl isoluminol, which shows a high level of light emission, has been extensively used in immunoassays using a luminescent tracer. The present report describes new derivatives of isoluminol which exhibit particularly high luminescent efficiency and, moreover, possess functional groups that permit ready coupling with steroids and proteins, for example with human chorionic gonadotropin; particulars will be communicated later. Hence, these compounds present an excellent potential for use as tracers in immunoassays.

1. H. O. ALBRECHT. Z. Phys. Chem. **136**, 321 (1928).
2. R. B. BRUNDRETT, D. F. ROSWELL, and E. H. WHITE. J. Am. Chem. Soc. **94**, 7536 (1972).
3. R. B. BRUNDRETT and E. H. WHITE. J. Am. Chem. Soc. **96**, 7497 (1974).
4. H. R. SCHROEDER and F. M. YEAGER. Anal. Chem. **50**, 1114 (1978).
5. M. PAZZAGLI, J. B. KIM, G. MESSERI, G. MARTINAZZO, F. KOHEN, F. FRANCESCHETTI, A. TOMMASI, R. SALERNO, and M. SERIO. Clin. Chim. Acta, **115**, 287 (1981).
6. F. KOHEN, H. R. LINDNER, and S. GILAD. J. Steroid Biochem. **19**, 413 (1983).
7. J. DE BOEVER, F. KOHEN, D. VANDEKERCKHOVE, and G. VAN MAALE. Clin. Chem. **30**, 1637 (1984).
8. P. J. CHENG, I. HEMMILÄ, and T. LÖVGREN. J. Immunol. Methods, **48**, 159 (1982).
9. G. J. BARDNARD, J. B. KIM, J. L. BROCKELBANK, W. P. COLLINS, B. GAIER, and F. KOHEN. Clin. Chem. **30**, 538 (1984).
10. H. R. SCHROEDER, F. M. YEAGER, R. C. BOGUSLASKI, and P. O. VOGELHUT. J. Immunol. Methods, **25**, 275 (1979).
11. H. R. SCHROEDER, R. C. BOGUSLASKI, R. J. CARRICO, and R. T. BUCKLER. Methods Enzymol. **57**, 424 (1978).
12. T. H. CHAN and G. J. KANG. Tetrahedron Lett. **23**, 3011 (1982).
13. N. J. LEONARD and J. A. ADAMCIK. J. Am. Chem. Soc. **81**, 595 (1959).
14. H. SATOH, M. TONEGAWA, K. KITAHARA, and R. AOYAGI. Tokyo Ika Digaku Kiyo, **5**, 71 (1979).

Can. J. Chem. Downloaded from www.nrcresearchpress.com by 72.64.146.136 on 09/07/12
For personal use only.

15. R. D. CLARK and C. H. HEATHCOCK. Synthesis, 47 (1974).
16. L. GRUBER, I. TÖMÖSKOZI, and L. RADICZ. Synthesis, 708 (1975).
17. P. N. NATARAJAN and S. T. CHEW. Can. J. Pharmacol. Sci. **8**, 61 (1973).
18. C. V. WILSON and J. F. SEINBERG. Org. Synth. **36**, 48 (1956).
19. H. D. K. DREW and F. H. PEARMAN. J. Chem. Soc. 26 (1937).
20. K. D. GUNDERMAN and M. DRAWERT. Chem. Ber. **95**, 2018 (1962).
21. E. J. COREY and A. VENKATESWARLU. J. Am. Chem. Soc. **94**, 6190 (1972).
22. S. LJUNGGREN, G. MERENYI, and J. LIND. J. Am. Chem. Soc. **105**, 7662 (1983).
23. J. LIND, G. MERENYI, and T. E. ERICKSON. J. Am. Chem. Soc. **105**, 7655 (1983).
24. T. PROLL and W. WALTER. Chem. Ber. **116**, 1564 (1983).
25. M. YOSHIMOTO, N. ISHIDA, and T. HIRAOKA. Tetrahedron Lett. 39 (1973).

Can. J. Chem. Downloaded from www.nrcresearchpress.com by 72.64.146.136 on 09/07/12
For personal use only.

Adsorption de l'azote sur l'amiante chrysotile phosphaté et lixivié

JALEH KHORAMI, LUC NOEL ET HUGUES MÉNARD
Département de chimie, Université de Sherbrooke, Sherbrooke (Qué.), Canada J1K 2R1

Received October 23, 1986

JALEH KHORAMI, LUC NOEL, and HUGUES MÉNARD. Can. J. Chem. **65**, 1397 (1987).

Le tracé des isothermes d'adsorption et de désorption de l'azote par la méthode volumétrique (B.E.T.), nous a permis de déterminer la surface spécifique et la porosité d'une série de fibres de l'amiante chrysotile avant et après des traitements chimiques. Nous avons démontré que les composés phosphatés formés durant la réaction entre le $POCl_3$ et l'amiante chrysotile encapsulent la surface des fibrilles et obstruent les pores entre les fibrilles. Ces modifications chimiques diminuent d'une façon significative la surface spécifique et la porosité des fibres. Les résultats de lessivage des fibres avec HCl 0,1 *M* montrent l'accroissement de la surface spécifique et de la porosité. La solvatation des impuretés et la lixiviation de la surface brucitique des fibres en fonction du temps sont responsables de cette augmentation.

JALEH KHORAMI, LUC NOEL et HUGUES MÉNARD. Can. J. Chem. **65**, 1397 (1987).

Adsorption and desorption isotherms of nitrogen, obtained by the volumetric (B.E.T.) method, have been used to determine the specific surface and the porosity of a series of chrysotile asbestos fibers, before and after chemical treatments. It was shown that the phosphorus compounds that are formed by the reaction of $POCl_3$ and chrysotile asbestos seal the surface of the fibrils and block the pores between the fibrils. These chemical modifications result in an important diminution of the specific surface and of the porosity of the fibers. Washing the fibers with 0.1 *M* HCl results in an increase of the specific surface and of the porosity. Solvation of the impurities and leaching of the brucitic surface of the fibers are responsible for this increase.

[Journal translation]

Can. J. Chem. Downloaded from www.nrcresearchpress.com by 72.64.146.136 on 09/07/12
For personal use only.

Introduction

L'amiante chrysotile, $Mg_3Si_2O_5(OH)_4$, est souvent associé à des impuretés que l'on retrouve entre les fibrilles ou à l'intérieur de celles-ci (1). Ses principaux minerais sont la brucite $Mg(OH)_2$, la magnésite $MgCO_3$, la dolomite $MgCO_3 \cdot CaCO_3$, la calcite $CaCO_3$, le talc $Mg_3Si_4O_{10}(OH)_2$ et la magnétite Fe_3O_4.

Nauman et Dresher (2) ont déterminé la surface spécifique et la porosité de quelques grades de fibres chrysotile d'origine canadienne. Ils ont observé que les fibres soumises aux traitements thermiques (100–200 et 400°C) et mécaniques par les voies humide et sèche, possèdent une surface spécifique plus grande.

La surface spécifique apparente des fibres traitées à plus haute température est plus élevée à cause de l'élimination totale de l'eau capillaire. L'augmentation de la surface des fibres qui ont subi des traitements mécaniques est attribuée à la défibrillation et libération des fibrilles individuelles. Une défibrillation complète est constatée pour les fibres traitées par la voie humide. Ces fibres possèdent alors la plus grande surface spécifique dûe aux surfaces externes des fibrilles accessibles pour l'adsorption des gaz. Nauman et Drescher (2) ont aussi étudié les isothermes d'adsorption de l'azote des fibres de chrysotile Cassiar avant et après la défibrillation. Le procédé d'adsorption et de désorption s'effectue réversiblement dans le cas des matériaux non-poreux. Avec les solides poreux, dans un intervalle précis de pression relative (P/P_0[1]), les deux tracés des isothermes d'adsorption et désorption se déplacent pour former une boucle qu'on appelle hysteresis.

Parmi les deux échantillons de fibres non traitées et défibrillées, nous constatons que ceux-ci possèdent des isothermes caractéristique des matériaux poreux. De ceci, nous pouvons conclure que les pores sont associés à la surface des fibrilles et à leurs dispositions spatiales et non pas à l'intérieur des fibrilles. De cette façon l'amiante chrysotile défibrillé a une surface plus élevée que les mêmes fibres non traitées.

Les études sur la porosité de l'amiante chrysotile avaient été poursuivies par Gorski et Steller (3, 4). Ces auteurs ont étudié les isothermes d'adsorption et de désorption de molécules telles que l'eau et le benzène.

Nos travaux sont orientés vers les fibres modifiées avec le $POCl_3$, suivant le procédé Lalancette et Dunnigan (5), les propriétés physico-chimiques de ces fibres ayant été étudiées auparavant par Kimmerle *et al.* (6).

Huber (7) a démontré que les fibres d'amiante chrysotile traitées à l'acide subissaient une augmentation de porosité proportionnelle au temps de traitement.

Nous avons entrepris ces travaux en lixiviant les fibres originales d'une part et les fibres modifiées au $POCl_3$ d'autre part. Les résultats obtenus démontrent que pour les fibres traitées au $POCl_3$ nous avons une diminution de la surface spécifique et de la porosité. Pour les fibres lixiviées nous notons une augmentation de la porosité proportionnelle au temps de traitement.

Partie expérimentale

Un appareil Quantsorb (modèle No QS-10) de Quantachrome Corp. est utilisé dans ces travaux. Les analyses sont effectuées selon la méthode décrite (8) et suivant les instructions données par Gregg et Sing (9).

Les mélanges des gaz d'azote et d'hélium de qualité pure sont fournis par « Liquid Carbonic Canada Ltd ».

Tous les échantillons sont conditionnés et dégazés pendant 16 h à 110°C sous atmosphère d'hélium. La pesée exacte des échantillons est nécessaire avant et après les analyses. Nous avons utilisé un intégrateur modèle 3390A de Hewlett Packard Co. pour les mesures de la surface des pics. Une valeur de 16,2 Å^2 comme surface de projection de l'azote a été utilisé lors de la détermination de la surface spécifique des matériaux. Les isothermes de désorption sont tracés avec 25 points en utilisant 25 mélanges de différents pourcentages d'azote dans l'hélium. Un appareil de Technicon Auto-Analyzer II est utilisé pour le dosage de phosphore.

Les fibres utilisées sont de la compagnie Johns Manville 4T-30. Les fibres courtes sont isolées selon le procédé Jolicœur *et al.* (10). Toutes les fibres ont été chauffées à 300°C pendant 150 min avant les traitements chimiques.

Partie théorique

De l'équation de Kelvin, telle que démontrée par Gregg et Sing (9) lorsque p_0 est la pression de saturation de la vapeur à

1. P = pression partielle; P_0 = pression de saturation à une température donnée.

TABLEAU 1. Identification des fibres

Nature des fibres	Surface spécifique ($m^2 g^{-1}$)	Pourcentage de phosphore
Fibres courtes	31	—
Fibres courtes modifiées avec $POCl_3$	24	2,7
Fibres longues chauffées à 300°C	18,5	—
Fibres longues modifiées avec $POCl_3$	5,4	1,6
Fibres longues modifiées avec $POCl_3$ et lixiviées 5 h	31,4	0,4
Fibres longues lixiviées 5 h	43,7	—
Fibres longues lixiviées 72 h	110	—

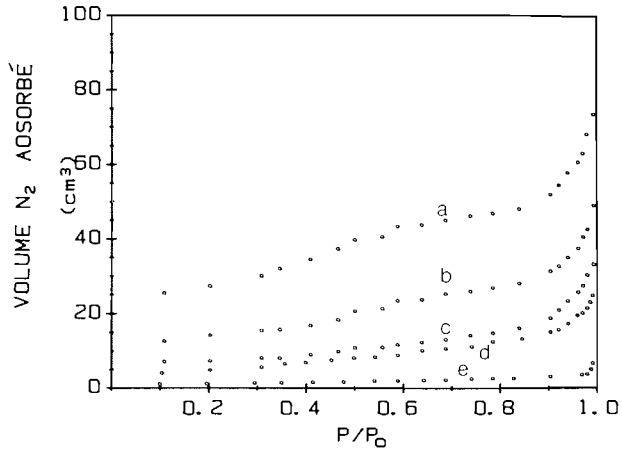

FIG. 1. Isothermes d'adsorption de l'azote sur des fibres longues : (*a*) longues lixiviées 72 h, (*b*) longues lixiviées 5 h, (*c*) phosphatées et lixiviées 5 h, (*d*) originales, (*e*) longues phosphatées.

la température T (K), V le volume molaire de l'adsorbat sous la forme liquide (azote = 89,2 $cm^3 mol^{-1}$), γ la tension interfaciale (azote = 28,9 dyne cm^{-1}), R la constante des gaz parfaits

$$[1] \quad \ln p/p_0 = \frac{-2\gamma V}{rRT} \cos \phi$$

($R = 8{,}31 \times 10^7$ erg $mol^{-1} K^{-1}$), ϕ l'angle de mouillage que fait l'azote liquide avec la surface qui, dans bien des cas, est dite $\phi = 0$, ce qui donne un $\cos \phi = 1$, et r représente le rayon d'un capillaire cylindrique très souvent appelé rayon de Kelvin.

Cependant, de la théorie il découle que dépendamment de la forme du pore il y a une certaine épaisseur, t, d'azote liquide qui reste sur les parois d'où la détermination du rayon r peut être biaisée.

Le rayon des pores sera donc :

$$[2] \quad r_p = r_K + t$$

lorsque cette épaisseur t d'azote sur la parois s'exprime

$$[3] \quad t = \sigma_N \left[\frac{5}{2.303 \log_{10}(p_0/p)} \right]^{1/3}$$

lorsque σ_N est l'épaisseur d'une monocouche d'azote (σ_N = 3.54 Å).

Au fur et à mesure que les pores se vident, le volume d'azote libéré par un même pore variera, car en réalité, comme la pression partielle (p/p_0) diminue, cette épaisseur d'azote liquide va elle aussi diminuer. Ceci aura donc pour effet de donner un volume de pore qui augmentera avec cette diminution de la pression partielle. Pour tenir compte de cette variation, de l'équation [4] nous aurons

$$[4] \quad \Delta V_p = \left[\frac{\bar{r}_p}{r_K} \right]^2 (V_{liq} - \Delta t \Sigma A)$$

lorsque A représente l'aire obtenue pour chaque pression partielle. Cette aire, A, se calcule de la façon suivante, soit :

$$[5] \quad A = \frac{2V_p}{r_p}$$

et la variation du volume azote liquide selon l'équation [6]

$$[6] \quad \Delta V_{liq} = \frac{\Delta V_{gaz} P}{T}$$

lorsque P et T représentent la pression atmosphérique et la température lors de l'expérience.

En construisant un graphique de $\Delta V_p/\Delta r_p$ en fonction de $\bar{r}_p$ nous aurons la distribution des pores en fonction de leur grosseur.

Résultats et discussion

La surface spécifique des fibres

Le tableau 1 illustre les mesures de la surface spécifique ainsi que le pourcentage de phosphore des fibres. On peut constater que la surface spécifique des fibres courtes et longues modifiées avec le $POCl_3$ a diminuée. La diminution est plus remarquable pour les fibres longues. D'autre part la lixiviation des fibres en fonction du temps augmente la surface spécifique des fibres. Cependant, la comparaison des résultats des fibres lixiviées pendant 5 h et les fibres modifiées avec le $POCl_3$ et lixiviées pendant 5 h montrent que la surface spécifique des fibres modifiées–lixiviées est moins grande que celle des fibres uniquement lixiviées.

L'augmentation de la surface spécifique des fibres lixiviées est due à la solvatation des impuretés types carbonate et brucite qui sont associées entre les fibrilles. La solvatation de ces impuretés aboutit à la libération des fibrilles. Cette attaque acide partielle à court terme, peut se compléter en fonction du temps avec la solvatation totale des impuretés et puis la lixiviation des couches brucitiques de l'amiante. Johan *et al.* (11) montrent que la lixiviation du chrysotile conduit à un changement considérable des propriétés physico-chimiques de ce minéral. L'augmentation de la surface spécifique des fibres est particulièrement frappante, allant de 46 $m^2 g^{-1}$ à 450 $m^2 g^{-1}$ environ pour le chrysotile lessivé à 95%.

En ce qui concerne les fibres modifiées avec le $POCl_3$, les études précédentes (6) montrent un changement des caractéristiques physico-chimiques qui est dû à la formation des composés phosphatés et en grande partie des polyphosphates. La réaction de phosphorylation se produit préférentiellement avec les couches brucitiques de l'amiante et la probabilité d'une réaction entre le $POCl_3$ et les impuretés ($Mg(OH)_2$, les carbonates, etc.) n'est pas écartée.

D'après ces résultats, la surface des fibrilles de l'aminante chrysotile modifié avec le $POCl_3$ est encapsulée par les composés phosphatés et les produits formés durant la réaction peuvent obstruer les pores existant entre les fibrilles. La diminution de la surface spécifique des fibres ainsi modifiées illus-

Can. J. Chem. Downloaded from www.nrcresearchpress.com by 72.64.146.136 on 09/07/12
For personal use only.

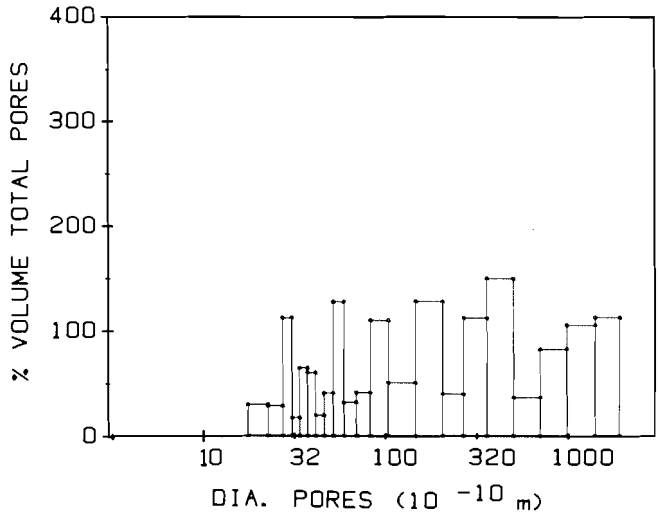

FIG. 2. Histogrammes représentant le pourcentage de volume total des pores en fonction du diamètre des fibres longues originales.

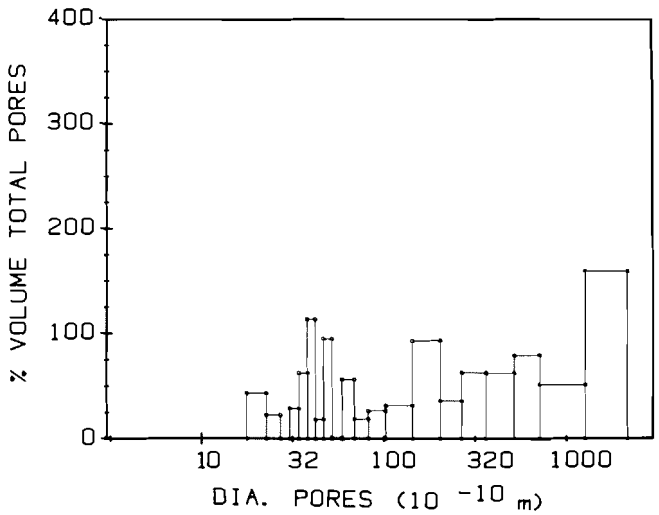

FIG. 3. Histogrammes représentant le pourcentage de volume total des pores en fonction du diamètre des fibres longues lixiviées 5 h.

tre bien les effets de l'encapsulation de la surface et l'obstruction des pores entre les fibrilles.

Sur le tableau 1, on peut constater que le pourcentage de phosphore sur les fibres courtes (2,7% de phosphore) est plus élevé comparativement aux fibres longues 1,65%. Cependant, la diminution de la surface spécifique est plus remarquable pour les fibres longues phosphatées. Il faut noter que les fibres courtes utilisées sont en grande partie sous forme de fibrilles individuelles dont leur surface brucitique est plus disponible et la réaction de la phosphatation est plustôt effectuée sur la surface des fibrilles pour encapsuler ces dernières. Dans le cas des fibres longues il faut signaler les deux effets: d'une part l'encapsulation de la surface brucitique (moins disponible) et d'autre part l'obstruction des pores.

Isotherme d'adsorption de l'azote et volume des pores

La figure 1 montre l'isotherme d'adsorption de l'azote pour les fibres longues originales (courbe *d*) en comparaison avec les mêmes fibres lixiviées (courbes *a* et *b*) et modifiées avec le $POCl_3$ (courbe *e*) ainsi que les fibres modifiées et lixiviées pendant 5 h (courbe *c*). Les figures 2–6 montrent les histogrammes représentant le pourcentage de volume total des pores

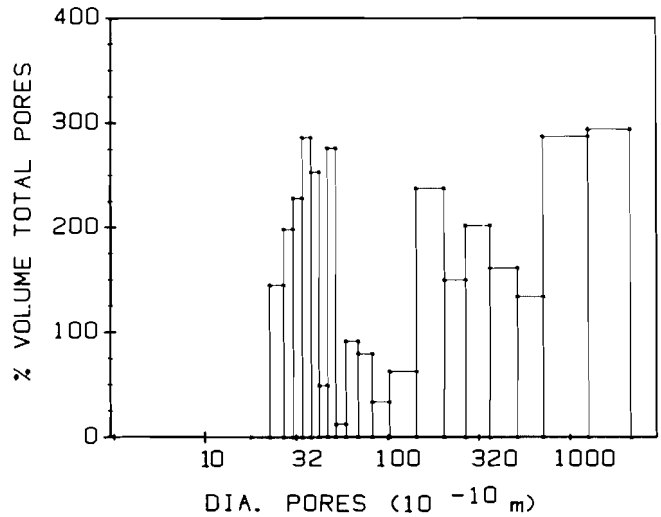

FIG. 4. Histogrammes représentant le pourcentage de volume total des pores en fonction du diamètre des fibres longues lixiviées 72 h.

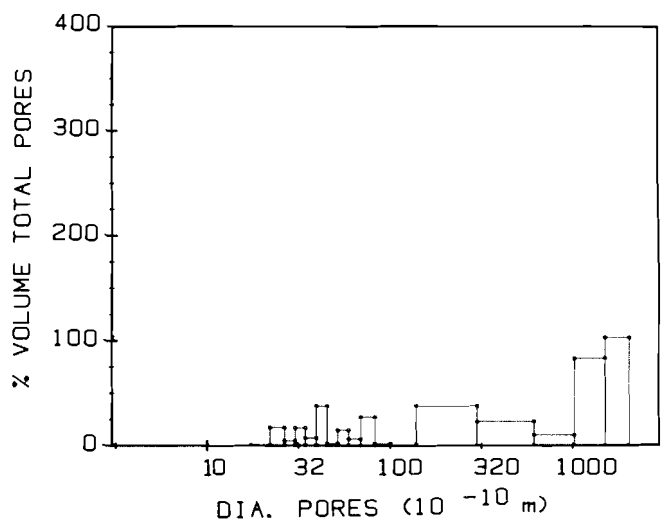

FIG. 5. Histogrammes représentant le pourcentage de volume total des pores en fonction du diamètre des fibres longues phosphatées.

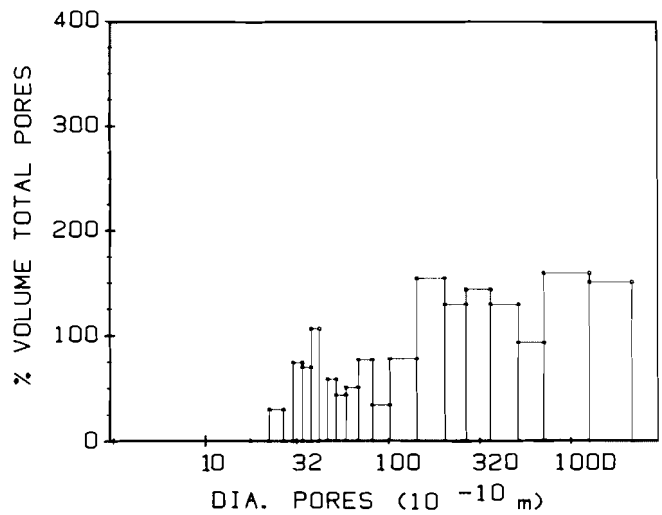

FIG. 6. Histogrammes représentant le pourcentage de volume total des pores en fonction du diamètre des fibres longues phosphatées et lixiviées.

Can. J. Chem. Downloaded from www.nrcresearchpress.com by 72.64.146.136 on 09/07/12
For personal use only.

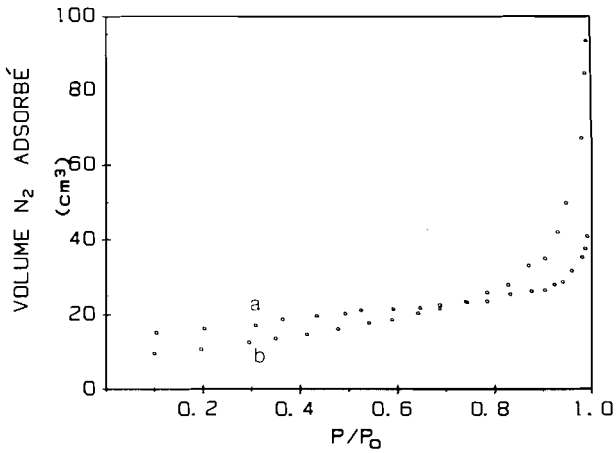

FIG. 7. Isothermes d'adsorption de l'azote des fibres (*a*) courtes originales, (*b*) courtes phosphatées.

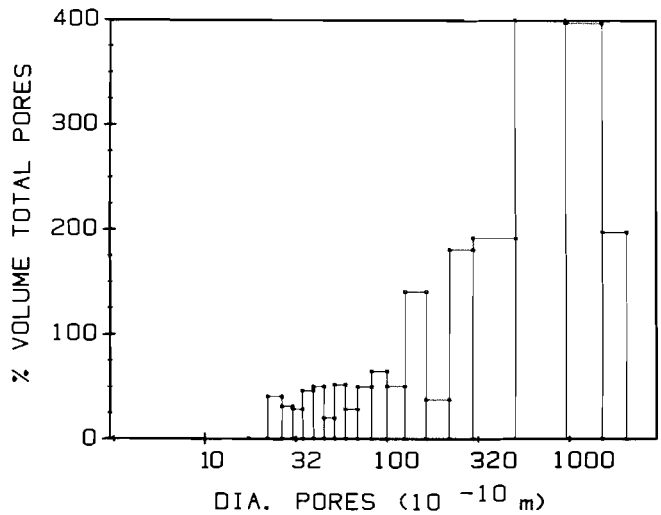

FIG. 8. Histogrammes représentant le pourcentage de volume total des pores en fonction du diamètre des fibres courtes originales.

en fonction du diamètre pour les fibres longues originales (fig. 2), lixiviées (fig. 3 et 4), phosphatées (fig. 5) et phosphatées et lixiviées (fig. 6).

Si on se base sur la description donnée par Gregg et sing (9), on peut classifier les courbes des isothermes d'adsorption. À la figure 1, les courbes *a* et *b* des fibres lixiviées montrent un point d'inflection vers $P/P_0 = 0{,}5$ correspondant aux matériaux poreux. D'après Brunauer *et al.* (12, 13), ces courbes peuvent être classées comme type IV. Les deux courbes des isothermes d'adsorption *c* et *d* présentées sont plutôt à la limite du type IV et II d'après la classification de Brunauer *et al.* La courbe *e* est plutôt typique de la classification type II.

La comparaison des histogrammes des fibres originales et des fibres lixiviées montre une nette augmentation de volume de pore sur toute l'échelle de diamètre présentée. Cependant, pour les fibres lixiviées 72 h, cette augmentation est plus considérable entre 20 et 50 Å de diamètre, ce qui explique l'augmentation appréciable de la surface spécifique de ces fibres.

Si nous comparons les deux histogrammes des fibres originales (fig. 2) et phosphatées (fig. 5), nous pouvons constater une diminution remarquable de volume de pore sur toute l'échelle de diamètre et même la disparition des pores sur l'histogramme illustré. Les résultats obtenus pour les fibres phosphorylées et

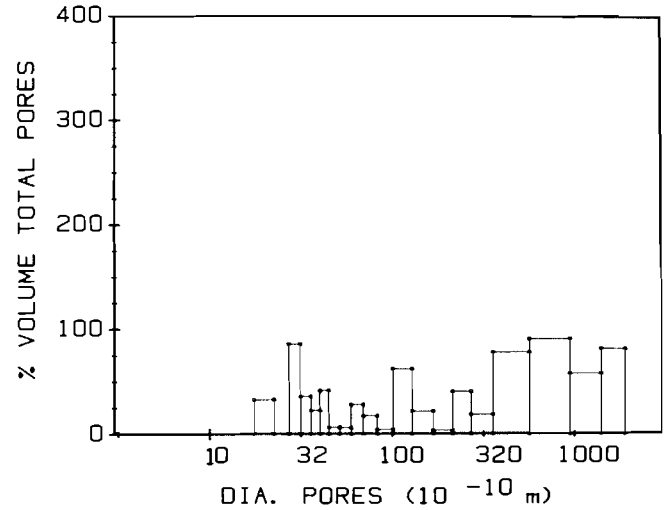

FIG. 9. Histogrammes représentant le pourcentage de volume total des pores en fonction du diamètre des fibres courtes phosphatées.

lixiviées montrent une certaine similarité entre ces fibres et les fibres originales.

La figure 7 ainsi que les figures 8 et 9 représentent les isothermes d'adsorption de l'azote et les histogrammes pour les fibres courtes et les fibres courtes phosphatées. On peut remarquer sur la figure 7 que les fibres courtes phosphatées (*b*) adsorbent une quantité plus élevée d'azote en comparaison avec les fibres courtes non traitées (*a*). Sur les histogrammes nous observons une diminution de volume global des pores.

Les résultats obtenus par les isothermes d'adsorption et le volume de pore des fibres étudiées confirment les interprétations mentionnées dans la partie précédente de nos études.

La lixiviation en fonction du temps des fibres longues originales aboutit à la création des nouveaux pores et surtout des mésopores.

De plus la phosphatation des fibres longues a comme effet d'encapsuler les fibrilles et de créer l'obturation des pores. Donc, les résultats des isothermes d'adsorption de l'azote et l'histogramme présenté pour ces fibres démontrent d'une façon plus claire les effets mentionnés.

Les résultats pour les fibres phosphatées et lixiviées montrent que les fibres phosphatées subissent l'attaque acide plus difficilement que les fibres originales qui sont plus poreuses (tableau 2). On peut constater que le pourcentage de surface par unité de surface n'est que de 97% pour les fibres longues modifiées avec $POCl_3$ et lixiviées 5 h en comparaison à 180% pour les fibres longues lixiviées 5 h. Le pourcentage de pore par unité de volume est de 121% pour ces fibres traitées au $POCl_3$ et lixiviées 5 h tandis que pour les fibres lixiviées 5 h nous obtenons 175%. Cet écart entre les fibres longues lixiviées 5 h et 72 h est considérablement augmenté, passant de 180 à 280% et de 175 à 236% pour les fibres lixiviées 5 h et 72 h respectivement.

Dans le cas des fibres courtes, comme on a déjà mentionné dans la partie précédente, ces fibres sont en grande partie sous forme de fibrilles et l'effet d'encapsulation est plus probable pour ces fibres. Cependant, les études précédentes effectuées par la microscopie électronique en transmission (14) montrent une aggrégation des fibres courtes après la phosphatation. Ce phénomène explique une légère augmentation de volume d'azote adsorbé sur ces fibres et l'apparition de certains pores.

Can. J. Chem. Downloaded from www.nrcresearchpress.com by 72.64.146.136 on 09/07/12
For personal use only.

TABLEAU 2. Comparaison de la surface et du volume des pores

Nature des fibres	Surface des pores ($m^2 g^{-1}$)	Volume de pore ($cm^3 g^{-1}$)	Pourcentage de surface par unité de surface	Pourcentage de pore par unité de volume
Fibres courtes	33	0,127	100	100
Fibres courtes modifiées avec $POCl_3$	22,9	0,044	72	35
Fibres longues chauffées	17,8	0,036	100	100
Fibres longues modifiées avec $POCl_3$	3,3	0,0089	18,7	25
Fibres longues modifiées avec $POCl_3$ et lixiviées 5 h	17,2	0,043	97	121
Fibres longues lixiviées 5 h	32	0,062	180	175
Fibres longues lixiviées 72 h	49,7	0,084	280	236

Conclusion

Les mesures de la surface spécifique ainsi que les études effectuées sur la porosité des fibres de l'amiante chrysotile modifié avec le $POCl_3$ montrent l'encapsulation des fibrilles et l'obturation des pores disponibles entre les fibrilles par les composés phosphatés formés durant la réaction. Ces modifications ont comme effet la diminution de la porosité et la surface spécifique des fibres.

Les résultats de l'attaque d'acide HCl 0,1 *M* montrent la solvatation des impuretés et la lixiviation de la surface brucitique des fibres en fonction du temps. L'augmentation de la surface spécifique et la porosité des fibres ainsi lessivées est frappante. La lixiviation du chrysotile augmente plutôt la quantité des mésopores situés entre 20 et 50 Å de diamètre. Nous avons aussi démontré que les fibres modifiées avec le $POCl_3$ sont plus résistantes à l'attaque d'acide.

Remerciements

Les auteurs remercient pour l'appui financier le Conseil national de recherches en sciences naturelles et en génie du Canada, l'Institut de l'amiante et l'Institut de recherche en santé et sécurité au travail.

1. J. KHORAMI, D. CHOQUETTE et F. M. KIMMERLE. Thermochimica Acta, **76**, 87 (1984).
2. A. W. NAUMAN et W. H. DRESCHER. Am. Mineral. **51**, 711 (1966).
3. C. H. GORSKI et L. E. STELLER. J. Am. Ind. Hyg. Assoc. **34**, 345 (1974).
4. C. H. GORSKI et L. E. STELLER. J. Am. Ind. Hyg. Assoc. **36**, 292 (1975).
5. J. M. LALANCETTE et J. DUNNIGAN. Phosphated asbestos fibers. U.K. Patent GB076-383A.
6. F. M. KIMMERLE, J. KHORAMI et C. CHOQUETTE. Therm. Anal. Proc. Int. Conf. 7th. 1982. p. 164.
7. O. HUBER. Modified chrysotile asbestos sorption agents. U.K. Patent 1,342,102.
8. Instruction Manual of the Quantachrome Company, Quantasorb Sorption System.
9. S. J. GREGG et K. S. W. SING. Adsorption surface area and porosity. Academic Press, New York. 1967. p. 121.
10. C. JOLICŒUR, P. ROBERGE et J. L. FORTIER. Can. J. Chem. **59**, 1140 (1981).
11. Z. JOHAN, J. GONI et C. SARCIA. Advances in inorganic geochemistry. Technip, Paris. 1973. p. 883.
12. S. BRUNAUER, L. S. DEMMING, W. S. DEMMING et E. TELLER. J. Am. Chem. Soc. **62**, 1723 (1940).
13. S. BRUNAUER, P. H. EMMET et E. TELLER. J. Am. Chem. Soc. **60**, 309 (1938).
14. Rapport interne. Programme de recherche sur l'amiante, Université de Sherbrooke (PRAUS). Effet du traitement $POCl_3$ sur le degré d'agglomération des fibres, 28 octobre 1981.

Can. J. Chem. Downloaded from www.nrcresearchpress.com by 72.64.146.136 on 09/07/12
For personal use only.

Heat capacities and isentropic compressibilities of electrolytes in propylene carbonate at 25°C[1]

GÉRALD PERRON, GUYLAINE TRUDEAU, AND JACQUES E. DESNOYERS[2]

Department of Chemistry, Université de Sherbrooke, Sherbrooke, P.Q., Canada J1K 2R1 and INRS-Energie, 1650 Montée Ste-Julie, Varennes, P.Q., Canada J0L 2P0

Received October 24, 1986

GÉRALD PERRON, GUYLAINE TRUDEAU, and JACQUES E. DESNOYERS. Can. J. Chem. **65**, 1402 (1987).

The heat capacities per unit volume and sound velocities of many solutions of 1:1 electrolytes in propylene carbonate (PC) were measured at 25°C. Combining these data with previously published densities, apparent molar heat capacities and isentropic compressibilities were calculated. By extrapolation to infinite dilution, the corresponding standard partial molar quantities were obtained. The heat capacities and compressibilities of water in PC were also calculated. Through ionic additivity, it was possible to calculate these functions for all alkali and tetraalkylammonium halides. The magnitude and trends with ionic size of the heat capacities of electrolytes in PC are similar to those in other aprotic solvents such as acetonitrile (ACN) and dimethylformamide (DMF) and significantly different from those in water. On the other hand, with compressibilities, the magnitudes are the same in PC and in water for alkali halides but significantly different for tetraalkylammonium halides. The trends with ionic size are similar to those in ACN. These effects can be interpreted through ion–solvent interactions. The separation of these thermodynamic functions into their ionic contributions is also discussed.

GÉRALD PERRON, GUYLAINE TRUDEAU et JACQUES E. DESNOYERS. Can. J. Chem. **65**, 1402 (1987).

Les capacités calorifiques volumiques et les vitesses ultrasonores de plusieurs solutions d'électrolytes 1:1 dans le propylene carbonate (PC) ont été mesurés à 25°C. En combinant ces données avec les densités déjà publiées, les capacités calorifiques et compressibilités isentropiques apparentes molaires ont été obtenues. Les capacités calorifiques et compressibilités de l'eau dans le PC ont aussi été mesurées. Les quantités molaires partielles standard ont aussi été obtenues par extrapolation à dilution infinie. Grâce au principe d'additivité ionique, ces fonctions ont été calculées pour les halogénures alcalins et de tetraalkylammonium. L'ordre de grandeur et la dépendance sur la taille des ions des capacités calorifiques dans la PC sont semblables à celles dans d'autres solvants aprotiques tels que l'acétonitrile (ACN) et le diméthylformamide (DMF) mais différentes des valeurs dans l'eau. Par contre, pour les compressibilités, l'ordre de grandeur est le même dans le PC et dans l'eau pour les halogénures alkalins mais pas pour les sel quaternaires d'ammonium. La dépendance sur le taille des ions est la même que dans l'ACN. Ces résultats peuvent être interprétés au moyen d'interactions soluté–solvant. La séparation des données thermodynamiques standard en valeurs ioniques est aussi discutée.

Introduction

Propylene carbonate (PC) is a very interesting solvent for electrolytes, in view of its high dielectric constant (64.9), wide liquid range, good solubilizing power for many electrolytes, and its inertness towards metals as reactive as lithium (1). As such, it is a useful solvent, alone or in combination with other aprotic solvents, for high energy batteries (2). It is also often suggested as a reference solvent for the study of solvation of ions (3).

Thermodynamic data are very useful for the prediction of the temperature and pressure dependences of equilibrium properties, e.g. the emf of cells, and for the understanding of solvation effects. Good data exist in the literature for free energies and enthalpies of solvation (3) and for apparent molar volumes (4) of electrolytes in PC. In the present work, we will extend these systematic studies to apparent molar heat capacities and isentropic compressibilities. Since these properties have been well studied for electrolytes in water (5, 6), methanol (MeOH) (7, 8), acetonitrile (ACN) (9, 10), and dimethylformamide (DMF) (11). The present study should be a good complement for a study of the solvating power of various solvents.

Experimental

The PC for the heat capacity measurements is the same as that used previously for density measurements (4). Moreover, the heat capacities per unit volume were measured with the same solutions and at the same time as the density measurements. The PC was redistilled for sound velocity measurements.

Most electrolytes, and their purification, are the same as those used in previous studies (4, 9, 10). $LiClO_4$ (ALFA INORGANIC VENTRON) was recrystallized in ACN, Et_4NCl in a mixture of ethanol and ether, and Et_4NI was prepared from Et_4NOH and HI and recrystallized from water. The water content of the electrolyte solutions and pure PC was analyzed by the Karl Fischer technique (Aqua-test II by Photovolt). The PC used for heat capacity measurements had 0.002% of water and for sound velocities 0.014% of water.

The relative change in heat capacities per unit volume were measured with a Picker flow microcalorimeter as described previously (12) and converted to specific heat capacities with the known densities (4). The induced change in temperature was 1.50 K for a flow rate of 0.45 mL per min. The specific heat capacity of the reference PC was determined in two ways. Against pure water, c_p^* was found to be $1.6220\ J\ g^{-1}\ K^{-1}$. If heptane and benzene were used as reference, as described previously (13), c_p^* was $1.6192\ J\ g^{-1}\ K^{-1}$. As it will be shown elsewhere (14), a small heat loss can occur with some commercial flow calorimeter, and this loss is a function of the flow rate. This source of error can account for the difference in the two above values. The literature value is $1.642\ J\ g^{-1}\ K^{-1}$ (1). For the calculation of apparent molar heat capacities, the value 1.6192 was used, and for densities, $1.19965\ g\ cm^{-3}$.

The procedure followed for the measurement of compressibilities was the same as the one for electrolytes in ACN (10). Sound velocities were measured with the "sing around" method using a Nusonic Model

[1]This paper is dedicated to Professor Douglas E. Ryan on the occasion of his 65th birthday.

[2]To whom correspondence should be addressed at Institut National de la Recherche Scientifique, P.O. Box 7500, Ste.-Foy, P.Q., Canada G1V 4C7.

Can. J. Chem. Downloaded from www.nrcresearchpress.com by 78.46.186.204 on 09/07/12
For personal use only.

TABLE 1. Apparent molar heat capacities and isentropic compressibilities of some electrolytes in propylene carbonate at 25°C: parameters in eq. [5]

Electrolyte	$C_{p,2}^0$ (J/K mol)	A_C (J/K mol $m^{1/2}$)	$10^4 K_{s,2}^0$ (cm^3/bar mol)	A_K (cm^3/bar mol $m^{1/2}$)
LiBr	81.2±1.5	−13.9	−17.7 ±0.4	20.7 ± 3.0
$LiClO_4$	130.0		−23.9 ±0.2	10.0 ± 1.0
NaI	92.0±0.3	27.5± 1.0	−30.2 ±0.2	7.0 ± 0.6
$NaClO_4$	160.0±1.2	2.2± 5.0	−31.1 ±0.2	8.0 ± 0.5
$Na\phi_4B$	554.5±3.1		35.0 ±0.5	2.5 ± 2.0
KI	81.7±1.4	12.4± 5.6	−26.2 ±0.2	8.4 ± 8.0
$KClO_4$	141.8±3.3	3.9±26.3	−28.1 ±1.1	4.8 ± 8.2
RbI	77.3±3.0	6.4±17.3	−27.2 ±1.0	
CsI	80.1±1.8		−29.4 ±1.1	18.6 ± 6.0
Me_4NClO_4	262.9±1.5	4.4± 6.4	4.9 ±0.1	12.9 ± 0.7
Et_4NCl	312.3±0.6		35.3 ±0.3	0.1 ± 1.1
Et_4NBr	312.0±1.3	8.4± 4.4	29.7	
Et_4NI	308.7±3.7		38.0 ±0.4	
Et_4NClO_4	370.6±0.7	8.0± 2.9	36.2 ±0.3	26.0 ± 1.0
Pr_4NCl	428.7±2.4	0.9± 8.9	80.4	−16.6
Pr_4NBr	428.2±1.2	5.7± 4.1	79.6 ±0.4	1.2 ± 1.4
Bu_4NBr	541.2±3.3	8.2±11.2	126.0 ±0.2	−1.2 ± 0.8
n-Pen_4NBr	660.2±1.5		163.3 ±0.2	
i-Pen_4NBr	644.0±3.7	1.2±12.0		
ϕ_4PBr	539.8±1.8		62.4 ±0.2	
ϕ_4AsCl	557.2±0.7		59.9 ±1.5	5.7 ±12.8
ϕ_3CH	381.5±2.3		83.4 ±0.6	
H_2O	82.4±0.4	13.0± 1.1	5.51±0.06	1.80± 0.2

6105 solution monitor (Mapco Inc). With the exception of RbI, CsI, $KClO_4$, and sodium tetraphenylboride ($NaB\phi_4$), the electrolytes were sufficiently soluble to proceed by addition of a stock solution to the pure solvent. Otherwise, the measurements were made by successive dilutions of the stock solution. The temperature of the measurements was 25.00°C and monitored with a thermistor placed directly in the cell.

The probe of the velocimeter was calibrated with water using the data of Del Grosso (15) and Millero (6). The drift in the sound velocities over a one day period was about 0.03 m s^{-1}. The isentropic compressibility of pure PC was obtained as $40.14 \pm 0.01 \times 10^{-6}$ bar^{-1}, which is in reasonably good agreement with the value of Hoiland (16), 40.08×10^{-6} bar^{-1}. However, this value did change from run to run, and it was found that better apparent molar compressibilities could be obtained if the sound velocity or isentropic compressibility of the pure solvent was obtained by extrapolation of the data to infinite dilution in each set of experiments.

Results

The apparent molar heat capacities and isentropic compressibilities were calculated from the heat capacities at constant volume σ and the isentropic compressibilities β_s using the following relations:

$$[1] \quad C_{p,2,\phi} = Mc_p + (1000(c_p - c_p^*))/m$$

$$[2] \quad c_p = c_p^*(1 + \Delta\sigma/\sigma^*)d^*/d$$

$$[3] \quad K_{s,2,\phi} = V_{2,\phi}\beta_s + (1000(\beta_s - \beta_s^*))/md^*$$

$$[4] \quad \beta_s = 100/du^2$$

where M is the solute molecular mass, c_p the specific heat capacity, d the density, $V_{2,\phi}$ the apparent molar volume of the solute, $K_{s,2,\phi}$ the apparent isentropic compressibility and u the sound velocity. The superscript * refers to the pure solvent. The densities required for the calculation of the apparent molar values were all taken from our previous work (4).

TABLE 2. Partial molar heat capacities $C_{p,2}^0$ of ions in propylene carbonate at 25°C based on the assumption $C_{p,Br^-}^0 = 45$ J K^{-1} mol^{-1}

Ion	$C_{p,2}^0$	Ion	$C_{p,2}^0$
Li^+	26	ϕ_4P^+	496
Na^+	56	ϕ_4As^+	512
K^+	38	ϕ_4B^-	498
Rb^+	35	Cl^-	45
Cs^+	35	Br^-	45
Me_4N^+	159	I^-	42
Et_4N^+	267	ClO_4^-	104
Pr_4N^+	383		
Bu_4N^+	496		
Pen_4N^+	610		
i-Pen_4N^+	599		

The original data and derived $C_{p,2,\phi}$ and $K_{s,2,\phi}$ are given in Tables 1 and 2.[3] The Debye–Hückel limiting slopes for electrolytes in PC are not available since sufficiently precise dielectric constant data as a function of temperature and pressure are not available. The standard partial molar quantities Y_2^0 were therefore obtained by extrapolation to infinite dilution using the Masson equation

$$[5] \quad Y_{2,\phi} = Y_2^0 + A_Y m^{1/2}$$

The conductivity results (17) which were reinterpreted by Zana *et al.* (4), show that 1:1 electrolytes are largely dissociated in PC, and under such conditions extrapolation with the Masson equation is valid.

[3]Complete set of data may be purchased from the Depository of Unpublished Data, CISTI, National Research Council of Canada, Ottawa, Ont., Canada K1A 0S2.

Can. J. Chem. Downloaded from www.nrcresearchpress.com by 78.46.186.204 on 09/07/12
For personal use only.

Can. J. Chem. Downloaded from www.nrcresearchpress.com by 78.46.186.204 on 09/07/12
For personal use only.

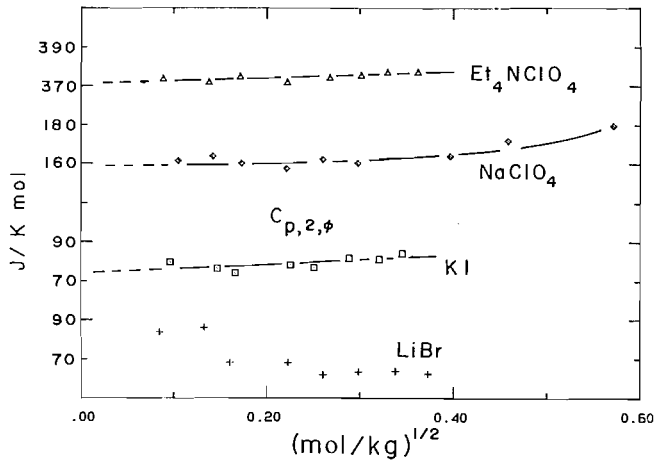

FIG. 1. Some typical plots of $C_{p,2,\phi}$ against the square root of the molality in PC at 25°C. Except for LiBr, all the plots are regular.

TABLE 3. Partial molar isentropic compressibilities $K_{s,2}^0$ of ions in propylene carbonate at 25°C based on the assumption $K_{s,Br^-}^0 = -6$ $10^4\,cm^3\,bar^{-1}\,mol^{-1}$

Ion	$K_{s,2}^0$	Ion	$K_{s,2}^0$
Li^+	−24	ϕ_3P^+	68
Na^+	−33	ϕ_4As^+	66
K^+	−30	ϕ_4B^-	68
Rb^+	−30	Cl^-	−6
Cs^+	−32	Br^-	−6
Me_4N^+	5	I^-	3
Et_4N^+	34	ClO_4^-	−2
Pr_4N^+	86		
Bu_4N^+	132		
Pen_4N^+	172		

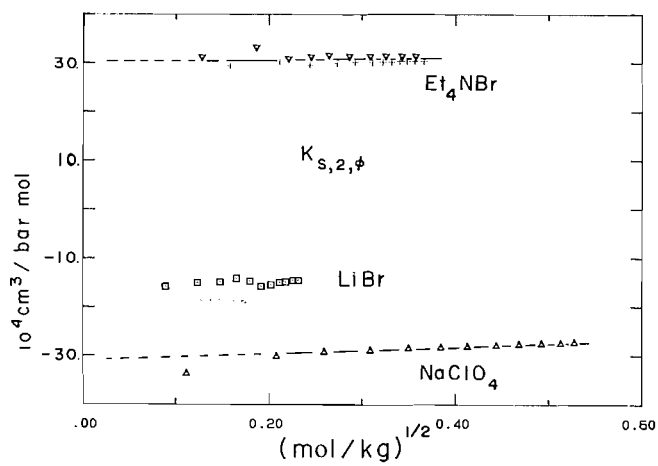

FIG. 2. Some typical plots of $K_{s,2,\phi}$ against the square root of the molality in PC at 25°C. Two sets of measurements were made with Et_4NBr and the presence of water in the LiBr solution affects the extrapolation.

Some examples of heat capacity data are shown in Fig. 1. These data were analyzed by least-squares and the derived parameters are given in Table 3. It should be noted that in the case of fully dissociated electrolytes the slopes A_c are on the average close to 6 $J\,K^{-1}\,mol^{-3/2}\,kg$, which is significantly smaller than in ACN.

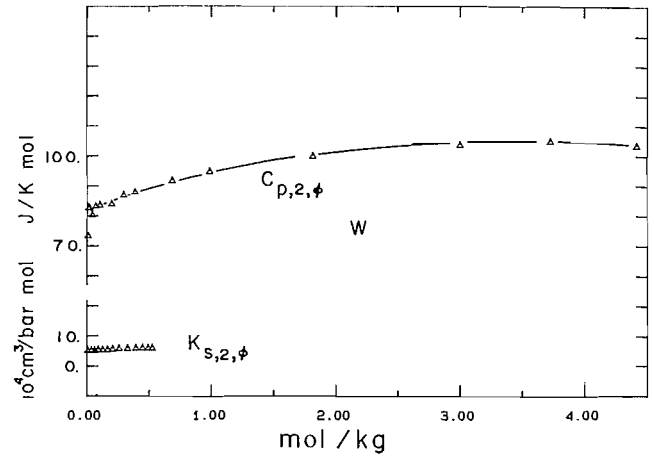

FIG. 3. The concentration dependence of $K_{s,2,\phi}$ and $C_{p,2,\phi}$ of water in PC at 25°C.

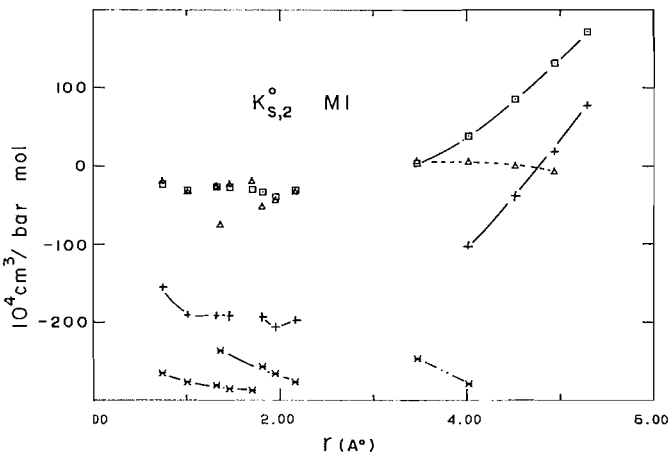

FIG. 4. The dependence of $K_{s,2}^0$ of alkali and tetraalkylammonium iodides on the cation ionic size: △ in water; + in ACN; □ in PC; * in MeOH.

Since very few reliable data exist in the literature on these systems, the only way of estimating the accuracy of the present data is through an ionic additivity scheme. The couples that could be used to check the additivity indicate a maximum error on heat capacities of 4 $J\,K^{-1}\,mol^{-1}$. The uncertainty on the data for LiBr seem somewhat larger than this value, probably because of the presence of water in the solid electrolyte. Also, the $K_{s,2}^0$ of Et_4NBr seems to be 5 to 10 × $10^{-4}\,cm^3\,bar^{-1}\,mol^{-1}$ too low when $K_{s,2}^0$ is plotted against the cations molecular weight.

Some difficulties were observed in some cases as a result of high viscosities, namely with $LiClO_4$ above 0.17 mol kg^{-1}, NaI and Pr_4NCl over the whole concentration range. Some LiBr seems to precipitate out above 0.10 mol kg^{-1} after standing for about 12 h. Also the solutions of Et_4NCl, below 0.3 mol kg^{-1} were slightly cloudy.

Some examples of plots of $K_{s,2,\phi}$ are shown in Fig. 2, and the derived parameters are given in Table 3. By the repetition of experiments and the additivity rule, the uncertainty on $K_{s,2}^0$ can be fixed at about 5 × $10^{-4}\,cm^3\,bar^{-1}\,mol^{-1}$. As in ACN (10), the data for LiBr are very sensitive to the presence of water, and $K_{s,2,\phi}$ seems to go through a maximum at low concentration. The infinite dilution value was therefore taken from the additivity rule. Other salts, such as Pr_4NCl and ϕ_4AsCl are also less reliable due to the presence of some water in the salts. As in the

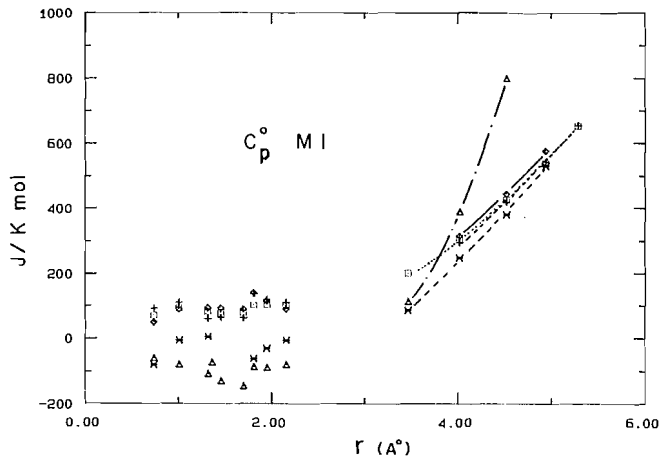

FIG. 5. The dependence of $C_{p,2}^0$ of alkali and tetraalkylammonium iodides on the cation ionic size: △ in water; + in ACN; □ in PC; * in MeOH; ◇ in DMF.

case of heat capacities, the parameters A_K are much smaller in PC than they were in ACN.

The heat capacities and compressibilities of water were also measured in PC and are shown in Fig. 3. As it was observed in other non-aqueous solvents (4, 18), $C_{p,2,\phi}$ has the same magnitude as the molar heat capacity of pure water and increases with increasing water concentration. The values of $K_{s,2,\phi}$, on the other hand remain fairly constant with water concentration in opposition to the corresponding values in lower alcohols (19).

Discussion

Thermodynamic properties can be quite informative on solute–solvent interactions. For this, it is important to examine the effect of solvent and different properties for the same electrolytes and, for each system, examine the effect of ionic size and compare anions with cations (20). It is with these objectives in mind that the present results will be examined.

Effect of ionic size

Through the additivity principle it is possible to obtain $K_{s,2}^0$ of most 1:1 electrolytes using the present results. For a common I^-, the effect of varying the cationic size on compressibilities is shown in Fig. 4 for the electrolytes in PC and compared with those in other typical solvents: water, ACN, and MeOH. Two main observations can be made on the PC data. Firstly, the data for alkali halides are very nearly the same in water and in PC but diverge significantly with tetraalkylammonium halides. Secondly, the trends with ionic size are similar for tetraalkylammonium halides in ACN and PC. The data in MeOH are much lower.

Criss and co-workers (8) have shown that with small ions there is a simple relationship between $K_{s,2}^0$ and β_s^* of the solvent and that, with the exception of lithium salts, $K_{s,2}^0$ increases slightly with ionic size in solvents of low compressibility. The present results on alkali halides are consistent with this. Since the compressibility of PC is similar to that of water, the similarity between $K_{s,2}^0$ of alkali halides in PC and in water is not unexpected and suggests that the particular structural effects that are characteristic of aqueous solutions are either not too sensitive to compressibilities or that they are largely accounted for in the compressibility of the pure solvent. With large organic ions like the tetraalkylammonium ions the increase with ionic size is, as in the case of other nonaqueous solvents, much more pronounced. These organic ions have a large intrinsic compressibility which is due primarily to the presence of compressible free space between the molecules. In this respect, the compressibility of these organic ions are not too different from those of a corresponding organic liquid. The observed difference between the $K_{s,2}^0$ of tetraalkylammonium iodides in PC and in ACN would then largely be due to I^-. In the case of aqueous solutions, the situation is quite different. Compressibilities are sensitive to hydrophobic hydration, and this hydration contribution largely cancels the intrinsic compressibility of the ions.

Through the additivity principle, the values of $C_{p,2}^0$ of most 1:1 electrolytes were also calculated and are plotted for the iodides against the cationic size in Fig. 5. The data in PC are now very similar to those in ACN and in DMF. The data in water are more negative with alkali halides and more positive with the tetraalkylammonium iodides. The data in MeOH fall somewhere in between water and the aprotic solvents.

The trends in Figs. 4 and 5 show that compressibilities and heat capacities are not sensitive to the same type of solvation effects. On the one hand, it appears that heat capacities are relatively insensitive to coulombic-type of ion–solvent interactions but very sensitive to structural hydration effects (structure-breaking and hydrophobic hydration) (20). The values of $C_{p,2}^0$ in non-aqueous solvents primarily reflect the intrinsic heat capacity and the Born polarization. This Born polarization (negative contribution) is much larger in MeOH than in aprotic solvents. In water, at low temperatures, the structure-breaking effect is at the origin of the negative $C_{p,2}^0$ of alkali ions and the hydrophobic effect predominates with R_4N^+. On the other hand, compressibilities are sensitive both to coulombic solvation and to structural effects. With alkali halides, the electrostatic interactions prevail in all solvents, while with R_4N^+ the hydrophobic hydration takes over in water.

Ionic contributions

Contrary to partial molar volumes (21), there are no direct methods of separating heat capacities and compressibilities into ionic contributions. As in the case of electrolytes in other non-aqueous solvents (4, 7–10), various approximate techniques can be used. For example, for heat capacities; (*1*) the method based on $C_{p,2}^0(\phi_4P^+) = C_{p,2}^0(\phi_4B^-)$ gives a value of $43\,J\,K^{-1}\,mol^{-1}$ for Br^-; (*2*) the extrapolation method of $C_{p,2}^0$ (R_4NBr) to zero cationic molecular weight gives a value for Br^- of $47\,J\,K^{-1}\,mol^{-1}$. (*3*) a comparison of $C_{p,2}^0$ (ϕ_4P^+) with $(4/3)C_{p,2}^0$ (ϕ_3CH) should also give an approximate value for Br^- in PC if the large ions and molecules are not solvated. The value obtained is $45\,J\,K^{-1}\,mol^{-1}$. All these approximate methods suggest that cations and anions of the same size have similar heat capacities in PC. Using the mean value $45\,J\,K^{-1}\,mol^{-1}$ for Br^-, ionic heat capacities in PC are given in Table 2. It should be stressed that this absolute scale is only approximate. For example, French and Criss (22) have presented evidence to show that the heat capacity of ϕ_4P^+ and ϕ_4B^- should actually differ by some $18\,J\,K^{-1}\,mol^{-1}$. These values are thus essentially conventional values which at the same time give the magnitude of the absolute values.

Essentially the same procedures used for heat capacities can be extended to compressibilities, if it can be assumed that large organic ions are unsolvated in PC: (*1*) the technique based on $K_{s,2}^0(\phi_4P^+) = K_{s,2}^0(\phi_4B^-)$ gives a value of $-5.6 \times 10^{-4}\,cm^3\,bar^{-1}\,mol^{-1}$ for Br^-; (*2*) the extrapolation method of $K_{s,2}^0$ (R_4NBr) gives $-58 \times 10^4\,cm^3\,bar^{-1}\,mol^{-1}$ for Br^-; (*3*) the comparison of $K_{s,2}^0(\phi_4P^+)$ with $(4/3)K_{s,2}^0(\phi_3CH)$ gives $-48 \times 10^{-4}\,cm^3\,bar^{-1}\,mol^{-1}$ for Br^-.

The agreement between the various techniques is far less

Can. J. Chem. Downloaded from www.nrcresearchpress.com by 78.46.186.204 on 09/07/12
For personal use only.

satisfactory with compressibilities than it was with heat capacities. This is a consequence of the larger dependence of compressibilities on solvation. Therefore, only conventional ionic values can be given. Since the compressibilities of dissociated acids in PC are not known the usual convention of taking the value for H^+ as zero is not possible and we have chosen the first procedure above to prepare Table 3.

Properties of water in non-aqueous solvents

The high heat capacity of liquid water is associated with the fluctuating structure of the liquid. Since no such structure exists in dilute solutions of water in non-aqueous solvent, a much lower value for $C_{p,2}^0$ of water in non-aqueous solvents is expected. As it is generally observed, the heat capacity of water remains comparable to that of the pure liquid down to very low concentrations. A possible explanation could be in terms of dimers or trimers of water in these systems. As the temperature is changed the concentration of dimers changes and this causes a relaxational contribution to $C_{p,2}$. Another approach is that of Berti *et al.* (23), who have investigated the volumes of water in a large number of solvents and have shown that V_w^0 are lower than the molar volume of water in polar solvents where the interactions are primarily with the polar group. In non-polar solvents the interactions are primarily with the hydrophobic part of the molecule and V_w^0 becomes larger than the molar volume. Such an approach can probably be extended to heat capacities and compressibilities but, unfortunately, most data in the literature has been extrapolated to infinite dilution from rather high water concentrations and no systematic trends can be observed with the polarity of the solvent. Further work along these lines is certainly desirable.

Acknowledgement

The authors are grateful to the Natural Sciences and Engineering Research Council of Canada for financial help.

1. W. H. Lee. Chemistry of non-aqueous solvents. Vol. 4. *Edited by* J. T. Lagoski. Academic Press, New York. 1976. Chap. 6.
2. H. V. Venkatasetty (*Editor*). Lithium battery technology. John Wiley, New York. 1984.
3. C. V. Krishnan and H. L. Friedman. Solute–solvent interactions. Vol. 2. *Edited by* J. F. Coetzee and C. D. Ritchie. Marcel Dekker, New York. 1976. Chap. 9.
4. R. Zana, J. E. Desnoyers, G. Perron, R. L. Kay, and K. Lee. J. Phys. Chem. **86**, 3996 (1982).
5. J. L. Fortier, P. A. Leduc, and J. E. Desnoyers. J. Solution Chem. **3**, 323 (1974).
6. F. J. Millero, G. K. Ward, and P. V. Chetirkin. J. Acoust. Soc. Am. **61**, 1492 (1977) and references cited therein.
7. A. J. Pasztor and C. M. Criss. J. Solution Chem. **7**, 27 (1978); C. Shin and C. M. Criss. J. Solution Chem. **7**, 205 (1978).
8. J. I. Lankford, W. T. Holladay, and C. M. Criss. J. Solution Chem. **13**, 699 (1984).
9. R. Zana, G. Perron, and J. E. Desnoyers. J. Solution Chem. **8**, 729 (1979).
10. I. Davidson, G. Perron, and J. E. Desnoyers. Can. J. Chem. **59**, 2212 (1981).
11. Y. S. Choi and C. M. Criss. Discuss. Faraday Soc. **64**, 204 (1978).
12. P. Picker, P. A. Leduc, P. R. Philip, and J. E. Desnoyers. J. Chem. Thermodyn. **3**, 631 (1971); J. E. Desnoyers, C. DeVisser, G. Perron, and P. Picker. J. Solution Chem. **5**, 605 (1976).
13. J. L. Fortier, G. C. Benson, and P. Picker. J. Chem. Thermodyn. **8**, 289 (1976).
14. G. Perron, F. Yamashita, M. A. Simard, and A. H. Roux. To be published.
15. V. A. Del Grosso and C. W. Mader. J. Acoust. Soc. Am. **52**, 1442 (1972).
16. H. Hoiland. J. Solution Chem. **6**, 291 (1977).
17. M. Jansen and H. L. Yeager. J. Phys. Chem. **77**, 3089 (1973); **78**, 1830 (1974).
18. C. De Visser, W. J. M. Heuvelslands, L. A. Dunn, and G. Somsen. J. Chem. Soc. Faraday Trans. I **74**, 1159 (1978).
19. J. Lara and J. E. Desnoyers. J. Solution Chem. **10**, 465 (1981).
20. J. E. Desnoyers and C. Jolicoeur. Treatise of electrochemistry. *Edited by* J. O'M. Bockris, B. E. Conway, and E. Yeager. Plenum Press, New York. 1982. Chap. 1.
21. R. Zana and E. Yeager. J. Phys. Chem. **71**, 521 (1967).
22. R. N. French and C. M. Criss. J. Solution Chem. **11**, 625 (1982).
23. P. Berti, S. Cabani, and V. Mollica. Fluid Phase Equil. To be published.

Can. J. Chem. Downloaded from www.nrcresearchpress.com by 78.46.186.204 on 09/07/12
For personal use only.

The structures of some sulphur-stabilized carbanions and stereoelectronic requirements for the formation of α-sulphonyl carbanions[1]

J. Stuart Grossert,[2] Jeffrey Hoyle,[3] T. Stanley Cameron,[2] Stephen P. Roe, and Beverly R. Vincent
Department of Chemistry, Dalhousie University, Halifax, N.S., Canada B3H 4J3

Received October 29, 1986

This paper is dedicated to Professor Douglas E. Ryan in honour of his 65th birthday

J. Stuart Grossert, Jeffrey Hoyle, T. Stanley Cameron, Stephen P. Roe, and Beverly R. Vincent. Can. J. Chem. **65**, 1407 (1987).

Relatively few structure determinations of α-sulphonyl stabilized carbanions have been reported. The salient features of these are summarized and discussed in the light of the X-ray crystal structures of the potassium salt from bis(methylsulfonyl)-3-(2,6-dimethoxypyridyl)sulfonylmethane (**5**), the carbon acid bis(methylsulphonyl-4-(1,3-dimethoxyphenyl)sulphonylmethane (**6**), the triethylammonium salt of 2-methylsulphonyl-2-phenylthio-1-(3-pyridyl)-1-ethanone (**7**), the carbon acid 2-methylsulphonyl-2-phenylthio-1-phenylethanone (**8**), and its triethylammonium salt (**9**). Results of these structure determinations show that the α-sulphonyl carbanion has a significantly shorter $^{-}C—SO_2$ bond distance than the free sulphone, but that the S—O bond distances are essentially unchanged. The coordination about the carbanionic carbon atoms is planar; these atoms can be described as interacting with the sulphur atoms in an ylid-like manner, with a barrier to rotation about the $^{-}C—SO_2$ bond. The sulphonyl oxygen atoms do interact to a significant degree with the counterion, but there is no close contact between the counterion and the carbanionic carbon atom. A comparison of the structures of **6** and **5**, or of **8** and **9**, permits an assessment to be made concerning the stereoelectronics of deprotonation reactions on carbon atoms adjacent to sulphones.

J. Stuart Grossert, Jeffrey Hoyle, T. Stanley Cameron, Stephen P. Roe et Beverly R. Vincent. Can. J. Chem. **65**, 1407 (1987).

Il y a relativement peu de structures de carbanions stabilisés par un groupement sulfonyle en α qui ont été déterminées. On résume leurs caractéristiques principales et on en discute en fonction des structures, déterminées par diffraction des rayons-X, du sel de potassium du bis(méthylsulfonyl) (diméthoxy-2,6 pyridyl)-3 sulfonylméthane (**5**), de l'acide carboné bis(méthylsulfonyl) (diméthoxy-1,3 phényl)-4 sulfonylméthane (**6**), du sel de triéthylammonium de la méthylsulfonyl-2 phénylthio-2 (pyridyl-3)-1 éthanone-1 (**7**), de l'acide carboné méthylsulfonyl-2 phénylthio-2 phényl-1 éthanone (**8**) et de son sel de triéthylammonium (**9**). Les résultats obtenus lors de ces déterminations de structure démontrent que la distance $^{-}C—SO_2$ est beaucoup plus courte dans l'anion que dans la sulfone libre; toutefois, les distances S—O sont essentiellement inchangées. La coordination autour des atomes de carbones carbanioniques est plane; on peut imaginer que ces atomes interagissent avec les atomes de soufre d'une manière qui ressemble à celle qui existe dans les ylides et il en résulte une barrière à la rotation autour de la liaison $^{-}C—SO_2$. Les atomes d'oxygène du sulfonyle interagissent beaucoup avec le contre-ion; toutefois, il n'y a pas de contact direct entre le contre-ion et l'atome de carbone carbanionique. Une comparaison des structures des composés **5** et **6** ou **8** et **9** permet de faire une évaluation relative aux facteurs stéréoélectroniques influencant les réactions de déprotonations qui se produisent sur des atomes de carbones adjacents à des sulfones.

[Traduit par la revue]

Can. J. Chem. Downloaded from www.nrcresearchpress.com by 72.64.146.136 on 09/07/12
For personal use only.

Introduction

The stabilization of carbanions by adjacent sulphur-containing moieties has been the subject of numerous studies (1–18). Calculations are at present limited to addressing the problem in the gas phase (10–14), and it would be useful to compare the results from calculations with data from the actual structures of anions in the solid state. It is, however, not a simple matter to gain insight into the actual structures of these carbanions (15, 17) and a limited number of solid-state structural studies have been reported (19–24). Since the reactions of sulphur-stabilized carbanions continue to attract the interest of synthetic chemists (8), further work on their structural features is merited. This paper reports on structural evidence obtained for two types of sulphur-stabilized carbanions, in one case involving only sulphonyl groups and, in the other, a combination of sulphenyl and sulphonyl groups. A brief summary of the structures of anions stabilized by these groups follows.

[1]Taken in part from the Ph.D. thesis of J.H., Dalhousie University, August 1984.

[2]General communications regarding this paper may be addressed to J.S.G.; communications regarding crystallographic details should be addressed to T.S.C.

[3]Current address: Nova Scotia College of Agriculture, Truro, N.S., Canada B2N 5E3.

Sulphenyl-stabilized carbanions

Recent theoretical calculations (10, 13) suggest that the optimum geometry of a sulphenyl-stabilized carbanion has a pyramidal structure at the carbanion, with the adjacent S—C bond being oriented in an *anti* conformation, **1***a*. This is

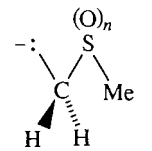

1*a* : $n = 0$
1*b* : $n = 2$

reminiscent of molecules that show an anomeric effect (hyperconjugative interaction). When the carbanion is formed, the anionic $^{-}C—S$ bond is shortened, while the adjacent S—C bond is lengthened. Experiment shows that dithiane rings are preferentially deprotonated and alkylated in an equatorial orientation (15, 16), but it is difficult to obtain detailed structural evidence since sulphenyl-stabilized carbanions are highly reactive species that are invariably formed by the use of strong organolithium bases. This results in the formation of complexed lithiated anions, for which calculations have not, so far as we are aware, been published. A crystal structure determination has been made on a lithiated dithiane derivative (23). It shows that the bonding about the lithiated carbon forms a distorted tetra-

Can. J. Chem. Downloaded from www.nrcresearchpress.com by 72.64.146.136 on 09/07/12
For personal use only.

hedron, and that the lithium atom interacts equally with the carbanionic carbon atom and a sulphur atom.

Carbanions stabilized by one sulphonyl group

The structures of sulphonyl-stabilized carbanions in solution have also been the subject of extensive experimental work (2, 6), but much of the recent chemical literature on these carbanions has emphasized their use as synthetic intermediates (4, 7, 8), after which the sulphur atom is discarded. Some recent papers (11, 13, 14, 17) have sought to shed further light on the structural problems, but these are not as yet completely solved. The experimental work comes from a group who have reported extensive spectroscopic studies (17) on the nature of carbanions (and associated counterions) adjacent to sulphinyl and sulphonyl groups. For the latter group of anions, the data provided reflect a lengthening of the S—O bond length with concomitant shortening of the C—S bond length. Chassaing *et al.* (17) interpreted these data as being due to delocalization of negative charge between the carbon and sulphonyl oxygen atoms, and suggested that these atoms are involved in a tridentate complex with a lithium cation, with the bonding about the carbanionic carbon showing tetrahedral character.

Two recent notes from Wolfe's laboratory address the structure of both free and lithiated carbanions stabilized by a sulphonyl group (11). The calculations suggested a shortening of the $^{-}$C—S bond of the free carbanion, **1***b*, as compared to the calculated C—S bond length in dimethyl sulphone.

Very recently, Bors and Streitwieser (14) have published their calculations on Me_2SO_2, on its monoanion (**1***b*), on $LiCH_2SO_2Me$ (**1***c*), and on the dilithio salts of the 1,1- and 1,3-dianions. The conclusion of these calculations is that *two* potential energy minima exist in **1***c*, one similar to the structure described by Wolfe *et al.* (11), and a second in which the lithium cation is complexed to both sulphone oxygen atoms, but not to the carbanionic carbon atom. In **1***c*, the structure of C_s symmetry with the lithium cation complexed to both sulphonyl oxygen atoms has an LiC—S bond that is 8.6% shorter, an S—Me bond that is 1.0% longer, and S—O bonds that are 4.4% longer than the corresponding bonds calculated for Me_2SO_2 (14).

Two recent communications (19, 20) report on determinations of the crystal structures of carbanions stabilized by only a single sulphonyl group; such species are unstable and are difficult to isolate as crystalline solids suitable for X-ray work. It is also of interest to note that the crystal structures of three lithium ester enolates (25), of two phenyl-stabilized free carbanions (26), and of several ketone enolates, with a range of metal counterions (27), have been published recently.

The lithium cations of $[TMEDA–Li]^+[Ph^-CHSO_2Ph]$ (**1***d*) (19),[4] a dimer complex, are coordinated by the two TMEDA nitrogen atoms and by both sulfonyl oxygen atoms; there is no bonding to be observed between the carbanionic carbon and the Li cation (cf. ref. 14). The $^{-}$C—S bond length is only 1.1% longer than the C=S bond in thioformaldehyde (19) and the S—O bond length "is only a little larger than that in sulphones," which is in accord with both spectroscopic results (17) and calculations (11, 14). In addition, coordination about the anionic carbon is planar.

The second structure to be reported on (20) is $[TMEDA–Li]^+[^-CH_2SO_2Ph]$ (**1***e*),[4] which likewise exists in the solid state as a dimer. The authors of this communication did succeed in finding both the hydrogen atoms on the anionic carbon atom, these three atoms being located in a plane that is orthogonal to the plane described by the anionic carbon and the Ph—S bond, in agreement with calculations (11, 14). Likewise, **1***e* has a short $^{-}$C—S bond[4] that is 12.2% shorter than the corresponding bond in its conjugate acid and is essentially identical with the length of a C=S bond (20). No increase in length of the S—O or S—Ph bonds could be detected when compared to those in $MeSO_2Ph$. As with **1***d*, the lithium cation is complexed only by the TMEDA and by the sulphonyl oxygen atoms.

Carbanions stabilized by several sulphonyl groups

There are three earlier reports of structures (21, 22, 24) having been determined for anions stabilized by multiple sulphonyl groups. The first of these, due to Hoogsteen (21), is not readily accessible, but reports carefully determined atomic parameters for the salt, $^{+}NH_4\ ^{-}C(SO_2Me)_3$, **2**.[4] The environ-

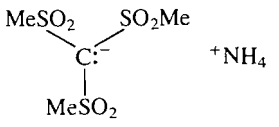

2

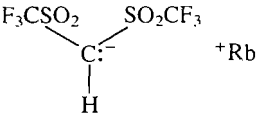

3

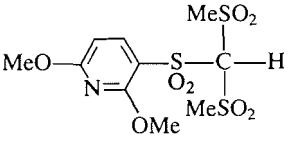

4

ment of the carbanionic carbon atom exhibits C_1 symmetry. The $^{-}$C—S bonds have lengths that can be compared with 1.83(1) Å for the HC—S bonds in the disordered structure of $(MeSO_2)_3CH$ (28), or with 1.834(4) Å for the equivalent C—S bond in $(EtSO_2)_3CH$ (29). These data suggest an approximate shortening of the C—S bond of 7% when the anion, **2**, is formed, which is about 2/3 of the bond shortening that occurs when only a single sulphone stabilizes the negative charge. The six S—O bonds are quite similar in length to the mean value of 1.434 Å quoted in ref. 19.[4] The three S—Me bonds in **2** may be compared to the S—Me bond length of 1.73(2) Å in its conjugate acid (28) or with 1.757(2) Å in $(MeSO_2CH_2)_2$ (30); this small increase when the anion is formed may be significant and is in accord with calculations (11, 14). Hoogsteen found that four of the sulphonyl oxygen atoms are located within a range of 2.85–2.93 Å from the ammonium ion, evidence of an $^{+}$N—H···O hydrogen bonding network in the crystal (31).

The second reported structure determination was carried out on the salt, $Rb^+\ ^{-}CH(SO_2CF_3)_2$, **3**, (22).[4] In this molecule, the rubidium cations are coordinated by the sulphonyl oxygen atoms, but not to the anionic carbon atoms. The third report is a preliminary communication from this laboratory (24) in which the preparation of bis(methylsulfonyl)-3-(2,6-dimethoxypyridyl)-sulfonylmethane (**4**) and the X-ray crystal structure determination of its potassium salt (**5**) were reported. We now present full details of this structure, plus the structures of bis(methylsulphonyl-4-(1,3-dimethoxyphenyl)sulphonylmethane (**6**), the triethylammonium salt of 2-methylsulphonyl-2-phenylthio-1-(3-pyridyl)-1-ethanone (**7**), the carbon acid 2-methylsulphonyl-2-

[4]Selected structural features are collected in Table 1. See footnote 6.

TABLE 2. Crystal data for compounds **5–9**

Parameter	Compound				
	5	**6**	**7**	**8**	**9**
Formula wt.	429.50	372.42	408.57	306.39	407.58
a (Å)	17.826(3)	8.888(3)	8.882(4)	8.184(2)	8.905(2)
b (Å)	6.919(3)	13.096(5)	9.175(5)	17.326(2)	9.386(3)
c (Å)	15.085(2)	14.983(3)	13.974(5)	10.831(2)	14.363(2)
α, deg	—	68.01(3)	97.56(4)	—	92.59(2)
β, deg	111.90(1)	81.45(2)	91.09(3)	106.92(3)	100.45(2)
γ, deg	—	72.60(3)	112.59(4)	—	113.75(2)
Z	4	4	2	4	2
V (Å^3)	1726.3(8)	1541.8(9)	1039.3(9)	1469.3(5)	1071.2(9)
d_c, g cm^{-3}*	1.652(1)	1.604(1)	1.305(1)	1.385(1)	1.264(1)
Space group	$P2_1/c$	$P\bar{1}$	$P\bar{1}$	$P2_1/a$	$P\bar{1}$
F(000), e′	888	776	436	640	436
μ, cm^{-1}†	6.99	5.06	2.75	3.59	2.66
Reflections:					
counted	2750	4355	4206	2346	3321
unique	2343	4170	3857	1989	3037
used (>3 esd)	1150	3060	2427	1520	2525
G	0.007092‡	0.0§	0.009726‡	0.0§	0.0§
R	0.033	0.0374	0.055	0.0384	0.0368
R_w	0.0331	0.0397	0.053	0.0382	0.0409

*Calculated density.
†MoK_{α_1} (λ = 0.70926 Å).
‡Structure solved by the SHELX program, weight = $[\sigma^2(F) + G(F)^2]^{-1}$; the value of G is initially set to 0.01 and is refined by the program; details can be found in ref. 38.
§Structure solved by the CRYSTALS program, weight = $[\sigma^2(F)]^{-1}$.

phenylthio-1-phenylethanone (**8**), and its triethylammonium salt (**9**).

Experimental

The compound **8** was prepared using a previously published procedure (32) and **9** was prepared by the treatment of **8** with triethylamine followed by recrystallization from aqueous ethanol. Compounds **4–7** were prepared by published methods (24, 33). Full details are available (34).[5] A Nonius CAD-4 four-circle diffractometer with an ω/2θ scan was used for all crystals to establish unit-cell dimensions and in the intensity data collections. Reflection data were reduced by routine procedures described previously (35). Lorentz and polarization factors were applied, but not absorption or extinction corrections. Partial structures were determined by the MULTAN-80 program (36), in which the E-maps having the highest figure-of-merit were chosen, and the maxima corresponding with nearly all non-hydrogen atoms were located. Other atoms were found on subsequent difference-Fourier maps. Scattering factors were taken from ref. 37. Full matrix least-squares refinements ($w\Delta F^2$ = min) were preformed with anisotropic temperature factors on the non-hydrogen atoms and isotropic temperature factors on the hydrogens. The converged refinements were based on reflections with $I > 3\sigma(I)$, where σ is the individual reflection e.s.d. derived from the counting statistics and the weighting schemes used are defined in Table 2. The SHELX-76 system (38) was used for the structure refinement calculations for compounds **5–7**. The CRYSTALS system (Issue V) (39) was used for the structure refinement calculations for compounds **8** and **9**.

Results and discussion

Crystal data for the five compounds investigated in this study are recorded in Table 2, selected bond lengths are given in Table 3, selected bond angles are in Table 4, while selected torsion angles are provided in Tables 5 and 6.[6] Figures 1–5 contain stereoscopic drawings to show the geometries of compounds **5–9**.[7] Examination of the structures of the five molecules reveals a number of interesting features. Foremost amongst these is the acidic central carbon atom in the carbon acid, **8**. This atom is bonded to electron-withdrawing groups and has an approximately tetrahedral bonding geometry. When the proton on this carbon atom is removed, the geometry about the resulting carbanionic carbon atom in **9** becomes approximately planar. Similar geometries, as appropriate, pertain to the anions **5** and **7**, and in the carbon acid **6**. Unfortunately, the structure of the carbon acid **4** could not be determined and the conjugate acid of **7** could not be isolated, thus preventing some direct comparisons. The planar environment of the carbanion carbon atom is consistent with theory (11, 13, 14), with the structure of Hoogsteen's salt (21), and with the structure of other stabilized carbanions (19, 20). The carbon acid, **6**, crystallized with two different molecules in each unit. These were quite similar, but some bond lengths are significantly different; these have been noted in Table 3, which provides values of selected bond lengths

[5]Complete details of the preparation, spectral characterization, and reactions of these compounds remain to be reported: J. S. Grossert, J. Hoyle, and P. K. Dubey, to be published.

[6]Selected bond lengths and angles as reported for compounds **1***d* (19), **1***e* (20), **2** (21), and **3** (22) have been collected and deposited (Table 1); sets of the positional parameters and isotropic thermal parameters (Tables 7–11), of the complete anisotropic thermal parameters (Tables 12–16), of the structure factor tables (Tables 17–21), plus full details of distances, bond angles, and torsion angles (Tables 22–26) for each molecule are available and may be purchased from the Depository of Unpublished Data, CISTI, National Research Council of Canada, Ottawa, Ont., Canada K1A 0S2.

[7]The stereoscopic drawings were produced by the SNOOPI program, a part of the CHEMGRAF system (Chemical Designs, Oxford, U.K.).

Can. J. Chem. Downloaded from www.nrcresearchpress.com by 72.64.146.136 on 09/07/12
For personal use only.

TABLE 3. Selected bond lengths (Å) for compounds **5–9**

Bond	Compound					
	5	**6**	**6′**	**7**	**8**	**9**
S1—C1	1.754(8)	1.732(6)	1.747(4)	1.755(3)	1.762(4)	1.769(4)
S1—C2	1.718(8)	1.848(4)	1.821(4)	1.744(3)	1.808(4)	1.742(3)
S2—C11	—	—	—	1.770(3)	1.771(4)	1.772(3)
S2—C2	—	—	—	1.734(3)	1.801(4)	1.736(3)
S3—C2	1.703(8)	1.815(4)	1.813(4)	—	—	—
S3—C4	1.757(8)	1.752(6)	1.752(6)	—	—	—
S4—C2	1.718(8)	1.837(4)	1.845(4)	—	—	—
S4—C21	1.762(6)	1.730(4)	1.748(4)	—	—	—
S1—O11	1.438(5)	1.427(4)	1.426(4)	1.446(2)	1.434(3)	1.445(2)
S1—O12	1.437(5)	1.423(4)	1.427(4)	1.433(2)	1.426(3)	1.445(2)
S3—O31	1.434(5)	1.426(3)	1.430(3)	—	—	—
S3—O32	1.437(5)	1.415(4)	1.426(3)	—	—	—
S4—O41	1.440(5)	1.426(3)	1.415(4)	—	—	—
S4—O42	1.431(5)	1.433(3)	1.431(3)	—	—	—
C2—H2	—	0.92(4)	0.91(4)	—	0.95(2)	—
C3—C2	—	—	—	1.396(4)	1.540(4)	1.403(4)
C3—C21	—	—	—	1.494(3)	1.501(4)	1.503(4)
C3—O3	—	—	—	1.263(3)	1.171(4)	1.266(3)

TABLE 4. Selected bond angles (in deg) for compounds **5–9**

Bond angle	Compound				
	5	**6**	**7**	**8**	**9**
O12—S1—O11	116.7(3)	119.6(2)	115.9(1)	118.1(2)	115.9(1)
O31—S3—O32	115.7(3)	116.1(2)	—	—	—
O42—S4—O41	116.3(3)	119.3(2)	—	—	—
C1—S1—C2	109.1(4)	106.4(2)	106.2(1)	107.5(2)	106.7(2)
C2—S2—C11	—	—	106.8(1)	103.9(2)	107.5(1)
C2—S3—C4	107.6(4)	105.8(2)	—	—	—
C2—S4—C21	108.0(3)	105.3(2)	—	—	—
C3—C2—H21	—	—	—	114(2)	—
C3—C2—S1	—	—	117.7(2)	113.5(3)	118.0(2)
C3—C2—S2	—	—	124.3(2)	107.5(3)	123.0(2)
C21—C3—C2	—	—	120.9(2)	116.6(3)	119.9(3)
C26—C21—C3	—	—	124.9(2)	116.9(4)	119.1(3)
C22—C21—C3	—	—	118.5(2)	123.3(4)	121.6(3)
S1—C2—S2	—	—	116.8(1)	112.5(2)	117.1(2)
S1—C2—S3	120.9(5)	112.0(2)	—	—	—
S1—C2—S4	118.6(5)	110.8(2)	—	—	—
S1—C2—H21	—	107(3)	—	103(2)	—
S2—C2—H21	—	—	—	107(2)	—
S3—C2—S4	120.9(5)	112.4(3)	—	—	—
O3—C3—C2	—	—	123.6(2)	120.0(3)	123.7(3)
O3—C3—C21	—	—	115.6(2)	123.3(4)	116.5(3)

in the molecules. Different aspects of the structures are detailed below.

Bond lengths

The S—Me bond lengths in $(MeSO_2CH_2)_2$ and $MeSO_2CH_2CH_2SO_2Ph$ are 1.757(2) Å (30) and 1.759(3) Å (40), respectively. These values are very similar to the S—Me bond lengths in a series of four substituted sulfones studied previously (33, 41), which average 1.759 Å. Examination of the seven S—Me bond lengths in **5–9** shows lengths that range from 1.732(6) to 1.769(4) Å (mean = 1.758 Å). The reason for one apparently short S—Me bond is not obvious.

In general, S—O bond lengths in sulphones are remarkably constant at a value of 1.439(14) Å (42), while a recent analysis of 53 bond lengths from the Cambridge Crystallographic Data Base gives a mean value of 1.434 Å (19). The nine S—O bond lengths in $(MeSO_2CH_2)_2$ (30), $MeSO_2CH_2CH_2SO_2Ph$ (40), $(EtSO_2)_3CH$ (29), and Me_2SO_2 (43) range from 1.439(3) to 1.452(2) Å with a mean of 1.445 Å. The mean of the six S—O bond lengths in the anion **5** was 1.436 Å, but that of the six S—O bond lengths in the carbon acid **6** was 1.425 Å. Both the *t*-test and analysis of variance show that these lengths are statistically different at the 0.5% confidence level. A similar set of tests on the S—O bonds in **7**, **8**, and **9** revealed that these bond lengths could not be distinguished with confidence as being different. Calculations (11, 14) suggest a lengthening of

Can. J. Chem. Downloaded from www.nrcresearchpress.com by 72.64.146.136 on 09/07/12
For personal use only.

TABLE 5. Selected torsion angles (in deg) for compounds **5** and **6**

Torsion angle*	**5**	**6**
S3—C2—S1—C1	121(1)	73(1)
S4—C2—S1—C1	−67(1)	−161(1)
S3—C2—S1—O11	−121(1)	−43(2)
S4—C2—S1—O11	51(1)	83(2)
S3—C2—S1—O12	7(1)	−172(1)
S4—C2—S1—O12	179(4)	−45(1)
S1—C2—S3—C4	−74(1)	76(1)
S4—C2—S3—C4	114(1)	−49(1)
S1—C2—S3—O31	43(1)	−166(1)
S1—C2—S3—O32	171(5)	−41(1)
S4—C2—S3—O31	−128(5)	68(2)
S4—C2—S3—O32	−1(1)	−166(1)
S1—C2—S4—C21	134(5)	73(1)
S3—C2—S4—C21	−54(1)	160(1)
S1—C2—S4—O41	−111(5)	−169(2)
S1—C2—S4—O42	17(1)	−42(1)
S3—C2—S4—O41	61(1)	−43(2)
S3—C2—S4—O42	−171(4)	84(1)
C2—S4—C21—C22	−115(1)	−119(2)
C2—S4—C21—C26	65(1)	63(2)
O41—S4—C21—C22	4(1)	128(2)
O41—S4—C21—C26	−176(1)	−50(2)
O42—S4—C21—C22	129(1)	−5(2)
O42—S4—C21—C26	−51(1)	177(2)

*Negative rotation is anticlockwise in A4—A3—A2—A1 when viewed down A2—A3.

TABLE 6. Selected torsion angles (in deg) for compounds **7–9**

Torsion angle*	**7**	**8**	**9**
S2—C2—S1—C1	−102(2)	−55(2)	99(2)
C3—C2—S1—C1	66(3)	67(2)	−66(1)
H21—C2—S1—C1	—	−169(2)	—
C3—C2—S1—O11	51(3)	−177(2)	51(2)
S2—C2—S1—O11	−142(2)	60(2)	−144(2)
H21—C2—S1—O11	—	−54(2)	—
C3—C2—S1—O12	179(2)	−51(2)	179(1)
S2—C2—S1—O12	−14(2)	−173(2)	−16(1)
H21—C2—S1—O12	—	73(2)	—
S1—C2—C3—C21	−178(2)	147(2)	−176(2)
S2—C2—C3—C21	15(3)	−88(1)	20(2)
H21—C2—C3—C21	—	30(2)	—
S1—C2—C3—O3	3(3)	−36(2)	5(2)
S2—C2—C3—O3	−164(2)	89(4)	−159(2)
H21—C2—C3—O3	—	−153(3)	—
S1—C2—S2—C11	87(2)	−114(2)	85(1)
C3—C2—S2—C11	−106(2)	121(2)	−111(1)
H21—C2—S2—C11	—	−2(3)	—
C2—C3—C21—C22	−141(3)	4(2)	55(2)
C2—C3—C21—C26	44(4)	−176(2)	−130(2)
O3—C3—C21—C26	−137(3)	7(2)	49(2)
C2—S2—C11—C12	−175(3)	51(2)	7(2)
C2—S2—C11—C16	5(2)	−133(2)	−173(1)

*Negative rotation is anticlockwise in A4—A3—A2—A1 when viewed down A2—A3.

the S—O bonds on the formation of an α-sulphonyl carbanion and this was possibly observed in the case of anion **1***d* (19), but not in the case of **1***e* (20). In addition, the spectroscopic results of Chassaing *et al.* (17, *vide supra*) must be considered; these offer carefully documented experimental evidence for the lengthening of the S—O bonds in α-lithio sulphones.

The salts **5**, **7**, and **9** offer an interesting series of compounds with which to compare the interaction of the cationic and anionic moieties. In the case of **5**, the potassium cation is separated from five of the sulphonyl oxygen atoms by distances varying between 2.695(5) and 3.125(5) Å. Water of crystallization coordinates to the potassium cation from two different sites, with the H_2O–K^+ distances being 2.860(5) and 2.780(5) Å respectively. There is no bonding between the potassium ion and the anionic carbon atom; in fact, the potassium ion is closer to two sulphur atoms and a second potassium cation (distances about 3.5 Å) than it is to any of the carbon atoms. The $^-$O–K^+ distances in the potassium enolate of pinacolone range from 2.568(2) to 2.661(3) Å (27), which are significantly shorter than those in **5**. This presumably, at least partly, reflects the high electron density on the oxygen atom of an enolate anion. Hydrogen-bonded interactions are apparent in the triethylammonium salts, **7** and **9**. Compound **7** exhibits an N(1)—H···O(3) distance of 1.972(4) Å and associated N—H—O angle of 165.3°, while **9** exhibits an N(1)—H···O(3) distance of 1.848(4) Å and associated N—H—O angle of 169.7°; these data are comparable to hydrogen bonds in other species between other trialkylammonium cations and oxygen atoms in various types of acceptor groups (31). Thus there is interaction between the triethylammonium ion and the enolate anion, but not to the sulphonyl oxygen atoms.

The shortening of the anionic carbon–sulphur bond vis-à-vis the C—S bond in sulphones became apparent even in the earlier crystal structure determinations of Hoogsteen (21) and Davøy *et al.* (22) despite relatively large uncertainties in the atomic positions. The mean of the $^-$C—SO_2Me bond lengths in Hoogsteen's salt (**2**) (1.701 Å) is not significantly different from the two $^-$C—SO_2Me bond lengths in structure **5**. Comparison of these bonds with the equivalent bond lengths in the carbon acid **6** shows an averaged decrease of 6.6% in the $^-$C—SO_2Me bond length on the formation of the anion (stabilized by three sulphonyl groups). This decrease can be compared to the corresponding decrease of 7% between $(MeSO_2)_3CH$ and Hoogsteen's salt (**2**), and the decrease of 12.2% between $MeSO_2Ph$ and **1***e* (*vide supra*). Calculations (11, 14) suggest a decrease of about 7.5% for the $^-$C—S bond length in an anion stabilized by a single sulphonyl group.

The anions **7** and **9** are more complex than the anion **5** in which the negative charge is only stabilized by sulphonyl groups. The $^-$C—SO_2Me bonds in the anions **7** and **9** average to a length of 1.743 Å, which is 3.6% shorter than the length of the equivalent C—S bond in the carbon acid **8**. In **7** and **9** the charge is also delocalized into the carbonyl, as is manifested by the 9.1% decrease in the C(2)—C(3) bond length, when compared to that in **8**. This may be compared with a shortening of about 11% in the corresponding C—C bond when ester lithium enolates are formed (25); given other sites for delocalization of charge in **7** and **9**, it is quite likely that this C—C bond shortening should be less than in an ester enolate. Of more interest is the fact that the phenylsulphenyl group also contributes to the charge stabilization since the mean of the $^-$C—SPh bond lengths in **7** and **9** is 3.7% shorter than the corresponding bond in **8**. The fact that phenylsulphenyl groups can stabilize negative charge has been discussed previously by Bordwell *et*

Can. J. Chem. Downloaded from www.nrcresearchpress.com by 72.64.146.136 on 09/07/12
For personal use only.

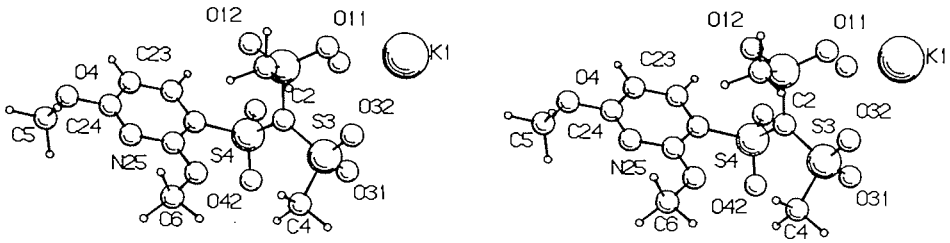

FIG. 1. The crystal structure of the potassium salt of bis(methylsulfonyl)-3-(2,6-dimethoxypyridyl)sulfonylmethane, **5**, as seen in a stereoscopic view.

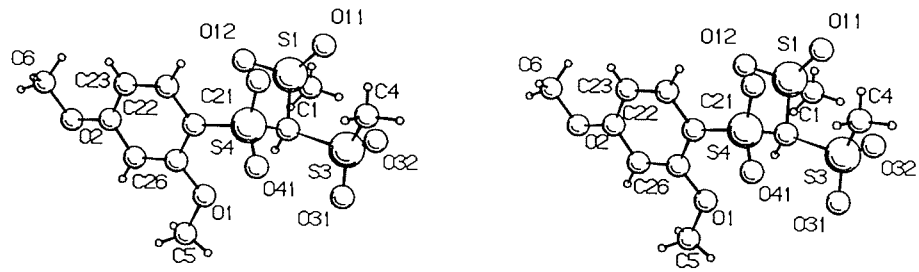

FIG. 2. A stereoscopic view of the crystal structure of bis(methylsulfonyl)-4-(1,3-dimethoxyphenyl)sulfonylmethane, **6**.

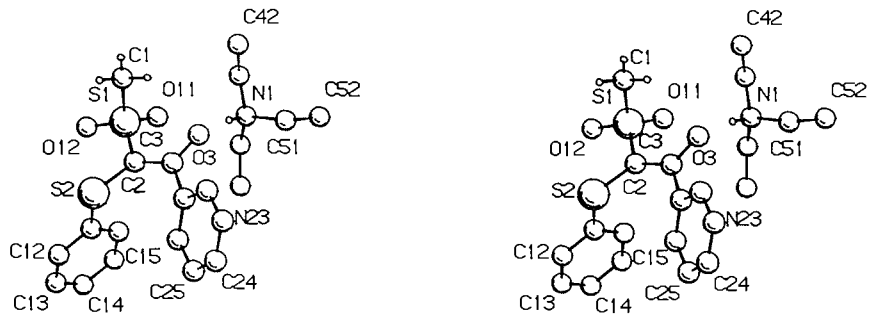

FIG. 3. The crystal structure of the triethylammonium salt of 2-methylsulphonyl-2-phenylthio-1-(3-pyridyl)-1-ethanone, **7**, as seen in a stereoscopic view.

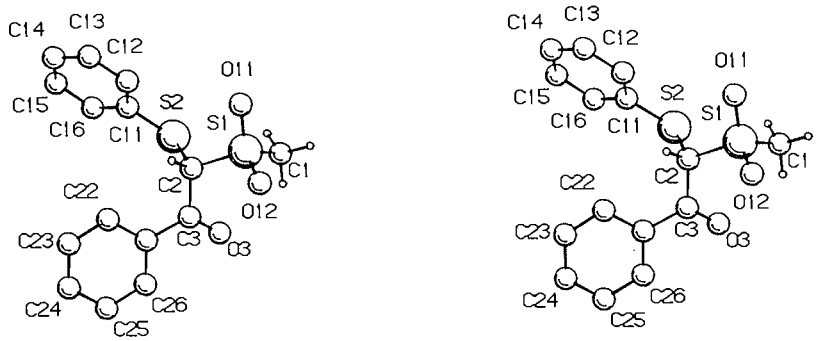

FIG. 4. A stereoscopic view of the crystal structure of 2-methylsulphonyl-2-phenylthio-1-phenylethanone, **8**.

al. (44). Wolfe's calculations (10) on Me_2S suggest a 4.7% shortening of the C—S bond when the anion is formed, but this is for a pyramidal anion, whereas the anionic carbon atoms in **7** and **9** are almost planar. We did not find any evidence for a lengthening of the S—Ph bond when comparing **7** and **9** with **8**. A 3.4% increase was found by Wolfe *et al.* (10) when comparing Me_2S and **1***a*, but this small increase could be diffused by more complex interactions with the phenyl ring. Finally, the mean of the carbonyl C=O bond lengths in **7** and **9** is 8.0% longer than the C=O bond in **8**. This may be compared to a 10% increase in the lengths of the corresponding bonds in ester lithium enolates (25) or an approximately 8% increase in the case of pinacolone enolates (27).[8]

Bond angles

Selected bond angles are summarized in Table 4.[6] The

[8]The length of the C=O bond in these enolates is dependent on the nature of the cation.

Can. J. Chem. Downloaded from www.nrcresearchpress.com by 72.64.146.136 on 09/07/12
For personal use only.

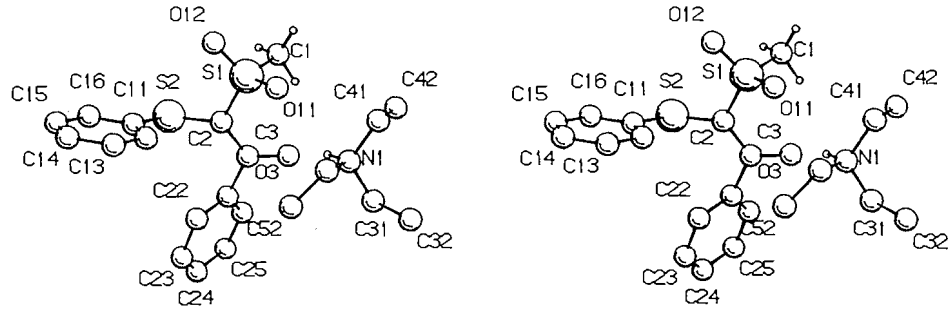

FIG. 5. The crystal structure of the triethylammonium salt of 2-methylsulphonyl-2-phenylthio-1-phenylethanone, **9**, as seen in a stereoscopic view.

S—C—S angles about the central anionic carbon atom in **5** total 359.5°, which is indicative of the fact that the bonding geometry about this atom is planar. Similar results obtain for the corresponding carbon atom in **7** and **9**, but in these cases the anion is much less symmetrical. The corresponding angles in Hoogsteen's anion, **2**, total 359.7° (21). All other angles are as expected, based on past precedent.

Torsion angles

A study of the dihedral angles in these five compounds (Tables 5 and 6) provides some interesting information,[6] especially when the projections outwards from C(2) along the three non-hydrogen bonds in structures **5**–**9** are compared. It is useful also to examine the orientations of the various aromatic rings with respect to their bonding to the remainder of the molecules. In a previous paper (33), we have commented on the considerable number of structures in which a polar group bound to one of the α carbon atoms is found to be *gauche* only to one of the oxygen atoms in a sulphone. This fact must reflect the strongly polar nature of the sulphonyl S—O bonds, although this is not the only factor that influences the orientation of groups in a structure, as not all sulphones exhibit this phenomenon (42, 45).[9]

Nonetheless, neither Hoogsteen's anion, **2** (21), nor **5** exhibit C_3 symmetry for the sulphonyl groups around the central carbon atom, but rather have the sulphonyl groups oriented so that one OSCS dihedral angle is essentially in an eclipsed conformation; no sulphur atom lies on the bisector of the OSO angle of any of the sulphonyl groups. However, in both the conjugate acid of **2**, and in **6**, at least one sulphur atom is *gauche* to any oxygen atom on an adjacent sulphonyl group. Importantly, the acidic proton is *gauche* to both oxygen atoms with respect to one sulphonyl group. It is noteworthy that there are three sulphonyl groups in **6**, yet H(21) is *gauche* to both oxygen atoms *only in the case of the C(2)—S(3) bond.* In **8**, H(21) is *gauche* to both oxygen atoms along the C(2)—S(1) bond. This orientation of a proton with respect to sulphonyl oxygen atoms is suggested to lead to greater kinetic acidity, both by calculation (11) and by experiment (1).

One of the C(2)—S bonds is almost eclipsed with an S(1)—O bond in the anions **5**, **7**, and **9**, the dihedral angles ranging from 7° to 16°, which is in contrast to the more symmetrical orientation for α-sulphonyl carbanions found by calculations (11, 14). Furthermore, the other two sulphonyl groups in **5** are arranged with S—C(2)—S—O dihedral angles of 1° and 17°, which

[9]J. S. Grossert, S. Sotheeswaran, and T. S. Cameron, to be published.

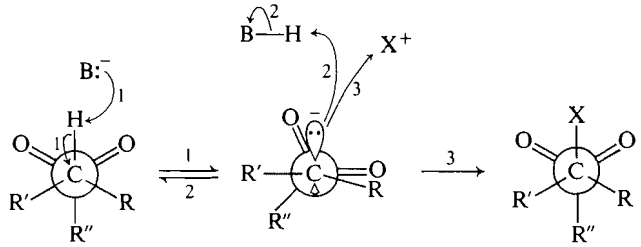

FIG. 6. Stereoelectronic requirements in the formation and reactions of α-sulphonyl carbanions from the species $RR'CHSO_2R''$ ($R \neq R'$), as viewed by means of Newman projections.

suggest some generality to the phenomenon. The anion of benzyl phenyl sulphone, **1***d*, shows the same asymmetry in the environment about the carbanionic center (19), whereas $^-CH_2SO_2Ph$, **1***e*, (20) is much more symmetrically oriented. As commented on by Boche *et al.* (19), this local chirality in unsymmetrically substituted, α-sulphonyl carbanions is undoubtedly the key factor in the retention of configuration in their formation, followed by subsequent protonation or alkylation reactions. These structures therefore provide good evidence for the stereoelectronic requirements of these reactions, as is illustrated in Fig. 6.

Finally, it should be noted that the carbanions represented by **7** and **9** indeed contain enolate anions, since atoms S(1)—C(2)—S(2) are coplanar with atoms C(21)—C(3)—O(3). However, *the aryl rings are twisted out of conjugation at angles of 40°–50° to the enolate anion system*, whereas the phenyl ring in **8** is almost coplanar with the carbonyl group, as expected for a benzoyl group. The aryl groups in both **5** and **6** are similarly arranged with respect to their adjacent sulphonyl groups, viz., essentially eclipsed with one of the S—O bonds; this is not so in the case of **1***e* (20).

Conclusions

It is interesting to recognize how earlier experimental results, which could be interpreted in terms of a planar, chiral structure for α-sulphonyl carbanions (1, 6), can now be understood from the series of structural studies reviewed and discussed in this paper. The general trends established by calculations (10–14), experiments (15, 17, 18), and crystal structure determinations (19–24) are in agreement. Results from calculations are increasingly becoming closer to experimental results, and will no doubt improve further when it is possible to do calculations on cations with a complete set of coordinating ligands.

The most acidic proton α to a sulphonyl group is that which lies in the bisector of the OSO angle; removal of such a proton is

Can. J. Chem. Downloaded from www.nrcresearchpress.com by 72.64.146.136 on 09/07/12
For personal use only.

both kinetically and thermodynamically favoured. On removal of this proton, it is necessary for one of the ^{-}C—R bonds to be able to become approximately coplanar with one of the S—O bonds (see Fig. 6), and the inability to achieve this is the likely cause of a recently announced cleavage reaction in the attempted formation, in a five-membered ring, of an anion between two sulphonyl groups (46). It is apparently possible to remove protons in other conformations with respect to the sulphonyl oxygen atoms, but such a reaction must be less facile.

Once formed in its preferred conformation, the anion is configurationally stable under normal conditions due to a kinetic barrier to rotation about the $^{-}C—SO_2$ bond. The anions are chiral if the carbanionic carbon is disubstituted with different ligands, the carbanionic carbon atom being stabilized by a polar interaction between the sulphur and carbon atoms. The concept that the anion is ylid-like, with greater electron density on the carbon atom (4), is a good working model for the structure of these species. Reaction of the anion with an electrophile would normally take place along the same trajectory as that along which the proton was removed, as shown in Fig. 6.

Finally, the interactions between the sulphonyl oxygen atoms and the cation must be considered. The Li^{+}—O distances in the sulphur-stabilized anions **1***d* and **1***e* (19, 20) are very similar to the corresponding distance in lithium enolates (25, 27), which suggests a significant concentration of electron density on the oxygen atoms in α-sulphonyl carbanions. However, the oxygen atoms in neutral sulphones are very weakly basic (7), and nucleophilic interactions with electrophiles are also very weak (7, 47), except in special circumstances (48).

The results presented in this work show quite clearly that the formation of an α-sulphonyl carbanion does not produce a significant change in the electron density *between* the sulphur and the oxygen atoms. The carbanionic carbon atom is electron rich and, if this atom is substituted with two different ligands, has a chiral environment. These are the facts that distinguish α-sulphonyl carbanions from enolate anions.

Acknowledgements

The authors gratefully acknowledge financial support from NSERC of Canada in the form of operating grants (to J.S.G. and T.S.C.), an infrastructure grant (to T.S.C.), and a graduate research fellowship (to B.R.V.). The Izaak Walton Killam Memorial Trust awarded predoctoral fellowships to J.H. and B.R.V., and Mrs. Wanda Tacreiter gave expert technical assistance.

1. E. J. Corey and T. H. Lowry. Tetrahedron Lett. 793 (1965).
2. B. S. Thyagarajan. Mech. React. Sulfur Compd. **4**, 115 (1969).
3. S. Wolfe. Acc. Chem. Res. **5**, 102 (1972).
4. P. D. Magnus. Tetrahedron, **33**, 2019 (1977).
5. W. Tagaki, S. Oae, W. E. Truce, T. C. Klinger, and W. W. Brand. *In* Organic chemistry of sulphur. *Edited by* S. Oae. Plenum, New York. 1977.
6. E. Block. Reactions of organosulfur compounds. Academic Press, New York. 1978. pp. 36–56.
7. T. Durst. *In* Comprehensive organic chemistry. Vol. 3. *Edited by* D. N. Jones. Pergamon, Oxford. 1979. pp. 171–195.
8. B. M. Trost and N. R. Schmuff. J. Am. Chem. Soc. **107**, 395 (1985); J. B. Hendrickson, G. J. Boudreaux, and P. S. Palumbo. J. Am. Chem. Soc. **108**, 2358 (1986); B. M. Trost and M. R. Ghadiri. J. Am. Chem. Soc. **108**, 1098 (1986).
9. N. D. Epiotis, W. R. Cherry, S. Shaik, R. Yates, and F. Bernardi. Fortschr. Chem. Forsch. **70**, 185 (1977); J. M. Lehn and G. Wipff. J. Am. Chem. Soc. **98**, 7498 (1976).
10. S. Wolfe, L. A. LaJohn, F. Bernardi, A. Mangini, and G. Tonachini. Tetrahedron Lett. **24**, 3789 (1983).
11. S. Wolfe, A. Stolow, and L. A. LaJohn. Tetrahedron Lett. **24**, 4017 (1983); S. Wolfe, L. A. LaJohn, and D. F. Weaver. Tetrahedron Lett. **25**, 2863 (1984).
12. S. Wolfe, A. Stolow, and L. A. LaJohn. Can. J. Chem. **62**, 1470 (1984).
13. S. Wolfe. Stud. Org. Chem. (Amsterdam), **19**, 133 (1985).
14. D. A. Bors and A. Streitwieser, Jr. J. Am. Chem. Soc. **108**, 1397 (1986).
15. A. G. Abatjoglou, E. L. Eliel, and L. F. Kuyper. J. Am. Chem. Soc. **99**, 8262 (1977).
16. D. Seebach. Synthesis, 11 (1969); E. J. Corey. J. Org. Chem. **40**, 231 (1975); B.-Th. Grobel and D. Seebach. Synthesis, 357 (1977).
17. G. Chassaing, A. Marquet, J. Corset, and F. Froment. J. Organomet. Chem. **232**, 293 (1982).
18. F. G. Bordwell, J. C. Branca, C. R. Johnson, and N. R. Vanier. J. Org. Chem. **45**, 3884 (1980).
19. G. Boche, M. Marsch, K. Harms, and G. D. Sheldrick. Angew. Chem. Int. Ed. Engl. **24**, 573 (1985).
20. H.-J. Gais, H. J. Lindner, and J. Vollhardt. Angew. Chem. Int. Ed. Engl. **24**, 859 (1985).
21. K. Hoogsteen. Ph.D. thesis, Rijksuniversiteit te Groningen, The Netherlands. 1957.
22. K. T. Davøy, T. Gramstad, and S. Husebye. Acta. Chem. Scand. Ser. A, **33**, 359 (1979).
23. R. Amstutz, D. Seebach, P. Seiler, B. Schweizer, and J. D. Dunitz. Angew. Chem. Int. Ed. Engl. **19**, 53 (1980).
24. J. S. Grossert, J. Hoyle, M. M. Bharadwaj, and T. S. Cameron. J. Chem. Soc. Chem. Commun. 1175 (1982).
25. D. Seebach, R. Amstutz, T. Laube, W. B. Schweizer, and J. D. Dunitz. J. Am. Chem. Soc. **107**, 5403 (1985).
26. M. M. Olmstead and P. P. Power. J. Am. Chem. Soc. **107**, 2174 (1985).
27. P. G. Williard and J. M. Salvino. J. Chem. Soc. Chem. Commun. 153 (1986); P. G. Williard and G. B. Carpenter. J. Am. Chem. Soc. **108**, 462 (1986).
28. J. V. Silverton, D. T. Gibson, and S. C. Abrahams. Acta Crystallogr. **19**, 651 (1965).
29. D. T. McGregor and J. C. Speakman. Acta Crystallogr. Sect. B: Struct. Crystallogr. Cryst. Chem. **25**, 540 (1969).
30. F. Mo and Ø. Berg. Acta Chem. Scand. Ser. A, **36**, 6557 (1982).
31. R. Taylor and O. Kennard. Acc. Chem. Res. **17**, 320 (1984).
32. J. S. Grossert and P. K. Dubey. J. Chem. Soc. Chem. Commun. 1183 (1982).
33. J. S. Grossert, P. K. Dubey, G. H. Gill, T. S. Cameron, and P. A. Gardner. Can. J. Chem. **62**, 798 (1984).
34. J. Hoyle. Ph.D. thesis, Dalhousie University, Halifax. August 1984.
35. T. S. Cameron and R. E. Cordes. Acta Crystallogr. Sect. B: Struct. Crystallogr. Cryst. Chem. **35**, 748 (1979).
36. G. Germaine, P. Main, and M. M. Woolfson. Acta Crystallogr. Sect. A: Cryst. Phys. Diffr. Theor. Gen. Crystallogr. **27**, 368 (1971).
37. International tables for X-ray crystallography. Vol. 3. The Kynoch Press, Birmingham, England. 1962.
38. G. Sheldrick. X-ray system report. University Chemical Laboratory, Cambridge, England. 1976.
39. J. R. Carruthers and D. J. Watkin. Acta Crystallogr. Sect. A: Cryst. Phys. Diffr. Theor. Gen. Crystallogr. **35**, 698 (1979).
40. F. Mo and A. Gaasdal. Acta Crystallogr. Sect. B: Struct. Crystallogr. Cryst. Chem. **36**, 2349 (1980).
41. J. S. Grossert, M. M. Bharadwaj, J. B. Faught, and A. Terzis. Can. J. Chem. **58**, 1106 (1980).
42. I. Hargittai. Sulphone molecular structures. Springer Verlag, Berlin. 1978.

Can. J. Chem. Downloaded from www.nrcresearchpress.com by 72.64.146.136 on 09/07/12
For personal use only.

43. D. A. LANGS, J. V. SILVERTON, and W. M. BRIGHT. J. Chem. Soc. Chem. Commun. 1653 (1970).
44. F. G. BORDWELL, G. E. DRUCKER, and G. J. MCCOLLUM. J. Org. Chem. **47**, 2504 (1982).
45. G. D. ANDREETTI, G. BOCELLI, and P. SGARABOTTO. Cryst. Struct. Commun. **6**, 89 (1977).
46. A. BERLIN, S. BRADAMANTE, R. FERRACCIOLI, and G. A. PAGANI. J. Chem. Soc. Chem. Commun. 1191 (1986).
47. J. W. DALLINGA and J. B. F. N. ENGBERTS. Spectrochim. Acta, Part A, **30**, 1923 (1974); W. KARZIJN and J. B. F. N. ENGBERTS. Recl. Trav. Chim. Pays-Bas, **96**, 95 (1977).
48. J. I. G. CADOGAN, D. K. CAMERON, I. GOSNEY, R. M. HIGHCOCK, and S. F. NEWLANDS. J. Chem. Soc. Chem. Commun. 766 (1986).

Can. J. Chem. Downloaded from www.nrcresearchpress.com by 72.64.146.136 on 09/07/12
For personal use only.

Two dimensional fluorescent sensors: the different dependences of the fluorescence band position and the fluorescence quantum yield of 1,5-diphenyl-3-vinyl-Δ^2-pyrazoline upon solvent dipolarity and hydrogen bond acidity

MERINNAGE DAYAL PREMAKUMARA DE COSTA, AMILRA PRASANNA DE SILVA,[1] AND SURAM THERESE PATHIRANA

Chemistry Department, Queen's University, Belfast BT9 5AG, Northern Ireland and Chemistry Department, University of Colombo, P.O. Box 1490, Colombo 3, Sri Lanka

Received November 4, 1986

MERINNAGE DAYAL PREMAKUMARA DE COSTA, AMILRA PRASANNA DE SILVA, and SURAM THERESE PATHIRANA. Can. J. Chem. **65**, 1416 (1987).

1,5-Diphenyl-3-vinyl-Δ^2-pyrazoline (**1**) has a fluorescence quantum yield (ϕ_F) which is strongly controlled by the hydrogen bond acidity of the solvent (α) and to a minor extent by the dipolarity of the solvent (π^*) according to the equation:

$$\log [(\phi_{F\text{aprotic}}/\phi_F) - 1] = 0.44(\pi^* + 6.1\alpha) - 2.03$$

The wavenumber of the fluorescence band maximum ($\bar{\nu}_F$) is controlled nearly equally by π^* and α according to the equation:

$$\bar{\nu}_F = -1.9(\pi^* + 1.1\alpha) + 23.7$$

Thus the fluorescence spectrum of **1** delivers two distinct and independent parameters of its microenvironment while its electronic absorption spectrum is essentially solvent invariant.

MERINNAGE DAYAL PREMAKUMARA DE COSTA, AMILRA PRASANNA DE SILVA et SURAM THERESE PATHIRANA. Can. J. Chem. **65**, 1416 (1987).

Le rendement quantique de la fluorescence (ϕ_F) de la diphényl-1,5 vinyl-3 Δ^2-pyrazoline (**1**) est fortement assujetti au contrôle de l'acidité de la liaison hydrogène du solvant (α) et, à un degré moindre, à celui du caractère dipolaire du solvant (π^*); ces facteurs sont reliés par l'équation suivante:

$$\log [(\phi_{F\text{aprotique}}/\phi_F) - 1] = 0{,}44(\pi^* + 6{,}1\alpha) - 2{,}03$$

Le nombre d'onde du maximum de la bande de fluorescence ($\bar{\nu}_F$) est assujetti à un contrôle à peu près égal de la part de π^* et de α: ces divers facteurs sont reliés entre eux par l'équation suivante:

$$\bar{\nu}_F = -1{,}9(\pi^* + 1{,}1\alpha) + 23{,}7$$

Ainsi, le spectre de fluorescence du composé **1** fournit deux paramètres distincts et indépendants de son microenvironnement: par ailleurs, son spectre d'absorption électronique ne varie pratiquement pas avec le solvant.

[Traduit par la revue]

Introduction

Fluorescent molecular sensors possess several advantageous features which are well suited to the study of dynamic microheterogeneous systems (1), examples of which are common in many areas of chemistry and biology. The features are (*a*) high spatial resolution (nanometer), (*b*) high temporal resolution (nanosecond), (*c*) extreme sensitivity (single molecule detection is now possible (2)), (*d*) good selectivity of detection, and (*e*) non-destructive and virtually non-invasive nature (mainly in the biological, rather than chemical context).

A fluorescent sensor molecule delivers information about its immediate microenvironment to a remote controller/observer. However, in general the exact location of the sensor is unknown (except for highly qualitative hydrophilicity/hydrophobicity arguments) and so the information remains uninterpretable. Thus (*a*) the lack of methods to determine the location of the sensor, or (*b*) the lack of specific targeting/anchoring strategies for sensors hamper the widespread rational use of fluorescent sensors. The latter problem can be tackled in specific instances by covalently binding the sensor to a chemically reactive location or by building the sensor into a specific point in a building block of the microheterogeneous system by organic synthesis (as in functionalized micelles (3)). The former problem remains unsolved in general.

A corollary of these general problems can be appreciated when we recognize that many fluorescent (and other) sensors deliver only one microenvironmental property per sensor. Two microenvironmental properties determined by two sensors bear no relation to one another because they concern two different locations. One solution to this is to employ a sensor molecule which can be operated on by two spectroscopic methods, several such sensors being available (4). However, to be useful the two spectroscopic methods must deliver two different kinds of microenvironmental information and that has not been always appreciated. We now improve this approach by demonstrating that a single sensor molecule operated in a single spectroscopic (fluorescence emission) mode can be made to simultaneously deliver information about two distinct and independent microenvironmental properties, i.e. fluorescent sensing in two dimensions. These two microenvironmental properties will show a one-to-one correspondence since both refer to the same location. A steady state fluorescence emission spectrum is a data file from which at least three quasi-independent spectral parameters (position of band maximum, maximum band height (or quantum yield) and band width)) can be extracted. In judiciously chosen cases each one of these can be made to be sensitive to a specific microenvironmental property or a combination of several. The utility of this concept of multidimensional fluorescent sensors can be further enhanced with the availability of time as an additional spectral parameter.

Results and discussion

Perusal of Table 1 indicates the essential invariance of the fluorescence quantum yield (ϕ_F) of 1,5-diphenyl-3-vinyl-Δ^2-

[1]To whom all correspondence should be addressed at Queen's University.

Can. J. Chem. Downloaded from www.nrcresearchpress.com by 78.46.186.204 on 09/07/12
For personal use only.

TABLE 1. Electronic spectral data of **1**[a]

Entry	Medium	π^*[b]	α[b]	$\bar{\nu}_{abs}$[c] (10^3 cm^{-1})	$\bar{\nu}_F$[d] (10^3 cm^{-1})	ϕ_F
1	Hexane	−0.08	0.00	29.2	23.8	0.59
2	Toluene	0.54	0.00	29.2	23.1	0.61
3	Ethyl Acetate	0.55	0.00	29.2	22.5	0.66
4	Dichloromethane	0.80	0.22	29.0	22.0	0.68
5	Acetonitrile	0.85	0.15	29.2	21.7	0.60
6	Dimethylformamide (DMF)	0.88	0.00	29.2	21.5	0.72
7	Formamide	0.98	0.66	29.2	20.5	0.25
8	*t*-Butanol	0.41	0.62	29.1	21.4	0.37
9	*i*-Propanol	0.46	0.78	29.0	21.2	0.24
10	Methanol	0.60	0.98	29.2	20.5	0.07
11	DMF–Water (1:1, v/v)	—	—	29.2	19.5	0.20[e]
12	DMF–D_2O (1:1, v/v)	—	—	29.2	19.5	0.33[e]
13	SLS micelles[f]	—	—	29.4	21.0	0.18

[a] 10^{-5} *M* solutions of **1** at 29°C in aerated solvents purified according to ref. 22.
[b] From ref. 7.
[c] The extinction coefficient is essentially solvent invariant with $\epsilon_{max} = 20\,000 \pm 3\,000\,M^{-1}\,cm^{-1}$.
[d] Excitation wavelength = 342 nm; uncertainty in $\bar{\nu}_F = 0.2 \times 10^3\,cm^{-1}$.
[e] The kinetic isotope effect (k_H/k_D) is calculated using the expression $k_H/k_D = (1/\phi_{FH} - 1)/(1/\phi_{FD} - 1)$ neglecting all radiationless processes except hydrogen bonding and is found to be 2.0.
[f] 0.02 *M* sodium lauryl sulphate in water, critical micellar concentration = 0.0081 *M*, from ref. 23.

pyrazoline (**1**) in aprotic solvents whereas the protic solvents possessing O—H or N—H bonds cause significant quenching. In particular, we note that ϕ_F in all of the aprotic solvents (entries 1–6 in Table 1) obeys the relation [1]

[1] $\phi_F = 0.64$
SD = 0.048, $n = 6$

$\phi_{Faprotic}$ is obtained by averaging the ϕ_F values in all of the aprotic solvents. The scatter of ϕ_F values within this group of solvents appears random (see the aprotic solvent region in Fig. 1) and is in accord with the model given below. The scatter is attributed to the experimental error of 10% in the determination of quantum yields due to the spectral correction procedure. The constancy of ϕ_F values of 1-phenyl-Δ^2-pyrazolines in aprotic solvents is supported by the data in Table 2 for **2**, X = H.

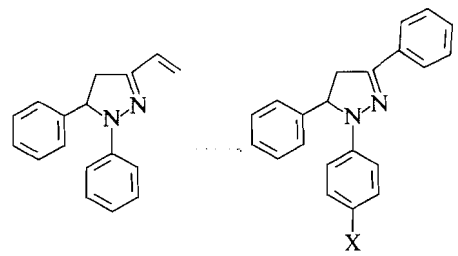

1 **2**

In order to quantitatively interpret the variation of ϕ_F in protic solvents and the variation of $\bar{\nu}_F$ in all solvents we make use of the following reasonable model. 1,3-Diaryl-Δ^2-pyrazolines show a significant degree of internal charge transfer in their lowest excited singlet state (refs. 5*a–d*, internal charge transfer states are discussed in ref. 5*e*). In particular, the charge separation is such that a substantial negative charge builds up on the N(2) and C(3) centres, which in turn should lead to an enhanced availability of the lone electron pair on N(2) towards a hydrogen bond donor solvent. Thus, excitation of **1** leads to the strengthening of the hydrogen bond between N(2) and the protic solvent, which results in the radiationless

TABLE 2. Electronic spectral data of **2**, X = H[a]

Solvent	$\bar{\nu}_{abs}$ (10^3 cm^{-1})	$\bar{\nu}_F$ (10^3 cm^{-1})	ϕ_F
Hexane	28.2	23.5	0.62
Toluene	27.6	22.6	0.57
Ethyl acetate	28.0	21.9	0.62
Dichloromethane	27.9	21.8	0.66
Dimethylformamide	27.6	21.5	0.68

[a] All conditions as for Table 1, except for excitation wavelength = 358 nm.

deactivation of the singlet state of **1**. Radiationless deactivations involving hydrogen bonding are known (6). The ϕ_F values of **1** are expected to remain uniformly high in aprotic solvents where such powerful hydrogen bonding effects are absent. Equation [2] therefore applies to protic solvents whereas eq. [3] is valid for aprotic solvents where k_H is absent (Scheme 1).

[2] $\phi_F = k_F/(k_F + k_d + k_H)$

[3] $\phi_{Faprotic} = k_F/(k_F + k_d)$

k_F, k_H, and k_d are the rate constants for excited state decay via fluorescence, solvent hydrogen bonding and other radiationless channels respectively. It is assumed that k_F and k_d are solvent independent to a first approximation (in spite of eq. [10]). Fluorescence lifetime (τ_F) data, if available, would obviate the need for this assumption by evaluation of eqs. [2]–[5].

[4] $\tau_F = (k_F + k_d + k_H)^{-1}$

[5] $\tau_{Faprotic} = (k_F + k_d)^{-1}$

The above model is justified by the observation of a solvent kinetic (deuterium) isotope effect of 2.0 on k_H (entries 11 and 12 in Table 1) which clearly shows the stretching of the O—H bond of the solvent by interaction with the lowest excited singlet state of **1**.

From Scheme 1 we see that k_H will be controlled largely by

Can. J. Chem. Downloaded from www.nrcresearchpress.com by 78.46.186.204 on 09/07/12
For personal use only.

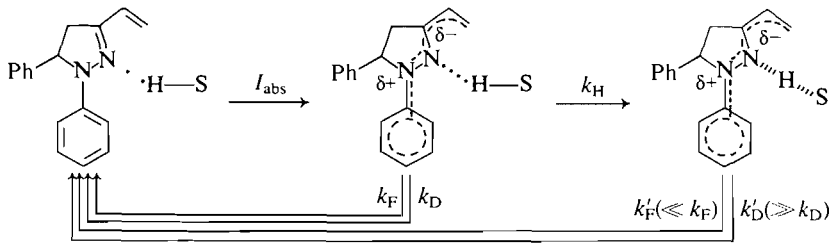

SCHEME 1

the solvent hydrogen bond acidity, α (7), though a minor dependence on the solvent dipolarity, π^* (7) is also to be expected in view of the orientation of the solvent molecule by dipole–dipole interaction which would maximize the hydrogen bonding. Casting this statement into the form of a linear free energy relationship gives eq. [6].

$$[6] \quad \log k_H = A(\pi^* + k\alpha) + B'$$

where A, k, and B' are adjustable parameters. The combination of eqs. [2], [3], and [6] gives eq. [7].

$$[7] \quad \log [(\phi_{Faprotic}/\phi_F) - 1] = A(\pi^* + k\alpha) + B$$

where $B = B' - \log (k_F + k_d)$. We have evaluated the three-parameter eq. [7] in a preliminary manner by the use of the four protic solvents (entries 7–10 in Table 1) which yields eq. [8] (with the aid of eq. [1]).

$$[8] \quad \log [(\phi_{Faprotic}/\phi_F) - 1] = 0.44(\pi^* + 6.1\alpha) - 2.03$$

$$SD = 0.058, \quad r = 0.994, \quad n = 4$$

It is important to note that eq. [7] can be tested with reasonable accuracy only for those solvents which give ϕ_F values which clearly deviate from $\phi_{Faprotic}$ and zero. The logarithmic term cannot be evaluated with confidence as these two limits are approached. Figure 1 combines equations [1] and [8] and clearly shows the difference between protic and aprotic solvent classes. Further work is planned with more solvents as well as with other fluors with instrumentation which will allow the determination of ϕ_F with lower error limits, which should reduce the scatter in $\phi_{Faprotic}$.

Among the Δ^2-pyrazolines (8, 9), **1** shows this hydrogen bonding-induced fluorescence quenching to an extreme extent because of the limited delocalization afforded by the 3-vinyl group which leaves much of the negative charge concentrated on N(2) in the excited state of **1**. **1** shows nearly complete switching ("on–off") behaviour when compared in hexane and methanol (a switching factor of 9 in ϕ_F — entries 1 and 10 in Table 1). Many other Δ^2-pyrazolines give lower switching factors (8, 9) though there are several exceptions in **2**, X = $NHCOCH_3$, NH_2, and OCH_3 (9). However, these have not received close scrutiny.

As seen from Scheme 1, the fluorescent state of **1**, in contrast to ground state (**1**), has substantial charge separation which leads to considerable stabilization by the dipole–dipole interactions with the solvent. Thus the energy gap between these two states, as measured by $\bar{\nu}_F$ (see ref. 10 for the difference in behaviour of $\bar{\nu}_{abs}$) is expected to be controlled by the solvent dipolarity, π^*. A degree of control by α is also to be expected since the fluorescent state of **1** may also be stabilized by weak hydrogen bonding to N(2). The corresponding linear free energy relationship is eq. [9].

$$[9] \quad \bar{\nu}_F = C(\pi^* + k'\alpha) + D$$

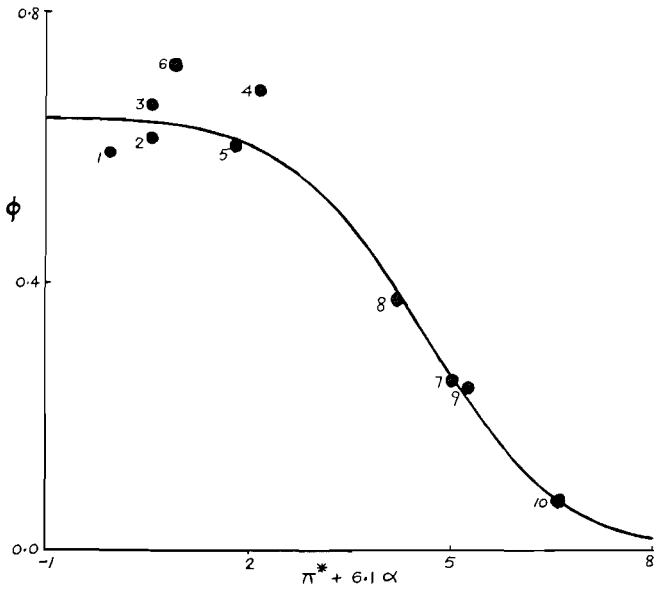

FIG. 1. Variation of the fluorescence quantum yield of **1** with the solvent polarity function ($\pi^* + 6.1\alpha$). Full line calculated from eqs. [1] and [8]. The numbers correspond to the entries in Table 1.

where C, k', and D are adjustable parameters. Equation [9] has been evaluated with data from all the solvents (entries 1–10 in Table 1) which gives eq. [10].

$$[10] \quad \bar{\nu}_F = -1.90(\pi^* + 1.1\alpha) + 23.7$$

$$SD = 0.283, \quad r = 0.968, \quad n = 10$$

Solvent-dependent fluorescence band positions of many 1,3-diaryl-Δ^2-pyrazolines have been previously analyzed via Lippert–Mataga type equations and yield excited state dipole moments (5, 11). The universal interaction function used therein (11) is quite closely related to solvent dipolarity (7). In particular, the Koppel–Palm treatment of solvent effects (12) employs a variant of the universal interaction function as the counterpart of solvent dipolarity of the Kamlet–Taft treatment used here (7). For our purposes it is more profitable to use the present correlation of $\bar{\nu}_F$ with π^* and α (eq. [10]) rather than the Lippert–Mataga equation since the present correlation allows a direct comparison with the ϕ_F correlation (eq. [8]). It is essential to consider α for a successful correlation of ϕ_F.

Many fluors with twisted internal charge transfer states (13) such as anilino naphthalene sulphonates (14) and dialkylamino phenyl triazines (15) as well as exciplexes (16) show solvent dependent $\bar{\nu}_F$ and ϕ_F. However, these two quantities show a large degree of correlation, i.e. the microenvironmental properties sensed via $\bar{\nu}_F$ and ϕ_F cannot be easily dissected into independent parameters as can be done for **1**. The Δ^2-pyrazolines in general and **1** in particular differ from the twisted

Can. J. Chem. Downloaded from www.nrcresearchpress.com by 78.46.186.204 on 09/07/12
For personal use only.

internal charge transfer systems in that the twisting of the donor (N(1)) and acceptor (N(2) and C(3)) moieties is prevented by the pyrazoline ring. The suitability of **1** as a two dimensional fluorescent sensor is enhanced by the fact that its electronic absorption spectral parameters are essentially solvent independent (Table 1), i.e. the variations in emission properties are not trivially caused by variations in excitation properties.

Entry 13 in Table 1 illustrates the utility of **1** in microenvironmental studies. **1** senses a hydrogen bond acidity of 0.82 and a dipolarity of 0.52 as deduced from the ϕ_F and $\bar{\nu}_F$ data in sodium lauryl sulphate micelles with the aid of eqs. [8] and [10]. These values of α and π^* lie in between those of ethanol and 2-propanol (7). **1** therefore resides at a location which is accessible to hydroxyl groups, i.e. water (1, 3, 17) though the moderate α value indicates the moderate concentration of water molecules at this location. The intermediate π^* value suggests that **1** is located in the region between the micellar core and the surface region which is exposed to non-electrostricted water. The conclusion therefore is that there is substantial penetration of water into the interior of the micelle.

Experimental

1 was prepared according to a known procedure (18). The following instruments were used in this work: Varian DMS90 ultraviolet–visible spectrophotometer, Aminco-Bowman SPF spectrophotofluorimeter, and Data General eclipse minicomputer. The fluorescence spectral data in Table 1 were determined as follows. The wavelength response function of the emission monochromator – photomultiplier tube combination of the spectrofluorimeter was determined over the range 340–590 nm by the well-known procedure of Lippert *et al.* (19) and Argauer and White (20). In particular, we employed 2-naphthol in acetate buffer (pH = 4.5), quinine sulphate in 0.1 *M* H_2SO_4, and 3-nitrophenyl dimethylamine in hexane:toluene (7:3 v/v) as the fluorescence emission spectral standards. The wavelength response function (which showed a maximum at 411 nm) was employed to correct the raw fluorescence emission spectra of **1** in various solvents. The excitation wavelength was maintained at 342 nm for all these cases since the ultraviolet absorption spectra were essentially solvent invariant. Even though the excitation spectra were not corrected, the band maxima in excitation and in absorption were nearly identical in all cases at 342 ± 3 nm. The optical densities of all these solutions of **1** at 342 nm were adjusted to 0.20 before the raw emission spectra were obtained. The corrected fluorescence intensity (at arbitrary but constant gain) versus wavenumber plots directly gave the wavenumber of maximum fluorescence emission $\bar{\nu}_F$ and their areas are directly proportional to the corresponding fluorescence quantum yields (ϕ_F). Such relative ϕ_F values were converted to absolute ϕ_F values by comparison with the area of a corrected fluorescence emission spectrum 1,3,5-triphenyl-Δ^2-pyrazoline, **2**, X = H, in aerated methanol obtained under identical conditions. This has $\phi_F = 0.37$ (8), obtained by comparison with the primary standard 9,10-diphenylanthracene which has $\phi_F = 0.95$ (21). Refractive index corrections were not applied since the refractive indices of various solvents at the required wavelengths are not accessible. Anyway, these corrections are expected to be small (8) and are of the order of the limits of experimental error in ϕ_F which are about 10%.

The three-parameter equations [8] and [10] were obtained by optimizing the blend of π^* and α with a linear least squares computer program which maximized the coefficient of correlation (r) between $\log [(\phi_{Faprotic}/\phi_F) - 1]$ or $\bar{\nu}_F$ and $(\pi^* + k\alpha)$ where k was adjusted by increments of 0.1.

Acknowledgements

This work would not have been possible without the facilities of the Centre for Analytical Research and Development at the University of Colombo which was directed by Professors D. E. Ryan and R. S. Ramakrishna. We also thank Dr. K. Seneviratne, G. N. Wickramanayake, L. P. Jayasinghe, R. Fernando and Ms. I. Campbell for help with aspects of this work. The referees are also thanked for their suggestions for improving the presentation of this paper.

1. J. H. Fendler. Membrane mimetic chemistry. Wiley, New York. 1982.
2. N. J. Dovichi, J. C. Martin, J. H. Jett, M. Trukla, and R. A. Keller. Anal. Chem. **56**, 348 (1984); For a comprehensive account see, J. Chem. Educ. No. 11 (1982).
3. D. G. Whitten, J. C. Russel, and R. H. Schmehl. Tetrahedron, **38**, 2455 (1982).
4. J. H. Fendler and E. J. Fendler. Catalysis in micellar and macromolecular systems. Academic Press, New York. 1975. Chap. 3.
5. (*a*) L. M. Kutsyna, L. V. Voevoda, V. G. Tischenko, and A. V. Shepel. Opt. Spectrosc. **26**, 91 (1969); (*b*) S. V. Tsukerman, E. G. Buryakovskaya, and V. F. Lavrushin. Opt. Spectrosc. **26**, 299 (1969); (*c*) H. Gusten, G. Heinrich, and H. Fruhbeis.Ber. Bunsenges. Phys. Chem. **81**, 810 (1977); (*d*) F. Pragst and F. G. Weber. J. Prakt. Chem. **318**, 51 (1976); (*e*) H. Shizuka. Acc. Chem. Res. **18**, 141 (1985).
6. J. Grimshaw and A. P. De Silva. J. Chem. Soc. Perkin II, 1010 (1981); P. Markov. Chem. Soc. Rev. **13**, 69 (1984).
7. M. J. Kamlet, J. L. M. Abboud, and R. W. Taft. Prog. Phys. Org. Chem. **13**, 485 (1981).
8. I. H. Leaver and D. E. Rivett. Mol. Photochem. **6**, 113 (1974).
9. D. E. Rivett, J. Rosevear, and J. F. K. Wilshire. Aust. J. Chem. **32**, 1601 (1979).
10. H. Langhals. Angew. Chem. Int. Ed. **21**, 724 (1982).
11. J. B. Birks. Photophysics of aromatic molecules. Wiley, New York. 1970. p. 115.
12. I. A. Koppel and V. A. Palm. *In* Advances in linear free energy relationships. *Edited by* N. B. Chapman and J. Shorter. Plenum, London. 1972. Chap. 5.
13. Z. R. Grabowski, K. Rotkiewicz, A. Siemiarczuk, D. J. Cowley, and W. Baumann. Nouv. J. Chim. **3**, 443 (1979).
14. E. M. Kosower. Acc. Chem. Res. **15**, 259 (1982).
15. D. J. Cowley. J. Chem. Soc. Perkin II, 281 (1984).
16. A. Weller. Pure Appl. Chem. **16**, 115 (1968).
17. F. M. Menger and D. W. Doll. J. Am. Chem. Soc. **106**, 1109 (1984).
18. R. Andrisano and L. Chierici. Gazz. Chim. Ital. **89**, 505 (1959); Chem. Abstr. **54**, 12116e (1960).
19. E. Lippert, W. Nagele, I. Seibold-Blankenstein, U. Staiger, and W. Voss. Z. Anal. Chem. **17**, 1 (1964).
20. R. J. Argauer and C. E. White. Anal. Chem. **36**, 368 (1964).
21. A. Maciejewski and R. P. Steer. J. Photochem. **35**, 59 (1986).
22. J. A. Riddick and W. B. Bunger. Organic solvents. Wiley, New York. 1970.
23. L. J. C. Love, J. G. Habarta, and J. G. Dorsey. Anal. Chem. **56**, 1132A (1984).

Can. J. Chem. Downloaded from www.nrcresearchpress.com by 78.46.186.204 on 09/07/12
For personal use only.

Photoacoustic infrared spectra (250–10 000 cm^{-1}) of partially deuterated kaolinite #9

K. H. MICHAELIAN, K. BUKKA, AND D. N. S. PERMANN

Energy, Mines and Resources Canada, CANMET, Coal Research Laboratory, P.O. Bag 1280, Devon, Alta., Canada T0C 1E0

Received September 26, 1986

K. H. MICHAELIAN, K. BUKKA, and D. N. S. PERMANN. Can. J. Chem. **65**, 1420 (1987).

Partial deuteration of kaolinite #9 was accomplished by grinding lumps to a size of 9 μm and refluxing a D_2O suspension for periods ranging from 8 to 146 h. Photoacoustic infrared spectra were obtained and compared with previously published infrared and Raman spectra of undeuterated kaolinite and with infrared spectra of deuterated kaolinite. Data from this investigation indicate an extent of deuteration of about 20%; with the exception of the OD stretching bands near 2700 cm^{-1}, most of the bands observed are attributable to undeuterated kaolinite. The infrared band at 2718 cm^{-1}, which was previously assigned to uncoupled inner surface OD stretching, is the analogue of the 3684 cm^{-1} band observed in Raman and photoacoustic infrared spectra of undeuterated kaolinite. The results support assignment of the 3684 cm^{-1} band to uncoupled inner surface hydroxyl stretching vibrations.

K. H. MICHAELIAN, K. BUKKA et D. N. S. PERMANN. Can. J. Chem. **65**, 1420 (1987).

On a réalisé une deutération partielle de la kaolinite #9 en broyant des morceaux pour les réduire en poudre de 9 μm et en portant ensuite cette poudre en suspension dans le D_2O au reflux pour des périodes allant de 8 à 146 h. On a déterminé les spectres infrarouges photoacoustiques et on les a comparé avec les spectres rapportés antérieurement tant pour les régions infrarouges et Raman de la kaolinite non-deutérée que pour la région infrarouge de la kaolinite deutérée. Les résultats de cette comparaison indiquent que le niveau de deutération atteint est d'environ 20%; à l'exception des bandes d'élongation OD que l'on retrouve près de 2700 cm^{-1}, la plupart des bandes observées peuvent être attribuées à la kaolinite qui n'est pas deutérée. La bande infrarouge que l'on retrouve à 2718 cm^{-1} avait été attribuée antérieurement à la bande d'élongation du OD non-couplé de la surface interne; elle est analogue à la bande à 3684 cm^{-1} qui est observée dans les spectres Raman et infrarouge photoacoustique de la kaolinite non-deutérée. Les résultats suggèrent que l'on doit attribuer la bande à 3684 cm^{-1} aux vibrations de l'élongation de l'hydroxyle non-couplé de la surface interne.

[Traduit par la revue]

Can. J. Chem. Downloaded from www.nrcresearchpress.com by 72.64.146.136 on 09/07/12
For personal use only.

Introduction

Infrared spectra of kaolinite, a common dioctahedral layer silicate of composition $Al_2Si_2O_5(OH)_4$, and its deuterated analogue have been reported by a number of authors (1–9). For well-crystallized samples, there is a general consensus (4–7, 9) that the four OH stretching bands at 3620, 3651, 3669, and 3695 cm^{-1} are shifted to 2675, 2698, 2710, and 2725 cm^{-1} respectively upon deuteration. These frequencies yield an average value of 1.354 for the ratio $\nu(OH)/\nu(OD)$. Deuteration experiments have also played an important role in the assignment of the hydroxyl stretching frequencies to particular OH groups in kaolinite; the comparative ease with which the three high frequency bands are shifted led to their assignment to inner surface hydroxyls, whereas the 3620 cm^{-1} band was attributed to the less readily exchanged inner hydroxyl groups (5). (A description and illustration of the different types of hydroxyl groups in kaolinite is given in ref. 4.)

Despite the common belief that kaolinite possesses four hydroxyl stretching bands, it is now known that a fifth band exists. Raman spectra of kaolinite #9 obtained in our laboratory (10) and elsewhere (11), Georgia kaolinite (11), and Keokuk kaolinite (12), all contain a band at approximately 3684 cm^{-1} in addition to four bands at frequencies corresponding to those in the infrared. Moreover, we have recently shown (13)[1] that the 3684 cm^{-1} band is active in the photoacoustic infrared spectrum of kaolinite. Thus it is firmly established that undeuterated kaolinite (kaolinite-H) has OH stretching bands at 3620, 3651, 3669, 3684, and 3695 cm^{-1}. Possible origins of the 3684 cm^{-1} band have been discussed previously (10), and it is of interest to observe the corresponding frequency for deuterated kaolinite (kaolinite-D) using infrared and (or) Raman spectroscopy so as to establish the correct assignment of this band.

[1]J. C. Zwinkels, J. C. Donini, and K. H. Michaelian. Paper in preparation.

In the present study, photoacoustic (PA) infrared spectra of partially deuterated kaolinite #9 have been obtained in the infrared spectral region between approximately 250 and 10 000 cm^{-1}. Because the samples studied were only partially deuterated, the spectra are generally quite similar to that of kaolinite-H. Nevertheless, the region near 2700 cm^{-1} does contain several OD stretching bands, which arise from deuterated kaolinite: in particular, bands at 2675 cm^{-1} and 2718 cm^{-1} are well defined in spectra of samples that were subjected to the exchange reaction for a prolonged time. As is discussed below, observation of the 2718 cm^{-1} band is consistent with its previous assignment (9) to uncoupled inner-surface hydroxyl vibrations.

Experimental

D_2O was purchased from MSD Isotopes, and had a reported isotopic purity of 99.8 at.% deuterium. Kaolinite #9, from Mesa Alta, New Mexico, U.S.A., was obtained from Ward's Natural Science Establishment, Inc.; the purity of this clay was described previously (10). The large lumps provided were reduced to an average size of ~9 μm with a ball grinder.

The exchange reaction was carried out by refluxing a ~4% suspension of kaolinite in D_2O for extended periods of time. The reaction mixture was contained in a round bottom flask isolated from atmospheric moisture by means of a drying tube filled with Drierite. Portions of kaolinite were withdrawn from the flask at 8, 24, 50, 74, 100, and 146-h intervals. These deuterated samples were dried several hours before their spectra were recorded.

Photoacoustic (PA) infrared spectra were obtained using an evacuable Bruker 113V Fourier transform infrared spectrometer and a Princeton Applied Research Corporation photoacoustic cell and preamplifier. The use of this equipment in the mid-infrared (15) and near-infrared (16) regions has been discussed previously. Far-infrared spectra were obtained using the same procedure as that for the mid-infrared, except that a 3.5-μm Mylar beamsplitter was used instead of the standard Ge/KBr beamsplitter. A CsI window was used on the PA cell for all spectral regions. Typical 4 cm^{-1} resolution spectra were obtained by coadding 500 interferograms. To improve the signal-

Can. J. Chem. Downloaded from www.nrcresearchpress.com by 72.64.146.136 on 09/07/12
For personal use only.

to-noise ratio in the mid-infrared region, a number of spectra were recorded at a specific interferometer mirror velocity and subsequently averaged; results for several velocities were then averaged to produce the final spectrum.

Results and discussion

OH/OD stretching region

Spectra of two partially deuterated samples of kaolinite #9 have been chosen to illustrate typical results. Figure 1 shows the OD stretching region of spectra obtained for samples exchanged for 8 and 100 h, while Fig. 2 displays the OH stretching bands in the same spectra. Band positions are summarized in Table 1.

Spectral characteristics of the isotopic exchange

Two observations indicate the relatively slow progress of the exchange reaction. First, comparison of the intensities in the OD region (Fig. 1) or in the OH region (Fig. 2) reveals little difference between the two samples; secondly, the amount of exchange estimated from the relative intensities of the OD and OH bands and the assumption that the absorption coefficient per OH group is approximately twice that per OD group (9) shows a slight increase from 18% at 8 h to 22% after 100 h. It can be noted here that most previous deuteration studies included intercalation (expansion) of the kaolinite, which makes the inner surface hydroxyls more accessible, or hydrothermal treatment of synthetic kaolinite. These procedures appear to effect exchange more readily than the method used in the present work, and can lead to a much higher proportion of deuterated kaolinite.

As deuteration proceeds, definition of the individual bands near 2700 cm^{-1} becomes progressively more complete. Initially one observes a weak, rather broad, featureless band centred at ~2700 cm^{-1}. After several hours a significant amount of exchange has occurred, particularly for the inner surface hydroxyl groups. Thus the lower curve in Fig. 1, obtained for a sample refluxed 8 h, shows a broad band centred near 2700 cm^{-1} with several barely identifiable features superimposed. After approximately two days, the exchange has apparently proceeded almost as far as is possible by this method, and one obtains a spectrum similar to the upper curve in Fig. 1. It can be seen that the features are more well developed, although the individual bands still overlap more than in the OH stretching region. This lack of definition appears to be characteristic of the OD stretching region in spectra of deuterated natural kaolinites (4–7, 9).

The 2675 cm^{-1} band in Fig. 1 is intensified relative to the other bands after prolonged deuteration. The counterpart of this band in the spectrum of kaolinite-H falls at 3620 cm^{-1} (Table 1). Thus, our results are consistent with the conclusion of Ledoux and White (5) that the 3620 cm^{-1} band arises from hydroxyls that are less readily exchanged, i.e., inner hydroxyl groups.

Comparison of Fig. 1 with previously published (4–7) infrared spectra of deuterated kaolinite reveals a significant difference with regard to the selectivities of the exchange reactions. When kaolinite is intercalated prior to deuteration, the inner surface hydroxyl groups become much more accessible to the D_2O molecules; it is for this reason that these OH groups are first replaced by OD groups. In contrast, the inner hydroxyls are situated in such a way (Fig. 1, ref. 4) that they may not be readily approached, even by small molecules. Because of this situation, deuteration of intercalated kaolinite readily shifts the inner surface hydroxyl bands at 3651, 3669, and 3695 cm^{-1} to 2691, 2706, and 2725 cm^{-1} respectively (cf. Table 1). On the other hand, the reflux exchange reaction used in the current investigation affects the hydroxyl groups approximately equally, with only a slight preference for exchange of inner surface hydroxyls (Fig. 1).

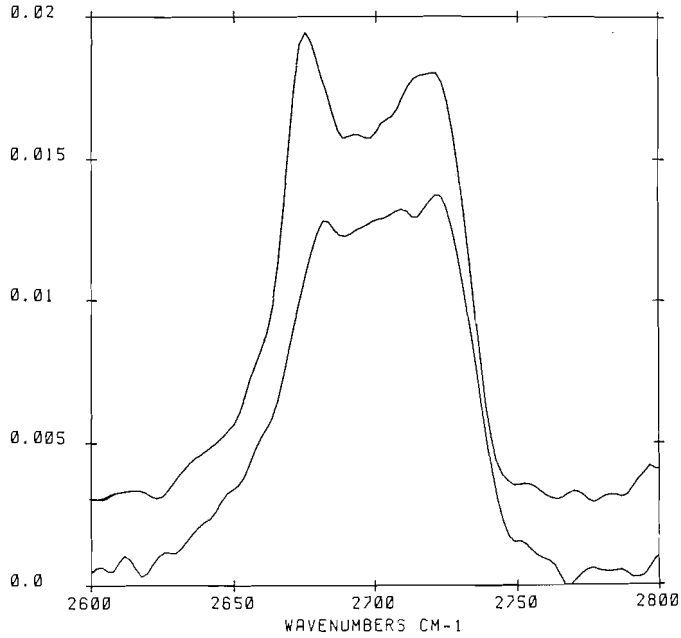

FIG. 1. OD stretching region of PA spectra of partially deuterated kaolinite #9; spectra have been baseline-linearized and smoothed. Lower curve: coaddition of 11 500-scan files; exchange reaction time 8 h. Upper curve: average of 3 coadditions (each corresponding to a different mirror velocity) of 10 500-scan files; reaction time 100 h. Spectra are displaced vertically for clarity.

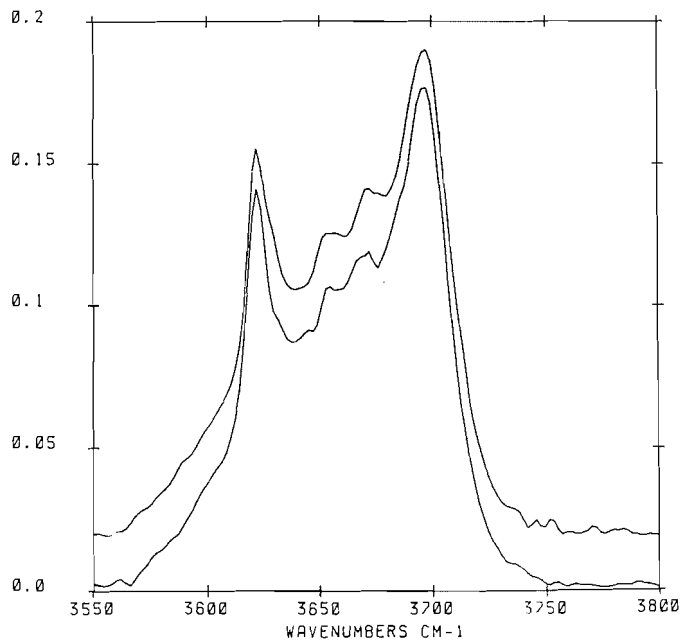

FIG. 2. Baseline-linearized OH stretching region of PA spectra of partially deuterated kaolinite #9. Lower curve: coaddition of 11 500-scan files; exchange reaction time 8 h. Upper curve: coaddition of 10 500-scan files; reaction time 100 h. Spectra are displaced vertically for clarity.

Assignment of the OH/OD stretching bands

Following the convention of Miller and Oulton (17), the

TABLE 1. Effect of deuteration on the OH stretching bands of kaolinite

Band	ν/cm^{-1} Kaolinite-H[a,b]	ν/cm^{-1} Kaolinite-D[a]	$\nu(OH)/\nu(OD)$
D	3620	2675	1.353
C	3651	2691	1.357
B	3669	2706	1.356
A′	3684	2718	1.355
A	3695	2725	1.356

[a]Infrared data (this work).
[b]Raman data (ref. 10).

four principal maxima in Fig. 2 are designated D, C, B, and A (Table 1); in agreement with our previous practice (10), the 3684 cm^{-1} band will be referred to as band A′ in the following discussion.

We have previously noted (16) that the PA spectrum of kaolinite has an intensity distribution somewhat different than that in transmission or diffuse reflectance spectra. These differences will be discussed in more detail elsewhere (19); the important point that should be mentioned here is that band A′ is weakly active in the PA spectrum, giving rise to a shoulder in Fig. 1*a* of ref. 16 and a less prominent change of slope in Fig. 2 in this paper. (Band A′ is clearly visible after deconvolution of PA spectra of kaolinite (13).) Different kaolinite samples were employed in these investigations; the relative intensity of band A′ in the PA spectrum thus appears to be sample dependent. Nevertheless, its PA activity facilitates its observation in spectra of weakly deuterated kaolinite.

The OD stretching region of the PA infrared spectrum of partially deuterated kaolinite #9 contains well-defined bands at 2675 and 2718 cm^{-1} (Fig. 1, upper curve). In addition, three weak, barely identifiable features were observed at approximately 2691, 2706, and 2725 cm^{-1} for several samples exchanged for longer periods. These band positions and their correlation to kaolinite-H frequencies (4, 5) are given in Table 1. As mentioned above, identification of the bands at 2675, 2691, 2706, and 2725 cm^{-1} as bands D, C, B, and A, respectively, is generally accepted. On the other hand, assignment of the 2718 cm^{-1} band requires further analysis.

As shown in Table 1, the 2718 cm^{-1} band in the PA spectrum of kaolinite-D corresponds to the 3684 cm^{-1} frequency (band A′) for kaolinite-H. These frequencies yield a $\nu(OH)/\nu(OD)$ ratio of 1.355, in close agreement with the values calculated for the other four bands.

The only previous observation of band A′ in spectra of kaolinite-D was reported by Rouxhet *et al.* (9) for both synthetic and natural kaolinites. Spectra of synthetic samples, in which the degree of deuteration ranged from a few per cent up to 73%, showed a band at 2714 cm^{-1} for isotopically dilute kaolinite-D, which is replaced by bands at 2708 and 2723 cm^{-1} when the deuteration is more complete. This led to the reasonable conclusion that the 2714 cm^{-1} band arises from uncoupled inner surface OD stretching vibrations; when these vibrations are coupled at higher concentrations, the antisymmetric and symmetric vibrations at 2708 and 2723 cm^{-1} are observed instead. In other words, band A′ is due to the uncoupled vibration, whereas bands A and B originate from the coupled vibrations.

The results of the present deuteration study support the conclusions of Rouxhet *et al.* (9), so far as the existence of

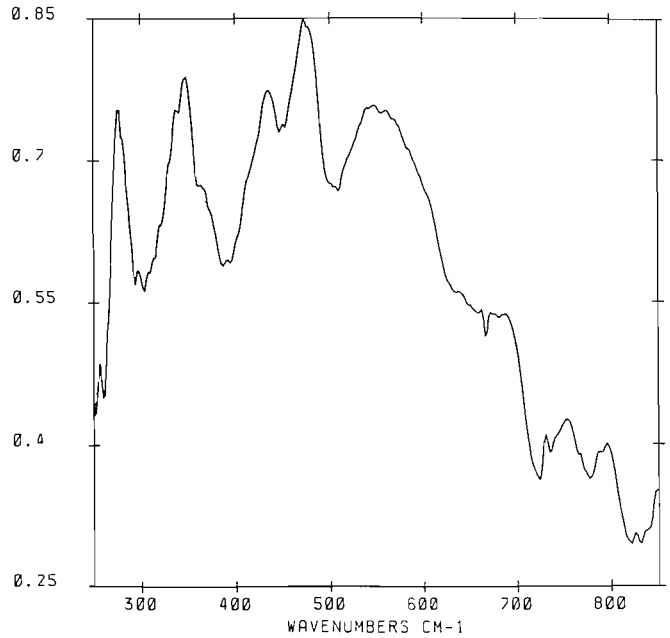

FIG. 3. Far infrared PA spectrum of partially deuterated kaolinite #9 merged from two 1000-scan spectra, each obtained at a different mirror velocity. Exchange reaction time 100 h.

band A′ has been confirmed in spectra of weakly deuterated kaolinite. As mentioned above, the extent of exchange realized in the present investigation is not very high; therefore, we have no data that verify that band A′ is *replaced* by bands A and B when the degree of deuteration is high. It is to be expected that spectra of highly deuterated kaolinite #9, or other kaolinites, would confirm the earlier observations (9) for synthetic kaolinite. Results of both the current study and previous investigations suggest, however, that it may be difficult to achieve a sufficient degree of deuteration for a natural kaolinite to verify this conclusion.

The activity of band A′ in Raman spectra of undeuterated kaolinite (10–12), which suggests that uncoupled inner surface hydroxyl vibrations occur even in the absence of isotopically dilute species, points to the need for a Raman investigation of kaolinite-D. Several Raman spectra of partially deuterated kaolinite were recorded in our laboratory in conjunction with the present infrared study; although the OH stretching bands were readily visible in the Raman spectra, the OD bands were too weak to be detected. Successful observation of the Raman bands near 2700 cm^{-1}, the need for which has been mentioned previously (11), is anticipated to provide further evidence confirming the conclusions of Rouxhet *et al.* (9).

Lattice vibration region

The kaolinite bands below 2000 cm^{-1} arise primarily from vibrations involving the heavier atoms (Si, O, and Al) in the lattice. Nevertheless, some participation of the lighter atoms in several vibrations is implied by earlier deuteration studies (2, 8). For simplicity, the region from 250 to 2000 cm^{-1} will be referred to as the lattice vibration region in the present discussion.

Results for the far-infrared region are shown in Fig. 3 and summarized in Table 2. Ten bands have been identified in the low frequency (~250–800 cm^{-1}) region of the PA spectrum of partially deuterated kaolinite; comparison of these frequencies with those from our earlier diffuse reflectance study of undeuterated kaolinite (18) shows that the two sets of frequencies are

Can. J. Chem. Downloaded from www.nrcresearchpress.com by 72.64.146.136 on 09/07/12
For personal use only.

TABLE 2. Far-infrared frequencies (cm^{-1}) in PA spectra of partially deuterated kaolinite and diffuse reflectance spectra of undeuterated kaolinite

Partially deuterated (PA)	Undeuterated[a] (Diffuse reflectance)
277	279
338	339
347	347
366	367
436	434
474	472
550	545
~640	
~690	
750	
797	

[a]Reference 18.

substantially the same in the common region up to 700 cm^{-1}. (The weaker bands in the diffuse reflectance spectrum have been omitted from Table 2 because they are not identifiable in the slightly noisier PA spectrum in Fig. 3.) This similarity arises because of the relatively small percentage of deuteration, as well as the fact that many of the bands (e.g. those at ~434, 472, 545, 701, and 797 cm^{-1} (2)) are shifted by only a few cm^{-1}, even when the degree of deuteration is high.

In the remainder of the lattice vibration region, bands of medium to strong intensity were observed at 918, 939, 1016, 1042, and 1117 cm^{-1}. These frequencies agree within a few cm^{-1} with those in transmission spectra of kaolinite-H, again presumably because of the relatively small degree of deuteration. According to familiar assignments of the spectrum of undeuterated kaolinite (14), the first two bands are due to AlOH bending vibrations, while the latter three arise from SiO stretching. In addition to these five bands, three weak bands at approximately 1637, 1823, and 1933 cm^{-1} were observed. The first band may indicate the presence of a small amount of H_2O, while the latter two can be assigned to combination transitions involving the strong bands at lower frequencies.

Near-infrared region

Near-infrared (nir) spectra of layer silicates typically display only a few bands. For kaolinite, these bands are due to combination transitions involving various OH stretching vibrations and an AlOH bending mode, or to overtones of the OH stretches. Thus one expects substantial changes in this region when kaolinite-H is converted to kaolinite-D.

The nir spectra of partially deuterated samples of kaolinite #9 obtained in this investigation display all of the bands observed previously (16) for international kaolinite; in addition one new band, presumably attributable to the isotopic exchange, is present. The bands reported in our earlier work are situated at 4526, 4620, 7065, and 7160 cm^{-1}. The first two arise from combination of bands D and A with the 915 cm^{-1} AlOH bending vibration, while the latter two frequencies are assigned to overtones of D and A, respectively. The overtone frequencies suggest (16) anharmonicities of ~100 cm^{-1} for the OH stretching vibrations. Using this value and the observed fundamental OD stretching frequencies (Table 1), one predicts that the overtones of the OD stretching vibrations will occur near 5200 cm^{-1}: this is, in fact, the approximate frequency of the weak new band in the nir spectrum of partially deuterated kaolinite. Therefore it is logical to conclude that this broad band is due to overtones of several of the OD stretching vibrations in kaolinite-D.

Conclusions

Partial conversion of kaolinite #9 to its deuterated form by refluxing the coarsely ground clay in D_2O for several days is described in this paper. Photoacoustic infrared spectra of samples exchanged for up to 146 h indicate that the degree of deuteration is of the order of 20%; consequently, the spectra resemble those of undeuterated kaolinite rather closely, except that several OD stretching bands near 2700 cm^{-1} are identifiable.

In the OD stretching region, a band at 2718 cm^{-1} was observed, in agreement with previously published data for partially deuterated synthetic and natural kaolinites. This band is the analogue of the 3684 cm^{-1} band recently observed in Raman and photoacoustic infrared spectra of undeuterated kaolinite. The most straightforward interpretation of both current and published data is that the 3684 cm^{-1} band arises from an uncoupled inner surface hydroxyl stretching vibration, whereas the bands at 3669 and 3695 cm^{-1} (2706 and 2725 cm^{-1} for deuterated kaolinite) are, respectively, due to the corresponding antisymmetric and symmetric coupled vibrations.

1. D. M. ROY and R. ROY. Geochim. Cosmochim. Acta, **11**, 72 (1957).
2. V. STUBICAN and R. ROY. Z. Kristallogr. **115**, 200 (1961).
3. J. J. FRIPIAT and F. TOUSSAINT. J. Phys. Chem. **67**, 30 (1963).
4. R. L. LEDOUX and J. L. WHITE. Science, **143**, 244 (1964).
5. R. L. LEDOUX and J. L. WHITE. Science, **145**, 47 (1964).
6. R. L. LEDOUX and J. L. WHITE. Clay and clay minerals. Proceedings of the Thirteenth National Conference on Clays and Clay Minerals. *Edited by* W. F. Bradley and S. W. Bailey. Pergamon Press, Oxford. 1966. p. 289.
7. R. L. LEDOUX and J. L. WHITE. Proceedings of the International Clay Conference, Jerusalem. 1966. p. 361.
8. H. JACOBS and M. STERCKX. Reun. Hisp.-Belga Miner. Arcilla, An. 154 (1970).
9. P. G. ROUXHET, N. SAMUDACHEATA, H. JACOBS, and O. ANTON. Clay Miner. **12**, 171 (1977).
10. K. H. MICHAELIAN. Can. J. Chem. **64**, 285 (1986).
11. C. T. JOHNSTON, G. SPOSITO, and R. R. BIRGE. Clays Clay Miner. **33**, 483 (1985).
12. A. WIEWIORA, T. WIECKOWSKI, and A. SOKOLOWSKA. Arch. Mineral. **35**, 5 (1979).
13. W. I. FRIESEN and K. H. MICHAELIAN. Infrared Phys. **26**, 235 (1986).
14. V. C. FARMER. *In* Data handbook for clay materials and other non-metallic minerals. *Edited by* H. van Olphen and J. J. Fripiat. Pergamon Press, London. 1979. p. 285.
15. J. C. DONINI and K. H. MICHAELIAN. Infrared Phys. **24**, 157 (1984).
16. J. C. DONINI and K. H. MICHAELIAN. Infrared Phys. **26**, 135 (1986).
17. J. G. MILLER and T. D. OULTON. Clays Clay Miner. **18**, 313 (1970).
18. J. C. ZWINKELS and K. H. MICHAELIAN. Infrared Phys. **25**, 629 (1985).

Can. J. Chem. Downloaded from www.nrcresearchpress.com by 72.64.146.136 on 09/07/12
For personal use only.

Electroionization study of ethane: ionization and appearance energies, ion-pair formations and negative ions

PIERRE PLESSIS AND PAUL MARMET

Herzberg Institute of Astrophysics, National Research Council of Canada, Ottawa, Ont., Canada K1A 0R6

Received October 9, 1986

PIERRE PLESSIS and PAUL MARMET. Can. J. Chem. **65**, 1424 (1987).

Threshold region ionization efficiency curves of ethane, of all singly charged fragments consisting of at least one carbon atom, and of $C_2H_5^{2+}$ and $C_2H_3^{2+}$ are presented and analysed. An energy filtered monoenergetic electron beam apparatus capable of producing very high signal-to-noise ratio data was used to study these ions. The C_2H_6 ionization energy is evaluated to be 11.57 ± 0.02 eV and structures due to competition with $C_2H_4^+$ fragment production are observed at higher energy in the $C_2H_6^+$ curve. As a result of the high apparatus sensitivity several of the measured appearance energies are lower (some by several eV) than previously reported. $C_2H_3^+ + H^-$, $CH_3^+ + CH_3^-$, and $C_2H_5^{2+} + H^-$ ion pair formations are observed. The $C_2H_5^+ + H^-$ ion pair formation, previously reported by several studies, is shown to be obscured by the isotopic $C_2H_4^+$ fragment signal.

PIERRE PLESSIS et PAUL MARMET. Can. J. Chem. **65**, 1424 (1987).

Les régions du seuil des courbes d'efficacité d'ionisation d'éthane, de tous les fragments simplement ionisés composés d'au moins un atome de carbone, et du $C_2H_5^{2+}$ et $C_2H_3^{2+}$, sont présentées et analysées. Ces ions, produits par bombardement avec un faisceau d'électrons monoénergétiques, sont étudiés avec un montage qui permet d'accumuler des données de très grand rapport signal sur bruit. L'énergie d'ionisation du C_2H_6 estimé à 11,57 ± 0,02 eV et des structures, causées par un mécanisme de compétition avec la production du $C_2H_4^+$, sont observées à plus haute énergie dans la courbe du $C_2H_6^+$. La haute sensibilité de l'appareil a permis de mesurer des seuils d'apparition à des énergies inférieures, quelques uns par plusieurs eV, aux valeurs des études antérieures. Les formations de paires d'ions $C_2H_3^+ + H^-$, $CH_3^+ + CH_3^-$ et $C_2H_5^{2+} + H^-$ sont observées. Il est démontré que la formation de paires d'ions $C_2H_5^+ + H^-$, rapportée par des travaux précédents, est masquée par l'isotope du fragment $C_2H_4^+$.

1. Introduction

In this paper the onset region electroionization efficiency (EIE) curves for ethane and all fragments composed of at least one carbon atom are presented and analysed. These curves have very high signal-to-noise ratio and have been obtained using an energy filtered monoenergetic electron beam. Ethane's ground state configuration is generally accepted as being $(1a_{1g})^2(1a_{2u})^2(2a_{1g})^2(2a_{2u})^2(1e_u)^4(3a_{1g})^2(1e_g)^4$, $^1A_{1g}$ for the staggered D_{3d} symmetry (1). The ionization and appearance curves of this molecule and its fragments have been studied considerably by photon and electron impact techniques (2, 3), but until now only Suzuki and Maeda (4) have studied this gas by a monoenergetic electron beam method. The present work shows a great improvement in the electron impact data for the ethane ions. Previous studies of CH_4 (5), C_2H_2 (6), C_2H_4 (7), and other atoms and molecules have clearly shown that our instrument is capable of producing high resolution data having very high signal-to-noise ratio, which yield more accurate threshold energies and the observation of new structures. This article deals with the initial threshold region of each curve. New features have been observed in the region up to 10 eV above threshold in each curve and these will be the subject of another paper (manuscript in preparation).

2. Apparatus and method

The apparatus is described in greater detail elsewhere (5). The ions are produced by intersecting electron and molecular beams. A large quadrupole mass filter provides the mass discrimination. The transmitted ions are detected by a dynode electron multiplier and counted individually as a function of the electron beam energy. Data acquisition is computer controlled and fully automated. The electron beam is produced by two 127° cylindrical selectors in series capable of giving a current of 10^{-8} A for an energy distribution of 30 meV full width at half maximum (FWHM). The high transmission characteristics of the mass filter combined with an efficient detection system allows for high counting rates (>10^6/s). Therefore, with integration times ranging from 100 to 200 h, electroionization efficiency curves of very high signal-to-noise ratio (>10^4) can be obtained. Energy calibration of each curve was done periodically (typically every 24 h) using the intense narrow threshold structure of argon (15.760 eV). The energy drift of the apparatus, after an initial stabilizing period of 2 days, was usually less than 10 meV per 24 h. At energies above 19 eV photon and (or) metastable neutral particle signal could be detected. This was done by taking data with the quadrupole mass filter adjusted so that no ions are transmitted. The stated purity of the ethane gas used was 99.96%. The gas pressure just outside the ion source region was generally maintained near 10^{-6} Torr. The pressure inside the ion source where the gas is introduced is approximately one to two orders of magnitude higher. Non-linear effects as a function of pressure, attributed to ion–molecule reactions, were seen in the threshold region curves of some fragment ions by comparing data taken at different pressures.

Structures in some of the threshold region curves were made more evident by taking the first derivative or by filtering the data with a specialized Fourier filtering technique (8–10) whose transmission factor for the mth frequency component is given by

$$[1] \quad T_{m,S} = 1 - \left(\cos\frac{\pi m}{N}\right)^{2S}$$

S is a parameter controlling the amount of low frequency component that is eliminated and N is the number of channels used. For the special case of $S = 1$ and eq. [1] multiplied by -1, the result is identical to the second derivative. It has been shown qualitatively that for small values of S ($S \leq 100$) the result is similar to the second derivative but contains a larger amount of low frequency components (11). In order to have direct resemblance with the second derivative, the vertically inverted filtered curves are presented in this paper.

2.1. *Factors affecting the shape of thresholds*

Ionization and appearance thresholds of ethane or of any other molecules are not as sharp as one would like. This can be attributed to various factors:

(*1*) The energy spread of the electron beam produces of course some broadening of the threshold structure. In the present work this is not the main cause since this contribution is only about 30 meV.

Can. J. Chem. Downloaded from www.nrcresearchpress.com by 78.46.186.204 on 09/07/12
For personal use only.

Can. J. Chem. Downloaded from www.nrcresearchpress.com by 78.46.186.204 on 09/07/12
For personal use only.

(2) There is also a doppler broadening due to the velocity distribution of the molecules, i.e. translational energy of the molecules. This effect makes a noticeable contribution (as much as 50 meV) in the case of low energy electron beams colliding with light molecules such as hydrogen, but is negligible when the mass of the particle is greater than about 20.

(3) Another cause of broadening of ionization or appearance thresholds results from the electron impact on thermally excited molecules. If the target molecules are previously vibrationally or rotationally excited, such vibrational or rotational quanta can be added to the electron energy so that the total energy reaches the threshold energy even if the electron energy alone is still slightly below the ionization or appearance threshold. In such a case, ions appear below the true threshold. This is easily observed experimentally in that the ionization thresholds of atoms (having no vibrational or rotational quanta) are sharper than those of molecules.

(4) It is also quite generally observed that the ionization thresholds of molecules show a longer and longer tail below the threshold as the number of atoms in the molecules increases. The importance of the thermal effect at a given temperature thus seems to be proportional to the number of atoms in the molecule. This is easily explained by the fact that larger molecules have a greater number of degrees of freedom and consequently possess a larger amount of internal energy which can contribute to ionization or to dissociative ionization.

(5) There is finally another very important factor which can lead to the absence of a clear threshold and this is the molecular structure of the molecule itself. Let us consider the case of a molecule for which the ionization mechanism is related to multiple structures existing just above the ionization threshold. This can be, for example, a series of vibrational states that are not quite resolved due to thermal effects as explained above. If, for the first five states, the relative ionization cross section increases by a factor of ten when one passes from one to the next, the four first states will not be clearly visible in the data and might be undistinguishable from pure thermal broadening effects. In such a case the ionization threshold will appear as a vertical ionization potential and not the adiabatic. However, when one has some knowledge of the structure of the molecule being studied, this information can be taken into acount in order to provide some guidance on the location or the shape of the ionization threshold.

3. Results and discussion

The ionization and appearance energies measured in this work are listed in Table 1 with those of other studies. The errors associated with our values are estimated by taking into account the error in calibration (±0.01 eV) and the estimated precision with which a threshold energy can be evaluated. This depends on the sharpness of the threshold structure and the statistical fluctuation in that region. The expression "threshold" in this paper refers to the true threshold of a reaction in which all products are in their ground state and possess no kinetic energy.

Activation energy may exist in some cases. Quantum mechanically, the probability for a process to occur at threshold can be many orders of magnitude smaller than when activation energy is present. Our instrument can detect cross sections as much as 10^{10} times smaller than some other cross sections, therefore it is possible to measure processes which are less probable by as much as ten orders of magnitude than those that are easily observed. It is this extreme sensitivity that allows us to measure such very low probability thresholds. This is illustrated by the fact that for most of our data it is possible to observe the formation of fragment ions at an electron energy which is so low that energy conservation according to thermochemistry does not allow the existence of any appreciable kinetic or internal (electronic, rotational, or vibrational) energy of the fragments. There is of course some curvature at threshold

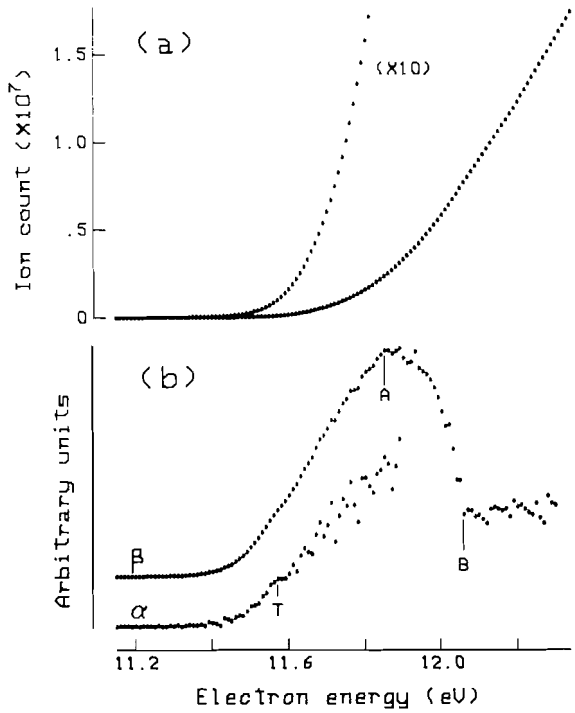

FIG. 1. (*a*) $C_2H_6^+$ EIE threshold region curve (10 meV/point). Resolution ≈ 30 meV FWHM. (*b*) Above curve high pass filtered with $S = 5$ (curve α) and $S = 50$ (curve β).

which is caused by the various phenomena described in section 2.1 and this has been taken into account in determ ining the position of the thresholds.

One must also recall that before a collision, one has an electron which is independent of the target molecule. Later, during the interaction of the electron with the target, there can be only quantum transitions in which the number of charges is conserved. Therefore only negative ion states are involved where these correspond to discrete states (Feshbach resonances), shape resonances, or continua. When a transition occurs, a new state of the negative ion complex is formed. This state may be repulsive leading to autoionization, dissociation, or photon emission. After autoionization or dissociation has occurred, which takes a relatively long time since slow particles are involved, one may again deal with independent neutrals and (or) ions. Finally, it must be realized that the number of charges of the negative complex is not the same as the number of charges of the initial neutral molecule, and therefore the states differ in these two cases. Consequently, by electron impact, the states involved are not the states of the neutral molecule as in photoionization. For this reason the negative ion complex $C_2H_6^{-*}$ is included in the reactions given below.

3.1. $C_2H_6^+$

The raw EIE threshold curve of ethane, presented in Fig. 1(*a*), shows fairly uniform curvature in the onset region making it difficult to accurately determine the ionization energy. The absence of any clear break at the ionization threshold can be attributed to two main factors: thermally excited vibrational states of ethane (hot bands) which produce ions below the true adiabatic threshold (such hot bands have been observed in C_2H_2 (6) and C_2H_4 (7)), and a low probability for going from the ethane ground state to the ion ground state (1). However, filtering the above curve with a high pass filter does reveal some interesting features. Previous studies have shown that an

TABLE 1. Ionization and appearance energies of ethane (in eV)

$C_2H_6 \rightarrow$	Present study	Others	
		Method[a]	Results
$C_2H_6^+$	11.56±0.02	PES	11.56 (18), 11.57±0.01 (19), 11.51 (20), 11.56 (21)
		PIMS	11.521±0.007 (22), 11.65±0.03 (23)
		EM	11.5±0.1 (4)
		RPD	11.66 (24)
		EDD	11.45±0.09 (13)
		RPI	11.45±0.05 (25)
		EI	11.4±0.4 (12)
$C_2H_5^+ + H^-$	(Obscured by $^{13}C^{12}CH_4^+$)	PIMS	12.00±0.05 (26)
		EM	12.0±0.1 (4)
		EDD	12.08±0.05 (13)
		TC	11.69±0.07
$C_2H_5^+ + H$	12.45±0.08	PIMS	12.65±0.08 (26)
		EM	12.5±0.1 (4)
		RPD	12.66 (24)
		EDD	12.79±0.02 (13)
		EI	12.1±0.4 (12)
		TC	12.45±0.07
$C_2H_4^+ + H_2$	11.81±0.05	PIMS	12.08±0.03 (26)
		EM	12.1±0.1 (4)
		EDD	12.15±0.08 (13)
		EI	12.1±0.4 (12)
		TC	11.846±0.011
$C_2H_3^+ + H_2 + H^-$	13.76±0.08	TC	13.72±0.18
$C_2H_3^+ + H_2 + H$	14.50±0.04	EM	14.6±0.1 (4)
		EDD	15.02±0.02 (13)
		EI	14.5±0.4 (12)
		TC	14.48±0.18
$C_2H_2^+ + 2H_2$	14.51±0.04	EM	14.7±0.1 (4)
		EDD	14.95±0.05 (13)
		EI	15.2±1.0 (12)
		TC	14.46±0.018
$C_2H^+ + 2H_2 + H$	22.4 ±0.3[b]	EM	25.6±0.2 (4)
		EI	27.0±1.0 (14)
		TC	19.4±0.8
$C_2^+ + 3H_2$	22.9 ±0.3[b]	EM	31.5±0.2 (4)
		EI	31.5±1.0 (14)
		TC	21.22±0.12
$CH_4^+ + CH_2$	(Obscured by impurities)	EM	20.4±0.3 (4)
		TC	16.63±0.06
$CH_3^+ + CH_3^-$	13.56±0.04	EM	14.1±0.1 (4)
		TC	13.59±0.05
$CH_3^+ + CH_3$	13.65±0.04	EM	14.9±0.1 (4)
		RPD	13.46 (24)
		EI	14.2±0.3 (14), 14.2±2.0 (12)
		TC	13.67±0.02
$CH_2^+ + CH_4$	14.69±0.05	EM	17.3±0.15 (4)
		EI	16.2±1.0 (14), 17.0±2.0 (12)
		TC	14.41±0.05
$CH^+ + CH_3 + H_2$	20.10±0.08[b]	EM	26.7±0.5 (4)
		EI	24.5±1.0 (14)
		TC	19.03±0.02
$C^+ + CH_4 + H_2$	20.3 ±0.2[b]	EM	29.6±0.2 (4)
		EI	30.4±1.5 (14)
		TC	18.645±0.011

Can. J. Chem. Downloaded from www.nrcresearchpress.com by 78.46.186.204 on 09/07/12
For personal use only.

TABLE 1 (*concluded*)

$C_2H_6 \rightarrow$	Present study	Others	
		Method[a]	Results
$C_2H_5^{2+} + H^-$	31.60±0.15		
$C_2H_5^{2+} + H$	32.3 ±0.2	EI	32.0±1.5 (14), 31.4 (15)
$C_2H_3^{2+} + H_2 + H$	35.5 ±0.3	EI	34.5 (15)

[a]Method: EDD, energy distribution difference; EI, electron impact (non-monoenergetic); EM, electron monochromator; PES, photoelectron spectroscopy; PIMS, photoionization mass spectrometry; RPD, retarding potential difference; RPI, resonance photoionization; TC, thermochemically. Data used to determine TC values are given in Table 4.

[b]Upper limit for this appearance energy.

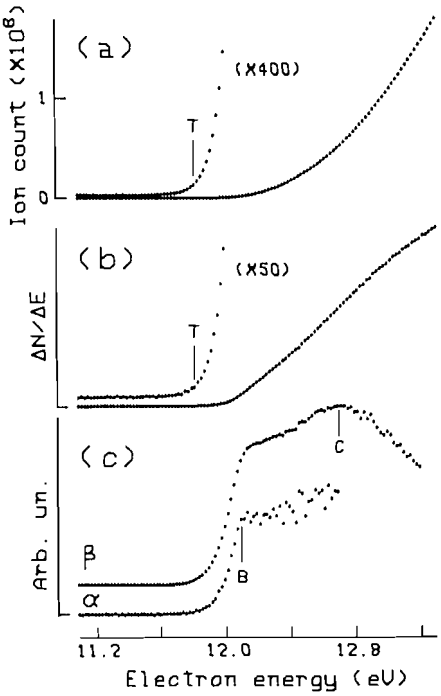

FIG. 2. (*a*) $C_2H_4^+$ appearance curve (20 meV/point). (*b*) First derivative of curve (*a*). (*c*) Curve (*a*) high pass filtered with $S = 2$ (curve α) and $S = 30$ (curve β).

TABLE 2. Structures observed in the $C_2H_6^+$ and $C_2H_4^+$ curves

Ion	Structure	Energy (eV)	Interpretation
$C_2H_6^+$	**T**	11.57	Ionization energy $(1e_g)^{-1}$
	A	11.85	Competition with $C_2H_4^+$(**T**) + H_2
	B	12.06	Competition with $C_2H_4^+$(**B**) + H_2
$C_2H_4^+$	**T**	11.81	Appearance energy ($C_2H_4^+ + H_2$)
	B	12.09	
	C	12.70	

ionization threshold often manifests itself by an initial maximum in the filtered curve (5–7). The weak but statistically valid local maximum at 11.57 ± 0.02 eV (structure **T**) of curve α of Fig. 1(*b*) corresponds very likely to the ionization energy of ethane and is in excellent agreement with the values reported by most photoelectron spectroscopy works (see Table 1). No other feature is observed below 11.57 eV in our filtered curves.

Curve β ($S = 50$) of Fig. 1(*b*), which contains a larger amount of low frequency components than curve α ($S = 5$),

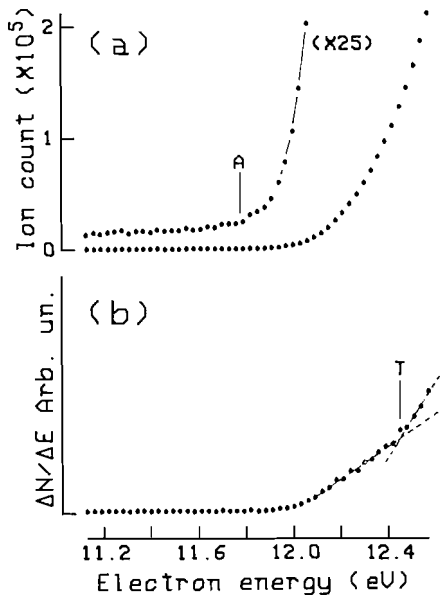

FIG. 3. (*a*) $C_2H_5^+$ appearance curve (30 meV/point). (*b*) First derivative of above curve.

increases gradually with energy up to 11.85 eV (structure **A**). The amplitude then diminishes at an increasing rate, stopping suddenly at 12.06 eV (structure **B**) where a distinct break is observed. The shape of curve β can be understood by comparing with the $C_2H_4^+$ fragment curves of Fig. 2. The initial $C_2H_4^+$ onset occurs at 11.81 ± 0.05 eV (structure **T**). The filtered $C_2H_4^+$ curve (α) shows that the rate of increase of the $C_2H_4^+$ signal rapidly reaches a maximum at 12.09 eV (structure **B**). The energies of structures **T** and **B** of the $C_2H_4^+$ curve correspond reasonably well with those of structures **A** and **B** of the $C_2H_6^+$ curve, respectively. These values are recorded in Table 2. Also, the shape of these two curves in the region between the indicated structures resembles the inverse of the other. This comparison indicates the presence of a competitive mechanism between the $C_2H_6^+$ and the $C_2H_4^+$ production channels. Structures **A** and **B** of the $C_2H_6^+$ curve are therefore attributed to the onset of the $C_2H_4^+$ fragment production. This fragmentation channel is highly probable. It is observed that the $C_2H_4^+$ peak height intensity is more than twice that of the $C_2H_6^+$ peak for 35 eV electrons.

3.2. $C_2H_5^+$

The $C_2H_5^+$ appearance curve of Fig. 3 shows an initial onset structure, **A**, at 11.76 eV with evidence of another structure

Can. J. Chem. Downloaded from www.nrcresearchpress.com by 78.46.186.204 on 09/07/12
For personal use only.

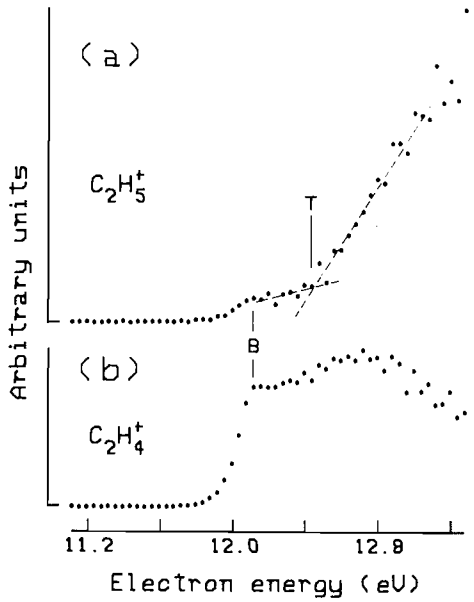

FIG. 4. (*a*) $C_2H_5^+$ appearance curve filtered using $S = 1$ (second derivative). (*b*) $C_2H_4^+$ appearance curve filtered using $S = 1$ (40 meV/point).

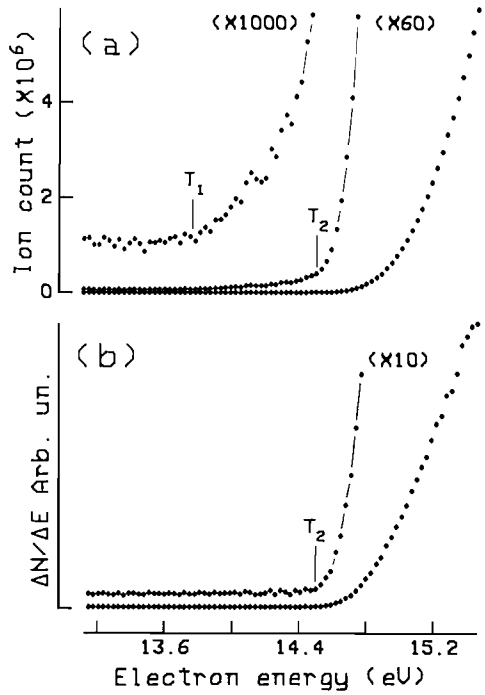

FIG. 5. (*a*) $C_2H_3^+$ appearance curve (30 meV/point). Ion pair formation is observed. (*b*) First derivative of above curve.

near 11.85 eV. This curve was taken at a reduced pressure (6×10^{-7} Torr) in order to minimize the effects of ion–molecule reactions which were relatively important at higher pressures. The energy of structure **A** coincides fairly well with the reaction energy of 11.69 ± 0.07 eV for the ion-pair formation

[2] $C_2H_6 + e^- \rightarrow C_2H_6^{-*} \rightarrow C_2H_5^+ + H^- + e^-$

Values of 12.0 eV or greater are reported for this process (see Table 1) which are inconsistent with the above values.

In spite of the good agreement between our value of structure **A** and the above stated thermochemical value, it is uncertain that structure **A** corresponds to the onset of reaction [2]. The second derivative $C_2H_5^+$ curve, shown in Fig. 4(*a*), reveals a step-like feature near 12.09 eV (structure **B**). From thermochemistry the appearance energy for the ion–neutral process

[3] $C_2H_6 + e^- \rightarrow C_2H_6^{-*} \rightarrow C_2H_5^+ + H + 2e^-$

is estimated to be 12.45 ± 0.07 eV (see Table 1). Feature **B** does not concur with the values of either reaction [2] or [3]. However, structure **T** at 12.45 ± 0.08 eV, seen in both the first and second derivative curves of $C_2H_5^+$ (Figs. 3(*b*) and 4(*a*), respectively), is in excellent agreement with the thermochemical value of process [3], indicating that this feature corresponds to the appearance threshold of the ion–neutral formation. This value is lower than most measurements for the onset of this reaction (Table 1).

No precise mechanism is known which can produce a distinct structure (**B**) between the thresholds of processes [2] and [3]. Figure 4 compares the $C_2H_5^+$ and $C_2H_4^+$ second derivative curves. It is observed that, in the range up to 12.45 eV, the two curves are similar except for the amplitudes. For the same source conditions the ratio of the $C_2H_5^+$ signal to the $C_2H_4^+$ signal at 12.1 eV is 0.02, which is precisely the isotopic concentration of $^{13}C^{12}CH_4^+$. It therefore appears evident that most if not all the signal below 12.45 eV is due to the mass 29 isotope of $C_2H_4^+$. If there is ion-pair production in this region it is much weaker than the $C_2H_4^+$ isotopic signal. It is probably this latter signal that the previous works measured near 12.0 eV.

3.3. $C_2H_4^+$

This fragment is by far the most abundant of the ethane ions at 35 eV (a table of the relative intensities will be published in another paper). The raw data $C_2H_4^+$ EIE curve is presented in Fig. 2(*a*). A weak slope has been subtracted to compensate for the ethylene impurity (0.03%) signal. An onset (**T**) is observed at 11.81 ± 0.05 eV. The same structure is more apparent in the first derivative curve (Fig. 2(*b*)). The high pass filtered curves of Fig. 2(*c*) reveal a clear break, **B**, at 12.09 eV and a broad maxima, **C**, at 12.70 eV. The energy of structure **T** agrees well with the energy of formation (11.846 ± 0.011 eV) of process

[4] $C_2H_6 + e^- \rightarrow C_2H_6^{-*} \rightarrow C_2H_4^+ + H_2 + 2e$

and corresponds to the appearance energy of the $C_2H_4^+$ fragment. This interpretation is supported by the aforementioned comparison between the $C_2H_6^+$ and $C_2H_4^+$ curves where structures due to competition with $C_2H_4^+$ production are seen in the $C_2H_6^+$ curve starting from 11.85 eV (see Table 2). The previously reported values for this appearance energy, listed in Table 1, are all near 12.1 eV, coinciding very well with the energy of the steo like feature **B** of our filtered curve. It is probable that these studies lacked sufficient sensitivity to measure the $C_2H_4^+$ signal below 12.1 eV. The $C_2H_4^+$ fragment cross section increases significantly from 12.09 eV on. It is presently unclear what processes are associated with structures **B** and **C**.

3.4. $C_2H_3^+$

The $C_2H_3^+$ fragment appearance curve, presented in Fig. 5, shows evidences of two processes. A weak slope caused by ion–molecule reactions has been subtracted from the curve. The onset of the first process occurs at 13.76 ± 0.08 eV (structure T_1) and corresponds to the threshold of the ion pair formation

[5] $C_2H_6 + e^- \rightarrow C_2H_6^{-*} \rightarrow C_2H_3^+ + H^- + H_2 + e$

This is in good agreement with the heat of reaction of 13.72 ±

Can. J. Chem. Downloaded from www.nrcresearchpress.com by 78.46.186.204 on 09/07/12
For personal use only.

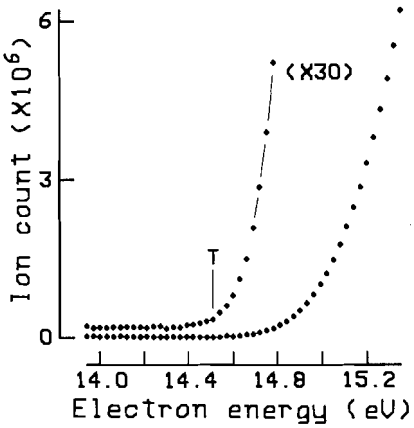

FIG. 6. $C_2H_2^+$ appearance curve (30 meV/point).

0.18 eV for this process. No other study reports observing this ion pair formation. The onset of the second process, indicated by $\mathbf{T}_2$, appears at 14.50 ± 0.04 eV. The first derivative curve (Fig. 5(*b*)) also clearly displays this feature which corresponds to the threshold of the ion–neutral process

[6] $C_2H_6 + e^- \rightarrow C_2H_6^{-}* \rightarrow C_2H_3^+ + H + H_2 + 2e^-$

Our value is in excellent agreement with the thermochemical value of 14.48 ± 0.18 eV for this process and compares well with Suzuki and Maeda's (4) value of 14.6 ± 0.1 eV and Chatham *et al.*'s (12) value of 14.5 ± 0.4 eV, but not with Selim's (13) value of 15.02 ± 0.02 eV. The 0.74 eV difference between $\mathbf{T}_1$ and $\mathbf{T}_2$ coincides very well with the hydrogen electron affinity (0.754 eV) and this supports the above interpretations of these two structures. The weak feature observed near 14.2 eV is probably due to statistical fluctuations.

3.5. $C_2H_2^+$

The $C_2H_2^+$ fragment EIE curve is shown in Fig. 6. A very weak slope, caused mainly by the $C_2H_2^+$ fragment signal of the ethylene impurity and by acetylene residual gas, was subtracted to render the baseline horizontal. The indicated structure **T**, at 14.5 ± 0.04 eV, corresponds very likely to the threshold of reaction

[7] $C_2H_6 + e^- \rightarrow C_2H_6^{-}* \rightarrow C_2H_2^+ + 2H_2 + e^-$

By comparing the values given in Table 1 it is seen that the above value concurs with the energy of formation of process [7] but is significantly lower than other measured values except for that of Chatham *et al.* (12) which has a large error. This discrepancy is indicative of the lack of sensitivity of these previous works.

3.6. C_2H^+

The appearance curve of this fragment (abundance: 0.63% of the $C_2H_4^+$ peak at 35 eV) presented in Fig. 7 shows a break at 22.4 ± 0.3 eV (structure **T**). The weak but long tail below this feature is attributed principally to the ethylene impurity and to the acetylene residual gas. Photon emission or metastable excited neutral particles also contribute to the signal with increasing intensity starting from about 19.7 eV. Structure **T** is associated with reaction

[8] $C_2H_6 + e^- \rightarrow C_2H_6^{-}* \rightarrow C_2H^+ + H + 2H_2 + 2e^-$

but because of the large discrepancy between the energy of this structure and the calculated heat of reaction for this purpose (19.4 ± 0.8 eV), it is doubtful that feature **T** corresponds to the

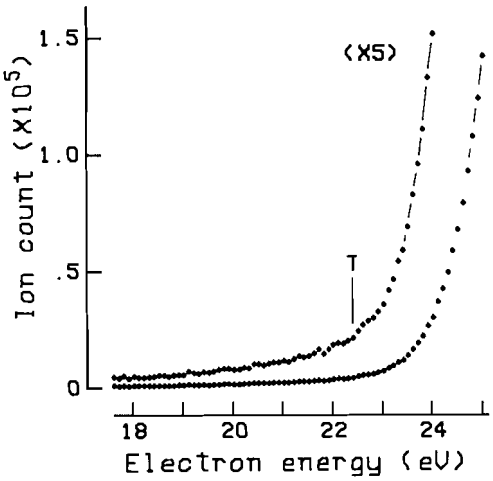

FIG. 7. C_2H^+ appearance curve (100 meV/point).

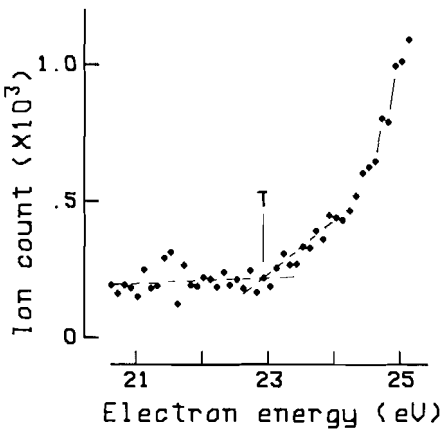

FIG. 8. C_2^+ appearance curve (100 meV/point).

minimum energy required to produce the C_2H^+ fragment. The genuine C_2H^+ signal may extend below 22.4 eV but is obscured by the signal produced by impurities. It is clear that if this is the case the C_2H^+ cross section below 22.4 eV is very small. At 22.4 eV it is likely that the products of reaction [8] possess excitation and (or) kinetic energy. Structure **T** is considered to be an upper limit for the C_2H^+ appearance energy. Previous results (Table 1) are several eV higher in energy.

3.7. C_2^+

Figure 8 presents the C_2^+ fragment appearance curve. A weak slope has been subtracted, caused by the factors given above for C_2H^+. Structure **T**, at 22.9 ± 0.3 eV, is associated with process

[9] $C_2H_6 + e^- \rightarrow C_2H_6^{-}* \rightarrow C_2^+ + 3H_2 + 2e^-$

and, for the same reasons that are given for C_2H^+, is considered to be an upper limit for the C_2^+ appearance energy. The value of 31.5 eV reported by Suzuki and Maeda (4) and Hipple (14) for this threshold is 8.6 eV higher than our value, indicating a severe limitation in the sensitivity of these measurements. There appears to be an increase in the C_2^+ cross section near 24.3 eV.

3.8. CH_4^+

An attempt was made to measure the appearance energy of the CH_4^+ fragment but, because of residual gases and gas impurities, no clear onset for this fragment could be observed.

Can. J. Chem. Downloaded from www.nrcresearchpress.com by 78.46.186.204 on 09/07/12
For personal use only.

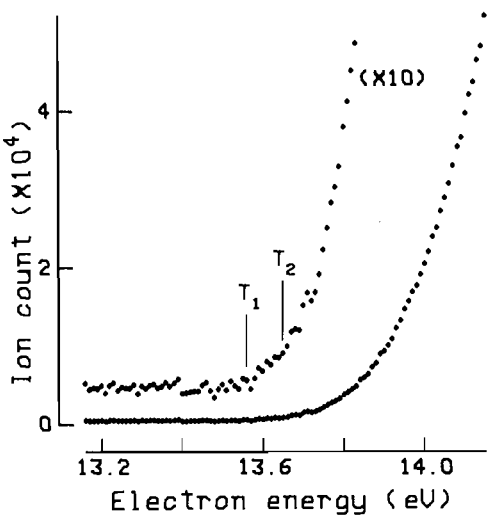

FIG. 9. CH_3^+ appearance curve (10 meV/point). Ion pair formation is observed.

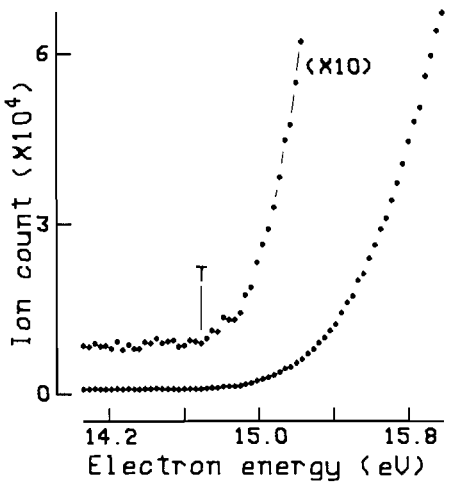

FIG. 10. CH_2^+ appearance curve (30 meV/point).

Suzuki and Maeda (4) report a value of 20.4 ± 0.3 eV for this threshold. No significant feature was seen at this energy in our curve and given that an ethane gas of higher purity was used in this work (99.96% as opposed to 99.7%), we suspect that impurities contributed significantly to their signal.

3.9. CH_3^+

The onset region of the CH_3^+ appearance curve presented in Fig. 9 has an initial break at 13.56 ± 0.04 eV and a second break at 13.65 ± 0.04 eV (structures $\mathbf{T}_1$ and $\mathbf{T}_2$, respectively). The energy difference between these two features is 0.09 eV which agrees very well with the CH_3 electron affinity of 0.08 ± 0.03 eV (see Table 4). Therefore it is probable that structures $\mathbf{T}_1$ and $\mathbf{T}_2$ correspond to the thresholds of reactions

[10] $C_2H_6 + e^- \rightarrow C_2H_6^{-*} \rightarrow CH_3^+ + CH_3^- + e^-$

and

[11] $C_2H_6 + e^- \rightarrow C_2H_6^{-*} \rightarrow CH_3^+ + CH_3 + 2e^-$

respectively. The respective energies of formation are 13.59 ± 0.05 and 13.67 ± 0.02 eV, in good agreement with our measured values. The electron affinity of 0.08 eV claimed by Suzuki and Maeda (4) for CH_3 is evidently much too large

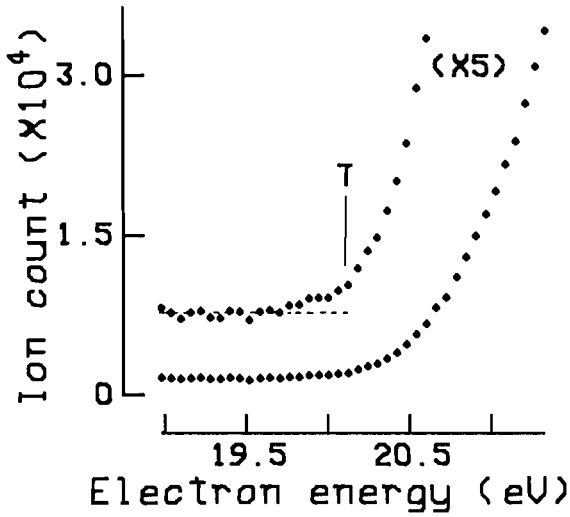

FIG. 11. CH^+ appearance curve (60 meV/point).

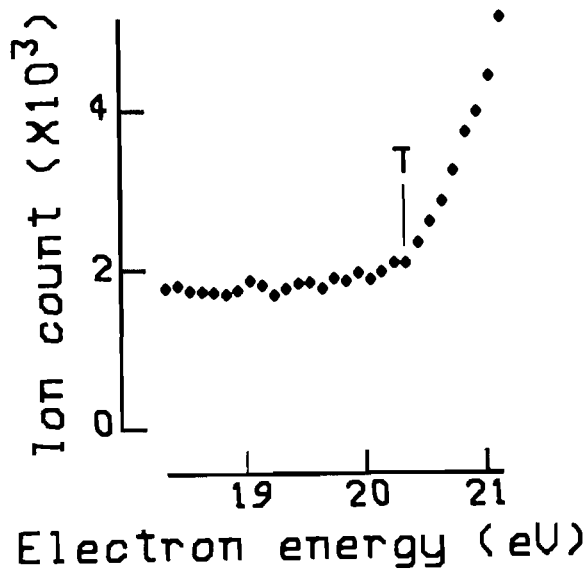

FIG. 12. C^+ appearance curve (100 meV/point).

(Table 1). The irregularities observed just above $\mathbf{T}_2$ are probably due to statistical scatter.

3.10. CH_2^+

The EIE curve of this fragment shown in Fig. 10 has a distinct onset at 14.69 ± 0.05 (structure **T**) which likely corresponds to the threshold of process

[12] $C_2H_6 + e^- \rightarrow C_2H_6^{-*} \rightarrow CH_2^+ + CH_4 + 2e^-$

The calculated energy of formation for this reaction is somewhat lower (14.41 ± 0.05 eV) while the values of previous works listed in Table 1 are all more than 1.5 eV higher in energy. The CH_2^+ curve shows an increase in cross section near 14.9 eV.

3.11. CH^+

The CH^+ appearance curve of Fig. 11 has an onset energy of 20.10 ± 0.08 eV (structure **T**). The weak tail below this energy, starting from 19.7 eV, is due to photon emission and (or) to metastable excited neutral molecules or atoms. Structure **T** is associated with processes

Can. J. Chem. Downloaded from www.nrcresearchpress.com by 78.46.186.204 on 09/07/12
For personal use only.

TABLE 3. Deduced double ionization energies (in eV)

Molecule	Ionization energy	
	Present study	Others
C_2H_3	30.0±0.4	29.6±0.3 (7), 29.1±0.5 (16), 29.9±0.3 (17)
C_2H_5	28.3±0.2	27.5±0.5 (16), 28.6±0.3 (17)

[13] $C_2H_6 + e^- \rightarrow C_2H_6^{-*} \rightarrow CH^+ + CH_4 + H + 2e^-$

and

[14] $C_2H_6 + e^- \rightarrow C_2H_6^{-*} \rightarrow CH^+ + CH_3 + H_2 + 2e^-$

which have energies of formation of 19.02 ± 0.02 and 19.03 ± 0.02 eV, respectively. Reaction [14] is the more probable process as it requires less hydrogen rearrangement. The discrepancy between these values and that of structure **T** leads us to consider 20.10 ± 0.08 eV to be an upper limit for the CH^+ appearance energy. Much higher values have been reported for this threshold (Table 1).

3.12. C^+

The C^+ EIE curve (Fig. 12) shows a relatively clear onset at 20.3 ± 0.2 eV. The weak tail below structure **T** is again due to the photon/metastable signal. Process

[15] $C_2H_6 + e^- \rightarrow C_2H_6^{-*} \rightarrow C^+ + CH_4 + H_2 + 2e^-$

is the only one that can be associated with this feature even though its energy of formation is 18.645 ± 0.011 eV. The C^+ fragment intensity is very weak (abundance: 0.02% of the $C_2H_4^+$ peak at 35 eV) and the value of structure **T** is considered as an upper limit for this appearance energy. Previously reported values for this threshold are higher by more than 9 eV (Table 1) indicating the very limited sensitivity of these measurements.

3.13. Doubly charged ions

Electroionization efficiency curves of the $C_2H_5^{2+}$ and the $C_2H_3^{2+}$ fragments (respective abundances: 0.33% and 0.015% of the $C_2H_4^+$ peak at 50 eV) were obtained and these are shown in Figs. 13 and 14, respectively. A slope caused by the photon/metastable signal has been subtracted from each curve. The $C_2H_5^{2+}$ onset region shows evidence for two processes. Structures $\mathbf{T}_1$ and $\mathbf{T}_2$ at 31.60 ± 0.15 eV and 32.3 ± 0.2 eV, respectively, correspond to the threshold of the following respective reactions:

[16] $C_2H_6 + e^- \rightarrow C_2H_6^{-*} \rightarrow C_2H_5^{2+} + H^- + 2e^-$

and

[17] $C_2H_6 + e^- \rightarrow C_2H_6^{-*} \rightarrow C_2H_5^{2+} + H + 3e^-$

The ion pair process is measured here for the first time. The 0.7 eV difference between $\mathbf{T}_1$ and $\mathbf{T}_2$ is in good agreement with the hydrogen electron affinity (0.754 eV). Our value for the ion neutral process is in good agreement with that of Hipple (14) (32.0 ± 1.5 eV) but higher than the value reported by Jones *et al.* (15) (31.4 eV). Given that the ion pair formation is observed, it is unlikely that the $C_2H_5^{2+}$ threshold occurs at lower energy. Our value of 31.60 ± 0.15 eV for the threshold of reaction [16] yields a value of 28.3 ± 0.2 eV for the C_2H_5 double ionization energy. By comparison, Rabrenovic and Beynon's (16) and Cooks *et al.*'s (17) values of 19.1 ± 0.5 and 20.3 ± 0.3 eV, respectively, for the $C_2H_5^+$ to $C_2H_5^{2+}$

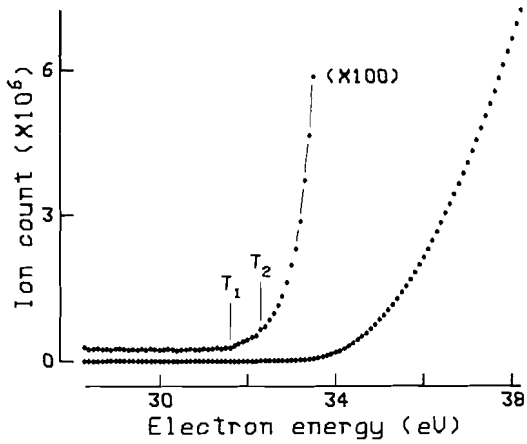

FIG. 13. $C_2H_5^{2+}$ appearance curve (100 meV/point). Ion pair formation is observed.

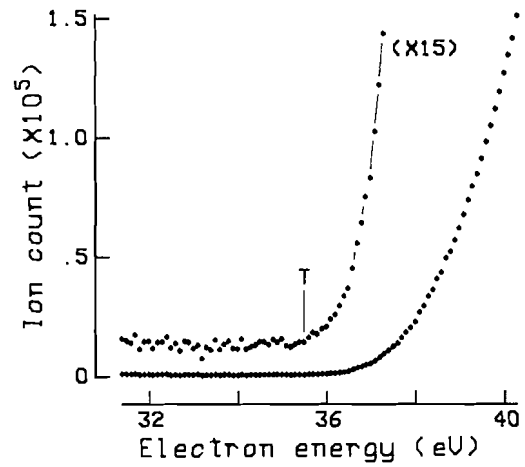

FIG. 14. $C_2H_3^{2+}$ appearance curve (100 meV/point).

ionization energy, combined with the ionization energy of C_2H_5 (8.39 ± 0.02, Table 4), give 27.5 ± 0.5 and 28.6 ± 0.3 eV, respectively, for the C_2H_5 double ionization energy. The above values are listed in Table 3.

The $C_2H_3^{2+}$ appearance energy is evaluated at 35.5 ± 0.3 eV, corresponding to the threshold of process

[18] $C_2H_6 + e^- \rightarrow C_2H_6^{-*} \rightarrow C_2H_3^{2+} + H + H_2 + 3e^-$

Jones *et al.* (15) reports a value of 34.5 eV for this threshold. A value of 30.0 ± 0.4 eV is deduced for the C_2H_3 double ionization potential which is in good agreement with the value of 29.6 ± 0.3 deduced from the work on ethylene (7) and also with the deduced values of Rabrenovic and Beynon (16) and Cooks *et al.* (17) (see Table 3).

Can. J. Chem. Downloaded from www.nrcresearchpress.com by 78.46.186.204 on 09/07/12
For personal use only.

TABLE 4. Data used in thermochemical calculations (in eV)

Gas	ΔH^0_{f0}	Ionization energy	Electron affinity
C	7.371±0.005 (27)	11.26039±0.00001 (3)	1.2629±0.0003 (34)
CH	6.123±0.004 (28)	10.64±0.01 (3)	1.238±0.008 (35)
CH_2	4.00±0.04 (29)	10.396±0.003 (3)	0.210±0.03 (35)
CH_3	1.558±0.007 (30)	9.842±0.002 (3)	0.08±0.03 (35)
CH_4	−0.693±0.003 (28)	12.615±0.010 (3)	
C_2	8.59±0.04 (28)	11.92±0.09 (6)	
C_2H	4.9±0.3 (28)[a]	11.6±0.5 (33)	
C_2H_2	2.356±0.008 (28)	11.401±0.007 (3)[b]	
C_2H_3	2.58±0.13 (31)[c,d]	8.95±0.05 (3)[d]	
C_2H_4	0.632±0.003 (28)	10.509±0.005 (2, 3)[e]	
C_2H_5	1.11±0.05 (32)[c]	8.39±0.02 (32)	
C_2H_6	−0.707±0.003 (30)		
H	2.23911±0.00004 (27)	13.598±0.001 (3)	0.754209(3) (34)

[a]Large uncertainty, but $4.5 \leq \Delta H^0_{f298} \leq 5.3$ eV (32).
[b]Average of first 11 values reported by ref. 3.
[c]ΔH^0_{f298} value
[d]Error estimated by present authors.
[e]Average of first 11 non-vertical values of ref. 2 and first 10 values of ref. 3.

Acknowledgements

Gratitude is expressed to Drs. M. Proulx and R. Dutil for their contribution to this work. Measurements were carried out at the Laboratoire de physique atomique et moléculaire at Laval University, Québec, and supported by grants from the Natural Sciences and Engineering Research Council of Canada.

1. J. BERKOWITZ. Photoabsorption, photoionization and photoelectron spectroscopy. Academic Press, New York. 1979. p. 295.
2. R. D. LEVIN and S. G. LIAS. Natl. Stand. Ref. Data Ser. NBS (U.S.) **71** (1982).
3. H. M. ROSENSTOCK, K. DRAXL, B. W. STEINER, and J. T. HERRON. J. Phys. Chem. Ref. Data, **6**, 11 (1977) suppl.1.
4. I. H. SUZUKI and K. MAEDA. Int. J. Mass Spectrom. Ion Phys. **24**, 147 (1977).
5. P. PLESSIS, P. MARMET, and R. DUTIL. J. Phys. B: At. Mol. Phys. **16**, 1283 (1983).
6. P. PLESSIS and P. MARMET. Int. J. Mass Spectrom. Ion Proc. **70**, 23 (1986).
7. P. PLESSIS and P. MARMET. Can. J. Phys. In press.
8. R. CARBONNEAU, E. BOLDUC, and P. MARMET. Can. J. Phys. **51**, 505 (1973).
9. P. MARCHAND and P. VEILLETTE. Can. J. Phys. **54**, 1309 (1976).
10. H. H. ARSENAULT and P. MARMET. Rev. Sci. Instrum. **48**, 512 (1977).
11. M. PROULX and P. MARMET. Int. J. Mass Spectrom. Ion Phys. **50**, 129 (1983).
12. H. CHATHAM, D. HILS, R. ROBERTSON, and A. GALLAGHER. J. Chem. Phys. **81**, 1770 (1984).
13. E. T. M. SELIM. Ind. J. Pure Appl. Phys. **14**, 547 (1976).
14. J. A. HIPPLE. Phys. Rev. **53**, 530 (1938).
15. B. E. JONES, L. E. ABBEY, H. L. CHATHAM, A. W. HANNER, L. A. TELESHEFSKY, E. M. BURGESS, and T. F. MORAN. Org. Mass Spectrom. **17**, 10 (1982).
16. M. RABRENOVIC and J. H. BEYNON. Int. J. Mass Spectrom. Ion. Proc. **54**, 79 (1983).
17. R. G. COOKS, T. AST, and J. H. BEYNON. Int. J. Mass Spectrom. Ion Phys. **11**, 490 (1973).
18. G. BIERI and L. ASBRINK. J. Elec. Spectros. Rel. Phenom. **20**, 149 (1980).
19. J. W. RABALAIS and A. KATRIB. Mol. Phys. **27**, 923 (1974).
20. M. J. S. DEWAR and S. D. WORLEY. J. Chem. Phys. **50**, 654 (1969).
21. A. D. BAKER, C. BAKER, C. R. BRUNDLE, and D. W. TURNER. Int. J. Mass Spectrom. Ion Phys. **1**, 285 (1968).
22. A. J. C. NICHOLSON. J. Chem. Phys. **43**, 1171 (1965).
23. K. WATANABE, T. NAKAYAMA, and J. MOTTL. J. Quant. Spectrosc. Radiat. Transfer, **2**, 369 (1962).
24. J. M. WILLIAM and W. H. HAMILL. J. Chem. Phys. **49**, 4467 (1968).
25. R. STOCKBAUER and M. G. INGHRAM. J. Chem. Phys. **54**, 2242 (1971).
26. W. CHUPKA and J. BERKOWITZ. J. Chem. Phys. **47**, 2921 (1967).
27. M. W. CHASE, J. L. CURNUTT, J. R. DOWNEY, R. A. MCDONALD, A. N. SYVERUD, and E. A. VALENZUELA. J. Phys. Chem. Ref. Data **11**, 695 (1982).
28. D. R. STULL and H. PROPHET. JANAF Thermochemical Tables. 2nd ed., Natl. Stand. Ref. Data Ser. **37** (1971).
29. M. W. CHASE, J. L. CURNUTT, H. PROPHET, R. A. MCDONALD, and A. N. SYVERUD. J. Phys. Chem. Ref. Data, **4**, 1 (1975).
30. K. M. PAMIDIMUKKALA, D. ROGERS, and G. B. SKINNER. J. Phys. Chem. Ref. Data, **11**, 83 (1982).
31. F. P. LOSSING. Can. J. Chem. **49**, 357 (1971).
32. F. A. HOULE and J. L. BEAUCHAMP. J. Am. Chem. Soc. **101**, 4067 (1979).
33. J. R. WYATT and F. E. STAFFORD. J. Phys. Chem. **76**, 1913 (1972).
34. H. HOTOP and W. C. LINEBERGER. J. Phys. Chem. Ref. Data, **14**, 731 (1985).
35. B. K. JANOUSEK and J. I. BRAUMAN. *In* Gas phase ion chemistry. Vol. 2. *Edited by* M. T. Bowers. Academic Press, New York. 1979. p. 53.

Can. J. Chem. Downloaded from www.nrcresearchpress.com by 78.46.186.204 on 09/07/12
For personal use only.

Isolation and structure of rolliniastatin 1 from the South American tree *Rollinia mucosa*[1]

GEORGE R. PETTIT,[2] GORDON M. CRAGG, JUDITH POLONSKY,[3] DELBERT L. HERALD, ANIMESH GOSWAMI, CECIL R. SMITH, CHRISTIAN MORETTI,[3] JEAN M. SCHMIDT, AND DAVID WEISLEDER[4]

Cancer Research Institute and Department of Chemistry, Arizona State University, Tempe, AZ 85287, U.S.A.

Received August 20, 1986

GEORGE R. PETTIT, GORDON M. CRAGG, JUDITH POLONSKY, DELBERT L. HERALD, ANIMESH GOSWAMI, CECIL R. SMITH, CHRISTIAN MORETTI, JEAN M. SCHMIDT, and DAVID WEISLEDER. Can. J. Chem. **65**, 1433 (1987).

Rollinia mucosa (Annonaceae), known in primitive medical practices of Indonesia and the West Indies as a treatment for tumors, has been investigated employing the seeds from a South American variety and the murine P388 lymphocytic leukemia (PS) for bioassay. The principal antineoplastic constituent (PS, 28% life extension, at 0.25 mg/kg and ED_{50} 4.5×10^{-5} μg/mL) was found to be a new *bis*-tetrahydrofuran designated rolliniastatin 1. Structural elucidation of rolliniastatin 1 was accomplished by a combination of high resolution nuclear magnetic resonance (300 MHz), mass spectral, and X-ray crystal structure techniques.

GEORGE R. PETTIT, GORDON M. CRAGG, JUDITH POLONSKY, DELBERT L. HERALD, ANIMESH GOSWAMI, CECIL R. SMITH, CHRISTIAN MORETTI, JEAN M. SCHMIDT et DAVID WEISLEDER. Can. J. Chem. **65**, 1433 (1987).

Utilisant les graines d'une variété sud-américaine de la plante et la murine P388 de leucémie lymphocitaire (PS) pour des bioessais, on a étudié les propriétés de la *Rollinia mucosa* (Annonaceae), qui est connue dans les pratiques médicales primitives de l'Indonésie et des Antilles pour le traitement des tumeurs. On a trouvé que le principal constituant actif (PS, augmentation de vie de 28%, à 0,25 mg/kg et ED_{50} de $4,5 \times 10^{-5}$ μg/mL) est un nouveau bis-tétrahydrofuranne que l'on a appelé rolliniastatine 1. On a déterminé la structure de la rolliniastatine 1 en combinant les techniques de la résonance magnétique nucléaire à haute résolution (300 MHz), du spectre de masse et de la diffraction des rayons-X par des cristaux uniques.

[Traduit par la revue]

The Annonaceae (ca. 2,100 species) is composed of shrubs and trees found mainly in tropical regions. The genus *Rollinia* generally occurs in Central and South America, and *R. mucosa* (Jacq.) Vaill, also known as *Annona mucosa* (Jacq.), has been used for the primitive medical treatment of tumors in the West Indies and in Indonesia (2). To assess the potential of this plant in respect to potentially useful antineoplastic components, seeds of *Rollinia mucosa* were collected in French Guiana in 1979. The lipophilic extract of these seeds showed activity in the P388 lymphocytic leukemia system, and fractionation of this extract was guided by bioassay using the murine P388 system in vitro.

Extraction of *Rollinia mucosa* seed (600 g) with hexane afforded 136 g of oily extract from which rolliniastatin 1 was isolated by a series of chromatographic steps. Steric exclusion chromatography was followed by gradient elution chromatography on silica gel with hexane – ethyl acetate. Rolliniastatin 1 (1.75 g, 0.29% yield) was isolated as a wax, mp 81–83°C from acetone: $[\alpha]_{589}$ +25.2°, $[\alpha]_{578}$ +26.2°, $[\alpha]_{546}$ +30.1°, $[\alpha]_{436}$ +48.5°, $[\alpha]_{365}$ +76.70° (t = 28°C, c 1.03, CH_2Cl_2); uv λ_{max} (CH_3OH): 224 nm (log ε, 3.93) (α,β-unsaturated carbonyl; ir ν_{max} ($CHCl_3$): 3580, 3460 (OH), 2928, 2855, (C—H), and 1748 cm^{-1}; SO-SIMS (3), m/z 645 $[M + Na]^+$, 730 $[M + Ag]^+$; and SP-SIHRMS, m/z 623.4917 (calcd. for $C_{37}H_{66}O_7$ + H: 623.4887). In deuterioglycerol SP-SIMS (3) gave m/z 627 $[M + D]^+$, indicating three exchangeable protons.

Spectral characteristics suggested that rolliniastatin 1 was a member of a new class of bioactive *bis*-tetrahydrofurans ("acetogenins"), which include uvaricin (4*a*), rollinicin (4*c*), isorollicin (4*b*), rollinone (4*b*), desacetyluvaricin (4*d*), cherimoline (4*e*), dihydrocherimoline (4*e*), 14-hydroxy-25-desoxyrollinicin (4*f*), and, most recently, asimicin (4*g*). These compounds characteristically contain 37 carbons, and have a γ-lactone moiety (usually α,β-unsaturated) and two tetrahydrofuran rings with a long hydrocarbon chain attached.

The ^{13}C and ^1H nmr spectra (Tables 1 and 2), elaborated by COSY and heteronuclear correlation experiments, established the α,β-unsaturated γ-lactone moiety of rolliniastatin 1. The following features were documented by ^{13}C shifts: the carbonyl group at C-1 (δ 174.5, singlet), the double bond between C-2 (δ 131.1, singlet) and C-35 (δ 151.7, doublet), a δ 77.9 doublet for C-36, and a δ 19.1 quartet for the C-37 methyl group. A heteronuclear correlation experiment connected C-35 with a downfield proton at δ 7.16, and C-36 with another at δ 5.02. Chemical shifts reminiscent of fatty acids were observed: ^1H and ^{13}C signals (Tables 1 and 2) for C-32, C-33, and C-34, and for a number of nearly equivalent methylene groups.

A DEPT nmr experiment revealed eight ^{13}C doublets associated with oxygenated carbons (δ 69.9, 71.8, 74.0, 77.9, and four more δ 81.0–83.0). One of these is in the lactone ring, and three others bear hydroxy groups that account for the three exchangeable protons. The presence of three secondary hydroxyl groups was confirmed by observing spectral changes induced by acetylation. The remaining four oxygen-bearing carbons were assigned to the tetrahydrofuran rings. Methine proton resonances complementing each of the doublet ^{13}C shifts occurred in the region δ 3.38–3.85, except for the C-36 proton signal at δ 5.02.

A high resolution mass spectrum of rolliniastatin 1 yielded a fragmentation pattern (Fig. 1) strikingly parallel to that of rol-

[1]Series part 132 of Antineoplastic Agents; for the preceding part see ref. 1.

[2]Correspondence may be addressed to this author.

[3]Institut de Chimie des Substances Naturelles, C.N.R.S., 91190 Gif-sur-Yvette, France.

[4]Northern Regional Research Center, ARS–USDA, Peoria, IL 61604, U.S.A.

Printed in Canada / Imprimé au Canada

Can. J. Chem. Downloaded from www.nrcresearchpress.com by 78.46.186.204 on 09/07/12
For personal use only.

TABLE 1. ^{1}H nuclear magnetic resonance chemical shifts and proton couplings for rolliniastatin 1[a]

Carbon no.	Chemical shifts (δ)	Couplings (J, Hz)	
3a	2.50 dddd	3a, 3b	15.1
		3a, 4	3.5
		3a, 35	1.5
		3a, 36	1.6
3b	2.36 dddd	3a, 3b	15.1
		3b, 4	8.1
		3b, 35	1.2
		3b, 36	1.4
4	3.85 m		
5	1.45		
6–13	1.25		
14	1.50 m		
15	3.38 m		
16	3.85 m		
17, 18	1.7–1.9 m		
19, 20	3.85 m		
21, 22	1.7–1.9 m		
23, 24	3.85 m		
25	1.45 m		
26–33	1.25 br, s		
34	0.85 t		
35	7.16 ddd	35, 36	1.5
36	5.02 dddq	36, 37	1.5
37	1.41 d		

[a]Chemical shifts in ppm (δ) at 300 MHz are reported relative to tetramethylsilane using a deuteriochloroform solution.

linone (4*b*), an isomeric *bis*-tetrahydrofuran that has a 14-oxo group and a saturated lactone moiety. Furthermore, the mass spectral fragmentation pattern allowed location of the presumptive *bis*-tetrahydrofuran system with its two α-hydroxyl groups between C-15 and C-24. Corroborative evidence for the α-hydroxy tetrahydrofuran system was provided by ^{1}H nmr. COSY experiments established couplings between the following sets of protons: H-14–H-15 (δ 1.45 → 3.38), H-15–H-16 (δ 3.38 → 3.85). The relationships between H-23, H-24, and H-25 were discerned by the same method. The following C-13/H-1 connections were delineated by heteronuclear connectivity experiments: C-14–H-14a + 14b (δ 34.1 → 1.45), C-15–H-15 (δ 74.0 → 3.38), C-16–H-16 (δ 83.0 → 3.85), and C-19–H-19 (δ 81.0 → 3.85). Corresponding connections were noted among protons and carbons from C-20 through C-25.

The plausible assumption that rolliniastatin 1, like rollinone, has an oxygen function at C-14 proved erroneous despite their similar mass spectra. Surprisingly, mass spectral results gave no hint of the third hydroxyl group location. By means of nmr experiments (including COSY, heteronuclear correlation, and simulation by PANIC) the third hydroxyl was located in relation to the lactone ring and placed at C-4. Allylic couplings (J = 1.5, 1.2 Hz) between the two nonequivalent protons, 3a and 3b (δ 2.50 and 2.36), and H-35 (δ 7.16) supported this assignment. In addition, protons 3a and 3b exhibited long range couplings (J = 1.6, 1.4 Hz) with H-36 (δ 5.02). Protons 3a and 3b were also found coupled (J = 3.4, 8.1 Hz) to H-4 (δ 3.85). In turn H-4 was found connected to a carbon appearing as a doublet at δ 69.9. Thus, the ^{13}C and ^{1}H shifts both indicated that C-4 was bonded to oxygen. Also established were appropriate connections between carbons and protons at C-3 (δ 2.36 + 2.50 → 33.2) and C-5 (δ 1.45 → 37.4).

TABLE 2. ^{13}C nuclear magnetic resonance chemical shifts of asimicin and rolliniastatin 1[a]

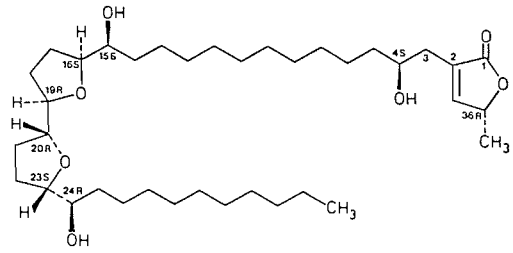

Carbon no.	Rolliniastatin	Asimicin
1	174.5 s	174.6 s
2	131.1 s	131.1 s
3	33.2 t	33.4 t
4	69.9 d	69.9 d
5	37.4 t	37.5 t
6	26.0 t	25.6 t
7	29.5 t	29.6 t
12	29.3 t	29.3 t
13	25.7 t	25.6 t
14	34.1 t[b]	33.6 t[b]
15	74.0 d[c]	74.1 d[c]
16	83.0 d	83.1 d
17	28.7 t	28.4 t
18	27.8 t	28.4 t
19	81.1 d	81.7 d
20	81.0 d	81.7 d
21	27.8 t	28.4 t
22	28.4 t	28.4 t
23	83.0 d	82.8 d
24	71.8 d[c]	74.1 d[c]
25	32.8 t[b]	33.4 t[b]
26	25.5 t	25.6 t
27	29.6 t	29.6 t
31		29.3 t
32	31.9 t	31.9 t
33	22.6 t	22.7 t
34	14.1 q	14.1 q
35	151.7 d	151.6 d
36	77.9 d	77.9 d
37	19.1 q	19.1 q

[a]Both spectra were determined in deuteriochloroform solution and chemical shifts are expressed in ppm (δ) from tetramethylsilane.
[b,c]These shifts may be interchanged.

The structure herein assigned rolliniastatin 1 was confirmed and stereochemical details were elucidated by an X-ray crystal structure (Fig. 2) determination of rolliniastatin 1 15-*O*-*p*-bromophenylurethane: needles from ethyl acetate melting at 91–92°C; $[\alpha]_D^{28}$ +38.3° (*c* 0.9, $CHCl_3$): ir ν_{max} (KBr): 3531, 3444, 1737, 1716 cm^{-1}; HREIMS, *m/z*, [M$^+$] 819.4223 (calcd. for $C_{44}H_{70}{}^{79}BrNO_8$: 819.4285). The X-ray structure determination (ρ(density) 1.067 g/cm^3 and *V* (cell volume) 4311.65 Å^3; $P2_12_12_1$; crystal dimension 0.13 × 0.37 × 0.08 mm; 4007 reflections; 2117 reflections observed (3σ cutoff); and R = 9.40, Rw = 7.92) of rolliniastatin 1 15-*O*-*p*-bromophenylurethane provided the following relative stereochemistry (Fig. 2) for the eight chiral centers: 4*S**, 15*S**, 16*S**, 19*R**, 20*R**, 23*S**, 24*R**, 36*R**. The absolute configuration was not unequivocally established on the basis of present X-ray data and is presently being investigated.

Can. J. Chem. Downloaded from www.nrcresearchpress.com by 78.46.186.204 on 09/07/12
For personal use only.

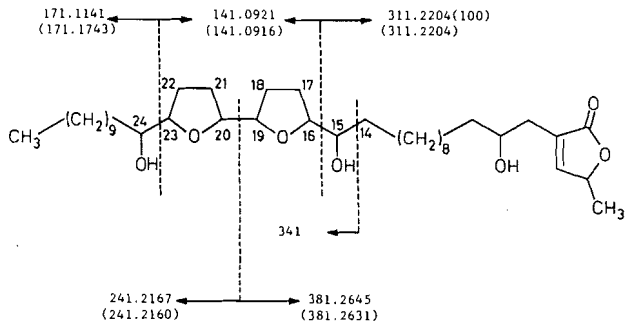

FIG. 1. HREIMS fragmentation of rolliniastatin 1 with calculated values in parentheses.

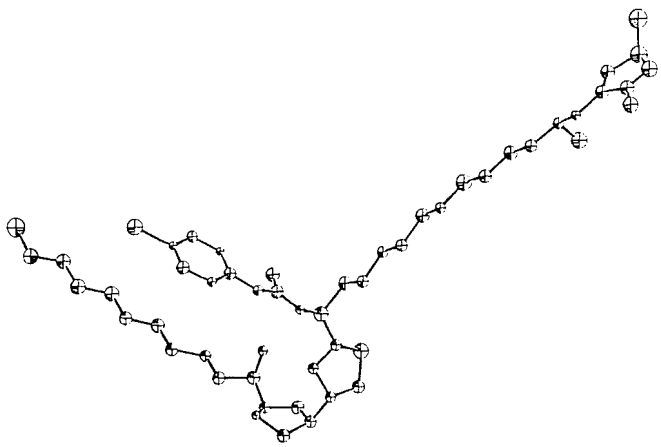

FIG. 2. The 15-*O*-*p*-Bromophenylurethane derivative of rolliniastatin 1, as depicted by ORTEP II (62% probability thermal ellipsoids) and viewed down the *X*-axis.

The rolliniastatin 1 spectral data suggest that asimicin[5,6] (4*g*) is a diastereomer of this bis-tetrahydrofuran. The ^{13}C nmr shifts for rolliniastatin 1 and asimicin (Table 2) are almost identical except those for C-14, C-24, and C-25 (alternatively, C-14, C-15, and C-25). The carbon nmr data indicate that the two compounds are diastereomers differing in configuration at a chiral center(s) in or near the bis-tetrahydrofuran systems. Asimicin's ^{13}C shifts for carbons 14–19 are virtually identical with those for carbons 20–25, suggesting that asimicin is pseudosymmetrical about the midpoint of the bond connecting C-19 and C-20. In contrast, rolliniastatin 1 is not symmetrical in this respect. These observations, and results herein of the first crystal structure determination for a member of this relatively new class of natural products, indicate that the rolliniastatin 1 isomer asimicin reported (4*g*) as this manuscript was being prepared receives further structural support. But a few of the other six known compounds (4) of this class may require some additional structural refinements. Presently we are investigating a series of *Rollinia mucosa* constituents related to rolliniastatin 1.

Biological evaluation (5) of rolliniastatin 1 (PS, 28% life extension, and ED_{50} 4.5×10^{-5} μg/mL) from *Rollinia mucosa* is continuing and includes an assessment of insecticidal activity well known for tropical American plants of this family, such as *Annona muricata* L. and *A. reticulata* L (6), and just noted for asimicin (4*g*).

[5]We thank Dr. J. L. McLaughlin, Purdue University, for a reference sample of asimicin.

[6]When compared by tlc, rolliniastatin 1 and asimicin initially were barely resolved, but were convincingly separated (when minimal amounts of sample were applied) on a silica plate using triple development with methylene chloride – methanol (95:5) as mobile phase. In this system the R_f for rolliniastatin 1 is slightly higher than that for asimicin.

Acknowledgments

For the *sine qua non* of this research our appreciation is extended to the Arizona Disease Control Research Commission, Eleanor W. Libby, the Waddell Foundation (Donald Ware), the Fannie E. Rippel Foundation, Herbert K. and Dianne Cummings (The Nathan Cummings Foundation), Polly J. Trautman, Lotte Flugel, Jack W. Whiteman, Mary Dell Pritzlaff, the Olin Foundation (Spencer T. and Ann W.), the Robert B. Dalton Endowment Fund, and Grant CA-30311-01A3 awarded by the National Cancer Institute, DHHS. We are also pleased to thank Drs. John E. Leet and Roland Riesen and Mr. Phillip J. Daschner for other assistance with this research.

1. G. R. PETTIT, S. B. SINGH, M. L. NIVEN, E. HAMEL, and J. M. SCHMIDT. J. Nat. Prod. **50**, 119 (1987).
2. J. L. HARTWELL. Plants used against cancer. Quarterman Publications, Inc., Lawrence, MA. 1982. p. 28.
3. C. W. HOLZAPFEL, G. R. PETTIT, and G. M. CRAGG. J. Nat. Prod. **48**, 513 (1985).
4. (*a*) S. D. JOLAD, J. J. HOFFMANN, K. H. SCHRAM, M. S. TEMPESTA, G. R. KREIK, and R. B. BATES. J. Org. Chem. **47**, 3151 (1982); (*b*) T. T. DABRAH and A. SNEDEN. J. Nat. Prod. **47**, 652 (1984); (*c*) T. T. DABRAH and A. T. SNEDEN. Phytochemistry, **23**, 2013 (1984); (*d*) S. D. JOLAD, J. J. HOFFMANN, J. R. COLE, C. E. BARRY III, R. B. BATES, and W. A. KONIG. J. Nat. Prod. **48**, 644 (1985); (*e*) D. CORTES, J. L. RIOS, A. VILLAR, and S. VALVERDE. Tetrahedron Lett. **25**, 3199 (1984); (*f*) J. D. ETSE and P. G. WATERMAN. J. Nat. Prod. **49**, 684 (1986); (*g*) J. K. RUPPRECHT, C.-J. CHANG, J. L. MCLAUGHLIN, K. L. MIKOLAJCZAK, and D. WEISLEDER. Heterocycles, **24**, 1197 (1986).
5. J. M. SCHMIDT and G. R. PETTIT. Experientia, **34**, 659 (1978).
6. J. M. WATT and M. G. BREYER-BRANDWIJK. Medicinal and poisonous plants of southern and eastern Africa. 2nd ed. E. and S. Livingston, Ltd., London. 1962. p. 58.

Can. J. Chem. Downloaded from www.nrcresearchpress.com by 78.46.186.204 on 09/07/12
For personal use only.

High-yield regioselective synthesis of 9-glycosyl guanine nucleosides and analogues via coupling with 2-*N*-acetyl-6-*O*-diphenylcarbamoylguanine[1]

RUIMING ZOU AND MORRIS J. ROBINS
Department of Chemistry, University of Alberta, Edmonton, Alta., Canada T6G 2G2

Received January 6, 1987

RUIMING ZOU and MORRIS J. ROBINS. Can. J. Chem. **65**, 1436 (1987).

Treatment of 2-*N*,9-diacetylguanine with diphenylcarbamoyl chloride followed by heating with aqueous ethanol gave 2-*N*-acetyl-6-*O*-diphenylcarbamoylguanine (2-acetamido-6-diphenylcarbamoyloxypurine). Bis-trimethylsilylation of this product followed by coupling with glycosyl acetates (trimethylsilyl triflate catalysis) or α-haloethers in *anhydrous toluene* gave 9-substituted guanine compounds in high yields with no 7-isomers detected.

RUIMING ZOU et MORRIS J. ROBINS. Can. J. Chem. **65**, 1436 (1987).

La réaction de la diacétyl-2-*N*,-9 guanine avec le chlorure de diphénylcarbamoyle, suivie d'un chauffage avec de l'éthanol aqueux, conduit à la *N*-acétyl-2 *O*-diphénylcarbamoyl-6 guanine (acétamido-2 diphénylcarbamoyloxy-6 purine). La bis-triméthylsilylation de ce produit, suivie d'un couplage avec soit les acétates de glycosyle (catalyse par le triflate de triméthylsilyle) ou les α-haloéthers dans le *toluène anhydre*, conduit aux composés de la guanine substitués en position 9; les rendements sont élevés et on ne détecte pas la présence d'isomères 7.

[Traduit par la revue]

Can. J. Chem. Downloaded from www.nrcresearchpress.com by 72.64.146.136 on 09/07/12
For personal use only.

Of the five heterocyclic bases commonly found in DNA and RNA, guanine (**1**) causes markedly enhanced experimental problems. Guanosine and its analogues are amphoteric ($pK_a1 \sim 1.7$, $pK_a2 \sim 9.2$) polyfunctional compounds that are sparingly soluble in water and polar aprotic solvents, and effectively insoluble in all other common solvents. They often self-associate in solution to form viscous gels and hydrate tenaciously in the crystalline state. Direct coupling with guanine-type bases produces N7/N9 isomeric mixtures (*1*) that are frequently difficult to separate for the above reasons. Changes in experimental variables affect the isomer ratios, but do not eliminate contamination of the desired thermodynamic N9 product by significant quantities of the kinetic N7 isomer (2).

Discovery (3) of the potent activity against herpes simplex type 1 and 2 viruses and low mammalian toxicity of 9-[(2-hydroxyethoxy)methyl]guanine (acyclovir) triggered a massive worldwide effort to synthesize and test guanine nucleosides and "acyclic nucleoside" analogues. Very recent syntheses of acyclovir analogues have employed 2-amino-6-alkoxypurines (4, 5) to enhance selectivity for N9 coupling.

Reese and Ubasawa (6) and Hata and co-workers (7) had observed O6 functionalization of guanine during phosphate activation for oligonucleotide synthesis, and Hata and co-workers have exploited O6 diphenylcarbamoylation of guanosine derivatives as a protection strategy (8). We now report regioselective coupling of bis-trimethylsilylated 2-*N*-acetyl-6-*O*-diphenylcarbamoylguanine (**2**) with acetylated pentofuranoses and α-haloethers as a convenient new route to guanine N9 products.

A suspension of 30.22 g (0.2 mol) of guanine (**1**) in 250 mL of dry DMAc and 50 mL of Ac_2O was stirred at 160°C for 7 h. The brown solution was cooled and crystalline 2-*N*,9-diacetylguanine[2,3] (9) was filtered and washed with EtOH. A second crop raised the yield to 42.53 g (90%). A stirred suspension of 5.88 g (25 mmol) of 2-*N*,9-diacetylguanine in 8.7 mL of $EtN(i\text{-}Pr)_2$ and 120 mL of dry C_5H_5N was treated with 6.37 g (27.5 mmol) of Ph_2NCOCl for 1 h at ambient temperature. H_2O (10 mL) was added and stirring continued for 10 min. Evaporation *in vacuo* and coevaporation (3 × 20 mL of $PhCH_3$) was followed by heating (steam bath) the residue with 300 mL of 50% $EtOH/H_2O$ for 1.5 h. Cooling, filtration, washing (EtOH), and drying gave 8.93 g (92%) of **2**.[3,4]

N,*O*-Bis(trimethylsilyl)acetamide (0.5 mL) was added to a suspension of 388 mg (1 mmol) of **2** in 10 mL of dry 1,2-dichloroethane. Stirring at 80°C for 15 min gave a clear solution that was evaporated *in vacuo*. The residue was dissolved in 5 mL of dry $PhCH_3$ and 0.25 mL of $CF_3SO_3SiMe_3$, and 382 mg (1.2 mmol) of 1,2,3,5-tetra-*O*-acetyl-β-D-ribofuranose in 5 mL of dry $PhCH_3$ was added. The solution was stirred at 80°C for 1 h and cooled, 50 mL of EtOAc was added, and the solution was worked up in the usual manner. The crude product was chromatographed (25 g silica, 2 × 15 cm; Et_2O/Me_2CO 8:2) to give 589 mg (91%) of **3**: ms (FAB) m/z 647 ($M + 1$); ^1H and ^{13}C nmr spectra were compatible with structure **3**.

Trace quantities (<3%) of a more rapidly migrating bis-ribosylated product (2-N,9 by nmr) were separated from **3** by the column chromatography. Deprotection of **3** with NH_3/H_2O/MeOH gave 75% (68% from **2**) of guanosine (**4**) hemihydrate[3] after recrystallization from water.

Analogous coupling reactions with $\mathbf{2}(SiMe_3)_2$ and tetra-*O*-acetyl-D-furanosyl derivatives of arabinose and xylose gave good yields of the corresponding 9-α- and 9-β-guanine nucleosides, respectively. Coupling of $\mathbf{2}(SiMe_3)_2$ and (2-acetoxyethoxy)methyl bromide (10) in toluene proceeded readily at ambient temperature without catalyst. The resulting acyclovir derivative was obtained in 63% yield after column chromatography and crystallization. X-ray crystallographic analysis of this intermediate confirmed the 6-diphenylcarbamoyloxy structure.[5] Deprotection gave acyclovir hemihydrate[3] (10) in 91% yield after recrystallization (H_2O).

[1](*a*) This paper constitutes "Nucleic acid related compounds. 52." For the previous paper in this series, see ref. 12. (*b*) A preliminary account was presented at the Annual Chemical Congress of the Royal Society of Chemistry, University of Warwick, U.K. April 11, 1986.

[2]Mass spectrum, m/z 235.0706 (M^+ 235.0706); ^1H nmr (Me_2SO-d_6) δ: 2.20 (2NAc), 2.80 (N9Ac), 8.42 (H8).

[3]These compounds had elemental analyses (C, H, N) within ±0.3% of theory.

[4]Mass spectrum, m/z 388.1283 (M^+ 388.1284); ^1H nmr (Me_2SO-d_6) δ: 2.18 (2NAc), 7.26–7.56 (NPh_2), 8.46 (H8).

[5]We thank Dr. R. Ball of the Structure Determination Laboratory of this Department for the X-ray analysis. Details will be published separately.

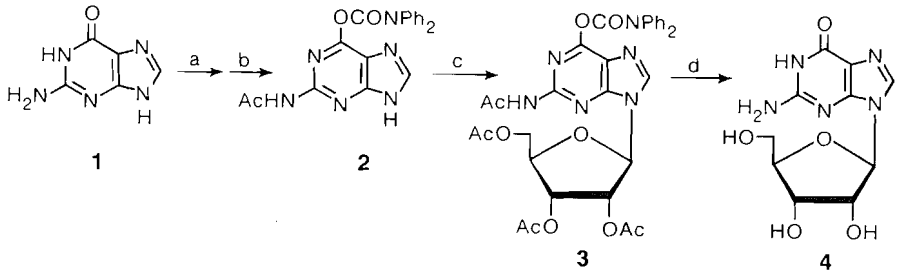

(a) Ac_2O/DMAc/Δ. (b) (i) Ph_2NCOCl/EtN(i-Pr)$_2$/Pyridine. (ii) EtOH/H_2O/Δ.
(c) (i) BSA/$ClCH_2CH_2Cl$/Δ/Evaporate. (ii) Tetraacetylribose/$CF_3SO_3SiMe_3$/$PhCH_3$/Δ.
(d) NH_3/H_2O/MeOH/60° C.

Vorbrüggen *et al.* (11) had reported coupling of tris-trimethylsilylated 2-*N*-acetylguanine and 1-*O*-acetyl-2,3,5-tri-*O*-benzoyl-β-D-ribofuranose in 1,2-dichloroethane at reflux with trimethylsilyl triflate as catalyst. The crude product was deprotected to give "pure guanosine" in 66% yield after recrystallization from water. Careful repetition of this sequence gave 66% of crystalline product that comigrated (tlc) with guanosine as described (11). However, the 400-MHz ^1H nmr spectrum of this material in Me_2SO-d_6 revealed a mixture of **4** and its N7 isomer. The nmr analysis of the crude coupling product showed a N9/N7 ratio of ~3:1.

Analysis (400-MHz ^1H and 100-MHz ^{13}C nmr) of our crude coupling product and the recrystallized deprotected nucleoside showed only **3** (plus trace amounts of the bis-ribosyl by-product) and **4**, respectively, with no detected N7 contaminant. Therefore, coupling of glycosyl acetate (and chloride) derivatives and α-haloethers with the readily accessible **2**$(SiMe_3)_2$ under *anhydrous* conditions in *toluene* as described herein represents a new and experimentally convenient route to 9-glycosyl guanine derivatives and analogues. These can be purified and manipulated readily and deprotected under mild conditions. It represents the method of choice among presently published alternatives for the preparation of guanine N9 nucleosides.[6] Further investigations on selective syntheses of N7 products and kinetic/thermodynamic isomer studies will be reported in detail.

Acknowledgments

We thank the Natural Sciences and Engineering Research Council of Canada, the National Cancer Institute of Canada, and the University of Alberta for generous support. We thank the Alberta Heritage Foundation for Medical Research for a Graduate Studentship to R.Z. 1982–1985.

[6]Alkylation of **2**$(SiMe_3)_2$ did not proceed satisfactorily under comparable conditions with "unactivated" alkyl halides. The use of salts of 2-amino-6-alkoxypurines (4, 5) appears to be favorable for preparation of 9-alkylguanines.

1. (*a*) L. Goodman. *In* Basic principles in nucleic acid chemistry. Vol. I. *Edited by* P. O. P. Ts'o. Academic Press, New York. 1974. Chap. 2; (*b*) M. Imazawa and F. Eckstein. J. Org. Chem. **43**, 3044 (1978); (*c*) K. K. Ogilvie, U. O. Cheriyan, B. K. Radatus, K. O. Smith, K. S. Galloway, and W. L. Kennell. Can. J. Chem. **60**, 3005 (1982); (*d*) G. E. Wright and L. W. Dudycz. J. Med. Chem. **27**, 175 (1984).
2. L. W. Dudycz and G. E. Wright. Nucleosides Nucleotides, **3**, 33 (1984).
3. G. B. Elion, P. A. Furman, J. A. Fyfe, P. de Miranda, L. Beauchamp, and H. J. Schaeffer. Proc. Natl. Acad. Sci. U.S.A. **74**, 5716 (1977).
4. M. MacCoss, A. Chen, and R. L. Tolman. Tetrahedron Lett. **26**, 1815 (1985).
5. J. Kjellberg, M. Liljenberg, and N. G. Johansson. Tetrahedron Lett. **27**, 877 (1986).
6. C. B. Reese and A. Ubasawa. Tetrahedron Lett. **21**, 2265 (1980).
7. H. P. Daskalov, M. Sekine, and T. Hata. Tetrahedron Lett. **21**, 3899 (1980).
8. (*a*) T. Kamimura, M. Tsuchiya, K. Koura, M. Sekine, and T. Hata. Tetrahedron Lett. **24**, 2775 (1983); (*b*) T. Kamimura, M. Tsuchiya, K. Urakami, K. Koura, M. Sekine, K. Shinozaki, K. Miura, and T. Hata. J. Am. Chem. Soc. **106**, 4552 (1984).
9. Y. Ishido, A. Hosono, S. Isome, A. Maruyama, and T. Sato. Bull. Chem. Soc. Jpn. **37**, 1389 (1964).
10. M. J. Robins and P. W. Hatfield. Can. J. Chem. **60**, 547 (1982).
11. H. Vorbrüggen, K. Krolikiewicz, and B. Bennua. Chem. Ber. **114**, 1234 (1981).
12. E. De Clercq, J. Balzarini, D. Madej, F. Hansske, and M. J. Robins. J. Med. Chem. **30**, 481 (1987).

Can. J. Chem. Downloaded from www.nrcresearchpress.com by 72.64.146.136 on 09/07/12
For personal use only.

Total synthesis of leukotriene B_4 analogues: 3-thia-LTB_4 and 3-thia-20,20,20-trifluoro-LTB_4

YVAN GUINDON AND DANIEL DELORME[1]

Merck Frosst Canada Inc., P.O. Box 1005, Pointe Claire – Dorval, P.Q., Canada H9R 4P8

Received December 11, 1986

YVAN GUINDON and DANIEL DELORME. Can. J. Chem. **65**, 1438 (1987).

Using *C*-furanosides as chiral precursors of (*Z*,*E*) 1,3-dienes has permitted the synthesis of two leukotriene B_4 analogues: 3-thia-LTB_4 and 3-thia-20,20,20-trifluoro-LTB_4.

YVAN GUINDON et DANIEL DELORME. Can. J. Chem. **65**, 1438 (1987).

L'utilisation de *C*-furanosides comme précurseurs chiraux de diènes-1,3 de stéréochimie (*Z*,*E*) a permis de synthétiser divers analogues du leucotriène B_4, en particulier le thia-3 LTB_4 et le thia-3 trifluoro-20,20,20 LTB_4.

LTB_4 **1** (Scheme 1) is an oxygenated metabolite of arachidonic acid that has been recently isolated (1), characterized, and synthesized by us and others (2, 3). Putative important roles in allergic, inflammatory (4), and immunological reactions (5) have been attributed to LTB_4. This local hormone is rapidly and extensively metabolized in vivo first by hydroxylation at C-20 to give **2** (ω-oxidation), followed by oxidation to the diacid **3** and subsequent β-oxidation of the two acidic chains (6). Metabolically stable analogues (7) of LTB_4 would lead to a better comprehension of the biological effects of this important mediator. This would also permit the elaboration of in vivo assays suitable for the evaluation of chemical entities as potential therapeutic agents. We would like to report herein on the total synthesis of two such analogues, 3-thia-LTB_4 **4** and 3-thia-20,20,20-trifluoro-LTB_4 **5**.

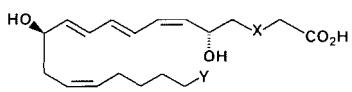

1. X = CH_2, Y = CH_3 : LTB_4
2. X = CH_2, Y = CH_2OH : 20-OH-LTB_4
3. X = CH_2, Y = CO_2H : 20-CO_2H-LTB_4
4. X = S, Y = CH_3 : 3-thia-LTB_4
5. X = S, Y = CF_3 : 3-thia-20-CF_3-LTB_4

SCHEME 1

Our approach to the synthesis of LTB_4 analogues is based on the utilization of properly substituted tetrahydrofurans as masked dienic functionalities. Recently, we described the transformation of *C*-furanosides (e.g. **6**) (Scheme 2) to chiral (*E*,*E*)-dienic precursors (e.g. **7**) in the synthesis of LTB_4 (2*a*). Our initial success was based on consecutive retro-Michael reaction followed by elimination of an activated oxygen in one chemical step. In this paper we present another alternative, which consists of using structurally similar tetrahydrofuran derivatives (e.g. **8**) as precursors of the (*Z*,*E*)-dienic functionality **9**. In this case the elimination of the leaving group is accomplished first, using the tetrahydrofuran ring as a template for the formation of the *cis* double bond (e.g. **13**). Our synthesis is summarized in Scheme 3.

The *C*-furanosides **12** were prepared from a known synthetic sequence using 2-deoxy-D-ribose **10** (8). The intracyclic olefin **13** was obtained, in 78% yield, through the formation of a secondary triflate ester **8** (9) followed by treatment, in the same

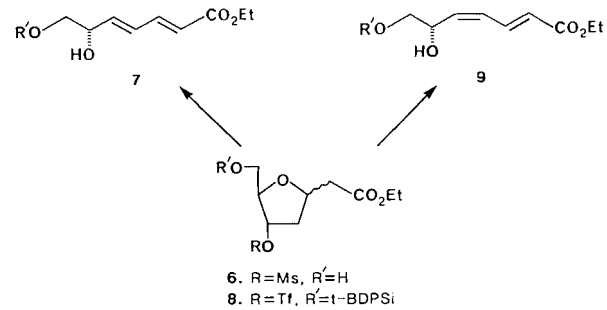

6. R=Ms, R′=H
8. R=Tf, R′=t-BDPSi

SCHEME 2

reaction mixture, with DBU. We were pleased to note that the efficient opening of **13** by LDA in THF (for LDA induced retro-Michael reactions see refs. 8, 10) led cleanly and exclusively to the optically active (*Z*,*E*)-diene ester **14**, $[\alpha]_D$ + 73.9° (*c* 1.33, $CHCl_3$), in very high yield.[2] It should be noted that the same *C*-furanosides may be expediently transformed to the optically active (*E*,*E*)-diene **7** by simply adding sodium ethoxide directly to the triflate ester reaction mixture. This latter transformation underscores the versatility of this approach and confirms the synthetic utility of tetrahydrofurans as masked 1,3-dienes.[3]

The allylic alcohol in **14** was to become the hydroxyl group at C-5 of our LTB_4 analogues, so that an inversion of configuration at this centre was necessary. This was achieved using a well-known procedure (DEAD, triphenylphosphine, benzoic acid, ref. 12) to give the benzoate **16**[4] in 89% yield,

[1]Author to whom correspondence may be addressed.

[2]^{1}H nuclear magnetic resonance (250 MHz, $CDCl_3$) δ 1.09 (s, 9H, $(CH_3)_3$), 1.34 (t, 3H, *J* = 7.5 Hz, CH_2CH_3), 2.68 (m, 1H, OH), 3.63 (ddd, 2H, *J* = 11 Hz, *J* = 8.0 Hz, *J* = 4.2 Hz, $SiOCH_2$), 4.22 (q, 2H, *J* = 7.5 Hz, CH_2CH_3), 4.78* (m, 1H, C*H*—OH), 5.73 (dd, 1H, *J* = 11 Hz, *J* = 8 Hz, H-5), 5.90 (d, 1H, *J* = 15 Hz, H-2), 6.20 (t, 1H, *J* = 11 Hz, H-4), 7.55 (dd, 1H, *J* = 12 Hz, *J* = 15 Hz, H-3), 7.35–7.71 (m, 10H, 2Ph).

*Decoupling experiment: 5.73 (d, 1H, *J* = 11 Hz, H-5); *Z* olefin; ir (neat); 3440, 2930, 2860, 1700, 1640, 1610 cm^{-1}. High resolution mass spectrum, *m*/*z* calcd. for $C_{25}H_{30}O_3Si$ (M^+ H_2O) 406.1964; found: 406.1986.

[3]A procedure for obtaining chiral (*Z*,*E*)-diene using a Wittig reaction on pseudoglucal was recently reported (11).

[4]The extent of the inversion of the allylic alcohol has been verified in the following way. In trityl series the benzoate **17** was treated sequentially with sodium ethoxide and LDA to give the corresponding alcohol with $[\alpha]_D$ −77.2° (*c* 1.55, $CHCl_3$) as opposed to $[\alpha]_D$ +79.4° (*c* 1.11, $CHCl_3$) for **15** (Scheme 3). Mosher esters (13) of both alcohols were, as well, made and ^{1}H nmr indicated that **17** was obtained with >97% inversion.

Can. J. Chem. Downloaded from www.nrcresearchpress.com by 78.46.186.204 on 09/07/12
For personal use only.

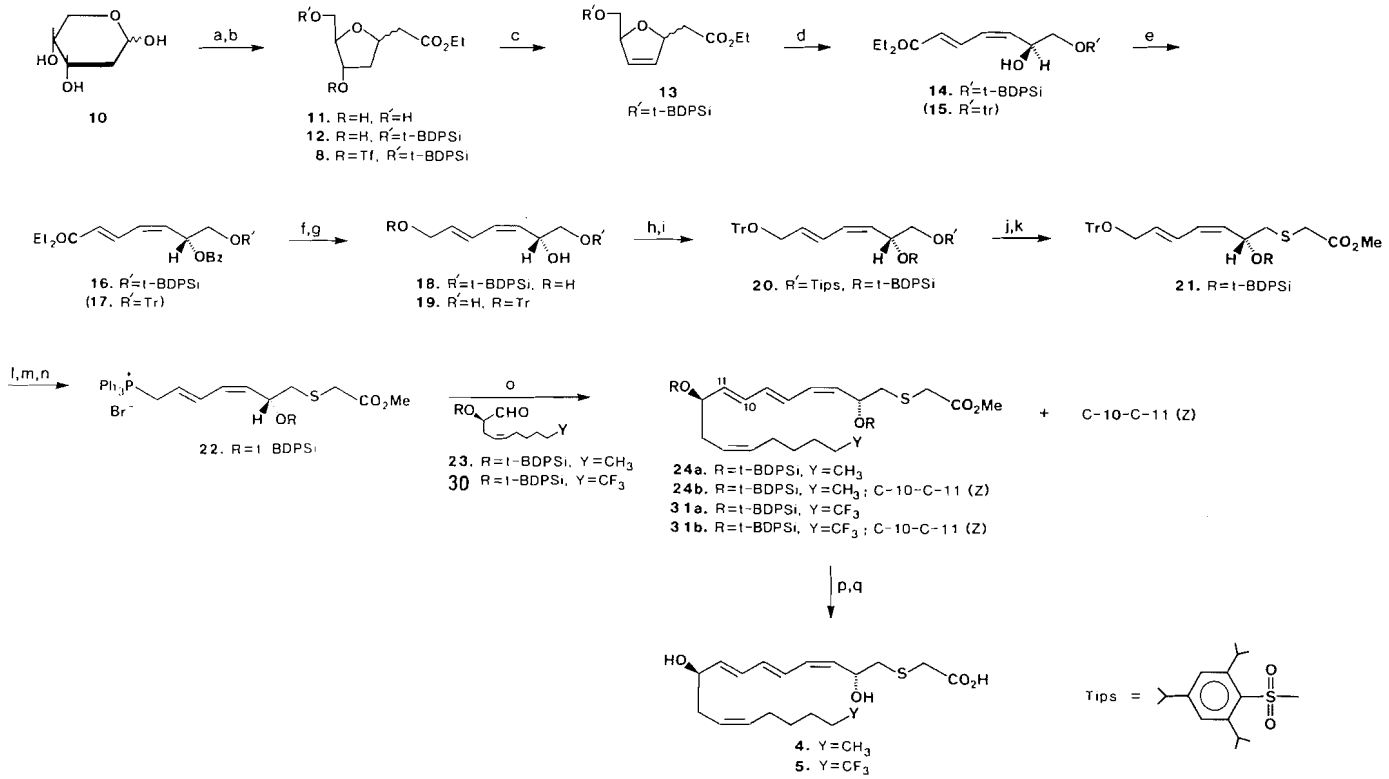

(a) See ref. 8; (b) *t*-BDPSiCl, iPr_2NEt, DMAP, CH_2Cl_2; (c) trifluoromethanesulfonic anhydride, (2 equiv.) pyridine, CH_2Cl_2; then DBU (6 equiv.), 78% (isolated yield); (d) LDA (1.2 equiv.), THF, 0°C, 92% (isolated yield)[2]; (e) Ph_3P, benzoic acid, DEAD, THF, r.t., 89% (isolated yield); (f) DIBAH, toluene, −10°C → r.t., 79% (isolated yield); (g) TrCl, pyr., DMAP, 50°C; then $nBu_4N^+F^-$, THF, r.t., 61% (isolated yield); (h) 2,4,6-triisopropylbenzenesulfonyl chloride, Et_3N, CH_2Cl_2, r.t., 63% (i) *t*-BDPSiCl, CH_2Cl_2, iPr_2NEt, r.t., 87%; (j) NaI, MEK, 70°C, 83%; (k) methylthioglycolate, NaH, THF, 50°C, 96%; (l) 20% aq. TFA, CH_2Cl_2, 63%; (m) CBr_4, DIPHOS, CH_2Cl_2, 0°C → r.t., 82%; (n) Ph_3P, CH_3CN, r.t.; (o) LiHMDS, THF, −78°C; then 23 → 0°C, 56%; (p) Bu_4NF, AcOH, THF, −10°C → r.t.; then CH_2N_2, then K_2CO_3, MeOH, r.t.; (q) NaOH, MeOH, 0°C → r.t.

SCHEME 3

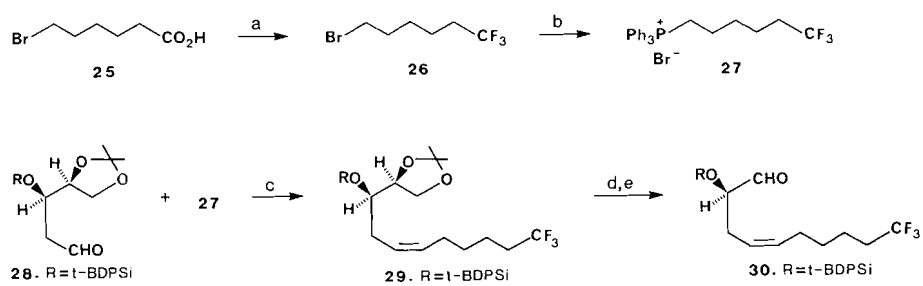

(a) SF_4, 130°C; (b) Ph_3P, CH_3CN, reflux; (c) BuLi, THF, −78°C → r.t.; (d) TFA, THF, H_2O, 0.4:4:1, 60°C, 91%; (e) $Pb(OAc)_4$, CH_2Cl_2, K_2CO_3, −78°C, 87%.

SCHEME 4

$[\alpha]_D$ +74.8° (*c* 1.01, $CHCl_3$). DIBAH reduction (14) of both esters led to the dienediol **18**, $[\alpha]_D$ −42.0° (*c* 1.24, $CHCl_3$). The resulting primary alcohol was then tritylated, followed by desilylation using nBu_4 N^+F^- in THF, affording **19** in 61% yield from **16**. Selective primary sulfonylation of **19** with triisopropylbenzenesulfonyl chloride (15) in the presence of triethylamine was then followed by protection of the secondary alcohol as *tert*-butyldiphenylsilyl ether (16) to give **20**. Successive displacement of the sulfonate **20** with sodium iodide in hot 2-butanone, followed by sodium thiolate of methylthioglycolate in THF at 50°C for 4 h, led to C-1—C-10 unit **21** in 79% yield.

Completion of the synthesis of 3-thia-LTB_4 was then performed in the following way. Regeneration of the primary hydroxyl group from **21** was achieved with 20% aqueous trifluoroacetic acid (17) in CH_2Cl_2. The resulting primary alcohol was converted to the corresponding bromide and treated with triphenylphosphine in acetonitrile to give the phosphonium salt **22**. The Wittig coupling between **22** and the aldehyde **23** (2*b*) was then achieved through ylide formation at −78°C (THF) using LiHMDS, followed by the addition of aldehyde **23** and warming of the reaction mixture to 0°C. Trienes **24***a* and **24***b* were thus obtained in a 1:1 ratio. Removal of both silyl ethers using nBu_4 N^+F^- in the presence of acetic acid, followed by

Can. J. Chem. Downloaded from www.nrcresearchpress.com by 78.46.186.204 on 09/07/12
For personal use only.

separation of the isomers using hplc,[5] led to the 3-thia-LTB_4 methyl ester. Subsequent saponification gave the 3-thia-LTB_4, **4**.

The introduction of a metabolically stable group such as trifluoromethyl (CF_3) at C-20 of 3-thia-LTB_4 **4** was then achieved as follows. Treatment of 6-bromohexanoic acid **25** with sulfur tetrafluoride (18) gave the trifluoro derivative **26** (Scheme 4). The corresponding phosphonium salt **27** was treated with butyllithium in dry THF followed by addition of aldehyde **28** (19) to afford the *Z*-olefin **29**. Selective removal of the acetonide and cleavage of the resulting diol in the presence of potassium carbonate gave the aldehyde **30**, $[\alpha]_D$ −14.7° (*c* 1.02, $CHCl_3$), in 79% isolated yield from **29**.

The aldehyde **30** was then coupled with the phosphonium bromide **22** (the C-1—C-10 unit) as described previously (Scheme 3). Removal of silyl ethers followed by separation of the resulting trienes and saponification gave 3-thia-20,20,20-trifluoro-LTB_4 **5**.[6] Both analogs **4** and **5** were shown to be biologically active in a PMN aggregation assay (20), with similar potency to LTB_4 itself. Functional effects and in vivo activities will be reported elsewhere.

In conclusion, the potential usefulness of optically active tetrahydrofurans as masked stable precursors of stereochemically well-defined 1,3-dienes has been illustrated in the synthesis of 3-thia-LTB_4 and 3-thia-20,20,20-trifluoro-LTB_4.

Acknowledgements

We are grateful to the Natural Sciences and Engineering Research Council of Canada for an Industrial Postdoctoral Fellowship to D. Delorme. We wish to thank Dr. J. Evans and S. Çharleson for biological testing, and Drs. A. O. King and D. K. Rupprecht from Merck Rahway Laboratories for the SF_4 reaction in the preparation of compound **26**.

1. P. Borgeat and B. Samuelsson. J. Biol. Chem. **254**, 2643 (1979).
2. (*a*) Y. Guindon, R. Zamboni, C. K. Lau, and J. Rokach. Tetrahedron Lett. **23**, 739 (1982); (*b*) R. Zamboni and J. Rokach. Tetrahedron Lett. **23**, 2631 (1982).
3. (*a*) E. J. Corey, A. Marfat, G. Goto, and F. Brion. J. Am. Chem. Soc. **102**, 7984 (1980); (*b*) E. J. Corey, A. Marfat, J. Monroe, K. S. Kim, P. B. Hopkins, and F. Brion. Tetrahedron Lett. **22**, 1077 (1981); (*c*) C. J. Sih, C. Q. Han, D. Ditullio, and Y. F. Wang. J. Org. Chem. **51**, 1253 (1986).
4. (*a*) A. W. Ford-Hutchinson, M. A. Bray, M. V. Poig, M. E. Shipley, and M. J. H. Smith. Nature, **286**, 264 (1980); (*b*) P. M. Simmons, J. A. Salmon, and S. Moncado. Biochem. Pharmacol. **32**, 1353 (1983).
5. D. G. Payan, A. Missirian-Bastian, and E. J. Goetzl. Proc. Natl. Acad. Sci. U.S.A. **81**, 3501 (1984); M. Rola-Pleszczynski, P. Borgeat, and P. Sirois. Biochem. Biophys. Res. Commun. **108**, 1531 (1982).
6. (*a*) T. W. Harper, M. J. Carrity, and R. C. Murphy. J. Biol. Chem. **261**, 5414 (1986); (*b*) R. J. Soberman, T. W. Harper, R. C. Murphy, and K. F. Austen. Proc. Natl. Acad. Sci. U.S.A. **82**, 2292 (1985); (*c*) M. Nadeau, B. Fruteau De Laclos, S. Picard, P. Braguet, E. J. Corey, and P. Borgeat. Can. J. Biochem. Cell Biol. **62**, 1321 (1984).
7. (*a*) Adv. Prostaglandin, Thromboxane, Leukotriene Res. **14**, 220 (1985); (*b*) G. A. Tolstikov, M. S. Miftakhov, and A. G. Tolstikov. Tetrahedron Lett. **26**, 3867 (1985).
8. J. Rokach, C. K. Lau, R. Zamboni, and Y. Guindon. Tetrahedron Lett. **22**, 2763 (1981).
9. R. W. Binkley, M. G. Ambrose, and D. G. Hehemann. J. Org. Chem. **45**, 4387 (1980).
10. R. H. Grubbs and J. R. Stille. J. Am. Chem. Soc. **108**, 855 (1986).
11. D. B. Tulshian and B. Fraser-Reid. J. Am. Chem. Soc. **103**, 474 (1981).
12. (*a*) G. Grynkiewicz and H. Burzynska. Tetrahedron Lett. **32**, 2109 (1976); (*b*) O. Mitsunobu. Synthesis, 1 (1981).
13. J. A. Dale, D. L. Dull, and H. S. Mosher. J. Org. Chem. **34**, 2543 (1969).
14. N. M. Yoon and Y. S. Gyoung. J. Org. Chem. **50**, 2443 (1985).
15. R. Lohrmann and H. G. Khorana. J. Am. Chem. Soc. **88**, 829 (1966).
16. S. Hanessian and P. Lavallée. Can. J. Chem. **53**, 2975 (1975).
17. J. D. Prugh, C. S. Rooney, A. A. Deana, and H. G. Ramjit. J. Org. Chem. **51**, 648 (1986).
18. (*a*) W. R. Hasek, W. C. Smith, and V. A. Engelhardt. J. Am. Chem. Soc. **82**, 543 (1960); (*b*) W. R. Hasek. Org. Synth. **41**, 104 (1961).
19. M. Y. H. Wong and G. R. Gray. J. Am. Chem. Soc. **100**, 3548 (1978).
20. J. Evans, D. Nathaniel, S. Charleson, C. Leveillé, R. Zamboni, Y. Leblanc, R. Frenette, B. J. Fitzsimmons, S. Leger, P. Hamel, and A. W. Ford-Hutchinson. Prostaglandins, Leukotrienes Med. In press.

[5]The hplc condition: Waters μ-Porasil column, 30% ethyl acetate in hexanes. In this system the 3-thia-LTB_4 methyl ester is more polar as the C-10—C-11 (*Z*) isomer.

[6]For the corresponding methyl ester: $[\alpha]_D$ +11.3° (*c* 0.23, $CHCl_3$); uv (MeOH); λ_{max}: 271.2 nm; ^1H nmr (250 MHz, acetone-d_6) δ: 2.20 (m, H-13, H-16, H-19), 2.83 (m, 2H, CH_2S), 3.43 (s, 2H, SCH_2CO), 3.70 (s, 3H, CO_2Me), 4.20 (m, 1H, H-12), 4.80 (m, 1H, H-5), 5.48 (m, 3H, H-6, H-14, H-15), 5.83 (dd, 1H, $J_{10,11}$ = 14.6 Hz, $J_{11,12}$ = 6.3 Hz, H-11), 6.12 (t, 1H, $J_{6,7} = J_{7,8}$ = 11 Hz, H-7), 6.32 (m, 2H, H-9, H-10), 6.65 (t, 1H, $J_{8,9}$ = 12.5 Hz, H-8).

Can. J. Chem. Downloaded from www.nrcresearchpress.com by 78.46.186.204 on 09/07/12
For personal use only.

ADDITIONS AND CORRECTIONS / AJOUTS ET CORRECTIONS

J. B. Paine III, D. Dolphin, J. Trotter, and T. J. Greenhough. Correlations between carbon-13 nuclear magnetic resonance and X-ray crystallography for pyrroles containing electron-withdrawing groups. Can. J. Chem. **63**, 2683 (1985).

Page 2684. Procedure for the preparation of **3** omitted methyl cyanoacetate (8 g). The yield of 21 g represents an 81% yield (not 87%).

Page 2687, third paragraph, line 5, "erros" should read "errors", and fourth paragraph, line 1, "is" should read "in".

Page 2690, third paragraph, lines 4 and 5, "methyl cyanoacrylate" should read "methyl cyanoacetate".

Can. J. Chem. Downloaded from www.nrcresearchpress.com by 78.46.186.204 on 09/07/12
For personal use only.

A chiral approach to 2-deoxystreptamine[1]

HANS H. BAER, ISAMU ARAI, BRUNO RADATUS, JUNE RODWELL, AND NGUYEN CHINH
Ottawa–Carleton Institute for Research and Graduate Studies in Chemistry, Department of Chemistry, University of Ottawa, Ottawa, Ont., Canada K1N 9B4

Received May 27, 1986[2]

HANS H. BAER, ISAMU ARAI, BRUNO RADATUS, JUNE RODWELL, and NGUYEN CHINH. Can. J. Chem. **65**, 1443 (1987).

A new synthesis of 2-deoxystreptamine (**21**), a component of numerous antibiotics, was developed. Starting from D-mannose, it proceeds through chiral intermediates and is designed to furnish starting points for the preparation of stereospecifically modified derivatives of the *meso* compound **21**. 1,2-Dideoxy-1-nitro-D-*manno*-heptitol (**2**), obtainable from mannose by the nitromethane method, was protected as the 4,5:6,7-di-*O*-isopropylidene derivative **4**, which was mesylated or triflated in position 3. From the sulfonic esters (**5** and **6**) two different routes involving displacement by azide, partial deacetonation at O-6,7, periodate oxidation, and cyclization of the resulting nitroaldohexose derivatives converged to give 1L-(1,3/2,4,6)-6-azido-1,2-*O*-isopropylidene-4-nitro-1,2,3-cyclohexanetriol (**19**) as a key intermediate. Catalytic hydrogenation then afforded optically active 4,5-*O*-isopropylidene-2-deoxystreptamine (**23**), isolated as its *N,N'*-diacetyl derivative **24**. Deacetonation of **19** gave the azidonitrotriol **15**, which was reduced to **21**. The potential utility of the chiral intermediates for stereospecific syntheses of deoxystreptamine-containing aminoglycosides is discussed.

HANS H. BAER, ISAMU ARAI, BRUNO RADATUS, JUNE RODWELL et NGUYEN CHINH. Can. J. Chem. **65**, 1443 (1987).

On a mis au point une nouvelle synthèse de la désoxy-2 streptamine (**21**), un composant de plusieurs antibiotiques. Utilisant le D-mannose comme produit de départ, cette synthèse procède par le biais d'intermédiaires chiraux et il est prévu qu'elle pourra fournir des points de départ pour la préparation de dérivés modifiés d'une façon stéréospécifique du composé *méso* **21**. Le didésoxy-1,2 nitro-1 D-*manno*-heptitol (**2**), que l'on peut obtenir à partir du mannose en faisant appel à la méthode au nitrométhane, a été protégé sous la forme du dérivé di-*O*-isopropylidène-4,5:6,7 (**4**) et l'on a ensuite transformé en dérivé mésylé ou triflé en position 3. À partir des esters sulfoniques (**5** et **6**), deux voies différentes impliquant une substitution par un ion azoture, une déacétonation partielle en O-6,7, une oxydation periodique et une cyclisation des dérivés nitroaldohexoses qui en résultent convergent pour donner l'azido-6 *O*-isopropylidène-1,2 nitro-4 cyclohexanetriol-1,2,3 1L(1,3/2,4,6) (**19**), un intermédiaire clé. L'hydrogénation catalytique fournit ensuite la *O*-isopropylidène-4,5 désoxy-2 streptamine optiquement active (**23**) qui a été isolée sous la forme de son dérivé *N,N'*-diacétylé (**24**). La déacétonation du composé **19** fournit l'azidonitrotriol **15** qui est réduit en **21**. On discute de l'utilité potentielle d'intermédiaires chiraux dans les synthèses stéréospécifiques d'aminoglycosides contenant la désoxystreptamine.

[Traduit par la revue]

Can. J. Chem. Downloaded from www.nrcresearchpress.com by 72.64.146.136 on 09/07/12
For personal use only.

Introduction

2-Deoxystreptamine (**21**) is a pivotal component of numerous important aminoglycoside antibiotics, several of which are in clinical use (1). Early syntheses in the laboratories of Nakajima *et al.* (2) and Suami *et al.* (3) embodied elegant concepts in certain stages but, being predicated on the use of achiral starting materials such as "benzeneglycols" (cyclohexadienediols) and *myo*-inositol, they did not lend themselves to, nor were they intended for, the synthesis of stereospecifically substituted, chiral derivatives of **21**. The same was true for an approach departing from 4,6-dinitropyrogallol (4) and for the more recent and convenient, high-yielding synthesis from 4,5-epoxycyclohexene reported by Prinzbach *et al.* (5). By contast, any approach based on the conversion of a sugar into an aminocyclitol inherently offers the possibility of generating asymmetrically structured derivatives. This is a desirable feature, for although **21** itself is achiral, as a constituent of antibiotics it invariably bears a substituent (i.e., a glycosyl residue) at one or other of its chemically equivalent but enantiotopic positions 4 and 6, or unequal substituents at both. Similarly, either one of the amino groups may occur alkylated, rendering the compound chiral. For example, the *N*-methyl-2-deoxystreptamine (hyosamine) present in destomycin A is levorotatory, whereas hygromycin B contains the dextrorotatory enantiomer (1). With their classical streptamine synthesis, Wolfrom *et al.* (6) have paved the way from *N*-acetyl-D-glucosamine into the diaminocyclitol series, utilizing the nitroalkane cyclization methodology (7), and by further elaboration of this approach Suami and Rinehart and co-workers (8) did in fact avail themselves of the chirality present in this amino sugar to synthesize optically active inosadiamines including (−)-hyosamine, the 1*S*-amino-3*R*-methylamino analog of **21**. Géro and co-workers (9) used carbohydrate-related D-(−)-quinic acid as an alternative resource for chiral aminocyclitol syntheses.

We report here a chiral synthesis of **21**, which departs from commercial D-mannose and proceeds through a number of intermediates that are potentially suitable for the stereospecific preparation of both *O*- and *N*-substituted derivatives.

Results and discussion

Known 1-deoxy-1-nitro-D-*glycero*-D-*galacto*-heptitol hexaacetate (**1**) was prepared from D-mannose by the nitromethane method (10). Although **1** can be dehydroacetoxylated (with sodium bicarbonate), and the resulting 1-nitroalkene then hydrogenated to give 1,2-dideoxy-1-nitro-D-*manno*-heptitol pentaacetate (**2**) (10, 11), we chose to perform this transformation in one step by reductive elimination with sodium borohydride in acetonitrile solution. Subsequent *O*-deacetylation (Zemplén) gave the pentaol **3**, which was acetonated to furnish

[1]This project was initiated by I.A. during a postdoctoral sojourn (1978), and preliminary results were communicated at the 62nd Canadian Chemical Conference, Vancouver, June 1979 (Abstract OR-91). Completion of the work was reported by H.H.B. and B.R. at the 191st ACS National Meeting, New York City, April 1986 (Abstract CARB-45).

[2]Revision received February 9, 1987.

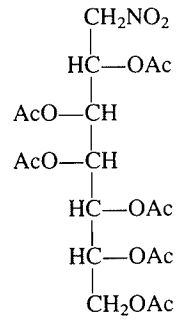

1

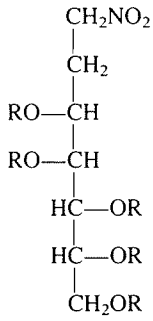

2 R = Ac
3 R = H

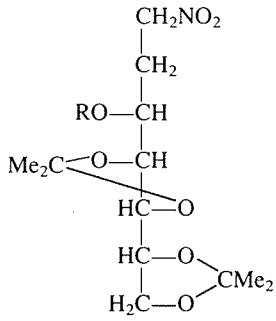

4 R = H
5 R = SO_2Me
6 R = SO_2CF_3

the 4,5;6,7-di-*O*-isopropylidene derivative **4**.[3] Mesylation and triflation of **4** afforded, respectively, the sulfonates **5** and **6**. In the 300-MHz ^1H nmr spectrum of **5**, the proton signal that occurred at lowest field and was, therefore, attributable to the hydrogen atom at the sulfonylated position was determined to be coupled to the two methylene protons H-2 and -2′, which resonated at high field, both on account of the mutual splitting patterns and by homonuclear shift correlation. This established C-3 as the site of sulfonylation. Overall yields of **5** and **6** from D-mannose were in the range of 20–25%. Two alternative routes toward the synthetic goal were elaborated from here, differing in the order by which the carbocycle was generated and the second nitrogen function introduced.

For route A (see Scheme 1), the mesylate **5** was selectively deacetonated at the 6,7 position by trifluoroacetic acid in toluene, and the resulting 4,5-mono-*O*-isopropylidene derivative **7** was cleaved with sodium metaperiodate to afford 5,6-dideoxy-2,3-*O*-isopropylidene-4-*O*-methylsulfonyl-6-nitro-*al*-D-*arabino*-hexose (**8**). Nitroalkane cyclization of this sugar, effected by sodium methoxide in methanolic solution, led to a mixture of epimeric cyclitols that could be isolated crystalline upon chromatographic separation. The structures **9** (for the less-mobile, higher-melting, and slightly preponderant epimer) and **10** (for the other component) followed from clearly resolved and readily interpretable ^1H nmr spectra. At first glance, one might have expected the axial-OH epimer **10** to exceed the equatorial-OH epimer **9** by approximately 0.9 kcal/mol in conformational energy, and since the reaction conditions employed for the cyclization probably favored thermodynamic control,[4] one should have anticipated an equilibrium of 85:15 (at 25°C) in favor of **9**, the desired epimer. Such a selectivity was not obtained, and inspection of Dreiding models suggests a possible explanation. It can be seen that, because of the considerable distortion imposed, in both compounds, on the cyclohexane chair by the *trans*-fused dioxolane ring, the axial OH group in **10** recedes in an outward direction from the opposing, coaxial hydrogen atoms. This may diminish nonbonding interaction and, consequently, the energy difference to the equatorially substituted counterpart **9**. Fortunately, it proved possible to isolate **9** directly from the mixture by fractional crystallization, thanks to its lower solubility, and, by doing so under epimerizing conditions (in the presence of a catalytic amount of base), part of **10** could be converted into **9**, which was thus obtained in 70% yield without resort to chromatography.

The *trans*-fused cyclic ketal groups in **9** and **10** were very acid labile, as was to be expected. When, in an early experiment, the alkaline mixture from the cyclization was processed with a sulfonic acid-type resin for deionization, loss of acetone occurred. Similarly, partial deacetonation was observed after prolonged exposure of the crystalline compounds to the laboratory atmosphere. Although not required for the present synthesis, a sample of **10** was deliberately methanolyzed under acid catalysis, and the highly crystalline triol **11** so obtained was characterized further through its triacetate **12**. Similar deacetonation of **9** gave the (amorphous) triol **13**, characterized likewise as its crystalline triacetate **14**. Unambiguous ^1H nmr data obtained for **12** and **14** reaffirmed the structures of the epimers.

With the nitrocyclitol **9** and its progeny **13** in hand, we proceeded to introduce the second nitrogen function. Both mesylates underwent displacement by azide ion, **13** with lithium azide in *N*,*N*-dimethylformamide (3 h at 100°C), and **9** also in this fashion or, more cleanly, under phase transfer conditions in benzene–water (3 days at 80°C) that entailed less decomposition. Unfortunately, the vicinal hydroxy-nitro groupings in **9** and **13** lost their stereochemical integrity in these displacement reactions; partial epimerization occurred at the carbinol positions, which vitiated the epimer separation previously performed. Thus, **13** gave a mixture from which the desired azidonitrotriol **15** was isolated crystalline by chromatography. This product was identical with **15** prepared from **19** (see later on). A second product, although not isolated pure, was judged to be the 3-epimer since it showed a similar infrared spectrum and was partly converted into **15** by base-catalyzed epimerization. Similarly, **9** furnished a mixture of the corresponding 1,2-*O*-isopropylidene derivatives **19** and[5] **20**. The products **15**, **19**, and **20** constitute a junction with the synthetic route B that is now to be delineated, and it will be seen in that context that separation of **19** and **20**, although somewhat laborious, is not a serious problem.

For route B, the mesylate **5** was first converted into the 3-azido-3-deoxy-D-*gluco*-heptitol derivative **16**. As reported by us elsewhere (12), treatment of **5** with tetrabutylammonium azide in boiling toluene had provided **16**, but only in 46% yield owing to interference of a competing reaction. This side reaction, which led to nitrocyclopropane derivatives, was of much interest in its own right (12); however, for the present purpose it was desirable to suppress it as far as possible to improve the yield of **16**. After considerable experimentation, displacement under phase transfer conditions using sodium azide and tetrabutylammonium hydrogen sulfate in benzene–water at 56°C was found to give a 76% yield and to minimize the

[3]Care should be exercised in the deionization of the alkaline reaction mixture obtained from **2**, which contains the nitronate of **3**, to avoid Nef reaction (10). In one large-scale experiment, in which the precaution of cooling was not observed and the crude product acetonated directly, the yield of **4** was diminished and a by-product, isolated in 7% yield, arose, which on spectroscopic evidence was judged to be methyl 2-deoxy-3,4:6,7-di-*O*-isopropylidene-α,β-D-*manno*-heptopyranoside.

[4]Prolongation of the reaction time did not seem to change the product ratio significantly.

[5]In the hope of forestalling such epimerization, we examined a mesylate displacement by azide in the 3-(trimethylsilyl) ether that was readily prepared from **9**. The attempt failed completely, giving a mixture of unidentified, chromatographically slow-moving products and no trace of the expected, fast-moving trimethylsilyl ether of **19**. The latter had been prepared for comparison from pure **19** (see route B), and when subjected to the same reaction conditions it, too, suffered similar degradation. A mixture of **19** and **20** can probably be prepared more rationally from crude **9** + **10** without their prior separation.

Can. J. Chem. Downloaded from www.nrcresearchpress.com by 72.64.146.136 on 09/07/12
For personal use only.

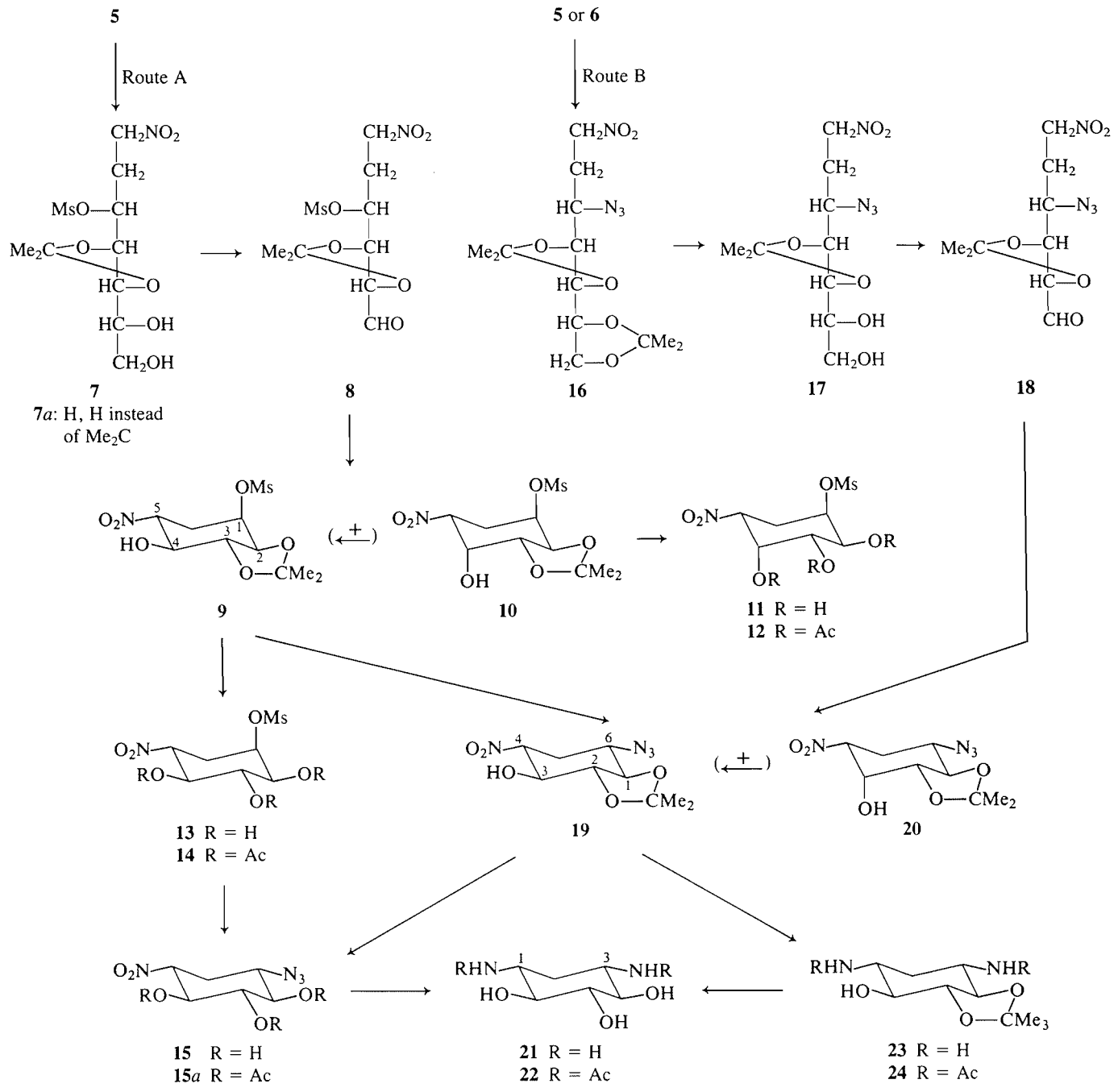

SCHEME 1

proportions of by-products, but the conversion was very slow, requiring 6 days for completion. Its performance at 80 or 100°C led to larger proportions of the unwanted products. A great improvement resulted from use of the triflate **6**, which, under similar phase transfer conditions but applied at room temperature for a few hours only, gave **16** in yields of 84% or better, and no cyclopropano by-products were detected. Compound **16** was then selectively 6,7-deacetonated with trifluoroacetic acid in toluene; a certain amount of full deacetonation occurred in the process, but the resulting tetraol could be reacetonated for recycling, and the 4,5-mono-*O*-isopropylidene derivative **17** was thus obtained in 88% yield. Subsequent periodate oxidation produced the aldehydo sugar **18** as an unstable intermediate that was not characterized but immediately subjected to methoxide-catalyzed ring closure, which furnished a mixture of **19** and its epimer **20**, similar in composition to that obtained from **9** by route A. The more stable isomer **19** was isolated from the mixture in 69% yield by direct crystallization, performed under conditions that allowed part of **20** to epimerize. The well-resolved ^{1}H nmr spectrum of **19** unambiguously indicated the all-equatorial substituent orientation in the compound. The epimer **20** that remained in the mother liquor was not isolated pure on a preparative scale, but a small sample was procured by column chromatography for nmr analysis, which ascertained its structure and configuration. Deacetonation of **19** quantitatively afforded crystalline **15**.

Hydrogenation over Adams catalyst converted **15** into 2-deoxystreptamine (**21**), and **19** into the latter's optically active, 4,5-*O*-isopropylidene derivative **23** that was isolated as a crystalline *N*,*N*′-diacetyl compound (**24**), which had previously

Can. J. Chem. Downloaded from www.nrcresearchpress.com by 72.64.146.136 on 09/07/12
For personal use only.

Can. J. Chem. Downloaded from www.nrcresearchpress.com by 72.64.146.136 on 09/07/12
For personal use only.

been obtained (13) in racemic form.[6] *N*-Acetylation of **21** and deacetonation of **24** yielded identical *N,N'*-diacetyl-2-deoxystreptamine (**22**).

Conclusion

With the preparation of 2-deoxystreptamine the ultimate success of our synthetic design has been demonstrated. It is to be stressed, however, that chemical synthesis of such chiral intermediates as **15**, **19**, **23**, and **24** was the primary goal of the enterprise.[7] These intermediates or conventionally prepared analogs such as the *N,N'*-diethoxycarbonyl or -dibenzyloxycarbonyl derivatives of **23**, which are known in racemic form only (16), are expected to open new avenues to stereospecific, total syntheses of deoxystreptamine-containing aminoglycosides where glycosylations specifically at O-4 or O-6 are required. Syntheses in that area have previously been accomplished (1) by use of racemic synthons of type **24**, but the necessary separation of diastereomers was generally troublesome and yields were often modest, as may be gleaned from several examples (16–18). Furthermore, it is to be expected that the unequal nitrogen functions present in **15** or **19** can be reduced to the amine stage in a stepwise fashion, which should allow mono-*N*-alkylation or -acylation to be effected stereospecifically. Such a protocol should prove valuable for synthetic designs in the area of destomycin A, hygromycin B, and the butirosins. Studies to exploit this chemistry along the lines indicated are in progress in our laboratory.

Experimental

Melting points were determined in capillaries with a Gallenkamp apparatus and are uncorrected. Optical rotations were measured at ~25°C in a Perkin–Elmer 241 polarimeter. Infrared (ir) data were recorded with a Perkin–Elmer 783 instrument from Nujol mulls for solid samples, and from neat films for syrups. Proton magnetic resonance (^{1}H nmr) spectra were taken at 300 MHz with a Varian XL 300 spectrometer from solutions in deuteriochloroform ($CHCl_3$ lock signal at δ 7.23), unless noted otherwise. Signal patterns are given as s = singlet, d = doublet, q = quartet, t = triplet, quin = quintet, sx = sextet, or m = multiplet, occasionally modified by prefixes b = broad, c = complex, or n = narrow. The ^{13}C nmr data were recorded with the same instrument, at 75.43 MHz. Column chromatography was performed with silica gel Merck 9385 (particle size, 20–45 μm), and analytical thin-layer chromatography (tlc) with precoated plates Si250F of J. T. Baker Chemical Co. The following solvent combinations (v/v) were used for chromatography, unless otherwise specified: A, methanol–$CHCl_3$ 1:2; B, the same, but 1:3; C, ether–hexane 1:1; D, EtOAc–hexane 1:1; E, the same, but 1:1.5; F, the same, but 1:2; G, the same, but 1:3; H, the same, but 1:4; and I, the same, but 1:19.

*1,2-Dideoxy-1-nitro-*D*-*manno*-heptitol pentaacetate (**2**)*

Crystalline 1-deoxy-1-nitro-D-*glycero*-D-*galacto*-heptitol hexaacetate (**1**) (10) (7.00 g) was dissolved in CH_3CN (70 mL, dried over molecular sieve), and to the chilled (0°C) solution was added $NaBH_4$ (0.56 g) followed by a few drops of ethanol. Gradual replacement of **1** by slightly less-mobile **2** was seen in tlc (Et_2O). The mixture was processed after 1 h by stirring it with Amberlite IR-120(H^+) resin until H_2 evolution ceased, decolorizing the filtrate with activated charcoal, and evaporating it with several sequential additions of methanol. The dry residue was dissolved in 5 mL of warm ethanol from which **2** crystallized on refrigeration. The mother liquor was evaporated, and the residue similarly crystallized from ethanol, to give a second crop of **2**, for a total of 5.241 g (85%), mp 91–93°C (lit. (11) mp 98–99°C); ν_{max}: 1740 (OAc) and 1555 (NO_2) cm^{-1}; no OH band. The product was sufficiently pure for further use, although a trace contaminant was present (tlc).

*1,2-Dideoxy-1-nitro-*D*-*manno*-heptitol (**3**)*

To a chilled (0°C) solution of **2** (14.2 g) in absolute methanol (650 mL) was added solid $NaOCH_3$ (10.34 g), and the mixture was stirred for 3 h at 0°C, after which tlc (solvent A) indicated complete replacement of **2** (R_f 0.95) by product ($R_f \sim 0.6$, with tailing due to the presence of base). The continuously chilled mixture was deionized with Dowex 50-X8(H^+) resin, and the clear, yellowish solution evaporated to dryness *in vacuo*, with portionwise addition of fresh methanol towards the end. The crude, dry product weighed 5.555 g (76%); in several runs performed on a 1–2 g scale, yields of 80–85% were obtained. Crude **3** was usable for the next step. An analytical sample, crystallized and recrystallized from ethanol, showed mp 116–118°C (lit. (11) mp 116–117°C); $[\alpha]_D$ +15° (*c* 3.2, water); ν_{max}: 3300 (bd, OH) and 1550 (NO_2) cm^{-1}; no ester CO band.

*1,2-Dideoxy-4,5;6,7-di-*O*-*isopropylidene-1-nitro-*D*-*manno*-heptitol (**4**)*

To a suspension of **3** (5.612 g) in reagent-grade acetone (280 mL) containing 2,2-dimethoxypropane (15 mL) was added freshly dried, anhydrous $CuSO_4$ (20 g). The mixture was stirred under ice cooling, and when it had reached +4°C, concentrated H_2SO_4 (2.0 mL) was added dropwise. Stirring was then continued at room temperature for 18–20 h. The formation of **4** ($R_f \sim 0.4$) was indicated by tlc (solvent G; R_f 0 for **3**). After neutralization of the mixture by stirring it with solid $NaHCO_3$, the supernatant was filtered through sintered glass with the aid of Celite, and evaporated to give a brownish oil. This was chromatographed on a column (4 × 10 cm) of silica gel, with solvent H as the eluant. The yield of chromatographically homogeneous, oily **4** (dried in high vacuum) was 6.16 g (81%); $[\alpha]_D$ +18° (*c* 1, $CHCl_3$); ν_{max}: 3450 (sharp, OH), 1545 (NO_2), 1430, 1370, 1250–1200, 1150, 1065, and 840 cm^{-1}; δ ($CDCl_3$): 4.56 (cm, 2H, AB part of ABMX system, H-1,1'), 4.19 (octet, H-6), 4.00 and 3.65 (m, 2 and 3H, H-3,4,5,7,7'), 3.75 (~s, exchangeable, OH), 2.48 (dtd, *W* 34 Hz, H-2), and 2.12 (dtd, *W* 36 Hz, H-2'); 1.42, 1.34, 1.335, 1.33 (s, 4 × 3H, $2Me_2C$). *Anal.* calcd. for $C_{13}H_{23}NO_7$ (305.3): C 51.14, H 7.59, N 4.59; found: C 51.21, H 7.65, N 4.40.

In several experiments using **3** of variable purity, the early chromatographic fractions of **4** contained a slightly more mobile by-product (see footnote 3), which was removed by rechromatography with solvent C.

*1,2-Dideoxy-4,5;6,7-di-*O*-*isopropylidene-3-*O*-*methylsulfonyl-1-nitro-*D*-*manno*-heptitol (**5**)*

Methanesulfonyl chloride (8 mL) in dry pyridine (26 mL) was added dropwise to a solution of **4** (6.16 g) in dry pyridine (50 mL), stirred at 0°C. After 1.5 h the reaction was complete (tlc, solvent D). The mixture was stirred for 10 min with some added water, poured onto crushed ice, and extracted with chloroform (2 × 120 mL). The extract was washed twice with $NaHCO_3$ solution, dried with Na_2SO_4, and evaporated with several added portions of toluene. The crude, oily **5** so obtained was chromatographed on silica gel (200 g) with solvent H. The fractions containing the product gave an oil (6.60 g, vacuum dried; 85%) that crystallized partially on storage in a desiccator overnight. Recrystallization from a minimum aount of EtOAc – petroleum ether gave pure **5** (5.874 g, 76%) as large, colorless plates, mp 74–75°C; $[\alpha]_D$ +24.3° (*c* 1.3, $CHCl_3$); ν_{max}($CHCl_3$): 1554 (NO_2), ~1370 (several bands, including NO_2 and OMs), and 1178 (OMs) cm^{-1}; OH band absent; ^{1}H nmr data (assignments confirmed by HOMCOR method), δ: 5.00 (septet, $J_{3,4}$ = 2.7, $J_{2,3}$ = 4.35; $J_{2',3}$ = 8.0 Hz, H-3), 4.58 (cm, 2H, H-1,1'), 4.22 (dd, $J_{3,4}$ = 2.7, $J_{4,5}$ = 7.2 Hz, H-4), 4.15

[6]According to regular organic nomenclature, **24** is 1L-(1,3/2,4,6)-4,6-diacetamido-1,2-*O*-isopropylidene-1,2,3-cyclohexanetriol; its enantiomer would receive the prefix 1D. In terms of the nomenclature (14) usually employed in the field of aminoglycoside antibiotics, **24** is 1,3-di-*N*-acetyl-4,5-*O*-isopropylidene-2-deoxystreptamine, and its enantiomer would be the corresponding 5,6-*O*-isopropylidene derivative.

[7]An analogous chiral compound, the 5,6-*O*-cyclohexylidene derivative of **21**, has been prepared semisynthetically from natural neamine (15).

Can. J. Chem. Downloaded from www.nrcresearchpress.com by 72.64.146.136 on 09/07/12
For personal use only.

(dd, $J_{6,7}$ = 6.1, J_{gem} = 8.55 Hz, H-7), 4.03 (dt, $J_{5,6}$ = 8.6, $J_{6,7}$ = 6.1, $J_{6,7'}$ = 5.2 Hz, H-6), 3.93 (dd, J = 5.2 and 8.5 Hz, H-7′), 3.78 (dd, J = 7.2 and 8.55 Hz, H-5), 3.08 (s, 3H, OSO_2Me), 2.45 (cm, 2H, H-2,2′), and 1.40s, 1.36s, 1.31s (6, 3, and 3H, $2Me_2C$). *Anal.* calcd. for $C_{14}H_{25}NO_9S$ (383.4): C 43.85, H 6.57, S 8.36; found: C 43.67, H 6.51, S 8.19.

*1,2-Dideoxy-4,5;6,7-di-*O*-isopropylidene-1-nitro-3-*O*-(trifluoromethylsulfonyl)-*D*-*manno*-heptitol (**6**)*

A solution of trifluoromethanesulfonic anhydride (5.7 mL) in dry CH_2Cl_2 (20 mL) was added dropwise, over a period of 45 min, to a solution of **4** (8.70 g) in dry CH_2Cl_2 (60 mL) and pyridine (10 mL), stirred at 0°C. After an additional 15 min, tlc (solvent: CH_2Cl_2) indicated complete conversion of **4** (R_f 0.15) into **6** (R_f 0.40). The mixture was poured into, and shaken with, ice water; after phase separation, the aqueous phase was extracted once with CH_2Cl_2, and the combined organic phase was washed with 2% H_2SO_4 followed by ice-cold $NaHCO_3$ solution and water, dried (Na_2SO_4), and evaporated at room temperature to give a syrup which, upon trituration with 5 mL of methanol, afforded a crystalline material. Isolated after short refrigeration, washed with methanol, and dried *in vacuo*, this first crop of **6** (7.385 g, 59%) melted at 77–79°C with decomposition (prior darkening from 68°C); $[\alpha]_D$ +23.9° (*c* 1, $CHCl_3$). Processing of the mother liquor furnished a second crop of crystalline **6** (1.05 g, 8.4%). The mother liquor therefrom, processed as before, left a syrup (~2 g) still rich in **6** (tlc); it could also be used in a subsequent operation (see preparation of **16**).

Compound **6** is rather unstable and tends to decompose rapidly at room temperature. It may be stored for some weeks at −20°C but is best utilized immediately. The ^{1}H nmr data, δ: 5.30 (m, $J_{3,4}$ = 2.3, $J_{2,3}$ ~ 4, $J_{2',3}$ ~ 8 Hz, H-3), 4.56 (cm, 2H, H-1,1′), 4.28 (dd, $J_{3,4}$ = 2.3, $J_{4,5}$ = 7.5 Hz, H-4), 4.17 (dd, $J_{6,7}$ = 6.1, J_{gem} = 8.6 Hz, H-7), 4.03 (~dt, $J_{5,6}$ =8.8 Hz, H-6), 3.92 (dd, $J_{6,7'}$ = 5.2, J_{gem} = 8.6 Hz, H-7′), 3.70 (dd, $J_{4,5}$ = 7.5, $J_{5,6}$ = 8.7 Hz, H-5), 2.57 (cm, 2H, H-2,2′), and 1.42s, 1.39s, 1.37s, 1.32s (4 × 3H, $2Me_2C$).

*1,2-Dideoxy-4,5-*O*-isopropylidene-3-*O*-methylsulfonyl-1-nitro-*D*-manno-heptitol (**7**)*

A solution of **5** (1.24 g) in toluene (9 mL) was cooled to −20°C, and 90% CF_3CO_2H (0.7 mL) was added. Oily **7** began to separate within a few minutes. The mixture was stirred magnetically for 30 min, then made homogeneous by the addition of a small amount of EtOAc, and immediately neutralized by agitation with solid sodium carbonate. The filtered solution was evaporated to give an oil that, according to tlc (solvent D), was a 3:1 mixture of **7** (R_f 0.25) and unreacted **5** (R_f 0.7). Chromatography of the material on a column (25 × 2 cm) of silica gel with solvent D as the eluant produced **5** (0.355 g), and subsequent elution with EtOAc furnished **7**. The recovered **5** was subjected to an identical hydrolysis (but on one-quarter scale), which gave an additional crop of **7** for a combined yield of 1.012 g (92%); $[\alpha]_D$ +9° (*c* 2.3, water), +25° (*c* 0.5, EtOAc); ir data, ν_{max}: 3400 (bd, OH), 1550 (NO_2), 1380–1330, 1250, 1175 (OMs), 1060, 925, 875, and 800 cm^{-1}; ^{1}H nmr ($CDCl_3$), δ: 5.02 (dt, $J_{2,3}$ = 3.4, $J_{3,4}$ = 3.5, $J_{2,3'}$ = 8.4 Hz, H-3), 4.58 (m, 2H, H-1,1′), 4.30 (dd, $J_{3,4}$ = 3.5, $J_{4,5}$ = 7.2 Hz, H-4), 3.9–3.6 (m, 4H, H-5,6,7,7′), 3.09 (s, 3H, CH_3SO_3), 3.02 (bs, 2H, OH), 2.47 (cm, 2H, H-2,2′), 1.40 and 1.37 (s, 3H each, Me_2C). *Anal.* calcd. for $C_{11}H_{21}NO_9S$ (343.4): C 38.47, H 6.16, N 4.08; found: C 38.70, H 5.91, N 3.86.

When a sample of **7** that had been stored at +4°C for 2 months was triturated with EtOAc it failed to dissolve fully, and part of the material crystallized, mp 97–98°C. Recrystallized from hot methanol, the fine needles showed mp 98°C; $[\alpha]_D$ +12° (*c* 1.2, water); ν_{max}: 3540 (sharp) and 3400–3250 (bd, OH), 1540 (NO_2), and multiple sharp bands in the 1200–800 cm^{-1} region. An ^{1}H nmr spectrum (D_2O) indicated retention of the mesyl function but absence of isopropylidene methyl groups. It was concluded that slow deacetonation, perhaps catalyzed by traces of acid left in the sample of **7**, had generated the tetraol **7***a*. *Anal.* calcd. for $C_8H_{17}NO_9S$ (303.3): C 31.68, H 5.65, S 10.58; found: C 31.95, H 5.79, S 10.44.

*5,6-Dideoxy-3,4-*O*-isopropylidene-4-*O*-methylsulfonyl-6-nitro-*al*-*D*-arabino-hexose (**8**)*

Sodium metaperiodate (0.60 g) was dissolved in an ice-cooled solution of **7** (1.012 g) in water (50 mL). The oxidation of **7** to give more mobile **8** (tlc, solvent D) was complete within 15 min. After addition of ethylene glycol (5 drops) the solution was concentrated by evaporation, with several sequential additions of ethanol, whereby solid $NaIO_3$ was deposited. The latter was removed by filtration and washed with ethanol, and the filtrate evaporated to give a colorless syrup. The syrup was taken up in $CHCl_3$ and the filtered solution was washed with a small amount of water, dried ($MgSO_4$), and evaporated. The resulting, chromatographically homogeneous syrup (0.95 g) showed broad ir absorption at 3400 cm^{-1} (presumably due to aldehyde hydrate); other prominent peaks were at 1555 (NO_2), ~1350, 1180, 1170, and 930 cm^{-1}. An ^{1}H nmr spectrum ($CDCl_3$) showed an aldehydic proton signal, δ 9.51, integrating to only 0.3 H. However, an analytical sample dried in high vacuum at 56°C for 18 h gave C,H values in agreement with the free-aldehyde structure **8**. *Anal.* calcd. for $C_{10}H_{17}NO_8S$ (311.3): C 38.58, H 5.50; found: C 38.60, H 5.53.

*1L-(1,2,4/3,5)-2,3-*O*-Isopropylidene-1-O-(methylsulfonyl)-5-nitro-1,2,3,4-cyclohexanetetrol (**9**) and 1L-(1,2/3,4,5)-2,3-*O*-isopropylidene-1-*O*-(methylsulfonyl)-5-nitro-1,2,3,4-cyclohexanetetrol (**10**)*

A solution of aldehyde **8** (2.33 g) in dry methanol (100 mL) containing $NaOCH_3$ (1 g) was allowed to stand at 25°C for 30 min, during which period **8** (R_f ~ 0.2, elongated spot) was consumed and two products having R_f 0.50 and 0.55 were formed, with the less mobile one (**9**) predominating slightly over the other (**10**) (tlc, solvent D). The solution was neutralized by stirring it with a *carboxylic acid*-type cation exchange resin (Amberlite IRC-50, H^+, or equivalent), which after filtration was washed exhaustively with methanol. The filtrate was evaporated and the resulting syrup dried in a high vacuum to give a mixture of **9** and **10** as a fluffy foam (2.193 g, 94%). Although for the preparation of **9** this mixture was processed as described in a subsequent paragraph, a mixture obtained in a similar experiment was partially separated by column chromatography on silica gel with solvents G and F, to characterize **9** and **10**. Pure and almost-pure fractions of either epimer were obtained.

The fractions of **9** (R_f 0.50) gave crystalline product, mp 147–148°C (dec.), after recrystallization from 99% ethanol; $[\alpha]_D$ −20.7° (*c* 1.4, $CHCl_3$); δ ($CDCl_3$): 5.25 (nm, H-1), 4.69 (ddd, $J_{5,6e}$ = 5, $J_{4,5}$ = 9.5, $J_{5,6a}$ = 12.5 Hz, H-5), 4.42 (td, $J_{4,OH}$ = 4, $J_{3,4}$ = $J_{4,5}$ = 9.5 Hz, H-4), 3.88 (t, $J_{2,3}$ = 10, $J_{3,4}$ = 9.5 Hz, H-3), 3.62 (dd, $J_{1,2}$ = 2, $J_{2,3}$ = 10 Hz, H-2), 3.09 (s, 3H, CH_3SO_3), 2.78 (d, J = 4 Hz, OH-4, superposed on ddd, which is clearly revealed after D_2O exchange, $J_{1,6e}$ = 3, $J_{5,6e}$ = 5, $J_{6a,6e}$ = 14.5 Hz, H-6e), 2.25 (quin, $J_{1,6a}$ = 3, $J_{5,6a}$ = 12.5, $J_{6a,6e}$ = 14.5 Hz, H-6a), 1.46 and 1.445 (s, 3H each, Me_2C). *Anal.* calcd. for $C_{10}H_{17}NO_8S$ (311.3): C 38.58, H 5.50, S 10.30; found: C 38.34, H 5.65, S 10.29.

Fractions of pure **10** (R_f 0.55) gave crystals from CH_2Cl_2–hexane, mp 130°C, and 130–131°C after recrystallization; $[\alpha]_D$ +6° (*c* 0.8, $CHCl_3$); δ ($CDCl_3$): 5.26 (nm, H-1), 5.09 (nm, H-4), 4.69 (ddd, $J_{4,5}$ = 2.5, $J_{5,6e}$ = 5.5, $J_{5,6a}$ = 12 Hz, H-5), 4.11 (dd, $J_{3,4}$ = 2.7, $J_{2,3}$ = 9.9 Hz, H-3), 3.86 (dd, $J_{1,2}$ = 2.2, $J_{2,3}$ = 9.8 Hz, H-2), 3.07 (s, 3H, CH_3SO_3), 2.65 (cm, 2H, H-6a,6e), 2.43 (d, $J_{4,OH}$ = 3 Hz, OH), 1.44 and 1.425 (s, 3H each, Me_2C). *Anal.* calcd. as for **9**; found: C 38.42, H 5.43, S 10.37.

Preparative isolation of **9** in good yield was achieved by fractional crystallization, coupled with base-catalyzed epimerization of the epimer **10**. Thus, the aforementioned amorphous mixture of **9** and **10** (2.19 g) was dissolved in 99% ethanol (2.5 mL), and seeded with **9**. Crystallization was allowed to proceed, undisturbed, at room temperature for 2 h. The mixture was diluted with ethanol (15 mL), the supernatant decanted, and the first crop of **9** (209 mg) washed with ethanol and collected. The combined supernatant and washings were evaporated with addition of CH_2Cl_2 to give a syrupy residue, which was dissolved in 2.5 mL of ethanol containing 10 mg of $NaOCH_3$. Seeding with **9** and storage of the mixture at room temperature

Can. J. Chem. Downloaded from www.nrcresearchpress.com by 72.64.146.136 on 09/07/12
For personal use only.

overnight produced a second crop of **9** (1.147 g), isolated after dilution with ethanol as described before. Three repetitions of the procedure, using progressively smaller volumes of solvent, gave additional crops (191, 125, and 43 mg), for a total of 1.715 g of **9** (78.3% of the original mixture). The crops melted in the range 136–143°C (dec.) and were contaminated by small amounts of **10**. For further purification, the material was dissolved in CH_2Cl_2 and the solution washed twice with water, dried (Na_2SO_4), and evaporated. One or two recrystallizations from ethanol of the recovered material gave chromatographically pure **9**, mp 147–148°C (dec.). All mother liquors were combined and reprocessed with $NaOCH_3$ as described, and a total of 1.54 g (70%) of pure **9** was eventually obtained.

It was observed that both **9** and **10** slowly underwent partial deacetonation when exposed to the laboratory air for prolonged periods. Such samples became incompletely soluble in $CHCl_3$ and showed a new, immobile spot in tlc (solvent D).

*1L-(1,2/3,4,5)-1-O-(Methylsulfonyl)-5-nitro-1,2,3,4-cyclohexanetetrol (**11**) and its 2,3,4-triacetate **12***

A solution of **10** (100 mg) in methanol (3 mL) was acidified with 3 drops of 1 *M* HCl and left overnight at room temperature, then heated briefly (2 min) to 60°C for a completion of the hydrolysis, which was monitored by tlc (solvent D). Evaporation with several added portions of methanol followed by 95% ethanol quantitatively gave crystalline **11**, which was recrystallized from hot methanol; mp 173°C (dec.), $[\alpha]_D$ −32.7° (*c* 1.4, 1:1 MeOH–DMF); ν_{max}: 3470 and 3410 (OH), 1335 (NO_2), 1170 (MsO), 1090–1070, 1030, 1000, 980, 900, and 870 cm^{-1}. *Anal.* calcd. for $C_7H_{13}NO_8S$ (271.2): C 30.99, H 4.83, N 5.16, S 11.82; found: C 31.19, H 4.85, N 4.92, S 11.89.

To a suspension of **11** (20 mg) in acetic anhydride (1 mL) was added BF_3–Et_2O (5 drops), with initial ice-cooling. All of **11** dissolved rapidly. The solution was kept at ambient temperature for 1 h and then brought to dryness. Trituration of the residue with a small amount of 95% ethanol gave **12** as fine needles, mp 191–192°C; $[\alpha]_D$ −71° (*c* 0.4, $CHCl_3$); ν_{max}: 1750 (ester CO) and 1553 (NO_2) cm^{-1}; ^1H nmr ($CDCl_3$; assignments confirmed by HOMCOR method), δ: 6.19 (nm, H-4), 5.31 (nm, H-1), 5.26 (dd, $J_{1,2}$ = 2.8, $J_{2,3}$ = 10.9 Hz, H-2), 5.15 (dd, $J_{3,4}$ = 3.0, $J_{2,3}$ = 10.9 Hz, H-3), 4.85 (ddd, $J_{4,5}$ = 2.7, $J_{5,6e}$ = 5, $J_{5,6a}$ = 12.5 Hz, H-5), 3.08 (s, 3H, CH_3SO_3), 2.77 (dtd, $J_{4,6e}$ = −1.2, $J_{5,6e}$ = 5, $J_{1,6e}$ = 4, $J_{6a,6e}$ = 15 Hz, H-6e), 2.64 (quin, $J_{1,6a}$ = 2.3, $J_{5,6a}$ = 12.5, $J_{6a,6e}$ = 15 Hz, H-6a), and 2.08, 2.07, 2.00 (s, 3H each, OAc). *Anal.* calcd. for $C_{13}H_{19}NO_{11}S$ (397.4): C 39.29, H 4.82, S 8.07; found: C 39.50, H 4.83, S 7.97.

*1L-(1,2,4/3,5)-1-O-(Methylsulfonyl)-5-nitro-1,2,3,4-cyclohexanetetrol (**13**) and its 2,3,4-triacetate **14***

A suspension of the acetonide **9** (300 mg) in ether (15 mL) containing 90% CF_3CO_2H (0.3 mL) was boiled under reflux. Deacetonation monitored by tlc (solvent D), to give nearly immobile **13**, was slow under these conditions but was accelerated upon addition of several drops of methanol to render the medium homogeneous, and it was complete after 3 h. Solvent removal and evaporation of several added portions of ether–methanol, followed by pure ether, from the material gave **13** (262 mg, quantitative) as a white, low-melting (50–60°C), amorphous powder after drying *in vacuo* over KOH; $[\alpha]_D$ −30° (*c* 1.2, methanol); ν_{max}: 3500–3200 (OH), 1550 (NO_2), 1170 (MsO), 1120–1070, 1000 (weak), 975, 900, 860–820, 780, and 720 cm^{-1}. *Anal.* calcd. for $C_7H_{13}NO_8S$ (271.2): C 30.99, H 4.83; found: C 30.91, H 4.82.

A sample of **13** (20 mg) was treated with acetic anhydride (1 mL) and BF_3–Et_2O (2 drops). The reaction mixture was allowed to dry in the air, leaving **14** as a crust of beautiful crystals that were washed with a small amount of cold methanol; mp 197–198°C, unchanged on recrystallization from methanol; $[\alpha]_D$ −61.9° (*c* 0.8, $CHCl_3$); ν_{max}: 1740 (ester CO) and 1563, 1543 cm^{-1} (a doublet for NO_2; compare the single band in **12**). The fingerprint region was clearly distinct from that of **12**. The ^1H nmr ($CDCl_3$; assignments confirmed by HOMCOR method), δ: 5.61 (~t, $J_{3,4}$ = 9.5, $J_{4,5}$ = 10 Hz, H-4), 5.40 (~t, $J_{2,3}$ = 10.5, $J_{3,4}$ = 9.5 Hz, H-3), 5.27 (nm, H-1), 5.00 (dd, $J_{1,2}$ = 3, $J_{2,3}$ = 10.5 Hz, H-2), 4.94 (ddd, $J_{5,6e}$ = 4.5, $J_{4,5}$ = 10, $J_{5,6a}$ = 13 Hz, H-5), 3.13 (s, 3H, CH_3SO_3), 2.76 (dt, $J_{1,6e}$ = $J_{5,6e}$ = 4.5, $J_{6a,6e}$ = 14.5 Hz, H-6e), 2.35 (quin, $J_{1,6a}$ = 2.2, $J_{5,6a}$ = 13, $J_{6a,6e}$ = 14.5 Hz, H-6a), and 2.06, 2.01, 2.00 (s, 3H each, OAc). *Anal.* calcd. for $C_{13}H_{19}NO_{11}S$ (397.4): C 39.29, H 4.82, S 8.07; found: C 39.37, H 4.65, S 8.21.

*6-Azido-4-nitro-1,2,3-cyclohexanetriol (**15**)*

*(a) From **13***

Compound **13** (200 mg) and LiN_3 (100 mg) were heated in dry *N,N*-dimethylformamide (2 mL) at 100°C for 3 h, under exclusion of atmospheric moisture. Thin-layer chromatography with solvent B indicated conversion of **13** (R_f 0.55) into products giving a strong spot (R_f 0.65) for **15** and a weaker spot (R_f ~ 0.57) attributed to the 3-epimer, differentiated from **13** by its color shade (5% H_2SO_4 spray, heat). The solvent was removed *in vacuo* at 50°C and by several coevaporations with added toluene. The brown syrup obtained was mixed with a few drops of water and triturated with $CHCl_3$ containing a small amount of methanol. The organic solution was washed with water, dried ($MgSO_4$), concentrated, and applied to a column of silica gel (6 g) for chromatography with solvent B. Colorless crystalline material was obtained from several fractions, totalling 115 mg (72%). Chromatographically homogeneous **15** (R_f 0.65) showed mp 163–166°C (dec.); $[\alpha]_D$ −21.0° (*c* 2.5, methanol); ν_{max}: 3400 (OH), 2110 (N_3), and 1550 (NO_2) cm^{-1}. Fractions in which the less abundant product (R_f 0.57) was enriched were dissolved in a small volume of methanol containing a catalytic amount of $NaOCH_3$, seeded with **15**, and allowed to dry slowly in an open vessel placed over KOH in an unevacuated desiccator. The dry residue then indicated (tlc) preponderance of **15**. *Anal.* calcd. for $C_6H_{10}N_4O_5$ (218.2): C 33.03, H 4.62, N 25.68; found: C 33.11, H 4.66, N 25.68.

*(b) From **19***

Slow evaporation (overnight) of a solution of **19** (100 mg) in methanol (2 mL) containing 5 drops of 1 *M* HCl, in a lightly covered Petri dish, gave a dry crust of stout crystals of **15** (84 mg after washing with small amounts of ether, EtOAc, and ether again); mp 169–170°C with decomposition from 165°C; $[\alpha]_D$ −20° (*c* 1.1, methanol). The ir spectrum was identical with that of **15** obtained from **13**.

*(c) Triacetate **15**a*

An analytical sample of **15** was treated on a watchglass with a few drops of acetic anhydride and a droplet of BF_3–Et_2O. Slow evaporation of the reagent in the air left **15***a* as a dry residue of long needles that were washed with ether–hexane; mp 140°C; ν_{max}: 2100 (N_3), 1750 (ester CO), and 1560 (NO_2) cm^{-1}; δ ($CDCl_3$): 5.59 (t, $J_{2,3}$ = $J_{3,4}$ = 10 Hz, H-3), 5.10 (septet, 2H, H-1,2), 4.66 (ddd, $J_{4,5e}$ = 4.5, $J_{3,4}$ = 10.7, $J_{4,5a}$ = 13.1 Hz, H-4), 3.63 (ddd, $J_{5e,6}$ = 4.5, $J_{1,6}$ = 9.5, $J_{5a,6}$ = 12.8 Hz, H-6), 2.63 (dt, $J_{4,5e}$ = $J_{5,6e}$ = 4.5, $J_{5a,5e}$ = 13.1 Hz, H-5e), 2.10 (q, line separation ~ 13 Hz, H-5a), 2.08, 2.00, and 1.99 (s, 3H each, OAc), and 1.55 (bs, H_2O). The presence of water of crystallization, not removed after drying the substance *in vacuo* at 80°C, was surprising, but was confirmed also by a broad ir band at 3200 cm^{-1} and by the combustion data. *Anal.* calcd. for $C_{12}H_{16}N_4O_8 \cdot 1.5\ H_2O$ (371.3): C 38.81, H 5.16, N 15.09; found: C 38.89, H 4.97, N 14.97.

*3-Azido-1,2,3-trideoxy-4,5;6,7-di-O-isopropylidene-1-nitro-D-glucoheptitol (**16**)*

*(a) From mesylate **5** by an improved procedure*

A mixture of mesylate **5** (9.59 g), NaN_3 (14 g), $Bu_4N^+HSO_4^-$ (8 g), water (50 mL), and benzene (250 mL) was efficiently stirred in a jacketed reaction vessel, the outer chamber of which contained boiling acetone. Monitored by tlc (solvent H), the reaction was estimated to be about 50% complete after 3 days. Additional NaN_3 (6 g) and $Bu_4N^+HSO_4^-$ (4 g) was introduced, and after a further 3 days only traces of **5** (R_f 0.12) were visible. The main product **16** (R_f 0.42) was accompanied by small proportions of by-products having R_f 0.49 and 0.29. The benzene layer was washed 4 times with water, dried (Na_2SO_4), and evaporated. The amber syrup so obtained (9.08 g) was chromatographed on a column of silica gel (83 × 2.5 cm) with solvent I. Mixture fractions were rechromatographed on a similar column. The combined fractions of **16**, homogeneous in tlc with solvent H, nevertheless contained a slow-moving impurity (R_f 0.03) as revealed

Can. J. Chem. Downloaded from www.nrcresearchpress.com by 72.64.146.136 on 09/07/12
For personal use only.

by tlc with CH_2Cl_2. This impurity was removed by passage of the product through a column (20 × 2.8 cm) by means of CH_2Cl_2. The evaporated eluate was decolorized with activated charcoal in ethanol, and final evaporation gave **16** as a syrup (6.281 g, vacuum dried; 76%), $[\alpha]_D$ +15° (*c* 0.7, $CHCl_3$), indistinguishable by ir and nmr spectra from the preparation previously described (12).

The by-products having R_f 0.49 and 0.29 were isolated in amounts of 501 and 47 mg, respectively. Both lacked N_3 absorption in the ir and were identical with the cyclopropano derivatives previously encountered (12), according to their ^1H nmr spectra.

(b) From triflate 6

To a solution of NaN_3 (15 g) and $Bu_4N^+HSO_4^-$ (8 g) in water (30 mL) was added crystalline **6** (8.374 g) followed by benzene (60 mL). The mixture was efficiently stirred at room temperature. Monitoring of the reaction by tlc was difficult because of similar mobilities of **6** and **16**; however, with CH_2Cl_2 as the solvent, **16** was seen to migrate marginally more slowly. (It also charred to a darker spot than **6**, after spraying the plate with dilute sulfuric acid and heating it on a hot-plate.) Although the reaction was close to completion after 1 h, stirring was continued overnight. The phases were then separated, the aqueous phase was extracted with benzene, and the combined benzene phases were washed 5 times with water, dried (Na_2SO_4), and evaporated, to give crude **16** (6.79 g), $[\alpha]_D$ +13.1° (*c* 0.8, $CHCl_3$). The colored syrup was purified by passage through silica gel (25 g) with CH_2Cl_2 as the solvent. The eluate gave on evaporation pure **16** (5.308 g, 84.1%) as a colorless syrup, $[\alpha]_D$ +14.6° (*c* 0.9, $CHCl_3$). The ^1H nmr data were the same as those for the product obtained under (*a*).

The mother liquor that had remained in the preparation of the crystalline batch of **6** (*vide supra*) here utilized was subjected to azide displacement in the same way, furnishing an additional 434 mg of **16**. Based on alcohol **4**, the yield was therefore 61%. In a similar operation (but on one-half scale), a two-step yield of 71% was achieved. Finally, a 93% yield from **4** was obtained when the alcohol was triflated as described but isolation of crystalline **6** was dispensed with and the entire, crude triflate syrup was used for azide displacement. The product was less pure (tlc; $[\alpha]_D$ +13.4°), but could be used for the preparation of **19**.

*3-Azido-1,2,3-trideoxy-4,5-*O*-isopropylidene-1-nitro-*D*-*gluco*-heptitol (17)*

Pure **16** (8.55 g) in toluene (80 mL) was treated at −30°C with 90% CF_3CO_2H (5 mL). After 15 min, tlc (solvent E) showed **17** (R_f 0.2) and a considerable amount of remnant **16** (R_f 0.75). Further acid (5 mL) was added, and after another 15 min the formation of immobile product was observed, even though some **16** was still present. The reaction was quenched by stirring the mixture for 0.5 h with solid $NaHCO_3$ (25 g), then shaking it with added water (40 mL) and ethyl acetate (10 mL). The phases were separated, and the organic phase was washed exhaustively with water. The organic phase contained unreacted **16**, which was isolated and subjected to an identical acid treatment (with appropriately adjusted volumes). All aqueous extracts were combined; they contained **17** as well as tetraol resulting from over-hydrolysis. Neutralization of excess $NaHCO_3$ with acetic acid followed by exhaustive extraction of the aqueous phase with ethyl acetate gave an extract that, after concentration to a volume of 100 mL, washing once with water at that stage, drying, and complete solvent removal, furnished the main crop of **17** as a syrup (6.38 g). The remaining aqueous phase was evaporated to dryness, to give a residue of salts containing tetraol. By acetonation of this material (compare the preparation of **4** from **3**), 580 mg of regenerated **16** was obtained, which yielded another 250 mg of **17** upon partial hydrolysis as just described. The total yield of **17** was therefore 6.63 g (88%); $[\alpha]_D$ +18.8° (*c* 0.9, EtOAc); ν_{max}: 3500–3200 (OH), 2110 (N_3), and 1550 (NO_2) cm^{-1}; δ ($CDCl_3$): 4.55 (dd, 2H, J = 6.4 and 7.1 Hz, H-1,1′), 4.08 (dd, $J_{3,4}$ = 3, $J_{4,5}$ = 7.2 Hz, H-4), 3.98 (~t, $J_{4,5}$ = 7.2, $J_{5,6}$ = 7.3 Hz, H-5), 3.85 (m, H-6), ~3.70 (two partially overlapping dd, $J_{6,7}$ and $J_{6,7'}$ = 5.1–5.2 Hz, H-7,7′), 3.49 (ddd, W = 17 Hz, H-3), ~2.40 (cm, 2H, H-2,2′), 1.9 (broad band, 2H, exchangeable with D_2O, 2OH), 1.44 and 1.36 (s, 3H each, Me_2C). *Anal.* calcd. for $C_{10}H_{18}N_4O_6$ (290.3): C 41.38, H 6.25, N 19.30; found: C 41.23, H 6.41, N 19.09.

*1L-(1,3/2,4,6)-6-Azido-1,2-*O*-isopropylidene-4-nitro-1,2,3-cyclohexanetriol (19)*

(a) From 17 via 18

A solution of diol **17** (6.63 g) in water (100 mL) was mixed with a solution of $NaIO_4$ (5.35 g) in water (50 mL), at 25°C. Oxidation was complete within a few minutes (tlc with EtOAc: R_f 0.7 → R_f 0.85). Ethylene glycol (0.3 g) was added after 10 min, and the solution was then extracted with EtOAc (4 × 100 mL), concentrated to a small volume, and extracted twice more with EtOAc. The dried extracts were evaporated to give syrupy aldehyde **18** (5.58 g, 95%, dried under oil-pump vacuum).

The entire syrup (**18**) was immediately dissolved in reagent-grade methanol (100 mL), and $NaOCH_3$ (0.5 g) in methanol (50 mL) was added with swirling. Thin-layer chromatography with solvent H indicated that the inhomogeneous starting material (R_f 0.0–0.25), which may have contained aldehyde hydrate or hemialdal, or already some cyclization product, was converted after 1 h into product(s) giving a single spot (R_f 0.25). The reaction mixture was concentrated to a small volume and then distributed between water and EtOAc. Repeated extractions of the water phase, and washing (H_2O), drying (Na_2SO_4), and evaporation of the EtOAc extracts gave syrupy product (5.0 g). Concentration of the combined water phases to a small volume, addition of 0.2 mL of glacial acetic acid, and several further extractions performed alternately with benzene and with EtOAc gave an additional crop of syrup (570 mg). Excess CH_2Cl_2 was added to, and evaporated from, the combined syrupy material, which was then taken up in 5 mL of 95% ethanol. After brief heating to dispel remnant CH_2Cl_2 the solution was stored overnight at ambient temperature for crystallization. A first crop of white crystals (1.181 g) of slightly impure **19**, mp 162–167°C, was collected and washed with 95% ethanol. The mother liquor was evaporated to a syrup, which was briefly heated (5 min; steam bath) with 2-propanol (3 mL) containing 10 mg of $NaOCH_3$. On subsequent seeding and standing (20 h) a second crop of crystals (0.834 g) was formed. The process was repeated several times, using 2-propanol or 95% ethanol as the solvent, until 4.11 g of crystalline product was eventually accumulated (73.6% from **18**, or 69.7% from **17**). The various fractions melted in the range of 147–167°C and contained small proportions of the epimer **20** as evidenced by nmr spectra. (In tlc with solvent E the epimers had similar R_f values of 0.55–0.60, but mixtures tended to give a double spot, with **19** migrating marginally faster.) For further purification, the material was dissolved in 4:1 benzene–CH_2Cl_2 and the solution was washed once with water, dried, and evaporated. The recovered crystalline product was then recrystallized once more from 95% ethanol, to give 3.60 g of pure **19**, mp 171°C; $[\alpha]_D$ −12.7° (*c* 0.8, $CHCl_3$). Processing of the mother liquor with $NaOCH_3$ as described above, and recrystallization of the crystals obtained, gave another 250 mg of pure **19**, for a total yield of 3.85 g (65% from **17**); ir, ν_{max}: 3500 (OH), 2100 (N_3), and 1550 (NO_2) cm^{-1}; ^1H nmr ($CDCl_3$), δ: 4.46 (ddd, $J_{4,5e}$ = 5, $J_{3,4}$ = 9, $J_{4,5a}$ = 12.5 Hz, H-4), 4.39 (dt; t after D_2O exchange; $J_{3,OH}$ = 3,3 $J_{2,3}$ = $J_{3,4}$ = 9.2 Hz, H-3), 3.72 (ddd, $J_{5e,6}$ = 4.8, $J_{1,6}$ = 9.6, $J_{5a,6}$ = 11.5 Hz, H-6), 3.50 (~t, $J_{1,2}$ = 9.3, $J_{1,6}$ = 9.6 Hz, H-1), 3.41 (t, $J_{1,2} \approx J_{2,3}$ = 9.35, H-2), 2.92 (d, exchangeable, J = 3.3 Hz, OH), 2.65 (dt, $J_{4,5e} \approx J_{5e,6}$ = 4.85, $J_{5a,5e}$ = 13.4 Hz, H-5e), 1.95 (ddd, $J_{5a,6}$ = 11.5, $J_{4,5a}$ = 12.6, $J_{5a,5e}$ = 13.4 Hz, H-5a), 1.47 and 1.46 (s, 3H each Me_2C). *Anal.* calcd. for $C_9H_{14}N_4O_5$ (258.3): C 41.85, H 5.46, N 21.70; found: C 41.61, H 5.77, N 21.52.

For additional characterization, a 50-mg sample of **19** was converted quantitatively into its *3-(trimethylsilyl) ether* by treatment for 2 h with hexamethyldisilazane (0.3 mL) in refluxing EtOAc (3 mL), in the presence of 3 mg of powdered $(NH_4)_2SO_4$. The ether was isolated by evaporation of the solution with added, excess EtOAc followed by toluene, washing with water, and drying of the colorless syrup obtained, *in vacuo*, whereupon it readily and completely crystallized on scratching. The ether had mp 76°C; R_f 0.85 (tlc, solvent F); ν_{max}:

Can. J. Chem. Downloaded from www.nrcresearchpress.com by 72.64.146.136 on 09/07/12
For personal use only.

2100 (N_3), 1550 (NO_2), and 1250, 850 (Si-C) cm^{-1}; ^1H nmr ($CDCl_3$), δ: 4.44 (ddd, $J_{4,5e}$ = 5, $J_{3,4}$ = 8.9, $J_{4,5a}$ = 12.9 Hz, H-4), 4.26 (~t, width 18.7 Hz, H-3), 3.66 (ddd, $J_{5e,6}$ = 4.8, $J_{1,6}$ = 10.1, $J_{5a,6}$ = 11.4 Hz, H-6), 3.46 (dd, $J_{1,2}$ = 9, $J_{1,6}$ = 10.1 Hz, H-1), 3.31 (dd, $J_{1,2}$ = 9.1, $J_{2,3}$ = 9.7 Hz, H-2), 2.52 (dt, $J_{4,5e} \approx J_{5e,6}$ = 4.9 Hz, $J_{5a,5e}$ = 13.3 Hz, H-5e), 1.98 (~sx, J = 11.5, 12.8, and 13.3 Hz, H-5a), 1.44 and 1.42 (s, 3H each, Me_2C), and 0.08 (s, 9H, Me_3Si).

Mother liquors remaining after the aforedescribed procedures of isolation and recrystallization of **19** contained **19** together with comparable amounts of its 3-epimer **20**, as was clearly revealed by ^1H nmr spectra that showed good separation of signals for the two components, except for overlapping H-4 signals. Epimerism at C-3 was indicated for **20** by a downfield shift and small splittings for the signal of equatorial H-3, and by deshielding of the H-1 and H-5a signals caused by an axial OH-3 group. Although attempted preparative separation of the epimers by column chromatography was inefficient, a small fraction containing virtually pure **20** could so be secured for spectral analysis; δ: 4.99 (nm, H-3), 4.44 (ddd, $J_{3,4}$ = 2.85, $J_{4,5e}$ = 4.9, $J_{4,5a}$ = 12.7 Hz, H-4), 3.99 (~t, $J_{1,2} \approx J_{1,6} \approx$ 9.8 Hz, H-1), 3.60 (ddd, $J_{5e,6}$ = 4.7, $J_{1,6}$ = 10.1, $J_{5a,6}$ = 11.7 Hz, H-6), 3.38 (dd, $J_{2,3}$ = 1.9, $J_{1,2}$ = 9.4 Hz, H-2), 2.49 (dt, H-5e), 2.33 (~sx, J = 11.7 and 12.7, and $J_{5a,5e}$ = 13.5 Hz, H-5a), ~1.5 (broad, exchangeable; OH), 1.46 and 1.445 (s, 3H each, Me_2C).

It was found that crystalline samples of **19** sometimes gave a weak spot (R_f ~ 0.33) in addition to the main spot (R_f 0.6) in tlc with solvent E. The intensity of the former, though always low, seemed to vary with the solvent of application and with the time span of the sample's exposure to silica gel. The phenomenon was probably due to reversal of the cyclization occurring to a minor extent under certain conditions. A substance (presumably **18**) that had the same R_f value accumulated in mother liquors of **19** and was found to be reconvertible into the mixture of epimeric cyclitols by treatment with $NaOCH_3$ in methanol.

(b) From **9**

To a solution of **9** (100 mg) in warm benzene (8 mL) was added NaN_3 (200 mg), $Bu_4N^+HSO_4^-$ (135 mg), and water (2 mL). The vigorously stirred mixture was boiled under reflux for 3 days. The mixture was then diluted with water and benzene, and the benzene phase was washed several times with water, dried ($MgSO_4$), treated with activated charcoal, and evaporated to give a colorless syrup; R_f 0.6 (strong) and 0.35–0.45 (traces; tlc with solvent E). The slow-moving contaminants were removed by passage of the material through a small column of silica gel (6 g) by means of solvent F. The purified syrup (60 mg, 72%) crystallized on trituration with a few drops of 95% ethanol and seeding with **19**. The ir spectrum matched that of pure **19** in all of its features, but additional peaks present in the fingerprint region were attributable to accompanying **20** (by comparison with the spectrum of isolated **20**). The ^1H nmr spectrum was a superposition of those of **19** and **20**, suggesting a ratio of roughly 4:1 for these components.

*2-Deoxystreptamine (**21**) and N,N'-diacetyl-2-deoxystreptamine (**22**)*

Azidonitrotriol **15** (125 mg) in water (20 mL) containing 1 *M* HCl (1.5 mL) was hydrogenated overnight, at ordinary temperature and pressure, with prehydrogenated Adams catalyst (from 90 mg of PtO_2). Evaporation of the optically inactive filtrate, followed by trituration of the residue with 95% ethanol, gave **21** as the crystalline dihydrochloride (136 mg, 100%); it partially sublimed above 300°C and decomposed at about 325°C (lit. (19) mp 325°C (dec.)). The ir spectrum was identical in every detail with that of an authentic sample kindly provided by Bristol Laboratories, Syracuse, N.Y.

A sample of the dihydrochloride was converted into the *N,N'*-diacetyl derivative **22** by treatment with acetic anhydride and triethylamine in methanol–water. Washed with methanol–ether, the crystalline **22** melted with decomposition at 297–300°C, with prior darkening from 290°C (lit. (20) mp 292°C (dec.)). The ir spectrum was identical with that of **22** prepared from an authentic sample of **21**, as well as with that of **22** obtained from the acetonide **24** in the following way. Compound **24** (144 mg) was dissolved in methanol (0.6 mL) with the aid of sonication, and 1:4 concentrated HCl – methanol (5 drops) was then added. After 5 min the reaction appeared to be largely finished (tlc with 1:4 methanol–EtOAc), and **22** began to crystallize. Collected after 2 days and washed with methanol, the crystals (109 mg, 88%) showed mp 299–301°C (dec., with darkening from ~292°C); ^{13}C nmr data (D_2O, dioxane reference signal at 67.4 ppm), δ: 174.8 (CO), 76.7 (C-5), 75.1 (C-4,6), 50.5 (C-1,3), 33.3 (C-2), and 22.9 (Me), in excellent agreement with reported (21) data; [α] 0.0° in the spectral region 365–589 nm (*c* 1.4, water).

*1L-(1,3/2,4,6)-4,6-Diacetamido-1,2-O-isopropylidene-1,2,3-cyclohexanetriol (N,N'-diacetyl-4,5-O-isopropylidene-2-deoxystreptamine, **24**)*

Platinum dioxide (775 mg) suspended in ethanol (12 mL) was prehydrogenated. Glacial acetic acid (1.08 g, 18 mmol) was then added to the suspension, followed by a solution of **19** (775 mg, 3 mmol) in warm ethanol (8 mL). The mixture was vigorously shaken under hydrogen at ordinary temperature and pressure for 5 h. Progress of the reaction was monitored by tlc (1:4 methanol–EtOAc), which indicated gradual disappearance of **19** (R_f 0.9) and formation of nearly immobile diamine **23**, with several intermediary products of intermediate mobilities being visible. The catalyst was filtered off and washed exhaustively with ethanol, and acetic anhydride (1.3 mL) was added to the filtrate. After 30 min the solution was evaporated *in vacuo* (bath temperature 30°C), and several portions of added ethanol were evaporated from the residue until the acidic smell had vanished. Crystallization of the syrup from about 2 mL of ethanol to which 4 drops of saturated, methanolic ammonia had been added gave a first crop (392 mg) of **24**. Processing of the mother liquor by use of ethanol, ethanol–acetone, and acetone as solvents gave several additional crops for a total of 608 mg (70.8%). The crops melted with decomposition in the range of 250–260°C, dependent on the rate of heating. Recrystallized from ethanol, **24** had mp 253–255°C (lit. (13) mp 193–195°C for racemic compound); ν_{max}: 3350 and 3280 (OH, NH), 1660, 1630 and 1560, 1530 (amide I and II) cm^{-1}; δ ($CDCl_3$): 5.57 and 5.49 (bd, 1H each, J = 7–8 Hz, exchangeable, NH), 3.98, 3.85, and 3.75 (bm, 1H each, H-1,3,6), 3.47 (cm, 2H, H-4,5), 2.52 (dt, $J_{1,2e} = J_{2e,3}$ = 4.8, $J_{2a,2e}$ = 12.9 Hz, H-2e), 2.00 and 1.96 (s, 3H each, Ac), and 1.43 (s, 6H, Me_2C). The optical rotation in methanol (*c* = 6.8, and in parentheses, *c* = 1.36) was noticeably concentration dependent: $[\alpha]_{365}$ −12.7° (−10.3°), $[\alpha]_{436}$ −3.8° (−2.4°), $[\alpha]_{546}$ −0.25° (+0.40°), $[\alpha]_{578}$ +0.1° (+0.65°), $[\alpha]_D$ +0.15° (+0.80°). *Anal.* calcd. for $C_{13}H_{22}N_2O_5 \cdot 0.5\,H_2O$ (295.3): C 52.87, H 7.85, N 9.48; found: C 52.65, H 7.78, N 9.30.

A sample of **24** was *O*-acetylated (acetic anhydride – pyridine); the *acetate* (R_f 0.45, tlc with 1:4 methanol–EtOAc) showed $[\alpha]_{365}$ +53.9°, $[\alpha]_{436}$ +38.6°, $[\alpha]_{546}$ +24.4°, $[\alpha]_{578}$ +21.9°, $[\alpha]_D$ +21.3° (*c* 1.5, $CHCl_3$).

Acknowledgements

This work was initiated with support from the National Research Council of Canada (Grant A-1350). Its continuation was made possible by Grant GM-35244 from the United States Public Health Service.

1. (*a*) S. UMEZAWA. Adv. Carbohydr. Chem. Biochem. **30**, 111 (1974); (*b*) K. L. RINEHART, JR. and T. SUAMI. Aminocyclitol antibiotics. ACS symposium series. 125. Washington, DC. 1980.
2. M. NAKAJIMA, A. HASEGAWA, and N. KURIHARA. Justus Liebigs Ann. Chem. **689**, 325 (1967).
3. T. SUAMI, F. W. LICHTENTHALER, S. OGAWA, Y. NAKASHIMA, and H. SANO. Bull. Chem. Soc. Jpn. **41**, 1014 (1968); T. SUAMI, S. OGAWA, S. NAITO, and H. SANO. J. Org. Chem. **35**, 2831 (1968); S. OGAWA, T. UEDA, Y. FUNAKI, Y. HONGO, A. KASUGA, and T. SUAMI. J. Org. Chem. **42**, 3083 (1977).
4. H. H. BAER and R.-J. YU. Tetrahedron Lett. 807 (1967); D. DIJKSTRA. Recl. Trav. Chim. Pays-Bas, **87**, 161 (1968).
5. H. PRINZBACH, R. KELLER, and R. SCHWESINGER. Angew. Chem. **87**, 626 (1975).
6. M. L. WOLFROM, S. M. OLIN, and W. J. POLGLASE. J. Am. Chem. Soc. **72**, 1724 (1950).
7. H. H. BAER. Adv. Carbohydr. Chem. Biochem. **24**, 67 (1969).

8. T. SUAMI, S. OGAWA, N. TANNO, M. SUGURO, and K. L. RINEHART, JR. J. Am. Chem. Soc. **95**, 8734 (1973); S. OGAWA, K. L. RINEHART, JR., G. KIMURA, and R. P. JOHNSON. J. Org. Chem. **39**, 812 (1974).
9. J. CLÉOPHAX, S. D. GÉRO, J. LEBOUL, M. AKHTAR, J. E. G. BARNETT, and C. J. PEARCE. J. Am. Chem. Soc. **98**, 7110 (1976); J. CLÉOPHAX, A. ROLAND, C. COLAS, L. CASTELLANOS, S. D. GÉRO, A. M. SEPULCHRE, and B. QUICLET. *In* Aminocyclitol antibiotics. ACS symposium series. 125. Washington, DC. 1980. pp. 392–411.
10. M. B. PERRY and D. T. WILLIAMS. Methods Carbohydr. Chem. **7**, 44 (1976).
11. C. SATOH and A. KIYOMOTO. Carbohydr. Res. **23**, 450 (1972).
12. B. RADATUS, U. WILLIAMS, and H. H. BAER. Carbohydr. Res. **157**, 242 (1986).
13. A. HASEGAWA, N. KURIHARA, D. NISHIMURA, and M. NAKAJIMA. Agric. Biol. Chem. **32**, 1123 (1968); M. NAKAJIMA, A. HASEGAWA, N. KURIHARA, H. SHIBATA, T. UENO, and D. NISHIMURA. Tetrahedron Lett. 623 (1968).
14. M. HICHENS and K. L. RINEHART, JR. J. Am. Chem. Soc. **85**, 1547 (1963).
15. A. CANAS-RODRIGUEZ, S. GALAN RUIZ-POVEDA, A. GOMEZ SANCHEZ, and E. BLANCO GONZALEZ. Carbohydr. Res. **59**, 240 (1977).
16. S. KOTO, K. TATSUTA, E. KITAZAWA, and S. UMEZAWA. Bull. Chem. Soc. Jpn. **41**, 2769 (1968); Y. NISHIMURA, T. TSUCHIYA, and S. UMEZAWA. Bull. Chem. Soc. Jpn. **43**, 2960 (1970).
17. R. U. LEMIEUX, T. L. NAGABHUSHAN, K. J. CLEMETSON, and L. C. N. TUCKER. Can. J. Chem. **51**, 53 (1973).
18. A. HARAYAMA, T. TSUCHIYA, and S. UMEZAWA. Bull. Chem. Soc. Jpn. **52**, 3626 (1979).
19. S. TATSUOKA, H. HITOMI, S. HORII, T. YAMAGUCHI, and A. MIYAKE. Chem. Pharm. Bull. **9**, 541 (1961).
20. E. AKITA, T. TSURUOKA, N. EZAKI, and T. NIIDA. J. Antibiot. **23**, 173 (1970).
21. S. OMOTO, S. INOUYE, M. KOJIMA, and T. NIIDA. J. Antibiot. **26**, 717 (1973).

Can. J. Chem. Downloaded from www.nrcresearchpress.com by 72.64.146.136 on 09/07/12
For personal use only.

The synthesis and structure of $Fe[\eta^5\text{-}C_5H_3(CHMeNMe_2)\overline{SiCl_2\text{-}1,2}][\overline{C_5H_4}\text{-}\eta^5]$

IAN R. BUTLER, WILLIAM R. CULLEN,[1] AND STEVEN J. RETTIG[2]

Chemistry Department, University of British Columbia, Vancouver, B.C., Canada V6T 1Y6

Received September 4, 1986

IAN R. BUTLER, WILLIAM R. CULLEN, and STEVEN J. RETTIG. Can. J. Chem. **65**, 1452 (1987).

The novel ferroceneophane $Fe[C_5H_3(CHMeNMe_2)\overline{SiCl_2\text{-}1,2}][\overline{C_5H_4}]$, **1***c*, is the product of the reaction of silicon tetrachloride with the dilithio derivative of *N,N*-dimethyl-α-ferrocenylethylamine. Crystals of **1***c* are monoclinic, space group $C2/c$, $a = 15.275(2)$, $b = 9.0869(4)$, $c = 22.363(2)$ Å, $\beta = 95.814(5)°$, $Z = 8$, $R = 0.037$ for 2274 reflections. The tilt angle between the cyclopentadieneyl rings is 19.0(2)° and the bridge-head angle at silicon is 100.7(1)°. Other angles at silicon indicate some repulsive interaction with the $CHMeNMe_2$ group. Silica rapidly reacts with **1***c* to give materials which have essentially the same Mössbauer spectra as the starting material. **1***c* reacts with methanol to give $Fe(C_5H_3(CHMeNMe_2)Si(OMe)_3\text{-}1,2)(C_5H_5)$ and other products.

IAN R. BUTLER, WILLIAM R. CULLEN et STEVEN J. RETTIG. Can. J. Chem. **65**, 1452 (1987).

Le nouveau ferrocènephane $Fe[C_5H_3(CHMeNMe_2)\overline{SiCl_2\text{-}1,2}][\overline{C_5H_4}]$, **1***c*, est produit par la réaction du chlorure de silicium avec le dérivé dilithié de la *N,N*-diméthyl α-ferrocènyléthylamine. Les cristaux de **1***c* sont monocliniques, groupe d'espace $C2/c$, avec $a = 15,275(2)$, $b = 9,0869(4)$ et $c = 22,363(2)$ Å, $\beta = 95,814(5)°$, $Z = 8$ et $R = 0,037$ pour 2274 réflexions. L'angle de déviation entre les noyaux cyclopentadiènеyles est de 19,0(2)° et l'angle à la tête de pont du silicium est de 100,7(1)°. Les autres angles au niveau du silicium indiquent qu'il existe des interactions répulsives avec le groupement $CHMeNMe_2$. La silice réagit rapidement avec le composé **1***c* pour conduire à des produits qui ont essentiellement les mêmes spectres de Mossbauer que le produit de départ. Le composé **1***c* réagit avec le méthanol pour donner du $Fe[C_5H_3(CHMeNMe_2)Si(OMe)_3\text{-}1,2][C_5H_5]$ ainsi que d'autres produits.

[Traduit par la revue]

The reaction of ferrocenophanes such as **1***a* with an electrode surface is a useful means of attaching a ferrocenyl group (1–4). In the case of **1***a* and **1***b* one Si—C bond is believed to be cleaved during attachment so that the final product, **2***a* = **3***a*, is as shown in reaction [1].

We are interested in preparing polymers functionalized with chiral ferrocene groups for use as "heterogenized" catalysts (5, 6). We also have an interest in exploring the electrochemistry of chiral surfaces (7, 8). For these reasons the synthesis of **1***c*, which contains both a chiral center and planar chirality, and its binding to silica, was an attractive target since, if necessary, it could readily be prepared as an optically pure enantiomer (9, 10).

We now report the successful synthesis of **1***c*, its binding to silica, and its solid state structure. Unfortunately, model studies indicate that a ring cleavage reaction would not be stereospecific so that both **2***c* and **3***c* could be expected from a reaction such as described by reaction [1].

Experimental section

General procedures

Unless otherwise stated all air- or moisture-sensitive materials were manipulated under a nitrogen atmosphere using standard Schlenk techniques. Mössbauer spectra were recorded and processed as described previously (11). Isomer shifts are listed relative to iron foil. Nuclear magnetic reosnance spectra were run on Bruker WP-80 and WH-400 instruments. Microanalyses were performed by Mr. Peter Borda of this Department.

*(1) Reaction of 2,1'-dilithio-*N,N*-dimethyl-α-ferrocenylethylamine with silicon tetrachloride. Preparation of the ferrocenophane* **1***c*

The dilithio derivative of *N,N*-dimethyl-α-ferrocenylethylamine (3.0 g, 7.8 mmol), prepared and isolated as the TMED adduct according to the literature procedure (12), was suspended in diethyl ether (20 mL) and added slowly to a chilled (−70°C) solution of silicon tetrachloride (5 g, 29.4 mmol) in diethyl ether (50 mL).

The reaction mixture was allowed to warm slowly to room temperature (~1 h) and was further stirred for 3 h. The solvent and excess $SiCl_4$ were removed by vacuum transfer to leave a yellow/brown powder. The powder was extracted with a 1:1 mixture of dry diethyl ether and dichloromethane (50 mL) and filtered through a *thin* layer of grade 1 activity, neutral alumina to give a clear yellow/orange solution. The solvent volume was reduced under vacuum until an oil began to form. Diethyl ether (10 mL) was then added carefully. The solution was chilled for 3–4 days at −20°C and large yellow crystals of the ferrocenophane **1***c* were obtained (yield ~ 40%, not optimised). These crystals were washed with dry hexane and vacuum dried. *Anal.* calcd. for $C_{14}H_{17}Cl_2FeNSi$: C 47.48, H 4.84, N 3.95; found: C 47.29, H 4.90, N 3.99. Mass spectrum, *m/e* (relative intensity) 357 (1.48), 355 (7.30), 353 (10.83)M^+; 342, 340, 338 (P − Me)$^+$, 314, 312, 310 (P − NMe_2 + H)$^+$. ^1H nmr ($CDCl_3$, 80 MHz) δ 1.50 (d, 3, J = 7 Hz), 2.25 (bs, 6), 3.92 (m, 1), 4.25 (m, 2), 4.70 (2m, 4). Mössbauer δ 0.52, Δ 2.38.

[1] 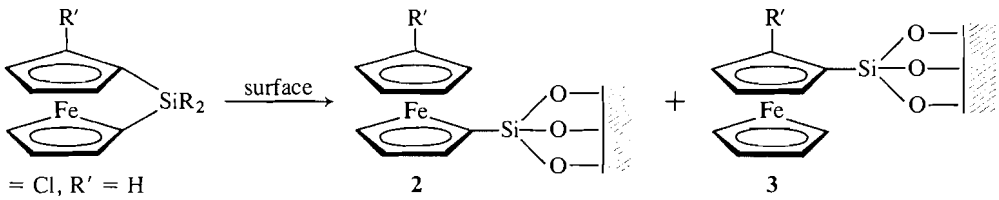

1*a*: R = Cl, R′ = H
b: R = Me, R′ = H
c: R = Cl, R′ = $CHMeNMe_2$
d: R = Ph, R′ = H

2 **3**

[1]Author to whom correspondence may be addressed.
[2]Experimental officer, U.B.C. Crystal Structure Service.

Can. J. Chem. Downloaded from www.nrcresearchpress.com by 72.64.146.136 on 09/07/12
For personal use only.

Can. J. Chem. Downloaded from www.nrcresearchpress.com by 72.64.146.136 on 09/07/12
For personal use only.

TABLE 1. Crystallographic data[a]

Compound	$[(C_5H_3(CH(NMe_2)CH_3))Fe(C_5H_4)]SiCl_2$
Formula	$C_{14}H_{17}Cl_2FeNSi$
fw	354.13
Crystal system	Monoclinic
Space group	$C2/c$
a	15.275(2)
b	9.0869(4)
c (Å)	22.363(2)
β (deg)	95.814(5)
V (Å^3)	3088.0(5)
Z	8
D_c (g/cm^3)	1.524
F(000)	1456
μ(Mo-K_α) cm^{-1}	13.87
Crystal dimensions (mm)	0.10 × 0.55 × 0.65
Transmission factors	0.482–0.872
Scan type	ω–θ
Scan range (deg in ω)	1.00 + 0.35 tan θ
Scan speed (deg/min)	1.55–10.06
Data collected	$\pm h, +k, +l$
$2\theta_{max}$ (deg)	55
Unique reflections	3539
Reflections with $I \geq 3\sigma(I)$	2274
Number of variables	240
R	0.037
R_w	0.041
S	1.597
Mean Δ/σ (final cycle)	0.02
Max Δ/σ (final cycle)	0.24
Residual density (e/Å^3)	−0.79 to +0.37

[a]Temperature 22°C, Enraf-Nonius CAD4-F diffractometer, Mo-K_α radiation ($\lambda_{K\alpha 1}$ = 0.70930, $\lambda_{K\alpha 2}$ = 0.71359 Å), graphite monochromator, takeoff angle 2.7°, aperature (2.00 + tan θ)° × 4.0 mm at a distance of 173 mm from the crystal, scan range extended by 25% on both sides for background measurement, $\sigma^2(I) = S + 2B + [0.04(S - B)]^2$ (S = scan count, B = normalized background count), function minimized $\Sigma w(|F_o| - |F_c|)^2$ where $w = 1/\sigma^2(F)$, $R = \Sigma||F_o| - |F_c||/\Sigma|F_o|$, $R_w = (\Sigma w(|F_o| - |F_c|)^2/\Sigma w|F_o|^2)^{1/2}$, $S = (\Sigma w(|F_o| - |F_c|)^2/(m - n))^{1/2}$. Values given for R, R_w, and S are based on those reflections with $I \geq 3\sigma(I)$.

TABLE 2. Final positional (fractional × 10^4; Fe, Cl, and Si × 10^5, H × 10^3) and isotropic thermal parameters ($U \times 10^3$ Å^2) with estimated standard deviations in parentheses

Atom	x	y	z	U_{eq}/U_{iso}
Fe	38583(3)	43896(5)	34666(2)	35
Cl(1)	17864(6)	30644(10)	43174(4)	58
Cl(2)	12968(6)	61044(11)	35605(5)	61
Si	22737(6)	46173(9)	37774(4)	38
N	3470(2)	9089(3)	3970(1)	50
C(1)	3319(2)	5380(3)	4142(1)	36
C(2)	3837(2)	6438(3)	3835(1)	38
C(3)	4726(2)	5907(4)	3889(2)	44
C(4)	4776(2)	4578(4)	4212(2)	48
C(5)	3928(2)	4251(4)	4375(1)	46
C(6)	2664(2)	3717(4)	3113(1)	43
C(7)	3062(2)	4644(4)	2692(1)	44
C(8)	3852(3)	3994(4)	2551(2)	50
C(9)	3971(3)	2657(4)	2876(2)	52
C(10)	3252(3)	2467(4)	3216(2)	47
C(11)	3528(2)	7874(3)	3537(1)	41
C(12)	4107(3)	8351(4)	3051(2)	52
C(13)	4265(4)	9307(6)	4373(3)	80
C(14)	2696(4)	8969(5)	4293(3)	78
H(3)	515(2)	625(4)	371(1)	39(9)
H(4)	530(2)	409(4)	435(1)	41(9)
H(5)	377(2)	340(4)	461(1)	34(8)
H(7)	283(2)	563(4)	256(2)	63(11)
H(8)	418(2)	422(4)	233(1)	37(10)
H(9)	443(2)	204(4)	288(1)	48(10)
H(10)	318(2)	173(4)	349(1)	45(9)
H(11)	292(2)	778(3)	335(1)	21(7)
H(12a)	468(2)	863(3)	319(1)	37(9)
H(12b)	383(3)	925(5)	282(2)	73(12)
H(12c)	413(2)	764(4)	275(2)	48(10)
H(13a)	437(3)	849(5)	468(2)	83(14)
H(13b)	415(3)	1015(6)	460(2)	82(14)
H(13c)	479(3)	953(5)	411(2)	96(17)
H(14a)	264(2)	981(5)	451(2)	60(11)
H(14b)	210(3)	884(5)	400(2)	93(16)
H(14c)	284(3)	816(6)	460(2)	116(19)

(2) Attachment of **1c** *to silica gel*

To 1.0 g of Kieselgel 60 (Fisher), which had been heated under vacuum at 110°C (oil bath) for 2 h then cooled, was added a stirred solution of **1c** (0.5 g, 1.4 mmol) in dry $CHCl_3$ (20 mL). The solution colour was rapidly discharged (~1 min). The coated silica was filtered off, and washed with chloroform (2 × 10 mL), and vacuum dried. *Anal.* C 6.77, H 1.10, N 0.49. Subsequent experiments showed that loadings of up to 1 g of **1c** per g of silica could be achieved.

Similarly, Aerosil 200 (Degussa), after drying at 180°C under vacuum, was added to a solution of **1c** in dry $CHCl_3$. The color was slowly discharged. Mössbauer δ 0.53; Δ 2.36.

(3) Reaction of **1c** *with MeOD*

A solution of **1c** (1.0 g, ~28 mmol) in CH_2Cl_2 was added to a mixture of MeOD (10.0 mL) in CH_2Cl_2 (10 mL). The solvent volume was reduced to a few mL and a top layer of diethyl ether was added. A yellow oil was obtained by this procedure. The oil was extracted with chloroform and the extracts were concentrated under vacuum. Addition of hexene resulted in the formation of pale yellow diamond shaped crystals. Mass spectrum, m/e (relative intensity) 378 (82.55) P, 363 (68.35) P − Me, 334 (100.00) P − NMe_2; 302 (80.95), 270, 121, 91, 72. ^{1}H nmr ($CDCl_3$, 400 MHz) δ 1.85 (bm), 1.97 (d, CH*Me*), 2.3–2.9 (bm), 3.49 (s, Si(O*Me*)$_3$), 3.71 (s, Si(O*Me*)$_3$), 4.1–4.6 (series of multiplets including 4.23 (s, C_5H_5 or C_5H_4D)).

(4) X-ray crystallographic analysis of **1c**

Crystallographic data are presented in Table 1. The final unit-cell parameters were obtained by least squares on 2 sin θ/λ values of 25 reflections (with 2θ = 35–41°) measured with MoKα_1 radiation. The intensities of three check reflections, measured each hour of X-ray exposure time throughout the data collection, showed only small random variations. The data were corrected for absorption using the Gaussian integration method (13, 14) the range of transmission factors being given in Table 1.[3]

The centrosymmetric space group $C2/c$ was suggested by the E-statistics and by the Patterson function from which the coordinates of the Fe, Cl, and Si atoms were determined. All remaining atoms, including hydrogen, were positioned from subsequent difference maps. In the final stages of refinement the non-hydrogen atoms were refined with anisotropic thermal parameters and the hydrogen atoms with isotropic thermal parameters. Neutral atom scattering factors and anomalous scattering corrections for Fe, Cl, and Si were taken from ref. 15.

Final atomic coordinates and equivalent isotropic (U_{eq} = (1/3) trace diagonalized U) or isotropic thermal parameters are given in Table 2.

[3]The computer programs used include locally written programs for data processing and locally modified versions of the following: ORFLS, full matrix least-squares, and ORFFE, function and errors, by W. R. Busing, K. O. Martin, and H. A. Levy; FORDAP, Patterson and Fourier Syntheses, by A. Zalkin; ORTEP II, illustrations, by C. K. Johnson.

TABLE 3. Bond lengths (Å) with estimated standard deviations in parentheses

Bond	Length (Å)	Bond	Length (Å)
Fe—C(1)	2.006(3)	N—C(13)	1.451(6)
Fe—C(2)	2.037(3)	N—C(14)	1.451(6)
Fe—C(3)	2.073(3)	C(1)—C(2)	1.461(4)
Fe—C(4)	2.074(3)	C(1)—C(5)	1.446(4)
Fe—C(5)	2.028(3)	C(2)—C(3)	1.435(5)
Fe—C(6)	2.008(3)	C(2)—C(11)	1.518(4)
Fe—C(7)	2.026(3)	C(3)—C(4)	1.405(5)
Fe—C(8)	2.077(4)	C(4)—C(5)	1.413(5)
Fe—C(9)	2.074(4)	C(6)—C(7)	1.443(5)
Fe—C(10)	2.030(3)	C(6)—C(10)	1.451(5)
Cl(1)—Si	2.046(1)	C(7)—C(8)	1.407(5)
Cl(2)—Si	2.035(1)	C(8)—C(9)	1.417(5)
Si—C(1)	1.852(3)	C(9)—C(10)	1.409(5)
Si—C(6)	1.847(3)	C(11)—C(12)	1.531(5)
N—C(11)	1.478(4)		

Bond lengths and angles involving non-hydrogen atoms appear in Tables 3 and 4, respectively.[4]

Results and discussion

The ferrocenophane **1***c* was prepared as outlined in reaction [2]:

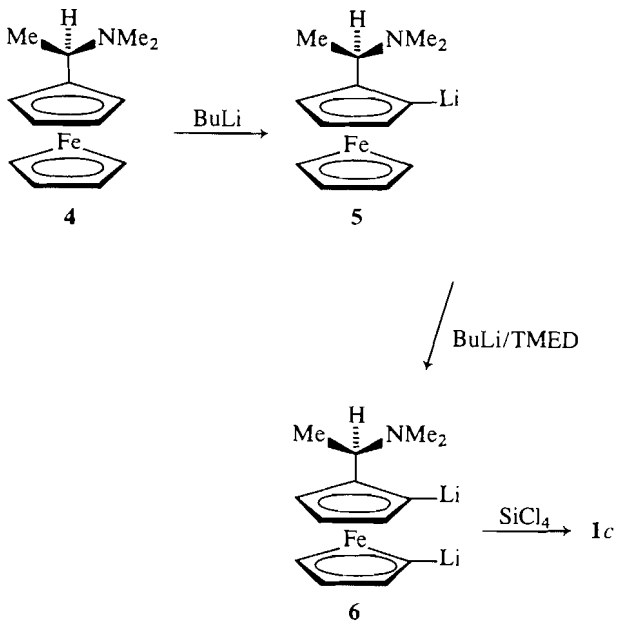

The amine **4** is easily resolved into its enantiomers and the initial lithiation to give **5** is essentially stereospecific (16, 17) and introduces a new chiral center because of planar chirality. For the synthesis of **1***c* a second lithiation of **4** affords a dilithio derivative **6** which easily reacts with $SiCl_4$ to give the ferrocenophane **1***c*, reaction [2]. This procedure in principal, allows the synthesis of chiral **1***c* from chiral **4**. The simpler ferrocenophane **1***a* was prepared by an analogous route from dilithioferrocene (3). The formulation of **1***c* is established by the microanalytical data and the spectroscopic properties, and confirmed by an X-ray structure determination. A view of the molecule is shown in Fig. 1.

Only one diastereomer is produced because of the directing effect of the NMe_2 group on the initial lithiation, reaction [2] (17). That the "correct" isomer is obtained is seen by rotating the $CHMeNMe_2$ group about the C(11)—C(2) bond. This brings the NMe_2 group in proximity to C(2) when the methyl group of C(12) is in the "less hindered" position outside the two η^5-rings (18). Recent studies indicate that this is a rather simplistic rationalization of the experimental observations (19).

Both the cyclopentadienyl rings are planar within experimental error, and, as has been previously established (20), ring bonds to substituted atoms (1.435(5)–1.461(2), mean 1.447(10) Å) are longer than those between unsubstituted atoms (1.405(5)–1.417(5) Å, mean 1.410(5) Å).

The crystal structure of a related [**1**]ferrocenophane **1***d* has been determined (21). The general features of the two structures are very similar and are tabulated in Table 5. The strain in the compounds is mainly reflected in the large value of $\overline{\beta}$. Other [**1**]ferrocenophanes containing Group V bridging atoms have smaller β values but their rings are tilted more and the α values range from 22.9–26.7° (12).

Strain in **1***c* does not seem to cause a shortening of the Si—C_5H_X bonds where the two values are not significantly different at 1.852(3) and 1.847(3) Å. The same distance in **1***d* is 1.881(11) Å (20). In a similar molecule where a $SiMe_2$ group (essentially tetrahedral) bridges two Cp rings which are separated by *two* Fe atoms (and bridging carbonyl groups) the Si—Cp distances seem to be longer at 1.876(7) Å (21), although they are still within the normal Si—C range. For example, in the compound $Fe(C_5H_3(CHMeNMe_2)(SiMe_3)_2$-1,2,3)$(C_5H_4SiMe_3)$ the bond lengths are 1.846(6), 1.862(5), and 1.880(5) Å (22). The angles at Si in **1***c* and **1***d* show departure from idealized tetrahedral geometry. In **1***d* the smallest angle at Si is 99.1(3)° (θ) whilst the largest is 114.4(4)° for the Ph—Si—Ph angle; one is probably the consequence of the other. In **1***c*, however, although θ is relatively unchanged at 100.70(14)° the Cl—Si—Cl angle is also small (107.26(6)°). The C—Si—Cl angles involving Cl(1) and Cl(2) are significantly different with average values of 110.0° (to Cl(1)) and 114.4° (to Cl(2)). Since Cl(2) is on the same side of the molecule as the $CHMeNMe_2$ substituent it is probably a repulsive interaction which opens up the angles. Certainly the H(11)---Cl(2) and H(14b)---Cl(2) distances at 2.99(3) and 2.90(5) Å are less than van der Waals contacts.

As mentioned in the Introduction, it was of interest to study the reaction of **1***c* with a surface.

Silica (two different brands) easily reacts with **1***c* at room temperature, and high loadings can be achieved. It was hoped to establish if a reaction such as described in reaction [*1*] had occurred by measuring the ^{57}Fe Mössbauer spectrum of the bound material. The basis for this expectation being the work of Clemance *et al.* (23) who report that the ring tilt of certain ferrocenophanes such as **1***d* correlates with the quadrupole splitting value, Δ. Thus for **1***d* this value is 1.97 mm s^{-1} whereas that for ferrocene is 2.40. The present results show that this is not a general phenomenon since the Mössbauer parameters for **1***c*, δ 0.52 and Δ 2.38 are in the range found for ferrocene derivatives with parallel rings. Moreover, the parameters are only slightly changed (δ 0.53 and Δ 2.36) after binding to silica has taken place. These results give little information about the occurrence of a reaction such as expected from reaction [1].

[4]Tables and anisotropic thermal parameters, bond lengths involving hydrogen, bond angles involving hydrogen, torsion angles, and measured and calculated structure factor amplitudes (Tables 5–9) (21 pages) have been deposited and may be purchased from the Depository of Unpublished Data, CISTI, National Research Council of Canada, Ottawa, Ont., Canada K1A 0S2.

Can. J. Chem. Downloaded from www.nrcresearchpress.com by 72.64.146.136 on 09/07/12
For personal use only.

TABLE 4. Bond angles (deg) with estimated standard deviations in parentheses

Bonds	Angle (deg)	Bonds	Angle (deg)
Cl(1)—Si—Cl(2)	107.3(1)	C(3)—C(2)—C(11)	125.2(3)
Cl(1)—Si—C(1)	110.3(1)	C(2)—C(3)—C(4)	109.5(3)
Cl(1)—Si—C(6)	109.6(1)	C(3)—C(4)—C(5)	108.1(3)
Cl(2)—Si—C(1)	115.8(1)	C(1)—C(5)—C(4)	109.3(3)
Cl(2)—Si—C(6)	113.0(1)	Si—C(6)—C(7)	117.3(2)
C(1)—Si—C(6)	100.7(1)	Si—C(6)—C(10)	117.7(2)
C(11)—N—C(13)	114.0(3)	C(7)—C(6)—C(10)	105.4(3)
C(11)—N—C(14)	112.1(3)	C(6)—C(7)—C(8)	109.1(3)
C(13)—N—C(14)	111.9(4)	C(7)—C(8)—C(9)	108.3(4)
Si—C(1)—C(2)	121.5(2)	C(8)—C(9)—C(10)	108.3(4)
Si—C(1)—C(5)	112.8(2)	C(6)—C(10)—C(9)	108.8(3)
C(2)—C(1)—C(5)	106.1(3)	N—C(11)—C(2)	113.1(3)
C(1)—C(2)—C(3)	107.0(3)	N—C(11)—C(12)	109.3(3)
C(1)—C(2)—C(11)	127.8(3)	C(2)—C(11)—C(12)	112.2(3)

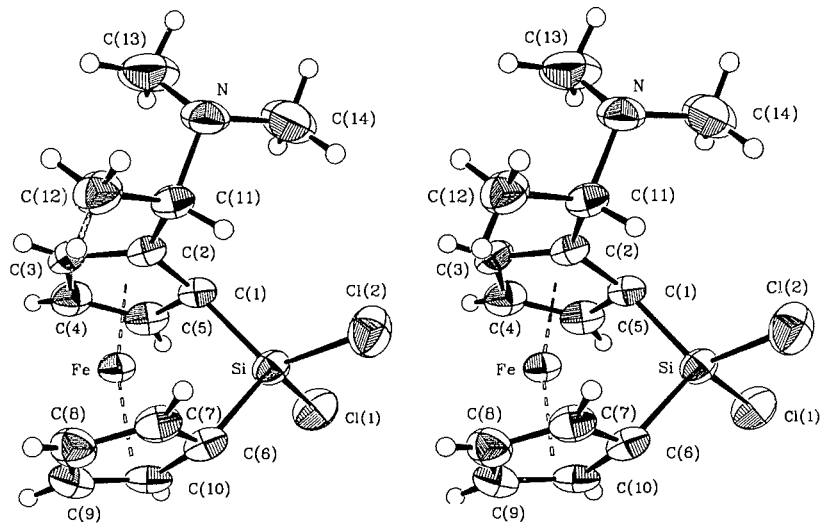

FIG. 1. Stereoscopic view of the structure of **1***c* (50% probability thermal ellipsoids are shown for non-hydrogen atoms).

In order to probe the stability of **1***c* further, it was treated with MeOD at 25°C. The initial product is an oil from which a yellow solid can be extracted. A ferrocenophane cleavage reaction would be expected to proceed according to reaction [3]. The isolated product has a mass spectrum with a parent peak of *m/e* 378 and fragmentation pattern expected for both **7** and **8**. (The pattern is similar to that of **1***c*.) The nmr spectrum of the yellow product is complicated and shows the presence of more than one compound. The principal features of the spectrum can be assigned to **7** or better its DCl derivative since the —NMe_2 resonances are very broad whereas the rest of the spectrum is sharp. If **8** is present, its amount is approximately 25% that of **7** as judged by the ratio of the *two* compounds present with $Si(OMe)_3$ groups. However, there is a problem in that only one compound with a —CH*Me*NMe_2 appear to be present, i.e. **7**. The very complicated set of resonances in the cyclopentadienyl region confirm that **7** is present in addition to other compounds which are *in higher concentration*.

Some samples of the yellow solid also show mass spectra with peaks of *m/e* 710, 696, 665, 651, 622--- corresponding to a siloxane such as **9**.

In conclusion, it seems that any cleavage reaction of **1***c* which might take place on binding to a surface (reaction [1]), is likely to result in more than one product. This is not a desirable property and calls into question the potential use of ferrocenophanes such as **1***c* for the preparation of chiral surfaces of known composition.

[3] 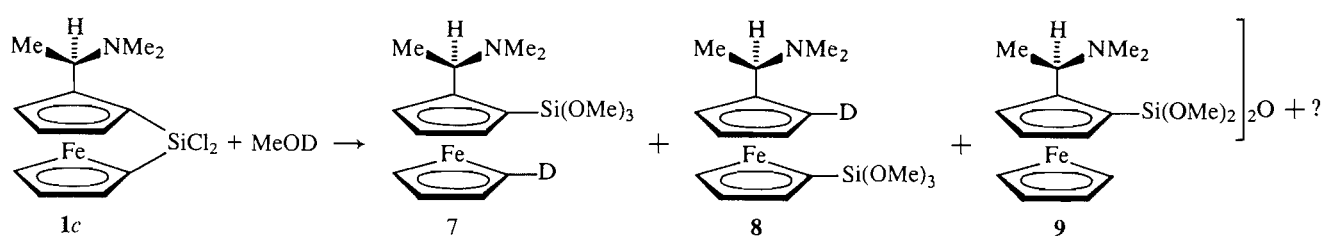

1*c* 7 **8** **9**

Can. J. Chem. Downloaded from www.nrcresearchpress.com by 72.64.146.136 on 09/07/12
For personal use only.

TABLE 5. Selected structural data for the [1]ferrocenophanes **1***c* and **1***d*

Parameter	**1***c*[a]	**1***d*[b]
Fe...Cp* (1)[c]	1.641(2) Å	1.65 Å
Fe...Cp* (2)	1.644(2) Å	1.65 Å
Cp(1)...Fe...Cp(2)	166.3(1)°	167.3°
C(1)...C(6)	2.849(4) Å	2.86 Å
Fe...Si	2.593(1) Å	2.636(5) Å
C(1)—Si—C(6) [= θ]	100.70(14)°	99.1(3)°
α[c]	19.0(2)°	19.2°
$\bar{\beta}$[c]	40.96(2)°	40°

[a]This work.
[b]From ref. 22.
[c]Cp* is the centroid of cyclopentadienyl ring, α = tilt angle between Cp rings, $\bar{\beta}$ = mean angle between Cp plane and Cp—Si bond.

Acknowledgments

We thank the Natural Sciences and Engineering Research Council of Canada for financial support for this work. We also thank Dr. J. Trotter for the use of equipment and the U.B.C. computing center for funds. Mössbauer spectra were recorded with the help of Dr. J. R. Sams and Mrs. A. Sallos.

1. A. B. FISCHER, J. A. BRUCE, D. R. MCKAY, G. E. MACIEL, and M. S. WRIGHTON. Inorg. Chem. **21**, 1766 (1982).
2. S. CHAO, J. L. ROBBINS, and M. S. WRIGHTON. J. Am. Chem. Soc. **105**, 181 (1983).
3. J. M. BOLTS, A. B. BOCARSLY, M. C. PALAZZOTTO, E. G. WALTON, N. S. LEWIS, and M. S. WRIGHTON. J. Am. Chem. Soc. **101**, 1378 (1979).
4. M. V. ROSENTHAL, T. SKOTHEIM, and J. WARREN. J. Chem. Soc. Chem. Commun. 342 (1985).
5. I. R. BUTLER, W. R. CULLEN, N. F. HAN, F. G. HERRING, N. R. JAGANNATHAN, and J. NI. Appl. Organomet. Chem. To be published.
6. W. R. CULLEN and N. F. HAN. J. Organomet. Chem. In press.
7. S. ABE and T. NONAKA. Chem. Lett. 1541 (1983).
8. S. ABE, T. NONAKA, and T. FUCHIGAMI. J. Am. Chem. Soc. **105**, 3630 (1983).
9. D. MARQUARDING, H. KLUSACEK, G. GOKEL, P. HOFFMANN, and I. K. UGI. J. Am. Chem. Soc. **92**, 3589 (1970).
10. W. R. CULLEN and J. D. WOOLLINS. Coord. Chem. Rev. **39**, 1 (1982).
11. J. R. SAMS and T. B. TSIN. Inorg. Chem. **14**, 1573 (1975).
12. I. R. BUTLER, W. R. CULLEN, F. W. B. EINSTEIN, S. J. RETTIG, and A. J. WILLIS. Organometallics, **2**, 128 (1983).
13. P. COPPENS, L. LEISEROWITZ, and D. RABINOVICH. Acta Crystallogr. **18**, 1035 (1965).
14. W. S. BUSING and H. A. LEVY. Acta Crystallogr. **22**, 457 (1967).
15. International tables for X-ray crystallography. Vol. IV. Kynoch Press, Birmingham. 1974.
16. D. W. SLOCUM, T. R. ENGELMANN, C. ERNST, C. A. JENNINGS, W. JONES, B. KOONSVITSKY, J. LEWIS, and P. SHENKIN. J. Chem. Ed. **46**, 144 (1969).
17. A. W. LANGER (*Editor*). Polyamine-chelated alkali metal compounds. Am. Chem. Soc. Symp. Ser. No. 130. 1974.
18. L. F. BATTELLE, R. BAU, G. W. GOKEL, R. T. OYAKAWA, and I. K. UGI. J. Am. Chem. Soc. **95**, 482 (1973).
19. I. R. BUTLER, W. R. CULLEN, F. G. HERRING, and N. R. JAGANNATHAN. Can. J. Chem. **64**, 667 (1986).
20. H. STEOCKLI-EVANS, A. G. OSBORNE, and R. H. WHITELEY. Helv. Chim. Acta, **59**, 2402 (1976).
21. P. A. WEGNER, V. A. USKI, R. P. KIESTER, S. DABESTANI, and V. W. DAY. J. Am. Chem. Soc. **99**, 4846 (1977).
22. I. R. BUTLER, W. R. CULLEN, and S. J. RETTIG. Organometallics. **5**, 1320 (1986).
23. M. CLEMANCE, R. M. G. ROBERTS, and J. SILVER. J. Organomet. Chem. **243**, 461 (1983).

Can. J. Chem. Downloaded from www.nrcresearchpress.com by 72.64.146.136 on 09/07/12
For personal use only.

Structural studies of organoboron compounds. XXVI.[1] 8-Methyl-6,6-diphenyl-5,7-dioxa-8-azonia-6-borata-6,7-dihydro-5*H*-benzocycloheptene

W. KLIEGEL AND U. LAUTERBACH

Institut für Pharmazeutische Chemie, der Technischen Universität Braunschweig, 3300 Braunschweig, Beethovenstraße 55, Bundesrepublik Deutschland

AND

STEVEN J. RETTIG AND JAMES TROTTER

Department of Chemistry, University of British Columbia, 2036 Main Mall, Vancouver, B.C. V6T 1Y6

Received September 4, 1986

W. KLIEGEL, U. LAUTERBACH, STEVEN J. RETTIG, and JAMES TROTTER. Can. J. Chem. **65**, 1457 (1987).

Crystals of 8-methyl-6,6-diphenyl-5,7-dioxa-8-azonia-6-borata-6,7-dihydro-5*H*-benzocycloheptene are triclinic, a = 12.917(1), b = 13.285(1), c = 10.567(1) Å, α = 94.183(8), β = 90.094(5), γ = 72.176(6)°, Z = 4, space group $P\bar{1}$. The structure was solved by direct methods and was refined by full-matrix least-squares procedures to R = 0.045 and R_w = 0.042 for 2914 reflections with $I \geq 2\sigma(I)$. The envelope-like conformation adopted by the seven-membered chelate ring places one *B*-phenyl group above the plane of the fused-ring system facilitating a thermally-induced 1,4-migration of a *B*-phenyl group to the nitrone carbon atom. Mean bond lengths (corrected for libration) are (N)O—B = 1.559(6), (C)O—B = 1.496(3), C—B = 1.610(4) Å.

W. KLIEGEL, U. LAUTERBACH, STEVEN J. RETTIG et JAMES TROTTER. Can. J. Chem. **65**, 1457 (1987).

Les cristaux du méthyl-8 diphényl-6,6 dioxa-5,7 azonia-8 borata-6 dihydro-6,7 5*H*-benzocycloheptène sont tricliniques, a = 12,917(1), b = 13,285(1) et c = 10,567(1) Å, α = 94,183(8), β = 90,094(5) et γ = 72,176(6)°, Z = 4 et groupe d'espace $P\bar{1}$. On a résolu la structure par des méthodes directes et on l'a affinée par la méthode des moindres carrés (matrice complète) jusqu'à des valeurs de R = 0,045 et R_w = 0,042 pour 2914 réflexions avec $I \geq 2\sigma(I)$. La conformation en forme d'enveloppe qu'adopte le cycle chélaté à sept chaînons conduit à placer un groupement *B*-phényle au-dessus du plan du système de cycles condensés et ainsi à faciliter la migration-1,4, induite thermiquement, d'un groupement *B*-phényle vers l'atome de carbone de la nitrone. Les longueurs moyennes des liaisons (corrigées pour la libration) sont : (N)O—B = 1,559(6), (C)O—B = 1,496(3) et C—B = 1,610(4) Å.

[Traduit par la revue]

Introduction

The diphenylboron chelate of *N*-methylsalicylaldonitrone (8-methyl-6,6-diphenyl-5,7-dioxa-8-azonia-6-borata-6,7-dihydro-5*H*-benzocycloheptene, **1**) reacts with phenylboronic acid upon heating, eliminating water to give the tricyclic compound **4**. The phenylboronate structure of **4** has been established by an earlier X-ray crystallographic analysis (1). The mechanism of this reaction involves an inter- or intramolecular shift of one phenyl group which results in the oxidation of the diphenylborinate group to a phenylboronate group and an associated reduction of the nitrone moiety to a hydroxylamine function. A combined theoretical and experimental approach to the question of the reaction mechanism (2) suggests an intramolecular 1,4-shift of one *B*-phenyl group occurs. The same type of phenyl group shift has also been observed in the thermal rearrangement of open-chain triphenylborane-adducts of nitrones (1, 3). Such a 1,4-migration of a phenyl group in **1** would require a conformation of the seven-membered ring which would bring one of the phenyl groups close enough to the nitrone group to allow a transition state such as **2**. This would favor the reaction via the intermediate **3** which has not as yet been isolated but rather reacts immediately with phenylboronic acid (or its anhydride) to give **4**. In order to determine the conformation of the seven-membered ring in **1** and, more importantly, the orientation of the *B*-phenyl groups, an X-ray crystallographic analysis was undertaken.

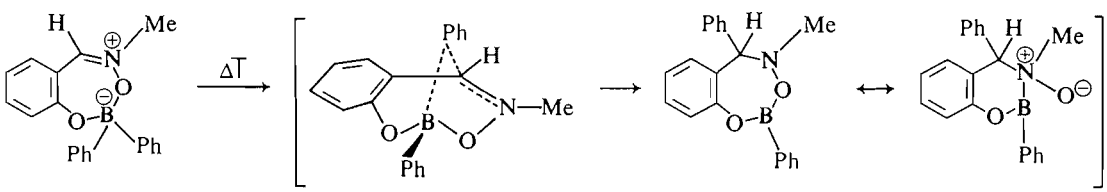

1 2 3

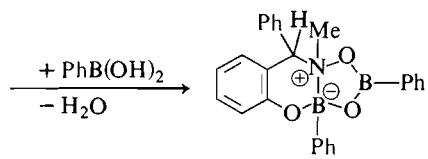

4

[1]For Part XXV, see ref. 26.

Can. J. Chem. Downloaded from www.nrcresearchpress.com by 118.98.75.50 on 09/07/12
For personal use only.

Can. J. Chem. Downloaded from www.nrcresearchpress.com by 118.98.75.50 on 09/07/12
For personal use only.

Experimental

8-Methyl-6,6-diphenyl-5,7-dioxa-8-azonia-6-borata-6,7-dihydro-5H-benzocycloheptene, 1

Compound **1** was prepared as described previously (4). Crystals suitable for X-ray analysis were obtained as described below. Dichloromethane was added to a suspension of the newly synthesized and purified substance in ethanol until complete dissolution was achieved at room temperature. The solution was slowly evaporated at room temperature until crystallization began after 2 weeks. The compound decomposes at 160–161°C (4).

X-ray crystallographic analysis

A crystal ca. 0.2 × 0.3 × 0.4 mm in size was mounted in a general orientation. Unit-cell parameters were refined by least-squares on 2 sin θ/λ values for 25 reflections (2θ = 56–81°) measured on a diffractometer with Cu-$K\alpha$ radiation ($\lambda(K\alpha_1) = 1.540562$, $\lambda(K\alpha_2) = 1.544390$ Å). Crystal data at 22°C are:

$C_{20}H_{18}BNO_2$ fw = 315.2

Triclinic, $a = 12.917(1)$, $b = 13.285(1)$, $c = 10.567(1)$ Å, $\alpha = 94.183(8)$, $\beta = 90.094(5)$, $\gamma = 72.176(6)°$ (cell with $c < a < b$ and two obtuse angles conforms to the conventions of ref. 5; the Buerger reduced cell is the same cell reoriented: $00\bar{1}/100/010$), $V = 1721.2(3)$ Å^3, $Z = 4$, $\rho_c = 1.216$ Mg m^{-3}, $F(000) = 664$, μ(Cu-$K\alpha$) = 5.8 cm^{-1}. Absent reflections: none, space group $P\bar{1}$ from structure analysis.

Intensities were measured with nickel-filtered Cu-$K\alpha$ radiation on an Enraf-Nonius CAD4-F diffractometer. An ω–2θ scan at 1.06–10.06° min^{-1} over a range of (0.65 + 0.14 tan θ) degrees in ω (extended by 25% on both sides for background measurement) was employed. Data were measured to 2θ = 150°. The intensities of three check reflections, measured every 3600 s throughout the data collection, remained constant to within 4%. After data reduction,[2] no absorption correction was made due to irregularity of the crystal surface. Of the 7071 independent reflections measured, 2914 (41.2%) had intensities greater than or equal to $2\sigma(I)$ above background where $\sigma^2(I) = S + 2B + (0.04(S - B))^2$ with S = scan count and B = normalized background count.

The structure was solved by direct methods, all non-hydrogen atoms of each of the two crystallographically independent molecules being positioned from an E-map and hydrogen atoms from subsequent difference maps. In the final stages of refinement the non-hydrogen atoms were refined with anisotropic thermal parameters and the hydrogen atoms with isotropic thermal parameters. The scattering factors of ref. 6 were used for non-hydrogen atoms and those of ref. 7 for hydrogen atoms. The weighting scheme $w = 1/\sigma^2(F)$, where $\sigma^2(F)$ is derived from the previously defined $\sigma^2(I)$, gave uniform average values of $w(|F_o| - |F_c|)^2$ over ranges of both $|F_o|$ and sin θ/λ and was employed in the final stages of full-matrix refinement of 577 variables. Reflections with $I < 2\sigma(I)$ were not included in the refinement. Convergence was reached at $R = 0.045$ and $R_w = 0.042$ for 2914 reflections with $I \geq 2\sigma(I)$. For all 7071 reflections $R = 0.155$. The function minimized was $\Sigma w(|F_o| - |F_c|)^2$, $R = \Sigma||F_o| - |F_c||/\Sigma|F_o|$ and $R_w = (\Sigma w(|F_o| - |F_c|)^2/\Sigma w|F_o|^2)^{1/2}$.

On the final cycle of refinement the mean and maximum parameter shifts corresponded to 0.02 and 0.47σ, respectively. The mean error in an observation of unit weight was 1.463. A final difference map showed maximum fluctuations of −0.32 to +0.21 e Å^{-3}. The final positional and thermal parameters appear in Tables 1 and 5,[3] respectively. Measured and calculated structure factors have been placed in the Depository of Unpublished Data.[3]

TABLE 1. Final positional (fractional × 10^4) and isotropic thermal parameters ($U \times 10^3$ Å^2) with estimated standard deviations in parentheses

Atom	x	y	z	U_{eq}
O(1)	8772(2)	2695(2)	7629(2)	59
O(2)	9730(1)	3845(1)	8703(2)	48
N	10710(2)	3607(2)	8093(3)	47
C(1)	9336(2)	2364(3)	6533(3)	54
C(2)	10341(2)	2511(2)	6250(3)	48
C(3)	10824(3)	2117(3)	5046(4)	64
C(4)	10357(3)	1600(4)	4171(4)	83
C(5)	9378(4)	1455(4)	4466(4)	90
C(6)	8874(3)	1830(3)	5620(4)	76
C(7)	10963(3)	3026(3)	7041(3)	51
C(8)	11432(4)	4130(4)	8749(5)	68
C(9)	8256(2)	3455(3)	9840(3)	47
C(10)	7409(3)	4323(3)	9513(4)	57
C(11)	6527(3)	4807(4)	10329(5)	77
C(12)	6483(4)	4433(4)	11489(6)	92
C(13)	7303(4)	3597(4)	11850(5)	82
C(14)	8189(3)	3103(3)	11037(4)	62
C(15)	10187(3)	1911(3)	9275(3)	55
C(16)	10355(5)	895(3)	8721(5)	88
C(17)	11145(9)	45(6)	9180(10)	145
C(18)	11772(6)	156(8)	10161(10)	161
C(19)	11639(4)	1154(7)	10739(7)	119
C(20)	10850(3)	2014(4)	10292(5)	78
B	9257(3)	2924(3)	8860(3)	46
O(1′)	3831(1)	2561(2)	6823(2)	49
O(2′)	4703(1)	3814(2)	6040(2)	47
N′	5684(2)	3610(2)	6608(2)	46
C(1′)	4350(2)	2310(2)	7896(3)	45
C(2′)	5322(2)	2523(2)	8258(3)	44
C(3′)	5771(3)	2198(3)	9439(3)	60
C(4′)	5287(3)	1709(3)	10238(4)	78
C(5′)	4343(3)	1505(3)	9874(4)	77
C(6′)	3889(3)	1797(3)	8736(4)	62
C(7′)	5942(3)	3041(3)	7559(3)	48
C(8′)	6384(3)	4141(4)	6034(5)	65
C(9′)	3307(2)	3331(3)	4768(3)	48
C(10′)	2461(3)	4222(3)	5220(4)	62
C(11′)	1572(3)	4669(4)	4474(6)	84
C(12′)	1523(4)	4261(5)	3269(7)	103
C(13′)	2347(4)	3393(5)	2778(5)	97
C(14′)	3225(3)	2936(3)	3527(4)	68
C(15′)	5315(2)	1892(2)	5054(3)	45
C(16′)	5670(3)	882(3)	5494(4)	60
C(17′)	6538(3)	86(4)	4916(5)	80
C(18′)	7065(4)	274(4)	3869(4)	77
C(19′)	6738(3)	1254(4)	3412(4)	68
C(20′)	5885(3)	2052(3)	4002(3)	56
B′	4309(3)	2837(3)	5667(3)	45

The ellipsoids of thermal motion for the non-hydrogen atoms are shown in Fig. 1. The thermal motion has been analysed in terms of the rigid-body modes of translation, libration, and screw motion (8). The rms standard error in the temperature factors σU_{ij} (derived from the

[2]The computer programs used include locally written programs for data processing and locally modified versions of the following: MULTAN 80, multisolution program by P. Main, S. J. Fiske, S. E. Hull, L. Lessinger, G. Germain, J. P. Declercq, and M. M. Woolfson; AGNOST, absorption corrections, by J. A. Ibers; ORFLS, full-matrix least-squares, and ORFFE, function and errors, by W. R. Busing, K. O. Martin and H. A. Levy; FORDAP, Patterson and Fourier syntheses, by A. Zalkin; ORTEP II, illustrations, by C. K. Johnson.

[3]The structure factor table, Table 1 (including H atom coordinates), Table 5 (anisotropic thermal parameters), and other material mentioned in the text may be purchased from the Depository of Unpublished Data, CISTI, National Research Council of Canada, Ottawa, Ont., Canada K1A 0S2.

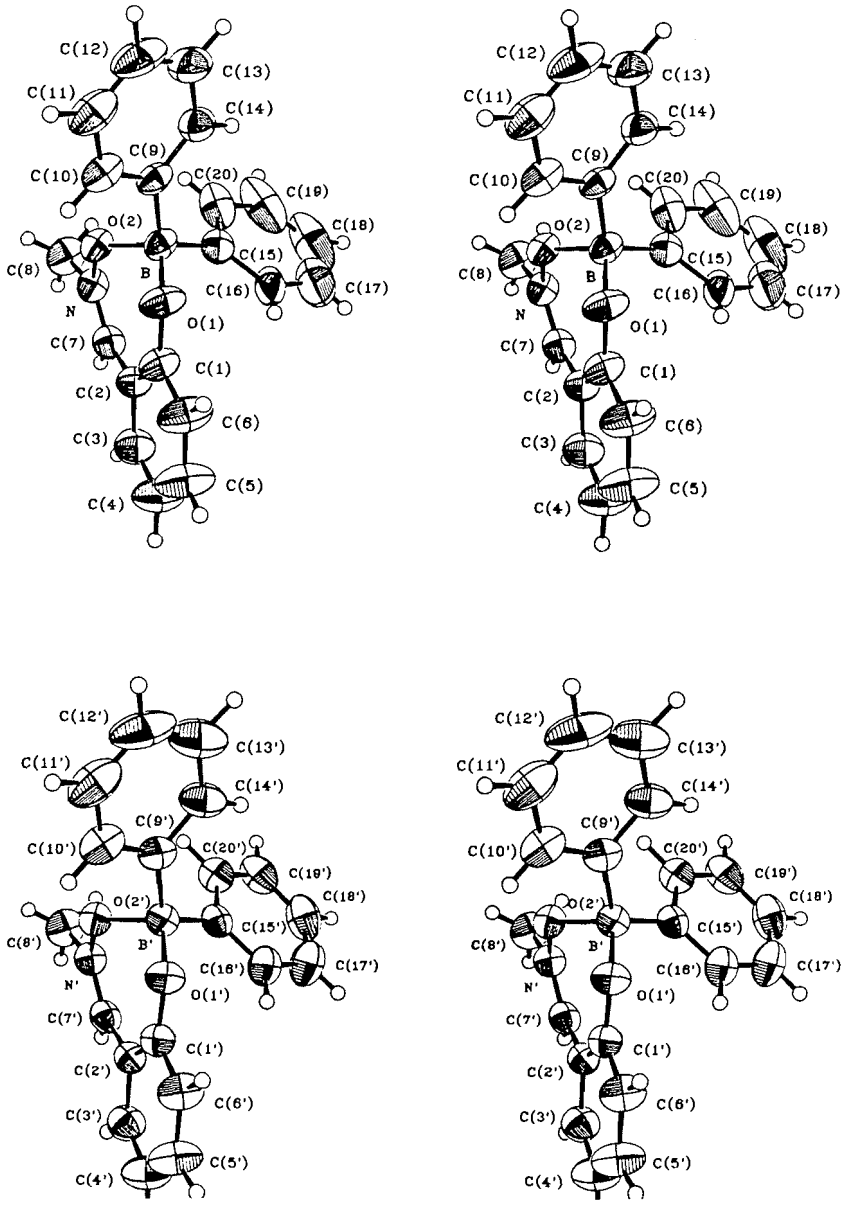

FIG. 1. Stereoscopic views of the two independent 8-methyl-6,6-diphenyl-5,7-dioxa-8-azonia-6-borata-6,7-dihydro-5*H*-benzocycloheptene molecules; 50% probability thermal ellipsoids are shown for the non-hydrogen atoms. Hydrogen atoms have been assigned arbitrary thermal parameters for the sake of clarity. The mirror image of the primed molecule is shown for ease of comparison.

Can. J. Chem. Downloaded from www.nrcresearchpress.com by 118.98.75.50 on 09/07/12
For personal use only.

least-squares analysis) is 0.0028 Å^2. The subunits PhB and "methylbenzocycloheptene" of each of the two independent molecules were analysed separately (rms ΔU_{ij} = 0.0025–0.0065 Å^2). The appropriate bond distances have been corrected for libration (8, 9), using shape parameters q^2 of 0.08 for all atoms involved. Corrected bond lengths appear in Table 2 along with the uncorrected values; corrected bond angles do not differ by more than 1 σ from the uncorrected values given in Table 3. Intra-annular torsion angles defining the conformations of the seven-membered chelate rings are listed in Table 4. Bond lengths and angles involving hydrogen and a complete listing of torsion angles (Tables 6–8) are included as supplementary material.

Results and discussion

The crystal structure of 8-methyl-6,6-diphenyl-5,7-dioxa-8-azonia-6-borata-6,7-dihydro-5*H*-benzocycloheptene, **1**, consists of discrete molecules separated by normal van der Waals distances. The shortest intermolecular contact between non-hydrogen atoms is C···C = 3.336(5) Å. The two crystallographically independent molecules in the asymmetric unit are virtually identical (Fig. 1, Tables 2–4) and are related to one another in the crystal lattice by a pseudo-glide plane. The coordinates of the primed molecule are related to those of the unprimed molecule by the approximate operation: $-1/2 + x, y, 1.45 - z$.

The X-ray analysis confirms the seven-membered chelate structure of **1**. Only a few stable seven-membered chelate rings involving bidentate ligands have been reported in the literature (4). This is the first crystallographic example of a boron chelate with such a ring system although the structures of compounds with seven-membered rings containing 4-coordinate (10) and 3-coordinate (11, 12) boron have been reported. A similar

TABLE 2. Bond lengths (Å) with estimated standard deviations in parentheses

Bond	Length		Bond	Length	
	Uncorr.	Corr.		Uncorr.	Corr.
O(1)—C(1)	1.341(3)	1.345	O(1′)—C(1′)	1.327(3)	1.331
O(1)—B	1.494(4)	1.499	O(1′)—B′	1.489(4)	1.493
O(2)—N	1.358(3)	1.363	O(2′)—N′	1.361(3)	1.365
O(2)—B	1.545(4)	1.553	O(2′)—B′	1.557(4)	1.564
N—C(7)	1.287(4)	1.291	N′—C(7′)	1.284(4)	1.288
N—C(8)	1.469(4)	1.472	N′—C(8′)	1.462(4)	1.465
C(1)—C(2)	1.406(4)	1.414	C(1′)—C(2′)	1.416(4)	1.421
C(1)—C(6)	1.396(4)	1.401	C(1′)—C(6′)	1.395(4)	1.400
C(2)—C(3)	1.409(4)	1.414	C(2′)—C(3′)	1.415(4)	1.419
C(2)—C(7)	1.436(4)	1.442	C(2′)—C(7′)	1.440(4)	1.445
C(3)—C(4)	1.360(5)	1.365	C(3′)—C(4′)	1.362(5)	1.366
C(4)—C(5)	1.376(5)	1.382	C(4′)—C(5′)	1.375(5)	1.381
C(5)—C(6)	1.369(5)	1.372	C(5′)—C(6′)	1.366(5)	1.370
C(9)—C(10)	1.390(4)	1.398	C(9′)—C(10′)	1.397(4)	1.405
C(9)—C(14)	1.392(4)	1.401	C(9′)—C(14′)	1.393(4)	1.406
C(9)—B	1.607(4)	1.613	C(9′)—B′	1.605(4)	1.612
C(10)—C(11)	1.389(5)	1.396	C(10′)—C(11′)	1.392(5)	1.399
C(11)—C(12)	1.363(6)	1.371	C(11′)—C(12′)	1.357(7)	1.370
C(12)—C(13)	1.357(6)	1.365	C(12′)—C(13′)	1.377(7)	1.385
C(13)—C(14)	1.393(5)	1.399	C(13′)—C(14′)	1.388(5)	1.395
C(15)—C(16)	1.385(5)	1.403	C(15′)—C(16′)	1.393(4)	1.407
C(15)—C(20)	1.398(5)	1.410	C(15′)—C(20′)	1.399(4)	1.406
C(15)—B	1.595(5)	1.605	C(15′)—B′	1.603(4)	1.609
C(16)—C(17)	1.387(10)	1.398	C(16′)—C(17′)	1.389(5)	1.394
C(17)—C(18)	1.342(11)	1.354	C(17′)—C(18′)	1.378(6)	1.385
C(18)—C(19)	1.380(11)	1.397	C(18′)—C(19′)	1.364(5)	1.378
C(19)—C(20)	1.389(6)	1.401	C(19′)—C(20′)	1.385(5)	1.390

structure, **5**, was suggested by Balaban *et al.* (13) for the catecholatoborate complex of salicylaldoxime but has been ruled out by the X-ray analysis of the diphenylboron chelate of salicylaldoxime, **6** (14), and by chemical findings (15). The seven-membered ring in **1** has an "envelope-like" conformation in which the boron atom is displaced (by 0.751(4), 0.740(4) Å) from the mean plane formed by the remaining ring atoms (maximum deviations from these six-atom mean planes are 0.091(3) and 0.123(3) Å for the two molecules). The O—C—C—C—N—O portion of the seven-membered ring actually consists of a pair of planar 4-atom groups, O(1)—C(1)—C(2)—C(7) and C(2)—C(7)—N—O(2), which are rotated about the C(2)—C(7) bond with respect to one another (by 11.8(6) and 15.8(6)°). The ring conformation places one *B*-phenyl group distinctly above the mean plane of the fused-ring system, the mean[4] distance between the boron-bound phenyl carbon atom C(16) and the nitrone carbon atom C(7) being 3.190(4) Å. This distance, which corresponds to a van der Waals contact, is probably sufficiently short to facilitate the 1,4-migration of the phenyl group via a transition state **2**. The aromatic rings in **1** are all planar to within experimental error, their geometry being consistent with normal substituent effects (16).

The C=N and N—O bond distances in the nitrone group of **1** (mean values of 1.290(2) and 1.364(1) Å, respectively) are comparable to those reported for the boron chelate **7** containing a nitrone ligand[5] (1.286(6) and 1.355(5) Å) (17). In both cases the relatively short C=N and the long N—O bond distances indicate an increased iminium salt character of the nitrone moiety within a *B*,*N*-betaine complex. The C=N bond lengths in free (uncomplexed) nitrones are somewhat longer in most cases while the N—O bonds are generally shorter (17–22).

As in other diphenylboron chelates with an *N*-oxide ligand (18, 23–25), the O—B bond between the nitrone oxygen atom and boron in **1** (mean 1.559(6) Å) is longer than the O—B bond to the phenolate (mean 1.496(3) Å) or, in other examples, alcoholate ligand. The sum of bond lengths involving the boron

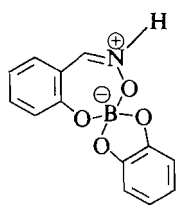

5

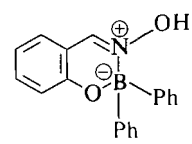

6

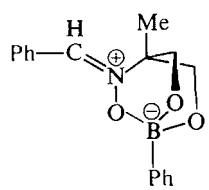

7

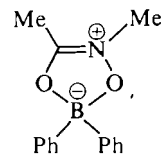

8

[4]Here and elsewhere in this report mean values refer to weighted means with rms deviations from the mean in parentheses.

[5]Libration corrected bond lengths (esd's assumed equal to those of the uncorrected values) are employed in the discussion of the geometry of the boron atom and are compared with similarly treated (8) distances unless otherwise stated.

Can. J. Chem. Downloaded from www.nrcresearchpress.com by 118.98.75.50 on 09/07/12
For personal use only.

TABLE 3. Bond angles (deg) with estimated standard deviations in parentheses

Bonds	Angle (deg)	Bonds	Angle (deg)
C(1)—O(1)—B	124.5(2)	C(1′)—O(1′)—B′	125.3(2)
N—O(2)—B	117.3(2)	N′—O(2′)—B′	116.4(2)
O(2)—N—C(7)	124.3(2)	O(2′)—N′—C(7′)	123.3(2)
O(2)—N—C(8)	111.7(3)	O(2′)—N′—C(8′)	112.1(3)
C(7)—N—C(8)	123.9(3)	C(7′)—N′—C(8′)	124.6(3)
O(1)—C(1)—C(2)	125.1(3)	O(1′)—C(1′)—C(2′)	125.6(3)
O(1)—C(1)—C(6)	116.2(3)	O(1′)—C(1′)—C(6′)	116.7(3)
C(2)—C(1)—C(6)	118.7(3)	C(2′)—C(1′)—C(6′)	117.6(3)
C(1)—C(2)—C(3)	117.9(3)	C(1′)—C(2′)—C(3′)	118.3(3)
C(1)—C(2)—C(7)	128.1(3)	C(1′)—C(2′)—C(7′)	127.8(3)
C(3)—C(2)—C(7)	114.0(3)	C(3′)—C(2′)—C(7′)	113.9(3)
C(2)—C(3)—C(4)	122.4(4)	C(2′)—C(3′)—C(4′)	122.1(4)
C(3)—C(4)—C(5)	119.0(4)	C(3′)—C(4′)—C(5′)	119.0(4)
C(4)—C(5)—C(6)	120.7(4)	C(4′)—C(5′)—C(6′)	120.7(4)
C(1)—C(6)—C(5)	121.3(4)	C(1′)—C(6′)—C(5′)	122.2(4)
N—C(7)—C(2)	131.0(3)	N′—C(7′)—C(2′)	130.6(3)
C(10)—C(9)—C(14)	116.8(3)	C(10′)—C(9′)—C(14′)	116.4(3)
C(10)—C(9)—B	119.8(3)	C(10′)—C(9′)—B′	119.6(3)
C(14)—C(9)—B	123.4(3)	C(14′)—C(9′)—B′	124.0(3)
C(9)—C(10)—C(11)	121.8(4)	C(9′)—C(10′)—C(11′)	121.4(4)
C(10)—C(11)—C(12)	119.8(5)	C(10′)—C(11′)—C(12′)	120.4(5)
C(11)—C(12)—C(13)	120.2(4)	C(11′)—C(12′)—C(13′)	120.2(5)
C(12)—C(13)—C(14)	120.5(5)	C(12′)—C(13′)—C(14′)	119.5(5)
C(9)—C(14)—C(13)	120.9(4)	C(9′)—C(14′)—C(13′)	122.1(4)
C(16)—C(15)—C(20)	116.4(4)	C(16′)—C(15′)—C(20′)	116.0(3)
C(16)—C(15)—B	123.6(4)	C(16′)—C(15′)—B′	124.0(3)
C(20)—C(15)—B	119.9(3)	C(20′)—C(15′)—B′	120.0(3)
C(15)—C(16)—C(17)	120.2(7)	C(15′)—C(16′)—C(17′)	121.7(4)
C(16)—C(17)—C(18)	122.7(9)	C(16′)—C(17′)—C(18′)	120.4(5)
C(17)—C(18)—C(19)	119.2(8)	C(17′)—C(18′)—C(19′)	119.5(4)
C(18)—C(19)—C(20)	118.8(7)	C(18′)—C(19′)—C(20′)	120.0(4)
C(15)—C(20)—C(19)	122.7(6)	C(15′)—C(20′)—C(19′)	122.4(4)
O(1)—B—O(2)	108.1(3)	O(1′)—B′—O(2′)	108.0(2)
O(1)—B—C(9)	106.4(2)	O(1′)—B′—C(9′)	106.1(2)
O(1)—B—C(15)	111.7(3)	O(1′)—B′—C(15′)	113.4(3)
O(2)—B—C(9)	102.5(2)	O(2′)—B′—C(9′)	102.0(2)
O(2)—B—C(15)	110.0(2)	O(2′)—B′—C(15′)	108.8(2)
C(9)—B—C(15)	117.4(3)	C(9′)—B′—C(15′)	117.5(3)

TABLE 4. Intra-annular torsion angles (deg) standard deviations in parentheses

Atoms	Value (deg)
B—O(1)—C(1)—C(2)	−22.4(5)
O(1)—C(1)—C(2)—C(7)	0.2(6)
C(1)—C(2)—C(7)—N	−11.8(6)
O(2)—N—C(7)—C(2)	1.0(5)
B—O(2)—N—C(7)	46.5(4)
N—O(2)—B—O(1)	−78.8(3)
C(1)—O(1)—B—O(2)	62.4(4)
B′—O(1′)—C(1′)—C(2′)	17.5(4)
O(1′)—C(1′)—C(2′)—C(7′)	−0.1(5)
C(1′)—C(2′)—C(7′)—N′	15.8(6)
O(2′)—N′—C(7′)—C(2′)	−1.7(5)
B′—O(2′)—N′—C(7′)	−50.0(4)
N′—O(2′)—B′—O(1′)	80.8(3)
C(1′)—O(1′)—B′—O(2′)	−58.4(3)

atom in *O,O*-chelates of diphenylboron is essentially constant for a given chelate ring size: 6.328(7) and 6.28(1) Å for five-and six-membered rings, respectively (26, and references therein). In **1**, with a seven-membered chelate ring, the corresponding sum is 6.276 Å. The average O—B and C—B bond lengths in **1** (1.528 and 1.610 Å), when compared with those in similar compounds having six-membered chelate rings, indicate relatively strong overall binding of the *O,O*-chelate to the Ph_2B moiety (26). Compound **1** may be regarded formally as a ring-enlarged analog (by *o*-phenyl insertion) of the *N*-methylacethydroximate **8** which shows comparable bond distances in the ring system and in the diphenylboron moiety (27).

Acknowledgements

We thank the Natural Sciences and Engineering Research Council of Canada and the Fonds der Chemischen Industrie, Frankfurt am Main, for financial support and the University of British Columbia Computing Centre for assistance.

Can. J. Chem. Downloaded from www.nrcresearchpress.com by 118.98.75.50 on 09/07/12
For personal use only.

1. W. KLIEGEL, D. NANNINGA, S. J. RETTIG, and J. TROTTER. Can. J. Chem. **62**, 845 (1984).
2. W. KLIEGEL and U. LAUTERBACH. Unpublished results.
3. P. PAETZOLD and G. SCHIMMAL. Z. Naturforsch. **35**b, 568 (1980).
4. W. KLIEGEL and D. NANNINGA. J. Organomet. Chem. **243**, 373 (1983).
5. J. D. H. DONNAY and H. M. ONDIK. Crystal data. Vol. 2. 3rd ed. p. 2. Natl. Bur. Stand., Washington. 1973.
6. D. T. CROMER and J. B. MANN. Acta Crystallogr. Sect. A, **24**, 321 (1968).
7. R. F. STEWART, E. R. DAVIDSON, and W. T. SIMPSON. J. Chem. Phys. **42**, 3175 (1965).
8. V. SCHOMAKER and K. N. TRUEBLOOD. Acta Crystallogr. Sect. B, **24**, 63 (1968).
9. D. W. J. CRUICKSHANK. Acta Crystallogr. **9**, 747 (1956); **9**, 754 (1956); **14**, 896 (1961).
10. I. CYNKIER and H. HOPE. Acta Crystallogr. Sect. B, **34**, 2990 (1978).
11. B. AURIVILLIUS. Acta Chem. Scand. Ser. B, **28**, 998 (1974).
12. I. CYNKIER and N. FURMANOVA. Cryst. Struct. Commun. **9**, 307 (1980).
13. A. T. BALABAN, C. N. RENTEA, and M. BACETSCU-ROMAN. Rev. Roum. Chim. **10**, 865 (1965).
14. W. KLIEGEL, S. J. RETTIG, and J. TROTTER. Can. J. Chem. **62**, 1363 (1984).
15. W. KLIEGEL and D. NANNINGA. Monatsch. Chem. **114**, 465 (1983).
16. A. DOMENICANO, P. MURRAY-RUST, and A. VACIAGO. Acta Crystallogr. Sect. B, **39**, 457 (1983) and references therein.
17. W. KLIEGEL, L. PREU, S. J. RETTIG, and J. TROTTER. Can. J. Chem. **63**, 509 (1985).
18. K. FOLTING, W. N. LIPSCOMB, and B. JERSLEV. Acta Crystallogr. **17**, 1263 (1964).
19. K. G. JENSEN and B. JERSLEV. Acta Crystallogr. Sect. B, **25**, 916 (1969).
20. J. N. BROWN and L. M. TREFONAS. Acta Crystallogr. Sect. B, **29**, 237 (1973).
21. L. GRECI and P. SGARABOTTO. J. Chem. Soc. Perkin Trans. II, 1281 (1984).
22. C. P. FALSHAW, N. A. HASHI, and G. A. TAYLOR. J. Chem. Soc. Perkin Trans. I, 1837 (1985).
23. S. J. RETTIG, J. TROTTER, and W. KLIEGEL. Can. J. Chem. **52**, 2531 (1974).
24. W. KLIEGEL, H.-W. MOTZKUS, S. J. RETTIG, and J. TROTTER. Can. J. Chem. **62**, 838 (1984).
25. S. J. RETTIG, J. TROTTER, and W. KLIEGEL. In preparation.
26. C. ORVIG, S. J. RETTIG, and J. TROTTER. Can. J. Chem. **65**, 590 (1987).
27. S. J. RETTIG, J. TROTTER, W. KLIEGEL, and D. NANNINGA. Can. J. Chem. **56**, 1676 (1978).

Can. J. Chem. Downloaded from www.nrcresearchpress.com by 118.98.75.50 on 09/07/12
For personal use only.

Azides. Part VIII. Thermolysis of ethyl azidoformate in acetic and propionic anhydrides: facilitation of intramolecular cyclization of the resultant carbethoxynitrene to 2-oxazolidinone[1]

N. R. AYYANGAR, K. C. BRAHME, AND K. V. SRINIVASAN
National Chemical Laboratory, Poona 411008, India

Received March 19, 1986[2]

N. R. AYYANGAR, K. C. BRAHME, and K. V. SRINIVASAN. Can. J. Chem. **65**, 1463 (1987).

The thermolysis of ethyl azidoformate in acetic and propionic anhydrides as solvents yielded the corresponding *N*-acyl-2-oxazolidinones (**2***a*,*b*) in relatively significant yields. The other major products isolated were *N*-carboxyethyl-*N*,*O*-diacyl hydroxylamine (**1***a*,*b*) and *N*,*N*,*O*-triacetyl hydroxylamine (**3**). The intramolecular cyclization is facilitated by the solvent.

N. R. AYYANGAR, K. C. BRAHME et K. V. SRINIVASAN. Can. J. Chem. **65**, 1463 (1987).

La thermolyse de l'azidoformate d'éthyle, dans les anhydrides acétique ou propionique comme solvants, conduit aux *N*-acyl oxazolidinones-2 correspondantes (**2***a*,*b*), avec des rendements relativement importants. Les autres produits majeurs qui ont pu être isolés sont les *N*-carboxyéthyl *N*,*O*-diacyl hydroxylamines (**1***a*,*b*) et la *N*,*N*,*O*-triacétyl hydroxylamine (**3**). La cyclisation intramoléculaire est facilitée par le solvant.

[Traduit par la revue]

Introduction

The facile synthesis of 2,5-dicarbomethoxy-*N*,*p*-toluenesulphonyl-1*H*-azepine in high yield (60%) by the thermal reaction of *p*-toluenesulphonylazide with dimethyl terephthalate (DMT) in refluxing propionic anhydride was reported earlier by our group (1). Likewise, the thermolysis of ethyl azidoformate with DMT in refluxing acetic anhydride yielding *N*-carbethoxy-2,5-dicarbomethoxy-1*H*-azepine and a new diazabicyclooctadiene derivative in 1 and 2.2% yields respectively has been reported in a recent communication (2). Although considerably lower yields of the products in the latter reaction may be attributed in part to the loss of singlet nitrene through triplet pathways, we thought that the parallel reaction of the nitrene with acetic anhydride itself is worth a closer scrutiny. The study of the thermolytic reaction of ethyl azidoformate with acetic anhydride is discussed in this communication.

Intramolecular cyclizations involving nitrenes as intermediate species have resulted in the synthesis of interesting heterocyclic systems and natural products (3–6). Azidoformates containing a C—H bond at a sterically favourable position relative to the azido group cyclize upon thermolysis or photolysis to yield 2-oxazolidinones (3). The photolysis of *tert*-butyl azidoformate in *tert*-butanol yielded 5,5-dimethyl-2-oxazolidinone in 60–75% yields (7). In this case, the shielding of the nitrene generated by the *tert*-butyl group and the close proximity of the methyl group promoted the cyclization. In this communication, we wish to report the formation of *N*-acyl-2-oxazolidinones in significant yields when ethyl azidoformate is thermolysed in acetic and propionic anhydrides as solvents. The only other instance involving the intramolecular cyclization of carbethoxy nitrene in an organic solvent is the thermolysis of ethyl azidoformate in methyl cyanoacetate and ethyl cyanoformate to yield 2-oxazolidinone and *N*-ethoxycarbonyl-2-oxazolidinone in 2 and 14% yields respectively (8).

Results and discussion

The thermolysis of ethyl azidoformate was carried out in an excess of acetic and propionic anhydrides as solvents. The decomposition of the azido group to the nitrene was complete in 0.5 h as revealed by the ir spectrum of an aliquot of the reaction mixture, which showed absence of the absorption frequency at 2128–2135 cm^{-1} due to the azido group. The reaction was continued for a further 11 h and the concentration profile of the reaction products was plotted (Fig. 1) by careful glc analysis of aliquots of the reaction mixture at regular intervals of time. The *N*-carboxyethyl-*N*,*O*-diacyl hydroxylamine (**1***a*,*b*) was obtained as a major product along with significant amounts of the *N*-acyl-2-oxazolidinone (**2***a*,*b*) (Scheme 1). Thermolysis in acetic anhydride also resulted in the formation of the *N*,*N*,*O*-triacetyl hydroxylamine (**3**). Although this product could not be isolated from the reaction mixture, its presence was detected by gc–ms and was characterized by comparison with the superposable mass spectra and identical glc retention times of an authentic sample synthesized by the acetylation of hydroxylamine. The thermolysis of ethyl azidoformate was also carried out in the corresponding carboxylic acids, viz. acetic and propionic acids. The products were isolated by column chromatography and characterized by spectral and elemental analysis.

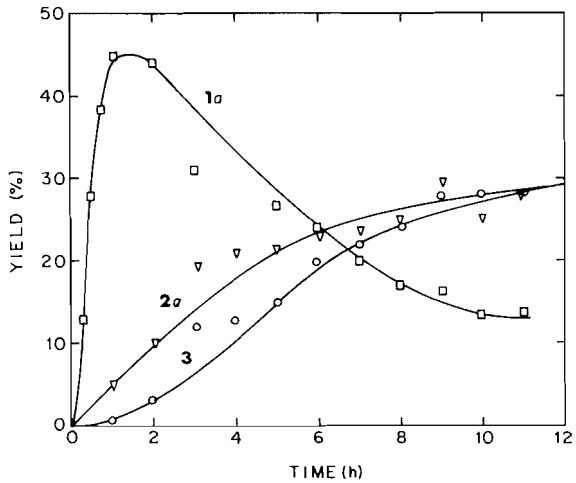

□, HYDROXYLAMINE DERIVATIVE (**1***a*); ▽, OXAZOLIDINONE (**2***a*); ○, TRIACETYL HYDROXYLAMINE (**3**)

FIG. 1. A plot of % yield of products of thermolysis in acetic anhydride versus time.

[1]NCL Communication No. 4017.
[2]Revision received February 3, 1987.

Printed in Canada / Imprimé au Canada

Can. J. Chem. Downloaded from www.nrcresearchpress.com by 118.98.75.50 on 09/07/12
For personal use only.

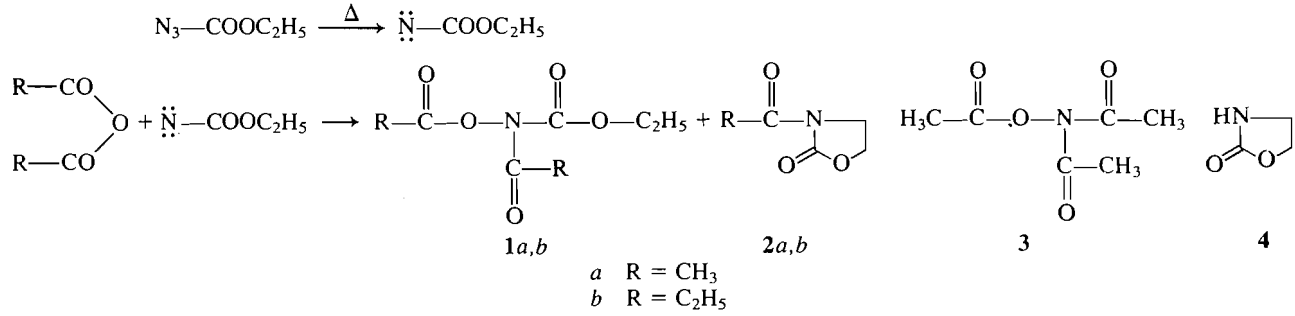

1*a*,*b* 2*a*,*b* 3 4

a R = CH_3
b R = C_2H_5

SCHEME 1

TABLE 1. Yield data on the products of thermolysis/photolysis of ethyl azidoformate in various solvents

Solvent	Reaction temperature (°C)	Reaction time (h)	Product	Yield[a] (%)
Acetic anhydride	140	11	**1***a*	12.5
			2*a*	28.9
			3	29.5
	28[b]	11	**1***a*	86.1
	i. 28[b]	*i.* 6		
	ii. 140[c]	*ii.* 11	**1***a*	88.3
			2*a*	2.0
			3	3.2
Propionic anhydride	140	4	**1***b*	54.3[d]
			2*b*	32.2[d]
Acetic acid[e]	118	11	**1***a*	75.2
Propionic acid[e]	140	11	**1***b*	20.0
			2*b*	4.6

[a]Yield by glc analysis unless otherwise stated.
[b]Photolysis.
[c]Thermolysis of photolysed reaction mixture.
[d]Isolated as propionyl derivatives.
[e]Products isolated as acetyl and propionyl derivatives respectively.

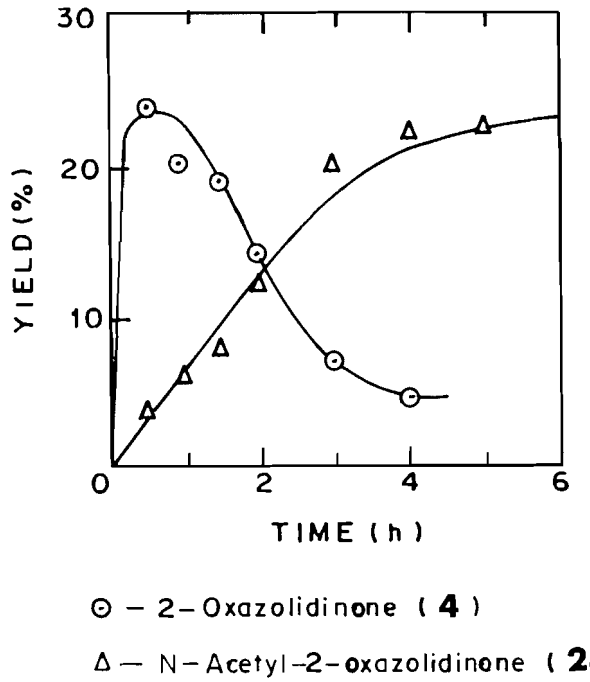

FIG. 2. A plot of % yields of **4** and **2***a* versus time.

The yields of the products are summarized in Table 1. Reaction products of the thermolysis of ethyl azidoformate in acetic acid did not contain 2-oxazolidinone (**4**) as indicated by careful glc analysis. In this reaction the major component was the hydroxylamine derivative (**5**), which was isolated in 75.2% yield. In the case of the thermolysis in propionic acid, however, *N*-acyl-2-oxazolidinone (**2***b*) was isolated in minor amounts (4.6%) (Table 1). The employment of an organic base such as triethylamine as catalyst for the thermolysis reactions in the anhydrides resulted in the lowering of yields of both the compounds **1***a*,*b* and **2***a*,*b*, and the formation of substantial amounts of polymeric material. Similar results were obtained when the thermolysis in propionic anhydride was carried out at the higher reflux temperature (165°C). Thus, the reaction temperature appears to be a critical parameter for maximizing the yields of **1***a*,*b* and **2***a*,*b*.

The photolysis of ethyl azidoformate in acetic anhydride resulted in the formation of **1***a* as a major product with no trace of the oxazolidinone **2***a*. In another experiment, the photolysis of the ethyl azidoformate in acetic anhydride was carried out for 6 h until the azide completely decomposed to the carbethoxy nitrene as indicated by the ir spectra. The photolysed reaction mixture was then refluxed (140°C) for 11 h and the products analysed by glc. The product analysis (Table 1) indicated formation of **2***a* to an extent of 2%. This indicates that thermal energy is required for activating the carbethoxy nitrene for intramolecular cyclization to the 2-oxazolidinone **2***a*. The low yields of **2***a* could be due to formation of **1***a* as the major product during the photolysis process itself. A major proportion of the remaining singlet nitrene might have been lost by triplet pathways. A careful examination of the products of thermolysis of ethyl azidoformate in *o*-dichlorobenzene, an inert solvent providing only the necessary temperature, did not reveal any oxazolidinone formation. The products of the reaction were not characterized. This observation highlights the role of anhydrides in favouring intramolecular cyclization to the oxazolidinones.

The concentration profiles of the reaction products with respect to time are shown in Figs. 1 and 2. To detect and estimate 2-oxazolidinone **4**, initially formed in the reaction (Fig. 2), a set of several experiments were performed for a period of 0.5, 1.0, 1.5, 2.0, 3.0, 4.0, and 5.0 h respectively under identical thermolysis conditions. The solvent was removed at 40°C under reduced pressure (2 Torr; 1 Torr = 133.3 Pa) in each case. The residue was made up to the required minimum volume (2 mL) and analysed by glc. This elaborate procedure became necessary to avoid the possible acetylation of 2-oxazo-

Can. J. Chem. Downloaded from www.nrcresearchpress.com by 118.98.75.50 on 09/07/12
For personal use only.

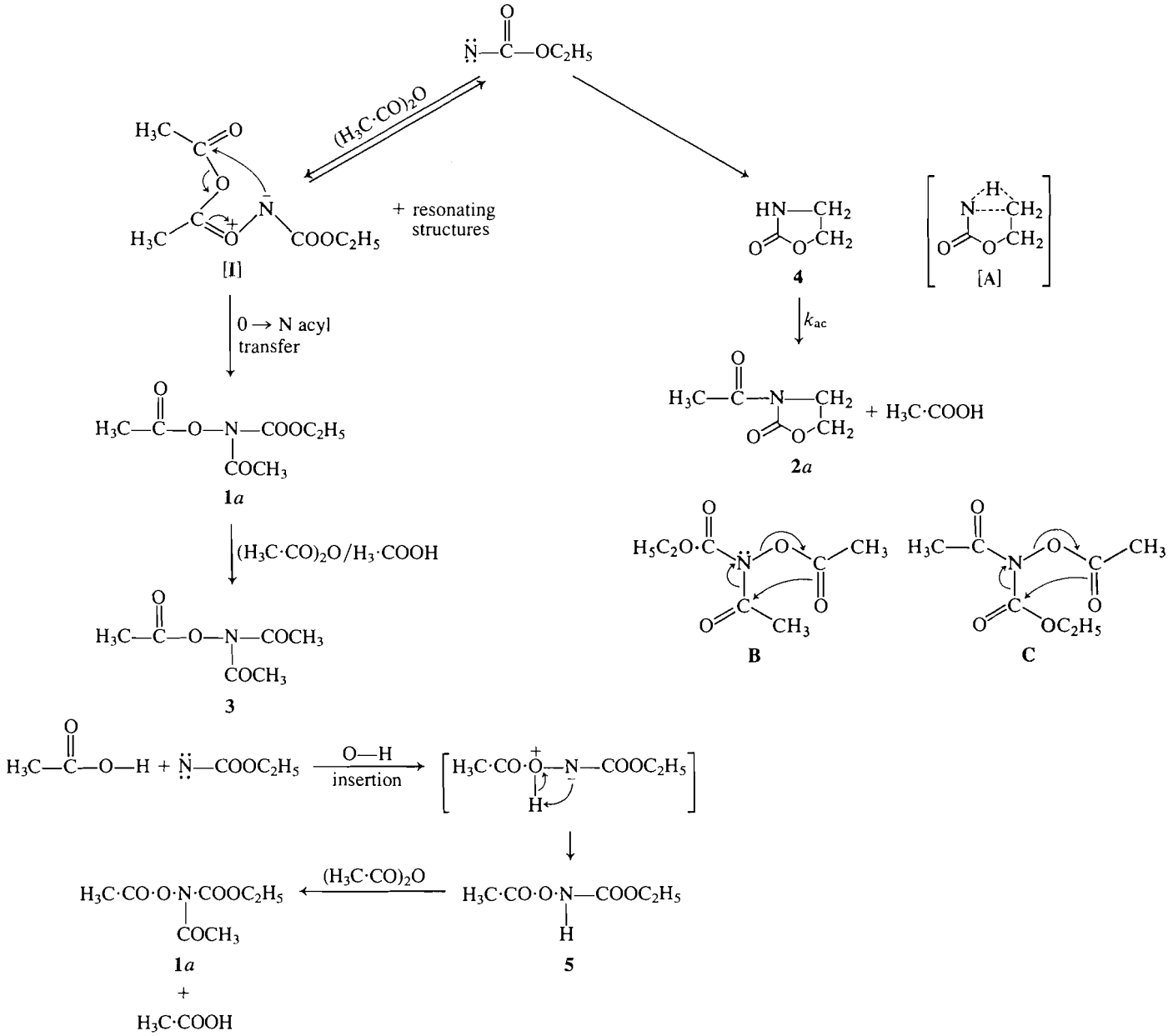

SCHEME 2

lidinone by acetic anhydride at the injection port temperature conditions of the glc instrument and due to the poor response of the compound during the glc analysis. It can be seen from Fig. 2 that the formation of **4** has reached a maximum value of 24.5% at 0.5 h and falls off subsequently as the process of acetylation starts taking place at a significant rate. Together with 4.5% of *N*-acetyl 2-oxazolidinone **2***a*, it is quite apparent that almost the entire intramolecular cyclization is complete within 0.5 h. The yield of **1***a* rapidly reaches a maximum value of 45.6% (in ca. 1 h) after the decomposition of all the azide at 140°C. The reduction in the yield of **1***a* to 12% after 11 h is accounted for by the subsequent formation of the triacetyl derivative **3** (29%). The compound **3** is formed by the *N*-acetylation of **1***a*, accompanied by the acid-catalysed elimination of carbethoxy substituent. This has been established by separate experiments in which **1***a* was refluxed with acetic anhydride in the presence and absence of acetic acid respectively. It was found that the yield of **3** increased by 15% when acetic acid was added to acetic anhydride. As can be seen (Scheme 2), there is a continuous formation of acetic acid in the reaction catalysing the decarboxylation of **1***a* to **3**. It was initially thought that an intermediate such as **1***a*, a truly covalently bonded species having stability at 140°C, could slowly give singlet nitrene on heating via the cyclic transition states such as **B** and **C** (Scheme 2), which may provide low-energy pathways to the singlet nitrenes. However, this hypothesis has been ruled out by the fact that under similar conditions there was no formation of 2-oxazolidinone from **1***a* as starting material (see Experimental).

Thermolysis of ethyl azidoformate in acetic anhydride at 140°C was found to follow first-order kinetics (Fig. 3). The rate constant k_t was evaluated as 0.111 ± 0.001 min^{-1}. The rate of acetylation of 2-oxazolidinone (**4**) was also followed kinetically at 140°C and was found to be first order (Fig. 4). The rate constant k_{ac} was evaluated as 0.081 ± 0.0005 min^{-1}. The azide decomposition is completed in approximately 0.5 h. Likewise, the acetylation of 2-oxazolidinone to **2***a* is completed in approximately 50 min.

In separate experiments, ethyl azidoformate was thermolysed

Can. J. Chem. Downloaded from www.nrcresearchpress.com by 118.98.75.50 on 09/07/12
For personal use only.

Can. J. Chem. Downloaded from www.nrcresearchpress.com by 118.98.75.50 on 09/07/12
For personal use only.

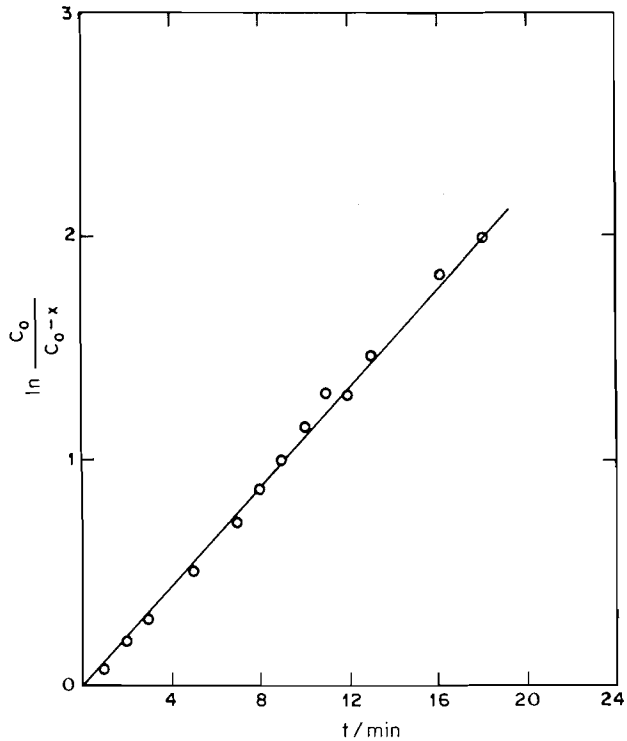

FIG. 3. First-order plot for the decomposition of ethyl azidoformate in acetic anhydride at 140°C.

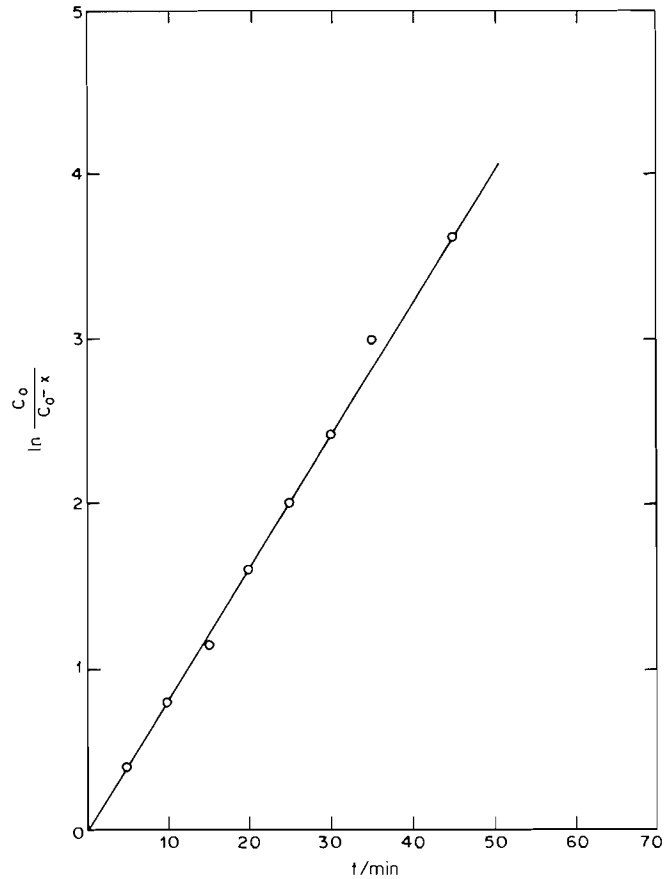

FIG. 4. First-order plot for the acetylation of 2-oxazolidinone at 140°C.

at 140°C with 0.4 and 1 molar equivalents of acetic acid, respectively, in excess of acetic anhydride under similar reaction conditions. The concentration profiles of products **1***a* and **2***a* are shown in Figs. 5 and 6. The above reactions have resulted in significantly lowering the yield of **2***a* to approximately 12% in both cases.

Based on the above observations, a probable pathway for the thermolysis of ethyl azidoformate in acetic anhydride is shown in Scheme 2. The nucleophilic carbonyl oxygen of acetic anhydride forms an ylidic bond with the electrophilic nitrene in a reversible equilibrium to form the reosnance stabilized intermediate [$\mathbf{I}_1$]. However, in the case of carboxylic acids such as acetic acid, the nitrene is trapped by an irreversible O—H insertion process, which by the sequence of reactions generates the hydroxylamine derivative **1***a* (Scheme 2). This explains the nonformation or insignificant formation of the 2-oxazolidinone derivative when the thermolysis was carried out in acetic and propionic acids, respectively, as well as the reduction in the yields of **2***a* in Figs. 5 and 6. The product **1***a* is formed by an O to N acetyl transfer from the initial ylide adduct [$\mathbf{I}_1$]. The compound **1***a*, by a process of acetylation accompanied by decarboxylation, yields **3**. The carbethoxy nitrene, whose intersystem crossing from a singlet to triplet state is probably retarded by acetic anhydride, undergoes intramolecular cyclization by a C—H insertion via [**A**] (9) to give rise to 2-oxazolidinone (**4**) (Fig. 2). The 2-oxazolidinone, on acetylation, yields *N*-acetyl-2-oxazolidinone (**2***a*).

Further confirmation for the mechanism is obtained from the kinetic data (Figs. 1–4), which indicate first-order decomposition of the azide to the nitrene, followed by rapid cyclization to 2-oxazolidinone (**4**), then pseudo first-order acetylation to give **2***a*. The rate of acetylation is slower than that of azide decomposition and cannot occur at a significant rate until the

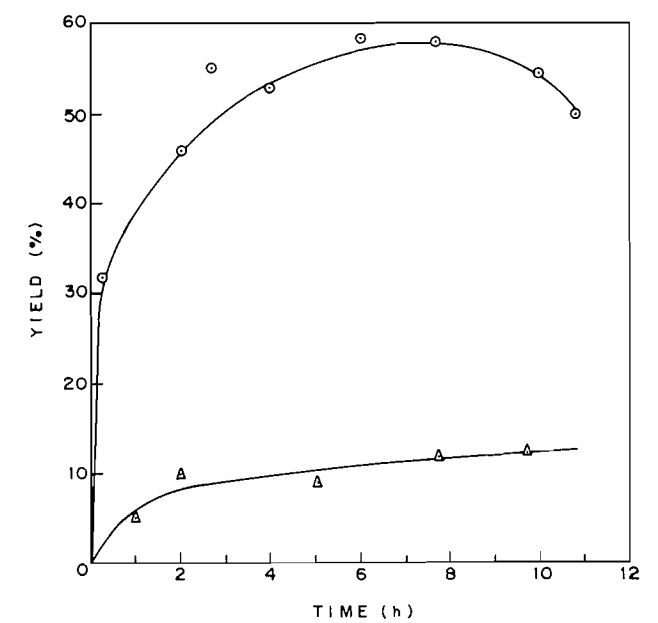

○, Hydroalymine derivative (**1***a*); Δ, N-Acetyl-2-Oxazolidinone(**2***a*)

FIG. 5. A plot of % yield versus time of products of thermolysis of ethyl azidoformate with 0.4 molar equivalent acetic acid in acetic anhydride.

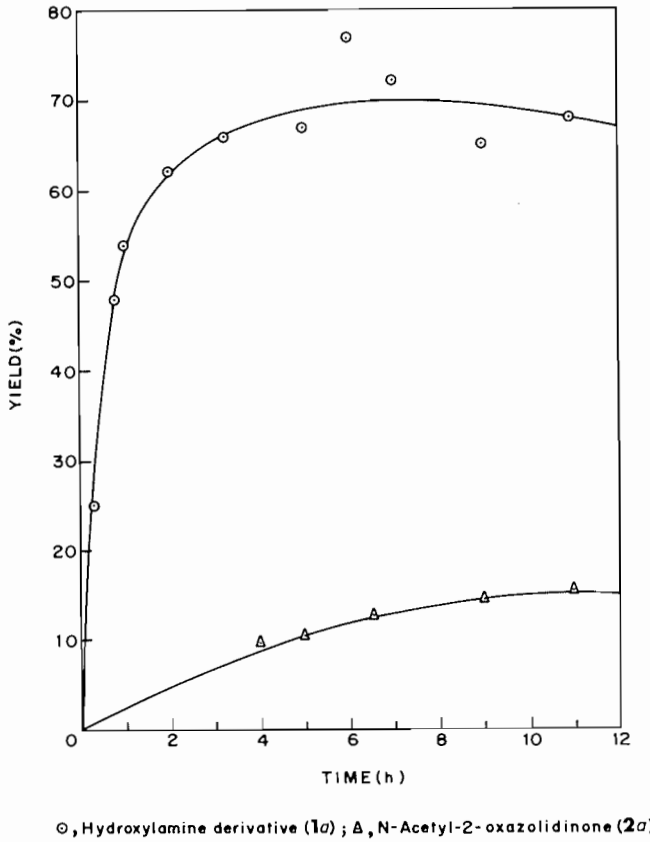

FIG. 6. A plot of % yield versus time of products of thermolysis of ethyl azidoformate with equimolar acetic acid in acetic anhydride.

concentration of 2-oxazolidinone builds up. The observed plots for **2***a* and **4** in Figs. 1 and 2 are quite consistent with these mechanistic considerations.

Experimental

Melting points were recorded in capillary tubes. Infrared spectra were recorded on a Perkin–Elmer 221 spectrophotometer, and proton nmr spectra on Varian FT-80 and Varian T-60 spectrometers using TMS as internal standard; mass spectra were recorded on a Finnigan MAT 1020 Automated GC/MS, gc–ms on an AEI MS 3074 gc–ms spectrometer, and glc analysis was carried out on a Hewlett Packard 700 laboratory chromatograph with Hewlett Packard 3380A integrator.

General procedure for the thermolysis

Ethyl azidoformate (43 mmol) was added dropwise to an excess of the anhydride (500 mmol) at 140°C over a period of 0.5 h with good stirring. The decomposition of the azide to the nitrene was complete (evident from the ir spectra showing the absence of frequency at 2128 cm^{-1} due to the azido group) after stirring for 0.5 h at 140°C. The reaction was continued further for 11 h at 140°C. At the end, the solvent was removed by distillation at 2 Torr pressure. The residue was dissolved in acetone, adsorbed on silica gel, and chromatographed through a column of silica gel. Elution with benzene:petroleum ether (1:1) initially yielded the hydroxylamine derivative (**1***a*,*b*) followed by *N*-acyl-2-oxazolidinone (**2***a*,*b*).

The thermolyses in other solvents were carried out in the same manner as described above. After removal of the solvent, the residue was refluxed with an excess of the anhydride for 3 h. The anhydride was removed by distillation under reduced pressure (2 Torr). The residue was dissolved in acetone and the products analysed by gas chromatography. The yield data are recorded in Table 1.

N-*Carboxyethyl*-N,O-*diacetyl hydroxylamine* (**1**a): bp 83°C/6 Torr: ir (Nujol): 1820, 1765, 1740, 1485, 1445, 1388, 1310, 1250, 1195, 1130, and 1095 cm^{-1}; ^1H nmr ($CDCl_3$) δ: 1.2 (t, 3H, CH_3), 2.2 (s, 3H, $NCOCH_3$), 3.0 (s, 3H, $OCOCH_3$), and 4.3 (q, 2H, $-CH_2$); ms, *m/e*: 189 (M^+) (73.6%), 163 (62%), 148 (76%), 147 (100%, base), 144 (69%), 118 (36%), 117 (86%), 105 (77%), 103 (77%), 78 (77%), 76 (71%), 70 (43%), 61 (42%), and 44 (99%). *Anal.* calcd. for $C_7H_{11}NO_5$: C 44.5, H 5.8, N 7.4; found: C 44.9, H 6.0, N 7.3%.

N-*Carboxyethyl*-N,O-*dipropionyl hydroxylamine* (**1**b): bp 103°C/6 Torr; ir (Nujol): 1800, 1755, 1730, 1465, 1412, 1380, 1360, 1305, 1240, 1190, 1175, and 1100 cm^{-1}; ^1H nmr ($CDCl_3$) δ: 1.2 (m, 9H, CH_3), 2.5 (m, 4H, $COCH_2$), and 4.3 (q, 2H, $COOCH_2$; ms, *m/e*: 217 (M^+) (51%), 205 (34%), 175 (8%), 164 (12%), 146 (10%), 117 (10%), 90 (32%), 89 (37%), 88 (22%), and 70 (30%). *Anal.* calcd. for $C_9H_{15}NO_5$: C 49.7, H 6.9, N 6.5; found: C 49.6, H 7.3, N 6.3%.

N-*Acetyl-2-oxazolidinone* (**2**a): mp 70°C (lit. (10) mp 69–70°C); ir (Nujol): 1775, 1700, 1460, 1385, 1375, 1265, 1210, 1130, 1090, and 1050 cm^{-1}; ^1H nmr ($CDCl_3$) δ: 2.5 (s, 3H, $COCH_3$), 4.0 (q, 2H, $-NCH_2$), and 4.5 (q, 2H, OCH_2); ms, *m/e*: 129 (M^+) (55%), 101 (95%), 88 (36%), 86 (12%), and 56 (100%). *Anal.* calcd. for $C_5H_7NO_3$: C 50.3, H 6.3, N 9.8; found: C 50.7, H 6.5, N 9.5%.

N-*Propionyl-2-oxazolidinone* (**2**b): mp 83°C; ir (Nujol): 1775, 1695, 1470, 1460, 1385, 1375, 1265, 1210, 1130, and 1090 cm^{-1}; ^1H nmr ($CDCl_3$) δ: 1.2 (t, 3H, CH_3), 2.9 (q, 2H, $COCH_2$), 4.0 (q, 2H, $-NCH_2$), and 4.5 (q, 2H, $-OCH_2$); ms, *m/e*: 143 (M^+) (87%), 117 (18%), 116 (80%), 108 (14%), 101 (15%), 90 (28%), 89 (93%), 88 (35%), 87 (42%), 71 (57%), and 58 (base) (100%). *Anal.* calcd. for $C_6H_9NO_3$: C 50.3, H 6.3, N 9.8; found: C 50.7, H 6.5, N 9.4%.

N,N,O-*Triacetyl hydroxylamine* (**3**): The compound **3** was synthesized by a known procedure (11); bp 110°C/14 Torr (lit. (12) bp 109–111°C/14 Torr); ms, *m/e*: 159 (M^+), 117, 75, 61, and 43. Retention time (gc): 1.57 min.

Photolysis of ethyl azidoformate in acetic anhydride

Ethyl azidoformate (86 mmol) was dissolved in acetic anhydride (2000 mmol) and the solution was transferred to a quartz tube. It was irradiated in an atmosphere of nitrogen by a 450-W high pressure mercury lamp at 28°C for a period of 11 h. The reaction was followed by ir spectroscopy. The reaction mixture was worked up as per the general procedure described above. The product analysis was carried out by glc. The yield data is given in Table 1.

Ethyl azidoformate (87 mmol) was dissolved in acetic anhydride (1863 mmol) and subjected to photolysis in the usual manner until the ir spectra indicated complete decomposition of the azido group to the nitrene (6 h). The reaction mixture was then transferred to a round-bottomed flask and refluxed further at 140°C for 11 h. The reaction products were analysed by glc. The yield data are recorded in Table 1.

Gas–liquid chromatographic (glc) analysis

The glc analysis was carried out on a column consisting of OV-17 as the stationary phase on Chromosorb WAW-DMCS (60–80 mesh) with a loading of 5% w/w. The following operating parameters were employed: column temperature 150°C, injection temperature 190°C, detector (FID) temperature 300°C, and carrier gas (Nitrogen) flow rate 40 mL min^{-1}. The composition of the products in the reaction mixture was then determined using the external standard quantitation method with the aid of the data processor unit present in the instrument. The eluted components with their retention times in parentheses are as follows: *N*-carboxyethyl-*N*,*O*-diacetyl hydroxylamine (**1***a*) (2.54 min); *N*-carboxyethyl-*N*,*O*-dipropionyl hydroxylamine (**1***b*) (7.67 min); *N*-acetyl-2-oxazolidinone (**2***a*) (3.59 min); *N*-propionyl-2-oxazolidinone (**2***b*) (12.15 min); *N*,*N*,*O*-triacetyl hydroxylamine (**3**) (1.57 min); 2-oxazolidinone (**4**) (10.96 min).

Attempts at conversion of **1**a *to* **2**a

(*i*) The hydroxylamine derivative (**1***a*) (5.3 mmol) was refluxed in acetic anhydride (49 mmol) for 11 h. (*ii*) The compound **1***a* (5.3 mmol) was refluxed in acetic anhydride (49 mmol) in the presence of acetic acid (5 mmol) for 11 h. In both the experiments, the solvents were distilled off under reduced pressure (2 Torr).

Can. J. Chem. Downloaded from www.nrcresearchpress.com by 118.98.75.50 on 09/07/12
For personal use only.

A careful glc analysis of the products did not reveal any trace of oxazolidinone **2***a*. The triacetyl compound **3** was formed to an extent of 2 and 17% yield, respectively, in the two experiments (as determined by glc analysis).

Attempts at conversion of ***3*** *to* ***2***a

N,N,O-Triacetyl hydroxylamine **3** (25 mmol) was dissolved in acetic anhydride (392 mmol) and refluxed for 11 h. On work-up as described above, the unreacted **3** was completely recovered and a careful glc analysis also did not reveal any trace of the oxazolidinone **2***a*.

2-Oxazolidinone: The compound was synthesized by the reaction of monoethanolamine with diethyl carbonate by a reported procedure (7).

Kinetic measurements

(i) Thermolysis of ethyl azidoformate in acetic anhydride at 140°C

(*a*) Ethyl azidoformate (130 mmol) was added quickly to refluxing acetic anhydride (1470 mmol) at 140°C with good stirring. Aliquots of the reaction mixture were withdrawn at regular time intervals and rapidly cooled externally to ambient temperatures. The samples were analysed by glc for the quantitative estimation of *N*-carbethoxy-*N,O*-diacetyl hydroxylamine (**1***a*), *N*-acetyl-2-oxazolidinone **2***a*, and *N,N,O*-triacetyl hydroxylamine **3**. A plot of their yields versus time is shown in Fig. 1.

(*b*) Ethyl azidoformate (10.87 mmol) was added quickly to refluxing acetic anhydride (123 mmol) at 140°C with good stirring. The reaction mixture was stirred for 0.5 h at 140°C and rapidly cooled externally to room temperature. Acetic anhydride was distilled off at 40°C under reduced pressure (2 Torr). The residue was diluted to 2 mL with acetone and the solution was analysed by glc for the quantitative estimation of 2-oxazolidinone (**4**) and *N*-acetyl-2-oxazolidinone (**2***a*).

The reactions were performed under exactly similar conditions over a period of 1.0, 1.5, 2.0, 3.0, 4.0, and 5.0 h respectively. The reaction mixtures were worked up as described above. The samples were analysed by glc for the quantitative estimation of **4** and **2***a*. The plot of % yields of **4** and **2***a* versus time in the above experiments is shown in Fig. 2.

(ii) Thermolysis of ethyl azidoformate

Ethyl azidoformate (27.4 mmol) was added quickly to refluxing acetic anhydride (304 mmol). The rate of decomposition of azide was determined by measurement of the volume of nitrogen evolved as a function of time (Fig. 3).

(iii) Acetylation of 2-oxazolidinone

2-Oxazolidinone (23 mmol) was added in one lot to refluxing acetic anhydride (196 mmol). Aliquots of samples were taken out at 5-min intervals, the reaction quenched by external cooling, and then were analysed by glc. The plot of percentage yield of **2***a* versus time is given in Fig. 4.

(iv) Thermolysis of ethyl azidoformate in the presence of 0.4 and 1.0 molar equivalent of acetic acid respectively in acetic anhydride at 140°C

Ethyl azidoformate (41 mmol) was added quickly with stirring to a mixture of 16.4 mmol or 41 mmol of acetic acid, as the case may be, and acetic anhydride (465 mmol) at 140°C. The reaction mixture was stirred at 140°C for 11 h. Aliquots of the reaction mixture were withdrawn at regular time intervals. The samples were cooled rapidly by external means to room temperature. They were subjected to glc analysis for the quantitative estimation of **1***a* and **2***a*. Plots of their % yields versus time are shown in Figs. 5 and 6.

1. N. R. AYYANGAR, R. B. BAMBAL, and A. G. LUGADE. Heterocycles, **18**, 77 (1982).
2. N. R. AYYANGAR, R. B. BAMBAL, K. V. SRINIVASAN, T. N. GURUROW, V. G. PURANIK, S. S. TAVALE, and P. S. KULKARNI. Can. J. Chem. **64**, 1969 (1986).
3. O. E. EDWARDS. *In* Nitrenes. *Edited by* W. Lwowski. Interscience Publishers, John Wiley & Sons, New York. 1970. p. 225.
4. T. SHERADSKY. *In* Chemistry of the azido group. *Edited by* S. Patai. Interscience Publishers, John Wiley & Sons, New York. 1971. p. 331.
5. J. APSIMON and O. E. EDWARDS. Proc. Chem. Soc. 461 (1961).
6. H. W. MOORE and D. M. GOLDISH. *In* Supplement D: The chemistry of halides, pseudo-halides and azides. *Edited by* S. Patai and Z. Rappoport. Interscience Publishers, John Wiley & Sons, New York. 1983. p. 362.
7. R. KREHER and G. H. BOCKHORN. Angew. Chem. Int. Ed. Engl. **3**, 589 (1964).
8. R. HUISGEN and H. BLASCHKE. Ann. Chem. **686**, 145 (1965).
9. W. LWOWSKI (*Editor*). Nitrenes. Interscience Publishers, John Wiley & Sons, New York. 1970. p. 203.
10. A. H. HOMEYER. U.S. Patent 2,399,118. April 23, 1946; Chem. Abstr. **40**, 4084^5 (1946).
11. T. URBANSKI. J. Chem. Soc. 3374 (1949).
12. R. LUKES and F. SORM. Collect. Czech. Chem. Commun. **12**, 440 (1947).

Can. J. Chem. Downloaded from www.nrcresearchpress.com by 118.98.75.50 on 09/07/12
For personal use only.

Deuterium isotope effects on the ^{119}Sn shielding constants and spin–spin coupling constants in stannane and the stannonium cation

KEVIN L. LEIGHTON AND RODERICK E. WASYLISHEN[1]
Department of Chemistry, Dalhousie University, Halifax, N.S., Canada B3H 4J3

Received December 5, 1986

KEVIN L. LEIGHTON and RODERICK E. WASYLISHEN. Can. J. Chem. **65**, 1469 (1987).

Deuterium induced isotope effects on the ^{119}Sn chemical shielding constants have been measured for stannane and the stannonium cation; they are found to be approximately -0.403 ppm/D and -0.05 ppm/D respectively. The ^{119}Sn shifts in the series SnD_nH_{4-n} ($n \leq 4$) deviate from additivity as predicted by Jameson and Osten. The primary and secondary isotope effects on Sn–H spin–spin coupling for stannane were obtained and are -2.8 Hz and -1.7 Hz respectively. The primary isotope effect for Sn–H spin–spin coupling for the stannonium cation was found to be -11.6 ± 7 Hz; an accurate value for the secondary isotope effect on the spin–spin coupling could not be obtained. The derivative of the ^{119}Sn shielding constant and J (Sn,H) with respect to extensions in the equilibrium bond length have been calculated for stannane.

KEVIN L. LEIGHTON et RODERICK E. WASYLISHEN. Can. J. Chem. **65**, 1469 (1987).

Pour le stannane et le cation stannonium, on a mesuré les effets isotopiques induits par le deutérium sur les constantes de blindage chimique du ^{119}Sn; on a trouvé qu'ils sont respectivement d'environ $-0{,}403$ ppm/D et de $-0{,}05$ ppm/D. Les déplacements du ^{119}Sn, dans la série des composés SnD_nH_{4-n} ($n \leq 4$), dévient de l'additivité comme prédité par Jameson et Osten. Pour le stannane, on a déterminé les effets isotopiques primaire et secondaire sur le couplage spin–spin Sn–H et ces valeurs sont respectivement de $-2{,}8$ Hz et $-1{,}7$ Hz. On a trouvé que l'effet isotopique primaire, pour le couplage spin–spin Sn–H du cation stannonium est de $-11{,}6 \pm 7$ Hz; on n'a pas pu obtenir de valeur précise pour l'effet isotopique secondaire sur le couplage spin–spin. Dans le cas du stannane, on a calculé la dérivée de la constante de blindage du ^{119}Sn et du J (Sn,H) par rapport aux extensions dans la longueur de la liaison en équilibre.

[Traduit par la revue]

Introduction

Isotope effects on chemical shifts have been known for many years and have been the subject of several reviews (1–4). For an observed nucleus, A, substitution of the directly bonded nucleus, ^{m}X, with a heavier isotope, $^{m'}$X, causes a shortening of the A—X bond that leads to a greater shielding in the heavier isotopomer. If the one-bond isotope shift is defined as

$$[1] \quad {}^1\Delta A(^{m'/m}X) = \sigma^A(A^{m}X\ldots) - \sigma^A(A^{m'}X\ldots) \qquad (m' > m)$$
$$= \sigma - \sigma'$$

where the prime indicates the heavier isotopomer, the one-bond isotope shift is normally negative (4). In this study we have measured isotope effects on the ^{119}Sn shielding constants in stannane, SnD_nH_{4-n} ($n \leq 4$) and the stannonium cation, $SnD_nH_{3-n}^+$ ($n \leq 3$). Also, we have obtained experimental values of ^1J (Sn,H) and ^1J (Sn,D) for each isotopomer of these two compounds.

Jameson and Osten have recently made significant contributions to the interpretation of isotope effects on both shielding constants (4–8) and spin–spin coupling constants (9). Our experimental results are discussed in terms of the theoretical models developed by these authors and we briefly outline their results as they pertain to stannane.

Chemical shielding

For a symmetric molecule of the type AX_n, where mean bond angle deformations have a negligible effect on the isotope shift, the one-bond isotope shift may be written as

$$[2] \quad {}^1\Delta A(^{m'/m}X) = (\partial\sigma^A/\partial\Delta r)_e \sum_n [\langle\Delta r_n\rangle - \langle\Delta r_n\rangle'] + \ldots$$

where $\langle\Delta r_n\rangle$ is the mean bond length displacement of bond n (5). If secondary isotope effects on $\langle\Delta r\rangle$ of other bonds caused by isotopic substitution of the A—X bond are neglected, then the one-bond isotope shift may be approximated (6) as

$$[3] \quad {}^1\Delta A(^{m'/m}X) = (\partial\sigma^A/\partial\Delta r_{AX})_e[\langle\Delta r_{Am}\rangle - \langle\Delta r_{Am'}\rangle]$$

where $\langle\Delta r_{Am}\rangle$ and $\langle\Delta r_{Am'}\rangle$ are the mean bond displacements of the A—^{m}X and A—$^{m'}$X bonds, respectively. Jameson and Osten (7) have shown that the difference in mean bond displacements can be expressed as a product of $\langle\Delta r_{Am}\rangle$ and a ratio of masses; thus eq. [3] becomes

$$[4] \quad {}^1\Delta A(^{m'/m}X) = (\partial\sigma^A/\partial\Delta r_{AX})_e\langle\Delta r_{Am}\rangle[(m' - m)/m'] \times (1/2)[m_A/(m_A + m)]$$

The mass term in this equation indicates that the $^{2/1}$H substitution of SnH_4 should provide a good case for the observation of an isotope shift on σ (^{119}Sn), since the fractional change in mass on isotopic substitution is large; $(m' - m)/m'$ is 0.5 and $m_A/(m_A + m)$ is $\simeq 1$. Also the magnitude of the electronic factor, $(\partial\sigma^A/\partial\Delta r_{AX})_e$, has been found to be related to the chemical shift range of A. Since tin has a relatively large chemical shift range, ~2700 ppm (10), $^1\Delta$Sn($^{2/1}$H) is expected to be relatively large.

For a symmetric molecule, such as CH_4 (11) or NH_4^+ (12), the isotope shift has been found to be proportional to the number of isotopically substituted atoms in equivalent positions; several examples are given in ref. 7. Deviations from strict additivity have been noticed in a few cases (4, 12); however, in general the experimental error associated with measuring isotope shifts is larger than any deviation from additivity. If secondary isotope effects on mean bond displacement are not neglected, deviations from additivity may be predicted. For a tetrahedral species AD_nH_{4-n} ($n \leq 4$) Jameson and Osten have predicted deviations from additivity to be in the ratio 0:3:4:3:0 (4, 7, 12). In the case of $ND_nH_{4-n}^+$ ($n \leq 4$) the ratio was observed to be 0:2.8:4:2.8:0. Here we present another case, SnD_nH_{4-n} ($n \leq 4$), where the deviations from additivity are much greater than the experimental error.

[1]Author to whom correspondence may be addressed.

Can. J. Chem. Downloaded from www.nrcresearchpress.com by 72.64.146.136 on 09/07/12
For personal use only.

Can. J. Chem. Downloaded from www.nrcresearchpress.com by 72.64.146.136 on 09/07/12
For personal use only.

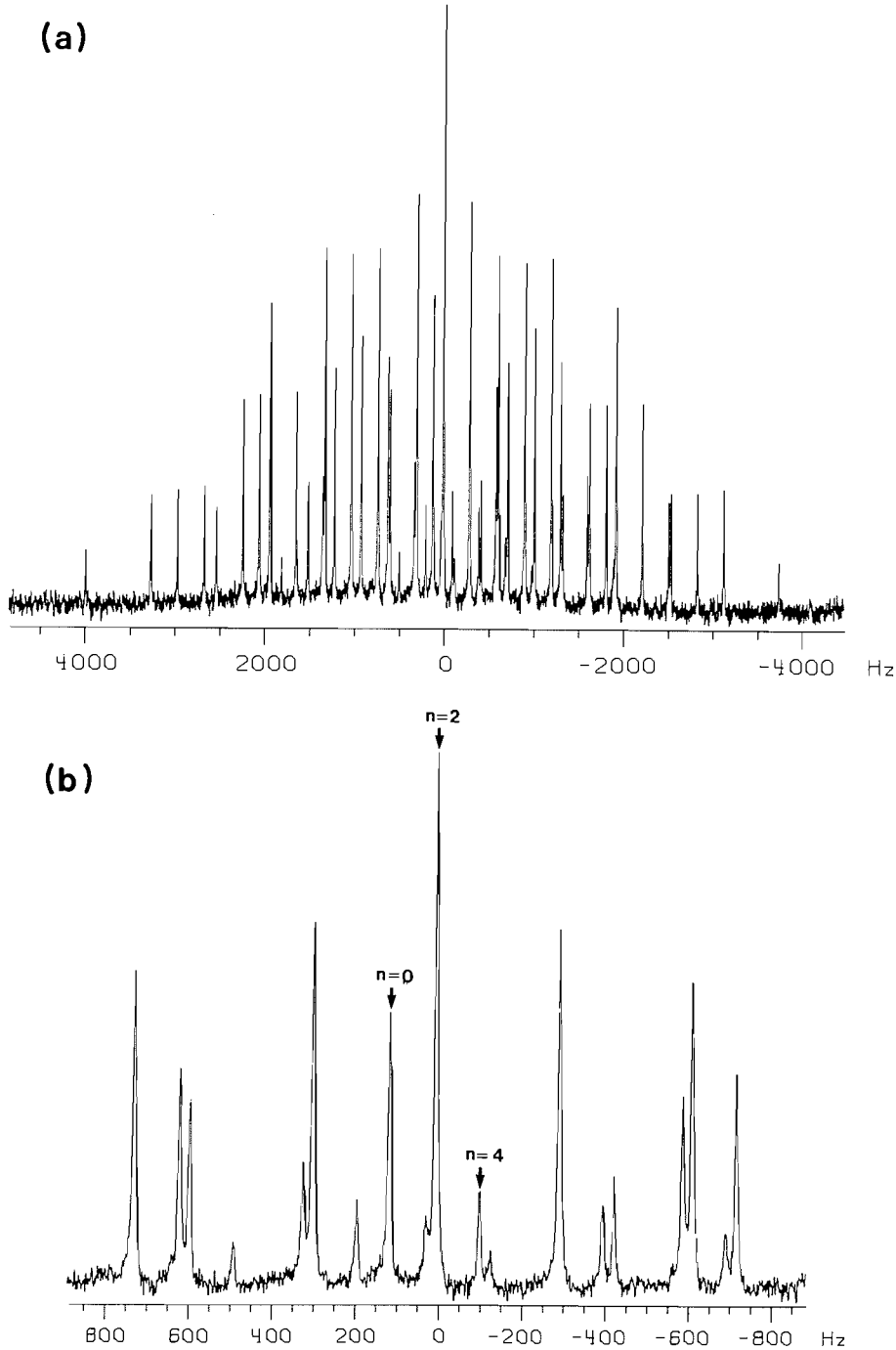

FIG. 1. (*a*) Tin-119 nmr spectrum of stannane, SnD_nH_{4-n} ($n \leq 4$) at 134.5735 MHz and −50°C. (*b*) Expansion of the central region of the spectrum in Fig. 1*a*. The arrows indicate the relative chemical shifts of each isotopomer.

Spin–spin coupling constants

Recently Jameson and Osten have summarized isotope effects on spin–spin coupling (9), of which there have been relatively few reports. In many cases the observed effects are comparable to the experimental error. The primary isotope effect on spin–spin coupling involving H is defined (9) as follows:

$$[5] \quad \Delta_p{}^nJ(A,{}^{2/1}H) \equiv |{}^nJ(A,D)|(\gamma_H/\gamma_D) - |{}^nJ(A,H)|$$

This is the change in coupling constant between two nuclei caused by isotopic substitution of one of the nuclei; n indicates the number of bonds separating the two coupled nuclei. The largest primary isotope effect on ^1J has been observed in phosphine (13) where $\Delta_p{}^1J(^{31}P,^{2/1}H)$ is +12 Hz, approximately 6% of the coupling constant. In general, the primary isotope effect is much smaller; for example in methane the primary isotope effect on $^1J(^{13}C,^{2/1}H)$ is approximately −0.3 Hz, or less than 0.5% of the carbon–proton coupling constant (11). In molecules where neither of the coupled nuclei have a lone pair, the primary isotope effect on the reduced coupling constant, $^1K(A,X)$, appears to be negative (9). Here the reduced coupling constant is independent of the magnetogyric ratios of the two coupled nuclei, γ_A and γ_X, and is defined by eq. [6].

$$[6] \quad K(A,X) = 4\pi^2J(A,X)/h\gamma_A\gamma_X$$

Can. J. Chem. Downloaded from www.nrcresearchpress.com by 72.64.146.136 on 09/07/12
For personal use only.

The rovibrational model of Jameson and Osten (9) predicts the $^{2/1}H$ isotope effect on $^1K(A,^{2/1}H)$ to depend on both an electronic factor (independent of mass) and a dynamic factor, eq. [7],

$$[7]\quad \Delta_p{}^1K(A^{2/1}H) = (\partial K/\partial \Delta r_{AH})_e[\langle \Delta r_{AD}\rangle - \langle \Delta r_{AH}\rangle] + 1/2(\partial^2 K/\partial \Delta r_{AH}{}^2)_e[\langle (\Delta r_{AD})^2\rangle - \langle (\Delta r_{AH})^2\rangle] \ldots$$

The terms of eq. [7] that involve the difference in mean bond length and the mean square amplitudes are generally negative (9). For one-bond carbon–proton spin–spin coupling constants both the partial derivatives in eq. [7] are positive (9); thus, as observed, a negative isotope effect is predicted. By analogy, a negative value for $\Delta_p{}^1K(Sn,^{2/1}H)$ in stannane is predicted.

Secondary isotope effects on spin–spin coupling constants are often smaller than primary effects and can be of either sign (9). The secondary isotope effect is defined as the change in observed coupling between two nuclei, A and B, caused by isotopic substitution of a neighbour X. The largest secondary isotope effect reported is in hydrogen selenide where $^1J(^{77}Se,H)$ in H_2Se is 0.9 Hz larger than the value observed for this same coupling in HDSe (14). The theoretical interpretation of secondary isotope effects on J is more difficult (9) and will not be discussed further here.

Stannane and the stannonium cation have been chosen for this study because the value of $^1J(^{119}Sn,^1H)$ is large for each, approximately −1930 Hz and −2910 Hz, respectively (15); with such large coupling constants, these two compounds represent a unique opportunity to investigate 1° and 2° isotope effects on spin–spin coupling constants and not be restricted by large experimental error.

Experimental

SnD_nH_{4-n} ($n \leq 4$) was prepared (16) from anhydrous $SnCl_4$ (BDH Chemicals, 98%) by reduction with a mixture of $LiAlH_4$ (Aldrich, 95%) and $LiAlD_4$ (MSD Isotopes, 99%). The mole ratio, hydrogen:deuterium, employed was 3:2; 0.006 mol of SnD_nH_{4-n} were condensed into a 10-mm od thick-walled nmr tube containing 5 mL of degassed CS_2 (BDH Chemicals, Spec. Grade) at −196°C; then the tube was sealed under vacuum. The sample tube was stored at liquid nitrogen temperature.

$SnD_nH_{3-n}{}^+$ ($n \leq 3$) was prepared (15, 17) by the reaction of 0.01 mol of SnD_nH_{4-n} (H:D mole ratio = 2:3) and 4 mL of HSO_3F (Aldrich), which had been distilled under nitrogen, in a 10-mm o.d. thick-walled nmr tube. The hydrogen evolved was pumped off periodically. After 2.5 h at −78°C, no further hydrogen was produced and the tube was sealed under vacuum. To avoid decomposition the sample was never warmed above −78°C.

The ^{119}Sn nmr spectra were recorded on a Nicolet 360 NB spectrometer (B_0 = 8.48 T) using a broad band variable temperature 10-mm probe. The spectrum of stannane was recorded at −50°C, and that of the stannonium ion at −80°C. The temperature was maintained at ±1.0°C by a nitrogen gas flow.

Results and discussion

Isotope effects on σ

(a) Stannane

The ^{119}Sn nmr spectrum of SnD_nH_{4-n} ($n \leq 4$) is shown in Fig. 1*a*; in Fig. 1*b*, the central region of the spectrum has been expanded and the chemical shifts of each isotopomer have been indicated. Replacement of each ^1H by ^2H in stannane results in an isotope shift of approximately −0.4 ppm/deuterium; however, as indicated in Table 1 the isotope shifts are not strictly additive. The deviations from additivity are 0.0:3.0:4.0:2.9:0.0, in excellent agreement with the predictions of Jameson and Osten (4, 7).

TABLE 1. ^{119}Sn chemical shifts (in ppm) and deviations from additivity for SnD_nH_{4-n} ($n \leq 4$)

	Experimental value	Perfect additivity	Difference	Ratio
SnH_4	0.0000	0.0000	0.0000	0.00
SnH_3D	−0.4266	−0.4026	0.0240	3.03
SnH_2D_2	−0.8369	−0.8052	0.0317	4.00
$SnHD_3$	−1.2306	−1.2077	0.0229	2.89
SnD_4	−1.6103	−1.6103	0.0000	0.00

Using the model of Jameson and Osten (4–6) one can estimate the partial derivative $(\partial\sigma^{Sn}/\partial\Delta r_{SnH})_e$. To obtain this derivative one must first obtain an estimate of $\Delta r_{Sn,H}$; see eq. [4]. For symmetrical AX_n molecules where isotopic substitution takes place at the terminal position (i.e., X) Jameson and Osten (4, 6) have suggested that to a first approximation one can associate $\langle \Delta r_{A,H}\rangle$ with $\langle \Delta r_{A,H}\rangle_{vib}$ where the latter term can be estimated using eq. [8].

$$[8]\quad \langle \Delta r\rangle_{vib} \simeq 22 \times 10^{-3}\, \mu^{-1/2}\, 10^{-D}$$

Here μ is the reduced mass in atomic units and D is given by eq. [9] where r_e

$$[9]\quad D \equiv (r_e - a_3)/b_3 - 3(r_e - a_2)/2b_2$$

is the equilibrium bond length and a_2, a_3, b_2, and b_3 are the Herschbach–Laurie parameters, which are tabulated in refs. 4 and 18. An accurate value of r_e in stannane is available from a recent microwave study of three different deuterated stannanes (19).

Using this procedure we find that $\langle \Delta r_{Sn-H}\rangle \simeq 17.65 \times 10^{-3}$ Å and substitution into eq. 4 gives $(\partial\sigma^{Sn}/\partial\Delta r_{SnH})_e = -92$ ppm/Å. This is to be compared with a value of −38 ppm/Å derived for $(\partial\sigma^C/\partial\Delta r_{CH})_e$ in methane (4, 8).

The magnitude of $(\partial\sigma^{Sn}/\partial\Delta r_{SnH})_e$ calculated here for stannane is smaller than the value one might intuitively expect. Previously, values of $(\partial\sigma^A/\partial\Delta r_{AH})_e$ for the first-row hydrides, AH_n, have been found to be proportional to $\langle a_0{}^3/r^3\rangle_A$ of the p orbitals (4, 5). Applying this argument to Group IV hydrides one estimates

$$[10]\quad (\partial\sigma^{Sn}/\partial\Delta r_{Sn-H})_e \simeq \frac{\langle a_0{}^3/r^3\rangle_{Sn}}{\langle a_0{}^3/r^3\rangle_C}(\partial\sigma^C/\partial\Delta r_{C-H})$$

Using values of $\langle a_0{}^3/r^3\rangle$ given by Barnes and Smith (20) one would predict the shielding derivative for Sn in SnH_4 to be approximately 9 times that for C in CH_4. Using the above arguments one predicts $^1\Delta Sn(^{2/1}H) = -1.6$ ppm/D in stannane, approximately four times the observed value. Thus the results here suggest that in the case of Sn factors other than $\langle a_0{}^3/r^3\rangle$ must play a significant role in accounting for variations in the electronic factor.

Recent theoretical calculations and shielding derivatives for the first- and second-row hydrides by Chesnut and Foley (21) indicate that the relative polarity of the heavy atom with respect to hydrogen plays an important role in determining the behaviour of the heavy atom shielding derivative. If the heavy atom is highly positive, e.g., NaH, the derivative is positive; however, if the central nucleus is highly negative, e.g., HCl, the derivative is large and negative (21). The derivative observed in this study for stannane appears to be consistent with the systematic change of derivatives reported in ref. 21.

Can. J. Chem. Downloaded from www.nrcresearchpress.com by 72.64.146.136 on 09/07/12
For personal use only.

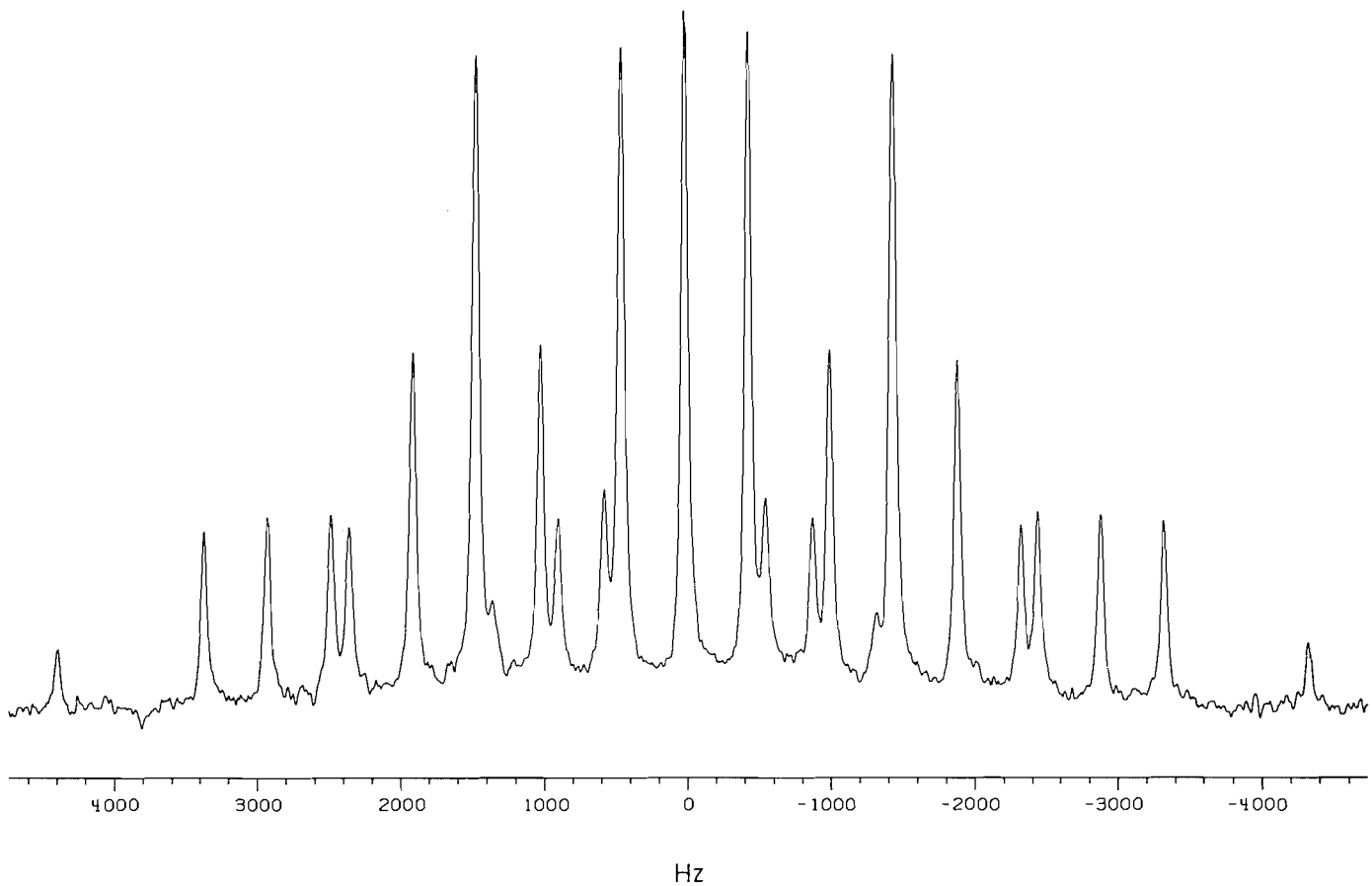

FIG. 2. Tin-119 nmr spectrum of the stannonium cation, $SnD_nH_{3-n}^+$ ($n \leq 3$) at 134.613 MHz and −80°C.

TABLE 2. Primary isotope effect on ^1J(Hz) in stannane

	$^1J(^{119}Sn,H)$	$^1J(^{119}Sn,D)$	$^1J(^{119}Sn,H)$*	$\Delta_p{}^1J(^{119}Sn,^{2/1}H)$
SnH_4	−1933.3 ± 0.1	—	—	—
SnH_3D	−1931.6 ± 0.1	−296.1 ± 0.1	−1928.9 ± 0.6	−2.7 ± 0.6
SnH_2D_2	−1929.9 ± 0.1	−295.8 ± 0.1	−1926.9 ± 0.6	−3.0 ± 0.6
$SnHD_3$	−1928.3 ± 0.2	−295.6 ± 0.1	−1925.6 ± 0.6	−2.7 ± 0.6
SnD_4	—	−295.2 ± 0.2	−1923.0 ± 1	—

*The value of $^1J(^{119}Sn,D)$ has been multiplied by the ratio, γ_H/γ_D, 6.51440.

Previously a $^{2/1}H$ induced isotope shift of −1.62 ppm had been reported for the tin chemical shift of Bu_3SnH (22).

(b) The stannonium cation

The ^{119}Sn nmr spectrum of $SnD_nH_{3-n}^+$ ($n \leq 3$) is much more symmetrical than that of stannane and is shown in Fig. 2. This indicates that the isotope shift is much smaller; $^1\Delta^{119}Sn(^{2/1}H)$ was found to be −0.05 ± 0.03 ppm/D, compared with −0.403 ± 0.001 ppm/D obtained for stannane. The ^{119}Sn nmr linewidths were 25 Hz, and not all of the lines of the spectrum could be resolved; thus the errors associated with this experiment were much larger than those for stannane. It is not possible to decide if the isotope shifts deviate from additivity because of the uncertainties in the experimental data.

It is possible to obtain a crude estimate of the shielding derivative for SnH_3^+; since the bond length is not known we must assume that it is about 1.7 Å. A value of −10 ppm/Å is obtained, which indicates the relative insensitivity of the ^{119}Sn nuclear shielding to Sn—H bond extension in the stannonium ion.

TABLE 3. Secondary isotope effect on ^1J(Hz) in stannane

Compounds	$\Delta_s{}^1J(^{119}Sn,H)[^1H]$	$\Delta_s{}^1J(^{119}Sn,D)[^2H]$
SnH_4–SnH_3D	−1.7 ± 0.1	—
SnH_3D–SnH_2D_2	−1.7 ± 0.1	−0.3 ± 0.1
SnH_2D_2–$SnHD_3$	−1.6 ± 0.2	−0.2 ± 0.1
$SnHD_3$–SnD_4	—	−0.4 ± 0.2

The small isotope shift and shielding derivative observed for the stannonium cation can be explained in terms of the charge argument mentioned above. Consideration of BH_3, BH_4^- and AlH_3, AlH_4^- indicates derivatives of +3.5, −27.0 and +84.2, +11.6 ppm/Å, respectively; thus in going from SnH_3^+ to SnH_4 one expects the derivative to decrease algebraically as observed.

Isotope effects on spin–spin coupling

(a) Stannane

Table 2 lists the observed coupling constants and values of

TABLE 4. Primary isotope effects on ^1J in the stannonium ion (Hz)

	$^1J(^{119}Sn,H)$	$^1J(^{119}Sn,D)$	$^1J(^{119}Sn,H)$*	$\Delta_p{}^1J(^{119}Sn,^{2/1}H)$
SnH_3^+	-2906.8 ± 5	—	—	
SnH_2D^+	-2907.2 ± 1	-444.5 ± 1	-2895.6 ± 6.5	-11.6 ± 7
$SnHD_2^+$	-2906.8 ± 1.5	-444.5 ± 1.5	-2895.6 ± 9.8	-11.2 ± 10
SnD_3^+	—	-443.6 ± 2	-2889.8 ± 24	—

*The value of $^1J(^{119}Sn,D)$ has been multiplied by the ratio γ_H/γ_D, 6.51440.

the primary isotope effect on spin–spin coupling in stannane. $^1J(^{119}SnH)$ for SnH_4 was found to be -1933.3 ± 0.1 Hz, in very good agreement with the value of -1933 Hz that has been reported (15). $\Delta_p{}^1J(^{119}Sn^{2/1}H)$ was found to be between -2.7 and -3.0 Hz, the average value being -2.8 ± 0.7 Hz, which is approximately 0.15% of the total coupling constant. Assuming that the first term of eq. [7] is much larger than the second, one can obtain an estimate of $(\partial J/\partial \Delta r_{SnH})_e$. The value we obtain is -640 Hz/Å, compared with $+190$ Hz/Å, the value calculated for $^1J(C,H)$ in methane using semiempirical molecular orbital calculations (9, 23). To compare these two values it is necessary to use the reduced coupling constant, K, since this eliminates the nuclear γ factor. The partial derivative of the reduced coupling constant in stannane is found to be 1.43×10^{21} kg m^{-2} s^{-2} A^{-2}/Å compared to a value of 3.5×10^{21} kg m^{-2} s^{-2} A^{-2}/Å in methane, an indication that the C–H coupling in methane is more sensitive to bond extension than is the Sn–H coupling in stannane.

The secondary isotope effect on $^1J(^{119}Sn,H)$ is -1.7 ± 0.2 Hz (see Table 3), about 0.09% of the total coupling constant. Unfortunately there is not enough information to reliably calculate the unknown derivative in eq. [14] of ref. 9. As expected, the secondary isotope effect on $^1J(^{119}Sn,D)$ is -0.3 ± 0.2 Hz, approximately 1/6.514 of the isotope effect on $^1J(^{119}Sn,H)$.

(b) The stannonium cation

The primary isotope effect on the spin–spin coupling for the stannonium ion is -11.7 ± 7 Hz (see Table 4). From this we obtain an estimate for the coupling derivative, $(\partial J/\partial \Delta r_{SnH})_e$, of -2680 Hz/Å, significantly larger than the value obtained for stannane, an indication that the coupling constant is more sensitive to bond extension. The secondary isotope is smaller than the experimental error and so an estimate of its magnitude would be meaningless.

Since the value of $\Delta_p{}^1J(^{31}P^{2/1}H)$ is positive in phosphine (13), a positive value of $\Delta_p{}^1J(^{119}Sn^{2/1}H)$ is anticipated for the isoelectronic SnH_3^- ion.

Acknowledgements

We thank the Natural Sciences and Engineering Research Council of Canada for financial support in the form of a summer undergraduate research scholarship (K.L.L.) and for operating and equipment grants (R.E.W.). Also, we thank Professor C. J. Jameson for a preprint of ref. 4, and a referee for several helpful comments.

1. H. BATIZ-HERNANDEZ and R. A. BERNHEIM. Prog. Nucl. Magn. Reson. Spectrosc. **3**, 63 (1967).
2. P. E. HANSEN. Annu. Rep. NMR Spectrosc. **15**, 105 (1983).
3. D. A. FORSYTH. *In* Isotopes in organic chemistry. Vol. 6. *Edited by* E. Buncel and C. C. Lee. Elsevier, Amsterdam. 1984. p. 1.
4. C. J. JAMESON and H. J. OSTEN. Annu. Rep. NMR Spectrosc. **17**, 1 (1986).
5. C. J. JAMESON and H. J. OSTEN. J. Am. Chem. Soc. **107**, 4158 (1985).
6. C. J. JAMESON and H. J. OSTEN. J. Chem. Phys. **81**, 4300 (1984). (Erratum: J. Chem. Phys. **83**, 915 (1985).)
7. C. J. JAMESON and H. J. OSTEN. J. Chem. Phys. **81**, 4293 (1984).
8. H. J. OSTEN and C. J. JAMESON. J. Chem. Phys. **81**, 4288 (1984).
9. C. J. JAMESON and H. J. OSTEN. J. Am. Chem. Soc. **108**, 2497 (1986).
10. B. WRACKMEYER. Annu. Rep. NMR Spectrosc. **16**, 73 (1985).
11. M. ALEI and W. E. WAGEMAN. J. Chem. Phys. **68**, 783 (1978).
12. R. E. WASYLISHEN and J. O. FRIEDRICH. J. Chem. Phys. **80**, 585 (1984).
13. A. K. JAMESON and C. J. JAMESON. J. Magn. Reson. **32**, 455 (1978).
14. H. J. JAKOBSEN, A. J. ZUZULIN, P. D. ELLIS, and J. D. ODOM. J. Magn. Reson. **38**, 219 (1980).
15. T. BIRCHALL and V. MANIVANNAN. J. Chem. Soc. Dalton Trans. 2671 (1985).
16. A. D. NORMAN, J. R. WEBSTER, and W. L. JOLLY. Inorg. Synth. **11**, 170 (1968).
17. J. R. WEBSTER and W. L. JOLLY. Inorg. Chem. **10**, 877 (1971).
18. D. R. HERSCHBACH and V. W. LAURIE. J. Chem. Phys. **35**, 458 (1961).
19. K. OHNO, H. MATSUURA, Y. ENDO, and E. HIROTA. J. Mol. Spectrosc. **118**, 1 (1986).
20. R. G. BARNES and W. V. SMITH. Phys. Rev. **93**, 95 (1954).
21. (*a*) D. B. CHESNUT. Chem. Phys. **110**, 415 (1986); (*b*) D. B. CHESNUT and C. K. FOLEY. J. Chem. Phys. **85**, 2814 (1986).
22. J. P. QUINTARD, M. D. CASTAING, G. DUMARTIN, B. BARBE, and M. PETRAUD. J. Organomet. Chem. **234**, 27 (1982).
23. N. M. SERGEYEV and U. N. SOLKAN. J. Chem. Soc. Chem. Commun. 12 (1975).

Can. J. Chem. Downloaded from www.nrcresearchpress.com by 72.64.146.136 on 09/07/12
For personal use only.

Enthalpies and heat capacities of solution for *tert*-butyl chloride and bromide in alcohols. Application of SPT, SRMR, and MS

R. M. C. GONÇALVES AND A. M. N. SIMÕES

CECUL, Instituto Bento da Rocha Cabral, Cd. Bento da Rocha Cabral, 14, 1200 Lisboa, Portugal

Received October 30, 1986

R. M. C. GONÇALVES and A. M. N. SIMÕES. Can. J. Chem. **65**, 1474 (1987).

Enthalpies and heat capacities of solution at infinite dilution for *tert*-butyl chloride and bromide in several alcohols are reported at 30, 35, and 40°C.

The Scaled Particle Theory (SPT), the Sinanoglu, Reiss, and Moura Ramos (SRMR) and the Model Solute (MS) methods were applied to the enthalpies of solvation. Significant differences in the results calculated from these theories were analysed and data discussed in terms of solute–solvent–solvent interactions.

R. M. C. GONÇALVES et A. M. N. SIMÕES. Can. J. Chem. **65**, 1474 (1987).

Les valeurs des enthalpies et capacités calorifiques de solution sont présentées pour les chlorure et bromure de tertiobutyle dans plusieurs alcools étudiés à 30, 35 et 40°C.

On a appliqué la "Scaled Particle Theory" (SPT) et les méthodes "Sinanoglu, Reiss et Moura Ramos" (SRMR) et "Model Solute" (MS). Les désaccords entre les valeurs obtenues par les différentes approches sont analysés dans cette article. On discute les resultáts en tenant compte des interactions solvant–solvant–soluté.

Can. J. Chem. Downloaded from www.nrcresearchpress.com by 72.64.146.136 on 09/07/12
For personal use only.

Introduction

Information about solute–solvent–solvent interactions occurring in the initial state of *tert*-butyl halides (*t*-BuX) solvolysis was first achieved by Arnett *et al.* (1) who reported thermodynamic quantities of solution in water–ethanol mixtures for *t*-BuCl.

Recently, Abraham (2) and Gonçalves and Simões (3) reported enthalpies of solution for *tert*-butyl chloride and bromide in several alcohols at 25°C. However, while kinetic studies of these reactions have been made at other temperatures, corresponding values for the enthalpies of solution do not appear to be available.

The first objective of this paper is to extend this study to other temperatures. Enthalpies of solution at infinite dilution, $\Delta_s H^\infty$, are now given for those substrats in *n*-alcohols (methanol to pentanol) and isopropanol and *tert*-butanol, at 30, 35, and 40°C. Together with previously reported values (3) heat capacities of solution were estimated, $\Delta_s C_p^\infty$.

The effect of hydroxylic solvents on the solvolysis of *t*-BuCl has been interpreted earlier, based on determinations of Gibbs' energy (4). The Scaled Particle Theory (SPT), the Sinanoglu, Reiss, and Moura Ramos (SRMR) and the Model Solute (MS) methods were used to calculate the terms due to the formation of cavities into the solvent and to decompose the transfer Gibbs' energy in a non-electrostatic and an electrostatic term.

Some large differences in the results from SPT and SRMR were noted although not leading to contradictory interpretations. A parallel development for the enthalpy has not yet been made.

The second purpose of this paper is to examine the results of the application of SPT, SRMR, and MS methods to the enthalpies of solvation $\Delta_{solv} H^\infty$, of *t*-BuCl and *t*-BuBr in water and in straight-chain and branched mono-alcohols.

Experimental

All enthalpies of solution were measured in a calorimeter previously described (3). The calorimetric technique, tests, calibration, and calculations were performed as earlier (3). Heats of empty ampoule breaking were negligible and corrections for condensation of solute vapour were performed in all cases. $\Delta_s H^\infty$ are the averages of the results from at least five measurements.

TABLE 1. $\Delta_s H^\infty$ and $\Delta_{solv} H^\infty$ for *t*-BuCl in alcohols/kJ mol^{-1}

Solvent	T/°C	$\Delta_s H^\infty$	Reference	$-\Delta_{solv} H^\infty$
H_2O	25	1.05[a]	1	27.93
MeOH	25	1.56 ± 0.03	3	27.42
		1.51	2	27.47
	30	2.34 ± 0.06		
	35	2.65 ± 0.06		
	40	3.04 ± 0.07		
EtOH	25	1.50 ± 0.03	3	27.48
		1.42	2	27.56
	30	1.93 ± 0.06		
	35	2.42 ± 0.05		
	40	2.70 ± 0.07		
1-PrOH	25	1.62 ± 0.03	3	27.36
		1.77	2	27.21
	30	2.49 ± 0.06		
	35	2.86 ± 0.05		
	40	3.25 ± 0.04		
1-BuOH	25	2.10 ± 0.03	3	26.88
		2.22	2	26.76
	30	2.68 ± 0.06		
	35	3.01 ± 0.06		
	40	3.38 ± 0.03		
1-PeOH	25	2.56 ± 0.04	3	26.42
	30	2.81 ± 0.04		
	35	3.14 ± 0.08		
	40	3.52 ± 0.03		
i-PrOH	25	3.57 ± 0.02	3	25.41
		3.50	2	25.48
	30	4.32 ± 0.05		
	35	5.11 ± 0.07		
	40	5.34 ± 0.07		
t-BuOH	27	6.32 ± 0.08	3	22.65
	30	6.56 ± 0.07		
	35	7.17 ± 0.06		
	40	7.25 ± 0.05		

[a]Extrapolated value.

Printed in Canada / Imprimé au Canada

Can. J. Chem. Downloaded from www.nrcresearchpress.com by 72.64.146.136 on 09/07/12
For personal use only.

TABLE 2. $\Delta_s H^\infty$ and $\Delta_{solv} H^\infty$ for *t*-BuBr in alcohols/kJ mol^{-1}

Solvent	T/°C	$\Delta_s H^\infty$	Reference	$-\Delta_{solv} H^\infty$
MeOH	25	2.20±0.03	3	29.61
		1.99	2	29.82
	30	2.43±0.03		
EtOH	25	1.75±0.03	3	30.06
		1.68	2	30.13
	30	2.07±0.03		
	35	2.26±0.04		
	40	2.69±0.08		
1-PrOH	25	2.00±0.04	3	29.81
		1.89	2	29.92
	30	2.39±0.03		
	35	2.79±0.04		
	40	2.97±0.02		
1-BuOH	25	2.37±0.05	3	29.44
	30	2.75±0.08		
	35	3.00±0.08		
	40	3.24±0.04		
1-PeOH	25	2.62±0.01	3	29.18
	30	3.02±0.05		
	35	3.28±0.02		
	40	3.59±0.07		
i-PrOH	25	4.12±0.07	3	27.69
	30	4.47±0.04		
	35	4.77±0.08		
	40	5.13±0.08		
t-BuOH	27	7.26±0.08	3	24.55
	30	7.25±0.08		
	35	7.29±0.09		
	40	7.40±0.06		

TABLE 3. Selected properties and molecular parameters of *t*-BuX at 25°C

Solute	$\Delta_{vap} H$/kJ mol^{-1}	Ref.	V_2/cm^3 mol^{-1}	Ref.	$\sigma_2{}^a$/Å
t-BuCl	28.98±0.06	5	111	6	5.69
t-BuBr	31.81±0.12	5	113	6	5.72

[a]Calculated from the Stearn and Eyring expression (7): $\sigma = 2\sqrt[3]{V/8N}$.

Numerical results

The solution enthalpies of *t*-BuCl and *t*-BuBr in several straight-chain and branched mono-alcohols, at 30, 35, and 40°C, are shown in Tables 1 and 2, except for the system *t*-BuBr in methanol at the higher temperatures, since the following solvolytic reaction path was found to significantly influence the solution process. Previous results for the same systems at 25°C from two different sources of data (2, 3), both obtained by a calorimetric technique, were also included as well as the solution enthalpy of *t*-BuCl in water, extrapolated from Arnett's values (1). $\Delta_s H^\infty$ are given along with twice the standard deviation of the mean. The solvation enthalpies at 25°C are also listed in Tables 1 and 2 and were obtained by subtracting the enthalpies of vaporization (Table 3) from the solution enthalpies.

The values $\Delta_s C_p^\infty$ in Table 4 were estimated as the slope of the linear regression analysis performed on the ($\Delta_s H^\infty$, T) pairs of points. $\sigma(\Delta_s C_p^\infty)$ is the standard deviation obtained directly from the least-squares method. Although it should be possible to fit a polynomial of higher order to our results, the coefficients would have questionable significance.

Application of SPT, SRMR, and MS

Before we discuss the application of SPT, SRMR, and MS methods to the solvation enthalpies of *t*-BuX in water and alcohols, we would like to emphasize that this study will be restricted to the temperature of 25°C due to the lack of fundamental properties and molecular values to perform this kind of analysis at other temperatures.

Application of SPT

According to the SPT (8), the enthalpy of creating a spherical cavity in a hard-sphere fluid is

$$[1]\quad H_c = y\alpha RT^2(1-y)^{-3}[(1-y)^2 + 3(1-y)r + 3(1+2y)r^2] + y(Rp/\rho\kappa)r^3 \qquad (r = \sigma_2/\sigma_1;\ \rho = N/V_1;\ y = \pi\rho\sigma_1^3/6)$$

where σ_1 and σ_2 are the diameter of the solvent and solute, respectively, and ρ is the number density of the solvent. For pressures around 1 atm the contribution of the pressure term was found to be negligible (8). Tables 3 and 5 give the values of the several parameters used in the calculations of H_c. The cavity formation term together with the interaction term, H_i, obtained from eq. [2],

$$[2]\quad \Delta_{solv} H^\infty = H_c + H_i + RT(\alpha T - 1)$$

where α is the coefficient of thermal expansion of the solvent, are listed in Table 6. The enthalpies of transfer to methanol, ∂H_i, are summarized in Table 7.

Application of SRMR

According to the SRMR method (15),

$$[3]\quad H_c/\text{J mol}^{-1} = 40.840KV_2^{2/3}\gamma\left[1 - \left(\frac{T}{\gamma}\frac{\partial\gamma}{\partial T} + \frac{2T}{3}\alpha\right)\right]$$

where γ is the surface tension of the solvent (dyne cm^{-1}) and K is a correction term due to the microscopic curvature of the cavity surface.

K may be calculated through eq. [4] proposed by Halicioglu and Sinanoglu (16):

$$[4]\quad K = 1 + (V_1/V_2)^{2/3}[K(1) - 1]$$

TABLE 4. $\Delta_s C_p^\infty \pm \sigma(\Delta_s C_p^\infty)$ for *t*-BuX in alcohols/J mol^{-1} K^{-1} $T\epsilon$|25, 40|°C

	Solvent						
Solute	MeOH	EtOH	1-PrOH	1-BuOH	1-PeOH	*i*-PrOH	*t*-BuOH
t-BuCl	95±15	82±6	105±17	83±8	64±4	122±18	76±16
t-BuBr	(46)	60±6	66±7	57±5	63±4	67±2	109±4

Can. J. Chem. Downloaded from www.nrcresearchpress.com by 72.64.146.136 on 09/07/12
For personal use only.

TABLE 5. Selected properties and molecular parameters of water and alcohols at 25°C

Solvent	σ_1/Å	Ref.	$10^3\alpha/K^{-1}$	Ref.	V_1/cm^3 mol^{-1}	Ref.	γ	$\Delta_{vap}H$/kJ mol^{-1}	Ref.	$K(1)$	γ/dyne cm^{-1}	Ref.	$-\partial\gamma/\partial T$[a]	Ref.
Water	2.77	2,8	0.257	8	18.07	8	0.371	43.9897	11	1.366	71.97	2	0.155	11
MeOH	3.71	2,8	1.195	9	40.74	9	0.395	37.28 ± 0.08	12	1.811	22.20	2	0.086	11
EtOH	4.36	2	1.093	9	58.69	9	0.445	42.30 ± 0.08	12	1.627	21.85	2	0.084	11
1-PrOH	4.85	2	0.995	9	75.17	9	0.479	47.32 ± 0.08	12	1.518	23.30	2	0.081	11
1-BuOH	5.32	2	0.932	9	91.99	9	0.516	52.30 ± 0.08	12	1.424	24.16	2	0.082	11
1-PeOH	5.77[b]	—	0.893	9	108.72	9	0.557	56.94 ± 0.16	12	1.304	25.16[a]	11	0.088	11
i-PrOH	4.87	2	1.064	9	76.96	9	0.473	45.23 ± 0.12	12	1.847	21.24	2	0.055	11
t-BuOH	5.33	2	1.335	10	97.76[c]	—	0.504	46.61 ± 0.08	12	1.217	20.02[d]	11	0.102	11

[a]Interpolated from γ values at 20 and 30°C, assuming linear behaviour.
[b]Extrapolated from σ_1 of normal alcohols.
[c]Extrapolated from values in refs. 13 and 14.
[d]T = 26°C.

TABLE 6. H_c and H_i of *t*-BuX in water and alcohols at 25°C/kJ mol^{-1}

		H_c		$-H_i$	
Solvent	Solute	SPT	SRMR	SPT	SRMR
Water	*t*-BuCl	7.499	119.80	33.14	114.44
MeOH	*t*-BuCl	24.97	56.86	50.80	82.68
	t-BuBr	25.23	57.34	53.24	85.36
EtOH	*t*-BuCl	25.58	56.06	51.39	81.87
	t-BuBr	25.86	56.52	54.25	84.91
1-PrOH	*t*-BuCl	26.17	56.55	51.79	82.17
	t-BuBr	26.46	57.04	54.53	85.11
1-BuOH	*t*-BuCl	27.50	57.20	52.59	82.29
	t-BuBr	27.80	57.71	55.45	85.36
1-PeOH	*t*-BuCl	29.67	57.55	54.27	82.15
	t-BuBr	30.00	57.88	57.36	85.24
i-PrOH	*t*-BuCl	25.71	52.01	49.43	75.73
	t-BuBr	25.99	52.40	51.99	78.40
t-BuOH	*t*-BuCl	35.22	50.86	56.38	72.02
	t-BuBr	35.61	51.38	58.67	77.42

V_1 and V_2 are the molar volumes of the solvent and the solute, respectively. $K = K(1)$ when the cavity has the solvent molecule dimensions.

Following Eyring (17), the enthalpy associated with the formation of such a cavity is given by the vaporization enthalpy of the solvent. $\Delta_{vap}H$ and $K(1)$ as well as γ and $\partial\gamma/\partial T$ for the different alcohols and water are shown in Table 5. H_c and the corresponding H_i values, obtained from eq. [2], are given in Table 6. For transfer to methanol, values of ∂H_i were calculated (Table 7).

Application of MS

Another approach to the study of solvent effects involves the decomposition of the transfer solvation enthalpy from one solvent to another in two terms, one concerned with the electrostatic contribution ∂H_e, and the other with the non-electrostatic contribution, ∂H_{ne} (6):

$$[5] \quad \partial\Delta_{solv}H^\infty = \partial H_e + \partial H_{ne}$$

This method makes use of reference molecules in order to evaluate ∂H_{ne}. ∂H_{ne} is assumed to be equal to $\partial\Delta_{solv}H^\infty$ of a model solute, rare gases or alkanes of identical molar volume. The hydrocarbons 2-methylpropane (2-mp) and 2,2-dimethylpropane (2,2-dmp) seem to be suitable model solutes for *tert*-butyl halides. Calorimetric enthalpy values for these two alkanes in water were reported by Dec and Gill (18). Unfortunately, solvation enthalpies in other solvents are only available from low precision gas-solubility measurements (19). The enthalpies of solvation of 2-mp and 2,2-dmp are given in Table 8. Table 7 shows ∂H_c values for *t*-BuCl, using 2-mp as model solute.

Discussion

The enthalpy term associated with the cavity formation in the solvents is a function of the cohesive properties of the solvents and the molar volumes of the solutes. The cohesive energy of the solvent may be characterized by its internal pressure, cohesive energy density, or surface tension. The two first cases lead to the cavity term to be proportional to the cavity volume, as it happens in the Scaled Particle Theory (8), while, in the last

TABLE 7. ∂H_i and ∂H_e of t-BuX in water and alcohols at 25°C/kJ mol^{-1}

Parameter	Solute	Value in solvent							
		Water	MeOH	EtOH	1-PrOH	1-BuOH	1-PeOH	i-PrOH	t-BuOH
∂H_i (SPT)	t-BuCl	17.7	0	−0.59	−0.99	−1.79	−3.56	+1.37	−5.58
	t-BuBr	—	0	−1.01	−1.29	−2.21	−4.12	+1.25	−5.43
∂H_i (SRMR)	t-BuCl	−62.8	0	+0.81	+0.51	+0.39	+0.53	+6.95	+10.66
	t-BuBr	—	0	+0.45	+0.25	0.00	+0.12	+6.96	+7.94
∂H_e (MS)	t-BuCl	+5.77	0	−0.19	—	—	—	+0.46	—
	t-BuBr	—	0	−0.58	—	—	—	+0.37	—

TABLE 8. $\Delta_{solv}H^{\infty}$ of alkanes in water and alcohols at 25°C/kJ mol^{-1}

Solute	$\Delta_{solv}H^{\infty}$ in solvent			
	Water[a]	MeOH[b]	EtOH[b]	i-PrOH[b]
2-mp	−24.19	−17.91	−17.78	−16.36
2,2-dmp	−24.15[c]	—	—	−20.50

[a]Reference 18.
[b]Reference 19.
[c]Value correctly reported in ref. 18*b*.

case, H_i is proportional to the cavity surface, as stated by the Sinanoglu, Reiss, and Moura Ramos method (15).

The comparison of the two sets of H_c and H_i results in Table 6 and of ∂H_i in Table 7 show that values calculated from SPT and SRMR differ quite considerably. In spite of the numerical discrepancies, the sign and the order of magnitude of the transfer Gibbs' functions calculated for t-BuCl in some hydroxylic solvents, using both SPT and SRMR models, led to a common interpretation of solvent effects (2). Unfortunately, this is not true for our ∂H_c and ∂H_i values. The theories may even lead to opposite interpretations and this is particularly relevant in water. As Desrosiers and Morel (20) pointed out recently, SPT and SRMR should not be expected to give the same H_c values, since SPT is based on statistical mechanics and uses molecular parameters, while SRMR is a macroscopic theory, relating the bulk surface tension to the energy of formation of a molecular sized cavity. In their opinion, SPT terms are probably the best we can get at present and SRMR can just be used to get gross approximations of the cavity terms. It is true that SPT calculations are very much dependent on the uncertainty of the molecular diameters. However, if a coherent choise of σ_1 and σ_2 is made, the comparison of thermodynamic data relative to the formation of cavities and, consequently, to the solute–solvent–solvent interactions is still valid. It is also true that according to the hypothesis of the SPT (8), the theory could not be used, in principle, for polar liquids. Tests of the validity of SPT, even when applied to solvents involving strong interactions such as alcohols and water, however, show that, provided the studied molecule is of small size and as hard sphere as possible, SPT can be used to calculate H_c whatever the solvent (20). We wish to emphasize that the solute molecules used in this work satisfy these conditions.

From now on we shall only analyse values calculated through SPT. Data in Table 6 show that there are positive and large solute–solvent–solvent interactions. As expected, a parallel behaviour is observed for both solutes in several media. Two exothermic contributions to H_i should be considered: one, due to the interaction of hydrophilic centers of the solute with solvent molecules and the other, due to the enhancement of hydrogen bonding of water or alcohol near the non–polar groups of the substrats. However, less hydrogen bond disruption and subsequent less strong solvent reorganization should take place in alcohols rather than in water, attending to the structural differences of these solvents. H_i and ∂H_i for water compared with values for other solvents are in accordance with this explanation (Tables 6 and 7).

The variation in the solvation of a certain compound in different solvents is reflected directly by the enthalpies of transfer from a chosen reference solvent.

The results in Table 7, using MeOH as reference solvent, show that, for normal alcohols, the larger the solvent molecule becomes the more exothermic is the solute–solvent–solvent interaction. A solute molecule dissolved in an alkanol with a short alkyl chain will probably disturb easily the hydrogen bonding in the solvent. On the other hand, in alkanols with large molecules a solute which is approximately of the same volume may fit into the solvent structure without substantial disruption of hydrogen bonding. ∂H_i for branched alcohols do not follow the same tendency (Table 7). At the moment we have no satisfactory explanation for this. ∂H_e and ∂H_i values in Table 7 differ considerably, which is not surprising bearing in mind that ∂H_i includes not only electrostatic effects covered by ∂H_e but also dispersive interactions (2). The same kind of variation seems to be observed for ∂H_i values calculated through SPT and ∂H_e from MS in alcohols. The few data available in the literature do not allow further interpretations.

Although this study has only been performed at 25°C, we don't see any reason to consider a different explanation at other temperatures. $\Delta_s C_p^{\infty}$ is always positive and the order of magnitude seems to be reasonable for this kind of compounds. As we could expect, based on the charge density of both substrate and consequent solute–solvent interactions, the selectivity towards the solvent is higher for t-BuCl, which is mainly revealed on the higher $\Delta_s C_p^{\infty}$ values for this compound.

In conclusion, from the application of SPT and SRMR to the solvation enthalpies of t-BuX (X = Cl, Br) in water and alcohols, we found that, though SPT may lead to some uncertainty in the results, if a coherent choise of the molecular diameters of the involved species is made, this theory seems to be a useful approach to compare the thermodynamic data relative to the formation of cavities and, consequently, to the solute–solvent–solvent interactions.

These results are consistent with similar conclusions based on recent applications of SPT to polar systems (21, 22). It should

Can. J. Chem. Downloaded from www.nrcresearchpress.com by 72.64.146.136 on 09/07/12
For personal use only.

be of main interest to obtain more calorimetric data for model hydrocarbons, specially gaseous ones, in a larger variety of solvents and at different temperatures (18, 23).

Acknowledgements

We thank one of the referees for the useful comments. We are grateful to the Instituto Nacional de Investigação Científica for financial support.

1. E. M. ARNETT, W. G. BENTRUDE, J. J. BURKE, and P. McC. DUGGLEBY. J. Am. Chem. Soc. **87**, 1541 (1965).
2. M. H. ABRAHAM. J. Chem. Soc. Perkin Trans. 2, 1028 (1977).
3. R. M. C. GONÇALVES and A. M. N. SIMÕES. J. Sol. Chem. **16**, 39 (1987).
4. M. H. ABRAHAM, A. NASEHZADEH, J. J. MOURA RAMOS, and J. REISS. J. Chem. Soc. Perkin Trans. 2, 854 (1980).
5. I. WADSÖ. Acta Chem. Scand. **22**, 2438 (1968).
6. M. H. ABRAHAM and G. F. JOHNSTON. J. Chem. Soc. (A), 1610 (1971).
7. A. E. STEARN and H. EYRING. J. Chem. Phys. **5**, 113 (1937).
8. R. A. PIEROTTI. Chem. Rev. **76**, 717 (1976).
9. J. L. HALES and J. H. ELLENDER. J. Chem. Thermodyn. **8**, 1177 (1976).
10. G. ALLEN, G. GEE, and G. J. WILSON. Polymer, **1**, 456 (1960).
11. J. A. RIDDICK and W. B. BURGER. Techniques of chemistry — organic solvents. John Wiley. 1970.
12. I. WADSÖ. Acta Chem. Scand. **20**, 544 (1966).
13. G. J. JANZ and R. P. T. TOMKINS. Nonaqueous electrolytes handbook. vol. 1. Academic Press, New York. 1972.
14. W. DANNHAUSER and L. W. BAHE. J. Chem. Phys. **40**, 3058 (1964).
15. J. J. MOURA RAMOS, M. LEMMERS, R. OTTINGER, M. L. STIEN, and J. REISSE. J. Chem. Res. (S), 56; (M), 658 (1977).
16. T. HALICIOGLU and O. SINANOGLU. An. New York Acad. Sci. **158**, 308 (1969).
17. H. EYRING. J. Chem. Phys. **4**, 283 (1936).
18. S. F. DEC and S. J. GILL. J. Sol. Chem. (*a*) **3**, 27 (1984); (*b*) **14**, 827 (1985).
19. M. H. ABRAHAM. J. Am. Chem. Soc. **104**, 2085 (1968).
20. N. M. DESROSIERS and J.-P. MOREL. Can. J. Chem. **59**, 1 (1981).
21. C. TREINER. Can. J. Chem. **59**, 2518 (1981).
22. N. H. SAGERT and D. W. P. LAU. Can. J. Chem. **62**, 81 (1984).
23. P. P. S. SALUJA, T. M. YOUNG, R. F. RODEWALD, F. H. FUCHS, D. KOHLI, and R. FUCHS. J. Am. Chem. Soc. **99**, 2949 (1977).

Can. J. Chem. Downloaded from www.nrcresearchpress.com by 72.64.146.136 on 09/07/12
For personal use only.

Interactions du Cu(II), du Hg(II) et du Pt(II) avec les formes monomères et dimères de la thymine, de la thymidine et de l'acide orotique

RAOUL M'BOUNGOU, MICHELLE PETIT-RAMEL ET GERMAINE THOMAS-DAVID
Laboratoire de chimie analytique II, Université Claude Bernard, Lyon I, 43 boulevard du 11 Novembre 1918, 69622 Villeurbanne CEDEX, France

ET

GÉRARD PERICHET ET BERNARD POUYET
Laboratoire de photochimie, Université Claude Bernard, Lyon I, 43 boulevard du 11 Novembre 1918, 69622 Villeurbanne CEDEX, France

Reçu le 24 septembre 1986

RAOUL M'BOUNGOU, MICHELLE PETIT-RAMEL, GERMAINE THOMAS-DAVID, GÉRARD PERICHET et BERNARD POUYET. Can. J. Chem. **65**, 1479 (1987).

Les constantes de protonation du monomère (TM) et du dimère (TD) de la thymine, du monomère (OM) et du dimère (OD) de l'acide orotique et de la thymidine (TY) ont été calculées à 25 et à 37°C et à force ionique $\mu = 0,1(NaNO_3)$. Dans les mêmes conditions, les constantes de stabilité des complexes formés avec le Cu(II), le Hg(II) et le Pt(II) ont été déterminées par protométrie. Les résultats sont discutés en termes de sites de liaison : azote N3 pour la thymine monomère et dimère et la thymidine; anion carboxylate en C6 et azote adjacent N1 pour l'acide orotique monomère et dimère.

RAOUL M'BOUNGOU, MICHELLE PETIT-RAMEL, GERMAINE THOMAS-DAVID, GÉRARD PERICHET, and BERNARD POUYET. Can. J. Chem. **65**, 1479 (1987).

The protonation constants of monomeric (TM) and dimeric (TD) forms of thymine and monomeric (OM) and dimeric (OD) forms of orotic acid and thymidine (TY) have been calculated at 25 and 37°C and at ionic strength $\mu = 0.1(NaNO_3)$. Under the same conditions the stability constants of their Cu(II), Hg(II), and Pt(II) complexes have been determined by protometric methods. The results have been discussed and a comparison has been established in terms of binding sites: nitrogen N3 for monomeric and dimeric forms of thymine and thymidine; carboxylate anion at C6 and adjacent ring nitrogen N1 for monomeric and dimeric forms of orotic acid.

Introduction

Sous l'action d'une irradiation monochromatique, la thymine (une des quatre bases azotées de l'ADN) peut se dimériser (fig. 1*a*) et donner lieu à une réaction autodéfensive de l'organisme qui utilise alors des enzymes de photoréactivation pour monomériser le dimère de la thymine. Des articles précédents (1, 2) ont montré, à titre d'exemple, une analogie de mécanisme réactionnel lorsque l'enzyme est remplacé par les ions Hg^{2+}.

Dans ce mémoire, nous étendrons cette première approche à l'acide orotique et à son espèce dimérisée (fig. 1*b*), qui, transformée par voie métabolique en nucléotide, entre dans la biosynthèse des bases pyrimidiques, classe à laquelle appartient la thymine (3). De plus, la substitution des ions Hg^{2+} par les ions Cu^{2+} et par les ions Pt^{2+}, issus du *cis*-platine, conduit à des complexes qui présentent non seulement les caractéristiques souhaitées en photochimie, mais sont susceptibles de plusieurs applications dans le domaine des traitements antitumoraux (4).

Outre l'intérêt évident de ces complexes dans de nombreux processus physiologiques, le choix de ces deux dérivés de la pyrimidine pose, lors de la formation des complexes métalliques monomères et dimères, un problème au niveau de la liaison métal–coordinat, notamment en ce qui concerne l'atome d'azote donneur d'électrons.

Dans la même ligne, nous aborderons l'étude des interactions du Cu(II) et du Hg(II) avec la thymidine, nucléoside correspondant à la thymine (fig. 1*c*), qui a la propriété de s'incorporer à l'ADN sans subir de modification (3).

La démarche suivie pour la mise en évidence des espèces protonées, puis des espèces complexes $M_pH_qA_r$, ainsi que le calcul de leurs constantes de stabilité β_{pqr} découle directement du protocole développé dans un précédent mémoire (1) : (*i*) examen des courbes de formation $\bar{n} = f(pL)$ où $\bar{n}$ représente le nombre moyen de ligands L déprotonés; (*ii*) affinement

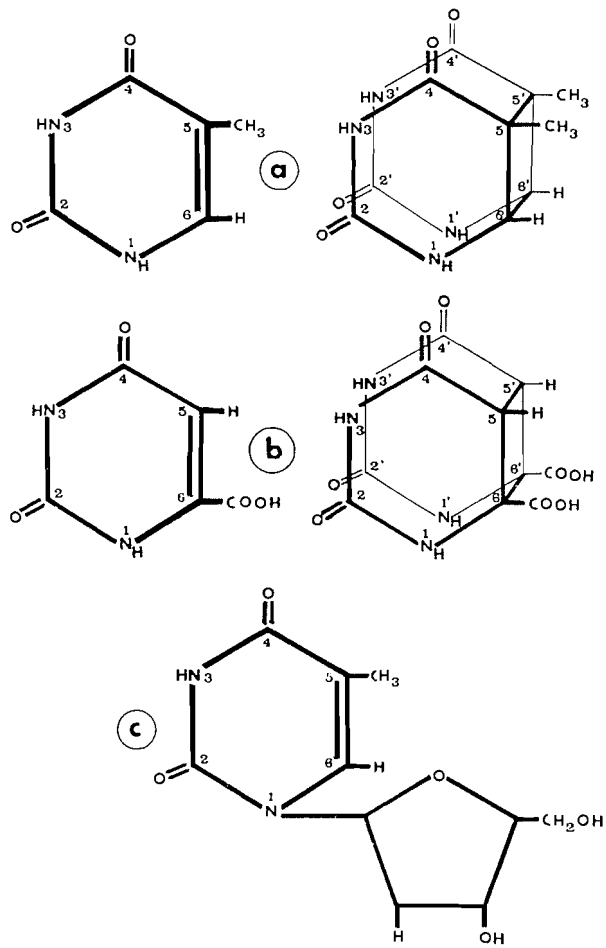

FIG. 1. (*a*) Thymine monomère et dimère. (*b*) Acide orotique monomère et dimère. (*c*) Thymidine.

Printed in Canada / Imprimé au Canada

Can. J. Chem. Downloaded from www.nrcresearchpress.com by 118.98.75.50 on 09/07/12
For personal use only.

TABLEAU 1. Constantes de formation des complexes de la thymine (monomère et dimère)

Espèce	*pqr*	log β_{pqr}	Domaine de formation	Référence 1	8	9	23	31	34
	t = 25°C	μ = 0,1				t = 45°C			t = 20°C
H(TM)	011	9,76(0,001)		9,8 (0,01)		9,1(0,1)	9,9	9,8	9,65(0,01)
$[Cu(TM)]^+$	101				6,08	5,8(0,1)			
$[Cu_2(TM)_2]^{2+}$	202	14,59	pH 5–8						
$[Cu_2(TM)_4]$	204	25,69	pH 5,5–10						
$[Hg(TM)]^+$	101		pH 2–5	10,65(0,02)					
$[Hg(TM)_2]$	102		pH 2–11	20,70(0,03)					
$[Hg\ H_{-1}]^+$	1-10		pH 2–4	−3,10(0,02)					
	t = 37°C	μ = 0,1							
H(TM)	011	9,8 (0,02)*							
cis-$[Pt(TM)(NH_3)_2]^+$	101	5,52(0,001)	pH 6–10						
cis-$[Pt(TM)_2(NH_3)_2]$	102	9,71(0,004)	pH 7–10						
	t = 25°C	μ = 0,1							
H(TD)	011	9,86(0,07)							
H_2(TD)	021	19,9 (0,2)							
[Cu(TD)]	101	8,8 (0,2)	pH 6,5–10,5						
$[CuH(TD)]^+$	111	16,08(0,2)	pH 6,5–10,5						
[Hg(TD)]	101		pH 3,5–8,5	13,55(0,02)					
$[Hg\ H_{-1}(TD)]^-$	1-11		pH 5–11	6,73(0,03)					
$[Hg\ H_{-2}(TD)]^{2-}$	1-21		pH 7–11	−1,69(0,04)					
$[Hg\ H_{-1}]^+$	1-10		pH 3,5–6,5	−3,10(0,03)					
	t = 37°C	μ = 0,1							
H(TD)	011	9,2 (0,3)							
H_2(TD)	021	18,2 (0,3)							

*Écarts-types correspondants aux constantes.

par minimisation d'écart-type sur les points expérimentaux et calculés des transformées des courbes de titration, $\bar{q} = f(\text{pH})$, rendues linéaires, où $\bar{q}$ est le nombre moyen de protons neutralisables par mole de ligand.

Résultats

Les bases puriques et pyrimidiques monomères composant des acides nucléiques sont susceptibles de complexer de nombreux cations tels que Hg^{2+}, Pt^{2+}, Cu^{2+}, Ni^{2+}, Zn^{2+}, Co^{2+}, Mg^{2+}, Ca^{2+} et Pb^{2+} bien que les constantes de stabilité correspondantes ne soient pas calculées (1, 2, 5–8). Excepté les travaux que notre laboratoire a publiés nous n'avons repertorié aucune donnée bibliographique relative à la déprotonation et aux stabilités thermodynamiques de ces mêmes bases sous forme dimérisée.

1. Thymine monomère et dimère

Bien qu'il y ait dans chaque molécule de thymine (5-méthyl-2,4 (1*H*, 3*H*) pyrimidinedione) monomère deux possibilités d'échange relatives aux hydrogènes portés par les fonctions amines N1 et N3, seule la déprotonation N3 est observable dans le domaine de pH envisagé. Par voie de conséquence la molécule de dimère subira deux déprotonations en N3 et N3′ (1).

(a) Interactions avec le cuivre

Thymine monomère, H(TM). En ce qui concerne la complexation du cuivre, seul le complexe $[Cu(TM)]^+$ est mentionné (8, 9). Pour notre part, nous observons que la variation systématique dans les limites de solubilité, de la concentration en ions cuivriques met en évidence d'autres espèces complexes. Les interactions thymine–cuivre se situent dans le domaine $6 < \text{pH} < 9$ et pour les deux rapports coordinat–métal considérés, l'examen des courbes de formation $\bar{n} = f(\text{p[TM]})$ conduit à deux remarques :

L'ensemble des courbes de formation tend vers $\bar{n} = 2$, ce qui implique la formation d'espèces faisant intervenir une, puis deux molécules de ligand par métal.

Le déplacement de ces courbes $\Delta(\text{p[TM]})$ avec l'accroissement de la concentration en métal, Δm, indique de plus, la formation d'espèces polynucléaires M_2L_2 et M_2L_4 (10, 11).

$$2Cu^{2+} + 2H(TM) \rightleftarrows [Cu_2(TM)_2]^{2+} + 2H^+$$

$$2Cu^{2+} + 4H(TM) \rightleftarrows [Cu_2(TM)_4] + 4H^+$$

La bonne convergence du processus d'affinement permet de vérifier les hypothèses émises. Les valeurs définitives des constantes affinées par la méthode de «pit-mapping», ainsi que les données bibliographiques sont rassemblées dans le tableau 1.

Thymine dimère, H_2(TD). La faible solubilité de la thymine dimère impose rapidement une limite supérieure à la concentration en coordinat ($\sim 10^{-4}$ *M*). Pour ce système il est possible de mettre en évidence (tableau 1) une espèce protonée $[CuH(TD)]^+$ due au départ du premier proton neutralisable en N3, puis une espèce complexe simple [Cu(TD)] répondant aux équilibres :

$$Cu^{2+} + H_2(TD) \rightleftarrows [CuH(TD)]^+ + H^+$$

$$Cu^{2+} + H_2(TD) \rightleftarrows [Cu(TD)] + 2H^+$$

(b) Interactions avec le platine

Thymine monomère. Si de nombreuses publications (1, 2, 13–17) détaillent la préparation de complexes de Pt(II) avec la presque totalité des bases constitutives de l'ADN, il faut noter que certains auteurs (18, 19) précisent que le *cis*-$[PtCl_2(NH_3)_2]$ n'a aucune réactivité directe vis-à-vis de la thymine ou de la thymidine même à 37°C. De plus dans chaque cas l'ion hydraté

Can. J. Chem. Downloaded from www.nrcresearchpress.com by 118.98.75.50 on 09/07/12
For personal use only.

TABLEAU 2. Constantes de stabilité des complexes de l'acide orotique (monomère et dimère); $t = 25°C$, $\mu = 0,1$ ($NaNO_3$)

Espèce	*pqr*	log β_{pqr}	Domaine de formation	Référence 23	Référence 24	Référence 25
H(OM)	011	9,33(0,01)*		9,45		9,45
H_2(OM)	021	11,77(0,3)		12,25		12,52
[Cu(OM)]	101	8,39(0,02)	pH 4–8		9,48	
[Hg(OM)]	101	8,6 (0,1)	pH 3–7			
$[Hg_2(OM)_3]^{2-}$	203	20,03(0,1)	pH 4,5–6,5			
cis-$[Pt(OM)(NH_3)_2]$	101	6,61(0,003)	pH 3,5–9			
cis-$[Pt(OM)_2(NH_3)]^{2-}$	102	11,59(0,003)	pH 5–9			
H(OD)	011	10,56(0,03)				
H_2(OD)	021	19,4 (0,04)				
H_3(OD)	031	23,8				
H_4(OD)	041	26,6				
$[Cu(OD)]^{2-}$	101	12,27(0,2)	pH 4,5–11			
$[Hg(OD)]^{2-}$	101	13,2 (0,6)	pH 4–10			
cis-$[Pt(OD)(NH_3)_2]^{2-}$	101	11,8 (0,4)	pH 4,5–10			

*Écarts-types correspondants aux constantes.

cis-$[Pt(H_2O)_2(NH_3)_2]^{2+}$ est beaucoup plus réactif que le composé chloré *cis*-$[PtCl_2(NH_3)_2]$.

Cette anomalie nous a semblé d'autant plus intéressante à étudier que quelques travaux récents (4, 20, 21) font état d'interactions *cis*-$[PtCl_2(NH_3)_2]$ avec l'ADN à 25°C. Et pour mieux cerner l'influence des ligands chlorés, nous avons procédé en deux temps en suivant par des mesures protométriques à 25 et à 37°C :

les interactions *cis*-$[PtCl_2(NH_3)_2]$ – thymine monomère

les interactions *cis*-$[Pt(H_2O)_2(NH_3)_2]^{2+}$ – thymine monomère

La constante de déprotonation de la thymine monomère a été recalculée à 37°C. Nous avons vérifié que le *cis*-$[PtCl_2(NH_3)_2]$ se complexait très difficilement avec la thymine monomère quelle que soit la température. Par contre l'ion substitué *cis*-$[Pt(H_2O)_2(NH_3)_2]^{2+}$ conduit à des mesures expérimentales fiables et reproductibles permettant le calcul précis des constantes de stabilité pour deux complexes successifs mixtes, uniquement identifiés par Lippert (22).

$$cis\text{-}[Pt(H_2O)_2(NH_3)_2]^{2+} + H(TM) \rightleftarrows cis\text{-}[Pt(TM)(NH_3)_2]^{+} + H^+ + 2H_2O$$

$$cis\text{-}[Pt(H_2O)_2(NH_3)_2]^{2+} + 2H(TM) \rightleftarrows cis\text{-}[Pt(TM)_2(NH_3)_2] + 2H^+ + H_2O$$

Thymine dimère. En ce qui concerne la thymine dimère, l'addition de *cis*-$[Pt(H_2O)_2(NH_3)_2]^{2+}$ n'a pas d'incidence sur les déplacements protométriques : il n'y a donc pas de formation d'espèce complexe dans nos conditions expérimentales. En outre, les modèles de Dreiding qui permettent une bonne visualisation des composés moléculaires montrent aisément l'impossibilité d'insertion «sandwich» de l'ion métallique entre les deux plans de la molécule dimère.

2. Acide orotique monomère et dimère

L'acide orotique (acide 6-uracilcarboxylique) n'est pas une base de l'ADN, et bien que possédant un groupement carboxylique en C6 il s'intègre dans l'ensemble des dérivés pyrimidiques dont nous avons souligné l'importance physiologique.

La première dissociation protonique concerne l'hydrogène du groupement carboxylique en C6. De plus il existe dans chaque molécule de monomère deux possibilités d'échange relatives aux hydrogènes portés par les fonctions amines en N1 et N3 (fig. 1*b*).

(a) Interactions avec le cuivre

Acide orotique monomère, H_2(OM). Nous avons calculé dans un premier temps, les constantes de stabilité protonique β_{011} et β_{021} de l'acide orotique monomère à 25°C (tableau 2). Bien qu'il y ait dans chaque molécule de monomère, deux possibilités d'échange protonique relatives aux hydrogènes portés par les fonctions amines N1 et N3 (fig. 1*b*), les mesures protométriques se révélant inopérantes pour une telle différenciation, nous pouvons supposer que le fort effet inductif du groupement carboxylique porté par C6 active préférentiellement l'hydrogène porté par N1 en position α, la seconde déprotonation de l'hydrogène porté par N3 se situant vers pH 13 (23).

Dans le domaine de pH où l'hydrolyse des métaux est négligeable, l'acide orotique monomère complexe les ions Ni^{2+} et Cu^{2+} en formant les chélates du type [Ni(OM)] et [Cu(OM)]. Pour chacun de ces chélates la liaison coordinat–métal passe par l'intermédiaire du groupement carboxylique et l'atome d'azote N1 (24–26).

En accord avec ces données, la complexation des ions Cu^{2+} par le monomère et pour deux rapports coordinat–métal se traduit par la formation d'une seule espèce complexe répondant à l'équilibre :

$$Cu^{2+} + H_2(OM) \rightleftarrows [Cu(OM)] + 2H^+$$

Dans ce cas, il y a formation d'un chélate par liaison coordinante entre le groupement carboxylique et l'azote adjacent N1 (27–30).

Acide orotique dimère, H_4(OD). Nous ne disposons d'aucune donnée bibliographique chiffrant les stabilités protoniques et les stabilités des complexes et nous avons suivi le même protocole d'étude que pour le monomère. La transformée des courbes de neutralisation $\bar{q} = f(pH)$ correspond bien à la présence de quatre protons neutralisables H_4(OD) relatifs aux constantes β_{011}, β_{021}, β_{031}, β_{041} du tableau 2.

Le traitement des données potentiométriques relatives au système Cu^{2+} – acide orotique dimère fait apparaître la formation d'une seule espèce complexe de type $[Cu(OD)]^{2-}$ qui répond à l'équilibre :

$$Cu^{2+} + H_4(OD) \rightleftarrows [Cu(OD)]^{2-} + 4H^+$$

Can. J. Chem. Downloaded from www.nrcresearchpress.com by 118.98.75.50 on 09/07/12
For personal use only.

Can. J. Chem. Downloaded from www.nrcresearchpress.com by 118.98.75.50 on 09/07/12
For personal use only.

(b) Interactions avec le mercure

Acide orotique monomère. En présence des ions Hg^{2+}, l'acide orotique monomère conduit à la formation simultanée du complexe simple [Hg(OM)] et de l'espèce complexe polynucléaire $[Hg_2(OM)_3]^{2-}$ dont les équilibres correspondants sont :

$$Hg^{2+} + H_2(OM) \rightleftarrows [Hg(OM)] + 2H^+$$

$$2Hg^{2+} + 3H_2(OM) \rightleftarrows [Hg_2(OM)_3]^{2-} + 6H^+$$

Les phénomènes secondaires qui accompagnent généralement la complexation des ions Hg^{2+} (hydrolyse et dismutation (1, 31, 32)) en présence d'un excès de métal, n'ont pas été pris en compte lors de l'affinement des constantes. L'introduction, dans le cycle d'affinement de la constante β_{1-10}, relative à la formation d'espèce hydroxylée soluble $[Hg\ H_{-1}]$ n'améliore pas sensiblement la convergence.

Acide orotique dimère. La solubilité importante de l'acide orotique dimère ne favorise pas l'hydrolyse des ions mercuriques que nous considérons comme négligeable. Les interactions de l'acide orotique dimère avec les ions Hg^{2+} se traduisent par la formation d'une seule espèce complexe de type $[Hg(OD)]^{2-}$ dont l'équilibre est :

$$Hg^{2+} + H_4(OD) \rightleftarrows [Hg(OD)]^{2-} + 4H^+$$

(c) Interactions avec le platine

Acide orotique monomère. Le platine complexé sous forme d'ions *cis*-$[Pt(H_2O)_2(NH_3)_2]^{2+}$ conduit à la formation de deux espèces chélates mixtes successives :

$$cis\text{-}[Pt(H_2O)_2(NH_3)_2]^{2+} + H_2(OM) \rightleftarrows cis\text{-}[Pt(OM)(NH_3)_2] + 2H^+ + 2H_2O$$

$$cis\text{-}[Pt(H_2O)_2(NH_3)_2]^{2+} + 2H_2(OM) \rightleftarrows cis\text{-}[Pt(OM)_2(NH_3)_2]^{2-} + 4H^+ + 2H_2O$$

Acide orotique dimère. Contrairement à la thymine dimère, la présence du groupement carboxylate en C6 favorise la formation d'un chélate externe impliquant l'azote N1 adjacent :

$$cis\text{-}[Pt(H_2O)_2(NH_3)_2]^{2+} + H_4(OD) \rightleftarrows cis\text{-}[Pt(OD)(NH_3)_2]^{2-} + 4H^+ + 2H_2O$$

3. Thymidine H(TY)

De nombreux travaux mentionnent les interactions de la thymidine avec les ions métalliques tels que Hg^{2+}, Cu^{2+}, Co^{2+}, Cd^{2+} et Mn^{2+} (12, 14, 18, 31, 33–35), mais fort peu se rapportent aux calculs des stabilités thermodynamiques permettant de chiffrer les équilibres de complexation.

Si l'introduction du groupe sucre sur l'azote N1 confère à la thymidine une plus grande solubilité que celle de la thymine, elle n'a pratiquement pas d'incidence sur la stabilité protonique de l'hydrogène porté par N3. La constante calculée (tableau 3) concorde avec les rares données bibliographiques que nous possédons (14, 31).

(a) Interactions avec le cuivre

Comme dans le cas de la thymine, l'obtention d'espèces polynucléaires se confirme rapidement selon les équilibres :

$$2Cu^{2+} + 2H(TY) \rightleftarrows [Cu_2(TY)_2]^{2+} + 2H^+$$

$$2Cu^{2+} + 4H(TY) \rightleftarrows [Cu_2(TY)_4] + 4H^+$$

(b) Interactions avec le mercure

Ferreira *et al.* (31) font état d'un complexe stable $[Hg(TY)_2]$ engageant deux molécules de ligands.

Dans nos conditions expérimentales (excès de ligand) nous avons détecté dès pH 3 la présence de la première espèce successive $[Hg(TY)]^+$. L'introduction de la constante correspondante à cette dernière améliore sensiblement la convergence de l'affinement relatif aux points expérimentaux de deux rapports coordinat:métal.

$$Hg^{2+} + H(TY) \rightleftarrows [Hg(TY)]^+ + H^+$$

$$Hg^{2+} + 2H(TY) \rightleftarrows [Hg(TY)_2]^{2+} + 2H^+$$

TABLEAU 3. Constantes de formation des complexes de la thymidine; $t = 25°C$, $\mu = 0{,}1$ ($NaClO_4$)

Espèce	*pqr*	log β_{pqr}	Domaine de formation	Référence 14	Référence 31
H(TY)	011	9,78		9,6	9,6
$[Cu_2(TY)_2]^{2+}$	202	12,78	pH 5,5–8,5		
$[Cu_2(TY)_4]$	204	23,1	pH 6–8,5		
$[Hg(TY)]^+$	101	7,88	pH 2–4		
$[Hg(TY)_2]$	102	14,94	pH 2–10		21,2

Conclusion

L'examen comparé des complexes du cuivre, du mercure et du platine, que nous venons d'explorer appelle plusieurs remarques en ce qui concerne les coordinats.

En outre, les constantes de formation consignées dans le tableau 1 donnent accès aux concentrations de toutes les espèces en solution et la figure 2, un exemple de leur répartition et précisent très exactement les conditions expérimentales de concentration et de pH nécessaires au bon déroulement de la transformation photochimique.

1. Thymine et thymidine

Thymine monomère, thymidine

La thymine monomère et la thymidine, coordinats monodentates, donnent préférentiellement des complexes polynucléaires avec le cuivre et le mercure, l'interaction unique en N3 favorisant l'apparition de liaisons métal–métal, notamment avec le cuivre tétracoordinant. Dans le cas du platine, les espèces mixtes mononucléaires obtenues par substitution successives des molécules d'eau satisfont totalement la tétracoordinence du métal. Ces espèces apparaissent dans un domaine de pH essentiellement plus alcalin que celui du milieu biologique et par là même indécelables dans les expérimentations «in vivo» rapportées par J. L. Butour (4) qui signale que seule la guanine est susceptible de complexer l'ion *cis*-platine.

Thymine dimère

La géométrie de la molécule favorise l'inclusion de l'atome métallique (cuivre ou mercure) entre les deux cycles adjacents. Par contre, aucun complexe n'a été détecté avec le platine, ce qui semble confirmé à l'aide des modèles de Dreiding par l'impossibilité stérique d'immiscer l'ion *cis*-$[Pt(H_2O)_2(NH_3)_2]^{2+}$ substitué entre les cycles uracile parallèles.

2. Acide orotique

Acide orotique monomère

Quel que soit le métal, les espèces mononucléaires sont les plus fréquentes avec le coordinat bidentate, chélatant par l'azote N1 et le groupement carboxylate porté par C6.

La comparaison des constantes de stabilité des complexes du cuivre et du mercure avec celles des complexes correspondants obtenus avec l'acide picolinique déjà étudiées dans notre laboratoire (respectivement $\beta_{101} = 7{,}76$, $\beta_{102} = 14{,}70$ (36) et $\beta_{101} = 7{,}70$, $\beta_{102} = 15{,}4$ (37)), corrobore les observations de Tucci *et al.* (25). Bien que dans le cas de l'acide picolinique, les sites de fixation soient identiques, l'azote adjacent en N1 n'étant

Can. J. Chem. Downloaded from www.nrcresearchpress.com by 118.98.75.50 on 09/07/12
For personal use only.

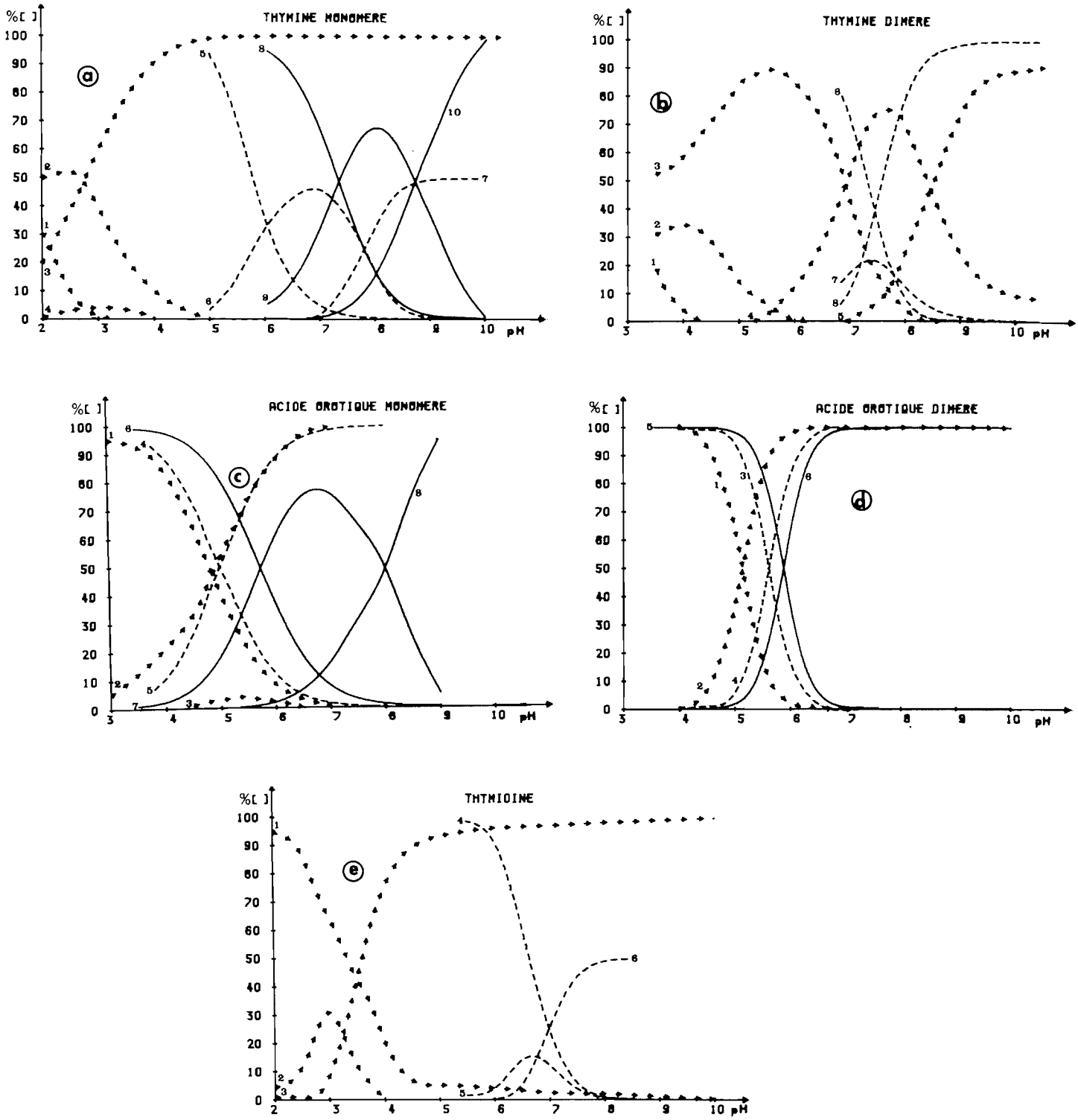

FIG. 2. (*a*) Thymine monomère : ▲▲ [HTM] = 2×10^{-3} *M*; [Hg^{2+}] = $4{,}750 \times 10^{-4}$ *M*; --[HTM] = 10^{-2} *M*; [Cu^{2+}] = $2{,}976 \times 10^{-3}$ *M*; —[HTM] = 10^{-3} *M*; [Pt^{2+}] = 2×10^{-4} *M*. 1, Hg^{2+}; 2, [Hg(TM)]$^{+}$; 3, [$Hg(TM)_2$]$^{+}$;4,[HgH_{-1}]$^{+}$;5,Cu^{2+};6,[$Cu_2(TM)_2$]$^{2+}$;7,[$Cu_2(TM)_4$]; 8, *cis*-[$Pt(H_2O)_2(NH_3)_2$]$^{2+}$; 9, *cis*-[Pt(TM)$(NH_3)_2$]$^{2+}$; 10, *cis*-[$Pt(TM)_2(NH_3)_2$].

(*b*) Thymine dimère : ▲▲ [HTD] = $9{,}96 \times 10^{-5}$ *M*; [Hg^{2+}] = $9{,}5 \times 10^{-5}$ *M*; -- [HTD] = 2×10^{-4} *M*; [Cu^{2+}] = 10^{-4} *M*. 1, Hg^{2+}; 2, [HgH_{-1}]$^{+}$; 3, [Hg(TD)]; 4, [HgH_{-1}(TD)]$^{-}$; 5, [HgH_{-2}(TD)]$^{2-}$; 6, Cu^{2+}; 7, [CuH(TD)]$^{+}$; 8, [Cu(TD)].

(*c*) Acide orotique monomère : ▲▲ [H_2OM] = 10^{-4} *M*; [Hg^{2+}] = $4{,}99 \times 10^{-5}$ *M*; -- [H_2OM] = 10^{-4} *M*; [Cu^{2+}] = $5{,}145 \times 10^{-5}$ *M*; — [H_2OM] = $8{,}966 \times 10^{-4}$ *M*; [Pt^{2+}] = 5×10^{-4} *M*. 1, Hg^{2+}; 2, [HgOM]; 3, [$Hg_2(OM)_3$]$^{2-}$; 4, Cu^{2+}; 5, [Cu(OM)]; 6, *cis*-[$Pt(H_2O)_2(NH_3)_2$]$^{2+}$; 7, *cis*-[Pt(OM)$(NH_3)_2$]; 8, *cis*-[$Pt(OM)_2(NH_3)_2$]$^{2-}$.

(*d*) Acide orotique dimère : [H_4OD] = $1{,}68 \times 10^{-4}$ *M*; ▲▲ [Hg^{2+}] = $3{,}352 \times 10^{-5}$ *M*; -- [Cu^{2+}] = $3{,}375 \times 10^{-5}$ *M*; — [Pt^{2+}] = $3{,}129 \times 10^{-5}$ *M*. 1, Hg^{2+}; 2, [Hg(OD)]$^{2-}$; 3, Cu^{2+}; 4, [Cu(OD)$^{2-}$]; 5, *cis*-[$Pt(H_2O)_2(NH_3)_2$]$^{2+}$; 6, *cis*-[Pt(OD)$(NH_3)_2$]$^{2-}$.

(*e*) Thymidine : ▲▲ [HTY] = $1{,}98 \times 10^{-3}$ *M*; [Hg^{2+}] = $5{,}92 \times 10^{-4}$ *M*; -- [HTY] = 10^{-2} *M*; [Cu^{2+}] = $2{,}976 \times 10^{-3}$ *M*. 1, Hg^{2+}; 2, [Hg(TY)]$^{+}$; 3, [$Hg(TY)_2$]; 4, Cu^{2+}; 5, [$Cu_2(TY)_2$]$^{2+}$; 6, [$Cu_2(TY)_4$].

pas chargé induit la formation d'un chélate moins stable que le complexe correspondant de l'acide orotique.

Acide orotique dimère

La chélation du cuivre, du mercure et du platine ne présente aucune difficulté dans un rapport coordinat:métal 1:1. Il faut noter que la chélation du platine (sous forme d'ion *cis*-$[Pt(H_2O)_2(NH_3)_2])^{2+}$, non observable avec la thymine dimère reste un phénomène externe à la «cage» formée par les deux cycles adjacents.

En ce qui concerne la transposition à une réaction photochimique reversible entre les complexes mercuriques dimère et monomère, nous avons précédemment montré l'intérêt (2) du complexe dimère [HgTD] de la thymine dont l'irradiation à 280–300 nm entraîne la formation des espèces monomères $[HgTM]^+$ ou $[Hg(TM)_2]$. La présence d'espèces hydroxylées $[HgH_{-1}TD]^-$ et $[HgH_{-2}TD]^{2-}$ observées dans ce cas, et susceptibles de gêner le processus de monomérisation, est écartée par l'utilisation de l'acide orotique dimère, qui, plus soluble, favorise beaucoup moins l'hydrolyse de l'ion Hg^{2+}.

Partie expérimentale

Nous disposons d'une chaîne de mesure étalonnée avec précision :

électrode en verre | solution thermostatée | NaCl saturé | électrode au calomel

Le jeu d'électrodes est relié à un potentiomètre ISIS 20000 Tacussel et les mesures sont effectuées que des solutions aqueuses thermostatées à 25 ± 0,1°C et sous atmosphère d'azote. La force ionique de chaque solution est maintenue constante à l'aide d'une solution de $NaNO_3$ 0,1 *M*.

Sels métalliques

Les sels de cuivre et de mercure sont préparés par dissolution de $Cu(NO_3)_2 \cdot 3H_2O$ et $Hg(NO_3)_2 \cdot H_2O$ Prolabo et dosés par complexométrie à l'EDTA notamment à l'aide d'une électrode reversible aux ions Hg^{2+} couplée à une électrode de référence au sulfate mercureux pour le mercure.

La solution de *cis*-$[Pt(H_2O)_2(NH_3)_2](NO_3)_2$ est préparée à partir de *cis*-$[PtCl_2(NH_3)_2]$ R. Bellon par substitution stoechiométrique des ions Cl^- effectuée à l'aide d'une solution titrée de nitrate d'argent (38–41). Une triple centrifugation du chlorure d'argent permet de garantir la reproductibilité de l'échange qui n'affecte en rien la liaison Pt—N (41).

Coordinats

La thymine monomère, l'acide orotique monomère et la thymidine proviennent respectivement des laboratoires Merck, Sigma Chemical Company et Boehringer Mannheim GMBH.

La thymine dimère est préparée par irradiation de solutions de monomère dans l'eau (10^{-3} *M*) gelée à −10°C. L'irradiation est effectuée à l'aide d'une lampe à vapeur de mercure haute pression et les solutions sont évaporées à sec. Le résidu est ensuite dissous dans l'eau bouillante puis filtré. Le filtrat est concentré et les cristaux de thymine dimère cristallisent avant ceux du monomère (1).

En ce qui concerne la préparation de l'acide orotique dimère, le processus général reste le même, les irradiations ayant lieu à 20°C, sur des solutions amenées à pH 1 sous barbotage d'azote pour éliminer l'oxygène. Dans chaque cas, deux rapports de concentration ligand:ion métallique (~2 et ~5) ont été considérés pour chaque système, soit environ 100 points expérimentaux.

Remerciements

Nous remercions vivement les laboratoires Roger Bellon, 159 avenue du Roule, 92200 Neuilly sur Seine de nous avoir fourni gracieusement le *cis*-$[PtCl_2(NH_3)_2]$.

1. M. Petit-Ramel, G. Thomas-David, G. Perichet et B. Pouyet. Can. J. Chem. **62**, 22 (1984).
2. G. Perichet, P. Meallier, B. Pouyet, M. Petit-Ramel et G. Thomas-David. J. Photochem. **29**, 375 (1985).
3. H. A. Harper. Précis de Biochimie. Université de Laval, Québec. 1977.
4. J. L. Butour. Thèse, Doctorat d'État, Toulouse. 1980.
5. P. Zaplatynsky, H. Neubacher et W. Lohmann. Z. Naturforsch. B: Anorg. Chem. Org. Chem. **34**, 1466 (1979).
6. D. M. L. Goodgame et I. Jeeves. Z. Naturforsch. C: Biosci. **34**, 1287 (1979).
7. J. D. Woollins et B. Rosenberg. Inorg. Chem. **21**, 1280 (1982).
8. Ya. D. Fridman, Z. M. Pulatova et M. G. Levina. Koord. Khim. **7**, 1 (1981).
9. M. M. Taqui Khan et C. R. Krishnamoorthy. J. Inorg. Nucl. Chem. **36**, 711 (1974).
10. A. Ringbom. Les complexes en chimie analytique. Dunod, Paris. 1967.
11. L. C. Van Poucke et H. F. Debrabander. Talanta, **20**, 733 (1973).
12. C. M. Flynn, Jr., T. S. Viswanathan et R. B. Martin. J. Inorg. Nucl. Chem. **39**, 437 (1977).
13. J. P. Davidson, P. J. Faber et R. G. Fischer. Cancer Chemother. Rep. Part 1, **59**, 2 (1975).
14. D. J. Nelson, P. L. Yeagle, T. L. Miller et R. B. Martin. Bioinorg. Chem. **5**, 353 (1976).
15. R. Faggiani, B. Lippert et C. J. L. Lock. Inorg. Chem. **19**, 295 (1980).
16. B. Lippert, R. Pfab et D. Neugebauer. Inorg. Chim. Acta, **37**, L 494 (1979).
17. A. B. Robins. Chem. Biol. Interact. **6**, 35 (1973).
18. G. Y. H. Chu, R. E. Duncan et R. S. Tobias. Inorg. Chem. **16**, 10 (1977).
19. I. A. G. Ross, A. J. Thomson et S. Mansy. J. Am. Chem. Soc. **96**, 20 (1974).
20. M. J. Cleare. Coord. Chem. Rev. **12**, 349 (1974).
21. J. P. Macquet et T. Theophanides. Bioinorg. Chem. **5**, 59 (1975).
22. B. Lippert. Biochimie, **60**, 9 (1978).
23. D. Shagar et J. J. Fox. Biochim. Biophys. Acta, **9**, 199 (1952).
24. Br. E. Doody, E. R. Tucci, R. Scruggs et N. C. Li. J. Inorg. Nucl. Chem. **28**, 833 (1966).
25. E. R. Tucci, Br. E. Doddy et N. C. Li. J. Phys. Chem. **65**, 1570 (1961).
26. E. R. Tucci, C. H. Ke et N. C. Li. J. Inorg. Nucl. Chem. **29**, 1657 (1967).
27. I. Mutikainen et P. Lumme. Acta Crystallogr. Sect. B: Struct. Crystallogr. Cryst. Chem. **36**, 2233 (1980).
28. P. Arrizabalaga, P. Castan et J. P. Laurent. Inorg. Chim. Acta, **92**, 203 (1984).
29. I. Mutikainen. Finn. Chem. Lett. **5**, 193 (1985).
30. P. Arrizabalaga, P. Castan et F. Duhan. Inorg. Chem. **22**, 2245 (1983).
31. R. Ferreira et E. Ben-Zvi. Adv. Chem. Coord. Compd. 457 (1961).
32. Y. Tetsuo et N. Davidson. J. Am. Chem. Soc. **83**, 12, (1961).
33. G. L. Eichborn, P. Clark et E. D. Becker. Biochemistry, **5**, 1 (1966).
34. A. M. Fiskin et M. Beer. Biochemistry, **4**, 7 (1965).
35. M. Goodgame et W. J. Keith. J. Chem. Soc. Dalton Trans. 1294 (1977).
36. L. Moyne. Thèse, Doctorat d'État, Lyon. 1966.
37. G. Anderegg. Helv. Chim. Acta, **43**, 414 (1960).
38. H. J. S. King. J. Chem. Soc. 1338 (1938).
39. J. K. Barton, S. A. Best, S. J. Lippard et R. A. Walton. J. Am. Chem. Soc. **100**, 12 (1978).
40. C. J. L. Lock, H. J. Peresie, B. Rosenberg et G. Turner. J. Am. Chem. Soc. **100**, 11 (1978).
41. J. K. Barton, H. N. Rabinowitz, D. J. Szalda et S. J. Lippard. J. Am. Chem. Soc. **99**, 8 (1977).
42. S. E. Livingstone. Comprehensive inorganic chemistry. Vol. 3. Pergamon Press, Oxford. 1975.

Can. J. Chem. Downloaded from www.nrcresearchpress.com by 118.98.75.50 on 09/07/12
For personal use only.

Binuclear metal chelate complexes of anthraquinones having a MO_4 chromophore. Part 1. Quinizarin

M. N. BAKOLA-CHRISTIANOPOULOU[1]
Department of Chemical Engineering, College of Engineering, Aristotelian University of Thessaloniki, GR – 540 06 Thessaloniki, Greece

P. D. AKRIVOS
Department of General and Inorganic Chemistry, Faculty of Chemistry, Aristotelian University of Thessaloniki, GR – 540 06 Thessaloniki, Greece

AND

M. BAUMGARTEN
Institut für Organische Chemie, Freie Universität, Berlin, Deutschland

Received August 29, 1986[2]

M. N. BAKOLA-CHRISTIANOPOULOU, P. D. AKRIVOS, and M. BAUMGARTEN. Can. J. Chem. **65**, 1485 (1987).

Homobinuclear metal chelate complexes having 1,4-dihydroxy-9,10-anthracenedione (quinizarin) as a bridging unit have been prepared with four bivalent first row transition elements, namely cobalt, nickel, copper, and zinc. The coordination spheres of the metal ions consist of two nearly equivalent six-membered rings with oxygen donor atoms derived from the quinizarin and the terminal ligands which are either β-diketones or salicylic aldehyde. TG, spectroscopic (ir, uv–vis, epr), and magnetic measurements have been applied to an investigation of the geometry adopted by the MO_4 chromophores. The results are consistent with varying degrees of distortion from the ideal square planar toward a tetrahedral arrangement around the metal ions, closely related to the specific metal center involved.

M. N. BAKOLA-CHRISTIANOPOULOU, P. D. AKRIVOS et M. BAUMGARTEN. Can. J. Chem. **65**, 1485 (1987).

On a préparé les complexes homobinucléaires métal/chélate de quatre éléments bivalents de la première rangée des éléments de transition (soit le cobalt, le nickel, le cuivre et le zinc) couplés à de la dihydroxy-1,4 anthracènedione-9,10 (quinizarine) agissant comme unité de pont. Les sphères de coordination des ions métalliques comportent deux cycles à six chaînons qui sont pratiquement équivalents et dans lesquels les atomes d'oxygène donneurs proviennent de la quinizarine alors que les ligands terminaux sont soit des β-dicétones ou de l'aldéhyde salicylique. On a utilisé des mesures de TG, de spectroscopie (ir, uv–visible et rpe) et de magnétisme pour étudier la géométrie adoptée par les chromophores MO_4. D'après ces résultats, l'arrangement autour des ions métalliques implique divers degrés de distorsion du plan carré idéal vers un arrangement tétraédrique; cet arrangement autour des ions métalliques ressemble beaucoup à celui qui existe autour du centre métallique spécifique impliqué.
[Traduit par la revue]

Introduction

Quinones, hydroxyquinones, and their substituted derivatives form an extended class of compounds that has attracted the interest of chemists and has been studied thoroughly. The investigations reported cover practically every topic of synthetic and experimental chemistry, including isolation from natural products (1), total synthesis (2), testing of antimicrobial activity (3), and preparation and identification of metal chelates and polymers (4). Metal chelates of hydroxyquinones with both first row transition metal elements and Pt(II) have been the main part of our research in recent years, both theoretical (5) and spectroscopic methods (6, 7) having been applied in our effort to gain insight into the chelating ability of hydroxyquinones and their subsequent modifications following coordination to different metal ion spheres. The formation of coordination compounds has attracted much more interest since the observation that many of the commercially used antibiotics possess active hydroxyquinonic sites (8), and the suspicion that this local structure might be responsible for the detected biological activity. As our contribution in this line of research, we have reported both the preparation and chemical (9) as well as biological (10) justification of such an activity of naphthazarinato bridged binuclear Pt(II) complexes. In the present paper we report on the synthesis and characterization of a series of mixed ligand neutral homobinuclear complexes of first row transition elements with the dianion 1,4-dihydroxy-9,10-anthracenedione (quinizarin) as the bridging unit, β-diketonates as terminal ligands (acetylacetone, benzoylacetone, and salicylic aldehyde), and the bivalent metal ions Co(II), Ni(II), Cu(II), and Zn(II) (Fig. 1).

Experimental

Materials and instruments

Quinizarin obtained from Bayer was recrystallized from hot benzene prior to its use in the preparation while no purification was performed on the diketones used (Aldrich). All the solvents used were of reagent grade. The ir spectra were recorded in the region 4000–250 cm^{-1} on a Perkin–Elmer 467 spectrophotometer, using KBr discs (1:100 in KBr) while the electronic spectra were obtained (900–250 nm) on a Perkin–Elmer–Hitachi 200 spectrophotometer. Magnetic measurements were carried out with a Faraday-type magnetometer equipped with a Cahn RG-HV electrobalance and the complex $Hg[Co(SCN)_4]$ as standard. Electron paramagnetic resonance spectra were recorded on a Bruker 200D X-band spectrometer equipped with a 100 kHz field modulator and a variable temperature control unit (120–400 K). Calibration of the magnetic field was done using a Bruker NMR Gaussmeter (BNM 12) or an nmr probe (Bruker) coupled to an AEG rf-oscillator. The frozen solution spectra were recorded at 130 K with a typical modulation depth of 4 Gpp.

Elemental analyses for C and H were carried out on a Perkin–Elmer 240 Elemental Analyzer. Results are given in Table 1.

TG measurements were carried out on a Dupont Instruments Series 99 Thermal Analyzer and DTG on the same instrument connected to

[1]Author to whom correspondence should be addressed.
[2]Revision received February 11, 1987.

Printed in Canada / Imprimé au Canada

Can. J. Chem. Downloaded from www.nrcresearchpress.com by 84.22.46.98 on 09/08/12
For personal use only.

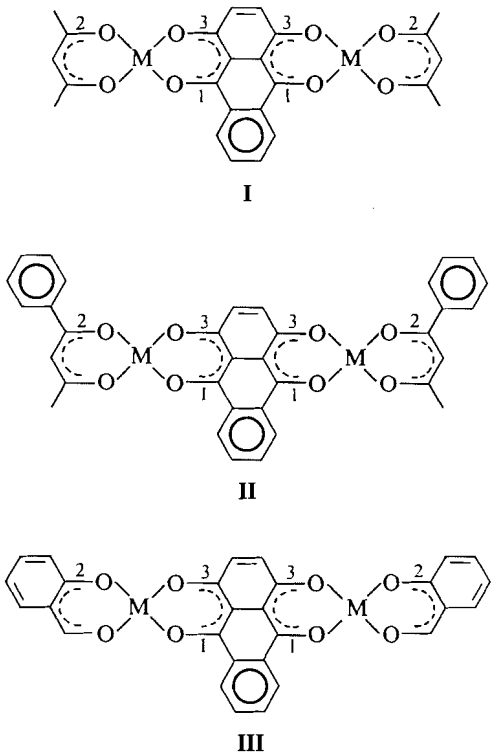

FIG. 1. The three classes of compounds prepared: **I**, acetylacetonates; **II**, benzoylacetonates; and **III**, salicylates. M:a for Zn(II); b for Cu(II); c for Ni(II), and d for Co(II).

a Dupont Instruments Series 951 thermogravimetric analyzer. The measurements were performed in a dynamic nitrogen atmosphere at a flow rate of 60 mL/min, up to 900°C, using a chromel/alumel thermocouple to measure the temperature. The heating rate was 10 deg/min and the sample weights about 10 mg.

Preparative

First, digestion of the β-diketone was performed with the stoichiometric amount of NaOH under moderate heating, in order to prepare the corresponding sodium salt. The process did not last for more than 15 min (for benzoylacetone). The filtered solution of the β-diketonate salt (2 mmol in 20 mL EtOH) was then added to a stirred solution of 2 mmol of the appropriate metal perchlorate in ethanol. To the resulting dark coloured mixture, an ethanolic solution containing 1 mmol of 1,4-dihydroxy-9,10-anthracenedione disodium salt was added over 5 min under vigorous stirring and moderate heating. The reaction mixture was allowed to stir for a further 15 min, filtered after cooling and the microcrystalline products were washed successively with water, ethanol, and diethylether, and finally dried in a vacuum desiccator over P_2O_5.

Results and discussion

The complexes were obtained in yields of 60–75%. They are microcrystalline substances of deep colour, stable in air, and insoluble in water and most of the common organic solvents. They are only slightly soluble in hot DMF and $CHCl_3$, a fact that does not allow molecular weight determination or ^1H nmr to be carried out. TG results presently discussed reveal the low temperature dissociation occurring within the β-diketonato groups, which precludes study of the mass spectra of the complexes. A number of recordings did not show the molecular ion peak but only indicated the presence of the organic ligands and their fragmentation patterns (11, 12).

TG measurements carried out on the Zn, Cu, and Co members of the series clearly showed that the thermal decomposition

TABLE 1. Analytical data for the complexes studied

	H%		C%		M%*	
Compound	Calcd	Obsd	Calcd	Obsd	Calcd	Obsd
I*a*	3.55	3.61	50.83	51.08	23.06	23.19
II*a*	3.50	3.52	59.08	59.37	18.92	19.12
III*a*	2.64	2.69	55.03	54.84	21.40	21.27
I*b*	3.58	3.60	51.16	51.29	22.56	22.44
II*b*	3.52	3.54	59.39	59.48	18.48	18.55
III*b*	2.66	2.70	55.37	55.68	20.92	20.79
I*c*	3.64	3.60	52.05	52.33	21.28	21.06
II*c*	3.52	3.59	59.45	59.16	17.37	17.62
III*c*	2.70	2.65	56.26	56.59	19.70	19.58
I*d*	3.64	3.58	52.01	52.28	21.27	21.03
II*d*	3.52	3.58	59.41	59.08	17.38	17.56
III*d*	2.70	2.66	56.22	56.52	19.71	19.50

*Titration with 10^{-2} *M* EDTA.

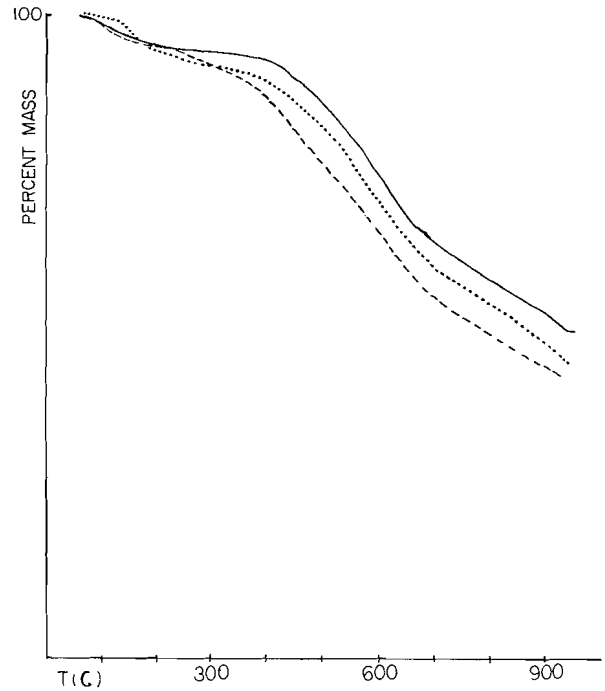

FIG. 2. TG curves for the three Zn(II) complexes: (—) acac, (---) bzac, and (···) sal.

of the complexes is a rather complicated phenomenon, taking place in several steps and is affected by the central metal ion (Figs. 2–4). The temperature ranges, percent mass losses (observed and theoretically predicted) are presented in Table 2. Only in two cases did the final residue at 900°C correspond to purely metallic substance (i.e. **I***b* and **I***d*), while in the rest it must be ascribed to the metal plus a portion of the hydroxyquinone bridging unit. In all three classes of compounds investigated, the first stage of decomposition is clearly a cleavage occurring in the β-diketonato group and corresponds to a $CH_3C{=}O$ fragment in classes **I** and **II** and $HC{=}O$ for class **III**. The remaining part of the diketone then undergoes further fragmentation, which is completed in several steps in the region 400–700°C. In the case of cobalt complexes, apart from the observation of the maximum rate of decomposition at

Can. J. Chem. Downloaded from www.nrcresearchpress.com by 84.22.46.98 on 09/08/12
For personal use only.

TABLE 2. The most relevant data obtained from the TG measurements*

Compound	Temperature range	Percent mass loss (obsd)	Percent mass loss (calcd)	Fragment	Maximum rate decomposition
I*a*	300–570	17.56	15.18	CH_3CO	475
	570–680	16.32	19.77	CH_2CH_3CO	635
	680–900	15.29	—	M(quin)	—
II*a*	30–450	12.65	12.46	CH_3CO	430
	450–650	21.31	22.31	$2C_6H_5$	465, 570
	650–900	20.55	—	M(quin)	—
III*a*	30–380	9.28	9.50	CHO	220
	380–700	29.17	30.14	C_6H_5O	475, 565, 625
	700–900	10.92	—	M(quin)	—
I*b*	30–450	38.86	35.18	$C_5H_7O_2$	235, 425
	450–640	41.64	42.26	$C_{14}H_6O_4$	530
II*b*	30–400	11.64	12.52	CH_3CO	305
	400–600	20.65	22.43	C_6H_5	360
		12.65	11.94	Bzac residue	540
	600–900	29.74	—	M(quin)	—
III*b*	30–540	88.92	9.56	CHO	255
		31.35	30.22	Sal residue	445, 520
	540–900	33.26	—	M(quin)	—
I*d*	30–550	34.38	35.77	$C_5H_7O_2$	385, 440
	550–750	42.72	42.96	$C_{14}H_6O_4$	580, 635, 700
II*d*	30–650	12.10	12.69	CH_3CO	275
		21.62	22.44	C_6H_5	450, 555
	650–900	43.02	—	M(quin)	—
III*d*	30–600	9.16	9.70	CHO	280
		13.40	13.76	$C_4H_2O_2$	440
		31.42	30.79	Sal residue	550
	600–900	23.42	—	M(quin)	—

*The fragment notation holds for all the equivalent fragments in a molecule (e.g. C_6H_5 means both phenyl groups of a benzoylacetonate). M(quin) is used in the case of dissociation of the metal–quinizarin polymer. A smoothly descending curve is obtained and therefore no maximum rate decomposition temperature is reached and no theoretical mass loss may be calculated (it would correspond to the total mass of quinizarin).

slightly lower temperatures, quinizarin fragments appear also in this region of temperatures (e.g. **II***d*).

The bonding scheme expressed by both the bridging and the terminal ligands is revealed to an extent by the ir spectra (Table 3). The main bands of interest are those connected to the C=O stretching modes, which are coded as $\nu(C\cdots O)_1$ and $\nu(C\cdots O)_3$ for quinizarin and $\nu(C\cdots O)_2$ for the β-diketones (13), respectively. More information is gained by considering the shifts of these bands relative to the corresponding ones in the free ligands. The absence of detectable bands higher than 1600 cm^{-1} is evidence for a bidentate chelation of the anthraquinonic unit (14). The shift of this band to lower frequencies is accompanied by an analogous shift to higher ones of the $\nu(C\cdots O)_3$ band which further confirms the above-mentioned bidentate coordination. The regular band of the coordinated acetylacetone carbonyl group can be clearly seen in group **I** members (15), while those of benzoylacetone and salicylic aldehyde are often hard to distinguish from the other constituents of the envelope present at 1595–1565 cm^{-1}. In accordance with the elemental analyses and the molecular conductivity measurements, no perchlorate anion band is present in the region 1050–1130 cm^{-1} (16). Therefore no coordination or semicoordination may occur through this anion, a fact enabling us to focus only on coordination number four arrangements coordination number four arrangements around the metal ions. Thus the possible local geometries are limited to tetrahedral, square planar, or any intermediate which is more likely to be adopted.

Unfortunately the solution electronic spectra do not offer sufficient evidence for either of the aforesaid coordination schemes. This is a consequence of both the low solubility of the complexes and the widespread $\pi \rightarrow \pi^*$ and $n \rightarrow \pi^*$ transitions of the extended aromatic rings of the organic substituents. Therefore the $d \rightarrow d$ absorptions can not offer their valuable information as they are masked by the more intense and broad intraligand or CT bands. The lowest energy CT bands should appear around 575 nm as this is the lowest energy band observed for the zinc members of the series. The shoulders therefore detected for a number of Co(II) and Ni(II) complexes in the region 600–630 nm (Table 3) may be assigned to $d \rightarrow d$ transitions and would be consistent with a distorted tetrahedral environment around the metal ions, though no unambiguous assignment or detailed analysis is possible.

The magnetic measurements become therefore more essential for our study as they offer stronger evidence in account with the ligand orientation around the metal ions.

Of course the most interesting are the μ_{eff} of cobalt and nickel complexes, since it has been firmly established that relatively small structural changes affect in a dramatic way their *d*-orbital splitting and occupation, giving rise to detectable changes in

Can. J. Chem. Downloaded from www.nrcresearchpress.com by 84.22.46.98 on 09/08/12
For personal use only.

TABLE 3. The characteristic ir bands (cm^{-1}), uv–vis absorption bands (nm), and μ_{eff} values of the complexes; the notation of Fig. 1 is being followed in coding the complexes*

	Infrared bands				Ultraviolet visible bands					
Compound	$(CO)_1$	$(CO)_2$	$(CO)_3$	M—O	I	II	III	IV	V	μ_{eff} (BM)
I*a*	1580b	1540	1270	570, 480	330sh	471, 486	515sh	571		
I*b*	1575b	1543	1277	550, 460	323sh	470, 484	515sh	567		1.96
I*c*	1580b	1547	1274	570, 480	313sh	485	521sh	553		1.69
I*d*	1570b	1532	1266	470, 380	308sh	462, 482	512	552, 576		4.48
II*a*	1580b		1268	460	325sh	468, 483	513sh	570		
II*b*	1585	1540	1274	475, 455	331	490	507sh	577	625sh	1.91
II*c*	1590b		1272	460	322sh	487	520sh	572		1.71
II*d*	1575b	1545	1262	470, 390	305sh	490	516sh	555	600, 615sh	4.38
III*a*	1575b		1262	490, 460	323sh	482	510sh	572		
III*b*	1580b		1278	560, 465	331	490	505sh	575	620sh	1.92
III*c*	1602	1560b	1255	465	320sh	480	517sh	588	612sh	1.74
III*d*	1600	1565b	1257	480, 470	312sh	500	515	582sh	622sh	4.36

*b indicates a broad band of which the approximate maximum is tabulated; sh indicates a shoulder of a main band.

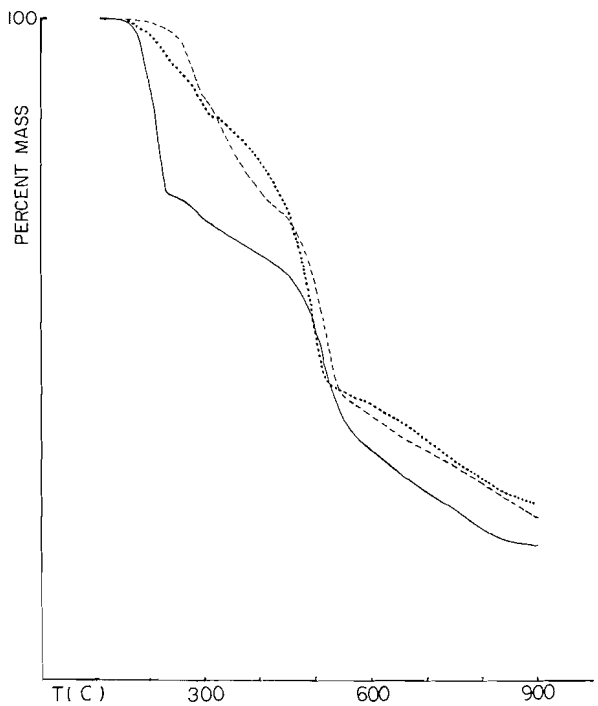

FIG. 3. TG curves for the three Cu(II) complexes. Notation as in Fig. 2.

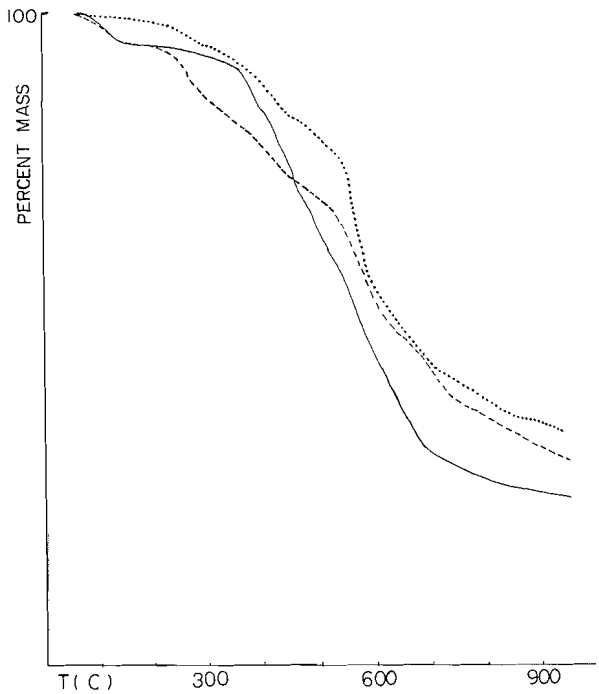

FIG. 4. TG curves for the three Co(II) complexes. Notation as in Fig. 2.

the values of the recorded μ_{eff}. For cobalt, the μ_{eff} values are indicative of an approximately tetrahedral Co^{2+} coordination sphere, since all the known planar Co^{2+} complexes are of low spin, their μ_{eff} values being less than half (16) of those observed (Table 3). Quite similar arguments may be applied in the case of Ni^{2+} compounds, where the measured μ_{eff} are in agreement with the general observation that small changes in the ligand field strength or chromophore geometry tend to decrease the spin-only value of 4.2 BM. The lower values obtained may be attributed to the compressed tetrahedral environment present in the complexes. In such a ligand field, the $d_{x^2-y^2}$ and d_{z^2} atomic orbitals lie close in energy, allowing spin singlet, triplet, and quintet states to be thermally populated at room temperature.

Low temperature magnetic measurements were not performed because it has been verified through a number of investigations that this and analogous bridging units (naphthazarin, anthrarufin) do not allow magnetic exchange phenomena to be propagated through their extended π systems (17).

Electron paramagnetic resonance spectroscopy has been applied to determine the local environment of the Cu^{2+} lone electron. The epr spectra were recorded in pyridine and exhibit the characteristic features of tetragonally distorted complexes ($g_{\parallel} \gg g_{\perp} > g_e$) with a $d_{x^2-y^2}$ ground state (18) (Figs. 5–8). This is not surprising in view of the well established fact that pyridine readily forms adducts through the heterocyclic nitrogen lone pair. It must therefore be assumed that two pyridine molecules occupy the axial positions in the coordination sphere of Cu^{2+} thus forcing the two chelate rings to adopt a coplanar orientation.

Can. J. Chem. Downloaded from www.nrcresearchpress.com by 84.22.46.98 on 09/08/12
For personal use only.

TABLE 4. Electron paramagnetic resonance parameters obtained by fitting procedure*

Compound	$g_\parallel$	$g_\perp$	$A_\parallel$	$A_\perp$	α^2	k	ΔE	
I*b*	2.302	2.058	486	36	0.827	0.314	18.28	25.04
II*b*	2.303	2.058	489	36	0.826	0.314	18.31	25.05
III*b*	2.284	2.062	515	40	0.832	0.323	19.56	23.08

*The hyperfine tensor components are listed in units ($\times 10^{-4}$ cm^{-1}) while ΔE is measured in kK and its two values represent the $xy \rightarrow x^2 - y^2$ and $xz,yz \rightarrow x^2 - y^2$ transitions respectively.

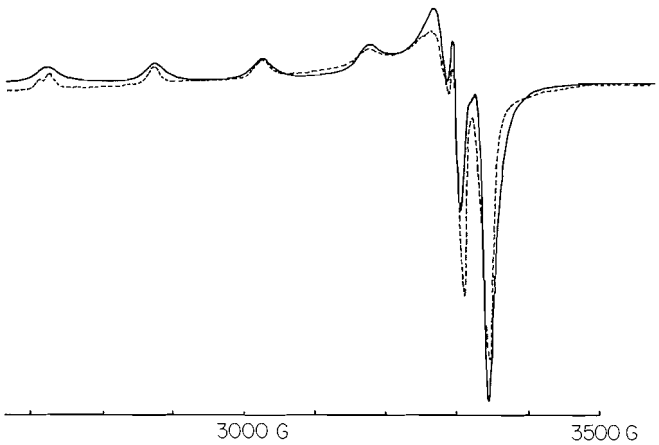

FIG. 5. The experimental (dashed line) and computer simulated (solid line) epr spectrum of **I***b* in pyridine.

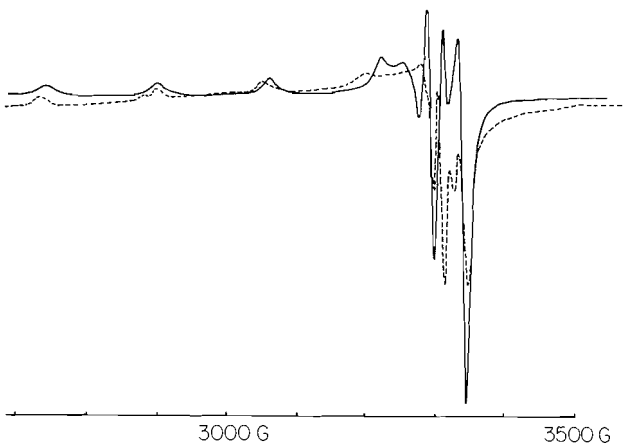

FIG. 6. The experimental and computer simulated epr spectrum of **II***b* in pyridine.

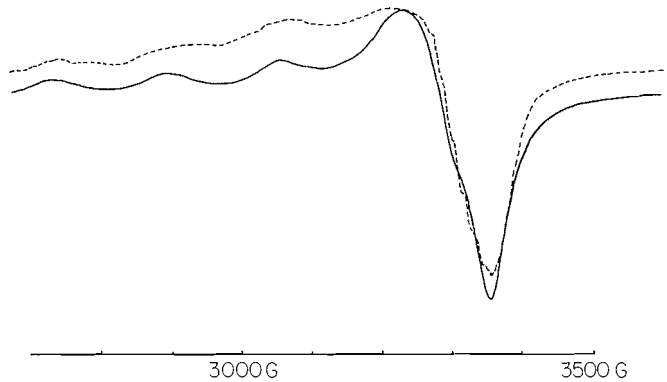

FIG. 7. The experimental and computer simulated epr spectrum of **III***b* in pyridine.

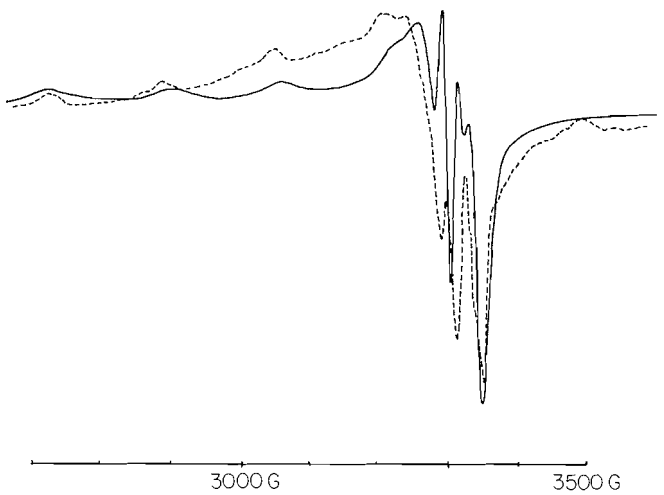

FIG. 8. The experimental and computer simulated epr spectrum of **II***b* in $CHCl_3$.

The parallel region of the spectra (lowfield) clearly shows the resolved Cu–hyperfine interaction while the perpendicular (highfield) is less resolved or even unresolved as in **III***b*. Furthermore, this region often renders additional difficulties in its analysis, as a result of the occurrence of extra splitting (19) or to a lesser extent from the nuclear quadruple splitting of the copper ion and the forbidden transitions ($\Delta M = \pm 1, \pm 2$) (20).

Regarding the terminal ligands, there seems to be no detectable change in the nature and parameters of the acac and bzac complexes, a fact readily understood since they both possess identical binding sites, the perturbation provoked by the aromatic ring in bzac being negligible. The case for sal is different though, owing to the strong π-withdrawing ability of the ligand. The consequence is a more electron deficient copper center, thus being more available for pyridine coordination and thus approaching a more regular elongated octahedral environment (Table 4).

More evidence is offered by the calculated $\Delta E(xy \rightarrow x^2 - y^2)$ and $\Delta E(xz,yz \rightarrow x^2 - y^2)$ transition energies where the effect of narrowing the gap between the d_{xy} and $d_{xz,yz}$ levels is quite clear. These data emerged via an analysis of the recorded spectra based on the expressions proposed by Vänngard (21) and McGarvey (22) for the $d_{x^2-y^2}$ ground state. The formulae used in the fitting procedure are:

$$g_\parallel = g_e - 8\lambda\alpha^2/\Delta E(xy \rightarrow x^2 - y^2)$$

$$g_\perp = g_e - 2\lambda\alpha^2/\Delta E(xz,yz \rightarrow x^2 - y^2)$$

$$A_\parallel = P|-K - 4\alpha^2/7 + \Delta g_\parallel + 3\Delta g_\perp/7|$$

$$A_\perp = P|-K + 2\alpha^2/7 + 11\Delta g_\perp/14|$$

During this procedure, λ and P were kept fixed at -828 and

Can. J. Chem. Downloaded from www.nrcresearchpress.com by 84.22.46.98 on 09/08/12
For personal use only.

350×10^{-4} cm^{-1}, respectively, while both α^2 and E were allowed to vary.

Frozen solution spectra in chloroform have also been recorded for the sake of comparison. The general characteristics of the spectra remain the same as those already discussed but now all three complexes were nearly identical (for **I***b*: $g_\parallel$ 2.279, $g_\perp$ 2.064, $A_\parallel$ 512, $A_\perp$ 47, and α^2 0.814, ΔE 19.49 and 21.85 respectively). This is a consequence of the weak coordinating ability of chloroform relative to that of pyridine, which allows the complexes to retain their originally distorted structures. The distortion, a common one in copper acetylacetonates, namely the stepped type distortion in which the chromophore remains essentially planar through the two heterocyclic rings form a dihedral angle that ranges from a few degrees to a few decades degrees (23).

The above assumption is further verified through the calculated E values which are less separated than those calculated from the spectra in pyridine (Table 4). Such a depression in energy separation of the d_{xy} and d_{xz} atomic levels is apparently the result of a small structural distortion away from the planar arrangement of the chromophore.

Conclusions

Quinizarin has proved to form readily homobinuclear mixed ligand complexes with first row transition elements. These complexes, neutral in character (uncharged) are characterized by two nearly identical six-membered heteroatomic chelate rings both with terminal oxygen atoms originating from the coordination of both the bridging and the peripheral ligands which are β-diketones or salicylic aldehyde. The two planes defined by quinizarin and the β-diketone, respectively, adopt an orientation intermediate between planar and tetrahedral relative to one another, the dihedral angle between them tending to lower in value on going from cobalt to copper as it can be deduced from the magnetic measurements and the epr spectral data presented.

Acknowledgment

The authors wish to express their thanks to Professor C. A. Tsipis for encouragement throughout this work.

1. T. Hanumaiah, G. S. R. Rao, C. P. Rao, K. V. J. Rao, H. J. Cowe, P. J. Cox, R. A. Howie, D. S. Marshall, and R. H. Thomson. Tetrahedron, **41**, 635 (1985).
2. F. Farina, M. T. Molina, and M. C. Paredes. Tetrahedron Lett. **26**, 111 (1985).
3. (*a*) E. M. Acton and G. L. Tong. J. Med. Chem. **24**, 669 (1981); (*b*) B. L. Van Duuren, A. Segal, S. S. Tseng, G. M. Rush, G. Loewengart, U. Mate, D. Roth, A. Smith, S. Melchionne, and I. Seidman. J. Med. Chem. **21**, 26 (1978).
4. (*a*) A. M. Tolati and V. W. Mistry. Labdev, Part A, **10**, 141 (1972); (*b*) J. J. O'Connell. U.S. Patent 3,192,236 (1965).
5. C. A. Tsipis, M. Sigalas, V. P. Papageorgiou, and M. N. Christianopoulou. Can. J. Chem. **61**, 1500 (1983).
6. C. A. Tsipis, E. Bakalbassis, V. P. Papageorgiou, and M. N. Christianopoulou. Can. J. Chem. **60**, 2477 (1982).
7. M. N. Christianopoulou. Polyhedron, **3**, 729 (1984).
8. H. S. El Khadem (*Editor*). Anthracycline antibiotics. Academic Press, New York. 1982.
9. V. P. Papageorgiou, M. N. Christianopoulou, L. L. Boutis, A. Papageorgiou, and C. A. Tsipis. Inorg. Chim. Acta, **124**, 203 (1986).
10. V. P. Papageorgiou, M. N. Christianopoulou, and C. A. Tsipis. U.S. Patent 4,560,782. 1985.
11. H. Budzikiewicz, C. Djerassi, and D. H. Williams. Structure elucidation of natural products by mass spectrometry. Vol. 2. Holden-Day, S. Fransisco. 1964. Chap. 28.
12. J. H. Bowie and P. Y. White. J. Chem. Soc. B, 89 (1969).
13. F. P. Dwyer and D. P. Mellor (*Editors*). Chelating agents and metal chelates. Academic Press, New York. 1964.
14. M. St. C. Flett. J. Chem. Soc. 1441 (1948).
15. (*a*) L. J. Bellamy and R. F. Branch. J. Chem. Soc. 4491 (1954); (*b*) K. Nakamoto, P. J. McCarthy, and A. E. Martell. J. Am. Chem. Soc. **83**, 1272 (1961).
16. R. J. Fitzgerald and G. R. Brubaker. Inorg. Chem. **8**, 2265 (1969).
17. D. N. Hendrickson. *In* Magnetostructural correlations in exchange coupled systems. *Edited by* R. D. Willett, D. Gatteschi, and O. Kahn. Reidel. 1985. p. 523.
18. E. I. Solomon, K. W. Penfield, and D. E. Wilcox. Struct. Bonding, **53**, 1 (1983).
19. I. V. Ovchinnicov and V. N. Konstantinov. J. Magn. Reson. **32**, 179 (1978).
20. R. L. Belford and D. C. Duan. J. Magn. Reson. **29**, 293 (1978).
21. T. Vanngard. *In* Biological applications of electron spin resonance. *Edited by* H. M. Swartz, J. R. Bolton, and D. C. Borg. John Wiley and Sons. 1972.
22. B. McGarvey. Transition metal chemistry. Vol. 3. *Edited by* R. L. Carlin. Dekker, New York. 1966. p. 90.
23. P. C. de Brun, W. D. Lyon, and H. A. Kuska. Inorg. Chem. **25**, 3106 (1986).

Can. J. Chem. Downloaded from www.nrcresearchpress.com by 84.22.46.98 on 09/08/12
For personal use only.

Mécanisme de réaction de mélanges méthane–chlore à haute température et faible taux de chlore

MARC CHAMBON, PAUL-MARIE MARQUAIRE ET GUY-MARIE CÔME[1]

Département de chimie physique des réactions, Centre national de la recherche scientifique (Unité associée 328), Institut national polytechnique de Lorraine (École nationale supérieure des industries chimiques) et Université de Nancy I, 1, rue Grandville, 54000 Nancy, France

Reçu le 11 août 1986

MARC CHAMBON, PAUL-MARIE MARQUAIRE et GUY-MARIE CÔME. Can. J. Chem. **65**, 1491 (1987).

Un brevet déposé par S. W. Benson en 1980 indique qu'une flamme chlore–méthane produit de l'éthane et de l'éthylène. Suite à ce brevet, nous avons effectué une étude fondamentale de la réaction à l'aide d'un réacteur continu agité isotherme, à des températures comprises entre 800 et 1000°C, à pression subatmosphérique, à faible taux de chlore (1% environ en volume) et à des temps de passage de l'ordre de 1 s. Dans ces conditions, la réaction conduit aux produits carbonés CH_3Cl, C_2H_4, C_2H_6 et C_3H_6 essentiellement. Le pourcentage du méthane converti transformé en hydrocarbures non chlorés croît avec la température et atteint 77% à 1000°C. Un mécanisme radicalaire qui rend compte des présentes observations est proposé et analysé.

MARC CHAMBON, PAUL-MARIE MARQUAIRE, and GUY-MARIE CÔME. Can. J. Chem. **65**, 1491 (1987).

A patent of Benson (1980) states that a methane/chlorine flame produces some ethane and some ethylene. A fundamental study of the reaction has been carried out using an isothermal, continuous, stirred reactor operated at temperatures varying from 800 to 1000°C, at subatmospheric pressures, at low concentrations of chlorine (about 1% by volume), and with reaction times of about 1 s. Under these conditions, the reaction leads mainly to the formation of the following carbon compounds: CH_3Cl, C_2H_4, C_2H_6, and C_3H_6. The percentage of methane that is transformed into non-chlorinated hydrocarbons rises with the temperature and reaches a level of 77% at 1000°C. A radical mechanism which takes into account all the data is proposed and analysed.

[Journal translation]

Introduction

La valorisation chimique du méthane, compte-tenu notamment des disponibilités en gaz naturel, suscite actuellement un vif intérêt et des recherches dans de nombreuses directions (cf. par exemple, réfs. 1 et 2).

En particulier, un procédé, suggéré par Benson en 1980 (3), consiste à faire une flamme de méthane et de chlore dans des rapports molaires compris entre 1:1 et 10:1, dont la température adiabatique est comprise entre 700 et 1710°C, la pression voisine de 1 atmosphère (101,3 kPa), et la durée de réaction de quelques millisecondes; la réaction conduite dans ces conditions est réputée conduire essentiellement à de l'*ethane* et à de l'*éthylène* d'une part, et à de l'*hydrogène* et de l'*acide chlorhydrique* d'autre part. Comme il est d'usage dans les brevets, aucune explication théorique n'est avancée pour rendre compte des revendications.

Dans une publication (4) postérieure au brevet, Weissmann et Benson présentent les résultats d'une étude de la *pyrolyse du chlorure de méthyle* effectuée de 924 à 1127°C en réacteur continu avec des temps de passage de 0,03 à 0,3 s. Les produits principaux de la réaction sont HCl, CH_4, C_2H_2 et C_2H_4, des produits mineurs étant C_6H_6, C_3H_6, C_2H_5Cl, $C_2H_4Cl_2$, etc.; du charbon, de la suie sont observés. Weissmann et Benson (4) proposent un mécanisme réactionnel détaillé pour rendre compte de leurs observations expérimentales relatives à la pyrolyse de CH_3Cl. À la suite de cette analyse, ils estiment que la réaction décrite dans le brevet (3) a lieu en *deux phases consécutives, la chloration du méthane en chlorure de méthyle, suivie de la pyrolyse de ce dernier*; l'argument essentiel avancé est que la formation de CH_3Cl à partir de chlore et de méthane s'effectue par une réaction en chaînes très rapide. Cette conclusion constitue évidemment une justification de leur étude.

En 1983, lorsque nous avons entrepris nos travaux sur la réaction de mélanges Cl_2/CH_4 à «haute» température, il n'existait alors aucune tentative d'élucidation dans ces conditions du mécanisme de la réaction, et ce fait persiste dans une large mesure. L'importance pratique potentielle du procédé (2) incitait, et incite toujours, à une meilleure compréhension des phénomènes.

Protocole expérimental

L'élucidation d'un mécanisme réactionnel nécessite de bien maîtriser les variables d'état du système. Ceci explique que nous ayons fait choix du réacteur continu agité, fonctionnant en régime permanent, à température et à pression constantes, et mis en oeuvre selon une technique maintenant classique au laboratoire (6).

La réaction des mélanges méthane–chlore a été étudiée à des températures comprises entre 1081 et 1273 K, des pressions de 170 et 577 Torr (1 Torr = 133,3 Pa), des temps de passage compris entre 0,8 et 1,6 s et des taux de chlore $[Cl_2]_0/[CH_4]_0$ compris entre 0,42 et 1,2%, c'est-à-dire dans des conditions très différentes à certains égards du brevet (3).

À titre de référence, la pyrolyse de méthane pur a été étudiée à 1181 K, 570 Torr et des temps de passage compris entre 0,8 et 2 s.

Les réactifs chlore et méthane ont été fournis par la Société «L'Air Liquide» et contiennent des teneurs très faibles en impuretés.

L'analyse des produits de réaction a été effectuée par chromatographie en phase gazeuse.

Résultats expérimentaux

Les produits suivants, par ordre d'importance décroissante, ont été mis en évidence : CH_3Cl, C_2H_4, C_2H_6, C_3H_6, C_2H_2, des traces de $CH_3—C{\equiv}CH$ et d'un composé qui pourrait être $CH_3—CH_2—CH_2—CH_3$ ou $CH_3—CH_2—CH{=}CH_2$. Du «charbon» se forme en quantités variables selon les conditions opératoires.

On ne peut pas conclure si $CH_2{=}C{=}CH_2$ est formé ou non, car il n'est pas séparé de CH_3Cl en chromatographie. On n'a pas recherché de produits ayant plus de 4 atomes de carbone. HCl, Cl_2 et H_2 n'ont pas été analysés quantitativement jusqu'à présent.

Les produits suivants n'ont pas été décelés, au moins

1. Auteur à qui adresser toute correspondance.

Can. J. Chem. Downloaded from www.nrcresearchpress.com by 72.64.146.136 on 09/07/12
For personal use only.

TABLEAU 1. Influence de la température et du taux de chlore sur les concentrations des produits carbonés de la réaction en sortie du réacteur, pour un temps de passage de 1 seconde

P(Torr)	T(K)	x(%)	$[CH_3Cl]$	$[C_2H_6]$	$[C_2H_4]$	$[C_2H_2]$	$[C_3H_6]$
300	1023	0,4	$1,5\times10^{-5}$	$7,5\times10^{-8}$	$3,7\times10^{-8}$	0	0
	1181		$1,1\times10^{-5}$	$1,3\times10^{-6}$	$2,1\times10^{-6}$	$4,9\times10^{-8}$	$1,3\times10^{-7}$
577	1181	0	0	$2,4\times10^{-7}$	0	0	0
		0,4	$2,0\times10^{-5}$	$3,7\times10^{-6}$	$4,6\times10^{-6}$	$1,9\times10^{-7}$	$3,4\times10^{-7}$
		0,8	$3,7\times10^{-5}$	$5,0\times10^{-6}$	$1,1\times10^{-5}$	$3,8\times10^{-7}$	$8,1\times10^{-7}$

NOTA : P, pression totale dans le réacteur; T, température de réaction; x, pourcentage molaire de chlore à l'entrée du réacteur, $x = [Cl_2]_0/([CH_4]_0 + [Cl_2]_0)$. Les concentrations sont exprimées en mol L^{-1}.

dans quelques expériences : CH_3—CH_2Cl, CH_2Cl—CH_2Cl, CH_2=$CHCl$, CH_2Cl_2, $CHCl_3$, CCl_4, C_3H_8.

La pyrolyse du méthane «pur» (sans chlore ajouté), dans des conditions similaires, conduit uniquement à de l'éthane.

Des résultats typiques, mettant en évidence l'influence de la température et du taux de chlore sur la réaction sont présentés dans le tableau 1.

Toutes choses égales par ailleurs, on constate que la quantité de méthane chloré décroît avec la température, tandis que les quantités de méthane transformées en hydrocarbures non chlorés croissent fortement, ainsi que la proportion d'hydrocarbures insaturés parmi ces derniers.

Toutes choses égales par ailleurs, l'accroissement du pourcentage de chlore à l'entrée du réacteur entraîne un accroissement important du taux de transformation du méthane. C'est ainsi qu'à 577 Torr, 1181 K, l'addition de 0,4% de chlore au méthane entraîne une multiplication par un facteur de l'ordre de 50 de la quantité de méthane transformée. Par ailleurs, le chlore a pour effet d'augmenter les quantités de méthane chloré ou transformées en hydrocarbures non chlorés et spécialement parmi ceux-ci les hydrocarbures insaturés.

Mécanisme réactionnel

Le mécanisme de pyrolyse du méthane pur paraît bien établi (cf. par exemple, réf. 7), de même que celui de chloration du méthane à «basse» température (cf. par exemple, réf. 5). D'une manière plus générale, les mécanismes de chloration d'hydrocarbures ou de pyrolyse d'hydrocarbures chlorés paraissent compris dans leurs grandes lignes, même si de nombreux points restent ouverts à la discussion (4, 5, 8–10).

Il paraît raisonnable, dans un premier temps, de chercher à rendre compte de nos résultats par un mécanisme radicalaire homogène. Nous discuterons tout d'abord le mécanisme primaire.

1. Mécanisme primaire

Il comporte les processus suivants :

Amorçages

[1] $CH_4 \rightarrow CH_3\cdot + H\cdot$

[2] $Cl_2 + M \rightarrow 2Cl\cdot + M$

Transferts

[3] $H\cdot + CH_4 \rightarrow H_2 + CH_3\cdot$

[4] $H\cdot + Cl_2 \rightarrow HCl + Cl\cdot$

Propagations

[5] $CH_3\cdot + Cl_2 \rightarrow CH_3Cl + Cl\cdot$

[6] $Cl\cdot + CH_4 \rightarrow HCl + CH_3\cdot$

Terminaison

[7] $2\,CH_3\cdot \rightarrow C_2H_6$

Les processus de terminaison consistent en principe en la recombinaison 2 à 2 des radicaux libres H·, Cl· et CH_3·. Mais, d'une part, les combinaisons d'atomes libres nécessitent des triples chocs et peuvent donc être négligées par rapport aux autres processus de terminaison. Il ne reste donc en compétition que les processus

[7′] $CH_3\cdot + Cl\cdot \rightarrow CH_3Cl$

et

[7″] $CH_3\cdot + H\cdot \rightarrow CH_4$

et le processus [7]. Les réactivités des radicaux libres Cl·, H· et CH_3· sont du même ordre de grandeur, mais la concentration de méthane étant très supérieure à celle du chlore, il s'ensuit que Cl· et H· sont beaucoup moins concentrés que CH_3·. La terminaison prépondérante s'effectue donc par le processus [7].

En appliquant l'approximation de l'état quasi stationnaire aux atomes et radicaux libres, on obtient les expressions suivantes des vitesses de formation des deux produits carbonés :

$$r_{C_2H_6} = k_1[CH_4] + k_2[Cl_2][M]$$

$$r_{CH_3Cl} = \frac{k_5}{k_7^{1/2}}(k_1[CH_4] + k_2[Cl_2][M])^{1/2}[Cl_2]$$

d'où l'on déduit :

$$\lambda = \frac{r_{CH_3Cl}}{r_{C_2H_6}} = \frac{k_5[Cl_2]}{k_7^{1/2}(k_1[CH_4] + k_2[Cl_2][M])^{1/2}}$$

C'est essentiellement à la discussion des variations du rapport λ avec la température que nous allons nous attacher, $[Cl_2]$, $[CH_4]$ et [M] étant supposés constants. Les valeurs des énergies d'activation E_5, E_7, E_1 et E_2 étant de l'ordre de 2, 0, 108 et 49 kcal mol^{-1} respectivement (7–10), il est clair que l'énergie d'activation «apparente» E_λ du terme λ est fortement négative, et ceci quelles que soient les importances respectives des vitesses d'amorçage par les processus [1] et [2]. On peut donc tirer les conclusions suivantes :

À basse température, le produit primaire principal carboné est CH_3Cl et la réaction a lieu en *chaînes longues*, comme il est bien connu, ce qui conduit à la stoechiométrie principale :

$$CH_4 + Cl_2 = CH_3Cl + HCl$$

Au fur et à mesure que la température augmente, le rapport λ diminue et, à haute température, le produit primaire principal carboné de la réaction devient C_2H_6, la *réaction par stades*

Can. J. Chem. Downloaded from www.nrcresearchpress.com by 72.64.146.136 on 09/07/12
For personal use only.

Can. J. Chem. Downloaded from www.nrcresearchpress.com by 72.64.146.136 on 09/07/12
For personal use only.

d'équation stoechiométrique

$$2CH_4 + Cl_2 = C_2H_6 + 2HCl$$

étant alors prépondérante, ce qui signifie que la vitesse du processus [5] est négligeable par rapport à celle du processus [7].

2. Mécanisme secondaire

Les deux produits primaires carbonés sont CH_3Cl et C_2H_6, ils interviennent donc comme réactifs dans le mécanisme secondaire, il s'ensuit que les radicaux libres secondaires sont $CH_2Cl\cdot$ et $C_2H_5\cdot$. Ces radicaux sont impliqués dans les processus de propagation suivants, où RH désigne n'importe quelle molécule possédant un atome d'hydrogène labile :

[8] et [-8] $CH_2Cl\cdot + RH \rightleftarrows CH_3Cl + R\cdot$

[9] $CH_2Cl\cdot + Cl_2 \rightarrow CH_2Cl_2 + Cl\cdot$

[10] $C_2H_5\cdot \rightarrow C_2H_4 + H\cdot$

[11] et [-11] $C_2H_5\cdot + RH \rightleftarrows C_2H_6 + R\cdot$

[12] $C_2H_5\cdot + Cl_2 \rightarrow C_2H_5Cl + Cl\cdot$

Parmi les produits secondaires nouveaux issus de processus de propagation, nous avons observé uniquement la formation de C_2H_4, mais ni celle de CH_2Cl_2, ni celle de C_2H_5Cl. Nous sommes donc amenés à conclure que, dans nos conditions, les processus [9] et [12] sont négligeables, et que le processus [10] est au minimum compétitif par rapport au processus [11].

L'explication de ces faits réside pour une part importante dans le caractère β ou μ (11) des radicaux libres, caractère susceptible du reste d'évoluer selon les conditions expérimentales (12). C'est ainsi que le radical $CH_2Cl\cdot$ est de caractère β, c'est-à-dire qu'il ne peut réagir que dans des processus bimoléculaires, alors que le radical $C_2H_5\cdot$ possède également un caractère μ, c'est-à-dire qu'il peut se décomposer monomoléculairement en donnant naissance à une molécule insaturée. Toutes choses égales par ailleurs, et notamment les concentrations des réactifs moléculaires impliqués dans les métathèses, le caractère μ du radical $C_2H_5\cdot$ l'emporte de plus en plus sur son caractère β lorsque la température augmente. Ceci permet de comprendre que, la température étant assez élevée et la concentration de chlore assez faible dans nos conditions, le processus [10] conduisant à l'éthylène soit prépondérant par rapport au processus [12] qui conduit au chlorure d'éthyle.

Le caractère essentiellement μ du radical $C_2H_5\cdot$ *dans nos conditions* comporte également des conséquences importantes au niveau des processus de terminaison qui ne peuvent faire intervenir que des radicaux de type β. Ceci conduit notamment à l'exclusion des recombinaisons des radicaux éthyles donnant du *n*-butane ou des radicaux éthyle et méthyle conduisant au propane, conclusion compatible avec nos résultats expérimentaux. Il reste donc uniquement à considérer les combinaisons des radicaux $CH_3\cdot$ et $CH_2Cl\cdot$, soit :

[13] $CH_3\cdot + CH_2Cl\cdot \rightarrow C_2H_5Cl$

[14] $2\,CH_2Cl\cdot \rightarrow CH_2Cl{-}CH_2Cl$

Or nous n'observons ni la formation de C_2H_5Cl ni celle de $CH_2Cl{-}CH_2Cl$, ce qui revient à dire que les processus de terminaison [13] et [14] sont négligeables par rapport au processus de terminaison [7], ou, ce qui revient au même, que *la concentration du radical $CH_2Cl\cdot$ est négligeable par rapport à celle de $CH_3\cdot$*. Cette conclusion est confortée par l'absence de formation de CH_2Cl_2 par le processus [9], à comparer avec la formation importante de CH_3Cl par le processus [5].

Pour les raisons déjà évoquées lors de l'analyse du mécanisme primaire, il n'y a pas lieu de tenir compte des terminaisons impliquant les atomes libres $Cl\cdot$ et $H\cdot$.

Nous examinerons en dernier lieu les réactions de HCl et H_2, produits primaires non carbonés. Ils peuvent intervenir par les processus de métathèse :

$$R\cdot + HCl \rightarrow RH + Cl\cdot$$

$$R\cdot + H_2 \rightarrow RH + H\cdot$$

ce qui n'introduit ni produits, ni radicaux libres nouveaux, mais peut éventuellement modifier la répartition entre ces derniers. Il en sera de même dans les mécanismes tertiaire et quaternaire. En outre, dans nos conditions, les concentrations de HCl et H_2 sont faibles, par rapport à CH_4 tout au moins, ce qui devrait limiter leurs effets. Par ailleurs, HCl est réputé avoir peu ou pas d'effet sur les pyrolyses de CH_3Cl (4) et de C_2H_6 (13).

3. Mécanisme tertiaire

L'analyse faite ci-dessus montre que, dans nos conditions, le seul produit secondaire nouveau est l'éthylène. Ce corps peut donner lieu, non seulement à des réactions de métathèse, mais également à des réactions d'additions ce qui n'était pas le cas des hydrocarbures saturés impliqués dans les mécanismes primaires et secondaires.

Les processus d'addition ne font intervenir que les radicaux libres prépondérants du milieu réactionnel, c'est-à-dire essentiellement $CH_3\cdot$ et, dans une certaine mesure, $C_2H_5\cdot$, soit :

[15] et [-15] $CH_3\cdot + C_2H_4 \rightleftarrows CH_3{-}CH_2{-}CH_2\cdot$

[16] et [-16] $C_2H_5\cdot + C_2H_4 \rightarrow CH_3{-}CH_2{-}CH_2{-}CH_2\cdot$

Les radicaux formés étant de type μ vont se décomposer monomoléculairement :

[17] $CH_3{-}CH_2{-}CH_2\cdot \rightarrow CH_3{-}CH{=}CH_2 + H\cdot$

[18] $CH_3{-}CH_2{-}CH_2{-}CH_2\cdot \rightarrow CH_3{-}CH_2{-}CH{=}CH_2 + H\cdot$

On observe bien la formation de propène, mais seulement celle de traces d'un composé susceptible d'être le butène-1. Ces résultats confirment à nouveau le caractère μ du radical $C_2H_5\cdot$ dans nos conditions, et le fait que l'on peut négliger le processus [16] et par conséquent [18].

REMARQUE : L'addition de l'atome de chlore sur l'éthylène suivie de la décomposition monomoléculaire du radical libre formé par perte d'un atome d'hydrogène aboutit à la formation de chlorure de vinyle, non détecté dans nos conditions. Ceci confirme l'hypothèse faite lors de l'élaboration du mécanisme primaire, à savoir que l'atome de chlore est en concentration négligeable par rapport aux radicaux libres méthyles.

L'éthylène peut également réagir par métathèse :

[19] $R\cdot + C_2H_4 \rightarrow RH + C_2H_3\cdot$

[20] $C_2H_3\cdot \rightarrow C_2H_2 + H\cdot$

On observe bien effectivement la formation d'acétylène.

REMARQUE : Il est logique que $CHCl_3$ ne soit pas formé, dans la mesure où son précurseur «secondaire» CH_2Cl_2 ne l'est pas.

4. Mécanisme quaternaire

Il y aurait lieu de considérer ici systématiquement les réactions d'addition et de métathèse impliquant le propène et l'acétylène et les décompositions monomoléculaires subséquentes de radicaux libres, comme il a été fait pour l'éthylène, mais nous nous limiterons aux quelques processus conduisant à des produits observés ou potentiellement formés.

Additions

[21] et [-21] $CH_3\cdot + C_2H_2 \rightleftarrows CH_3—CH{=}CH\cdot$

Métathèses

[22] $R\cdot + CH_3—CH{=}CH_2 \rightarrow RH + \cdot CH_2—CH{=}CH_2$

[23] $R\cdot + C_2H_2 \rightarrow RH + CH{\equiv}C\cdot$

Décompositions

[24] $CH_3—CH{=}CH\cdot \rightarrow CH_3—C{\equiv}CH + H\cdot$

[25] $CH{\equiv}C\cdot \rightarrow$ «charbon» + $H\cdot$

[26] $\cdot CH_2—CH{=}CH_2 \rightarrow CH_2{=}C{=}CH_2 + H\cdot$

REMARQUE : Le processus [25] décrit la formation de «charbon» de manière très formelle, bien qu'il soit clair que l'acétylène soit le précurseur habituel des suies, etc. (cf. par exemple ref. 14).

5. Discussion du mécanisme global

Le mécanisme radicalaire construit ci-dessus, selon les principes généraux de la cinétique des réactions en phase gazeuse, conduit au *schéma réactionnel* suivant indiquant la «filiation» des différents produits carbonés de réaction observés dans nos conditions :

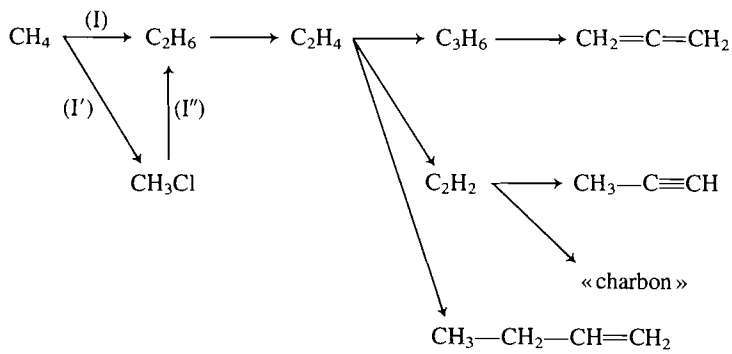

Le mécanisme, et le schéma qui en est déduit, rendent compte de façon remarquable des caractéristiques que nous avons observées, au minimum d'un point de vue qualitatif; ils permettent notamment de comprendre l'influence de la température sur la sélectivité de la réaction.

En effet, le premier fait important, dans la réaction thermique de mélanges méthane–chlore, consiste dans la *diminution de la longueur de chaînes primaire avec la température*, qui se traduit par une production primaire croissante de C_2H_6 (voie I) au détriment de CH_3Cl (voie I'). Cette évolution est du reste «aggravée» par le fait que CH_3Cl donne également potentiellement naissance, dans nos conditions du moins, à C_2H_6 (voie I''), par les processus suivants :

$$CH_3Cl \rightarrow CH_3\cdot + Cl\cdot$$

$$Cl\cdot + CH_4 \rightarrow HCl + CH_3\cdot$$

$$2CH_3\cdot \rightarrow C_2H_6$$

Par ailleurs, le schéma réactionnel ci-dessus montre que tous les hydrocarbures non-chlorés proviennent du précurseur C_2H_6.

À partir de ces deux faits, il est immédiat de déduire que le pourcentage de méthane converti transformé en hydrocarbures non-chlorés croît avec la température, toutes autres choses égales par ailleurs, en accord avec nos constatations expérimentales.

Le mécanisme réactionnel explique la formation des diverses molécules insaturées par des réactions de métathèse et d'addition radicalaires suivies d'une décomposition unimoléculaire des radicaux libres ainsi formés. Ceci est dû à un deuxième fait important, très caractéristique des réactions radicalaires, et qui est le *caractère μ prédominant des radicaux libres alcoyles* (à l'exclusion des radicaux méthyle) *à température suffisamment élevée*. Il n'est donc pas étonnant que le pourcentage de molécules insaturées parmi les hydrocarbures non-chlorés formés croisse avec la température.

Enfin, on peut observer que le processus d'amorçage [2] et les processus de propagation impliquant Cl_2 et $Cl\cdot$ permettent de comprendre aisément l'effet fortement accélérateur de Cl_2 sur le taux de transformation de CH_4.

Conclusion

Le mécanisme réactionnel radicalaire proposé ici permet de rendre compte, de façon qualitative au moins, des observations que nous avons effectuées sur la réaction chlore–méthane vers 900°C et à faible taux de chlore. Il n'est pas possible d'appliquer tel quel ce mécanisme, compte-tenu des nombreuses simplifications résultant des conditions opératoires particulières pour lesquelles il a été établi, à des domaines expérimentaux différents : la flamme chlore–méthane (3), la pyrolyse du chlorure du méthyle (4), bien qu'il soit évident que de nombreuses conclusions soient déjà aisément transposables, telles que nature des produits formés, influence de la température sur les sélectivités. Il sera nécessaire de procéder à l'écriture d'un mécanisme beaucoup plus complet et à une identification quantitative du modèle ainsi créé, appuyée éventuellement sur des résultats expérimentaux ad hoc. Ce mécanisme, généralisant celui présenté dans cet article, permettra de répondre à la question évoquée en la référence 4 de l'importance relative des voies [I] et [I', I''] dans la formation de l'éthane, selon les niveaux de température et de taux de chlore. La simulation à partir d'un tel modèle permettrait également de prévoir l'exis-

Can. J. Chem. Downloaded from www.nrcresearchpress.com by 72.64.146.136 on 09/07/12
For personal use only.

tence de conditions opératoires, probablement très restrictives, où les produits formés seraient différents; on peut citer ici le chlorure de vinyle, et on comprend alors aisément l'importance d'une telle approche mécanistique.

Remerciements

La recherche a été financée en partie par le Ministère de la Recherche et de la Technologie (DDSTI), Action «Procédés de Fabrication de Produits Chimiques» (Contrat n° 82 F 0832).

1. H. GUERIN, L. PAUGAM et R. BOULITROP. Encyclopaedia Universalis, Supplément I, Le Savoir. 1981. pp. 282–290.
2. M. E. FRANCK et C. J. MIKULKA. Functionalization of methane. The American Institute of Chemical Engineers, Spring National Meeting, New Orleans, Louisiana, U.S.A. 1986.
3. S. W. BENSON. Brevet U.S. N° 4 199 533 (1980).
4. M. WEISSMANN et S. W. BENSON. Int. J. Chem. Kinet. **16**, 307 (1984).
5. B. E. KURTZ. Ind. Eng. Chem. Process Des. Dev. **11**, 332 (1972).
6. P. M. MARQUAIRE et G. M. CÔME. React. Kinet. Catal. Lett. **9**, 165 (1978); P. AZAY et G. M. CÔME. Ind. Eng. Chem. Process Des. Dev. **18**, 754 (1979); P. AZAY, P. M. MARQUAIRE, P. POMMIER et G. SCACCHI. J. Chem. Educ. **5**, 441 (1981).
7. M. H. BACK et R. A. BACK. *Dans* Pyrolysis : theory and industrial practice. Academic Press, New York. 1983. p. 1.
8. G. CHILTZ, P. GOLDFINGER, G. HUYBRECHTS et G. VERBEKE. Chem. Rev. **63**, 355 (1963).
9. A. MACCOLL. Chem. Rev. **69**, 33 (1969).
10. A. C. LLOYD. Int. J. Chem. Kinet. **3**, 39 (1971).
11. P. GOLDFINGER, M. LETORT et M. NICLAUSE. *Dans* Contribution à l'étude de la structure moléculaire. Desoer, Liège, Belge. 1947–1948. p. 283.
12. D. A. LEATHARD. Communication au premier symposium international «Gas Kinetics», Szeged, Hongrie. Preprints. 1969. p. 263.
13. J. MULLER, F. BARONNET, G. SCACCHI, M. DZIERZYNSKI et M. NICLAUSE. Int. J. Chem. Kinet. **9**, 425 (1977).
14. D. L. TRIMM. *Dans* Pyrolysis : theory and industrial practice. Academic Press, New York. 1983. p. 203.

Can. J. Chem. Downloaded from www.nrcresearchpress.com by 72.64.146.136 on 09/07/12
For personal use only.

The structure and internal rotational barrier of 3-phenyl-1-propyne by molecular orbital calculations and the *J* method

TED SCHAEFER AND GLENN H. PENNER
Department of Chemistry, University of Manitoba, Winnipeg, Man., Canada R3T 2N2

Received January 7, 1987

TED SCHAEFER and GLENN H. PENNER. Can. J. Chem. **65**, 1496 (1987).

The ^1H nuclear magnetic resonance spectral parameters are reported for 3-phenyl-1-propyne dissolved in CCl_4, C_6D_6, and in acetone-d_6. The long-range spin–spin coupling constants imply very small and perhaps vanishing barriers to internal rotation about the C_{sp^2}—C_{sp^3} bond in all three solutions, in contrast to benzyl cyanide in which there exist significant solvent perturbations of the internal barrier. STO 3G MO computations, utilizing geometry optimization procedures, imply an internal rotational potential of $V/\text{kJ mol}^{-1} = -2.8 \sin^2\psi - 0.6 \sin^2 2\psi$; the angle ψ is 90° when the C≡C bond lies in a plane perpendicular to the benzene plane. 6-31G MO energies imply $V/\text{kJ mol}^{-1} = -0.3 \sin^2\psi - 0.4 \sin^2 2\psi$, the fourfold component being larger than the twofold. A flat minimum occurs near $\psi = 50°$.

TED SCHAEFER et GLENN H. PENNER. Can. J. Chem. **65**, 1496 (1987).

On a déterminé les paramètres spectraux, en résonance magnétique nucléaire du ^1H, du phényl-3 propyne-1 dissous dans le CCl_4, le C_6D_6 ou dans l'acétone-d_6. Les constantes de couplage spin–spin à longue distance impliquent que, dans le trois solutions, les barrières à la rotation interne autoure de la liaison C_{sp^2}—C_{sp^3} sont très faibles ou inexistantes; ces résultats contrastent avec ceux obtenus avec le cyanure de benzyle, dans lequel les solvants perturbent fortement la barrière interne. Des calculs d'OM STO 3G, faisant appel à des procédés d'optimisation de la géométrie, impliquent que le potentiel à la rotation interne $V/\text{kJ mol}^{-1} = -2{,}8 \sin^2\psi - 0{,}6 \sin^2 2\psi$; l'angle ψ est égal à 90° lorsque la liaison C≡C se trouve dans un plan qui est perpendiculaire au plan du benzène. Les énergies évaluées à l'aide de calculs d'OM 6-31G impliquent que $V/\text{kJ mol}^{-1} = -0{,}3 \sin^2\psi - 0{,}4 \sin^2 2\psi$; la composante quaternaire est plus importante que la composante binaire. On retrouve un minimum aplati autour de $\psi = 50°$.

[Traduit par la revue]

Introduction

The internal barriers to rotation about the C_{sp^2}—C_{sp^3} bond in a number of benzyl X compounds (e.g. X = F, Cl, CN) have been measured in solution by means of the *J* method (1–3). For $^1H,^1H$ couplings the latter depends on the relationship, $^6J(H,CH_2) = {}^6J_{90}\langle\sin^2\theta\rangle$, where $^6J(H,CH_2)$ is the long-range spin–spin coupling constant over six bonds between the *para* and methylene protons (4, 5).

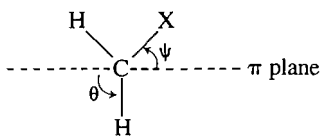

1

The angle θ is the angle by which the α C—H bond twists out of the benzene plane, as in **1**, and $^6J_{90}$ is the value of $^6J(H,CH_2)$ when $\theta = 90°$. The expectation value of $\langle\sin^2\theta\rangle$ can be related to the internal barrier by a hindered rotor model (5) or by a classical averaging procedure.

For X = F, Cl, CN the internal barrier depends on the polarity of the solvent (1–3). Although the twofold barriers for X = F, Cl are quite different in magnitude, being about 1 kJ/mol for benzyl fluoride and about 9 kJ/mol for benzyl chloride in CS_2 solution, the conformations with $\psi = 90°$ are both stabilized by about 2 kJ/mol in passing from CS_2 to the polar acetone-d_6 solutions. Presumably these phenomena are a consequence of electrostatic stabilization of the more polar perpendicular conformer, that with $\psi = 90°$ (6). In benzyl cyanide the internal barrier is rather small in CS_2 solution, in the vicinity of 1 kJ/mol, and contains an appreciable fourfold component (3). Again, polar solvents increase the stability of the perpendicular conformer.

Some molecular orbital computations (1–3) agree rather well with the barriers deduced in solution for X = F, Cl, CN. Furthermore, for hydrocarbons such as styrene, quantitative agreement exists between experiment and results at the 6-31 G level of *ab initio* molecular orbital theory (7). While benzyl cyanide is rather polar, its dipole moment being about 3.5 D (8), that of 3-phenyl-1-propyne must be rather smaller, while retaining a triple bond in the X substituent. This paper reports molecular orbital computations of the structure and internal rotational barrier in the latter molecule. In addition, the ^1H nmr spectra in CCl_4, C_6D_6, and acetone-d_6 are analyzed. The spectral parameters indicate a very small barrier, essentially independent of solvent, and in agreement with the molecular orbital results.

Results and discussion

Molecular orbital calculations

Energies for optimized geometries, but holding the carbon framework as a planar hexagon, were computed at 15° intervals of ψ (seven values) at the STO 3G level of *ab initio* molecular orbital theory (409 m of cpu time). The minimum energy of −341.197 092 au occurred at $\psi = 90°$. The relative energies are represented by eq. [1]. The errors in the twofold and fourfold

$$[1] \quad V/\text{kJ mol}^{-1} = -2.78(4) \sin^2\psi - 0.64(4) \sin^2 2\psi$$

components are given at the 95% confidence level. At 300 K a classical averaging procedure then yields $\langle\sin^2\psi\rangle$ as 0.626, $\langle\sin^2\theta\rangle$ as 0.437, and $\langle\psi\rangle$ as 54.1°.

It is known that 6-31G computations may be more reliable for hydrocarbons than are those with minimal basis sets, as for styrene, for example (7, 9). They are also much more expensive. Hence the 6-31G calculations were performed with geometry optimization only at $\psi = 0$, 45, and 90° (total cpu time of 32 h). The three energies yield eq. [2]

$$[2] \quad V(\psi)/\text{kJ mol}^{-1} = -0.27 \sin^2\psi - 0.43 \sin^2 2\psi$$

implying $\langle\sin^2\psi\rangle$ as 0.513, $\langle\sin^2\theta\rangle$ as 0.494, and $\langle\theta\rangle$ as 47.6° at

Can. J. Chem. Downloaded from www.nrcresearchpress.com by 72.64.146.136 on 09/07/12
For personal use only.

TABLE 1. The ^{1}H nmr spectral parameters of 3-phenyl-1-propyne at 300.135 MHz and 300 K

Parameter	CCl_4[a]	C_6D_6[b]	Acetone-d_6[c]
ν(C≡C—H)	605.331(1)[d]	573.315(1)[d]	776.329(1)[d]
$\nu(CH_2)$	1059.732(1)	974.940(1)	1085.000(1)
ν_2	2179.202(1)	2152.285(1)	2209.947(1)
ν_3	2167.225(1)	2129.353(1)	2195.048(1)
ν_4	2141.826(1)	2107.542(1)	2168.858(1)
^4J(C≡C—H,CH_2)	−2.775(1)[e]	−2.760(1)[e]	−2.776(1)[e]
$^3J_{23}$	7.736(1)	7.735(1)	7.741(1)
$^3J_{34}$	7.458(1)	7.458(1)	7.458(1)
$^4J_{26}$	1.973(1)	1.974(1)	1.969(1)
$^4J_{24}$	1.248(1)	1.246(1)	1.244(1)
$^4J_{35}$	1.450(1)	1.459(1)	1.460(1)
$^5J_{25}$	0.592(1)	0.594(1)	0.599(1)
^4J(H,CH_2)	−0.782(1)	−0.779(1)	−0.774(1)
^5J(H,CH_2)	0.320(1)	0.321(1)	0.316(1)
^6J(H,CH_2)	−0.601(1)	−0.593(1)	−0.591(1)
Calculated transitions	768	772	768
Assigned transitions	550	621	571
Largest difference	0.021	0.022	0.021
Root mean square deviation	0.007[f]	0.007[f]	0.007[f]

[a]Solution is 5.0 mol% in CCl_4, containing 10 mol% of C_6D_{12} and 0.5 mol% of tetramethylsilane (TMS).
[b]Solution is 5.0 mol% in benzene-d_6 with 0.5 mol% of TMS.
[c]Solution is 5.0 mol% in acetone-d_6 with 0.5 mol% of TMS.
[d]To high frequency of internal TMS at 300.135 MHz (carrier frequency), numbers in parentheses being standard deviations in the last significant figure.
[e]No evidence was observed for coupling interactions between the methine and ring protons.
[f]No significant correlations were observed between the spectral parameters.

300 K. In other words, the internal rotation is very nearly free[1] (the total energy at $\psi = 45°$ was computed as −345.287 029 au).

The experimental barriers

For benzyl cyanide, INDO MO FPT calculations yield a $^6J_{90}$ insignificantly different from that in toluene, so that it was taken as −1.20 Hz, as discussed previously (3). For 3-phenyl-1-propyne, such calculations with a standard geometry, as also used for toluene (4), give $^6J_{90}$ as −1.24 Hz, as compared to −1.22 Hz for toluene. For the latter, $^6J_{90}$ is actually −1.20 Hz (10). Accordingly, the assumption that $^6J_{90}$ is -1.21 ± 0.01 Hz for the propyne derivative implies $\langle \sin^2 \theta \rangle$ values of (Table 1) 0.497(4), 0.490(4), and 0.488(4) in CCl_4, C_6D_6, and acetone-d_6 solutions, respectively. The hindered rotor model (5) then indicates *apparent* twofold barriers as large as 0.4 ± 0.2 kJ/mol in the acetone solution, dropping essentially to zero in CCl_4 solution (a vanishing barrier corresponds to a $\langle \sin^2 \theta \rangle$ of 0.5). Of course, the small 6-31G barrier, which has a larger fourfold than a twofold component, implies $\langle \sin^2 \theta \rangle$ as 0.494. It is probably sensible to conclude that the internal barrier in 3-phenyl-1-propyne is indeed very small and that it is largely independent of solvent. In the polar benzyl cyanide, by way of contrast, the internal rotational barrier is also small but is significantly solvent dependent (3). In an *n*-propyl benzene derivative the barrier about the C_{sp^2}—C_{sp^3} bond in the *anti* form of the molecule is apparently greater than 5 kJ/mol (11) with θ as 30° for the conformation of lowest energy ($\psi = 90°$).

^{4}J(H,CH_2) and ^{5}J(H,CH_2)

In toluene ^5J(H,CH_3) is 0.329(1) Hz(10). It has been written as $0.366 \langle \sin^2 \theta \rangle + 0.322 \langle \sin^2 (\theta/2) \rangle$, where the first term is the σ–π contribution, and the second term is the σ electron component of ^5J(H,CH_3) and is absent in ^6J(H,CH_3). Because $^6J_{90}^{\pi}$ in toluene and the present compound are almost identical and because $\langle \sin^2 \theta \rangle$ in the latter is very nearly 0.5, as in toluene, ^5J(H,CH_2) should be just a little smaller in the propyne. It is, by about 0.01 Hz (Table 1).

On the other hand, ^4J(H,CH_2) is −0.782(1) Hz in CCl_4 solution, rather larger in magnitude than the −0.702(1) Hz in toluene (10). ^4J(H,CH_3) in the latter was taken (12) as $-1.08 \langle \sin^2 \theta \rangle - 0.32 \langle \cos^2 \theta \rangle$. For toluene this sum becomes −0.70 Hz. The second term is considered (12) to be a σ electron contribution to ^4J. The 10% increase in the magnitude of ^4J in the phenylpropyne is not understood.

The computed structure of 3-phenyl-1-propyne

Figure 1 displays the 6-31G structure of 3-phenyl-1-propyne for the conformation in which the acetylenic group lies in the benzene plane. Steric crowding is indicated by the large exocyclic bond angles of 123.3° and 115.6°. The internal *ipso* angle of 118.7° is similar to that observed, 118.1°, for a methyl substituent (13). In methyl acetylene, the triple bond length is 1.206 Å, according to microwave spectroscopy (14), and presumably refers to the ground vibrational state.

Experimental

3-Phenyl-1-propyne was prepared from 1-phenyl-1-propyne, exactly as described in the literature (15). Solutions, 5.0 mol% in CCl_4, benzene-d_6, and acetone-d_6, containing 0.5 mol% tetramethylsilane and an additional 10 mol% of cyclohexane-d_{12} in the CCl_4 mixture, were prepared and transferred to 5-mm od nmr tubes. These solutions were degassed by the freeze–pump–thaw technique and the sample tubes were then flame-sealed. The ^{1}H nmr spectra were obtained on a Bruker AM300 spectrometer at a probe temperature of 300 K. The procedure was identical to that recently described in detail for toluene (10). The ^{1}H nmr spectra were analyzed with the computer program NUMARIT (16), as modified by R. Sebastian. Figure 2 displays the

[1]For benzyl cyanide V_2 and V_4 are −1.1 and −0.29 kJ/mol for 6-31G level calculations (3).

Can. J. Chem. Downloaded from www.nrcresearchpress.com by 72.64.146.136 on 09/07/12
For personal use only.

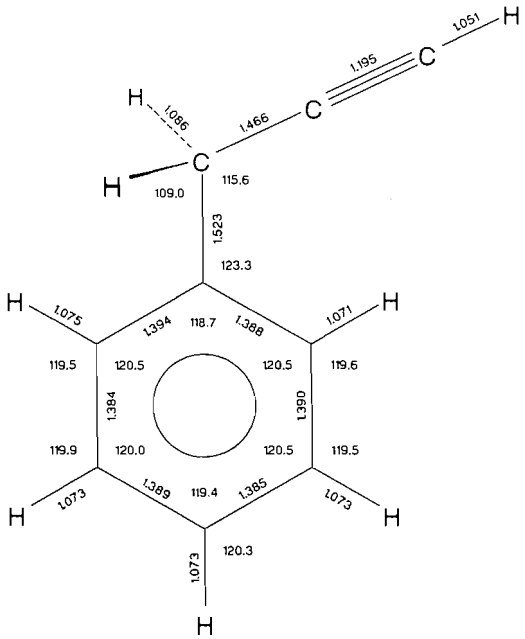

FIG. 1. The geometry-optimized structure of 3-phenyl-1-propyne at the 6-31G level of molecular orbital theory is shown for the conformation in which the acetylenic group lies in the benzene plane ($\psi = 0°$ for **1** in the text). The total energy is −345.286 817 au and is not the minimum energy, which occurs near $\psi = 50°$ (see text). Bond lengths are given in angstroms and bond angles in degrees. The phenyl group was constrained to planarity during the optimization procedure. Although the exocyclic bond angles imply significant crowding for this structure, it is only 0.5$_6$ kJ/mol less stable than that at $\psi = 50°$C.

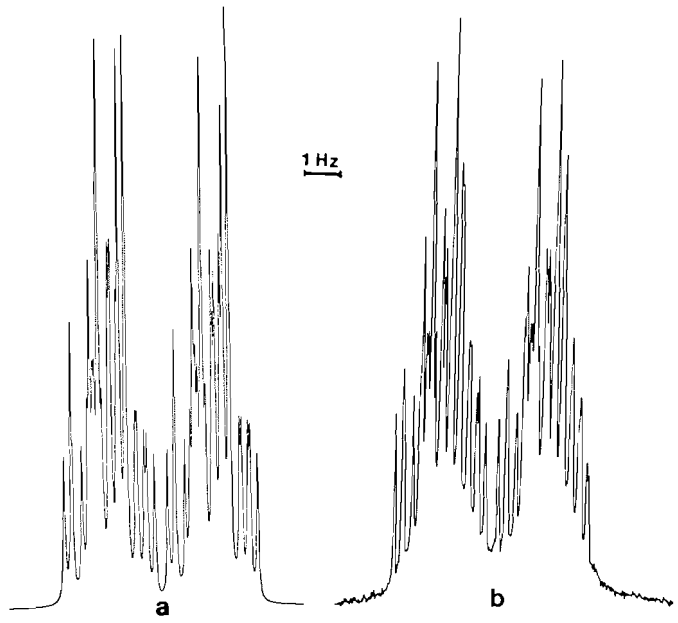

FIG. 2. The calculated (*a*) and observed (*b*) ^{1}H nmr spectrum of the methylene protons of 3-phenyl-1-propyne as a 5 mol% solution in acetone-d_6 at 300 K and 300 MHz. The linewidths at half-height are approximately 0.08 Hz. The intensity differences between some peaks in the two spectra have their origin in the presence of many transitions lying within, say, 0.01 Hz of each other in a given observed peak, but which cannot be distinguished in an assignment. Of course, the long-range coupling constants also appear in the ring proton spectrum, so that, in fact, they can be extracted precisely from an 8-spin analysis.

observed and computed ^{1}H nmr spectra of the methylene protons in acetone-d_6 solution. Table 1 presents the spectral parameters for 3-phenyl-1-propyne in the three solutions.

STO 3G MO computations utilized the program MONSTERGAUSS (17) and the 6-31G calculations employed GAUSSIAN 82 (18), both on an Amdahl 470 system. INDO MO FPT computations (19) of $^6J(H,CH_2)$ on 3-phenyl-1-propyne were also done. The dipole moments at $\psi = 0°$ and 90° (see **1**) were 0.37 and 0.47 D at the 6-31G level of MO theory, so that electrostatic interactions with the solvent (7) differ very little for the two forms.

Acknowledgments

We are grateful to the Natural Sciences and Engineering Research Council of Canada for a grant-in-aid of this research.

1. T. SCHAEFER, J. PEELING, and R. SEBASTIAN. Can. J. Chem. **63**, 3219 (1985).
2. T. SCHAEFER, R. SEBASTIAN, and G. H. PENNER. Can. J. Chem. **64**, 1372 (1986).
3. T. SCHAEFER and G. H. PENNER. Can. J. Chem. **64**, 2013 (1986).
4. R. WASYLISHEN and T. SCHAEFER. Can. J. Chem. **50**, 1852 (1972).
5. W. J. E. PARR and T. SCHAEFER. Acc. Chem. Res. **13**, 400 (1980).
6. R. J. ABRAHAM and E. BRETSCHNEIDER. *In* Internal rotation in molecules. *Edited by* W. J. Orville-Thomas. J. Wiley and Sons, New York. 1974. Chap. 13.
7. C. W. BOCK, M. TRACHTMAN, and P. GEORGE. Chem. Phys. **93**, 431 (1985).
8. C. P. SMYTH and W. S. WALLS. J. Am. Chem. Soc. **54**, 1854 (1932).
9. T. SCHAEFER and G. H. PENNER. Chem. Phys. Lett. **114**, 526 (1985).
10. T. SCHAEFER, R. SEBASTIAN, and G. H. PENNER. Can. J. Chem. **63**, 2597 (1985).
11. T. SCHAEFER, L. J. KRUCZYNSKI, B. KRAWCHUK, R. SEBASTIAN, J. L. CHARLTON, and D. M. MCKINNON. Can. J. Chem. **58**, 2452 (1980).
12. M. BARFIELD, C. J. FALLICK, K. HATA, S. STERNHELL, and P. W. WESTERMAN. J. Am. Chem. Soc. **105**, 2178 (1983).
13. A. DOMENICANO and P. MURRAY-RUST. Tetrahedron Lett. 2283 (1979).
14. C. C. COSTAIN. J. Chem. Phys. **29**, 864 (1958).
15. R. WEST and G. A. GORNOWICZ. J. Am. Chem. Soc. **93**, 1720 (1971).
16. A. R. QUIRT and J. S. MARTIN. J. Magn. Reson. **5**, 318 (1971); J. S. MARTIN, A. R. QUIRT, and K. E. WORVILL. The nmr program library. Daresbury Laboratory, Daresbury, U.K.
17. M. R. PETERSEN and R. A. POIRIER. MONSTERGAUSS. Department of Chemistry, University of Toronto, Toronto, Ontario. 1981.
18. J. S. BINKLEY, M. J. FRISCH, D. J. DEFREES, K. RAGHAVACHARA, R. A. WHITESIDE, H. B. SCHLEGEL, E. M. FLUDER, and J. A. POPLE. GAUSSIAN 82. Department of Chemistry, Carnegie–Mellon University, Pittsburgh, PA.
19. P. A. DOBOSH and N. S. OSTLUND. QCPE, **11**, 281 (1975).

Can. J. Chem. Downloaded from www.nrcresearchpress.com by 72.64.146.136 on 09/07/12
For personal use only.

A new procedure for the *in situ* generation of methylene ketenes

ANDREW P. MASTERS, TED S. SORENSEN,[1] AND PHU MANH TRAN
The Department of Chemistry, University of Calgary, Calgary, Alta., Canada T2N 1N4

Received October 21, 1986

ANDREW P. MASTERS, TED S. SORENSEN, and PHU MAHN TRAN. Can. J. Chem. **65**, 1499 (1987).

The reaction of pentacarbonylmanganate anion **3** and 2-bromopropenoyl chlorides **2** leads to 2,4-alkylidenecyclobutane-1,3-diones **5**. The latter are formed from dimerization of the corresponding methylene ketenes **1** so that the reaction of **2** and **3** constitutes a new synthetic procedure for the *in situ* generation of these very reactive intermediates. Acid chlorides **2** are readily available from α,β-unsaturated acids via bromination–dehydrobromination – thionyl chloride sequences.

ANDREW P. MASTERS, TED S. SORENSEN et PHU MAHN TRAN. Can. J. Chem. **65**, 1499 (1987).

La réaction de l'anion pentacarbonylmanganate (**3**) et des chlorures de bromo-2 propènoyles (**2**) conduit aux dialkylidène-2,4 cyclobutanediones-1,3 (**5**). Ces derniers composés se forment par dimérisation des méthylène cétènes correspondants (**1**); il en résulte que la réaction des composés **2** et **3** constitue une nouvelle voie de synthèse pour la préparation *in situ* de ces intermédiaires très réactifs. Les chlorures d'acides **2** sont facilement disponibles à partir des acides α,β-insaturés, par le biais de la série de réaction de bromation/d'élimination de HBr/chlorure de thionyle.

[Traduit par la revue]

Methylene ketenes **1** are extremely reactive and short-lived compounds, nevertheless some knowledge of their chemistry has developed in the past fifteen years (1). Present procedures for preparing **1** generally involve either photochemistry (2)

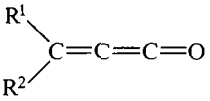

1

or high-temperature pyrolysis (most often of Meldrum's acid derivatives) (3). Neither method is particularly well suited for preparative chemistry (although clearly useful for directly observing **1**) and in this paper we present a new synthetic procedure capable of the convenient *in situ* generation of **1** at subambient temperatures.

Results

The overall stoichiometry for this methylene ketene synthesis is shown in eq. [1]. A closely related reaction has recently been

[1] 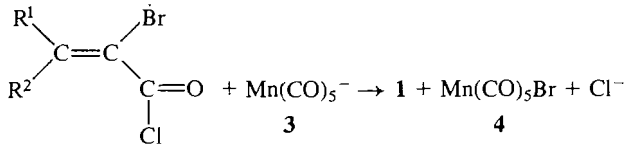

2*a* $R^1 = R^2 = CH_3$
2*b* $R^1 = R^2 = \phi$
2*c* $R^1 = R^2$ = 2-adamantylidene
2*d* $R^1 = H$, $R^2 = CH_3$

used for the preparation of ketenes and vinyl ketenes, where the bromine atom in these cases is located on an sp^3 centre (4). Surprisingly, 2-bromopropenoyl chlorides **2** (sp^2-bromine) are, if anything, even more reactive towards **3**, the eq. [1] reaction appearing to proceed at temperatures as low as −80°C in some cases. The pentacarbonylmanganate **3** has been used in this work as the sodium salt in tetrahydrofuran solvent or as the partially air-stable bistriphenylphosphineiminium (PPN^+) salt (5) in chloroform or methylene chloride solvent. The latter method is somewhat more convenient but can involve work-up problems in some cases.

[1]Author to whom correspondence may be addressed.

To detect the *in situ* formation of **1**, one must have a trapping procedure that unequivocally indicates that **1** was indeed formed. Because of the acid chloride functionality in **2**, as well as the triviality of the trapping product, we have steered clear of trapping agents such as alcohols, amines, etc. and have looked for suitable $\pi^2 + \pi^2$ or $\pi^4 + \pi^2$ trapping reactions. Unfortunately, only the $\pi^2 + \pi^2$ self-dimerization has so far been successful, and this only in cases where R^1 and R^2 are alkyl or aryl. Three representative examples are described, involving $R^1 = R^2 = CH_3$, $R^1 = R^2$ = phenyl, and the cyclic 2-adamantyl case. In the latter case, we had hoped to also observe directly the monomer species. The reactions are shown in eq. [2].

[2] 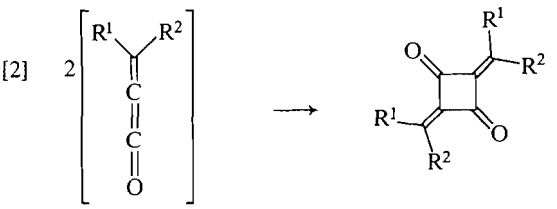

1*a* $R^1 = R^2 = CH_3$
1*b* $R^1 = R^2 = \phi$
1*c* $R^1 = R^2$ = 2-adamantylidene

5*a–c*

Both **5***a* and **5***b* have previously been reported as the sole dimerization products of the corresponding methylene ketenes (3), so that the *in situ* generation of **1***a–c* cannot really be in doubt in our examples. In each case, dimer **5** is initially formed in high yield (ir measurements), but only **5***b* and **5***c* have been isolated in good yield. Compound **5***a* decomposes extensively on silica gel flash chromatography and the pure solid has consequently been isolated in only about 40% yield.

The acid chloride **2***d* reacts rapidly at subambient temperatures with **3** to give $Mn(CO)_5Br$ (characteristic ir bands), but the also characteristic ir stretching frequencies expected for **5***d* ($R^1 = H$, $R^2 = CH_3$) are completely absent (the assumption here is that **5***d* would have very similar frequencies to **5***a* and **5***c*). The ^1H nmr spectrum of the crude reaction mixture is broad (paramagnetic Mn species) and uninformative (insoluble material precipitates out with time). This failure to observe **5***d* is not entirely unexpected since previous pyrolysis work, intended to give methylene ketene **1***d* ($R^1 = H$, $R^2 = CH_3$), gave no **5***d* (3) on warming the pyrolysate.

Can. J. Chem. Downloaded from www.nrcresearchpress.com by 118.98.75.50 on 09/07/12
For personal use only.

Can. J. Chem. Downloaded from www.nrcresearchpress.com by 118.98.75.50 on 09/07/12
For personal use only.

Since **1***d* could not be trapped as an observable self-dimer, attempts were made to trap this ketene with cyclopentene, acrolein, 2,3-dimethylbutadiene, ethyl vinyl ether, and dihydropyran. In the first four cases, part of the tetrahydrofuran solvent volume was replaced with the potential trapping agent (corresponding to about an 80-fold molar excess compared to **2***d*) and the reactions were then performed in the normal way (sodium salt procedure). In the case of dihydropyran and ethyl vinyl ether, the reaction was also carried out under dilute addition conditions using a syringe pump to add **2***d* to the solution of **3**. However, in all cases, the crude reaction mixture, on glc analysis, failed to show the presence of any 1:1 adduct (or indeed of any volatile material). Significantly, when the acid chloride **2***a* is reacted with **3** in tetrahydrofuran – ethyl vinyl ether solvent mixtures, one also obtains no 1:1 adduct with the ether (but one gets the usual ir spectrum of **5***a* in good yield). Previous workers in this area (1) have also failed to trap methylene ketenes with a range of alkenes and dienes, although ketenes and methylene ketenes have been coreacted, and we plan to conduct experiments in this area since both ketenes and methylene ketenes can be prepared using the same synthetic procedure, i.e. with **3** and mixed bromoacyl chlorides.

Discussion

The 2-adamantylidene ketene **1***c* is, from molecular models, reasonably hindered, but even this appears (ir) to dimerize faster than it is formed from the acid chloride **2***c*, i.e. typical *in situ* generation conditions. However, such conditions are often ideally suited for trapping experiments (cf. numerous studies of vinyl ketene cycloadditions where the ketene is generated *in situ* in the presence of the trapping agent) (for two recent examples see ref. 6). Hopefully, the experimental ease of the present methylene ketene synthesis will enable a testing of a much wider range of potential trapping species, including cases with internal "built-in" trapping functionality.

The mechanism of the methylene ketene formation is quite obviously related to the more general reaction of **3** with all α-bromoacyl chlorides, i.e., the crucial functionality is the partial structure **6**, and it does not matter whether the remaining

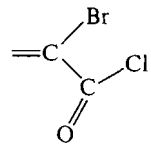

6

structure is part of a double bond (sp^2) or is directly bonded to R or H substituents (sp^3). As before (4), one can formulate the reaction as a HOMO–LUMO interaction between **3** and **2**, the LUMO on **2** having a significant C—Br σ* component. Interaction of **3** with the C1—C2 pseudo π-bond could lead to an intermediate π-complex and eventually to a methylene ketene (mechanism 1). Alternatively, and perhaps more likely, is a direct interaction of **3** with the α-bromine. This could

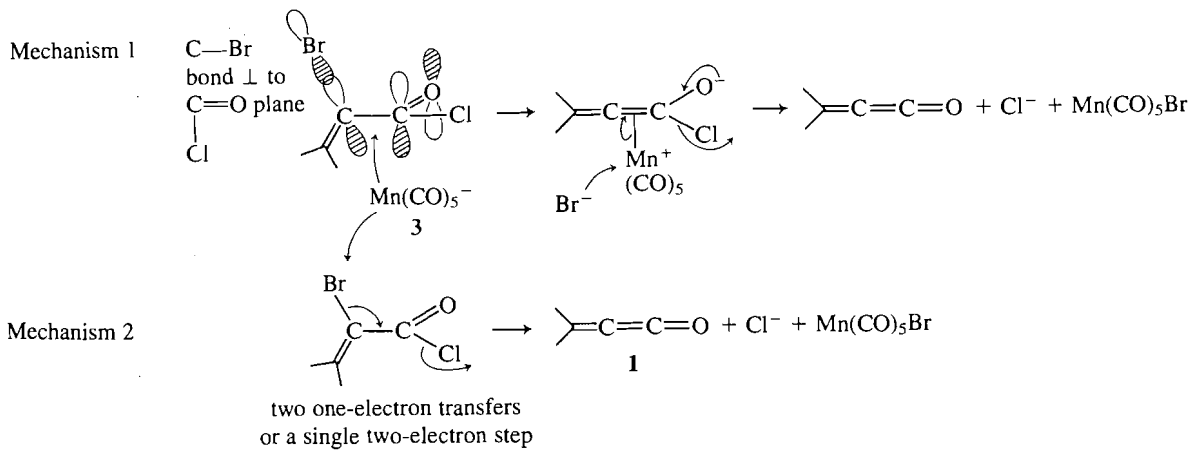

involve either two one-electron steps or a single two-electron process (mechanism 2). We have previously ruled out the initial formation of an acyl manganese intermediate, e.g. **7**, in the simple sp^3-Br cases and believe that such an intermediate is even less likely in the present case.

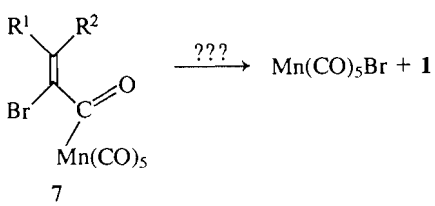

7

Future prospects

The reaction used to prepare **1** can possibly be extended to the formation of two virtually unknown types of ketenes, butatrienones **8** (7) and acetylenic ketenes **9**, the former from α-bromobutadienoyl chlorides, the latter from the γ-bromo

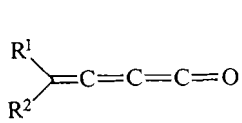

8

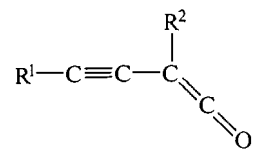

9

isomer (cf. vinyl ketene formation from γ-bromocrotonyl chlorides (4)).

Experimental

All melting and boiling point values are uncorrected. Gas chromatography analyses were performed on 6 ft × 4 mm columns of OV-1 or OV-17. Mass spectrometric analyses were obtained on a Kratos MS80, infrared spectra on a Nicolet 5DX FT instrument, and ^1H and ^{13}C nmr spectra on a Varian XL-200 spectrometer.

2-Bromo-3-methyl-2-butenoyl chloride **2**a, bp 72–73°C/12 Torr (1 Torr = 133.3 Pa); ^1H nmr, δ: 2.07 and 2.09 (3H each), was prepared by the standard thionyl chloride procedure (8).

Can. J. Chem. Downloaded from www.nrcresearchpress.com by 118.98.75.50 on 09/07/12
For personal use only.

2-Bromo-2-butenoyl chloride **2**d was prepared from the *E*-acid and was obtained as a 1:2 *E–Z* mixture (by ^{1}H nmr) of acid chlorides, bp 65°C/10 Torr (9).

Tricyclo[3.3.1.1^{3,7}]decylideneacetic acid

The title compound was prepared by a variant of the literature routes (10), involving the direct condensation (11) of 2-adamantanone and ethyl acetate, in near quantitative yield. The hydroxy ester so formed (15 g) was both hydrolyzed and dehydrated by dissolving it in 75 mL of methylene chloride and adding this to 75 mL of stirred 96% sulfuric acid (ice bath). After 3 h at 20°C, the sulfuric acid layer was slowly added to a large excess of ice. The resulting solid acid was filtered (extraction of the filtrate with methylene chloride provides a small additional amount) and dried. Recrystallization from hexane–CCl_4 provided the title acid in high overall yield.

2-Bromo-2-tricyclo[3.3.1.1^{3,7}]decylideneacetic acid

The preceding acid was quantitatively brominated in CCl_4 solution at 0°C (left overnight in the refrigerator). A sample recrystallized from CCl_4 had mp 153–154°C; ^{1}H nmr, δ: 5.66, H—C(Br)(COOH)—. The crude dibromide (2.00 g, 5.68 mmol) was added in portions to 15 mL of 10% KOH – 95% ethanol cooled to 0°C in ice. After 3 h at 20°C, the solid was filtered and the filtrate acidified with 5% HCl. This heterogeneous aqueous phase was extracted (3 × 25 mL) with methylene chloride, which was dried and concentrated until the title acid began to crystallize out. Two crops were collected, 0.83 g (54%), mp 201–203°C; ^{1}H nmr $(CD_3)_2CO$, δ: 3.55 and 3.23 (1H, each, nonequivalent allylic), 1.7–2.0 (remaining hydrogens); ^{13}C nmr, $(CD_3)_2CO$, δ: 28.3 (d × 2), 36.9 (t), 37.1 (d), 38.9 (t × 2), 39.0 (d), 39.6 (t × 2), 102.7 (?, q), 135.6 (q), 159.5 (q). *Exact Mass* calcd. for $C_{12}H_{15}O_2{}^{79}Br$: 270.0277; found: 270.0254.

2-Bromo-2-tricyclo[3.3.1.1^{3,7}]decylideneacetyl chloride **2**c

The above acid, 4.00 g, 14.7 mmol, was refluxed for several hours with an excess of thionyl chloride (6 mL). After the excess thionyl chloride was distilled off, the acid chloride was distilled, bp 174–177°C/9 Torr, 3.61 g (85%). It solidifies in the refrigerator; ^{1}H nmr $(CD_3)_2CO$, δ: 3.23 and 3.18 (1H each, allylic), 1.8–2.05 (remaining H); ^{13}C nmr ($CDCl_3$), δ: 27.9 (d × 2), 36.8 (t), 37.6 (d), 39.1 (t × 2), 39.6 (t × 2), 105.8 (q), 162.1 (q). *Exact Mass* calcd. for $C_{12}H_{12}{}^{35}Cl^{79}BrO$: 287.9916; found: 287.9900.

3,3-Diphenyl-2-bromopropenoyl chloride **2**b

The bromoacid (12) (3.00 g; 9.90 mmol), 5 mL of thionyl chloride, and two drops of dimethylformamide were stirred at ca. 20°C for 1 h. A few millilitres of methylene chloride were added and the excess thionyl chloride and solvent removed on the Rotovap. This procedure was repeated twice with the fresh addition of solvent each time. Addition of carbon tetrachloride and crystallization gave two crops of **2***b*, 2.35 g (74%). A sample was recrystallized from the same solvent, mp 86–88°C. Application of the ordinary thionyl chloride procedure to prepare **2***b* yielded a mixture of the acid chloride and a red compound with an ir C=O stretch at 1721 cm^{-1}, which likely corresponds to 3-phenyl-2-bromoindenone formed by intramolecular acylation. Acid chloride **2***b* has a C=O stretch at 1764 cm^{-1} (CH_2Cl_2); ^{13}C nmr ($CDCl_3$), δ: 112.5 (q), 128.2 (d × 2), 128.6 (d × 2), 129.3 (d × 3), 129.5 (d × 2), 129.6 (d), 138.95 (q), 139.2 (q), 150.6 (q), 165.2 (l). *Exact Mass* calcd. for $C_{15}H_{10}O^{79}Br^{35}Cl$: 319.9604; found: 319.9605.

2,4-Bis(tricyclo[3.3.1.1^{3,7}]decylidene)-cyclobutane-1,3-dione **5**c

Under an argon atmosphere, a solution of $Na^+Mn(CO)_5^-$ was prepared by stirring 0.15 g (0.77 mmol) of $Mn_2(CO)_{10}$ in 7 mL of tetrahydrofuran (distilled from benzophenone ketyl) over 1.5 mL of 1% sodium amalgam for 20 min. The solution was then transferred under argon via a hollow needle to a filter tube containing Celite. After filtering, the tube was washed with 2 mL of tetrahydrofuran. The pale yellow anion solution contained in a round bottom flask was removed from the filter tube and quickly fitted with a serum cap. This solution was cooled to −78°C and 0.2167 g (0.749 mmol) of the adamantyl acid chloride **2***c* in 2 mL of tetrahydrofuran was added dropwise via syringe, with stirring, over 3 min. The solution was then allowed to warm to 20°C, a precipitate forming. The solution was filtered through Celite, and extraction of the Celite with hot methylene chloride and the removal of solvent yielded 57.5 mg of pure **5***c*. From the filtrate, an additional 21.2 mg of dimer **5***c* was eventually obtained by concentrating the volume, total 78.7 mg (60% recovery). Eventually $Mn(CO)_5Br$ cocrystallizes with **5***c*. A recrystallized sample (yellow plates) had mp ca. 330°C (dec.); ir: characteristic peaks at 1683 and 1615 cm^{-1}; ^{1}H nmr ($CDCl_3$), δ: 3.63 (allylic), 1.90–2.10 (remaining protons); ^{13}C nmr ($CDCl_3$), δ: 27.7 (d × 4), 36.7 (t × 2), 40.7 (d × 8), 144.1 (q × 2), 176.4 (q × 2), 192.0 (q × 2). In the off-resonance spectrum, the quaternary carbon at 176.5 is broader than the one at 144.1 and is probably the carbon at the 2-position of the adamantane ring. *Anal.* calcd. for $C_{24}H_{28}O_2$: C 82.72, H 8.10; found: C 82.99, H 8.13.

2,4-Bis(diphenylmethylene)-cyclobutane-1,3-dione **5**b

To a stirred, −78°C, solution of $PPN^+Mn(CO)_5^-$ (2.521 g; 3.44 mmol), in 25 mL of methylene chloride, contained in a 100-mL round bottom flask and protected by a rubber septum, was added dropwise from a syringe over a 5-min period a solution of acid chloride **2***b* in 10 mL of methylene chloride. Even at −78°C, the solution appears to darken and become somewhat murky. After a few minutes at −78°C, the solution was gradually allowed to warm to room temperature (ca. 0.5 h). The infrared spectrum of the dark red solution taken immediately on warming showed characteristic peaks for $Mn(CO)_5Br$ and the dimer **5***b*. About one-half of the methylene chloride was removed on the Rotovap and the solution was stored overnight in a refrigerator. This treatment converts most of the $Mn(CO)_5Br$ to a polar species with lower frequency infrared peaks, probably $PPN^+Mn(CO)_4ClBr^-$. Most of the remaining methylene chloride was removed and the residue subjected to flash chromatography on silica gel using hexane – methylene chloride elution. A small first fraction of $Mn(CO)_5Br$ is followed by essentially pure **5***b*, 0.454 g (71%), as dark red crystals; mp ca. 307°C (dec.) (lit. (3) mp 315°C (dec.)); ir (CH_2Cl_2): 1684 and 1541 cm^{-1} (lit. (3) ir (Nujol) 1694 and 1537 cm^{-1}); ^{13}C nmr ($CDCl_3$), δ: 127.9 (d × 8), 131.7 (d × 4), 132.3 (d × 8), 136.1 (q × 4), 152.4 (q × 2), 156.0 (q × 2), 186.6 (q × 2); ms, *m/e* (% base): 412 (36, M^+), 178 (100) (lit. (3) ms *m/e* 412 (50, M^+), 178 (100)).

2,4-Di(1'-methyl-1'-ethylidene)cyclobutane-1,3-dione **5**a

Using acid chloride **2***a*, the methylene ketene dimer **5***a* could be prepared using either the sodium salt method (see above for **5***c*) or the PPN^+ salt procedure used for **5***b*. The infrared spectra in each case, taken immediately on warming the reaction solutions, showed a carbonyl region containing only peaks for $Mn(CO)_5Br$ (2005, 2047, and 2136 cm^{-1}) and the dimer **5***a* (see below). Weighed samples of pure **5***a* and $Mn(CO)_5Br$ were prepared as mixtures for infrared calibration, indicating that the ketene dimer **5***a* yield is about 90% based on $Mn(CO)_5Br$. Using the sodium salt procedure, $Mn(CO)_5Br$ and **5***a* could be cosublimed (0.01 Torr, 20 → 60°C) from the crude reaction mixture and the combined weight was close to that expected for 100% $Mn(CO)_5Br$ and ca. 90% **5***a*. Attempts to sublime the crude PPN^+ salt mixture gave no **5***a*, an indication that the latter reacts rapidly with PPN^+Cl^- under these conditions. Using the sodium salt procedure (1.00-mmol scale), the crude products after filtration could be flash chromatographed on silica gel (methylene chloride solvent), whereby one obtains about 40% overall recovery of pure, crystalline **5***a* as orange-yellow needles (this **5***a* fraction is preceded by a very small $Mn_2(CO)_{10}$ fraction and then $Mn(CO)_5Br$ in 83% yield). Streaking on the chromatography column or tlc plates indicated that decomposition to a more polar compound was occurring on the column. Alternative attempts at an aqueous work-up procedure resulted in the immediate loss of **5***a*. Dimer **5***a* is characterized by a pair of strong infrared peaks at (THF) 1694 and 1632 cm^{-1} (lit. (3) ir (Nujol) 1680 and 1621 cm^{-1}); mp 150–151°C (lit. (3) mp 135°C; lit (13) mp 143°C); ^{1}H nmr: δ 2.26 (s) (lit. (3) δ 2.25); ms, *m/e* (% base peak): 164 (61, M^+), 136 (55), 93 (70), 83 (64), 67 (100) (lit. (3) ms *m/e*: 164 (36, M^+), 67 (100)). Attempted trapping reactions were carried out using the sodium salt

procedure. In all cases the infrared spectrum of the crude reaction solution indicated that **5***a* was formed in about 90% yield.

Reaction of acid chloride **2** d *with* $Na^+Mn(CO)_5^-$

This reaction was carried out as described for the preparation of **5***c*. Immediately on warming, an infrared spectrum was taken, showing peaks for $Mn(CO)_5Br$, no peaks for $Mn(CO)_5^-$, and only broad low intensity "bumps" in the rest of the carbonyl region. The reaction was repeated with five different potential trapping agents (see Results), giving similar results. The latter reactions were also analyzed by glc, showing $\leq 1\%$ of any volatile 1:1 trapping products.

Acknowledgement

We thank the Natural Sciences and Engineering Research Council of Canada for generous financial support.

1. R. F. C. BROWN and F. W. EASTWOOD. The chemistry of ketenes, allenes and related compounds. Part 2. *Edited by* S. Patai. John Wiley and Sons, New York. 1980. Chap. 19.
2. O. L. CHAPMAN, C. C. CHANG, J. KOLC, N. R. ROSENQUIST, and H. TOMIOKA. J. Am. Chem. Soc. **97**, 6586 (1975).
3. R. F. C. BROWN, F. W. EASTWOOD, and K. J. HARRINGTON. Aust. J. Chem. **27**, 2373 (1974).
4. A. P. MASTERS, T. S. SORENSEN, and T. ZIEGLER. J. Org. Chem. **51**, 3559 (1986).
5. (*a*) D. N. DUFFY and B. K. NICHOLSON. J. Organometal. Chem. **164**, 227 (1979); (*b*) J. A. GLADYSZ, G. M. WILLIAMS, W. TAM, D. L. JOHNSON, D. W. PARKER, and J. C. SELOVER. Inorg. Chem. **18**, 553 (1979).
6. (*a*) R. L. DANHEISER, S. K. GEE, and H. SARD. J. Am. Chem. Soc. **104**, 7670 (1982); (*b*) D. A. JACKSON, M. REY, and A. S. DREIDING. Helv. Chim. Acta, **66**, 2330 (1983).
7. R. D. BROWN, R. F. C. BROWN, F. W. EASTWOOD, P. D. GODFREY, and D. J. MCNAUGHTON. J. Am. Chem. Soc. **101**, 4705 (1979).
8. D. PITRE. Farm. Sci. Tec. (Pavia), **4**, 657 (1949); Chem. Abstr. **44**, 4866e (1950).
9. N. H. CROMWELL and F. PELLETIER. J. Org. Chem. **15**, 877 (1950).
10. (*a*) J. BURKHARD, J. VAIS, and S. LANDA. Collect. Czech. Chem. Commun. **38**, 1263 (1973); (*b*) V. L. NARAYANAN and L. SETESCAK. J. Org. Chem. **36**, 4127 (1971).
11. M. W. RATHKE. J. Am. Chem. Soc. **92**, 3222 (1970).
12. D. D. E. NEWMAN and L. N. OWEN. J. Chem. Soc. 4722 (1952).
13. B. ROSEBEEK. Ph.D. thesis, Rijksuniversiteit, Groningen, The Netherlands. 1961.

Can. J. Chem. Downloaded from www.nrcresearchpress.com by 118.98.75.50 on 09/07/12
For personal use only.

The synthesis of 3-carboxymethyleneazetidinones

WERNER HINZ AND GEORGE JUST[1]
Department of Chemistry, McGill University, Montreal, P.Q., Canada H3A 2K6

Received September 30, 1986

WERNER HINZ and GEORGE JUST. Can. J. Chem. **65**, 1503 (1987).

A series of novel azetidinones bearing the methoxycarbonylmethylene, thioethoxycarbonylmethylene, and alkylaminocarbonylmethylene side chain in their three position have been synthesized from the reaction of the potassium salt of 4,4′-bis(thioethoxy)-3-butenoic acid with a number of Schiff bases.

WERNER HINZ et GEORGE JUST. Can. J. Chem. **65**, 1503 (1987).

Faisant appel à la réaction du sel de potassium de l'acide bis(thioéthoxy)-4,4′ butène-3 oïque avec un certain nombre de bases de Schiff, on a synthétisé une série de nouvelles azétidinones portant les chaînes latérales méthoxycarbonylméthylène, thioéthoxycarbonylméthylène et alkylaminocarbonylméthylène en position 3.

[Traduit par la revue]

Introduction

The mechanism of β-lactam action on bacterial cell wall enzymes has been at the centre of much interest over many years (1). Recently, Keith *et al.* (2) put forward the oxazolone structure **2** for the reactive intermediate directly preceding acylation of the penicillin-sensitive enzyme and this report prompted us to explore possible syntheses of azetidinones of type **3**. Their mode of action in biological systems should, by analogy, involve the intermediate **4**, and comparing the biological activities of β-lactam compounds of types **1** and **3** could provide evidence either in support of or against the suggested mechanism of β-lactam activity. We here wish to describe a short and efficient synthesis of these novel 3-substituted azetidinones.

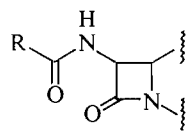

1

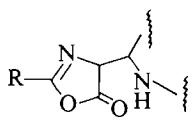

2

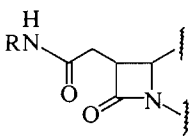

3

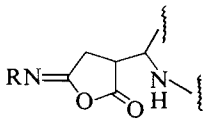

4

Results and discussion

Several years ago, the reaction of crotonyl chloride with various Schiff bases was developed in this laboratory to yield 3-vinylazetidinones in good yield (3). Based on this approach, we investigated the use of appropriately substituted crotonic acid derivatives, which, employed in cyclization reactions with corresponding imines, should lead to precursors for 3-carboxymethyleneazetidinones.

To obtain the desired oxidation state (carboxylic acid) at the β-carbon of the azetidinone (C-3) side chain, it was evident that the methyl group (C-4) of our starting crotonic acid had to be converted into an aldehyde functionality and suitably protected.

Aldehyde **5** was readily available, although only in moderate yield, both via the selenium dioxide oxidation of methyl crotonate (4) and via ozonolysis of methyl sorbate (5). The dimethyl acetal **6** (5, 6) and the protected cyanohydrin derivatives **8** and **9** (7–9) were readily prepared following standard procedures; however, neither **6** nor **8** and **9** underwent cyclization reactions with **12***a* under a number of reaction conditions. We observed either no reaction (with **6**) or facile decomposition of the substrate (with **8** and **9**).

As a third approach, the reaction of **5** with ethanethiol and zinc chloride gave **7** in near quantitative yield. The thioacetal functionality proved to be the protecting group of choice, and the possible use of **8** or **9** was not further explored in detail.

During the hydrolysis of the methyl ester of **7** to give the free carboxylic acid **10**, the double bond migrated to form the thioketeneacetal functionality. This migration was most easily followed by ^{1}H nmr spectroscopy showing the disappearance of the alkene proton resonances of **7** and the appearance of a triplet resonance (1H) at 6.17 ppm and of a doublet resonance (2H) at 3.51 ppm. Since this shift had not been observed when the ester grouping of **6** was hydrolysed, it was evident that the acidity of the C-4 proton in **7** was considerably higher than the acidity of the corresponding proton in **6**, and we were confident that the reaction of **10** with Schiff bases **12** to give azetidinones **13** should proceed well.

Reaction of potassium salt **11** with imine **12***a*, obtained from cinnamaldehyde and *p*-anisidine (10), in the presence of cyanuric chloride and triethylamine, gave **13***a* in 50% yield. Only the *cis* isomer was isolated, the configuration being confirmed by the coupling constant between the azetidinone ring protons, which was $^3J_{H3-H4} = 6$ Hz. In an analogous fashion, **13***b* was obtained as its *cis* isomer from the reaction of **11** with Schiff base **12***b*. However, the reaction of **12***c* (11) and of **12***d* (12), prepared from benzaldehyde and 2-naphthaldehyde, with **11** gave considerably lower yields of azetidinones **13***c* and **13***d* under identical reaction conditions (ca. 7%); both *cis* and *trans* isomers were present in the product mixture in an approximately 1:1 ratio (*trans*:$^3J_{H3-H4} = 2$ Hz, *cis*:$^3J_{H3-H4} = 6$ Hz), and **13***c* and **13***d* as well as **15***c* and **15***d* were found to be rather unstable compounds.

Key intermediates **13***a*–**13***d* required chemical transformations at three sites: conversion of the thioketeneacetal grouping into the amide functionality; transformation of the styryl side chain into the methyl substituent common in many biologically active monobactams (13); reduction of the styryl and the phenylpropargyl side chains, and removal of the N-protecting group with subsequent sulfonation.

Treatment of **13***a* with boron trifluoride etherate and methanol yielded the methyl ester **14***a*. Alternatively, the considerably more reactive thioesters **15** were obtained from the hydrolysis of **13** with trifluoroacetic acid and aqueous ethanol.

[1]Author to whom correspondence may be addressed.

Can. J. Chem. Downloaded from www.nrcresearchpress.com by 72.64.146.136 on 09/07/12
For personal use only.

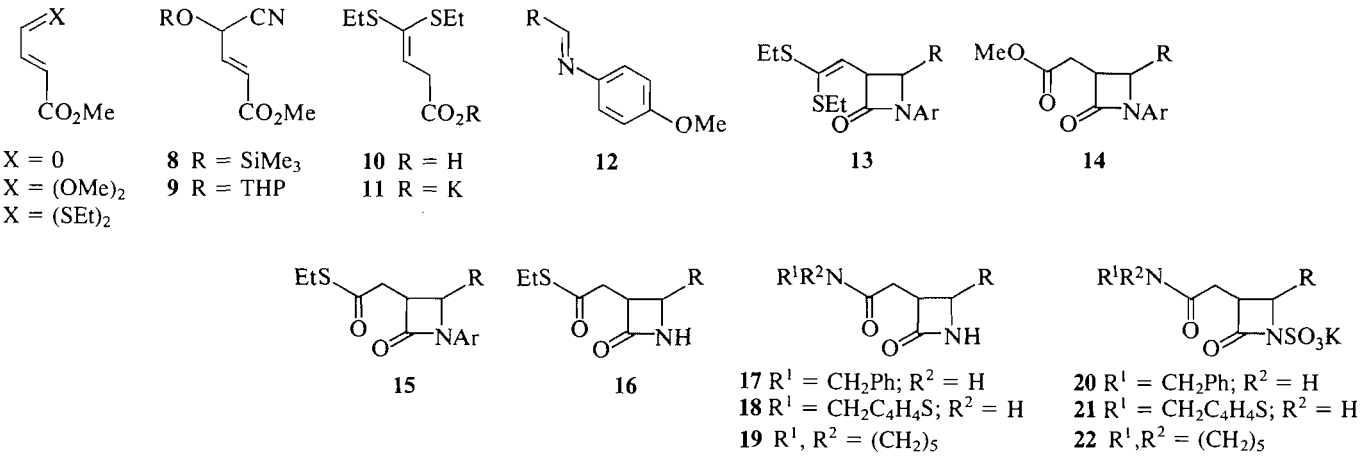

5 X = 0
6 X = $(OMe)_2$
7 X = $(SEt)_2$

8 R = $SiMe_3$
9 R = THP

10 R = H
11 R = K

12

13

14

15

16

17 $R^1 = CH_2Ph$; R^2 = H
18 $R^1 = CH_2C_4H_4S$; R^2 = H
19 R^1, $R^2 = (CH_2)_5$

20 $R^1 = CH_2Ph$; R^2 = H
21 $R^1 = CH_2C_4H_4S$; R^2 = H
22 R^1,$R^2 = (CH_2)_5$

12–22: *a*: R = *trans*-styryl *b*: R = C≡CPh *c*: R = CH_3
d: R = 2-naphthyl *e*: R = CH_2OMs *f*: R = CH_2I *g*: R = CH_3
h: R = CH_2CH_2Ph *i*: R = *cis*-styryl

This reaction provided surprisingly good yields, even with our rather sensitive substrates, when the reaction was carried out under gentle conditions over a period of several days.

Transformation of the styryl side chain of **15***a* into the C-4 methyl substituent of **15***g* was carried out at the thioester stage since the attempted ozonolysis of **13***a* had led to a multitude of products. Ozonolysis of **15***a* gave a reasonably clean aldehyde, which was reduced without purification with sodium borohydride, followed by mesylation, to give **15***e*. The mesylate **15***e* was readily converted into the iodomethylene derivative **15***f* using tetra-*n*-pentylammonium iodide – potassium iodide. In the ^{13}C nmr spectrum, an upfield shift of the methylene resonance of 65 ppm accompanied this substitution reaction, with the iodomethylene resonance observed distinctly at −0.02 ppm. Tributyltin hydride reduction of **15***f* gave **15***g* in good yield.

Similarly, removal of the N-protecting group was not possible in the presence of the thioketeneacetal functionality of **13***a*. However, it was a rapid and clean reaction once the hydrolysis to the thioester group of **15** had been carried out. Oxidation with ceric ammonium nitrate in acetonitrile and water yielded the N-unsubstituted β-lactams **16**.

Simply warming a mixture of the deprotected thioesters **16** and an excess of the appropriate alkylamine (benzylamine, 2-thiophenemethylamine, piperidine) in the absence of any solvent to 70°C yielded the azetidinones **17**, **18**, and **19** with the desired "reversed amide" side chain. The reactions employing the primary amines appeared cleaner than those with the secondary amine.

At this point of the synthetic scheme, two new C-4 side chains were introduced. The *trans*-styryl group of **17***a* was reduced to the phenylethyl substituent of **17***h* via hydrogenation using platinum as the catalyst. Only a small degree of debenzylation was observed. Similarly, hydrogenation of the triple bond of **17***b* using nickel boride as a catalyst (14) led to the formation of the *cis*-styryl derivative **17***i*. The ^1H nmr spectrum showed three-bond coupling constants of 11 Hz across the double bond, as compared to $^3J_{H,H}$ = 17 Hz, observed for the *trans*-styryl substituent.

Sulfonation using the pyridine – sulfur trioxide complex was followed by treatment with tetrabutylammonium hydrogen sulfate and passing of the intermediate ammonium salt through a short column of Dowex 50X8-200 ion exchange resin. The resulting potassium salts **20–22** were identified by their FAB (fast atom bombardment) low and high resolution mass spectra in which $M + 1$ and $M + 39$ peaks were always prominent.

All sulfonium salts **20–22** were tested for their activity against strains of Gram-positive and Gram-negative bacteria. Some promising initial results unfortunately were not confirmed when a larger number of compounds were submitted to the testing process. The lack of biological activity of course implies that support for the "Keith mechanism" was not produced, although these negative testing results do not necessarily disprove the proposed mechanism.

Compounds were tested by the standard agar dilution method of Mueller Hinton. Plates were inoculated with $1–5 \times 10^4$ CFU using the STERS replicator and incubated 18 h at 35°C. The lowest concentration for inhibition of growth is the MIC (minimum inhibitory concentration). Although styrylmonobactam **17** initially showed activity against various strains of *Staphylococcus aureus* and *Streptococcus faecalis* at a MIC of 0.12–4 mg/mL, inducing us to prepare the other analogues, these biological results were not reproducible.

Experimental

Melting points were determined on a Gallenkamp melting point apparatus and are uncorrected. Infrared spectra were recorded on a Perkin–Elmer infrared spectrometer, model 297, or a Nicolet 7000 FT-IR spectrometer as thin films in bromoform between potassium bromide plates. Nuclear magnetic resonance spectra were measured on Varian XL-200 or Varian XL-300 FT-NMR spectrometers using deuterated chloroform or dimethylsulfoxide-d_6 as the solvent. All chemical shift values are quoted in ppm (δ) downfield from tetramethylsilane, which was used as an internal standard. Mass spectra were recorded on a Hewlett Packard mass spectrometer, model 5984A, with the chemical ionization mode (isobutane, source pressure 1 Torr (1 Torr = 133.3 Pa)) or the FAB mode (matrix: glycerol, atom energy 8 kV, 1 mA) being used as indicated. Column chromatography was carried out on silica gel 60 (230–400 mesh, Merck No. 9485).

Methyl 4,4'-bis(thioethoxy)but-2-enoate 7

Aldehyde **5** (2.28 g, 20 mmol), ethanethiol (5 mL), and zinc chloride (400 mg) were stirred at −15°C for 1 h. Hydrochloric acid (0.5 *N*, 5 mL) was added and stirring was continued at room temperature for 15 min. Excess ethanethiol was removed and the residue dissolved in water and dichloromethane. The organic layer was washed with aqueous sodium hydrogen carbonate (5%), dried ($MgSO_4$), and the solvent removed. Column chromatography (dichloromethane:hexanes 2:1) or distillation gave **7** as a yellow oil, bp 90–100°C/0.1 Torr

Can. J. Chem. Downloaded from www.nrcresearchpress.com by 72.64.146.136 on 09/07/12
For personal use only.

(3.4 g, 77%); ir: 1730, 1645 cm^{-1}; ^1H nmr ($CDCl_3$): 1.26 (t, 6H), 2.61 (m, 4H), 3.77 (s, 3H), 4.41 (d, 1H, J = 9 Hz), 5.92 (d, 1H, J = 16 Hz), 6.87 (dd, 1H, J = 16 Hz, J = 9 Hz); ^{13}C nmr ($CDCl_3$): 14.27 (q), 24.98 (t), 44.80 (d), 51.63 (q), 120.55 (d), 144.72 (d), 166.24 (s); ms (ei): 220 (M^+).

4,4'-Bis(thioethoxy)-3-butenoic acid ***10***

The ester **7** (22 g, 0.1 mol), potassium hydroxide (6.72 g, 0.12 mol), water (100 mL), and ethanol (100 mL) were heated under reflux for 3 h. The mixture was concentrated, and water (100 mL) was added and extracted with dichloromethane (50 mL). It was then acidified with hydrochloric acid and extracted with dichloromethane (3 × 50 mL). The combined organic layers were dried ($MgSO_4$) and the solvent removed to yield the acid **10** as an oil (19.2 g, 93%); ir: 3700–2500, 1690 cm^{-1}; ^1H nmr ($CDCl_3$): 1.21 (t, 6H), 2.72 (q, 4H), 3.47 (d, 2H, J = 7 Hz), 6.12 (t, 1H, J = 7 Hz), 11.25 (bs, 1H); ^{13}C nmr ($CDCl_3$): 14.05 (q), 14.35 (q), 26.98 (t), 27.32 (t), 35.73 (t), 127.65 (d), 134.47 (s), 177.50 (s). *Exact Mass* calcd.: 207.0514; found: 207.0513.

The acid **10** (6.76 g, 32.8 mmol), potassium hydroxide (1.84 g, 32.8 mmol), and water (50 mL) were left at room temperature for 30 min. Removal of the solvent gave the potassium salt **11** (8 g, 100%), which was used without further purification.

Schiff base ***12***b

Phenylprogargylaldehyde (2.8 g, 21.5 mmol) and dichloromethane (50 mL) were added dropwise to anisidine (2.65 g, 21.5 mmol), magnesium sulfate (5 g), and dichloromethane (100 mL) at 0°C. After 24 h at the same temperature, the mixture was filtered and the solvent removed. Recrystallization from ethyl acetate and hexanes gave the Schiff base ***12b*** as a yellow solid (4.3 g, 85%); mp 107–109°C; ir: 2160, 1590 cm^{-1}; ^1H nmr ($CDCl_3$): 3.82 (s, 3H), 6.90 (d, 2H), 7.23 (d, 2H), 7.34–7.39 (m, 3H), 7.56–7.61 (m, 2H), 7.94 (s, 1H). *Exact Mass* calcd.: 236.1076; found: 236.1075.

3-[2,2-Bis(thioethoxy)ethenyl]azetidinones ***13***a–d*: General procedure*

Cyanuric chloride (368 mg, 2 mmol) and dichloromethane (10 mL) were added to the potassium salt **11** (488 mg, 2 mmol), triethylamine (0.3 mL, 2 mmol), dichloromethane (80 mL), and the corresponding imine (2 mmol) at −40°C. This temperature was maintained for 4 h and the mixture was allowed to warm to −18°C overnight. The solution was washed with water and brine, dried ($MgSO_4$), and the solvent was removed. Column chromatography (dichloromethane:hexanes 2:1) gave the azetidinone.

Azetidinone ***13***a: 52%; mp 95–96°C; ir: 1740, 1510 cm^{-1}; ^1H nmr ($CDCl_3$): 1.07 (t, 3H), 1.25 (t, 3H), 2.64 (m, 2H), 2.76 (m, 2H), 3.76 (s, 3H), 4.82 (dd, 1H, J = 16 Hz, J = 6 Hz), 4.89 (dd, 1H, J = 17 Hz, J = 6 Hz), 6.12 (d, 1H, J = 16 Hz), 6.17 (d, 1H, J = 17 Hz), 6.70 (d, 1H, J = 16 Hz), 6.81 (d, 2H), 7.25–7.41 (m, 7H); ^{13}C nmr ($CDCl_3$): 13.84 (q), 15.04 (q), 27.07 (t), 55.33 (q), 55.81 (d), 58.49 (d), 114.31 (d), 118.24 (d), 124.90 (d), 126.62 (d), 128.29 (d), 128.63 (d), 131.67 (s), 135.24 (d), 135.75 (s), 137.73 (s), 156.04 (s), 164.97 (s). *Exact Mass* calcd.: 426.1562; found: 426.1553.

Azetidinone ***13***b: 33%; mp 63–65°C; ir: 2240, 1745, 1500 cm^{-1}; ^1H nmr ($CDCl_3$): 1.21 (t, 3H), 1.28 (t, 3H), 2.76 (q, 2H), 2.85 (q, 2H), 3.79 (s, 3H), 4.98 (m, 2H), 6.31 (m, 1H), 6.89 (d, 2H), 7.25–7.43 (m, 5H), 7.51 (d, 2H); ^{13}C nmr ($CDCl_3$): 13.91 (q), 15.05 (q), 27.28 (t), 28.26 (t), 47.57 (d), 55.24 (d), 55.50 (q), 82.97 (s), 89.29 (s), 114.39 (d), 118.28 (d), 121.86 (s), 125.74 (d), 128.36 (d), 128.94 (d), 131.04 (s), 131.81 (d), 138.31 (s), 156.34 (s), 163.89 (s). *Exact Mass* calcd.: 424.1404; found: 424.1405.

Azetidinone ***13***c: 7%; oil; ir: 1740 cm^{-1}; ^1H nmr ($CDCl_3$): 1.18 (t, 3H), 1.24 (t, 3H), 2.70 (m, 2H), 2.80 (m, 2H), 3.78 (s, 3H), 4.48 (dd, J = 10 Hz, J = 2 Hz), 4.72 (d, J = 2 Hz), 5.25 (d, J = 6 Hz), 6.18 (d, J = 10 Hz), 6.85 (d, 2H), 7.20–7.39 (m, 7H). *Exact Mass* calcd.: 400.1419; found: 400.1405.

Azetidinone ***13***d: 7%; oil; ir: 1730 cm^{-1}; ^1H nmr ($CDCl_3$): 1.08 (t, 3H), 1.21 (t, 3H), 2.62 (m, 2H), 2.81 (m, 2H), 3.77 (s, 3H), 4.54 (dd, J = 10 Hz, J = 2 Hz), 4.86 (d, J = 2 Hz), 6.39 (d, 1H, J = 10 Hz), 6.80 (d, 2H), 7.21–7.90 (m, 9H); ms (ci): 450 (M^+ + 1).

3-(Methoxycarbonylmethylene)azetidinone ***14***a

Borontrifluoride etherate (0.2 mL) was added to azetidinone ***13a*** (280 mg, 0.66 mmol) and methanol (10 mL) at room temperature and stirring was continued for 48 h. The solvent was removed and column chromatography (dichloromethane) gave the methyl ester ***14a*** as an oil that solidified on standing (180 mg, 78%); mp 165–167°C; ir: 1740 cm^{-1}; ^1H nmr ($CDCl_3$): 2.68 (dd, 1H), 2.86 (dd, 1H), 3.54 (s, 3H), 3.69 (s, 3H), 3.91 (m, 1H), 4.83 (t, 1H), 6.19 (dd, 1H), 6.68 (d, 1H), 6.83 (d, 2H), 7.27–7.42 (m, 7H); ^{13}C nmr ($CDCl_3$): 29.56 (t), 50.12 (q), 51.93 (d), 55.42 (d), 56.59 (q), 114.30 (d), 118.22 (d), 123.23 (d), 126.59 (d), 128.40 (d), 128.70 (d), 131.43 (s), 135.66 (s), 135.80 (d), 156.06 (s), 165.11 (s), 171.53 (s). *Exact Mass* calcd.: 352.1549; found: 352.1549.

3-(Thioethoxycarbonylmethylene)azetidinones ***15***a–d*: General procedure*

Trifluoroacetic acid (5 mL), ethanol (130 mL), water (50 mL), and the corresponding azetidinone **13** (3.8 mmol) were kept at 40°C for 72 h. The solution was concentrated, water (300 mL) was added, and the resulting emulsion extracted with dichloromethane (4 × 50 mL). The combined organic layers were dried ($MgSO_4$) and the solvent removed. Column chromatography (dichloromethane) gave azetidinone **15** as a solid.

Azetidinone ***15***a: 61%; mp 121–124°C; ir: 1740, 1685, 1510 cm^{-1}; ^1H nmr ($CDCl_3$): 1.11 (t, 3H), 2.80 (dq, 2H), 2.98 (dd, 1H, J = 17 Hz, J = 10 Hz), 3.08 (dd, 1H, J = 17 Hz, J = 5 Hz), 3.77 (s, 3H), 4.04 (m, 1H), 4.84 (t, 1H, J = 6 Hz), 6.19 (dd, 1H, J = 16 Hz, J = 6 Hz), 6.68 (d, 1H, J = 16 Hz), 6.84 (d, 2H), 7.25–7.39 (m, 7H); ^{13}C nmr ($CDCl_3$): 14.47 (q), 23.44 (t), 38.94 (t), 50.41 (d), 55.45 (q), 56.67 (d), 114.32 (d), 118.24 (d), 123.18 (d), 126.71 (d), 128.36 (d), 128.62 (d), 131.42 (s), 135.66 (s), 135.79 (d), 156.08 (s), 165.05 (s), 196.82 (s). *Exact Mass* calcd.: 382.1476; found: 382.1463.

Azetidinone ***15***b: 68%; mp 77–79°C; ir: 2220, 1745, 1690 cm^{-1}; ^1H nmr ($CDCl_3$): 1.19 (s, 3H), 2.90 (dd, 2H), 3.18 (dd, 1H), 3.36 (dd, 1H), 3.77 (s, 3H), 4.08 (m, 1H), 4.97 (d, 1H, J = 6 Hz), 6.88 (d, 2H), 7.25–7.43 (m, 5H), 7.48 (d, 2H); ^{13}C nmr ($CDCl_3$): 14.67 (q), 23.50 (t), 39.97 (t), 46.70 (d), 49.59 (d), 55.49 (q), 82.22 (s), 89.07 (s), 114.40 (d), 118.24 (d), 121.70 (s), 128.32 (d), 129.02 (d), 130.88 (s), 131.94 (d), 156.40 (s), 164.13 (s), 196.53 (s). *Exact Mass* calcd.: 380.1321; found: 380.1320.

Azetidinone ***15***c: 56%; oil; ir: 1745 cm^{-1}; ^1H nmr ($CDCl_3$): 1.23 (t, 3H), 2.89 (q, 2H), 3.11 (m, 2H), 3.73 (s, 3H), 4.16 (m, 1H), 4.83 (d, 1H, J = 6 Hz), 5.24 (d, 1H, J = 2 Hz), 6.76 (d, 2H), 7.20 (d, 2H), 7.34 (s, 5H). *Exact Mass* calcd.: 356.1321; found: 356.1320.

Azetidinone ***15***d: 70%; oil; ir: 1740 cm^{-1}; ^1H nmr ($CDCl_3$): 1.23 (t, 3H), 2.88 (q, 2H), 3.13 (m, 2H), 3.71 (s, 3H), 4.22 (m, 1H), 5.00 (d, 1H, J = 2 Hz), 5.39 (d, 1H, J = 6 Hz), 6.75 (d, 2H), 7.24 (m, 3H), 7.47 (m, 3H), 7.78–7.87 (m, 3H). *Exact Mass* calcd.: 406.1478; found: 406.1477.

Ozonolysis of the 4-styryl substituent to give ***15***e

Azetidinone ***15a*** (381 mg, 1 mmol) and dichloromethane (60 mL) were ozonized at −78°C during 30 min. The excess ozone was removed with a stream of nitrogen gas, dimethyl sulfide (2 mL) was added, and the solution was kept at room temperature for 48 h. The excess dimethyl sulfide was removed, sodium borohydride (111 mg, 3 mmol) was added, and the mixture was stirred for 24 h. The solution was washed with buffer solution (pH 7), with brine, and dried ($MgSO_4$). The solvent was removed and the crude alcohol dried under high vacuum. Methanesulfonyl chloride (228 mg, 2 mmol) and dichloromethane (20 mL) were added to this crude alcohol, triethylamine (0.5 mL), and dichloromethane (60 mL) at −78°C. This temperature was maintained for 1 h and the mixture was left to warm to room temperature. The solvent was removed and column chromatography (dichloromethane:ethyl acetate 20:1) gave the product as colourless needles (240 mg, 61%); mp 112°C; ir: 1750, 1680, 1510, 1140 cm^{-1}; ^1H nmr ($CDCl_3$): 1.27 (s, 3H), 2.84 (s, 3H), 2.92 (q, 2H), 3.01 (dd, 1H), 3.32 (dd, 1H), 3.78 (s, 3H), 3.96 (m, 1H), 4.53 (m, 3H), 6.87 (d, 2H), 7.33 (d, 2H); ^{13}C nmr ($CDCl_3$): 14.56 (q),

Can. J. Chem. Downloaded from www.nrcresearchpress.com by 72.64.146.136 on 09/07/12
For personal use only.

23.73 (t), 37.53 (q), 38.34 (t), 47.81 (d), 53.11 (d), 55.48 (q), 65.56 (t), 114.61 (d), 118.89 (d), 130.13 (s), 156.67 (s), 164.52 (s), 197.00 (s). *Exact Mass* calcd.: 388.0889; found: 388.0889.

4-(Iodomethylene)azetidinone ***15*** f

Azetidinone **15***e* (194 mg, 0.5 mmol), tetrapentylammonium iodide (425 mg, 1 mmol), potassium iodide (166 mg, 1 mmol), and dry benzene (40 mL) were heated under reflux for 20 h. The solvent was removed and column chromatography (dichloromethane:ethyl acetate 30:1) gave the iodo compound (190 mg, 89%); mp 120°C; ir: 1750, 1510, 1140 cm^{-1}; ^1H nmr ($CDCl_3$): 1.28 (t, 3H), 2.94 (q, 2H), 3.07–3.30 (m, 3H), 3.59 (dd, 1H), 3.78 (s, 3H), 4.00 (m, 1H), 4.45 (m, 1H), 6.87 (d, 2H), 7.26 (d, 2H); ^{13}C nmr ($CDCl_3$): −0.02 (t), 14.62 (q), 23.75 (t), 37.67 (t), 48.36 (d), 54.87 (d), 55.53 (q), 114.61 (d), 118.91 (d), 129.93 (s), 156.59 (s), 164.74 (s), 196.59 (s). *Exact Mass* calcd.: 420.0124; found: 420.0130.

4-Methylazetidinone ***15***g

The 4-iodomethyleneazetidinone **15***f* (21 mg, 0.05 mmol), tributyltin hydride (29 mg, 0.03 mmol), AIBN (catalyst), and dry benzene (10 mL) were heated under reflux for 3 h. The solvent was removed, and the residue was dissolved in acetonitrile (20 mL) and washed with hexanes (6 × 20 mL). The acetonitrile was removed and column chromatography (dichloromethane:ethyl acetate 50:1) gave **15***g* as an oil that solidified on standing (12 mg, 81%); mp 73–75°C; ir: 1740, 1690, 1510, 1390 cm^{-1}; ^1H nmr ($CDCl_3$): 1.26 (t, 3H), 1.37 (d, 3H, J = 6 Hz), 2.92 (q, 2H), 2.95 (dd, 1H), 3.12 (dd, 1H), 3.78 (s, 3H), 3.82 (m, 1H), 4.32 (m, 1H), 6.86 (d, 2H), 7.27 (d, 2H); ^{13}C nmr ($CDCl_3$): 13.99 (q), 14.64 (q), 23.55 (t), 38.17 (t), 48.10 (d), 50.86 (d), 114.48 (d), 118.49 (d), 130.72 (s), 156.13 (s), 165.08 (s), 197.16 (s). *Exact Mass* calcd.: 294.1163; found: 294.1163.

N-deprotected azetidinones ***16****: General procedure*

Ceric ammonium nitrate (1.64 g, 3 mmol) and water (80 mL) were added to the N-protected azetidinone **15** (1 mmol) and acetonitrile (80 mL) at −10°C. After 30 min at this temperature, water (400 mL) was added and the mixture was extracted with ethyl acetate (5 × 50 mL). The combined organic layers were dried ($MgSO_4$) and the solvent removed. Column chromatography (dichloromethane:ethyl acetate 2:1) yielded **16**.

Azetidinone ***16***a: 65%; mp 141–142°C; ir: 3420, 1765, 1680 cm^{-1}; ^1H nmr ($CDCl_3$): 1.14 (t, 3H), 2.82 (dq, 2H), 2.88 (dd, 1H), 2.98 (dd, 1H), 3.94 (m, 1H), 4.54 (t, 1H, J = 6 Hz), 5.94 (bs, 1H), 6.15 (dd, 1H), 6.63 (d, 1H), 7.28–7.38 (m, 5H); ^{13}C nmr ($CDCl_3$): 14.53 (q), 23.44 (t), 38.96 (t), 51.76 (d), 53.12 (d), 124.75 (d), 126.63 (d), 128.22 (d), 128.66 (d), 133.97 (d), 135.81 (s), 168.87 (s), 196.91 (s). *Exact Mass* calcd.: 276.1064; found: 276.1064.

Azetidinone ***16***b: 60%; mp 109–112°C; ir: 3400, 2220, 1765 cm^{-1}; ^1H nmr ($CDCl_3$): 1.18 (t, 3H), 2.88 (dq, 2H), 3.11 (dd, 1H), 3.30 (dd, 1H), 3.99 (m, 1H), 4.69 (d, 1H, J = 5 Hz), 6.21 (bs, 1H), 7.27–7.35 (m, 3H), 7.42 (m, 2H); ^{13}C nmr ($CDCl_3$): 14.65 (q), 23.49 (t), 40.04 (t), 43.25 (d), 51.72 (d), 83.86 (s), 87.81 (s), 121.84 (s), 128.35 (d), 128.93 (d), 131.85 (d), 168.36 (s), 196.49 (s). *Exact Mass* calcd.: 274.0903; found: 274.0909.

Azetidinone ***16***g: 84%; mp 60–63°C; ir: 1770, 1560 cm^{-1}; ^1H nmr ($CDCl_3$): 1.24 (d, 3H, J = 6 Hz), 1.24 (t, 3H), 2.88 (q, 2H), 2.92–3.05 (m, 2H), 3.68 (m, 1H), 3.95 (quintet, 1H, J = 6 Hz), 5.92 (bs, 1H); ^{13}C nmr ($CDCl_3$): 14.63 (q), 16.47 (q), 23.52 (t), 38.28 (t), 47.67 (d), 49.25 (d), 169.04 (s), 197.04 (s). *Exact Mass* calcd.: 188.0746; found: 188.0745.

Reaction with alkylamines to give ***17–19****: General procedure*

The thioester **16** (1 mmol) and the corresponding amine (2 mL) were heated to 70°C for 2 h. The excess amine was removed under high vacuum and the residue triturated with carbon tetrachloride to yield the product.

Azetidinone ***17***a: 87%; mp 187–191°C; ir: 3320, 1765, 1635, 1140 cm^{-1}; ^1H nmr ($CDCl_3$): 2.44 (dd, 1H), 2.71 (dd, 1H), 3.87 (m, 1H), 4.41 (dq, 2H), 4.58 (t, 1H, J = 6 Hz), 6.01 (bs, 1H), 6.16 (dd, 1H), 6.64 (d, 1H), 6.71 (s, 1H), 7.19–7.34 (m, 10H); ^{13}C nmr (DMSO-d_6): 30.65 (t), 42.07 (t), 50.95 (d), 51.79 (d), 126.33 (d), 126.58 (d), 126.95 (d), 127.06 (d), 127.64 (d), 128.09 (d), 129.59 (d), 131.98 (d), 136.17 (s), 139.17 (s), 169.33 (s), 169.59 (s). *Exact Mass* calcd.: 321.1604; found: 321.1603.

Azetidinone ***17***b: 80%; mp 141–142°C; ir: 1750 cm^{-1}; ^1H nmr ($CDCl_3$): 2.82 (m, 2H), 3.92 (m, 1H), 4.42 (d, 1H), 4.82 (d, 2H), 7.16–7.45 (m, 8H), 7.78 (m, 2H), 8.39 (s, 1H). *Exact Mass* calcd.: 319.1447; found: 319.1449.

Azetidinone ***17***g: 98%; mp 120–121°C; ir: 1750 cm^{-1}; ^1H nmr ($CDCl_3$): 1.24 (d, 3H), 2.56 (m, 2H), 3.02 (bs, 1H), 3.56 (m, 1H), 3.91 (m, 1H), 4.44 (d, 2H), 6.20 (bs, 1H), 7.29 (s, 5H). *Exact Mass* calcd.: 233.1291; found: 233.1290.

Azetidinone ***18***a: 85%; mp 199–201°C; ir: 3300, 1765, 1640 cm^{-1}; ^1H nmr ($CDCl_3$): 2.41 (dd, 1H), 2.65 (dd, 1H), 3.82 (m, 1H), 4.55 (m, 3H), 6.03 (bs, 1H), 6.15 (dd, 1H), 6.62 (d, 1H), 6.78 (bs, 1H), 6.90 (d, 1H), 7.17 (t, 1H), 7.30 (s, 5H). *Exact Mass* calcd.: 327.1168; found: 327.1182.

Azetidinone ***19***a: 70%; mp 152°C; ir: 3400, 1760 cm^{-1}; ^1H nmr ($CDCl_3$): 1.22–1.64 (m, 6H), 2.54 (dd, 1H), 2.66 (dd, 1H), 2.92 (bs, 1H), 3.16–3.34 (m, 2H), 3.57 (bs, 1H), 3.91 (m, 1H), 4.59 (t, 1H, J = 6 Hz), 6.17 (dd, 1H), 6.34 (bs, 1H), 6.60 (d, 1H), 7.19–7.36 (m, 5H). *Exact Mass* calcd.: 299.1761; found: 299.1760.

Azetidinone ***19***g: 75%; mp 99–102°C; ir: 1755 cm^{-1}; ^1H nmr ($CDCl_3$): 1.21 (d, 3H), 2.58 (dd, 1H), 2.77 (dd, 1H), 2.88 (bs, 1H), 3.41 (bs, 1H), 3.53 (bs, 1H), 3.75 (m, 1H), 4.05 (m, 1H). *Exact Mass* calcd.: 211.1473; found: 211.1470.

Hydrogenation of 4-styryl substituent: azetidinone ***17***h

Azetidinone **17***a* (32 mg, 0.1 mmol), platinum (catalyst), and ethanol (5 mL) were hydrogenated at normal pressure for 30 min. The mixture was filtered and the solvent removed. Column chromatography (dichloromethane:ethyl acetate 3:2) yielded **17***h* (18 mg, 56%); mp 149°C; ir: 1750 cm^{-1}; ^1H nmr ($CDCl_3$): 1.73 (m, 1H), 1.97 (m, 1H), 2.49 (dd, 1H), 2.60–2.77 (m, 3H), 3.61 (m, 1H), 3.81 (m, 1H), 4.44 (d, 2H), 5.78 (bs, 1H), 7.15–7.39 (m, 10H). *Exact Mass* calcd.: 323.1760; found: 323.1744.

Hydrogenation of 4-alkynyl substituent: ***17***i

Azetidinone **17***b* (32 mg, 0.1 mmol), nickel(II) acetate (50 mg, 0.2 mmol), sodium borohydride (7.6 mg, 0.2 mmol), ethylene diamine (0.3 mL), and ethanol (2 mL) were hydrogenated at normal pressure for 6 h. The mixture was filtered and the solvent removed. Column chromatography (dichloromethane:ethyl acetate 1:1) yielded the *cis*-styryl derivative **17***i* (7 mg, 20%); mp 170°C; ir: 1755 cm^{-1}; ^1H nmr ($CDCl_3$): 2.53 (dd, 1H), 2.78 (dd, 1H), 3.89 (m, 1H), 4.43 (d, 2H), 4.78 (dd, 1H, J = 9 Hz, J = 6 Hz), 5.62 (dd, 1H, J = 11 Hz, J = 9 Hz), 5.95 (bs, 1H), 6.77 (d, 1H, J = 11 Hz), 7.16–7.41 (m, 5H). *Exact Mass* calcd.: 321.1581; found: 321.1571.

N-sulfonation of azetidinones to give ***20–22****: General procedure*

The N-deprotected azetidinone **17–19** (0.1 mmol), pyridine sulfur trioxide complex (48 mg, 0.3 mmol), and pyridine (0.5 mL) were heated to 80°C for 2 h. Buffer solution (sodium hydrogen phosphate, 0.5 *N*, 5 mL) was added, the mixture extracted with dichloromethane (3 × 10 mL), and the combined organic layers reextracted with buffer solution (3 × 10 mL). Tetrabutylammonium hydrogen sulfate (0.1 mmol) was added to the combined aqueous layers and these were then extracted with dichloromethane (3 × 20 mL). The combined organic layers were dried ($MgSO_4$) and the solvent removed to yield the tetrabutylammonium salt as an oil that was dried under high vacuum. The crude salt was passed through Dowex 50X8-200 ion exchange resin (6 mL, potassium form) to yield, after lyophylization, **20–22** as colourless solids.

Azetidinone ***20***a: 52%; mp 170–175°C; ir: 1760 cm^{-1}; ^1H nmr (DMSO-d_6): 3.14 (bs, 2H), 3.63 (dd, 1H), 4.12 (bs, 2H), 4.48 (t, 1H, J = 6 Hz), 6.23 (dd, 1H), 6.67 (d, 1H), 7.02–7.42 (m, 10H); ^{13}C nmr (DMSO-d_6): 30.55 (t), 41.99 (t), 48.62 (d), 57.62 (d), 125.93 (d), 126.36 (d), 126.54 (d), 127.03 (d), 127.51 (d), 128.05 (d), 128.48 (d), 132.85 (d), 136.48 (d), 138.93 (s), 165.60 (s), 169.26 (s); ms (FAB): 477 (M^+ + 39), 439 (M^+ + 1).

Can. J. Chem. Downloaded from www.nrcresearchpress.com by 72.64.146.136 on 09/07/12
For personal use only.

Azetidinone ***20***b: 34%; mp 158–160°C; ir: 1760 cm^{-1}; ^1H nmr (DMSO-d_6): 2.67 (m, 2H), 3.76 (m, 1H), 4.24 (s, 2H), 4.69 (d, 1H, J = 6 Hz), 7.16–7.44 (m, 10H), 8.46 (bs, 1H); ms (FAB): 475 (M^+ + 39), 437 (M^+ + 1).

Azetidinone ***20***g: 64%; mp 217–225°C; ir: 1755 cm^{-1}; ^1H nmr (DMSO-d_6): 1.16 (d, 3H, J = 6 Hz), 2.43 (m, 2H), 3.86 (m, 1H), 4.24 (d, 2H), 7.25 (s, 5H), 8.43 (bs, 1H). *Exact Mass* calcd.: 351.0417; found: 351.0343.

Azetidinone ***20***h: 36%; mp 120–123°C; ir: 1760 cm^{-1}; ^1H nmr (DMSO-d_6): 1.71 (m, 1H), 2.11 (m, 1H), 2.61 (m, 4H), 3.50 (m, 1H), 3.79 (m, 1H), 4.25 (d, 2H), 7.07–7.29 (m, 10H), 8.47 (bs, 1H). *Exact Mass* calcd.: 479.0398; found: 479.0445.

Azetidinone ***20***i: 42%; mp 205–210°C; ir: 1760 cm^{-1}; ^1H nmr (DMSO-d_6): 2.56 (m, 2H), 3.78 (m, 1H), 4.15 (m, 2H), 4.72 (dd, 1H), 5.74 (dd, 1H), 6.61 (d, 1H), 7.24 (s, 5H), 7.26–7.40 (m, 5H), 8.42 (bs, 1H); ms (FAB): 477 (M^+ + 39), 439 (M^+ + 1).

Azetidinone ***21***a: 52%; mp 173–175°C; ir: 1765 cm^{-1}; ^1H nmr (DMSO-d_6): 2.38 (d, 2H), 3.60 (m, 1H), 4.26 (d, 2H), 4.47 (t, 1H, J = 6 Hz), 6.16 (dd, 1H), 6.68 (d, 1H), 6.78 (s, 3H), 7.21–7.36 (m, 6H), 8.40 (bs, 1H); ms (FAB): 483 (M^+ + 39), 445 (M^+ + 1).

Azetidinone ***22***a: 38%; mp 182–185°C; ir: 1755 cm^{-1}; ^1H nmr (DMSO-d_6): 1.22–1.39 (m, 6H), 2.45 (dd, 1H), 2.58 (dd, 1H), 2.72 (bs, 1H), 3.01 (m, 2H), 3.45 (bs, 1H), 3.58 (m, 1H), 4.44 (t, 1H, J = 6 Hz), 6.20 (dd, 1H), 6.58 (d, 1H), 7.16–7.44 (m, 5H); ms (FAB): 455 (M^+ + 39), 417 (M^+ + 1).

Azetidinone ***22***g: 41%; mp 190–195°C; ir: 1760 cm^{-1}; ^1H nmr (DMSO-d_6): 1.13 (d, 3H, J = 6 Hz), 1.30–1.59 (m, 6H), 2.51 (m, 2H), 2.72 (bs, 1H), 3.32–3.40 (m, 4H), 3.85 (quintet, 1H, J = 6 Hz); ms (FAB): 367 (M^+ + 39), 329 (M^+ + 1).

Acknowledgements

We wish to thank Dr. O. Mamer for an excellent mass spectral service; Miss N. Kuck, Lederle Laboratories, for biological tests; and the Natural Sciences and Engineering Research Council of Canada, Lederle Laboratories, and Fonds pour la formation de chercheurs et l'aide à la recherche (FCAR), Province de Québec, for financial support.

1. J. Ghuysen, J. Frere, M. Leyh-Bouille, and O. Dideberg. *In* β-Lactam antibiotics—mode of action, new developments and future prospects. *Edited by* M. Salton and G. D. Stockman. Academic Press, New York. 1981.
2. D. D. Keith, J. Fengi, P. Rossman, L. Todoro, and M. Weigele. Tetrahedron, **39**, 2445 (1983).
3. R. Zamboni and G. Just. Can. J. Chem. **57**, 1945 (1979).
4. F. Bohlmann and E. Inhoffen. Chem. Ber. **89**, 1276 (1956).
5. P. L. Stotter and J. B. Eppner. Tetrahedron Lett. 2417 (1973).
6. J. Klein and E. D. Bergmann. J. Am. Chem. Soc. **79**, 3452 (1957).
7. W. Lidy and W. Sundermeyer. Chem. Ber. **106**, 587 (1973).
8. P. G. Gassman and J. J. Tally. Tetrahedron Lett. 3773 (1978).
9. W. Dumont, C. Vermeyen, and A. Krief. Tetrahedron Lett. **25**, 2883 (1984).
10. D. R. Kronenthal, C. Y. Han, and M. N. Taylor. J. Org. Chem. **47**, 2765 (1982).
11. H. Miller, E. Plochl, and H. Scheitz. Chem. Ber. **31**, 2701 (1898).
12. E. Massarami, D. Nardi, and L. Mauri. Boll. Chim. Farm. **104**, 155 (1965).
13. W. H. Koster, C. M. Cimarusti, and R. B. Sykes. Monobactams. *In* β-Lactam antibiotics, chemistry and biology. Vol. 3. *Edited by* R. B. Morin and M. Gorman. Academic Press, New York. 1982.
14. C. A. Brown and V. K. Akuja. J. Org. Chem. **38**, 2226 (1973); J. Chem. Soc. Chem. Commun. 553 (1973).

Can. J. Chem. Downloaded from www.nrcresearchpress.com by 72.64.146.136 on 09/07/12
For personal use only.

A proton nuclear magnetic resonance relaxation study of the glycine, alanine, and lactate complexes of gadolinium(III) in aqueous solution

R. Stephen Reid and Benjamin Podányi

Department of Chemistry, University of Saskatchewan, Saskatoon, Sask., Canada S7N 0W0

Received October 17, 1986

R. Stephen Reid and Benjamin Podányi. Can. J. Chem. **65**, 1508 (1987).

The ^{1}H nuclear magnetic resonance spin-lattice and spin–spin relaxation rate enhancements induced by the gadolinium(III) ion were measured in solutions of glycine, alanine, and sodium lactate containing different amounts of Gd(III). The proton relaxation rates in the Gd(III) complexes were calculated from these data, and were used to calculate metal–hydrogen atom distances. Comparison of these data with corresponding distances calculated from literature X-ray crystallographic data for model compounds shows that in the two amino acid complexes the Gd(III) ion is coordinated in a four-membered ring through the two oxygen atoms of the carboxylate group. By contrast, in the lactate complex coordination is via a five-membered ring involving one oxygen atom of the carboxylate group and the α-hydroxyl oxygen.

R. Stephen Reid et Benjamin Podányi. Can. J. Chem. **65**, 1508 (1987).

Opérant dans des solutions de glycine, d'alanine et de lactate de sodium contenant diverses quantités de Gd(III), on a mesuré les rehaussements que provoquent les ions gadolinium(III) sur les vitesses de relaxation spin–spin et spin–réseau, en résonance magnétique nucléaire du ^{1}H. En se basant sur ces données, on a calculé les vitesses de relaxation des protons dans ces complexes de Gd(III) et on a utilisé ces vitesses pour calculer les distances entre le métal et l'hydrogène. Une comparaison de ces données avec les distances correspondantes calculées à partir des données de diffraction des rayons-X de composés modèles démontre que, dans les deux complexes d'acides aminés, l'ion Gd(III) est impliqué dans un cycle de coordination à quatre membres par le biais des deux atomes d'oxygène du carboxylate. Par ailleurs, dans le complexe du lactate, la coordination se fait par le biais d'un cycle à cinq chaînons impliquant un atome d'oxygène du groupement carboxylate et l'oxygène de l'hydroxyle en α.

[Traduit par la revue]

Introduction

The gadolinium(III) ion has the longest electronic relaxation time amongst the lanthanide(III) cations, and is therefore well suited to use as a paramagnetic relaxation agent (1). Gd(III) complexes are now widely used as "contrast agents" in magnetic resonance imaging (2). Because Gd(III) has a similar ionic radius to Ca(II), the aquo Gd(III) ion has also been used as an nmr probe in the structural investigation of Ca(II) complexes in solution (3). For these reasons, a detailed understanding of the behaviour of Gd(III) complexes with biologically relevant small molecules is of some interest. Such understanding necessitates investigation of the stability and structure of such complexes in aqueous solution.

X-ray crystallographic studies have shown that in the Gd(III) complexes of simple carboxylic acids coordination is through both oxygen atoms of the carboxylic acid group (4). Solution studies using ^{13}C nmr relaxation rate enhancement reached the same conclusion. By contrast, the α-hydroxy acid complexes in solution involve coordination via the hydroxy group and one carboxylic acid group oxygen atom (5).

Some controversy has surrounded the structure of lanthanide(III) – amino acid complexes. Early results from cd (circular dichroism) studies suggested involvement of the amino group (6); however, this was questioned by later workers (7). Proton and ^{13}C chemical shift changes induced by lanthanide ions suggested that for the alanine complexes of light lanthanides coordination was via only one oxygen, but for heavier lanthanides via two (8). Another nmr study reported the opposite trend (9). Later studies by Elgavish and Reuben on the sarcosine complexes show that this entire series is isostructural, coordinating through both oxygens (10, 11). A similar conclusion was reached in another ^{13}C relaxation rate study of the conformation of leucine, lysine, and methionine (12).

Because of the lack of proton relaxation rate data in the literature, it was decided to investigate the complexation of Gd(III) by glycine, alanine, and lactic acid using this technique. All three of these molecules can be readily observed by nmr in biological systems such as the erythrocyte (13); lactic acid was one of the first compounds to be detected using in vivo proton nmr (14).

The relaxation rate enhancement induced by a paramagnetic ion is described by the Solomon–Bloembergen equation (15, 16). In the present study the metal ion and the protons are separated by 4 or 5 bonds, so contact contributions may be neglected. Equations [1] and [2] describe the spin-lattice (R_{1c}) and the spin–spin (R_{2c}) relaxation rates in the complex:

$$[1] \quad R_{1c} = \frac{5.17 \times 10^{-43}}{r^6}\left(\frac{3\tau_c}{1 + \omega_I^2\tau_c^2} + \frac{7\tau_c}{1 + \omega_S^2\tau_c^2}\right)$$

$$[2] \quad R_{2c} = \frac{2.58 \times 10^{-43}}{r^6}\left(4\tau_c + \frac{3\tau_c}{1 + \omega_I^2\tau_c^2} + \frac{13\tau_c}{1 + \omega_S^2\tau_c^2}\right)$$

where r is the distance between the paramagnetic ion and the proton under observation and ω_I and ω_S are the proton and the electron Larmor precession frequencies, 1.88×10^9 Hz and 1.24×10^{12} Hz respectively, at an applied magnetic field of 7 T. τ_c is the correlation time of the dipole–dipole interaction between the paramagnetic electron spin and the proton nuclear spin, which is expected to be in the 10^{-9}–10^{-11} s time range.

Since $\omega_S^2\tau_c^2 \gg 1 \simeq \omega_I^2\tau_c^2$ in the whole correlation time range, the terms containing the electronic Larmor precession frequency can be neglected. τ_c can be described by eq. [3]:

$$[3] \quad \frac{1}{\tau_c} = \frac{1}{\tau_S} + \frac{1}{\tau_b} + \frac{1}{\tau_d}$$

where τ_S is the electron-spin relaxation time, τ_b is the lifetime of the coordinated ligand, and τ_d is the rotational correlation time of the complex.

The lower limit of τ_S of the Gd(III) ion can be estimated to be 2×10^{-7} s at 5 T or higher magnetic fields (17), based on esr data (18). τ_b can be estimated by Lenkinski's method to be in the range of 10^{-5}–10^{-7} s for the ligands under investigation

Can. J. Chem. Downloaded from www.nrcresearchpress.com by 72.64.146.136 on 09/07/12
For personal use only.

(17). The observed correlation time τ_c is therefore ultimately dominated by the rotational correlation time of the complex (τ_d), so in our case the relaxation rates in the complex can be described by eqs. [4] and [5]:

$$[4] \quad R_{1c} = \frac{1.55 \times 10^{-42} \cdot \tau_d}{r_6 \cdot (1 + 3.55 \times 10^{18} \cdot \tau_d^2)}$$

$$[5] \quad R_{2c} = \frac{2.58 \times 10^{-43}}{r^6} \cdot \left(4\tau_d + \frac{3\tau_d}{1 + 3.55 \times 10^{18} \cdot \tau_d^2}\right)$$

Dividing [4] by [5] gives:

$$[6] \quad \frac{R_{1c}}{R_{2c}} = \frac{6.01}{3 + 4(1 + 3.55 \times 10^{18} \cdot \tau_d^2)}$$

from which the correlation time may be calculated.

The relationship between the observed relaxation rates (R_{io}) and those in the complex (R_{ic}) in a chemically exchanging ligand system was first described by Luz and Meiboom (19) and Swift and Connick (20); the problem of the two-site exchanging system was later solved without restrictions by Leigh (21). Leigh also derived an approximate solution (eq. [7]) assuming no contribution of the outer sphere relaxation, dilute solution of the paramagnetic spins, and that the shift caused by the complexation is much less then the reciprocal of the lifetime of the coordinated ligand ($\Delta\omega \ll 1/\tau_b$):

$$[7] \quad R_{io} = R_{if} + \frac{N_f}{N_b(T_{ic} + \tau_b)} \qquad (i = 1, 2)$$

where T_{ic} is $1/R_{ic}$, R_{if} is the relaxation rate of the free ligand and N_f/N_b is the mole fraction of the ligand in the free and in the coordinated state.

All the above assumptions apply in our case, where small amounts of Gd(III) ions have been added to dilute solutions of small ligands, which are in fast exchange between the free and the coordinated state. Equation [7] can be further simplified, because $T_{ic} \gg \tau_b$, so the effect of the lifetime of the coordinated ligand can be neglected, and because $N_f \simeq N_L$ (the total amount of ligands in solution). Rearrangement of the equation then gives

$$[8] \quad R_{ic} = \frac{R_{io} - R_{if}}{q \cdot p} \qquad (i = 1, 2)$$

where q is the average coordination number of the metal ion (i.e., $N_b = N_M \times q$) and p is the molar ratio of the metal ion to ligand in the solution (i.e., $p = N_M/N_L$). The determination of these quantities and of τ_d, and the calculation of Gd(III)–proton distances for the three complexes, is described below.

Experimental

Chemicals

Glycine, *l*-alanine (US Biochemical Corporation), sodium-*l*-lactate (Fluka AG), and gadolinium nitrate (Alfa Products) were used as received.

Preparation of solutions

A. For measurements at variable p: Stock solutions (0.013–0.020 *M*) were prepared in D_2O. pH* was adjusted to 4.5 by adding DCl to the solution. The pH* was measured using a Beckman SS-2 pH meter equipped with a glass combination electrode and calibrated in the usual manner. Samples (0.4 mL) were taken for the nmr measurements. Different Gd(III) concentrations were obtained by the successive addition of small volumes (3–6 μL) of a stock solution of 0.001 *M* $Gd(NO_3)_3$ in D_2O to the ligand solutions. The exact amount of Gd(III) solution added was determined by weight.

B. For measurements at constant p: The pH* of a stock solution 0.1 *M* in alanine and 0.002 *M* in Gd(III) was adjusted to 4.5. Samples were obtained by dilution of this solution and readjustment of pH* to 4.5.

^{1}H nuclear magnetic resonance measurements

The 300-MHz ^{1}H nmr spectra were obtained on a Bruker AM300 spectrometer, and 400-MHz data on a Bruker WH400 instrument. All data were collected at a proble temperature of 30 ± 1°C. Spin-lattice relaxation time measurements were made by the standard inversion–recovery method, with 10–12 different delay values. Relaxation times were calculated by the standard Bruker routine, and checked by a linearized plot and a weighted linear least-squares analysis. The standard deviation of the T_1 values yielded by the latter program was less than ±3% in all cases. Spin–spin relaxation time measurements on the glycine solutions were performed using the standard CPMG technique, and the relaxation times calculated using the Bruker routine. The spin–spin relaxation times of the sodium lactate solutions were estimated from the measured line-broadening caused by the Gd(III) ions. Experimental spectra were compared to simulations calculated by the Bruker routine PANIC, adjusting parameters in the latter to achieve the closest agreement. To correct for variations in field homogeneity, a small amount of TMS was added to the solutions, and the linewidth of the TMS signal was subtracted from the linewidth of the lactate signals in each case.

Calculations

The relaxation rates in the glycine and lactate complexes were calculated by linear least-squares regression from the observed relaxation rate measurements at 4 different p values. The relaxation rates in the complex of alanine, as well as the formation constants K_1 and K_2, were calculated by the MINPACK nonlinear least-squares regression program (36). The seven measurements with different p values and (or) alanine concentrations gave 14 experimental points, from which the 4 parameters were calculated. Different starting values gave identical solutions. The standard deviation of the parameters was estimated from the diagonal elements of the covariance matrix of the regression.

The gadolinium–hydrogen distances in the model compounds were calculated by the BONDLA program, which is a part of the XTAL83 program system (37). The crystal coordinates and the appropriate symmetry operations were loaded in, and the distances of all atoms within 1 nm of the metal ion were returned. Molecular connectivities were checked from the bond-distance list. The conformations in the solid state were investigated by calculating the torsion angles around all the important bonds using the program.

Results

Lactate

The proton relaxation rate enhancements for sodium lactate were measured at various Gd(III) concentrations. Figure 1 shows the results as a function of p. The response appears linear. From literature formation constants (22) the effective coordination number q was calculated to be 1.87 at the 0.02 *M* lactate concentration used. The resultant R_{1c} and R_{2c} values are shown in Table 1, together with the values of τ_d calculated from eq. [6]. The close agreement between the two τ_d values supports the assumption that a single correlation time can be used. The calculated distances between the Gd(III) ion and the protons, based upon the mean of the measured correlation times, are also given in Table 1.

Glycine

Relaxation rate data are shown in Fig. 1. Using literature formation constants (23), q was calculated to be 0.066 at the 0.013 *M* glycine concentration used. Because of the short correlation time of the small glycine molecule, both the R_{1c}/R_{2c} ratio and the ratio of R_{1c} measured at 7.0 and 9.4 T are close to

Can. J. Chem. Downloaded from www.nrcresearchpress.com by 72.64.146.136 on 09/07/12
For personal use only.

TABLE 1. Relaxation rates, correlation times, and calculated Gd(III)–proton distances for the complexes

Ligand	Resonance	R_{1c} (kHz)	R_{2c} (kHz)	τ_d ($s \times 10^{-10}$)	Distance (pm)
Lactate	CH	34.4 ± 1.5	47 ± 3	2.8 ± 0.6	470 ± 30
Lactate	CH_3	13.6 ± 0.3	19.2 ± 1.4	3.2 ± 0.7	540 ± 30
Glycine	CH_2	9.6 ± 0.5	10.2 ± 0.6	≦1.4	530[a]
Alanine	CH	15.7 ± 1.0	—	2.4 ± 1.0	520 ± 20
Alanine	CH_3	8.9 ± 0.5	—	2.2 ± 0.5	570 ± 20

[a]See text.

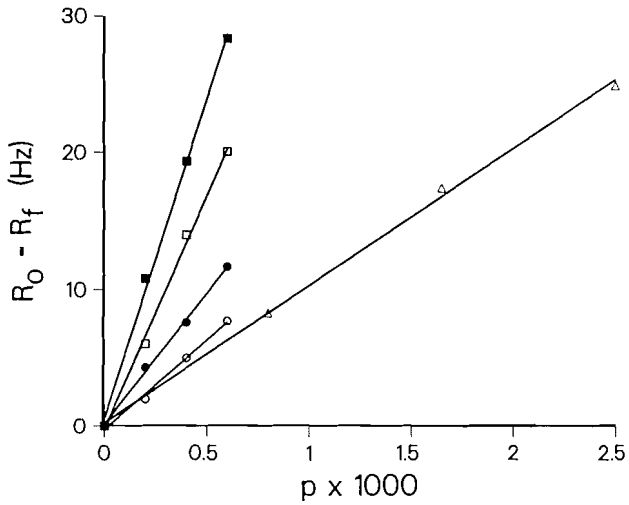

FIG. 1. Relaxation rates of the lactate and the glycine resonances at different gadolinium(III)/ligand ratios (p). ■: R_2 (lactate CH); □: R_1 (lactate CH); ●: R_2 (lactate CH_3); ○: R_1 (lactate CH_3); △: R_1 (glycine CH_2).

TABLE 2. Solution concentrations and observed and calculated proton relaxation rates for Gd(III)–alanine solutions

$p^a \times 10^3$	[L] (M)	$R_{1o}(CH_3)^a$ (Hz)		$R_{1o}(CH)^a$ (Hz)	
		Measured	Calculated	Measured	Calculated
0.00	0.020	0.50	—	0.21	—
0.69	0.020	0.87	0.89	0.85	0.89
1.25	0.020	1.17	1.19	1.41	1.44
1.95	0.020	1.58	1.58	2.22	2.12
2.00	0.100	6.83	6.86	11.41	11.44
2.00	0.050	3.50	3.49	5.44	5.50
2.00	0.015	1.27	1.32	1.55	1.66
2.00	0.010	1.07	1.04	1.16	1.16

[a]Terms defined in text.

unity. The upper limits of the correlation time gained from these measurements are 2.0×10^{-10} and 1.4×10^{-10} s respectively. On the basis of the difference in size of the glycine and alanine molecules, a difference in correlation times in excess of 30% would not be expected. The latter upper limit was used therefore in the calculation of Gd–hydrogen distance (Table 1).

Alanine

The R_{1o} data, collected at different Gd(III) and alanine concentrations, are given in Table 2. No reliable formation constant data are available in the literature, but known stepwise formation constants of the complexes of alanine with other lanthanide ions (11) suggest that, at most, only the first and second stepwise complexation processes are of importance in the concentration range used in our investigations. In this case, eq. [8] becomes:

$$[9] \quad R_{1c} = \frac{(R_{1o} - R_{1f})}{p} \cdot \frac{(1 + K_1[L] + K_1K_2[L]^2)}{(K_1[L] + 2K_1K_2[L]^2)}$$

where K_1 and K_2 are the first and second stepwise formation constants respectively, and [L] is the equilibrium ligand concentration. The experimental data were fitted to eq. [9] using nonlinear least-squares analysis. Both K_1 and K_2 were approximately 3 M^{-1}, although these values are imprecise due to the relatively small number of data points, and the strong interaction between these parameters in the fitting process. The resultant R_{1c} values (shown in Table 1) are, however, fairly precise. Agreement between experimental R_{1c} values and those calculated from the fit parameters is good (see Table 2). Attempts to fit to a model involving only K_1 failed. This means that under the experimental conditions used here both 1:1 and 1:2 complexes are formed between Gd(III) and alanine. The correlation time of the complex was calculated from the field strength dependence of R_{1c}. The ratios of R_{1c} measured at 7.0 T and at 9.4 T were 0.90 ± 0.03 and 0.88 ± 0.07 for the CH_3 and the CH protons respectively. The close agreement between these again supports the assumption of a single correlation time. The calculated correlation time together with calculated Gd(III)–proton distances are given in Table 1.

Discussion

To use the distance data calculated above to determine the mode of coordination in these complexes, corresponding data must be predicted for the various possibilities illustrated in Fig. 2. These could be determined using X-ray crystallographic data. According to a search of the Cambridge Crystallographic Data Bank, there are only 43 Gd(III) complex structures in the literature, only one (the glycolic acid complex (24)) being relevant to the present study. However, comparison of ion–oxygen distances in the Gd(III) complexes of acetate (4), propionate (25), and EDTA (26) with those in the Ca(II) complexes (27–29) shows that corresponding distances are very similar. This similarity in size has already been exploited in solution nmr work, as mentioned above (3). It is therefore possible to use appropriate Ca(II) compounds, for which an extensive crystallographic literature exists (30), as models for the Gd(III) analogues.

The crystal structure of Ca(II)–*l*-glutamate includes two modes of coordination: via both oxygens of the carboxylate group next to the amino group (Mode I in Fig. 2), and via one

Can. J. Chem. Downloaded from www.nrcresearchpress.com by 72.64.146.136 on 09/07/12
For personal use only.

TABLE 3. Experimentally derived Gd(III)–proton distances and $R_{1c}(CH_3)/R_{1c}(CH)$ ratios, and predicted values for different modes of coordination[a]

(*a*) Experimental values

Ligand	Gd...CH (pm)	Gd...CH_3 (pm)	$R_{1c}(CH_3)/R_{1c}(CH)$
Lactate	470	540	0.39
Glycine	530 (CH_2)	—	—
Alanine	520	570	0.57

(*b*) Predicted values

Mode of coordination	Gd...CH (pm)	Gd...CH_3 (pm)	$R_{1c}(CH_3)/R_{1c}(CH)$
Mode I	521	575	0.55
Mode IIa	433	528	0.31
Mode IIc	471	465	1.08
Mode III	389	534	0.15

[a]See Figs. 2 and 3 for definitions.

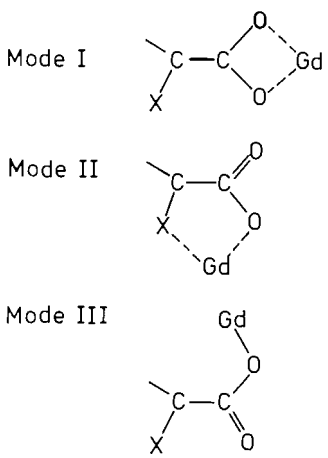

FIG. 2. The three possible coordination modes in the α-hydroxy- or α-amino acid complexes of gadolinium(III). X = O or NH_2.

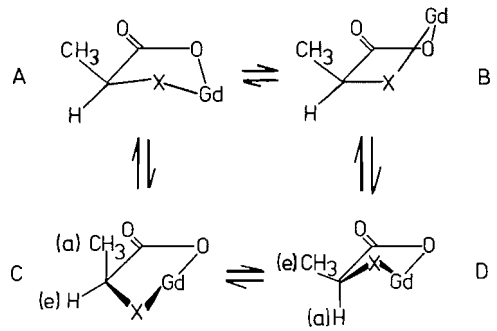

FIG. 3. The four envelope conformations of the five-membered chelate ring in Mode-II coordination. X = O or NH; a: axial; e: equatorial.

oxygen of this carboxylate group and the amino group (31) (Mode II). The latter mode is also shown in the crystal structure of the Ca(II)–di-*dl*-glycerate complex (32). Selection of a model for coordination through one oxygen only (Mode III) requires care. In the amino-acid complexes, the positively charged amino group and the metal ion will be as far as possible from each other, so a suitable model structure requires an antiperiplanar arrangement of the coordinating oxygen atom and the α-substituent. A suitable compound is a mixed calcium – cobalt aspartic acid complex (33).

The Gd(III)–proton distances predicted using these models have been calculated. A quick evaluation can also be performed using the ratios $R_{1c}(CH_3)/R_{1c}(CH)$. The average distance of the three methyl hydrogens was calculated according to eq. [10].

$$[10] \quad \frac{3}{r_{av}^6} = \frac{1}{r_1^6} + \frac{1}{r_2^6} + \frac{1}{r_3^6}$$

The experimental distances were generally shorter than those calculated from the crystal structures. It has been previously observed that the experimental relaxation rates of gadolinium complexes of amino acids (12) and of dipeptides (34) are described satisfactorily by the Solomon–Bloembergen equation only if the coordinating Gd—O bond length is set to be somewhat longer than it is expected to be from crystallographic data. In the present case, if the coordinating bond lengths are increased by 15% and the metal ion is placed onto the axis of the C1—C2 bond in Mode I, then good agreement is obtained with experimental values, as shown in Table 3. It is clear that the amino acid complexes involve coordination through both oxygens of the carboxylate group, and the lactate complex coordination through one oxygen of the carboxylate group and the hydroxyl group.

In the lactate case, the possible conformational equilibrium of the chelate ring makes the situation more complex. In a five-membered ring, with planarity of the carboxylate group, there are four possible envelope conformations and two half-chairs. The latter were not observed in any of the X-ray structures. The four possible envelope conformations are shown in Fig. 3. The metal–proton distances calculated for the di-*dl*-glycerate and glutamic acid complexes correspond to conformations A and C respectively. In terms of metal–proton distances these represent the extremes, conformations B and D being intermediate. The experimentally determined distances are also intermediate, indicating a probable equilibrium between two or more of these forms. However, the possibility of contributions from other forms not suggested by X-ray studies cannot be excluded. The rate of interchange, as expected (35), is fast, since no line-broadening not ascribable to paramagnetic relaxation was observed.

Can. J. Chem. Downloaded from www.nrcresearchpress.com by 72.64.146.136 on 09/07/12
For personal use only.

Acknowledgements

We are grateful to the Natural Sciences and Engineering Research Council of Canada for financial support of this work. Thanks are due also to Glen Bigam (Department of Chemistry, University of Alberta) for the 400-MHz nmr measurements, and to Dr Kálmán Simon (Chinoin Pharmaceutical and Chemical Works Ltd., Budapest, Hungary) for the search of the Cambridge Crystallographic Data Bank.

1. R. A. DWEK. Nuclear magnetic resonance in biochemistry. Clarendon Press, Oxford. 1975.
2. D. H. CARR. Physiol. Chem. Phys. Med. NMR, **16**, 137 (1985).
3. R. J. P. WILLIAMS. Struct. Bonding, **50**, 79 (1982).
4. M. C. FAVAS, D. L. KEPERT, B. W. SKELTON, and A. H. WHITE. J. Chem. Soc. Dalton Trans. 454 (1980).
5. C. A. M. VIJVERBERG, J. A. PETERS, A. P. G. KIEBOOM, and H. VAN BEKKUM. Tetrahedron, **42**, 167 (1986).
6. (*a*) L. I. KATZIN. Inorg. Chem. **8**, 1649 (1968); (*b*) L. I. KATZIN and E. GULYAS. Inorg. Chem. **7**, 2442 (1968).
7. R. PRADOS, L. G. STADTHERR, H. DONATO, and R. B. MARTIN. J. Inorg. Nucl. Chem. **36**, 689 (1974).
8. A. D. SHERRY and E. PASCUAL. J. Am. Chem. Soc. **99**, 5871 (1977).
9. B. A. LEVINE and R. J. P. WILLIAMS. Proc. R. Soc. Ser. A, **345**, 5 (1975).
10. G. A. ELGAVISH and J. REUBEN. J. Am. Chem. Soc. **100**, 3617 (1978).
11. G. A. ELGAVISH and J. REUBEN. J. Magn. Reson. **42**, 242 (1981).
12. C. CHACHATY, B. PERLY, and G. LANGLET. J. Magn. Reson. **50**, 125 (1982).
13. F. F. BROWN, I. D. CAMPBELL, P. W. KUCHEL, and D. L. RABENSTEIN. FEBS Lett. **82**, 12 (1977).
14. K. L. BEHAR, J. A. DEN HOLLANDER, M. E. STROMSKI, T. OGINO, R. G. SHULMAN, O. A. C. PETROFF, and J. W. PRICHARD. Proc. Natl. Acad. Sci. U.S.A. **80**, 4945 (1983).
15. I. SOLOMON. Phys. Rev. **99**, 559 (1959).
16. N. BLOEMBERGEN. J. Chem. Phys. **27**, 572 (1957).
17. R. E. LENKINSKI. *In* Biological magnetic resonance. Vol. 6. *Edited by* L. J. Berliner and J. Reuben. Plenum Press, New York. 1984. p. 36. ff.
18. J. REUBEN and M. COHN. Biochemistry, **10**, 2834 (1971).
19. Z. LUZ and S. MEIBOOM. J. Chem. Phys. **40**, 2686 (1964).
20. T. J. SWIFT and R. E. CONNICK. J. Chem. Phys. **37**, 307 (1962).
21. J. S. LEIGH, JR. J. Magn. Reson. **4**, 308 (1971).
22. H. DEELSTRA and F. VERBEEK. Anal. Chim. Acta, **31**, 251 (1964).
23. Z. KONTEATIS and H. G. BRITTAIN. J. Inorg. Nucl. Chem. **43**, 1675 (1981).
24. I. GRENTHE. Acta Chim. Scand. (*a*) **23**, 1752 (1969); (*b*) **26**, 1479 (1972).
25. G. V. ROMANENKO, N. V. PODBEREZSKAYA, and V. V. BAKAKIN. Zh. Strukt. Khim. **11**, 46 (1981).
26. L. K. TEMPLETON, D. H. TEMPLETON, A. ZALKIN, and H. W. RUBEN. Acta Crystallogr. Sect. B: Struct. Crystallogr. Cryst. Chem. **38**, 265 (1982).
27. M. M. BOREL and M. LEDESERT. J. Inorg. Nucl. Chem. **37**, 2334 (1975).
28. H. MARUYAMA, Y. TOMIIE, I. MIZUTANI, Y. YAMAZAKI, Y. UESU, N. YAMADA, and J. KOBAYASHI. J. Phys. Soc. Jpn. **23**, 889 (1967).
29. A. A. BALCHIN and C. H. CARLISLE. Acta Crystallogr. **19**, 103 (1965).
30. H. EINSPAHR and C. E. BUGG. Acta Crystallogr. Sect. B: Struct. Crystallogr. Cryst. Chem. **37**, 1044 (1981).
31. H. EINSPAHR and C. E. BUGG. Acta Crystallogr. Sect. B: Struct. Crystallogr. Cryst. Chem. **30**, 1037 (1974).
32. E. J. MEEHAN, H. EINSPAHR, and C. E. BUGG. Acta Crystallogr. Sect. B: Struct. Crystallogr. Cryst. Chem. **35**, 828 (1979).
33. I. OONISHI, M. SHIBATA, F. MARUMO, and Y. SAITO. Acta Crystallogr. Sect. B: Struct. Crystallogr. Cryst. Chem. **29**, 2448 (1973).
34. B. PERLY and C. CHACHATY. J. Magn. Reson. **49**, 397 (1982).
35. D. G. LISTER, J. N. MACDONALD, and N. L. OWEN. Internal rotation and inversion. Academic Press, London. 1978.
36. MINPACK-1 Fortran program. Argonne National Laboratory, Report Number: AN-80-74. 1974.
37. J. M. STEWART, S. R. HALL, R. A. ALDEN, R. OLTHOF-HAZENKAMP, and R. M. DOHERTY. The XTAL system of crystallographic programs. Computer Science Center, University of Maryland, College Park, MD. 1983.

Can. J. Chem. Downloaded from www.nrcresearchpress.com by 72.64.146.136 on 09/07/12
For personal use only.

A new series of mono- and dipiperidine, oxazoline, and oxazolidine crown ethers. Stability constants, ion transport rates, and nuclear magnetic resonance studies

J. DESROCHES, H. DUGAS,[1] AND M. BOUCHARD
Department of Chemistry, Université de Montréal, C.P. 6128, Succ. A, Montréal, P.Q., Canada H3C 3J7

AND

T. M. FYLES AND G. D. ROBERTSON
Department of Chemistry, University of Victoria, Victoria, B.C., Canada V8W 2Y2

Received September 29, 1986

This paper is dedicated to Professor Zdenek Valenta on the occasion of his 60th birthday

J. DESROCHES, H. DUGAS, M. BOUCHARD, T. M. FYLES, and G. D. ROBERTSON. Can. J. Chem. **65**, 1513 (1987).

A series of monopiperidine, **1**, dipiperidine **2**, **3** (*syn* and *anti*), as well as the corresponding oxazoline and oxazolidine crown ethers have been prepared and their ionophoric properties evaluated. The *syn*-dipiperidine **2***c* turned out to be a particularly efficient Ca^{2+} ligand (log $K = 9.7$). ^{13}C and ^{23}Na nuclear magnetic resonance spectroscopy was used to evaluate the nature of the complex between the monopiperidine **1***c*, the *syn*-dipiperidine **2***c*, and Ca^{2+} and Na^+ ions. In methanol–water solution, the dimeric salt $(\mathbf{2}c)_2Ca$ exhibits both a tight or asymmetric and a symmetric or loose ion pair between the cation and the carboxylate groups. Sodium-23 chemical shifts and line-width variation both support a 1:1 complex with **1***c* and **2***c*. The structural results correlate with observations from ion transport experiments.

J. DESROCHES, H. DUGAS, M. BOUCHARD, T. M. FYLES et G. D. ROBERTSON. Can. J. Chem. **65**, 1513 (1987).

On a préparé une série de monopipéridines (**1**), de dipipéridines (**2** et **3**) (*syn* et *anti*) ainsi que les éthers couronnes oxazolines et oxazolidines correspondantes et on a évalué leurs propriétés ionophoriques. La dipipéridine *syn* (**2***c*) est un ligand particulièrement efficace pour le Ca^{2+} (log $K = 9{,}7$). On a utilisé la spectroscopie de résonance magnétique nucléaire du ^{13}C et du ^{23}Na pour évaluer la nature du complexe qui se forme entre la monopipéridine **1***c*, la dipipéridine-*syn* (**2***c*) et les ions Ca^{2+} et Na^+. Dans une solution méthanol–eau, le sel dimère $(\mathbf{2}c)_2Ca$ se présente à la fois sous la forme d'une paire intime (ou asymétrique) d'ions et d'une paire symétrique (ou lâche) d'ions entre le cation et les groupements carboxylates. Les déplacements chimiques du ^{23}Na ainsi que les variations de la largeur des raies sont tous les deux en accord avec l'existence d'un complexe 1:1 avec **1***c* et **2***c*. Les résultats structuraux permettent d'établir une corrélation avec les expériences de transport d'ions.

[Traduit par la revue]

Introduction

A number of research groups have devoted some effort to the synthesis of nitroxide crown ethers in recent years (1–4). We have also been involved in this endeavor, particularly the preparation of dinitroxide (spin label) crown ethers **2***a*,*b* and **3***a*,*b* (5). The *syn* compound **2***a* turned out to be a good epr monitor of K^+ ion binding in the cavity because of the observable spin–spin exchange interaction between the two nitroxide groups. As the presence of a nitroxide function on these systems makes any nmr study rather tedious, we have decided to prepare the piperidine analogues **1***c*,*d*, **2***c*,*d*, and **3***c*,*d*. Furthermore, the corresponding oxazolines **1***f*, **2***f* and oxazolidines **1***g*, **2***g* have been prepared. The syntheses of these compounds were undertaken in view of their potential as new ion carriers and consequently their rates of transport of Na^+, K^+, and Ca^{2+} ions have been evaluated. This work is complemented by a ^{13}C nmr study of **1***c* and **2***c* in the presence of Ca^{2+} ion and a ^{23}Na nmr study in the presence of Na^+ ion. Data such as those provided by nmr experiments are useful and complementary to earlier epr results (5) to confirm the pH dependency of the solution conformation of *syn* **2***a*.

These compounds were studied to have a better understanding of the role played by one or two carboxylic groups near an ion complexing cavity such as a crown ether. Factors such as charge-to-size ratio and the concept of hole-size selectivity in macrocyclic chemistry will be examined.

Results and discussion

Syntheses

The syntheses and purification of **1***c*, **2***c*, and **3***c* involved the condensation of 2,2,6,6-tetramethyl-4-aminopiperidine with the corresponding mono- or dianhydride [18]-crown-6-*R*,*R*-tartaric acid following known procedures (6, 7). For instance, the addition of 2 equivalents of 2,2,6,6-tetramethyl-4-aminopiperidine to the [18]-crown-6 monoanhydride in CH_2Cl_2 gave, after stirring for 2 h at room temperature, the monoacid **1***c* in 90% yield. The *syn* adduct **2***c* was prepared similarly in the presence of an excess of triethylamine. In the absence of triethylamine, 4 equiv. of the aminopiperidine were needed and a 2:8 mixture of *syn*-**2***c* and *anti*-**3***c* diacids was obtained. The assignment of the configuration of the *syn* and *anti* isomers was based on the polarity and mobility on tlc, spectral data, and comparison with previous work (6). The corresponding methyl esters **1***d*, **2***d*, and **3***d* were made by treatment with a large excess of ethereal CH_2N_2.

In parallel with this study, the corresponding crown ether anilide mono- and diacids were prepared as before (6) and treated with CH_2N_2 to obtain **1***e* in 80% yield and **2***e* in 78% yield. The monooxazoline **1***f* was synthesized in 80% yield by refluxing 2 equiv. of 2-amino-2-methyl-1-propanol with the methyl ester **1***e* in xylene (8, 9). The dioxazoline **2***f* was prepared similarly using 4 equiv. of the amino alcohol. The corresponding oxazolidines **1***g* and **2***g* were obtained in 50% yield by reduction of **1***f* and **2***f* with 1.0 equiv. of $NaBH_4$ at −30°C, pH 7, for 2 h (10).

Ion transport rates

In all cases, the transport of cations across a chloroformic liquid membrane was studied using a U-shaped cell, where typically a 10^{-3} *M* solution of a crown ether carrier and a 10^{-2} *M* solution of metal picrate produce transport behavior that can be described as zero order (linear increase in picrate

[1]Author to whom correspondence may be addressed.

Can. J. Chem. Downloaded from www.nrcresearchpress.com by 118.98.75.50 on 09/07/12
For personal use only.

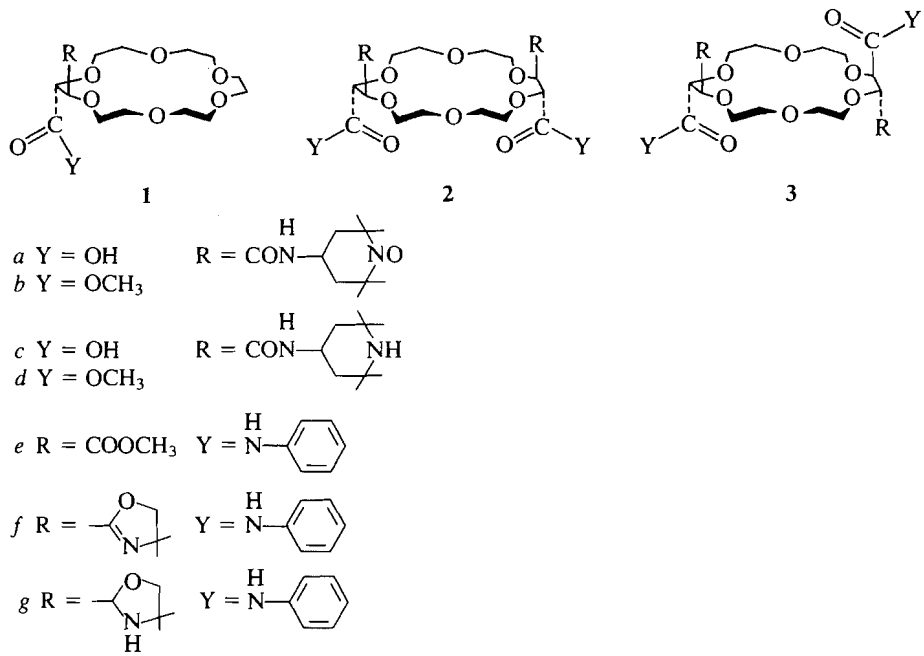

concentration in the receiving phase) (11). In such a situation, the transfer of the metal salt is considered to be a carrier-facilitated process whereby the species are moved down a concentration gradient across the organic liquid phase by the organic carrier molecule that resides in this artificial membrane. Without a carrier, no transfer of ions is observed in this system. Under these conditions, a diffusion mechanism of the [metal–carrier] complex can safely be regarded as the rate limiting step, the organic layer being magnetically stirred at a rate of 400 rpm. However, at this stirring rate a related system is kinetically limited by adsorption/desorption processes at the interface (12). A similar phenomenon may be applicable to some of the new carboxylic acid carriers prepared here, but for neutral macrocycles a diffusion-limited treatment is more appropriate in the sense that, to date, all related cases known are diffusion limited (13, 14). We therefore discuss our results in terms of a diffusion mechanism.

The transport rates of Na^+, K^+ and Ca^{2+} ions for the various crown ether carriers are presented in Table 1, and the corresponding nitroxide crown ethers were also evaluated for comparison. From these results, the following general observations can be made. Firstly, values obtained for the transport rates are quite comparable to those obtained for similar crown ethers with aliphatic chains (17). Secondly, very little selectivity is observed for Ca^{2+} ions and most compounds exhibit a marked preference for K^+ over the other cations. Thirdly, a comparison between the oxazoline and oxazolidine series indicates that neither seems to favor any ion selectivity. Lastly, an appreciable change in relative rate of transport is detected for the *syn*/*anti* pair and K^+ transport only in the case of the *anti*-dipiperidine ester **3***d*. The larger values in rate of transport for the *syn*-dinitroxide ester **2***b* over the *syn*-dipiperidine ester **2***d* are also noteworthy.

One might expect that relative rates in ion transport can be explained simply in terms of the selectivity of complexation, which is determined from stability constants (discussed in the next section). Basically, as the overall extraction constant gets bigger (in parallel with the stability constant) the rate goes up. This means that the systems lie on the low side of the optimal extraction constant (13); in this case, selectivity and relative rate will come out the same in a competitive experiment, but this has yet to be done. Furthermore, the selectivity of a crown ether for a given ion has often been intuitively attributed to a matching of the cavity size and the metal ion diameter. However, more recent investigations (15) have revealed that such a single "cavity-size" selectivity concept is not always applicable.

In the present paper, the general trend found in Table 1

TABLE 1. Transport rates for the various carriers at 10^{-3} *M*

Crown ether carrier	Metal ion* (rate, μmol/h)		
	Na^+	K^+	Ca^{2+}
1*a*†	1.2	5.6	2.0
1*d*	4.9	9.3	1.7
1*e*	2.3	9.0	0.3
1*f*	0.1	0.4	0.1
1*g*	0.3	0.8	0.1
2*a*†	2.2	1.9	2.0
2*b*	3.4	7.8	0.6
2*d*	0.4	0.3	0.1
2*e*	0.4	3.6	1.0
2*f*	0.1	0.4	0.1
2*g*	0.1	0.4	0.2
3*a*†	2.3	2.1	0.6
3*d*‡	0.8	2.8	0.6

*As picrate salts using the procedure of refs. 18 and 19. The experiments were conducted in a U-tube cell (diam. 1.7 cm) with $CHCl_3$ as the organic liquid membrane and 0.05 *M* diethanolamine·HCl, pH 9.7, for the receiving aqueous phase at 20°C. The initial concentration of picrate salts was 10^{-2} *M*. The mono- and diacid crown ethers **1***c*, **2***c*, and **3***c* were much too soluble in water and insoluble in $CHCl_3$ to perform an experiment under such conditions. Error estimates ± 10%.

†Determined at pH 7.0 (water, unbuffered) rather than 9.7 because of the solubility of the crown ethers in basic solution.

‡Even after repeated chromatography, it was not possible to obtain the *anti* isomer completely devoid (20%) of *syn* isomer **2***d*.

Can. J. Chem. Downloaded from www.nrcresearchpress.com by 118.98.75.50 on 09/07/12
For personal use only.

Can. J. Chem. Downloaded from www.nrcresearchpress.com by 118.98.75.50 on 09/07/12
For personal use only.

indicates that for the series of [18]-crown-6 mono derivative, the anticipated preference for K^+ ion is observed. In the [18]-crown-6 di-derivatives series, a similar behavior is maintained except for compounds **2***a* and **2***d*, where little selectivity is shown.

It is worthwhile to point out that the presence of carboxylate groups close to the crown ether cavity could have a profound effect on the stability of the corresponding ion complex as well as on the ionophoric properties of such macrocyclic compounds. Indeed, other carboxylic acid crown ethers have been described (16) and found to form substantially more stable complexes, when deprotonated. One might thus expect that the replacement of the ionic carboxylic function in **2***a* by a neutral methyl ester, **2***b*, should modify the stability constant and eventually lead to a difference in the ion transport rate. Comparing compounds **2***a* and **2***b* (Table 1) exemplified such expectation. In the case of **2***a*, the low transport rate and the lack of transport selectivity can be rationalized primarily in terms of electrostatic interaction with a favorable stabilizing effect of the carboxylate groups on the complexation. However, in **2***b*, a pole–dipole interaction of the cation with the crown ether is the main stabilizing factor, leading to a less tightly bound ion, but with a greater hole-size selectivity.

Another point to be considered is how the carboxylate crowns actually do the transport. For the neutral crowns it is just a simple example of cotransport of a pair of ions (M^+ and picrate$^-$). For the acids it is not so clear. We assume that there is a *countertransport* of cations and protons, forming some picric acid on the source side of the membrane, which diffuses to the receiving side without intervention of the carrier. The pH of the source phase changes from 6.9 to 6.6 over 19 h of experiment. Similarly, the receiving phase varies from pH 6.8 to 7.0 because of the countertransport of picric acid, which forms picrate ion (Pic^-). The net result is the same as with the neutral crowns: a cotransport of M^+ and Pic^-. Therefore, in the biochemical sense the acid crown behaves as an electrically neutral transporter while the picric acid becomes an uncoupler of the proton gradient. The following diagram summarizes the observations:

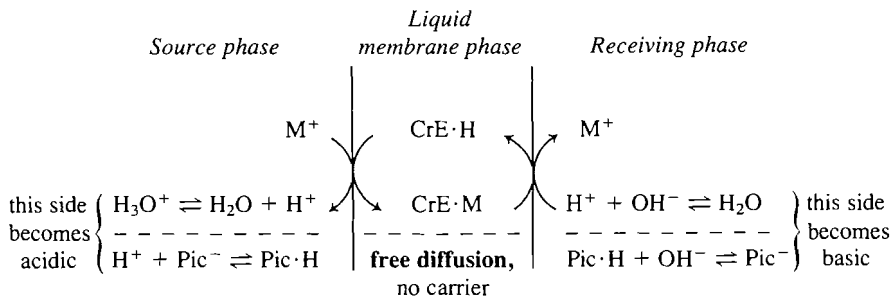

Finally, the introduction of oxazoline (**1***f*, **2***f*) or oxazolidine (**1***g*, **2***g*) groups as potentially active ion ligands seems to decrease appreciably the ion transport rate of the corresponding crown ether carriers. Although the stability constants have not been determined, this behavior might be attributed to the participation of the oxygen or the nitrogen atom of the heterocycle in the ion complexation.

Ionization and association constants

The values obtained by potentiometric titration (7, 21) for the pK_a and association constants with K^+, Na^+, or Ca^{2+} and mono-, *syn*-di-, and *anti*-dinitroxide crown ethers **1***a*, **2***a*, **3***a* are summarized in Table 2, and compared to values for mono- and *syn*-dipiperidines **1***c* and **2***c*. Noteworthy is the observation that for the *anti* series, ΔpK_a has a value close to one log unit. The *syn* series, however, has a ΔpK_a value larger than 2 log units. This general trend has previously been noticed in similar dialiphatic chain [18]-crown-6 diacids (18). Among the various compounds synthesized, the *syn* arrangement is unique in the sense that the two carboxylate groups are attached on the same side of the macrocyclic ring and converge to provide two identical sites by which binding information can be passed on. The presence of two acidic groups oriented *syn* and facing one another thus increases considerably the pK_a of the second carboxylic function. There could very well be a water molecule trapped between the two carboxylic groups to ensure proper proton transfer. This is reminiscent of the differences in pK_a values found for fumaric acid ($pK_1 = 3.02$, $pK_2 = 4.39$, $\Delta pK = 1.37$) and maleic aicd ($pK_1 = 1.92$, $pK_2 = 6.22$, $\Delta pK = 4.30$). The *syn* orientation of the two carboxylic groups in **2***c* directly affected their reactivity, since diazomethane esterification never resulted in high yield of **2***d*. Such behavior was also noticed in other systems where two carboxylic functions facing each other are separated by a rigid naphthyl moiety (20).

Stability constants for complexation with Na^+ and K^+ ions were in the 10^4–10^6 M^{-1} range for all three crown compounds examined. For the **2***c*·Ca^{2+} complex, however, much higher

TABLE 2. Ionization and association constants*

Crown ether ligand (L)	pK_a	log *K*		
		K^+	Na^+	Ca^{2+}
1*a*	6.18	3.8 (L^-)		
1*c*	6.28		4.3 (LH)	5.0 (LH)
	8.68 (NH)	5.0 (L^-)	4.4 (L^-)	5.1 (L^-)
2*a*	5.67	4.4 (LH^-)		
	8.05	5.4 (L^{2-})		
	$\Delta pK_a = 2.38$			
2*c*	4.20			
	6.17	4.2 (LH_2)	4.5 (LH_2)	7.8 (LH_2)
	8.15	4.3 (LH^-)	4.7 (LH^-)	8.3 (LH^-)
	10.61 (NH)	5.4 (L^{2-})	5.6 (L^{2-})	9.7 (L^{2-})
	$\Delta pK_a = 1.98$			
3*a*	6.09	5.1 (LH^-)		
	7.02	6.8 (L^{2-})		
	$\Delta pK_a = 0.93$			

*Measured in $MeOH/H_2O$ (9:1), 0.05 *M* Me_4NCl, 25°C. Error in pK_a, ±0.1; in log *K*, ±0.2. L stands for fully deprotonated crown ether ligand. The equilibria involved are $LH \rightleftharpoons L^-$ for **1***a* and **1***c*, and $LH_3^+ \rightleftharpoons LH_2 \rightleftharpoons LH^- \rightleftharpoons L^{2-}$ for **2***a*, **2***c*, and **3***a*. The species implicated with the corresponding log *K* are indicated in the parentheses.

Can. J. Chem. Downloaded from www.nrcresearchpress.com by 118.98.75.50 on 09/07/12
For personal use only.

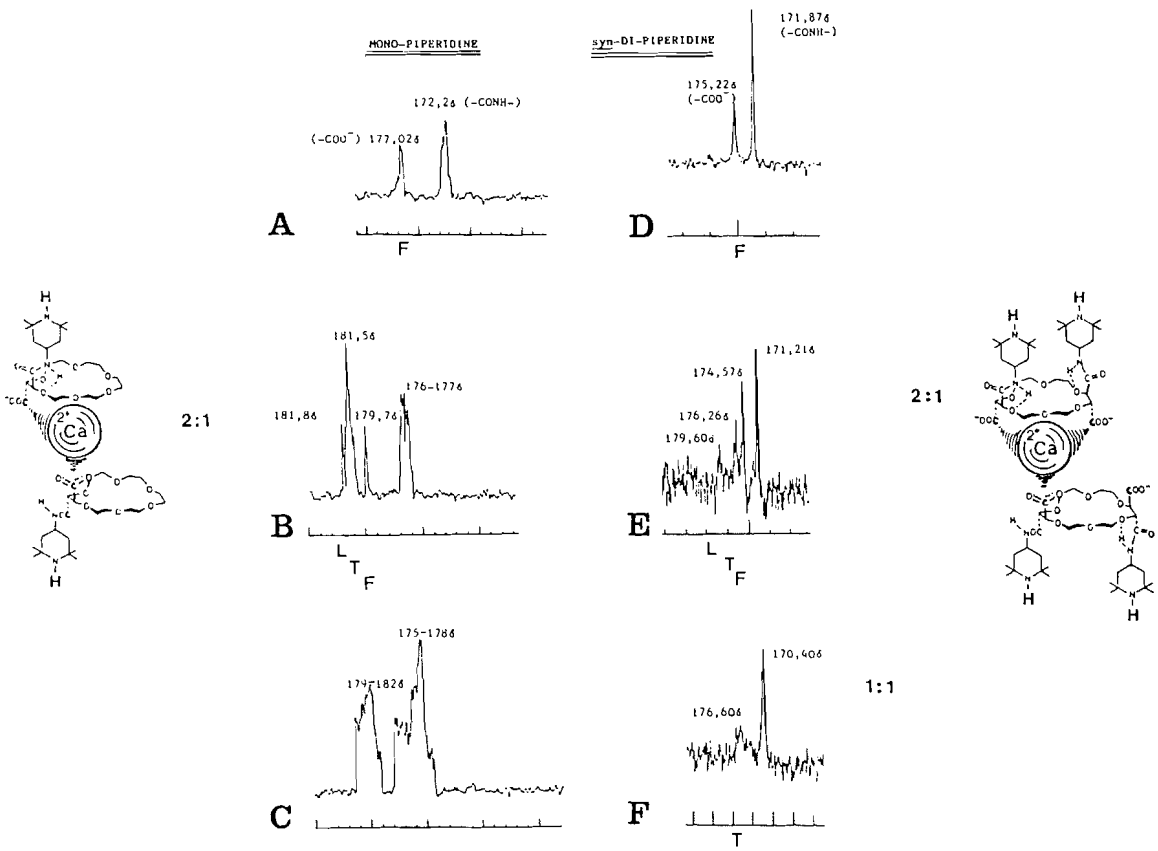

FIG. 1. Carbonyl region of the ^{13}C nmr spectra of monopiperidine **1***c* and *syn*-dipiperidine **2***c* in CD_3OD/D_2O (90:10 v/v), Me_4NOH, pH 11.6. A and D, free form (mono- and dicarboxylate); B and E, in the presence of Ca^{2+} [$Ca(SCN)_2$] ion at a 2:1 ratio of crown ether:metal ion, C and F, at a 1:1 ratio of crown ether:metal ion. The letters F, L, and T under the spectra mean *free*, *loose*, and *tight* bound ions respectively (see text).

values were obtained (from 10^7 to almost 10^{10}) depending on the degree of ionization of the carboxylic groups. Therefore, *syn* crown ether diacids are particularly good Ca^{2+} ligands (17). This observation reflects the correlation in the electrostatic attraction to be made between the charge of the crown ether carrier (dicarboxylate vs. monocarboxylate) and the nature and charge of the ion involved in the complexation (16). As noted above, there is no simple relationship between stability and extraction constants. The slow Ca^{2+} transport rate could be due to a high value of extraction constant (complex too stable) or might be related to the slow diffusion of the picric acid uncoupler down its concentration gradient.

Finally, in the dicarboxylic crown molecule **2***c*, the complexation selectivity could be controlled by the charge-to-size (Q/r) ratio. For Ca^{2+}, this ratio is larger than for Na^+ or K^+ and the complexation constant is consequently much larger.

These findings generally agree with earlier considerations (7) that binding selectivity does not directly result in transport selectivity of the same magnitude, although overall complex stability and selectivity both play a role in the transport process (17).

Nuclear magnetic resonance studies

These studies were undertaken to gain more structural information on the nature of the [crown ether·Ca^{2+}] complex, particularly with the mono- and *syn*-dipiperidine acids **1***c* and **2***c*.

From previous ^1H nmr studies on analogous compounds (5, 21), the following general observations on the conformation of the crown ether have been made. Firstly, the observable vicinal coupling constant (^3J = 2–3 Hz) of the chiral center is consistent with a diaxial orientation of the amide and carboxyl groups. Such conformation was also noted in X-ray crystal structures of related compounds (6, 21). Secondly, this chiral barrier fragment (—O—$\overset{*}{C}$HX—$\overset{*}{C}$HY—O—) is relatively rigid, suggesting that any conformational change in the molecule should implicate the ethylenedioxy segments of the crown ether ring. Thirdly, the amide N*H* proton is involved in a strong intramolecular hydrogen bond to the adjacent ether oxygen of the crown. Although ^1H nmr spectroscopy can provide a powerful tool for the investigation of the conformation of crown ether carriers and their ion complexes, it gives no direct information on the environment of the carboxylate group itself. Furthermore, the estimation of T_1 relaxation times of the $-CH_2O-$ group of the crown is rather tedious since the spectral bands highly overlap in the region of interest and provide relatively little information.

As noted in the previous section, the main forces involved in the complexation process are electrostatic interactions between the carboxylate groups of the crown and its bound cation. Therefore, there is a particular interest in exploring this region to gain more structural information on the nature of the complex formed, particularly with the Ca^{2+} ion.

Figure 1 demonstrates that ^{13}C nmr spectroscopy is a reliable technique for the investigation of the carboxylate environment of our crown ether molecules **1***c* and **2***c*, since the spectra exhibit two well-separated resonances in the carbonyl region. The free salts (pH 11.6) show two narrow resonances: the amide

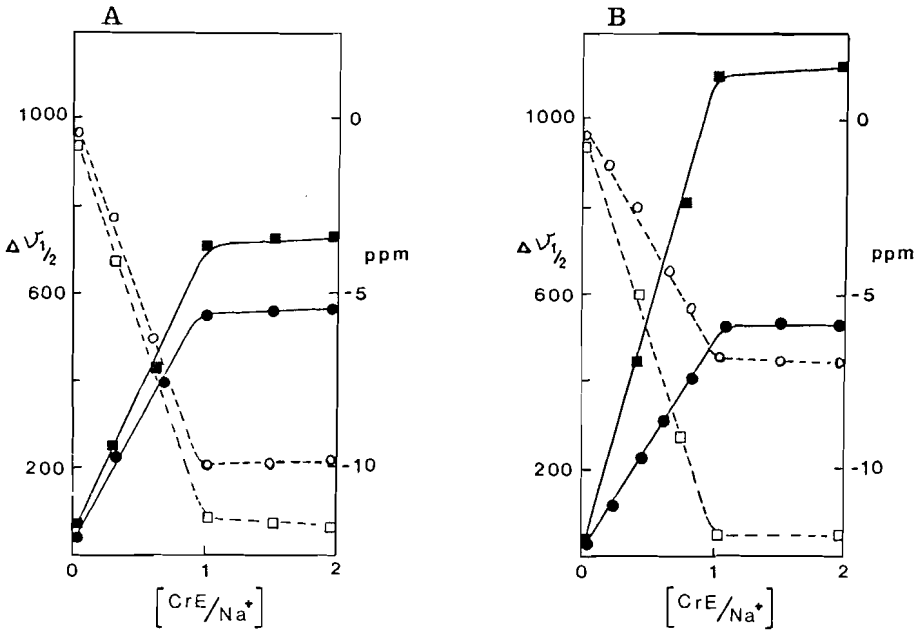

FIG. 2. ^{23}Na chemical shift (dashed lines) and line width ($\Delta\nu_{1/2}$) (solid lines) as a function of added monopiperidine **1***c* (A) and *syn*-dipiperidine **2***c* (B); $[Na^+] = 0.1$ *M* in CD_3OD/D_2O (90:10 v/v); circles, pH = 2.0 (HCl); squares, pH = 10.0 (Me_4NOH). CrE means the corresponding crown ether.

band between 171 and 173 ppm and the carboxylate band near 175–177 ppm (spectra A and D). Addition of $Ca(SCN)_2$ to give a 2:1 ratio (CrE/Ca^{2+}) changes appreciably the appearance of the spectra. Figure 1B clearly shows a downfield shift coupled with the appearance of two new resonances at 181.8 and 181.5 ppm. The same trend is observed for **2***c* (Fig. 1E), which also suggests the presence of three discrete carboxylate forms in solution: a tight (T), a loose (L), and a free carboxylate (F). These carboxylate – metal ion interactions have been described previously by Fyles and Whitfield (21), where an asymmetric or tight carboxylate–cation pair might be viewed as a purely electrostatic interaction involving the carboxylate charge fully localized on one oxygen atom and interaction with a proximal cation. In the more symmetrical or loose ion pair interaction, however, the charge could be seen as more delocalized on the carboxylate and with the metal ion more distant. Under the conditions of concentration used, we expect to be looking at the 2:1 crown ether – calcium complex. Indeed, both **1***c* and **2***c* exist mainly as a dimer with the metal being coordinated with both the crown and the carboxylate groups of one molecule but assisted by only the carboxylate group of the other macrocycle. In fact, this behavior is quite similar to naturally occurring linear carboxylic acid ionophores such as A-23187 and X-14547A, which form 2:1 complexes with calcium ion (23).

In the 1:1 complexes (Figs. 1C and 1F), where a stoichiometric amount of metal ion leads to a preferential coordination with the crown carboxylate groups, only a tight carboxylate–cation interaction seems to dominate. In such a situation, the metal ion nuclear quadrupole typically broadens the lines.

Information on the structure and molecular motion can also be obtained by nmr relaxation time (T_1) measurements. Studies using this approach (24) have been carried out on neutral [18]-crown-6 compounds, and typical values in 9:1 $MeOH/D_2O$ were in the order of 1.3 s for the free ligand and of 1.1 s for the corresponding Na^+ complexes. In our case, we found that the $-CH_2O-$ crown carbons of **2***c* had a value of 0.05 s and a value of 0.16 s for **1***c*. Consequently, these surprisingly low values seem to indicate that these species in solution are in an aggregated form. A recent study on aliphatic monoacid [18]-crown-6 analogs showed no evidence of such aggregated species (21).

In a complementary approach, we became interested in looking directly at the magnetic resonance of the ion bound to the crown ether. For this, ^{23}Na nmr ($I = 3/2$, 100% abundance) is known to be a very direct probe for evaluating the degree of symmetry of the crown ether – ion complex (25). Indeed, ^{23}Na chemical shifts are directly related to the perturbation of the electrons of the sodium atom and consequently are expected to be very sensitive to the immediate environment of the ion (26). Furthermore, in the solvated form, the nmr relaxation rate of ^{23}Na is relatively long if the ion is symmetrically solvated, while when bound to a crown ether, the symmetry around the cation could be considerably reduced, resulting in a faster nuclear relaxation (27).

Figure 2 illustrates the ^{23}Na chemical shift and line-width ($\Delta\nu_{1/2}$) variations of the sodium nucleus upon addition of **1***c* (Fig. 2A) or **2***c* (Fig. 2B) to a 0.1 *M* NaSCN solution at two different pH values. These data clearly show that the complexes are completely formed after the addition of one equivalent of the crown ether to the solution, in both acidic or basic media. For compound **1***c*, the expected upfield variation in the chemical shifts observed for a complex of 1:1 stoichiometry is comparable in either acidic or basic solution, indicating a similar coordination and shielding electron density at the metal nucleus. However, the chemical shifts in compound **2***c* are significantly different for the two different pH's. This larger variation is probably related to the concerted effect of the two *syn* dicarboxylic acid functions.

It is noteworthy that the line-width variations of **1***c* and **2***c* in acidic condition are also comparable, indicating a preferential coordination by the crown ether ring without participation of the oxygens of the carboxylic groups. However, a much larger variation is observed under basic conditions, indicating clearly that the carboxylate forms increase the asymmetry about the sodium nucleus. This asymmetry change is especially seen in

Can. J. Chem. Downloaded from www.nrcresearchpress.com by 118.98.75.50 on 09/07/12
For personal use only.

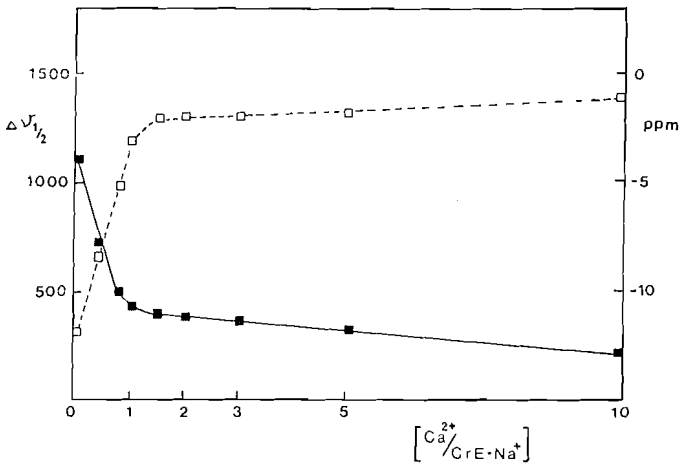

FIG. 3. Variation in the ^{23}Na chemical shift (dashed lines) and line width ($\Delta\nu_{1/2}$) (solid lines) as a function of Ca^{2+} ion added to *syn*-dipiperidine **2***c* complexed to Na^+ ion at a 1:1 [CrE·Na^+] ratio, pH = 10.0.

syn **2***c* where a difference of almost 600 Hz is observed between acidic and basic conditions.

Since the stability constant (Table 2) for **2***c* and Ca^{2+} ion in basic solution is 10^4-fold more important than for Na^+ ion, one would expect that addition of a Ca^{2+} solution to a stoichiometric [**2***c*·Na^+] complex should induce a narrowing of the observed ^{23}Na resonance as well as a downfield shift. Figure 3 illustrates this behavior for *syn* **2***c* and clearly indicates that the calcium ion is strongly complexed into the crown dicarboxylate system, even in the presence of sodium in the medium.

In general, the addition of any competitive cation to a 1:1 complex should induce a downfield shift and a narrowing of the observed ^{23}Na resonances in going from a fully complexed state to a lower (less than 1:1) complex state. However, the magnitude of the change in $\Delta\nu_{1/2}$ and chemical shift is very dependent upon the stability constants of the ions implicated in the competition experiment. For instance, if no preferential complexation for Ca^{2+} ion is taking place, the chemical shift of ^{23}Na should take a value around −6.5 ppm after the addition of one equivalent of Ca^{2+}; i.e., the value observed in a situation where 50% of the crown ether is complexed with sodium ion. In the case of *syn* **2***c*, the observed chemical shift after addition of Ca^{2+} was around −4 ppm. Clearly, the crown discriminates in favor of Ca^{2+} ion over Na^+ ion. For [**1***c*·Na^+] in competition with Ca^{2+}, a similar situation occurred, but to a smaller extent. The ^{23}Na resonance after addition of one equivalent of Ca^{2+} was at −5 ppm as compared to a value of −6.2 ppm for a 50% sodium–crown solution. This indicates again that the stability constant of **1***c* for Ca^{2+} is higher than for Na^+ ion.

In summary, our ^{23}Na nmr results indicate that both mono- and dicarboxylic derivatives (**1***c* and **2***c*) complex sodium in a similar fashion in acidic medium, and the results can be rationalized in terms of protonation of the carboxylic groups with Na^+ ion near the center of the macrocycle, with only a small participation of the adjacent acidic function. However, in basic medium, a shift in the position of the Na^+ ion within the macrocycle towards the carboxylate is a plausible explanation for the differences noted in ^{23}Na nmr experiments.

Experimental

Reagents

Sodium thiocyanate (Anachemia Inc.) was twice recrystallized from MeOH and dried under vacuum at 50°C for 2 days. Calcium thiocyanate was purchased as a 62% aqueous solution (Pfaltz and Bauer Inc.) and was dried *in vacuo* at 50°C for 4 days.

Methanol-d_4 and D_2O (Cambridge Isotope Lab.) were used directly from the manufacturer's sealed vials without further purification.

Macrocyclic polyethers **1***c* and **2***c* were passed over DOWEX 50-X8 (H^+ form) resin and stored into a carefully washed vessel.

Tetramethylammonium hydroxide pentahydrate (Aldrich) was dried at 40°C under vacuum for 1 day. All glassware used in this study was washed with concentrated HCl to remove any remaining cations.

*(2R,3R)-(+)-N-4′-(2′,2′,6′,6′-Tetramethylpiperidine)-2-carboxamido-1,4,7,10,13,16-hexaoxacyclooctadecane-3-carboxylic acid (**1**c)*

2,2,6,6-Tetramethyl-4-aminopiperidine (187.2 mg, 1.2 mmol) was dissolved in 15 mL of anhydrous dichloromethane. To this solution was added a solution of the monoanhydride [18]-crown-6 (200 mg, 0.6 mmol) (7) in 15 mL of dichloromethane, under a N_2 atmosphere. After 2 h of stirring at ambient temperature, the monopiperidine monoacid **1***c* precipitated as a white solid (yield: 90%, mp 161–163°C). The product was then eluted from a Dowex 50W-X8 column (H^+ form) with water and recrystallized from acetone–methanol mixture; $[\alpha]_D^{25}$ +29.0° (*c* 1.0, MeOH); ir (KBr), cm^{-1}: 1625, 1400, 1100; ^1H nmr (D_2O, 90 MHz) δ: 8.41 (s, 1H, acid), 7.43 (s, 1H, N*H* amide), 4.23 and 4.02 (dd, 2H, J_{ab} = 3.5 Hz), 3.73 (m, 20H, crown), 1.65 and 1.52 (s, 12H, methyl); ms (EI) *m/e*: 490 (M^+). *Anal.* calcd. for $C_{23}H_{42}N_2O_9$: C 56.31, H 8.63, N 5.71; found: C 55.89, H 8.47, N 5.60.

The corresponding methyl ester **1***d* was obtained by dissolving the compound (348 mg, 0.71 mmol) in 1 mL of MeOH, cooling to 0°C, and adding 2 mL of an ethereal CH_2N_2 solution. The progress of the reaction was followed by tlc (MeOH). The solvent was evaporated after completion of the reaction and the product purified on a silica gel column. A white solid (271 mg, 0.54 mmol) was obtained in 76% yield (mp 79–81°C); $[\alpha]_D^{25}$ +25.1° (*c* 1.0, $CHCl_3$); ir ($CHCl_3$), cm^{-1}: 1750 (ester), 1670 (amide), 1350 (*gem*-CH_3), 1110; ^1H nmr ($CDCl_3$, 90 MHz) δ: 4.41 and 4.25 (dd, 2H, J_{ab} = 2.9 Hz), 3.82 (s, 3H, OCH_3), 3.61 (m, 21H, crown, C*H*—N), 1.30 (m, 4H, CH_2—N—CH_2), 1.35 and 1.43 (2s, 12H, CH_2); ms (EI) *m/e*: 505 ($M + H^+$).

*(2R,3R)-(+)-2-Carbomethoxy-3-carboxanilide-1,4,7,10,13,16-hexaoxacyclooctadecane (**1**e) and its precursor, the corresponding acid*

The monoanhydride [18]-crown-6 (565 mg, 1.7 mmol) (7) was dissolved in 15 mL of dichloromethane and, to this solution, aniline (0.7 mL in 15 mL CH_2Cl_2) was added dropwise. After 2 h of stirring at ambiant temperature under a N_2 atmosphere, the reaction mixture was washed twice with 5 mL of 5% HCl solution and three times with 5 mL of 5% NMe_4OH solution. The aqueous phase was acidified with 5% HCl and the desired product extracted with chloroform. The volume of the chloroformic extract was reduced and 60 mL of heptane was added to precipitate the product. This acid was recrystallized from a dichloromethane–toluene mixture to give 622.6 mg (1.5 mmol) of a white solid (yield, 88%; mp 143–145°C); $[\alpha]_D^{25}$ +85.7° (*c* 1.0, $CHCl_3$); ir ($CHCl_3$), cm^{-1}: 1750 (amide), 1100; ^1H nmr ($CDCl_3$, 90 MHz) δ: 8.91 (s, 1H, N*H* amide), 7.33 (m, 5H, phenyl), 4.52 and 4.40 (dd, 2H, J_{ab} = 2.7 Hz), 3.63 (m, 20H); ms (CI) *m/e* 428 ($M + H^+$).

This monoanilide monoacid [18]-crown-6 (316 mg, 0.7 mmol) was dissolved in 1 mL THF, cooled to 0°C, and to this solution was added 2 mL of an ethereal CH_2N_2 solution. The reaction was followed by tlc ($MeOH/CHCl_3$, 1:2) and, after completion, the solvent was evaporated and the resulting methyl ester **1***e* purified by column chromatography on silica gel. A pale yellow oil (314 mg, 0.7 mmol) was obtained in 96% yield; ir ($CHCl_3$), cm^{-1}: 3000, 2900, 1750, 1680, 1140; ^1H nmr ($CDCl_3$, 90 MHz) δ: 9.42 (s, 1H, N*H* amide), 7.31 (m, 5H, phenyl), 4.52 and 4.40 (dd, 2H, J_{ab} = 2.35 Hz), 3.83 (s, 3H, OCH_3), 3.90 (m, 20H, crown); ms (CI) *m/e*: 442 ($M + H^+$).

*(2R,3R)-(+)-2-(4′,4′-Dimethyl-2-oxazoline-2-yl)-3-carboxanilide-1,4,7,10,13,16-hexaoxacyclooctadecane (**1**f)*

A mixture of the monoanilide monoethyl ester [18]-crown-6 **1***e*

Can. J. Chem. Downloaded from www.nrcresearchpress.com by 118.98.75.50 on 09/07/12
For personal use only.

Can. J. Chem. Downloaded from www.nrcresearchpress.com by 118.98.75.50 on 09/07/12
For personal use only.

(57.8 mg, 0.12 mmol), 2-amino-2-methyl-propanol (0.3 mL, 0.52 mmol), and P_2O_5 (150 mg) in 10 mL of xylene was refluxed for 30 h under a N_2 atmosphere. After filtration, the solvent was evaporated and the residue chromatographed on a silica gel column. A yellow oil (42.8 mg, 0.09 mmol) was recovered in 69% yield; ir ($CHCl_3$), cm^{-1}: 1680 (amide), 1600 (C=N—C), 1100; ^1H nmr ($CDCl_3$, 90 MHz) δ: 7.39 (m, 5H, phenyl), 4.35 (m, 2H), 3.68 (m, 22H, crown and CH_2 of oxazoline), 1.40 (m, 6H, CH_3); ms (CI) *m/e*: 481 ($M + H^+$). *Exact Mass* calcd. for $C_{24}H_{36}N_2O_8$: 480.2471; found: 480.2456.

(2R,3R)-(+)-2-(4',4'-Dimethyl-2-oxazolidine)-3-carboxanilide-1,4,7,10,13,16-hexaoxocyclooctadecane (1g)

The monooxazoline **1***f* (33.9 mg, 0.07 mmol) was dissolved in 5 mL of a 1:1 THF/MeOH mixture. The temperature of the solution was brought to −30°C and the pH was ajusted to 7 with 9 *N* HCl. $NaBH_4$ (3 mg, 0.07 mmol), dissolved in cool water, was added dropwise and the conditions maintained for 2 h. If the reaction was not complete, 0.25 equiv. of $NaBH_4$ was added again and the reaction continued for another hour. The reaction was stopped by addition of few millilitres of EtOH and the solution made alkaline by addition of a small amount of 10% NaOH. The aqueous phase was then separated and the organic layer washed with water. After a silica gel column purification, 17.7 mg (0.04 mmol) of a yellow semisolid material (57%) was recovered; ir ($CHCl_3$), cm^{-1}: 1740, 1260, 1120; ^1H nmr ($CDCl_3$, 400 MHz) δ: 9.50 (s, 1H, N*H* amide), 7.33 (m, 5H, phenyl), 3.63 (m, 22H, crown, CH_2 of oxazolidine), 1.25 (m, 7H, CH_3, N*H* oxazolidine); ms (CI) *m/e*: 483 ($M + H^+$). *Exact Mass* calcd. for $C_{24}H_{38}N_2O_8$: 482.2628; found: 482.2622.

Procedure for the preparation of only the syn *isomer (2c): (2R,3R,11R,12R)-(+)-N,N'-di-4'-(2',2',6',6'-tetramethyl-piperidine)-2,11-dicarboxamido-1,4,7,10,13,16-hexaoxacyclo-octadecane-3,12-dicarboxylic acid*

A solution of the dianhydride [18]-crown-6 (418 mg, 1.2 mmol (6) in 15 mL of dichloromethane was slowly added to 2,2,6,6-tetramethyl-4-aminopiperidine (374.4 mg, 2.4 mmol) dissolved also in 15 mL of dichloromethane, and containing 1 mL of triethylamine. After a few hours, the product precipitated out of the solution. It was filtered and recrystallized from acetone–water to obtain 616 mg (1.1 mmol) of *syn* **2***c* in 95% yield (mp 190°C (dec.)); $[\alpha]_D^{25}$ +31.4° (*c* 1.0, $CHCl_3$); ir (KBr), cm^{-1}: 3400, 1650, 1390, 1145; ^1H nmr (D_2O, 400 MHz) δ: 4.10 and 3.93 (dd, 2H, J_{ab} = 5.58 Hz), 3.71 (m, 18H, crown, -C*H*), 2.22 (m, 10H, CH_2 piper., N*H*), 1.53 and 1.52 (s, 12H, CH_3), 1.45 and 1.43 (s, 12H, CH_3); ms (CI) *m/e*: 717 ($M + H^+$). *Anal.* calcd. for $C_{34}H_{60}N_4O_{12}$: C 56.97, H 8.44, N 7.82; found: C 56.57, H 8.09, N 7.70.

The corresponding *syn*-dimethyl ester **2***d* was obtained in 80% yield by treating **2***c* with an ethereal CH_2N_2 solution (mp 200°C (dec.)); $[\alpha]_D^{25}$ +45.6° (*c* 1.0, $CHCl_3$); ir ($CHCl_3$), cm^{-1}: 1650, 1400, 1130; ^1H nmr ($CDCl_3$, 400 MHz) δ: 4.31 and 4.11 (s, 4H), 3.73 (m, 18H), 3.25 (s, 24H, CH_3); ms (CI) *m/e*: 745 ($M + H^+$).

Procedure for the preparation of the anti *isomer (3c)*

The dianhydride [18]-crown-6 (242.4 mg, 0.6 mmol) (6) in 10 mL of dichloromethane was added to a solution of 2,2,6,6-tetramethyl-4-aminopiperidine (416.4 mg, 2.7 mmol), also in 10 mL of dichloromethane. During the reaction, 385.7 mg (0.5 mmol) of a mixture of *syn* and *anti* isomers precipitated (yield, 83%). Even after repeated chromatography, the *anti* isomer **3***c* was always contaminated by 20% of **2***c*. The corresponding *anti* dimethyl ester **3***d* was obtained as an oil.

syn-*(2R,3R,11R,12R)-(+)-2,11-Dicarboxanilide-1,4,7,10,13,16-hexaoxacyclooctadecane (2e)*

The precursor dianilide diacid has already been reported (6). It was dissolved in THF, mixed with ethereal CH_2N_2, and left at 0°C overnight. It was then purified by chromatography to yield a yellowish oil (81%); $[\alpha]_D^{25}$ +67.6° (*c* 1.0, $CHCl_3$); ir ($CHCl_3$), cm^{-1}: 1750, 1680, 1120; ^1H nmr ($CDCl_3$, 90 MHz) δ: 9.22 (s, 2H, N*H* amide), 7.40 (m, 10H, phenyl), 4.41 (s, 4H), 3.85 (s, 6H, OCH_3), 3.73 (m, 16H, crown); ms (CI) *m/e*: 619 ($M + H^+$).

syn-*(2R,3R,11R,12R)-(+)-2,11-Bis(4',4'-dimethyl-2-oxazoline-2-yl)-3,12-dicarboxanilide-1,4,7,10,13,16-hexaoxocycloocta-decane (2f)*

Under reflux for 24 h, a mixture of the dianilide dimethyl ester **2***e* (42.3 mg, 0.07 mmol) and 2-amino-2-methyl-propanol (0.12 mL, 0.3 mmol) was treated in 10 mL of xylene in the presence of P_2O_5. After reflux, the solution was filtered, most of the solvent evaporated, and the residue chromatographed on silica gel to obtain 41.3 mg (0.06 mmol) of a yellow oil (yield, 86%); $[\alpha]_D^{25}$ +47.8° (*c* 1.0, $CHCl_3$); ir ($CHCl_3$), cm^{-1}: 1670, 1600, 1100; ^1H nmr ($CDCl_3$, 90 MHz) δ: 7.42 (m, 10H, phenyl), 4.51 (m, 4H), 3.63 (m, 20H, crown, CH_2 oxazoline), 1.42 (m, 12H, CH_3); ms (CI) *m/e*: 349 ($M + 2H^+/2$). *Exact Mass* calcd. for $C_{36}H_{48}N_4O_{10}$: 696.3370; found: 696.3312.

syn-*(2R,3R,11R,12R)-(+)-2,11-Bis(4',4'-Dimethyl-2-oxazolidine)-3,12-dicarboxanilide-1,4,7,10,13,16-hexaoxacyclooctadecane (2g)*

The same procedure as for the synthesis of **1***g* was followed to obtain **2***g* as a semi-solid yellow material (yield, 50%); ^1H nmr ($CDCl_3$, 90 MHz) δ: 9.02 (s, 2H, N*H* amide), 7.41 (m, 10H, phenyl), 4.48 and 4.41 (dd, 4H, J_{ab} = 1.99 Hz), 3.72 (m, 20H, crown, C*H* and CH_2 oxazolid.), 1.32 (m, 14H, CH_3, N*H* oxazolid.). *Exact Mass* calcd. for $C_{36}H_{52}N_4O_{10}$: 700.3683; found: 700.3598.

Transport studies

Transport experiments were performed in a thermostated room (20 ∓ 1°C), using a U-shaped cell constructed of 17-mm id tubing. The tube had a total capacity of 55 mL and consisted of a 10-mL membrane phase interfaced to both a 15-mL source phase of 0.01 *M* picrate salts solution at pH 9.7 (diethanolamine HCl 0.05 *M*) and a 15-mL blank buffer receiving phase. The membrane phase was made of alcohol-free spectroscopic grade chloroform containing 10^{-3} *M* carrier. The aqueous phases were stirred at a constant rate of 80 rpm and the organic phase at 400 rpm for all the experiments. Blank experiments (no carrier present) were performed to determine the membrane leakage. No detectable movement of cation across the chloroform membrane was found in the blank unit within 8 h. The rates of ion transport were determined by monitoring the picrate concentration in the receiving phase by visible spectroscopy at 354 nm. Samples were withdrawn from the receiving phase at 30-min intervals for 8 h and the absorption of picrate recorded. For low concentration of metal picrate in the receiving phase the solution samples could be removed, analysed, and replaced. For high concentration, it was necessary to dilute the samples from the receiving phase to calculate the concentration. Therefore, for high concentrations, a 100-μL sample of the receiving phase was removed, diluted as necessary, and subsequent experimental readings were corrected for the resulting change in volume. It should be noted that in the case of calcium transport experiments, the apparent rate of picrate transport was divided by two, to take into acount the divalent nature of the cation. A plot of moles of cation transported into the receiving phase vs. time was made for each system. The data were fitted to a straight line, the slope of which gave values of transport rate. Linear fits of the data (zero-order regime) and agreement between different runs of the same system was within ± 10%.

Determination of pK_a and pK_s

The methods used have been previously described in detail (7).

^{13}C, ^{23}Na nuclear magnetic resonance studies

Noise decoupled, natural abundance ^{13}C nmr spectra were obtained at 20.17 MHz using a Bruker WP-80 spectrometer in the pulsed transform mode.

The sample solution was placed in a 9-mm id nmr tube and chemical shifts were referred to Me_4Si. Solutions were 0.17 *M* (**1***c*) and 0.25 *M* (**2***c*) in CD_3OD:D_2O 9:1 v/v, and acid (HCl) or base (tetramethylammonium hydroxyde pentahydrate) was added to give a target value of pH (2 and 11.6). All solutions were prepared by weighing the desired amount of the ligand and salt.

^{13}C relaxation times (T_1's) were measured by the fast inversion–recovery technique $(180°\tau-90°-t)_n$ where 15 different pulse intervals,

τ, were used for each individual measurement and were chosen so that at least 10 points were included for each T_1 calculation (28). Usually 1000–3000 scans were necessary for each τ value to obtain a reasonable signal-to-noise ratio. On the average, each run required 48 h.

Sodium-23 nmr measurements were obtained on the same instrument at 21.21 MHz. Samples solutions were 0.1 *M* NaSCN in $CD_3OD:D_2O$ 9:1 v/v and were pH adjusted to give target values of 2 (HCl) and 10 ($Me_4NOH \cdot 5H_2O$). Sodium complexes of **1***c* and **2***c* were made by adding weighed amounts of the crown ethers into the 9-mm nmr tube. A 3 *M* deuterated aqueous sodium chloride solution was used as reference and the reported sodium-23 chemical shifts were referred to this solution. Relaxation times for ^{23}Na were determined from the line widths of the absorption spectra.

Dry calcium thiocyanate was used in the competition experiment.

Acknowledgements

We thank the Formation de chercheurs et action concertée of the Ministère de l'Éducation du Québec for a scholarship to M.B., and the Natural Sciences and Engineering Research Council of Canada for financial support.

1. K. Ishizu, H. Kohama, and K. Mukai. Chem. Lett. 227 (1978).
2. M. P. Eastman, D. E. Patterson, R. A. Bartsch, Y. Liu, and P. G. Eller. J. Phys. Chem. **86**, 2052 (1982).
3. J. F. W. Keana, J. Cuomo, L. Lex, and S. E. Seyedrezai. J. Org. Chem. **48**, 2647 (1983).
4. Yu. G. Mamedova and Z. O. Tuarsheva. J. Org. Chem. USSR Engl. Transl. **19**, 1715 (1983).
5. H. Dugas and M. Ptak. J. Chem. Soc. Chem. Commun. 710 (1982); H. Dugas, P. Keroack, and P. Ptak. Can. J. Chem. **62**, 489 (1984).
6. J. P. Behr, J. M. Lehn, D. Moras, and J. Thierry. J. Am. Chem. Soc. **103**, 701 (1981).
7. L. A. Frederick, T. M. Fyles, N. P. Gurprassad, and D. M. Whitfield. Can. J. Chem. **59**, 1724 (1981).
8. A. I. Meyers and E. D. Mihelich. J. Am. Chem. Soc. **97**, 7383 (1975).
9. G. R. Newkome and C. R. Marston. Tetrahedron, **39**, 2001 (1983).
10. A. I. Meyers and A. Nabeya. J. Chem. Soc. Chem. Commun. 1163 (1967).
11. T. M. Fyles, V. A. Malik-Diemer, and D. M. Whitfield. Can. J. Chem. **59**, 1734 (1981).
12. T. M. Fyles. J. Membr. Sci. **24**, 229 (1985).
13. J. P. Behr, M. Kirch, and J. M. Lehn. J. Am. Chem. Soc. **107**, 241 (1985).
14. J. D. Lamb, J. J. Christensen, J. L. Oscarson, B. L. Nielsen, B. W. Assay, and R. M. Izatt. J. Am. Chem. Soc. **102**, 6820 (1980).
15. G. W. Gokel, D. M. Goli, C. Minganti, and L. Echegoyen. J. Am. Chem. Soc. **105**, 6786 (1983).
16. C. A. Chang, J. Twu, and R. A. Bartsch. Inorg. Chem. **25**, 396 (1986).
17. L. M. Dulyea, T. M. Fyles, and D. M. Whitfield. Can. J. Chem. **62**, 498 (1984).
18. T. M. Fyles, C. A. McGavin, and D. M. Whitfield. J. Org. Chem. **49**, 753 (1984).
19. M. Kirch and J. M. Lehn. Angew. Chem. Int. Ed. Engl. **14**, 555 (1973).
20. J. Rebek, Jr., L. Marshall, R. Wolak, K. Parris, M. Killoran, B. Askew, D. Nemeth, and N. Islam. J. Am. Chem. Soc. **107**, 7476 (1985).
21. T. M. Fyles and D. M. Whitfield. Can. J. Chem. **62**, 507 (1984).
22. J. J. Daly, P. Schonhelzer, J. P. Behr, and J. M. Lehn. Helv. Chim. Acta, **64**, 1444 (1981).
23. R. W. Taylor, R. F. Kauffman, and D. R. Pfeiffer. *In* Polyether antibiotics, naturally occurring acid ionophores. Vol. 1. *Edited by* J. W. Westley. M. Dekker, Inc., New York. 1982. pp. 103–184.
24. L. Echegoyen, A. Kaifer, H. Durst, R. A. Schultz, D. M. Dishong, D. M. Goli, and G. W. Gokel. J. Am. Chem. Soc. **106**, 5100 (1984).
25. P. Laszlo. Angew. Chem. Int. Ed. Engl. **17**, 254 (1978).
26. A. J. Popov. Pure Appl. Chem. **51**, 101 (1979).
27. J. D. Lin and A. I. Popov. J. Am. Chem. Soc. **103**, 3773 (1981).
28. D. Canet, G. C. Levy, and I. R. Peat. J. Magn. Reson. **18**, 199 (1975).

Can. J. Chem. Downloaded from www.nrcresearchpress.com by 118.98.75.50 on 09/07/12
For personal use only.

Resonance Raman spectroscopic evidence for the formation of covalent complexes between *N*-acylamino acid dithioesters and mercury papain[1]

HO-HI LEE, RONALD H. ANGUS, PAUL R. CAREY, AND ANDREW C. STORER
Division of Biological Sciences, National Research Council of Canada, Ottawa, Ont., Canada K1A 0R6

Received December 31, 1986

HO-HI LEE, RONALD H. ANGUS, PAUL R. CAREY, and ANDREW C. STORER. Can. J. Chem. **65**, 1521 (1987).

Ethyl dithioesters of *N*-acylglycine and *N*-acylalanine are shown to bind tightly to the active site of papain in which the side chain of cysteine-25 is in the mercurated form. Although both classes of dithioester bind to the active site mercury via their thiono (C=S) sulfur atoms, the resulting adducts are quite different. Absorption and resonance Raman data, supported by comparison with model compounds and by ^{15}N and $^{13}C{=}S$ isotopic substitutions, show that the glycine and alanine dithioesters are converted to enethiolates and 4-methyloxazolin-5-thiones, respectively. The difference in product formation is explained by a mechanism in which stereospecific proton removal is brought about by the $-COO^-$ side chain of Asp-158, which is situated in the vicinity of the active site. For glycine dithioesters the Asp-158 catalyses the removal of a C_α proton whereas for alanine dithioesters the alanine's NH proton is removed.

HO-HI LEE, RONALD H. ANGUS, PAUL R. CAREY et ANDREW C. STORER. Can. J. Chem. **65**, 1521 (1987).

On a démontré que les dithioesters éthyliques de la *N*-acylglycine et de la *N*-acylalanine se lient intimement au site actif de la papaïne dans laquelle la chaîne latérale de la cystéine-25 est mercurée. Même si le deux classes de dithioesters se lient au mercure du site actif par le biais de leurs atomes de soufre thiono (C=S), les adduits qui en résultent sont très différents. Les données d'absorption et de résonance Raman, appuyées par une comparaison avec des composés modèles et par des substitutions isotopiques avec du ^{15}N et du $^{13}C{=}S$, démontrent que les dithioesters de la glycine et de l'alanine se transforment respectivement en thioénolates et en méthyl-4 oxazolinethiones-5. On explique cette différence de comportement par un mécanisme impliquant un enlèvement stéréospécifique d'un proton par le COO^- de la chaîne latérale de l'Asp-158, qui est située près du site actif. Dans le cas des dithioesters de la glycine, l'Asp-158 catalyse l'enlèvement d'un proton du C_α alors que, pour les dithioesters de l'alanine, c'est le proton du NH de l'alanine qui est enlevé.

[Traduit par la revue]

Can. J. Chem. Downloaded from www.nrcresearchpress.com by 72.64.146.136 on 09/07/12
For personal use only.

Introduction

Active papain can be reversibly converted to an inactive form by treatment with mercuric chloride. It has been shown that inactivation is the result of the binding of a single mercury atom to the essential cysteine (Cys-25) in the active site (1). The enzymatic activity can be regenerated readily by the addition of a thiol reducing agent, e.g. β-mercaptoethanol.

As well as possessing proteinase activity, papain also acts as an esterase and recent work from this laboratory has centered on resonance Raman (RR) studies of transient covalent enzyme–substrate complexes formed during the hydrolysis of thionoesters (2, 3). The transient complexes studied are dithioesters formed between the enzyme's active site cysteine residue and the acyl portion of the thionoester:

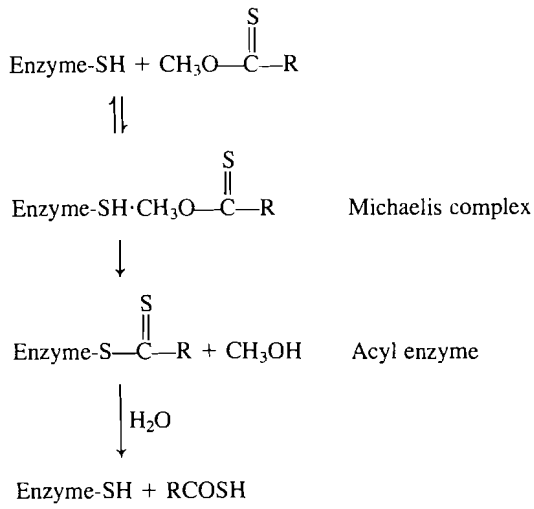

Initially the enzyme binds the substrate to give a Michaelis complex, which reacts to form an acyl enzyme (in this case a chromophoric dithioester, λ_{max} 315 nm), which then deacylates to enzyme and thiolacid. We have acquired considerable information on the acyl enzyme, but none as yet on the Michaelis complex. Therefore, it was decided to test dithioesters in place of thionoesters as substrates to produce chromophoric Michaelis complexes to study by RR spectroscopy. Although we have shown (unpublished data) that dithioesters are bound to papain without significant hydrolysis, we decided initially to use inactive Hg-papain. This proved to be a poor choice as a model for a Michaelis complex since the thiocarbonyl groups of the dithioesters were found to interact quite strongly with the enzyme-bound mercury. Interestingly, however, *N*-acylglycine and *N*-acylalanine dithioesters showed differential binding behaviour; this report describes the different products resulting from binding the two dithioesters and focuses on the ability of Asp-158 to perform stereospecific proton removal from the bound dithioesters.

Experimental

Papain was purchased from the Sigma Chemical Co. as a suspension in 50 m*M* sodium acetate pH 4.5. Mercury papain was prepared from this source by affinity chromatography on a mercurial-agarose column according to the method of Sluyterman and Wijdenes (4). Papain concentrations were estimated using an A^{280} 1% of 25 and a MW of 23 000.

The unlabelled and ^{15}N and $^{13}C{=}S$ labelled *N*-acyl glycine ethyl dithioesters were prepared and characterized as described in Lee *et al.* (5). The *N*-benzoyl-DL-alanine ethyl dithioester (and its $^{13}C{=}S$ labelled analogue) were synthesized as described in Angus *et al.* (6). 4-Ethyl-2-phenyloxazolin-5-one was supplied by Dr. C. Chuaqui. The RR spectra were obtained using 324 or 337-nm Kr^+ laser excitation and a diode array based detection system described previously (7).

[1]NRCC Publication No. 27521.

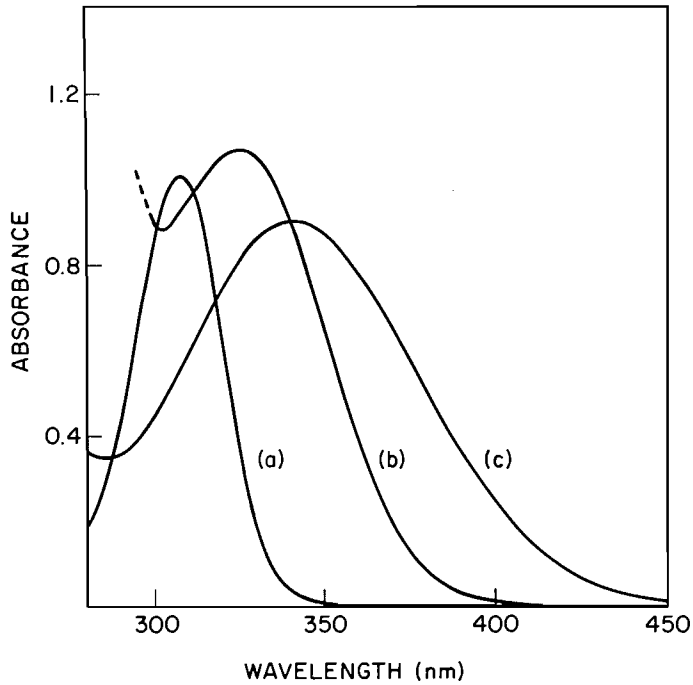

FIG. 1. Absorption spectra of *N*-benzoylglycine ethyl dithioester (1.0×10^{-4} *M*) (*a*) in acetate buffer (pH 4.5); (*b*) in the presence of 1.57×10^{-4} *M* Hg-papain, pH 4.5; (*c*) in 0.1 *N* NaOH (as the enethiolate form).

Results and discussion

(i) N-Benzoylglycine or N-(β-phenylpropionyl)glycine ethyl dithioester bound to Hg-papain

When either *N*-benzoylglycine or *N*-(β-phenylpropionyl)glycine ethyl dithioester is mixed with Hg-papain, in the pH range 4–7, marked changes occur in the absorption and RR spectral properties of the dithioester chromophore. These changes indicate that a complex is formed between the dithioester and Hg-papain, and the spectral data allow us to discuss the molecular details of each complex. The absorption spectrum of *N*-benzoylglycine ethyl dithioester, λ_{max} 308 nm in acetate buffer pH 4.5, is compared in Fig. 1 with the absorption spectrum of its complex formed with Hg-papain, which has a λ_{max} at 326 nm. Included in Fig. 1 is the spectrum of the enethiolate, λ_{max} 340 nm, formed from the dithioester at pH 13 in the absence of Hg-papain (8). Formation of both the complex and the enethiolate results in a red shift in λ_{max} and a broadening of the absorption band, both effects being more pronounced for the enethiolate. A red shift in λ_{max}, from 308 nm to 312 nm, and band broadening are also observed for *N*-(β-phenylpropionyl)glycine ethyl dithioester upon complexing with Hg-papain (data not shown). However, it should be noted that the absorption spectral data for this complex is less precise due to the fact that the shifted band near 312 nm is broad and appears as an unresolved shoulder on the main protein peak near 280 nm. The enethiolate produced at pH 13 from this dithioester has a blue shifted (λ_{max} 298 nm) and broadened absorption peak (8). It has been established that the electronic transition giving rise to the absorption band near 305 nm in dialkyl dithioesters and *N*-acylglycine dithioesters is localized on the -C(=S)S- group. The red shift and broadening of the absorption peaks for *N*-benzoylglycine and *N*-(β-phenylpropionyl)glycine ethyl dithioesters upon binding to Hg-papain suggest that, upon complexation, the electronic transition giving rise to the chromophore becomes delocalized over a larger region of the molecule. The RR data for the complexes provide some information as to the nature of this delocalization.

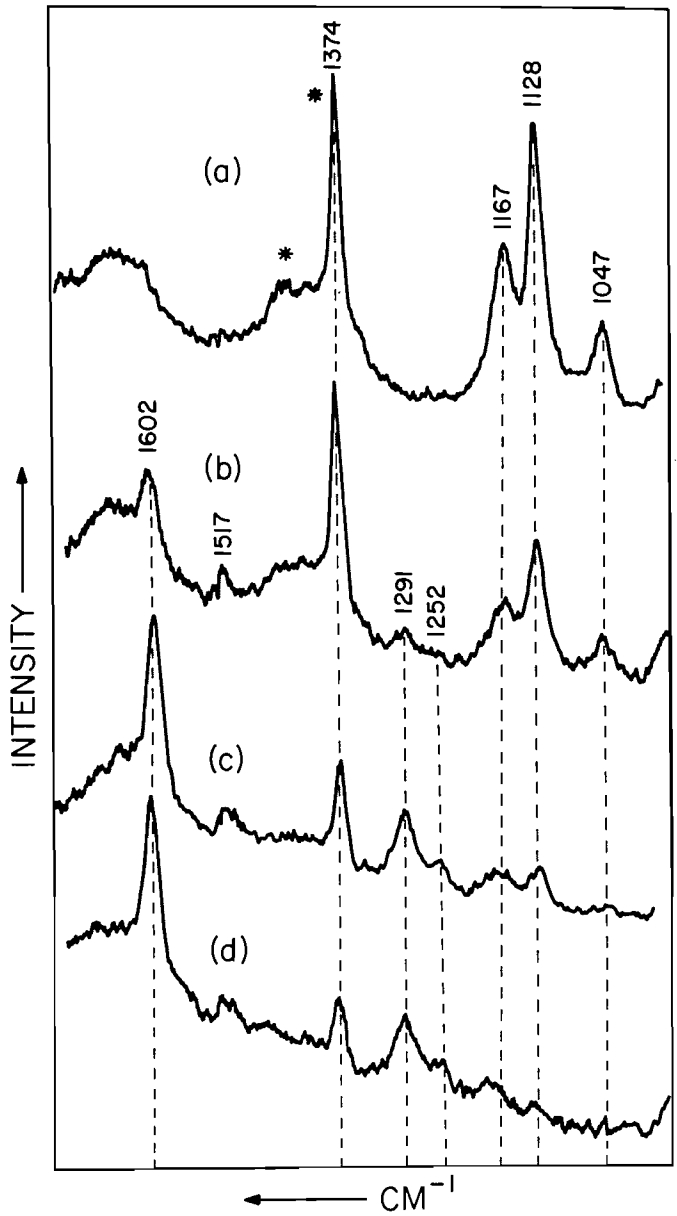

FIG. 2. Resonance Raman spectra of *N*-benzoylglycine ethyl dithioester (1.2×10^{-4} *M*) (*a*) in 10% CH_3CN and in the presence of (*b*) 3.0×10^{-5} *M* Hg-papain, (*c*) 9.0×10^{-5} *M* Hg-papain, (*d*) 2.6×10^{-4} *M* Hg-papain. All solutions contain acetate buffer, pH 4.5. Asterisks denote CH_3CN features. The broad feature near 1650 cm^{-1} is due to water.

Figure 2 shows the 324-nm excited RR spectra of solutions containing different ratios of *N*-benzoylglycine ethyl dithioester and Hg-papain. In each spectrum the peak near 1375 and the shoulder near 1425 cm^{-1} are due to the presence of 10% CH_3CN, used to keep the dithioester in solution. In traces (*a*) and (*b*) the peaks at 1167, 1128, and 1047 cm^{+1} are due to free, unbound dithioester. As the relative amount of Hg-papain increases, the features due to the free dithioester become relatively less intense (trace (*c*)) and in the presence of a twofold excess of Hg-papain it is difficult to detect any peaks due to free dithioester (trace (*d*)). Concomitant with the

Can. J. Chem. Downloaded from www.nrcresearchpress.com by 72.64.146.136 on 09/07/12
For personal use only.

Can. J. Chem. Downloaded from www.nrcresearchpress.com by 72.64.146.136 on 09/07/12
For personal use only.

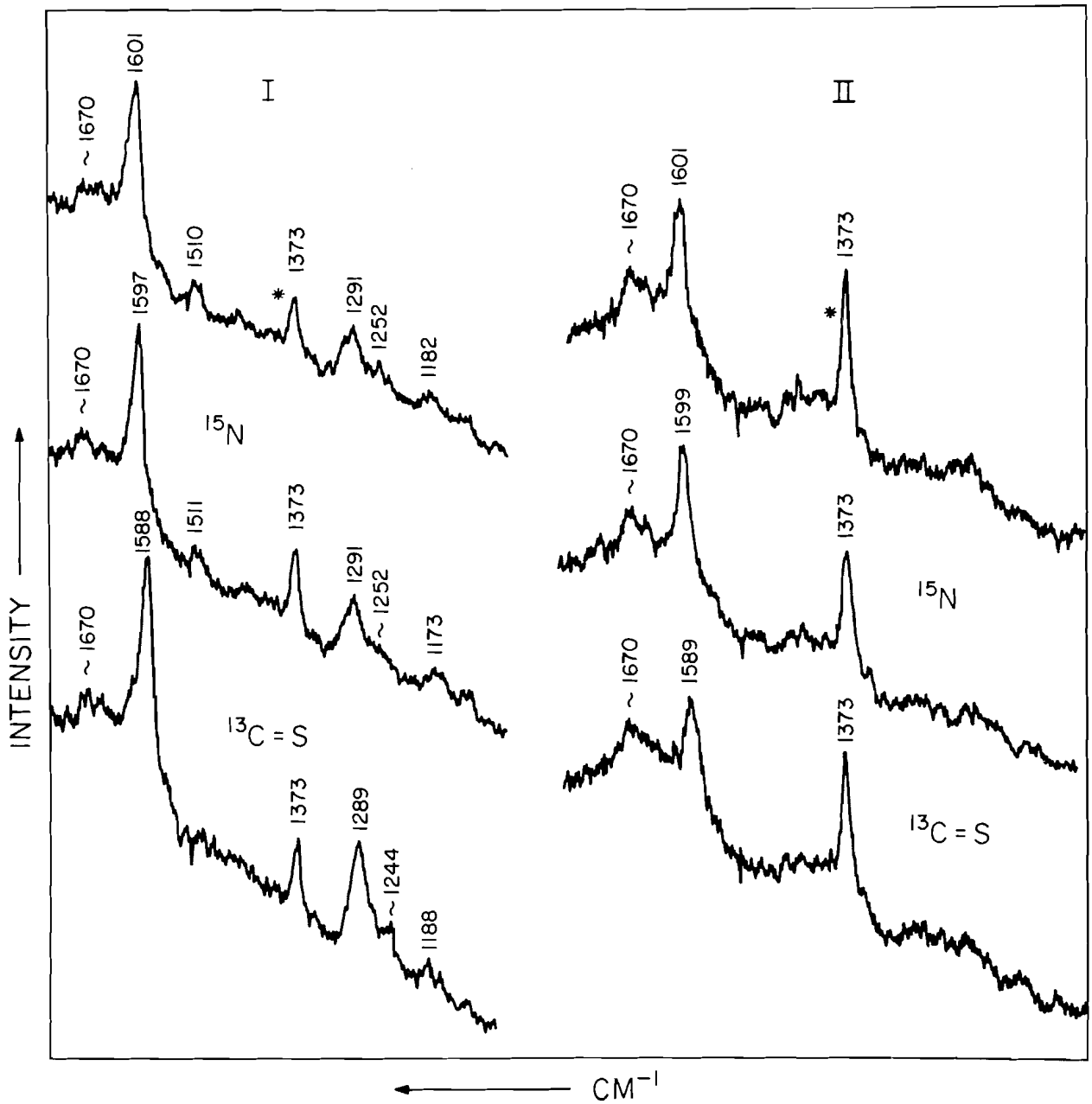

FIG. 3. Resonance Raman spectra of dithioesters *N*-benzoyl (I), and *N*-(β-phenylpropionyl) (II) glycine dithioesters and their ^{13}C, ^{15}N analogs in the presence of Hg-papain. Dithioesters, 1.0×10^{-4} *M*; Hg-papain, 2.73×10^{-4} *M*; in 10% CH_3CN, pH 4.5 acetate buffer.

decrease in free dithioester features, peaks due to the Hg-papain–dithioester complex appear at 1602, 1291, and 1252 cm^{-1} with increasing intensity. The data in Fig. 2 allow us to estimate, semiquantitatively, the dissociation constant, K_d, for the Hg-papain – *N*-benzoylglycine ethyl dithioester complex. Assuming a 1:1 stoichiometry in the complex, K_d is in the range 10^{-4}–10^{-5} *M*, indicating fairly tight binding between the ligand and the protein.

Further information on the origin of the RR features due to the enzyme–dithioester complex comes from the results of isotopic substitution experiments. Figure 3 shows the RR spectra of isotopically labelled, ^{15}N or $^{13}C{=}S$, *N*-benzoylglycine (I) and *N*-(β-phenylpropionyl)glycine (II) ethyl dithioesters bound to Hg-papain. ^{15}N substitution brings about a shift of 2–4 cm^{-1} for the intense feature near 1600 cm^{-1} in both complexes (Fig. 3) while $^{13}C{=}S$ substitution results in a 12–13 cm^{-1} decrease for this band in both cases. These results are compared in Table 1 to those for the enethiolates formed from the dithioesters at pH 13.0 in aqueous solution in the absence of enzyme (8). There is a marked similarity, both in the general appearance of the enethiolate (8) and dithioester–Hg-papain complex RR spectra (Figs. 2 and 3) and in their response to ^{15}N and $^{13}C{=}S$ substitution. However, the correspondence is not complete; the intense feature near 1590 cm^{-1} occurs at slightly higher wavenumbers for the dithioester–Hg-papain complexes. For the enethiolates the 1590 cm^{-1} band was assigned to a double bond-like mode partially delocalized through the glycinic linkages (8). Thus, it is likely that the 1601 cm^{-1} peaks seen in Figs. 2 and 3 for the dithioesters bound to Hg-papain arise from an analogous delocalized "double bond" mode, but that the degree of delocalization is slightly less for these species in the enzyme–substrate complexes. This conclusion is consistent

TABLE 1. Comparison of the isotope shifts of the major spectral features for the enethiolate and Hg-papain bound form of the dithioesters

	N-Benzoylglycine ethyl dithioester		*N*-(β-Phenylpropionyl)glycine ethyl dithioester	
	At pH 13.0[a]	Complexed with Hg-papain	At pH 13.0[a]	Complexed with Hg-papain
Unlabelled	1593	1601 cm^{-1}		
	1293	1291	1598	1601 cm^{-1}
^{15}N	1587	1597		
	1292	1291	1590	1599
$^{13}C{=}S$	1579	1588		
	1285	1289	1585	1589

[a]From ref. 8.

with the absorption data shown in Fig. 1 since the red shift for *N*-benzoylglycine ethyl dithioester bound to Hg-papain is less than that for the enethiolate formed from this dithioester (8). Further evidence for the differing degrees of delocalization comes from the observation that phenyl ring modes could be observed near 1500 and 1000 cm^{-1} for the enethiolate but not for the Hg-papain complex formed from *N*-benzoylglycine ethyl dithioester, indicating that delocalization into the phenyl ring is important only for the enethiolate.

The spectroscopic data indicate, therefore, that both *N*-benzoylglycine and *N*-(β-phenylpropionyl)glycine ethyl dithioesters bind to Hg-papain in a form resembling, but not identical to, the corresponding enethiolate species. Additional experiments were undertaken to investigate the mode of binding. The dithioester and enzyme could not be separated by passage of the complex down a 1 × 20 cm Sephadex G-15 chromatography column, which is consistent with the tight binding indicated by $K_d = 10^{-4}$–10^{-5} *M* (see above). Significantly, papain can be denatured by reducing the pH to 2.0 or less and this was performed on a solution containing Hg-papain – *N*-benzoylglycine ethyl dithioester complex that had been formed near neutral pH. The denatured Hg-papain dithioester complex showed a shift in λ_{max} from 326 to 320 nm. When the solution containing the denatured complex at pH 2.0 was passed down the G-15 column, preequilibrated at this pH, again no separation of protein and dithioester occurred. This demonstrates that tight binding still exists between the dithioester and the denatured enzyme and that the binding includes a covalent linkage.

The spectroscopic properties of the Hg-papain complexes could not be mimicked by mixing aqueous $HgCl_2$ with either *N*-benzoylglycine or *N*-(β-phenylpropionyl)glycine ethyl dithioester; thus, the enzyme appears to be required for the formation of the observed complexes. Moreover, no complex was formed by adding either dithioester to denatured Hg-papain. In an additional experiment, β-mercaptoethanol was shown to displace the dithioesters from Hg-papain. The β-mercaptoethanol (50 m*M*) was added to a 1.1×10^{-4} *M* solution of Hg-papain – *N*-benzoylglycine ethyl dithioester complex. The λ_{max} of the Hg-papain–dithioester complex changed from 326 nm to 308 nm and the RR spectrum (not shown) became equivalent to that for the dithioester in the absence of Hg-papain (Fig. 2*a*). Thus, the interaction between the dithioester and Hg-papain is broken by β-mercaptoethanol and the spectral properties revert to those of the free dithioester.

The following proposed mechanism incorporates all of the above observations:

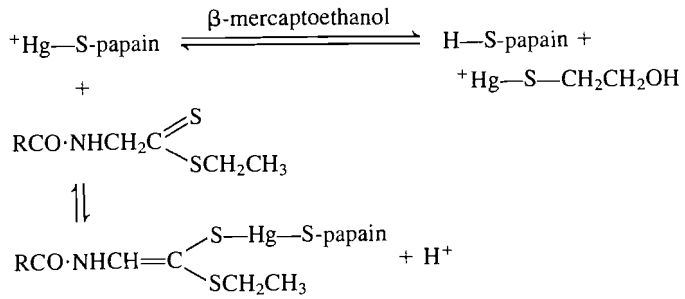

The analogy of the dithioester adduct formed in the Hg-papain–dithioester complex to an enethiolate

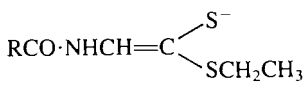

is immediately clear.

(ii) N-*Benzoylalanine ethyl dithioester bound to Hg-papain*

Changes also occur in the absorption and RR spectra of *N*-benzoyl-DL-alanine ethyl dithioester upon mixing with Hg-papain. The absorption spectrum of *N*-benzoylalanine ethyl dithioester in solution has a λ_{max} at 311 nm, which broadens and shifts to 320 nm on addition of Hg-papain and to 349 nm upon subsequent addition of β-mercaptoethanol. This contrasts with the behaviour of *N*-benzoylglycine ethyl dithioester, which on addition of Hg-papain exhibits a red shift from 308 to 326 nm that is reversed by the addition of β-mercaptoethanol. The RR spectrum of the *N*-benzoylalanine ethyl dithioester – Hg-papain adduct is shown in Fig. 4*b* along with the spectrum of the free dithioester, Fig. 4*a*. From a comparison of Figs. 4*b* and *c* it can be seen that the substitution of a ^{13}C label into the thiocarbonyl group results in a decrease in relative intensity of a feature at 1579 cm^{-1} and very small shifts in other peaks in the spectrum of the adduct.

RR spectra of the unlabelled and ^{13}C labelled enethiolates formed from *N*-benzoylalanine ethyl dithioester at high pH are shown in Fig. 5. From a comparison of the adduct (Figs. 4*b* and *c*) and enethiolate spectra (Fig. 5) and their differential responses to ^{13}C substitution it is clear that, unlike the glycine case, *N*-benzoylalanine ethyl dithioester does not form an enethiolate type adduct with Hg-papain. However, there are marked similarities between the RR spectrum of the Hg-enzyme

Can. J. Chem. Downloaded from www.nrcresearchpress.com by 72.64.146.136 on 09/07/12
For personal use only.

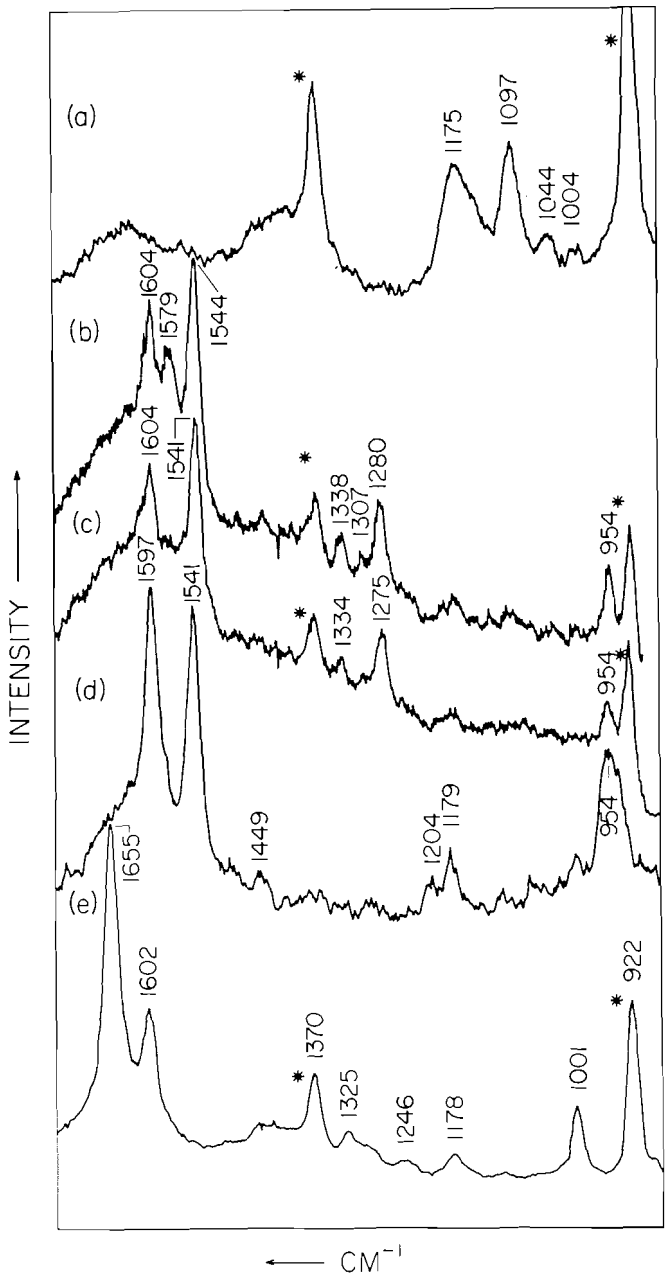

FIG. 4. Resonance Raman spectra of (*a*) *N*-benzoylalanine ethyl dithioester (1.6×10^{-4} *M*) in acetate buffer pH 4.5; (*b*) unlabelled and (*c*) $^{13}C{=}S$ labelled *N*-benzoylalanine ethyl dithioester (0.8×10^{-4} *M*) and Hg-papain (2.3×10^{-4} *M*) in acetate buffer pH 4.5; and 4-ethyl-2-phenyl oxazolin-5-one (*d*) 0.6 m*M* in 0.01 *N* NaOH and (*e*) 60 m*M* in 40% CH_3CN. Asterisks denote CH_3CN features.

complex and the spectra of oxazolin-5-one type compounds. The RR spectra of oxazolin-5-ones that have their conjugated π-electron chain extended by the presence of a benzylidene group at the 4-position are dominated by two or three intense features in the 1550–1610 cm^{-1} region (9, 10). The analogy to Figs. 4*b* and 4*c* is further strengthened by the fact that these benzylidene substituted oxazolin-5-ones show only small frequency shifts but large changes in peak intensities when ^{13}C is substituted into the oxazolinone ring (9, 10). The correspondence of Fig. 4*b* to the RR spectrum of a highly conjugated oxazolinone-type species is reinforced by comparison with the RR spectrum of the ionized form of 4-ethyl-2-phenyl oxazolin-5-one (structure **b**) recorded in 0.01 *N* NaOH.

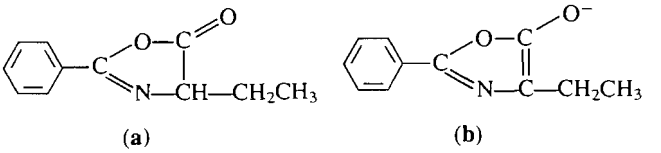

(a) (b)

The RR spectra of 4-ethyl-2-phenyl oxazolin-5-one at pH 12 and neutral solution are shown in Figs. 4*d* and *e* respectively. Several similarities exist between the spectra of the enzyme adduct (Fig. 4*b*) and the ionized oxazolinone (Fig. 4*d*); intense peaks occur near 954, 1540, and 1600 cm^{+1} in both spectra. Although there is not a one-to-one correspondence between the spectra in Figures 4*b* and 4*d*, the similarities in the major features are sufficient to indicate that the *N*-benzoylalanine ethyl dithioester in the Hg-papain complex is in a form resembling that of an oxazolin-5-one at high pH. A suggested mechanism giving rise to such a species on the enzyme is:

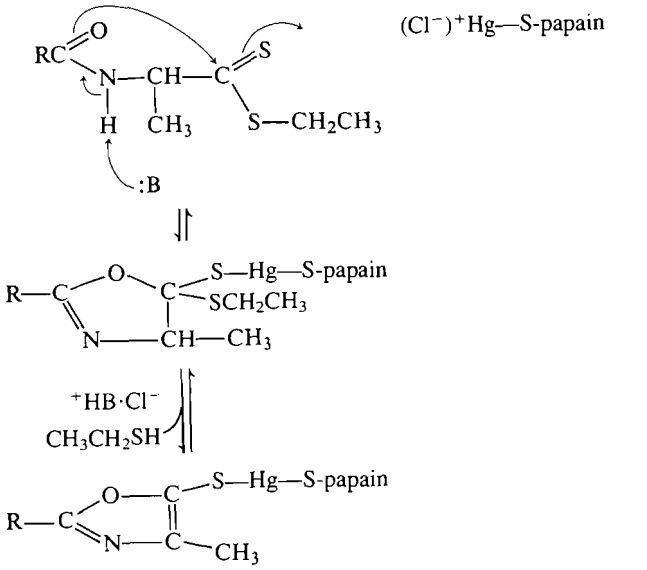

Treatment of this complex with β-mercaptoethanol would result in the release of the corresponding oxazolin-5-thione rather than in regenerating the dithioester. Thus this mechanism explains the lack of reversibility of adduct formation involving the alanine dithioester. Attempts at obtaining the RR spectrum of the product formed by the addition of β-mercaptoethanol were thwarted by very high fluorescence from the sample. Also, since papain is capable of catalysing the hydrolysis of both esters and thionoesters (11), i.e., the activity of the enzyme is not adversely affected by the S for O substitution, and since oxazolin-5-ones are substrates for papain (12), it is probable that the active enzyme, generated in the presence of β-mercaptoethanol, would rapidly hydrolyse the oxazolin-5-thione formed.

Papain must be participating actively in the formation of the dithioester–Hg-papain complexes since in the absence of native enzyme similar complexes are not formed between Hg and the dithioesters. There are two ways in which the enzyme can assist in complex formation. Firstly, it can utilize its specificity for *N*-acylamino acid esters to orient the dithioesters in order to favour their reaction with the enzyme-bound mercury. That this effect does indeed occur is supported by the observation that denatured Hg-papain does not form complexes with dithioesters. The second way in which papain can assist in complex formation is to provide a base to specifically abstract a proton, from the α-CH group in the case of glycine or from the NH group in the case of the alanine dithioesters. In all

Can. J. Chem. Downloaded from www.nrcresearchpress.com by 72.64.146.136 on 09/07/12
For personal use only.

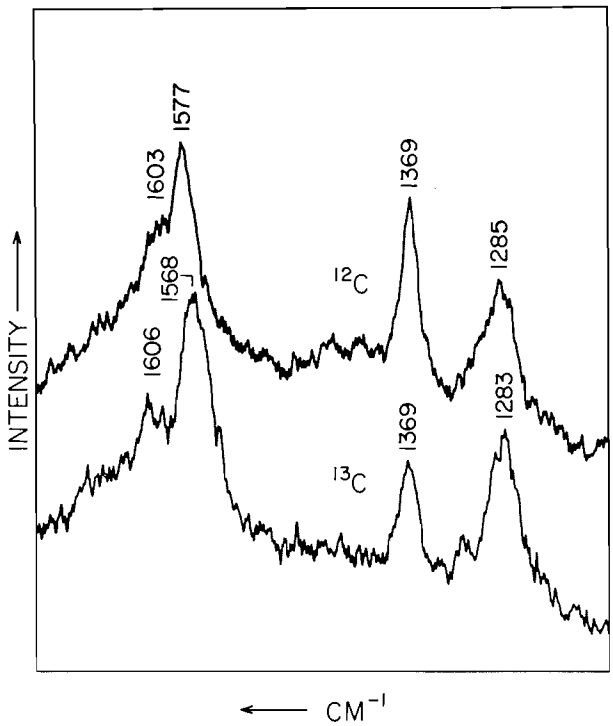

FIG. 5. Resonance Raman spectra of labelled and unlabelled *N*-benzoylalanine ethyl dithioester (5×10^{-4} *M*) in 1 *N* NaOH. These spectra were obtained using 337-nm laser excitation.

likelihood both steric complementarity and proton abstraction operate to stabilize the observed complexes; the mechanism of base-catalysed proton removal is discussed further below. Finally it should be remembered that both the D and L forms of the alanine dithioester are available for binding to papain. However, papain's strong preference for the L form of the amino acid binding at the S_1–P_1 site is well established (13) and it has been further demonstrated that papain shows no detectable binding capacity for D-amino acid esters or thionoesters (unpublished results, this laboratory). Thus it is assumed that only the L form of *N*-benzoylalanine ethyl dithioesters is bound in the active site. It is expected therefore that on mixing *N*-benzoyl-DL-alanine dithioester with excess Hg-papain only 50% of the dithioester should be converted to oxazolin-5-thione. This is consistent with the broad feature obtained in the absorption spectrum of the mixture. However, it is apparently inconsistent with the data in Figs. 4*b* and *c*. In these figures it appears that greater than 50% of the dithioester is converted to the cyclic oxazolin-5-thione. However, due to differences in concentration and resonance intensity enhancement it can be calculated that the dithioester features in Figs. 4*b* and *c* in the 1100–1200 cm^{-1} range are $\gg 10$ times weaker than the corresponding features in Fig. 4*a*.

The different Hg-papain complexes formed by the glycine and alanine dithioesters tested can be explained readily by a mechanism in which an enzyme side chain acts as a base to catalyse formation of the adducts. Examination of a 3-dimensional model of papain identifies the carboxylate side chain of Asp-158 as a prime candidate for this base. If it is assumed that the benzoylamido portion of the dithioesters bind to the enzyme in the manner proposed for substrates (14), i.e., the carbonyl group is hydrogen bonded to the NH of Gly-66, and also that the thiocarbonyl sulphur is directed towards the sulphur of Cys-25, then both the amide proton and the α-CH proton in the L-configuration lie in close proximity to the side chain of Asp-158. For the glycine-based dithioesters it is apparent that the $-COO^-$ group of Asp-158 preferentially removes the α-CH proton to form an enethiolate. However, for the alanine-based dithioester the position taken up by the labile glycine α-CH proton is occupied by alanine's CH_3 side chain. Thus in the alanine case the amide proton is removed, catalysing the formation of a 4-methyl-2-phenyloxazolin-5-thione complex in the active site.

Acknowledgment

We thank Dr. C. Chuaqui for the gift of 4-ethyl-2-phenyl-oxazolin-5-one.

1. A. N. GLAZER and E. L. SMITH. *In* The enzymes. Vol. 3. *Edited by* P. D. Boyer. Academic Press, New York. 1971. pp. 501–546.
2. P. R. CAREY and A. C. STORER. Acc. Chem. Res. **16**, 455 (1983).
3. P. R. CAREY and A. C. STORER. Ann. Rev. Biophys. Eng. **13**, 25 (1984).
4. L. A. AE. SLUYTERMAN and J. WIJDENES. Biochim. Biophys. Acta, **200**, 593 (1970).
5. H. LEE, A. C. STORER, and P. R. CAREY. Biochemistry, **22**, 4781 (1983).
6. R. H. ANGUS, P. R. CAREY, H. LEE, A. C. STORER, and K. I. VARUGHESE. Can. J. Chem. **63**, 2169 (1985).
7. P. R. CAREY and L. R. SANS CARTIER. J. Raman Spectrosc. **14**, 271 (1983).
8. H. LEE, P. R. CAREY, and A. C. STORER. Can. J. Chem. **62**, 763 (1984).
9. K. KUMAR, D. J. PHELPS, and P. R. CAREY. Can. J. Chem. **56**, 232 (1978).
10. D. J. PHELPS, R. G. CARRIERE, K. KUMAR, and P. R. CAREY. Can. J. Chem. **56**, 240 (1978).
11. A. C. STORER and P. R. CAREY. Biochemistry, **24**, 6808 (1985).
12. J. DE JERSEY. Biochemistry, **9**, 1761 (1970).
13. I. SCHECHTER and A. BERGER. Biochem. Biophys. Res. Commun. **27**, 157 (1967).
14. J. DRENTH, K. H. KALK, and H. M. SWEN. Biochemistry, **15**, 3731 (1976).

Can. J. Chem. Downloaded from www.nrcresearchpress.com by 72.64.146.136 on 09/07/12
For personal use only.

Crystal chemistry of complex indium(III) and other M(III) halides, with a discussion of M—Cl bond lengths in complex M(III) chlorides and of the structures of and hydrogen bonding in $(NH_4)_2[InCl_5(H_2O)]$, $K_3InCl_6 \cdot nH_2O$, $(MeNH_3)_4[InCl_6]Cl$, and $(Me_2NH_2)_4[InCl_6]Cl$

OSVALD KNOP,[1] T. STANLEY CAMERON, D. ADHIKESAVALU, BEVERLY R. VINCENT,[2] AND JAMES A. JENKINS
Department of Chemistry, Dalhousie University, Halifax, N.S., Canada B3H 4J3

Received March 21, 1986[3]

OSVALD KNOP, T. STANLEY CAMERON, D. ADHIKESAVALU, BEVERLY R. VINCENT, and JAMES A. JENKINS. Can. J. Chem. **65**, 1527 (1987).

The crystal chemistry of complex In(III) halides is discussed and compared with that of other Group III elements and Fe(III), with critical comments and analysis of the available information. The cation/anion packing types occurring among $A^+[M^{3+}X_4]$ halides are classified according to volume per formula unit and the relative ionic sizes of M, X, and A, and the structural trends in this class of compounds are identified. The effect of systematic factors responsible for variation in M(III)—Cl bond lengths is examined in detail. It is shown that the *mean* M(III)—Cl bond lengths in $[MCl_nL_m]^\epsilon$ (M = Al, Ga, Fe, In, Tl; L = Cl or a neutral ligand) complexes can be approximated, to within about 0.02 Å, by a linear function of the coordination number CN = $n + m$ and the charge ϵ over the range $3 \leq CN \leq 6$ and $-3 \leq \epsilon \leq 2$. This analytical expression provides a norm for comparing M(III)—Cl bond lengths and demonstrates that the CN is always a more important factor than ϵ in determining the variation in the mean bond length and that it becomes dominant when M is small. The crystal structure of $(Me_2NH_2)_4[InCl_6]Cl$ ($P2_12_12$, a = 10.156(4) Å, b = 13.007(4) Å, c = 8.751(3) Å, Z = 2) has been determined and those of $(NH_4)_2[InCl_5(H_2O)]$ (*Pnma*, a = 13.953(4) Å, b = 10.086(5) Å, c = 7.152(3) Å, Z = 4), $K_3InCl_6 \cdot nH_2O$ (*I*4*mm*, a = 15.659(8) Å, c = 18.106(5) Å, Z = 14) and $(MeNH_3)_4[InCl_6]Cl$ ($P2/n$, a = 16.113(3) Å, b = 7.446(2) Å, c = 16.163(4) Å, β = 103.75(2)°, Z = 4) redetermined. The water in $K_3InCl_6 \cdot nH_2O$ appears to be in part zeolitic; the hydrate examined contained more water than the monohydrate reported previously. Hydrogen bonding in these and related structures is described and discussed in detail; descriptions of the hydrogen-bonding schemes in $(NH_4)_2[InCl_5(H_2O)]$ and $(MeNH_3)_4[InCl_6]Cl$ constitute the main improvement over earlier structure determinations.

OSVALD KNOP, T. STANLEY CAMERON, D. ADHIKESAVALU, BEVERLY R. VINCENT et JAMES A. JENKINS. Can. J. Chem. **65**, 1527 (1987).

On discute de la chimie des cristaux des complexes des halogénures de l'In(III) et on la compare à celle des complexes du Fe(III) et des autres éléments du groupe III; on fait des commentaires critiques ainsi qu'une analyse des informations disponibles. On a classifié les divers types d'empillements cation/anion que l'on retrouve dans les halogénures $A^+[M^{3+}X_4]$ d'après les volumes par unité de formule ainsi que d'après les grosseurs relatives des ions M, X et A et l'on a identifié les tendances structurales dans cette classe de composés. On a étudié en détail l'effet des facteurs systématiques qui sont responsables de la variation des longueurs des liaisons M(III)—Cl. On démontre qu'on peut faire une approximation valable (à ±0,02 Å) des longueurs moyennes des liaisons M(III)—Cl dans les complexes $[MCl_nL_m]^\epsilon$ (M = Al, Ga, Fe, In, Tl; L = Cl ou un ligand neutre) en utilisant une fonction linéaire du nombre de coordination (NC = $n + m$) et de la charge (ϵ) pour des écarts de $3 \leq NC \leq 6$ et $-3 \leq \epsilon \leq 2$. Cette expression analytique fournit une norme pour comparer les longueurs des liaisons M(III)—Cl et démontre que le NC est toujours un facteur plus important que ϵ dans la détermination de la variation de la longueurs moyenne de la liaison et que ce facteur devient dominant lorsque M est petit. On a déterminé la structure cristalline de $(Me_2NH_2)_4[InCl_6]Cl$ ($P2_12_12$, a = 10,156(4), b = 13,007(4) et c = 8,751(3) Å, Z = 2) et on a redéterminé celles de $(NH_4)_2[InCl_5(H_2O)]$ (*Pnma*, a = 13,953(4), b = 10,086 et c = 7,152(3) Å, Z = 4), $K_3InCl_6 \cdot nH_2O$ (*I*4*mm*, a = 15,659(8) et c = 18,106(5) Å, Z = 14) et $(MeNH_3)_4[InCl_6]Cl$ ($P2/n$, a = 16,113(3), b = 7,446(2) et c = 16,163(4) Å, β = 103,75(2)°, Z = 4). La molécule d'eau du $K_3InCl_6 \cdot nH_2O$ semble être partiellement zéolithique; l'hydrate examiné contenait plus d'eau que le monohydrate qui avait été examiné antérieurement. On décrit et on discute en détail des liaisons hydrogènes qui existent dans ces structures et dans des composés apparentés; les descriptions des schémas des liaisons hydrogènes des complexes $(NH_4)_2[InCl_5(H_2O)]$ et $(MeNH_3)_4[InCl_6]Cl$ constituent la principale amélioration par rapport aux déterminations de structures faites antérieurement.
[Traduit par la revue]

In this contribution to the structural chemistry of In–halogen compounds we offer (**A**) a *catalogue raisonné* of the crystal chemistry of halogeno complexes of In(III) and related compounds; (**B**) a detailed analysis of the systematic factors responsible for variation in M—Cl bond lengths in Group III and Fe(III) complex chlorides, and a resulting scheme which permits these bond lengths to be rationalized and predicted; (**C**) crystal-structure determinations or re-determinations of the four title compounds; and (**D**) a discussion of hydrogen bonding in these and other In(III) halides. Our discussion of the crystal chemistry attempts not merely to unify results published to date, but also to offer critical comment and identify gaps in our present knowledge. It therefore includes complex In(III) fluorides, which are usually treated as belonging to the solid-state rather than to the coordination chemistry of indium, even though their structures often contain recognizable InF_n^ϵ units (some of which may exist in fluoride melts). A few pseudo-halogeno complexes are also mentioned. On the other hand, halogeno complexes containing In—C bonds have been deliberately excluded; the presence of the covalent In—C bond introduces factors, additional to the coordination number (CN) and the charge ϵ on the complex, which affect the In—Hal bond lengths but which we are not prepared to discuss at present.

The four topics are presented in the above order. Most of the In(III) halides discussed in the following and for which

[1]To whom correspondence may be addressed.

[2]Holder of NSERC (1983–1986) and Killam (1984–1986) graduate fellowships.

[3]Revision received February 11, 1987.

Can. J. Chem. Downloaded from www.nrcresearchpress.com by 72.64.146.136 on 09/07/12
For personal use only.

Can. J. Chem. Downloaded from www.nrcresearchpress.com by 72.64.146.136 on 09/07/12
For personal use only.

crystallographic information exists, are listed in Table 1. The literature references for these are not repeated in the text. The structural results for the four title compounds are described in **C**, but they will be drawn upon in **A** and **B**; details of the crystal structure analysis have been relegated to the end of this paper (Experimental).

A. Crystal chemistry of complex In(III) and related halides

The crystal chemistry of complex In(III) halides exhibits a considerable variety. Apart from the well-represented six-coordinate species, examples of which occur in the four title compounds, structures containing In in four-, five-, and seven-coordination are known (Table 1). Indium analogs of almost all the types of complex halides of other Group III elements are known. Among the species not yet reported for In are those containing isolated single M—X—M bridges, such as occur in the bent $[X_3MXMX_3]^-$ (M = Al, Ga; X = Cl, Br, I) ions, but their absence from the chemical literature may simply be due to accident rather than to their reluctance to form.

By and large the crystal chemistry of In^{vi} and In^{iv}, relative to that of other M(III) elements in halides of corresponding compositions, is determined by the position of In^{3+} in the sequence of the effective ionic radii; the extent of structural similarity in relation to ionic size will emerge more clearly from the discussion below. From the limited data available at present it would appear that the upper size limit for isostructural behaviour is between Tl and Y, although a cubic elpasolite Cs_2KYF_6 isostructural with Cs_2KInF_6 has been reported (56). Some of the fluoride structures are quite insensitive to the size of M and tolerate substitutions ranging over most of the M^{3+} sequence, e.g. Cs_2KMF_6 (M = Al, Ga, Co, Fe, Sc, In, Tl, Y) (56) or the chiolites $K_5M_3F_{14}$ (M = Al, In, Tl). In many respects the crystal chemistry of In(III) resembles closely that of Fe^{3+} and Tl^{3+}, but there are exceptions. Thus the $A_2[MCl_5(H_2O)]$ chlorides have *Pnma* structures for M = Fe, Sc, In and A = K, Rb, NH_4. However, the Cs salt is *Pnma* for In and Tl, but *Cmcm* for Fe. Occasional differences are found for In/Tl pairs of compounds, not only in regard to structure but also to properties. For example, Cs_2KTlF_6 is stated to be very hygroscopic, while Cs_2KInF_6 can be handled in atmospheric air (56).

Isolated octahedra

The structures of A_3InF_6 cryolites derive from the idealized cubic ($Fm3m$, $Z = 4$) $A^{xii}{}_2A^{vi}[MF_6]$ aristotype, which may be viewed as an ordered $AA_{0.5}M_{0.5}F_3$ perovskite arrangement.

TABLE 1. Complex In(III) halides with known or presumed crystal structures or symmetries[a]

Compound	Space group	Z	References
	Seven-coordinated In		
Sr_2InF_7	$P2_1/c$	4	1
$N_2H_5InF_4\cdot H_2O$	$P2_12_12_1$	4	2
KIn_2F_7	$P2_1/m$	4	3
α-$Ba_3In_2F_{12}$	$P4/mbm$	2	4
$RbIn_3F_{10}$	$P222_1$	2	5
$Rb_2In_3F_{11}$	$P2_1/m$	4	6
	Six-coordinated In: identical ligands		
$AInF_4$ (A = Na, K, Rb), see text			
A_3InX_6 (X = F, Cl), see text			
A_2BInX_6 (X = F, Cl, Br), see text	$Fm3m$	4	7, 8
$(Me_3NH)_3InCl_6$	$I4_1/acd$	16	9
$(Ph_4As)_3In(NCS)_6$	$C2/c$	8	10
Na_2MgInF_7	$Imm2$	4	11
$(MeNH_3)_4InCl_7$	$P2/c$	4	12; this work
$(MeNH_3)_4InBr_7$[b]	$P2/c$	4	13
$(Me_2NH_2)_4InCl_7$	$P2_12_12$	4	This work
In_2Cl_3	$Pnma$	32	14
$A_3In_2X_9$ (X = Cl, Br), see text			
$Na_3Li_3In_2F_{12}$	$Ia3$	8	15
$A_5In_3F_{14}$ (A = K, NH_4)	$P4/mnc$ or $P4_22_12$	2	16, 17
	Six-coordinated In: mixed ligands		
$KInBr_4\cdot 2H_2O$	$P2_1/c$	2	18–20
$K_2InCl_5\cdot H_2O$[c]	$Pnma$	4	18, 21, 22
$Cs_2InCl_5\cdot H_2O$	$Pnma$	4	23; this work
$(NH_4)_2InCl_5\cdot H_2O$	$Pnma$	4	24; this work
$A_2InBr_5\cdot H_2O$ (A = K, NH_4)[d]	$Pnma$	4	4, 18, 20, 25, 26
$K_3InCl_6\cdot nH_2O$	$I4mm$	14	18, 27, 28; this work
$K_3InBr_6\cdot\frac{3}{2}H_2O$	$I4mm$	14	18, 20, 27
$(S_4N_3)[cis\text{-}InCl_4(H_2O)_2]$	$Pnma$	4	29
$[fac\text{-}InCl_3(H_2O)_3]\cdot(dioxan)_3$	$P2_1/c$	4	30
$[mer\text{-}InCl_3(terpy)]$	$P2_1/c$	4	31, 32
$[mer\text{-}InCl_3(py)_3]\cdot(py)$	$C222_1$	4	33
$[mer\text{-}InBr_3(py)_3]\cdot(py)$	$P2_1$	2	34
$[cis\text{-}InCl_2(acac)(bipy)]$[e]	$P2_1/c$	4	35
$[cis\text{-}InCl_2(py)_2(OOCPh)]$[e]	$Pna2_1$	4	36
$[cis\text{-}InI_2(dmso)_4]InI_4$[e]	$C2/c$	8	37

TABLE 1 (*concluded*)

Compound	Space group	Z	References
	Five-coordinated In		
$(Me_4N)_2InCl_5$	Monoclinic		38
$(Et_4N)_2InCl_5$	$P4/n$ or $P\bar{4}$	2	39, 40
$InCl_3 \cdot 4H_2O$	$Pnma$	4	20
[*trans*-$InCl_3(PPh_3)_2$]	$Pbca$	8	41
{*trans*-$InCl_3[OP(NMe_2)_3]_2$}	$P2_1/c$	4	42
$(n\text{-}Bu_4N)_2\{InX[SC(CN)=C(CN)S]_2\}$ (X = Cl, Br)	$P2_1/c$	4	43
	Four-coordinated In		
InX_2 (X = Cl, I)	$Pnna$	4	44–46
$AInCl_4$ (A = K, Rb, NH_4), see text	$I4_1/a$	4	47
$KInBr_4$	$Pnna$	4	48
Et_4NInCl_4, $Et_4NInClBr_3$	$P\bar{6}_3mc$	2	49, 50
$Et_4NInClI_3$	$F\bar{4}3m$	4	50
$n\text{-}Bu_4NInCl_{4-n}Br_n$ (n = 0, 1, 3, 4)	$Pnna$	4	51
$Ph_4AsInCl_4$	$I\bar{4}$	2	52, 53
$(BEDT\text{—}TTF)_2InBr_4$[f]	$P\bar{1}$	2	54
Me_3SInI_4	"Anisotropic"		38
Et_3SInI_4	Monoclinic		38

[a] See **A** for structural representation and a more detailed treatment. Compounds containing In—C and other covalent bonds are not included. Z is number of formula units per unit cell.

[b] Space group in ref. 13 wrongly stated as $P2_1/c$.

[c] The Tl and Rb analogs are isostructural on powder diffraction evidence (23). The compound analyzing to $(Me_4N)_2InCl_5 \cdot H_2O$ (25) is presumably of this type, but no structural or spectroscopic evidence for this has so far been presented.

[d] The Rb and Cs analogs are isostructural on powder diffraction evidence (55).

[e] *cis* relative to the halogen atom.

[f] BEDT—TTF = 3,4;3′,4′-bis(ethylenedithio)-2,2′,5,5′-tetrathiafulvalene.

The symmetries of the actual structures are lower owing to rotational displacements of the InF_6 octahedra, and the crystal chemistry is complicated by the occurrence of polymorphic transitions (57). The monoclinic, antiferrorotatory ($P2_1/n$, Z = 2) α-Na_3InF_6 is isostructural with the mineral cryolite, Na_3AlF_6, and the corresponding Tl and Sc analogs (16, 58, 59). The K, Rb, Cs, Tl, and NH_4 compounds have been examined (60–62), but the structural relationships in this family cannot be regarded as firmly established even for the room-temperature phases. The Rb compound has been reported as $Fm3m$ (60) as well as $I4/mmm$ (62); the K compound as $Fd3$ (60), $Fd3m$ (63), and isostructural with K_3TlF_6 (59); the Cs compound as tetragonal, probably $P4/mnc$ (60, 62), c/a = 1.011 (63); and the NH_4 compound as $P4/mnc$ (60) or $P2_1/n$ (64) below $T_{tr} \sim$ 355 K, and $Pa3$ or $Fm3m$ above T_{tr} (64).

No A_3InCl_6 cryolites with cubic or near cubic unit cells and Z = 4 seem to be known, although a cubic phase with a P or I lattice was obtained (47) by quenching molten Ag_3InCl_6; for a = 16.650 Å a Z of 16 would seem appropriate. The same authors indexed an X-ray powder pattern of Na_3InCl_6 as orthorhombic, Z = 6. The literature statements concerning A_3InCl_6 (A = K, Rb, Cs, NH_4) require a more detailed comment and are discussed separately below. The orthorhombic, pseudotrigonal In_2Cl_3 ($Pnma$, Z = 32) is essentially $In_3[InCl_6]$ (14), isostructural with α-$Tl_3[TlCl_6]$ (65).

The cubic elpasolites, $A^{xii}{}_2B^{vi}[MX_6]$, are a variant of the cryolite structure and may be regarded as ordered perovskites, $AB_{0.5}M_{0.5}X_3$. This populous family is well represented by In halides. The fluorides A_2BInF_6 (A = K, Rb, Cs, NH_4, Tl; B = Na, K, Ag, Tl; not in all A, B combinations) (56, 62, 66–68), the chlorides $Rb_2LiInCl_6$, $In_2LiInCl_6$, $Rb_2NaInCl_6$, Cs_2BInCl_6 (B = Li, Na, K) (7, 8, 14, 69, 70) and $Cs_2NaInBr_6$ (71) all have this structure under ordinary conditions. The slight tetragonal distortion of Rb_2TlInF_6 (68), c/a = 1.008, points to the existence of a transition to the cubic form above room temperature. $Cs_2In[InCl_6]$ exhibits three phases: *III* ($Fm3m$, Z = 4), *II* ($P4/nbm$, Z = 4), and *I* ($Pban$?, Z = 4); $Cs_2TlInCl_6$ (*III*) and $Cs_2TlInCl_6$ (*II*) are analogous (70).

The hexagonal (12L) elpasolite structure typified by $Cs_2Na[CrF_6]$ (72) is adopted by Cs_2LiMCl_6, M = In or Sc (73). Other structure types encountered among In fluorides are represented by the weberite $Na_2Mg[InF_6]F$ (11); $LiMg[InF_6]$, presumed to be related to the hexagonal ($P\bar{3}1m$) $Li_2[ZrF_6]$ (74); and the garnet ($Ia3$) $Na_3Li_3In_2F_{12}$, which can be formulated as $Na_3Li_3[InF_6]_2$ and is isostructural with its Al (cryolithionite), Sc, and Rh analogs (15).

In $(Ph_4As)[In(NCS)_6]$ the ions are both too large and unwieldy to give a classical cryolite packing. It would be interesting to see whether $(Me_4N)_3[In(NCS)_6]$, hitherto unreported, is isostructural with its Fe(III) analog, the structure of which ($C2/c$, Z = 8) has been determined (75).

The structures of the four alkylammonium salts containing InX_6^{3-} ions (Table 1) are interesting mainly for their hydrogen bonding and are discussed in **D**.

Infrared and Raman spectra of $[Co(NH_3)_6]InCl_6$ indicate (76) that this salt contains isolated $InCl_6$ groups and is isostructural with the cubic ($Pa3$) $[Co(NH_3)_6][TlX_6]$ (X = Cl, Br) (77) and probably also (apart from possible orientational ordering) with $[Co(NH_3)_4(H_2O)_2][TlCl_6]$ (78). The cation/anion packing in these crystals is of the NaCl type.

A number of compounds containing In^{vi} complexes with mixed ligands have also been studied. The octahedral complexes in $[InI_2(dmso)_4][InI_4]$ and $(S_4N_3)[InCl_4(H_2O)_2]$ have *cis* configurations. Similar situations are encountered in

Can. J. Chem. Downloaded from www.nrcresearchpress.com by 72.64.146.136 on 09/07/12
For personal use only.

TABLE 2. Crystal data of complex In chlorides studied in this work[a]

Parameter	Value					
		$K_3InCl_6 \cdot nH_2O$		$(MeNH_3)_4InCl_7$		
	$(NH_4)_2InCl_5 \cdot H_2O$[b]	This work	Ref. 27[c]	This work	Ref. 12[d]	$(Me_2NH_2)_4InCl_7$
Formula	$Cl_5H_{10}InN_2O$	See text	$Cl_6H_2InK_3O$	$C_4H_{24}Cl_7InN_4$		$C_8H_{32}Cl_7InN_4$
fw	346.18	See text	462.85	491.26		547.36
μ_{Mo}, cm^{-1}	33.7	40.2	37.6	20.8		18.2
a, Å	13.953(4)	15.659(8)	15.723(9)	16.113(3)	16.113(3)	10.156(4)
b, Å	10.086(5)	—	—	7.446(2)	7.466(5)	13.007(4)
c, Å	7.152(3)	18.106(5)	18.069(18)	16.163(4)	20.300(8)	8.751(3)
β, deg	—	—	—	103.75(2)	127.9(4)	—
V, $Å^3$	1006.5(12)	4440(6)	4467(10)	1883.6(13)	1927(3)	1156.0(12)
Z	4	14	14	4	4	2
ρ_o, g/cm^3	2.281(50)	2.49	2.420	1.72		
ρ_c, g/cm^3	2.284(28)	2.48	2.415[e]	1.731(16)	1.693(25)	1.572(10)
Space group	*Pnma* (no. 62)	*I*4*mm* (no. 107)		*P*2/*n* (no. 13)	*P*2/*c* (no. 13)	$P2_12_12$ (no. 18)
$F(000)$, e	664	See text	3052	976		552
Reflections:						
Total measured	1463	1737	5073	2932	834[h]	1255
Unique used[f]	902[g]	880[g]	2208[f]	2075[g]	834[h]	1176[f]
$100R$; $100R_w$	4.07; 3.93	5.7; 5.5	2.9; 3.6	5.44; 5.14	7.6	4.92; 6.35

[a]Mo $K\alpha_1$, λ = 0.70926 Å (graphite monochromator); θ-range, 2–23°.
[b]Reference 24: a = 14.07 Å, b = 10.17 Å, c = 7.16 Å. Reference 23; a = 13.988 Å, b = 10.150 Å, c = 7.174 Å.
[c]λ = 0.7107 Å.
[d]On conversion to *P*2/*n*: a = 16.113(3) Å, b = 7.466(5) Å, c = 16.427(12) Å, β = 102.8°.
[e]Recalculation from the data of ref. 27 gives 2.409.
[f]$I \geq 3\sigma(I)$.
[g]$I \geq 2\sigma(I)$.
[h]Visual intensity estimates.

other M(III) compounds: the *cis* configuration is found in $[FeCl_2(H_2O)_4][FeCl_4] \cdot H_2O$ (79), $[AlCl_2(bipy)_2]Cl$ (80), and $[GaCl_2(bipy)_2][GaCl_4]$ (81), while in $[FeCl_2(dmso)_4][FeCl_4]$ (82), $[FeCl_2(H_2O)_4]Cl \cdot 2H_2O$ (83), $[FeCl_2(H_2O)_4][SbCl_6] \cdot 4H_2O$ (84), and $[MCl_2(py)_4][MCl_4]$ (M = Al, Ga) (85, 86) the configuration is *trans*.

In $[InCl_3(H_2O)_3] \cdot (dioxan)_3$ the configuration is *fac*, as it is in $[AlCl_3(py)_3]$ (85), and similar to that in $[Cl_3(H_2O)Sn—OH—]_2 \cdot (dioxan)_3$, but without the formation of a di-μ-O dimer (cf. ref. 87). In $[InX_3(py)_3] \cdot (py)$ (X = Cl, Br), $[TlBr_3(py)_3]$ (88), and $[TlCl_3(py)_3] \cdot (py)$ (33), however, the configuration is *mer*; predictably, it is *mer* also in the isomorphous $[MCl_3(terpy)]$ (M = Al, Ga, In, Tl, and probably Fe) group of complexes (31, 32, 80, 89).

A_3InX_6 and $A_3InX_6 \cdot nH_2O$ (X = Cl, Br)

The ready formation of hydrates and the difficulty in retaining the high-temperature phases by quenching are responsible for a number of inconsistencies in the literature statements concerning anhydrous A_3InX_6.

X-ray powder patterns of A_3InCl_6 (A = Na, K, Rb, Cs, NH_4, Ag; α, annealed low-temperature phase; β, quenched high-temperature phase) have been reported by Atkinson and Field (47), who indexed them all as tetragonal except for the Na and β-Ag salts (see above). The β-K, Rb, and α-Cs unit cells are obviously of the same type, and the α-K cell is dimensionally similar when transformed by taking $a\sqrt{2}$ instead of a. These authors also state (23) to have obtained, by evaporation of aqueous solutions of the chlorides at 0°C under vacuum, α-K_3InCl_6 from a K/In = 1:2 solution and β-K_3InCl_6 from a K/In = 1:1 solution. The product obtained by evaporation at −20°C under vacuum gave a powder pattern "similar to that of the α-K_3InCl_6 but with a slightly larger and distorted unit cell. This product, which probably contained lattice water, could be converted to β-K_3InCl_6 by heating to above 150°C." Furthermore, Atkinson *et al.* (90) observed that their β-K_3InCl_6 changed, on prolonged X-irradiation, to a material with a powder pattern of their α-K_3InCl_6. However, Wignacourt (18) has shown that neither form of Atkinson's K_3InCl_6 was in fact the anhydrous high-temperature form. Wignacourt's quenched β-K_3InCl_6, also tetragonal, had a = 8.031 Å, c = 9.572 Å, while his low-temperature α-K_3InCl_6 had unit-cell dimensions very similar to those of the β-K_3InCl_6 of ref. 47.

Indeed, when the unit-cell volumes of Atkinson's β-K, Rb, and α-Cs and Wignacourt's α-K phases are plotted against c, the four points fall on a smooth curve (Fig. 1, top), while the point for Atkinson's α-K (transformed cell) is completely off. Furthermore, three of the four $\bar{a} = (V/Z)^{1/3}$ (Z taken as 8, see below) values plotted against Shannon's (91) ionic radii $r^{xii}(A^+)$ fall on a straight line, with the point for β-K lying somewhat above and that for Atkinson's α-K appreciably below that line (Fig. 1, bottom). This can be taken as evidence that Atkinson's β-K, Rb, and α-Cs and Wignacourt's α-K have unit cells of the same type and are in all likelihood the authentic anhydrous low-temperature A_3InCl_6 phases. Although $(NH_4)_3InCl_6$ in ref. 47 is considered to be isostructural with β-K, Rb, and α-Cs, barring a mispring in Table 1 of that paper the unit-cell dimensions do not support this claim.[4]

Comparison of the unit-cell dimensions of Atkinson's α-

[4]The NH_4 and β-Cs phases were somewhat unstable and showed evidence of decomposition on cooling from the melt (47).

Can. J. Chem. Downloaded from www.nrcresearchpress.com by 72.64.146.136 on 09/07/12
For personal use only.

Can. J. Chem. Downloaded from www.nrcresearchpress.com by 72.64.146.136 on 09/07/12
For personal use only.

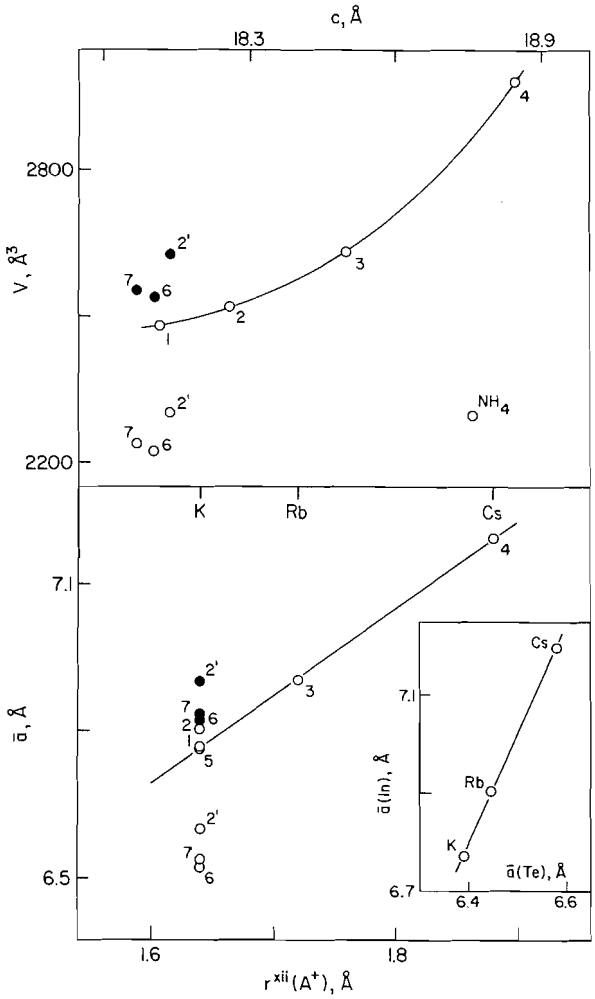

FIG. 1. Tetragonal A_3InCl_6 chlorides. (*Top*) Variation of the unit-cell volume with c. (*Bottom*) Variation of the mean unit-cell dimension $\bar{a} = (V/Z)^{1/3}$ with Shannon's effective ionic radius $r^{xii}(A^+)$. Open circles: *1*, α-K_3InCl_6 (18); *2*, β-K_3InCl_6 (47, 90); *3*, Rb_3InCl_6 (47); *4*, Cs_3InCl_6 (47); *5*, high-temperature (β) K_3InCl_6 (18); *6*, $K_3InCl_6 \cdot nH_2O$ (this work); *7*, $K_3InCl_6 \cdot H_2O$ (18, 27); *2′*, α-K_3InCl_6 (47, 90); NH_4, $(NH_4)_3InCl_6$ (47). Full circles: (16/14)V of *2′*, *6*, and *7* (see text). *Inset*: $\bar{a}(A_3InCl_6)$ plotted against $\bar{a}(A_2TeCl_6)$.

K_3InCl_6 with those of $K_3InCl_6 \cdot nH_2O$ (Table 2) shows that, allowing for a reasonable variation and taking into account the preparative circumstances, the presumed anhydrous α phase must have been a K_3InCl_6 hydrate. From the structure determinations we know (see **C**) that for $K_3InCl_6 \cdot nH_2O$ Z is 14. At the same time, the volume V_1 per formula unit of the hydrate should not be smaller than the V_1 of anhydrous K_3InCl_6. We also know, from comparison with In_3InCl_6 and Tl_3TlCl_6 (14, 65), that $V_1(K_3InCl_6)$ must be of the order of 290 Å^3. This indicates that for the anhydrous low-temperature phases $Z = 8$, i.e. to compare the unit-cell volumes in Fig. 1 the value for Atkinson's α-K_3InCl_6 must be multiplied by 16/14. The adjusted value is about 6% larger than Wignacourt's V(α-K_3InCl_6), a reasonable increment. The similarly treated V values for the hydrate (Table 2) fall in the same region of the plot as Atkinson's V(α-K_3InCl_6).

Unlike in $K_3InCl_6 \cdot nH_2O$ (see **C**), in the anhydrous A_3InCl_6 the In coordination polyhedra can only be $InCl_6$. The above volume and other relationships therefore suggest that, in spite of the initial appearance to the contrary, the structures of the α-A_3InCl_6 (A = K, Rb, Cs) chlorides do derive from the cubic cryolite aristotype (In in 000 etc., A^{vi} in $\frac{1}{2}00$ etc., A^{xii} in $\frac{1}{4}\frac{1}{4}\frac{1}{4}$ etc.), by distortions such that the $InCl_6$ octahedra are tilted away from the a as well as from the c axis so as to double but simultaneously shorten the c period. The tilt must be appreciable, as the observed tetragonal c/a ratios for the K, Rb, and Cs compounds are 1.548, 1.550, and 1.498, respectively. Since no cryolite chlorides of a similar type are known, we compare in Fig. 1 (inset) the $\bar{a}$(α-A_3InCl_6) values with those for the closest available cognates of the cubic cryolite structure, the $Fm3m$ A_2TeCl_6; these hexachlorides may be viewed as defect cryolites, $A^{xii}{}_2\square^{vi}[TeCl_6]$. The resulting linear relationship supports the suggested derivation.

The hydrated A_3MX_6 (M = In, Tl) cryolites might be expected to be analogous to the stoichiometric hydrate $K_3RhCl_6 \cdot H_2O$, the structure of which consists of a distorted fcc array of $[RhCl_6]^{3-}$ octahedra interspersed with K^+ and H_2O (92, 93). However, the three salts reported to date, $K_3InCl_6 \cdot nH_2O$, $K_3InBr_6 \cdot nH_2O$, and $K_3TlCl_6 \cdot nH_2O$ (Table 1 and **C**), are zeolitic and, as discussed in detail in **C**, their $I4mm$ structures ($Z = 14$) are characterized by the simultaneous presence of $[MX_6]^{3-}$ and $[MX_5(H_2O)]^{2-}$ ions. These structures can be derived from the cryolite structure presumed for the anhydrous A_3MX_6 as follows. The idealized cubic A_3MX_6 cryolite structure may be formally regarded as a combination of the NaCl and the *anti*-CaF_2 structure types, $A'A''_2[MX_6]$: the $[MX_6]^{3-}$ anions form a fcc array with A′ in positions corresponding to Na in NaCl and A″ in positions corresponding to F in CaF_2 (cryolite if A′ = A″, elpasolite if A′ ≠ A″). When the cubic cryolite cell ($Z = 4$) is quadrupled to form a tetragonal bc cell with $a_{tet} = a_{cub}\sqrt{2}$, $c_{tet} \sim 2c_{cub}$, omission of two of the sixteen $K_3[MX_6]$ units from this cell and conversion of two of the remaining fourteen $[MX_6]^{3-}$ ions to $[MX_5(H_2O)]^{2-}$ ions generate the framework of the hydrated cryolite:

$$K_3MX_6 = \quad K_{48} \quad [MX_6]_{12} \quad [MX_6]_4$$

$$K_3MX_6 \cdot \tfrac{1}{7}H_2O = K_{42}\square_6 \quad [MX_6]_{12} \quad [MX_5(H_2O)]_2X_2$$

The X^- ions take the place of the removed $[MX_6]^{3-}$ ions. The resulting readjustment of one of the K positions (K(6), see **C**) produces additional space in the structure which, together with one third of the □ vacancies (those at 2(*a*) in $I4mm$, see **C**), permit the zeolitic water molecules to be incorporated. It is remarkable that the conversion of $[MX_6]^{3-}$ to $[MX_5(H_2O)]^{2-} + X^-$ on hydration should stop, in all three cases, at the $[MX_5(H_2O)]/[MX_6] = \frac{1}{6}$ ratio and that any extra water entering the structure should remain uncoordinated to M.

Connected octahedra

The layer perovskites $AInF_4$ (A = K, Rb, Cs) (16, 61, 62) can be represented as $A[InF_2F_{4/2}]$ structures (cf. ref. 94 for possible derivation from the $P4/mmm$ $TlAlF_4$ aristotype). The ambiguity of the space-group assignment of the K and Rb compounds from X-ray diffraction (*Pbam* or *Pba*2 ⊂ *Pbam*, ref. 61) was resolved, on ir and Raman evidence, in favour of *Pbam* (62). The Cs compound ($Pca2_1$, $Z = 4$) is stated (61) to be isostructural with α-$RbFeF_4$ and α-$CsFeF_4$.

$NaInF_4$ has been indexed as hexagonal ($P3_112$ or $P3_121$, $Z = 8$), isostructural with $NaScF_4$ (16, 58), but in ref. 62 it is stated to be orthorombic, $Pca2_1$, $Z = 4$. Attempts to quench the high-temperature form were unsuccessful (16).

Shared octahedra of *two* types occur in the tetragonal $A_5In_3F_{14}$ (A = K, NH_4), which have the chiolite-type structure, $A_5[InF_2F_{4/2}][InF_4F_{2/2}]_2$, as does $K_5Tl_3F_{14}$ (59).

Can. J. Chem. Downloaded from www.nrcresearchpress.com by 72.64.146.136 on 09/07/12
For personal use only.

The $A_3In_2X_9$ halides (95, 96) contain isolated $In_2X_9^{3-}$ groups consisting of two InX_6 octahedra sharing a face, i.e. tri-μ-$[X_3InX_3InX_3]^{3-}$. The two classes reported to date represent different stacking variants. The rhombohedral ($R\bar{3}c$, Z = 6) $A_3[In_2Cl_9]$ (A = Rb, Cs, In, Tl), $Cs_3[In_2Cl_8Br]$ and $Cs_3[In_2Cl_7Br_2]$(*I*) are not isostructural with $Cs_3Fe_2Cl_9$ but related to $Cs_3Fe_2F_9$; $Cs_3M_2X_9$ (MX = ScCl, TlCl, YCl, YBr) are of the same type (96, 97). The hexagonal ($P6_3/mmc$, $Z = 2$) $Cs_3[In_2Cl_7Br_2]$(*II*) and $Cs_3[InCl_{9-n}Br_n]$ (n = 3, 6, 9) are isostructural with $Cs_3Cr_2Cl_9$.

Five-coordinated In

The $[InCl_5]^{2-}$ complex in $(Et_4N)_2InCl_5$ is an almost regular square pyramid of C_2 symmetry (39, 40), as is the $[TlCl_5]^{2-}$ complex in the isostructural Tl compound (40).[5] $(Et_2NH_2)_2TlCl_5$ has been prepared and analyzed (98) and may be of this type. Square-pyramidal geometry is also present in $(n\text{-}Bu_4N)_2$-{InX[SC(CN)=C(CN)S]$_2$} (X = Cl, Br) and their isostructural Tl analogs (43). As would be expected, in $[InCl_3(PPh_3)_2]$ the coordination figure is a *trans* trigonal bipyramid, as it also is in $InCl_3\cdot 4H_2O = [InCl_3(H_2O)_2]\cdot 2H_2O$ and in $\{InCl_3$-$[OP(NMe_2)_3]_2\}$; the Tl complexes $[TlBr_3(py)_2]$ (99), $[TlBr_3$-$(OPPh_3)_2]$ (100), and $[TlBr_3(Opy)_2]$ (101) are of the same coordination type.

Indium analogs of compounds containing $[X_3M—MX_3]^{2-}$ ions (e.g. $(Me_4N)_2[Ga_2Cl_6]$ (102), $(n\text{-}Pr_4N)_2[Ga_2Br_6]$ (103), and $Ga_2[Ga_2I_6]$ (104)) have been prepared and authenticated by vibrational spectroscopy ($(n\text{-}Bu_4N)_2[In_2X_6]$, X = Cl, Br, I (105)), but their crystal structures have not been determined.

An $[InCl_5]^{2-}$ complex is presumed to exist also in the primitive cubic $BaInCl_5$ (47) (Z = 16?), crystallographically different from $BaInF_5$, $BaFeF_5$, $SrFeF_5$ (106), $BaGaF_5$, or any of the three known forms of $BaAlF_5$ (107). While the existence of $BaInCl_5$ was confirmed in the dry $BaCl_2$–$InCl_3$ system (108), no double salt was found in the $BaCl_2$–$InCl_3$–H_2O system at 24°C (109).

Seven-coordinated In

It is mainly the emergence of this coordination that signals a division between the structural chemistry of In(III) and Fe(III) halides. Only fluoride structures have been reported to date.

Isolated irregular InF_7 polyhedra are found in Sr_2InF_7, which is isostructural with K_2NbF_7 (ref. 1; cf. also ref. 106).

Edge- and vertex-sharing pentagonal InF_7 bipyramids connected to form three-dimensional frameworks occur alone (KIn_2F_7) or in combination with InF_6 octahedra ($RbIn_3F_{10}$, $Rb_2In_3F_{11}$). Thus $K_2InF_7 = K[InF^{eq}{}_{4/2}F^{eq}{}_{1/2}F^{ax}{}_{2/2}]_2$ can also be represented as $K[\mu\text{-}F^{eq}{}_{4/2}F^{ax}{}_{2/2}InF^{eq}InF^{ax}{}_{2/2}F^{eq}{}_{4/2}]$ (3). $RbIn_3F_{10}$ can be formulated as $Rb[InF_{4/2}F_{2/2}][InF_{2/2}F_{2/2}F_{1/2}F_{2/2}]_2$ (5); the NH_4 compound (17) is probably isostructural. The related $Rb_2In_3F_{11}$ contains two nonequivalent InF_7 units: $Rb_2[InF_{2/2}F_2F_{2/2}][InF^{eq}{}_{4/2}F^{eq}{}_{1/2}F^{ax}{}_{2/2}]_2$ (6). Each InF_7 bipyramid in these structures shares four equatorial corners to form characteristic infinite chains reminiscent of those found in $PaCl_5$; the chains are cross-linked in different ways to form sheets and stacking sequences perpendicular to the sheets. A simpler variant of this type of arrangement occurs in $N_2H_5InF_4\cdot H_2O = N_2H_5[InF^{eq}{}_{4/2}F^{eq}{}_{1/1}F^{ax}{}_{1/1}(H_2O)^{ax}]$, where the coordination polyhedron is a *trans*-$InF_6(H_2O)$ bipyramid.

Yet another arrangement is found in α-$Ba_3[In_2F_{12}]$ (ref. 4; cf. also ref. 106). In this structure two trigonal In coordination prisms sharing a vertical edge, each augmented on the far vertical face, form isolated [di-μ-$F_5InF_2InF_5]^{6-}$ groupings. The structure differs from that of low $Ba_3Al_2F_{12} = Ba_6F_4[Al_4F_{20}]$ (*Pnnm*, Z = 4), which contains "isolated" $[F_{4/1}AlF_{2/2}]_4$ rings similar to $[MF_5]_4$ (M = Nb, Ru (110).

Isolated tetrahedra

With the exception of the fluorides (see above), all the $AInX_4$ halides with known structures contain isolated InX_4^- tetrahedra. No example of linked InX_4 tetrahedra seems to have been reported to date.

The K, β-Rb, and NH_4 chlorides (47), which crystallize with tetragonal structures of the scheelite type, are isostructural with the corresponding Tl(III) (111, 112) but not Ga(III) or Fe(III) (52, 113) chlorides.[6] The hydrogen-bonding scheme in NH_4InCl_4 is thus almost certain to correspond to that in NH_4TlCl_4 (111): each of the four equivalent H atoms participates in a bifurcated, almost symmetric N—H···2Cl bond, d(H···Cl) ~ 2.5 Å.

Only powder patterns were available for the Na, β-Cs (water-quenched high-temperature form), and the annealed, low-temperature α-Rb and α-Cs chlorides (47). Assuming that the indexing in ref. 47 corresponds to the actual structure, the following can be noted. The $(b + c)/4 = a'$ mean for the orthorhombic $NaInCl_4$ defines a tetragonal cell dimensionally similar ($a/a' = 2.395$) to the scheelite cells and a volume V_I per formula unit which is compatible with $V_I(KInCl_4)$ and V_I(β-$RbInCl_4$). The $NaInCl_4$ structure may thus turn out to be a variant of the scheelite structure.[7] The large tetragonal cells reported in ref. 47 for α-$RbInCl_4$ and α-$CsInCl_4$ are consistent with Z = 28.

The orthorhombic $KInBr_4$ (48) and In[InI_4] (45), which have cation/anion packings of a distorted CsCl type, are isostructural with Ga[$GaCl_4$] (114),[8] $KTlBr_4$ (116), NH_4TlBr_4 (116), and Tl[$TlBr_4$] (117), while Tl[$TlCl_4$] has the scheelite structure (111) and Ga[GaI_4] (104) has an unusual, complex rhombohedral ($R3c$, Z = 6) structure. The existence of In[$InCl_4$] is in dispute. Low- (α) and high-temperature (β) forms of $InInCl_4$ are claimed (44, 118) to have been obtained; the powder pattern of the β phase was indexed as orthorhombic, on a unit cell dimensionally similar to that of Ga[$GaCl_4$] (and of β-$TlInCl_4$, ref. 118). However, no phase of the composition $InCl_2$ was found in a recent re-investigation (97) of the system In–Cl. The unit-cell volume of $InGaCl_4$ ($BaSO_4$ type, ref. 113) would suggest that the In and Ga atoms in this crystal are disordered.

No other $AInBr_4$ or $AInI_4$ structures with simple cations have so far been reported, though one would expect them to be similar to those of the corresponding Tl compounds, which have been studied in some detail. The existence of peritectic transformations makes investigation of the bromides difficult. $CsTlBr_4$ at room temperature has $P2_12_12_1$ symmetry (116).[9]

[5]The crystal symmetry of $(Et_4N)_2InBr_5$ from optical investigation is reported (38) as cubic. Spectroscopic evidence (25) seems to suggest that this bromide is in fact $(Et_4N)_2[InBr_4]Br$.

[6]The observation (47) that the powder patterns of the K, NH_4, and β-Rb salts could also be indexed on cubic cells with $a_{cub} = a_{tet}\sqrt{5} = c_{tet}$ has its root in the fortuitous circumstance that the c/a ratios of these salts are very close to $\sqrt{5}$. This is not so for scheelites in general.

[7]Attempts to prepare $NaTlCl_4$ and $CsTlCl_4$ by the method which yielded the K, Rb, and NH_4 chlorides failed (111).

[8]^{35}Cl nqr spectra indicate that Ga[$GaCl_4$] undergoes a transition, at ca. 320 K, in which the $GaCl_4$ tetrahedron, of low symmetry in the high-temperature phase, *increases* its symmetry in the low-temperature phase (115). An analogous transition, at ca. 250 K, is observed in $KGaCl_4$ (115); the phase above 250 K has been reported as monoclinic, $P2_1$ (113).

[9]It is interesting to note that $V_I(CsTlBr_4)$ is 4.2% *smaller* than $V_I(NH_4TlBr_4)$. A monoclinic form of $CsTlBr_4$ is mentioned in ref. 119; cubic symmetry ($Fm3c$) is reported in ref. 120 (also for $CsTlI_4$).

Can. J. Chem. Downloaded from www.nrcresearchpress.com by 72.64.146.136 on 09/07/12
For personal use only.

The pseudohexagonal mixed halide $Tl[TlCl_2Br_2]$ crystallizes in the same space group ($Z = 4$), but its unit-cell dimensions are not related to those of $CsTlBr_4$; the packing in this crystal is of the *anti*-NiAs type (121). The cubic ($Z = 24$) $ATlI_4$ iodides can be prepared by direct synthesis under anhydrous conditions or by dehydrating the respective cubic $ATlI_4 \cdot nH_2O$ hydrates. The latter can lose water already at temperatures well below ambient, with retention of the cubic structure and almost without change in the unit-cell dimensions (119, 122). While a structure of an anhydrous $ATlI_4$ has not yet been reported, it would seem that the nonaqueous part of the hydrate structure (see *Hydrated species*) is preserved. This receives some support from ^{127}I nqr spectra (122), which at room temperature contain a *single* ν_1 resonance line for $KTlI_4 \cdot 2H_2O$ (and also for the Rb, Cs, and NH_4 salts) as well as for $KTlI_4$; the resonance in the room-temperature spectrum of NH_4TlI_4, however, was a doublet. For $CsGaI_4$ at room temperature the ν_1 resonance is a quartet (123), which excludes a cubic structure.

The tetrahalides $Et_4N[InX_4]$ have the *anti*-NiAs ($P6_3mc$) ion packing for $X_4 = Cl_4$ (49), $ClBr_3$ (ordered) (50), and probably Br_4 (38), with the ethyl groups orientationally disordered. Et_4NTlBr_4, Et_4NTlBr_3I (124),[10] Et_4NFeCl_4,[11] and $Me_4SbGaCl_4$ (125) are also of this type.[12] The structure of $Et_4NInClI_3$, however, is of the NaCl type,[13] with Cl and I disordered, and so are the structures of $Et_4NTlBr_2I_2$, $Et_4NTlBrI_3$, Et_4NTlI_4 (124), and $Et_4NFeI_4(I)$ (127).[14] Interestingly, $Et_4NGaClI_3$ (Cl and I disordered) (128) and the isostructural $Et_4NFeI_4(II)$ (127) are of yet another type: the orthorhombic (*Pnnm*) unit cell is pseudohexagonal, $a \sim c\sqrt{3}$, and the structure is based on a distorted NiAs packing arrangement.

The n-$Bu_4N[InCl_{4-n}Br_n]$ ($n = 0, 1, 3, 4$) salts are orthorhombic (*Pnna*), as are the isostructural Tl compounds ($n = 0, 4$) (126), but n-Bu_4NTlI_4 is monoclinic ($P2_1/n \subset Pnna$) (129).[15] The cation/anion packing in the *Pnna* structures is of the NaCl type.

$Ph_4As[InCl_4]$ is isostructural with the corresponding Ga, Fe, and Tl chlorides (52, 53, 126). The ion packing in these crystals (and in Ph_4AsI) is of the tetragonally distorted zincblende type; the structure reflects the symmetries of the two ions.

With the possible exception of Et_4NTlI_4, in none of the $A[MX_4]$ compounds mentioned here (and included in Fig. 2) has the MX_4^- ion the T_d symmetry, though in some of them it is very nearly a regular tetrahedron. Unless significantly pertured by the orientational disorder of the ethyl group, a regular tetrahedron can, however, be expected for InI_4^- in Et_4NInI_4, as yet not investigated.

The cation/anion packing type for $A[InX_4]$ halides can be related, in a general way, to ionic size, but for this to be instructive the In compounds are best considered in the overall context of the $A[M(III)X_4]$ structures. A plot of the volume V_1 per formula unit against Shannon's (91) $r^{iv}(M^{3+})$ (Fig. 2) involves a minimum of assumptions, as V_1 derives directly from experiment and reflects the effective size of both A and X, and the sequence (though not necessarily the values) of $r^{iv}(M^{3+})$ is reasonably well established.[16] The relevance of relative ionic size is evident. The boundary, at low V_1, between the 6:6 ($BaSO_4$) and the 8:8 ($CaWO_4$ and $GaGaCl_4$) packing types is quite sharp, although $GaGaCl_4$ itself falls in the 6:6 region of the plot; the $GaGaCl_4$ type appears to be favoured as V_1 increases.[17] Above $V_1 \sim 300$ Å^3 (ignoring $ATlI_4$, with structures not yet known) only 6:6 packing types occur. The exception is $Ph_4As[MCl_4]$, which are of the 4:4 zincblende type, but this is probably because of the particular, more or less rigid geometry of the Ph_4As group which requires the tetrahedral anion to fit with economy of space between the phenyl rings of adjacent cations. Moreover, the increasing cation size tends to give rise to packing of the NaCl type, and the importance of the relative size of the anion disappears. The reason for the occurrence of *both* the NiAs and the *anti*-NiAs packing types as alternatives to the NaCl-type packing is not obvious, although it may have its origin in the tendency to minimize X–X repulsions between neighbouring anions. In the hexagonal *anti*-NiAs structure the MX_4 tetrahedra are aligned, at $c/2$ intervals, in polar columns on threefold axes, the successive orientations alternating so as to produce staggered sequences $\|c$; the perpendicular spacing between the columns is a, hence X–X contacts are possible only between adjacent tetrahedra in a column. In the orthorhombic NiAs-type structure, however, the interval between the eclipsed anions on a threefold axis is the full $b \sim 14$ Å translation, hence X–X contacts are possible only *between* columns, which have perpendicular separations of ca. $c/\sqrt{3} \sim a/3$.

A more detailed, though more presumptive, distribution of the packing types is obtained when the effective cation radius $r^{vi}(A^+)$ is plotted against the sum of Shannon's $r^{iv}(M^{3+})$

[10]The unindexed powder patterns given in ref. 124 can be indexed as hexagonal and consistent with $P6_3mc$ for Et_4NTlBr_4 ($a = 8.43$ Å, $c = 13.73$ Å) and Et_4NTlBr_3I ($a = 8.55$ Å, $c = 13.99$ Å), and fcc for $Et_4NTlBr_2I_2$ ($a = 12.17(2)$ Å), $Et_4NTlBrI_3$ ($a = 12.29(3)$ Å), and Et_4NTlI_4 ($a = 12.44(1)$ Å).

[11]B. R. Vincent, T. S. Cameron, and O. Knop. To be published.

[12]Salts analyzing to Me_4NTlX_4 and Et_4NTlX_4 (X = Cl, Br) have been prepared but apparently not examined by X-ray diffraction (126).

[13]Figure 1 of ref. 50 does not agree with x(N) of Table I of that paper; it shows a zincblende arrangement of the ions. The $V(Et_4NInClBr_3)$ in Table I and the In—Cl distance in that compound in Table III are in error. One would also expect U_{iso}(Cl) to be larger than U_{iso}(Br) and U_{iso}(I) in Table II.

[14]In ref. 127 the structure of $Et_4NFeI_4(I)$ is described as tetragonal ($a = 8.652(2)$ Å, $c = 12.236(2)$ Å, $Z = 2$) and refined in $I\bar{4}m2$. However, $a\sqrt{2} = 12.236(3)$ Å $= c$, $x(I)\sqrt{2} = z(I)$, and the positions of the Fe, N, and I atoms are equally well described in the cubic group $F\bar{4}3m$. These relationships hold too well to be fortuitous, and in the absence of any reference to them in that paper, and in view of ref. 50, it must be assumed that the true space group is in fact $F\bar{4}3m$, expressed in ref. 127 as the $I\bar{4}m2$ setting of $F\bar{4}2m \subset F\bar{4}3m$.

[15]The ^{35}Cl, ^{81}Br, and ^{127}I nqr spectra of the n-Bu_4NGaX_4 halides (130, 131) indicate trigonal symmetry for the $GaCl_4^-$ and $GaBr_4^-$ ions and the existence of disordered $GaCl_nBr_{4-n}^-$ ions in the $X_4 = Cl_nBr_{4-n}$ compounds. The tetraiodide is not isostructural with the tetrachloride and tetrabromide.

[16]The differences between the V_1 values for corresponding In,Tl pairs of $A[MX_4]$ halides (AX = KCl, NH_4Cl, RbCl, KBr, Et_4NBr, n-Bu_4NCl, n-Bu_4NBr; cf. Fig. 2) would suggest that $r^{iv}(Tl^{3+})$ relative to $r^{iv}(In^{3+})$ is not constant but is larger than the latter when $V_1 < 250$ Å^3 and smaller when $V_1 > 250$ Å^3: $V_1(Tl) = 8.23 + 0.968V_1(In)$, $r^2 = 1.00$, $\sigma = 3$ Å^3. For the difference $V_1(In) - V_1(Tl)$ at either end of the V_1 range to arise from poor experimental accuracy the lattice parameters would have to be in error by an appreciable amount, ~0.5% on the average. The differences are therefore likely to be real and possibly connected with the greater polarizability, by external charges, of the Tl—X bond, which in the isolated ion may be shorter than the corresponding In—X bond. Unfortunately, a direct comparison of In—X and Tl—X bond lengths in MX_4^- is precluded by the lack of structure determinations of matched $A[MX_4]$ pairs; theoretical estimates of these bond lengths do not seem to exist.

[17]A formal relationship between the $BaSO_4$ (*Pnma*) and $GaGaCl_4$ (*Pnna*) structure types is derived, via the common supergroup *Imma*, in ref. 132. However, an argument based on symmetry alone does not account for the difference in the cation/anion coordination in the two structures.

Can. J. Chem. Downloaded from www.nrcresearchpress.com by 72.64.146.136 on 09/07/12
For personal use only.

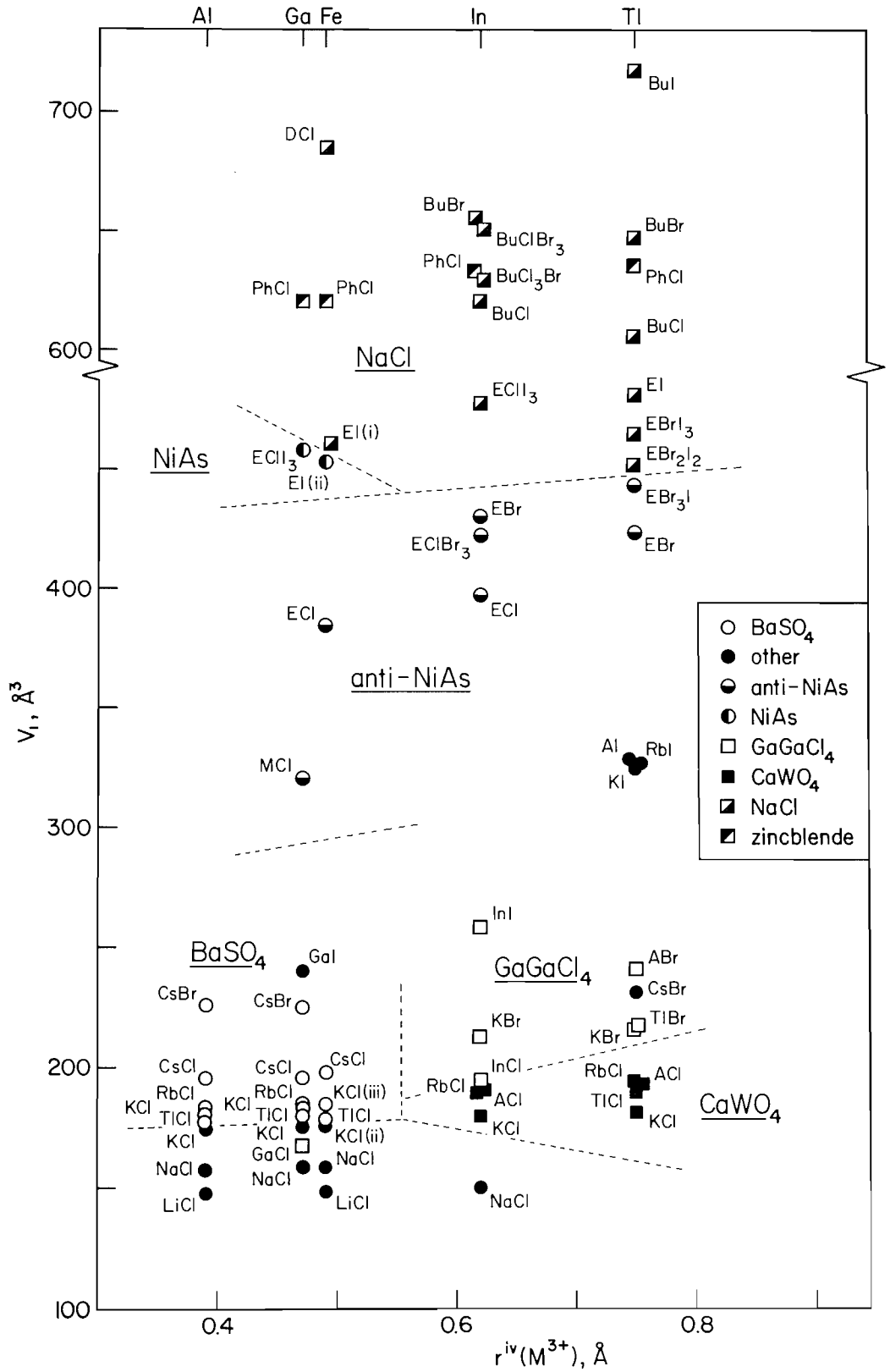

FIG. 2. Cation/anion packing types occurring among $A^+[MX_4]^-$ halides (X = Cl, Br, I). V_1, volume per formula unit; $r^{iv}(M^{3+})$, Shannon's effective ionic radius. The boundaries drawn for the existence fields (broken lines) are provisional. A = NH_4, M = Me_4Sb, E = Et_4N, Bu = n-Bu_4N, Ph = Ph_4As, D = $[FeCl_2(dmso)_4]$. Type symmetries: $BaSO_4$, $CaWO_4$, $GaGaCl_4$, *anti*-NiAs. Reduced type symmetries: NiAs, *Pnnm*; NaCl, $F\bar{4}3m$, *Pnna* (or $P2_1/n$); zincblende, $I\bar{4}$.

Can. J. Chem. Downloaded from www.nrcresearchpress.com by 72.64.146.136 on 09/07/12
For personal use only.

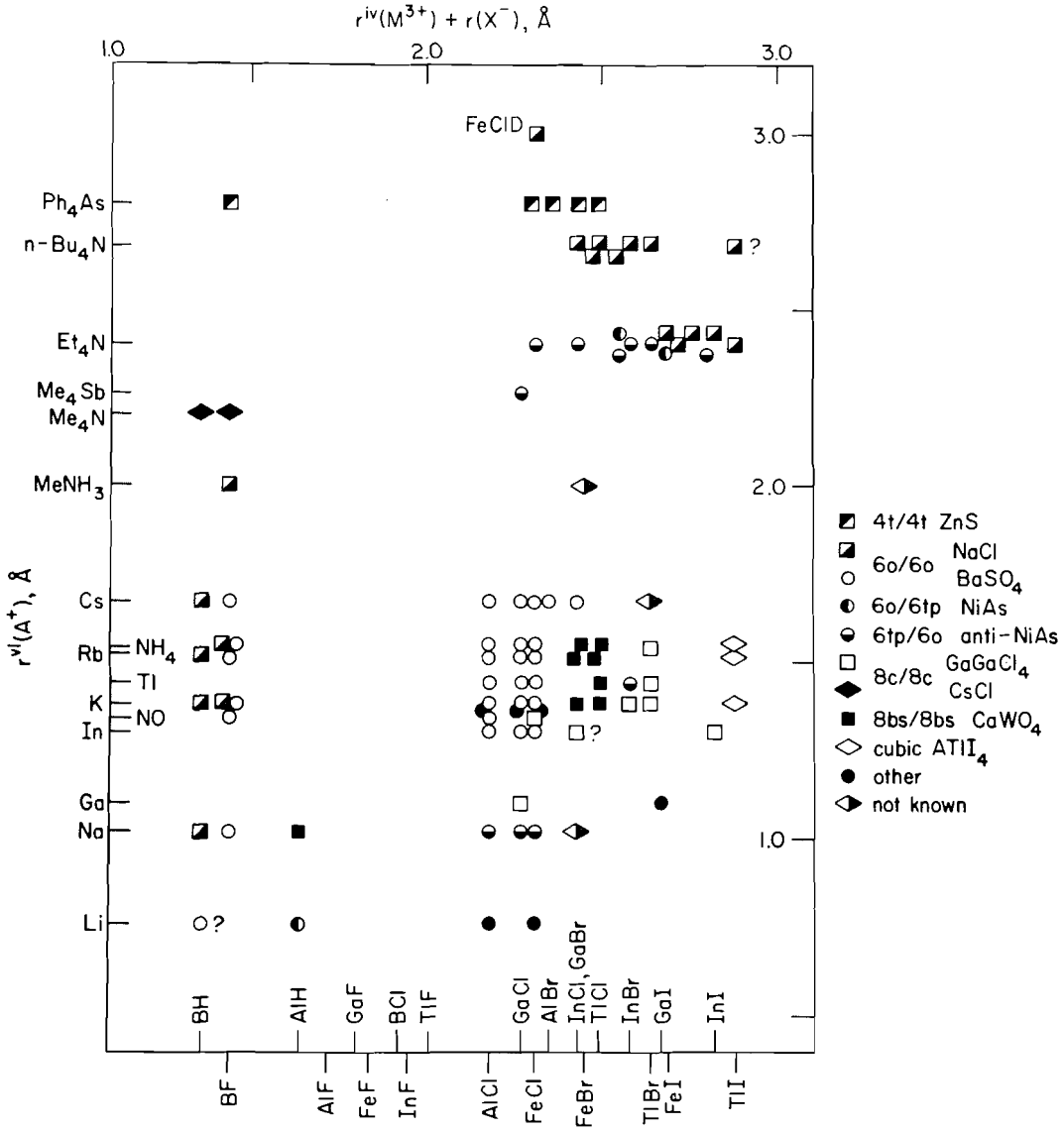

FIG. 3. Distribution of the gross-structure (cation/anion packing) types among $A[M(III)X_4]$ halides according to Shannon's $r^{iv}(M^{3+}) + r(X^-)$ and $r^{iv}(A^+)$ (the value used for $r^{iv}(Tl^{3+})$ is 0.68 Å). The cation/anion coordination ratios and polyhedra are represented by *6tp/6o* etc., where *bs* = combination of square and tetragonal bisphenoid of overall symmetry D_{2d}, *c* = cube, *o* = octahedron, *t* = tetrahedron, *tp* = trigonal prism. Although distinguished in the plot, the $BaSO_4$ and NaCl packing types differ only in the degree of distortion of the coordination octahedra, and similarly for the coordination cubes of the CsCl and $GaGaCl_4$ packing types. The structures of the Me_4N, $MeNH_3$, Ph_4As, and Ph_4Bi tetrafluoroborates (not yet determined) are assumed to be of the same type as those of the corresponding perchlorates. FeClD = $[trans\text{-}FeCl_2(dmso)_4]^+$.

and $r(X^-)$ (Fig. 3).[18] This plot involves, in addition to the deficiencies of Fig. 2, uncertainty about the size of A^+, both because of differences in the CN of A^+ between compounds and because the size estimates assigned to the composite cations are of necessity somewhat arbitrary. Furthermore, the radius sum is not an entirely satisfactory substitute for a representative M—X bond length, which would be preferable to use if it could be obtained with confidence for all the M,X combinations in the plot. Including ABF_4, ABH_4 and $AAlH_4$ serves to strengthen the conclusion from Fig. 2, viz. 6:6 packing types prevail over a surprisingly wide range of cation and anion sizes, with 8:8 types occurring only with combinations of large simple (and NH_4^+) cations and large anions, and with combinations of composite cations and very small anions. The last-named set requires further investigation, for apart from Me_4NBH_4 it contains only one other compound, Me_4NBF_4, the structure of which has not yet been determined but has been inferred from similarity with Me_4NClO_4. Low packing coordination ratios have so far been found only with $LiAlCl_4$ and $LiFeCl_4$ (ratios not clearly defined), and with the Ph_4AsMCl_4 chlorides mentioned above.

Hydrated species

The binary halide hydrates, $InCl_3 \cdot 4H_2O$ and $InBr_3 \cdot 2H_2O$, are reported (18, 20) as orthorhombic, the chloride as *Pnma* ($Z = 4$), the bromide as *Pmcm* or $Pmc2_1$ or $P2cm$. The chloride is almost certainly isostructural with $TlCl_3 \cdot 4H_2O$ and $TlBr_3 \cdot 4H_2O$ (133), hence by implication the In complex is a slightly distorted $[trans\text{-}InCl_3(H_2O)_2]$ trigonal bipyramid (see above).

[18]Here and in what follows $r^{iv}(Tl^{3+})$ is taken as 0.68 Å (see footnote 16). The other $r^{iv}(M^{3+})$ values are Shannon's: 0.39, 0.47, 0.49, and 0.62 Å for Al, Ga, Fe, and In, respectively.

TABLE 3. The $X_{ax}MX_{eq}$ angle (deg) of the $[MX_5(H_2O)]^{2-}$ anion in $A_2[MX_5(H_2O)]$ and $K_3MX_6 \cdot nH_2O$

	$A_2[MX_5(H_2O)]$			$K_3MX_6 \cdot nH_2O$	
Compound[a]	Max.[b]	Mean angle	Reference	Angle	Reference
KInCl	92.4	91.8(7)	18, 22	95.4(2)	18, 27, this work
KInBr	93.0	92.4(7)	18	96.4(3)	18
NH_4InCl	94.0	92.3(17)	This work		
NH_4InBr	94.2	92.8(14)	26		
KTlCl				95.9(3)	18
RbTlCl	93.6	92.2(15)	134		
RbFeCl	94.4	92.3(21)	135		
NH_4FeCl	94.4	92.4(20)	136		
H_3OFeCl	94.4	92.4(20)	137		
CsFeCl	94.4(2)	94.4(2)	135, 138		

[a]The site symmetry at the M atoms in $A_2[MX_5(H_2O)]$ is *m* except in $Cs_2[FeCl_5(H_2O)]$, where it is *mm*; in $K_3MX_6 \cdot nH_2O$ the site symmetry at M(3) is *4mm*.

[b]Maximum $X_{ax}MX_{eq}$ angle. The average uncertainty of this angle is of the order of 0.1°. This angle always involves the X atoms related by the plane of reflection through M.

The orthorhombic (*Pnma*) $A_2[InX_5(H_2O)]$ (X = Cl, Br; for A, see Table 1) salts belong to a large family of $A_2MX_5 \cdot H_2O$ compounds, many of which are isostructural and which have been studied in detail for a variety of reasons (the main features of the *Pnma* structure are described in **C**; new spectroscopic results on some of these salts will be reported elsewhere). The nonplanarity of the In or Tl atom in the $[MX^{ax}X^{eq}_4(H_2O)]^{2-}$ octahedron with the four X^{eq} atoms is not due to any special tendency of In and Tl to formation of MX_5 complexes. As Table 3 shows, the nonplanarity is present not only in the In and Tl compounds but in their Fe(III) analogs as well, and although the *mean* $X^{ax}MX^{eq}$ angle in the octahedron is ~92.4°, the *largest* of the four $X^{ax}MX^{eq}$ angles is ~94° and thus not much inferior to that in $K_3MX_6 \cdot nH_2O$, ~96°C. The deviation of the $X^{ax}MX^{eq}$ angle from 90° is attributable to the electrostatic repulsion of the X atoms and the compression of the $X^{eq}MO$ angle as a consequence of the smaller effective size of the oxygen atom: in the truly five-coordinate, square-pyramidal $InCl_5^{2-} = [InCl^{ax}Cl^{eq}_4\square]^{2-}$ ion in $(Et_4N)_2InCl_5$ (39) the $Cl^{ax}InCl^{eq}$ angle is 103.9(4)°.

Although we were not successful in duplicating the preparation (23) of $K_2InCl_5 \cdot 2H_2O$ (see **C**), our failure does not mean that this hydrate does not exist, even though a phase of this composition was not found in the $KCl–InCl_3–H_2O$ system at room temperature (18, 20, 139). Rather it reflects the delicate nature of the phase relationships in that system, for in the corresponding Tl system the dihydrate $K_2TlCl_5 \cdot 2H_2O$ forms under conditions of crystallization which in the other $ACl–TlCl_3–H_2O$ systems (A = Rb, Cs, NH_4) lead without difficulty to the monohydrates (134). The crystal structure of $K_2TlCl_5 \cdot 2H_2O$ ($P2_1/c$, $Z = 4$) contains isolated centrosymmetric pairs of $TlCl_6$ octahedra sharing an edge, with the water molecules interspersed between them, i.e. the compound is $K_4[di\text{-}\mu\text{-}Tl_2Cl_{10}] \cdot 4H_2O$. In flowing N_2 the crystal loses water completely already at 72°C; the freshly dehydrated material retains the X-ray powder diffraction pattern of the dihydrate. However, on heating the dihydrate under static conditions (in a Guinier–Simon camera) a powder pattern "identical" with that of the tetragonal $K_3TlCl_6 \cdot 2H_2O$ was observed above 110°C (134). Since the presence of lines of a second phase ($KTlCl_4$) is not mentioned, it seems quite likely that this pattern was in fact that of $(K_{8/3}Tl^+_{1/3})TlCl_6$ formed by solid-state conversion with the loss of two Cl atoms.[19] In contrast, the $K_2InCl_5 \cdot 2H_2O$ of ref. 23 is stated to have dehydrated, by heating to 150°C, to $K_2InCl_5 \cdot H_2O$, which was stable up to >400°C.[20] The difference between the Tl and the In compound on heating thus appears to reflect the much greater reluctance of In(III) to reduce to In(I). Evidently a much more extensive and systematic effort will be required to establish beyond doubt the full range of species in the $KCl–InCl_3–H_2O$ system. The monoclinic $(Me_3S)_4In_2Cl_{10} \cdot 3H_2O$ of ref. 38 may very well turn out to be an analog of the above Tl compound, $(Me_3S)_4[In_2Cl_{10}] \cdot 3H_2O$.

The monoclinic $KInBr_4 \cdot 2H_2O$ is $K[trans\text{-}InBr_4(H_2O)_2]$ (19). In contrast, the cubic ($F\bar{4}3c$) Tl bromides and iodides of the corresponding empirical formula are in fact $A[TlX_4] \cdot nH_2O$, with structures consisting of threedimensional frameworks of TlX_4 tetrahedra and AX_{12} cuboctahedra, and with the extra A atoms and the zeolitic water molecules distributed at random over the available interstices, though not necessarily in the same manner for the different A elements (119). In the $A[TlI_4] \cdot nH_2O$ (A = K, Rb, Cs, NH_4) iodides, $0 \leq n \leq 2$; existence of transitions between room temperature and −90°C in the Rb, Cs, and NH_4 salts has been detected by ^{127}I nqr spectroscopy (119, 122). Other isostructural compounds described in ref. 119 are $KTlBr_4 \cdot 2H_2O$ (cf. also ref. 140, where the structure is refined in $Fm3c$), $RbTlBr_4 \cdot H_2O$, $CsTlBr_4 \cdot H_2O$, and $NH_4TlBr_4 \cdot 2H_2O$ as well as the Li and Na bromide dihydrates.[21] While the iodides can be dehydrated to $ATlI_4$ with retention of the cubic structure, complete dehydration of the bromides results in structural change (119, 122). Analogous compounds of In(III), if they exist, do not appear to have been studied.

The reported In—O distances in aquo complexes range from ~2.13 to ~2.36 Å (Table 4). The values are too few, and in part not sufficiently accurate, to detect with confidence any trends

[19]Thermal degradation of $(NH_4)_2TlCl_5 \cdot H_2O$ in a stream of N_2 led to a loss of water in one step at 270°C. Further heating produced, at 320–325°C, a residue of TlCl (134).

[20]According to ref. 18, $K_2InCl_5 \cdot H_2O$, under dynamic heating conditions, loses its water between 190 and 230°C to yield K_2InCl_5.

[21]According to ref. 141, $KTlBr_4 \cdot 2H_2O$ is obtained from solutions with K/Tl > 1, while solutions with K/Tl = 1 yield $KTlBr_4 \cdot H_2O$.

Can. J. Chem. Downloaded from www.nrcresearchpress.com by 72.64.146.136 on 09/07/12
For personal use only.

TABLE 4. Uncorrected In—OH_2 bond lengths in aquo complexes on In(III)

Compound	In—O, Å	References
$K_2[InCl_5(H_2O)]$	2.210(5); 2.224(9)	18, 22; 21
$(NH_4)_2[InCl_5(H_2O)]$	2.229(5)	This work
$[InCl_5(H_2O)]^{2-}$ in $K_3InCl_6 \cdot nH_2O$	2.278(13); 2.15(5)	18, 27; this work
$K_2[InBr_5(H_2O)]$	2.256(14)	18
$(NH_4)_2[InBr_5(H_2O)]$	2.29	26
$[InBr_5(H_2O)]^{2-}$ in $K_3InBr_6 \cdot \frac{3}{2}H_2O$	2.36(11)	18
$N_2H_5[InF_2F_{4/2}(H_2O)]$	2.183(5)	2
$(S_4N_3)[cis\text{-}InCl_4(H_2O)_2]$	2.264(7)	29
$K[trans\text{-}InBr_4(H_2O)_2]$	2.261(6)	19
$(H_3O)[trans\text{-}In(SO_4)_2(H_2O)_2] \cdot 2H_2O$	2.134(5), 2.143(5)	142
$(H_5O_2)[trans\text{-}In(SO_4)_2(H_2O)_2]$	2.172(5)	143
$In(OH)(SO_4)(H_2O)_2$	2.16(4), 2.19(4)	144
$InPO_4 \cdot 2H_2O$	2.12(4), 2.28(4)	145
$[fac\text{-}InCl_3(H_2O)_3] \cdot (dioxan)_3$	2.199(7), 2.250(7), 2.283(7)	30

that may exist with respect to charge on the complex and the nature, size and configuration of the co-ligands.

B. M—Cl bond lengths in complex M(III) chlorides

If comparisons of available In—Cl bond lengths (as determined by X-ray diffraction) are to have any meaning in relation to the chemistry of the complexes, it must be shown that the differences that may exist between complexes are significant and attributable to systematic rather than accidental causes.

The limits to meaningful comparisons are set by the following considerations. The *accuracy* of an individual In—Cl bond length in a routine structure determination is probably not much better than ±0.01 Å. This represents about 2% of the total spread, ~0.5 Å, of observed uncorrected In—Cl distances (see below). Variation in the In—Cl bond length in the same complex in a particular crystal amounts to perhaps another 0.01 Å, except where the bond lengths are constrained to a single value by symmetry. Differences of less than 0.02 Å between uncorrected bond lengths in different compounds can therefore rarely be regarded as chemically significant; strong asymmetry of the crystal environment of the complex and hydrogen bonding may double this limit even without contribution from special factors (e.g. the "*trans*" effect). Corrections for thermal motion are model dependent and in general not likely to increase the reliability of bond-length comparisons. For such comparisons to reveal rather than obscure the trends that may exist, they must be systematic but not too detailed, and they must encompass the widest possible variety of crystal structures.

Effect of coordination number and ionic charge

The primary systematic factors determining the In—Cl bond lengths in $[InCl_nX_m]^\epsilon$ complexes are the CN = $n + m$ and the charge ϵ on the complex. When the size disparity of the ligands is appreciable, the effect of the CN may be difficult to ascertain; ligand configuration may also be a significant factor. In an attempt to improve on previous comparisons of In—Cl bond lengths, the present examination draws upon all the available information we could locate as well as on our extensive SCF calculations at the 6-31G* level (split-valence basis set with polarization functions included for all atoms) for free $[AlCl_n]^\epsilon$ and $[AlF_n]^\epsilon$ species,[22] but even so, consideration of X other than Cl remains restricted largely to H_2O in five- and six-coordinated aquochloro complexes. The paucity of information on mixed-ligand complexes is regrettable, as their inclusion is essential if the effect of ϵ is to be investigated separately from the effect of CN.

To investigate the trends in the variation of the In—Cl bond lengths we have compiled (Table 5) the *mean* uncorrected In—Cl distances $D(CN,\epsilon)$ for all the chloro complexes listed in Table 1 and elsewhere in this paper. Examination of the $\sigma(D)$ values and sample sizes for the individual CN,ϵ combinations shows that the $[InCl_6]^{3-}$ and $[InCl_5(H_2O)]^{2-}$ samples are of reasonable size and that the mean bond length in $[InCl_6]^{3-}$ in particular varies surprisingly little from structure to structure (cf. similar constancy in other halogeno complexes, e.g. $[AlF_6]^{3-}$ (146) and $[SnCl_6]^{2-}$ (147, 148)). For the other CN,ϵ combinations the spread is somewhat larger but still not appreciable, considering that the mean for CN,ϵ = 5,2−, for example, is obtained from complexes as different as the trigonal-bipyramidal $[InCl_5]^{2-}$ and the square-pyramidal $\{InCl[SC(CN)=C(CN)S]_2\}^{2-}$. However, owing to the very small sample sizes the D values of Table 5 for such CN,ϵ combinations must be regarded as less representative.

In the CN,ϵ = 6,ϵ series the D/ϵ increment is approximately constant and ~0.025 Å. This suggested that D might, in the first approximation, be representable as a linear function of ϵ and possibly also of CN. Regressing D on CN and ϵ showed that this supposition indeed is plausible. When D was mapped on CN and ϵ along the gradient of $D_{calcd} = c_0 + c_\epsilon\epsilon + c_{CN}CN$ (i.e. perpendicular to the constant-D contours), the points for $D(CN,\epsilon)$ fell very close to the appropriate points of the CN,ϵ lattice. This could, of course, be fortuitous owing to the restrictive distribution of the available CN,ϵ combinations (CN ≥ 4, $\epsilon \leq 0$). Similar, separate regressions were therefore obtained for Al, Ga, Fe(III), and Tl(III) chloro complexes (Table 5).[23] With the exception of Ga, for which only three D values were available, the D were in each case reasonably approximated by D_{calcd}. Furthermore, it was found that c_0, c_ϵ, and c_{CN} could all be adequately represented, in the M size range under consideration, by $c_i = k_{i0} + k_{i2}r_M^2$, where r_M is short for $r^{iv}(M^{3+})$.[18] These findings strongly suggested that D(M—Cl) could be approximated by a linear function of r_M^2,

[22] S. C. Choi, R. J. Boyd, and O. Knop. To be published.

[23] The compounds included in the regressions and the pertinent references are listed in Table 6, see footnote 24.

Can. J. Chem. Downloaded from www.nrcresearchpress.com by 72.64.146.136 on 09/07/12
For personal use only.

TABLE 5. The mean values $D(CN,\epsilon)$ of M—Cl bond lengths (Å) in complex M(III) chlorides[a]

		$D(CN,\epsilon)$				
CN	ϵ	Al	Ga	Fe	In	Tl
6	2+	2.196(4)/1	—	—	—	—
	1+	2.267(12)/2	2.289(24)/2	2.279(35)/4	—	—
	0	2.286(12)/1	2.322(84)/1	2.325(13)/3	2.432(17)/3	—
	1−	—	—	—	2.460(31)/1	—
	2−	—	—	2.365(6)/5	2.487(9)/4	2.565(31)/2
	3−	—	—	2.385(7)/1	2.512(4)/6	2.580(10)/3
5	1+	—	—	2.198(30)/2	—	—
	0	2.157(18)/3	—	2.226(23)/4	2.371(12)/2	2.423(33)/3
	2−	—	—	—	2.436(18)/2	—
4	0	2.110(11)/4	—	—	—	—
	1−	2.125(9)/9	2.170(12)/7	2.188(19)/10	2.346(13)/2	2.419(3)/4
3	0	2.068(4)/1[b]	[b]	2.14(3)/1[b]	—	—

[a]The mean bond length $\bar{d}_k$ in complex k is $\Sigma w_i d_i/\Sigma w_i$, with a standard deviation $\sigma(d_k)$, where d_i is an individual uncorrected M—Cl bond length in that complex and $w_i = \sigma^{-2}(d_i)$ is calculated from the esd's quoted. The aggregate mean bond length $D(CN,\epsilon)$ in a sample of p CN,ϵ-complexes is $(\Sigma\bar{d}_k)/p$, with a standard deviation $\sigma[D(CN,\epsilon)]$; in the table, p is the number after the oblique stroke. When $p = 1$, $D = \bar{d}_k$ and $\sigma(D) = \sigma(\bar{d}_k)$.

[b]See text for values actually used in the regression of D on r_M^2, CN, and ϵ.

CN, and ϵ. Before proceeding with the triple regression, the aggregate of D values (Table 5) was examined in detail, taking into account observations made on the separate regressions for each M.

The CN,ϵ combinations in each D(M—Cl) set are distributed nonuniformly, favouring high CNs. The regression function can therefore be expected to approximate D less well at low CNs and positive ϵ charges. Inclusion of $D(3,0)$ values, from MCl_3 monomers, in the regression is thus particularly important. However, M—Cl bond lengths in MCl_3 (determined by electron diffraction in the gas phase) appear to be available only for Al and Fe; for Fe the quoted uncertainty is ±0.03 Å (Table 6).[24] To obtain an estimate for $GaCl_3$ and an improved value for $FeCl_3$, the d values for the AlF_3, $AlCl_3$, AlI_3, $GaBr_3$, and GaI_3 monomers (cf. ref. 149) were regressed on r_M and $r^{vi}(X^-)$.[25] The regression equation gave d_{calcd}(Al—F) = 1.627(8) Å and d_{calcd}(Al—Cl) = 2.077(8) Å, both in excellent agreement with the corresponding d_{SCF} values, 1.621 and 2.077 Å, respectively. For $GaCl_3$ and $FeCl_3$ the d_{calcd} values are 2.098(8) and 2.103(8) Å, respectively. These values for the free MCl_3 monomers would correspond, in the crystal, to the M—Cl bond lengths *corrected for thermal motion*. For inclusion in the aggregate D set they were therefore adjusted by subtracting 0.05 Å from D_{calcd}(Al—Cl), 0.04 Å from D_{calcd}(Ga—Cl), and 0.03 Å from D_{calcd}(Fe—Cl) (see below).

The function resulting from the triple regression was

$$[1]\quad D_{calcd} = 1.5273 + 1.4092r_M^2 + 0.10531(1 - 1.1556r_M^2)CN - 0.01693(1 + 2.2918r_M^2)\epsilon$$

($r^2 = 0.990$, $\sigma = 0.016$ Å). The overall agreement of D_{calcd} and D is shown in Fig. 4. The rates of change of D_{calcd} with CN and ϵ are $\partial D_{calcd}/\partial CN = 5.4\sigma$ for Al but 3.1σ for Tl, and $\partial D_{calcd}/\partial\epsilon = -1.4\sigma$ for Al and -2.2σ for Tl (Table 7). This

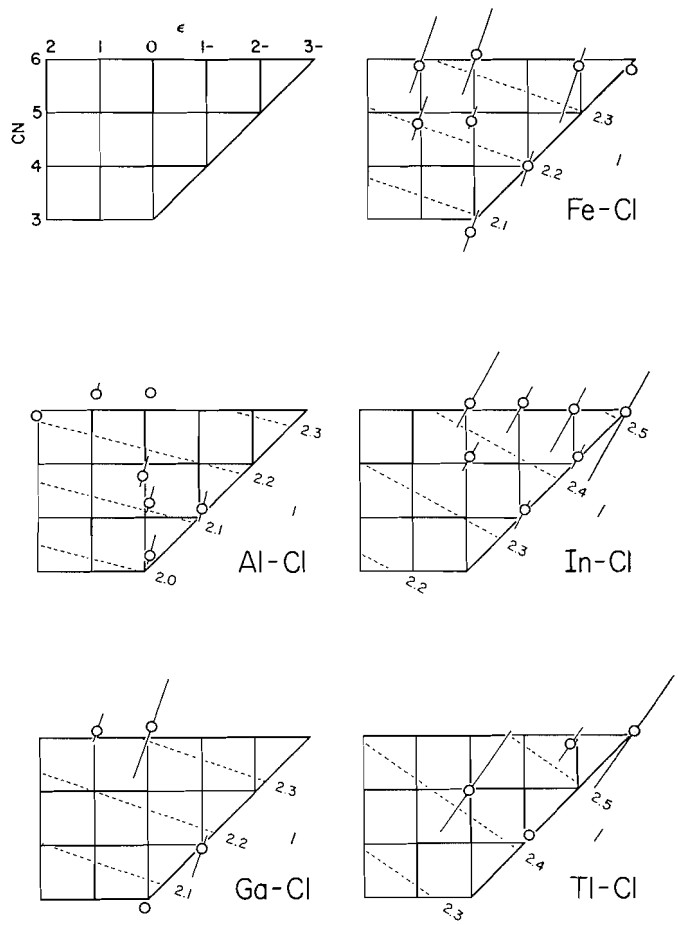

FIG. 4. The mean observed M—Cl bond length D in $[MCl_nX_m]^\epsilon$ complexes mapped on the CN = $n + m$ and the charge ϵ. Lengths of the bars represent the longest and the shortest d(M—Cl) reported for that CN,ϵ combination. The lengths of the small bars on the right-hand side of each plot represent 1σ of the D regression. The constant-D_{calcd} contours (in Å) are defined by the regression of D on CN and ϵ (Table 7; eq. [1]). Distances from the appropriate CN,ϵ lattice points measure the difference $D_{calcd} - D$.

[24]Copies of these tables can be purchased from the Depository of Unpublished Data, CISTI, National Research Council of Canada, Ottawa, Ont., Canada K1A 0S2.

[25]$d_{calcd} = 0.2816 + 0.2544r_M + 0.9372r^{iv}(X^-)$, $r^2 = 1.00$, $\sigma = 0.008$ Å.

Can. J. Chem. Downloaded from www.nrcresearchpress.com by 72.64.146.136 on 09/07/12
For personal use only.

TABLE 7. Linear regression of the mean M—Cl bond length D in M(III) chloro complexes (Table 6) on $r_M^2 = [r^{iv}(M^{3+})]^2$, CN, and ϵ[a]

M	r^2	σ, Å	c_0	c_ϵ	c_{CN}	$\lvert c_{CN}/c_\epsilon \rvert$
Al	0.950	0.023	1.7416	−0.0228	0.0868	3.81
Ga	0.999	0.004	1.8386	−0.0255	0.0784	3.07
Fe	0.994	0.009	1.8657	−0.0262	0.0761	2.90
In	0.996	0.005	2.0690	−0.0318	0.0585	1.84
Tl	0.986	0.013	2.1789	−0.0349	0.0491	1.41

[a] $D_{calcd} = c_0 + c_\epsilon\epsilon + c_{CN}CN$, c_0 (Å) = $1.5273 + 1.4092r_M^2$, c_ϵ (Å/charge) = $-0.0169 - 0.0389r_M^2$, c_{CN} (Å/CN) = $0.1053 - 0.1216r_M^2$. The r^2 and σ refer to $D_{calcd} - D$ calculated for each M separately from eq. [1].

TABLE 8. $(NH_4)_2[InCl_5(H_2O)]$: positional and thermal parameters ($\times 10^4$)

Atom	x[a] / y / z	x / y / z	U_{11} / U_{22} / U_{33}	U_{12} / U_{13} / U_{23}
In	110	1154(0)	251(3)	0
	¼	¼	178(4)	−17(2)
	187	1920(1)	215(3)	0
Cl(1)	000	0027(2)	363(10)	0
	¼	¼	371(11)	110(10)
	465	4608(3)	374(11)	0
Cl(2)	262	2545(1)	304(9)	0
	¼	¼	332(10)	−67(8)
	420	4069(3)	264(9)	0
Cl(3)	234	2244(2)	467(12)	0
	¼	¼	451(12)	76(9)
	−081	−0794(3)	242(9)	0
Cl(4)	116	1042(1)	475(9)	−1(6)
	000	0036(1)	193(8)	−115(7)
	139	1808(2)	459(9)	−26(6)
O	000	−0082(5)	434(33)	0
	¼	¼	278(31)	−229(33)
	−038	−0058(10)	540(40)	0
H_w[b]		−036(9)	135(51)	
		174(4)		
		−072(6)		
N	134	1436(5)	463(29)	−29(25)
	000	0005(6)	319(28)	−73(28)
	639	6587(8)	425(30)	46(25)
HN(1)[b]		180(8)	164(66)	
		−036(13)		
		545(11)		
HN(2)[b]		183(8)	141(62)	
		−016(13)		
		779(10)		
HN(3)[b]		078(5)	316(165)	
		−016(13)		
		669(19)		
HN(4)[b]		133(10)	157(73)	
		101(3)		
		642(18)		

[a] Positional parameters ($\times 10^3$) from ref. 24 converted to match the present set.

[b] Positional parameters ($\times 10^3$); isotropic temperature factors $U_{iso} \times 10^3$.

implies that individual $\bar{d}$ for neighbouring CN,ϵ combinations may be statistically indistinguishable.

As far as the goodness of fit is concerned, the price to pay for approximating D(M—Cl) by a single equation, and the coefficients c_i by a two-term quadratic in r_M, is the relatively high σ, which amounts to ~3% of the D spread. Separate regressions of D on CN and ϵ for each M resulted in lower σ's (0.013, 0.014, 0.003, and 0.008 Å for Al, Fe, In, and Tl, respectively), and it is possible (although we have not investigated this) that the c_i could be approximated more closely by another function of r_M.[26] For In in particular the individual regression gave a noticeably better fit, though this improvement may be without physical significance (see below).

The simplicity of eq. [1] has the advantage of bringing to light the effects of CN and ϵ in a straightforward manner (Table 7). The effect of CN decreases and that of ϵ increases from Al to Tl; the effect of CN relative to that of ϵ, i.e. the ratio $\lvert c_{CN}/c_\epsilon \rvert$, decreases from ~3.8 for Al to ~1.4 for Tl. The CN is thus always a more important factor than ϵ in determining the variation in D; it becomes dominant when the M atom is small.

The five c_{CN} values obtained in the separate regressions, i.e. without involving r_M, could be represented as $c_{CN} = k_{CN,0} + k_{CN,2}r_M^2$ to a high degree of correlation ($r^2 = 0.98$, σ = 0.0025), hence the two-term quadratic must be a good local approximation function and its inclusion in the triple regression is justified. The variation of c_{CN} with r_M^2 can be interpreted as a dependence of c_{CN} on the "effective surface area" of the atom M: the larger M, the less D varies with CN. If the expression for c_{CN} in Table 7 held past Tl, it would imply that in $[YCl_n]^{3-n}$ ($n \leq 6$) complexes D would be independent of n.

Is a linear *approximation of* D *appropriate over the entire CN, ϵ range?*

The functional dependence of D on CN and ϵ, and hence the suitability of the linear approximation, could be investigated properly only if a D value were available for every point of the CN,ϵ lattice of Fig. 4. The covering of the lattice is, however, quite incomplete, only about 40% for Fe and less for the other M, for many of the CN,ϵ combinations are not accessible under ordinary chemical conditions and of those that are accessible some have not been investigated structurally. For example, very little information exists on species such as $[MCl_{4-n}X_n]^\epsilon$ (n = 1–3) or $[MCl_{3-n}X_n]^\epsilon$ (n = 1, 2), where X is not a halogen; $AlCl_6^{3-}$ does not appear to form; seven-coordinate indium in halogeno complexes occurs only in combination with fluorine; MCl_2^+ and MCl^{2+} have not been reported.[27] However, some assistance comes from SCF calculations for the chemically inaccessible species of interest here. At present, calculations at the 6-31G* level (lowest-level basis set deemed adequate for realistic comparisons with experiment) have been found practicable only for free $[AlF_n]^\epsilon$ ($n \leq 6$) and $[AlCl_n]^\epsilon$ ($n \leq 4$) species. Within this limitation, optimized d values are now available for $\epsilon = 3 - n$ and for a number of other ϵ values as well.[22]

The $\bar{d}_{SCF}$ values[28] for $[AlF_n]^{3-n}$ and $[AlCl_n]^{3-n}$ are compared in Fig. 5 with the D and D_{calcd} values. Two experimental values are available to check the validity of the Al–F set, d = 1.63(1) Å for free AlF_3 (cf. ref. 149) (smoothed to 1.627(8) Å, see above) and D = 1.807(1) Å for $[AlF_6]^{3-}$ (146), and two for the Al–Cl set, d = 2.068(4) Å for free $AlCl_3$ (cf. ref. 149) (smoothed to 2.077(8) Å, see above) and D = 2.125(9) Å for $[AlCl_4]^-$ (Table 5). As pointed out above, the d for AlF_3

[26] The quadratic approximations obviously are valid only locally, in the limited range of r_M, for r_M does not increase indefinitely.

[27] Formation of $FeCl_2^+$ and $FeCl^+$ in gas-phase reactions has been detected by mass spectrometry (150), but no other information on these species is available.

[28] Except for n = 5, all the d values in an $[AlX_n]^{3-n}$ complex are identical, i.e. $d = \bar{d}$; for n = 5, $\bar{d} = \frac{3}{5}d_{eq} + \frac{2}{5}d_{ax}$.

Can. J. Chem. Downloaded from www.nrcresearchpress.com by 72.64.146.136 on 09/07/12
For personal use only.

Can. J. Chem. Downloaded from www.nrcresearchpress.com by 72.64.146.136 on 09/07/12
For personal use only.

and $AlCl_3$ are in excellent agreement with the $\bar{d}_{SCF}$ values, 1.621 and 2.077 Å, respectively. However, the $\bar{d}_{SCF}$ values for $[AlF_6]^{3-}$ and $[AlCl_4]^-$, 1.857 and 2.169 Å, respectively, are about 0.05 Å above the corresponding D. Although the uncertainty in $\bar{d}_{SCF}$ is difficult to estimate, it is highly probable that the discrepancy has its cause in the experimental bond-length values and can be attributed, at least in part, to the effect of thermal motion. The $\bar{d}_{SCF}$ values are to be compared with the fully corrected $\bar{d}$ values in the crystal, whereas the D are the means of *uncorrected* $\bar{d}$ values.[29] For $[AlCl_4]^-$ the magnitude of the correction has been considered in detail by Mairesse *et al.* (151), who found that the uncorrected Al—Cl bond lengths in $A[AlCl_4]$ (A = Li, Na, K, Cs, NH_4, NO)[30] were increased by as much as 0.05 Å, depending on the model (rigid-body or riding motion), the particularities of the crystal structure, and the inclusion of absorption correction. The corrected Al—Cl bond lengths averaged 2.156(6) Å for the rigid-body model and 2.146(3) Å for the riding-motion model. When a correction of this order is applied to $D(AlCl_4^-)$, the difference between D and $\bar{d}_{SCF}$ disappears, hence the $\bar{d}_{SCF}$ curve of Fig. 5 for Al—Cl may be regarded as consistent with observation. The $[AlF_6]^{3-}$ ion presents more difficulty. Here the correction for thermal motion has been found to amount to only about 0.005 Å (146); the reasons for the residual difference of ~0.04 Å between D and $\bar{d}_{SCF}$ are not fully understood at present.[31]

The important feature in Fig. 5 is the *shape* of the $\bar{d}_{SCF}$ curves. The Al—F curve becomes quasi-linear past CN 4, and the shape of the Al—Cl curve suggests that this curve, too, becomes quasi-linear in the CN 4–6 range. The two lines are roughly parallel, and their quasi-linear portions are roughly parallel to the D_{calcd} lines. This provides circumstantial support for our initial assumption that $D(CN,\epsilon)$ can be approximated by a linear function of CN and ϵ for CN $\geq$ 4. At CN 3 the faithfulness of the linear approximation begins to deteriorate, and at CN < 3 a nonlinear regression function would be required.

While the mean bond length D agrees quite well with D_{calcd} (Fig. 4), the individual $\bar{d}$, and even more the individual d, bond lengths may deviate from D_{calcd} appreciably. The largest and the smallest d implicit in D are indicated in Fig. 4 by the lengths of the bars associated with the D points. The high–low spread of d for a particular CN,ϵ combination may amount to as much as 0.17 Å, i.e. ~10σ of the D regression. It is most pronounced in *mer*-MCl_3X_3 complexes, where in an extreme case, that of [*mer*-$GaCl_3$(terpy)] (89), the difference between the d involving a *trans*-Cl and the d involving the middle Cl amounts to 0.168(4) Å, i.e. the difference in that complex alone accounts for the maximum spread in d shown in Fig. 4. The $\bar{d}$ spread in *cis*/*trans* pairs is smaller, less than ~0.06 Å or ~4σ of the D regression: 0.056(23) Å for $[FeCl_2(H_2O)_4]^+$ (79, 83), and 0.024(4) Å for Al and 0.048(8) Å for Ga in the [*cis*-$MCl_2(bipy)_2$]/[*trans*-$MCl_2(py)_4$] pairs (80, 81, 85, 86). High–low d spread of ~3σ or more is also noted in $[MCl_5(H_2O)]^{2-}$, [*cis*-$FeCl_2$(PIH)(H_2O)]$^+$ (153), and α-Tl_3TlCl_6 (65).

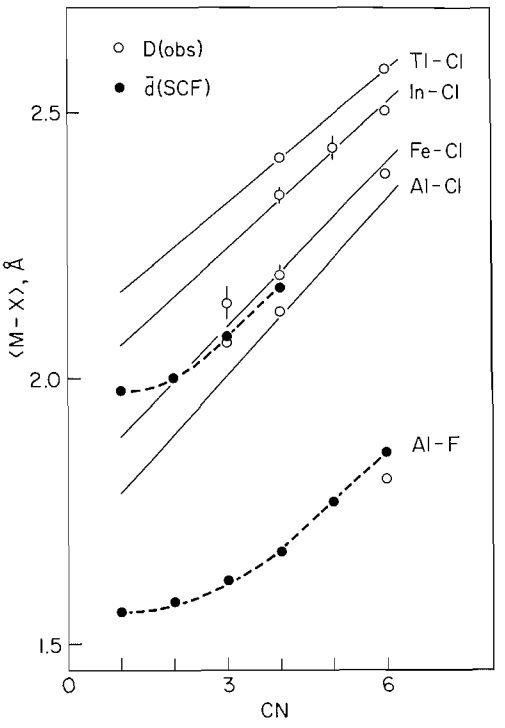

FIG. 5. Comparison of D, D_{calcd}, and $\bar{d}_{SCF}$ values for $[AlF_n]^{3-n}$ and $[MCl_n]^{3-n}$ (M = Al, Fe, In, Tl) complexes. The straight lines represent D_{calcd}; the broken lines indicate the trends in the $\bar{d}_{SCF}$ series for Al—Cl and Al—F. The d and $\bar{d}_{SCF}$ points for $[AlF_3]^0$ are not distinguishable on the scale of this drawing.

Binuclear complexes

The complexes so far considered have been almost all mononuclear in M(III). In *isolated* binuclear chloro complexes the terminal M—Cl bonds are shorter than the bridging M—Cl bonds, typically by about 0.2 Å,[32] but the number of reliable determinations is too small to permit a detailed treatment. Complexes for which bond lengths are available are the MCl_3 dimers [di-μ-$Cl_2MCl_2MCl_2$]^0 (also electron diffraction data for the gas phase); the [tri-μ-$Cl_3MCl_3MCl_3$]$^{3-}$ ions; and the [di-μ-Tl_2Cl_{10}]$^{4-}$ ion in $K_2TlCl_5 \cdot 2H_2O$ (134). While the CN of the M atom is clearly defined, it is not self-evident what *charge* is appropriate when using eq. [1] to evaluate D_{calcd}. Since changing ϵ by one unit produces a change in $\bar{d}$ of only about 0.025 Å, the bond lengths must be known with good accuracy if one is to determine the formal charge to be used. Examination of the $\bar{d}$ values for the above binuclear complexes shows that the best agreement between $\bar{d}$ and D_{calcd} is obtained when the complex $[Cl_xMCl_yMCl_x]^{6-2x-y}$ is partitioned in such a way that the mononuclear entity is $[Cl_xMCl_y]^{3-x-y}$, CN = x + y; i.e. $[M_2Cl_6]^0 \rightarrow MCl_4^-$, $[M_2Cl_9]^{3-} \rightarrow MCl_6^{3-}$, and $[M_2Cl_{10}]^{4-} \rightarrow MCl_6^{3-}$. The agreement between $\bar{d}$ and D_{calcd} is good for Ga_2Cl_6, Fe_2Cl_6, $[In_2Cl_9]^{3-}$, and $[Tl_2Cl_{10}]^{4-}$, and also for $[Y_2Cl_9]^{3-}$ (97) if $r^{iv}(Y^{3+})$ is taken as 0.72 Å. It is less good for Al_2Cl_6.

Conclusions

In sum, eq. [1] is capable of reproducing the mean uncor-

[29]The Tl—Cl bond lengths determined for $TlCl_4^-$ and $TlCl_6^{3-}$ *in solution* (152) agree with the corresponding bond lengths in crystals corrected for thermal motion.

[30]All of these are included in the D of $AlCl_4^-$ in Table 5.

[31]The $\bar{d}_{SCF}$ value for $[AlF_6]^{3-}$ may in fact be an overestimate. In general, larger basis sets are required to calculate the equilibrium geometries of anions to the same accuracy as obtained for neutral molecules with smaller basis sets. Within a series of anions, a given basis set is expected to become less adequate as the charge increases, with the resulting progressive overestimation of bond lengths.

[32]As pointed out in ref. 149, $d_{terminal}$ in free M_2X_6 dimers is the same as d in free MX_3, for which CN,ϵ = 3,0.

TABLE 9. $(NH_4)_2[InCl_5(H_2O)]$: bond distances (Å) and angles (deg)

Atoms	Distance: This work[a]	Distance: Ref. 24	Atoms	Angle
In—Cl(1)	2.484(2)/10	2.52	Cl(1)—In—Cl(2)	90.92(5)
In—Cl(2)	2.476(1)/8	2.71	Cl(1)—In—Cl(3)	178.79(5)
In—Cl(3)	2.466(2)/10	2.59	Cl(1)—In—Cl(4)	89.17(5)
In—Cl(4) 2×	2.491(2)/8	2.57	Cl(1)—In—O	90.09(13)
In—Cl mean[b]	2.480(9)/10	2.59(7)	Cl(2)—In—Cl(3)	90.30(5)
In—O	2.229(5)/8	2.23	Cl(2)—In—Cl(4)	93.95(5)
O···Cl(4B)	3.148(5)	3.11	Cl(2)—In—O	178.99(13)
H_w···Cl(4B)	2.18(7)		Cl(3)—In—Cl(4)	90.75(6)
			Cl(3)—In—O	88.70(13)
			Cl(4)—In—Cl(4′)	171.96(6)
			Cl(4)—In—O	86.07(13)
			O—H_w—Cl(4B)	172(6)

[a]Number after oblique stroke: correction to be added ($\times 10^3$, rigid-body motion model).
[b]Weighted by σ^{-2}.

rected M—Cl bond lengths D in the $[M(III)Cl_nX_m]^\epsilon$ complexes studied to date to about 0.02 Å, regardless of the nature of X, except when X forms an M—C bond. In that case the M—Cl distance increases with m, adding roughly 0.05 Å per X. Thus in $\{InCl[-2-(Me_2NCH_2)C_6H_4-]_2\}$ (32), d is 2.465(1) Å compared to $D(5,0)$ = 2.371(12) Å (Table 5) and $D_{calcd}(5,0)$ = 2.362(16) Å. Similarly, in $Me_4As[MeInCl_3]$ and $Me_4Sb[MeInCl_3]$, $\bar{d}$ = 2.401(7) Å (154), compared to $D(4,1-)$ = 2.346(13) Å and $D_{calcd}(4,1-)$ = 2.335(16) Å; and for Ga—Cl in $Me_4Sb[GaCl_{4-n}Me_n]$ (125), $\bar{d}$ = 2.172(30) Å for n = 0, 2.223 Å for n = 1, 2.277 Å for n = 2, and 2.381 Å for n = 3, compared to $D(4,1-)$ = 2.170(12) Å and $D_{calcd}(4,1-)$ = 2.178(16) Å. The reason for the lengthening of the M—Cl bond is to be looked for in the covalency of the M—C bond: the increase in $\bar{d}$ with n in the Ga complexes correlates with an increase in the Ga—C bond length, a decrease in the ESCA Ga(3d) ionization potential, and an increase in the relative negative charge on the Ga atom (125).

Perhaps the most useful feature of the regression exemplified by eq. [1] is that in D_{calcd} it provides a hitherto lacking but much needed reference standard for judging the "normalcy" of experimental M—Cl bond lengths in $[M(III)Cl_nX_m]^\epsilon$ complexes. The validity of this standard will improve as the sample on which the D values of Table 5 are based becomes chemically and structurally more representative: the present sample reflects both the vagaries of, and changes in emphasis in, the natural accumulation of structural information. The composition of the existing sample (Tables 1 and 6[24]) may serve to show where further work is needed.

Before recalculating the D regression at some future date consideration might be given to the possibility of finding an $r^{iv}(M^{3+})$ set that would suit the purpose better than Shannon's set. One should keep in mind that $r^{iv}(M^{3+})$ as used in eq. [1] is merely an artificial parameter introduced to order the M^{3+} according to their relative contribution to the M—Cl bond length in a particular $[MCl_n]^{3-n}$ series, irrespective of the actual CN, even though for CN 4 it has direct relevance for tetrahedral species. In this context it will be desirable to investigate the effect of the spin state of Fe^{3+} on this parameter and on D calculated from the regression equation.

C. Crystal structures of the title compounds

Crystal data of the four compounds will be found in Table 2. Details of the structure determinations are described in Experimental at the end of this paper.

$(NH_4)_2[InCl_5(H_2O)]$

The only ternary compound in the system NH_4Cl–$InCl_3$–H_2O at 25°C is stated (139) to be $(NH_4)_2InCl_5 \cdot H_2O$, therefore not surprisingly it was a product of this composition that was obtained by crystallization from an aqueous solution of NH_4/In = 2 at room temperature. A determination of the crystal structure by photographic methods was reported in 1948 (24), but as it yielded In—Cl distances longer than 2.5 Å, a redetermination was indicated.

The hydrogen atoms were located from a difference Fourier map. The only constraint applied in the refinement was to the N—H and O—H bond lengths, 1.02 and 0.98 Å, respectively, and to the HNH and HOH angles.

As would be expected, the atomic positions in this structure (Table 8) are very similar to those in the K salt (22). The σ^{-2}-weighted mean of the In—Cl distances, 2.480(9) Å, is indistinguishable within 1σ from that for the K salt, 2.482(7) Å, and the In—O distances are the same within 3σ (Table 9). The hydrogen-bonding system (Table 10) is illustrated in Figs. 6 and 7. Each two neighbouring $InCl_5(H_2O)$ octahedra not on the same mirror plane are linked together by two strong and almost straight O—H_w···Cl(4) bonds (related by a centre of symmetry) to form infinite zigzag chains $\| b$ (Fig. 6*A*). These chains are cross-linked by N—H···Cl bonds (Fig. 6*B*), with H···Cl distances ranging from 2.52(11) Å to ~3.2 Å (corresponding to NHCl > 90°) (Fig. 7). Each Cl atom is an acceptor of at least four hydrogen bonds (Table 10). All the N—H···Cl bonds are asymmetrically bifurcated, although additional, more distant Cl atoms probably participate as weak partners in these bonds.

$(NH_4)_2[InCl_5(H_2O)]$ is isostructural with its Fe analog (136), but the orientation of the ammonium ion is slightly different, the result being that the hydrogen-bonding features in the two compounds are not identical. Direct comparison of H···Cl distances and NHCl angles is not possible, as the N—H distances in the refinement of the Fe compound were not constrained and the reported apparent bond lengths are as short as 0.78(5) Å. When the N—H distances in the structure of ref. 136 are adjusted to 1.02 Å by extending the N—H vectors,

Can. J. Chem. Downloaded from www.nrcresearchpress.com by 72.64.146.136 on 09/07/12
For personal use only.

Can. J. Chem. Downloaded from www.nrcresearchpress.com by 72.64.146.136 on 09/07/12
For personal use only.

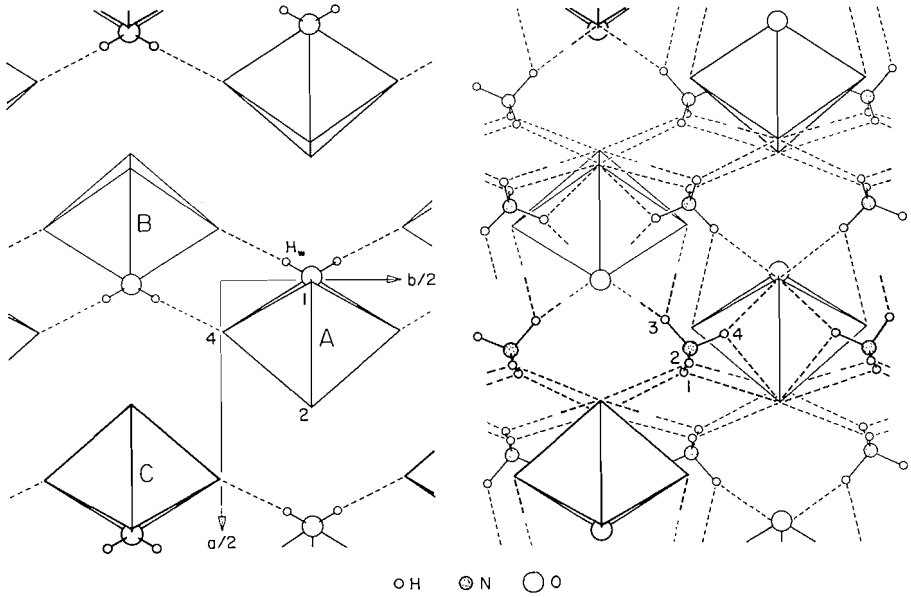

FIG. 6. $(NH_4)_2[InCl_5(H_2O)]$: projection of a portion of the structure on (001). *A* (*left*), the O—H_w···Cl bond system. *B* (*right*), the N—H···Cl bond system. Hydrogen bonds are indicated by broken lines.

TABLE 10. $(NH_4)_2[InCl_5(H_2O)]$: N···Cl and H···Cl distances (Å) and NHCl angles (deg)[a]

HN	Cl	N···Cl[b]	H···Cl[c]	NHCl[d]
1A	3C	3.562	2.69	143
	4A	3.462	2.84	119
	4C	3.523	3.18	101
	2A	3.461	3.22	95
2A	2C	3.400	2.68	127
	3Aa	3.334	2.93	104
	4C	3.523	3.05	109
	4Aa	3.774	3.08	126
3A	1Ba	3.357	2.52	138
	4Ba	3.642	2.80	140
	1A	3.492	3.24	95
4A	1A	3.492	2.69	135
	2A	3.461	2.83	120
3Ba	1A	3.357	2.52	138
4A		3.492	2.69	135
3A		3.492	3.24	95
2Cb	2A	3.400	2.68	127
4A		3.461	2.83	120
1A		3.461	3.22	95
1Cb	3A	3.562	2.69	143
2Ab		3.334	2.93	104
H_w(B)	4A		2.18(7)	
3Ba		3.642	2.80	140
1A		3.462	2.84	119
2Cb		3.523	3.05	109
2Ab		3.774	3.08	126
1Cb		3.523	3.18	101

[a]Symmetry code: A, x, y, z; B, $-x, -y, -z$; C, $\frac{1}{2} - x, -y, \frac{1}{2} + z$; a, $X + (0, 0, 1)$; b, $X + (0, 0, -1)$.
[b]esd = 0.006 Å.
[c]esd ~ 0.11 Å.
[d]esd ~ 7°.

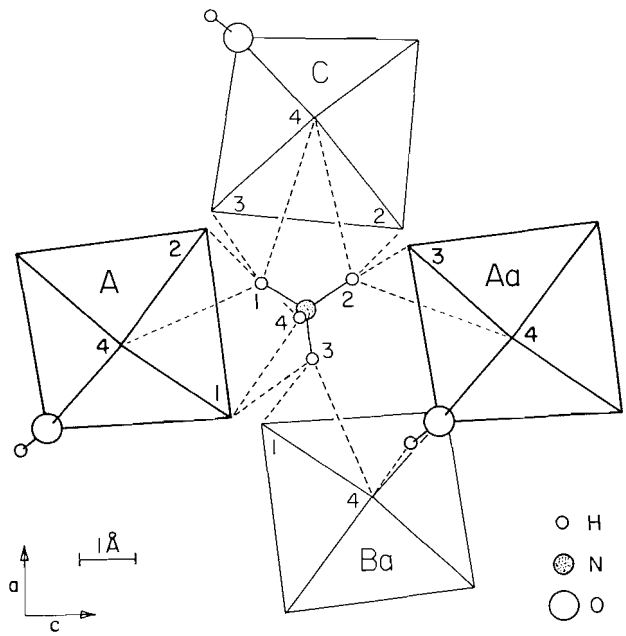

FIG. 7. $(NH_4)_2[InCl_5(H_2O)]$: environment of the ammonium ion (projection on (010)). For symmetry code and H···Cl distances and NHCl angles see Table 10. The H(4)···Cl(2A) bond is partially omitted for clarity.

the corrected H···Cl distances and NHCl angles are seen to be distributed somewhat differently from those in the In salt (Fig. 8). They follow the same trend but the overall H_N-bonding scheme seems to be somewhat stronger in the Fe compound. In both crystals the shortest H_N···Cl distance is H(3A)···Cl(1Ba); the O—H···Cl(4) bond has practically the same geometry.

Detailed comparison of the (uncorrected) bond lengths and angles in the MCl_5O octahedron in the NH_4In, NH_4Fe (136),

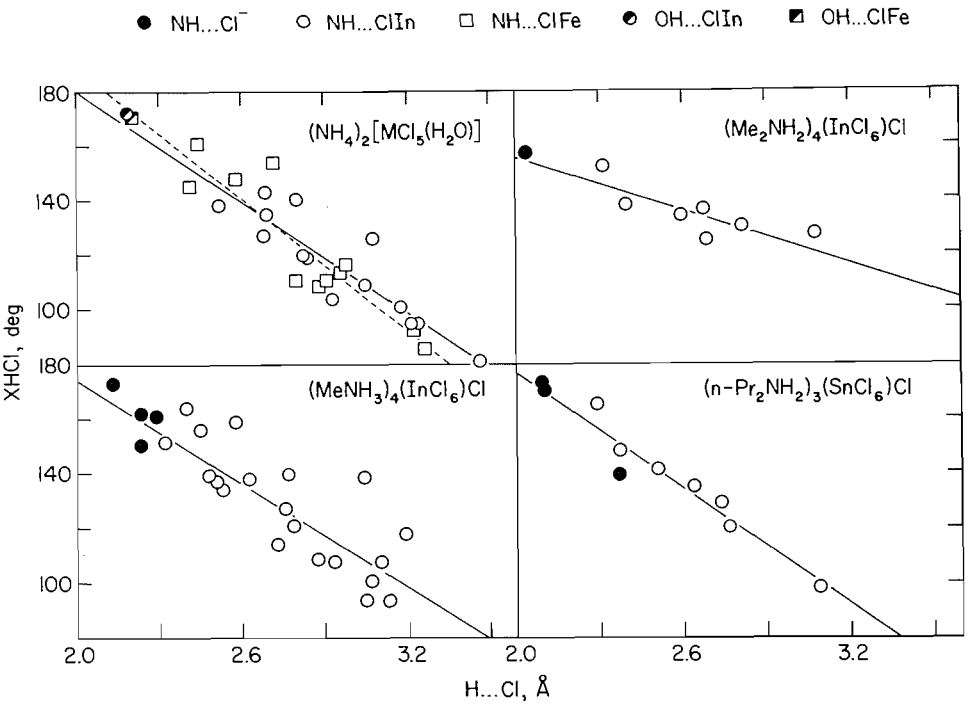

FIG. 8. Variation of the XHCl angle with the H···Cl distance in $(NH_4)_2[MCl_5(H_2O)]$ (solid regression line, M = In; broken regression line, M = Fe, from data of ref. 136, see text), $(MeNH_3)_4[InCl_6]Cl$, $(Me_2NH_2)_4[InCl_6]Cl$, and $(n\text{-}Pr_2NH_2)_3[SnCl_6]Cl$ (from ref. 148).

and KIn (22) salts reveals that, apart from an overall shortening of the bond lengths by about 0.12 Å in the NH_4Fe salt, the octahedra in the two ammonium salts are dimensionally closely similar, while significant differences in some of the angles exist between NH_4In and KIn. This indicates that the geometry of the octahedron is affected more by the N—H···Cl bonding than by any possible differences resident in the central atom.

The ir spectra of the H-containing entities in $(NH_4)_2[InCl_5(H_2O)]$ will be reported elsewhere (cf. ref. 155).

$K_3InCl_6 \cdot nH_2O$

The hydrates reported to exist in the system $KCl–InCl_3–H_2O$ correspond to K/In ratios of 2 and 3. The existence of $K_2InCl_5 \cdot H_2O$ is well established (18, 20, 21, 23, 55, 139, 156), but the K/In = 3 phase has been formulated variously as $K_3InCl_6 \cdot H_2O$ (18, 27, 28), $K_3InCl_6 \cdot \frac{3}{2}H_2O$ (157, 158), and $K_3InCl_6 \cdot 2H_2O$ (139, 159). In addition, a material analyzing to $K_2InCl_5 \cdot 2H_2O$ and dehydrating to $K_2InCl_5 \cdot H_2O$ when heated to 150°C, is stated (23) to have been obtained by evaporation of an aqueous solution of the chlorides (K/In = 2) at room temperature. Being curious about the mode of incorporation of the extra molecule of water in the structure of this dihydrate, we repeated the preparation as closely as the description in ref. 23 permitted, even though a phase of this composition had not been found in the ternary system at room temperature (20, 139).

The first crop of crystals was dried carefully by repeated pressing between layers of filter paper and then in air until the crystals were completely free-flowing. Structure analysis on a crystal selected from this visually uniform crop was carried, without prejudice as to composition, to $R = 11\%$. At this stage 14 octahedrally coordinated In atoms were identified in the tetragonal unit cell, plus a number of atoms taken to be potassium. The In atoms in 8(*c*)–*xxz* etc. and 4(*b*)–$0\frac{1}{2}z$ etc. formed isolated $InCl_6$ anions, while those in 2(*a*)–00*z* etc. appeared to be inside $InCl_5O$ octahedra. These features, the unit-cell dimensions and the unusual *Z* value showed that the compound had to be either identical with or closely similar to the $K_3InCl_6 \cdot H_2O$ of Wignacourt *et al.* (18, 27) (Table 2). This salt was formulated as $K_{21}[InCl_6]_4[InCl_6]_2[InCl_5(H_2O)]Cl \cdot 6H_2O$ and related to the dimensionally similar $K_3TlCl_6 \cdot 2H_2O$, for which a structure had been proposed many years ago by Hoard and Goldstein (160). The K/In ratio of our product being consistent with the expectation from the phase diagram and not 2:1, it was clear that the conditions leading to $K_2InCl_5 \cdot 2H_2O$ would have to be stated much more explicitly than in ref. 23 for the duplication to succeed, and we did not pursue the preparative efforts further. However, the structure proposed in refs. 18 and 27 was of such an unexpected complexity that we thought it worthwhile to verify the structure of our compound in detail, especially in view of the conflicting reports as to the degree of hydration of the K/In = 3 chloride.

The positions of the $InCl_6$ and $InCl_5O$ octahedra and of the K(1) to K(5) atoms being virtually the same in both cases (Table 11,[24] Fig. 9), we placed the remaining nonhydrogen atoms as in refs. 18 and 27 (cf. Fig. 10). The isotropic refinement converged at $R = 9.2\%$, but a number of discrepancies became evident. The K(6) atom in 2(*a*) and the O(2) atom in 8(*d*),[33] both at half occupancy, did not refine properly, giving unsatisfactory temperature factors and leaving residual electron density in a difference map. Furthermore, repeated density measurements on our material gave values consistently higher than quoted in ref. 27 but close to 2.483 reported for $K_3InCl_6 \cdot 2H_2O$ by Wallace (159).

Wignacourt (18), in addition to $K_3InCl_6 \cdot H_2O$, also determined the structure of $K_3InBr_6 \cdot \frac{3}{2}H_2O$ ($R = 7.5\%$) and redetermined the structure of $K_3TlCl_6 \cdot 2H_2O$ ($R = 4.0\%$), taking the water content of the Tl compound to be $\frac{3}{2}H_2O$

[33] Numbering as in refs. 18 and 27.

Can. J. Chem. Downloaded from www.nrcresearchpress.com by 72.64.146.136 on 09/07/12
For personal use only.

Can. J. Chem. Downloaded from www.nrcresearchpress.com by 72.64.146.136 on 09/07/12
For personal use only.

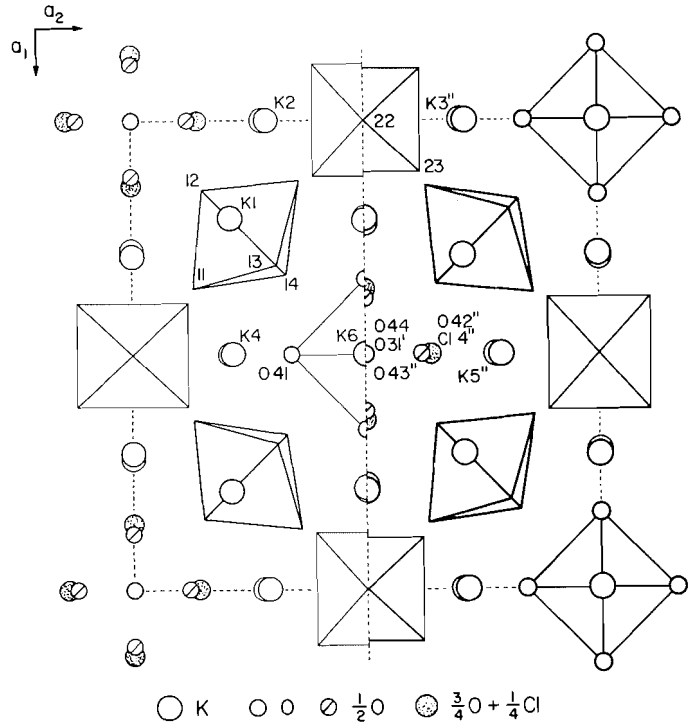

FIG. 9. $K_3InCl_6 \cdot nH_2O$: projection of the lower (*left*) and the upper (*right*) half of the unit cell on (001). X, *xyz*; X′ is related to X by bc translation; X″ is related to X by rotation about C_4. The octahedra are projections of $In(1)Cl_6$, $In(2)Cl_6$, and $In(3)Cl_5O$, respectively.

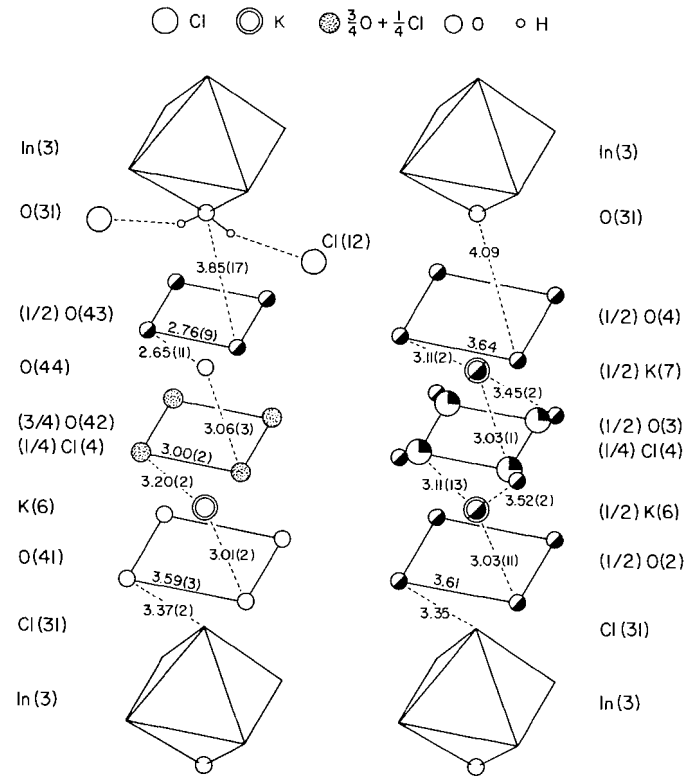

FIG. 10. $K_3InCl_6 \cdot nH_2O$: atoms on or closest to the C_4 axis defined by $(\frac{1}{2}, \frac{1}{2}, z)$ (Table 15). (*Left*), this work; (*right*), ref. 27.

TABLE 12. Number of water molecules in tetragonal A_3MX_6 (A = In, Tl) hydrates

	Number of water molecules					
Reference	KInCl	KInBr	KTlCl	NH_4TlCl	KTlBr	RbTlBr
157	$\frac{3}{2}$[a]	—	—	—	—	—
161	—	—	2	2	—	—
158	$\frac{3}{2}$[a]	—	2[a,b]	—	—	—
162	—	—	—	2	1	~1.3[a]
141	—	—	2[c]	0[d]	—	—
159	~1.8[a]	(2)[e]	2[a]	2[a]	—	2[a]
160	—	—	2	—	—	$\frac{8}{7}$
139	2	—	—	—	—	—
111	—	—	—	1	—	—
27	1	1	2	—	—	—
163	—	—	$\frac{13}{7}$	—	—	$\frac{13}{7}$
18	1	$\frac{3}{2}$	$\frac{3}{2}$	—	—	—
20	1[a]	$\frac{3}{2}$	—	—	—	—

[a]Analyzed for water.
[b]But mixed crystals $K_3(Tl, In)Cl_6$, Tl/In ~ 4, contained $\frac{3}{2}H_2O$.
[c]From solutions with K/Tl ≥ 3.
[d]From solutions with NH_4/Tl > 1.
[e]In the air the crystals lost water so rapidly that crystal measurements were not possible; water could not be determined.

and assuming that both compounds were isostructural with $K_3InCl_6 \cdot H_2O$.[34] The differences in the degree of hydration of these hexahalides suggested to us that some of the discrepancies we observed could be due to a difference in the water content.

Examination of the literature evidence bearing on the water content (Table 12), the axial ratio (Table 13) and the density (Table 14) of tetragonal A_3MX_6 (M = In, Tl; X = Cl, Br) hydrates indeed supports the view that some of the water in these crystals is zeolitic and can be lost by spontaneous dehydration at room temperature (cf. in particular KInBr, Table 12). It also suggests that these hydrates can be formulated as $A_3MX_6 \cdot nH_2O$, $1 \leq n \leq 2$. The loss of water appears to be reflected in the c/a ratio (cf. KInCl, Table 13) and significantly affects the density (Table 14). We therefore concluded that our crystal had essentially the structure proposed in ref. 27 but a higher water content.

The highest peak in a difference map which was computed with Wignacourt's O(2), O(3), Cl(4), K(6), and K(7) omitted, was at the 2(*a*) position corresponding to K(6). The strength of the peak in the 2(*a*) position corresponding to K(7) was less than 2/3 of the highest peak. Similarly, the strength of the peak corresponding to O(2) in 8(*d*) was about twice that of the peak corresponding to O(4) in 8(*d*). This, combined with consideration of stoichiometry and interatomic distances, led us to the following modification of Wignacourt's model (Table 15, Fig. 10):

The O(4) atom is in 8(*d*) at half occupancy as O(43) (renamed). K(6) is in 2(*a*) with full occupancy; this satisfies the potassium stoichiometry for K_3InCl_6. Wignacourt's K(7), in

[34]The composition of the bromide was established from a phase equilibrium study of the system KBr–$InBr_3$–H_2O at 21°C (18); it is not clear how the water content of the Tl compound was arrived at. In ref. 27 the compositions of these two hydrates are stated as $K_3InBr_6 \cdot H_2O$ and $K_3TlCl_6 \cdot 2H_2O$. The presence of a $[TlCl_5(H_2O)]^{2-}$ ion in the K_3TlCl_6 hydrate crystal was suggested on Raman evidence already in ref. 76, although possibly on grounds that may not be valid (cf. ref. 18).

TABLE 13. Axial ratio c/a of tetragonal A_3MX_6 hydrates of Table 12

	c/a					
Reference	KInCl	KInBr	NH_4InCl	KTlCl	NH_4TlCl	RbTlBr
161	—	—	—	—	1.1249[a]	—
158	1.1578[a]	—	—	1.1191[a,b]	—	—
162	—	—	—	—	—	1.1417[a]
159	1.1558[a]	—	—	1.1230[a]	1.1451[a]	1.1367[a]
160	—	—	—	1.1366(27)	—	1.1475(65)
47	1.139 (α)	—	1.190	—	—	—
27	1.1492(18)	—	—	—	—	—
18, 20	—	1.1433(8)	—	1.1426(8)	—	—
[c]	1.1563(9)	—	—	—	—	—

[a]Converted from the axial ratio obtained from crystal measurement.
[b]1.1277 for $K_3(Tl, In)Cl_6$, Tl/In ~ 4.
[c]This work.

TABLE 14. Density of tetragonal A_3MX_6 hydrates of Table 12[a]

	Density				
Reference	KInCl	KInBr	KTlCl	NH_4TlCl	RbTlBr
159	2.483	[3.140][b]	2.859	2.389	4.077
	—	—	—	—	—
	—	—	—	—	—
47	—	—	—	—	—
	2.432 (α)	—	—	—	—
	2.341 (α)	—	—	—	—
160	—	—	2.90(10)	—	—
	—	—	2.935(11)	—	4.06(3)
	—	—	2.842(11)	—	3.99(3)
27	2.420	—	—	—	—
	2.503(17)	—	—	—	—
	2.409(16)[c]	—	—	—	—
18, 20	—	3.34	2.90	—	—
	—	3.348(4)	2.921(3)	—	—
	—	3.267(4)	2.828(3)	—	—
[d]	2.49(2)	—	—	—	—
	2.518(10)	—	—	—	—
	2.424(10)	—	—	—	—

[a]First line, ρ_o; second line, ρ_c for a dihydrate; third line, ρ_c for a monohydrate; in g/cm^3.
[b]See footnote *e* of Table 12.
[c]Our recalculation; ref. 27 gives 2.415.
[d]This work.

the second 2(*a*) position at half occupancy, is now replaced by O(44) at full occupancy, and O(2) = O(41) is in 8(*d*) at full occupancy. The remaining two Cl atoms, Cl(4), are placed in 8(*d*) in statistical disorder with O(3) = O(42), but while only four oxygens are accommodated in this equipoint in ref. 27, to agree with the composition $K_3InCl_6 \cdot H_2O$, up to six oxygens are located there now. The present model therefore contains six more water molecules, as O(41) and O(44), per unit cell plus an additional zero to two as O(42), compared with ref. 27. This corresponds to $1.43 \leq n \leq 1.57$.

The occupancy factors of O(41), O(43), O(44), and Cl(4) refined to values close to those assumed (Table 15). Placing 2Cl(4) + 4O(42) in the mixed 8(*d*) site left, on refinement, significant electron density in a difference map. The calculated crystal density for this occupancy is 2.464 g/cm^3, that for six O(42) is 2.477 g/cm^3, a difference of 0.013(4) g/cm^3. Since the measured density was 2.49(1) g/cm^3, we assumed full occupancy for the mixed site, i.e. $n = 1.57$.

All the atoms (hydrogens always excluded) were refined anisotropically. The final difference map showed a residual peak (of approximate strength 1 e/Å^3) very close to Cl(4), but attempts to resolve the O(42) from the Cl(4) position were unsuccessful. These two atoms were therefore refined together, yielding a final R of 5.7%.

The dimensions of the $In(1)Cl_6$ and $In(2)Cl_6$ octahedra agree well with those of ref. 27 (Table 16). The In(1)—Cl(12) bond in $In(1)Cl_6$ is significantly longer, by 0.076(14) Å, than the mean of the other five bonds, 2.501(11) Å, i.e. the distortion along the In(1)—Cl(12) axis is of approximately C_{4v} symmetry (Fig. 9). The lengthening of the In(1)—Cl(12) bond may be attributable to the hydrogen bond presumed to exist between Cl(12) and O(31). The orthorhombically distorted $In(2)Cl_6$ octahedron is

Can. J. Chem. Downloaded from www.nrcresearchpress.com by 72.64.146.136 on 09/07/12
For personal use only.

Can. J. Chem. Downloaded from www.nrcresearchpress.com by 72.64.146.136 on 09/07/12
For personal use only.

TABLE 15. $K_3InCl_6 \cdot nH_2O$: positional ($\times 10^4$) and thermal ($\times 10^3$) parameters of atoms for which comparison with ref. 27 requires comment[a]

	Reference 27[b]					This work				
Site	Atom	f	x y z	U_{11} U_{22} U_{33}	U_{12} U_{13} U_{23}	Atom	f	x y z	U_{11} U_{22} U_{33}	U_{12} U_{13} U_{23}
2(*a*)	K(6)	½	½ ½ 3618(7)	73(1) 73(1) 35(6)	0 0 0	K(6)	1	½ ½ 3623(16)	101(13) 101(13) 52(15)	0 0 0
2(*a*)	K(7)	½	½ ½ 6187(8)	136(10) 136(10) 36(7)	0 0 0	O(44)	1	½ ½ 6164(36)	106(39) 106(39) 24(34)	0 0 0
2(*a*)	O(1)	1	0 0 3907(7)	106(4) 106(4) 26(6)	0 0 0	O(31)	1	0 0 3982(24)	53(20) 53(20) 5(23)	0 0 0
8(*d*)	O(2)	½	½ 3378(6) 2711(5)	28(3) 61(6) 58(6)	0 0 40(4)	O(41)	1	½ 3381(21) 2727(17)	49(17) 66(19) 61(20)	0 0 32(15)
8(*d*)	O(3)	½	½ 3346(9) 4935(12)	71(10) 48(11) 41(8)	0 0 −5(10)	O(42)	¾	½ 3645(14) 4948(12)	47(10) 90(14) 21(8)	0 0 17(11)
8(*d*)	O(4)	½	½ 3362(15) 7149(11)	35(5) 108(13) 63(9)	0 0 −32(9)	O(43)	½	½ 3754(72) 7151(44)	57(39) 170(91) 67(50)	0 0 17(52)
8(*d*)	Cl(4)	¼	½ 3718(6) 4931(6)	48(4) 28(3) 21(3)	0 0 −2(3)	Cl(4)	¼	½ 3645(14) 4948(12)	47(10) 90(14) 21(8)	0 0 17(11)

[a]The z coordinates are referred to z[In(2)] = ½; f, site occupancy factor. Atoms O(42) and Cl(4) share the same equipoint.
[b]U_{ij} obtained from the β_{ij} of ref. 18.

TABLE 16. $K_3InCl_6 \cdot nH_2O$: bond lengths (Å) and angles (deg)

Atoms	Distance[a]	Δ[b]	Atoms	Angle
In(1)—Cl(11) 2×	2.490(7)/6	5	Cl(11)—In(1)—Cl(11′)	178.44(24)
Cl(12)	2.577(8)/6	−5	Cl(12)	89.89(24)
Cl(13)	2.512(8)/6	4	Cl(13)	89.23(24)
Cl(14)	2.516(8)/6	7	Cl(14)	90.12(24)
Cl(15)	2.498(8)/7	7	Cl(15)	90.77(25)
In(2)—Cl(21)	2.415(5)/6	12	Cl(12)—In(1)—Cl(13)	87.82(25)
Cl(22)	2.430(5)/6	9	Cl(14)	179.74(26)
Cl(23) 4×	2.543(7)/6	9	Cl(15)	91.64(26)
In(3)—Cl(31)	2.421(6)/9	3	Cl(13)—In(1)—Cl(14)	92.44(25)
Cl(32) 4×	2.514(6)/6	11	Cl(15)	179.46(27)
O(31)	2.146(44)/8	132[c]	Cl(14)—In(1)—Cl(15)	88.09(26)
			Cl(21)—In(2)—Cl(22)	180
In(1)—Cl mean	2.512(31)[d]	6(29)[e]	Cl(23)	90.42(20)
In(2)—Cl mean	2.483(62)[d]	29(62)[e]	Cl(22)—In(2)—Cl(23)	89.58(19)
In(3)—Cl mean	2.495(42)[d]	10(45)[e]	Cl(23)—In(2)—Cl(23′)	89.26(22)
			Cl(23″)	90.73(22)
			Cl(23*)	179.17(12)
			Cl(31)—In(3)—Cl(32)	95.40(20)
			O(31)	180
			Cl(32)—In(3)—Cl(32)	89.49(20)
			Cl(32′)	169.19(21)
			O(31)	84.60(42)

[a]Number after oblique stroke: correction to be added ($\times 10^3$, rigid-body motion model).
[b]$\Delta = [d(\text{ref. 27}) - d(\text{this work})] \times 10^3$ Å.
[c]esd of d[In(3) − O(31)] of ref. 27, 0.013 Å.
[d]Weighted by abundance and σ^{-2}.
[e]Weighted by abundance.

TABLE 17. $K_3InCl_6 \cdot nH_2O$: interatomic distances (Å)

Atoms	Distance	Δ^a
K(1)···Cl(23Ea) 2×	3.112(10)	19(2)
Cl(14Cc)	3.168(10)	−28(3)
Cl(13)	3.257(10)	9(3)
Cl(12)	3.300(10)	−19(3)
Cl(32) 2×	3.396(9)	0(1)
Cl(15Cc)	3.474(11)	−26(3)
K(2)···Cl(11D) 2×	3.135(9)	12(2)
Cl(32)	3.208(9)	17(3)
Cl(21)	3.251(8)	10(2)
Cl(12) 2×	3.302(10)	13(2)
Cl(23Bb) 2×	3.323(9)	3(3)
K(3)···Cl(22)	3.202(8)	17(2)
O(41Bd)	3.21(3)	−3(1)[b]
Cl(11Cc) 2×	3.231(9)	−7(2)
Cl(32)	3.235(8)	0(3)
Cl(14Cc) 2×	3.332(9)	8(2)
Cl(23Bb) 2×	3.365(9)	12(3)
K(4)···O(41)	2.68(3)	2(1)[b]
Cl(4), O(42)	3.17(2)	11(1)[b], −31(2)[b]
Cl(23D) 2×	3.303(10)	6(3)
Cl(13) 2×	3.353(10)	19(2)
Cl(21D)	3.379(8)	−6(2)
Cl(11) 2×	3.470(9)	−19(3)
K(5)···O(43)	2.96(7)	−45(2)[b]
Cl(4), O(42)	3.20(2)	12(1)[b], −28(2)[b]
Cl(15Bc) 2×	3.220(10)	32(2)
Cl(23D) 2×	3.280(10)	−2(3)
Cl(11Fc) 2×	3.340(9)	−3(3)
Cl(22D)	3.466(10)	−7(3)
K(6)···O(41) 4×	3.01(3)	2(1)[b]
Cl(4), O(42) 4×	3.20(2)	−9(13)[b], 32(2)[b]
O(31)···Cl(12) 4×	3.52(2)	−1[b]
O(43Af) 4×	3.85(17)	24[b]
O(41)···K(4)	2.68(3)	2(1)[b]
K(6)	3.01(3)	2(11)[b]
K(3Be)	3.21(3)	−3(1)[b]
Cl(14) 2×	3.25(3)	0[b]
Cl(31Ae)	3.37(3)	−2[b]
Cl(13) 2×	3.47(3)	3[b]
O(41D) 2×	3.59(3)	2[b]
O(42), Cl(4) ··· O(42D), Cl(4D) 2×	3.00(2)	68[b], −15[b]
O(42), Cl(4) ···O(44)	3.06(3)	39[b], −2[b]
O(42), Cl(4) ···K(4)	3.17(2)	−31(2)[b], 11(1)[b]
O(42), Cl(4) ···K(5)	3.20(2)	−28(2)[b], 12(1)[b]
O(42), Cl(4) ···K(6)	3.20(2)	32(2)[b], −9(13)[b]
O(43)···O(44)	2.65(7)	46(2)[b]
O(43D) 2×	2.76(9)	88[b]
K(5)	2.96(7)	−45(2)[b]
Cl(12Bc) 2×	3.19(7)	0[b]
Cl(15Cc) 2×	3.26(7)	−6[b]
O(44)···O(43) 4×	2.65(7)	46(2)[b]
O(42), Cl(4) 4×	3.06(3)	39[b], −2[b]

TABLE 17 (*concluded*)

Atoms					Distance
Symmetry code[c]					
A	x	y	z	a	X + (1, 0, 0)
B	x	$-y$	z	b	X + (0, 1, 0)
C	$-x$	$-y$	z	c	X + (½, ½, ½)
D	y	x	z	d	X + (−½, ½, ½)
E	$-y$	x	z	e	X + (½, ½, −½)
F	$-y$	$-x$	z	f	X + (−½, −½, −½)

[a] $\Delta = [d(\text{ref. 27}) - d(\text{this work})] \times 10^3$; values in parentheses, esd of ref. 27.
[b] $\times 10^2$.
[c] Where there is no letter designation, *xyz* are as per Tables 11 and 15.

compressed along the Cl(21)—Cl(22) axis, i.e. $\|c$; the difference between the equatorial and the axial bond lengths is 0.12(1) Å ~ 5%. These distortions contrast with the almost regular $InCl_6$ octahedral geometry in $(MeNH_3)_4[InCl_6]Cl$ and $(Me_2NH_2)_4[InCl_6]Cl$.

The K···Cl distances in the well-defined $K(1)Cl_8$, $K(2)Cl_8$, and $K(3)Cl_8O$ coordination polyhedra range from 3.11(1) to 3.47(1) Å (Table 17). Their mean, 3.27(10) Å, can be compared with the K^{viii}···Cl distances calculated from Shannon's ionic radii, 3.32 Å. The shortest of the K···Cl distances, K(1)···Cl(23Ea) = 3.11(1) Å, is shorter than the K^{vi}···Cl separation in KCl, 3.147 Å (Shannon's radii give 3.19 Å), but as the ionic charges in $K_3InCl_6 \cdot nH_2O$ are not symmetrically balanced, the distance is marginally still in the range expected. The mean difference between our K···Cl distances and those of refs. 18 and 27 is |0.013| Å, i.e. on the average within slightly more than one esd.

The shortest K···O distances to clearly defined oxygens, 2.68(3), 2.96(7), 3.01(3), and 3.21(3) Å, agree to within |0.03| Å with refs. 18 and 27 except for K(5)···O(43) = 2.96(7) Å. This distance in refs. 18 and 27, 2.51(2) Å, is far too short: K^{vi}···O_w in the alums $KM(SO_4)_2 \cdot 12H_2O$ (M = Al, Cr) is 2.94–2.97 Å, but the CN of K(5) is 8–9. The K(4)···O(41) distance, which is 2.68(3) Å in this work and 2.70(1) Å in refs. 18 and 27, is too short in both cases.

In the analysis of the single-crystal Raman spectrum of $K_3InCl_6 \cdot H_2O$ (28) it is pointed out that the chlorine closest to O(31) is Cl(12), at 3.51 Å (3.52(2) Å in Table 17) and that the $H_2O(31)$ molecule is therefore not involved in hydrogen bonding. However, if this molecule is oriented so that its hydrogens point symmetrically at the Cl(12) atoms (two equivalent positions are possible, Figs. 9 and 10), then $d(H \cdots Cl) \sim 2.60$ Å and O(31)H(31)Cl(12) ~ 156°. This implies that weak hydrogen bonding is possible and indeed likely (cf. Fig. 8), even though the H atoms have not been located by X-rays and spectroscopic evidence of the hydrogen bond is lacking. Given the low relative abundance of $H_2O(31)$ in the crystal (⅐ of the total water) and the incomplete resolution of the $\nu(H_2O)$ and $\delta(H_2O)$ features in the ir and Raman spectra, it is doubtful that features specific to $H_2O(31)$ could be distinguished in the spectra of ref. 28 and pertinent frequency comparisons made. The other water molecules in the crystal almost certainly participate in hydrogen bonding, but the

Can. J. Chem. Downloaded from www.nrcresearchpress.com by 72.64.146.136 on 09/07/12
For personal use only.

Can. J. Chem. Downloaded from www.nrcresearchpress.com by 72.64.146.136 on 09/07/12
For personal use only.

particulars of their involvement cannot be determined from the evidence at hand.

Although the main features of the $K_3InCl_6 \cdot nH_2O$ structure proposed by Wignacourt and confirmed here may be regarded as established, the exact distribution and location of the K^+, Cl^-, and H_2O constituents occurring in the columns with In(3)—O(31) as axes (Fig. 10) are still somewhat uncertain and, indeed, may vary with the overall water content of the crystal. The distribution we propose for our crystal is consistent with the X-ray evidence and has the polar character appropriate to the *I*4*mm* space group, but the distribution of charges is better balanced in Wignacourt's model for the monohydrate. It is unfortunate that the Rb and Cs analogs of $K_3InCl_6 \cdot nH_2O$ do not appear to exist. If they did, the location of K(6) (and Wignacourt's K(7)) could be established with considerably more confidence. Hoping that $Tl_3InCl_6 \cdot nH_2O$ *might* exist and be isostructural with the K compound, we attempted to obtain crystals of this chloride from aqueous TlCl + $InCl_3$ solutions with Tl/In ≥ 3 at room temperature. However, the crystals that formed were those of $Tl_2[InCl_5(H_2O)]$.

$(MeNH_3)_4[InCl_6]Cl$

This salt was originally described as tetragonal (38). Its structure was determined from visually estimated photographic intensities by Schlimper and Ziegler (12) (Table 2). Our redetermination, in the less oblique $P2/n$ setting, confirms their result in all but detail (Tables 18 and 19,[24] Fig. 11) and supplements it by establishing the hydrogen-bonding scheme. The hydrogen atoms were located from a difference Fourier map; the C—H and N—H bond lengths were constrained in the refinement to 1.08 and 1.02 Å, respectively, and the HCH and HNH angles to tetrahedral.

TABLE 18. $(MeNH_3)_4(InCl_6)Cl$: positional and thermal parameters ($\times 10^4$) of atoms other than hydrogen

Atom	x / y / z This work	x / y / z Reference 12[a]	U_{11} / U_{22} / U_{33}	U_{12} / U_{13} / U_{23}
In(1)	0	0	297(5)	22(4)
	0	0	179(5)	89(3)
	0	0	160(4)	−4(4)
Cl(11)	1582(1)	1578(5)	305(11)	9(12)
	0156(4)	0175(29)	494(15)	51(9)
	0630(1)	0630(8)	296(11)	11(12)
Cl(12)	−0126(2)	−0130(8)	455(14)	10(11)
	−2591(3)	−2606(23)	309(13)	132(10)
	0951(1)	0936(12)	166(11)	115(10)
Cl(13)	−0259(2)	−0262(8)	506(15)	25(11)
	2177(3)	2164(21)	334(13)	174(11)
	1105(1)	1110(11)	292(12)	−134(10)
In(2)	½	½	270(5)	11(4)
	0	0	186(4)	84(3)
	0	0	189(4)	9(4)
Cl(21)	5654(1)	5653(5)	398(12)	50(13)
	−0139(4)	−0158(30)	564(16)	43(9)
	1568(1)	1560(9)	187(10)	22(12)
Cl(22)	3976(2)	3978(9)	434(14)	181(12)
	2348(4)	2391(23)	398(14)	132(11)
	0265(2)	0266(14)	387(13)	−24(12)
Cl(23)	3973(2)	3976(10)	445(14)	−144(12)
	−2437(4)	−2460(24)	366(14)	151(11)
	0146(2)	0136(15)	398(13)	34(11)
Cl(1)	¼	¼	790(31)	0
	3786(7)	3681(41)	613(28)	−17(21)
	¼	¼	373(21)	0
Cl(2)	¼	¼	474(23)	0
	−3782(7)	−3754(37)	571(27)	−33(21)
	−¼	−¼	655(27)	0
N(1)	4306(3)	4315(17)	666(60)	101(55)
	4979(5)	4875(85)	530(58)	194(45)
	8615(3)	8629(27)	350(47)	69(48)
C(1)	4773(5)	4774(25)	832(89)	100(84)
	4982(10)	4824(113)	748(88)	323(63)
	7930(4)	7883(40)	397(60)	19(69)
N(2)	1387(3)	1356(18)	413(48)	3(43)
	−5259(5)	−5321(76)	427(54)	116(42)
	0673(3)	0651(28)	501(52)	−43(45)
C(2)	2072(4)	2168(26)	442(61)	7(62)
	−4787(10)	−4708(124)	583(78)	266(61)
	0246(5)	0282(40)	748(83)	133(70)
N(3)	1172(3)	1213(34)	646(70)	−67(66)
	0770(8)	0756(99)	955(91)	281(54)
	2808(3)	2886(51)	474(60)	67(61)
C(3)	1458(5)	1465(36)	554(74)	−111(68)
	−1120(10)	−1052(126)	754(94)	82(56)
	2828(5)	2800(60)	390(65)	44(63)
N(4)	2753(3)	2758(27)	526(61)	−94(53)
	−0684(8)	−0701(66)	747(74)	262(51)
	6145(3)	6213(35)	555(62)	−26(57)
C(4)	2868(5)	2904(37)	519(71)	−70(65)
	1192(9)	1296(102)	798(97)	135(52)
	6453(4)	6573(57)	315(57)	50(59)

[a]The coordinates from ref. 12 have been converted from $P2/c$ to $P2/n$ (cf. Table 2) and the atoms renumbered as follows (ref. 12 → this work): In(1) → In(2), In(2) → In(1), Cl(1) → Cl(22), Cl(2) → Cl(23), Cl(3) → Cl(13), Cl(4) → Cl(2), Cl(5) → Cl(21), Cl(6) → Cl(11), Cl(7) → Cl(12), Cl(8) → Cl(1), N(3) → N(4), N(4) → N(3), C(1) → C(2), C(2) → C(1), C(3) → C(4), C(4) → C(3). Equivalent positions have been substituted where required.

The structure consists of $MeNH_3^+$, $InCl_6^{3-}$, and Cl^- ions. It may be viewed as a highly distorted CsCl-type packing of $[(MeNH_3)_4Cl]^{3+}$ and $[InCl_6]^{3-}$ units. The $[Cl(\cdots HNMeH_2)_4]^{3+}$ "cation" is hydrogen-bonded to the eight $InCl_6^{3-}$ anions which surround it at the corners of a monoclinic coordination prism. All the In atoms are in the *ac* plane. The two sets of Cl^- atoms occupy the 2(*e*) and 2(*f*) positions of $P2/n$, but their refined $|y|$ coordinates are indistinguishable, so that the $[InCl_6^{3-} + Cl^-]$ anion sublattice may be regarded as a monoclinic (subgroup) distortion of a higher-symmetry arrangement, viz. $Pmna \supset P2/n$ with In in 2(*a*) and 2(*b*) and Cl^- in 4(*g*), and with the $InCl_6$ octahedra of approximately $2/m$ symmetry.

The In(1)Cl_6 and In(2)Cl_6 octahedra are more regular than reported in ref. 12 (Table 20). The mean uncorrected In—Cl distance is 2.509(6) Å, with a high–low spread of only 0.015(8) Å, and the In(1)—Cl(11) and In(2)—Cl(22) distances,

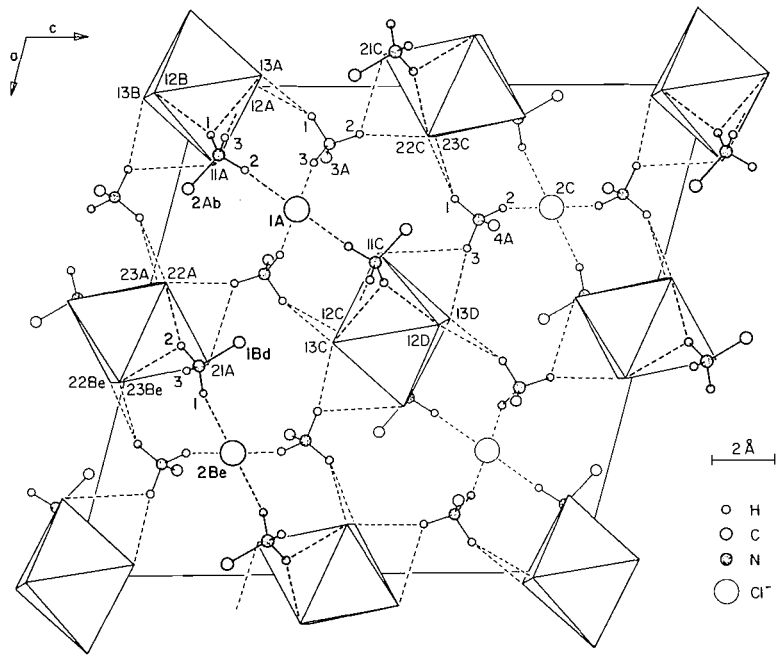

FIG. 11. $(MeNH_3)_4[InCl_6]Cl$: projection of the structure on (010). Hydrogen bonds are indicated by broken lines. For symmetry code, H···Cl distances and NHCl angles see Table 21. The bonds from H(13Bd) to Cl(22Bb), Cl(21Ab), Cl(23Ab), and the H(21Ab)···Cl(11A) bond are not shown. The Me hydrogens are omitted for clarity.

TABLE 20. Bond lengths (Å) and angles (deg) in $(MeNH_3)_4[InCl_6]Cl$ and $(Me_2NH_2)_4[InCl_6]Cl$

Atoms	Distance[a] This work	Distance[a] Ref. 12[b]	Atoms	Angle
		$(MeNH_3)_4[InCl_6]Cl$		
In(1)—Cl(11)	2.513(2)/9	2.569	Cl(11)—In(1)—Cl(12)	89.5(1)
In(1)—Cl(12)	2.504(2)/8	2.500	Cl(11)—In(1)—Cl(13)	89.7(1)
In(1)—Cl(13)	2.519(3)/10	2.517	Cl(12)—In(1)—Cl(13)	89.4(1)
In(1)—Cl mean[c]	2.512(8)	[2.529(36)]	Cl(21)—In(2)—Cl(22)	89.5(1)
In(2)—Cl(21)	2.505(2)/10	2.507	Cl(21)—In(2)—Cl(23)	89.8(1)
In(2)—Cl(22)	2.510(2)/11	2.551	Cl(22)—In(2)—Cl(23)	89.3(1)
In(2)—Cl(23)	2.505(2)/11	2.533		
In(2)—Cl mean[c]	2.507(3)	[2.530(22)]		
In—Cl mean[c]	2.509(6)/10	[2.530(27)][d]		
		$(Me_2NH_2)_4[InCl_6]Cl$		
In—Cl(1)	2.504(2)/10		Cl(1)—In—Cl(2)	88.56(8)
In—Cl(2)	2.515(2)/8		Cl(1)—In—Cl(3)	89.38(8)
In—Cl(3)	2.515(2)/11		Cl(2)—In—Cl(3)	90.20(9)
In—Cl mean[c]	2.511(5)/10		C(11)—N(1)—C(12)	113(1)
N(1)—C(11)	1.479(9)		C(21)—N(2)—C(22)	114(1)
N(1)—C(12)	1.476(8)			
N(2)—C(21)	1.478(9)			
N(2)—C(22)	1.480(8)			

[a]Number after oblique stroke: correction to be added ($\times 10^3$, rigid-body motion model).
[b]Numbering of atoms converted, see Table 18.
[c]Weighted by σ^{-2}.
[d]In—Cl mean quoted in ref. 12: 2.523(14) Å.

both unusually long in ref. 12, are close to the mean.[35] The differences in the In—Cl bond lengths and ClInCl angles arise mainly from the significant differences in the unit-cell dimensions between the two determinations.

[35]In this the $InCl_6$ geometry closely resembles the dimensional homogeneity of the $InBr_6$ octahedra in the isostructural $(MeNH_3)_4[InBr_6]Br$, where the In—Br mean is 2.670(11) Å, with a high–low spread of 0.023(4) Å (13).

The H···Cl distances and NHCl angles are distributed quite uniformly (Fig. 8). All H_N atoms are engaged in N—H···Cl bonds (Fig. 11, Table 21). One hydrogen in each of the four nonequivalent $—NH_3$ groups has a Cl^- ion as acceptor. The other two hydrogens are bonded to Cl atoms of the $InCl_6^{3-}$ anions by highly bent, bifurcated, or trifurcated bonds. The bifurcated and trifurcated bonds are always to Cl atoms of the same complex anion. Each Cl^- is hydrogen-bonded to four cations, and each Cl in an $InCl_6^{3-}$ anion acts as acceptor to at

Can. J. Chem. Downloaded from www.nrcresearchpress.com by 72.64.146.136 on 09/07/12
For personal use only.

Can. J. Chem. Downloaded from www.nrcresearchpress.com by 72.64.146.136 on 09/07/12
For personal use only.

TABLE 21. $(MeNH_3)_4[InCl_6]Cl$: N···Cl and H···Cl distances (Å) and NHCl angles (deg)[a]

N	HN	Cl	N···Cl	H···Cl	NHCl
1Bd	11Bd	2B	3.174(5)	2.23(11)	150(9)
		23Be	3.277(5)	3.04(11)	94(7)
	12Bd	22A	3.539(5)	2.57(11)	159(8)
		23Be	3.277(5)	2.72(11)	114(7)
	13Bd	22Bd	3.450(5)	2.62(11)	138(8)
		21Ab	3.618(5)	2.77(11)	140(8)
		23Ab	3.555(5)	3.10(11)	108(7)
2Ab	21Ab	12B	3.323(5)	2.47(9)	139(7)
		13A	3.471(5)	2.75(9)	127(6)
		11A	3.431(5)	2.78(9)	121(6)
	22Ab	1A	3.150(5)	2.12(9)	173(8)
	23Ab	12Ab	3.257(5)	2.31(11)	151(9)
		13Bb	3.788(5)	3.19(11)	118(7)
3A	31A	13A	3.313(6)	2.52(10)	134(7)
		21C	3.398(6)	3.06(10)	101(6)
		12A	4.082(7)	3.23(11)	141(3)
	32A	22C	3.389(6)	2.39(12)	164(9)
		21C	3.398(6)	2.93(12)	108(7)
	33A	1A	3.221(5)	2.22(12)	162(10)
4A	41A	23C	3.320(6)	2.50(7)	137(5)
		22C	3.875(6)	3.04(7)	139(5)
		11C	3.352(6)	3.13(7)	94(4)
	42A	2C	3.272(6)	2.28(11)	161(8)
	43A	13D	3.407(6)	2.44(10)	156(8)
		11C	3.352(6)	2.87(10)	109(6)
	21Ab			2.78(9)	121(6)
	43C	11A		2.87(10)	109(6)
	41C			3.13(7)	94(4)
	23A			2.31(11)	151(9)
	21Bi	12A		2.47(9)	139(7)
	31A			3.23(11)	141(3)
	43Dg			2.44(10)	156(8)
	31A	13A		2.52(10)	134(7)
	21Ab			2.75(9)	127(6)
	23B			3.19(11)	118(7)
	13Bj			2.77(11)	140(8)
	32C	21A		2.93(12)	108(7)
	31C			3.06(10)	101(6)
	32C			2.39(12)	164(9)
	12Bd	22A		2.57(11)	159(8)
	13Af			2.62(11)	138(8)
	41C			3.04(7)	139(5)
	41C			2.50(7)	137(5)
	12Ah	23A		2.72(11)	114(7)
	11Ah			3.04(11)	94(7)
	13Bj			3.10(11)	108(7)
	22Ab			2.12(9)	173(8)
	22C	1A		2.12(9)	173(8)
	33A			2.22(12)	162(10)
	33C			2.22(12)	162(10)
	11Ah			2.23(11)	150(9)
	11Ci	2A		2.23(11)	150(9)
	42Af			2.28(11)	161(8)
	42C			2.28(11)	161(8)

A	x	y	z	a	X + (−1, 0, 0)
B	$-x$	$-y$	$-z$	b	X + (0, 1, 0)
C	$\frac{1}{2}-x$	y	$\frac{1}{2}-z$	c	X + (0, 0, 1)
D	$\frac{1}{2}+x$	$-y$	$\frac{1}{2}+z$	d	X + (1, 1, 1)

TABLE 21 (*concluded*)

N	HN	Cl	N···Cl	H···Cl	NHCl
			e	X + (1, 0, 0)	
			f	X + (0, 0, −1)	
			g	X + (−1, 0, −1)	
			h	X + (0, −1, −1)	
			i	X + (0, −1, 0)	
			j	X + (1, 0, 1)	

[a]H···Cl distances up to 3.2 Å.

least two N-hydrogens. The hydrogen bonds to the Cl^- ions are strong, as indicated both by the short H···Cl^- distances and the large NHCl angles, and by the low NH stretching frequency in the ir spectrum (Fig. 12; see next paragraph).

$(Me_2NH_2)_4[InCl_6]Cl$

Attempts to obtain an aquopentachloroindate(III) of Me_2NH from aqueous solutions of Me_2NH/In ratio of 2:1 resulted in products the ir spectra of which contained no indication of the presence of H_2O. However, the spectra of undeuterated and deuterated samples (Fig. 12) showed clearly that the complex NH stretching absorption fell in two groups centering at approximately 3140 and 2730 cm^{-1}. Such separation is characteristic of mixed-anion halides (e.g. alkylammonium hexachlorostannate(IV) chlorides, cf. refs. 147 and 148 and work in progress) and indicative of the simultaneous presence of long and short N—H···Cl bonds, the latter involving the Cl^- ion. This made us suspect that the product was in fact the $(Me_2NH_2)_4InCl_7$ salt first described by Ekeley and Potratz (38) and believed (13, 25) to be an analog of $(MeNH_3)_4[InCl_6]Cl$. Our suspicion was vindicated by the crystal-structure analysis (Tables 2 and 22).

The salt crystallizes in the relatively uncommon chiral group $P2_12_12$. The hydrogen atoms were placed from geometric considerations and refined isotropically (Tables 22 and 23).[24] The structure consists of $Me_2NH_2^+$ cations of two types, Cl^- and almost regular $InCl_6^{3-}$ anions (Table 20). The In atoms and the Cl^- ions are situated on twofold axes. If the $[InCl_6^{3-} + Cl^-]$ complex is regarded as the anion sublattice (distorted fcc), then the cation/anion arrangement may be described as a distorted *anti*-CaF_2 packing. The symmetry of the heterogeneous anion sublattice approaches $Pbam \supset P2_12_12$.

The structure is built up from alternating layers $\parallel(001)$ of two kinds (Fig. 13). One (at $z \sim \frac{1}{2}$) contains the $InCl_6$ octahedra and cations 2 joined by bifurcated N(2)—H(21)···2Cl and N(2)—H(22)···2Cl bonds, the bifurcation involving Cl atoms of the same octahedron (Table 24). In layers of the second kind (at $z \sim 0$) Cl^- ions and the C(1)—N(1)—H(11) portions of cations 1 form an almost planar system held together by very short H(11)···Cl^- bonds. Adjacent layers are cross-linked by trifurcated N(1)—H(12)···3Cl bonds to three *fac*-Cl atoms.

The involvement of the Cl^- ion in the two short hydrogen bonds related by the twofold axis through Cl^- is reflected in the strong anisotropy of the thermal motion of the ion, $U_{11} \sim U_{33}$, $2U_{22}/(U_{11} + U_{33}) \sim 2.2$, as well as in the magnitude of the mean amplitude perpendicular to the H(11)···Cl^-···H(11′) bond, ~0.4 Å. This is in marked contrast to the motion of the Cl^- ions in $(MeNH_3)_4[InCl_6]Cl$, where the presence of a *second*

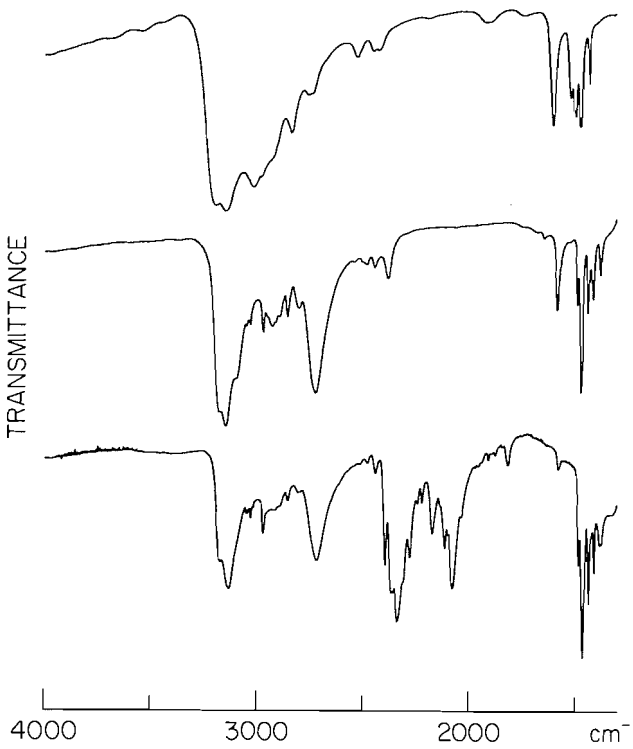

FIG. 12. Infrared spectra of $(MeNH_3)_4InCl_7$ (*top*), $(Me_2NH_2)_4InCl_7$ (*middle*), and $(Me_2NH_2)_4InCl_7$ (~60% D) (*bottom*).

pair of C_2-related N—H···Cl^- bonds resulted in a more nearly isotropic motion (Table 18, Fig. 11).

D. Hydrogen bonding

$(Me_3NH)_3[InCl_6]$

The Me_3NH^+ cation is too large to be readily accommodated in the octahedral (minority) sites of the cubic cryolite structure, and the molecular symmetry of the cation does not coincide with the site symmetry of either cation site in that structure. Moreover, the N-hydrogens can be expected to form N—H···Cl bonds and cause the cation to assume preferential orientation. As a result, the structure of $(Me_3NH)_3InCl_6$ (9) resembles only remotely the cryolite structure. It is dominated by the effect of the hydrogen bonding and by the requirement that each anion be engaged in hydrogen bonds to three cations. The structure may be regarded as consisting of columns of centrosymmetric $InCl_6$ groups $\|c$. The positions of the N-hydrogens have not been determined, but it is clear from the positions of the Me groups that each anion is associated with two N(1) cations related by the centre in the In atom and with their N-hydrogens pointing into opposite faces of the octahedron, i.e. forming trifurcated N—H···3Cl bonds. Because of the disorder in the structure the third cation (N(2) of ref. 9) can occupy one of the two available positions to form a third trifurcated N—H···3Cl bond, the three bonds being in a *mer* configuration. The columns, which are "insulated" from one another by the outwardly oriented Me groups, are vertically related by the 4_1 axes inside the channels formed by the columns. The $\{(Me_3NH)_3[InCl_6]\}$ units do not appear to be linked by hydrogen bonds to their neighbours within a column or between columns. The crystal may thus be regarded as consisting of neutral $\{(Me_3NH)_3[InCl_6]\}$ "molecules".

In forming exclusively trifurcated N—H···3Cl bonds $(Me_3NH)_3InCl_6$ resembles $(Me_3NH)_2SnCl_6$ (147). In the latter, completely ordered structure the centrosymmetric neutral $\{(Me_3NH)[SnCl_6](HNMe_3)\}$ units form a fcc array; in the former, a similar array of In atoms is severely compressed along the *c* axis.

TABLE 22. $(Me_2NH_2)_4[InCl_6]Cl$: positional and thermal parameters ($\times 10^4$) of atoms other than CH_3 hydrogens

Atom	*x* *y* *z*	U_{11} U_{22} U_{33}	U_{12} U_{13} U_{23}
In	0	208(4)	3(3)
	0	193(4)	0
	5727(1)	301(4)	0
Cl(1)	−0783(2)	338(11)	37(10)
	1275(2)	295(11)	−32(11)
	3785(3)	415(11)	82(9)
Cl(2)	2211(2)	203(10)	−40(8)
	0869(2)	325(11)	−14(11)
	5679(3)	552(13)	−7(11)
Cl(3)	−0745(3)	441(14)	50(12)
	1194(2)	517(15)	40(13)
	7817(3)	484(13)	−211(13)
Cl^-	½	629(27)	450(38)
	0	1396(53)	0
	10124(6)	653(26)	0
N(1)	2337(9)	371(47)	−37(43)
	0948(7)	561(58)	−15(38)
	9574(9)	357(47)	4(42)
C(11)	2553(16)	856(97)	−65(70)
	2071(8)	456(73)	−100(80)
	9485(17)	681(88)	−92(71)
C(12)	1710(17)	790(98)	−150(97)
	0630(15)	1305(133)	247(77)
	11020(14)	506(80)	120(82)
N(2)	1347(9)	374(48)	26(37)
	3182(7)	271(41)	−143(55)
	4737(11)	1002(86)	8(47)
C(21)	0701(15)	661(81)	73(70)
	3613(10)	656(79)	−29(78)
	6108(13)	680(85)	107(67)
C(22)	0862(12)	435(67)	−52(58)
	3619(9)	456(70)	−96(60)
	3280(12)	740(83)	51(63)
H(11)	3219(9)	936(546)[a]	
	0566(7)		
	9456(9)		
H(12)	1719(9)	820(444)[a]	
	0749(7)		
	8690(9)		
H(21)	2346(9)	466(227)[a]	
	3312(7)		
	4817(11)		
H(22)	1172(9)	349(227)[a]	
	2402(7)		
	4732(11)		

[a] U_{iso}.

$(MeNH_3)_4[InCl_6]Cl$ and $(Me_2NH_2)_4[InCl_6]Cl$

The most interesting aspect of hydrogen bonding in these mixed-anion salts is the competition for hydrogen-bond forma-

Can. J. Chem. Downloaded from www.nrcresearchpress.com by 72.64.146.136 on 09/07/12
For personal use only.

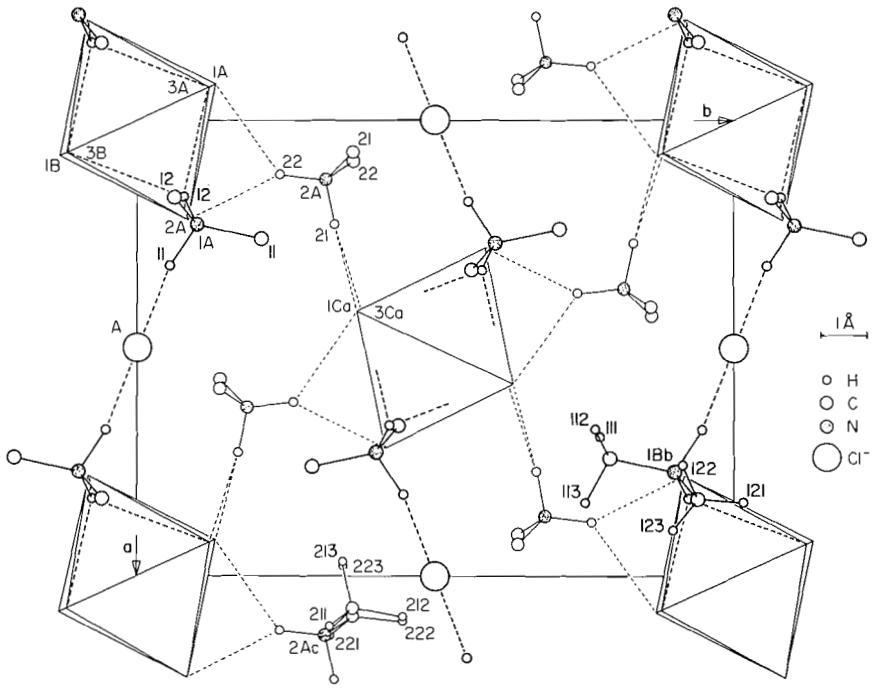

FIG. 13. $(Me_2NH_2)_4[InCl_6]Cl$: projection of the structure on (001). Hydrogen bonds are indicated by broken lines. For symmetry code, H···Cl distances and NHCl angles see Table 24. Only one set of Me hydrogens each is shown for clarity. The H(12A)···Cl(2A) bond is barely visible in this projection.

tion between the triply-charged $InCl_6^{3-}$ anion, with a formal charge of $\frac{1}{2}-$ on each Cl atom, and the compact Cl^- ion. The number of N-hydrogens bonded to Cl^- is $\frac{1}{4}$ of the total number of N-hydrogens in both compounds, but the Cl atoms of $InCl_6^{3-}$ (Cl_M for short) in $(Me_2NH_2)_4[InCl_6]Cl$ are less strongly involved in hydrogen bonding than the Cl_M atoms in $(MeNH_3)_4[InCl_6]Cl$. To show that the hydrogen bonding to Cl^- occurs, preferentially, at the expense of the bonding to Cl_M, the two salts are compared, in Table 25 and Fig. 14, to each other and to other suitable salts for which the hydrogen-bonding schemes are known. It is seen that non-hydrogen-bonded Cl_M occur already at an H_N/Cl_{total} ratio of $\frac{6}{7}$ for the mixed-anion salts (**3**), whereas in the pure hexachloro salts non-bonded Cl_M does not appear until $H_N/Cl_{total} = \frac{1}{3}$ (**10**). Even then it occurs only in the Et compound (**10**) but not in the corresponding Me compound (**9**), which has a structure of a different type. It would be interesting to know whether a similar situation exists between $(Me_3NH)_3[InCl_6]$ (**11**) and $(Et_3NH)_3[InCl_6]$ (structure as yet not determined). In **4**, which contains *two* Cl^- ions per formula unit, the $SnCl_6$ octahedron is involved only in two normal $H\cdots Cl_M$ bonds, with the other four Cl_M non-bonded.

The connection that may exist between the extent of hydrogen bonding and the tendency of alkylammonium hexachloro compounds to form mixed-anion salts has not yet been explored. For a salt $(R_nNH_{4-n})_{6-p+m}[M^pCl_6]Cl_m$, $H_N/Cl_{total} = (4 - n)[1 - p/(6 + m)]$; if each Cl^- engages $2r$ N-hydrogens to form $H\cdots Cl^-$ bonds, $H_N/[MCl_6] = (4 - n)(6 - p) + (4 - n - 2r)m$. Hence $H_N^{max}/[MCl_6] = 12 + (4 - 2r)m$ ($n_{min} = 0$, $p_{min} = 3$), $H_N^{max}/Cl_M = 2 + m(4 - 2r)/6$, e.g. for $(NH_4)_{3+m}[InCl_6]Cl_m$; $H_N^{min}/[MCl_6] = 1 + (1 - 2r)m$, $H_N^{min}/Cl_M = [1 + m(1 - 2r)]/6$, e.g. for $(R_3NH)_{1+m}[SbCl_6]Cl_m$. For H_N/Cl_M to be zero, $m = (4 - n)(p - 6)/(4 - n - 2r)$, in which case the octahedra are non-bonded, and it is possible that in such circumstances the mixed-anion salt will not form. To determine how far this formalism is relevant to the existence of mixed-anion salts will require additional experimental effort.

TABLE 24. $(Me_2NH_2)_4[InCl_6]Cl$: N···Cl and H···Cl distances (Å) and NHCl angles (deg)

N	H	Cl	N···Cl	H···Cl[a]	NHCl
1A	11A	A	3.015(8)	2.04	157(2)
	12A	3A	3.492(6)	2.68	136(2)
		2A	3.389(5)	2.69	125(2)
		3B	3.559(9)	2.82	130(2)
2A	21A	1Ca	3.266(6)	2.32	152(2)
		3Ca	3.792(6)	3.08	127(3)
	22A	2A	3.240(9)	2.40	138(2)
		1A	3.395(5)	2.60	134(2)
	11A	A		2.04	157(2)
	21Ca }	1A		2.32	152(2)
	22A }			2.60	134(2)
	22A }	2A		2.40	138(2)
	12A }			2.69	125(2)
	12A }	3A		2.68	136(2)
	12B }			2.82	130(2)
	21Cd }			3.08	127(3)

Symmetry code:

A	x	y	z	a	X + (0, 0, 1)
B	$-x$	$-y$	z	b	X + (1, 1, 2)
C	$\frac{1}{2} + x$	$\frac{1}{2} - y$	$-z$	c	X + (1, 1, 0)
				d	X + (−1, 0, 1)

[a]Estimated standard deviation, 0.01 Å.

The simple X^- anion in mixed-anion salts most often is either located on an element (or pseudoelement) of symmetry (e.g. $4/m$ in $(NH_4)_3[SiF_6]F$ and $Cs_3[MCl_4]Cl$, m in $(NH_4)_3[ZnCl_4]Cl$)

Can. J. Chem. Downloaded from www.nrcresearchpress.com by 72.64.146.136 on 09/07/12
For personal use only.

TABLE 25. Connectivity of hydrogen-bonding systems in mixed-anion and related salts

Compound	Number of H_N	Acceptors per formula unit		H_N per total Cl	H_N engaged per each[a]			Reference
		Cl^-	Cl_M		Cl^-	$[MCl_6]$	Cl_M	
1 $(MeNH_3)_4[InCl_6]Cl$	12	1	6	$\frac{12}{7}$	1 × 4	8	$(\frac{2}{2}+\frac{2}{3})$ (2×), $(\frac{1}{2}+\frac{2}{3})$ (4×)	This work
2 $(Me_2NH_2)_4[InCl_6]Cl$	8	1	6	$\frac{8}{7}$	1 × 2	6	$(\frac{1}{2}+\frac{2}{3})$ (2×), $\frac{2}{2}$ (2×), $(\frac{1}{2}+\frac{1}{3})$ (2×)	This work
3 $(n\text{-}Pr_2NH_2)_3[SnCl_6]Cl$	6	1	6	$\frac{6}{7}$	1 × 2 + $\frac{1}{2}$ × 1	$\frac{7}{2}$	$(1+\frac{1}{2})$ (1×), $\frac{1}{2}$ (4×), 0 (1×)	148
4 $[(CH_2)_8NH_2]_4[SnCl_6]Cl_2$	8	2	6	1	1 × 3	2	1 (2×), 0 (4×)	[b]
5 $(MeNH_3)_2[SnCl_6]$	6	—	6	1	—	6	$\frac{3}{3}$ (6×)	Cf. ref. 147
6 $(EtNH_3)_2[SnCl_6]$	6	—	6	1	—	6	$\frac{3}{3}$ (6×)	147
7 $(Me_2NH_2)_2[SnCl_6]$	4	—	6	$\frac{2}{3}$	—	4	$\frac{2}{3}$ (6×)	147
8 $(Et_2NH_2)_2[SnCl_6]$	4	—	6	$\frac{2}{3}$	—	4	1 (2×), $\frac{1}{2}$ (4×)	148
9 $(Me_3NH)_2[SnCl_6]$	2	—	6	$\frac{1}{3}$	—	2	$\frac{1}{3}$ (6×)	147
10 $(Et_3NH)_2[SnCl_6]$	2	—	6	$\frac{1}{3}$	—	2	$\frac{1}{2}$ (4×), 0 (2×)	164
11 $(Me_3NH)_3[InCl_6]$	3	—	6	$\frac{1}{2}$	—	3	$\frac{2}{3}$ (3×), $\frac{1}{3}$ (3×)	9

[a] $\frac{1}{2}$ represents contribution from a bifurcated, $\frac{1}{3}$ from a trifurcated N—H···Cl bond; $\frac{2}{2} = 2 \times \frac{1}{2}$, $\frac{2}{3} = 2 \times \frac{1}{3}$.
[b] B. R. Vincent, T. S. Cameron, and O. Knop. To be published.

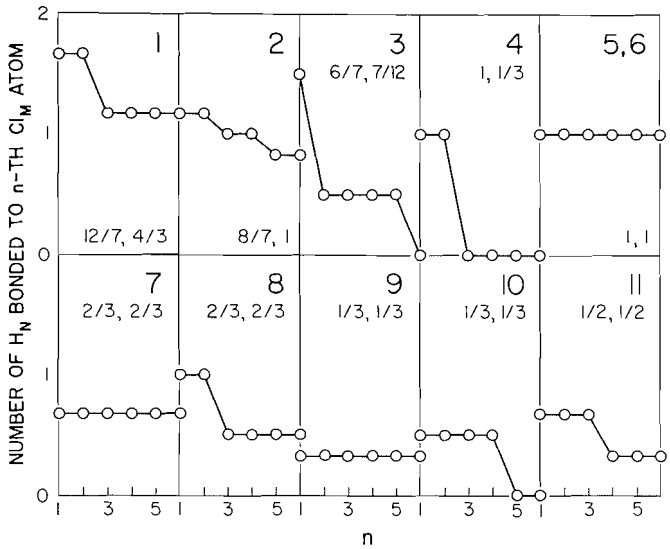

FIG. 14. The extent to which an MCl_6 octahedron in compounds **1–11** of Table 25 is involved in hydrogen bonding. The first number refers to the number of H_N atoms per total Cl; the second number refers to the mean number of H_N atoms bonded to a Cl atom (Cl_M) in the MCl_6 octahedron.

or paired with another X^- through a symmetry operation to form an identifiable substructure entity. In this $(MeNH_3)_4[InCl_6]Cl$ and $(Me_2NH_2)_4[InCl_6]Cl$ are no exception: the Cl^- ion in both is located on a twofold axis. In compounds **3** and **4** it forms almost planar $(\cdots Cl\cdots H—N—H\cdots)_2$ rings, centrosymmetric and $\|(001)$ in **3**, and of C_2 symmetry and $\|(010)$ in **4**; the stacks of these rings define channels $\|c$ in **3** and $\|b$ in **4**.

The distributions of H···Cl,NHCl pairs (including H···Cl,OHCl pairs for $(NH_4)_2[MCl_5(H_2O)]$) are shown in Fig. 8. As would be expected, the H···Cl^- bonds are stronger than the H···Cl_M bonds, but this does not make the H···Cl^-,$NHCl^-$ points stand out in the distributions, and the appearance of each distribution is such that a linear regression can be attempted. Although the legitimacy of a linear relationship between the NHCl bond angle and the H···Cl distance may not be unassailable, the coefficients of determination r^2 for the linear regressions are sufficiently high to suggest that significant correlation exists: 0.75 for $(MeNH_3)_4[InCl_6]Cl$, 0.81 for $(Me_2NH_2)_4[InCl_6]Cl$, 0.91 for the cognate $(n\text{-}Pr_2NH_2)_3[SnCl_6]Cl$ (148), and 0.84 and 0.87, respectively, for $(NH_4)_2[InCl_5(H_2O)]$ and $(NH_4)_2[FeCl_5(H_2O)]$. The increased opportunity for hydrogen bonding is reflected in the number of dissimilar H···Cl distances, which is larger for the low-symmetry $(MeNH_3)_4[InCl_6]Cl$ ($H_N/Cl_{total} = \frac{12}{7}$) than in the somewhat higher-symmetry $(Me_2NH_2)_4[InCl_6]Cl$ ($H_N/Cl_{total} = \frac{8}{7}$).

The H···Cl,NHCl distributions show that whatever may be the principle which governs the distribution and the most probable value of the XHY angle in *molecular* crystals (cf. for ex. refs. 165 and 166), in ionic crystals containing X^+—H···Y^- bonds, such as those under consideration here, the H···Y^-,XHY^- distribution appears to be the result of optimization of the overall hydrogen-bonding energy within the geometric framework determined primarily by Coulombic forces, with the XHY^- angle and the type of hydrogen bond (normal, bifurcated, trifurcated) incidental to the particulars of the cation/anion packing. Secondly, the linear regressions of Fig. 8 hold over the approximate 90–180° interval, hence there is no natural cut-off d(H···Cl) value for effective hydrogen-bonding interaction that could be determined from the properties of the distribution alone. In some cases the longest H···Cl distance that, *geometrically*, may qualify as corresponding to a hydrogen bond, occurs at an NHCl angle appreciably larger than 90° and may therefore be taken as the cut-off value: in $(Me_2NH_2)_4[InCl_6]Cl$ this is observed at ~3.1 Å and ~125°, but the H···Cl distance is too long on conventional criteria for effective hydrogen bonding. In most cases, however, there are H···Cl,NHCl points in the distribution down to NHCl = 90–100° and d(H···Cl) > 3.2 Å. It is possible that our traditional notions about hydrogen bonding between charged entities may require revision, but for the problem of the cut-off angle to be treated meaningfully, experimental as well as theoretical assessments of charge-density distribution in the H···Cl region of such presumed hydrogen bonds must first be obtained. In the

Can. J. Chem. Downloaded from www.nrcresearchpress.com by 72.64.146.136 on 09/07/12
For personal use only.

meantime, comparison of H···Cl and NHCl means in the distributions for different compounds and of the slopes of the regression lines can be used to estimate the *relative* strength of the overall hydrogen bonding in a crystal. These matters will be elaborated elsewhere.

Experimental

$(MeNH_3)_4InCl_7$ and $(Me_2NH_2)_4InCl_7$ resulted from room-temperature crystallization of solutions containing the alkylammonium chloride and $InCl_3$ in a molar ratio of 2:1. The solutions were prepared by dissolving $In(OH)_3$ in conc. HCl, evaporating, redissolving in a minimum amount of water and adding a methanolic solution of $MeNH_3Cl$ or Me_2NH_2Cl. The products were recrystallized from MeOH. For the preparation of $(NH_4)_2[InCl_5(H_2O)]$ and $K_3InCl_6 \cdot nH_2O$ see **C**.

Densities were determined by flotation in suitable liquid mixtures. Infrared spectra were obtained on a Bomem DA3.02 Fourier transform spectrometer, using fluorolube mulls supported between CaF_2 plates.

Structure determination

A CAD-4 four-circle diffractometer was used in the determination (at ~19°C) of the unit-cell dimensions and in the intensity collection. As nearly equiaxial crystals as could be found, typically 0.01–0.02 mm^3 in volume, were used. The intensities were reduced by routine procedures (167). Lorentz and polarization corrections were applied but no absorption or extinction corrections. The scattering factors for neutral atoms were taken from ref. 168. The structures were solved using the SHELX (169) and CRYSTALS (170) systems.

After the nonhydrogen atoms had been located, full-matrix least-squares ($w\Delta F^2$ = min) refinement was carried out with isotropic temperature factors until R was reduced to a reasonably low value. The hydrogen atoms were then located from a difference map or from structural considerations, and the refinement was continued with anisotropic temperature factors on the nonhydrogen atoms and isotropic factors on the hydrogens. The anisotropic temperature factor is defined as $T = \exp[-2\pi^2(U_{11}h^2a^{*2} + U_{22}k^2b^{*2} + U_{33}l^2c^{*2} + 2U_{23}klb^*c^* + 2U_{13}hla^*c^* + 2U_{12}hka^*b^*)]$. The least-squares weights were of the type $w^{-1} = a\sigma^2|F_o| + b|F_o|^2$ (SHELX) or $w^{-1} = \sigma^2|F_o|$ (CRYSTALS, $(Me_2NH_2)_4InCl_7$). The crystal data on the title compounds are given in Table 2 and the structure factors in Tables 26–29.[24]

Acknowledgments

We thank Dr. M. Falk for obtaining the ir spectra and Dr. S. P. Deraniyagala for assistance with some of the preparative work. We are also indebted to Dr. J.-P. Wignacourt for providing us with a copy of ref. 18. This investigation was supported by grants from the Natural Sciences and Engineering Research Council of Canada to O.K. and T.S.C.

1. J. Scheffler and R. Hoppe. J. Fluor. Chem. **25**, 27 (1984).
2. P. Bukovec and L. Golič. Acta Crystallogr. B, **32**, 948 (1976).
3. J.-C. Champarnaud-Mesjard and B. Frit. Acta Crystallogr. B, **33**, 3722 (1977).
4. J. Scheffler and R. Hoppe. Z. Anorg. Allg. Chem. **521**, 79 (1985).
5. J.-C. Champarnaud-Mesjard, D. Mercurio, and B. Frit. J. Inorg. Nucl. Chem. **39**, 947 (1977).
6. J.-C. Champarnaud-Mesjard and B. Frit. Acta Crystallogr. B, **34**, 736 (1978).
7. L. R. Morss, M. Siegal, L. Stenger, and N. Edelstein. Inorg. Chem. **9**, 1771 (1970).
8. G. Meyer and E. Dietzel. Rev. Chim. Min. **16**, 189 (1979).
9. J. G. Contreras, F. W. B. Einstein, M. M. Gilbert, and D. G. Tuck. Acta Crystallogr. B, **33**, 1648 (1977).
10. F. W. B. Einstein, M. M. Gilbert, D. G. Tuck, and P. L. Vogel. Acta Crystallogr. B, **32**, 2234 (1976).
11. J. Chassaing. C.R. **268**C, 2188 (1969).
12. H.-U. Schlimper and M. L. Ziegler. Z. Naturforsch. **27**b, 377 (1972).
13. M. A. Khan and D. G. Tuck. Acta Crystallogr. B, **37**, 683 (1981).
14. G. Meyer. Z. Anorg. Allg. Chem. **478**, 39 (1981).
15. R. de Pape, J. Portier, J. Grannec, G. Gauthier, and P. Hagenmuller. C.R. **269**C, 1120 (1969).
16. J. Grannec, J.-C. Champarnaud, and J. Portier. Bull. Soc. Chim. Fr. 3862 (1970).
17. J.-C. Champarnaud-Mesjard, J. Grannec, and B. Gaudreau. C.R. **278**C, 171 (1974).
18. J.-P. Wignacourt. Thèse d'Etat. Université de Lille. 1981.
19. J.-P. Wignacourt, G. Mairesse, and P. Barbier. Acta Crystallogr. B, **36**, 669 (1980).
20. J.-P. Wignacourt, G. Mairesse, P. Barbier, A. Lorriaux-Rubbens, and F. Wallart. Can. J. Chem. **60**, 1747 (1982); (errata) **61**, 1227 (1983).
21. J.-P. Wignacourt, G. Mairesse, and P. Barbier. Cryst. Struct. Commun. **5**, 293 (1976).
22. J.-P. Wignacourt, A. Lorriaux-Rubbens, P. Barbier, G. Mairesse, and F. Wallart. Spectrochim. Acta, **36**A, 403 (1980).
23. A. W. Atkinson and B. O. Field. J. Inorg. Nucl. Chem. **32**, 2601 (1970).
24. H. P. Klug, E. Kummer, and L. Alexander. J. Am. Chem. Soc. **70**, 3064 (1948).
25. J. Gislason, M. H. Lloyd, and D. G. Tuck. Inorg. Chem. **10**, 1907 (1971).
26. K. Yamada, N. Weiden, and A. Weiss. J. Mol. Struct. **111**, 217 (1983).
27. J.-P. Wignacourt, G. Nowogrocki, G. Mairesse, and P. Barbier. Rev. Inorg. Chem. **2**, 207 (1980).
28. A. Lorriaux-Rubbens, F. Wallart, J.-P. Wignacourt, P. Barbier, and G. Mairesse. Spectrochim. Acta, **37**A, 1021 (1981).
29. M. L. Ziegler, H.-U. Schlimper, B. Nuber, J. Weiss, and G. Ertl. Z. Anorg. Allg. Chem. **415**, 193 (1975).
30. S. H. Whitlow and E. J. Gabe. Acta Crystallogr. B, **31**, 2534 (1975).
31. G. Beran, K. Dymock, H. A. Patel, A. J. Carty, and P. M. Boorman. Inorg. Chem. **11**, 896 (1972).
32. M. Khan, R. C. Steevensz, D. G. Tuck, J. G. Noltes, and P. W. R. Corfield. Inorg. Chem. **19**, 3407 (1980).
33. S. E. Jeffs, R. W. H. Small, and I. J. Worrall. Acta Crystallogr. C, **40**, 1329 (1984).
34. R. W. H. Small and I. J. Worrall. Acta Crystallogr. B, **38**, 932 (1982).
35. J. G. Contreras, F. W. B. Einstein, and D. G. Tuck. Can. J. Chem. **52**, 3793 (1974).
36. M. A. Khan, C. Peppe, and D. C. Tuck. Acta Crystallogr. C, **39**, 1339 (1983).
37. F. W. B. Einstein and D. G. Tuck. J. Chem. Soc. Chem. Commun. 1182 (1970).
38. J. B. Ekeley and H. A. Potratz. J. Am. Chem. Soc. **58**, 908 (1936).
39. D. S. Brown, F. W. B. Einstein, and D. G. Tuck. Inorg. Chem. **8**, 14 (1969).
40. G. Joy, A. P. Gaughan, Jr., I. Wharf, D. F. Shriver, and J. P. Dougherty. Inorg. Chem. **14**, 1795 (1975).
41. M. V. Veidis and G. J. Palenik. J. Chem. Soc. Chem. Commun. 586 (1969).
42. S. P. Sinha, T. T. Pakkanen, T. A. Pakkanen, and L. Niinistö. Polyhedron, **1**, 355 (1982).
43. R. O. Day and R. R. Holmes. Inorg. Chem. **21**, 2379 (1982).
44. J. R. Chadwick, A. W. Atkinson, and B. G. Huckstepp. J. Inorg. Nucl. Chem. **28**, 1021 (1966).
45. H. P. Beck. Z. Naturforsch. **39**b, 310 (1984).
46. M. A. Khan and D. G. Tuck. Inorg. Chim. Acta, **97**, 73 (1985).

Can. J. Chem. Downloaded from www.nrcresearchpress.com by 72.64.146.136 on 09/07/12
For personal use only.

Can. J. Chem. Downloaded from www.nrcresearchpress.com by 72.64.146.136 on 09/07/12
For personal use only.

47. A. W. ATKINSON and B. O. FIELD. J. Inorg. Nucl. Chem. **32**, 2615 (1970).
48. J.-P. WIGNACOURT, G. MAIRESSE, and F. ABRAHAM. Acta Crystallogr. C, **40**, 2006 (1984).
49. J. TROTTER, F. W. B. EINSTEIN, and D. G. TUCK. Acta Crystallogr. B, **25**, 603 (1969).
50. A. R. AMIL, S. M. CARRERA, S. GARCÍA-BLANCO, and M. L. BECERRA. An. Quím. **78**, 396 (1982).
51. M. A. KHAN and D. G. TUCK. Acta Crystallogr. B, **38**, 803 (1982).
52. R. C. GEARHART, JR., J. D. BECK, and R. H. WOOD. Inorg. Chem. **14**, 2413 (1975).
53. F. A. COTTON and C. A. MURILLO. Inorg. Chem. **14**, 2467 (1975).
54. M. A. BENO, D. D. COX, J. M. WILLIAMS, and J. F. KWAK. Acta Crystallogr. C, **40**, 1334 (1984).
55. K. YAMADA and A. WEISS. Ber. Bunsenges. **87**, 932 (1983).
56. R. HOPPE and S. SCHNEIDER. Z. Anorg. Allg. Chem. **361**, 113 (1968).
57. O. KNOP, W. J. WESTERHAUS, M. FALK, and W. MASSA. Can. J. Chem. **63**, 3328 (1985).
58. R. E. THOMA and R. H. KARRAKER. Inorg. Chem. **5**, 1933 (1960).
59. J. GRANNEC, J. PORTIER, and P. HAGENMULLER. J. Solid State Chem. **3**, 227 (1971).
60. H. BODE and E. VOSS. Z. Anorg. Allg. Chem. **290**, 1 (1957).
61. J. GRANNEC, J.-C. CHAMPARNAUD-MESJARD, J. P. COSTY, J. C. COUSSEINS, and B. GAUDREAU. Rev. Chim. Minér. **9**, 569 (1972).
62. G. CUVEILLER, J.-C. CHAMPARNAUD-MESJARD, G. GAUDREAU, and S. TURRELL. J. Mol. Struct. **79**, 345 (1982).
63. R. HOPPE. *In* 20 Jahre Fonds der Chemischen Industrie. *Edited by* Verband der Chemischen Industrie, Frankfurt. Verlag Chemie, Weinheim. 1970. p. 97.
64. S. SCHWARZMANN. Fortschr. Mineral. **42**, 231 (1966).
65. R. BÖHME, J. RATH, B. GRUNWALD, and G. THIELE. Z. Naturforsch. **35**b, 1366 (1980).
66. J. GRANNEC and J. RAVEZ. C.R. **271**C, 1084 (1970).
67. S. SCHNEIDER and R. HOPPE. Z. Anorg. Allg. Chem. **376**, 277 (1970).
68. J. SETTER and R. HOPPE. Z. Anorg. Allg. Chem. **423**, 125 (1976).
69. G. BAUD, L. BARADUC, P. GAILLE, and J.-C. COUSSEINS. C.R. **272**C, 1328 (1971).
70. G. MEYER. Naturwissenschaften, **67**, 143 (1980).
71. G. MEYER and H.-C. GAEBELL. Z. Naturforsch. **33**b, 1476 (1978).
72. D. BABEL and R. HAEGELE. J. Solid State Chem. **18**, 39 (1976).
73. G. MEYER and H.-C. GAEBELL. Z. Anorg. Allg. Chem. **445**, 147 (1978).
74. J. PORTIER, F. MENIL, and P. HAGENMULLER. Bull. Soc. Chim. Fr. 3485 (1970).
75. U. MÜLLER. Acta Crystallogr. B, **33**, 2197 (1970).
76. T. BARROWCLIFFE, I. R. BEATTIE, P. DAY, and K. LIVINGSTON. J. Chem. Soc. A, 1810 (1967).
77. T. WATANABÉ, M. ATOJI, and C. OKAZAKI. Acta Crystallogr. **3**, 405 (1950).
78. M. LINHARD, W. MANTHEY, and K. PLIETH. Z. Elektrochem. **57**, 862 (1953).
79. J. T. SZYMAŃSKI. Acta Crystallogr. B, **35**, 1958 (1979).
80. P. L. BELLAVANCE, E. R. COREY, and G. W. HEY. Inorg. Chem. **16**, 462 (1977).
81. R. RESTIVO and G. J. PALENIK. J. Chem. Soc. Dalton, 341 (1972).
82. M. J. BENNETT, F. A. COTTON, and D. L. WEAVER. Acta Crystallogr. **23**, 581 (1967).
83. M. D. LIND. J. Chem. Phys. **47**, 990 (1967).
84. A. FERRARI, L. CAVALCA, and M. E. TANI. Gazz. Chim. Ital. **87**, 22 (1957).
85. P. PULLMANN, K. HENSEN, and J. W. BATS. Z. Naturforsch. **37**b, 1312 (1982).
86. I. SINCLAIR, R. W. H. SMALL, and I. J. WORRALL. Acta Crystallogr. B, **37**, 1290 (1981).
87. T. S. CAMERON, O. KNOP, and B. R. VINCENT. Can. J. Chem. **63**, 759 (1985).
88. S. E. JEFFS, R. W. H. SMALL, and I. J. WORRALL. Acta Crystallogr. C, **40**, 1827 (1984).
89. G. BERAN, A. J. CARTY, H. A. PATEL, and G. J. PALENIK. J. Chem. Soc. Chem. Commun. 222 (1970).
90. A. W. ATKINSON, J. R. CHADWICK, and E. KINSELLA. J. Inorg. Nucl. Chem. **30**, 401 (1968).
91. R. D. SHANNON. Acta Crystallogr. A, **32**, 751 (1976).
92. P. J. CRESSWELL, J. E. FERGUSSON, B. R. PENFOLD, and D. E. SCAIFE. J. Chem. Soc. Dalton, 254 (1972).
93. P. MURRAY-RUST and J. MURRAY-RUST. Acta Crystallogr. B, **31**, 1037 (1975).
94. O. KNOP, T. S. CAMERON, S. P. DERANIYAGALA, D. ADHIKESAVALU, and M. FALK. Can. J. Chem. **63**, 516 (1985).
95. F. J. BRINKMANN. J. Inorg. Nucl. Chem. **34**, 394 (1972).
96. G. MEYER. Z. Anorg. Allg. Chem. **445**, 140 (1978).
97. G. MEYER and R. BLACHNIK. Z. Anorg. Allg. Chem. **503**, 126 (1983).
98. R. A. WALTON. Inorg. Chem. **7**, 640 (1968).
99. S. E. JEFFS, R. W. H. SMALL, and I. J. WORRALL. Acta Crystallogr. C, **40**, 65 (1984).
100. S. E. JEFFS, R. W. H. SMALL, and I. J. WORRALL. Acta Crystallogr. C, **40**, 381 (1984).
101. W. HILLER, M. E. GARCÍA-FERNANDEZ, M. R. BERMEJO, and M. V. CASTANO. Acta Crystallogr. C, **42**, 60 (1986).
102. K. L. BROWN and D. HALL. J. Chem. Soc. Dalton, 1843 (1973).
103. H. J. CUMMING, D. HALL, and C. E. WRIGHT. Cryst. Struct. Commun. **3**, 107 (1974).
104. G. GERLACH, W. HÖNLE, and A. SIMON. Z. Anorg. Allg. Chem. **486**, 7 (1982).
105. B. H. FREELAND, J. L. HENCHER, D. G. TUCK, and J. G. CONTRERAS. Inorg. Chem. **15**, 2144 (1976).
106. J. GRANNEC and J. RAVEX. C.R. **270**C, 2059 (1970).
107. R. DOMESLE and R. HOPPE. Z. Anorg. Allg. Chem. **495**, 16 (1982).
108. R. BLACHNIK and J. E. ALBERTS. Z. Anorg. Allg. Chem. **490**, 235 (1982).
109. E. M. KARTZMARK. Can. J. Chem. **58**, 539 (1980).
110. R. DOMESLE and R. HOPPE. Z. Anorg. Allg. Chem. **495**, 25 (1982).
111. G. THIELE, B. GRUNWALD, W. RINK, and D. BREITINGER. Z. Naturforsch. **34**b, 1512 (1979).
112. J. GLASER. Acta Chem. Scand. A, **34**, 75 (1980).
113. G. MEYER and E. SCHWAN. Z. Naturforsch. **35**b, 117 (1980).
114. G. GARTON and H. M. POWELL. J. Inorg. Nucl. Chem. **4**, 84 (1957).
115. T. DEEG and A. WEISS. Ber. Bunsenges. **79**, 497 (1975).
116. H. W. ROTTER and G. THIELE. Z. Anorg. Allg. Chem. **499**, 175 (1983).
117. A. C. HAZELL. J. Chem. Soc. 3459 (1963).
118. A. W. ATKINSON and B. O. FIELD. J. Inorg. Nucl. Chem. **30**, 3177 (1968).
119. H. W. ROTTER and G. THIELE. Z. Naturforsch. **37**b, 995 (1982).
120. T. WATANABÉ, Y. SAITO, R. SHIONO, and M. ATOJI. Struct. Repts. **11**, 393 (1951).
121. G. THIELE and W. RINK. Z. Anorg. Allg. Chem. **414**, 47 (1975).
122. H. KASHIWAGI, D. NAKAMURA, and M. KUBO. J. Phys. Chem. **71**, 4443 (1967).
123. W. FICHTNER and A. WEISS. Z. Naturforsch. **35**b, 170 (1980).
124. R. W. MATTHEWS and R. A. WALTON. J. Chem. Soc. A, 1639 (1968).
125. H.-D. HAUSEN, H. BINDER, and W. SCHWARZ. Z. Naturforsch. **33**b, 567 (1978).

126. F. A. COTTON, B. F. G. JOHNSON, and R. M. WING. Inorg. Chem. **4**, 502 (1965).
127. S. POHL and W. SAAK. Z. Anorg. Allg. Chem. **523**, 25 (1985).
128. A. RUIZ AMIL, S. MARTÍNEZ CARRERA, S. GARCÍA-BLANCO, and M. LOPEZ BECERRA. An. Quím. **78**, 400 (1982).
129. J. GLASER, P. L. GOGGIN, M. SANDSTRÖM, and V. LUTSKO. Acta Chem. Scand. A, **37**, 437 (1983).
130. I. M. ALYMOV, E. V. BRYUKHOVA, A. N. GRIGOR'EV, L. M. MIKHEEVA, and L. N. KOMISSAROVA. Izv. Akad. Nauk SSSR, Ser. Khim. 982 (1975).
131. I. M. ALYMOV, T. L. KHOTSYANOVA, E. V. BRYUKHOVA, A. N. GRIGOR'EV, L. M. MIKHEEVA, and L. N. KOMISSAROVA. Zh. Neorg. Khim. **20**, 2276 (1975).
132. H. PRINZ, K. DEHNICKE, and U. MÜLLER. Z. Anorg. Allg. Chem. **488**, 49 (1982).
133. J. GLASER. Acta Chem. Scand. A, **33**, 789 (1979).
134. G. THIELE and B. GRUNWALD. Z. Anorg. Allg. Chem. **498**, 105 (1983).
135. C. J. O'CONNOR, B. S. DEAVER, JR., and E. SINN. J. Chem. Phys. **70**, 5161 (1979).
136. B. N. FIGGIS, C. L. RASTON, R. P. SHARMA, and A. H. WHITE. Aust. J. Chem. **31**, 2717 (1978).
137. I. SØTOFTE and K. NIELSEN. Acta Chem. Scand. A, **35**, 821 (1981).
138. J. E. GREEDAN, D. C. HEWITT, R. FAGGIANI, and I. D. BROWN. Acta Crystallogr. B, **36**, 1927 (1980).
139. E. M. KARTZMARK. Can. J. Chem. **55**, 2792 (1977).
140. J. GLASER. Acta Chem. Scand. A, **34**, 157 (1980).
141. R. J. MEYER. Z. Anorg. Allg. Chem. **24**, 321 (1900).
142. R. CAMINITI, G. MARONGIU, and G. PASCHINA. Cryst. Struct. Commun. **11**, 955 (1982).
143. P. J. TUDO, B. JOLIBOIS, G. LAPLACE, G. NOWOGROCKI, and F. ABRAHAM. Acta Crystallogr. B, **35**, 1580 (1979).
144. G. JOHANSSON. Acta Chem. Scand. **15**, 1437 (1961).
145. R. C. L. MOONEY-SLATER. Acta Crystallogr. **14**, 1140 (1961).
146. D. ADHIKESAVALU, T. S. CAMERON, and O. KNOP. **63**, 3322 (1985).
147. O. KNOP, T. S. CAMERON, M. A. JAMES, and M. FALK. Can. J. Chem. **61**, 1620 (1983); (errata) **62**, 1227 (1984).
148. T. S. CAMERON, M. A. JAMES, O. KNOP, and M. FALK. Can. J. Chem. **61**, 2192 (1983).
149. C. E. SJØGREN, P. KLAEBOE, and E. RYTTER. Spectrochim. Acta, **40**A, 457 (1984).
150. W. L. GRADY and M. M. BURSEY. Int. J. Mass Spect. Ion Proc. **56**, 161 (1984).
151. G. MAIRESSE, P. BARBIER, and J.-P. WIGNACOURT. Acta Crystallogr. B, **35**, 1573 (1979).
152. J. GLASER. Acta Chem. Scand. A, **36**, 451 (1982).
153. T. B. MURPHY, D. K. JOHNSON, N. J. ROSE, A. A. ARUFFO, and V. SCHOMAKER. Inorg. Chim. Acta, **66**, L67 (1982).
154. H. J. GUDER, W. SCHWARZ, J. WEIDLEIN, H. J. WIDLER, and H.-D. HAUSEN. Z. Naturforsch. **31**b, 1185 (1976).
155. M. FALK, C.-H. HUANG, and O. KNOP. Can. J. Chem. **53**, 51 (1975).
156. D. M. ADAMS and D. C. NEWTON. J. Chem. Soc. Dalton, 681 (1972).
157. R. E. MEYER. Lieb. Ann. Chem. Pharm. **150**, 149 (1869).
158. A. FOCK. Z. Kristallogr. **6**, 160 (1882).
159. R. C. WALLACE. Z. Kristallogr. **49**, 417 (1911).
160. J. L. HOARD and L. GOLDSTEIN. J. Chem. Phys. **3**, 645 (1935).
161. C. RAMMELSBERG. Pogg. Ann. Phys. **146**, 598 (1872).
162. J. H. PRATT. Am. J. Sci. [3] **49**, 398 (1895).
163. J. GLASER and U. HENRIKSSON. J. Am. Chem. Soc. **103**, 6642 (1981).
164. O. KNOP, T. S. CAMERON, M. A. JAMES, and M. FALK. Can. J. Chem. **59**, 2550 (1981).
165. M. D. NEWTON, G. A. JEFFREY, and S. TAKAGI. J. Am. Chem. Soc. **101**, 1997 (1979).
166. R. TAYLOR and O. KENNARD. Acc. Chem. Res. **17**, 320 (1984).
167. T. S. CAMERON and R. E. CORDES. Acta Crystallogr. B, **35**, 748 (1979).
168. International tables for X-ray crystallography. Vol. IV. The Kynoch Press, Birmingham, England. 1974.
169. G. M. SHELDRICK. SHELX system report. University Chemical Laboratories, Lensfield Road, Cambridge, England. 1976.
170. J. R. CARRUTHERS and D. L. WATKINS. CRYSTALS, issue 5. Chemical Crystallography Laboratory, Oxford, England. 1981.

Can. J. Chem. Downloaded from www.nrcresearchpress.com by 72.64.146.136 on 09/07/12
For personal use only.

^{13}C magnetic resonance studies. 131.[1,2] An examination of β-enolization in an unsaturated [3.2.1] system: 3,3-dimethylbicyclo[3.2.1]oct-6-en-2-one

GREG A. ANTONIADIS, MICHAEL T. M. CLEMENTS,[3] SRIYAWATHIE PEIRIS, AND J. B. STOTHERS
Department of Chemistry, University of Western Ontario, London, Ont., Canada N6A 5B7

Received January 8, 1987

GREG A. ANTONIADIS, MICHAEL T. M. CLEMENTS, SRIYAWATHIE PEIRIS, and J. B. STOTHERS. Can. J. Chem. **65**, 1557 (1987).

Under homoenolization conditions (*t*-BuO$^-$/*t*-BuOH/185°C), 3,3-dimethylbicyclo[3.2.1]oct-6-en-2-one (**5**) is converted into six products through three reaction pathways. The major product, 3,3-dimethylbicyclo[3.3.0]octan-2-one, arises by unidirectional β-enolate rearrangement of **5** to the isomeric unsaturated [3.3.0] ketones, which (*a*) undergo efficient reduction to **2**, by single electron transfer, and (*b*) suffer Haller–Bauer cleavage to two isomeric 2,2-dimethyl-3-cyclopentenylpropanoic acids. In competition with these processes is the reversible conjugate addition of *t*-BuO$^-$ to **5** to furnish the 6-*tert*-butoxy derivative, which undergoes β-enolate rearrangement to two isomeric ketones. The structures of these products were established primarily from their ^1H and ^{13}C magnetic resonance spectra.

GREG A. ANTONIADIS, MICHAEL T. M. CLEMENTS, SRIYAWATHIE PEIRIS et J. B. STOTHERS. Can. J. Chem. **65**, 1557 (1987).

Dans des conditions d'homoénolisation (*t*-BuO$^-$/*t*-BuOH/185°C), la diméthyl-3,3 bicyclo[3.2.1]octène-6 one-2 (**5**) se transforme en six produits, par le biais de trois voies réactionnelles. Le produit principal, la diméthyl-3,3 bicyclo[3.3.0]octanone-2, provient d'une transposition unidirectionnelle du β-énolate du composé **5** en cétones [3.3.0] insaturées isomères (*a*) qui subissent une réduction efficace en **2** par un transfert unique d'électron et (*b*) qui subissent un clivage de Haller–Bauer pour conduire à deux acides diméthyl-2,2 cyclopentène-3 yl propanoïques isomères. Ces processus sont en compétition avec l'addition conjuguée réversible de l'anion *t*-BuO$^-$ au composé **5** qui conduit au derivé *tert*-butylate-6 qui subit une transposition β-énolique conduisant à deux cétones isomères. Pour déterminer les structures, on a principalement fait appel aux spectres de résonance magnétique nucléaire du ^1H et du ^{13}C.

[Traduit par la revue]

Introduction

Over the past several years, the rearrangements of several polycyclic ketones have been found to occur by homoenolization through proton abstraction from carbons remote from the carbonyl group (1), generally from β-carbons via β-enolates, although there are a few examples of γ-enolization leading to rearrangement (2). In a few cases we have utilized β-enolate rearrangements for the generation of the ring systems of some interesting natural products (3). In each of these cases, the key step was patterned after the known conversion of 3,3-dimethylbicyclo[3.2.1]octan-2-one (**1**) to its [3.3.0] isomer **2** (4), as exemplified by the conversion of **3** → **4** (3*a*). Thus, it was of interest to examine the possible isomerization of an unsaturated system analogous to **1** as a potential synthetic route to substituted 3,3-dimethylbicyclo[3.3.0]octane derivatives, several of which have been employed in the syntheses of a variety of natural products (5). Consequently, the behavior of 3,3-dimethylbicyclo[3.2.1]oct-6-en-2-one (**5**) has been studied under typical homoenolization conditions (*t*-BuO$^-$/*t*-BuOH at elevated temperatures) to determine whether its transformation to **6** proceeds in a manner similar to that exhibited by **1**. The results of these experiments are presented in this paper.

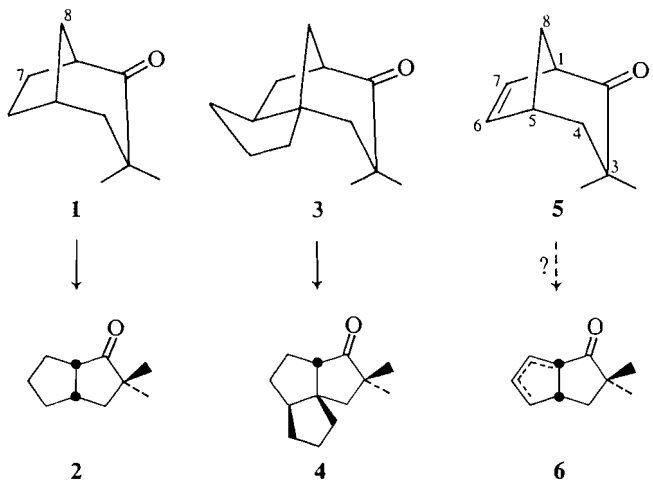

Results

Ketone **5** was prepared from norbornenone (**7**) as outlined in Scheme 1. This route is less efficient than a directed ring expansion by homoketonization of the cyclopropoxide derived from **7**, a route that we had found to be effective for several other bicyclic ketones (6) but this sequence follows a different course with **7** (7). Reaction of **7** with trimethylsilyl cyanide (8) gave **8** in 96% yield and reduction with LAH furnished **9** in 86% yield. Tiffeneau–Demjanov rearrangement (9) of **9** yielded a 1:1 mixture of **10** and **11** (70%), which were readily identified by ^{13}Cmr (10). Although this mixture is separable by glc, it was methylated to furnish the corresponding mixture of **5** and **12**, which was more readily separated by flash chromatography (11); these ketones were identified by their ^1H, ^{13}Cmr, and mass spectra. The ^{13}C data are collected in Table 1.

Following our usual procedures (4), ketone **5** was dissolved in anhydrous *t*-BuO$^-$/*t*-BuOH (1.25 *M*) to furnish a solution 0.30 *M* in **5**. Aliquots of this solution were transferred to glass tubes under nitrogen, sealed under vacuum, and heated to 185°C for varying periods of time (24, 48, and 96 h). The neutral product from each tube was isolated by pentane extraction in yields that steadily decreased with increased reaction time. Each product was analyzed by glc after passing each, in pentane, through a short silica column to remove apparently polymeric material. Over the course of 96 h, glc revealed the

[1]For Part 130 see ref. 20; for Part 129 see ref. 21.
[2]Taken in part from the honors B.Sc. thesis of G.A.A.
[3]Present address: Chemistry Department, Trinity College, Dublin 2, Ireland.

Can. J. Chem. Downloaded from www.nrcresearchpress.com by 72.64.146.136 on 09/07/12
For personal use only.

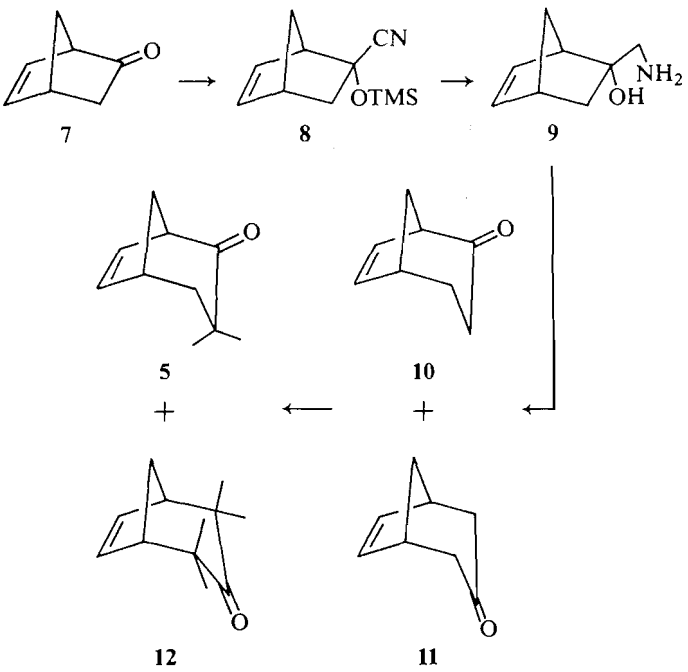

SCHEME 1

smooth conversion of **5** to four new components, of which the major one constituted 50% of the neutral product. Samples of each were obtained by preparative glc and each gave rise to strong carbonyl absorption in the infrared showing all to be ketones. From its carbonyl absorption at 1740 cm^{-1} and its ^{13}Cmr spectrum the major component was readily shown to be **2** (4). The distribution of the components in the neutral fractions as a function of time is given in Table 2. An acidic fraction was isolated in ca. 20% yield from the 96 h runs by ether extraction of the aqueous phase; glc analysis of this material indicated the presence of a single band.

The second new ketone (1695 cm^{-1}, $CHCl_3$), constituting 15% of the neutral fraction after 24 h but only 8% after 96 h, was found to have the molecular formula $C_{14}H_{24}O_2$ and lacked olefinic absorption in its ^1H and ^{13}Cmr spectra. The presence of a *tert*-butoxyl group was evident from the 9-proton singlet at δ 1.190 and ^{13}C absorption at δ_C 28.3 (Me_3) and 73.5 (quat C). The proton spectrum also contained two methyl singlets (1.097, 1.148) and two one-proton doublets of doublets at δ 3.99 and 2.80, each of which was coupled to a pattern at δ 1.80 with couplings of 3.3 and 7.5 Hz, respectively. The δ 1.80 multiplet also contained couplings of 15.0 and 1.8 Hz of which the larger interaction was readily ascribed to geminal coupling with a proton at δ 2.20. The latter pattern also exhibited splittings of 7.0 Hz (common to the δ 3.99 pattern) and 1.8 Hz. The requisite decoupling experiments confirmed these interactions and led to structure **13** for this ketone, for which the *endo*-6 proton absorbs at δ 3.99, H-1 at 2.80, and the *exo*- and *endo*-7 protons at 1.80 and 2.20, respectively. In addition, the *syn*- and *anti*-8 proton absorptions appeared at δ 1.66 and 2.10 (J_{gem} = 12 Hz) with the latter containing a 4.5-Hz coupling to H-1. A partially obscured multiplet near δ 2.24 (H-5) and a two-proton pattern centred at 1.75 (H-4) were also apparent. The ^{13}C shieldings are listed in Table 1.

The third ketone (1690 cm^{-1}, $CHCl_3$) also had the molecular formula $C_{14}H_{24}O_2$ by precise mass measurement and could be assigned structure **14** on the basis of its spectral data. Both the ^1H and ^{13}Cmr spectra lacked olefinic absorption. In addition to methyl singlets at δ 1.049 (3H), 1.156 (3H), and 1.165 (9H), the proton spectrum contained a singlet at δ 3.73 (*syn* H-8), a doublet, δ 2.68, J = 7.5 Hz (H-1), a broad multiplet, δ 2.30, $\nu_{1/2}$ = 14 Hz (H-5), and complex multiplets centred at 2.15 (2H) and 1.70 (4H). The ^{13}C shieldings are collected in Table 1. The assignment of the *anti* orientation for the *tert*-butoxyl group followed from the lack of coupling of the carbinyl proton, since a *syn* proton in this system has a dihedral angle with respect to each bridgehead proton of ca. 90°.

The minor, fourth ketone (1730 cm^{-1}, $CHCl_3$; δ_C 224.8) was found to be isomeric with **13** and **14** by precise mass measurement. The proton spectrum exhibited three methyl singlets (1.012 (3H), 1.139 (3H), 1.164 (9H)), carbinyl proton absorption (3.75, m, $\nu_{1/2} \sim$ 14 Hz), bridgehead proton patterns at δ 3.00 ("dt", J = 4, 10 Hz) and 2.60 ("dq", J = 2.5, 10 Hz) with complex multiplets centred at 2.08 (2H) and 1.65 (4H). Decoupling at δ 3.75 collapsed the 2.60 pattern to an apparent 1:3:3:1 quartet without affecting the 3.00 absorption, while simultaneous irradiation of the latter pattern changed the 2.60 multiplet to a doublet of triplets without altering the carbinyl absorption at 3.75. On the basis of these data, we conclude that this ketone is *exo*-6-*tert*-butoxy-3,3-dimethylbicyclo[3.3.0]octan-2-one (**15**) and the ^{13}C shieldings fit nicely upon comparison with those for **2** with due allowance for the effects of the 6-alkoxy substituent (Table 1).

The acidic fraction, isolated from the 96-h product, was esterified with diazomethane and, although glc analysis indicated a single component, the ^1H and ^{13}C spectra revealed the presence of a 1:2 mixture of isomeric methyl esters. The molecular formula was found to be $C_{11}H_{18}O_2$ by precise mass measurement. The olefinic proton absorption consisted of a broadened singlet, δ 5.65, and a pair of doublets of "quartets", δ 5.60 (J = 5.6 and 2.1 Hz) and 5.70 (J = 5.6 and 2.4 Hz), each with comparable intensities. The ^{13}C spectrum contained three equally intense signals for monoprotonated olefinic carbons, which were comparable to a methine and four methylene signals in the higher field region. The latter were accompanied by one methine and one methylene signals, each of which was half as intense as the others. At highest field, three methyl signals in a 1:1:1 ratio were found, each somewhat less intense than the single methoxyl signal. These data led to the assignment of structures **16***a* and *b* to the minor and major esters, respectively; the ^{13}C data are listed in Table 1.

Hydrogen–deuterium exchange in **5** under these strongly basic conditions was briefly examined. The total ^2H content in samples of **5**-d_x recovered after 2, 4, and 16 h was determined by mass spectrometry and the labelling level at the various sites undergoing exchange was obtained by integration of the ^2Hmr signals. The earlier samples exhibited strong signals at δ 2.9, 5.8, and 6.1, readily assigned to deuterium at C-1, -7, and -6, respectively, upon comparison with the proton data (see Experimental) and, after 16 h, weak signals in a 3:1 ratio appeared at 1.00 and 1.05, indicative of much slower *exo*- and *endo*-methyl exchange. The incorporation results are summarized in Table 3 from which it is apparent that rapid exchange occurs at the α-bridgehead and both olefinic positions with significantly slower exchange at both methyl sites, the more rapid of which is presumably the *exo*-methyl by analogy with several other related systems (1). It may be noted that an additional sample of **5**-d_x recovered after 50 h showed no evidence of ^2H exchange at C-8.

The ^{13}C spectrum of a 1:1 mixture of **5** with **5**-d_x isolated after 2 h in deuterated base revealed the characteristic ^2H-induced

Can. J. Chem. Downloaded from www.nrcresearchpress.com by 72.64.146.136 on 09/07/12
For personal use only.

TABLE 1. ^{13}C magnetic resonance shielding data[a] for **2**, **5**, and **12–16**

Compound	C-1	C-2	C-3	C-4	C-5	C-6	C-7	C-8	Me	Me_3C-
5[b]	55.3	213.3	43.4	40.4	39.3	140.1	131.1	39.5	31.3 34.7	
12	49.7	50.0	221.3	50.0	49.7	136.4	136.4	35.0	25.1 28.2	
2	50.4	224.6	47.7	43.5	36.3	33.6	25.0	29.5	23.1 25.3	
13	50.9	218.5	41.9	42.7	44.2	75.4	32.7	40.2	30.8 31.2	28.3 (Me_3) 73.5
14	58.9	215.5	41.6	43.0	42.9	26.3	26.3	77.2	29.7 31.2	28.5 (Me_3) 73.8
15	49.3	224.8	47.4	41.3	45.6	79.1	34.0	26.8	23.3 25.3	28.6 (Me_3) 73.4
				C-1′	C-2′	C-3′	C-4′	C-5′		MeO
16*a*	178.8	42.3	47.5	35.4	39.9	130.1	130.1	39.9	25.8(2)	51.7
b	178.8	42.4	47.3	42.3	135.5	130.1	31.6	32.1	25.8 25.9	51.7

[a]In ppm from internal TMS for $CDCl_3$ solutions.
[b]Assignments were confirmed by the deuterium-induced shifts found for **5**-d_x (see text).

TABLE 2. Composition[a] of the neutral product obtained upon homoenolization of **5** (*t*-BuO^-/*t*-BuOH at 185°C)

Compound	Time (h)	Yield (%)	**5**	**2**	**13**	**14**	**15**
5	24	85–90	60	18	15	6	1
	48	75–80	47	30	12	9	2
	96	55–60	25	50	8	12	5

[a]Determined as % of the total neutral product by glc with a 6% FFAP column.

TABLE 3. Deuterium incorporation in **5** at 185°C

		% exchange/hydrogen by ^2Hmr (±2%)				
					Methyl	
Time (h)	Atoms D/molecule	H-1	H-6	H-7	*exo*	*endo*
2	1.63	36	41	86	—	—
4	1.85	43	50	92	—	—
16	2.59	83	83	83	~3	~1

effects (12) that served to confirm the assignments listed in Table 1. The methylene absorptions at δ_C 40.4 and 39.5 arising from C-4 and -8, respectively, differed in that the latter contained a component shifted by 75 ppb (1 ppb = 0.001 ppm), owing to deuterium at C-1. The C-5 pattern at δ_C 39.3 included components ascribable to species having ^2H at C-6 (110 ppb) and C-7 (30 ppb, $J \sim 1.4$ Hz), while the C-1 absorption, δ_C 55.3, exhibited components shifted by 76 ppb (^2H-7) and 16 ppb, $J \sim 1.2$ Hz (^2H-6). Deuterium incorporation at C-6 and C-7 was evident from the appearance of the characteristic triplets, $J_{CD} = 26$ Hz, shifted upfield by 290 and 270 ppb, respectively. The C-6 pattern also contained components shifted by 25 ppb (^2H-1) and 150 ppb (^2H-7); these were indistinguishable from the noise for C-7 because of the high level of incorporation (86%) at this centre. Other isotope shifts observed were 24 ppb (C-3, ^2H-1) and 16 ppb (*endo*-Me, ^2H-1).

An examination of **12** under homoenolization conditions showed that it is stable; even after 240 h at 185°C, **12** was recovered in >85% yield with no evidence (glc and ^{13}Cmr) of the presence of any isomeric material.

Discussion

The reactivity of **5** under homoenolization conditions contrasts sharply with that of the isomeric bicyclooctenones **17** and **18**, which are cleanly equilibrated under the same conditions with negligible side reactions (13). In fact, the most striking feature of the **17** ⇌ **18** equilibration is the enhanced rate relative

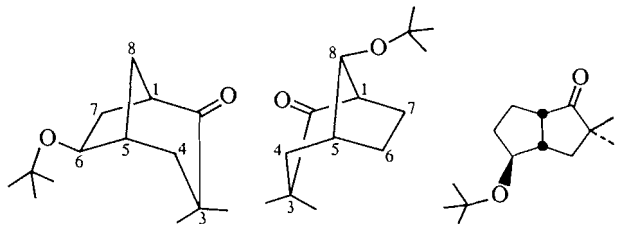

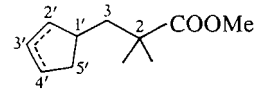

16*a* $\Delta^{3'}$
b $\Delta^{2'}$

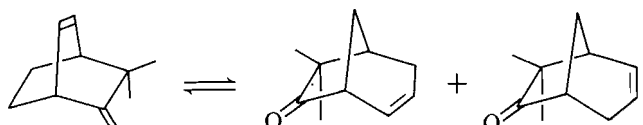

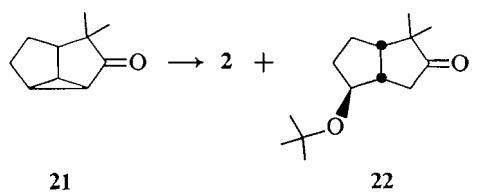

Can. J. Chem. Downloaded from www.nrcresearchpress.com by 72.64.146.136 on 09/07/12
For personal use only.

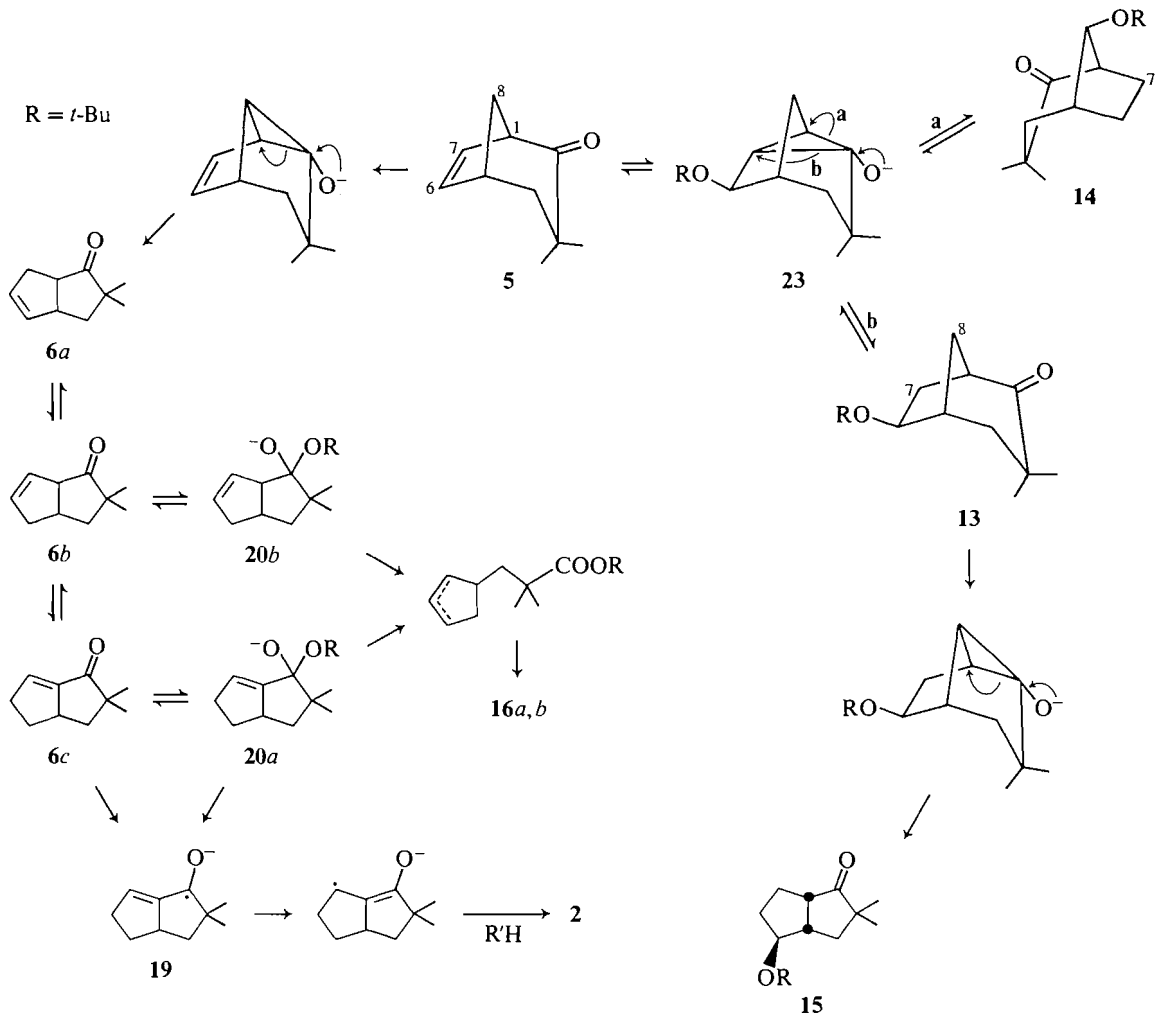

SCHEME 2

to the behavior of several other bicyclic ketones, since equilibrium is established in ca. 20 h. It may be noted that the rate of rearrangement of **17** is more than 100 times faster than that found for its saturated analog (14). At the outset of this study of **5** it was anticipated that a significant rate enhancement over that exhibited by **1** → **2** might be realized, with the formation of one or more of the **6** isomers. However, while the rate of disappearance of **5** is faster than that found for **1** (4), a multicomponent product results. The generation of the products obtained from **5** upon treatment with *t*-BuO$^-$/*t*-BuOH at 185°C can be explained as outlined in Scheme 2.

Since **2** is the predominant product from **5** it is clear that proton abstraction at C-8 is the major process, but the isomeric unsaturated ketones **6** do not survive the reaction conditions. It is apparent that reduction occurs but we were unable to detect an oxidized product. We suggest that the α,β-unsaturated isomer **6***c* undergoes reduction by electron transfer from the *tert*-butoxide anion, either directly from ketyl **19** or by homolysis of the addition product **20***a*. A similar reduction process was observed earlier for the related ketone **21**, which is smoothly converted to a mixture of **2** and its 6-*tert*-butoxy derivative **22** under the same conditions (15). The absence of 8-*tert*-butoxy-**2** among the products from **5** indicates that **22** may arise from Michael addition of *t*-BuO$^-$ to **21** rather than by reaction with a *tert*-butoxide radical as suggested earlier (15). Haller–Bauer cleavage of **20***a* to form an ester could also occur (Scheme 2) but the addition product **20***b* from **6***b* may be more susceptible to cleavage since the process leads to an allylic carbanion. Upon formation of the monocyclic ester(s), equilibration of the $\Delta^{2'}$ and $\Delta^{3'}$ isomers can occur readily in the strongly basic medium via allylic anions. It has been shown previously that *tert*-butyl esters from such ketonic cleavages do not survive the reaction conditions and are isolated as the corresponding carboxylic acids (16). Since the samples of **5**-d_x recovered from the experiments in deuterated base lacked detectable deuterium at C-8, proton abstraction from this site must be irreversible such that opening of the resulting β-enolate leads only to **6***a*. This is exactly analogous to the result for its saturated analog **1** (4).

Approximately one-fourth of the neutral fractions consisted of material containing a *tert*-butoxyl substituent. Thus, addition of *t*-BuO$^-$ to the double bond of **5** is a competitive process. The addition of *t*-BuO$^-$ can lead directly to β-enolate **23** (Scheme 2), which can open in two other ways: path **a** leading to **14** and path **b** to **13**. Proton abstraction from C-8 in **13** provides a route to **15** and may be expected to be unidirectional by analogy with the findings for **1** and **5** upon proton abstraction from the methano bridge. Proton abstraction from C-7 in **13** and **14** to form **23** is also analogous to the findings for **1** (4). Elimination of *tert*-butyl alcohol from **13**-*d*, formed in deuterated base, would account for the relatively rapid deuterium incorporation at C-7 in **5** (Table 3). In contrast to **1** for which bridgehead

Can. J. Chem. Downloaded from www.nrcresearchpress.com by 72.64.146.136 on 09/07/12
For personal use only.

exchange of H-1 is nearly complete in 1 h at 185°C, the corresponding process in **5** is much slower, perhaps owing to increased strain imposed by the 6,7 double bond in the α-enolate. It may also be noted that exchange at the methyl sites in **5** is 3–5 times slower than the rates of methyl exchange in **1**. Exchange at C-6 may involve homoconjugative deuteronation at C-6 with subsequent loss of the original 6-hydrogen or direct vinyl exchange; the process occurs at a rate comparable to that of bridgehead exchange (Table 3).

In summary, ketone **5** undergoes β-enolization at C-8 leading irreversibly to the isomeric unsaturated [3.3.0] system **6**, which, unfortunately in terms of the original premise for this study, does not survive under the reaction conditions but suffers reduction and Haller–Bauer ring cleavage. Reversible conjugate addition of *tert*-butoxide also occurs at C-6 in **5** to generate **13**, which exhibits β-enolization to both C-7 and C-8 leading to **14** and **15**, respectively. Furthermore, the material balance is much lower than is usually found upon similar treatment of several closely-related ketones, indicating that other unidentified processes consume starting material in significant amounts, perhaps by polymerization.

Experimental

Gas–liquid chromatography was carried out on a Varian 920 instrument using columns of 6% FFAP or 20% DEGS on Chromosorb W, as indicated. Ether was dried over sodium and freshly distilled before use; methyl iodide was dried over 4A sieves. Norbornenone (**7**) was employed as starting material and its preparation had been described earlier (7).

Infrared spectra were recorded with a Beckman 4250 instrument and mass spectra were obtained on a Varian MAT-311A system at 70 eV (direct inlet). Routine ^{1}Hmr spectra were recorded with a Varian EM-360 instrument while data for pure samples were collected with a Varian XL-200 instrument. The ^{2}H and ^{13}Cmr spectra were obtained at 46.1 and 75.4 MHz, respectively, with a Varian XL-300 system, and comparison of the fully decoupled ^{13}C spectra with those recorded with either the APT (17) or DEPT (18) sequences identified the number of hydrogen atoms on each carbon.

*Bicyclo[3.2.1]oct-6-en-2- and -3-ones (**10**, **11**)*

Trimethylsilyl cyanide (7.14 g, 0.072 mol) was added slowly to a stirred mixture of norbornenone (8.2 g, 0.066 mol) and ZnI_2 (20 mg) under N_2 at ice temperature. The ice bath was removed after the addition and stirring was continued for 20 h at room temperature. Removal of the excess reagents afforded the cyanohydrin ether **8** (15.1 g, 96%); ir ($CHCl_3$): 2400 cm^{-1}; ^{13}Cmr ($CDCl_3$) δ_C: 1.2 ($SiMe_3$), 44.9, 47.8 (2 × CH_2), 43.7, 54.7, 131.4, 139.0 (4 × CH), 73.5 (quat C), 123.2 (CN).

Cyanohydrin ether **8** (8.3 g, 0.040 mol) in Et_2O (50 mL) was added to a stirred suspension of LAH (1.9 g, 0.050 mol) in anhydrous Et_2O (50 mL) under N_2 at a rate that maintained gentle reflux and the mixture was heated under reflux for 16 h before the destruction of excess LAH by the addition of water. The precipitate was removed by filtration, washed with Et_2O, and the washings added to the filtrate before drying over $MgSO_4$. Evaporation of the solvent furnished the aminoalcohol **9** (4.8 g, 86%); ir ($CHCl_3$): 3450, 1610 cm^{-1}; ^{13}Cmr ($CDCl_3$) δ_C: 41.4, 48.7, 50.9 (3 × CH_2), 42.3, 49.4, 133.4, 139.2 (4 × CH), 80.9 (quat C).

A solution of aminoalcohol **9** (10.1 g, 0.073 mol) in glacial HOAc (5.2 mL) and water (80 mL) was cooled to 0°C with stirring before a solution of $NaNO_2$ (6.2 g, 0.090 mol) in water (80 mL) was slowly added dropwise over a period of 45 min. Stirring was continued for 1 h before the reaction mixture was heated under reflux for 1 h. Upon cooling to room temperature, the acidic solution was neutralized with aqueous $NaHCO_3$ solution before isolation of the product by ether extraction (8 × 100 mL). The combined extracts were dried over $MgSO_4$. Evaporation of the solvent gave a yellow oil (6.3 g, 70%) that was a 1:1 mixture of two major components, by glc analysis (DEGS), which were identified as **10** and **11** by ^{13}Cmr (10). The crude product was subjected to flash chromatography (Et_2O – petroleum ether, 20:80) to remove traces of minor impurities before the methylation step.

*3,3-Dimethylbicyclo[3.2.1]oct-6-en-2-one (**5**)*

To a vigorously stirred suspension of $NaNH_2$ (8.25 g, 0.2 mol) in Et_2O (200 mL) under N_2 was slowly added a solution of the mixture of **10** and **11** (2.5 g) in Et_2O (25 mL) at room temperature before the mixture was refluxed for 3 h. After cooling, methyl iodide (9.4 mL, 0.15 mol) was added slowly before the mixture was heated under reflux overnight. After cooling to room temperature, a second portion of MeI (3.2 mL, 0.05 mol) was added and refluxing continued for 3.3 h before the addition of a third portion of MeI (3.2 mL, 0.05 mol). After a reflux period of 3.3 h, the reaction mixture was cooled to room temperature before the slow addition of water (50 mL). The ether layer was separated and the aqueous layer extracted with ether (5 × 100 mL). The combined extracts were dried over $MgSO_4$, and the product, recovered by evaporation of the solvent as a yellowish oil (2.6 g, 77%), was found to be a 1:1 mixture of two major components, by glc analysis (FFAP), that was readily separable by flash chromatography (Et_2O – petroleum ether, 10:90). The first major component was obtained as a crystalline solid, mp 77–78°C, by preparative glc (FFAP) and found to be **5**; ir ($CHCl_3$): 1690, 1380 cm^{-1}; ^{1}Hmr ($CDCl_3$) δ: 1.012 (s, 3H, Me), 1.045 (s, 3H, Me), 1.48 (ddd, 1H, *endo*-H-4, J_{gem} = 13.5, $J_{4,5}$ = 2.3, $J_{4,8}$ = 2.3 Hz), 1.70 (dd, J = 13.5, 4.3 Hz, 1H, *exo*-H-4), 1.91 (bd, J = 11.3 Hz, 1H, *syn*-H-8), 2.17 (dddd, J = 11.3, $J_{8,1}$ = 4,5, $J_{8,5}$ = 5.4 Hz, $J_{8,4}$ = 2.3 Hz, *anti*-H-8), 2.68 (m, 1H, H-5), 2.90 (dd, $J_{1,8}$ = 4.5, $J_{1,7}$ = 3.0 Hz, 1H, H-1), 5.77 (dd, $J_{7,6}$ = 5.5, $J_{7,1}$ = 3.0 Hz, 1H, H-7), 6.12 (dd, $J_{6,7}$ = 5.5, $J_{6,5}$ = 2.5 Hz, 1H, H-6); ^{13}Cmr: see Table 1. *Exact Mass* calcd. for $C_{10}H_{14}O$: 150.1045; found: 150.1040.

*2,2,4,4-Tetramethylbicyclo[3.2.1]oct-6-en-3-one (**12**)*

The second component isolated from the methylation product mixture by flash chromatography was shown to be **12**; mp 25–26°C; ir ($CHCl_3$): 1695, 1380 cm^{-1}; ^{1}Hmr ($CDCl_3$) δ: 0.887 (s, 6H, Me), 1.099 (s, 6H, Me), 1.760 (dt, J = 5.2, 11.6 Hz, 1H, *anti*-H-8), 2.263 (bd, J = 11.6 Hz, 1H, *syn*-H-8), 2.270 (bm, 2H, H-1,5), 6.08 (bs, 2H, H-6,7); ^{13}Cmr: see Table 1. *Exact Mass* calcd. for $C_{12}H_{18}O$: 178.1358; found: 178.1355.

Homoenolization experiments

The general procedures described previously (19) were followed, whereby a solution of **5** in *t*-BuO$^-$/*t*-BuOH, prepared from potassium metal and *t*-BuOH (water content < 200 μg/mL), was prepared under N_2 (mole ratio: ketone/*t*-BuO$^-$/*t*-BuOH; 1:4:40) and aliquots were quickly transferred to predried, thick-walled glass tubes. The solutions were degassed before the tubes were sealed under vacuum and then heated at 185°C for varying periods of time. After cooling, the reaction mixture was washed from the tube with water and the neutral products were isolated by pentane extraction. Evaporation of the solvent gave a black oil, which was passed through a short column of silica gel before glc analysis (DEGS) that revealed the presence of four significant bands in addition to that for remaining starting material. Samples of these five bands were obtained by preparative glc (DEGS) and each exhibited strong carbonyl absorption in the ir and was identified, primarily from the nmr data. These ketones were eluted, in this order: **2**, **5**, **14**, **15**, and **13**. The basic aqueous phase was acidified with 5% HCl solution before ether extraction. The extracts were dried over $MgSO_4$ before evaporation of the solvent. The resulting product was treated with diazomethane, generated from Diazald in the usual fashion, and allowed to stand overnight before evaporation of the solvent. Gas–liquid chromotographic analysis (FFAP) indicated the presence of a single major band, which consisted of a 2:1 mixture of isomeric methyl esters by ^{13}Cmr, after isolation by preparative glc.

An analogous series of experiments was carried out with **12** as the starting material. In all cases, the neutral product, >85% recovery, contained only the initial ketone; there was no evidence (glc, ^{13}Cmr) of the presence of a new component.

Can. J. Chem. Downloaded from www.nrcresearchpress.com by 72.64.146.136 on 09/07/12
For personal use only.

A series of samples of **5** with *tert*-butylalcohol-O-d_1 (99% deuterated; H_2O content < 200 μg/mL) was also run to examine the exchange processes of **5** under the same reaction conditions; the results are described in the text.

exo-*6*-tert-*Butoxy-3,3-dimethylbicyclo[3.2.1]octan-2-one (13)*

The second ketonic product from **5** was assigned structure **13** on the basis of the following data: ir ($CHCl_3$): 1695, 1035 cm^{-1}; ^{1}Hmr ($CDCl_3$) δ: 1.097 (s, 3H, CH_3), 1.148 (s, 3H, CH_3), 1.190 (s, 9H, $3CH_3$), 3.99 (dd, J = 3.3, 7.0 Hz, *endo*-H-6), 2.80 (dd, J = 4.5, 7.5 Hz, H-1), 2.20 (ddd, J = 1.8, 7.0, 15.0 Hz, *endo*-H-7), 2.24 (m, H-5), 2.10 (bdt, $J \sim 4.5$, 12 Hz, *anti*-H-8), 1.80 (dddd, J = 1.8, 3.3, 7.5, 15.0 Hz, *exo*-H-7), 1.66 (bd, $J \sim 12$ Hz, *syn*-H-8), 1.75 (m, 2H, H-4), ^{13}Cmr: Table 1. *Exact Mass* calcd. for $C_{14}H_{24}O_2$: 224.1776; found: 224.1771.

anti-*8*-tert-*Butoxy-3,3-dimethylbicyclo[3.2.1]octan-2-one (14)*

The third ketone isolated from the neutral product from **5** was assigned structure **14** from the following data: ir ($CHCl_3$): 1690, 1067 cm^{-1}; ^{1}Hmr ($CDCl_3$) δ: 1.049 (s, 3H, CH_3), 1.156 (s, 3H, CH_3), 1.165 (s, 9H, $3CH_3$), 3.73 (bs, *syn*-H-8), 2.68 (bd, $J \sim 7.5$ Hz, H-1), 2.30 (m, $\nu_{1/2} \sim 14$ Hz, H-5), 2.15 (m, 2H), 1.70 (m, 4H); ^{13}Cmr: Table 1. *Exact Mass* calcd. for $C_{14}H_{24}O_2$: 224.1776; found: 224.1769.

exo-*6*-tert-*Butoxy-3,3-dimethylbicyclo[3.3.0]octan-2-one (15)*

The minor ketone from the homoenolization of **5** was found to be **15** from the following data: ir ($CHCl_3$): 1730, 1195 cm^{-1}; ^{1}Hmr ($CDCl_3$) δ: 1.012 (s, 3H, CH_3), 1.139 (s, 3H, CH_3), 1.164 (s, 9H, $3CH_3$); 3.75 (m, $\nu_{1/2} \sim 14$ Hz, *endo*-H-6), 3.00 (ddd, $J \sim 4$, 10, 10 Hz, H-1), 2.60 (dddd, J = 2.5, 10, 10, 10 Hz, H-5), 2.08 (m, 2H), 1.65 (m, 4H); ^{13}Cmr: Table 1. *Exact Mass* calcd. for $C_{14}H_{24}O_2$: 224.1776; found: 224.1772.

*Methyl $\Delta^{2'}$ and $\Delta^{3'}$-3-cyclopentenyl-3,3-dimethylpropanoates (16*a, b*)*

The acidic fraction isolated from the 96-h runs with **5** was esterified with diazomethane in the usual fashion. The single major band indicated by glc (FFAP) to represent >95% of the product was purified by preparative glc; the ^{1}H and ^{13}Cmr spectra showed the presence of two components in an approximately 1:2 ratio. The following spectral data for these compounds led to the assignments of structures **16***a* and *b*, respectively; ir ($CHCl_3$): 3050, 1720 cm^{-1}; ^{1}Hmr ($CDCl_3$) δ: 1.204 (s, 3H, CH_3), 1.214 (s, 3H, CH_3), 3.668 (s, 3H, OCH_3), 2.70 (m, ~1H), 1.25–2.5 (complex patterns, ~6H), 5.65 (bs, H-3′,4′ minor isomer) 5.60 (ddt, $J \sim 5.6$, 2.1, 2.1 Hz), and 5.70 (ddd, $J \sim 5.6$, 2.4, 2.4 Hz, H-2′ and 3′) in the major isomer; ^{13}Cmr: Table 1. *Exact Mass* calcd. for $C_{11}H_{18}O_2$: 182.1307; found: 182.1300.

Acknowledgements

We are grateful for the financial support provided by the Natural Sciences and Engineering Research Council of Canada.

1. N. H. Werstiuk. Tetrahedron, **39**, 305 (1983).
2. A. K. Cheng, A. K. Ghosh, and J. B. Stothers. Can. J. Chem. **62**, 1385 (1984).
3. (*a*) J. L. Jurlina, H. A. Patel, and J. B. Stothers. Can. J. Chem. **62**, 1159 (1984); (*b*) H. A. Patel and J. B. Stothers. Can. J. Chem. **62**, 1926 (1984); (*c*) B. A. Dawson, A. K. Ghosh, J. L. Jurlina, A. J. Ragauskas, and J. B. Stothers. Can. J. Chem. **62**, 2521 (1984).
4. A. L. Johnson, N. O. Petersen, M. B. Rampersad, and J. B. Stothers. Can. J. Chem. **52**, 4143 (1974).
5. S. Nozoe, J. Furukawa, U. Sankawa, and S. Shibata. Tetrahedron Lett. 195 (1976); A. G. Greene. Tetrahedron Lett. **21**, 3059 (1980); S. Kagawa, S. Matsumoto, S. Nishida, S. Yu, J. Morita, A. Ichihara, H. Shirahama, and T. Matsumoto. Tetrahedron Lett. 3913 (1969); L. A. Paquette, H. Schostarez, and G. D. Annis. J. Am. Chem. Soc. **103**, 6526 (1981); L. A. Paquette and G. D. Annis. J. Am. Chem. Soc. **105**, 7358 (1983); W. K. Bornack, S. S. Bhagwat, J. Ponton, and P. Helquist. J. Am. Chem. Soc. **103**, 4647 (1981); S. Danishefsky, R. Zamboni, M. Kahn, and S. J. Etheredge. J. Am. Chem. Soc. **103**, 3460 (1981); J. Froborg and G. Magnusson. J. Am. Chem. Soc. **100**, 6728 (1978).
6. V. Patel, A. J. Ragauskas, and J. B. Stothers. Can. J. Chem. **64**, 1440 (1986).
7. A. J. Ragauskas and J. B. Stothers. Can. J. Chem. **61**, 2254 (1983).
8. D. A. Evans, G. L. Carroll, and L. K. Truesdale. J. Org. Chem. **39**, 914 (1974).
9. M. A. McKinney and P. P. Patel. J. Org. Chem. **38**, 4059 (1973).
10. J. B. Stothers, J. R. Swenson, and C. T. Tan. Can. J. Chem. **53**, 581 (1975).
11. W. C. Still, M. Kahn, and A. Mitra. J. Org. Chem. **43**, 2923 (1978).
12. J. L. Jurlina and J. B. Stothers. J. Am. Chem. Soc. **104**, 4677 (1982); R. Aydin, J. R. Wesener, H. Gunther, R. L. Santillan, M. E. Garibay, and P. Joseph-Nathan. J. Org. Chem. **49**, 3845 (1984).
13. A. K. Cheng and J. B. Stothers. Can. J. Chem. **56**, 1342 (1978).
14. A. K. Cheng, J. B. Stothers, and C. T. Tan. Can. J. Chem. **55**, 447 (1977).
15. A. K. Cheng, A. K. Ghosh, and J. B. Stothers. Can. J. Chem. **62**, 1385 (1984).
16. A. Nickon, J. L. Lambert, J. E. Oliver, D. F. Covey, and J. Morgan. J. Am. Chem. Soc. **98**, 2593 (1976); R. A. Dyllick-Brenzinger and J. B. Stothers. J. Chem. Soc. Chem. Commun. 108 (1979), and references therein.
17. S. L. Patt and J. N. Shoolery. J. Magn. Reson. **46**, 535 (1982).
18. D. M. Doddrell, D. T. Pegg, and M. R. Bendall. J. Magn. Reson. **48**, 323 (1982).
19. A. L. Johnson, J. B. Stothers, and C. T. Tan. Can. J. Chem. **53**, 212 (1975).
20. A. Stoessl, J. B. Stothers, and R. C. Zimmer. J. Chem. Soc. Chem. Commun. 508 (1987).
21. S. Peiris, A. J. Ragauskas, and J. B. Stothers. Can. J. Chem. **65**, 789 (1987).

Can. J. Chem. Downloaded from www.nrcresearchpress.com by 72.64.146.136 on 09/07/12
For personal use only.

Selected-ion flow tube studies of reactions of the carbene cation $:C_4N^+$ and their implications for interstellar gas cloud chemistry

DIETHARD K. BOHME, STANISŁAW WŁODEK, AND ASIT B. RAKSIT

Department of Chemistry and Centre for Research in Experimental Space Science, York University, Downsview, Ont., Canada M3J 1P3

Received December 1, 1986

DIETHARD K. BOHME, STANISŁAW WŁODEK, and ASIT B. RAKSIT. Can. J. Chem. **65**, 1563 (1987).

The carbene cation $:C_4N^+$ was generated in a Selected-Ion Flow Tube (SIFT) apparatus from allyl cyanide by electron impact and reacted at room temperature in helium buffer gas at ca. 0.33 mm Hg with the molecules H_2, CO, HCN, CH_4, CD_4, H_2O, HC_3N, C_2H_2, CH_3CN, CD_3CN, H_2S, NH_3, ND_3, and C_4H_2. The reactions were observed to exhibit a range in reactivity and a variety of reaction products. The observed products are consistent with expectations based on the carbene character of $:C_4N^+$. The results have implications for the role of $:C_4N^+$ as a reaction intermediate in the chemistry of interstellar gas clouds. Possible synthetic routes initiated by $:C_4N^+$ are proposed for the formation of dicyanoacetylene, cyanodiacetylene, and several acyclic as well as cyclic neutral carbenes.

DIETHARD K. BOHME, STANISŁAW WŁODEK et ASIT B. RAKSIT. Can. J. Chem. **65**, 1563 (1987).

Opérant à la température ambiante, dans de l'hélium à environ 0,33 Torr comme gaz tampon et utilisant du cyanure d'allyle soumis à un impact électronique que l'on fait réagir avec des molécules de H_2, CO, HCN, CH_4, CD_4, H_2O, HC_3N, C_2H_2, CH_3CN, CD_3CN, H_2S, NH_3, ND_3 et C_4H_2, on a produit le cation carbènique $:C_4N^+$ dans un tube à écoulement à sélectif pour les ions (SIFT). On a observé que les réactivités varient beaucoup et que les réactions conduisent à un grand nombre de produits. Les produits obtenus correspondent à ceux que l'on peut espérer en se basant sur le caractère carbènique du $:C_4N^+$. Les résultats ont des implications concernant le rôle du $:C_4N^+$ comme intermédiare dans la chimie des nuages gazeux interstellaires. On propose diverses voies de synthèse, initiées par le $:C_4N^+$, pour la formation du dicyanoacétylène, du cyanodiacétylène et de plusieurs carbènes neutres tant acycliques que cycliques.

[Traduit par la revue]

Introduction

A recent experimental study in our laboratory of ion/molecule reactions with cyanoacetylene has suggested a pivotal role for this molecule in the chemical evolution of interstellar gas clouds (1, 2). The presence of cyanoacetylene in a number of these clouds has been firmly established by radioastronomers (3). Gas phase cyanoacetylene is destroyed in these clouds predominantly by reaction with carbon ions (4, 5). This destruction reaction has been shown in our laboratory to proceed with an extremely high specific rate, $k = 6.1 \times 10^{-9}$ cm^3 molecule^{-1} s^{-1} at 296 ± 2 K, and to establish both C_3H^+ and C_4N^+ as product ions in the relative amounts indicated by reaction [1].

$$[1] \quad C^+ + HC_3N \xrightarrow{0.8} C_3H^+ + CN$$

$$\xrightarrow{0.2} C_4N^+ + H$$

This result in turn points towards a pivotal role for C_3H^+ and C_4N^+ as intermediate reactant ions in the further chemical evolution of these environments by ion/molecule reactions. We have explored the interesting chemistry of C_3H^+ in a separate study (6–8). Here we report the results of measurement directed towards the characterization of the chemistry of C_4N^+.

The C_4N^+ was produced from allyl cyanide by electron impact and is likely to have the resonance structure indicated in [2]. The ion has carbene character and a charge which is

$$[2] \quad :C^+—C{\equiv}C—C{\equiv}N: \leftrightarrow :C{=}C{=}C^+—C{\equiv}N:$$

$$\leftrightarrow :C{=}C{=}C{=}C{=}N^+:$$

delocalized. There is one report of an ionization energy for C_4N (9) and it indicates a moderate recombination energy for C_4N^+ of 11.9 ± 0.5 eV. The high value reported for the heat of formation of C_4N^+, 449 kcal mol^{-1} (9), is suggestive of a high chemical reactivity. We are not aware of any previous laboratory measurements of this reactivity.

The reactivity of C_4N^+ is of interest in interstellar cloud chemistry because of its possible role in the synthesis of cyanopolyacetylenes, cyanoacetylene itself, cumulated and disubstituted carbenes (10), and other molecules not yet identified in the interstellar medium.

Experimental

The measurements were performed with the Selected-Ion Flow Tube (SIFT) apparatus in the Ion Chemistry Laboratory (8, 11). The C_4N^+ was generated in an axial electron impact ionizer (Extranuclear Model 0413) from allyl cyanide, CH_2CHCH_2CN, either pure or diluted with helium, at electron energies in the range from 50 to 55 eV. The ion spectrum recorded downstream when C_4N^+ is selected upstream is shown in Fig. 1. The major impurity ion was C_3^+ which is thought to arise from the collisional dissociation of C_4N^+. The CHO^+ and $C_3H_2N^+$ ions may arise from reactions of C_4N^+ with water impurities in the helium buffer gas, while H_3O^+ will be formed by the further reaction of CHO^+ with water. The ions were injected into helium buffer gas at ca. 12 to 50 V. The total pressure was in the range from 0.32 to 0.35 mm Hg and the ambient temperature was 296 ± 2 K. The reagent gases and vapours as well as the helium buffer gas were generally of high purity with a minimum purity of 99.5 mol%. Hydrogen cyanide was prepared according to the procedure described by Glemser (12).

Results

Table 1 summarizes the rate constants and product distributions obtained in this study. It includes all the primary product ions which were observed to contribute 5% or more to the total products. The reactions are listed in order of decreasing ionization energy of the neutral substrate. Rate constants and product distributions were derived in the usual manner (6, 13). In the derivation of minor product distributions complications were introduced by reactions of the C_3^+ initially present in the flow tube which in some instances gave products in common with the products of the C_4N^+ reactions. These reactions of C_3^+

Can. J. Chem. Downloaded from www.nrcresearchpress.com by 118.98.75.50 on 09/07/12
For personal use only.

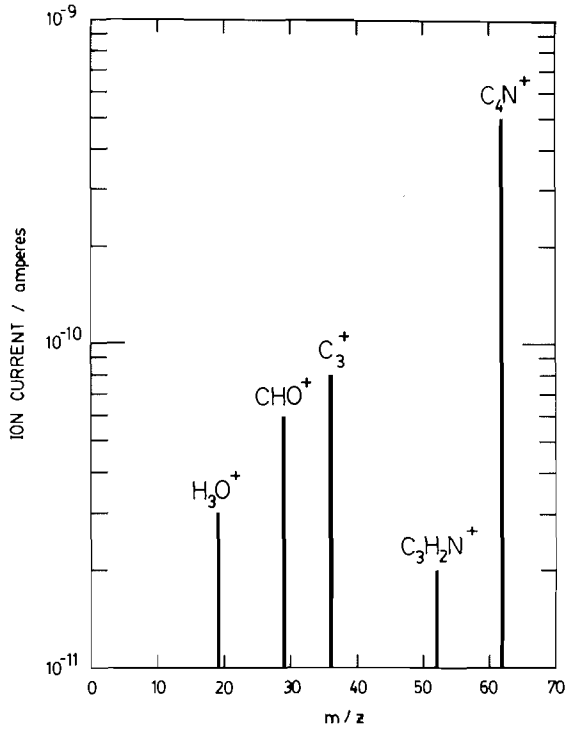

FIG. 1. SIFT spectrum for C_4N^+ derived from pure allyl cyanide by electron ionization at 50 eV. The buffer gas is helium at 0.35 mm Hg and the ion injection energy is ca. 50 V. The background "chemical noise" arises from the collisional dissociation of C_4N^+ and from reactions with water impurity in the buffer gas.

were measured separately and their contributions to the C_4N^+ product spectrum were subtracted where required.

H_2

Molecular hydrogen was observed to react with C_4N^+ only slowly with a specific rate of 2.2×10^{-11} cm^3 molecule^{-1} s^{-1}. The only product which was apparent is indicated in reaction [3]. There was no evidence for hydrogen atom transfer or the

[3] $C_4N^+ + H_2 \rightarrow C_3H^+ + HCN$

addition of molecular hydrogen to C_4N^+. The C_3H^+ product ion reacted further to add molecular hydrogen in a manner reported elsewhere (8).

CO

Only addition was observed with carbon monoxide as shown in reaction [4]. The effective bimolecular rate constant obtained

[4] $C_4N^+ + CO \rightarrow C_5NO^+$

from the decay of C_4N^+ at a total pressure of 0.323 mm Hg and a helium density of 1.05×10^{16} atoms cm^{-3} was 9.3×10^{-11} cm^3 molecule^{-1} s^{-1}. The reaction can be presumed to proceed in a termolecular fashion under these operating conditions but no measurements were made as a function of pressure. The C_5NO^+ ion did not appear to add a second molecule of CO.

HCN, HC_3N

Hydrogen cyanide and cyanoacetylene were observed to react with C_4N^+ in a similar fashion. Adduct formation was the predominant channel observed with both molecules at the moderate helium pressures employed. For the addition reaction [5] with HCN an effective bimolecular rate constant of

[5] $C_4N^+ + HCN \rightarrow C_5HN_2^+$

TABLE 1. Summary of rate constants (in units of 10^{-9} cm^3 molecule^{-1} s^{-1}) and product distributions measured for reactions of :C_4N^+ with the SIFT technique at 296 ± 2 K

Neutral reactant	Products	Branching[a] ratio	k_{exp}[b]	k_c[c]
H_2	$C_3H^+ + CHN$	1.0	0.022	1.5
CO	C_5NO^+	1.0	0.093[d]	0.78
HCN	$C_5HN_2^+$	1.0	0.84[d]	3.2
CH_4	$C_3H_2N^+ + C_2H_2$	0.35	0.57	1.05
	$C_4H_3^+ + CHN$	0.30		
	$C_2H_3^+ + C_3HN$	0.25		
	$CH_2N^+ + C_4H_2$	0.05		
	$C_5H_2N^+ + H_2$	0.05		
H_2O	$C_3H_2N^+ + CO$	0.5	1.5[d]	2.4
	$CHO^+ + C_3HN$	0.4		
	$C_4H_2NO^+$	0.1		
HC_3N	$C_7HN_2^+$	1.0	1[d]	3.3
C_2H_2	$C_5H^+ + CHN$	≥0.7	0.80[d]	1.0
	$C_6H_2N^+$	≤0.3		
CH_3CN	$C_2H_3^+ + C_4N_2$	0.6	3.1	3.7
	$C_4HN_2^+ + C_2H_2$	0.4		
H_2S	$CHS^+ + C_3HN$	0.60	0.89[d]	1.4
	$C_2NS^+ + C_2H_2$	0.25		
	$C_3HS^+ + CHN$	0.10		
	$C_4H_2NS^+$	0.15		
ND_3	$ND_3^+ + C_4N$	0.65	1.2	
	$C_3D_2N^+ + CDN$	0.20		
	$CD_2N^+ + C_3DN$	0.15		
C_4H_2	$C_7H^+ + CHN$	0.4	1.6[d]	1.1
	$C_8H_2N^+$	0.6		

[a]Primary product ions which contribute more than 5%. The branching ratio has been rounded off to the nearest 5% and is estimated to be accurate to ±30%.

[b]The accuracy of the rate constants is estimated to be better than ±30%.

[c]Collision rate constants derived from the combined variational transition state theory — classical trajectory study of Su and Chesnavich (14).

[d]In helium buffer gas at a total pressure of ca. 0.3 mm Hg and concentration of ca. 1×10^{16} atoms cm^{-3}.

8.4×10^{-10} cm^3 molecule^{-1} s^{-1} was measured at a total pressure of 0.33 mm Hg and a helium density of 1.1×10^{16} atoms cm^{-3}. A second molecule of HCN was observed to add, but more than 10 times slower. A third molecule was also observed to add slowly at higher additions of HCN. Previous experiments reported from our laboratory have shown that one molecule of cyanoacetylene also adds rapidly to C_4N^+ according to reaction [6] when the C_4N^+ is generated from the

[6] $C_4N^+ + HC_3N \rightarrow C_7HN_2^+$

reaction of C^+ with HC_3N at a total pressure of 0.31 mm Hg and a helium density of 1.0×10^{16} atoms cm^{-3} (2).

CH_4, CD_4

The product ions observed for the reaction of C_4N^+ with methane are indicated in reaction [7] along with their relative

[7] $C_4N^+ + CH_4 \xrightarrow{0.35} C_3H_2N^+ + C_2H_2$

$\xrightarrow{0.30} C_4H_3^+ + CHN$

$\xrightarrow{0.25} C_2H_3^+ + C_3HN$

$\xrightarrow{0.05} CH_2N^+ + C_4H_2$

$\xrightarrow{0.05} C_5H_2N^+ + H_2$

Can. J. Chem. Downloaded from www.nrcresearchpress.com by 118.98.75.50 on 09/07/12
For personal use only.

Can. J. Chem. Downloaded from www.nrcresearchpress.com by 118.98.75.50 on 09/07/12
For personal use only.

yields. The overall rate constant determined from the decay of C_4N^+ was 5.7×10^{-10} cm^3 molecule^{-1} s^{-1}. Measurements with CD_4 excluded $C_4H_4^+$, CHN^+, and $C_2H_4^+$ as possible product ions. C_3HN^+, which has the same mass as $C_4H_3^+$, could not be completely excluded. Some $m/z = 52$ ions were observed with CD_4. The source for this ion was uncertain. For example, it may be produced from the C_3^+ impurity ions. In any case, the observed ion signals for this ion correspond to a maximum contribution to the products of 5%. The reaction with CD_4 has a measured rate constant of 5.0×10^{-10} cm^3 molecule^{-1} s^{-1}.

The reaction with CH_4 was also investigated using the reaction of C^+ with cyanoacetylene as a source for C_4N^+. Sufficient cyanoacetylene was added into the flow tube to quench most of the C^+ and methane was then added further downstream. The major ion in the flow tube under these conditions was C_3H^+ but the addition of methane did allow an assessment of the products of the C_4N^+ reaction since the products of the reaction of C_3H^+ with methane were known from previous measurements in our laboratory (8). The experiment was carried out at low resolution and products were observed at $m/z = 51 + 52$, $27 + 28$, and 76, in approximately the same proportions as those observed when C_4N^+ was derived directly from allyl cyanide. Also the rate constant determined under these conditions for the decay of C_4N^+, $k = 5.5 \times 10^{-10}$ cm^3 molecule^{-1} s^{-1}, is consistent with the rate constant determined when C_4N^+ was derived by electron impact on allyl cyanide. Finally, both the adduct ions $C_3H^+.HC_3N$ and $C_4N^+.HC_3N$ present under these operating conditions were observed not to react with CH_4, $k \leq 10^{-11}$ cm^3 molecule^{-1} s^{-1}.

H_2O

Two major bimolecular channels were observed for the reaction with H_2O. Adduct formation was observed as a minor channel. The reaction was rapid overall, $k = 1.5 \times 10^{-9}$ cm^3 molecule^{-1} s^{-1}. The product distribution is indicated in reaction [8]. There was no evidence for the occurrence of

$$[8]\quad C_4N^+ + H_2O \xrightarrow{0.5} C_3H_2N^+ + CO$$
$$\xrightarrow{0.4} CHO^+ + C_3HN$$
$$\xrightarrow{0.1} C_4H_2NO^+$$

hydrogen atom or oxygen atom abstraction. The CHO^+ reacted further with H_2O to establish H_3O^+.

C_2H_2

C_4N^+ appeared to react with acetylene to produce predominantly C_5H^+ as shown in reaction [9]. The reaction was rapid,

$$[9]\quad C_4N^+ + C_2H_2 \rightarrow C_5H^+ + CHN$$

$k = 8.0 \times 10^{-10}$ cm^3 molecule^{-1} s^{-1}. The C_5H^+ rapidly reacted further by adding acetylene to produce $C_7H_3^+$. Because of insufficient resolution at the signal intensities of these experiments it was not possible to exclude the possibility of some (less than about 30%) formation of the $C_6H_2N^+$ adduct from the reaction of C_4N^+. There was no evidence for the occurrence of charge transfer or the formation of C_3H^+.

CH_3CN, CD_3CN

A rapid reaction was observed between C_4N^+ and acetonitrile, $k = 3.1 \times 10^{-9}$ cm^3 molecule^{-1} s^{-1}. Two products were formed in about equal amounts according to reaction [10].

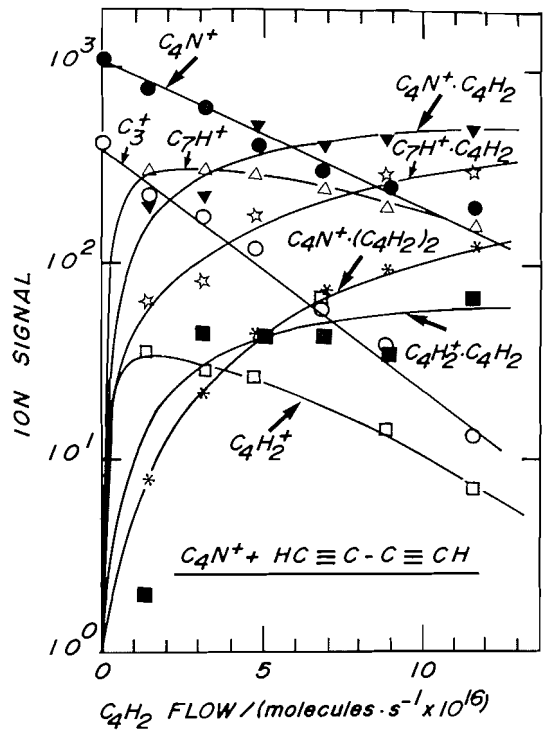

FIG. 2. The variations in ion signals observed for the addition of diacetylene into the reaction region of the SIFT apparatus in which the C_4N^+ cation is initially established in helium buffer gas. $P = 0.348$ mm Hg, $\bar{v} = 6.5 \times 10^3$ cm s^{-1}, $L = 46$ cm, and $T = 295$ K. The C_4N^+ is derived from allyl cyanide at an electron energy of 55 eV.

$$[10]\quad C_4N^+ + CH_3CN \xrightarrow{0.6} C_2H_3^+ + C_4N_2$$
$$\xrightarrow{0.4} C_4HN_2^+ + C_2H_2$$

Experiments with CD_3CN excluded CHN^+ and $C_5H_3N^+$ as possible reaction products. Trace amounts (about 1%) of an ion corresponding to the adduct $C_4N^+.CH_3CN$ were also observed to be formed as a primary product. The predominant primary products $C_2H_3^+$ and $C_4HN_2^+$ both were observed to react further by proton transfer to form CH_3CNH^+ which in turn rapidly added a molecule of acetonitrile to form the protonated dimer $(CH_3CN)_2H^+$.

H_2S

The reaction with hydrogen sulphide was observed to be rapid, $k = 8.9 \times 10^{-10}$ cm^3 molecule^{-1} s^{-1}, and to lead to a variety of products in the yields indicated in reaction [11].

$$[11]\quad C_4N^+ + H_2S \xrightarrow{0.60} CHS^+ + C_3HN$$
$$\xrightarrow{0.25} C_2NS^+ + C_2H_2$$
$$\xrightarrow{0.10} C_3HS^+ + HCN$$
$$\xrightarrow{0.05} C_4H_2NS^+$$

The occurrence of some charge transfer ($\lesssim 5\%$) could not be ruled out.

NH_3, ND_3

Charge transfer was the predominant reaction channel observed with ammonia. Other products observed were $C_3H_2N^+$ and CH_2N^+ and trace amounts ($\lesssim 1\%$) of the adduct $C_4H_3N_2^+$. The specific rate for the total reaction with ammonia was

1.5×10^{-9} cm^3 molecule^{-1} s^{-1}. Experiments with deuterated ammonia excluded $C_2N_2^+$, N_2^+, and $C_2H_4^+$ as possible reaction products. The branching ratios were determined with ND_3 to be as indicated in reaction [12]. The total rate constant with ND_3

$$[12]\quad C_4N^+ + ND_3 \xrightarrow{0.65} ND_3^+ + C_4N$$
$$\xrightarrow{0.20} C_3D_2N^+ + CDN$$
$$\xrightarrow{0.15} CD_2N^+ + C_3DN$$

was measured to be 1.2×10^{-9} cm^3 molecule^{-1} s^{-1}.

C_4H_2

The reaction of C_4N^+ with diacetylene was observed to be rapid, $k = 1.6 \times 10^{-9}$ cm^3 molecule^{-1} s^{-1}. The predominant channels were as indicated in reaction [13]. Figure 2 shows

$$[13]\quad C_4N^+ + C_4H_2 \xrightarrow{0.4} C_7H^+ + CHN$$
$$\xrightarrow{0.6} C_8H_2N^+$$

representative data. In determining the branching ratio for C_7H^+ account had to be taken of the production of some of the C_7H^+ ion from the C_3^+ ion which is initially present. The $C_4H_2^+$ observed in Fig. 2 could be attributed entirely to charge transfer with C_3^+. The adduct ion $C_4N^+.C_4H_2$ ($C_8H_2N^+$) was seen to add a second molecule of diacetylene.

Discussion and conclusions

The observed reactions of $:C_4N^+$ exhibit an interesting variety of products. Many of these products are consistent with the carbene character of this ion and may be rationalized in terms of σ bond insertion or in terms of coordination with an unbonded electron pair. The structure of the $:C_4N^+$ generated from allyl cyanide by electron impact is taken to be that in which the atom sequence is CCCCN as given in [2]. The heavy atom backbone of allyl cyanide is assumed to be maintained in the dissociative ionization and not to rearrange to a different atom sequence such as CCCNC, for example.

Possible coordination with an unbonded electron pair is evident from the high specific rate of the association reaction with carbon monoxide for which the product ion may be O=C=C=C=C=C=N:$^+$. The C_4N^+ also has nitrene character so that formation of :C=C=C=C=N$^+$=C=O is also plausible.

The reactions between $:C_4N^+$ and molecules of type HX are likely to proceed by carbene insertion into the H—X bond to give the substituted propargyl-like ion NC—C≡C—C$^+$(H)X which may then rearrange, dissociate or be collisionally stabilized. The collisionally stabilized adduct was observed as a partial product in the reactions with HX = H_2O, H_2S, C_2H_2, and C_4H_2, and as the exclusive product in the reactions with HX = HCN and HC_3N. Rearrangement to a substituted cyclopropenyl-like ion with subsequent decomposition or collisional stabilization has been advanced earlier as a possible reaction mechanism for the analogous reactions with the carbene cation $:C_3H^+$ (7, 8, 15). For reactions with $:C_4N^+$ the rearrangement with subsequent decomposition may be expressed in the following manner:

[14] NC—C≡C—C:$^+$ + HX → [NC—C≡C—C$^+$(H)X] → [cyclopropenyl-like ion] → NC—C≡C—H + :CX$^+$

A more direct mechanism involving 1,2 hydrogen migration in which the cyclopropenyl-like ion does not participate as an intermediate is also feasible and indeed may be preferred. The reaction products observed with CH_3CN are more consistent with a mechanism involving C—C bond insertion.

An inspection of the observed products suggests that the intermediate reaction complex is sufficiently long-lived in these reactions to allow proton transfer to occur before the products separate. This appears to be the case in the formation of $C_3H_2N^+$ and CHO^+ from H_2O and in the formation of $C_3D_2N^+$ and CD_2N^+ from ND_3. Also, two sets of ionic products in the reaction with methane may be connected in this manner, viz. $C_3H_2N^+/C_2H_3^+$ and $C_4H_3^+/CH_2N^+$. A long life-time for the intermediate complex may also have the consequence of allowing secondary carbene insertion steps before the products separate. Such steps would provide ready explanations for the observation of the bimolecular product ions other than $:CX^+$ (and ions derived from $:CX^+$ by proton transfer). For example, the products observed with H_2 may be accounted for by the following reaction sequence:

[15] $:C_4N^+ + H_2 \rightarrow$ [NC—C≡C$^+$H$_2$] → [cyclopropenyl-like ion] → [H—C≡C—H + :C_2N^+] → [H—C≡C—CH$^+$—CN] → :C_3H^+ + HCN

The reaction of C_2N^+ with acetylene has been measured separately in our laboratory and has been observed to produce C_3H^+ and HCN with high efficiency. A similar mechanism may apply to the formation of C_5H^+ from C_2H_2, C_7H^+ from C_4H_2, C_3HS^+ from H_2S, and $C_4H_3^+$ from CH_4.

Several of the reactions which have been identified in this study have implications for the chemistry of interstellar gas clouds where C_4N^+ is expected to be a likely reaction intermediate due to reaction [1]. First, the observed low reactivity of C_4N^+ towards molecular hydrogen suggests that this ion may be available for reaction with other, less abundant, constituents in interstellar gas clouds which are rich in molecular hydrogen. The degree to which this is the case will depend on the magnitude of the rate constant of reaction [3] at cloud temperatures which may be much less than the small rate constant of 2.2×10^{-11} cm^3 molecule^{-1} s^{-1} measured at 296 K if the reaction has a small activation energy. The availability of C_4N^+ in interstellar gas clouds may be much more sensitive to the presence of atomic hydrogen. Known heats of formation (16) indicate that the channels in reaction [16] are about

Can. J. Chem. Downloaded from www.nrcresearchpress.com by 118.98.75.50 on 09/07/12
For personal use only.

Can. J. Chem. Downloaded from www.nrcresearchpress.com by 118.98.75.50 on 09/07/12
For personal use only.

[16] $C_4N^+ + H \rightarrow C_4H^+ + N$
$\rightarrow C_3H^+ + CN$

70 kcal mol^{-1} and 4 ± 8 kcal mol^{-1} exothermic, respectively, and so may be important loss processes in cloud regions richer in atomic hydrogen.

The measurements reported here indicate that the reaction with the second most abundant molecular gas CO can lead to loss of C_4N^+ in dense interstellar gas clouds only by radiative association as indicated in reaction [17]. The efficiency of this

[17] $C_4N^+ + CO \rightarrow C_5NO^+ + h\nu$

radiative association is uncertain but it may be noted that the specific rate of association observed at the higher pressures of our SIFT experiments is moderately large, viz. within a factor of ten of the collision rate. This result implies the formation of a moderately strong bond (17–19) and consequently a moderately high efficiency for radiative association (20).

The specific rates of association of C_4N^+ with HCN and HC_3N are within a factor of four of the collision rate. We have argued elsewhere that such high rates may be indicative of covalent bond formation in the adduct ion by C—H bond insertion (21). The much lower specific rates observed for the addition of a second molecule of HCN or HC_3N (which is more likely to lead to weaker electrostatic bonding) are consistent with such an interpretation. Covalent bonding with one molecule of HCN or HC_3N may result in acyclic or cyclic structures as indicated by ions **I** and **II** where R = CN or C_3N.

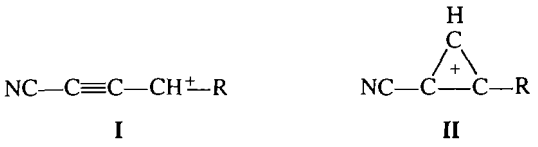

I **II**

Neutralization of these structures may lead to the acyclic disubstituted carbenes :C(CN)C_3N and :C$(C_3N)_2$ or the cyclic carbenes **III** and **IV** (10).

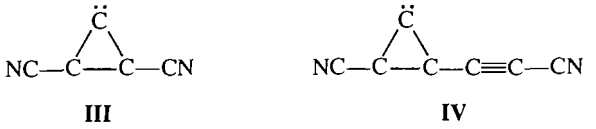

III **IV**

Interestingly, the reaction observed in the SIFT experiments with CH_3CN has quite different implications for molecular synthesis. The reaction between C_4N^+ and CH_3CN appears to be a suitable source for dicyanoacetylene. Sixty percent of this reaction leads directly to the neutral molecule C_4N_2 which is likely to be dicyanoacetylene. The remainder of the reaction leads to the protonated form of C_4N_2 which may subsequently neutralize to yield C_4N_2. One such neutralization event was observed in the proton transfer reaction between $C_4HN_2^+$ and CH_3CN. The proton affinity of dicyanoacetylene is not known but the latter observation establishes that PA (C_4N_2) < PA (CH_3CN) = 188.4 kcal mol^{+1} (22).

The rapid charge transfer reaction observed between C_4N^+ and ammonia provides a direct neutralization route for this ion in interstellar clouds which contain ammonia and is therefore a source for neutral C_4N.

The reaction with methane also has implications for molecular growth. In particular it appears to provide a source for diacetylene and cyanodiacetylene: 35% of the reaction either leads to C_4H_2 directly or to its protonated form, 5% of the reaction leads to $C_5H_2N^+$ which is likely to be protonated cyanodiacetylene, the remaining 60% appears to generate neutral or protonated cyanoacetylene. In the interstellar chemistry these latter products lead to chemical feedback in the sense that the cyanoacetylene will become available for reaction with C^+ which regenerates the C_4N^+.

The reactions of C_4N^+ with acetylene and diacetylene have the potential to lead to unsaturated or slightly saturated carbon chains and so represent contributing pathways to interstellar carbon and hydrocarbon molecules. Neutralization of the product ions C_5H^+ and C_7H^+ by proton transfer or electron/ion recombination may lead to C_5 and C_7, respectively, while neutralization by charge transfer will lead to the C_5H and C_7H radicals. Neutralization reactions of this type with interstellar molecules have been observed with C_3H^+, for example (8). The observation of the pentynylidyne radical C_5H has recently been reported for the circumstellar envelope of IRC + 10216 (23).

Acknowledgements

We thank the Natural Sciences and Engineering Research Council of Canada and the donors of the Petroleum Research Fund, administered by the American Chemical Society, for partial support of this research.

1. D. K. Bohme and A. B. Raksit. Mon. Not. R. astr. Soc. **213**, 717 (1985).
2. A. B. Raksit and D. K. Bohme. Can. J. Chem. **63**, 854 (1985).
3. B. E. Turner. Astrophys. J. **163**, L35 (1971).
4. R. C. Woods. Molecular ions. *Edited by* J. Berkowitz and K. O. Groeneveld. Plenum Publication Corporation. 1983.
5. T. J. Millar and A. Freeman. Mon. Not. R. astr. Soc. **207**, 405 (1984).
6. A. B. Rakshit and D. K. Bohme. Int. J. Mass Spectrom. Ion Phys. **49**, 275 (1983).
7. D. K. Bohme, A. B. Raksit, and A. Fox. J. Am. Chem. Soc. **105**, 5481 (1983).
8. A. B. Raksit and D. K. Bohme. Int. J. Mass Spectrom. Ion Processes, **55**, 69 (1984).
9. V. H. Dibeler, R. M. Reese, and J. L. Franklin. J. Am. Chem. Soc. **83**, 1813 (1961).
10. D. K. Bohme. Nature, **319**, 473 (1986).
11. G. I. Mackay, G. D. Vlachos, D. K. Bohme, and H. I. Schiff. Int. J. Mass Spectrom. Ion Phys. **36**, 259 (1980).
12. O. Glemser. *In* The handbook of preparative inorganic chemistry. *Edited by* G. Brauer. Academic Press, New York. 1963. p. 658.
13. N. G. Adams and D. Smith. J. Phys. B, **9**, 1439 (1976).
14. T. Su and W. J. Chesnavich. J. Chem. Phys. **76**, 5183 (1982).
15. A. C. Hopkinson and M. H. Lien. J. Am. Chem. Soc. **108**, 2843 (1986).
16. J. L. Franklin, J. G. Dillard, H. M. Rosenstock, J. T. Herron, K. Draxl, and F. H. Field. Natl. Stand. Ref. Data Ser. Natl. Bur. Stand. **26**, 41 (1969).
17. A. Good. Trans. Faraday Soc. **67**, 3495 (1971).
18. E. Herbst. J. Chem. Phys. **70**, 2201 (1979).
19. E. E. Ferguson, N. G. Adams, and D. Smith. Chem. Phys. Lett. **128**, 84 (1986).
20. D. R. Bates. Astrophys. J. **270**, 564 (1983).
21. D. K. Bohme, S. Dheandhanoo, S. Włodek, and A. S. Raksit. J. Phys. Chem. In press.
22. S. G. Lias, J. F. Liebman, and R. D. Levin. J. Phys. Chem. Ref. Data, **13**, 695 (1984).
23. J. Cernicharo, C. Kahane, J. Gomez-Gonzalez, and M. Guelin. Astron. Astrophys. **164**, L1 (1986).

The reaction of chloro(triphenylphosphine)gold(I) with 1-methylthymine

R. FAGGIANI, H. E. HOWARD-LOCK, C. J. L. LOCK,[1] AND M. A. TURNER
The Laboratories for Inorganic Medicine, Institute for Materials Research, McMaster University, Hamilton, Ont., Canada L8S 4M1

Received September 8, 1986

R. FAGGIANI, H. E. HOWARD-LOCK, C. J. L. LOCK, and M. A. TURNER. Can. J. Chem. **65**, 1568 (1987).

1-Methylthyminato-N^3-triphenylphosphinegold(I) was prepared by reacting chloro(triphenylphosphine)gold(I) with 1-methylthymine in aqueous methanol at pH 11. The product was examined by X-ray crystallography and was found to have the orthorhombic space group $C222_1$ (no. 20) with cell dimensions a = 12.760(7) Å, b = 11.530(2) Å, c = 31.893(5) Å, and eight formula units in the unit cell. Data were collected with use of MoKα radiation and a Syntex $P2_1$ diffractometer. The crystal structure was determined by standard methods and refined to R = 0.112 and R_w = 0.076 on the basis of 4760 unique reflections. Bond lengths and bond angles are normal. Packing in the crystal lattice is dominated by the triphenylphosphine rings which arrange roughly as blades of a propellor and are the source of the crystal's chirality. The title and related compounds were also examined by ^{1}H nmr, ^{13}C nmr, and vibrational spectroscopy.

R. FAGGIANI, H. E. HOWARD-LOCK, C. J. L. LOCK et M. A. TURNER. Can. J. Chem. **65**, 1568 (1987).

On a préparé le méthyl-1 thyminato N^3-triphénylphosphineor(I) en faisant réagir le chloro(triphénylphosphine)or(I) avec la méthyl-1 thymine, en solution méthanolique aqueuse et à un pH de 11. On a étudié le produit par diffraction des rayons-X et on a trouvé que les cristaux sont orthorhombiques, groupe d'espace $C222_1$ (no. 20), avec a = 12,670(7), b = 11,530(2) et c = 31,893(5) Å et Z = 8. On a recueilli les données en utilisant la radiation MoKα et un diffractomètre Syntex $P2_1$. On a déterminé la structure par les méthodes standards et on l'a affinée jusqu'à des valeurs de R = 0,112 et R_w = 0,076 pour 4760 réflexions indépendantes. Les longueurs et les angles de liaisons sont normaux. L'empillement dans le réseau cristallin est dominé par les cycles triphénylphosphines qui s'arrangent approximativement comme des hélices d'avion et qui sont la source de la chiralité des cristaux. On a aussi étudié le composé mentionné dans le titre ainsi que d'autres composés apparentés à l'aide de la spectroscopie rmn du ^{1}H et du ^{13}C ainsi que par spectroscopie vibrationnelle.

[Traduit par la revue]

Can. J. Chem. Downloaded from www.nrcresearchpress.com by 72.64.146.136 on 09/07/12
For personal use only.

Introduction

The phosphine coordinated gold(I) complex, auranofin, is used in the treatment of rheumatoid arthritis (1). Unlike the other anti-arthritis gold drugs, auranofin has also shown evidence for anti-cancer activity in *in vivo* studies of P388 lymphocytic leukemia and sarcoma 180 tumors in mice (2–4). These results have prompted further investigation of the interaction of auranofin and analogous gold compounds with DNA both *in vivo* and *in vitro* (5–7).

Gel electrophoresis studies of compounds analogous to auranofin ([1,2-bis(diphenylphosphino)ethane]bis[chlorogold(I)] and chloro(triethylphosphine)gold(I), the synthetic precursor to auranofin), show an alteration in the mobility of pBR322 circular DNA, indicating *in vitro* binding of the gold complex to reactive sites on the DNA strand (8, 9). Auranofin itself showed no activity. These results complement those of Blank and Dabrowiak (10) who investigated changes in the absorption and CD spectra of nucleosides and calf thymus DNA in the presence of gold compounds. Again, activity was observed only when an easily displaced ligand was bound to gold (i.e. Cl^- or Br^- but not SR^-). Actual products of reaction were not isolated in these studies although interaction with DNA was observable *in situ*.

The characterization of gold compounds with nucleobases was begun on the basis of the electronic and structural similarity of Au(III) to Pt(II) (11). However, evidence obtained in XANES experiments (12) suggests that Au(III) is reduced to Au(I) *in vivo* (probably by free thiol groups on transport proteins such as albumin) before it enters the cell and becomes available for interaction with DNA. Gold(I) complexes with nucleobases have also been prepared and characterized by Mössbauer, nmr, and infrared spectroscopies (13–15). Beck *et al.* (16) have determined the structure of the complex of (triphenylphosphine)gold(I) with adenine, where the metal binds to the deprotonated N(9) position, a site occupied by the sugar group in biological systems. We have investigated the interaction of chloro(triphenylphosphine)gold(I) with 1-methylthymine and have characterized the resulting complex both by spectroscopic methods and X-ray diffraction.

[1]To whom all correspondence should be addressed.

Experimental section

1-Methylthymine (Fluka) was used without further purification. Analyses were performed by Atlantic Microlab, Atlanta, GA.

Potassium 1-methylthyminate

1-Methylthymine (0.2 g) was dissolved in 15 mL of distilled water. The pH of this solution was raised to 12 by addition of 5 *N* KOH. After heating for several minutes, the solvent was evaporated under reduced pressure and the residue was dried *in vacuo* at 80°C for 3 h. The resulting solid was used without further purification in infrared spectroscopy.

Chloro(triphenylphosphine)gold(I)

$HAuCl_4.3H_2O$ (1.00 g, 2.5 mmol) was dissolved in 20 mL distilled water and cooled in an ice bath. To this was added, dropwise, a solution of 500 μL (5.0 mmol) of thiodiglycol in 1 mL ethanol. An ethanol solution (20 mL) of 0.70 g (2.5 mmol) triphenylphosphine was added and the mixture was stirred for 30 min. The product was filtered and dried *in vacuo* for 12 h then recrystallized twice from dichloromethane/hexane. Yield 86%.

*1-Methylthyminato-N^3-triphenylphosphinegold(I) (**A**)*

1-Methylthymine (0.70 g, 5.0 mmol) was dissolved in 20 mL of distilled water and the pH was raised to 11.1 by addition of 0.5 *N* NaOH. A methanol solution (20 mL) of chloro(triphenylphosphine)gold(I) (2.47 g, 5.0 mmol) was added and the covered solution was stirred. After 6 h, all but 10 mL of the solvent was removed under reduced pressure and the resulting suspension was filtered, the precipitate washed with cold water, and dried *in vacuo*. Crystals suitable for diffraction were obtained by slow recrystallization from methanol/water (50/50 v/v) at 4°C. Yield 74%: (*Anal.* calcd. for $C_{24}H_{22}AuN_2O_2P$: C 48.2, H 3.7, N 4.7; found: C 48.3, H 3.9, N 4.6.

Both proton magnetic resonance and natural abundance carbon-13

Can. J. Chem. Downloaded from www.nrcresearchpress.com by 72.64.146.136 on 09/07/12
For personal use only.

TABLE 1. Crystal data

Compound	$C_{24}H_{22}AuN_2O_2P$
Formula weight	598.369
Crystal size (mm)	0.13 × 0.13 × 0.16
Systematic absences	hkl; $h + k = 2n + 1$
Space group	$C222_1$ (no. 20)
Unit cell parameters (Å)	a = 12.760(1)
	b = 11.530(2)
	c = 31.893(5)
Volume (Å^3)	4692(3)
Z	8
μ linear absorption coefficient (cm^{-1})	65.74
ρ_{calcd}, ρ_{obs} (g/cm^3)	1.694, 1.69(1)
max 2θ, reflections measured	55°, h, k, $\pm l$
Standard reflections (esd %)	−3 1 3 (1.0%), 2 0 8 (1.0%)
Temperature (°C)	22
Total number of reflections measured	6629
Number of independent reflections	4760
no. with $I > 0$ (used)	4760
R_{int}[a]	0.0306
Final R[b], R_w[c]	0.1117, 0.0761
Final shift/error max (ave.)	0.155 (0.011)
Final difference map;	
Highest peak, lowest valley (e Å^{-3})	4.2, −3.4
Weighting	$w = (\sigma^2(F) + 0.0004F^2)^{-1}$
F(000)	2301
No. of variables	27
Error in obs. of unit wt., S	1.3575

[a] $R_{int} = (\Sigma(N\Sigma(w(\langle F\rangle - F)^2))/\Sigma(N-1)\Sigma wF^2)^{1/2}$.
[b] $R = \Sigma||F_o| - |F_c||/\Sigma|F_o|$.
[c] $R_w = (\Sigma w(|F_o| - |F_c|)^2/\Sigma wF_o^2)^{1/2}$.

magnetic resonance spectra were recorded on a Bruker WM-500 spectrometer. Samples for infrared spectroscopy (4000–250 cm^{-1} range) were prepared as KBr pellets (5–10% w/w) and spectra were recorded on a Perkin Elmer 283 spectrometer with use of polystyrene for calibration. Spectra in the 500–100 cm^{-1} range were obtained on an indene calibrated Nicolet 7199 FT-IR spectrometer from Nujol mulls between polyethylene plates. Raman spectra of powder samples excited by the λ 514.5 nm line from a Coherent Radiation Argon Laser Model 52 were recorded on a SPEX 14018. The spectra were calibrated against $HgCl_2$.

Collection of diffraction data and solution of the structure

The crystal of **A** used for diffraction was a colourless prism. Precession photographs showed the crystal to be orthorhombic. Cell parameters were obtained by least-squares refinement of the setting angles of 15 automatically centered reflections (19° < 2θ < 26°) on a Syntex $P2_1$ diffractometer with use of graphite monochromatized MoKα radiation (λ 0.71069 Å). Crystal data and other information related to data collection are given in Table 1. The crystal density was measured by flotation in an aqueous zinc chloride solution. Intensity data were measured at 22°C on the $P2_1$ diffractometer. The methods of selection of scan rates and initial data treatment have been described (17, 18). Corrections were made for Lorentz and polarization effects but not for absorption. Absorption corrections were attempted, but the crystal was of such a shape that an analytical correction was not possible. In addition, it was not possible to get adequately spaced strong high angle reflections for a proper χ-scan correction. Such a correction was attempted, but gave results no better than those presented here. Attempts to grow better crystals were unsuccessful. Ignoring the absorption correction will introduce a maximum error in F_o of 8%.

A three dimensional Patterson map was used to locate the Au atom. The positions of all the other non-hydrogen atoms were obtained from subsequent electron density difference maps. Further refinement of all parameters, including anisotropic temperature factors for all atoms, was done by full-matrix least-squares methods, and minimized the function $\Sigma w(|F_o| - |F_c|)^2$. Refinement was terminated when the maximum (shift/error) was less than 0.2. Peaks of residual electron density were very close to the Au atom. No attempts were made to locate the hydrogen atoms. Corrections were made for secondary extinction by the method used in SHELX.[2]

Since the space group was chiral, an alternative refinement was tested where $-x$, $-y$, $-z$ replaced x, y, z for all atoms. The structure converged to the larger R and R_w factors of 0.1213 and 0.0899; evidence that the correct enantiomorph had been chosen. Parameters were also refined to convergence with use of a truncated set of data where $I > 3\sigma$ (2685 reflections). The resulting R factors of 0.0594 and R_w of 0.0627 were significantly improved because of the deletion of a large number of weak reflections; however, esd's and consequent errors in bond lengths and angles increased. The parameters of the more accurate solution are reported as suggested by Seiler *et al.* (22). The atom parameters are listed in Table 2.[3]

TABLE 2. Atomic positional coordinates (× 10^4) and temperature factors (Å^2 × 10^3)

Atom	x	y	z	U_{eq}*
Au	2849.0(5)	6644.6(6)	3665.8(2)	47.4
N(1)	2065(15)	3107(12)	3359(6)	74
C(1)	1596(23)	2139(18)	3561(11)	132
C(2)	2266(15)	4157(15)	3591(6)	52
O(2)	1980(16)	4239(13)	3950(5)	92
N(3)	2648(10)	5098(11)	3383(4)	41
C(4)	2904(15)	5018(16)	2949(6)	54
O(4)	3234(11)	5953(11)	2759(5)	77
C(5)	2784(18)	3910(16)	2751(6)	58
C(5′)	3157(18)	3792(19)	2285(7)	85
C(6)	2419(14)	3020(16)	2955(8)	64
P	3108(3)	8351(5)	3985(1)	42
C(7)	3862(13)	9336(14)	3669(6)	45
C(8)	3912(19)	10507(23)	3783(7)	87
C(9)	4431(28)	11395(38)	3543(15)	160
C(10)	4986(29)	10956(30)	3216(13)	125
C(11)	4986(16)	9758(36)	3071(8)	113
C(12)	4371(16)	8921(21)	3321(8)	82
C(13)	1907(15)	9097(13)	4094(6)	50
C(14)	1027(14)	8902(15)	3795(6)	63
C(15)	90(16)	9536(17)	3877(8)	71
C(16)	−5(20)	10301(20)	4223(7)	82
C(17)	817(22)	10467(17)	4489(8)	92
C(18)	1800(17)	9897(17)	4442(6)	73
C(19)	3797(15)	8188(14)	4488(5)	50
C(20)	3205(21)	7570(21)	4797(7)	92
C(21)	3660(24)	7296(30)	5193(12)	129
C(22)	4626(37)	7799(26)	5246(8)	136
C(23)	5294(20)	8470(23)	4937(10)	116
C(24)	4790(17)	8659(16)	4542(6)	64

*$U_{eq} = (1/3)(U_{11} + U_{22} + U_{33})$.

Results and discussion

Gold(I) is considered a soft or class b metal ion (24) and likely to interact with the relatively soft sites on DNA

[2]All calculations were carried out on CYBER 170/730 and 815 computers. The programs DATCO5 and DATRDN from the XRAY76 package (18) were used for preliminary treatment of data. The structure solution and refinement were done with use of the SHELX package (19), geometry calculations were done with NRC 22 (20), and diagrams were prepared with use of ORTEP (21).

[3]Tables of anisotropic temperature factors, dihedral and torsional angles, and moduli of F_o and F_c are available, at a nominal charge, from the Depository of Unpublished Data, CISTI, National Research Council of Canada, Ottawa, Ont., Canada K1A 0S7.

TABLE 3. Selected interatomic distances (Å) and angles (deg)

Atoms	Distance	Atoms	Distance	Atoms	Distance
Au—P	2.240(5)	Au—N(3)	2.20(1)	N(1)—C(2)	1.44(2)
C(2)—N(3)	1.36(2)	N(3)—C(4)	1.42(2)	C(4)—C(5)	1.43(2)
C(5)—C(6)	1.30(2)	C(6)—N(1)	1.37(2)	N(1)—C(1)	1.42(3)
C(2)—O(2)	1.20(2)	C(4)—O(4)	1.31(2)	C(5)—C(5′)	1.57(3)
Au....O(2)	3.12(2)	Au....O(4)	3.04(2)		

Bonds	Angle	Bonds	Angle	Bonds	Angle
P—Au—N(3)	178.7(4)	Au—N(3)—C(2)	122(1)	Au—N(3)—C(4)	118(1)
Au—P—C(7)	112.3(6)	Au—P—C(13)	112.5(6)	Au—P—C(19)	112.1(6)
C(6)—N(1)—C(2)	119(2)	N(1)—C(2)—N(3)	119(2)	C(2)—N(3)—C(4)	120(1)
N(3)—C(4)—C(5)	118(2)	C(4)—C(5)—C(6)	121(2)	C(5)—C(6)—N(1)	122(2)
C(6)—N(1)—C(1)	121(2)	C(1)—N(1)—C(2)	120(2)	N(1)—C(2)—O(2)	120(2)
O(2)—C(2)—N(3)	121(2)	N(3)—C(4)—O(4)	118(2)	O(4)—C(4)—C(5)	124(2)
C(4)—C(5)—C(5′)	118(2)	C(5′)—C(5)—C(6)	121(2)		

bases. In studies involving *cis*-dichlorodiammine platinum(II), (*cis*-DDP), Pt(II) binds preferentially at the N(7) position of guanine residues (25). However, in other experiments, when attempts are made to strip platinum off the DNA strand with cyanide ion, the small fraction of the metal which remains is bound to thymine residues (26). Reaction of Pt(II) with deprotonated thymine is apparently not reversible as with other bases. The pH at which this reaction occurs *in vitro* is higher than physiological pH and whether the reaction with thymine can occur *in vivo* is not known. Nevertheless, the possibility of metal assisted pK shifts or enzyme assistance can not be ruled out. We have shown that interactions of DNA bases with metals at one site can markedly affect the pK of another site. Thus the interaction of Pt(II) with N(7) of guanine causes an acid shift of the N1 proton of 1.6 pK units and Pt(II) can bind at pH 7 to the exocyclic O(4) or N(4) groups of 1-methylthymine, 1-methylcytosine, and 1-methyluracil by a process of deprotonation, even though the pK of the NH_2 group in 1-methylcytosine is formally >12. (The pK's of the OH groups in the enol forms of 1-methyluracil and 1-methylthymine are unknown.) This reaction apparently involves initial binding of another Pt(II) atom at N3 of cytosine (27). Because of evidence for the stability of a platinum–thyminate interaction, it was expected that gold would also form a stable compound, and it does.

The structure of 1-methylthyminato-N^3-triphenylphosphinegold(I) is shown in Fig. 1 and selected bond distances and angles are given in Table 3. The molecule itself is chiral because of the propellor-like arrangement of the phenyl rings on phosphorus. Bond lengths and angles involving gold, phosphorus, and the phenyl rings (C—C ave 1.42(3) range 1.35(4)–1.52(4), C—C—C ave 119(3)°, range 112(3)–125(2)°) are consistent with results for chloro(triphenylphosphine)gold(I) (28). Coordination to (triphenylphosphine)gold(I) which involves deprotonation at N3 has the effect on 1-methylthymine of lengthening the C(4)—O(4) bond distance to 1.31(2) Å in A vs. 1.237(4) Å in 1-methylthymine (29). In neutral 1-methylthymine, C(4)=O(4) is involved in hydrogen bonding and is therefore already a relatively long bond (cf. C(2)=O(2) 1.20(2) Å. The Au....O(4) distance is slightly shorter (3.04(2) Å) than the Au....O(2) distance (3.12(2) Å) which may indicate a slightly stronger Van der Waals interaction of the Au with the negative, more polarizable O(4). The C(5)—C(6) distance in the gold complex is shortened (1.30(2) Å) compared to that for 1-methylthymine

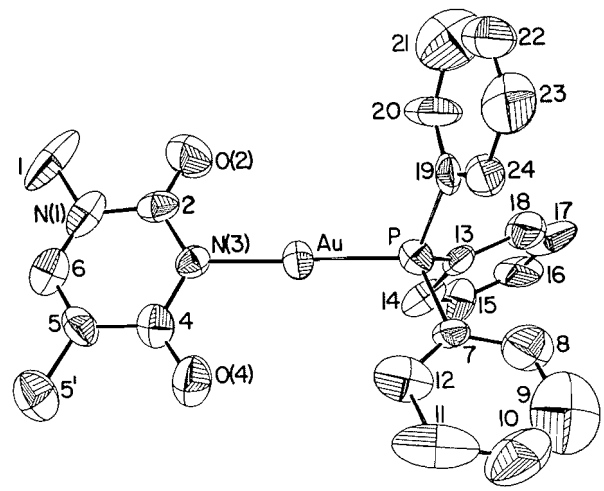

FIG. 1. 1-Methylthyminato-N^3-triphenylphosphinegold(I) showing the atom numbering. Carbon atoms are indicated by numbers only.

(1.346 Å (29)). A possible explanation may be that, since the hydrogen bonding holding the dimers together in 1-methylthymine is disrupted in the process of deprotonation in order to form the (triphenylphosphine)gold(I) complex, there is no longer electron delocalization from the C(5)=C(6) bond into the carbonyl group (see Fig. 3). No firm conclusions should be made, however, until the structure of 1-methylthyminate ion has been determined.

Other effects of gold binding on interatomic distances are the lengthening of the N(3)—C(4) (1.42(2) Å vs. 1.375(4) Å (29)) and N(1)—C(2) (1.44(2) Å vs. 1.379(4) Å (29)) distances. The C(4)—N(3)—C(2) angle (126.2(4)° in 1-methylthymine (28)) narrows to 122(2)° in **A**. Other angles (C(6)—N(1)—C(2), N(1)—C(2)—N(3), N(3)—C(4)—C(5), C(4)—C(5)—C(6)) in the ring open accordingly to compensate. (Triphenylphosphine)gold(I) is apparently more able to stabilize N(3) in an sp^2 form than the proton as it is a poorer electron acceptor. It has been observed for Pt(II) binding to cytosine that angle opening is not as great as that caused by protonation (30).

The packing is shown in Fig. 2. The molecules are arranged in sets of bilayers parallel to the ***ab*** plane. Within a given bilayer, molecules are oriented such that the thyminate–gold–

Can. J. Chem. Downloaded from www.nrcresearchpress.com by 72.64.146.136 on 09/07/12
For personal use only.

Can. J. Chem. Downloaded from www.nrcresearchpress.com by 72.64.146.136 on 09/07/12
For personal use only.

TABLE 4. Nuclear magnetic resonance data

	1-Methylthymine[a]			1-Methylthyminate[b]			1-Methylthyminatotriphenylphosphine gold(I)[c]		
	Chemical shift (ppm)	Multiplicity (J Hz)	Assignment	Chemical shift (ppm)	Multiplicity (J Hz)	Assignment	Chemical shift (ppm)	Multiplicity (J Hz)	Assignment
^{1}Hmr	1.7709	d($^4J_{CH_3(5')—H(6)}$ 1.00)	CH(5')[d]	1.6757	d($^4J_{CH_3(5')—H(6)}$ 1.00)	CH_3(5')	1.8616	s	CH_3(5')
	3.2413	s	CH_3(1)	3.1464	s	CH_3(1)	3.2714	s	CH_3(1)
	7.3560	q($^4J_{H(6)—CH_3(5')}$ 1.00)	H(6)	7.1707	q($^4J_{H(6)—CH_3(5')}$ 1.00)	H(6)	6.8765	s	H(6)
							7.4140	m	C(7)—C(12)[e]
							7.5620	m	"
^{13}Cmr	12.32	s	C(5')	13.40	s	C(5')	13.45	s	C(5')
	36.80	s	C(1)	37.57	s	C(1)	36.67	s	C(1)
	111.44	s	C(5)	111.62	s	C(5)	110.93	s	C(5)
	145.32	s	C(6)	144.48	s	C(6)	140.27	s	C(6)
	154.00	s	C(2)	159.99	s	C(2)	157.71	s	C(2)
	168.17	s	C(4)	175.92	s	C(4)	172.06	s	C(4)
				168.37	s	K_2CO_3[f]	129.25	d($^3J_{P—C(9)}$ 11.31)	C(9)C(1)
							129.38	d($^1J_{P—C(7)}$ 61.56)	C(7)
							131.74	s	C(10)
							134.40	d($^2J_{C(8)—P}$ 13.82)	C(8)C(12)

[a]Sample run in D_2O.
[b]Sample run in D_2O made basic with K_2CO_3 (pH 11).
[c]Sample run in $CDCl_3$.
[d]See numbering scheme in Fig. 1 (molecule).
[e]Refers to carbons listed in this table and their equivalents on the other two phenyl rings (see Fig. 1).
[f]K_2CO_3 in D_2O (pH 11) was run alone to confirm this peak assignment.

TABLE 5. Vibrational spectra of 1-methylthyminato-N^3-triphenylphosphine gold(I) and related species

K thyminate		Chloro(triphenyl-phosphine)gold(I)		1-Methylthyminato-N^3-triphenylphosphinegold(I)		
Infrared[a]	Raman[b]	Infrared	Raman	Infrared	Raman	Assignment
		3080m	3060(37)			νC—H(ph)[c]
3062m	3052(10)	3060m	3052(29)	3050w	3056(4)	νC—H(ph), νC(6)—H
3020m	3027(5)					ν_aNC—H_3, ν_aCC—H_3
2980sh	2980(5)					νC—H_3
2960m	2959(7)					νC—H_3
2940m	2938(7)					νC—H_3
2924w	2921(7)			2920w		ν_sCC—H_3
2900vw	2904(10)					νC—H_3
2840w						
		1980w		1980w		νC=C(ph), phenyl ring overtones
		1900w		1900w		
		1820w		1820w		
1702w						
1663br	1659(22)			1655s	1648(13)	νC(2)=O(2)
1610s	1624(41)			1590s	1586(52)	In-phase, νC(4)=O(4), νC(5)=C(6)
		1585w	1590(53)		1586(52)	νC=C(ph)
			1573(10)		1574(10)	νC=C(ph)
1570s				1580s		Out-of-phase, νC(4)=O(4), νC(5)=C(6)
1525vs	1525(20)					"Alternate bond stretch"
		1480m	1479(2)	1479m	1481(8)	νC=C(ph)
1460s	1480(7)			1454w		ν_aC—CH_3, ν_aN—CH_3
		1439s	1435(3)	1432s	1432(20)	νC=C(ph)
		1432s		1425sh		νC=C(ph)
1430s	1431(20)					δ_aC—CH_3, δ_aN—CH_3
1415s	1417(20)			1418s		δ_sN—CH_3, ν-ring(thy)[d]
		1381m		1381m	1380(8)	
1375m	1372(10)			1360sh		δ_sC—CH_3
1352s	1356(50)			1354m	1359(10)	δ_sN—CH_3, ν-ring(thy)
1327s	1323(10)			1323m		δCH(ph), ν-ring(thy)
1277m	1278(10)			1274w		
1232w				1240w	1244(13)	ν-ring(thy)
1200s				1213m		ν-skel(thy)
		1179s	1182(5)	1184w	1183(10)	δCH(ph) (in-plane)
1158s	1158(7)		1160(10)	1163m	1160(6)	ν-skel(thy)
		1100s	1100(38)	1101s	1100(39)	νP—C (q-vib)[e]
1060m	1060(10)			1060w		rN—CH_3
1040mw						
		1021s	1028(20)	1026w	1027(32)	δCH(ph) (in-plane)
			1024(30)			δ CH(ph) (in-plane)
1002m	1002(10)					rC-CH_3
		995m	996(100)	996m	999(100)	Ring breathing, νC=C(ph)
					984sh	
948w						
900m	900(35)			922vw	920(10)	ν-skel(thy)
888s	882(5)			896vw		ν-ring(thy)
780s	777(86)			773m	781(20)	δ,ν-ring(thy)
758sh				761m		δ,ν-ring(thy)
		750m	745(10)	745m		δCH(ph) (out-of-plane)
		741s		743m		δCH(ph) (out-of-plane)
		736m		721m		δCH(ph) (out-of-plane)
		705s	711(6)	705m	709(5)	r-vib
697m				690sh		
689s	689(33)	688s	689(12)	688s	692(13)	δ-ring(thy), r-vib
657m	661(7)			655vw	660(5)	δC=O (in-plane)
		615vw	615(14)		612(17)	δ-ring(thy), δC—C—C(ph) (in-plane)
548w	543(90)					δ-ring(thy)
		545s	540(4)	548s	537(15)	y-vib
		505s	520vw	511m		y-vib
		500s	505w	503m		y-vib
468v	466(23)					δ-ring(thy)
455m		452w		458s	457(7)	t-vib
		448w	450vw	452w		t-vib
		438w	438vw	444m		

Can. J. Chem. Downloaded from www.nrcresearchpress.com by 72.64.146.136 on 09/07/12
For personal use only.

TABLE 5 (*concluded*)

K thyminate		Chloro(triphenylphosphine)gold(I)		1-Methylthyminato-N^3-triphenylphosphinegold(I)		
Infrared[a]	Raman[b]	Infrared	Raman	Infrared	Raman	Assignment
426vs	421(10)			435w	430(5)br	δC═O (in-plane)
		390w	393w	354w		δC—CH_3
	325(7)			330mw	328w	
		325s	327(30)			ν Au—^{35}Cl
		316m	319(20)			ν Au—^{37}Cl
283w	283(10)			285m		δN—CH_3
			272(10)			
			262(10)		261(10)	ν Au—N, ν Au—P, *x*-vib
			253(20)	256w	257(20)	ν Au—N, ν Au—P, *x*-vib
254w						δ-ring(thy)
			229(16)		224(10)	
		217vw	216(15)	218w	216(10)	*u*-vib
		205vw	203(22)	194w	194(6)	*u*-vib
186m	192(10)					δ-ring(thy)
			181(23)			δ AuCl
157m	149(13)		158(3)	164w	156(11)	δ-ring(thy), δ PAuN
131m	122(13)			128w	123(10)	δ-ring(thy), δ PAuN

[a]Abbreviations: s = strong, m = medium, w = weak, v = very, sh = shoulder, br = broad.
[b]Raman peak intensity relative to strongest peak taken as 100.
[c](ph) refers to phenyl rings of triphenylphosphine.
[d](thy) refers to the thymine ring.
[e]For definition of q, r, t, u, y and *x*-vib (36) see Fig. 4.

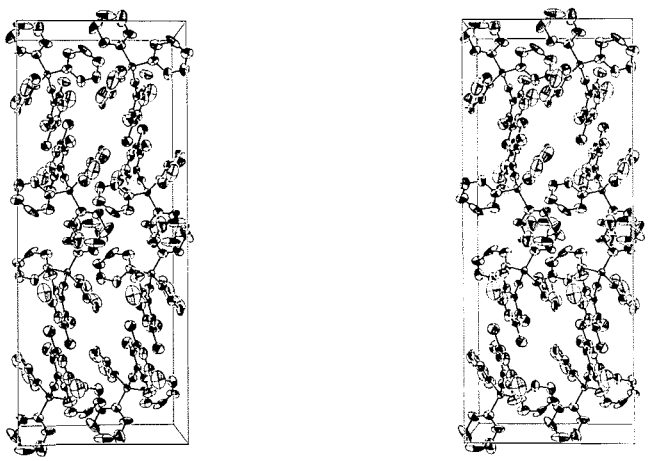

FIG. 2. The packing of 1-methylthyminato-N^3-triphenylphosphinegold(I) within the unit cell. ***a*** and ***c*** are parallel to the bottom and sides of the page and the view is down ***b***.

phosphine dipole is roughly in the ***b*** direction which will maximize any dipole–dipole interaction. In the adjacent bilayer in the ***c*** direction, dipoles are in the opposite direction along the ***b*** axis. The molecules are inclined from the ***b*** direction, however, such that there are hydrophobic layers formed by the phenyl groups at $z = 0, 1/2$ and hydrophilic layers formed by the thyminate groups at $z = 1/4, 3/4$.

The question arises as to why this crystal is chiral (as is the crystal of the starting compound, chloro(triphenylphosphine)gold(I)) (2), since the preparative reaction should give a racemic product. Surprisingly, in a compound with so many aromatic rings, there is very little evidence of any $\pi-\pi$ interaction of the rings, except for the small interaction of the thyminate group in one molecule with the C(7–12) ring of the adjacent molecule in the ***a*** direction related by the C centering operation. This interaction may be responsible for the rather small Au—P—C(7)—ring(C(7)) dihedral angle of 14°, but it is then unlikely to be the main cause of the chirality, since when the dihedral angle is 0° the phenyl ring exerts no selective force on the other rings in determining their configuration. Indeed, apart from the above interaction, there is no evidence of any interactions, other than van der Waals, which could cause the crystal to be chiral and we can see no good reason why the chiral space group is preferred.

The proton and carbon-13 nmr data for 1-methylthymine, potassium 1-methylthyminate, and 1-methylthyminato-N^3-triphenylphosphinegold(I) are given in Table 4. The positions of the peaks arising from methyl protons are similar in the three compounds. Small upfield shifts in the methyl resonances of the 1-methylthyminate ion (1.77 to 1.68 ppm and 3.24 to 3.15 ppm) compared to 1-methylthymine may be because the larger amount of electron density delocalized around the thymine ring has a shielding effect. On the other hand, (triphenylphosphine)gold(I) appears to be a better electron-withdrawing group than the proton, as the methyl peaks of the complex are shifted slightly downfield compared to those of the neutral ligand (1.77 to 1.86 ppm and 3.24 to 3.27 ppm). The effects of removal of the H(3) proton and its substitution by gold are more pronounced for H(6), the proton bound to C(6) than for the methyl groups. An upfield shift is observed (7.36 to 7.17 ppm) on deprotonation, again explained by the larger electron density in the ring. In the gold-substituted case, however, a further upfield shift (to 6.88 ppm) is observed, opposite to that noticed for the methyl groups external to the ring. We speculate that the downfield shift of the methyl resonances upon gold binding is an inductive effect caused by the electronegativity of the (triphenylphosphine)gold cation, whereas the upfield shift of H(6) is a result of increased electron density at the *para* position. Complexation to gold has also affected the electronic structure of thymine enough to eliminate the small coupling

Can. J. Chem. Downloaded from www.nrcresearchpress.com by 72.64.146.136 on 09/07/12
For personal use only.

(^4J 1 Hz) between H(6) and the C(5′) methyl protons observed in both neutral and anionic 1-methylthymine spectra.

Assignment of peaks in the carbon-13 nmr spectrum of 1-methylthymine in D_2O is in agreement with literature assignments for DMSO-d_6 solutions of thymine (31, 32).[4] The positions of peaks caused by the C(5′), C(1), and C(5) atoms change very little in the three compounds. The C(6) signal shows a significant upfield shift in the gold complex compared to the neutral and anionic species which is further evidence of the shielding power of electron density from the gold atom at the *para* position. Deprotonation has a marked effect on the resonance of C(2) and C(4). The electronegativity of the oxygen atoms appears to increase and deshield these carbon atoms. Complexation with gold partially compensates for the absence of the N(3) proton. C(4) is the carbon which shows the greatest sensitivity to changes in the electronic structure.

The vibrational spectra of 1-methylthyminato-N^3-triphenylphosphine gold(I) and related species are summarized in Table 5. Assignments were facilitated by previous vibrational analyses by Susi and Ard (34) on 1-methylthymine, Guay *et al.* (35) on 1-methylthyminate, and Whiffen (36) on monosubstituted benzenes, Shobatake and Nakamoto (37) on metal triphenylphosphines, and Shobatake *et al.* (38) on triphenyl compounds of group Va elements. Deprotonation at N(3) of 1-methylthymine, or substitution of this proton by a heavy metal ion, is expected to result in the disappearance of the N(3)—H modes (νN(3)—H at 3155 cm^{-1} and γN(3)—H at 897 cm^{-1}) of 1-methylthymine. Potassium thyminate bands occurring in the 2800 cm^{-1} to 3100 cm^{-1} region, caused by various C—H stretches, are unaffected by deprotonation or binding to gold.

The three peaks for 1-methylthymine in the 1600–1700 cm^{-1} region assigned to νC(2)=O(2) (1698 cm^{-1}), νC(4)=O(4), νC(5)=C(6) in-phase (1654 cm^{-1}), νC(4)=O(4), νC(5)=(6) out-of-phase (1638 cm^{-1}) (34) are all shifted to lower frequency (1663, 1610, and 1570 cm^{-1}, respectively) upon N(3) deprotonation. This can be explained by a decrease in double bond character because of electron delocalization throughout the O—C—N—C—O system, resulting from N(3) deprotonation.

The peak at 1525 cm^{-1} assigned to the "alternate bond stretch" (38) shows a very large increase in intensity in the infrared and Raman spectra of the anion compared to 1-methylthymine and agrees with results obtained for the anion (39). A similar assignment was made for the 1462 cm^{-1} peak in uracil (40). The increase in absorption is probably a result of a large dipole moment being created upon loss of the proton. Further changes in the frequencies of these bands are observed when gold is bound to 1-methylthyminate. It is expected that binding a heavy metal to N(3) would result in the release of electron density into the thymine ring, increasing the basicity of the carbonyl groups in agreement with nmr results. For the purpose of comparison, spectra of potassium 1-methylthyminate are more suitable than those of the neutral ligand, since 1-methylthymine exists in the solid as a dimer whose hydrogen bonding affects the nature of its conjugated bonds (see Fig. 3). At 1580 cm^{-1}, the peak arising from the νC(4)=O(4), νC(5)=C(6) out-of-phase mode is found 10 cm^{-1} higher in the complex than in the anion, and the in-phase mode at 1590 is 20 cm^{-1} lower (1610 cm^{-1} in the anion). The extent of lowering of the νC(2)=O(2) frequency (1663 cm^{-1} in 1-methylthyminate to 1655 cm^{-1} in **A** from 1698 cm^{-1} in neutral 1-methylthymine) is somewhat surprising in light of the C(2)=O(2) bond length. Such shifts indicate more single bond character in both the 1-methylthyminate ion and the ion bound to gold. It must be remembered, however, that the structure reported here is not particularly accurate, and the errors are such that the C(2)—O(2) bond in **A** may well be sufficiently longer than in the neutral molecule to explain the shift. There is no close interaction between Au and O(2) and O(4), as there is in the Ag complex (41).

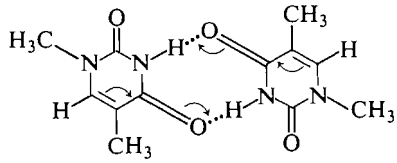

FIG. 3. Hydrogen bonding in the 1-methylthymine dimer (29).

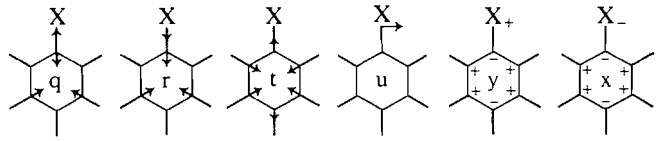

FIG. 4. Whiffen's *q*, *r*, *t*, *u*, *y* and *x* modes (36).

As an approximation, certain bands in the vibrational spectra of triphenylphosphine and triphenylphosphine gold chloride and the thyminato complex can be interpreted in terms of the spectra of monosubstituted benzene. Whiffen (36) has categorized the bands of monosubstituted benzenes into those vibrations which are and are not affected by changes in the substituent group. Six of the fundamental modes (Whiffen's *q*, *r*, *t*, *u*, *y*, and *x* bands, depicted in Fig. 4) are sensitive to substituent change. In the *q*, *r*, and *t* modes, there is vibration along the Ph—X bond (X = substituent), whereas *u*, *y*, and *x* are Ph—X bending vibrations. When triphenylphosphine is coordinated to either chlorogold(I) or 1-methylthyminato-N^3-gold(I), the *q*, *r*, and *t* bands are shifted to higher frequency, while the *u*, *y*, and *x* bands are not significantly shifted. The *q*-band at 1089 cm^{-1} in triphenylphosphine shifts to 1100 cm^{-1} in chloro(triphenylphosphine)gold(I), the *r*-bands shift from 688, 680 cm^{-1} to 705, 688 cm^{-1} and the *t*-bands shift from 425, 413 cm^{-1} to ≈450, 440 cm^{-1}. Of these, the *t*-bands show the larger shift.

In general, it is difficult to assign metal–phosphorus stretching bands because triphenylphosphine itself exhibits a number of bands in the low frequency region. In the past, the metal isotope substitution technique has been used for some complexes; for example, *trans*-Pd[P(C_6H_5)$_3$]$_2$$Cl_2$, and the bands having the larger isotopic shifts have been assigned to Pd—Cl and Pd—P stretching vibrations (37). The latter at 191 and 155 cm^{-1} seem to us to be very low and are more typical of metal–chlorine bending motions. Indeed, our experience with force constant analyses shows that bending vibrations can have a larger isotopic shift than stretching vibrations, depending on the interactions of force constants and the potential energy distribution. In the present work no bands can be assigned to purely Au—P or Au—N stretching modes. We expect the

[4]There is confusion in the literature about the assignment of the C4 and C6 ^{13}C nmr peaks. The Sadtler index (33) interprets the results of Krugh (31) such that the C4 and C6 peaks are interchanged compared to the assignment of Goldstein and Tarpley (32). Part of the problem arises because there is no explicit statement about the pyrimidine ring numbering in the work by Krugh; if it is assumed, however, that I.U.P.A.C. numbering is used the two sets of results are consistent.

Can. J. Chem. Downloaded from www.nrcresearchpress.com by 72.64.146.136 on 09/07/12
For personal use only.

Au—P modes to be strongly coupled to the vibrations of the triphenylphosphine ligand, and because the phenyl rings are "tilted" there will be a component of motion along the Au—P bond even for the ligand-bending vibrations. The ligand *t*-band is essentially P—phenyl stretch, and it will be coupled to the Au—P and Au—N stretching vibrations. In the ligand *x*-vibration, two of the phenyl rings contribute a component of motion along the P—Au—N axis and hence one can assume Au—N as well as Au—P coupling. It is reasonable for this "out-of-plane" phenyl ring bend to be at higher wavenumber than the "in-plane" *u*-vibration because it contains more phenyl–phenyl ring interaction.

The band at 181 cm^{-1}, absent in the thyminate complex, is typical of metal–chlorine bending vibrations, and is so assigned. Other low frequency bands are likely δNAuP, in-plane and out-of-plane motions (with respect to the plane of thyminate ring).

It is apparent that Au(I) can bind to DNA bases at similar positions to Pt(II) although, because of geometric requirements, any interactions with more than one base on a DNA strand will be different to those for *cis*-DDP. Thus, while any anti-cancer activity of gold(I) complexes may be the result of DNA base interaction, it is unlikely to be of the same type as *cis*-DDP. It will be worthwhile examining these differences in more complex polynucleotide systems.

Can. J. Chem. Downloaded from www.nrcresearchpress.com by 72.64.146.136 on 09/07/12
For personal use only.

Acknowledgements

We acknowledge, with thanks, financial support from the Natural Sciences and Engineering Research Council of Canada and the grant of a Graduate Fellowship (M.A.T.). We thank Dr. D. W. Hughes for helpful discussions.

1. A. E. Finkelstein, D. T. Walz, U. Batista, M. Mixraji, F. Roisman, and A. Misher. Ann. Rheum. Dis. **35**, 251 (1976).
2. A. E. Finkelstein, O. R. Burrone, D. T. Walz, and A. Misher. J. Rheumatol. **4**, 245 (1977).
3. T. M. Simon, D. H. Kunishima, G. J. Vibert, and A. Lorber. Cancer, **44**, 1965 (1979).
4. T. M. Simon, D. H. Kunishima, G. J. Vibert, and A. Lorber. Cancer Res. **41**, 94 (1981).
5. C. K. Mirabelli, J. P. Zimmerman, H. R. Barkus, C.-M. Sung, and S. T. Crooke. Biochem. Pharm. **35**, 1435 (1986).
6. H. S. Allaudeen, R. M. Snyder, M. H. Whitman, and S. T. Crooke. Biochem. Pharm. **34**, 3243 (1985).
7. C. K. Mirabelli, R. K. Johnson, D. T. Hill, L. F. Faucette, G. R. Girard, G. Y. Kuo, C. M. Sung, and S. T. Crooke. J. Med. Chem. **29**, 218 (1986).
8. C. K. Mirabelli, C.-M. Sung, J. P. Zimmerman, D. T. Hill, S. Mong, and S. T. Crooke. Biochem. Pharm. **35**, 1427 (1986).
9. C. J. L. Lock and M. A. Turner. Unpublished results.
10. C. E. Blank and J. C. Dabrowiak. J. Inorg. Biochem. **21**, 21 (1984).
11. N. Hadjiliadis, G. Pneumatikakis, and R. Basosi. J. Inorg. Biochem. **14**, 115 (1981).
12. R. C. Elder, M. K. Eidsness, M. J. Heeg, K. G. Tepperman, C. F. Shaw, and N. Schaeffer. *In* Platinum, gold and other metal chemotherapeutic agents. *Edited by* S. J. Lippard. ACS Symposium Series, American Chemical Society. 1983. p. 385.
13. G. H. M. Calis and N. Hadjiliadis. Inorg. Chim. Acta, **79**, 241 (1983).
14. F. Bonati, A. Burini, and B. R. Pietroni. Z. Naturforsch. **40B**, 1749 (1985).
15. K. C. Agrawal, K. B. Bears, D. Marcus, and H. B. Jonassen. Proc. Am. Soc. Cancer Res. **19**, 23 (1978).
16. N. Beck, U. Nagel, and Y. Rosopulos. Chem. Ber. **118**, 931 (1985).
17. B. Lippert, C. J. L. Lock, B. Rosenberg, and M. Zvagulis. Inorg. Chem. **16**, 1525 (1977).
18. R. P. Hughes, N. Krishnamachari, C. J. L. Lock, J. Powell, and G. Turner. Inorg. Chem. **16**, 314 (1977).
19. J. M. Stewart. The XRAY 76 System Tech. Rept. TR-446, Computer Science Center, University of Maryland, College Park, MD. 1976.
20. G. M. Sheldrick. SHELX; Program for crystal structure determination. University of Cambridge, England, 1976.
21. F. A. Ahmed and M. E. Pippy. NRC-22, Mean plane and torsional angles. National Research Council of Canada, Ottawa, Canada. 1976.
22. C. K. Johnson. ORTEP-II, Report ORNL-5138, Oak Ridge National Laboratory, TN. U.S.A. 1976.
23. P. Seiler, W. B. Schweizer, and J. D. Dunitz. Acta Crystallogr. **40B**, 319 (1984).
24. S. Ahrland, J. Chatt, and N. R. Davies. Q. Rev. Chem. Soc. **12**, 265 (1958).
25. S. Mansy, B. Rosenberg, and A. J. Thomson. J. Am. Chem. Soc. **95**, 1633 (1973).
26. G. Raudaschl-Sieber and B. Lippert. Inorg. Chem. **24**, 2426 (1985).
27. R. Faggiani, B. Lippert, C. J. L. Lock, and R. A. Speranzini. Inorg. Chem. **21**, 3216 (1982).
28. N. C. Baenziger, W. E. Bennett, and D. M. Soboroff. Acta Crystallogr. **32B**, 962 (1976).
29. K. Hoogsteen. Acta Crystallogr. **16**, 28 (1963).
30. C. J. L. Lock, R. A. Speranzini, and J. Powell. Can. J. Chem. **54**, 53 (1976).
31. T. R. Krugh. J. Am. Chem. Soc. **95**, 4761 (1973).
32. J. H. Goldstein and A. R. Tarpley, Jr. J. Am. Chem. Soc. **93**, 3573 (1971).
33. Sadtler ^{13}C NMR Index, No. CNMI 3215.
34. H. Susi and J. S. Ard. Spectrochim. Acta, **30A**, 1843 (1974).
35. F. Guay, A. L. Beauchamp, C. Gilbert, and R. Savoie. Can. J. Spectrosc. **28**, 13 (1983).
36. D. H. Whiffen. J. Chem. Soc. 1350 (1956).
37. K. Shobatake and K. Nakamoto. J. Am. Chem. Soc. **92**, 3332 (1970).
38. K. Shobatake, C. Postmus, J. R. Ferraro, and K. Nakamoto. Appl. Spectrosc. **23**, 12 (1969).
39. K. L. Wierzchowski, E. Litonska, and D. Shugar. J. Am. Chem. Soc. **87**, 4621 (1965).
40. M. Tsuboi, S. Takahashi, and I. Harada. Physico-chemical properties of nucleic acids. vol. 2. *Edited by* J. Duschesne. Academic Press, New York. 1973. p. 91.
41. F. Guay and A. L. Beauchamp. J. Am. Chem. Soc. **101**, 6260 (1979).

A ^{13}C and ^{15}N nuclear magnetic resonance study of the protonation of a retinal Schiff base by acids of different pK_as and in solvents of different polarities

DANIEL COSSETTE AND DANIEL VOCELLE[1]

Département de chimie, Université du Québec à Montréal, C.P. 8888, Succ. A, Montréal (Qué.), Canada H3C 3P8

Received September 5, 1986

DANIEL COSSETTE and DANIEL VOCELLE. Can. J. Chem. **65**, 1576 (1987).

^{13}C and ^{15}N nuclear magnetic resonance spectra of mixtures of all-*trans*-retinylidene *tert*-butylamine (RtBA) and substituted acetic acids in equimolar concentrations in both $CDCl_3$ and CD_3OD were studied in relation to two questions: the nature of the state of protonation of a retinal Schiff base in the presence of carboxylic and mineral acids in solvents of different polarities, and secondly, to determine the nature of the interactions (if any) between the polar groups located on the acids and the polyenic chain of the retinal derivative. Using carboxylic acids of different pK_as and three mineral acids, we present results that indicate that, in solvents of low polarity, weak acids can only partially protonate RtBA while, in a more polar milieu, the protonation percentages are higher. With polar groups such as NO_2, Cl, Br, I, and CN, no specific interaction could be found between the polyenic chain of the imine and these groups. Variations in the intensity of certain peaks of RtBA were noted and these could possibly be related to the presence of the polar groups on the acids. Comparisons of our results with those obtained on rhodopsin and bacteriorhodopsin indicate that the milieu surrounding the chromophore must be polar if protonation is complete, while in a less polar environment partial protonation can be expected.

DANIEL COSSETTE et DANIEL VOCELLE. Can. J. Chem. **65**, 1576 (1987).

Les spectres de résonance magnétique nucléaire de ^{13}C et de ^{15}N de mélanges de tout-*trans*-rétinylidène *tert*-butylamine (RtBA) et d'acides acétiques substitués, en concentrations équimolaires dans des solvants comme $CDCl_3$ et CD_3OD, ont été étudiés relativement à deux questions : la nature de l'état de protonation d'une base de Schiff du rétinal en présence d'acides carboxyliques dans des solvants de polarités différentes, et deuxièmement, de déterminer la nature des interactions (si elles existent) entre les groupes polaires localisés sur les acides et la chaîne polyénique. Par l'utilisation d'acides carboxyliques ayant des pK_as variés et également de trois acides minéraux, nous montrons des résultats qui indiquent que dans des solvants de faibles polarités, les acides faibles ne peuvent protoner RtBA que partiellement tandis qu'en des milieux plus polaires, la protonation peut être complète. Avec des groupes comme NO_2, Cl, Br, I et CN, aucune interaction spécifique n'a pu être trouvée entre la chaîne polyénique de l'imine et ces groupes. Des variations dans l'intensité de certains pics de RtBA ont été aperçues qui peuvent possiblement être reliées à la présence des groupes polaires des acides. Des comparaisons de nos résultats avec ceux obtenus à partir de rhodopsine et de bactériorhodopsine indiquent que le milieu entourant le chromophore doit être polaire pour une protonation complète tandis qu'en milieu moins polaire une protonation partielle est probable.

Introduction

Several ^{13}C and ^{15}N nmr studies of visual and bacterial (1, 2) pigments and of related model systems (3–11) have been made recently and these techniques have been successful in revealing some important facts about the structure of these protein membranes. Still, the exact interactions between the chromophore (a Schiff base of retinal) and its surrounding protein moiety are not known. These interactions come, first, from protonation and the subsequent formation of a salt bridge between the protonated Schiff base and its counterion and, second, from interactions between the chromophore and some charged groups of the protein. In this last respect, negatively charged groups (probably carboxylate anions) located near C11–C13 for rhodopsin (12) and near C5 for bacteriorhodopsin have been proposed (13), as well as some positively charged groups around C7 for bacteriorhodopsin (2*d*). These works have relied heavily on studies made of model systems, especially those by Blatz *et al.* (14), and used all-*trans*-retinylidene *n*-butylamine (RnBA) and many strong acids as protonating agents. Blatz *et al.* were able to show that the λ_{max} of RnBA was strongly influenced by the strength of the binding between the counterion and the positively charged nitrogen atom of the azomethine function. As for the secondary interactions with charged groups, often called "the opsin shift" by the group headed by Nakanishi (13), several model systems have been built to show how these charges could operate and under what conditions (15).

For, interesting as they are, these models have inherent weaknesses: the shifts obtained are very small or the acids used are too strong or in too large excesses. It appears then especially important to devise a model system where the protonating acid would have an acidity strength similar to glutamic (pK_a 4.25) or aspartic acids (pK_a 3.89) since these two acids are likely candidates for both the protonation of the Schiff base and for secondary interactions (16). The question of the solvent to be used in these models is also highly important. It is not known as yet what is the polarity of the milieu surrounding the chromophore in both rhodopsin and bacteriorhodopsin. Some are proposing a nonpolar environment (17) while others (18) advocate a more polar one. At this stage, it appears interesting to conduct studies in both mediums.

Finally, ^{13}C and ^{15}N nmr spectroscopies are eminently suited for this type of work since both nuclei respond readily to the influences of charges. For all these reasons then, we have devised a model system of rhodopsin and bacteriorhodopsin that consists of all-*trans*-retinylidene *tert*-butylamine (RtBA) and several carboxylic acids having a large spectrum of pK_as (Fig. 1). The solvents used were chloroform, since it is a good nonpolar solvent, and methanol, because of its solvating capacity and its greater polarity. Since, in the pigments, it is probable that both the protonating agent and the charged group are in a 1:1 molar ratio with the chromophore, the same ratio was also used in our study. Finally, our model was investigated by high resolution ^{13}C nmr (at 100 MHz) and ^{15}N nmr (40.4 MHz) to detect as precisely as possible any effect by polar groups. This study follows a similar one made on a much simpler imine, *trans*,*trans*-2,4-heptadienylidene *tert*-butylamine (HBA), and many references will be made to it (19).

[1]Author to whom correspondence may be addressed.

Can. J. Chem. Downloaded from www.nrcresearchpress.com by 72.64.146.136 on 09/07/12
For personal use only.

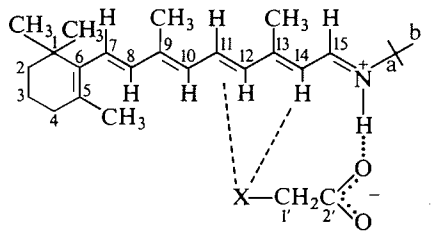

FIG. 1. All-*trans*-retinylidene *tert*-butylamine in the presence of a substituted acetic acid with numerotation used in the text.

Experimental

All-*trans*-retinylidene *tert*-butylamine (RtBA) was prepared according to a method already described (20). The use of the *tert*-butyl derivative instead of the more customary *n*-butylamine (RnBA) in the model of the visual pigment is based on the rationale that it is far more stable. Many hours are needed to take the ^{15}N nmr spectra, and this added stability becomes quite an important asset. It must be remembered that aldimines can enter into many reactions: among them, hydrolysis and polymerization can become a real nuisance, especially in acidic solutions (21). In this study, great care has been taken to prevent these secondary reactions and ^{13}C nmr spectra were obviously free of them (absence of unrelated peaks), while for ^{15}N nmr spectra this question is less clear. The facts that the chemical shifts found were linearly correlated with the pK_as of the acids (see Results and discussion), that often only a few hundred scans were necessary, and that visual inspection of the sample after the nmr analysis showed only slight increase in coloration, are good indications that RtBA was fairly stable during the time required to take the spectra. Nevertheless, completely anhydrous conditions (dry box, N_2 atmosphere), freshly distilled imine, absence of direct light, and relatively rapid time of analysis are important parameters in taking good nmr spectra of this Schiff base.

Solution concentrations for ^{13}C nmr spectra were of the order of 0.07 *M* and of 0.6–1 *M* for ^{15}N spectra; the ratio of Schiff base to acid was always 1:1. In the case of RtBA – propionic acid, the conditions used differed slightly since good spectra are surprisingly difficult to achieve with this acid; 0.05 *M* chromium acetate was added to the solution to assure better contacts. Deuterated chloroform and deuterated methanol were used as solvents and to ensure a good lock. The spectra were taken on a high resolution Bruker WH 400 instrument at a frequency of 100 MHz for ^{13}C and 40.4 MHz for ^{15}N. The ^{13}C proton noise-decoupled spectra resulted from 400–600 scans taken with rf pulses of 5 μs, a pulse angle of 45°, at intervals of 3.2 s. The unprotonated NtBA ^{15}N proton noise-decoupled spectra resulted from 2000–5000 scans with rf pulses of 12 μs, an angle of 90°, a pulse delay of 1.6 s, and an acquisition time of 0.4 s; the protonated Schiff base permited the use of the INEPT sequence (22) and only 200–400 scans were then necessary.

All ethylenic ^{13}C atoms were obtained as separate peaks for the protonated Schiff base. Identification of all peaks was done as follows. First of all, the ^{13}C nmr spectrum of RnBA in $CDCl_3$ has already been analyzed by Mateescu and co-workers (3*c*) and all the peaks have been identified. Since RtBA is an imine quite similar to RnBA, the same assignations could have been made. Nevertheless, a complete analysis was done using 2D nmr. Figure 1 shows our model with the numerotation of carbon atoms retained in this paper. Carbon atoms a, b, 15, 13, 9, 6, 1′, and 2′ are easily identified by their specific chemical shifts or by their intensities. Carbon atoms at 14, 12, 11, 10, 8, and 7 are somewhat more difficult to assign. First, it must be remembered that all odd-numbered atoms are deshielded while all even-numbered ^{13}C are shielded (zigzag pattern, see Results and disscusion). To ascertain the exact position of the protons, a normal proton–proton COSY 2D (23) was done followed by a long-range cross-section proton–proton COSY 2D. These two operations allowed the right assignations of all protons located at 14, 12, 11, 10, 8, and 7. Following these proton assignations, a 2D proton–carbon correlation allowed the proper identification of all carbon atoms. The assignations were identical with those published.

Results and discussion

^{13}C nuclear magnetic resonance results

Chemical shifts of C5–C15 are presented in Table 1 for spectra of RtBA and acids in equimolar concentrations in $CDCl_3$ and in Table 2 when the solvent was CD_3OD. In parentheses are given the differences in chemical shifts ($\Delta\delta$) obtained by subtracting, for a given carbon atom, the chemical shift of that carbon from the corresponding system with acid (e.g. C15[RtBA–acid] − C15[RtBA]). As typical examples, ^{13}C nmr spectra of RtBA – 3-nitropropanoic acid in CD_3OD and RtBA–TCA appear in Figs. 2*a* and 2*b* respectively.

In deuterated chloroform, Table 1 indicates deshielding (positive sign) for all odd-carbon atoms and shielding (negative sign) for even-numbered ones. Deshielding is greatest for C13 and it decreases as the distance of the carbon atom from the azomethine group increases. Figure 3 shows the zigzag pattern obtained when, for a given acid (in this case trichloroacetic acid (TCA) in $CDCl_3$), the $\Delta\delta$ are plotted against the position of the carbon atoms. This pattern originates from the fact that all odd-numbered carbon atoms are in a resonance position. If a curve is drawn by joining the tips in the zigzag pattern (dash line in Fig. 3) or, even better, if curves between ln $\Delta\delta$ and the carbon atoms are drawn (Fig. 4), the expected deshielding for C15 should be far more important than the one actually measured. It is worth mentioning that curves such as the one shown in Fig. 4 have correlation coefficients of 0.98 and more. For TCA, HCl, HBr, and HI, these calculated deshieldings are shown in Table 3. The difference between the expected C15 deshieldings and the actual values can be evaluated by subtracting values of Table 1 from those of Table 3. The actual very weak deshieldings experienced by C15 have been explained by Sharma and Roels (24) on the basis of a shielding effect due to a marked decrease in the anisotropy of the C=N bond on protonation, a shielding that is counterbalanced by the strong deshielding effect of having a C^+—N bond (resonance position). This difference between the expected value and what is actually obtained is then a measure of the loss of anisotropy of the C=N bond and consequently is a measure of the degree of protonation. From a previous study of these same systems by FTIR (25) and from works done on HBA (19), we can safely postulate that mineral acids are able to completely protonate NtBA. Consequently, a difference of 26 ppm between the expected and the actual deshieldings signifies full protonation. For the medium strong acids (like chloroacetic acid), the difference is about 16 ppm, which implies a percentage of protonation of 60–70%, while for the weak acids the value is about 5–10%.

Another way of calculating these degrees of protonation is by comparing the $\Delta\delta$ of C13 (or C11) for all the systems studied. Again, from Table 1, it is possible to postulate that a deshielding value of approximately 17.5 ppm corresponds to complete protonation. From the same table, it is quite easy to measure the degree of protonation caused by propionic acid (9% protonation) and by chloro, fluoro, and cyanoacetic acids (60–70% protonation). Both methods give the same value.

Now, if we compare the degrees of protonation of RtBA with the simpler imine HBA (19), we find that propionic acid gives different values for both imines (10 and 20% respectively) while monohalogenated acids give the same percentages (60–70%) and cyanoacetic acid also gives similar values (70–80%). The

Can. J. Chem. Downloaded from www.nrcresearchpress.com by 72.64.146.136 on 09/07/12
For personal use only.

TABLE 1. Chemical shifts of RtBA in presence of acids in deuterated chloroform at 25°C

System studied[a]	pK_a / C10	C15 / C9	C14 / C8	C13 / C7	C12 / C6	C11 / C5
RtBA		153.82	130.38	143.35	136.11	127.34
	129.92	137.69	137.34	127.54	137.61	129.53
RtBA–CH_3CH_2COOH	4.90	154.45	129.10	144.90	135.91	128.10
		(+0.63)	(−1.28)	(+1.55)	(−0.20)	(+0.76)
	129.87	138.14	137.32	127.88	137.60	129.79
	(+0.05)	(+0.45)	(+0.02)	(+0.34)	(−0.01)	(+0.26)
RtBA–$ClCH_2COOH$	2.85	156.36	123.96	153.93	134.59	132.95
		(+2.54)	(−6.42)	(+10.58)	(−1.52)	(+5.61)
	129.56	141.84	136.96	129.96	137.56	130.63
	(−0.36)	(+4.15)	(−0.38)	(+2.42)	(−0.05)	(+1.10)
RtBA–FCH_2COOH	2.60	156.39	123.79	153.97	134.55	133.08
		(+2.57)	(−6.59)	(+10.62)	(−1.56)	(+5.74)
	129.53	141.92	136.95	130.01	137.53	130.66
	(−0.39)	(+4.23)	(−0.39)	(+2.47)	(−0.08)	(+1.13)
RtBA–$NCCH_2COOH$	2.45	156.49	123.37	155.22	134.42	133.58
		(+2.67)	(−7.01)	(+11.87)	(−1.69)	(+6.24)
	129.58	142.37	136.92	130.20	137.49	130.83
	(−0.34)	(+4.68)	(−0.42)	(+2.66)	(−0.11)	(+1.30)
RtBA–Cl_3CCOOH	0.66	157.88	120.61	160.61	133.68	136.56
		(+4.06)	(−9.77)	(+17.26)	(−2.47)	(+9.22)
	129.36	144.83	136.78	131.70	137.07	131.55
	(−0.56)	(+7.14)	(−0.66)	(+4.16)	(−0.54)	(+2.02)
RtBA–HCl	−6.90	157.38	120.21	160.78	133.64	136.68
		(+3.56)	(−10.17)	(+17.43)	(−2.47)	(+9.34)
	129.33	144.74	136.78	131.62	137.32	131.40
	(−0.59)	(+7.05)	(−0.56)	(+4.08)	(−0.29)	(+1.87)
RtBA–HBr	−8.90	157.70	119.48	162.02	133.50	137.38
		(+3.88)	(−10.90)	(+18.67)	(−2.61)	(+10.04)
	129.32	145.33	136.61	131.92	137.31	131.58
	(−0.60)	(+7.64)	(−0.73)	(+4.38)	(−0.30)	(+2.05)
RtBA–HI	−9.20	158.06	118.19	165.75	133.02	139.93
		(+4.24)	(−12.19)	(+22.40)	(−3.09)	(+12.59)
	130.10	147.56	136.62	133.52	137.38	132.54
	(+0.18)	(+9.87)	(−0.72)	(+5.98)	(−0.23)	(+3.01)

[a]In parentheses, the difference in chemical shifts between RtBA and RtBA–acids.

similarity of both systems makes HBA, even though much simpler, a reasonable model of the chromophore of rhodopsin. The reason for this similarity can be found by comparing Tables 1 and 2; it appears clear that in NtBA the perturbation caused by the presence of the acid is felt by all ethylenic carbon atoms but the effect is stronger for C11–C15, a region that corresponds to HBA. These two methods of calculating the percentages of protonation appear theoretically valid since all $\Delta\delta$ for all carbon atoms are linearly correlated with the pK_as of the carboxylic acids (measured in water). Correlation coefficients of 0.996 for C15, 0.998 for C14, 0.994 for C13, 0.990 for C11, and 0.995 for C9 are good examples of this behavior. These good correlation coefficients between $\Delta\delta$ and the pK_as imply also that the polar groups located on the acids (like Cl, F, etc.) do not significantly alter the chemical shifts of the ethylenic carbons of the retinal Schiff base.

The interaction of the polar groups with the polyenic chain might possibly be revealed by the peak intensities of C11 and C14. Depending on the acids and solvents used, the intensities of the peaks of RtBA in the ethylenic region vary considerably. Table 4 shows the ratio obtained by relating the integration of the peak relative to that of C8. That carbon atom was chosen because it is located rather far away from the azomethine function and its intensity remained constant for all cases studied. In deuterated chloroform, the intensity of the C15 peak is slightly affected (as based on its surface integration) by the presence of acids. The C14 and C11 peaks behave similarly: their intensities decrease more than half in the presence of acids substituted by polar groups. In deuterated methanol the C14, C11, and C15 peaks are affected when in the presence of weak to medium strong acids. It is difficult to ascribe these losses of intensity to one particular cause. However, since mineral acids affect very slightly the intensities of these peaks in both $CDCl_3$ and CD_3OD while substituted acetic acids are able to do so more strongly, this could possibly indicate an interaction of the polar groups with the ethylenic carbon atoms of RtBA. With HBA these losses of peak intensities were not present since the molecule is much smaller than RtBA. Pattaroni and Lauterwein (11), in their remarkable ^1H and ^{13}C nmr studies of protonated and unprotonated RnBA, present spectra that show the same variation in peak intensities. In conclusion then, polar groups attached to the protonating agents do not alter significantly the

Can. J. Chem. Downloaded from www.nrcresearchpress.com by 72.64.146.136 on 09/07/12
For personal use only.

TABLE 2. Chemical shifts of RtBA in presence of acids in deuterated methanol at 25°C

System studied[a]	pK_a / C10	C15 / C9	C14 / C8	C13 / C7	C12 / C6	C11 / C5
RtBA		156.87	128.49	147.18	137.01	129.53
	131.25	139.01	139.01	129.93	139.36	130.52
RtBA–CH_3CH_2COOH	4.90	159.10	125.57	155.25	135.95	133.85
		(+2.23)	(−2.92)	(+8.07)	(−1.06)	(+4.32)
	130.53	142.42	138.61	130.90	138.92	131.17
	(−0.72)	(+3.41)	(−0.40)	(+0.97)	(−0.44)	(+0.65)
RtBA–$NO_2CH_2CH_2COOH$	3.90	160.82	122.83	161.11	135.39	136.79
		(+3.95)	(−5.66)	(+13.93)	(−1.62)	(+7.26)
	130.94	144.63	138.54	131.76	138.93	131.76
	(−0.31)	(+5.62)	(−0.47)	(+1.83)	(−0.43)	(+1.24)
RtBA–ICH_2COOH	3.15	161.57	121.49	163.59	134.96	138.10
		(+4.70)	(−7.00)	(+16.41)	(−2.08)	(+8.57)
	130.74	145.64	138.33	132.25	138.83	131.92
	(−0.51)	(+6.63)	(−0.68)	(+2.32)	(−0.53)	(+1.40)
RtBA–Cl_3CCOOH	0.66	162.30	120.37	166.19	132.79	139.42
		(+5.43)	(−8.12)	(+19.01)	(−4.22)	(+9.89)
	130.83	146.61	138.37	134.79	138.88	132.22
	(−0.42)	(+7.60)	(−0.64)	(+4.86)	(−0.48)	(+1.70)
RtBA–HCl	−6.90	162.40	120.27	166.33	132.87	139.55
		(+5.53)	(−8.22)	(+19.15)	(−4.14)	(+10.02)
	130.84	146.70	138.40	134.77	138.91	132.24
	(−0.41)	(+7.69)	(−0.61)	(+4.84)	(−0.45)	(+1.72)
RtBA–HBr	−8.90	162.38	120.29	166.33	132.77	139.48
		(+5.51)	(−8.20)	(+19.24)	(−4.24)	(+9.93)
	130.89	146.60	138.40	134.82	138.89	132.19
	(−0.36)	(+7.59)	(−0.61)	(+4.89)	(−0.47)	(+1.67)

[a]In parentheses, the difference in chemical shifts between RtBA and RtBA–acids.

Can. J. Chem. Downloaded from www.nrcresearchpress.com by 72.64.146.136 on 09/07/12
For personal use only.

spectra of the retinal Schiff base except by possibly reducing the peak intensity of some carbon atoms of the polyenic chain. We have indicated in a previous paper (26) that ^1H nmr data obtained from these same systems could be interpreted by assuming point-charge interactions between the polar groups of the acids and the polyenic chain of the Schiff base. There is no inconsistency between both statements since proton nmr may well be more sensitive to such effects than ^{13}C nmr. This can be shown by looking at the nmr data for position 14. Table 1 shows that C14 is not as shielded as C13 is deshielded while ^1H nmr indicated that it was H14 that was the most strongly deshielded proton.

The mineral acids induce chemical shifts on RtBA that do not correlate well with those of the carboxylic acids, and Table 1 shows that TCA, HCl, and HBr affect RtBA roughly the same way even though their pK_as are quite different. It seems that when the Schiff base is fully protonated, as undoubtedly it is with these acids, the chemical shifts of the carbon atoms respond weakly to other effects. HI behaves somewhat differently since its action on RtBA is much stronger than the others (but still in the right direction). We do not know why this is so but it must be remembered that, compared to the others, iodide is a very big counterion, which binds weakly with the protonated Schiff base in chloroform (*2a*).

In deuterated methanol, the ^{13}C nmr data show the same zigzag pattern as previously described and Table 2 indicates that this solvent, compared to $CDCl_3$, induces a more pronounced deshielding by some 3 ppm for C15. Furthermore, protonation is much more important. Using the same methods as described earlier, we find that all three strong acids (TCA, HCl, and HBr) have roughly the same chemical shifts (levelling effects) and that protonation is complete. Considering that a $\Delta\delta$ of 10 ppm for C11 indicates 100% protonation (see Table 2), we then find the following protonation percentages: propionic acid, 43%; 3-nitropropanoic acid, 73%; and iodoacetic acid, 86%. For HBA, the protonation percentages for these same systems were 20–30%, 60–70%, and 80–90% respectively. RtBA is then slightly more protonated than HBA under the same conditions, quite probably because of increased stabilization of the protonated Schiff base due to more extended conjugation. Nevertheless, HBA again appears a good model for the more complexed RtBA and the same conclusions can be applied for both systems.

^{15}N nuclear magnetic resonance data

Values obtained by this method appear in Table 5. Since more than 100 ppm separates the values of protonated and unprotonated Schiff base (27, 28), ^{15}N nmr is particularly good in calculating precise protonation percentages. In deuterated chloroform, if we accept that a chemical shielding of approximately 150 ppm (between NtBA and NtBa–HCl) corresponds to 100% protonation, then the protonation percentages are the following: propionic acid, 25%; chloroacetic acid 75%; TCA 95%. Again we note that HI exerts a very strong shielding effect and the same reasoning that we advanced before can also be applied here. It is also comforting to observe the close similarity of these results with those obtained by ^{13}C nmr. The percentage is greater than expected for propionic acid but still it is the one that protonates RtBA the least. Shielding, as

Can. J. Chem. Downloaded from www.nrcresearchpress.com by 72.64.146.136 on 09/07/12
For personal use only.

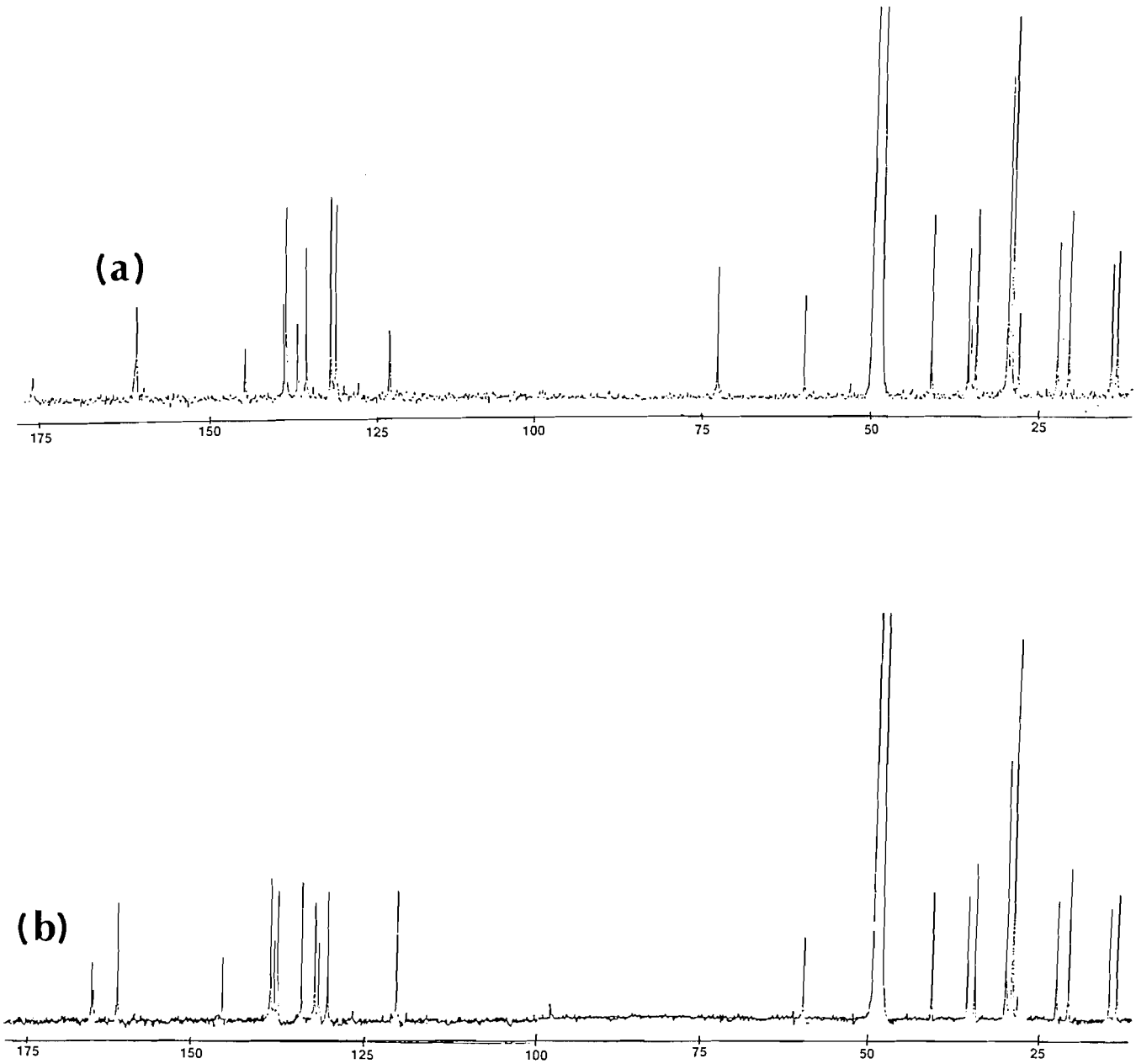

FIG. 2. The ^{13}C nmr spectra of (*a*) RtBA – 3-nitropropanoic acid and (*b*) RtBA – trichloroacetic acid in equimolar concentrations in CD_3OD.

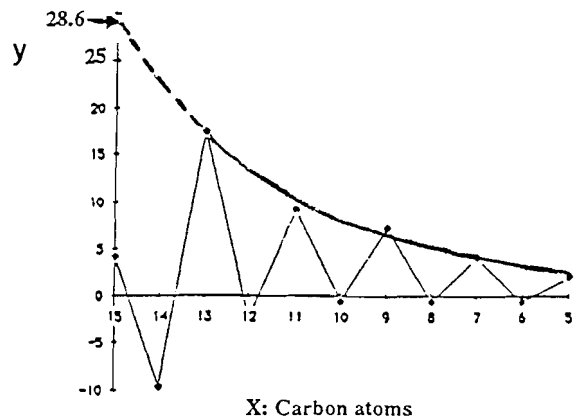

FIG. 3. Zigzag pattern representing the actual deshielding values (y) of specific carbon atoms (x) of RtBA when in the presence of an equimolar concentration of trichloroacetic acid in $CDCl_3$. The dashed line represents the expected deshielding for C15.

expected, is more important in deuterated methanol. There is some 14 ppm difference between the nonpolar $CDCl_3$ and the polar CD_3OD for RtBA. Protonation is also more pronounced in methanol. By using the same method as described before, the percentages of protonation are 39% for propionic acid, 90% for iodoacetic acid, and all three strong acids are evidently 100% protonated. These degrees of protonation compare remarkably well with those found by ^{13}C nmr or when compared with the related HBA system.

Comparisons with other systems

The usual model system of rhodopsin and bacteriorhodopsin is all-*trans*-retinylidene *n*-butylamine (RnBA) and its salts, usually the hydrochloride. The fact that we used a *tert*-butyl group implies that a correction must be made to account for the difference in structure. This correction factor can be determined by comparing our ^{13}C nmr results with those obtained on RnBA. The unprotonated Schiff base has been studied using ^{13}C nmr by

TABLE 3. Expected deshielding of C15 upon protonation. Figures represent the difference between the RtBA and RtBA–acid systems

System studied	C15[a]	C15[b]	$a - b$	C15[a]	C15[b]	$a - b$
RtBA (**1**)						
1–CH_3CH_2COOH	2.50	0.63	1.87	16.92	2.23	14.69
1–$NO_2CH_2CH_2COOH$				27.11	3.95	23.16
1–ICH_2COOH				31.97	4.70	27.27
1–$ClCH_2COOH$	18.19	2.54	15.65			
1–FCH_2COOH	18.36	2.57	15.79			
1–$CNCH_2COOH$	20.15	2.67	17.48			
1–Cl_3CCOOH	28.62	4.06	24.56	34.99	5.43	29.56
1–HCl	30.27	3.56	26.71	35.12	5.53	29.59
1–HBr	31.98	3.88	28.10	35.58	5.51	30.07
1–HI	36.01	4.24	31.77			

[a]Extrapolated value.
[b]From Tables 1 and 2.

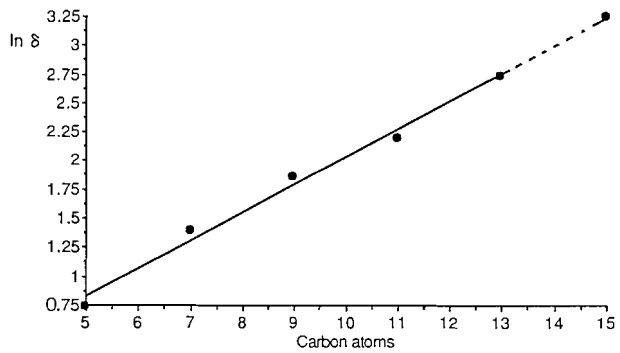

FIG. 4. Graph representing the deshielding (δ) of certain carbon atoms (x) and showing the extrapolated value for C15 for RtBA in the presence of an equimolar concentration of a carboxylic acid (TCA); $y = 0.241x \pm 0.381$; $R^2 = 0.994$.

TABLE 4. Integration ratio of C15, C14, C11 in deuterated chloroform and deuterated methanol relative to C8

	$CDCl_3$			CD_3OD		
System studied	C15	C14	C11	C15	C14	C11
RtBA (**1**)	0.89	1.09	1.08	0.86	0.99	0.97
1–CH_3CH_2COOH	0.92	0.90	0.90	0.45	0.40	0.42
1–$NO_2CH_2CH_2COOH$				0.50	0.60	0.64
1–ICH_2COOH				0.53	0.46	0.36
1–$ClCH_2COOH$	0.74	0.53	0.31			
1–FCH_2COOH	0.76	0.64	0.45			
1–$CNCH_2COOH$	0.75	0.55	0.45			
1–Cl_3CCOOH	0.73	0.69	0.62	0.87	0.88	0.92
1–HCl	0.92	0.94	0.95	0.85	0.82	0.92
1–HBr	0.85	0.91	0.98	0.89	0.94	0.97
1–HI	0.85	1.10	0.90			

Mateescu and co-workers (3*c*), by Pattaroni and Lauterwein (11), by Rabiller and Danho (10) (in this case, the all-*trans*-retinylidene Schiff base made with $H_2N(CH_2)_3CO_2t$-Bu was used as a reference), and finally by Inoue *et al.* (5). All these groups measured the chemical shifts of RnBA (or analogs) for C5–C15 and the solvents used were $CDCl_3$, CD_2Cl_2, and CCl_4. Comparisons with their results indicate that the chemical shifts of C5–C14 are all very similar except for the data found by Inoue in CCl_4. Harbison *et al.* (2*b*) also published data on the solid-state ^{13}C nmr of RnBA; again the values differed considerably from those obtained in CD_2Cl_2 or $CDCl_3$. Because of these differences we used as a base of comparison only those data obtained in these two solvents. For RnBA, C15 values were also very similar: the average value was 159.5 ppm. When this chemical shift is compared to that for RtBA (153.8), a difference of 5.7 ppm is found. It represents the shielding brought by the *tert*-butyl group on C15. In deuterated methanol, the correction for the *tert*-butyl can be determined by comparing our results with those of Inoue *et al.* (5) on RnBA. Again values for C5–C14 are very similar except for C11, where there is a difference of 1.8 ppm. For C15, a correction factor of 4.6 ppm is needed. Spectra of RnBA–HCl were also recorded by Mateescu in both $CDCl_3$ (1*d*) and CD_2Cl_2 (3*c*), by Harbison for solid-state samples (4), and by Inoue in CD_3OD (5). In deuterated methanol the C5–C14 region has chemical shifts that are similar to the data of Table 2. For RnBA–HCl in $CDCl_3$ and in CD_2Cl_2, all odd-numbered carbon atoms had chemical shifts that were different in these two nonpolar solvents, the difference being smaller as the distance from the azomethine function increased. When these two spectra were compared to those of RtBA, the same situation arose. Since both RtBA–HCl and RnBA–HCl spectra were taken in $CDCl_3$ we can evaluate the impact of the *tert*-butyl group on the polyenic chain. The values are 6.27 ppm for C15, 1.55 for C13, 0.59 for C9, 0.45 for C7 and 0.37 ppm for C5. Finally, a comparison can be established between our RtBA–TCA system in $CDCl_3$ and Pattaroni and Lauterwein's system of RnBA–TFA in CD_2Cl_2. Since the chemical shifts are very similar in these two solvents, TCA and trifluoroacetic acid should induce similar effects on the Schiff base since their pK_as are very close. This being the case, the differences between both systems are for C15 = 5.6, C13 = 1.62, C11 = 1.08,

TABLE 5. ^{15}N chemical shifts of RtBA in presence of acids in deuterated chloroform and deuterated methanol at 25°C

System studied	pK_a	Chloroform	Methanol
RtBA		238.99	225.03
RtBA–CH_3CH_2COOH	4.90	199.06	170.09
RtBA–ICH_2COOH	3.15		98.99
RtBA–$ClCH_2COOH$	2.85	126.01	87.30
RtBA–Cl_3CCOOH	0.66	95.69	87.41
RtBA–HCl	−6.90	90.37	87.46
RtBA–HI	−9.20	71.12	85.19

Can. J. Chem. Downloaded from www.nrcresearchpress.com by 72.64.146.136 on 09/07/12
For personal use only.

Can. J. Chem. Downloaded from www.nrcresearchpress.com by 72.64.146.136 on 09/07/12
For personal use only.

C9 = 0.78, C7 = 0.36, and C5 = 0.51 ppm. These differences are similar to those found previously for HCl.

Let us compare now our results with those obtained with the natural pigments. Mateescu *et al.* (1*f*) found, for rhodopsin solubilized in octyl β-glucoside, 165.9 ppm for C15, 130.0 ppm for C14, 168.1 ppm for C13, 148.8 ppm for C9, and 137.0 ppm for C6. For bacteriorhodopsin, the values were 166.0, 130.0, 168.9, 148.5, and 135.6 ppm respectively. By CP-MAS, these same authors found 150 for C15 and 143.7 ppm for C13. Yamaguchi *et al.* (6) found, for bacteriorhodopsin in octyl β-glucoside, 118.9 ppm for C14 and 169 ppm for C15. Harbison *et al.* (2*b*), using the CP-MAS technique, found 122.0 ppm for C14, 134.3 for C12, 139.1 for C11, and 133.0 ppm for C10 for the all-*trans* isomer of bacteriorhodopsin. From these works we note immediately that thin films give chemical shifts that differ considerably from those in solutions. With models, the same differences were also noted. Another discrepancy can be seen for C14: Mateescu finds a value of 130 ppm for this atom, while for Yamaguchi the value is 118 ppm. Since there is little doubt that the chromophore of bacteriorhodopsin is protonated (29), a value of 130.0 ppm simply cannot fit. By comparison with models (including our own presented in this paper), a protonated chromophore must have a chemical shift in the 120-ppm region. For these reasons, we prefer retaining a value near 120 ppm for C14. For solubilized rhodopsin the following comparisons can be made. In deuterated chloroform, C15 has values ranging from 160.72 to 164.33 ppm after applying a correction factor of 6.27 ppm uniformly from propionic acid to HI in Table 1. In deuterated methanol, C15 has values ranging from 164.0 to 167.4 ppm (correction factor of 4.9 ppm) for the protonated species. Since Mateescu finds 166 ppm for this carbon atom in rhodopsin, it follows that our model in deuterated methanol resembles rhodopsin much more than it resembles the one in $CDCl_3$. It could possibly signify that the environment surrounding the chromophore in rhodopsin has a polarity similar to methanol. This statement can be extended to bacteriorhodopsin, which must have an environment even more polar than rhodopsin since a value of 169 ppm is found for C15. This is in concordance with the works of Rafferty and Shichi (30) and Hildebrandt and Stockburger (31), which indicated water molecules around the chromophore. If we compared the value of 118 ppm obtained by Yamaguchi for C14 of bacteriorhodopsin with our own C14 values in CD_3OD (no correction needed here), we find that C14 has values ranging from 125.57 to 120.27 ppm. These data mean that for medium strong acids, the Schiff base in CD_3OD is more shielded than in $CDCl_3$. This implies that if the environment surrounding the chromophore is more polar than methanol, shielding could well reach 118 ppm.

What can we say about the protonating agent? For rhodopsin, Glu and Asp have pK_as similar to 3-nitro propanoic acid. In CD_3OD, this acid induces a corrected chemical shift for C15 of 165.7 ppm (that is, 160.82 + 4.9). This compares very well with the 165.9 ppm found by Mateescu. This similarity in the results indicates that Glu and Asp can partially protonate the Schiff base (around 75%). For bacteriorhodopsin, Glu and Asp can well be the protonating agents, since in a very polar milieu these two acids are able to fully protonate a Schiff base. It is interesting to note that if we extrapolate the chemical shift of C14 for the system RtBA – propionic acid to a solvent like water, a value of 119.8 ppm is found. For a stronger acid this value could well reach 118 ppm and even less.

Studies of our ^{15}N nmr with those obtained on models or on natural pigments are limited by two facts: many different sample states have been used so that comparisons with other works are difficult and there has been, to our knowledge, no study done on the solubilized pigments. The ^{15}N nmr spectra of bacteriorhodopsin were obtained by CP-MAS techniques using lyophilized samples. Mateescu *et al.* (1*d*) and Harbison *et al.* (2*a*) used this technique and obtained different results, probably because of differences in the way of preparing the samples. Mateescu *et al.* (1*f*) mentions a fact that we consider highly important: the degree of protonation of the chromophore seems to be regulated by the degree of hydration of the sample. This statement is in line with what we think of the environment surrounding the chromophore in both rhodopsin and bacteriorhodopsin. If water molecules do exist near the Schiff base, lyophilization under high vacuum should extract much of it and, consequently, will affect the degree of protonation of the Schiff base since the milieu will become less polar. Correspondingly, if water molecules are used in a proton transfer relay (32, 33), its absence will also cause the Schiff base to become unprotonated. Our data in deuterated chloroform confirm this fact, that rather weak acids like Glu and Asp can fully protonate a retinal Schiff base only in a very polar milieu. This does not prove that there are water molecules in the vicinity of the chromophore but indirectly suggests that water could create conditions favorable to full protonation. If we compare our results with those of Mateescu and co-workers (3*c*) in dichloromethane, we find that a correction of some 20 ppm is needed for the *tert*-butyl group of unprotonated RtBA and of 14 ppm for the hydrochloride salt.

Acknowledgements

The authors wish to express their sincere thanks to Professor Camille Sandorfy for helpful discussions and to the Laboratoire régional de RMN à haut champ (Dr Phan Viet Minh Tan) of the Université de Montréal for all ^{13}C and ^{15}N nmr spectra. It is a pleasure to acknowledge the financial help of the National Research Council of Canada (grant A0943) and of the Université du Québec à Montréal.

1. (*a*) J. W. Shriver, E. Abrahamson, and G. D. Mateescu. J. Am. Chem. Soc. **98**, 2407 (1976); (*b*) J. W. Shriver, G. D. Mateescu, R. Fager, D. Torchia, and E. W. Abrahamson. Nature (London), **270**, 271 (1977); (*c*) J. W. Shriver, G. D. Mateescu, and E. W. Abrahamson. Biochemistry, **18**, 4785 (1979); (*d*) G. D. Mateescu, W. G. Copan, D. D. Muccio, D. V. Waterhous, and E. W. Abrahamson. *In* Proceedings of International Symposium on Synthesis and Applications of Isotopically Labeled Compounds, Kansas City, MO. June 1982. *Edited by* W. P. Duncan and A. Susan. Elsevier, Amsterdam. 1983; (*e*) J. W. Shriver, G. D. Mateescu, and E. W. Abrahamson. Methods Enzymol. **81**, 698 (1982); (*f*) G. D. Mateescu, E. W. Abrahamson, J. W. Shriver, W. Copan, D. Muccio, M. Iqbal, and V. Waterhous. *In* Spectroscopy of biological molecules. *Edited by* C. Sandorfy and T. Theophanides. D. Reidel Publishing Co., Boston, MA. 1984. pp. 257–290.
2. (*a*) G. S. Harbison, J. Herzfeld, and R. G. Griffin. Biochemistry, **22**. 1 (1983); (*b*) G. S. Harbison, S. O. Smith, J. A. Pardoen, P. P. J. Mulder, J. Lugtenburg, J. Herzfeld, R. Mathies, and R. G. Griffin. Biochemistry, **23**, 2662 (1984); (*c*) G. S. Harbison, S. O. Smith, J. A. Pardoen, C. Winkel, J. Lugtenburg, J. Herzfeld, R. Mathies, and R. G. Griffin. Proc. Natl. Acad. Sci. U.S.A. **81**, 1706 (1984); (*d*) G. S. Harbison, S. O. Smith, J. A. Pardoen, J. M. L. Courtin, J. Lugtenburg, J. Herzfeld, R. Mathies, and R. G. Griffin. Biochemistry, **24**, 6955 (1985).

3. (*a*) J. W. SHRIVER, G. D. MATEESCU, and E. W. ABRAHAMSON. Biochemistry, **18**, 4785 (1979); (*b*) G. D. MATEESCU and M. IQBAL. Biochemistry, **23**, 3357 (1984); (*c*) G. D. MUCCIO, W. G. COPAN, E. W. ABRAHAMSON, and G. D. MATEESCU. Org. Magn. Reson. **22**, 121 (1984).
4. G. S. HARBISON, P. P. J. MULDER, H. PARDOEN, J. LUGTENBURG, J. HERZFELD, and R. G. GRIFFIN. J. Am. Chem. Soc. **107**, 4809 (1985).
5. Y. INOUE, Y. TOKITÔ, R. CHÛJO, and Y. MYIOSHI. J. Am. Chem. Soc. **99**, 5592 (1977).
6. A. YAMAGUCHI, T. UNEMOTO, and A. A. IKEGAMI. Photochem. Photobiol. **33**, 511 (1981).
7. R. S. BECKER, S. BERGER, D. K. DALLING, D. M. GRANT, and R. J. PUGMIRE. J. Am. Chem. Soc. **96**, 7008 (1974).
8. R. ROWAN III and B. D. SYKES. J. Am. Chem. Soc. **96**, 7000 (1974).
9. H. S. RODMAN, B. A. WALLACE, A. CROTEAU, and B. H. HONIG. Biophys. J. **47**, 92a (1985).
10. C. RABILLER and D. DANHO. Helv. Chim. Acta, **67**, 1254 (1984).
11. C. PATTARONI and J. LAUTERWEIN. Helv. Chim. Acta, **64**, 1969 (1981).
12. B. HONIG, Ù. DINUR, K. NAKANISHI, V. BALOGH-NAIR, M. A. GAWINOWICZ, M. ARNABOLDI, and M. G. MOTTO. J. Am. Chem. Soc. **101**, 7084 (1979).
13. K. NAKANISHI, V. BALOGH-NAIR, M. ARNABOLDI, K. TSUJIMOTO, and B. HONIG. J. Am. Chem. Soc. **102**, 7945 (1980).
14. (*a*) P. E. BLATZ and J. M. MOHLER. Biochemistry, **14**, 2304 (1975); (*b*) P. E. BLATZ, J. M. MOHLER, and H. V. NAVANGUL. Biochemistry, **11**, 848 (1972).
15. (*a*) M. SHEVES, K. NAKANISHI, and B. HONIG. J. Am. Chem. Soc. **101**, 7086 (1979); (*b*) M. SHEVES and K. NAKANISHI. J. Am. Chem. Soc. **105**, 4033 (1983); (*c*) F. DERGUINI, C. G. CALDWELL, M. G. MOTTO, V. BALOGH-NAIR, and K. NAKANISHI. J. Am. Chem. Soc. **105**, 646 (1983).
16. E. A. DRATZ and P. A. HARGRAVE. Trends Biochem. Sci. Pers. Ed. **8**, 128 (1983).
17. B. HONIG, T. EBREY, R. H. CALLENDER, U. DINUR, and M. OTTOLENGHI. Proc. Natl. Acad. Sci. U.S.A. **76**, 2503 (1979).
18. A. WARSHEL and N. BARBOY. J. Am. Chem. Soc. **104**, 1469 (1982).
19. D. COSSETTE and D. VOCELLE. Can. J. Chem. **65**, 661 (1987).
20. M. BISSONNETTE, H. LE THANH, and D. VOCELLE. Can. J. Chem. **62**, 1459 (1984).
21. R. TIOLLAIS. Bull. Soc. Chim. Fr. 708 (1947); 716 (1947).
22. R. K. HARRIS. *In* Nuclear magnetic resonance spectroscopy. Marshfield, MA. 1983. pp. 173–175, and references therein.
23. (*a*) A. BAX and R. FREEMAN. J. Magn. Reson. **42**, 164 (1981); (*b*) J. Magn. Reson. **44**, 542 (1983).
24. G. M. SHARMA and O. A. ROELS. J. Org. Chem. **38**, 3648 (1973).
25. L. S. LUSSIER, C. SANDORFY, H. LE THANH, and D. VOCELLE. Photochem. Photobiol. **45**, 801 (1987).
26. M. BISSONNETTE, H. LE THANH, and D. VOCELLE. Can. J. Chem. **63**, 1480 (1985).
27. (*a*) M. ALLEN and J. D. ROBERTS. J. Org. Chem. **45**, 130 (1980); (*b*) J. Org. Chem. **43**, 2590 (1978); (*c*) M. ALLEN, J. D. ROBERTS, and R. O. DUTHELER. J. Am. Chem. Soc. **100**, 3882 (1978).
28. D. D. MUCCIO, W. G. COPAN, E. W. ABRAHAMSON, and G. D. MATEESCU. Fed. Proc. Fed. Am. Soc. Exp. Biol. **39**, 2096 (1980).
29. R. R. BIRGE. Annu. Rev. Biophys. Bioeng. **10**, 315 (1981).
30. C. N. RAFFERTY and H. SHICHI. Photochem. Photobiol. **33**, 229 (1984).
31. P. HILDEBRANDT and M. STOCKBURGER. Biochemistry, **23**, 5539 (1984).
32. J. P. ROSENBUSCH. Bull. Inst. Pasteur, **83**, 207 (1985).
33. G. ZUNDEL and H. MERZ. *In* Information and energy transduction in biological membranes. Alan R. Liss, New York. 1984. p. 153.

Can. J. Chem. Downloaded from www.nrcresearchpress.com by 72.64.146.136 on 09/07/12
For personal use only.

The characterisation and X-ray crystal structure of pentabromodiselenium hexafluoroarsenate, $Se_2Br_5AsF_6$; some thermodynamic considerations and the nonexistence of $Se_2I_5AsF_6$

MICHAEL P. MURCHIE, JACK PASSMORE, AND PETER S. WHITE

Department of Chemistry, University of New Brunswick, Fredericton, N.B., Canada E3B 6E2

Received September 26, 1986[1]

MICHAEL P. MURCHIE, JACK PASSMORE, and PETER S. WHITE. Can. J. Chem. **65**, 1584 (1987).

The crystal structure of $Se_2Br_5AsF_6$ was determined by low-temperature X-ray diffraction methods. Single crystals of $Se_2Br_5AsF_6$ are rhombohedral, space group $R3$ with $a = 13.367(4)$ Å, $c = 19.000(6)$ Å, $V = 2940$ Å^3, and $Z = 9$. The structure was refined to final agreement indices of $R = 0.087$, $R_w = 0.093$ for 604 observed ($I > 3\sigma(I)$) reflections and 71 parameters. The structure consists of essentially discrete $Se_2Br_5^+$ cations and AsF_6^- anions with some cation–anion interaction. The $Se_2Br_5^+$ cation, of essentially C_{2h} symmetry contains two *trans* $SeBr_2$ units, linked by a bridging bromine atom. The two terminal selenium–bromine bond distances are 2.291(7) and 2.268(6) Å, of bond order 1, and the angle between them is 100.0(3)°. The bridging bromine atom lies at the inversion centre of the $Se_2Br_5^+$ cation, with an Se—Br distance of 2.582(3) Å, corresponding to a bond order of about 0.5. The two angles between the bridging Se—Br and terminal Se—Br bonds are 97.4(1)° and 98.9(2)°. $Se_2Br_5AsF_6$ decomposes slowly at room temperature and rapidly at 100°C leading to the formation of $SeBr_3AsF_6$, $SeBr_4$, and elemental selenium. It reacts with Br_2 to give $SeBr_3AsF_6$ and $SeBr_4$. $Se_2Br_5AsF_6$ is prepared by the reaction of $Se_4(AsF_6)_2$ and the appropriate quantity of Br_2. The analogous reaction with I_2 leads to $I_2SeSeSeSeI_2(AsF_6)_2$ and not $Se_2I_5AsF_6$. These differences have been accounted for on the basis of estimates of the appropriate bond and crystal lattice energies. The ^{77}Se nmr of $SeBr_3^+$ and $Se_2Br_5^+$ in SO_2 solution, and the Raman spectrum of $SeBr_4$ are reported.

MICHAEL P. MURCHIE, JACK PASSMORE et PETER S. WHITE. Can. J. Chem. **65**, 1584 (1987).

Faisant appel à des méthodes de diffraction des rayons-X à basse température, on a déterminé la structure cristalline du composé $Se_2Br_5AsF_6$. Les monocristaux de $Se_2Br_5AsF_6$ sont rhomboédriques, groupe d'espace $R3$, avec $a = 13{,}367(4)$ et $c = 19{,}000(6)$ Å, $V = 2940$ Å^3 et $Z = 9$. On a affiné la structure jusqu'à des valeurs finales de $R = 0{,}087$ et $R_w = 0{,}093$ pour 604 réflexions indépendantes avec ($I > 3\sigma(I)$) et 71 paramètres. La structure comporte essentiellement des cations $Se_2Br_5^+$ et des anions AsF_6^- individuels qui interagissent faiblement l'un avec l'autre. Le cation $Se_2Br_5^+$, dont la symétrie est essentiellement C_{2h}, contient deux unités $SeBr_2$ *trans* qui sont liées par un atome de brome. Les distances des deux liaisons sélénium/brome terminales sont égales à 2,291(7) et 2,268(6) Å, d'ordre de liaison 1, et l'angle entre ces liaisons est égal à 100,0(3)°. L'atome de brome qui agit comme pont se trouve au centre d'inversion du cation $Se_2Br_5^+$ et la distance Se—Br de 2,582(3) Å correspond à un ordre de liaison d'environ 0,5. Les deux angles entre les liaisons Se—Br (servant de pont) et Se—Br (terminale) égalent 97,41(1)° et 98,9(2)°. Le $Se_2Br_5AsF_6$ se décompose lentement à la température ambiante et rapidement à 100°C pour conduire à la formation de $SeBr_3AsF_6$, de $SeBr_4$ et de sélénium élémentaire. Il réagit avec le Br_2 pour conduire au $SeBr_3AsF_6$ et au $SeBr_4$. Le $Se_2Br_5AsF_6$ se prépare par réaction du $Se_4(AsF_6)_2$ avec une quantité appropriée de Br_2. La réaction analogue avec du I_2 conduit au $I_2SeSeSeSeI_2(AsF_6)_2$, non pas au $Se_2I_5AsF_6$. On peut expliquer ces différences en se basant sur une évaluation des énergies de liaison et de réseau cristallin appropriées. On rapporte aussi les spectres rmn du ^{77}Se du $SeBr_3^+$ et du $Se_2Br_5^+$, en solution dans le SO_2, ainsi que le spectre Raman du $SeBr_4$.

[Traduit par la revue]

Introduction

Various neutral selenium bromides are known (ref. 1, p. 219) reminiscent of the chlorides (ref. 1, p. 134), and in contrast to the iodides (ref. 1, p. 272) which are nonexistent. The structures of the neutral selenium bromides α- and β-$SeBr_4$ (4) and α- and β-SeBr (5, 6) have been determined by X-ray crystallography, while $SeBr_2$ has been identified by Raman and uv–visible spectroscopy (7). The selenium–bromine anion, $SeBr_6^{2-}$, has been shown to have an octahedral structure by infrared and Raman spectroscopy (8), and X-ray crystal structures of the novel anions $SeBr_4^{2-}$ and $Se_2Br_6^{2-}$ (with $[P(C_6H_5)_4^+]_2$ counterions) have been determined (9). The only binary selenium–bromine cation to be characterised fully is $SeBr_3^+$, prepared as the salt of the weakly basic AsF_6^-, SbF_6^- (10), $AlCl_4^-$ and $AlBr_4^-$ (11) anions. The Raman spectra of $SeBr_3MF_6$ (M = As, Sb) (10) showed the $SeBr_3^+$ cation to have essentially C_{3v} symmetry, with stretching frequencies and force constants somewhat higher in energy than those of the isoelectronic $AsBr_3$ (12). More recently, the structure of crystalline $SeBr_3SbF_6$ has been determined by X-ray diffraction (13).

In addition, we have previously reported the preparation of $Se_2Br_5AsF_6$ (10) according to reactions [1] and [2].

$$[1]\quad 4Se + 5Br_2 + 3AsF_5 \xrightarrow{\text{liquid } SO_2} 2Se_2Br_5AsF_6 + AsF_3$$

$$[2]\quad Se_4(AsF_6)_2 + 5Br_2 \xrightarrow{\text{liquid } SO_2} 2Se_2Br_5AsF_6$$

In this paper, the identity and structure of $Se_2Br_5AsF_6$ is established by a low-temperature X-ray crystal structure determination. The $Se_2Br_5^+$ cation is the first reported example of a $M_2Hal_5^+$ species (M = main group (VI) element; Hal = halogen).

Experimental

Except where otherwise stated, apparatus, reagents, and techniques are as previously described (14, 15). Elemental selenium (B.D.H.) was used without further purification. Literature methods were used to prepare $Se_4(AsF_6)_2$ (16) and $SeBr_4$ (17). Infrared spectra were obtained with a Perkin–Elmer 687 spectrometer using AgCl plates. Nuclear magnetic resonance spectra were recorded at room tempera-

[1]Revision received March 4, 1987.

Can. J. Chem. Downloaded from www.nrcresearchpress.com by 118.98.75.50 on 09/07/12
For personal use only.

TABLE 1. Comparison of the Raman spectral data for the: (**I**) combined precipitate, (**II**) more soluble product, and (**III**) least soluble product in the 1:7.1 reaction of $Se_4(AsF_6)_2$ with bromine[a]

Reaction products[b]				$SeBr_3AsF_6$		
I	**II**	**III**	$SeBr_4$[c]	Crystalline[d]	Powder[e]	Tentative assignments[f]
677(0.5)	677(0.5)			677(6.5)	676(1.0)	$\nu_1(AsF_6^-)$
				570(1.0)	570 sh	$\nu_2(AsF_6^-)$
				560 sh	560(<0.5)	
367(<0.5)	366(<0.5)			366(2.0)	365(<0.5)	$\nu_5(AsF_6^-)$
303 sh	304 sh			303 sh	303 sh	$\nu_3(SeBr_3^+)$
291(3.0)	292(10.0)			292(10.0)	292(10.0)	$\nu_1(SeBr_3^+)$
266(1.5)	263(0.5)	265(1.5)	264(4.0)			$\nu_1(SeBr_4)$
244(10.0)	243(3.0)	243(10.0)	242(10.0)			$\nu_3(SeBr_4)$
		229 sh	228 sh			
136(1.0)	135(3.0)	138(1.5)	138(2.0)	136(4.5)	138(2.0)	$\nu_2(SeBr_3^+)$, $\nu_2(SeBr_4)$
[g]	108(4.0)	[g]	[g]	109(5.0)	[g]	$\nu_4(SeBr_3^+)$, $\nu_4(SeBr_4)$

[a]All spectra were recorded at room temperature. Vibrational frequencies are in cm^{-1}.
[b]Product **I** is a mixture of the more soluble product **II** and the least soluble product **III**.
[c]$SeBr_4$ was prepared according to ref. 17. Raman vibrational frequencies and intensities are those obtained in this work.
[d]Raman spectral data for crystalline $SeBr_3AsF_6$ were obtained from ref. 10.
[e]Raman spectral data for powdered $SeBr_3AsF_6$ are as recorded in this work. The intensities of $\nu_1(AsF_6)$ and $\nu_5(AsF_6)$ for samples of powdered $SeBr_3AsF_6$ were observed to be lower than those for crystalline $SeBr_3AsF_6$.
[f]Assignments for $SeBr_3AsF_6$ are those quoted in ref. 10. Assignments for $SeBr_4$ and made by comparison with those cited for the infrared of $SeBr_4$ and the infrared and Raman of solid $SeCl_4$, $TeCl_4$, and $TeBr_4$ (20).
[g]The region below 136 cm^{-1} was obscured by the exciting line.

ture on a Varian XL-200 spectrometer using a 10-mm probe (broad-band over the frequency range 20–125 MHz) tuned to 38.164 MHz to observe ^{77}Se. Fluorine-19 spectra were obtained on the same probe by using the ^1H decoupler coil retuned to 188.220 MHz as the observe coil. Typically, for ^{77}Se and ^{19}F nmr spectra, the free induction decays were accumulated in 32 kwords of memory over a spectral width of 100 kHz (6.1 Hz/data point, line broadening of 5 Hz, pulse repetition time 0.16 s) with pulse widths of 20 and 6 μs, in 2000–7000 and 1000–3000 scans, respectively. Samples were run unlocked (field drift, <1 Hz/h) and were referenced externally to $(CH_3)_2Se$ and CCl_3F. The samples were prepared in 10-mm od thick-walled nmr tubes fitted with J. Young (o-ringette PTFE stopcock; model BST/2) valves.

Preparation of single crystals of $Se_2Br_5AsF_6$

The preparation of $Se_2Br_5AsF_6$, briefly referred to in an earlier publication (10), was repeated in order to obtain single crystals and a sample for ^{77}Se and ^{19}F nmr spectroscopy. Typically, AsF_5 (1.21 g, 7.14 mmol) and Br_2 (1.94 g, 12.14 mmol) were condensed onto a mixture of Se (0.76 g, 9.66 mmol) and liquid SO_2 (4.67 g). An intense red–brown solution over a dark solid was formed on warming to room temperature. This red–brown solution was filtered after 1 day, leaving a dark purple precipitate which was washed through the sintered-glass frit by 10 extractions with about 2 mL of the solvent. The volatile products were very slowly removed over a 5-h period by pumping under dynamic vacuum with the valve opened very slightly, leaving 3.59 g of a highly-crystalline dark purple solid (calculated yield for $Se_2Br_5AsF_6$, based on Se is 3.61 g). Single crystals were quickly mounted in well-dried capillaries in the dry box, which were then rapidly flame-sealed when taken out of the dry box, as described in ref. 15, and stored at −20°C prior to the X-ray crystal structure determination.

Characterisation of $Se_2Br_5AsF_6$

The $Se_2Br_5AsF_6$ product was identified in solution by ^{77}Se and ^{19}F nmr spectroscopy at room temperature only, since the solubility of $Se_2Br_5AsF_6$ decreases rapidly with decrease in temperature. The ^{77}Se nmr spectrum for a solution of $Se_2Br_5AsF_6$ (0.83 g) in SO_2 (3.85 g) contained a broad singlet at $\delta(Me_2Se)$ = 1331.1 ppm. The ^{19}F nmr spectrum contained a 1:1:1:1 quartet (J_{As-F} = 892 ± 6 Hz) at $\delta(CCl_3F)$ = −57.2 ppm which confirmed the presence of the AsF_6^- anion (18). The ^{77}Se and ^{19}F nmr spectra, obtained *in situ*, for a fresh sample of $Se_2Br_5AsF_6$ prepared by the reaction of $Se_4(AsF_6)_2$ and Br_2 according to reaction [2] were identical to those described above. The infrared spectrum of solid $Se_2Br_5AsF_6$ also showed the presence of the AsF_6^- anion (19). Attempts to obtain Raman spectra (exciting line 5145 Å) of solid $Se_2Br_5AsF_6$ at room temperature and at −196°C (with and without spinning) were unsuccessful. Good elemental analyses have already been obtained (10) for $Se_2Br_5AsF_6$.

Thermal stability of $Se_2Br_5AsF_6$

Samples of $Se_2Br_5AsF_6$ were sealed in glass sample tubes and stored at ca. −20°C without noticeable decomposition for >1.5 years. However, at room temperature, samples of $Se_2Br_5AsF_6$ slowly decomposed after periods ranging from 2 h to 2 days. The thermal instability was indicated by the formation of a red–brown liquid film on the crystals and loss of crystallinity of the sample. The thermal instability of $Se_2Br_5AsF_6$ made it necessary to carry out all room-temperature manipulations of the solid as quickly as possible and to determine its X-ray crystal structure at low temperature. A sample of $Se_2Br_5AsF_6$ (1.11 g, 1.49 mmol) was held at 100°C and subjected to a dynamic vacuum for 3 h. The volatile product was collected in a U-tube at −196°C and identified as $SeBr_4$ (0.30 g) by comparison of its Raman spectrum with that of a sample prepared by published (17) methods. The weight and colour of the remaining solid (0.82 g), a mixture of pale yellow and gray–black material, were consistent with the presence of $SeBr_3AsF_6$ and elemental selenium in a 2:1 mole ratio. The Raman spectrum of the yellow solid was identical to that reported (10) for $SeBr_3AsF_6$.

Attempted synthesis of $Se_2Br_7AsF_6$

(a) Reaction of $Se_4(AsF_6)_2$ with bromine. $Se_4(AsF_6)_2$ (0.87 g, 1.25 mmol) and Br_2 (1.42 g, 8.89 mmol) were reacted at a 1:7.1 mole ratio in liquid SO_2 (9.72 g) in a two-bulbed reaction vessel. A yellow–orange precipitate beneath an intense red–brown solution was formed immediately. The Raman spectrum of the combined precipitate (**I**) (i.e. before separating the more soluble product (**II**) from the least soluble product (**III**)), obtained *in situ*, indicated the presence of a mixture of $SeBr_3AsF_6$ and $SeBr_4$ (Table 1). The solution was filtered, and the more soluble product (**II**) was extracted by washing the combined precipitate (**I**) approximately ten times with 1–2 mL of the solvent. The

Can. J. Chem. Downloaded from www.nrcresearchpress.com by 118.98.75.50 on 09/07/12
For personal use only.

Can. J. Chem. Downloaded from www.nrcresearchpress.com by 118.98.75.50 on 09/07/12
For personal use only.

TABLE 2. Crystal data for $Se_2Br_5AsF_6$

Formula	$Se_2Br_5AsF_6$
System	Rhombohedral (hexagonal setting)
Space group	$R3$
a (Å)	13.367(4)
c (Å)	19.000(6)
V (Å^3)	2940
Z	9
λ (CuK$\bar{\alpha}$), Å	1.5418
μ (mm^{-1})	28.80
Crystal size (mm)	0.30 × 0.30 × 0.30
Temperature (K)	100(5)
$2\theta_{max}$ (deg)	110
Scan mode	ω–2θ
Scan range (deg 2θ)	2.0 (corrected for dispersion)
Scan speed (deg 2θ min^{-1})	2.0
$R = \Sigma\Delta F^2/\Sigma\|F\|^2$	0.087
$R_w = \Sigma(w\Delta F)^2/\Sigma w^2\|F\|^2$	0.093
No. of unique reflections	829
No. of observed reflections ($I > 3\sigma(I)$)	604

TABLE 3. Atomic parameters X, Y, Z, and B_{iso},[a] esd (in parentheses) refer to the last digit printed

Atom	X	Y	Z	B_{iso}
Br(1)	1/2	0	1/2	4.17
Se(1)	0.7178(3)	0.1438(3)	0.48394(20)	4.25
Br(2)	0.7230(4)	−0.2155(3)	0.43697(20)	5.12
Br(3)	0.7468(4)	0.0738(4)	0.38199(20)	4.97
As(1)	0	0	0.2955(4)	4.16
F(11)	0	0	0.2066(19)	5.05
F(12)	0	0	0.3868(21)	5.25
F(13)	−0.002(5)	0.126(4)	0.302(3)	3.21
F(14)	0.139(5)	0.133(6)	0.280(3)	3.59
F(15)	0.083(5)	0.154(5)	0.294(3)	3.83
F(16)	−0.076(7)	0.067(7)	0.285(3)	4.62
As(2)	0	0	0	3.98
F(21)	0.7863(15)	0.3762(16)	0.3854(12)	4.54

[a]The mean of the principal axes of the thermal ellipsoid.

solvent was slowly condensed back onto the least soluble product (**III**), thus isolating the more soluble product. The Raman spectrum of the more soluble product (**II**) (Table 1) indicated that it was predominantly $SeBr_3AsF_6$ with a small amount of $SeBr_4$. The solvent was slowly removed from the vessel by pumping under dynamic vacuum. The Raman spectrum of the least soluble product (**III**) indicated the presence of only $SeBr_4$.

(b) Reaction of $Se_2Br_5AsF_6$ with bromine. In one reaction, Br_2 (0.25 g, 1.59 mmol) was condensed onto a frozen solution of $Se_2Br_5AsF_6$ (1.03 g, 1.38 mmol) and SO_2 (3.79 g) in a 10 mm od nmr tube. An intense red–brown solution over a yellow–orange precipitate was noted on warming to room temperature. No change in the solution or precipitate was noted after standing at room temperature for 4 days. The ^{77}Se nmr spectrum, obtained at room temperature, contained a singlet at $\delta(Me_2Se)$ = 1323.1 ppm which indicated the presence of $SeBr_3^+$ (cf. $\delta(Me_2Se)$ = 1326.1 ppm for a solution of $SeBr_3AsF_6$ (0.55 g, 1.07 mmol) in SO_2 (3.11 g)). The Raman spectrum, obtained *in situ*, of the yellow–orange precipitate contained several peaks which indicated the presence of a mixture of $SeBr_3AsF_6$ and $SeBr_4$. The volatile material was removed by pumping under vacuum. The infrared spectrum of the yellow–orange solid indicated the presence of the AsF_6^- anion (19). An elemental analysis of the yellow–orange precipitate was consistent with a 1:1 mixture of $SeBr_3AsF_6$ and $SeBr_4$. *Anal. calcd.*: Se 17.43, Br 61.73, As 8.27, F 12.58; found: Se 15.91, Br 63.25, As 7.36, F 12.9. Empirical formula $Se_{2.0}Br_{7.9}As_{1.0}F_{6.7}$.

The X-ray crystal structure of $Se_2Br_5AsF_6$ [2]

Initial attempts to examine single crystals of $Se_2Br_5AsF_6$ at room temperature failed because of decomposition of the compound, which seemed to be accelerated by exposure to the X-ray beam. Even at 100 K, crystals exposed to MoKα radiation fluoresced heavily and only diffracted for about 1 h. It was therefore decided to undertake the structure determination at low temperature using CuKα radiation, even though the absorption coefficient for this wavelength radiation is extremely high. A number of crystals were used to determine possible space groups (Rc or $R3$) and approximate cell parameters. The procedure used the search program of the Enraf-Nonius CAD-4 diffractometer as well as a number of axial photographs and the cell reduction program of LePage (21). The intensity data collection and final cell parameter determination was made on one crystal from a fresh sample of the compound. Because the crystals do not possess well-defined faces, an effort was made to select one with equal dimensions in three directions. The data were collected using an Enraf-Nonius low-temperature device, which cools the crystal in a stream of cold N_2. Two unique sets of data were collected. A summary of the crystallographic data is given in Table 2.

The structure was solved using the MULTAN-80 (22) suite of direct methods programs. A spherical absorption correction was applied to the data and after refining with isotropic thermal parameters the empirical absorption routine DIFABS (23) was used. One of the AsF_6^- units was found to be disordered and was modelled as three rigid octahedra with a common F—As—F axis. The final least-squares refinement included all atoms except for the disordered fluorines with anisotropic thermal parameters. The final atomic coordinates are given in Table 3. The least-squares refinement was performed using SHELX-76 (24); all other calculations used a local implementation of the NRCVAX system of programs (25), on a Wicat S-160 computer.

Results and discussion

Preparation and properties of $Se_2Br_5AsF_6$

Highly crystalline purple $Se_2Br_5AsF_6$ was prepared quantitatively as previously described (10) either by reaction of the appropriate amounts of Se, Br_2, and AsF_5, according to reaction [1], or $Se_4(AsF_6)_2$ and $5Br_2$, according to reaction [2]. It is possible that the $Se_2Br_5^+$ cation exists as such in sulphur dioxide solution and is characterised by a broad singlet in the ^{77}Se nmr spectrum at $\delta(Me_2Se)$ = 1331.1 ppm at room temperature. It is also possible that it is in equilibrium with $SeBr_2$ and $SeBr_3^+$ in solution.

$Se_2Br_5AsF_6$ decomposes slowly at room temperature and rapidly at 100°C into $SeBr_3AsF_6$, $SeBr_4$, and elemental selenium. This is consistent with the initial evolution of $SeBr_2$, according to reaction [3], followed by its disproportionation into $SeBr_4$ and elemental selenium (1), reaction [4].

[3] $Se_2Br_5AsF_6(s) \rightarrow SeBr_3AsF_6(s) + SeBr_2(g)$

[4] $2SeBr_2(g) \rightarrow SeBr_4(s) + Se(s)$

On addition of bromine to a solution of $Se_2Br_5AsF_6$ in sulphur dioxide solution, a mixture of $SeBr_3AsF_6$ and $SeBr_4$ are obtained, according to reaction [5]. We could find no evidence for the formation of $Se_2Br_7AsF_6$.

[5] $Se_2Br_5AsF_6(s) + Br_2(l) \rightarrow SeBr_3AsF_6(s) + SeBr_4(s)$

[2]Complete set of data may be purchased from the Depository of Unpublished Data, CISTI, National Research Council of Canada, Ottawa, Ont., Canada K1A 0S2.

Can. J. Chem. Downloaded from www.nrcresearchpress.com by 118.98.75.50 on 09/07/12
For personal use only.

A comparison of the products of reactions of Se_4^{2+} with iodine and bromine in SO_2 solution and an explanation for the nonexistence of $Se_2I_5AsF_6$

Reactions of $Se_4(AsF_6)_2$ and varying amounts of iodine in SO_2 solution, followed by ^{77}Se nmr spectroscopy, produced $Se_4I_4^{2+}$ (34, 35) according to reaction [6].

$$[6]\quad Se_4^{2+} + 2I_2 \xrightarrow{SO_2} Se_4I_4^{2+}$$

The $Se_4I_4^{2+}$ cation itself was in equilibrium with small amounts of $Se_6I_2^{2+}$ and SeI_3^+ according to reaction [7].

$$[7]\quad 2Se_4I_4^{2+} \rightleftharpoons Se_6I_2^{2+} + 2SeI_3^+$$

The same peaks appeared in the ^{77}Se nmr spectrum at all mole ratios of $Se_4(AsF_6)_2$:I_2, i.e. $Se_4I_4^{2+}$ did not react further with iodine and did not form $Se_2I_5^+$.

In contrast, the ^{77}Se nmr spectra for the products obtained in the reactions of $Se_4(AsF_6)_2$ with bromine showed a large number of peaks at ratios of $Se_4(AsF_6)_2$:Br_2 less than 1:5. The number of peaks varied with the particular value of the mole ratio. Most of the peaks were broad and unidentified and are presently under investigation. At a $Se_4(AsF_6)_2$:Br_2 mole ratio of 1:5, corresponding to the formation of $2Se_2Br_5^+$, only one peak in the ^{77}Se nmr spectrum was observed. Thus, whereas the reaction of Se_4^{2+} with iodine is completed with the formation of $Se_4I_4^{2+}$, the $Se_4Br_4^{2+}$ cation, if it is formed at all, reacts with more bromine to give $Se_2Br_5^+$. The reason for this is that the reaction of $Se_4I_4^{2+}$ and more iodine, according to reaction [8], is not thermodynamically favourable (ΔH[8] $\simeq$ +15 kcal mol^{-1}) whereas the reaction of the hypothetical $Se_4Br_4^{2+}$ and bromine, according to reaction [9], is favourable (ΔH[9] $\simeq$ −9 kcal mol^{-1}).

$$[8]\quad I_2Se^+SeSeSe^+I_2 + I_2(s) \rightarrow 2I_2Se^+SeI$$

$$\Delta H[8] = -2\Delta H[\text{Se—I}] + \Delta H[\text{atomisation energy of } I_2(s)] + \Delta H[\text{Se—Se}]$$
$$\simeq -82 + 51 + 46 \text{ (ref. 36)}$$
$$\simeq +15 \text{ kcal mol}^{-1}$$

$$[9]\quad Br_2Se^+SeSeSe^+Br_2 + Br_2(l) \rightarrow 2Br_2Se^+SeBr$$

$$\Delta H[9] = -2\Delta H[\text{Se—Br}] + \Delta H[\text{atomisation energy of } Br_2(l)] + \Delta H[\text{Se—Se}]$$
$$\simeq -108 + 53 + 46 \text{ (ref. 36)}$$
$$\simeq -9 \text{ kcal mol}^{-1}$$

Br_2Se^+SeBr and/or its disproportionation products may then react with one more molecule of bromine to give the observed $Se_2Br_5^+$.

Consistently, the energy cycles below show that the formation of $Se_2Br_5AsF_6$ from selenium, bromine, and AsF_5 according to reaction [11] is much more favourable (ΔH[11] $\simeq$ −161 kcal mol^{-1}) than the corresponding formation of $Se_2I_5AsF_6$ (ΔH[10] $\simeq$ −19 kcal mol^{-1}). The estimates of some of the thermodynamic quantities involved in Table 4 are in the nature of guesstimates. Nevertheless the difference in ΔH values for reactions [10] and [11] is clearly substantial, and is almost entirely due to the Se—Br bond energy being greater than the Se—I bond energy (ΔH_5 below). The free energy change in these reactions will be less favourable than the estimated enthalpy values given here, as entropy favours the reactants, not the products. Thus the ΔG value for reaction [10] could be approximately zero, in contrast to ΔG for reaction [11] which will undoubtedly be substantially negative.

$$[10]\quad 4Se(s) + 5I_2(s) + 3AsF_5(g) \rightarrow 2Se_2I_5AsF_6(s) + AsF_3(l)$$

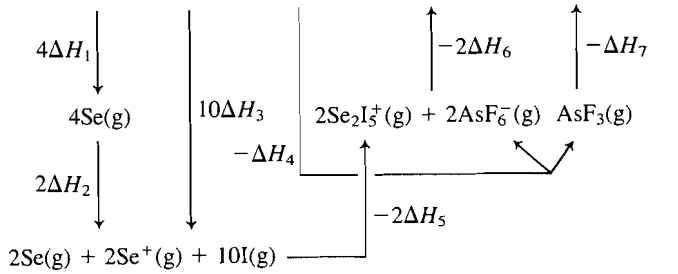

$$\Delta H[10] = 4\Delta H_1 + 2\Delta H_2 + 10\Delta H_3 - \Delta H_4 - 2\Delta H_5 - 2\Delta H_6 - \Delta H_7$$
$$\simeq 216 + 450 + 255 - 233 - 2\Delta H_5 - 228 - 9$$
$$\simeq 451 - 2\Delta H_5 \simeq 451 - 470 \simeq -19 \text{ kcal mol}^{-1}$$

$$[11]\quad 4Se(s) + 5Br_2(l) + 3AsF_5(g) \rightarrow 2Se_2Br_5AsF_6(s) + AsF_3(l)$$

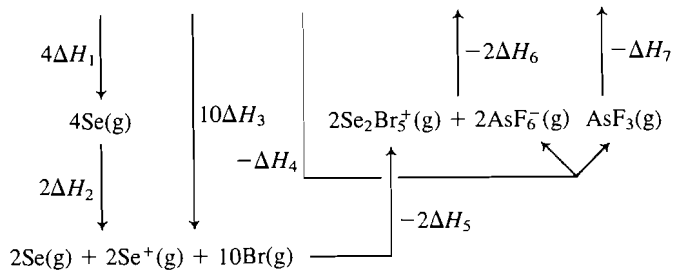

$$\Delta H[11] = 4\Delta H_1 + 2\Delta H_1 + 2\Delta H_2 + 10\Delta H_3 - \Delta H_4 - 2\Delta H_5 - 2\Delta H_6 - \Delta H_7$$
$$\simeq 216 + 450 + 265 - 233 - 2\Delta H_5 - 234 - 9$$
$$\simeq 455 - 2\Delta H_5 \simeq 455 - 616 \simeq -161 \text{ kcal mol}^{-1}$$

Crystal structure

The structure of the $Se_2Br_5^+$ cation, including bond distances and angles, is illustrated in Fig. 1, and a packing diagram is given in Fig. 2. Relevant bond distances and angles are presented in Table 5. The shortest cation–anion contact is 2.75(8) Å (Table 5) which suggests that $Se_2Br_5AsF_6$ essentially consists of $Se_2Br_5^+$ and AsF_6^- ions, with cation–anion interactions. The $Se_2Br_5^+$ cation is the first example of an $M_2Hal_5^+$ species (M = main group (VI) element; Hal = halogen) but is related to the $O_2H_5^+$ cation shown to be present in H_5O_2Br (38) and *o*-$C_6H_4(COOH)SO_3H\cdot 3H_2O$ (39) by neutron diffraction.

The $Se_2Br_5^+$ cation contains two $SeBr_2$ units linked by Br(1) which is on an inversion centre and has approximately C_{2h} symmetry. The two terminal selenium–bromine bond distances in $Se_2Br_5^+$ (2.291(7) and 2.268(6) Å) are comparable to those distances (Table 6) in other species where the selenium–bromine bond order is ca. 1.0. In $Se_2Br_5^+$, the bridging selenium–bromine bond distance of 2.582(3) Å is roughly the same order of magnitude as other related bridging selenium–bromine distances (Table 6), and corresponds to a bond order of approximately 0.5. In valence bond terms, the structure may be represented by a combination of resonance structures **I** and **II** of equal weight, and lesser amounts of resonance structure **III**. The resultant charge on selenium may be somewhat higher than 0.5, depending upon the importance of structure **III**. The Se—Br—Se bond angle of 180° is consistent with the structure being represented by **I** and **II** or **III** where the bridging bromine atom has, in VSEPR terms, an AX_2E_3 configuration (42), or the bonding in the bridging region being represented by a three-centre four-electron bond.

Comparison of Figs. 1 and 3 shows that the overall geometry

Can. J. Chem. Downloaded from www.nrcresearchpress.com by 118.98.75.50 on 09/07/12
For personal use only.

TABLE 4. Thermodynamic data

Reaction	ΔH (kcal mol^{-1})	Reference
$Se(s) \rightarrow Se(g)$	54	26
$Se(g) \rightarrow Se^+(g)$	225	26
$I_2(s) \rightarrow 2I(g)$	51	26
$Br_2(l) \rightarrow 2Br(g)$	53	26
$AsF_3(l) \rightarrow AsF_3(g)$	9	27
$Se(s) + Br_2(l) \rightarrow SeBr_2(g)$	−5	27
$Se(s) + 2Br_2(l) \rightarrow SeBr_4(s)$	−18	28
$3AsF_5(g) + 2e^- \rightarrow 2AsF_6^-(g) + AsF_3(g)$	−233	*a*
$Se_2Br_5^+(g) \rightarrow Se^+(g) + Se(g) + 5Br(g)$	308	*b*
$Se_2I_5^+(g) \rightarrow Se^+(g) + Se(g) + 5I(g)$	235	*b*
$SeBr_3^+(g) \rightarrow Se^+(g) + 3Br(g)$	162	*b*
$Se_2Br_5AsF_6(s) \rightarrow Se_2Br_5^+(g) + AsF_6^-(g)$	117 ± 5	*c*
$Se_2I_5AsF_6(s) \rightarrow Se_2I_5^+(g) + AsF_6^-(g)$	114 ± 5	*c*
$SeBr_3AsF_6(s) \rightarrow SeBr_3^+(g) + AsF_6^-(g)$	127 ± 5	*c*

[a]The heat of reaction for the formation of $2AsF_6^-(g)$ and $AsF_3(g)$ may be estimated as follows:

	ΔH (kcal mol^{-1})
$As(s) + (3/2)F_2(g) \rightarrow AsF_3(g)$	−187.8 (ref. 27)
$AsF_5(g) \rightarrow As(s) + (5/2)F_2(g)$	295.6 (ref. 29)
$F_2(g) + 2e^- \rightarrow 2F^-(g)$	−119 (ref. 29)
$2AsF_5(g) + 2F^-(g) \rightarrow 2AsF_6^-(g)$	−222 (ref. 30)
$3AsF_5(g) + 2e^- \rightarrow 2AsF_6^-(g) + AsF_3(g)$	−233 kcal mol^{-1}

[b]The atomization energies of $Se_2Br_5^+(g)$ and $Se_2I_5^+(g)$ were estimated from the sums of the respective bond dissociation energies. It is assumed that the selenium–bromine single bond energy in cations containing a positively charged terminal Se(IV)—Br bond is the same as that in neutral $SeBr_2$ (54.0 kcal mol^{-1}, ref. 26). Since neutral selenium–iodine compounds are nonexistent (ref. 3) the selenium–iodine bond energy for SeI_2, calculated by Sanderson (41.2 kcal mol^{-1}, ref. 31), was used and assumed to be about the same as that for the terminal $Se(IV)^+$—I in $Se_2I_5^+$. It is likely that the $Se(IV)^+$—Br bond strength is slightly stronger than that for Se(II)—Br, since Se—Br bond lengths in $Se(IV)^+$—Br species are slightly shorter than in Se(II)—Br species. The Se—Br bond lengths in $[SeBr_3^+][SbF_6^-]$ and $SeBr_2$ are 2.269(8) and 2.32(2), respectively (Table 5) and are likely significantly different. However, the $Se(IV)^+$—I bond length in SeI_3AsF_6 (2.510(3) Å; ref. 33) is essentially the same as that estimated for the Se(II)—I bond length in SeI_2 (2.50 Å, ref. 33), indicating that the $Se(IV)^+$—I and Se(II)—I bond strengths are the same. The linear Se—Br—Se and Se—I—Se bridging bonds in $Se_2Br_5^+$ and $Se_2I_5^+$ are similar to the linear I—I—I bridging bonds in I_3^-, Topol (ref. 32) has shown that there is a gain in energy of 24 kcal mol^{-1} in the formation of $I_3^-(g)$ according to the following equation: $I^-(g) + I_2(g) \rightarrow I_3^-(g)$. Therefore, the sum of the bridging I—I bond energies in I_3^- equals 24 plus 36.1 (I—I bond energy in $I_2(g)$) kcal mol^{-1}, and the ratio of bridging bond energies in $I_3^-(g)$ to the bond energy in $I_2(g)$ is (24 + 36.1)/36.1 = 1.7.

Assuming that the bridging bond energies in $Se_2Br_5^+$ and $Se_2I_5^+$ may be estimated in a similar fashion, then their atomization energies may be estimated as follows:

$Se_2Br_5^+$	$Se_2I_5^+$
4(Se—Br) = 4(54.0)	4(Se—I) = 4(41.2)
+ bridging bonds = 1.7(54.0)	+ bridging bonds = 1.7(41.2)
$\therefore \Delta H_5$ = 308 kcal mol^{-1}	$\therefore \Delta H_5$ = 235 kcal mol^{-1}

The values of ΔH_5 may in fact be somewhat higher than estimated here, especially in the $Se_2Br_5^+$ case.

[c]Bartlett *et al.* (ref. 30) have shown that there is an essentially linear relationship, for simple A^+B^- salts (e.g. NaCl, KBr, KI) between the lattice energies and (molecular volume)$^{-1/3}$, where the equation of the line may be represented by: $\Delta H_L = 556.3(\text{molecular volume})^{-1/3} + 26.31$ kcal mol^{-1}. Therefore, the crystal lattice energy of $Se_2Br_5AsF_6$ (molecular volume is 326.7 Å^3) is estimated as 107 ± 5 kcal mol^{-1}. However, Bartlett *et al.* noted that for species such as ClO_2BF_4 and SF_3BF_4 there was a positive deviation (6–8 kcal mol^{-1}) from the line, which was attributed to the dispersion energies of these salts being greater than those of the simple salts (e.g. NaCl, KBr). A conservative estimate of 10 kcal mol^{-1} has been used for the positive deviation of $Se_2Br_5AsF_6$, and therefore, ΔH_L (corrected) for $Se_2Br_5AsF_6$ is estimated as 117 ± 5 kcal mol^{-1}. Similarly, the crystal lattice energy of $SeBr_3AsF_6$ (molecular volume 232.0 Å (ref. 13)) is estimated as 127 ± 5 kcal mol^{-1}.

The ratio of the molecular volume of the hypothetical $Se_2I_5AsF_6$ to SeI_3AsF_6 is assumed to be similar to that of $Se_2Br_5AsF_6$ to $SeBr_3AsF_6$. Therefore

$$V_{Se_2I_5AsF_6} = \frac{V_{SeI_3AsF_6} \times V_{Se_2Br_5AsF_6}}{V_{SeBr_3AsF_6}} = \frac{265.0 \text{ Å}^3 \text{ (ref. 33)} \times 326.7 \text{ Å}^3}{232.0 \text{ Å}^3 \text{ (ref. 13)}} = 373.2 \text{ Å}^3$$

The lattice energy of $Se_2I_5AsF_6$ is therefore estimated to be 114 ± 5 kcal mol^{-1}.

TABLE 5. (*a*) Bond distances (esd's in parentheses)[a,b]

Bond	Distance (Å)	Bond	Distance (Å)
	$Se_2Br_5^+$		
Se(1)—Br(1)	2.582(3)	Se(1)—Br(3)	2.268(6)
Se(1)—Br(2)	2.291(7)		
	AsF_6^-'s		
As(1)—F(11)	1.69(4)	As(1)—F(15)	1.79(5)
As(1)—F(12)	1.73(4)	As(1)—F(16)	1.66(12)
As(1)—F(12)	1.73(4)	As(1)—F(16)	1.66(12)
As(1)—F(13)	1.71(7)		
As(1)—F(14)	1.84(5)	As(2)—F(21)	1.72(2)
	Interionic distances		
Se(1)—F(11k)	3.12(1)	Br(1)—F(21f)	3.30(2)
Se(1)—F(14f)	2.75(8)	Br(1)—F(21g)	3.30(2)
Se(1)—F(15f)	3.02(7)		
Se(1)—F(16h)	3.22(12)	Br(2)—F(131)	3.10(9)
Se(1)—F(21k)	3.34(2)	Br(2)—F(14f)	3.12(12)
Se(1)—F(21f)	2.98(3)	Br(2)—F(15f)	3.14(12)
		Br(2)—F(151)	3.26(8)
Br(1)—F(14f)	3.23(5)		
Br(1)—F(14g)	3.23(5)	Br(3)—F(14m)	2.94(11)
Br(1)—F(16h)	3.15(9)	Br(3)—F(15m)	3.30(11)
Br(1)—F(16i)	3.15(9)	Br(3)—F(16n)	3.04(10)

(*b*) Angles (esd's in parentheses)[b]

Bonds	Angle (deg)	Bonds	Angle (deg)
	$Se_2Br_5^+$		
Se(1)—Br(1)—Se(1a)	180.0	Br(1)—Se(1)—Br(3)	98.9(2)
Br(1)—Se(1)—Br(2)	97.4(2)	Br(2)—Se(1)—Br(3)	100.0(3)
	AsF_6^-'s		
F(11)—As(1)—F(12)	180.0	F(12)—As(1)—F(13)	85.6(18)
—F(13)	94.4(18)	—F(14)	99.4(18)
—F(14)	80.6(18)	—F(15)	90.9(19)
—F(15)	89.1(19)	—F(16)	97.0(23)
—F(16)	83.0(23)	F(21)—As(2)—F(21q)	180.0
		—F(21o)	90.1(11)
		—F(21r)	89.9(11)
	Interionic angles		
Br(1)—Se(1)—F(11k)	86.6(1)	Br(3)—Se(1)—F(21f)	80.6(6)
—F(14f)	74.4(12)	F(11k)—Se(1)—F(14f)	45.3(22)
—F(15f)	92.7(12)	—F(15f)	46.7(25)
—F(16h)	64.7(8)	—F(16h)	40.0(3)
—F(21k)	116.2(4)	—F(21k)	60.4(7)
—F(21f)	72.4(3)	—F(21f)	64.4(8)
Br(2)—Se(1)—F(11k)	117.5(6)	F(14f)—Se(1)—F(15f)	18.4(20)
—F(14f)	75.9(25)	—F(16h)	12.0(3)
—F(15f)	70.8(24)	—F(21k)	104.6(18)
—F(16h)	85.0(3)	—F(21f)	102.0(3)
—F(21k)	145.4(4)	F(15f)—Se(1)—F(16h)	29.7(22)
—F(21f)	169.7(3)	— F(21k)	98.5(16)
Br(3)—Se(1)—F(11k)	141.1(7)	—F(21f)	110.0(3)
—F(14f)	171.4(10)	F(16h)—Se(1)—F(21k)	101.0(3)
—F(15f)	166.1(22)	—F(21f)	91.0(3)
—F(16h)	163.4(9)	F(21k)—Se(1)—F(21f)	44.8(4)
—F(21k)	83.2(4)		

[a]All interactions less than the sum of the van der Waal's radii are included (r_{Se} = 1.90 Å, r_{Br} = 1.85 Å, r_F = 1.47 Å from Bandi, ref. 37).

[b]Fluorine atoms F(13), F(14), F(15), and F(16) are disordered (33% occupancy).

Can. J. Chem. Downloaded from www.nrcresearchpress.com by 118.98.75.50 on 09/07/12
For personal use only.

TABLE 6. Comparison of selenium–bromine bond distances (Å)

Molecule	Se—Br (terminal)	Average	Se—Br (bridging)	Average	Reference
$Se_2Br_5AsF_6$	2.291(7) 2.268(6)	2.28	2.582(3)		This work
$SeBr_3SbF_6$	2.280(8) 2.254(7) 2.272(8)	2.27			1,13
α-$SeBr_4$[a]	2.44 2.35 2.31	2.37	3.05 3.02 2.87	2.98	1,4
α-SeBr	2.357(2)				1,6
β-SeBr	2.366(1) 2.369(1)	2.37			1,5,6
$SeBr_2$[b]	2.32(2)				1,40
$[P(C_6H_5)_4]_2SeBr_4$	2.595(1) 2.596(1)	2.60			9
$[P(C_6H_5)_4]_2Se_2Br_6$	2.485(1) 2.399(1)	2.44	2.887(1) 2.710(1)	2.80	9
$SeBr_2$(tmtu)[c]	2.569(3) 2.620(3)	2.70	3.34		41

[a] β-$SeBr_4$ is isostructural, but not isomorphous, with α-$SeBr_4$ (1, 4).
[b] The Se—Br bond length in $SeBr_2$ was determined by electron diffraction studies of the decomposition products at 200°C of $SeBr_4$(g) which are presumably $SeBr_2$(g) and Br_2(g) according to ref. 40.
[c] tmtu = tetramethyl thiourea ($C_5H_{12}N_2S$).

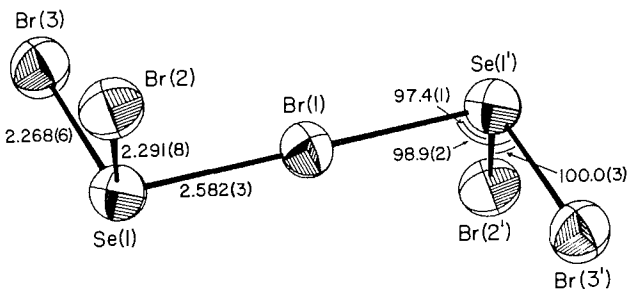

FIG. 1. The structure of the $Se_2Br_5^+$ cation in $Se_2Br_5AsF_6$.

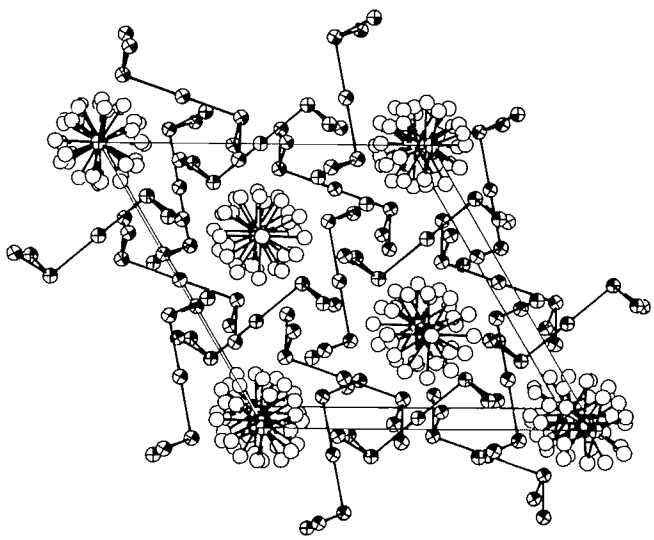

FIG. 2. Crystal packing in $Se_2Br_5AsF_6$.

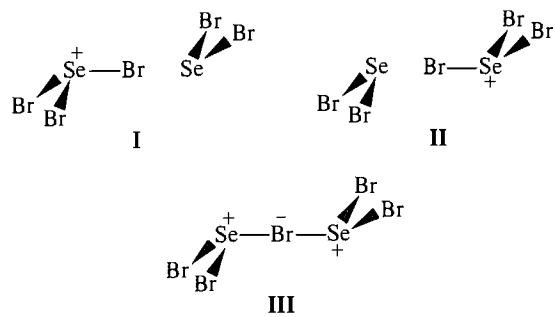

of the $Se_2Br_5^+$ cation is similar to that in the *trans* cation in (α)$6SbF_3 \cdot 5SbF_5$ (43) and $5SbF_3 \cdot 3SbF_5$ (44) and about the bridging iodine atom in the $[(S_7I)_2I]^{3+}$ cation (45). Interestingly, $Se_2Br_5^+$ may be viewed as isolating the bridging halogen unit in $[(S_7I)_2I]^{3+}$ by replacing the chalcogen–chalcogen bonds of the rings with terminal chalcogen–halogen bonds. This geometry minimises both the repulsion between the lone pairs on the two selenium atoms and the electro-static repulsions between the terminal bromine atoms that certainly carry some partial positive charge. Calculations performed on Cl_5^+, as a model for I_5^+, have shown that electrostatic repulsion between the terminal atoms are responsible for the transplanar geometry of Cl_5^+ and hence that of I_5^+ (15). The $O_2H_5^+$ cations in H_5O_2Br (38) and *o*-$C_6H_4(COOH)SO_3H \cdot 3H_2O$ (39) contain OH_2 units joined by a bridging hydrogen atom with a bridging angle of almost 180°. The bridging bond distances are almost equal. However, the overall structure is staggered.

The average terminal selenium–bromine bond distance of 2.280(7) Å found in $Se_2Br_5^+$ is somewhat shorter than that found in the neutral and anionic selenium–bromine species, but it is slightly longer, though not significantly different, than the average 2.269(8) Å selenium–bromine distance in $SeBr_3^+$ (see Table 6). The longer bond in $Se_2Br_5^+$ may be accounted for by

Can. J. Chem. Downloaded from www.nrcresearchpress.com by 118.98.75.50 on 09/07/12
For personal use only.

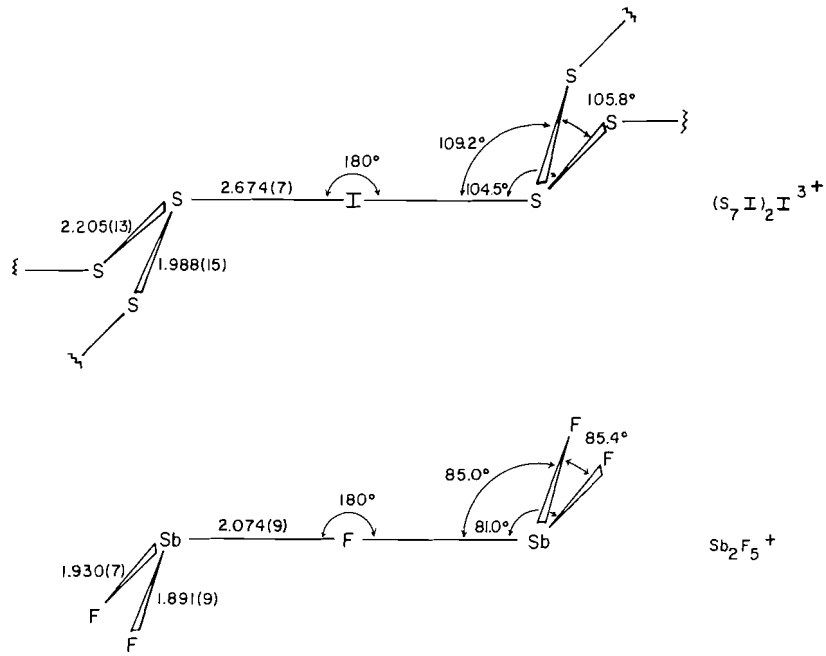

FIG. 3. Geometries about the bridging halogen atoms in $[(S_7I)_2I]^{3+}$ and $Sb_2F_5^+$ (in $5SbF_3 \cdot 3SbF_5$); analogous to geometry about Br(1) in $Se_2Br_5^+$.

TABLE 7. Comparison of the terminal and bridging linear M—X bond lengths (M = S, Se, Sb, Br, I; X = F, Br, I)

Compound	M—X(terminal) (Å)	M—X(bridging) (Å)	M—X(terminal) / M—X(bridging)	References
$Se_2Br_5AsF_6$	2.28	2.582(3)	0.88	This work
$((S_7I)_2I)(SbF_6)_3$	2.34	2.674(7)	0.87	45
$(Se_6I_2)(AsF_6)_2/(Se_6I)_n \cdot n(AsF_6)$	2.45	2.736(3)	0.90	46
$Sb_2F_5^+$ in $5SbF_3 \cdot 3SbF_5$	1.91	2.074(9)	0.92	44
$Br_2/(C_6H_5N_2)(Br_3)$	2.28	2.54	0.90	2
$I_2/((C_2H_5)_4N)(I_3)$	2.67	2.928(3)	0.91	2
I_5AsF_6	2.65	2.895(1)	0.91	15

the contribution of $SeBr_2$ (valence bond structures **I** and **II**), which has a longer (2.32(2) Å) bond length, and the lower charge of 0.5 on the Se atom. The bridging selenium–bromine bond length of 2.582(3) Å is also shorter than other bridging selenium–bromine distances found in the neutral or anionic species (Table 6). This is expected as distances are shorter in species containing positively charged selenium atoms than in those that are formally neutral. Nevertheless, the ratio of M—X (terminal) to M—X (bridging) (M = S, Se, Sb, Br, I; X = F, Br, I) distances in a variety of species are all very similar (see Table 7).

The relative sizes of the Br—Se—Br bond angles in $Se_2Br_5^+$ are consistent with a VSEPR model, i.e. the smaller angle is associated with the longer adjacent bonds (42). Consistently, the Br—Se—Br bond angles in $SeBr_3^+$ are larger than those in $Se_2Br_5^+$ (Figs. 1 and 4).

There are two unique AsF_6^- anions in the crystal structure of $Se_2Br_5AsF_6$. The anion containing As(2) is a regular octahedron with an average As—F bond distance of 1.72 Å and F—As—F bond angle of 90.0° (Table 5). The anion containing As(1), which is disordered in the equatorial plane such that each equatorial fluorine atom has only ca. 33% occupancy, has an average As—F bond distance of 1.74 Å, the bond angles were fixed by the disorder model.

There are weak interactions between the selenium atoms in the cation in $Se_2Br_5AsF_6$ and the fluorine atoms in the anion (Table 5, Figs. 4 and 5) that are significantly less than the sum of the van der Waals radii (3.37 Å) (37). The very weak contact Se(1)—F(21k) is only 1% shorter than the sum of the van der Waals radii and will not be discussed further. Three of the contacts are to disordered fluorine atoms of ca. 33% occupancy (i.e. F(14), F(15), F(16)). Since their environments with respect to the cation are very similar, they may be qualitatively considered as one contact. Therefore, the bond distances and angles of Se(1)—F(14), Se(1)—F(15), and Se(1)—F(16) have been averaged such that the Se(1)—F(ave) bond distance is 3.00 Å and the bond angles are Br(3)—Se(1)—F(ave), 167.0°; Br(2)—Se(1)—F(ave), 77.4°; Br(1)—Se(1)—F(ave), 77.3°; and F(21f)—Se(1)—F(ave), 101.2°. The strongest contacts Se(1)—F(21f) and Se(1)—F(ave) are opposite to the Se(1)—Br(2) and Se(1)—Br(3) bonds in the cation, i.e. F—Se—Br bond angles are both about 180° (Figs. 4 and 5). The Se—F contact distances in $Se_2Br_5AsF_6$ (i.e. F(21f), 2.98; F(ave), 3.00; F(11k), 3.12 Å) are considerably longer than those in

Can. J. Chem. Downloaded from www.nrcresearchpress.com by 118.98.75.50 on 09/07/12
For personal use only.

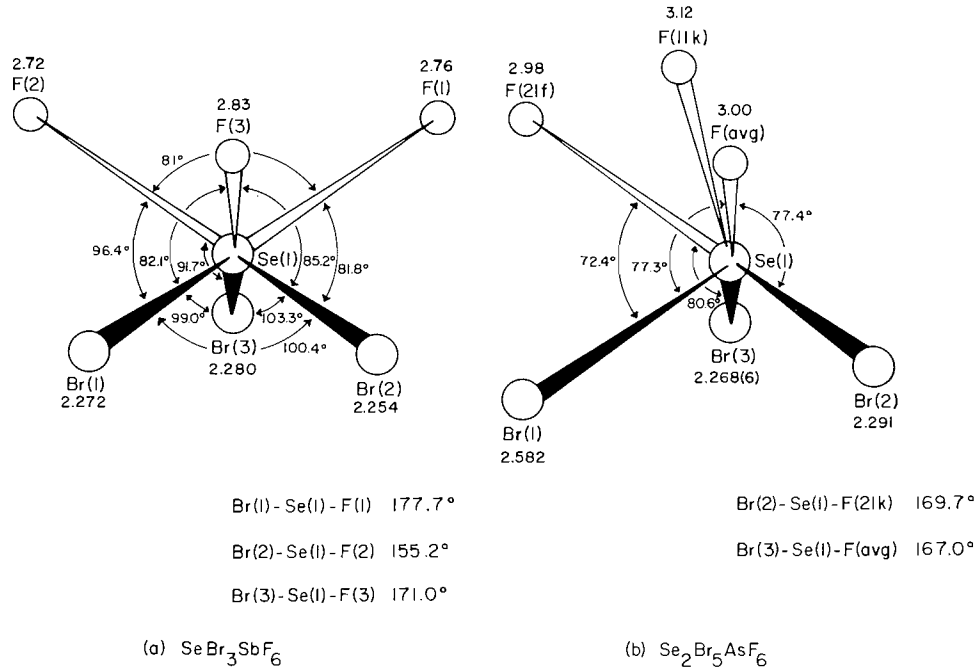

FIG. 4. Comparison of the environment around the selenium atoms in (*a*) $SeBr_3SbF_6$ and (*b*) $Se_2Br_5AsF_6$.

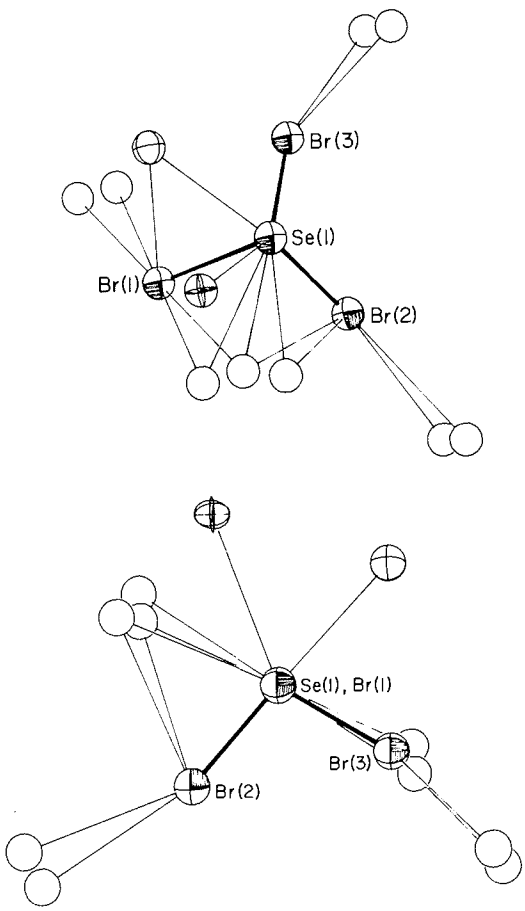

FIG. 5. Fluorine atom contacts to the selenium and bromine atoms in $Se_2Br_5AsF_6$ (all Se---F ≦ 3.330 Å; Br---F ≦ 3.290 Å). Partially filled, unlabelled circles represent fluorine atoms of 100% occupancy and empty circles represent fluorine atoms of ca. 33% occupancy.

$SeBr_3SbF_6$ (2.72, 2.83, and 2.76 Å (13)) which is consistent with each selenium atom in $Se_2Br_5AsF_6$ having a positive charge of less than 1.

It is not altogether easy to describe the stereochemistry about the selenium atoms in VSEPR terms (42). The positively charged selenium atoms of valence bond structures **I**, **II**, and **III** are clearly AX_3E whereas the neutral selenium atoms in **I** and **II** are AX_2E_2. Presumably each selenium atom is a combination of AX_3E and AX_2E_2. However, assuming a primary coordination of AX_3E, the complete geometry around Se(1) in $Se_2Br_5AsF_6$ can be expressed as $AX_3Y_2Y'E$ where the secondary contacts F(21f) and F(ave) designated Y_2, cap two of the faces of the tetrahedron around the lone pair (see Figs. 4 and 5), and the weakest of the contacts (Se(1)—F(11k)), designated Y', lies between edge bridging and face capping positions. Alternatively the geometry around Se(1) in $Se_2Br_5^+$ may also be regarded as AXY_4E (see Figs. 4 and 5), but in compounds having a similar AXY_4E environment around the central atom, the shortest bond in the molecule or ion is *trans* to the lone pair.

The bonding in the $Se_2Br_5^+$ cation may be regarded as involving only *p*-orbitals, with the selenium 4*s* orbital inert. The two strongest contacts to Se(1) at 180° to the strong Se—Br bonds therefore may involve donation of charge from the fluorine atoms to the σ* Se—Br orbitals. The three-centre four-electron bond in the bridging region, places non-bonding electron density in 4*p* lobes along the Se(1)—Br(1)—Se(1a) axis, consistent with the absence of atoms in this region (see Figs. 4 and 5). There is a similar empty region *trans* to the bridging bonds in I_5^+ and I_{15}^{3+} in I_5AsF_6 (15) and $I_{15}(SbF_6)_3$ (3) which may also be considered as containing three-centre four-electron bonds. It is also possible that the bonds in the bridging region may involve *sp* hybrid orbitals on the Se(1) atom, increasing the steric activity of the two lone pairs *trans* to the colinear Se(1)—Br(1)—Se(1*a*) bond.

The Br—F contact distances in $Se_2Br_5AsF_6$ (Table 4) are

Can. J. Chem. Downloaded from www.nrcresearchpress.com by 118.98.75.50 on 09/07/12
For personal use only.

longer than those in $SeBr_3SbF_6$ (i.e. 3.01, 2.85, and 3.02 Å) (13); consistent with the higher charge per selenium atom in $SeBr_3^+$ than $Se_2Br_5^+$.

Acknowledgements

We gratefully thank the Natural Sciences and Engineering Research Council for financial support and Mr. Chi-Ming Wong for help with the estimations of the energy changes.

1. Gmelin handbook of inorganic chemistry. 8th ed. Selenium (supplement volume B2). Springer-Verlag, Berlin. 1984.
2. A. F. WELLS. Structural inorganic chemistry. 5th ed. Clarendon, Oxford. 1984.
3. J. PASSMORE, P. TAYLOR, T. WHIDDEN, and P. S. WHITE. Can. J. Chem. **57**, 968 (1979).
4. VON P. BORN, R. KNIEP, and D. MOOTZ. Z. Anorg. Allg. Chem. **451**, 12 (1979).
5. D. KATRYNIOK and R. KNIEP. Angew. Chem. Int. Ed. Engl. **19**, 645 (1980).
6. R. KNIEP, L. KORTE, and D. MOOTZ. Z. Naturforsch. **38**b, 1 (1983).
7. J. MILNE. Polyhedron, **4**, 65 (1985).
8. P. J. HENDRA and Z. JOVIC. J. Chem. Soc. (A), 600 (1968).
9. B. KREBS, A. SCHÄFFER, and S. POHL. Z. Naturforsch. **39**b, 1633 (1984).
10. W. V. F. BROOKS, J. PASSMORE, and E. K. RICHARDSON. Can. J. Chem. **57**, 3230 (1979).
11. A. FINCH, P. N. GATES, and D. R. NETHERTON. Inorg. Chim. Acta, **32**, L91 (1979).
12. J. E. D. DAVIES and D. A. LONG. J. Chem. Soc. (A), 1273 (1971) and references therein.
13. J. PASSMORE, E. K. RICHARDSON, T. K. WHIDDEN, and P. S. WHITE. Can. J. Chem. **58**, 851 (1980).
14. M. MURCHIE and J. PASSMORE. Inorg. Synth. **24**, 76 (1986).
15. A. APBLETT, F. GREIN, J. P. JOHNSON, J. PASSMORE, and P. S. WHITE. Inorg. Chem. **25**, 422 (1986).
16. M. MURCHIE and J. PASSMORE. To be submitted.
17. G. BRAUER (*Editor*). Handbook of preparative inorganic chemistry. 2nd ed. Vol. 1. Academic Press, New York. 1963. p. 427.
18. P. A. W. DEAN, R. J. GILLESPIE, R. HULME, and D. A. HUMPHRIES. J. Chem. Soc. (A), 341 (1971).
19. G. M. BEGUN and A. C. RUTENBERG. Inorg. Chem. **6**, 2212 (1967).
20. J. W. GEORGE, N. KATSAROS, and J. K. WYNNE. Inorg. Chem. **6**, 903 (1967); G. C. HAYWARD and P. J. HENDRA. J. Chem. Soc. (A), 643 (1967).
21. Y. LEPAGE. J. Appl. Crystallogr. **15**, 255 (1982).
22. P. MAIN. "MULTAN-80", University of York: York, England. 1980.
23. N. WALKER and D. STUART. Acta Crystallogr. A**39**, 158 (1983).
24. G. M. SHELDRICK. SHELX-76, Program for crystal structure determination. Cambridge University. 1976.
25. E. J. GABE, F. L. LEE, and Y. LEPAGE. *In* Crystallographic computing 3: data collection, structure determination, proteins and databases. *Edited by* G. M. Sheldrick, C. Kruger, and R. Goddard. Clarendon Press, Oxford. 1985.
26. D. A. JOHNSON. Some thermodynamic aspects of inorganic chemistry. 2nd ed. Cambridge University Press, New York. 1982, and reference therein.
27. D. D. WAGMAN, W. H. EVANS, V. B. PARKER, R. H. SCHUMM, I. HALOW, S. M. BAILEY, K. L. CHURNEY, and R. L. NUTTALL. J. Phys. Chem. Ref. Data, **11**, Supplement 2 (1982).
28. A. D. WESTLAND and R. MAKHIJA. Can. J. Chem. **56**, 1586 (1978).
29. R. BOUGON, T. BUI-HUY, J. BURGESS, K. O. CHRISTIE, and R. D. PEACOCK. J. Fluorine Chem. **19**, 263 (1982).
30. (*a*) T. E. MALLOUK, G. L. ROSENTHAL, G. MÜLLER, R. BRUSASCO, and N. BARTLETT. Inorg. Chem. **23**, 3167 (1984); (*b*) T. J. RICHARDSON, F. L. TANZELLA, and N. BARTLETT. J. Am. Chem. Soc. **108**, 4937 (1986).
31. R. T. SANDERSON. Chemical bonds and bond energy. Academic Press, New York. 1971.
32. L. E. TOPOL. Inorg. Chem. **10**, 736 (1971).
33. J. P. JOHNSON, M. MURCHIE, J. PASSMORE, M. TAJIK, and C.-M. WONG. To be submitted.
34. M. M. CARNELL, F. GREIN, M. MURCHIE, J. PASSMORE, and C.-M. WONG. J. Chem. Soc. Chem. Commun. 225 (1986).
35. M. MURCHIE and J. PASSMORE. To be submitted.
36. W. E. DASENT. Inorganic energetics. 2nd ed. Cambridge University Press, New York. 1982. pp. 107–114.
37. A. BONDI. J. Phys. Chem. **68**, 441 (1964).
38. R. ATTIG and J. M. WILLIAMS. Angew Chem. Int. Ed. Engl. **15**, 491 (1976).
39. R. ATTIG and J. M. WILLIAMS. Inorg. Chem. **15**, 3057 (1976).
40. P. A. AKISHIN, V. P. SPIRIDONOV, and R. A. MISHULINA. Vestn. Mosk. Univ. Khim. **17**, 23 (1962).
41. K. J. WYNNE, P. S. PEARSON, M. G. NEWTON, and J. GOLEN. Inorg. Chem. **11**, 1192 (1972).
42. R. J. GILLESPIE. Molecular geometry. Van Nostrand-Reinhold, London. 1972.
43. A. J. EDWARDS and D. R. SLIM. J. Chem. Soc. Chem. Commun. 178 (1974).
44. W. A. S. NANDANA, J. PASSMORE, P. S. WHITE, and C.-M. WONG. J. Chem. Soc. Dalton Trans. Submitted.
45. J. PASSMORE, G. SUTHERLAND, and P. S. WHITE. Inorg. Chem. **21**, 2717 (1982).
46. W. A. S. NANDANA, J. PASSMORE, and P. S. WHITE. J. Chem. Soc. Chem. Commun. 526 (1983).

Can. J. Chem. Downloaded from www.nrcresearchpress.com by 118.98.75.50 on 09/07/12
For personal use only.

Specific patterns of short range solvation — aliphatic amines in benzene–dimethylsulfoxide mixed solvents

EDWARD D. BERMAN, ROSEMARIE THOMAS, PHILIP STAHL, AND RONALD M. SCOTT[1]
Department of Chemistry, Eastern Michigan University, Ypsilanti, MI 48197, U.S.A.

Received October 30, 1986

EDWARD D. BERMAN, ROSEMARIE THOMAS, PHILIP STAHL, and RONALD M. SCOTT. Can. J. Chem. **65**, 1594 (1987).

The trends in the values of equilibrium constants for the formation of proton transfer complexes between 2,4-dinitrophenol and various aliphatic amines are used to infer the nature of the short range solvation of the amines in benzene–DMSO solvent mixtures. Hydrogen bonds between the DMSO oxygen and the amine proton increase the basicity of the primary and secondary amines. Equilibrium constants for this bond formation are estimated for secondary amines.

EDWARD D. BERMAN, ROSEMARIE THOMAS, PHILIP STAHL et RONALD M. SCOTT. Can. J. Chem. **65**, 1594 (1987).

On utilise les tendances dans les valeurs des constantes d'équilibre pour la formation de complexes de transfert de protons entre le dinitro-2,4 phénol et diverses amines aliphatiques pour tirer des conclusions relatives à la nature de la solvatation à courte distance d'amines dans des mélanges de solvants formés de benzène et de DMSO. Les liaisons hydrogènes entre l'oxygène du DMSO et le proton de l'amine augmente avec la basicité des amines primaires et secondaires. On a évalué les constantes d'équilibre pour la formation de cette liaison dans des amines secondaires.

[Traduit par la revue]

Can. J. Chem. Downloaded from www.nrcresearchpress.com by 118.98.75.50 on 09/07/12
For personal use only.

Introduction

Solvation influences on dissolved reactants fall into two categories: long range and short range effects. Long range solvation effects depend on solvent polarity and the resultant ability of the solvent to disperse charge, facilitating the separation of unlike charges. Various terms have been generated to describe or quantify this solvent property. Terms such as dielectric constant are based on a physical measurement made on either pure solvent or a solvent mixture and depend for their usefulness on the existence of a close correlation between the property measured and the ability of the solvent to disperse charge. Other terms such as Taft's π value are based on the relative degree to which model reactions occur in the solvent (1). Short range solvation effects depend on specific interaction as by hydrogen bonding between the reactant and the solvent. Tendencies for specific solvents to interact by hydrogen bond formation with solutes have been described by such constants as the α and β values of Taft (2).

We are here studying the formation of a proton-transfer complex in which a phenolate ion is hydrogen bonded to an aliphatic ammonium ion. Such a structure occurs by the formation first of a phenol-amine hydrogen bonded adduct followed by the transfer of the proton of the phenol to the amine along the hydrogen bond axis. Clearly charge separation is involved and the effect of long range solvation on this reaction has been reported in several papers (3).

Solvent systems used to study solvation effects on this reaction often have not allowed a differentiation of long range from short range effects. Mixtures of dioxane and water are frequently used because these two miscible liquids allow a vast range (approximately 2.2 to 80) of dielectric constant to be studied. However, both dioxane and water have electrons to donate, water has protons to donate, and the two compounds can and do interact with one another in a potentially complex fashion (4).

We wish as much as possible to isolate for study specific short range interactions. For this purpose the benzene–dimethylsulfoxide (DMSO) solvent system has been selected. The two liquids are miscible. Benzene is very non-polar ($\epsilon = 2.3$) and is capable of only very weak electron donation, yet it will dissolve the reactants under study. DMSO is an electron donor but is not a proton donor ($\epsilon = 45$, $\beta = 0.764$). The solvents therefore do not interact appreciably with one another, and self interaction does not extend to hydrogen bonding. Attention is focused on the effect of the electron-donating properties of DMSO on the proton-transfer complex reaction. Amounts of DMSO added are kept small so as to minimize the change in the long range solvation environment of the solution.

The reaction used as a model, the formation of a proton-transfer complex between 2,4-dinitrophenol (DNP) and a variety of aliphatic amines, is selected for the following reasons. DNP has sufficient strength as an acid to form a proton-transfer complex with aliphatic amines in pure benzene. Unfortunately in DNP there is an internal hydrogen bond between the phenolic-OH and the *ortho* nitro group. Although this hydrogen bond would break in favor of an external bond to DMSO, the DMSO will be displaced as the more basic amines are added to solution. However, DNP presents no other opportunities for hydrogen bonding to DMSO and is therefore considered free of short range solvation effects in this solvent system. Tertiary aliphatic amines present only one site for short range interaction with the solvent, that being the unshared amine electrons. Since these are involved in the interaction with DNP, tertiary amines are also free of short range interactions with the solvent. Interactions between tertiary amines and DNP are used as control studies illustrating the long range solvation effects on the formation of the proton-transfer complex as the composition of solvent is altered.

Primary and secondary amines are capable through their amine proton of forming a hydrogen bond with DMSO. It is the effect of this specific short range solvation interaction on the formation of the proton-transfer complex that we report.

Experimental

The benzene was Aldrich spectra grade and was used without further purification. DMSO was Eastman spectra grade and was stored over calcium hydride after opening. DNP (Aldrich) was dissolved in benzene, dried with $MgSO_4$, and recrystallized. The amines studied were triethylamine (TEA), diethylamine (DEA), *n*-butylamine (*n*BA), Diisopropylamine (DIpA), morpholine (Mo), and *N*-methylmorpho-

[1]To whom all correspondence should be addressed.

TABLE 1. Equilibrium constants for proton transfer formation at 25°C between various amines and 2,4-dinitrophenol in benzene and benzene plus DMSO

	Equilibrium constants with			
Wt.% DMSO	*n*-Butylamine	Diethylamine	Triethylamine	Diisopropylamine
20	$(2.52\pm0.76)\times10^{7}$			
10	$(5.16\pm1.39)\times10^{5}$			
5	$(9.69\pm2.27)\times10^{4}$	$(5.76\pm0.39)\times10^{4}$	$(7.45\pm1.40)\times10^{3}$	
3	$(6.16\pm0.11)\times10^{4}$	$(5.28\pm0.08)\times10^{4}$	$(3.51\pm0.18)\times10^{3}$	
1.2				$(3.55\pm0.13)\times10^{4}$
1	$(2.60\pm0.17)\times10^{4}$	$(4.50\pm0.19)\times10^{4}$	$(2.68\pm0.05)\times10^{3}$	
0.8				$(3.43\pm0.23)\times10^{4}$
0.6				$(2.27\pm0.59)\times10^{4}$
0.5				$(1.66\pm0.55)\times10^{4}$
0.4				$(1.46\pm0.12)\times10^{4}$
0.3	$(3.28\pm0.30)\times10^{3}$	$(1.31\pm0.07)\times10^{4}$	$(4.89\pm0.86)\times10^{3}$	$(1.22\pm0.18)\times10^{4}$
0.2				$(6.14\pm0.46)\times10^{3}$
0.1	$(8.79\pm0.38)\times10^{2}$	$(6.76\pm0.28)\times10^{3}$	$(4.23\pm0.45)\times10^{3}$	$(5.38\pm0.16)\times10^{3}$
0.03	$(3.87\pm0.21)\times10^{2}$	$(3.07\pm0.08)\times10^{3}$	$(3.45\pm0.12)\times10^{3}$	
0.00	$(7.52\pm0.26)\times10^{1}$	$(1.19\pm0.05)\times10^{3}$	$(2.93\pm0.21)\times10^{3}$	$(8.41\pm0.70)\times10^{2}$

line (NMM). All amines were purified by distillation, then stored under nitrogen.

All samples for spectral analysis were assembled by weight. The five solutions used in each study included a constant amount of DNP, one had no amine and the four others contained differing amounts of amine. Quantities of solvent mixture were prepared on a percent by weight of DMSO basis and were then used to prepare all solutions used in sample preparation. All spectra except those involving morpholines were measured using a Perkin–Elmer Lamba 7 uv–visible spectrophotometer. Temperature was regulated by a Perkin–Elmer electronic temperature control accessory. For runs where thermodynamic parameters were to be calculated the spectra were run at five temperatures ranging from 15 to 55°C. Morpholine data were measured using a Beckman DK-2A spectrophotometer, temperature being regulated by use of a jacketed cell and circulating water bath.

In each solvent mixture and for each amine studied, the spectrum for the pure proton-transfer complex was taken. Absorbances were read from all samples at 365, 370, 430, and 440 nm. Equilibrium constants were calculated from the absorbances at each wavelength by two methods. In one the composition of the mixture was calculated directly from the known concentrations of reactants and the minimum, maximum, and sample absorbances. In the other, the iterative method, only the minimum and sample readings were used. A deliberately low value for maximum absorbance at that wavelength was estimated and the equilibrium constants for all samples were determined using that value. Then the estimated maximum absorbance was slightly incremented and the constants again were determined. This was repeated until the calculated equilibrium constant values showed no tendency to increase or decrease with increasing amine concentration. The measured maximum absorbances and those predicted by the iterative technique were in good agreement. The set of equilibrium constants for each reaction was averaged and the standard deviation was calculated.

The equilibrium constants for the formation of the hydrogen bond between DMSO and DEA or DIpA were estimated by assuming that the plateau in the increase in K_{eq} with increasing DMSO concentration that occurs at around (0.8–1.0) wt.% DMSO represents complete hydrogen bonding. From concentrations of reactants added and the fraction of the plateau absorbance obtained at each DMSO concentrations the K_{eq} was calculated (see Fig. 1).

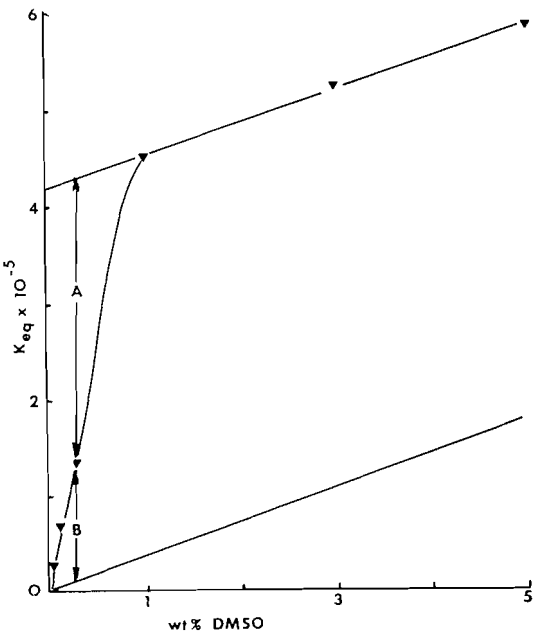

FIG. 1. Equilibrium constant values are plotted versus wt.% DMSO from DEA showing the assumptions made in calculating the equilibrium constant for DMSO–amine hydrogen bond formation. The ratio of A to B is assumed to be the ratio of non-hydrogen bonded amine to hydrogen bonded amine.

Results

The values obtained for equilibrium constants for the formation of proton-transfer complexes between DNP and the amines studied in benzene solution to which varying amounts of DMSO have been added are presented in Table 1. Corresponding values for morpholine are shown in Table 2. The data are plotted for the aliphatic amines in Fig. 2 and for the morpholines in Fig. 3. The equilibrium constants for the formation of a hydrogen bond between DMSO and the amine protons of DEA and DIpA are 9.87 M^{-1} and 15.52 M^{-1}, respectively. Thermodynamic parameters obtained are shown in Table 3.

Discussion

A few of the constants determined in this study had been reported previously. Our equilibrium constant values for the proton-transfer reaction in benzene for DEA and TEA are very

Can. J. Chem. Downloaded from www.nrcresearchpress.com by 118.98.75.50 on 09/07/12
For personal use only.

TABLE 2. Equilibrium constants for proton transfer complex formation at 25°C between morpholine or *N*-methylmorpholine and 2,4-dinitrophenol in benzene and benzene plus DMSO

	Equilibrium constants with	
Wt.% DMSO	Morpholine	*N*-Methylmorpholine
0	126± 22	34.0±11.2
1.24	4637±2684	51.4± 9.1
3.7	8835±3854	62.9±16.7
6.16	9805± 751	79.8± 7.5

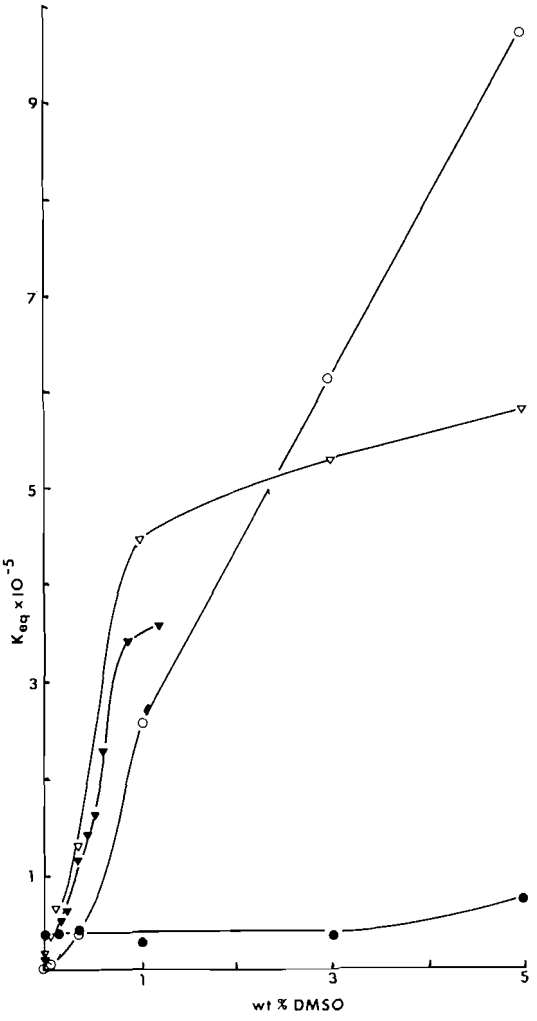

FIG. 2. Trends in the values of equilibrium constants are plotted here for the addition of the 5 wt.% DMSO. The amines are TEA (solid circles), *n*BA (open circles), DEA (open triangles), and DIpA (solid triangles).

similar to those reported by Pearson and Vogelsong (1240 vs. 1190 M^{-1} and 2940 vs. 2930 M^{-1}, respectively (6)). We are less close to the thermodynamic parameters reported by Bayles and Taylor for *n*BA in benzene ($\Delta H^0 = -11.86$ vs. -10.9 kcal/mol, $\Delta G^0 = -2.56$ vs. 4.04 kcal/mol, and $\Delta S^0 = -26.2$ vs. -28 esu, respectively (8)). Our values in pure benzene and 5 wt.% DMSO also closely reproduce those of an earlier unpublished study.[2]

A previous study was made in this laboratory using the

[2]G. Laird and R. M. Scott. Unpublished results.

TABLE 3. Thermodynamic parameters of hydrogen bond formation between 2,4-dinitrophenol and the indicated amines

Wt.% DMSO in benzene	ΔH^0 (kcal/mol)	ΔG^0 (kcal/mol)	ΔS^0 (eu)
	n-Butylamine		
5	−10.2±1.19	−6.70±0.10	−11.9
3	−12.5±0.156	−6.54±0.011	−19.8
1	−16.1±0.307	−6.02±0.032	−33.9
0.3	−18.6±0.114	−4.89±0.046	−46.0
0.1	−16.7±0.733	−4.02±0.026	−42.6
0.03	−13.3±1.01	−3.53±0.031	−32.8
0.00	−10.9±1.23	−2.56±0.021	−28.0
	Diethylamine		
5	−11.4±0.779	−6.52±0.16	−16.4
3	−11.0±1.80	−6.47±0.12	−15.2
1	−13.6±1.56	−6.36±0.076	−24.3
0.3	−14.8±1.01	−5.62±0.10	−30.8
0.1	−15.5±0.412	−5.23±0.074	−34.5
0.03	−14.0±1.10	−4.76±0.045	−31.0
0.00	−13.1±2.57	−4.20±0.74	−29.9
	Triethylamine		
5	−7.52±0.215	−5.27±0.062	−7.55
3	−12.5±0.137	−4.84±0.030	−25.7
1	−12.6±0.733	−4.68±0.010	−26.6
0.3	−12.9±0.504	−5.01±0.095	−26.5
0.1	−12.9±0.202	−4.95±0.062	−26.7
0.03	−11.9±0.642	−4.83±0.020	−23.7
0.00	−12.9±0.449	−4.75±0.036	−27.3

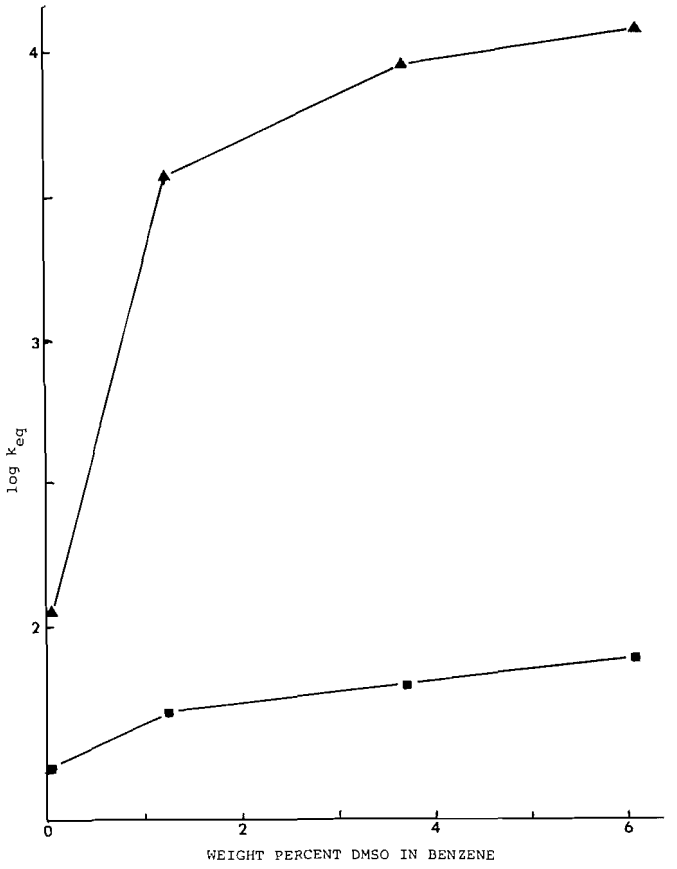

FIG. 3. Data are presented for the change in log k_{eq} versus wt.% DMSO for morpholine (solid triangles) and *N*-methylmorpholine (solid squares).

Can. J. Chem. Downloaded from www.nrcresearchpress.com by 118.98.75.50 on 09/07/12
For personal use only.

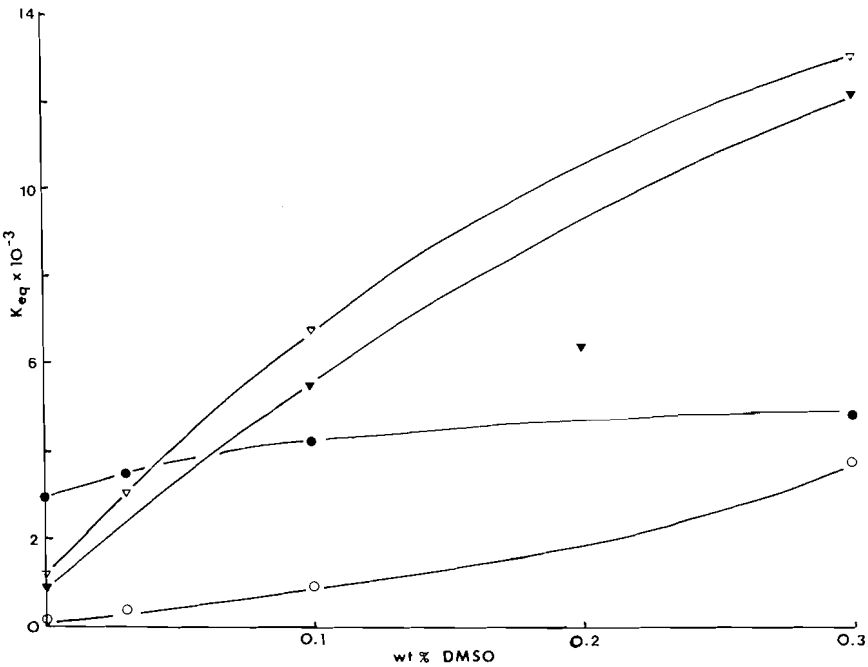

FIG. 4. Trends in the values of equilibrium constants are displayed for the addition of the first 0.3 wt.% DMSO. Legend is as in Fig. 2.

benzene–DMSO solvent system (5). In that study the acid used was *p*-nitrophenol (*p*NP) but in other respects the system was the same. Because *p*NP is a much weaker acid than DNP (pK_a = 7.21 vs. 4.09), it was not possible to perform a proton-transfer reaction to a measurable degree in pure benzene, or in fact in any mixture with less than 30 wt.% DMSO. The DMSO concentration ranged from 30 wt.% to 100 wt.% in that study. Under these conditions there was a large change in solvent dielectric constant, making the observation of the separate contribution of short range solvation forces impossible. However, it was then established by proton nmr that hydrogen bonding does occur between amine protons and DMSO, and there was a clear indication using the *p*NP–TEA interaction as a reference that DMSO does increase the reactivity of both DEA and *n*BA in the proton-transfer reaction.

The data presented in this report show that TEA and NMM, the tertiary amines, show a relatively small increase in the value of the equilibrium constant for the formation of the proton-transfer complex as the solvent is varied from pure benzene to benzene with 5 wt.% DMSO (Figs. 2, 3). Since there are no groups available for hydrogen bond formation between TEA and DMSO, we attribute this small change to the increase in dielectric constant of the solvent with increasing DMSO content. Assuming that a change in dielectric constant would affect all of the amines in the same fashion, this curve allows us to estimate the portion of the increase in equilibrium constant observed with the other amines that is due to long range solvation forces.

A comparison of the TEA and DEA data reveals that the equilibrium constant for DEA rises very sharply at concentrations of DMSO up to 1.0 wt.%. Beyond this the value increases less rapidly, in fact with a slope comparable to that seen for TEA or NMM. Data for *n*BA display a similar increase in equilibrium constant as DMSO is added to that observed with DEA, but the increase continues beyond 1 wt.% DMSO.

The effect of DMSO on the reactivity of primary and secondary amines in both the earlier and the present study is due to the formation of a hydrogen bond between the DMSO oxygen and the amine proton. To the degree that such bonding withdraws the proton from the nitrogen of the unreacted amine the electron density around the nitrogen becomes higher, and the basicity of the amine is enhanced. Once the proton transfer complex is formed and the amine is positively charged, the hydrogen bond to DMSO is even more favored. The hydrogen bond with DMSO would then correct the charge somewhat, stabilizing and so encouraging the formation of the complex. Notice that exactly the same effect is obtained with DIpA and Mo, the other two secondary amines in this study. In the case of primary amines there is an opportunity for two hydrogen bonds to form between the amine and DMSO. The first such DMSO–amine hydrogen does not form as readily as is the case with the secondary amines. In support of this statement we offer a plot of the addition of the first 0.3 wt.% DMSO to the system (Fig. 4). Here we see the shift in the order of basicity of the amines from that determined by the inductive effect of the alkyl groups, such that the tertiary amine is the stronger as has previously been reported for non-polar solvent systems (6), toward one determined by the short range solvation of the amines, such that the primary amine is the stronger as also has been observed previously (3, 7). Notice here that the slope of the change in K_{eq} as DMSO is added is considerably smaller for *n*BA than for DEA. Once the first DMSO has hydrogen bonded to the primary amine, its effect is similar to the inductive effect of the alkyl group, i.e. electron density on the nitrogen is increased, and the slope of increased K_{eq} with increased DMSO concentration approaches that displayed by the secondary amine (Fig. 2). Due to the ability of the primary amine to hydrogen bond two molecules of DMSO the K_{eq} for the primary amine continues to rise, surpassing that of the secondary amines. In an attempt to observe a plateau in the primary amine data higher concentrations of DMSO were added (Table 1) but no plateau was observed. At these higher levels of DMSO long-range solvation may well have become a significant factor. Under these circumstances no effort was made to estimate an equilibrium constant for hydrogen bond formation between DMSO and *n*BA amine protons.

Can. J. Chem. Downloaded from www.nrcresearchpress.com by 118.98.75.50 on 09/07/12
For personal use only.

Summary

Equilibrium constants for the formation of proton-transfer complexes between 2,4-dinitrophenol and various aliphatic amines have been measured in benzene and benzene with small additions of DMSO as solvent. These have been used to infer the nature and relative importance of short range solvation in this reaction. Using interactions with tertiary amines as a non-reacting reference system, a sharp rise in the equilibrium constant is observed on the addition of up to 1 wt.% DMSO, after which the increase is less pronounced. It is proposed that the formation of a hydrogen bond between the secondary amine hydrogen and the DMSO oxygen increases the basicity of the amine and thus the value of the equilibrium constant. By 1 wt.% DMSO this bond formation is complete. Based on this assumption equilibrium constants for the hydrogen bond formation have been estimated. Primary amines show similar behavior but continue to display an increase in equilibrium constant beyond 1 wt.% DMSO due to their ability to bond to two DMSO molecules. The response to increasing DMSO concentration indicates that the hydrogen bond formation with primary amines goes less readily than with secondary amines.

1. M. J. KAMELT, J. L. M. ABBOUD, and R. W. TAFT. Progress in physical organic chemistry. Vol. 13. Wiley-Interscience, New York. 1981. p. 485; M. J. KAMLET and R. W. TAFT. J. Chem. Soc. Perkin II, 349 (1979).
2. R. W. TAFT and M. J. KAMLET. J. Am. Chem. Soc. **98**, 2886 (1976); M. J. KAMLET, A. SOLOMONOYICI, and R. W. TAFT. J. Am. Chem. Soc. **101**, 3734 (1979).
3. R. SCOTT, D. DEPALMA, and S. N. VINOGRADOV. J. Phys. Chem. **72**, 3192 (1968); R. SCOTT and S. VINOGRADOV. J. Phys. Chem. **73**, 1890 (1969).
4. A. B. MILLER and R. M. SCOTT. Spectrochim. Acta, **30**A, 459 (1980).
5. A. REYES and R. M. SCOTT. J. Phys. Chem. **84**, 3600 (1980).
6. R. G. PEARSON and D. C. VOGELSONG. J. Am. Chem. Soc. **80**, 1038 (1957); J. P. BRIGGS and R. YAMDAGNI. J. Am. Chem. Soc. **87**, 2332 (1965); J. I. BRAVMAN, J. M. RIVEROS, and L. K. BLAIR. J. Am. Chem. Soc. **93**, 3914 (1971).
7. S. N. VINOGRADOV, R. A. HUDSON, and R. M. SCOTT. Biochim. Biophys. Acta, **214**, 6 (1970).
8. J. W. BAYLES and A. F. TAYLOR. J. Chem. Soc. 417 (1961).

Can. J. Chem. Downloaded from www.nrcresearchpress.com by 118.98.75.50 on 09/07/12
For personal use only.

Substituent effects on homolytic versus heterolytic photocleavage of (1-naphthylmethyl)trimethylammonium chlorides

B. Foster, B. Gaillard,[1] N. Mathur, A. L. Pincock, J. A. Pincock,[2] and C. Sehmbey
Department of Chemistry, Dalhousie University, Halifax, N.S., Canada B3H 4J3

Received October 10, 1986

This paper is dedicated to Professor Douglas E. Ryan on the occasion of his 65th birthday

B. Foster, B. Gaillard, N. Mathur, A. L. Pincock, J. A. Pincock, and C. Sehmbey. Can. J. Chem. **65**, 1599 (1987).

Singlet excited state rate constants have been measured for both the heterolytic and homolytic photocleavage of 3- and 4-methoxy and 3- and 4-cyano (1-naphthylmethyl)trimethylammonium chlorides, **6**–**10**. The results are interpreted in terms of the *meta* effect or changes in charge distribution upon excitation and the competition between bond cleavage, electron transfer, and hydrogen atom transfer in the contact pairs resulting from the two types of cleavage.

B. Foster, B. Gaillard, N. Mathur, A. L. Pincock, J. A. Pincock et C. Sehmbey. Can. J. Chem. **65**, 1599 (1987).

On a mesuré les constantes de vitesse de l'état excité singulet pour la photoclivage tant hétérolytique qu'homolytique des chlorures des méthoxy-3 (et -4) et des cyano-3 (et -4) (naphtyl-1 méthyl)triméthylammonium (**6**–**10**). On interprète les résultats en fonction de l'effet *méta* ou de changements dans la distribution de charge lors de l'excitation ainsi que par la compétition qui se développe entre le clivage des liaisons, les transferts électroniques et les transferts d'atomes d'hydrogène dans les paires de contact qui proviennent de deux types différents de clivage.

[Traduit par la revue]

Can. J. Chem. Downloaded from www.nrcresearchpress.com by 72.64.146.136 on 09/07/12
For personal use only.

Introduction

The subject of excited state cleavage of a σ bond between a leaving group and a benzylic carbon has recently been reviewed (1). The results compiled clearly indicate that the processes leading to products derived from homolytic and heterolytic cleavage are in competition and that this competition is controlled by factors such as multiplicity, solvent, leaving group, and substituent. In a recent paper (2), we have reported a detailed, excited singlet state rate study of leaving group effects for 1-naphthylmethyl compounds. We now present a similar study on the effect of ring substituents on these reactions.

In their pioneering work on photo-benzylic cleavages, Zimmerman *et al.* (3, 4) observed the "*meta*" effect. As shown in eq. [1], photolysis of benzyl acetates in aqueous dioxane gave

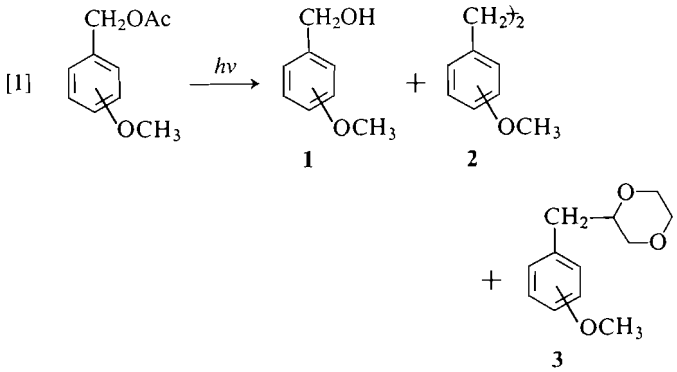

benzyl alcohols, **1**, derived from trapping of the corresponding benzyl cation, and two products, **2** and **3**, which are formed from the related benzyl radical. In contrast to ground state predictions, the *meta* methoxy substrate gave an increased yield ($\phi = 0.13$) of the alcohol **1** relative to the *para* isomer ($\phi = 0.016$). Several other examples of this effect were reported at the same time. Moreover, the observation could be rationalized by HMO calculations of the change in charge distribution that results from excitation of a benzylic substrate.

Since that time, several reports supporting this observation have appeared. For instance, the quantum yield for photosolvolysis of benzyltrimethylammonium salts is much reduced, relative to other substituents, for an electron-withdrawing cyano group at the *meta* position (5). Moreover, irradiation of several substituted benzyloxycarbonyl glycines gives a maximum in the quantum yield for the *meta* methoxy substituent (6). Of course, these changes in quantum yield do not necessarily reflect true changes in the reactivity of the substrate since they are determined by ratios of reactive to nonreactive pathways. Since all rates may be affected by substitution, some care must be exercised in interpreting results of this type.

More detailed studies involving rate constant evaluation have been attempted as well. Cristol and Bindel (7, 8) have reported an extensive study of benzylic chlorides. Unfortunately, these substrates react from both the singlet and triplet state, and sorting out the relative reactivity of the two is not easy. Moreover, the reactivity of excited triplet states is inherently more complex because heterolytic cleavage must involve a triplet to singlet conversion. Because of these difficulties, rate data could only be obtained for the triplet state; the lifetimes of these excited states are at, or beyond, the limit for reliable measurement using normal quenching techniques. Wan and Turro (9, 10) have reported enhanced rates of proton quenching of fluorescence for 3-CH_3O, 3-CH_3, and 3-F substituted benzyl alcohols but a complete study was impossible due to the low reactivity of the unsubstituted and 4-substituted cases. Perhaps the best quantitative confirmation of the *meta* effect or, more precisely, changes in charge distribution upon excitation controlling the rate of heterolytic bond cleavage is the work of Seiler and Wirz (11, 12) for the photohydrolysis of trifluoromethyl substituted 1- and 2-naphthols, eq. [2] being an example. In a reaction assumed to proceed by an initial ionic

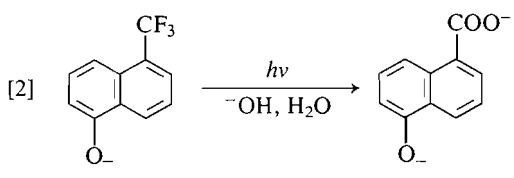

[1]Department of Chemistry, University of Texas at Austin, Austin, TX 78712, U.S.A.

[2]Author to whom correspondence may be addressed.

cleavage of the carbon–fluorine bond, rates as a function of the relative position of the naphthoxide oxygen and the trifluoromethyl group were well correlated with calculated charge density changes upon excitation.

In contrast to these observations supporting the original *meta* effect argument, there are a few opposing reports. Givens and Matuszewski (13) have observed a normal ground state order for the photosolvolysis of a series of benzylic phosphates and McKenna and co-workers (14) report decreased yields of ionic cleavage for 3,5-dimethoxybenzylammonium salts.

In this paper, we report a complete, excited state rate study for both heterolytic and homolytic cleavage for the 1-naphthylmethylammonium chlorides, **6–10**, a series that contains both

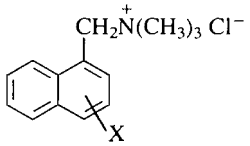

6 (X = H), **7** (X = 4-CH_3O), **8** (X = 3-CH_3O), **9** (X = 4-CN), **10** (X = 3-CN)

electron-donating and electron-withdrawing substituents. As outlined in detail previously (2), these compounds were chosen because the parent compound, **6**, gave mixtures of products resulting from ionic and radical intermediates, the triplet state was unreactive, the singlet state had a lifetime that was within the range of nanosecond single-photon counting measurement, and the quantum yield of reaction was high enough to measure conveniently.

Results and discussion

Synthesis of 1-naphthylmethyltrimethylammonium chlorides

The salts were prepared from the corresponding chlorides using anhydrous gaseous trimethylamine. The initial plan was to prepare the chlorides from methylnaphthalene derivatives by *N*-chlorosuccinimide free radical substitution but this only worked satisfactorily for the cyano cases. The methoxy compounds gave complex product mixtures that included ring chlorination, presumably because these naphthalene derivatives are overly activated toward electrophilic chlorination. For these cases the chlorides were prepared from the corresponding alcohols using HCl. The synthetic routes are outlined: Scheme 1 for **7**, Scheme 2 for **8**, Scheme 3 for **9**, and Scheme 4 for **10**. The unsubstituted compound, **6**, has been reported previously (2). Details and appropriate references are in the experimental section.

The ultraviolet spectra in methanol are plotted in Fig. 1 and are sufficiently different to confirm clearly the substitution pattern, since they agree well with absorption maxima and extinction coefficients in methanol for sample analogues: 4-methoxy-1-methylnaphthalene, λ_{max} 295 nm (ε 4530); 3-methoxy-1-methylnaphthalene, λ_{max} 327 (ε 1110), 315 (ε 620), 286 (ε 3160), 272 (ε 3840), 262 (ε 3450); 4-cyano-1-methylnaphthalene, λ_{max} 299 (ε 6110); and 3-cyano-1-methylnaphthalene, λ_{max} 334 (ε 2540), 320 (ε 1550), 294 (ε 5420), 282 (ε 7140). There are two transitions above 250 nm for naphthalene derivatives (15), a longitudinal polarized ^1L_b band and a transverse polarized ^1L_a band. Substitution in the 4 position by the conjugating methoxy or cyano groups causes bathochromic and hyperchromic effects on the ^1L_a band so that the weaker ^1L_b band is obscured. In contrast, substitution in the 3 position has a similar effect on the ^1L_b band so that it is now readily observable; this is particularly true for the methoxy group.

Preparative scale photolysis of the salts, 7–10

Irradiation of the salts in methanol with nitrogen purging using a Pyrex filtered 200-W Hanovia medium pressure mercury lamp gave clean conversion to the methyl ether, **11**, and the methylnaphthalene, **12** (2), eq. [3]. Calibrated hplc analysis of the reaction mixtures, Table 1, showed excellent mass balance and no evidence for other products. These reactions were irradiated until no further increase in product peaks was obvious and therefore the yields represent mass balance with essentially complete conversion of starting material. Continuous monitoring by hplc during photolysis indicated that the product ratios were independent of extent of conversion and controls showed that there was no conversion of **11** to **12**.

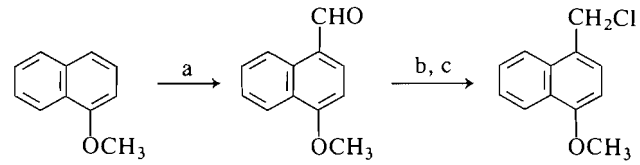

a, $(CH_3)_2NCOH$, $POCl_3$; b, $NaBH_4$; c, HCl

SCHEME 1. Synthesis of chloro-(4-methoxy-1-naphthyl)methane.

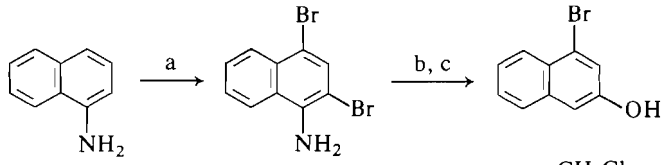

a, Br_2; b, $NaNO_2$, HOAc; c, $NaBH_4$; d, NaH/DMF, CH_3I; e, Mg, $CH_2{=}O$; f, HCl

SCHEME 2. Synthesis of chloro-(3-methoxy-1-naphthyl)methane.

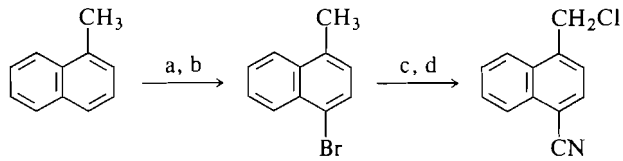

a, $ClSO_3H$; KOH; b, Br_2; c, CuCN, DMF; d, NCS

SCHEME 3. Synthesis of chloro-(4-cyano-1-naphthyl)methane.

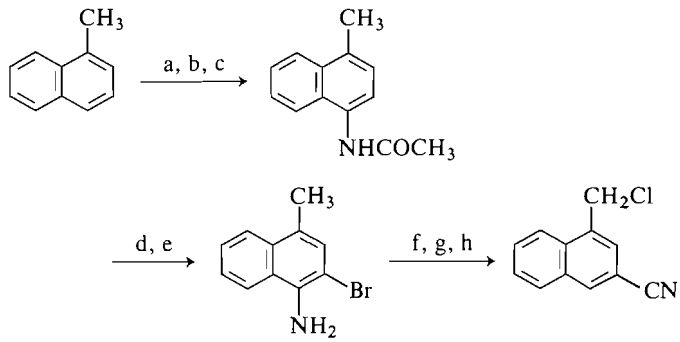

a, CH_3COCl, $AlCl_3$; b, NH_2OH; c H_2SO_4; d, HCl, H_2O; e, Br_2, dioxane; f, $NaNO_2$, HCl, Cu, CH_3CH_2OH; g, CuCN, DMF; h, NCS.

SCHEME 4. Synthesis of chloro-(3-cyano-1-naphthyl)methane.

[3]

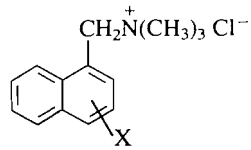

$\longrightarrow$ N*p*-CH_2OCH_3 + N*p*-CH_3

11 **12**

Can. J. Chem. Downloaded from www.nrcresearchpress.com by 72.64.146.136 on 09/07/12
For personal use only.

TABLE 1. Product yields and singlet and triplet parameters for **6–10**

Compound	**11**[a]	**12**[a]	$\tau_S \times 10^{9}$ [b] (s^{-1})	$\tau_T \times 10^{6}$ [c] (s^{-1})	E_S[d] (kcal/mol)	E_T[e] (kcal/mol)
6 (H)	72	21	3.82 (0.07)	8.8 (0.6)	90	62.0
7 (4-CH_3O)	90	<5	1.50 (0.02)	16.6 (0.2)	85	62.4
8 (3-CH_3O)	61	35	4.0 (0.1)	7.0 (0.7)	84	59.4
9 (4-CN)	34	62	3.54 (0.03)	7.1 (0.3)	85	56.2
10 (3-CN)	48	46	12.3 (0.4)	7.4 (0.1)	85	58.1

[a]% Yield by calibrated hplc for high conversion runs.
[b]Determined at 1°C by single photon counting at CFKR, University of Texas, Austin.
[c]Determined at room temperature by flash photolysis at CFKR, University of Texas, Austin.
[d]Determined in methanol by overlap of the excitation and emission spectra.
[e]Determined from the phosphorescence spectra at 77 K in 4:1 ethanol/methanol.

Can. J. Chem. Downloaded from www.nrcresearchpress.com by 72.64.146.136 on 09/07/12
For personal use only.

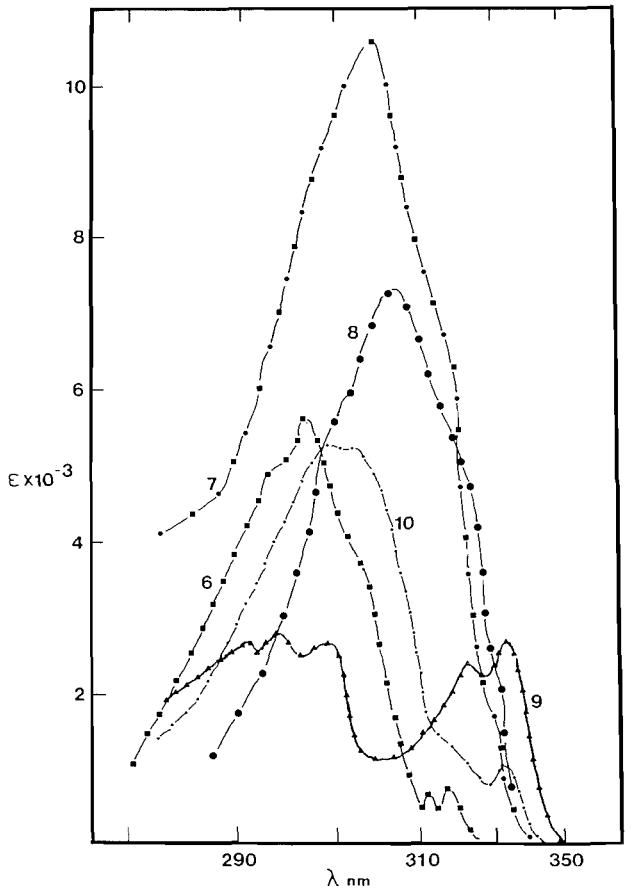

FIG. 1. Ultraviolet absorption spectra of **6–10** in methanol; **6** (H), **7** (4-CH_3O), **8** (3-CH_3O), **9** (4-CN), **10** (3-CN).

Reaction multiplicity; quantum yields and singlet reaction rates

Before attempting quantum yield and rate studies for these salts, information on reaction multiplicity was necessary to insure that only the singlet was reacting. As reported previously (2), this is straightforward for **6** (X = H) since xanthone sensitization gives no reaction; direct irradiations must be singlet reactions. For the other substrates this experiment is more difficult since their ultraviolet spectra, Fig. 1, extend to longer wavelengths and compete for absorption with xanthone, λ_{max} 338 nm (ε 6800). Using a $BiCl_3$ filter solution with a cut-off at 342 nm, xanthone concentration of 8.5×10^{-4} *M* (*A* = 2 at 350 nm), and the 4-methoxy compound **7** at 2.5×10^{-3} *M* (*A* = 0 at 350 nm), clean conversion to the methyl ether **11** was observed. That xanthone does transfer triplet energy to the salt in methanol was confirmed by flash photolysis studies. The transient triplet–triplet absorption spectrum of xanthone with λ_{max} 610 nm (16) is quenched by the salts **6–10**, leading to the appearance of the triplet–triplet absorption of the salt with a broad structureless band centered at approximately 440 nm. Decay of this band was first order and allowed calculation of the triplet lifetimes in methanol, which are reported in Table 1. Since we wished to examine the singlet reactivity of these salts, we did not pursue these sensitization studies but rather chose to quench any possible triplet state reaction.

Triplet quenching of these substrates (E_T = 56–62 kcal/mol, Table 1) should be close to the diffusion controlled rate (1.8×10^{10} M^{-1} s^{-1} in methanol (17*a*)) by 2,5-dimethylhexadiene (E_T = 58.7 kcal/mol (17*b*)). However, singlet state quenching of naphthalene derivatives by this diene is also very rapid (18) and a value of 9.3×10^{9} M^{-1} s^{-1} has been reported previously for **6** (2). Stern–Volmer fluorescence intensity quenching plots for **6–10** are shown in Fig. 2 and the $k_q\tau_S$ values from the slopes are listed in Table 2 along with the k_q values calculated using τ_S values from Table 1. The k_q values for the singlet are close to the diffusional value for the cyano cases but there is obviously a small substituent effect. This effect is as expected, based on the observation (18) that this singlet quenching represents exciplex formation involving electron transfer from the diene to the naphthalene derivative.

Fortunately, the more than three orders of magnitude difference between the singlet, τ_S, and triplet lifetimes, τ_T, of the naphthylammonium salts makes selective quenching possible. The quantum yields for formation of **11** and **12** for all five substrates **6–10** are given in Table 3. These values were obtained at the specific concentration of the diene given.

The percent of triplet excited states quenched, Table 3, at this concentration of diene is calculated from the known triplet lifetimes (Table 1) by the relationship, eq. [4], assuming $k_q = k_{diff} = 1.8 \times 10^{10} M^{-1} s^{-1}$.

$$[4] \quad \%T = 100\, k_q[D] \Big/ \left(\frac{1}{\tau_T} + k_q[D]\right)$$

Because the triplet energy gap between the naphthalenes and the

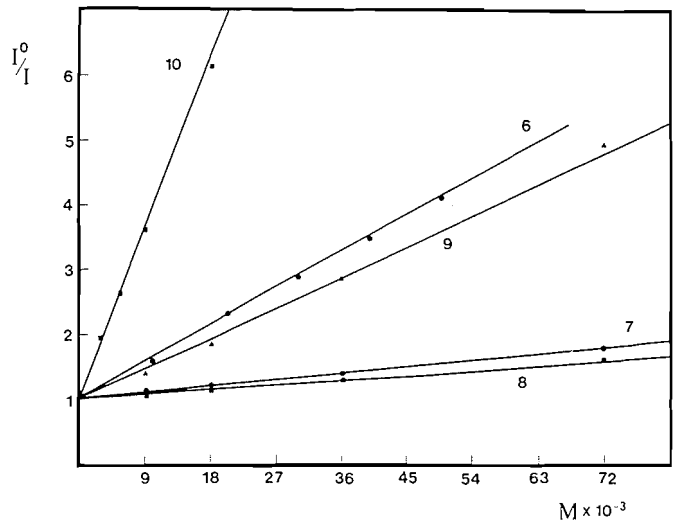

FIG. 2. Stern–Volmer quenching plots by 2,5-dimethyl-2,4-hexadiene of **6**–**10** in methanol: **6** (H), **7** (4-CH_3O), **8** (3-CH_3O), **9** (4-CN), **10** (3-CN).

TABLE 2. Stern–Vollmer quenching data by 2,5-dimethyl-2,4-hexadiene for **6**–**10** in methanol

Compound	$k_q\tau_S$ (M^{-1})	$k_q \times 10^{-10}$ (M^{-1} s^{-1})	ϕ_F	$k_F \times 10^{-7}$ (s^{-1})
6 (H)	64	0.93	0.06	1.6
7 (4-CH_3O)	11.3	0.75	0.17	11
8 (3-CH_3O)	8.7	0.22	0.10	2.5
9 (4-CN)	55	1.6	0.40	11
10 (3-CN)	28	2.3	0.48	3.9

diene is not exothermic for all cases, the k_q values are likely to be less than diffusional (19). The diene concentration used for the quantum yields was deliberately chosen to be high enough so there was no ambiguity about the quenching of essentially all the excited triplets.

The percent of singlet excited states quenched at this concentration of diene can be calculated from an expression identical to eq. [4] except that the k_q values are known. These values are also in Table 3. They range from 3 to 20%. The measured quantum yields of singlet reaction to form **11** and **12** are therefore lower than the real quantum yields by this amount. Corrected values are given in Table 3.

The mechanism of photocleavage

The mechanistic steps required to discuss the bond cleavage reactions are shown in Scheme 5. These steps will now be discussed in detail.

The light absorption step 1 is the ^1L_b transition under conditions used for the quantum yields since the wavelengths chosen were 280 nm for **6**, **8**, and **10** and 300 nm for **7** and **9** (see Fig. 1). For the 4-methoxy and 4-cyano salts this transition is very close in energy to the ^1L_a one and, although difficult to tell, this may be S_1. For the other three compounds rapid internal conversion from S_2 to S_1 is expected to give the ^1L_a state. Although there has been some suggestion from flash photolysis experiments that S_1 for chloromethylnaphthalene does not dissociate efficiently and that bond cleavage occurs more efficiently upon excitation to S_2 (19), more recently results (20) have shown that the 1-naphthylmethyl radical can be

1. $S_0 + h\nu \rightarrow S_1$
2. k_F $S_1 \rightarrow S_0 + h\nu_F$
3. k_{ISC} $S_1 \rightarrow T_1$
4. k_R^T $T_1 \rightarrow ArCH_2^{\bullet} + {}^{\bullet}\overset{+}{N}(CH_3)_3$
5. k_Q^T $T_1 + Q \rightarrow S_0$
6. k_Q^S $S_1 + Q \rightarrow S_0$
7. k_I $S_1 \rightarrow [ArCH_2^+ :N(CH_3)_3]$
8. k_R $S_1 \rightarrow [ArCH_2^{\bullet} {}^{\bullet}\overset{+}{N}(CH_3)_3]$
9. k_D $S_1 \rightarrow S_0$
10. k_{HT} $[ArCH_2^{\bullet}\ H{-}CH_2{-}\overset{+}{N}(CH_3)_2 \rightarrow ArCH_3 + CH_2{=}\overset{+}{N}(CH_2)$
11. k_{ET} $[ArCH_2^{\bullet} {}^{\bullet}\overset{+}{N}(CH_3)_3] \rightarrow ArCH_2^+ + :N(CH_3)_3$
12. k_{RD} $[ArCH_2^{\bullet} {}^{\bullet}\overset{+}{N}(CH_3)_3] \rightarrow ArCH_2^{\bullet} + {}^{\bullet}N(CH_3)_3$
13. k_{ID} $[ArCH_2^+ :N(CH_3)_3] \rightarrow ArCH_2 + :N(CH_3)_3$
14. $ArCH_2^+ + CH_3OH \rightarrow ArCH_2OCH_3 + H^+$

SCHEME 5. Mechanistic scheme for the photolysis of the naphthylmethyl ammonium salts, **6**–**10**.

generated from S_1. We have not examined wavelength effects for the efficiency of photocleavage, but the fluorescent quantum yield for **6** was independent of excitation wavelength from 280 to 320 nm.

The S_1 fluorescence step 2 is efficient for all of these naphthyl derivatives and the quantum yields are listed in Table 2. The associated rate constants for fluorescence, $k_F = \phi_F/\tau_S$, are also listed in Table 2 and we note that the order is at least qualitatively as expected from the absorption spectra in Fig. 1 (2). The 4-methoxy and 4-cyano compounds with the highest extinction coefficient have the fastest fluorescence rate and the unsubstituted compound has the slowest. From the absorption and fluorescence spectra the position of the (0,0) band can be estimated to give the singlet energies listed in Table 1.

The intersystem crossing efficiency, step 3, is unknown for these naphthyl derivatives. It is worth noting, however, that the sum of the quantum yields of fluorescence and singlet reaction for these substrates (ϕ_T) is similar to, but usually somewhat larger than, that for the ϕ_F of the corresponding unreactive cases: **6**, $\phi_T = 0.31$, naphthalene, $\phi_F = 0.24$ (2); **7**, $\phi_T = 0.45$, 1-methoxynaphthalene, $\phi_F = 0.43$ (21); **8**, $\phi_T = 0.49$, 2-methoxynaphthalene, $\phi_F = 0.33$ (21); **9**, $\phi_T = 0.53$, 1-cyanonaphthalene, $\phi_F = 0.37$ (21); **10**, $\phi_T = 0.64$, 2-cyanonaphthalene, $\phi_F = 0.53$ (21). Moreover, for unreactive naphthalene derivatives the sum of $\phi_F + \phi_{ISC}$ is close to unity; for instance, naphthalene (0.20 + 0.80), 1-methylnaphthalene (0.21 + 0.77), and 1-methoxynaphthalene (0.43 + 0.50) (17*c*). Therefore, it is probable that the photoprocess unaccounted for in the case of **6**–**10** is intersystem crossing rather than internal conversion of S_1 to the ground state.

That intersystem crossing does occur from these substrates is well established since they all show phosphorescence in a rigid matrix at 77 K. This phosphorescence can be used to calculate the triplet energies in Table 1. Furthermore, the triplet state of these substrates can be observed by flash photolysis in methanol at room temperature as a broad transient absorption centered at about 440 nm. Decay of this transient was difficult to monitor as it always overlapped with another transient with a maximum at 360 nm, which we have assigned to the naphthylmethyl radical. Similar observations have been made for 1-chloromethylnaphthalene (19, 20). In that case, decay of the triplet was much faster than decay of the radical and the method was used to study the chemistry of the radical. For these ammonium salts the two transients decayed with similar lifetimes. Cleaner spectra of the triplets could be generated by xanthone sensitization as described above.

Can. J. Chem. Downloaded from www.nrcresearchpress.com by 72.64.146.136 on 09/07/12
For personal use only.

TABLE 3. Quantum yields and derived rate constants in methanol for photolysis of **6**–**10** and formation of **11** and **12**

Compound	Diene[a] ($M \times 10^3$)	%T[b]	%S[c]	**11**[d]	**12**[d]	**11**[e]	**12**[e]	$k_{11}^f \times 10^{-7}$ (s^{-1})	$k_{12}^f \times 10^{-7}$ (s^{-1})
6 (X = H)	0.92	99.3	3.1	0.18 (0.02)	0.53 (0.005)	0.19 (0.02)	0.055 (0.005)	4.9 (0.5)	1.4 (0.1)
7 (X = 4-CH_3O)	4.6	99.9	4.9	0.27 (0.01)	<0.01 —	0.28 (0.01)	<0.01 —	18.7 (0.5)	<0.1 —
8 (X = 3-CH_3O)	2.3	99.7	16.2	0.21 (0.01)	0.125 (0.005)	0.24 (0.01)	0.145 (0.006)	6.0 (0.2)	3.6 (0.2)
9 (X = 4-CN)	2.3	99.6	11.5	0.037 (0.002)	0.083 (0.001)	0.041 (0.002)	0.092 (0.001)	1.15 (0.07)	2.59 (0.04)
10 (X = 3-CN)	0.85	99.1	20.1	0.075 (0.007)	0.055 (0.009)	0.090 (0.008)	0.066 (0.011)	0.73 (0.09)	0.53 (0.10)

[a]2,5-Dimethyl-2,5-hexadiene.
[b]Calculated from eq. [4] assuming $k_q = 1.8 \times 10^{10}\ M^{-1}\ s^{-1}$.
[c]Calculated from known k_q values in Table 2.
[d]Observed quantum yields at low conversion (<10%) at 1°C. They are the average of two determinations and (errors) are mean deviations.
[e]Quantum yields corrected for % of quenched.
[f](Errors) are standard deviations.

Bond cleavage from the excited triplet as in step 4 can only give a radical pair since heterolytic cleavage leading to a pair of singlet products must be a singlet process. For the unsubstituted naphthylmethylammonium salt, **6**, no reaction occurs upon sensitization with xanthone (2). Since the rate of triplet decay is $1.1 \times 10^5\ s^{-1}$, the rate of reaction must be considerably slower to be undetected. A reasonable explanation for this slow rate is the high bond strength expected for these salts. An estimate of the carbon–nitrogen bond strength in (1-naphthylmethyl)amine is 61 kcal/mol, based on a value of 64 kcal/mol for benzylamine (22) minus about 3 kcal/mol for the stabilization of the naphthylmethyl radical relative to benzyl (23). Substitution of the methyl groups at the nitrogen will weaken the bond further but quaternization of an amine to an ammonium salt is known, by MO calculations, to lead to large increases in bond strength.[3] For instance, using third-order Møller–Plesset perturbation theory at the 6-31G** level and the 6-31G* optimized geometry yields a calculated bond dissociation energy for CH_3—NH_2 of 87 kcal/mol, which increases to 117 kcal/mol for CH_3—$^+NH_3$. The bond strength of **6** is therefore likely higher than the available triplet energy of 62 kcal/mol. Despite the expected endothermicity of this process, xanthone sensitized irradiation of **7** did in fact result in the methyl ether expected from ionic cleavage of the carbon–nitrogen bond (see above). It seems unlikely therefore that this represents reactivity of the triplet state of this substrate and adds support to Schuster's suggestion that sensitization of these naphthylmethyl compounds results in exciplex formation (24). Further work on this topic of sensitization is obviously required before definite conclusions can be reached.

The steps 5 and 6 represent quenching of the excited triplet and singlet state, respectively, of the naphthyl derivatives. Both of these rates are rapid but, as discussed above, the irradiations were done with concentration of the quencher chosen so that triplets were quenched effectively but singlets were not (see Table 3). Consequently, the results reflect only the reactivity of the excited singlet state.

Steps 7 and 8 are therefore the rates of interest, the first is for heterolytic cleavage of the carbon–nitrogen bond to give the 1-naphthylmethyl cation and trimethylamine, the second for homolytic cleavage to the 1-naphthylmethyl radical and the trimethylamine radical cation. (In both cases, the dissociated species are shown as contact pairs; the diffusion to solvent separated pairs is shown in steps 12 and 13.) Both of these processes could be rapid since the singlet energies (Table 1) are above the expected bond strengths. It is these two rate constants, k_I and k_R, that are required to assess substituent effects properly and to confirm whether charge distribution changes upon excitation control the two rates of photocleavage. However, there are complications that make unambiguous determination of these values difficult.

The quantum yields of formation of the ethers **11** in eq. [3] and the singlet lifetimes, τ_S, of the substrates allow evaluation of an operational rate constant for product formation, k_{11}, according to eq. [5]. A similar expression is used for k_{12}. The

$$[5] \quad \phi_{11} = \frac{k_{11}}{k_F + k_D + k_{ISC} + k_{11}} = k_{11}\tau_S$$

values are in Table 3 for the substrates **6**–**10**. The complications in relating these operational rate constants to k_I and k_R are outlined in steps 9–13 of Scheme 5.

The first of these, step 9, is the internal conversion of S_1 to S_0. For unreactive naphthalene derivatives, as discussed above, the quantum yields of fluorescence plus intersystem crossing are usually close to unity, therefore internal conversion is not an important component of singlet decay. This is presumably a result of the large energy gap in a rigid molecule, making vibrational overlap poor. For these reactive naphthalene cases, this step could, in contrast, be quite important. For instance, reversal of either k_I or k_R, that is, internal return from the intimate pair resulting from either heterolytic or homolytic cleavage, would be a method of excited state decay that would only be detectable as k_D. If this were true, measured k_{11} and k_{12} would be smaller than k_I and k_R. There are two pieces of evidence that suggest that internal return is not important. The first is that, as discussed above, the sum of the quantum yields of reaction plus fluorescence for these substrates is larger than that for unreactive models where the only other mode of excited singlet decay is intersystem crossing. The second is the observation that no racemization of starting material is observed

[3]R. J. Boyd, M. Glover, W. Brandon, and J. A. Pincock. Manuscript in preparation.

Can. J. Chem. Downloaded from www.nrcresearchpress.com by 72.64.146.136 on 09/07/12
For personal use only.

Can. J. Chem. Downloaded from www.nrcresearchpress.com by 72.64.146.136 on 09/07/12
For personal use only.

for the photolysis of an analogous chiral benzylammonium salt (25).

Steps 10 and 11 are two processes that may well be competitive with each other. Step 10 is hydrogen atom transfer from the radical ion of trimethylamine to the naphthylmethyl radical. Since the C—H bond strength in this radical ion is much lower (34 kcal/mol) (26) than that expected for 1-methylnaphthalene (82 kcal/mol) (22), this process should be exothermic by approximately 48 kcal/mol and therefore rapid. In fact, this process must be faster than step 12, which is the diffusional separation of the contact pair to give the free 1-naphthylmethyl radical. Photolysis of 1-naphthylmethyl derivatives in methanol normally gives the dimer of the 1-naphthylmethyl radical as a major product derived from homolytic cleavage (2, 24). Only with trimethylamine as the leaving group is 1-methylnaphthalene the exclusive product. This observation suggests that, for this leaving group, the radical never gets free of the contact pair. In the case of the corresponding benzylic substrates, a related observation is that formation of the dimer occurs only from the triplet excited state (27) in which hydrogen atom transfer should be slower because of the spin restriction in a process leading from triplet contact pairs to singlet products. Diffusional separation now occurs.

Step 11 is electron transfer in the contact pair. If this process is important, then there is a pathway for formation of the 1-naphthylmethyl cation by a route that initially involved homolytic cleavage of the carbon–nitrogen bond. The operational rate constant k_{11} would then be greater than the real rate constant for heterolytic cleavage. In fact, solution oxidation potentials for the benzyl radical (+0.40 V vs. $Ag/AgNO_3$ in CH_3CN) (28) and trimethylamine (+0.82 V vs. $Ag/AgNO_3$ in CH_3CN) (29) indicate that electron transfer like that for Step 11 would be exothermic by 10 kcal/mol. The oxidation potential for the 1-naphthylmethyl radical itself is not known and therefore an exact determination of the exothermicity for the particular electron transfer involved with these substrates cannot be made. Moreover, the substituted naphthalene derivatives would have differing oxidation potentials depending on the substituent. At any rate, it appears that electron transfer in the contact pair derived from homolytic cleavage should be favorable. Possibly this effect is being most strongly observed for the 4-methoxy substrate, **7**, where the only observable product is the ether **11**, derived from the 1-naphthylmethyl cation.

This point concerning electron transfer should, in fact, be important for all photochemical benzylic cleavages. Many of the usual leaving groups have oxidation potentials higher than that for trimethylamine: bromide (0.7 V vs. SCE in CH_3CN) (30), chloride (1.1 V vs. SCE in CH_3CN) (30), dimethylsulfide (1.4 V vs. $Ag/AgNO_3$ in CH_3CN) (31), and alcohols (no oxidation in CH_3CN up to solvent limit) (32). This implies that electron transfer in the pair generated from homolytic cleavage should, in general, be favorable. It is perhaps surprising that products derived from the benzylic radical are ever observed, since the process in competition with electron transfer is diffusion from the solvent cage. In the case of trimethylamine studied by us, the process in competition with electron transfer is hydrogen atom transfer. Both should be exothermic and it is very difficult to predict their relative rates. Cases of slow exothermic electron transfer are now well established (32) and seem to be attributed to the solvent reorganization required according to Marcus theory as the charge moves from one site to the other. Since complete electron transfer is not observed, it is possibly correct to assume that electron transfer does not compete with hydrogen atom transfer. If this is true, then the product ratios and quantum yields observed are a direct reflection of the initial homolytic and heterolytic cleavage steps, and the calculated rates k_{11} and k_{12} do correspond to k_I and k_R.

Before discussing these rate variations, it is worth mentioning that the original *meta* effect was attributed to charge distribution changes on excitation using SHMO calculations (3, 4). The prediction was not only that an electron-donating substituent *meta* to the reactive site would be activating for heterolytic cleavage but also that a *para* substituent would be deactivating relative to the unsubstituted case. The converse would be true for an electron-withdrawing substituent: activation for the *para* substitution and deactivation for the *meta*. The idea was that these effects would be most important for generation of the cationic intermediate and that the radical intermediate would perhaps form at a more or less constant rate independent of substituent. Calculations at the SHMO level for excited states are, of course, very naive and, for instance, do not even take into account that the degeneracies of both the HOMO and LUMO, which predict only one transition, are lost by differing electron correlation in the various possible configurations. The result is three transitions: ^1L_b, ^1L_a, and ^1B (15*b*). In methoxynaphthalenes, the 2-isomer has the lowest lying state as ^1L_b, but for the 1-isomer, S_1 is more likely to be ^1L_a (see Fig. 1). Excited state electron densities have been calculated for 1- and 2-methoxynaphthalene (33). The results suggest that for a 1-methoxy substituent the electron density *para* should decrease for both the ^1L_b and the ^1L_a states; for a 2-methoxy substituent, the electron density increases *meta* in the ^1L_b state. In other words, the *meta* effect is still predicted.

The first fact that should be pointed out concerning the rate constants k_{11} and k_{12} in Table 3 is the relatively small total range of the values, a factor of about 20 for the heterolytic process, k_{11}, and about 40 for the homolytic one, k_{12}. This point is particularly interesting when compared to analogous ground state processes. For instance, the solvolysis of substituted cumyl chlorides by an S_N1 mechanism to generate a carbocation has a predicted rate spread of 10^8 going from the activating 4-methoxy group to the deactivating 4-cyano group, giving a ρ^+ value of -4.5 (34). The much lower rate spread for the photochemical process is probably a reflection of the exothermic nature of the rate-determining step so the substituent selectivity is lost. For ground state processes leading to benzylic radicals the range of substituent effects is quite variable because of the changing polarity of the transition state. For instance, hydrogen abstraction from substituted toluenes by bromine atoms gives a rate spread of 10^2 and a ρ^+ value of -1.4 (35), but the substituent effect drops to almost zero for the pyrolysis of benzylic azo compounds (35). In processes that truly reflect radical stability, both 4-methoxy and 4-cyano are rate accelerating and 3-methoxy and 3-cyano are rate retarding, as predicted by the $\sigma^\cdot$ scale (36). Again substituent effects are very small, for instance, a range of only three for the methylenearylcyclopropane rearrangement (37). Not surprisingly, rationalizing these small rate changes has been considerably more difficult since more than just transition state stability will be important. The rate range for the exothermic photochemical homolytic cleavages of **6**–**10** is then actually quite large by comparison. The second point to mention is this: the spread in rate constants is greater for the homolytic process than it is for the heterolytic one. As mentioned above, the original concept of the *meta* effect was directed at electron density changes upon excitation

having major effects on heterolytic bond cleavage, with no mention made of the homolytic one. It is in fact difficult to predict the way in which substituent effects should influence the homolytic cleavage of the quite polar carbon–nitrogen bond in these ammonium salts. Quite possibly a neutral leaving group might lead to considerably different results.

Examination of the values reveals that, if the 4-methoxy substrate is omitted for the moment, the *meta* effect may be controlling the rate constants. For the heterolytic process, the rates are close to the expected order: 3-methoxy > hydrogen > 4-cyano > 3-cyano with only 4-cyano too slow to fit the scheme. Surprisingly, the homolytic process follows exactly the order predicted by the *meta* effect for a heterolytic cleavage. Possibly, the electron density changes on excitation are influencing the rate of bond cleavage, and the final product distribution is actually a function of electron transfer distribution in the two developing fragments.

Finally, the 4-methoxy compound, **7**, reacts with both a rate constant (higher) and a product partitioning (exclusively heterolytic) that seem out of line with the other substituents. Similar high yields of ionic cleavage have been observed for a related 4-methoxybenzylammonium salt (25). Their results are, of course, not predicted by the *meta* effect. Perhaps, in fact, the mechanism changes because of direct interaction between the electron-donating methoxy group and the inductively electron-withdrawing trimethylammonium group. The ground state probably has considerable charge delocalization, as in **12**. This is seen in the absorption spectrum where the extinction coefficient for **7** increases to 10500 from 4500 for the corresponding 4-methoxy-1-methylnaphthalene. This effect should be most pronounced for a very electronegative group like a positively charged nitrogen, although, contrary to this prediction, positively charged oxygens as leaving groups still seem to retain the *meta* effect (9, 10). At any rate, internal charge transfer of this type may modify the nature of the charge changes on excitation and favour heterolytic cleavage. Cristol and Bindel (1) have made this suggestion for some substituted benzyl compounds and have even applied the Weller equation to rationalize observed bond cleavages.

Since the *meta* effect arguments do not rationalize these rate constants very well, it was obviously of interest to look at Hammett type substituent approaches. Four scales of σ value should be considered: normal σ and σ^+, $\sigma^\cdot$ (36) for radical stability, and σ^{ex} (38) derived from the excited singlet state pK_a of phenols. Differentiating between σ and σ^+ is probably impossible with the substituents available since only 4-methoxy will have a different value on the two scales. However, the plot of log k_{11} (the heterolytic process) versus σ gives $\rho = -1.4 \pm 0.2$ ($r = 0.96$) and versus σ^+ gives $\rho^+ = -0.9 \pm 0.2$ ($r = 0.94$). In both cases it is perhaps significant that the 3-methoxy value is above the line and the 3-cyano below the line (the *meta* effect?). The negative ρ values indicate that, in general, electron-donating groups favour this process as expected for a ground state cation-forming reaction. For k_{11} (the homolytic process) there is no obvious σ or σ^+ correlation. The $\sigma^\cdot$ scale for radical stability is also of little help since it predicts that both 4-methoxy and 4-cyano should be rate accelerating and 3-methoxy about equal in reactivity to the unsubstituted case. Finally, consideration of the σ^{ex} scale reveals that there is no value for 3-cyano but that the remaining four points give a correlation for k_{11}, $\rho = 0.52 \pm 0.1$ ($r = 0.94$), that is dominated by the large σ^{ex} value of 1.6 for 4-cyano but again shows the trend of negative ρ value.

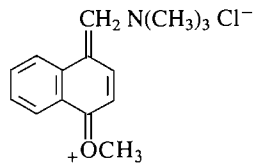

13

Independent of the reason for the enhanced heterolytic cleavage observed for **7**, one of the objectives of this study was to learn enough about substituent effects in photochemical benzylic cleavages to be able to design synthetically useful reagents for controlling the partitioning between the two possible pathways. This objective has been reached and uses of the 4-methoxynaphthyl methyl group are currently being studied.

Experimental

Preparation of (1-naphthylmethyl)trimethylammonium chlorides

6, (X = H): Prepared as described previously (2): mp 251–252°C. The melting point reported previously (231–232°C) was a typographical error.

7, (X = 4-CH_3O): 4-Methoxy-1-naphthaldehyde was prepared from 1-methoxynaphthalene by the previously reported method (39); bp 178–179°C at 3 Torr (1 Torr = 133.3 Pa) (lit. (39) bp 205–206°C at 16 Torr); nmr ($CDCl_3$) δ: 9.90 (s, 1H), 8.0–8.2 (m, 1H), 7.2–7.7 (m, 5H), 6.53 (d, J = 8 Hz, 1H), 3.83 (s, 3H).

4-Methoxy-1-naphthaldehyde was reduced to 4-methoxy-1-naphthylmethanol as follows. To a solution of 4.6 g (0.12 mol) of sodium borohydride in 50 mL of ethanol was slowly added a solution of 44.5 g (0.24 mol) of the aldehyde in 30 mL of ethanol with the temperature kept below 50°C. After 1 h, 1000 mL of water was added and the mixture extracted with 2 × 200 mL of ether. The ether layer was washed with 2 × 200 mL of water, dried with $MgSO_4$, and evaporated to give 43.3 g (0.23 mol, 96%) of crude alcohol. Recrystallizing from benzene gave the pure alcohol, mp 76–77°C; nmr ($CDCl_3$) δ: 8.0–8.2 (m, 1H), 7.6–7.8 (m, 1H), 7.2–7.45 (m, 2H), 7.00 (d, J = 7 Hz, 1H), 6.35 (d, J = 7 Hz, 1H), 3.70 (s, 3H), 2.95 (br s, exchangeable, 1H).

The alcohol (2 g, 0.011 mol) was dissolved in 80 mL of ether and hydrogen chloride gas was bubbled for 1 h. The ether solution was then washed with 50 mL of water and 50 mL of 5% sodium bicarbonate, dried over $MgSO_4$, and concentrated to give 2.01 g (8.7 mmol, 88%) of crude chloro-(4-methoxy-1-naphthyl)methane; nmr ($CDCl_3$) δ: 7.75–8.2 (m, 2H), 7.2–7.5 (m, 2H), 7.13 (d, J = 8 Hz, 1H), 6.43 (d, J = 8 Hz, 1H), 4.80 (s, 2H), 3.75 (s, 3H).

The crude chloride was dissolved in 100 mL of ether and trimethylamine was bubbled through the solution slowly for 3 h. The reaction was left overnight and the white solid filtered to give 2.34 g (8.5 mmol, 77% based on the alcohol) of crude (4-methoxy-1-naphthyl)methyltrimethylammonium chloride, **7**. This salt was purified by recrystallization from acetonitrile; mp 219–220°C; ultraviolet (Fig. 1); nmr (220 MHz, D_2O) δ: 8.24 (d, J = 8.5 Hz, 1H), 8.08 (d, J = 8.5 Hz, 1H), 7.75 (t, 1H), 7.62 (t, 1H), 7.60 (d, J = 8.1 Hz, 1H), 7.00 (d, J = 8.1 Hz, 1H), 4.81 (s, 2H), 4.11 (s, 3H), 3.13 (s, 9H); mass spectrum: 216 (41), 215 (67), 214 (51), 209 (30), 208 (60), 207 (48), 206 (84), 200 (40), 184 (38), 173 (45), 172 (71), 171 (100), 157 (17), 142 (37), 141 (55), 129 (36), 128 (49), 127 (27), 115 (34), 59 (37), 58 (46), 57 (19), 52 (11), 50 (24). *Anal.* calcd. for $C_{15}H_{20}NOCl$: H 7.59, N 5.27, Cl 13.34; found: H 7.90, N 5.38, Cl 13.33.

8, (X = 3-CH_3O): 1-Bromo-3-methoxynaphthalene was prepared as described previously (40); nmr ($CDCl_3$) δ: 7.1–8.0 (m, 5H), 6.77 (d, J = 2 Hz, 1H), 3.63 (s, 3H).

A Grignard reagent was prepared from 5.3 g (23 mmol) of the bromo derivative, 0.60 g (25 mmol) of magnesium, and 15 mL of ether, and then 12 mL of benzene was added. To this solution was added formaldehyde, generated from the pyrolysis of 0.80 g (26 mmol) of dried paraformaldehyde. The solution was refluxed for 1 h after the addition and then poured into a solution of 5 mL of HCl in 500 mL of water. This mixture was extracted with 3 × 50 mL of ether. The ether

Can. J. Chem. Downloaded from www.nrcresearchpress.com by 72.64.146.136 on 09/07/12
For personal use only.

Can. J. Chem. Downloaded from www.nrcresearchpress.com by 72.64.146.136 on 09/07/12
For personal use only.

was washed with 2 × 50 mL of saturated $NaHCO_3$, dried over $MgSO_4$, and concentrated to give 3.4 g of a crude mixture of starting bromide and product alcohol. Chromatography using silica gel and benzene eluent gave 1.9 g (10 mmol, 46%) of the alcohol, which was recrystallized from low boiling petroleum ether to give pure (3-methoxy-1-naphthyl)methanol; mp 88–89°C, nmr ($CDCl_3$) δ: 7.99 (d, J = 8.3 Hz, 1H), 7.77 (d, J = 8.2 Hz, 1H), 7.44–7.50 (t, 1H), 7.36–7.42 (t, 1H), 7.23 (d, J = 2.3 Hz, 1H), 7.09 (d, J = 2.4 Hz, 1H), 5.12 (s, 2H), 3.92 (s, 3H), 2.67 (br s, exchangeable, 1H).

The alcohol, 2.2 g (12 mmol), was placed in a round-bottomed flask and melted in an oil bath. To it was added 20 mL of concentrated HCl and the mixture was stirred for 2 h. After cooling, 120 mL of $CHCl_3$ was added and the mixture was washed with 60 mL of water and 60 mL of saturated $NaHCO_3$. The $CHCl_3$ layer was dried with $MgSO_4$ and concentrated to give 2.2 g (11 mmol, 92%) of crude chloro-(3-methoxy-1-naphthyl)methane as a yellow solid. The chloride was dissolved in 100 mL of anhydrous ether and trimethylamine was bubbled slowly through the solution for 3 h and then the reaction was left overnight. Filtration of the white solid gave 1.75 g (6.6 mmol, 55% based on starting alcohol) of crude (3-methoxy-1-naphthyl)methyltrimethylammonium chloride, **8**. Recrystallization from acetonitrile gave the pure salt; mp 174–176°C; ultraviolet (Fig. 1); nmr (220 MHz, D_2O) δ: 8.03 (m, 1H), 7.87 (m, 1H), 7.5–7.7 (m, 2H), 7.38 (d, J = 2.4 Hz, 1H), 7.21 (d, J = 2.4 Hz, 1H), 4.73 (s, 2H), 3.99 (s, 3H), 3.12 (s, 9H); mass spectrum: 215 (37), 209 (20), 208 (57), 207 (44), 206 (70), 173 (40), 172 (70), 171 (100), 158 (21), 157 (49), 156 (42), 141 (22), 129 (45), 128 (59), 127 (39), 115 (15), 59 (46), 58 (50), 57 (23), 50 (17). *Anal.* calcd. for $C_{15}H_{20}NOCl$: H 7.59, N 5.27, Cl 13.34; found: H 7.82, N 5.65, Cl 13.44.

9, (X = 4-CN): 4-Cyano-1-methylnaphthalene, mp 50–51°C (lit. (41) mp 53–54°C), was prepared as described previously (41) from 4-bromo-1-methylnaphthalene (42).

A solution of 5.0 g (30 mmol) of 4-cyano-1-methylnaphthalene and 5.3 g (40 mmol) of *N*-chlorosuccinimide in 10 mL of chlorobenzene was irradiated for 8 h using a 300-W tungsten lamp (43). The reaction refluxed during the irradiation from the heat of the lamp. Monitoring by nmr indicated no further conversion was occurring. The mixture was allowed to cool and then filtered. The solid was washed with CCl_4 and the filtrate evaporated to give 5.4 g of material, which, by nmr analysis, consisted of 50% chloro-(4-cyano-1-naphthyl)methane and 50% 4-cyano-1-methylnaphthalene.

The mixture was dissolved in 50 mL of ether and trimethylamine was bubbled through the solution for 3 h. The reaction mixture was filtered after standing overnight to give 3.5 g of the ammonium salt. Recrystallization from acetonitrile gave the pure salt, **9**; mp 243–245°C; ultraviolet (Fig. 1); nmr (220 MHz, D_2O) δ: 8.29 (d, J = 8.2 Hz, 1H), 8.04 (m, 1H), 8.01 (d, J = 7.6 Hz, 1H), 7.7–7.9 (m, 3H), 5.06 (s, 2H), 3.20 (s, 9H); mass spectrum: 210 (45), 202 (29), 201 (17), 200 (58), 181 (49), 180 (30), 167 (53), 166 (99), 165 (18), 164 (36), 140 (47), 139 (45), 65 (33), 59 (35), 58 (48), 57 (18), 50 (15). *Anal.* calcd. for $C_{15}H_{17}N_2Cl$: H 6.57, N 10.74, Cl 13.61; found: H 6.48, N 10.32, Cl 13.40.

10, (X = 3-CN): 1-Acetamido-4-methylnaphthalene; mp 166–168°C (lit. (43) 168–169°C) was prepared by Beckmann rearrangement of the oxime derived from 1-acetyl-4-methylnaphthalene (44). All attempts to brominate this compound gave mixtures that could not be separated. However, 1-amino-4-methylnaphthalene was cleanly brominated by the procedure of Kosolapoff (45).

The amide, 10 g (51 mmol), was dissolved in 12 mL of 95% ethanol, 12 mL of concentrated HCl was added, and the mixture refluxed for 3 h. To the cooled solution was added 200 mL of water and NaOH pellets until the pH was 10. The aqueous layer was extracted with 2 × 100 mL of chloroform and the extract washed with water, dried over $MgSO_4$, and concentrated to give 8.0 g (100%) of the amine; nmr ($CDCl_3$) δ: 7.7–8.1 (m, 2H), 7.3–7.6 (m, 2H), 7.1 (d, J = 8 Hz, 1H), 6.67 (d, J = 8 Hz, 1H). To the amine dissolved in 16 mL of dioxane, 21 mL of water, and 6 g of potassium hydroxide was added over 2 h a solution of 2.6 mL (50 mmol) of bromine in 85 mL of dioxane. Then 100 mL of H_2O was added and the mixture extracted with 2 × 100 mL of $CHCl_3$. The extracts were washed with 50 mL of 40% KOH and 50 mL of H_2O, dried over $MgSO_4$, and concentrated to give 8.8 g (74%) of 1-amino-2-bromo-4-methylnaphthalene; nmr ($CDCl_3$) δ: 7.3–8.0 (m, 5H), 4.4 (br s, 2H), 2.50 (s, 3H).

The amine was deaminated as follows (46). To 21 g (89 mmol) of the amine in 55 mL of 95% ethanol, 90 mL of H_2O, and 37 mL of concentrated H_2SO_4 cooled to 10°C was added dropwise a solution of 10.4 g of sodium nitrite in 18 mL of H_2O. The mixture was stirred for 2 h and then 2.5 g of copper powder was added, followed by heating at 60°C for 1 h and then in a boiling water bath for 10 min. The reaction mixture was left overnight at room temperature. The reaction was diluted with 100 mL of H_2O and extracted with 2 × 100 mL of benzene. The benzene extract was washed with 50 mL of H_2O, 50 mL of 5% NaOH, 50 mL of 10% HCl, 50 mL of H_2O, and dried over $MgSO_4$. Concentration gave 18 g of a dark oil, which was distilled, 100–104°C at 0.5 Torr, to give 10.5 g (54%) of 3-bromo-1-methylnaphthalene; nmr ($CDCl_3$) δ: 7.3–8.1 (m, 6H), 2.67 (s, 3H); mass spectrum: 222 (95), 221 (16), 220 (100), 141 (71), 139 (25), 115 (19), 71 (15).

The cyanation procedure was that of Friedman and Schechter (47). A solution of 6.4 g (29 mmol) of the bromide and 3.0 g of cuprous cyanide in 6 mL of dimethyl formamide was refluxed for 4 h. The reaction mixture was poured into a solution of 25 mL of H_2O, 4 mL of concentrated HCl, and 20 g of ferric chloride, and heated at 65°C for 20 min. The mixture was extracted with 2 × 20 mL of benzene and the extract washed with 40 mL of 10% HCl and 40 mL of 5% NaOH, dried over $MgSO_4$, and concentrated to give 2.7 g of crude product. Recrystallization from hexane gave 2.0 g (41%) of 3-cyano-1-methylnaphthalene; mp 67–68°C; nmr ($CDCl_3$) δ: 7.3–7.9 (m, 4H), 7.18 (s, 1H), 2.47 (s, 3H); mass spectrum: 167 (100), 166 (61), 140 (32), 139 (16).

The 3-cyano-1-methyl derivative was chlorinated as follows (43). To 0.87 g (5.2 mmol) of the cyano derivative in 15 mL of chlorobenzene was added 0.91 g (7.8 mmol) of *N*-chlorosuccinimide. The mixture was irradiated with a 300-W tungsten lamp for 14 h. The reaction mixture was diluted with 20 mL of CH_2Cl_2 and extracted with 2 × 10 mL of H_2O, dried over $MgSO_4$, and concentrated by pumping in a warm water bath to give 0.84 g of material, which by nmr analysis consisted of 83% chloro-(3-cyano-1-naphthyl)methane and 17% 3-cyano-1-methylnaphthalene.

This mixture was dissolved in 40 mL of ether and trimethylamine was bubbled through the solution for 4 h. After standing overnight, the reaction mixture was filtered to give 425 mg of the ammonium salt. Recrystallization from acetonitrile gave the pure salt, **10**; mp 254–255°C; ultraviolet (Fig. 1); ir (KBr): 2210 cm^{-1}; nmr (220 MHz, D_2O) δ: 8.56 (s, 1H), 8.33 (d, J = 8.2 Hz, 1H), 8.10 (d, J = 8.1 Hz, 1H), 7.97 (d, J = 1.4 Hz, 1H), 7.91 (t, 1H), 7.78 (t, 1H), 5.04 (s, 2H), 3.18 (s, 9H); mass spectrum: 210 (51), 209 (20), 203 (33), 202 (16), 201 (73), 167 (74), 166 (100), 164 (43), 152 (15), 140 (69), 139 (61), 115 (20), 113 (23), 87 (21), 75 (17), 74 (21), 69 (21), 63 (31), 59 (55), 58 (66), 57 (37), 51 (19), 50 (37).

Preparative scale photolyses of 1-naphthylmethyltrimethylammonium chlorides, 7–10

Preparative scale irradiations were done using a Pyrex filtered 200-W medium pressure Hanovia mercury lamp in a 300-mL immersion well with nitrogen purging. The reactions were monitored by hplc with a Brownlee 10-μm RP-8 reverse phase column using 80% methanol/water as eluant and detection at 280 nm. Yields are shown in Table 1. The photoproduct mixtures were obtained from the photolysis solution by adding 300 mL of H_2O and extracting with hexane (3 × 300 mL). The hexane was dried with $MgSO_4$ and concentrated. The residue was then chromatographed on silica gel to isolate the photoproducts.

The products and their isolated yields are as follows:

7, X = 4-CH_3O; 300 mg (1.13 mmol); methoxy-(4-methoxy-1-naphthyl)methane; bp 70–72°C, 0.2 Torr; nmr ($CDCl_3$) δ: 7.85–8.1 (m, 1H), 7.6–7.85 (m, 1H), 6.4 (d, J = 7 Hz, 1H), 4.60 (s, 2H), 3.77 (s, 3H), 3.58 (s, 3H); 184 mg (82%).

8, X = 3-CH_3O; 190 mg (0.71 mmol); 3-methoxy-1-methylnaph-

thalene; mp 45–46°C; nmr ($CDCl_3$) δ: 6.73–7.90 (m, 6H), 3.78 (s, 3H), 2.58 (s, 3H); 71 mg (50%); methoxy-(3-methoxy-1-naphthyl)methane; nmr ($CDCl_3$) δ: 6.85–7.98 (m, 6H), 4.75 (s, 2H), 3.80 (s, 3H), 3.57 (s, 3H).

9, X = 4-CN; 151 mg (0.60 mmol): 4-cyano-1-methylnaphthalene; *vide supra*; 49 mg (38%); methoxy-(4-cyano-1-naphthyl)methane; mp 70.5–71°C; nmr ($CDCl_3$) δ: 7.1–8.15 (m, 6H), 4.86 (s, 2H), 3.48 (s, 3H); 41 mg (35%).

10, X = 3-CN; 114 mg (0.45 mmol): 3-cyano-1-methylnaphthalene; nmr ($CDCl_3$) δ: 7.3–8.1 (m, 6H), 2.72 (s, 3H); 20 mg (31%); methoxy-(3-cyano-1-naphthyl)methane; nmr ($CDCl_3$) δ: 7.6–8.3 (m, 6H), 4.90 (s, 2H), 3.50 (s, 3H); 14 mg (16%).

Quantum yields and fluorescence measurements were determined as described previously (2).

Acknowledgements

We thank the Natural Sciences and Engineering Research Council of Canada for financial assistance and the CFKR (Centre for Fast Kinetics Research), University of Texas, Austin, and in particular M. Rogers and S. Atherton, for the excited state lifetime measurements. The CFKR is supported jointly by the Biomedical Resources Technology of the Division of Research Resources of NIH (RR 00886) and the University of Texas at Austin. J.A.P. and A.L.P. thank Professor M. A. Fox for her hospitality at the University of Texas.

1. S. J. Cristol and T. H. Bindel. Organic photochemistry. Vol. 6. Marcel Dekker, New York. 1983. p. 327.
2. B. Arnold, L. Donald, A. Jurgens, and J. A. Pincock. Can. J. Chem. **63**, 3140 (1985).
3. H. E. Zimmerman and V. R. Sandel. J. Am. Chem. Soc. **85**, 915 (1963).
4. H. E. Zimmerman and S. Somasekhara. J. Am. Chem. Soc. **85**, 922 (1963).
5. M. A. Ratcliff, Jr. and J. K. Kochi. J. Org. Chem. **36**, 3112 (1971).
6. J. A. Barltrop and P. Schofield. J. Chem. Soc. 4758 (1965).
7. S. J. Cristol and T. H. Bindel. J. Org. Chem. **45**, 951 (1980).
8. S. J. Cristol and T. H. Bindel. J. Am. Chem. Soc. **103**, 7287 (1981).
9. P. Wan. J. Org. Chem. **50**, 2583 (1985).
10. N. J. Turro and P. Wan. J. Photochem. **28**, 93 (1985).
11. P. Seiler and J. Wirz. Tetrahedron Lett. 1683 (1971).
12. P. Seiler and J. Wirz. Helv. Chim. Acta, **55**, 2693 (1972).
13. R. S. Givens and B. Matuszewski. J. Am. Chem. Soc. **106**, 6860 (1984).
14. D. C. Appleton, D. C. Bull, R. S. Givens, V. Lillis, J. McKenna, J. M. McKenna, S. Thackery, and A. R. Walley. J. Chem. Soc. Perkin Trans. 2, 77 (1980).
15. H. H. Jaffé and M. Orchin. Theory and applications of ultraviolet spectroscopy. J. Wiley and Sons, Inc., New York. 1962. (*a*) p. 303; (*b*) p. 101.
16. J. C. Scaiano. J. Am. Chem. Soc. **102**, 7747 (1980).
17. S. L. Murov. Handbook of photochemistry. Marcel Dekker, Inc., New York. 1973. (*a*) p. 55; (*b*) p. 4; (*c*) pp. 5, 50.
18. D. A. Labianca, G. N. Taylor, and G. S. Hammond. J. Am. Chem. Soc. **94**, 3679 (1972).
19. E. F. Hilinski, D. Huppert, D. F. Kelley, S. V. Milton, and R. M. Rentzepis. J. Am. Chem. Soc. **106**, 1951 (1984).
20. L. J. Johnston and J. C. Scaiano. J. Am. Chem. Soc. **107**, 6368 (1985).
21. H. Shizuka. Acc. Chem. Res. **18**, 141 (1985).
22. S. W. Benson. J. Chem. Educ. **42**, 502 (1965).
23. W. C. Herndon. J. Org. Chem. **46**, 2119 (1981).
24. G. H. Slocum and G. B. Schuster. J. Org. Chem. **49**, 2177 (1984).
25. V. Lillis, J. McKenna, J. M. McKenna, M. J. Smith, P. S. Taylor, and I. H. Williams. J. Chem. Soc. Perkin Trans. 2, 83 (1980).
26. D. D. M. Wayner, J. J. Danenberg, and D. Griller. J. Am. Chem. Soc. Submitted.
27. V. Lillis, J. McKenna, J. M. McKenna, and I. H. Williams. Chem. Commun. 474 (1974).
28. D. D. M. Wayner and D. Griller. J. Am. Chem. Soc. **107**, 7764 (1985).
29. C. K. Mann. Anal. Chem. **36**, 2424 (1964).
30. I. M. Kolthoff and J. F. Coetzee. J. Am. Chem. Soc. **79**, 870 (1957).
31. P. T. Cottrell and C. K. Mann. J. Electrochem. Soc. **116**, 1499 (1969).
32. (*a*) J. R. Miller, L. T. Calcaterra, and G. L. Closs. J. Am. Chem. Soc. **106**, 3047 (1984); (*b*) J. R. Miller, J. V. Beitz, and R. K. Huddleston. J. Am. Chem. Soc. **106**, 5057 (1984).
33. H. Shizuka and S. Tobita. J. Am. Chem. Soc. **104**, 6919 (1982).
34. H. C. Brown and Y. Okamoto. J. Am. Chem. Soc. **80**, 4979 (1958).
35. B. K. Bandish, A. W. Garner, M. L. Hodges, and J. W. Timberlake. J. Am. Chem. Soc. **97**, 5856 (1975).
36. D. D. M. Wayner and D. R. Arnold. Can. J. Chem. **63**, 2378 (1985).
37. J. M. Dust and D. R. Arnold. J. Am. Chem. Soc. **105**, 1221, 6531 (1983).
38. P. J. Baldry. J. Chem. Soc. Perkin Trans. 2, 951 (1979).
39. N. P. Buu-Hoi and D. Lavit. J. Chem. Soc. 2777 (1955).
40. M. S. Newman, V. Sankaran, and D. R. Olson. J. Am. Chem. Soc. **98**, 3237 (1976).
41. H. G. Rule, N. Campbell, A. G. McGregor, and A. A. Woodham. J. Chem. Soc. 1816 (1950).
42. L. F. Fieser and D. M. Bowen. J. Am. Chem. Soc. **62**, 2103 (1940).
43. M. F. Hebbelynck and R. H. Martin. Bull. Soc. Chim. Belg. **59**, 193 (1950).
44. J. Sauer, R. Huisgen, and A. Hauser. Ber. **91**, 1461 (1958).
45. G. M. Kosolapoff. J. Am. Chem. Soc. **75**, 3596 (1953).
46. L. A. Bigelow, J. R. Johnson, and L. T. Sandborn. Org. Synth. Coll. Vol. 1, 133 (1932).
47. L. Friedman and H. Schechter. J. Org. Chem. **26**, 2522 (1961).

Can. J. Chem. Downloaded from www.nrcresearchpress.com by 72.64.146.136 on 09/07/12
For personal use only.

Benzodiazepine stereochemistry: crystal structures of the diazepam antagonist Ro 15-1788 and the anomalous benzodiazepine Ro 5-4864

ANDREW HEMPEL AND NORMAN CAMERMAN
Biochemistry Department, University of Toronto, Toronto, Ont., Canada M5S 1A8

AND

ARTHUR CAMERMAN
Departments of Medicine (Neurology) and Pharmacology, University of Washington, Seattle, WA 98195

Received August 28, 1986[1]

ANDREW HEMPEL, NORMAN CAMERMAN, and ARTHUR CAMERMAN. Can. J. Chem. **65**, 1608 (1987).

The crystal and molecular structures of the benzodiazepine antagonist Ro 15-1788, and of Ro 5-4864, a diazepam derivative with low affinity for central benzodiazepine receptors, have been determined. Stereochemical comparisons with diazepam have resulted in the conclusion that the steric bulk of the 4′-chlorine atom alone is responsible for the lowered activity of Ro 5-4864, and have suggested possible structural reasons for the antagonist/weak agonist activities of Ro 15-1788.

ANDREW HEMPEL, NORMAN CAMERMAN et ARTHUR CAMERMAN. Can. J. Chem. **65**, 1608 (1987).

On a déterminé les structures cristalline et moléculaire de l'antagoniste de la benzodiazépine, le composé Ro 15-1788, et du composé Ro 5-4864, un dérivé du diazépam possédant une faible affinité pour les récepteurs centraux de la benzodiazépine. En se basant sur des comparaisons stéréochimiques avec le diazépam, on peut conclure que l'encombrement stérique de l'atome de chlore en position 4′ est le seul responsable de l'activité plus faible du composé Ro 5-4864 et on peut suggérer des raisons structurales possibles pour les activités antagoniste/faible agoniste du composé Ro 15-1788.

[Traduit par la revue]

Can. J. Chem. Downloaded from www.nrcresearchpress.com by 118.98.75.50 on 09/07/12
For personal use only.

Introduction

A large number of benzodiazepine (BZ) derivatives have been synthesized in attempts to achieve compounds specific for a particular pharmacological effect in the benzodiazepine spectrum of activities, such as anxiolytic or anticonvulsant action. Two analogues of considerable interest are Ro 15-1788 (ethyl-8-fluoro-5,6-dihydro-5-methyl-6-oxo-4*H*-imidazo[1,5-*a*][1,4]benzodiazepine-3-carboxylate), an antagonist of BZ binding, and Ro 5-4864 (7-chloro-1,3-dihydro-1-methy-5-(*p*-chlorophenyl)-2*H*-1,4-benzodiazepine-2-one), a compound that demonstrates a number of effects upon BZ-receptors. Ro 15-1788 is a representative of a novel class of BZ derivatives which have the unique pharmacological activity of selectively antagonizing the behavioral and neurological effects of diazepam through specific inhibition of BZ receptor-binding (1–3),

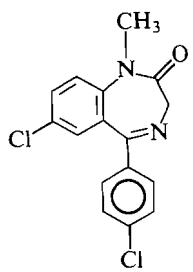

Ro 5-4864

a property which could make them useful as antidotes to BZ-induced intoxications. Although initial studies indicated that Ro 15-1788 was a pure antagonist, more recent results suggest that at high doses it possesses partial agonist activity (4). These properties make Ro 15-1788 a useful model to compare with the more standard BZ's in order to define the stereochemical characteristics of agonist/antagonist activities. Ro 5-4864 is a compound that has aroused interest for many years, partly because of conflicting reports of its actions.

[1]Revision received February 18, 1987.

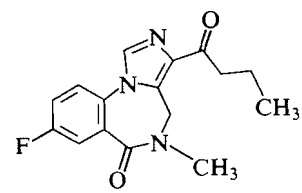

Ro 15-1788

Differing from diazepam structurally only in the possession of a 4′-Cl atom, Ro 5-4864 binds only very weakly to high affinity CNS (central nervous system) BZ-binding sites (5) but demonstrates strong specific binding to peripheral-type BZ receptors (6). In addition, other Ro 5-4864 binding sites in brain and spinal cord which differ pharmacologically from classical BZ receptors have been reported recently (7).

We have determined the crystal and molecular structures of Ro 15-1788 and Ro 5-4864 and compared their three-dimensional structures with diazepam in an attempt to correlate pharmacological properties with stereochemical characteristics in BZ derivatives; we now report the results of these studies.

Experimental section

A. Ro 15-1788

Crystals were obtained from aqueous solution. Crystal data are given in Table 1; the space group was established from the systematically absent reflections on Weissenberg and precession photographs. A prism 0.3 × 0.2 × 0.3 mm was selected and intensities of reflections with $2\theta < 130°$ (corresponding to a minimum interplanar spacing of 0.85 Å) were measured on an automated four-circle diffractometer with Ni-filtered CuKα radiation using the $2\theta/\theta$ scan technique. One octant of reciprocal space was measured and equivalent reflections merged ($R = 0.047$). No absorption corrections were applied. A total of 1194 unique reflections were considered to be observed ($I > 3\sigma(I)$) out of 2264 measured and were used in the refinement. The structure was solved using the direct phasing program MULTAN80 (16). Atomic positional and anisotropic thermal parameters were refined by full-matrix least squares. All hydrogen atoms were located on difference electron-density plots and their coordinates were refined with fixed isotropic temperature factors. The final discrepancy index converged

Can. J. Chem. Downloaded from www.nrcresearchpress.com by 118.98.75.50 on 09/07/12
For personal use only.

TABLE 1. Crystal data

Parameter	Value	
	Ro 15-1788	Ro 5-4864
Formula	$C_{15}H_{14}O_3N_3F$	$C_{16}H_{12}N_2OCl_2$
Molecular weight	309	318
Crystal system	Tetragonal	Orthorhombic
a (Å)	19.444 (8)	28.434 (12)
b (Å)	19.444 (8)	13.907 (8)
c (Å)	7.349 (5)	7.480 (6)
Volume of unit cell (Å^3)	2778	2958
Density calcd (g/cm^3)	1.43	1.41
No. of molecules in cell	8	8
Space group	$P4_2/n$	$Pbca$
Absorption coefficient (cm^{-1})	9.4	39.2

to $R = 0.047$ with $S = 1.41$. (R for all measured reflections = 0.12.) The highest features in the final difference electron density map were −0.33 and +0.30 e Å^{-3}.

B. Ro 5-4864

Crystals were obtained from acetone; crystal data are given in Table 1. A plate, 0.3 × 0.08 × 0.2 mm was used for X-ray data collection in a procedure similar to that described above. A total of 2200 unique reflections were recorded ($2\theta_{max} = 120°$) in the positive hkl octant of which 876 were considered to be observed ($I > 3\sigma(I)$). In addition to the usual data reduction procedure, an empirical correction for absorption based on ϕ angle was applied (transmission factors ranged from 0.61–0.99). The space group was established by the systematic absences on Weissenberg and precession photographs. The structure was solved and refined as described for Ro 15-1788. The final discrepancy index R was 0.068 (observed reflections) and 0.14 (all reflections). $S = 1.84$. The highest features in the final difference map were ±0.50 e Å^{-3}. In both structures, unit weights were used in the least-squares calculations and the function minimized was $\Sigma(|F_o| - |F_c|)^2$. The atomic scattering factors used were as cited for nonhydrogen (8) and hydrogen (9) atoms. Computer programs used were XFLS (17) and some local programs.

Table 2 lists the atomic fractional coordinates and equivalent isotropic thermal parameters; the anisotropic thermal parameters, hydrogen positional parameters, and a list of the observed and calculated structure factors are available.[2]

Results and discussion

Description of the structures

Figure 1 shows the molecular structures of Ro 15-1788[3] and Ro 5-4864 and the atomic numbering schemes. Bond lengths and angles are given in Table 3. The halogenated-phenyl rings in both compounds are planar, as is the five-membered heterocycle in Ro 15-1788; the bond lengths confirm that

TABLE 2.

(*A*) Fractional atomic coordinates (× 10^4) and equivalent isotropic temperature factors for Ro 15-1788

Atom	X	Y	Z	B_{eq} (Å^2)
C1	7378(3)	−498(2)	3900(6)	5.0
C2	6982(2)	80(2)	3733(6)	4.6
C3	7307(2)	691(2)	3337(6)	3.6
C4	8020(2)	707(2)	3130(5)	3.0
C5	8416(2)	109(2)	3261(6)	3.2
C6	8071(3)	−504(2)	3681(7)	4.4
N7	8330(1)	1356(1)	2773(4)	2.8
C8	8948(2)	1585(2)	3464(5)	2.8
C9	9378(2)	1095(2)	4521(6)	2.9
N10	9600(1)	534(1)	3353(4)	3.0
C11	9168(2)	34(2)	2813(6)	3.5
C12	8044(2)	1899(2)	1870(7)	3.6
N13	8425(1)	2450(1)	1940(5)	3.7
C14	8999(2)	2251(2)	2930(5)	3.0
C15	9558(2)	2750(2)	3207(6)	3.4
O16	10141(1)	2437(1)	3690(4)	3.7
C17	10751(2)	2870(2)	3883(8)	4.0
C18	11329(3)	2402(4)	4371(9)	5.5
O19	9502(1)	3362(1)	2999(5)	5.3
O20	9358(1)	−472(1)	1975(4)	5.1
C21	10308(2)	542(3)	2657(9)	4.1
F22	7067(1)	−1103(1)	4348(4)	7.8

(*B*) Fractional atomic coordinates (× 10^4) and equivalent isotropic temperature factors for Ro 05-4864

Atom	X	Y	Z	B_{eq} (Å^2)
C1	6060(3)	1740(7)	1086(15)	3.9
C2	6490(4)	1999(7)	1820(14)	4.5
C3	6854(3)	1391(9)	1755(15)	4.1
C4	6823(3)	507(8)	869(14)	3.6
C5	6414(3)	243(7)	45(13)	2.7
C6	6023(3)	878(7)	164(14)	3.3
N7	7244(3)	−80(7)	778(12)	4.7
C8	7232(5)	−1056(9)	1175(16)	5.6
C9	6745(4)	−1480(8)	1393(17)	5.0
N10	6514(3)	−1494(6)	−335(13)	4.9
C11	6350(4)	−682(7)	−876(14)	4.0
C12	6074(3)	−699(7)	−2578(15)	3.5
C13	6062(3)	66(8)	−3781(16)	4.2
C14	5817(3)	45(7)	−5376(14)	3.7
C15	5562(4)	−770(8)	−5710(13)	4.2
C16	5568(4)	−1539(9)	−4571(18)	5.5
C17	5806(4)	−1523(8)	−3305(15)	4.2
C18	7694(4)	381(9)	665(16)	6.9
O19	7594(3)	−1499(7)	1298(13)	9.0
Cl20	5583(1)	2476(2)	1257(4)	5.6
Cl21	5242(1)	−829(2)	−7714(4)	5.7

C12—N13 (1.30 Å) and C8—C14 (1.36 Å) in that ring are formal double bonds. The bond lengths and angles in Ro 5-4864 do not differ significantly from the corresponding values in diazepam (10). The N10—C11 bond in Ro 15-1788 is 1.34 Å vs. 1.29 Å in Ro 5-4864 and diazepam reflecting loss of formal double bond character concomitant with N10 methylation and the carbonyl function at C11; the angles at N10 are still trigonal, however, and nitrogen lone-pair electrons undoubtedly contribute to the amide nature of the bond. The seven-membered diazepine rings in both compounds adopt boat-shaped conformations, as is the case in diazepam, with the C11 carbonyl

[2]Complete set of data may be purchased from the Depository of Unpublished Data, CISTI, National Research Council of Canada, Ottawa, Ont., Canada K1A 0S2.

[3]After this work was completed an independent structure determination of Ro 15-1788 was reported (ref. 13). That determination is of extremely low precision: fewer than 600 data with $I > 2\sigma(I)$ were obtained, vs. 1194 data with $I > 3\sigma(I)$ here; atomic equivalent isotropic thermal parameters ranged from 8.5–25.8 Å^2 with a mean of 14.0 Å^2, vs. 2.8–7.8 Å^2 with a mean of 4.0 Å^2 in the present determination; and the final R was 0.071 vs. 0.047 here. In addition, no hydrogen atoms were located in that structure determination and nonhydrogen atom bond parameters are not given. The structural basis for agonist activity proposed therein is different from our postulations. See Discussion.

Can. J. Chem. Downloaded from www.nrcresearchpress.com by 118.98.75.50 on 09/07/12
For personal use only.

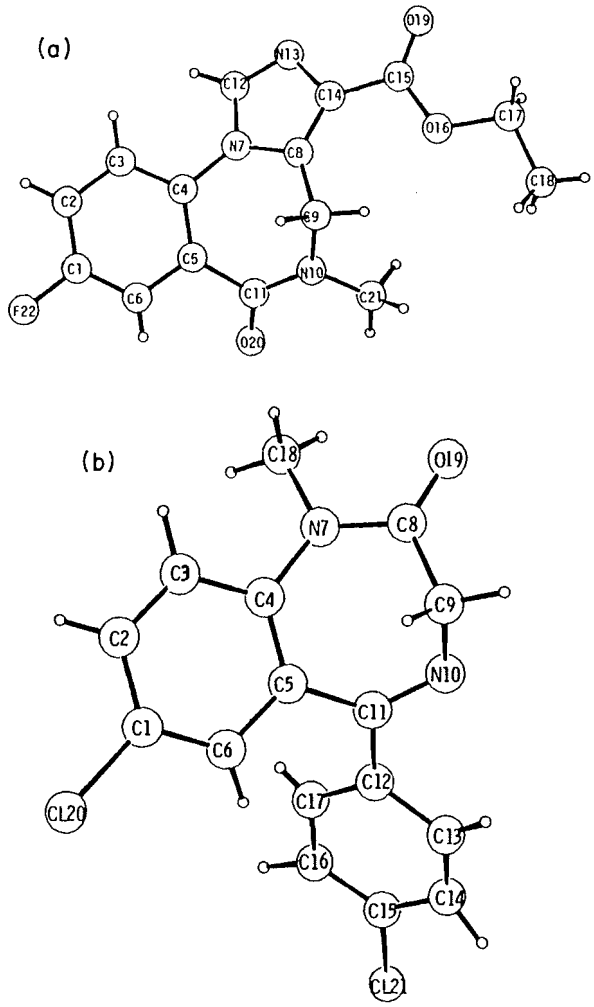

FIG. 1. Molecular conformations and atomic numbering schemes for (*a*) Ro 15-1788 and (*b*) Ro 5-4864.

group causing the boat to be somewhat shallower in Ro 15-1788 than in the other two molecules. There are no hydrogen bond donors in either molecule and the intermolecular interactions in both crystals consist only of van der Waals contacts.

Stereochemical comparisons with diazepam

A superposition of the Ro 5-4864 structure with that of diazepam (not shown) demonstrates that in addition to the close similarity in molecular parameters, the two molecules share virtually identical conformations. There appear to be no transmitted effects of the 4′-chloro substitution in Ro 5-4864 and differences in receptor binding must be attributable to the steric effects of the 4′-chlorine atom. The high affinity CNS BZ-binding sites must accommodate the extra bulk of the chlorine only with difficulty, while the peripheral and the uncharacterized brain and spinal cord Ro-4864 sites are sufficiently different structurally to allow entry of the *p*-chloro substituent.

This hypothesis is supported by animal data available for two other 4′-substituted diazepam derivatives. Although receptor-binding studies have not been performed for 4′-fluoro and 4′-methoxy nordiazepam, these drugs have been tested for efficacy against metrazol-, minimal electroshock-, and maximal electroshock-induced convulsions in mice (11). Both compounds were ineffective at the highest dose measured against metrazol and minimal electroshock tests (the usual experimental

TABLE 3. Bond lengths (Å) and bond angles (deg) with esd's in parentheses

Ro 15-1788		Ro 5-4864	
Bond	Length	Bond	Length
C1—C2	1.368 (7)	C1—C2	1.386 (13)
C1—C6	1.357 (7)	C1—C6	1.387 (13)
C1—F22	1.364 (5)	C1—Cl20	1.704 (10)
C2—C3	1.375 (6)	C2—C3	1.337 (14)
C3—C4	1.395 (6)	C3—C4	1.399 (14)
C4—C5	1.397 (5)	C4—C5	1.368 (13)
C4—N7	1.424 (5)	C4—N7	1.451 (13)
C5—C6	1.404 (6)	C5—C6	1.422 (13)
C5—C11	1.506 (6)	C5—C11	1.470 (13)
N7—C8	1.378 (5)	N7—C8	1.390 (15)
N7—C12	1.366 (5)	N7—C18	1.434 (13)
C8—C9	1.487 (5)	C8—C9	1.512 (16)
C8—C14	1.357 (5)	C8—O19	1.203 (12)
C9—N10	1.455 (5)	C9—N10	1.450 (15)
N10—C11	1.344 (5)	N10—C11	1.288 (12)
N10—C21	1.468 (5)	C11—C12	1.495 (14)
C11—O20	1.218 (5)	C12—C13	1.394 (14)
N13—C12	1.303 (6)	C12—C17	1.412 (14)
N13—C14	1.387 (5)	C13—C14	1.382 (14)
C14—C15	1.472 (6)	C14—C15	1.369 (13)
C15—O19	1.204 (5)	C15—C16	1.368 (15)
C15—O16	1.334 (5)	C15—Cl21	1.755 (11)
O16—C17	1.461 (4)	C16—C17	1.353 (15)
C17—C18	1.489 (8)		

Ro 15-1788		Ro 5-4864	
Bonds	Angle	Bonds	Angle
C2—C1—C6	123.7 (5)	C2—C1—C6	119 (1)
C2—C1—F22	118.8 (5)	C2—C1—Cl20	121 (1)
C6—C1—F22	117.5 (6)	C6—C1—Cl20	120 (1)
C1—C2—C3	118.1 (5)	C1—C2—C3	120 (1)
C2—C3—C4	119.9 (5)	C2—C3—C4	122 (1)
C3—C4—C5	121.5 (4)	C3—C4—C5	120 (1)
C3—C4—N7	117.4 (4)	C3—C4—N7	118 (1)
C5—C4—N7	121.1 (3)	C5—C4—N7	122 (1)
C4—C5—C6	117.2 (4)	C4—C5—C6	118 (1)
C4—C5—C11	127.0 (4)	C4—C5—C11	123 (1)
C6—C5—C11	115.5 (4)	C6—C5—C11	118 (1)
C1—C6—C5	119.6 (5)	C1—C6—C5	121 (1)
C4—N7—C8	126.0 (3)	C4—N7—C8	121 (1)
C4—N7—C12	127.0 (3)	C4—N7—C18	119 (1)
C8—N7—C12	106.6 (3)	C8—N7—C18	118 (1)
N7—C8—C9	118.4 (3)	N7—C8—C9	115 (1)
N7—C8—C14	105.4 (3)	N7—C8—O19	120 (1)
C9—C8—C14	136.2 (4)	C9—C8—O19	125 (1)
C8—C9—N10	109.8 (3)	C8—C9—N10	109 (1)
C9—N10—C11	122.0 (4)	C9—N10—C11	116 (1)
C9—N10—C21	118.4 (4)	C5—C11—N10	125 (1)
C11—N10—C21	119.4 (4)	C5—C11—C12	119 (1)
C5—C11—N10	118.2 (4)	N10—C11—C12	116 (1)
C5—C11—O20	118.9 (4)	C11—C12—C13	123 (1)
N10—C11—O20	122.9 (4)	C11—C12—C17	119 (1)
N7—C12—N13	112.6 (4)	C13—C12—C17	117 (1)
C12—N13—C14	104.4 (4)	C12—C13—C14	124 (1)
C8—C14—N13	111.1 (4)	C13—C14—C15	116 (1)
C8—C14—C15	130.0 (4)	C14—C15—C16	122 (1)
N13—C14—C15	118.9 (4)	C14—C15—Cl21	118 (1)
C14—C15—O16	111.4 (3)	C16—C15—Cl21	120 (1)
C14—C15—O19	124.5 (4)	C15—C16—C17	122 (1)
O16—C15—O19	124.1 (4)	C12—C17—C16	119 (1)
C15—C16—C17	117.0 (3)		
O16—C17—C18	106.5 (4)		

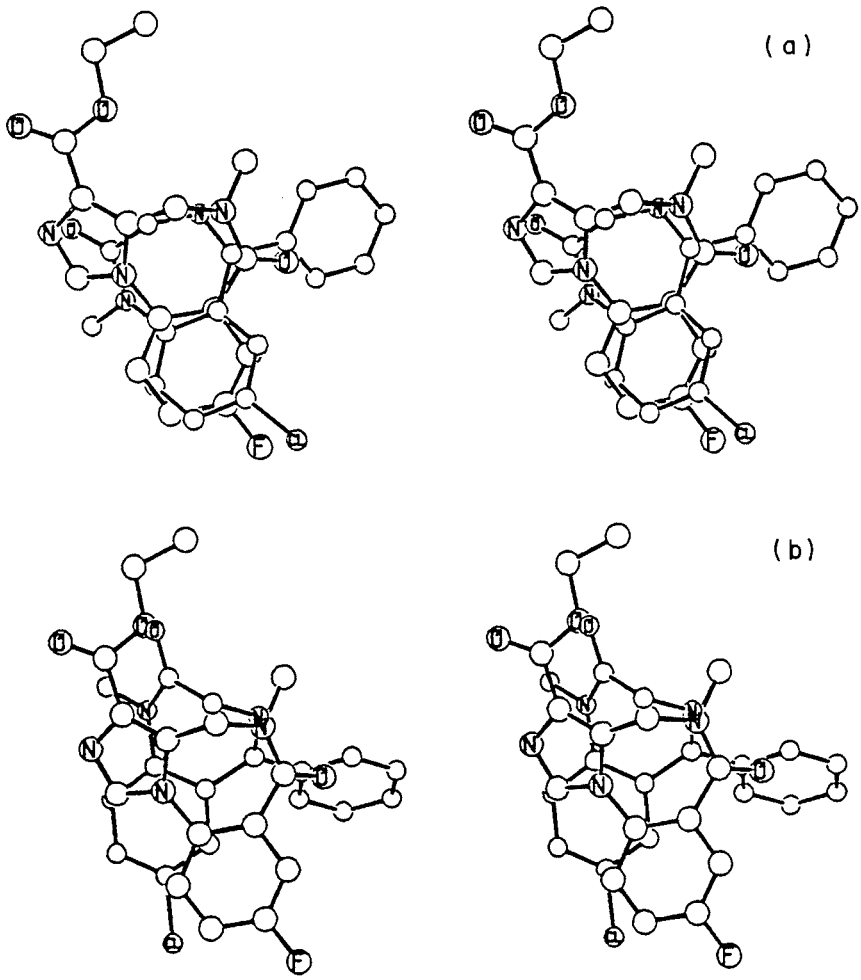

FIG. 2. Stereoscopic superpositions of Ro 15-1788 (large circles, light bonds) and diazepam so that (*a*) atoms N10 and N13 of Ro 15-1788 are maximally fitted to N10 and O19 of diazepam; (*b*) atoms N10 and O16 of Ro 15-1788 are maximally fitted to N10 and O19 of diazepam. The atomic numbering scheme for diazepam is identical to that used for Ro 5-4864 (Fig. 1).

model for petit mal seizures) but showed some activity against the maximal electroshock procedure (the usual experimental model for grand mal or generalized seizures). Median effective doses (ED_{50}) for the fluoro and methoxy substituted BZ's were 50 and 400 mg/kg, respectively. Since protection against electrically induced convulsions is mediated through binding to CNS receptors and since the steric effects of methoxy are considerably greater than for fluorine, these data are consistent with the conclusion we draw about the steric effects of the Ro 5-4864 4′-chlorine from the crystal structure analysis.

A superposition of the benzodiazepine portions of Ro 15-1788 and diazepam has been deposited. Our previous structure-activity studies on BZ's and other antiepileptic drugs (12) have suggested that when corresponding hydrophobic regions are superposed, two hydrogen bond acceptor atoms occupy similar positions in each molecule and are very likely necessary for the central nervous system receptor-mediated anticonvulsant properties of these compounds. Assuming that N10 and the C8 carbonyl oxygen are required for receptor interactions which trigger the pharmacological response, one can rationalize the BZ antagonist properties of Ro 15-1788 in terms of substitution of a carbon atom (C14) in the position of the carbonyl oxygen. Receptor binding could still occur through hydrophobic interactions and hydrogen bonding to N10, probably with extra interactions involving the ester grouping, but the lack of a correctly-positioned carbonyl oxygen or other hydrogen bond acceptor could prevent the interaction necessary to effect pharmacological action.

There are a number of ways the structural results could be interpreted to rationalize the partial agonist activity observed at high concentrations of Ro 15-1788. There are some electronegative atoms in Ro 15-1788 whose vectoral separations approximate that of N10-019 of diazepam and whose superpositions onto these latter atoms results in an overall Ro 15-1788 conformation which loosely approximates diazepam, including gross similarities in distribution of hydrophobic moieties. Two examples are shown in Fig. 2: the N10...N13 distance is 4.50 Å and the N10...O16 separation is 3.86 Å while the corresponding N...O distance in diazepam is 3.35 Å. Although receptor binding in either of these modes may not be favored for Ro 15-1788, in high concentrations this may occur sufficiently to explain the weak agonist properties of the compound. Additionally, if some hydrolysis of the ester takes place (speculation) this could facilitate the occurrence of a binding mode such as shown in Fig. 2; higher concentrations of Ro 15-1788 would result in higher amounts of the hydrolyzed species and increased "agonist" mode binding.

We explain the partial agonist properties of Ro 15-1788 at high concentrations by postulating that it can bind weakly to the BZ receptor in a second orientation in which the gross conformation (distribution of hydrophobic and hydrophillic groups) resembles diazepam and in which two electronegative

Can. J. Chem. Downloaded from www.nrcresearchpress.com by 118.98.75.50 on 09/07/12
For personal use only.

atoms superpose with the two electronegative sites in diazepam putatively involved in the pharmacological response. A model for BZ receptor binding has been suggested by Codding and Muir (13) in which all agonists, antagonists, and inverse agonists occupy the same BZ receptor site in one common orientation and exert their diverse effects through combinations of seven different interactions with unspecified receptor groups. This model does not explain how Ro 15-1788 can show both antagonist and weak agonist behaviour. In addition, as pointed out by Dodd *et al.* (14), the model does not distinguish between antagonists and inverse agonists, and moreover, fails for agonists in the case of the agonist β-carboline-3-carboxylates ZK91296 and ZK93423 (15).

Acknowledgments

Samples of Ro 15-1788 and Ro 5-4864 were gifts from Hoffmann La Roche, Inc. Support was from NIH grant NSO9839 from the NINCDS. A.C. is a Klingenstein Senior Fellow in the Neurosciences.

1. W. HUNKELER, M. MOHLER, L. PIERI, P. DOLE, E. P. BONETTI, R. CUMIN, R. SCHAFFNER, and W. HAEFELY. Nature (London), **290**, 514 (1981).
2. T. E. ALBERTSON, J. F. BOWYER, and M. G. PAULE. Life Sci. **31**, 1597 (1982).
3. D. J. NUTT, P. J. COWN, and H. J. LITTLE. Nature (London), **295**, 436 (1982).
4. J. H. SKERRITT and R. L. MACDONALD. Neurosci. Lett. **43**, 321 (1983) and references therein.
5. R. F. SQUIRES and C. BRAESTRUP. Nature (London), **266**, 732 (1977).
6. H. SCHOEMAKER, R. G. BOLES, W. D. HORST, and H. I. YAMAMURA. J. Pharm. Exp. Ther. **225**, 61 (1983).
7. J. H. SKERRITT, M. A. WERZ, M. J. MCLEAN, and R. L. MACDONALD. Brain Res. **310**, 99 (1984) and references therein.
8. D. T. CROMER and J. B. MANN. Acta Crystallogr. Sect. A, **24**, 321 (1968).
9. R. F. STEWART, E. R. DAVIDSON, and W. T. SIMPSON. J. Chem. Phys. **42**, 3175 (1965).
10. A. CAMERMAN and N. CAMERMAN. J. Am. Chem. Soc. **94**, 268 (1972).
11. L. H. STERNBACH, L. O. RANDALL, R. BANIZER, and H. LEHR. Drugs affecting the central nervous system. *Edited by* A. Burger. Marcel Dekker, New York. 1968. p. 237.
12. A. CAMERMAN and N. CAMERMAN. Mechanisms of action of antiepileptic drugs. *Edited by* G. H. Glaser, J. K. Penry, and D. M. Woodbury. Raven Press, New York. 1980. p. 223.
13. P. W. CODDING and A. K. MUIR. Mol. Pharmacol. **28**, 178 (1985).
14. R. H. DODD, L. C. OUANNES, A. CHIARONI, C. RICHE, G. POISSONNET, J. ROSSIER, G. DEVAUX, and P. POTIER. Mol. Pharmacol. **31**, 74 (1987).
15. D. N. STEPHENS, G. T. SHEARMAN, and W. KEHR. Psychopharmacology, **83**, 233 (1984).
16. P. MAIN, S. J. FISKE, S. E. HULL, L. LESSINGER, G. GERMAIN, J.-P. DECLERCQ, and M. M. WOOLFSON. Multan 80. A system of computer programs for the automatic solution of crystal structures from X-ray diffraction data. Universities of York, England, and Louvain, Belgium. 1980.
17. W. R. BUSING and H. A. LEVY. ORFLS. Oak Ridge National Laboratory Report ORNL-TM-305. 1962.

Can. J. Chem. Downloaded from www.nrcresearchpress.com by 118.98.75.50 on 09/07/12
For personal use only.

Caractérisation et spectres de vibration du sulpiride

LUC MAURY[1] ET JEAN-LOUIS DELARBRE
Laboratoire de physique industrielle pharmaceutique, Faculté de pharmacie, 11 avenue Charles Flahault, 34060 Montpellier CEDEX, France

ET

JOËLLE RAMBAUD ET BERNARD PAUVERT
Groupe polymorphisme et biodisponibilité, Faculté de pharmacie, 11 avenue Charles Flahault, 34060 Montpellier CEDEX, France

Reçu le 14 novembre 1986

LUC MAURY, JEAN-LOUIS DELARBRE, JOËLLE RAMBAUD et BERNARD PAUVERT. Can. J. Chem. **65**, 1613 (1987).

Les auteurs ont caractérisé deux formes du sulpiride par absorption infrarouge et diffusion Raman (vibrations du réseau). L'analyse des spectres a permis de proposer une attribution des vibrations caractéristiques des groupements amide et sulfonamide en relation avec les longueurs des liaisons hydrogène inter ou intra-moléculaires. La comparaison des spectres du chlorhydrate de sulpiride et du sulpiride indique que le chlorhydrate lui-même se présenterait sous forme chélatée.

LUC MAURY, JEAN-LOUIS DELARBRE, JOËLLE RAMBAUD, and BERNARD PAUVERT. Can. J. Chem. **65**, 1613 (1987).

The authors have characterized two forms for sulpiride by infrared spectroscopy and Raman scattering (lattice vibrations). An assignment of the fundamental vibrations of the amide and sulfonamide groups involved in the inter or intramolecular hydrogen bonds has been proposed. Comparison of the sulpiride chlorhydrate spectra with those of sulpiride indicates that the chlorhydrate itself will be in the chelated form.

Introduction

Lors de travaux antérieurs (1, 2), nous avons mis en évidence la nécessité de mettre en oeuvre des techniques variées et complémentaires afin de pouvoir distinguer polymorphisme et isomérie, notions très souvent confondues ou ignorées. Nous poursuivons actuellement ce même type d'études en série orthométhoxybenzamide et plus particulièrement sur le *N*-[(éthyl-1 pyrrolidinyl-2 méthyl]méthoxy-2 sulfamoyl-5 benzamide ou sulpiride.

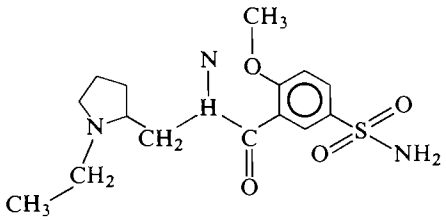

Le sulpiride, utilisé en thérapeutique comme régulateur de la vasomotricité de la muqueuse gastrique et comme antipsychotique majeur non sédatif, a fait l'objet d'études en relation avec le polymorphisme (3); cependant, la détermination des structures des deux formes a révélé qu'il s'agissait non de polymorphisme mais d'isomérie. Par ailleurs, il a été démontré que l'efficacité neuroleptique du sulpiride est en relation avec la stéréochimie de l'énantiomère (4–6) et qu'il existe une analogie de structure chimique (7) entre les orthométhoxybenzamides et d'autres familles de neuroleptiques. Le centre actif serait le noyau aromatique avec présence obligatoire d'un substituant, dont la position et la nature sont importantes, et un groupement azoté situé à une certaine distance du nuage électronique. Ces analogies structure–activité seraient liées à la formation d'une liaison hydrogène intramoléculaire, entre les groupements méthoxy et amide, constituant ainsi un pseudo-cycle à 6 chaînons, partiellement plan, branché sur le cycle aromatique (7–9). Il nous a donc paru intéressant d'entreprendre une étude spectrale des deux formes du sulpiride, racémique (R) et énantiomère dextrogyre (E) (les spectres du lévogyre et du dextrogyre ne pouvant être distingués), qui correspondent aux deux types de cristaux obtenus par recristallisation. Après les avoir caractérisés, nous discuterons l'attribution de certains modes fondamentaux, en relation avec les liaisons hydrogène inter- ou intramoléculaires. Par ailleurs, dans le domaine 4000–2000 cm^{-1}, nous envisagerons le cas des deux chlorhydrates correspondants.

1. Auteur à qui adresser toute correspondance.

Matériel et méthode

Produits

Le sulpiride base, racémique et énantiomère, est un produit Delagrange; à partir de ces produits nous avons préparé les deux chlorhydrates.

Des recristallisations à partir du sulpiride base ont été effectuées dans différents solvants : eau; alcools méthylique, éthylique, propylique, isopropylique, butylique, amylique; dioxanne; tétrahydrofuranne; acétone; chloroforme; dichloroéthane et dans deux mélanges de solvants : eau–éthanol et eau–acétone.

Spectrométrie d'absorption infrarouge

Les spectres infrarouges ont été enregistrés à température ambiante sur un spectromètre Perkin–Elmer 983 G; les échantillons étaient placés sous forme de pastille KBr.

Spectrométrie de diffusion Raman

Les spectres Raman des poudres cristallines ont été enregistrés sur un spectromètre Jobin Yvon «Ramanor HG2 S». La technique utilisée était celle de la diffusion à 90° en incidence normale. La radiation excitatrice est la raie 514.5 nm d'un laser Spectra Physics, modèle 164, à argon ionisé; la puissance sur l'échantillon était maintenue à 200 mW et aucune modification des échantillons n'a été observée.

Résultats et discussion

Recristallisations

Les recristallisations à froid des différentes solutions n'ont généralement donné que des résultats médiocres. En revanche, à partir de solutions saturées à chaud, trois types de cristallisations ont été obtenues : (*i*) cristallisation homogène : formée de cristaux d'aspect cubique (cristaux I) isolés à partir de solutions dans l'eau, l'acétone et les mélanges eau–éthanol ou eau–

Can. J. Chem. Downloaded from www.nrcresearchpress.com by 118.98.75.50 on 09/07/12
For personal use only.

Can. J. Chem. Downloaded from www.nrcresearchpress.com by 118.98.75.50 on 09/07/12
For personal use only.

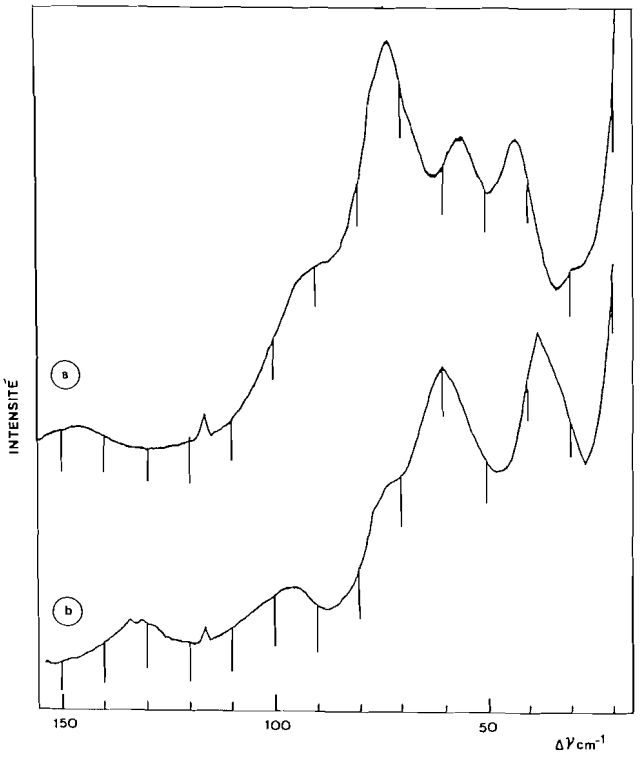

FIG. 1. Spectres Raman des vibrations du réseau du sulpiride; (*a*) racémique; (*b*) énantiomère.

acétone; ces cristaux correspondent au sulpiride racémique; (*ii*) cristallisation homogène : constituée de cristaux en forme de lamelles (cristaux II) obtenus à partir de solutions dans le méthanol ou le chloroforme; ils correspondent au sulpiride énantiomère; (*iii*) cristallisation hétérogène : apparaît comme un mélange des deux formes cristallines précédentes.

L'identification des cristaux I et II respectivement au racémique et à l'énantiomère a pu être réalisée grâce aux produits dont nous disposions : le sulpiride racémique et le sulpiride dextrogyre.

Diffusion Raman : vibrations du reseau cristallin

Les spectres Raman des vibrations du réseau (phonons) représentés sur la figure 1 permettent immédiatement de distinguer les formes (R) et (E); la première est caractérisée par quatre raies principales à 42, 55, 73 et 93 cm^{-1} alors que la seconde présente deux raies très intenses, à 38 et 60 cm^{-1}, accompagnées de massifs moins intenses à 72, 96 et 132 cm^{-1}.

Analyse vibrationnelle

Les spectres Raman (fig. 2) et infrarouge (fig. 3) du racémique et de l'énantiomère, dans le domaine des vibrations internes, présentent de très nombreuses différences à l'inverse de ce que l'on observe dans le cas de polymorphisme. Toutefois, les différences essentielles se manifestent au même niveau, c'est-à-dire au niveau des groupements impliqués dans des liaisons hydrogène. C'est pourquoi nous discuterons principalement les attributions de ces groupements, l'ensemble de nos propositions d'attribution étant reporté dans le tableau 1.

Structure cristalline

L'analyse des structures cristallines (8, 9) révèle que dans le racémique comme dans l'énantiomère, il existe une liaison hydrogène intramoléculaire de type N—H...O entre le proton amide et un doublet électronique de l'oxygène du groupement méthoxy, comme d'ailleurs dans un autre composé de cette série, le métoclopramide (7). Ces liaisons sont «bifurquées», les distances NH...O étant respectivement de 1,88 (R) et 2,10 Å (valeur moyenne pour les énantiomères). En outre, dans le racémique, deux liaisons hydrogène intermoléculaires sont présentes par l'intermédiaire des deux protons du groupement $-SO_2—NH_2$: ces deux liaisons, la première de type N---O, la seconde de type N---N, ont des longueurs de 2,88 et 2,94 Å. En revanche, dans l'énantiomère, une seule liaison de type N---O de longueur 2,86–3,00 Å se manifeste; dans les deux cas l'atome accepteur est l'oxygène du groupement carbonyle.

Analyse spectrale

Domaine 4000–2000 cm^{-1} : Les spectres Raman et infrarouge des deux composés (R) et (E) révèlent d'importantes modifications dans ce domaine spectral. Les vibrations de valence ν CH des groupements alkyle, méthoxy et aromatique (observées en deçà de 3100 cm^{-1}) ne seront pas discutées. Par contre, les vibrations de valence des groupements NH et NH_2 qui se traduisent par de fortes bandes infrarouges nécessitent une discussion.

En effet, si des corrélations entre les fréquences des vibrations de valence ν NH_2 d'un groupement amine et les longueurs des liaisons N---X (X = O, N) ont été établies (13), il n'en est pas de même pour ce qui concerne les vibrations de valence d'un groupement sulfonamide. Les résultats obtenus sur le sulpiride

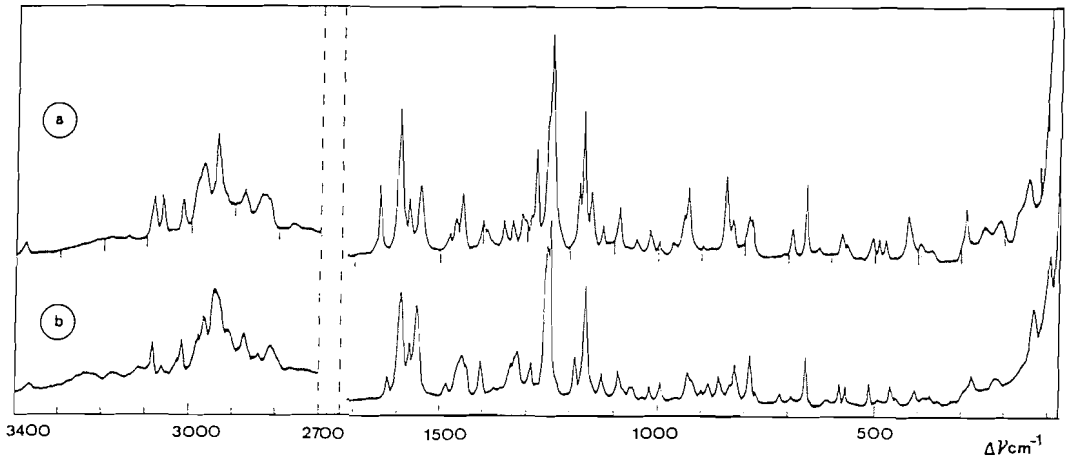

FIG. 2. Spectres Raman des vibrations internes du sulpiride; (*a*) racémique; (*b*) énantiomère.

Can. J. Chem. Downloaded from www.nrcresearchpress.com by 118.98.75.50 on 09/07/12
For personal use only.

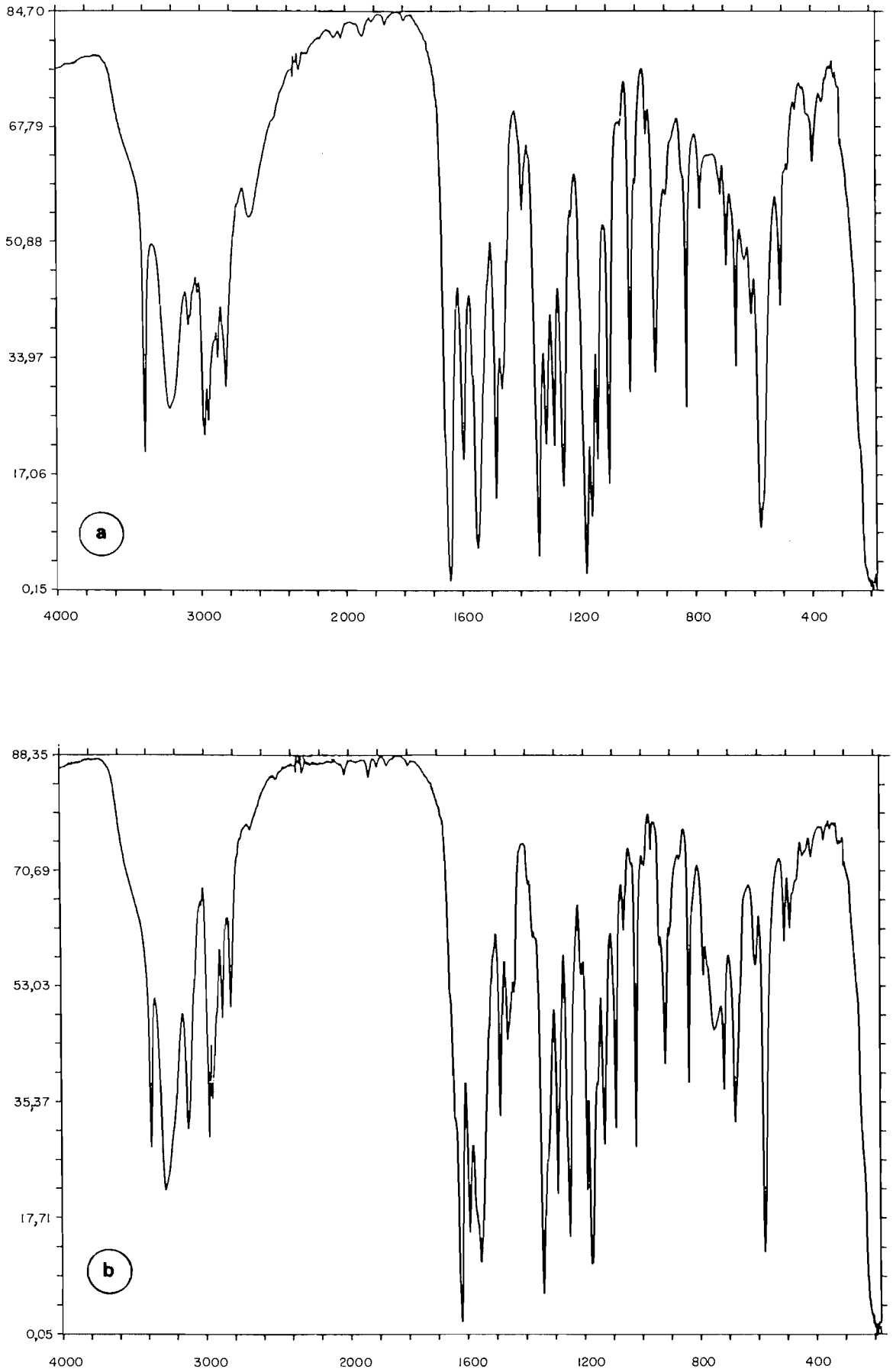

FIG. 3. Spectres infrarouge du sulpiride; (*a*) racémique; (*b*) énantiomère.

Can. J. Chem. Downloaded from www.nrcresearchpress.com by 118.98.75.50 on 09/07/12
For personal use only.

TABLEAU 1. Fréquences fondamentales et propositions d'attribution du sulpiride racémique et enantiomère[a]

Racémique				Enantiomère				
Raman		Infrarouge		Raman		Infrarouge		Attributions[b]
3387	M	3387	FF	3365	M	3374	F	ν_{as} NH_2
		3220	FL			3280	FL	ν_s NH_2 + 2ν C=O
		3195	ep			3200	ep	
				3112	M	3120	F	ν NH
3081	M	3084	f	3082	F			ν ϕ CH
3065	M							
3017	M	3027	f	3015	F	3020	ep	ν CH (OCH_3)
2985	ep	2982	f	2977	ep	2970	F	ν CH_2, CH_3
2970	F	2969	M	2965	M			
2940	F	2942	M	2940	FF	2942	F	
				2907	M			
2875	M	2850	f	2872	F	2878	M	
2832	M	2824	M	2840	M			
				2812	M	2818	M	
1640	M	1643	FF	1622	M	1620	FF	Amide I
1580	FF			1590	FF	1590	F	ν 8a
1570	M			1567	M	1570	ep	ν 8b
1542	M	1548	FF	1552	FF	1555	FF	Amide II
1475	f	1481	F	1482	f	1488	F	
1462	M	1459	M	1450	F	1461	M	δ CH_2, δ CH_3
1447	M					1455	ep	
1400	M					1440	f	
1390	ep	1392	M	1405	F			
1352	M	1336	FF	1337	ep	1340	FF	ν_{as} SO_2
1332	M							
1310	M	1309	F	1325	M	1320	ep	Amide III
1290	ep	1291	F	1290	M	1290	F	ν_I ϕ—O—CH_3
1277	F							
1254	ep	1250	F	1255	F	1250	FF	ν_{II} ϕ—O—CH_3 + w CH_2
1242	FF			1247	F			
				1190	F	1190	F	ν_s SO_2
1177	M	1173	FF	1165	FF	1176	FF	
1167	F	1152	F					ν 9a
1152	M							
1135	M	1132	M	1127	M	1130	M	tw CH_2, w CH_2
1090	M	1091	F	1090	M	1090	F	r CH_2
1050	f	1050	f	1062	M	1060	M	ν C—N, tw NH_2
1017	M	1019	F	1017	f	1020	M	r CH_3
1000	f	1002	f	992	f	995	f	ν C—C
965	f	966	f			970	f	ν C—C (cycle pyrrolidine)
942	ep	934	F	930	M	930	ep	r CH_2
932	F			920	ep	920	F	
900	tf	900	f	900	tf	902	ep	Pulsation du cycle pyrrolidine
		875	ep	870	M	870	f	ν 17a
				860	M			ν 17b
845	F	840	ep	832	f	840	F	ν S—N
827	M	828	F	822	M			ν_{11}
790	M	782	M	785	M	790	M	ν_{III} ϕ—O—CH_3 + γ NH_2
785	ep					785	M	
		712	M	717	tf	717	F	

TABLEAU 1 (*concluded*)

Racémique				Enantiomère				Attributions[b]
Raman		Infrarouge		Raman		Infrarouge		
690	M	692	M	690	tf			ν_4
						678	F	
660	F	658	F	657	M			ν 6b
		607	M	610	f	610	M	Déformation du cycle pyrrolidine
575	M	580	FF	580	M	580	FF	δSO_2
565	f	570	ep	552	M			
505	f	506	M	510	M	510	M	ν_V ϕ—O—CH_3
490	f			487	tf			
		480	ep			490	M	Déformation
475	f			460	M			
420	M					420	f	ν_{IV} ϕ—O—CH_3
392	f	394	M	407	M			ν_{VI} ϕ—O—CH_3

[a]FF = très fort; F = fort; M = moyen; f = faible; ep = épaulement.
[b]Pour les bandes attribuées au noyau aromatique (ϕ) on a adopté la notation de Wilson.

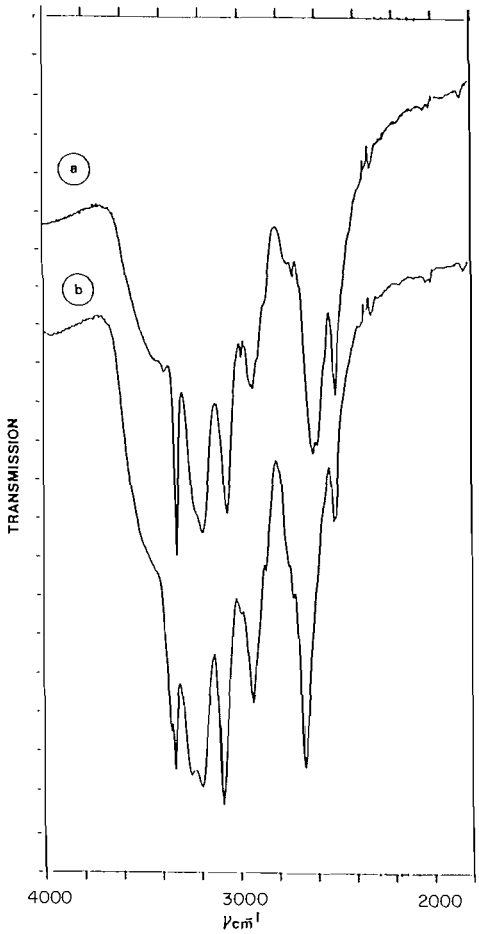

FIG. 4. Spectres infrarouge du sulpiride chlorhydrate (4000–2000 cm^{-1}); (*a*) racémique; (*b*) énantiomère.

peuvent toutefois être rapprochés de ceux obtenus sur des composés renfermant le même groupement $-SO_2 \cdot NH_2$ (10).

Contrairement à ce qui est observé dans les sulfamides (1, 2, 10) les spectres du sulpiride, qui renferme également un groupement sulfonamide, ne révèlent pas deux bandes fines et intenses caractéristiques des vibrations ν_{as} NH_2 et ν_s NH_2. La raie fine et intense située entre 3320 et 3380 cm^{-1} selon le composé (base ou chlorhydrate (fig. 4), racémique ou énantiomère), est attribuée au mode antisymétrique ν_{as} NH_2. La bande large et intense vers 3200 cm^{-1} rend compte du mode symétrique ν_s NH_2; cette bande présente un épaulement qui est attribué à l'harmonique 2ν C=O qui vient perturber le mode ν_s NH_2. Les attributions de ces modes du groupement sulfonamide sont en accord avec celles proposées par Novak *et al.* (10) dans le cas du benzènesulfonamide et du sulfanilamide dans lesquels les liaisons N.....O ont des longueurs comparables à celles de type $NH_2 \ldots X$ (X = O, N) présentes dans le sulpiride.

Dans le cas du chlorhydrate (E), les modes sont dédoublés ce qui pourrait traduire l'existence de dimères cycliques comme cela a déjà été observé sur le sulfaméthoxypyridazine (11) ou le pentobarbital (12). Le mode ν NH amide, engagé dans la liaison hydrogène intramoléculaire, se manifeste par la bande située vers 3120 cm^{-1} (E), valeur proche de celle trouvée dans le sulfaméthoxozole (2), cette fréquence étant absente du spectre du sulpiride (R). Ceci peut être relié au fait que la distance NH....O est beaucoup plus courte dans le racémique (1,88 Å) que dans les énantiomères (moyenne des distances 2,10 Å).

La présence de cette bande dans les deux chlorhydrates est donc en faveur de l'existence de ces deux composés sous forme chélatée, ce que la détermination des structures devrait nous permettre de confirmer. Signalons que les bandes observées sur les spectres des chlorhydrates à 2627, 2600 et 2506 cm^{-1} (R) et à 2656 et 2512 cm^{-1} (E) sont caractéristiques des absorptions $NH^+ \ldots Cl^-$ (13, 14).

Domaine 2000–200 cm^{-1} : De très nombreuses vibrations apparaissent communes aux deux espèces et traduisent les vibrations du noyau aromatique (10) ou pyrrolidine (15). On observe toutefois que les fréquences traduisant les modes amide et sulfonamide sont perturbées.

Quelle que soit la forme (R ou E) du sulpiride, la bande amide I se traduit par des raies d'intensité forte ou moyenne en infrarouge ou en Raman. Cette bande apparaît à 1643 cm^{-1} (R) et à 1620 cm^{-1} (E) par suite de l'existence de liaisons N—H...O différentes.

En accord avec Toppart *et al.* (16) nous attribuons la bande 1548 cm^{-1} (R) et 1555 cm^{-1} (E) à la bande amide II.

Dans le domaine 1305–1250 cm^{-1} se situe la bande amide III mettant en jeu les modes δ NH et ν CN (17). L'attribution de cette bande est ici rendue difficile par suite de la présence, dans

Can. J. Chem. Downloaded from www.nrcresearchpress.com by 118.98.75.50 on 09/07/12
For personal use only.

ce domaine, du mode ν_{as} SO_2; cependant, il nous semble possible d'attribuer les bandes 1310 cm^{-1} (R) et 1320 cm^{-1} (E) à l'amide III, la raie très intense 1340 cm^{-1} traduisant le mode ν_{as} SO_2. Le mode ν_s SO_2 apparaît, comme cela est généralement observé, sous forme d'un doublet (10) très net à 1190–1176 cm^{-1} (E) et sous forme d'une raie intense 1177 cm^{-1} munie d'un épaulement à 1190 cm^{-1} (R). Le dernier mode du groupement sulfone concerne la déformation δ SO_2 très intense en absorption vers 580 cm^{-1} quel que soit le composé, alors que dans tous les sulfamides étudiés, ce mode se traduisait par un doublet très intense vers 540–576 cm^{-1}.

Les attributions proposées pour le groupement SO_2 montrent que ses vibrations apparaissent dans les deux composés aux mêmes fréquences, ce qui confirme l'absence de liaison hydrogène intéressant les atomes d'oxygène de ce groupement.

Les dernières vibrations discutées concernent le groupement méthoxy dont l'oxygène participe à la liaison hydrogène intramoléculaire. Pour le chaînon ϕ—O—CH_3, mis à part les modes des protons, on attend deux vibrations de valence, deux déformations dans le plan et deux hors du plan. Comme les masses des atomes C et O sont sensiblement voisines, ces vibrations provoquent des déplacements des atomes de carbone du cycle aromatique : en conséquence, des couplages sont observés (18) entre les vibrations du groupe méthoxy et celles du noyau aromatique, couplages qui donnent les vibrations d'ensemble notées de I à IV dont les attributions (tableau 1) sont en accord avec celles proposées sur des composés analogues (19–21).

1. L. Maury, J. Rambaud, B. Pauvert, Y. Lasserre, G. Berge et M. Audran. J. Pharm. Sci. **74**, 422 (1985).
2. L. Maury, J. Rambaud, B. Pauvert, Y. Lasserre, G. Berge et M. Audran. Can. J. Chem. **63**, 3012 (1985).
3. K. S. Kim et M. H. Lee. Yakhak Nommunjip, Seoul National University, **5**, 42 (1980).
4. C. O. Andrews, A. Davis, H. S. Freeman, J. D. McDermed, J. A. Poat et G. N. Woodruff. Br. J. Pharmacol. **64**, 433 (1978).
5. L. Garau, S. Govoni, E. Stefanini, M. Trabucchi et P. F. Spano. Life Sci. **23**, 1745 (1978).
6. L. I. Goldberg, J. D. Kohli, J. J. Litinsky et J. D. McDermed. Catecholamines: Basic and clinical frontiers: usdin. Pergamon Press, New York. 1979.
7. M. Cesaric, C. Pascard, M. El Moukhtari et L. Sung. Eur. J. Med. Chem. **16**, 13 (1981).
8. C. Houttemane, J. C. Boivin, G. Nowogrocki, D. J. Thomas et J. P. Bonte. Acta Crystallogr. Sect. B: Struct. Crystallogr. Cryst. Chem. **37**, 981 (1981).
9. L. Y. Y. Ma, N. Camerman et A. Camerman. Acta Crystallogr. Sect. B: Struct. Crystallogr. Cryst. Chem. **38**, 2861 (1982).
10. A. Novak, J. Lascombe et M. L. Josien. J. Phys. Colloq. **5**, 38 (1966).
11. L. Maury, J. Rambaud, B. Pauvert, G. Berge, M. Audran et Y. Lasserre. Pharm. Acta Helv. **60**, 22 (1985).
12. M. Draguet-Brughmans, R. Bouche, J. P. Flandre et A. Van den Bulcke. Pharm. Acta Helv. **54**, 140 (1979).
13. A. Novak. Struct. Bonding (Berlin), **18**, 177 (1974).
14. J. Bellamy. The infrared spectra of complex molecules. Chapman and Hall, London. 1975.
15. J. C. Evans et J. C. Wahr. J. Chem. Phys. **31**, 655 (1959).
16. J. Topart, M. Hanocq, M. Van Damme et L. Molle. Pharm. Acta Helv. **51**, 314 (1976).
17. S. Blanchard. J. Mol. Struct. **38**, 63 (1977).
18. K. W. F. Kohlrausch. Phys. Z. **30**, 58 (1936).
19. J. M. Lebas. J. Chim. Phys. **59**, 1072 (1962).
20. M. T. Forel, C. Garrigou-Lagrange, J. Gemin et M. L. Josien. J. Chim. Phys. **1**, 1047 (1963).
21. M. Brigodiot et J. M. Lebas. J. Chim. Phys. **1**, 347 (1965).

Can. J. Chem. Downloaded from www.nrcresearchpress.com by 118.98.75.50 on 09/07/12
For personal use only.

Chemical and electrochemical reduction of pyrazino[2,3-*g*]quinoxalines and of their benzo and dibenzo derivatives; the structure of fluorindine and the formation of tetraanion

JOSEPH ARMAND AND LINE BOULARES
Laboratoire de physicochimie des solutions, E.N.S.C.P., 11 Rue Pierre et Marie Curie, 75231 Paris CEDEX 05, France

CHRISTIAN BELLEC
Laboratoire de chimie des hétérocycles, Université Pierre et Marie Curie, 4 Place Jussieu, 75230 Paris CEDEX 05, France

AND

JEAN PINSON
Laboratoire d'électrochimie, Université Paris VII, 2 Place Jussieu, 75251 Paris CEDEX 05, France

Received October 22, 1986

JOSEPH ARMAND, LINE BOULARES, CHRISTIAN BELLEC, and JEAN PINSON. Can. J. Chem. **65**, 1619 (1987).

The structure of fluorindine is established by nmr as the 5,14-dihydroquinoxalino[2,3-*b*]phenazine. The catalytic hydrogenation of 2,3-di(*p*-methoxyphenyl)pyrazino[2,3-*b*]phenazine **2***a* leads to the 6,11-dihydro derivative **4***a*. The electrochemical reduction in an hydroorganic medium furnishes **4***a* and then the 1,4,6,11-tetrahydro derivative **8***a*. In dry DMSO the voltammogram shows four monoelectronic reversible systems corresponding to the successive formation of a radical anion, dianion, radical trianion, and tetraanion. Thus **2***a* appears as a new example of the very restricted class of compounds leading to tetraanions upon electrochemical reduction. The catalytic hydrogenation of 2,7-diphenylpyrazino[2,3-*g*]quinoxaline **1***a* or the reaction of $LiAlH_4$ with 1,2,7,8-tetramethylpyrazino[2,3-*g*]quinoxaline **1***b* leads to 1,2,3,4-tetrahydro compounds. The electrochemical reduction of **1***a* and **1***b* in hydroorganic medium leads successively to 1,4-dihydro and then to 1,4,6,9-tetrahydro compounds which undergo a further rearrangement. In dry DMSO **1***a* and **1***b* behave differently from **2***a*: one only observes two reversible monoelectronic systems.

JOSEPH ARMAND, LINE BOULARES, CHRISTIAN BELLEC et JEAN PINSON. Can. J. Chem. **65**, 1619 (1987).

Par rmn on montre que la fluorindine est la dihydro-5,14 quinoxalino [2,3-*b*] phénazine. Par hydrogénation catalytique la di(*p*-methoxyphenyl)-2,3 pyrazino [2,3-*b*] phenazine **2***a* fournit le dérivé dihydro-6,11 **4***a*. La réduction électrochimique en milieu hydroorganique fournit **4***a* puis le dérivé tétrahydro-1,4,6,11 **8***a*. Dans le DMSO très sec le voltamogramme montre la présence de quatre pics monoélectroniques réversibles correspondant à la réduction successive en radical anion, dianion, radical trianion et enfin tétraanion : **2***a* est un nouvel exemple de composés – très peu nombreux – susceptibles d'engendrer un tétraanion par réduction électrochimique. L'hydrogénation catalytique de la diphényl-2,7 pyrazino [2,3-*g*] quinoxaline **1***a* ou l'action de $AlLiH_4$ dans le cas de la tétraméthyl-1,2,7,8 pyrazino [2,3-*g*] quinoxaline **1***b* conduit au dérivé tétrahydro-1,2,3,4. La réduction électrochimique en milieu hydroorganique de **1***a* et **1***b* conduisent successivement aux dérivés dihydro-1,4 puis tétrahydro-1,4,6,9, ce dernier se réarrangeant. Dans le DMSO très sec **1***a* et **1***b* ont un comportement différent de celui de **2***a* puisqu'on observe seulement la présence de 2 pics monoélectroniques réversibles.

Can. J. Chem. Downloaded from www.nrcresearchpress.com by 72.64.146.136 on 09/07/12
For personal use only.

We have been interested for sometime in the chemical and electrochemical reduction of *N*-heterocyclic compounds (1, 2). We now report the behaviour of pyrazino[2,3-*g*]quinoxalines **1**, pyrazino[2,3-*b*]phenazines **2**, and quinoxalino[2,3-*b*]phenazines **3**. Through the examination of such a series of compounds, we intend to observe the modification of chemical and physicochemical properties with the increased number of cycles.

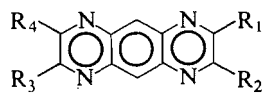

1

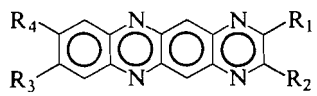

2

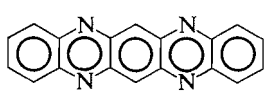

3

To our knowledge the reduction of **1** has not been studied previously, whereas that of **2** has been investigated for analytical purposes (3–5). In order to titrate traces of α-dicarbonyl derivatives, these compounds were reacted with 2,3-diaminophenazine to give **2** which was reduced by hypophosphorus acid into a dihydro derivative **4**. This last compound presents a strong visible absorption ($\lambda_{max} \simeq 600$ nm). The structure **4′** of **4**, i.e., a quinonoïd 1,6-dihydro derivative, was assigned on the basis of this visible absorption (3–5).

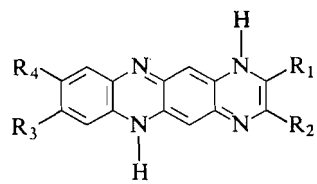

4′

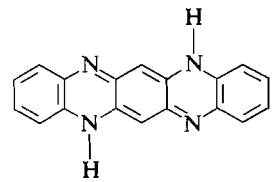

5′

In the same way a quinonoïd structure was assigned to fluorindine **5** and its derivatives which have been used as a drug (8) and as an acid–base indicator (9). Fluorindine **5** has been given a 5,12-dihydroquinoxalino[2,3-*b*]phenazine structure **5′** by all previous authors (6–9).

Structure of fluorindine **5**

This compound is a dihydro derivative of quinoxalino-[2,3-*b*]phenazine **3** which has not yet been prepared; the oxidation of **5** leads only to a quinone (6, 7), and **5** is very slightly soluble in all solvents. It was, however, possible to

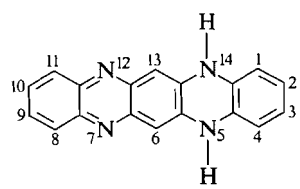

5

TABLE 1. Nuclear magnetic resonance data[a] for **4***a* and **5**

Compound		δ		
4*a*	O—CH_3	3.75	s	6H
	5-H,12-H	6.25	s	2H
	7-H,8-H	6.10–6.60	AA′BB′	4H
	9-H,10-H		pattern	
	3′-H,5′-H	6.82	d	4H
	3″-H,5″-H			
	2′-H,2″-H	7.25	d	4H
	6′-H,6″-H			
	6-H,11-H	8.80	s[b]	2H
5	6-H,13-H	6.34	s	2H
	8-H,9-H	6.50–6.60	AA′BB′	4H
	10-H,11-H		pattern	
	1-H,2-H	7.42–7.66	AA′BB′	4H
	3-H,4-H		pattern	
	7-H,12-H	9.75	s[b]	2H

[a]Solvent DMSO-d_6; δ values in ppm relative to internal TMS.
[b]Broad signal exchanged with D_2O.

obtain a well-resolved 250-MHz spectrum in DMSO-d_6 after 1000 accumulations. The nmr data are given in Table 1.

This spectrum unambiguously shows that fluorindine has structure **5**, i.e., it is a 5,14-dihydro derivative and not a 5,12-dihydro compound as previously stated.

Protons 1, 2, 3, and 4 form an AA′BB′ pattern analogous to that of 5,10-dihydrophenazine (6.06–6.70 ppm); the chemical shifts of these protons are significantly lower than that of benzene (7.23 ppm). It is known that in a benzene ring the electronic effects of the amino groups on the *ortho* and *meta* protons amount to a shielding of several tenths of a ppm (e.g., in *o*-phenylene diamine the benzene protons give a singlet at 6.70 ppm). This also explains the chemical shift of H_6 and H_{13} at 6.34 ppm. The 8, 9, 10, and 11 protons also give rise to an AA′BB′ pattern but at lower field and in the same region as the benzene protons of quinoxaline (δ = 7.7–8.2 ppm).

Neutral solutions of **5** are pink–violet whereas acidic solutions are blue. The pK_a of the protonated form measured by spectrophotometry is 2.30. Fluorindine can be reduced by Zn + Ac_2O to give 5,7,12,14-tetraacetyl 5,7,12,14-tetrahydroquinoxalino[2,3-*b*]phenazine (6).

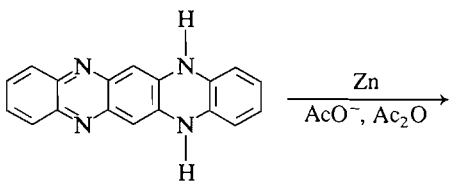

5

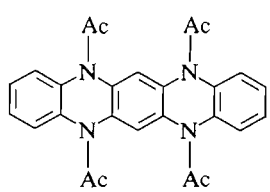

*Reduction of pyrazino[2,3-*b*]phenazine*

Catalytic hydrogenation in the presence of Pd/C of 2,3-di(*p*-methoxyphenyl)pyrazino[2,3-*b*]phenazine **2***a* gives a dihydro compound **4***a*. The nmr spectrum shows that **4***a* is the 6,11-dihydro-2,3-di(*p*-methoxyphenyl)pyrazino[2,3-*b*]phenazine.

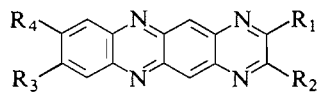

2*a*
$R_1 = R_2 = p\text{-}OCH_3C_6H_4$
$R_3 = R_4 = H$

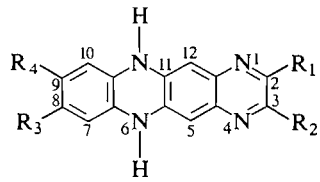

4*a*
$R_1 = R_2 = p\text{-}OCH_3C_6H_4$
$R_3 = R_4 = H$

The equivalence of 5-H and 12-H protons and the observation of an AA′BB′ pattern for 7-H, 8-H, 9-H, 10-H permit one to exclude structure **4′** which corresponds to a 1,6-dihydro derivative. Besides, the chemical shifts of 7-H, 8-H, 9-H, and 10-H are located between 6.10 and 6.60 ppm; this demonstrates that the two NH protons are on the 6 and 11 positions. If they had been on the 1,4 positions, protons 7-H, 8-H, 9-H, and 10-H would have shown an AA′BB′ pattern between 7.4 and 7.7 ppm (as in the case of **5** discussed above).

Reduction of **2***a* in dilute solution by zinc in acetic acid, by electrochemistry, or by H_3PO_2 — following the experimental procedure used during the titration of α-dicarbonyl compounds (3–5) — also leads to **4***a* (as shown by polarography) and not to a 1,6-dihydro derivative as had been postulated before. Reductions with $LiAlH_4$ furnished complex mixtures which could not be separated.

Electrochemical reduction of **2***a* has also been investigated.

In a water–DMF medium (40–60), **2***a* shows a two-electron wave which is pH dependent between pH 4 and 10 ($E_{1/2}$(V) = +0.30–0.06 pH). In more acidic or more basic media, **2***a* becomes unstable. The first wave is followed by a second pH-dependent two-electron wave: $E_{1/2}$(V) = +0.06–0.06 pH. Electrolysis of a dilute solution of **2***a* at pH 8 at a potential corresponding to the first plateau gives the dihydro derivative **4***a* as shown by comparison of the polarogram of the solution with that of the hydrogenation product under the same conditions. Electrolysis on the second plateau of **2***a*, i.e., at a potential corresponding to the reduction of **4***a*, furnishes an easily oxidizable compound which gives an anodic wave whose $E_{1/2}$ value is near that of the second cathodic wave of **2***a*.

The voltammogram of **2***a* at pH 7 ($v = 0.2\ V\ s^{-1}$) shows two reversible two-electron peaks at $E^0 = -0.075$ V and $E^0 =$

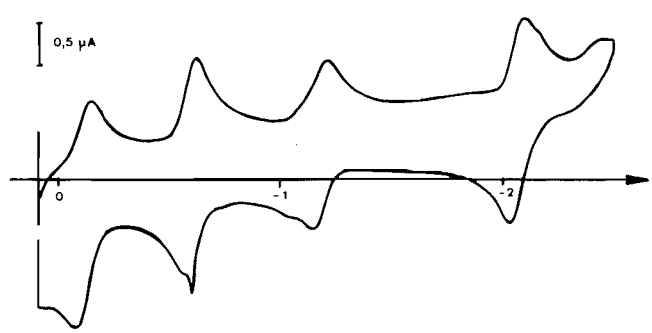

FIG. 1. Voltammogram of **2***a*, $c = 5 \times 10^{-4}$ *M*, in DMSO dried over Al_2O_3, 10^{-1} *M* NEt_4ClO_4, $v = 250\ mV\ s^{-1}$; reference: sce.

Can. J. Chem. Downloaded from www.nrcresearchpress.com by 72.64.146.136 on 09/07/12
For personal use only.

Can. J. Chem. Downloaded from www.nrcresearchpress.com by 72.64.146.136 on 09/07/12
For personal use only.

-0.825 V, the first one showing a spiky shape indicative of a reactant adsorbed on the electrode.

In view of our preceding results concerning the electrochemical reduction of compounds containing a pyrazine ring (1, 10, 11), we propose the following reduction scheme for **2***a*:

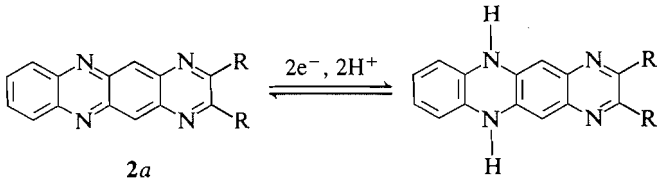

2*a*
R = *p*-$OCH_3C_6H_4$

4*a*

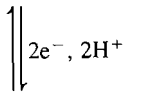

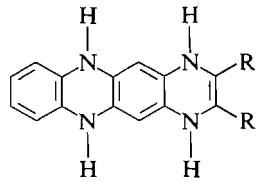

8*a*

The first reversible system observed on the voltammogram corresponds to the reduction **2***a* $\rightleftharpoons$ **4***a* whereas the second reversible system corresponds to **4***a* $\rightleftharpoons$ **8***a*. We have indeed shown previously (1, 10, 11) that compounds with a pyrazine ring are reversibly reduced to 1,4-dihydro pyrazines. Thus, at the difference of most 1,4-dihydro-compounds, no rearrangement of the primary reduction product is observed in pyrazino[2,3-*b*]phenazines. In aprotic medium (very dry DMSO) the cyclic voltammogram of **2***a* shows four perfectly reversible one-electron peaks ($E_{p_c} - E_{p_i} = 60$ mV) located at $E_1^0 = -0.03$ V, $E_2^0 = -0.51$ V, $E_3^0 = -1.09$ V, $E_4^0 = -2.00$ V corresponding to the successive formation of a radical anion, a dianion, a radical trianion, and a tetraanion (Fig. 1). We are presently trying to obtain these species in order to investigate their charge distribution through the examination of their nmr and esr spectra.

Reduction of pyrazino[2,3-g]quinoxalines: 1

Catalytic hydrogenation (Pd/C) of 2,7-diphenylpyrazino-[2,3-*g*]quinoxaline **1***a* furnishes a 1,2,3,4-tetrahydro derivative **6***a*.

In the case of 1,2,7,8-tetramethylpyrazino[2,3-*g*]quinoxaline **1***b*, one obtains only decomposition products, one of which is biacetyl.

Reduction by $LiAlH_4$ leads to the *cis*-1,2,3,4-tetrahydro **6***b* in the case of **1***b* and to a complex mixture in the case of **1***a*.

Reduction by zinc and acetic acid leads to a compound which can also be obtained by electrochemical reduction (see below); the polarograms of both solutions are identical. This compound, which is very oxidizable and could not be isolated without reoxidation, is most likely the 1,4-dihydro derivative **7**.

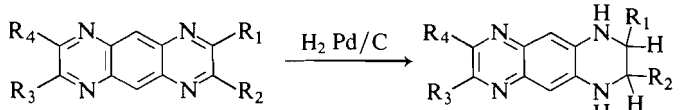

1*a* $R_1 = R_3 = C_6H_5$, $R_2 = R_4 = H$
1*b* $R_1 = R_2 = R_3 = R_4 = CH_3$

6*a* $R_1 = R_3 = C_6H_5$, $R_2 = R_4 = H$
6*b* $R_1 = R_2 = R_3 = R_4 = CH_3$

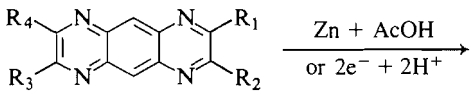

1*a*
1*b*

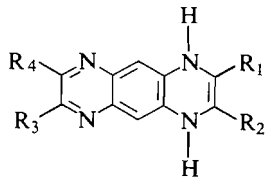

7*a*
7*b*

Electrochemical reduction of **1***a* and **1***b* has also been investigated.

In a water–DMF medium (50–50) **1***a* presents a two-electron wave which is pH dependent between pH 2 and 12: $E_{1/2}$ (V) = $+0.1 - 0.090$ pH from pH 2 to pH 3.7, corresponding to reduction to a protonated form of **7**, and $E_{1/2}$ (V) = 0.00–0.063 pH from pH 3.7 to pH 12, where **7** is obtained. This wave is followed by a second two-electron wave distorted by adsorption phenomena; this wave is pH-dependent between pH 2 and 12: $E_{1/2}$ (V) = $-0.37 - 0.073$ pH. Electrolysis of a dilute solution of **1***a* at pH 7.25 at a potential corresponding to the first plateau gives a readily oxidizable compound which presents an anodic wave whose $E_{1/2}$ is near that of the first cathodic wave of **1***a*. Electrolysis at a potential corresponding to the second plateau of **1***a* furnishes a compound which does not give any anodic wave. A voltammogram of **1***a* at pH 7.25 (0.06 V s^{-1}) shows two reversible 2e peaks located at $E^0 = -0.44$ V and $E^0 = -0.91$ V. Compound **1***b* shows similar behaviour: the first two-electron wave is pH-dependent between pH 2 and 12: $E_{1/2}$ (V) = 0.08–0.095 pH from pH 2 to pH 5.75 and $E_{1/2}$ (V) = $-0.11 - 0.062$ pH from pH 5.75 to pH 12. This first wave is followed by a second two-electron wave which is pH-dependent between pH 2 and 12: $E_{1/2}$ (V) = $-0.55 - 0.060$ pH, and this wave is distorted by adsorption phenomena. Electrolysis of **1***b* in dilute solution gives the same results as **1***a*. A voltammogram of **1***b* at pH 7.25 ($v = 0.06$ V s^{-1}) shows a first set of cathodic–anodic waves where the cathodic peak is located at $E_{p_c} = -0.60$ V and the anodic peak at $E_{p_a} = -0.49$ V; the lack of reversibility of this system is probably due both to a slow electron transfer and to adsorption phenomena, the cathodic peak is broad and symmetrical. The second set of cathodic–anodic waves is reversible: $E^0 = -0.95$ V.

In view of the similarity of these results with those already obtained for **2***a*, it appears that **1***a* and **1***b* are first reduced to a 1,4-dihydro derivative and then to a 1,4,6,9-tetrahydro compound. The 1,4-dihydro compound is responsible for the first anodic wave observed during electrolysis in dilute solutions and for the first anodic wave on the voltammogram. The 1,4,6,9-tetrahydro derivative corresponds to the second anodic peak on the voltammogram but rearranges to nonoxidizable compound as shown by the electrolysis of the dilute solution. Indeed, we have shown before (1, 10, 11) that pyrazine rings are reduced in a protic medium to 1,4-dihydropyrazine rings, giving rise to a more or less reversible system. The very low solubility of **1***a* and **1***b* prevented us from carrying out a preparative electrolysis in order to isolate the rearranged products.

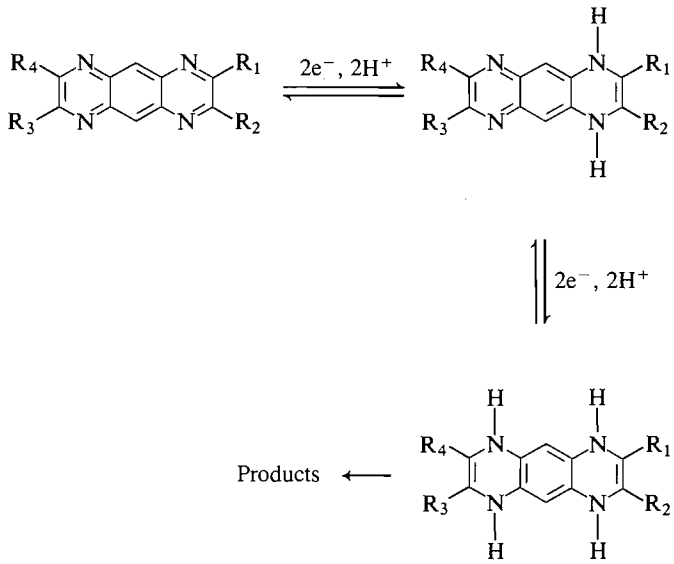

In aprotic medium (DMSO or DMF) **1***a* presents (at 0.2 V s^{-1}) two reversible waves located at $E_1^0 = -0.90$ V (DMSO and DMF) and at $E_2^0 = -1.51$ V (DMF) or $E_2^0 = -1.46$ V (DMSO) corresponding to the formation of a radical anion and a dianion. An electrolysis in dry DMSO on the second wave of this system leads to a dark solution which can be reoxidized by air. **1***a* is recovered as shown by cyclic voltammetry and thin-layer chromatography. In acetonitrile two reversible waves are observed at $E_1^0 = -0.89$ V and $E_2^0 = -1.37$ V followed by a two-electron irreversible wave at $E_{p_c} = -2.12$ V. In DMSO **1***b* gives rise to two reversible electron-transfer processes at $E_1^0 = -1.30$ V and $E_2^0 = -1.85$ V.

Discussion

Although the study of such highly conjugated nitrogen heterocycles is rendered difficult by their low solubility and the oxidability of the reduced compounds, some interesting features can be seen. In a hydroorganic medium, the pyrazine rings are reduced one by one, always leading to compounds where the two nitrogens of the same ring are hydrogenated. In an aprotic medium, they lead when the conjugation is extended enough (i.e., with four cycles) through the stepwise addition of electrons to a tetraanion. Very few such species are known: bianthryl (12) leads to a tetraanion through a pair of two-electron transfers, the two anthracene rings behaving independently. Other examples include acepleiadylene (13), cyclophanes (14), and annulenes (15) which have been obtained by addition of alkali metals. Electrochemical methods should permit us to prepare more selectively the different reduced species. This is currently in progress in our laboratories.

Experimental

Melting points are uncorrected. ^{1}H-nmr spectra were recorded on a Bruker WH 80, a Varian A 60, and a Bruker 250-MHz spectrometer using tetramethylsilane (TMS) as internal standard. The apparatus and techniques used for the electrochemical studies and pH measurements have been described previously (11). All potentials referred to saturated calomel electrode (sce); the temperature of the solution was 20°C. Dimethylsulfoxide used in the cyclic voltammetric experiments was distilled under vacuum, deoxygenated with nitrogen, and dried over phosphorus pentoxide. The calomel electrode was separated from the solution by a bridge filled with dry DMSO. The microanalyses were performed by the "Service de microanalyse, Université Pierre et Marie Curie". The following abbreviations are used in reporting nmr results: s = singlet, d = doublet, t = triplet, q = quadruplet, m = multiplet. All the described compounds gave correct elemental analysis.

Preparation of **1**a, **1**b, **2**a, *and* **5**

2,7-Diphenylpyrazino[2,3-g]quinoxaline **1**a. A mixture of phenylglyoxal hydrate (1.07 g), 1,2,4,5-tetraaminobenzene tetrahydrochloride (1 g), and sodium acetate trihydrate (1.92 g) in 50 mL of ethanol was stirred at room temperature for 2 h. The solid material was filtered, washed with water and ethanol, and dried to give 930 mg (79%) of **1***a*. Melting point 215°C dec. ^{1}H-nmr ($CDCl_3$): 2-Ph + 7-Ph, m, 7.55 ppm (6H) and 8.26 ppm (4H); 5-H, 10-H, s, 8.88 ppm (2H); 3-H, 8-H, s, 9.40 ppm (2H).

1,2,7,8-Tetramethylpyrazino[2,3-g]quinoxaline, **1**b was obtained (16) by condensation of diacetyl and 1,2,4,5-tetraamino benzene.

2,3-Di(p-Methoxyphenyl)pyrazino[2,3-b]phenazine, **2**a was prepared according to ref. 17, using 4,4′-dimethoxybenzil instead of benzil. Yield 11%, mp 220°C dec. ^{1}H-nmr ($CDCl_3$): O-CH_3, s, 3.91 ppm (6H); 3′-H, 5′-H, 3″-H, 5″-H, d, 6.91 ppm (4H); 2′-H, 2″-H, 6′-H, 6″-H, d, 7.65 ppm (4H); 7-H, 8-H, 9-H, 10-H, AA′BB′ pattern at 7.82 and 8.27 ppm (2 × 2H); 5-H, 12-H, s, 9.17 ppm (2H).

Fluoridine **5** was prepared according to ref. 6.

Hydrogenation of **2**a*: preparation of* **4**a. A catalytic hydrogenation was carried out at room temperature with 150 mg of **2***a* in 25 mL of dimethylformamide in the presence of 100 mg of 10% Pd/C. After 3 h of stirring and consumption of one mole of H_2 per mole of **2***a*, the solution was filtered, poured into 150 mL of water, and then extracted with $CHCl_3$. The extracts were dried over Na_2SO_4 and evaporated to give 60 mg of **4***a*. Melting point 230°C dec.

Hydrogenation of **1**a*: preparation of* **6**a. A catalytic hydrogenation was carried out at room temperature with 250 mg of **1***a* in 70 mL of dimethylformamide in the presence of 100 mg of Pd/C. After 5 h of stirring and consumption of two moles of H_2 per mole of **1***a*, the solution was filtered, washed with water, and dried to give 195 mg of **6***a* (77%). Melting point 263–265°C dec. ^{1}H-nmr (DMSO-d_6 + D_2O): 3-CH_2, m, 4.52 ppm (2H); 5-H + 10-H, 2d, 6.81 ppm and 6.94 ppm (2H); 2-H + 2-Ph + 7-Ph, m, 7.0–8.2 ppm (11H); 8-H, s, 8.76 ppm (1H).

Reduction with $LiAlH_4$ *of* **1**b*: preparation of* **6**b. $LiAlH_4$ (400 mg) was added slowly to a solution of **1***b* (300 mg) in freshly distilled tetrahydrofuran (50 mL). After 7 h of stirring at room temperature, the mixture was quenched with 5 mL of water and filtered. Tetrahydrofuran was evaporated and the solid which precipitated was filtered, washed with water, and dried. Compound **6***b*: 200 mg (65%). Melting point 268–270°C dec. ^{1}H-nmr ($CDCl_3$): N_1—H + N_2—H, br.s. exchanged with D_2O, 2.20 ppm (2H); 7-CH_3 + 8-CH_3, s, 2.65 ppm (6H); 2-H, 3-H, m, 3.70 ppm (2H); 5-H, 7-H, s, 7.00 ppm (2H).

1. (*a*) J. Armand, L. Boulares, C. Bellec, and J. Pinson. Can. J. Chem. **60**, 2797 (1982); **62**, 1028 (1984); (*b*) J. Armand and J. Pinson. Physical methods in heterocyclic chemistry. John Wiley, New York. 1984. p. 427.
2. J. Armand, K. Chekir, N. Ple, G. Queguiner, and M. P. Simonnin. J. Org. Chem. **46**, 4754 (1981) and references therein.
3. J. M. Dechary, E. Kun, and H. C. Pitot. Anal. Chem. **26**, 449 (1954).
4. E. Sawicki, T. R. Hauser, and R. Wilson. Anal. Chem. **34**, 505 (1962).
5. T. Kawashima and M. Tanaka. Anal. Chim. Acta, **40**, 137 (1968).
6. G. M. Badger and R. Pettit. J. Chem. Soc. 3211 (1952).
7. M. A. Fox and T. A. Voynick. J. Org. Chem. **46**, 1235 (1981).
8. C. Tie-Min, F. Zhao-Xia, and C. Ji-Quiao. Pei Ching I. M. Sueh Ydan Hsuem Pao, **12**, 262 (1980); Chem. Abstr. **94**, 175048*q* (1981).

Can. J. Chem. Downloaded from www.nrcresearchpress.com by 72.64.146.136 on 09/07/12
For personal use only.

9. R. R. GUPTA, S. K. JAIN, and K. G. OJHA. Ann. Soc. Sci. Bruxelles, Ser. 1, **92**, 233 (1978).
10. J. ARMAND, L. BOULARES, K. CHEKIR, and C. BELLEC. Can. J. Chem. **59**, 3237 (1981).
11. J. ARMAND, K. CHEKIR, and J. PINSON. Can. J. Chem. **56**, 1804 (1978) and references therein.
12. (*a*) O. HAMMERICH and J. M. SAVEANT. J. Chem. Soc. Chem. Commun. 938 (1979); (*b*) W. HUBER and K. MÜLLEN. J. Chem. Soc. Chem. Commun. 698 (1980).
13. B. CH. BECKER, W. HUBER, and K. MÜLLEN. J. Am. Chem. Soc. **102**, 7805 (1980).
14. K. MÜLLEN, W. HUBER, T. MEUL, M. NAGAKAWA, and M. IYODA. J. Am. Chem. Soc. **104**, 5403 (1982).
15. K. MÜLLEN, H. UNTERBERG, W. HUBER, O. WENNERSTÖM, U. NORINDER, D. TANNER, and B. THULIN. J. Am. Chem. Soc. **106**, 7514 (1984).
16. R. NIETZKI and E. MÜLLER. Ber. **20**, 440 (1889).
17. O. FISCHER and E. HEPP. Ber. **23**, 841 (1890).

Can. J. Chem. Downloaded from www.nrcresearchpress.com by 72.64.146.136 on 09/07/12
For personal use only.

Electron transfer reactions. Reaction of Δ^2-oxazoline-5-ones and related substrates with potassium[1]

MOHAMMED MUNEER AND RAVINDRA K. TIKARE
Department of Chemistry, Indian Institute of Technology, Kanpur 208016, India

PRASHANT V. KAMAT
Radiation Laboratory, University of Notre Dame, Notre Dame, IN 46556, U.S.A.

AND

MANAPURATHU V. GEORGE
Department of Chemistry, Indian Institute of Technology, Kanpur 208016, India, and Radiation Laboratory and Department of Chemistry, University of Notre Dame, Notre Dame, IN 46556, U.S.A.

Received July 24, 1986[2]

MOHAMMED MUNEER, RAVINDRA K. TIKARE, PRASHANT V. KAMAT, and MANAPURATHU V. GEORGE. Can. J. Chem. **65**, 1624 (1987).

The reaction of several Δ^2-oxazolin-5-ones (**1***a–c*, **12**) and bioxazolinones (**17**, **26**) with potassium in THF has been investigated. Treatment of **1***a* with potassium in THF gave a mixture of dibenzamide (**11***a*), *N*-benzoyl-*C*-phenylglycine (**6***a*), and *C*-phenylglycine (**10***a*). A higher yield of **11***a* was obtained, together with benzoic acid (**9**), when the reaction of **1***a* was carried out in THF saturated with oxygen. The reaction of **1***b* gave a mixture of β-phenylalanine (**10***b*) and **9**, whereas **1***c* gave a mixture of *N*-benzoyl-*C*,*C*-diphenylglycine (**6***c*) and *N*-benzoyl-*C*,*C*-diphenylmethylamine (**5***c*). Similarly, the reaction of **12** gave a mixture of α-benzamidocinnamic acid (**15**) and **9**. The reaction of the bioxazolinone **17** with potassium gave a mixture of **11***a*, **6***a*, and **10***a*, along with an appreciable yield of 2,3,5,6-tetraphenylpyrazine (**25**), whereas **26** under analogous conditions gave a mixture of **15**, **6***b*, and benzamide (**29**). Reasonable mechanisms, involving the initial formation of radical anion intermediates and their subsequent transformation to give the observed products, have been suggested. Potassium superoxide oxidation of some of these substrates gives similar product mixtures. Cyclic voltammetric studies have been carried out to measure the reduction potentials of **1***a–c*, **12**, **17**, and **26** in the generation of their radical anions. The radical anions of these substrates were also generated pulse radiolytically in methanol and their spectra showed absorption maxima in the region 295–350 nm.

MOHAMMED MUNEER, RAVINDRA K. TIKARE, PRASHANT V. KAMAT et MANAPURATHU V. GEORGE. Can. J. Chem. **65**, 1624 (1987).

On a étudié la réaction de plusieurs Δ^2-oxazolinones-5 (**1***a–c*, **12**) et bioxazolinones (**17**, **26**) avec le potassium dans le THF. La réaction de **1***a* avec le potassium dans le THF conduit à un mélange de dibenzamide (**11***a*), de *N*-benzoyl *C*-phénylglycine (**6***a*) et de *C*-phénylglycine (**10***a*). Lorsqu'on a effectué la réaction de **1***a* dans du TFH saturé en oxygène, on a obtenu de l'acide benzoïque (**9**) et un meilleur rendement de **11***a*. La réaction du produit **1***b* conduit à un mélange de β-phénylalanine (**10***b*) et de composé **9**; par ailleurs, le composé **1***c* conduit à un mélange de *N*-benzoyl *C*,*C*-diphénylglycine (**6***c*) et de *N*-benzoyl *C*,*C*-diphénylméthylamine (**5***c*). De la même manière, la réaction du composé **12** conduit à un mélange d'acide α-benzamidocinnamique (**15**) et de composé **9**. La réaction de la bioxazolinone **17** avec le potassium conduit à un mélange de composés **11***a*, **6***a* et **10***a* aux côtés d'une quantité appréciable de tétraphényl-2,3,5,6 pyrazine (**25**); par ailleurs, le composé **26** soumis aux mêmes conditions conduit à un mélange des composés **15**, **6***b* et de benzamide **29**. On suggère des mécanismes raisonnables impliquant la formation initiale d'intermédiaires anions radicaux et leurs transformations subséquentes pour donner les produits observés. L'oxydation de quelques-uns de ces substrats par le superoxyde de potassium conduit à des mélanges réactionnels semblables. On a effectué des études de voltamétrie cyclique pour mésurer les potentiels de réduction des composés **1***a–c*, **12**, **17** et **26** lors de la génération de leurs radicaux anions. On a aussi généré les radicaux anions de ces substrats par radiolyse pulsée dans le méthanol; leurs spectres présentent des maxima d'absorption dans la région de 295–350 nm.

[Traduit par la revue]

Introduction

In a recent investigation (1), we examined the reactions of several 2(3*H*)-furanones and bifurandiones with potassium in THF and showed that several products, arising through the initial formation of radical anions and their subsequent reaction with oxygen, are formed in these cases. Thus the reaction of 3,3,5-triphenyl-2(3*H*)-furanone with potassium in THF, for example, gave a mixture of 4-oxo-2,2,4-triphenylbutanoic acid, 1,3,3-triphenyl-2-propen-1-one, and benzoic acid. The reaction of a bifurandione such as 2,2′,3,3′,4,4′-hexaphenyl-2,2′-bifuran-5,5′(2*H*,2′*H*)-dione with potassium, on the other hand, gave a mixture of a 2(5*H*)-furanone, 2,3-diphenylpropenoic acid, and benzoic acid. In this context, it was felt worthwhile to investigate the reaction of some representative Δ^2-oxazolin-5-ones and bioxazolinones with potassium in THF, to study the type of products formed in these cases and also their reaction pathways.

Results and discussion

We have examined, in the present studies, the reactions of 2,4-diphenyl-Δ^2-oxazolin-5-one (**1***a*), 4-benzyl-2-phenyl-Δ^2-oxazolin-5-one (**1***b*), 2,4,4-triphenyl-Δ^2-oxazolin-5-one (**1***c*), and 4-benzylidene-2-phenyl-Δ^2-oxazolin-5-one (**12**). In addition, the reactions of two bioxazolinones such as bi-4,4′-(2,4-diphenyl-Δ^2-oxazolin-5-one) (**17**) and bi-4,4′-(4-benzyl-2-phenyl-Δ^2-oxazolin-5-one) (**26**) have been investigated.

The reaction of **1***a* with potassium in THF, for example, gave

[1]Document No. NDRL-2793 from the Notre Dame Radiation Laboratory.

[2]Revision received February 25, 1987.

Can. J. Chem. Downloaded from www.nrcresearchpress.com by 118.98.75.50 on 09/07/12
For personal use only.

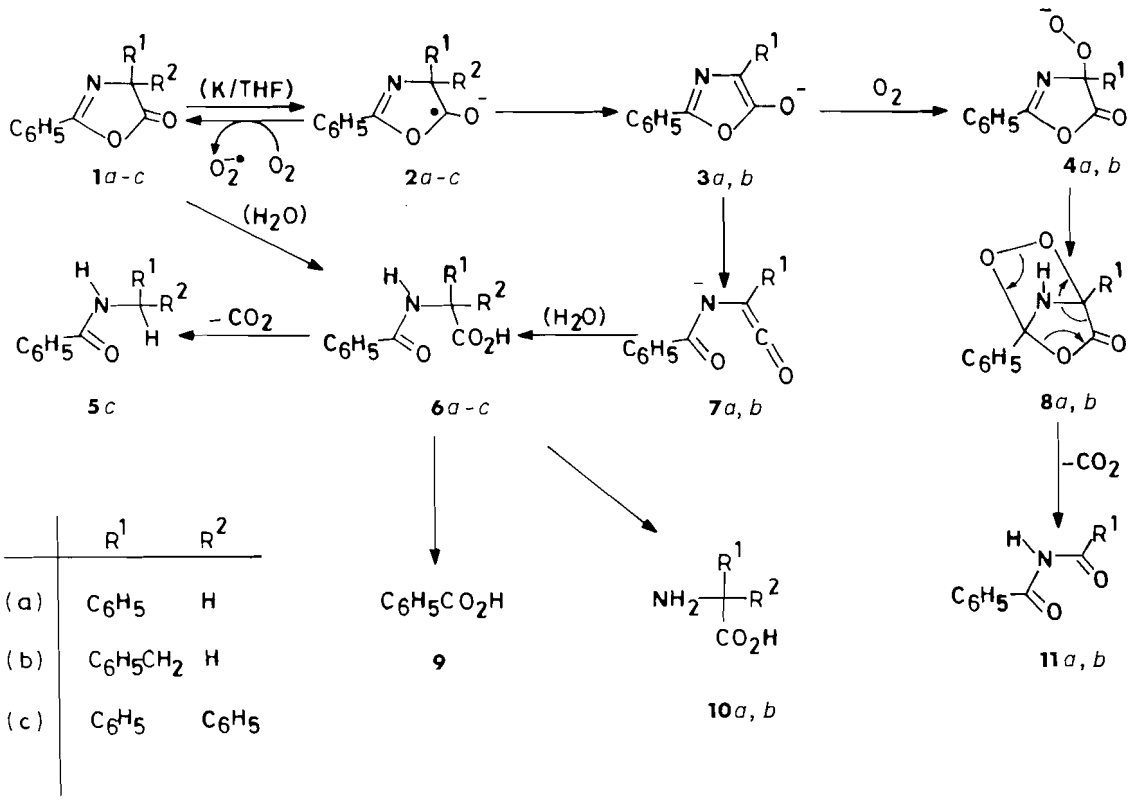

SCHEME 1.

a mixture of dibenzimide (**11***a*), *N*-benzoyl-*C*-phenylglycine (**6***a*), and *C*-phenylglycine (**10***a*). When the reaction of **1***a* with potassium, however, was carried out in THF saturated with oxygen, a much higher yield of **11***a* was obtained, along with appreciable amounts of benzoic acid (**9**). The reaction of **1***b* with potassium in THF gave a mixture of β-phenylalanine (**10***b*) and benzoic acid. Under analogous conditions, the reaction of **1***c* with potassium in THF gave a mixture of *N*-benzoyl-*C*,*C*-diphenylglycine (**6***c*) and *N*-benzoyl-*C*,*C*-diphenylmethylamine (**5***c*). On the other hand, when the reaction of **1***c* with potassium was carried out in THF saturated with oxygen, a mixture of **6***c*, **5***c*, and benzoic acid was formed.

The formation of the different products in the reaction of **1***a–c* with potassium in THF could be understood in terms of the pathway shown in Scheme 1. It has been assumed that the initial step in the reaction involves an electron transfer process leading to the formation of the radical anions **2***a–c*, which can, through the loss of a hydrogen atom, give the anionic intermediates **3***a*,*b*. These intermediates **3***a*,*b*, in turn, can lead to the carboxylic acids **6***a*,*b*, through the corresponding ketene intermediates **7***a*,*b*. The carboxylic acids **6***a–c* can also be directly formed from **1***a–c*, under hydrolytic conditions of work-up. Products such as **5***c*, **9**, and **10***a*,*b* in these reactions, however, could arise through the further transformations of **6***a–c*. The formation of **11***a*,*b*, on the other hand, could be understood in terms of the reaction of **3***a*,*b* with oxygen, under work-up conditions, to give the hydroperoxy intermediates **4***a*,*b*, which will then lead to the observed products through the endoperoxides **8***a*,*b*. The fact that enhanced yields of **11***a* were obtained in the reaction of **1***a* with potassium in THF saturated with oxygen, and also when treated with potassium superoxide in benzene containing 18-crown-6, would support the involvement of oxygen and superoxide in the transformations of **1***a–c*, as implicated in Scheme 1. It may be pointed out here that recent studies by Bates *et al.* (2) have shown that 4-isopropyl-2-phenyl-Δ^2-oxazolin-5-one and 4-benzyl-2-phenyl-Δ^2-oxazolin-5-one are readily converted to the corresponding acyclic imides, *N*-isobutyrylbenzimide and *N*-(phenylacetyl)benzamide, respectively, on bubbling oxygen gas through their solutions in dimethyl sulfoxide. The formation of the cyclic imides corresponding to **11***a*,*b* in these reactions has been explained in terms of hydroperoxy intermediates, analogous to **4***a*,*b* (Scheme 1). Similarly, Warnhoff and co-workers (3) have shown that oxygen reacts with 4-alkylidene-2-phenyl-Δ^2-oxazolin-5-ones in the presence of triethylamine to give the corresponding imides, again arising through hydroperoxy intermediates, analogous to **4***a*,*b*, shown in Scheme 1. The reaction of **1***b* with potassium superoxide and 18-crown-6 in benzene likewise gave a mixture of the oxygenated products *N*-benzoylphenylacetamide (**11***b*), *N*-benzoyl-β-phenylalanine (**6***b*), and benzoic acid (**9**), whereas the reaction of **1***c* with potassium superoxide and 18-crown-6, under analogous conditions, gave an excellent yield of *N*-benzoyl-*C*,*C*-diphenylglycine (**6***c*). It may be mentioned in this connection that recent studies by Chuaqui *et al.* (4) have shown that the reaction of potassium superoxide with Δ^2-oxazolin-5-ones gives different products depending on the substituents present in the oxazolinone ring system. Thus, the reaction of 4,4-dimethyl-2-phenyl-Δ^2-oxazolin-5-one with potassium superoxide gave the ring-opened product, *N*-benzoyl-α-aminoisobutyric acid, whereas the reaction of 4-ethyl-2-phenyl-Δ^2-oxazolin-5-one gave a mixture of *N*-benzoyl-α-aminobutyric acid and *N*-benzoylpropionamide. The formation of the ring-opened α-aminoacid derivatives in these reactions has been explained in terms of the initial nucleophilic attack of the superoxide on the starting Δ^2-oxazolin-5-ones, followed by further transformation. The formation of *N*-benzoylpropionamide in the reaction of 4-ethyl-2-phenyl-Δ^2-oxazolin-5-one, however, has been explained in

Can. J. Chem. Downloaded from www.nrcresearchpress.com by 118.98.75.50 on 09/07/12
For personal use only.

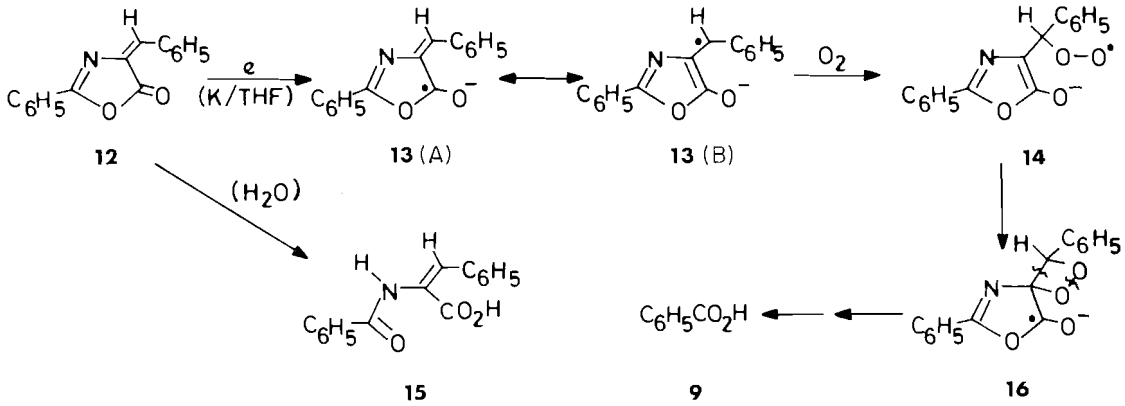

SCHEME 2.

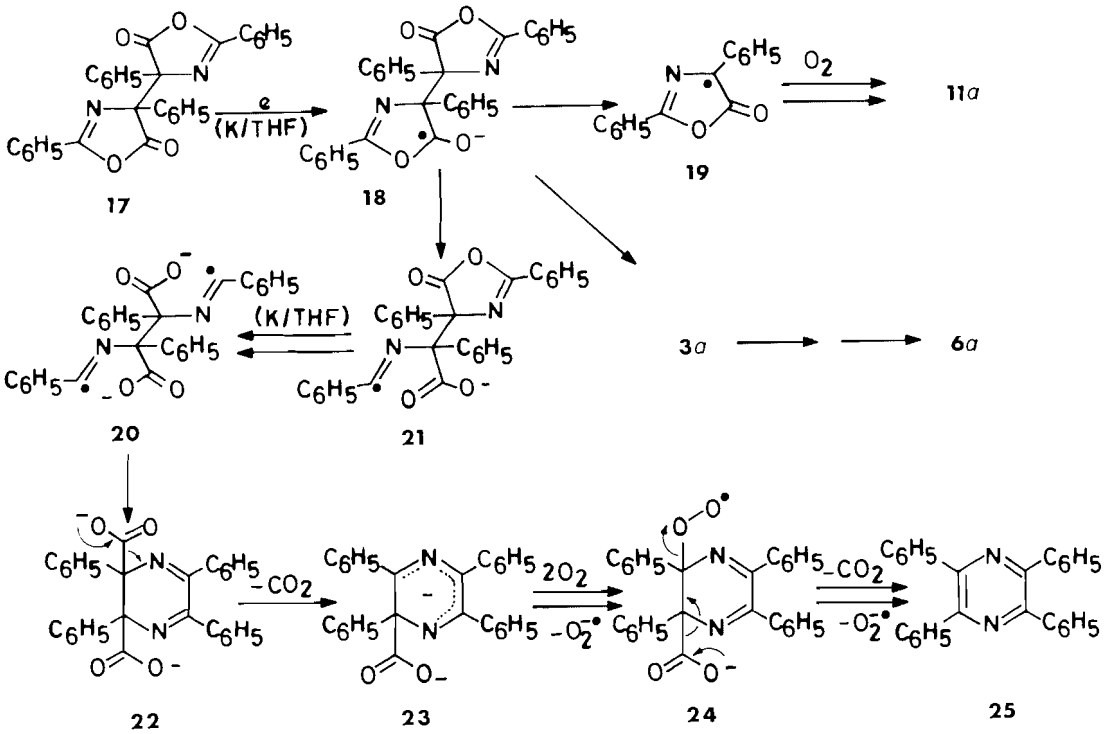

SCHEME 3.

terms of a 1,3-dipolar cycloaddition of singlet oxygen to the N-protonated zwitterionic form of the oxazolinone, followed by the loss of CO_2 and further transformations. We feel that under our reaction conditions the pathway shown in Scheme 1, involving the radical anion intermediates **2***a–c*, may be operative (see later reports on cyclic voltammetric and pulse radiolysis studies).

The reaction of 4-benzylidene-2-phenyl-Δ^2-oxazolin-5-one (**12**) with potassium in THF gave a mixture of α-benzamidocinnamic acid (**15**) and benzoic acid (**9**). The formation of these products, on the basis of analogy to the reactions of other Δ^2-oxazolinones, can be rationalized in terms of the pathway shown in Scheme 2.

The reaction of a bioxazolinone such as **17** with potassium in THF gave a mixture of dibenzimide (**11***a*), *N*-benzoyl-*C*-phenylglycine (**6***a*), *C*-phenylglycine (**10***a*), and 2,3,5,6-tetraphenylpyrazine (**25**) (Scheme 3), whereas the reaction of **26** with potassium in THF gave a mixture of α-benzamidocinnamic acid (**15**), *N*-benzoyl-β-phenylalanine (**6***b*), and benzamide (**29**) (Scheme 4). The reaction of **26** with potassium superoxide and 18-crown-6, however, gave a mixture of **15** and benzoic acid (**9**). The formation of the different products in the reaction of **17** and **26** with potassium in THF could be rationalized in terms of the pathways shown in Schemes 3 and 4. The initially formed radical anion **18** in the case of **17**, for example, could undergo fragmentation to give both the radical **19** and the anionic species **3***a*, which in turn could lead to **11***a* and **6***a*, respectively, as shown in Scheme 3. The radical anion intermediate **18** could also undergo transformation to give **21**, which could ultimately lead to 2,3,5,6-tetraphenylpyrazine (**25**), through the intermediates **20**, **22**, **23**, and **24**, as shown in Scheme 3. It may be pointed out here that **25** has also been reported to be formed from **17** in small amounts under thermal conditions (5). Similarly the radical anion **27**, formed from **26**, could lead to the different products as shown in Scheme 4.

Cyclic voltammeric studies

As highlighted in our earlier studies (20), electrochemical investigations would prove valuable in the characterization of radical anions, the primary intermediates involved in the

Can. J. Chem. Downloaded from www.nrcresearchpress.com by 118.98.75.50 on 09/07/12
For personal use only.

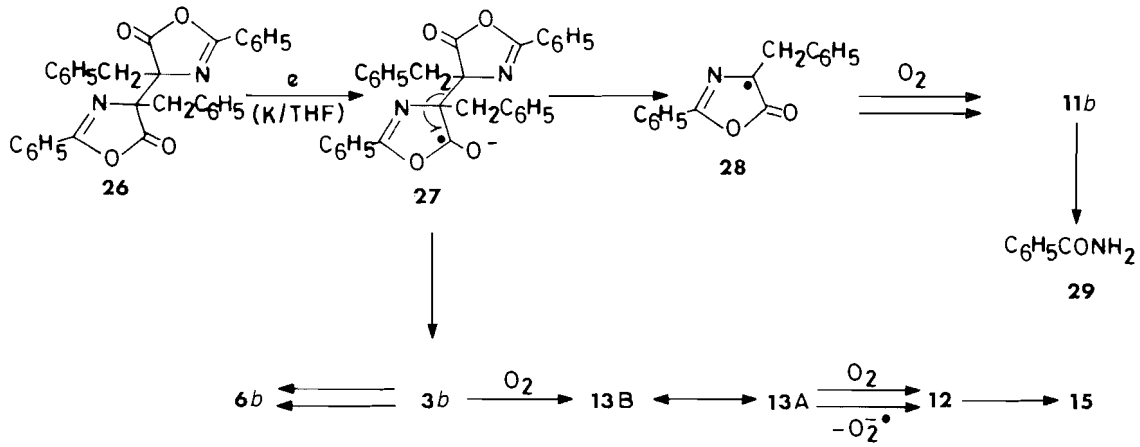

SCHEME 4.

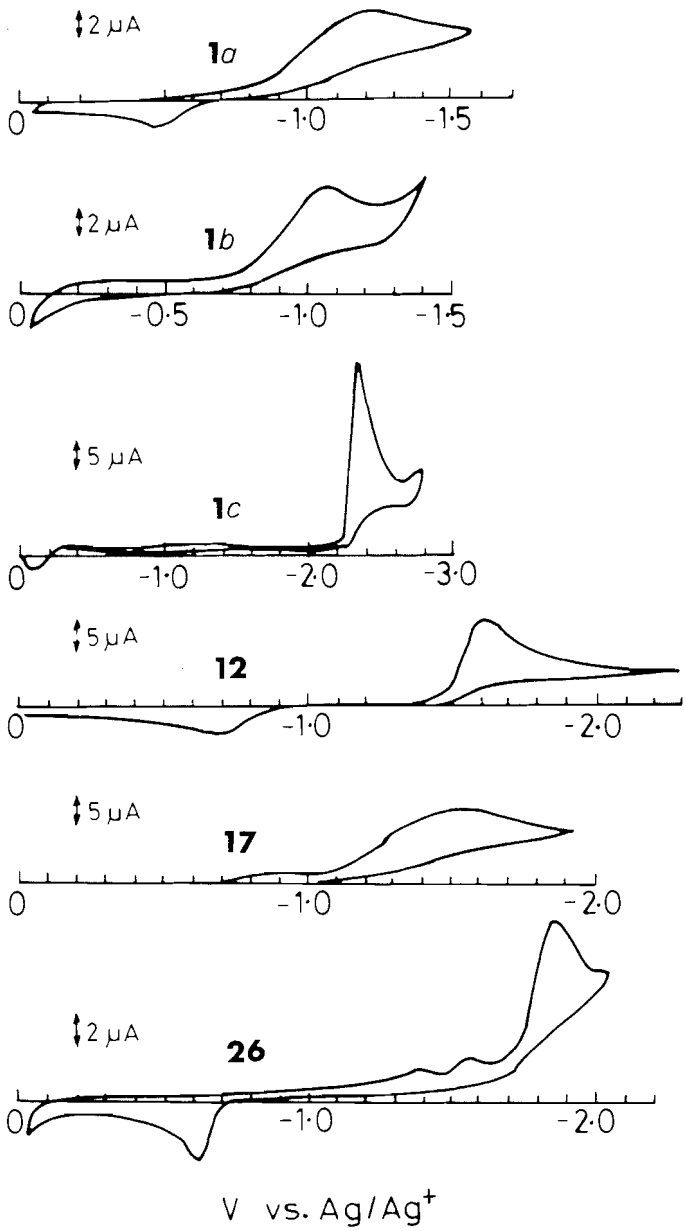

FIG. 1. Cyclic voltammograms of **1***a–c*, **12**, **17**, and **26** in deaerated acetonitrile containing 0.1 *M* tetrabutylammonium perchlorate (TBAP). Sweep rate was 200 mV/s.

reaction of different unsaturated organic substrates with potassium in THF. In the present study, we have generated electrochemically the radical anions of the Δ^2-oxazolin-5-ones **1***a–c*, **12**, and the bioxazolinones **17** and **26**, the substrates under investigation. The cyclic voltammograms of **1***a–c*, **12**, **17**, and **26** are shown in Fig. 1 and the reduction peak potentials are summarized in Table 1. All the substrates exhibited irreversible reduction peaks with the reduction potentials in the range of -0.9 to -2.35 V versus Ag/Ag^+ reference.

Pulse radiolysis studies

It has been reported earlier that the radical anions of unsaturated organic compounds can be generated through their reaction with solvated electrons (e_s^-) under pulse radiolytic conditions (6–8). In the present study, the radical anions of the Δ^2-oxazolin-5-ones **1***a–c* and **12** and the bioxazolinones **17** and **26** were generated pulse radiolytically in methanol, and their absorption spectra are presented in Fig. 2. These radical anions exhibited strong absorption maxima in the region of 295–350 nm and were shortlived in methanol ($\tau_{1/2}$ = 2.3–214 μs). As is evident from Table 1, these radical anions are formed from their appropriate precursors through reaction with solvated electrons under diffusion controlled rates.

Experimental

All melting points are uncorrected and were determined on a Mel-Temp apparatus. Petroleum ether was the fraction with bp 60–80°C. THF was dried over sodium and distilled immediately before use. Gold label (Aldrich) acetonitrile was used for cyclic voltammetric studies and spectral grade methanol (Fisher Scientific) was used for pulse radiolysis.

Starting materials

2,4-Diphenyl-Δ^2-oxazolin-5-one (**1***a*) (5*b*), mp 104–105°C; 4-benzyl-2-phenyl-Δ^2-oxazolin-5-one (**1***b*) (9), mp 69–70°C; 2,4,4-triphenyl-Δ^2-oxazolin-5-one (**1***c*) (10), mp 136–137°C; 4-benzylidene-2-phenyl-Δ^2-oxazolin-5-one (**12**) (11), mp 165–166°C; bi-4,4′-(2,4-diphenyl-Δ^2-oxazolin-5-one) (**17**) (12, 13), mp 193–194°C; and bi-4,4′-(4-benzyl-2-phenyl-Δ^2-oxazolin-5-one) (**26**) (12, 13), mp 209–210°C, were prepared by reported procedures.

Reaction of Δ^2-oxazolin-5-ones **1**a–c *with potassium in THF*

A general procedure was to shake 5.0 mmol of the appropriate Δ^2-oxazolin-5-one with potassium (10 mmol) in dry THF (125 mL) for several hours in a stoppered flask. A few clean, broken glass pieces were added to the mixture to ensure a fresh surface of the metal throughout the reaction. The reaction mixture underwent pronounced color changes, indicative of the formation of radical anion inter-

Can. J. Chem. Downloaded from www.nrcresearchpress.com by 118.98.75.50 on 09/07/12
For personal use only.

TABLE 1. Electrochemical, spectral, and kinetic data of **1***a–c*, **12**, **17**, and **26**

	Reduction peak potential,[a] E_p (V vs. Ag/Ag^+)	Absorption maxima (nm)		$k^{b,c}$ (10^{10} M^{-1} s^{-1})	$\tau_{1/2}{}^{b,d}$ (μs)
		Starting material[a]	Radical anion[b]		
1*a*	−1.05	235	315	1.1	4.5
1*b*	−1.10	240, 340, 360, 380	295	1.6	2.6
1*c*	−2.35	247	295	1.6	2.3
12	−1.56	258, 344, 360, 380	390	2.0	2.3
17	−0.9, −1.33, −1.55	222	310	1.1	5.3
26	−1.4, −1.58, −1.87	244	350	1.5	214.0

[a]In acetonitrile containing 0.1 *M* tetrabutylammonium perchlorate.
[b]In methanol.
[c]Rate constant for the reaction of the substrate with solvated electron in methanol.
[d]Half-life of the radical anion in methanol.

Can. J. Chem. Downloaded from www.nrcresearchpress.com by 118.98.75.50 on 09/07/12
For personal use only.

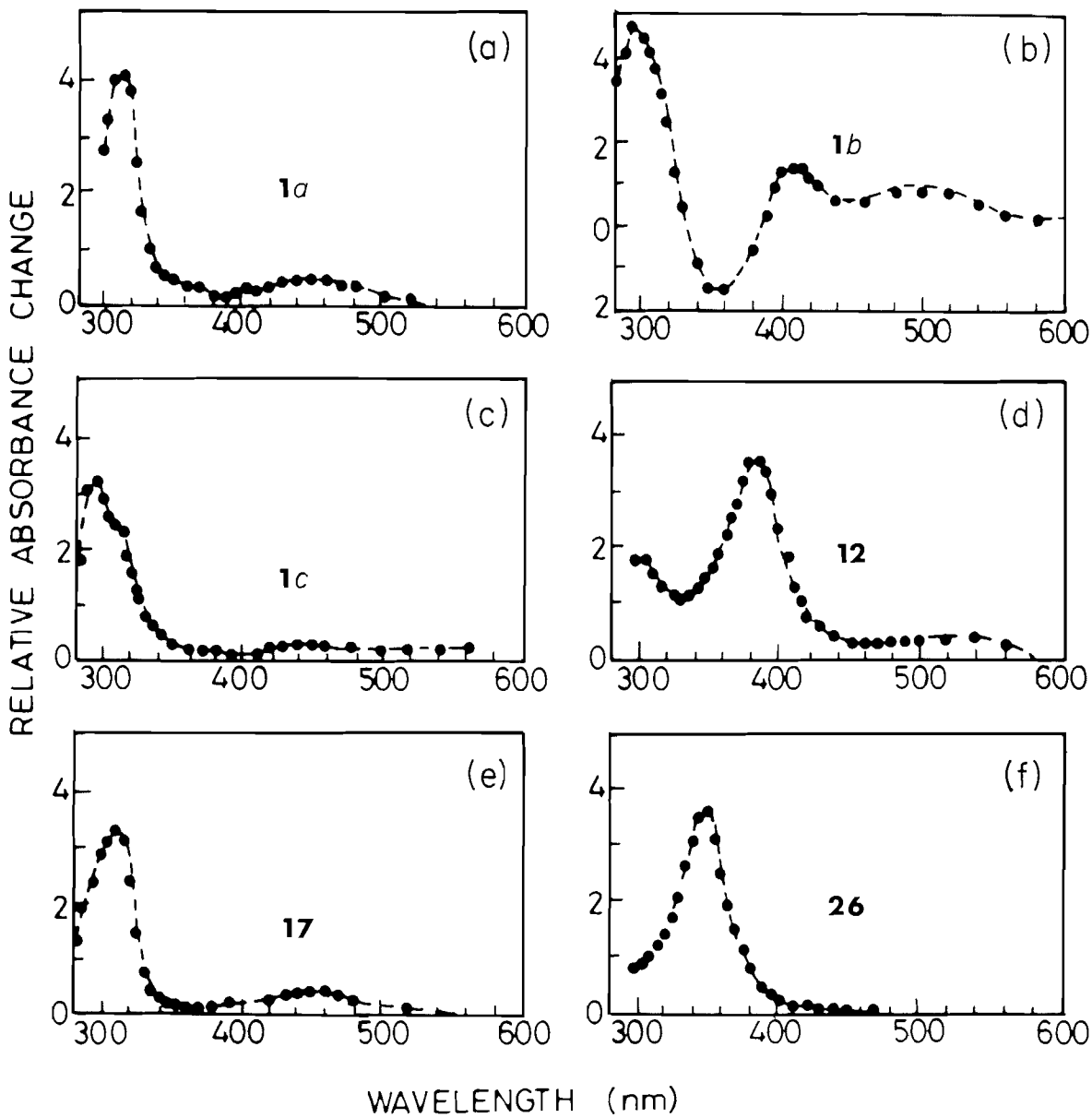

FIG. 2. Absorption spectra of the pulse radiolytically generated radical anions from **1***a* (a), **1***b* (b), **1***c* (c), **12** (d), **17** (e), and **26** (f) in nitrogen saturated methanol, observed at 0.04 μs after the electron pulse.

Can. J. Chem. Downloaded from www.nrcresearchpress.com by 118.98.75.50 on 09/07/12
For personal use only.

mediates. On completion of the reaction, the mixture was poured into moist THF (100 mL) to destroy any unchanged potassium and the solvent was removed under vacuum. The residual solid was treated with water (10 mL) and extracted with ethyl acetate. Work-up of the organic layer by removal of the solvent under vacuum and fractional crystallization from suitable solvents gave some of the reaction products. Acidification of the aqueous layer with dilute hydrochloric acid, followed by work-up in the usual manner, gave some of the acidic products, which were purified by recrystallization from suitable solvents.

Reaction of **1**a

Treatment of **1***a* (1.2 g, 5.0 mmol) with potassium (0.39 g, 10 mmol) in THF for 4 h and work-up in the usual manner gave 140 mg (12%) of dibenzamide (**11***a*) (solid from ethyl acetate extract was fractionally crystallized from benzene), mp 144–145°C (mixture mp) (14); 250 mg (33%) of *C*-phenylglycine (**10***a*) (mother liquor after removal of **11***a* was evaporated under vacuum and the residual solid was recrystallized from ethanol), mp 270–280°C (mixture mp) (15); and 350 mg (27%) of *N*-benzoyl-*C*-phenylglycine (**6***a*) (acidification of the aqueous layer with dilute hydrochloric acid and recrystallization from ethanol), mp 117–178°C (mixture mp) (5*b*).

Treatment of **1***a* (500 mg, 2.1 mmol) with potassium (160 mg, 4.1 mmol) in THF saturated with oxygen (100 mL) for 10 h and work-up in the usual manner gave 190 mg (40%) of **11***a* (extraction of the reaction mixture with methylene chloride, chromatographing the residual solid over alumina, elution with ethyl acetete – benzene (4:6), and recrystallization from benzene), mp 144–145°C (mixture mp), and 80 mg (32%) benzoic acid (**9**) (acidification of the aqueous layer with dilute hydrochloric acid and recrystallization from hot water), mp 120–121°C (mixture mp).

Reaction of **1**b

Treatment of **1***b* (1.25 g, 5.0 mmol) with potassium (0.39 g, 10 mmol) in THF for 4 h and work-up in the usual manner gave 200 mg (33%) of benzoic acid (**9**) (acidification of the aqueous layer with dilute hydrochloric acid and recrystallization from hot water), mp 120–121°C (mixture mp); 300 mg (37%) of β-phenylalanine (**10***b*) (removal of the solvent under vacuum from the ethyl acetate extract and fractional crystallization from ethanol), mp 284–288°C (mixture mp); and 70 mg (6%) of recovered starting material **1***b* (mother liquor after removal of **10***b* was evaporated under vacuum and recrystallized from petroleum ether).

Reaction of **1**c

Treatment of **1***c* (1.56 g, 5.0 mmol) with potassium (0.39 g, 10 mmol) in THF for 45 h and work-up in the usual manner gave 0.5 g (30%) of *N*-benzoyl-*C*,*C*-diphenylglycine (**6***c*) (extraction of the reaction mixture with methylene chloride, removal of the solvent under vacuum, and recrystallization from benzene), mp 166–167°C (mixture mp) (10), and 0.81 g (57%) of *N*-benzoyl-*C*,*C*-diphenylmethylamine (**5***c*) (acidification of the aqueous layer with dilute hydrochloric acid and recrystallization from ethanol), mp 191–192°C (mixture mp) (10).

Treatment of **1***c* (0.4 g, 1.28 mmol) with potassium (80 mg, 2 mmol) in THF saturated with oxygen (100 mL) for 6 h and work-up in the usual manner gave 80 mg (19%) of **6***c*, mp 166–167°C (mixture mp); 250 mg (68%) of **5***c*, mp 191–192°C (mixture mp); and 50 mg (32%) of benzoic acid (**9**), mp 120–121°C (mixture mp).

*Reaction of 4-benzylidene-2-phenyl-Δ^2-oxazolin-5-one (**12**) with potassium in THF*

A mixture of **12** (1.15 g, 4.6 mmol) and potassium (0.39 g, 10 mmol) was shaken in THF (125 mL) for 3 h and poured into moist THF (100 mL). Removal of the solvent under vacuum gave a solid, which was treated with water (10 mL) and extracted with methylene chloride. Acidification of the aqueous layer gave 0.48 g (39%) of α-benzamidocinnamic acid (**15**), mp 222–224°C (mixture mp) (16), after recrystallization from ethanol. The mother liquor on concentration gave 0.22 g (39%) of benzoic acid (**9**), mp 120–121°C, after recrystallization from hot water. Removal of the solvent from the methylene chloride extract gave 0.1 g (9%) of the unchanged starting material (**12**), mp 165–166°C (mixture mp).

*Reaction of bi-4,4'-(2,4-diphenyl-Δ^2-oxazolin-5-one) (**17**) with potassium in THF*

A mixture of **17** (0.94 g, 2.0 mmol) and potassium (0.25 g, 6.4 mmol) was shaken in THF for 5 h. Work-up as in the earlier cases by treatment with moist THF and removal of the solvent under vacuum gave a solid, which was treated with water (10 mL) and extracted first with benzene and later with ethyl acetate. Removal of the solvent from the benzene extract gave 0.15 g (17%) of dibenzimide **11***a*, mp 144–145°C (mixture mp). Removal of the solvent from the ethyl acetate extract gave 80 mg (14%)[3] of *C*-phenylglycine (**10***a*), mp 270–280°C (mixture mp), after recrystallization from ethanol. The mother liquor on evaporation gave 0.31 g (41%) of 2,3,5,6-tetraphenylpyrazine (**25**), mp 248–249°C (mixture mp) (17), after recrystallization from ethanol. Acidification of the aqueous layer with dilute hydrochloric acid gave 80 mg (8%)[3] of *N*-benzoyl-*C*-phenylglycine (**6***a*), mp 177–178°C (mixture mp).

*Reaction of bi-4,4'-(4-benzyl-2-phenyl-Δ^2-oxazolin-5-one) (**26**) with potassium in THF*

A mixture of **26** (0.95 g, 1.9 mmol) and potassium (0.25 g, 6.4 mmol) in THF (125 mL) was shaken for 5 h. Work-up in the usual manner by treatment of the reaction mixture with moist THF and removal of the solvent under vacuum gave a solid, which was treated with water (10 mL) and extracted with benzene and later with ethyl acetate. Removal of the solvent from the benzene extract gave 0.2 g (20%)[3] of **15**, mp 222–224°C (mixture mp), after recrystallization from ethanol. Removal of the solvent from the ethyl acetate extract gave 0.15 g (15%) of **6***b*, mp 186–187°C (mixture mp), after recrystallization from methanol. The mother liquor was concentrated to give a solid, which was recrystallized from methanol to give 50 mg (11%)[3] of benzamide (**29**), mp 128–129°C (mixture mp).

Reaction of Δ^2-oxazolin-5-ones **1**a–c *with potassium superoxide*

A general procedure was to stir a mixture of 2 mmol of the appropriate Δ^2-oxazolin-5-one, 4 mmol of potassium superoxide, and 2 mmol of 18-crown-6 in benzene (100 mL) for 24 h at room temperature. On completion of the reaction, the excess of superoxide was destroyed by adding water (20 mL) and extracted with an aqueous solution of sodium chloride. The aqueous layer was acidified with dilute hydrochloric acid and extracted with suitable solvents to give some of the products. Work-up of the organic layer gave the remaining products.

Reaction of **1**a

A mixture of **1***a* (0.5 g, 2 mmol), potassium superoxide (0.29 g, 4.1 mmol), and 18-crown-6 (0.53 g, 2.1 mmol) was stirred for 24 h and worked up in the usual manner. The aqueous layer was acidified with dilute hydrochloric acid and extracted with ethyl acetate. Removal of the solvent under vacuum gave 40 mg (7%) of **6***a*, mp 177–178°C (mixture mp), after recrystallization from ethanol. Removal of the solvent from the organic layer gave 260 mg (55%) of **11***a*, mp 144–145°C (mixture mp), after recrystallization from benzene.

Reaction of **1**b

Treatment of **1***b* (0.4 g, 1.6 mmol) with potassium superoxide (0.22 g, 3.1 mmol) and 18-crown-6 (0.4 g, 1.6 mmol) in benzene (60 mL) for 24 h and work-up as in the earlier case gave 100 mg (23%) of **6***b* (acidification of the aqueous layer with dilute hydrochloric acid, extraction with ethyl acetate, and recrystallization from methanol), mp 186–187°C (mixture mp); 90 mg (46%) of **9** (concentration of the mother liquor and fractional crystallization from hot water), mp 120–121°C (mixture mp); and 80 mg (21%) of **11***b* (from organic layer), mp 129–130°C, after recrystallization from benzene (lit. (18) mp 129–130°C).

[3]Yield based on the assumption that one mole of the starting material gives two moles of the product.

Reaction of **1***c*

Treatment of a mixture of **1***c* (0.67 g, 2.1 mmol), potassium superoxide (0.56 g, 7.9 mmol), and 18-crown-6 (1.0 g, 3.9 mmol) in benzene for 24 h and work-up in the usual manner gave 0.6 g (85%) of **6***c* (acidification of the aqueous layer with dilute hydrochloric acid and recrystallization from ethanol), mp 166–167°C (mixture mp), and 70 mg (10%) of recovered starting material **1***c* (removal of the solvent from the organic layer under vacuum and recrystallization from ethanol).

*Reaction of bi-4,4'-(4-benzyl-2-phenyl-Δ^2-oxazolin-5-one) (**26**) with potassium superoxide*

A mixture of **26** (0.5 g, 1.0 mmol), potassium superoxide (0.14 g, 2.0 mmol), and 18-crown-6 (0.26 g, 1.0 mmol) in benzene (80 mL) was stirred at room temperature for 24 h. Work-up of the mixture as in the earlier cases gave 0.15 g (28%)[3] of **15** (acidification of the aqueous layer with dilute hydrochloric acid and recrystallization from ethanol), mp 222–224°C (mixture mp); 50 mg (21%)[3] of **9** (from mother liquor), mp 120–121°C (mixture mp); and 200 mg (40%) of recovered starting material **26** (removal of the solvent from the organic layer and recrystallization from benzene – petroleum ether (1:9)), mp 209–210°C (mixture mp).

Cyclic voltammetry

Measurements were made with a Princeton Applied Research (PAR) Model 173 potentiostat/galvanostat, a PAR Model 175 universal programmer, and a Kipp and Zonen X–Y recorder. Experiments were performed in a standard three-compartment cell equipped with a Pt-disc working electrode, a Pt-wire counter electrode, and a Ag/Ag^+ reference electrode. The cyclic voltammograms were recorded in a deaerated acetonitrile containing 0.1 *M* tetrabutylammonium perchlorate (TBAP). The direction of the initial scan was cathodic and the scan rate was 200 mV/s.

Pulse radiolysis

The description of the pulse radiolysis apparatus, which allows the determination of the transient spectra at various time intervals after the pulse and the kinetic measurements of the spectral changes, has been reported earlier (19). The irradiation was carried out with 5-ns electron pulses from the Notre Dame 8-MeV ARCO LP-7 linear accelerator, using dose rates of $\sim 2 \times 10^{16}$ eV/g per pulse. The solutions of the appropriate substrates in methanol were deaerated before pulse radiolysis by bubbling nitrogen for at least 30 min and the deaeration was continued in the reservoir from which the solution was allowed to flow slowly and continuously through the cell. The rate constants for the reactions with solvated electrons (e_s^-) were determined from the kinetic analysis of the enhanced rate of decay of e_s^- in the presence of the appropriate substrate or from the growth rate of the radical anion.

Acknowledgments

We thank the Department of Science and Technology, Government of India, Indian Institute of Technology, Kanpur, and the Office of Basic Energy Sciences of the U.S. Department of Energy for financial support of this work.

1. B. Pandey, R. K. Tikare, M. Muneer, P. V. Kamat, and M. V. George. Chem. Ber. **119**, 917 (1986).
2. R. B. Bates, F. A. Fletcher, K. D. Janda, and W. A. Miller. J. Org. Chem. **49**, 3038 (1984).
3. R. Bisson, R. B. Yeats, and E. W. Warnhoff. Can. J. Chem. **50**, 2851 (1972).
4. C. A. Chuaqui, S. Delaney, and J. Merritt. Tetrahedron, **39**, 2947 (1983).
5. (*a*) V. M. Dixit, V. Bhat, A. M. Trozzolo, and M. V. George. J. Org. Chem. **44**, 4169 (1979); (*b*) H. Gotthardt, R. Huisgen, and H. O. Bayer. J. Am. Chem. Soc. **92**, 4340 (1970); (*c*) N. Gakis, M. Märky, H.-J. Hansen, H. Heimgartner, H. Schmid, and W. E. Oberhänsli. Helv. Chim. Acta, **59**, 2149 (1976).
6. K. B. Patel and R. L. Willson. J. Chem. Soc. Faraday Trans. 1, **69**, 814 (1973).
7. J. H. Baxendale and P. Wardman. Natl. Stand. Ref. Data Ser. (U.S. Natl. Bur. Stand.), **54**, 1 (1975).
8. N. V. Raghavan, P. K. Das, and K. Bobrowski. J. Am. Chem. Soc. **103**, 4569 (1981).
9. E. Mohr and F. Stroschein. Ber. **42**, 2521 (1909).
10. (*a*) K. H.-Oehringen. Monatsh. Chem. **93**, 639 (1962); (*b*) F. R. Japp and A. Findley. Proc. Chem. Soc. **15**, 165 (1899).
11. H. B. Gillespie and H. R. Snyder. Org. Synth. Coll. Vol. II, 489 (1943).
12. V. Bhat. Ph.D. thesis, Indian Institute of Technology, Kanpur. 1978.
13. C. S. Cleaver and B. C. Pratt. J. Am. Chem. Soc. **77**, 1544 (1955).
14. A. W. Titherley. J. Chem. Soc. **85**, 1673 (1904).
15. R. E. Steiger. Org. Synth. Coll. Vol. III, 84 (1955).
16. R. E. Buckles, R. Filler, and L. Hilfman. J. Org. Chem. **17**, 233 (1952).
17. F. R. Japp and W. D. Davidson. J. Chem. Soc. **67**, 32 (1895).
18. C. D. Hurd and A. G. Praps. J. Org. Chem. **24**, 388 (1959).
19. L. K. Patterson and J. Lilie. Int. J. Radiat. Phys. Chem. **6**, 129 (1974).
20. K. Ashok, P. M. Scaria, P. V. Kamat, and M. V. George. Can. J. Chem. In press.

Can. J. Chem. Downloaded from www.nrcresearchpress.com by 118.98.75.50 on 09/07/12
For personal use only.

The α(C—C)/β(C—H) ratio of the primary processes in the 184.9 nm photolysis of gaseous *cis*- and *trans*-2-butene

HÉLÈNE DESLAURIERS, WLODZIMIERCZ MAKULSKI,[1] AND GUY J. COLLIN[2]
Département des Sciences fondamentales, Université du Québec à Chicoutimi, Chicoutimi (Qué.), Canada G7H 2B1

Received October 6, 1986

HÉLÈNE DESLAURIERS, WLODZIMIERCZ MAKULSKI, and GUY J. COLLIN. Can. J. Chem. **65**, 1631 (1987).

A complete study of the 184.9 nm photolysis of *cis*- and *trans*-2-butene has been done in the gas phase. The main primary processes (>90%) are the α(C—C) and β(C—H) bond ruptures. Both processes have similar quantum yield values in *cis*-2-butene: ϕ(C—C)/β(C—H) ≅ $0.95_7 \pm 0.13$. Conversely, the α(C—C) bond rupture is more important in *trans*-2-butene: ϕ(C—C)/β(C—H) ≅ $1.34_6 \pm 0.20$. These values are compared with those measured in propene (0.57) and isobutene (0.95). No simple molecular property seems sufficient to explain such an effect.

HÉLÈNE DESLAURIERS, WLODZIMIERCZ MAKULSKI et GUY J. COLLIN. Can. J. Chem. **65**, 1631 (1987).

Une étude complète de la photolyse à 184,9 nm des *cis*- et *trans*-butènes-2 a été réalisée en phase gazeuse. Les principaux processus primaires (>90%) sont les ruptures des liaisons α(C—C) et β(C—H). Les deux processus ont des importances similaires dans le cas du *cis*-butène-2 : ϕ(C—C)/β(C—H) ≅ $0{,}95_7 \pm 0{,}13$. Dans le cas du *trans*-butène-2, le même rapport est de $1{,}34_6 \pm 0{,}20$, donc plus important. Ces valeurs sont rapprochées de celles mesurées dans le propène (0,57) et l'isobutène (0,95). Aucune propriété moléculaire simple ne semble appropriée pour expliquer un tel effet.

Can. J. Chem. Downloaded from www.nrcresearchpress.com by 118.98.75.50 on 09/07/12
For personal use only.

Introduction

The vacuum and the very far uv photolysis of 2-butene is relatively well known. Chesick used a zinc lamp (202.6–206.2 nm) (1), and Borrell *et al.* a mercury one (184.9 nm) (2). Both laboratories investigated the effects of pressure on the total product yields and the product distributions. We also reported the yields of primary products as well as the yields of products formed from the decomposition of primary fragments at 123.6 nm, 147.0 nm (3), and ca. 174 nm (9, 20). The aim of the present authors is to measure the primary photochemical processes occurring in the 184.9 nm photolysis of *cis*-2-butene and *trans*-2-butene, particularly in view of the effect of the geometry of the starting molecule. For example, some differences were noticed in our previous studies at 174 nm (9, 20). More recently, we have studied the 184.9 nm photolysis of propene and isobutene. In this class of alkenes which do not have a C—C bond located in the β position relative to the double bond, the primary fragmentation processes involve the rupture of either an α(C—C) bond or a β(C—H) bond. The α(C—C)/β(C—H) ratios are 0.57 (σ = 0.054) and 0.95 (σ = 0.10) in propene and isobutene, respectively (4). We had no firm explanation for the observed values of the above-mentioned ratios. Obviously, it is interesting to try to measure the same ratio in the two 2-butene molecules.

Experimental

All the experimental techniques are well known and are described in the literature (3, 4, 9, 20).

Materials

2-Butenes are Phillips 66 products. *cis*-2-Butene (stated purity: 99.94 mol%) contains 1,3-butadiene, 24–26 ppm; *n*-butane, 1.4–2.0 ppm; isobutene, 17–19 ppm; 1-butene, 21–22 ppm; and *trans*-2-butene, 406–432 ppm. *trans*-2-Butene (stated purity: 99.48 mol%) contains *cis*-2-butene, 0.45%; *n*-butane, 150 ppm; and 1,3-butadiene + 1-butene, 2.5 ppm.

Oxygen (99.98%), Research purity, and nitric oxide, C.P. (99.0%) are from Matheson and are used as received. Deuterium sulfide and deuterium iodide (rather than H_2S or HI) are used as radical scavengers. They are from Merck, Sharp, and Dohme of Canada. They are also used as received after being degassed under high vacuum and at liquid nitrogen temperature.

Photolysis

All the photolyses are performed in a 90.3 cm^3 Pyrex cell (equipped with two 1 mm-thick suprasil quartz windows) placed in front of a low pressure mercury lamp (Philips) (5). The emission of the lamp as well as the absorption through the cell were checked with a 0.5-m McPherson monochromator (5). Chemical actinometry was used as comparing the formation of *n*-butane in the 184.9 nm photolysis of ethylene: $\Phi(n\text{-}C_4H_{10}) = 0.153$ (6, 7). In some experiments we used an 185 nm Acton Research filter in order to eliminate emission from the 253.7 nm line.

Typical rates of photon input in the cell are in the ranges (2–6) × 10^{13} or (6–10) × 10^{13} photons s^{-1}. The absorption coefficients of the mercury line (184.9 nm) by olefins are very high (8). For example, at a pressure of 0.3 Torr, ca. 99% of the incident beam is absorbed by *cis*-2-butene. Thus, it may be assumed that no correction for absorption is needed, provided the pressure is higher than 0.5 Torr in the 25 cm-long cell. In order to make the appropriate corrections for partial absorption at low pressures ($P < 0.5$ Torr), the photon beam was collimated and resulted in a lower intensity. Photolytic times were adjusted so that the number of photons injected in the cell never exceeded 0.5% of the total number of butene molecules in order to avoid back reactions.

Analysis

Photolysis materials were analyzed on two different gas chromatographs equipped with a dual flame ionization detector and either a squalane (6 m × ϕ6 mm; 25%) or UCON LB 550X (7 m × ϕ6 mm; 20%) column (4).

Results

Fifteen product quantum yields are reported in Table 1 for various selected butene pressures. Except for methane which is only slightly affected, the quantum yield values for the C_2 and C_3 hydrocarbons decrease with an increase in the pressure. For the C_4, C_5, and C_6 products, the quantum yield values are roughly independent of the pressure. The situation is similar in the photolysis of *trans*-2-butene:Nitric oxide mixtures, except that there is no formation of C_5 and C_6 products and the propyne quantum yield is constant over the 0.5–100 Torr pressure scale. In the presence of DI, there is a large increase in the methane quantum yields (Table 3). Conversely, there is no difference in the quantum yields of acetylene, propyne, and allene measured

[1]Present address: Department of Chemistry, Warsaw University, Zwirki i Wigury 101, 02-089 Warsaw, Poland.

[2]To whom all correspondence should be addressed.

either in the presence of nitric oxide oxide or DI. There is more 1,3-butadiene formed in the presence of DI than in that of nitric oxide.

Similar results are obtained in the photolysis of *cis*-2-butene either in the absence or the presence of the same additives (Tables 4–6).

Discussion

The behavior of the photoexcited molecules is relatively well known as far as gaseous alkenes are concerned. As was stated above, fragmentation involves mainly the rupture of either an α(C—C) or a β(C—H) bond (1–5).

[1] $2\text{-}C_4H_8 + h\nu \rightarrow {}^1(2\text{-}C_4H_8)^* \rightarrow 2\text{-}C_4H_8^{**}$

[2][3] $CH_3CH{=}CHCH_3^{**} \rightarrow CH_3CH{=}\dot{C}H^* + CH_3$

$\Delta H = 389$ kJ mol^{-1}

[3] $CH_3CH{=}CHCH_3^{**} \rightarrow CH_3\overline{CHCHCH_2}^* + H$

$\Delta H = 355$ kJ mol^{-1} (10)

$^1(M)^*$ is a singlet electronic excited state and $2\text{-}C_4H_8^{**}$ represents the photoexcited molecule in its fundamental electronic state, where all the energy of the incident photon is transferred in its vibrational framework. These primary processes are followed by secondary processes, in which the excited fragments, the 1-propenyl and α-methallyl radicals may suffer either further fragmentation, isomerization, and/or stabilization through collisions. The energy of the incident photon is 644 kJ einstein^{-1} (154 kcal einstein^{-1}). Thus, there is an excess energy of at least 260 kJ mol^{-1} available to energize the fragments. This excess energy must be partitioned in both sets of radicals formed in processes [2] and [3].

It may be assumed that the partitioning is roughly proportional to the number of internal degrees of freedom of each partner (ref. 11, pp. 240–242; ref. 12). Thus, on the ground of energetic considerations, both unsaturated radicals formed in processes [2] and [3] have many open channels.

[4*a*] $CH_3CH{=}\dot{C}H^* \rightarrow CH_3 + CH{\equiv}CH$

$\log A = 13.95$ and $E_A = 171$ kJ mol^{-1} (13)

[4*b*] $CH_3CH{=}\dot{C}H^* \rightarrow H + CH_3C{\equiv}CH$

$\log A = 13.7$ and $E_A = 184$ kJ mol^{-1} (13)

[4*c*] $CH_3CH{=}\dot{C}H^* \rightarrow \overline{CH_2CHCH_2}^*$

$E_A = 147$ kJ mol^{-1} (13, 14)

[5] $\overline{CH_2CHCH_2}^* \rightarrow H + CH_2{=}C{=}CH_2$

[6] $C_3H_5^* + M \rightarrow M + C_3H_5$

[7] $CH_3\dot{C}HCHCH_2^* \xrightarrow{k_d} H + CH_2{=}CHCH{=}CH_2$

$E_A \cong 210$ kJ mol^{-1} (15)

[8] $CH_3\dot{C}HCHCH_2^* + M \xrightarrow{k_s} M + CH_3CHCHCH_2$

These secondary processes are followed by the usual radical–radical disproportionation/combination reactions and the addition of hydrogen atoms to the starting material (16).

[9*a*] $H + 2\text{-}C_4H_8 \rightarrow CH_3\dot{C}HCH_2CH_3^{\ddagger}$

[9*b*] $H + 2\text{-}C_4H_8 \rightarrow H_2 + C_4H_7$

[10*a*] $CH_3\dot{C}HCH_2CH_3^{\ddagger} \rightarrow CH_3 + CH_3CH{=}CH_2$

[10*b*] $CH_3\dot{C}HCH_2CH_3^{\ddagger} \rightarrow CH_3CH_2CH_2\dot{C}H_2^{\ddagger}$

[11] $CH_3CH_2CH_2\dot{C}H_2^{\ddagger} \rightarrow CH_3\dot{C}H_2 + CH_2{=}CH_2$

[12] $C_4H_9^{\ddagger} + M \rightarrow M + C_4H_9$

[13] $CH_3 + CH_3 \rightarrow C_2H_6$

[14*a*] $CH_3 + CH_3\dot{C}HCH_2CH_3 \rightarrow CH_4 + C_4H_8$

[14*b*] $\rightarrow CH_3CH(CH_3)CH_2CH_3$

[15*a*] $CH_3 + CH_3\overline{CHCHCH_2} \rightarrow CH_3CH(CH_3)CH{=}CH_2$

[15*b*] $\rightarrow CH_3CH{=}CHCH_2CH_3$ (*cis* + *trans*)

[15*c*] $\rightarrow CH_4 + CH_2{=}CHCH{=}CH_2$

[16*a*] $CH_3 + CH_3CH{=}\dot{C}H \rightarrow CH_4 + C_3H_4$

[16*b*] $\rightarrow CH_3CH{=}CHCH_3$ (*cis* + *trans*)

[17*a*] $CH_3 + \overline{CH_2CHCH_2} \rightarrow CH_4 + C_3H_4$

[17*b*] $\rightarrow CH_3CH_2CH{=}CH_2$

[18*a*] $2C_4H_9 \rightarrow n\text{-}C_4H_{10} + n\text{-}C_4H_8$

[18*b*] $\rightarrow C_8H_{18}$

[19] $2\overline{CH_2CHCH_2} \rightarrow CH_2{=}CHCH_2CH_2CH{=}CH_2$

[20] $2CH_3\overline{CHCHCH_2} \rightarrow C_8H_{14}$

...etc.

All these reactions are almost sufficient to explain the formation of the products reported in Tables 1, 2, 4, and 5. This mechanism finds very good support from the experiments performed in the presence of a few percent of a radical scavenger, such as D_2S or DI (Tables 3 and 6). In these experiments, a stable, thermalized radical abstracts an hydrogen (deuterium) atom from the additive (17, 18).

[21] $R + XH(D) \rightarrow RH(D) + X$; $X \equiv I$, H(D)S

This process is efficient in all cases except in the case of allylic radicals where only hydrogen iodide is efficient (17). This particular behaviour (Table 3) explains the lower propene yields, measured in the presence of hydrogen sulfide, in comparison with what is observed in the presence of hydrogen iodide, and gives very strong support to the isomerization process of 1-propenyl radicals: process [4*c*].

At this time we would not like to explain systematically all the above-mentioned reactions, preferring to ask the interested reader to go back to the original papers (1–3, 18, 19). We would prefer to focus our attention on the main differences occurring between *cis*- and *trans*-2-butene. Obviously this goal will force us to emphasize the main features and even in some cases, to stress some minor characteristics.

From Tables 2 and 5, the main products observed in the presence of either oxygen or nitric oxide are propene and 1,3-butadiene. Both products are clearly related to the presence of hydrogen atoms: processes [7]–[10]. From this mechanism, the inverse of the 1,3-butadiene (B) quantum yield is a linear function of pressure (ref. 11, pp. 235–245)

[I] $[\Phi(B)]^{-1} = [\Phi_0(B)]^{-1}(1 + k_s[M]/k_d)$

The agreement with the Stern–Volmer line observed in Fig. 1 is good except for a strong negative curvature observed at pressures higher than 10 Torr. Eventually, a plateau region is established at pressures around or higher than ≅70 Torr. From the extrapolation of the quantum yields to zero pressure (Fig. 2*A*), one can extract the quantum yields of process [7], i.e. in the absence of a stabilizing process [8]: the $\Phi_0(1,3\text{-}C_4H_6)$ values are 0.29 and 0.21 in *cis*- and *trans*-2-butene, respec-

[3] $\Delta H_f^0(CH_3CH{=}\dot{C}H) = 56.8$ kcal mol^{-1}, see ref. 14.

Can. J. Chem. Downloaded from www.nrcresearchpress.com by 118.98.75.50 on 09/07/12
For personal use only.

TABLE 1. Pressure dependence of hydrocarbon quantum yields in the 184.9 nm photolysis of pure *trans*-2-butene

Product	Quantum yield when pressure in Torr is					
	0.5[a]	1.0	5.0	10	50	100
Methane	0.050	0.062	0.056	0.061	0.057	0.058
Acetylene	0.075	0.087	0.074	0.063	0.040	0.028
Ethylene	0.017	0.018	0.014	0.012	0.010	0.008
Ethane	0.152	0.145	0.118	0.110	0.091	0.081
Propene	0.193	0.158	0.091	0.078	0.069	0.060
Propyne	0.022	0.018	0.024	0.022	0.021	0.019
Allene	0.018	0.018	0.012	0.009	0.005	0.004
1-Butene	0.076	0.125	0.11	0.11	0.10	0.10
n-Butane	0.024	n.m.[b]	n.m.	n.m.	n.m.	n.m.
3-Methyl-1-Butene	0.025	0.031	0.037	0.038	0.037	0.025
Isopentane[c]	0.092	0.102	0.098	0.094	0.079	0.066
trans-2-Pentene	0.035	0.044	0.050	0.052	0.053	0.040
cis-2-Pentene	0.026	0.027	0.031	0.033	0.031	0.026
1,4-Pentadiene	0.005	0.005	0.007	0.005	0.006	—
1,5-Hexadiene	—	0.012	0.018	0.018	—	—

[a]1 Torr ≡ 133 N m^{-2}.
[b]n.m. ≡ not measured.
[c]Traces of *n*-pentane were also observed: $\Phi \leqq 0.01$.

TABLE 2. Pressure dependence of hydrocarbon quantum yields in the 184.9 nm photolysis of *trans*-2-butene: nitric oxide mixtures (100:5)[a]

Product	Quantum yield when butene pressure in Torr is					
	0.5	1.0	5.0	10	50	100
Methane	0.037	0.042	0.033	0.038	0.040	0.011
Acetylene	0.075	0.085	0.070	0.067	0.043	0.032
Ethylene	0.016	0.018	0.010	0.011	0.010	0.007
Propene	0.157	0.144	0.053	0.040	0.020	0.015
Propyne	0.020	0.016	0.020	0.021	0.020	0.018
Allene	0.019	0.018	0.012	0.09	0.006	0.004
1,3-Butadiene	0.203	0.166	0.107	0.088	0.048	0.036

[a]There is no formation of ethane, C_5, and C_6 products: $\Phi < 0.001$.

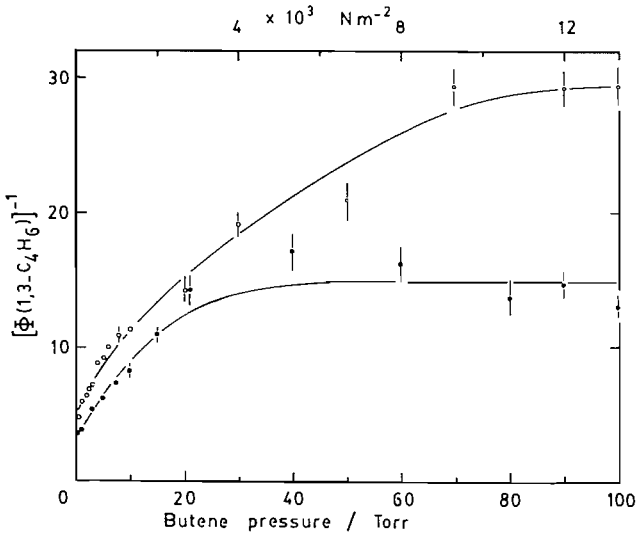

FIG. 1. The inverse of the 1,3-butadiene quantum yields vs. the 2-butene pressure in the presence of a radical scanvenger such as NO or O_2: $\Phi_0 \cong 0.29$ and 0.12 in *cis*- (●) and *trans*-2-butene (○), respectively.

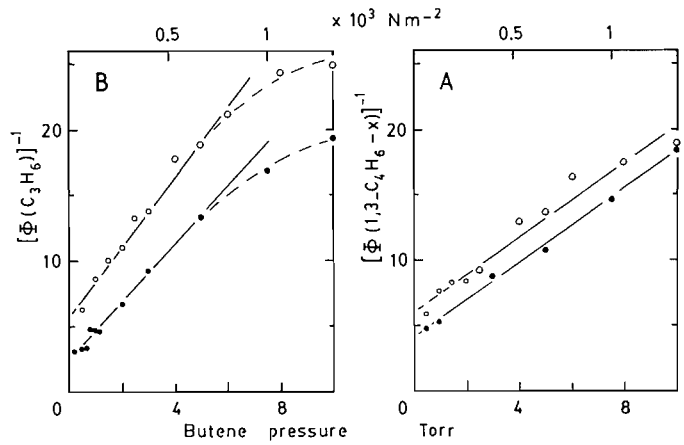

FIG. 2. The inverse of quantum yields vs. the *cis*- (●) or *trans*-2-butene (○) pressure in the presence of O_2 or NO, respectively. *A*: $[\Phi(1,3\text{-}C_4H_6) - 0.067]^{-1}$, (●), $y = 4.06 + 1.43x$, $r^2 = 0.99$ and $[\Phi(1,3\text{-}C_4H_6) - 0.035]^{-1}$, (○), $y = 6.08 + 1.43x$, $r^2 = 0.96$; *B*: $[\Phi(\text{propene})]^{-1}$, (●), $y = 2.61 + 2.15x$, $r^2 = 0.99$ and (○), $y = 5.95 + 2.67x$, $r^2 = 0.98$.

tively. Thus, at first sight, it seems that the β(C—H) bond rupture (process [3]) is more important in *cis*-2-butene. A similar behavior can be expected from the propene quantum yields (Fig. 2*B*). The evaluation of zero pressure quantum yields of propene leads to the Φ_0(propene) values: they are 0.40 and 0.17 in *cis*- and *trans*-2-butene, respectively. Again, there are more hydrogen atoms formed from *cis*- than from *trans*-2-butene. However, several processes add to the hydrogen atom formation: see for example, processes [4*b*], [5], [7]. Moreover, the above mechanism assumes that for each 1,3-butadiene molecule, two hydrogen atoms are formed. If this were the case, one would expect a hydrogen quantum yield larger than, or at least equal to 0.58 at zero pressure in *cis*-2-butene. Since the zero pressure quantum yield of propene is only 0.40, there is a deficit in the hydrogen atom budget. At least two corrections must be applied to this mechanism. The first one involves the

Can. J. Chem. Downloaded from www.nrcresearchpress.com by 118.98.75.50 on 09/07/12
For personal use only.

TABLE 3. Pressure dependence of hydrocarbon quantum yields in the 184.9 nm photolysis of *trans*-2-butene in the presence of either D_2S (15%) or DI (5%)

Product	Quantum yield when butene pressure in Torr is						
	1	2	5	10	20	50	100
Additive D_2S							
Propene	0.206	0.183	0.154	0.141	0.146	0.140	0.149
Additive DI							
Methane	0.70	0.76	0.73_8	0.72_8	0.66_2	0.65_2	0.57
Acetylene	0.078	0.081	0.075	0.066	0.051	0.039	0.028
Ethylene	0.034	0.031	0.024	0.019	0.020	0.021	0.020
Ethane	0.014	0.012	0.012	0.012	0.011	0.011	0.015
Propene	0.276	0.314	0.354	0.354	0.341	0.374	0.320
Propyne	0.022	0.023	0.024	0.023	0.021	0.022	0.025
Allene	0.021	0.018	0.014	0.013	0.010	0.006	0.004
1,3-Butadiene	0.208	0.193	0.175	0.155	0.145	0.152	0.131
n-Butane	0.235	0.360	0.368	n.m.	n.m.	0.414	n.m.

TABLE 4. Pressure dependence of hydrocarbon quantum yields in the 184.9 nm photolysis of pure *cis*-2-butene

Product	Quantum yield when butene pressure in Torr is					
	0.4[a]	1.0	5.0	10	50	100
Methane	0.07	0.061	0.053	0.060	0.052	0.054
Acetylene	0.067	0.068	0.064	0.05	0.042	0.032
Ethylene	0.026	0.025	0.016	0.013	0.010	0.008
Ethane	0.182	0.14	0.104	0.081	0.086	0.074
Propene	0.28	0.21	0.124	0.095	0.082	0.077
Propyne	0.042	0.030	0.012	0.019	0.020	0.015
Allene	0.016	0.015	0.010	0.011	0.004	0.002
1,3-Butadiene	0.32	0.295	0.24	0.20	0.176	0.157
trans-2-Butene	0.026	0.036	n.m.	n.m.	n.m.	n.m.
n-Butane	Trace	0.009	0.021	0.013	0.03	0.015
1-Butene	0.072	n.m.	0.135	0.136	0.128	0.117
3-Methyl-1-Butene	0.019	0.033	0.041	0.035	0.040	0.036
Isobutane	0.036	0.077	0.077	0.077	0.098	0.086
trans-2-Pentene	0.061	0.045	0.050	0.062	0.052	0.042
cis-2-Pentene	0.034	0.035	0.041	0.054	0.044	0.036

[a]Propane was also observed in this experiment: $\Phi \cong 0.02$.

TABLE 5. Pressure dependence of hydrocarbon quantum yields in the 184.9 nm photolysis of *cis*-2-butene: oxygen mixtures (100:10)[a]

Product	Quantum yield when butene pressure in Torr is					
	0.5	1.0	5.0	10	50[b]	100
Methane	0.028	0.035	0.042	0.040	0.031	0.030
Acetylene	0.072	0.073	0.065	0.062	0.050	0.026
Ethylene	0.038	0.036	0.014	0.011	0.010	0.007
Propene	0.292	0.212	0.075	0.052	0.024	0.012
Propyne	0.020	0.021	0.024	0.021	0.018	0.011
Allene	0.017	0.017	0.012	0.009	0.004	0.003
1,3-Butadiene	0.274	0.255	0.160	0.121	0.078	0.078
trans-2-Butene	0.053	0.049	0.13	n.m.[b]	n.m.	n.m.

[a]There is no formation of ethane, *n*-butane, 1-butene, C_5 and C_6 hydrocarbons: $\Phi < 0.002$.

[b]High intensity experiment: $I \cong 8\ 10^{13}$ photons s^{-1}; elsewhere: $I \cong 2\text{–}6\ 10^{11}$ photons s^{-1}.

hydrogen atom abstraction process (reaction [9*b*]) with a k_{9a}/k_{9b} ratio much higher than the one measured for thermalized systems: $0.23 \leqq k_{9b}/k_{9a} \leqq 0.117$ (21). The second adds a new fragmentation process for the photoexcited molecule:

[22] $\quad 2\text{-}C_4H_8{}^{**} \rightarrow H_2 + 1,3\text{-}C_4H_6$

One may assume that such a concerted process is not pressure dependent: in other words that the photoexcited molecule has a lifetime shorter than the time available between two collisions, at least at sub-atmospheric pressures (22). From the plateau regions observed in Fig. 1, the quantum yields for process [22] may be evaluated at 0.067 and 0.035 in *cis*- and *trans*-2-butene, respectively. This correction lowers the ϕ(process [7]) values to 0.246 and 0.165 in *cis*- and *trans*-2-butene, respectively.

The formation of acetylene is linked to the primary α(C—C) bond rupture: processes [2] and [4*a*]. In agreement with a chemical activation study (13), the hot 1-propenyl radicals may either decompose, giving rise to the formation of acetylene and

Can. J. Chem. Downloaded from www.nrcresearchpress.com by 118.98.75.50 on 09/07/12
For personal use only.

TABLE 6. Pressure dependence of hydrocarbon quantum yields in the 184.9 nm photolysis of *cis*-2-butene in the presence of DI (5%)

Product	Quantum yield when butene pressure in Torr is							
	1.2	5.0	10	20	30	40	50	60
Methane	0.72	0.646	0.60	0.58	0.565	0.56	0.53	0.51
Acetylene	0.100	0.065	0.057	0.041	0.025	0.022	0.017	0.014
Ethylene	0.030	0.026	0.022	0.017	0.010	0.010	0.012	0.009
Ethane	0.013	0.008	0.021	0.012	0.011	0.011	0.011	0.02
Propene	0.387	0.423	0.44	0.44	0.48	0.478	0.46	0.45
Propyne	0.014	0.023	0.014	0.021	0.015	0.013	0.011	0.008
Allene	0.020	0.007	n.m.	0.003	0.002	Trace	Trace	Trace
1-Butene	0.107	0.202	0.203	0.227	0.29	0.33	n.m.	n.m.
1,3-Butadiene	0.26	0.12	n.m.	n.m.	0.08	0.07	n.m.	n.m.
n-Butane	0.137	0.25	0.25	0.26	0.359	n.m.	n.m.	n.m.

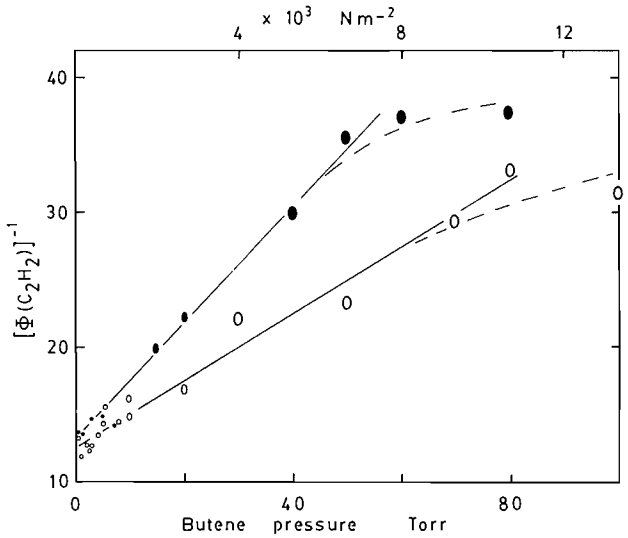

FIG. 3. The inverse of acetylene quantum yields vs. the 2-butene pressure in the presence of a radical scavenger such as NO or O_2 in *cis*-2-butene (●), $y = 13.16 + 0.42x$, $r^2 = 0.98$ and *trans*-2-butene (○), $y = 12.58 + 0.248x$, $r^2 = 0.98$.

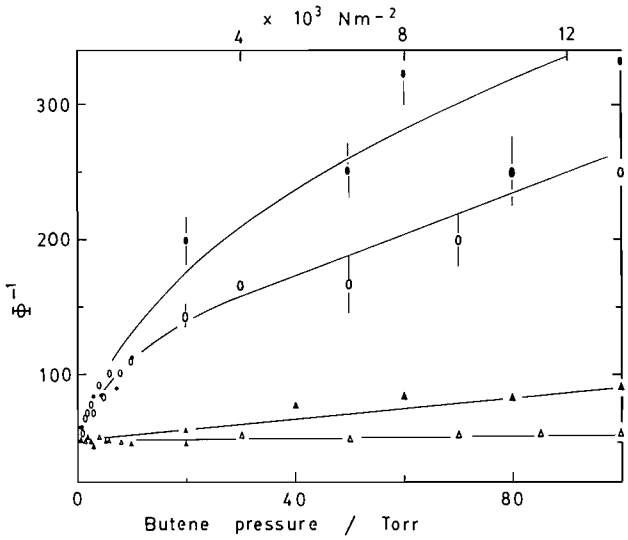

FIG. 4. The inverse of quantum yields of propyne (lower curves: △,▲) and allene (upper curves: ○,●) vs. the 2-butene pressure in the presence of a radical scavenger such as NO or O_2 in *cis*- (●,▲) and *trans*-2-butene (○,△).

propyne or isomerize to the allyl structure. With an internal energy of 266 kJ mol^{-1}, the relative rate constants, $k_{4a}/k_{4b}/k_{4c}$ are 1.0/0.2/0.2 (13) and are likely to be dependent on the internal energy content of the precursor. In the present study, the maximum available energy is 644 − 385 = 259 kJ mol^{-1}. This excess energy is divided in both methyl and 1-propenyl radicals, more precisely in the vibrational degrees of freedom of each fragment (11). On statistical ground, the mean energy content of the 1-propenyl radicals is only 18/27 of this maximum energy, E^*(1-propenyl) ≅ 173 kJ mol^{-1} (11). Thus, in comparison with the activation study mentioned above, and from the known energy barriers for processes [4*a*]–[4*c*], the isomerization process must be favored, and the ratio k_{4a}/k_{4b} must be increased. Acetylene is the major compound (Tables 2 and 5) and Figs. 3 and 4 show the Stern–Volmer plots of the acetylene and C_3H_4 quantum yields. It is obvious from these figures that the acetylene quantum yield is much more dependent on pressure than that of propyne. This observation indicates that both products are not entirely formed from the same precursor. It must be added that the main fate of hot allyl radicals is isomerization towards the 2-propenyl and 1-propenyl radicals (13). Thus, the hot C_3H_5* radicals is a complex mixture of the three isomers. Finally, the molecular elimination of methane concurrently with propyne from the photoexcited molecules must be questioned. The low pressure dependence of the propyne quantum yield is consistent with this process and a large fraction of the propyne formation may be ascribed to the following process.

[23] $\quad 2\text{-}C_4H_8^{**} \rightarrow CH_4 + CH_3C{\equiv}CH$

This process explains part of the formation of methane observed in the presence of either NO or O_2.

The formation of ethylene may derive from at least two different processes (Fig. 5). At low pressures, the very strong inverse dependence of its quantum yield on the pressure supports the involvement of vibrationally excited 1-butyl radicals (processes [9]–[12]), and does not demand more explanations (23). At high pressures ($P > 50$ Torr), a fragmentation process involving a photoexcited C_4H_8** molecule cannot be precluded. One of the two following processes may be proposed:

[24] $\quad 2\text{-}C_4H_8^{**} \rightarrow 2C_2H_4$

Can. J. Chem. Downloaded from www.nrcresearchpress.com by 118.98.75.50 on 09/07/12
For personal use only.

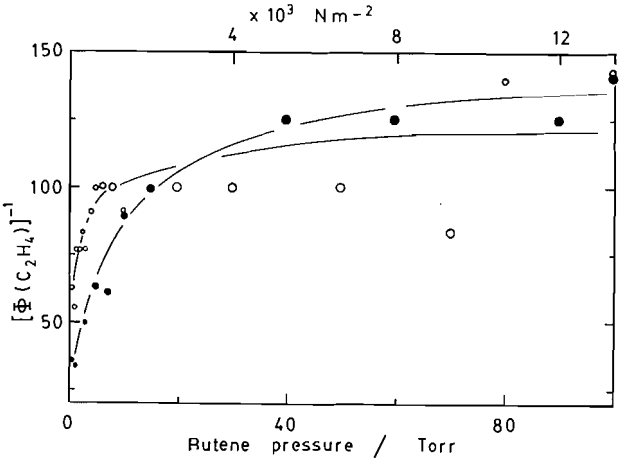

FIG. 5. The inverse of the ethylene quantum yields vs. the *cis*- (●) or *trans*-2-butene (○) pressure in the presence of O_2 or NO, respectively.

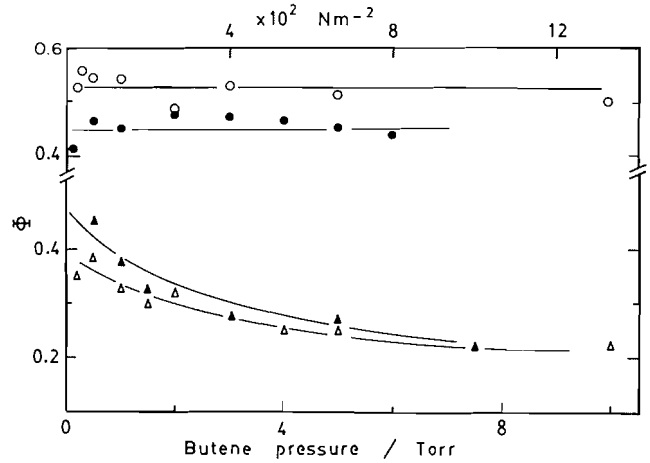

FIG. 6. The pressure dependence of the $\Phi[\beta(C—H)]$ values (relationships [II‴], lower part) and $\Phi[\alpha(C—C)]$ values ([IV′], upper part) in the 184.9 nm photolysis of *cis*- (●,▲) and *trans*-2-butene (○,△); see text. For clarity, the *y*-axis has been displaced.

$$[25a]^4 \quad 2\text{-}C_4H_8{}^{**} \rightarrow (C_4H_8)^{**} \rightarrow C_2H_5{}^* + C_2H_3 \qquad \Delta H = 428 \text{ kJ mol}^{-1}$$

$$[26] \quad C_2H_5{}^* \rightarrow C_2H_4 + H \qquad \Delta H = 151.5 \text{ kJ mol}^{-1}$$

The molecular process (reaction [24]) involves an internal rearrangement of the photoexcited molecules. Processes [25] and [26] are supported by the small increase in the ethylene yield in the presence of DI (Tables 3 and 6). The difference between the $\Phi_{DI}(C_2H_4)$ and $\Phi_{O_2,NO}(C_2H_4)$ values may be linked through process [21] to the formation of vinyl radicals: $\Phi(C_2H_3) \cong 0.01$. A similar process may lead to the formation of acetylene and ethyl radicals.

$$[25b] \quad 2\text{-}C_4H_8{}^{**} \rightarrow (C_4H_8)^{**} \rightarrow C_2H_5 + C_2H_3{}^*$$

$$[27] \quad C_2H_3{}^* \rightarrow C_2H_2 + H \qquad \Delta H = 143.4 \text{ kJ mol}^{-1} \text{ (25)}$$

This mechanism is supported by the formation of a small amount of ethane in the presence of DI: $\Phi(C_2H_5) \cong 0.012$ and adds to the formation of acetylene. One must add that on energetic consideration acetylene, ethylene, and two hydrogen atoms cannot be formed from the same photoexcited molecule. Finally, isomerization of *cis*-2-butene to *trans*-2-butene is observed at low pressures (Table 5) as well as at high pressures (2) with low quantum yields.

From Tables 2 and 5, it is obvious that the total of the product quantum yields observed in the presence of either NO or O_2 is less than 0.5 (Φ(propene) is not included in this sum). Thus, the majority of the primary products are probably radicals. This observation is corroborated in Tables 1 and 4, where many products are formed in pure butene through radical–radical processes. For example, processes [15*a*], [15*b*], and [17*b*] are simple reactions to explain the 3-methyl-1-butene, 2-pentene, and 1-butene formations, respectively. By looking at these products, one may have access to the quantum yield of the primary β(C—H) bond rupture: $\phi[\beta(C–H)]$. This quantum yield is given by the following relationship:

$$[II] \quad \phi[\beta(C—H)] = \phi(\text{process [7]}) + \phi(\text{process [8]})$$

ϕ(process [7]) is equal to the difference between the quantum yield of 1,3-butadiene measured in the presence of either NO or O_2, Φ_{NO,O_2}(1,3-butadiene), and the quantum yield of process [22]. As far as ϕ(process [8]) is concerned, it may be obtained from the sum of radical–radical reactions involving α-methallyl radicals:

$$[II'] \quad \phi[\beta(C—H)] = \Phi_{NO,O_2}(1,3\text{-}C_4H_6) - \phi(\text{process [22]}) + \phi(R + \alpha\text{-}C_4H_7) + 2\phi(\alpha\text{-}C_4H_7 + \alpha\text{-}C_4H_7)$$

Unfortunately, only the $\phi(CH_3 + \alpha\text{-}C_4H_7)$ values have been measured (Tables 1 and 4). Thus, the best estimate of $\phi(R + \alpha\text{-}C_4H_7)$ that can be made will happen when the methyl radical quantum yield is maximum, i.e. at zero pressure where the fragmentation of the vibrationally excited *s*-butyl radical is maximum. As far as the last term of II′ is concerned it may be calculated from the following ratio (26):

$$[III] \quad \frac{[\Phi(CH_3 + CH_3)]^2}{\Phi(CH_3 + \alpha\text{-}C_4H_7)\Phi(\alpha\text{-}C_4H_7 + \alpha\text{-}C_4H_7)} = 4.0$$

Thus, at 0.4–5.0 Torr, Φ(process [20]) are 0.073 and 0.067 in *cis*- and *trans*-2-butene, respectively.

$$[II'''] \quad \phi[\beta(C—H)] \cong \Phi_{NO,O_2}(1,3\text{-}C_4H_6) - \Phi(\text{process [22]}) + \phi(CH_3 + \alpha\text{-}C_4H_7) + 2\phi(\alpha\text{-}C_4H_7 + \alpha\text{-}C_4H_7) \quad \text{at } P \rightarrow 0$$

The results are displayed in Fig. 6. At zero pressure, the $\phi[\beta(C—H)]$ values may be estimated at 0.47 ± 0.04 and 0.39 ± 0.04 in *cis*- and *trans*-2-butene, respectively.

The combination reaction between 1-propenyl and methyl radicals yields the starting material or its isomer. Thus, it is difficult to evaluate the $\phi[\alpha(C—C)]$ values from the reaction processes of the 1-propenyl radicals. An easier way for this evaluation resides in the measurement of the quantum yields of the primary methyl radicals.

$$[IV] \quad \phi[\alpha(C—C)] = \Phi_{pr}(CH_3) = \Phi(CH_3) - \Phi_{O_2}(C_3H_6) - \Phi(C_2H_2)$$

The quantum yield of the methyl radical may be equated to the difference between the methane quantum yield measured in the presence of DI and the one measured in the presence of either O_2 or NO. Equation [IV] must be corrected for the formation of propene and acetylene, since both products are formed concurrently with secondary methyl radicals.

[4] $\Delta H_f^0(C_2H_5) = 118.5 \pm 1.7$ kJ mol^{-1} (24*a*) and $\Delta H^0(C_2H_3) = 301 \pm 8$ kJ mol^{-1} (24*b*).

Can. J. Chem. Downloaded from www.nrcresearchpress.com by 118.98.75.50 on 09/07/12
For personal use only.

TABLE 7. The 184.9 nm photofragmentation of *cis*- and *trans*-2-butene

Process $2\text{-}C_4H_8^{**} \rightarrow$	Φ^a *cis*	Φ^a *trans*
$CH_3 + CH_3\dot{C}H{=}\dot{C}H^*$	0.45 ± 0.03	$0.52_5 \pm 0.03$
$H + CH_3\dot{C}HCHCH_2^*$	0.47 ± 0.04	0.39 ± 0.04
$H_2 + CH_2{=}CHCH{=}CH_2$	0.067	0.035
$CH_3C{\equiv}CH + CH_4$	0.013	0.02
$C_2H_4 + C_2H_3 + H$	0.007	0.01
$C_2H_5 + C_2H_2 + H$	0.012	0.012
Total	1.019	0.992

[a]Quantum values are extrapolated to zero pressure.

$$[IV'] \quad \phi[\alpha(C{-}C)] = \Phi_{DI}(CH_4) - \Phi_{O_2,NO}(CH_4) - \Phi_{O_2}(C_3H_6) - \Phi_{O_2}(C_2H_2)$$

The so-calculated $\phi[\alpha(C{-}C)]$ values are $0.52_5 \pm 0.03$ and 0.45 ± 0.03 in *trans*- and *cis*-2-butene, respectively, on the 1–10 Torr pressure scale (Fig. 6). The 184.9 nm processes are summarized in Table 7. Owing to the relatively larger uncertainties arising from the methods used above, the quantum yields for fragmentation are unity. Both systems are similar except for a larger difference in the $\alpha(C{-}C)/\beta(C{-}H)$ ratio.

Taking into account the error limits indicated in Table 7, the $\alpha(C{-}C)/\beta(C{-}H)$ ratios measured in *cis*- and *trans*-2-butene are $0.95_7 \pm 0.13$ and $1.34_6 \pm 0.20$, respectively. These values must be compared with 0.57 and 0.95 obtained in propene and isobutene, respectively. A very interesting and intriguing effect appears to be attached to the number and location of the methyl substituents. This effect may be due to the electrophilic property of the methyl group. Unfortunately, it is difficult to link the increase in this ratio from propene to *trans*-2-butene to any simple molecular property of these molecules. In fact, it is likely that the $\alpha(C{-}C)/\beta(C{-}H)$ ratio is not dependent on one parameter only.

The above mechanism is consistent with the view that the internal conversion of electronic excitation energy to vibrational energy is preceding the bond cleavage processes. However, it cannot be precluded that bond cleavage is part of the conversion process itself. In that case, the geometry (symmetry, ...) of the molecule may play a role in the redistribution of energy.

The difference for this ratio may be discussed in terms of the spectroscopy of these compounds. Both Rydberg and valence states are populated at 184.9 nm. Do the two fragmentation pathways result from the same excited state or different ones? If each exit channel is linked to one electronic excited state, the $\alpha(C{-}C)/\beta(C{-}H)$ ratio can be explained in terms of differences in the absorption processes. It is apparent from Fig. 6 that the primary $\alpha(C{-}C)$ process is pressure independent on the 0–10 Torr pressure scale. On the other hand, the primary $\beta(C{-}H)$ quantum yield decreases on the same pressure scale. Given that the extinction coefficient of a Rydberg transition decreases with increasing pressure, while that of a valence transition is pressure independent (27), the above data suggest that the $\alpha(C{-}C)$ process is π,π^*-derived and the $\beta(C{-}H)$ process, $\pi,3s(R)$-derived. Since the $\alpha(C{-}C)/\beta(C{-}H)$ ratio is pressure dependent, then it indicates that both processes do not occur from a common excited state. This proposal is somewhat different from that given by Borrel *et al.* (2). The Rydberg state was proposed to break down to a variety of products unless they are collisionally deactivated. Conversely, isomerization is the only reaction path for the V state (2).

However, it must be recalled that the quantum yield of the primary $\beta(C{-}H)$ process is measured through eq. [II‴], that is strictly valid at zero pressure. In fact, products arising from $s\text{-}C_4H_9 + \alpha\text{-}C_4H_7$ interactions were not measured: the larger the pressure, the more important are these reactions. Thus, the decrease of the primary $\beta(C{-}H)$ bond rupture reported on Fig. 6 may be the result of the way this quantum yield is measured. It must be said that the pressure dependence of the $\beta(C{-}H)$ quantum yield is rather strong in comparison with the decrease in extinction coefficient of a Rydberg transition (28). Conversely, the ethylene (a product mainly originating from the decomposition of hot *s*-butyl radicals) is strongly pressure dependent on the 0–20 Torr pressure scale (Fig. 5). Thus, stabilization of hot *s*-butyl radical–radical is very efficient at moderate pressure and part of $\alpha\text{-}C_4H_7$ radicals disappear in radical–radical reactions and, as such, are not included in [II‴].

Acknowledgments

The authors would like to thank the Natural Sciences and Engineering Research Council of Canada (programme de Développement de la recherche) for the support given to this project and the salary to one of us (W.M.). We would also like to thank Dr. R. Back (NRCC, Ottawa) for the gift of one *trans*-2-butene sample. We are also indebted to an unknown referee who made very valuable comments.

1. J. P. CHESICK. J. Chem. Phys. **45**, 3934 (1966).
2. P. BORRELL and F. C. JAMES. Trans. Faraday Soc. **62**, 2452 (1966); P. BORELL, P. CASHMORE, A. CERVENKA, and F. C. JAMES. J. Chim. Phys. 229 (1970).
3. G. J. COLLIN and P. M. PERRIN. Can. J. Chem. **50**, 2823 (1972).
4. H. DESLAURIERS and G. J. COLLIN. J. Chim. Phys. **82**, 1033 (1985).
5. H. DESLAURIERS, G. J. COLLIN, and A. WIĘCKOWSKI. J. Phys. Chem. **85**, 944 (1981).
6. P. POTZINGER, L. C. GLASGOW, and G. VON BÜNAU. Z. Naturf. **27**a, 628 (1972).
7. H. OKABE. *In* Photochemistry of small molecules. J. Wiley and Sons, New York. 1978. p. 126.
8. F. H. WATSON, JR. and S. P. MCGLYNN. Theoret. Chim. Acta, **21**, 309 (1971).
9. A. WIĘCKOWSKI and G. J. COLLIN. J. Phys. Chem. **81**, 2592 (1977).
10. W. TSANG. Int. J. Chem. Kinet. **5**, 929 (1973).
11. W. FORST. *In* Theory of unimolecular reactions. Academic Press, New York. 1973.
12. G. J. COLLIN and H. DESLAURIERS. Int. J. Chem. Kinet. **12**, 17 (1980); D. HOUDE, H. DESLAURIERS, and G. J. COLLIN. Can. J. Chem. **61**, 962 (1983).
13. J. NIEDZIELSKI, J. GAWLOWSKI, and T. GIERCZAK. J. Photochem. **21**, 195 (1983).
14. T. IBUKI, T. MARATA, and Y. TAKEZAKI. J. Phys. Chem. **78**, 2543 (1974).
15. P. I. ABELL. Campr. Chem. Kinet. **18**, 111 (1976); C. H. BAMFORD and C. F. H. TIPPER. Elsevier, Amsterdam; W. TSANG. Int. J. Chem. Kinet. **5**, 929 (1973).
16. B. S. RABINOVITCH and D. W. SETSER. *In* Advances in photochemistry. *Edited by* W. A. Noyes, G. S. Hammond, and J. N. Pitts, Jr. Vol. 3. 1964. p. 1 and references therein.
17. P. AUSLOOS, R. E. REBBERT, and S. G. LIAS. J. Photochem. **2**, 267 (1974).
18. G. J. COLLIN and K. BUKKA. J. Photochem. **6**, 381 (1976/77).
19. G. J. COLLIN and H. DESLAURIERS. Nouv. J. Chim. **3**, 701 (1979).

Can. J. Chem. Downloaded from www.nrcresearchpress.com by 118.98.75.50 on 09/07/12
For personal use only.

20. A. WIĘCKOWSKI and G. J. COLLIN. Can. J. Chem. **55**, 3636 (1977).
21. K. R. JENNINGS and R. J. CVETANOVIĆ. J. Chem. Phys. **35**, 1233 (1961).
22. J. GAWLOWSKI and G. J. COLLIN. J. Photochem. **23**, 241 (1983).
23. S. W. BENSON and H. E. O'NEAL. NSRDS-NBS **21**, 576 (1970) and references therein.
24. (*a*) M. BROUARD, P. D. LIGHTFOOT, and M. J. PILLING. J. Phys. Chem. **90**, 445 (1986); (*b*) R. B. SHARMA, N. M. SEMO, and W. S. KOSKI. Int. J. Chem. Kinet. **17**, 831 (1985).
25. D. G. KEIL, K. P. LYNCH, J. A. COWFER, and J. V. MICHAEL. Int. J. Chem. Kinet. **8**, 825 (1976).
26. S. W. BENSON and W. B. DEMORE. Ann. Rev. Phys. Chem. **16**, 397 (1965) and references therein.
27. M. B. ROBIN. *In* Higher excited states of polyatomic molecules. Vol. II, 1975. pp. 1–50; Vol. III, 1985. pp. 227–236.
28. M. B. ROBIN and N. A. KUEBLER. J. Mol. Spectrosc. **33**, 274 (1970).

Can. J. Chem. Downloaded from www.nrcresearchpress.com by 118.98.75.50 on 09/07/12
For personal use only.

Collisional energy transfer in non-reactive systems

WENDELL FORST
Département de chimie physique des réactions, UA 328 CNRS, INPL-ENSIC, 1 rue Grandville, 54042 Nancy CEDEX, France

GUO-YING XU
Department of Chemistry and CRAM, Laval University, Quebec, P.Q., Canada G1K 7P4

AND

GRIGORIOS GIDIOTIS
Department of Chemistry, Stanford University, Stanford, CA 94305, U.S.A.

Received October 16, 1986

WENDELL FORST, GUO-YING XU, and GRIGORIOS GIDIOTIS. Can. J. Chem. **65**, 1639 (1987).

If the internal energy of target molecules highly dispersed in a heat bath is monitored as a function of time, their one-photon laser excitation and subsequent bulk collisional relaxation yields information only about energy transfer in the bulk system (a macroscopic time-dependent property). This paper discusses three special cases when $\langle \Delta E \rangle$, the average energy transferred in a collision (a microscopic property) can be deduced from bulk relaxation data without knowledge of the collisional transition probability: (*i*) initial excitation is a δ function; (*ii*) relaxation of bulk average energy follows simple exponential law; or (*iii*) it is linear in time. The implications of exponential relaxation is that $\langle \Delta E \rangle$, which is the first moment of the collisional transition probability, is a linear function of internal energy. These conclusions are illustrated using available laser relaxation data on azulene, benzene, and hexafluorobenzene, and are compared with similar data on toluene and two cycloheptatrienes. Some inconsistencies are noted, the probable origin of which is discussed.

WENDELL FORST, GUO-YING XU et GRIGORIOS GIDIOTIS. Can. J. Chem. **65**, 1639 (1987).

Si l'on suit, en fonction du temps, l'énergie interne des molécules-cible excitées par l'absorption d'un photon laser et hautement dispersées dans un bain à température constante, leur relaxation subséquente par collisions ne fournit l'information que sur le transfert d'énergie-en-masse (une propriété macroscopique, fonction du temps). Dans ce travail l'on discute de trois cas spéciaux qui permettent d'obtenir $\langle \Delta E \rangle$, l'énergie moyenne transférée par collision (une propriété microscopique) sans connaître la forme de la probabilité de transition par collision : (*i*) la distribution initiale d'énergie est une fonction δ; (*ii*) la relaxation-en-masse suit une loi exponentielle simple, ou (*iii*) est linéaire dans le temps. L'implication de la relaxation exponentielle est que $\langle \Delta E \rangle$, soit le premier moment de la probabilité de transition par collision, est une fonction linéaire de l'énergie. Ces conclusions sont illustrées à l'aide des données disponibles dans la littérature au sujet de la relaxation de l'azulène, du benzène et de l'hexafluorobenzène excités au laser, et qu'on compare ensuite à des données semblables sur le toluène et deux cycloheptatriènes. On note un certain manque de consistence entre les données, dont on discute la source probable.

Can. J. Chem. Downloaded from www.nrcresearchpress.com by 118.98.75.50 on 09/07/12
For personal use only.

Introduction

In a gaseous system, intermolecular collisional energy transfer takes place in principle whenever the pressure is finite, which is the case of every process of practical interest; therefore the quantitative characterization of such energy transfer is an important element in the understanding and modelling of gas phase reaction processes. We shall focus here on the particular case of energy transfer in a bulk system: it is a thermal system, i.e. one in contact with a heat bath, in which some average system property is monitored; an obvious example is a thermal reaction. Historically, thermal reactions were the first to be used for extracting energy transfer information (1).

It is clear that bulk systems cannot provide any insight into state-to-state dynamics, but this is not too serious a handicap in the present context since the principal information necessary for modelling purposes is $\langle \Delta E \rangle$, the average energy transferred in a collision (defined below in eq. [3]), and for this purpose bulk systems can yield the necessary data. However, energy transfer in bulk systems is often accompanied by some other process (e.g. chemical reaction), and as a result extracting energy transfer data from bulk experiments is not as straightforward and unambiguous as one might wish (1), except in special circumstances. One such special circumstance (a somewhat idealized experimental version of which is described below) is the object of much current interest since it is experimentally realizable and allows a more direct access to $\langle \Delta E \rangle$.

In this version of a bulk experiment, the molecule of interest (henceforth referred to as the "target" molecule) is highly dispersed in an inert gas heat bath, large enough so that bath properties (temperature in particular) remain constant throughout. A laser pulse of short duration excites the target molecule, by one-photon absorption, to a high energy state (or states), preferably not high enough to open a reactive channel. The system is then left undisturbed and its time history is monitored by recording the average internal (i.e. vibrational) energy $\langle\langle y \rangle\rangle$ of the target molecules as a function of time.

Under these conditions the excitation energy deposited initially in the molecule is dissipated exclusively by binary collisions between target and heat bath molecules, so that such a system represents the case of "pure" bulk relaxation, uncomplicated by the simultaneous occurrence of any other process, e.g. chemical reaction. If the heat bath consists of a large excess of rare gas, then the process taking place in such a bulk system is pure V–T (vibration-to-translation) energy transfer.

Theory

It is important at the outset to make clear the distinction between a microscopic and macroscopic property. The internal energy y of a molecule, for instance, is an intrinsic molecular property at the microscopic level; similarly $\langle \Delta E \rangle$ (the information sought in the present context) represents the average outcome of single-collision events and thus is likewise a microscopic property. In a bulk system, however, what is accessible to measurement in the type of experiment described

Can. J. Chem. Downloaded from www.nrcresearchpress.com by 118.98.75.50 on 09/07/12
For personal use only.

above are not the *microscopic* molecular properties, but instead only average properties of the whole (bulk) system, i.e. bulk observables, which represent the *macroscopic* properties of the system. Such macroscopic properties are bulk averages (2) (defined below in eqs. [1] and [2]), and will be denoted here by double brackets $\langle\langle \ldots \rangle\rangle$ in order to distinguish them from per-collision averages denoted by single brackets $\langle \ldots \rangle$; this notation and nomenclature follows that of ref. 2. A lucid exposition of the general concepts developed here for the specific case of collisional energy transfer may be found in van Kampen (3).

Let $c(y,t)$ represent the time-dependent population density, i.e. the probability, per unit energy, that a molecule shall have internal energy y at time t. The assumption is that the molecule is sufficiently large and the energy sufficiently high so that there is a quasi-continuum of molecular energy levels. The macroscopic bulk observable which corresponds to a given (energy-dependent) microscopic property is defined as the average of the latter over $c(y,t)$. Thus, in particular, the observable or bulk-average energy is given by

$$[1] \quad \langle\langle y \rangle\rangle = \int y\, c(y,t)\, \mathrm{d}y$$

and the macroscopic or bulk-average energy transfer by

$$[2] \quad \langle\langle \Delta E \rangle\rangle = \int \langle \Delta E \rangle\, c(y,t)\, \mathrm{d}y$$

which represents the average energy transferred per collision in the bulk system.

The intrinsic or microscopic energy transfer $\langle \Delta E \rangle$ is defined by

$$[3] \quad \langle \Delta E \rangle = \int (x - y)\, q(x,y)\, \mathrm{d}x$$

where $q(x,y)$ is the collisional transition probability, i.e. the probability, per collision and per unit energy, that if a molecule had energy y before the collision, it shall have energy x after the collision. Equation [3] shows that $\langle \Delta E \rangle$ is in fact the first moment of the transition probability $q(x,y)$. Note that $\langle \Delta E \rangle$, which represents the total energy transferred in a collision, may be positive ("up-collision") or negative ("down-collision") depending on the pre-collision energy y.

It can be shown that if the collision frequency in the relaxing system is ω, then (3, 4)

$$[4] \quad \mathrm{d}\langle\langle y \rangle\rangle/\mathrm{d}t = \omega \langle\langle \Delta E \rangle\rangle$$

so that $\langle\langle \Delta E \rangle\rangle$ is obtainable directly from the time decay of $\langle\langle y \rangle\rangle$. In the case of the experimental laser system described in the Introduction, $\langle\langle \Delta E \rangle\rangle$ will be always negative because, overall, the target molecules are losing energy to the heat bath. Clearly $\langle\langle \Delta E \rangle\rangle$ depends not only on $q(x,y)$, i.e. on the intrinsic (microscopic) properties of the collision partners, but also on the particular experimental conditions: excitation level, pressure, etc. In addition, $\langle\langle \Delta E \rangle\rangle$ is a function of time (cf. eq. [2]).

The obvious difficulty here is that the quantity accessible to measurement (via the decay of $\langle\langle y \rangle\rangle$) is $\langle\langle \Delta E \rangle\rangle$, whereas the information desired is $\langle \Delta E \rangle$. This amounts to the classic problem of recovering a function from its average.

The standard way to deal with a relaxation problem of the kind described above is first to write down the master equation for a polyatomic molecule having a quasi-continuum of energy levels in the form (5)

$$[5] \quad \mathrm{d}\, c(x,t)/\mathrm{d}t = \omega \int q(x,y)\, c(y,t)\, \mathrm{d}y - \omega\, c(x,t)$$

Equation [5] is solved for $c(x,t)$, either analytically (4–6) or numerically (7), using several assumed models of the transition probability $q(x,y)$ (gaussian, stepladder, exponential, etc.). Whichever model leads to the best fit between the calculated (via eq. [1]) and experimental decay of $\langle\langle y \rangle\rangle$ is then used to obtain $\langle \Delta E \rangle$ from eq. [3]. Models of $q(x,y)$ usually contain adjustable parameters, so that several models can be made to fit a given relaxing system, with the result that $\langle \Delta E \rangle$ so obtained is model-dependent, and consequently ambiguous.

There are in principle three special cases which do not require the master equation be actually solved in order to determine $\langle \Delta E \rangle$. Thus no model for $q(x,y)$, parametrized or not, need be postulated, with the result that the $\langle \Delta E \rangle$ so obtained is model-independent. The three special cases are set out below and are the main subject of this work.

(*i*) One special case arises when the initial distribution is a δ function at, say, y_0: $c(y,0) = \delta(y - y_0)$. From the record of the time dependence of $\langle\langle y \rangle\rangle$ one can easily obtain $\mathrm{d}\langle\langle y \rangle\rangle/\mathrm{d}t$, which, when extrapolated back to $t = 0$, yields $\langle\langle \Delta E \rangle\rangle_0$, the initial value of $\langle\langle \Delta E \rangle\rangle$, since (cf. eq. [4]) $\lim_{t\to 0} \mathrm{d}\langle\langle y \rangle\rangle/\omega\, \mathrm{d}t = \langle\langle \Delta E \rangle\rangle_0$. From eq. [2], we then have directly $\langle\langle \Delta E \rangle\rangle_0 \equiv \langle \Delta E \rangle$; in other words, for an initial δ function distribution, $\langle\langle \Delta E \rangle\rangle_0$ becomes identical with the microscopic $\langle \Delta E \rangle$. Thus $\langle \Delta E \rangle$ can be obtained at y_0, but its energy dependence is unknown; to do that it would be necessary to run a number of experiments with different initial δ function excitation energies y_0.

(*ii*) The second way to deal with the relaxation problem is represented by the special case, much discussed in the literature (3, 8, 9), when $\langle\langle y \rangle\rangle$ decays via a simple exponential (Bethe–Teller law):

$$[6] \quad \langle\langle y \rangle\rangle_\infty - \langle\langle y \rangle\rangle = (\langle\langle y \rangle\rangle_\infty - \langle\langle y \rangle\rangle_0) \exp(-t/\tau)$$

where $\langle\langle y \rangle\rangle_0$ and $\langle\langle y \rangle\rangle_\infty$ are, respectively, the initial and final (= equilibrium) values of $\langle\langle y \rangle\rangle$ (at $t = 0$ and $t \to \infty$), and τ is the relaxation time. A well-known theorem due to Shuler, Weiss, and Andersen (9) states that when the system relaxes via a simple exponential, the first moment of the transition probability (i.e. $\langle \Delta E \rangle$) must be a linear function of energy (this is the so-called "linear sum rule"), a relation that is valid for all y:

$$[7] \quad \langle \Delta E \rangle = a + by$$

where a and b are constants. Taking the bulk average of both sides of eq. [7], we get

$$[8] \quad \langle\langle \Delta E \rangle\rangle = a + b\langle\langle y \rangle\rangle$$

which holds at all times, in particular at $t \to \infty$, which in a non-reactive system represents equilibrium with the heat bath. Under these conditions, $\langle\langle y \rangle\rangle \to \langle\langle y \rangle\rangle_\infty$ and $\langle\langle \Delta E \rangle\rangle \to 0$ since at equilibrium there is no net energy transfer in the bulk system. Thus $a = -b\langle\langle y \rangle\rangle_\infty$, and so

$$[9] \quad \langle\langle \Delta E \rangle\rangle = -b(\langle\langle y \rangle\rangle_\infty - \langle\langle y \rangle\rangle)$$

These considerations show clearly that this analysis is inapplicable in a reactive system. The (observable) relaxation time is commonly defined by

$$[10] \quad \tau = \frac{\langle\langle y \rangle\rangle_\infty - \langle\langle y \rangle\rangle}{\mathrm{d}\langle\langle y \rangle\rangle/\mathrm{d}t}$$

Can. J. Chem. Downloaded from www.nrcresearchpress.com by 118.98.75.50 on 09/07/12
For personal use only.

which, in view of eq. [4], can be written equivalently as

$$[11] \quad \tau = \frac{\langle\langle y\rangle\rangle_\infty - \langle\langle y\rangle\rangle}{\omega\langle\langle \Delta E\rangle\rangle}$$

Combining eqs. [6] and [11] we get

$$[12] \quad \langle\langle \Delta E\rangle\rangle = \langle\langle \Delta E\rangle\rangle_0 \exp(-t/\tau)$$

where $\langle\langle \Delta E\rangle\rangle_0 = \langle\langle y\rangle\rangle_\infty - \langle\langle y\rangle\rangle_0$. From the comparison of [9] and [11] it follows that $-b = 1/\omega\tau$, so that eq. [7] becomes

$$[13] \quad \langle \Delta E\rangle = \frac{1}{\omega\tau}(\langle\langle y\rangle\rangle_\infty - y)$$

Thus the microscopic property $\langle \Delta E\rangle$ is given entirely in terms of the macroscopic observable $\langle\langle y\rangle\rangle$ and its time derivative which defines the relaxation time τ (via eq. [10]). Unlike in the preceding special case, the functional dependence of $\langle \Delta E\rangle$ on energy is now known for all energies. To achieve this, it was not necessary to solve the master equation, and therefore no assumption had to be made as to the nature of the model for the transition probability $q(x,y)$. Hence the result shown in eq. [13] is model-independent, but applies only if the decay of $\langle\langle y\rangle\rangle$ in a non-reactive system follows the simple exponential (eq. [6]).

It is of some interest to note that when $y = 0$, eq. [13] indicates a positive intercept, i.e. under these conditions $\langle \Delta E\rangle$ is not zero but is positive. This means that at low energies the energy dependence of $\langle \Delta E\rangle$ does not become much smaller than implied by eq. [13], as is sometimes suggested, but merely shows that in the vicinity of $y = 0$ only up-collisions occur. This is understandable since a molecule whose pre-collision energy is zero can only gain energy in a collision.

Inasmuch as $\langle\langle y\rangle\rangle_\infty$ can be easily calculated (e.g. from the Einstein function for a collection of harmonic oscillators), the only other parameter necessary to completely characterize $\langle \Delta E\rangle$ of eq. [13] (in addition to pressure which determines ω) is τ, which is readily obtainable from the experimentally observed time decay of $\langle\langle y\rangle\rangle$. Taking the logarithm of both sides of eq. [6] we see that a plot of $\ln(\langle\langle y\rangle\rangle - \langle\langle y\rangle\rangle_\infty)$ vs. time will yield a straight line of slope $-1/\tau$.

(*iii*) The third way to deal with the relaxation problem on hand concerns the special case when the decay of $\langle\langle y\rangle\rangle$ is *linear* over a time span that covers the dissipation of an *appreciable* fraction of initial excitation energy (clearly any decay will look linear if the time span corresponds to the dissipation of a small enough fraction of excitation energy). It can be shown (10) that this is an unmistakeable sign that the transition probability $q(x,y)$ is exponential. The consequence of this is that $\langle \Delta E\rangle$ is an energy-independent constant over the time span that corresponds to the linear portion of the $\langle\langle y\rangle\rangle$ decay. It follows from eq. [2] that consequently $\langle \Delta E\rangle \equiv \langle\langle \Delta E\rangle\rangle$ since $c(y,t)$ is normalized to unity.

Under these conditions there is therefore no distinction between the microscopic and macroscopic average energy transfers, and thus (cf. eq. [4]) the slope of the linear portion of the $\langle\langle y\rangle\rangle$ decay, divided by ω, gives $\langle \Delta E\rangle$ directly. However, as the system gets closer to equilibrium, $\langle \Delta E\rangle$ and $\langle\langle \Delta E\rangle\rangle$ do become distinct from one another, and $\langle\langle \Delta E\rangle\rangle$ eventually decays to zero, as of course it must when the system reaches equilibrium (cf. Fig. 3*b* in ref. 10).

Experimental results

The common feature of laser experiments that lend themselves to the analysis presented above is that the excitation of the target molecule (carefully selected for its "clean" photophysics) is achieved by one-photon absorption, first to an excited electronic state, which is then followed by fast internal conversion to produce the vibrationally excited target molecule in the ground electronic state. It is the relaxation of this vibrationally excited ground electronic state, immersed in a heat bath, that provides the signal which is a measure the internal energy as a function of time.

Two different methods were used to monitor the time-dependence of the internal energy of the excited molecule: infrared fluorescence from C—H stretch modes in the case of azulene, and uv absorbance measurements in all other cases. Details of the experiments can be found in the cited literature, and therefore only the most salient features will be mentioned here. The results shown below in the figures were recalculated from published data when necessary.

Probably the best-documented case of collisional relaxation is that of azulene studied by Barker and co-workers (1). Several thousand experiments were performed repetitively using signal-averaging in order to improve the signal/noise ratio, and the "calibration", i.e. the method for converting the measured signal (ir fluorescence in this particular case) into $\langle\langle y\rangle\rangle$ was carefully analysed (12). Arguments were presented to show that the ensemble of excited ground electronic state azulene molecules had a distribution of vibrational energies no wider than room temperature Boltzmann distribution, i.e. essentially a microcanonical (δ-function) distribution.

Two results of experiments performed with a nitrogen laser (excitation energy 337 nm = 29674 cm^{-1}) are shown in Fig. 1. In this and following figures a semi-logarithmic plot is used to provide a rapid visual check on exponential decay. The signal in Fig. 1 is seen to be quite free of noise over more than half the energy range, showing the relaxation to be clearly exponential, until increasing noise in the system makes interpretation uncertain. Similar experiments (not shown) were also performed at the lower excitation energy of 600 nm = 16667 cm^{-1}.

Time-resolved uv absorption measurements on excited benzene (B) were reported by Nakashima and Yoshihara (13), and on excited hexafluorobenzene (HFB) by Nakashima and Yoshihara (14), both using an ArF laser (excitation energy 193 nm = 51813 cm^{-1}). In this case the "calibration" was based on the modified Sulzer–Wieland model (15) of high-temperature spectra, with the assumption that the microcanonical distribution of excitation energy deposited in ground-state B or HFB produces absorption spectra that can be represented by a high-temperature Boltzmann (canonical) distribution involving all the vibrational modes, the average energy of which is equal to excitation energy. The time decay of the system is thus described by a series of Boltzmann distributions of progressively lower temperatures.

Figure 2 shows the relaxation of benzene in the presence of a number of bath gases, and generally shows exponential decay, except perhaps in the benzene–argon case (panel *a*) where there appears to be some drift. It is noteworthy that benzene self-relaxation shows good exponential decay all the way down to ~2000 cm^{-1}.

Similarly, Fig. 3 shows the relaxation of HFB, where there is some deviation from exponential behavior after about one-half of the excitation energy has decayed (using only the initial clearly linear parts of the plots would decrease the slopes by about 10%). Panel *a* of Fig. 3 also shows that in the case of HFB self-relaxation there is some small dependence on the observing frequency. All the data published in refs. 13 and 14 were based on the evaluation of oscilloscope traces of single experiments.

A summary of the experimental data on azulene, benzene, and HFB evaluated according to eq. [13] (linear energy dependence of $\langle \Delta E\rangle$) is shown in Table 1 where listed separately are the parameters $a = \langle\langle y\rangle\rangle_\infty/\omega\tau$, $b = -1/\omega\tau$ and $\omega\tau$. The dimensionless relaxation time $\omega\tau$ can be considered to represent roughly the number of collisions necessary to dissipate the excitation energy. For the purpose of comparing the various results at the same energy, the last column of Table 1 gives the absolute value of $\langle \Delta E\rangle$ calculated from eq. [7] for the arbitrarily chosen reference energy of $y = 30\,000$ cm^{-1}.

These results can be compared with those obtained by the Göttingen group (16–18) on the same or similar molecules at comparable excitation energies (KrF laser excitation at 248 nm = 40323 cm^{-1}).

Can. J. Chem. Downloaded from www.nrcresearchpress.com by 118.98.75.50 on 09/07/12
For personal use only.

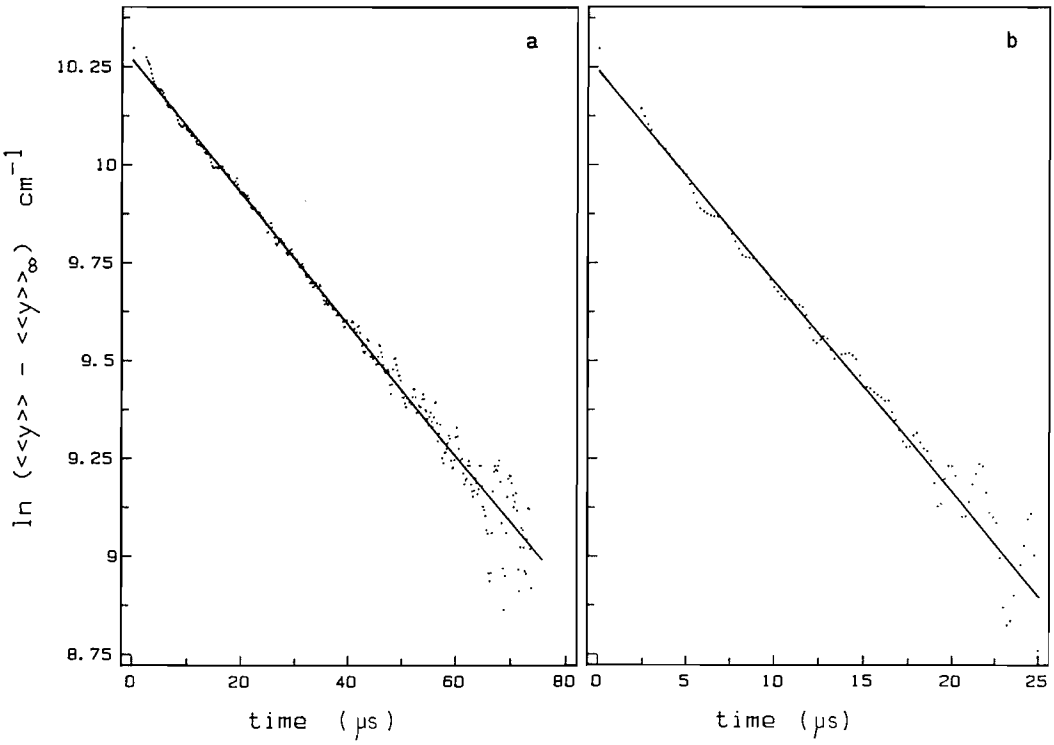

FIG. 1. Relaxation of azulene: (*a*) azulene self-relaxation, 8.9 mTorr (7306 laser shots); (*b*) azulene–argon mixture, 298 mTorr total pressure (9832 laser shots). Vertical scale is the same for both (*a*) and (*b*). Dots represent output from multichannel analyzer, converted into $\langle\langle y\rangle\rangle$; continuous line is the least-squares line calculated from smoothed experimental $\langle\langle y\rangle\rangle$ (data of refs. 11 and 12).

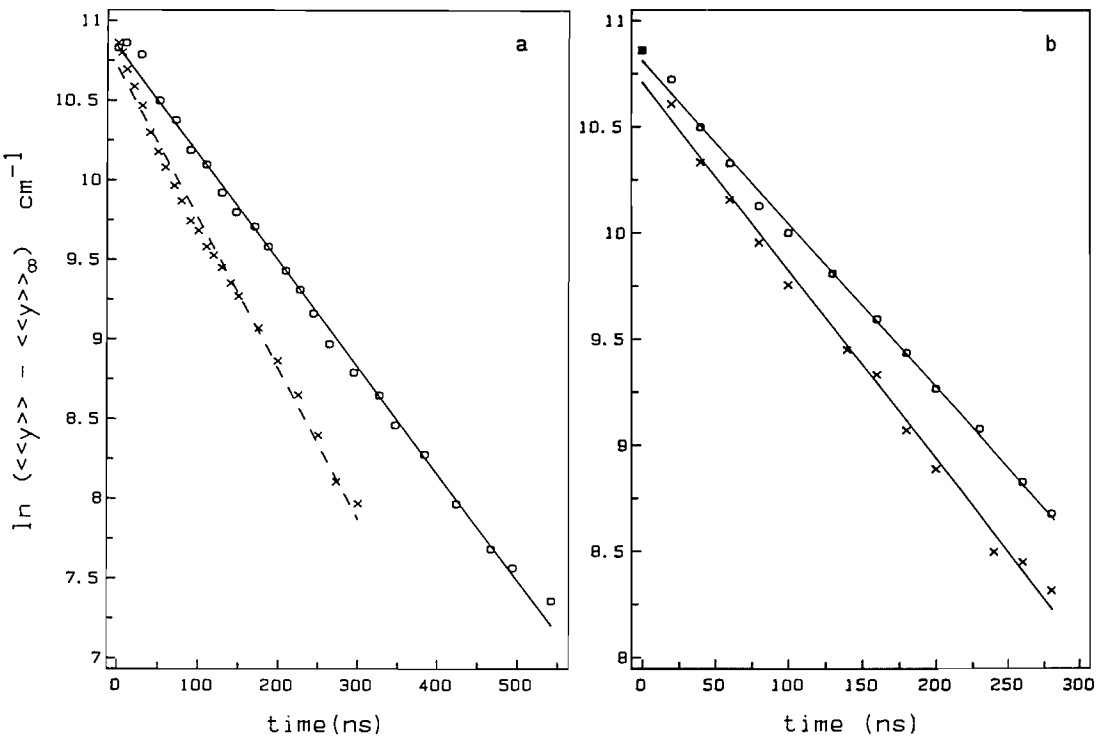

FIG. 2. Relaxation of benzene, observing frequency 220 nm: (*a*) ○: benzene self-relaxation, 8 Torr, ×: benzene–argon mixture, 802 Torr total pressure; (*b*) ○: benzene–N_2 mixture, 418 Torr total pressure; ×: benzene–isopentane mixture, 14 Torr total pressure. Straight lines calculated by least squares from experimental points (data of ref. 13).

They also used the calibration procedure based on the Sulzer–Wieland model and found, from the evaluation of single oscilloscope traces, that the decay of $\langle\langle y\rangle\rangle$ was linear in time, and therefore $\langle\Delta E\rangle$ was energy-independent (except, presumably, at very low energies; however, *vide supra*). This suggests an exponential transition probability. The molecules studied were azulene (16), toluene (17), ethylcycloheptatriene (18), and isopropyl cycloheptatriene (18).

A selection of these results is shown in Table 2, and it may be seen immediately that in spite of the disagreement about the energy dependence of $\langle\Delta E\rangle$, these results are roughly comparable (and for

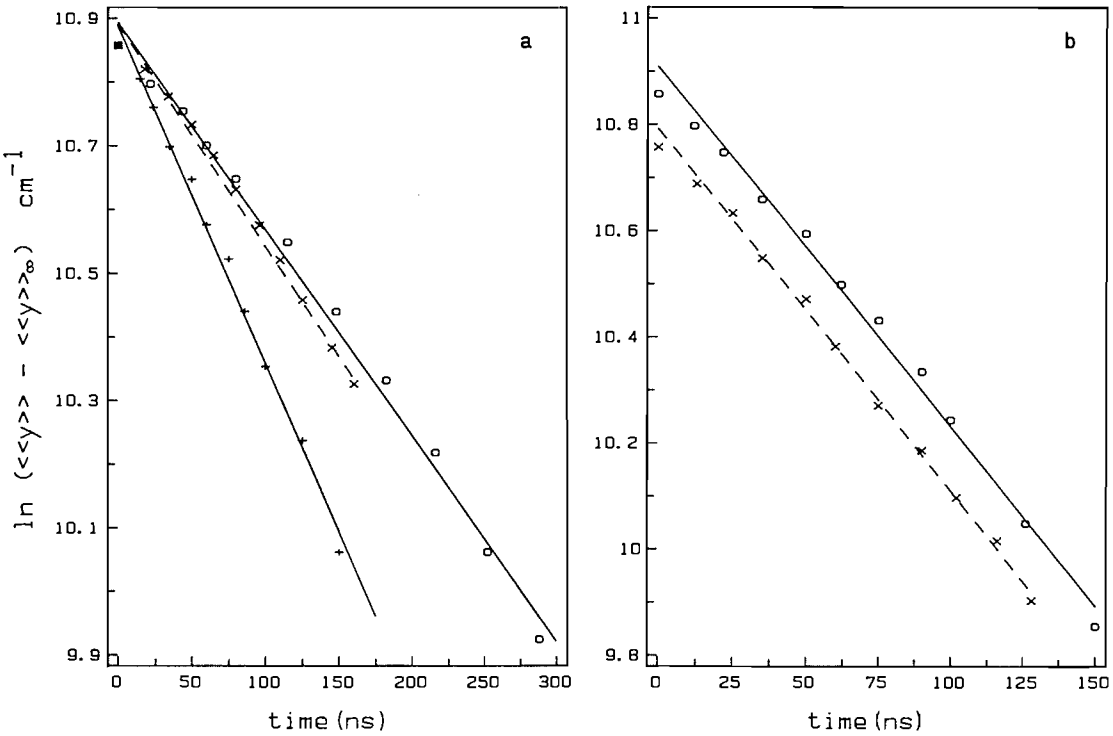

FIG. 3. Relaxation of hexafluorobenzene (HFB) observing frequency 300 nm except where noted: (*a*) ○: HFB self-relaxation, 6 Torr, ×: HFB self-relaxation, 6 Torr (350 nm observing frequency), +: HFB–argon mixture, 26 Torr total pressure; (*b*) ○: HFB–O_2 mixture, 27 Torr total pressure, ×: HFB–N_2 mixture, 28 Torr total pressure (displaced downward 0.1 $\log_e$ units for clarity). Straight lines calculated by least squares from experimental points (data of ref. 14).

TABLE 1. Parameters in equation $\langle \Delta E \rangle = a + by$ (eq. [7]) (all energies in cm^{-1})[a]

System	a	$-b$	$\omega\tau$	$\lvert\langle \Delta E \rangle\rvert$ at $y = 3 \times 10^4$
Az–Az	46.24	4.72×10^{-2}	21.2	1270
Az–Ar	8.22	8.40×10^{-3}	119	244
B–B	14.29	3.91×10^{-2}	25.6	1159
B–Ar	0.324	8.87×10^{-4}	1127	26
B–N_2	0.429	1.17×10^{-3}	855	35
B–ip*	10.13	2.77×10^{-2}	36.1	820
HFB–HFB	49.0	3.23×10^{-2}	30.9	920
HFB–Ar	5.57	3.68×10^{-3}	272	105
HFB–N_2	7.08	4.67×10^{-3}	214	133
HFB–O_2	6.70	4.43×10^{-3}	226	126

[a] $\omega\tau = -1/b$; Az = azulene, B = benzene, HFB = hexafluorobenzene, ip* = isopentane.

azulene–argon almost identical) to those shown in Table 1: larger colliders (this includes self-relaxation) yield for $\langle \Delta E \rangle$ values of the order of 1000 cm^{-1}, and diatomic or monoatomic colliders yield $\langle \Delta E \rangle$ roughly in the 200–300 cm^{-1} range. This comparison also reinforces the impression that the results in Table 1 for benzene–Ar and benzene–N_2 show anomalously low values of $\langle \Delta E \rangle$.

Discussion

In a very general way, and with the exceptions noted below, the results shown in Table 1 are roughly mutually consistent, in that the $\langle \Delta E \rangle$ values for self-relaxation are all in the 1000 cm^{-1} range, whereas relaxations involving argon and the diatomics lead to $\langle \Delta E \rangle$ in the range 100 to 200 cm^{-1}. This is also reflected in the dimensionless relaxation time $\omega\tau$ (third column in Table 1), inasmuch as $\omega\tau\langle \Delta E \rangle \sim y$. It is interesting to note in this connection that ultrasonic measurements yield (19) $\omega\tau \sim 50$ for benzene self-relaxation, which is within a factor of 2 of the value given in Table 1.

TABLE 2. Selection of Göttingen (16–18) results[a]

System	$\lvert\langle \Delta E \rangle\rvert$, cm^{-1}	System	$\lvert\langle \Delta E \rangle\rvert$, cm^{-1}
Az–Ar	210	CHT–Ar	180
		CHT–N_2	250
T–T	770	CHT–O_2	230
T–Ar	130	CHT–np	800
T–N_2	130		
T–np	740	iCHT–Ar	240
		iCHT–np	940

[a] Az = azulene, T = toluene, CHT = ethylcycloheptatriene, iCHT = isopropyl cycloheptatriene, np = *n*-pentane.

The exceptions seem to be the results involving benzene–Ar and benzene–N_2 where $\langle \Delta E \rangle$ appears to be too small by an order of magnitude. There is no obvious explanation for this discrepancy: although there seems to be some drift from exponential decay in these cases (Fig. 2), it is no worse (argon perhaps excepted) than in the case of HFB.

Given that — with the exceptions noted above — the numerical results in Table 1 and 2 are approximately comparable, the main disagreement between the results in Tables 1 and 2 is really only about the *form* of the energy dependence of $\langle \Delta E \rangle$. The question whether the decay of $\langle\langle y \rangle\rangle$ is linear, or exponential, or of some other form — which, as we have seen, determines ultimately the energy dependence of $\langle \Delta E \rangle$ — hinges crucially on the *shape* of the decay curve, which must therefore be well characterized. One of the difficulties is that we are dealing here with what are inherently noisy systems, especially if the data are obtained from a single oscilloscope trace at a single excitation

Can. J. Chem. Downloaded from www.nrcresearchpress.com by 118.98.75.50 on 09/07/12
For personal use only.

Can. J. Chem. Downloaded from www.nrcresearchpress.com by 118.98.75.50 on 09/07/12
For personal use only.

energy (as is the case of the work reported in refs. 13, 14, 16–18), so that judging the shape of the decay curve of $\langle\langle y\rangle\rangle$ is difficult at best. (Note, however, that it is shown in ref. 13 that assumption of constant $\langle\Delta E\rangle$ leads to decay curves that despite the noise are in clear disagreement with experiment.)[1]

In addition, toluene and the cycloheptatrienes are reactive systems where collisional relaxation occurs in competition with unimolecular reaction (e.g. toluene fragments into benzyl + H) which was assumed to be unimportant at the excitation energies used, but which nevertheless introduces an element of uncertainty into the interpretation of the experiments.[2] In this respect the azulene work is clearly superior, both on account of the signal averaging used and the absence of a reactive channel, and also because the energy dependence of $\langle\Delta E\rangle$ as shown in Table 1 could be approximately confirmed directly in the separate series of experiments using 600 nm excitation energy (11) (an example of special case (*i*)).

A more fundamental difficulty resides in the "calibration", i.e. in the fact that the signal actually measured is not $\langle\langle y\rangle\rangle$ but uv absorbance (or ir fluorescence intensity in the azulene work) which must then be converted into $\langle\langle y\rangle\rangle$. The shape of the calibration curve, i.e. the $\langle\langle y\rangle\rangle$ dependence of the signal, clearly has a major influence on the shape of the time decay of $\langle\langle y\rangle\rangle$, and thus on the energy dependence of $\langle\Delta E\rangle$. None of the calibration methods used so far are entirely free of objections. In principle, the question of the energy dependence of $\langle\Delta E\rangle$ could be settled more or less without calibration problems by experiments at a number of different excitation energies.[2]

Finally, a word about exponential decay which, as we have seen, is the macroscopic consequence of the linear dependence of $\langle\Delta E\rangle$ on y. It implies such severe restrictions (21) on the nature of the microscopic transition probability $q(x,y)$ as to make *strictly* exponential decay the exception rather than the rule, and therefore rather suspect. However, it can be shown (22) that *approximately* exponential decay (and this is all that can be ascertained in noisy systems) is very much less restrictive (23), and results in a $\langle\Delta E\rangle$ *approximately* linear in y. The corresponding dimensionless relaxation time $\omega\tau$ is then related to an *average* eigenvalue that characterizes the initial decay of the nonequilibrium ensemble.

[1]These experiments will be repeated using signal-averaging. (N. Nakashima, private communication).

[2]In a very recent series of experiments, Chung and Carr (20) have re-examined the collisional deactivation of ethylcycloheptatriene, this time excited to four different excitation energies. Master equation calculations using the stepladder model for collisional deactivation and RRKM theory for the fragmentation rate constant show that, within experimental error, $\langle\Delta E\rangle$ is an increasing *linear* function of energy in the range 35 000 to 43 000 cm^{-1}. Since this is a reactive system, the interpretation of $\langle\Delta E\rangle$ in terms of the constants that appear in eq. [13] does not apply here. It is also not clear what distortion (if any) has been introduced into the energy dependence of $\langle\Delta E\rangle$ by use of the stepladder model. This study is nevertheless significant in that it avoids the calibration difficulties associated with the other cited work.

Acknowledgments

This work has received financial support from the Natural Sciences and Engineering Research Council of Canada, and is hereby dedicated to Douglas E. Ryan on the occasion of his 65th birthday. The authors are grateful to N. Nakashima and R. W. Carr for correspondence and for providing preprints of refs. 14 and 21, respectively, in advance of publication.

1. D. C. Tardy and B. S. Rabinovitch. J. Chem. Phys. **45**, 3720 (1966); Chem. Rev. **77**, 369 (1977).
2. I. Procaccia and R. D. Levine. J. Chem. Phys. **62**, 2496 (1975).
3. N. G. van Kampen. Stochastic processes in physics and chemistry. North-Holland, Amsterdam. 1981. Chap. V.
4. W. Forst. J. Chem. Phys. **80**, 2504 (1984).
5. A. P. Penner and W. Forst. J. Chem. Phys. **67**, 5296 (1977); W. Forst and A. P. Penner. J. Chem. Phys. **72**, 1435 (1980).
6. C. A. Brau, J. D. Keck, and D. F. Carrier. Phys. Fluids, **9**, 1885 (1966).
7. B. J. Gaynor, R. G. Gilbert, and K. D. King. Chem. Phys. Lett. **55**, 40 (1978); R. G. Gilbert and K. D. King. Chem. Phys. **49**, 367 (1980); H. W. Schranz and S. Nordholm. Chem. Phys. **74**, 365 (1983).
8. K. E. Shuler. Phys. Fluids, **2**, 442 (1959); N. G. van Kampen. Adv. Chem. Phys. **15**, 65 (1969).
9. K. E. Shuler, G. H. Weiss, and K. Andersen. J. Math. Phys. **3**, 550 (1962).
10. W. Forst and G.-Y. Xu. J. Chem. Phys. **86**, 1269 (1987).
11. M. J. Rossi, J. R. Pladziewicz, and J. R. Barker. J. Chem. Phys. **78**, 6695 (1983); J. R. Barker. J. Phys. Chem. **88**, 11 (1984).
12. W. Forst and J. R. Barker. J. Chem. Phys. **83**, 124 (1985).
13. N. Nakashima and K. Yoshihara. J. Chem. Phys. **79**, 2727 (1983).
14. T. Ichimura, Y. Mori, N. Nakashima, and K. Yoshihara. J. Chem. Phys. **83**, 117 (1985).
15. H. Hippler, J. Troe, and H. J. Wendelken. J. Chem. Phys. **78**, 5351 (1983); L. Brouwer, H. Hippler, L. Lindemann, and J. Troe. J. Phys. Chem. **89**, 4608 (1985).
16. H. Hippler, L. Lindemann, and J. Troe. J. Chem. Phys. **83**, 3906 (1985).
17. H. Hippler, J. Troe, and H. J. Wendelken. J. Chem. Phys. **78**, 6709 (1983).
18. H. Hippler, J. Troe, and H. J. Wendelken. J. Chem. Phys. **78**, 6718 (1983).
19. J. D. Lambert. J. Chem. Soc. Faraday II, **68**, 364 (1972).
20. G.-Y. Chung and R. W. Carr, Jr. 9th International Symposium on Gas Kinetics. Bordeaux, July 1986. Preprint.
21. G. Gidiotis and W. Forst. J. Phys. Chem. **90**, 3496 (1986).
22. R. I. Cukier and K. E. Shuler. J. Chem. Phys. **57**, 302 (1972); R. I. Cukier and J. T. Hynes. J. Chem. Phys. **64**, 2674 (1976).
23. G. Gidiotis and W. Forst. To be published.

Synthesis of oligosaccharide structures unique to pituitary glycoprotein hormones

VANDANA AND OLE HINDSGAUL[1]
Department of Chemistry, University of Alberta, Edmonton, Alta., Canada T6G 2G2

AND

JACQUES U. BAENZIGER
Department of Pathology, Washington University School of Medicine, St. Louis, MO 63310, U.S.A.

Received January 5, 1987

VANDANA, OLE HINDSGAUL, and JACQUES U. BAENZIGER. Can. J. Chem. **65**, 1645 (1987).

The trisaccharide βDGalNac(1→4)βDGlcNAc(1→2)αDMan (**2**) and its 4″-*O*-sulfate ester (**3**) have been chemically synthesized as their 8-methoxycarbonyloctyl glycosides. Structures **2** and **3** contain oligosaccharide sequences unique to the asparagine-linked carbohydrate chains of pituitary glycoprotein hormones. The characteristic chemical shift for H-4 of the βDGalNAc residue in the sulfate ester **3** (4.692 ppm) is identical to that in the ^{1}H nuclear magnetic resonance spectrum of glycopeptides isolated from bovine lutropin (luteinizing hormone), thus establishing the position of sulfation in the natural structures.

VANDANA, OLE HINDSGAUL et JACQUES U. BAENZIGER. Can. J. Chem. **65**, 1645 (1987).

On a synthétisé chimiquement le trisaccharide βDGalNAc(1→4)βdGlcNAc(1→2)αDMan (**2**) et son ester *O*-sulfate-4″ (**3**), sous la forme de glycosides de méthoxycarbonyl-8 octyle. Les structures **2** et **3** contiennent la séquence oligosaccharide qui est unique aux chaînes d'hydrates de carbones des hormones glycoprotéines pituitaires qui sont liées à l'asparagine. Le déplacement chimique caractéristique pour le H-4 du résidu βDGalNAc, du sulfate de l'ester **3** (4,692 ppm), est identique à celui observé dans le spectre de résonance magnétique nucléaire du ^{1}H des glycopeptides isolés de la lutropine bovine (hormone de lutéinisation); ces résultats établissent donc la position de la sulfatation dans les structures naturelles.

[Traduit par la revue]

Introduction

Green *et al.* (1, 2) have recently reported the structural elucidation of the asparagine (Asn)-linked carbohydrate chains of the pituitary glycoprotein hormone lutropin (luteinizing hormone). The carbohydrates were found to contain varying amounts of DGalNAc and sulfate, which occurred in both complex and hybrid oligosaccharide structures. The major ionic oligosaccharide isolated was the disulfated biantennary structure **1**, which accounted for 31% of the total carbohydrate. This structure contains the unusual sequence $SO_3 \rightarrow$ βDGalNAc(1→4)βDGlcNAc(1→2)αDMan---, which appears unique to pituitary glycoprotein hormones. The position of the sulfate ester could not be established but was restricted to either the 3 or 4 position of the βDGalNAc residues in both **1** and related hybrid structures. These unusual oligosaccharides are found on lutropin and in small amounts of follitropin but not on other glycoproteins synthesized by the pituitary gonadotroph (3).

To aid in assessing the functional significance of this unique hormonal glycosylation we have chemically synthesized the lutropin trisaccharide terminus βDGalNAc(1→4)βDGlcNAc-(1→2)αDManOR (**2**) and its 4″-*O*-sulfate ester (**3**), as their 8-methoxycarbonyloctyl glycosides (R = $(CH_2)_8COOCH_3$) (4). Compound **2** should be useful as an acceptor in assaying the pituitary sulfotransferase activity, which we expect will catalyze its conversion to **3** in the presence of adenosine 3′-phosphate 5′-phosphosulfate (3). Compound **3**, as its synthetic glycoconjugates, will be used in the production and isolation (5) of antibodies directed to the "completed" hormonal structures.

Results and discussion

The target trisaccharides **2** and **3** were prepared from the key intermediate **16**, which was protected in a manner that allowed the selective liberation of the 4″-OH group for sulfation prior to deblocking. Two different routes were examined for the preparation of **16**. In the first approach, **16** was prepared by addition (using **11**) of the terminal DGalNAc residue to the preformed disaccharide derivative **15**. Since at the time this work began the position of the sulfate ester on the terminal DGalNAc was not known, this route offered the advantage of allowing the terminal addition of a DGalNAc derivative different from **11**, which could then later be sulfated at the 3- instead of the 4-position. The second route examined involved the addition of the preformed βDGalNAc(1→4)DGlcNAc disaccharide derivative **22** to the mannose residue **13**. While this route would be less efficient, it could be easily extended to the construction of larger oligosaccharides terminating in the required βDGalNAc(1→4)βDGlcNAc--- sequence should the need for such structures arise.

Reductive opening of the benzylidene ring in the readily accessible DGlcNAc derivative **4** (6), using $NaCNBH_3$/HCl (7), gave the 3,6-di-*O*-benzyl derivative **5** (8) (89%). Glycoside **5** was acetylated to provide **6** whose allyl group was removed by sequential isomerization using tris(triphenylphosphine)rho-

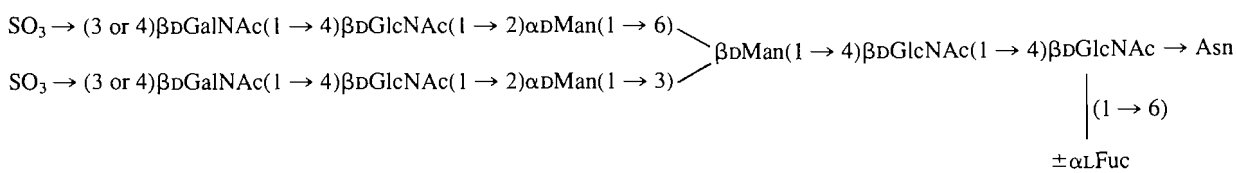

1

[1]Author to whom correspondence may be addressed.

Can. J. Chem. Downloaded from www.nrcresearchpress.com by 72.64.146.136 on 09/07/12
For personal use only.

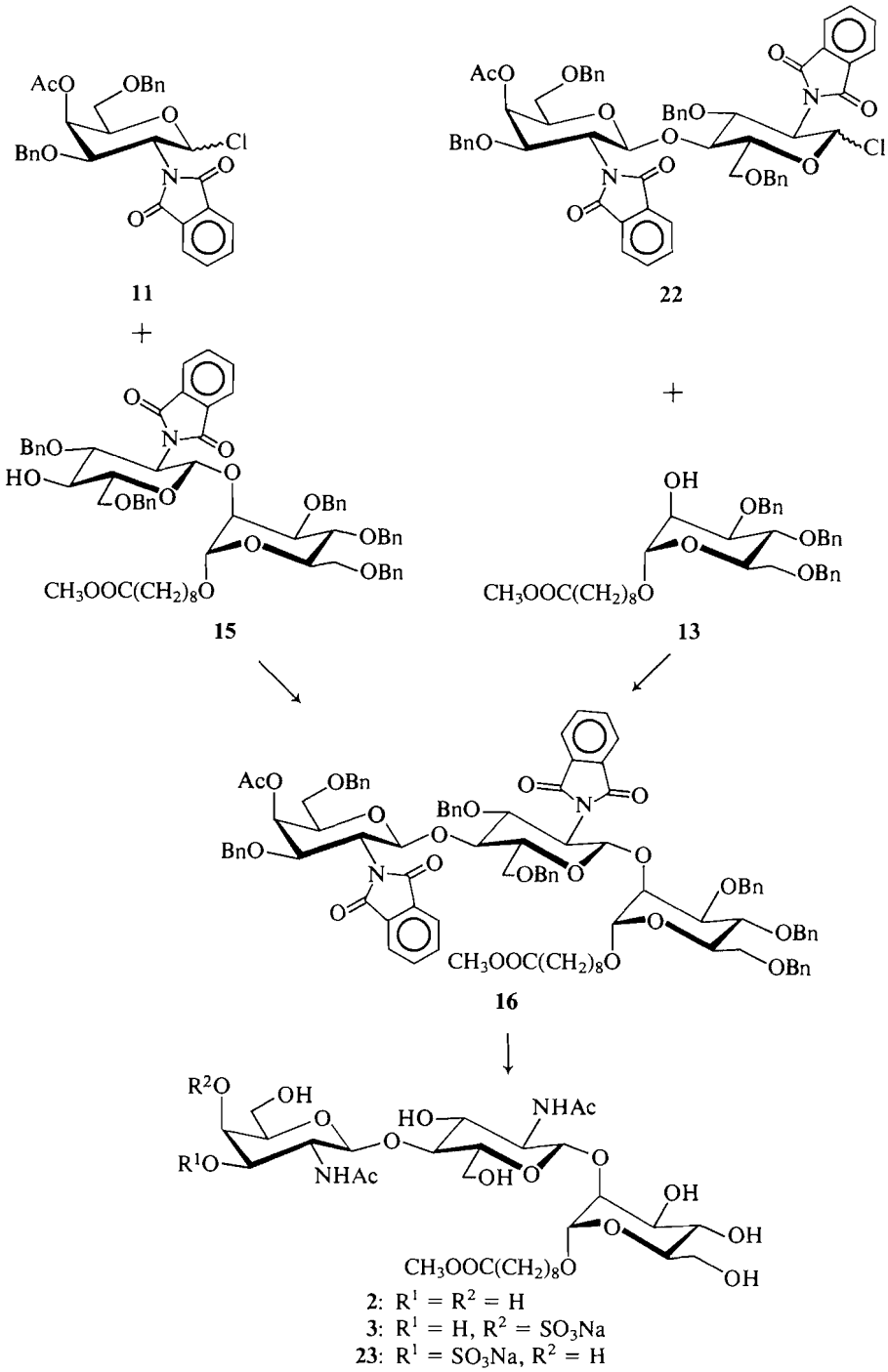

dium(I) chloride (9) and mercuric ion catalyzed hydrolysis to provide an anomeric mixture of reducing sugars **7** (86%). Reaction of **7** with oxalyl chloride (10), in the presence of dimethylformamide, then gave the glycosyl chlorides **8** (8).

Condensation of **8** and **13**, prepared by de-*O*-acetylation of previously reported **12** (11), in the presence of silver trifluoromethanesulfate and *sym*-collidine, gave the expected (12) β-linked disaccharide **14** in 69% yield. The β configuration of the new glycosidic linkage in **14** was evident from the observation of the signal for the H-1′ (5.286 ppm, $J_{1',2'}$ = 8.0 Hz) in its ^{1}H nmr spectrum. De-*O*-acetylation of **14**, with sodium methoxide in methanol, then gave the alcohol **15**.

The glycosyl chloride **11**, required for the homologation of **15** to **16**, was conveniently prepared from the DGlcNAc derivative **5**. Reaction of **5** with trifluoromethanesulfonic anhydride (13), in dichloromethane–pyridine, gave the 4-*O*-trifluoromethanesulfonate, which was not characterized but converted directly to the DGalNAc derivative **9** (83%) by reaction of tetraethylammonium acetate in dimethylformamide. Removal of the allyl group in **9** gave the reducing sugars **10**, which were converted, as before, to the glycosyl chlorides **11**.

Condensation of **11** and **15** gave the β-linked key intermediate **16** (64%) whose structure was supported by its ^{1}H nmr spectrum, which showed the presence of two signals for anomeric protons at 5.337 and 5.104 ppm with coupling constants of 8.5 and 8.0 Hz, respectively. Reaction of **16** with hydrazine acetate in refluxing methanol (14) gave the di-*N*-acetyl derivative **17** in acceptable (69%) yield. Attempted

Can. J. Chem. Downloaded from www.nrcresearchpress.com by 72.64.146.136 on 09/07/12
For personal use only.

Can. J. Chem. Downloaded from www.nrcresearchpress.com by 72.64.146.136 on 09/07/12
For personal use only.

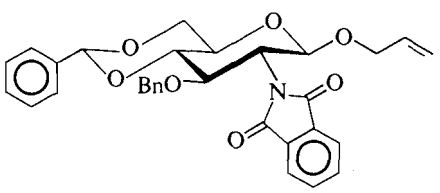

4

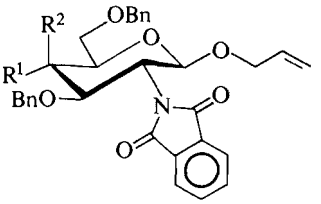

5: R^1 = OH, R^2 = H
6: R^1 = OAc, R^2 = H
9: R^1 = H, R^2 = OAc

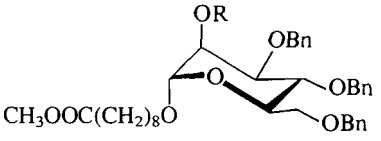

12: R = Ac
13: R = H

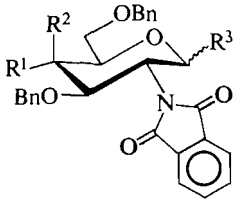

7: R^1 = OAc, R^2 = H, R^3 = OH
8: R^1 = OAc, R^2 = H, R^3 = Cl
10: R^1 = H, R^2 = OAc, R^3 = OH
11: R^1 = H, R^2 = OAc, R^3 = Cl

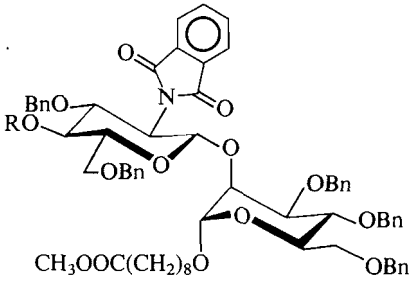

14: R = Ac
15: R = H

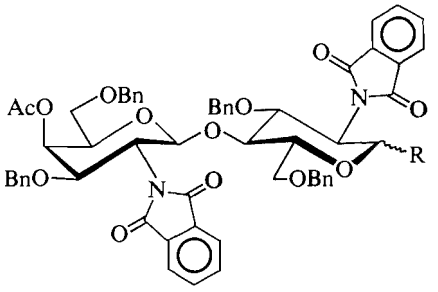

20: R = $OCH_2CH{=}CH_2$ (β)
21: R = OH
22: R = Cl

conversion of **16** to **17** using hydrazine hydrate in refluxing methanol (15) gave only low (15–40%) yields that were not reproducible. The major side products in these latter reactions appeared to be derived from attack of hydrazine on the methyl ester, based on the absence of the methoxy signal in the ^{1}H nmr spectra of the crude products. De-*O*-acetylation of **17** gave the 4″-OH compound **18**.

Sulfation of **18** proceeded smoothly using sulfur trioxide – pyridine (16) complex in dimethylformamide at room temperature to yield **19** (93%) as its sodium salt after ion exchange. Removal of the remaining benzyl ether protecting groups in **18** and **19** using hydrogenolysis over palladium on charcoal gave the target trisaccharides **2** (82%) and **3** (84%).

The alternate route to **16** required the preparation of the disaccharidic glycosyl chloride **22** and its condensation with **13**. Glycosylation of **5** with **11** gave the β(1→4)-linked disaccharide **20** (66%) (H-1′, 5.329 ppm, $J_{1',2'}$ = 8.2 Hz), which was easily elaborated into **22** by allyl group removal followed by conversion of the reducing sugar **21** (85%) to the glycosyl chloride **22** in conventional fashion. Condensation of **13** with **22** (1.4 equiv.) then gave the β-linked trisaccharide **16** in 47% yield. It is expected that this yield could be substantially improved by use of a larger excess of **22** in the glycosylation since hydrolysis and elimination of HCl to form the glycal are known (12) to be major side reactions of phthalimido-halo sugars such as **22**. Such conditions were, however, not explored in this work since sufficient **16** had already been generated by the previous stepwise route.

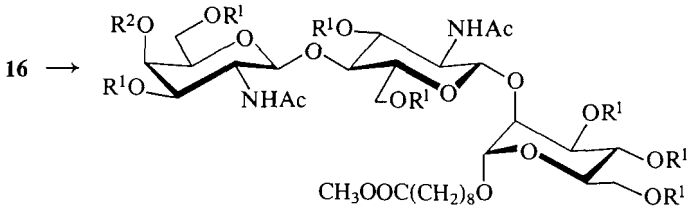

17: R^1 = Bn, R^2 = Ac
2: R^1 = R^2 = H ← **18**: R^1 = Bn, R^2 = H
3: R^1 = H, R^2 = SO_3Na ← **19**: R^1 = Bn, R^2 = SO_3Na

Comparison of the ^{1}H nmr spectra of **2** and **3** showed that sulfation of OH-4″ of **2** produced a large downfield shift in the signal for H-4″ in **3**. This signal is a characteristic doublet of doublets ($J_{3,4} \approx 3.2$ Hz, $J_{4,5} < 1$ Hz) in simple βDGalNAc glycosides (17) and is found near 3.9 ppm in such structures, as well as in **2**, where it is obscured by other ring protons. In the sulfated structure **3**, however, a doublet for H-4″ (4.692 ppm, $J_{3'',4''} = 2.3 \pm 0.2$ Hz) was clearly visible in the "anomeric region" of the spectrum, which coupled to H-3″ at 3.91 ppm. The observed decrease in $J_{3'',4''}$ is expected (18) as a result of the antiperiplanar orientation of the electronegative sulfate group to

Can. J. Chem. Downloaded from www.nrcresearchpress.com by 72.64.146.136 on 09/07/12
For personal use only.

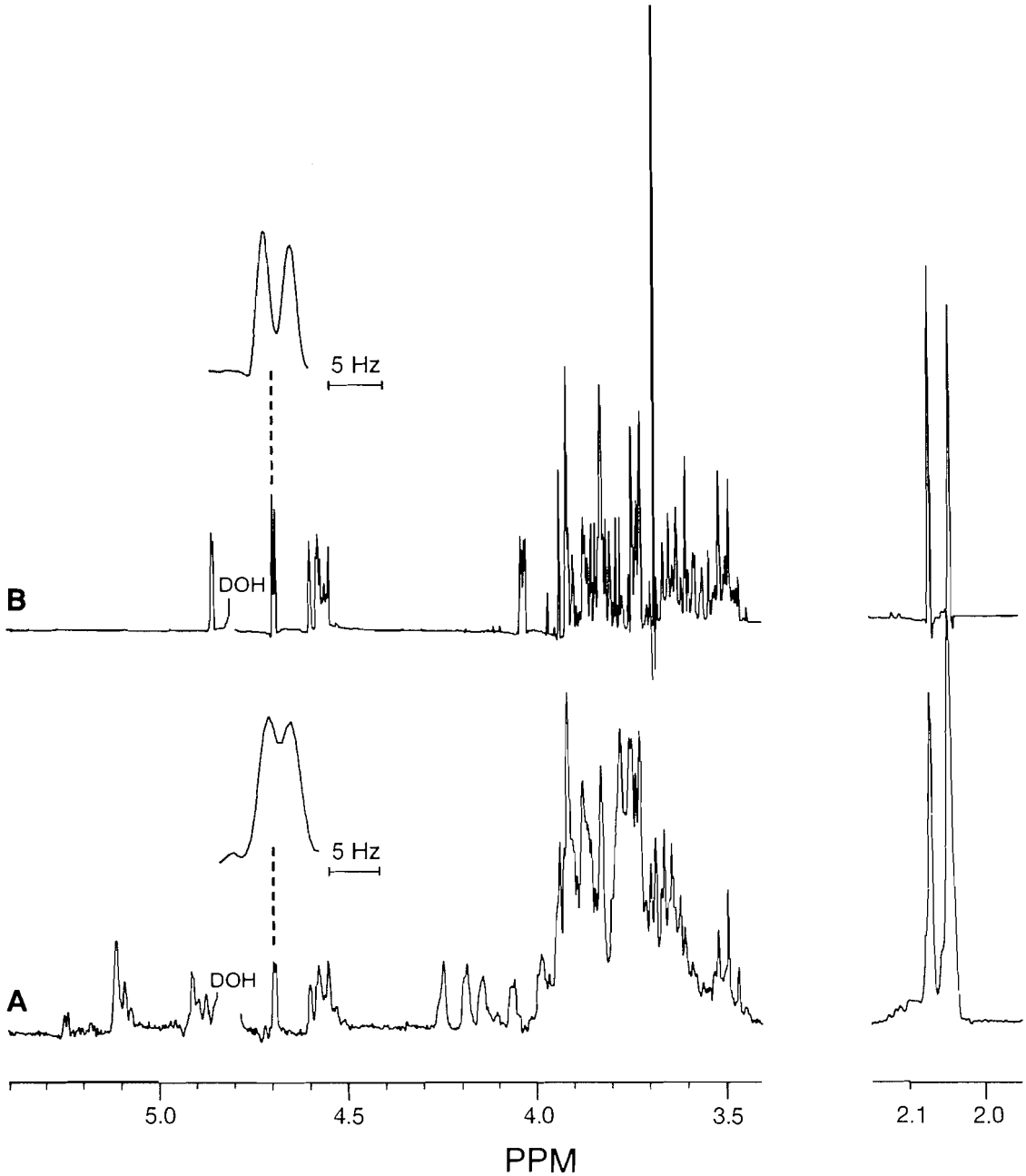

FIG. 1. Comparison of the resolution-enhanced 360-MHz ^{1}H nmr spectra of a glycopeptide mixture isolated from bovine lutropin (2) (A) and the synthetic 4″-O-sulfated trisaccharide **3** (B). The inset expansions show the signals assigned to H-4 of the terminal sulfated βDGalNAc residues. Spectra were recorded in D_2O at 296 K, acetone internal standard (δ 2.225 ppm).

H-3″. $J_{4'',5''}$ could not be resolved and was therefore significantly less than 1 Hz.

The characteristic shift of H-4″ in synthetic **3** could be used to unequivocally establish the position of sulfation of the βDGalNAc residues in the naturally occurring structures. In Fig. 1 the ^{1}H nmr spectrum of a mixture of monosulfated hybrid and complex lutropin glycopeptides (2, 3) is compared with a spectrum of **3** recorded under identical conditions. The glycopeptides show the expected anomeric signals for additional αDMan and βDGlcNAc residues not present in **3** but the key feature is the appearance of the characteristic βDGalNAc H-4 doublet at δ 4.692 ppm ($J_{3,4} \approx 2.2$ Hz) in both spectra. This signal collapsed to a singlet on irradiation at 3.91 ppm in both samples. Signals corresponding to the *N*-acetyl methyl groups of **3**, at 2.071 and 2.044 ppm, are also present in the glycopeptide spectrum.

Comparison of the spectra shown in Fig. 1 leaves no doubt that the βDGalNAc residues in the major lutropin glycopeptides are sulfated at the 4-position. The possibility that a minor fraction of these structures bear 3-*O*-sulfated βDGalNAc residues cannot be excluded on the basis of this evidence. We have, however, recently synthesized the 3″-sulfate ester of **2**,[2] namely 8-methoxycarbonyloctyl 2-*O*-[2-acetamido-4-*O*-(2-acetamido-2-deoxy-3-*O*-sulfo-β-D-galactopyranosyl)-2-deoxy-β-D-glucopyranosyl]-α-D-mannopyranoside sodium salt (**23**). The ^{1}H nmr spectrum of **23** displays characteristic signals for

[2]Vandana and O. Hindsgaul. Manuscript in preparation.

Can. J. Chem. Downloaded from www.nrcresearchpress.com by 72.64.146.136 on 09/07/12
For personal use only.

H-3″ (dd, 4.437 ppm, $J_{2'',3''}$ = 11.0 and $J_{2'',4''}$ = 3.0 Hz), H-4″ (d, 4.254 ppm, $J_{4'',5''} < 1$ Hz), and H-1″ (d, 4.675 ppm, $J_{1'',2''}$ = 8.8 Hz). The absence of a signal for H-3 of an αDGalNAc residue near 4.4 ppm in Fig. 1, A, strongly suggests that Asn-linked oligosaccharides are exclusively 4-*O*-sulfated on the terminal βDGalNAc residues.

Experimental

All solvents and reagents used were reagent grade. All solid reactants for glycosylation were dried overnight over phosphorus pentoxide in a high vacuum prior to use. Solution transfers where anhydrous conditions were required were done under nitrogen using standard syringe techniques. Unless otherwise stated, all reactions were performed at ambient temperatures. Molecular sieves were purchased from BDH Chemicals.

Thin-layer chromatograms (tlc) were performed on precoated silica gel 60-F254 plates (E. Merck, Darmstadt) and visualized by quenching of fluorescence and (or) by charring after spraying with 5% sulfuric acid in ethanol. Unless otherwise stated, chromatography was performed on silica gel 60 (40-63 μm, E. Merck No. 9385). Organic solutions were dried over sodium sulfate prior to solvent removal on a rotary evaporator under the vacuum of a water aspirator with bath temperatures of 40°C or lower. For gel filtration, Bio-Gel P-2 (200–400 mesh) (Bio-Rad Laboratories, Richmond, CA) was used.

Proton nuclear magnetic resonance (^{1}H nmr) spectra were recorded at either 300 MHz (Bruker AM-300) or 360 MHz (Bruker WM-360) with either tetramethylsilane (δ = 0 in $CDCl_3$ and CD_3OD) or acetone (δ = 2.225 in D_2O) as internal standard at ambient temperature. Carbon-13 nuclear magnetic resonance (^{13}C nmr) spectra were recorded at either 75.5 MHz (Bruker AM-300) or 90.56 MHz (Bruker WM-360) with either internal tetramethylsilane (δ = 0 in $CDCl_3$ or CD_3OD) or external 1% 1,4-dioxane (δ = 67.4 in D_2O) as reference standard. Only partial nmr data are reported. Other spectra features were in accord with the proposed structures. The ^{1}H nmr coupling constants are reported as though they were first order. Assignments of ^{13}C resonances are tentative. Optical rotations were determined on a Perkin–Elmer 241 polarimeter in a 1-dm cell at ambient temperatures (23 ± 1°C).

*Allyl 3,6-di-*O*-benzyl-2-deoxy-2-phthalimido-β-D-glucopyranoside (**5**)*

A mixture of allyl 3-*O*-benzyl-4,6-*O*-benzylidene-2-deoxy-2-phthalimido-β-D-glucopyranoside (**4**) (6.50 g, 12.3 mmol), sodium cyanoborohydride (4.42 g, 70.3 mmol), and a crystal of methyl orange in tetrahydrofuran (80 mL) was stirred at 0°C under nitrogen atmosphere. To this clear solution was added dropwise over 0.5 h a solution of diethyl ether saturated with hydrogen chloride (10 mL) until the red color of the indicator persisted. The reaction mixture was diluted with dichloromethane (100 mL), solids were removed by filtration, and the filtrate was washed with saturated $NaHCO_3$ followed by water. Solvent removal left a residue, which was dissolved in a mixture of methanol–dichloromethane (1:1) and passed through a deionized mixed bed ion-exchange resin (Amberlite MB-1, 20 mL). The resin was washed with methanol–CH_2Cl_2 (1:1) and the solvent was evaporated to provide a syrup, which was purified by chromatography using ethyl acetate – toluene (1:6) as eluent. The title compound, **5**, was obtained as a clear syrup (5.80 g, 89%); $[\alpha]_D$ +31.4° (*c* 1.0, chloroform); R_f 0.36 in ethyl acetate – toluene, 1:3; ^{1}H nmr ($CDCl_3$) δ: 5.666 (m, 1H, CH_2=C*H*CH_2), 5.190 (d, 1H, $J_{1,2}$ = 8.0 Hz, H-1), 3.123 (d, 1H, $J_{4,OH}$ = 3.0 Hz, D_2O exchangeable, OH); ^{13}C nmr ($CDCl_3$) δ: 117.26 (*C*H_2=CHCH_2), 97.31 (C-1), 69.69 (C-6), 55.30 (C-2). *Anal.* calcd. for $C_{31}H_{31}NO_7$: C 70.30, H 5.90, N 2.64; found: C 70.51, H 5.84, N 2.56.

*Allyl 4-*O*-acetyl-3,6-di-*O*-benzyl-2-deoxy-2-phthalimido-β-D-glucopyranoside (**6**)*

Acetic anhydride (5 mL) was added to a solution of **5** (1.25 g, 2.36 mmol) in dry pyridine (10 mL) and the solution was kept for 2 h. Excess acetic anhydride was decomposed by dropwise addition of ethanol (2 mL) to the ice-cold reaction mixture and the solvent was evaporated. The residue was dissolved in dichloromethane (20 mL), washed with water, and the aqueous layer was extracted with dichloromethane. The combined dichloromethane extracts were washed with 5% HCl, and with saturated $NaHCO_3$ followed by water. Solvent removal left a white solid (1.30 g, 96%); $[\alpha]_D$ +65.4° (*c* 0.37, chloroform); R_f 0.39 (ethyl acetate – hexane, 2:3); ^{1}H nmr ($CDCl_3$) δ: 5.678 (m, 1H, CH_2=C*H*CH_2), 5.192 (d, $J_{1,2}$ = 8.5 Hz, H-1), 5.135 (dd, $J_{3,4}$ = 9.0 Hz, $J_{4,5}$ = 10.0 Hz, H-4), 1.940 (s, 3H, $COCH_3$); ^{13}C nmr ($CDCl_3$) δ: 169.64 (*C*OCH_3), 117.46 (*C*H_2=CHCH_2), 97.27 (C-1), 55.45 (C-2), 20.90 (CO*C*H_3). *Anal.* calcd. for $C_{33}H_{33}NO_8$: C 69.34, H 5.82, N 2.45; found: C 69.04, H 5.82, N 2.55.

*4-*O*-Acetyl-3,6-di-*O*-benzyl-2-deoxy-2-phthalimido-α,β-D-glucopyranose (**7**)*

A solution of **6** (1.30 g, 2.27 mmol), tris(triphenylphosphine)rhodium(I) chloride (295 mg, 0.32 mmol), and 1,8-diazabicyclo[2.2.2]-octane (107.3 mg, 0.96 mmol) in ethanol–benzene–water (7:3:1; 80 mL) was heated at reflux for 24 h. Solvent was removed and the residue dissolved in acetone (50 mL) containing mercuric oxide (10 mg). To this solution was added a solution of mercuric chloride (3.09 g) in acetone–water (9:1, 50 mL) and the mixture was stirred for 2 h. Following solvent evaporation the residue was dissolved in dichloromethane (100 mL) and washed with 30% KBr followed by water. Evaporation left a syrup, which was purified by chromatography using ethyl acetate – hexane (2:3) as eluent. The title compound was obtained as a white solid (1.04 mg, 86%); R_f 0.36–0.40 (ethyl acetate – hexane, 1:1); ^{1}H nmr ($CDCl_3$) δ: 5.36 (1H, H-1β ($J_{1,2}$ = 8.5 Hz) and H-1α), 3.489 (d, ≈0.15H, D_2O exchangeable, $J_{1,OH}$ = 5.5 Hz, OHα), 3.179 (d, ≈0.85H, D_2O exchangeable, J = 8.0 Hz, OHβ), 1.939 (s, ≈2.5H, $COCH_3$β), 1.915 (s, ≈0.5H, $COCH_3$α). *Anal.* calcd. for $C_{30}H_{29}NO_8$: C 67.78, H 5.50, N 2.64; found: C 67.78, H 5.76, N 2.47.

*4-*O*-Acetyl-3,6-di-*O*-benzyl-2-deoxy-2-phthalimido-α,β-D-glucopyranosyl chloride (**8**)*

A solution of oxalyl chloride (394 μL, 4.52 mmol) in dichloromethane (1 mL) was added dropwise to a stirring solution of **7** (800 mg, 1.51 mmol) and *N*,*N*-dimethylformamide; (35 μL, 0.45 mmol) in dichloromethane (2 mL). After stirring for 2 h the mixture was diluted with dichloromethane (10 mL) and poured into ice water. The organic layer was washed with cold water (3 × 25 mL), dried (Na_2SO_4), and concentrated to a pale yellow foam that showed the presence of two compounds by tlc. The major anomer (**8**β) had R_f 0.45 and the minor anomer (**8**α) had R_f 0.55 in ethyl acetate – hexane (7:10); ^{1}H nmr ($CDCl_3$) δ: 6.224 (d, ≈0.3H, $J_{1,2}$ = 3.5 Hz, H-1α), 5.981 (m, ≈0.7H, $J_{1,2}$ = 9.0 Hz, H-1β), 1.942 (s, ≈2H, $COCH_3$β), 1.898 (s, ≈1H, $COCH_3$α).

*Allyl 4-*O*-acetyl-3,6-di-*O*-benzyl-2-deoxy-2-phthalimido-β-D-galactopyranoside (**9**)*

Compound **5** (1.27 g; 2.40 mmol) was dissolved in dry dichloromethane (20 mL), dry pyridine (1 mL) was added, and the mixture was cooled to −5°C. To this stirring mixture was added dropwise a solution of trifluoromethanesulfonic anhydride (0.97 mL; 5.76 mmol) in dry dichloromethane (2 mL) and the reaction mixture was stirred for 0.5 h. After dilution with dichloromethane (20 mL) and washing with ice-cold 5% HCl and ice water, solvent was evaporated at 0°C to leave a foam that showed a single spot on tlc examination (R_f 0.31 in ethyl acetate – hexane, 2:5), presumably the trifluoromethanesulfonyl ester of **5**. To this residue was added a solution of tetraethylammonium acetate (2.27 g, 11.98 mmol) in dry dimethylformamide (22 mL) and the resulting mixture was stirred for 4 h. Solvent was evaporated and the residue was dissolved in chloroform and washed with cold water (3 × 20 mL). Solvent removal left a syrup, which was purified by chromatography using ethyl acetate – hexane (2:5) as eluent. The title compound was obtained as a foam (1.14 g, 83%); $[\alpha]_D$ +54.9° (*c* 0.89, chloroform); R_f 0.34 in ethyl acetate – hexane 1:2; ^{1}H nmr ($CDCl_3$) δ: 5.668 (m, 2H, CH_2=C*H*CH_2) and H-4 (dd, $J_{3,4}$ = 3.2 Hz, $J_{4,5}$ = 1.0 Hz)), 5.182 (d, 1H, $J_{1,2}$ = 8.5 Hz, H-1), 2.138 (s, 3H, $COCH_3$);

^{13}C nmr ($CDCl_3$) δ: 170.44 ($COCH_3$), 117.45 (CH_2=$CHCH_2$), 97.56 (C-1), 52.92 (C-2), 20.92 ($COCH_3$). *Anal.* calcd. for $C_{33}H_{33}NO_8$: C 69.34, H 5.82, N 2.45; found: C 69.16, H 5.81, N 2.46.

*4-O-Acetyl-3,6-di-O-benzyl-2-deoxy-2-phthalimido-α,β-D-galactopyranose (**10**)*

The allyl group in **9** (870 mg, 1.52 mmol) was removed exactly as described for the preparation of **7**. Purification by chromatography using ethyl acetate – hexane (7:10) as eluent gave **10** as a white solid (690 mg, 85%) that showed the presence of both anomers on tlc; R_f 0.30 (**10β**) and R_f 0.37 (**10α**) in ethyl acetate – hexane (1:1); ^{1}H nmr ($CDCl_3$) δ: 5.660 (dd, >0.9H, $J_{3,4}$ = 3.2 Hz, $J_{4,5}$ = 1.0 Hz, H-4β), 5.326 (dd, >0.9H, $J_{1,2}$ = 8.5 Hz, $J_{1,OH}$ = 8.0 Hz, H-1β), 3.092 (d, >0.9H, D_2O exchangeable, OHβ), 2.142 (s, >2.7H, $COCH_3$β), 2.108 (s, <0.3H, $COCH_3$α). *Anal.* calcd. for $C_{30}H_{29}NO_8$: C 67.78, H 5.50, N 2.64; found: C 67.46, H 5.50, N 2.73.

*4-O-Acetyl-3,6-di-O-benzyl-2-deoxy-2-phthalimido-α,β-D-galactopyranosyl chloride (**11**)*

Compound **10** (800 mg, 1.51 mmol) was reacted with oxalyl chloride as described for the conversion of **7** to **8**. The product was obtained as a yellowish foam (800 mg, 97%) that showed the presence of both anomers by tlc: R_f 0.41 (**11β**) and R_f 0.48 (**11α**) in ethyl acetate – hexane (7:10); ^{1}H nmr ($CDCl_3$) δ: 6.329 (≈0.2H, $J_{1,2}$ = 3.5 Hz, H-1α), 5.986 (d, ≈0.8H, $J_{1,2}$ = 9.0 Hz, H-1β), 2.160 (s, ≈2.4H, $COCH_3$β), 2.080 (s, ≈0.6H, $COCH_3$α).

*8-Methoxycarbonyloctyl 3,4,6-tri-O-benzyl-α-D-mannopyranoside (**13**)*

8-Methoxycarbonyloctyl 2-*O*-acetyl-3,4,6-tri-*O*-benzyl-α-D-mannopyranoside (**12**, 1.10 g, 1.66 mmol) was dissolved in dry methanol (20 mL) containing sodium methoxide (10 mg). After 4 h, the solution was neutralized by addition of Amberlite IR-120 (H) resin, resin was removed by filtration, and solvent was evaporated to provide **13** as a clear syrup (1.0 g, 97%); $[\alpha]_D$ +38.6° (*c* 0.36, chloroform); R_f 0.38 in ethyl acetate – hexane 7:10; ^{1}H nmr ($CDCl_3$) δ: 4.881 (d, 1H, $J_{1,2}$ = 1.5 Hz, H-1), 4.025 (ddd, 1H, $J_{2,3}$ = 3.2, $J_{2,OH}$ = 2.5 Hz, H-2), 3.685 (s, OCH_3), 2.469 (d, 1H, D_2O exchangeable, OH), 2.291 (t, 2H, *J* = 7.5 Hz, CH_2COO); ^{13}C nmr ($CDCl_3$) δ: 174.26 ($COOCH_3$), 99.16 (C-1, $^1J_{C,H}$ = 167.5 Hz), 51.43 (OCH_3), 34.07 (CH_2COO). *Anal.* calcd. for $C_{37}H_{48}O_8$: C 71.58, H 7.79; found: C 71.50, H 7.95.

*8-Methoxycarbonyloctyl 2-O-(4-O-acetyl-3,6-di-O-benzyl-2-deoxy-2-phthalimido-β-D-glucopyranosyl)-3,4,6-tri-O-benzyl-α-D-mannopyranoside (**14**)*

A mixture of **13** (1.10 g, 1.77 mmol) and silver trifluoromethanesulfonate (1.71 g, 6.65 mmol) was dried *in vacuo* over P_2O_5, dry dichloromethane (2 mL) was added followed by *sym*-collidine (0.87 mL, 6.61 mmol) and 4Å molecular sieves (0.5 g), and the mixture was stirred at −20°C for 0.5 h. The α,β-mixture **8** (2.92 g, 5.32 mmol) in dichloromethane (2 mL) was then added and after 2 h at −20°C the reaction mixture was warmed to room temperature and stirring was continued for an additional 14 h. The mixture was then diluted with dichloromethane (100 mL), solids were removed by filtration, and the organic solution was washed with water, 5% HCl, saturated $NaHCO_3$, and water. Solvent evaporation left a syrup that was purified by chromatography using ethyl acetate – toluene (1:10) as eluent to provide **14** (1.39 g, 69%) as a clear syrup; $[\alpha]_D$ +12.1° (*c* 0.66, chloroform); R_f 0.33 in ethyl acetate – toluene 1:6; ^{1}H nmr ($CDCl_3$) δ: 5.286 (m, 1H, $J_{1',2'}$ = 8.0 Hz, virtual coupling to H-3', H-1'), 5.153 (m, 1H, $J_{3',4'} \approx J_{4',5'} \approx$ 9.5 Hz, virtual coupling to H-2', H-4'), 3.647 (s, OCH_3), 2.278 (t, 2H, *J* = 7.5 Hz, CH_2COO), 1.953 (s, 3H, $COCH_3$); ^{13}C nmr ($CDCl_3$) δ: 174.25 ($COOCH_3$), 96.97 and 96.90 (C-1 and C-1'), 55.36 (C-2'), 51.41 (OCH_3), 34.07 (CH_2COO), 20.91 ($COCH_3$). *Anal.* calcd. for $C_{67}H_{75}NO_{15}$: C 70.94, H 6.67, N 1.23; found: C 70.65, H 6.61, N 1.13.

*8-Methoxycarbonyloctyl 2-O-(3,6-di-O-benzyl-2-deoxy-2-phthalimido-β-D-glucopyranosyl)-3,4,6-tri-O-benzyl-α-D-mannopyranoside (**15**)*

De-*O*-acetylation of **14** (200 mg, 0.18 mmol), as described for the preparation of **13**, gave the title compound as a clear syrup (190 mg, 99%); $[\alpha]_D$ −3.2° (*c* 0.79, chloroform); R_f 0.31 in ethyl acetate – hexane, 2:3); ^{1}H nmr ($CDCl_3$) δ: 5.266 (d, 1H, $J_{1',2'}$ = 8.0 Hz, H-1'), 4.454 (d, 1H, $J_{1,2}$ = 1.8 Hz, H-1), 3.652 (s, 3H, OCH_3), 3.017 (d, D_2O exchangeable, $J_{4',OH}$ = 2.0 Hz, OH), 2.282 (t, 2H, *J* = 7.5 Hz, CH_2COO); ^{13}C nmr ($CDCl_3$) δ: 174.29 ($COOCH_3$), 97.02 (2 × C, C-1 and C-1'), 55.20 (C-2'), 51.43 (OCH_3), 34.09 (CH_2COO). *Anal.* calcd. for $C_{65}H_{73}NO_{14}$: C 71.47, H 6.74, N 1.28; found: C 71.01, H 6.61, N 1.24.

*8-Methoxycarbonyloctyl 2-O-[4-O-(4-O-acetyl-3,6-di-O-benzyl-2-deoxy-2-phthalimido-β-D-galactopyranosyl)-3,6-di-O-benzyl-2-deoxy-2-phthalimido-β-D-glucopyranosyl)-3,4,6-tri-O-benzyl-α-D-mannopyranoside (**16**)*

A. From **11** and **15**: A mixture of **15** (300 mg, 0.27 mmol), silver trifluoromethanesulfonate (155 mg, 0.60 mmol), *sym*-collidine (80 μL, 0.60 mmol), and 4Å molecular sieves (0.2 g) in dichloromethane (1.0 mL) was stirred for 0.5 h and a solution of α,β-mixture **11** (302 mg, 0.55 mmol) in dichloromethane (1.0 mL) was then added dropwise. After 12 h, the reaction was diluted with dichloromethane (50 mL), solids were removed by filtration, and the filtrate was washed sequentially with water, 5% HCl, saturated $NaHCO_3$, and water. After solvent evaporation the residue was purified by chromatography using ethyl acetate – toluene (1:8) as eluent to provide **16** as a white foam (283 mg, 64%); $[\alpha]_D$ 0° (*c* 0.95, chloroform); R_f 0.37 in ethyl acetate – toluene, 1:6; ^{1}H nmr ($CDCl_3$) δ: 5.622 (dd, 1H, $J_{3'',4''}$ = 3.0 Hz, $J_{1'',2''} \approx$ 1.0 Hz, H-4''), 5.337 (d, 1H, $J_{1'',2''}$ = 8.5 Hz, H-1''), 5.104 (d, 1H, $J_{1',2'}$ = 8.0 Hz, H-1'), 4.379 (H-1 and H-2''), 4.252 (H-2'), 3.942 (dd, 1H, $J_{1,2}$ = 1.5 Hz, $J_{2,3}$ = 3.0 Hz, H-2), 3.649 (s, OCH_3), 2.261 (t, 2H, CH_2COO), and 2.028 (s, 3H, $COCH_3$); ^{13}C nmr ($CDCl_3$) δ: 174.25 ($COOCH_3$), 170.24 ($COCH_3$), 97.51 (C-1''), 96.88 and 96.79 (C-1 and C-1'), 55.55 (C-2'), 53.74 (C-2''), 51.40 (OCH_3), 34.05 (CH_2COO), and 20.82 ($COCH_3$). *Anal.* calcd. for $C_{95}H_{100}N_2O_{21}$: C 71.05, H 6.28, N 1.74; found: C 70.96, H 6.29, N 1.77.

B. From **13** and **22**: Alcohol **13** (82 mg, 0.132 mmol), silver trifluoromethane sulfonate (53 mg, 0.21 mmol), *sym*-collidine (30 μL, 0.228 mmol), 4Å molecular sieves (85 mg), and the α,β-mixture **22** (187 mg, 0.18 mmol) were mixed and stirred in dichloromethane for 24 h as described in procedure A above. Trisaccharide **16** (100 mg, 47%) was isolated in the same manner and had identical ^{1}H nmr and optical rotation as the material characterized in procedure A.

*8-Methoxycarbonyloctyl 2-O-[2-acetamido-4-O-(2-acetamido-4-O-acetyl-3,6-di-O-benzyl-2-deoxy-β-D-galactopyranosyl)-3,6-di-O-benzyl-2-deoxy-β-D-glucopyranosyl]-3,4,6-tri-O-benzyl-α-D-mannopyranoside (**17**)*

A mixture of **16** (150 mg, 0.093 mmol) and hydrazine acetate (258 mg, 2.80 mmol) was refluxed in dry methanol (15 mL) for 3 h, more hydrazine acetate (258 mg, 2.80 mmol) was then added, and the refluxing was continued for a further 20 h. The reaction was then taken to dryness, the residue was dissolved in pyridine (3 mL), and acetic anhydride (2 mL) was added. After stirring for 16 h, excess of acetic anhydride was decomposed by dropwise addition of ethanol to the reaction mixture at 0°C. Solvent was evaporated and toluene (2 × 5 mL) was added to and evaporated from the residue, which was then dissolved in dichloromethane and washed with 5% HCl, saturated $NaHCO_3$, and cold water. Evaporation left a white solid, which was purified by chromatography using acetone–hexane (2:3) as eluent. The title compound was obtained as a clear syrup (92 mg, 69%); $[\alpha]_D$ +6.9° (*c* 0.72, chloroform); R_f 0.33 in acetone–hexane, 2:3; ^{1}H nmr ($CDCl_3$) δ: 5.791 (d, 1H, D_2O exchangeable, $J_{NH',2'}$ = 8.0 Hz, NH'), 5.562 (d, 1H, $J_{3'',4''}$ = 3.0 Hz, $J_{4'',5''}$ < 1 Hz, H-4''), 5.032 (d, 1H, $J_{1',2'}$ = 7.4 Hz, H-1'), 4.985 (d, 1H, D_2O exchangeable, $J_{NH'',H-2''}$ = 7.5 Hz, NH''), 4.771 (d, $J_{1'',2''}$ = 8.0 Hz, H-1''), 4.095 (H-2), 3.655 (s, OCH_3), 3.492 (m, H-2''), 3.235 (m, H-2'), 2.291 (t, 2H, CH_2COO), 2.004 (s, 3H, $OCOCH_3$), 1.786 and 1.740 (each s, 3H, $NHCOCH_3$); ^{13}C nmr ($CDCl_3$) δ: 174.32 ($COOCH_3$), 171.17, 170.42, and 170.24 (3 × C, $COCH_3$), 99.47 (C-1''), 97.69 (2 × C, C-1 and C-1'), 56.50 (C-2'), 54.41 (C-2''), 51.45 (OCH_3), 23.55 and 23.37 (2 × C, $NHCOCH_3$), 20.84 ($OCOCH_3$). *Anal.* calcd. for $C_{83}H_{100}O_{19}N_2$: C 69.73, H 7.05, N 1.96; found: C 69.47, H 6.91, N 2.07.

Can. J. Chem. Downloaded from www.nrcresearchpress.com by 72.64.146.136 on 09/07/12
For personal use only.

Can. J. Chem. Downloaded from www.nrcresearchpress.com by 72.64.146.136 on 09/07/12
For personal use only.

8-Methoxycarbonyloctyl 2-O-[2-acetamido-4-O-(2-acetamido-3,6-di-O-benzyl-2-deoxy-β-D-galactopyranosyl)-3,6-di-O-benzyl-2-deoxy-β-D-glucopyranosyl]-3,4,6-tri-O-benzyl-α-D-mannopyranoside (18)

Compound **17** (60 mg, 0.042 mmol) was de-*O*-acetylated as described for the preparation of **13** to provide a clear syrup (55 mg, 95%); R_f 0.35 in ethyl acetate – hexane, 3:1; ^{1}H nmr ($CDCl_3$) δ: 5.844 (br d, 1H, D_2O exchangeable, $J_{NH',2'}$ = 8 Hz, NH′), 5.074 (br d, 1H, D_2O exchangeable, $J_{NH'',2''}$ = 8 Hz, NH″), 5.008 (d, 1H, $J_{1',2'}$ = 7.5 Hz, H-1′), 4.754 (H-1), 4.714 (d, $J_{1'',2''}$ = 8.0 Hz, H-1″), 3.654 (s, OCH_3), 2.475 (br s, 1H, D_2O exchangeable, OH), 2.295 (t, 2H, J = 7.5 Hz, CH_2COO), 1.788 and 1.733 (each s, 3H, $NHCOCH_3$). This material was not further characterized but was used directly in the preparation of **19**.

8-Methoxycarbonyloctyl 2-O-[2-acetamido-4-O-(2-acetamido-3,6-di-O-benzyl-2-deoxy-4-O-sulfo-β-D-galactopyranosyl)-3,6-di-O-benzyl-2-deoxy-β-D-glucopyranosyl]-3,4,6-tri-O-benzyl-α-D-mannopyranoside sodium salt (19)

Compound **18** (50 mg, 0.036 mmol) was dissolved in dry dimethylformamide (1.0 mL) and sulfur trioxide – pyridine complex (29 mg, 0.182 mmol) in dry dimethylformamide (2 mL) was added dropwise. The resulting solution was stirred for 4 h and excess of reagent was destroyed by the addition of methanol (1 mL). Solvent was evaporated and the residue was dissolved in chloroform and washed with cold water. Chloroform evaporation left a white solid, which was dissolved in methanol and passed through Dowex 50-X8 (Na^+) (10 mL) in methanol. Solvent removal provided the title compound as a hygroscopic white solid (50 mg, 93%); $[\alpha]_D$ +15.1° (*c* 0.86, methanol); R_f 0.41 in dichloromethane–methanol, 9:1; ^{1}H nmr (CD_3OD) δ: 4.994 (d, 1H, $J_{3'',4''}$ = 3.0 Hz, $J_{4'',5''}$ < 1 Hz, H-4″), 4.744 (d, 1H, $J_{1,2}$ = 1.8 Hz, H-1), 4.139 (dd, 1H, $J_{2,3}$ = 3.2 Hz, H-2), 3.668 (s, OCH_3), 3.304 (dd, 1H, $J_{2'',3''}$ = 11.0 Hz, H-3″), 2.307 (t, 1H, J = 7.5 Hz, CH_2COO), 1.860 and 1.810 (each s, 3H, $NHCOCH_3$); ^{13}C nmr (CD_3OD) δ: 175.94 ($COOCH_3$), 173.48 (2 × C, $NHCOCH_3$), 101.77, 101.01, and 98.69 (C-1, C-1′, and C-1″), 81.55 (C-4″), 56.46 (C-2′), 54.24 (C-2″), 51.96 (OCH_3), 34.77 (CH_2COO), and 23.30 (2 × C, $NHCOCH_3$). *Anal.* calcd. for $C_{81}H_{97}N_2O_{21}SNa\cdot 2.5\,H_2O$: C 63.39, H 6.37, N 1.82; found: C 63.21, H 6.39, N 1.66.

8-Methoxycarbonyloctyl 2-O-[2-acetamido-4-O-(2-acetamido-2-deoxy-β-D-galactopyranosyl)-2-deoxy-β-D-glucopyranosyl]-α-D-mannopyranoside (2)

Compound **18** (16 mg, 0.012 mmol) was dissolved in 95% ethanol (3 mL) containing 5% palladium on carbon (20 mg) and was stirred under hydrogen (1 atm (101.3 kPa)) for 20 h. Catalyst was removed by filtration, washed with 95% ethanol, and the solvent was evaporated to dryness. The residue was then passed through a column of Bio-Gel P2 (200–400 mesh) (2.5 × 50 cm) using 10% aqueous ethanol as eluent. The carbohydrate containing fractions were pooled, concentrated, and lyophilized to provide a white powder (7.2 mg, 82%); $[\alpha]_D$ +9.6° (*c* 0.99, water); R_f 0.32 in chloroform–methanol–water, 60:35:6; ^{1}H nmr (D_2O) δ: 4.854 (d, 1H, $J_{1,2}$ = 1.6 Hz, H-1), 4.559 (m, 1H, $J_{1',2'}$ = 8.2 Hz, virtual coupling to H-3′, H-1′), 4.514 (d, 1H, $J_{1'',2''}$ = 8.4 Hz, H-1″), 4.032 (dd, 1H, $J_{2,3}$ = 3.4 Hz, H-2), 3.94 (H-2″), 3.73 (H-2′), 3.687 (s, OCH_3), 2.387 (t, 2H, J = 7.5 Hz, CH_2COO), 2.068 and 2.045 (each s, 3H, $COCH_3$); ^{13}C nmr (D_2O) δ: 178.67 ($COOCH_3$), 175.55 (2 × C, $COCH_3$), 102.60, 100.24, and 97.55 (C-1, C-1′, and C-1″), 68.88 (OCH_2CH_2), 62.32, 61.75, and 60.69 (C-6, C-6′, and C-6″), 55.50 (C-2′), 53.35 (C-2″), 52.88 (OCH_3), 34.53 (CH_2COO), 23.15 and 23.01 ($NHCOCH_3$). *Anal.* calcd. for $C_{32}H_{56}N_2O_{18}\cdot 2H_2O$: C 48.48, H 7.12, N 3.53; found: C 48.06, H 6.94, N 3.82.

8-Methoxycarbonyloctyl 2-O-[2-acetamido-4-O-(2-acetamido-2-deoxy-4-O-sulfo-β-D-galactopyranosyl)-2-deoxy-β-D-glucopyranosyl]-α-D-mannopyranoside sodium salt (3)

Compound **19** (46 mg, 0.031 mmol) was hydrogenated as described for the preparation of **2**. After passage through a column of Bio-Gel P-2 and lyophilization, the residue was dissolved in water and passed through Dowex 50-X8 (Na^+) (10 mL). Lyophilization of the eluate gave a hygroscopic white powder (22.2 mg, 84%); $[\alpha]_D$ +2.5° (*c* 0.81, water); R_f 0.23 in chloroform–methanol–water, 60:35:6; ^{1}H nmr (D_2O) δ: 4.856 (d, 1H, $J_{1,2}$ = 1.5 Hz, H-1), 4.692 (d, 1H, $J_{3'',4''}$ = 2.3 Hz, H-4″), 4.587 (m, 1H, $J_{1'',2''}$ = 8.2 Hz, virtual coupling to H-3″, H-1″), 4.558 (m, 1H, $J_{1',2'}$ = 8.3 Hz, virtual coupling to H-3′, H-1′), 4.032 (dd, 1H, $J_{2,3}$ = 3.4 Hz, H-2), 3.91 (m, H-2″ and H-3″), 3.76 (H-2′ and H-3′), 3.687 (s, OCH_3), 2.386 (t, 2H, J = 7.5 Hz, CH_2COO), 2.071 and 2.044 (each s, 3H, $COCH_3$); ^{13}C nmr (D_2O) δ: 178.66 ($COOCH_3$), 175.61 (2 × C, $COCH_3$), 102.61, 100.31, and 97.61 (C-1, C-1′, and C-1″), 80.48 (C-4″), 68.94 (OCH_2CH_2), 62.38, 61.83, and 60.97 (C-6, C-6′, and C-6″), 55.52 (C-2′), 53.78 (C-2″), 52.94 (OCH_3), 34.58 (CH_2COO), 23.21 and 23.08 (2 × C, $COCH_3$). *Anal.* calcd. for $C_{32}H_{55}N_2O_{21}SNa\cdot 2H_2O$: C 42.95, H 6.20, N 3.13; found: C 42.75, H 6.00, N 2.94.

Allyl 4-O-(4-O-acetyl-3,6-di-O-benzyl-2-deoxy-2-phthalimido-β-D-galactopyranosyl)-3,6-di-O-benzyl-2-deoxy-2-phthalimido-β-D-glucopyranoside (20)

Condensation of **5** (307 mg, 0.58 mmol) with **11** (450 mg, 0.82 mmol) in the presence of silver trifluoromethanesulfonate (235 mg, 0.92 mmol) and *sym*-collidine (130 μL, 0.98 mmol), as described for the preparation of **16**, provided a crude syrupy product, which was purified by chromatography using ethyl acetate – toluene (1:8) as eluent. Compound **20** was obtained as a white foam (397 mg, 66%); $[\alpha]_D$ +27.1° (*c* 0.30, chloroform); R_f 0.30 in ethyl acetate – toluene, 1:6; ^{1}H nmr ($CDCl_3$) δ: 5.616 (dd, $J_{3',4'}$ = 3.0 Hz, $J_{4',5'} \approx$ 1.0 Hz, H-4′), 5.605 (m, $CH_2{=}CHCH_2$), 5.329 (d, 1H, $J_{1',2'}$ = 8.2 Hz, H-1′), 4.999 (d, $J_{1,2}$ = 8.2 Hz, H-1), 2.030 (s, 3H, $COCH_3$); ^{13}C nmr ($CDCl_3$) δ: 170.23 ($COCH_3$), 117.15 ($CH_2{=}CHCH_2$), 97.47 and 97.18 (C-1 and C-1′, 55.67 (C-2), 53.72 (C-2′), 20.82 ($COCH_3$). *Anal.* calcd. for $C_{61}H_{58}N_2O_{14}$: C 70.23, H 5.60, N 2.69; found: C 70.23, H 5.58, N 2.78.

4-O-(4-O-Acetyl-3,6-di-O-benzyl-2-deoxy-2-phthalimido-β-D-galactopyranosyl)-3,6-di-O-benzyl-2-deoxy-2-phthalimido-α,β-D-glucopyranose (21)

Reaction of **20** (235 mg, 0.23 mmol) under the conditions described for the conversion of **6** to **7** gave, after chromatographic purification using ethyl acetate – toluene (1:4) as eluent, the title compound as a white solid (193 mg, 85%); R_f 0.20 (**21**α) and R_f 0.14 (**21**β) in ethyl acetate – toluene, 1:3; ^{1}H nmr ($CDCl_3$) δ: 5.622 (dd, 1H, $J_{3',4'}$ = 3.0, $J_{4',5'} \approx$ 1.0 Hz, H-4′), 5.323 (d, ≈0.8H, $J_{1',2'}$ = 8.0 Hz, H-1′β), 5.300 (d, ≈0.2H, $J_{1',2'}$ = 8.0 Hz, H-1′α), 5.232 (dd, ≈0.2H, $J_{1,OH}$ = 4.0, $J_{1,2}$ = 4.0 Hz, H-1α), 5.157 (dd, ≈0.8H, $J_{1,OH}$ = 8.5, $J_{1,2}$ = 8.5 Hz, H-1β), 4.752 (d, ≈0.2H, D_2O exchangeable, OHα), 2.824 (d, ≈0.8H, D_2O exchangeable, OHβ), 2.021 (s, ≈2.4H, $COCH_3$β), 2.001 (s, ≈0.6H, $COCH_3$α).

4-O-(4-O-Acetyl-3,6-di-O-benzyl-2-deoxy-2-phthalimido-β-D-galactopyranosyl)-3,6-di-O-benzyl-2-deoxy-2-phthalimido-α,β-D-glucopyranosyl chloride (22)

Reaction of **21** (193 mg, 0.192 mmol) with oxalyl chloride/dimethylformamide, as described for the preparation of **8**, gave **22** as a pale yellow foam (190 mg, 97%); R_f 0.36 in ethyl acetate – toluene, 1:6; ^{1}H nmr ($CDCl_3$) δ: 6.131 (d, ≈0.2H, $J_{1,2}$ = 3.5 Hz, H-1α), 5.809 (d, ≈0.8H, $J_{1,2}$ = 8.0 Hz, H-1β), 5.654 (dd, ≈0.2H, $J_{3',4'}$ = 3.0 Hz, $J_{4',5'} \approx$ 1.0 Hz, H-4′α), 5.616 (dd, ≈0.8H, $J_{3',4'}$ = 3.0 Hz, $J_{4',5'} \approx$ 1.0 Hz, H-4′β), 5.334 (d, $J_{1',2'}$ = 8.2 Hz, H-1′α), 5.328 (d, $J_{1',2'}$ = 8.2 Hz, H-1′β), 2.01 (3H, $COCH_3$ α and β).

Acknowledgements

The authors gratefully acknowledge the ongoing financial support of the Natural Sciences and Engineering Research Council of Canada and the Alberta Heritage Foundation for Medical Research. We are also grateful to Dr. J. J. Krepinsky for suggesting the use of hydrazine acetate for phthalimido group removal prior to publication of the procedure.

1. E. D. GREEN, H. VAN HALBEEK, I. BOIME, and J. U. BAENZIGER. J. Biol. Chem. **260**, 15263 (1985).

2. E. D. GREEN, I. BOIME, and J. U. BAENZIGER. J. Biol. Chem. **261**, 16309 (1986).
3. E. D. GREEN, I. BOIME, and J. U. BAENZIGER. Mol. Cell. Biochem. **72**, 81 (1987).
4. R. U. LEMIEUX, D. R. BUNDLE, and D. A. BAKER. J. Am. Chem. Soc. **97**, 4076 (1975).
5. R. U. LEMIEUX, D. A. BAKER, and D. R. BUNDLE. Can. J. Biochem. **55**, 507 (1977).
6. Jpn. Kokai Tokkyo Koho JP 60 51, 702 [85 51, 702]; Chem. Abstr. **104**, 34298j (1986).
7. P. J. GAREGG and H. HULTBERG. Carbohydr. Res. **93**, C-10 (1981).
8. T. OGAWA, T. KITAJIMA, and T. NUKADA. Carbohydr. Res. **123**, C-5 (1983).
9. E. J. COREY and J. W. SUGG. J. Org. Chem. **38**, 3224 (1983).
10. T. IVERSON and D. R. BUNDLE. Carbohydr. Res. **103**, 29 (1982).
11. P. J. GAREGG, H. HULTBERG, and T. NORBERG. Carbohydr. Res. **96**, 59 (1981).
12. R. U. LEMIEUX, T. TAKEDA, and B. Y. CHUNG. Am. Chem. Soc. Symp. Ser. **39**, 90 (1976).
13. R. W. KINKLEY and M. G. AMBROSE. J. Carbohydr. Chem. **3**, 1 (1984).
14. H.-H. LEE, D. A. SCHWARTZ, J. F. HARRIS, J. P. CARVER, and J. J. KREPINSKY. Can. J. Chem. **64**, 1912 (1986).
15. D. R. BUNDLE and S. JOSEPHSON. Can. J. Chem. **57**, 662 (1979).
16. R. L. WHISTLER, W. W. SPENCER, and J. N. BEMILLER. Methods Carbohydr. Chem. **2**, 298 (1963).
17. K. BOCK and H. THØGERSEN. Annu. Rep. NMR Spectrosc. **13**, 1 (1982).
18. C. ALTONA and C. A. G. HAASNOOT. Org. Magn. Reson. **13**, 417 (1980).

Can. J. Chem. Downloaded from www.nrcresearchpress.com by 72.64.146.136 on 09/07/12
For personal use only.

Rotating frame nuclear magnetic resonance experiments on metal complexes

RICHARD J. BUIST AND DONALD R. EATON[1]
Department of Chemistry, McMaster University, Hamilton, Ont., Canada L8S 4M1

Received September 3, 1986

RICHARD J. BUIST and DONALD R. EATON. Can. J. Chem. **65**, 1653 (1987).

Measurements of the rate of nuclear magnetic relaxation in the rotating frame ($T_{1\rho}$) have the potential to provide significant information not readily available by other nmr methods. Some applications to metal complex chemistry are described. The method has been applied to ^{59}Co nmr and used to obtain ^{59}Co–^{14}N spin–spin coupling constants for the tris(ethylenediamine)cobalt(III) and hexanitrocobaltate(III) ions. The larger coupling constant in the latter compound is related to the different hybridization of the nitrogen atom. Proton $T_{1\rho}$ measurements on thiourea and its zinc complex have demonstrated that at room temperature broadening of the ^{1}H resonance is very largely ascribable to scalar relaxation rather than to chemical exchange processes.

RICHARD J. BUIST et DONALD R. EATON. Can. J. Chem. **65**, 1653 (1987).

Les mesures de taux de relaxation magnétique nucléaire dans le référentiel tournant ($T_{1\rho}$) peuvent éventuellement fournir des informations importantes qui ne sont pas facilement accessibles par d'autres méthodes rmn. On décrit quelques applications à la chimie des complexes métalliques. On a appliqué la méthode à la rmn du ^{59}Co et on l'a utilisée pour déterminer les constantes de couplage spin–spin ^{59}Co–^{14}N des ions tris(éthylènediamine)cobalt(III) et hexanitrocobaltate(III). On relie la constante de couplage qui est plus grande dans le dernier composé avec une hybridation différente de l'atome d'azote. Des mesures de $T_{1\rho}$ sur la thiourée et son complexe de zinc ont démontré que, à la température ambiante, l'élargissement de la résonance du ^{1}H est principalement dû à une relaxation scalaire plutôt qu'à des processus d'échanges chimiques.

[Traduit par la revue]

Introduction

Most nmr relaxation studies have involved measurement of either the spin-lattice relaxation time, T_1, or the spin–spin relaxation time T_2. There is, however, a third relaxation time which can be rather easily obtained using a pulsed nmr instrument. This is the relaxation time in the rotating frame, commonly designated $T_{1\rho}$. Measurements of this parameter can yield chemically significant information not easily obtained by other methods. The present paper describes some applications of $T_{1\rho}$ measurements to metal complex chemistry.

$T_{1\rho}$ is the relaxation time of transverse magnetization measured in the presence of a strong radiofrequency field which is known as the spin-locking field (B_1). The basic experiment used to measure $T_{1\rho}$ is quite straightforward (1). A 90° pulse along the x axis in the rotating frame rotates the magnetization to the y axis. As soon as this pulse is completed, the phase of the radio frequency is changed by 90° so that B_1 also lies along the y axis also. Since the magnetization is now in the same direction as the rf field, no torque is exerted and it remains in that direction. The spins are said to be "locked" along the y axis. This magnetization will, however, still decay and the rate at which this occurs is a measure of $T_{1\rho}$. Since it is difficult to measure the magnetization in the presence of the spin locking field, the normal procedure is to carry out a series of experiments with B_1 applied for increasing periods of time and measure the initial height of the FID after the spin-locking field is turned off. It is also usual to measure $T_{1\rho}$ as a function of B_1. It is obvious that if B_1 becomes small $T_{1\rho}$ approaches T_2. However, at large values of B_1, $T_{1\rho}$ does not equal T_2 but rather approaches the value of T_1. In the intermediate region $T_{1\rho}$ lies between T_1 and T_2 and the measurements provide information on any processes which cause these two relaxation times to differ. In solution scalar relaxation and chemical exchange are the usual causes of such differences (2).

The first use of $T_{1\rho}$ measurements was reported by Solomon (3). This was a proton study of formamide and provided information on scalar relaxation of the second kind resulting from coupling to the quadrupolar ^{14}N nucleus. Both the N–H coupling constant and the ^{14}N T_1 were obtained. A paper by Meiboom (4) and several subsequent papers (5–7) report $T_{1\rho}$ measurements on water. The situation is quite complicated and both proton exchange and scalar relaxation by ^{17}O contribute to the observed results. Chemical exchange studies include work by Deverell *et al.* (8) on chair to chair isomerization of cyclohexane, Ohuchi *et al.* (9) on isomerization of decalin, Hennig and Limbach (10) (tautomers of *meso*-tetraphenylporphine), Stilbs and Moseley (11) (ureas), and Dodrell *et al.* (12) (benzaldehydes). There has also been a number of studies of scalar relaxation caused by quadrupolar nuclei including those by Mlynarik (13) (nitrobenzene and pyridine), Ohuchi *et al.* (9) (chlorocarbons), and Morgan and Strange (14) (liquid HCl and HBr). Chopra, McClung, and Jordan (15) have used $T_{1\rho}$ measurements to analyze the relaxation of solvent molecules by paramagnetic ions. These authors showed that, under the appropriate conditions, the number of molecules in the solvation shell can be determined as well as the paramagnetic chemical shift and the exchange lifetime. To our knowledge this was the first application of $T_{1\rho}$ measurements in the area of transition metal chemistry.

Experimental

The nmr experiments were performed on Bruker CXP-200 and WM-250 instruments. The CXP-200 instrument is best equipped for this type of experiment since the broad-band transmitter power is directly attenuable from the console. This means that $T_{1\rho}$'s can be determined for any nucleus observable on this instrument. For ^{1}H experiments the high power decoupler was used to provide the variable strength spin-locking field. Since the attenuation available directly on the decoupling unit was limited to about 10 dB, additional attenuation was obtained by inserting a variable attenuator with settings ranging from 3 to 100 dB into the decoupler line. Excessive sample heating was not found to be a problem if spin-locking times were kept below 2 s and if a 30-s cooling time was inserted between experiments. In the case of the Bruker WM-250 instrument, cooling air was passed over the

[1]Author to whom correspondence should be addressed.
[2]Revision received March 11, 1987.

Can. J. Chem. Downloaded from www.nrcresearchpress.com by 118.98.75.50 on 09/07/12
For personal use only.

Can. J. Chem. Downloaded from www.nrcresearchpress.com by 118.98.75.50 on 09/07/12
For personal use only.

sample. On this instrument the spin-locking field was applied through the decoupler channel. The decoupler and receiver leads on the computer were connected together to ensure a constant phase relationship between the two. Since the decoupler is used the power available for spin locking is much more limited on the WM-250 than on the CXP-200. All ^{59}Co measurements were made on the CXP-200. Proton measurements were made on both instruments and good agreement between the two sets of data was obtained in the region at low B_1 levels where comparison was possible. Except for a few ^{59}Co runs, all measurements on both instruments were taken with one scan. The decoupler power was measured by finding the 180° null or averaging the results obtained from a 180° null with that from a 360° null. This gives B_1 by using the relationship $(\pi/t180) = \gamma B_1$. $T_{1\rho}$'s were either calculated from a log I vs. time plot or obtained directly from the instrument using the Bruker T_2 calculation routine. Since the T_1's and $T_{1\rho}$'s measured were quite short, no attempt was made to remove O_2 from the solutions. It was estimated that in these circumstances relaxation by the paramagnetic O_2 should not result in significantly large errors. The probe temperature was 293 K for the CXP-200 and 294 K for the WM-250. Estimated errors are around 15% for the ^{59}Co data and 10% for ^{1}H data. Random errors are considerably less than this. T_1's were measured using the standard inversion–recovery pulse sequence.

The cobalt complexes studied were obtained commercially and used without further purification. Unbuffered aqueous solutions of approximately 0.2 M concentration were used. The pH's of these solutions were approximately 5 for the cobaltinitrite and 6 for the ethylenediamine complex. The zinc thiourea complex was prepared in a manner described previously (16). Nuclear magnetic resonance spectra were obtained using approximately 0.1 M solutions in acetone-d_6.

^{59}Co measurements

For cobalt complexes of low symmetry, quadrupolar or chemical shift anisotropy relaxation mechanisms are very effective, leading to short relaxation times and very broad lines. For complexes of higher symmetry these relaxation mechanisms become less important and if the metal is bonded to a nucleus with $I > 0$ scalar relaxation of the second kind must be considered. This mechanism is only effective if the relaxation time of the coupled nucleus is short. This is usually the case for quadrupolar nuclei. The most common such ligand nucleus is ^{14}N with $I = 1$. Spin–spin coupling constants between two such directly bonded nuclei potentially provide information on the bonding but multiplets cannot be directly observed because of the short relaxation times. $T_{1\rho}$ measurements provide an indirect approach to these coupling constants.

Two other methods are available for obtaining the ^{59}Co–^{14}N coupling constant indirectly. The first involves isotopic substitution with ^{15}N. The latter nucleus has $I = 1/2$ and the nitrogen resonance is therefore reasonably narrow allowing the cobalt coupling to be observed. Yamasaki *et al.* (17) have performed such an experiment on the tris(ethylenediamine) complex and report $^1J(^{59}\text{Co}–^{15}\text{N}) = 63.8$ Hz which corresponds to an ^{14}N coupling constant of 45.5 Hz. The ^{15}N spectra were significantly broadened by scalar relaxation with the ^{59}Co and computer simulation of the experimental curves was necessary. From this curve fitting these authors obtained a T_1 for the cobalt of 13 ms. The second possible method is to measure both T_1 and T_2 for the ^{59}Co and T_1 for the coupled nucleus (in this case ^{14}N) and then calculate J from

$$1/T_{1I} - 1/T_{2I} = (1/3)\{(2\pi J)^2 T_{1S} n_s S(S + 1)\}$$

In this equation n_s is the number of ^{14}N nuclei coupled to the Co, the subscript I refers to Co, and the subscript S to N. The formula is only valid when $(\omega_1^2 - \omega_S^2)(T_{1S})^2 \gg 1$. This condition is satisfied in the case of ^{59}Co and ^{14}N. Since the T_2's are more difficult to measure by pulse methods it is usual to obtain them from linewidths and to assume that for ^{14}N, $T_1 = T_2$. This neglects instrumental line broadening and also the possibility that scalar relaxation of the ^{14}N by the ^{59}Co will contribute to the ^{14}N linewidth. It is also possible that coupling with other nuclei, e.g. the protons in the tris(ethylenediamine) complex, will contribute to the Co linewidth. Dodrell *et al.* (18) have demonstrated that this occurs by showing that the linewidth of the hexamminne complex was reduced by both ^{14}N and ^{1}H decoupling. Rose and Bryant (19, 20) have used this second method to obtain ^{59}Co–^{14}N coupling constants for several Co complexes.

TABLE 1. ^{59}Co $T_{1\rho}$ data on tris(ethylenediamine)cobalt(III)[a] and hexanitrocobaltate(III)[b] ions $T = 294$ K

$Co(en)_3^{3+}$		$Co(NO_2)_6^{3-}$	
B_1 (rad/s)	$T_{1\rho}$ (s)	B_1 (rad/s)	$T_{1\rho}$ (s)
7660	0.00796	12300	0.0209
5150	0.00733	10600	0.0188
4030	0.00653	9130	0.0171
3270	0.00611	7480	0.0156
3140	0.00580	6283	0.0139
2530	0.00557	5067	0.0121
2090	0.00495	4080	0.0111
1750	0.00481		
1050	0.00410		

[a]Aqueous solution pH 6.
[b]Aqueous solution pH 5.

As is apparent from the above discussion both of these methods for obtaining coupling constants have limitations and $T_{1\rho}$ measurements may have advantages. We have therefore carried out such measurements for the two complex ions $Co(en)_3^{3+}$ and $Co(NO_2)_6^{3-}$. The results for the former complex may be compared with the literature values obtained indirectly. They therefore constitute a check on the reliability of the method. The measured $T_{1\rho}$'s for different values of B_1 are given in Table 1. Values of T_1 are also required and these were found to be 9.5 and 34.1 ms for the ethylenediamine and nitrite complexes, respectively. Following the treatment of Morgan and Strange (14) we obtain

$$[1] \quad \frac{1}{T_{1\rho}} - \frac{1}{T_1} = \frac{8(\pi J)^2 T_1^N}{3(1 + \omega_1^2 T_1^{N2})}$$

This equation contains two unknowns, J and T_1^N (the nitrogen relaxation time) and the linear plots shown in Figs. 1 and 2 enable both to be obtained. As a check the ^{14}N T_1's have also been measured directly by inversion recovery. They are quite short (less than a millisecond) but can be obtained reasonably accurately using the CXP-200 high power instrument. All of these data are presented in Table 2. The scatter of the experimental data is quite small, as is apparent from Figs. 1 and 2, and the major source of error may well lie in the use of eq. [1] which is strictly only valid over a restricted range of B_1 values.

The internal consistency of these results is good as shown by a comparison of the calculated and directly measured nitrogen T_1's. In the case of the ethylenediamine complex they are 0.431 and 0.445 ms, respectively, and in the case of the nitrite complex 0.140 and 0.150 ms, respectively. The agreement in both cases is well within the possible errors. The intercepts of Figs. 1 or 2 can be used to calculate T_2 for the Co and hence

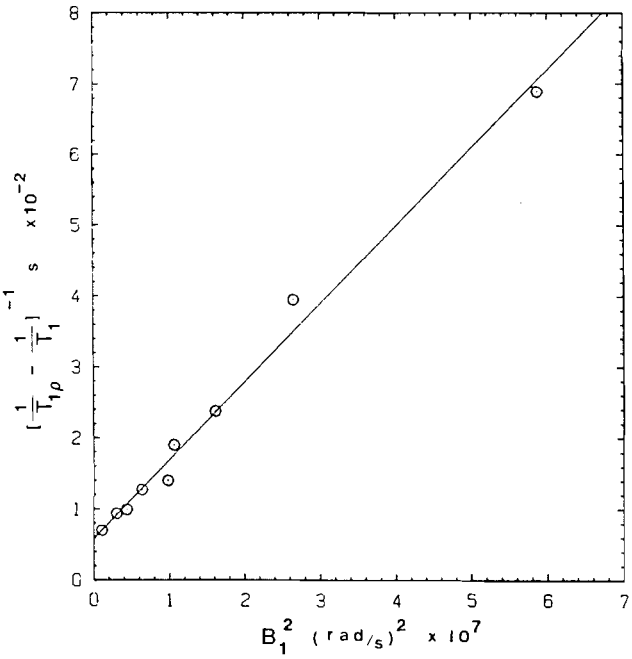

FIG. 1. Plot of $\left(\frac{1}{T_{1\rho}} - \frac{1}{T_1}\right)^{-1}$ vs. B_1^2 for $Co(en)_3^{3+}$. ^{59}Co data. Axes marked in units of s $\times$ 10^{-2} and $(rad/s)^2 \times 10^7$.

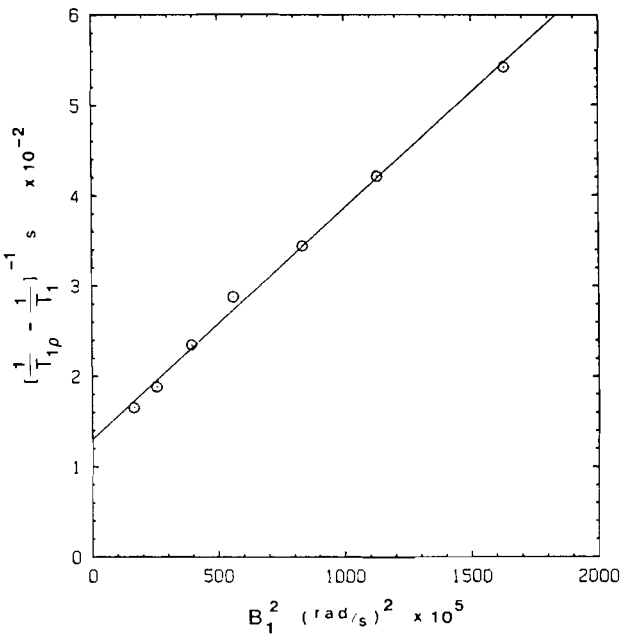

FIG. 2. Plot of $\left(\frac{1}{T_{1\rho}} - \frac{1}{T_1}\right)^{-1}$ vs. B_1^2 for $Co(NO_2)_6^{3-}$. ^{59}Co data.

the linewidth. For the ethylenediamine complex the calculated linewidth is 87.1 Hz and the experimental value 90 Hz, which is acceptable agreement. Additional broadening due to unresolved coupling with the protons can be no more than a few hertz in agreement with the findings of Doddrell *et al.* (18). For the cobaltinitrite a value of 23.9 Hz is calculated compared to the experimental 55 Hz. It is not clear whether this discrepancy arises from magnetic field inhomogeneity, or from other factors but in this case use of the linewidth to obtain T_2 and hence J leads to a large error (a value of J = 80 Hz was reported previously (21) based on this assumption). If it is assumed that

TABLE 2. Analysis of ^{59}Co $T_{1\rho}$ data

Parameter	Value	
	$Co(en)_3^{3+}$	$Co(NO_2)_6^{3-}$
$T_1(^{59}Co)$ (ms)	9.5[a]	34.1[a]
$T_2(^{59}Co)$ (ms)	2.8 (3.65)[b]	5.3[b] (9.41)
$J(^{59}Co—^{14}N)$ (Hz)	49.8 (lit. 45.5)[c]	58.9
$T_1(^{14}N)$ (ms)	0.431 (lit. 0.445)[d]	0.140 (0.150)[a]

[a]Measured directly in this work by inversion–recovery.
[b]Obtained from the measured linewidth; B_0 inhomogeneity unknown (values in parentheses calculated from the intercept and T_1).
[c]Reference 17.
[d]Reference 29.

TABLE 3. Proton $T_{1\rho}$ data on thiourea and $Zn(tu)_4(ClO_4)_2$[a] T = 294 K

Thiourea		$Zn(tu)_4(ClO_4)_2$	
B_1 (rad/s)	$T_{1\rho}$ (s)	B_1 (rad/s)	$T_{1\rho}$ (s)
6040	0.235		
4250	0.130	3490	0.058
3930	0.111	3080	0.048
3490	0.0886	2830	0.044
3270	0.078	2690	0.041
2560	0.056	2310	0.037
2140	0.045	1800	0.032
1530	0.029	1500	0.0273
532	0.0138		

[a]Solvent acetone-d_6.

$T_1 = T_2$ for the ^{14}N resonance of cobaltinitrite the calculated linewidth of 2195 Hz agrees well with the observed value of 2200 Hz.

The coupling constant obtained for the tris(ethylenediamine) complex, 49.8 Hz, agrees satifactorily with the literature values of 45.5 Hz (17) and 50 Hz (19) obtained by other methods. The cobaltinitrite value of 58.9 Hz does not agree with that reported in the literature (20) (46 Hz) but the latter value was based on an incorrect ^{14}N assignment (21). The correctness of the revised assignment is further supported by the good agreement between the ^{14}N linewidth calculated from the relaxation time and that observed experimentally. The significantly larger coupling constant for the nitro complex than for ammine complexes can be correlated with the change in the hybridization of the nitrogen (22). For the ammines, the N is sp^3 hybridized but for the nitro group it is closer to sp^2. The increase in s character would be expected to lead to an increase in coupling constant.

Proton measurements on thiourea and its zinc complex

The above ^{59}Co measurements can only be interpreted in terms of scalar relaxation. In other systems, there are possibilities for either scalar relaxation or chemical exchange effects. An example of such a case is provided by the proton spectra of thiourea and its metal complexes. The linewidths of these compounds have been examined at low temperatures (16, 23–26) and the variations have been ascribed to chemical exchange

Can. J. Chem. Downloaded from www.nrcresearchpress.com by 118.98.75.50 on 09/07/12
For personal use only.

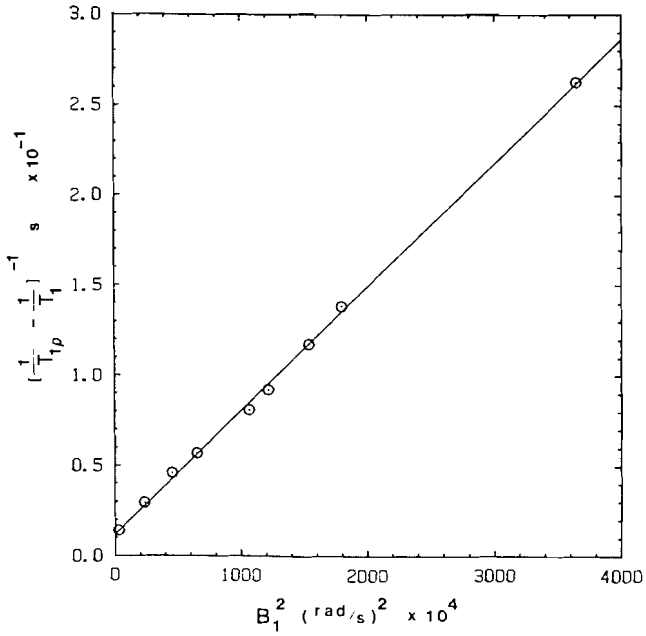

FIG. 3. Plot of $\left(\frac{1}{T_{1\rho}} - \frac{1}{T_1}\right)^{-1}$ vs. B_1^2 for thiourea. ^{1}H data.

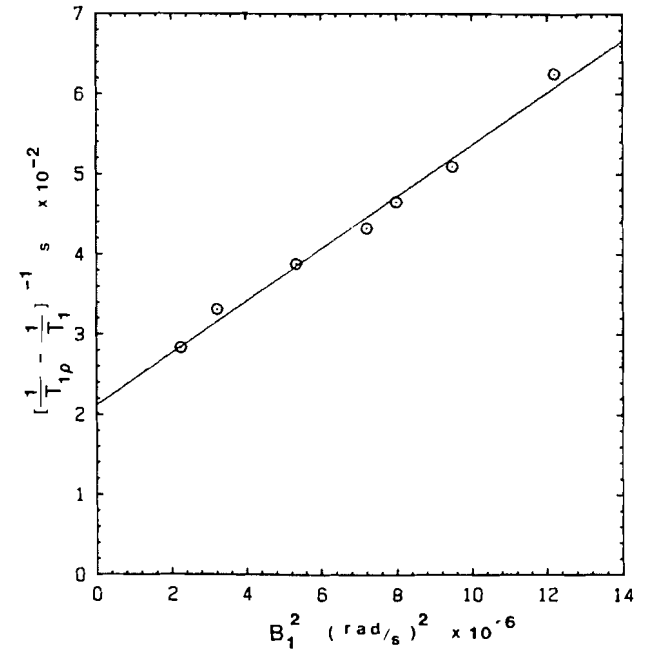

FIG. 4. Plot of $\left(\frac{1}{T_{1\rho}} - \frac{1}{T_1}\right)^{-1}$ vs. B_1^2 for Zn thiourea perchlorate. ^{1}H data.

processes attributable to restricted rotation about the C—N bond or to ligand exchange. The possible contribution of scalar relaxation due to coupling with the ^{14}N has not been explicitly considered. Generally the effects of rapid chemical exchange will be more pronounced at low temperatures, since the inverse of the chemical shift difference is then small enough to be comparable with the rate of the reaction. Scalar relaxation effects, on the other hand, usually become more pronounced at high temperatures, since relaxation times increase with increasing temperature and this leads to more effective scalar relaxation (1). $T_{1\rho}$ measurements on these compounds have therefore been carried out at room temperature, which is considerably higher than the temperatures employed in the chemical exchange studies.

TABLE 4. Analysis of proton $T_{1\rho}$ data

Parameter	Value	
	Thiourea	$Zn(tu)_4(ClO_4)_2$
$T_1(^1H)$ (s)	2.2	0.815
$T_2(^1H)$ (s)	0.011	0.023
$J(^1H-^{14}N)$ (Hz)	64.9	67.7
$T_1(^{14}N)$ (ms)	0.761	0.396

Data, obtained at 21°C, illustrating the variation of $T_{1\rho}$ with B_1 for both thiourea and its zinc perchlorate complex are given in Table 3. Appropriate plots of these data are shown in Figs. 3 and 4. These plots are expected to be linear no matter whether the variation of $T_{1\rho}$ is caused by chemical exchange or by scalar relaxation. There is a rather simple experiment to settle the origin of the effect. If chemical exchange is responsible for line broadening and hence the variation of $T_{1\rho}$, the widths of the ^{15}N satellite lines of the NH_2 resonance should be equal to that of the main line corresponding to ^{14}N. If scalar relaxation is the cause, the widths should be markedly different since the T_1 of ^{15}N ($I = 1/2$) will be much longer than that of ^{14}N with $I = 1$. The rate of relaxation of the ^{15}N is too slow to effectively relax the coupled proton. The width of the main resonance in acetone-d_6 at 21°C is 30 Hz. Since ^{15}N has only 0.365% natural abundance the satellites are difficult to observe in the normal spectrum. However, a SEFT experiment (28) which magnifies small sharp peaks with long T_2's at the expense of large broad peaks with short T_2's (run with τ = 0.05 s) gave a very well-resolved low noise spectrum of the two satellites separated by 90.8 Hz with widths of 1.9 Hz. Clearly, the broadening of the central line is primarily due to scalar relaxation. The data of Fig. 3 can therefore be analysed in the same manner as that used for the ^{59}Co data. The results of this analysis and a similar one for the zinc complex are shown in Table 4. The ^{14}N–^{1}H coupling constantof 64.9 Hz obtained from the $T_{1\rho}$ measurements may be compared with the value of 64.7 Hz calculated from the ^{15}N satellite spectrum. This agreement confirms that the variation of $T_{1\rho}$ has been correctly attributed to scalar relaxation. The T_2 value obtained from the intercept of Fig. 3 also agrees well with the value calculated from the linewidth which confirms this conclusion.

Having demonstrated that chemical exchange does not contribute to the nmr spectrum at room temperature for the thiourea ligand one might ask whether the same is true for metal complexes. The data for the Zn perchlorate complex is particularly pertinent since the rate of ligand exchange may be very rapid and contribute to line broadening at higher temperatures than does restricted rotation. This complex is an effective catalyst for anil formation transimination reactions (27) and the rate of ligand exchange is of significance to the understanding of the mechanisms of catalysis. The $T_{1\rho}$ data (Fig. 4) are quite similar to those obtained for the free ligand and show no anomalies attributable to chemical exchange effects. The N–H coupling constant obtained from the analysis (67.7 Hz) is slightly larger than that for free thiourea and the relaxation times are shorter as expected for a larger molecule.

Conclusion

The application of $T_{1\rho}$ measurements to the study of scalar relaxation in metal complexes has been demonstrated. This

Can. J. Chem. Downloaded from www.nrcresearchpress.com by 118.98.75.50 on 09/07/12
For personal use only.

experiment is useful in the determination of spin–spin coupling constants when one or both of the nuclei are quadrupolar. The major advantage is that linewidth measurements are not required and errors arising from B_0 inhomogeneity are avoided. Both of the significant variables are determined in one set of experiments on the same sample at the same temperature. It is not necessary to measure the T_1 of the coupled nucleus which, in the case of nuclei with small magnetogyric ratios, such as ^{14}N, can be difficult. The same general method can also be applied to chemical exchange problems. Low temperature measurements in the slow exchange region are not necessary and no assumptions about the temperature dependence of the chemical shift differences are required. In principle, if both chemical exchange and scalar relaxation are present, the two can be separated by measuring $T_{1\rho}$ as a function of temperature since the effect of the former on $T_{1\rho}$ decreases with temperature while the latter increases. Calculations of rotation barriers in the thioureas and similar molecules based on line broadening data may be in error since no allowance is usually made for the effect of scalar relaxation. For the determination of chemical exchange rates the technique complements the various forms of spin saturation transfer and two dimensional nmr now available for rate determinations. The former method applies in the region of fast exchange following line coalescence and the latter methods are useful in the slow exchange region.

Acknowledgements

We are indebted to Dr. S. C. F. Au-Yeung for help with the ^{14}N T_1 measurements, to the South West Ontario High Field NMR Centre for use of the CXP-200 instrument, and to the Natural Sciences and Engineering Research Council of Canada for financial support of the research.

1. T. C. Farrar and E. D. Becker. Pulse and Fourier transform NMR. Academic Press, New York. 1971.
2. A. Abragam. The principles of nuclear magnetism. Oxford University Press, Oxford. 1961.
3. I. Solomon. C.R. Acad. Sci. **249**, 1631 (1959).
4. S. Meiboom. J. Chem. Phys. **34**, 375 (1961).
5. L. J. Burnett and A. H. Zeltmann. J. Chem. Phys. **60**, 4636 (1974).
6. R. R. Knispel and M. M. Pintar. Chem. Phys. Lett. **32**, 238 (1975).
7. W. Lamb, D. R. Brown, and J. Jonas. J. Phys. Chem. **85**, 3883 (1981).
8. C. Deverell, R. E. Morgan, and J. H. Strange. Mol. Phys. **18**, 553 (1970).
9. M. Ohuchi, T. Fujito, and M. Imanari. J. Magn. Reson. **35**, 415 (1979).
10. J. Hennig and H. Limbach. J. Chem. Soc. Faraday Trans. II, **75**, 752 (1979).
11. P. Stilbs and M. E. Moseley. J. Magn. Reson. **31**, 55 (1978).
12. D. M. Doddrell, M. R. Bendall, P. F. Barron, and D. T. Pegg. J. Chem. Soc. Chem. Commun. 77 (1979).
13. V. Mlynarik. J. Magn. Reson. **49**, 534 (1982).
14. R. E. Morgan and J. H. Strange. Mol. Phys. **17**, 397 (1969).
15. S. Chopra, R. E. D. McClung, and R. B. Jordan. J. Magn. Reson. **59**, 361 (1984).
16. D. R. Eaton and K. Zaw. J. Inorg. Nucl. Chem. **38**, 1007 (1976).
17. A. Yamasaki, Y. Miyakoshi, M. Fujita, Y. Yoshikawa, and H. Yamatera. J. Inorg. Nucl. Chem. **41**, 473 (1979).
18. D. M. Doddrell, M. R. Bendall, P. C. Healey, G. Smith, C. H. L. Kennard, C. L. Raston, and A. H. White. Aust. J. Chem. **32**, 1219 (1979).
19. K. D. Rose and R. G. Bryant. Inorg. Chem. **18**, 1332 (1979).
20. K. D. Rose and R. G. Bryant. Inorg. Chem. **18**, 2130 (1979).
21. R. J. Buist, S. C. F. Au-Yeung, and D. R. Eaton. Can. J. Chem. **63**, 3558 (1985).
22. K. Frei and H. Bernstein. J. Chem. Phys. **38**, 1216 (1963).
23. A. S. Tompa, R. D. Barefoot, and E. Price. J. Phys. Chem. **73**, 435 (1969).
24. W. S. Stewart and T. H. Siddall, III. Chem. Rev. **70**, 517 (1970).
25. L. M. Jackman. *In* Dynamic nuclear magnetic resonance spectroscopy. *Edited by* L. M. Jackman and F. A. Cotton. Academic Press, New York. 1975. Chapt. 7.
26. B. M. Pinto, W. A. Szarek, and T. B. Grindley. Org. Magn. Reson. **22**, 676 (1984).
27. A. R. Boate and D. R. Eaton. Can. J. Chem. **55**, 2426 (1977); **55**, 2432 (1977).
28. D. L. Rabenstein and T. T. Nakashima. Anal. Chem. **51**, 1465A, (1979).
29. S. C. F. Au-Yeung, R. J. Buist, and D. R. Eaton. J. Magn. Reson. **55**, 24 (1983).

Can. J. Chem. Downloaded from www.nrcresearchpress.com by 118.98.75.50 on 09/07/12
For personal use only.

Bond angle variations in XCY fragments and their relationship to the anomeric effect

B. Mario Pinto[1]
Department of Chemistry, Simon Fraser University, Burnaby, B.C., Canada V5A 1S6

H. Bernhard Schlegel
Department of Chemistry, Wayne State University, Detroit, MI 48202, U.S.A.

AND

Saul Wolfe
Department of Chemistry, Queen's University, Kingston, Ont., Canada K7L 3N6

Received March 11, 1986[2]

B. Mario Pinto, H. Bernhard Schlegel, and Saul Wolfe. Can. J. Chem. **65**, 1658 (1987).

The crystal structures of 2-substituted heterocyclohexanes containing exocyclic X and endocyclic Y exhibit systematic variations in their XCY bond angles. When X is in the more stable axial orientation, corresponding to the anomeric effect, the XCY angle is larger than tetrahedral; when X is in the equatorial orientation the XCY angle is smaller than tetrahedral. These geometrical effects are predicted by the perturbational molecular orbital analysis employed previously to account for the existence of the anomeric effect and its variation with changes in X and Y. *Ab initio* molecular orbital calculations, with full geometry opimization, of selected conformations of XCH_2YH molecules also reproduce this geometrical effect.

B. Mario Pinto, H. Bernhard Schlegel et Saul Wolfe. Can. J. Chem. **65**, 1658 (1987).

Les structures cristallines d'hétérocyclohexanes substitués en position 2 et contenant un groupement X exocyclique et un groupement Y endocyclique présentent des variations systématiques de leurs angles de liaisons XCY. Lorsque X se trouve dans l'orientation axiale la plus stable, correspondant à l'effet anomère, l'angle XCY est plus grand que celui d'un tétraèdre; par ailleurs, lorsque X est dans l'orientation équatoriale, l'angle XCY est plus petit que celui d'un tétraèdre. On peut prédire ces effets géométriques en faisant appel à l'analyse des orbitales moléculaires perturbationnelle qui a été utilisée antérieurement pour expliquer l'existence de l'effet anomère ainsi que sa variation avec des changements dans X et Y. On peut aussi reproduire cet effet géométrique en faisant appel à des calculs d'orbitales moléculaires *ab initio*, impliquant une optimisation complète de la géométrie, de conformations choisies de molécules XCH_2YH.

[Traduit par la revue]

Introduction

Molecules of the type XYCAB, in which X and Y are heteroatoms, exhibit interesting geometries. When AB is a double bond ($XYC{=}CH_2$), the XCY angle is substantially smaller than the 120° angle associated with sp^2-hybridized carbon: X = Y = F, ∠XCY = 109.4°; X = F, Y = Cl, ∠XCY = 112.0°; X = Y = Cl, ∠XCY = 114.4° (1).[3] For A = B = H, a shortening (strengthening) of the C—X and C—Y bonds, compared to CH_3X and CH_3Y, is normally observed (2, 3). The magnitude of this shortening is attenuated by torsion about the C—X and (or) C—Y bonds when X and (or) Y are rotors (XR, YR) and is a manifestation of the Edward–Lemieux (anomeric) effect (4).

The bond strengthening observed in $XYCH_2$ is an electrostatic (coulombic) effect in which one substituent causes a change in the charge density at the central carbon and this, in turn, causes a change in the length of the bond to the second substituent (5–7). The XCY bond angles in $XYC{=}CH_2$ and the torsional behaviour and bond length variations in $RXCH_2YR'$ have been rationalized, both qualitatively (1, 6, 8) and quantitatively (1, 6, 9), by a perturbational molecular orbital (PMO) treatment that focuses on the two-orbital two-electron stabilizing orbital interactions that contribute to the HOMO of XYCAB. In this treatment the relevant interaction involves a doubly occupied nonbonding orbital on X and an unoccupied acceptor orbital on YCAB or, alternatively, a doubly occupied nonbonding orbital on Y and an unoccupied acceptor orbital on XCAB (1, 9). The magnitude of this interaction is proportional to the square of the overlap between the interacting orbitals, and is inversely proportional to their energy difference.

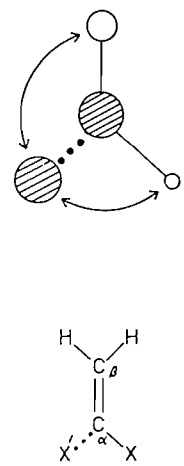

FIG. 1. The stabilizing orbital interaction that contributes to the HOMO of a 1,1-disubstituted ethylene.

Figure 1 illustrates the application of this procedure to $X'XC{=}CH_2$, with the interaction taken as $X'\cdots CX{=}CH_2$. The acceptor orbital of $CX{=}CH_2$ has nodal planes between X and C_α, and between C_α and C_β, and the coefficient of C_β is larger than the coefficient at X (1). For $X'CX{=}CH_2$ to be formed from the interaction of X′ with $CX{=}CH_2$, the primary overlap, of X′ with C_α ($\cdots$), must be in-phase (positive). With this requirement, it can be seen that the secondary overlap (depicted by double-headed arrows), between X′ and C_β, and between X′ and X, is out-of-phase (negative). Maximum

[1]Author to whom correspondence may be addressed.
[2]Revision received January 6, 1987.
[3]Also, S. Wolfe and M. H. Whangbo, unpublished results.

Can. J. Chem. Downloaded from www.nrcresearchpress.com by 72.64.146.136 on 09/07/12
For personal use only.

TABLE 1. Experimental O_5—C_1—X_1 bond angles in 1-axially and 1-equatorially substituted oxacyclohexanes[a]

Compound	Substituent at C_1 axial	Substituent at C_1 equatorial	O_5—C_1—X_1 bond angle (°)	Reference
Methyl α-D-pyranosides (8 X-ray studies)	OCH_3	H	112.3 (mean angle)	14
Methyl α-D-pyranosides (3 neutron studies)	OCH_3	H	112.5 (mean angle)	14
Methyl β-D-pyranosides (8 X-ray studies)	H	OCH_3	107.9 (mean angle)	14
Methyl β-D-xylopyranoside (neutron study)	H	OCH_3	107.4	14
α-D-Pyranoses (10 X-ray studies)	OH	H	111.9 (mean angle)	14
α-D-Pyranoses (3 neutron studies)	OH	H	111.1 (mean angle)	14
β-D-Pyranoses (5 X-ray studies)	H	OH	106.8 (mean angle)	14
2-*R*-Methylcyclohexyl α-D-glucopyranoside	2-*R*-Methylcyclohexyl	H	112.3, 113.1	15
2-*S*-Methylcyclohexyl β-D-glucopyranoside	H	2-*S*-Methylcyclohexyl	108.2	15
Methyl α-D-glucopyranoside	OCH_3	H	112.6	16
Methyl β-D-glucopyranoside	H	OCH_3	108.1	16
Phenyl α-D-glucopyranoside	OPh	H	112.5	16
Phenyl β-D-glucopyranoside	H	OPh	107.4	16
Penta-*O*-acetyl-α-D-glucopyranoside	OAc	H	110.2	16
Penta-*O*-acetyl-β-D-glucopyranoside	H	OAc	105.8	16
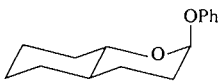	OPh	H	111.6	16
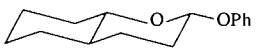	H	OPh	107.0	16
α-D-Glycosides (39 cases)	OR	H	113.5 (mean angle)	17
β-D-Glycosides (30 cases)	H	OR	111.8 (mean angle)	17
Tri-*O*-acetyl-β-D-xylopyranosylfluoride	H	F	105.7	18
Tri-*O*-benzoyl-β-D-xylopyranosylfluoride	F	H	110.7, 109.9	18

[a]Compounds have been numbered according to the convention for carbohydrate derivatives.

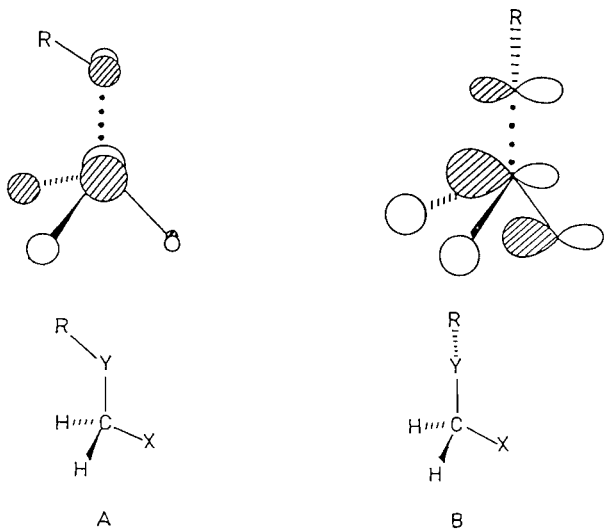

FIG. 2. The stabilizing orbital interaction that contributes to the HOMO of XCH_2YR. A, antiperiplanar conformation; B, perpendicular conformation.

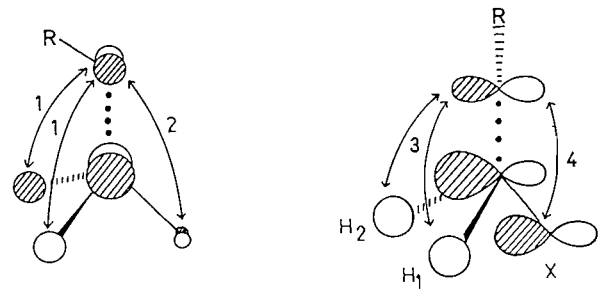

FIG. 3. The primary (···) and secondary (↷) overlap in the stabilizing orbital interactions of Fig. 2.

overlap between X′ and $CX{=}CH_2$ will therefore be achieved by an increase in the $C_\beta C_\alpha X'$ angle, and a concomitant decrease in the $X'C_\alpha X$ angle.

Figure 2 illustrates the application of the PMO procedure to C—Y torsion in XCH_2YR, with the interaction taken as $RY\cdots CH_2X$. In each conformation shown, the doubly occupied orbital is n_p, the *p*-type nonbonding orbital on Y, and the acceptor orbital is the unoccupied orbital of CH_2X that has the proper symmetry for non-zero primary overlap with n_p. In the antiperiplanar conformation, this is $\pi^*_{CH_2X}$, and in the perpendicular conformation, the acceptor orbital is $\sigma^*_{CH_2X}$. Since the σ* orbital lies lower than the π* orbital (6, 10), there is greater stabilization in the n–σ* interaction than in the n–π* interaction. This analysis accounts for the greater stability of the *gauche* conformations of XCH_2YR molecules in comparison to the *syn* or antiperiplanar conformations (4, 6); it also predicts a longer C—X bond in the more stable *gauche* conformation, because there is greater charge transfer to the antibonding C—X region in this case. Furthermore, if the CYR moiety of XCH_2YR is incorporated into a heterocyclohexane, the analysis can account for the existence of the anomeric and related (11) effects, and for the trends in these effects as both X and Y are varied (8).

Results and discussion

The purpose of this manuscript is to point out that the analysis of Fig. 1 can be incorporated into Fig. 2 to predict that the XCY bond angles of XCH_2YR molecules will differ systematically in the *gauche* and antiperiplanar conformations. Figure 3 is similar to Fig. 2, but now emphasizes the primary (····) and secondary

Can. J. Chem. Downloaded from www.nrcresearchpress.com by 72.64.146.136 on 09/07/12
For personal use only.

TABLE 2. Relative energy, C—X and C—Y bond lengths, and X—C—Y bond angles in selected conformations of XCH_2YH molecules[a]

Compound		Relative energy (kcal mol^{-1})	Bond length r_{C-X}, r_{C-Y} (Å)		Bond angle (°) X—C—Y
X = F, Y = O	**2***a*	0.0	r_{C-O} r_{C-F}	1.384 1.406	110.6
	2*e*	6.46	r_{C-O} r_{C-F}	1.398 1.386	106.6
X = Cl, Y = O	**2***a*	0.0 (0.0)[b]	r_{C-O} r_{C-Cl}	1.378 (1.401)[b] 1.912 (1.831)[b]	111.4 (111.9)[b]
	2*e*	6.37 (5.12)[b]	r_{C-O} r_{C-Cl}	1.401 (1.422)[b] 1.863 (1.789)[b]	107.1 (107.1)[b]
X = F, Y = S	**2***a*	0.0	r_{C-S} r_{C-F}	1.861 1.401	111.1
	2*e*	4.02	r_{C-S} r_{C-F}	1.886 1.396	106.2
X = Cl, Y = S	**2***a*	0.0 (0.0)[b]	r_{C-S} r_{C-Cl}	1.850 (1.800)[b] 1.877 (1.811)[b]	113.5 (114.2)[b]
	2*e*	2.95 (2.19)[b]	r_{C-S} r_{C-Cl}	1.873 (1.818)[b] 1.862 (1.799)[b]	108.1 (108.8)[b]
X = OH, Y = O	**4***a*	0.0	r_{C-O_1} r_{C-O_2}	1.411 1.411	112.3
	4*e*	4.51	r_{C-O_1} r_{C-O_2}	1.421 1.398	107.8
X = SH, Y = O	**4***a*	0.0	r_{C-O} r_{C-S}	1.406 1.892	113.0
	4*e*	3.86	r_{C-O} r_{C-S}	1.417 1.867	108.4
X = OH, Y = S	**4***a*	0.0	r_{C-O} r_{C-S}	1.406 1.891	112.9
	4*e*	4.02	r_{C-O} r_{C-S}	1.403 1.909	109.0
X = SH, Y = S	**4***a*	0.0 (0.00)[b]	r_{C-S_1} r_{C-S_2}	1.872 (1.819)[b] 1.872 (1.819)[b]	115.2 (115.8)[b]
	4*e*	1.80 (1.02)[b]	r_{C-S_1} r_{C-S_2}	1.882 (1.826)[b] 1.867 (1.816)[b]	110.5 (111.1)[b]
X = NH_2, Y = O	**6***a*	0.0	r_{C-O} r_{C-N}	1.439 1.423	115.3
	6*e*	0.71	r_{C-O} r_{C-N}	1.444 1.415	110.4
X = NH_2, Y = S	**6***a*	0.0	r_{C-S} r_{C-N}	1.937 1.412	116.1
	6*e*	1.08	r_{C-S} r_{C-N}	1.945 1.413	111.6
X = F, Y = NH	**8***a*	0.0	r_{C-N} r_{C-F}	1.395 1.437	113.1
	8*e*	9.05	r_{C-N} r_{C-F}	1.427 1.409	107.5
X = Cl, Y = NH	**8***a*	0.0	r_{C-N} r_{C-Cl}	1.374 1.994	113.6
	8*e*	10.3	r_{C-N} r_{C-Cl}	1.425 1.891	108.5

Can. J. Chem. Downloaded from www.nrcresearchpress.com by 72.64.146.136 on 09/07/12
For personal use only.

TABLE 2 (*concluded*)

Compound	Relative energy (kcal mol^{-1})	Bond length r_{C-X}, r_{C-Y} (Å)		Bond angle (°) X—C—Y
X = OH, Y = NH **8***a*	0.0	r_{C-N} r_{C-O}	1.419 1.440	115.4
8*e*	7.89	r_{C-N} r_{C-O}	1.440 1.422	110.6

[a]From *ab initio* MO calculations employing full geometry optimization and the 4-31G basis set.
[b]Values in parentheses are those obtained with the 3-21G(*)//3-21G(*) basis set (20).

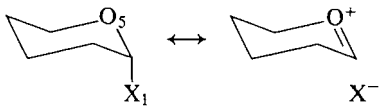

FIG. 4. The hyperconjugative interaction proposed for a 1-axially substituted pyranoside.

(↷) overlap in the $n-\pi^*$ interaction of the antiperiplanar conformation and the $n-\sigma^*$ interaction of the perpendicular conformation. In the antiperiplanar conformation, although the interaction is stabilizing and attractive with respect to the CH_2X group as a whole, the secondary overlap interactions 1 and 2 are both out-of-phase, and result in a repulsive force. If the CH_2X group is assumed to be rigid, the YCH and YCX angles cannot both increase.[4] Because the hydrogen atoms of $\pi^*_{CH_2X}$ have larger coefficients than X (6, 10), 1 is more repulsive than 2: the YCH angles increase, and the YCX angle decreases. Maximum overlap between RY and CH_2X is achieved by a *decrease* in the XCY angle from the idealized tetrahedral angle depicted in Fig. 3. This decrease reduces the secondary overlap 1 at the expense of a small increase in the secondary overlap 2.

In the perpendicular conformation, the secondary overlaps 3 and 4 are both negative, but 4 is more repulsive than 3. Maximum overlap between RY and CH_2X in this conformation can be achieved by minimizing overlap 4 at the expense of an increase in 3.[5] This leads to an *increase* in the XCY angle from the idealized tetrahedral angle depicted in Fig. 3.

Variations of the foregoing argument have been employed to account for methyl tilt angles in CH_3X molecules (12), and for bond angle trends in lactones and lactams (13).

To check the validity of the argument in the present case, quantitative PMO analyses (6) were performed on FCH_2OH in its antiperiplanar and perpendicular conformations, with particular reference to the interactions depicted in Fig. 3 and the charge distributions in the acceptor orbitals. At the 4-31G level, the optimized perpendicular structure is 5.27 kcal/mol more stable, and the optimized geometrical parameters are, perpendicular: C—F 1.404 Å, C—O 1.383 Å, ∠FCO 110.8°, $\angle OCH_1$ 107.7°, $\angle OCH_2$ 112.9°; antiperiplanar: C—F 1.386 Å, C—O 1.398 Å, ∠FCO 106.6°, ∠OCH 111.9°.

In the antiperiplanar conformation, the $2p$ atomic orbital coefficients on carbon and on fluorine in $\pi^*_{CH_2F}$ are C, 1.49; F, −0.18, and the $1s$ atomic orbital coefficients on the hydrogens are ±1.61 (out-of-phase with C_{2p}). In the perpendicular structure, the hybrid orbital depicted for carbon in Figs. 2 and 3 comprises C_{2s}, 0.45, and C_{2px}, −1.29; the hybrid orbital depicted for, e.g., fluorine in Figs. 2 and 3 comprises F_{2s}, 0.74, and F_{2px}, −0.42; the $1s$ coefficients are H_1, −0.73; H_2, −0.76. The secondary overlap associated with the $2s$ component of fluorine approximately cancels the secondary overlap associated with H_1 and H_2, because the fluorine is in the plane of the oxygen donor orbital and the hydrogens are not. Interaction 4 therefore dominates because of the $2px$ component of fluorine.

To carry this latter point further, additional quantitative PMO analyses were performed on the perpendicular structure, with the FCO angle decreased to 106.6°, the value in the antiperiplanar structure. At the smaller angle, the hydrogen atomic orbital coefficients increase, to H_1, −0.81; H_2, −0.88; the $2s$ component of the fluorine decreases, to 0.72, and the total overlap between O_{2px} and $\sigma^*_{CH_2F}$ decreases from 0.298 to 0.282. The changes in the atomic orbital coefficients on H_1, H_2, and on F reflect the adjustment of the charge distribution and secondary overlap to the smaller FCO angle.

Table 1 summarizes experimental data, taken from X-ray and neutron diffraction crystal structures, of α- and β-pyranoses and pyranosides (14–17), 1-axially and 1-equatorially oriented β-D-xylopyranosyl fluorides (18), and axial and equatorial tetrahydropyranyl acetals (16). In all of these structures the $O_5—C_1—X_1$ valence bond angle is systematically larger than the tetrahedral value when X is axial, and systematically smaller than the tetrahedral value when X is equatorial.

The larger than tetrahedral X—C—Y bond angle in 1-axially substituted pyranoses has been commented upon previously by Lemieux *et al.* (15), and rationalized in terms of the greater trigonal character of the central carbon atom (C_1) associated with the hyperconjugative interaction depicted in Fig. 4. However, such an argument would not account for the decrease in the X—C—Y bond angle that is observed in 1-equatorially substituted pyranoses. The PMO argument, on the other hand, anticipates both effects.

To probe these trends further, the bond angle variations in X—C—Y fragments were examined computationally on the model compounds XCH_2YH, in which X = NH_2, OH, SH, Cl, F, and Y = O, S, NH. The calculations were performed using GAUSSIAN 80 (19) with the 4-31G basis set, and full geometry optimization of all structures. To facilitate the discussion, Fig. 5 shows the conformations of XCH_2YH that correspond to local minima on the potential energy surface, and their relationship to the conformations of heterocyclohexanes.

Table 2 summarizes the relative energies of the XCH_2YH conformations, the optimized C—X and C—Y bond lengths, and the optimized X—C—Y bond angles. Although the individual values of these geometrical parameters are basis set

[4]An alternate argument supposes that the interaction of X with $RYCH_2$ tends to open the XCH angles. This interaction is the same in both conformations, and it will cause the XHC angles to be the same in both conformations, i.e., a rigid CH_2X group.

[5]For small changes in the XCY angle, the change in the primary overlap will be negligible.

Can. J. Chem. Downloaded from www.nrcresearchpress.com by 72.64.146.136 on 09/07/12
For personal use only.

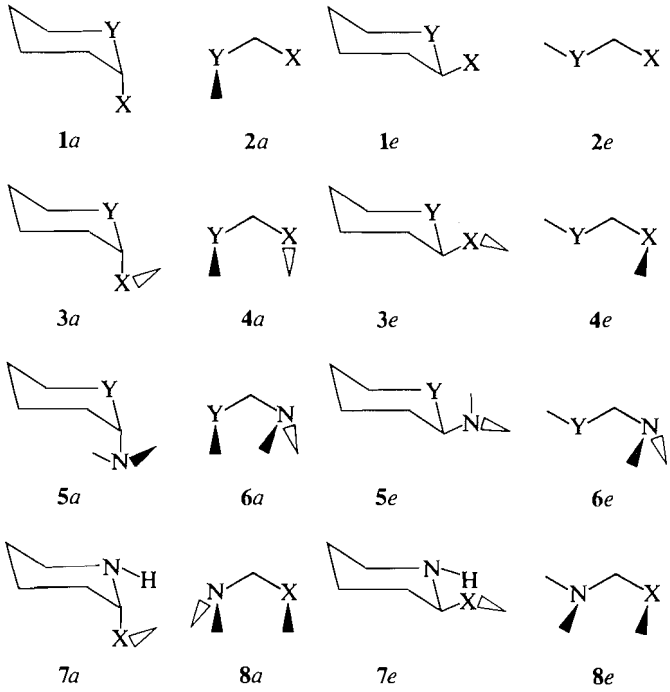

FIG. 5. Conformations of XCH_2YH molecules and their relationship to the conformations of 2-substituted heterocyclohexanes.

dependent, the trends are not (20–22). In each case, the minimum energy conformation of XCH_2YH corresponds to that conformation of the heterocyclohexane in which the substituent is axially oriented, in accord with the anomeric effect, and the bond length variations are consistent with the analysis of Fig. 2. The trends in the X—C—Y bond angles are also clear: the angle is larger than tetrahedral in conformations of the "*a*" series, and close to or smaller than tetrahedral in conformations of the "*e*" series in most cases.

Acknowledgements

The authors thank the Natural Sciences and Engineering Research Council of Canada, the National Science Foundation, and the donors of the Petroleum Research Fund, administered by the American Chemical Society, for support of this research.

1. M. H. WHANGBO, D. J. MITCHELL, and S. WOLFE. J. Am. Chem. Soc. **100**, 3698 (1978).
2. J. HINE. J. Am. Chem. Soc. **85**, 3239 (1963).
3. G. A. JEFFREY, J. A. POPLE, S. BINKLEY, and S. VISHVESHWARA. J. Am. Chem. Soc. **100**, 373 (1978).
4. S. WOLFE, A. RAUK, L. M. TEL, and I. G. CSIZMADIA. J. Chem. Soc. B, 136 (1971).
5. E. SHUSTOROVICH. J. Am. Chem. Soc. **100**, 7513 (1978).
6. S. WOLFE, M. H. WHANGBO, and D. J. MITCHELL. Carbohydr. Res. **69**, 1 (1979).
7. A. PROSS and L. RADOM. J. Comput. Chem. **1**, 295 (1980).
8. B. M. PINTO and S. WOLFE. Tetrahedron Lett. **23**, 3687 (1982).
9. M. H. WHANGBO, H. B. SCHLEGEL, and S. WOLFE. J. Am. Chem. Soc. **99**, 1296 (1977).
10. W. L. JORGENSEN and L. SALEM. The organic chemist's book of orbitals. Academic Press, New York. 1973.
11. N. J. CHU. Ph.D. thesis. University of Ottawa, 1959; A. J. KIRBY. The anomeric effect and related stereoelectronic effects at oxygen. Springer Verlag, Berlin. 1983.
12. A. PROSS, L. RADOM, and N. V. RIGGS. J. Am. Chem. Soc. **102**, 2253 (1980).
13. L. NORSKOV-LAURITSEN, H.-B. BÜRGI, P. HOFMANN, and H. R. SCHMIDT. Helv. Chim. Acta, **68**, 76 (1985).
14. G. A. JEFFREY. *In* Anomeric effect origin and consequences. *Edited by* W. A. Szarek and D. Horton. ACS Symp. Ser. No. 87, American Chemical Society, Washington, DC. 1979. p. 50, and references cited therein.
15. R. U. LEMIEUX, S. KOTO, and D. VOISIN. *In* Anomeric effect origin and consequences. *Edited by* W. A. Szarek and D. Horton. ACS Symp. Ser. No. 87, American Chemical Society, Washington, DC. 1979. p.17, and references cited therein.
16. A. J. BRIGGS, R. GLENN, P. G. JONES, A. J. KIRBY, and P. RAMASWAMY. J. Am. Chem. Soc. **106**, 6200 (1984), and references cited therein.
17. B. FUCHS, L. SCHLEIFER, and E. TARTAKOVSKY. Nouv. J. Chim. **8**, 275 (1984), and references cited therein.
18. G. KOTHE, P. LUGER, and H. PAULSEN. Acta Crystallogr. Sect. B: Struct. Crystallogr. Cryst. Chem. **35**, 2079 (1979).
19. J. S. BINKLEY, R. A. WHITESIDE, R. KRISHNAN, R. SEEGER, D. J. DEFREES, H. B. SCHLEGEL, S. TOPIOL, L. R. KAHN, and J. A. POPLE. QCPE, **13**, 406 (1981).
20. P. v. R. SCHLEYER, E. D. JEMMIS, and G. W. SPITZNAGEL. J. Am. Chem. Soc. **107**, 6393 (1985).
21. P. v. R. SCHLEYER and A. J. KOS. Tetrahedron, **39**, 1141 (1983).
22. C. VAN ALSENOY, L. SCHÄFER, J. N. SCARSDALE, J. O. WILLIAMS, and H. J. GEISE. J. Mol. Struct. **76**, 11 (1981); L. SCHÄFER, C. VAN ALSENOY, J. O. WILLIAMS, J. N. SCARSDALE, and H. J. GEISE. J. Mol. Struct. **76**, 349 (1981).

Can. J. Chem. Downloaded from www.nrcresearchpress.com by 72.64.146.136 on 09/07/12
For personal use only.

Acid-catalyzed rearrangement of cyclobutanols. A novel rearrangement

E. LEE-RUFF AND FRED J. ABLENAS
Department of Chemistry, York University, Toronto, Ont., Canada M3J 1P3

Received July 29, 1986[1]

E. LEE-RUFF and FRED J. ABLENAS. Can. J. Chem. **65**, 1663 (1987).

The acid-catalysed dehydration–rearrangement reaction of α-thienyl cyclobutanols **3** and **4** resulted in the formation of tetrahydronaphtho[2,3-*b*]thiophenes **5***a* and **6***a*. The rearrangement to the linearly fused PAH system instead of the expected angularly fused system reflects α-scission of the cyclobutyl ring. A mechanism based on deuterium labelling studies is proposed to account for the product formation.

E. LEE-RUFF et FRED J. ABLENAS. Can. J. Chem. **65**, 1663 (1987).

La réaction acid-catalysée de transposition–deshydratation des α-thiénylcyclobutanols **3** et **4** conduit à la formation des tétrahydronaphto[2,3-*b*]thiophènes **5***a* et **6***a*. La transposition conduisant à un système PAH comportant une fusion linéaire plutôt qu'au système attendu comportant une fusion angulaire est le reflet d'une scission en α du noyau cyclobutyle. Afin d'expliquer la formation des produits observés, on propose un mécanisme qui est basé sur des études impliquant des atomes de deutérium comme marqueurs.

[Traduit par la revue]

Can. J. Chem. Downloaded from www.nrcresearchpress.com by 118.98.75.50 on 09/07/12
For personal use only.

Bicyclic cyclobutanones with an α-aryl substituent undergo selective β-scission under acid catalysis to give tricyclic ketones by way of intramolecular orthoannelation of an intermediate carbocation (1–3). This observation has been used as a general approach towards the synthesis of polynuclear aromatic hydrocarbons (PAH) in which non-benzenoid and heterocyclic rings are incorporated in the PAH ring system as terminal units. These studies were also extended to bicyclic cyclobutanols bearing at least one α-aryl substituent. Acid reaction of typical bicyclic cyclobutanols effects dehydration and rearrangement to give angularly fused hydroarenes that are readily dehydrogenated to PAH's (4) (Scheme 1). The intermediate carbocations are the result of selective β-scission of the cyclobutanol ring and are stabilized by positive charge delocalizing groups such as a vinyl or heteroatom group. The cyclobutanols are readily obtained from the corresponding cyclobutanones, which in turn are prepared from aryl ketene cycloadditions to cycloolefins. As an extension to these studies we were interested in the possibility of cyclobutanols with α-heteroaromatic substituents undergoing similar transformations to give heteroaromatic PAH's. Both α- and β-thienylketene precursors are commercially available and such transformations would constitute a general synthetic route to PAH's incorporating a terminal thiophene nucleus. A number of these compounds are of interest in environmental chemistry and toxicology due to their presence in fossil fuel and coal sources and their mutagenic activity (5). In this study we report a different and heretofore unreported acid-catalyzed dehydration–rearrangement of two α-thienyl bicyclic cyclobutanols in which regiospecific α-ring opening is involved.

Results and discussion

The preparation of cyclobutanones **1** and **2** was accomplished by generating 2- or 3-thienylketene *in situ* by dehydrochlorination of the acid chloride with triethylamine in the presence of 1,3-cyclohexadiene. In each case a stereoisomeric mixture was obtained in which the *endo*-substituted product predominates and column chromatography on silica gel causes the equilibration to the thermodynamic *exo*-substituted product (6). The *endo*-substituted derivative is predicted to be the kinetic product based on orbital symmetry considerations of the $2\pi a + 2\pi s$ transition state (7).

Reduction of ketones **1** and **2** with excess lithium aluminum hydride gave alcohols **3** and **4** (X = H, Y = H) respectively as a mixture of diastereomers in 78–80% yields. The relative distribution of the diastereomers **3** and **4** is reflected by the diastereomeric distribution of the starting ketones **1** and **2**, indicating that hydride addition takes place stereospecifically. It would be anticipated from steric considerations that hydride addition proceeds from the *exo* face of the carbonyl group, giving the *endo* bicyclic alcohols **3** and **4**, although the stereochemistry of the alcohols could not be unequivocally assigned on the basis of the nmr data.

Reaction of a diastereomeric mixture of alcohol **3** in a 50:50 mixture of 10% aqueous H_2SO_4 and 95% ethanol proceeded to give a single product identified as the tetrahydronaphthothiophene **5***a*. The regiochemistry of the ring opening and annelation reaction was established by conversion of **5***a* to the known naphtho[2,3-*b*]thiophene (8) (7) upon dehydrogenation with DDQ. The assignment of **5***a* was based on the proton nmr spectrum, which exhibited a singlet at δ 6.3 ppm assigned to the *meso* vinylic proton. Labelling experiments and synthesis confirmed the assigned regiochemistry of **5***a*. Reduction of ketone **1** with lithium aluminum deuteride gave the reduced alcohol **3** in 81% yield with 100% retention of deuterium at the α-position, as was evident by mass spectrometry and nmr. Acid dehydration of 2-d_1-**3** with a 50:50 mixture of aqueous 10%

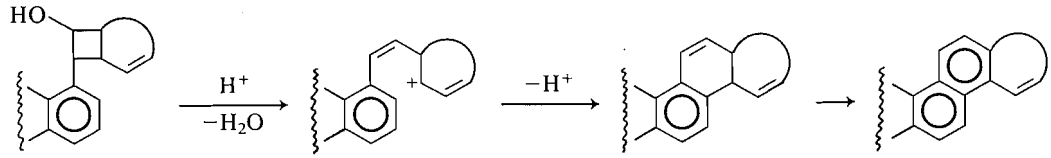

SCHEME 1

[1]Revision received March 10, 1987.

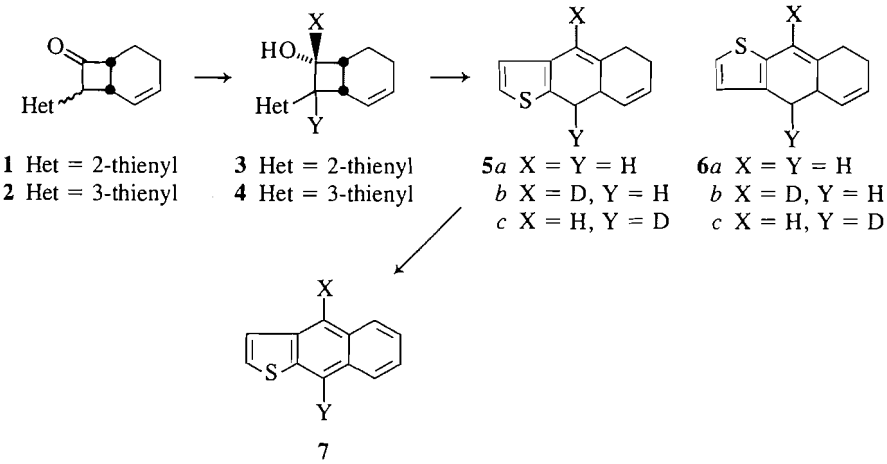

1 Het = 2-thienyl
2 Het = 3-thienyl

3 Het = 2-thienyl
4 Het = 3-thienyl

5*a* X = Y = H
b X = D, Y = H
c X = H, Y = D

6*a* X = Y = H
b X = D, Y = H
c X = H, Y = D

7

H_2SO_4 and 95% ethanol gave **5***b* in 49% yield, identical in all respects to **5***a* except that the singlet peak associated with the *meso* vinyl proton in **5***a* was absent. Mass spectrometric analysis of **5***b* indicated a 100% deuterium retention. Dehydrogenation of **5***b* provided **7** (X = D, Y = H) with 99% deuterium retention. The singlet signal at δ 8.32 ppm associated with the C-9 proton in **7** was absent in the monodeuterated derivative. Alternatively, the monodeuterated alcohol **3** (Y = D, X = H, 76% d_1 retention), in which the β-position was labelled, was prepared. This alcohol was available by lithium aluminum hydride reduction of the corresponding ketone **1** (d_1), which was obtained from the cycloaddition of 2-thienylketene (α-d_1) with 1,3-cyclohexadiene. The deuterated ketene precursor, the α,α-dideutero-2-thienylacetyl chloride, could be prepared by the sequence shown in Scheme 2.

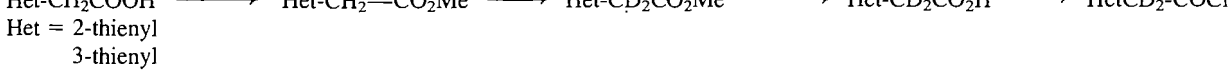

a, $SOCl_2$; b, CH_3OH; c, NaOMe, MeOD; d, NaOD, D_2O; e, H_3O^+; f, $SOCl_2$.

SCHEME 2

It is interesting to note that the deuteration exchange step c in the above scheme resulted not only in the exchange of the benzylic hydrogens but also the aromatic hydrogen at C-5 in the thiophene ring. Not surprisingly, this ring deuteration was reversed during the acid-catalyzed rearrangement of the resultant cyclobutanol **3** to the tetrahydroarene **5***b*. The 3-thienyl derivative did not undergo ring deuteration under these conditions.

Reaction of **3** (d_1, Y = D) with acid gave exclusively **5***c* (76% d_1 retention), which was converted to **7** (Y = D, X = H) with 47% d_1 retention. The position of the label was assigned on the basis of reduction in the intensity of the singlet at δ 8.37 ppm in the nmr spectrum when compared with the perhydroderivative **7** (X = Y = H). Further confirmation of structure **5***a* was obtained by independent synthesis. Ketone **1** was subjected to α-ring opening with sodium hydroxide in 1,2-dimethoxyethane to give carboxylic acid **8**. Ring closure to the ketone **9** was effected by converting **8** to the acid chloride with thionyl chloride and reaction of the acid chloride with $TiCl_4$ in dichloromethane. Standard reduction of ketone **9** with $LiAlH_4$ and acid-catalyzed dehydration provided **5***a*, identical in all respects with the sample obtained from the acid-catalyzed dehydration and rearrangement of alcohol **3**.

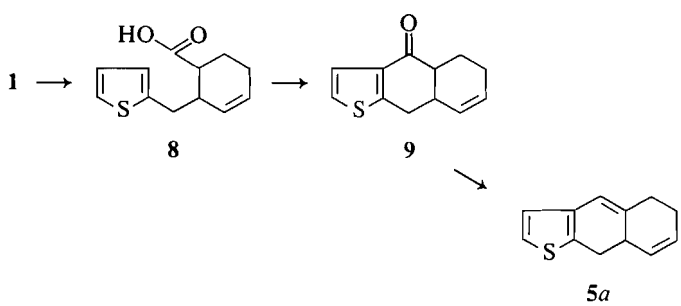

8 **9** **5***a*

Similarly the acid-catalyzed dehydration and rearrangement of cyclobutanol **4** provided the tetrahydronaphthothiophene **6***a* in 80% yield. The regiochemistry of the ring-opening reaction and olefinic sites was established by similar specific deuterium labelling experiments using the sequence:

4 (X = D, Y = H) → **6***b* → **7** (Y = D, X = H)

and

4 (X = H, Y = D) → **6***c* → **7** (Y = H, X = D)

The regiospecific formation of the tetrahydronaphthothiophenes can be rationalized according to the following scheme (Scheme 3). The bicyclic cyclobutyl cation **10** formed upon acid dehydration could undergo β-alkylation giving ion **11**. Deprotonation of **11** would give the cross-conjugated system **12**, which would be expected to equilibrate to the heteroaromatic compound **5***a*. The alternate mechanism that could account for α-ring opening of cyclobutyl cation **10** would involve a hydride shift to the bridgehead bicyclic cation **13** (Scheme 4). Its valence tautomeric form **14** could undergo β-alkylation giving **15**. However, analysis of the product obtained from the acid rearrangement of alcohols **3** and **4** indicated the exclusive formation of regioisomers **5** and **6** respectively, with no indication of the thermodynamic product **15** being present. The labelling experiments point to the absence of any equilibration of ion **10** by way of non-classical species (9) or hydride transfer

Can. J. Chem. Downloaded from www.nrcresearchpress.com by 118.98.75.50 on 09/07/12
For personal use only.

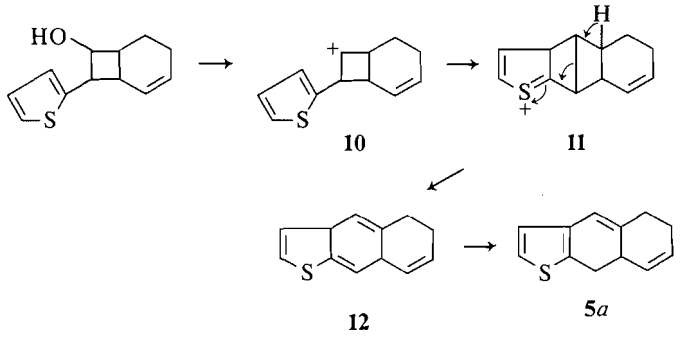

SCHEME 3

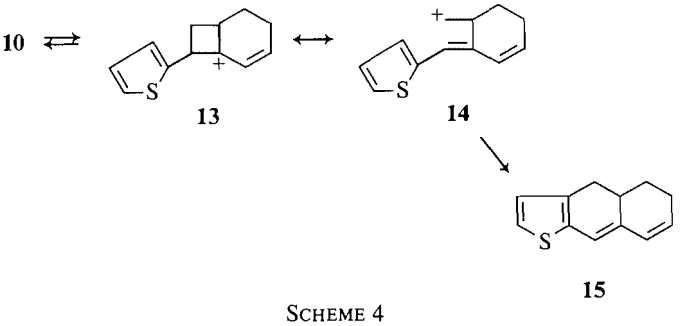

SCHEME 4

processes. The regiochemistry of the ring-opening reactions of these α-thienylbicyclic alcohols is in sharp contrast to the observed β-ring-opening reactions associated with the corresponding α-naphthyl and α-phenylbicyclic alcohols. The difference may be due in part to the greater nucleophilic character of the thiophene ring relative to a phenyl group. This greater nucleophilicity of thiophene would impart substantial stabilization to ions such as **11** leading to the observed α-ring-opening processes. Further studies are in progress to establish the generality of these unique rearrangements and to develop this methodology as a route to linear annelated thiopheno and related heterocyclic PAH's.

Experimental

The ^{1}H nmr spectra were recorded in $CDCl_3$ solution with TMS as an internal reference on a CFT-20 or AM-300 nmr spectrometer. Infrared spectra were recorded neat on NaCl discs on a Unicam SP1000 instrument, low resolution mass spectra were obtained on a VG Micromass 16F instrument, and high resolution mass spectra were obtained on a VG ZAB-E instrument. Deuterium incorporations based on mass spectra were corrected for natural isotopic abundances.

Anhydrous methanol was obtained by distilling A.C.S. grade methanol from magnesium methoxide. Methanol-*d* (99.5% *d*: CH_3OD) and LAD (98 at.% *d*) were obtained from the Aldrich Chemical Company. Toluene, triethylamine, and diethyl ether were dried with sodium.

Elemental analyses were performed by Guelph Chemical Laboratories.

2-Thienylacetyl chloride

This compound was prepared by the procedure of Miller *et al.* (10). Distillation at 39°C (0.05 Torr; 1 Torr = 133.3 Pa) afforded the acid chloride (95% yield); ir ν: 1805 cm^{-1}.

3-Thienylacetyl chloride

3-Thienylacetic acid (4.50 g, 32 mmol) was combined with thionyl chloride (3.5 mL, 1.5 equiv.) and heated at 60°C for 2 h. The oil was cooled and excess thionyl chloride evaporated off. Distillation afforded the acid chloride, bp 36°C (0.005 Torr) (lit. (11) bp 112°C), (4.90 g, 95%).

Methyl thienylacetates

2-Thienylacetyl chloride (1.25 g, 7.8 mmol) was added to dry methanol (3 mL) with stirring. After 30 min, saturated sodium bicarbonate solution (5 mL) was added and the solution extracted with dichloromethane (10 mL). The organic layer was dried ($MgSO_4$), filtered, and solvent removed to yield the crude ester, which was distilled, bp 50°C (0.06 Torr), to yield methyl 2-thienylacetate (0.99 g, 82%); ir ν: 1730 cm^{-1}; ^{1}H nmr δ: 7.2 (d, J = 5.4 Hz, H5), 6.9–7.2 (m, 2H), 3.83 (s, CH_2), 3.71 (s, CH_3) ppm.

Methyl 3-thienylacetate was obtained by a similar procedure. The crude ester was used for further reactions without purification; ir ν: 1730 cm^{-1}; ^{1}H nmr δ: 7.28 (dd, J = 5.4, 0.9 Hz, H5), 7.14 (m, H2), 7.04 (d, J = 5.4 Hz, H4), 3.70 (s, CH_3), 3.66 (s, CH_2) ppm.

α,α-d$_2$-Thienylacetyl chlorides

Methyl 2-thienylacetate (0.99 g, 6.4 mmol) was dissolved in methanol-*d* (1.0 mL) and added to a solution of sodium methoxide (0.3 *M*) in methanol-*d* (3.0 mL). After refluxing for 1 h, the methanol-*d* was evaporated off and the red oil redissolved in methanol-*d* (3.0 mL). After a further 1 h reflux, the solution was diluted with dichloromethane (10 mL) and washed with water (3 × 5 mL), dried ($MgSO_4$), filtered, and the solvent removed to yield the crude α,α-d_2 ester (0.784 g, 78%), ^{1}H nmr showing disappearance of the peak at δ 3.83 ppm due to the methylene group.

The ester was refluxed in sodium deuteroxide/deuterium oxide (4 *M*, 5 mL) for 1.5 h, cooled, and poured into ice/1 *M* hydrochloric acid. The resulting aqueous solution was extracted with dichloromethane (3 × 10 mL), and the organic layers combined, washed with water (10 mL), dried ($MgSO_4$), filtered, and solvent removed to yield the d_3-acid (0.61 g, 85%), mp 59–61°C (lit. (12) mp 62°C); ^{1}H nmr δ: 6.96 (s, H3, H4), 11.21 (s, O*H*) ppm; ms *m/z*: 145 (47), 144 (4), 100 (100).

The d_3-acid was converted to 5,α,α-trideuterio-(2-thienyl)-acetyl chloride by reaction with thionyl chloride (*vide supra*).

α,α-d_2-3-Thienylacetyl chloride was prepared by a similar sequence, although in this isomer the ^{1}H nmr shifts of the corresponding methyl ester occurred at δ 3.66 and 3.70 ppm (CH_2 and CH_3 respectively).

*8-(2-Thienyl)-bicyclo[4.2.0]oct-2-ene-7-one (**1**)*

2-Thienylacetyl chloride (1.00 g, 6.2 mmol) and 1,3-cyclohexadiene (3.0 mL, 5 equiv.) were dissolved in dry toluene (30 mL) and the solution warmed to 50°C. Triethylamine (0.98 mL, 7.0 mmol) was added dropwise and the solution stirred for 1 h.

The solution was poured onto ice and the organic layer removed. The aqueous layer was extracted with dichloromethane (30 mL) and the organic layers combined and washed successively with water (20 mL), 2 *M* hydrochloric acid (20 mL), saturated sodium bicarbonate solution (10 mL), and water (10 mL), dried ($MgSO_4$), filtered, and solvent removed to afford an oil (1.1 g).

The oil was chromatographed on silica gel (41 g) (dichloromethane:carbon tetrachloride (50:50) eluant) to yield **1** as an oil (0.40 g, 32%); ir ν: 1780 cm^{-1}; ^{1}H nmr δ, (*endo* isomer): 7.20 (d, J = 5.6 Hz, H5), 6.97 (m, 1H), 6.90 (m, 1H), 5.95 (m, 1H), 5.55 (m, 1H), 4.88 (d, J = 7.0 Hz, H8), 3.70 (m, 1H), 3.30 (m, 1H), 1.5–2.2 (m, 4H); (*exo* isomer): 7.20 (d, J = 5.6 Hz, H5), 6.97 (m, 1H), 6.90 (m, 1H), 6.10 (m, 1H), 5.97 (m, 1H), 4.27 (m, H8), 3.67 (m, 1H), 3.05 (m, 1H), 1.7–2.2 (m, 4H) ppm; *m/z*: 204 (100), 176 (38), 148 (55), 124 (96), 97 (91). This compound was air and light sensitive. *Exact Mass* calcd. for $C_{12}H_{12}OS$: 204.0609; found: 204.0618.

*8,5′-Dideuterio-8-(2-thienyl)-bicyclo[4.2.0]oct-2-ene-7-one (8,5′-d$_2$-**1**)*

Addition of triethylamine (0.41 mL, 1.0 equiv.) to a solution of 5′,α,α-trideuterio-(2-thienyl)-acetyl chloride (2.99 mmol) and 1,3-cyclohexadiene (1.50 mL, 5.2 equiv.) in dry toluene (20 mL) ultimately afforded the 8,5′-dideuterio cyclobutanone (186.5 mg, 30%). Integration of the ^{1}H nmr peak at δ 4.88 ppm indicated 88% deuterium retention at C8, as well as at C5 of the thiophene ring; ms *m/z*: 206 (100), 205 (91), 204 (24).

*8-(3-Thienyl)-bicyclo[4.2.0]oct-2-ene-7-one (**2**)*

The 3-thienyl isomer **2** of **1** was obtained by a similar procedure; **2** was obtained as an oil (33%); ir ν: 1790 cm^{-1}; ^{1}H nmr δ (endo isomer):

Can. J. Chem. Downloaded from www.nrcresearchpress.com by 118.98.75.50 on 09/07/12
For personal use only.

Can. J. Chem. Downloaded from www.nrcresearchpress.com by 118.98.75.50 on 09/07/12
For personal use only.

7.24 (d, J = 5.6 Hz, H5), 7.18 (s, H2), 6.88 (d, J = 5.6 Hz, H4), 5.99 (m, 1H), 5.50 (m, 1H), 4.70 (d, J = 7.0 Hz, H8), 3.70 (m, 1H), 3.25 (m, 1H), 1.5–2.2 (m, 4H); (*exo* isomer): 7.30 (d, J = 5.6 Hz, H5), 7.15 (m, H2), 7.00 (d, J = 5.6 Hz, H4), 6.13 (m, 1H), 5.99 (m, 1H), 4.17 (m, H8), 3.62 (m, 1H), 3.00 (m, 1H), 1.5–2.2 (m, 4H) ppm; ms m/z: 204 (100), 176 (35), 148 (58), 124 (98), 97 (95). This compound was air and light sensitive. *Exact Mass* calcd. for $C_{12}H_{12}OS$: 204.0609; found: 204.0615.

8-d_1-***2***

The 8-d_1 analogue of **2** was obtained by the cycloaddition reaction of the ketene derived from α,α-dideuterio-(3-thienyl)acetic acid. 8-d_1-**2** was obtained as an oil (10%), estimated by ^{1}H nmr to be 69% d_1, based on the integration of the H8 signal.

*8-(2-Thienyl)-bicyclo[4.2.0]oct-2-ene-7-ol (**3**)*

The diastereomeric mixture of cyclobutanones **1** (205.5 mg, 1.01 mmol) was dissolved in dry diethyl ether (3 mL), lithium aluminum hydride (43.0 mg, 4.5 equiv.) was added, and the solution stirred 1 h.

Ethyl acetate (1.0 mL) was added and the solution diluted with dichloromethane (5 mL) and washed with 2 *M* hydrochloric acid (5 mL), followed by saturated sodium bicarbonate solution (5 mL). The organic layer was dried ($MgSO_4$), filtered, and solvent removed to yield a diastereomeric mixture of cyclobutanols (192.9 mg).

Flash chromatography (silica gel, 21 g, dichloromethane eluant) afforded the *exo* isomer, followed by the *endo* isomer (161.3 mg total, 78%), white needles, mp 70–70.5°C (EtOH); ir ν: 3450 (br), 2950, 1430, 1130 cm^{-1}; ^{1}H nmr δ (*exo* isomer): 7.16 (dd, J = 5.1, 1.2 Hz, H5), 6.96 (dd, J = 5.1, 2.4 Hz, H4), 6.87 (m, H3), 5.85 (m, 2H), 4.30 (q, H7), 3.42 (t, H8), 2.67 (m, 1H), 2.35 (m, 1H), 1.65–2.2 (m, 5H); (*endo* isomer): 7.19 (dd, J = 5.1, 1.2 Hz, H5), 7.04 (m, H3), 6.98 (dd, J = 5.1, 3.6 Hz, H4), 6.02 (m, 1H), 5.70 (m, 1H), 4.70 (q, H7), 4.23 (t, H8), 3.12 (m, 1H), 2.84 (m, 1H), 2.33 (m, 1H), 1.6–2.1 (m, 4H) ppm; ms m/z: 206 (2), 188 (2), 148 (96), 126 (100). *Anal.* calcd. for $C_{12}H_{14}OS$: C 69.86, H 6.85, S 15.54; found: C 69.08, H 6.80, S 15.44. *Exact Mass* calcd. for $C_{12}H_{14}OS$: 206.0765; found: 206.0763.

7-d_1-***3***

Reduction of the diastereomeric cyclobutanones (198.8 mg, 0.975 mmol) by lithium aluminum deuteride (28.7 mg, 3.1 equiv.) afforded the 7-d_1 alcohols (163.4 mg, 81%); no ^{1}H nmr peak observed at δ 4.70 or 4.30 ppm; ms m/z: 207 (2), 189 (1), 149 (100), 127 (100), indicating 100% d_1.

8-d_1-***3***

Reduction of d_2-**1** (97.8 mg, 0.475 mmol) by LAH (21.1 mg, 4.7 equiv.) in diethyl ether (3 mL) afforded the d_2-alcohols (74.9 mg, 76%) determined by ^{1}H nmr to be 30% 8-d_1 and 57% 5′-d_1; ms m/z: 208 (11), 207 (20), 206 (20), 57 (100).

*8-(3-Thienyl)-bicyclo[4.2.0]oct-2-ene-7-ol (**4**)*

Reduction of the diastereomeric ketones **2** (270.8 mg, 1.33 mmol) by LAH (49.2 mg, 3.9 equiv.) in diethyl ether (4 mL) ultimately afforded the *endo* and *exo* isomers of **4** (85.1 and 101.8 mg, respectively, 68% total yield), mp 64.5–65.0°C (EtOH); ir ν: 3450 (br) (OH), 2950, 1430, 1130 cm^{-1}; ^{1}H nmr δ (*endo* isomer): 7.36 (m, H2), 7.30 (d, J = 5.4 Hz, H5), 7.05 (d, J = 5.4 Hz, H4), 6.00 (m, 1H), 5.75 (m, 1H), 4.70 (q, H7), 4.05 (t, H8), 3.10 (m, 1H), 2.82 (m, 1H), 2.35 (m, 1H), 1.6–2.1 (m, 4H); (*exo* isomer): 7.31 (d, J = 5.4 Hz, H5), 7.28 (s, H2), 7.03 (d, J = 5.4 Hz, H4), 5.83 (m, 2H), 4.30 (q, H7), 3.27 (t, H8), 2.68 (m, 1H), 2.30 (m, 1H), 1.7–2.2 (m, 5H) ppm; ms m/z: 206 (11), 188 (21), 148 (96), 126 (100). *Anal.* calcd. for $C_{14}H_{14}OS$: C 69.86, H 6.84, S 15.54; found: C 69.62, H 7.05, S 15.28.

7-d_1-***4***

Reduction of the diastereomeric mixture of ketones **2** (92.4 mg, 0.453 mmol) with lithium aluminum deuteride (20.0 mg, 4.2 equiv.) in diethyl ether (3.0 mL) ultimately afforded the 7-d_1 alcohol (84.4 mg, 90%); ^{1}H nmr indicated 100% d_1-labelling at the 7-position; ms m/z: 207 (5), 206 (2), 149 (30), 97 (100), 148 (2).

8-d_1-***4***

Reduction of the diastereomeric mixture of 69% d_1-**2** (53.0 mg, 0.259 mmol) with LAH (10.5 mg, 4.3 equiv.) in diethyl ether (2.0 mL) afforded 8-d_1-**4** (50.3 mg, 94%), determined to be 60% d_1 at position 8; ms m/z: 207 (1.2), 206 (0.5), 188 (1.2), 127 (100).

*4,4a,7,8-Tetrahydronaphtho[2,3-b]thiophene (**5**a)*

The alcohol **3** (62.9 mg, 0.305 mmol) was dissolved in 95% ethanol (4 mL) and added to refluxing 10% sulfuric acid (4 mL). After 1 h the solution was cooled and extracted with dichloromethane (3 × 5 mL), the organic layers combined and washed with water (5 mL), dried ($MgSO_4$), filtered, and solvent removed to provide an oil (59.5 mg), which was flash chromatographed (silica gel, petroleum ether) to afford ***5a*** (55.0 mg, 96%), mp 41–45°C; ^{1}H nmr δ: 7.04 (d, J = 5.0 Hz, H2), 6.83 (d, J = 5.0 Hz, H1), 6.27 (s, H9), 5.88 (m, 1H), 5.68 (m, 1H), 2.1–3.2 (m, 7H) ppm; ms m/z: 188 (100), 171 (66), 159 (23), 147 (57). *Anal.* calcd. for $C_{12}H_{12}S$: C 76.54, H 6.44, S 17.03; found: C 76.46, H 6.86, S 16.88.

5a *from **9***

The ketone **9** (53.1 mg, 0.260 mmol) in dry diethyl ether (3 mL) was reduced with LAH (12.1 mg, 0.318 mmol) to afford the crude 4,4,7,8,8a,9-hexahydro-9-hydroxynaphtho[2,3-*b*]thiophene (49.1 mg, 92%); ^{1}H nmr δ: 6.90 (s, 2H), 5.75 (m, 1H), 5.50 (m, 1H), 4.1–4.5 (m, 2H), 1.6–3.0 (m, 6H) ppm.

The crude alcohol was dissolved in dry toluene (10 mL) and refluxed in the presence of *p*-toluenesulfonic acid (4.2 mg, 0.020 mmol) for 1 h, cooled, basic alumina (3 g) added, and the solvent removed. The residue was placed on a column of basic alumina (10 g), and petroleum ether eluted ***5a*** (23.4 mg, 48% from **9**).

*4-Deuterio-4,4a,7,8-tetrahydronaphtho[2,3-b]thiophene (**5**c)*

The 8,5′-d_2-alcohol **3** was rearranged to yield ***5c*** (87%), determined to be 50% d_1 at position 4 only, due to a doublet of decreased intensity at δ 3.03 ppm in the ^{1}H nmr.

*9-Deuterio-4,4a,7,8-tetrahydronaphtho[2,3-b]thiophene (**5**b)*

The 7-d_1-alcohol **3** was rearranged to afford 100% d_1-***5c*** (49%), lacking the vinylic ^{1}H nmr signal of ***5a*** at δ 6.27 ppm.

*5,6,8a,9-Tetrahydronaphtho[2,3-b]thiophene (**6**a)*

The alcohol **4** (82.4 mg, 0.400 mmol) in 95% ethanol (3 mL) was rearranged in refluxing 10% sulfuric acid (3 mL) to afford ***6a*** (61.7 mg, 82%), mp 37–39°C; ^{1}H nmr δ: 7.01 (d, J = 5.0 Hz, H2), 6.84 (d, J = 5.0 Hz, H3), 6.27 (s, H4), 5.85 (m, 1H), 5.65 (m, 1H), 2.1–3.2 (m, 7H) ppm; ms m/z: 188 (100), 171 (56), 147 (51). This compound was not stable to air or light. *Exact Mass* calcd. for $C_{12}H_{12}S$: 188.0648; found: 188.0654.

*4-Deuterio-5,6,8a,9-tetrahydronaphtho[2,3b]thiophene (**6**b)*

The 7-d_1 alcohol **3** was rearranged to afford 100% d_1-***6b*** (53.3 mg, 98%), lacking a vinylic singlet at δ 6.27 ppm; ms m/z: 189 (100), 188 (1).

*9-Deuterio-5,6,8a,9-tetrahydronaphtho[2,3-b]thiophene (**6**c)*

The 8-d_1 alcohol **3** was rearranged to afford ***6c*** (16.1 mg, 36%), with a decreased ^{1}H nmr doublet at δ 2.92 ppm; ms m/z: 189 (82), 188 (100), indicating 45% d_1-labelling.

*Naphtho[2,3-b]thiophene (**7**)*

From ***5a***: The tetrahydroarene ***5a*** (35.6 mg, 0.189 mmol) was dissolved in dry toluene (40 mL) together with DDQ (103.9 mg, 2.4 equiv.) and refluxed 2 h. The slurry was cooled, concentrated on the rotovap, and passed through a column of basic alumina (10 g, petroleum ether:toluene (75:25)) to yield the arene **7** (86%), mp 187–188.5°C (pet. ether) (lit. (8) mp 189–190°C); ^{1}H nmr δ: 8.37 (s, H4), 8.33 (s, H9), 7.90–8.00 (m, H5,8), 7.51 (d, J = 5.6 Hz, H2), 7.45–7.50 (m, H6,7), 7.43 (d, J = 5.6 Hz, H1) ppm; ms m/z: 184 (100), 139 (16), 92 (11).

7 from **6**a

6*a* was dehydrogenated to yield the arene **7** (82%), identical to the arene derived from **5***a*.

4-d_1-*7 from* **6**b

6*b* was dehydrogenated to yield 100% 4-d_1-**7** (19%), lacking a signal for H4 at δ 8.37 ppm in the ^{1}H nmr; ms *m/z*: 185 (100), 184 (0).

4-d_1-*7 from* **5**b

5*b* was dehydrogenated to yield 41% 4-d_1-**7** (76%), with a signal at δ 8.37 ppm corresponding to 0.50 proton in the ^{1}H nmr; ms *m/z*: 185 (100), 184 (97).

9-d_1-*7 from* **5**c

5*c* was dehydrogenated to yield 100% 9-d_1-**7** (95%), lacking a signal at δ 8.33 ppm in the ^{1}H nmr; ms *m/z*: 185 (100), 184 (0).

9-d_1-*7 from* **6**c

6*c* was dehydrogenated to yield 9-d_1-**7** (19%), with a signal at δ 8.33 ppm corresponding to 0.59 proton in the ^{1}H nmr; ms *m/z*: 185 (89), 184 (100).

2-(2-Thenyl)-cyclohex-3-ene-1-carboxylic acid (8)

The cyclobutanone **1** (410.0 mg, 2.01 mmol) in 1,2-DME (3 mL) was refluxed with sodium hydroxide solution (1 *M*, 4.20 mL) for 2 h, cooled, diluted with water (50 mL), and acidified to pH 2. The resultant solution was extracted with dichloromethane (3 × 15 mL), the organic layers combined, washed with water, and then extracted with saturated sodium bicarbonate solution (5 × 15 mL).

The aqueous layers were combined and acidified to pH 5, causing a flocculant tan precipitate that was collected by vacuum filtration to afford **8** (231.4 mg, 50%), mp 94.0–94.5°C (EtOH:H_2O (50:50)); ir ν: 1660 cm^{-1}; ^{1}H nmr δ: 9.80 (br s, 1H), 7.20 (d, *J* = 5.1 Hz, H5), 7.00 (m, H4), 6.90 (m, H3), 5.60 (br s, 2H), 2.5–3.1 (m, 3H), 1.7–2.2 (m, 5H) ppm; ms *m/z*: 222 (1), 204 (11), 124 (11), 96 (61). *Anal.* calcd. for $C_{12}H_{14}O_2S$: C 64.83, H 6.34, S 14.42; found: C 64.41, H 6.40, S 14.65.

8a-H-*4,4a-7,8-Tetrahydro-9-oxonaphtho[2,3-*b*]thiophene (9)*

The carboxylic acid **8** (131.9 mg, 0.594 mmol) was dissolved in thionyl chloride (0.08 mL, 1.9 equiv.) and warmed to ca. 70°C for 2 h, cooled, and excess thionyl chloride removed on the rotovap by repeatedly dissolving the viscous oil in dichloromethane (1.0 mL) and removing volatiles on the rotovap (three times).

The crude acid chloride was dissolved in dry dichloromethane (3.0 mL) and titanium tetrachloride (0.07 mL, 1.1 equiv.) added at room temperature with stirring.

After 1 h, the solution was diluted with dichloromethane (10 mL) and washed with 2 *M* hydrochloric acid (10 mL), water (10 mL), then dried ($MgSO_4$), filtered, and solvent removed to afford an oil (147.8 mg), which was flash chromatographed (silica gel, dichloromethane:carbon tetrachloride (50:50)) to afford the ketone **9** (60.6 mg, 50%), mp 104–104.5°C (EtOH); ir ν: 1655, 1261 cm^{-1}; ^{1}H nmr δ: 7.02 (d, *J* = 5.0 Hz, H2), 6.81 (d, *J* = 5.0 Hz, H3), 5.80 (m, 1H), 5.52 (d, *J* = 6.3 Hz, 1H), 3.12 (m, 1H), 2.68 (m, 2H), 2.48 (m, 1H), 2.0–2.3 (m, 3H), 1.40 (m, 1H) ppm.

Acknowledgements

We would like to thank the Natural Sciences and Engineering Research Council of Canada and the Ministry of Environment, Air Resources Branch, Ontario, for financial support.

1. E. Lee-Ruff, A. C. Hopkinson, and L. H. Dao. Can. J. Chem. **59**, 1675 (1981).
2. P. Duperrouzel and E. Lee-Ruff. Can. J. Chem. **58**, 51 (1980).
3. L. H. Dao, A. C. Hopkinson, and E. Lee-Ruff. Tetrahedron Lett. 1413 (1978).
4. E. Lee-Ruff, A. C. Hopkinson, and H. Kazarians-Moghaddam. Can. J. Chem. **60**, 154 (1982).
5. R. A. Pelroy, D. L. Stewart, Y. Tominaga, M. Iwao, R. N. Castle, and M. L. Lee. Mutat. Res. **117**, 31 (1983).
6. M. Rey, S. M. Roberts, A. S. Dreiding, A. Roussel, H. Vanlierde, S. Toppet, and L. Ghosez. Helv. Chim. Acta, **65**, 703 (1982).
7. L. A. Burke. J. Org. Chem. **50**, 3149 (1985).
8. (*a*) A. M. Willputte and J. Martin. Bull. Soc. Chim. Belg. **65**, 874 (1956); (*b*) H. Wynberg, J. deWit, and H. J. M. Sinnige. J. Org. Chem. **35**, 711 (1970).
9. J. S. Staral, I. Yavari, J. D. Roberts, G. K. S. Prakash, D. J. Donovan, and G. A. Olah. J. Am. Chem. Soc. **100**, 8016 (1978).
10. W. H. Miller, A. M. Dessert, and G. W. Anderson. J. Am. Chem. Soc. **70**, 500 (1948).
11. P. Cagniant and G. Merle. C.R. Seances Acad. Sci. Ser. C, **264**, 112 (1967).
12. R. C. Weast (*Editor*). CRC handbook of chemistry and physics. 55th ed. CRC Press, Cleveland, OH. 1974.

Can. J. Chem. Downloaded from www.nrcresearchpress.com by 118.98.75.50 on 09/07/12
For personal use only.

Preparation and thermal rearrangement of 2-(*tert*-butyldimethylsiloxy)-5-methyl-6-*exo*-[(*Z*)-3-methyl-1-butenyl]-4-*exo*-vinylbicyclo[3.1.0]hex-2-ene. A total synthesis of (±)-sinularene

EDWARD PIERS AND GRACE L. JUNG

Department of Chemistry, University of British Columbia, 2036 Main Mall, University Campus, Vancouver, B.C., Canada V6T 1Y6

Received December 24, 1986

EDWARD PIERS and GRACE L. JUNG. Can. J. Chem. **65**, 1668 (1987).

A total synthesis of the marine sesquiterpenoid (±)-sinularene (**1**) is described. The alcohol **19** was converted via an 8-step sequence into the bicyclic enone **28**. Conjugate addition of lithium divinylcuprate to the latter substance afforded mainly the ketone **30**, which was transformed into the enol silyl ether **6**. Thermolysis (220°C, 4.5 h) of **6** provided cleanly the bicyclic triene **7**, which, in two steps, was converted into the tricyclic olefinic ketone **34**. Hydrogenation of **34** and subsequent Wittig olefination of the resultant ketone **4** with methylenetriphenylphosphorane provided (±)-sinularene (**1**).

EDWARD PIERS et GRACE L. JUNG. Can. J. Chem. **65**, 1668 (1987).

On décrit une synthèse totale du sesquiterpénoïde marin (±)-sinularène (**1**). Utilisant une séquence de réactions impliquant 8 étapes, on a transformé l'alcool **19** en l'énone bicyclique **28**. L'addition conjuguée de divinylcuprate de lithium à cette dernière substance conduit principalement à la cétone **30** qui a été transformé en l'éther énolique silylé **6**. La thermolyse (220°C, 4,5 h) du composé **6** conduit proprement au triène bicyclique **7** qui, en deux étapes, est transformé en la cétone tricyclique oléfinique **34**. L'hydrogénation du composé **34** fournit la cétone **4** qui, par oléfination subséquente à l'aide du méthylènetriphénylphosphore et selon la méthode de Wittig, conduit au (±)-sinularène (**1**).

[Traduit par la revue]

Can. J. Chem. Downloaded from www.nrcresearchpress.com by 72.64.146.136 on 09/07/12
For personal use only.

Introduction

The hydrocarbon (−)-sinularene was isolated some ten years ago from the soft coral *Sinularia mayi*, obtained from Telukdalam, Nias Island, Indonesia. This structurally unusual natural product was shown to possess the constitution and absolute stereochemistry depicted by structural formula **1** (1). Subsequently, two oxygenated sinularane-type sesquiterpenoids, (−)-12-acetoxysinularene (**2**) and (+)-12-acetoxycyclosinularene (**3**), were obtained from a dichloromethane extract of

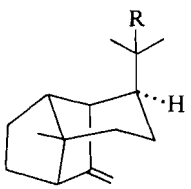

1 R = H
2 R = OAc

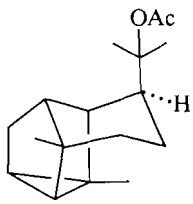

3

Clavularia inflata, collected near Laing Island, Papua – New Guinea (2). To our knowledge, three total syntheses of (±)-sinularene (**1**) have been reported (3–5) in addition to that described herein. A preparation of (±)-12-acetoxysinularene (**2**) has also been accomplished (6). We report herein the details of our total synthesis of racemic sinularene (**1**).[1]

Results and discussion

(a) General considerations

If, in a retrosynthetic sense, one "converts" the olefinic double bond of **1** into a carbonyl group (to provide the ketone **4**) and then disconnects the C-8—C-9 single bond with concomitant functionalization at C-9, one would arrive at the substituted bicyclo[3.2.1]octanone **5** (X = leaving group). The conversion, in a synthetic sense, of **5** into the tricyclic ketone **4** would involve a straightforward intramolecular alkylation. Compound **4** had already served as an intermediate in the Collins–Wege total synthesis of (±)-sinularene (**1**) (3).

[1]For a preliminary account of this work, see ref. 7.

In view of the results obtained from our earlier studies (8, 9) on the thermal rearrangement of 6-*exo*-(1-alkenyl)bicyclo[3.1.0]hex-2-ene systems as a method for preparing substituted bicyclo[3.2.1]octa-2,6-dienes, we envisaged that an interesting total synthesis of (±)-sinularene (**1**) might be effected via a route in which the key step would involve thermal (Cope) rearrangement of a highly functionalized bicyclo[3.1.0]hex-2-ene such as **6**. If this reaction were to proceed in the desired manner, the product would be the substituted bicyclo[3.2.1]octa-2,6-diene **7**. It seems evident that suitable functional group manipulations would readily transform **7** into the required ketone **5**.

Presumably, the desired Cope rearrangement of **6** would involve isomerization of **6**, via a diradical intermediate (10*a*), into the epimer **8**, which would then undergo a concerted bond reorganization (10*b*, 11–13) to produce **7**. However, it should be noted that, in theory, thermolysis of **6** could lead to rearrangement processes other than the desired Cope reaction. For example, it is possible that a homo-[1,5]-sigmatropic hydrogen migration (13, 14) from the angular methyl group to C-2 of the (*Z*)-3-methyl-1-butenyl side chain could occur. This process would form, at least initially, the highly substituted (and probably unstable) cyclopentene **9**.

A clear-cut prediction as to which rearrangement pathway would be preferred is not straightforward. For the thermal conversion of (*Z*)-1-methyl-2-vinylcyclopropane (**10**) into (*Z*)-1,4-pentadiene (**11**), the energy of activation E_a is 31.2 kcal/mol ($\log A = 11.03\ s^{-1}$) (15). Presumably, this "simplest" homo-[1,5]-sigmatropic hydrogen shift is a concerted process that proceeds by way of a transition state that can be represented by **A** (13, 14). The presumed transition state (see **B**) for the analogous transformation of **6** into **9** would be destabilized by a notable steric interaction between the isopropyl group and H_X and, therefore, the energy of activation for this reaction would be expected to be significantly larger than that of **10** → **11**.

Turning now to Cope rearrangements, it is well known (10–13) that the rate-determining step of rearrangement of most *trans*-divinylcyclopropane systems is the epimerization of the *trans* compound to the corresponding *cis*-divinylcyclopropane.

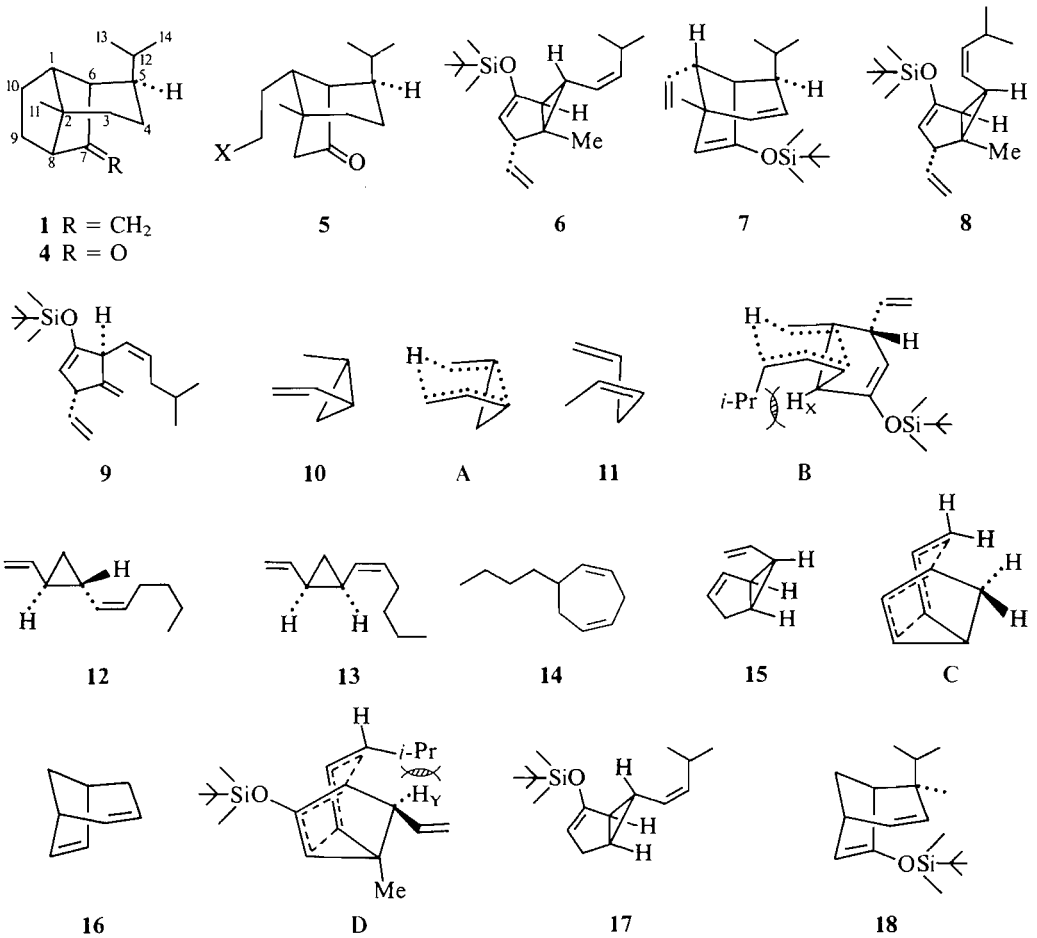

1 R = CH_2
4 R = O

5 **6** **7** **8**

9 **10** **A** **11** **B**

12 **13** **14** **15** **C**

16 **D** **17** **18**

For example, the E_a values associated with the thermal conversions of **12** and **13** into the cycloheptadiene **14** are 32.8 (log A = 14.54 s^{-1}) and 20.5 kcal/mol (log A = 10.70 s^{-1}), respectively (16).

For the thermal rearrangement of 6-*endo*-vinylbicyclo-[3.1.0]hex-2-ene (**15**) into bicyclo[3.2.1]octa-2,6-diene (**16**), presumably via transition state **C** (10*b*, 11–13), the energy of activation (E_a) is 22.9 kcal/mol (log A = 11.7 s^{-1}) (17). Even though the Cope transition state for the conversion of **8** into **7** would suffer from a significant nonbonded interaction between the isopropyl group and H_Y (see **D**), it is unlikely that this repulsion would raise the value of E_a for this process to the region of 32–35 kcal/mol. Therefore, it seems reasonable to propose that the slow step of the overall conversion of **6** into **7** would be the isomerization of **6** into **8**. Furthermore, if one assumes (*a*) that the E_a value associated with the latter conversion would be similar to that for **12** → **13** (32.8 kcal/mol) and (*b*) that E_a for **6** → **9** (via transition state **B**) would be significantly *higher* than that of **10** → [**A**] → **11** (31.2 kcal/mol), then it does not appear unreasonable to conclude that thermolysis of **6** would proceed in the desired (Cope) sense to provide **7**. In this connection, it is pertinent to point out that earlier work (9, 18) had shown that thermolysis of **17** proceeded smoothly to give the diene **18**. Of course, the substrate **17** lacked an angular (C-5) methyl group and, therefore, a homo-[1,5]-sigmatropic hydrogen migration (cf. **6** → **9**) was precluded. Nevertheless, the successful conversion of **17** into **18** showed that a Cope rearrangement via a transition state resembling **D** was, indeed, a viable process.

(b) Synthesis and thermolysis of compound **6**

Treatment of a tetrahydrofuran (THF) solution of 1-lithio-3-methyl-1-butyne with 2-methylpropenal provided, in excellent yield, the alcohol **19** (see Scheme 1). Subjection of the latter substance to a triethyl orthoacetate-based Claisen rearrangement process (19) gave, stereoselectively, the expected ester **20** (58%), which was hydrolyzed with base to give the acid **21**. Conversion (oxalyl chloride, hexane) of **21** into the corresponding acid chloride **22**, followed by reaction of the latter compound with diazomethane in diethyl ether, gave the diazo ketone **23**. Copper(II) acetylacetonate-catalyzed cyclization of **23** produced, in 52% overall yield from the ester **20**, the substituted bicyclo[3.1.0]hexan-2-one **24**. In the ^1H nmr spectrum of **24**, the protons H_X and H_Y give rise to a doublet (δ 1.69, J_{XY} = 3 Hz) and a doublet of doublets (δ 1.87, J_{XY} = 3 Hz, J_{YZ} = 1.7 Hz), respectively. The magnitude of the H_X–H_Y coupling constant shows that, as expected, these two cyclopropyl protons have a *trans* relationship (20). The long-range coupling between H_Y and H_Z was confirmed by an appropriate decoupling experiment (see Experimental).

Hydrogenation of **24** in the presence of Lindlar's catalyst (21) provided the keto alkene **25**. The expected stereochemistry of the alkene double bond in **25** was confirmed by the ^1H nmr spectrum, which shows that J_{XY} = 11.5 Hz, a coupling constant typical of mutual coupling between *cis* vicinal alkene protons.

To allow for the introduction of an *exo* vinyl group to the C-4 position of the bicyclic ketone **25**, it was necessary to transform **25** into the corresponding enone **28**. To this end, **25** was subjected to Reich's (22) "one-pot" selenenylation – selenoxide

Can. J. Chem. Downloaded from www.nrcresearchpress.com by 72.64.146.136 on 09/07/12
For personal use only.

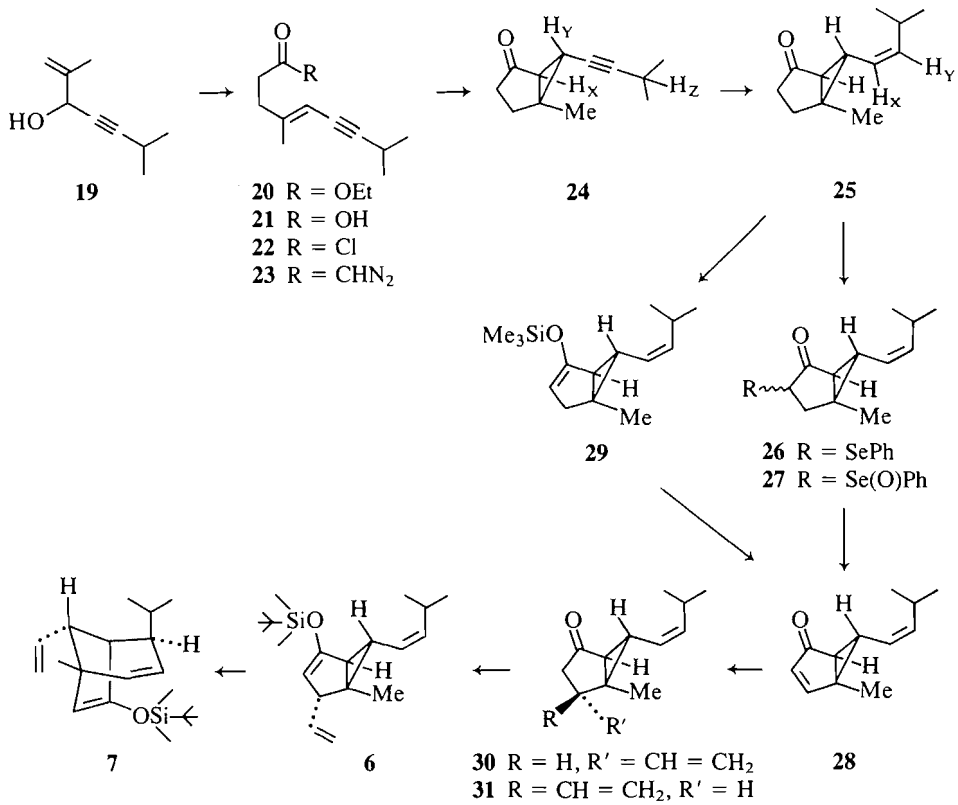

SCHEME 1

elimination sequence involving the intermediates **26** and **27**. However, this procedure provided the enone **28** in mediocre yield (50% at best). Other procedures, in which the α-phenylseleno ketone **26** was isolated prior to oxidation, were even less efficient.

Better results were obtained by application of the method reported by Saegusa and co-workers (23). Thus, conversion (Me_3SiI, Et_3N, CH_2Cl_2, −78°C) of the ketone **25** into the rather unstable enol silyl ether **29**, followed by immediate treatment of the latter substance with palladium(II) acetate in dry acetonitrile, gave, in 78% yield, a colorless oil. Analysis of this material by gas–liquid chromatography (glc) showed that it consisted of a mixture of the desired enone **28** (~85%) and the ketone **25** (~15%). Since efforts to effect efficient chromatographic separation of **25** and **28** proved fruitless, the mixture was employed for the next synthetic step.

Reaction of an 85:15 mixture of **28** and **25** with lithium divinylcuprate in diethyl ether (−30°C to room temperature) provided an oil that, on the basis of an analysis by glc, consisted of an 83:9:8 mixture of the desired product **30**, the epimer **31**, and the ketone **25**, respectively.[2] Separation of this mixture by column chromatography on silica gel provided the pure products **30** (46% from **25** via **29** and **28**) and **31** (6% from **25**).

Conjugate addition of divinylcuprate to the enone **28** would be expected to take place primarily from the less hindered convex face of the molecule to provide **30** as the predominant product. This expectation was confirmed by ^1H nmr spectroscopy. Thus, analysis of the ^1H nmr spectrum of the major product **30**, along with suitable decoupling experiments, showed that the resonances due to H_J, H_K, H_L, H_M, and H_N appear at δ 2.25, 1.89, 2.91, 2.15, and 2.67, respectively. In a nuclear Overhauser enhancement (nOe) difference experiment, irradiation at δ 2.15 (H_M) caused enhancement of the signals at δ 2.25, 2.91, and 2.67 (H_J, H_L, H_N, respectively). This result showed that, in the major conjugate addition product, H_L is *endo* to the bicyclic ring system and, therefore, the vinyl group must have an *exo* orientation.

Further evidence for the stereochemistry of **30** and **31** was provided by the magnitude of the mutual coupling constants associated with the protons H_J, H_K, and H_L in the two compounds. A molecular model indicates that, in compound **30**, the dihedral angle between H_K and H_L is close to 90° and, therefore, these protons would be expected to be only weakly coupled. Indeed, in a decoupling experiment, irradiation at δ 2.91 (H_L) caused the signal due to H_J (δ 2.55) to collapse from a pair of doublets (J_{JK} = 18.5 Hz, J_{JL} = 8 Hz) to a doublet (J_{JK} = 18.5 Hz), but did not affect the resonance (δ 1.89) derived from H_K, which remained a doublet with J_{JK} = 18.5 Hz. On the other hand, analysis of the ^1H nmr spectrum of the minor conjugate addition product **31**, along with appropriate decoupling experiments, showed that proton H_L (δ 2.91) is coupled to both H_J (δ 2.08, J_{JL} = 9.5 Hz) and H_K (δ 2.20–2.29, overlapped with the signal due to H_M, J_{KL} = 9.0 Hz). Considering the size of the H_J—H_L and H_K—H_L dihedral angles in compound **31** (molecular model), the magnitudes of these coupling constants are reasonable.

Routine conversion of the ketone **30** into the enol silyl ether **6** (96%) set the stage for investigating the "crucial" thermolysis of the latter substance. In the event, when a benzene solution of **6** was heated (sealed tube) at 220°C for 4.5 h, a single product was formed in 86% yield. It was gratifying to find that this material

[2]Interestingly, reaction of **28** with vinylmagnesium bromide in the presence of a catalytic amount of copper(I) bromide – dimethyl sulfide complex was somewhat less stereoselective, producing (63% yield) epimers **30** and **31** in a ratio of about 70:30, respectively.

Can. J. Chem. Downloaded from www.nrcresearchpress.com by 72.64.146.136 on 09/07/12
For personal use only.

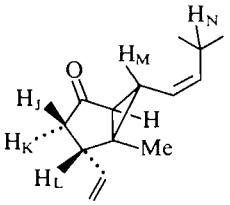

30

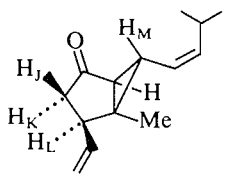

31

was the desired bicyclo[3.2.1]octa-2,6-diene **7**. No evidence could be found for the formation of compound **9**, which would have been derived from a homo-[1,5]-sigmatropic hydrogen migration (*vide supra*). Therefore, our expectation (hope?) that the Cope rearrangement process would be energetically more favorable than the sigmatropic hydrogen shift proved to be valid.

The constitution and relative stereochemistry of **7** was fully corroborated by the spectral data derived from this substance. For confirmation of the stereochemical assignment, the ^{1}H nmr spectrum was particularly useful. For example, suitable decoupling experiments showed that H_K, H_L, and H_M give rise to a doublet (δ 2.46, J_{JK} = 9.0 Hz), a broad singlet (δ 2.26), and a multiplet (δ 1.92–1.97), respectively, and that the H_K–H_L and H_L–H_M couplings are very weak. The latter obervations are in accord with the stereochemistry shown in **7**, since, in the conformationally rigid structure of this molecule, the H_K–H_L and H_L–H_M dihedral angles are both close to 90° (molecular model).

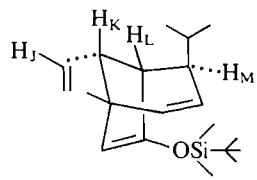

7

(c) Conversion of compound 7 into (±)-sinularene (1)

Treatment of the triene **7** with disiamylborane (24) in THF (0°C to room temperature), followed by oxidation of the resultant trialkylborane with alkaline hydrogen peroxide, effected clean, chemoselective functionalization of the vinylic double bond. When the resultant primary alcohol **32** (see Scheme 2) was treated with *p*-toluenesulfonyl chloride and 4-dimethylaminopyridine in dichloromethane at room temperature, the product was not the initially expected *p*-toluenesulfonate **33**, but proved to be the tricyclic ketone **34** (68% from the triene **7**). Evidently, under the conditions of the *p*-toluenesulfonylation reaction or during the subsequent work-up procedure, the initially formed product **33** underwent a solvolytic ring closure with accompanying cleavage of the silyl ether linkage. In any case, the direct, efficient conversion of **32** into **34** was a pleasing result.

Hydrogenation of **34** in methanol in the presence of palladium-on-carbon gave, in 91% yield, the ketone **4**. The ^{1}H nmr and infrared (ir) spectra of this material were found to be identical with those derived from the same compound previously prepared by Collins and Wege (3).[3]

The ketone **4** had previously been converted into (±)-sinularene (**1**) via a three-step sequence of reactions (3). However, we have found that this transformation could be performed conveniently in a single operation by treatment of **4** with an

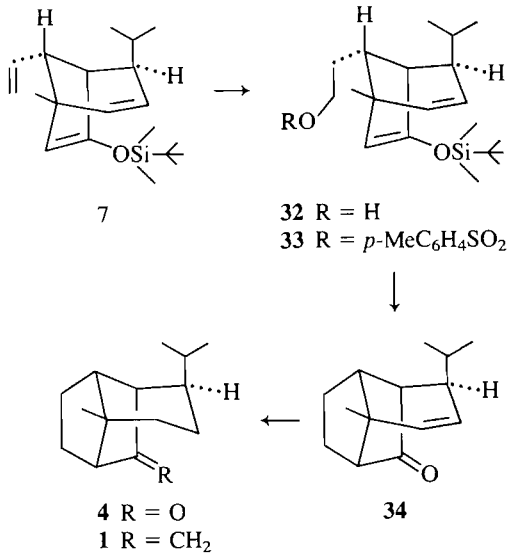

7

32 R = H
33 R = *p*-$MeC_6H_4SO_2$

4 R = O
1 R = CH_2

34

SCHEME 2

excess of methylenetriphenylphosphorane in refluxing THF. Although the Wittig reaction was slow, (±)-sinularene (**1**) was formed cleanly and efficiently (78%). The material thus obtained was spectrally identical with (±)-sinularene previously prepared by Oppolzer *et al.* (4).[4]

Experimental

General

Distillation temperatures are uncorrected. Infrared (ir) spectra were recorded on a Perkin–Elmer model 710B spectrophotometer and were calibrated using the 1601 cm^{-1} band of polystyrene film. Proton (^{1}H) and carbon (^{13}C) nuclear magnetic resonance (nmr) spectra were recorded on deuteriochloroform solutions using tetramethylsilane as an internal standard. In cases of compounds containing a *tert*-butyldimethylsilyl group, the resonance positions were determined relative to the chloroform signal (δ 7.25). Analytical gas–liquid chromatography (glc) was performed with Hewlett–Packard models 5832A (columns: 6 ft × 0.125 in., 5% OV-17 on 80–100 mesh Chromosorb W (HP); 6 ft × 0.125 in., 5% OV-210 on 80–100 mesh Chromosorb W (HP); 10 ft × 0.125 in., 10% SE-30 on 80–100 mesh Chromosorb W (HP)) and 5880A (column: 25 m × 0.21 m fused silica column coated with cross-linked SE-54) gas chromatographs. Thin-layer chromatography (tlc) was accomplished using commercial aluminum-backed silica gel plates (E. Merck, Type 5539). Unless otherwise noted, conventional column chromatography was performed using 70–230 mesh silica gel (E. Merck), while flash column chromatography was carried out with 230–400 mesh silica gel (E. Merck). High resolution mass spectrometric measurements were recorded on a Kratos/AEI MS-50 mass spectrometer.

2,6-Dimethyl-1-hepten-4-yn-3-ol (19)

To a cold (−78°C), stirred solution of 3-methyl-1-butyne (0.375 mL, 3.67 mmol) in dry THF (5 mL) (argon atmosphere) was added a solution of *n*-butyllithium (4.04 mmol) in hexane, and the mixture was stirred at −30°C for 1 h. 2-Methylpropenal (0.34 mL, 4.04 mmol) was added dropwise, the mixture was stirred for 1 h at −30°C, and then was poured into saturated aqueous ammonium chloride. The resultant mixture was extracted thoroughly with ether. The combined extract was washed successively with saturated aqueous ammonium chloride, saturated aqueous sodium bicarbonate, and brine, and then was dried ($MgSO_4$). Removal of the solvent (water aspirator), followed by distillation (air-bath temperature 67–72°C/0.1 Torr; 1 Torr = 133.3 Pa) of the residual yellow oil, provided 480 mg (95%) of the alcohol **19** as a

[3]We thank Professor Wege for copies of the ^{1}H nmr and ir spectra of (±)-**4**.

[4]We thank Professor Oppolzer for copies of the ^{1}H nmr, ir, and mass spectra of (±)-sinularene (**1**).

Can. J. Chem. Downloaded from www.nrcresearchpress.com by 72.64.146.136 on 09/07/12
For personal use only.

clear, colorless oil that exhibited ir (film): 3350, 2220, 1650 cm^{-1}; ^1H nmr (80 MHz) δ: 1.17 (d, 6H, J = 7 Hz), 1.77 (br s, 1H, exchanges with D_2O), 1.85 (br s, 3H), 2.61 (d septet, 1H, J = 2, 6.5 Hz), 4.77 (br s, 1H), 4.90 (br s, 1H), 5.15 (br s, 1H). *Exact Mass* calcd. for $C_9H_{14}O$: 138.1045; found: 138.1044.

*Ethyl (*E*)-4,8-dimethyl-4-nonen-6-ynoate (**20**)*

A stirred mixture of the alcohol **19** (460 mg, 3.33 mmol), triethyl orthoacetate (3.05 mL, 16.6 mmol), and propanoic acid (0.015 mL, 0.2 mmol) was heated at 130°C for 20 h. Most of the triethyl orthoacetate was removed by fractional distillation at atmospheric pressure. The residual oil was subjected to flash column chromatography (125 g of silica gel, elution with 1:25 ether – petroleum ether). Distillation (air-bath temperature 81–86°C/0.1 Torr) of the oil obtained from the appropriate fractions gave 402 mg (58%) of the ester **20** as an odoriferous, colorless oil that exhibited ir (film): 1730 cm^{-1}; ^1H nmr (400 MHz) δ: 1.19 (d, 6H, J = 7 Hz), 1.25 (t, 3H, J = 7 Hz), 1.87 (s, 3H), 2.36–2.45 (m, 4H), 2.70 (septet, 1H, J = 7 Hz), 4.13 (q, 2H, J = 7 Hz), 5.29 (br s, 1H). *Exact Mass* calcd. for $C_{13}H_{20}O_2$: 208.1463; found: 208.1453.

*(*E*)-4,8-Dimethyl-4-nonen-6-ynoic acid (**21**)*

A stirred mixture of the ester **20** (500 mg, 2.4 mmol), potassium hydroxide (276 mg, 2.88 mmol), water (1 mL), and methanol (10 mL) was refluxed for 4 h. The solution was cooled to room temperature, washed twice with petroleum ether, filtered through a layer of Celite, cooled to 0°C, and acidified with 10% hydrochloric acid. The resultant mixture was extracted thoroughly with ether. The combined extract was dried ($MgSO_4$) and the solvent was removed under reduced pressure. The residual oil was crystallized from hexane at −78°C to furnish 294 mg (68%) of the acid **21** as a colorless oil that exhibited ir (film): 3300–2500 (br), 1705 cm^{-1}; ^1H nmr (80 MHz) δ: 1.22 (d, 6H, J = 7 Hz), 1.90 (s, 3H), 2.30–3.00 (m, 5H), 5.30 (br s, 1H), 10.85 (br s, 1H). *Exact Mass* calcd. for $C_{11}H_{16}O_2$: 180.1150; found: 180.1151.

*(*E*)-4,8-Dimethyl-4-nonen-6-ynoyl chloride (**22**)*

A stirred solution of the acid **21** (9.75 g, 54.1 mmol) and oxalyl chloride (14.2 mL, 162.4 mmol) in dry hexane (235 mL) was refluxed under an atmosphere of argon for 1 h. The solvent and excess oxalyl chloride were removed under reduced pressure (water aspirator) and the brown residue was distilled (air-bath temperature 94–99°C/0.1 Torr) to afford 10.3 g (95%) of the acid chloride **22** as a pale yellow oil. This material exhibited ir (film): 2200, 1790, 1623 cm^{-1}; ^1H nmr (80 MHz) δ: 1.20 (d, 6H, J = 7 Hz), 1.88 (s, 3H), 2.32–3.13 (m, 5H), 5.31 (br s, 1H). *Exact Mass* calcd. for $C_{11}H_{15}{}^{37}ClO$: 200.0782; found: 200.0783.

*5-Methyl-6-*exo*-(3-methyl-1-butynyl)bicyclo[3.1.0]hexan-2-one (**24**)*

To a cold (0°C), stirred solution of diazomethane (240 mg, 5.67 mmol) in ether (15 mL) was added dropwise, via a flame-polished pipette, a solution of the acid chloride **22** (250 mg, 1.26 mmol) in ether (3 mL). The resulting solution was stirred at 0°C for 30 min and at room temperature for 1 h. The residual diazomethane was dispelled by bubbling argon through the yellow solution, via a flame-polished pipette, for 30 min. Removal of the solvent gave 250 mg of the crude diazo ketone **23** as a viscous yellow oil. This material, which was not purified further, exhibited ir (film): 2200, 2085, 1633 cm^{-1}.

To a stirred suspension of $Cu(acac)_2 \cdot H_2O$ (24 mg, 0.092 mmol) in refluxing dry benzene (7 mL), under an atmosphere of argon, was added dropwise a solution of the crude diazo ketone **23** (250 mg, 1.23 mmol) in dry benzene (3 mL). The resulting dark brown mixture was refluxed for 1 h and then was cooled to room temperature. Most of the benzene was removed carefully under reduced pressure (water aspirator) and the residual material was subjected to flash column chromatography (70 g of silica gel, elution with 1:3 ether – petroleum ether). Disillation (air-bath temperature 85–88°C/0.1 Torr) of the oil thus obtained provided 178 mg (81% from the acid chloride **22**) of the bicyclic ketone **24** as a colorless oil that exhibited ir (film): 1725, 1172 cm^{-1}; ^1H nmr (400 MHz) δ: 1.14 (d, 6H, J = 7 Hz), 1.44 (s, 3H), 1.69 (d, 1H, J = 3 Hz), 1.87 (overlapped dd, 1H, J = 3, 1.7 Hz), 1.94–2.14 (m, 4H), 2.53 (d septet, 1H, J = 1.7, 7 Hz). Decoupling experiment: irradiation at δ 1.87 caused the signals at δ 1.69 and 2.53 to collapse to a singlet and a septet (J = 7 Hz), respectively. *Anal.* calcd. for $C_{12}H_{16}O$: C 81.76, H 9.16; found: C 81.69, H 9.20. *Exact Mass* calcd.: 176.1201; found: 176.1196.

*5-Methyl-6-*exo*-[(*Z*)-3-methyl-1-butenyl]bicyclo[3.1.0]hexan-2-one (**25**)*

A suspension of 5% palladium on calcium carbonate (49 mg, prepared with lead acetate as described by Lindlar and Dubois (21)) in dry pentane (7 mL) was prehydrogenated at room temperature and atmospheric pressure. To the mixture was added dropwise a solution of the alkyne **24** (973 mg, 5.53 mmol) in dry pentane (3 mL) and the reaction mixture was stirred efficiently under an atmosphere of hydrogen. The progress of the reaction was monitored by glc, which showed that the starting material had been consumed after a period of 3 h. Filtration of the mixture through a layer of Celite and concentration of the filtrate gave a colorless oil that was subjected to flash column chromatography (125 g of silica gel, elution with 1:5 ether – petroleum ether). Distillation (air-bath temperature 78–80°C/0.1 Torr) of the oil thus obtained afforded 900 mg (91%) of the keto alkene **25** as a colorless oil, which exhibited ir (film): 1719, 1650 cm^{-1}; ^1H nmr (400 MHz) δ: 0.98, 1.00 (d, d, 3H each, J = 7 Hz), 1.32 (s, 3H), 1.57 (poorly resolved d, 1H, J = 2 Hz), 1.90–2.25 (m, 5H), 2.60–2.73 (m, 1H), 4.91 (overlapped dd, 1H, J = 11.5, 10 Hz), 5.36 (overlapped dd, 1H, J = 11.5, 10 Hz). *Exact Mass* calcd. for $C_{12}H_{18}O$: 178.1358; found: 178.1357.

*5-Methyl-6-*exo*-[(*Z*)-3-methyl-1-butenyl]bicyclo[3.1.0]hex-3-en-2-one (**28**)*

(a) Via selenoxide elimination

To a cold (−78°C), stirred solution of lithium diisopropylamide (2.3 mmol) in dry THF (15 mL), under an atmosphere of argon, was added dropwise a solution of the ketone **25** (273 mg, 1.53 mmol) in dry THF (3 mL), and the mixture was stirred at −78°C for 30 min. A solution of phenylselenenyl chloride (440 mg, 2.30 mmol) in dry THF (4 mL) was added dropwise and the solution was stirred at 0°C for 30 min. After acetic acid (0.175 mL, 3.06 mmol) had been introduced, a solution of 30% aqueous hydrogen peroxide (0.868 g) in 2 mL of water was added dropwise. The reaction mixture was stirred at 0°C for 30 min, diluted with 1:1 ether – petroleum ether, and then was poured into saturated aqueous sodium bicarbonate. The layers were separated and the aqueous phase was extracted thoroughly with ether. The combined extract was washed twice with brine, dried ($MgSO_4$), and concentrated. Subjection of the residual material to flash column chromatography (70 g silica gel, elution with 1:7 ether – petroleum ether), concentration of the appropriate fractions, and distillation (air-bath temperature 76–80°C/0.1 Torr) of the oil thus obtained furnished 136 mg (50%) of the enone **28** as a colorless oil. This material exhibited ir (film): 1690 cm^{-1}; ^1H nmr (400 MHz) δ: 0.97, 0.98 (d, d, 3H each, J = 7 Hz), 1.45 (s, 3H), 1.99 (poorly resolved d, 1H, J = 3 Hz), 2.36 (dd, 1H, J = 9.5, 3 Hz), 2.60–2.73 (m, 1H), 4.91 (overlapped ddd, 1H, J = 12, 9.5, 1 Hz), 5.40 (overlapped ddd, 1H, J = 12, 9, <1 Hz), 5.66 (dd, 1H, J = 5.5, 1 Hz), 7.52 (dd, 1H, J = 5.5, 1 Hz). Decoupling experiments: irradiation at δ 4.91 caused the signal at δ 2.60–2.73 to sharpen and the resonances at δ 2.36 and 5.40 to collapse to doublets (J = 3, 9 Hz, respectively); irradiation at δ 7.52 caused the signals at δ 1.99 and 5.66 to collapse to a dd (J = 3, 1 Hz) and a d (J = 1 Hz), respectively. *Exact Mass* calcd. for $C_{12}H_{16}O$: 176.1201; found: 176.1203.

*(b) Via $Pd(OAc)_2$ oxidation of the enol silyl ether **29***

To a cold (−78°C), stirred solution of the ketone **25** (713 mg, 4.0 mmol) and triethylamine (4.46 mL, 32.0 mmol) in dry dichloromethane (40 mL), under an atmosphere of argon, was added, dropwise, freshly prepared (25) trimethylsilyl iodide (14 mmol). The resulting dark orange suspension was stirred at −78°C for 30 min. The reaction mixture was diluted with ether and then was poured into a 1:1 mixture of 5% aqueous sodium thiosulfate and saturated aqueous sodium bicarbonate. The layers were separated and the organic layer was dried ($MgSO_4$) and concentrated. The residual material, which was shown by glc analysis to be a 12:1 mixture of the enol silyl ether **29** and the

Can. J. Chem. Downloaded from www.nrcresearchpress.com by 72.64.146.136 on 09/07/12
For personal use only.

Can. J. Chem. Downloaded from www.nrcresearchpress.com by 72.64.146.136 on 09/07/12
For personal use only.

starting material **25**, was dissolved in dry acetonitrile (3 mL) and the resultant solution was added, dropwise, to a stirred suspension of palladium(II) acetate (1.80 g, 8.0 mmol) in dry acetonitrile (3 mL). The mixture was stirred at room temperature for 1 h and then was filtered. The filtrate was washed twice with saturated aqueous sodium bicarbonate, dried ($MgSO_4$), and concentrated to give a dark brown oil. Subjection of this material to flash column chromatography (70 g of silica gel, elution with 1:7 ether – petroleum ether) and concentration of the appropriate fractions afforded 554 mg (78%) of a colorless oil. On the basis of glc analyses and the ^{1}H nmr spectrum, this material consisted of an 85:15 mixture of the desired enone **28** and the ketone **25**, respectively. Since attempts to separate these two compounds by chromatography were not successful, the mixture was used for the next reaction.

*5-Methyl-6-*exo*-[(Z)-3-methyl-1-butenyl]-4-*exo*-vinylbicyclo[3.1.0]-hexan-2-one (**30**) and the C-4 epimer **31***

To a stirred solution of tetravinyltin (258 mg, 1.14 mmol) in dry ether (5 mL), under an atmosphere of argon, was added dropwise a solution of phenyllithium (4.54 mmol) in a mixture of ether and cyclohexane. A white precipitate formed almost immediately and the resulting reaction mixture was stirred for 30 min. The stirring was stopped and the white precipitate was allowed to settle to the bottom of the flask. The pale yellow solution was transferred (syringe) to another dry flask (argon atmosphere) and then was cooled with stirring to −63°C. Copper(I) bromide – dimethyl sulfide complex (467 mg, 2.27 mmol) was added and the mixture was stirred at −63°C for 20 min to furnish a dark grey suspension. A solution of an 85:15 mixture of the enone **28** and the ketone **25**, respectively, (200 mg) in dry ether (3 mL) was added dropwise and the resultant dark purple mixture was stirred at −30°C for 15 min and at room temperature for 1 h. Saturated aqueous ammonium chloride (pH 8) (6 mL) and ether (5 mL) were added and the mixture was stirred vigorously until the aqueous layer became deep blue. The layers were separated and the aqueous phase was extracted twice with ether. The combined organic extract was washed successively with saturated aqueous ammonium chloride (pH 8) and brine, and then was dried ($MgSO_4$). Removal of the solvent, column chromatography (50 g silica gel, elution with 1:5 ether – petroleum ether) of the resultant oil, and distillation (air-bath temperature 91–97°C/0.1 Torr) of the two oils thus obtained afforded 136 mg (46% from **25**) of the ketone **30** and 19 mg (6% from **25**) of the epimeric substance **31**.

Compound **30** exhibited ir (film): 1722, 1635, 920 cm^{-1}; ^{1}H nmr (400 MHz) δ: 1.00, 1.01 (d, d, 3H each, J = 6.5 Hz), 1.20 (s, 3H), 1.63 (br s, 1H, $w_{1/2}$ = 5.5 Hz), 1.89 (d, 1H, J = 18.5 Hz), 2.15 (ddd, 1H, J = 8.5, 3, 1 Hz), 2.55 (dd, 1H, J = 18.5, 8 Hz), 2.67 (dd septet, 1H, J = 9.5 Hz, <1, 6.5 Hz), 2.91 (overlapped dd, 1H, J = 10, 8 Hz), 4.91 (overlapped ddd, 1H, J = 10.5, 8.5, <1 Hz), 5.04–5.12 (m, 2H), 5.39 (overlapped ddd, 1H, J = 10.5, 9.5, 1 Hz), 5.72 (overlapped ddd, 1H, J = 17, 10, 10 Hz). Difference nuclear Overhauser enhancement (nOe) experiment: irradiation at δ 2.15 caused enhancement of the signals at δ 2.55, 2.67, and 2.91. Decoupling experiments: irradiation at δ 5.39 caused the signals at δ 2.15, 2.67, and 4.91 to collapse to a dd (J = 8.5, 3 Hz), a poorly resolved septet (J = 6.5 Hz), and a poorly resolved d (J = 8.5 Hz), respectively; irradiation at δ 4.91 caused the resonances at δ 2.15, 2.67, and 5.39 to change to an overlapped dd (J = 3, 1 Hz), a d septet (J = 9.5, 6.5 Hz), and a poorly resolved d (J = 9.5 Hz), respectively; irradiation at δ 2.15 sharpened the signal at δ 1.63 and collapsed the signals at δ 4.91 and 5.39 to a d (J = 10.5 Hz) and a dd (J = 10.5, 9.5 Hz), respectively; irradiation at δ 2.91 simplified the multiplet at δ 5.04–5.12 and changed the resonances at δ 2.55 and 5.72 to a d (J = 18.5 Hz) and a dd (J = 17, 10 Hz), respectively. *Exact Mass* calcd. for $C_{14}H_{20}O$: 204.1514; found: 204.1517.

Compound **31** exhibited ^{1}H nmr (400 MHz) δ: 1.00 (d, 6H, J = 6.5 Hz), 1.31 (s, 3H), 1.63 (br s, 1H, $w_{1/2}$ = 5.5 Hz), 2.08 (dd, 1H, J = 18, 9.5 Hz), 2.20–2.29 (m, 2H), 2.68 (dd, septet, 1H, J = 9.5, <1, 6.5 Hz), 2.91 (overlapped ddd, 1H, J = 9.5, 9, 7 Hz), 4.89 (overlapped ddd, 1H, J = 10.5, 9, <1 Hz), 5.10–5.17 (m, 2H), 5.38 (overlapped ddd, 1H, J = 10.5, 9.5, 1 Hz), 5.83 (ddd, 1H, J = 17.5, 10, 7 Hz). Decoupling experiments: irradiation at δ 4.89 simplified the signal at δ 2.20–2.29 and caused the signals at δ 2.68 and 5.38 to change to a dd (J = 9.5, 6.5 Hz) and a br d (J = 9.5 Hz), respectively; irradiation at δ 2.91 simplified the multiplets at δ 2.20–2.29 and 5.10–5.17, and collapsed the signals at δ 2.08 and 5.83 to a d (J = 18 Hz) and a dd (J = 17.5, 10 Hz), respectively; irradiation at δ 5.10–5.17 caused the signal at δ 2.91 to sharpen and the resonance at δ 5.83 to collapse to a d (J = 7 Hz). *Exact Mass* calcd. for $C_{14}H_{20}O$: 204.1514; found: 204.1510.

*2-(*tert*-Butyldimethylsiloxy)-5-methyl-6-*exo*-[(Z)-3-methyl-1-butenyl]-4-*exo*-vinylbicyclo[3.1.0]hex-2-ene (**6**)*

To a cold (−78°C), stirred solution of lithium diisopropylamide (3.35 mmol) in dry THF (16 mL), under an atmosphere of argon, was added a solution of the ketone **30** (623 mg, 3.05 mmol) in dry THF (4 mL) and the solution was stirred at −78°C for 30 min. A solution of freshly sublimed *tert*-butyldimethylsilyl chloride (690 mg, 4.57 mmol) and hexamethylphosphoramide (6.1 mmol) in dry THF (6 mL) was added and the solution was stirred at −78°C for 30 min and at room temperature for 2 h. The reaction mixture was poured into saturated aqueous sodium bicarbonate and the layers were separated. The aqueous layer was extracted with ether, the combined organic extract was washed thrice with brine, and dried ($MgSO_4$). Removal of the solvent, followed by column chromatography of the residual oil on a short column of neutral alumina (80–200 mesh, elution with petroleum ether) and distillation (air-bath temperature 118–123°C/0.1 Torr) of the oil thus obtained, gave 933 mg (96%) of the enol silyl ether **6** as a colorless oil. This material exhibited ir (film): 1635, 1620, 960, 920, 790 cm^{-1}; ^{1}H nmr (400 MHz) δ: 0.17 (s, 6H), 0.94 (s, 9H), 0.99 (d, 6H, J = 7 Hz), 1.13 (s, 3H), 1.34 (overlapped dd, 1H, J = 2.5, 1 Hz), 1.40 (br dd, 1H, J = 9, 2.5 Hz), 2.71 (dd septet, 1H, J = 9, 1, 7 Hz), 3.10 (br d, 1H, J = 9 Hz), 4.20 (dd, 1H, J = 2.5, 1 Hz), 4.92 (overlapped ddd, 1H, J = 11, 9, 1 Hz), 4.98 (dd, 1H, J = 10, 2 Hz), 5.04 (ddd, 1H, J = 17, 2, 1 Hz), 5.29 (overlapped ddd, 1H, J = 11, 9, 1 Hz), 5.74 (ddd, 1H, J = 17, 10, 9 Hz). *Exact Mass* calcd. for $C_{20}H_{34}OSi$: 318.2379; found: 318.2370.

*6-(*tert*-Butyldimethylsiloxy)-4-*exo*-isopropyl-1-methyl-8-*exo*-vinylbicyclo[3.2.1]octa-2,6-diene (**7**)*

A solution of the enol silyl ether **6** (170 mg, 0.534 mmol) in 3 mL of dry benzene was placed in a glass pyrolysis tube (2-mm wall thickness) and the solution was degassed. The tube was cooled with liquid nitrogen and was sealed under vacuum (0.1 Torr). After the tube had been heated at 220°C for 4.5 h in a steel container packed with sand, it was cooled to room temperature and then was unsealed. Removal of the solvent, column chromatography of the residual oil on neutral alumina that had been pretreated with a solution of triethylamine (elution with petroleum ether), and distillation (air-bath temperature 88–99°C/0.1 Torr) of the oil thus obtained afforded 146 mg (86%) of the bicyclic triene **7**, which exhibited ir (film): 1630, 1620, 940, 915, 784 cm^{-1}; ^{1}H nmr (400 MHz) δ: 0.13, 0.15, 0.92, 0.95 (s, s, s, s, 3, 3, 9, 3H, respectively), 0.97, 1.00 (d, d, 3H each, J = 7 Hz), 1.67–1.79 (m, 1H), 1.92–1.97 (m, 1H), 2.26 (br s, 1H), 2.46 (d, 1H, J = 9 Hz), 4.74 (s, 1H), 5.01 (dd, 1H, J = 10, 2.5 Hz), 5.08 (ddd, 1H, J = 17, 2.5, <1 Hz), 5.35 (ddd, 1H, J = 9.5, 3, 2 Hz), 5.96 (ddd, 1H, J = 17, 10, 9 Hz), 6.00 (dd, 1H, J = 9.5, 2 Hz). Decoupling experiments: irradiation at δ 5.35 caused the signals at δ 1.92–1.97 and 6.00 to collapse to a br d (J = 7 Hz) and a d (J = 2 Hz), respectively, and the signal at δ 2.26 to sharpen; irradiation at δ 1.95 caused the signals at δ 1.67–1.79, 5.35, and 6.00 to collapse to a septet (J = 7 Hz), a dd (J = 9.5, 2 Hz), and a d (J = 9.5 Hz), respectively, and the signal at δ 2.26 to sharpen; irradiation at δ 2.26 changed the signals at δ 1.92–1.97 and 5.35 to an overlapped ddd (J = 7, 3, 2 Hz) and a dd (J = 9.5, 3 Hz). *Exact Mass* calcd. for $C_{20}H_{34}OSi$: 318.2379; found: 318.2365.

*6-(*tert*-Butyldimethylsiloxy)-8-*exo*-(2-hydroxyethyl)-4-*exo*-isopropyl-1-methylbicyclo[3.2.1]octa-2,6-diene (**32**)*

To a cold (0°C), stirred solution of disiamylborane (0.346 mmol) in dry THF (2 mL), under an atmosphere of argon, was added a solution of the triene **7** (50 mg, 0.157 mmol) in dry THF (2 mL) and the resulting

Can. J. Chem. Downloaded from www.nrcresearchpress.com by 72.64.146.136 on 09/07/12
For personal use only.

mixture was allowed to warm to room temperature over a period of 1.5 h. The reaction mixture was recooled to 0°C and a solution of sodium hydroxide (13.8 mg, 0.346 mmol) in water (1 mL) and a 30% aqueous solution of hydrogen peroxide (0.106 mL, 1.04 mmol) were added. The stirred mixture was allowed to warm to room temperature over a period of 1 h. The reaction mixture was diluted with a 1:1 mixture of ether – petroleum ether and then was poured into saturated aqueous ammonium chloride. The layers were separated, the aqueous layer was extracted thoroughly with ether, and the combined organic extract was washed with brine and dried ($MgSO_4$). Removal of the solvent gave a light yellow oil, which was subjected to column chromatography on 18 g of 80–200 mesh neutral alumina. Elution of the column with petroleum ether (30 mL), and ether (30 mL), followed by concentration of the appropriate fractions, provided 45 mg (86%) of the alcohol **32** as a colorless, odoriferous oil that exhibited ir (film): 3300, 1622 cm^{-1}; ^1H nmr (400 MHz) δ: 0.11, 0.13, 0.90, 0.99 (s, s, s, s, 3, 3, 9, 3H, respectively), 0.95, 0.97 (d, d, 3H each, J = 6.5 Hz), 1.49–1.70 (m, 3H), 1.73–1.82 (m, 1H), 1.85–1.91 (m, 1H), 1.94 (dd, 1H, J = 10, 3.5 Hz), 2.28 (br s, 1H), 3.63–3.79 (m, 2H), 4.69 (s, 1H), 5.30 (ddd, 1H, J = 9.5, 3, 2 Hz), 5.98 (dd, 1H, J = 9.5, 2 Hz). *Exact Mass* calcd. for $C_{20}H_{36}O_2Si$: 336.2485; found: 336.2486.

10-exo-*Isopropyl-7-methyltricyclo[4.4.0.0^{3,7}]dec-8-en-2-one (**34**)*

To a cold (0°C), stirred solution of 4-dimethylaminopyridine (236 mg, 1.93 mmol) in dry dichloromethane (5 mL) was added a solution of *p*-toluenesulfonyl chloride (184 mg, 0.964 mmol) in dry dichloromethane (2 mL) and the mixture was stirred at room temperature, under an atmosphere of argon, for 30 min. A solution of the alcohol **32** (216 mg, 0.643 mmol) in dry dichloromethane (3 mL) was added, the reaction mixture was stirred at room temperature for 1.3 h, and then was diluted with ether and poured into saturated aqueous sodium bicarbonate. The layers were separated and the aqueous layer was extracted thoroughly with ether. The combined organic extract was washed successively with brine, 5% hydrochloric acid, saturated aqueous sodium bicarbonate and brine, and then was dried ($MgSO_4$). Removal of the solvent, followed by distillation (air-bath temperature 83–87°C/0.1 Torr) of the residual yellow oil, furnished 103 mg (79%) of the olefinic ketone **34**, a colorless oil that exhibited ir (film): 1743, 1630 cm^{-1}; ^1H nmr (400 MHz) δ: 0.95, 0.98 (d, d, 3H each, J = 7 Hz), 1.09 (s, 3H), 1.35–1.43 (m, 1H), 1.52–1.66 (m, 2H), 1.90–1.96 (m, 1H), 1.98–2.07 (m, 3H), 2.28 (br s, 1H, $w_{1/2}$ = 5.5 Hz), 2.35 (br d, 1H, J = 3 Hz), 5.59 (d, 1H, J = 10 Hz), 5.63 (ddd, 1H, J = 10, 3.5, 1.5 Hz). Decoupling experiment: irradiation at δ 5.61 caused the signals at δ 1.90–1.96 and 2.28 to collapse to a dd (J = 9.5, 2.5 Hz) and a d (J = 2.5 Hz), respectively. *Exact Mass* calcd. for $C_{14}H_{20}O$: 204.1514; found: 204.1526.

10-exo-*Isopropyl-7-methyltricyclo[4.4.0.0^{3,7}]decan-2-one (**4**)*

To a vigorously stirred, prehydrogenated suspension of 10% palladium-on-carbon (4 mg) in methanol (2 mL), under an atmosphere of hydrogen, was added a solution of the olefinic ketone **34** (43 mg, 0.21 mmol) in methanol (2 mL). The mixture was stirred at room temperature and reaction progress was monitored by glc. After 24 h, the hydrogenation had become quite sluggish and another 3 mg of the palladium catalyst was introduced. The reaction mixture was stirred for another 3 h and then was filtered through a layer of Celite. Concentration of the filtrate and distillation (air-bath temperature 93–98°C/0.1 Torr) of the residual oil gave 40 mg (91%) of the ketone **4** as a colorless oil that exhibited ir (film): 1740 cm^{-1}; ^1H nmr (400 MHz) δ: 0.89, 0.92 (d, d, 3H each, J = 6.5 Hz), 1.00 (s, 3H), 1.38–1.64 (m, 6H), 1.66–1.77 (m, 2H), 1.91–2.00 (m, 2H), 2.02–2.11 (m, 2H), 2.14 (br d, 1H, J = 4.5 Hz). The ir and ^1H nmr spectra of **4** were identical with those of a sample of this ketone prepared previously by Collins and Wege (3).[3] *Exact Mass* calcd. for $C_{14}H_{22}O$: 206.1671; found: 206.1671.

*(±)-Sinularene (**1**)*

To a stirred, yellow solution of methylenetriphenylphosphorane (1.05 mmol) (prepared by treatment of a suspension of methyltriphenylphosphonium bromide (376 mg, 1.05 mmol) in 10 mL of dry THF with a hexane solution of 1.05 mmol of *n*-butyllithium) was added a solution of the ketone **4** (21.7 mg, 0.105 mmol) in dry THF and the resulting mixture was heated under reflux. Reaction progress was monitored by glc, which indicated that, after 46.5 h, starting material was still present and the reaction had become quite sluggish. Consequently, a solution of 1.05 mmol of methylenetriphenylphosphorane in 10 mL of dry THF was added (syringe) and the reaction mixture was refluxed for an additional 22.5 h. A few drops of water were added and most of the solvent was removed under reduced pressure (water aspirator). The residue (white solid plus an oil) was treated with petroleum ether and the resultant mixture was dried ($MgSO_4$) and then was filtered through a column of silica gel (2.5 g, 6 × 160 mm column, elution with petroleum ether). Removal of the solvent from the eluate gave 17 mg (78%) of (±)-sinularene (**1**), which exhibited one peak on glc and one spot on tlc analyses; ir (film): 3060, 1661, 1462, 1385, 1382, 1370, 878 cm^{-1}; ^1H nmr (400 MHz) δ: 0.90, 0.92 (d, d, 3H each, J = 6.5 Hz), 0.91 (3H, s), 1.05–1.32 (m, 5H), 1.46–1.51 (m, 2H), 1.56–1.81 (m, 3H), 1.85–1.95 (m, 1H), 2.14 (br d, 1H, J = 3.5 Hz), 2.20 (br s, 1H, $w_{1/2}$ = 7 Hz), 4.58 (br s, 1H, $w_{1/2}$ = 3 Hz), 4.78 (br s, 1H, $w_{1/2}$ = 4 Hz); ^{13}C nmr (100.6 MHz): three methyl carbons (δ 20.7, 20.8, 21.4), four methylene carbons (δ 22.4, 26.0, 30.2, 31.7), five methine carbons (δ 29.1, 42.9, 49.2, 50.2, 53.5), one quaternary carbon (δ 46.9), two alkene carbons (δ 101.2, 163.3). The ir and ^1H nmr spectra of (±)-**1** were identical with those of racemic sinularene prepared previously by Oppolzer, Strauss, and Simmons (4).[4] *Exact Mass* calcd. for $C_{15}H_{24}$: 204.1878; found: 204.1880.

Acknowledgements

We are grateful to the Natural Sciences and Engineering Research Council of Canada for financial support and for a Postgraduate Scholarship (to G.L.J.).

1. C. M. Beechan, C. Djerassi, J. S. Finer, and J. Clardy. Tetrahedron Lett. 2395 (1977).
2. J. C. Braekman, D. Daloze, A. Dupont, B. Tursch, J. P. Declercq, G. Germain, and M. Van Meerssche. Tetrahedron, **37**, 179 (1981).
3. P. A. Collins and D. Wege. Aust. J. Chem. **32**, 1819 (1979).
4. W. Oppolzer, H. F. Strauss, and D. P. Simmons. Tetrahedron Lett. **23**, 4673 (1982).
5. K. Antczak, J. F. Kingston, and A. G. Fallis. Can. J. Chem. **63**, 993 (1985); K. Antczak, J. F. Kingston, A. G. Fallis, and A. W. Hanson. Can. J. Chem. **65**, 114 (1987).
6. W. Oppolzer, T. Begley, and A. Ashcroft. Tetrahedron Lett. **25**, 825 (1984).
7. E. Piers and G. L. Jung. Can. J. Chem. **63**, 996 (1985).
8. E. Piers and E. H. Ruediger. J. Org. Chem. **45**, 1725 (1980).
9. E. Piers, G. L. Jung, and E. H. Ruediger. Can. J. Chem. **65**, 670 (1987).
10. J. J. Gajewski. Hydrocarbon thermal isomerizations. Academic Press, Inc., New York, NY. 1981. (*a*) pp. 215–216; (*b*) pp. 258–260.
11. J. E. Baldwin and K. E. Gilbert. J. Am. Chem. Soc. **98**, 8283 (1976).
12. S. J. Rhoads and N. R. Raulins. Org. React. **22**, 1 (1975).
13. E. M. Mil'vitskaya, A. V. Tarakanova, and A. V. Plate. Russ. Chem. Rev. **45**, 469 (1976).
14. C. W. Spangler. Chem. Rev. **76**, 187 (1976).
15. R. J. Ellis and H. M. Frey. J. Chem. Soc. 5578 (1964).
16. W. Pickenhagen, F. Näf, G. Ohloff, P. Muller, and J.-C. Perlberger. Helv. Chim. Acta, **56**, 1868 (1973).
17. J. M. Brown. Chem. Commun. 226 (1965).
18. E. Piers, G. L. Jung, and N. Moss. Tetrahedron Lett. **25**, 3959 (1984).
19. W. S. Johnson, L. Werthemann, W. R. Bartlett, T. J. Brocksom, T. Li, D. J. Faulkner, and M. R. Petersen. J. Am. Chem. Soc. **92**, 741 (1970); K. A. Parker and R. W. Kosley, Jr. Tetrahedron Lett. 691 (1975).
20. D. H. Williams and I. Fleming. Spectroscopic methods in

organic chemistry. 2nd ed. McGraw–Hill Book Co. (U.K.) Ltd., London. 1973. pp. 107–108.
21. H. LINDLAR and R. DUBOIS. Org. Synth. **46**, 89 (1966).
22. H. J. REICH, I. L. REICH, and J. M. RENGA. J. Am. Chem. Soc. **95**, 5813 (1973); H. J. REICH, J. M. RENGA, and I. L. REICH. J. Am. Chem. Soc. **97**, 5434 (1975).
23. Y. ITO, T. HIRAO, and T. SAEGUSA. J. Org. Chem. **43**, 1011 (1978).
24. H. C. BROWN and G. ZWEIFEL. J. Am. Chem. Soc. **83**, 1241 (1961).
25. D. E. SEITZ and L. FERREIRA. Synth. Commun. **9**, 931 (1979).

Can. J. Chem. Downloaded from www.nrcresearchpress.com by 72.64.146.136 on 09/07/12
For personal use only.

Metallacyclohexasulfanes: the crystal and molecular structures of $(\eta^5\text{-}C_5H_5)_2MS_5$, M = Zr and Hf

ALAN SHAVER AND JAMES M. MCCALL
Department of Chemistry, McGill University, 801 Sherbrooke St. W., Montreal, Que., Canada H3A 2K6

AND

VICTOR W. DAY AND SARAH VOLLMER
The Crystalytics Company, Lincoln, NE 68501, U.S.A., and Department of Chemistry, University of Nebraska, Lincoln, NE 68588, U.S.A.

Received August 25, 1986[1]

ALAN SHAVER, JAMES M. MCCALL, VICTOR W. DAY, and SARAH VOLLMER. Can. J. Chem. **65**, 1676 (1987).

The crystal and molecular structures of $(\eta^5\text{-}C_5H_5)_2ZrS_5$, **2**, and $(\eta^5\text{-}C_5H_5)HfS_5$, **3**, have been determined by single crystal diffractometry methods. Both compounds crystallized with four molecules in a monoclinic unit cell of dimensions: a = 8.984(3) Å, b = 13.336(4) Å, c = 11.421(2) Å, β = 93.10(2)° for **2**, and a = 9.012(2) Å, b = 13.291(2) Å, c = 11.381(2) Å, β = 93.25(1)° for **3**; the space group is $P2_1/n$ for both. These crystals of **2** and **3** are thus isomorphous with those of $(C_5H_5)_2TiS_5$, **1**, studied by Epstein *et al.* (3*a*). The structures of all three complexes are very similar consisting of a cyclohexane-like six-membered MS_5 ring with two C_5H_5 rings attached to the metals in an axial and equatorial position. The coordination spheres of **2** and **3** are less crowded than that of **1**. The consequences of this are discussed with respect to the barriers to ring inversion in these complexes.

ALAN SHAVER, JAMES M. MCCALL, VICTOR W. DAY et SARAH VOLLMER. Can. J. Chem. **65**, 1676 (1987).

Utilisant des méthodes de diffractométrie sur des cristaux uniques, on a déterminé les structures cristallines et moléculaires des composés $(\eta^5\text{-}C_5H_5)_2ZrS_5$ (**2**) et $(\eta^5\text{-}C_5H_5)_2HfS_5$ (**3**). Chacun des composés cristallise avec quatre molécules dans une cellule unitaire monoclinique avec a = 8,984(3), b = 13,336(4) et c = 11,421(2) Å et β = 93,10(2)° pour le composé **2** et a = 9,012(2), b = 13,291(2) et c = 11,381(2) Å et β = 93,25(1)° pour le composé **3**; dans chacun des cas, le groupe d'espace est $P2_1/n$. Les cristaux des composés **2** et **3** sont donc isomorphes avec ceux du composé $(C_5H_5)_2TiS_5$ (**1**) étudié par Epstein et ses collaborateurs (3*a*). Les structures de ces trois complexes sont très semblables; elles comportent chacune un cycle à six chaînons de MS_5 qui adopte une forme semblable à celle d'un cyclohexane ainsi que deux cycles de C_5H_5 qui sont attachés aux métaux dans les positions axiale et équatoriale. Les sphères de coordination des composés **2** et **3** sont moins encombrées que celles du composé **1**. On discute de ces résultats en fonction des barrières à l'inversion de cycle dans ces complexes.

[Traduit par la revue]

Introduction

Recently a general method for the preparation of metallacyclosulfanes (i.e. species of the type MS_x) was reported (1). Treatment of the appropriate dichloro precursors with non-aqueous solutions of Li_2S_x, prepared in situ, gave the series Cp_2MS_5 and $Cp^*_2MS_3$, where M = Ti, Zr, and Hf, Cp = C_5H_5, and Cp* = C_5Me_5. The complex Cp_2TiS_5, **1**, had been reported previously (2) and had been shown (3) to have a cyclohexane-like six-membered ring with axial and equatorial Cp rings. At room temperature ring inversion is slow on the nmr time scale for the titanium complex (4); however, only upon cooling the zirconium, **2**, and hafnium, **3**, analogues it was possible to resolve two signals for their Cp rings (1). The X-ray structures of the latter two complexes have been determined in order to compare their structures to that of **1** seeking an explanation for their relative ease of ring inversion. The availability of these three complexes also provided an opportunity to compare the structures for the complete series.

Experimental

Crystal data

$C_{10}H_{10}S_5Zr$ fw = 381.7

Monoclinic, $P2_1/n$, a = 8.984(3), b = 13.336(4), c = 11.421(2), β = 93.10(2), V = 1366.3 Å^3, Z = 4, ρ_c = 1.86 g cm^{-3}, (MoK_α λ = 0.71073 Å, μ = 1.50 mm^{-1} (6*a*)).

$C_{10}H_{10}S_5Hf$ fw = 468.9

Monoclinic, $P2_1/n$, a = 9.012(2), b = 13.291(2), c = 11.382(2), β = 93.25(1), V = 1360.9 Å^3, Z = 4, ρ_c = 2.29 g cm^{-3}, (MoK_α = 0.71073 Å, μ = 8.77 mm^{-1} (6*a*)).

Large-well shaped single crystals of **2** and **3** suitable for X-ray diffraction studies were obtained as previously described (1). Both compounds crystallize in the centrosymmetric monoclinic space group $P2_1/n$ (an alternate setting of $P2_1/c$-C_{2h}, No. 14) (5). Intensity measurements were made on a computer-controlled Nicolet PĪ autodiffractometer for a spherical specimen of **2** which had a diameter of 0.69 mm (μr = 0.52) and an irregularly shaped crystal of **3**. Intensity measurements for both compounds utilized graphite-monochromated MoKα radiation and full (1.0°) wide ω scans and gave a total of 5096 independent reflections having $2\theta_{MoK\alpha} < 71.0°$ for **2** and 4663 reflections having $2\theta_{MoK\alpha} < 63.7°$ for **3**. For all reflections of **2** a scanning rate of 3° min^{-1} was employed for the scan between ω settings 0.50° above and below the calculated Kα doublet value (λ = 0.71073 Å). Similar scans for those reflections of **3** having $2\theta_{MoK\alpha} <$ 43° utilized a scanning rate of 4° min^{-1} while a scanning rate of 3° min^{-1} was used for all the other reflections. Each 1.0° scan of both compounds was divided into 19 equal time intervals, and those 13 contiguous intervals which had the highest single accumulated count at their midpoint were used to calculate the net intensity from scanning. Background counts, each lasting for one-half (**2**) or one-fourth (**3**) of the total time used for the net scan (13/19ths of the total scan time), were measured at omega settings 1.0° above and below the calculated Kα doublet value for each reflection. Since the absorption of X-rays by a spherical crystal having μr = 0.90 is virtually independent of scattering angle (7), the data for **2** were not corrected for absorption. The intensity data of **3** were corrected empirically for variable absorption using χ scans for five reflections having 2θ values between 11° and 31°.

The non-hydrogen atoms of **2** were located using Patterson and difference Fourier techniques, and those of the isomorphous hafnium compound, **3**, were derived from the parameters of **2**. Atomic positions were calculated for all hydrogens of both compounds assuming sp^2 hybridized geometry for the cyclopentadienyl carbons and a C—H bond length of 0.95 Å. The non-hydrogen parameters initially used for these calculations were those resulting from the full-matrix least-squares refined model (R_1 (8) (unweighted, based on F) = 0.029 and 0.035 for **2** and **3** respectively) which incorporated

[1]Revision received February 27, 1987.

Can. J. Chem. Downloaded from www.nrcresearchpress.com by 72.64.146.136 on 09/07/12
For personal use only.

Can. J. Chem. Downloaded from www.nrcresearchpress.com by 72.64.146.136 on 09/07/12
For personal use only.

TABLE 1. Atomic coordinates for non-hydrogen atoms in crystalline $(C_5H_5)_2ZrS_5$, **2**, and $(C_5H_5)_2HfS_5$, **3**[a]

Atom[b] type	Fractional coordinates			Equivalent isotropic thermal parameter,[c] B, Å^2
	10^4 x	10^4 y	10^4 z	
M	−82.9(2)	2004.8(1)	2225.4(2)	2.69
	−57.0(2)	1991.3(2)	2233.9(2)	2.57
S_1	−2610.5(7)	2746.8(5)	2635.1(6)	4.39
	−2561.7(19)	2727.7(13)	2625.6(15)	4.10
S_2	−3965.2(7)	1501.4(6)	2629.8(6)	5.28
	−3944.3(20)	1486.3(17)	2637.1(17)	5.01
S_3	−4226.3(8)	1031.6(7)	923.6(7)	5.68
	−4218.0(20)	1016.2(18)	930.6(18)	5.48
S_4	−2363.6(8)	205.8(5)	582.0(6)	5.12
	−2358.3(22)	187.5(13)	585.9(16)	4.80
S_5	−785.7(7)	1266.8(4)	235.0(5)	3.94
	−784.0(18)	1263.2(12)	257.7(12)	3.65
C_{a1}	−201(4)	1170(3)	4192(3)	6.9
	−204(11)	1158(7)	4184(7)	6.5
C_{a2}	1286(4)	1421(2)	4067(3)	6.3
	1272(11)	1418(6)	4078(7)	6.1
C_{a3}	1791(3)	843(3)	3166(3)	6.1
	1799(8)	838(7)	3177(8)	5.8
C_{a4}	627(4)	229(2)	2739(3)	5.7
	649(11)	227(6)	2735(7)	5.6
C_{a5}	−579(4)	434(2)	3374(3)	6.1
	−584(9)	431(7)	3373(8)	5.8
C_{b1}	284(7)	3456(4)	868(5)	9.6
	345(19)	3412(11)	842(10)	9.5
C_{b2}	139(5)	3854(2)	1907(6)	8.8
	155(14)	3804(7)	1845(18)	9.9
C_{b3}	1297(5)	3579(3)	2640(3)	7.6
	1315(15)	3552(8)	2642(8)	7.7
C_{b4}	2210(4)	2989(3)	2007(5)	8.2
	2217(10)	2968(8)	2020(14)	8.2
C_{b5}	1552(7)	2913(4)	893(4)	9.7
	1608(19)	2874(9)	905(12)	9.7

[a]Numbers in parentheses are the estimated standard deviations in the last significant digit.
[b]For each atom type, the coordinates are reported in two lines corresponding to complexes **2** and **3**, respectively. Atoms are labeled in agreement with Figs. 1 and 2.
[c]This is one-third of the trace of the orthogonalized B_{ij} tensor.

unit-weighting and anisotropic thermal parameters for all non-hydrogen atoms and reflections having $2\theta_{MoK\alpha} < 43°$ and $I > 3\sigma(I)$. They were periodically updated. The R values are defined as $R_1 = \Sigma||F_o| - |F_c||/\Sigma|F_o|$ and $R_2 = \{\Sigma\omega(|F_o| - |F_c|)^2/\Sigma\omega|F_o|^2\}^{1/2}$, where ω is the weight given each reflection. The function minimized is $\Sigma\omega(|F_o| - K|F_c|)^2$, where K is the scale factor. All structure factor calculations for both compounds employed recent tabulations of atomic form factors (6*b*) and an anomalous dispersion correction (6*c*) to the scattering factors of the Hf, Zr, and sulfur atoms. A least-squares refinable extinction correction (8) of the form $1/(1 + gIc)^{1/2}$ was employed for structure factors of **2**. A careful examination of the final F_o and F_c values for **3** indicated the absence of extinction effects. The final cycles of empirically-weighted[2] full-matrix least-squares refinement which employed isotropic thermal parameters for fixed hydrogen atoms and anisotropic thermal parameters for all other atoms converged to values of 0.029 and 0.036 for R_1 and R_2 (weighted, based on F), respectively, for 4465 independent reflections of **2** having $2\theta_{MoK\alpha} < 71.0°$ and $I > 3\sigma(I)$. Similar refinement cycles for **3** gave $R_1 = 0.037$ and $R_2 = 0.045$ for 3635 independent reflections having $2\theta_{MoK\alpha} < 63.7°$ and $I > 3\sigma(I)$. Hydrogen atom parameters were not varied for either **2** or **3**.

Results and discussion

The final atomic coordinates for the non-hydrogen atoms of **2** and **3** are presented with estimated standard deviations in Table 1.[3] A perspective ORTEP drawing illustrating the numbering scheme is given in Fig. 1. The crystals of **2** and **3** used in this study are isomorphous with the crystal of **1** studied by Epstein *et al.* (3*a*). The volume of the unit cells follow the expected order Ti < Hf < Zr. The volumes for the isostructural and isomorphous indenyl series $(\eta^5\text{-}C_9H_7)_2M(CH_3)_2$, M = Ti, Zr, and Hf followed the same order; this has been attributed to the lanthanide contraction effect (9).

[2]Empirical weights were calculated from the equation $\rho = \sum_0^2 a_n|F_o|^n = 0.548 - (2.23 \times 10^{-3})|F_o| + (1.00 \times 10^{-4})|F_o|^2$ for **2** and $\sigma = \sum_0^3 a_n|F_o|^n = 1.91 - (1.66 \times 10^{-2})|F_o| + (2.36 \times 10^{-4})|F_o|^2 - (4.94 \times 10^{-8})|F_o|^3$, the a_n being coefficients derived from the least-square fitting of the curve $||F_o| - |F_c|| = \sum_0^2 a_n|F_o|^n$, where F_c values were calculated from the fully refined model using unit weighting and an $I > 3\sigma(I)$ rejection criterion.

[3]Crystal structure analysis reports for **2** and **3**, Fig. 2 (ORTEP drawing of **3**), Table 2 (anisotropic thermal parameters for the non-hydrogen atoms of **2** and **3**), Table 3 (hydrogen atom coordinates for **2** and **3**), Table 5 (bond lengths and angles about the non-hydrogen atoms of the cyclopentadienyl rings in **2** and **3**), Table 7 (structure factors for **2**), Table 8 (structure factors for **3**), (56 pages) may be purchased from the Depository of Unpublished Data, CISTI, National Research Council of Canada, Ottawa, Ont., Canada K1A 0S2.

Can. J. Chem. Downloaded from www.nrcresearchpress.com by 72.64.146.136 on 09/07/12
For personal use only.

TABLE 4. Bond lengths (Å) and angles (deg) subtended at the metal and sulfur atoms in crystalline $(C_5H_5)_2MS_5$, where M = Ti, **1**; Zr, **2**; and Hf, **3**[a]

Type[b]	**1**[c]	**2**	**3**
		Bond lengths, Å	
M—S_1	2.448 (1)	2.544 (1)	2.523 (2)
M—S_5	2.422 (1)	2.526 (1)	2.501 (1)
M—S (average[d])	2.435 (1, 13, 13, 2)	2.535 (1, 9, 9, 2)	2.512 (2, 11, 11, 2)
M—C_{a1}	2.376 (4)	2.514 (3)	2.491 (8)
M—C_{a2}	2.374 (4)	2.502 (3)	2.477 (8)
M—C_{a3}	2.367 (4)	2.489 (3)	2.469 (8)
M—C_{a4}	2.388 (4)	2.515 (3)	2.488 (8)
M—C_{a5}	2.398 (4)	2.523 (2)	2.505 (9)
M—C_{b1}	2.392 (5)	2.513 (3)	2.504 (14)
M—C_{b2}	2.380 (6)	2.503 (3)	2.458 (10)
M—C_{b3}	2.348 (5)	2.472 (3)	2.445 (11)
M—C_{b4}	2.341 (6)	2.467 (3)	2.449 (10)
M—C_{b5}	2.370 (6)	2.487 (3)	2.484 (15)
M—C (average[d])	2.373 (5, 14, 32, 10)	2.499 (3, 16, 32, 10)	2.477 (10, 17, 32, 10)
M—C_{ga}[e]	2.066 (—)	2.216 (—)	2.190 (—)
M—C_{gb}[e]	2.071 (—)	2.206 (—)	2.188 (—)
M—C_g (average[d])	2.069 (—, 3, 3, 2)	2.211 (—, 5, 5, 2)	2.189 (—, 1, 1, 2)
S_1—S_2	2.059 (2)	2.059 (1)	2.068 (3)
S_2—S_3	2.056 (2)	2.048 (1)	2.042 (3)
S_3—S_4	2.067 (2)	2.057 (1)	2.062 (3)
S_4—S_5	2.059 (2)	2.057 (1)	2.063 (2)
S—S (average[d])	2.060 (2, 3, 7, 4)	2.055 (1, 4, 7, 4)	2.059 (3, 8, 17, 4)
$S_1 \ldots S_5$	3.58	3.82	3.76
$S_2 \ldots S_4$	3.31	3.30	3.29
		Angles, deg	
S_1MS_5	94.6 (1)	97.8 (1)	96.8 (1)
$C_{ga}MC_{gb}$[e]	133.7 (—)	131.3 (—)	131.5 (—)
MS_1S_2	107.4 (1)	102.7 (1)	103.7 (1)
MS_5S_4	108.6 (1)	103.7 (1)	104.7 (1)
MSS (average)	108.0 (1, 6, 6, 2)	103.2 (1, 5, 5, 2)	104.2 (1, 5, 5, 2)
$S_1S_2S_3$	105.2 (1)	106.7 (1)	106.2 (1)
$S_2S_3S_4$	106.7 (1)	107.0 (1)	106.8 (1)
$S_3S_4S_5$	102.7 (1)	104.2 (1)	103.8 (1)
SSS (average)	104.9 (1, 14, 22, 3)	106.0 (1, 12, 18, 3)	105.6 (1, 12, 18, 3)
$C_{ga}MS_1$	110.7 (—)	111.7 (—)	111.5 (—)
$C_{ga}MS_5$	110.7 (—)	111.2 (—)	111.5 (—)
$C_{gb}MS_1$	100.5 (—)	100.2 (—)	101.4 (—)
$C_{gb}MS_5$	99.6 (—)	99.1 (—)	98.5 (—)
$S_1MS_5/S_1S_2S_4S_5$[f]	58 (—)	61 (—)	60 (—)
$S_1S_2S_4S_5/S_2S_3S_4$[f]	72 (—)	74 (—)	73 (—)

[a]Numbers in parentheses following individual entries are the estimated standard deviations in the last significant digit.

[b]Atoms are labeled in agreement with Figs. 1 and 2.

[c]The data given for **1** were taken or calculated from ref. 3*a*.

[d]See footnote 4.

[e]The least-squares mean planes for the following groups of atoms in **2** and **3** are defined by the equation: $aX + bY + cZ = d$ where X, Y, and Z are orthogonal coordinates measured along $\boldsymbol{a}$, $\boldsymbol{b}$, and $\boldsymbol{c}^*$, respectively, of the crystal system: (*a*) C_{a1}, C_{a2}, C_{a3}, C_{a4}, and C_{a5} for **2**, $a = 0.287$; $b = -0.707$, $c = 0.646$, $d = 1.947$; (*b*) C_{b1}, C_{b2}, C_{b3}, C_{b4}, and C_{b5} for **2**, $a = 0.505$, $b = 0.809$, $c = -0.302$, $d = 3.563$; (*c*) C_{ga}, Zr, and C_{gb}, $a = -0.402$, $b = 0.526$, $c = 0.749$, $d = 3.341$; (*d*) S_1, Zr, and S_5, $a = 0.257$, $b = 0.856$, $c = -0.449$, $d = 1.128$; (*e*) S_1, S_2, S_4, and S_5 for **2**, $a = 0.624$, $b = -0.419$, $c = 0.660$, $d = -0.934$; (*f*) S_2, S_3, and S_4 for **2**, $a = 0.454$, $b = 0.830$, $c = -0.324$, $d = -0.987$; (*g*) C_{a1}, C_{a2}, C_{a3}, C_{a4}, and C_{a5} for **3**, $a = 0.282$, $b = -0.709$, $c = 0.646$, $d = 1.943$; (*h*) C_{b1}, C_{b2}, C_{b3}, C_{b4}, and C_{b5} for **3**, $a = 0.504$, $b = 0.811$, $c = -0.298$, $d = 3.548$; (*i*) C_{ga}, Hf, and C_{gb}, $a = -0.383$, $b = 0.538$, $c = 0.751$, $d = 3.355$; (*j*) S_1, Hf, and S_5, $a = 0.257$, $b = 0.855$, $c = -0.450$, $d = 1.105$; (*k*) S_1, S_2, S_4, and S_5 for **3**, $a = 0.622$, $b = -0.422$, $c = 0.660$, $d = -0.917$; (*l*) S_2, S_3, and S_4 for **3**, $a = 0.451$, $b = 0.830$, $c = -0.327$, $d = -1.008$; where C_{ga} and C_{gb} refer to the center of gravity of the five membered rings of the cyclopentadienyl rings of *a* and *b*, respectively.

[f]This is the dihedral angle between the least-square mean planes through the two groups of atoms listed.

Can. J. Chem. Downloaded from www.nrcresearchpress.com by 72.64.146.136 on 09/07/12
For personal use only.

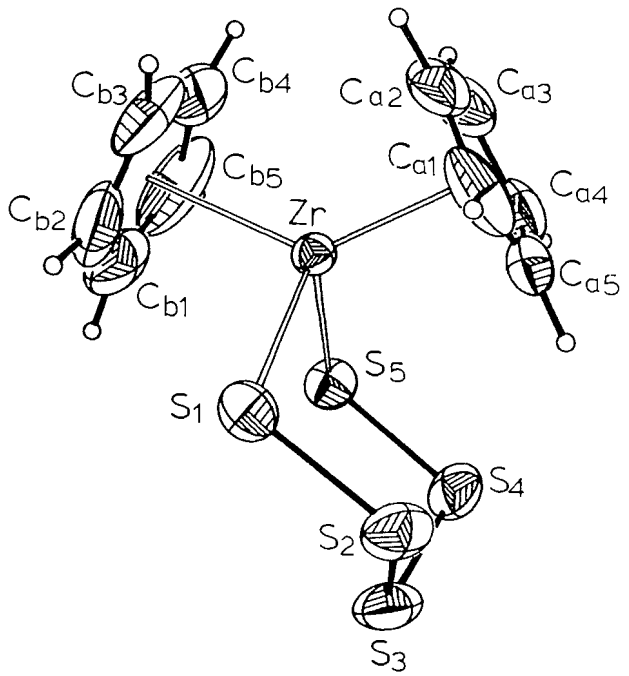

FIG. 1. A perspective ORTEP drawing of $(\eta^5\text{-}C_5H_5)_2ZrS_5$, **2**, showing the atom labelling scheme used for **2** and **3**. A similar drawing of **3** is shown in Fig. 2. (see footnote 3). All nonhydrogen atoms are represented by thermal vibration ellipsoids drawn to encompass 50% of the electron density; hydrogen atoms are represented by arbitrarily-sized spheres for purposes of clarity.

All three compounds **1**, **2**, and **3** are isostructural being discrete, mononuclear Cp_2MX_2 species in which the metal ions adopt the familiar pseudotetrahedral "bent sandwich" configuration. The X groups in these cases are the terminal atoms of the bidentate pentasulfide chain thus forming a six-membered ring which adopts a chair conformation. The molecules approximate C_s-*m* point symmetry with the idealized mirror plane passing through the two Cp ring centroids (C_{ga} and C_{gb}), the metal atom and the central sulfur atom (S_3). Selected bond lengths and angles about the metal and sulfur atoms in **1**, **2**, and **3** are given in Table 4. The bond lengths and angles for the non-hydrogen atoms of the cyclopentadienyl rings in **2** and **3** are given in Table 5.[3]

Parameters describing the Cp_2M portion of the coordination spheres of **2** and **3** differ little from those of **1** and correspond well with other group IVB Cp_2MX_2 moieties. The average metal-to-carbon bond distances for **2** and **3** (2.499(3,16,32,10)[4] Å for **2** and 2.477(10,17,32,10) Å for **3**) are about 0.12 Å larger than the average (2.376(1) Å) for **1**; this is consistent with the approximately 0.12 Å smaller covalent radius of titanium. These distances correspond closely with other group IVB Cp_2MX_2 species for a variety of X ligands and cyclopentadienyl ligands (9) wherein the metal-to-carbon distances are remarkably constant for each metal. In **2** and **3**, the five carbon atoms of the cyclopentadienyl ligands are coplanar to within 0.005 Å and those carbon atoms nearest the sulfur atoms are slightly but significantly further from the metal atom. This was also observed for **1** (3*a*) and probably reflects the steric bulk of the pentasulfido-ligand.

[4]The first number in parentheses following an averaged value of a bond length or angle is the root-mean-square estimated standard deviation of an individual datum. The second and third numbers, when given, are the average and maximum deviations from the averaged value, respectively. The fourth number represents the number of individual measurements which are included in the average value.

TABLE 6. Intramolecular nonbonded contacts in crystalline $(C_5H_5)_2ZrS_5$, **2**

Type[a]	Distance, Å	Type[a]	Distance, Å
Zr...S_3	4.14	S_5...C_{a5}	3.75
		S_2...C_{a1}	3.76
S_1...S_5	3.82	S_2...H_{a1}	3.60
		S_2...C_{a5}	3.42
S_2...S_4	3.30	S_2...H_{a5}	2.92
		S_4...C_{a4}	3.55
S_1...C_{b2}	3.03	S_4...H_{a4}	3.22
S_1...H_{b2}	2.77	S_4...C_{a5}	3.51
S_5...C_{b1}	3.15	S_4...H_{a5}	3.13
S_5...H_{b1}	3.05		
S_5...C_{b5}	3.10	H_{a2}...H_{b3}	2.78
S_5...H_{b5}	2.97	H_{a2}...H_{b4}	3.03
S_1...C_{a1}	3.44	H_{a3}...H_{b4}	2.56
S_1...H_{a1}	3.30		
S_1...C_{a5}	3.66	C_{a2}...C_{b3}	3.31
S_1...H_{a5}	3.70	C_{a2}...C_{b4}	3.29
S_5...C_{a4}	3.36	C_{a3}...C_{b4}	3.19
S_5...H_{a4}	3.18		

[a]Atoms are labeled in agreement with Figs. 1 and 2 and Tables 1–3.

The plane determined by the metal atom and the two cyclopentadienyl ring centers intersects the plane of the metal, S_1 and S_5 atoms in dihedral angles of 90.5°, 90.6°, and 90.8° for **1**, **2**, and **3**, respectively. However, the bidentate sulfur ligand is displaced from the "equatorial girdle" (the plane passing through the metal and bisecting the C_{ga}—M—C_{gb} angle) towards the ring *b* such that the intramolecular contacts between ring *b* and S_1 and S_5 atoms are considerably shorter than those for ring *a* (Table 6). This distortion has been previously noted (3*a*) for **1** and was attributed to a combination of steric repulsions between the axial cyclopentadienyl ring (*a*) and the sulfur atoms S_2 and S_4 and attractive interactions between ring *b* and sulfur atoms S_1 and S_5. These contacts provide a structural rationale for the novel migration of one of the cyclopentadienyl rings in **1** to the sulfur ligand as observed by Giolando and Rauchfuss (10).

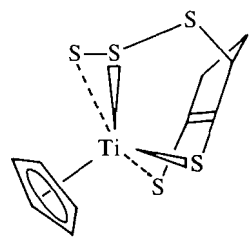

In **2** and **3** the sulfur atoms S_1, S_2, S_4, and S_5 are coplanar to within 0.01 Å. The dihedral angles for the pairs of planes $S_1MS_5/S_1S_2S_4S_5$ and $S_1S_2S_4S_5/S_2S_3S_4$ are similar (Table 4) and indicate similar MS_5 ring shapes. The shortest S—S bond length is the S_2—S_3 bond in all three compounds. Although the S_1—S_2 and S_4—S_5 bond lengths are equal within experimental error in **1**, **2**, and **3**, the two M—S bonds and the central S_2—S_3 and S_3—S_4 bonds are unequal in length. In each case the longer M—S_1 bond is opposite the longer S_3—S_4 bond, and the shorter M—S_5 bond lies opposite the shorter S_2—S_3 bond. Unequal Ti—S distances were also found for $Cp_2Ti(SPh)_2$ (11) which are on average shorter (2.410 Å) than the average Ti—S

distance in **1**. The inequality of S—S bond lengths found in **1**, **2**, and **3** was also observed in Cp_2VS_5 (3*b*) and in Cp_2WS_4 (12). The salts $M_2'S_5$ ($M' = NH_4$ (13), K (14), Rb (15), Tl (16) which contain discrete S_5^{2-} chains, also displayed a variation in bond lengths. For the rubidium salt the two inner bond lengths were 2.054(8) Å and 2.109(7) Å, and the two outer bond lengths were 2.019(7) Å and 2.036(8) Å with the longest S—S bond adjacent to the shortest S—S bond. The S—S bonds in the Cp_2MS_5 molecules, with the exception of the short S_2—S_3 bonds, are all longer than those found in Rb_2S_5. Cyclohexasulfur, S_6, crystallizes in the chair conformation with all S—S bond lengths equal at 2.068(2) Å (17). This distance is marginally greater than the average S—S distances of 2.060 Å for **1**, 2.055 Å (1, 4, 7, 4) for **2**, and 2.059 Å (3, 8, 17, 4) for **3**, respectively. The S—S—S angles are larger in the Cp_2MS_5 molecules than those in S_6 (102.61(6)°) (17). The non-bonded *trans*-annular sulfur–sulfur distances $S_1 \cdots S_5$ follow the order Ti < Hf < Zr, consistent with the trend in the S_1—M—S_5

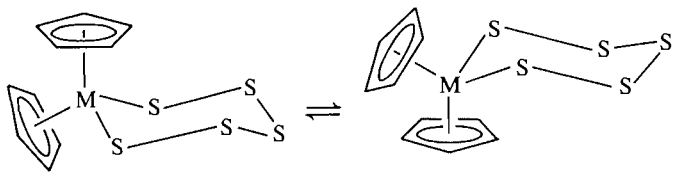

M = Ti, Zr, Hf

angles, and the M—S bond distances; however the $S_2 \cdots S_4$ distances are nearly the same. The "end-to-end" $M \cdots S_3$ distances in the **2** and **3** are only slightly shorter than for **1**.

Clearly the structures of **1**, **2**, and **3** are quite similar with any significant differences being attributed to differences in the size of the metal atoms. Given this close similarity, the differences observed for their barriers to ring inversion (kJ mol^{-1}: 76.3, **1** (4*b*); 48.6, **2** (1); 58.0, **3** (1)) might initially seem surprising. However, while the coordination spheres of all three compounds are sterically quite conjested, that of **1** is more conjested than those for **2** and **3** due to the smaller covalent radius of titanium. If the non-bonded contacts between the cyclopentadienyl rings and the sulfur atoms were due, at least in part, to attractive forces, then the MS_5 ring in **1** might be expected to have a higher barrier to ring inversion than those in **2** and **3**. Consistent with this, it was found (1) that reducing the cyclopentadienyl ring – sulfur interaction by "tying-back" the C_5 rings with a bridging methylene group in $CH_2(C_5H_4)_2TiS_5$ lowered the barrier to 66.5 kJ mol^{-1} (the C_gTiC_g angle is 121° in $CH_2(C_5H_4)_2TiCl_2$(18) and 131° in Cp_2TiCl_2 (19)). Finally it is noted that the structures of **1**, **2**, and **3** are clearly different from that of $(C_5Me_5)_2ThS_5$ which contains a twist-boat conformation of the ThS_5 ring with a 1,2,4,5-tetrahapto S_5 ligand (20).

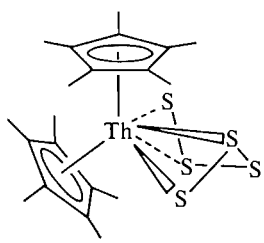

Acknowledgements

This research was supported by grants from the Natural Sciences and Engineering Research Council of Canada, the Quebec Department of Education, and Imperial Oil Co. of Canada. Predoctoral fellowships awarded to J.M.M. by NSERC and the Noranda Group of Companies are gratefully acknowledged.

1. A. SHAVER and J. M. MCCALL. Organometallics, **3**, 1823 (1984).
2. E. SAMUEL. Bull. Soc. Chim. Fr. 3548 (1966).
3. (*a*) E. F. EPSTEIN, I. BERNAL, and H. KÖPF. J. Organomet. Chem. **26**, 229 (1971); (*b*) E. G. MULLER, J. L. PETERSEN, and L. F. DAHL. J. Organomet. **111**, 91 (1976).
4. (*a*) H. KÖPF, B. BLOCK, and M. SCHMIDT. Chem. Ber. **101**, 272 (1968); (*b*) E. W. ABEL, M. BOOTH, and K. G. ORRELL. J. Organomet. Chem. **160**, 75 (1978).
5. International tables for X-ray crystallography. Kynoch Press. Birmingham, England. Vol. 1. 1969. p. 99.
6. International tables for X-ray crystallography. Kynoch Press. Birmingham, England. Vol. IV. 1969. (*a*) p. 55; (*b*) p. 99; (*c*) p.149.
7. International tables for X-ray crystallography. Kynoch Press. Birmingham, England. Vol. 11. 1967. p. 302.
8. H. H. ZACHARIASEN. Acta Crystallogr. **23**, 558 (1967).
9. (*a*) J. L. ATWOOD, W. E. HUNTER, D. C. HRNCIR, E. SAMUEL, H. ALT, and M. D. RAUSCH. Inorg. Chem. **14**, 1757 (1975); (*b*) B. R. DAVIS and I. BERNAL. J. Organomet. Chem. **30**, 75 (1971); (*c*) E. F. EPSTEIN and I. BERNAL. Inorg. Chim. Acta, **7**, 211 (1973); (*d*) D. J. SIKORA, M. D. RAUSCH, R. D. ROGERS, and J. L. ATWOOD. J. Am. Chem. Soc. **103**, 1265 (1974); (*e*) C. H. SALDARRIAGA-MOLINA, A. CLEARFIELD, and I. BERNAL. Inorg. Chem. **13**, 2880 (1974).
10. D. M. GIOLANDO and T. B. RAUCHFUSS. J. Am. Chem. Soc. **106**, 6455 (1984).
11. E. G. MULLER, S. F. WALKINGS, and L. F. DAHL. J. Organomet. Chem. **111**, 73 (1976).
12. B. R. DAVID and I. BERNAL. J. Cryst. Mol. Struct. **2**, 135 (1972).
13. N. K. GOH and H. G. VON SCHNERING, cited by ref. 12.
14. B. KELLY and P. WOODWARD. J. Chem. Soc. Dalton Trans. 1314 (1976).
15. P. BÖTTCHER. Zeit. für Kristall. **150**, 65 (1979).
16. B. P. LECLERC and T. S. KABRÉ. Acta Crystallogr. **31B**, 1675 (1975).
17. J. STEIDEL, J. PICKARDT, and R. STEUDEL. Z. Naturforsch. **33B**, 1554 (1978).
18. J. A. SMITH, J. VON SEYERL, G. HUTTNER, and H. H. BRINTZINGER. J. Organomet. Chem. **173**, 175 (1979).
19. A. CLEARFIELD, D. K. WARNER, C. H. SALDARRIAGA-MOLINA, R. ROPAL, and I. BERNAL. Can. J. Chem. **53**, 1622 (1975).
20. D. A. WROBLESKI, D. T. CROMER, J. V. ORTIG, T. B. RAUCHFUSS, R. R. RYAN, and A. P. SATTELBERGER. J. Am. Chem. Soc. **108**, 174 (1986).

Can. J. Chem. Downloaded from www.nrcresearchpress.com by 72.64.146.136 on 09/07/12
For personal use only.

Synthesis and Diels–Alder reactions of 1-((*E*)-2-*tert*-butyldimethylsiloxy)ethylidene-4a-carbomethoxy-1,2,3,4,4a,5,6,7-octahydronaphthalene and related substances. Preparation of functionalized decahydro-1*H*-phenalenes

EDWARD PIERS AND RICHARD W. FRIESEN

Department of Chemistry, University of British Columbia, 2036 Main Mall, University Campus, Vancouver, B.C., Canada V6T 1Y6

Received February 10, 1987

EDWARD PIERS and RICHARD W. FRIESEN. Can. J. Chem. **65**, 1681 (1987).

The preparation of the structurally novel dienes **7** and **8** is described. The results of a study of the Diels–Alder reactivity of these substances and the "parent" diene **9** are summarized and the potential use of the resultant Diels–Alder adducts in organic synthesis is demonstrated.

EDWARD PIERS et RICHARD W. FRIESEN. Can. J. Chem. **65**, 1681 (1987).

On décrit la préparation des dièmes **7** et **8** qui sont nouveaux par leur structure. On présente un résumé des résultats obtenus au cours d'une étude sur la réactivité, vis-à-vis de la réaction de Diels–Alder, de ces composés ainsi que de leur hydrocarbure de base (**9**); on démontre aussi l'utilité potentielle des adduits de Diels–Alder qui en résultent dans le domaine de la synthèse organique.

[Traduit par la revue]

Can. J. Chem. Downloaded from www.nrcresearchpress.com by 72.64.146.136 on 09/07/12
For personal use only.

The amphilectane-type diterpenoids (e.g. 8,15-diisocyano-11(20)-amphilectene, **A**; 8-isocyano-10-cycloamphilectene, **B**)

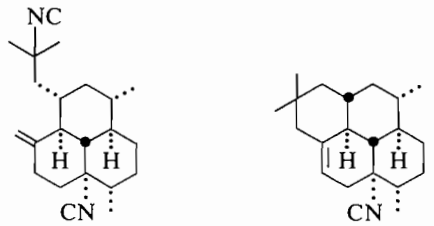

A **B**

are structurally unusual natural products that have been isolated from sponges (1, 2). In connection with an investigation into the preparation and chemical reactivity of novel bicyclic dienes, with the goal of effecting a total synthesis of substances such as **A** and **B**, we outline herein (*a*) the efficient synthesis of the structurally unique dienes **7** and **8**, (*b*) the Diels–Alder reactivity of these substances along with that of the "parent" diene **9** (3), and (*c*) the synthetic utility of (some of) the resultant Diels–Alder adducts.

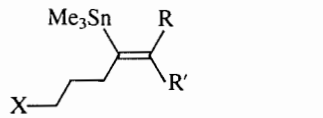

1 R = H, R′ = CO_2Me, X = Cl
2 R = CO_2Me, R′ = H, X = Cl
3 R = H, R′ = $CH_2OSiMe_2Bu^t$, X = I
4 R = $CH_2OSiMe_2Bu^t$, R′ = H, X = I

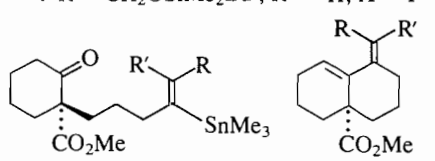

5,6 **7,8,9**

5,7 R = H, R′ = $CH_2OSiMe_2Bu^t$
6,8 R = $CH_2OSiMe_2Bu^t$, R′ = H
9 R = R′ = H

Conversion of methyl 6-chloro-2-hexynoate[1,2] into the geometrically isomeric α,β-unsaturated esters **1** and **2** via known methods (4), followed, in each case, by suitable functional group modifications (*i*-Bu_2AlH, Et_2O; *t*-$BuMe_2SiCl$, imidazole, dimethylformamide; NaI, acetone), provided the alkylating agents **3** and **4** (45–50% overall). Alkylation (KH, THF) of 2-carbomethoxycyclohexanone with **3** and **4** gave compounds **5** (88%) and **6** (69%). Conversion of the latter substances into the corresponding bicyclic dienes **7** (61%) and **8** (65%) was accomplished via a "one-pot" sequence of reactions involving deprotonation (lithium diisopropylamide, THF, −40°C), enol triflate formation ($PhN(SO_2CF_3)_2$, THF, −40°C → room temperature) (5) and palladium(0)-catalyzed ring closure (addition of 3 mol% $(Ph_3P)_4Pd$, THF, reflux) (6, and refs. cited therein). Thus, importantly, the cyclization step is stereospecific and even the formation of the *cisoid cis* diene **8** is clean and efficient. Furthermore, use of alkylating agents related to **2** (X = I in place of Cl) and **4** (R = CH_2OCH_2OMe in place of $CH_2OSiMe_2Bu^t$) affords dienes **8** (R = CO_2Me or CH_2OCH_2OMe in place of $CH_2OSiMe_2Bu^t$) as single products. The stereochemistry of the various diene systems that we have prepared was confirmed by suitable ^1H nmr nuclear Overhauser enhancement (nOe) difference experiments.[3]

In connection with exploring the chemical reactivity of the structurally unique dienes **7** and **8** and related substances, we have thus far investigated the Diels–Alder reactivity of **7**, **8**, and the "parent" diene **9** (3). Some of the results obtained to date are summarized in Table 1 (see Chart 1 for structural formulas).

[1]This material was prepared from 5-chloro-1-pentyne: MeLi, tetrahydrofuran(THF), −20°C; $ClCO_2Me$, THF, −20°C → room temperature (69%).

[2]All compounds reported herein gave spectral data in full accord with structural assignments. New compounds gave satisfactory molecular mass determinations (high resolution mass spectrometry) and (or) microanalytical data.

[3]For example, in the ^1H nmr spectrum of **8** (R = CH_2OCH_2OMe instead of $CH_2OSiMe_2Bu^t$), irradiation at δ 5.59 (signal due to cyclohexene olefinic proton) caused enhancement of the signal (δ 4.20) due to the CH_2OCH_2OMe protons.

TABLE 1. Diels–Alder reactions of dienes **7–9**

Entry	Diene	Dienophile[a]	Reaction conditions	Product(s) (ratio;[b] combined yield,[c] %)
1	**9**	**C**	THF, room temperature, 30 min	**10**,[d] **13** (96:4;83)
2	**7**	**C**	THF, room temperature, 30 min	**11**, **14** (88:12;74)[e]
3	**8**	**C**	Et_2O, reflux, 15 h	**12**[d] (72)
4	**7**	**D**	PhH, reflux, 18 h	**15** (63)
5	**8**	**D**	PhH, reflux, 3 days	**16** (18)
6	**9**	**E**	Et_2O, room temperature, 3 h	**17**, **18**, **25** (3:1:2;83)
7	**7**	**E**	Et_2O, room temperature, 3 h	**19**,[d] **20**, **26**[d] (70:tr:30;81)
8	**8**	**E**	Et_2O, reflux, 7 h	**19**,[d] **20**, **26**[d] (69:4:27;78)
9	**9**	**F**	PhH, reflux, 3 days	**21**,[d] **22**, **27**[d] (3:1:2;85)
10	**7**	**F**	PhH, reflux, 3 days	**23**, **24**, **28** (47:16:35;88)[f]

[a]Dienophiles: **C**, tetracyanoethylene; **D**, maleic anhydride; **E**, nitroethylene; **F**, methyl acrylate.
[b]Ratios were determined by careful analysis of the crude product mixtures by ^1H nmr spectroscopy and gas–liquid chromatography.
[c]Isolated yield of (combined) purified product(s).
[d]The constitution and relative stereochemistry of each of these compounds was confirmed by single crystal X-ray analysis of the substance itself (**10**, **12**, **26**) or of a suitable derivative (**19**, **21**, **27**).
[e]When this reaction was carried out at −78°C for 2 h, **11** was obtained as a single product (84%).
[f]Another unidentified isomer was formed in about 2% yield.

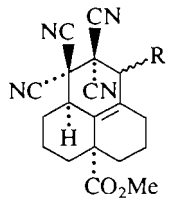

10 R = H
11 R = β-$CH_2OSiMe_2Bu^t$
12 R = α-$CH_2OSiMe_2Bu^t$

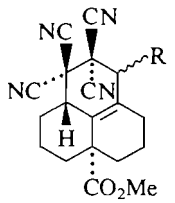

13 R = H
14 R = α-$CH_2OSiMe_2Bu^t$

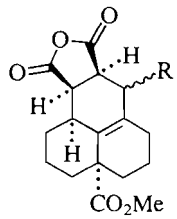

15 R = β-$CH_2OSiMe_2Bu^t$
16 R = α-$CH_2OSiMe_2Bu^t$

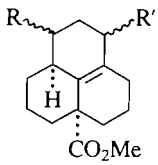

17 R = β-NO_2, R′ = H
18 R = α-NO_2, R′ = H
19 R = β-NO_2, R′ = β-$CH_2OSiMe_2Bu^t$
20 R = α-NO_2, R′ = β-$CH_2OSiMe_2Bu^t$
21 R = β-CO_2Me, R′ = H
22 R = α-CO_2Me, R′ = H
23 R = β-CO_2Me, R′ = β-$CH_2OSiMe_2Bu^t$
24 R = α-CO_2Me, R′ = β-$CH_2OSiMe_2Bu^t$

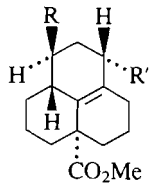

25 R = NO_2, R′ = H
26 R = NO_2, R′ = $CH_2OSiMe_2Bu^t$
27 R = CO_2Me, R′ = H
28 R = CO_2Me, R′ = $CH_2OSiMe_2Bu^t$

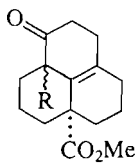

29 R = β-H
30 R = α-H

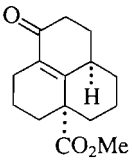

31

CHART 1

A number of points should be made regarding the data given in Table 1. (*a*) The structures of a number of "key" products (**10**, **12**, **19**, **21**, **26**, **27**) were determined by X-ray crystallography.[4] Other structural assignments were made on the basis of analogy, chemical correlation, and (or) spectral (mainly ^1H nmr) comparisons. (*b*) Reactions of **7–9** with unsymmetrical dienophiles are completely regioselective (Entries 6–10). These results are in accord with predictions based on biradical arguments (7) or frontier orbital postulates (8). (*c*) Sterically demanding dienophiles (e.g. tetracyanoethylene (**C**)) or dienophiles having a high predilection for an *endo* transition state (e.g. maleic anhydride (**D**)) approach the diene systems of **7–9** largely or completely from the side opposite to the angular CO_2Me function (β-attack) (Entries 1–5). However, with other dienophiles (e.g. nitroethylene (**E**), methyl acrylate (**F**), dimethyl acetylenedicarboxylate[5]) β-attack is favored over α-attack to a lesser degree (1.8–3:1, respectively) (Entries

[4]We are very grateful to Dr. S. J. Rettig for these structure determinations, the details of which will be reported elsewhere.

[5]Reaction (PhH, reflux, 6 h) of **9** with this dienophile provided (78%) the β- and α-attack products in a ratio of 3:1, respectively. The structure of the major product was confirmed by X-ray crystallography.

Can. J. Chem. Downloaded from www.nrcresearchpress.com by 72.64.146.136 on 09/07/12
For personal use only.

6–10). (*d*) Approach of the dienophiles **D–F** from the β face of the dienes **7–9** occurs exclusively (Entries 4, 5) or primarily (Entries 6, 7, 9, 10) via *endo* transition states. In contrast, α-attack of the dienophiles proceeds exclusively via *exo* transition states presumably because α-face *endo* transition states are significantly destabilized by steric interaction of the dienophile substituent with the angular CO_2Me group of the dienes. (*e*) Base-catalyzed equilibration of compounds **17**, **19**, **21**, and **23** (*t*-BuOK, *t*-BuOH, 80°C for **17**, **19**; MeONa, MeOH, reflux for **21**, **23**) affords, in each case, predominately or exclusively the corresponding epimers **18**, **20**, **22**, and **24**, respectively. (*f*) Not unexpectedly, the Diels–Alder reactivity of the *cisoid cis* diene **8** is much lower than that of the geometric isomer **7**. Indeed, only reaction of **8** with very reactive dienophiles (e.g. **C**, **D**) gave normal Diels–Alder products (Entries 3, 5) and, even then, the yield was low in one case (Entry 5). An anomalous reaction occurred when **8** was treated with nitroethylene (**E**) in refluxing ether (Entry 8), since the product mixture obtained was essentially identical with that derived from reaction of **7** with **E**. It appears that, in the former process, a rate-determining, nitroethylene-promoted isomerization of **8** into **7** (electron-transfer mechanism?) precedes a normal Diels–Alder transformation. When a solution of **8** in ether was refluxed in the absence of **E**, the diene could be recovered unchanged in high yield.

The (potential) synthetic utility of the Diels–Alder adducts was demonstrated as follows. Treatment of the *mixture* of **17**, **18**, and **25** (Table 1, Entry 6) with MeONa in MeOH, followed by addition of aqueous $TiCl_3$–NH_4OAc (9), afforded a *single* product **30** (90%). Apparently, under the reaction conditions, compound **29**, which would have been present in the initial product mixture, epimerized to the more stable epimer **30**.[6]

[6]The stereochemistry of **30** was confirmed by a ^1H nmr nOe difference experiment, in which irradiation at δ 3.69 (CO_2Me) caused enhancement of the signal (δ 2.82) due to the angular proton adjacent to the ketone carbonyl group. Calculations (MM2) (see ref. 10) indicate that isomer **30** should be ~2.6 kcal/mol more stable than **29**. We are very grateful to Professor L. Weiler for carring out these calculations.

Treatment of **30** with *t*-BuOK–*t*-BuOH provided the α,β-unsaturated ketone **31** (uv λ_{max}(MeOH) = 242 nm).

Further extensions to this work, including the possible application of the methods to the total synthesis of amphilectane-type diterpenoids (e.g. **A**, **B**), are being actively pursued.

Acknowledgements

We are grateful to the Natural Sciences and Engineering Research Council of Canada for financial support and for a 1967 Science and Engineering Scholarship (to R.W.F.).

1. S. J. Wratten, D. J. Faulkner, K. Hirotsu, and J. Clardy. Tetrahedron Lett. 4345 (1978).
2. P. Kazlauskas, P. T. Murphy, R. J. Wells, and J. F. Blount. Tetrahedron Lett. **21**, 315 (1980).
3. E. Piers, R. W. Friesen, and B. A. Keay. J. Chem. Soc. Chem. Commun. 809 (1985).
4. E. Piers and H. E. Morton. J. Org. Chem. **45**, 4263 (1980); E. Piers, J. M. Chong, and H. E. Morton. Tetrahedron Lett. **22**, 4905 (1981).
5. J. E. McMurry and W. J. Scott. Tetrahedron Lett. **24**, 979 (1983).
6. E. Piers and R. W. Friesen. J. Org. Chem. **51**, 3405 (1986).
7. M. J. S. Dewar, S. Ollivella, and J. J. P. Stewart. J. Am. Chem. Soc. **108**, 5771 (1986).
8. I. Fleming. Frontier orbitals and organic reactions. John Wiley & Sons, Inc., New York, NY. 1976. pp. 87–181.
9. J. E. McMurry and J. Melton. J. Org. Chem. **38**, 4367 (1973).
10. U. Burkert and N. L. Allinger. Molecular mechanics. American Chemical Society, Washington, DC. 1982.

Can. J. Chem. Downloaded from www.nrcresearchpress.com by 72.64.146.136 on 09/07/12
For personal use only.

^{39}K and ^{13}C nuclear magnetic resonance studies of the potassium cation – dibenzo-30-crown-10[1] complex in solution

CHRISTIAN DETELLIER[2] AND MARC ROBILLARD

Ottawa–Carleton Chemistry Institute, University of Ottawa Campus, Ottawa, Ont., Canada K1N 9B4

Received March 10, 1987

CHRISTIAN DETELLIER and MARC ROBILLARD. Can. J. Chem. **65**, 1684 (1987).

The structure and microdynamics in solution of the dibenzo-30-crown-10 – potassium thiocyanate complex have been studied by ^{39}K and ^{13}C nuclear magnetic resonance. In the four solvents studied (nitromethane, acetonitrile, acetone, and pyridine), the large crown ether wraps around the potassium cation and expels the conjugate anion and the solvent molecules from the cation coordination sphere. Measurements of ^{39}K quadrupolar and ^{13}C dipole–dipole relaxation times in acetone-d_6 gave the effective correlation time of the complex and the ^{39}K quadrupolar coupling constant (1.4 ± 0.3 MHz). The comparison between ^{23}Na and ^{39}K quadrupolar coupling constants for the complexes Na^+–dibenzo-24-crown-8 and K^+–dibenzo-30-crown-10 showed that the electric field gradients at the metal nucleus sites are quasi identical ($q(^{39}K)/q(^{23}Na) \simeq 0.9$) in the two complexes.

CHRISTIAN DETELLIER et MARC ROBILLARD. Can. J. Chem. **65**, 1684 (1987).

Nous avons étudié la structure et la microdynamique en solution du complexe dibenzo-30-couronne-10 – thiocyanate de potassium par la résonance magnétique nucléaire du ^{39}K et du ^{13}C. Dans les quatre solvants étudiés (nitrométhane, acétonitrile, acétone et pyridine), le grand éther en couronne s'enroule autour du cation potassium, expulsant de la couche de coordination l'anion conjugué et les molécules de solvant. La mesure des temps de relaxation quadripolaire en ^{39}K et dipole–dipole en ^{13}C dans l'acétone deutérée a permis de calculer le temps de corrélation effectif du complexe et la constante de couplage quadripolaire du ^{39}K (1.4 ± 0.3 MHz). La comparaison entre les constantes de couplage quadripolaires du ^{23}Na et du ^{39}K des complexes Na^+–dibenzo-24-couronne-8 et K^+–dibenzo-30-couronne-10 a montré que les gradients de champ électrique au site du noyau métallique sont quasi identiques ($q(^{39}K)/q(^{23}Na) \simeq 0{,}9$) dans les deux complexes.

Introduction

Large crown ethers, such as dibenzo-30-crown-10 (DB30C10, **1**) (1) show some analogies with cryptands (2) in their complexation behaviour. They selectively complex alkali metal cations, creating a three-dimensional cavity during the complexation process. The equilibrium constants for the formation of the complexes M^+–DB30C10, in acetone, are 3.5×10^2 for Na^+, 2×10^4 for K^+, and 1.7×10^4 for Cs^+ (3). DB30C10, like dibenzo-18-crown-6 (DB18C6) (4), cryptand [2,2,2] (5, 6), and the antibiotic ionophore valinomycin (7), selectively complexes K^+. The recognition of K^+ by DB30C10 is conformationally controlled, whereas in the case of cryptands the control is mainly constitutional because their cavity was built during the synthesis. This makes DB30C10 a good model for valinomycin and others for which the cation recognition also relies mainly on conformational controls (7).

X-ray results on the KSCN–DB30C10 complex have shown that the large crown ether wraps around K^+. The ligand has a stable conformation with a majority of "*trans*" C—O and "*gauche*" C—C bonds (8). Live and Chan have shown by ^1H and ^{13}C nmr that the complex in acetone-d_6 solutions has a structure analogous to the crystalline one (3). A ^{13}C nmr study by Shamsipur and Popov supported this conclusion (9). We have shown previously that a 2:1 K^+–DB30C10 complex (10) and 2:1 and 3:2 Na^+–DB30C10 complexes (11) are formed in nitromethane.

In this paper, we show that a 1:1 K^+–DB30C10 complex is quantitatively formed in several nonaqueous solvents with the complete expulsion of solvent molecules from the first coordination shell of the cation. This is very similar to what was observed previously for the Na^+–DB24C8 complex (12). The electric field gradients of ^{23}Na–DB24C8 and ^{39}K–DB30C10 are identical within the limits of the experimental errors. This shows the quasi identity of the coordination shells of Na^+ and K^+ in the two complexes.

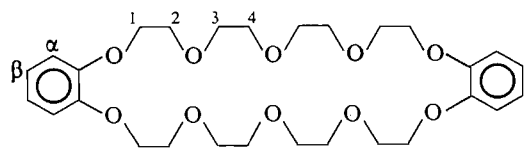

1

SCHEME 1

Experimental

Dibenzo-30-crown-10 (Parish Chemical Co.) was recrystallized in a minimum of acetone; after cooling and washing by a few millilitres of acetone, it was dried under vacuum for several hours (mp 105–106°C). Potassium thiocyanate (Aldrich, 99+%) and potassium hexafluorophosphate (Aldrich, 98%) were vacuum dried (60°C) over P_2O_5 for at least 4 h prior to use.

Nitromethane (Aldrich, gold label) and acetonitrile (BDH, assured) were dried under reflux over calcium hydride, fractionally distilled, and stored over 4 Å molecular sieves under argon. Pyridine (Aldrich, gold label) and acetone (Fisher, spectranalyzed) were stored over 4 Å molecular sieves under argon at least two days prior to use. The nmr tubes were tightly capped under argon. All the spectra were recorded within 24 h of preparation of the samples.

The ^{39}K nmr spectra were obtained at 13.997 MHz (Varian XL-300). The chemical shifts were measured with respect to a 0.1 *M* KCl solution in D_2O–H_2O 10:90. The lineshapes were Lorentzian in all cases, and linewidths at half-height were measured graphically. The 90° pulse width was 90 μs.

^{13}C T_1 measurements were done at 75.43 MHz in acetone-d_6 on degassed samples (argon bubbling) containing an excess of salt over the crown. The inversion–recovery 180°–τ–90° pulse sequence was

[1]Dibenzo-30-crown-10: 6,7,9,10,12,13,15,16,23,24,26,27,29,-30,32,33-hexadecahydrodibenzo[*b*,*q*][1,4,7,10,13,16,19,22,25,28]-decaoxacyclotriacontin.

[2]Author to whom correspondence may be addressed.

Can. J. Chem. Downloaded from www.nrcresearchpress.com by 72.64.146.136 on 09/07/12
For personal use only.

Can. J. Chem. Downloaded from www.nrcresearchpress.com by 72.64.146.136 on 09/07/12
For personal use only.

used. The 90° pulse width was 22 μs. The T_1 was obtained from a three-parameter nonlinear regression analysis on nine experimental data points. Nuclear Overhauser enhancement measurements were done using a gated decoupling technique, with a recycling time more than ten times larger than T_1.

Results

Figure 1 shows the ^{39}K chemical shifts of a 0.050 *M* KSCN solution in four solvents (nitromethane (NM), acetonitrile (AN), acetone (AC), pyridine (PY)) as a function of ρ, the ratio [DB30C10]/[KSCN]. In the cases of acetone, acetonitrile, and pyridine, a quasi-linear variation of the chemical shift was observed, until a plateau value was reached for $\rho \geq 1.0$. This is characteristic of the formation of a 1:1 complex with an equilibrium constant of formation larger than 10^4 (3). In acetone, $\log K_f = 4.3$ (3). For $0.0 < \rho < 1.0$, the chemical shift observed was the average mean between the two limiting values for solvated and complexed potassium. In nitromethane, the chemical shift variation was not linear. This has been shown to be indicative of the 2:1 K^+–DB30C10 complex formation (10). In all four solvents, the complex exhibited the same characteristic chemical shift value (−13.3 ± 0.2 ppm). A slight deviation was observed in pyridine at high crown concentrations. The value of the chemical shift of the complex (−13.3 ppm) is in the range expected for a potassium in an oxygen environment: we measured the chemical shift of a 0.1 *M* KSCN solution in methanol as being −8.9 ppm. This value is similar to the one previously published by Shih and Popov (13). The linewidths of the complex span a range of values between 49 Hz (AN) and 95 Hz (PY) (Table 1). These values are close to those measured in ^{23}Na nmr for sodium complexed by DB24C8 (12), and both are linearly related to the viscosity of the solvent. Figure 2 shows the relationship between the solvent viscosity and the measured linewidth of ^{39}K or ^{23}Na in the complexes K^+–DB30C10 and Na^+–DB24C8 respectively. The slopes of the linear relationships are in the same order of magnitude (11.4 Hz/mP for ^{23}Na and 7.2 Hz/mP for ^{39}K).

In the absence of chemical exchange contributions, and because of the effectiveness of the quadrupolar relaxation, the observed linewidth of a quadrupolar nucleus depends only upon the inhomogeneity and the quadrupolar contributions to the relaxation rate (eq. [1]) (16).

$$[1] \quad \frac{1}{T_{2,\text{obs}}} = \pi\nu_{1/2} = \frac{1}{T_{2,\text{inh}}} + \frac{1}{T_{2,\text{q}}}$$

$(T_{2,\text{inh}})^{-1}$ is given by eq. [2] (17, 18).

$$[2] \quad (T_{2,\text{inh}})^{-1} = (T_{2,\text{obs}})^{-1} - (T_{1,\text{obs}})^{-1}$$

The comparison between T_2 and T_1 (eq. [2]) gave $(T_{2,\text{inh}})^{-1} = 21 \pm 4$ Hz. This is comparable to the values of $(T_{2,\text{obs}})^{-1} - (T_{1,\text{obs}})^{-1}$ previously determined in nitromethane under similar experimental conditions (10). Under extreme narrowing conditions, and neglecting the asymmetry parameter, the quadrupolar contribution to the transverse relaxation rate $(T_{2,\text{q}})^{-1}$ is given by eq. [3] (16), where τ_c is the correlation time characteristic of

$$[3] \quad \frac{1}{T_{2,\text{q}}} = \frac{3\pi^2}{10}\frac{2I+3}{I^2(2I-1)}\chi^2\tau_c$$

the quadrupolar relaxation and χ is the quadrupolar coupling constant (QCC), which is given by eq. [4]:

$$[4] \quad \chi = \frac{e^2qQ(1+\gamma_\infty)}{h}$$

Q is the quadrupole moment, q the electric field gradient at

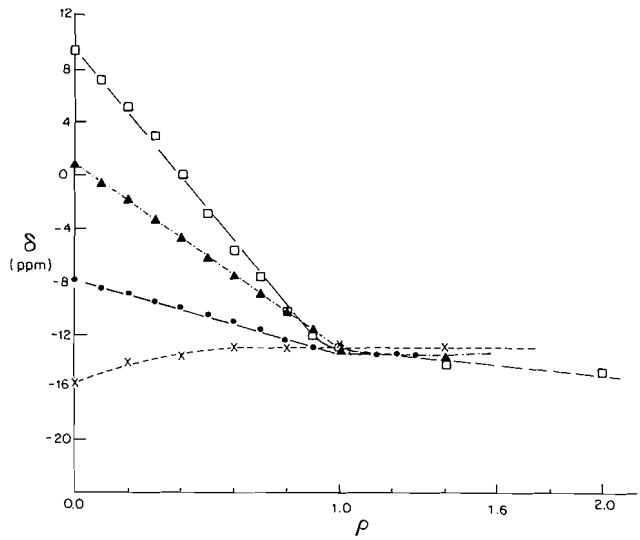

FIG. 1. ^{39}K chemical shifts as a function of the ratio ρ = [DB30C10]/[KSCN] in some nonaqueous solvents: □: pyridine; ▲: acetonitrile; ●: acetone, ×: nitromethane. [KSCN] = 0.050 *M*.

TABLE 1. Values of the ^{39}K chemical shifts and linewidths for the complex K^+–DB30C10 in nitromethane (NM), acetone (AC), acetonitrile (AN), and pyridine (PY) at 294 K. The viscosities of the four solvents are also indicated

Solvent	δ (ppm) (±0.1)	$\nu_{1/2}$ (Hz)	η (mP)
NM	−13.0	71 ± 4	6.20[a]
AC	−13.4	53 ± 3	3.24[b]
AN	−13.4	49 ± 3	3.57[b]
PY	−13.4	95 ± 8	9.52[c]

[a] 298 K; ref. 14.
[b] 294 K, interpolation between 288 and 298 K; ref. 14.
[c] 293 K; ref. 15.

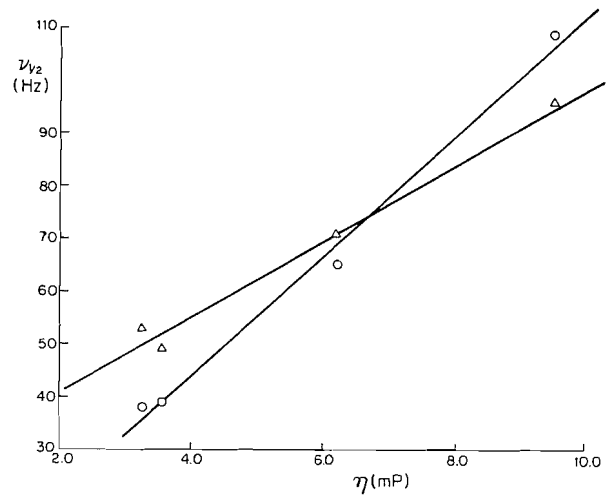

FIG. 2. Linewidths at half-height of the ^{39}K nmr signals (△) and of the ^{23}Na nmr signals (○; ref. 11) for the complexes K^+–DB30C10 and Na^+–DB24C8 respectively, as a function of the solvent viscosity (for acetone, acetonitrile, nitromethane, pyridine).

TABLE 2. Results of ^{13}C measurements in deuterated acetone

Complex[a]	Parameter	C(1)	C(2–4)[d]	α	β
DB30C10–KSCN	δ (ppm)[b,c]	69.13	69.29	116.48	123.11
	$T_{1,obs}$[e] (s)	0.96 ± 0.05	0.95 ± 0.05	1.61 ± 0.09	1.49 ± 0.09
	nOe[f]	1.59	1.71	1.62	1.87
	τ_{eff}[g] (ps)	19	21	23	29
DB30C10–KPF_6	δ (ppm)[b,c]	68.82	69.00	116.26	122.85
	$T_{1,obs}$[e] (s)	1.06 ± 0.05	1.06 ± 0.05	1.97 ± 0.08	1.84 ± 0.08
	nOe[f]	1.44	1.33	1.31	1.62
	τ_{eff}[g] (ps)	16	14	15	20

[a]In $(CD_3)_2CO$ at 294 K.
[b]±0.03 ppm; reference: TMS.
[c]The chemical shift of the nonprotonated aromatic carbon was 149.47 (DB30C10–KSCN) and 149.20 (DB30C10–KPF_6).
[d]The resonances of C(2), C(3), and C(4) were undistinguishable in $(CD_3)_2CO$.
[e]The error was taken as 3σ, σ being obtained from a three-parameter linear regression.
[f]±5%.
[g]Calculated from eq. [8]. $\overline{\tau_{eff}}$ = (23 ± 4) ps (KSCN) and (16 ± 3) ps (KPF_6).

the quadrupolar nucleus site, and $(1 + \gamma_\infty)$ the Sternheimer antishielding factor.

For a spin 3/2 nucleus, such as ^{23}Na or ^{39}K, eq. [3] is reduced to eq. [5]:

$$[5] \quad \frac{1}{T_{2,q}} = \frac{2\pi^2}{5}\chi^2\tau_c$$

If the correlation time, τ_c, characteristic of the electric field gradient fluctuation, has an origin purely reorientational, it should obey the Debye–Stokes–Einstein relationship (eq. [6])

$$[6] \quad \tau_c = \frac{4}{3}\pi a^3 \frac{\eta}{kT} f_r$$

(16). This condition is fulfilled if the lifetime of a spatially well-defined coordination shell of the complex is long with respect to the time characteristic of the molecular reorientation.

In eq. [6], a is the molecular radius, η the medium macroscopic viscosity, and f_r the microviscosity coefficient (19). The experimentally observed linear relationship between the ^{39}K linewidth and the viscosity of the solvent can be easily interpreted from eqs. [1], [5], and [6]. If χ, the quadrupolar coupling constant, were independent of the solvent nature, one would expect a direct relationship between $(T_{2,q})^{-1}$ and τ_c, which is proportional to the viscosity of the solvent. One can assume that, at first approximation, a, the molecular radius of the complex, is independent of the solvent. Moreover, f_r, the microviscosity coefficient, which depends mainly upon the relative size of the complex and of the solvent molecule (19), should also be, at first approximation, independent of the solvent. In the case of Na^+–DB24C8, we have estimated f_r to be ~0.24 in a series of nonaqueous solvents (12).

At this point, two independent observations indicate that the solvent molecules do not participate in the K^+ coordination shell of the complex: the ^{39}K chemical shifts are independent of the solvent, and the linewidths are linearly related to the solvent macroscopic viscosity. The latter behaviour is expected only if the ^{39}K quadrupolar coupling constant does not depend upon the solvent and, consequently, if the symmetry of the electric charges around K^+ is identical in all the solvents. This would be the case if the crown oxygen donor atoms were the only coordinating atoms of K^+.

To evaluate the quadrupolar coupling constant, χ, we need to know τ_c (eq. [5]). We have to make the approximation that τ_c is identical to a reorientational correlation time measured on other nuclei of the supramolecule, the ligand ^{13}C for example. This approach has been used previously and has permitted the calculation of the ^{23}Na quadrupolar coupling constants of Na^+ complexed by some cryptands (20), by the large crown ether DB24C8 (12), and by 15C5 and 18C6 (21). Under extreme narrowing conditions, the ^{13}C dipole–dipole relaxation rate $(1/T_{1,DD})$ is given by eq. [7], where N_H is the number of directly attached hydrogens, r_{CH} the C—H bond length, and τ_{eff} the effective correlation time (22).

$$[7] \quad \frac{1}{T_{1,DD}} = \left(\frac{\mu_0}{2\pi}\right)^2 N_H \gamma_H^2 \gamma_c^2 \hbar^2 r_{CH}^{-6} \tau_{eff}$$

Taking $r_{C—H}$ = 0.1085 nm, eq. [7] is reduced to eq. [8] (the constant term has s^{-2} units).

$$[8] \quad \frac{1}{T_{1,DD}} = 2.2086 \times 10^{10} N_H \tau_{eff}$$

The dipole–dipole contribution to the observed longitudinal relaxation time, $T_{1,obs}$, can be obtained from the measurement of the nuclear Overhauser enhancement (nOe), as shown by eq. [9].

$$[9] \quad T_{1,DD} = T_{1,obs} \times \frac{1.98}{(nOe)_{obs}}$$

Table 2 shows the results of the ^{13}C measurements in the cases of DB30C10–KSCN and DB30C10–KPF_6 in deuterated acetone. Within the limits of the experimental errors, the ^{13}C correlation times, τ_{eff}, are identical for the two complexes (23 ± 4 ps and 16 ± 3 ps respectively). Making the approximation that $\tau_{eff} = \tau_c$, the knowledge of τ_c permits the calculation of χ from eq. [5]. The values of χ for $^{39}K^+$–DB30C10 in $(CD_3)_2CO$ are 1.4 ± 0.3 MHz (SCN^-) and 1.6 ± 0.3 MHz (PF_6^-).

Discussion

The complex K^+–DB30C10 is characterized by the same ^{39}K chemical shift (−13.3 ppm) in each of the four solvents of this study: nitromethane, pyridine, acetone, and acetonitrile. When an excess of crown is present with respect to K^+ the chemical

Can. J. Chem. Downloaded from www.nrcresearchpress.com by 72.64.146.136 on 09/07/12
For personal use only.

shift is constant, showing the absence of complexes other than the 1:1. The slight deviation observed in the case of pyridine for high [crown]:[K^+] ratios could be due to a slight concentration of the sandwich complex. Chemical shift values of K^+ complexed by other ionophores have been reported by Neurohr *et al.* (23). They are given relative to KSCN in a methanol–D_2O 95:5 mixture. The valinomycin–KSCN complex resonates 14.3 ppm highfield from K^+ in methanol, which corresponds to −24 ppm from K^+ in water (K^+ in methanol resonates at −10 ppm from K^+ in water (13)). In the cryptand [2,2,2] – K^+ complex, the ^{39}K chemical shift is +1 ppm relative to K^+ in water (23). In the same study, the ^{39}K quadrupolar coupling constants of the valinomycin–K^+ and of the [2,2,2]–K^+ complexes were measured to be respectively 1.2 MHz and 2.6 MHz (23). A proportionality between the ^{23}Na chemical shifts and the quadrupolar coupling constants has been found for Na^+ encaged in cryptands (20) and was corroborated by the chemical shift and the quadrupolar coupling constant values of $^{23}Na^+$–DB24C8 (12). On the basis of that correlation, assuming that it can be applied to ^{39}K parameters, we can roughly estimate the ^{39}K QCC of the KSCN–DB30C10 complex: the interpolation between the two data from ref. 23 gives 1.7 MHz. The agreement with the value that we have experimentally measured is excellent: 1.7 MHz, to be compared with 1.4 ± 0.3 MHz or 1.6 ± 0.3 MHz! ^{39}K QCC's of 15C5–$KClO_4$ and 15C5–KI in CD_3CN have been determined by Eliasson *et al.* to be 1.4 MHz (21). In the same study, much higher values (3.4 and 3.5 MHz) were attributed to the systems 18C6–$KClO_4$ and 18C6–KI (21).

It is particularly interesting to compare ^{23}Na and ^{39}K QCC's in the two complexes Na^+–DB24C8 and K^+–DB30C10. In the two cases, we have strong indications of the similarity of the cationic environment. The coordination sphere is made of ether oxygens only, since all the solvent molecules and the counter-anion have been expelled from the sodium or the potassium coordination sphere during the complexation process. This similarity should be reflected in the electric field gradient at the site of the metal cation. From eq. [4], and from known values (16) of the quadrupole moment (Q = 0.055 barn (^{39}K) and 0.12 barn (^{23}Na)) and of the Sternheimer antishielding factor (24) ($|(1 + \gamma_\infty)|$ = 5.26 for ^{23}Na and 19.96 for ^{39}K), one can estimate the ratio of the two electric field gradients: $q(^{39}K)/q(^{23}Na) \simeq 0.9$ (KSCN complex) and $\simeq 1.1$ (KPF_6 complex). The similarity of the two electric field gradients is thus remarkable and confirms that the environment of Na^+ and K^+ in DB24C8 and DB30C10 complexes, respectively, consists only of oxygen atoms from the ligand. The structure of the complex in solution is similar to the structure in the crystal where DB30C10 has been shown to wrap around K^+ (8). ^{13}C and ^1H nmr studies of the ligand have suggested the same conclusion (3, 9). Moreover, the crown ether coordination shell is rigid on the time scale of the molecular reorientation of the complex. This means that the chemical exchange of K^+ between different ligands is not responsible for the quadrupolar relaxation. This is expected on the basis of the known time scale for such processes, 10^4–$10^6\ s^{-1}$ (18), much slower than molecular tumbling. But it means also that no internal fluctuations in the potassium coordination shell can be detected from the quadrupolar relaxation rate, $(T_{2,q})^{-1}$. In the complex, the crown ether segmental motions and the cation mobility into the cavity are frozen in the time scale of the overall molecular reorientation. When complexing K^+, DB30C10 appears as a rigid matrix, with its oxygen ether atoms pointing to the inside and surrounding K^+, tightly maintained in the cavity.

Acknowledgements

We are grateful to the Natural Sciences and Engineering Research Council of Canada (NSERCC) for financial support.

1. C. J. Pedersen. J. Am. Chem. Soc. **89**, 7017 (1967).
2. J. M. Lehn. Acc. Chem. Res. **11**, 49 (1978).
3. D. Live and S. I. Chan. J. Am. Chem. Soc. **98**, 3769 (1976).
4. H. K. Frensdorff. J. Am. Chem. Soc. **93**, 600 (1971).
5. E. Kauffmann, J. M. Lehn, and J. P. Sauvage. Helv. Chim. Acta, **59**, 1099 (1976).
6. A. F. Danil de Namor and L. Ghousseini. J. Chem. Soc. Faraday Trans. 1, **81**, 781 (1985).
7. R. Hilgenfeld and W. Saenger. Top. Curr. Chem. **101**, 1 (1982).
8. J. D. Owen, M. R. Truter, and J. N. Wingfield. Acta Crystallogr. Sect. C: Cryst. Struct. Commun. **40**, 1515 (1984).
9. M. Shamsipur and A. I. Popov. J. Am. Chem. Soc. **101**, 4051 (1979).
10. H. D. H. Stover, M. Robillard, and C. Detellier. Polyhedron, **6**, 577 (1987).
11. H. D. H. Stover, L. J. Maurice, A. Delville, and C. Detellier. Polyhedron, **4**, 1091 (1985).
12. M. Bisnaire, C. Detellier, and D. Nadon. Can. J. Chem. **60**, 3071 (1982).
13. J. S. Shih and A. I. Popov. Inorg. Nucl. Chem. Lett. **13**, 105 (1977).
14. R. C. Weast (*Editor*). Handbook of chemistry and physics. 66th ed. CRC Press, Cleveland, OH. 1985–1986.
15. J. A. Dean (*Editor*). Lange's handbook of chemistry. 13th ed. McGraw–Hill, New York. 1985.
16. C. Detellier. *In* NMR of newly accessible nuclei. Vol. 2. *Edited by* P. Laszlo. Wiley, New York. 1983. Chap. 5.
17. H. D. H. Stover, A. Delville, and C. Detellier. J. Am. Chem. Soc. **107**, 4167 (1985).
18. A. Delville, H. D. H. Stover, and C. Detellier. J. Am. Chem. Soc. **107**, 4172 (1985).
19. A. Gierer and K. Wirtz. Z. Naturforsch. Teil A, **8**, 532 (1953).
20. J. P. Kintzinger and J. M. Lehn. J. Am. Chem. Soc. **96**, 3313 (1974).
21. B. Eliasson, K. M. Larsson, and J. Kowalewski. J. Phys. Chem. **89**, 258 (1985).
22. R. K. Harris. Nuclear magnetic resonance spectroscopy. Pitman, London. 1983. Chap. 3.
23. K. J. Neurohr, T. Drakenberg, S. Forsen, and H. Lilja. J. Magn. Reson. **51**, 460 (1983).
24. P. C. Schmidt, K. D. Sen, T. P. Das, and A. Weiss. Phys. Rev. B: Condens. Matter, **22**, 4167 (1980).

Can. J. Chem. Downloaded from www.nrcresearchpress.com by 72.64.146.136 on 09/07/12
For personal use only.

Kinetic and equilibrium study of the ring opening of 2-aryl-1-methyl-1-pyrrolinium ions in aqueous solution

ROBERT A. MCCLELLAND AND N. ESTHER SEAMAN
Department of Chemistry, University of Toronto, Toronto, Ont., Canada M5S 1A1

Received August 11, 1986

This paper is dedicated to Professor John T. Edward

ROBERT A. MCCLELLAND and N. ESTHER SEAMAN. Can. J. Chem. **65**, 1689 (1987).

Ultraviolet spectral and kinetic measurements are reported for the transformations in aqueous solution undergone by the cyclic iminium ion, the 2-aryl-1-methyl-1-pyrrolinium ion $\mathbf{I}^+$. In solutions with pH < 9.5 this ion equilibrates with a ring-opened hydrated form, the protonated 4-methylaminobutyrophenone $\mathbf{SH}^+$. The concentration of the latter at equilibrium is small, but it can be observed using nuclear magnetic resonance spectroscopy. A kinetic analysis provides a measure of the $\mathbf{I}^+ \rightleftarrows \mathbf{SH}^+$ equilibrium constant. Values range from 0.06 for 4-methoxyphenyl to 0.17 for 3-chlorophenyl. In acid solutions (pH < 5) the equilibration is slow (half-life ≈ 20 min for phenyl) and pH independent. Above pH 5 this process becomes first order in hydroxide ion. In strongly basic solutions a neutral species is formed in equilibrium with these two cations, with pK(app) for the transformation cations ⇄ neutral + H^+ ranging from 11.8 to 11.3. Spectral arguments imply that the base species is the ring-opened 4-methylaminobutyrophenone **S**, with less than ten percent of the pseudobase of I^+ present.

ROBERT A. MCCLELLAND et N. ESTHER SEAMAN. Can. J. Chem. **65**, 1689 (1987).

On a mesuré les spectres ultraviolets et la cinétique des transformations que subit l'ion cyclique iminium, l'ion aryl-2 méthyl-1 pyrrolinium I^+, dans des solutions aqueuses. Dans des solutions de pH < 9,5, cet ion s'équilibre avec la forme hydratée qui est ouverte, soit la méthylamino-4 butyrophénone protonée SH^+. À l'équilibre, la concentration de ce composé est faible; toutefois, on peut l'observer par rmn. Une analyse cinétique fournit une mesure de la constante d'équilibre $I^+ \rightleftarrows SH^+$. Les valeurs de cette constante varient de 0,06 pour le méthoxy-4 phényle à 0,17 pour le chloro-3 phényle. Dans des solutions acides (pH < 5), l'équilibre est lent (demi-vie ≈ 20 min pour le phényle) et ne dépend pas du pH. Au-dessus d'un pH de 5, ce processus devient du premier ordre en ions hydroxydes. Dans des solutions fortement basiques, il se forme une espèce neutre qui est en équilibre avec ceux deux cations; le pK(app) pour la transformation des cations ⇄ forme neutre + H^+ varie de 11,8 à 11,3. Les arguments basés sur les spectres indiquent que l'espèce basique est la méthylamino-4 butyrophénone à chaîne ouverte S; il y aurait moins de dix pourcent de la pseudobase de I^+ qui serait présente.

[Traduit par la revue]

The reversible addition of hydroxide ion to heterocyclic cations is well documented (1). The pseudobase product of this reaction is usually also the tetrahedral adduct of an intramolecular nucleophilic addition to a carbonyl (or acyl) group. As

[1] 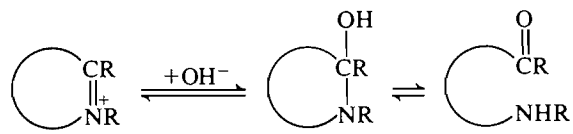

such, the pseudobase frequently exists in equilibrium with a ring-opened form, a phenomenon which has been termed "ring-chain tautomerism" (1). As part of a program of study of tetrahedral intermediates (2, 3) we have investigated a series of cyclic iminium ions I^+. This study was prompted by suggestions that

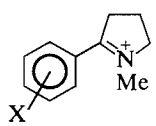

I^+; X = 4-MeO, 4-Me, H, 4-Cl, 3-Cl

nitrosamines derived from nicotine are forming by way of iminium salts, one of which has a structure analogous to I^+ (4, 5).

As our analysis will demonstrate, the I^+ system has the interesting property of having the cation in equilibrium with a ring-opened amino ketone. This may explain the ease of formation of the ring-opened N-nitroso derivative of nicotine.

[2] 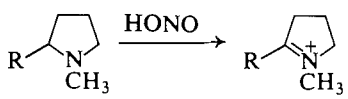

R = 3-pyridyl

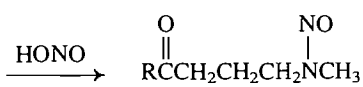

Experimental

2-Aryl-1-methyl-1-pyrrolinium trifluoromethanesulfonates

2-Aryl-1-pyrrolines (6, 7) were dissolved in methylene chloride freshly distilled from concentrated H_2SO_4; an equivalent amount of methyl trifluoromethanesulfonate was slowly added, with the solution being cooled in an ice bath. Anhydrous ether was then added and the resultant white solid collected by filtration. This was purified by redissolving in methylene chloride and reprecipitation with ether. Proof of structure was accomplished through ^1H nmr spectroscopy. The spectrum of the unsubstituted compound was identical to that reported for the perchlorate salt (8).

Kinetic and ultraviolet spectral measurements were made on a Cary 2390 spectrophotometer and a Durrum–Gibson stopped-flow spectrophotometer. In general, stock solutions of the I^+ salt of concentrations $1–2 \times 10^{-4}$ M in water were used to initiate studies. For reactions in base this stock solution was mixed with an equivalent volume of sodium hydroxide solution; kinetics were studied on the stopped-flow apparatus, with final spectra being recorded on the Cary. The kinetic measurements reported in weakly basic, neutral, and acidic solutions were performed by adding the stock solution to an equivalent volume of 0.20 M NaOH. This solution was then mixed with an equal volume of solution of the appropriate pH, also containing 0.10 M HCl. First-order rate constants were obtained as the average of 3–8 runs, by least-squares analysis of plots of $\ln(A - A_\infty)$ or $\ln(A_\infty - A)$ versus time. Wavelengths employed for kinetic studies were 305 nm (4-$MeOC_6H_4$), 276 nm (4-MeC_6H_4), 265 nm (C_6H_5), 280 nm (4-ClC_6H_4), and 275 nm (3-ClC_6H_4).

Results

The analysis principally involved uv spectral and kinetic measurements; observations are presented in detail here for the unsubstituted ion, which was examined most thoroughly. The

Can. J. Chem. Downloaded from www.nrcresearchpress.com by 118.98.75.50 on 09/07/12
For personal use only.

TABLE 1. Observed constants for the transformations of 2-aryl-1-methyl-1-pyrrolinium ions (25°C, ionic strength = 0.1)

Aryl group	pK(app)	A	B	C
4-MeOC$_6$H$_4$	11.89	1.94	161	6.76×10^{-4}
4-MeC$_6$H$_4$	11.86	3.01	294	6.46×10^{-4}
C$_6$H$_5$	11.67	4.52	496	7.41×10^{-4}
4-ClC$_6$H$_4$	11.53	5.04	799	7.59×10^{-4}
3-ClC$_6$H$_4$	11.39	5.95	1395	6.03×10^{-4}

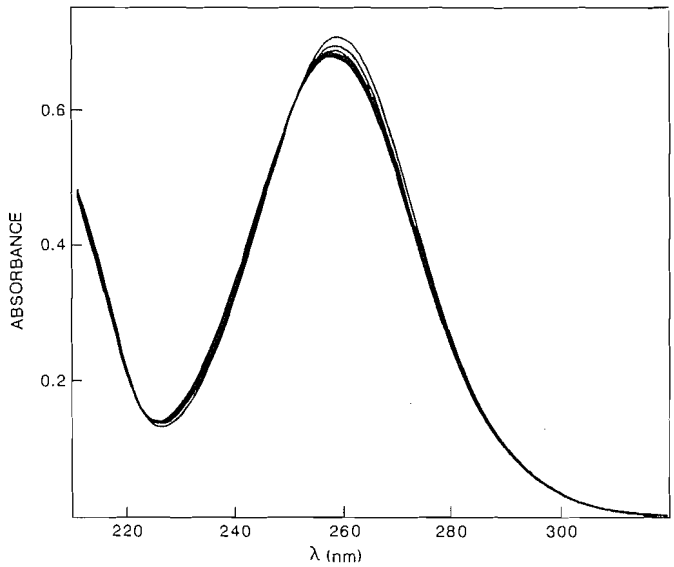

FIG. 1. 1-Methyl-2-phenyl-1-pyrrolinium trifluoromethanesulfonate ($7.5 \times 10^{-5} M$) in $10^{-3} M$ HCl, with spectra recorded every 20 min. The absorbance decreases with time at 260 nm, and increases at 240 nm.

other derivatives behave qualitatively the same. The empirical constants presented in this section are symbolized as K(app) (app = apparent) or $A, B \ldots$, while the rate and equilibrium constants derived on the basis of a mechanistic scheme in the discussion section are symbolized as $k_1, K_1 \ldots$ A summary of the empirical constants obtained for all the ions is given in Table 1.

Figure 1 shows uv spectra observed on dissolving iminium salt in weakly acidic solution. There is a small but reproducible spectral change with the intensity at the 257-nm λ_{max} decreasing slightly and an accompanying absorbance increase at lower wavelengths. More dramatic spectral changes are observed in strongly basic solutions, and they occur very quickly, requiring stopped-flow spectroscopy for the change actually to be observed (see kinetics, later). A typical spectrum in base is that shown as the initial spectrum in Fig. 2, with λ_{max} at 245 nm. (Although the actual solution here is acidic, the transformation that is occurring is quite slow, and the starting spectrum is that of a base solution.)

As might be expected, the absorption spectra in base are pH dependent, ranging from the 245-nm λ_{max} at high hydroxide ion concentrations to the 257-nm λ_{max} at very low hydroxide concentrations. Figure 3 shows absorbance dependencies at 240 nm and 265 nm, wavelengths slightly off the λ_{max} being chosen in order to have larger overall absorbance changes. These describe acid–base titration curves, and acidity constants were calculated as

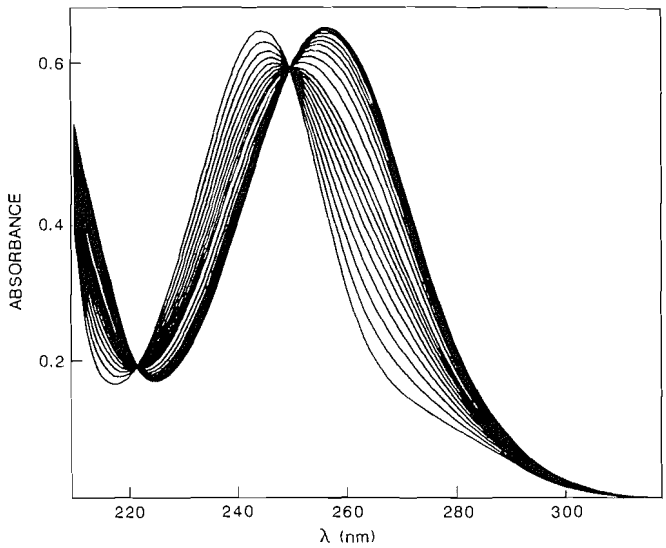

FIG. 2. 1-Methyl-2-phenyl-1-pyrrolinium trifluoromethanesulfonate added to $0.10 M$ NaOH, followed by acidification to pH 2 by addition of HCl. Final concentration of substrate is $7.5 \times 10^{-5} M$. The first ten spectra were recorded with 8-min intervals, thereafter 20 min.

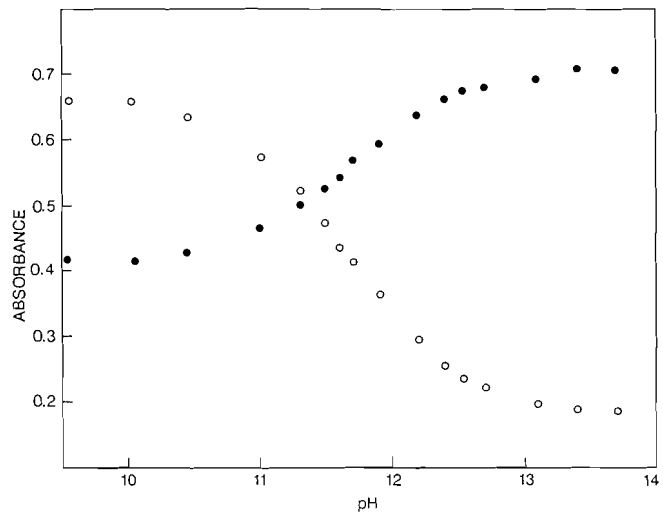

FIG. 3. 1-Methyl-2-phenyl-1-pyrrolinium ion absorbances in base solution; ●, 265 nm; ○, 240 nm. All solutions were $7.5 \times 10^{-5} M$ substrate, and up to $0.1 M$ NaOH had ionic strength (μ) of 0.1 maintained with NaCl. Solutions below pH 11 were carbonate buffers, and above pH 11 they contained sodium hydroxide. The pH in solutions containing more than $0.01 M$ NaOH was calculated with pK_w of 13.7 at $\mu = 0.1$ (9).

$$[3] \quad K(\text{app}) = \frac{A_{base} - A}{A - A_{acid}} [H^+]$$

where A, A_{base}, and A_{acid} are absorbances in the solution in question, base ($1 M$ NaOH), and acid (pH < 10) respectively.

That a reversible acid–base type of equilibrium exists throughout the pH range is demonstrated by the experiment described in Fig. 2. This shows the spectral changes that occur when a basic solution with the 245-nm absorbance is reacidified, with the result that the 257-nm absorbance is regenerated. The change is quite slow, at least in strong acids. The rate, within experimental error, is identical with that of the much smaller

Can. J. Chem. Downloaded from www.nrcresearchpress.com by 118.98.75.50 on 09/07/12
For personal use only.

Can. J. Chem. Downloaded from www.nrcresearchpress.com by 118.98.75.50 on 09/07/12
For personal use only.

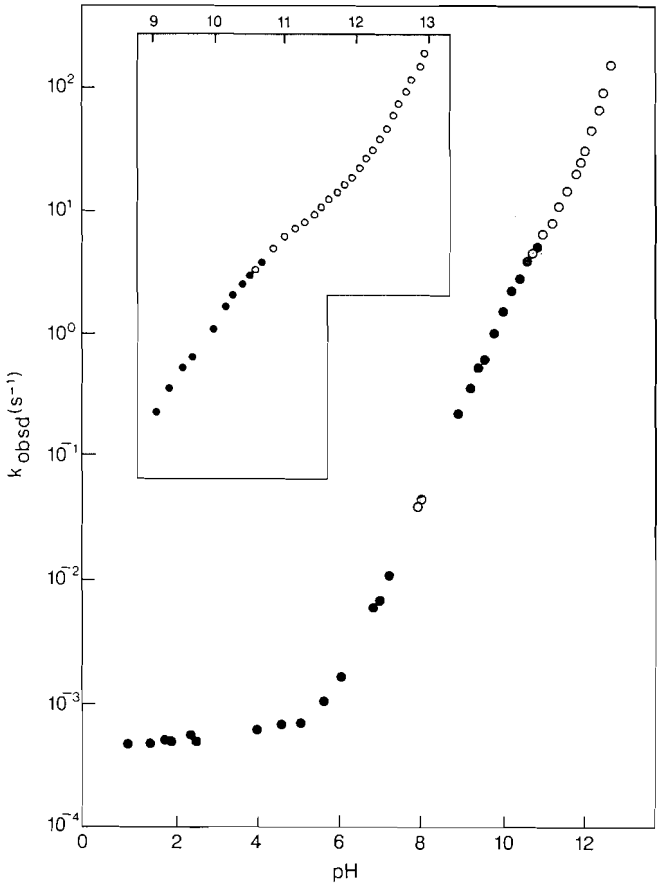

FIG. 4. Observed rate constants (s^{-1}, 25°C, 0.1 ionic strength) for transformations of the 1-methyl-2-phenyl-1-pyrrolinium ion; ○, starting with neutral solution of ion; ●, starting with 0.1 *M* NaOH solution. Rate constants in buffer solutions (pH 4–11) were based upon extrapolation to zero buffer concentration or were determined in dilute (0.002 *M*) buffers. The insert is an expansion of the high pH region.

spectral change found on adding iminium ion directly to a solution of the same pH.

The various transformations all obey excellent first-order kinetics, with no evidence for intermediates. First-order rate constants are shown in Fig. 4. Those in strongly basic solutions were obtained by mixing, on a stopped-flow spectrophotometer, a neutral solution of iminium ion with aqueous sodium hydroxide. Other rate constants were obtained using the procedure described in Fig. 2, by preparing an 0.1 *M* NaOH solution and mixing this with an appropriate neutralizing buffer, either on the stopped-flow apparatus or in a conventional uv cuvette.

The rate constants in base (pH > 7) accurately follow the empirical relationship

$$[4] \quad k_{obsd} = \frac{A[OH^-] + B[OH^-]^2}{C + [OH^-]}$$

and values of the three coefficients were determined by a non-linear least-squares fit of the experimental data to this equation. The quantity A/C is the slope of the approximately linear plot of k_{obsd} vs. $[OH^-]$ in the pH 7–10 region, while the quantity B is the limiting slope of a similar plot at high hydroxide ion concentration. In acid solution (pH < 5) the rate constants level, with $k_{obsd} = D = 5.0 \times 10^{-4}\ s^{-1}$ for the unsubstituted compound. (The other derivatives were not studied in detail in acids.) Catalysis by the buffer is also observed in acids, but this was not investigated in detail.

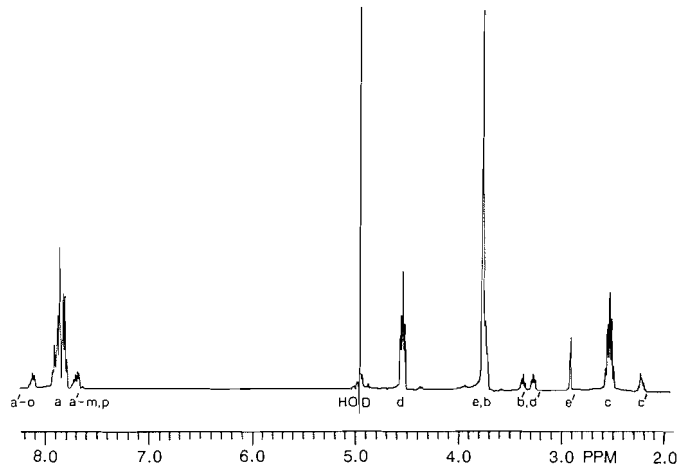

FIG. 5. The 400-MHz ^1H nmr spectrum in D_2O solution, pD ~ 2, of the 1-methyl-2-phenyl-1-pyrrolinium ion, recorded 24 h after solution preparation.

Figure 5 shows a 400-MHz nmr spectrum in weakly acidic D_2O, a day after solution preparation. A spectrum recorded immediately consisted only of the larger signals, with the smaller signals indicated by primes appearing with time. No further change occurred beyond that shown in the figure. It can be noted that the kinetics show that the equilibration, whatever it represents, is complete within a day.

Discussion

Nature of the acid species

Both uv (Fig. 1) and nmr (Fig. 5) show that the iminium ion is not completely stable in acids, but that another minor species is formed in equilibrium. We propose that this is the ring-opened protonated amino ketone SH^+.

$$[5] \quad C_6H_5\overset{a}{C}{=}\overset{+}{N}(\overset{e}{CH_3})\overset{b}{CH_2}\overset{c}{CH_2}\overset{d}{CH_2} \rightleftharpoons C_6H_5\overset{a'}{C}(=O)\overset{b'}{CH_2}\overset{c'}{CH_2}\overset{d'}{CH_2}\overset{+}{N}H_2\overset{e'}{CH_3}$$

SH^+

Peak assignments for the nmr spectrum in Fig. 5 are shown in eq. [5]. The spectrum assigned to I^+ is very similar to that recorded in a nonhydroxylic solvent (8). The ketone spectrum is characterized by the two triplets for the b′ and d′ methylene groups, as well as the separation of the aromatic *ortho* hydrogen signals from the *meta*:*para* signals, which is typical of the C_6H_5CO grouping. As will become apparent in the next section, the small uv change of Fig. 1 is also consistent with the formation of a small amount of the butyrophenone derivative. The nmr integration shows that at equilibrium the ketone is formed to the extent of about ten percent. A more accurate figure will be derived through the kinetic analysis.

Nature of the base species

There are two candidates for the product that is formed in base, the pseudobase IOH of the iminium ion or the neutral

$$[6] \quad Ar\text{-}\underset{HO\ CH_3}{N} \rightleftharpoons ArC(=O)CH_2CH_2CH_2NHCH_3$$

IOH S

amino ketone S. The uv spectrum of the latter should resemble that of acetophenone or butyrophenone, while the spectrum for the former should be like that of benzene or toluene, being much weaker in intensity (10). In fact, the spectrum is virtually identical to that of a benzoyl ketone. It is, of course, impossible to exclude the presence of a small amount of IOH, but there is likely less than 10% of this.

With the structural assignments, predominantly I^+ in acid and predominantly S in base, the K(app) approximately represents the equilibrium $I^+ \rightleftarrows S + H^+$. With p$K$(app) around 12 and [IOH]/[S] less than 0.1, pK_R for the equilibrium $I^+ \rightleftarrows IOH + H^+$ must be 13 or greater. Perhaps the closest analog of I^+ that has been studied in this regard is the 2-methyl-3,4-dihydroisoquinolinium cation, which has a pK_R value of 11.0

[7] 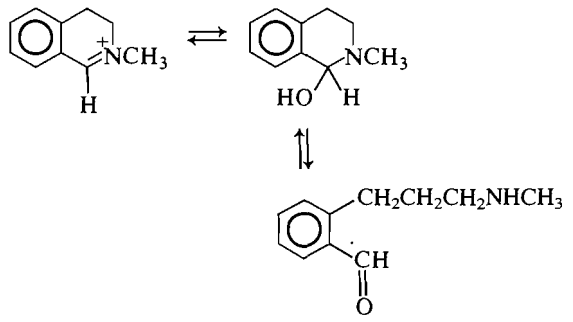

(11). This cyclic cation has a phenyl ring at the position of OH attachment. Its major difference is the presence of a hydrogen at that carbon, while I^+ has the methylene unit that is part of the ring. The effect of substituting hydrogen for alkyl cannot be determined with certainty, but it is likely to be such that a 2-log unit increase in pK_R is not improbable. The hydration of ketones and aldehydes, for example, shows large effects of substituting hydrogen for methyl (12). An example in a heterocyclic context is that shown in eq. [8] where the addition equilibrium is 350 times less favourable for R = CH_3 than for R = H (13).

[8] 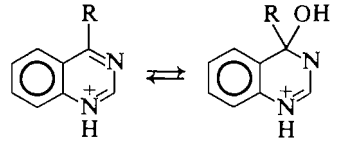

Interestingly, with the cation in eq. [7], the base equilibrium apparently favours the pseudobase form. This is likely a reflection of the generally more favourable additions to aldehydes, although ring size may also be important.

Kinetic analysis

[9] 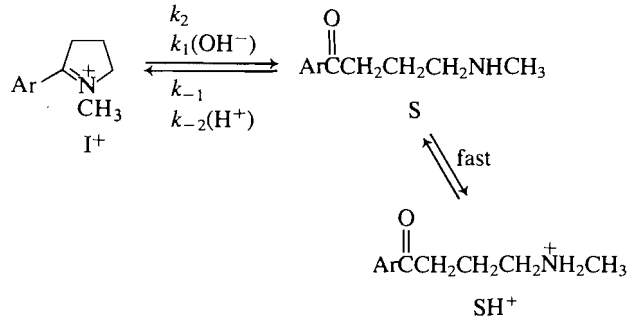

A scheme that satisfies the observed kinetics, as well as the previous discussion, is presented in eq. [9]. Three species are involved, I^+, S, and SH^+, with the simple protonation equilibrium involving the last two being very fast. The pseudobase IOH must also be involved but, since it is not present in significant amounts, it can be taken as a steady-state intermediate. There is a question as to whether the $I^+ \rightleftarrows$ IOH stage or the IOH $\rightleftarrows$ S stage is rate limiting, but for the analysis this does not need to be known, the kinetics being satisfied by eq. [9]. The following definitions are made:

$$[10] \quad K_{I^+} = \frac{[S][H^+]}{[I^+]} = \frac{k_1 K_w}{k_{-1}} = \frac{k_2}{k_{-2}}$$

$$[11] \quad K_{SH^+} = \frac{[S][H^+]}{[SH^+]}$$

$$[12] \quad K_+ = \frac{[SH^+]}{[I^+]} = \frac{K_{I^+}}{K_{SH^+}}$$

$$[13] \quad K(\text{app}) = \frac{[S][H^+]}{([I^+] + [SH^+])} = \frac{K_{I^+} K_{SH^+}}{K_{I^+} + K_{SH^+}}$$

The last quantity defines the spectroscopic acidity constant based upon this scheme.

Ignoring the k_2, k_3 terms and their reverse, and recognizing that the kinetics refer to an approach to equilibrium, the following expression is obtained:

$$[14] \quad k_{obsd} = \frac{k_1 \dfrac{K_w}{K(\text{app})}[OH^-] + k_1[OH^-]^2}{\dfrac{K_w}{K_{SH^+}} + [OH^-]}$$

(The derivation makes use of the relationship between k_1 and k_{-1} noted in eq. [10].) Equation [14] has the same form as the empirical eq. [4], and we can set $A = k_1 K_w/K(\text{app})$, $B = k_1$, and $C = K_w/K_{SH^+}$. The observed values of A, B, C then provide the three constants k_1, K(app), and K_{SH^+}, and these in turn provide other constants, all of which are listed in Table 2. The identity, within experimental error, of the K(app) values derived kinetically and spectroscopically points to the consistency in the analysis. The ammonium pK_{SH^+} values lie within the range expected, and show little effect associated with the remote aromatic substituent. As expected, pK_{I^+} values indicate stabilization of the iminium ion form by electron-donating substituents. This is also true for the K_+ values. These are all small, consistent with the nmr analysis, but they do show increasing amounts of the protonated ketone form with electron-withdrawing substituents in the aromatic ring.

In terms of the rate–pH profile of Fig. 4, the region at very high pH has k_{obsd} approaching $k_1[OH^-]$. This represents conversion of the iminium ion to the amino ketone S. The other region of linearity in hydroxide ion (pH 7–10) has

$$[15] \quad k_{obsd}(\text{pH } 7\text{–}10) = \frac{k_1 K_{SH^+}}{K(\text{app})}[OH^-] = \left(k_1 + k_{-1}\frac{K_{SH^+}}{K_w}\right)[OH^-]$$

Here k_{obsd} refers to the kinetics of approach to equilibrium of the two ions I^+ and SH^+. The last part of eq. [15] is written in terms of forward and reverse rate constants. Since $[I^+] > [SH^+]$ at equilibrium, it is the rate constant for the reverse process $SH^+ \rightarrow I^+$, $k_{-1}K_{SH^+}[OH^-]/K_w$, which makes the greater contribution to k_{obsd}. The hydroxide ion dependency arises because of the requirement for SH^+ deprotonation.

Can. J. Chem. Downloaded from www.nrcresearchpress.com by 118.98.75.50 on 09/07/12
For personal use only.

TABLE 2. Rate and equilibrium constants for the transformations of 2-aryl-1-methyl-1-pyrrolinium ions (25°C, ionic strength = 0.1)

	4-$MeOC_6H_4$	4-MeC_6H_4	C_6H_5	4-ClC_6H_4	3-ClC_6H_4
k_1, M^{-1} s^{-1} [a]	1.6×10^2	2.9×10^2	5.0×10^2	8.0×10^2	1.4×10^3
k_{-1}, s^{-1} [b]	1.8	2.8	4.2	4.4	5.1
pK_{SH^+} [c]	10.53	10.51	10.57	10.58	10.48
pK(app), kinet [d]	11.78	11.71	11.66	11.50	11.32
pK(app), spect [e]	11.89	11.86	11.67	11.53	11.39
pK_{I^+} [f]	11.76	11.68	11.62	11.44	11.26
K_+ [g]	0.059	0.067	0.089	0.137	0.165

[a] B from Table 1.
[b] k_1K_w/K_{I^+}.
[c] K_w/C.
[d] BK_wA.
[e] Taken directly from Table 1.
[f] $K_{SH^+}K(app)/(K_{SH^+} - K(app))$.
[g] K_{I^+}/K_{SH^+}.

The plateau region in acid also represents I^+–SH^+ equilibration, occurring by the k_2/k_{-2} process in eq. [9], so that

$$[16] \quad k_{obsd}(pH < 5) = \frac{k_2K_{SH^+}}{K(app)} = k_2 + k_{-2}K_{SH^+}$$

Now the need for SH^+ deprotonation in the reverse direction is exactly balanced by the H^+ catalysis of the S → I^+ reaction.

Mechanism

Mechanisms of the reversible formation of imines and iminium ions from amines and carbonyl compounds are well established (14). A carbinolamine (the pseudobase of this study) is an intermediate and, for the reaction written in the hydrolysis

[17]

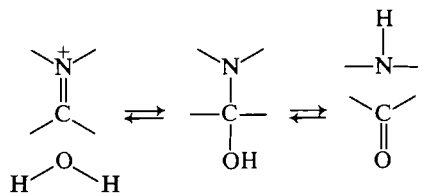

direction, breakdown of the intermediate to products is usually found to be rate limiting in acid solution, with formation of the intermediate rate limiting in neutral and basic solutions. The change in rate-limiting step is explained in terms of H^+ catalysis of the reverse of the formation, while the breakdown to products requires no catalysis.

The change in rate-limiting step is characterized experimentally by the appearance of a downward break in the rate–pH profile at some pH (14). For the I^+ system the absence of such a break, other than that associated with amine protonation, implies that there is no change in rate-limiting step. This makes the actual mechanistic assignment somewhat uncertain. Equation [18] is written with the iminium ion – pseudobase interconversion rate limiting throughout.

[18]

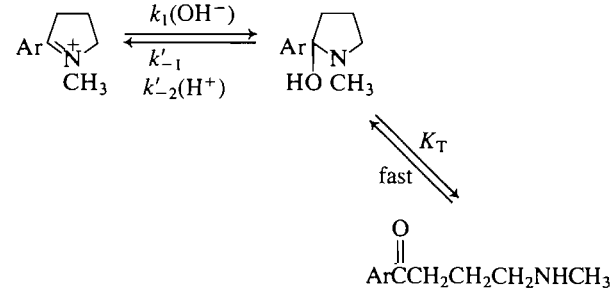

This reaction occurs in the forward direction with addition of hydroxide ion and addition of water coupled with H^+ loss. The microscopic reverse of the latter process has H^+ assisting OH departure from the pseudobase. This mechanism corresponds to the more general eq. [9], with k_1 and k_2 having the same meaning, and $k_{-1} = k'_{-1}/K_T$ and $k_{-2} = k'_{-2}/K_T$.

The alternative mechanism where pseudobase–aminoketone equilibration is rate limiting is written as

[19]

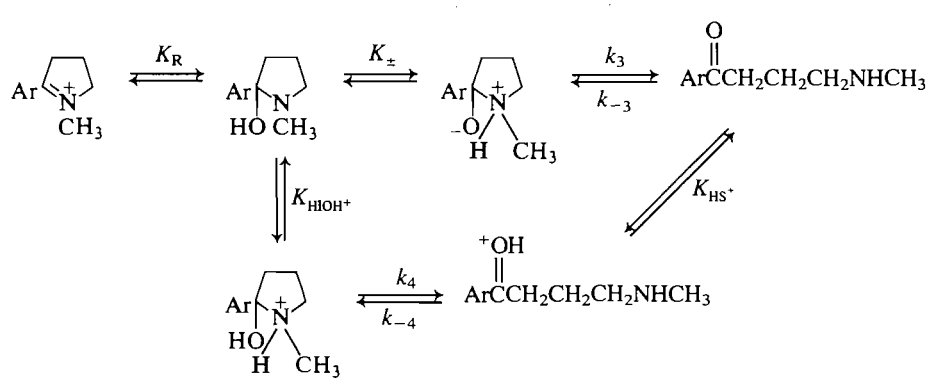

Can. J. Chem. Downloaded from www.nrcresearchpress.com by 118.98.75.50 on 09/07/12
For personal use only.

Here the reaction in neutral and base solution is that proceeding by way of the zwitterion with k_1 of eq. [9] = $k_3K_{\pm}K_R/K_w$ and $k_{-1} = k_3$. The acid reaction involves the N-protonated pseudobase and O-protonated amino ketone, with $k_2 = k_4K_R/K_{HIOH^+}$ and $k_{-2} = k_{-4}/K_{HS^+}$.

The mechanisms of eqs. [18] and [19] are kinetically equivalent, and both satisfy the observed kinetics. Precedence would suggest eq. [17] to better represent the correct mechanism, since the addition stage is normally rate limiting in base. However, hydrolysis of the 1,3-diphenyl-2-imidazolinium ion, a cyclic ion not unlike I^+, has the breakdown stage rate limiting (15), so that it may be dangerous to generalize with a cyclic system.

[20] 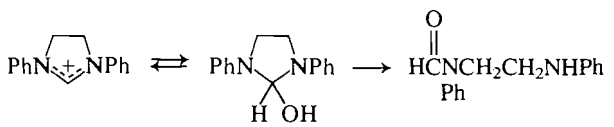

The experimental k_{obsd} in acid requires for the mechanism of eq. [18] a k_2' value greater than $10^8 M^{-1} s^{-1}$, since $K_T < 0.1$. For the mechanism of eq. [19], k_{-4} is required to be of the order of $10^{11} s^{-1}$, since pK_{HS^+} for protonated acetophenones is of the order of -4 (16).

Summary

Despite the mechanistic ambiguity, the basic features of the aqueous chemistry of I^+ are clear. In solutions with pH < 10, equilibration occurs to produce a small amount (6–14% depending upon substituent) of the ring-opened protonated amino ketone. The equilibration is quite slow in acids (pH < 5), where it occurs by a pH independent reaction, but it rapidly accelerates above pH 6 due to a process with a hydroxide ion dependency. In strongly basic solutions, a neutral species is produced very rapidly in a pH dependent equilibrium with apparent pK values ranging from 11.3 to 11.9. Spectral comparisons suggest that the neutral form is amino ketone, with the pseudobase of I^+ being present to, at best, only a very small amount.

Acknowledgement

Continued financial support of the Natural Sciences and Engineering Research Council of Canada is gratefully acknowledged.

1. J. W. BUNTING. Adv. Heterocycl. Chem. **25**, 1 (1979).
2. R. A. MCCLELLAND and L. J. SANTRY. Acc. Chem. Res. **16**, 394 (1983).
3. O. S. TEE, M. TRANI, R. A. MCCLELLAND, and N. E. SEAMAN. J. Am. Chem. Soc. **104**, 7219 (1982).
4. S. S. HECHT, C. B. CHEN, and D. HOFFMANN. Acc. Chem. Res. **12**, 92 (1979).
5. S. S. HECHT, C. B. CHEN, R. M. ORNAF, E. JACOBS, J. D. ADAMS, and D. HOFFMANN. J. Org. Chem. **43**, 72 (1978).
6. L. C. CRAIG, H. BULBROOK, and R. M. HIXON. J. Am. Chem. Soc. **53**, 1831 (1931).
7. A. E. KEMPPAINEN, M. J. THOMAS, and P. J. WAGNER. J. Org. Chem. **41**, 1294 (1976).
8. P. S. MARIANO, J. STAVINOHA, and E. BAY. Tetrahedron, **37**, 3385 (1981).
9. H. S. HARNED and B. B.OWEN. The physical chemistry of electrolytic solutions. 3rd ed. Reinhold, New York. 1958.
10. J. HARRON, R. A. MCCLELLAND, C. THANKACHAN, and T. T. TIDWELL. J. Org. Chem. **46**, 903 (1981).
11. J. W. BUNTING, V. S. F. CHEW, and G. CHU. J. Org. Chem. **47**, 2308 (1982).
12. R. P. BELL. Adv. Phys. Org. Chem. **4**, 1 (1966).
13. J. W. BUNTING and D. D. PERRIN. J. Chem. Soc. (B), 436 (1966).
14. T. H. LOWRY and K. S. RICHARDSON. Mechanism and theory in organic chemistry. 2nd ed. Harper and Row, New York. 1981. pp. 635–641, and references therein.
15. D. R. ROBINSON. Tetrahedron Lett. 5007 (1968); J. Am. Chem. Soc. **92**, 3138 (1970).
16. A. LEVI, G. MODENA, and G. SCORRANO. J. Am. Chem. Soc. **96**, 6585 (1974).

Can. J. Chem. Downloaded from www.nrcresearchpress.com by 118.98.75.50 on 09/07/12
For personal use only.

Keto ethers. IV.[1] Products formed on reaction of dihydro-2,2,5,5-tetramethyl-3(2*H*)-furanone with strong acids

PETER YATES AND PATRICK MICHAEL BURKE[2]

Lash Miller Chemical Laboratories, University of Toronto, Toronto, Ont., Canada M5S 1A1

Received August 20, 1986

This paper is dedicated to Professor John T. Edward

PETER YATES and PATRICK MICHAEL BURKE. Can. J. Chem. **65**, 1695 (1987).

Reaction of tetrahydro-2,2,5,5-tetramethyl-3(2*H*)-furanone (**1**) with 96 or ca. 100% sulfuric acid or hot polyphosphoric acid followed by aqueous quenching gave the following products: 2-hydroxy-2,5-dimethyl-4-hexen-3-one (**3**), 2,4,4-trimethyl-2-cyclopenten-1-one (**7**), 3,5,5-trimethyl-2-cyclopenten-1-one (**8**), tetrahydro-3,4,5,5-tetramethylfuran-2,3-diol (**11**), 2,5-dihydro-3,5,5-trimethyl-2-methylenefuran (**17**) and its dimer **20**, 2,5-dihydro-2,3,5,5-tetramethyl-2-furanol (**18**), 4-hydroxy-2,4-dimethyl-2-pentenoic acid γ-lactone (**22**), 2,3,5-trimethyl-2-cyclopenten-1-one (**23**), and tetramethylfuran (**25**). In 96% sulfuric acid the products arise by ring opening, ring opening followed by reclosure to carbocyclic products, methyl migration from C-2 to C-3 to give rearranged furan derivatives, and oxidation. In ca. 100% sulfuric acid or hot polyphosphoric acid further methyl migrations can occur to give **23** and **25**.

PETER YATES et PATRICK MICHAEL BURKE. Can. J. Chem. **65**, 1695 (1987).

La réaction de la tétrahydro tétraméthyl-2,2,5,5 2*H*-furannone-3 (**1**) avec de l'acide sufurique à 96 ou à environ 100% ou avec de l'acide polyphosphorique à chaud, suivie par un piégeage avec de l'eau, conduit aux produits suivants : l'hydroxy-2 diméthyl-2,5 hexène-4 one-3 (**3**), la triméthyl-2,4,4 cyclopentène-2 one-1 (**7**), la triméthyl-3,5,5 cyclopentène-2 one-1 (**8**), le tétrahydro tétraméthyl-3,4,5,5 furannediol-2,3 (**11**), le dihydro-2,5 triméthyl-3,5,5 méthylène-2 furanne (**17**) et son dimère **20**, le dihydro-2,5 tétraméthyl-2,3,5,5 furannol-2 (**18**), la γ-lactone de l'acide hydroxy-4 diméthyl-2,4 pentène-2 oïque (**22**), la triméthyl-2,3,5 cyclopentène-2 one-1 (**23**) et le tétraméthylfuranne (**25**). Dans l'acide sulfurique à 96%, les produits proviennent d'ouvertures de cycle, d'ouvertures de cycle suivies d'une recyclisation conduisant à des produits carbocycliques, de transpositions de groupements méthyles de la position C-2 à la position C-3 conduisant à des dérivés furanniques transposés et d'oxydations. Dans l'acide sulfurique à environ 100% ou dans l'acide polyphosphorique à chaud, il se produit d'autres migrations de groupements méthyles qui conduisent aux composés **23** et **25**.

[Traduit par la revue]

There have been many investigations of the reactions of organic compounds with strong acids (3, 4). Several of these have concerned substrates with saturated or unsaturated carbonyl functions. Less attention has been paid to carbonyl compounds containing other functional groups. We report on an investigation of the variety of reactions undergone by the keto ether **1** in strongly acidic media.[3] We describe here the isolation and determination of the structures of the products formed in such reactions and plan, in a subsequent publication, to discuss the formation of these products in terms of the site(s) of protonation of **1** and the nature of the cationic intermediates.

Compound **1** is readily available from the ynediol **2** (6). Reactions in strongly acidic media followed by aqueous quenching gave mixtures of products whose composition was dependent on both the nature of the medium and the time of reaction. These products were isolated by standard procedures and identified by their spectra (Tables 1 and 2) and by comparison in most cases with independently synthesized samples.

Vapor phase chromatographic (vpc) analyses of product mixtures from 96% sulfuric acid showed that one compound was formed rapidly and that the amount of this product reached a maximum after 2 h and then fell to zero after several days. This compound was shown to be **3** by comparison with an authentic sample prepared as in Scheme 1 (2, 7). It has been reported that **3** fails to form a 2,4-dinitrophenylhydrazone (7); our attempts to form such a derivative in ethanol gave the 2,4-dinitrophenylhydrazone of the *O*-ethyl analogue of **3**.

A second product that was detected by vpc analysis increased in amount gradually to a maximum of about 5% after 6 h and then remained essentially constant in amount. This compound was shown to be **7** by comparison with an authentic sample (Scheme 1). Treatment of **2** with hot 50% sulfuric acid gave the dienyne **4** (8) in 45–50% yield, accompanied by a complex mixture of other products, three of which were identified as **1**, **3**, and **5**; the structural assignment **5** is based on spectroscopic data (see Experimental). Cuprous ion-catalyzed addition of hydrogen chloride to **4** gave a product whose ^{1}H nmr spectrum

TABLE 1. The ir and uv spectra of the products from the reactions of compound **1** with sulfuric acid and of related compounds

Compound[a]	λ_{max}, μm[b]	λ_{max} (ε), nm[c]
3	5.87, 5.96 (s), 6.19	240 (12 600)
7	5.85 (s), 6.10	229 (12 000)
8	5.85 (s), 6.15	229 (12 600)
9	5.84 (s), 5.90 (sh), 6.15	229 (12 000)
11	2.75, 2.78, 2.85–2.95	—
17	6.04, 6.12	254 (7000)
18	2.75, 2.85, 2.95, 6.05	End absorption
20	6.04, 6.09	261 (7200)
23	5.87 (s), 6.04	236 (13 200)
25	6.05, 6.25	222 (7000)

[a]For structures, see Table 2.
[b]In CCl_4; s = strong, sh = shoulder.
[c]In 95% EtOH; only π–π* bands recorded.

[1]This series of papers was originally designated as α-Keto Ethers (1); to avoid ambiguity we now use the term Keto Ethers. Reference 2 is considered to be paper III in this series.

[2]Present address: E. I. du Pont de Nemours and Co., Petrochemicals Department, Wilmington, DE 19898, U.S.A.

[3]Part of this work was carried out some years ago (5); where other workers have in the meantime reported related results we give only a cursory account of our own observations.

Can. J. Chem. Downloaded from www.nrcresearchpress.com by 118.98.75.50 on 09/07/12
For personal use only.

TABLE 2. The ^{1}H and ^{13}C nmr spectra of the products from the reactions of compound **1** with sulfuric acid and of related compounds

Compound	$^{H}\delta$[a]		$^{C}\delta$[b]		
1	1.18	CH_3-2	26.1	CH_3-2	76.1 C-5
	1.32	CH_3-5	32.1	CH_3-5	80.8 C-2
	2.40	H-4	46.4	C-4	218.8 C-3
3	1.27	CH_3-2	21.3	CH_3-5$_Z$	117.7 C-4
	1.96 (d, *J* 1.5)	CH_3-5$_Z$	26.7	CH_3-2	160.1 C-5
	2.18 (d, *J* 1.5)	CH_3-5$_E$	28.2	CH_3-5$_E$	203.3 C-3
	3.75 (br s)	OH	75.3	C-2	
	6.20 (m)				
7	1.18	CH_3-4	9.8	CH_3-2	138.7 C-2
	1.68 (d, *J* 1.5)	CH_3-2	28.3	CH_3-4	167.5 C-3
	2.13	H-5	38.6	C-4	209.6 C-1
	6.92 (q, *J* 1.5)	H-3	50.2	C-5	
8	1.05	CH_3-5			
	2.09 (d, *J* 1)	CH_3-3			
	2.48 (br s)	H-4			
	5.78 (m)	H-2			
9	1.22	CH_3-4			
	2.01 (d, *J* 1.5)	CH_3-3			
	2.17	H-5			
	5.68 (q, *J* 1.5)	H-2			
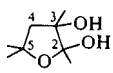 **11**	1.20 } 1.25 } 1.29 }	CH_3-3 CH_3-5			
	1.34	CH_3-2			
	1.95 (AB, *J* 12)	H-4			
	2.70 (br s)	OH			
17	1.29	CH_3-5	11.2	CH_3-3	131.8 C-3
	1.76 (d, *J* 2)	CH_3-3	26.8	CH_3-5	138.1 C-4
	3.67 } 3.99 }	H-1	76.2	C-1	166.3 C-2
			88.1	C-5	
	5.80 (q, *J* 2)	H-4			
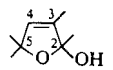 **18**	1.20 } 1.30 }	CH_3-5			
	1.40	CH_3-2			
	1.71 (d, *J* 2)	CH_3-3			
	3.00	OH			
	5.42 (q, *J* 2)	H-4			
20[c]	1.20 } 1.28 }	{ CH_3-5′ CH_3-5	11.3 } 12.2 }	{ CH_3-3 CH_3-3′	84.6 } 88.3 } { C-5 C-2′
	1.45	CH_3-2′	26.8 }	CH_3-5	89.0 } C-5′
	1.64 (d, *J* 2) }	{ CH_3-3′	26.9 }		98.9 C-1
	1.71 (d, *J* 2) }	{ CH_3-3	27.6 }	CH_3-2′	127.7 C-4′
	4.15	H-1	29.2 }	CH_3-5′	132.3 C-3
	5.13 (q, *J* 2)	H-4′	30.0 }		136.1 C-4
	5.72 (q, *J* 2)	H-4			141.1 C-3′
					158.4 C-2

Can. J. Chem. Downloaded from www.nrcresearchpress.com by 118.98.75.50 on 09/07/12
For personal use only.

TABLE 2. (*concluded*)

Compound	$^{H}\delta$[a]		$^{C}\delta$[b]			
21[c]	1.18 1.24 1.27 1.57 (br s) 1.60 (d, *J* 2) 2.20 2.30 5.17 (q, *J* 2)	CH_3-5 CH_3-2′ CH_3-5′ CH_3-3 CH_3-3′ H-1 H-4 H-4′				
23	1.08 (d, *J* 7) 1.61 2.01 2.0–3.0 (m)	CH_3-5 CH_3-2 CH_3-3 H-4 H-5	8.0 16.6 17.0 39.6	CH_3-2 CH_3-3 CH_3-5 CH-5	40.8 135.0 137.9 212.0	C-4 C-2 C-3 C-1
25	1.75 2.08	CH_3-3,4 CH_3-2,5				

[a] In CCl_4; signals are singlets unless otherwise specified, and have relative intensities in accord with assignments; *J* values are in hertz.
[b] In $CDCl_3$; multiplicities in SFORD spectra are in accord with assignments.
[c] For numbering see structure below:

20 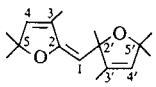 **21** 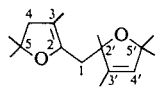

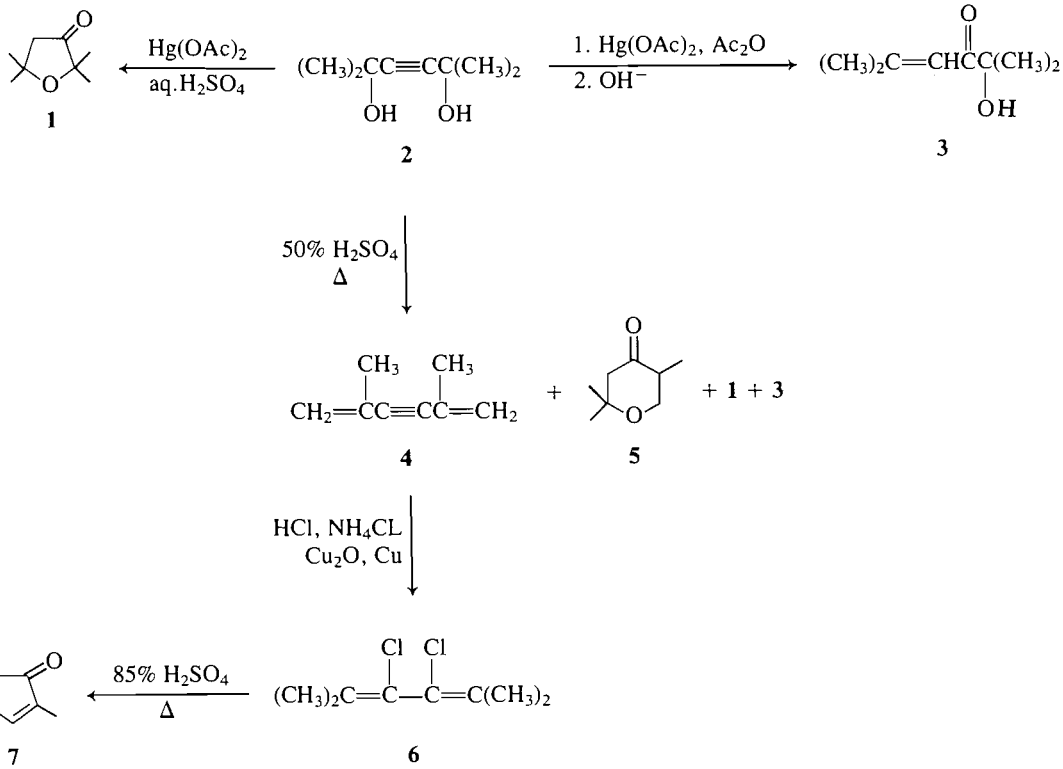

1 **2** **3** **4** **5** **6** **7**

SCHEME 1

Can. J. Chem. Downloaded from www.nrcresearchpress.com by 118.98.75.50 on 09/07/12
For personal use only.

showed it to be 3,4-dichloro-2,5-dimethyl-2,4-hexadiene (**6**) and not the corresponding 1,3-dichloro compound as earlier considered (8).[4] Treatment of **6** with hot 85% sulfuric acid gave **7**.

A second cyclopentenone was detected among the reaction products from treatment of **1** with 96% sulfuric acid; it was present in only trace amounts, but was formed in greater, albeit still small, amounts from **1** on treatment with ca. 100% sulfuric acid (*vide infra*). This product was shown to be 3,5,5-trimethyl-2-cyclopenten-1-one (**8**) by comparison with an authentic sample (10), obtained as a 2:3 mixture with 3,4,4-trimethyl-2-cyclopenten-1-one (**9**). The individual structural assignments

8 **9**

are based on an alternative, unambiguous synthesis of **9** (11) and are confirmed by comparison of the ^{1}H nmr spectra of these compounds and **7** (Table 2).

Work-up of the reaction mixture of **1** and 96% sulfuric acid after short reaction times gave, in addition to compounds **3**, **7**, and **8**, a crystalline, highly water-soluble compound, $C_8H_{16}O_3$, which could only be isolated by continuous extraction. The yield of this product increased in the first two hours and decreased to zero after 12 days. It is assigned the gross structure **11** on the following basis. Its ir spectrum shows the presence of one or more hydroxyl groups and the absence of a carbonyl group. Oxidation with lead tetraacetate followed by basic hydrolysis gave diacetone alcohol (**14**) (Scheme 2). It was independently synthesized by treatment of the hydroxy lactone **10** (12) with methylmagnesium iodide. This reaction also gave **12**, identified by comparison with an authentic sample prepared by treatment of **1** with methylmagnesium iodide (13), and a high-melting crystalline product **13**. The structure of the latter was not established, but it may be related to 2,3,5-trimethyl-2,3,5-hexanetriol since it gave **12** on treatment with 50% sulfuric acid. While **11** was obtained as a crystalline solid with a 2° melting range, its ^{1}H and ^{13}C nmr spectra exhibit a complex series of peaks in the methyl proton region, indicating that in solution it exists as a mixture of diastereomers (the ^{1}H nmr data given in Table 2 are the signals assigned to the major tautomer). These diastereomers should be readily interconvertible via ring–chain tautomerization, although none of the ketonic tautomer could be observed spectroscopically.

Two interesting reactions of the diol **11** were observed. When injected onto a vpc column (see Experimental) at 140°C it underwent pinacol rearrangement to give **1**; this reaction appears to be catalyzed by acid sites on the column, since no reaction was observed on heating **11** alone at 150°C. When a solution of **11** in benzene was boiled in the presence of a catalytic amount of *p*-toluenesulfonic acid, bimolecular dehydration occurred to give a high-melting crystalline product lacking hydroxyl or carbonyl groups. This is assigned the gross structure **15**, the head-to-tail isomer being preferred on mechanistic grounds and because both **15** and **11** dissolve in 96% sulfuric acid to give rapidly and quantitatively the same cationic species, as shown by ^{1}H nmr spectroscopy.

After long reaction times (5–12 days) the ^{1}H nmr spectrum of the reaction mixture of **1** and 96% sulfuric acid indicated that only one major cationic species was present. However, the usual work-up conditions (quenching in water) gave rise to a complex mixture of "infinity" products. It soon became evident that this was because the product initially formed on quenching was extremely sensitive both to acids and to atmospheric oxygen. When the reaction mixture was quenched in aqueous base and precautions were taken during work-up to avoid contact of the product with adventitious acid and to minimize contact with air, a volatile product was obtained. This was shown to be **17** by comparison with an authentic sample prepared by treatment of the enynol **16** (14, 15) with aqueous mercuric acetate (Scheme 3).[5]

When the base-quenched reaction mixture of **1** and 96% sulfuric acid was worked up without precautions to avoid contact with adventitious acid the major product isolated was not **17**, but a compound that decomposed to give **17**. This compound is assigned structure **18** on the basis of its conversion on standing to **17** and the fact that the latter in the presence of water is converted to the former. On longer standing both **17** and **18** formed the same bimolecular product, **17** via dimerization and **18** via dehydration and dimerization. This product was also isolated from the mixture of infinity products from **1** and 96% sulfuric acid on quenching with water (*vide supra*). It is assigned structure **20** on spectroscopic grounds and because of its conversion on hydrogenation to a dihydro derivative considered to be **21** (Scheme 3). The ir spectrum of **20** shows ethylenic stretching bands analogous to those of **17** and its uv spectrum shows a maximum at 261 nm (ε 7100) with a small bathochromic shift as expected in relation to the maximum of **17** at 254 nm. Its ^{1}H nmr spectrum shows the presence of five CH_3—C(sp^3) and two CH_3—C(sp^2) groups, the latter each being allylically coupled to a vinyl proton; in addition, a one-proton singlet at δ 4.15 ppm is attributable to the HC=C—O proton of **20**, analogous to the H_2C=C—O proton signals of **17** at δ 3.67 and 3.99 ppm. The relationship of the ^{13}C spectra of **20** and **17** (Table 2) confirms the structural assignment.

The hydrogenation of **20** is considered to occur in 1,4 fashion giving **21**, whose ^{1}H nmr spectrum shows the presence of five CH_3—C(sp^3) groups, two CH_3—C(sp^2) groups, and a single vinyl proton, coupled to one of the latter CH_3 groups. It is considered that the conversion of **17** and **18** to **20** is effected by traces of adventitious acids, involving reversible protonation of **17** to give the cation **19** and attack of this on **17** followed by loss of a proton. The ease of conversion of **17** to **20** is shown by the fact that treatment of **16** with mercuric acetate in 2% sulfuric acid gives **20** rather than **17** (Scheme 3).

It was noted above that the nature of the product mixture from **1** and 96% sulfuric acid is affected by the presence of atmospheric oxygen. This led to the formation of an additional product, whose relative amount was increased when the reaction mixture was exposed to air *after* quenching and work-up. This product was identified as the lactone **22** by comparison with an authentic sample obtained by dehydration of **10** (Scheme 2) (12). It is clear that this product arises by autoxidation of either **17** or its cationic precursor.

When **1** was treated with 99.5–100.3% sulfuric acid, the

[4]Loewenthal (9) has reached the same conclusion regarding the structure of this intermediate.

[5]This synthesis is based on that of 2,5-dialkylfurans (16). Arens and Brandesma and co-workers have prepared **17** by base-catalyzed cyclization of **16** (17) and rearrangement of 4,5-epoxy-3,5-dimethyl-1-hexyne (18).

Can. J. Chem. Downloaded from www.nrcresearchpress.com by 118.98.75.50 on 09/07/12
For personal use only.

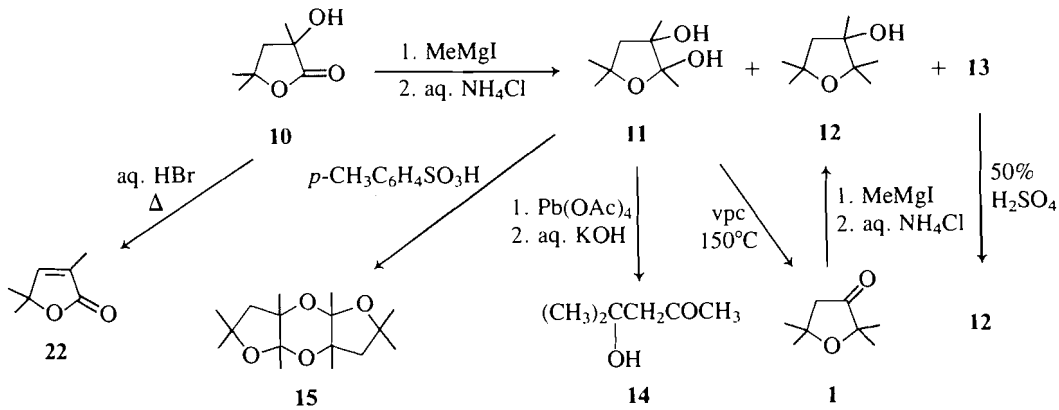

SCHEME 2

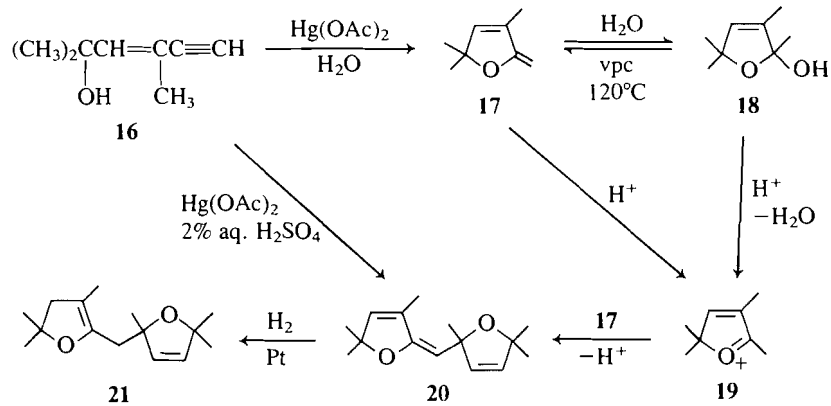

SCHEME 3

product distribution after quenching was markedly different from that observed on treatment with 96% sulfuric acid. The amount of the diene **17** was greatly reduced and the product mixture consisted largely of the cyclopentenones **7** and **8**, together with a new product, which in the case of 100.3% sulfuric acid was the preponderant product. This was isomeric with **7** and **8** and was identified as the cyclopentenone **23** on the following basis. Its spectra indicated that it is either 2,3,5-trimethyl-2-cyclopenten-1-one (**23**) or 2,3,4-trimethyl-2-cyclopenten-1-one. The latter compound has been prepared previously (19) and the melting point of its semicarbazone does not correspond with that of the semicarbazone prepared from the product obtained in the present work. Furthermore, ozonolysis of this product followed by oxidative work-up gave a mixture of α-methyllevulinic acid (**24**) (20) and its tautomeric lactol. Thus the product from **1** and 99.5–100.3% sulfuric acid has structure **23**.[6]

When **1** was heated with polyphosphoric acid for 2 h at 100°C the diene **17** and the cyclopentenone **7** were observed after quenching, together with a major additional product. When the reaction mixture was heated for 6 h at 120°C, this new product was formed almost exclusively. It was identified as tetramethylfuran (**25**) by comparison of it and its *exo* adduct with maleic anhydride with authentic samples (22, 23).

In summary, **1** on treatment with 96% sulfuric acid followed by quenching gives the products shown in Scheme 4. The hydroxy enone **3** and the diol **11** are isolated only after relatively short reaction times, while the diene **17** is the major product after long reaction times. The cyclopentenones **7** and **8** are formed in relatively small amounts but persist after long reaction times. Autoxidation gives the lactone **22**. Reaction of **1** with 99.5–100.3% sulfuric acid followed by quenching gives increased amounts of the cyclopentenones **7** and **8** together with the diene **17** and the cyclopentenone **23**. In hot polyphosphoric acid **1** gives, after quenching, tetramethylfuran (**25**) together

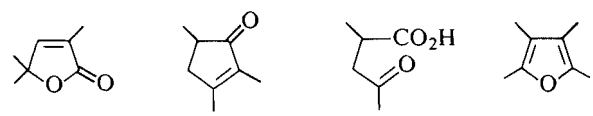

22 **23** **24** **25**

with cyclopentenone products. Thus in 96% sulfuric acid the products arise by (*i*) ring opening,[7] (*ii*) ring opening followed by reclosure to carbocyclic products, (*iii*) methyl migration to give rearranged furan derivatives, and (*iv*) autoxidation. In 99.5–100.35% sulfuric acid or hot polyphosphoric acid solutions further methyl migrations can occur to give **23** and **25**.

Experimental

Melting points were determined on a Fisher–Jones micro hot stage and are uncorrected. Infrared spectra were recorded in CCl_4, unless otherwise indicated; ultraviolet spectra were recorded in 95% EtOH.

[6]The fact that the ir carbonyl stretching band of **9** has a shoulder while those of **7**, **8**, and **23** do not is in accord with expectation, based on our studies of Fermi resonance in the spectra of 2-cyclopenten-1-ones (21).

[7]We have shown that cleavage of **1** to **3** is reversible (2).

Can. J. Chem. Downloaded from www.nrcresearchpress.com by 118.98.75.50 on 09/07/12
For personal use only.

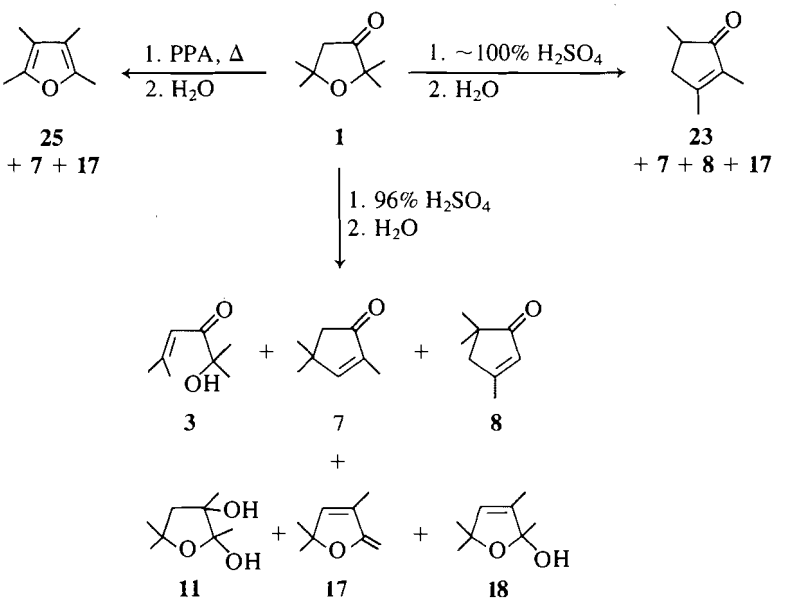

25 + **7** + **17** — **1** — **23** + **7** + **8** + **17**

3 + **7** + **8** + **11** + **17** + **18**

SCHEME 4

The ^1H and ^{13}C nmr spectra were recorded in CCl_4 and $CDCl_3$, respectively.

Vapor phase chromatographic (vpc) analyses were carried out on an F and M Model 500 gas chromatograph. Helium was used as carrier gas and the flow rate was adjusted to 35–45 mL/min. The columns used were commercially available (F and M Scientific Corporation) and consisted of coiled stainless steel tubes with 0.25-in. od containing one of the following packings (10% substrate in each case): diisodecyl phthalate (DIDP) on 60–80 mesh Chromsorb P (6 ft); neopentylglycol sebacate (NPGS) on 60–80 mesh Chromsorb P (8 ft); fluorosilicone on 60–80 mesh Diatoport S (6 ft); Carbowax 1500 on 60–80 mesh Chromsorb P (6 ft). Preparative vapor phase chromatographic separations were performed on an F and M Model 770 automatic preparative gas chromatograph with helium at a rate of 1.5–2.0 L/min as carrier gas. The column consisted of two 4-ft, 0.75-in. od stainless steel tubes connected at the bottom with a 0.25-in. jumper tube. The column packing consisted of NPGS supported on 60–80 mesh Chromsorb W (10% substrate). Dry Ice – acetone was used in the cooling bath.

The 96% H_2SO_4 used in this work was C.P. reagent grade concentrated H_2SO_4, specified to contain a minimum of 95.5% by weight H_2SO_4. The 100.3% H_2SO_4 was made by addition of 30% oleum (Fisher reagent grade fuming H_2SO_4 specified to contain 30–33% free SO_3; 80 g) to 96% H_2SO_4 (120 g). Its strength was determined by titration. The 99.5% H_2SO_4 was made in similar fashion.

Dihydro-2,2-5,5-tetramethyl-3(2H)-furanone (1)

Compound **1** was prepared from 2,5-dimethyl-3-hexyne-2,5-diol by the method of Leonard *et al.* (6). The product was distilled to give a colorless liquid, bp 54–55°C (22 Torr; 1 Torr = 133.3 Pa); n_D^{23} 1.4192 (lit. (6) bp 150–151°C; n_D^{20} 1.4211); ir, λ_{max}: 5.68, 8.67 μm; uv, λ_{max}: 295 (ε 32), 245 nm (sh, ε 88). *The 2,4-dinitrophenylhydrazone of 1* was prepared by the method of Shriner, Fuson, and Curtin (24); recrystallization from 95% EtOH gave yellow plates, mp 179.5–180.5°C (lit. (6) mp 178–179°C).

Reactions of compound 1 in 92–96% sulfuric acid

(i) Isolation of products formed after 10 min – 25 h

Solutions of **1** in 96% H_2SO_4 were allowed to stand for the following periods: 10 min, 2 h, 6 h, 12 h, 18 h, 25 h, and 12 days. The following procedure was used in carrying out the reactions and working up the reaction mixtures.

Compound **1** (2.00 g) was added dropwise with gentle swirling to 96% H_2SO_4 (20 g), which was cooled in ice-water. The reaction mixture was allowed to stand at room temperature in a stoppered flask. The initially light yellow solution slowly darkened on standing for some hours and finally became black after ca. 2 days. After being allowed to stand for a specified time, the solution was poured in a thin stream into a rapidly stirred ice–water mixture (200 g). The aqueous solution was extracted with ether (2 × 100 mL) and the extract was dried over a mixture of anhydrous $MgSO_4$ (10 g) and K_2CO_3 (2 g). Removal of the solvent gave an oil (Extract I). The remaining aqueous solution was contiguously extracted with ether for 2 days. The extract was dried over $MgSO_4$–K_2CO_3 and the solvent was evaporated. The residue (Extract II) generally crystallized on standing in petroleum ether or cyclohexane.

Extract I was analyzed by vpc on a DIDP column at 150°C. The products were isolated by allowing the effluent carrier gas stream from the exit port to pass through U-tubes cooled in Dry Ice – acetone as each peak appeared on the chromatogram.

The following results for a reaction time of 6 h exemplify those obtained with the procedure described above. Extract I consisted of a pale yellow oil (0.72 g) that slowly turned dark red on being exposed to air. Its ir spectrum showed bands at 2.75, 2.8–2.9, 5.68, 5.84, 5.95, and 6.0–6.17 μm. Vapor phase chromatography on a DIDP column at 150°C showed the presence of three components.[8] These were (with retention times given in parentheses) residual compound **1** (3.7 min), *2,4,4-trimethyl-2-cyclopenten-1-one* (**5**)[9] (6.8 min), and *2-hydroxy-2,5-dimethyl-4-hexen-3-one* (**3**)[9] (11.1 min). Quantitative comparison of the vpc peak area produced by a known volume of compound **1** with that produced by the same volume of Extract I indicated that ca. 54% of the latter was retained on the column.

Extract II consisted of a viscous yellow oil (0.66 g). Its ir spectrum showed prominent bands at 2.75, 2.8–2.9, 9.15, and 10.5–1.07 μm. On standing alone or in petroleum ether, the oil deposited long, needle-like crystals of *tetrahydro-2,3,5,5-tetramethylfuran-2,3-diol* (**11**).[9]

Analysis by vpc of Extract I from the 12-, 18-, and 25-h reactions revealed the presence of an additional product with longer retention time (13.8 min), which was found to be *4-hydroxy-2,4-dimethyl-2-pentenoic acid γ-lactone* (**22**).[9] These analyses were carried out on samples that had stood in air for several days. It was subsequently found that the relative amount of this component in the mixtures increased with time of standing. Moreover, reexamination of a sample

[8]Thin-layer chromatography on silica gel with chloroform – 10% methanol as eluent and iodine vapor as developer indicated the presence of at least four components in the mixture; it was subsequently found that trace amounts of compound **8** (*vide infra*) were present.

[9]Identified by comparison with an authentic sample (*vide infra*).

Can. J. Chem. Downloaded from www.nrcresearchpress.com by 118.98.75.50 on 09/07/12
For personal use only.

Can. J. Chem. Downloaded from www.nrcresearchpress.com by 118.98.75.50 on 09/07/12
For personal use only.

of Extract I from the 6-h reaction that had stood for 2 weeks now indicated the presence of ca. 5% of **22**.

The composition of Extract I, as indicated by the vpc and spectroscopic analyses, varied with the reaction time as follows: the amount of compound **3** increased to a maximum at 2 h and then decreased gradually to zero after 12 days; that of compound **7** increased in the first 6 h and then remained constant. The amount of product retained on the vpc column increased with time, becoming ca. 94% of Extract I after 12 days. The composition of Extract II, as indicated by spectroscopic analysis, remained essentially constant for the different reaction times. The yield of **11** increased during the first 2 h, then remained approximately constant up to a reaction time of 25 h and decreased to zero after 12 days.

Each of compounds **3**, **7**, and **11** was isolated in pure form by vpc of a sample of Extract I in which it appeared in optimum concentration. With the use of temperatures 10–20°C lower than those used for the analytical runs, it was found that sample sizes up to 100 μL could be separated on the analytical columns without serious loss of resolution.

(ii) Isolation of infinity products

(a) Work-up under acidic conditions. A solution of **1** (10.0 g) in 92% H_2SO_4[10] (100 g) was allowed to stand at room temperature for 5 days in a loosely stoppered flask. The solution was then poured in a thin stream into rapidly stirred ice-water (1 kg). A black scum that formed on the surface of the aqueous solution was filtered and the brown filtrate was extracted with ether (500 mL; 2 × 250 mL). The extract was washed with saturated aqueous $NaHCO_3$, 250 mL) and water (250 mL) and dried over $MgSO_4$. Evaporation of the solvent gave a pale yellow liquid (6.2 g); ir, λ_{max}: 5.84, 6.02–6.10, 10.5 μm. Vapor phase chromatographic analysis on an NPGS column at 120°C indicated the presence of three components with low retention times (3.2, 4.2, and 7.6 min) and one component that gave rise to a broad peak with a very long retention time (54.2 min; ca. 65% of total). Distillation of the product mixture gave a colorless liquid (1.25 g), bp 85–87°C (0.65 Torr). This slowly turned red on exposure to air. Two further distillations gave pure *compound 20*,[9] bp 73–74°C (0.35 Torr).

(b) Work-up under basic conditions. A solution of **1** (50 g) in 94% H_2SO_4[10] (1 kg) was allowed to stand at room temperature for 3 weeks. Part of this solution (200 g) was added through a capillary to the periphery of a rapidly stirred solution of NaOH (200 g) in water (1 L) cooled to ca. 5°C and surrounded by an ice bath. When the addition was complete the alkaline solution was steam distilled. The distillate (250 mL) was saturated with NaCl and extracted with ether (200 mL; 2 × 150 mL). The extract was dried over K_2CO_3 and the solvent was evaporated to give *2,5-dihydro-2,3,5,5-tetramethyl-2-furanol* (**18**) as a pale yellow, mobile liquid (6.82 g). Distillation, which was accompanied by much decomposition, gave **18** as a colorless liquid (1.6 g), bp 80–81°C (27 Torr).

When compound **18** was allowed to stand in a tightly stoppered flask for 2 weeks globules of water were formed. The ^1H nmr spectrum of the resulting organic product was identical with that of compound **20**.

In a second experiment all glassware with which the extract from the basified reaction mixture was to come into contact was soaked in aqueous 10% NaOH before use. Under these conditions the product (15.7 g) from 400 g of a similar acid reaction solution to that above showed much reduced absorption in the 2.75–2.9 μm region of its ir spectrum. Distillation gave two well-separated fractions: (*i*) bp 46–48°C (30 Torr) (5.3 g) and (*ii*) bp 103°C (2 Torr) (3.7 g). The latter was shown to be compound **20**. Fraction (*i*) was a clear, colorless liquid with a strong mint-like odor; ir, λ_{max}: 5.85, 6.05–6.10, 10.45 μm; uv (EtOH), λ_{max}: 254 nm. Analysis by vpc (NPGS, 85°C) and collection of fractions showed the presence of compound **7** and *2,5-dihydro-3,5,5-trimethyl-2-methylenefuran* (**17**),[9] the latter being the major product.

Reactions of compound 1 in 99.5–100.3% sulfuric acid

(i) 100.3% sulfuric acid

(a) Work-up under acidic conditions. Compound **1** (10.0 g) was added slowly with stirring to 100.3% H_2SO_4 (200 g) cooled to 10°C at such a rate that the temperature did not rise above 20°C. The solution rapidly developed a deep red color, which darkened slowly on standing. The reaction mixture was allowed to stand for 4 h and was then added through a capillary to rapidly stirred ice-water (2 kg). The aqueous acid solution was extracted with ether (3 × 300 mL) and the extract was washed with saturated aqueous $NaHCO_3$ (100 mL) and dried over $MgSO_4$. Removal of the solvent gave a light yellow, sweet-smelling liquid (4.1 g); ir, λ_{max}: 5.84, 6.10 μm. Analysis by vpc (NPGS, 130°C) showed the presence of three compounds (retention times and relative yields are in parentheses): compound **1** (6.0 min; 44%), *3,5,5-trimethyl-2-cyclopenten-1-one* (**8**)[9] (12.0 min; 1.7%), and *2,3,5-trimethyl-2-cyclopenten-1-one* (**23**)[9] (12.0 min; 54%). These were separated by preparative vpc (NPGS, 120°C).

(b) Work-up under basic conditions. The reaction of **1** (10.0 g) with 100.3% H_2SO_4 (200 g) was allowed to proceed as above for 5 h. The reaction mixture was then added through a capillary to aqueous 10% NaOH (2 L) and cooled to 5°C in an ice bath. Steam distillation and extraction with ether gave a yellow liquid (6.0 g); ir, λ_{max}: 5.84, 6.10 μm. Analysis by vpc (NPGS, 130°C) indicated the presence of the same three components, in the same relative yields, as above. These were separated by preparative vpc.

(ii) 99.5% H_2SO_4

The following results exemplify those obtained. Compound **1** (20.0 g) was added dropwise with swirling to 99.5% H_2SO_4 (200 g), which was cooled to 5°C in an ice bath. The deep red mixture was allowed to stand at 5°C for 24 h and then at room temperature for a further week. Work-up under basic conditions as described above gave a yellowish liquid (14.9 g); ir, λ_{max}: 2.75, 2.90, 5.84, 6.05–6.10 μm. Analysis by vpc (NPGS, 110°C) indicated the presence of four compounds: **7** (65%), **8** (1.4%), **17** (25%), and **23** (8.4%).

Reactions of compound 1 in polyphosphoric acid

A mixture of **1** (2.00 g) and polyphosphoric acid (PPA; Victor Chemical Co.; 25 g) was heated at 100°C for 7 h in a 3-necked flask fitted with a condenser, thermometer, and $CaCl_2$ drying tube. The reddish-brown reaction mixture was allowed to cool to room temperature and poured into water (100 mL), and the flask was washed out with further water (100 mL). The combined aqueous solutions were extracted with ether (2 × 200 mL) and the extract was washed with saturated aqueous $NaHCO_3$ (100 mL) and water (2 × 200 mL) and dried over Na_2SO_4. Evaporation of the ether gave a pale yellow liquid (1.45 g); ir, λ_{max}: 2.85–2.95, 5.84, 6.09 μm. Its ^1H nmr spectrum showed strong signals at δ 1.75 and 2.08. Vapor phase chromatographic analysis (NPGS, 110°C) indicated the following composition (retention times and relative yields in parentheses): compound **17** (4.5 min; 8%),[11] compound **1** (7.0 min; 5%), *tetramethylfuran* (**25**)[9] (87.7 min; 81%), compound **7** (14.3 min; 6%).

Compounds **1**, **7**, and **17** were collected from the analytical column. Compound **25** was isolated by preparative vpc (NPGS, 100°C) as a colorless liquid (0.54 g).

The yields of the three products when **1** was heated with PPA under different conditions are given in Table 3.

2-Hydroxy-2,5-dimethyl-4-hexen-3-one (3)

2-Acetoxy-2,5-dimethyl-4-hexen-3-one was prepared from 2,5-dimethyl-3-hexyne-2,5-diol (**2**) and hydrolyzed to give **3**, as previously described (2, 7).

2-Ethoxy-2,5-dimethyl-4-hexen-3-one-2,4-dinitrophenylhydrazone

To a solution of **3** (200 mg) in 95% EtOH (2 mL) was added 2,4-dinitrophenylhydrazine reagent (24) (8 mL). The mixture was allowed to stand for 24 h and filtered to give orange-yellow crystals (340 mg), mp 93–98°C. Four recrystallizations from aqueous 70% EtOH gave orange needles, mp 108–110°C; ir, λ_{max}: 3.02, 6.18 μm; uv, λ_{max}: 360 nm (ε 22 600); ^1H nmr, δ: 1.18 (t, J = 7 Hz, 3H), 1.48 (s, 6H), 1.67 (s, 3H), 2.08 (s, 3H), 3.40 (q, J = 7 Hz, 2H), 5.81 (s, 1H), 7.9–8.4 (m, 2H), 9.08 (d, J = 3 Hz, 1H), 11.20 (s, 1H). *Anal.* calcd. for $C_{16}H_{22}N_4O_5$: C 54.84, H 6.33, N 15.99; found: C 54.99, H 6.28, N 16.04.

[10]Similar results were obtained in 96% H_2SO_4.

[11]Variable amounts of **17** were retained on the vpc column.

TABLE 3. Yields of products from the reactions of compound **1** with PPA

Reaction time (h):	4	7	8.5	6
Temperature (°C):	100	100	110	120
Combined yield (%):	77	80	82	81
Relative yield (%): **7**	13	6.6	6.0	1.0
17[a]	14.5	8.4	0	0
25	72.5	85	94	99

[a]See footnote 10.

2,4,4-Trimethyl-2-cyclopenten-1-one (7)

A mixture of 2,5-dimethyl-3-hexyne-2,5-diol (**2**) (71 g; 0.50 mol) and 50% H_2SO_4 (90 g) was stirred rapidly and heated at 50°C for 2 h under nitrogen. The organic layer (53.0 g) was removed, dried, and distilled. The major fraction was *2,5-dimethyl-1,5-hexadien-3-yne* (**4**), obtained as a pale yellow liquid (27.0 g), bp 40°C (28 Torr); ir, λ_{max}: 6.20 (w), 11.20 μm; ^{1}H nmr, δ: 1.90 (t, J = 2 Hz, 6H), 5.25 (m, 4H). On standing for 2 days this product polymerized to a viscous yellow oil. Subsequent distillation fractions were shown by vpc analysis (Carbowax, 120°C) to contain five components. The major component was isolated by vpc and is considered to be *tetrahydro-2,2,5-trimethyl-4-pyrone* (**5**); ir, λ_{max}: 5.81 μm; ^{1}H nmr, δ: 0.92 (d, J = 7 Hz, 3H), 1.14 (s, 3H), 2.28 (br s, 2H), 2.50 (m, 1H), 3.2–4.2 (m, 2H). The *2,4-dinitrophenylhydrazone of 5* was prepared in the usual manner (24); after five recrystallizations from 95% EtOH it was obtained as yellow needles, mp 151.5–153°C. *Anal.* calcd. for $C_{14}H_{18}N_4O_5$: C 52.17, H 5.61, N 17.38; found: C 51.85, H 5.67, N 17.47.

Two of the other products from the higher-boiling fractions from the original reaction mixture were identified by vpc and ^{1}H nmr analysis as compounds **1** and **3**.

A mixture of **4** (19.2 g), concentrated hydrochloric acid (150 mL), cuprous oxide (0.5 g), ammonium chloride (1.0 g), and copper bronze (0.50 g) was heated at 60–65°C for 4.5 h under nitrogen. The reaction mixture was cooled to room temperature, diluted with water (100 mL), and extracted with ether (3 × 60 mL). The combined extracts were washed with saturated aqueous $NaHCO_3$ (2 × 30 mL) and water (50 mL), and dried. Distillation of the residue after removal of solvent gave *3,4-dichloro-2,5-dimethyl-2,4-hexadiene* (**6**) (12.8 g), bp 29–31°C (0.65 Torr); n_D^{20} 1.4940); ^{1}H nmr, δ: 1.73 (s, 6H), 1.88 (s, 6H).

Compound **6** (12.0 g) was stirred rapidly with 85% H_2SO_4 (100 g) at 60°C for 2 h. The mixture was cooled, diluted with water (50 mL), and extracted with ether (2 × 100 mL). The extract was washed with saturated aqueous $NaHCO_3$ (50 mL) and dried. Distillation of the residue after removal of the solvent gave a colorless liquid (5.5 g), bp 42–52°C (3 Torr), which was shown by ^{1}H nmr spectroscopic analysis to be a mixture of **6** and *2,4,4-trimethyl-2-cyclopenten-1-one* (**7**). The latter was separated by the use of Girard's Reagent T (25) and obtained as a colorless liquid, bp 52°C (10 Torr); n_D^{25} 1.4606 (lit. (19*a*) bp 66°C (20 Torr); n_D^{25} 1.4573). The *2,4-dinitrophenylhydrazone of 7* was prepared in the usual manner (24); after recrystallization from EtOAc–EtOH it was obtained as orange crystals, mp 211.5–223°C. *Anal.* calcd. for $C_{14}H_{16}N_4O_4$: C 55.25, H 5.30, N 18.41; found: C 55.33, H 5.43, H 18.14.

3,5,5-Trimethyl-2-cyclopenten-1-one (8) and 3,4,4-trimethyl-2-cyclopenten-1-one (9)

A solution of redistilled 2-methyl-2-butene (47 g) in $CHCl_3$ (140 mL) was cooled in an ice bath and rapidly stirred. Nitrosyl chloride was slowly bubbled through this solution until a permanent green color was produced (ca. 2 h). Removal of the solvent gave crude *3-chloro-3-methyl-2-butanone oxime* as a bright blue viscous liquid (85 g; 95%); ir ($CHCl_3$), λ_{max}: 2.80, 2.90–3.10 μm; ^{1}H nmr, δ: 1.75 (s, 6H), 2.01 (s, 3H), 9.6 (s, 1H).

Sodium (15.0 g, 0.65 mol) was dissolved in dry EtOH (250 mL) and freshly distilled ethyl acetoacetate (81 g, 0.7 mol) was added to the solution. The mixture was cooled in ice-water and the crude oxime (85 g, 0.63 mol) in dry EtOH (50 mL) was added slowly over 25 min. The mixture was allowed to stand overnight and the precipitated NaCl was filtered. Removal of the EtOH from the filtrate gave a pale brown crystalline mess. This was heated with boiling 50% aqueous KOH (1200 g) under reflux for 4 h. The resulting solution was steam distilled and the steam distillate was extracted with ether (2 × 200 mL). Evaporation of the ether gave a pale brown liquid (20.5 g), which on distillation gave a colorless liquid (9.5 g), bp 62–85°C (10 Torr), consisting of the cyclopentenones **8** and **9** (2:3 by vpc analysis); these were readily separated by preparative vpc (NPGS, 120°C).

3,5,5-Trimethyl-2-cyclopenten-1-one (**8**) (2.04 g), n_D^{20} 1.4670, the component with the lower retention time, was obtained as a colorless liquid. The *2,4-dinitrophenylhydrazone of 8* was prepared in the usual manner (24). Two recrystallizations from EtOAc–EtOH gave orange needles, mp 227.5–228.5°C. *Anal.* calcd. for $C_{14}H_{16}N_4O_2$: C 55.25, H 5.30, N 18.41; found: C 55.27, H 5.32, N 18.51.

3,4,4-Trimethyl-2-cyclopenten-1-one (**9**) was obtained as a colorless liquid, n_D^{20} 1.4737. The *semicarbazone of 9* was prepared in the usual manner (24); on recrystallization from EtOH it was obtained as white platelets, mp 201–202°C (dec.) (lit. (10) mp 199–200°C).

Tetrahydro-2,3,5,5-tetramethyl-2,3-furandiol (11)

To a solution of 2,4-dihydroxy-2,4-dimethylpentanoic acid γ-lactone (**10**; 7.2 g, 0.050 mol) (26) in dry ether (100 mL) was added 1.24 *M* ethereal methylmagnesium iodide (110 mL, 0.15 mol). The mixture was allowed to stand overnight and worked up with aqueous NH_4Cl. The clear supernatant layer was separated, and the inorganic cake was washed with ether (2 × 50 mL). The ethereal solutions were combined, dried, and freed of solvent to give **11** as an oil (2.9 g, 36%). This slowly crystallized on standing in petroleum ether – cyclohexane. Two recrystallizations from this solvent mixture gave **11** as colorless crystals, mp 72–74°C. *Anal.* calcd. for $C_8H_{16}O_3$: C 59.98, H 10.07; found: C 60.11, H 10.17.

Extraction of the inorganic cake with hot $CHCl_3$ (3 × 30 mL) and evaporation of the combined extracts gave *compound 13* as a white solid (3.9 g), which was insoluble in ether, CH_2Cl_2, and $CHCl_3$. It was recrystallized from acetone–EtOAc to give white prisms, mp 227–229°C (dec.); ir (Nujol), λ_{max}: 3.02 (m) μm. Compound **13** was converted to **12** (*vide infra*) on treatment with 50% H_2SO_4.

The inorganic cake remaining after the above extraction was dissolved in 50% H_2SO_4, and the solution was extracted with $CHCl_3$ (3 × 100 mL). A pale brown crystalline product (1.03 g) was obtained on removal of the solvent. Purification by vpc (fluorosilicone, 100°C) gave *tetrahydro-2,2,3,5,5-pentamethyl-3-furanol* (**12**) as a white crystalline solid, mp 75–76°C (lit. (13) mp 76–77°C); ir, λ_{max}: 2.75 (w), 2.90 (m) μm. This was shown to be identical with an authentic sample of **12** prepared by treatment of **1** with methylmagnesium iodide (13).

Lead tetraacetate cleavage of 14. Formation of diacetone alcohol (14)

To a solution of **11** (100 mg) in water (3 mL) was added a suspension of lead tetraacetate (346 mg) in glacial acetic acid (3 mL). After 2 h the mixture was filtered, and the filtrate was made strongly alkaline with aqueous KOH and allowed to stand for a further 90 min. The solution acquired a strong odor of diacetone alcohol (**14**). 2,4-Dinitrophenylhydrazine reagent (24) was added and the solution was allowed to stand for 2 days, giving orange-yellow crystals, mp 198–202°C. Recrystallization from 80% EtOH gave *diacetone alcohol, 2,4-dinitrophenylhydrazone* as yellow needles, mp 202–204°C (lit. (24) mp 203°C).

Rearrangement of 11 to 1 on vapor phase chromatography

When a 10% solution of **11** in $CHCl_3$ was injected on a vpc column (DIDP or NPGS) at 140°C a peak with retention time equal to that of **1** was produced. Collection from the column gave a colorless liquid, the ir spectrum of which was identical with that of authentic **1**. Peak area measurements indicated a yield of ca. 30%. No change was observed when **1** was heated alone at 150°C.

Acid-catalyzed self-condensation of 11. Formation of 15

A solution of **11** (0.60 g) in benzene (50 mL) containing a crystal of

Can. J. Chem. Downloaded from www.nrcresearchpress.com by 118.98.75.50 on 09/07/12
For personal use only.

Can. J. Chem. Downloaded from www.nrcresearchpress.com by 118.98.75.50 on 09/07/12
For personal use only.

p-toluenesulfonic acid was boiled under reflux for 30 min. The solution was washed with water (30 mL) and dried. Evaporation of the solvent gave a crystalline product that showed no hydroxyl or carbonyl absorption in its ir spectrum. Three recrystallizations from hexane gave *compound* ***15*** as colorless crystals, mp 190.5–191.5°C (sealed cap); ir, λ_{max}: 8.5–8.6, 8.85, 10.55 μm; ^{1}H nmr, δ: 1.25 (s, 6H), 1.32 (s, 6H), 1.39 (s, 6H), 1.47 (s, 6H), 1.90 (J = 13 Hz, H), 2.00 (d, J = 13 Hz, 2H). *Anal.* calcd. for $C_{16}H_{28}O_4$: C 67.57, H 9.93, *Mol. Wt.* 284; found: C 67.66, H 9.93. *Mol. Wt.* (Rast) 284.

*2,5-Dihydro-3,5,5-trimethyl-2-methylenefuran (**17**)*

A solution of lithium acetylide was prepared from acetylene and lithium wire (1.73 g, 0.25 mol) in liquid ammonia (250 mL) in the presence of hydrated ferric nitrate (50 mg). Mesityl oxide (24.5 g, 0.25 mol) in dry ether (25 mL) was added with stirring and cooling. A slow stream of acetylene was passed continuously through the solution, which was stirred and cooled for a further 2.5 h. Ammonium chloride (20 g) was cautiously added and the ammonia was allowed to evaporate overnight. Extraction with ether and evaporation of the solvent gave a mixture (1.76 g) consisting only of *3,5-dimethyl-4-hexen-1-yn-3-ol* and unconsumed mesityl oxide (28.5% conversion from vpc analysis). A pure sample of the product was collected from a vpc column (NPGS, 85°C); ir, λ_{max}: 2.78, 3.02, 4.75, 6.0–6.1, 10.9 μm; ^{1}H nmr, δ: 1.51 (s, 3H), 1.71 (s, 3H), 1.87 (s, 3H), 2.33 (s, 1H), 2.38 (s, 1H), 5.32 (s, 1H).

The mixture (15 g) of the above ynol and mesityl oxide from a larger scale run was dissolved in ether (150 mL) and the solution was shaken for 30 min with 50% H_2SO_4 (150 mL). The ethereal layer was separated and the aqueous solution was extracted with ether (150 mL). The combined ethereal solutions were washed with water (2 × 50 mL), dried over $CaCl_2$, and concentrated. Fractional distillation with a spinning band column gave *2,4-dimethyl-3-hexen-5-yn-3-ol* (**16**) (1.2 g), bp 59–61°C (15 Torr) (lit. (14) bp 65–66°C (20 Torr)); ir, λ_{max}: 2.78, 3.02, 4.78, 6.17, 10.5 μm; ^{1}H nmr, δ: 1.34 (s, 6H), 1.86 (s, 3H), 2.71 (s, 1H), 3.25 (s, 1H), 5.89 (s, 1H).

A solution of **16** (180 mg) in ether (5 mL) was shaken for 3 min with a solution of mercuric acetate (30 mg) in water (5 mL). The organic layer was separated and the aqueous layer was washed with ether (10 mL). The combined ethereal solutions were dried over K_2CO_3 and the solvent was removed. The residue (120 mg) exhibited a single peak on vpc analysis (NPGS, 75°C). Collection of the product from the vpc column gave *2,5-dihydro-3,5,5-trimethyl-2-methylenefuran* (**17**). *Anal.* calcd. for $C_8H_{12}O$: C 77.37, H 9.74; found: C 76.51, H 9.94.

Shaking an ethereal solution of **16** with mercuric sulfate in 2% w/v sulfuric acid gave **20**, the dimer of **17** (*vide infra*).

*Dimerization of **17**. Formation of **20***

On standing, compound **17** neat or in solution in CCl_4 underwent dimerization to give **20**, which was also formed via spontaneous dehydration of **18** on standing. Repeated distillation, with precautions to minimize contact with air, gave **20** as a colorless liquid, bp 73–74°C (0.35 Torr). An analytical sample was prepared by vpc on an NPGS column at 150°C. *Exact Mass* calcd. for $C_{15}H_{21}O_2$ (M − CH_3): 233.1542; found: 233.1542. *Anal.* calcd. for $C_{16}H_{24}O_2$: C 77.37, H 9.74; found: C 76.90, H 9.58.

*Hydrogenation of **20**. Formation of **21***

A solution of **20** (3.07 g) in EtOH (50 mL) containing reduced platinum oxide (120 mg) was stirred under hydrogen at a slight positive pressure. One molar equivalent of hydrogen was adsorbed in 100 min. Further uptake of hydrogen was extremely slow (0.28 molar equiv. after 12 h). The solution was filtered and the solvent was removed. Distillation of the residue gave **21** as a colorless liquid, bp 66–70°C (0.7 Torr). *Exact Mass* calcd. for $C_{16}H_{26}O_2$ (M), $C_{15}H_{23}O_2$ (M − H): 250.1983, 249.1854; found: 250.1900, 249.1862.

*4-Hydroxy-2,4-dimethyl-2-pentenoic acid γ-lactone (**22**)*

2,4-Dihydroxy-2,4-dimethylpentanoic acid γ-lactone (**10**) (26) was heated for 14 h with boiling 47% hydrobromic acid under reflux (12) to give **22** in almost quantitative yield. Recrystallization from heptane gave white needles, mp 54.5–55°C (lit. (12) mp 55–56°C).

*Ozonolysis of **23**. Formation of α-methyllevulinic acid (**24**)*

A stream of ozonized oxygen (ca. 20% O_3; 15 L/h) was passed into a solution of **23** (0.47 g) in CH_2Cl_2 (100 mL) cooled in a Dry Ice – acetone bath, until the solution had turned deep blue (45 min). The excess ozone was removed by passing a stream of nitrogen through the solution for 5 min. The solution was added dropwise to water (30 mL) and the mixture was shaken vigorously and allowed to stand overnight. Aqueous 40% NaOH (10 mL) and aqueous 6% H_2O_2 (15 mL) were added. The mixture was shaken for 5 min and allowed to stand at room temperature for 20 h. The organic layer was separated and the aqueous solution was acidified with 10% H_2SO_4. Extraction of the acid solution with ether (4 × 50 mL) and removal of the solvent gave a mixture of **24** and its tautomeric lactol as an oil (0.59 g); ir, λ_{max}: 2.75–2.80, 3–4.1, 5.62–5.70, 5.80 μm. The remainder of the acidic product from the ozonolysis (ca. 0.5 g) was mixed with a solution of semicarbazide hydrochloride (400 mg) and sodium acetate (300 mg) in water (0.3 mL) and the solution was allowed to stand overnight. The resulting solid (147 mg) was filtered and twice recrystallized from 70% aqueous EtOH to give the *semicarbazone of **24*** as colorless prisms, mp 178–178.5°C, undepressed when mixed with an authentic sample prepared from ethyl 2-bromoproprionate and ethyl acetoacetate (20).

*Maleic anhydride adducts of tetramethylfuran (**25**)*

The mixture of adducts (22, 23) was repeatedly crystallized from heptane to give the *exo* adduct as long needles, mp 96.5–97.5°C (lit. (22) mp 95–96°C); ir, λ_{max}: 5.37, 5.62, 9.24 μm; ^{1}H nmr, δ: 1.60 (s, 6H), 1.64 (s, 7.3H), 1.69 (s, 1.3H), 3.01 (s, 2H), 3.48 (s, 0.42H). *Anal.* calcd. for $C_{12}H_{14}O_4$: C 64.85, H 6.35; found: C 64.76, H 6.39.

Equimolar solutions of maleic anhydride and tetramethylfuran in $CHCl_3$ were mixed and the ^{1}H nmr spectrum of the resulting solution was recorded after approximately 1, 3, and 6 min. The ratios of the peak heights at δ 3.01 and 3.48 were 2.05, 2.95, and 4.6, respectively. This ratio remained constant after 6 min and was the same as that observed when the pure *exo* isomer was dissolved in $CHCl_3$.

Acknowledgments

We thank Mr. Baldev Gambhir for technical assistance and the Natural Sciences and Engineering Research Council of Canada for support of this work.

1. P. Yates, D. G. Farnum, and G. H. Stout. J. Am. Chem. Soc. **80**, 196 (1958); P. Yates, S. Lipinsky, and D. Vossius. Can. J. Chem. **59**, 1977 (1961).
2. P. M. Burke, W. F. Reynolds, J. C. L. Tam, and P. Yates. Can. J. Chem. **59**, 1449 (1976).
3. G. A. Olah, G. K. S. Prakash, and J. Sommer. Superacids. John Wiley and Sons Inc., New York, NY. 1985; G. A. Olah, A. M. White, and D. A. O'Brien. *In* Carbonium ions. Vol. 4. *Edited by* A. Olah and P. v. R. Schleyer. Wiley–Interscience, Inc., New York, NY. 1973. pp. 1734–1748.
4. M. Liler. Reaction mechanisms in sulfuric acid. Academic Press, New York, NY. 1971.
5. P. M. Burke. Ph.D. Thesis, University of Toronto, Toronto, Ontario, 1966.
6. F. Leonard, A. Wajngurt, and H. Horn. J. Org. Chem. **21**, 1402 (1956).
7. W. Lozac'h. Bull. Soc. Chim. Fr. **11**, 416 (1944).
8. G. F. Hennion and R. B. Davis. J. Org. Chem. **16**, 1289 (1951).
9. H. J. R. Loewenthal. Isr. J. Chem. **4**, 31 (1966).
10. H. Sargent. J. Org. Chem. **7**, 154 (1942).
11. E. R. Buchman and H. Sargent. J. Org. Chem. **7**, 148 (1942).
12. C. Sandris, G. Ourisson, and G. Dupont. Bull. Soc. Chim. Fr. 1079 (1954).
13. P. Yates and N. Yoda. Tetrahedron, **19**, 849 (1963).
14. J. Cymerman, I. M. Heilbron, and E. R. H. Jones. J. Chem. Soc. 90 (1945).

15. W. OROSHNIK and A. D. MEBANE. J. Am. Chem. Soc. **71**, 2062 (1962).
16. I. M. HEILBRON, E. R. H. JONES, P. SMITH, and B. C. L. WEEDON. J. Chem. Soc. 54 (1946).
17. W. G. GALESLOOT, L. BRANDSMA, and J. F. ARENS. Recl. Trav. Chim. Pays-Bas, **88**, 671 (1969); P. H. M. SCHREURS, W. G. GALESLOOT, and L. BRANDSMA. Recl. Trav. Chim. Pays-Bas, **94**, 70 (1975).
18. P. H. M. SCHREURS, A. J. DE JONG, and L. BRANDSMA. Recl. Trav. Chim. Pays-Bas, **95**, 75 (1976).
19. I. N. NAZAROV and I. I. ZARETSKAYA. Bull. Acad. Sci. URSS, Cl. Sci. Chim. 529 (1946); Chem. Abstr. **42**, 7731 B (1948); A. V. KOPERINA and B. A. KAZANSKII. Izv. Akad. Nauk SSSR Otd. Khim. Nauk, 302 (1948); Chem. Abstr. **43**, 156 a (1949).
20. E. A. BRAUDE and C. J. TIMMONS. J. Chem. Soc. 3313 (1953).
21. P. YATES, G. D. ABRAMS, and L. L. WILLIAMS. Tetrahedron Lett. 4341 (1969).
22. R. GAERTNER and R. G. TONKYN. J. Am. Chem. Soc. **73**, 5872 (1951).
23. F. A. L. ANET. Tetrahedron Lett. 1219 (1962).
24. R. L. SHRINER, R. C. FUSON, and D. Y. CURTIN. The systematic identification of organic compounds. 5th ed. John Wiley and Sons Inc., New York, NY. 1964.
25. L. F. FIESER. Experiments in organic chemistry. 3rd ed. D. C. Heath and Co., Boston, MA. 1955. p. 88.
26. K. KOHN. Monatsch. **30**, 401 (1909).

Can. J. Chem. Downloaded from www.nrcresearchpress.com by 118.98.75.50 on 09/07/12
For personal use only.

The syntheses of mono- and disubstituted phthalocyanines using a dithioimide

CLIFFORD C. LEZNOFF,[1] SHAFRIRA GREENBERG, BEN KHOUW, AND A. B. P. LEVER
Department of Chemistry, York University, North York (Toronto), Ont., Canada M3J 1P3

Received September 30, 1986

This paper is dedicated to Professor John T. Edward

CLIFFORD C. LEZNOFF, SHAFRIRA GREENBERG, BEN KHOUW, and A. B. P. LEVER. Can. J. Chem. **65**, 1705 (1987).

Hydrolysis of 5-neopentoxy-1,3-diiminoisoindoline gave 5-neopentoxy-1*H*-isoindole-1,3(2*H*)-dione (4-neopentoxyphthalimide), which, on treatment with Lawesson's reagent, yielded the thiophthalimides, 5-neopentoxy-1*H*-isoindole-1,3(2*H*)-dithione, 2,3-dihydro-6-neopentoxy-3-thioxo-1*H*-isoindol-1-one, and 2,3-dihydro-5-neopentoxy-3-thioxo-1*H*-isoindol-1-one. Attempted S-alkylations of the thiophthalimides resulted in the formation of β-isoindigos and N-alkylation products. In a new phthalocyanine synthesis crossed condensations of 1,3-diiminoisoindoline with 5-neopentoxy-1*H*-isoindole-1,3(2*H*)-dithione yielded mixtures of phthalocyanines from which 2-neopentoxyphthalocyanine and 2,16-dineopentoxyphthalocyanine could be purified in part from other phthalocyanines.

CLIFFORD C. LEZNOFF, SHAFRIRA GREENBERG, BEN KHOUW et A. B. P. LEVER. Can. J. Chem. **65**, 1705 (1987).

L'hydrolyse de la néopentoxy-5 diimino-1,3 indoline conduit à la néopentoxy-5 1*H*-isoindole (2*H*)-dione-1,3 (néopentoxy-4 phtalimide) qui, par traitement avec le réactif de Lawesson, fournit les thiophtalimides, néopentoxy-5 1*H*-isoindole (2*H*)-dithione-1,3, dihydro-2,3 néopentoxy-6 thioxo-3 1*H*-isoindolone-1 et dihydro-2,3 néopentoxy-5 thioxo-3 1*H*-isoindolone-1. Des essais de S-alkyler les thiophtalimides ont conduit à la formation de β-isoindigos et de produits de N-alkylation. Dans une nouvelle synthèse de la phtalocyanine, des condensations de la diimino-1,3 isoindoline avec la néopentoxy-5 1*H*-isoindole (2*H*-dithione-1,3 ont conduit à des mélanges de phtalocyanines à partir desquels on a pu purifier en partie la néopentoxy-2 phtalocyanine et la dinéopentoxy-2,16 phtalocyanine.

[Traduit par la revue]

Although symmetrical tetra (1–3) and octasubstituted (4–6) phthalocyanines are well known, the synthesis of simple mono- (7), disubstituted (8), and other unsymmetrical phthalocyanines (9, 10) remains a difficult problem. A typical symmetrical phthalocyanine synthesis involves the self-condensation of 5-substituted or 4,5-disubstituted-1,3-diiminoisoindolines (4, 11). A simple strategy available to form unsymmetrical phthalocyanines is the mixed condensation of two different 1,3-diiminoisoindolines to obtain the desired mono-, di-, or trisubstituted phthalocyanines. In fact, condensation of 1,3-diiminoisoindoline (**1**) and 5-neopentoxy-1,3-diiminoisoindoline (**2**) does give mixtures of unsubstituted, mono-, di-, tri-, and tetraneopentoxyphthalocyanines (**3**–**8**) as expected when analyzed by mass spectroscopy.[2]

We envisioned that a completely new approach to phthalocyanine synthesis was required. If we could perform a crossed condensation of substrates in which one of the substrates is unable to self-condense and if we could lower the temperature of phthalocyanine formation so that crossed condensation is favoured over self-condensation of the other substrate, then specifically substituted phthalocyanines could be formed as shown in Scheme 1.

Although phthalic anhydrides self-condense, probably via phthalimides to form phthalocyanines in the presence of urea (12) at very high temperatures, phthalimides are inert to self-condensation under 150°C. On the other hand, 1,3-diiminoisoindoline (**1**) and its derivatives readily form phthalocyanines at 150°C but only slowly below 100°C unless special catalytic bases are used (13). We believed that if we used thiophthalimides in crossed condensation reactions, then the nucleophilic addition of the 1,3-diiminoisoindoline (**1**) to a dithiophthalimide such as 1*H*-isoindole-1,3(2*H*)-dithione (**9**) or 5-neopentoxy-1*H*-isoindole-1,3(2*H*)-dithione (**10**) would in fact be much faster than self-condensation of **1**, as the high reactivity of the thiocarbonyl group is well known (14). It is thus possible that a crossed condensation of **1** and **10** could occur even at ambient temperature to form exclusively the desired 2,16-dineopentoxyphthalocyanine (**5**) (along with 2,17-dineopentoxyphthalocyanine), but no other compounds. In addition, any self-condensation of **1** would yield the highly insoluble unsubstituted phthalocyanine (**3**), which may then be separable from the organic solvent-soluble **5**. Another attractive feature of this strategy is the fact that only **5** (the "*para*" disubstituted isomer) would be formed and not 2,9-dineopentoxyphthalocyanine (**6**) (the "*ortho*" disubstituted isomer).

The first step in the realization of the strategy outlined in Scheme 1 is the preparation of the required thiophthalimide. Thus treatment of 4-nitrophthalimide (**11**) with neopentoxides led only to the recovery of **11**, and no 4-neopentoxyphthalimide (**12**) was formed (Scheme 2). Indeed, the preparations of 4-alkoxyphthalimides are known in the literature (15) but only through a lengthy 5-step synthesis from diethyl 4-nitrophthalate. Since it is known that 1,3-diiminoisoindolines can be hydrolyzed to phthalimides (16) and since we readily had available 5-neopentoxy-1,3-diiminoisoindoline (**2**) from previous studies on binuclear phthalocyanines (17), **2** was converted to 4-neopentoxyphthalimide (**12**) by refluxing **2** in aqueous dioxane (Scheme 2). Treatment of **12** with excess 2,4-bis(4-methoxyphenyl)-1,3-dithia-2,4-diphosphetane-2,4-disulfide (**13**) (Lawesson's reagent) (18) gave 5-neopentoxy-1*H*-isoindole-1,3(2*H*)-dithione (**10**) in 82% yield while the reaction of **12** with only 0.5 equivalents of **13** gave **10**, admixed with the two possible monothionated products, 2,3-dihydro-6-neopentoxy-3-thioxo-1*H*-isoindol-1-one (**14**) and 2,3-dihydro-5-neopentoxy-3-thioxo-1*H*-isoindol-1-one (**15**) in 37, 16, and 24% yields respectively. The new thiophthalimides **10**, **14**, and **15** were fully characterized by elemental analysis and spectroscopic data and compared with the known **9** and monothiophthalimide by uv–vis (Table 1) (19) and ^{13}C nmr (Table 2) (20) spectroscopy.

[1]Author to whom correspondence may be addressed.
[2]S. Greenberg and C. C. Leznoff, unpublished results.

Can. J. Chem. Downloaded from www.nrcresearchpress.com by 118.98.75.50 on 09/07/12
For personal use only.

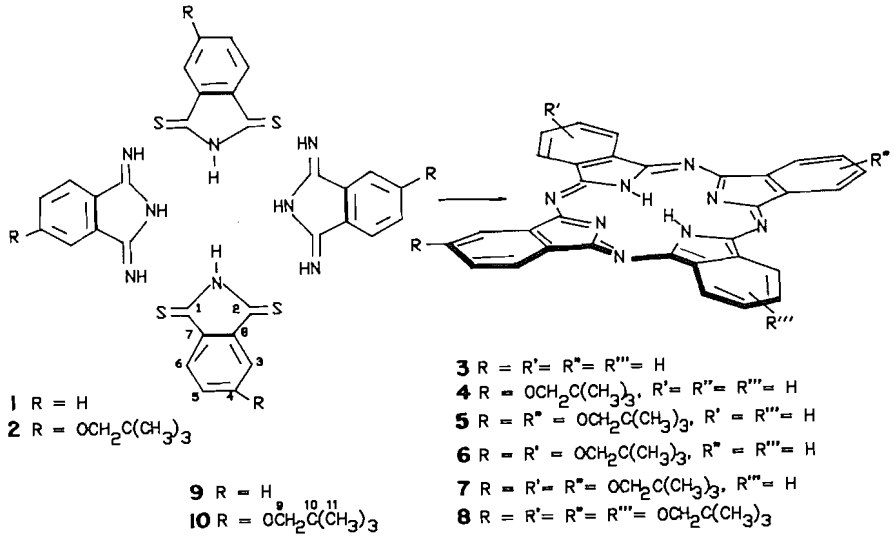

SCHEME 1

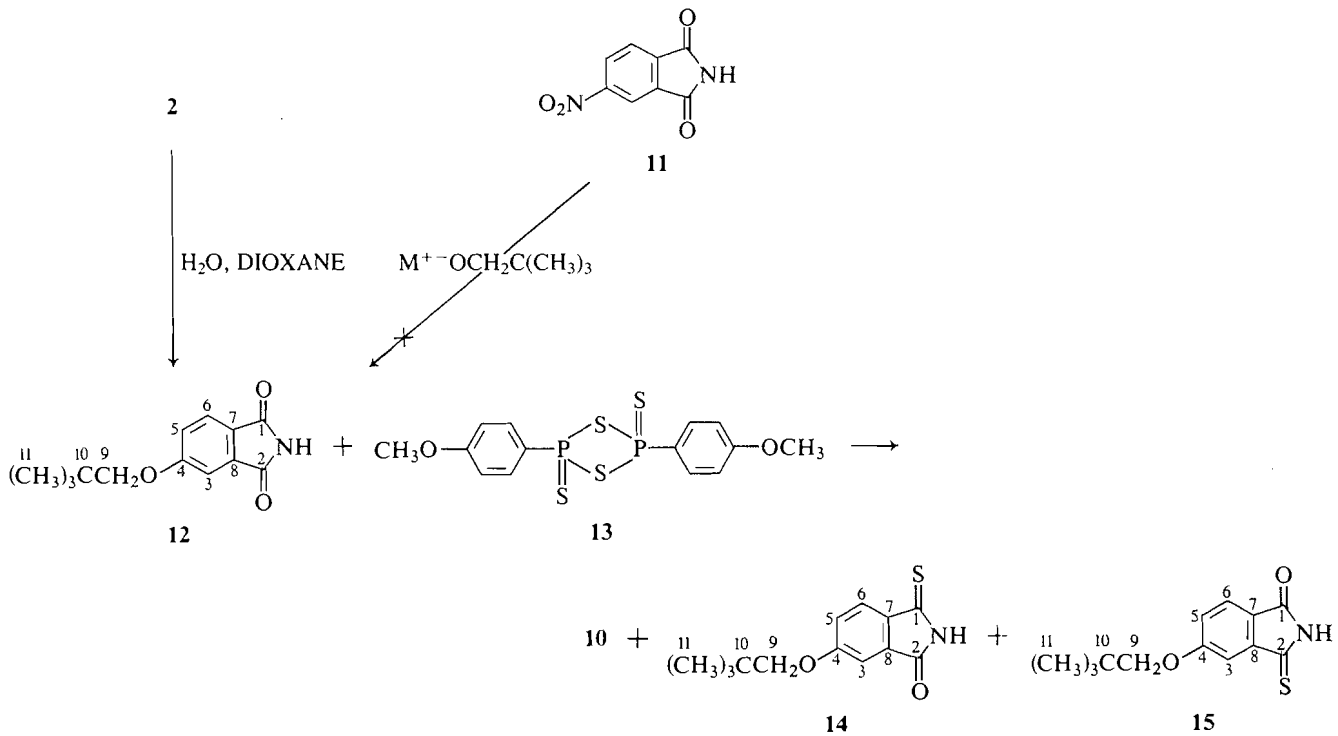

SCHEME 2

In previous studies (17) we had shown that **2** readily self-condenses to 2,9,16,23-tetraneopentoxyphthalocyanine (**8**) at 150°C in 2-*N*,*N*-dimethylaminoethanol. Control studies conducted to determine the maximum temperature at which **1** will not exhibit phthalocyanine formation showed that **1** was stable in 2-*N*,*N*-dimethylaminoethanol at 70°C or below and only reacted slowly below 95°C. Thus, **1** was dissolved in 2-*N*,*N*-dimethylaminoethanol at 50°C and **10** was added to this mixture and stirred at 80–90°C for 24 h to give, after precipitation with water, a dark-coloured residue containing phthalocyanines (Experiment 1) (Scheme 1). Extraction of the residue with methanol removed most non-phthalocyanine impurities. Thus the formation of phthalocyanines by the crossed condensation of a dithiophthalimide with a 1,3-diiminoisoindoline has been demonstrated for the first time. Further extraction of the residue with tetrahydrofuran (THF) (first phthalocyanine extract) yielded a solution of phthalocyanines that contained a mixture of **3**–**8** as revealed by mass spectroscopy (Table 3). The mixture contained 2,16-dineopentoxyphthalocyanine (**5**) (and possibly the 2,9-dineopentoxyphthalocyanine isomer (**6**)) as desired but significant quantities of phthalocyanine (**3**), 2-neopentoxyphthalocyanine (**4**), and 2,9,16-trineopentoxyphthalocyanine (**7**) were also produced, while 2,9,16,23-tetraneopentoxyphthalocyanine (**8**) was formed in traces only. Of course, the relative ratio of the parent ions of **3**–**8** is not necessarily an accurate representation of the relative abundances of **3**–**8**, but it does give us a strong indication that the exclusive formation of **5** did not occur. As phthalocyanines give strong parent ions in their mass spectra (21) and pure **8** does not give fragment ions corresponding to **3**–**7** (17), we can be confident that the

Can. J. Chem. Downloaded from www.nrcresearchpress.com by 118.98.75.50 on 09/07/12
For personal use only.

TABLE 1. Absorption spectra of phthalimides, thiophthalimides, and β-isoindigos in $CHCl_3$ at 24°C

Compound	λ_{max}(nm) (ε log)	Reference
Phthalimide[a]	240 (3.28), 296 (3.32)	19
Thiophthalimide[a]	244 (3.71), 298 (4.15), 334 (4.05)	25[b]
9[a]	246 (4.05), 264 (3.83), 376 (4.36)	25
10	282 (4.25), 292 (4.15), 380 (4.40)	
12	248 (4.23), 282 (3.32), 326 (3.54)	
14	256 (4.22), 304 (4.18), 344 (4.09), 366 (4.04)	
15	256 (4.38), 306 (4.17), 370 (3.54)	
16	248 (4.14), 362 (4.30), 390 (4.22)	
17	256 (4.59), 336 (4.25), 421 (4.71), 442 (4.84), 464 (4.79)	36[b]
18	246 (4.00), 356 (4.06), 394 (3.92)	
19	256 (4.09), 336 (3.75), 424 (4.22), 444 (4.37), 468 (4.30)	36[b]
22	246 (4.12), 320 (3.84), 420 (4.23), 440 (4.43), 466 (4.23)	

[a]The absorption spectra of these known compounds were recorded for comparison with the other unknown compounds.
[b]The spectra of closely related compounds are described.

TABLE 2. ^{13}C nuclear magnetic resonance chemical shifts in ppm (δ) of some phthalimides and thiophthalimides

	Carbon[a]										
Compound	1	2	3	4	5	6	7	8	9	10	11
Phthalimide[b]	167.60	167.60	123.50	134.10	134.10	123.50	132.50	132.50	—	—	—
Thiophthalimide[b]	170.06	197.01	123.01	133.69	134.30	123.92	127.92	137.33	—	—	—
9	197.32	197.32	123.10	133.56	133.56	123.10	135.08	135.08	—	—	—
10	196.68[c]	197.27[c]	107.01	164.52	120.76	125.03	128.38	137.48	78.76	31.91	26.49
12	168.57	168.57	108.46	164.69	120.52	125.09	124.18	135.18	78.65	31.77	26.36
14	196.76	170.05	107.38	164.46	120.97	125.80	130.40[c]	130.46[c]	78.85	31.89	26.45
15	170.18	197.24	108.70	164.76	120.25	124.71	119.71	139.76	78.63	31.85	26.44
16[d]	197.46	197.46	123.03	132.95	132.95	123.03	134.76	134.76	—	—	—

[a]The numbering of the carbon atoms in the listed compounds follows that given for these structures in the schemes and does not follow from the names of the compounds.
[b]The ^{13}C nmr spectra of these and related known compounds (20) were recorded and used to help assign the chemical shifts of the other unknown compounds.
[c]These values may be interchanged.
[d]The chemical shift of the N-methyl group is 31.04 ppm. In comparison, the chemical shift of the S-methyl group of **17** is 13.49 ppm.

ions observed are parent ions due to **3**–**8** and not fragment ions corresponding to **3**–**7**. Further extraction of the crude residue with toluene and, finally, with more tetrahydrofuran gave, again by mass spectroscopic analysis (Table 3), smaller quantities of phthalocyanines but fractions richer in the mono- and unsubstituted phthalocyanines **4** and **3** respectively. From previous work in our laboratory (9) we knew that mixtures of substituted mononuclear phthalocyanines are almost impossible to separate by flash chromatography (22) or even preparative thin-layer chromatography (tlc), probably because of aggregation phenomena. Since we had some phthalocyanine extracts that were already partially rich in **5** and **4**, we felt that vacuum liquid chromatography (vlc) (23), a very powerful separation technique, may give us pure samples of **5** and **4**. Thus further efforts to purify the first extract by vlc were attempted. Although it appeared that several blue-green bands readily separated on the column, again mass spectroscopic examination of each band (Table 3) showed that substantial contamination of each fraction remained. Some fractions obtained by vlc were rich in 2,16-dineopentoxyphthalocyanine (**5**) and one fraction contained almost pure 2-neopentoxyphthalocyanine (**4**) (with a trace of **5**) (Table 3), again by mass spectroscopic analysis of each chromatographic fraction. It should be noted that our previously reported (9) synthesis of an unsymmetrical phthalocyanine was based on a polymer support method yielding only the desired product, and no exhaustive chromatography was necessary to isolate the desired product. In addition mass spectroscopy revealed the presence of the desired product only. As a word of caution, other workers have recently reported the preparation of a mononitrophthalocyanine (7), a dicarboxyphthalocyanine (8), and an unsymmetrical octasubstituted phthalocyanine (10). Although the products were purified by flash chromatography in some cases (10) and the compounds gave sometimes acceptable elemental analysis (7, 10), no mass spectral data were recorded in detail (7, 8, 10) and in these instances mixtures of phthalocyanines may have been obtained. For example, an elemental analysis of a disubstituted phthalocyanine could be identical to that of a mixture of unsubstituted, mono-, di-, tri-, and tetrasubstituted phthalocyanines, especially since a mixture of this type usually shows up as one spot on tlc examination.[2]

In another experiment (Table 3, Experiment 2), we tried to optimize the formation of 2-neopentoxyphthalocyanine (**4**) by partially self-condensing an excess of **1** at 120°C and then adding a minimal quantity of **10** in a crossed phthalocyanine condensation (Scheme 1). The dark residue, obtained after the

Can. J. Chem. Downloaded from www.nrcresearchpress.com by 118.98.75.50 on 09/07/12
For personal use only.

TABLE 3. Mass spectroscopic data on the mixtures of phthalocyanines **3–8** in crossed condensation reactions of **1** and **10**

Experiment	Extract No.[a]	Fraction (vlc)	Mass spectrum[b] *m/z* (relative intensity %)
1	1	[c]	858(1), 772(22), 686(100), 600(45), 514(15)
1	1	2	858(5), 772(41), 686(10)
1	1	4	858(1), 772(87), 686(100), 600(11)
1	1	5	772(4), 686(100), 600(17)
1	1	6	772(7), 686(100), 600(6)
1	1	9	686(12), 600(100), 514(100)
1	2	[c]	772(1), 686(54), 600(100), 514(32)
1	2	1a[d]	772(3), 686(100)
1	2	1b[d]	686(100), 600(27)
1	2	1c[d]	686(84), 600(100)
1	2	2	686(16), 600(100)
1	2	3	686(8), 600(100)
1	2	3[e]	686(1), 600(100)
1	3[f]	—	686(18), 600(92), 514(100)
1	3[g]	—	686(1), 600(66), 514(100)
1	R[h]	—	600(29), 514(100)
2	1	—	772(1), 686(26), 600(80), 514(100)
2	2	—	772(1), 686(41), 600(100), 514(72)
2	3*f*	—	686(48), 600(100),
2	3[g]	—	686(1), 600(35), 514(100)
2	R[h]	—	600(12), 514(100)

[a]Extractions of phthalocyanines were performed as follows; extract 1 with THF for 5 h, extract 2 with THF for 19 h (In Expt. 1 a prior extraction with toluene for 10 h was performed), extract 3 with THF for 48 h.

[b]The peaks at 514, 600, 686, 772, and 858 are assigned as the parent peaks of **3**, **4**, **5** + **6**, **7**, and **8** respectively.

[c]Before further purification.

[d]Further flash chromatography of vlc fraction 1 gave fractions 1a, 1b, and 1c, which were analyzed by mass spectroscopy.

[e]This fraction is the same as the above entry (vlc fraction 3) but has been recrystallized.

[f]This sample is the evaporated filtrate.

[g]This sample is a precipitate formed before evaporation of the filtrate.

[h]Unextracted residue.

reaction, was purified as before to give a blue phthalocyanine solid. Extraction with THF for 5, 19, and 48 h gave extracts 1–3 respectively. From extract 3 a blue product precipitated. Mass spectroscopic analysis (Table 3) of extracts 1, 2, 3 (precipitate) and 3 (filtrate) and the remaining residue again showed that extracts 1 and 2 contained varying amounts of **3–7**, extracts 3 (precipitate) contained mostly **3** and **4**, while extract 3 (filtrate) contained mostly **4** and **5**. The solid blue residue contained mostly **3**. Further purifications by vlc on these extracts were not attempted.

Although we had succeeded in developing a new phthalocyanine synthesis at moderate temperatures based on thioimides, the yields of phthalocyanines in the key crossed condensation steps were low and the desired selectivity leading to mono- or disubstituted phthalocyanines was at best only partially achieved. Since 1-alkoxy-3-iminoisoindolines have been implicated as intermediates in phthalocyanine formation (24), we believed that 1-thioalkoxy-3-thioisoindolines could be used as a reactive partner instead of dithiophthalimides in phthalocyanine synthesis. Alkylation of thioamide-type compounds has been accomplished in many studies (25–29) giving exclusive S-alkylation as opposed to N-alkylation. In a model study of alkylations on dithiophthalimide (**9**) by a wide variety of methods encompassing basic (25–27), Lewis acid (27, 28), or neutral (29) conditions (Table 4), only N-alkylation or the formation of dialkyldithio-β-isoindigos took place (Scheme 3, Tables 1, 2, and 4). Thus methylation (25) of **9** with dimethyl sulfate and base gave *N*-methyldithiophthalimide (**16**) in 25–63% yield but the use of iodomethane and base (26, 27) gave mostly *S,S'*-dimethyldithio-β-isoindigo (**17**) (30) in 12–60% yield (Table 4). Another method using **9** and triethylorthoformate (29) at 180°C gave *N*-ethyldithiophthalimide (**18**) and *S,S'*-diethyldithio-β-isoindigo (**19**) (30), but again no simple S-alkylation occurred (Table 4). Still other alkylation methods (27, 28) exhibited no reaction or gave intractable products (Table 4).

Since the desired S-alkylated dithiophthalimide could not be prepared and since 3-ethoxyisoindol-1-one (**20**) was known (31), then simple treatment of **20** with Lawesson's reagent (**13**) (18) should yield 3-ethoxyisoindol-1-thione (**21**), which could be used in a cross-condensation reaction with **1**. Treatment of **20** with **13** did not give the desired **21**, but an unstable red compound **22**, which we tentatively assign by spectroscopic data (Tables 1 and 2) to 3-(3-ethoxy-1*H*-isoindol-1-ylidene)-2,3-dihydro-1*H*-isoindol-1-thione (**22**) as shown in Scheme 4. This last experiment indicates to us that the use of thiocarbonyl compounds in phthalocyanine synthesis is invariably complicated by the concomitant formation of isoindigos.

There have only been a few studies on the mechanism of phthalocyanine formation from phthalonitriles (32) or via amine–imidine condensations (24, 33). The formation of phthalocyanines **4–8** from condensation of **1** and the dithione **10** must obviously result from the displacement and hence removal of

Can. J. Chem. Downloaded from www.nrcresearchpress.com by 118.98.75.50 on 09/07/12
For personal use only.

TABLE 4. Alkylation reactions of dithiophthalimide (**9**) under different conditions

Alkylating agent	Base	Solvent	Temperature (°C)	Time (h)	Products (% yield)	Reference[a]
$(CH_3O)_2SO_2$	2 *M* NaOH	EtOH	0	0.17	**16** (25)	25
$(CH_3O)_2SO_2$	Et_3N	Toluene–THF	22	20	**16** (63)	
CH_3I	—	Dioxane	110	20	**9**	
$(CH_3O)_2SO_2$	—	Toluene	110	20	dec.[b]	
CH_3I	—	Acetone	22	20	**9**	
$(CH_3)_3\overset{+}{O}BF_4^-$	—	CH_2Cl_2	22	20	**17** (16)	28
CH_3I	0.8 *M* NaOH	MeOH	22	18	**17** (60)	27
$BF_3 \cdot OEt_2$	—	Toluene	120	2	**9**	27
$BF_3 \cdot OMe_2$	—	Toluene	60[c]	18	dec.[b]	27
CH_3I	$(Bu)_4NOH$	THF	22	18	**16** (22)[d]	
CH_3I	1 *M* CsOH	MeOH	22	18	**17** (12)	
CH_3I	1 *M* CsOH	MeOH	−20	5	**9**	
$HC(OEt)_3$	—	$HC(OEt)_3$	90	60	**9**	29
$HC(OEt)_3$	—	$HC(OEt)_3$	180	5	**18** (13)[e]	29

[a]The references refer to published methods of achieving S-alkylation.
[b]Decomposition of the starting material to an unresolvable mixture of compounds has occurred.
[c]At 22°C only **9** was recovered.
[d]Some **17** and other spots were detected on tlc.
[e]In addition **19** (8) was isolated.

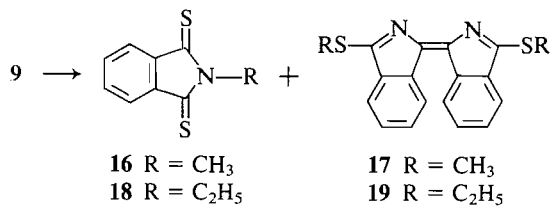

16 R = CH_3 **17** R = CH_3
18 R = C_2H_5 **19** R = C_2H_5

SCHEME 3

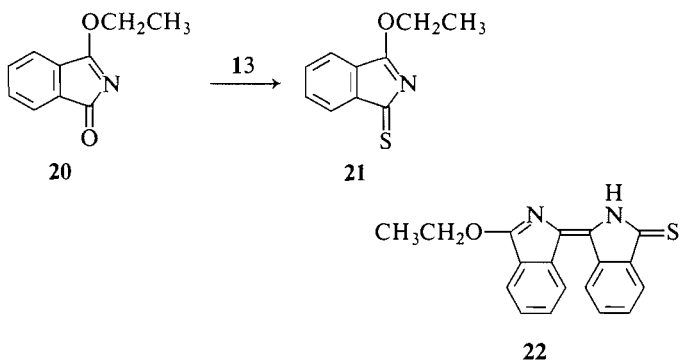

20 **21** **22**

SCHEME 4

the thione functional groups by ammonia, amines, or imines. The original hypothesis assumed that condensation of **1** and **10** would give in the first step an intermediate trimeric species (**23**) (Scheme 5), which on reaction with a 2nd equivalent of **10** would lead to **5**. Indeed, the lower temperature at which phthalocyanine formation is initiated (as low as 20°C) indicates that this first step is a likely possibility. It could happen, however, that although we have lowered the *initiation* step of phthalocyanine formation, the *propagation* step can still proceed rapidly at these modest temperatures. Thus intermediate **23** may react with more **10** giving 2,16-dineopentoxyphthalocyanine (**5**), but it could also react with more **1** giving the monosubstituted 2-neopentoxyphthalocyanine (**4**). In addition, **23** may undergo a N–H tautomeric shift giving the trimeric intermediate **24**. Trimeric intermediate **24** could react with **1** in two ways, giving two dimeric intermediates **25** and **26**, the former possessing a neopentoxy substituent. A N–H tautomeric shift of **25** could give a different dimeric intermediate **27**. The unsubstituted dimeric intermediate **26** could self-condense or react with **1** or **27** to give the phthalocyanine (**3**) or more **4**. The substituted dimeric intermediate **27** could react with **1** or **26** to give **2** or more **4** and with itself to give **5** and 2,9-dineopentoxyphthalocyanine (**6**). The generation of the monomeric 5-neopentoxy-1,3-diiminoisoindoline (**2**) in this reaction opens the door to other pathways of phthalocyanine formation. Thus **2** could react with **25** to generate 2,9,16-trineopentoxyphthalocyanine (**7**), or to form a new dimeric intermediate **28** containing two neopentoxy substituents. Intermediate **28** can further self-condense or react with **2** to give 2,9,16,23-tetraneopentoxyphthalocyanine (**8**). Alternatively **28** can condense with **26** to give **6** directly. Further condensation of **28** with **1** or **26** could give a new trimeric intermediate **29**, containing two neopentoxy substituents. Condensation of **29** with **2**, **10**, or even **25** could give more **7**, while condensation with **1**, **26**, or **27** could give **6**. Although Sato *et al.* (34) have shown that elemental sulfur (perhaps as thiolate anions) can act as a catalyst in the formation of 1,3-diiminoisoindolines from phthalonitriles, there was no report that phthalocyanine formation occurred under their conditions. We did notice in our reactions of **1** with **10** that a small amount of elemental sulfur was produced and this sulfur could account for the catalytic self-condensation of **1** to **3**. Indeed, control experiments conducted on **1** and elemental sulfur showed phthalocyanine formation starting at 50°C.[2] Elemental sulfur could not account directly for the formation of **4**–**8** but could further catalyze the reactions outlined in Scheme 5. Another complication not outlined in Scheme 5 is the possible production of ammonia gas, which could form **2** directly from **10**. The fact that the condensations of **1** and **10** are conducted under a steady stream of argon somewhat vitiates against this possibility. A full description of phthalocyanine formation is still clouded by the multiplicity of

Can. J. Chem. Downloaded from www.nrcresearchpress.com by 118.98.75.50 on 09/07/12
For personal use only.

Can. J. Chem. Downloaded from www.nrcresearchpress.com by 118.98.75.50 on 09/07/12
For personal use only.

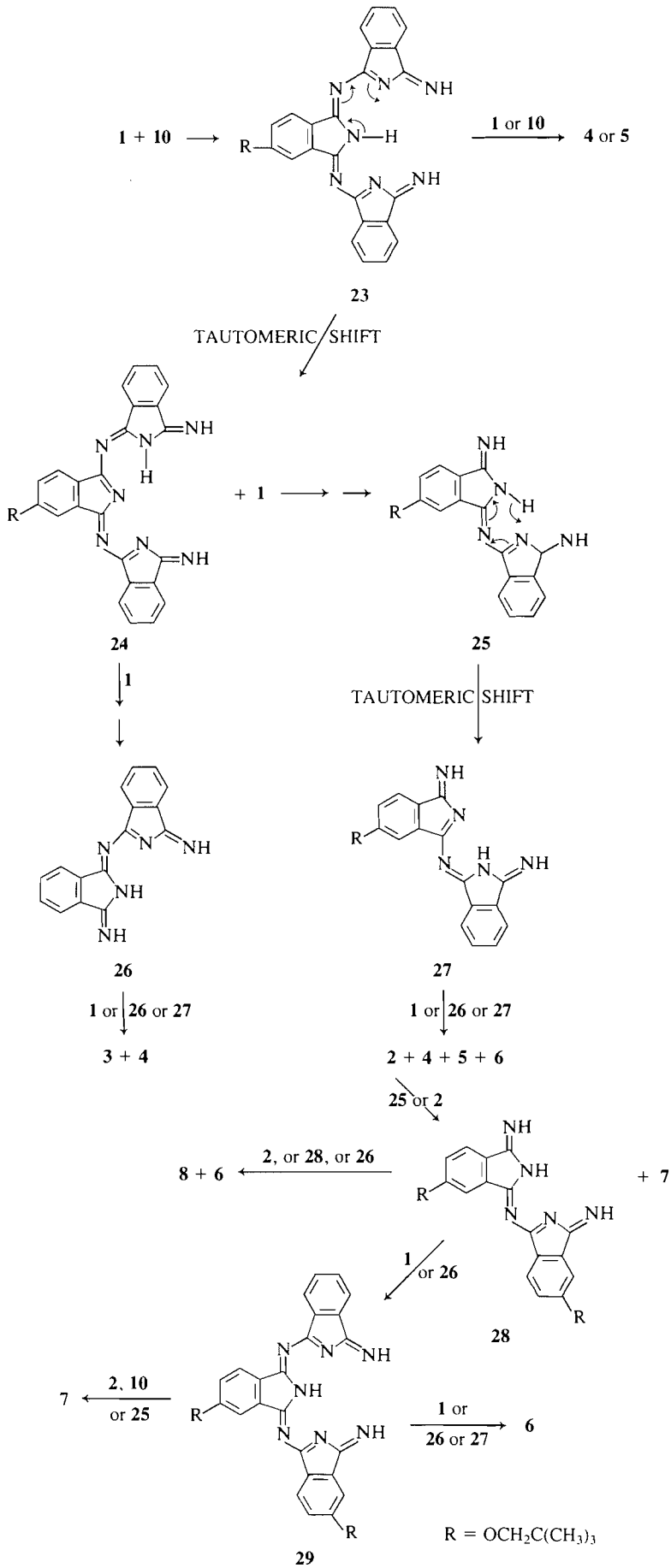

SCHEME 5

Can. J. Chem. Downloaded from www.nrcresearchpress.com by 118.98.75.50 on 09/07/12
For personal use only.

possible intermediates and catalysis by intermediates and by-products.

In this paper we have demonstrated that phthalocyanine formation readily occurs at modest temperatures from a 1,3-diiminoisoindoline and a dithiophthalimide, but that selective formation of mono- or disubstituted phthalocyanines was only partially achieved.

Experimental

Matheson high-purity argon was used to maintain inert atmosphere conditions. Infrared (ir) spectra were recorded on a Pye Unicam SP1000 infrared spectrophotometer using KBr discs for solids or as neat films between NaCl discs. Nuclear magnetic resonance (nmr) spectra for carbons and protons were recorded on a Bruker AM300 nmr spectrometer using deuterochloroform as solvent and tetramethylsilane as the internal standard unless otherwise stated. The positions of the signals are reported in δ units. (The splittings of the signals are described as singlets (s), doublets (d), triplets (t), quartets (q), or multiplets (m).)

The visible–ultraviolet spectra (uv) were recorded on a Hewlett Packard HP8451A Diode Array spectrophotometer. Mass spectra (ms) were recorded at 70 eV on a VG Micromass 16F mass spectrometer in the EI mode.

Melting points (mp) were determined using a Kofler hot stage melting point apparatus and are uncorrected. Thin-layer chromatography (tlc) was performed using silica gel G as the adsorbent. Flash chromatography was performed using silica gel of particle size 20–45 μm. All reactions were stirred with a magnetic stirrer. All solvents were freshly distilled before use. Microanalyses were performed by Guelph Chemical Laboratories Ltd., Guelph, Ont.

4-Neopentoxyphthalimide (12)

A suspension of 5-neopentoxydiiminoisoindoline (**2**) derived from 134 mg (0.63 mmol) of 4-neopentoxyphthalonitrile in 3 mL of a 1:1 mixture of water–dioxane was refluxed for 22 h. Since the crude diiminoisoindoline contained sodium methoxide (from the method of preparation), 28 mg of ammonium chloride (0.52 mmol) was added to the mixture. During the first 2–3 h ammonia was evolved and the suspension turned clear, and later a precipitate was formed. After cooling to room temperature the crude product was diluted with ethyl acetate and the organic layer was washed thoroughly with water, dried over anhydrous magnesium sulfate, filtered, and concentrated to a small volume. The crude product was purified using silica gel column chromatography and elution with ethyl acetate – petroleum ether (1:4). The product was recrystallized from a mixture of ethyl acetate – hexanes to give, in 75% yield, 110 mg of 5-neopentoxyphthalimide (**12**) as white crystals, mp 170–171°C (with previous darkening at 151–153°C); ir (cm^{-1}): 3240 (NH), 1780 (CO), 1740 (CO), 1630, 1370, 1240, 1020, 760; ^1H nmr δ: 7.75 (d, J = 8.3, 1H), 7.73 (br, 1H, NH), 7.32 (d, J = 2.2, 1H), 7.20 (dd, J = 8.3, 2.2, 1H), 3.75 (s, 2H, CH_2O), 1.07 (s, 9H, $(CH_3)_3C$); ms m/z: 233 (M^+, 10), 218 ($M^+ - 15$, 2.5), 175 (11), 164 (12), 71 (65), 43 (100). *Anal.* calcd. for $C_{13}H_{15}NO_3$: C 66.94, H 6.48, N 6.00; found: C 66.84, H 6.64, N 5.96.

5-Neopentoxy-1H-isoindole-1,3(2H)-dithione (10), 2,3-dihydro-6-neopentoxy-3-thioxo-1H-isoindol-1-one (14), and 2,3-dihydro-5-neopentoxy-3-thioxo-1H-isoindol-1-one (15)

A suspension of 192 mg (0.83 mmol) of **12** and 177 mg (0.44 mmol) of Lawesson's reagent (**13**) (18) in 2 mL of dry toluene was stirred at 90°C for 2.5 h. The reaction was followed by tlc (eluant toluene) and was stopped after 2.5 h, due to the formation of blue material at the base line when examined by tlc, even though not all of the starting material had reacted. After cooling to room temperature the crude product was purified by flash chromatography (22) using toluene as eluant. The first dark moving band gave, in 37% yield, 80 mg of 5-neopentoxy-1*H*-isoindole-1,3(2*H*)-dithione (**10**) as dark red-brown needles, mp 194–196°C (with previous softening); ir (cm^{-1}): 3260 (NH), 1625, 1480, 1450, 1350, 1230, 1120, 930, 840; ^1H nmr δ: 9.95 (br, 1H, NH), 7.78 (d, J = 8.4, 1H), 7.26 (d, J = 2.1, 1H), 7.20 (dd, J = 8.4, 2.1, 1H), 3.75 (s, 2H, CH_2O), 1.07 (s, 9H, $(CH_3)_3C$); ms m/z: 265 (M^+, 90), 250 ($M^+ - 15$, 10), 195 (93), 162 (60), 71 (45), 43 (100). *Anal.* calcd. for $C_{13}H_{15}NOS_2$: C 58.83, H 5.70, N 5.28; found: C 58.89, H 5.89, N 5.30.

Continued elution with toluene gave a yellow moving band. After evaporation of the solvent 2,3-dihydro-6-neopentoxy-3-thioxo-1*H*-isoindol-1-one (**14**) was isolated in 16% yield (33.5 mg) as orange crystals, mp 159–160°C; ir (cm^{-1}): 3240 (NH), 1745 (C=O), 1610, 1310, 1250, 1110, 830; ^1H nmr δ: 9.08 (br, 1H, NH), 7.86 (d, J = 8.4, 1H), 7.23 (d, J = 2.1, 1H), 7.18 (dd, J = 8.4, 2.1, 1H), 3.72 (s, 2H, CH_2O), 1.07 (s, 9H, $(CH_3)_3C$); ms m/z: 249 (M^+, 44), 179 (71), 71 (44), 43 (100). *Anal.* calcd. for $C_{13}H_{15}NO_2S$: C 62.62, H 6.07, N 5.62; found: C 62.77, H 6.00, N 5.79.

Continued elution with toluene gave a pink moving band. After evaporation of the solvent, 2,3-dihydro-5-neopentoxy-3-thioxo-1*H*-isoindol-1-one (**15**) was isolated in 23% yield (48.4 mg) as pink crystals, mp 139–142°C; ir (cm^{-1}): 3260 (NH), 1745 (C=O), 1605, 1490, 1310, 1085, 860, 775, 700; ^1H nmr δ: 9.45 (br, 1H, NH), 7.69 (d, J = 8.3, 1H), 7.40 (d, J = 2.1, 1H), 7.18 (dd, J = 8.3, 2.1, 1H), 3.74 (s, 2H, CH_2O), 1.07 (s, 9H, $(CH_3)_3C$); ms m/z: 249 (45), 179 (57), 71 (53), 43 (100). *Anal.* calcd. for $C_{13}H_{15}NO_2S$: C 62.62, H 6.07, N 5.62; found: C 62.40, H 5.99, N 5.84.

Some unreacted **12** was not recovered.

N-Methyldithiophthalimide (16)

A solution of 110 mg of dithiophthalimide (**9**) (0.61 mmol) in 1 mL of 95% ethanol and 0.3 mL of 2 *M* sodium hydroxide (0.6 mmol) was diluted with 1 mL water and cooled to 0°C according to the procedure of Baguley and Elvidge (25). The red solution was stirred while 0.15 mL of dimethylsulfate was added dropwise during 2–5 min. After a further 5 min the solution was diluted with 2 mL water. The crude product was extracted with ether and the organic layer was washed with water, dried over anhydrous magnesium sulfate, and evaporated to give 157 mg of crude product. The crude product was chromatographed using normal grade silica gel. Elution with toluene gave, in 25% yield, 30 mg of pure dark needles, mp 103–104°C (lit. (35) mp 98–100°C, 91–92°C); ir (cm^{-1}): 1460, 1410, 1355, 1330–1310, 1050, 960, 760, 750, 650; ^1H nmr δ: 7.78 (dd, J = 8.6, 2.5, 2H), 7.60 (dd, J = 8.6, 2.5, 2H), 3.77 (s, 3H, N-CH_3); ms m/z: 193 (M^+, 100), 117 ($M^+ - CS_2$, 28).

S,S-Dimethyldithio-β-isoindigo (17)

To a solution of 207 mg of **9** (1.16 mmol) in 3 mL of 0.8 *M* sodium hydroxide and 1 mL methanol, 0.06 mL of methyl iodide was added (0.96 mmol). The red solution became less intense in color and after a while a precipitate was formed. The suspension was stirred at room temperature for 18 h during which a red precipitate of *S,S*-dimethyldithio-β-isoindigo (**17**) appeared and the solution became clear. The methanol was evaporated under reduced pressure, water was added, and the insoluble material was filtered and washed with water. The crude product was dissolved in hot ethyl acetate and the hot suspension was filtered to remove 20 mg of insoluble material, which by mass spectra and ^1H nmr was shown to have a structure corresponding to an isoindigo trimer. This fraction was not further characterized. The crude **17** was recrystallized from ethyl acetate to give, in 60% yield, 92.8 mg of pure **17** as red or golden needles according to the concentration of the crystallizing solution, mp 260–263°C (lit. (30) mp 258°C); ir (cm^{-1}): 1470, 1455, 1340, 1265, 1030, 755, 660; ^1H nmr δ: 8.79 (d, J = 7.5, 2H), 7.60–7.40 (m, 6H), 2.95 (s, 6H, SCH_3); ^{13}C nmr δ: 172.70, 145.56, 139.80, 137.82, 129.22, 128.16, 126.56, 119.81, 13.49; ms m/z: 322 (M^+, 100), 307 ($M^+ - 15$, 80), 274 ($M^+ - SCH_3$, 73), 161 (M^{+2}, 10), 146 ($M - 15$, 25).

The fine structure of **17** regarding geometrical isomerism is not clear. Elvidge and Golden (36) suggested the *trans* form for dialkylimino-β-isoindigos since these compounds did not form complexes with metals. Dithio-β-isoindigo, on the other hand, did form metal complexes and was suggested by Drew and Kelly (30) to be in the *cis* form.

N-Ethyldithiophthalimide (18) and S,S-diethyldithio-β-isoindigo (19)

A solution of 125 mg of dithiophthalimide (**9**) (0.70 mmol) and

Can. J. Chem. Downloaded from www.nrcresearchpress.com by 118.98.75.50 on 09/07/12
For personal use only.

10 mL of triethylorthoformate was heated to 160°C for 3 h and then to 180°C according to the procedure of Rutavichyus and Iokubaitite (29). The volatile material (5–7 mL) had been removed by distillation through a fractionating column at 180°C. The solution was cooled and the excess triethylorthoformate was removed under pressure at 60°C/0.1 Torr (1 Torr = 133.3 Pa). Preliminary purification of the crude reaction mixture was done by column chromatography using normal grade silica gel. Elution with ether – petroleum ether (1:9) gave some elemental sulfur and 18.3 mg of *N*-ethyldithiophthalimide **18** (13% yield) as red needles, mp 51–53°C (lit. (35) mp 47–48°C, 81–83°C); ir (cm^{-1}): 1465, 1355, 1065, 765, 720, 700; ^1H nmr δ: 7.85 (dd, J = 8.7, 2.5, 2H), 7.66 (dd, J = 8.7, 2.5, 2H), 4.50 (q, J = 7, 2H, N-CH_2), 1.29 (t, J = 7, 3H, CH_2CH_3), ms m/z: 207 (M^+, 100), 191 (29), 179 (31).

Further elution of the silica gel gave 88 mg of a mixture consisting of *N*-ethyldithiophthalimide **18**, *S,S*-diethyldithio-β-isoindigo, **19**, and unreacted starting material, **9**. This mixture was further purified by preparative tlc using ether – petroleum ether (1:9) as eluting solvent. The yellow moving band consisting of **19** was extracted with ether in a Soxhlet apparatus to give, after solvent evaporation, 10 mg of pure **19** as golden needles in 8% yield, mp 126–128°C (with previous softening) (lit. (30) mp 162°C); ir (cm^{-1})): 1470, 1450, 1330, 1270, 1245, 1020, 745, 650; ^1H nmr δ: 8.78 (d, J = 7.3, 2H), 7.67–7.40 (m, 6H), 3.57 (q, J = 7.4, 4H, S-CH_2), 1.62 (t, J = 7.4, 6H, CH_2CH_3); ms m/z: 350 (M^+, 80), 321 ($M^+ - 29$, 100).

The unreacted dithiophthalimide was not recovered.

*3-(3-Ethoxy-1*H*-isoindol-1-ylidene)-2,3-dihydro-1*H*-isoindol-1-thione (**22**)*

A suspension of 1.08 g (6.09 mmol) of 3-ethoxy-isoindol-1-one (**20**) (31) and 1.36 g (3.36 mmol) of Lawesson's reagent (**13**) (18) in 10 mL of dry toluene was refluxed under argon for 2 h. After cooling to room temperature the crude product was purified by flash chromatography using toluene as eluant to give, in 12% yield, 111 mg of **22** as red crystals, mp >300°C; ir (cm^{-1}): 1635, 1530, 1340, 1140, 1080, 750; ^1H nmr (acetone-d_6) δ: 8.97 (d, J = 7.7, 1H), 8.63 (d, J = 7.8, 1H), 8.02 (d, J = 7.7, 1H), 7.78–7.54 (m, 5H), 4.79 (q, J = 7.0, 2H, CH_2O), 1.57 (t, J = 7.0, CH_3CH_2); ^{13}C nmr (DMSO-d_6) δ: 190.88, 170.66, 137.04, 136.03, 135.28, 132.73, 132.13, 131.64, 130.34, 129.75, 129.66, 128.41, 126.80, 124.44, 123.73, 120.56, 65.30, 14.38; ms m/z: 306 (M^+, 100), 277 ($M^+ - 29$, 87).

*A synthesis of 2-neopentoxyphthalocyanine (**4**) and 2,16-dineopentoxyphthalocyanine (**5**) (Experiment 1)*

The crude 1,3-diiminoisoindoline derived from 200 mg of phthalonitrile (1.56 mmol) in 2 mL of *N,N*-dimethylaminoethanol was heated to 50°C until completely dissolved. After 1 h, 274 mg of **10** (1.03 mmol) was added. The very light green solution turned red and then dark. The solution was stirred at 80–90°C under an argon atmosphere for 24 h. The mixture was cooled to room temperature, diluted with water, filtered, and washed thoroughly with water and then with methanol until the filtrate was almost clear. The crude product (112 mg) was extracted with methanol in a Soxhlet extractor for 10 h until the extract was almost clear. This process removed brown impurities. The desired product was then extracted for 5 h (extract 1) with freshly distilled THF to give 42 mg of a mixture of phthalocyanines. Mass spectra (Table 3) of the mixture showed that it consisted of mainly the 2,16-dineopentoxyphthalocyanine (**5**) (with perhaps 2,9-dineopentoxyphthalocyanine (**6**)) with a trace of the 2,9,16,23-tetraneopentoxyphthalocyanine (**8**) and some 2,9,16-trineopentoxyphthalocyanine (**7**), 2-neopentoxyphthalocyanine (**4**), and phthalocyanine (**3**). This fraction was purified by vacuum liquid chromatography (vlc) (23) using hexane (200 mL) as the eluting solvent, followed by hexane–toluene (1:1 × 700 mL) hexane–toluene (1:4 × 200 mL), toluene (500 mL), and finally 2-methoxyethanol–toluene (1:9 × 700 mL). The different fractions were examined by mass spectra (Table 3). Only partial separation was achieved.

The original mixture of phthalocyanines was subsequently extracted with toluene for 10 h and with THF for 19 h (extract 2) to give 27 mg of a mixture of phthalocyanines consisting mainly of monosubstituted phthalocyanine (**4**) and some unsubstituted, disubstituted, and a trace of trisubstituted phthalocyanines (Table 3). Further purification by vlc as above removed all trineopentoxyphthalocyanine but did not completely separate the dineopentoxyphthalocyanine from the mononeopentoxyphthalocyanine (Table 3). However, most of the unsubstituted phthalocyanine (**3**) was left on the column. The monosubstituted phthalocyanine (**4**) was recrystallized from toluene from a fraction (vlc fraction 3, Table 3) containing a trace amount of disubstituted phthalocyanine (**5**) but the crystallized product (**4**) still contained a trace of the disubstituted phthalocyanine (vlc fraction 3[e], Table 3).

Subsequent extraction of the original mixture with THF for 48 h (extract 3) removed 12.6 mg of a fraction consisting mainly of unsubstituted phthalocyanine (**3**) along with some **4** and a trace of **5** (Table 3). The phthalocyanines remaining in the thimble after the three extractions were the unsubstituted one and some monosubstituted (Table 3).

*A synthesis of 2-neopentoxyphthalocyanine (**4**) (Experiment 2)*

The crude 1,3-diiminoisoindoline derived from 2.0 g of phthalonitrile (15.6 mmol) in 15 mL of *N,N*-dimethylaminoethanol was heated to 120°C under an argon atmosphere for 2 h. Compound **10**, 135 mg (0.51 mmol), was then added and the mixture was kept at 120°C for an additional 3 h. The mixture was cooled to room temperature, diluted with water, filtered, and washed thoroughly with water followed by methanol until the filtrate was almost clear. The crude product was extracted with methanol in a Soxhlet apparatus until the extract was almost clear to remove brown and yellow impurities. The 1.56 g of the desired product was fractionally extracted with freshly distilled THF for 5 days. At intermittent times the solvent was evaporated, the phthalocyanines mixture was examined by mass spectra (Table 3), more solvent was added, and the extraction continued. The total amount of phthalocyanines removed by extraction after 5 days was 63.4 mg; 1.50 g was left in the thimble. The first extract contained a trace of **7**, some **5** (plus **6**), mainly **4** and **3** (Table 3). Subsequent extractions contained increasing amounts of the **5** and **4** without **7** (Table 3). During the last extraction a precipitate was formed which was filtered off to give 19.1 mg of mainly **3**, some **4**, and a trace of **5** (Table 3). The filtrate, 12.2 mg, contained **5** and **4** (Table 3).

Acknowledgements

We are grateful to the Natural Sciences and Engineering Research Council of Canada for financial support of this research.

1. F. H. Moser and A. L. Thomas. The phthalocyanines. Vols. I and II. CRC Press, Boca Raton, FL. 1983; A. B. P. Lever. Adv. Inorg. Chem. Radiochem. **7**, 27 (1965).
2. S. A. Mikhalenko, S. V. Barkanova, O. L. Lebedev, and E. A. Luk'yanets. Zh. Obshch. Khim. **41**, 2735 (1971); I. G. Oksengendler, N. V. Kondratenko, E. A. Luk'yanets, and L. M. Yagupol'skii. Zh. Org. Khim. **13**, 1554 (1977); V. I. Gavrilov, L. G. Tomilova, V. M. Derkacheva, E. V. Chernykh, N. T. Ioffe, I. V. Shelepin, and E. A. Luk'yanets. Zh. Obshch. Khim. **53**, 1347 (1983).
3. R. C. Graham, E. M. Eyring, and G. H. Henderson. J. Chem. Soc. Perkin Trans. 2, 765 (1981); M. Hanack, J. Metz, and G. Pawlowski. Chem. Ber. **115**, 2836 (1982); S. W. Oliver and T. D. Smith. Heterocycles, **22**, 2047 (1984); A. W. Snow and N. L. Jarvis. J. Am. Chem. Soc. **106**, 4706 (1984).
4. G. Pawlowski and M. Hanack. Synthesis, 287 (1980).
5. Z. Witkiewicz, R. Dabrowski, and W. Waclawek. Mater. Sci. II, 39 (1976); L. I. Solov'eva and E. A. Luk'yanets. Zh. Obshch. Khim. **50**, 1122 (1980); D. Wöhrle and B. Wahl. Tetrahedron Lett. **20**, 227 (1979); M. J. Camenzind and C. L. Hill. J. Heterocycl. Chem. **22**, 575 (1985); N. Kobayashi, M. Koshiyama, Y. Ishikawa, T. Osa, H. Shirai, and N. Hojo. Chem. Lett. 1633 (1984).
6. C. Piechocki, J. Simon, A. Skoulios, D. Guillon, and P. Weber. J. Am. Chem. Soc. **104**, 5245 (1982).
7. M. Hedayatullah. C. R. Acad. Sci. Ser. 2, **296**, 621 (1983).

8. H. SHIRAI, K. HANABUSA, M. KITAMURA, and E. MASUDA. Makromol. Chem. **185**, 2537 (1984); E. M. IDELSON. U.S. Patent No. 4 061 654 (1977); Chem. Abstr. **88**, 171797 m (1978).
9. C. C. LEZNOFF and T. W. HALL. Tetrahedron Lett. **23**, 3023 (1982); T. W. HALL, S. GREENBERG, C. R. MCARTHUR, B. KHOUW, and C. C. LEZNOFF. Nouv. J. Chim. **6**, 653 (1982); D. WÖHRLE and G. KRAWCZYK. Polym. Bull. **15**, 193 (1986).
10. C. PIECHOCKI and J. SIMON. J. Chem. Soc. Chem. Commun. 259 (1985).
11. P. J. BRACH, S. J. GRAMMATICA, O. A. OSSANNA, and L. WEINBERGER. J. Heterocycl. Chem. **7**, 1403 (1970).
12. F. H. MOSER and A. L. THOMAS. Phthalocyanine compounds. Reinhold, New York. 1963; K. KASUGA and M. TSUTSUI. Coord. Chem. Rev. **32**, 67 (1980).
13. H. TOMODA, S. SAITO, S. OGAWA, and S. SHIRAISHI. Chem. Lett. 1277 (1980); H. TOMODA, S. SAITO, and S. SHIRAISHI. Chem. Lett. 313 (1983).
14. E. E. REID. Organic chemistry of bivalent sulfur. Vol. 3. Chemical Publishing Co., New York. 1960. Chap. 2.
15. S. I. KANEVSKAYA and V. B. BRASYUNAS. Zh. Obshch. Khim. **29**, 1930 (1959).
16. G. E. FICKEN and R. P. LINSTEAD. J. Chem. Soc. 3525 (1955); R. P. LINSTEAD and M. WHALLEY. J. Chem. Soc. 3530 (1955).
17. C. C. LEZNOFF, S. GREENBERG, S. M. MARCUCCIO, P. C. MINOR, P. SEYMOUR, A. B. P. LEVER, and K. B. TOMER. Inorg. Chim. Acta, **89**, L35 (1984); C. C. LEZNOFF, S. M. MARCUCCIO, S. GREENBERG, A. B. P. LEVER, and K. B. TOMER. Can. J. Chem. **63**, 623 (1985); S. M. MARCUCCIO, P. I. SVIRSKAYA. S. GREENBERG, A. B. P. LEVER, C. C. LEZNOFF, and K. B. TOMER. Can. J. Chem. **63**, 3057 (1985); S. GREENBERG, S. M. MARCUCCIO, C. C. LEZNOFF, and K. B. TOMER. Synthesis, 406 (1986).
18. B. S. PEDERSEN, S. SCHEIBYE, N. H. NILSSON, and S.-O. LAWESSON. Bull. Soc. Chim. Belg. **87**, 223 (1978); R. A. CHERKASOV, G. A. KUTYREV, and A. N. PUDOVIK. Tetrahedron, **41**, 2567 (1985); M. P. CAVA and M. I. LEVINSON. Tetrahedron, **41**, 5061 (1985).
19. P. F. CLARK, J. A. ELVIDGE, and R. P. LINSTEAD. J. Chem. Soc. 3593 (1953).
20. R. L. MARKEZICH and O. S. ZAMEK. J. Org. Chem. **42**, 3431 (1977); L. I. SPIESSENS and M. J. O. ANTEUNIS. Bull. Soc. Chim. Belg. **92**, 965 (1983).
21. D. E. GAMES, A. H. JACKSON, and K. T. TAYLOR. Org. Mass Spectrom. **9**, 1245 (1974); S. M. SCHILDCROUT. J. Am. Chem. Soc. **105**, 3852 (1983).
22. W. C. STILL, M. KAHN, and A. MITRA. J. Org. Chem. **43**, 2923 (1978).
23. N. M. TARGETT, J. P. KILCOYNE, and B. GREEN. J. Org. Chem. **44**, 4962 (1979).
24. T. J. HURLEY, M. A. ROBINSON, and S. I. TROTZ. Inorg. Chem. **6**, 389 (1967).
25. M. E. BAGULEY and J. A. ELVIDGE. J. Chem. Soc. 709 (1957).
26. W. KÖHLER, M. BUBNER, and G. ULBRICHT. Chem. Ber. **100**, 1073 (1967).
27. M. LEMPERT-SRÉTER and K. LEMPERT. Acta Chim. Hung. **117**, 121 (1984).
28. M. A. CASADEI, B. DI RIENZO, and F. M. MORACCI. Synth. Commun. **13**, 753 (1983).
29. A. I. RUTAVICHYUS and S. P. IOKUBAITITE. Zh. Org. Khim. **12**, 2604 (1984).
30. H. D. K. DREW and D. B. KELLY. J. Chem. Soc. 625 (1941).
31. D. R. ANDERSON, J. S. KEUTE, T. H. KOCH, and R. H. MOSELEY. J. Am. Chem. Soc. **99**, 6332 (1977).
32. V. F. BORODKIN. Zh. Prikl. Khim. (Leningrad), **31**, 813 (1958); F. BAUMANN, B. BIENERT, G. RÖSCH, H. VOLLMANN, and W. WOLF. Angew. Chem. **68**, 133 (1956).
33. J. A. ELVIDGE and N. R. BAROT. *In* The chemistry of double-bonded functional groups. Part 2. *Edited by* S. Patai. John Wiley & Sons, London. 1977. p. 1167.
34. R. SATO, T. SENZAKI, Y. SHIKAZAKI, T. GOTO, and M. SAITO. Chem. Lett. 1423 (1984); R. SATO, M. NAKAYAMA, Y. YUZAWA, T. GOTO, and M. SAITO. Saito. Chem. Lett. 1887 (1985).
35. M. MACHIDA, K. ODA, E. YOSHIDA, and Y. KANAOKA. J. Org. Chem. **50**, 1681 (1985); J. P. BROWN. British Pat. 1261817 (1971); Chem. Abstr. **76**, 85574g (1972).
36. J. A. ELVIDGE and J. H. GOLDEN. J. Chem. Soc. 4144 (1956).

Can. J. Chem. Downloaded from www.nrcresearchpress.com by 118.98.75.50 on 09/07/12
For personal use only.

Enolization of the benzocyclohexadienone formed during the bromination of 1-naphthol in aqueous solution

OSWALD S. TEE[1] AND N. RANI IYENGAR

Department of Chemistry, Sir George Williams Campus, Concordia University, Montréal, P.Q., Canada H3G 1M8

Received November 17, 1986

This paper is dedicated to Professor John T. Edward

OSWALD S. TEE and N. RANI IYENGAR. Can. J. Chem. **65**, 1714 (1987).

Benzo-4-bromo-2,5-cyclohexadienone (**5**) has been observed in the aqueous bromination of 1-naphthol and the kinetics of its enolization to 4-bromo-1-naphthol have been studied in the pH range 0–7. This process is catalyzed by the proton, hydroxide ion, water, buffer acids, and by buffer bases. For catalysis by general bases the Brønsted $\beta = 0.59$ whereas catalysis by general acids has a value of $\alpha \sim 0$. These findings are very similar to those obtained previously for the 4-bromo-2,5-cyclohexadienone **2***b*, formed during the aqueous bromination of 2,6-dimethylphenol. The mechanistic implications of the results are discussed. The enolization of the related dienone **8**, formed from bromine and 1-naphthol-2-carboxylic acid, was also studied. At acidic pHs the dienone **8** is much more reactive than **5**, with the 2-COOH behaving as an internal catalyst having an "effective molarity" of about 110 *M*. The enolization of **8** is also catalyzed by buffer bases.

OSWALD S. TEE et N. RANI IYENGAR. Can. J. Chem. **65**, 1714 (1987).

On a observé la formation de benzo bromo-4 cyclohexadiène-2,5 one (**5**) au cours de la bromation du naphtol-1 en milieu aqueux; opérant à des pH allant de 0 à 7, on a étudié la cinétique de son énolisation en bromo-4 naphthol-1. La réaction est catalysée par les protons, les ions hydroxydes, l'eau, les tampons acides ainsi que basiques. Dans le cas de la catalyse générale par les bases, la valeur β de Brønsted = 0,59 alors que pour la catalyse générale par les acides, la valeur $\alpha \sim 0$. Ces résultats sont semblables à ceux obtenus antérieurement pour la bromo-4 cyclohexadiène-2,5 one (**2***b*) qui se forme au cours de la bromation du diméthyl-2,6 phénol, en milieu aqueux. On discute des implications mécanistiques de ces résultats. On a aussi étudié l'énolisation de la dièнone **8** apparentée qui se forme à partir du brome et de l'acide naphtol-1 carboxylique-2. À des pH acides, la dièнone **8** est beaucoup plus réactive que **5** à cause du COOH en position 2 qui agit comme catalyseur interne et qui aurait un « molarité efficace » d'environ 110 *M*. L'énolisation de **8** est aussi catalysée par les tampons basiques.

[Traduit par la revue]

In acidic aqueous solution the bromination of phenol (1) leads largely to *para* substitution (**1***a* → **2***a* → **3***a*) (2). The cyclohexadienone (**2***a*) that is involved in this reaction can be observed (3) but detailed study of its behaviour is difficult because of its short half-life (<44 ms) and because the difference between its rates of formation and decay is not large (3, 4). Several methylated dienones have been generated and studied, particularly the 2,6-dimethyl derivative **2***b*, which is formed much more quickly and decays more slowly than does **2***a* (3, 4). Cyclohexadienones cannot be observed during the aqueous bromination of phenols bearing electron-withdrawing substituents (4). Such phenols react slowly with bromine (1, 2, 5, 6) whereas the intermediate dienones must enolize more rapidly than **2***a* (4).

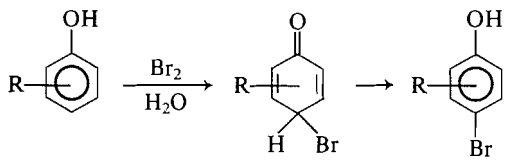

1 **2** **3**

a: R = H; *b*: R = 2,6-dimethyl

Enolization of the cyclohexadienone **2***b* shows catalysis by general acids and general bases (4). Catalysis by the latter is quite straightforward with a Brønsted $\beta = 0.54$. This value, together with primary and solvent isotope effects, can be explained by simple rate-limiting deprotonation of **2** leading to the anion of the product **3**. In contrast, the general acid catalysis has a Brønsted $\alpha \sim 0$, which cannot be explained by simple mechanisms. It was attributed to a termolecular transition state (water, dienone, general acid HA) in which proton transfer from the dienone to the base (water) is far in advance of that from HA to the dienone oxygen (4).

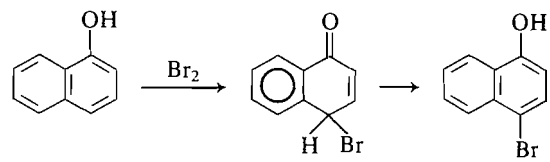

4 **5** **6**

Since this type of mechanism is not usual for ketone enolization (7), we have sought another phenol from which a dienone of reasonable lifetime could be formed and which could, therefore, be studied in detail. A good candidate appeared to be 1-naphthol (**4**) for two reasons. Firstly, since it is a naphthalene, in which each benzenoid ring is less "aromatic" than benzene (8), 1-naphthol should be much more reactive towards bromine[2] than is phenol. Secondly, the benzo ring in the dienone **5** should be a stabilizing feature and so give rise to an intermediate having a longer lifetime than **2***a*. These expectations have been realized and the present paper describes studies of the enolization of **5**. In addition we have also studied the dienone **8** formed from 1-naphthol-2-carboxylic acid (**7**) and bromine. The intention here was to see if the 2-COOH functions as an internal catalyst in the enolization of **8**.

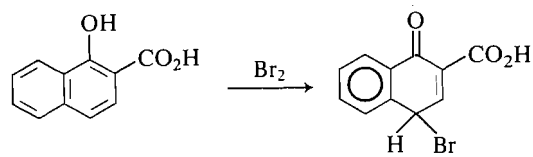

7 **8**

[1]Author to whom correspondence may be addressed.

[2]Naphthalene is much more reactive than benzene towards various electrophiles (9).

Can. J. Chem. Downloaded from www.nrcresearchpress.com by 118.98.75.50 on 09/07/12
For personal use only.

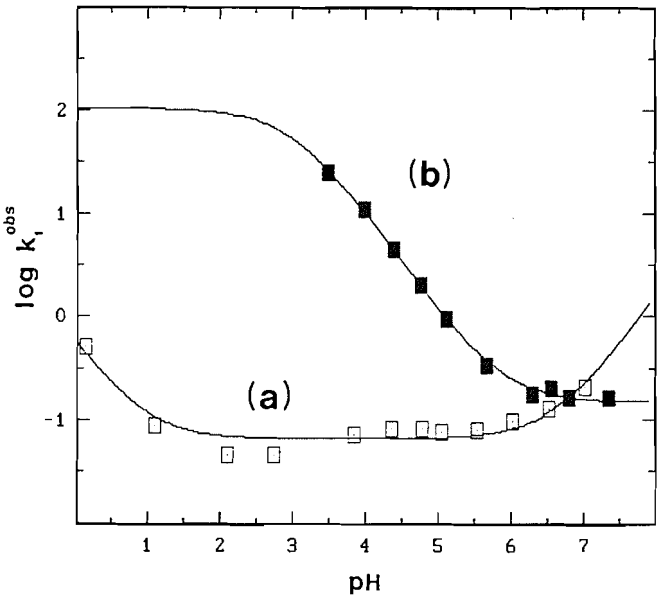

FIG. 1. pH–rate profiles for the enolization of (*a*) dienone **5** (open symbols); (*b*) dienone **8** (closed symbols).

Results

As anticipated, 1-naphthol reacts rapidly with aqueous bromine. Indeed, even at spectrophotometric concentrations the uv absorption bands of bromine and tribromide ion[3] disappear within the dead time of the stopped-flow apparatus. At longer times, however, one can observe a decrease in absorbance around 270 nm that is ascribed[4] to the enolization of the dienone **5** to **6**. The product of the overall reaction is 4-bromo-1-naphthol (**6**), as one expects from synthetic brominations (12).

First-order rate constants (k_{obs}) for the conversion of **5** to **6** vary with pH as shown in Fig. 1*a*. In the pH range 2–6 these values are essentially constant but they rise at higher and lower pHs. The results may be represented by eq. [1] in which k_H is the catalytic coefficient for hydronium ion catalysis, k_0 is the rate constant for a "spontaneous" or "water-catalyzed" reaction, and k_{OH} is for hydroxide ion catalysis.

$$[1] \quad k_{obs} = k_H[H^+] + k_0 + k_{OH}K_w/[H^+]$$

For the data shown in Fig. 1*a* appropriate constants are $k_H = 0.52 M^{-1} s^{-1}$, $k_0 = 0.065 s^{-1}$, and $k_{OH}K_w = 1.6 \times 10^{-8} M s^{-1}$. From this last value and $pK_w = 13.80$ (13) a value of $k_{OH} = 1.0 \times 10^6 M^{-1} s^{-1}$ is estimated. The data in the central region do not conform well to a constant value of k_0, due to buffer catalysis (see below). Consequently, a better estimate of k_0 (for the purposes of analysis) was obtained from the intercepts of buffer plots.

Catalysis by carboxylic acid buffers was found at pHs spanning the range 1.90–4.92. Individual buffer plots are linear over the concentration range used, with no upward curvature indicative of second-order terms in the buffer. Analysis of the slopes of the buffer plots in terms of the fractions of the acidic and basic components of the buffers yielded the catalytic coefficients (k_{HA} and k_A) given in Table 1. Also given there are values for the hydronium ion, hydroxide ion, and water.[5] The value of k_A for water[6] is taken as $k_0/(55.5 M)$, where $k_0 = 0.0463 s^{-1}$ was obtained from the average of the intercepts of all the buffer plots. The catalytic constant for hydronium ion in Table 1 was estimated from the data point at highest acidity and the value of k_0, just given.

Clearly, the conversion of **5** to **6** is catalyzed by general acids and general bases, as was found earlier for the enolization of the dienone **2***b* (4). Figure 2 shows the Brønsted plots generated from the values of k_A and k_{HA} in Table 1. They are both very

TABLE 1. Catalytic constants for enolization of the dienone **5**

Acid (HA)	pK_a	k_A	k_{HA}
Hydronium ion	−1.74	8.34×10^{-4}	0.626
Cyanoacetic	2.23	0.198	0.459
Chloroacetic	2.74	0.472	0.439
Methoxyacetic	3.52	0.855	0.966
3-Chloropropionic	3.93	2.29	2.05
Acetic	4.65	4.02	3.04
Water	15.54[b]	(1.0×10^6)[c]	—

[a]At 25°C, $I = 1.0 M$ (NaCl); pK_a values as in ref. 4. Units of k_A and k_{HA} are $M^{-1} s^{-1}$.
[b]Equals log 55.5 + pK_w, where $pK_w = 13.80$ (13).
[c]Not included in Fig. 2.

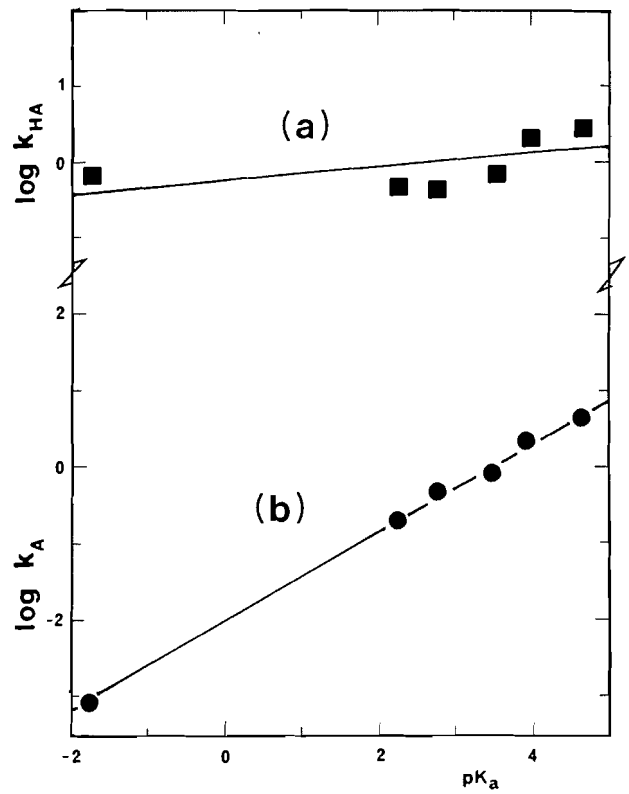

FIG. 2. Brønsted plots for catalysis of the enolization of the dienone **5** by (*a*) general acids, HA; (*b*) general bases, A^-.

[3]For various reasons (10) kinetic studies of bromination reactions are usually carried in the presence of a large excess of added bromide ion (1, 2, 6, 10). Consequently, a considerable fraction of the initial bromine is present as Br_3^- (1, 10).

[4]Naphthalenones similar to **5** have 3 or 4 absorption maxima in the region 230–300 nm (11).

[5]The values for hydronium ion and hydroxide ion are not particularly accurate as they are based on limited data (Fig. 1*a*). However, they are probably within a factor of two of the correct values.

[6]The k_0 term in eq. [1] is ascribed to water acting as a general base. As previously (3, 4), it cannot be due to OH^- attacking the protonated form of the dienone. Such would require an unrealistically large second-order rate constant.

Can. J. Chem. Downloaded from www.nrcresearchpress.com by 118.98.75.50 on 09/07/12
For personal use only.

similar to the analogous plots obtained for **2***b* (4). The values of k_A (excluding the value for OH^-) give $\beta = 0.59$ (sd = 0.02, r = 0.9979) for general base catalysis.[7]

The values of k_{HA} for the buffer acids show little variation and are not very different from the value for H_3O^+. Taken as a whole these data give $\alpha = -0.09$ (sd = 0.06). Without the point for H_3O^+ the data for the carboxylic acids give a negative value: $\alpha = -0.38$ (sd = 0.06)!

The benzocyclohexadienone **8** was generated from 1-naphthol-2-carboxylic acid (**7**) and bromine. The pH–rate profile for its decomposition is shown in Fig. 1*b*. At pH > 6 the profile is essentially flat and **8** shows a reactivity very similar to that shown by the unsubstituted dienone **5** in its pH-independent region. However, below pH 6 the profile for **8** rises steeply, indicating an enhanced reactivity relative to that of **5**. Unfortunately, the solubility of undissociated **7** in water is very low and it was not possible to extend the profile below pH 3.5.

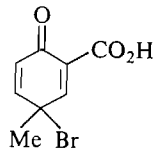

9

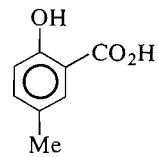

10

For the structurally similar dienone **9**, generated from 5-methylsalicylic acid (**10**), the pK_a of the carboxyl group is 3.06 (14, 15). Therefore, the pK_a of the carboxyl group of **8** should be about 3 and, as shown in Fig. 1*b*, the rate profile should have an inflection in the region that is not accessible due to low solubility (see above). The profile for **8** can be represented by eq. [2], where k_1 describes the flat portion of the profile and the second term assumes that the reactive species at low pH is the undissociated form of **8** reacting with rate constant k_2.

$$[2] \quad k_{obs} = (k_1 K_a + k_2[H^+])/(K_a + [H^+])$$

The data conform well to this equation with $k_1 = 0.14\ s^{-1}$ and $k_2 = 110\ s^{-1}$, assuming that the pK_a is 3.[8]

The enolization of the dienone **8** was also studied in two buffers. Around pH 5, where the second term of eq. [2] is dominant, there is strong catalysis by acetate buffers that corresponds to attack of acetic acid on the anion of **8**, with $k_{HA} = 78\ M^{-1}\ s^{-1}$ and no detectable catalysis by acetate ion. Above pH 6, in the region where k_1 becomes dominant in eq. [2], catalysis was found in phosphate buffers. Analysis of the buffer plots indicates catalysis by both buffer components with catalytic constants of $46\ M^{-1}\ s^{-1}$ for $H_2PO_4^-$ and $22\ M^{-1}\ s^{-1}$ for HPO_4^{2-}.

Discussion

The present results for the enolization of the benzocyclohexadienone **5** are very similar to those obtained earlier for the 2,6-dimethyl derivative **2***b*, with **5** being slightly less reactive. Thus, the various catalytic constants for **5** (Table 1) are about 5 times smaller than those for **2***b* (4) and so the Brønsted exponents (α and β) for the two dienones are virtually the same.

For general base catalysis of the enolization of **5** by carboxylate ions and water the value of β equals 0.59. It is possible that hydroxide ion also follows the same correlation.[7] As found previously for **2***b* (4), the results are quite consistent with simple rate-limiting deprotonation of the dienone by the general base to give the anion of the product (Scheme 1).

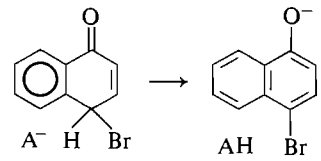

5

SCHEME 1. General base-catalyzed enolization of dienone **5**.

The value of α for general acid catalysis is essentially zero,[9] much lower than is normally found for ketone enolization (7). As argued earlier, this difference in behaviour is probably due to the fact that the enolization of cyclohexadienones is highly *exo*thermic (4, 16)[10] whereas that of simple ketones is significantly *endo*thermic (7, 17, 18). In explanation, we suggested that the transition state contains water, dienone, and the general acid (HA) (Scheme 2) and that transfer of the C4 proton of the dienone to water is far in advance of the proton transfer from HA to the dienone oxygen. This mechanism effectively avoids the protonated form of the dienone, which should be a relatively high energy species (4).

A mechanism that is kinetically indistinguishable from that just described involves A^- as the base and hydronium ion as the acid. For this mechanism the data for **2***b* and **5** require β to be about 1, which is not reasonable. Simple proton abstraction from **5** by general bases (Scheme 1) has $\beta = 0.59$ and so a *lower* value than this should be obtained for proton abstraction assisted by hydrogen bonding or by proton transfer from the hydronium ion.

A disturbing feature of the present data for general acid catalysis (Fig. 2*a*), as with the previous data (4), is that without the point for hydronium ion the value of α is decidedly *negative*. While it is conceivable that catalysis by H_3O^+ and by carboxylic acids is due to different mechanisms, we have no detailed explanation of why catalysis by carboxylic acids should have a negative α value. In view of the accumulated errors involved (see Experimental), the value of α should probably be taken as zero. For the mechanism outlined in the previous paragraph, a value of $\beta > 1$ would be required, equally anomalous.

Anomalous Brønsted exponents have been discussed by various authors (19). They cite several studies of the ionization of nitroalkanes in which it was found that structural change *in the nitroalkane* corresponds to an α value outside the normal range. However, for a given nitroalkane and a series of bases,

[7]If hydroxide ion is included in the plot, $\beta = 0.42$ (sd = 0.06, r = 0.9472). Thus, it may well be that OH^- also belongs on the correlation for general bases but that the Brønsted plot shows some curvature over 17 pK_a units.

[8]Nonlinear fitting of eq. [2] to the data gives $k_1 = 0.147\ s^{-1}$, $k_2 = 104\ s^{-1}$, and $K_a = 9.74 \times 10^{-4}\ M$ (pK_a = 3.01).

[9]As pointed out by a referee, water must fall off the line with $\alpha = 0$ since it does not swamp the effect of other general acids. This is reasonable, we believe, for the proposed mechanism in Scheme 2. We visualize that proton transfer from HA occurs after some negative charge has built up the dienone oxygen (4). This transfer can be thermodynamically favourable for carboxylic acids ($\alpha \sim 0$) but *must* be unfavourable ($\alpha \sim 1$) for water since the product pK_a is less than 10. Consequently, over the range of pK_a −2 to 16 the Brønsted plot for general acids must be curved.

[10]In our earlier paper (4) we employed pKs to estimate that phenol is favoured over 2,5-cyclohexadienone by a factor of 10^{11} (equivalent to 15 kcal/mol) in aqueous solution. More recently, using gas phase measurements, Shiner *et al.* have deduced that the dienone is less stable than phenol by 10 ± 3 kcal/mol (16).

Can. J. Chem. Downloaded from www.nrcresearchpress.com by 118.98.75.50 on 09/07/12
For personal use only.

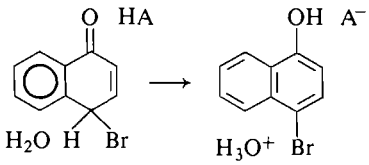

SCHEME 2. General acid-catalyzed enolization of dienone **5**.

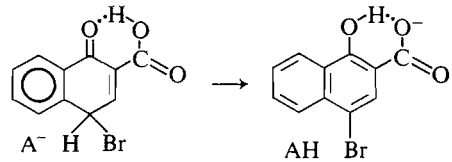

8

SCHEME 3. Enolization of dienone **8** catalyzed by the *internal* acid group and an *external* base.

normal β values were found (19). In contrast, our work on the dienones **2***b* and **5** yields unusual α values for a series of general acid catalysts. It is probably the case that the proton transfers, electronic reorganization, and solvation changes are appreciably asynchronous[11] so that the transition state for dienone enolization in Scheme 2 does not strongly resemble either reactants *or* products. In such a case, normal Brønsted exponents may not be appropriate (19).

In an attempt to provide additional information about the mechanism of enolization of cyclohexadienones we have studied the behaviour of the dienone **8**. This molecule contains a carboxyl group adjacent to the dienone oxygen that might function in place of the external general acid HA required by the mechanism depicted in Scheme 2. Earlier attempts in this laboratory to observe enolizable cyclohexadienone intermediates in the bromination of salicylic acids were unsuccessful (14), and so it was concluded that they were too transient to be detected by stopped-flow technique. The present results for the dienone **8** support this conclusion, since over most of the pH range studied it is much more reactive than **5**. This implies that the analogous dienone derived from salicylic acid would be significantly more reactive than the dienone **2***a* and so it would not have been observable at the pHs used.

The rate profile for the enolization of the carboxyl-bearing dienone **8** has two distinct regions (Fig. 1*b*), which can be described by the two terms in eq. [2]. The first term is attributed to water abstracting the C4 proton from the anion of **8**, since its value ($0.14\,s^{-1}$) is similar to k_0 ($0.046\,s^{-1}$) for the water-catalyzed deprotonation of **5**.[6] There may also be proton abstraction by general bases, since buffer catalysis was observed in phosphate buffers, as discussed later.

The second term in eq. [2] is attributed to reaction of the undissociated form of the carboxylic acid, **8**. However, the increase in rate at pH < 6 could be due to a proton-catalyzed reaction of the anion of **8**. If such were the case, the rate constant for H^+ catalysis would be $1.1 \times 10^5\,M^{-1}\,s^{-1}$, meaning that the anion of **8** is 200 000 times more reactive than the dienone **5** in acid-catalyzed enolization. This factor is not reasonable for a simple substituent effect of a *meta* carboxylate group, since the appropriate substituent constant is virtually zero (20). Likewise, the rate enhancement is much too large for an electrostatic effect of the carboxylate ion on the rate of proton transfer; such effects are relatively small (less than a factor of 100) for monoanions It is also unreasonable to ascribe the rate increase to hydrogen-bond stabilization of the incipient protonated dienone oxygen, since in energy terms this would have to be 7.2 kcal/mol.

We conclude, therefore, that **8** reacts as its undissociated form at pH < 6 and that the 2-carboxyl group functions as an intramolecular general acid catalyst. It is envisaged that water (or another general base) abstracts the C4 proton of **8** and there is proton transfer from the 2-carboxyl group to the dienone oxygen (Scheme 3), the two processes not necessarily being synchronous. This mechanism is an intramolecular analogue of that proposed for the general acid-catalyzed enolization of **5** (Scheme 2), with the 2-carboxyl replacing HA. Moreover, the mechanism in Scheme 3 is similar to that for the debromination of the "*ipso* dienone" **9**, which also exhibits intramolecular catalysis (14, 15).

From the value of $\alpha = -0.09$ for the enolization of **5** it is estimated that an acid of $pK_a = 3$ (appropriate for **8**) should have a value of k_{HA} of $1.0\,M^{-1}\,s^{-1}$. Therefore, since the dienone **8** reacts with $k_2 \sim 110\,s^{-1}$, the *effective molarity* (EM) (22) of the internal carboxyl group is about $110\,M$.[12] This EM is within the normal range of values found for intramolecular general acid catalysis (22) and is similar to the value of $58\,M$ that we found for the debromination of **9** (14, 15).

If, as depicted in Scheme 3, general bases other than water can be involved in the enolization of **8**, then catalysis by buffers is to be expected. Indeed, strong catalysis was found in acetate and phosphate buffers. Operationally, the catalysis in acetate buffers appears as acetic acid catalysis on the anion of **8** ($k_{HA} = 78\,M^{-1}\,s^{-1}$). However, this is ascribed to the kinetic equivalent: acetate ion acting as the base on undissociated **8** with $k_A = 3500\,M^{-1}\,s^{-1}$ (Scheme 3).

In phosphate buffers (pH near 6) there is catalysis by both the acidic and basic components. The apparent catalysis by the dihydrogen phosphate ion ($k_{HA} = 46\,M^{-1}\,s^{-1}$) is assigned to the attack of the hydrogen phosphate dianion on undissociated **8** (Scheme 3) with $k_A = 1.6 \times 10^5\,M^{-1}\,s^{-1}$. The catalysis by HPO_4^{2-} is most probably due to direct attack by that ion on the anion of **8** ($k_A = 22\,M^{-1}\,s^{-1}$); the alternative of the triphosphate trianion attacking undissociated **8** would need to have an unrealistic rate constant of $5 \times 10^{10}\,M^{-1}\,s^{-1}$.

Conclusions

The kinetics of enolization of the benzocyclohexadienone **5** are very similar to those found earlier (4) for the monocyclic derivative **2***b*. Consequently, similar mechanistic conclusions are drawn. The enolization of the derivative of **5** bearing a carboxyl group at C_2, viz. **8**, exhibits intramolecular general acid catalysis (EM ~ $110\,M$) and catalysis by buffer bases.

Experimental

The substrates 1-naphthol and 1-naphthol-2-carboxylic acid (both from Aldrich) were recrystallized before use.

Procedures for carrying out kinetics experiments were as described in previous publications (3, 4, 6, 10, 14, 15). The transient cyclohexadienones (**5** and **8**) were generated *in situ* in the stopped-flow apparatus by mixing equal volumes of substrate solution (0.20 or 0.50 mM) and bromine solution (0.05 or 0.10 mM). For acetate and chloroacetate buffers both of these solutions contained the buffer. For the other

[11]Very recently, Bernasconi has proposed a "Principle of Imperfect Synchronization" and discussed it in relation to proton transfer reactions (23).

[12]Using the value of $\alpha = -0.38$ (for carboxylic acids), as a referee suggested, gives a higher EM of $150\,M$.

Can. J. Chem. Downloaded from www.nrcresearchpress.com by 118.98.75.50 on 09/07/12
For personal use only.

buffers, which react slowly with bromine, only the initial substrate solution contained buffer (of twice the desired strength); the bromine solution was simply prepared in aqueous NaCl. For the pH–rate profiles (Fig. 1) $I = 0.11\,M$ ($0.1\,M$ KBr + $0.01\,M$ buffer salt) except in dilute acid where pH < 2. The studies of buffer catalysis were all carried out with $I = 1.0\,M$ (NaCl + buffer salt).

The decays of the dienones **5** and **8** were monitored at 270 nm relative to little or no change at 360 nm.

The individual "observed" rate constants, reported in the Supplementary Material,[13] are the averages of 3–5 determinations; they are reproducible within 5%. The standard deviations of the slopes of the buffer plots varied from 1 to 8% of the slope value. The derived values of k_{HA} have standard deviations of 3–15%. Accordingly, the probable error in α is such that its value should be taken as zero.

Acknowledgements

One of us (O.S.T.) thanks the Natural Sciences and Engineering Research Council of Canada for an operating grant, and Professors J.-M. Lehn and J. A. Osborn (Université Louis Pasteur, Strasbourg) for their hospitality and the use of facilities during a sabbatical leave.

1. R. P. Bell and D. J. Rawlinson. J. Chem. Soc. 63 (1961).
2. M. Paventi. Ph.D. thesis, Concordia University, Montreal, Canada. 1984; O. S. Tee, M. Paventi, N. R. Iyengar, and J. M. Bennett. Manuscript in preparation.
3. O. S. Tee, N. R. Iyengar, and M. Paventi. J. Org. Chem. **48**, 759 (1983).
4. O. S. Tee and N. R. Iyengar. J. Am. Chem. Soc. **107**, 455 (1985).
5. J. Kulic and M. Vecera. Collect. Czech. Chem. Commun. **39**, 71 (1974).
6. O. S. Tee, N. R. Iyengar, and B. Kraus. J. Org. Chem. **50**, 973 (1985).
7. J. Toullec. Adv. Phys. Org. Chem. **18**, 1 (1982); W. J. Albery. J. Chem. Soc. Faraday Trans. 1, **78**, 1579 (1982).
8. A. Streitwieser, Jr. Molecular orbital theory for organic chemists. John Wiley, New York. 1961. p. 241.
9. R. O. C. Norman and R. Taylor. Electrophilic substitution in benzenoid compounds. Elsevier, Amsterdam. 1965. pp. 88, 150, 219.
10. O. S. Tee and C. G. Berks. J. Org. Chem. **45**, 830 (1980).
11. P. B. D. de la Mare and H. Suziki. J. Chem. Soc. (C), 648 (1968).
12. W. Militzer. J. Am. Chem. Soc. **60**, 256 (1938); L. A. Yanovskaya, A. P. Terent'ev, and L. I. Belen'kii. Zh. Obshch. Khim. **22**, 1594 (1952); L. Forliano. Synthesis, 487 (1980).
13. R. Fischer and J. Byé. Bull. Soc. Chim. Fr. 2920 (1964).
14. O. S. Tee and N. R. Iyengar. J. Org. Chem. **50**, 4468 (1985).
15. O. S. Tee, N. R. Iyengar, and J. M. Bennett. J. Org. Chem. **51**, 2585 (1986).
16. C. S. Shiner, P. E. Vorndam, and S. R. Kass. J. Am. Chem. Soc. **108**, 5699 (1986).
17. E. Tapuhi and W. P. Jencks. J. Am. Chem. Soc. **104**, 5758 (1982); B. Capon and C. Zucco. J. Am. Chem. Soc. **104**, 7567 (1982).
18. Y. Chiang, A. J. Kresge, and P. A. Walsh. J. Am. Chem. Soc. **104**, 6122 (1982); Y. Chiang, A. J. Kresge, Y. S. Tang, and J. Wirz. J. Am. Chem. Soc. **106**, 460 (1984); Y. Chiang, A. J. Kresge, and J. Wirz. J. Am. Chem. Soc. **106**, 6392 (1984); P. Pruszynski, Y. Chiang, A. J. Kresge, N. P. Schepp, and P. A. Walsh. J. Phys. Chem. **90**, 3760 (1986); J. R. Keefe, A. J. Kresge, and J. Toullec. Can. J. Chem. **64**, 1224 (1986).
19. R. P. Bell. The proton in chemistry. 2nd ed. Chapman and Hall, London, U.K. 1973. p. 216; A. J. Kresge. *In* Proton transfer reactions. *Edited by* E. F. Caldin and V. Gold. Chapman and Hall, London, U.K. 1975. Chap. 7. pp. 188–194; H. Maskill. The physical basis of organic chemistry. Oxford University Press, Oxford, U.K. 1985. pp. 440–441; R. Stewart. The proton: applications to organic chemistry. Academic Press, Orlando, FL. 1985. pp. 278–280.
20. J. E. Leffler and E. Grunwald. Rates and equilibria of organic reactions. John Wiley, New York. 1963. p. 204; A. J. Hoefnagel, M. A. Hoefnagel, and B. M. Wepster. J. Org. Chem. **43**, 4720 (1978).
21. M. Eigen. Angew. Chem. Int. Ed. Engl. **3**, 1 (1964); W. P. Jencks. Catalysis in chemistry and enzymology. McGraw–Hill, New York. 1969. pp. 97–98; A. Fehrst. Enzyme structure and mechanism. 2nd ed. W. H. Freeman, New York. 1985. pp. 64–65; Y. Chiang, M. J. Cho, B. A. Euser, and A. J. Kresge. J. Am. Chem. Soc. **108**, 4192 (1986).
22. A. J. Kirby. Adv. Phys. Org. Chem. **17**, 183 (1980).
23. C. F. Bernasconi. Tetrahedron, **41**, 3219 (1985).

[13]The original data have been deposited as Supplementary Material (Tables S1–S5, 6 pages). Copies may be purchased from the Depository of Unpublished Data, CISTI, National Research Council of Canada, Ottawa, Ont., Canada K1A 0S2.

Can. J. Chem. Downloaded from www.nrcresearchpress.com by 118.98.75.50 on 09/07/12
For personal use only.

Hydration reactivity of ketenes generated by flash photolysis

ANNETTE D. ALLEN, A. JERRY KRESGE, NORMAN P. SCHEPP, AND THOMAS T. TIDWELL
Department of Chemistry, University of Toronto, Toronto, Ont., Canada M5S 1A1

Received December 15, 1986

This paper is dedicated to Professor John T. Edward

ANNETTE D. ALLEN, A. JERRY KRESGE, NORMAN P. SCHEPP, and THOMAS T. TIDWELL. Can. J. Chem. **65**, 1719 (1987).

The ketenes *n*-BuCH=C=O, PhCH=C=O, and Ph_2C=C=O have been generated by flash photolysis and their reactivities toward water, including acid and base catalysis, have been measured in wholly aqueous media by ultraviolet spectrophotometry. The phenyl group electronically enhances the reactivity of ketenes relative to *n*-butyl toward water and hydroxide, but retards reaction with protic acids. The presence of bulky groups, including phenyls, on each side in the ketene plane sterically retards nucleophilic attack. The reactions are interpreted as involving in-plane attack by nucleophilic water or hydroxide in the neutral and base-induced reactions, and electrophilic protonation perpendicular to the ketene plane for the acid-catalyzed reaction.

ANNETTE D. ALLEN, A. JERRY KRESGE, NORMAN P. SCHEPP et THOMAS T. TIDWELL. Can. J. Chem. **65**, 1719 (1987).

Faisant appel à la photolyse éclair, on a préparé les cétènes *n*-BuCH=C=O, PhCH=C=O et Ph_2C=C=O; utilisant la spectrophotométrie ultraviolette et opérant dans des milieux aqueux, on a mesuré leurs réactivités vis-à-vis de l'eau, tant sous l'influence de catalyseurs acides que basiques. Par comparaison avec le groupement *n*-butyle, le groupement phényle augmente la réactivité des cétènes vis-à-vis de l'eau et de l'ion hydroxyde; toutefois, il retarde la réaction avec les acides protiques. La présence de groupements encombrants, y compris les groupements phényles, de chaque côté du plan du cétène retarde l'attaque nucléophile. Pour expliquer les réactions qui se produisent en milieux neutre ou basique, on fait appel à un mécanisme impliquant une attaque, par l'eau du l'hydroxyde nucléophiles, qui se produirait dans le plan; par ailleurs, les réactions catalysées par les acides se produiraient par le biais d'une protonation électrophile qui se ferait d'une façon perpendiculaire au plan du cétène.

[Traduit par la revue]

The kinetic study of the hydration of ketenes in wholly aqueous media is complicated not only by the strong tendency of the ketenes to dimerize but also by their high reactivity with water. Previously, only by using *in situ* generation of ketenes by flash photolysis of diazoketones to give arylketenes (1) or of cyclobutanone to give ketene (2), together with fast measurement techniques, have such studies been accomplished (eqs. [1], [2]) for these ketenes.

[1] $ArCOCHN_2 \xrightarrow{h\nu} ArCH{=}C{=}O \xrightarrow{H_2O} ArCH_2CO_2H$

[2] 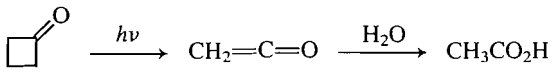

In these previous flash photolytic studies (1, 2), the reactions were monitored by measuring changes in conductivity of the reacting solutions brought about by ionization of the carboxylic acid products. This technique could be used only over a limited pH range: high background conductivity made it inapplicable below pH 4 and above pH 11. Consequently, only the uncatalyzed hydration reaction could be studied; acid and base catalysis remained undetected.

Other studies of ketene hydration have utilized mixed solvents to circumvent the high reactivity of ketenes in pure water; these include diphenylketene and dimethylketene in H_2O/dioxane or ether (3, 4), and a variety of alkylketenes in H_2O/acetonitrile (5, 6). The very crowded di-*tert*-butylketene has also recently been found to be sufficiently unreactive towards water that its hydration may be studied in pure water at 25°C by conventional spectrophotometric methods (6). In these systems acid (3–6) and base (6) catalysis have been observed. The hydration of ketenes has also been studied in the gas phase (7) and by theoretical methods (8).

At least partly because of the diversity of methods and conditions that have been used for these studies of ketene hydration there are also widely divergent views of the mechanisms of these processes, and these have been recently reviewed (10). We have advocated (5, 6) the processes shown in eqs. [3]–[5]

[3] 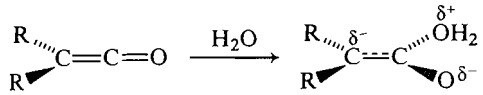

1

[4] 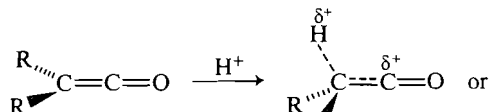

2*a*

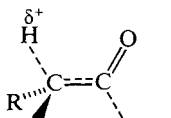

2*b*

[5] 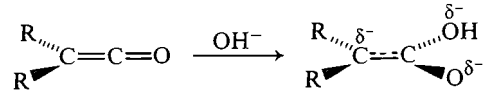

3

with transition states **1**–**3** for the neutral, acid, and base induced processes, respectively, whereas cyclic transition state **4** has been proposed for the neutral hydration in mixed solvents (3, 4), and transition states **5** (8) and **6** (9) have been advanced in the theoretical studies.

In eq. [3] attack by water in the plane of the ketene is envisaged (6), and for the acid catalyzed reaction proton attack

Can. J. Chem. Downloaded from www.nrcresearchpress.com by 118.98.75.50 on 09/07/12
For personal use only.

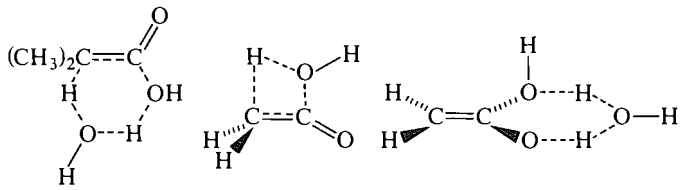

4 5 6

occurs perpendicular to the ketene plane, either to give an acylium-ion-like transition state **2***a*, or possibly with concerted "enforced" attack of water via **2***b* (5, 6). The hydroxide induced reaction (eq. [3]) resembles that for the neutral hydration (eq. [1]) (6). The nucleophilic attack of H_2O and OH^- occur on the LUMO **7** of ketenes, whereas electrophilic protonation occurs on the HOMO **8** (11).

7 8

In contrast to the transition states **1**–**3**, in the concerted additions to the C=C bond via **4** and **5**, attack would have to occur in the plane perpendicular to the ketene, while **6** resembles the well-studied hydration transition state of aldehydes and ketones (12).

To help resolve these highly discordant interpretations, we have begun a study of ketene hydration using flash photolysis with spectrophotometric detection. This technique allows us to measure reaction rates over the entire pH range from strongly acidic to strongly basic solutions and to examine the acid and base catalyzed processes as well as the uncatalyzed reactions. In this paper we report results for *n*-butylketene (**9**), phenylketene (**10**), and diphenylketene (**11**); the first of those was

n-BuCH=C=O PhCH=C=O Ph_2C=C=O

9 **10** **11**

generated by photolyzing cyclohexanone (eq. [6]) (13), while the latter two were made by photo-Wolff rearrangement (eq. [7], R = H, Ph) (1, 14).

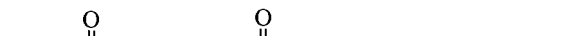

[6]

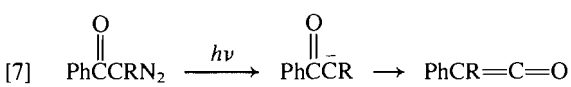

[7]

Results

n-*Butylketene*

Rates of hydration of this ketene were measured in aqueous perchloric acid solutions over the concentration range $[HClO_4]$ = 0.01–0.10 *M* and in aqueous sodium hydroxide solutions over the concentration range [NaOH] = 0.002–0.06 *M*; the ionic strength was maintained constant at 0.10 *M* by adding sodium chloride as required. These data are summarized in Tables S1 and S2.[1]

The hydration reaction showed both acid and base catalysis, with observed first-order rate constants accurately proportional to acid or base concentrations. Linear least-squares analysis gave the catalytic coefficients $k_{H^+} = (3.98 \pm 0.09) \times 10^3 M^{-1} s^{-1}$ and $k_{HO^-} = (3.29 \pm 0.04) \times 10^4 M^{-1} s^{-1}$. Both sets of data also showed significant zero-catalyst-concentration intercepts or "uncatalyzed" reactions, and gave uncatalyzed rate constants in good agreement with each other: $k_0 = (8.85 \pm 0.49) \times 10^1 s^{-1}$ from the acidic solutions and $k_0 = (9.61 \pm 0.93) \times 10^1 s^{-1}$ from the basic solutions.

Rates of hydration of *n*-butylketene were also measured in aqueous $H_2PO_4^-/HPO_4^{2-}$ buffer solutions. These measurements were made in a series of solutions of constant buffer ratio ($[H_2PO_4^-]/[HPO_4^{2-}] = 0.60$) and constant ionic strength (0.10 *M*), with buffer concentration changing over the range [buffer] = 0.009–0.05 *M*. These data are summarized in Table S3.[1]

Hydration rates in these buffer solutions showed little variation with buffer concentration. Linear least-squares analysis of the relationship between observed first-order rate constants and buffer concentration gave a catalytic coefficient just barely greater than its standard deviation: $k_{cat} = \Delta k_{obs}/\Delta[buffer] = (8.7 \pm 5.8) \times 10^1 M^{-1} s^{-1}$. The zero-buffer-concentration intercept, on the other hand, was well defined, $k_0 = (1.01 \pm 0.02) \times 10^2 s^{-1}$, and consistent with the less precise determinations of this quantity in perchloric acid and sodium hydroxide solutions. The weighted average of all three values is $k_0 = 99.4 \pm 1.6 M^{-1} s^{-1}$.

Phenylketene

Rates of hydration of phenylketene were measured in aqueous perchloric acid solutions over the concentration range $[HClO_4]$ = 0.01–0.10 *M* and in aqueous sodium hydroxide solutions over the concentration range [NaOH] = 0.001–0.10 *M*; the ionic strength was maintained at 0.10 *M* by adding sodium chloride as required. These data are summarized in Tables S4 and S5.[1]

This hydration reaction showed no acid catalysis. Linear least-squares analysis of the relationship between observed first-order rate constants measured in perchloric acid solutions and the acid concentration gave a negative hydronium catalytic coefficient with absolute magnitude comparable to its standard deviation: $k_{H^+} = \Delta k_{obs}/\Delta[HClO_4] = -(4.6 \pm 2.1) \times 10^3 M^{-1} s^{-1}$. The rate constant of the uncatalyzed reaction, however, was well defined by these experiments: $k_0 = (4.65 \pm 0.14) \times 10^3 s^{-1}$.

Observed rate constants determined in sodium hydroxide solutions, on the other hand, increased strongly with base concentration. The relationship between these two variables was linear, and least-squares analysis gave $k_{HO^-} = (1.22 \pm 0.05) \times 10^6 M^{-1} s^{-1}$, and an uncatalyzed rate constant, $k_0 = (5.50 \pm 0.03) \times 10^3 s^{-1}$, consistent with the result from perchloric acid solutions.

Some measurements of the rate of hydration of phenylketene were also made in H_2O and D_2O solutions with no added acid or base. The ionic strength of these solutions was fixed at 0.10 *M* by adding sodium chloride. These data are summarized in Table S6.[1] They provide the solvent isotope effect $k_{H_2O}/k_{D_2O} = 1.44 \pm 0.14$ for the uncatalyzed reaction.

The measurements in H_2O give another estimate of the rate constant for the uncatalyzed hydration of phenylketene: $k_0 = (4.54 \pm 0.30) \times 10^3 s^{-1}$. This result is in agreement with the determinations made in perchloric acid and sodium hydroxide

[1]Tables S1–S8 of rate data may be purchased from the Depository of Unpublished Data, CISTI, National Research Council, Ottawa, Ont., Canada K1A 0S2.

Can. J. Chem. Downloaded from www.nrcresearchpress.com by 118.98.75.50 on 09/07/12
For personal use only.

solutions, and the weighted average of all three values is $k_0 = (4.77 \pm 0.12) \times 10^3\ s^{-1}$.

Diphenylketene

Rates of hydration of this ketene were measured in aqueous perchloric acid solutions over the concentration range $[HClO_4] = 0.002–0.10\ M$ and in aqueous sodium hydroxide solutions over the concentration range $[NaOH] = 0.001–0.10\ M$. Ionic strength was maintained at $0.10\ M$ by adding sodium chloride as required. These data are summarized in Tables S7 and S8.[1]

This hydration reaction also showed no acid catalysis. Linear least-squares analysis gave $k_{H^+} = \Delta k_{obs}/\Delta[HClO_4] = -(1.18 \pm 0.98) \times 10^2\ M^{-1}\ s^{-1}$ and $k_0 = (2.74 \pm 0.04) \times 10^2\ s^{-1}$. Catalysis by hydroxide ion, on the other hand, was strong, with observed rate constants accurately proportional to base concentration. Linear least-squares analysis gave the hydroxide ion catalytic constant $k_{HO^-} = (6.11 \pm 0.11) \times 10^4\ M^{-1}\ s^{-1}$ and a rate constant for the uncatalyzed process, $k_0 = (1.97 \pm 0.48) \times 10^2\ s^{-1}$, consistent with the more precise determination of this quantity in perchloric acid solutions.

Some additional measurements of the rate of hydration of diphenylketene were also made in H_2O and D_2O containing sodium chloride ($0.10\ M$). These data are summarized in Table S6.[1] They give a solvent isotope effect of $k_{H_2O}/k_{D_2O} = 1.74 \pm 0.13$ on the uncatalyzed reaction. The measurements in H_2O provide another estimate of the rate constant for the uncatalyzed reaction, $k_0 = (2.85 \pm 0.12) \times 10^2\ s^{-1}$, which is consistent with the results obtained in perchloric acid and sodium hydroxide solutions. The weighted average of all three values is $k_0 = 275 \pm 3\ s^{-1}$.

Our value of $4770\ s^{-1}$ for k_{H_2O} for PhCH=C=O measured by uv spectrophotometry at 25°C is in good agreement with that of $4900\ s^{-1}$ at 26°C obtained previously (1) by conductivity (Table 1). Similarly, our measurement of the solvent isotope effect $k_{H_2O}/k_{D_2O} = 1.44 \pm 0.14$ for PhCH=C=O is probably within the experimental uncertainty of the previously reported (1) value of 2.

Our measured value of k_{H_2O}/k_{D_2O} of 1.74 for $Ph_2C{=}C{=}O$ in pure water is in good agreement with the reported (4*b*) values of 1.7–2.0 in dioxane/water mixtures.

Discussion

The observed value of k_{H_2O} for *n*-BuCH=C=O may be usefully compared to those of other aliphatic ketenes (2, 6) as given by Table 2.

The comparative data in Table 2 show that *n*-BuCH=C=O is more reactive than $CH_2{=}C{=}O$ by a factor of 2.2, and this small difference appears reasonable for the differential effect of the *n*-butyl substituent, compared to hydrogen, on the ground states and transition states for the mechanism of eq. [3]. Similarly *n*-BuCH=C=O is more reactive than the isomeric *t*-BuCH=C=O by a small factor of 2.6, and this result shows that the presence of a single bulky group has no major effect on the reactivity. This result is expected for the transition state **1** in eq. [3] in which the nucleophilic water can attack in the ketene plane opposite the bulky group. The small retardation for *t*-BuCH=C=O may arise from steric hindrance to solvation of the polar transition state.

The reactivity of *n*-BuCH=C=O is greater than that of $Et_2C{=}C{=}O$ and *t*-$Bu_2C{=}C{=}O$ by factors of 12 and 6×10^5, respectively. In the case of $Et_2C{=}C{=}O$ each side of the ketone possesses a moderate sized substituent, and so a rate decrease is expected due to the hindrance to the nucleophile in the transition state **1**, regardless of the side of approach in the plane. When two very bulky *tert*-butyl groups are present the rate is enormously decreased; this distinctively nonadditive effect of the second *tert*-butyl group is exactly what is expected if hydration occurs by in-plane attack of the nucleophile, but is *not* the behaviour expected for attack perpendicular to the ketene plane as shown in the cyclic transition state **4**, where the effect of the *tert*-butyl groups would be close to additive.

TABLE 1. Summary of rate constants for ketene hydration in aqueous solution at 25°C, ionic strength = $0.10\ M$

	Ketene		
Rate constant	*n*-Butyl	Phenyl	Diphenyl
$k_{H^+}/M^{-1}\ s^{-1}$	3 980	—	—
$k_{HO^-}/M^{-1}\ s^{-1}$	32 900	1 220 000	61 100
$(k_0)_{H_2O}/s^{-1}$	99.4[a]	4 770[a]	275[a]
$(k_0)_{D_2O}/s^{-1}$	—	3 150	164
$(k_0)_{H_2O}/(k_0)_{D_2O}$	—	1.44[b]	1.74[a]
K_{HO^-}/k_{H_2O}	330	260	220

[a]Weighted average, see text.
[b]Derived from reactions without added acid or base.

Thus the comparative rate data for the aliphatic ketenes shown in Table 2 give evidence that substituent effects of aliphatic groups on ketene hydration by neutral water are rather small, insofar as these arise from electronic influences on the stabilities of the ground states and transition states, and from effects on solvation. However, steric effects are large when nucleophilic attack by water in the ketene plane is impeded, and this provides strong support for the mechanism of eq. [3], as we have proposed previously (6, 10).

The observed solvent isotope effects for the hydration of *n*-BuCH=C=O, PhCH=C=O, and $Ph_2C{=}C{=}O$ (Table 1) are similar to the values of 1.45–2.58 found for alkylketenes in mixed solvents (6). Solvent isotope effects for rate-limiting attack of water on the carbonyl carbon of a variety of ketones, esters, and carboxylic anhydrides have been observed in the range of 2.2–4.0 (15), and these have been generally interpreted in terms of general base assistance by a second water molecule to attack on the carbonyl carbon. If this interpretation is correct, then the observed solvent isotope effects for *n*-BuCH=C=O, PhCH=C=O, and $Ph_2C{=}C{=}O$ may indicate that such general base catalysis by a second water molecule is also involved in the ketene hydration transition state **1** (eq. [3]).

The reaction of ketenes with hydroxide has been proposed (6) to occur through attack of the nucleophile in the plane of the ketene as shown in eq. [5], and there is little doubt that the reaction of *n*-BuCH=C=O proceeds by this path as well. However for *t*-$Bu_2C{=}C{=}O$ the reaction with HO^- was so slow that it could not be reliably detected, whereas less crowded aliphatic ketenes were so reactive that it was necessary to use mixed solvents to measure their reaction rates using conventional uv spectrophotometry (6). Thus the current measurements are the first reported reaction rates of ketenes with hydroxide in wholly aqueous media.

The reactivity of PhCH=C=O towards H_2O is significantly greater than that of the alkylketenes, and exceeds the values in Table 2 by factors of 48 (*n*-BuCH=C=O), 130 (*t*-BuCH=C=O), 580 ($Et_2C{=}C{=}O$), and 110 ($CH_2{=}C{=}O$). The rate of PhCH=C=O towards hydroxide exceeds that of *n*-BuCH=

Can. J. Chem. Downloaded from www.nrcresearchpress.com by 118.98.75.50 on 09/07/12
For personal use only.

TABLE 2. Rate data for hydration of aliphatic ketenes in H_2O, 25°C (μ = 0.1, NaCl)

Ketene:	*n*-BuCH=C=O	*t*-BuCH=C=O[a]	Et_2C=C=O[a]	CH_2=C=O[c]	*t*-Bu_2C=C=O[a]
k_{H_2O} (s^{-1}):	99	37.9[b]	8.26[b]	44	1.57×10^{-4}

[a]Reference 6.
[b]Extrapolated from values measured in H_2O/CH_2CN mixtures.
[c]Reference 2.

C=O in reactivity by a factor of 37, and the resemblance of the rate factors towards H_2O and HO^- argues for a similarity in mechanism. The high reactivity of PhCH=C=O is consistent with a polar, enolate-like transition state, such as **1**, in which there is significant negative charge buildup adjacent to the phenyl ring. A relatively nonpolar cyclic transition state such as **4** is difficult to reconcile with the high reactivity of PhCH=C=O; not only would the phenyl stabilization of charge development at C_β be absent in such a transition state, but also the ground state of PhCH=C=O is stabilized by conjugation of phenyl with the C=C double bond, and this conjugation is diminished in the cyclic transition state, and reduced reactivity would be expected. Invocation of a highly polar cyclic transition state appears unjustified, as such a transition state does not explain the steric effects. Little steric or electronic effect of substituents is expected in the carbonyl hydration transition state **6**, so this path is also evidently unimportant in solution.

The 20-fold greater reactivity of PhCH=C=O compared to Ph_2C=C=O in both the neutral and OH^- induced reactions provides a further significant indication as to the mechanism of these reactions. There is evidently no conflict of opinion that the OH^- induced reaction proceeds by nucleophilic attack in the plane of the ketenes as depicted in eq. [5], and the similarity in the rate differences for the two reactions is suggestive that the H_2O reaction follows a similar path, namely that of eq. [3]. The second phenyl is expected to stabilize both the ground state and an enolate-like transition state, but the most important effect is a large steric barrier in the plane of the ketene that cannot be avoided when two bulky phenyl groups are present. Such steric barriers are well documented both in preparative (10) and kinetic (5, 6) studies. While there might be a small steric barrier to a cyclic transition state such as **4**, there is little evidence for such effects for attack perpendicular to alkenes (16) and these effects would also be cumulative, whereas for attack in the plane there is an abrupt change to a high steric barrier when two bulky groups are present, as is observed. Thus the observed reactivity of PhCH=C=O and Ph_2C=C=O towards H_2O and OH^- favours reaction occurring in the plane through transition states such as **1** and **3**, respectively, and argues against the intervention in solution of cyclic transition states such as **4**–**6**.

The pK_a values of the enols Ph_2CH=CHOH and PhCH=CHOH have recently been determined as 9.4 and 9.5, respectively.[2] As shown in eq. [8], the proton dissociation of enols

[8] 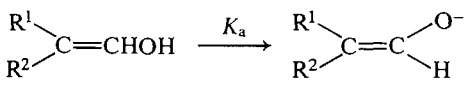

involves conversion of a neutral to an anionic species *without* a change in hybridization from sp^2 of the carbon bearing the substituents, and this is closely analogous to the additions of water and hydroxide to ketenes shown in eqs. [3] and [5]. The slightly greater acidity of Ph_2C=CHOH is supportive that in the absence of a steric barrier to in-plane nucleophilic attack Ph_2C=C=O would be more reactive than PhCH=C=O.

The observed ratios of k_{HO^-}/k_{H_2O} of 330, 260, and 220 for *n*-BuCH=C=O, PhCH=C=O, and Ph_2C=C=O, respectively, are noticeably less than those reported for many carbonyl group hydrations, including 1.6×10^6 for $PhCOCF_3$ (12*a*), 1.2×10^7 for 3-ClC_6H_4CHO (12*b*) and 5.0×10^5 for CH_2O (12*c*) (k_{OH^-} in units of $M^{-1}\,s^{-1}$, k_{H_2O} in s^{-1}). Similar small values of this ratio have been observed for other ketenes (6), and for the α,β-unsaturated carbonyl compounds shown below (12 h), but the origin of the variation in this ratio has not been elucidated. However, the relative constancy of the ratio for ketenes is supportive of the similarity of mechanisms for the neutral and hydroxide induced reactions shown in eqs. [1] and [3], respectively.

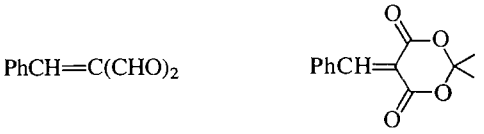

k_{HO^-}/k_{H_2O} 3.3×10^3 1.3×10^3

The value of k_{H^+}/k_{H_2O} of 40 (Table 1) obtained for *n*-BuCH=C=O is comparable to values of 140 and 280 for Et_2C=C=O and *t*-BuCH=C=O, respectively, which we obtained previously in mixed solvents at lower temperatures (6). No acid catalyzed reaction at all could be detected for PhCH=C=O and Ph_2C=C=O, and this is consistent with the large rate retarding effect expected for protonation next to phenyl, as illustrated by the average deceleration of 690 relative to hydrogen observed for the *cis*- and *trans*-2-phenylvinyl methyl ethers (eq. [9]) (17). There must be a sizeable rate retardation for k_{H^+} of PhCH=C=O as well, or this reaction would have been detected in the current experiments.

[9] $PhCH{=}CHOCH_3 \xrightarrow{H^+} PhCH_2\overset{+}{C}HOCH_3$

In summary, the generation of ketenes by flash photolysis combined with uv spectrophotometric measurement of reaction rates has been shown to be a valuable technique for examining these intermediates. These initial studies on *n*-BuCH=C=O, PhCH=C=O, and Ph_2C=C=O demonstrate the polar and steric influences of substituents on ketene hydration reactivity, and provide strong evidence for the mechanisms of eqs. [3]–[5] involving in-plane attack of nucleophilic water or hydroxide, and perpendicular attack at C_β in acid.

Experimental

Materials

The ketene precursor $PhCOCHN_2$ was prepared by reaction of PhCOCl with CH_2N_2 in ether with added triethylamine (14), while $PhCOCN_2Ph$ was obtained by the reaction of $PhCOC(NNH_2)Ph$ (Aldrich) with HgO (18).

[2]A. J. Kresge, Y. Chiang, and E. T. Krogh. Unpublished results.

Can. J. Chem. Downloaded from www.nrcresearchpress.com by 118.98.75.50 on 09/07/12
For personal use only.

Flash photolysis

A kinetic flash photolysis system of conventional design (19) was employed. The excitation flash of 50-μs width at half-length was produced by electrical discharge of 2000-J energy from a Xenon Corporation Model A Micro Pulser power supply through two Xenon Corporation FPA-5-100C xenon flash lamps. The monitoring light was supplied by an Osram Model XBO 150-W xenon lamp, operating from an Oriel Model 68700 universal arc lamp power supply. This light was passed first through a 10-cm water-jacketed (25.0 ± 0.05°C) sample cell and then through an Oriel Model 77250 grating monochrometer, and the output from that was detected by an Oriel Model 77341 photomultiplier. The signal from the photomultiplier was sent to a Biomation Model 805 transient recorder and A-D converter, and the digitized output was fed into a Commodore PC 10 microcomputer.

First-order rate constants were calculated by fitting time and absorbance data to an exponential function by nonlinear least-squares analysis.

Acknowledgements

We are grateful to the Natural Sciences and Engineering Research Council of Canada and the Donors of the Petroleum Research Fund administered by the American Chemical Society for financial support of this research.

1. E. BOTHE, H. MEIER, D. SCHULTE-FROHLINDE, and C. VON SONNTAG. Angew. Chem. Int. Ed. Engl. **15**, 380 (1976).
2. E. BOTHE, A. M. DESSOUKI, and D. SCHULTE-FROHLINDE. J. Phys. Chem. **84**, 3270 (1980).
3. P. J. LILLFORD and D. P. N. SATCHELL. J. Chem. Soc. B, 889 (1968).
4. (*a*) N. L. POON and D. P. N. SATCHELL. J. Chem. Soc. Perkin Trans. 2, 1381 (1983); (*b*) J. Chem. Soc. Perkin Trans. 2, 1485 (1986).
5. S. H. KABIR, H. R. SEIKALY, and T. T. TIDWELL. J. Am. Chem. Soc. **101**, 1059 (1979).
6. A. D. ALLEN and T. T. TIDWELL. J. Am. Chem. Soc. **109**, 2774 (1987).
7. P. G. BLAKE and H. H. DAVIES. J. Chem. Soc. Perkin Trans. 2, 321 (1972).
8. M. T. NGUYEN and A. F. HEGARTY. J. Am. Chem. Soc. **106**, 1552 (1984).
9. J. Y. CHOI and I. LEE. Kich'o Kwahak Yonguso Nonmunjip, **5**, 61 (1984); Chem. Abstr. **101**, 54096h (1984).
10. H. R. SEIKALY and T. T. TIDWELL. Tetrahedron, **42**, 2587 (1986).
11. K. N. HOUK, R. W. STROZIER, and J. A. HALL. Tetrahedron Lett. 897 (1974).
12. (*a*) C. D. RITCHIE. J. Am. Chem. Soc. **106**, 7187 (1984); (*b*) R. A. MCCLELLAND and M. COE. J. Am. Chem. Soc. **105**, 2718 (1983); (*c*) L. H. FUNDERBURK, L. ALDWIN, and W. P. JENCKS. J. Am. Chem. Soc. **100**, 5444 (1978); (*d*) J. L. KURZ and J. I. COBURN. J. Am. Chem. Soc. **89**, 3528 (1967); (*e*) I. H. WILLIAMS, D. SPANGLER, D. A. FEMEC, G. M. MAGGIORA, and R. L. SCHOWEN. J. Am. Chem. Soc. **105**, 31 (1983); (*f*) R. P. BELL. Adv. Phys. Org. Chem. **4**, 1 (1966); (*g*) R. P. BELL and P. E. SÖRENSEN. J. Chem. Soc. Perkin Trans. 2, 1740 (1972); (*h*) C. F. BERNASCONI and M. F. STRONACH. J. Org. Chem. **51**, 2144 (1986).
13. M. ANPO and Y. KUBOKAWA. Bull. Chem. Soc. Jpn. **50**, 1913 (1977); M. Y. ENCINAS and J. C. SCAIANO. J. Chem. Soc. Perkin Trans. 2, 56 (1980).
14. K.-P. ZELLER. Chem. Ber. **112**, 678 (1979).
15. (*a*) R. D. GANDOUR, M. COYNE, V. J. STELLA, and R. L. SCHOWEN. J. Org. Chem. **45**, 1733 (1980); (*b*) F. M. MENGER and K. S. VENKATASUBBAN. J. Org. Chem. **41**, 1868 (1976); (*c*) J. M. ALLEN and K. S. VENKATASUBBAN. J. Org. Chem. **50**, 1508 (1985); (*d*) K. S. VENKATASUBBAN, K. R. DAVIES, and J. L. HOGG. J. Am. Chem. Soc. **100**, 6125 (1978); (*e*) R. P. BELL and J. E. CRITCHLOW. Proc. R. Soc. London, Ser. A, **325**, 35 (1971); (*f*) B. ROSSALL and R. E. ROBERTSON. Can. J. Chem. **53**, 869 (1975); (*g*) H. NEUVONEN. J. Chem. Soc. Perkin Trans. 2, 1141 (1986).
16. T. T. TIDWELL. Tetrahedron, **34**, 1855 (1978).
17. Y. CHIANG, A. J. KRESGE, and C. I. YOUNG. Can. J. Chem. **56**, 461 (1978).
18. E. C. HORNING (*Editor*). Org. Synth. Coll. Vol. 3. Wiley, New York. 1955. p. 356.
19. M. A. WEST. *In* Techniques of chemistry. Vol. VI. *Edited by* C. F. Bernasconi. Wiley–Interscience, New York. 1986. Part II. Chap. VIII.

Can. J. Chem. Downloaded from www.nrcresearchpress.com by 118.98.75.50 on 09/07/12
For personal use only.

Effect of mercerization on the crystallite size and crystallinity index in cellulose from different sources

J. F. REVOL, A. DIETRICH, AND D. A. I. GORING

Department of Chemistry, Pulp and Paper Building, McGill University, Montreal, P.Q., Canada H3A 2A7

Received November 4, 1986

This paper is dedicated to Professor John T. Edward

J. F. REVOL, A. DIETRICH, and D. A. I. GORING. Can. J. Chem. **65**, 1724 (1987).

Native cellulose samples having a wide range of crystallinity and crystallite size were mercerized by treatment with sodium hydroxide. The resultant cellulose II samples showed only a narrow range of crystallinity and an essentially constant crystallite size. For the low-crystallinity samples, crystallinity and crystallite size actually increased on mercerization. These results are in line with the proposal that mercerization involves the mingling of chains from adjacent and antiparallel cellulose I *microfibrils* to form cellulose II crystals of antiparallel chains.

J. F. REVOL, A. DIETRICH et D. A. I. GORING. Can. J. Chem. **65**, 1724 (1987).

Utilisant de l'hydroxyde de sodium, on a mercerisé divers échantillons de cellulose naturelle possédant un large éventail de cristallinités et de grosseurs de cristaux. Les échantillons de cellulose II qui en résultent ne présentent qu'un éventail restreint de cristallinités et la grosseur des cristaux est pratiquement constante. Pour des échantillons de faible cristallinité, la cristallinité et la grosseur des cristaux augmente avec la mercerisation. Ces résultats sont en accord avec l'hypothèse selon laquelle la mercerisation implique un mélange des *microfibres* de cellulose I adjacentes et antiparallèles pour former des cristaux de cellulose II de chaînes antiparallèles.

[Traduit par la revue]

Introduction

Although the conversion of cellulose I to cellulose II in mercerization has been studied by a variety of methods (1–4), its mechanism is not yet fully understood. It has been shown that the alkali-induced conversion of cotton from cellulose I to cellulose II is governed by the swelling of the fibre (5). More recently it was found that, in wood and in bamboo, the degree of mercerization of cellulose depends on the degree of swelling (6, 7). There is, therefore, no doubt that swelling is necessary to convert cellulose I to cellulose II on mercerization.

There seems to be a growing body of opinion that, in native cellulose, each elementary microfibril contains chains of the same polarity (parallel chains) (8–11), while regenerated and mercerized cellulose contains chains of alternating polarity (antiparallel chains) (12). The mechanism by means of which such chain reversal occurs in mercerization has been discussed by Blackwell *et al.* (1), by Revol and Goring (6), and more recently by Okano and Sarko (13, 14). Their explanation is as follows. Single microfibrils in native cellulose contain chains of the same polarity, but they can point alternately up and down. This hypothesis was confirmed recently by Revol and Goring (15) who showed that in the Valonia cell wall, cellulose microfibrils in close proximity have their fibre *c* axis alternately up and down (in opposite directions). Two neighbouring microfibrils of opposite polarity may coalesce during swelling in alkali, and allow the chains to adopt the antiparallel arrangement needed to form cellulose II. Recent X-ray diffraction studies seem to indicate that an antiparallel arrangement is already present in the alkali cellulose (14) found as an intermediate state during the conversion.

If the above concepts are correct, the cellulose I crystal structure will be entirely destroyed by swelling during mercerization and the subsequent cellulose II crystal structure created when the alkali is removed. Thus we would not expect to find a correlation between the crystallinity and crystallite size in the native cellulose and those parameters in the corresponding mercerized product. The purpose of the present work was to test this hypothesis. Native celluloses, having a wide range of crystallite size and crystallinity index, were selected from different sources. These were then mercerized conventionally. The crystallite size and crystallinity index were determined on the resulting cellulose II and compared with the corresponding parameters of the original native cellulose.

Experimental

The different native celluloses chosen are listed in Table 1. Each sample was refluxed in an aqueous solution of 4% sodium hydroxide for 12 h, rinsed with water, and refluxed in an aqueous solution of 1% HCl for 4 h. It was then rinsed with water until neutral in pH. For Valonia cellulose, an additional treatment of reflux in an aqueous solution of 4% HCl for 5 h was given. Such a treatment allows better mercerization of the sample, which is otherwise very resistant to alkali. This Valonia sample was then stretched as much as possible to orient the microfibrils in one direction, and twisted to eliminate any preferential orientation that is known to exist in the original cell wall. For mercerization, the samples were treated for 1 h in an aqueous solution of 18% sodium hydroxide at room temperature. They were then thoroughly washed until the wash water was neutral in pH. In the case of Valonia, this treatment was repeated 3 times.

X-ray diffraction patterns were recorded on flat film in a Warhus camera: Ni-filtered Cu-Kα radiation was used. The X-ray patterns were then analyzed with a microdensitometer (MK III CS. Joyce Loebl).

The degree of crystallinity or crystallinity index (C.I.) for cellulose I was determined (16) by

$$[1] \quad \text{C.I.} = \frac{I_{020} - I_{18.5°}}{I_{020}}$$

and for cellulose II (17) by

$$[2] \quad \text{C.I.} = \frac{I_{110} - I_{15.0°}}{I_{110}}$$

The crystal size was determined (18) from

$$[3] \quad t = \frac{0.9\lambda}{\beta \cos \theta}$$

where t is the thickness of the crystallite, λ the wavelength, β the corrected angular width at half maximum intensity, and θ the Bragg angle. The value of β was obtained (18) from

$$[4] \quad \beta = B^2 - b^2$$

Can. J. Chem. Downloaded from www.nrcresearchpress.com by 118.98.75.50 on 09/07/12
For personal use only.

TABLE 1. Crystallinity parameters for the various cellulose samples before and after mercerization

Cellulose sources	*d* spacing of the (020) planes (nm)	C.I. (crystallinity index)	Crystal size perpendicular to the (020) planes (nm)
Valonia ventricosa	0.387	0.95	15.4
Mercerized *Valonia ventricosa*		0.66	3.6
Ramie	0.387	0.83	5.8
Mercerized ramie		0.65	4.0
Kraft pulp (black spruce)	0.393	0.67	4.0
Mercerized kraft pulp (black spruce)		0.66	3.7
Celery	0.407	0.41	3.0
Mercerized celery		0.50	3.4
Swiss chard	0.403	0.43	2.9
Mercerized Swiss chard		0.60	4.4

where *B* is the observed angular width at half maximum intensity, and *b* the angular width at half maximum intensity of the reflection given by crystals of hexamethylenetetramine. The crystal size, *t*, was determined perpendicular to the (020) plane for both cellulose I and cellulose II. The amorphous contribution of cellulose has been evaluated and subtracted by hand according to a procedure used previously (19). For cellulose II, the overlapping of the 110 and 020 reflections was resolved by a technique similar to that of Patil *et al.* (20).

Results and discussion

The *d* spacing of the (020) planes is listed in Table 1 for the different celluloses. Values of *d* for *Valonia* and ramie were equal. However, the spacing becomes larger for the kraft pulp and still larger for celery and Swiss chard. Changes in the crystallinity index and in the size of the crystals perpendicular to the (020) plane follow a reversed tendency. Spacings of more than 0.4 nm for the (020) planes as shown in Table 1 for celery and Swiss chard have been reported previously for the primary wall of cotton fibres and in the wall of rose cells cultured in vitro (21, 22). These correspond generally to cellulose microfibrils of low crystallinity and small lateral size, as seen in Table 1, which contrasts with the high crystallinity and large size of the cellulose microfibrils contained in the *Valonia* cell wall. The least crystalline specimens are obviously more distorted, which results in a looser packing of the chains and hence larger unit cell dimensions.

After conversion to cellulose II by mercerization, crystallinity index and crystal size tend toward similar values for all the celluloses as shown in Table 1. The crystallinity index for the mercerized celluloses remains in a narrow range of 0.50–0.66 while it varies from 0.41 to 0.95 for the native celluloses. The crystal size is approximately constant for the mercerized celluloses, from 3.4 nm to 4.4 nm, while it varies from 2.9 nm to 15.4 nm in native celluloses. There is thus an evident convergence of the crystallinity and of the crystal size during the conversion from cellulose I to cellulose II by mercerization of native cellulose from different sources.

The present results indicate clearly that in native cellulose of high crystallinity, mercerization reduces crystallinity and crystal size, while for low crystallinity celluloses the reverse occurs. These trends would not be expected if the conversion of cellulose I to cellulose II was simply a change in conformation of the chain or arrangement of atoms in the unit cell. The present results are more in line with the idea that mercerization involves a complete destruction of the cellulose I structure by separation of the molecular chains followed by a reforming of the crystal structure as cellulose II. And this concept is compatible with the proposal that mingling of chains from the adjacent and antiparallel *microfibrils* of cellulose I to give the antiparallel *chains* of cellulose II occurs during mercerization.

Of course, we have no definitive proof that the picture presented above is correct. However, as far as the authors are aware, the present paper is the first report that larger crystals and higher crystallinity may be obtained by mercerizing cellulose. This finding will help to elucidate the ultrastructure of cellulose in its natural state as well as the way in which it is mercerized.

1. J. BLACKWELL, F. J. KOLPAK, and K. H. GARDNER. Tappi, **61**(1), 71 (1978).
2. F. J. KOLPAK, M. WEIH, and J. BLACKWELL. Polymer, **19**, 123 (1978).
3. F. J. KOLPAK and J. BLACKWELL. Polymer, **19**, 132 (1978).
4. J. O. WARWICKER, R. JEFFRIES, R. L. COLBRAN, and R. N. ROBINSON. Shirley Institute Pamphlet No. 93, Dicksbury, Manchester, U.K. 1966.
5. R. JEFFRIES and J. O. WARWICKER. Text Res. J. **39**, 548 (1969).
5. J.-F. REVOL and D. A. I. GORING. J. Appl. Polym. Sci. **26**, 1275 (1981).
7. S. J. KUANG, J.-F. REVOL, and D. A. I. GORING. Cellul. Chem. Technol. **19**, 113 (1985).
8. K. H. GARDNER and J. BLACKWELL. Biopolymers, **13**, 1975 (1974).
9. C. WOODCOCK and A. SARKO. Macromolecules, **13**, 1183 (1980).
10. K. HIETA, S. KUGA, and M. USUDA. Biopolymers, **23**, 1807 (1984).
11. H. CHANZY and B. HENRISSAT. FEBS Lett. **184**, 285 (1985).
12. A. SARKO and R. MUGGLI. Macromolecules, **7**, 486 (1974).
13. T. OKANO and A. SARKO. J. Appl. Polym. Sci. **29**, 4175 (1984).
14. T. OKANO and A. SARKO. J. Appl. Polym. Sci. **30**, 325 (1985).
15. J.-F. REVOL and D. A. I. GORING. Polymer, **24**, 1547 (1983).
16. L. SEGAL, J. J. CREELY, A. E. MARKIN, JR., and C. M. CONRAD. Text. Res. J. **29**, 786 (1959).
17. G. CENTOLA and D. BORRUSO. Ind. Carta, **16**, 87 (1962).
18. A. M. HINDELEH and D. J. JOHNSON. Polymer, **13**, 423 (1972).
19. O. ELLEFSEN, E. WANG LUND, B. A. TONNESEN, and K. OIEN. Nor. Skogind. **11**, 284 (1957); **11**, 349 (1957).
20. N. B. PATIL, N. E. DWELTZ, and T. RADHAKRISHNAN. Text. Res. J. **32**, 460 (1962).
21. H. CHANZY, K. IMADA, and R. VUONG. Protoplasma, **94**, 299 (1978).
22. H. CHANZY, K. IMADA, A. MOLLARD, R. VUONG, and F. BARNOUD. Protoplasma, **100**, 303 (1979).

Can. J. Chem. Downloaded from www.nrcresearchpress.com by 118.98.75.50 on 09/07/12
For personal use only.

Thermodynamics of ionization of aqueous alkanolamines

JIN-HO KIM,[1] CELINA DOBROGOWSKA, AND LOREN G. HEPLER
Department of Chemistry, University of Alberta, Edmonton, Alta., Canada T6G 2G2

Received December 22, 1986

This paper is dedicated to Professor John T. Edward

JIN-HO KIM, CELINA DOBROGOWSKA, and LOREN G. HEPLER. Can. J. Chem. **65**, 1726 (1987).

We have made electrochemical measurements with a glass electrode that have yielded pK values at T = 298.15 K for monothanolamine (MEA), triethanolamine (TEA), diisopropanolamine (DIPA), and methyldiethanolamine (MDEA) relative to the already well-known pK for diethanolamine (DEA), with all pK values referring to equilibria of the type $AmH^+(aq)$ = $Am(aq) + H^+(aq)$ in which Am(aq) represents an alkanolamine in aqueous solution and $AmH^+(aq)$ represents the corresponding protonated alkanolamine. We have also made calorimetric measurements leading to ΔH^0 values for dissociation of the protonated species of all five of these alkanolamines in aqueous solution at T = 298.15 K. These pK and ΔH^0 values have led to ΔG^0 and ΔS^0 values for the corresponding dissociation reactions of all five $AmH^+(aq)$ species.

JIN-HO KIM, CELINA DOBROGOWSKA et LOREN G. HEPLER. Can. J. Chem. **65**, 1726 (1987).

On a effectué des mesures électrochimiques à l'aide d'une électrode de verre qui ont permis d'obtenir, à 298,15 K, des valeurs de pK de la monoéthanolamine (MEA), de la triéthanolamine (TEA), de la diisopropanolamine (DIPA) et de la méthyldiéthanolamine (MDEA) relatives à la valeur bien connue du pK de la diéthanolamine (DEA); toutes les valeurs de pK se réfèrent à des équilibres du type $AmH^+(aq)$ = $Am(aq) + H^+(aq)$ dans lesquels Am(aq) représente une alkanolamine en solution aqueuse et $AmH^+(aq)$ représente l'alkanolamine protonée correspondante. On a aussi effectué des mesures calorimétriques qui ont conduit à des valeurs de ΔH^0 pour la dissociation des espèces protonées de chacune de ces cinq alkanolamines, en solutions aqueuses, à 298,15 K. Ces valeurs de pK et de ΔH^0 ont permis de déterminer les valeurs de ΔG^0 et de ΔS^0 pour les réactions de dissociation correspondantes de chacune des cinq espèces $AmH^+(aq)$.

[Traduit par la revue]

Introduction

Investigations of the acid–base properties of many organic substances have contributed in important ways to our understanding of relationships between molecular structures, properties of individual atoms or groups of atoms within molecules, and "chemical reactivity" as measured by equilibrium constants or by rate constants. In this connection the need for and uses of thermodynamic data (equilibrium constants or free energies, enthalpies, and entropies) for acid–base reactions in solution (where solvation effects occur along with "intrinsic" acid–base effects) and in the gas phase (no solvent) has been discussed recently in a perceptive paper (1) by Professor Edward.

Our general interest in the thermodynamic properties of organic acids and bases comes from considerations discussed in the paper (1) by Edward and as also reviewed elsewhere (2). Our specific interest in alkanolamines is derived partly from our general interest in thermodynamics of aqueous acids and bases and also comes partly from the present and potential uses of aqueous solutions of alkanolamines in removing acidic gases from industrial gas streams (3, 4).

As a result of the interests summarized above, we have made potentiometric and calorimetric measurements leading to pK, ΔG^0, ΔH^0, and ΔS^0 values for reactions of the general type represented by

[1] $AmH^+(aq) = Am(aq) + H^+(aq)$

in which Am(aq) represents an alkanolamine and $AmH^+(aq)$ represents the protonated alkanolamine, all in aqueous solution.

Experimental

Monoethanolamine (MEA, from Aldrich), diethanolamine (DEA, from Aldrich), triethanolamine (TEA, from Fisher), methyldiethanolamine (MDEA, from Aldrich), and diisopropanolamine (DIPA, from Eastman) were distilled twice at reduced pressure in an atmosphere of nitrogen and then stored over silica gel in desiccators filled with nitrogen.

Perchloric acid solutions were prepared from concentrated stock solution (≈70%, from Fisher) and double distilled water. These solutions, which were used in potentiometric titrations to check purities of the alkanolamines, in preparation of solutions used in determining equilibrium constants for reactions of type [1], and in calorimetric measurements, were standardized by potentiometric titrations in which tris(hydroxymethyl)aminoethane (from Fisher) was used as an alkalimetric standard.

Potentiometric titrations and measurements leading to pK values for reactions of type [1] were carried out with a Fisher Model 825 MP Accumet pH meter and Fisher electrodes (glass and calomel).

The method (5) used for determination of pK values for reactions of type [1] was based on calibration of the glass electrode – pH meter system with reference buffer solutions of Am/AmH^+ type. As shown previously (5), this convenient method minimizes common problems associated with junction potentials and activity coefficients. A fundamental requirement for application of this method is that we must have a reliable value (based on proper considerations of activity coefficients) for the pK of some reference compound that is similar to the compounds of interest. We have chosen diethanolamine (DEA) as our reference, because this substance is similar to the other alkanolamines of interest and because Bower, Robinson, and Bates (6) have provided an accurate and reliable pK = 8.883 for

[2] $DEAH^+(aq) = DEA(aq) + H^+(aq)$

at T = 298.15 K.

All calorimetric measurements have been made with a "home made" isoperibol calorimeter, which consisted of a glass Dewar vessel (370 cm^3 capacity) suspended in a brass can that was immersed in a constant temperature bath maintained at 25.00 ± 0.01°C and held constant during each calorimetric measurement to ±0.001°C, using a Tronac temperature controller (Model TPC-41) with an auxiliary cooling system maintained at 24.80 ± 0.05°C. Temperature changes in the calorimeter were measured with a thermistor (YSI 44045) combined with a Current Comparator Resistance Bridge (Guildline 9975). Our method of calorimetric measurement involved placing a weighed sample of alkanolamine in a small glass ampoule that was fastened to

[1]Visiting research scientist from Department of Chemistry, Kangweon National University, Chuncheon, Korea.

Can. J. Chem. Downloaded from www.nrcresearchpress.com by 118.98.75.50 on 09/07/12
For personal use only.

TABLE 1. Equilibrium constants ($pK = -\log K$) for ionizations of type [1], enthalpies of solution as in eq. [3], enthalpies of reaction as in eq. [4], and standard enthalpies of proton ionization (ΔH^0, as in eq. [1]) of alkanolamines at $T = 298.15$ K

Amine[a]	pK	ΔH_3 (kJ mol^{-1})	ΔH_4 (kJ mol^{-1})	ΔH^0 (kJ mol^{-1})
MEA	9.508±0.01	−11.43±0.09	−61.98±0.11	50.55±0.14
DEA	[b]	−14.50±0.06	−56.43±0.10	41.93±0.12
TEA	7.80 ±0.03	−14.38±0.08	−48.29±0.13	33.91±0.15
DIPA	8.88 ±0.03	−4.5 ±0.14	−47.2 ±0.16	42.7 ±0.2
MDEA	8.52 ±0.03	−20.5 ±0.2	−55.7 ±0.2	35.2 ±0.3

[a]Abbreviations are as follows: MEA = monoethanolamine, DEA = diethanolamine, TEA = triethanolamine, DIPA = diisopropanolamine, and MDEA = methyldiethanolamine.

[b]We have used $pK = 8.883$ from ref. 6 as reference or standard for calibration (5) of our glass electrode – pH meter system.

the end of the stirrer in the calorimeter. Gentle pressure on the top of the stirrer caused the bulb to break on the bottom of the Dewar vessel, thus introducing the alkanolamine to the solution in the calorimeter. The calorimeter was calibrated electrically for each experiment.

We have checked the accuracy of the calorimetric system described above by way of measurements of the enthalpy of solution of KCl(c) in distilled water, the enthalpy of solution of 4-aminopyridine in excess aqueous acid (7, 8) and the enthalpy of neutralization of tris(hydroxymethyl)aminomethane by excess aqueous acid. Results of these measurements, as fully reported elsewhere (9) along with a more detailed description of the calorimeter, agreed to within 0.5%, 0.04%, and 0.02%, respectively, with the "best" values from the literature.

Results and calculations

Results of our pH measurements leading to pK values (based on molal standard states for solutes) for equilibria of type [1] at $T = 298.15$ K are summarized in Table 1.

We have measured enthalpies of solution of pure alkanolamines (DIPA is solid at 298.15 K, others are liquid) into dilute aqueous sodium hydroxide. Results of these measurements (after small "corrections" for the enthalpy effect due to hydrolysis) are the enthalpies of solution represented by

[3] $\mathrm{Am(pure)} = \mathrm{Am(aq)} \qquad \Delta H_3$

We have also measured enthalpies of solution and reaction of pure alkanolamines in excess dilute perchloric acid as represented by

[4] $\mathrm{Am(pure)} + \mathrm{H^+(aq)} = \mathrm{AmH^+(aq)} \qquad \Delta H_4$

Results of all these calorimetric measurements are summarized in Table 1, where ΔH_3 and ΔH_4 values refer to $T = 298.15$ K.

Combinations of our ΔH_3 and ΔH_4 values in Table 1 for reactions of types [3] and [4] as in

[5] $\Delta H_1 = \Delta H_3 - \Delta H_4$

lead to ΔH_1 values for reactions of type [1]. Because the enthalpies of solution of alkanolamines as in reaction [3] were independent of concentration in dilute solutions and because of the electrical symmetry of reactions represented by eqs. [1] and [4], we take these calculated ΔH_1 values to be equal to the desired standard state enthalpies (ΔH^0) of reactions of type [1], as listed in the fifth column in Table 1.

Results of our measurements, as summarized in Table 1, can be related to results of earlier investigators as follows.

Two excellent electrochemical investigations (10, 11) have led to $pK = 9.498$ and 9.500 for dissociation of $MEAH^+$(aq) at 298.15 K. Other investigators (12–14) have reported $pK = 9.51$, 9.52 (interpolation between 20 and 30°C), and 9.50. All of these results are in good agreement with our $pK = 9.508$. Two investigations (10, 11) that led to pK values at several temperatures also led by way of $d \ln K/dT = \Delta H^0/RT^2$ to $\Delta H^0 = 50.54$ and 50.88 kJ mol^{-1} for the dissociation of $MEAH^+$(aq) as in reaction [1], in excellent agreement with our calorimetric $\Delta H^0 = 50.55$ kJ mol^{-1}. Some earlier calorimetric measurements (15–18) have led to $\Delta H^0 = 50.50$, 50.50, 50.38, and 50.63 kJ mol^{-1}, also in good agreement with our calorimetric result. Two other calorimetric investigations (19, 20) and one $d \ln K/dT$ investigation (13) have led to ΔH^0 values in poor agreement with the "best" results above (10, 11, 15–18).

We have already selected $pK = 8.883$ for the dissociation of $DEAH^+$(aq), based on the measurements of Bower, Robinson, and Bates (6), as our reference or standard for calibrating our glass electrode – pH meter system; other values having larger uncertainties have been reported (14, 21). The $\Delta H^0 = 42.40$ kJ mol^{-1} calculated from application of $d \ln K/dT$ to the results of Bower, Robinson, and Bates (6) is in reasonable agreement with our calorimetric $\Delta H^0 = 41.93$ kJ mol^{-1} and with $\Delta H^0 = 41.88$ kJ mol^{-1} from earlier calorimetric measurements (17), but is in poor agreement with ΔH^0 values from one other $d \ln K/dT$ investigation (21) and one other calorimetric (20) investigation.

Careful electrochemical measurements by Bates and Allen (22) have led to $pK = 7.762$ and (from $d \ln K/dT$) $\Delta H^0 = 33.45$ kJ mol^{-1} for dissociation of $TEAH^+$(aq). We also have $\Delta H^0 = 34.14$ kJ mol^{-1} from calorimetric measurements by Christensen and colleagues (17). All of these results are in satisfactory agreement with our $pK = 7.80$ and $\Delta H^0 = 33.91$ kJ mol^{-1}. Other pK (14, 23, 24) and ΔH^0 (20, 24) values have been reported, but we consider all of these to be less accurate than those listed above in this paragraph.

For dissociation of $DIPAH^+$(aq) the only earlier results we can cite are from equilibrium measurements (in 1.00 M KCl) by Blauwhoff and Bos (25), who have reported that pK values for $DIPAH^+$(aq) and $DEAH^+$(aq) are "essentially equal" over the temperature range 293–323 K. The resulting implications that $pK \approx 8.88$ and that $\Delta H^0 \approx 42$ kJ mol^{-1} for dissociation of $DIPAH^+$(aq) are consistent with our $pK = 8.88$ and $\Delta H^0 = 42.7$ kJ mol^{-1}.

Our $pK = 8.52$ for dissociation of $MDEAH^+$(aq) is in good agreement with $pK = 8.52$ at 298 K from Schwabe, Graichen, and Spiethoff (26); the ΔH^0 value that can be obtained by

Can. J. Chem. Downloaded from www.nrcresearchpress.com by 118.98.75.50 on 09/07/12
For personal use only.

TABLE 2. Selected "best" thermodynamic properties at $T = 298.15$ K for reactions of alkanolamines represented by $AmH^+(aq) = Am(aq) + H^+(aq)$

Amine[a]	pK	ΔG^0 (kJ mol^{-1})	ΔH^0 (kJ mol^{-1})	ΔS^0 (J K^{-1} mol^{-1})
MEA	9.500	54.225	50.52	−12.43
DEA	8.883	50.703	41.90	−29.53
TEA	7.762	44.305	34.01	−34.53
DIPA	8.88	50.69	42.7	−26.8
MDEA	8.52	48.63	35.2	−45.0

[a]Abbreviations are identified below Table 1.

application of $d \ln K/dT$ to their results has a very large uncertainty. Douheret and Pariaud (14) have reported pK values that are larger than values mentioned above.

In addition to the pK and ΔH^0 values that have been cited, we also have some information about ΔC_p^0 for reactions of type [1]. The only "direct" evaluation by way of heat capacity measurements that we know about is $\Delta C_p^0 = -13\,J\,K^{-1}\,mol^{-1}$ for dissociation of $MEAH^+(aq)$ from the work of Cabani, Matteoli, and Selli (27). Levi, McEwan, and Wolfenden (15) have made calorimetric measurements leading to ΔH^0 values at 10, 20, and 30°C and thence to $\Delta C_p^0 = +17\,J\,K^{-1}\,mol^{-1}$ for dissociation of $MEAH^+(aq)$ at 298.15 K. Only a few of the investigations leading to pK values at different temperatures permit meaningful evaluation of ΔH^0 at several temperatures by way of $d \ln K/dT$ and then evaluation of ΔC_p^0 by way of $d\Delta H^0/dT$. In this connection we cite (10, 11) $\Delta C_p^0 = -5$ and $+45\,J\,K^{-1}\,mol^{-1}$ for dissociation of $MEAH^+(aq)$. We also have $\Delta C_p^0 = +49\,J\,K^{-1}\,mol^{-1}$ (6) for dissociation of $DEAH^+(aq)$ and $\Delta C_p^0 = +52\,J\,K^{-1}\,mol^{-1}$ (22) for dissociation of $TEAH^+(aq)$. Because of the uncertainties in these values and the observation that ΔC_p^0 values for isocoulombic reactions such as [1] are commonly small (as is the case for all the values listed here), the best that we can do now is say that $\Delta C_p^0 \approx 0$ for the reactions under present consideration.

On the basis of our results in Table 1 and the other results (pK values, ΔH^0 values from $d \ln K/dT$, and ΔH^0 values from calorimetric measurements) already cited, we have selected what we consider to be the best available thermodynamic quantities for dissociation of the five $AmH^+(aq)$ species that we have investigated. These selected thermodynamic values are listed in Table 2.

Detailed analysis of the thermodynamic results reported here for alkanolamines in terms of such useful equations as those proposed and developed by Hammett and Taft or analysis of the relationships between thermodynamic data that apply to aqueous solutions and similar data that apply to the gas phase as discussed by Edward (1) are subjects for continuing research.

Acknowledgements

We all thank the Natural Sciences and Engineering Research Council of Canada for support of this research. We also thank Professor A. E. Mather for background information and useful advice. J.-H. K. thanks Kangweon National University for providing leave of absence from his duties there.

1. J. T. EDWARD. J. Chem. Educ. **59**, 354 (1982).
2. L. G. HEPLER. Thermochim. Acta, **100**, 171 (1986).
3. G. ASTARITA, D. W. SAVAGE, and A. BISIO. Gas treating with chemical solvents. John Wiley and Sons, New York. 1983.
4. R. D. DESHMUKH and A. E. MATHER. Chem. Eng. Sci. **36**, 355 (1981).
5. W. F. O'HARA, T. HU, and L. G. HEPLER. J. Phys. Chem. **67**, 1933 (1963).
6. V. E. BOWER, R. A. ROBINSON, and R. G. BATES. J. Res. Natl. Bur. Stands. **66A**, 71 (1962).
7. T. E. BURCHFIELD and L. G. HEPLER. J. Chem. Thermodyn. **13**, 513 (1981).
8. M. J. AKELLO, M. I. PAZ-ANDRADE, and G. PILCHER. J. Chem. Thermodyn. **15**, 949 (1983).
9. C. DOBROGOWSKA and L. G. HEPLER. In preparation.
10. R. G. BATES and G. D. PINCHING. J. Res. Natl. Bur. Stands. **46**, 349 (1951).
11. S. P. DATTA and A. K. GRZYBOWSKI. J. Chem. Soc. 3068 (1962).
12. V. SIVERTZ, R. E. REITMEIER, and H. V. TARTAR. J. Am. Chem. Soc. **62**, 1379 (1940).
13. J. R. LOTZ, B. P. BLOCK, and W. C. FERNELIUS. J. Phys. Chem. **63**, 541 (1959).
14. G. DOUHERET and J. C. PARIAUD. J. Chim. Phys. **59**, 1013 (1962).
15. D. L. LEVI, W. S. MCEWAN, and J. H. WOLFENDEN. J. Chem. Soc. 760 (1949).
16. G. OJELUND and I. WADSO. Acta Chem. Scand. **22**, 2691 (1968).
17. J. C. CHRISTENSEN, R. M. IZATT, D. P. WRATHALL, and L. D. HANSEN. J. Chem. Soc. A, 1212 (1969).
18. D. C. TYSON, JR., W. H. MCCURDY, JR., and C. E. BRICKER. Anal. Chem. **13**, 1640 (1961).
19. D. J. EATOUGH. Anal. Chem. **42**, 6351 (1970).
20. E. POPPER, L. ROMAN, and P. MARCU. Talanta, **14**, 1163 (1967).
21. G. CHREMOS and H. K. ZIMMERMAN. Texas J. Sci. **11**, 467 (1959); Chem. Abstr. **54**, 11655a (1960).
22. R. G. BATES and G. F. ALLEN. J. Research Natl. Bur. Stands. **64A**, 343 (1960).
23. H. SIGEL, K. H. SCHELLER, and B. PRIJS. Inorg. Chim. Acta, **66**, 147 (1982).
24. H. WEIDMAN and H. K. ZIMMERMAN. Texas J. Sci. **11**, 212 (1959); Chem. Abstr. **54**, 1987a (1960).
25. P. M. BLAUWHOFF and M. BOS. J. Chem. Eng. Data, **26**, 7 (1981).
26. K. SCHWABE, W. GRAICHEN, and D. SPIETHOFF. Z. phys. Chem. N.F. **20**, 68 (1959).
27. S. CABANI, E. MATTEOLI, and E. SELLI. J. Chem. Soc. Faraday Trans. 1, **75**, 363 (1979).

Can. J. Chem. Downloaded from www.nrcresearchpress.com by 118.98.75.50 on 09/07/12
For personal use only.

Arylphosphonic acids. I. Substituent effects on their first and second dissociations

K. NAGARAJAN, KEVIN P. SHELLY, R. R. PERKINS, AND ROSS STEWART
Department of Chemistry, University of British Columbia, Vancouver, B.C., Canada V6T 1W5

Received November 24, 1986

This paper is dedicated to Professor John T. Edward

K. NAGARAJAN, KEVIN P. SHELLY, R. R. PERKINS, and ROSS STEWART. Can. J. Chem. **65**, 1729 (1987).

Thermodynamic pK_1 and pK_2 values of 36 arylphosphonic acids have been determined. The pK values of the *meta* and *para* compounds are correlated well by the σ^n parameter, suggesting that there is little conjugation between the phosphonic group and the aromatic ring; the ρ values of the first and second dissociations are 0.923 and 1.140, respectively. The $-PO_3H^-$ group itself appears to be electron donating, contrary to earlier literature reports. The effect of *ortho* groups has been examined using multivariate analysis; the steric component of the proximity effect is acid weakening and has a larger effect on the second dissociation than on the first, presumably because a greater change in degree of solvation accompanies the second dissociation than the first.

K. NAGARAJAN, KEVIN P. SHELLY, R. R. PERKINS et ROSS STEWART. Can. J. Chem. **65**, 1729 (1987).

On a déterminé les valeurs des pK_1 et pK_2 thermodynamiques de 36 acides arylphosphoniques. On a pu établir une bonne corrélation entre les valeurs des pK des composés *méta* et *para* et le paramètre σ^n; ce résultat suggère qu'il existe peu de conjugation entre le groupement phosphonique et le cycle aromatique; les valeurs de ρ pour les première et deuxième dissociations sont respectivement 0,923 et 1,140. Contrairement à ce qui a pu être publié antérieurement, le groupement $-PO_3H^-$ semble être électrodonneur. Faisant appel à une analyse multi-variable, on a aussi examiné l'effet des groupements en *ortho*; la composante stérique de l'effet de proximité a pour effet de diminuer l'acidité et cet effet est plus important sur la deuxième dissociation que sur la première; ce résultat est probablement causé par le fait que le changement dans le degré de solvatation qui accompagne la deuxième dissociation est plus important que celui qui accompagne la première.

[Traduit par la revue]

Can. J. Chem. Downloaded from www.nrcresearchpress.com by 118.98.75.50 on 09/07/12
For personal use only.

Introduction

As part of a study of general acid and general base catalysis of protolytic reactions we have prepared a series of arylphosphonic acids, $ArPO_3H_2$, and examined the effectiveness of the three catalytic species, $ArPO_3H_2$, $ArPO_3H^-$, and $ArPO_3^{2-}$, on the enolization of acetone (1); the present paper deals with the acid dissociation constants of the first two of these species.

There are a number of reports in the literature of the effect of substituents on the pK_1 and pK_2 values of arylphosphonic acids, most notably those of Jaffé *et al.* (2, 3) and of Nualláin (4). We are particularly concerned with proximity effects in prototropic reactions and we needed pK data for *ortho*, *meta*, and *para* derivatives. The data of Jaffé *et al.* include such compounds but the pK values are not thermodynamic values; the data of Nualláin, which are much less extensive, have been corrected for ionic strength effects but include only two *ortho* compounds. Since we needed a set of self-consistent pK values for our catalytic work we have measured the first and second dissociation constants of a considerable number of arylphosphonic acids and corrected them to the standard state. The effects of substituents on the dissociation constants are interesting in their own right, first with respect to the degree of conjugation between the ring and the phosphonic acid unit, and secondly with respect to pK_1/pK_2 variations and associated solvent and related effects.

Results and discussion

The pK_1 and pK_2 values of 36 arylphosphonic acids are reported in Table 1. For those compounds whose pK values have been previously determined by Jaffé *et al.* (2, 3) the agreement is, in general, satisfactory, when account is taken of concentration effects. Seven of the compounds have had their pK values determined by Nualláin and corrected to zero ionic strength. The agreement here is good, except that we find the strongest acids, which contain nitro groups, to be slightly less acidic than did he.

Meta *and* para *compounds, substituent effects*

The π-bonding abilities of phosphorus and carbon are known to be quite different (5–7). With regard to arylphosphonic acids, the degree of conjugation between aryl ring and the acidic functional group appears to be considerably less than is the case with aryl carboxylic acids, judging from the *ortho* effects to be discussed later. Accordingly, one might expect that ordinary Hammett σ values would overestimate the electron-releasing capacity of groups such as alkoxy in the *para* position and that the modified substituent constant σ^n, which is intended for use with systems that have no through conjugation, would be better for correlating arylphosphonic acid pK values (8–10). In deriving values of σ^n, Hoefnagel and Wepster had examined the then existing data for pK_2 and noted that the substituent constant for the 4-amino substituent was high in comparison with other systems in which through conjugation was not possible at all (10). They concluded, therefore, that σ^n did not correlate with log K_2 of arylphosphonic acids. (Zwitterion formation in neutral 4-aminophenylphosphonic acid prevents a similar test being made on log K_1.) Along similar lines, reported correlations of pK with σ for ring-substituted phosphonic acids led Hudson to conclude that π bonding with the phosphorus atom is significant (5*a*), although others have reached different conclusions (5*b*, *c*).

We find that our data for log K_2 are correlated very well by σ^n (Fig. 1 and eq. [1]) and rather poorly by σ (eq. [2]), indicating the degree of π bonding between ring and phosphorus to be small.

$$[1] \quad \log K_2 = 1.140\sigma^n + 7.55 \text{ (corr. coeff. 0.9970)}$$

$$[2] \quad \log K_2 = 0.980\sigma + 7.48 \text{ (corr. coeff. 0.9778)}$$

The situation with respect to K_1 is less clear, partly because the bellwether amino substituent is, perforce, absent and partly because the precision of the K_1 values is less (see Experimental). Indeed the correlation between log K_1 and σ^n (Fig. 1 and

Can. J. Chem. Downloaded from www.nrcresearchpress.com by 118.98.75.50 on 09/07/12
For personal use only.

TABLE 1. Dissociation constants of arylphosphonic acids[a]

Substituent	pK_1	pK_2
H	1.86	7.51
3-CH_3	1.95	7.64
4-CH_3	2.00	7.68
4-C_2H_5	1.99	7.65
3-CH_3O	1.74	7.42
4-CH_3O	2.00	7.68
4-C_2H_5O	2.00	7.65
3-F	1.53	7.16
3-Cl	1.53	7.10
4-Cl	1.58	7.23
4-Br	1.54	7.18
4-CN	1.27	6.79
3-NO_2	1.20	6.69
4-NO_2	1.19	6.67
4-NH_2	—	7.84
β-naphthyl	—[b]	7.42
3-carboxy	1.55	7.78[c,d]
4-carboxy	1.51	7.64[c,e]
3,4-$(CH_3)_2$	2.04	7.76
3,5-$(CH_3)_2$	2.01	7.73
2-CH_3	2.08	7.92
2-C_2H_5	2.11	8.09
2-$(CH_3)_2CH$	2.13	8.18
2-CH_3O	2.21	8.21
2-C_2H_5O	2.32	8.42
2-F	1.49	7.19
2-Cl	1.56	7.39
2-Br	1.53	7.37
2-I	1.56	7.46
2-NO_2	1.28	7.05
α-naphthyl	—[b]	7.64
2,3-$(CH_3)_2$	2.17	8.07
2,4-$(CH_3)_2$	2.17	8.07
2,5-$(CH_3)_2$	2.10	8.00
2,6-$(CH_3)_2$	2.39	8.62
2,4,6-$(CH_3)_3$	2.53	8.82

[a]Corrected to zero ionic strength; in water, 25°C.
[b]Erratic values obtained, likely because of low solubility.
[c]pK_3.
[d]pK_2 = 4.37.
[e]pK_2 = 4.27.

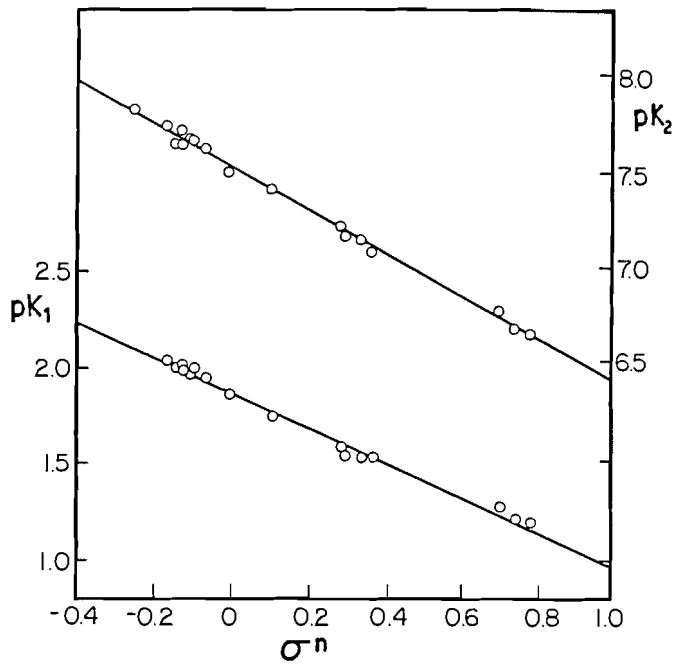

FIG. 1. Plot of pK_1 (lower curve and left-hand axis) and pK_2 (upper curve and right-hand axis) for arylphosphonic acids against the substituent constant σ^n.

eq. [3]) is not dramatically better than that for σ (eq. [4]) when all points are included. However, when lines are drawn with respect to the *meta* compounds and the *para* nitro and cyano compounds (those for which $\sigma \approx \sigma^n$), the values of slope and intercept are 1.143 and 7.55, respectively, for K_2 and 0.926 and 1.89 for K_1. These values are almost identical to those given in eqs. [1] and [3] and are considerably different from those given in eqs. [2] and [4], showing conclusively that σ^n, not σ, is the parameter of choice for both pK_1 and pK_2.

[3] $\log K_1 = 0.924\sigma^n + 1.88$ (corr. coeff. 0.9954)

[4] $\log K_1 = 0.856\sigma + 1.84$ (corr. coeff. 0.9872)

The pK_2 values of the 3- and 4-carboxyphenylphosphonic acids refer to the dissociation of the carboxyl group and this allows a check to be made of the previously reported substituent effect of the $-PO_3H^-$ group. Jaffé *et al.* measured pK values for these compounds some time ago (2) but the values of the derived substituent constants (σ_m and σ_p) appear to have been transposed in their paper, an error that has been retained in several recent compilations of Hammett substituent constants. (See, for example, ref. 11*a*.) Furthermore, their pK values were not corrected for ionic strength effects, which can be quite large for the second and higher dissociations of polyprotic acids. Their uncorrected pK results indicated that the $-PO_3H^-$ group is electron withdrawing, with the effect being greater from the *para* than from the *meta* position. After being corrected to zero ionic strength our results suggest that the $-PO_3H^-$ group is electron donating relative to hydrogen rather than electron withdrawing, with the relative ordering for *meta* and *para* being the same as that indicated by the pK values of Jaffé *et al.* Since charged groups are notorious for the inconstancy of their Hammett substituent values (11*b*, *c*), the significance of the values we can derive for the $-PO_3H^-$ group ($\sigma_m = -0.17$ and $\sigma_p = -0.07$) is uncertain.

Reaction constants for K_1 *and* K_2

The reaction constant for the first dissociation is smaller than that for the second, $\rho_1^n = 0.924$, $\rho_2^n = 1.140$ (Fig. 1). (Nualláin found ρ_1 to be 0.902 and ρ_2 to be 1.023 (4).) We find it difficult to rationalize the somewhat greater effect of substituents on K_2 than on K_1 and, because of our concern that the first ionization constants for the most acidic phosphonic acids might be greater than the measured values (*vide infra*), thus lowering the observed value of ρ, we cast about for analogous systems to which the present system could be compared. There is, in fact, little known about the electronic effect of aryl substituents on successive dissociations of oxygen acids. The ρ_1 and ρ_2 values for 5-substituted isophthalic acids are virtually identical (12). The limited precise data available for *meta* and *para* arylarsonic acids indicate that ρ_1 is larger than ρ_2 (2, 13, 14). The successive dissociation constants of $C_6H_5CO_2H_2\cdot$ have been determined (15, 16) but, unfortunately, their *meta* and *para* derivatives do not appear to have been studied. Successive additions of electrons to a neutral molecule to give the mono and dianion are in

Can. J. Chem. Downloaded from www.nrcresearchpress.com by 118.98.75.50 on 09/07/12
For personal use only.

many ways analogous to successive deprotonations; evidence here is also sparse but there are indeed cases where the ρ of the second step is considerably larger than that of the first, e.g., the stepwise reduction of maleimide (17).

Our concern regarding the pK_1 values of the most acidic compounds, in particular the nitro substituted phenylphosphonic acids, stems from observations of differences in the degrees of ionization and dissociation of strong and moderately strong acids (18, 19). The pertinent equilibria are shown in eq. [5]

[5] $ArPO_3H_2 + H_2O \rightleftharpoons ArPO_3H^- \cdot H_3O^+ \rightleftharpoons ArPO_3H^- + H_3O^+$

For weaker acids ionization and dissociation are synonymous and so pK values measured potentiometrically will correspond to the ionization process; for stronger acids this may not be so. It would be expected that the reaction constant of a Hammett type correlation would correspond to the ionization process, which would mean that the ρ we have measured for the first dissociation might be slightly low. Since our main concern is the determination of catalytic effects in prototropic reactions of the A-2 type, which depend on dissociative phenomena, the potentiometrically determined pK_1 values are all we require. It should be noted, however, that in acid catalyzed reactions of the A-S_E2 type (ref. 19, p. 260; refs. 20 and 21), in which a proton is transferred in the rate-controlling step, the pertinent catalytic species for strong and moderately strong acids may be the ion pair or the non-ionized acid and it is not known if the use of potentiometric pK values is appropriate.

Ortho *effects*

Unlike benzoic acids, where virtually any *ortho* group has a marked acid-strengthening effect, most arylphosphonic acids with *ortho* substituents have acidities that are very roughly comparable to those of their *para* analogues, at least when direct interactions such as hydrogen bonding are absent, and this has been remarked upon previously (3). Since the generally accepted explanation for the acid-strengthening effect of *ortho* groups in benzoic acids involves steric hindrance to conjugation in the neutral molecule, it is to be expected that arylphosphonic acids, in which conjugation between the acid unit and the ring is slight (*vide supra*), would not exhibit the marked acid-strengthening effect of *ortho* groups that is characteristic of benzoic acids. The proximity effects that do appear in arylphosphonic acid ionizations were analyzed by the multivariate analysis method of Bijloo and Rekker (23), which is based on the work of Fujita and Nishioka (24; see also ref. 25).

Their method assigns a value to the electronic effect of an *ortho* group by taking the effect of the corresponding *para* substituent and augmenting it by a special *ortho* inductive effect σ_I^o; the well-known steric parameter E_S is assumed to make the other contribution to the *ortho* effect. Equation [5] should correlate the pK values of all ring substituted arylphosphonic acids, σ^n being used for the electronic effect since it gives a superior correlation for *para* substituents.

[6] $pK_0 - pK = \Delta pK = \rho\sigma^n + \rho_I\sigma_I^o + \delta E_S^o$

where pK_0 is the value for the unsubstituted compound (experimental values 1.86 and 7.51 for the successive dissociations); σ^n for *ortho* and *para* groups are taken as identical; ρ_I is the reaction constant for the special *ortho* inductive effect; and δ is the corresponding quantity for the steric effect.

When all the data of Table 1 were subjected to multivariate analysis using eq. [6], satisfactory correlations could be obtained provided the *ortho* alkoxy groups were omitted; these compounds show anomalously high pK_1 and pK_2 values, presumably because of hydrogen bonding between the oxygen of the alkoxy unit and the proton(s) of the phosphonic groups (4). The results are shown in eqs. [7] and [8].

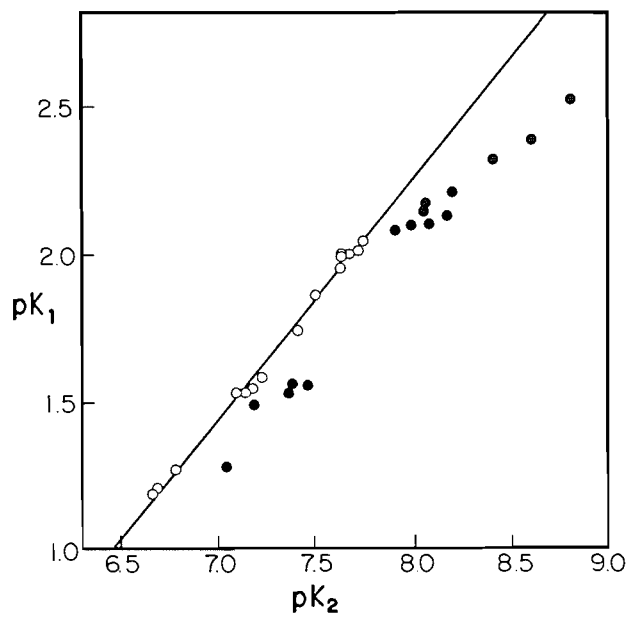

FIG. 2. Plot of pK_1 against pK_2 for arylphosphonic acids; *meta* and *para* compounds (open circles) and *ortho* compounds (filled circles).

[7] $1.86 - pK_1 = 0.87\sigma^n + 0.32\sigma_I^o + 0.13E_S^o$

(corr. coeff. 0.986, 29 acids)

[8] $7.52 - pK_2 = 1.07\sigma^n + 0.29\sigma_I^o + 0.33E_S^o$

(corr. coeff. 0.988, 30 acids)

The high correlation coefficients, the closeness of the ρ values to those found when *meta* and *para* compounds only are used (eqs. [3] and [1]), and the close agreement between the experimental and calculated pK values of the unsubstituted compound suggest that *ortho* effects can be successfully treated using eq. [6]. (The agreement is not nearly as good when ρ values for the *meta*/*para* and *ortho* series are directly compared (23), although satisfactory correlation coefficients are obtained in all cases.)

What is the significance of the other coefficients? The values of ρ_I are fairly modest, much smaller than those found for benzoic acids (eq. [9]) (23). The values of δ are positive, meaning that steric effects are acid weakening, the reverse of the situation found with benzoic acids. The values of −0.13 and −0.33 for the first and second dissociation can be compared with the value of +0.40 for benzoic acids.

[9] $4.21 - pK = 0.96\sigma + 1.32\sigma_I^o - 0.40E_S^o$

The steric effect of *ortho* groups is probably associated principally with hindrance to solvation and, if this be so, the larger δ for K_2 than for K_1 is reasonable, indicating a greater change in solvation going from anion to dianion than from neutral acid to monoanion (5*b*). Indeed, the neutral molecule, being highly acidic, may be quite highly solvated, particularly if the ion-pair form is present in significant amounts (eq. [5]). The differential steric effect of *ortho* groups can be seen in Fig. 2, where pK_1 is plotted against pK_2. The horizontal displacement

of the *ortho* compounds from the line for the *meta* and *para* compounds can be considered to be a measure of the enhanced steric effect on the second dissociation.

Experimental

Materials

Most of the arylphosphonic acids were prepared in good yields by a published method that involves the treatment of the aryl iodide or bromide with triethyl phosphite at 180°C in the presence of anhydrous nickel bromide (26, 27). The diethyl arylphosphonates so produced were hydrolyzed to the corresponding acids by refluxing them with concentrated hydrochloric acid for 6–8 h. The 3- and 4-carboxyphenylphosphonic acids were prepared in quantitative yields by starting with the corresponding methyl iodobenzoates. Dimethyl 2,6-dimethylphenylphosphonate was obtained by photolysis of a mixture of 2,6-dimethyliodobenzene and trimethyl phosphite (28).

The acid hydrolysis route to the phosphonic acids is not suitable for those esters having an acid-sensitive group, e.g., cyano, or for those phosphonic acids that undergo dephosphonation under the drastic conditions employed during hydrolysis, e.g., the 2,6-dimethyl, 2,4,6-trimethyl, 2-methoxy, and 2-ethoxy compounds. In such cases the acid hydrolysis route produced a very poor yield of the desired products and so an alternative route, based on the method of Blackburn and Ingleson (29), was developed. This involves dealkylating the esters by treatment with iodotrimethylsilane to give the trimethylsilyl esters, which undergo hydrolysis in water at room temperature to give the phosphonic acids in excellent yields. The detailed procedure follows.

The dialkyl arylphosphonate (20 mmol) in 25 mL of anhydrous carbon tetrachloride cooled to 0°C was treated with 6 mL iodotrimethylsilane (42 mmol) in small portions. The mixture was allowed to warm to room temperature and was stirred for 30 min. The volatiles were removed by evaporation, 50 mL water was added, and the mixture stirred overnight. A pinch of sodium bisulfite was used to remove the dark colour caused by the presence of iodine, the water evaporated off, and the resulting white crystalline mass recrystallized from a 1-propanol/ethyl acetate/petroleum ether mixture.

The halo and 4-nitro phenylphosphonic acids were prepared from the corresponding diazonium fluoroborates (30). In the case of 2-bromophenylphosphonic acid, phosphorus tribromide was employed, since the use of phosphorus trichloride, as suggested by Freedman *et al.* (31), produced a mixture containing a significant amount of 2-chlorophenylphosphonic acid impurity. When phosphorus tribromide is used in the synthesis of 2-iodophenylphosphonic acid, as recommended by Doak and Freedman (32), the product was contaminated with 2-bromophenylphosphonic acid. Here the use of phosphorus trichloride produced the desired product, 2-iodophenylphosphonic acid, cleanly. 4-Aminophenylphosphonic acid was prepared from the 4-bromo compound by the method of Grummit *et al.* (33).

3-Nitrophenylphosphonic acid was prepared by nitrating phenylphosphonic acid with fuming nitric acid followed by crystallization of the magnesium salts of the isomeric nitration mixture (34).

2-Nitrophenylphosphonic acid was prepared by the method of Cadogan *et al.* (35).

Table 2 lists the melting points and analytical data for the arylphosphonic acids that are not well documented in the literature, some having been previously unreported, and some reported without analytical data.

pK Measurements

The dissociation constants were obtained from potentiometric titrations of the arylphosphonic acid with standardized sodium hydroxide solutions using a Radiometer Model 26 pH meter and a Radiometer GK 2421C combined glass electrode. The pH meter was standardized with aqueous buffer solutions over the range 2–7. Titrations were done in a jacketed container fitted with a cover having holes to accommodate a nitrogen bleed, the electrode, and the tip of the microburette. A temperature of 25.0 ± 0.1°C was maintained by circulating water from a thermostated water bath through the jacket. A nitrogen atmosphere was maintained over the solution during the titrations; an Ascarite guard tube kept over the microburette eliminated absorption of carbon dioxide by the alkali.

TABLE 2. Melting point and analytical data for substituted phenylphosphonic acids[a]

Substituent	Melting point, °C[b]	Analysis: Calculated C	Calculated H	Found C	Found H
2-Isopropyl	173–174	54.00	6.55	54.12	6.48
2,3-Dimethyl	218–220	51.62	5.96	51.48	5.88
3,4-Dimethyl	150–151	51.62	5.96	51.64	5.98
3,5-Dimethyl	196–198	51.62	5.96	51.79	5.88
2,6-Dimethyl	188–190[c]	51.62	5.96	51.43	5.97
2,4,6-Trimethyl	171–172[d]	54.00	6.55	54.27	6.65
2-Methoxy	201–202[e]	44.69	4.82	44.89	4.95
2-Ethoxy	180–182	47.53	5.49	47.39	5.50
4-Ethoxy	168	47.53	5.49	47.72	5.52
2-Fluoro	153–155[f]	40.93	3.44	40.87	3.50
3-Fluoro	102–103[g]	40.93	3.44	40.93	3.41

[a]Compounds that are not well documented in the literature.
[b]Uncorrected.
[c]Reference 38 gives 174–179°C.
[d]Reference 39 gives 177°C.
[e]Reference 27 gives 179–182°C; ref. 31 gives 202–203°C.
[f]Reference 22 gives 146–149°C.
[g]Reference 27 gives 95–98°C.

The dissociation constants were calculated using the method of Speakman (36) as adapted by Albert and Serjeant; the calculations were done on a computer using their Fortran IV programme (35). The above method was preferred over the conventional equations, to overcome problems in the estimation of very low pK values. For the same reason the titrations were performed in different concentration regions wherever solubility permitted, as suggested by Albert and Serjeant (37). The pK_2 values could be reproduced within ± 0.03 unit whereas pK_1 values below 2.0 could be reproduced only within ± 0.08 unit. Accordingly, a large number of determinations were made in the latter cases and averages taken.

Acknowledgements

One of the authors (K.N.) thanks Ramakrishna Mission Vivekananda College Madras, India, for granting sabbatical leave during this period. We acknowledge the work of three summer students, Alex Lee, Lisa Wong, and Lakhbir Rai, who helped with the pK determinations. We also thank Dr. U. Maciejewska for preparing one of the arylphosphonic acids used in the work. Finally, we acknowledge the financial support of the Natural Sciences and Engineering Research Council of Canada.

1. K. P. SHELLY, K. NAGARAJAN, and R. STEWART. Can. J. Chem. **65**, 1734 (1987).
2. H. H. JAFFÉ, L. D. FREEDMAN, and G. O. DOAK. J. Am. Chem. Soc. **75**, 2209 (1953).
3. H. H. JAFFÉ, L. D. FREEDMAN, and G. O. DOAK. J. Am. Chem. Soc. **76**, 1548 (1954).
4. C. Ó. NUALLÁIN. J. Inorg. Nucl. Chem. **36**, 339 (1974).
5. (*a*) R. F. HUDSON. Structure and mechanism in organo-phosphorus chemistry. Academic Press, London. 1965. pp. 82–83; (*b*) D. J. MARTIN and C. E. GRIFFIN. J. Organomet. Chem. **1**, 292 (1964); (*c*) H. H. JAFFÉ. J. Chem. Phys. **22**, 1430 (1954).
6. B. J. WALKER. Organophosphorus chemistry. Penguin, London. 1972. p. 108.
7. T. A. MODRO. Phosphorus Sulfur, **5**, 331 (1979).
8. R. W. TAFT, S. EHRENSON, I. C. LEWIS, and R. E. GLICK. J. Am. Chem. Soc. **81**, 5352 (1959).
9. R. W. TAFT. J. Phys. Chem. **64**, 1805 (1960).
10. A. J. HOEFNAGEL and B. M. WEPSTER. J. Am. Chem. Soc. **95**, 5357 (1973).

Can. J. Chem. Downloaded from www.nrcresearchpress.com by 118.98.75.50 on 09/07/12
For personal use only.

11. (*a*) D. D. PERRIN, B. DEMPSEY, and E. P. SERJEANT. pK_a predictions for organic acids and bases. Chapman and Hall, London. 1981. p. 111; (*b*) A. J. HOEFNAGEL, M. A. HOEFNAGEL, and B. M. WEPSTER. J. Org. Chem. **43**, 4720 (1978); (*c*) J. HINE. Structural effects on equilibria in organic chemistry. Wiley–Interscience, New York. 1975; pp. 66, 67.
12. S. J. GUMBLEY and R. STEWART. J. Chem. Soc. Perkin Trans. 2, 529 (1984).
13. C. Ó. NUALLÁIN and S. Ó. CINNÉIDE. J. Inorg. Nucl. Chem. **35**, 2871 (1973).
14. D. PRESSMAN and D. H. BROWN. J. Am. Chem. Soc. **65**, 540 (1943).
15. M. SIMIC and M. Z. HOFFMAN. J. Phys. Chem. **76**, 1398 (1972).
16. E. HAYON and M. SIMIC. Acc. Chem. Res. **7**, 114 (1974).
17. P. ZUMAN. Substituent effects in organic polarography. Plenum Press, New York. 1967. p. 145, and personal communication from Professor Zuman.
18. R. I. GELB, L. M. SCHWARTZ, and D. A. LAUFER. J. Am. Chem. Soc. **103**, 5664 (1981).
19. R. STEWART. The proton. Applications to organic chemistry. Academic Press, Orlando, FL. 1985. pp. 11–14, and references therein.
20. T. A. MODRO and K. YATES. J. Am. Chem. Soc. **98**, 4247 (1976).
21. R. TAYLOR. *In* Comprehensive chemical kinetics. Vol. 13. *Edited by* C. H. Bamford and C. F. H. Tupper. Elsevier, Amsterdam. 1972.
22. G. O. DOAK and L. D. FREEDMAN. J. Am. Chem. Soc. **75**, 1379 (1973).
23. G. J. BIJLOO and R. F. REKKER. Quant. Struct.-Act. Relat. Pharmacol. Chem. Biol. **3**, 91 (1984).
24. T. FUJITA and T. NISHIOKA. Prog. Phys. Org. Chem. **12**, 49 (1976).
25. V. A. BARANSKII and B. I. ISTONWIN. J. Gen. Chem. U.S.S.R. **49**, 409 (1979).
26. P. TAVS. Chem. Ber. **103**, 2428 (1970).
27. R. C. GRABIAK, J. A. MILES, and G. M. SCHWENZER. Phosphorus Sulfur, **9**, 197 (1980).
28. R. OBRYCKI and C. E. GRIFFIN. J. Org. Chem. **33**, 632 (1968).
29. G. M. BLACKBURN and D. INGLESON. J. Chem. Soc. Perkin Trans. 1, 1150 (1980).
30. G. O. DOAK and L. D. FREEDMAN. J. Am. Chem. Soc. **73**, 5658 (1951).
31. L. D. FREEDMAN, H. TAUBER, G. O. DOAK, and H. J. MAGNUSON. J. Am. Chem. Soc. **75**, 1379 (1953).
32. G. O. DOAK and L. D. FREEDMAN. J. Am. Chem. Soc. **75**, 683 (1953).
33. O. GRUMMITT, N. VOURLOGIANES, J. MEHAFFEY, and R. TEBBE. Org. Prep. Proced. **2**, 5 (1970).
34. G. O. DOAK and L. D. FREEDMAN. J. Am. Chem. Soc. **77**, 6221 (1955).
35. J. I. G. CADOGAN, D. J. SEARS, and D. M. SMITH. J. Chem. Soc. (C), 1314 (1969).
36. J. C. SPEAKMAN. J. Chem. Soc. 855 (1940).
37. A. ALBERT and E. P. SERJEANT. The determinations of ionisation constants. A laboratory manual. 3rd ed. Chapman and Hall, London. 1984. pp. 25, 35, 57–68.
38. TH. VAN DER KNAAP, TH. C. KLEBACH, R. LOURENS, M. VOS, and F. BICKELHAUPT. J. Am. Chem. Soc. **105**, 4026 (1983).
39. I. SIGAL and L. LOEW. J. Am. Chem. Soc. **100**, 6394 (1978).

Can. J. Chem. Downloaded from www.nrcresearchpress.com by 118.98.75.50 on 09/07/12
For personal use only.

Arylphosphonic acids. II. General acid and general base catalysis of acetone enolization

KEVIN P. SHELLY, K. NAGARAJAN, AND ROSS STEWART
Department of Chemistry, University of British Columbia, Vancouver, B.C., Canada V6T 1Y6

Received November 24, 1986

This paper is dedicated to Professor John T. Edward

KEVIN P. SHELLY, K. NAGARAJAN, and ROSS STEWART. Can. J. Chem. **65**, 1734 (1987).

We have measured the rate constants for the enolization of acetone catalyzed by 29 arylphosphonate dianions ($ArPO_3^{2-}$) and by 20 arylphosphonic acids ($ArPO_3H_2$). An excellent Brönsted correlation is found for the former reaction, with most *ortho* substituted compounds falling on the line drawn for the *meta* and *para* compounds ($\beta = 0.72$). The largest deviation is found for *o*-iodo, whose small positive deviation is ascribed to a polarizability effect in the transition state. The arylphosphonic acids give a fairly good Brönsted plot ($\alpha = 0.37$) but here the *ortho* substituents tend to react slightly faster than would be expected on the basis of their equilibrium acid strengths. Catalysis by the monoanion $ArPO_3H^-$ is difficult to detect; such ions appear to be acting as general acids, not general bases, and do not appear to act as bifunctional catalysts; it is shown that protonating acetone is 3.4×10^4 times as effective as deprotonating $ArPO_3H^-$. The Brönsted coefficients (β) for the rate-controlling steps for the enolization of acetone by the principal routes are shown to be inversely related to the magnitude of the rate constants.

KEVIN P. SHELLY, K. NAGARAJAN et ROSS STEWART. Can. J. Chem. **65**, 1734 (1987).

On a mesuré les constantes de vitesse pour l'énolisation de l'acétone, catalysée par 29 dianions arylphosphonates ($ArPO_3^{2-}$) et par 20 acides arylphosphoniques ($ArPO_3H_2$). On a obtenu une excellent corrélation de Brönsted pour la première réaction; la plupart des composés substitués en *ortho* se retrouvent sur la courbe obtenue à l'aide des composés *méta* et *para* ($\beta = 0{,}72$). On a trouvé que le dérivé *o*-iodo conduit à la plus grande déviation et on attribue sa petite déviation positive à un effet de polarisabilité dans l'état de transition. Les acides arylphosphoniques ont conduit à une courbe de Brönsted assez bonne ($\alpha = 0{,}37$); toutefois, dans ce cas, les vitesses de réaction des composés portant des substituants en position *ortho* sont généralement plus grandes que celles que l'on pourrait attendre en se basant sur les forces de leur équilibre acide. Il est difficile de détecter la présence de catalyse par le monoanion $ArPO_3H^-$; ces ions semblent agir par catalyse acide générale, non par catalyse basique générale, et ils ne semblent pas agir comme catalyseurs bifonctionnels; on démontre que la protonation de l'acétone est $3{,}4 \times 10^4$ fois plus efficace que la déprotonation de $ArPO_3H^-$. On démontre qu'il existe une corrélation inverse entre l'amplitude des constantes de vitesse et les coefficients de Brönsted (β) des étapes contrôlant la vitesse d'énolisation de l'acétone par le principales voies.

[Traduit par la revue]

Introduction

Enolization of carbonyl compounds is one of the most important catalytic processes in organic chemistry, being the first step in a number of condensation, racemization, halogenation, and oxidation processes. As part of our study of prototropic reactions we have examined the catalytic effect of a series of arylphosphonic acids **1** on the enolization of acetone, a substance that has come to be regarded as the prototypical carbonyl compound.

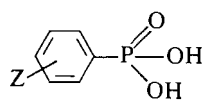

1

There are good reasons for choosing arylphosphonic acids as the catalytic species. We have shown previously that proton removal from activated methyl groups in a number of cyclic conjugated systems is catalyzed by general acids and bases and exhibits steric activation. Activation by adjacent alkyl groups in the substrate has been demonstrated in many cases (1–5) and in two instances (involving general base catalysis) by adjacent groups in the base (6, 7). The latter reactions are the deprotonations of 1,2,3-trimethylpyrazinium ion and methylcreatininium ion by carboxylate ions (eqs. [1] and [2]), in which the more hindered bases, e.g. *ortho*-substituted benzoate ions, exhibit marked positive deviations from the Brönsted line drawn for the least hindered carboxylate ions (see also ref. 8).

The substrates in eqs. [1] and [2], being cationic, are for all practical purposes subject only to general base catalysis, not to general acid catalysis. We have encountered difficulties in trying to assess the effects of hindered carboxylic acids and carboxylate bases on substrates such as acetone, mainly because of acute solubility problems. For a number of reasons these problems are less severe with phosphonic acids; they have the further advantage of providing three catalytic entities for study, the neutral acid, the monoanion, and the dianion, enabling us to pursue another matter of particular interest to us: the effect on the reaction rate of changing the charge on catalyst or substrate (9, 10).

[1] $RCO_2^- +$ 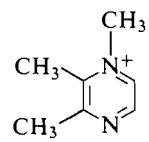 $\longrightarrow RCO_2H +$ 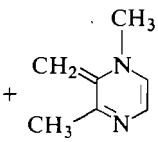

[2] $RCO_2^- +$ 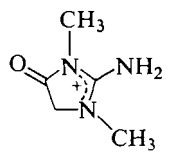 $\longrightarrow RCO_2H +$ 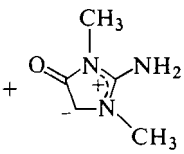

Results and discussion

The mechanism of the enolization of acetone catalyzed by general acids (HA) and their conjugated bases (A^-) is given in eqs. [3] and [4] (11, 12).

In the case of catalysis by neutral phosphonic acids eq. [3] (general acid catalysis) is operative; in the case of catalysis by phosphonate dianions eq. [4] (general base catalysis) is operative. In the case of phosphonate monoanions either route might

Can. J. Chem. Downloaded from www.nrcresearchpress.com by 118.98.75.50 on 09/07/12
For personal use only.

Can. J. Chem. Downloaded from www.nrcresearchpress.com by 118.98.75.50 on 09/07/12
For personal use only.

[3a] $CH_3—\overset{\overset{O}{\|}}{C}—CH_3 + HA \rightleftharpoons CH_3—\overset{\overset{+OH}{\|}}{C}—CH_3 + A^-$

[3b] $CH_3—\overset{\overset{+OH}{\|}}{C}—CH_3 + A^- \rightarrow CH_3—\overset{\overset{OH}{|}}{C}=CH_2 + HA$

[4] $CH_3—\overset{\overset{O}{\|}}{C}—CH_3 + A^- \rightarrow CH_3—\overset{\overset{O-}{|}}{C}=CH_2 + HA$

be followed. Indeed, since such species could act simultaneously as both acid and base, the possibility of bifunctional catalysis exists (eq. [5]).

[5] $CH_3—C(=O)—CH_3 + HO—P(—Ar)(—O^-)=O \rightarrow CH_3—C(—OH)=CH_2 + {}^-O—P(—Ar)(—HO)=O$

In this connection Spaulding *et al.* (13) showed that the dianion of phosphoric acid, HPO_4^{2-}, does not appear to function as a bifunctional catalyst for the enolization of acetone, despite earlier indications to the contrary.

Brönsted relation

The catalytic constants for enolization of acetone by arylphosphonic acids $ArPO_3H_2$ and their dianions $ArPO_3^{2-}$ are given in Table 1. The Brönsted plot for catalysis by arylphosphonic acids (the composite reaction [8]) is shown in Fig. 1, the Brönsted coefficient α being equal to 0.390 for *meta* and *para* compounds (correlation coefficient 0.9901). The Brönsted plot for catalysis by arylphosphonate dianions (eq. [9]) is shown in Fig. 2, the Brönsted coefficient β being equal to 0.718 (correlation coefficient 0.9954), again for the *meta* and *para* compounds. (We use α when the variable species is the proton donor and β when it is the proton acceptor; we have also applied standard statistical corrections to rate and equilibrium constants (14, 15).)

[6] $ArPO_3H_2 + CH_3—\overset{\overset{O}{\|}}{C}—CH_3 \rightleftharpoons ArPO_3H^- + CH_3—\overset{\overset{+OH}{\|}}{C}—CH_3$

[7] $ArPO_3H^- + CH_3—\overset{\overset{+OH}{\|}}{C}—CH_3 \rightarrow ArPO_3H_2 + CH_3—\overset{\overset{OH}{|}}{C}=CH_2$

Adding eqs. [6] and [7] gives eq. [8].

[8] $ArPO_3H_2 + CH_3—\overset{\overset{O}{\|}}{C}—CH_3 \rightarrow CH_3—\overset{\overset{OH}{|}}{C}=CH_2 + ArPO_3H_2$

[9] $ArPO_3^{2-} + CH_3—\overset{\overset{O}{\|}}{C}—CH_3 \rightarrow CH_3—\overset{\overset{O^-}{|}}{C}=CH_2 + ArPO_3H^-$

For catalysis by the neutral phosphonic acids the Brönsted plot shows some divergence between the *meta* and *para* compounds on the one hand and the *ortho* compounds on the other. The latter deviate to a small extent in the positive direction. That is, they tend to be slightly more effective catalysts than would be suggested by their equilibrium acid strengths. The deviations, which are not large, are more pronounced for the

TABLE 1. Rate constants for the enolization of acetone catalyzed by substituted phenylphosphonic acids and dianions; water, 25°C

Substituent	pK_1	$10^5 k_{H_2A}\ M^{-1}\ s^{-1}$	pK_2	$10^5 k_{A^{2-}}\ M^{-1}\ s^{-1}$
4-NO_2	1.19	3.17	6.67	0.670
3-NO_2	1.20	3.26	6.69	0.732
4-CN	1.27	3.02	6.79	0.788
3-Cl	1.53	2.32	7.10	1.48
3-F	1.53	2.50	7.16	1.42
4-Br	1.54	—	7.18	1.77
4-Cl	1.58	—	7.23	1.67
2-Naph	—	—	7.42	2.24
H	1.86	1.78	7.51	2.95
3-CH_3	1.95	1.73	7.64	3.22
4-CH_3	2.00	—	7.68	3.48
4-C_2H_5	1.99	—	7.65	3.48
3,5-$(CH_3)_2$	2.01	—	7.73	3.88
3,4-$(CH_3)_2$	2.04	1.46	7.76	4.21
3-COOH	1.55	2.44	7.64[a]	2.34[b]
4-COOH	1.51	—	7.78[a]	2.36[b]
3-CH_3O	1.74	1.90	7.42	—
2-NO_2	1.28	3.24	7.05	1.09
2-F	1.49	2.65	7.19	1.42
2-Cl	1.56	2.46	7.39	1.96
2-Br	1.53	2.87	7.37	2.35
2-I	1.56	2.75	7.46	3.17
1-Naph		—	7.64	3.44
2-CH_3	2.08	1.65	7.92	4.99
2,5-$(CH_3)_2$	2.10	—	8.00	5.72
2,3-$(CH_3)_2$	2.15	—	8.07	6.20
2,4-$(CH_3)_2$	2.17	—	8.07	6.51
2-C_2H_5	2.11	1.45	8.09	6.52
2-$CH(CH_3)_2$	2.13	1.31	8.18	7.85
2,6-$(CH_3)_2$	2.39	1.05	8.62	15.9
2-CH_3O	2.21	1.37	8.21	—

[a] pK_3.
[b] $k_{A^{3-}}$.

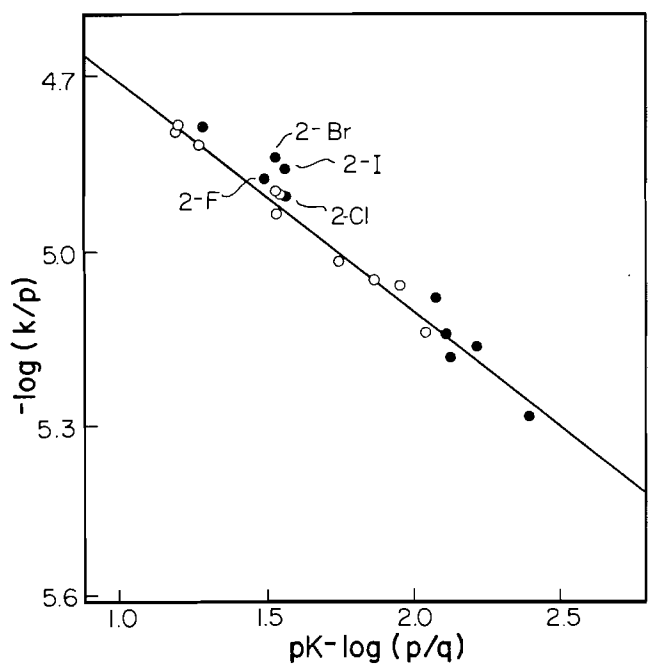

FIG. 1. Brönsted plot for catalysis of acetone enolization by arylphosphonic acids; *meta* and *para* compounds (open circles) and *ortho* compounds (filled circles); line drawn with respect to the *meta* and *para* compounds.

Can. J. Chem. Downloaded from www.nrcresearchpress.com by 118.98.75.50 on 09/07/12
For personal use only.

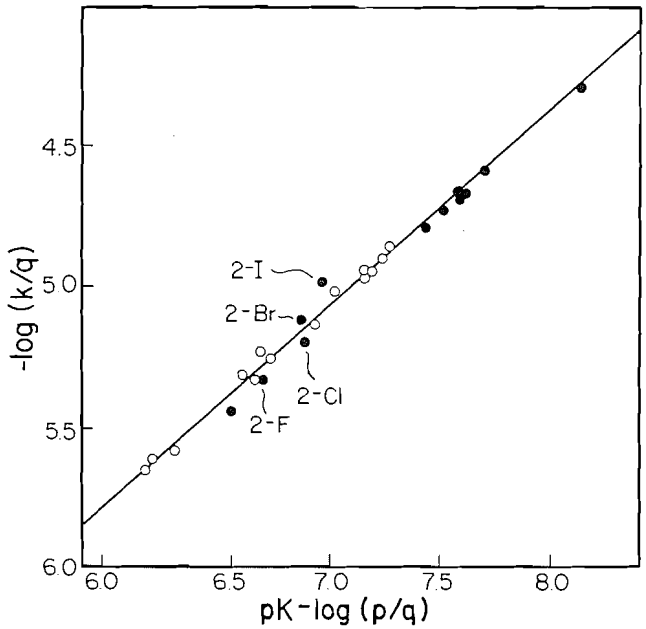

FIG. 2. Brönsted plot for catalysis of acetone enolization by arylphosphonate dianions; *meta* and *para* compounds (open circles) and *ortho* compounds (closed circles); line drawn with respect to the *meta* and *para* compounds.

more acidic compounds, suggesting that a slightly larger Brönsted coefficient may govern the reactivity of the *ortho* rather than that of the *meta* and *para* compounds. (For reasons that are unclear to us, the precision of the rate constant derived for the *o*-bromo compound was less than those of the other halogen compounds.) Even when the *ortho* compounds are omitted, there is more scatter in the Brönsted plot for catalysis by $ArPO_3H_2$ (Fig. 1) than in that for catalysis by $ArPO_3^{2-}$ (Fig. 2), an effect that is probably due to the precision of the measurements of both pK_1 and k_{H_2A} being somewhat lower than the measurements of pK_2 and $k_{A^{2-}}$. The Brönsted equations for catalysis by neutral arylphosphonic acids are summarized in eqs. [10]–[12], where n = number of compounds and r = correlation coefficient.

$$[10] \quad (m, p) \qquad \log k_{H_2A}/p = 0.390 \log (p/qK) - 4.32 \qquad n = 10,\ r = 0.9901$$

$$[11] \quad (o) \qquad \log k_{H_2A}/p = 0.444 \log (p/qK) - 4.20 \qquad n = 10,\ r = 0.9861$$

$$[12] \quad (m, p, o) \qquad \log k_{H_2A}/p = 0.405 \log (p/qK) - 4.28 \qquad n = 20,\ r = 0.9795$$

For the phosphonate dianions a very good Brönsted relationship is obtained when the points for the charged substituent $-CO_2^-$ are omitted (Fig. 2). This group shows marked negative deviations from the Brönsted plot for both the *meta* and *para* positions. Similar deviations for dicarboxylate ions compared to monocarboxylate ions have been observed previously (6, 13).

Ortho substituents in the dianion conform well to the Brönsted line drawn with respect to the *meta* and *para* compounds. The largest deviations occur with the *o*-iodo and *o*-bromo groups, which appear to confer small but real degrees of activation, particularly when they are compared to the other halogens. (A similar effect is present in the case of acid catalysis, Fig. 1.) The greater polarizabilities of iodo and bromo, compared to chloro and fluoro, are probably responsible for these effects.

With the exception of iodo and bromo, there appears to be no special proximity effect on the rate of reaction. That is, *ortho* groups exert essentially the same effect on the dissociation equilibrium of the monoanions as on the rate of proton abstraction by the arylphosphonate dianions (eqs. [13]–[15]). This is in sharp contrast to the effect that neighbouring groups produce in reactions [1] and [2], where significant positive deviations from Brönsted plots are observed. We conclude that proton transfer from acetone to the ion $ArPO_3^{2-}$ is normal in the sense that the effect of nearby substituents on the transition state and on the product is similar. In the case of proton transfer from the conjugate acid of acetone to the ion $ArPO_3H^-$, *ortho* groups show a small degree of activation.

We have shown elsewhere (16) that the effect of *ortho* groups on pK_1 and pK_2 of arylphosphonic acids is largely electronic with the steric component being relatively small, particularly for pK_1. Thus, proton transfer to and from arylphosphonic acids and their anions is not subject to major steric effects, either with respect to rate or equilibrium.

$$[13] \quad (m, p) \qquad \log k_{A^{2-}}/q = 0.718 \log (p/qK) - 10.09 \qquad n = 14,\ r = 0.9954$$

$$[14] \quad (o) \qquad \log k_{A^{2-}}/q = 0.712 \log (p/qK) - 10.06 \qquad n = 13,\ r = 0.9907$$

$$[15] \quad (m, p, o) \qquad \log k_{A^{2-}}/q = 0.703 \log (p/qK) - 9.99 \qquad n = 27,\ r = 0.9944$$

Catalysis by the monoanion is difficult to observe, although it has been detected in the pH range 3.1–5.5 in the case of the *meta*-nitro, the 3,4-dimethyl, and the unsubstituted compounds. Using nearly saturated solutions of these phosphonic acids and making use of the known catalytic constants for H^+, HO^-, water, the neutral acids, and the dianions, a residual contribution, presumably made by the monoanions, could be observed.

The catalytic rate constants for these monoanions are approximately $10^{-7} M^{-1} s^{-1}$, values that suggest that they are acting as general acids, not as general bases, since they correspond much more closely to an extension of the Brönsted plot for $ArPO_3H_2$ than to that for $ArPO_3^{2-}$. (The calculated values for these monoanions acting as bases is in the range of 10^{-9}–10^{-8} $M^{-1} s^{-1}$; acting as acids they should be in the range of 10^{-6}–$10^{-7} M^{-1} s^{-1}$). Furthermore, if bifunctional catalysis of the sort shown in eq. [5] (tautomeric catalysis (17, 18)) were important, the catalytic constants would be expected to be considerably increased over the values calculated on the basis of the Brönsted plots for both $ArPO_3H_2$ and $ArPO_3^{2-}$.

As one proceeds along the series to weaker acids there should come a point where the monoanion $ArPO_3H^-$ is found to act predominantly as a base rather than as an acid. Assuming the Brönsted lines for $ArPO_3H_2$ and $ArPO_3^{2-}$ also govern the catalytic activity of the species $ArPO_3H^-$, one can show that such a role reversal will not take place with even the weakest of the arylphosphonic acids we have examined.

What is the significance of the Brönsted coefficients found in this work? It is generally agreed that for systems of like structure the coefficient should increase in size as reactivity decreases. This would lead to a curved Brönsted plot if a sufficiently wide span of reactivities were produced by changing substituents. In practice, curvature is usually undetectable

TABLE 2. Brönsted coefficients and rate constants of reactions [7] and [9]

Reaction	Reactants	β^a	k^b
[7]	$(CH_3)_2C{=}\overset{+}{O}H + ArPO_3H^-$	0.61	0.83[c]
[9]	$(CH_3)_2C{=}O + ArPO_3^{2-}$	0.72	2.95×10^{-5}

[a] $1 - \alpha$; see text.
[b] Ar = C_6H_5; $M^{-1}s^{-1}$, in water at 25°C.
[c] Calculated value; see text.

for a single series although Bell, by combining several kinds of substrate and catalyst, produced a distinctly curved plot, albeit one with considerable scatter (19). More frequently, the inverse relationship between Brönsted coefficient and reactivity is sought by comparing Brönsted coefficients for related series whose reactivities are considerably different. In the case of acetone enolization catalyzed by arylphosphonic acids, the Brönsted coefficients of the two important rate-controlling steps (reactions [7] and [9]) can be compared. They are shown in Table 2 together with the rate constants for the unsubstituted compounds.

The Brönsted coefficient for the first reaction in Table 2 (eq. [7]) has been taken as $1.00 - \alpha$, where α is the measured value for eq. [8]. This follows from eq. [6] being a protolytic equilibrium with an effective constant of unity. That is, the effect of substituents on the equilibrium acid strengths of $ArPO_3H_2$ is identical to that on the equilibrium shown in eq. [6]. The rate constant has been calculated as shown in the following section.

It can be seen from the results in Table 2 that there is, indeed, an inverse relationship between reactivity and Brönsted coefficient. Unfortunately, the Brönsted coefficient for the reaction between $ArPO_3H^-$ and $(CH_3)_2C{=}O$ cannot be determined because, as we have seen, the reaction of most members of the series is too slow to be detected.

Activation by protonation or deprotonation

In prototropic reactions activation can be achieved either by protonating the substrate or by deprotonating the catalytic species that removes a proton from the substrate. In the cases of enolization of acetone by water, the activation conferred by protonating the substrate (proton activating factor, *paf*) is about 10^7, whereas that conferred by deprotonating the base (deprotonating factor, *dpf*) is about 10^{10} (9).

As we have seen, reaction between phenylphosphonate monoanion, $C_6H_5PO_3H^-$, and acetone is slow. As in the case referred to above, activation can be achieved by either protonating the substrate (to give $(CH_3)_2C{=}\overset{+}{O}H$) or by deprotonating the catalyst (to give $C_6H_5PO_3^{2-}$). It can be shown that the former is much more effective than the latter. Consider eqs. [16*a*]–[16*c*].

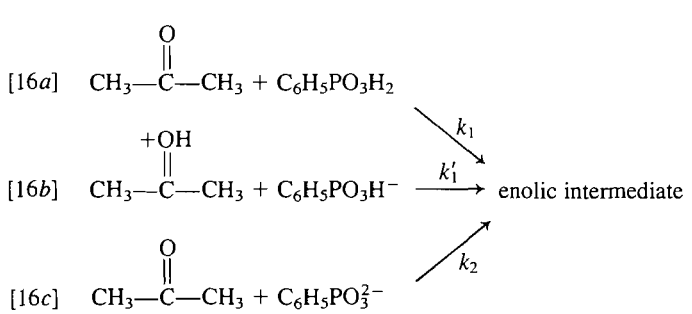

If we assume that the actual pathway for catalysis by phenylphosphonic acid (eq. [16*a*]) is given by eq. [16*b*], and letting Z and ZH^+ represent acetone and its conjugate acid, then $k_1[Z][C_6H_5PO_3H_2] = k_1'[ZH^+][C_6H_5PO_3H^-]$. Substituting the following values for the pertinent protolytic equilibria (eqs. [17] and [18]) gives eq. [19].

[17] $K_{ZH^+} = [Z][H^+]/[ZH^+] = 8 \times 10^2$ (see ref. 12, p. 121)

[18] $K_1 = [H^+][C_6H_5PO_3H^-]/[C_6H_5PO_3H_2] = 1.4 \times 10^{-2}$

[19] $k_1'/k_1 = [Z][C_6H_5PO_3H_2]/[ZH^+][C_6H_5PO_3H^-] = 5.7 \times 10^4$

Since $k_1 = 0.60k_2$ (Table 1), then

$$k_1' = 3.4 \times 10^4 k_2 \text{ (or } 1.0\,M^{-1}s^{-1})$$

Thus, using the reaction between acetone and the phenylphosphonate monoanion as a reference point, protonating the substrate (to form $(CH_3)_2C{=}\overset{+}{O}H$) is 3.4×10^4 times as effective as deprotonating the catalyst (to form $C_6H_5PO_3^{2-}$). On the other hand, when the base is water protonating the substrate is only 10^{-3} times as effective as deprotonating the base (to form HO^-).

Experimental

Materials

The preparation of the arylphosphonic acids has been described elsewhere (16). Acetone was refluxed with potassium permanganate, fractionally distilled, and stored overnight over calcium carbonate. The liquid was filtered and fractionally distilled a second time.

Rate measurements

The rates of enolization of acetone were determined iodometrically by following the decrease in the absorbance of the triiodide ion at 353 nm, 400 nm, or 440 nm. In general, aliquots from stock solutions of phosphonate buffer were mixed in 5- or 10-mL volumetric flasks with sodium chloride and acetone. The ionic strength was adjusted to 0.1 *M* for the measurement of the diacid catalytic constants (k_{H_2A}) and to 0.05 *M* for the measurement of the dianion catalytic constants ($k_{A^{2-}}$) by adding the appropriate quantities of sodium chloride. A 3-mL sample of this solution was temperature equilibrated at 25°C for 15 min in a closed cuvette. The iodination was initiated by the addition of 50 μL of triiodide ion solution. The decrease in absorbance was followed with a Cary 16 spectrophotometer equipped with a cell holder thermostated at 25 ± 0.1°C. The concentrations of acetone that were used varied from 0.1 to 0.5 *M* and those of iodide plus triiodide ion varied from 4×10^{-5} to 5×10^{-4} *M*. Each observed first-order rate constant (k_{obs}) was calculated from the linear slope of the plot of absorbance against time by use of the equation k_{obs} = slope/($\varepsilon_{I_3^-}$[acetone]) where $\varepsilon_{I_3^-}$ is the extinction coefficient of triiodide ion at the chosen wavelength. The values of $\varepsilon_{I_3^-}$ used were $2.45 \times 10^4 M^{-1}cm^{-1}$ at 353 nm (20), $5.9 \times 10^3 M^{-1}cm^{-1}$ at 400 nm (value determined in this work), and $1818\,M^{-1}cm^{-1}$ at 440 nm (5). The fact that all plots were linear from the time of the first reading (about 30 s after the addition of the triiodide aliquot) until at least 70% of the iodine had reacted showed that the kinetics of iodine consumption were zero order. The pH values of buffer solutions before and after rate measurements were unchanged. The catalytic constants calculated from rate measurements at 353 nm, 400 nm, and 440 nm were identical. The catalytic constants calculated from a number of rate measurements where acetone concentration was varied were identical. For phosphonate dianion catalysis a number of buffers reacted with triiodide. We were unable to study the enolization in these cases except for 2-iodophenylphosphonate dianion, where in the absence of acetone the disappearance of iodine was a slow first-order reaction that could be satisfactorily corrected for. The enolization process is zero order in iodine and it could be shown that the reaction of iodine with the buffer anion has a

Can. J. Chem. Downloaded from www.nrcresearchpress.com by 118.98.75.50 on 09/07/12
For personal use only.

Can. J. Chem. Downloaded from www.nrcresearchpress.com by 118.98.75.50 on 09/07/12
For personal use only.

negligible effect on the measured rate of enolization. For phosphonic acid catalysis a relatively concentrated solution of buffer is needed for the neutral acid to make a significant contribution to the observed rate; in the case of several of these compounds low solubility prevented values of k_{H_2A} being obtained.

(a) Phosphonate dianion catalysis: all the phosphonate buffers were prepared by the addition of between 4/3 and 5/3 equivalents of sodium hydroxide to the free acid. The proportion of dianion in the buffer was taken to be the fraction in excess of one equivalent, that of monoanion to be unity minus this fraction, and that of the diacid to be zero. Since $K_1/K_2 > 10^5$, the concentrations obtained in this way are quite accurate. The dependence of k_{obs} upon the composition of the buffers (at moderately low buffer concentrations) is given by eq. [20] where k_{sum} is the contribution from hydronium ion, water, and hydroxide ion. Equation [20] can be rewritten as eqs. [21] or [22], where r is the buffer ratio of monoanion to dianion ($[HA^-]/[A^{2-}]$).

$$[20] \quad k_{obs} = k_{sum} + k_{HA^-}[HA^-] + k_{A^{2-}}[A^{2-}]$$

$$[21] \quad k_{obs} = k_{sum} + [HA^-]\left\{k_{HA^-} + \frac{1}{r}\cdot k_{A^{2-}}\right\}$$

$$[22] \quad k_{obs} = k_{sum} + [A^{2-}]\{k_{A^{2-}} + r\cdot k_{HA^-}\}$$

Plots of k_{obs} against $[HA^-]$ at a given buffer ratio were found to be linear, the slopes s being equal to $k_{HA^-} + k_{A^{2-}}/r$ and the intercepts to k_{sum}. For phenylphosphonate and 3,4-dimethylphenylphosphonate, s was determined at 3 buffer ratios. Plots of s against $1/r$, which were found to be linear, give a slope of $k_{A^{2-}}$ and an intercept k_{HA^-}. However, the intercept values were too small to be detected, indicating the absence of any significant catalysis by the monoanions. Accordingly, for the other buffer systems, $k_{A^{2-}}$ was simply determined from the slopes of the lines obtained from plots of k_{obs} against $[A^{2-}]$ using eq. [22]. At least two buffer ratios were studied (r = 2, 1, or 0.5); the values of $k_{A^{2-}}$ from these determinations generally agreed within ±3% of the average value. The $k_{A^{2-}}$ values obtained in this manner for phenylphosphonate and 3-4-dimethyl phenylphosphonate agreed with those obtained by plotting s against $1/r$. Generally, four different concentrations at each buffer ratio were examined, and the pH of each solution was found to be the same. Rates of iodination were measured at 353 nm except in the case of nitrosubstituted phosphonates, which were measured at 400 nm because of significant absorption of same at 353 nm.

(b) Phosphonic diacid catalysis: upon the addition of between 1/2 and 2/3 equivalent of sodium hydroxide to the free acid, in an analogous treatment to that described above, the dependence of k_{obs} on the species present was expected to be given by eq. [23]. This can be rewritten as eq. [24], where n is the buffer ratio of diacid to monoanion $\{[H_2A]/[HA^-]\}$.

$$[23] \quad k_{obs} = k_{sum} + k_{H_2A}[H_2A] + k_{HA^-}[HA^-]$$

$$[24] \quad k_{obs} = k_{sum} + [H_2A]\{k_{H_2A} + 1/nk_{HA^-}\}$$

Unlike the case of $[HA^-]/[A^{2-}]$ buffers, we found that with $[H_2A]/[HA^-]$ buffers the pH varied with concentration. Thus the treatment used to determine the dianion catalytic constants was of no avail in these cases. For each particular solution at a particular pH, the concentration of the diacid was determined from eq. [25], where $[H_2A]_0$ is the initial concentration of free acid and B is the number of equivalents of sodium hydroxide added. Equation [24] reduced to eq. [26].

$$[25] \quad [H_2A] = [H_2A]_0 - [B] - [H^+]$$

$$[26] \quad k_{obs} = k_{H^+}[H^+] + k_{H_2A}[H_2A]$$

Knowing $k_{H^+} = 2.84 \times 10^{-5} M^{-1} s^{-1}$ (21), values of k_{H_2A} are determined at different pH values and varying quantities of base. The good agreement between catalytic constants so determined shows there is no significant catalysis by the monoanion. Generally four values of k_{H_2A} were obtained, each being within ±5% of the average value. Because of the speed of these reactions, a wavelength of 440 nm was generally used for the kinetic determinations.

(c) Catalysis by phosphonic–carboxylic trianions: the buffers were prepared by the addition of between 7/3 and 8/3 equivalents of sodium hydroxide to the free acid. The proportion of trianion in the buffers was taken to be the fraction in excess of two equivalents, that of dianion to be one minus this fraction, and that of the monoanion and triacid to be zero. In these cases $K_2/K_3 > 10^3$. The dependence of k_{obs} upon the buffer composition is given by eq. [27] where y is the buffer ratio of dianion to trianion ($[HA^{2-}]/[A^{3-}]$).

$$[27] \quad k_{obs} = k_{sum} + [A^{3-}]\{k_{A^{3-}} + yk_{HA^{2-}}\}$$

The trianion catalytic constants were determined from the slopes of the lines obtained from plots of k_{obs} against $[A^{3-}]$. The consistency of results obtained in this way at different buffer ratios, y, indicates the absence of any significant catalysis by the dianion, HA^{2-}.

(d) Catalysis by phosphonic–carboxylic triacids: a similar treatment to that used for the diacid catalysis using eqs. [28] and [29] afforded the triacid catalytic constant.

$$[28] \quad [H_3A] = [H_3A]_0 - [B] - [H^+]$$

$$[29] \quad k_{obs} = k_{H^+}[H^+] + k_{H_3A}[H_3A]$$

Acknowledgement

The financial support of the Natural Sciences and Engineering Research Council of Canada is gratefully acknowledged.

1. T. W. S. Lee and R. Stewart. Can. J. Chem. **64**, 1085 (1986).
2. R. Stewart and S. J. Gumbley. Can. J. Chem. **63**, 3290 (1985).
3. R. Stewart and T. W. S. Lee. J. Org. Chem. **47**, 2075 (1982).
4. R. Stewart, S. J. Gumbley, and R. Srinivasan. J. Am. Chem. Soc. **102**, 6168 (1980).
5. R. Stewart, R. Srinivasan, and S. J. Gumbley. Can. J. Chem. **59**, 2755 (1981).
6. R. Srinivasan and R. Stewart. J. Chem. Soc. Perkin Trans. 2, 674 (1976).
7. K. Nagarajan, T. W. S. Lee, R. R. Perkins, and R. Stewart. Can. J. Chem. **64**, 1090 (1986).
8. R. P. Bell, E. Gelles, and E. Moller. Proc. R. Soc. London, A: **198**, 308 (1949).
9. R. Stewart and R. Srinivasan. Acc. Chem. Res. **11**, 271 (1978).
10. R. Stewart and R. Srinivasan. Can. J. Chem. **59**, 957, 3318 (1981).
11. J. Toullec. *In* Advances in physical organic chemistry. Vol. 18. *Edited by* V. Gold and D. Bethell. Academic Press, London. 1982. p. 1.
12. R. Stewart. The proton. Applications to organic chemistry. Academic Press, Orlando, FL. 1985. pp. 259–263.
13. J. Spaulding, J. E. Stein, and J. E. Meany. J. Phys. Chem. **81**, 1359 (1977).
14. R. P. Bell and P. G. Evans. Proc. R. Soc. London, A: **291**, 297 (1966).
15. D. M. Bishop and K. J. Laidler. J. Chem. Phys. **42**, 1688 (1965).
16. K. Nagarajan, K. P. Shelly, R. R. Perkins, and R. Stewart. Can. J. Chem. **65**, 1729 (1987).
17. P. Rony. J. Am. Chem. Soc. **91**, 6090 (1969).
18. K-A. Engdahl, H. Biveheb, P. Ahlberg, and W. H. Saunders. J. Am. Chem. Soc. **105**, 4767 (1983).
19. R. P. Bell. The proton in chemistry. 2nd ed. Cornell University Press, Ithaca, NY. 1973. p. 203.
20. W. J. Albery, R. P. Bell, and A. L. Powell. Trans. Faraday Soc. **61**, 1194 (1965).
21. R. P. Bell and O. M. Lidwell. Proc. R. Soc. London, A: **176**, 88 (1940).

Binding of magnesium and lanthanum ions to heparin in the presence of sodium ions. A relationship between ^{13}C chemical shift displacements and counterion condensation theory

PHOTIS DAIS,[1] QIN-JI PENG,[2] AND ARTHUR S. PERLIN
Department of Chemistry, McGill University, Montreal, P.Q., Canada H3A 2A7

Received December 19, 1986

This paper is dedicated to Professor John T. Edward

PHOTIS DAIS, QIN-JI PENG, and ARTHUR S. PERLIN. Can. J. Chem. **65**, 1739 (1987).

Interactions between beef lung heparin and Mg^{2+} and La^{3+} counterions, in the presence of sodium ions, have been investigated by ^{13}C-nmr spectroscopy. The chemical shift displacements observed for the carbons of the main disaccharide unit of heparin, when analysed on the basis of counterion condensation theory, indicate that the association between the heparin polyanion and Mg^{2+} is a delocalized process. This is analogous to the Ca^{2+}/Na^{+}/heparin system, despite the fact that the binding affinity of heparin for Ca^{2+} is stronger than that for Mg^{2+}. By contrast, the interaction with La^{3+} is in excess of the theoretical predicted, which suggests that there is at least a partial site-binding of this counterion. In Ca^{2+}/M^{+}/heparin systems in which $M^{+} = Na^{+}$ or K^{+}, the selective binding preference of heparin for the univalent cations may be related to the order of their crystallographic ionic radii. A critical assessment is offered of the validity of this nmr spectroscopic approach to the study of counterion binding to heparin.

PHOTIS DAIS, QIN-JI PENG et ARTHUR S. PERLIN. Can. J. Chem. **65**, 1739 (1987).

Faisant appel à la rmn du ^{13}C, on a étudié les interactions entre l'héparine de poumon de bœuf et des ions Mg^{2+} et La^{3+}, en présence d'ions sodium. Une analyse des déplacements chimiques observés pour les carbones de l'unité dissacharidique principale de l'héparine en faisant appel à la théorie de condensation des contre-ions indique que l'association entre le polyanion de l'héparine et le Mg^{2+} est un processus délocalisé. Ceci est analogue au système Ca^{2+}/Na^{+}/héparine, même si l'affinité de l'héparine pour le Ca^{2+} est plus forte que pour le Mg^{2+}. Par ailleurs, l'interaction avec le La^{3+} est plus importante que celle prévue sur une base théorique; ceci suggère qu'il existe au moins un site de liaison partiel pour ce contre-ion. Dans les systèmes Ca^{2+}/M^{+}/héparine, dans lesquels $M^{+} = Na^{+}$ ou K^{+}, on peut établir une corrélation entre la liaison sélective préférentielle pour les cations univalents et l'ordre de leurs rayons ioniques cristallographiques. On offre une évaluation critique de la validité de cette approche par spectroscopie rmn pour étudier la liaison de contre-ions avec l'héparine.

[Traduit par la revue]

Introduction

In a previous study (1), the binding of calcium ions (Ca^{2+}) by heparin in the presence of sodium ions was examined by monitoring ^{13}C chemical shift displacements as a function of the calcium ion concentration and total ionic strength. The results (1) are consistent with the counterion condensation model (2–4), thereby indicating that the association between the heparin polyanion and calcium ions is a delocalized process, rather than one involving specific binding.

We now report the results obtained for the interaction of beef lung heparin with magnesium (Mg^{2+}) or lanthanum (La^{3+}) ion, in the presence of sodium (and chloride) ions. Studies (5–8) on the binding of Mg^{2+} to heparin have shown that this cation interacts less strongly than Ca^{2+} and, in accord with the counterion condensation model, binds in a delocalized or territorial fashion. Although it has been suggested (9) that $Co(NH_3)_6^{3+}$, a trivalent cation, forms localized ion pairs with heparin and other acidic polysaccharides, the binding observed was treated as a mass-action type of process, and the possibility that it is territorial was not evaluated. The main objectives of this study were: (*a*) to examine whether the order of binding to heparin, $Ca^{2+} > Mg^{2+}$ established by other methods (5–8), is also reflected in ^{13}C chemical shifts; (*b*) whether Mg^{2+} and La^{3+} binding conform to the Manning two-variable approach (2–4); and (*c*) to probe the binding preference between divalent and trivalent metal ions by performing competitive experiments with the La^{3+}/Ca^{2+}/heparin system. In addition, the selectivity between univalent cations, Na^{+} and K^{+}, first addressed theoretically by Manning (4) and observed experimentally for heparin, by Mattai and Kwak (5), is examined with systems containing heparin in the presence of Ca^{2+} and either Na^{+} or K^{+} (Ca^{2+}/Na^{+}/HEP or Ca^{2+}/K^{+}/HEP).

Experimental

Samples of sodium heparin, extracted from beef lung, were furnished by Upjohn Co. of Canada. The samples were purified by dialysis against distilled water and freeze-dried. Equivalent weights were determined by passage through a column of Amberlite IR-120 (H^{+}) resin, and subsequent conductimetric titration of the acidic eluate with NaOH (0.1 *M*). The equivalent weight of the beef lung heparin was found to be 178, whereas the sulfate to carboxylate ratio was 2.4. Potassium and calcium heparin were prepared from the heparinic acid solution by neutralization with 0.1 *M* solutions of KOH and $Ca(OH)_2$, respectively, and further purification by dialysis against distilled water, followed by freeze-drying. Polymer concentrations were 0.025, 0.05, and 0.1 *M*, depending on the experiment. Magnesium and lanthanum ions were introduced in the form of solid $MgCl_2$ and $LaCl_3$, respectively, in appropriate amounts.

The ^{13}C nmr experiments were conducted with a Varian XL-300 spectrometer operating at 75.4 MHz for carbon. Spectra were recorded in D_2O at 70°C and ^{13}C chemical shifts (reproducibility ±2 Hz) were referred to TSP as an external reference.

Results and discussion

Table 1 lists the ^{13}C chemical shift displacements for all carbons of the main disaccharide unit of heparin (**1**), for the systems Mg^{2+}/Na^{+}/HEP, La^{3+}/Na^{+}/HEP, La^{3+}/Ca^{+2}/HEP,

[1]Present address: Department of Chemistry, University of Crete, 71110 Iraklion Crete, Greece.

[2]Present address: Analytical Centre, Dalian Institute of Technology, Dalian, China.

Can. J. Chem. Downloaded from www.nrcresearchpress.com by 118.98.75.50 on 09/07/12
For personal use only.

TABLE 1. ^{13}C chemical shift displacements[a] (in Hz) induced by interaction of various metal ions (M^{N+}) with the system M^{N+}/HEP in D_2O at 70°C

	^{13}C chemical shift							
Carbon	Mg^{2+}/Na^+/HEP		La^{3+}/Na^+/HEP		Ca^{2+}/Na^+/HEP		La^{3+}/Ca^{2+}/HEP	Ca^{2+}/K^+/HEP
I-1	−3.0	−1.9	−53.6	−53.3	−15.2	−17.2	−24.8	−16.4
I-2	−1.2	+3.5	−37.2	−31.7	−32.1	−29.7	+11.7	−33.1
I-3	−2.4	+1.0	−62.6	−62.5	−47.5	−42.7	+5.2	−48.0
I-4	−1.4	+1.7	−3.0	−4.2	+1.6	+2.0	−6.5	+4.2
I-5	+15.5	+16.0	+18.7	+24.1	+11.9	+13.4	+11.7	+20.1
I-6	+8.2	+4.6	+87.1	+80.5	+28.6	+29.6	+35.7	+38.1
A-1	+6.1	+8.7	+48.5	+40.5	+27.1	+27.7	+2.4	+36.0
A-2	−3.1	−2.5	−4.8	−5.7	−2.9	−0.5	−2.5	+2.8
A-3	−1.6	0.0	−10.4	−18.9	+12.4	+12.1	−27.0	+12.2
A-4	+9.1	+8.0	−0.4	−6.5	+12.5	+13.1	−21.9	+19.9
A-5	−6.0	−1.0	−3.6	−4.9	−5.9	−5.2	+4.1	−3.0
A-6	−1.0	+0.4	+15.5	+11.1	+3.0	+4.1	+4.7	+10.7
C_p[b]	0.05	0.10	0.025	0.05	0.05	0.10	0.05	0.10
I[c]	0.20	0.40	0.175	0.35	0.20	0.40	0.425	0.40

[a]Negative values denote an upfield shift.
[b]At $X = C_2/C_p = 1.0$ where C_2 is $[M^{N+}]$ and C_p is $[M^{N+}/HEP]$.
[c]Total ionic strength in molarity units.

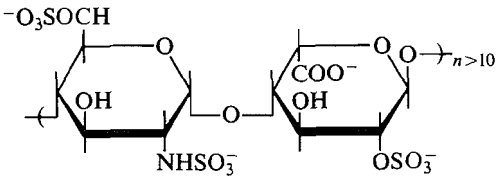

1

and Ca^{2+}/K^+/HEP at two total ionic strengths of ~0.2 and 0.4 M, and a constant ratio ($X = C_2/C_p = 1.0$) of metal ion (C_2) to heparin (C_p) concentration. In addition, Table 1 contains comparative data (1) for the system Ca^{2+}/Na^+/HEP. In general, the chemical shift displacements for all carbons of the system Mg^{2+}/Na^+/HEP at a given ionic strength, reflecting the extent of binding, are smaller than those for the Ca^{2+}/Na^+/HEP system. This indication of stronger binding to heparin by calcium than magnesium, in accord with earlier findings (5–8), may be explained on the basis that the hydrated Ca^{2+} is better able to displace Na^+ from the polyanion surface than is the comparatively larger hydrated Mg^{2+}.

For the system La^{3+}/Na^+/HEP (Table 1), the opposite effect is observed. The chemical shift displacements are larger than those for the system Ca^{2+}/Na^+/HEP, the greatest differential being observed for carbon I-6, i.e., the carboxyl carbon of the α-L-idopyranosyluronic acid 2-sulfate residue. A stronger binding of La^{3+} relative to Ca^{2+} also is seen in the chemical shift changes for the system La^{3+}/Ca^{2+}/HEP (Table 1). Displacement by La^{3+} of the Ca^{2+} condensed onto the polyanion surface is a direct consequence of the charge-density rule (2–4), because the introduction of the trivalent cation shifts the minimum of the charge-density parameter to $\xi = 1/3$, which is well below the minimum of $\xi = 1/2$ for calcium binding.

The effect of the total ionic strength on the binding of La^{3+} to heparin is recorded in Table 2, which summarizes chemical shift displacements as a function of La^{3+} concentration (X-ratio) at two ionic strengths.

A noteworthy feature of these data is the gradual decrease in the differential between chemical shift displacements with increasing concentration of La^{3+}, that reflects a decrease in binding as the X-ratio increases. This anti-cooperative behavior, also observed in the Ca^{2+}/Na^+/HEP (1) and Mg^{2+}/Na^+/HEP systems (not shown) is attributable, according to Manning's two-variable theory (2–4), to an entropy effect. At low concentrations of divalent (θ_2) and/or trivalent (θ_3) counterion, the concentration gradient of univalent ions between the "condensed" region surrounding the polyanion and the bulk solution is high. With the addition of more La^{3+} (or Ca^{2+}), i.e., increasing θ_3 (or θ_2), this concentration gradient decreases, and hence the entropy gain accompanying the release of Na^+ ions decreases with increasing θ_3 (or θ_2). Consequently, the extent of metal ion binding decreases with increasing θ_3 (or θ_2). The anti-cooperativity is more noticeable at lower ionic strengths and at low θ_3 (or θ_2), where the inequality $I \gg C_2$ holds (2). This is in agreement with the experimental data in Table 2. At high concentrations of La^{3+} (or Ca^{2+}), i.e. for θ_3 (or θ_2) near saturation, the inequality $I \gg C_2$ becomes invalid and then reversed (2), indicating that the polyanion is in an aqueous environment of La^{3+} (or Ca^{2+}) with negligible amounts of Na^+. In this region, where counterion binding is minimal, the magnitude of the chemical shift displacements is expected to remain unchanged, or even to decrease when the aforementioned inequality is reversed. Although such effects are not apparent in the chemical shift displacements of the systems Ca^{2+}/Na^+/HEP and Mg^{2+}/Na^+/HEP, it is noticeable for some carbons in the system La^{3+}/Na^+/HEP (Table 2). For instance, the magnitude of the chemical shift displacements for carbons I-1, A-3, and A-5 decreases from $X = 0.5$ onwards, whereas it remains practically constant for the I-5 and A-6 carbons in the same region of concentration. By contrast, other carbons (e.g. I-3) show a definite trend of increasing chemical shift displacements. No satisfactory explanation for these diverse observations is apparent at present.

As already noted, the thermodynamic driving force for metal ion binding is regarded (2) to be almost entirely entropic. The free energy gradient for the release of univalent counterions by trivalent ions is from the "condensed" volume around the

Can. J. Chem. Downloaded from www.nrcresearchpress.com by 118.98.75.50 on 09/07/12
For personal use only.

TABLE 2. ^{13}C chemical shift displacements[a] (in Hz) induced by interaction of heparin with La^{3+} ions as a function of lanthanum ion concentration and ionic strength[b] in D_2O at 70°C

	I-1[d]		I-2[d]		I-3[d]		I-5[e]		I-6[e]	
X[c]	0.175[b]	0.350[b]	0.175	0.350	0.175	0.350	0.175	0.350	0.175	0.350
0.2	43.5	41.8	14.9	15.6	25.0	28.8	1.3	6.5	33.6	31.9
0.5	70.3	66.2	28.4	26.1	49.8	51.9	18.3	22.4	66.3	64.5
0.7	61.9	61.0	31.8	29.3	53.3	57.0	18.8	24.5	75.9	74.2
1.0	53.6	53.3	37.2	31.7	62.6	62.5	18.7	24.1	87.1	80.5

	A-1[e]		A-3[d]		A-5[e]		A-6[e]	
X[c]	0.175	0.350	0.175	0.350	0.175	0.350	0.175	0.350
0.2	16.4	12.5	13.0	24.7	4.6	5.0	8.5	6.2
0.5	30.9	29.0	28.9	36.1	8.9	7.7	12.4	12.1
0.7	37.9	33.6	21.2	27.9	7.0	6.7	13.1	12.1
1.0	48.5	40.5	10.4	18.9	3.6	4.9	15.5	11.1

[a]Data for I-4, A-2, and A-4 are not included, as these nuclei did not exhibit significant chemical shift changes.
[b]Total ionic strength was kept constant by adding NaCl.
[c]Ratio of La^{3+} ion to heparin concentration (C_2/C_p; C_p = 0.025 and 0.05 M for I = 0.175 and 0.35 M, respectively).
[d]Negative values (upfield shifts).
[e]Positive values (downfield shifts).

polyanion to the bulk solution. At low ionic strength, this concentration gradient is large; hence, La^{3+} binding and a release of univalent counterions is a favorable entropic process. At high ionic strength, the smaller gradient should lead to a reduced binding of La^{3+}. Overall, a change in this direction is observed (Table 2) for most of the carbons affected by an increase in the ionic strength from 0.175 to 0.350, although carbons A-3 and I-5 are atypical in that they exhibit an increase in chemical shift displacement. Perhaps this inconsistency is related to such questions (see later) as the applicability of counterion condensation theory at high concentration levels, and the influence on chemical shift of conformational changes induced in the polyanion by the binding of metal ions.

Binding selectivity of univalent counterions to heparin

In their study of the binding of Ca^{2+} and Mg^{2+} to heparin by a dye spectrophotometric method, Mattai and Kwak (5) showed that either cation binds to a greater extent in the presence of Na^+, than of K^+. This tendency was rationalized on the basis of size selectivity (10) in the hydrated form, with Na^+ being larger than K^+. Therefore, the smaller hydrated K^+ is more difficult to replace than Na^+, and hence the number of bound divalent counterions (θ_2) for the system $M^{2+}/Na^+/HEP$ must be greater than that in the system $M^{2+}/K^+/HEP$. However, it should be emphasized that the difference found between $\theta_2(M^{2+}/Na^+/HEP)$ and $\theta_2(M^{+2}/K^+/HEP)$ was quite small. For instance, at I = 0.001 M, C_p = 0.001 M, and C_2/C_p = 0.5, the values of θ_2 for the systems $Ca^{2+}/Na^+/HEP$ and $Ca^{2+}/K^+/HEP$ were 0.282 and 0.267, respectively (5). This small difference was attributed (5) to the presence of two types of charged groups in heparin that have different binding affinities for univalent counterions: delocalized binding to the sulfate groups, for which the order of preference depends on hydrated size (K^+ over Na^+), and partial site binding to the carboxylate groups, for which the order of preference depends on the crystallographic radius (Na^+ over K^+). Because the heparin has a high sulfate content (the sulfate/carboxylate ratio was ca. 2.7 (5)), the overall preference was in favor of a decreasing size of the hydrated ion.

Recent experimental findings by the same authors (10), on divalent metal ion binding to polyelectrolytes having different structures and functional groups, show that the greater interaction of divalent counterions with carboxyl than with sulfate groups is not related to specificity in the replacement of the univalent counterion. Nevertheless, polymers having sulfonate groups, which exhibit delocalized binding, do discriminate slightly between the univalent counterions.

By contrast, Manning's theoretical (11) and experimental (12) studies on species selectivity suggest that site-binding mechanisms play no role in the association between univalent counterions and polyelectrolytes, and that ion-selectivity may be attributed to the local dielectric constant of the medium surrounding the polyelectrolyte. This dielectric constant is, perhaps, equivalent to a 1 M aqueous ionic solution (the local concentration of territorially-bound univalent counterions is estimated (2, 11) to be of the order of 1 M for polyanions of typical charge-densities). Manning, using the Born approximation, was able to calculate the contribution of the molar free energy of transfer of a counterion from the bulk dilute solution of dielectric constant D_{H_2O} = 78.3 to the local polyanion environment with dielectric constants (13) D_{Cs^+} = 70.6 and D_{Na} = 66.7 corresponding to their respective 1 M ionic solution. The results indicated (11) that the polyelectrolyte selects the larger Cs^+ counterion (in terms of crystallographic radius) than the smaller Na^+, because the positive free energy of transfer to an environment of lower dielectric constant was found to be less for the larger ion. However, it is possible to interpret (14) these results in terms of the direct size selectivity proposed by Mattai and Kwak (5, 10), because Na^+ is the larger of the two counterions in their hydrated form.

Data in Table 1 indicate a trend in selectivity opposite to that reported by Mattain and Kwak for heparin (5), because the chemical shift displacements for the system $Ca^{2+}/Na^+/HEP$ are smaller than those observed for the system $Ca^{2+}/K^+/HEP$. Although this differential in the chemical shifts is slightly above the experimental error (±2–3 Hz), it is reproducible, indicating that the binding preference of heparin follows the order of the ions' crystallographic radii. This discrepancy may

Can. J. Chem. Downloaded from www.nrcresearchpress.com by 118.98.75.50 on 09/07/12
For personal use only.

Can. J. Chem. Downloaded from www.nrcresearchpress.com by 118.98.75.50 on 09/07/12
For personal use only.

be due to the following: firstly, our measurements required more concentrated solutions in order to obtain nmr spectra of acceptable quality (see below), whereas species selectivity generated by tiny differential free energies (0.2 to 0.5 kcal at 25°C (11)) is better manifested in dilute solution. Secondly, as the sulfate/carboxylate ratio of our sample of heparin (ca. 2.4) is smaller than those of Mattai and Kwak, the lower proportion of sulfate groups might lead to the overall binding preference for the ion of lesser crystallographic radius. Also, the small difference between the θ_2 values for these two systems, which is comparable to the experimental uncertainty of the measurements, may not exhaust the range of differences possible among heparin samples from various sources. Consequently, a more systematic study with various alkali metal counterions and heparin samples is required before definite conclusions on species selectivity of heparin are justified.

Quantitative interpretation of the chemical shift data

Further information about the nature of Mg^{2+} and La^{3+} binding to heparin was obtained by comparing the experimental data with quantitative predictions of the two-variable theory (2–4). According to this theory, a counterion–polyanion interaction is a function of the charge-density parameter ($\xi = 2.43$ for heparin (15)), and is independent of the nature of the charged group. The counterions are bound in a delocalized or territorial manner, retaining the fully hydrated state, although moving in an unrestricted and random way along the length of the polyanion chain. To describe the effect of Na^+ on the extent of binding of N-valent ion, M^{N+}, the following parameter has been defined (1, 16, 17)

$$[1] \quad n = \frac{\theta_1^0 - \theta_1}{\theta_N}$$

θ_1^0 and θ_1 are the fractions of the bound Na^+ ions before and after the addition of the M^{N+} ions, respectively, and θ_N is the fraction of the bound N-valent ions. According to the counterion condensation theory, θ_1^0 is invariant, or moderately different, for high ionic strengths up to 1.0 M. For the present system, θ_1^0 equals 0.59 (1). Although n may not remain constant as the cation is added incrementally, it can be interpreted as a stoichiometric coefficient in the stoichiometric ion-exchange equilibrium,

$$[2] \quad n\mathrm{Na}_b^+ + \mathrm{M}_f^{N+} \rightarrow n\mathrm{Na}_f^+ + \mathrm{M}_b^{N+}$$

in which the subscripts b and f refer to bound and free states of heparin, respectively, with respect to Na^+ and M^{N+}. Calculations based on either the Poisson–Boltzmann equation or the counterion condensation theory have shown (16) that $n < N$ (N equals 2 and 3 for Mg^{2+} and La^{3+}, respectively). Therefore, if the binding of M^{N+} to heparin can be described satisfactorily by the counterion condensation model, then the stoichiometry of the bound M^{N+} should not be a constant quantity, but should vary with the M^{N+} concentration, to a maximum value of N. Following our earlier (1) mathematical treatment relating the observed chemical shift, ν^{obs}, with the chemical shifts of the bound and free states of heparin, ν^b and ν^f, respectively, we obtain the following expression for the observed chemical shift displacements.

$$[3] \quad \nu^{obs} - \nu^{Na^+/HEP} = (\nu_M^b - \nu_{Na}^b) n\theta_N$$

where $\nu^{Na^+/HEP}$ is the chemical shift of Na^+/HEP salt before the addition of M^{N+}. It appears from eq. [3] that the observed chemical shift displacements depend not only on θ_N, but also on the stoichiometry of the M^{N+} binding.

Provided that the quantity $(\nu_M^b - \nu_{Na}^b)$ is constant, the chemical shift displacement $(\nu^{obs} - \nu^{Na^+/HEP})$ will be a linear function of the product $n\theta_N$. This, indeed, is observed in Fig. 1 for the system Mg^{2+}/Na^+/HEP, at $I = 0.2\,M$ and $C_p = 0.05\,M$, which also illustrates the nonlinear behavior of the chemical shift displacements vs. θ_2 alone, also predicted by eq. [3]. Values of θ_2 and n for the system M^{2+}/Na^+/HEP were calculated using the two-variable theory of Manning (2–4), as expressed by eqs. [6]–[9] in ref. 1. By numerical iteration of those equations and using $\xi = 2.43$, $N = 3$, theoretical values of θ_3, θ_1, and n were obtained for the system La^{3+}/Na^+/HEP at $C_p = 0.025$, $0.05\,M$ and ionic strengths 0.175 and $0.35\,M$, respectively. These values, and the values for the product $n\theta_3$ and the association constant $K_3 = \theta_3/C_{3f}$ (C_{3f} is the concentration of the free La^{3+} in the bulk), are summarized in Table 3. The smaller degree of binding to heparin by Mg^{2+} than by Ca^{2+} is reflected in the slopes of the linear plots $(\nu^{obs} - \nu^{Na^+/HEP})$ vs. $n\theta_2$ for their respective carbons. For example, the slopes for carbons I-1 and A-1 in the system Mg^{2+}/Na^+/HEP are 13.0 and 26.4, respectively, whereas the corresponding values for Ca^{2+}/Na^+/HEP are 59.5 and 107.1, respectively. The characteristics of the chemical shift displacements for carbons I-2, I-3, I-6, and A-1 in the system La^{3+}/Na^+/HEP vs. $n\theta_3$ (or θ_3) are depicted in Fig. 2. The observed nonlinear behavior of the quantity $(\nu^{obs} - \nu^{Na^+/HEP})$, particularly vs. $n\theta_3$, is in excess of theoretical predictions, suggesting that at least part of the bound La^{3+} is site bound. Apparently, La^{3+} binds to a much larger extent than would be predicted on the basis of long-range electrostatic forces, although the charge-density requirement of the binding appears valid.

We conclude that such divalent metal ions as Ca^{2+} and Mg^{2+}, interact with heparin, in a delocalized manner, whereas the trivalent La^{3+} counterion is characterized by some specific binding to heparin. This view is reinforced by consideration of the following questions in terms of the nmr data in Table 1. (*a*) Does the divalent or trivalent counterion bind to a unique site? For divalent counterions the answer is in the negative, because Ca^{2+} and Mg^{2+} induce chemical shift displacements for most of the carbons of the disaccharide unit. By contrast, binding to a unique site is expected to influence the chemical shifts of only a limited number of carbons near the site of binding (18). Although the same is true for La^{3+}, the fact that it induces a much larger chemical shift displacement of I-6, relative to the other carbons, than is brought about by Mg^{2+} and Ca^{2+}, is indicative of preferential binding to the carboxyl group of the iduronic acid residue. On the basis of this discussion a positive response can be given to the second question: (*b*) are there other binding sites? The first type of binding site is the carboxylate or sulfate group. Binding to either of these sites is expected to induce chemical shift changes for carbons that bear the charged groups, and/or are influenced by electrostatic effects due to the bound counterion (18). Hence, chemical shift changes are expected to be larger for La^{3+} than Ca^{2+} (or Mg^{2+}), because the local electrostatic potential should be higher for trivalent than divalent counterions. From these considerations and the data in Table 1, one could attempt to classify the sulfate groups on the basis of their relative affinity for binding, as may be reflected in the respective chemical shift displacements for carbons I-2, A-2, and A-6. However, the binding process is too complex a phenomenon for such a simplistic interpretation since it, itself, may induce conformational changes in heparin that independently affect the magnitude of its chemical shifts (1). A second type of binding site is offered by the hydroxyl groups. Nevertheless, as there is only one hydroxyl

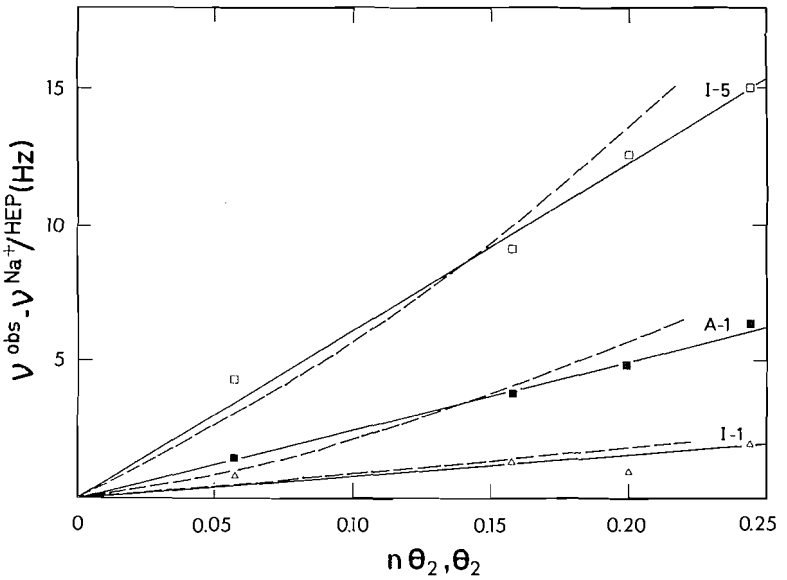

FIG. 1. $n\theta_2$ vs. ^{13}C chemical shift displacements ($\nu^{obs} - \nu^{Na^+/HEP}$) for I-1, I-5, and A-1 carbon resonances of beef lung heparin (C_p = 0.05 M, I = 0.2 M) induced by Mg^{2+} counterion binding. The non-linear behavior of the chemical shift displacements vs. θ_2 alone is illustrated by the dotted lines.

TABLE 3. Number of bound counterions (θ_1 and θ_3) per charged group of beef lung heparin, association constants (K_3), and stoichiometry (n), as a function of La^{3+} ion concentration and ionic strength (I)[a]

C_2 (mol/L)	I (mol/L)	θ_1	θ_3	K_3	n	$n\theta_3$
	0.350[b]					
0.050		0.363	0.160	3.8	1.414	0.225
0.035		0.400	0.140	5.0	1.355	0.189
0.025		0.435	0.121	6.4	1.273	0.154
0.010		0.526	0.074	11.6	0.816	0.060
	0.175[c]					
0.0250		0.247	0.192	9.5	1.780	0.341
0.0175		0.277	0.175	13.3	1.780	0.312
0.0125		0.309	0.158	18.4	1.770	0.279
0.0050		0.414	0.105	43.8	1.670	0.175

[a]Two variable approach from eqs. [8] and [9] (ref. 1).
[b]C_p = 0.05 M.
[c]C_p = 0.025 M.

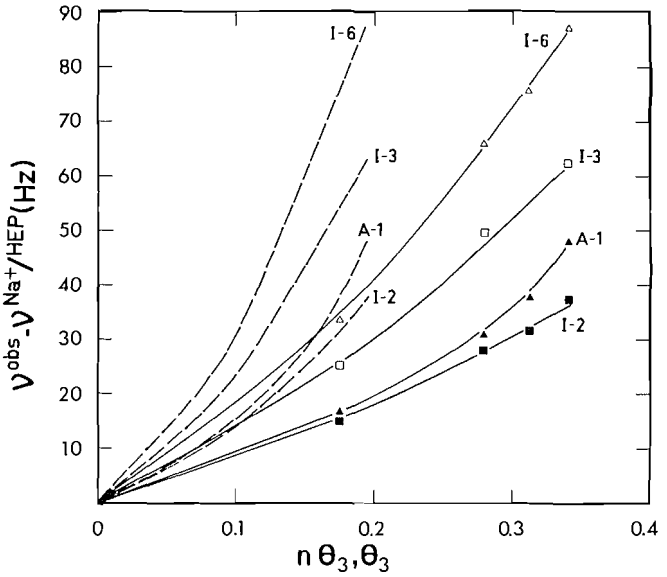

FIG. 2. $n\theta_3$ vs. ^{13}C chemical shift displacements ($\nu^{obs} - \nu^{Na^+/HEP}$) for I-2, I-3, I-6, and A-1 carbon resonances of beef lung heparin (C_p = 0.025 M, I = 0.175 M) induced by La^{3+} counterion binding. The behavior of the chemical shift displacements vs. θ_3 alone is illustrated by the dotted lines.

group per monosaccharide unit, these sites are fewer than the charged groups and likely play no more than a minor role in the concept of electrostatic interactions addressed here. (*c*) Do the counterions spend a large part of their time in privileged sites? This question cannot be answered on the basis of the ^{13}C nmr data cited in Table 1. ^{13}C, and possibly ^{33}S, spin–lattice relaxation times of the I-6 carbon and the sulfate groups as a function of counterion concentration and ionic strength, may be an appropriate probe. That is, if the counterions are trapped preferentially by the carboxylate groups most of the time, they will not relax the sulfate groups efficiently. Only a high concentration of counterions will relax the sulfate groups more, because the stronger sites will then be saturated. Uniform relaxation, on the other hand, would reflect equal mobility of the counterions over the charged groups of heparin.

An assessment of nmr measurements of binding interactions

It is worthwhile to comment here on the validity of the nmr approach and the various approximations used in this study and earlier (1) to interpret the binding behavior of heparin in mixed counterion systems. Evidently, the nmr method is very useful for this type of application at the molecular level, because it provides a large number of parameters, i.e., chemical shifts, coupling constants, spin–lattice relaxation times, and line widths. In particular, the sensitivity of the observed ^{13}C chemical shifts to electrostatic effects caused by the bound counterions, is a direct measure of the local counterion subpopulations surrounding the polyanion surface, and an indirect probe of conformational changes induced in the polyanion. However, owing to the low natural isotopic abundance of the ^{13}C nucleus (~1.1%), the ^{13}C nmr spectra were recorded at relatively high concentrations, so as to give acceptable S/N ratios. The laws governing counterion condensation in polyelectrolyte solutions are "limiting laws", referring to the "limit of infinite dilution" (2–4, 10). This mathematical limit, attained when $C \rightarrow 0$, is a

Can. J. Chem. Downloaded from www.nrcresearchpress.com by 118.98.75.50 on 09/07/12
For personal use only.

Can. J. Chem. Downloaded from www.nrcresearchpress.com by 118.98.75.50 on 09/07/12
For personal use only.

necessary condition under which exponential terms in the electrostatic free energy can be linearized. For practical cases, linearization can be achieved as well, if the condition (2–4, 11)

$$[4] \quad kb \ll 1$$

is fulfilled. For many polyelectrolytes, b, the average axial separation between charged groups (in Å) is so small as compared to the Debye screening length, k^{-1}, that eq. [4] holds even at ionic strengths that are not especially low. The Debye screening parameter depends on the ionic strength, and for aqueous solutions of 1:1 electrolytes at 70°C is given by (19).

$$[5] \quad k^{-1} = (3.07 \times 10^{-8}) I^{-1/2} \text{ cm}$$

An equivalent, and appealing, criterion for the applicability of the counterion condensation model over a range of ionic strengths is (2–4)

$$[6] \quad \frac{I}{C_s^{loc}} = 2.7k^2b^2 \ll 1$$

in which the invariant local concentration, C_s^{loc}, of territorially bound counterions is much greater than the bulk ionic strength. For heparin in aqueous solution of 1:1 electrolytes, and $I = 0.4M$, k^{-1} equals 4.85 Å according to eq. [5], and b equals 2.9 Å (15), so that $kb = 0.60$ and $I/C_s^{loc} = 0.98$. The range of allowable ionic strengths is seen to approach $0.4M$ in a 1:1 salt solution. Consequently, our nmr measurements were conducted at close to the limit imposed by the counterion condensation theory.

The validity of our conclusion from Figs. 1 and 2 (and Fig. 5 of ref. 1) implies that the quantity $(\nu_M^b - \nu_{Na}^b)$ in eq. [3] is constant. Moreover, ν_M^b and ν_{Na}^b must be individually constant, unless their variations are exactly compensated for at least over the range of concentration studied here. Coincidental compensation cannot be disproved without an independent means of determining ν_M^b and ν_{Na}^b. A theoretical basis for examining this assumption is offered by eq. [18] of ref. 1, which can be generalized to

$$[7] \quad \nu^{M^{N+}}/\text{HEP} = \nu^f + (\nu_M^b - \nu^f)\theta_N^0$$

for the system $M^{N+}/M^{N+}/HEP$. This equation was derived on the basis of a general conclusion about the counterion condensation model, which is that the addition of a simple electrolyte to a salt–polyanion solution containing the same counterion does not change the fraction of bound counterions, θ_N^0. This conclusion in relation to eq. [7] implies that ν_M^b must be a constant quantity. Indeed, addition of NaCl or $CaCl_2$ salts to Na^+/HEP and Ca^{2+}/HEP, respectively, showed insignificant chemical shift changes for all the carbons of the heparin. These findings, in agreement with earlier (7) c.d. measurements for the same systems, constitute clear evidence that ν_M^b and ν_{Na}^b must individually be constant, regardless of the composition of the solution.

An important quantity in the counterion condensation theory is the charge-density parameter given by (2–4)

$$[8] \quad \xi = \frac{e^2}{b\epsilon kT}$$

which controls the onset of condensation and the fraction of condensed counterions. This non-adjustable parameter is determined by the structure of the polyelectrolyte, namely, the axial separation, b, between charged groups. For heparin, the latter quantity was determined from molecular models of the disaccharide repeat sequence in its most extended form, from which a value of 2.9 Å was obtained (15). This compares with a value of 3.0 Å from X-ray scattering measurements (20). The determination of the quantity, b, and hence, ξ, assumes an idealized repeating structure of heparin, which may not be true, since heparin is a highly heterogeneous polymer (21), and its composition may vary substantially with the source. This means that the SO_3^-/CO_2^- ratio may vary from sample to sample, and so b (or ξ) also can vary (15). Moreover, the linear charge-density parameter chosen is for a polyelectrolyte in its most extended form. This assumption, inherent in Manning's theory, is in contrast to experimental evidence (8, 22, 23) that heparin in solution exists in a less fully extended conformation.

The counterion condensation theory of Manning is intuitively attractive, and yields a soundly analytical description of various properties of polyelectrolyte–salt solutions. Applications, including the present study, have been made to a large number of polyelectrolyte systems (1–3, 5, 10, 12, 14, 15). However, as an approximate theory in its mathematical treatment, it has received several criticisms (24–34) based on discrepancies with experimental observations. These have resulted in the development of extended treatments of the polyelectrolyte theory, by application of the Poisson–Boltzmann (24–30) or Gouy–Chapman (31) equations. An extension of Manning's theory without an explicit reference to the condensed phase has been considered as well (32).

In relation to the particular system, La^{3+}/Na^+/HEP, Manning's theory does not take into account specific interactions nor the case in which a polyanion, such as heparin, bears charged groups of different types. The latter property is fundamental in the sense that one group may show site-binding affinity to counterions, whereas the affinity of another group on the same polyanion is consistent with the requirements characterizing delocalized or territorial binding. As noted by Mattai and Kwak (10), one possible approach for including specific interactions in the condensation theory is modification of the entropy of mixing terms of the bound counterions (in eq. [28] of ref. 2) and/or the use of the condensation volume, V_p, as an adjustable parameter in the two-variable theory to account for the restricted nature of the counterion in the condensed phase. The need for a variable, V_p, parameter has already been stressed by other authors (24, 34). However, these suggestions do not go beyond a qualitative prediction of localized counterion binding. A quantitative description of site binding can be approached on the basis of Mass-Action Law (24, 25, 31) for mixed counterions. Accordingly, the extent of site-binding for the La^{3+}/Na^+/HEP system can be evaluated by methods presented in the appendices of refs. 24 and 25, with the appropriate equations adjusted for a solution of univalent and trivalent counterions. An isolated model for measuring the binding constant would be a disaccharide corresponding to the main unit of heparin, and the binding constant determined would actually be a weighted average of those for the carboxylate and sulfate groups.

In summary, this nmr study presents evidence that the binding affinity of heparin is stronger for Ca^{2+} than Mg^{2+} ions, in agreement with earlier observations, and that Mg^{2+} ions bind in a territorial manner consistent with the counterion condensation model. For La^{3+}, counterion binding exceeds predictions of the two-variable theory, indicating at least partial site-binding. ^{13}C chemical shift displacements in the systems Ca^{2+}/Na^+/HEP and Ca^{2+}/K^+/HEP show that the binding preference of hepa-

rin for univalent Na^+ and K^+ cations follows the order of their crystallographic radii, although other experiments in progress may help to clarify this aspect of species selectivity. Finally, the validity of our nmr approach for studying the binding of counterions to heparin has been critically assessed.

Acknowledgements

The authors express their gratitude to the Natural Sciences and Engineering Research Council of Canada, and to McGill University for generous support.

1. P. DAIS, Q.-J. PENG, and A. S. PERLIN. Carbohydr. Res. In press.
2. G. S. MANNING. Q. Rev. Biophys. **2**, 179 (1978).
3. G. S. MANNING. *In* Polyelectrolytes. *Edited by* E. Selegny. D. Reidel Publishing Co., Dordrecht, Holland. 1974.
4. G. S. MANNING. Acc. Chem. Res. **12**, 443 (1979).
5. J. MATTAI and C. T. KWAK. Biochim. Biophys. Acta, **677**, 303 (1981).
6. C. VILLIERS, C. BRAUD, and M. VERT. Carbohydr. Res. **83**, 335 (1980).
7. C. BRAUD, C. VILLIERS, and M. VERT. Carbohydr. Res. **86**, 165 (1980).
8. M. C. M. CHUNG and N. F. ELLERTON. Biopolymers, **15**, 1409 (1976).
9. M. B. MATHEWS. Arch. Biochem. Biophys. **104**, 394 (1964).
10. J. MATTAI and C. T. KWAK. Macromolecules, **19**, 1663 (1986).
11. G. S. MANNING. J. Phys. Chem. **88**, 6654 (1984).
12. G. S. MANNING. Biopolymers, **20**, 2337 (1981).
13. R. POTTEL. *In* Water, Vol. 3. *Edited by* F. Franks. Plenum Press, New York. 1973.
14. G. E. BOYD and D. P. WILSON. Macromolecules, **15**, 78 (1982).
15. G. P. DIAKUM, H. E. EDWARDS, D. J. WEDLOCK, J. C. ALLEN, and G. O. PHILLIPS. Macromolecules, **6**, 1110 (1978).
16. M. L. BEAM, C. F. ANDERSON, and M. T. RECORD, JR. Biochemistry, **22**, 5418 (1983).
17. W. H. BRAUNLIN, C. F. ANDERSON, and M. T. RECORD, JR. Biopolymers, **25**, 205 (1986).
18. L. W. JAQUES, J. B. MACASKILL, and W. WELTNER, JR. J. Phys. Chem. **83**, 1412 (1979).
19. H. S. HARNED and B. B. OWEN. The physical chemistry of electrolyte solutions. 3rd ed. Reinhold Publ. Co., New York. 1958. p. 60.
20. S. S. STIVALA, M. HERBST, O. KRATKY, and J. PILZ. Arch. Biochem. Biophys. **127**, 795 (1968).
21. A. S. PERLIN, M. MAZUREK, L. B. JAQUES, and L. W. KAVANAGH. Carbohydr. Res. **7**, 369 (1968).
22. L. YUAN, T. J. DOUGHERTY, and S. S. STIVALA. J. Polym. Sci. Part A, **10**, 171 (1972).
23. L. YUAN and S. S. STIVALA. Biopolymers, **11**, 2079 (1972).
24. M. GUERON and G. WEISBUCH. Biopolymers, **19**, 353 (1980).
25. G. WEISBUCH and M. GUERON. J. Phys. Chem. **85**, 517 (1981).
26. C. P. WOODBURY, JR. and G. V. RAMANATHAN. Macromolecules, **15**, 82 (1982); and references therein.
27. S. ENGSTROM and H. WENNERSTROM. J. Phys. Chem. **82**, 2711 (1978).
28. B. JONSSON, H. WENNERSTROM, and B. HALLE. J. Phys. Chem. **84**, 2179 (1980).
29. G. GUNNARSON, B. JONSSON, and H. WENNERSTROM. J. Phys. Chem. **84**, 3114 (1980).
30. M. LE BRET and B. H. ZIMM. Biopolymers, **23**, 287 (1984).
31. D. STIGTER. J. Phys. Chem. **82**, 1603 (1978); and references therein.
32. M. SATOH, J. KOMIYAMA, and T. IIJIMA. Macromolecules, **18**, 1195 (1985).
33. J. A. MARINSKY. J. Phys. Chem. **89**, 5294 (1985).
34. J. A. MARINSKY. J. Phys. Chem. **89**, 5303 (1985).

Can. J. Chem. Downloaded from www.nrcresearchpress.com by 118.98.75.50 on 09/07/12
For personal use only.

General solution to axially symmetric quadrupole interaction in nuclear magnetic resonance of solids

B. C. SANCTUARY AND G. CAMPOLIETI
Department of Chemistry, 801 Sherbrooke St. W., Montreal, P.Q., Canada H3A 2K6

Received November 24, 1986

This paper is dedicated to Professor John T. Edward

B. C. SANCTUARY and G. CAMPOLIETI. Can. J. Chem. **65**, 1746 (1987).

Spins with magnitude I greater than $\frac{1}{2}$ have nuclear electric quadrupole interactions that perturb the Zeeman splitting. To calculate the spin dynamics of multipulse sequences, it is necessary to know how the system evolves between pulses under the quadrupole. Prior work gave specific solution for $\frac{1}{2} < I \leq \frac{9}{2}$ in tabulated form. In this paper, a single expression is obtained, which is valid for all I.

B. C. SANCTUARY et G. CAMPOLIETI. Can. J. Chem. **65**, 1746 (1987).

Les spins dont l'amplitude I est plus grande que $\frac{1}{2}$ possèdent des interactions quadrupolaires électriques nucléaires qui perturbent le couplage Zeeman. Dans le but de calculer la dynamique des spins dans des séquences multispins, il est nécessaire de connaître comment le système évolue entre les pulsations, sous l'effet du quadrupole. Un travail antérieur a fourni une solution spécifique, sous la forme de tableau, du cas où $\frac{1}{2} < I \leq \frac{9}{2}$. Dans le présent travail, on a obtenu une expression unique qui est valide pour toutes les valeurs de I.

[Traduit par la revue]

I. Introduction

Spin dynamic calculations of multipulse sequences require knowledge of the evolution of the spin system under the interaction Hamiltonian. For solids containing spin $I > \frac{1}{2}$, the nuclear quadrupole interaction often dominates (1). Typically, a principle axis frame is chosen so that two parameters e^2qQ *and* η are required. Solution of this problem in the presence of a magnetic field is difficult as a consequence of the two different symmetries of the Zeeman and quadrupole Hamiltonians. When the asymmetry term η is zero and the principal axis lies along the magnetic field direction, an exact solution is possible. In a previous paper (2) the solutions were given for specific I values from $I = 1$ to $\frac{9}{2}$. Hence the evolution of the full density matrix was obtained from arbitrary initial conditions.

The difficulty with the solutions of ref. 2, although exact, is that they are specific for each I magnitude. No general transformation was found that solved the complete problem for any I. In contrast, knowledge of the transformation that diagonalizes the quadrupole Hamiltonian would allow the symmetry properties to be studied and these, in turn, would aid in finding perturbation solutions when $\eta \neq 0$, that is, when the field and principal axis do not coincide.

In this paper we report the general solution, using the multipole formulations, to the axially symmetric quadrupole problem in which the principal axis and magnetic field direction coincide. The solutions are valid for all I magnitudes. Table 1 of ref. 2 is obviated and a simple expression for all the transformations is given. The results of Table 3 of ref. 2 reduce to one simple equation.

II. Background

The Hamiltonian in question is given by

$$[1] \quad H_Q = -\gamma\hbar I_Z H_Z + \hbar Q_I\{3I_Z^2 - I(I+1)\}$$

where

$$[2] \quad Q_I = \tilde{Q}/[2I(2I-1)]$$

The object is to calculate the full spin density matrix, $\sigma_I(t)$, which evolves according to

$$[3] \quad i\hbar \frac{\partial\sigma_I(t)}{\partial t} = [H_Q, \sigma_I]$$

To proceed, the spin density operator is expanded in terms of spherical tensor operators (3, 4),

$$[4] \quad \sigma_I = \frac{1}{2I+1}\left[E_I + \sum_{k=1}^{2I}\sum_{q=-k}^{k} \phi_q^k(t)\mathcal{Y}^{kq}(I)\right]$$

The problem is then to obtain the coefficients $\phi_q{}^k(t)$. These are loosely referred to as polarizations with multipole magnitude k and multiquantum coherence q. More exactly, the k even quantities are alignments while the k odd are polarizations. Moreover, $q = 0$ are not coherences but incoherent superpositions of populations for the single spin case. The $q \neq 0$ terms are correctly coherences. These distinctions are not made in this work and all $\phi_q{}^k(t)$ are considered polarizations with coherence q.

In the rotating frame, defined by

$$[5] \quad \hat{\phi}_q{}^k(t) = \exp(-iq\omega_0 t)\phi_q{}^k(t)$$

where $\omega_0 = \gamma H_Z$, the Hamiltonian [1] gives

$$[6] \quad \frac{\partial\hat{\phi}_q^k}{\partial t} = \frac{3}{2}q\tilde{Q}\left[\frac{(2I+k+2)(2I-k)[(k+1)^2-q^2]}{I^2(2I-1)^2(2k+1)(2k+3)}\right]^{1/2}\hat{\phi}_q^{k+1} - \frac{3}{2}q\tilde{Q}\left[\frac{(2I+k+1)(2I-k+1)[k^2-q^2]}{I^2(2I-1)^2(2k-1)(2k+1)}\right]^{1/2}\hat{\phi}_q^{k-1}$$

It is these sets of coupled equations which have been solved from initial conditions $\phi_q{}^k(0)$ for special cases of I and q and which are reported in ref. 2, Tables 1 and 3. As I increases, the dimensionality of the resulting matrices increases. The unitary transformations required to diagonalize these become increasingly difficult to obtain. From Tables 1 and 3 of ref. 2 some inherent symmetries appear to be present, but these are not obvious.

Can. J. Chem. Downloaded from www.nrcresearchpress.com by 118.98.75.50 on 09/07/12
For personal use only.

III. Alternate solutions

From eq. [3], the solution to $\sigma(t)$ is

$$[7] \quad \sigma(t) = \exp\left(\frac{-i}{\hbar} H_Q t\right) \sigma(0) \exp\left(\frac{i}{\hbar} H_Q t\right)$$

where

$$\sigma(0) = |\psi(0)\rangle\langle\psi(0)|$$

Using eq. [3] and the orthogonality of the spherical tensor operators

$$[8] \quad \mathrm{Tr}\{\mathcal{T}^{k'q'\dagger}\mathcal{T}^{kq}\} = (2I + 1)\delta_{kk'}\delta_{qq'}$$

where † is the operator adjoint, the density operator becomes

$$[9] \quad \phi_q^k(t) = \frac{1}{2I+1} \sum_{k'q'} \langle\langle \mathcal{T}^{kq}| \, e^{-iH_Q t/\hbar} \mathcal{T}^{k'q'} \, e^{iH_Q t/\hbar} \rangle\rangle \phi_{q'}^{k'}(0)$$

The inner product is defined

$$[10] \quad \langle\langle A|B\rangle\rangle = \mathrm{Tr}\{A^+ B\}$$

The Wigner–Eckart theorem (5, 6) gives

$$[11] \quad \langle IM|\mathcal{T}^{kq}|I'M'\rangle = \delta_{II'}(-1)^{I-M} \begin{pmatrix} I & k & I \\ -M & q & M' \end{pmatrix} \times \langle I\|\mathcal{T}^k\|I\rangle$$

where the reduced matrix element is

$$[12] \quad \langle I\|\mathcal{T}^k\|I\rangle = i^k \cdot \sqrt{(2I+1)(2k+1)}$$

Using this, eq. [9] becomes

$$[13] \quad \hat{\phi}_q^k(t) = \sum_{k'=0}^{2I} \sum_{M=-I}^{I} (i)^{k'-k} \sqrt{(2k+1)(2k'+1)} \times \begin{pmatrix} I & I & k \\ M & -M-q & q \end{pmatrix} \begin{pmatrix} I & I & k' \\ M & -q-M & q \end{pmatrix} \times e^{i3\omega^I_Q q(q+2M)t} \phi_q^{k'}(0)$$

with

$$\omega^I_Q = -Q_I$$

which is the exact solution for the time evolution of the full density matrix under Hamiltonian [1] from arbitrary initial conditions $\phi^k{}_q(0)$.

IV. Discussion

The multipole operators (7) $\mathcal{T}^{kq}(I) \equiv |kq\rangle\rangle$ are useful for describing pulsed nmr primarily because they are rotated under the Zeeman interaction. In contrast, the quadrupole Hamiltonian is diagonal in the $|IM\rangle\langle IM'|$ basis. The relation between the $|kq\rangle\rangle$ and $|IM\rangle\langle IM'|$ basis is

$$[14] \quad |kq\rangle\rangle = i^k[(2I+1)(2k+1)]^{1/2} \sum_M (-1)^{I-M} \times \begin{pmatrix} I & k & I \\ -M & q & M-q \end{pmatrix} |IM\rangle\langle IM-q| \equiv (2I+1)^{1/2} \sum_M \mathcal{T}_q{}^{kM}(I)|IM\rangle\langle IM-q|$$

It then follows that the solution [13] can be written as

$$[15] \quad \hat{\phi}^k{}_q = \sum_{k'} \sum_{M=-I}^{I} (\mathcal{T}(I)^{-1})_q{}^{q+M,k} \times \exp[i3\omega^I_Q q(q+2M)t] \mathcal{T}^{k',q+M}(I)\phi_q^{k'}(0)$$

where

$$[16] \quad (\mathcal{T}(I)^{-1})_q{}^{Mk} \equiv \mathcal{T}_q{}^{kM}(I)^*$$

which is to be compared to [23] of ref. 2. Equation [15] generates all the results of Table 3 of ref. 2 while the expression for $\mathcal{T}_q{}^{kM}(I)$, eq. [14], generates Table 1 of ref. 2.

The symmetries of $\mathcal{T}$ are simply those of 3–j coefficients. Using these and the explicit expressions in eq. [9] will be useful in obtaining perturbative solutions to problems where the principal axis differs from the symmetry axis or when $\eta \neq 0$.

Acknowledgements

This work is supported by a Canadian Government grant (NSERC) and a Quebec Government grant (FCAC).

1. A. Abragam. The principles of nuclear magnetism. Clarendon Press, Clarendon, TX. 1961.
2. B. C. Sanctuary, T. K. Halstead, and P. A. Osment. Mol. Phys. **49**, 753 (1983).
3. U. Fano. Rev. Mod. Phys. **29**, 74 (1957).
4. B. C. Sanctuary. J. Chem. Phys. **64**, 4352 (1976).
5. A. R. Edmonds. Angular momentum in quantum mechanics. 3rd ed. Princeton University Press, Princeton, N.J. Third printing. 1974.
6. L. C. Biedenhard and J. D. Louck. Angular momentum in quantum physics: theory and application. Addison-Wesley Publishing Co., Reading, MA. 1981.
7. B. C. Sanctuary. J. Magn. Reson. **61**, 116 (1985).

Can. J. Chem. Downloaded from www.nrcresearchpress.com by 118.98.75.50 on 09/07/12
For personal use only.

Rate constant for hydroxylation of a primary alkyl radical by induced decomposition of an alpha hydroperoxyalkyl diazene

CHANDRA LAKHANI, LUKOSE MATHEW, AND JOHN WARKENTIN
Department of Chemistry, McMaster University, Hamilton, Ont., Canada L8S 4M1

Received December 11, 1986

This paper is dedicated to Professor John T. Edward

CHANDRA LAKHANI, LUKOSE MATHEW, and JOHN WARKENTIN. Can. J. Chem. **65**, 1748 (1987).

Rate constants for induced decomposition of 5-hexenyl(1-hydroperoxy-1-methylethyl) diazene ($(CH_3)_2C(OOH)N{=}N(CH_2)_4CH{=}CH_2$, **2**) have been estimated. Thermolysis of **2** at 50°C affords 5-hexenyl radicals which abstract the hydroxyl group from **2** in competition with cyclization of 5-hexenyl to cyclopentylmethyl radicals. The known rate constant (k_c) for that cyclization was used to clock the bimolecular hydroxyl abstraction process. For reaction in hexafluorobenzene at 50°C, the rate constant for abstraction of hydroxyl from **2** (k_{OH}) was found to be dependent on the concentration of **2**. For example, at [**2**] = 0.4 *M*, $k_{OH} = 3.2 \times 10^6 M^{-1} s^{-1}$ whereas, at [**2**] = 0.10 *M*, $k_{OH} = 1.8 \times 10^7 M^{-1} s^{-1}$. The concentration dependence of k_{OH} is attributed to the effects of intermolecular hydrogen bonding and the large absolute values of k_{OH} are ascribed to concerted induced decomposition, the O—O bond being broken in concert with scission of the nearest C—N bond of the azo function. The relevance of the results, to synthetic application of α-hydroperoxyalkyl diazenes in hydroxyalkylation reactions, is discussed.

CHANDRA LAKHANI, LUKOSE MATHEW et JOHN WARKENTIN. Can. J. Chem. **65**, 1748 (1987).

On a évalué les constantes de vitesse pour la décomposition induite de l'hexène-5 yl (hydroperoxy-1 méthyl-1 éthyl) diazène ($(CH_3)_2C(OOH)N{=}N(CH_2)_4CH{=}CH_2$, (**2**). La thermolyse du composé **2**, à 50°C, conduit à des radicaux hexène-5 yles qui enlèvent le groupement hydroxyle du composé **2**; cette réaction est en compétition avec la cyclisation de l'hexène-5 yle en radical cyclopentylméthyle. On a utilisé la constante de vitesse (k_c) de cyclisation qui est connue comme chronomètre pour mesurer la vitesse du processus d'enlèvement bimoléculaire de l'hydroxyle. Dans le cas de la réaction dans l'hexafluorobenzène, à 50°C, on a trouvé que la constante de vitesse pour l'enlèvement de l'hydroxyle du composé **2** (k_{OH}) dépend de la concentration du composé **2**. Par exemple, pour [**2**] = 0,4 *M*, $k_{OH} = 3{,}2 \times 10^6 M^{-1} s^{-1}$: par ailleurs, si [**2**] = 0,1 *M*, $k_{OH} = 1{,}8 \times 10^7 M^{-1} s^{-1}$. On attribue la relation entre k_{OH} et la concentration aux effets des liaisons hydrogènes intermoléculaires et on attribue les valeurs absolues élevées de k_{OH} à une décomposition induite concertée dans laquelle le bris de la liaison O—O se fait simultanément avec la scission de la liaison C—N la plus près de la fonction azo. On discute de l'influence que ces résultats pourraient avoir sur les possibilités d'utiliser les α-hydroxyalkyl diazènes dans les réactions d'hydroxyalkylation.
[Traduit par la revue]

Introduction

α-Hydroperoxyalkyl diazenes (**1**) are readily prepared in solution by autoxidation of hydrazones of aldehydes or ketones, reaction [1] (1–5). They undergo thermal homolysis reactions at moderate temperatures and have been used to initiate radical

[1] $R_2C{=}NNHR' \xrightarrow{O_2} \underset{\mathbf{1}}{R_2C(OOH)N{=}NR'}$

polymerization (6) and as sources of hydroxyl radicals for aromatic substitution (7) or monomer-addition studies (8).[1] Recently, it was shown that **1** are useful reagents for hydroxyalkylation of enol ethers and of some alkenes, reaction [2] (10), and that the overall reaction is a consequence of the radical chain chemistry shown in reactions [3]–[6].

[2] $R_2C(OOH)N{=}NR' + CH_2{=}CHY \rightarrow R'CH_2CH(Y)OH + R_2CO + N_2$

Initiation

[3] $\underset{\mathbf{1}}{R_2C(OOH)N{=}NR'} \rightarrow R_2CO + HO\cdot + N_2 + R'\cdot$

Propagation

[4] $R'\cdot + H_2C{=}CHY \rightarrow R'CH_2\dot{C}HY$

[5] $R'CH_2\dot{C}HY + \mathbf{1} \rightarrow R'CH_2CH(Y)OH + R_2CO + N_2 + R'\cdot$

Termination

[6] 2 Radicals → Non-radical products

The chain propagation step, in which the adduct radical, $R'CH_2\dot{C}HY$, induces decomposition of **1** by abstraction of hydroxyl, reaction [5], was particularly intriguing, not only because overall hydroxyalkylation is a new reaction but also because hydroxyl abstraction from **1** appeared to be much more facile than the analogous induced decomposition of simple hydroperoxides. It became of interest to us to estimate the rate constant for reaction [5] because that constant, and the rate constants for competing reactions (e.g., telomer formation) that consume $R'CH_2\dot{C}HY$, define the synthetic scope of **1** as hydroxyalkylating agents.

Methods, results, and discussion

A convenient technique for determining the rate constant of a bimolecular free radical – molecule reaction involves the use of an internal clock (11), which is usually a competing unimolecular reaction of that radical for which the rate constant is known. Cyclization of the 5-hexen-1-yl radical was chosen as the radical clock for this study not only because the rate constant for the reaction is a reliable number (11, 12) but also because it seemed to be of the right order of magnitude. Accordingly, 5-hexenyl(1-hydroperoxy-1-methylethyl)diazene (**2**) was synthesized and thermolyzed in hexafluorobenzene. Scheme 1 describes the major reactions and products.

The relationship between rate constants and concentrations (or

[1]Non-radical chemistry of α-hydroperoxyalkyl diazenes has been reviewed recently by Baumstark (9).

Can. J. Chem. Downloaded from www.nrcresearchpress.com by 118.98.75.50 on 09/07/12
For personal use only.

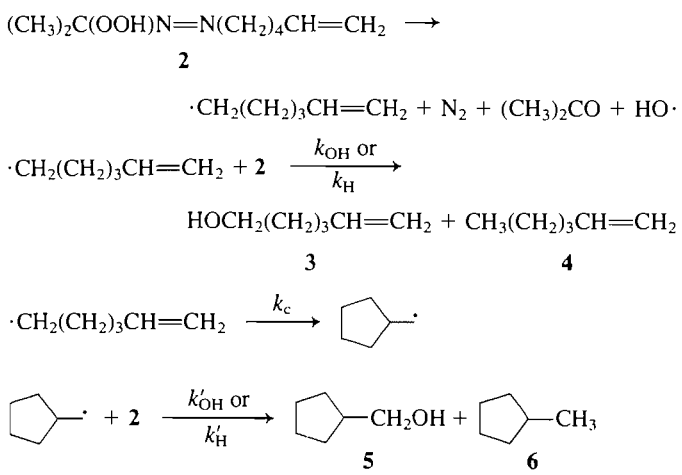

SCHEME 1

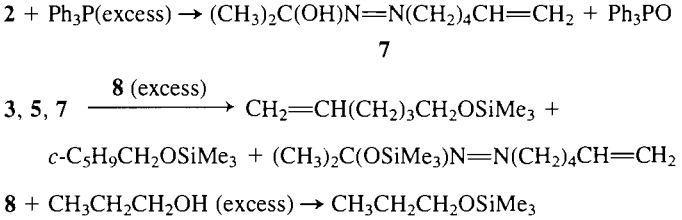

SCHEME 2

yields) of products is given by eq. [7], provided that there are no other products derived from cyclopentylmethyl radicals and that there are no appreciable differential losses resulting from reactions of the first-formed products in subsequent processes.

$$[7]\quad \frac{[\mathbf{3}]}{[\mathbf{5}]+[\mathbf{6}]} = \frac{k_{OH}[\mathbf{2}]_{ave}}{k_c}$$

Decomposition of **2** was stopped after about 10% conversion, by cooling the samples, in order to provide for pseudo-first-order conditions and to minimize attack by free radicals on the products. The remaining hydroperoxide was reduced by addition of triphenylphosphine in excess, and the resulting hydroxyalkyl diazene (**7**) as well as **3** and **5** were silylated with *N,O*-bis(trimethylsilyl)trifluoroacetamide (**8**), and excess **8** was destroyed by addition of propanol (Scheme 2). The reduction and silylation reactions were carried out under conditions that did not permit loss of 1-hexene and methylcyclopentane, the most volatile products in eq. [7], and the final solution was analyzed for the trimethylsilyl ethers (of **3**, **5**, **7**) and for **6** by glpc.[2]

An alternative, much simpler procedure was adopted initially. That procedure involved low temperature, high-vacuum, closed-system distillation of the products from 10% reaction of α-hydroperoxyalkyl diazene; essentially a bulb-to-bulb separation of solvent and products from unreacted hydroperoxide. The distillate was then analyzed for **3** and **5** (unsilylated) and for **6** by glpc. Although a large number of runs were completed in this way, the method was abandoned because of unacceptably large scatter in the values of k_{OH} so obtained.[3]

5-Hexen-1-ol (**3**) was the major product (60–70%) followed by methylcyclopentane (12–18%) and cyclopentylmethanol (9–11%). Those three products accounted for about 90% of the 5-hexenyl moieties from the **2** that had reacted. The remaining 10% included 1-hexene and some unidentified minor products. The yields of 1-hexene ranged from 2% to about 8%; those yields showed the greatest scatter but they never exceeded half the yields of methylcyclopentane from corresponding runs. In view of the poor reproducibility of the 1-hexene yields, discussion of their significance has to be tentative. Fortunately, those yields do not enter into the calculation of k_{OH} (eq. [7]), and the experimental scatter in those yields therefore does not affect k_{OH} values.

The low yields of 1-hexene are not surprising. Cyclization of 5-hexenyl radical (**12**) occurs with rate constant 5.4×10^5 s^{-1} at 50°C while abstraction of hydroperoxyl hydrogen from **2** by 5-hexenyl has a rate constant estimated to be near 2×10^4 $M^{-1}\,s^{-1}$ at 50°C.[4] It follows that the yield of 1-hexene should be less than 1% of the yield of cyclopentyl products from runs in which [**2**] = 0.2 *M*, and correspondingly smaller yet for lower concentrations of **2**.[5] The actual yields of 1-hexene, 2–8%, probably reflect errors in that estimate or significant H-abstraction from other sites in **2**.[5]

Before discussing the yields in Table 1, we turn briefly to potential problems besetting a system as complex as this one, where a series of reactions had to be used to turn excess starting material into a derivative that would not produce one or more of the products of interest during analysis for those products. Care was taken to assure that the product ratios were characteristic of the chemistry of Scheme 1 and not artifacts arising out of the subsequent chemistry of the assay procedure (Scheme 2). A distortion of the ratio could arise from thermolysis of **7** (formed from destruction of excess **2** with Ph_3P, Scheme 2) during analysis, if silylation of **7** were incomplete. The hydroxydiazene (**7**) but not its trimethylsilyl ether, decomposed partially under the gc analysis conditions forming, *inter alia*, **6**. To ensure that this potential source of error was

[2]This seemingly complex procedure was necessary because both the α-hydroperoxyalkyl diazene and the α-hydroxyalkyl diazene decompose on both hlpc and glpc columns to yield one or more of the products in eq. [7]. The trimethylsilyl ether derived from the α-hydroxyalkyl diazene was stable under the conditions of analysis.

[3]Careful examination of the distillates and of the residue showed that a trace of α-hydroperoxyalkyl diazene was actually being transferred to the receiving flask during long-time distillation and that some alcohols remained in the residue from short-time distillation. Whatever the reason for the scatter in values of k_{OH} for a given set of conditions, the simple approach also gave absolute values of k_{OH} ca. five-fold smaller than those obtained by the more elaborate method.

[4]The rate constant for abstraction of hydroperoxyl hydrogen from *t*-butyl hydroperoxide by a primary alkyl radical, ca. $2 \times 10^4\,M^{-1}\,s^{-1}$ at 50°C (13) was taken as the best model available.

[5]We assume that the hydroperoxyl group of **2** is the primary source of abstractable hydrogen. The allyl-type methylene groups of **2** (N=NCH$_2$ and CH$_2$CH=CH$_2$) are the next best H-donors but the rate constants, at least that for abstraction from the allylic methylene group by primary alkyls, are probably smaller (ca. $10^3\,M^{-1}\,s^{-1}$) (see footnote 6) than that for abstraction from the hydroperoxyl group (13).

[6]This estimate is based on the following data. 1-Pentene is 8.1-fold better as a H-donor than 2,2,4-trimethylpentane at 338 K, toward methyl radicals (14). The room temperature rate constant for abstraction by methyl from 2,2,4-trimethylpentane (15) is $20\,M^{-1}\,s^{-1}$. If the correction for the ca. 40°C difference in temperatures is taken to be about 2^4, then the rate constant for abstraction of allylic hydrogen by methyl at 338 K comes to about $2590\,M^{-1}\,s^{-1}$ and the value at 323 K to less than $1000\,M^{-1}\,s^{-1}$.

Can. J. Chem. Downloaded from www.nrcresearchpress.com by 118.98.75.50 on 09/07/12
For personal use only.

TABLE 1. Product distribution and derived rate constants for induced decomposition of **2** at 50°C

$[2]_i$, M[a]	Percent reaction[b]	$[2]_{ave}$, M[c]	Relative yields[d] **3**	**4**	**5**	**6**	Ratio **3**/(**5** + **6**)	$k_{OH}^{50°C}$ (M^{-1} s^{-1})[e]
	8.4		1.0	0.09	0.13	0.23	2.8	
0.10		0.095	1.0	0.04	0.11	0.17	3.6	$(1.8\pm0.3)\times10^7$
	10.4		1.0	nd	0.14	0.14	3.6	
			1.0	nd	0.14	0.19	3.0	
	10.2		1.0	0.08	0.14	0.34	2.1	
0.20		0.19	1.0	0.03	0.14	0.37	2.0	$(6.7\pm1.0)\times10^6$
	7.9		1.0	nd	0.17	0.20	2.7	
			1.0	nd	0.19	0.19	2.6	
	8.6		1.0	nd	0.15	0.28	2.3	
0.40		0.38	1.0	nd	0.18	0.33	2.0	$(3.0\pm0.2)\times10^6$
	10.1		1.0	0.11	0.19	0.32	2.0	
			1.0	0.13	0.19	0.30	2.0	

[a]Initial concentration of **2** in C_6F_6.

[b]Estimated by gc analysis of remaining **2**, as the trimethylsilyl ether, and of the products derived from the 5-hexenyl portion of **2**, not counting 1-hexene which was a minor product.

[c]Calculated from the average percent reaction for two experiments at each initial concentration.

[d]Duplicate experiments at each concentration of **2** and duplicate product analyses for each experiment. Compounds **3**, **4**, **5**, and **6** are 5-hexen-1-ol, 1-hexene, cyclopentylmethanol, and methylcyclopentane, respectively. The alcohols were analyzed as the corresponding trimethylsilyl ethers. Relative yields were determined from enlarged (3×) recorder traces by the "cut and weigh" method. Those of methylcyclopentane contain a correction factor (1.3) for its lower molar detector response compared to that of 5-hexenyl trimethylsilyl ether. Isomeric trimethylsilyl ethers were assumed to have the same detector response, within experimental error. The sum of the yields of **3**, **5**, and **6** was estimated to be 90% or greater. The symbol nd means "not determined."

[e]Calculated with the use of eq. [7], where $k_C^{50°C} = 5.4\times10^5\ s^{-1}$ (12). The single rate constant for each concentration was calculated from $[2]_{ave}$ for two runs and from the average product ratio **3**/(**5** + **6**) for that concentration. The error is the standard deviation of rate constants calculated from individuals product ratios and $[2]_{ave}$ for a particular $[2]_{initial}$.

eliminated, the silylation reactions themselves were monitored by gc and reaction solutions were subjected to the treatment with propanol (Scheme 2) and to subsequent analysis only after silylation of **3**, **5**, and **7** was complete.

The fact that methylcyclopentane was an important product is cause for additional concern about the validity of the yields of alcohols. If methylcyclopentane arose primarily from abstraction of hydroperoxyl hydrogen,[5] then the peroxyl radicals that resulted would have formed, in sequence, tetraoxide and oxygen. Oxygen so formed would have led to 5-hexenyl hydroperoxide and cyclopentylmethyl hydroperoxide which, in turn, would have led to **3** and **5** during the treatment with Ph_3P. Although this problem can not be dismissed, there are several reasons for believing that the distortion of the data, from formation of O_2, should be minor. First, the maximum possible yield of transient O_2 by the above mentioned mechanism is only about half that of methylcyclopentane. Second, the peroxyl radicals can follow pathways other than coupling, such as H-abstraction from the side chain of **2** and addition to the double bond. Those processes would produce radicals that would compete for the limited supply of oxygen, and that lead to products different from **3** and **5**. Third, since both alkyl radical precursors of **3** and **5** would react fast with oxygen, the distortion of the true yield ratio (eq. [7]) would be small because both the numerator and the denominator would be larger than they ought to be in view of the second source of the alcohols. The above factors, taken together, make it unlikely that our k_{OH} values for the 5-hexenyl radical should be too large by a factor as large as 1.1, from the incursion of tetraoxide-derived oxygen. Assuming that all potential sources of serious error have been dealt with, we turn to the discussion of the data in Table 1.

A striking feature of the analytical results (Table 1) is that the yields of **6** exceed those of **5** under all conditions that were studied. The reverse is true for the acyclic analogs, where the yields of **4** (although least accurately determined), were much below those of **3**. Thus, the ratio of rate constants, k_{OH}/k_H, must be substantially larger for the 5-hexenyl radical than for the cyclopentylmethyl radical. A rough estimate leads to $(k_{OH}/k_H)^{5\text{-hexenyl}} \geq 4.9(k_{OH}/k_H)^{\text{cyclopentylmethyl}}$, which was obtained as follows. The upper limit of the yield of **4** from any run is one half the yield of **6** for that run (see above). That upper limit leads to $(k_{OH}/k_H)^{5\text{-hexenyl}} > 7.8$, using the averaged data in Table 1, from all three concentrations. Averaged relative yields of **5** and **6** lead to $(k_{OH}/k_H)^{\text{cyclopentylmethyl}} = 1.6$ and $7.8/1.6 = 4.9$.

Although the reduced selectivity of cyclopentylmethyl could be the result of either a diminished k_{OH} or an enhanced k_H (or both) relative to corresponding rate constants for 5-hexenyl, there is a reasonable argument for a diminished k_{OH}. The hydroxy oxygen of **2** is undoubtedly more protected by steric hindrance than the hydroperoxy hydrogen and the cyclopentylmethyl radical, because it is β-branched and has two γ-hydrogens eclipsing the CH_2 group, could well be more sensitive toward steric hindrance than the isomeric 5-hexenyl radical.

A second striking feature of the yield data is the small decrease of the ratio, **3**/(**5** + **6**), attending a four-fold increase in the concentration of **2**. The expected result, based on Scheme 1,[7] is a four-fold increase in that ratio with a four-fold increase in [**2**]. The data can be accommodated within the framework of

[7]Loss of **3** at higher concentrations of **2**, by epoxidation (9) of **3**, is not likely to be serious because the conversions were kept to about 10%.

Can. J. Chem. Downloaded from www.nrcresearchpress.com by 118.98.75.50 on 09/07/12
For personal use only.

Can. J. Chem. Downloaded from www.nrcresearchpress.com by 118.98.75.50 on 09/07/12
For personal use only.

Scheme **1** only if k_{OH} is dependent on the concentration of **2**, as indicated in Table 1. We now turn to the examination of that dependence in mechanistic terms.

Induced decomposition of **2** and of analogous azohydroperoxides is presumably a concerted process involving the scission of the O—O bond and, at least, the nearest C—N bond (16). Such a concerted induced decomposition has a geometric requirement; the breaking σ bonds must be either *anti*- or *syn*-periplanar. The latter geometry is provided for, more or less, by virtue of intramolecular H-bonding in monomeric **2**, as in **9** and **10**. Intermolecularly, H-bonded species (e.g., **11**)

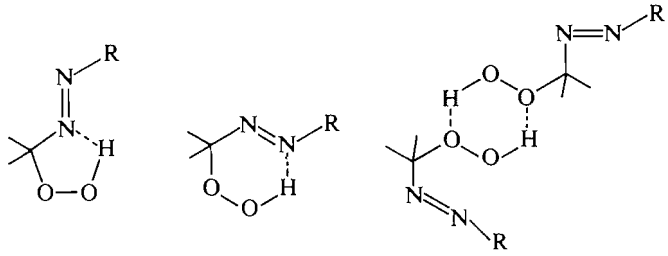

9 **10** **11**

which become prevalent at high [**2**], do not retain the alignment of orbitals required for facile induced decomposition and the observed rate constant, a composite of rate constants for monomeric and associated **2**, falls with increasing concentration of [**2**]. Steric hindrance to attack at hydroxy oxygen of associated **2**, already mentioned earlier, would operate in the same sense, to reduce k_{OH} below that applicable to the monomeric species.

Attempts to work with **2** at 0.02 *M* initial concentration were not rewarding, because the constraint of low conversion necessary to use eq. [7] (pseudo first order kinetics) led to very noisy data. Presumably, k_{OH} for attack on monomeric **2** by 5-hexenyl exceeds $1.8 \times 10^7 M^{-1} s^{-1}$ at 50°C. Whatever the limiting rate constant may be, it is clear that induced decomposition of azohydroperoxides by relatively unhindered carbon-centered radicals is very fast at commonly used concentrations of such peroxides.

Induced decomposition of simple hydroperoxides, as opposed to azo hydroperoxides, by free radicals is probably much less facile. Although absolute rate constants for the reaction, R·(alkyl) + R′OOH → ROH + R′O·, have not been reported, it is possible to estimate an upper limit for a model hydroperoxide. Thus, 5-hexenyl radical reacts with *t*-butyl hydroperoxide (**12**) to form 1-hexene rather than 5-hexen-1-ol (13). If it is assumed that some 5-hexen-1-ol was actually formed but in ≤5% yield, then it follows from $k_H = 2 \times 10^4 M^{-1} s^{-1}$ that $k_{OH} \leq 1 \times 10^3 M^{-1} s^{-1}$, for **12**.[8] *t*-Butyl hydroperoxide is a reasonable model for the steric effects to be expected in **2** and the fact that k^2_{OH} is larger by a factor ≥10^3 than k^{12}_{OH} therefore implies that there is a substantial electronic effect of the azo substituent or else that different mechanisms apply in the two cases. The latter explanation is more likely to be correct than the former. Induced decomposition of **12**, by radical attack at hydroxyl oxygen, affords alcohol and *t*-butoxyl. Analogous induced decomposition of **2** can lead to alcohol and either alkoxy radical or ketone plus diazenyl radical; the latter products are formed if O—O bond cleavage occurs in concert with scission of the nearest C—N bond. The thermochemistry for the concerted induced decomposition is considerably more favourable than that for induced scission of the O—O bond alone[9] and the extra driving force provided by partial formation of the strong carbonyl double bond at the transition state is presumably responsible for the facile induced decomposition of α-hydroperoxyalkyl diazenes as compared to their alkyl hydroperoxide counterparts.[8] Evidence for a concerted mechanism of unimolecular thermolysis of an α-benzoylperoxyalkyl diazene was presented earlier (17) and that result, reinforced with the present findings, suggests that concertedness may be a common mechanism for both induced and uninduced decomposition of α-hydroperoxyalkyl diazenes and some of their derivatives.

The implications of the present results to synthesis with α-hydroperoxyalkyl diazenes deserve brief discussion. At first sight, the large values of k_{OH} and the low yields of 1-hexene from 5-hexenyl radicals are encouraging. However, if α-hydroperoxyalkyl diazenes are to serve as reagents for hydroxyalkylating multiple bonds, then the rate constants of interest are those for attack of secondary and tertiary radicals[10] at the OH group. The results are less encouraging in the latter regard, for even a branched primary radical (cyclopentylmethyl) abstracts H faster than OH under some conditions. The sensitivity of OH abstraction to steric hindrance that this result implies was already suspected when it was found that norbornene is hydroxyalkylated in very low yield by α-hydroperoxyalkyl diazenes (18). For synthetic application there is nothing to be gained from the concentration dependence of k_{OH} because the increase in k_{OH} with dilution is cancelled, more or less, by the decrease in the value of the concentration term in the equation for the second order rate of hydroxyl abstraction. It is clear then that structural modification of the reagent is required, to reduce steric hindrance to approach at the hydroxyl oxygen and/or to hold the hydroperoxy function in a conformation better suited to concerted induced decomposition. We plan to test new reagents, having one or both of those modifications, in the future.

Experimental

5-Hexenyl[1-hydroperoxy-1-methylethyl]diazene (**2**) was prepared by the procedure described earlier (19), involving autoxidation of the 5-hexenyl hydrazone of acetone in light petroleum. It was stored as that solution in a freezer. Samples of **2** in hexafluorobenzene were prepared by removing the solvent from an aliquot of the solution of **2** in petroleum using a steam of dry N_2, weighing the residual **2**, and adding the appropriate volume of C_6F_6. Samples sizes were 0.6–1.0 mL of **2** in C_6F_6.

Thermolyses were carried out with degassed solutions of **2** in C_6F_6, in sealed Pyrex tubes. A solution of **2** was heated at 49.8 ± 0.2°C in an oil bath for 25–30 min. That time had been determined, by experiment with solutions of **2** in nmr tubes, to cause ca. 10% decomposition. The sample was chilled, the tube was cut and the cold contents were transferred to a small glass-stoppered flask containing triphenylphosphine in 50% excess over the hydroperoxide. The flask was left overnight in the refrigerator before *N*,*O*-bistrimethylsilyl trifluoro-

[8]5-Hexen-1-ol was not reported as a coproduct of the reaction of 5-hexenyl radicals with *t*-butyl hydroperoxide in chlorobenzene (13). In a personal communication one of the authors (J.A.H.) emphasized that, although 5-hexen-1-ol was not an important reaction product, small amounts could have been missed because they were not looking for it.

[9]For the concerted induced decomposition, R· + $(CH_3)_2C(OOH)$-N=N—R → ROH + $(CH_3)_2CO$ + ·N=NR, we estimate ΔH = −97 kcal mol^{-1} whereas, for the hypothetical induced decomposition, R· + $(CH_3)_2C(OOH)N{=}NR$ → ROH + $(CH_3)_2C(O\cdot)N{=}NR$, ΔH is about −50 kcal mol^{-1}.

[10]Except for the case of addition to ethylene or to an alkyne, the adduct of R· and acceptor will be either a 2°- or a 3°-radical, if the addition is to a C—C multiple bond.

acetamide (BSTFA), in 15- to 20-fold excess over initially present hydroperoxide, was added. The flask was again stoppered securely and the contents were kept at ca. 20°C until silylation of **3**, **5**, and **7** was complete, as judged by periodic gc analysis. Silylation of **7** was slowest, taking about 4 days, but solutions were left for a full week before excess propanol was added to destroy the remaining BSTFA. The solution was then analyzed by gc, with two columns. Column 1 (10′ × ⅛″, steel) packed with Carbowax 20M (5%) on Chromosorb P (100/120 mesh) separated 1-hexene and methylcyclopentane from the solvent and from other products. It was used with N_2 flowing at 10 mL min^{-1} at a temperature of 35°C until **4**, **6**, and the solvent had been eluted. The temperature was then raised to 200°C to purge the column. Column 2 (6′ × ⅛″, glass) packed with OV-17 (3%) on Chromosorb P (100/120 mesh) did not resolve **4** from **6** but it separated the silyl ethers of **3**, **5**, and **7** cleanly from other components. It was operated with N_2 flowing at 10 mL min^{-1} and with the following temperature program: 40°C (2 min) increased to 150°C at 5° min^{-1} and finally to 300°C at 25° min^{-1} to purge the column of Ph_3P and Ph_3PO. Calibration of the two column procedure with solutions of **6** and the trimethylsilyl ether of **5** showed that reproducibility of the volume injected was reliable and that only a multiplicative factor of 1.3, for the signal from **6**, was required. Detector response factors for isomers **4** and **6**, on the one hand, and for the trimethylsilyl ethers of **3** and **4**, on the other hand, were assumed to be the same.

Spectra of products

The following nmr spectra of authentic materials, synthesized form the alcohols by treatment with BSTFA, matched those of products formed from **2** by thermolysis and subsequent treatment. Nuclear magnetic resonance spectra were run at 90 MHz with C_6F_6 as solvent and with internal TMS. Mass spectra are the low resolution, ei, type. Peaks with intensities below 5% are not included unless they correspond to molecular ions.

Trimethylsilyl ether of **3**. ^{1}H nmr: δ 0.10 (s, 9H), 1.47 (m, 4H), 2.03 (m, 2H), 3.53 (*t*, J = 6 Hz, 2H), 4.90 (m, 2H), 5.50–6.10 (m, 1H). MS: m/z 172 (M^+, 0.5%), 157 ($M^+ - CH_3$, 50%), 129 (18%), 127 (14%), 103 (20%), 99 (12%), 83 (19%), 75 (100%), 73 (43%), 54 (12%), 41 (7%).

Trimethylsilyl ether of **5**. ^{1}H nmr: δ 0.07 (s, 9H), 1.53 (m, 9H), 3.77 (d, J = 6 Hz, 2H). MS: m/z 172 (M^+, 2%), 157 ($M^+ - CH_3$, 93%), 103 (30%), 75 (100%), 73 (48%), 70 (5%).

Trimethylsilyl ether of **7**. ^{1}H nmr: δ 0.10 (s, 9H), 1.23 (s, 6H), 1.24–2.24 (m, 6H), 3.80 (*t*, J = 7.5 Hz, 2H), 4.90 (m, 2H), 5.33–6.10 (m, 1H). MS: m/z ($M^+ - CH_3$, 25%), 153 (7%), 131 (100%), 73 (55%).

1. K. H. Pausacker. J. Chem. Soc. 348 (1950).
2. R. Criegee and G. Lohaus. Chem. Ber. **84**, 219 (1951).
3. A. J. Belamy and R. D. Guthrie. J. Chem. Soc. 2788 (1965).
4. W. F. Taylor, H. A. Weiss, and T. C. Wallace. J. Org. Chem. **34**, 1759 (1969).
5. M. Schulz and U. Missol. Z. Chem. **14**, 265 (1974).
6. R. E. MacLeay and O. L. Mageli. Ger. Offen. 2, 155,679 (Cl.08f), (1972). U.S. Appl. 88,248. (1970); Chem. Abstr. **77**, 125975t (1972).
7. (*a*) T. Tezuka, N. Narita, W. Ando, and S. Oae. J. Am. Chem. Soc. **103**, 3045 (1981); (*b*) T. Tezuka and N. Narita. J. Am. Chem. Soc. **101**, 7413 (1979).
8. R. D. Grant, E. Rizzardo, and D. H. Solomon. J. Chem. Soc. Perkin Trans. II, 379 (1985).
9. A. L. Baumstark. Bioorg. Chem. **14**, 336 (1986).
10. E. Y. Osei-Twum, D. McCallion, A. S. Nazran, R. Panicucci, P. A. Risbood, and J. Warkentin. J. Org. Chem. **49**, 336 (1984).
11. D. Griller and K. U. Ingold. Acc. Chem. Res. **13**, 317 (1980).
12. C. Chatgilialoglu, K. U. Ingold, and J. C. Scaiano. J. Am. Chem. Soc. **103**, 7739 (1981).
13. J. A. Howard and S. B. Tong. Can. J. Chem. **57**, 2755 (1979).
14. (*a*) M. Levy, M. Steinberg, and M. Szwarc. J. Am. Chem. Soc. **76**, 5978 (1954); (*b*) M. Levy and M. Szwarc. J. Am. Chem. Soc. **77**, 1949 (1955); (*c*) R. P. Buckley and M. Szwarc. Proc. R. Soc. (London) Ser. A, **240**, 396 (1957).
15. R. H. Schuler and R. R. Kuntz. J. Chem. Phys. **67**, 1004 (1963).
16. M. Schulz and U. Missol. J. Prakt. Chem. **322**, 417 (1980).
17. A. S. Nazran and J. Warkentin. J. Am. Chem. Soc. **104**, 6045 (1982).
18. E. Y. Osei-Twum and J. Warkentin. J. Org. Chem. **50**, 4725 (1985).
19. D. R. Jewell, L. Mathew, and J. Warkentin. Can. J. Chem. **65**, 311 (1987).

Can. J. Chem. Downloaded from www.nrcresearchpress.com by 118.98.75.50 on 09/07/12
For personal use only.

Vinyl ether hydrolysis. XVIII. The two-stage reaction of 2,3-dimethoxy-1,3-butadiene[1]

A. Jerry Kresge and Ya Yin

Department of Chemistry, University of Toronto, Toronto, Ont., Canada M5S 1A1

Received December 15, 1986

This paper is dedicated to Professor John T. Edward

A. Jerry Kresge and Ya Yin. Can. J. Chem. **65**, 1753 (1987).

The kinetics of acid-catalyzed hydrolysis of 2,3-dimethoxy-1,3-butadiene (**1**) to 3-methoxy-3-buten-2-one (**2**) and the subsequent 10^4 times slower conversion of the latter to biacetyl (**3**):

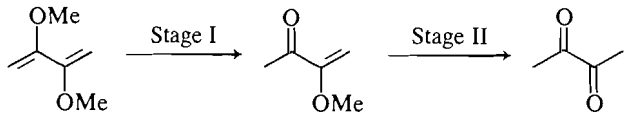

1 **2** **3**

were studied in aqueous solution at 25°C. Both stages of this process give substantial hydrogen ion isotope effects, k_{H^+}/k_{D^+} = 2.95 for Stage I and k_{H^+}/k_{D^+} = 1.83 for Stage II, and Stage I shows general acid catalysis in formic and acetic acid buffers; both stages are therefore assigned the conventional mechanism for vinyl ether hydrolysis involving rate-determining proton transfer from catalyzing acid to substrate. The second vinyl ether group of the initial substrate (**1**) is found to have only a slight (3-fold) accelerative effect on the reactivity of the first group, but the acetyl substituent present in the intermediate **2** decreases its reactivity by a factor of 10^4; the latter appears to be due largely to the electron-withdrawing inductive effect of acetyl, with little or no influence from a countervailing electron-supplying resonance effect.

A. Jerry Kresge et Ya Yin. Can. J. Chem. **65**, 1753 (1987).

Opérant à 25°C et dans des solutions aqueuses, on a déterminé la cinétique de l'hydrolyse acido-catalysée du diméthoxy-2,3 butadiène-1,3 (**1**) en méthoxy-3 butène-3 one-2 (**2**) et de la transformation subséquente de ce dernier, qui est 10^4 fois plus lente que la réaction précédente, en biacétyle (**3**). Pour chacune des étapes, on observe des effets isotopiques cinétiques de l'ion

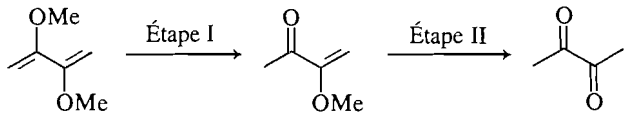

1 **2** **3**

hydrogène qui sont importants, k_{H^+}/k_{D^+} = 2,95 pour l'étape I et k_{H^+}/k_{D^+} = 1,83 pour l'étape II: de plus, l'étape I est soumise à une catalyse acide générale dans des tampons d'acide formique ou d'acide acétique. Pour chacune des étapes, on attribue donc le mécanisme conventionnel d'hydrolyse des éthers vinyliques impliquant une étape déterminante comportant un transfert de proton de l'acide agissant comme catalyseur vers le substrat. On a observé que le deuxième groupement éther vinylique du substrat original (**1**) n'a qu'une faible influence (facteur d'environ 3) sur le réactivité du premier groupement; toutefois, le groupement acétyle présent dans l'intermédiaire **2** diminue la réactivité par un facteur de 10^4. Il semble que ce dernier effet est principalement dû à l'effet inductif électro-affinitaire du groupement acétyle et que l'effet électro-donneur inverse provenant de la résonance n'a que peu ou pas d'influence.

[Traduit par la revue]

2,3-Dimethoxy-1,3-butadiene, **1**, contains two vinyl ether functional groups whose consecutive hydrolysis, eq. [1], might

[1]

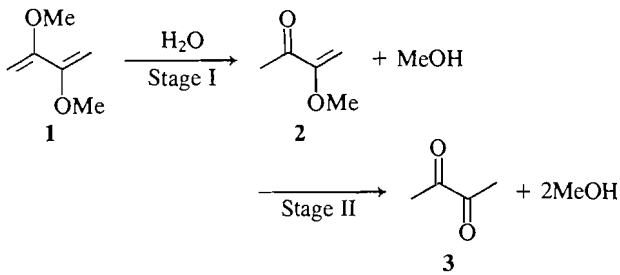

1 **2** **3**

be expected to occur in separate stages proceeding at rather different rates. This follows from the fact that the conventional mechanism for vinyl ether hydrolysis involves rate-determining proton transfer from a catalyzing acid to the substrate in a step that generates a carbocation intermediate (1), and α-acyl substituents such as that present in the product of the first hydrolysis stage, **2**, are likely to be carbocation destabilizing, eq. [2] (2).

[2]

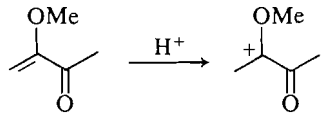

2

We wish to report that we have examined the kinetics of hydrolysis of 2,3-dimethoxy-1,3-butadiene and have found this to be the case. Our results provide a quantitative estimate of this α-acetyl effect on carbocation stability, a subject of some current interest (2), and also give information on the effect of one vinyl ether group in 2,3-dimethoxy-1,3-butadiene on the reactivity of the other.

Results

Reaction identification

2,3-Dimethoxy-1,3-butadiene has a strong uv absorption band

[1]Part XVII: ref. 21.

Can. J. Chem. Downloaded from www.nrcresearchpress.com by 213.166.140.6 on 09/07/12
For personal use only.

with λ_{max} = 230 nm. In acidic solutions this band gradually diminishes in intensity and is replaced, through a change showing a tight isosbestic point at λ = 255 nm, by a somewhat weaker but still strong absorbance at λ_{max} = 250 nm. This new absorption band then also diminishes, but much more slowly, to give a final spectrum with no apparent uv or visible absorbance; the final solution, however, has a faint yellow color.

These two spectral changes occur on time scales that differ by four orders of magnitude. We were therefore able to isolate the intermediate substance with λ_{max} = 250 nm and show, through comparison of its proton nmr spectrum with a published description (3), that it is indeed 3-methoxy-3-buten-2-one, **2**; in addition, the value λ_{max} = 250 nm agrees well with that expected for an α,β-unsaturated ketone with an α-methoxy substituent (4). We also isolated a yellow material as the final reaction product, and its nmr spectrum showed it to be biacetyl, **3**; a previous study (3) also found biacetyl to be the sole reaction product of the acid-catalyzed hydrolysis of 3-methoxy-3-butene-2-one.

These considerations thus demonstrate that 2,3-dimethoxy-1,3-butadiene does indeed hydrolyze by the two-stage process shown in eq. [1], and that the velocities of the two stages are sufficiently different to allow detailed kinetic examination of each.

Kinetics

We measured rates of the first stage of this hydrolysis reaction in perchloric acid solutions by stopped-flow techniques and in formic and acetic acid buffer solutions by conventional spectrophotometry. The determinations in perchloric acid solutions were done in H_2O and in D_2O, in H_2O over the acid concentration range 0.02–0.10 *M* and in D_2O over the acid concentration range 0.01–0.06 *M*. The ionic strength was maintained at 0.10 *M* by adding sodium chloride as required. These data are summarized in Table S1.[2]

The rate data obtained in both solvents adhered well to the first-order rate law, and observed first-order rate constants were accurately proportional to acid concentration. Linear least-squares analysis gave the catalytic coefficients k_{H^+} = 4.37 ± 0.03 M^{-1} s^{-1} and k_{D^+} = 1.48 ± 0.02 M^{-1} s^{-1}, which provide the isotope effect k_{H^+}/k_{D^+} = 2.95 ± 0.04. For both solvents, the zero-acid-concentration rate intercepts were less than their experimental uncertainty.

Rate measurements of the first stage of the hydrolysis reaction in formic and acetic acid buffers were performed in series of solutions of constant buffer ratio and constant ionic strength (0.10 *M*) but changing buffer concentration (fivefold variation). These data are summarized in Table S2.[2]

These rate data also adhered well to the first-order rate expression, and observed first-order rate constants were accurately proportional to buffer concentration. This is the expected behavior for a general acid-catalyzed reaction, such as vinyl ether hydrolysis (1), and the data were therefore fitted to the rate law that governs such a process, eq. [3]. Linear least-squares

$$[3] \quad k_{obs} = k_{H^+}[H^+] + k_{HA}[HA]$$

analysis gave formic acid catalytic coefficients determined at two different buffer ratios in good agreement with each other, k_{HA} = (2.24 ± 0.04) × 10^{-2} M^{-1} s^{-1} ([HA]/[A^-] = 0.91) and k_{HA} = (2.28 ± 0.05) × 10^{-2} M^{-1} s^{-1} ([HA]/[A^-] = 1.9), and hydrogen ion catalytic coefficients, k_{H^+} = 4.13 ± 0.08 and 4.17 ± 0.06 M^{-1} s^{-1}, consistent with the value determined in perchloric acid solutions, k_{H^+} = 4.37 ± 0.03 M^{-1} s^{-1}. Measurements in acetic acid buffers were made at only one buffer ratio ([HA]/[A^-] = 1.1); these data gave the acetic acid catalytic coefficient k_{HA} = (4.08 ± 0.05) × 10^{-3} M^{-1} s^{-1} and the hydrogen ion catalytic coefficient k_{H^+} = 4.34 ± 0.10 M^{-1} s^{-1}. Hydrogen ion concentrations of the buffer solutions needed for this analysis were obtained by calculation, using thermodynamic dissociation constants for formic (5) and acetic (6) acids and activity coefficients recommended by Bates (7).

TABLE 1. Summary of rate constants for the first and second stages in the hydrolysis of 2,3-dimethoxy-1,3-butadiene to biacetyl at 25°C

Rate constants/M^{-1} s^{-1}	Stage I	Stage II
k_{H^+}	4.37	0.000241
k_{D^+}	1.48	0.000132
k_{HCO_2H}	0.0226	—
$k_{CH_3CO_2H}$	0.00408	—

The second stage of this hydrolysis reaction, the conversion of 3-methoxy-3-buten-2-one (**2**) to biacetyl (**3**), was much slower than the first, and rate measurements were therefore made only in perchloric acid solutions. Concentrated as well as dilute acid solutions were used; the concentration range covered was 0.2–47 wt.% acid (0.02–6.3 *M*), and ionic strength was equal to the concentration of the acid. These data are summarized in Table S3.[2]

These data showed good first-order behavior, and observed first-order rate constants increased with increasing acidity, with the increase being somewhat stronger than in direct proportion to acid concentration. Such behavior is typical of reactions in which proton transfer to carbon is rate determining. The data are usually analyzed using acidity functions, and the X_0 scale (8) appears to be the best quantity currently available for this purpose (9). In the present case, a plot of log (k_{obs}/[H^+]) versus X_0 was accurately linear, and least-squares analysis gave slope = 0.71 ± 0.01 and intercept = −3.618 ± 0.007; the latter leads to the hydrogen ion catalytic coefficient k_{H^+} = (2.41 ± 0.04) × 10^{-4} M^{-1} s^{-1}.

A few measurements of the rate of the second hydrolysis stage were also made in D_2O solutions of perchloric acid over the concentration range 0.02–0.10 *M*, ionic strength = 0.10 *M*. These data are summarized in Table S4;[2] they give the hydrogen ion catalytic coefficient k_{D^+} = (1.31 ± 0.03) × 10^{-4} M^{-1} s^{-1}, which leads to the isotope effect k_{H^+}/k_{D^+} = 1.83 ± 0.05.

All of the catalytic coefficients determined here for both stages of this vinyl ether hydrolysis reaction are listed in Table 1.

Discussion

Reaction mechanism

The results obtained here show that the hydrolysis of 2,3-dimethoxy-1,3-butadiene to 3-methoxy-3-buten-2-one (eq. [1], Stage I) is a general acid-catalyzed process, which indicates that proton transfer occurs in the rate-determining step of this reaction. This conclusion is reinforced by the strong hydrogen-ion isotope effect, k_{H^+}/k_{D^+} = 2.95, and the two pieces of evidence together suggest that the conventional, rate-determining proton transfer mechanism for vinyl ether hydrolysis is operating. This hydrogen ion isotope effect in fact agrees remarkably well with the value, k_{H^+}/k_{D^+} = 3.12, predicted from a correla-

[2]Tables S1–S4 of rate data may be purchased from the Depository of Unpublished Data, CISTI, National Research Council of Canada, Ottawa, Ont., Canada K1A 0S2.

Can. J. Chem. Downloaded from www.nrcresearchpress.com by 213.166.140.6 on 09/07/12
For personal use only.

tion of isotope effects with free energy of activation for the hydrolysis of a large group of vinyl ethers known to react by the conventional mechanism (1*b*). It would appear safe to conclude, therefore, that this first stage in the hydrolysis of 2,3-dimethoxy-1,3-butadiene occurs as shown in eq. [4].

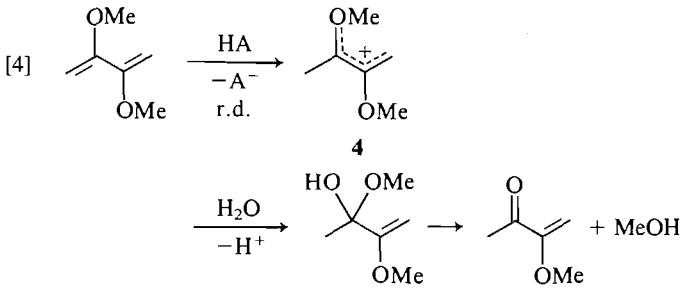

The hydrogen ion isotope effect on the second stage of the hydrolysis of 2,3-dimethoxy-1,3-butadiene, conversion of 3-methoxy-3-buten-2-one (**2**) to biacetyl (**3**), also agrees well with the value expected on the basis of this correlation: $(k_{H^+}/k_{D^+})_{obs} = 1.83$, $(k_{H^+}/k_{D^+}) = 1.57$. This suggests that this stage also occurs by the conventional mechanism, as shown in eq. [5].

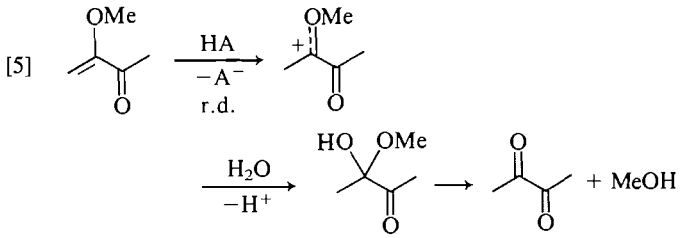

These mechanistic assignments are reinforced by the fact that examination of the proton nmr spectrum of the reaction mixture midway through the second stage of hydrolysis of 2,3-dimethoxy-1,3-butadiene conducted in D_2O solution showed only one deuterium atom in the methyl group of 3-methoxy-3-buten-2-one and no deuterium incorporation in its vinyl group. This indicates that neither of the carbon protonation steps of eqs. [4] and [5] is reversible. This is significant in view of the fact that the only variant on the conventional mechanism for vinyl ether hydrolysis ever proposed is a scheme in which the carbon protonation step is reversible (10).

The mechanisms of eqs. [4] and [5] show the carbocation products of carbon protonation as discrete intermediates; this implies that they are stable species with lifetimes at least as long as the period of a molecular vibration, $\tau \sim 10^{-13}$ s (11). There is no direct information on the lifetimes of carbocations such as these in aqueous solution, but an estimate may be made by extrapolating a σ^+ correlation of rates of reaction with water for a series of more stable carbocations (12). This method gives a lifetime of 1×10^{-8} s for the vinyl-substituted methoxymethyl cation (**4**), formed in the first stage of the hydrolysis reaction, eq. [4],[3] which is easily long enough to allow this species to be a viable intermediate in aqueous solution. The lifetime estimated in this way for the acetyl-substituted methoxymethyl cation (**5**) formed in the second hydrolysis step (eq. [5]), 5×10^{-12} s,[4] is much shorter but still safely over the 10^{-13} s limit. The latter lifetime, however, is just below the rotational correlation time of water, 1×10^{-11} s (15), which might be a measure of the time required for a water molecule solvating the vinyl ether substrate to rotate into correct position for bonding to the carbocationic center. If the lifetime of this carbocation is indeed too short to allow such repositioning of a water molecule to take place, then the repositioning would have to occur before proton transfer to carbon, and a preassociation mechanism would result.

Reactivity

The hydrogen ion rate constant determined here for the hydrolysis of 2,3-dimethoxy-1,3-butadiene, **1**, divided by two to allow for the fact that this molecule has two identical vinyl ether groups, is only 2.9 times the corresponding rate constant for the hydrolysis of methyl vinyl ether, **6** (1*b*). This weak effect of introducing a vinyl substituent indicates that allylic resonance of the type **7** → **8**, offset somewhat by the opposing inductive

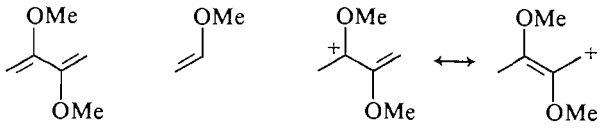

1 **6** **7** **8**

effect of the α-methoxyvinyl group, contributes very little more to the stability of the transition state of this reaction than does 1,3-butadienyl resonance (**9** → **10** → **11**) to the stability of its

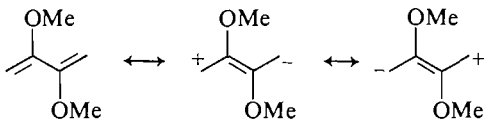

9 **10** **11**

initial state. This contrasts sharply with the effect of vinyl substituents on the rate of hydration of simple alkenes, a reaction that also occurs through rate-determining protonation of a carbon–carbon double bond to form a carbocationic intermediate (16). For example, the hydrogen ion catalytic coefficient for the hydration of 2-methyl-1,3-butadiene, **12** (13), is 10^4 times that for the hydration of propene, **13** (17), and a similar comparison of 1,3-butadiene itself, **14** (13), with ethene, **15** (17), gives the even greater rate factor 10^7. This

12 **13** **14** **15**

difference in behavior between vinyl ethers and simple alkenes may be attributed to the great effectiveness of methoxyl group resonance, **16** → **17**, at stabilizing the transition state of the

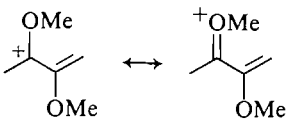

16 **17**

vinyl ether hydrolysis reaction: this type of conjugation is so effective that there is little demand for additional stabilization by the vinyl group. A similar, though attenuated, example of this phenomenon may be seen in the comparison of **12** and **13** on one hand with **14** and **15** on the other, where introduction of a cation-stabilizing methyl group reduces the vinyl substituent effect from 10^7 down to 10^4.

The second stage of the hydrolysis of 2,3-dimethoxy-1,3-butadiene is much slower than the first: the rate retardation calculated, making allowance for the presence of two vinyl ether groups in the diene, amounts to a factor of 9.1×10^3. This

[3]This estimate is based upon use of the σ^+ constant for $CH_2{=}CH{-}$ (ref. 13) in place of the (unknown) σ^+ constant of $CH_2{=}C(OMe){-}$.

[4]Estimated using $\sigma^+ = 0.47$ for $CH_3CO{-}$ (ref. 14).

Can. J. Chem. Downloaded from www.nrcresearchpress.com by 213.166.140.6 on 09/07/12
For personal use only.

may be attributed to a cation-destabilizing effect of the α-acetyl substituent in the cationic intermediate formed in the rate-determining step of this second reaction stage, eq. [2]. The electronic influence of acyl substituents on adjacent electron-deficient centers has traditionally been attributed to an electron-withdrawing inductive effect, but evidence has recently been supplied for a countervailing electron-supplying resonance effect, **18** → **19** (19). It is of interest to inquire whether or not such an

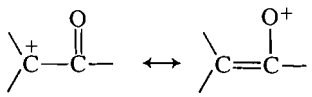

18 **19**

effect operates in the present system. This may be done by using a σ^+ correlation (16*b*, 18) to predict the rate constant of the present reaction. Although this correlation was originally based upon hydrogen-ion rate constants for the hydration of alkenes, it also works well for the hydrolysis of vinyl ethers; for example, it predicts $k_{H^+} = 0.29\,M^{-1}\,s^{-1}$ for the hydrolysis of methyl vinyl ether whereas the observed value is $k_{H^+} = 0.76\,M^{-1}\,s^{-1}$. The inductive effect of the acetyl group in the present reaction may be estimated using this correlation with only an inductive σ constant. Use of $\sigma_I = 0.30$ (20) gives $k_{H^+} = 6.0 \times 10^{-5}\,M^{-1}\,s^{-1}$, which is only 4 times less than the observed value, $k_{H^+} = 2.4 \times 10^{-4}\,M^{-1}\,s^{-1}$. This suggests that the countervailing electron-supplying resonance effect of acetyl is quite weak in the present system, and that is consistent with the strong electron-supplying resonance effect of methoxyl, which again leaves the system with little demand for additional resonance stabilization by other substituents.

Experimental

Materials

2,3-Dimethoxy-1,3-butadiene (Aldrich) was purified by distillation; its proton nmr spectrum was consistent with its structure. 3-Methoxy-3-buten-2-one was prepared by partial hydrolysis of 2,3-dimethoxy-1,3-butadiene: 1 g of the latter substance was dissolved in 25 mL 0.4 *M* $HClO_4$ and the solution was allowed to stand at room temperature for 2 min; the acid was then neutralized with sodium hydroxide, the product was extracted with ether, the ether was evaporated, and the residue was purified by gas chromatography. Its proton nmr spectrum was consistent with its structure and agreed with a literature description (3).

All other materials were best available commercial grades. Solutions were prepared with deionized water purified further by distillation; D_2O (Merck Sharp & Dohme, 99.8%) D) was used as received.

Kinetics

Rate determinations were made spectrophotometrically by monitoring the decrease in absorbance at λ = 230 nm for the first hydrolysis stage and at λ = 250 nm for the second hydrolysis stage. Measurements were made using a Cary 118 spectrometer with cell compartment thermostatted at 25.0 ± 0.02°C or a Durrum–Gibson stopped-flow spectrometer operating at 25.0 ± 0.1°C. Observed first-order rate constants were evaluated by least-squares fitting of the data to an exponential (Cary measurements) or a linear (Durrum–Gibson measurements) function.

Acknowledgements

We are grateful to the Natural Sciences and Engineering Research Council of Canada and the Donors of the Petroleum Research Fund, administered by the American Chemical Society, for financial support of this work.

1. (*a*) P. Salomaa, A. Kankaanpera, and M. Lajunen. Acta. Chem. Scand. **20**, 1790 (1966); A. J. Kresge and Y. Chiang. J. Chem. Soc. B, 53 (1967); 57 (1967); A. J. Kresge, H. L. Chen, Y. Chiang, E. Murrill, M. A. Payne, and D. S. Sagatys. J. Am. Chem. Soc. **93**, 413 (1971); (*b*) A. J. Kresge, D. S. Sagatys, and H. L. Chen. J. Am. Chem. Soc. **99**, 7228 (1977); (*c*) T. Okuyama, T. Fueno, H. Nakatsuji, and J. Furukawa. J. Am. Chem. Soc. **89**, 5826 (1967); M. M. Kreevoy and R. Eliason. J. Phys. Chem. **72**, 1313 (1968).
2. P. G. Gassman and T. T. Tidwell. Acc. Chem. Res. **16**, 279 (1983).
3. L. Brodsky and W. C. Agosta. J. Org. Chem. **39**, 2928 (1974).
4. A. I. Scott. Interpretation of the ultraviolet spectra of natural products. Pergamon, New York. 1964. pp. 55–59.
5. H. S. Harned and N. D. Embree. J. Am. Chem. Soc. **56**, 1042 (1934).
6. H. S. Harned and R. W. Ehlers. J. Am. Chem. Soc. **55**, 652 (1933).
7. R. G. Bates. Determination of pH. Theory and practice. Wiley, New York. 1973. p. 49.
8. R. A. Cox and K. Yates. Can. J. Chem. **59**, 2116 (1981).
9. A. J. Kresge, H. J. Chen, G. L. Capen, and M. F. Powell. Can. J. Chem. **61**, 249 (1983).
10. J. D. Cooper, V. P. Vitullo, and D. L. Whalen. J. Am. Chem. Soc. **93**, 6294 (1971).
11. W. P. Jencks. Chem. Rev. **72**, 705 (1972); Acc. Chem. Res. **9**, 425 (1976); Acc. Chem. Res. **13**, 161 (1980); Chem. Soc. Rev. **10**, 345 (1981); Y. Chiang and A. J. Kresge. J. Am. Chem. Soc. **107**, 6363 (1985).
12. Y. Chiang, W. K. Chwang, A. J. Kresge, M. F. Powell, and S. Szilagyi. J. Org. Chem. **49**, 5218 (1984).
13. W. K. Chwang, P. Knittel, K. M. Koshy, and T. T. Tidwell. J. Am. Chem. Soc. **99**, 3395 (1977).
14. T. T. Tidwell. Angew. Chem. Int. Ed. Engl. **23**, 20 (1984).
15. D. Eisenberg and W. Kauzmann. The structure and properties of water. Oxford University Press, New York. 1969. pp. 206–214.
16. (*a*) A. J. Kresge, Y. Chiang, P. H. Fitzgerald, R. S. McDonald, and G. H. Schmid. J. Am. Chem. Soc. **93**, 4907 (1971); (*b*) V. J. Nowlan and T. T. Tidwell. Acc. Chem. Res. **10**, 252 (1977).
17. W. K. Chwang, V. J. Nowlan, and T. T. Tidwell. J. Am. Chem. Soc. **99**, 7233 (1977).
18. K. Oyama and T. T. Tidwell. J. Am. Chem. Soc. **98**, 947 (1976).
19. X. Creary. J. Am. Chem. Soc. **103**, 2463 (1981); X. Creary and C. C. Geiger. J. Am. Chem. Soc. **104**, 4151 (1982); X. Creary. J. Am. Chem. Soc. **106**, 5568 (1984).
20. M. Charton. Prog. Phys. Org. Chem. **13**, 119 (1981).
21. R. A. Burt, Y. Chiang, A. J. Kresge, and S. Szilagyi. Can. J. Chem. **62**, 74 (1984).

Can. J. Chem. Downloaded from www.nrcresearchpress.com by 213.166.140.6 on 09/07/12
For personal use only.

Phase transitions and molecular motions in adamantane derivatives: 1-adamantanol

PIERRE D. HARVEY, DENIS F. R. GILSON,[1] AND IAN S. BUTLER[1]

Department of Chemistry, McGill University, 801 Sherbrooke St. W., Montreal, P.Q., Canada H3A 2K6

Received December 11, 1986

This paper is dedicated to Professor John T. Edward

PIERRE D. HARVEY, DENIS F. R. GILSON, and IAN S. BUTLER. Can. J. Chem. **65**, 1757 (1987).

An order–disorder transition occurs in 1-adamantanol at 359 K on heating and at 342 K on cooling, with transition entropies of 36 and 34 $J\,K^{-1}\,mol^{-1}$, respectively. FT-ir spectra show that free hydroxyl groups exist in the high temperature phase, but the majority of the O—H groups remain hydrogen bonded. The barrier to adamantyl group rotation in the low-temperature phase, determined from proton spin–lattice relaxation time measurements, is 20.9 $kJ\,mol^{-1}$, and the barrier to rotation in the high-temperature phase is 35.0 $kJ\,mol^{-1}$.

PIERRE D. HARVEY, DENIS F. R. GILSON et IAN S. BUTLER. Can. J. Chem. **65**, 1757 (1987).

Avec l'adamantanol-1, il se produit une transition ordre/désordre à 359 K lorsqu'on chauffe et à 342 K lorsqu'on refroidit: les entropies de transition sont respectivement 36 et 34 $J\,K^{-1}\,mol^{-1}$. Les spectres ir/TF démontrent que des groupements hydroxyles libres existent dans la phase à haute température; toutefois, des liaisons hydrogènes relient encore la majorité des groupements O—H. Dans la phase à basse température, la barrière à la rotation du groupement adamantyle, telle que déterminée à partir des temps de relaxation spin/réseau des protons, est égale à 20,9 $kJ\,mol^{-1}$; dans la phase à haute température, la barrière à la rotation est égale à 35,0 $kJ\,mol^{-1}$.

[Traduit par la revue]

Introduction

The cage hydrocarbon adamantane, $C_{10}H_{16}$, affords the best known example of an organic molecular crystal which undergoes an order–disorder phase transition. Simple substitution on the adamantyl skeleton does not prevent the transition from occurring, but can lead to a wide variation in the temperature and entropy of the transition. In many cases, the phase transitions occur below room temperature, and, therefore, the crystal structures of the ordered phases are seldom known. One particular exception is 1-adamantanol, in which the transition is reported to occur at 353 K with an entropy change of 40.6 $J\,K^{-1}\,mol^{-1}$ (1, 2). These values are very much higher than those of adamantane itself (3), 208 K and 16.2 $J\,K^{-1}\,mol^{-1}$, presumably due to the presence of the hydrogen-bonded substituent. The crystal structure of the room-temperature phase is tetragonal, space group $P4_2/n$, with eight molecules per unit

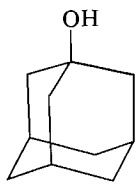

cell. Four adamantane molecules form a tetramer with the hydroxyl protons hydrogen bonded along the sides of a square, but the hydrogen atoms occupy one of two possible orientations, and the structure is, to this extent, disordered. The large entropy change is strong evidence of an order–disorder transition probably to a face-centered cubic structure in which the molecules undergo extensive molecular motion. The latter is confirmed by the observation of relatively narrow lines in the ^{13}C nmr spectrum of the high-temperature phase, narrow enough to observe the chemical shifts of different carbon atoms (4).

Phase transitions have also been observed in two other hydrogen-bonded adamantane derivatives. In the adamantyl carboxylic acid, the transition occurs at 251 K, with an entropy change of 8.97 $J\,K^{-1}\,mol^{-1}$ (5). In adamantanamine hydrochloride, the transition is at the remarkably low temperature of 124 K, with an entropy change of only 2.52 $J\,K^{-1}\,mol^{-1}$ (6). Studies of the Raman and ir spectra of these compounds showed that the vibrational peaks remain quite sharp and exhibit factor group splittings in the high-temperature phases and, therefore, do not involve a disordered high-temperature phase. This has been confirmed by a study of the crystal structure of adamantanamine hydrochloride (7). In both these compounds, the hydrogen bonding is sufficiently strong that the substituent group is held rigidly in the lattice, but the hydrocarbon portion of the molecule is capable of reorientation. The barriers to rotation have been determined from the proton spin–lattice relaxation times (5, 6). The aim of the present study was to examine the barrier to rotation and the temperature dependence of the vibrational spectrum of 1-adamantanol for comparison with the previously reported behaviour of the carboxylic acid and amine hydrochloride compounds.

Experimental

1-Adamantanol (Aldrich Chemical Co.) was purified by slow sublimation (60°C, 10^{-3} mm Hg). Differential scanning calorimetry studies were performed on a Perkin-Elmer DSC 2. For the ir spectroscopic studies, the sample was sealed between NaCl plates and the temperature controlled by a flow of heated nitrogen gas and measured with a digital thermometer. The spectra were recorded on a Nicolet model 6000 Ft-ir spectrometer. Proton spin–lattice relaxation times were measured (at 33 MHz) as described previously (5, 6).

Results and discussion

The differential scanning calorimetry results showed a transition, on heating, at 359 K with enthalpy and entropy of transition of 13 $kJ\,mol^{-1}$ and 36 $J\,K^{-1}\,mol^{-1}$, respectively. On cooling, the transition showed hysteresis, shifting to 342 K, with enthalpy and entropy changes of 12 $kJ\,mol^{-1}$ and 34 $J\,K^{-1}\,mol^{-1}$. No changes were observed upon cycling through the transition several times or by varying the scanning rate below 5° min^{-1}. The transition temperatures are in reasonable agreement with those reported by Amoureux *et al.* (1), except that the hysteresis was not, apparently, observed in that study, and the enthalpy and entropy changes are somewhat smaller. The transition properties of various substituted adamantyl derivatives are

[1]Authors to whom correspondence should be addressed.

Can. J. Chem. Downloaded from www.nrcresearchpress.com by 118.98.75.50 on 09/07/12
For personal use only.

TABLE 1. Transition temperatures, enthalpies, and entropies for selected 1-adamantyl derivatives

Derivative	T_{Tr} (K)	Enthalpy (kJ mol^{-1})	Entropy (J K mol^{-1})	Reference
—OH heating	359	13	36	This work
cooling	342	12	34	This work
	353	14.4	40.6	1
—CO_2H	251	2.25	9.0	5
—NH_3Cl	124	0.31	2.5	6

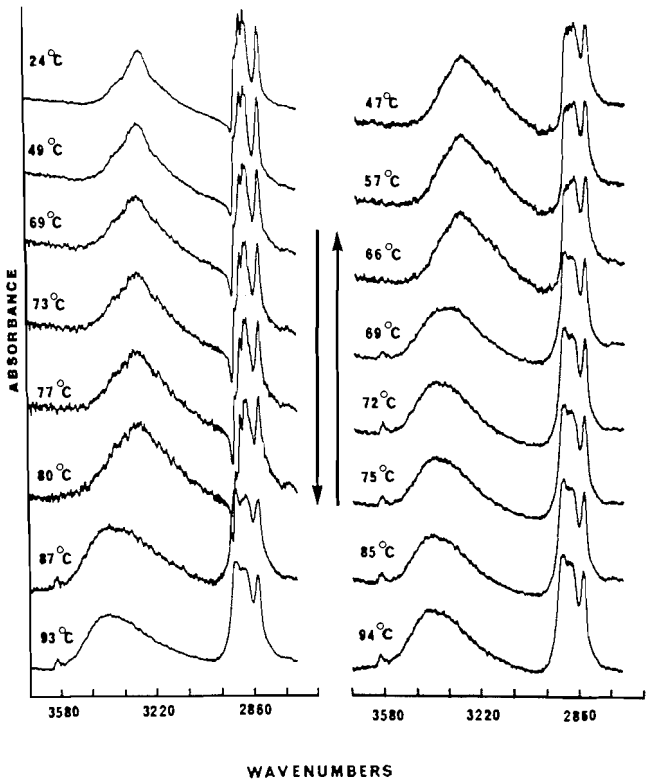

FIG. 1. The temperature dependence of the FT-ir spectra of 1-adamantanol in the 3700–2620 cm^{-1} region: 25 scans, 2 cm^{-1} resolution.

compared in Table 1. The transition temperature in 1-adamantanol is much higher than other adamantane derivatives. This is, at first sight, not surprising, since it can be attributed to the influence of the hydrogen bonding, but the entropy of transition in 1-adamantanol is also much larger than that of adamantane (3), or any other 1-substituted derivative, and resembles that of 2-adamantanone, which has a complicated phase behaviour (8) and also exhibits a large hysteresis. The crystal structure data indicate that the positions of the hydroxyl protons are already disordered and therefore the transition entropy is lowered by at least $R \ln 2$. Even allowing for an excess entropy of the type proposed by Clark *et al.* (9), an entropy change of (35 − approx. 10.5) J K^{-1} mol^{-1} is equivalent to a ratio of about 18:1 for the ratio of distinguishable positions in the ordered and disordered phases.

At room temperature, the vibrational spectra show sharp peaks with clear splittings due to the factor group effects. The frequencies and assignments are listed in Table 1. As the temperature is increased, the O—H stretching frequency shifts to higher energy, and, at the transition temperature, there is broadening and loss of splittings in the C—H vibrations and a

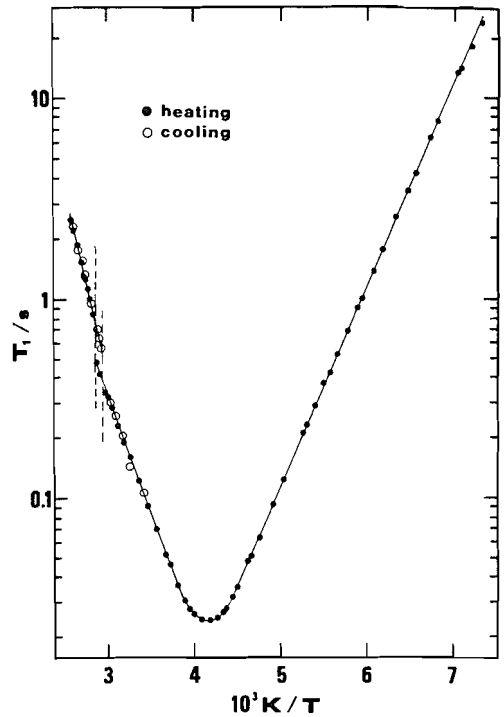

FIG. 2. Proton spin–lattice relaxation time versus reciprocal temperature. Heating (●), cooling (○).

weak absorption appears at 3593 cm^{-1} (Fig. 1). On cooling, this behaviour is reversed except that the temperature of the spectral changes exhibit a hysteresis similar to that observed in the dsc studies.

The sharp peaks observed in the vibrational spectra are consistent with the presence of an ordered phase at room temperature. Although it was not possible to confirm the eight molecules per unit cell given in the crystal structure report (1), the spectral splittings do indicate that there are several molecules per unit cell. Since one of the interests in the present study centered on the influence of hydrogen bonding on the properties of the solid phase, the FT-ir spectrum of the O—H stretching region was studied as a function of temperature. At room temperature, a broad absorption is observed at 3280 cm^{-1}, with shoulders located at 3360 and 3200 cm^{-1}. These correspond to the combination and hot band of the O—H and O···H vibrations. The latter can be evaluated to be about 80 cm^{-1} and may be observed in the Raman spectrum as a weak band at 77 cm^{-1}. The O—H frequency shifts to higher energy with increasing temperature, perhaps as a result of an increase in intensity of the hot band. Broad absorptions of medium intensity appear in the ir spectrum at 1453 and 1418 cm^{-1} and are assigned to O—H···O bending modes. In the vapour phase, the free molecule O—H stretching vibration occurs at 3637 cm^{-1} (10), shifting to 3606 cm^{-1} in dilute solution in carbon tetrachloride and 3595 cm^{-1} in carbon disulphide (11). From the appearance of the absorption at 3593 cm^{-1}, it is evident that free O—H groups are present in the disordered phase, but it is equally apparent that extensive hydrogen bonding persists.

The behaviour of the proton spin–lattice relaxation time with change of temperature is shown in Fig. 2. The T_1 measurements clearly show the phase transition and the hysteresis.

The spin–lattice relaxation time, assuming that dipolar relaxation is the dominant mechanism, is given by eq. [1]:

$$[1] \quad 1/T_1 = (2/3)C\tau\{1/(1 + \omega^2\tau^2) + 4/(1 + 4\omega^2\tau^2)\}$$

Can. J. Chem. Downloaded from www.nrcresearchpress.com by 118.98.75.50 on 09/07/12
For personal use only.

TABLE 2. Vibrational data (cm^{-1}) for 1-adamantanol

Raman	FT-ir	Assignments	Raman	FT-ir	Assignments
	3360 s sh	bonded OH stretch	1121 w	1118 s	CH bend
	3280 s		1113 w sh	1114 s	
	3200 s sh		1110 w	1112 s	
2954 m			1101 m	1102 m	CC stretch + CH_2 twist
2936 vs sh	2934 s		1087 m s	1088 s	
2930 vs				1078 w	
2924 vs sh	2924 vs sh			1034 w	
2919 vs sh	2916 vs	CH stretch		984 m	CCC bend
2901 s	2900 vs		982 s	982 m	
2892 s	2893 s			977 m	
2860 m sh	2858 s sh		936 w	936 m sh	CH_2 rock + CC stretch + CCC bend
2850 m	2850 s		933 w	933 m s	
2844 m sh	2834 s sh			926 m sh	CC stretch
				915 w	
	1474 w	CH_2 bend		880 v w	CH_2 rock
	1453 m br	bonded OH bend		814 w	CC stretch
1442 m w	1445 w	CH_2 bend		811 w	
	1440 w		777 v s	777 w	CC stretch
1432 m	1430 w		724 v s	722 w	
	1418 m br	bonded OH bend	656 v w	668 w	CCC bend
	1384 w	CH bend	642 w		
	1369 w		555 w	553 m w sh	CCC bend
1359 v w	1364 w sh			551 m w	
	1353 m s	CH bend + CH_2 waq.	466 m	465 w sh	CCC bend
	1344 m w			463 w	
	1335 m w		429 w	428 w	CCC bend
1318 n w	1316 m w			410 v w	
1304 w w	1303 m	CC stretch + CH_2 waq.	398 w	399 w	CCO bend
	1300 m			315 v w	
	1288 w sh	CH_2 twist + CH bend	296 w	295 w	
1281 v w	1281 w			272 w	
1264 m	1263 w		246 w		
1229 m br	1227 m br	C—O stretch	129 w br	117 w br?	OH torsion
1186 m	1183 w	CH_2 twist	77 v w		O···H stretch
1174 m	1175 w		64 v w		
	1171 w				

TABLE 3. Activation energies for rotation in 1-adamantyl derivatives

Low-temperature phase		High-temperature phase	
	E_a (kJ mol^{-1})	E_a (kJ mol^{-1})	Reference
—OH	20.7	35.0	This work
$—CO_2H$	32.0	19.3	5
$—NH_3Cl$[a]	—	33.6	6
—H	25.5	13.0	16

[a]Value of E_a not measured in the low-temperature phase.

where T is the resonance frequency, C is a constant dependent on the change in the second moment produced by the motion, and $\tau = \tau_0 \exp(E/RT)$ is a correlation time for the molecular motion. The low-temperature phase showed a V-shaped curve, typical of relaxation by dipolar mechanism, with a minimum in the spin–lattice relaxation time at value of $\omega\tau \simeq 0.62$. Rotation of the adamantyl group about the molecular 3-fold axis is assumed to be responsible for relaxation in the low-temperature phase of 1-adamantanol because the contribution to the total relaxation rate arising from rotation of the single hydroxyl proton is small compared with the fifteen protons of the cage and the value of the minimum in T_1 is similar (28 ms, $C = 7.9 \times 10^9$ rad^2 s^{-2}) to those observed for other compounds in which rotation about the 3-fold axis is believed to occur (6, 12–14). The internal barrier to rotation of the hydroxyl group has been determined by Craven (15) from far-ir studies to be 4.8 kJ mol^{-1}, and the energy required to break the hydrogen bond can be estimated from the O—H stretching frequency to be about 26 kJ mol^{-1}. Thus, the barrier to hydroxyl group rotation probably exceeds 30 kJ mol^{-1}.

In fitting eq. [1] to the experimental data, it was apparent that the slopes of the reciprocal temperature plots on either side of the minimum were not the same and thus gave slightly different values for the activation energy, 19.7 and 21.5 kJ mol^{-1}. However, as the crystal structure does not indicate any asymmetric units in the unit cell, the difference in activation energies does not arise from non-equivalent molecules. Therefore, we do not attribute any great significance to the difference except that it might arise from a distribution in correlation times as the hydrogen bonding arrangements dictate slight changes in local molecular positions.

In the high-temperature phase, the correlation times are too short to give a minimum in T_1, $\omega\tau \ll 1$, and the relaxation

Can. J. Chem. Downloaded from www.nrcresearchpress.com by 118.98.75.50 on 09/07/12
For personal use only.

time is inversely proportional to the correlation time. The activation energy for this phase was 35.0 kJ mol^{-1}. A comparison of barrier heights for various adamantane derivatives is given in Table 3. Note that the barrier in 1-adamantanol is quite low in the ordered phase, but highest in the disordered phase. Since no structural information exists for the disordered phase, we can only assume that the high entropy of transition indicates extensive disorder, but the evidence from the ir spectroscopic studies indicates that hydrogen bonding persists in the high-temperature phase. The residence times of certain molecular orientations are long compared with the vibrational time scale, while they may be short for the nmr scale. We assume that the measured barrier is that for isotropic rotation and, possibly, translational diffusion of 1-adamantanol molecules.

Acknowledgements

This work was supported by grants from the Natural Sciences and Engineering Research Council of Canada and the Government of Quebec. P.D.H. acknowledges the award of scholarships from NSERC and the McConnell Foundation (McGill University).

1. J. P. Amoureux, M. Bee, C. Gors, V. Martin, and F. Beart. Cryst. Struct. Commun. **8**, 449 (1979).
2. P. Cuvelier. Comp. Rend. Acad. Sci. Paris, **296**, 519 (1983).
3. S. S. Chang and E. F. Westrum. J. Phys. Chem. **64**, 1547 (1980).
4. R. E. Wasylishen and B. A. Pettitt. Can. J. Chem. **58**, 655 (1980).
5. P. D. Harvey, D. F. R. Gilson, and I. S. Butler. J. Phys. Chem. **90**, 136 (1986).
6. P. D. Harvey, D. F. R. Gilson, and I. S. Butler. J. Phys. Chem. **91**, 1267 (1987).
7. F. Gariepy-Belanger, F. Brisse, P. D. Harvey, I. S. Butler, and D. F. R. Gilson. Acta Crystallogr. In press.
8. I. S. Butler, H. B. R. Cole, D. F. R. Gilson, P. D. Harvey, and J. D. McFarlane. J. Chem. Soc. Faraday Trans. 2, **82**, 535 (1986).
9. T. Clark, T. Mc. O. Knox, H. Mackle, and M. A. McKervey. J. Chem. Soc. Faraday Trans. 1, **73**, 1224 (1977).
10. F. G. Dijkman. Mol. Phys. **36**, 705 (1978).
11. T. Visser and J. H. Van der Maas. Spectrochim. Acta, **38**A, 293 (1982).
12. M. Bee and J. P. Amoureux. Mol. Phys. **50**, 63 (1963).
13. I. Ursu, R. Grosescu, M. Lupu, and M. Lazarescu. Rev. Roum. Phys. **28**, 789 (1983).
14. J. Virlet, L. Quiroga, B. Boucher, J. P. Amoureux, and M. Castelain. Mol. Phys. **48**, 1289 (1983).
15. S. M. Craven. Spectrochim. Acta, **29**A, 679 (1973).
16. H. Resing. Mol. Cryst. Liq. Cryst. **9**, 101 (1969).

Can. J. Chem. Downloaded from www.nrcresearchpress.com by 118.98.75.50 on 09/07/12
For personal use only.

The conformational preference of methoxyl and acetoxyl groups in 3-oxycyclohexenes, 2-oxymethylenecyclohexanes, and 1-oxytetralins and the generalized anomeric effect[1]

ADAMA OUÉDRAOGO, MINH TAN PHAN VIET,[2] JOHN K. SAUNDERS,[3] AND JEAN LESSARD[4]

Département de chimie, Université de Sherbrooke, Sherbrooke (Qué.), Canada J1K 2R1

Received December 22, 1986

This paper is dedicated to Professor John T. Edward

ADAMA OUÉDRAOGO, MINH TAN PHAN VIET, JOHN K. SAUNDERS, and JEAN LESSARD. Can. J. Chem. **65**, 1761 (1987).

The ^{13}C and ^{1}H nuclear magnetic resonance data of 3-oxycyclohexenes, 2-oxymethylenecyclohexanes, and 1-oxytetralins show (*i*) that the pseudoaxial preference is larger for the acetoxyl group than for the methoxyl group in 3-oxycyclohexenes, (*ii*) that the methoxyl and the acetoxyl groups have the same pseudoaxial preference in 1-oxytetralins, and (*iii*) that in 2-oxymethylenecyclohexanes, the acetoxyl group prefers the equatorial orientation whereas the methoxyl group prefers to be axial. These results are interpreted in terms of the orbital picture ($\pi-\sigma^*$ stabilization of the axial conformer) of the generalized anomeric effect to which is opposed a conformational effect termed the "unsaturation effect" in 2-acetoxymethylenecyclohexane and probably also, but to a much smaller extent, in 1-acetoxytetralin. The results also show that *cis* and *trans tert*-butyl analogues of 3-oxycyclohexenes do not represent the true limit conformers whereas *cis* and *trans* 4-*tert*-butyl derivatives of 2-oxymethylenecyclohexanes do not differ drastically from the limit conformers.

ADAMA OUÉDRAOGO, MINH TAN PHAN VIET, JOHN K. SAUNDERS et JEAN LESSARD. Can. J. Chem. **65**, 1761 (1987).

Les données de la résonance magnétique nucléaire du ^{13}C et du ^{1}H montrent (*i*) que la préférence pseudo-axiale d'un groupe acétoxyle est supérieure à celle d'un groupe méthoxyle dans les oxy-3 cyclohexenes, (*ii*) que les groupements méthoxyle et acétoxyle des oxy-1 tétralines ont la même préférence pseudo-axiale et (*iii*) que, dans les oxy-2 méthylènecyclohexanes, le groupement acétoxyle préfère l'orientation équatoriale tandis que le groupement méthoxyle préfère l'orientation axiale. Ces résultats sont interprétés en termes des interactions orbitalaires (stabilisation $\pi-\sigma^*$ du conformère axial) de l'effet anomère généralisé auquel s'oppose un autre effet appelé « effet d'insaturation » dans l'acétoxy-2 méthylènecyclohexane; cet effet serait présent aussi dans l'acétoxy-1 tétraline mais serait beaucoup moins fort. Les résultats montrent encore que les dérivés *tert*-butyles *cis* et *trans* ne représentent pas les vrais conformères des oxy-3 cyclohexènes alors que les dérivés *tert*-butyles en position 4 des oxy-2 méthylènecyclohexanes ne diffèrent pas trop des vrais conformères.

Can. J. Chem. Downloaded from www.nrcresearchpress.com by 118.98.75.50 on 09/07/12
For personal use only.

Introduction

We reported earlier (1) that the methoxyl group of 3-methoxycyclohexene (**1***a*, X = H) and 2-methoxymethylenecyclohexane (**2***a*, X = H) exists preferentially in the pseudoaxial or axial orientation. This preference is increased upon introducing an electron-donating group (X = phenyl, methoxyl) on the double bond and decreased upon introducing an electron-withdrawing group (X = cyano) (1–3). Glycenoses and alkenes having the general formula $RCH(OCH_3)CH{=}CHX$ (**3**) show an analogous conformational behaviour (4). These observations have been explained by a stereoelectronic effect, namely the $\pi-\sigma^*_{C-O}$ stabilization of the axial (or its equivalent) orientation of the methoxyl group (1–5). In 4-methoxyspiro[5.2]octane (**4***a*), a similar electronic interaction involving orbitals of the cyclopropane ring and the σ^*_{C-O} orbital has been suggested to account for the axial preference of the methoxyl group (6). The axial preference (or its equivalent) of the alkoxyl group in compounds **1***a*–**4***a* is analogous to the preference for the axial conformation in 2-methoxytetrahydropyran (**5***a*) (7–9)—the anomeric effect (10)—and to the general preference for the *gauche* conformation about a carbon–heteroatom bond in R—X—C—Y systems—the generalized anomeric effect (11, 12)—and constitutes a *further generalization* of the anomeric effect (1, 13). The anomeric effect has been explained both in terms of an $n-\sigma^*_{C-O}$ interaction stabilizing the axial (*gauche*) orientation (14–18) and in terms of electrostatic interactions destabilizing the equatorial (*anti*) orientation (19–21). The two types of interactions are most probably involved in the anomeric effect (22, 23). In compounds **1***a*–**4***a*, however, electrostatic interactions (e.g. dipole–quadrupole interactions) are probably less important than in 2-methoxytetrahydropyran (**5***a*) and in systems R—X—C—Y in general (1), and probably also less important than the orbital ($\pi-\sigma^*_{C-O}$) interaction (1).

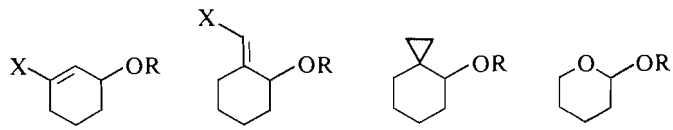

1 **2** **4** **5**

a, R = CH_3; *b*, R = $COCH_3$

The preference for the pseudoaxial or axial orientation is larger for the acetoxyl group (R = $COCH_3$) than for the methoxyl group (R = CH_3) in 4-oxyspirooctanes (**4**) (6) and in 2-oxytetrahydropyrans (**5**) (9, 24), as expected from the orbital interaction picture of the generalized anomeric effect: larger $\pi-\sigma^*_{C-O}$ or $n-\sigma^*_{C-O}$ stabilization (overlap) of the axial conformer in the case of the acetoxyl group, which is more electron withdrawing and thus a better electron acceptor (σ^*_{C-O} lower in energy) than the methoxyl group (1, 6, ref. 13, p. 71).

To evaluate further how general is the generalized anomeric effect and to obtain more quantitative data on the conformational preference of 3-oxycyclohexenes **1**, we studied the 3-oxycyclohexenes **1** (X = H), **6**, and **7**, the 2-oxymethylenecyclohexanes **2** (X = H), and the 1-oxytetralins **8** by ^{1}H and ^{13}C nmr spectroscopy. The results (*i*) confirm the pseudoaxial preference of the oxygenated substituent in 3-oxycyclohexenes (**1**, X = H) and establish the larger pseudoaxial preference of

[1]Abstracted in part from the Ph.D. thesis of A. Ouédraogo, Université de Sherbrooke, Sherbrooke (Québec), 1984.

[2]Present address: Département de chimie, Faculté des Arts et des Sciences, Université de Montréal, Montréal (Qué.), Canada H3C 3V1.

[3]Present address: Division of Biological Sciences, National Research Council, 100 Sussex Drive, Ottawa, Ont., Canada K1A 0R6.

[4]Author to whom correspondence may be addressed.

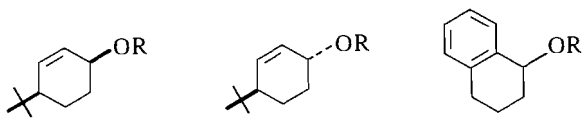

6 (*cis*) **7** (*trans*) **8**

a, R = CH_3; *b*, R = $COCH_3$

the acetoxyl group as compared to the methoxyl group. (*ii*) They emphasize further the fact that "model conformers" of cyclic compounds locked by a large *tert*-butyl group do not always represent the true limit conformers (26). (*iii*) They show that the *generalized anomeric effect is overrun by some other effect in 2-acetoxymethylenecyclohexane* (**2***b*, X = H), which prefers the equatorial conformation, but not in 2-acetoxytetralin (**8***b*), which exists preferentially as the axial conformer. (*iv*) In 1-oxytetralins **8**, however, the pseudoaxial preference of the acetoxyl group is similar to that of the methoxyl group.

Results and discussion

3-Oxycyclohexenes ***1*** *(X = H)*

The evidence for the pseudoaxial preference of the oxygenated substituent in 3-oxycyclohexenes **1***a* and **1***b* (X = H) comes from the chemical shift of C-5 (Table 1) and from the linewidth at half-height ($\Delta\nu_{1/2}$) of H-3 (Table 2) and has already been discussed (1). We want to emphasize here the larger pseudoaxial preference of the acetoxyl group (**1***b*, X = H) as compared to the methoxyl group (**1***a*, X = H). Indeed, C-5 is more shielded (Table 1) and $\Delta\nu_{1/2}$ is smaller (Table 2) for **1***b* than for **1***a*. Furthermore, the coupling constant $J_{H\text{-}2,H\text{-}3}$ is larger for **1***b* than for **1***a* (Table 2), showing that the dihedral angle between H-2 and H-3, $\Phi_{H\text{-}2,H\text{-}3}$, is smaller for **1***b*. From the Dreiding model of a 3-substituted cyclohexene, $\Phi_{H\text{-}2,H\text{-}3}$ is smaller in the pseudoaxial conformer (H-3 pseudoequatorial: $\Phi_{H\text{-}2,H\text{-}3} \simeq 40\text{–}45°$) than in the pseudoequatorial conformer (H-3 pseudoaxial: $\Phi_{H\text{-}2,H\text{-}3} \simeq 75\text{–}80°$).

Additional evidence for the greater pseudoaxial preference of the acetoxyl group is provided by the low-temperature dynamic ^1H nmr measurements on solutions of **1***a* and **1***b* (X = H) in a one-to-one (v/v) mixture of $CHFCl_2$ and CHF_2Cl down to 110 K.[5] The ^1H nmr spectrum of 3-methoxycyclohexene (**1***a*, X = H) at 100 MHz does show a coalescence of the H-3 proton between 125 and 120 K. At 110 K there are two broad and not fully resolved signals with the higher field one, corresponding to the pseudoequatorial conformer, being much smaller. The signals were too broad and the resolution too poor to allow a complete analysis of the spectrum. The approximate difference in chemical shifts ($\Delta\delta \simeq 3$ ppm) shows that the barrier to inversion should be lower than 27 kJ/mol and thus similar to the published values for other cyclohexene derivatives (27, 28). In the case of 3-acetoxycyclohexene (**2***b*, X = H), no coalescence could be detected down to 100 K presumably because there was essentially one conformer present, the pseudoaxial conformer. Again the signals were very broad at the lowest temperatures. Thus the pseudoaxial preference in 3-oxycyclohexenes **1** (X = H) is larger for the acetoxyl group than for the methoxyl group as in 4-oxyspirooctanes (**4**) (6) and in 2-oxytetrahydropyrans (**5**) (9, 24), and as predicted by the orbital picture of the generalized anomeric effect: a better $\pi\text{–}\sigma^*_{C\text{–}O}$ stabilization of the pseudoaxial orientation in the case of the more electron-withdrawing ($\sigma^*_{C\text{–}O}$ lower in energy) acetoxyl group.

[5]We are grateful to Professor C. H. Bushweller of the University of Vermont for carrying out the low-temperature ^1H nmr measurements.

TABLE 1. Selected ^{13}C chemical shift data for 3-oxycyclohexenes **1** (X = H), **6**, and **7**[a]

No.	OR	Solvent[b]	δ (ppm)[c] C-3 (C-α)	δ (ppm)[c] C-5 (C-γ)
1*a* (X = H)	OCH_3	$CDCl_3$	74.3	19.2
		CCl_4	73.6	19.1
		$CHFCl_2$	74.3	19.5
		CF_2Br_2	74.7	19.5
6*a*	OCH_3	$CDCl_3$	72.2	19.0
7*a*	OCH_3	$CDCl_3$	76.2	22.7
		$CHFCl_2$[d]	76.7	23.0
1*b* (X = H)	$OCOCH_3$	$CDCl_3$	68.2[e]	19.0
		CCl_4	67.6	18.8
		$CHFCl_2$	68.5	19.1
		CF_2Br_2	67.9	19.0
6*b*	$OCOCH_3$	$CDCl_3$	66.5	19.2
7*b*	$OCOCH_3$	$CDCl_3$	70.5	22.6
		$CHFCl_2$[d]	71.1	22.9

[a]At 62.89 MHz in $CDCl_3$ and at 100.62 Mz in $CHFCl_2$ and CF_2Br_2.
[b]$CDCl_3$ and CCl_4: 0.3 *M* solutions; *T* = 299 K. $CHFCl_2$ and CF_2Br_2: solutions 0.4 *M* in $CHFCl_2$ (CF_2Br_2)–CD_2Cl_2 80:20; *T* = 234 K.
[c]Relative to TMS; ±0.05 ppm.
[d]*T* = 243 K.
[e]Senda and Imaizumi (29) reported à $\delta_{C\text{-}3}$ value of 69.08 ppm (3 *M* solution).

TABLE 2. Linewidth at half-height of H-3 and $J_{H\text{-}2,H\text{-}3}$ in 3-oxycyclohexenes **1** (X = H), **6**, and **7**[a]

No.	OR	Solvent[b]	$\Delta\nu_{1/2}$ H-3[c] (Hz)	$J_{H\text{-}2,H\text{-}3}$[d] (Hz)
1*a* (X = H)	OCH_3	CCl_4	11.0[e]	2.6
		$CDCl_3$	11.7	2.9
6*a*	OCH_3	CCl_4	8.0	~4
		$CDCl_3$	9.0	4.1
7*a*	OCH_3	CCl_4	16.1	—
		$CDCl_3$	16.7	1.4
1*b* (X = H)	$OCOCH_3$	CCl_4	8.8	3.6
		$CDCl_3$	11.2[e]	3.6
6*b*	$OCOCH_3$	CCl_4	8.0	4.7
		$CDCl_3$	10.0	4.7
7*b*	$OCOCH_3$	CCl_4	15.5	2.7
		$CDCl_3$	17.5	2.7

[a]The 250-MHz spectra were taken at 299 K and at a concentration of 0.3% (w/v).
[b]CCl_4 = CCl_4–CD_3COCD_3 90:10.
[c]Linewidth at half-height, ±0.2 Hz.
[d]By homodecoupling, ±0.1 Hz.
[e]The value is larger than that reported in ref. 1.

As shown in Tables 1 and 2, we have studied the ^{13}C and ^1H nmr spectra of *cis* and *trans* 6-*tert*-butyl-3-oxycyclohexenes **6** and **7**. These compounds are expected to be conformationally rigid with the oxygen substituent pseudoaxial in the *cis* isomer **6** and pseudoequatorial in the *trans* isomer **7**. And indeed, C-5 is more shielded (Table 1), $\Delta\nu_{1/2}$ of H-3 is smaller, and $J_{H\text{-}2,H\text{-}3}$ is larger (Table 2) for *cis* **6** than for *trans* **7**. In Table 3 are listed pseudoaxial populations for the unsubstituted 3-oxycyclohexenes **1***a* and **1***b* (X = H) calculated from the nmr parameters of Tables 1 and 2. The ^{13}C chemical shifts of **6** and

Can. J. Chem. Downloaded from www.nrcresearchpress.com by 118.98.75.50 on 09/07/12
For personal use only.

TABLE 3. Pseudoaxial populations for 3-oxycyclohexenes **1***a* and **1***b* (X = H) calculated from the nmr data of Tables 1 and 2

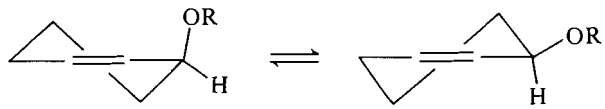

No.	Models used No.	OR	Solvent	% Pseudoaxial[a] From C-3 (C-α)[b]	From C-5 (C-γ)[b]	From $J_{H-2,H-3}$	From $\Delta\nu_{1/2}$
1*a* (X = H)	**6***a*, **7***a*	OCH_3	$CDCl_3$	65	41	56	65
			CCl_4				63
	(ref. 1)[c]		CCl_4				70
1*b* (X = H)	**6***b*, **7***b*	$OCOCH_3$	$CDCl_3$	75	47	45	84
			CCl_4			45	82
	9, **10**[d]		$CDCl_3$	88[e]			
	(ref. 1)[c]		CCl_4				77

[a]Calculated from $K_e = (\delta_{trans}-\delta)/(\delta-\delta_{cis})$ or $(J-J_{trans})/(J_{cis}-J)$, etc.

[b]The C-3 and C-5 chemical shifts of **6***a–c* and **7***a–c* were corrected for the effect of the *tert*-butyl group using the chemical shift differences between 3-*tert*-butylcyclohexene and cyclohexene: +0.7 ppm for C-3; −2.0 ppm for C-5.

[c]In ref. 1, $\Delta\nu_{1/2}$ for the pseudoequatorial conformer was estimated to be 17.0 Hz (close to the observed value for 5,5-dimethyl-3-oxycyclohexenes: 16.0 to 16.5 Hz) and 6.5 Hz for the pseudoaxial conformer. The $\Delta\nu_{1/2}$ values reported for **2***a* and **2***b* are 9.6 and 8.9 Hz respectively in CCl_4 (1).

[d]The C-3 chemical shifts of **9** and **10** were taken from ref. 29. The authors used the chemical shift difference between *tert*-butylcyclohexane and cyclohexane (+0.1 ppm on C-3) as a correction for the effect of the *tert*-butyl group.

[e]Senda and Imaizumi (29) reported 68% based on a chemical shift of 69.08 ppm for C-3 of **1***b*. We found 68.2 ppm (see Table 2).

7 were corrected for the effect of the *tert*-butyl group by using the chemical shift differences between 3-*tert*-butylcyclohexene and cyclohexene (see Table 3, footnote *b*). The calculated pseudoaxial populations based on the C-3 chemical shifts of *cis* and *trans* 5-*tert*-butyl-3-acetoxycyclohexenes **9** and **10**

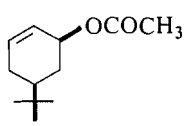

9 (*cis*)

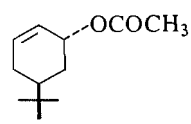

10 (*trans*)

reported by Senda and Imaizumi (29)[6] and those based on the $\Delta\nu_{1/2}$ values reported in ref. 1 are also included in Table 3. It is clear from the scattered values of Table 3 that the influence of the *tert*-butyl group varies according to its position on the ring and depending on the nmr parameter used. The large *tert*-butyl substituent must have an effect on the ring geometry. This effect cannot be evaluated accurately and the use of a *tert*-butyl group to lock the conformation of a cyclohexene ring is inaccurate, if not invalid, as already stressed (26).

According to δ_{C-5} (Table 1) and $J_{H-2,H-3}$ (Table 2) for **1***a* and **1***b* (X = H), the polarity of the solvents seems to have little effect on the pseudoaxial preference of the methoxyl and the acetoxyl groups of 3-oxycyclohexenes. The methoxyl group appears to be more pseudoaxial in $CDCl_3$ (C-5 more shielded, $J_{H-2,H-3}$ larger) than in CCl_4. This could be accounted for by a stronger solvation of the methoxyl group in $CDCl_3$ since solvation should lower the energy of the σ^*_{C-O} orbital and lead to an increase of the stabilizing $\pi-\sigma^*_{C-O}$ interaction.

[6]Senda and Imaizumi (29) reported 69.08 ppm for the C-3 chemical shift of **1***b* (X = H) and calculated a pseudoaxial population of 68% from this chemical shift value and those of C-3 of **9** and **10**. We found 68.2 ppm for the C-3 chemical shift of **1***b* (Table 1) and the calculated pseudoaxial population becomes 88%.

2-Oxymethylenecyclohexanes **2** *(X = H)*[7]

The nmr data of Table 4 and the conformational equilibria obtained from them show clearly the axial preference of the methoxyl group in 2-methoxymethylenecyclohexane (**2***a*, X = H). The value of ΔG_{e-a} in CF_2Br_2, 1.4 kJ/mol, is close to the value reported previously, 1.7 kJ/mol, from which the generalized anomeric effect has been estimated at 3 kJ/mol (1). Using the ΣJ_{H-2} value of 7.6 Hz for **2***a* (X = H) in CCl_4 at 310 K (Table 5) and the ΣJ_{H-2} values for *cis* (**11**) and *trans* (**12**) 4-*tert*-butyl-3-methoxymethylenecyclohexanes of 15 and 5.5 Hz respectively, the axial preference of the methoxyl group in **2***a* (X = H) was estimated to be 78% (ΔG^0_{e-a} = 3.2 kJ/mol). Zefirov and Baranenkov (3) found exactly the same axial preference at ca. 300 K using a $\Delta\nu_{1/2}$ value of 8.4 Hz in CCl_4 and $\Delta\nu_{1/2}$ values of 17.6 Hz (axial conformer) and 5.8 Hz (equatorial conformer) obtained from the low temperature ^1H nmr spectrum of **2***a* (X = H) in CS_2. Thus it would appear that the *tert*-butyl derivatives **11** and **12** do represent adequately the

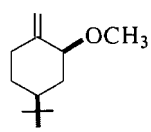

11 (*cis*)

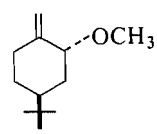

12 (*trans*)

true limit conformers of **2***a* (X = H), contrary to the 3-oxycyclohexene case discussed in the previous section. However, a ΔG^0_{e-a} of 3.2 kJ/mol in CCl_4 appears to be large compared to the value of 1.4 kJ/mol in CF_2Br_2. The latter is also a nonpolar solvent although it is probably more polar than CCl_4, and the axial preference of **2***a* does decrease as the polarity of the solvent increases (see Tables 4 and 5, and the discussion

[7]This section is abstracted from the Ph.D. thesis of M. T. Phan Viet, Université de Sherbrooke, Sherbrooke (Québec), 1979. Some of the results appeared in a preliminary communication (24).

Can. J. Chem. Downloaded from www.nrcresearchpress.com by 118.98.75.50 on 09/07/12
For personal use only.

TABLE 4. Conformational equilibria and C-4 and C-5 chemical shifts of 2-methoxy- (**2***a*) and 2-acetoxy- (**2***b*) methylenecyclohexanes (X = H)

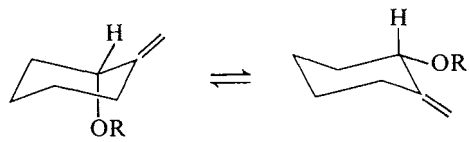

No.	OR	Solvent[a]	T (K)	δ (ppm)[b] C-4	δ (ppm)[b] C-6	% Axial by integration	% Axial from[c] δ_{C-4}	% Axial from[c] δ_{C-6}	$\overline{\Delta G^0_{e-a}}$[d] (kJ mol^{-1})
2*a* (X = H)	OCH_3	CF_2Br_2	160	eq 25.1	34.9	75			
				ax 20.3	30.3				
			217	21.9	31.8		67	67	1.4
			253	22.1	32.0		62	63	
			288	22.3	32.3		58	57	
		$CHFCl_2$	163	eq 25.2	35.1	67			
				20.7	30.5				
			213	22.4	32.1		63	65	0.8
			258	22.5	32.5		60	57	
			267	22.6	32.6		58	54	
2*b*[e] (X = H)	$OCOCH_3$	$CHFCl_2$	163	eq 24.9	34.7	≤5[f]			
			193	24.1	34.0		17	16	
			243	24.0	34.0		19	16	−3.0
			269	23.9	34.0		21	16	

[a]CF_2Br_2 and $CHFCl_2$ designate a mixture of CF_2Br_2–CD_2Cl_2 80:20 or $CHFCl_2$–CD_2Cl_2 80:20 containing 2% TMS and 4% (w/v) of **2***a* and **2***b*.

[b]From 22.63-MHz spectra, relative to TMS, ±0.05 ppm.

[c]Calculated from $K_e = (\delta_{eq} - \delta)/(\delta - \delta_{ax})$.

[d]ΔG^0 was more or less constant over the temperature range studied (from 160 to 270 K) and $\overline{\Delta G^0_{e-a}}$ represents the mean value (±15%) from the various determinations of K_e.

[e]Due to the insolubility of **2***b* in CF_2Br_2, it was not possible to record its nmr spectrum in this solvent at low temperatures.

[f]No signal corresponding to the axial conformer could be detected. For the determination of K_e, we assumed that the γ-effect was the same as in 3-methoxycyclohexene (**1***a*, X = H): $\delta_{eq} - \delta_{ax}$ = 4.7 ppm for C-4; $\delta_{eq} - \delta_{ax}$ = 4.4 ppm for C-6.

below). We believe that the conformational equilibria determined from ^{13}C chemical shifts (Table 4) are more reliable than those obtained from the ^1H nmr data ($\Delta\nu_{1/2}$ or ΣJ_{H-3}).

The similarity of the conformational behaviour of 2-methoxymethylenecyclohexane (**2***a*, X = H) and of 3-methoxycyclohexene (**1***a*, X = H) (they both show a generalized anomeric effect, which is enhanced upon the introduction of a methoxyl group on the double bond (1)) cannot be extended to the acetoxyl derivatives **2***b* and **1***b* (X = H). Indeed, we have seen in the preceding section that 3-acetoxycyclohexene (**1***b*, X = H) shows a larger axial preference than 3-methoxycyclohexene (**1***a*, X = H) as expected from the orbital picture of the generalized anomeric effect. On the contrary, 2-acetoxymethylenecyclohexane (**2***b*, X = H) exists preferentially as the equatorial conformer: $\Delta G^0_{e-a} = -4.0$ kJ/mol in $CHFCl_2$.[8] This does not mean that the $\pi-\sigma^*_{C-O}$ interaction is absent in **2***b* (X = H). In fact, Zefirov and Baranenkov (30) reported that the proportion of axial conformer in CS_2 at ca. 300 K increases from 40% for **2***b* (X = H) to 53% for 2-trifluoroacetoxymethylenecyclohexane (**2**, X = H, R = $COCF_3$). We consider this as evidence in favor of the presence of a $\pi-\sigma^*_{C-O}$ interaction in the axial conformer of 2-acyloxymethylenecyclohexanes (**2**, X = H, R = COR'), the interaction being stronger with the more electronegative trifluoroacetoyl group (σ^*_{C-O} lower in energy) than with the acetoxyl group. *We conclude therefore that, in* **2**b *(X = H), the generalized anomeric effect is overcome by another effect, which has yet to be identified.* Since other oxygenated substituents in which the oxygen is directly attached to an unsaturated system (e.g. vinyloxyl, phenoxyl) also show a smaller axial preference in 2-oxymethylenecyclohexanes **2** (X = H) than do alkoxyl substituents, the effect was termed the "unsaturated effect" (24).

As seen from Tables 4 and 5, the axial preference of the methoxyl group in **2***a* (X = H) decreases with the polarity of the solvent: ΔG_{e-a} = 1.4 kJ/mol in CF_2Br_2 and 0.8 kJ/mol in $CHFCl_2$ (Table 4); ΣJ and $\Delta\nu_{1/2}$ for H-2 are larger (Δ = 0.5–0.6 Hz), C-4 and C-6 are less shielded (Δ = 0.5–0.6 ppm), in $CHCl_3$ than in CCl_4 (Table 5). This is contrary to what has been observed with 3-methoxycyclohexene (**1***a*, X = H) where the axial preference of the methoxyl group increases with the polarity of the solvent. The solvent effect is much larger for **2***a* than for **1***a* and, if the small effect in the case of **1***a* is real, it would even be in the opposite direction. This could be explained if electrostatic interactions are more important in **2***a* than in **1***a* and destabilize the equatorial orientation (1). Then, these electrostatic interactions would be less important in a more polar solvent. The solvent effect is less pronounced in the case of 2-acetoxymethylenecyclohexane (**2***b*, X = H) ($\Delta\Delta\nu_{1/2}$ = 0.2 Hz; Δδ (C-4 and C-6) = 0.2 ppm) because the electrostatic interactions could be less important and (or) the solvation

[8]We were unable to record the ^{13}C nmr spectrum of **2***b* (X = H) in CF_2Br_2 at low temperature because of insolubility problems (see Table 4, footnote *e*).

Can. J. Chem. Downloaded from www.nrcresearchpress.com by 118.98.75.50 on 09/07/12
For personal use only.

Can. J. Chem. Downloaded from www.nrcresearchpress.com by 118.98.75.50 on 09/07/12
For personal use only.

TABLE 5. Linewidth at half-height ($\Delta\nu_{1/2}$) of H-2 and C-γ chemical shifts of 2-oxymethylenecyclohexanes **2** (X = H)[a]

No.	OR	Solvent[b]	$\Delta\nu_{1/2}$ H-2[c] (Hz)	δ (ppm)[d] C-4	δ (ppm)[d] C-6
2*a* (X = H)	OCH_3	CCl_4	9.0 (7.6[e])	21.6	31.6
		$CDCl_3$	9.6 (8.7[e])	22.2	32.2
2*b* (X = H)	$OCOCH_3$	CCl_4	13.6	23.1	33.1
		$CDCl_3$	13.8	23.4	33.4

[a]At 310 K. The ^1H nmr spectra were taken at 60 MHz, the ^{13}C nmr spectra at 22.63 MHz.
[b]CCl_4: solutions 0.3 *M*; $CDCl_3$: solutions 0.5 *M*.
[c]Linewidth at half height, ±0.2 Hz.
[d]Relative to TMS, ±0.5 ppm.
[e]Distance between the outside peaks of the broad triplet, $\Sigma J_{H\text{-}2}$, ±0.1 ppm.

weaker with the less basic acetoxyl group than with the methoxyl group.

1-Oxytetralins 8

The 1-oxytetralins **8** have an oxygenated substituent adjacent to an sp^2 alicyclic ring carbon, as do the 3-oxycyclohexenes **1** and the 2-oxymethylenecyclohexanes **2**. They resemble 3-oxycyclohexenes **1** in having two adjacent sp^2 carbons in the alicyclic ring[9] but at the same time they also bear some resemblance to 2-oxymethylenecyclohexanes **2** in having an exocyclic double bond. So we studied the 1-oxytetralins **8***a* and **8***b* to see if the generalized anomeric effect and the "unsaturation effect" (smaller axial preference of the acetoxyl group when compared to the methoxyl group) were operating on their conformational behaviour.

The ^{13}C nmr spectra of **8***a* and **8***b* at 100.62 MHz in CF_2Br_2 and $CHFCl_2$ showed no change with temperature down to 151 K. Thus either the barrier to inversion is lower than 30 kJ/mol and therefore similar to that of 3-methoxycyclohexene (**1***a*, X = H) ($\Delta G^{\ddagger} \leq 27$ kJ/mol) rather than similar to that of 3-methoxymethylenecyclohexane (**2***a*, X = H) ($\Delta G^{\ddagger} = 37$ kJ/mol) (1), or there is essentially one conformer present.

The nmr data of Table 6 show clearly the axial preference of the oxygenated substituent in **8***a* and **8***b*. Indeed, the signal of H-1 is a relatively narrow triplet ($J \approx 2.4$–4.6 Hz) implying that H-1 is essentially pseudoequatorial.[10] Thus the generalized anomeric effect is operating also in 1-oxytetralins **8**.

As seen from the $\Sigma J_{H\text{-}1}$ values of Table 6, the acetoxyl group of *cis* 1-acetoxy-3-phenyltetralin (**13**) is clearly pseudoequatorial (H-1 pseudoaxial: doublet of a doublet, J = 6.5 and 11 Hz) and that of the *trans* isomer **14**, pseudoaxial (H-1

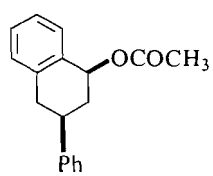

13 (*cis*)

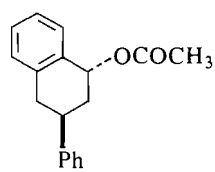

14 (*trans*)

pseudoequatorial: triplet J = 3.5 Hz) (34). Assuming that the phenyl group is nearly 100% pseudoequatorial and does not introduce any distortion in the ring, the pseudoaxial preference of the acetoxyl group of **8***b* in $CDCl_3$ would be ≤87%.

[9]The conformation of the alicyclic ring of tetralin is a half-chair as in cyclohexene (31, 32).

[10]Yamaguchi *et al.* (33) report 4.0 Hz for $J_{H\text{-}1}$ of **8***b* in $CDCl_3$. We obtained 4.2 Hz (see Experimental).

TABLE 6. C-3 chemical shift of 1-oxytetralins **8** and $\Sigma J_{H\text{-}1}$ of **8**, **13**, and **14**

No.	OR	Solvent	$\Sigma J_{H\text{-}1}$[a] (Hz)	$\delta_{C\text{-}3}$[b] (ppm)	$\delta_{C\text{-}5}$ of **1** (X = H)[b] (ppm)
8*a*	OCH_3	CCl_4[c]	9.3 (t)	18.7	19.1
		$CDCl_3$	8.8 (t)	18.8	19.2
		CF_2Br_2[d]		18.2	19.2
		$CHFCl_2$[d]		18.1	19.2
8*b*	$OCOCH_3$	CCl_4[c]	7.8 (t)	18.9	18.8
		$CDCl_3$	8.3 (t)	18.9	19.0
		CF_2Br_2[d]		18.1	18.5
		$CHFCl_2$[d]		18.2	18.4
13(*cis*)[e]	$OCOCH_3$	$CDCl_3$	17.5 (dd)		
14(*trans*)[e]	$OCOCH_3$	$CDCl_3$	7.0 (t)		

[a]Distance between the outside peaks of the signals (t = triplet, dd = doublet of a doublet). The spectra were taken at 250 MHz and at a concentration of 0.3% (w/v).
[b]At 299 K (62.89 MHz) in CCl_4 and $CDCl_3$ (0.3 *M* solutions). At 151 K (100.62 MHz) in CF_2Br_2 and $CHFCl_2$ (0.25 *M* solutions for **8**, 0.3 *M* solutions for **1**).
[c]CCl_4 = CCl_4–CD_3COCD_3 90:10.
[d]Mixtures of CF_3Br_2 ($CHFCl_2$)–CD_2Cl_2 80:20.
[e]Taken from ref. 34.

The C-3 chemical shift of **8***a* is about the same as that of **8***b* in a given solvent at a given temperature (Table 6). Thus, in 1-oxytetralins, **8**, the methoxyl group and the acetoxyl group have nearly the same axial preference. The narrower $\Sigma J_{H\text{-}1}$ for **8***b* is probably due, at least in part, to an electronegativity effect on the vicinal coupling constants (35).

The C-5 chemical shifts for 3-methoxycyclohexene (**1***a*, X = H) and 3-acetoxycyclohexene (**1***b*, X = H) are also included in Table 6 for comparison purposes and they are quite similar to the C-3 chemical shifts of **8***a* and **8***b*. This similitude reflects the similarity in structure of tetralins and cyclohexenes[9] and the pseudoaxial preference of the oxygenated substituent in both structures. However, there is a slight difference in the conformational behaviour of 1-oxytetralins **8** and 3-oxycyclohexenes **1** (X = H). In the latter, the axial preference of the acetoxyl group is greater than that of the methoxyl group but the two substituents have the same axial preference in the former. The "unsaturation effect" could be responsible for this small difference in the conformational behaviour of **8** and **1**. But, obviously, this effect would be much smaller in the 1-oxytetralins **8** than it is in the 2-oxymethylenecyclohexanes **2** (X = H). Judging from the C-3 chemical shifts of Table 6, the solvent effect ($CDCl_3$ vs. CCl_4, $CHFCl_2$ vs. CF_2Br_2) on the axial preference in 1-oxytetralins **8** is small, as in 3-oxycyclohexenes **1** (X = H).

Conclusion

The results of this paper confirm that the generalized anomeric effect is operating in allylic ethers like 3-methoxycyclohexene (**1***a*, X = H) and 2-methoxymethylenecyclohexane (**2***a*, X = H) and show that it is operating in benzylic ethers such as 1-methoxytetralin (**8***a*). The methoxyl group prefers the axial or pseudoaxial orientation as a result of π–σ^*_{C-O}

Can. J. Chem. Downloaded from www.nrcresearchpress.com by 118.98.75.50 on 09/07/12
For personal use only.

stabilization although a contribution from electrostatic interactions (e.g. dipole–quadrupole destabilizing the equatorial orientation) cannot be excluded (1). The pseudoaxial preference of the acetoxyl group is larger than that of the methoxyl group in the 3-oxycyclohexene series, as expected from a stronger $\pi-\sigma^*_{C-O}$ interaction in the case of the acetoxyl group (σ^*_{C-O} lower in energy). However, in 2-acetoxymethylenecyclohexane (**2***b*, X = H) where the equatorial conformer largely predominates (~80% at ca. 0°C), the generalized anomeric effect is overrun by another effect termed the "unsaturation effect." This effect might be operating to a small extent in 1-acetoxytetralin (**8***b*) where the axial preference is the same as in 1-methoxytetralin (**8***a*). In the seven-membered ring analogues of 1-oxytetralins **8**, 3-oxybenzocycloheptenes, the acetoxyl group has a smaller preference for the axial orientation than does the methoxyl group, probably as a result of the "unsaturation effect" playing against the generalized anomeric effect.[11]

tert-Butyl analogues of 3-oxycyclohexenes **1** cannot be used as models for the limit conformers because of distortions introduced in the cyclohexene ring, whereas in 4-*tert*-butyl analogues of 2-oxymethylenecyclohexanes **2** the ring does not appear to be seriously distorted.

It is interesting to compare the 2-oxymethylenecyclohexanes **2** (X = H) with the analogous 2-oxycyclohexanones **15**. The latter resemble 2-oxymethylenecyclohexanes **2** (X = H) in having an exocyclic double bond although they are quite different from **2** because a carbonyl group is strongly polarized and its π and π^* orbitals are much lower in energy than those of an exomethylene group. Nevertheless, the conformational behaviour of **2** (X = H) and **15** shows some similarity. In both structures, the methoxyl group prefers the axial orientation (~76% for **2***a* (X = H) and 63% for **15***a* (36) at ca. 300 K in CCl_4) and the acetoxyl group prefers the equatorial orientation (~65% for **2***b* (X = H) and ≤100% for **15***b* (37) at ca. 300 K),

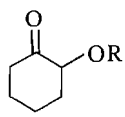

15 *a*, R = CH_3; *b*, R = $COCH_3$

although not to the same extent. The axial preference of the methoxyl group in **15***a* cannot be explained by a $\pi_{C=O}-\sigma^*_{C-O}$ interaction because of the low energy of the $\pi_{C=O}$ orbital.[12] But it can be explained in terms of a $\sigma_{C-O}-\sigma^*_{C=O}$ (38, 39) or an $n-\pi^*_{C=O}$ (40) interaction as proposed for 2-halogenocyclohexanones.[13] Such interactions would be less important in 2-acetoxycyclohexanone (**15***b*) because the energy of the σ_{C-O} and *n* orbitals should be lower in an acetoxyl group than in a methoxyl group. However, other effects (the "unsaturation effect" (?)) are probably operating in the strong equatorial preference of the acetoxyl group of **15***b*.

Experimental

Melting points were determined on a Buchi apparatus and are uncorrected. Infrared spectra were taken on a Perkin–Elmer 257 spectrometer. Mass spectra were recorded on a Hitachi RMU-6E or a VG-ZAB-1F spectrometer. Vapor phase chromatographic analyses were performed on a Hewlett Packard chromatograph, model 5710, equipped with a flame ionization detector using an OV-101 (dimethylsilicone on Carbowax 20 M) quartz column 12 m long. Preparative vapor phase chromatography was carried out on a Varian Aerograph chromatograph, model 2800, equipped with a thermal conductivity detector: OS-138 (10% polyphenylether on Chromosorb W) column with o.d. 0.125 in. and length 6 ft. Flash column chromatography was done on Merck silica gel 60 (230–400 mesh). Merck silica gel $60F_{254}$ was used for thin (0.25 mm) and preparative (1–2 mm) layer chromatography.

Nuclear magnetic resonance spectra

Routine proton spectra were obtained on a Varian A-60 spectrometer or a Bruker WP-60 Fourier transform spectrometer in deuterochloroform (solutions approximately 0.4 *M*) using TMS as internal standard. The linewidths and (or) coupling constants were determined on a Bruker HX-90 or WM-250 Fourier transform spectrometer. The temperature, solvent, and concentration are given in Tables 2, 5, and 6.

For carbon-13 spectra, TMS was used as internal standard. They were recorded on a Bruker HX-90 or WM-250 Fourier transform spectrometer. Variable temperature and low temperature data were obtained with a Bruker HX-90 (±3 K, see ref. 1) or Bruker WM-400 (±1 K, control unit BVT 1000 calibrated with methanol) Fourier transform spectrometer. The temperature, solvent, and concentration are indicated in Tables 1, 4, 5, and 6.

Materials

Compounds not commercially available were prepared either as described in the literature or by standard procedures. All compounds were pure (>98%) according to vpc analyses unless otherwise stated.

The preparation of 3-methoxycyclohexene (**1***a*, X = H), 3-acetoxycyclohexene (**1***b*, X = H), and 2-methoxymethylenecyclohexane (**2***a*, X = H) has already been described (1).

*2-Acetoxymethylenecyclohexane (***2**b, *X = H)*

2-Hydroxymethylenecyclohexane (see ref. 1) (1.12 g, 7.27×10^{-3} mol) was stirred overnight in acetic acid (5 mL) containing sodium acetate (0.4 g). The usual work-up followed by microdistillation (85°C/25 Torr; 1 Torr = 133.3 Pa) gave **2***b* (X = H) (1.45 g, 90%); ir (CCl_4) ν_{max}: 1750, 1657, 1360, and 1228 cm^{-1}; ^{1}Hmr ($CDCl_3$) δ: 1.4–2.4 (8H), 2.09 (s, CH_3CO), 4.80 (m, 2H-7), 5.20 (m, H-2) ppm; ^{13}Cmr ($CDCl_3$) δ: 21.2 (CH_3CO), 23.4 (C-4), 27.6 (C-5), 33.4 and 33.5 (C-6 and C-3), 74.3 (C-2), 107.2 (C-7), 146.6 (C-1), 170.0 (C=O) ppm; *m/e*: 154 (M^+).

cis *and* trans *4-*tert*-Butylcyclohexene-1-ols*

These were prepared from 4-*tert*-butylcyclohexanone according to a published procedure (25). The 29:71 mixture of *cis* and *trans* isomers (85% yield, mp 40.5–43°C) was separated by flash column chromatography (hexane and ethyl acetate – hexane mixtures as eluent) to yield the pure isomers, which were recrystallized from pentane. *Cis* isomer: mp 54.5–55°C (lit. (5) mp 51–54°C). *Trans* isomer: mp 37–38°C (lit. (5) mp 32–34°C).

cis *6-*tert*-Butyl-3-methoxycyclohexene (***6**a)*

cis 4-*tert*-Butylcyclohexen-1-ol (0.144 g, 0.94×10^{-3} mol) was methylated (5) to give **6***a* (0.105 g, 57%) after purification by preparative layer chromatography on silica gel; ir ($CHCl_3$) ν_{max}: 1070 cm^{-1}; ^{1}Hmr ($CDCl_3$) δ: 0.90 (s, 9H), 1.50 (m, H-5), 1.75 (m, H-4), 1.9–2.1 (m, H-6), 3.40 (s, CH_3O), 3.55 (m, H-3), 5.85 (br d, *J* = 10.2 Hz, H-2), 5.95 (d of t, *J* = 10.2 and 1.5 Hz, H-1) ppm; ^{13}Cmr ($CDCl_3$) δ: 19.0 (C-5), 27.2 (C-4), 27.4 and 32.7 (*tert*-butyl), 46.5 (C-6), 56.1 (OCH_3), 72.2 (C-3), 126.9 (C-1), 134.3 (C-2) ppm; *m/e*: 168 (M^+).

trans *6-*tert*-Butyl-3-methoxycyclohexene (***7**a)*

trans 4-*tert*-Butylcyclohexen-1-ol (1.04 g, 6.76×10^{-3} mol) was methylated (5) to give **6***b* (0.496 g, 44%) after microdistillation (90–

[11]M. St-Jacques, unpublished results. We thank professor Maurice St-Jacques for communicating these results to us.

[12]The energy of the π orbital of formaldehyde is lower than that of ethylene by 3.58 eV according to photoelectron spectroscopy (37).

[13]We have shown (2) that such interactions are not involved in 2-methoxymethylenecyclohexanes (**2***a*, X = OCH_3, H, CN) as expected from the fact that a $\pi^*_{C=C}$ orbital is higher in energy than a $\pi^*_{C=O}$ orbital.

Can. J. Chem. Downloaded from www.nrcresearchpress.com by 118.98.75.50 on 09/07/12
For personal use only.

105°C/15 Torr); ir ($CHCl_3$) ν_{max}: 1090 cm^{-1}; ^{1}Hmr ($CDCl_3$) δ: 0.90 (s, 9H), 1.2–1.5 (m, H-2), 1.90 (m, H-4), 2.15 (m, H-6), 3.40 (s, OCH_3), 3.75 (m, H-3), 5.7–5.8 (m, H-1 and H-2) ppm; ^{13}Cmr ($CDCl_3$) δ: 22.7 (C-5), 29.2 (C-4), 27.2 and 32.9 (*tert*-butyl), 46.3 (C-6), 53.4 (OCH_3), 76.2 (C-3), 129.6 (C-1), 131.6 (C-2) ppm; *m/e*: 168 (M^+).

cis 6-tert-*Butyl-3-acetoxycyclohexene (6b)*

cis 4-*tert*-Butylcyclohexen-1-ol (0.306 g, 1.99 × 10^{-1} mol) was acetylated at ca. 0°C (ice bath) with acetyl chloride (0.22 mL, 3.1 × 10^{-3} mol) in dry ether (4 mL) containing pyridine (0.28 mL, 3.48 × 10^{-3} mol) for 90 min. The reaction mixture was stirred at room temperature for 5 h. The usual work-up followed by preparative layer chromatography (ethyl acetate – hexane) gave **6***b* (0.37 g, 95%); ir ($CHCl_3$) ν_{max}: 1720 and 1250 cm^{-1}; ^{1}Hmr ($CDCl_3$) δ: 0.90 (s, 9H), 1.40 (m, H-5), 1.90 (m, H-4), 2.00 (s, CH_3CO), 2.15 (m, H-6), 5.10 (br s, H-3), 5.85 (br d, J = 10.2 Hz, H-2), 6.05 (d, J = 10.1 Hz, H-1) ppm; ^{13}Cmr ($CDCl_3$) δ: 19.2 (C-5), 21.4 (CH_3CO), 28.4 (C-4), 27.4 and 32.7 (*tert*-butyl), 46.2 (C-6), 66.5 (C-3), 125.9 (C-1), 135.9 (C-2), 170.8 (C=O) ppm; *m/e*: 196 (M^+).

trans 6-tert-*Butyl-3-acetoxycyclohexene (7*b)

trans 4-*tert*-Butylcyclohexen-1-ol (0.905 g, 5.88 × 10^{-3} mol) was acetylated as above to give **7***b* (1.15 g, 88%) after flash chromatography (ethyl acetate – hexane); bp 88–91°C/6 Torr; ir ($CHCl_3$) ν_{max}: 1720 and 1250 cm^{-1}; ^{1}Hmr ($CDCl_3$) δ: 0.90 (s, 9H), 1.40 (m, H-5), 1.7–2.0 (m, H-4), 2.10 (s, CH_3CO), 2.15 (m, H-6), 5.25 (m, H-3), 5.60 (br d, J = 10.6 Hz), 5.80 (d of q, J = 10.4 and 1.8 Hz) ppm; ^{13}Cmr ($CDCl_3$) δ: 21.4 (CH_3CO), 22.6 (C-5), 28.9 (C-4), 27.2 and 32.9 (*tert*-butyl), 45.9 (C-6), 70.5 (C-3), 128.1 (C-1), 133.0 (C-2), 170.9 (C=O) ppm; *m/e*: 196 (M^+). *Exact Mass* calcd. for $C_{12}H_{20}O_2$: 196.1463; found (ms): 196.1466.

*1-Methoxytetralin (8*a)

α-Tetralol (3.15 g, 0.02 mol) was treated with NaH, then with CH_3I in THF at 0°C (25), to give, after extraction with CH_2Cl_2, the methoxyl derivative **8***a* as a liquid (3.32 g, 96%). Flash chromatography and preparative layer chromatography on silica gel, and distillation (bp 94°C/4 Torr) did not improve the purity (96% by vpc); ir ($CHCl_3$) ν_{max}: 1600, 1495, 1080 cm^{-1}; ^{1}Hmr ($CDCl_3$) δ: 1.7–2.1 (H-2 and H-3), 2.7–2.9 (m, H-4), 3.40 (s, OCH_3), 4.30 (t, J = 4.5 Hz, H-1), 7.1–7.2 (H-5, H-6, and H-7), 7.35 (m, H-8) ppm; ^{13}Cmr ($CDCl_3$) δ: 18.8 (C-3), 27.5 (C-4), 29.1 (C-2), 56.1 (OCH_3), 76.9 (C-1), 125.7, 127.6, 129.0, 129.3 (C-5, C-6, C-7, C-8), 136.7 (C-10), 137.6 (C-9) ppm; *m/e*: 162 (M^+). *Exact Mass* calcd. for $C_{11}H_{14}O$: 162.1044; found: 162.1032.

*1-Acetoxytetralin (8*b)

α-Tetralol (2.08 g, 0.014 mol) was acetylated as described for **6***b* above to give **8***b* as a liquid (2.56 g, 96% yield). It was purified by preparative layer chromatography (ether–benzene); ir ($CHCl_3$) ν_{max}: 1720, 1600, 1495, 1370, 1240 cm^{-1}; ^{1}Hmr ($CDCl_3$) δ: 1.8–2.0 (H-2 and H-3), 2.10 (s, CH_3CO), 2.7–2.9 (m, H-4), 6.00 (t, J = 4.2 Hz, H-1), 7.1–7.3 (4 aromatic H) ppm; ^{13}Cmr ($CDCl_3$) δ: 18.9 (C-3), 21.4 (CH_3CO), 29.0 (C-4), 29.2 (C-2), 70.2 (C-1), 126.2, 128.1, 129.1, 129.5 (C-5, C-6, C-7, C-8), 134.7 (C-10), 138.0 (C-9), 170.8 (C=O) ppm; *m/e*: 190 (M^+). *Exact Mass* calcd. for $C_{12}H_{14}O_2$: 190.0993; found: 190.0996.

cis *and* trans *4-*tert*-Butyl-2-acetoxymethylene cyclohexanes (11 and 12)*

A mixture of *cis* and *trans* 4-*tert*-butyl-2-acetoxycyclohexanones was prepared as described in ref. 36. In a 250-mL three-necked flask, dry methyltriphenylphosphonium bromide (15.0 g, 0.042 mol) was suspended in dry THF (55 mL). The suspension was cooled to 0°C (ice bath), *n*-butyllithium 1.6 *M* in hexane (0.045 mol) was added, and the mixture was stirred at room temperature for 30 min. It was cooled to 0°C and the mixture of 4-*tert*-butyl-2-acetoxycyclohexanones (3.80 g, 0.02 mol) in dry THF (20 mL) was added dropwise. The reaction mixture was stirred at room temperature overnight, refluxed for 1 h, then concentrated in a rotatory evaporator. Pentane (150 mL) was added and the precipitate was filtered and washed with ether, then with a pentane–THF mixture. The resulting solution was passed through basic alumina (activity 1) and concentrated. Upon addition of pentane, a precipitate was formed again and was removed by filtration. Evaporation of the solvent gave a liquid mixture of **11** and **12** (3.09 g, 85%), which was separated by vpc.

11: ir (CCl_4) ν_{max}: 1650, 1360, 1130, 1110, 1077, 890 cm^{-1}; ^{1}Hmr ($CDCl_3$) δ: 0.87 (s, 9H), 1.4–2.4 (8H), 3.46 (s, OCH_3), 3.60 (m, H-2), 4.70–4.90 (m, 2H-7) ppm; ^{13}Cmr ($CDCl_3$) δ: 27.6 and 32.0 (*tert*-butyl), 29.0 (C-5), 34.2 (C-6), 35.7 (C-3), 47.1 (C-4), 57.4 (OCH_3), 82.1 (C-2), 103.8 (C-7), 148.9 (C-1) ppm; *m/e*: 182 (M^+).

12: ir (CCl_4) ν_{max}: 1648, 1360, 1100, 1080, 1070, 895 cm^{-1}; ^{1}Hmr ($CDCl_3$) δ: 0.85 (s, 9H), 1.2–2.4 (8H), 3.19 (s, CH_3O), 3.71 (br t, J = 2.7 Hz, H-2), 4.75–4.90 (m, 2H-7) ppm; ^{13}Cmr ($CDCl_3$) δ: 27.5 and 32.0 (*tert*-butyl), 28.6 (C-5), 30.5 (C-6), 34.3 (C-3), 41.0 (C-4), 55.2 (OCH_3), 81.6 (C-2), 110.6 (C-7), 147.7 (C-1); *m/e*: 182 (M^+).

Acknowledgements

We are grateful to the Natural Sciences and Engineering Research Council of Canada and to the "Fonds pour la Formation de Chercheurs et l'Aide à la Recherche" of Quebec for their financial support and to Mrs. S. Thériault for typing the manuscript.

1. J. Lessard, M. T. Phan Viet, R. Martino, and J. K. Saunders. Can. J. Chem. **55**, 1015 (1977).
2. J. Lessard, J. K. Saunders, and M. T. Phan Viet. Tetrahedron Lett. **23**, 2059 (1982).
3. N. S. Zefirov and I. V. Baranenkov. Tetrahedron, **39**, 1769 (1983), and references therein.
4. J. M. J. Tronchet and T. N. Xuan. Carbohydr. Res. **67**, 469 (1978).
5. R. S. Brown, R. W. Marcinko, and A. Tse. Can. J. Chem. **57**, 1890 (1979).
6. N. S. Zefirov, E. G. Chalenko, A. V. Aripovsky, J. G. Mursakulov, M. M. Guseinov, and E. A. Ramazanov. J. Chem. Soc. Chem. Commun. 147 (1978).
7. G. O. Pierson and O. A. Runquist. J. Org. Chem. **33**, 2572 (1968).
8. A. J. de Hoog, H. R. Buys, C. Altona, and E. Havinga. Tetrahedron, **25**, 3365 (1969).
9. C. B. Anderson and D. T. Sepp. Tetrahedron, **24**, 1707 (1968).
10. R. U. Lemieux and N. S. Chu. Abstracts of papers. Am. Chem. Soc. **133**, 31N (1958).
11. R. U. Lemieux. Pure Appl. Chem. **25**, 527 (1971).
12. E. L. Eliel. Angew. Chem. Int. Ed. Engl. **11**, 739 (1972).
13. A. J. Kirby. The anomeric effect and related stereoelectronic effects at oxygen. Springer Verlag, New York. 1983. pp. 20–23.
14. L. Radom, W. J. Hehre, and J. A. Pople. J. Am. Chem. Soc. **94**, 2371 (1972).
15. C. Altona. Ph.D. thesis, University of Leiden, The Netherlands. 1974.
16. C. Romers, C. Altona, H. R. Buys, and E. Havinga. *In* Topics in stereochemistry. Vol. 4. *Edited by* E. L. Eliel and N. L. Allinger. Wiley–Interscience, New York. 1969. p. 39.
17. S. David, O. Eisenstein, W. J. Hehre, L. Salem, and R. Hoffman. J. Am. Chem. Soc. **95**, 3806 (1973).
18. G. Baddeley. Tetrahedron Lett. 1645 (1973).
19. J. T. Edward. Chem. Ind. 1102 (1955).
20. M. A. Kabayama and D. Patterson. Can. J. Chem. **36**, 563 (1958).
21. R. U. Lemieux. *In* Molecular rearrangements. *Edited by* P. de Mayo. Interscience, New York. 1965. p. 45.
22. I. Tvarovska and T. Bleha. Can. J. Chem. **57**, 424 (1979).
23. P. Deslongchamps. Stereoelectronic effects in organic chemistry. Pergamon Press, New York. 1983. p. 6.
24. M. T. Phan Viet, J. Lessard, and J. K. Saunders. Tetrahedron Lett. 317 (1979).

25. E. U. DINER, F. SWEET, and R. K. BROWN. Can. J. Chem. **44**, 1591 (1966).
26. F. D. JENSEN and C. H. BUSHWELLER. *In* Advances in alicyclic chemistry. Vol. 3. *Edited by* H. Hart and G. Karabatsos. Academic Press, New York. 1971. pp. 153–161, and references therein.
27. F. R. JENSEN and C. H. BUSHWELLER. J. Am. Chem. Soc. **91**, 5774 (1969).
28. M. BERNARD and M. ST-JACQUES. Tetrahedron, **29**, 2539 (1973).
29. Y. SENDA and S. IMAIZUMI. Tetrahedron, **30**, 3813 (1974).
30. N. S. ZEFIROV and I. V. BARANENKOV. Zh. Org. Khim. **17**, 2364 (1981).
31. G. DREFAHL and K. PONSOLD. Chem. Ber. **91**, 266 (1958).
32. M. A. LASHEEN. Acta Crystallogr. **5**, 593 (1952).
33. S. YAMAGUCHI, K. KABATO, Y. NINOMIYA, and N. INOUE. Bull. Chem. Soc. Jpn. **43**, 3952 (1970).
34. S. MITSUI, A. KASAHARA, and K. KANAYA. Bull. Chem. Soc. Jpn. **41**, 2526 (1968).
35. L. M. JACKMAN and S. STERNHELL. Applications of nuclear magnetic resonance spectroscopy in organic chemistry. Pergamon Press, New York. 1969. pp. 283–284.
36. D. CANTACUZENE and M. TORDEUX. Can. J. Chem. **54**, 2759 (1976).
37. I. FLEMING. Frontier orbitals and organic chemical reactions. John Wiley and Sons, Ltd., New York. 1976. p. 22.
38. E. J. COREY and H. J. BURKE. J. Am. Chem. Soc. **77**, 5418 (1955).
39. N. L. ALLINGER, J. ALLINGER, L. A. FREIBERG, R. F. CZAJA, and N. A. LEBEL. J. Am. Chem. Soc. **82**, 5876 (1960).
40. O. EISENSTEIN, N. T. AHN, Y. JEAN, A. DEVAQUET, D. CANTACUZENE, and L. SALEM. Tetrahedron, **30**, 1717 (1974).

Can. J. Chem. Downloaded from www.nrcresearchpress.com by 118.98.75.50 on 09/07/12
For personal use only.

A carbon-13 nuclear magnetic resonance study of the basicities of aliphatic alcohols

DONALD G. LEE AND KENNETH J. DEMCHUK
Department of Chemistry, University of Regina, Regina, Sask., Canada S4S 0A2

Received October 4, 1986

This paper is dedicated to Professor John T. Edward

DONALD G. LEE and KENNETH J. DEMCHUK. Can. J. Chem. **65**, 1769 (1987).

Carbon-13 nmr chemical shifts have been used to determine the basicity constants for nine alcohols. The method involves comparing the chemical shifts for carbon atoms adjacent to the site of protonation with those for carbon atoms in a more remote position. The differences in the chemical shifts (Δ values) at different acidities are then used to calculate basicity constants for the alcohols. The pK_{BH^+} values, determined by use of the "X function" are as follows: ethanol −2.12, 1-propanol −2.12, 3-chloro-1-propanol −2.24, 2-chloroethanol −2.45, 2-bromoethanol −2.41, 2-nitroethanol −2.09, 2-methoxyethanol −1.93, 2-phenoxyethanol −1.87, and 2-propanol −2.06. The typical slope parameter, m^*, is 0.17. Two linear free energy correlations are obtained: when the alcohols are considered to be a series of monosubstituted ethanols, the Hammett plot has a slope of 0.65; when they are considered to be a series of mono- and disubstituted methanols, the slope is 1.7. Alcohols bearing oxygen-containing substituents are more basic than predicted by about 0.5 pK units, presumably because their conjugate acids can be stabilized by intramolecular hydrogen bonding.

DONALD G. LEE et KENNETH J. DEMCHUK. Can. J. Chem. **65**, 1769 (1987).

On a utilisé les déplacements chimiques de la rmn du ^{13}C pour déterminer les constantes de basicité de neuf alcools. La méthode implique une comparaison des déplacements chimiques des atomes de carbones adjacents au site de protonation avec ceux des atomes de carbones dans des positions plus éloignées. On utilise alors les différences dans les déplacements chimiques (valeurs Δ) à différentes acidités pour calculer les constantes de basicité des alcools. Les valeurs de pK_{BH^+}, déterminées en utilisant la « fonction X », sont: éthanol, −2,12; propanol-1, −2,12; chloro-3 propanol-1, −2,24; chloro-2 éthanol, −2,45; bromo-2 éthanol, −2,41; nitro-2 éthanol, −2,09; méthoxy-2 éthanol, −1,93; phénoxy-2 éthanol, −1,87 et propanol-2 −2,06. Le paramètre typique de la pente, m^*, est 0,17. On obtient deux corrélations linéaires d'énergie libre; lorsque les alcools sont considérés comme une série d'éthanols monosubstitués, la pente de la courbe de Hammett est égale à 0,65; lorsqu'on les considère comme une série de méthanols mono- ou disubstitués, la pente est égale à 1,7. Les alcools portant des oxygènes contenant des substituants sont plus basiques que les valeurs prédites, par environ 0,5 unités de pK; ce résultat est probablement dû au fait que leurs acides conjugués peuvent être stabilisés par des liaisons hydrogènes intramoléculaires.

[Traduit par la revue]

Introduction

A quantitative knowledge of the basicity of organic compounds is essential to an understanding of a myriad of acid-catalyzed reactions (1). As a consequence, numerous attempts have been made to develop methods to accurately determine equilibrium constants for the dissociation of the conjugate acids of various organic bases, B, as in reaction [1]. The pK_{BH^+} values, defined by eq. [3], may then be obtained if the terms on the right can be defined. The first of these can be obtained if it is possible to determine the ionization ratio, $I = [BH^+]/[B]$, experimentally — a measurement that is usually

[1] $$BH^+ \overset{K_{BH^+}}{\rightleftharpoons} B + H^+$$

[2] $$K_{BH^+} = a_B a_{H^+}/a_{BH^+}$$

[3] $$pK_{BH^+} = \log [BH^+]/[B] - \log [H^+] - \log \gamma_B\gamma_{H^+}/\gamma_{BH^+}$$

accomplished by employing some form of spectroscopy. For example, absorbances have been used to obtain ionization ratios for a variety of compounds that contain uv/vis-active chromophores (2–4).

Nuclear magnetic resonance is more appropriate for use with aliphatic compounds which lack chromophores (5–15). Furthermore, Edward has noted that medium effects on the absolute chemical shifts may be cancelled by using the difference between the shifts for two nuclei in the same molecule (16). In the present work, carbon-13 nuclear magnetic shifts were used to estimate the extent of protonation of a number of aliphatic alcohols. Since the chemical shift differences for a partly protonated compound, Δ, is a weighted average of the chemical shift for the neutral molecule, Δ_B, and its conjugate acid, Δ_{BH^+}, the ionization ratio is given by eq. [4], and the first term in eq. [3] is thereby obtained.

[4] $$I = (\Delta - \Delta_B)/(\Delta_{BH^+} - \Delta)$$

The third term on the right of eq. [3] has been called the "excess acidity," because it is the difference between the observed acidity of a solution and that which it would have if it were ideal (17, 18). Various approaches have been made to an evaluation of this term, with the most successful being that of Cox and Yates who defined an average acidity function, X, and included a slope parameter, m^*, to account for the observation that the activity coefficient ratios for most compounds are linearly related (19). Equation [3] can then be restated as in eq. [5], the form in which it is most commonly used.

[5] $$\log I - \log [H^+] = m^*X + pK_{BH^+}$$

Plots of ($\log I - \log [H^+]$) against the X function are consequently expected to be linear with a slope of m^* and an intercept of pK_{BH^+}.

Experimental

Materials

Certified reagent grade sulfuric acid (Fisher) was used to prepare the acidic solutions. Stock sulfuric acid, which had been titrated with a standard sodium hydroxide solution, was determined to be 95.90 wt.% H_2SO_4. The concentration of sulfuric acid in each of the solutions was calculated using this value and confirmed by titration.

All alcohols were reagent grade and were used as received without further purification.

Collection of nmr spectra

Carbon-13 nuclear magnetic resonance spectra were obtained using

Can. J. Chem. Downloaded from www.nrcresearchpress.com by 118.98.75.50 on 09/07/12
For personal use only.

TABLE 1. Carbon-13 nmr chemical shift data for ethanol[a]

% H_2SO_4	log $[H^+]$[b]	X-function[b]	C(1)	C(2)	Δ
0.0			60.27	19.61	40.66
12.12	0.202	0.294	60.49	19.61	40.88
23.09	0.536	0.703	60.81	19.56	41.25
36.32	0.777	1.397	61.36	19.31	42.05
48.05	0.925	2.195	62.15	18.92	43.23
59.37	1.028	3.176	63.40	18.40	45.00
64.54	1.066	3.741	64.23	18.11	46.12
69.48	1.094	4.386	65.24	17.82	47.42
71.94	1.108	4.752	65.83	17.67	48.16
74.67	1.122	5.195	66.52	17.46	49.06
77.74	1.135	5.734	67.51	17.28	50.23
78.95	1.140	5.957	67.95	17.20	50.75
81.37	1.144	6.411	68.77	17.03	51.74
83.74	1.135	6.860	69.55	16.87	52.68
88.65	1.047	7.753	71.03	16.81	54.22
93.21	0.812	8.577	72.10	16.62	55.48
95.90	0.552	9.258	72.85	16.51	56.34
Δ_{BH^+}					60

[a]Shifts in ppm, TMS = 0.
[b]From ref. 18.

a Bruker HX-90 spectrometer operating in the Fourier transform, proton noise decoupled mode at 22.63 MHz. In all cases, 8K of data were collected using a Nicolet 1080 series computer. The fluorine field lock signal was obtained from hexafluorobenzene in a coaxial insert of a 10 mm nmr tube. Tetramethylsilane was added to the locking compound for a spectrum reference. All spectra were recorded using a 3000 Hz sweep width, giving 2.7 data points per hertz resolution.

In a typical procedure, a 1.0 mL glass syringe was used to transfer a 0.20 mL aliquot of an alcohol to a clean dry 5.0 mL volumetric flask. The flask was then made up to volume at room temperature with an acid solution of known concentration. The nmr spectrum of the solution was obtained at a probe temperature of 22°C immediately after preparation. To obtain a reasonable spectrum in the shortest time, approximately 200 to 1000 scans were collected. The maximum time between sample preparation and the completion of data acquisition was approximately 30 min.

The procedure was then repeated using acid solutions with different concentrations.

Results

During the collection of the spectra for each alcohol, a phenomenon similar to that reported by McClelland and Reynolds (12) was observed; in stronger acid solutions, less time was required to obtain a good spectrum. It has been suggested that this is due to the shortened spin–lattice relaxation times in the more viscous sulfuric acid solutions.

Similar changes in the carbon-13 chemical shifts were observed for all alcohols as the concentrations of the sulfuric acid solutions increased. These changes were relatively small and regular. The carbon attached to the hydroxylic oxygen always shifted to lower and lower fields as the sulfuric acid concentrations increased. This indicated that the electron density at the carbon atom decreases as the extent of oxygen protonation increases.

The carbon β to the oxygen usually moved to slightly higher fields as the concentration of the acid solution was increased. This could possibly be the result of a solvent effect or an alternating resonance effect associated with the protonated oxygen (12). Since only chemical shift differences were used in subsequent calculations, the absolute magnitude of the shifts

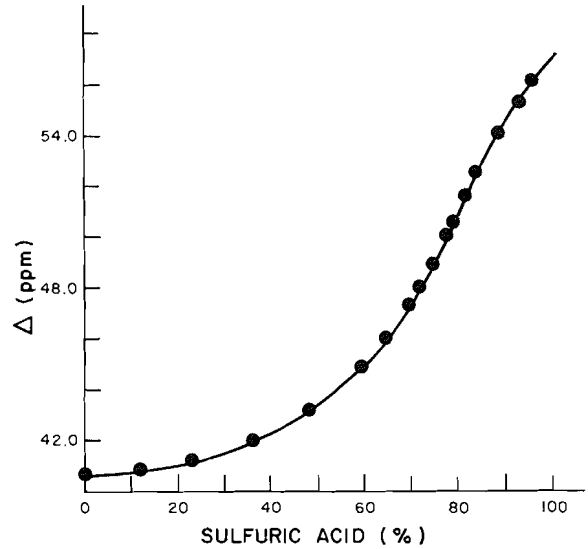

FIG. 1. Titration curve for the protonation of ethanol.

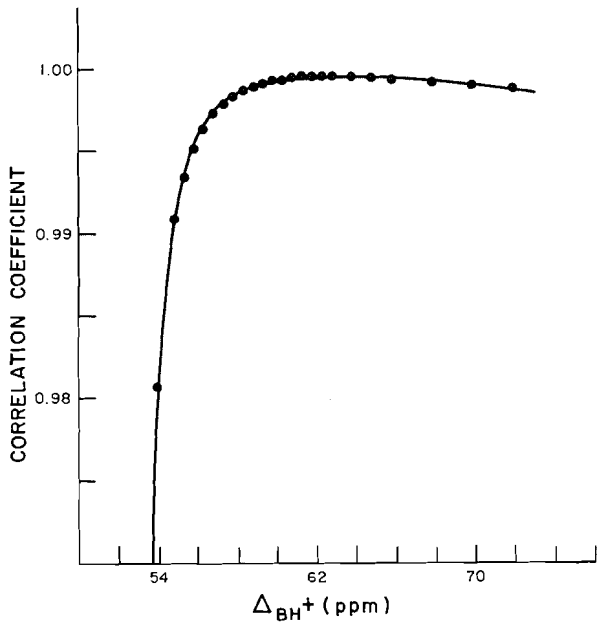

FIG. 2. Correlation coefficients of the X-function plot (eq. [4]) as a function of Δ_{BH^+} for the protonation of ethanol.

(relative to TMS) is not important. For all of the alcohols studied, the absolute value of the change in the shift of the α-carbon was always larger than the accompanying change in the β-carbon shift. Therefore, the chemical shift difference between these two, Δ, was found to become more positive with increasing sulfuric acid concentration.

Another phenomenon observed with all of the alcohols was esterification in concentrated sulfuric acid solutions. The tendency of alcohols to produce sulfate esters in highly concentrated sulfuric acid was first reported by Edward and co-workers (16) and later by Lee and Cameron (5). Although the appearance of sulfate ester proton nmr peaks interferes with the measurement of hydrogen-1 chemical shifts, such spectral interference is not a problem when carbon-13 nmr is used to monitor the extent of protonation. Carbon-13 signals for the sulfate esters were observed to be significantly different from those of the protonated alcohols. In very concentrated sulfuric acid solutions, only peaks for the sulfate esters could be found.

Can. J. Chem. Downloaded from www.nrcresearchpress.com by 118.98.75.50 on 09/07/12
For personal use only.

TABLE 2. Carbon-13 Δ values[a]

	Δ values							
% H_2SO_4	1-Propanol	3-Chloro-1-propanol	2-Chloro-ethanol	2-Bromo-ethanol	2-Nitro-ethanol	2-Methoxy-ethanol	2-Phenoxy-ethanol	2-Propanol
0.0	39.03	24.50	15.86	27.00	−19.51	−12.80	−8.91	40.58
12.12	39.28	24.74	15.90	27.01	−19.42	−12.73	−8.85	40.91
23.09	39.62	25.09	16.05	27.17	−19.31	−12.57	−8.68	41.50
36.32	40.35	25.68	16.38	27.56	−19.00	−12.28	−8.35	42.78
48.05	41.34	26.48	16.86	28.15	−18.66	−11.99	−7.79	44.65
59.37	42.88	27.66	17.64	29.09	−18.17	−11.65	−7.15	47.40
64.54	43.83	28.42	18.15	29.68	−17.87	−11.48	−6.80	49.09
69.48	44.92	29.31	18.76	30.40	−17.56	−11.28	−6.41	50.96
71.94	45.62	29.93	19.15	30.88	−17.33	−11.16	−6.23	52.02
74.67	46.42	30.60	19.63	31.42	−17.14	−11.06	−6.02	53.27
77.74	47.45	31.53	20.63	32.20	−16.85	−10.85	−5.73	54.81
78.95	47.92	32.05	20.66	32.64	−16.72	−10.74	−5.55	55.47
81.37	48.82	33.03	21.45	33.59	−16.41	−10.53		56.70
83.74	49.65	33.82	22.37	34.39	−16.13	−10.41		57.79
88.65	51.22	35.97	24.27	37.17	−15.22			59.79
93.21	52.39							61.40
95.90								62.44
Δ_{BH^+}	57	41	31	43	−12	−7	−4	65

[a]Shifts in ppm, TMS = 0.

The extent of protonation in each solution was monitored by calculating the difference in the chemical shifts of the α and β carbons. This difference increases as the acidity of the solutions increases, and a plot of Δ vs. % H_2SO_4 produces, in theory, a titration curve from which the pK_{BH^+} can subsequently be obtained. A typical example of the complete carbon-13 data for one alcohol, ethanol, is presented in Table 1 and the data for the other alcohols are summarized in Table 2.

When the data for ethanol is plotted, as in Fig. 1, it is apparent that the upper plateau of the titration curve is not defined; i.e., Δ values for the fully protonated alcohol (Δ_{BH^+} values), which are required for the calculation of the ionization ratios (I), are not available experimentally. Consequently, a procedure for calculating Δ_{BH^+} values, previously described in the literature (5, 20), was modified for use in the present study. In this procedure the best values are obtained by comparing the correlation coefficients of the X-function plots for a range of Δ_{BH^+} values. Since theory predicts that these plots should be linear, it can be assumed that the highest correlation coefficient would be obtained when the correct Δ_{BH^+} value is used in the calculation. Experimentally, it was found that the correlation coefficients increased sharply up to a certain point and then remained constant over a fairly broad range before declining slightly as in Fig. 2. The Δ_{BH^+} values corresponding to the point at which the maximum was first achieved were used in all subsequent calculations. The calculated values have been included in Tables 1 and 2.

Having calculated reliable values for Δ_{BH^+} it was then possible to prepare plots of (log I − log [H^+]) vs. the X function from which the pK_{BH^+} values can be obtained. Three typical plots have been reproduced in Fig. 3 and the data obtained for all of the alcohols has been summarized in Table 3.

For the most part, only ionization ratios which were within the range of log I = ±1.0 were used in the least-squares

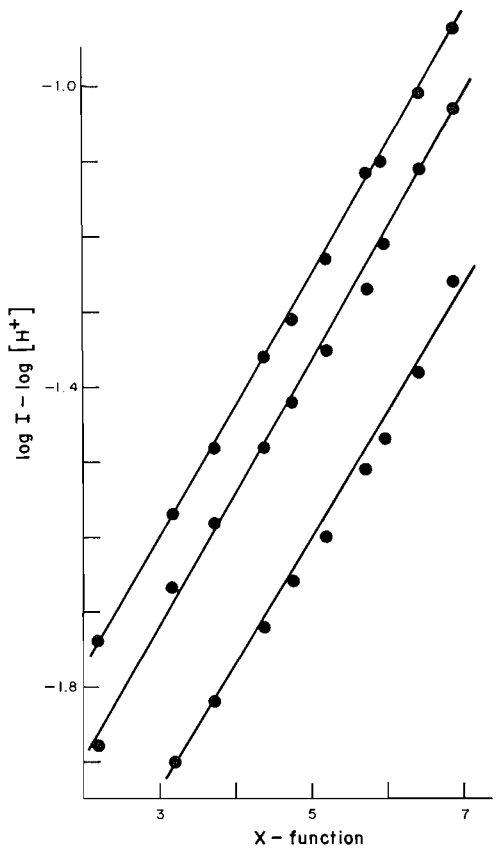

FIG. 3. X-function plots. Top: ethanol; slope = 0.17 ± 0.02, intercept = −2.12 ± 0.02, r = 0.999. Middle: 3-chloro-2-propanol; slope = 0.17 ± 0.02, intercept = −2.24 ± 0.02, r = 0.997. Bottom: 2-chloroethanol; slope = 0.17 ± 0.01, intercept = −2.45 ± 0.03, r = 0.997.

Can. J. Chem. Downloaded from www.nrcresearchpress.com by 118.98.75.50 on 09/07/12
For personal use only.

TABLE 3. Basicity data obtained by application of the X-function equation to the carbon-13 nmr shifts

Alcohol	m^*	pK_{BH^+}	r^a
Ethanol	0.17±0.02	−2.12±0.02	0.999
1-Propanol	0.16±0.02	−2.12±0.02	0.999
3-Chloro-1-propanol	0.17±0.02	−2.24±0.02	0.997
2-Chloroethanol	0.17±0.01	−2.45±0.03	0.997
2-Bromoethanol	0.17±0.02	−2.41±0.03	0.998
2-Nitroethanol	0.12±0.03	−2.09±0.08	0.998
2-Methoxyethanol	0.09±0.03	−1.93±0.13	0.992
2-Phenoxyethanol	0.18±0.07	−1.87±0.09	0.996
2-Propanol	0.18±0.02	−2.02±0.02	0.999

[a]Correlation coefficient of a linear regression analysis.

analyses. This was done to decrease the potential for errors in log I measurements, since it is known that errors in I increase with increasing distance from 50% ionization. Khaldna (21) has suggested that when the absolute value of log I is greater than 1.0 it is too inaccurate to use in sensitive calculations. Many other authors have followed this same convention (3, 5, 8, 12, 17, 18, 22).

Calculations were made only on data obtained in solutions of less than 85% sulfuric acid because it has been reported that acidity function equations fail in concentrated acid solutions. Cox and Yates have suggested that this is due to the presence of large amounts of undissociated sulfuric acid, and that an alternative formulation of the X function might be necessary for very concentrated sulfuric acid mixtures (10). Therefore, Δ values obtained in acid solutions greater than 85% were not incorporated into these calculations.

Other authors, particularly Cox and Yates, have reported that medium effects are of substantial importance when carbon-13 nmr data are used to measure the basicity of amides (11). The results for alcohols, reported in this paper, did not in themselves appear to require the application of any special corrections for medium effects. However, a referee has reported that the use of the program developed by Cox and Yates with our data gives pK_a values of similar magnitudes but substantially larger uncertainties. Consequently, because the final chapter on the analysis of protonation data does not appear to have been written, we have chosen to publish all of our Δ values, thus making them conveniently available to other workers who may in future develop better ways to handle the problem of medium effects.

Discussion

Much of the alcohol basicity data in the older literature is not reliable because the pK_{BH^+} values were often reported as the H_0 at which the alcohol was one-half protonated (21). As a consequence widely divergent values for the basicity constants of simple alcohols may be found in the literature (23). The difficulty arises, in part, because the acidity function plots were originally assumed to have a slope of 1.00 for all compounds. However, plots of log I versus $-H_0$ for alcohols resulted in slopes far from unity (5, 24). Thus the H_0 values at half ionization do not correspond to thermodynamic pK_{BH^+} values and should only be used as indicators of relative basicities, a fact early recognized by Edward and co-workers (16).

The basicities of two simple alcohols, ethanol and methanol, have been determined by use of the Bunnett–Olsen equation, which does not presume a similar slope for all compounds. The pK_{BH^+} value obtained from the carbon-13 nmr data of ethanol

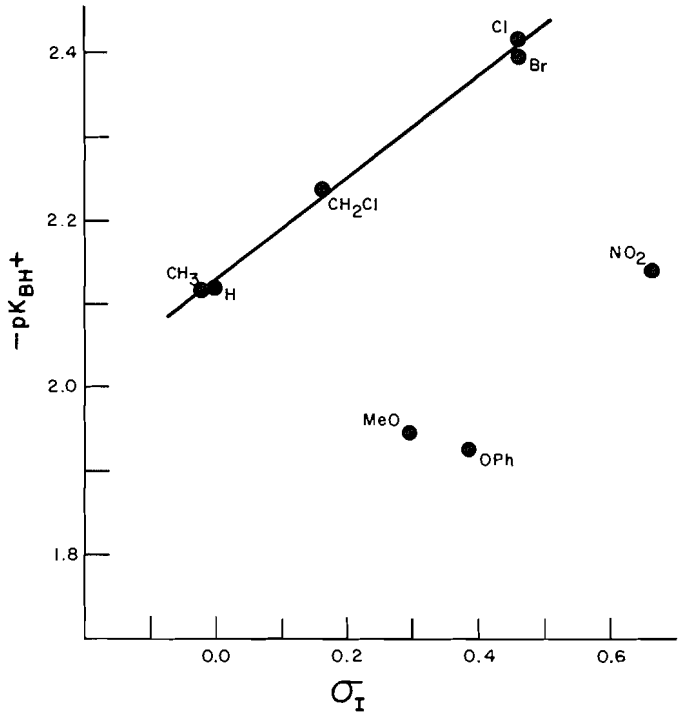

FIG. 4. Linear free energy plot for the basicity of a series of 2-substituted ethanols.

(−2.12) does not agree well with the value of −1.98 obtained by Lee and Cameron using H-nmr data (7). However, the comparison becomes much better when the original data is recalculated using the latest H_0 and log $[H^+]$ values (18, 25, 26). Application of the X-function method to the H-nmr data then gives a pK_{BH^+} of −2.12 with m^* equal to 0.23.

When Bonvicini and co-workers (20) applied the Bunnett–Olsen equation (27, 28) to the proton nmr data for methanol, a pK_{BH^+} of −1.98 was obtained. They used a method similar to the procedure described above to determine chemical shifts for the fully protonated alcohol.

The low values of m^* reported in Table 3 are very likely as a consequence of the high solvation requirements for the protonated alcohols relative to their neutral forms. Because each increase in acidity is necessarily accompanied by a decrease in the amount of water available in the solution, oxonium ions which require extensive solvation (through hydrogen bonding), are less readily formed than other cations. The consequence of this reality is low m^* values.

The alcohols in this study, with the exception of 2-propanol, can be considered to be a series of monosubstituted ethanols. The inductive effects of the substituents can then be observed from a plot of basicity constants against the substituent constants, σ_I, as in Fig. 4 (29, 30). From this plot it can be seen that the points for ethanol, 1-propanol, 3-chloropropanol, 2-chloroethanol, and 2-bromoethanol all fall on a single straight line. A linear regression analysis of the data gives a slope of +0.65 ± 0.06 and an intercept of 2.12. The correlation coefficient of this plot (0.996) can be considered as "excellent" (31). The positive slope indicates that the reaction is facilitated by electron-withdrawing substituent groups, as would be predicted since these reactions are defined in terms of the dissociation of the conjugate acids.

The plot in Fig. 4 also indicates that the basicities for the nitro-, methoxy-, and phenoxy-substituted ethanols do not

Can. J. Chem. Downloaded from www.nrcresearchpress.com by 118.98.75.50 on 09/07/12
For personal use only.

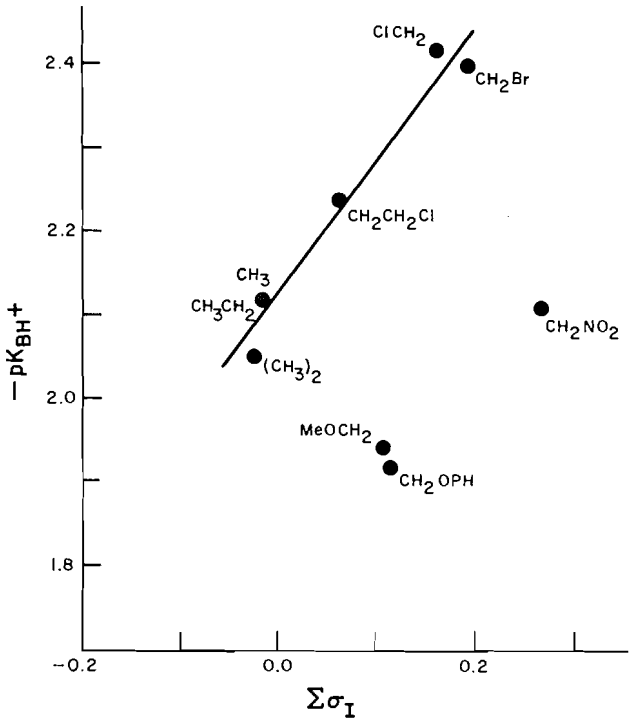

FIG. 5. Linear free energy plot for the basicity of a series of mono- and disubstituted methanols.

correlate with the other alcohols. Since the points for these three alcohols fall below the others it appears that alcohols which bear oxygen-containing substituents are more basic than would be predicted by about 0.5 pK units; i.e., for these alcohols equilibrium [1] appears to be shifted slightly to the left. The reason for this seems likely to be stabilization of the conjugate acids by internal hydrogen bonding, an effect that has previously been noted in the literature (32).

A similar inductive effect correlation can be made by treating the alcohols as a series of substituted methanols (Fig. 5). Since substituent constants have been shown to be additive (31, 33), the data for 2-propanol can also be included in this correlation. The plot has a slope of $+1.7 \pm 0.1$ and intercept of 2.11. Although the correlation coefficient (0.970) is not as good as that obtained for the plot in Fig. 4, it is typical of linear free-energy plots and still very acceptable (31). The more positive slope is obtained because the substituents are now considered to be one methylene group closed to the protonated center. This ρ value (+1.7) is similar to that found for the protonation of dialkyl ethers (+2.0), acetophenones (+1.69), and thiobenzoic acids (+1.4) (20, 34, 35).

The ratio of the ρ values from the plots in Figs. 3 and 4 is 0.4. This ratio, which has been called the methylene transmission coefficient (36), is an attenuation of the inductive effect by one methylene group. It has previously been calculated to be approximately 0.4 ± 0.1 (37), but often varies with the nature of the substituent (36).

The transmission coefficient can be used to estimate a σ_I value for the nitromethylene group from the value for NO_2. The σ_I value for the nitro group (0.67) times the transmission coefficient (0.4) gives an approximate σ_I value for O_2NCH_2 of +0.27. When this value is included in the plot for the substituted methanols (Fig. 4), it can be seen that the three alcohols bearing oxygen-containing substituents fall below the others, again by about 0.5 pK units.

Because extensive compilations of σ_I values are available in the literature (25, 26), the use of these correlations now permit the calculation of basicity constants for a large number of alcohols.

Conclusions

(1) The pK_{BH^+} values for aliphatic alcohols can be estimated from the equation, $pK_{BH^+} = 0.65\sigma_I + 2.12$, if the alcohols are considered to be a series of 2-substituted ethanols. If the alcohols are considered to be mono- or disubstituted methanols the correlation equation becomes $pK_{BH^+} = 1.7\sigma_I + 2.11$.

(2) Alcohols bearing oxygen-containing substituents on the β-carbon are more basic by about 0.5 pK units than predicted by the above correlations.

Acknowledgement

The authors are grateful for financial support from the Natural Sciences and Engineering Research Council of Canada.

1. M. LILER. Reaction mechanisms in sulfuric acid. Academic Press Inc., New York. 1971.
2. L. P. HAMMETT and A. J. DEYRUP. J. Am. Chem. Soc. **54**, 2721 (1932).
3. M. J. JORGENSON and D. R. HARTTER. J. Am. Chem. Soc. **85**, 878 (1963).
4. M. A. PAUL and F. A. LONG. Chem. Rev. **57**, 1 (1957).
5. D. G. LEE and R. CAMERON. J. Am. Chem. Soc. **93**, 4724 (1971).
6. D. G. LEE and M. H. SADAR. J. Am. Chem. Soc. **96**, 2862 (1974); Can. J. Chem. **54**, 3464 (1976).
7. D. G. LEE and R. CAMERON. Can. J. Chem. **50**, 445 (1972).
8. D. G. LEE. Can. J. Chem. **48**, 1919 (1970).
9. A. R. BUTLER. J. Chem. Soc. Perkin Trans. II, 959 (1976).
10. R. L. BENOIT and M. FRECHETTE. Can. J. Chem. **63**, 3053 (1985).
11. R. A. COX, L. M. DRUET, A. E. KLAUSNER, T. A. MODRO, P. WAN, and K. YATES. Can. J. Chem. **59**, 1568 (1981); R. A. COX and K. YATES. Can. J. Chem. **59**, 1560 (1981).
12. R. A. MCCLELLAND and W. F. REYNOLDS. Can. J. Chem. **54**, 718 (1976).
13. H. CERFONTAIN, A. KOEBERG-TELDER, and C. KRUK. Tetrahedron Lett. **42**, 3639 (1975).
14. Y. R. SIIGUR, M. MYAGI, Y. L. KHALDNA, and E. LIPPMAA. Reakts. Sposobn. Org. Soed. **8**, 267 (1971).
15. R. L. BENOIT and M. FRECHETTE. Can. J. Chem. **62**, 995 (1984).
16. J. T. EDWARD, J. B. LEANE, and I. C. WANG. Can. J. Chem. **40**, 1521 (1962).
17. R. A. COX and K. YATES. Can. J. Chem. **59**, 2116 (1981).
18. R. A. COX and K. YATES. J. Am. Chem. Soc. **100**, 3861 (1978).
19. R. A. COX and K. YATES. Can. J. Chem. **61**, 2225 (1983).
20. P. BONVICINI, A. LEVI, V. LUCCHINI, G. MODENA, and G. SCORRANO. J. Am. Chem. Soc. **95**, 5960 (1973).
21. Y. L. KHALDNA. Russ. Chem. Rev. **49**, 1174 (1980).
22. R. KOPPANG, C. G. RUSSELL, and D. G. LEE. Acta Chem. Scand. B, **31**, 491 (1977).
23. V. A. PALM. Tables of rate and equilibrium constants of heterocyclic organic compounds. Supplementary volume 1, Issue 3, Tartu State University Press. 1986. pp. 1091–1095.
24. R. E. WESTON, S. EHRENSON, and K. HEINZINGER. J. Am. Chem. Soc. **89**, 481 (1967).
25. C. D. JOHNSON, A. R. KATRITZKY, and S. A. SHAPIRO. J. Am. Chem. Soc. **91**, 6654 (1969).
26. W. F. GIAUQUE, E. W. HORNUNG, J. E. KUNZLER, and T. R. RUBIN. J. Am. Chem. Soc. **82**, 62 (1960).
27. J. F. BUNNETT and F. P. OLSEN. Can. J. Chem. **44**, 1899 (1966).

Can. J. Chem. Downloaded from www.nrcresearchpress.com by 118.98.75.50 on 09/07/12
For personal use only.

28. J. F. BUNNETT and F. P. OLSEN. Can. J. Chem. **44**, 1917 (1966).
29. M. CHARTON. Prog. Phys. Org. Chem. **13**, 119 (1981).
30. M. CHARTON. J. Org. Chem. **29**, 1222 (1964).
31. H. H. JAFFE. Chem. Rev. **53**, 191 (1953).
32. A. F. POPOV and ZH. P. GEL'BINA. Geol. Kim. Biol. Nauk. **4**, 328 (1977).
33. R. W. TAFT, JR. Steric effects in organic chemistry. *Edited by* M. S. Newman. John Wiley and Sons Inc., New York. 1956.
34. R. A. COX, C. R. SMITH, and K. YATES. Can. J. Chem. **57**, 2952 (1979).
35. R. A. COX and K. YATES. Can. J. Chem. **60**, 3061 (1982).
36. F. G. BORDWELL and J. E. BARTMESS. J. Org. Chem. **43**, 3103 (1978).
37. J. E. LEFFLER and E. GRUNWALD. Rates and equilibria of organic reactions. John Wiley and Sons Inc., New York. 1963.

Can. J. Chem. Downloaded from www.nrcresearchpress.com by 118.98.75.50 on 09/07/12
For personal use only.

Photooxygenation of nitrobenzyl derivatives. Mechanisms of photogeneration and hydrolysis of α-hydroperoxy nitrobenzyl ethers

PETER WAN,[1] S. MURALIDHARAN, IAIN MCAULEY, AND CHRISTOPHER A. BABBAGE
Department of Chemistry, University of Victoria, Victoria, B.C., Canada V8W 2Y2

Received November 30, 1986

This paper is dedicated to Professor John T. Edward

PETER WAN, S. MURALIDHARAN, IAIN MCAULEY, and CHRISTOPHER A. BABBAGE. Can. J. Chem. **65**, 1775 (1987).

The photooxygenation of nitrobenzyl derivatives **1–10** has been studied in aqueous solution as a function of pH. For *m*-nitrobenzyl ethers **2–4** and **9**, stable α-hydroperoxy ethers (**11–13**) are the primary photochemical products. Acid hydrolysis of **11–13** gives *m*-nitrobenzaldehyde and hydrogen peroxide. Quantum yields for photooxygenation are reported for a number of derivatives as a function of pH. Acid and base catalyses of photooxygenation are observed for several compounds. A mechanism involving photogenerated nitrobenzyl carbanion intermediates is proposed.

PETER WAN, S. MURALIDHARAN, IAIN MCAULEY et CHRISTOPHER A. BABBAGE. Can. J. Chem. **65**, 1775 (1987).

Opérant en solutions aqueuses, on a étudié la photo-oxydation des dérivés nitrobenzyliques (**1–10**) en fonction du pH. Dans les cas des éthers *m*-nitrobenzyliques (**2–4** et **9**), les produits photochimiques primaires sont les éthers α-hydroperoxylés stables (**11–13**). L'hydrolyse acide des composés **11–13** conduit au *m*-nitrobenzaldéhyde et au peroxyde d'hydrogène. Dans les cas d'un certain nombre de dérivés, on rapporte les rendements quantiques pour la photo-oxygénation en fonction du pH. Dans les cas de plusieurs composés, on a observé que la photo-oxygénation est soumise à une catalyse acide/base. On propose un mécanisme impliquant, comme intermédiaires, des carbanions nitrobenzyliques générés photochimiquement.
[Traduit par la revue]

Can. J. Chem. Downloaded from www.nrcresearchpress.com by 118.98.75.50 on 09/07/12
For personal use only.

The photochemistry of aliphatic and aromatic nitro compounds has received considerable attention and several reviews (1–4) have been published. Recently, we (5–7) and others (8, 9) have noted that some *m*- and *p*-nitro-substituted benzenes display unexpected reactivity when irradiated in aqueous solution, especially in the presence of hydronium and hydroxide ions as catalysts for the transformations (5–8). Whereas it is well known (1–4) that *o*-nitrobenzyl systems are photolabile due to the proximity to the substituent of the reacting nitro chromophore, resulting in initial intramolecular hydrogen abstraction via the n,π^* triplet excited state, it had been assumed for many years that the corresponding *meta* and *para* derivatives should not be photolabile, except for simple photoreduction. However, in aqueous solution, a number of *m*- and *p*-nitro-substituted derivatives have been found to react via new photochemical processes (5–9). In a preliminary report (10) we had demonstrated that molecular oxygen can react with photoexcited nitrobenzyl derivatives, which represent an additional example of the rich and sometimes unpredictable photochemistry of *m*- and *p*-substituted nitroaromatic compounds. In this work, we report the generality and proposed mechanisms for the photooxygenation reaction of a variety of *m*- and *p*-nitro-substituted derivatives. In addition, the thermal aqueous chemistry of several photogenerated α-hydroperoxy *m*-nitrobenzyl ethers isolated in these studies will be presented.

Results

Product studies

The compounds chosen for the study, **1–10**, are shown below. Both *m*- and *p*-nitrobenzyl alcohols **1** and **7**, respectively, are commercially available. In addition, their aqueous photochemistry under *deaerated* conditions has been reported by us (6, 7). Nitrobenzyl ethers **2–5** and **8** are available from their corresponding nitrobenzyl chlorides, via the appropriate Williamson ether synthesis. Acetate **6** was made by treating **1** with acetyl chloride in the presence of pyridine. 2-Methoxy-(*m*- and *p*-nitrophenyl)ethanols **9** and **10** were made via acid-catalyzed methanolysis of the corresponding nitrophenyl epoxides. The details of these syntheses are presented in the experimental section.

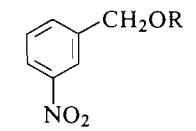

1 R = H
2 R = CH_3
3 R = CH_2CH_3
4 R = $CH_2CH_2CH_3$
5 R = Ph
6 R = $OCOCH_3$

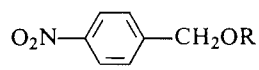

7 R = H
8 R = CH_3

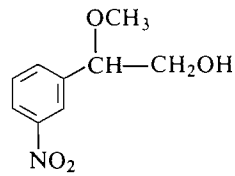

9

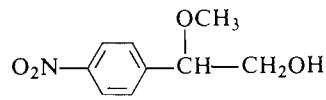

10

Rafizadeh and Yates (8) have reported that *m*-nitrobenzyl ethers **2**, **3**, **5**, and **9** (and related compounds not shown above) all reacted in *deaerated* aqueous solution to give *m*-nitrobenzaldehyde as the only isolable product in low quantum yield (0.011 for **2** in pH 7). In this study, we have found that when ethers **2–4** are irradiated in *aerated* aqueous solution (typical scale 200–500 mg; 20% CH_3CN/H_2O; oxygen purged; Hanovia 450-W medium pressure lamp; 30-min photolysis), the major products are the corresponding α-hydroperoxides, obtained in about 40% yield (eq. [1]). The minor product consists of about 5% of the corresponding alkyl *m*-nitrobenzoate and a trace (<5%) of *m*-nitrobenzaldehyde. The remainder of the photolysate is recovered starting material. When the same photolysis is carried out under an argon atmosphere, the only

[1]NSERC University Research Fellow. Correspondence may be addressed to this author.

[1] 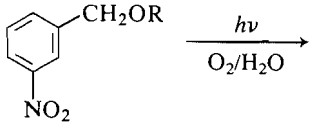

2–4

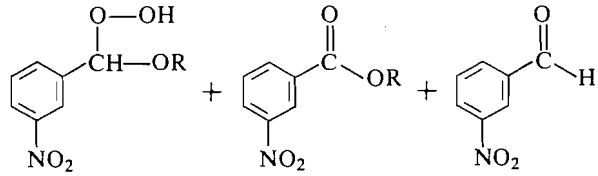

40% 5% <5%

11 R = CH_3 **14** R = CH_3
12 R = CH_2CH_3 **15** R = CH_2CH_3
13 R = $CH_2CH_2CH_3$ **16** R = $CH_2CH_2CH_3$

product is *m*-nitrobenzaldehyde, obtained in low yield, as was reported by Rafizadeh and Yates (8). The photooxygenation (eq. [1]) is not observed in oxygenated aqueous solution when kept in the dark, even for extended periods (>1 day). Thus, in the presence of oxygen, there is a new photochemical pathway that involves overall insertion of molecular oxygen into the benzylic C—H bond of **2–4**. Extended photolysis of **2–4** (>1 h) results in an increased proportion of esters **14–16** in the photolysate. Furthermore, independent photolysis of α-hydroperoxides **11–13** in aqueous solution or in pure CH_3CN (both under argon) results in the formation of **14–16**, respectively, as the only product. This is taken as evidence that esters **14–16** are secondary photoproducts of **11–13**, presumably via a mechanism involving initial O—O bond cleavage on excitation (eq. [2]). The small amount of *m*-nitrobenzaldehyde always ob-

[2] 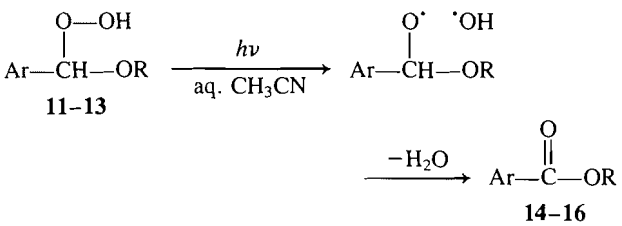

11–13 **14–16**

served in these photolyses is presumably due to the residual photoredox pathway (as observed in argon purged solutions) reported previously (8). Alternatively, it may be due to residual thermal hydrolysis of **11–13** (*vide infra*).

α-Hydroperoxides **11–13** are, as far as we are aware, new compounds. They are yellow oils and are relatively stable in hydrocarbon and nonhydroxylic solvents. For example, refluxing in benzene for several hours results in only about 20% conversion of **11–13** to the corresponding ester, via an overall dehydration of the compound. We have fully characterized **11–13** via standard spectroscopic techniques (see Experimental). For example, the methine proton is shifted downfield to δ 5.8 compared to δ 5.5 for the methine signal of *m*-nitrobenzaldehyde dimethyl acetal. The OOH proton resonates at δ 8.8 (exchangeable), considerably downfield shifted from alcoholic OH's, which resonate in the region δ 2–5. These α-hydroperoxides are reducible with either aqueous KI or Na_2SO_3, to give *m*-nitrobenzaldehyde cleanly as the only product (in addition to the alcohol fragment, which was not characterized), via eq. [3]. In aqueous KI, the course of the reduction may be judged by the increase in coloration (to a final deep yellow) due to the formation of I_2.

[3] 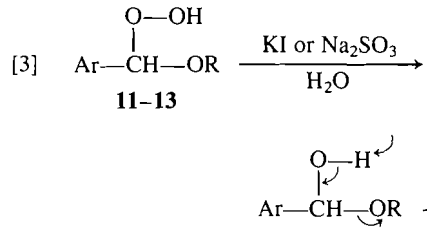

11–13

α-Hydroperoxides **11–13** are unstable in aqueous solution, especially in low pH. Below pH 3 they suffer acid-catalyzed hydrolysis, to give *m*-nitrobenzaldehyde, the corresponding alcohol fragment, and hydrogen peroxide (eq. [4]). Hydrogen peroxide was detected after complete hydrolysis, by its characteristic reaction with KI (to give I_2). To gain insight into the mechanism of hydrolysis, hydroperoxide **11** was solvolyzed in pure MeOH, with several drops of concentrated H_2SO_4 added as catalyst. The products were *m*-nitrobenzaldehyde dimethyl acetal and methyl *m*-nitrobenzoate in a 25:75 ratio (eq. [5]).

[4] 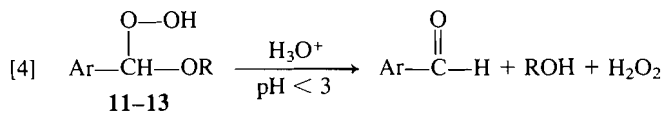

11–13

[5] 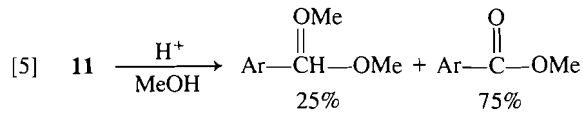

These products were characterized by comparison of the nmr signals with the authentic samples. Although methyl *m*-nitrobenzoate is probably formed via dehydration of **11** (as the simplest explanation), clearly the dimethyl acetal is formed via initial heterolytic cleavage of the C—OOH bond of **11**, i.e., the hydroperoxy group being the leaving group in the solvolysis. Additional discussion regarding the mechanism of hydrolysis of **11–13** will be given in the Discussion. Above pH 3, the hydrolysis pathway is very slow and only dehydration of **11–13** is observed, to give the corresponding alkyl *m*-nitrobenzoates.

Several observations provide insight into the mechanism of photooxygenation of **2–4**. The reaction does not take place in the commonly available organic solvents (CH_3CN, MeOH, EtOH, benzene, diethyl ether, etc., all oxygenated during photolysis). Rose Bengal sensitization for singlet oxygen (λ_{excit} > 400 nm) gives only low yields (<5%) of *m*-nitrobenzaldehyde and methyl *m*-nitrobenzoate for **2**; no α-hydroperoxide is observed, even under low conversion experiments. That singlet oxygen is responsible for these photooxygenations is therefore unlikely, especially considering the fact that singlet oxygen is not known to react with benzylic hydrogens to give hydroperoxides and additionally is not known to exhibit the drastic solvent dependence of reactivity as observed above.

The reaction requires an α-oxygen substituent in the structure since *m*-nitrotoluene does not undergo the reaction. However, the presence of an α-oxygen is not a sufficient requirement since both **5** and **6** are totally nonreactive. It is not clear at this time why **5** and **6** are not reactive. The reaction appears to be very sensitive to the presence of electron-withdrawing groups in R of **1–6**. As there are no accessible low energy states in the acetoxy or phenoxy chromophores, photophysical quenching of reaction of **5** and **6** appears unlikely.

The discovery that, in the presence of oxygen, certain *m*-nitrobenzyl ethers react via a new pathway led us to reinvestigate the photochemistry of *m*-nitrobenzyl alcohol **1**. We have

Can. J. Chem. Downloaded from www.nrcresearchpress.com by 118.98.75.50 on 09/07/12
For personal use only.

Can. J. Chem. Downloaded from www.nrcresearchpress.com by 118.98.75.50 on 09/07/12
For personal use only.

reported the aqueous redox photochemistry of both *m*- and *p*-nitrobenzyl alcohols **1** and **7** in deoxygenated aqueous solution (6, 7). For **1**, the products are *m*-nitrobenzaldehyde (70%) and *m*-azoxybenzaldehyde **17** (30%). Compound **17** is the

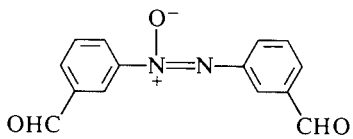

17

"reduction" product in the overall photoredox pathway, the mechanism of which has been discussed in some detail (6, 7). However, when **1** is irradiated in oxygenated aqueous solution, the only product is *m*-nitrobenzaldehyde, with a concurrent 20% increase in quantum efficiency (from 0.087 to 0.10). Additionally, hydrogen peroxide was detected in the aqueous portion (after CH_2Cl_2 extraction) by its characteristic reaction with KI. These observations are consistent with a photooxygenation pathway for **1** when irradiated in oxygenated aqueous solution (eq. [6]), analogous to that observed for ethers **2–4**.

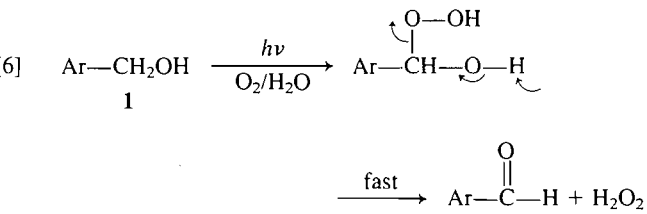

[6] $Ar{-}CH_2OH \xrightarrow[O_2/H_2O]{h\nu} Ar{-}CH(OOH){-}OH \xrightarrow{fast} Ar{-}C(=O){-}H + H_2O_2$

1

However, the initially formed α-hydroperoxy alcohol is unstable and decomposes to *m*-nitrobenzaldehyde and hydrogen peroxide. This reaction and the ones already described above for **2–4** offer a means for the photochemical activation of molecular oxygen, to give hydrogen peroxide. It is made more attractive by the fact that **1–4** absorb well beyond 300 nm (to about 370 nm), thus enabling solar radiation to effect the conversion.

p-Nitrobenzyl derivatives **7** and **8** showed no reaction in oxygenated solution in the pH region 0–11. In these cases, complete recovery of starting material was possible after photolysis. Above pH 11, photolysis of **7** and **8** gives *p*-nitrobenzoic acid as the only product (eq. [7]), the yield increasing

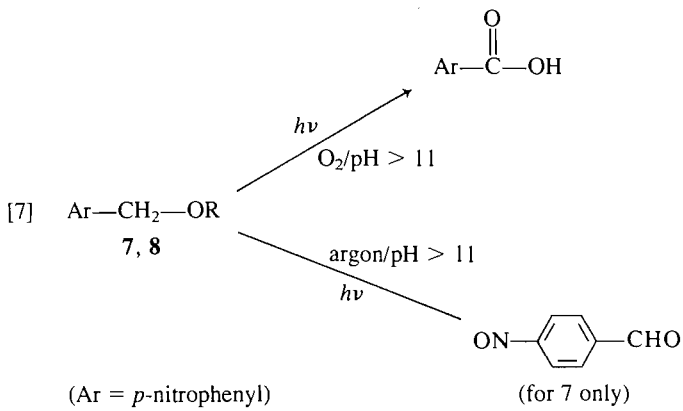

[7] $Ar{-}CH_2{-}OR$ (**7, 8**) → ($h\nu$, O_2/pH > 11) → $Ar{-}C(=O){-}OH$; ($h\nu$, argon/pH > 11) → $ON{-}C_6H_4{-}CHO$

(Ar = *p*-nitrophenyl) (for 7 only)

with pH (*vide infra*). We have reported (6, 7) that **7** gives *p*-nitrosobenzaldehyde when photolyzed above pH 11 in deoxygenated solutions (eq. [7]). Compound **8** is photoinert under the same conditions. It is apparent, however, that in the presence of oxygen, a different photochemical pathway is followed by **7**, whereas photoreaction is observed for **8** only in *oxygenated* aqueous base.

To gain additional insight into the mechanism of photooxygenation of **1–4** and **7**, **8**, nitrophenyl derivatives **9** and **10** were studied. We have recently reported (5) that both *m*- and *p*-nitrophenethyl alcohols (**18** and **19**, respectively) react via a retro-aldol type pathway in deoxygenated aqueous solution, to give *m*-nitrotoluene in the case of **18** and both *p*-nitrotoluene and *p,p'*-dinitrobibenzyl in the case of **19** (eq. [8]). The

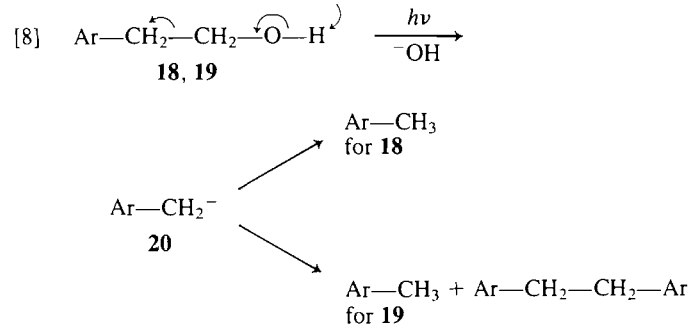

[8] $Ar{-}CH_2{-}CH_2{-}O{-}H$ (**18, 19**) $\xrightarrow[{}^-OH]{h\nu}$ $Ar{-}CH_2^-$ (**20**) → $Ar{-}CH_3$ for **18**; $Ar{-}CH_3 + Ar{-}CH_2{-}CH_2{-}Ar$ for **19**

reactions are base catalyzed. Arguments were presented (5) that support the intermediacy of photogenerated nitrobenzyl carbanions **20**. Based on this and previous studies (6, 7), we suspected that the present photooxygenation reactions of **1–4** and **7**, **8** also proceed via photogenerated nitrobenzyl carbanions. We find that when **9** is photolyzed in oxygenated aqueous solution, the only product is the α-hydroperoxy ether **11** obtained in good yields (>50%). The reaction is base catalyzed (*vide infra*). On extended photolysis, methyl *m*-nitrobenzoate is observed, which was shown to be a secondary photoproduct of **11**. However, photolysis of **10** in neutral or acidic media (pH 0–11; oxygenated) gave only methyl *p*-nitrobenzoate in low yields (<15%); the α-hydroperoxide corresponding to **11** is not observed. At high pH (pH > 11), *p*-nitrobenzoic acid is the only product, with increasing yields with increasing pH. Thus the dichotomy of reactivity observed for **9** and **10** some-

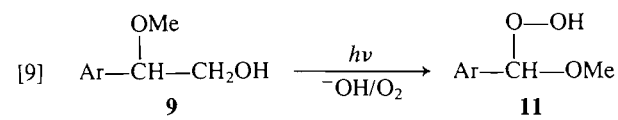

[9] $Ar{-}CH(OMe){-}CH_2OH$ (**9**) $\xrightarrow[{}^-OH/O_2]{h\nu}$ $Ar{-}CH(O{-}OH){-}OMe$ (**11**)

what parallels the results already observed for **1–4** and **7**, **8**. Corroborative evidence, which suggests that photogenerated nitrobenzyl carbanions can react with molecular oxygen to give reasonably stable hydroperoxides, is the recent finding[2] that both *m*- and *p*-nitrophenyl acetate ions (**21** and **22**, respectively) give the corresponding hydroperoxides in high quantum efficiency ($\Phi > 0.5$) on photolysis in oxygenated aqueous solution (eq. [10]). The photodecarboxylation of **21** and **22** has already been shown by Margerum and Petrusis (12) to proceed via nitrobenzyl carbanion intermediates, which in deoxygenated solutions give the corresponding toluenes and, in the case of the *para* isomer, significant yields of *p,p'*-dinitrobibenzyl.

Quantum yields and pH effects

The photooxygenation of **2–4** and **9** may be conveniently followed by uv spectrophotometry. For example, as shown in Fig. 1, photolysis of **2** in oxygenated pH 7 solution results initially in very little change in the uv absorption spectrum. However, on addition of several drops of 30% H_2SO_4 to the

[2]P. Wan and S. Muralidharan. Manuscript in preparation.

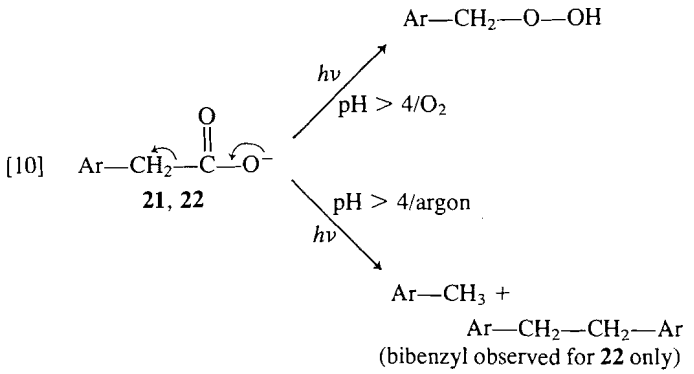

[10]

cuvette solution, a "grow-in" of a band at about 235 nm (assignable to *m*-nitrobenzaldehyde) takes place. This observation is consistent with the product studies reported above, in which the initially photogenerated α-hydroperoxides are relatively stable in neutral pH but suffer acid-catalyzed hydrolysis in acidic medium. That very little absorbance change occurs on initial generation of the α-hydroperoxide (trace 1 of Fig. 1) is consistent with the fact that **2** and **11** have nearly identical λ_{max} and ε_{max} (for **2**, λ_{max} = 266 nm, ε_{max} = 7 300; for **11**, λ_{max} = 264 nm, ε_{max} = 7 000). *m*-Nitrobenzaldehyde, of course, has a very different uv absorption spectrum, with λ_{max} = 235 nm (ε_{max} = 23 000).

Quantum yields for α-hydroperoxide formation were measured for **2**–**4** and **9** at pH 7 (λ_{excit} = 254 nm), using the known quantum yield for photoredox reaction of **1** in deoxygenated solution (Φ = 0.087), as measured by Rafizadeh and Yates (8), as an actinomer (Table 1). The procedure used involves measuring the amount of *m*-nitrobenzaldehyde produced via uv spectrophotometry after acidification of the initially photolyzed solution with aqueous H_2SO_4, as shown in Fig. 1. Sufficient time was allowed for complete hydrolysis of the initially generated α-hydroperoxide prior to final measurement. A dilution factor was incorporated in the calculations due to the dilution effect on addition of the acid. Using the same procedure, quantum yields were measured for **2** and **9** as a function of pH (from 0 to 14), to gain insight into the pH effect of reaction. The results of the pH study are shown in Fig. 2. Compound **9** shows strong base catalysis above pH 11, with a maximum quantum yield of 0.21 at pH 14. Compound **2**, on the other hand, does not show base catalysis, but both **2** and **9** exhibit weak acid catalysis below pH 2. Studies were not carried out in the H_0 acidity region since the generated α-hydroperoxides are quickly hydrolyzed to *m*-nitrobenzaldehyde, and also because a competitive redox pathway may be operative with significant quantums yields in the higher acidity region (6–8). It may not be possible to separate the oxygenation pathway from the internal redox pathway at these acidities, but studies are under way to explore the extent of the photooxygenation pathway at higher acidities.

The quantum yields for photooxygenation of the *p*-nitro-substituted compounds **7**, **8**, and **10** were much lower than the corresponding *meta* isomers. Thus for **10** at pH 7, Φ for methyl ester formation is about 0.02 and increases to about 0.08 at pH 14. There is no acid catalysis of reaction. For **7** and **8**, measurable quantum yields are observed only above pH 12 (the product is *p*-nitrobenzoic acid), reaching a quantum yield of about 0.05 at pH 14 for both **7** and **8**. The base catalysis of reaction is shown in Fig. 3. Again there is no measurable acid catalysis of reaction, both **7** and **8** being photoinert in the pH 0–11 region.

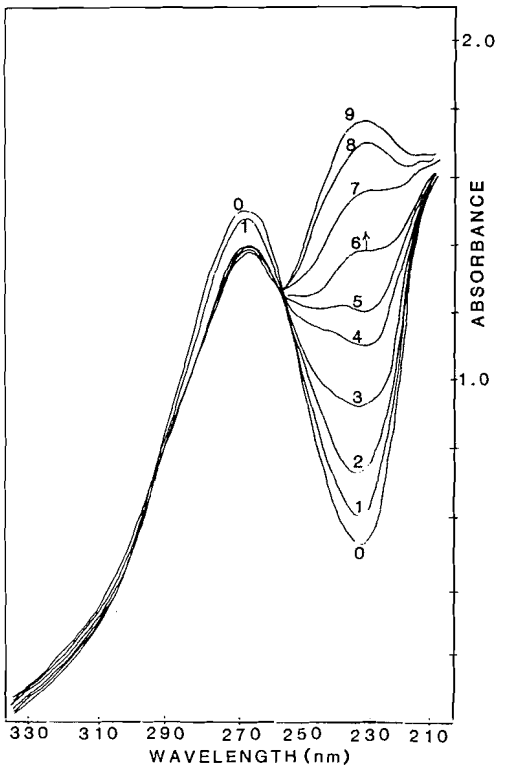

FIG. 1. Ultraviolet traces of the photooxygenation of **2** and subsequent acid-catalyzed hydrolysis of the α-hydroperoxy ether **11**. Trace 1 was taken immediately after photolysis at 254 nm (Rayonet reactor). Traces 2–9 were recorded initially about every 10 min after the addition of several drops of 30% H_2SO_4 to the cuvette solution, later increasing to every 20 min.

TABLE 1. Quantum yields for α-hydroperoxide formation for compounds **2**–**4** and **9** at pH 7 in oxygenated solution

Compound	Φ^a
2	0.042
3	0.049
4	0.067
9	0.040

[a]Errors are ±10%.

α,α-Dideutero-*m*- and *p*-nitrobenzyl alcohols (α,α-*d*-**1** and α,α-*d*-**7**, respectively) were readily available from a previous study (6, 7). We find that these compounds are less reactive than **1** and **7**, respectively, towards photooxygenation at pH 7. The values are Φ_H/Φ_D = 1.9 for the *para* isomer and 1.4 for the *meta* isomer, where Φ_H and Φ_D are the quantum yields for photooxygenation of the parent alcohol and the α,α-dideuterated compound, respectively.

Solvent isotope effects of photooxygenation were measured for ethers **1**–**4** and **9** and **10**. The results are shown in Table 2. All these compounds are less reactive in H_2O than in D_2O, which supports a mechanism involving solvent participation (see Discussion).

Reactivity of photogenerated α-hydroperoxy ethers

As was discussed above, α-hydroperoxy ethers **11**–**13** suffer acid-catalyzed hydrolysis, to give *m*-nitrobenzaldehyde (eq. [4]). Above pH 3, however, the hydrolysis pathway is very

Can. J. Chem. Downloaded from www.nrcresearchpress.com by 118.98.75.50 on 09/07/12
For personal use only.

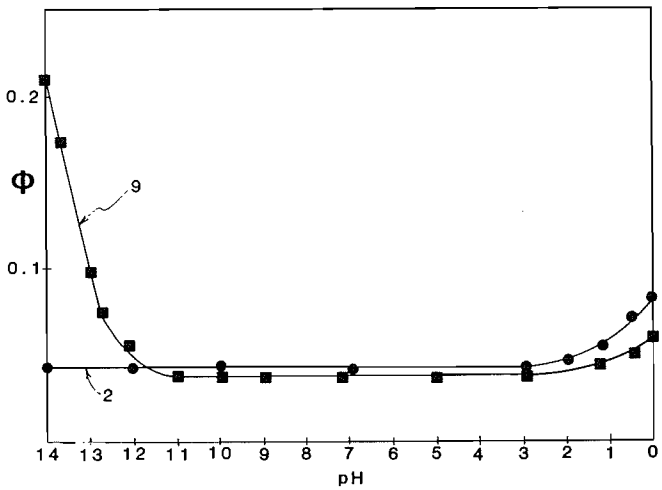

FIG. 2. Plot of quantum yield for α-hydroperoxide formation as a function of pH for **2** and **9**.

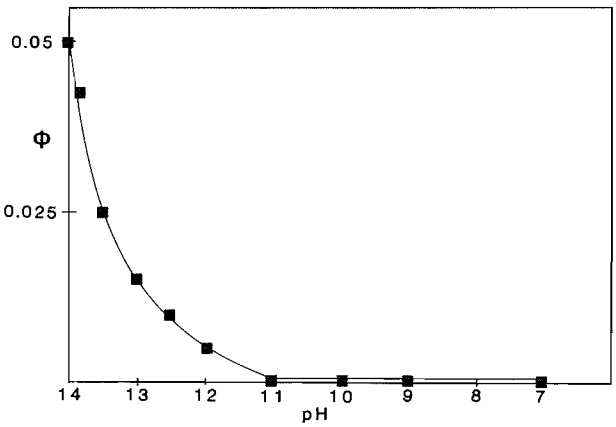

FIG. 3. Plot of quantum yield for photooxygenation as a function of pH for **7** and **8**.

TABLE 2. Solvent isotope effect on quantum yield of α-hydroperoxide formation of **2–4** and **9**, and photooxygenation of **10** (at pH 7)

Compound	Φ_H/Φ_D[a]
1	1.30±0.05
2	1.16±0.02
3	1.17±0.02
4	1.05±0.01
9	1.22±0.02
10	1.29±0.05

[a]Relative quantum yield for reaction in H_2O versus D_2O (pH 7).

slow and an overall dehydration pathway takes over, which gives the corresponding esters **14–16** as the product. Pseudo first-order rate constants of acid-catalyzed hydrolysis were measured as a function of pH for **11–13** via uv spectrophotometry, by monitoring for the formation of *m*-nitrobenzaldehyde. Also measured are the corresponding rates of hydrolysis of *m*-nitrobenzaldehyde dimethyl acetal **23** at selected pH's, for comparison purposes. These rates are tabulated in Table 3.

TABLE 3. Pseudo first-order rate constants for hydrolysis of **11–13** as a function of pH at 30 ± 2°C

	$k_{obs}(s^{-1})$[a]			
pH (or H_0)	**11**	**12**	**13**	**23**
3.0	—	—	—	1.9×10^{-4}
2.0	7.4×10^{-5}	1.4×10^{-4}	9.3×10^{-5}	1.7×10^{-3}
1.0	2.7×10^{-4}	5.1×10^{-4}	6.1×10^{-4}	1.0×10^{-2}
0.25	1.0×10^{-3}	2.3×10^{-3}	2.3×10^{-3}	—
−0.45	2.1×10^{-3}	6.2×10^{-3}	6.7×10^{-3}	—

[a]Via uv spectrophotometry at 235 nm. Errors ±5%.

TABLE 4. Observed first-order rate constants for dehydration of **11–13** in aqueous solution as a function of pH at 30 ± 2°C

	$k_{obs}(s^{-1})$[a]		
pH	**11**	**12**	**13**
3.0	2.9×10^{-5}	3.7×10^{-5}	3.4×10^{-5}
5.0	4.7×10^{-5}	4.3×10^{-5}	3.3×10^{-5}
7.0	4.4×10^{-5}	3.8×10^{-5}	4.8×10^{-5}
8.0	6.4×10^{-5}	4.4×10^{-5}	6.5×10^{-5}

[a]Via uv spectrophotometry at 254 nm. Errors ±10%.

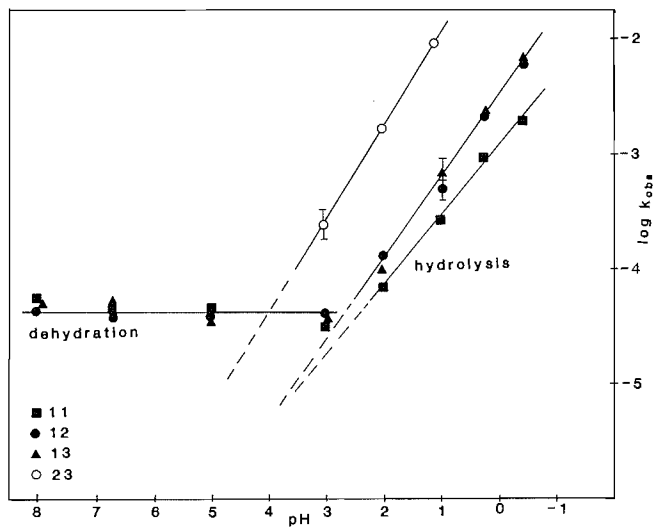

FIG. 4. Logarithmic plot of first-order rate constants for hydrolysis of **11–13** and **23**, and the dehydration of **11–13** as a function of pH.

Observed first-order rate constants for dehydration of **11–13** in the pH 3–8 region were also measured and are given in Table 4. Compound **23** does not react via a dehydration pathway. All of the above rate constants are plotted together in logarithmic form in Fig. 4. The hydrolysis rates of **11–13** are significantly slower (by more than one log unit) than for **23** at the same pH. However, they all exhibit the same dependence on acidity below pH 3 (slope ≃ 1). In the series **11–13**, the ethyl and propyl ethers (**12** and **13**) are measurably more reactive than the methyl ether **11** towards hydrolysis, but all have similar rates for dehydration in the pH 3–8 region.

Can. J. Chem. Downloaded from www.nrcresearchpress.com by 118.98.75.50 on 09/07/12
For personal use only.

Can. J. Chem. Downloaded from www.nrcresearchpress.com by 118.98.75.50 on 09/07/12
For personal use only.

Discussion

The photoretro-aldol type reaction of **18** and **19** and related compounds, as well as the photodecarboxylation of **21** and **22** (which may be formally regarded as a photoretro-aldol type reaction) are believed to proceed via nitrobenzyl carbanion intermediates (5, 12). Margerum and Petrusis (12) have observed a transient at 350 nm in the decarboxylation of *p*-nitrophenylacetate ion **22**, which has been assigned to the *p*-nitrobenzyl carbanion. The lifetime of this intermediate in neutral water is at least several seconds (12). The corresponding *m*-nitrobenzyl carbanion has not been observed and available data (12) indicate that it is much shorter lived, which is consistent with the expected relative stability of these two species (the *p*-nitrobenzyl carbanion can be stabilized via a resonance form in which the negative charge resides at the nitro group). It is well known that carbanions generated in the ground state react efficiently with oxygen (13–15), to give initially hydroperoxides, which readily dehydrate in many cases to give carbonyl compounds, which themselves may undergo further oxygenation to give carboxylic acids as the final oxidation product. Russell *et al.* (15) have shown that the base-catalyzed oxygenation of *p*-nitrotoluene in potassium *tert*-butoxide in *tert*-butanol gives *p*-nitrobenzoic acid, via reaction of *p*-nitrobenzyl carbanion with molecular oxygen. Since strong base is required to generate the *p*-nitrobenzyl carbanion in the ground state, the initially formed hydroperoxides are not isolable (15). However, when **21** and **22** are irradiated in oxygenated aqueous solution, the major products are the corresponding hydroperoxides (eq. [10]). The observation that these hydroperoxides are not formed when **21** and **22** are irradiated in oxygenated organic solvents or in oxygenated aqueous solution when pH $< pK_a$ of the substrate argues against a simple free radical autoxidation mechanism (16) for photooxygenation. These results indicate that when *m*- and *p*-nitrobenzyl carbanions are photogenerated in oxygenated aqueous solution, they react preferentially with oxygen, and not with protons from solvent water.

The base-catalyzed photooxygenation reaction of **9** (eq. [9]; Fig. 2) is also consistent with a mechanism involving an initial photoretro-aldol step to generate the α-methoxy-*m*-nitrobenzyl carbanion, followed by rapid reaction with oxygen to give **11**, and not with a free radical mechanism for oxygenation. Moreover, a simple free radical autoxidation pathway would give hydroperoxide **24** as the oxidation product (via reaction of the benzyl radical from hydrogen abstraction of **9** with oxygen), which is not observed. If **24** is formed, it should survive in the

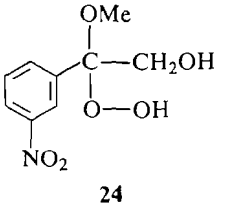

24

reaction mixture since very similar compounds (viz. hydroperoxides **11**–**13**) are isolable under the same reaction conditions.

We now turn our attention to a discussion of the photooxygenation mechanism for the parent nitrobenzyl systems **1**–**4** and **7**, **8**. The reactions of **1**–**4** and **7**, **8** are closely related to those of **9** and **21**, **22**. In addition, several observations rule out a free radical pathway. The photooxygenations are not observed at all in oxygenated organic solvents. A free radical mechanism would not exhibit such a drastic solvent dependence. Compounds **7** and **8** exhibited base catalysis of photooxygenation, and **1**–**4** exhibited acid catalysis, observations that are clearly incompatible with a radical pathway. The substantial solvent isotope effect for reaction (Table 2) for a number of these derivatives clearly implicates the involvement of solvent water in mediating the reaction, acting as a base (D_2O in a weaker base than H_2O) and also perhaps acting as a proton source (D_2O is a weaker acid than H_2O). Therefore, it is proposed that the mechanism of photooxygenation of **1**–**4** and **7**, **8** involves photogenerated nitrobenzyl carbanions, formed via deprotonation of the benzylic C—H bond by solvent water for **1**–**4**, where no base catalysis is observed, and by hydroxide ion for **7** and **8**, where base catalysis is observed. We propose also that the generated carbanions are "hydrogen bonded" species (to the departing proton) and not free carbanions, as shown by structure **25** for the *meta* derivatives. It reacts with

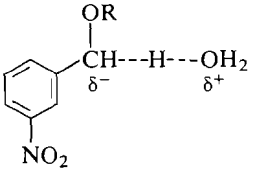

25

oxygen to give the corresponding hydroperoxides, but in the absence of oxygen returns to starting material without incorporation of deuterium from D_2O. It is not clear at this time whether **25** is an electronically excited or ground state species. However, deactivation to the ground state is expected to be very fast and subsequent reaction with oxygen could take place from there.

We are not aware of any precedents in the literature of photochemical mechanisms in which the primary photochemical event involves deprotonation of a C—H bond, except in a related reaction reported by us (6, 7), which also involves nitroaromatic compounds. We showed (6, 7) that deprotonation of a benzylic C—H bond of nitroaromatic compounds in aqueous solution is a viable mechanism, and leads to some interesting chemistry. Again, we were unable to observe deuterium incorporation from D_2O into recovered substrate (6, 7). Free nitrobenzyl carbanions are known to react with D_2O (if oxygen is not present in solution) to give the α-deuterated species. For example, when **21** and **22** are photodecarboxylated in D_2O, the nitrotoluene photoproducts are incorporated with deuterium at the benzylic position.[2] That free carbanions are probably not generated via simple photodeprotonation of C—H bonds is perhaps not surprising because it is well known that there is an inherent activation barrier for heterolytic C—H bond cleavage, which is believed to be due to the inability of the deprotonating base to initially form a hydrogen bonded complex with the departing proton prior to the actual deprotonation (17). This has the consequence of making rates of proton transfers to and from carbon slower than expected in most cases. Since excited states are short lived, simple deprotonation of a C—H bond would generally not be a competitive deactivational process, which is consistent with the lack of reported photochemical reactions via this mechanism. However, the results of this work along with those of a related reaction (6, 7) indicate that, in exceptionally reactive substrates such as nitrobenzyl systems, partial deprotonation of the benzylic C—H bond by solvent water or hydroxide ion in the excited state can lead to photochemical reaction.

The dichotomy of catalytic effects observed in this study and

Can. J. Chem. Downloaded from www.nrcresearchpress.com by 118.98.75.50 on 09/07/12
For personal use only.

in a previous study (6, 7), in which the simple *meta* nitro-substituted isomers exhibit acid catalysis and the simple *para* isomers exhibit base catalysis of reaction, is apparently a general phenomenon in the photochemistry of these nitroaromatic compounds in aqueous solution (6, 7). It is well known that there is better electronic transmission of charge at the *meta* than at the *para* position in the excited state of substituted benzenes (17–19). The acid catalysis observed for the *meta* derivatives may be due to assistance of the deprotonation step from the polarized excited state, via protonation of the electron-rich nitro group, as shown by structure **26**. Such a transition

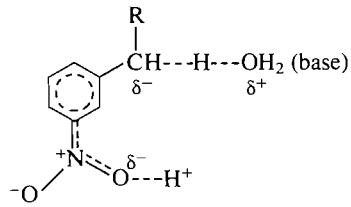

26

state structure would also account for the observed solvent isotope effect of greater than unity in these reactions (Table 2). It would also explain why these reactions are observed only in aqueous solution, since the reaction requires the solvent to act as a base and as a proton source, in addition to the requirement of high dielectric constant. Water is by far the most polar of all the known protic solvents. It is not clear at this time why acid catalysis of reaction for the *para* isomers is not observed.

We have not made any attempts to determine directly the multiplicity of the reactive state of these photooxygenations due to the fact that the solutions were saturated with oxygen during reaction. However, the close analogy of these reactions with the photoredox processes (6–8) and photoretro-aldol reactions (5) would suggest that the same reactive state is involved, viz. the triplet excited state.

The propensity for nitrobenzyl carbanion formation in these systems can be rationalized by considering the enhanced electron-withdrawing ability of photoexcited aromatic nitro groups (5–8, 18, 20). The *m*-nitro group, having better electron-withdrawing ability, accounts for the ease of reaction of the *meta* isomers in these reactions and in others requiring the same type of stabilization (5–8, 18, 20). The *p*-nitro group, on the other hand, does not have the same electron-withdrawing power (but enhanced compared to the ground state, nevertheless) and requires base catalysis for reaction in all cases.

Finally, the thermal hydrolysis of the photogenerated α-hydroperoxides **11–13** requires comment. As shown in Fig. 4, the α-hydroperoxy ethers hydrolyze more slowly than **23**, but with the same catalytic effect (slope of log k vs. pH = 1). Since we were able to demonstrate that methanol will substitute for the hydroperoxy group when the solvolysis is carried out in pure methanol (eq. [5]), the hydrolysis mechanism of **11–13** must involve initial loss of hydrogen peroxide in a specific acid-catalyzed mechanism (eq. [12]). This mechanism also accounts

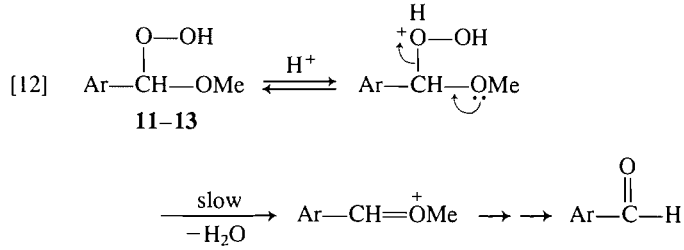

for the fact that the ethyl and propyl ethers **12** and **13**, respectively, are slightly more reactive than the methyl ether **11**, since they would be expected to have a better inductive electron-donating effect, thus speeding up the second step of eq. [12].

In summary, this study has shown that nitrobenzyl derivatives react via an oxygenation pathway when photolyzed in aqueous solution. In several cases, the initially formed α-hydroperoxides are isolable and therefore provide a convenient route to such species. Additionally, the study has provided insight into the general mechanistic behaviour of the photochemistry of nitrobenzyl derivatives in aqueous solution, opening up new avenues for further investigation.

Experimental

General

Ultraviolet spectra were recorded on Unicam SP8 and LKB Ultrospec II instruments. The ^{1}H nmr spectra were recorded on a Perkin–Elmer R32S instrument and the ^{13}C nmr spectra on a Bruker WM250 instrument. All nmr spectra were taken in $CDCl_3$ with TMS as internal standard. The ir spectra were recorded on a Perkin–Elmer 1320 instrument and mass spectra on a Finnigan 3300 spectrometer. Photolyses were carried out using a Hanovia 450-W medium pressure mercury arc housed in a water-cooled quartz jacket and placed inside a Pyrex immersion reaction vessel. The emission of the lamp was filtered through a Corex filter sleeve. Small scale photolyses and quantum yield measurements were carried out using a Rayonet RPR 100 photochemical reactor equipped with 254-nm lamps.

Materials

Nitrobenzyl ethers **2–5** were prepared by the reaction of the corresponding sodium alkoxides with *m*-nitrobenzyl chloride (Aldrich) in the appropriate alcohol solvent, or in THF for **5**.

m-*Nitrobenzyl methyl ether* **2**

To a 150-mL solution of dry MeOH was added 1.34 g (0.058 mol) of metallic sodium spheres. The solution was stirred until complete dissolution of the sodium metal. To this was added 5.0 g (0.029 mol) of *m*-nitrobenzyl chloride and the solution refluxed for 20 min, after which a fine precipitate of NaCl was observed. After a further 20 min, the reaction was quenched by pouring the solution into 200 mL ice-water. After acidification, the solution was extracted with CH_2Cl_2, which gave a yellow oil. Distillation gave the methyl ether in 70% yield, bp 81°C (2 Torr; 1 Torr = 133.3 Pa); ir (film): 2800–3100 (w), 1600 (m), 1520 (s), 1340 (s), 1200 (m), 1100 (s) cm^{-1}; ^{1}H nmr δ: 3.4 (s, 3H, OMe), 4.5 (s, 2H, $ArCH_2O$—), 7.3–8.3 (m, 4H, arom.); mass spectrum (CI): 168 ($M^+ + 1$). In a similar fashion, ethers **3** and **4** were prepared.

m-*Nitrobenzyl ethyl ether* **3**, bp 92–95°C (2 Torr); ir (film): 2810–3100 (w), 1603 (m), 1522 (s), 1340 (s), 1210 (m), 1105 (s) cm^{-1}; ^{1}H nmr δ: 1.25 (t, J = 8 Hz, 3H, OCH_2CH_3), 3.5 (q, J = 8 Hz, 2H, OCH_2CH_3), 4.5 (s, 2H, $ArCH_2O$—), 7.3–8.4 (m, 4H, arom.); mass spectrum (CI): 182 ($M^+ + 1$).

m-*Nitrobenzyl* n-*propyl ether* **4**, bp 85°C (1 Torr); ir (film): 2830–3090 (w), 1604 (m), 1530 (s), 1335 (s), 1200 (m), 1100 (s) cm^{-1}; ^{1}H nmr δ: 0.96 %t, J = 8 Hz, 3H, —CH_2CH_3), 1.65 (m, 2H, —CH_2-CH_2CH_3), 3.45 (t, J = 8 Hz, 2H, —$CH_2CH_2CH_3$), 4.6 (s, 2H, $ArCH_2O$—), 7.3–8.3 (m, 4H, arom.); mass spectrum (CI): 196 ($M^+ + 1$).

m-*Nitrobenzyl phenyl ether* **5**

This ether was made in a similar manner except that 2 equiv. of phenol was first dissolved in 150 mL dry THF prior to the addition of sodium metal. The solution was refluxed for 2 h immediately after the addition of sodium. The isolated material was a yellow viscous oil and was distilled at 120°C on a Kugelrohr apparatus (2 Torr); ir (film): 2800–3100 (w), 1600 (m), 1530 (s), 1330 (s), 1203 (m), 1100 (s) cm^{-1}; ^{1}H nmr δ: 5.05 (s, 2H, $ArCH_2O$—), 6.8–7.3 (m, 5H, —OPh), 7.3–8.3 (m, 4H, $ArCH_2$—); mass spectrum (CI): 230 ($M^+ + 1$).

Can. J. Chem. Downloaded from www.nrcresearchpress.com by 118.98.75.50 on 09/07/12
For personal use only.

p-*Nitrobenzyl methyl ether* **7**

This ether was made via the same procedure used for **2** (it should be noted that this procedure fails for the ethyl and *n*-propyl *p*-nitrobenzyl ethers; the only product from these reactions is *p,p'*-dinitrostilbene); ir (film): 2800–3100 (w), 1605 (s), 1525 (s), 1335 (s) cm^{-1}; ^1H nmr δ: 3.4 (s, 3H, OMe), 4.5 (s, 2H, $ArCH_2O$—), 7.45 (d, J = 9 Hz, 2H, arom.), 8.15 (d, J = 9 Hz, 2H, arom.); mass spectrum (CI): 168 (M^+ + 1).

(m-*Nitrobenzyl)acetate* **6**

This was readily prepared by reaction of **1** with acetic anhydride in pyridine, bp 70°C (2 Torr); ir (film): 2800–3100 (w), 1735 (s), 1600 (w), 1530 (s), 1335 (s) cm^{-1}; ^1H nmr δ: 2.2 (s, 3H, OCOMe), 5.3 (s, 2H, $ArCH_2O$—), 7.3–8.3 (m, 4H, arom.).

2-Methoxy(*m*- and *p*-nitrophenyl)ethanols **9** and **10** were prepared based on the procedure of Jacober and Hanzlik (21), via acid-catalyzed methanolysis of the corresponding nitrophenyl epoxides, which are known compounds (22–24).

2-Methoxy-(m-*nitrophenyl)ethanol* **9**

To a 50-mL solution of dry MeOH was added 2 g of *m*-nitrophenyl epoxide and 1 mL concentrated H_2SO_4 and refluxed for 1.5 h. The solution was quenched with solid sodium bicarbonate, cooled, and water was added. Extraction with CH_2Cl_2 gave an oil that could be recrystallized from ligroin in the cold to give a low melting solid, mp 10°C; ir (film): 3140–3700 (br, m), 2800–3100 (m), 1525 (s), 1350 (s), 1110 (s) cm^{-1}; ^1H nmr δ: 2.4 (br, 1H, OH), 3.35 (s, 3H, OMe), 3.65 (d, J = 8 Hz, 2H, —CH_2OH), 4.4 (t, J = 8 Hz, 1H, ArCH), 7.4–8.3 (m, 4H, arom.); mass spectrum (CI): 198 (M^+ + 1).

2-Methoxy-(p-*nitrophenyl)ethanol* **10**

Using the same procedure as for **9**, **10** was obtained as a solid from ligroin, mp 56°C; ir (Nujol): 3140–3700 (br, m), 1600 (m), 1520 (s), 1350 (s), 1100 (s) cm^{-1}; ^1H nmr δ: 2.7 (br, 1H, OH), 3.3 (s, 3H, OMe), 3.65 (d, J = 8 Hz, 2H, —CH_2OH), 4.4 (t, J = 8 Hz, 1H, ArCH), 7.5 (d, J = 9 Hz, 2H, arom.), 8.2 (d, J = 9 Hz, 2H, arom.); mass spectrum (CI): 198 (M^+ + 1).

m-Nitrobenzaldehyde dimethyl acetal **23** was readily prepared by refluxing *m*-nitrobenzaldehyde in excess methanol in the presence of trimethyl orthoformate as the dehydrating agent. Esters **14–16** were prepared by refluxing *m*-nitrobenzoic acid with the corresponding alcohols, with acid catalysis.

Preparative photolyses

Large scale photolyses of **1–10** were generally carried out on 0.5–1.0 g scales using a Hanovia 450-W immersion reactor, and smaller scale photolyses with 100–200 mg samples using a Rayonet RPR 100 reactor with 254-nm lamps.

α-*Hydroperoxy-*m-*nitrobenzyl methyl ether* **11**

In a typical photolysis, 500 mg of **2** was dissolved in 200 mL CH_3CN/800 mL distilled water. A pinch of sodium bicarbonate was added. The solution was transferred to the immersion well and purged with a stream of oxygen for 10 min, with stirring, prior to photolysis. The solution was also purged with oxygen during the photolysis. After 45 min, the lamp was switched off and the solution worked up by extraction with CH_2Cl_2, after addition of NaCl (to saturate the aqueous solution with salt). The ratios of the products were calculated by ^1H nmr integration, using the methoxy singlets of **2** (δ 3.4), **11** (δ 3.65), and **14** (δ 4.0), and the formyl proton of *m*-nitrobenzaldehyde (δ 10.1). It showed 54% substrate, 40% **11**, 5% **14**, and a trace of *m*-nitrobenzaldehyde. The crude mixture was separated by chromatography on silica gel (CH_2Cl_2) to give pure **11** (120 mg, 24% overall yield) as an oil; ir (film): 3150–3600 (br, m), 2800–3100 (w), 1610 (w), 1525 (s), 1350 (s), 1200 (s), 1100 (s) cm^{-1}; ^1H nmr δ: 3.65 (s, 3H, OMe), 5.8 (s, 1H, ArCH), 7.4–8.6 (m, 4H, arom.), 8.8 (br, 1H, OOH); ^{13}C nmr (^1H decoupled) δ: 56.59 (OMe), 105.88 (ArCH), 122.23, 123.93, 129.31, 133.08, 137.96, 148.18 (arom. C); mass spectrum (EI): 199 (M^+, very weak). Chemical analysis was not attempted due to the presence of small amounts of thermal decomposition products, which eluded separation.

α-*Hydroperoxy-*m-*nitrobenzyl ethyl ether* **12**

In a similar manner as above, **12** was isolated and characterized; ir (film): 3150–3600 (br, m), 2800–3100 (w), 1610 (w), 1530 (s), 1350 (s), 1205 (s), 1100 (s) cm^{-1}; ^1H nmr δ: 1.3 (t, J = 8 Hz, 3H, OCH_2CH_3), 3.7–4.3 (m, diastereomeric H, 2H, OCH_2CH_3), 5.9 (s, 1H, ArCH), 7.4–8.3 (m, 4H, arom.), 8.9 (br, 1H, OOH); mass spectrum (EI): 213 (M^+, very weak).

α-*Hydroperoxy-*m-*nitrobenzyl* n-*propyl ether* **13**

^1H nmr δ: 1.0 (t, J = 8 Hz, 3H, —$CH_2CH_2CH_3$), 1.75 (m, J = 8 Hz, 2H, —$CH_2CH_2CH_3$), 3.5–4.1 (m, diastereomeric H, 2H, —CH_2-CH_2CH_3), 5.9 (s, 1H, ArCH), 7.4–8.4 (m, 4H, arom.), 8.9 (br, 1H, OOH); ir (film): 3150–3600 (br, m), 2800–3100 (w), 1610 (w), 1530 (s), 1350 (s), 1200 (s), 1100 (s) cm^{-1}; mass spectrum (EI): 227 (M^+, very weak).

Rose Bengal sensitization of **2**

The light source used for this experiment consists of the above Hanovia 450-W lamp but filtered through a uranium glass filter and a filter solution consisting of 0.6 g $K_2Cr_2O_7$ in 1 L of water, which has a cutoff at 400 nm. A typical experiment using this setup consists of dissolving 100 mg of Rose Bengal (Aldrich) and 200 mg of **2** in 50 mL CH_3CN/350 mL water, and transferring this solution to a Pyrex vessel, which is placed adjacent to the light source. The solution is photolyzed with a stream of oxygen purging through the solution. That singlet oxygen is generated efficiently is shown by the fact that when 1 g of 2-methylfuran is used as the substrate, a 10-min photolysis using the above procedure results in complete conversion of the furan (to a hydroperoxide derivative), which is a known singlet oxygen trap (25). When **2** is irradiated under this setup for 30 min, no reaction is observed (similar time scale as for direct photolysis runs without Rose Bengal). On extended photolysis (4 h), the reaction gives 8% *m*-nitrobenzaldehyde and 2% methyl *m*-nitrobenzoate **14**. The rest of the photolysate is recovered starting material **2**. No trace of hydroperoxide **11** is detected. It is clear from this experiment that singlet oxygen can react with **2** but relatively inefficiently, and, more importantly, does not give hydroperoxides.

Reactivity of **11**

Hydrolysis of **11**

Two solutions each of 100 mg of **11** in 20 mL CH_3CN/80 mL pH 1 and 20 mL CH_3CN/80 mL pH 7 were prepared and left at room temperature with stirring in the dark for 2 days. After work-up, the pH 1 hydrolysis yielded 100% *m*-nitrobenzaldehyde whereas the pH 7 hydrolysis showed a mixture of 40% methyl *m*-nitrobenzoate **14** and 60% starting material **11**; no trace of *m*-nitrobenzaldehyde was observed. The aqueous layer of the pH 1 run was tested for H_2O_2 with KI, which gave a positive test. On the other hand, the test was negative for the pH 7 hydrolysis. As there is no convenient *in situ* method for detecting H_2O_2 (11), we have shown that our method works when authentic H_2O_2 is added to solutions of similar composition. The rate of reaction of authentic H_2O_2 with KI (monitored at 358 nm) is also similar to the rate obtained with the aqueous layer of the hydrolyzed **11**, as a further indication that hydrogen peroxide is produced. In a typical run with 10^{-4} *M* H_2O_2 and 10^{-2} *M* KI, the observed rate is 9.3×10^{-4} s^{-1} (25°C). The KI test is negative when **23** is used as the substrate.

Reduction of **11**

A solution of 100 mg of **11** in 20 mL CH_3CN and 500 mg of Na_2SO_3 (or KI) in 80 mL water was prepared and stirred for several hours. In the case of KI, the solution turned to a deep yellow with time. After work-up, the product was *m*-nitrobenzaldehyde.

Photolysis of **11**

A solution of 100 mg of **11** in 20 mL CH_3CN/80 mL water was photolyzed in a quartz reaction vessel in a Rayonet reactor (254-nm lamps) with argon purging for 2 h. After work-up, the nmr of the photolysate showed 30% methyl ester **14** and 70% starting material. Photolysis of **11** in pure CH_3CN gave the same product mixture. No reaction was observed without irradiation. Refluxing a solution of **11**

in benzene for 2 h in the dark gave 20% conversion to **14**. No reaction was observed without reflux.

Quantum yield measurements

Quantum yields for α-hydroperoxide formation for **2–4** and **9** were measured spectrophotometrically with 254-nm irradiation, using the known quantum yield (0.087) of photoredox reaction of **1** (in argon) as the actinometer (8). The major product of this reaction is *m*-nitrobenzaldehyde with *m*-azoxybenzaldehyde as the minor product. Both have λ_{max} at 235 nm with essentially the same ε (23 000 and 25 000). The reported quantum yield (7, 8) is for the total quantum yield of the two products. Solutions of **1–4** and **9** were prepared in quartz cuvettes, ensuring that they have the same OD at 254 nm. The solution containing **1** was saturated with argon while the solutions containing **2–4** and **9** were saturated with oxygen. The cuvettes were then irradiated at 254 nm in a merry-go-round apparatus for 3 min. After photolysis, the increase in OD at 235 nm for **1** was measured. For **2–4** and **9**, 1.0 mL was removed from each via a pipette and 1.0 mL of 30% H_2SO_4 added to effect hydrolysis of the photogenerated α-hydroperoxides. After complete hydrolysis (typically requiring 1 h), the OD's at 235 nm were measured and normalized back to the initial concentration, accounting for the dilution factor. Quantum yields for α-hydroperoxide formation were then calculated by equating it to the quantum yield for *m*-nitrobenzaldehyde formation measured in each solution, using **1** as the reference. This procedure is valid because essentially all the *m*-nitrobenzaldehyde formed is due to hydrolysis of the initially produced α-hydroperoxide (except for **1**, which was the reference). The same procedure was employed in the study of pH effect on reaction for **2** and **9**, as well as the solvent isotope effects given in Table 2.

Rate measurements

The hydrolysis and dehydration rates for **11–13** and **23** were measured by following the increase in OD at 235 nm. Kinetic runs were carried out by injecting a stock solution of the compound (dissolved in CH_3CN) into a solution of known pH and monitoring the OD at 235 nm at 30 ± 2°C in a spectrophotometer. Alternatively, the hydroperoxide may be photogenerated *in situ* by photolysis of the corresponding starting material and the rate of reaction obtained by following the increase in OD at 235 nm in the dark. In all cases, good pseudo first-order kinetics were observed.

Acknowledgments

The authors are grateful to the Natural Sciences and Engineering Research Council of Canada for an operating grant, a University Research Fellowship, and summer undergraduate scholarships to I.A. and C.A.B. We also acknowledge additional support from the University of Victoria.

1. H. A. Morrison. *In* The chemistry of the nitro and nitroso groups. *Edited by* H. Feuer. Wiley, New York. 1969. Chap. 4.
2. Y. L. Chow. *In* The chemistry of the amino, nitro and nitroso compounds and their derivatives. *Edited by* S. Patai. Wiley, New York. 1982. Chap. 6.
3. D. Döpp. Top. Curr. Chem. **55**, 49 (1975).
4. A. N. Frolov, N. A. Kuznetsova, and A. V. El'tsov. Russ. Chem. Rev. Engl. Transl. **45**, 1024 (1976).
5. P. Wan and S. Muralidharan. Can. J. Chem. **64**, 1949 (1986).
6. P. Wan and K. Yates. J. Org. Chem. **48**, 136 (1983).
7. P. Wan and K. Yates. Can. J. Chem. **64**, 2076 (1986).
8. K. Rafizadeh and K. Yates. J. Org. Chem. **51**, 2777 (1986).
9. G. G. Wubbels, T. F. Kalhorn, D. E. Johnson, and D. Campbell. J. Org. Chem. **47**, 4664 (1982).
10. P. Wan. Tetrahedron Lett. 2387 (1985).
11. J. R. Harbour, J. Tromp, and M. L. Hair. Can. J. Chem. **63**, 204 (1985).
12. J. D. Margerum and C. T. Petrusis. J. Am. Chem. Soc. **91**, 2467 (1969).
13. J. C. Stowell. Carbanions in organic synthesis. Wiley, New York. 1979.
14. J. R. Jones. The ionisation of carbon acids. Academic Press, London. 1973.
15. G. A. Russell, A. J. Moye, E. G. Janzen, S. Mak, and E. R. Talaty. J. Org. Chem. **32**, 137 (1967).
16. J. A. Howard, K. U. Ingold, and M. Symonds. Can. J. Chem. **46**, 1017 (1968).
17. A. J. Kresge. Acc. Chem. Res. **8**, 354 (1975).
18. H. E. Zimmerman and S. Somasekhara. J. Am. Chem. Soc. **85**, 922 (1963).
19. H. E. Zimmerman and V. R. Sandel. J. Am. Chem. Soc. **85**, 915 (1963).
20. J. Cornelisse and E. Havinga. Chem. Rev. **75**, 353 (1975).
21. S. P. Jacober and R. P. Hanzlik. J. Am. Chem. Soc. **108**, 1594 (1986).
22. K. Rafizadeh and K. Yates. Org. Prep. Proced. Int. **17**, 140 (1985).
23. C. O. Guss. J. Org. Chem. **17**, 678 (1952).
24. C. O. Guss and H. G. Mautner. J. Org. Chem. **16**, 887 (1951).
25. C. S. Foote, M. T. Wuesthoff, S. Wexler, I. G. Burstain, R. Denny, G. O. Schenck, and K.-H. Schulte-Elte. Tetrahedron, **23**, 2583 (1967).

Can. J. Chem. Downloaded from www.nrcresearchpress.com by 118.98.75.50 on 09/07/12
For personal use only.

^{1}H and ^{13}C nuclear magnetic resonance assignment of fluorescent olefinic sterol derivatives for use as membrane probes

JACINTA DREW[1]
Ottawa–Carleton Chemistry Institute, Department of Chemistry, University of Ottawa, Ottawa, Ont., Canada K1N 9B4

JEAN-ROBERT BRISSON[2]
Division of Biological Sciences, National Research Council of Canada, 100 Sussex Drive, Ottawa, Ont., Canada K1A 0R6

PETER MORAND[2]
Ottawa–Carleton Chemistry Institute, Department of Chemistry, University of Ottawa, Ottawa, Ont., Canada K1N 9B4

AND

ARTHUR G. SZABO
Division of Biological Sciences, National Research Council of Canada, 100 Sussex Drive, Ottawa, Ont., Canada K1A 0R6

Received December 15, 1986

This paper is dedicated to Professor John T. Edward

JACINTA DREW, JEAN-ROBERT BRISSON, PETER MORAND, and ARTHUR G. SZABO. Can. J. Chem. **65**, 1784 (1987).

A number of fluorescent steroids with unsaturated sidechains have been analyzed by high resolution ^{1}H and ^{13}C nmr spectroscopy. The geometry of the olefinic systems was assigned on the basis of ^{1}H–^{1}H shift-correlated spectra (COSY) and selected nOe difference experiments. For one of these compounds, a ^{13}C–^{1}H shift-correlated spectrum, a COSY spectrum, a ^{1}H *J*-resolved spectrum as well as nOe experiments on the angular methyl groups permitted complete ring proton assignment and coupling constant analysis. The high degree of similarity of the ring carbon ^{13}C chemical shifts of these steroids and cholesterol would indicate that the former have the potential for use as fluorescent probes of cholesterol domains in membranes.

JACINTA DREW, JEAN-ROBERT BRISSON, PETER MORAND et ARTHUR G. SZABO. Can. J. Chem. **65**, 1784 (1987).

Faisant appel à la rmn du ^{1}H et du ^{13}C, on a analysé un certain nombre de stéroïdes fluorescents qui portent des chaînes latérales qui ne sont pas saturées. On a attribué la géométrie des systèmes oléfiniques en se basant sur des spectres de corrélation homonucléaire ^{1}H–^{1}H (COSY) et sur des expériences sélectives d'eOn différentiel. Pour l'un de ces composés, un spectre de corrélation ^{13}C–^{1}H, un spectre COSY, un spectre de ^{1}H résolu pour *J* ainsi que des expériences d'eOn sur les groupements méthyles angulaires ont permis de faire une attribution complète pour les protons du cycle ainsi qu'une analyse complète des constantes de couplage. La grande similitude qui existe entre les déplacements chimiques ^{13}C des carbones du cycle de ces stéroïdes et ceux du cholestérol indiquerait que les premiers pourraient être utilisés comme sondes fluorescentes des domaines du cholestérol dans les membranes.

[Traduit par la revue]

Can. J. Chem. Downloaded from www.nrcresearchpress.com by 118.98.75.50 on 09/07/12
For personal use only.

Introduction

Cholesterol is an important lipid component of many membranes but its role in influencing the structure and function of membranes is not fully understood (1). This is partly due to the difficulty of monitoring any property of cholesterol when it is in such an inhomogeneous environment as a membrane. Hence, an external material with an easily measurable property is usually added to the system under question in order to probe the effect of cholesterol on the system.

Fluorescence is one of the most sensitive probe techniques available. Consequently, very little external fluorescent probe material needs to be added, thereby minimizing any possible perturbations of the system by the probe. Many fluorescent probes bearing no resemblance to natural membrane constituents have been used in cholesterol/membrane studies, particularly diphenylhexatriene (2). For our projected studies, we wished to have a fluorescent probe which resembled cholesterol closely, especially with regard to its amphipathic nature and molecular geometry.

We have synthesized the fluorescent cholesterol analogues **1** → **6** with conjugated unsaturation in the sidechain (3).[3] We believe that these analogues resemble cholesterol most closely of all the currently available fluorescent cholesterol-like probes (4). In the synthesis of compounds **1** → **6**, one of the double bonds in the sidechain was formed in a Wittig reaction, hence there was the possibility of the product being a mixture of two isomers. In order to be able to use these probes in fluorescence lifetime and anisotropy studies, it was important that they be a single isomer. So, 500 MHz ^{1}H nmr spectroscopy was used to determine which isomers were present, and the ratio of the isomers if applicable. This meant an analysis of the downfield region (~6 → 8 ppm) of the ^{1}H nmr spectrum. It was decided to analyze the upfield (ring proton) region of the spectrum as well, since few steroids have had their ^{1}H nmr spectrum fully assigned and analyzed for coupling constants. Comparison of the ring ^{13}C chemical shifts with those reported in the literature for cholesterol (5) could also give us an idea of how similar these cholesterol-type probes are to cholesterol.

[1]Commonwealth Scholar.

[2]To whom correspondence may be addressed.

[3]The complete details of the synthesis of these compounds will be reported elsewhere.

Results and discussion

(a) Olefinic and aromatic proton assignments of ***1*** → ***6***

The downfield portion of a one-dimensional (1D) ^{1}H nmr spectrum of a mixture of **1** and **2** is shown in Fig. 1. Due to the presence of the two geometrical isomers, straightforward analysis of the 1D spectrum was not possible. A ^{1}H–^{1}H shift-correlated spectrum (COSY) (6) of the same region is shown in Fig. 2. The 22-H resonances were recognized due to their coupling with the corresponding 21-methyl resonances at

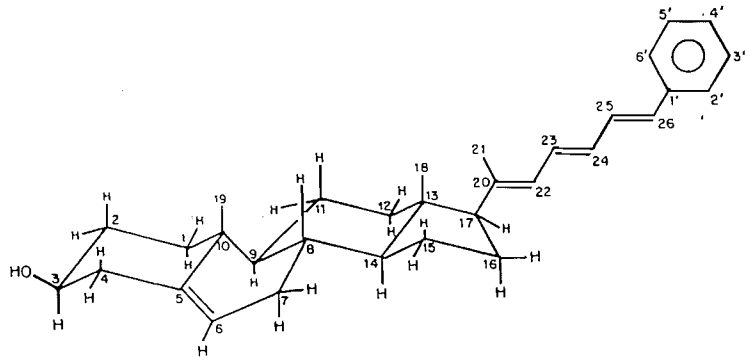

1

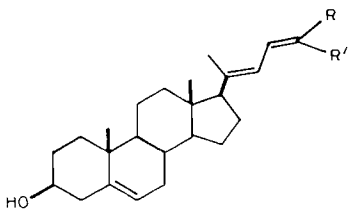

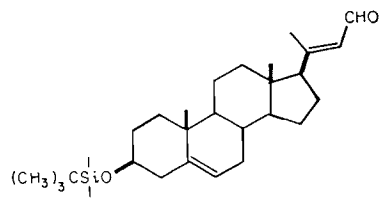

7

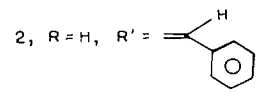

2, R = H, R' =

3, R = Phenyl, R'=H
4, R = H, R'= Phenyl
5, R = 2-Naphthyl, R'=H
6, R = H, R'= 2-Naphthyl

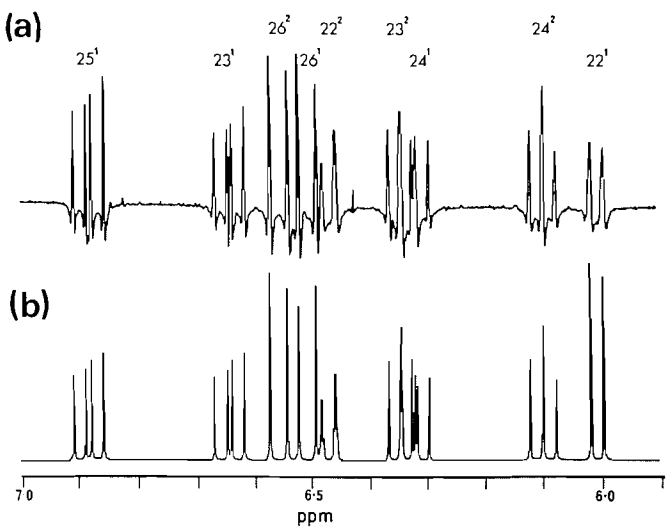

FIG. 1. Downfield region of the 500 MHz ^{1}H nmr spectrum of a mixture of **1** and **2**. (*a*) Experimental spectrum. (*b*) Simulated spectrum with parameters given in Table 1.

TABLE 1. ^{1}H nmr chemical shifts (ppm)[a] for the olefinic and aromatic protons of compounds **1** → **6** in $CDCl_3$

	Chemical shift (ppm)					
Proton	**1**	**2**[d]	**3**	**4**	**5**	**6**[d]
22	6.007[c]	6.468[c]	6.074	6.343	6.129	6.533
23	6.641[c]	6.343[c]	7.083	6.506	7.206	6.593
24	6.322[c]	6.101[c]	6.466	6.444	6.622	6.496
25	6.883[c]	7.260				
26	6.507[c]	6.557[c]				
1′	—		—	—	7.713	
2′	7.389		7.400	7.34[b]	—	
3′	7.299		7.295	7.32[b]	7.638	
4′	7.189		7.182	7.211	7.76[b]	
5′	7.299		7.295	7.32[b]	7.76[b]	
6′	7.389		7.400	7.34[b]	7.394	
7′					7.433	
8′					7.76[b]	

[a] ±0.002 ppm.
[b] ±0.01 ppm due to overlapping resonances.
[c] From iterative analysis.
[d] Aromatic ^{1}H chemical shifts not determined.

~1.9 ppm (not shown). The connectivities of the olefinic proton resonances in the two isomers was then easily established (for chemical shifts see Table 1). The COSY spectrum also confirmed the presence of an olefinic proton resonance under the aromatic envelope, a fact suspected from integration of the 1D spectrum.

By coupling constant analysis (Table 2) of the olefinic proton multiplets (J_{trans} ~ 15 Hz, J_{cis} ~ 11 Hz from numerous studies of carotene systems (7) for example), and from integration of the 22-H resonance of **1** versus the identical 6-H resonance of both isomers, it was determined that the isomers **1** and **2** were present in the ratio 40:60. Simulation of the olefinic proton resonances using a 50:50 ratio and the measured chemical shifts and coupling constants, produced a spectrum virtually identical to the experimental 1D spectrum except for the intensity ratios (Fig. 1). Although **1** and **2** had been obtained by a Wittig

Can. J. Chem. Downloaded from www.nrcresearchpress.com by 118.98.75.50 on 09/07/12
For personal use only.

Can. J. Chem. Downloaded from www.nrcresearchpress.com by 118.98.75.50 on 09/07/12
For personal use only.

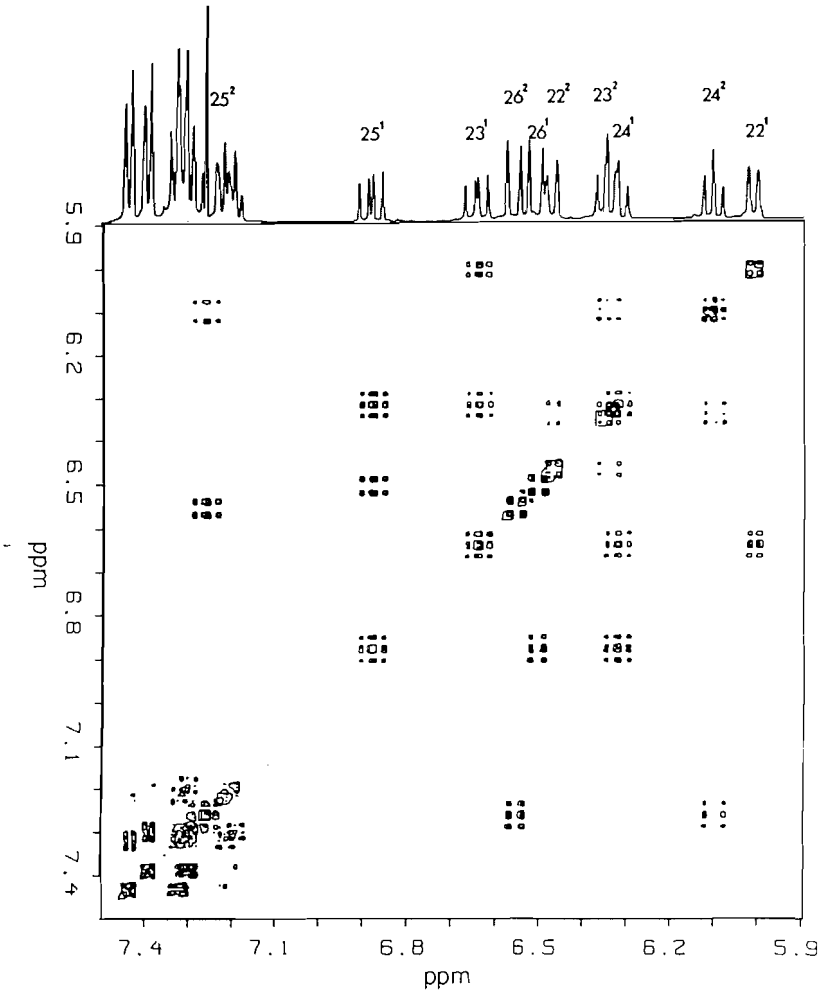

FIG. 2. Downfield region of the COSY spectrum of a mixture of **1** and **2**.

TABLE 2. $^1H-^1H$ nmr coupling constants (Hz) in the sidechain of compounds **1–6**

	Coupling constant (Hz)					
Proton pair	**1**[a]	**2**[a]	**3**	**4**	**5**	**6**
21,22	<0.5	1.2	<0.5	<0.5	<0.5	<0.5
22,23	11.1	11.6	11.0	11.3	10.9	11.4
23,24	14.7	11.2	15.6	11.3	15.4	11.2
24,25	10.1	11.1				
25,26	15.2	15.1				

[a]Values found from iterative analysis of the spectrum of **1** and **2** shown in Fig. 1.

TABLE 3. ^1H nuclear Overhauser enhancements

Compound	Saturated signal	Proton resonance enhanced (magnitude of nOe)[a]
1	18-CH_3	8β,11β(3);15β(1);21-CH_3(2);22(1).
	19-CH_3	2β(1);4β(2);8β,11β(3).
	22	16β(2);17α(3);18-CH_3(2);24(7).
	23	21-CH_3(5);25(6);2′,6′(1).
3	18-CH_3	8β,11β(6);15β(2);21-CH_3(2);22(2).
	19-CH_3	2β(1);4β(2);8β,11β(2).
	22	16β(7);17α(3);18-CH_3(2);24(13).
	23	21-CH_3(11);2′,6′(18).
4	22	16β(6);17α(2);2′,6′(1).
	23	21-CH_3(8);24(10).
5	22	16β(>1)[b];17α(3);24(7).
	23	21-CH_3(6);1′(2);3′(6).

[a]Intensity of saturated signal in difference spectrum set to −100.
[b]Overlap with incomplete cancellation of 21-methyl signal.

reaction on the 20(22) *E*-aldehyde **7** (3*a*), the geometry of the C-20, C-22 double bond of the two isomers was not confirmed as being *E* by the 1D or COSY experiments. This is because the similarity of transoid and cisoid allylic coupling constants does not allow unambiguous assignment (8).

Nuclear Overhauser effect (nOe) experiments (9) allowed us to determine the C-20, C-22 double bond geometry since the magnitude of this effect is dependent on internuclear distance to the inverse sixth power. In a 20(22)*E*-isomer of the compounds under study, one would expect to see an n0e enhancement of the 21-methyl resonance upon saturation of the 23-H resonance due to the proximity of these protons. Saturation of the 22-H resonance should not lead to an enhancement of the 21-methyl resonance since these protons are on opposite sides of a double bond and hence too far apart for a nOe to occur. On the other hand, in a 20(22)Z-isomer, an nOe enhancement of the 21-methyl resonance should occur upon saturation of the 22-H resonance but not the 23-H resonance. Nuclear Overhauser

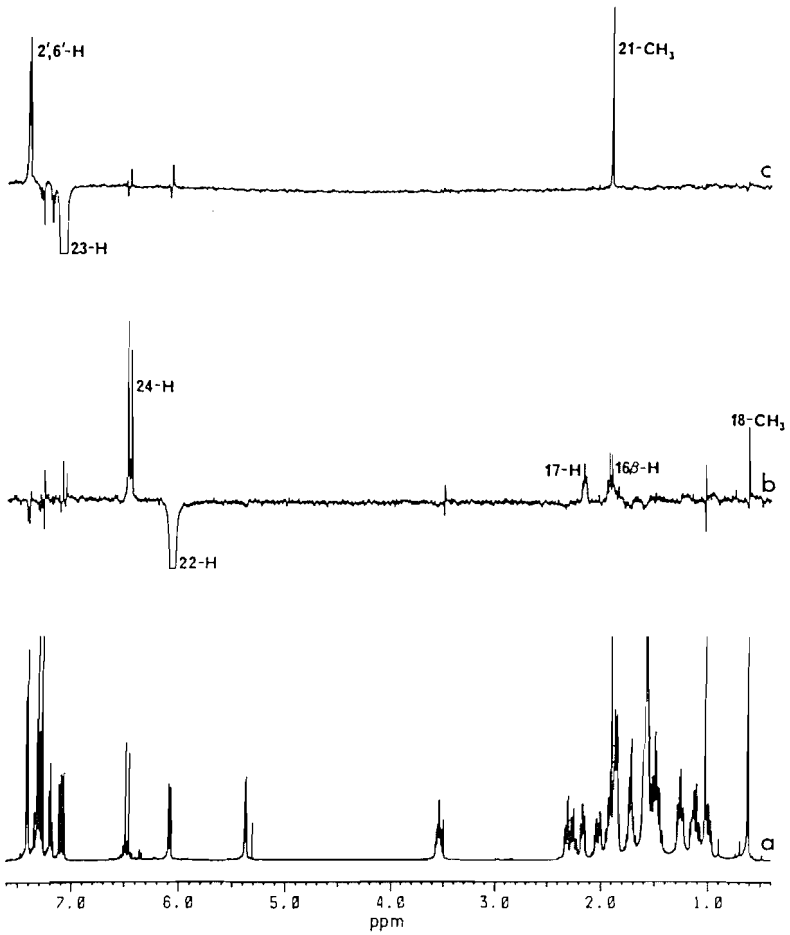

FIG. 3. (*a*) Complete ^{1}H nmr spectrum of **3**. (*b*) Nuclear Overhauser effect difference spectrum after saturation of 22-H at δ 6.07. (*c*) Nuclear Overhauser effect difference spectrum after saturation of 23-H at δ 7.08.

Can. J. Chem. Downloaded from www.nrcresearchpress.com by 118.98.75.50 on 09/07/12
For personal use only.

effect experiments were performed on a purified sample of **1** (Table 3) and since an enhancement of the 21-methyl resonance at 1.85 ppm was observed upon saturation of the 23-H resonance, the C-20, C-22 double bond geometry was confirmed as being *E*, as expected from the synthetic route to this compound (3*a*).

Analysis of the signals in the olefinic proton region of the 1D ^{1}H nmr spectra of the conjugated dienes **3** → **6** was straightforward after the geometry of the conjugated trienes **1** and **2** had been determined unequivocally. (For a diagram of the nOe experiments performed on **3**, see Fig. 3.) All that remained was to assign the aromatic proton resonances. The assignment of the *ortho*-, *meta*-, and *para*-proton resonances of **1**, **3**, and **4** followed from inspection of the multiplicity and integration of the three multiplets in the aromatic region (for **3**, see Fig. 3). The identical *ortho*-protons (2′-H,6′-H) should give a doublet resonance which integrates to two protons, the identical *meta*-protons (3′-H,5′-H) should give a triplet resonance which also integrates to two protons while the *para*-proton (4′-H) should give a triplet resonance which only integrates to one proton. Likewise the assignment of the naphthyl proton resonances in **5** came from multiplicity and integration arguments although the individual chemical shifts of the 4′-, 5′-, and 8′-naphthyl protons could not be extracted from the multiplet centred at 7.76 ppm. The relative order of the naphthyl proton chemical shifts agreed with that reported for 2-methylnaphthalene (10). All the downfield ^{1}H chemical shifts determined for compounds **1** → **6** are given in Table 1, while ^{1}H–^{1}H coupling constants are given in Table 2.

(b) Ring proton chemical shifts of 1

The cholesterol ring system with its Δ^5 double bond, 3β-OH and 17β substitution, as found in compounds **1** → **6**, presents quite a challenge to the nmr spectroscopist for proton assignment as there are 23 proton signals within 1.7 ppm. The only known attempts at ring proton resonance assignment of cholesterol are given in Table 4. These assignments were made by comparing spectra of deuterated cholesterol derivatives (11*a*) or by the use of lanthanide shift reagents (11*b*). Since compounds **1** → **6** do not possess the C_8H_{17} saturated sidechain of cholesterol, their ^{1}H nmr assignment was easier, especially with the aid of the recently acquired battery of two-dimensional (2D) nmr techniques (6, 12). These 2D nmr techniques have been successfully used to assign ring proton resonances of other steroids, usually those with a larger number of functional groups and (or) double bonds resulting in some simplification of the spectrum (ref. 13*a*–*f*, for a recent application of 2D NMR techniques to closely related triterpenes see ref. 13*g*).

The first step in the assignment was to distinguish the methine from the methylene proton resonances. This was achieved by performing a DEPT experiment (6*b*) to identify the methine and methylene carbons (Fig. 4). Then a ^{13}C–^{1}H shift correlated spectrum (6) with proton decoupling in both dimensions (Fig. 5) allowed determination of corresponding methine proton chemi-

TABLE 4. ^{1}H nmr chemical shifts for the ring protons and methyl groups of cholesterol and the steroids **1** and **3**

Proton	Cholesterol in pyridine-d_5[a]	Cholesterol in chloroform-d[b]	**1**[c] (±0.005)	**3**[d] (±0.008)
1α	1.83	—	1.088	1.102
1β		—	1.855	1.851
2α	2.07	1.90	1.845	1.854
2β	1.80	1.58	1.515	1.516
3α	3.82	3.47	3.530	3.526
4α	2.60	2.3	2.303	2.306[f]
4β			2.240	2.235[f]
6	5.41	5.30	5.361	5.362
7α	2.03	2.05	1.565	1.561
7β			2.008	2.002
8β			1.468	1.467
9α			0.976	0.982
11α			1.573	1.566
11β			1.447	1.455
12α			1.231	1.239
12β			1.840	1.841
14α			1.119	1.127
15α			1.709	1.699
15β			1.244	1.236
16α			1.687	1.702
16β			1.893	1.902
17α			2.135	2.152
18		0.68	0.589[e]	0.598
19		1.02	1.013[e]	1.009
21			1.848[e]	1.896

[a]From ref. 11*a*.
[b]From ref. 11*b*.
[c]$CDCl_3$ solution; from spin simulation.
[d]$CDCl_3$ solution; from CHORTLE analysis.
[e]Measured from the 1D spectrum.
[f]Measured from the 1D spectrum (CHORTLE analysis gave the average chemical shift of the 2 resonances).

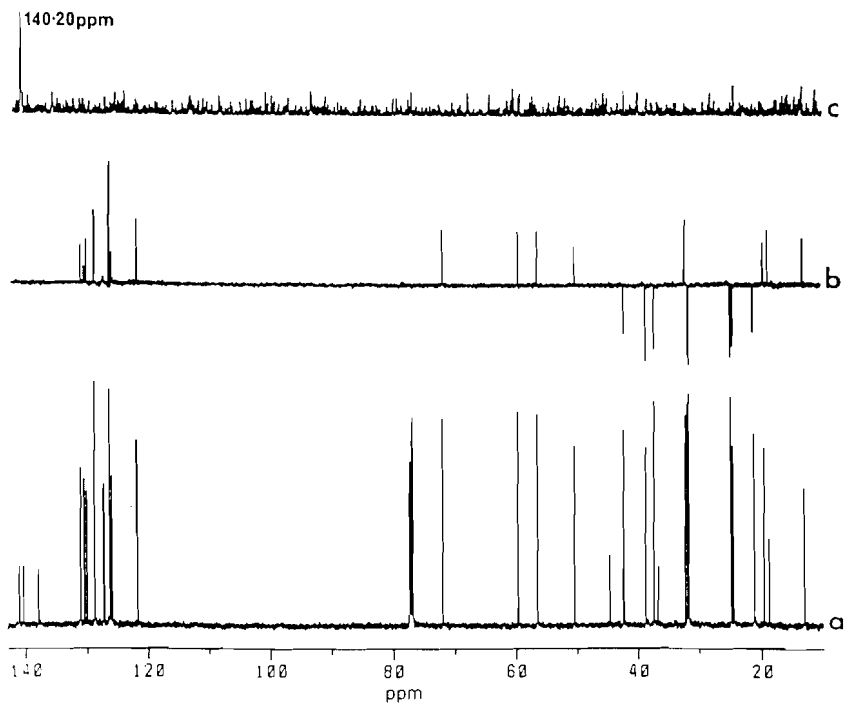

FIG. 4. (*a*) Complete ^{13}C nmr spectrum of **1**. (*b*) DEPT spectrum of **1** (methine, methyl resonances up; methylene resonances down). (*c*) Selective INEPT spectrum of **1** upon irradiation of 21-CH_3 at δ 1.85.

Can. J. Chem. Downloaded from www.nrcresearchpress.com by 118.98.75.50 on 09/07/12
For personal use only.

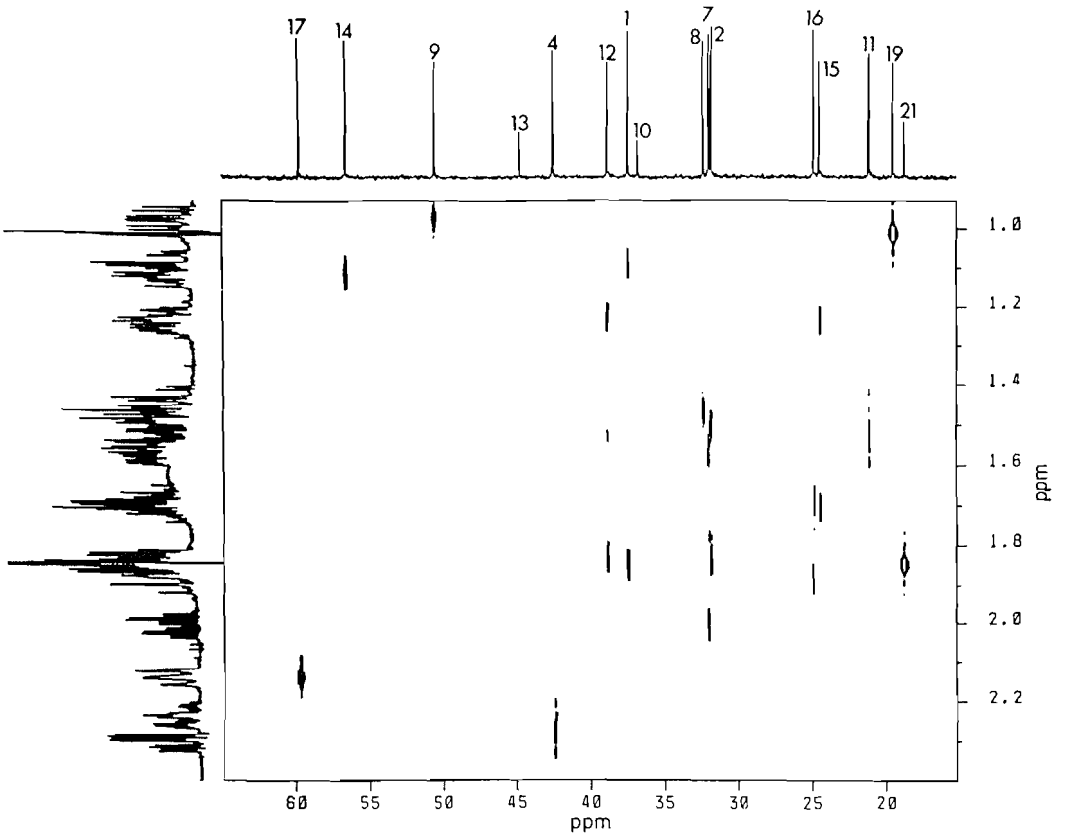

FIG. 5. Upfield region of the $^{13}C-^{1}H$ shift-correlated spectrum of **1**.

cal shifts. Of the four methine proton resonances, the most downfield one (2.135 ppm) was assigned to 17α-H because of its proximity to the 20(22) double bond. The three remaining methine proton resonances due to 8β-H, 9α-H, and 14α-H could only be assigned after analysis of nOe difference experiments and a COSY spectrum.

The second step in the assignment was to distinguish the axial methylene proton resonances from the equatorial proton resonances, since the chemical shifts of axial and equatorial protons in cyclohexyl ring systems differ due to the shielding effect of 1,3-diaxial interactions (13*e*). This was possible from the proton-decoupled $^{13}C-^{1}H$ shift correlated spectrum mentioned above since two non-equivalent methylene protons give two peaks in the ^{1}H dimension for each methylene carbon (Fig. 5). Because of the 1,3-diaxial interaction, the axial proton can be assigned to the more upfield of the two resonances.

The third step was to assign proton numbers to the observed chemical shifts (Table 4). This was achieved in large part by analysis of a COSY spectrum (Fig. 6), with the help of the few known resonances (3α-H, 6-H, and 17α-H). For example, the methine proton 14α-H was distinguished from the 8β and 9α methine protons through its coupling with the 15α and β protons (coupled weakly to 17α-H at 2.135 ppm). Then since 8β-H but not 9α-H couples with 14α-H, the two remaining methine proton resonances were assigned. However, the spin system 1α, 1β, 2α, 2β could not be easily distinguished from the 12α, 12β, 11α, 11β spin system. Furthermore, the methylene protons of the cyclopentyl D ring could not be simply assigned as α or β on the basis of the axial/equatorial proton chemical shift difference found for cyclohexyl systems.

Both of these problems were solved by selective nOe difference experiments. The rigid cholesterol ring system, with its two angular methyl groups at C-18 and C-19 makes it an ideal molecule for nOe experiments. Through saturation of the 18-methyl and 19-methyl resonances, the axial protons on the β face of the molecule can be observed (Table 3). Both the 11β and the 2β protons are axial, but while saturation of the 19-methyl resonance will lead to an enhancement of both these resonances, saturation of the 18-methyl resonance will only affect the 11β proton. On this basis, the spin systems 1α, 1β, 2α, 2β and 12α, 12β, 11α, 11β were assigned. These nOe difference experiments also allowed assignment of the 15β-H and confirmation of the assignment of the 4β and 8β axial protons. All that remained was to assign the 16-H resonances since the 16β-H had not been observed by the nOe experiment on the 18-methyl group.

It had been noted from the nOe experiment performed on the 22-H resonance to determine the 20(22) double bond geometry (see section A) that enhancements were seen to two ring proton resonances centred at 2.15 ppm and 1.90 ppm as well as to the 18-methyl group at 0.59 ppm (Table 3). From a Dreiding model it was determined that, upon rotation of the C-17, C-20 bond, the 22-H approaches the 17α and the 16β ring protons most closely. Since the nOe is dependent on internuclear distance to the inverse sixth power (9), the two resonance enhancements must be due to these two protons. The 2.15 ppm resonance had already been independently assigned to 17α-H, and the 1.90 ppm resonance did correspond to one of the 16-H chemical shifts previously determined so the 16β-H and hence 16α-H were assigned.

(c) Ring proton–proton coupling constants of ***1***

Our interest in obtaining proton–proton coupling constants from the multiplets in this crowded region of the spectrum was

Can. J. Chem. Downloaded from www.nrcresearchpress.com by 118.98.75.50 on 09/07/12
For personal use only.

Can. J. Chem. Downloaded from www.nrcresearchpress.com by 118.98.75.50 on 09/07/12
For personal use only.

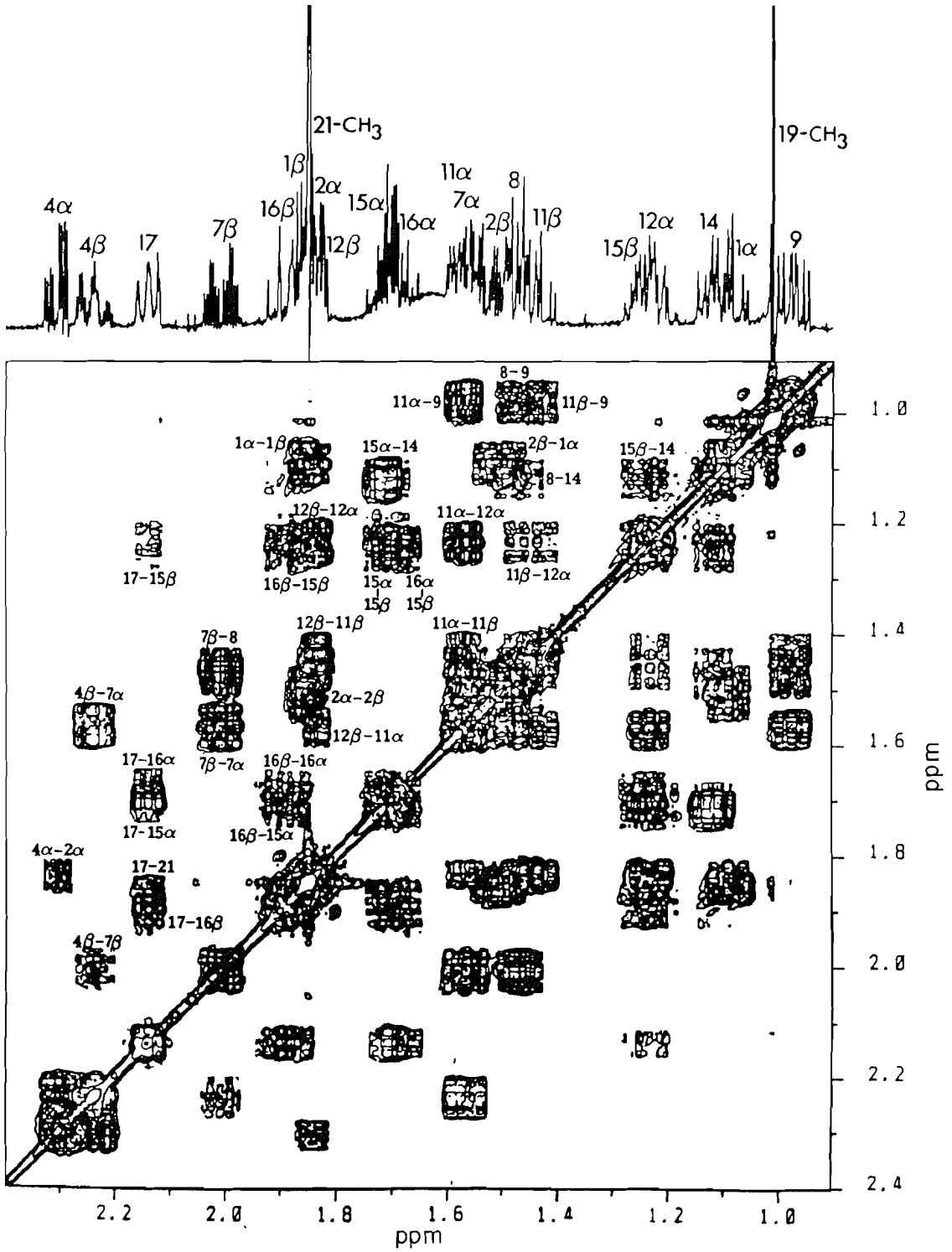

FIG. 6. Upfield region of the COSY spectrum of **1**.

threefold. Firstly, their determination would provide a further means of confirming the assigned proton chemical shifts, particularly for those geminal proton pairs whose axial proton was on the α-face of the molecule and hence had not been confirmed by nOe experiments. Secondly, given the precedence for allylic and homoallylic coupling (8) and the previously observed ^4J coupling to steroid angular methyl groups (8, 13*e*), it was of interest to determine the extent of long-range coupling in a cholesterol-type ring system. Lastly, due to the dependence of vicinal coupling constants on dihedral angle (14) a coupling constant analysis of the D ring protons could give us an idea of the D ring conformation of **1** in solution.

A ^{1}H homonuclear *J*-resolved spectrum (6) of **1** was measured. In such a spectrum, the various proton multiplets are seen as single lines in the second dimension f_2 (in this case allowing confirmation of the chemical shifts), and as separated multiplets in the first dimension f_1 allowing measurement of the various coupling constants. For those resonances that were

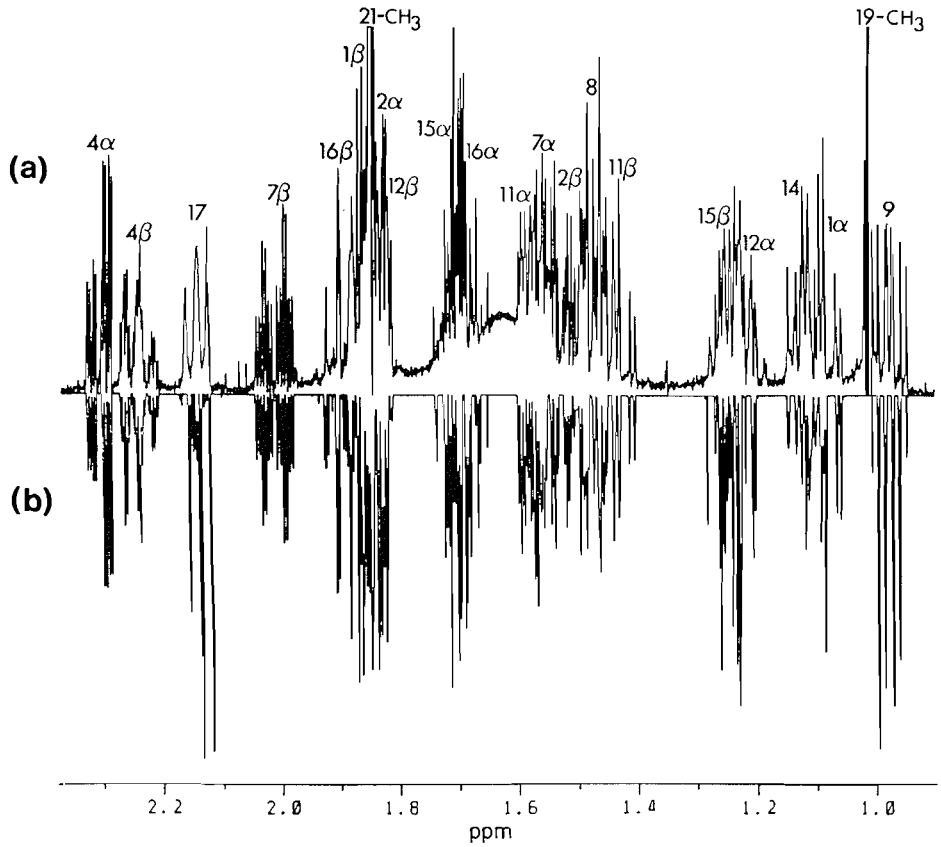

FIG. 7. Upfield region of the 500 MHz ^{1}H nmr spectrum of **1**. (*a*) Experimental spectrum. (*b*) Simulated spectrum.

overlapping in the ^{1}H 1D spectrum, the f_1 cross-sections of the *J*-resolved spectrum were plotted and the coupling constants determined. The chemical shifts and coupling constants were used as initial values to generate a simulated ^{1}H 1D spectrum in the region 0.9 → 2.4 ppm, excluding the methyl resonances at 1.01 pm and at 1.85 ppm (Fig. 7). The coupling constants obtained after spin simulation are given in Tables 5 and 6.

The simulated spectrum matched the experimental spectrum well except for the D ring proton resonances which were line broadened in the latter case. This line broadening is probably due to an intermediate exchange of the chemical shifts of these resonances (15), because of a somewhat hindered rotation about the C-17, C-20 bond of the sidechain modulating the environment of the ring D protons, in particular the 17 proton ($\delta_{17\alpha\text{-H}}$ = 2.135 ppm). The line broadening could also be a result of modulation of the coupling constants due to conformational flexibility of the D ring itself. Because of this line broadening and the strong overlap of the resonances due to the 15α and 16α protons, the error associated with the coupling constants of the D-ring protons is larger than for the other ring protons. However, these D-ring coupling constants are quite similar to those determined for other steroids (11*a*, *b*, *d*, *e*), for example there is a large difference in the coupling constants of the geminal protons 15α and 15β with the 16β proton (0.5 and 10.0 Hz, respectively).

As far as long-range coupling is concerned, there was evidence from the COSY spectrum of ^4J coupling between the 18-methyl group and both the 12α and 17α proton resonances (not shown in Fig. 6), and also between the 19-methyl group and the 1α and 9α protons (see Fig. 6) as found in some other steroids (8, 13*e*). However, there was no evidence of coupling between the 18-methyl group and the 14α proton, not even from a long-range COSY experiment (6). Long-range coupling between the 2α and 4α protons was also seen in the COSY spectrum (Fig. 6), and measured from the well-separated 4α proton resonance to be 1.2 Hz. These two protons and the four σ-bonds between them are in the familiar "W" arrangement, a condition found to be necessary for long-range coupling not involving a double bond. This is the first known example of a non-allylic/non-carbonyl long-range coupling in the steroid nucleus not involving one of the angular methyl groups.

Allylic couplings were seen between protons on either side of the C-5, C-6 double bond, as to be expected from similar studies of Δ^4-steroids (8). The magnitude of the allylic coupling was greater between the 6 and 4β protons than between the 6 and 4α protons (2.7, 2.3 Hz, respectively). This is in keeping with theoretical agruments (8) where the closer the angle between the plane of the double bond and the vinyl C—H bond is to 90°, the larger the coupling. Homoallylic coupling was also seen between the 4β proton and both the 7α and 7β protons (see Fig. 6). However, there was no coupling between the 4α (equatorial) proton and the 7α and 7β protons.

(d) ^{13}C chemical shifts of 1

Since the proton chemical shifts of **1** were known, assignment of the ^{13}C chemical shifts of **1** was straightforward from the ^{13}C–^{1}H shift-correlated spectrum (Fig. 5). However, of the five quaternary carbon resonances, only the C-10 and C-13 resonances could be assigned based on literature values for other steroids (5). The three remaining quaternary carbon resonances were separated by only 3 ppm (δ 140.85, δ 140.20, and δ 137.74). After measurement of the ^{13}C nmr spectrum for

Can. J. Chem. Downloaded from www.nrcresearchpress.com by 118.98.75.50 on 09/07/12
For personal use only.

TABLE 5. $^1H-^1H$ nmr coupling constants of **1**[a]

Proton pair	^2J	^3J	$^3J_{ax-ax}$	$^3J_{ax-eq}$	$^3J_{eq-eq}$	$\lvert^4J\rvert$	^5J
1α,1β	13.4						
1α,2α				3.5			
1α,2β			13.0				
1β,2α					1.8		
1β,2β				4.9			
2α,2β	14.6						
2α,3α				4.5			
2α,4α						1.2	
3α,4α				4.4			
3α,4β			11.4				
4α,4β	13.0						
4α,6						2.3	
4β,6						2.7	
4β,7α							2.2
4β,7β							2.8
6,7α		3.0					
6,7β		5.2					
7α,7β	17.6						
7α,8β			10.6				
7β,8β				5.2			
8β,9α			11.2				
8β,14α			11.2				
9α,11α				5.4			
9α,11β			12.2				
11α,11β	13.6						
11α,12α				2.5			
11α,12β					2.0		
11β,12α			13.0				
11β,12β				4.2			
12α,12β	12.8						
12α,18						1.2	
17α,18						Not measurable	
1α,19						1.2	
9α,19						0.8	

[a]Refined values after spin simulation (±0.5 Hz).

compounds **3**, **4**, and **5**, the 140.84 ppm resonance was assigned to C-5 due to its insensitivity to the structure of the sidechain (Table 7). The remaining two quaternary carbon resonances of **1** were due to C-20 and C-1′ and were assigned after performing a selective INEPT experiment (16). In this experiment, a specific proton resonance is saturated and the parameters for ^{13}C spectrum acquisition are such that only the carbon atom which is long-range coupled ($J_{CH} \sim 10$ Hz) to the irradiated proton is observed. In our case, upon saturation of the 21-methyl proton resonance, only the quaternary signal at 140.20 was observed and assigned to C-20 (Fig. 4). Hence the remaining quaternary carbon resonance at 137.74 ppm was assigned to C-1′.

*(e) Nuclear magnetic resonance assignments of **3**, **4**, and **5***

Ring ^{13}C resonances of **3**, **4**, and **5** were assigned by analogy to those determined for **1** due to the similarity of the chemical shifts of the carbon signals in the four compounds (Table 7). The only small differences (0.17 ppm at most, for C-17) occurred for the chemical shifts of the D ring carbons, as to be expected from the different sidechain structures.

Olefinic ^{13}C resonances of **3** were determined from a CHORTLE experiment (17) (not from a $^{13}C-^1H$ shift-correlated spectrum due to low sample concentration) by their correlation with the known olefinic proton resonances (Table 7). The CHORTLE experiment also allowed the ring proton resonances of **3** to be assigned. The resulting proton chemical shifts were very similar to those obtained for **1** by spin simulation (Table 4).

TABLE 6. $^1H-^1H$ nmr coupling constants (Hz) in the D ring of **1**[a]

	15α	15β	16α	16β	17α
14α	6.8	11.6			
15α		12.0	8.2	0.5	
15β			8.5	10.0	
16α				10.9	8.3
16β					10.2

[a]Refined values from spin simulation; average error ±1 Hz.

Finally, the ring ^{13}C chemical shifts of cholesterol (5) have been included in Table 7. Comparison of these values with those measured in this work for **1**, **3**, **4**, and **5** indicate that the effect of the unsaturated sidechains of these latter compounds on the cholesterol ring system is small. Hence these fluorescent steroids bear a close resemblance to cholesterol with their free 3β-OH, their cholesterol ring system and their hydrophobic sidechain, and should prove useful in fluorescence studies of cholesterol domains in membranes.

Can. J. Chem. Downloaded from www.nrcresearchpress.com by 118.98.75.50 on 09/07/12
For personal use only.

TABLE 7. ^{13}C nmr chemical shifts for cholesterol and the steroids **1**, **3**, **4**, and **5**

Carbon	^{13}C nmr chemical shift (ppm)				
	Cholesterol[a,b]	**1**[b]	**3**[b]	**4**[b,c]	**5**[b,c]
1	37.3	37.29	37.29	37.30	37.29
2	31.6	31.67	31.67	31.68	31.68
3	71.6	71.80	71.80	71.79	71.77
4	42.2	42.31	42.31	42.32	42.32
5	140.6	140.84	140.84	140.84	140.85
6	121.4	121.59	121.60	121.60	121.58
7	31.9	31.85	31.85	31.84	31.85
8	31.9	32.21	32.21	32.21	32.23
9	50.2	50.35	50.36	50.35	50.37
10	36.5	36.60	36.60	36.60	36.60
11	21.1	21.07	21.08	21.08	21.08
12	39.8	38.65	38.67	38.63	38.69
13	42.3	44.57	44.49	44.59	44.54
14	56.8	56.42	56.42	56.40	56.43
15	24.3	24.41	24.40	24.39	24.42
16	28.3	24.80	24.81	24.85	24.84
17	56.2	59.61	59.55	59.72	59.60
18	11.9	13.05	13.05	13.17	13.07
19	19.4	19.44	19.44	19.44	19.44
20		140.20	139.91	141.49	140.23
21	18.8	18.67	18.71	18.58	18.79
22		125.77	125.73		
23		130.28	130.03		
24		130.88	125.73		
25		129.85			
26		130.93			
1′		137.74	138.18		
2′		126.17	126.08		
3′		128.59	128.54		
4′		127.13	126.90		
5′		128.59	128.54		
6′		126.17	126.08		

[a]From ref. 5.
[b]$CDCl_3$ solutions.
[c]Olefinic and aromatic ^{13}C chemical shifts not determined.

Experimental section

All nmr measurements were performed with a Bruker AM-500 instrument at 300 K. Chemical shifts are relative to internal TMS. Sample concentrations were typically 3–5 mg/0.5 mL $CDCl_3$ for 1D experiments. The 2D experiments are outlined below.

The $^1H-^1H$ shift-correlated spectrum (COSY) of a mixture of **1** and **2** was acquired and processed using the standard software provided by Bruker. The f_2 spectral width was 4000 Hz or 8 ppm. The initial (t_1,t_2) matrix of 512 × 2K real data points was zero-filled to 2K × 2K data points to give a final resolution of 1.95 Hz/point. Processing was done using sine bell squared functions and a magnitude calculation. For each FID, 32 transients were accumulated requiring a total acquisition time of 16 h. Sample concentration was 25 mg/0.5 mL $CDCl_3$.

The COSY spectrum of **1** was acquired with an f_2 spectral width of 1400 Hz or 2.8 ppm. The initial (t_1,t_2) matrix of 256 × 1K real data points was zero-filled to 1K × 1K points to give a digital resolution of 1.37 Hz/point. Data manipulation was done using sine bell functions and a magnitude calculation. For each FID, 64 transients were accumulated. Sample concentration was 40 mg/0.5 mL $CDCl_3$.

The $^{13}C-^1H$ shift-correlated spectrum of **1** with proton decoupling in the F_1 domain was obtained with the usual pulse sequence (18). The spectral widths were 4000 Hz (8 ppm) in f_1 and 18500 Hz (~145 ppm) in f_2. The initial (t_1,t_2) matrix of 256 × 1K real data points was zero-filled to 1K × 2K data points to give a digital resolution of 4 Hz/point and 9 Hz/point in the f_1 and f_2 domains, respectively. Processing was done using gaussian functions and a power spectrum calculation. For each FID, 800 transients were accumulated for a total acquisition time of 60 h.

Nuclear Overhauser effect difference spectra of **1**, **3**, **4**, and **5** were obtained using spectral widths of 5000 Hz (10 ppm) and 8K real data points, to give a digital resolution of 0.6 Hz/point. Each line in a multiplet was irradiated sequentially (19) for a total irradiation time of 2 s per multiplet.

The ^1H *J*-resolved spectrum of **1** was acquired with spectral widths of 1000 Hz (2 ppm) and 31.25 Hz in the f_2 and f_1 domains, respectively. The initial (t_1,t_2) matrix of 32K × 2K real data points was zero-filled to 64 × 2K data points to give a digital resolution of 0.49 Hz/point in both dimensions. Processing was done with sine bell functions and a magnitude calculation.

The CHORTLE analysis of **3** (5 mg/0.5 mL $CDCl_3$) was performed using the pulse sequence of Pearson (17), with four proton evolution times of 0.24, 1.00, 2.40, and 3.20 ms and 14000 transients per point.

All ^{13}C spectra, including the DEPT spectrum of **1** (for the pulse sequence used see ref. 20), were acquired with spectral widths of 31250 Hz (250 ppm), 16K real data points and 12000 transients. The selective INEPT spectrum of **1** was acquired using the pulse sequence of Bax (16) except that there was no ^1H broadband decoupling and no refocussing of the ^{13}C resonances due to hardware restrictions in switching from high to low power. A total of 1680 transients was accumulated.

Spectral simulations were made using the PANIC program provided by Bruker.

Acknowledgements

We would like to thank Dr. David Bundle (NRC) for preliminary nmr measurements and Dr. André Simard (NRC) for computer programming. We are also grateful to the Canadian Commonwealth Scholarship Committee and the Natural Sciences and Engineering Research Council of Canada for financial support.

1. F. SCHROEDER. Prog. Lipid Res. **23**, 97 (1984).
2. (*a*) W. R. VEATCH and L. STRYER. J. Mol. Biol. **117**, 1109 (1977); (*b*) S. KAWATO, K. KINOSHITA, and A. IKEGAMI. Biochemistry, **17**, 5026 (1978); (*c*) B. R. LENTZ, D. A. BARROW, and M. HOECHLI. Biochemistry, **19**, 1954 (1980); (*d*) M. VINCENT and J. GALLEY. Biochem. Biophys. Res. Commun. **13**, 799 (1983); (*e*) M. STRAUME and B. J. LITMAN. Biophys. J. **49**, 310a (1986).
3. (*a*) J. DREW, G. GOWDA, P. MORAND, P. PROULX, A. G. SZABO, and D. WILLIAMSON. J. Chem. Soc. Chem. Commun. 901 (1985); (*b*) P. MORAND, J. DREW, A. G. SZABO, and P. PROULX. Canadian Patent application Serial No. 482,887, May 31 (1985); (*c*) P. MORAND, J. DREW, A. G. SZABO, and P. PROULX. U.S. Patent Application, Serial No. 867,565, May 28 (1986).
4. (*a*) R. R. RANDO, F. W. BANGERTER, and M. R. ALECIO. Biochim. Biophys. Acta, **684**, 12 (1982); (*b*) M. CRANNEY, R. B. CUNDALL, G. R. JONES, J. T. RICHARDS, and E. W. THOMAS. Biochim. Biophys. Acta, **735**, 418 (1983); (*c*) R. T. FISCHER, F. A. STEPHENSON, A. SHAFIEE, and F. SCHROEDER. Chem. Phys. Lipids, **36**, 1 (1984); (*d*) G. SMUTZER and P. L. YEAGLE. Biochim. Biophys. Acta, **814**, 274 (1985); (*e*) Y. J. KAO, A. K. SOUTAR, K.-Y. HONG, H. J. POWNALL, and L. C. SMITH. Biochemistry, **17**, 2689 (1978); (*f*) I. F. CRAIG, D. P. VIA, W. W. MANTULIN, H. J. POWNALL, A. M. GOTTO, and L. C. SMITH. J. Lipid Res. **22**, 687 (1981).
5. J. W. BLUNT and J. B. STOTHERS. Org. Magn. Reson. **9**, 439 (1977).
6. A. BAX. Two-dimensional nuclear magnetic resonance in liquids. D. Reidel, Holland. 1982; (*b*) R. BENN and H. GUNTHER. Angew. Chem. Int. Ed. Eng. **22**, 350 (1983).

Can. J. Chem. Downloaded from www.nrcresearchpress.com by 118.98.75.50 on 09/07/12
For personal use only.

7. (*a*) G. ENGLERT. Pure Appl. Chem. **57**, 801 (1985); (*b*) J. WERNLY and J. LAUTERWEIN. J. Magn. Reson. **66**, 355 (1986) and references therein.
8. (*a*) N. S. BHACCA and D. H. WILLIAMS. Applications of NMR spectroscopy in organic chemistry. Holden-Day, San Francisco. 1966. p. 108; (*b*) L. M. JACKMAN and S. STERNHELL. Applications of nuclear magnetic resonance spectroscopy in organic chemistry. Pergamon, Oxford. 1969. p. 316.
9. J. H. NOGGLE and R. E. SCHIRMER. The nuclear Overhauser effect. Academic Press, New York. 1971.
10. W. BRUGEL. Handbook of NMR spectral parameters. Vol. 2. Heyden, London. 1979. p. 455.
11. (*a*) S. P. SAWAN, T. L. JAMES, L. D. GRUENKE, and J. C. CRAIG. J. Magn. Reson. **35**, 409 (1979); (*b*) C. D. BARRY, C. M. DOBSON, D. A. SWEIGART, L. E. FORD, and R. J. P. WILLIAMS. *In* Nuclear magnetic resonance shift reagents. *Edited by* R. J. Sievers. Academic Press, New York. 1973. p. 173.
12. R. FREEMAN and G. A. MORRIS. Bull. Magn. Reson. **1**, 5 (1979).
13. (*a*) L. D. HALL and J. K. M. SANDERS. J. Am. Chem. Soc. **102**, 5703 (1980); (*b*) R. D. FARRANT, D. N. KIRK, J. D. MERSH, and J. K. M. SANDERS. J. Steroid Biochem. **19**, 181 (1983); (*c*) T. C. WONG and V. RUTAR. J. Am. Chem. Soc. **106**, 7380 (1984); (*d*) A. G. J. SEDEE, G. M. J. BEIJERSBERGEN VAN HENEGOUWEN, W. GUIJT, and C. A. G. HASNOOT. J. Chem. Soc. Perkin Trans. II, 1755 (1984); (*e*) H.-J. SCHNEIDER, U. BUCHHEIT, N. BECKER, G. SCHMIDT, and U. SIEHL. J. Am. Chem. Soc. **107**, 7027 (1985); (*f*) M. SAVIGNAC, G. JAOUEN, C. A. RODGER, R. E. PERRIER, B. G. SAYER, and M. J. MCGLINCHEY. J. Org. Chem. **51**, 2328 (1986); (*g*) W. F. REYNOLDS, S. MCLEAN, J. POPLAWSKI, R. G. ENRIQUEZ, L. I. ESCOBAR, and I. LEON. Tetrahedron, **42**, 3419 (1986).
14. M. KARPLUS. J. Chem. Phys. **30**, 11 (1959).
15. R. A. DWEK. Nuclear magnetic resonance in biochemistry. Clarendon, Oxford. 1975. p. 38.
16. A. BAX. J. Magn. Reson. **57**, 314 (1984).
17. G. A. PEARSON. J. Magn. Reson. **64**, 487 (1985).
18. (*a*) A. BAX. J. Magn. Reson. **53**, 517 (1983); (*b*) V. RUTAR. J. Magn. Reson. **58**, 306 (1984); (*c*) J. WILDE and P. H. BOLTON. J. Magn. Reson. **59**, 343 (1984).
19. (*a*) D. NEUHAUS. J. Magn. Reson. **53**, 109 (1983); (*b*) M. KINNS and J. K. M. SANDERS. J. Magn. Reson. **56**, 518 (1984).
20. D. T. PEGG, M. R. BENDALL, and D. M. DODDRELL. J. Magn. Reson. **44**, 238 (1981).

Can. J. Chem. Downloaded from www.nrcresearchpress.com by 118.98.75.50 on 09/07/12
For personal use only.

Pulse cyclic voltammetry. II. Flowing solutions

GORDON N. ECCLES AND WILLIAM C. PURDY[1]

Department of Chemistry, McGill University, 801 Sherbrooke St. West, Montreal, P.Q., Canada H3A 2K6

Received December 16, 1986

This paper is dedicated to Professor John T. Edward

GORDON N. ECCLES and WILLIAM C. PURDY. Can. J. Chem. **65**, 1795 (1987).

By the use of pulse cyclic chronovoltammetry, better analytical data are sometimes obtained during the reverse scans. This is demonstrated by a chronovoltammetric FIA study of the quinone–hydroquinone couple. A quantitative FIA pulse cyclic chronovoltammetric investigation of the ferri–ferrocyanide reversible couple showed linearity for time-integrated fourier-smoothed data for reduction scan currents as well as the total of the forward and reverse scan peak currents. The detection limit was found to be $2 \times 10^{-6} M$.

GORDON N. ECCLES et WILLIAM C. PURDY. Can. J. Chem. **65**, 1795 (1987).

Lorsqu'on utilise la chronovoltamétrie cyclique pulsée, on obtient quelquefois de meilleurs données analytiques durant les balayages inverses. On a mis cette propriété en évidence au cours d'une étude chronovoltamétrique FIA du couple quinone/hydroquinone. Une étude chronovoltamétrique cyclique pulsée FIA quantitative du couple réversible ferri/ferrocyanure présente une bonne linéarité pour les données, intégrées en fonction du temps et lissées par transformation de fourier, relatives aux courants de balayage pour la réduction ainsi que pour les courants totaux de balayage dans les deux sens. On a trouvé que la limite de détection est de $2 \times 10^{-6} M$.

[Traduit par la revue]

Can. J. Chem. Downloaded from www.nrcresearchpress.com by 118.98.75.50 on 09/07/12
For personal use only.

Introduction

Research on electrochemical detection methods for electroactive species in flowing streams is focussing on improving selectivity without compromising sensitivity or detection limits. This is one area of major concentration in our laboratory and this paper will describe a rapid scan detector that utilizes a modified cyclic voltammetry (CV) waveform as the applied signal. This development adds another dimension to the detector, the possibility of both qualitative and quantitative analysis.

Amperometric electrochemical detectors are the most common (1, 2) and offer high sensitivity, relatively simple instrumentation and reasonable selectivity through judicious selection of the applied potential. Pulse and square-wave linear sweep applied waveforms add the additional dimension of qualitative information to highly selective electrochemical detectors (3–8). Flow injection analysis and CV have been shown to be compatible and easily combined as a potentially new way to perform electrochemical experiments (9, 10).

To date the majority of electrochemical studies on organic compounds have involved oxidations; organic reductions await the development of a reliable mercury electrode (11, 12). The advantages of a mercury electrode are its relatively high hydrogen overpotential, its renewable surface that can discard adsorbed reaction products and its low capacitative background current. Disadvantages are its toxicity and the difficulties involved in controlling the drop in flowing streams. The use of carbon electrodes eliminates these two problems. Hepler, Weber, and Purdy evaluated Low-temperature Isotropic Carbon (LTIC) as an electrode material and found it to have higher hydrogen overpotentials when compared to electrodes made of carbon paste or glassy carbon impregnated with ceresin wax (13). This compares adequately as a substitute for a Hg electrode. Electrochemical cleaning of solid electrodes in situ can be accomplished by pulse methods (7, 14) but interference from electrode charging current remains a limitation with carbon.

In spite of this disadvantage, a wealth of voltammetric information can be obtained by applying a pulse cyclic voltammetric waveform as the excitation signal (15, 16). This work will show some of the merits achieved when applying this waveform to an LTIC electrode in flow-injection analysis (FIA) using the hydroquinone–quinone couple. In addition, a FIA quantative study of the ferri–ferrocyanide couple with integration and fourier-smoothing techniques will be illustrated.

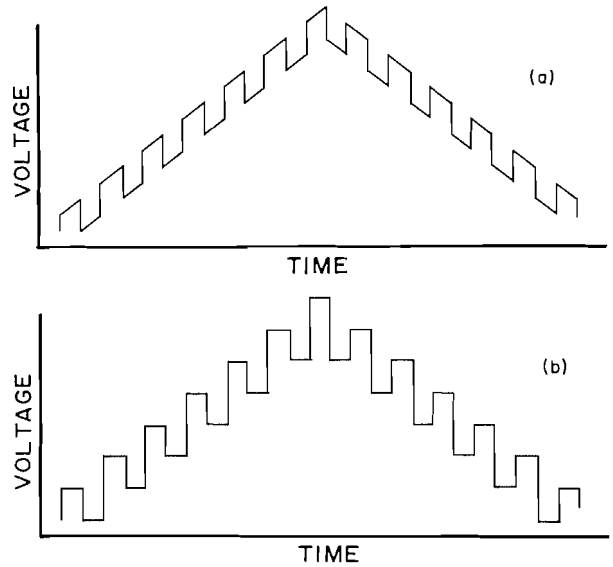

FIG. 1. Working electrode waveforms. (*a*) Pulse cyclic voltammetry. (*b*) Square-wave cyclic voltammetry.

Experimental

Flow injection apparatus

The flow injection system consisted of a constant flow reciprocating pump (Model 590 Waters Associates, Milford, MA) and a 20 μL loop injector (Model 7010, Rheodyne, Berkeley, CA). Coiled Teflon tubing measuring 195 cm in length and 0.292 in. in diameter with Teflon and stainless steel couplings was used. The mobile phase was 1 *M* sulfuric acid and the flow rate was 0.150 mL/min in all experiments.

Electrochemical apparatus

The microprocessor-controlled potentiostat used to carry out CV and pulse cyclic voltammetry (PCV) has been described previously (15). The work described in that paper was based on the waveform shown in Fig. 1*a*. This type of waveform offers electrochemical information in two time domains. In addition to the conventional CV time scale,

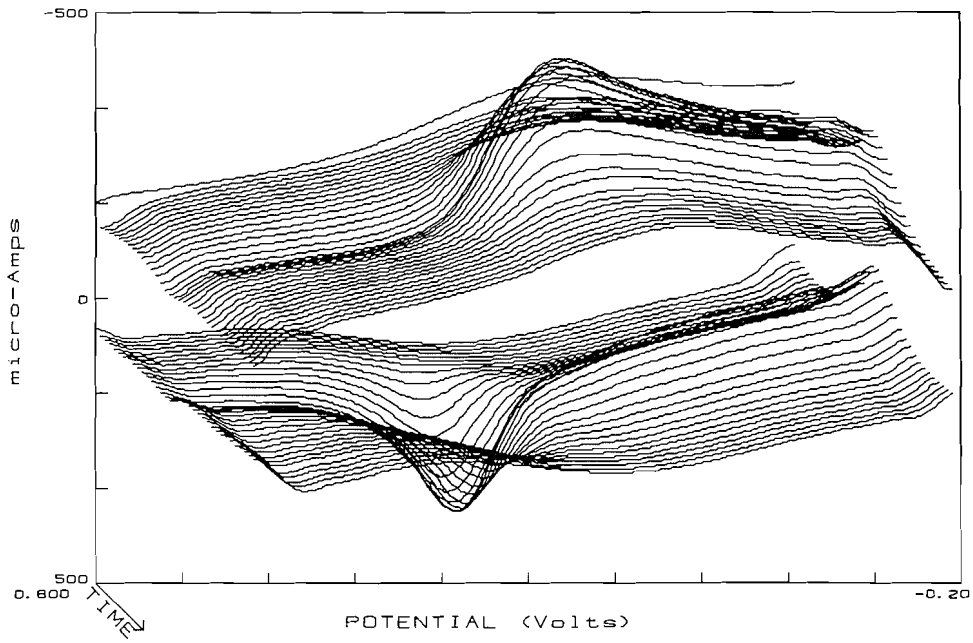

FIG. 2. Fourier-smoothed cyclic chronovoltammogram of 1 m*M* quinone in 1 *M* sulfuric acid. Initial time delay = 35 s. Number of cycles = 35. Data acquisition frequency = 120 Hz. Voltage ramp = 1 V/s.

Can. J. Chem. Downloaded from www.nrcresearchpress.com by 118.98.75.50 on 09/07/12
For personal use only.

another short time scale is obtained from the negative and positive going pulses. During the lifetime of a pulse in this waveform the potential continues to ramp, introducing a charging current component. Recently a modification to our instrument was undertaken to generate the waveform in Fig. 1*b* which is similar to the new waveform that was developed by Drake, Van Duyne, and Bond (17). The difference is that a square wave is applied as opposed to a pulse train and will be termed square-wave cyclic voltammetry. Preliminary results using this waveform indicate the expected decrease in the background current and consequently a relative increase in the faradaic component. The extent of the improvement at the LTIC electrode is currently under investigation.

Additional equipment that is required includes an IBM PC with 640 Kbytes of memory, an IBM colour monitor, a HP 7470 2-pen plotter, and a parallel opposed channel electrode flow cell (1 μL volume) consisting of a 2 mil Teflon spacer sandwiched between two LTIC (available from Carbomedics Inc., Austin, TX) plates with a downstream silver/silver chloride reference electrode. One plate was used as the working electrode and the other operated as the auxiliary. The data were obtained and stored in computer memory until each run was completed. Then the results were transferred to a hard disk.

The software language used to operate the instrument and manipulate the data was written in TURBO Pascal-87. The program is menu-driven and communicates interactively with the operator for smooth operation. The fourier-smoothing program was modified to handle our data format and translated to TURBO Pascal-87 from a routine written in BASIC (18).

Chemicals

Reagent grade chemicals were used in preparation of all solutions. A 2.00 m*M* stock solution of potassium ferricyanide was prepared by dissolving the salt in 1 *M* sulfuric acid. Solutions of 1.00, 0.400, 0.200, and 0.080 m*M* were subsequently prepared by diluting the appropriate volume of the stock solution in 1 *M* sulfuric acid. A solution of 1 m*M* quinone was prepared by dissolving the required weight in 1 *M* sulfuric acid.

Procedure

Cyclic and pulse cyclic chronovoltammograms were obtained for a 1 m*M* solution of quinone in 1 *M* sulfuric acid. The sequence was to inject 20 μL of the solution, hold the working electrode at 0.800 V vs. an Ag/AgCl reference for 35 s and then apply the waveform. The time delay was predetermined by an initial run at a faster sweep rate and was used to reduce the amount of blank cycles. One run containing several consecutive cycles was obtained for each mode of operation.

Pulse cyclic chronovoltammograms were obtained for various concentrations of ferricyanide in 1 *M* sulfuric acid. The sequence was identical to the one described above. A total of 3 runs containing 35 consecutive cycles was obtained for each concentration.

The data were stored on the hard disk in the computer. Later, the response current vs. potential curves were processed and smoothed prior to plotting.

Results and discussion

FIA of quinone using a rapid scan CV and PCV detector

In static solutions it was found that the residual current becomes reproducible after completion of the first cycle during a multiple scan CV (16). This behaviour is also observed in flowing streams and is illustrated by the results of a multiple scan CV of a 20 μL injection of 1 m*M* quinone in 1 *M* sulfuric acid shown in Fig. 2. The forward and reverse current traces are arbitrarily spaced apart to reduce overlapping lines. The upper curves represent the forward scans (peaks are reduction currents of quinone to hydroquinone) and the lower curves are results of the reverse scans (peaks are oxidation currents of hydroquinone to quinone). The oxidation peak is well defined in contrast to the broad reduction peak indicating that this couple is not electrochemically reversible.

The data in Fig. 3 were obtained from a multiple scan pulse cyclic chronovoltammogram of a 20 μL injection of 1 m*M* quinone in 1 *M* sulfuric acid. Again the upper and lower traces are arbitrarily spaced apart for clarity. The upper traces correspond to data acquired at the end of positive-going pulses, while the lower traces represent data from negative-going pulses. The current axis is of greater magnitude than in Fig. 2, indicating a sensitivity increase using PCV in contrast to CV. On the left of the switching potential (−0.200 V), the major peak in negative microampere range corresponds to reduction

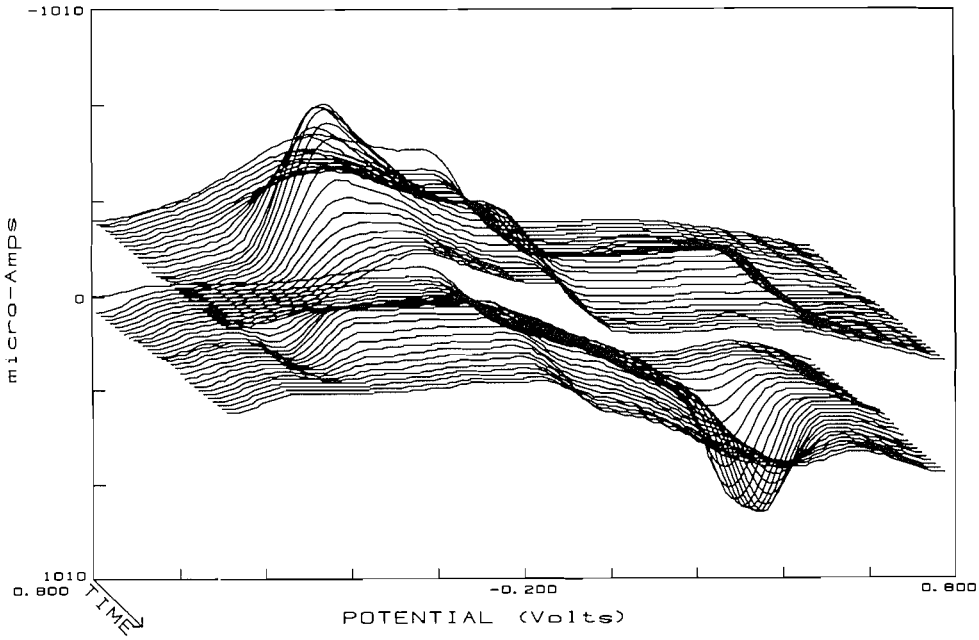

FIG. 3. Fourier-smoothed pulse cyclic chronovoltammogram of 1 m*M* quinone in 1 *M* sulfuric acid. Initial time delay = 35 s. Number of cycles = 30. Data acquisition frequency = 120 Hz. Square wave frequency = 60 Hz. Square wave amplitude = 100 mV. Voltage ramp = 1 V/s.

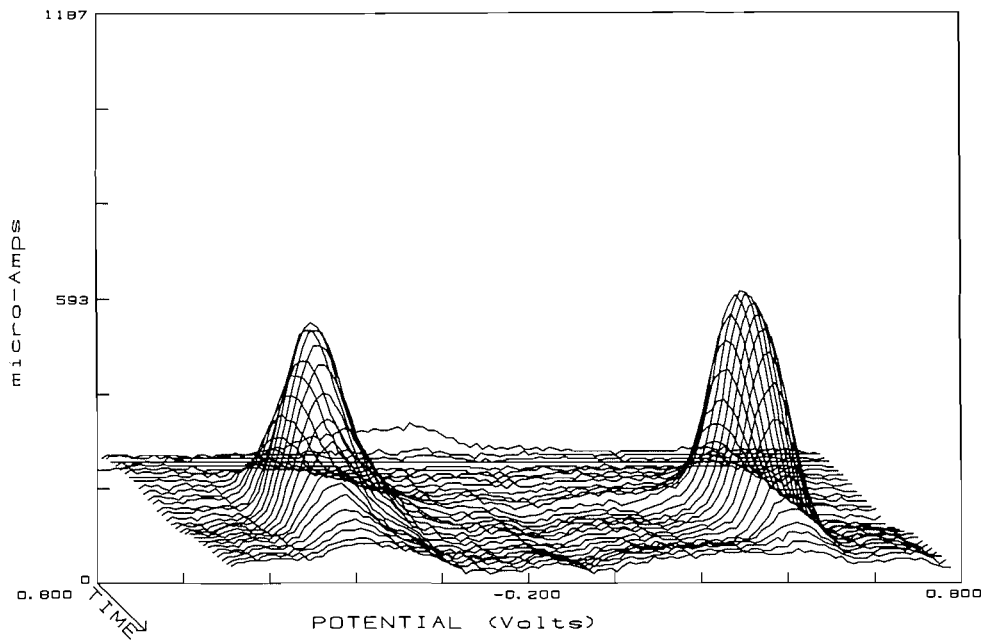

FIG. 4. Fourier-smoothed background corrected absolute difference plot obtained from the data in Fig. 3.

currents obtained from the conversion reaction of quinone to hydroquinone and the minor peak was constructed from oxidation currents obtained from the conversion of the generated hydroquinone to quinone (during the pulse time scale). On the right hand side of the switching potential the reverse scan voltammetric information displays a major peak in the positive microampere region for the oxidation of the generated hydroquinone during the long time scale of the process. Less electrochemical activity is observed here during the pulse time scale (upper traces) than during the forward scans.

It is shown in Fig. 3 that the oxidation currents during the short and long time scales predominate. Another way to display these data is by plotting the absolute current difference between a point acquired during a forward pulse and another during the respective reverse pulse; shown in Fig. 4. The peak on the right of this background corrected plot shows the major oxidation current obtained and the smaller peak on the left represents the major reduction current. Thus, it is clear that for an injected volume of quinone the oxidation current during the long time scale provides better analytical sensitivity. This demonstrates the analytical ability of a PCV detector in that better analytical data can sometimes be found in the reverse scan.

Can. J. Chem. Downloaded from www.nrcresearchpress.com by 118.98.75.50 on 09/07/12
For personal use only.

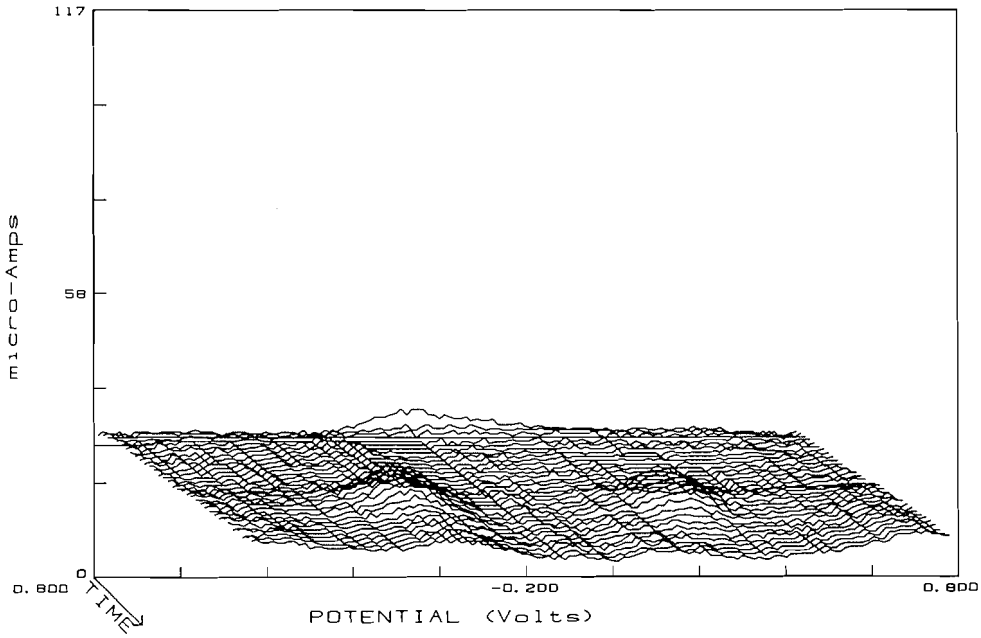

FIG. 5. Background corrected absolute PCV difference plot of 0.08 m*M* ferricyanide in 1 *M* sulfuric acid. Initial time delay = 35 s. Number of cycles = 35. Data acquisition frequency = 130 Hz. Square wave frequency = 65 Hz. Square wave amplitude = 100 mV. Voltage ramp = 1 V/s.

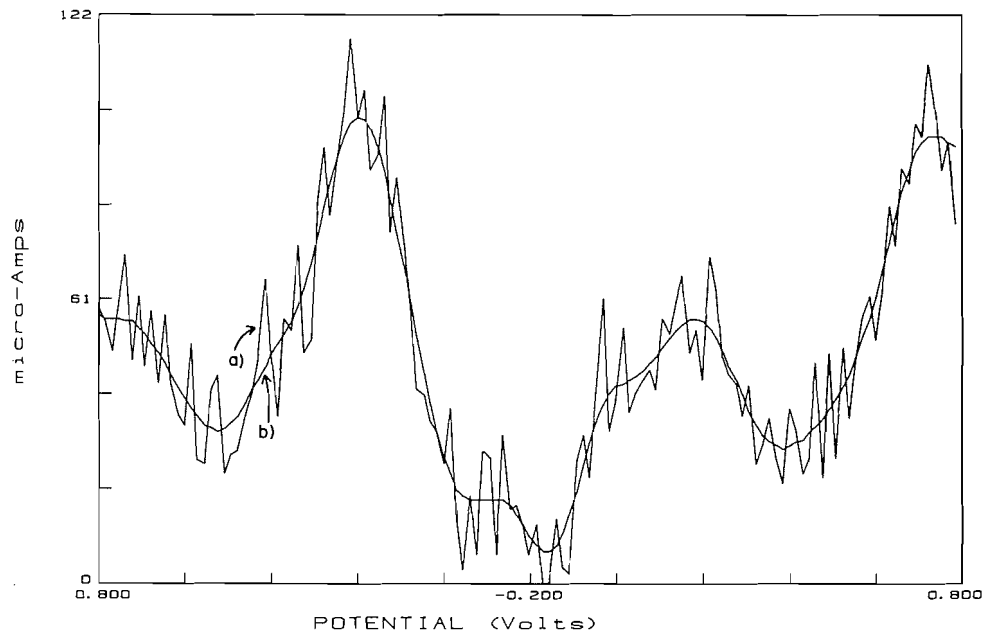

FIG. 6. Time-integrated plot of Fig. 4. (*a*) Before fourier smoothing. (*b*) After fourier smoothing.

Quantitative study of ferricyanide using FIA with a rapid scan PCV detector

A multiple scan PCV background corrected absolute difference plot is shown in Fig. 5 for 0.08 m*M* potassium ferricyanide in 1 *M* sulfuric acid. The major reduction currents obtained during the negative scans are shown on the left side of the switching potential and the major oxidation currents on the right. The signal is enhanced up to a factor of ten by integrating the pulse cyclic chronovoltammogram with respect to the time axis for those cycles containing a response; a plot of these results is shown in Fig. 6*a*. The outcome is a single total current response curve containing significant high frequency noise. After fourier smoothing, the noise is reduced considerably and peak currents are easily measured (see Fig. 6*b*). Plots of reduction scan currents, oxidation scan currents and the totals of these two against concentration of ferricyanide are shown in Fig. 7. Signal drop at the high concentration may be due to departure from the dynamic range of the technique. The equation of the line (high concentration omitted) for the reduction scans is $y = 11.25 + 499.9x$ with a correlation coefficient of 0.9903. The detection limit was found to be 2×10^{-6} *M*. The total current line equation (high concentration omitted) is $y = 44.69 + 773.0x$ with a correlation coefficient of 0.993. The separation that is observed between the reduction

Can. J. Chem. Downloaded from www.nrcresearchpress.com by 118.98.75.50 on 09/07/12
For personal use only.

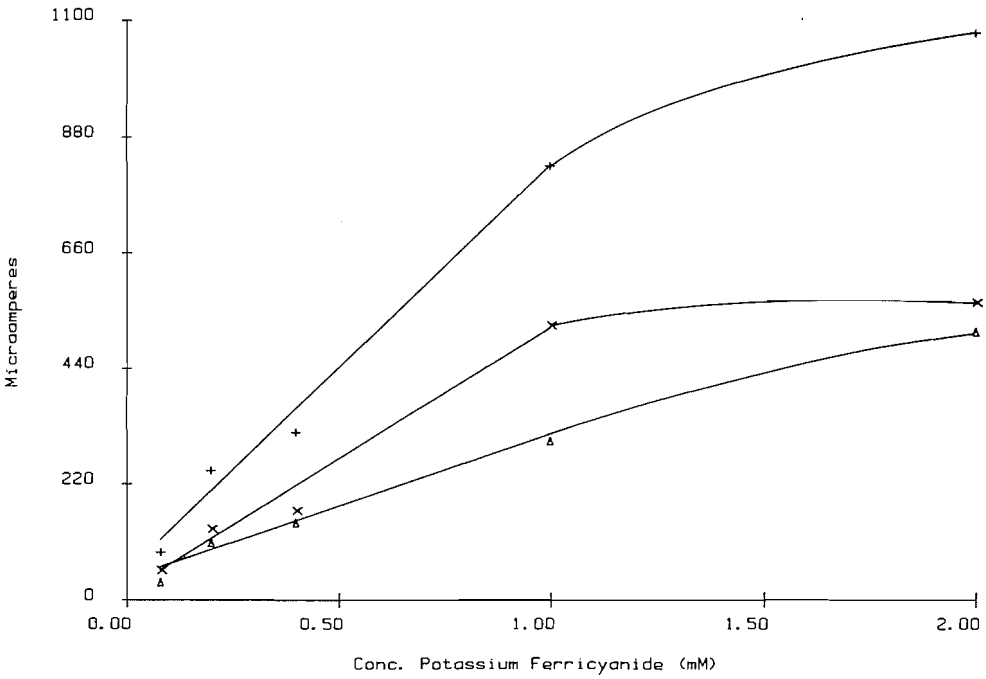

FIG. 7. Peak height vs. concentration of ferricyanide of various time-integrated fourier-smoothed difference plots. (×) Forward scan currents, (△) reverse scan currents, (+) total currents.

scan peak current and the oxidation scan peak current may be due to the timing involved with the flowing sample front, the electrode and the applied waveform. This is currently being investigated.

Conclusions

A rapid scan CV and PCV detector in FIA offers the advantage of generating an electroactive compound initially absent in the injected sample and studying its electroactive properties during the reverse scan. This was illustrated using the quinone hydroquinone redox couple. The relative sensitivity was shown to be greater for the PCV detector.

Linear calibration curves were obtained by plotting the time-integrated reduction scan peaks and the total forward and reverse scan peak currents against the concentration of ferricyanide. The detection limit was found to be $2 \times 10^{-6} M$.

Acknowledgment

The authors are indebted to the Natural Sciences and Engineering Research Council of Canada for financial support of this work.

1. A. D. ROSTON and P. T. KISSINGER. Anal. Chem. **54**, 1417A (1982).
2. S. A. MCCLINTOCK and W. C. PURDY. International Laboratory, **14**, No. 7, 70 (1984).
3. D. G. SWARTZFAGER. Anal. Chem. **48**, 2189 (1976).
4. J. WANG, E. OUZIEL, C. H. YARNITZKY, and M. ARIEL. Anal. Chim. Acta, **102**, 99 (1978).
5. R. SAMUELSON and J. OSTERYOUNG. Anal. Chem. **52**, 2215 (1980).
6. R. SAMUELSON and J. OSTERYOUNG. Anal. Chim. Acta, **123**, 97 (1981).
7. M. STASTNY, R. VOLF, H. BENADIKOVA, and I. VIT. J. Chrom. Sci. **21**, 18 (1983).
8. J. J. SCANLON, P. A. FLAQUER, G. W. ROBINSON, G. E. O'BRIEN, and P. E. STURROCK. Anal. Chim. Acta, **158**, 169 (1984).
9. J. JANATA and J. RUZICKA. Anal. Chim. Acta, **139**, 105 (1982).
10. N. THOEGERSEN, J. JANATA, and J. RUZICKA. Anal. Chem. **55**, 1669 (1983).
11. K. BRATIN, P. T. KISSINGER, and C. S. BRUNTLETT. J. Liq. Chromatogr. **4**(10), 1777 (1981).
12. K. BRATIN and P. T. KISSINGER. J. Liq. Chromatogr. **4** (Supp. 2), 321 (1981).
13. B. R. HEPLER, S. G. WEBER, and W. C. PURDY. Anal. Chim. Acta, **102**, 41 (1978).
14. S. HUGHES and D. C. JOHNSON. Anal. Chim. Acta, **132**, 11 (1981).
15. G. N. ECCLES and W. C. PURDY. Anal. Lett. **18**(A6), 657 (1985).
16. G. N. ECCLES and W. C. PURDY. Can. J. Chem. To be published.
17. K. F. DRAKE, R. P. VAN DUYNE, and A. M. BOND. J. Electroanal. Chem. **89**, 231 (1978).
18. E. E. AUBANEL and K. B. OLDHAM. Byte, Feb., 207 (1985).

Can. J. Chem. Downloaded from www.nrcresearchpress.com by 118.98.75.50 on 09/07/12
For personal use only.

Destabilized carbocations. Nuclear magnetic resonance detection and reactivities of aryl α-thioformamidyl cations

F. J. ABLENAS, B. E. GEORGE, M. MALEKI, R. JAIN, A. C. HOPKINSON, AND E. LEE-RUFF
Department of Chemistry, York University, North York, Ont., Canada M3J 1P3

Received December 14, 1986

This paper is dedicated to Professor John T. Edward

F. J. ABLENAS, B. E. GEORGE, M. MALEKI, R. JAIN, A. C. HOPKINSON, and E. LEE-RUFF. Can. J. Chem. **65**, 1800 (1987).

A series of α-aryl and diarylthioformamidyl cations were observed by low-temperature nuclear magnetic resonance spectroscopy. These ions undergo efficient cyclization and deprotonation to give benzothiophenes.

F. J. ABLENAS, B. E. GEORGE, M. MALEKI, R. JAIN, A. C. HOPKINSON et E. LEE-RUFF. Can. J. Chem. **65**, 1800 (1987).

Faisant appel à la résonance magnétique nucléaire à basse température, on a pu observer une série de cations α-aryl et diarylthioformamidyles. Ces cations subissent des réactions efficaces de cyclisation et de déprotonation pour conduire aux benzothiophènes.

[Traduit par la revue]

Can. J. Chem. Downloaded from www.nrcresearchpress.com by 118.98.75.50 on 09/07/12
For personal use only.

Introduction

The destabilization of carbocations with electron-withdrawing groups imparts certain properties that are unique to such systems, and has prompted a number of recent investigations of their structures and reactivities (1). An α-formyl group, when coplanar with a cationic carbon, functions as a π-donor and σ-acceptor with the overall effect being destabilizing (2). Higher level calculations show H_2C^+CHO to collapse without a barrier to the oxygen-bridged cyclic ion **2** (3) and this structure is very weakly stabilized relative to the open structure (4). However, it is expected that alkyl and (or) aryl substitution will stabilize the open form. Solvolytic studies of their α-keto-sulphonate precursors indicate that only minor rate-retarding effects are observed with a carbonyl group present (5). In certain cases (5) an α-keto substituent actually enhanced rates of solvolysis relative to hydrogen.

The stabilizing effect of a carbonyl group may be associated with two charge delocalization mechanisms. Delocalization of the positive charge via π-delocalization (mesomeric effect) would produce a vinyl oxenium ion **1**. Alternatively, neighboring group interaction (σ-bridging) would give a 3H-oxirenium cation **2**. Ionization of α-chloroepoxides has been shown to

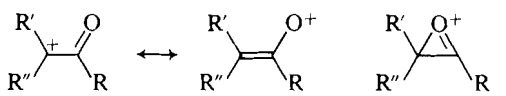

1 **2**

provide an alternate route to α-carbonyl cations (6). Although *ab initio* calculations for the parent ion (R, R′, R″ = H) indicate that the bridged species **2** is slightly more stable (3) for the formylmethyl cation, no experimental evidence is found either from solvolytic data (7) or from nmr observations of these species under stable ion conditions (8) of the substituted derivatives to indicate that these ions are bridged (4). Replacing the carbonyl group with a thiocarbonyl group would be expected to enhance charge delocalization by both mesomeric and σ-bridging mechanisms and perhaps stabilize adjacent cations.[1] MO calculations of the thioformyl methyl cation show that the bridged species is significantly more stable (4) and this is corroborated by product studies on chiral α-thiocarbomethoxymethyl mesylates (9). Furthermore, the stabilization by an α-thiocarbonyl group of an adjacent carbocation is indicated by rate enhancements in the solvolyses of these derivatives (9) relative to carbonyl substituents. Having previously observed diaryl α-carbonylcarbocations under stable ion conditions and studied their reactivity (10), we were interested in comparing aryl and diaryl α-thiocarboxamidyl carbocations with their oxygen analogues. In this study we report the low temperature nmr data and reactivity of six such derivatives.

Results and discussion

The precursors to the carbocations are the alcohols **3**, which were prepared by reaction of lithium *N*,*N*-dimethylthioformamide anion, generated *in situ* from LDA and *N*,*N*-dimethylthioformamide in THF, with the corresponding aryl aldehyde or ketone at −78°C.

The carbocations **4** were prepared by mixing either SO_2 or CD_2Cl_2 solutions of the alcohols and chlorosulphonic acid in a 10-mm nmr tube at −95°C. In all cases except **3***a*, red coloured solutions were observed. The ^{13}C nmr spectra of these ions were obtained and the chemical shifts for the thiocarbonyl and

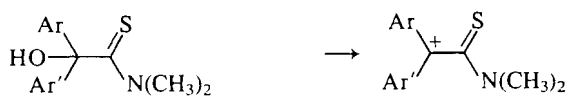

3*a* Ar = C_6H_5, Ar′ = H
b Ar = *p*-CH_3O—C_6H_4, Ar′ = H
c Ar = Ar′ = *p*-F—C_6H_4
d Ar = *p*-CH_3O—C_6H_4, Ar′ = C_6H_5
e Ar = *p*-F—C_6H_4, Ar′ = C_6H_5
f Ar = Ar′ = Ph

4

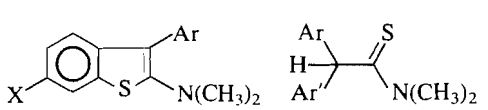

5*a* Ar = H, X = H
b Ar = H, X = CH_3O
c Ar = *p*-F—C_6H_4, X = F
d Ar = C_6H_5, X = CH_3O
e Ar = C_6H_5, X = F
f Ar = C_6H_5, X = H

6

[1] A. C. Hopkinson and M. H. Lien, unpublished results; calculations at the 6-31G* level using the equation

$$CH_3—\overset{+}{C}HX + CH_4 \rightarrow CH_3^+ + CH_3CH_2X$$

give ΔE = 0.7 kcal/mol for X = O and ΔE = 25.6 kcal/mol for X = S.

TABLE 1. ^{13}C chemical shifts of **4**[a] (δ ppm)

Ion	C^+	C=S (C=S for alcohol **3**)	
4*b*	151.0 or 148.7[b]	190.8	(203.8)
4*c*	131.1[c]	181.7	(205.7)
4*d*	169.4[d]	185.6 or 182.3[e]	(206.5)
4*e*	183.6[d]	181.8	(203)
4*f*	186.9[d]	185.3	(206.5)

[a]Full nmr data for ions **4***b–f* are reported in the experimental section.

[b]Assignment is based on H-coupled ^{13}C spectra. However, specific assignment between C^+ and C—H (arene) could not be made.

[c]Assignment is based on JMOD ^{13}C spectra.

[d]Assignment is based on specific ^{13}C labelling using alcohols **3***d–f* labelled at carbinol carbon.

[e]The thiocarbonyl carbon and the *p*-methoxy aryl carbon could not be differentiated.

cation carbons tabulated in Table 1. That a single species was present was evident from the high field signals associated with *N,N*-dimethyl carbons. The specific assignments of the chemical shifts for the thiocarbonyl and cationic carbons were based on H-coupled and JMOD ^{13}C nmr spectra[2] for ions **4***b* and *c* respectively. For ions **4***d–f* the specific assignments for these two carbons were based on specifically ^{13}C labelled alcohols **3***d–f* labelled at the carbinol carbon with tenfold enrichment. It is noteworthy that ion **4***c* exhibits an unusually high shifted cationic carbon signal relative to the other ions. This could be attributed to sulphur σ-bridging effects in this ion, in which the presence of two electron-withdrawing aryl groups would be expected to promote this type of interaction. However, caution must be exercised in extrapolating charge densities on the basis of nmr chemical shifts (11). Alcohol **3***a* did not readily undergo dehydrative ionization under these conditions (*vide infra*) as was evident from its inertness to unimolecular reaction. It would appear that one phenyl substituent in **4***a* is not sufficiently stabilizing for its observation.

Quenching of ions **4***c,e*, and *f* in SO_2 solution by addition to ice resulted in the formation of benzothiophenes **5** and the reduced products **6** in approximately equal amounts. In contrast, when the solutions of **4***b,c,e*, and *f* in CH_2Cl_2 and **4***b* in SO_2 were quenched in ice under identical conditions, no reduced product **6** could be detected and only products **5** were isolated. The formation of **6** in the presence of SO_2 may be associated with the reducing properties of H_2SO_3 formed upon the addition of water. That rearrangement of cation **4** to the corresponding protonated benzothiophene **5** had not occurred at −78°C was ascertained by obtaining ^{13}C nmr spectra of solutions of **5** in triflic acid/CD_2Cl_2 at room temperature.[3] The spectra of protonated **5** were completely different from those obtained from alcohols **3** in acid solution and it was evident that the protonation occurs exclusively at the expected β-position of the thiophene ring in **5** by the appearance of a CH_2 signal at high field for the aldehyde adducts.

The aromatic region in the ^{13}C nmr spectra of ions **4***b* and *d* was more complex than expected for a single isomer. The additional aromatic carbon signals for these ions can be attributed to geometric isomerism associated with the restricted

[2]"J" modulated spin-echo pulse sequence, which distinguishes CH/CH_3 carbon nuclei from quaternary/CH_2 nuclei.

[3]The ^{13}C chemical shifts of cations **4** were essentially independent of the choice of CD_2Cl_2 or SO_2 as cosolvents.

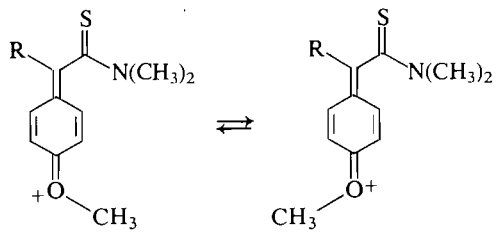

SCHEME 1

barrier to rotation of the methoxyl group (Scheme 1). Observation of a single methoxy and *N,N*-dimethyl carbon signals implies coincidental equivalence of these carbon centers in the two isomers. Such phenomena have been previously reported for protonated anisaldehyde in which the rotational barrier is sufficiently large that at room temperature two distinct species are observed (12).

The studies of the acid rearrangement product formation from alcohols **3** were performed using methanesulphonic acid in methylene chloride. The solutions of **3** in chlorosulphonic acid led to water soluble products, presumably due to sulphonation. Alcohols **3***b–f* underwent dehydrative cyclization to benzothiophenes **5** in quantitative yield within 5 min at ambient temperature. The reaction of alcohol **3***a* was sluggish under these conditions and **3***a* had to be heated to reflux in chlorobenzene solution with 5 equiv. of methanesulphonic acid to give the benzothiophene **5***a* in 31% yield. The spectral data for benzothiophene **5***a* were compared with those of a previously reported sample and were found to be identical (13). The molecular structural assignments for **5***b–f* were based on spectral and analytical data.

It is noteworthy that alcohol **3***a*, which did not undergo ionization in $ClSO_3H$ at −70°C, does undergo the cyclization reaction but at a significantly slower rate. This observation can be rationalized in terms of the low stabilization of the cation **4***a* by the substituents. Once the ion is formed, albeit under more vigorous conditions, the reactivity of **4***a* should be greater than those of ions **4***b–f*. Two mechanisms for the cyclization of ions **4** can be envisaged. Rearrangement of a bridged species **7** (Scheme 2) to **8** could proceed in similar fashion to a vinyl

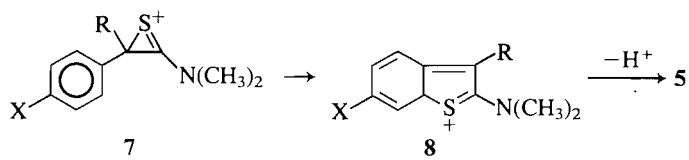

SCHEME 2

cyclopropane rearrangement (14) with sulphur attack on the ring. Alternatively (Scheme 3) the ions **4** can be regarded as 4π-thiapentadienyl cations **9** and cyclizations of these to thiacyclopentenyl cations in carbocyclic analogues are common (15). It is interesting to note that in the unsymmetrical ions **4***d* and *e* (where X = OCH_3, F) cyclization occurs to the

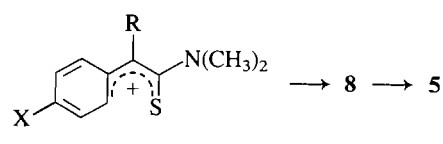

SCHEME 3

Can. J. Chem. Downloaded from www.nrcresearchpress.com by 118.98.75.50 on 09/07/12
For personal use only.

substituted aryl group. The regioselectivity of the cyclization ring suggests that a significant amount of positive charge is delocalized into the substituted aryl ring and that sulphur cyclization proceeds by a nucleophilic attack of S to this ring in both **4***d* and *e*. The corresponding diphenylacetamidyl methyl cation undergoes fluorene cyclization (10) in contrast to ion **4***f*. The lack of fluorene cyclization in ions **4***c–f* suggests that the nucleophilic reactivity of sulphur is greater than that for oxygen, thus leading exclusively to heteroatomic cyclization in these diaryl derivatives.

Experimental

The ^{1}H nmr spectra were recorded in $CDCl_3$ solution with TMS as an internal reference on a CFT-20 or AM-300 nmr spectrometer, and ^{13}C nmr spectra were recorded in $CDCl_3$ solution (unless otherwise noted). Infrared spectra were recorded on a Unicam SP1000 instrument, and mass spectra were obtained on a VG Micromass 16F instrument. Elemental analyses were performed by Guelph Chemical Laboratories.

Tetrahydrofuran was dried with sodium; *N*,*N*-dimethylthioformamide (Aldrich) was dried over 3A molecular sieves.

Carboxyl-^{13}C-labelled benzoic acid and d_2-dichloromethane were obtained from MSD Isotopes.

Preparation of α-hydroxy thioacetamides (general procedure)

A solution of the carbonyl compound (3.79 mmol) and *N*,*N*-dimethylthioformamide (0.32 mL, 3.78 mmol) in dry THF (2.0 mL) was added to a solution of LDA at −78°C, which was prepared by adding *n*-butyllithium (3.80 mmol) to diisopropylamine (0.53 mL, 3.79 mmol) in THF (40 mL). The resultant solution was allowed to slowly warm to room temperature over 3 h.

The reaction was quenched by adding saturated ammonium chloride solution (40 mL), and transferring the resultant two-phase mixture to a separatory funnel. The organic layer was removed, dried ($MgSO_4$), filtered, and solvent evaporated to yield the crude α-hydroxy thioacetamide. The desired product was purified either by recrystallization from 95% ethanol or flash chromatography (silica gel; petroleum ether:dichloromethane, 50:50).

N,N-*Dimethyl-2-hydroxy-2-phenylthioacetamide* **3**a

The benzaldehyde adduct was obtained as colourless crystals, mp 102–102.5°C (80%); ir (KBr) *ν*: 3420 (OH), 1540 (s), 1310 (s) (thioamide I and II), 1215 (C—O) cm^{-1}; ^{1}H nmr δ: 7.30–7.50 (m, 5H), 7.20 (s, O*H*), 5.30 (s, 1H), 3.55 (s, 3H), 3.10 (s, 3H) ppm; ^{13}C nmr δ: 203.6 (C=S); 139.8 (ArC1); 128.9, 127.3 (ArC2, C3); 128.4 (ArC4); 73.9 (C-OH); 45.5, 41.1 (NMe_2) ppm; ms *m/z*: 195 (31), 89 (77), 88 (100). *Anal.* calcd. for $C_{10}H_{13}NOS$: C 61.51, H 6.71, N 7.17, S 16.42; found: C 61.47, H 6.85, N 6.89, S 16.08.

N,N-*Dimethyl-2-anisyl-2-hydroxythioacetamide* **3**b

The adduct was obtained as pale yellow crystals, mp 103–103.5°C (83%); ir (KBr) *ν*: 3300 (OH), 1480 (s) and 1350 (s) (thioamide I and II) cm^{-1}; ^{1}H nmr δ: 7.35 (d, 2H, J = 8.6 Hz), 6.79 (d, 2H, J = 8.7 Hz), 5.18 (s, 2H), 3.72 (s, 3H), 3.45 (s, 3H), 3.04 (s, 3H) ppm; ^{13}C nmr δ: 203.8 (C=S); 159.5 (ArC4); 132.0 (ArC1); 128.6 (ArC2); 114.2 (ArC3); 73.3 (OMe); 55.2 (C-OH); 45.6 and 41.0 (NMe_2) ppm; ms *m/z*: 225 (8), 137 (70), 109 (40), 90 (87), 88 (30), 57 (85). *Anal.* calcd. for $C_{11}H_{15}NSO_2$: C 58.65, H 6.72, N 6.22, S 14.23; found: C 59.00, H 6.78, N 5.99, S 14.23.

N,N-*Dimethyl-2,2-di-(4-fluorophenyl)-2-hydroxythioacetamide* **3**c

This compound was obtained as white crystals, mp 95.0–95.5°C (64%); ir ($CHCl_3$) *ν*: 3240 (br) (OH); 1508, 1225 (s) (thioamide I and II), 1210 (C—F), 1160 (m) (C—O) cm^{-1}; ^{1}H nmr δ: 7.27 (dd, $J_{H,H}$ = 8.8 Hz, $J_{H,F}$ = 5.3 Hz, 4H), 6.98 (t, J = 8.7 Hz, 4H), 6.53 (s, OH), 3.53 (s, 3H), 2.73 (s, 3H) ppm; ^{13}C nmr δ: 205.7 (C=S); 162.2 (d, $^1J_{C,F}$ (16) = −256 Hz, C—F); 138.1 (d, $^4J_{C,F}$ = +3.2 Hz); 130.1 (d, $^3J_{C,F}$ = +8.1 Hz); 115.2 (d, $^2J_{C,F}$ = +21 Hz); 81.5 (C-OH); 47.9, 45.2 (NMe_2) ppm; ms *m/z*: 307 (7), 219 (24), 122 (100), 95 (40). *Exact Mass* calcd. for $C_{16}H_{15}F_2NOS$: 307.0842; found: 307.0847.

N,N-*Dimethyl-2-anisyl-2-hydroxy-2-phenylthioacetamide* **3**d

This compound was obtained as an oil that could not be crystallized (83%); ir ($CHCl_3$) *ν*: 3180 (OH), 1510, 1250 (s) (thioamide I and II), 1040 (C—O) cm^{-1}; ^{1}H nmr δ: 7.20–7.35 (m, 7H), 6.82 (d, J = 7.2 Hz, 2H), 6.53 (s, OH), 3.77 (s, OCH_3), 3.53 (s, 3H), 2.73 (s, 3H) ppm; ^{13}C nmr δ: 206.5 (C=S); 159.0 (anisyl C4); 142.5 (phenyl C1); 134.2 (anisyl C1); 129.7, 128.3, 128.2 (ArC); 127.7 (phenyl C4); 113.5 (anisyl C3); 82.1 (C-OH); 55.2 (OCH_3); 47.9, 45.2 (NMe_2) ppm; ms *m/z*: 301 (6), 213 (73), 135 (85), 105 (54), 90 (100). *Exact Mass* calcd. for $C_{17}H_{19}NO_2S$: 301.1137; found: 301.1136.

N,N-*Dimethyl-2-*p*-fluorophenyl-2-phenyl-2-hydroxythioacetamide* **3**e

This compound was obtained as pale yellow crystals, mp 98–98.5°C (85%); ir (KBr) *ν*: 3200 (OH), 1520 (s) and 1280 (s) (thioacetamide I and II) cm^{-1}; ^{1}H nmr δ: 7.37 (m, 7H), 7.06 (t, J = 8.6 Hz, 2H), 6.60 (s, OH), 3.6 (s, 3H), 2.8 (s, 3H) ppm; ^{13}C nmr δ: 203.1 (C=S); 161.5 (d, $^1J_{C,F}$ = 284 Hz, C—F); 142.1 (phenyl C1); 138.2 (d, $^4J_{C,F}$ = 3 Hz); 130.3 (d, $^3J_{C,F}$ = 8 Hz); 128.3, 128.2, and 127.9 (phenyl C2, C3, and C4); 105.1 (d, $^2J_{C,F}$ = 22 Hz); 81.9 (C-OH); 47.9 and 45.2 (NMe_2) ppm; ms *m/z*: 289 (10), 201 (30), 123 (60), 105 (34), 89 (30). *Anal.* calcd. for $C_{16}H_{16}FNOS$: C 66.41, H 5.57, F 6.56, N 4.84, S 11.08; found: C 66.59, H 5.55, F 6.72, N 5.09, S 11.39.

N,N-*Dimethyl-2-hydroxy-2,2-diphenylthioacetamide* **3**f

The benzophenone adduct was obtained as white crystals, mp 147–148°C (benzene) (80%); ir (KBr) *ν*: 3450 (OH), 1520, 1246 (s) (thioamide I and II), 1210 (C—O) cm^{-1}; ^{1}H nmr δ: 7.30–7.40 (m, 10H), 6.62 (s, O*H*), 3.58 (s, 3H), 2.76 (s, 3H) ppm; ^{13}C nmr δ: 206.5 (C=S); 142.3 (ArC1); 128.4, 128.2 (ArC2, C3); 127.8 (ArC4); 82.5 (C-OH); 47-9, 45.3 (NMe_2); ms *m/z*: 271 (13), 183 (38), 105 (100). *Exact Mass* calcd. for $C_{16}H_{17}NOS$: 271.1031; found: 271.1040.

Preparation of 10 at.% 2-^{13}C-2-hydroxythioacetamides

The ^{13}C-labelled compounds **3***d*, **3***e*, and **3***f* were prepared from the corresponding labelled benzophenones, which were in turn prepared from the Friedel–Crafts acylation of anisole (17*a*), fluorobenzene (17*c*), and benzene (17*b*), respectively, with 10 at.% carboxyl-^{13}C-benzoyl chloride. The ^{13}C content of **3***d*, *e*, and *f* was ascertained by mass spectrometry and nmr.

*Preparation of 2-dimethylaminobenzo[*b*]thiophenes (general procedure)*

The α-hydroxy thioacetamide (0.316 mmol) was dissolved in dichloromethane (10 mL) and cooled to 0°C. Methanesulfonic acid (0.10 mL, 1.54 mmol) was added, resulting in a green-brown solution that decolourized within 10 min, when tlc indicated the absence of starting material.

The solution was washed with saturated sodium bicarbonate solution (10 mL), water (10 mL), dried ($MgSO_4$), filtered, and solvent removed to yield the arene, which was recrystallized from 95% ethanol or petroleum ether.

*2-Dimethylaminobenzo[*b*]thiophene* **5**a

This compound was prepared by the rearrangement of **3***a* in refluxing chlorobenzene (2 h), affording the product as a brown solid that was sublimed to afford **5***a* as colourless crystals, mp 34–37°C (lit. (13) mp 35–36°C) (31%), identical to the authentic compound.

*2-Dimethylamino-6-methoxybenzo[*b*]thiophene* **5**b

Rearrangement of **3***b* afforded **5***b* as a pale yellow crystal, mp 69–70°C (pet. ether, 80%); ^{1}H nmr δ: 7.3 (d, J = 8.6 Hz, H4), 7.1 (d, J = 2.3 Hz, H7), 6.85 (dd, J = 8.6 and 2.3 Hz, H5), 5.95 (s, 1H), 3.8 (s, 3H), 2.95 (s, 6H) ppm; ms *m/z*: 207 (66), 192 (100), 164 (7), 150 (7). *Anal.* calcd. for $C_{11}H_{13}NOS$: C 63.43, H 6.29, N 6.72, S 15.39; found: C 63.65, H 6.33, N 6.42, S 15.13.

*6-Fluoro-3-(4-fluorophenyl)-2-dimethylaminobenzo[*b*]thiophene* **5**c

Rearrangement of **3***c* afforded **5***c* as white crystals, mp 56.0–57.5°C (pet. ether); ir (KBr) *ν*: 1590, 1500 (aryl C=C), 1212 (s) (C—F) cm^{-1}; ^{1}H nmr δ: 7.36–7.46 (m, 3H), 7.27–7.33 (m, H7), 7.15 (t, J = 8.8 Hz, H9,11), 6.83 (dt, J = 8.8, 2.3 Hz, 1H), 3.76 (s, 6H) ppm; ms *m/z*: 289 (100), 278 (21), 263 (33), 237 (24). *Anal.* calcd. for $C_{16}H_{13}F_2NS$: C 66.41, H 4.54, F 13.13, N 4.84, S 11.08; found: C 66.50, H 4.50, F 13.10, N 4.41, S 11.16.

Can. J. Chem. Downloaded from www.nrcresearchpress.com by 118.98.75.50 on 09/07/12
For personal use only.

Can. J. Chem. Downloaded from www.nrcresearchpress.com by 118.98.75.50 on 09/07/12
For personal use only.

*2-Dimethylamino-6-methoxy-3-phenylbenzo[*b*]thiophene* **5**d

Rearrangement of **3***d* afforded **5***d* as an oil that could not be crystallized (96%); ir ($CHCl_3$) ν: 1585, 1040 (s) (C—O) cm^{-1}; ^1H nmr δ: 7.20–7.45 (m, 6H), 7.15 (d, J = 2.1 Hz, H7), 6.79 (dd, J = 7.8, 2.1 Hz, H5), 3.78 (s, 6H) ppm; ms m/z: 283 (94), 268 (100). *Anal.* calcd. for $C_{17}H_{17}NOS$: C 72.04, H 6.06, N 4.94, S 11.31; found: C 72.24, H 5.89, N 4.78, S 11.00.

*2-Dimethylamino-3-phenyl-6-fluorobenzo[*b*]thiophene* **5**e

This was obtained from the rearrangement of **3***e* as a colorless crystal, mp 69–70°C (pet. ether, 80%); ^1H nmr δ: 7.40 (m, 5H), 7.30 (m, 1H), 7.1 (m, 1H), 6.9 (m, 1H), 2.70 (s, 6H) ppm; ms m/z: 271 (38), 149 (15), 97 (35), 85 (37), 68 (100). *Anal.* calcd. for $C_{16}H_{14}FNS$: C 70.82, H 5.20, F 7.00, N 5.16, S 11.81; found: C 70.91, H 5.13, F 7.20, N 4.88, S 11.68.

*2-Dimethylamino-3-phenylbenzo[*b*]thiophene* **5**f

This compound was prepared by the rearrangement of **3***f* at room temperature. **5***f* was obtained as white crystals, mp 86.5–88.5°C (95% EtOH, 80%); ^1H nmr δ: 7.67 (d, J = 7.0 Hz, 1H), 7.10–7.50 (m, 8H), 2.74 (s, 6H) ppm; ms m/z: 253 (100), 238 (13), 237 (16), 223 (26). *Exact Mass* calcd. for $C_{16}H_{15}NS$: 253.0925; found: 253.0925.

*The ^{13}C nmr spectra of carbocations (***4***) (general procedure)*

The alcohol (0.249 mmol) was dissolved in sulfur dioxide (0.50 mL) at −78°C in a 10-mm nmr tube, then frozen solid at −95°C. A solution of chlorosulfonic acid in sulfur dioxide (50%, 1.0 mL) at −95°C was added and the alcohol mixture dissolved at this temperature. The precooled deuterium lock (CD_2Cl_2) was then added to the pale red solution and the spectrum recorded at −75 to −65°C. Phasing of the signals in the JMOD spectrum is indicated by (+) for C-quaternary and CH_2, and (−) for CH and CH_3.

N,N-*Dimethyl-2-anisylthioacetamide-2-yl cation* **4**b: ^{13}C nmr δ: 190.8 (C=S); 178.1 (aryl C-OMe); 156.0 ($J_{C,H}$ = 181 Hz), 152.7 ($J_{C,H}$ = 177 Hz) (aryl C); 151.0 (J = 168 Hz), 148.7 (J = 188 Hz) (aryl C and C^+), 193.5 ($J_{C,H}$ = 173 Hz) (aryl C); 135.4 (aryl C1); 129.2 ($J_{C,H}$ = 176 Hz), 128.5 ($J_{C,H}$ = 179 Hz), 122.3 ($J_{C,H}$ = 179 Hz) (aryl C); 64.4 (OCH_3); 48.1 and 46.0 (NMe_2) ppm.

N,N-*Dimethyl-2,2-di-(4-fluorophenyl)thioacetamide-2-yl cation* **4**c: ^{13}C nmr δ: 181.7 (+) (C=S); 179.2 (+) (C4-F, $^1J_{C,F}$ (16) = −295 Hz); 153.5 (−), 146.1 (aryl C); 131.1 (+) (C^+); 124.2 (−) ($^3J_{C,F}$ = 18 Hz); 49.7 and 48.2 (NMe_2) ppm.

N,N-*Dimethyl-2-anisyl-2-phenylthioacetamide-2-yl cation* **4**d: ^{13}C nmr δ: 185.6 (+), 182.3 (+) (C=S and C4-OMe); 169.4 (+) (C^+); 153.1, 143.5, 140.4, 136.2, 131.8, and 130.1 (−) (aryl C—H); 129.9 (+) 127.2 (+) (phenyl and anisyl C1); 120.9 (−) (aryl C—H); 62.3 (−) (OCH_3); 48.2 and 47.0 (−) (NMe_2) ppm.

N,N-*Dimethyl-2-*p*-fluorophenyl-2-phenylthioacetamide-2-yl cation* **4**e: ^{13}C nmr δ: 184.8 (+) (C^+); 181.8 (+) (C=S); 180.6 (+) (C4-F, $^1J_{C,F}$ = −300 Hz); 155.4 (−) and 147.2 (−) (C2, $^3J_{C,F}$ = 15 and 18 Hz); 152.8 (−) (aryl C1); 134.9 (−) (aryl C1); 134.0 (+) and 131.8 (+) (aryl C1 and C1); 124.6 (−) (aryl C3, $^2J_{C,F}$ = 23 Hz); 49.7 and 48.1 (−) (NMe_2) ppm.

N,N-*Dimethyl-2,2-diphenylthioacetamide-2-yl cation* **4**f: ^{13}C nmr δ: 186.9 (+) (C^+); 181.2 (+) (C=S); 154.0 (−) (phenyl C—H); 149.9 (−) and 141.2 (−) (phenyl C2); 134.4 (−) (phenyl C—H); 133.6 (+) (phenyl C1); 48.9 and 47.3 (−) (NMe_2) ppm.

N,N-*Dimethyl-2,2-di-(4-fluorophenyl)thioacetamide* **6**c

The hydroxy thioacetamide **3***c* (93.4 mg, 0.304 mmol) was dissolved in SO_2 (0.50 mL) and, at −95°C, $SO_2/ClSO_3H$ (0.50 mL, ca. 5 equiv.) was added and the thioacetamide dissolved to afford a red solution.

The solution was poured onto ice, saturated sodium bicarbonate solution was added, and the ice allowed to melt. The aqueous layer was extracted with dichloromethane (10 mL), and the organic layer dried ($MgSO_4$), filtered, and solvent removed to afford an oil (76.5 mg), which was flash chromatographed to afford **5***c* (36.7 mg, 42%) followed by **6***c* (31.9 mg, 36%), obtained as white crystals, mp 109–110°C (EtOH); ir (KBr) ν: 1505, 1230 (thioamide I and II) cm^{-1}; ^1H nmr δ: 7.20 (dd, J = 8.8, 5.3 Hz, 4H), 7.0 (t, J = 8.8 Hz, 4H), 5.55 (s, 1H), 3.55 (s, 3H), 3.30 (s, 3H) ppm; ms m/z: 291 (9), 258 (8), 201 (27), 163 (100). *Exact Mass* calcd. for $C_{16}H_{15}F_2NS$: 291.0893; found: 291.0899.

N,N-*Dimethyl-2-*p*-fluorophenyl-2-phenylthioacetamide* **6**e

Quenching and work-up of the solution of the cation **4***e*, derived from **3***e* (87.3 mg), gave a mixture of the **5***e* and **6***e* (81.1 mg; yield of **6***e* estimated by ^1H nmr is 41%, **5***e* is 59%, based on the signals due to $CHC(S)NMe_2$ at δ 5.53 (s, 1H), 3.52 (s, 3H), and 3.15 (s, 3H) ppm for **6***e*, and the signal due to NMe_2 of **5***e* at δ 2.70 (s, 6H) ppm).

N,N-*Dimethyl-2,2-diphenylthioacetamide* **6**f

Quenching and work-up of the solution of cation **4***f*, derived from **3***f* (118.8 mg), afforded a mixture of **5***f* and **7***f* (94.1 mg; yield of **7***f* estimated by ^1H nmr is 21%); ^1H nmr δ: 7.30–7.10 (m, 10H), 5.60 (s, 1H), 3.52 (s, 3H), 3.32 (s, 3H) ppm.

Acknowledgements

We would like to thank the Natural Sciences and Engineering Research Council of Canada and the Ministry of the Environment (Air Resources Branch) for their generous financial support of this project. The assistance of Dr. K. Sharma in obtaining the low temperature nmr spectra is gratefully acknowledged.

1. (*a*) T. T. Tidwell. Angew. Chem. Int. Ed. Engl. **23**, 20 (1984); (*b*) P. G. Gassman and T. T. Tidwell. Acc. Chem. Res. **16**, 279 (1983); (*c*) J.-P. Begue and M. Charpentier-Morize. Acc. Chem. Res. **13**, 207 (1980); (*d*) X. Creary. Acc. Chem. Res. **18**, 3 (1985).
2. M. N. Paddon-Row, C. Santiago, and K. N. Houk. J. Am. Chem. Soc. **102**, 6561 (1980).
3. R. H. Nobes, W. J. Bouma, and L. Radom. J. Am. Chem. Soc. **105**, 309 (1983).
4. C. F. Rodriquez and A. C. Hopkinson. Org. Mass Spectrom. **20**, 691 (1985).
5. X. Creary. J. Am. Chem. Soc. **106**, 5568 (1984).
6. (*a*) M. Spraul and K. Griesbaum. Chem. Ber. **116**, 2641 (1983); (*b*) R. N. McDonald and R. N. Steppel. J. Am. Chem. Soc. **92**, 5664 (1970).
7. X. Creary and C. C. Geiger. J. Am. Chem. Soc. **104**, 4151 (1982).
8. A. C. Hopkinson, L. H. Dao, P. Duperrouzel, M. Maleki, and E. Lee-Ruff. J. Chem. Soc. Chem. Commun. 727 (1983).
9. (*a*) X. Creary and M. E. Mehrsheikh-Mohammadi. J. Org. Chem. **51**, 7 (1986); (*b*) X. Creary and P. A. Inocencio. J. Am. Chem. Soc. **108**, 5979 (1986).
10. L. H. Dao, M. Maleki, A. C. Hopkinson, and E. Lee-Ruff. J. Am. Chem. Soc. **108**, 5237 (1986).
11. H. C. Brown and E. N. Peters. J. Am. Chem. Soc. **99**, 1712 (1977).
12. J. Sommer, R. Jost, and T. Drakenberg. J. Chem. Soc. Perkin Trans. 2, 363 (1980).
13. N. O. Vesterager, E. B. Pedersen, and S.-O. Lawesson. Tetrahedron, **29**, 321 (1973).
14. R. Breslow. Mol. Rearrange. 1963–1964, **1**, 257 (1967).
15. R. Bladek and T. S. Sorensen. Can. J. Chem. **50**, 2806 (1972).
16. T. Schaefer, J. Peeling, and G. H. Penner. Can. J. Chem. **64**, 2162 (1986).
17. A. I. Vogel. Practical organic chemistry. 4th ed. Longman Group Ltd., New York. 1978. (*a*) p. 776; (*b*) p. 775; (*c*) R. D. Dunlop and J. H. Gardner. J. Am. Chem. Soc. **55**, 1665 (1933).

Structural studies of oligosilanes produced by catalytic dehydrogenative coupling of primary organosilanes

C. AITKEN, J. F. HARROD, AND U. S. GILL
Chemistry Department, McGill University, Montreal, P.Q., Canada H3A 2K6

Received October 26, 1986

This paper is dedicated to Professor John T. Edward

C. AITKEN, J. F. HARROD, and U. S. GILL. Can. J. Chem. **65**, 1804 (1987).

The structures of some poly(organosilylenes), -(SiRH)$_n$- (R = Ph, *p*-tolyl, *n*-hexyl, and benzyl), produced by catalytic dehydrogenative coupling of primary silanes have been studied by infrared, nuclear magnetic resonance, and mass spectroscopies. These results, combined with data on molecular weights and molecular weight distributions from vapour pressure osmometry and gel permeation chromatography, lead to the conclusion that the polymers are linear and have SiH_2R end groups. The polymers all have degrees of polymerization of ca. 10 and very narrow molecular weight dipersions. Some possible features of the mechanism that gives rise to this behaviour are discussed.

C. AITKEN, J. F. HARROD et U. S. GILL. Can. J. Chem. **65**, 1804 (1987).

Faisant appel aux spectroscopies d'infrarouge, de résonance magnétique nucléaire et de masse, on a étudié les structures de quelques poly(organosilylènes), -(SiRH)$_n$- (R = Ph, *p*-tolyl, *n*-hexyl et benzyl), qui sont produits par un couplage déshydrogénant de silanes primaires.Ces résultats, combinés aux données de poids moléculaires et de distributions des poids moléculaires obtenues par osmométrie de tension de vapeur et par chromatographie par perméation de gel, conduit à la conclusion que les polymères sont linéaires et qu'ils contiennent des groupements terminaux SiH_2R. Les degrés de polymérisation des polymères sont tous d'environ 10 et les dispersions de leurs poids moléculaires sont très étroites. On discute de quelques-unes des caractéristiques du mécanisme qui donne lieu à ce comportement.

[Traduit par la revue]

Can. J. Chem. Downloaded from www.nrcresearchpress.com by 118.98.75.50 on 09/07/12
For personal use only.

Introduction

We have recently described the dehydrogenative coupling of organosilanes catalyzed by titanocene and zirconocene derivatives (1, 2). A preliminary communication gave a brief description of the characterization of the oligosilanes produced (3). In the present paper we give a detailed description of the results of a number of physicochemical measurements that have been applied to determining the structure of these materials.

Synthetic methods for the catenation of silicon are few. The Wurtz-type coupling of halosilanes with highly electropositive metals is the most commonly used strategy and a fairly large number of papers describing this type of chemistry have appeared (for a review of the synthesis and properties of organopolysilanes see ref. 4). Despite the difficulty of controlling the heterogeneous Wurtz-type coupling, and the problems of by-products and of handling liquid alkali metals, these reactions are still the only source of high molecular weight polysilylenes. All of the information regarding the interesting properties of polysilanes as silicon carbide fibre precursors (5) and as photoactive materials (6) has been obtained with such materials. Recently, a report has appeared of the catalytic redistribution of di- and other oligosilanes to give higher molecular weight polysilanes (7).

Given the potential applications of polysilanes, new methods for their synthesis assume some importance. Therein lies the relevance of the catalytic dehydrogenative coupling reaction shown in eq. [1]. With titanocene and zirconocene based

$$[1]\quad n\mathrm{RSiH_3} \longrightarrow \mathrm{H}\text{-}\left(\mathrm{Si}(\mathrm{R})(\mathrm{H})\right)_n\text{-}\mathrm{H} + (n-1)\mathrm{H_2}$$

catalysts, the selectivity for removal of only two hydrogens from the silicon is very high and the yields of product are essentially quantitative. The structural characterization of the polymers produced in eq. [1] is not simple because each silicon is a stereo centre and the polymer, like all atactic polymers, is a mixture of a large number of stereoisomers.

Results and discussion

^{1}H and ^{29}Si nuclear magnetic resonance spectra

The ^{1}H nmr spectra of all of the polymers prepared so far show broad unresolved massifs in the regions characteristic of the functional group protons. In particular, there is a broad set of resonances in the region of 4–5 ppm due to Si—H, and others for the aryl and (or) alkyl protons of the R group. The spectrum of poly(phenylsilylene) is shown in Fig. 1. Although such spectra give little information on the fine structure of the polymer, they do consistently integrate in the manner expected for the stoichiometry of eq. [1]. The broadness of the resonances is most likely due to the presence of an envelope of Si—H species with different chemical shifts, which are in turn split by H–H coupling to vicinal Si—H groups. Stepwise replacement of the SiH_3 protons with silicon causes a progressive downfield shift of the residual proton resonances. For example, the shifts for $PhSiH_3$ and $PhSiH_2SiH_2Ph$ are 4.22 and 4.39 ppm respectively (C_6D_6). It is therefore tempting to conclude that the massif between 4.3 and 5.0 ppm in Fig. 1 is due to $Ph(Si)SiH_2$ and that the one above 5.0 ppm is due to $Ph(Si_2)SiH$. On the other hand, the fact that the integral for the downfield massif is always smaller than that for the high field argues against such a simple assignment.

^{29}Si nuclear magnetic resonance spectroscopy is similarly uninformative about the details of polymer structure. The normal mode spectrum is a complex massif of poorly resolved peaks in the range of −50 to −70 ppm. The application of a polarization transfer sequence (DEPT [8]) gives more useful information, since it can distinguish silicon atoms bearing two protons from those bearing one or three protons. Figure 2 shows the DEPT spectra of a poly(*n*-hexylsilylene) for different pulse angles. These spectra clearly show that the dominant species present is Si—H, but the presence of SiH_2 groups in the

Can. J. Chem. Downloaded from www.nrcresearchpress.com by 118.98.75.50 on 09/07/12
For personal use only.

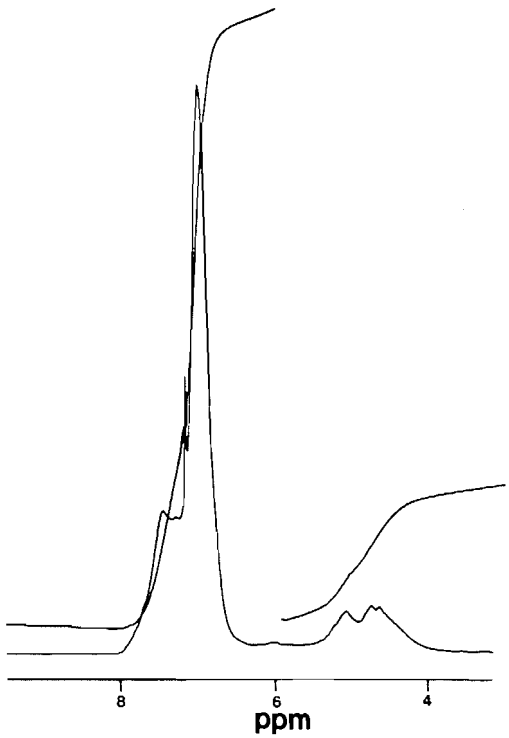

FIG. 1. 200-MHz ^{1}H nmr spectrum of poly(phenylsilylene) in C_6D_6.

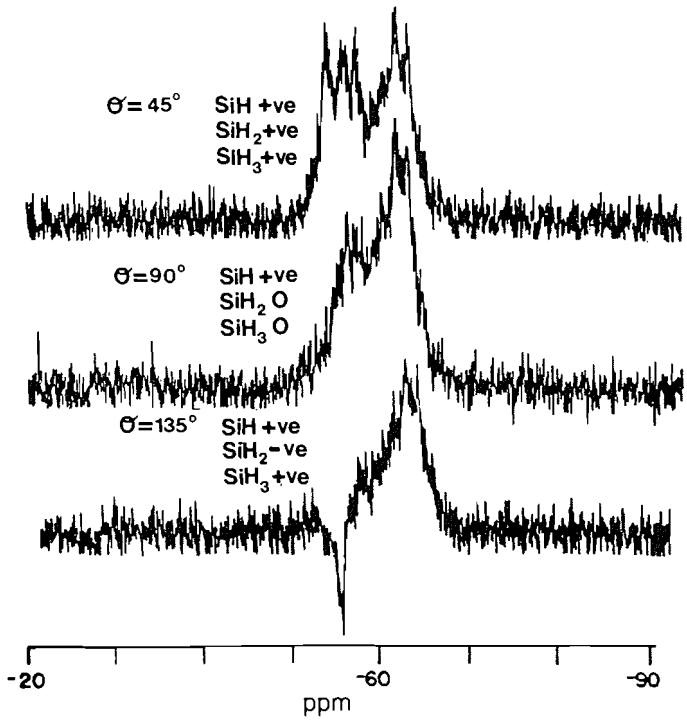

FIG. 2. Natural abundance ^{29}Si nmr DEPT spectra of poly(*n*-hexylsilylene) in C_6D_6.

polymer is also evident. Similar spectra were obtained for poly(phenylsilylene). It is interesting to note that the relative positions of the silicon resonances of SiH and SiH_2 are reversed relative to the positions of the proton resonances. Similar behaviour has been observed previously with SiH compounds.[1]

Infrared spectra

The ir spectra of all of the polysilylenes produced so far exhibit, in addition to the bands due to the alkyl or aryl substituents, an intense ν_{Si-H} band at ca. 2100 cm^{-1} and a strong band at ca. 910 cm^{-1}. The band at ca. 2100 cm^{-1} is at about 60 cm^{-1} lower frequency than that of the primary silane monomers. This shift to lower frequency typically occurs when the hydrogens of silane are progressively replaced by an alkyl or a silyl group (10). The frequencies observed for the polymers are in the right range for tertiary Si—H. The band at 910 cm^{-1} can be assigned to the bending mode of a SiH_2 group (11). This band is present in all primary and secondary alkyl and arylsilanes, but notably absent from tertiary silanes. Its presence in the polymers is further clear evidence for terminal $PhSiH_2$ groups. It is also relevant to note that these SiH_2 groups can be selectively hydrosilated by reaction of the polymer with a 1-alkene, or norbornadiene, in the presence of dimethyltitanocene as catalyst (14). Such hydrosilation results in the diminution, or disappearance, of the 910 cm^{-1} peak and little change in the 2100 cm^{-1} peak.

The position of the 2100 cm^{-1} band and the relative intensities of the 2100 and 910 cm^{-1} bands are both sensitive to molecular size in the range of molecular weight exhibited by these polymers. In Table 1 we show these values for a number of simple alkyl- and aryl-substituted silanes and for two oligomers,

TABLE 1. Values for ν_{Si-H} and intensity ratios I_ν/I_δ for some SiH compounds

Compound	ν_{Si-H}, cm^{-1}	I_ν/I_δ
$CyclohexylSiH_3$	2140	1.00
$BenzylSiH_3$	2145	[a]
$PhenylSiH_3$	2150	1.18
Ph_2SiH_2	2135	0.87
$PhMeSiH_2$	2135	0.88
n-$BuMeSiH_2$	2130	0.75
Et_3SiH	2090	0
Ph_3SiH	2120	0
$H(SiHPh)_5H$	2118	0.89
$H(SiHPh)_8H$	2095	0.47
$H(SiHHx)_{10}H$[b]	2080	[a]

[a]There is interference from a substituent mode in these cases.
[b]Hx = *n*-hexyl.

which were shown by mass spectroscopy (*vide infra*) to have degrees of polymerization of 5 and 8 respectively.

Molecular weight studies

In a preliminary report, the average degrees of polymerization ($\bar{D}_n$) of the poly(silylenes) were found by vapour pressure osmometry (vpo) to be about 10 (3). Some vpo results are shown in Table 2.

The molecular weight properties of the polymers have now been studied by gel permeation chromatography (gpc). The column used was able to clearly resolve a mixture of phenylmethylcyclotri- (D_3^{Ph}) and phenylmethylcyclotetrasiloxane (D_4^{Ph}). Calibration samples of nearly monodisperse polystyrene of $\bar{M}_n$ = 530, 950, and 2800 Da were also easily resolved. Unfortunately, the lack of correlation between retention times and molecular weights of these and other calibrants

[1]J. F. Harrod and E. Pelletier, unpublished results.

TABLE 2. Molecular weights of polysilylenes determined by vapour pressure osmometry[a]

Monomer	[Catalyst][b]	T, °C	Mol. Wt.[c]	No. of Si atoms
$PhSiH_3$	2	20	843	8
$PhSiH_3$	2	60	958	9
$PhSiH_3$	10	20	1358	13
$HxSiH_3$	1	20	984	9

[a]Reaction mixture: 2 mL silane + 7 mL toluene.
[b]Mole per cent based on silane.
[c]±30 dalton.

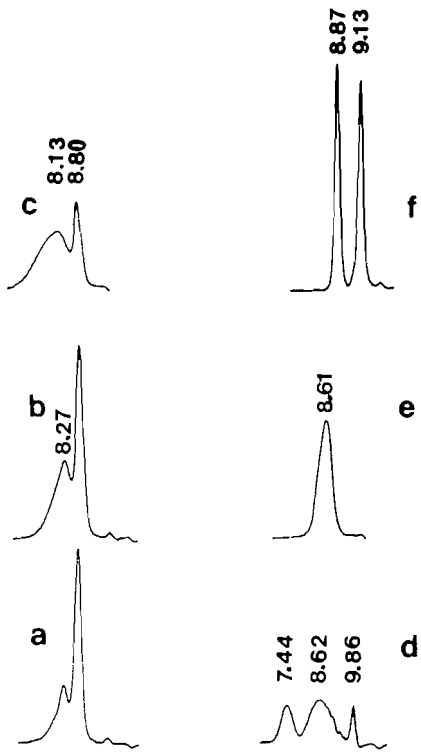

FIG. 3. Some gel permeation chromatograms of poly(phenylsilylenes) and of some standards. (*a*), (*b*), (*c*): Poly(phenylsilylenes) produced by reaction of $PhSiH_3$/toluene (volume ratios 1:2, 2:1, and 3:0 respectively) with dimethyltitanocene (10 mg) for 7 d. (*d*): Polystyrene standards of M_n = 2800, 950, and 525 dalton. (*e*) $Ph_8Ge_4H_2$. (*f*) An equimolar mixture of D_4^{Ph} and D_3^{Ph}. The numbers above the chromatograms are retention times in min.

highlighted the extreme difficulty of obtaining accurate estimates of molecular weight in this range by gpc. At best it can be concluded that the gpc results are not in disagreement with those of vpo.

Despite the failure to obtain accurate molecular weight, gpc does give other important information concerning molecular weight distribution and relative molecular size. Some relevant chromatograms are shown in Fig. 3. The distributions of the poly(phenylsilylenes) are bimodal. The distribution of the lighter fraction is narrow enough to indicate that it is a monodisperse species. The heavier fraction is due to at least two species. The relative amount of the higher molecular weight component increases with increasing monomer concentration for a constant reaction time. The character of the chromatogram is remarkably insensitive to variation in reaction conditions and does not vary significantly for catalysts as different from

TABLE 3. A comparison of the mass spectra of hexaphenylcyclohexasilane, **1**, and pentaphenylpentasilane, **2**

1[a]			**2**		
Ion	Mass	(%)	Ion	Mass	(%)
$Ph_6Si_6H_6$	636	30	$Ph_5Si_5H_7$	532	0.45
$Ph_5Si_5H_5$	530	20	$Ph_5Si_4H_5$	501	2.0
$Ph_4Si_5H_4$	452	50	$Ph_4Si_5H_4$	452	1.1
Ph_4Si_4H	421	40	$Ph_4Si_4H_2$	422	3.0
$Ph_3Si_5H_5$	376	16	$Ph_3Si_4H_3$	346	7.2
Ph_3Si_4H	344	75	Ph_3Si_4H	316	12.4
Ph_3Si_3	315	20	Ph_3Si_2	287	27.0
Ph_3Si	259	60	Ph_3Si	259	24.0
Ph_2Si_3	238	12	$Ph_2Si_3H_2$	240	25.0
Ph_2Si_2	209	16	Ph_2Si_2H	211	42.0
Ph_2SiH	183	80	Ph_2SiH	183	47.0
PhSi	105	100	PhSi	105	100.0

[a]Data from ref. 12.

each other as Cp_2TiMe_2, $Cp_2Ti(CO)_2$, and $CpCp^*TiMe_2$. This behaviour is unusual and points to an unusual mechanism for the polymerization reaction.

Mass spectroscopy

The mass spectra of the polysilylenes produced in this study were all successfully measured by direct inlet methods. In Table 3 we show a listing of ms data for a poly(phenylsilylene) produced by dehydrogenative coupling and for a previously reported hexaphenylcyclohexasilane, synthesized by Hengge and Lunzer by classical methods (12). The gross differences between the spectra are those expected for a linear and a cyclic molecule. In the cyclic case, the primary event is probably cleavage of a Si—Si bond, followed by an unzipping of the chain. The initial cleavage does not result in a mass loss and the parent ion is observed in high abundance. In the linear case, the primary event is also a Si—Si cleavage, but in this case cleavage leads to fragmentation and the parent ion is only observed at very low abundance. In both linear and cyclic cases the loss, and migration to adjacent silicon, of phenyl groups and loss of hydrogen are both important secondary processes, a behaviour typical of aryl silanes (13).

The linear pentasilylene whose spectrum is listed in Table 3 was obtained from a very slow reaction run at 0°C and was chosen for comparison with the cyclic compound because of the relative simplicity of its spectrum and because it is the only poly(phenylsilylene) for which the parent ion has been observed. Under all other experimental conditions investigated, polysilylenes of slightly higher degrees of polymerization were obtained. The mass spectra of a number of differently substituted polysilylenes are listed in Table 4. Most of the peaks listed are the most intense in a cluster that originates from a combination of isotope distribution and sequential hydrogen stripping. The peaks are due to a multiplicity of species and the listed ion assignments are those considered most likely to be a major component at a particular mass.

Apart from the increased complexity due to increased degree of polymerization, the fragmentation patterns for the phenyl and *p*-tolyl polymers are very similar to that of the pentamer listed in Table 3. The *n*-hexyl polymer behaves somewhat differently in that the (parent − 1) ion is highly abundant and fragmentation involves extensive cleavage of the alkyl side chain. The listing for the *n*-hexyl polymer is only partial below m/e = 400 since

Can. J. Chem. Downloaded from www.nrcresearchpress.com by 118.98.75.50 on 09/07/12
For personal use only.

TABLE 4. Mass spectra of some representative polysilylenes produced by dehydrogenative coupling

R[a] = Ph			R = To			R = Hx			R = Bz		
Ion	Mass	(%)	Ion	Mass	(%)	Ion	Mass	(%)	Ion	Mass	(%)
$R_7Si_8H_9$	771	0.2	$R_6Si_9H_8$	806	0.7	$R_{10}Si_{10}H_{11}$	1141	18	$R_5Si_7H_9$	660	0.5
$R_6Si_8H_9$	695	0.4	$R_6Si_8H_6$	776	1.2	$R_9Si_{10}H_{11}$	1056	10	$R_3Si_7H_4$	473	1.3
$R_5Si_8H_{10}$	619	0.4	$R_5Si_8H_6$	685	6.0	$R_9Si_8H_7$	996	9	$R_2Si_7H_{11}$	389	6.0
$R_4Si_8H_{11}$	543	0.5	$R_4Si_8H_7$	595	44.0	$R_8Si_8H_8$	912	9	$R_2Si_6H_6$	629	1.0
$R_7Si_7H_6$	741	0.3	$R_3Si_8H_9$	506	100.0	$R_7Si_7H_4$	795	8	$R_4Si_6H_7$	539	1.0
$R_6Si_7H_5$	663	0.7	$R_7Si_7H_2$	835	2.0	$R_6Si_6H_2$	680	8	$R_2Si_6H_5$	355	4.5
$R_5Si_7H_6$	587	0.8	$R_6Si_7H_4$	746	12.0	$R_5Si_6H_3$	596	9	$R_4Si_5H_5$	509	2.0
R_4Si_7H	505	0.9	$R_5Si_7H_5$	656	10.0	$R_4Si_6H_5$	513	10	$R_3Si_5H_4$	417	1.5
$R_6Si_6H_2$	632	0.7	$R_4Si_7H_7$	567	11.0	$R_3Si_6H_8$	431	9	$R_2Si_5H_5$	327	1.5
R_5Si_6H	556	2.0	$R_3Si_7H_8$	477	40.0	$R_3Si_5H_5$	400	7	$R_3Si_4H_6$	391	6.2
R_4Si_6H	478	2.7	$R_6Si_6H_2$	716	10.0	R_2SiH	199	38	$R_2Si_4H_7$	301	2.5
R_3Si_6	399	2.0	$R_5Si_6H_3$	626	44.0	$RSiH_2$	115	72	$R_3Si_3H_2$	359	2.0
R_5Si_5H	526	3.1	$R_4Si_6H_4$	536	45.0	$EtSiH_2$	59	100	$R_2Si_3H_6$	271	32.0
$R_4Si_5H_2$	450	6.1	$R_3Si_6H_4$	445	16.0	$PrSiH_2$	73	95	RSi_3H_4	179	4.0
R_3Si_5H	372	4.0	$R_5Si_5H_2$	597	32.0	$BuSiH_2$	87	24	R_2Si_2H	239	17.0
R_4Si_4H	421	5.2	$R_4Si_5H_2$	506	100.0	$PeSiH_2$	101	10	$[R_2Si_2]$-H	237	32.0
R_3Si_4	343	7.0	$R_3Si_5H_3$	416	87.0				RSi_2H_2	149	100.0
R_2Si_4	266	4.0	$R_2Si_5H_2$	324	24.0				RSi	119	76.0
R_3Si_3H	316	5.3	R_4Si_4	477	40.0				PhSi	105	32.0
R_2Si_3H	240	3.0	R_3Si_4	385	60.0						
R_3Si_2	287	8.0	R_3Si_3	357	15.0						
R_2Si_2	210	10.0	R_3Si_2	329	15.0						
RSi_2	133	3.0	R_3SiH	302	86.0						
R_3Si	259	68.0									
R_2SiH	183	71.0									
RSi	105	100.0									

[a]Radical abbreviations: Ph = phenyl; To = 3-methylphenyl; Hx = *n*-hexyl; Bz = benzyl; Et = ethyl; Pr = propyl; Bu = butyl; Pe = pentyl.

the spectrum becomes very complicated below this mass due to the increased presence of alkyl chain fragmentation products. The other listings are more or less complete down to the lowest cited mass.

The structure and molecular weights of the polymers

No single physical measurement cited in the preceding sections gives an unequivocal answer as to the structure and size of the polysilylenes. Although accurate quantitative determination of the relative proportions of SiH, SiH_2, and SiH_3 is not possible in a DEPT experiment, the spectrum shown in Fig. 2 allows the conclusions that most of the silicon hydride protons are present as Si—H, that there is an amount of SiH_2 present, which is not out of line with that expected for a linear polymer of the chain length indicated by the other measurements, and, by a process of elimination, there cannot be much Si of any other kind. The relatively high intensity of the 910 cm^{-1} band in the polymers also argues for the presence of SiH_2 end groups. That the polymers are not cyclics is strongly indicated by the mass spectra, but none of the evidence excludes the possibility that there may be a small amount of branching. The weight of the evidence is nevertheless against a significant amount of branching.

Given that we are dealing with essentially linear polymers with predominantly SiH_2 end groups, the next important question is, what are their molecular weight properties? The gpc results show that the polymers have molecular sizes comparable to that of polystyrene with a molecular weight of ca. 1000 Da ($\bar{D}_n$ ca. 10). This corresponds to a chain of ca. 20 C atoms. If we make the simplistic assumption that the size of a polysilicon chain relative to a polycarbon chain varies in relation to the covalent radius ratio for the two elements (C/Si = 0.6), it leads to the conclusion that most of the polysilylenes prepared with titanocene based catalysts are about 10–12 silicons long. Given the relative weakness of the underlying assumption, this is in good agreement with both the vpo (uncertainty ca. ±5%) and the ms results. A more careful analysis of the poly(phenylsilylene) chromatograms, using the same assumption, leads to the conclusion that the lighter fraction has a chain of 9 Si and the heavier fraction a chain of 14–16 Si. The vpo value for the molecular weight of the poly(phenylsilylene) produced at room temperature with 2 mol% catalyst agrees well with the gpc result, since the polymer consists mostly of the lighter fraction at the monomer concentration used in its preparation.

In the case of the ms results, the highest observed mass may only represent a lower limit if higher mass fragments are below the limit of detection, or if heavier fragments are too unstable to be observed. We consider these eventualities to be unlikely and believe that the highest observed masses represent in fact the *upper limit* on molecular weight.

The chromatograms shown in Fig. 3 show that the polysilylene molecular weight distributions are usually, if not always, polymodal; in the case of the poly(phenylsilylenes) the distributions are bimodal. The dispersity of the lighter component is so narrow as to indicate it is due to an essentially monodisperse molecular species. The heavier fraction is probably due to at least two species of differing molecular size. Perfect monodispersity in terms of molecular size is not expected since the average dimensions of the different stereoisomers at a particular degree of polymerization are not expected to be the same. The same is of course true of the polystyrene and the D_n^{Ph} standards, and their behaviour does not lend any support to the idea that

Can. J. Chem. Downloaded from www.nrcresearchpress.com by 118.98.75.50 on 09/07/12
For personal use only.

Can. J. Chem. Downloaded from www.nrcresearchpress.com by 118.98.75.50 on 09/07/12
For personal use only.

the two components of the poly(phenylsilylenes) are different stereoisomers. The mass spectra exclude the possibility that one of the components is cyclic and the other linear. This leaves only the possibility that we are dealing with two linear molecules differing in length by a few silicon atoms. From Fig. 3, it is evident that the higher molecular weight species is produced more abundantly as the monomer concentration is increased. This leads us to favour a hypothesis that the two fractions are the products of two different chain termination mechanisms operating on a common metal polysilylene species.

The mechanism of the polymerization reaction

The essential features of the catalytic dehydrogenative coupling reaction are the following: the polymerization is selective for primary silanes; it does not proceed by the production of measurable amounts of species of intermediate molecular weight; polydispersities are extremely narrow; high catalyst concentration leads to higher molecular weight; the limiting molecular weight is very insensitive to reaction variables; polymerization rates are very sensitive to steric factors (14). In general terms these facts point towards a mechanism in which propagation occurs very rapidly relative to termination until the growing chain reaches a certain size, at which point the propagation rate drops by a sufficient amount that virtually all growing chains are terminated before another monomer addition can occur.

Results reported elsewhere show that most of the catalyst remains in an inactive form during the polymerization, but the inactive species are probably in equilibrium with the active form (1, 14). This, coupled with the effect of catalyst concentration on molecular weight and lack of dependence of molecular weight on conversion, excludes a standard "living polymerization" mechanism (15).

Kinetic studies indicate that the active species is a mononuclear titanium complex, and we have previously suggested that propagation occurs through α-hydride elimination at a Ti(IV)silyl centre (14), thus:

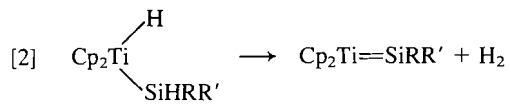

[2] $Cp_2Ti(H)(SiHRR') \longrightarrow Cp_2Ti{=}SiRR' + H_2$

where R′ = H or polysilyl.

A mechanism involving α-hydride elimination is attractive from the point of view of its analogy to similar eliminations observed with the alkyls of lighter transition element metallocenes (16) and from the fact that eq. [2] is not possible for a secondary silane beyond the first homologation step. A number of equally plausible mechanisms for the production of polymer from a silylene complex can be envisaged on the basis of present data. The simplest is the following:

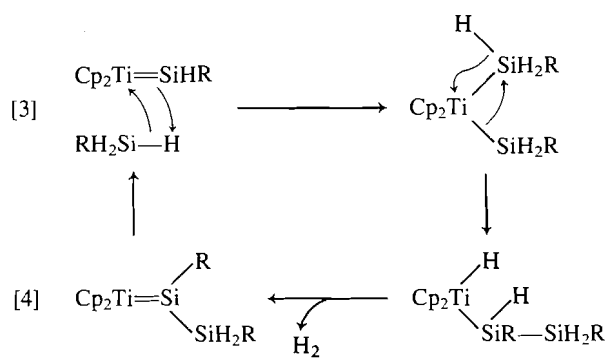

[3] $Cp_2Ti{=}SiHR$ / $RH_2Si{-}H$ → $Cp_2Ti(H)(SiH_2R)(SiH_2R)$

[4] $Cp_2Ti{=}Si(R)(SiH_2R)$ → H_2 + $Cp_2Ti(H)(H)(SiR{-}SiH_2R)$

It is unlikely that the silylene complex exists for any significant time as a terminal complex, if at all. We consider it more likely that it participates as a bridging silylene. The α-hydride elimination steps of a mechanism such as illustrated in eqs. [3] and [4] provide ample opportunity for the intervention of steric effects. The cyclopentadienyl ligands are sterically encumbering and could well impede the achievement of the eclipsed conformation that would favour the migration of the hydride from the silicon to the titanium. Further experiments to test this hypothesis are currently in progress.

Of several possible termination steps, only hydrogenolysis of the Ti—Si bond can be definitively excluded. Studies published elsewhere (14) showed that polymer molecular weights are unaffected by wide variations in the free hydrogen concentration in solution during the polymerization. The gpc results for poly(phenylsilylene) described above reveal the presence of at least two termination processes, one dependent on monomer concentration and the other independent. The monomer-independent termination could be either a spontaneous reductive elimination of silane from the bis(silyl) intermediate in eq. [3], or the hydridosilyl intermediate in eq. [4], or a simple homolysis of a Ti—Si bond followed by hydrogen atom abstraction by the silyl radical. At our present level of understanding of the mechanism it is not clear what kind of process could lead to a monomer dependent termination.

Experimental

Materials and reagents

All solvents were carefully dried and deoxygenated by standard procedures before use. Silanes were prepared by $LiAlH_4$ reduction of the appropriate chlorosilane using modifications of literature methods (17). Dimethyltitanocene was prepared by a literature procedure (9) and freshly recrystallized before use.

Spectroscopic methods

The nmr spectra were recorded on a Varian model XL-300 FT spectrometer. The DEPT pulse sequence for the acquisition of the spectra in Fig. 2 was as follows: 90°(H,Y)–τ–180°(H,X), 90°(Si,X)–τ–σ (H,X), 180°(Si,X)–τ–decouple, acquire. A τ value of 0.0025 s, based on a J_{Si-H} of 200 Hz, was used in conjunction with a θ array of 45°, 90°, and 135°.

Mass spectra were acquired with a ZAB-HS model 2F spectrometer using the direct inlet mode, an electron impact energy of 70 eV, and a probe temperature ranging from ca. 60 to 100°C.

Molecular weight determinations

Molecular weights by vpo were determined using a Corona/Wescan model 232 apparatus. All measurements were made in toluene at 50°C and care was taken to protect the samples from oxygen. Calibrations were performed with sucrose octaacetate and with Waters Associates calibration standard no. 41994. Measurements were estimated to be accurate to within ±40 Da. The gpc measurements were carried out on a Varian 5000 liquid chromatograph interfaced to a Varian Vista 402 data station and equipped with a Waters Associates 10^3 Å Ultrastyragel column. All gpc measurements were carried out using air-free, chromatographic grade THF as solvent. The calibrants used were made by Toyo Soda Manufacturing Co. Ltd. and supplied by Varian Associates. The molecular weight characteristics of the calibrants were [M_n, dalton (M_w/M_n)]: 5.26×10^2 (1.15); 9.5×10^2 (1.13); 2.8×10^3 (1.05).

Polymerization reactions

Polymerizations may be carried out under a wide range of conditions. The following is a representative example. Dimethyltitanocene (10.0 mg) was dissolved in toluene (1.0 mL) under argon. Phenylsilane (1.0 mL) was added to the solution. In a few minutes the color of the solution changed from pale yellow to dark blue and a rapid evolution of

hydrogen commenced. The effervescence continued at a progressively decreasing rate for several days. After 7 d at room temperature the effervescence had essentially ceased and the solution had become quite viscous. All volatile material was pumped off under vacuum to give a dark blue glassy solid. This solid was redissolved in ca. 1.5 mL of toluene and added to a 20 × 2 cm column of Florisil in toluene. The polymer was recovered by slow elution with toluene (80 mL) followed by vacuum evaporation of the eluent. After pumping the resulting solid for 1 h, the product was obtained as a colourless, brittle glass (750 mg).

Similar results were obtained with tetrahydrofuran as solvent, or with no solvent at all. A reaction identical to that described above, except that it was maintained at 0°C, yielded a gum (550 mg). This material was used to obtain the mass spectrum given in Table 3. Poly(*p*-tolylsilylene) was obtained as a glassy solid, but the benzyl and *n*-hexyl polymers were oils.

Acknowledgements

We thank the Natural Sciences and Engineering Research Council of Canada, the Fonds pour la formation de chercheurs et l'aide à la recherche de Québec, and the Dow Corning Corporation for financial support of this work. Thanks are also due to Dr. Francoise Sauriol for help with measurement of nmr spectra and Dr. Orval Mamer for measurement of the mass spectra.

1. C. T. AITKEN, J. F. HARROD, and E. SAMUEL. J. Am. Chem. Soc. **108**, 4059 (1986).
2. C. T. AITKEN, J. F. HARROD, and E. SAMUEL. Can. J. Chem. **64**, 1677 (1986).
3. C. T. AITKEN, J. F. HARROD, and E. SAMUEL. J. Organomet. Chem. **279**, C11 (1985).
4. R. WEST. J. Organomet. Chem. **300**, 327 (1986).
5. S. YAJIMA, T. SHISHODO, and H. KAYANO. Nature, **264**, 237 (1976).
6. R. D. MILLER, D. HOFER, D. R. MCKEAN, C. G. WILSON, R. WEST, and P. T. TREFONAS, III. ACS Symposium Series No. 266. American Chemical Society, Washington DC. 1984. pp. 293–310; G. C. GOBBI, W. W. FLEMING, R. SOORIYAKUMARAN, and R. D. MILLER. J. Am. Chem. Soc. **108**, 5624 (1986).
7. R. H. BANEY, J. H. GAUL, and T. K. HILTY. Organometallics, **2**, 859 (1983).
8. D. M. DODRELL, D. T. PEGG, and M. R. BENDALL. J. Magn. Reson. **48**, 323 (1982).
9. K. CLAUS and K. BESTIAN. Justus Liebigs Ann. Chem. **654**, 8 (1962).
10. A. L. SMITH. *In* Chemical Analysis. Vol. 41. *Edited by* P. J. Elving and I. M. Kolthoff. John Wiley and Sons, New York. 1976. p. 257.
11. F. HÖFLER, G. BAUER, and E. HENGGE. Spectrochim. Acta, **32A**, 1435 (1976).
12. E. HENGGE and F. LUNZER. Monatsh. Chem. **107**, 371 (1976).
13. J. E. COUTANT and R. J. ROBINSON. *In* Analysis of silicones. *Edited by* A. L. Smith. J. Wiley and Sons, New York. 1971. Chap. 12. pp. 338–375.
14. J. F. HARROD and S. S. YUN. Organometallics. In press.
15. F. W. BILLMEYER. Textbook of polymer science. 2nd ed. Wiley–Interscience, New York. 1971. p. 318.
16. L. R. CHAMBERLAIN, A. P. ROTHWELL, and I. P. ROTHWELL. J. Am. Chem. Soc. **106**, 1847 (1984), and references therein.
17. R. A. BENKESER, H. LANDESMAN, and D. FOSTER. J. Am. Chem. Soc. **74**, 648 (1952).

Can. J. Chem. Downloaded from www.nrcresearchpress.com by 118.98.75.50 on 09/07/12
For personal use only.

Photochemistry of substituted cyclic enones. Part 6. Photochemical reactions of 5-arylmethyl-3-phenylcyclopent-2-enones. A photostationary state[1,2]

MICHAEL T. M. CLEMENTS AND T. BRIAN H. MCMURRY[3]
University Chemical Laboratory, Trinity College, Dublin 2, Ireland

Received November 27, 1986

This paper is dedicated to Professor John T. Edward

MICHAEL T. M. CLEMENTS and T. BRIAN H. MCMURRY. Can. J. Chem. **65**, 1810 (1987).

Photolysis of 5-(1- and 2-naphthylmethyl)-3-phenylcyclopent-2-enones affords [2 + 2] cycloaddition products, the 7,8- and 5,6-benzo-fused 10-phenyltetracyclo[7.2.1.$0^{3,10}$.$0^{4,9}$]dodeca-5,7-dien-2-ones respectively, in equilibrium with the starting enones. A similar dibenzo-fused photoproduct is formed from the corresponding 9-phenanthrylmethyl substituted cyclopentenone. The photoproducts revert to the respective enones on acid treatment, or pyrolysis, and on photolysis.

MICHAEL T. M. CLEMENTS et T. BRIAN H. MCMURRY. Can. J. Chem. **65**, 1810 (1987).

La photolyse des (naphtyl-1 ou -2 méthyl)-5 phényl-3 cyclopentène-2 ones conduit à des produits de cycloadditions [2 + 2], soit respectivement les benzo-7,8 ou -5,6 phényl-10 tétracyclo[7.2.1.$0^{3,10}$.$0^{4,9}$] dodécadiène-5,7 ones-2, qui sont en équilibre avec les énones de départ. Si l'on part de la cyclopentènone correspondante substituée par une phénanthryl-9 méthyle, il se forme un photoproduit similaire qui est fusionné à un dibenzo. Par traitement avec des acides, par pyrolyse ou par photolyse, les photoproduits se retransforment dans leurs énones respectives.

[Traduit par la revue]

In recent publications (1, 3, 4) we have described the photochemical intramolecular cyclisation of 5-allyl and substituted 5-allylcyclopentenones. In all these cases the reactions were regiospecific, as far as the direction of addition, but in the case of the compounds with cinnamyl side chains there was loss of stereoselectivity of the phenyl substituent. We wished to discover whether aromatic "double bonds" could be incorporated into cycloaddition products and, if so, whether the regiospecificity would be affected. Furthermore, to our knowledge, no example is known where enone adds onto a naphthalene ring although, where two naphthalene rings are linked by a suitable chain, then photoaddition of the two rings is found (5).

Synthesis

The 5-arylmethyl-3-phenylcyclopentenones were synthesised by standard routes (Scheme 1). The ring closure of the diketo esters involves the hydrolysis of the ester and decarboxylation of the keto acid, followed by cyclisation of the resultant 1,5-diketone. In this way, 5-benzyl-, 5-(1-naphthylmethyl)-, 5-(2-naphthylmethyl)-, and 5-(9-phenanthrylmethyl)-3-phenylcyclopentenones (**1***a–d*) were prepared.

Photochemical rearrangements

We photolysed the ketones using a medium pressure Hg lamp and a Pyrex filter. Under these conditions, we could detect no photoproduct from the benzyl ketone **1***a* other than a mixture of dimers whose structures we have not investigated further. In the case of the 1-naphthylmethyl compound **1***b*, a photoproduct builds up in the reaction mixture to a concentration of about 22%, but the reaction does not appear to proceed further. The isolation of this product **2***b* proved difficult, as it was labile to acid and, indeed, partially decomposed on silica. However, it could be isolated in a pure state by chromatography on a basic alumina column, and we confirmed that it reverted to **1***b* on pyrolysis or acid treatment. Photolysis of pure **2***b* reverts mainly to **1***b*.

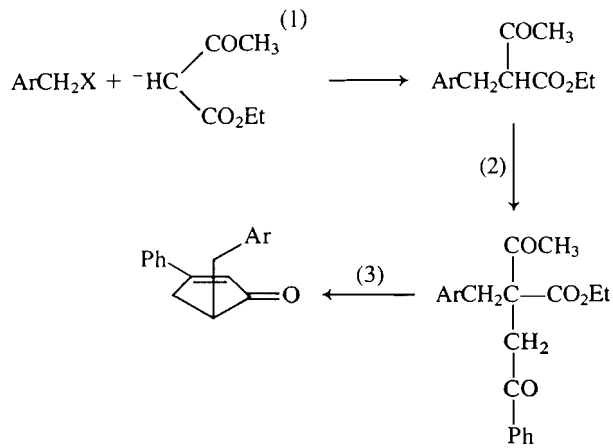

(1) From NaH, $CH_3OCH_2CH_2OCH_3$

(2) (a) NaH, $CH_3OCH_2CH_2OCH_3$
(b) $PhCOCH_2Br$

(3) KOH, 1%, then 10%

SCHEME 1

The structure of **2***b* follows from its infrared spectrum, which showed a peak at 1740 cm^{-1} characteristic of this ring system (1, 3, 4), and by its ^1H and ^{13}C nmr spectra. In the ^1H spectrum the 5- and 6-hydrogen signals both appear as double doublets, coupled to each other, and separately to the 4-proton, as found in other related photoproducts containing the dihydronaphthalene skeleton (6–8). Of the hydrogens in the 11- and 12-methylene groups, one proton signal lies at a lower field than any of the others, and is assigned to the 12-*exo* hydrogen as it is in the deshielding zone of the fused benzene ring.

The 2-naphthylmethyl derivative **1***c* behaves similarly on photolysis. In this case, the mixture contained 15% of the photoproduct **2***c*, which reverted to **1***c* on heating or acid treatment, and mainly to **1***c* on photolysis. The 7- and 8-proton signals in this case appeared as doublets coupled to each other. The 12-*exo* signal in this case lies at higher field than that of **2***b*,

[1]For part 5, see ref. 1.
[2]For preliminary communication, see ref. 2.
[3]Author to whom correspondence may be addressed.

Can. J. Chem. Downloaded from www.nrcresearchpress.com by 118.98.75.50 on 09/07/12
For personal use only.

Can. J. Chem. Downloaded from www.nrcresearchpress.com by 118.98.75.50 on 09/07/12
For personal use only.

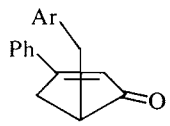

1*a* Ar = Ph

b Ar = 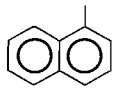

c Ar = 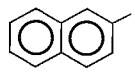

d Ar = 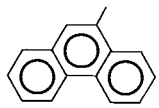

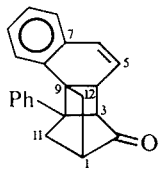

2*b*

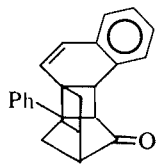

2*c*

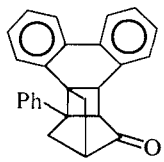

2*d*

as the fused benzene ring is not close enough to deshield it. The 4-H signal in **2***c* lies at lower field than the corresponding signal in **2***b*. This is to be expected, as it is benzylic in **2***c* but only allylic in **2***b*.

We have confirmed the structures **2***b* and **2***c* by using the lanthanide shift reagent, Eu(fod)$_3$. The 3-, 1-, and 4-hydrogens in this order show the greatest shift, followed by the 11-*exo* and 12-*endo* hydrogens. Had the alternative structures **3***b* and **3***c*

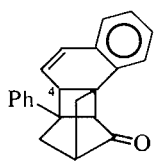

3*b*

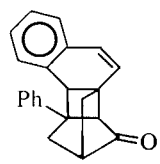

3*c*

been correct, the corresponding 4-hydrogen shift would have been much smaller than the shift of either of the 12-hydrogens and would be comparable to the shifts of the olefinic protons. It is significant that the europium reagent appears to complex more strongly with **2***b* than with **2***c*. In the latter case the fused aromatic ring would inhibit approach of the bulky reagent to the carbonyl group.

When the phenanthryl ketone **1***d* was irradiated, it afforded one product **2***d* in 14% yield. The ir spectrum showed a peak at 1745 cm^{-1} characteristic of the ring system and, in its ^{1}H nmr spectrum, the 12-*exo* proton appears downfield as in **2***b* but not **2***c*. As with the other compounds, **2***d* reverts to **1***d* on pyrolysis, on acid treatment, and on photolysis.

Discussion

It is interesting that the photocyclisation of 5-allylcyclopentenones is completely regiospecific (1, 3, 4, 9), with but a few exceptions (10), where there is an electron-donating group at the 3-position and further substituents at the 2-position. The photolysis reactions using a naphthalene or phenanthrene skeleton to provide the ene-component afford products with the same regiospecificity. This is to be compared with the case of the cycloaddition reaction of acrylonitrile with α- and β-naphthols and their trimethylsilyl ethers. In these cases, the regioselectivity is governed by the position of the oxygen substituent (8). In our cases, the position of the naphthalene substituent does not affect the regioselectivity.

Srinivasan and Carlough and Liu and Hammond (11) have offered an explanation of regioselectivity in ring closure reactions in terms of "the rule of five." Preferably, reactions proceed in such a way that the diradical intermediates lie in, or are external to, five-membered ring(s). Very recently a rationalisation of this rule has been given by Gleiter and Sander (12) in terms of molecular orbital theory. Of course the rule of five could explain either regioisomer of type **2** or **3**. The position of the carbonyl group must be crucial in determining the obtained regioselectivity.

We believe that the reverse reaction must proceed by excitation of the dihydronaphthalene chromophore, either directly, as happens with some of the photoadducts of acrylonitrile with naphthalenes (8), or by transfer of energy intramolecularly from the carbonyl triplet to the dihydronaphthalene or the corresponding dihydrophenanthryl chromophore.

Experimental

For general conditions, see Part 1 (ref. 13). Photolyses were carried out using a Hanovia 460-W medium pressure mercury lamp, and a Pyrex filter. In flash chromatographic separations, we employed silica Merck grade 9385 and a solvent mixture hexane:ethyl acetate (85:15) unless otherwise stated. Alumina chromatography employed Merck Grade 1076 (Basic). 1,2-Dimethoxyethane was dried over sodium hydroxide, followed by calcium hydride, and distilled before use. The ir spectra of liquids were measured as films, of solids in Nujol mulls. The nmr spectra were measured in deuteriochloroform solution.

Synthetic experiments

Ethyl 2-acetyl-2-benzyl-4-oxo-4-phenylbutanoate

Ethyl 2-benzyl-3-oxobutanoate (14) (1.4 g) in dry 1,2-dimethoxyethane (5 mL) was added dropwise to a suspension of sodium hydride (0.26 g) in dry 1,2-dimethoxyethane (5 mL) and the mixture heated at 25°C for 30 min. The mixture was cooled to room temperature, phenacyl bromide (1.27 g) in dry 1,2-dimethoxyethane (5 mL) added, and the mixture stirred for 18 h. Water was added, and the resulting solution extracted with ether (3 × 10 mL). The combined ether layers were washed and dried ($MgSO_4$). Removal of the solvent and flash chromatography of the residue gave ethyl 2-acetyl-2-benzyl-4-oxo-4-phenylbutanoate as an oil (1.53 g; 33%); ν_{max}: 1740, 1720, 1690 cm^{-1}; δ_H: 1.14 (t, *J* 7.7 Hz, ester CH_3), 2.38 (s, CH_3CO), 3.22 and 3.47 (ABq, *J* 13.5 Hz, PhCH_2), 3.45 (s, 3-H), 4.03 (q, *J* 7.9 Hz, ester CH_2), and 6.65–7.65 (m, aromatic H) ppm.

5-Benzyl-3-phenylcyclopent-2-en-1-one

Potassium hydroxide solution (1%, 630 mL, deoxygenated) and the above diketoester (7.9 g) were refluxed for 2 h under nitrogen. This mixture was cooled to room temperature, the strength of the potassium hydroxide increased to 10%, and the resulting mixture refluxed under nitrogen for a further 2.5 h. The cooled mixture was extracted with chloroform (3 × 75 mL). The combined organic layers were washed and dried ($MgSO_4$). Removal of solvent and flash chromatography of the residue afforded *5-benzyl-3-phenylcyclopent-2-en-1-one* **1***a* as needles (2.6 g; 42%), mp 70–71°C; λ_{max}: 285 and 224 nm (log ε 4.18 and 3.92 respectively); ν_{max}: 1690 and 1500 cm^{-1}; δ_H: 2.62–2.95 (m, 4- and 5-H), 3.15 (m, PhCH_2), 6.35 (t, *J* 2 Hz, 2-H), and 7.05–7.53 (m, aromatic H) ppm. *Anal.* calcd. for $C_{18}H_{16}O$: C 87.1, H 6.5; found: C 87.0, H 6.4%.

Ethyl 2-acetyl-2-(1-naphthylmethyl)-4-oxo-4-phenylbutanoate

Ethyl 2-(1-naphthylmethyl)-3-oxobutanoate (15) (23.1 g) in dry 1,2-dimethoxyethane (70 mL) was added dropwise to a suspension of sodium hydride (3.4 g) in dry 1,2-dimethoxyethane (50 mL) under

Can. J. Chem. Downloaded from www.nrcresearchpress.com by 118.98.75.50 on 09/07/12
For personal use only.

nitrogen. The mixture was stirred for 10 min, phenacyl bromide (16.9 g) in dry 1,2-dimethoxyethane (30 mL) added, and the resulting mixture stirred at 20°C for 12 h. Water was added and the solution extracted with chloroform (3 × 50 mL). The combined organic layers were washed and dried ($MgSO_4$). Removal of solvent afforded an oil, which on flash chromatography gave the *diketoester* (4.0 g) as needles, mp 116–117°C; δ_H: 1.10 (t, *J* 7.7 Hz, ester CH_3), 2.49 (s, CH_3CO), 3.53 (s, 1-H), 3.79 and 4.04 (ABq, *J* 14.0 Hz, $ArCH_2$), 4.08 (q, *J* 7.7 Hz, ester CH_2), and 7.08–7.96 (m, aromatic H) ppm. *Anal.* calcd. for $C_{25}H_{24}O_4$: C 77.3, H 6.0; found: C 77.3, H 6.2%.

5-(1-Naphthylmethyl)-3-phenylcyclopent-2-en-1-one **1**b

Potassium hydroxide solution (1%, 600 mL, deoxygenated) and the naphthylmethyl diketoester (10.5 g) were refluxed for 4 h under nitrogen. The mixture was cooled to room temperature, the potassium hydroxide concentration increased to 10%, and the refluxing continued for 4 h. The solution was extracted with chloroform (3 × 250 mL) and the combined organic layers were washed and dried ($MgSO_4$). Removal of solvent and flash chromatography of the residue afforded *5-(1-naphthylmethyl)-3-phenylcyclopent-2-en-1-one* **1***b* (3.2 g, 40%), as needles, mp 127–128°C; λ_{max}: 283 and 223 nm (log ε 4.46 and 4.59 respectively); ν_{max}: 1690, 1510, and 1500 cm^{-1}; δ_H: 2.88–3.19 (m, 4- and 5-H), 4.0 (s, $ArCH_2$), 6.62 (t, *J* 1.5 Hz, 2-H), and 7.32–8.34 (m, aromatic H) ppm. *Anal.* calcd. for $C_{22}H_{18}O$: C 88.55, H 6.1; found: C 88.9, H 5.8%.

Ethyl 2-acetyl-2-(2-naphthylmethyl)-4-oxo-4-phenylbutanoate

Ethyl 2-(2-naphthylmethyl)-3-oxobutanoate (15) (2.01 g) in dry 1,2-dimethoxyethane (30 mL) was added to a suspension of sodium hydride (330 mg) in dry 1,2-dimethoxyethane (20 mL) and the mixture stirred for 15 min. Phenacyl bromide (1.47 g) in dry 1,2-dimethoxyethane (20 mL) was added dropwise to the solution at 0°C and the resulting mixture stirred at 0°C for 1.5 h. Water was added and the aqueous solution extracted with ether (3 × 25 mL). The combined ether layers were washed and dried ($MgSO_4$). Removal of solvent and flash chromatography of the residue afforded ethyl 2-acetyl-2-(2-naphthylmethyl)-4-oxo-4-phenylbutanoate as an oil (1.3 g, 45%); δ_H: 1.15 (t, *J* 7.7 Hz, ester CH_3), 2.44 (s, CH_3CO), 3.31 (s, 3-H), 3.40 and 3.59 (ABq, *J* 7.6 Hz, $ArCH_2$), 4.17 (q, *J* 7.7 Hz, ester CH_2), and 6.99–7.82 (m, aromatic H) ppm.

5-(2-Naphthylmethyl)-3-phenylcyclopent-2-en-1-one **1**c

Aqueous potassium hydroxide (5%, 500 mL, deoxygenated) and ethyl 2-acetyl-2-(2-naphthylmethyl)-4-oxo-4-phenylbutanoate (10 g) were refluxed for 60 h under nitrogen. The solution was extracted with chloroform (3 × 100 mL). The combined organic layers were washed and dried, and the solvent removed. The residue was chromatographed to give the *2-naphthylmethyl cyclopentenone* **1***c* (1.9 g, 26%) as needles, mp 74–75°C; λ_{max}: 281 and 222 nm (log ε 4.51 and 4.64); ν_{max}: 1690, 1515, and 1500 cm^{-1}; δ_H: 2.59 and 3.03 (m, 4- and 5-H), 3.5 (m, $ArCH_2$), 6.56 (t, *J* 2 Hz, 2-H), and 7.23–7.87 (m, aromatic H) ppm. *Anal.* found: C 88.8, H 6.1%.

Ethyl 3-oxo-2-(9-phenanthrylmethyl)butanoate

Ethyl acetoacetate (4.85 g) in dry 1,2-dimethoxyethane (30 mL) was added slowly to a suspension of sodium hydride (1.48 g) in dry 1,2-dimethoxyethane (25 mL) under nitrogen, and the mixture stirred for 20 min. 9-Bromomethylphenanthrene (16) (10.3 g) in dry 1,2-dimethoxyethane (120 mL) was added dropwise, and the resulting mixture stirred at 60°C for 15 h. Water was added, and the solution extracted with ether (3 × 75 mL). The combined ether layers were washed and dried ($MgSO_4$). Removal of the solvent gave the ketoester, which was used without further purification; ν_{max}: 1740, 1715, 1650, and 1620 cm^{-1}.

Ethyl 2-acetyl-4-oxo-2-(9-phenanthrylmethyl)-4-phenylbutanoate

Ethyl 3-oxo-2-(9-phenanthrylmethyl)butanoate (11 g) in dry 1,2-dimethoxyethane (150 mL) was added dropwise to a suspension of sodium hydride (1.36 g) in dry 1,2-dimethoxyethane (30 mL) under nitrogen, and the mixture was stirred for 30 min. It was then cooled to 0°C, and phenacyl bromide (6.8 g) in dry 1,2-dimethoxyethane (35 mL) was added dropwise. The resulting solution was stirred at 0°C for 3 h and at 20°C for a further 1 h. Water was added, and the mixture extracted with ether (3 × 50 mL). The combined ether layers were washed and dried and the solvent removed to leave the residue, which was used unpurified in the next stage; ν_{max}: 1745, 1715, 1690, 1650, and 1620 cm^{-1}.

5-(9-Phenanthrylmethyl)-3-phenylcyclopent-2-en-1-one **1**d

The above diketoester (14.3 g) and 1% aqueous potassium hydroxide (600 mL, deoxygenated) were refluxed for 3 h with stirring under nitrogen. The concentration of potassium hydroxide was increased to 10%, and the refluxing continued for a further 3.5 h. The aqueous mixture was extracted with chloroform (3 × 250 mL). The combined organic layers were washed and dried ($MgSO_4$). The solvent was removed and the residue chromatographed to give *5-(9-phenanthrylmethyl)-3-phenylcyclopent-2-en-1-one*, **1***d* (680 mg; 6%) as needles, mp 134°C; λ_{max}: 290 (log ε 4.55), 278 (log ε 4.55), and 253 nm (log ε 4.82); ν_{max}: 1690, 1650, and 1500 cm^{-1}; δ_H: 2.71–3.28 (m, 4-H, 5-H), 4.10 (m, $ArCH_2$), 6.60 (t, *J* 1.5 Hz, 2-H), and 7.45–8.80 (m, aromatic H) ppm. *Anal.* calcd. for $C_{26}H_{20}O$: C 89.6, H 5.8; found: C 89.0, H 5.8%.

Photolysis experiments

Photolysis of 5-benzyl-3-phenylcyclopentenone **1**a

The cyclopentenone **1***a* (600 mg) in degassed benzene (550 mL) was irradiated for 5 h. Removal of solvent and flash chromatography (hexane 90: ethyl acetate 10) of the residue afforded a dimer mixture (210 mg; 35%), mp 174°C; λ_{max}: 228 nm (log ε 3.75); ν_{max}: 1750 cm^{-1}. The major dimer component had δ_H: 2.12 (m, 4-H), 3.0 (m, 3-H, $PhCH_2$), 3.35 (s, 1-H), 6.55–6.69, and 6.96–7.44 (m, aromatic H) ppm; δ_C: 34.7 (t, $PhCH_2$), 41.8 (t, 4-C), 47.2 (d, 1-C), 47.8 (d, 3-C), 52.8 (s, 5-C), 126.1, 129.3, 139.1, 143.8 (aromatic C), and 215.5 (s, 2-C) ppm. *Anal.* calcd. for $C_{36}H_{32}O_2$: C 87.1, H 6.5; found: C 86.9, H 6.4%.

Pyrolysis of dimer

The dimer mixture (100 mg) was heated to 120°C for 5 h. Flash chromatography of the residue afforded the starting enone (64 mg), mp 170°C, identified by its ^1H nmr spectrum.

Photolysis of 5-(1-naphthylmethyl)-3-phenylcyclopent-2-en-1-one **1**b

The cyclopentenone **1***b* (200 mg) in degassed benzene (600 mL) was irradiated for 2 h. The solvent was removed and the residue chromatographed on alumina to afford *7,8-benzo-10-phenyltetracyclo[7.2.1.0^{3,10}.0^{4,9}]dodeca-5,7-dien-2-one* **2***b* (44 mg; 22%), mp 131–132°C; ν_{max}: 3050, 3020, 2920, 2845, 1740, 1490, and 1480 cm^{-1}; δ_H: 1.75 (br d, *J* 11.7 Hz, 11 *endo*-H), 2.06 (d, *J* 11.7 Hz, 11 *exo*-H), 2.21 (br d, *J* 12.3 Hz, 12 *endo*-H), 2.98 (m, 1-H, 4-H, 12 *exo*-H), 3.25 (s, 3-H), 5.67 (dd, *J* 9.7 and 2.5 Hz, 5-H), 5.92 (dd, *J* 9.7 and 1.0 Hz, 6-H), and 6.67–7.33 (m, aromatic H) ppm; δ_C: 38.6 (t, 12-C), 44.3 (t, 11-C), 48.4 (d, 3- and 4-C), 48.8 (s, 9-C), 51.5 (d, 1-C), 61.8 (s, 10-C), 123.7–138.1 (aromatic and olefinic C), and 214.1 (2-C) ppm. *Exact Mass* calcd. for $C_{22}H_{18}O$: *m/z* 298.1358; found: M^+, *m/z* 298.1346.

Photolysis of the photoproduct **2**b

The photoproduct (30 mg) in [$^2H_6$]-benzene was irradiated for 20 min. The nmr spectrum of the resulting solution showed the presence of the cyclopentenone **1***b*.

Pyrolysis of the photoproduct **2**b

The photoproduct (20 mg) was heated at 120°C for 4 h. The product was identified by tlc and ^1H nmr as the enone **1***b*.

Acid catalysed rearrangement of **2**b

The photoproduct **2***b* (50 mg) was absorbed onto silica, and eluted with hexane – ethyl acetate (85:15). Analysis by tlc and ^1H nmr showed the presence of the enone **1***b*.

Photolysis of 5-(2-naphthylmethyl)-3-phenylcyclopent-2-en-1-one **1**c

The cyclopentenone **1***c* (200 mg) was irradiated in degassed benzene (600 mL) for 3 h. Removal of solvent and chromatography of the residue on alumina afforded *5,6-benzo-10-phenyltetracyclo[7.2.1.0^{3,10}.0^{4,9}]dodeca-5,7-dien-2-one* **2***c* (30 mg; 15%) as needles, mp 88–89°C; ν_{max}: 3060, 3020, 2920, 2845, 1740, 1490, and

1480 cm^{-1}; δ_H: 1.81 (ddd, *J* 11.5, 3.0, and 1.5 Hz, 11 *endo*-H), 2.11 (d, *J* 11.5 Hz, 11 *exo*-H), 2.20 (dd, *J* 12.3 and 3.0 Hz, 12 *endo*-H), 2.31 (dd, *J* 12.3 and 1.5 Hz, 12 *exo*-H), 2.96 (br t, *J* 1.5 Hz, 1-H), 3.34 (s, 4-H), 3.39 (s, 3-H), 5.52 (d, *J* 9.5 Hz, 8-H), 6.10 (d, *J* 9.5 Hz, 7-H), and 6.55–7.83 (m, aromatic H) ppm; δ_C: 43.5 (t, 11-C), 44.5 (t, 12-C), 48.7 (s, 9-C), 48.8 (d, 4-C), 49.7 (d, 3-C), 54.1 (d, 1-C), 63.6 (s, 10-C), 125.5–138.1 (aromatic and olefinic C), and 215.0 (2-C) ppm. *Exact Mass* found: M^+, *m/z* 298.1351.

Photolysis of the photoproduct **2**c

The photoproduct (20 mg) **2***c* in purified [$^2H_6$]-benzene was irradiated for 20 min. The resulting mixture contained **2***c* and **1***c*.

Pyrolysis of the photoproduct **2**c

The photoproduct (15 mg) was heated at 120°C for 4 h. The product was identified by tlc and ^1H nmr as the enone **1***c*.

Acid catalysed rearrangement of **2**c

The photoproduct **2***c* was absorbed onto silica. Elution with ethyl acetate – hexane (15:85) afforded a mixture; ^1H nmr showed the presence of **1***c*.

Photolysis of 5-(9-phenanthrylmethyl)-3-phenylcyclopent-2-en-1-one **1**d

The cyclopentenone **1***d* (200 mg) in degassed benzene (600 mL) was irradiated for 2.5 h. The solvent was removed and the residue chromatographed on alumina to give *5,6;7,8-dibenzo-10-phenyltetracyclo[7.2.1.0^{3,10}.0^{4,9}]dodeca-5,7-dien-2-one* **2***d* (28 mg; 14%), mp 112°C; ν_{max}: 3050, 2985, 2970, 1745, 1485, and 1445 cm^{-1}; δ_H: 1.85 (ddd, *J* 11.9, 2.0, and 1.0 Hz, 11 *endo*-H), 2.2 (d, *J* 11.9 Hz, 11 *exo*-H), 2.29 (dd, *J* 13.2 and 2.0 Hz, 12 *endo*-H), 3.09 (m, 1-H and 12 *exo*-H), 3.34 (s, 3-H), 3.54 (s, 4-H), and 6.46–7.56 (m, aromatic H) ppm; δ_C: 40.3 (t, 12-C), 44.6 (t, 11-C), 49.46 (s, 9-C), 49.49 (d, 4-C), 49.6 (d, 3-C), 54.1 (d, 1-C), 62.3 (s, 10-C), 122.8–137.9 (aromatic C), and 214.8 (s, 2-C) ppm. *Exact Mass* calcd. for $C_{26}H_{20}O$: *m/z* 348.1514; found: M^+, *m/z* 348.1504.

Photolysis of the photoproduct **2**d

The photoproduct **2***d* (10 mg) was irradiated in [$^2H_6$]-benzene (0.6 mL) for 2 h. The resulting solution was shown (tlc, ^1H nmr) to contain the enone **1***d*, and **2***d*.

Europium shift experiments

Aliquots of Eu(fod)$_3$ were added to a 0.1 *M* solution of **2***b* and **2***c* and the nmr spectra recorded.

$$\Delta M = \frac{\Delta\delta}{[\text{Eu(fod)}_3]/[\text{Ketone}]}$$

For **2***b*, ΔM values: 6.2 (3-H), 5.38 (1-H), 4.15 (4-H), 3.28 (11 *exo*-H), 3.15 (12 *endo*-H), 2.17 (12 *exo*-H), 2.12 (11 *endo*-H), 1.23 (5-H), and 0.75 (6-H).

For **2***c*, ΔM values: 5.1 (3-H), 4.43 (1-H), 3.31 (4-H), 2.5 (11 *exo*-H and 12 *endo*-H), 1.78 (11 *endo*-H), 1.73 (12 *exo*-H), 0.95 (8-H), and 0.69 (7-H).

Acknowledgement

We are grateful to the Department of Education, Republic of Ireland, for a maintenance award to M.T.M.C.

1. I. D. CUNNINGHAM, T. B. H. MCMURRY, M. P. NAPIER, and S. N. RAO. J. Chem. Soc. Perkin Trans. 1, 1235 (1986).
2. M. T. M. CLEMENTS and T. B. H. MCMURRY. J. Chem. Soc. Chem. Commun. 1104 (1986).
3. M. T. M. CLEMENTS, R. C. CATHCART, I. D. CUNNINGHAM, T. B. H. MCMURRY, and S. N. RAO. J. Chem. Res. (S), 223 (1984); (M) 2060 (1984).
4. G. GOWDA and T. B. H. MCMURRY. J. Chem. Soc. Perkin Trans. 1, 1516 (1980).
5. E. A. CHANDROSS and C. J. DEMPSTER. J. Am. Chem. Soc. **92**, 703 (1970); **92**, 705 (1970).
6. R. M. BOWMAN, C. CALVO, J. J. MCCULLOUGH, R. C. MILLER, and I. SINGH. Can. J. Chem. **51**, 1060 (1973); J. J. MCCULLOUGH, R. C. MILLER, and W-S. WU. Can. J. Chem. **55**, 2909 (1977); I. A. AKHTAR and J. J. MCCULLOUGH. J. Org. Chem. **46**, 1447 (1981); J. J. MCCULLOUGH, W. K. MACINNIS, C. J. L. LOCK, and R. FAGGIANI. J. Am. Chem. Soc. **104**, 4644 (1982).
7. T. R. CHAMBERLAIN and J. J. MCCULLOUGH. Can. J. Chem. **51**, 2578 (1973); K. MIZUNO, C. PAC, and H. SAKURAI. J. Chem. Soc. Perkin Trans. 1, 2221 (1975).
8. R. M. BOWMAN, T. R. CHAMBERLAIN, C-W. HUANG, and J. J. MCCULLOUGH. J. Am. Chem. Soc. **96**, 692 (1974).
9. S. WOLFF, S. AYRAL-KALOUSTIAN, and W. C. AGOSTA. J. Org. Chem. **41**, 2947 (1976).
10. W. OPPOLZER and S. C. BURFORD. Helv. Chim. Acta, **63**, 188 (1980); A. J. BARKER, M. J. BEGLEY, M. MELLOR, D. A. OTIENO, and G. PATTENDEN. J. Chem. Soc. Perkin Trans. 1, 1893 (1983); A. J. BARKER and G. PATTENDEN. J. Chem. Soc. Perkin Trans. 1, 1901 (1983).
11. R. SRINIVASAN and K. H. CARLOUGH. J. Am. Chem. Soc. **89**, 4932 (1967); R. S. H. LIU and G. S. HAMMOND. J. Am. Chem. Soc. **89**, 4936 (1967).
12. R. GLEITER and W. SANDER. Angew. Chem. Int. Ed. Engl. **24**, 566 (1985); M. OHSAKU. Tetrahedron Lett. **27**, 1797 (1986).
13. G. GOWDA and T. B. H. MCMURRY. J. Chem. Soc. Perkin Trans. 1, 274 (1979).
14. L. BOROWIECKI and Z. KAZUBSKI. Pol. J. Chem. **52**, 1447 (1978); S. AL HASSAN, R. J. KULICK, D. B. LIVINGSTONE, C. J. SUCKLING, H. C. S. WOOD, R. WRIGGLESWORTH, and R. FERONE. J. Chem. Soc. Perkin Trans. 1, 2645 (1980); V. DAVE and E. W. WARNHOFF. J. Org. Chem. **48**, 2590 (1983).
15. F. MAYER, A. SIEGLITZ, E. FISCHER, J. HAGEN, R. JUNG, W. KNIES, C. KOHL, F. LISTMANN, W. NEUGEBAUER, and T. SCHULTE. Chem. Ber. **55**, 1835 (1922).
16. W. E. BACKMANN and M. C. KLOETZEL. J. Am. Chem. Soc. **59**, 2207 (1937).

Can. J. Chem. Downloaded from www.nrcresearchpress.com by 118.98.75.50 on 09/07/12
For personal use only.

Principal property values for six non-natural amino acids and their application to a structure–activity relationship for oxytocin peptide analogues

SVANTE WOLD,[1] LENNART ERIKSSON, SVEN HELLBERG, JÖRGEN JONSSON, MICHAEL SJÖSTRÖM, BERT SKAGERBERG, AND CONNY WIKSTRÖM

Research Group for Chemometrics, Umeå University, S-901 87 Umeå, Sweden

Received December 30, 1986

This paper is dedicated to Professor John T. Edward

SVANTE WOLD, LENNART ERIKSSON, SVEN HELLBERG, JÖRGEN JONSSON, MICHAEL SJÖSTRÖM, BERT SKAGERBERG, and CONNY WIKSTRÖM. Can. J. Chem. **65**, 1814 (1987).

Previously derived principal property scales for the 20 coded amino acids have been extended to six noncoded amino acids, namely ornithine, norvaline, norleucine, O-methylated threonine, α-amino butyric acid, and citrulline. This has been done first, for the 20 coded amino acids, by developing PLS models for the relations between the previously derived scales (z_1, z_2, and z_3) and newly measured thin-layer chromatography data, proton nuclear magnetic resonance data, plus literature data describing amino acid "bulk" (van der Waals volume and molecular mass). Thereafter, z values for the noncoded amino acids were calculated by inserting the same measured data for these compounds into the PLS models. As a validation, the calculated z values were then used to describe the structural variation of a set of 60 oxytocin peptide analogues for which literature data on biological measurements existed. The models explain 71–81% of the variance of the biological data and are highly significant according to cross-validation. Prediction errors of about twice the estimated biological measurement error are obtained for the 11 peptide analogues containing noncoded amino acids.

SVANTE WOLD, LENNART ERIKSSON, SVEN HELLBERG, JÖRGEN JONSSON, MICHAEL SJÖSTRÖM, BERT SKAGERBERG et CONNY WIKSTRÖM. Can. J. Chem. **65**, 1814 (1987).

Des échelles de propriétés principales qui avaient été développées antérieurement pour les 20 acides aminés codés ont été étendues à six acides aminés non-codés, soit l'ornithine, la norvaline, la norleucine, la thréonine *O*-méthylée, l'acide α-aminobutyrique et la citrulline. Dans un premier temps, on a développé des modèles PLS pour les 20 acides aminés codés en se basant sur les relations entre les échelles développées antérieurement (z_1, z_2 et z_3) et les nouvelles données mesurées par chromatographie en couche mince et par résonance magnétique nucléaire ainsi que des données de la littérature décrivant le «volume» des acides aminés (volume de van der Waals et masse moléculaire). Ensuite, on a calculé les valeurs z des acides aminés non-codés en insérant les mêmes données pour ces composés dans les modèles PLS. Afin de valider nos conclusions, on a ensuite utilisé les valeurs z pour décrire la variation de structure d'un ensemble de 60 analogues du peptide oxytocine pour lesquels des données relatives aux mesures biologiques existent dans la littérature. Les modèles expliquent de 71 à 81% de la variance des données biologiques et, d'après des contre-validations, elles sont très significatives. Pour 11 des analogues peptidiques contenant des acides aminés qui ne sont pas codés, on peut prédire des erreurs qui sont le double de l'erreur évaluée pour les mesures biologiques.

[Traduit par la revue]

Introduction

We have earlier developed three scales summarizing a number of properties of the 20 coded amino acids, i.e., those coded by RNA in the protein synthesis (1–3). We called these three scales, z_1, z_2, and z_3, *principal properties* (PPs) of the amino acids. The PPs were used for a quantitative description of the variation in sequence in families of peptide analogues, thereby allowing the construction of models of the relation between structure and biological activity for these peptide families (3–5). Since amino acids other than the 20 coded ones are often included in synthetic peptide sequences, it is of interest to extend the z-scales to such noncoded acids.

The purpose of the present article is to outline a working procedure for this extension of z-scales, based on data measured on the amino acids (see Tables 1 and 2) and multivariate PLS models (partial least-squares projections to latent structures). Finally, the results are validated on a set of oxytocin peptide analogues varying in five of the nine amino acid positions. Five biological measurements were available for these compounds. Three of these were oxytocin-like (OT), and two vasopressin-like (VP), activity measurements. This set included 11 peptides containing one of the six noncoded amino acids. Two PLS models were developed, one for OT, and one for VP, relating the variation in peptide sequence in the training sets to the biological activity data. The training sets comprised peptides with coded amino acids only and with complete biological data.

Method

Data measured on a set of similar objects, here a set of amino acids, can be well approximated by a bilinear model, i.e., a principal components (PC) or a PLS model (6–8). PLS (partial least-squares projection to latent structures) was originally developed by H. Wold for the modeling of complex social science systems (8), and was later modified for solving a number of data analytic problems in chemistry and neighboring sciences (10–13). PLS allows the modeling of the relationship between any data measured on a set of similar objects and any other data or data aggregates relating to the same set.

We have previously shown that physicochemical data measured on the 20 coded amino acids are adequately summarized by a model with three PCs. The score vectors in this PC model were denoted z_1–z_3 and called *principal properties* (PPs) of the amino acids. Tentatively, we interpreted these three scales as related to lipophilicity, side chain bulk, and electronic properties of the amino acids.

The PPs have been found relevant for quantifying the variation in sequence within sets of similar peptides and the relation between this sequence variation and the variation in biological potency in such sets (2–4).

[1]Author to whom correspondence may be addressed.

Printed in Canada / Imprimé au Canada

Can. J. Chem. Downloaded from www.nrcresearchpress.com by 118.98.75.50 on 09/07/12
For personal use only.

TABLE 1. Conditions for the tlc and nmr experiments corresponding to variables 1–10, and the two "bulk" describing variables

Variable no.	Type	Eluent (tlc) or pD (nmr)
Thin-layer chromatography		
1	Silica gel	Ethanol–water (7:3)[a]
2	Silica gel	1-Butanol – acetic acid–water (4:1:1)
3	Silica gel	Phenol–water (3:1 weight/weight)
4	Silica gel	Butanone–pyridine – acetic acid – water (70:15:2:15)
5	Cellulose	Ethanol–water (7:3)
6	Cellulose	Pyridine–isoamylalcohol–water (7:6:6)
7	Kieselguhr	Butanone–water–phenol–acetone–ethanol (1:1:1:1:1)
Proton nmr		
8		pD = 2.0[b] α-Proton shift in ppm
9		pD = 7.0 α-Proton shift in ppm
10		pD = 12.5 α-Proton shift in ppm
11	van der Waals volume (cm^3/mol)	
12	Molecular weight (g/mol)	

[a]The composition of the eluents refers to parts by volume.
[b]The pD refers to measurements by a pH electrode in heavy water corrected by 0.45 units (see ref. 9).

PCA

The PC model for a matrix X with the n rows corresponding to objects, here amino acids or peptides, and the p columns containing different measurements made on these objects, is given by

$$[1] \quad X = 1\bar{x} + TP' + E$$

Here 1 denotes a column vector with elements of unity, and $\bar{x}$ denotes the vector of column averages of X. The $(n \times A)$ score matrix T contains information about the n objects expressed as A vectors, components, and the $(A \times p)$ loading matrix P' contains coefficients expressing how the original x-variables are combined to form T. The rows in P' are normalized to length one. The residual matrix E contains the deviation between data and model, i.e., the part unexplained by the model.

The number of statistically significant model dimensions, A, may be determined by cross-validation (12). This procedure is based on a repeated analysis of the data matrix, each time with part of its elements treated as missing observations. The model is developed on the remaining data and the pseudo-missing observations are then predicted from the model. The differences between the predicted and the actual values are used to evaluate whether the current model dimension improves the predictive power of the model.

From a model developed on a "training set" of objects, scores (t values) for new objects are simply calculated from their x-data, a row vector x, as

$$[1b] \quad t = xP$$

This also gives a measure of dissimilarity between a new object and the training set, calculated as the standard deviation of the residuals (rsd):

$$[1c] \quad e = x - tP'$$

The primary use of PCA is to get an overview of a data matrix in terms of a picture (the plot of columns in T against each other) and for estimating the number of "factors" in the matrix.

PLS

The predictive two-block PLS model relates a matrix X to a matrix Y with the purpose of predicting Y from X. For the X part the model is the same as for PCA (eq. [1]), but in addition a matrix W of PLS-weight vectors results from the computations. The Y block is modeled in the same way as the X block:

$$[2] \quad Y = 1\bar{y} + UC' + F$$

In addition, the Y-block score matrix U (dimension $n \times A$) is modeled by the "inner relation", where B is a diagonal coefficient matrix, and H is a $(n \times A)$ residual matrix:

$$[3] \quad U = TB + H$$

The number of model dimensions, A, is typically small (1, 2, or 3) as long as the modeled objects are similar to each other with respect to the measured data.

Inserting eq. [3] into eq. [2] gives the predictive model for Y (the asterisks indicate that C^* differs from C, etc.):

$$[4] \quad Y = 1\bar{y} + TC^{*\prime} + F^*$$

Similarly to PCA, the significance of the model dimensions is evaluated by cross-validation.

Predictions of the y values for new objects are obtained from the x-data for these objects inserted into the PLS model (W is the PLS-weight matrix):

$$[4a] \quad y = xW'(PW')^{-1}c$$

The main use of predictive two-block PLS models is for the same data analytical problems as multiple regression (MR), i.e., to get a predictive model of Y in terms of X. A difference between MR and PLS is that PLS can handle collinearities in X, even to the extent that the number of variables in X (p) can exceed the number of objects (n). Also, PLS does not assume that the x-variables are 100% relevant, but tolerates that X contains systematic and unsystematic parts that are unrelated to the problem of interest in the analysis, i.e., the modeling of Y.

Can. J. Chem. Downloaded from www.nrcresearchpress.com by 118.98.75.50 on 09/07/12
For personal use only.

TABLE 2. R_f values from tlc measurements, ^{1}H nmr shifts for α-proton (for experimental conditions, see Table 1), van der Waals volume (vdW), molecular weight (MW), and principal property values (z_1, z_2, and z_3). Values are given for the 20 natural amino acids (coded in mRNA) and six non-natural amino acids

No.	Code[a]	R_f							^{1}H nmr			vdW	MW	z_1	z_2	z_3
1	A Ala	60	24	29	9	52	23	37	4.13	3.77	3.30	13.7	89.1	0.07	−1.73	0.09
2	V Val	74	42	43	22	68	43	72	3.94	3.60	3.03	34.1	117.2	−2.69	−2.53	−1.29
3	L Leu	82	52	50	33	73	53	83	4.05	3.71	3.23	44.4	131.2	−4.19	−1.03	−0.98
4	I Ile	80	50	49	28	72	53	83	4.02	3.66	3.08	44.4	131.2	−4.44	−1.68	−1.03
5	P Pro	52	20	50	11	57	31	68	4.37	4.11	3.51	30.7	115.1	−1.22	0.88	2.23
6	F Phe	82	50	52	35	66	52	87	4.31	3.98	3.48	56.1	165.2	−4.92	1.30	0.45
7	W Trp	86	54	54	40	—	51	88	4.36	4.05	3.56	75.1	204.2	−4.75	3.65	0.85
8	M Met	77	45	50	29	63	49	79	4.20	3.84	3.30	45.0	149.2	−2.49	−0.27	−0.41
9	K Lys	1	7	2	1	19	7	1	4.05	3.74	3.27	51.1	147.0	2.84	1.41	−3.14
10	R Arg	1	9	6	1	19	7	1	4.06	3.76	3.20	64.9	175.0	2.88	2.52	−3.44
11	H His	9	6	16	1	16	20	2	4.29	4.00	3.47	45.1	156.0	2.41	1.74	1.11
12	G Gly	44	19	22	6	32	22	17	3.88	3.54	3.15	3.5	75.1	2.23	−5.36	0.30
13	S Ser	44	19	15	6	36	23	13	4.18	3.87	3.31	18.3	105.1	1.96	−1.63	0.57
14	T Thr	58	25	27	11	46	29	30	3.97	3.57	3.08	28.5	119.1	0.92	−2.09	−1.40
15	C Cys	—	23	27	—	46	—	—	4.30	3.97	3.00	25.0	121.2	0.71	−0.97	4.13
16	Y Tyr	81	50	47	32	68	51	80	4.30	3.90	3.40	61.6	181.2	−1.39	2.32	0.01
17	N Asn	39	14	25	5	21	12	12	4.33	4.00	3.56	32.5	132.1	3.22	1.45	0.84
18	Q Gln	53	16	37	7	32	20	23	4.10	3.76	3.24	42.7	146.1	2.18	0.53	−1.14
19	D Asp	—	16	9	2	38	20	19	4.34	3.89	3.51	30.0	132.1	3.64	1.13	2.36
20	E Glu	—	24	15	4	42	19	28	4.12	3.74	3.21	40.2	146.1	3.08	0.39	−0.07
21	Orn	1	6	2	1	17	8	1	4.07	3.77	3.22	41.2	133.0	4.11	0.51	−1.61
22	Cit	55	17	38	6	32	22	29	4.08	3.74	3.08	60.6	175.2	0.77	1.28	−1.58
23	Abu	69	34	37	15	58	33	55	4.05	3.69	3.17	23.9	103.1	−0.61	−2.51	−0.01
24	Nle	84	51	51	33	74	54	81	4.05	3.71	3.20	44.4	131.2	−3.62	−1.36	−0.88
25	Nva	77	46	46	24	69	48	73	4.06	3.71	3.22	34.1	117.1	−2.50	−1.92	−0.35
26	Omt	66	30	47	17	62	38	74	3.96	3.60	3.10	37.8	133.0	−1.43	−1.80	−1.78

[a]Orn = ornithine, Cit = citrulline, Abu = α-amino butyric acid, Nle = norleucine, Nva = norvaline, Omt = *O*-methyl threonine.

A PLS model relating PPs to newly measured physicochemical data

The previous PPs (2, 3) were derived by a PCA of values for the physicochemical data that were obtained mainly from the literature. This makes it difficult to extend the *z*-scales to amino acids for which the corresponding literature data are unavailable. To get around this problem, we have measured multivariate data on the individual amino acids with the hope that these data contain sufficient information to constitute a basis for the *z*-scales. These data comprise retention data in seven thin-layer chromatography (tlc) systems, and proton nmr data for the amino acid α-proton at three different conditions (see Table 1).

In addition, we have used the van der Waals volume and molecular weight to describe the variation in bulk between the amino acids.

With these 12 variables (Table 2) comprising the matrix *X*, a two-block single *y* PLS model (8, 10, 11) was developed for each *z*-scale as the dependent (*y*) variable.

For each *z*-scale, a measure of the explained variance and the predicted variance is obtained. If these measures are sufficiently small, the *z*-scales may be predicted from (i.e., calculated from) the physicochemical measurements used as *x*-variables in the present study.

Predicting PPs (z-scales) for new amino acids

Once a PLS model is developed for the relation between a *z*-scale and the 12 physicochemical variables, the *z* values for new amino acids may be predicted (calculated) from their 12 physicochemical measurements inserted in the earlier developed PLS model.

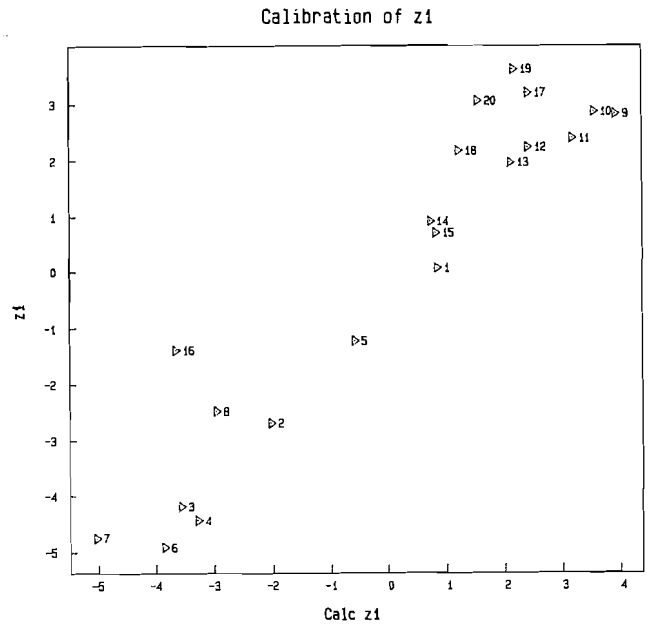

FIG. 1. A PLS model of the first PP, z_1, modeled as a linear combination of the 12 physicochemical variables, mainly nos. 1–7 (see Table 3). The model explains 89% of the variance in z_1. The amino acids are numbered according to Table 2.

Peptide QSAR

To develop a quantitative structure–activity relationship (QSAR) for a family of peptides, one essential problem to be solved first is the translation of the variation in sequence to the variation in one or several quantitative variables. Having the three PPs, i.e. *z*-scales, for the amino acids, we translate the

Can. J. Chem. Downloaded from www.nrcresearchpress.com by 118.98.75.50 on 09/07/12
For personal use only.

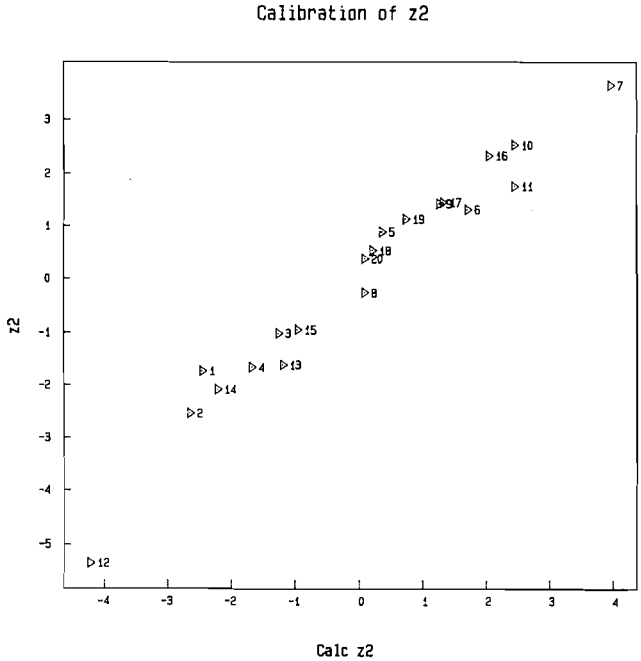

FIG. 2. A PLS model of the second PP, z_2, modeled as a linear combination of the 12 physicochemical variables, mainly nos. 8–12 (see Table 3). The model explains 95% of the variance in z_2. The amino acids are numbered according to Table 2.

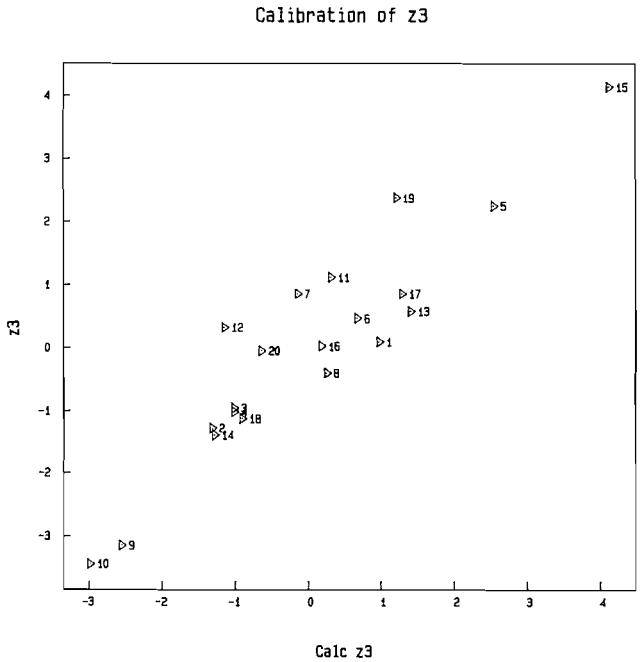

FIG. 3. A PLS model of the third PP, z_3, modeled as a linear combination of the 12 physicochemical variables (see Table 3). The model explains 85% of the variance in z_3. The amino acids are numbered according to Table 2.

variation in amino acid sequence into the variation in z values. Thus, each varying peptide position is translated to the values of the three z-scales.

This gives as the result a matrix (X) describing the sequence variation in the peptide family. This matrix has as many rows as there are peptides and as many columns as there are varying positions times three (three z-scales).

In a PLS model of a QSAR, the Y-matrix contains the measured activity values of a training set of peptides. The activity values for a set of oxytocin analogues were obtained from the literature (14). This Y-matrix is related to the X-matrix describing the structure by a PLS model. The appropriate number of model dimensions (PLS components) is determined by cross-validation (12, 13).

Predictions of the activities (Y) of new peptides may thereafter be obtained by first translating their peptide sequence to an x-vector using the z-scales, and then inserting the x-vector in the PLS model developed earlier.

TABLE 3. PLS regression coefficients for the combination of 12 physicochemical variables to predict z_1, z_2, and z_3

	$r(z_1)$	$r(z_2)$	$r(z_3)$
1	−0.13	−0.09	−0.33
2	−0.14	−0.02	−0.01
3	−0.14	−0.04	−0.11
4	−0.14	0.00	−0.15
5	−0.14	−0.07	−0.01
6	−0.14	−0.06	0.17
7	−0.14	−0.01	−0.03
8	−0.01	0.17	0.58
9	−0.01	0.15	0.45
10	0.00	0.15	−0.25
11	−0.06	0.36	−0.42
12	−0.04	0.35	−0.10

Results

Using PLS modeling and the measured data described above, we arrived at the following results:

PLS models relating previously developed z-scales to measured physicochemical data

Significant PLS models were obtained for each of z_1, z_2, and z_3, with 1, 3, and 4 model dimensions, respectively. The agreement between the previous z values and those predicted by the PLS model of the physicochemical data is shown in Figs. 1–3.

The explained variances of z_1–z_3 are 89, 95, and 85%, respectively, which we feel are adequate for the present purposes.

PPs (z-scales) for six new amino acids

By means of these PLS models (see above), z values were calculated for the six noncoded amino acids giving the values in Table 2 (nos. 21–26).

Oxytocin analogues QSAR

This quantitative structure relationship (QSAR) is an extension of the one previously reported (3) where only two biological activity variables were modeled for oxytocin related nonapeptides of the general structure: Cys-x-x-x-x-Cys-Pro-x-Gly-NH_2 (see Table 4). Here three additional biological effect variables were compiled and analysed (see Figs. 4–8).

1. PCA of five biological activities

First a PCA was made of the biological activity data for all peptides. Two highly significant PCs (cross-validation) were obtained. The loading plot of p_2 against p_1 shows that the biological variables are clustered in two groups containing nos. 1–3 and 4 and 5, respectively.

These two groups of activity variables were analyzed separately, as described below.

Can. J. Chem. Downloaded from www.nrcresearchpress.com by 118.98.75.50 on 09/07/12
For personal use only.

TABLE 4. Amino acid sequence for oxytocin analogs substituted in positions 2, 3, 4, 5, and 8 (Cys-X-X-X-X-Cys-Pro-X-Gly-NH_2). The sequence is given in one-letter code for the natural amino acids and three-letter code for non-natural amino acids

No.	Sequence	No.	Sequence	No.	Sequence
1	YIQNL	21	YFQNH	41	FFQN-Orn
2	FIQNL	22	YISNI	42	Y-Nva-QNL
3	YFQNL	23	SIQNL	43	Y-Nle-QNL
4	YYQNL	24	LIQNL	44	Y-Omt-QNL
5	FFQNL	25	YISNL	45	YIENL
6	YWQNL	26	YIQNG	46	YINNL
7	YLQNL	27	YIQNA	47	YI-Abu-NL
8	YVQNL	28	FYQNL	48	YIVNL
9	YIQNI	29	FIQNR	49	YIANL
10	YIQNV	30	YSQNK	50	YIGNL
11	YFQNK	31	YISNQ	51	YFNNK
12	YYQNK	32	FFQNR	52	YFANK
13	FFQNK	33	YFSNK	53	YIQQL
14	FYQNK	34	GIQNL	54	YIQAL
15	YIQNK	35	YGQNL	55	YIQSL
16	SIQNK	36	HFQNL	56	YFQSK
17	YWQNK	37	HFQNK	57	YIQN-Abu
18	FIQNK	38	YIQN-Orn	58	YIQN-Cit
19	YFQNR	39	FIQN-Orn	59	YFQN-Cit
20	YIQNR	40	YFQN-Orn	60	YINQL

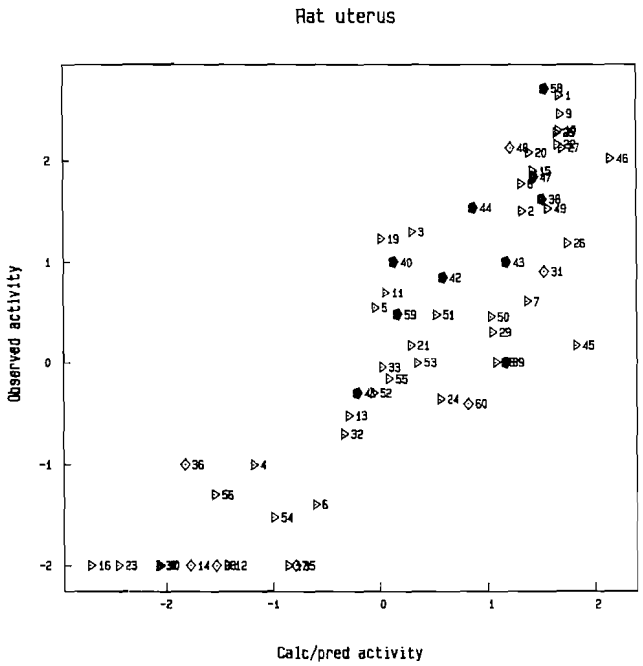

FIG. 4. PLS predictions of the first biological activity variable, rat uterus contractile activity, plotted against the observed values. The triangles denote the training set points for the 20 coded amino acids, rhombes denote predictions for the test set peptides with coded amino acids, and pentagons (filled) the predictions for test set peptides containing noncoded amino acids. The peptides are numbered according to Table 4.

2. PLS model for the three oxytocin-like activities (OT)

The variation in peptide sequence for the oxytocin analogues was translated to 15 *x*-variables by describing each varying position (nos. 2, 3, 4, 5, and 8) by the three *z*-scales derived as described above.

A training set of peptides was formed by those having only coded amino acids and all three biological activities defined.

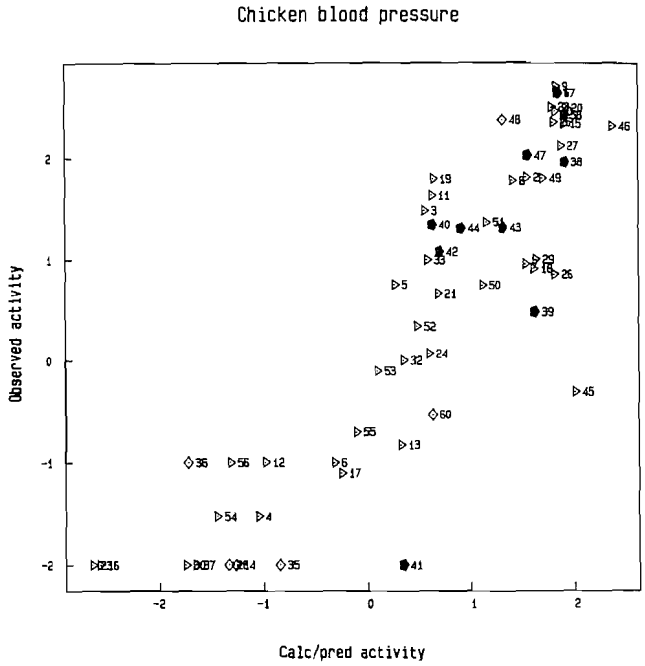

FIG. 5. PLS predictions of the second biological activity variable, chicken blood pressure, plotted against the observed values. Notation and numbering same as in Fig. 4.

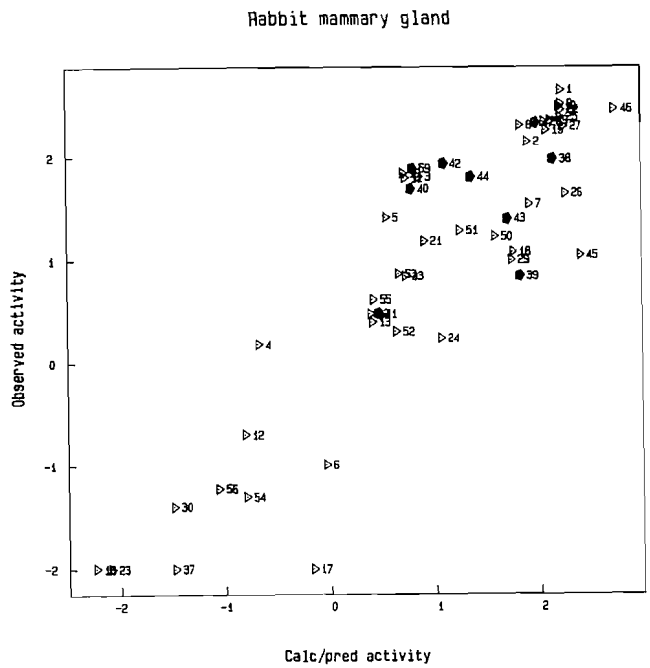

FIG. 6. PLS predictions of the third biological activity variable, rabbit mammary gland activity, plotted against the observed values. Notation and numbering same as in Fig. 4.

The test set thus contained peptides with coded amino acids and incomplete biological data, plus peptides with a noncoded amino acid in some position.

A highly significant three-dimensional PLS model resulted for the training set. The relations between observed activities and those predicted by the model are illustrated in Figs. 4–6.

The resulting PLS parameters (given as supplementary material) may be used to construct peptides that are likely to be more active than the present 60 analogues. However, since in the present case the experimental design, i.e., the selection of

Can. J. Chem. Downloaded from www.nrcresearchpress.com by 118.98.75.50 on 09/07/12
For personal use only.

Can. J. Chem. Downloaded from www.nrcresearchpress.com by 118.98.75.50 on 09/07/12
For personal use only.

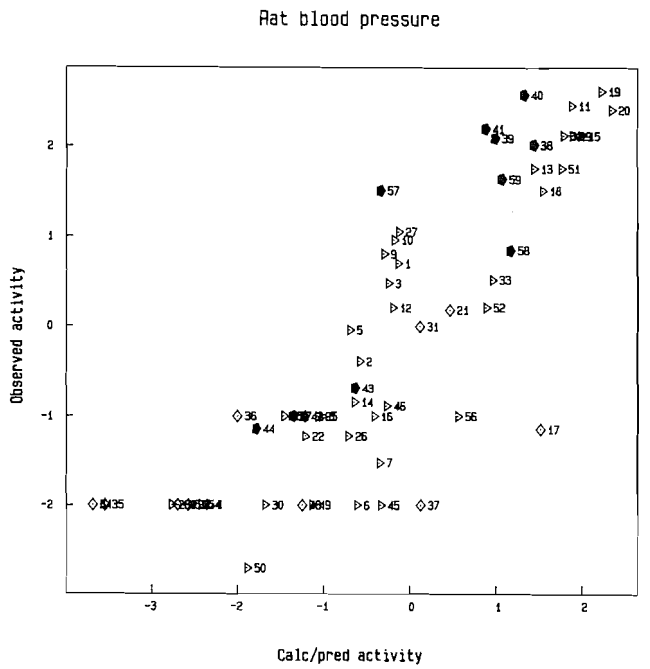

FIG. 7. PLS predictions of the fourth biological activity variable, rat blood pressure, plotted against the observed values. Notation and numbering same as in Fig. 4.

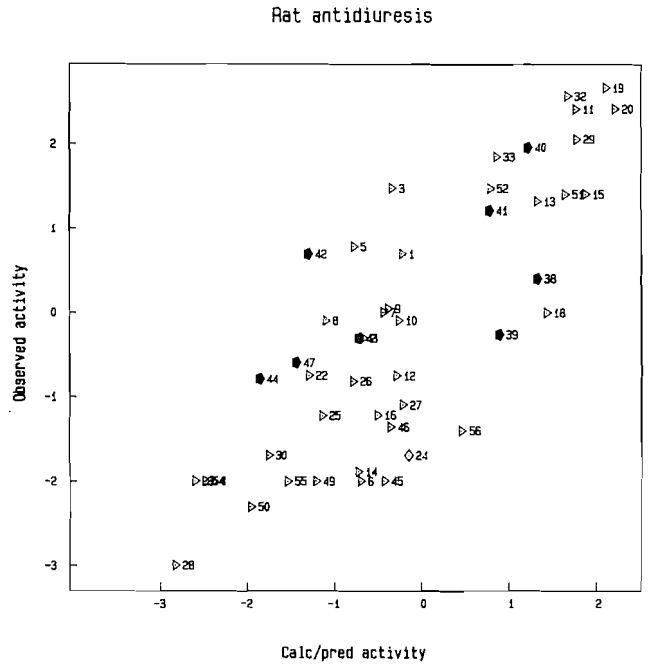

FIG. 8. PLS predictions of the fifth biological activity variable, rat antidiuresis, plotted against the observed values. Notation and numbering same as in Fig. 4.

training compounds, is highly unbalanced from the statistical point of view, such extrapolations are uncertain and should be regarded with caution. There are ways of constructing balanced training sets of compounds, which efficiently probe the chemical properties of several amino acid positions simultaneously (3, 5).

3. PLS model for the two vasopressin-like activities (VP)

In the same way, a PLS model was developed for the two VP-like biological activity variables. A PLS model with two significant dimensions was obtained, giving predictions plotted in Figs. 7 and 8.

Discussion

The multivariate modeling of chemical data may be used to find the number of "inherent factors" in a chemical system, and to obtain values for the factors (latent variables) for pertinent cases (objects). This approach has previously been used, for instance, by Edward *et al.* to investigate the complexity of the ionization of weak acids (15) and other interesting systems (16). Here it is used to get a quantitative description of amino acids, which then is utilized in models relating the variation in peptide sequence to the variation in biological activity.

We see in Figs. 4–8 that the models are not "perfect", but still the predictive power of the model is remarkably good considering the crudeness of the approach. These results are of some interest with respect to the traditional "lock-and-key" interpretation of the biological activity of organic molecules. The present results indicate either that shape is less important or that shape and conformation are in some way inherent in the z values. Regardless of the interpretation this has practical consequences in that, at least for small peptides, we may not need to go via the cumbersome three-dimensional structural approach with crystallography, molecular graphics, and similar methods.

The z values developed here are not final, and final values will perhaps never be obtained. The approach of soft modeling does not aim at final answers, if such exist, but rather to develop a working approach to the study of complexity. With the change in time and problem formulation, the perspective on a given system changes, and thereby its latent variables and their values. Hence, the z values should be taken as scales useful in a certain context, which may change tomorrow when a better understanding of peptide QSARs is reached.

Supplementary material

Tables of resulting PLS parameters for the peptide QSAR models are given as supplementary material to allow interested readers to check results and make their own predictions.[2]

Acknowledgements

This article is dedicated to our friend and colleague Jack Edward, whose wisdom, encouragement, and kind advice has made our work and life both easier and more enjoyable. The support from the Swedish Natural Science Research Council (NFR) and the Swedish Board of Technical Development (STU) has been most valuable.

1. M. SJÖSTRÖM and S. WOLD. J. Mol. Evol. **22**, 272 (1985).
2. S. HELLBERG, M. SJÖSTRÖM, and S. WOLD. Acta Chem. Scand. Ser. B, **40**, 135 (1986).
3. S. HELLBERG, M. SJÖSTRÖM, B. SKAGERBERG, and S. WOLD. J. Med. Chem. In press.
4. M. SJÖSTRÖM, S. WOLD, Å. WIESLANDER, and L. RILFORS. EMBO J. In press.
5. S. HELLBERG, M. SJÖSTRÖM, B. SKAGERBERG, C. WIKSTRÖM, and S. WOLD. Acta Pharm. Jugosl. In press.
6. S. WOLD. Chem. Scr. **5**, 97 (1974).
7. S. WOLD. Pattern Recognit. **8**, 127 (1976).
8. H. WOLD and K. G. JÖRESKOG (*Editors*). Systems under indirect observation. North-Holland, Amsterdam. 1982.
9. R. GARY, R. G. BATES, and R. A. ROBINSON. J. Phys. Chem. 3806 (1964).
10. S. WOLD, A. RUHE, H. WOLD, and W. J. DUNN, III. SIAM J. Sci. Stat. Comput. **5**, 735 (1984).

[2]These tables may be purchased from the Depository of Unpublished Data, CISTI, National Research Council of Canada, Ottawa, Ont., Canada K1A 0S2.

11. S. WOLD *et al.* Analusis (Paris), **12**, 477 (1984).
12. S. WOLD. Technometrics, **20**, 397 (1978).
13. S. WOLD. *In* Food research and data analysis. *Edited by* H. Martens and H. Russwurm, Jr. Appl. Sci. Publishing, London. 1983. p. 147.
14. B. BERDE and R. A. BOISSONNAS. *In* Handbuch der experimentellen Pharmakologie. Vol. 23. Springer, Berlin. 1968. p. 802.
15. J. T. EDWARD, M. SJÖSTRÖM, and S. WOLD. Can. J. Chem. **59**, 2350 (1981).
16. J. T. EDWARD, E. JOHANSSON, and S. WOLD. Discr. Appl. Math. In press.

Can. J. Chem. Downloaded from www.nrcresearchpress.com by 118.98.75.50 on 09/07/12
For personal use only.

A novel reaction of α-haloepoxides with trialkylstannates

L. D. COREY, S. M. SINGH, AND A. C. OEHLSCHLAGER
Department of Chemistry, Simon Fraser University, Burnaby, B.C., Canada V5A 1S6

Received November 25, 1986

This paper is dedicated to Professor John T. Edward

L. D. COREY, S. M. SINGH, and A. C. OEHLSCHLAGER. Can. J. Chem. **65**, 1821 (1987).

The reaction of α-haloepoxides with zinc powder or reagents containing the trialkylstannate anion yields allylic alcohols by *anti* elimination of the carbon halogen and adjacent carbon epoxy oxygen bonds. Appreciable $Z \rightarrow E$ isomerization occurs in both types of reactions but the experimental results indicate that the conversion of *erythro* α-bromoepoxides to *E* allylic alcohols by zinc or trialkylstannates shows sufficient stereospecificity to be synthetically useful.

L. D. COREY, S. M. SINGH et A. C. OEHLSCHLAGER. Can. J. Chem. **65**, 1821 (1987).

La réaction des α-haloépoxydes avec de la poudre de zinc ou avec des réactifs contenant l'anion trialkylstannate conduit à des alcools allyliques par une élimination *anti* des liaisons carbone/halogène et carbone adjacent/oxygène de l'époxyde. Dans chacun des types de réactions, il se produit une quantité appréciable d'isomérisation $Z \rightarrow E$; ce résultat indique que la conversion des α-bromo époxydes *érythro* en alcools allyliques *E*, sous l'influence du zinc ou des trialkylstannates, présente suffisamment de stéréospécificité pour être utile d'un point de vue de synthèse.

[Traduit par la revue]

The nucleophilic replacement of halogen by trialkylstannates (reaction *a*) is a well-documented process (1).

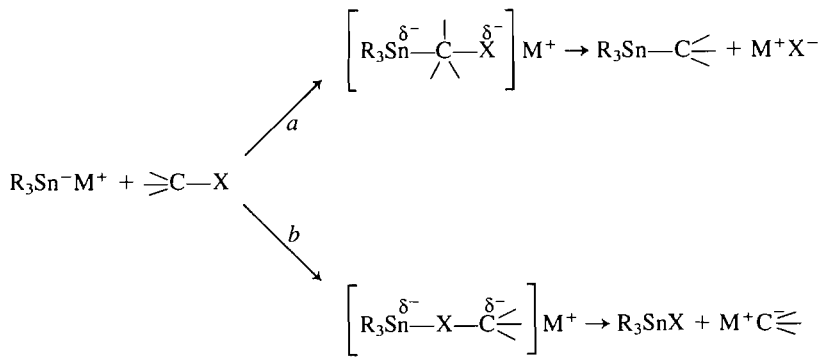

Less well known are the reactions of trialkylstannates with organohalides to give trialkylstannyl halides and organometallics (reaction *b*). Indeed, the latter process would not be expected to proceed in the direction shown unless the carbanionic center in the organic residue were stabilized by an appropriate electron withdrawing group.

Nozaki and co-workers (2) have recently discovered interesting examples of the latter reaction (*b*). His group has shown that α-haloketones (**1***a*) and α-haloesters (**1***b*) rapidly undergo reaction with tributylstannyl-diethylaluminum (**2**) to provide

$$n\text{-}Bu_3Sn\text{—}AlEt_2$$
2

tributyltin bromide (**3**) and the diethylaluminum enolates (**4**) of the dehalogenated α-halocarbonyl compounds. The synthetic utility of this reaction lies in the fact that conversion of **1** to **4** may be conducted in the presence of aldehydes that undergo *in situ* aldol reactions with **4**. The conversion of **1** to **4** was illustrated as a cyclic process (Scheme 1) involving the *syn* conformer of **1**.

The initial goal of the present investigation was to determine if **2** and related trialkylstannates would convert α-haloepoxides (**5**) to allylic alcohols (**6**). The envisioned process involved conversion of α-hydroxyepoxides (**7**) to α-haloepoxides (**5**) (via α-tosylepoxides, **8**) and thence to allylic alcohols (**6**). Such a process when used in conjunction with the Sharpless asymmetric epoxidation (3) of primary alcohols (**5**, $R^1 = R^2 = H$) would potentially allow preparation of chiral secondary alcohols (**6**, $R^1 = R^2 = H$) in yields higher than those achievable through the application of Sharpless kinetic resolution.

The second goal of this study was to compare the stereochemistry of the conversion of **5** ($R^1 \neq R^2$) to **6** ($R^1 \neq R^2$) by powdered zinc (4) with that effected by trialkylstannates. We considered it likely that the former reaction would proceed by an *anti* elimination whereas a trialkylstannate mediated elimination would proceed by a *syn* elimination.

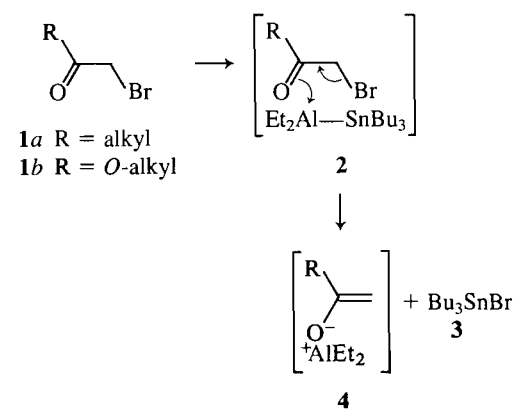

1*a* R = alkyl
1*b* R = *O*-alkyl

2

4

SCHEME 1

Can. J. Chem. Downloaded from www.nrcresearchpress.com by 118.98.75.50 on 09/07/12
For personal use only.

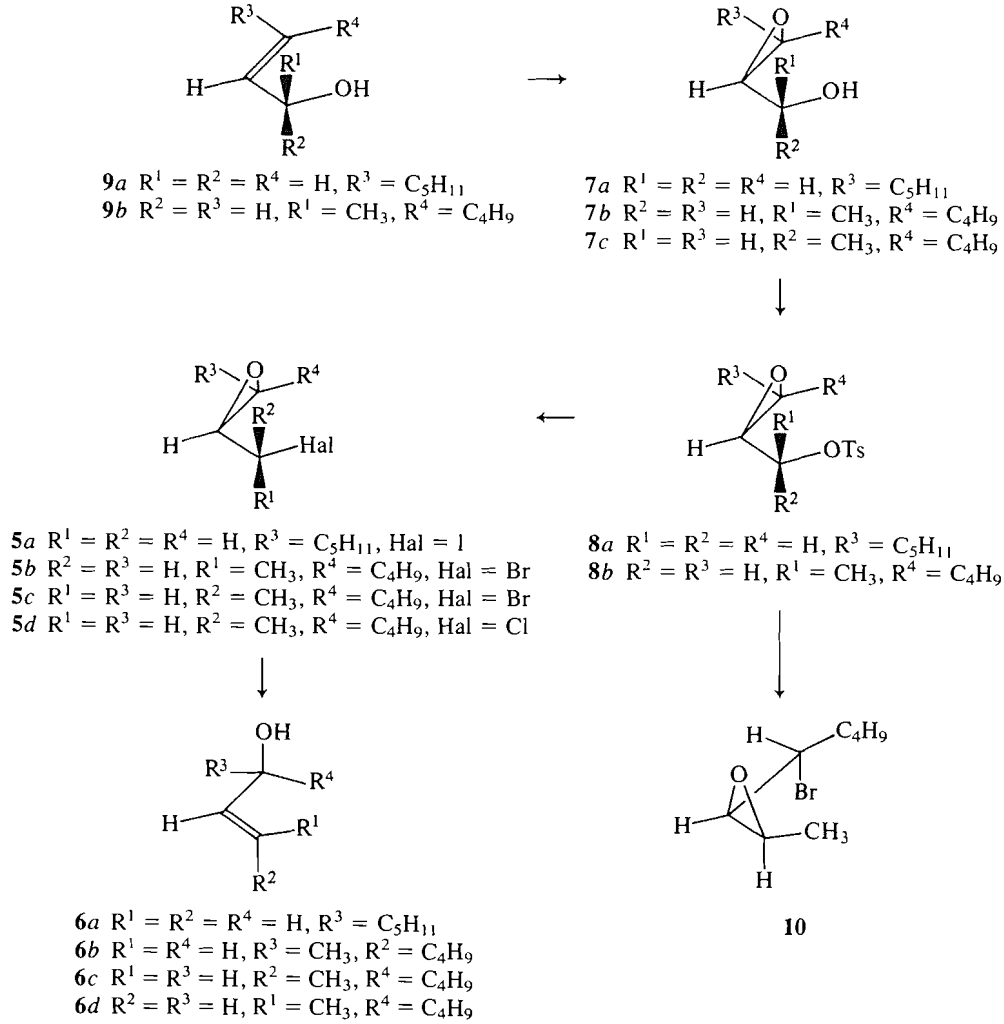

SCHEME 2

Results

We chose the conversion of *E*-2-octen-1-ol (**9***a*) to 1-octen-3-ol (**6***a*) as an initial test of the proposed strategy since the enantiomers of the desired product (**6***a*) were required for biological testing as pheromone synergist for *Oryzaephilus mercator* and *O. surinamensus* (5). Conversion of **9***a* to **5***a* proceeded cleanly for both the racemic series and the chiral series. Epoxidation of **9***a* (6, 7) with *m*-chloroperoxybenzoic acid gave (±)-**7***a* in 87% yield. The chiral enantiomers (2*S*,3*S*)-**7***a* and (2*R*,3*R*)-**7***a* were prepared from **9***a* by reaction under Sharpless asymmetric epoxidation conditions (8) using either (+) or (−)-diisopropyl tartrate as the chiral auxiliary ligand in 91 and 51% yield respectively. Preparation of the Mosher ester ((+)-α-methoxy-α-trifluoromethyl-phenylacetyl derivative) (9) of (2*S*,3*S*)-**7***a* and (2*R*,3*R*)-**7***a* followed by analysis of the resulting diastereoisomeric mixture by capillary gc revealed an enantiomeric excess of 90% for (2*S*,3*S*)-**7***a* and 80% for (2*R*,3*R*)-**7***a*. Racemic **7***a* and each enantiomer were converted to the corresponding tosylates, (±)-**8***a*, (2*S*,3*S*)-**8***a*, and (2*R*,3*R*)-**8***a* by treatment with *p*-toluenesulfonyl chloride and powdered potassium hydroxide in ether to yield 91, 61, and 98% respectively (10). The tosylates were each converted to the corresponding iodides, (±)-**5***a*, (2*R*,3*S*)-**5***a*, and (2*S*,3*R*)-**5***a*, by the reaction with sodium iodide in reagent grade acetone in yields of 91, 90, and 96% respectively (11).

Initially we examined the reaction of (±)-**8***a* with zinc powder and $Bu_3SnAlEt_2$ (**2**) to determine if these reagents would effect the conversion of **8***a* to 1-octen-3-ol (**6***a*). This reaction was of interest because, if successful with either reagent, it would allow the conversion shown in Scheme 2 without generation of the corresponding halogen substrate. Unfortunately, reaction of (±)-**8***a* with zinc powder failed to produce (±)-**6***a*. However, reaction of (±)-**5***a*, (2*R*,3*S*)-**5***a*, and (2*S*,3*R*)-**5***a* with zinc powder gave (±)-**6***a*, (*S*)-**6***a*, and (*R*)-**6***a* respectively in good yields. In the case of the reaction of (2*R*,3*S*)-**5***a*, the chemical yield of the zinc mediated reaction was 85%, and no diminution of chiral purity at C3 was detected during the reaction. In the case of (2*R*,3*S*)-**5***a*, the chemical yield was 75%.

We next examined the reaction of various α-substituted epoxides with $Bu_3SnAlEt_2$ (**2**). Of the several methods available to generate **2**,[1] we chose a route via reaction of tributyltin hydride and lithium diisopropylamide followed by addition of diethylaluminum chloride. We have found this to be the most efficient route to **2** of those reported.[1] Reaction of (±)-**8***a* with **2** in THF failed to give detectable amounts of **6***a*, and we

[1] Bu_3SnLi was prepared by BuLi + $SnCl_2$, Li + Bu_3SnCl, Li + Bu_6Sn_2 (ref. 1*b*), BuLi + Bu_6Sn_2, Li/NH_3 + Bu_3SnCl, Li/NH_3 + Bu_6Sn_2 (ref. 32*a*), and lithium diisopropylamide + Bu_3SnH (refs. 32*b*, 33).

Can. J. Chem. Downloaded from www.nrcresearchpress.com by 118.98.75.50 on 09/07/12
For personal use only.

Can. J. Chem. Downloaded from www.nrcresearchpress.com by 118.98.75.50 on 09/07/12
For personal use only.

recovered good yields of starting material. However, reaction of (±)-**5***a* with **2** gave **6***a* in 74% yield.

To determine the stereochemistry of the zinc powder and trialkylstannate mediated conversion of α-haloepoxides to allylic alcohols observed above, *erythro*-2-bromo-3,4-epoxyoctane, **5***b*, and *threo*-2-bromo-3,4-epoxyoctane, **5***c*, were prepared and subjected to reaction with zinc powder and selected trialkylstannate reagents. The choice of *Z* geometry in the epoxide group of these substrates was dictated by the reported *threo* selectivity of *m*-CPBA in the epoxidation of *Z* secondary allylic alcohols (12); this reaction would easily allow access to *threo*-3,4-epoxy-2-octanol, **7***b*. The reported *erythro* selectivity of the reduction of α-ketoepoxides would allow access to the corresponding *erythro*-3,4-epoxy-2-octanol, **7***c* (13).

The synthesis of **5***b* and **5***c* commenced with reaction of 1-hexynyllithium with ethanol (14) to give 3-octyn-2-ol in 49% yield. This alcohol was reduced to the *Z* allylic alcohol **9***b* by P-2 nickel and hydrogen in nearly quantitative yield (15). Epoxidation of **9***b* with *m*-CPBA gave **7***b*, which exhibited an ^{1}H nmr spectrum consistent with it being *threo*-3,4-epoxy-2-octanol, **7***b*, ($J_{2,3}$ coupling of 8.0 Hz). An epoxide hydrogen coupling ($J_{3,4}$) of 4.3 Hz indicated a *Z* epoxide.[2] The tosylate, **8***b*, was prepared by reaction of **7***b* with *p*-toluenesulfonyl chloride and potassium hydroxide in ether (10). When **8***b* was reacted with lithium bromide in acetone (11), the expected product was not obtained; instead the product of an S_N2' reaction, *threo*-4-bromo-2,3-epoxyoctane **10**, was obtained in 41% yield.

The structure **10** was verified by comparison of the calculated ^{1}H nmr chemical shifts of the hydrogens on the epoxide bearing carbons (δ 3.55 and 3.80 ppm) and for the hydrogen on the carbon bearing the bromine (4.23 ppm) (16) with the observed chemical shifts (3.14, 3.28, 3.77 ppm respectively). Associated coupling indicated these hydrogens to be on C3, C2, and C4 respectively. The observed coupling of 4.1 Hz for $J_{2,3}$ indicates that **10** has the *Z*-2,3 geometry.[2] *Threo* stereochemistry of the product is assigned since substitution of bromide at C4 would be expected to proceed with inversion as should tosylate displacement by oxygen at C2.

Reaction of **10** with zinc powder in methanol gave *E*-3-octen-2-ol, **6***b*, in 81% yield, which was independently generated by reduction of 3-octyn-2-ol with lithium tetrahydridoaluminate. The conversion of **10** to **6***b* by zinc powder requires the transformation to proceed via a formal *syn* elimination of the leaving groups. We suspect the elimination was actually *anti*, and **6***b* was formed by subsequent isomerization of the initially formed *Z* isomer of **6***b*.

The conversion of **7***b* to *erythro*-2-bromo-3,4-epoxyoctane, **5***b*, was achieved using Mitsunobu conditions in 49% yield (17). The observed ^{1}H nmr coupling constant between the C2 and C3 hydrogens for **5***b* is 8.9 Hz. Reaction of **5***b* with zinc powder produced a **6***c*:**6***d* ratio of 95:5. The ratio of **6***c* to **6***d* was determined by ^{1}H nmr analysis of the isolated mixture and by gc analysis. There was approximately 5% of **5***c* that could be found in **5***b*.

Authentic samples of **6***c* and **6***d* were prepared independently by reduction of 2-octyn-4-ol (14) with lithium tetrahydridoaluminate to give **6***c* or by P-2 nickel to give **6***d* (10).

[2]For (*Z*)-*threo*-3,4-epoxy-2-pentanol, the $J_{3,4}$ coupling is 4.3 Hz, and for (*E*)-*threo*-3,4-epoxy-2-pentanol, the $J_{3,4}$ coupling is 2.2 Hz (ref. 34).

To prepare *threo*-2-bromo-3,4-epoxyoctane (**5***c*), **7***b* was oxidized (71%) to *Z*-3,4-epoxy-2-octanone with oxalyl chloride in dimethylsulfoxide (18). *Erythro* selective reduction of this ketoepoxide with zinc borohydride (13) gave **7***c* in 88% yield. This product was assigned *erythro* stereochemistry on the basis of its ^{1}H nmr spectrum, which exhibited a $J_{2,3}$ coupling of 7.7 Hz. Comparison of the ^{1}H nmr spectra of **7***b* and **7***c* revealed that the chemical shifts of the hydrogens on C2, C3, and C4 are different and integration could be used to determine the *threo*:*erythro* ratio. The *threo*:*erythro* ratio for **7***b* is 94:6 and that for **7***c* is 4:96.

Conversion of **7***c* to the desired bromoepoxide, **5***c*, was achieved using hexamethylphosphorous triamide (HMPT) and carbon tetrabromide (CBr_4) at −78°C (19). The observed C2H–C3H coupling in the ^{1}H nmr of **5***c* is 9.4 Hz. Reaction of **5***c* with zinc powder produced a **6***c*:**6***d* ratio of 89:11. We also converted **7***c* to the corresponding chloride (**5***d*) by reaction with triphenylphosphine in carbon tetrachloride (CCl_4) in 62% yield (20). Subsequent reactions of **5***d* with zinc powder and $Bu_3SnAlEt_2$ resulted in recovered starting material without a trace of the expected product.

Most likely the zinc powder conversion of α-haloepoxides, **5***b* and **5***c*, to allylic alcohols, **6***c* and **6***d*, proceeds by *anti* elimination of the departing groups and, in the case of conversion of **5***c*, isomerization of the expected initial product (**6***d*) occurs.

The results of our study of the reaction of α-haloepoxides **5***b* and **5***c* with various trialkylstannates are shown in Table 1. Reaction of **5***b* or **5***c* with *n*-$Bu_3SnAlEt_2$ (**2**) gave predominantly **6***c* (Entries 1 and 2). *Anti* elimination of the departing groups in **5***b* would be expected to give **6***c*, which was in fact obtained in high (1:99) stereochemical purity from this reaction. Conversion of **5***c* by **2** to a mixture rich (11:89) in **6***c* suggested initial conversion to **6***d* followed by isomerization to **6***c*. Indeed, in an independent experiment **6***d* was shown to isomerize to a 1:1 mixture of **6***c* and **6***d* when treated with **2** at 0°C for 1 h. Entry 3 shows the failure of attempts to avoid the isomerization of **6***d* to **6***c* by conducting the reaction of **5***c* with **2** with BF_3–Et_2O as a Lewis acid catalyst. When the reaction shown in this entry was conducted below room temperature, no reaction occurred over 12 h.

The conversion of α-haloepoxides **5***b* and **5***c* to allylic alcohols **6***c* and **6***d* is also efficient with Bu_3SnLi, **11** (Entries 4–8). Conversion to products is most efficient when two molar equivalents of stannate reagent are used (compare Entries 4–7). As with **2**, conversion of **5***c* to **6***d* by **11** was accompanied by isomerization to **6***c*.

Reaction of Bu_2SnLi (**11**) with *B*-methoxy-9-borabicyclo-[3.3.1]nonane yields the stannylborate reagent, **12** (21). Reac-

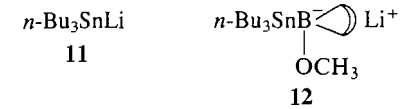

tion of **12** with **5***b* was carried out at 65°C for 4 h to provide **6***c* (Entries 9, 10). Conversion of **5***c* to **6***d* by **12** also required heating and gave isomerization to **6***c* (Entry 11).

The most efficient stannate induced conversion of α-haloepoxides to allylic alcohols investigated utilized Bu_3SnLi **11**. Reactions with this reagent were the most rapid and gave the cleanest products upon work-up.

The observation that α-tosylepoxide, **8***a*, and α-chloroepoxide, **5***d*, failed to react with $Bu_3SnAlEt_2$ (**2**) whereas

TABLE 1. Reaction of Bu_3SnM with α-haloepoxides **5***b* and **5***c*

Entry	Compound	nBu_3SnM (Molar ratio)	Reaction conditions (°C, h)	Conversion[b] (%)	Yield (%)	Product ratio[b] **6***d*:**6***c*
		$nBu_3SnAlEt_2$ (**2**)				
1	**5***b*	(1:2)	0, 1	100	60	<1:99
2	**5***c*	(1:15)	0 to 25, 18	100	70	11:89
3	**5***c*	(1:1)[a]	25, 12	100	C	11:89
		nBu_3SnLi (**11**)				
4	**5***b*	(1:1.1)	−20, 1	25		
5	**5***b*	(1:1.5)	−20, 1	73		
6	**5***b*	(1:2)	−20, 1	100	84	<1:99
7	**5***b*	(1:3)	−20, 1	100	82	<1:99
8	**5***c*	(1:2)	−20 to −15, 1	100	81	11:89
		nBu_3SnB[d] (**12**)				
9	**5***b*	(1:2)	−20 to 25, 12	37		
10	**5***b*	(1:2)	65, 4	100	75	<1:99
11	**5***c*	(1:2.5)	65, 6	100	78	11:89

[a]$BF_3 \cdot OEt_2$ (2 equiv.) was added.
[b]Conversion and the product ratio (*Z*-**6***d*:*E*-**6***c*) were determined on capillary gc.
[c]Product was not isolated.
[d]Bu_3SnB reagent was prepared by the treatment of Bu_3SnLi with *B*-methoxy-9-borabicyclo[3.3.1]nonane.

α-iodoepoxide, **5***a*, and α-bromoepoxides **5***b* and **5***c* underwent smooth reaction with this reagent suggests to us that stannate mediated conversion of α-haloepoxides to allylic alcohols (Scheme 2) proceeds via attack of stannate anion on halogen (Scheme 1, reaction *b*). The alternative possibility that stannate anion attack occurs at the epoxide carbon adjacent to the α-halogen followed by rapid elimination of stannyl halide cannot be ruled out.

Experimental

General procedures

Routine gc analyses were run on a Hewlett–Packard 5880A gas chromatograph using a DB-1 capillary column (0.2 mm id × 15 m) and suitable temperature control programs. Infrared spectra were determined on a Perkin–Elmer 599B spectrophotometer. Samples were run as neat films between NaCl plates or as KBr pellets. The CH stretching and CH bending absorptions are not reported for ir spectra. The ^1H nmr spectra were recorded on a Bruker 400 WM nmr spectrometer in $CDCl_3$ using the residual $CHCl_3$ for internal standard. Low resolution mass spectra were obtained either via direct insertion or via gc inlet on a Hewlett–Packard 5985B coupled gas chromatograph/mass spectrometer. All samples were run using an electron impact ionization voltage of 70 eV. All reactions requiring anhydrous and (or) oxygen-free conditions were conducted with a positive pressure of argon or nitrogen in flame-dried glassware. Tetrahydrofuran was freshly distilled from sodium or potassium metal with benzophenone as an indicator. Methylene chloride was dried by distillation over P_2O_5 or CaH_2. Acetonitrile was dried by distillation from CaH_2 and stored over 4A molecular sieves. Pyridine was dried by distillation and storing over KOH. Dimethylformamide was dried by distillation and stored over 4A molecular sieves. All boiling points and melting points are uncorrected. The enantiomeric excess of the chiral alcohols was determined by gc analysis of the derivatives of (+)-α-methoxy-α-trifluoromethylphenylacetic acid (MPTA).

Preparation of E-*2,3-epoxy-1-octanol ((±)-7*a)

This was obtained in 87% yield from *E*-2-octen-1-ol (6, 7) and 85% *m*-chloroperoxybenzoic acid, mp 28–29°C (lit. (22) mp 33–34°C).

*Preparation of (2*S*,3*S*)-2,3-epoxy-1-octanol ((2*S*,3*S*)-7*a)

To 18.2 mL (19.1 g, 67.2 mmol) of $Ti[OCH(CH_3)_2]_4$ in 200 mL of dry CH_2Cl_2 at −23°C (Dry Ice/CCl_4 bath) under argon was added 18.3 mL (16.4 g, 70 mmol) of diisopropyl L(+)-tartrate in 20 mL of dry CH_2Cl_2. After 10 min, 8.5 g (66.3 mmol) of **9***a* dissolved in 10 mL of dry CH_2Cl_2, followed by 135 mmol of dry *tert*-butylhydroperoxide (23) in CH_2Cl_2, was added to the solution and stirred for 10 min. The reaction was placed in the freezer at −23°C until complete, and quenched by dilution with 200 mL of ether and 18.2 mL of saturated aqueous Na_2SO_4 solution. The quenched reaction mixture was filtered through a bed of Celite and the filtrate was mixed with 100 mL of saturated aqueous NaCl in 2 *M* NaOH. The organic layer was separated and the aqueous layer was extracted with ether (4 × 50 mL), dried ($MgSO_4$), filtered, and concentrated *in vacuo* to give a liquid that crystallized upon refrigeration to yield 91% (8.66 g) of (2*S*,3*S*)-**7***a*, mp 33–34.5°C. The spectroscopic data were in agreement with those given for (±)-**7***a*. To 100 mg (0.69 mmol) of (2*S*,3*S*)-**7***a* in 1 mL of CH_2Cl_2 were added 5 drops of dry C_6H_5N and 200 mg (0.79 mmol) of MTPA-Cl. The solution was stirred to react overnight, then washed with 1 mL of H_2O. Gas chromatographic analysis of the organic layer showed two diastereoisomers of the ester in the ratio of 5:95 (R_t 10.5 and 10.24, 160°C isothermal). The molecular ions of the diastereoisomers were confirmed by CI/gc/ms.

*Preparation of (2*R*,3*R*)-7*a

The procedure was identical to that described above for the preparation of (2*S*,3*S*)-**7***a* except that diisopropyl D(−)-tartrate was used. The crude product was purified by chromatography on a silica gel column using hexane:ethyl acetate (1:1) as eluent to yield 51% (4.4 g) of (2*R*,3*R*)-**7***a* from **9***a*, mp 34–35°C. The spectroscopic data were in agreement with those given for (±)-**7***a*. Gas chromatographic analysis of the MTPA-ester of (2*R*,3*R*)-**7***a* showed two diastereoisomers of the ester in the ratio of 90:10 (R_t 10.05 and 10.24, 160°C isothermal). The molecular ions of the diastereoisomers were confirmed by CI/gc/ms.

Preparation of E-*2,3-epoxy-1-octanyl tosylate ((±)-8*a)

To 9.7 g (67.3 mmol) of (±)-**7***a* in 150 mL of anhydrous ether at −10°C was added 14.18 g (74.4 mmol, 1.1 equiv.) of *p*-toluenesulfonyl chloride and 47.5 g (338 mmol, 5 equiv.) of powdered KOH, which was divided in 5 portions and added over 20 min, keeping the temperature below 0°C. The solution was stirred at 0°C for 30 min and then poured into 400 mL of ice water. The organic layer was separated and the aqueous layer was extracted with ether (3 × 75 mL). The combined organic extract was backwashed with brine (2 × 50 mL),

Can. J. Chem. Downloaded from www.nrcresearchpress.com by 118.98.75.50 on 09/07/12
For personal use only.

dried ($MgSO_4$), filtered, and concentrated *in vacuo* to give a crystalline solid (18.3 g, 91%), mp 23–25°C; ir (KBr pellet): 1360, 1180, 960, 815, 770, 670, and 560 cm^{-1}; ^1H nmr ($CDCl_3$) δ: 0.87 (3H, C(8), t, J = 6.7 Hz), 1.28 (4H, C(7), C(6), m), 1.37 (2H, C(5), m), 1.50 (2H, C(4), m), 2.43 (3H, $ArCH_3$, s), 2.76 (1H, C(3), dt, J = 2.1, 11.1 Hz), 2.93 (1H, C(2), ddd, J = 2.1, 3.7, 6.0 Hz), 3.96 (1H, C(1)H(a), dd, J = 6.6, 12.0 Hz), 4.17 (1H, C(1)H(b), dd, J = 3.5, 12.0 Hz), 7.34 (2H, Ar, d, J = 8.0 Hz), 7.78 (2H, Ar, d, J = 8.0 Hz); ms, *m/e* (%, relative intensity): 155 (100%), 91 (57%), 55 (12%). *Anal.* calcd. for $C_{15}H_{22}O_3S$: C 60.38, H 7.43; found: C 60.43, H 7.67.

Preparation of (2S,3S)-8a

The procedure was identical to that described above for the preparation of (±)-**8***a*, except that (2*S*,3*S*)-**7***a* was used. The yield of (2*S*,3*S*)-**8***a* was 61% (10 g). The spectroscopic data were in agreement with those given above for (±)-**8***a*.

Preparation of (2R,3R)-8a

The procedure was identical to that described above for the preparation of (±)-**8***a*, except that (2*R*,3*R*)-**7***a* was used. The yield of (2*R*,3*R*)-**8***a* was 98% (8.7 g), mp 23–25°C. The spectroscopic data were in agreement with those given above for (±)-**8***a*.

Preparation of E-2,3-epoxy-1-iodooctane ((±)-7a)

To 10.0 g (33.5 mmol) of (±)-**8***a* in 200 mL of dry acetone was added 10.1 g (67 mmol, 2 equiv.) of dry NaI and the solution was stirred for 3 h. The solution was filtered and the filtrate concentrated to yield yellow crystals. The crystals were dissolved in a pentane:water (50 mL:50 mL) mixture. The organic layer was separated and the aqueous layer was extracted with pentane (4 × 50 mL). The combined organic extract was dried ($MgSO_4$), filtered, and concentrated *in vacuo* to give a liquid that crystallized upon refrigeration, mp 22.5–25°C. The yield of (±)-**5***a* was 97% (8.2 g); ir (KBr pellet): 1723, 1250, 1180, 892, 815, 750, 670, 610, and 560 cm^{-1}; ^1H nmr ($CDCl_3$) δ: 0.93 (3H, C(8), t, J = 6.7 Hz), 1.36 (4H, C(7), C(6), m), 1.47 (2H, C(5), m), 1.57 (2H, C(4), m), 2.81 (1H, C(3), dt, J = 1.8, 5.5 Hz), 3.03 (2H, C(2), C(1)H(a), m), 3.27 (1H, C(1)H(b), dd, J = 4.8, 8.9 Hz); ms, *m/e* (%, rel. int.): 127 (87%), 83 (100%), 57 (32%), 55 (86%), 41 (19%). *Anal.* calcd. for $C_8H_{15}IO$: C 37.81, H 5.95; found: C 38.07, H 6.00.

Preparation of (2R,3S)-5a

The procedure was identical to that described above for the preparation of (±)-**5***a* except that (2*S*,3*S*)-**8***a* was used. The yield of (2*R*,3*S*)-**5***a* was 90% (6.9 g), mp 23–25°C. The spectroscopic data were in agreement with those given above for (±)-**5***a*.

Preparation of (2S,3R)-5a

The procedure was identical to that described above for the preparation of (±)-**5***a* except that (2*R*,3*R*)-**8***a* was used. The yield of (2*S*,3*R*)-**5***a* was 96% (6.9 g), mp 23.5–26°C. The spectroscopic data were in agreement with those given above for (±)-**5***a*.

Preparation of (S)-1-octen-3-ol ((S)-6a) by reaction of (2R,3S)-5a with zinc powder

To 6.5 g (25.6 mmol) of (2*R*,3*S*)-**5***a* in 125 mL of absolute methanol was added 5.02 g (76.8 mmol, 3 equiv.) of powdered zinc and the solution was refluxed for 3 h. After cooling, 125 mL of pentane was added and the solution was filtered, backwashed with saturated aqueous NaCl solution (2 × 50 mL), dried ($MgSO_4$), filtered, and concentrated *in vacuo* to give 85% (2.8 g) of (*S*)-**6***a* as a liquid. The spectroscopic data were in agreement with those reported for (±)-**6***a* (24–26), bp 62.5–63.5°C (1.25 Torr; 1 Torr = 133.3 Pa). Gas chromatographic analysis of the MTPA-ester of (*S*)-**6***a* showed two diastereoisomers of the ester in the ratio of 96:4. The molecular ions of the diastereoisomers were confirmed by CI/gc/ms.

Preparation of (R)-1-octen-3-ol, (R)-6a

The procedure was identical to that described above for the preparation of (*S*)-**6***a*, except that (2*S*,3*R*)-**5***a* was used (2.6 g, 75%). The spectroscopic data were in agreement with those reported for (±)-**6***a*, bp 65–66°C (1.25 Torr); gc analysis of the MTPA-ester of (*R*)-**6***a* showed two diastereoisomers of the ester in the ratio of 90:10. The molecular ions of the diastereoisomers were confirmed by CI/gc/ms.

Preparation of 1-octen-3-ol ((±)-6a)

The procedure described above was applied using (±)-**5***a* and zinc powder, bp 50°C (0.25 Torr) (lit. (24) bp 62–65°C (1 Torr)) to yield 80% (61 mg) of (±)-**6***a*. The ^1H nmr (25) and ir (26) spectra were in agreement with those previously reported.

Preparation of 1-octen-3-ol ((±)-6a), by reaction of (±)-5a with $Bu_3SnAlEt_2$ (2)

To the LDA (10 mmol) (freshly prepared) in THF, was added 2.64 mL (10 mmol) of nBu_3SnH in 2.5 mL of THF at −70°C. The reaction was maintained at −78°C for 2 h and 10 mL of Et_2AlCl (1 *M*, 10 mmol) was slowly added. The temperature was increased to 0°C and maintained at this temperature for 1 h.[1] At this point, 2.55 g (10 mmol) of (±)-**5***a* in 5 mL of dry THF was added and the reaction was stirred for 1 h. The reaction was quenched with 10 mL of 1 *M* HCl, the organic layer was separated out, and the aqueous layer was extracted with ether (4 × 10 mL). The combined organic extract was dried ($MgSO_4$), filtered, and concentrated *in vacuo* to give a crude concentrate. The concentrate was purified by chromatography on a silica gel column using hexane:ethyl acetate (4:1) as eluent. The yield of (±)-**6***a* was 74% (0.94 g).

Preparation of Z-3-octen-2-ol (9b)

To 2.64 g (10.6 mmol) of $Ni(OAc)_2 \cdot 4H_2O$ in 50 mL of 95% ethanol with H_2 purge was added 10 mL (14.2 mmol) of a solution containing 0.5 g of $NaBH_4$ in 12 mL of absolute ethanol and 0.65 mL of 2 *M* NaOH. After 5 min, 1.6 mL (23.9 mmol) of ethylenediamine was added, followed by 11.5 g (91.1 mmol) of 3-octyn-2-ol (27). The reaction was stirred for 4 h under H_2 purge and monitored by gc analysis of aliquots. Just prior to total conversion, the reaction was quenched with 100 mL of brine and acidified with 1 *M* HCl (≈50 mL). The solution was extracted with ether (4 × 50 mL). The combined organic extract was backwashed with brine, with 2 mL of 1 *M* HCl, dried ($MgSO_4$), filtered, and concentrated *in vacuo* to provide 98% (11.5 g) of **9***b* as a liquid, bp 80–81°C (20 Torr) (lit. (27) bp 82°C (21 Torr)); ir (27) (film): 3360, 1712, 1280, 1110, 1055, 922, and 740 cm^{-1}; ^1H nmr ($CDCl_3$) δ: 0.91 (3H, C(8), t, J = 6.7 Hz), 1.25 (3H, C(1), d, J = 5.3 Hz), 1.35 (4H, C(7), C(6), m), 1.81 (1H, OH, br), 2.08 (2H, C(5), m), 4.65 (1H, C(2), quint, J = 6.7 Hz), 5.42 (2H, C(4), C(3), m); ms, *m/e* (%, rel. int.): 113 (31%), 110 (20%), 71 (100%), 68 (15%), 58 (32%), 57 (52%), 45 (29%), 43 (77%), 41 (33%).

Preparation of threo-3,4-epoxy-2-octanol (7b)

To 18.2 g (85.8 mmol) of 85% *m*-chloroperoxybenzoic acid (12) in 200 mL of CH_2Cl_2 at 0°C was added 11 g (85.8 mmol) of **9***b* in 10 mL of CH_2Cl_2. The solution was warmed to room temperature and stirred for 2 h. The reaction was quenched with 200 mL of saturated Na_2CO_3 and stirred for 1 h. The organic layer was separated and the aqueous layer extracted with pentane (4 × 50 mL). The combined organic extract was dried ($MgSO_4$), filtered, and concentrated *in vacuo* to give 95% (12.5 g) of **7***b* as a liquid, bp 60°C (0.2 Torr); ir (film): 3440, 1725, 1575, 1285, 1262, 1110, 1072, 900, 887, 828, 812, 758, and 735 cm^{-1}; ^1H nmr ($CDCl_3$) δ: 0.93 (3H, C(8), t, J = 7.3 Hz), 1.28 (3H, C(1), d, J = 7.0 Hz), 1.40 (4H, C(7), C(6), m), 1.57 (2H, C(5), m), 2.00 (1H, OH, br), 2.89 (1H, C(3), dd, J = 4.3, 8.0 Hz), 3.05 (1H, C(4), m), 3.67 (1H, C(2), d quint, J = 1.5, 7.0 Hz). From decoupling experiments, $J_{2,3}$ = 8.0 Hz; ms, *m/e* (%, rel. int.): 69 (49%), 58 (100%), 57 (58%), 55 (18%), 45 (37%), 43 (49%), 41 (46%).

Preparation of threo-3,4-epoxy-2-octanyl tosylate (8b)

To 11 g (76.3 mmol) of **7***b* in 150 mL of anahydrous ether at −10°C was added 15.8 g (82.7 mmol, 1.1 equiv.) *p*-toluenesulfonyl chloride and 21.4 g (381 mmol, 5 equiv.) of powdered KOH divided in five portions that were added over 20 min. The solution was stirred for 1 h and quenched with ice water. The organic layer was separated, and the

Can. J. Chem. Downloaded from www.nrcresearchpress.com by 118.98.75.50 on 09/07/12
For personal use only.

Can. J. Chem. Downloaded from www.nrcresearchpress.com by 118.98.75.50 on 09/07/12
For personal use only.

aqueous layer was extracted with ether (3 × 50 mL). The combined organic extract was backwashed with brine, dried ($MgSO_4$), filtered, and concentrated *in vacuo* without heating to give a liquid that crystallized upon refrigeration (mp 21–22°C). The yield of **8***b* was 83% (18.9 g); ir (KBr pellet): 1725, 1600, 1365, 1195, 1180, 910, 820, 790, 670, 580, and 562 cm^{-1}; ^1H nmr ($CDCl_3$) δ: 0.90 (3H, C(8), t, J = 6.7 Hz), 1.38 (4H, C(7), C(6), m), 1.44 (3H, C(1), d, J = 6.7 Hz, 2H, C(5), m), 2.44 (3H, $ArCH_3$, s), 2.92 (2H, C(4), C(5), m), 4.42 (1H, C(2), quint, J = 6.7 Hz), 7.33 (2H, Ar, d, J = 7.3 Hz), 7.83 (2H, Ar, d, J = 7.3 Hz); ms, *m/e* (%, rel. int.): 241 (4.5%), 212 (4.8%), 155 (83%), 127 (19%), 91 (100%), 69 (43%), 65 (50%), 57 (24%), 55 (19%), 43 (45%), 41 (85%). *Anal.* calcd. for $C_{15}H_{22}O_3S$: C 60.38, H 7.43; found: C 60.34, H 7.65.

Preparation of threo-*4-bromo-2,3-epoxyoctane (**10**)*

To 3.11 g (10.4 mmol) of **8***b* in 50 mL of dry acetone was added 7.22 g (83.3 mmol, 8 equiv.) of LiBr and the solution was stirred overnight in a darkened flask. Then 20 mL of water and 10 mL of pentane were added and the solution was stirred for 10 min. The organic layer was separated and the aqueous layer was extracted with pentane (4 × 10 mL). The combined organic extract was washed twice with water, dried ($MgSO_4$), and concentrated *in vacuo* to give a liquid that was purified by chromatography on a silica gel column using hexane:ethyl acetate (6:1) as eluent. The yield of **10** was 55% (1.19 g); bp 45–46°C (0.01 Torr); ir (film): 1725, 1260, 1185, 1120, 1060, 980, 930, 825, 755, 740, 705, and 645 cm^{-1}; ^1H nmr ($CDCl_3$) δ: 0.92 (3H, C(8), t, J = 7.3 Hz), 1.30 (3H, C(1), d, J = 5.6 Hz), 1.42 (4H, C(6), C(7), m), 1.83 (1H, C(5)H(a), m), 1.91 (1H, C(5)H(b), m), 3.14 (1H, C(3), dd, J = 4.0, 9.6 Hz), 3.28 (1H, C(2), qd, J = 4.1, 5.6 Hz), 3.77 (1H, C(4), ddd, J = 5.5, 8.0, 9.6 Hz); ms, *m/e* (%, rel. int.): 127 (75%), 109 (13%), 85 (22%), 83 (30%), 71 (13%), 69 (28%), 67 (15%), 57 (38%), 55 (100%), 45 (17%), 43 (30%), 41 (55%). *Anal.* calcd. for $C_{15}H_{22}BrO$: C 46.39, H 7.30; found: C 46.82, H 7.60.

Preparation of E-*3-octen-2-ol (**6**b) by reaction of **10** with zinc powder*

To 0.50 g (2.41 mmol) of **10** in 10 mL of absolute methanol was added 0.47 g (7.23 mmol, 3 equiv.) of powdered zinc and the solution was refluxed for 5 h. The flask was cooled to room temperature, then 5 mL of ether and 4 mL of 2 *M* HCl were added sequentially. The organic layer was separated and the aqueous layer was extracted with ether (3 × 10 mL). The combined organic extract was backwashed with brine, dried ($MgSO_4$), filtered, and concentrated *in vacuo* to give 81% (0.25 g) of **6***b* as a liquid, bp 79–81°C (12 Torr) (lit. (27) bp 82.3–83°C (15 Torr)); ir (27) (film): 3370, 1740, 1675, 1300, 1265, 1155, 1130, 1070, 975, 955, 927, 758, and 745 cm^{-1}; ^1H nmr ($CDCl_3$) δ: 0.84 (3H, C(8), t, J = 8.1 Hz), 1.20 (3H, C(1), d, J = 7.5 Hz), 1.29 (4H, C(6), C(7), m), 1.96 (2H, C(5), q, J = 7.8 Hz), 4.19 (1H, C(2), quint, J = 7.5 Hz), 5.45 (1H, C(3), tdd, J = 1.5, 7.5, 15.3 Hz), 5.57 (1H, C(4), dtd, J = 0.8, 7.5, 15.3 Hz); ms, *m/e* (%, rel. int.): 128 (0.4%), 113 (1.8%), 110 (0.6%), 85 (13%), 71 (100%), 59 (20%), 57 (38%), 55 (15%), 45 (15%), 43 (64%), 41 (37%).

Preparation of erythro-*2-bromo-3,4-epoxyoctane (**5**b)*

To 2.88 g (20 mmol) of **7***b* and 10.66 g (40 mmol, 2 equiv.) of triphenylphosphine in 100 mL of dry THF were added 2.25 g (10 mmol, 0.5 equiv.) of $ZnBr_2$ and 5.70 mL (40 mmol, 2 equiv.) of diisopropylazodicarboxylate in 50 mL of dry THF. The reaction was stirred for 3 h and then passed through a silica gel column using hexane as eluent to remove the inorganic by-products. The yield of **5***b* was 49% (2.01 g), bp 41–43°C (0.1 Torr); ir (film): 1780, 1270, 1250, 1175, 1005, 945, 920, 820, 810, and 640 cm^{-1}; ^1H nmr ($CDCl_3$) δ: 0.94 (3H, C(8), t, J = 7.3 Hz), 1.85 (3H, C(1), d, J = 6.8 Hz), 2.47 (6H, C(5), C(6), C(7), m), 3.06 (1H, C(4), td, J = 4.5, 7.5 Hz), 3.13 (1H, C(3), dd, J = 4.0, 9.5 Hz), 3.71 (1H, C(2), qd, J = 6.5, 9.5 Hz); ms, *m/e* (%, rel. int.): 127 (62%), 71 (38%), 69 (100%), 57 (18%), 41 (18%). *Anal.* calcd. for $C_{15}H_{22}BrO$: C 46.39, H 7.30; found: C 46.61, H 7.66.

*Reaction of **5**b with zinc powder*

To 0.50 g (2.41 mmol) of **5***b* in 15 mL of absolute methanol was added 0.47 g (7.23 mmol, 3 equiv.) of powdered zinc and the solution was refluxed for 3 h. The flask was cooled to room temperature and 5 mL of ether and 4 mL of 2 *M* HCl were added. The organic layer was separated and the aqueous layer was extracted with ether (3 × 10 mL). The combined organic extract was backwashed with saturated aqueous $NaHCO_3$ (2 × 10 mL). The ether extract was dried ($MgSO_4$), filtered, and concentrated *in vacuo* to give 68% (0.21 g) of **6***c* as a liquid, bp 120°C (15 Torr) (lit. (28) bp 91°C (11 Torr)); ir (28) (film): 3370, 1680, 1320, 1150, 1080, 1050, 1030, 1010, 972, 905, and 738 cm^{-1}; ^1H nmr (28) ($CDCl_3$) δ: 0.91 (3H, C(8), t, J = 7.4 Hz), 1.34 (4H, C(7), C(6), m), 1.50 (3H, C(5), OH, m), 1.72 (3H, C(1); dd, J = 1.7, 7.4 Hz), 4.02 (1H, C(4), q, J = 7.4 Hz), 5.48 (1H, C(3), qdd, J = 1.7, 7.2, 15.4 Hz), 5.66 (1H, C(2), dqd, J = 1.0, 7.4, 15.2 Hz); ms, *m/e* (%, rel. int.): 128 (0.4%), 113 (2.0%), 99 (1.0%), 95 (1.5%), 86 (18%), 71 (100%), 43 (10%).

Preparation of Z-*2-octen-4-ol (**6**d) from 2-octyn-4-ol*

To 2.49 g (10 mmol) of $Ni(OAc)_2 \cdot 4H_2O$ in 50 mL of 95% ethanol with H_2 bubbling through the solution was added 10 mL of a solution comprised of 0.5 g $NaBH_4$, 12 mL of 100% ethanol, and 0.65 mL 2 *M* NaOH. After 5 min, 1.6 mL (23.9 mmol) of ethylenediamine was added. This was followed by the addition of 1.0 g (7.92 mmol) of 2-octyn-4-ol (28). The reaction was followed by gc analysis of aliquots. After completion, the solution was diluted with 20 mL of saturated aqueous NaCl, acidified with 2 *M* HCl, and the layers were separated. The aqueous layer was extracted with ether (2 × 10 mL) and the combined extract was backwashed with brine, dried ($MgSO_4$), filtered, and concentrated *in vacuo* to yield 80% (0.83 g) of **6***d*, bp 64.5–67°C (18 Torr) (lit. (28) bp 63–65°C (20 Torr)). The ^1H nmr and ir spectra corresponded to those previously reported (28).

Preparation of Z-*3,4-epoxy-2-octanone*

To 6.35 mL (69 mmol) of oxalyl chloride in 50 mL of CH_2Cl_2 at −60°C was added 10.7 mL (138 mmol) of dry DMSO in 10 mL of CH_2Cl_2. After 2 min, 9 g (63 mmol) of **7***b* in 10 mL of CH_2Cl_2 was slowly added. After 15 min, 50 mL (357 mmol) of Et_3N was added and the reaction stirred for 5 min. It was warmed to room temperature and diluted with 100 mL of H_2O. The layers were separated, and the aqueous layer was extracted with hexane (2 × 30 mL). The combined extract was washed with saturated aqueous NaCl, 1 *M* HCl until acidic, H_2O, 5% aqueous Na_3CO_3 until basic, and finally H_2O. The organic layer was dried ($MgSO_4$), filtered, and concentrated *in vacuo* to give a liquid that distilled at 35°C (0.10 Torr) (lit. (29) bp 55–56°C (2 Torr)) to yield 71% (6.4 g) of Z-3,4-epoxy-2-octanone. The mass spectrum corresponded to that previously reported (30).

Preparation of erythro-*3,4-epoxy-2-octanol (**7**c)*

To 6 g (42.2 mmol) of Z-3,4-epoxy-2-octanone in 40 mL ether at 0°C under argon was added 88.6 mL (≈21.1 mmol) of $Zn(BH_4)_2$ (31). After 1 h the reaction was quenched with 20 mL of 1 *M* HCl and the organic layer was separated, dried ($MgSO_4$), filtered, and concentrated *in vacuo* to give 88% yield (5.35 g) of **7***c*, bp 66°C (0.45 Torr); ir (film): 3430, 1270, 1105, 1065, 955, and 810 cm^{-1}; ^1H nmr ($CDCl_3$) δ: 0.96 (3H, C(8), t, J = 7.3 Hz), 1.37 (3H, C(1), d, J = 7.0 Hz), 1.49 (7H, C(5), C(6), C(7), OH, m), 2.82 (1H, C(3), dd, J = 4.1, 7.7 Hz), 3.01 (1H, C(4), ddd, J = 4.0, 5.2, 7.0 Hz), 3.73 (1H, C(2), br, d quint, J = 1.9, 6.5 Hz). From decoupling experiments, $J_{2,3}$ = 7.7 Hz; ms, *m/e* (%, rel. int.): 69 (69%), 58 (100%), 57 (50%), 55 (18%), 45 (25%), 43 (32%), 41 (34%).

Preparation of threo-*2-bromo-3,4-epoxyoctane (**5**c)*

To 0.4 g (2.77 mmol) of **7***c* and 0.92 g (2.77 mmol) of CBr_4 in 12 mL of THF at −78°C was added dropwise 4.5 mL (24.9 mmol) of HMPT. The reaction was allowed to warm up to room temperature over a period of 12 h. Ice water (10 mL) was added to quench the reaction. The layers were separated and the aqueous layer was extracted with pentane (5 × 20 mL). The combined organic layer was backwashed with saturated aqueous NaCl, dried (Na_2SO_4), filtered, and concentrated *in vacuo*. The liquid was purified by silica gel chromatography using hexane:ethyl acetate (9:1) as eluent to yield 74% (0.42 g) of **5***c*, bp 42–44°C (0.01 Torr); ir (film): 1752, 1265, 1210, 1060, 1045, 1030, 990, 980, 918, 830, 815, 740, and 655 cm^{-1}; ^1H nmr ($CDCl_3$) δ: 0.91 (3H, C(8), t, J = 7.0 Hz), 1.46 (6H, C(5), C(6), C(7), m), 1.74 (3H, C(1), d, J = 7.2 Hz), 3.14 (2H, C(3), C(4), m), 3.86 (1H,

C(2), qd, J = 7.0, 9.3 Hz). The ^{1}H nmr did not show any signals corresponding to **5***b*; ms, *m/e* (%, rel. int.): 127 (67%), 109 (10%), 71 (38%), 69 (100%), 57 (19%), 43 (12%), 41 (27%); CI 209 (55%), 207 (53%), 191 (9%), 189 (10%), 127 (95%), 109 (100%), 85 (59%).

Reaction of **5**c *with zinc powder*

To 47 mg (0.72 mmol) of zinc powder in 5 mL of absolute methanol was added 50 mg (0.24 mmol) of **5***c*. The solution was refluxed for 5 h and then cooled to room temperature. The solution was diluted with 10 mL of ether and extracted with saturated aqueous NaCl (3 × 10 mL). The organic layer was dried ($MgSO_4$), filtered, and concentrated *in vacuo* to yield 75% (23 mg) of **6***c*. Gas chromatographic and ^{1}H nmr analysis indicated a 11:89 ratio of **6***d*:**6***c*.

Reaction of **5**b *and* **5**c *with stannates*

$Bu_3SnAlEt_2$ (Table 1, Entries 1 and 2)

To LDA (0.145 mmol) in 10 mL of THF was added 145 μL (0.145 mmol) of Bu_3SnH at −20°C. After 30 min, 145 μL of 1.0 *M* (0.145 mmol) Et_2AlCl was added. After 15 min, 0.5 or 1.0 equiv. of **5***b* or **5***c* was added and the reaction stirred for 1 h at the temperature indicated. The reaction was quenched with 20 mL of water. The organic layer was separated, and the aqueous layer was extracted with ether (5 × 20 mL). The extracts were combined, dried ($MgSO_4$), filtered, and concentrated *in vacuo* to give a liquid that was chromatographed on silica gel using hexane:ethyl acetate as eluent. The fractions shown to contain **6***c* and **6***d* by gc analysis were concentrated *in vacuo* and distilled at 120°C (15 Torr) to give **6***c* and **6***d* in the yields and isomeric ratios (gc) reported in Table 1.

$Bu_3SnAlEt_2/BF_3\cdot Et_2O$ (Table 1, Entry 3)

The reaction of **5***c* with $Bu_3SnAlEt_2$ was conducted as described above except that 2 equiv. of $BF_3\cdot Et_2O$ with respect to **5***c* were added and the reaction was stirred at room temperature for 12 h prior to work-up. The gc analysis of the **6***c*:**6***d* ratio is given in Table 1.

n-*Bu_3SnLi (Table 1, Entries 4–8)*

To 70 μL (0.50 mmol) of diisopropylamine in 2.0 mL of THF at −20°C was added 0.2 mL of 2.4 *M* (0.50 mmol) BuLi in *n*-hexane and the reaction was stirred for 15 min. Then 135 μL (0.50 mmol) of Bu_3SnH was added slowly. The reaction was stirred for 30 min at −20°C, then 0.33, 0.5, or 1 equiv. of **5***b* or **5***c* in 2.0 mL of THF was added and the reaction stirred for 1 h at the temperature indicated. The reaction mixture was quenched with 20 mL of ice water and the reaction mixture worked up as described above for entries 1 and 2. The isolated yields of **6***c* and **6***d* as well as the isomeric ratios (gc) obtained were recorded in Table 1.

Lithium B-*tributyltin*-B-*methoxy*-9B-*bicyclo[3.3.1]nonanylborate (12) (Table 1, Entries 9–11)*

To a solution of *n*Bu_3SnLi (0.50 mmol) in 2.0 mL of THF prepared as above, was added *B*-methoxy-9-borabicyclo[3.3.1]nonane (76 μL, 0.50 mmol) at −20°C. The reaction was stirred at this temperature for 45 min, then warmed to 0°C over 15 min. At this point 0.5 or 0.8 equiv. of **5***b* or **5***c* was added and the reaction was conducted for the time and at the temperature specified in Table 1. Each reaction was quenched by addition of 20 mL of ice water and worked up as described above for Entries 1 and 2. The isolated yields of **6***c* and **6***d* as well as the isomer ratios (gc) obtained are recorded in Table 1.

Isomerization of **6**d *with $Bu_3SnAlEt_2$*

To LDA (1 mmol) in 5 mL of THF was added 265 μL (1 mmol) of Bu_3SnH at −78°C. After 1 h, 1 mL of 1 *M* (1 mmol) Et_2AlCl was slowly added and the temperature was allowed to rise to 0°C for 30 min. Then 128 mg (1 mmol) of **6***d* was added and stirred for 1 h. The reaction was quenched with 1 mL of 1 *M* HCl and the layers separated. The aqueous layer was extracted with ether (3 × 5 mL) and the combined layers were dried ($MgSO_4$), filtered, and concentrated *in vacuo*. The gc analysis of the concentrate revealed a **6***c*:**6***d* ratio of 1:1.

Acknowledgements

We thank the Natural Sciences and Engineering Research Council of Canada for support of this work through an Operating Grant to A. C. Oehlschlager.

1. (*a*) M. Pereyre and J.-P. Quintard. Pure Appl. Chem. **53**, 2401 (1981), and references therein; (*b*) C. Tamborski, F. E. Ford, and E. J. Soloski. J. Org. Chem. **28**, 237 (1963).
2. N. Tsuboniwa, S. Matsubara, Y. Morizawa, K. Oshima, and H. Nozaki. Tetrahedron Lett. **25**, 2569 (1984).
3. K. B. Sharpless, C. H. Behrens, T. Katsuki, A. W. M. Lee, V. S. Martin, M. Takatani, S. M. Viti, F. J. Walker, and S. S. Woodard. Pure Appl. Chem. **55**, 589 (1983).
4. (*a*) K. Mori and H. Ueda. Tetrahedron, **37**, 2581 (1981); (*b*) N. Nakagawa and K. Mori. Agric. Biol. Chem. **48**, 2799 (1984).
5. A. M. Pierce, H. D. Pierce, Jr., A. C. Oehlschlager, and J. H. Borden. J. Agric. Food Chem. **33**, 848 (1985).
6. M. de Gaudemaris and P. Arnaud. Bull. Soc. Chim. Fr. 315 (1962).
7. N. A. Porter, C. B. Ziegler, Jr., F. F. Khouri, and D. H. Roberts. J. Org. Chem. **50**, 2252 (1985).
8. V. S. Martin, S. S. Woodard, T. Katsuki, Y. Yamada, M. Ikeda, and K. B. Sharpless. J. Am. Chem. Soc. **103**, 6237 (1981).
9. J. A. Dale, D. L. Dull, and H. S. Mosher. J. Org. Chem. **34**, 2543 (1969).
10. J. G. Miller and A. C. Oehlschlager. J. Org. Chem. **49**, 2332 (1984).
11. R. S. Tipson, M. A. Clapp, and L. H. Cretcher. J. Org. Chem. **12**, 133 (1947).
12. B. E. Rossiter, T. R. Verhoeven, and K. B. Sharpless. Tetrahedron Lett. 4733 (1979).
13. (*a*) J. L. Pierre and P. Chautemps. Tetrahedron Lett. 4371 (1972); (*b*) P. Chautemps and J. L. Pierre. Tetrahedron, **32**, 549 (1976); (*c*) T. Nakada, T. Tanaka, and T. Oishi. Tetrahedron Lett. **22**, 4723 (1981).
14. L. Brandsma. Preparative acetylenic chemistry. Elsevier Publishing Company, Amsterdam, London, New York. 1971.
15. A. C. Oehlschlager, J. W. Wong, V. G. Verigin, and H. D. Pierce, Jr. J. Org. Chem. **48**, 5009 (1983).
16. R. M. Silverstein, G. C. Bassler, and T. C. Morrill. Spectrometric identification of organic compounds. 4th ed. John Wiley & Sons, New York. 1981. p. 225.
17. P.-T. Ho and N. Davies. J. Org. Chem. **49**, 3027 (1984).
18. A. J. Mancuso, S.-L. Huang, and D. Swern. J. Org. Chem. **43**, 2480 (1978).
19. C. S. Wilcox and R. M. Otoski. Tetrahedron Lett. **27**, 1011 (1986).
20. (*a*) J. B. Lee and I. M. Downie. Tetrahedron, **23**, 359 (1967); (*b*) E. I. Snyder. J. Org. Chem. **37**, 1466 (1972).
21. S. Sharma and A. C. Oehlschlager. Tetrahedron Lett. Submitted.
22. E. J. Corey, G. W. J. Fleet, and M. Kato. Tetrahedron Lett. 3963 (1973).
23. J. G. Hill, B. E. Rossiter, and K. B. Sharpless. J. Org. Chem. **48**, 3607 (1983).
24. P. Gruenanger and D. Grieco. Gazz. Chim. Ital. **88**, 296 (1958).
25. K. Takabe, H. Tachikawa, and T. Katagiri. Synth. Commun. **10**, 89 (1980).
26. T. Oritani and K. Yamashita. Agric. Biol. Chem. **44**, 2707 (1980).
27. H. Sliwa and P. Maitte. Bull. Soc. Chim. Fr. 369 (1962).
28. W. G. Dauben and R. E. Wolf. J. Org. Chem. **35**, 374 (1970).
29. I. G. Tishchenko, O. N. Bubel, and I. P. Zyat'koc. Zh. Obshch. Khim. **33**, 2613 (1963).
30. W. Reusch and C. Djerassi. Tetrahedron, **23**, 2893 (1967).
31. W. J. Gensler, F. Johnson, and A. D. B. Sloan. J. Am. Chem. Soc. **82**, 6074 (1960).
32. W. C. Still. J. Am. Chem. Soc. (*a*) **99**, 4836 (1977); (*b*) **100**, 1481 (1978).
33. S. Sharma and A. C. Oehlschlager. Tetrahedron Lett. **27**, 6161 (1986).
34. W. Brugel. Handbook of NMR spectral parameters. Vol. 2. Heyden, London. 1972. p. 389.

Can. J. Chem. Downloaded from www.nrcresearchpress.com by 118.98.75.50 on 09/07/12
For personal use only.

Intramolecular rearrangements: Epimerization of bicyclic vinyl tertiary alcohols via a [2,3] sulfoxide sigmatropic rearrangement

WILLIAM L. BROWN AND ALEX G. FALLIS

Department of Chemistry, Memorial University of Newfoundland, St. John's, Nfld., Canada A1B 3X7

Received November 21, 1986

This paper is dedicated to Professor John T. Edward

WILLIAM L. BROWN and ALEX G. FALLIS. Can. J. Chem. **65**, 1828 (1987).

A general method for inverting the stereochemistry of bicyclic vinyl *endo* alcohols such as **6** and **12** to give the corresponding *exo* isomers **10** and **18** is described. The procedures employ a [2,3] sulfoxide rearrangement as a key step. In the case of the norbornene alcohol **12** the intermediate sulfenate ester **13** gives the oxetane **14** rather than the expected sulfoxide **17**. It was therefore prepared by thionyl chloride induced rearrangement of **12** to the allylic chloride **15** followed by displacement (PhSNa) and oxidation (*m*-chloroperbenzoic acid). The *exo* alcohol thus obtained underwent smooth anionic oxy-Cope rearrangement (KH, THF) to the *cis*-hydrindenone **19**.

WILLIAM L. BROWN et ALEX G. FALLIS. Can. J. Chem. **65**, 1828 (1987).

On décrit une méthode générale pour procéder à l'inversion de la stéréochimie des alcools vinyliques bicycliques *endo*, comme les produits **6** et **12**, pour obtenir les isomères *exo* correspondants (**10** et **13**). L'étape clé de ces méthodes implique une transposition [2,3] du sulfoxyde. Dans le cas particulier de l'alcool norbornénique **12**, l'ester sulfénique intermédiaire **13** conduit à l'oxétane **14** plutôt qu'au sulfoxyde **17** attendu. On l'a donc préparé par une transposition du composé **12**, induite par le chlorure de thionyle, en chlorure allylique **16** qui est suivie d'une substitution (PhSNa) et d'une oxydation (acide *m*-chloroperbenzoïque). L'alcool *exo* qui est ainsi obtenu donne lieu à une transposition oxy-Cope anionique (KH, THF) qui conduit à l'hydrindénone-*cis* (**19**).

[Traduit par la revue]

Introduction

The total synthesis of complex, multicyclic, natural products remains an area of fundamental importance and intense international activity. A particularly powerful transformation for the intramolecular construction of cyclohexanones in these systems is the anionic oxy-Cope rearrangement. This [3,3] sigmatropic rearrangement proceeds under mild conditions (1) and occupies a central role in the approach to ophiobolin A being developed by Paquette *et al.* (2), the route to taxusin under examination by

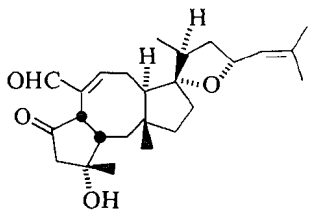

Ophiobolin A

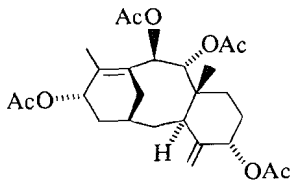

Taxusin

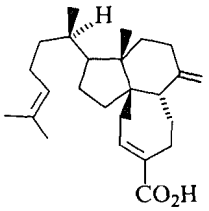

Gascardic acid

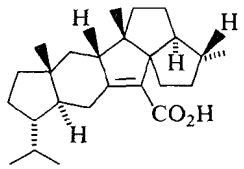

Retigeranic acid

Martin *et al.* (3), and our own studies directed toward the total syntheses of gascardic acid (4) and retigeranic acid (5). The general transformations **1** to **2** and **3** to **4** are representative of the type of multicyclic spiro-fused skeletons whose preparation may be envisaged using this chemistry. The versatility of this approach is further exemplified by the ease with which different functionality may be introduced on the periphery of the ring system.

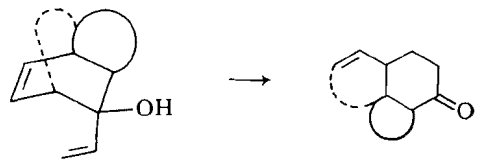

1 **2**

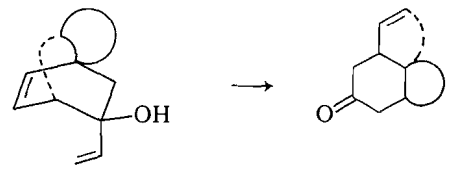

3 **4**

Successful [3,3] sigmatropic rearrangement clearly requires that the reactive components in the 1,5 diene unit bear a *cis* relationship. In cyclic systems this has frequently required the insertion of additional groups to control the stereochemistry. It is well established that nucleophilic addition to 2-norbornanone type ketones occurs preferentially from the *exo* face although products from *endo* attack predominate when an appropriate *syn* C-7 substituent is present. This procedure has been used by Jung *et al.* in their approach to steroids (6, 7) and to reserpine (8) via an anionic oxy-Cope pathway. A more general, alternative solution would involve the epimerization of the undesired isomer to afford the required *cis* diene stereochemistry.

It is known that configurational inversion of tertiary alcohols by the Mitsunobu method (diethyl azodicarboxylate–triphenylphosphine) is not feasible (9). However, previous inversions in prostaglandin intermediates (10) as well as earlier work by Evans *et al.* (11–13) with *tert*-butyl substituted cyclohexanes indicated that in these sterically biased systems the allylic sulfoxide rearrangement proceeded across the equatorial face of the cyclohexylidene ring to give predominantly the equatorial alcohol. These studies revealed that the transition state for these

Can. J. Chem. Downloaded from www.nrcresearchpress.com by 118.98.75.50 on 09/07/12
For personal use only.

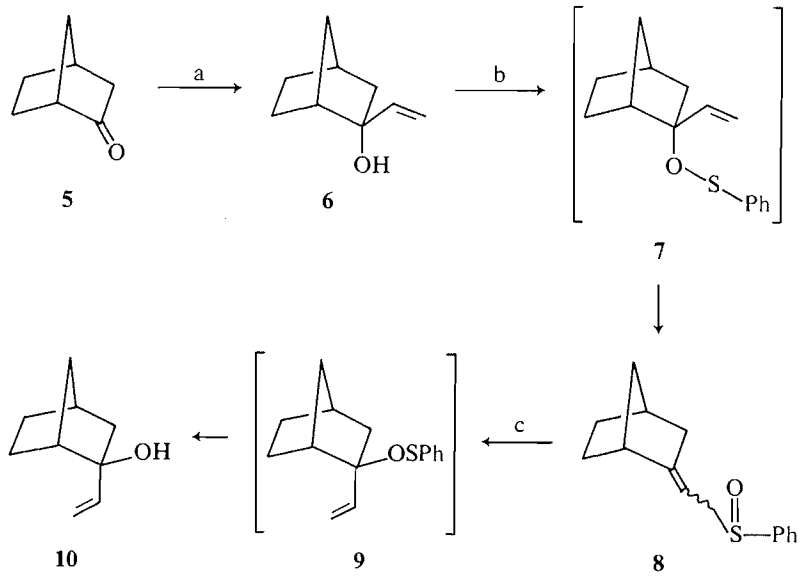

5 6 7 8 9 10

(a) CH_2 = CHMgBr, THF, 0°C, 1 h, 99%
(b) *n*-BuLi, THF, 0°C then −78°C, PhSCl, 1.5 h, 21°C, 12 h, 46%
(c) $(MeO)_3P$, MeOH, 65°C, 24 h, 56%

migrations was strongly influenced by steric effects as revealed by product geometry. Thus in ring systems in which there is a choice between the *exo* and *endo* surface it seemed likely that the normal preference for *exo* attack by vinyl nucleophiles could be reversed via a sulfenate–sulfoxide–sulfenate interconversion, since allylic sulfoxides such as **8** and **17** should rearrange preferentially across the less congested *exo* surface. The steroid nucleus possesses a related stereochemical bias and while our work was in progress Morera and Ortar reported an epimerization procedure based on this rearrangement pathway for the preparation of 17β-vinyl-17α-hydroxy steroids from the more accessible 17-epimers (14). We wish to report the details of a general procedure to epimerize allylic tertiary alcohols via a [2,3] sulfoxide sigmatropic rearrangement as illustrated for the two bicyclic alcohols **6** and **12**, described previously in preliminary form (15).

Results and discussion

The feasibility of this approach was established as follows. Addition of vinylmagnesium bromide to 2-bicyclo[2.2.1]heptanone (**5**) in tetrahydrofuran at 0°C gave, as expected, the *endo* alcohol **6** exclusively in quantitative yield. Treatment of **6** with *n*-butyllithium followed by freshly distilled benzenesulfenyl chloride at −78°C afforded, via the sulfenate ester **7** which was not isolated, the sulfoxide **8** in 45% yield after flash chromatography. Temperatures above −40°C resulted in rapid addition of benzenesulfenyl chloride to the double bond. Thermal rearrangement of **8** occurred smoothly in refluxing methanol containing trimethyl phosphite as a thiophile, to the desired *exo* alcohol **10** (ratio of *exo* alcohol **10** to *endo* alcohol **6** was 8:1). This result confirmed that the rearrangement had occurred in the desired manner with a high level of selectivity and should also suffice for norbornenones.

Similar Grignard addition of vinylmagnesium bromide to norbornenone **11** at −78°C gave only the *endo* alcohol **12** in 62% yield. In contrast to the results above, none of the sulfoxide **17** was formed when either the lithium or potassium alkoxide derived from **12** was exposed to PhSCl at −78°C. Instead, the tricyclic oxetane **14** was formed in 60% yield. The structure of this material was established by analogy with related examples of this ring system reported previously (16), and ruled out the alternative twistane isomer (17). The ^1H nmr coupling constant (J = 5 Hz) of the two methine hydrogens attached to the carbons bearing heteroatoms established that the thiophenyl and oxygen substituents bore a *cis* relationship and suggested that **14** arose via *syn* addition of the polarized sulfenate ester **13** (see following paper, ref. 19). Other sulfur transfer reagents (dimethyl disulfide, *N*-thiophenyl phthalimide, and succinimide) were also not effective for preparing the sulfoxide.

To circumvent these difficulties the following general solution was developed. Allylic (SNi′ type) rearrangement of the vinyl alcohol **12** with thionyl chloride in hexane afforded the unstable primary chloride **15** in 40% yield after chromatography. The chlorine was displaced with sodium thiophenolate to give **16** and this thioether oxidized at −78°C with *m*-chloroperbenzoic acid to the desired sulfoxide **17** (86%). Under these conditions no epoxides were detected although the sulfoxide was accompanied by some (7%) of the corresponding sulfone. This allylic sulfoxide was heated in refluxing methanol containing sodium thiophenolate to give the vinyl alcohols **18** and **12** in 46 and 5% yield respectively. Trimethyl phosphite was less effective as a thiophile and resulted in lower yields and significant decomposition. The *cis* hydrindenone **19** was obtained in 70% yield when the potassium anion of alcohol **18** was heated in refluxing THF for 20 min. As expected, treatment of the *endo* alcohol **12** under the same conditions caused no reaction.

These procedures are of general synthetic utility for adjusting the stereochemistry of vinyl alcohols and will facilitate the extended use of the oxy-Cope rearrangement to a variety of related ring systems. Direct rearrangement via a sulfenate ester intermediate may still be feasible with less reactive double bonds than norbornene. These concepts are under further investigation and their application to natural product synthesis is being developed.

Experimental

Melting points were determined in capillary tubes with a Thomas–Hoover Unit-Melt apparatus or on a Fisher–Johns melting point

Can. J. Chem. Downloaded from www.nrcresearchpress.com by 118.98.75.50 on 09/07/12
For personal use only.

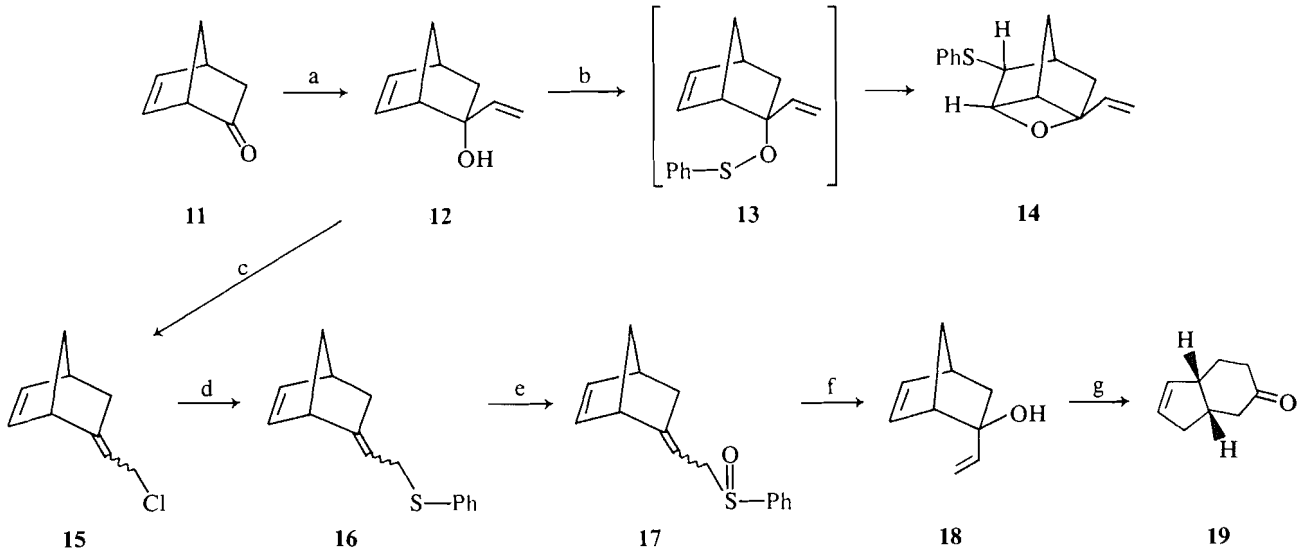

(a) CH_2 = CHMgBr, THF, −78°C, 1 h, 62%
(b) *n*-BuLi, THF, 0°C then −78°C, PhSCl, 1 h, 21°C, 16 h, 60%
(c) SO_2Cl_2, hexane, 0°C, 16 h, 40%
(d) PhSH, NaH, DME, 0°C, 21°C, 18 h, 41%
(e) *m*-$ClPhCO_3H$, CH_2Cl_2, −78°C, 5 h, 86%
(f) PhSNa, MeOH, 65°C, 24 h, 46%
(g) KH, THF, 0°C, 67°C, 20 min, 70%

apparatus and are uncorrected. Infrared spectra were recorded on a Perkin–Elmer 237B or 451 grating spectrophotometer and were calibrated with the 2850 and 1601 cm^{-1} bands of polystyrene film. Proton magnetic resonance spectra were measured at 80 MHz with a Bruker WP80 spectrometer employing a chloroform lock or at 60 MHz with a Varian EM 360 spectrometer. Signal positions are reported in ppm downfield from tetramethylsilane (δ scale) as an internal standard; multiplicity, the number of protons, coupling constants, and proton assignments are indicated in parentheses. Mass spectra were determined on a V.G. Micromass 7070 HS instrument using an ionization energy of 70 eV.

Thin-layer chromatographic analyses were carried out on commercial precoated silica gel plates with fluorescent indicator (Eastman Kodak silica gel 13181). Preparative thin-layer chromatography was conducted on 20 × 20 cm glass plates coated with silica gel $PF^{254+366}$ type 60 (E. Merck). Flash chromatography using BDH silica gel Kieselgel 60, 230–400 mesh, was employed for all column chromatography.

Petroleum ether refers to a fraction with boiling range 30–60°C. Anhydrous diethyl ether (ether), tetrahydrofuran (THF), dimethoxyethane (DME), and dioxane were obtained by distillation from lithium aluminium hydride or potassium/benzophenone. Absolute ethanol and methanol were dried by distillation from magnesium. Dry hexamethylphosphoramide (HMPA), dimethylformamide (DMF), dimethyl sulfoxide (DMSO), and diisopropylamine were prepared by distillation from calcium hydride. Solutions in organic solvents were dried over anhydrous magnesium sulfate and stripped of solvent with a Buchi rotary evaporator connected to a water aspirator. Unless otherwise indicated, all reactions were conducted under an atmosphere of dry nitrogen.

endo-*2-Vinyl-2-bicyclo[2.2.1]heptanol (6)*

Norcamphor (5.00 g, 45.40 mmol, Aldrich) in THF (100 mL) was added dropwise to a solution of vinylmagnesium bromide (45.40 mL, 45.40 mmol, 1.0 *M*, Aldrich) at 0°C. After stirring for 1 h the reaction mixture was quenched with 3 *M* HCl, extracted with ether, the combined ether extracts washed with water, brine, dried, concentrated, and the product purified by chromatography (50% ether/petroleum ether), to yield the *endo* alcohol **6**, 6.22 g (99%); ir (film): 3348 (O-H), 1645 (RCH=CH_2) cm^{-1}; ^1H nmr (CCl_4) δ: 0.90–2.65 (m, 10H), 3.40 (br s, 1H, OH), 4.80–4.98 (dd, 1H, *J* = 2 Hz, C=CH), 5.00–5.30 (dd, 1H, *J* = 2 Hz, 18.4, C=CH), 5.88–6.30 (dd, 1H, *J* = 11 Hz, 18.4 Hz, RCH=C).

Reaction of the lithium anion of alcohol 6 with benzenesulfenyl chloride

(a) From −40 to 21°C, endo-*2-(1-thiophenyl-2-chloroethanyl)-2-bicyclo[2.2.1]heptanol*

n-Butyllithium (0.49 mL, 4.96 mmol, 10.2 *M*, Aldrich) was added dropwise to a solution of alcohol **6** (0.57 g, 4.13 mmol) in THF (40 mL) at 0°C. After stirring for 10 min the reaction temperature was lowered to −40°C and an ether solution (20 mL) of benzenesulfenyl chloride (prepared from thiophenol (0.55 g, 5.00 mmol, Aldrich) and sulfuryl chloride (0.67 g, 5.00 mmol, Aldrich)) added dropwise. After the addition was complete the reaction mixture was warmed to 21°C, quenched with water, extracted with ether, the combined ether extracts washed with water, brine, dried, concentrated, and the product purified by chromatography (50% ether/petroleum ether) to give *endo*-2-(1-thiophenyl-2-chloroethanyl)-2-bicyclo[2.2.1]heptanol, 0.95 g (82%); ir (film): 3490 (O-H), 3050 (Ar-H), 2930 (C-H) cm^{-1}; ^1H nmr (CCl_4) δ: 1.00–2.50 (br m, 10H), 3.70 (m, 3H), 4.55 (t, 1H, CH(SPh)CH_2Cl), 7.28 (m, 5H, Ar-H). *Exact Mass* calcd. for $C_{15}H_{19}SOCl$: 282.0845; found: 282.0854.

(b) From −78 to 21°C, 2-(1-phenylsulfinylethenyl)bicyclo[2.2.1]-heptane (8)

n-Butyllithium (2.78 mL, 6.96 mmol, 2.5 *M*, Aldrich) was added dropwise to a solution of alcohol **6** (0.80 g, 5.80 mmol) in THF (25 mL) at 0°C. After stirring for 10 min the reaction was cooled to −78°C and a freshly distilled solution of benzenesulfenyl chloride (0.83 g, 5.80 mmol) in ether (25 mL) was added dropwise over 45 min. The reaction was stirred at −78°C for an additional 1.5 h and then allowed to warm to 21°C and stirred for a further 12 h. The reaction mixture was quenched with water and worked up as above. The product was purified by chromatography (50% ether/petroleum ether) to yield sulfoxide **8**, 0.66 g (46%); ir (film): 3045 (=C-H), 2930 (C-H), 1675 (C=C), 1040 (S=O) cm^{-1}; ^1H nmr (CCl_4) δ: 1.30 (br m, 7H), 2.10 (m, 2H), 2.58 (br s, 1H), 3.32 (d, 2H, *J* = 8 Hz, =CH-CH_2), 5.18 (t, 1H, *J* = 8 Hz, =CH-CH_2), 7.42 (m, 5H, Ar-H). *Exact Mass* calcd. for $C_{15}H_{16}SO$: 244.0922; found: 244.0934.

Can. J. Chem. Downloaded from www.nrcresearchpress.com by 118.98.75.50 on 09/07/12
For personal use only.

Can. J. Chem. Downloaded from www.nrcresearchpress.com by 118.98.75.50 on 09/07/12
For personal use only.

exo-2-*Vinyl-2-bicyclo[2.2.1]heptanol* (**10**)

The vinyl sulfoxide **8** (1.00 g, 4.07 mmol) and trimethylphosphite (4.78 mL, 40.65 mmol, Aldrich) in dry methanol (60 mL) were refluxed for 24 h. The solution was concentrated, the residue dissolved in ether, washed with water, brine, dried, and concentrated to yield a yellow oil. The oil was purified by chromatography (10% ethanol/hexanes) to give *exo* alcohol **10**, 0.32 g (56%) and some *endo* isomer **6**, 0.04 g (7%); ^{1}H nmr (CCl_4) δ: 0.90 (m, 10H), 3.40 (br s, 1H, O-H), 4.75–4.96 (dd, 1H, J = 1.5 Hz, J = 10 Hz, C=CH), 4.95–5.25 (dd, 1H, J = 1.5 Hz, J = 18 Hz, C=CH), 5.80–6.25 (dd, 1H, J = 10 Hz, J = 18 Hz, RCH=C).

Bicyclo[2.2.1]hept-5-en-one (**11**)

Bicyclo[2.2.1]hept-5-en-2-ol (mixture of *exo* and *endo* isomers) (10.00 g, 90.90 mmol, Aldrich) in dichloromethane (150 mL) was added in one aliquot to a slurry of pyridinium chlorochromate (29.30 g, 136.40 mmol) in dichloromethane (150 mL). It darkened immediately and, after stirring for 2 h, anhydrous ether (300 mL) was added and the supernatant solution decanted from the black gum. This residue was washed with ether, and the combined organic phases were filtered through Florisil and concentrated to give a yellow oil. The oil was purified by distillation, bp 60–62°C/12 Torr (lit. (18) bp 80–90°C/80 Torr) (1 Torr = 133.3 Pa) to yield **11**, 7.10 g (72%); ir (film): 3055 (=C-H), 2960 (C-H), 1740 (C=O), 1640 (C=C) cm^{-1}; ^{1}H nmr (CCl_4) δ: 1.75 (m, 2H, CH_2 bridge), 2.05 (m, 2H, CH_2C=O), 2.90 (m, 1H, CH bridgehead), 3.18 (m, 1H, CH-C=O), 6.05 (dd, 1H, J = 6 Hz, J = 3.6 Hz, CH=C), 6.52 (dd, 1H, J = 6 Hz, J = 3 Hz, CH=C). *Exact Mass* calcd. for C_7H_8O: 108.0575; found: 108.0559.

endo-2-*Vinylbicyclo[2.2.1]hept-5-en-2-ol* (**12**)

Ketone **11** (2.00 g, 18.52 mmol) in THF (50 mL) was added dropwise to a stirred solution of vinylmagnesium bromide (18.52 mL, 18.52 mmol, 1.0 *M*, Aldrich) in THF (80 mL) at −78°C. After stirring at −78°C for 1 h and warming to 21°C the reaction mixture was quenched with 3 *M* HCl and extracted with ether. The combined ether extracts were washed with water, brine, dried, concentrated, and the product purified by chromatography (50% ether/petroleum ether) to yield the *endo* alcohol **12**, 1.57 g (62%); ir (film): 3355 (O-H), 3050 (=C-H), 2910 (C-H), 1630 (C=C) cm^{-1}; ^{1}H nmr (CCl_4) δ: 1.10 (dt, 1H), 1.48 (d, 2H), 1.75–2.10 (dd, 1H), 2.49 (br s, 1H), 2.70 (m, 1H), 2.85 (br s, 1H, O-H), 4.88–5.05 (dd, 1H, J = 2 Hz, J = 11 Hz, RC=CH), 5.10–5.45 (dd, 1H, J = 2 Hz, J = 18 Hz, RC=CH), 5.87–6.50 (m, 3H, CH=CH, RCH=C).

2-Phenylthio-5-vinyl-4-oxatricyclo[3.2.1.0^{3,6}]octane (**14**)

n-Butyllithium (3.52 mL, 8.82 mmol, 2.5 *M*, Aldrich) was added slowly to a solution of alcohol **12** (1.00 g, 7.35 mmol) in THF (50 mL) at 0°C. After stirring for 10 min the reaction temperature was lowered to −78°C and a solution of benzenesulfenyl chloride (1.05 g, 7.35 mmol) in ether (40 mL) was added dropwise over 1 h. The reaction was warmed to 21°C, stirred for an additional 16 h, and the reaction mixture quenched with water. After ether extraction, the combined ether extracts were washed with water, brine, dried, concentrated, and product purified by chromatography (50% ether/petroleum ether) to yield the oxetane **14**, 1.08 g (60%); ir (film): 3050 (=C-H, Ar-H), 2940 (C-H), 1645 (C=C), 1090 (C-O-C), 960 (oxetane); ^{1}H nmr (CCl_4) δ: 1.20–2.10 (m, 4H), 2.85 (m, 1H, bridgehead H), 3.32 (dd, 1H, J = 5 Hz, J = 2 Hz, 1H, CHSPh), 3.60 (d, 1H, J = 2 Hz, bridgehead H), 4.25 (dd, 1H, J = 2, 5 Hz, HC-O), 5.00 (dd, 1H, J = 10 Hz, J = 2.5 Hz, RHC=C*H*H, *cis*), 5.15 (dd, 1H, J = 16 Hz, J = 16 Hz, J = 2.5 Hz, RHC=CH*H*, *trans*, 1H), 5.80 (dd, 1H, J = 10 Hz, J = 16 Hz, RC*H*R=CH_2), 7.20 (m, 5H, Ar-H). *Exact Mass* calcd. for $C_{15}H_{16}SO$: 244.0922; found: 244.0934.

2-(1-Chloroethenyl)bicyclo[2.2.1]hept-5-ene (**15**)

Alcohol **12** (0.44 g, 3.24 mmol) and thionyl chloride (0.46 g, 3.88 mmol, Aldrich) in hexane (25 mL) were stirred at 0°C. After 16 h the reaction mixture was quenched with cold water, extracted with hexane, and the combined organic extracts washed with water, brine, dried, and concentrated. The product was purified by chromatography (30% ether/petroleum ether) (compound decomposes slightly on the column), to give chloride **15**, 0.20 g (40%); ir (film): 3020 (=C-H) cm^{-1}; ^{1}H nmr (CCl_4) δ: 1.45 (br m, 2H), 2.00 (br m, 2H), 3.05 (m, 1H), 3.52 (br s, 1H), 3.92 and 4.08 (both d, together 2H, both *cis* and *trans* isomers, =CHC*H*$_2$Cl), 5.50 (m, 1H, RR′C=CHR), 6.00 (m, 2H, RCH=CHR).

2-(1-Phenylthioethenyl)bicyclo[2.2.1]hept-5-ene (**16**)

Thiophenyl (4.10 g, 37.22 mmol, Aldrich) in DME (25 mL) was added dropwise to a stirred suspension of sodium hydride (1.63 g, 40.93 mmol, 60% suspension in oil, Aldrich, previously washed with hexane) in DME (50 mL) at 0°C. The chloride **16** (5.21 g, 33.83 mmol) in DME (50 mL) was added dropwise to the sodium thiophenolate and after the addition was complete the temperature of the reaction was increased to 21°C and stirring was continued for 18 h. The reaction mixture was quenched by the addition of water, extracted with ether, the combined ether extracts washed with water, brine, dried, concentrated, and the product purified by distillation, bp 105–110°C/0.05 Torr, to yield thioether **16**, 3.13 g (41%); ir (film): 3048 (=C-H), 2910 (C-H), 1675 (R$_2$C=CRH) cm^{-1}; ^{1}H nmr (CCl_4) δ: 1.50 (br s, 4H), 2.75 (br s, 1H), 3.00 (br s, 1H), 3.30 and 3.48 (d, 2H, both *cis* and *trans* isomers, CH_2SPh), 5.20 (br m, 1H, RR′C=CHR), 5.90 (m, 2H, RCH=CHR), 7.10 (m, 5H, Ar-H). *Exact Mass* calcd. for $C_{15}H_{16}S$: 228.0973; found: 228.0985.

2-(1-Phenylsulfinylethenyl)bicyclo[2.2.1]hept-5-ene (**17**)

The bicyclic sulfide **16** (3.13 g, 13.87 mmol) and *m*-chloroperbenzoic acid (3.00 g, 13.87 mmol, 80%, Aldrich) in dichloromethane (50 mL) were stirred at −78°C for 5 h. The reaction mixture was filtered to remove *m*-chlorobenzoic acid. The filtrate was washed with water, 10% sodium sulfite, saturated sodium bicarbonate, brine, dried, concentrated, and the products purified by chromatography (60% ether/pentane) to yield sulfoxide **17**, 2.88 g (86%); ir (film): 3045 (=C-H, Ar-H), 2950 (C-H), 1675 (R$_2$C=CHR), 1040 (S=O) cm^{-1}; ^{1}H nmr (CCl_4) δ: 1.30 (br m, 4H), 2.75 (br m, 1H), 3.30 (br m, 3H, CH_2SOPh, CH bridgehead), 5.10 (br m, 1H, C=C*H*), 5.90 (m, 2H, CH=CH), 7.45 (br s, 5H, Ar-H).

2(1-Phenylsulfonylethenyl)bicyclo[2.2.1]hept-5-ene, 0.25 g (7%); ir (film): 3040 (=C-H, Ar-H), 2950 (C-H), 1676 (C=C), 1320, 1140 (SO_2) cm^{-1}; ^{1}H nmr (CCl_4) δ: 1.40 (br m, 4H), 2.85 (m, 1H), 3.10 (br s, 1H), 3.65 (two doublets, both isomers, 2H, CH_2SO_2Ph), 5.20 (br m, 1H, C=CH), 5.85 (br s, 2H, CH=CH), 7.55 (br m, 5H, Ar-H). *Exact Mass* calcd. for $C_{15}H_{16}SO_2$: 260.0871; found: 260.0830.

exo-2-*Vinylbicyclo[2.2.1]hept-5-en-2-ol* (**18**)

Thiophenol (6.06 g, 54.94 mmol, Aldrich) in methanol (30 mL) was added slowly to a stirred suspension of sodium hydride (2.20 g, 54.94 mmol, 60% suspension in oil, Aldrich, previously washed with hexane) in DME (30 mL) maintained at 0°C. This was followed by the addition of sulfoxide **17** (1.34 g, 5.49 mmol) in methanol (30 mL). The reaction mixture was refluxed for 24 h, quenched with water, and extracted with ether. The combined ether extracts were washed with water, brine, dried, concentrated, and the product purified by chromatography (30% ether/petroleum ether) to give the *exo* alcohol **18**, 0.34 g (46%), and the *endo* isomer **12**, 0.04 g (5%); ir (film): 3360 (O-H), 1630 (C=C) cm^{-1}; ^{1}H nmr (CCl_4) δ: 1.80–2.20 (m, 2H), 2.60 (m, 1H), 2.85 (br s, 1H, O-H), 4.65–4.70 (dd, 1H, J = 2 Hz, J = 11 Hz, RC=CH), 4.95–5.35 (dd, 1H, J = 2 Hz, J = 18 Hz, RC=CH), 5.50–6.20 (m, 3H, CH=CH, RHC=C).

cis-*Bicyclo[4.3.0]non-7-en-3-one* (**19**)

Alcohol **18** (0.10 g, 0.74 mmol) in THF (5 mL) was added to a mixture of potassium hydride (0.09 g, 0.81 mmol, 35% suspension in oil, Aldrich, previously washed with hexane) in THF (10 mL) at 0°C. The reaction mixture was refluxed for 20 min, quenched with water, and extracted with ether. The combined ether extracts were washed with water, brine, dried, concentrated, and the product purified by chromatography (20% ether/petroleum ether) to yield *cis*-bicyclo[4.3.0]non-7-en-3-one (**19**), 0.07 g (70%); ir (film): 3025 (=C-H), 2875 (C-H), 1715 (C=O) cm^{-1}; ^{1}H nmr (CCl_4) δ: 1.50–2.30 (m, 6H), 2.40–3.20 (m, 4H, CH_2COCH_2), 5.30–5.80 (m, 2H, CH=CH). *Exact Mass* calcd. for $C_9H_{12}O$: 136.0888; found: 136.0889.

Similar treatment of alcohol **12** afforded only recovered starting material.

Acknowledgements

We are grateful to Memorial University of Newfoundland and the Natural Sciences and Engineering Research Council of Canada for financial support of this research, and to B. Gregory for high resolution mass spectra.

1. D. A. EVANS and A. M. GOLOB. J. Am. Chem. Soc. **97**, 4765 (1975).
2. L. A. PAQUETTE, D. R. ANDREWS, and J. P. SPRINGER. J. Org. Chem. **48**, 1147 (1983).
3. S. F. MARTIN, J. B. WHITE, and R. WAGNER. J. Org. Chem. **47**, 3190 (1982).
4. S. J. ALWARD and A. G. FALLIS. Can. J. Chem. **62**, 121 (1984).
5. S. K. ATTAH-POKU, F. CHAU, V. K. YADAV, and A. G. FALLIS. J. Org. Chem. **50**, 3418 (1985); A. G. FALLIS, V. K. YADAV, and S. M. TULADHAR. 69th Canadian Chemical Conference of the C.I.C., Symposium on Synthetic Methods, Saskatoon, Sask., June 1–4, 1986. Abstract No. OR-B3-4.
6. M. E. JUNG and J. P. HUDSPETH. J. Am. Chem. Soc. **100**, 4309 (1978).
7. M. E. JUNG and G. L. HATFIELD. Tetrahedron Lett. **24**, 2931 (1983).
8. M. E. JUNG and L. A. LIGHT. J. Am. Chem. Soc. **106**, 7614 (1984).
9. O. MITSUNOBU. Synthesis, 1 (1981).
10. J. G. MILLER, W. KURZ, K. G. UNTCH, and G. STORK. J. Am. Chem. Soc. **96**, 6774 (1974).
11. D. A. EVANS, G. C. ANDREWS, and C. L. SIMS. J. Am. Chem. Soc. **93**, 4956 (1971).
12. D. A. EVANS and G. C. ANDREWS. J. Am. Chem. Soc. **94**, 3672 (1972).
13. D. A. EVANS and G. C. ANDREWS. Acc. Chem. Res. **7**, 147 (1974).
14. E. MORERA and G. ORTAR. J. Org. Chem. **48**, 119 (1983).
15. W. L. BROWN and A. G. FALLIS. Tetrahedron Lett. **26**, 607 (1985).
16. M. SHIBASAKI, A. NISHIDA, and S. IKEGAMI. Tetrahedron Lett. 3061 (1980).
17. A. K. SAKSENA, P. MANGIARACINA, and R. BRAMBILLA. Tetrahedron Lett. 1729 (1978).
18. S. RANGANATHAN, D. RANGANATHAN, and A. K. MEHROTRA. Synthesis, 289 (1977).
19. S. M. TULADHAR and A. G. FALLIS. Can. J. Chem. **65**, 1833 (1986).

Can. J. Chem. Downloaded from www.nrcresearchpress.com by 118.98.75.50 on 09/07/12
For personal use only.

Cyclic ether synthesis: sulfenyletherification with benzenesulfenyl chloride/*N,N*-diisopropylethylamine and sulfenate ester cycloadditions

SUDERSAN M. TULADHAR AND ALEX G. FALLIS

Department of Chemistry, Memorial University of Newfoundland, St. John's, Nfld., Canada A1B 3X7

Received November 23, 1987

This paper is dedicated to Professor John T. Edward

SUDERSAN M. TULADHAR and ALEX G. FALLIS. Can. J. Chem. **65**, 1833 (1987).

A general method for the formation of the cyclic ethers **9**, **10**, **13**, **14**, **16**, and **28** and the lactone **30** is described. The procedure employs benzenesulfenyl chloride prepared *in situ* in acetonitrile and *N,N*-diisopropylethylamine to generate a thiiranium (episulfonium) ion intermediate from which the cyclic products arise by internal nucleophilic displacement. In the special case of the norbornene alcohols **1** and **2** the oxetanes **5** and **6** are formed by intramolecular sulfenate ester cycloaddition.

SUDERSAN M. TULADHAR et ALEX G. FALLIS. Can. J. Chem. **65**, 1833 (1987).

On décrit une méthode générale de formation des éthers cycliques **9**, **10**, **13**, **14**, **16** et **28** ainsi que de la lactone **30**. La méthode est basée sur l'utilisation du chlorure de benzénesulfényle préparé *in situ* dans l'acétonitrile et de la *N,N*-diisopropyléthylamine pour préparer l'ion thiiranium (épisulfonium) intermédiaire à partir duquel les produits cycliques se forment par une réaction de substitution nucléophile interne. Dans le cas particulier des alcools norborniéniques **1** et **2**, les oxétanes **5** et **6** se forment par une cycloaddition intramoléculaire de l'ester sulfénique.

[Traduit par la revue]

Can. J. Chem. Downloaded from www.nrcresearchpress.com by 213.166.140.6 on 09/07/12
For personal use only.

Introduction

Marine species are a rich source of secondary metabolites containing cyclic ethers. Compounds such as acanthifolin (1) and brevetoxin (2, 3) are particularly challenging synthetic targets which require procedures for the facile construction of tetrahydrofuran and pyran rings with suitable functionality for further elaboration. Consequently there is considerable interest in devising viable synthetic methods for the preparation of cyclic ethers (3–6).

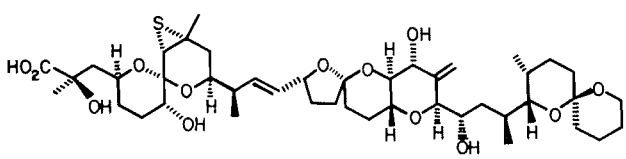

Acanthifolin

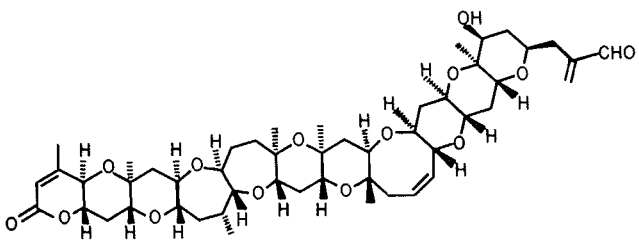

Brevetoxin

In the preceding paper we reported that the lithium alkoxide of the norbornene-alcohol **1** afforded the functionalized oxetane **5** via the likely intermediacy of the sulfenate ester **3** upon treatment with benzenesulfenyl chloride at −78°C (7). This observation, although unexpected, was of considerable synthetic interest since straightforward differential functionalization of norbornenes is difficult. In addition, it appeared that oxetanes of this type could be opened selectively, the oxidation level of the sulfur substituent altered as desired to facilitate alkylations, and thus they could be useful synthetic intermediates. We also wondered if *syn* addition of a polarized

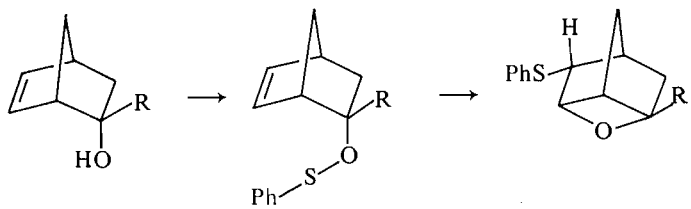

1 R = CH = CH_2 **3** R = CH = CH_2 **5** R = CH = CH_2
2 R = CH_3 **4** R = CH_3 **6** R = CH_3

sulfenate ester to a double bond was a general reaction. However, as described below it appears not to be, but we have developed a mild, general intramolecular route to cyclic ethers from unsaturated alcohols with benzene or methanesulfenyl chloride generated *in situ* in acetonitrile at room temperature (21°C) followed by the addition of *N,N*-diisopropylethylamine. These studies are related to the recent report of O'Malley and Cava (6) which employed dimethyl(methylthio)sulfonium fluoroborate for this type of transformation and provide access to the sulfur analogue of selenium based methods for cyclic etherification and lactonization (8–11).

Results and discussion

Initially, to examine the reactivity of simple sulfenate esters, methyl benzenesulfenate was prepared and mixed with norbornene but after several hours in refluxing THF the components were recovered unchanged. In order to ascertain if oxetane formation was limited to intramolecular examples the behaviour of sulfenate ester **8** derived from **7** was examined but it also did not form **9** at temperatures up to 85°C. Recently Edstrom and Livinghouse have described the addition of benzenesulfenates to alkenes in the presence of Lewis acids followed by arene annulation of the resulting thiiranium (episulfonium) ion intermediate (12). Treatment of the sulfenate ester **8** with either boron trifluoride etherate or silica gel afforded the tetrahydrofuran **9** in modest yield (~50%) accompanied by the alcohol **7**. Unfortunately this procedure may have limited synthetic potential as a preparative method, since it failed in the more complex case of the sulfenate ester derived from the bicyclic alcohol **26**.

In contrast to this behaviour, the substituted tetrahydrofuran **9**

Can. J. Chem. Downloaded from www.nrcresearchpress.com by 213.166.140.6 on 09/07/12
For personal use only.

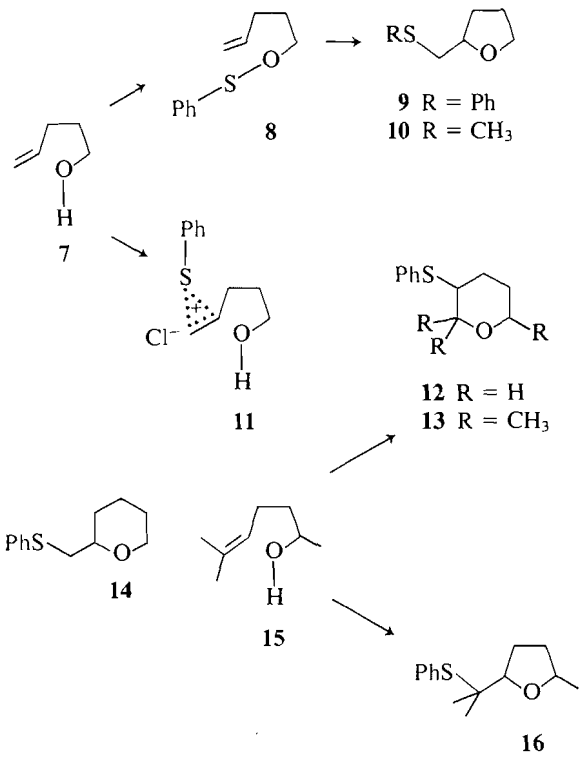

was formed from **7** in 84% yield when the alcohol was treated with a solution of benzenesulfenyl chloride generated *in situ* in acetonitrile at 21°C followed by *N*,*N*-diisopropylethylamine. (The yield was not improved when distilled benzenesulfenyl chloride was employed.) A parallel procedure employing methanesulfenyl chloride afforded the corresponding ether **10** (6). These results are consistent with the initial formation of a thiiranium (episulfonium) ion intermediate of type **11** which is displaced by the internal oxygen nucleophile. The products arise via a preferred 5-*exo-tet* cyclization of **11** (13, 14). The alternative 6-*endo-tet* mode of ring closure to the pyran **12** was not observed. However, six-membered rings were formed exclusively when the alternative choice was a 7-*endo-tet* ring closure, so that pyran **14** was formed from 5-hexen-1-ol in 85% yield. In the more highly substituted olefin **15** a 1:1 mixture of the two cyclic ethers **13** and **16** was obtained. One might expect, based on results from the addition of substituted benzenesulfenyl chlorides to alkenes (15), that the major kinetically controlled product should arise from attack at the least hindered carbon of the thiiranium ion. However, this product (**12**) was not observed from **7** and in the case of **15** where both modes of attack were encountered the product composition apparently reflects the sterically crowded environment in the intermediate and the relative ease of ring formation. Another route could involve the formation of addition product followed by cyclization in the presence of the amine base. However, cyclization did not occur to form the simple oxetane **21** from 3-buten-1-ol (**17**) but intermolecular attack by the chlorine nucleophile took precedence to give the Markovnikov addition product **19**. Furthermore, cyclization of **19** to **21** by treatment with additional bases was also not possible. In a similar fashion **18** was prepared from **7** (PhSCl, Et_2O, 21°C, 2 h). Although on standing it slowly formed a small amount of the tetrahydrofuran, treatment of **18** with sodium hydride at 21°C did not enhance cyclization and only starting material was recovered. In contrast, when *n*-butyllithium was employed (0–21°C) elimination to form **20** was observed, although, some of this enol ether may have arisen from the tetrahydrofuran **9**, since it opened cleanly to **20** at 0°C with *n*-butyllithium. As a route to protected aldehydes this may be of further synthetic utility.

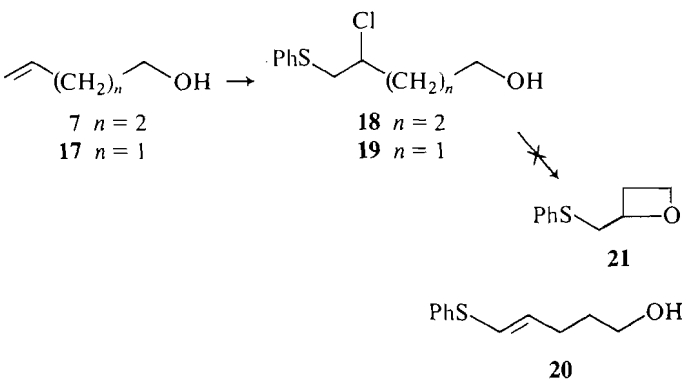

It was anticipated that examination of the behaviour of the two norbornene-type alcohols **2** and **26** would permit a distinction to be made between the sulfenate ester cycloaddition and the thiiranium ion pathways due to the different stereochemistry of the products which should result in each case. Thus alcohol **2** was treated at 0°C with *n*-butyllithium followed by PhSCl at −78°C. The products, other than alkene addition (46%), consisted of two unstable materials, the oxetane **6** (20%) and the thio-aldehyde **24** (14%) from the ring opening of **6**. The magnitude of the coupling constant (J = 5.0 Hz) between the two adjacent *exo* hydrogens of **6** was consistent with a *syn* addition as observed in the case of **1** above. Unfortunately the benzenesulfenyl chloride/diisopropylethylamine procedure did not afford the oxetane **23** that was expected from intermediate **22** but only a low yield (17%) of the ring-opened aldehyde **24**. In spite of the fact that the oxetane **23** was not detected it is the most probable intermediate. In the presence of the amine base the *endo* proton on the sulfur-bearing carbon may be readily abstracted leading to facile ether cleavage to form the enol followed by tautomerization. The geometry for this elimination-opening process is clearly more favourable for **23** than for either **5** or **6**. Previously the ring-opened aldehyde **25** from **1** was not encountered; however, examination (^{1}H nmr) of a sample of **1** which had been stored for more than a year at 0–5°C revealed that it contained a significant amount of aldehyde and indicated that even in storage these oxetanes undergo ring cleavage.

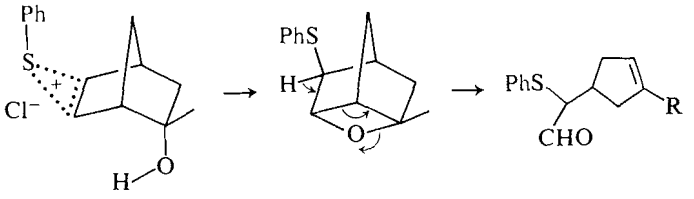

In principle the tetrahydrofuran ring that would be formed from **26** should exhibit greater stability and it was examined next. However, the sulfenate ester cycloaddition failed to give **27** even with added Lewis acids. It therefore appears that this intramolecular reaction is limited to reactive norbornene double bonds in which the sulfenate ester is aligned in the correct geometry. In contrast, the benzenesulfenyl chloride/diisopropylethylamine procedure gave the tricyclic tetrahydrofuran **28** in 83% yield. The stereochemistry was established on the basis of the *trans* coupling constant (J = 2.5 Hz) between the *endo*

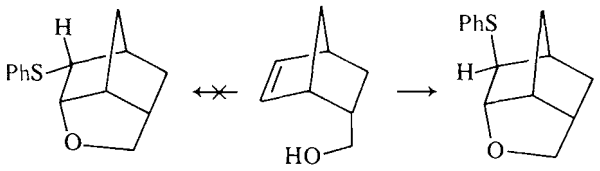

27 26 28

and *exo* hydrogens attached to the carbons bearing heteroatoms and by analogy with related selenium examples (11). As expected from related studies (16, 17) the procedure may also be employed for sulfenyllacetonization (**29**–**30**). The results of these studies and the examples discussed above are summarized in Table 1.

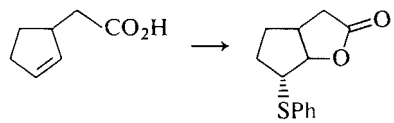

29 30

In conclusion this *in situ* benzenesulfenyl chloride/*N*,*N*-diisopropylethylamine procedure provides a general, mild route to sulfur-substituted cyclic ethers in which the sulfur functionality may be modified for further synthetic manipulations. Thus after oxidation of the sulfur moiety it may be reductively removed, alkylated at the adjacent carbon, or eliminated to give a substituted alkene, depending upon the ultimate synthetic objective. These features and the simplicity of this cyclization method should facilitate its extended use in synthesis.

Experimental

Infrared spectra were recorded on a Perkin–Elmer 237B or 451 grating spectrophotometer, and were calibrated with the 2850 and 1601 cm^{-1} bands of polystyrene film. Proton magnetic resonance spectra were measured at 80 MHz with a Bruker WP80 spectrometer employing a chloroform lock or at 60 MHz with a Varian EM 360 spectrometer. Signal positions are reported in ppm downfield from tetramethylsilane (δ scale) as an internal standard, multiplicity, the number of protons, coupling constants, and proton assignments are indicated in parentheses. Mass spectra were determined on a V.G. Micromass 7070 HS instrument using an ionization energy of 70 eV.

Thin layer chromatographic analyses were carried out on commercial precoated silica gel plates with fluorescent indicator (Eastman Kodak silica gel 13181). Preparative thin layer chromatography was conducted on 20 × 20 cm glass plates coated with silica gel $PF^{254+366}$ type 60 (E. Merck). Flash chromatography using BDH silica gel Kieselgel 60, 230–400 mesh was employed for all column chromatography. Additional chromatographic purification was achieved using a Harrison Research Chromatotron Model 7924T.

Petroleum ether refers to a fraction with boiling range 30–60°C. Anhydrous diethyl ether (ether), tetrahydrofuran (THF), dimethoxyethane (DME), and dioxane were obtained by distillation from lithium aluminium hydride or potassium/benzophenone. Absolute ethanol and methanol were dried by distillation from magnesium. Dry hexamethylphosphoramide (HMPA), dimethylformamide (DMF), dimethyl sulfoxide (DMSO), and diisopropylamine were prepared by distillation from calcium hydride. Solutions in organic solvents were dried over anhydrous magnesium sulphate and stripped of solvent with a Buchi rotary evaporator connected to a water aspirator. Unless otherwise indicated all reactions were conducted under an atmosphere of dry nitrogen.

General sulfenyletherification procedure

A solution of benzenesulfenyl chloride was prepared *in situ* in dry acetonitrile (10 mL) containing dry pyridine (2 drops) and diphenyldisulfide (0.634 g, 2.90 mmol) to which sulfuryl chloride (0.24 mL, 2.96 mmol) in acetonitrile (3 mL) was added dropwise. This solution was stirred at 21°C for 1 h and then added dropwise to a magnetically stirred solution of 4-penten-1-ol (0.50 g, 5.81 mmol, Aldrich) in dry acetonitrile (10 mL) at room temperature (21°C). Stirring was continued for 0.5 h after addition was complete, a solution of *N*,*N*-diisopropylethylamine (1.20 mL, 6.89 mmol) in acetonitrile (5 mL) was added, and the reaction mixture stirred for a further 0.5 h. The reaction mixture was concentrated under reduced pressure, extracted with ether (50 mL), the combined ether extracts washed with water (3 × 50 mL), saturated aqueous ammonium chloride (2 × 25 mL), dried, filtered, concentrated, and the product purified by chromatography (5% ethyl acetate/*n*-hexane), to give 2-phenylthiomethyltetrahydrofuran (**9**). Yield 0.94 g (84%); ir (film): 2900, 2880, 1580 (C=C), 1060 (C—O) cm^{-1}; ^1H nmr ($CDCl_3$) δ: 1.60–2.19 (m, 4H, CH_2CH_2), 3.06 (m, 2H, CH_2—S), 3.69–4.14 (m, 3H, HC—O, CH_2—O), 7.14–7.44 (m, 5H, ArH); ^{13}C nmr ($CDCl_3$) δ: 25.80, 31.01, 39.04, 68.26, 77.84, 126.11, 129.02, 129.44, 130.30. *Exact mass* calcd. for $C_{11}H_{14}OS$: 194.0764; found: 194.0753.

*2-Methylthiomethyltetrahydrofuran (**10**)*

A parallel procedure was used with methanesulfenyl chloride. A solution of methanesulfenyl chloride was prepared *in situ* in dry acetonitrile (10 mL) containing dry pyridine (2 drops) and dimethylsulfide (0.272 g, 2.90 mmol) to which sulfuryl chloride (0.24 mL, 2.96 mmol) in acetonitrile (3 mL) was added dropwise. This solution was stirred at 21°C for 1 h and then added dropwise to a magnetically stirred solution of 4-penten-1-ol (0.50 g, 5.81 mmol, Aldrich) in dry acetonitrile (10 mL) at room temperature (21°C) as described above to afford **10** in 86% yield (6); ir (film) 2880, 1580 (C=C), 1060 (C—O); ^1H nmr ($CDCl_3$) δ: 1.59–2.25 (m, 4H, CH_2CH_2), 2.17 (s, 3H, CH_3S), 2.64 (dd, 2H, CH_2—S), 3.70–4.13 (m, 3H, CH_2O, HC—O); ^{13}C nmr ($CDCl_3$) δ: 16.41, 25.81, 31.11, 39.40, 68.29, 78.63. *Exact mass* calcd. for $C_6H_{12}OS$: 132.0608; found: 132.0604.

*2-Phenylthiomethyltetrahydropyran (**4**)*

The above procedure with 5-hexen-1-ol (0.60 mL, 5.0 mmol, Aldrich) afforded the pyran **14**, 0.92 g (88%); ^1H nmr ($CDCl_3$) δ: 1.32–1.87 (m, 6H, —$(CH_2)_3$), 3.01 (m, 2H, CH_2S), 3.24–3.53 (m, 2H, CH_2O), 4.00 (m, 1H, HC—O), 7.13–7.43 (m, 5H, ArH); ^{13}C nmr ($CDCl_3$) δ: 23.41, 25.97, 31.35, 39.90, 68.78, 76.73, 126.03, 129.10, 129.36, 137.39. *Exact mass* calcd. for $C_{12}H_{16}OS$: 208.0921; found: 208.0947.

*5-Methyl-2-phenylthiomethyl(1,1-dimethyl)tetrahydrofuran (**16**) and 2,2,6-trimethyl-3-phenylthiotetrahydropyran (**13**)*

The above procedure with 6-methyl-5-hepten-2-ol (0.60 mL, 3.95 mmol, Aldrich) gave an inseparable 1:1 mixture of **16** and **13**, 0.78 g (84%); ir (film) 1585 (C=C), 1090 (C—O) cm^{-1}; ^1H nmr ($CDCl_3$) δ: 1.11 (d, 3H, J = 6.5 Hz, CH_3C—O), 1.25 (d, 3H, J = 6.5 Hz, CH_3C—O), 1.41 (s, 6H, 6H, $(CH_3)_2C$), 3.15 (t, 1H, J = 3 Hz, HC—SPh), 3.68 (m, 1H, HC—O); The ratio of **16**:**13** was 48:52 based on the ^{13}C nmr signals at 55.20 (CHS) and 53.49 (CH—O). *Exact mass* calcd. for $C_{14}H_{20}OS$: 236.1234; found: 236.1229.

*5-exo-Phenylthio-3-oxatricyclo[4.2.0.0^{4,8}]nonane (**28**)*

The above procedure with 5-norbornene-2-methanol (**26**) (0.60 mL, 4.96 mmol, 17% *endo*, Aldrich) provided the tricyclic ether **28**, 0.65 g (83% based on *exo* isomer); ir (film) 1595 (C=C), 1100 (C—O) cm^{-1}; ^1H nmr ($CDCl_3$) δ: 1.16–2.73 (m, 7H), 3.01 (d, 1H, J = 2.5 Hz, HC—S), 3.67–3.83 (m, 2H, CH_2—O), 4.18 (d, 1H, J = 5 Hz, HC—O), 7.23–7.41 (m, 5H, ArH); ^{13}C nmr ($CDCl_3$) δ: 36.06, 38.02, 38.28, 39.64, 46.48, 56.73, 74.76, 86.13, 125.77, 129.10, 130.04, 130.89. *Exact mass* calcd. for $C_{14}H_{16}OS$: 232.0921; found: 232.0935.

*3-Chloro-4-phenylthiobutanol (**19**)*

The above procedure with 3-buten-1-ol (0.50 mL, 5.81 mmol) gave the addition product **19**, 1.21 g (97%); ir (film) 3350 (br, OH), 1583 (C=C) cm^{-1}.

*8-Phenylthio-2-oxabicyclo[3.3.0]octan-3-one (**30**)*

The above procedure with 2-cyclopentene-1-acetic acid (0.60 mL, 4.98 mmol, Aldrich) afforded the lactone **30**, 0.98 g (87%) (16); ir

Can. J. Chem. Downloaded from www.nrcresearchpress.com by 213.166.140.6 on 09/07/12
For personal use only.

TABLE 1. Summary of experiments

Entry	Reactant	Reagent	Product	Isolated yield
1	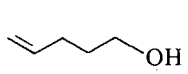 7	PhSCl $^{i}Pr_2NEt$	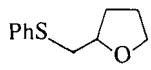 **9**	84%
2	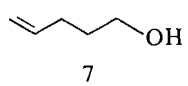 7	MeSCl $^{i}Pr_2NEt$	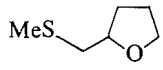 **10**	86%
3	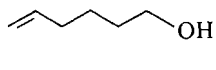	PhSCl $^{i}Pr_2NEt$	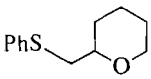 **14**	85%
4	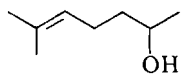 **15**	PhSCl $^{i}Pr_2NEt$	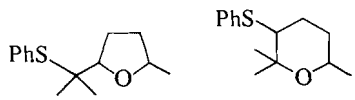 **16** 1 : 1 **13**	84%
5	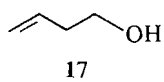 **17**	PhSCl $^{i}Pr_2NEt$	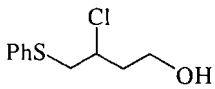 **19**	97%
6	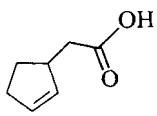 **29**	PhSCl $^{i}Pr_2NEt$	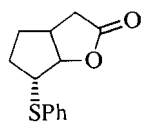 **30**	84%
7	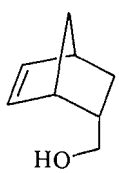 **26**	PhSCl $^{i}Pr_2NEt$	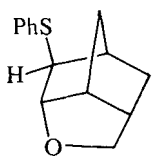 **28**	83%
8	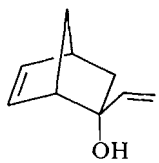 **1**	BuLi PhSCl	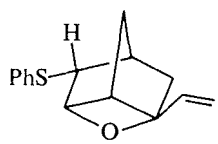 **5**	60% (ref. 7)
9	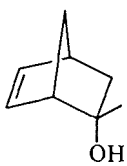 **2**	BuLi PhSCl	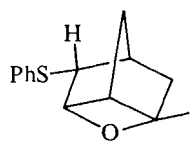 **6**	20%

(film) 1780 (C=O), 1590 (C=C), 1175 (C—O) cm^{-1}; ^{1}H nmr ($CDCl_3$) δ: 3.80 (m, 1H, HC—S), 4.81 (d, 1H, J = 6 Hz, HC—O), 7.35 (m, 5H); ^{13}C nmr ($CDCl_3$) δ: 30.07, 32.04, 35.63, 37.42, 51.44, 89.88, 128.14, 129.36, 130.64, 131.58, 176.69. *Exact mass* calcd. for $C_{13}H_{14}O_2S$: 218.0765; found: 218.0778.

4-Chloro-5-phenylthiopentanol (18)

A solution of benzenesulfenyl chloride was prepared *in situ* in dry diethyl ether (15 mL) containing dry pyridine (0.05 mL) and diphenyldisulfide (0.418 g, 1.91 mmol) to which sulfuryl chloride (0.255 g, 1.91 mmol) in ether (3 mL) was added dropwise. This solution was

Can. J. Chem. Downloaded from www.nrcresearchpress.com by 213.166.140.6 on 09/07/12
For personal use only.

stirred at 21°C for 2 h and then added dropwise to a magnetically stirred solution of 4-penten-1-ol (0.50 g, 5.81 mmol, Aldrich) in dry ether (15 mL) at 21°C. The reaction was stirred for a further 2 h, diluted with ether, quenched with saturated aqueous ammonium chloride solution, and extracted with ether (3 × 20 mL). The combined ether extracts were washed with water, brine, dried, filtered, concentrated, and the addition product **18** obtained as a pale yellow viscous oil, 0.804 g (62%); ir (film) 3400 (br, OH), 1585 (C=C) cm^{-1}; ^1H nmr ($CDCl_3$) δ: 1.40–2.20 (m, 4H, CH_2CH_2), 2.95–4.05 (m, 5H), 3.85 (br s, 1H, OH), 7.10–7.50 (m, 5H, ArH).

5-Phenylthio-4-penten-1-ol (20)

Treatment of **18** (0.80 g, 3.47 mmol) or **9** (0.357 g, 1.84 mmol) in dry ether (20–30 mL) at 0°C with *n*-butyllithium in hexane (2.20 mL, 3.52 mmol and 1.20 mL, 1.92 mmol respectively) for 1 h was followed by quenching with saturated aqueous ammonium chloride. The reaction was extracted with ether, the combined ether extracts washed with brine, dried, filtered, and concentrated and purified by chromatography (10% ether acetate/*n*-hexane) to give **20**, 0.412 g (66%) and 0.35 g (83%) respectively, ir (film) 3320 (OH), 1580 (C=C) cm^{-1}; ^1H nmr ($CDCl_3$) δ: 1.20–2.40 (m, 4H, CH_2CH_2), 3.55 (t, 2H, J = 7.0 Hz, CH_2—O), 3.90 (s, 1H, OH), 5.5–6.30 (m, 2H, HC=CH), 7.00–7.40 (m, 5H, ArH).

endo-*2-Phenylthio-5-methyl-4-oxatricyclo[3.2.1.0^{3,6}]octane (6) and 2-phenylthio-(3-methyl-3-cyclopentenyl)ethanal (24)*

n-Butyllithium in hexane (0.60 mL, 1.62 mmol, Aldrich) was added dropwise at 0°C to a stirred solution of *endo*-2-methyl-5-norbornen-2-ol (**2**, from norbornenone and methyllithium) (18) (0.20 g, 1.61 mmol) in dry ether (20 mL). After 4 h the reaction mixture was cooled to −78°C and a solution of benzenesulfenyl chloride (prepared as described above from sulfuryl chloride (0.11 g, 0.80 mmol) and diphenyldisulfide (0.18 g, 0.82 mmol) in dry ether (10 mL) containing dry pyridine (1 drop)) was added dropwise over 1 h. The reaction was stirred for a further 1 h at −78°C after addition was complete and allowed to rise to room temperature (21°C) and stirred for a further 15 h. Water was added, the reaction mixture extracted with ether, the combined ether extracts washed with water, saturated aqueous ammonium chloride, dried, filtered, concentrated, and the products purified by chromatography (5% ethyl acetate/*n*-hexane) to give the thioaldehyde **24** 0.052 g (14%); ir (film) 2720 (HC=O), 1715 (C=O), 1580 (C=C) cm^{-1}; ^1H nmr ($CDCl_3$) δ: 1.71 (br s, 3H, CH_3C=), 2.15–2.75 (m, 5H), 3.50 (m, 1H, HC—S), 5.30 (m, 1H, HC=C), 7.21–7.48 (m, 5H, ArH), 9.36 (d, 1H, J = 4.7 Hz, HC=O); ^{13}C nmr ($CDCl_3$) δ: 16.40, 36.99, 37.25, 41.35, 123.12, 123.29, 128.42, 129.36, 132.78, 139.44.

Oxetane **6**, 0.074 g (20%); ^1H nmr ($CDCl_3$) δ: 1.30 (s, 3H, CH_3C), 2.75 (m, 1H, bridehead H), 3.21 (m, 3H), 3.68 (br s, 1H, bridgehead H), 4.40 (dd, 1H, J = 2, 5 Hz, HC—O), 7.4 (m, 5H, ArH). The major products 0.20 g (46%) arose from addition to the norbornene double bond.

Phenylthio-4-pentenol (8)

A solution of *n*-butyllithium in hexane (2.90 mL, 4.65 mmol, 1.6 *M*, Aldrich) was added dropwise to a stirred solution of 4-penten-1-ol (0.5 g, 5.8 mmol, Aldrich) in dry ether (20 mL) at 21°C. An ether solution (10 mL) of benzenesulfenyl chloride (1.91 mmol) prepared as outlined above was added dropwise over 10 min, stirring was continued for a further 2 h at 21°C and the reaction quenched with aqueous saturated ammonium chloride solution. The solution was extracted with ether, the combined ether extracts were washed with water, brine, dried, filtered, and concentrated, to give the sulfenate ester **8**, 0.392 g 35% as a pale yellow liquid; ir (film) 3070 (=C—H), 1645 (C=C), 740, 695 cm^{-1}; ^1H nmr ($CDCl_3$) δ: 1.0–2.1 (m, 4H), 3.76 (t, 2H, J = 7 Hz, H_2C—O), 4.80 (m, 1H, C=CH), 5.00 (m, 1H, C=CH), 5.35–6.0 (m, 1H, RCH=C), 7.73 (m, 5H, ArH). This material was recovered unchanged after 3 h in refluxing dimethoxyethane (85°C). However, stirring at 21°C in ether with a 2:1 weight ratio of 60–120 mesh silica gel afforded a 50% yield of tetrahydrofuran **9** and the starting alcohol.

In the case of the sulfenate ester derived from **26** neither refluxing an ether – silica gel slurry (10 h) nor treatment at 21°C for 3 h in the presence of boron trifluoride etherate afforded any cyclic ether products.

Acknowledgements

We are grateful to Memorial University of Newfoundland and the Natural Sciences and Engineering Research Council of Canada for financial support of this research, B. Gregory for high resolution mass spectra, and the referees for their comments.

1. F. J. Schmitz, R. S. Prasad, Y. Gopichand, M. B. Hossain, and D. Helm. J. Am. Chem. Soc. **103**, 2467 (1981).
2. Y. Y. Lin, M. Risk, M. S. Ray, D. V. Engen, J. Clardy, J. Golik, J. C. James, and K. Nakanishi. J. Am. Chem. Soc. **103**, 6773 (1981).
3. K. C. Nicolaou, M. E. Duggan, C. Hwang, and P. K. Somers. J. Chem. Soc. Chem. Commun. 1358 (1985).
4. D. R. Williams and J. G. Phillips. Tetrahedron, **42**, 3013 (1986).
5. P. C. Ting and P. A. Bartlett. J. Am. Chem. Soc. **106**, 2668 (1984).
6. G. J. O'Malley and M. P. Cava. Tetrahedron Lett. **26**, 6159 (1985).
7. W. L. Brown and A. G. Fallis. Tetrahedron Lett. **26**, 607 (1985); Can. J. Chem. **65**, 1828 (1987).
8. K. C. Nicolaou and Z. Lysenko. Tetrahedron Lett. 1257 (1977).
9. D. L. J. Clive, G. Chittattu, N. J. Curtis, W. A. Kiel, and C. K. Wong. J. Chem. Soc. Chem. Commun. 725 (1977).
10. K. C. Nicolaou and N. A. Petasis. Selenium in natural products synthesis. Cis Inc., Philadelphia. 1984.
11. K. C. Nicolaou, R. L. Magolda, W. J. Sipio, W. E. Burnette, Z. Lysenko, and M. M. Joullie. J. Am. Chem. Soc. **102**, 3784 (1980).
12. E. D. Edstrom and T. Livinghouse. J. Am. Chem. Soc. **108**, 1334 (1986).
13. J. E. Baldwin. J. Chem. Soc. Chem. Commun. 734 (1976).
14. J. E. Baldwin, R. C. Thomas, L. I. Kruse, and L. Silberman. J. Org. Chem. **42**, 3846 (1977).
15. W. A. Smit, N. S. Zefirov, and I. V. Bodrikov. *In* Organic sulfur chemistry. *Edited by* R. Kh. Freidlina and A. E. Skorva. Pergamon Press, Oxford. 1981. p. 159.
16. K. C. Nicolaou and Z. Lysenko. J. Chem. Soc. Chem. Commun. 293 (1977).
17. R. Kimura, A. Ichihara, and S. Sakamura. Synthesis, 516 (1979).
18. H. C. Brown, E. N. Peters, and M. Ravindranathan. J. Am. Chem. Soc. **97**, 2900 (1975).

Can. J. Chem. Downloaded from www.nrcresearchpress.com by 213.166.140.6 on 09/07/12
For personal use only.

Synthesis, structure, and hydrolysis of esters of strained and unstrained *N*-phosphonylureas

RONALD KLUGER AND GREGORY R. J. THATCHER
The Lash Miller Chemical Laboratories, Department of Chemistry, University of Toronto, Toronto, Ont., Canada M5S 1A1

AND

WILLIAM C. STALLINGS
Biophysics Research Division, The University of Michigan, Ann Arbor, MI 48104, U.S.A.

Received December 22, 1986

This paper is dedicated to Professor John T. Edward

RONALD KLUGER, GREGORY R. J. THATCHER, and WILLIAM C. STALLINGS. Can. J. Chem. **65**, 1838 (1987).

Compounds **1–5** were prepared to compare reactivity patterns of cyclic and acyclic phosphonylurea esters. The rates and products of reactions of phosphonylurea esters (**1–3**) with hydroxide in aqueous acetonitrile were analyzed. In these compounds the phosphonate moiety is in a strained five-membered ring, which also contains the ureido group. Structural determination of **1** by X-ray crystallography indicates that the five-membered ring is planar and the internal ring angle at phosphorus is 93.1°. The endocyclic N—C—N angle of the ureido group is 111°. The compounds undergo hydrolysis in alkaline aqueous acetonitrile at 35°C with a rate about 10^6 times that of analogues (**4**, **5**) in which the phosphonate group is exocyclic to the ureido ring. Compound **1** undergoes alkaline hydrolysis ($k = 9.0 \times 10^3\ M^{-1}\ s^{-1}$) to release the phenoxy group to give **6**. The hydrolysis of alkyl esters **2** ($k = 2.4 \times 10^4\ M^{-1}\ s^{-1}$) and **3** ($k = 1.3 \times 10^3\ M^{-1}\ s^{-1}$) leads to cleavage of the endocyclic P—N bond, producing **7** and **8** respectively. The exocyclic alkyl esters (**4** and **5**) also cleave at the P—N bond with respective rate constants of $6.5 \times 10^{-3}\ M^{-1}\ s^{-1}$ and $4.4 \times 10^{-2}\ M^{-1}\ s^{-1}$. The data are consistent with a mechanism in which hydroxide adds to **1** to form a pentacoordinate phosphorus intermediate with the phenoxy group in an equatorial position and the ureido ring in apical and equatorial positions (with nitrogen apical). The departure of the urea group is slower than pseudorotation of the intermediate and expulsion of phenoxide. In the isomerized intermediate, phenoxy is apical but the methylene group of the ring, which has low apicophilicity, must also be apical. Reactions of **2** and **3**, which have more basic oxygen leaving groups, occur with P—N cleavage because expulsion from the isomerized intermediate in those cases is not sufficiently fast. These results fit reaction patterns at phosphorus that are determined by ring strain and electronegativity of ligands. Contributions from effects due to antiperiplanar interactions between bonding and nonbonding electrons are not detected.

RONALD KLUGER, GREGORY R. J. THATCHER et WILLIAM C. STALLINGS. Can. J. Chem. **65**, 1838 (1987).

Dans le but d'évaluer les comportements réactionnels des esters phosphonylurées cycliques ainsi qu'acycliques, on a préparé les composés **1–5**. On a analysé les vitesses ainsi que les produits des réactions des esters phosphonylurées (**1–3**) avec l'hydroxyde dans l'acétonitrile aqueux. Dans ces composés, la portion phosphonate se trouve dans un cycle à cinq chaînons qui est tendu et qui contient aussi le groupement uréido. En se basant sur une détermination de structure du composé **1** par diffraction des rayons-X, on peut en déduire que le cycle à cinq chaînons est plan et que l'angle interne du cycle au niveau du phosphore est de 93°. L'angle endocyclique N—C—N du groupement uréido est de 111°. À 35°C et en solution acétonitrile alcaline, les composés subissent une hydrolyse dont la vitesse est environ 10^6 fois celle de ses analogues **4** et **5** dans lesquels le groupement phosphonate est exocyclique par rapport au cycle uréido. Le composé **1** subit une hydrolyse alcaline ($k = 9{,}0 \times 10^3\ M^{-1}\ s^{-1}$) qui conduit à une élimination du groupement phénoxy et à la formation du composé **6**. L'hydrolyse des esters alkylés **2** ($k = 2{,}4 \times 10^4\ M^{-1}\ s^{-1}$) et **3** ($k = 1{,}3 \times 10^3\ M^{-1}\ s^{-1}$) conduit à une rupture de la liaison P—N et à la formation respectivement des composés **7** et **8**. Les esters alkylés exocycliques (**4** et **5**) se coupent aussi au niveau de la liaison P—N avec des vitesses respectives de réaction de $6{,}5 \times 10^{-3}\ M^{-1}\ s^{-1}$ et $4{,}4 \times 10^{-2}\ M^{-1}\ s^{-1}$. Ces données sont en accord avec un mécanisme dans lequel l'ion hydroxyde s'additionne au composé **1** pour former un intermédiaire phosphoré pentacoordonné comportant le groupement phénoxy dans une position équatoriale et le cycle uréido dans les positions apicale et équatoriale (avec l'azote apical). Le départ du groupement urée est plus lent que la pseudorotation de l'intermédiaire et l'expulsion du phénolate. Dans l'intermédiare isomérisé, le phénoxy est apical mais le groupement méthylène du cycle, qui a peu de tendance à prendre la position apicale, doit aussi être apical. Les réactions des composés **2** et **3**, qui portent des groupements nucléofuges oxygénés plus basiques, se produisent avec une rupture de la liaison P—N parce que, dans ces cas, l'expulsion de groupements à partir de l'intermédiaire isomérisé n'est pas suffisamment rapide. Ces résultats sont en accord avec les comportements réactionnels au niveau du phosphore qui sont déterminés par des tensions de cycles et par l'électronégativité des ligands. On n'a pas pu détecter de contributions des effets dus aux interactions antipériplanaires entre les électrons liants et non-liants.

[Traduit par la revue]

Introduction

The reactivity patterns of cyclic tetracoordinated phosphorus esters are dominated by effects due to ring strain and the electronegativity of groups attached to phosphorus (1, 2). The kinetic effects of competition between these and other factors in structurally defined systems provide a quantitative basis for evaluation of the factors controlling reactivity. In this paper we report the rate of hydrolytic reactions of esters of cyclic phosphonylureas (**1–3**) in alkaline aqueous acetonitrile and the reactions of analogues in which the phosphorus atom is not contained in a ring (**4**, **5**). An X-ray crystal study of the cyclic phosphonylurea ester (**1**) provides a basis for the necessary structural analysis. The identity of the reaction products (**6–8**) and the rates of the reactions provide information that can be used to understand general reactivity patterns for phosphorus esters.

Experimental

Materials

Deuterated materials were obtained from Merck Isotopes, Aldrich Chemical Company, and Norrell. Materials used for syntheses were

Can. J. Chem. Downloaded from www.nrcresearchpress.com by 118.98.75.50 on 09/07/12
For personal use only.

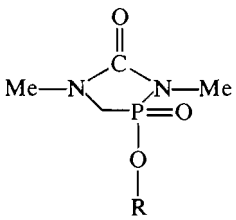

1 R = Ph
2 R = Me
3 R = Et
6 R = Na

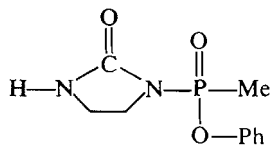

4

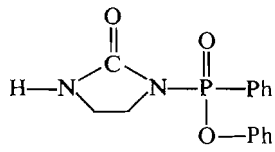

5

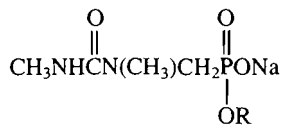

7 R = Me
8 R = Et

1: 1,4-dimethyl-2-phenoxy-1,4-diaza-2-phospholidine-2,5-dione (cyclic phenyl ester)
2: 1,4-dimethyl-2-methoxy-1,4-diaza-2-phospholidine-2,5-dione (cyclic methyl ester)
3: 1,4-dimethyl-2-ethoxy-1,4-diaza-2-phospholidine-2,5-dione (cyclic ethyl ester)
4: phenyl (1-imidazolidinone)methylphosphonate
5: phenyl (1-imidazolidinone)phenylphosphonate
6: sodium 1,4-dimethyl-2-oxy-1,4-diaza-2-phospholidine-2,5-dione
7: sodium methyl phosphono-(*N,N*-dimethylurea)
8: sodium ethyl phosphono-(*N,N*-dimethylurea)

Can. J. Chem. Downloaded from www.nrcresearchpress.com by 118.98.75.50 on 09/07/12
For personal use only.

purchased from the Aldrich Chemical Company and BDH Canada Limited. Inorganic chemicals were Fisher reagents.

Methods

Nuclear magnetic resonance spectra

Proton nmr spectra were recorded at 200 MHz using a Varian XL-200 spectrometer for samples in deuterated solvents. Carbon nmr spectra (20 MHz) were recorded on a Varian CFT-20 and phosphorus nmr spectra were recorded at 32 MHz using a Bruker WP-80.

Elemental analyses were determined by Galbraith Laboratories (Knoxville, Tennessee, U.S.A.).

Syntheses

1,4-Dimethyl-2-phenoxy-1,4,2-diazaphospholidine-2,5-dione (1)

The procedure is a modification of that reported by Birum (3). A mixture of 1,3-dimethylurea (4.4 g), paraformaldehyde (1.5 g), acetic anhydride (6 mL), and acetic acid (5 mL) was heated at 70°C for 4 h. Triphenyl phosphite (13.1 mL) was added and the mixture was kept at 90°C for 2 h. The mixture was concentrated *in vacuo* (1 Torr (133.3 Pa)). The residue was dissolved in 100 mL chloroform and washed with two 100-mL portions water. The chloroform layer was dried over magnesium sulfate and concentrated. Addition of anhydrous ether caused the product to precipitate. The material was recrystallized from chloroform–ether. Yield: 4.8 g (50%), mp 118–120°C; ir (KBr): 1713, 1591, 1490, 1288; ^{1}H nmr (chloroform-*d*, ppm downfield from Me_4Si) δ: 7.20, 7.15 (5H, 2s/m, ArH), 3.48 (2H, d, J = 15 Hz, N—CH_2P), 2.92 (3H, d, J = 2 Hz, C—N—CH_3), 2.82 (3H, d, J = 8 Hz, P—N—CH_3); ^{31}P nmr (chloroform-*d*, ppm downfield from phosphoric acid) δ: 23.46. *Anal.* calcd. for $C_{10}H_{13}N_2O_3P$: C 50.00, H 5.45, N 11.66, P 12.90; found: C 49.77, H 5.36, N 11.36, P. 12.68.

1,4-Dimethyl-2-methoxy-1,4,2-diazaphospholidine-2,5-dione (2)

This was prepared by the reaction of *N,N'*-dimethyl-*N*-methoxymethylurea and trimethyl phosphite using the method reported by Kluger *et al.* (4).

1,4-Dimethyl-2-ethoxy-1,4,2-diazaphospholidine-2,5-dione (3)

This was prepared by the reaction of *N,N'*-dimethyl-*N*-methoxymethylurea and triethyl phosphite (4).

Sodium 1,4-dimethyl-2-oxy-1,4,2-diazaphospholidine-2,5-dione (**6**) was prepared by reaction of sodium iodide (0.47 g) in 25 mL dry butanone with **2** with stirring and refluxing for 3 h (5). The white precipitate was collected by filtration, washed with butanone, dissolved in methanol, and precipitated by the addition of ether. The resulting powder was dried in a vacuum desiccator. Proton nmr (acetonitrile-d_3, relative to internal Me_4Si) δ: 3.21 (2H, d, J = 14 Hz, P—CH_2N), 2.80 (3H, s, N—CH_3), 2.66 (3H, d, J = 7 Hz, P—N—CH_3).

Phenyl phenylphosphonochloridate

Phenol (10.5 g) and pyridine (8.5 g) in 35 mL dry benzene were added to a stirred solution of phenylphosphonochloridate during 30 min. The solution was filtered and the filtrate distilled at 145°C, 2 Torr (6) in 60% yield.

Phenyl (1-imidazolidinone)methylphosphonate (4)

Imidazolidinone (1.67 g) and triethylamine (3.73 mL) were dissolved in 80 mL dry ether and added to a stirred solution of phenyl methylphosphonochloridate (3.7 g) in 20 mL dry ether at −5°C. The mixture was stirred for 5 h, then warmed to room temperature and allowed to stand for 24 h. The resulting precipitate was washed with ether. The filtrate and washings were concentrated *in vacuo*. The residue was dissolved in 50 mL chloroform and washed with two 50-mL portions of water. The chloroform layer was dried over magnesium sulfate and concentrated. The concentrate was placed on a column of silica gel (5 × 50 cm) and eluted with 10% methanol in chloroform. Fractions containing the product were detected by thin-layer chromatography. Evaporation yielded a white crystalline solid; uv (λ_{max}, acetonitrile): 262 nm; ^{1}H nmr (chloroform-*d*, relative to internal Me_4Si) δ: 7.17, 7.12 (5H, 2s, ArH), 5.98 (1H, s, NH), 3.05–3.8 (4H, m, NCH_2CH_2), 1.88 (3H, d, J = 18 Hz, P—CH_3). *Anal.* calcd. for $C_{10}H_{13}N_2O_3P$: C 50.00, H 5.45, N 11.66, P 12.90; found: C 49.76, H 5.40, N 11.52, P 12.89.

Phenyl (1-imidazolidinone)phenylphosphonate (5)

Imidazolidinone (0.34 g) and triethylamine (0.57 mL) in 20 mL methylene chloride were added to a stirred solution of phenyl phenylphosphonochloridate (0.97 g) in 5 mL methylene chloride during 20 min. This was stirred for an additional 20 min at room temperature followed by addition of benzene and methylene chloride, then concentrated. The precipitate was collected by filtration and washed with benzene. The filtrates were combined and concentrated *in vacuo* to yield a white powder, which was recrystallized from benzene (0.75 g), mp 145°C; ir spectrum (KBr): 1729, 1251 cm^{-1}; uv (λ_{max}, acetonitrile): 266 nm; ^{1}H nmr (chloroform-*d*, relative to internal Me_4Si) δ: 7.38 (5H, s, O—ArH), 7.1–8.3 (5H, m, P—ArH), 5.8 (1H, s, NH), 3.1–4.0 (4H, m, NCH_2CH_2N); ^{31}P nmr (chloroform-*d*) δ: 13.57.

Kinetics

Reactions were conducted in solutions of 60% acetonitrile–water (mixtures by volume) due to the low solubility of most of the substrates in water. Deuterated solvents were also used in the same proportion. Lower percentages of acetonitrile were used in some runs to determine solvent effects.

pH measurement

For solutions of low basicity, the apparent pH of the solution was

Can. J. Chem. Downloaded from www.nrcresearchpress.com by 118.98.75.50 on 09/07/12
For personal use only.

determined with a Canlab combination pH electrode and Radiometer pH meter 26. Jordan has shown that pH-meter readings give accurate measurements in acetonitrile–water mixtures (7). For solutions of moderate to high basicity, hydroxide concentration was determined by titration of the aqueous component, and the concentration reported is of that component. To arrive at values for second-order rate constants for the reactions of the acyclic compounds, the observed first-order rate constants were fit to a linear least-squares best fit as a function of aqueous hydroxide concentrations. However, for the cyclic compounds, the reactions were measured in solutions containing aqueous acetonitrile whose acidity was measured with a pH electrode. Therefore, an estimate of hydroxide concentration is necessary. We used the ion product for pure water at 35°C (13.68). The data were fit to the expression $k_{obs} = k_w + k_{OH^-}[OH^-]$.

Proton nuclear magnetic resonance spectroscopy

Products of the hydrolysis reaction of **1–5** were determined periodically by proton nmr analysis of deuterated reaction solutions and comparison of the product spectra with independently synthesized samples.

Ultraviolet kinetics

The production of phenoxide from the hydrolysis of **1**, **4**, and **5** was observed by its absorption at 259 nm using a Varian Cary 210 spectrophotometer with the sample in a cell contained in a jacketed cell holder maintained at 35°C with a Neslab Exacal circulator. Acetonitrile (1.8 mL) and the basic aqueous solution in water were equilibrated at 35.0°C. The substrate was added to the cell and the cell was stoppered, inverted, and shaken. Data were collected at intervals of 0.5 s using a microprocessor-controlled interface to the PET computer and collected in a memory array of the computer. These data were transferred to diskettes and analyzed using the kinetic overrelaxation algorithm (8), giving first-order rate constants with correlation coefficients of at least 0.99998 and confidence intervals of 1% (confidence intervals are two standard deviations). The effect of ionic strength was found to be very small since repetition of experiments using added potassium chloride (0.05 *M*) did not affect the observed rate in a test with each compound.

pH-stat method

Since the hydrolysis reactions of **1**, **2**, and **3** produce phosphonic acids rapidly, the rate of product formation can be followed using a pH-stat (Radiometer pH meter 28, titrator adapter TT11, and autoburette 12, volume 0.125 mL). A Heath potentiometric variable-voltage strip-chart recorder was connected to the apparatus via a 50-turn potentiometer against a 1-V reference cell (alkaline battery), which was connected to the rotating shaft of the autoburette. This converts volume of added titrant to voltage, which is recorded as a function of time. The reactions were conducted in a jacketed beaker maintained at 35°C by a circulating water bath. A mixture of 3 mL acetonitrile and 2 mL 0.1 *M* potassium chloride was stirred and equilibrated in the reaction vessel with the apparatus set to maintain the pH reading of the meter through the addition of 0.01 *M* or 0.05 *M* potassium hydroxide in water from the autoburette. The substrate was added and the pH of the solution maintained by the pH-stat. The substrate concentration ranged from 0.2 m*M* to 2.5 m*M*. The data from the chart were entered into the same program as was used for nmr and uv kinetics. Correlation coefficients of at least 0.9999 were obtained with an uncertainty of 1% (two standard deviations).

X-ray crystallography

1,4-Dimethyl-2-phenoxy-1,4,2-diazaphospholidine-2,5-dione (**1**) crystallized as long parallelepipeds in space group $P2_1/n$ with a = 12.461(3), b = 5.497(2), c = 16.889(4) Å, β = 97.24(2)°, and four molecules per unit cell. Three-dimensional diffraction data were measured at room temperature with a Nicolet diffractometer using graphite monochromated CuKα radiation; the $\theta/2\theta$ scan mode was employed, and the maximum value of θ was 64°. A 0.1 × 0.1 × 0.4-mm sample was sealed in an X-ray glass capillary. Of the 1919 unique reflections collected, 1594 had intensities, I, greater than an observation threshold of $2.0\sigma(I)$, where $\sigma(I)$ was derived from counting statistics. As indicated by the systematic decrease in intensity of three periodically monitored reflections (15% in 61 exposure-hours), the data were corrected for irradiation-induced decay. In addition, an empirically determined curve was used to correct the intensities for X-ray absorption. The data were converted to structure factor amplitudes by the application of Lorentz and polarization factors, and placed on an absolute scale using a Wilson plot. Values of $\sigma(F)$ were calculated from $\sigma(F) = (F/2)\{[\sigma^2(I)/I^2] + \delta^2\}^{1/2}$ where δ is an instrumental uncertainty determined from the variation of three periodically monitored reflections (δ = 0.0327).

The molecular skeleton was correctly positioned in an E-map calculated using phases derived from direct methods (9) and the structure, including hydrogen atoms located in intermediate Fourier syntheses, was refined (10, 11) by full-matrix least squares using published X-ray scattering factors (12, 13). The function minimized in the least-squares process was $\Sigma w(|F_o| - |F_o|)^2$ where the weights, w, were $\sigma^{-2}(F)$. The unweighted crystallographic residual for the observed data is 0.055 with a weighted residual of 0.049. Coordinates are listed in Table 1; refined temperature factors (anisotropic parameters for the non-hydrogen atoms and isotropic parameters for the hydrogen atoms) as well as observed and calculated structure factors have been deposited as supplementary material.[1] The crystals are a racemic mixture; the reported coordinates are for an arbitrarily selected isomer. Programs utilized in this study include ICRRMLS (10, 11), VIEW (14), and other programs from the crystallographic library at the Fox Chase Institute for Cancer Research, Philadelphia, PA.

Results

The observed rate constants for hydrolysis of the cyclic compounds (**1–3**) in 60% acetonitrile–water solutions are given in Table 2. The limited solubilities of the reactants and products in water necessitated the use of acetonitrile as a cosolvent. Deuterated solvents were used to permit us to follow the reactions by proton nmr spectroscopy. The rate constants for hydrolysis of the exocyclic phosphonates (**4** and **5**) in acetonitrile–water solutions are listed in Table 3. This table also contains data showing the effect of decreasing the proportion of acetonitrile on the reaction rate, and rates observed in deuterated media. Increasing the aqueous content of the solution increases the rate of reaction as expected, but only to a small degree. For example, the rate of hydrolysis of **5** in 60% acetonitrile containing 0.25 *M* hydroxide is about 1/5 the rate for the same compound in 0.5 *M* hydroxide in 23% acetonitrile. This shows that the solvent effect is not significant in terms of the comparisons of cyclic and acyclic compounds. The structural changes affect reactivity by many orders of magnitude in rate while the solvent effects cause rate changes within a single order of magnitude.

The data in Table 4 summarize second-order rate constants for the reactions of the five substrates with hydroxide in 60% aqueous acetonitrile. Since the activity of hydroxide and deuteroxide in the acetonitrile solutions is not known, the absolute values of the rate constants are subject to future correction but comparison of relative magnitudes should be valid. As expected, the cyclic phosphonates (**1–3**) are much more reactive toward hydrolysis than are the exocyclic phosphonates (**4**, **5**). However, the products and rates of the reactions depend on the solution conditions.

Base catalysis

The three cyclic phosphonates undergo hydrolysis that increases in rate with hydroxide concentration in solutions with pH > 6. The phenyl ester, **1**, undergoes hydrolysis with

[1]This material may be purchased from the Depository of Unpublished Data, CISTI, National Research Council of Canada, Ottawa, Ont., Canada K1A 0S2.

Can. J. Chem. Downloaded from www.nrcresearchpress.com by 118.98.75.50 on 09/07/12
For personal use only.

TABLE 1. Positional parameters, expressed as fractions of cell edges, for **1**. The numbers in parentheses represent the estimated standard deviation with respect to the last digit reported

Atom	*x*	*y*	*z*
P(1)	0.16575(6)	0.0390(2)	0.50176(5)
O(2)	0.0912(2)	0.2402(4)	0.5088(2)
O(3)	0.2013(2)	−0.0966(4)	0.5841(2)
C(4)	0.1311(3)	−0.1920(6)	0.4270(2)
N(5)	0.2267(5)	−0.2086(5)	0.3863(2)
C(6)	0.3075(3)	−0.4715(7)	0.4071(2)
N(7)	0.2823(2)	0.1008(5)	0.4692(2)
O(8)	0.3903(2)	−0.0317(6)	0.3776(2)
C(9)	0.2289(3)	−0.3764(7)	0.3207(3)
C(10)	0.3617(3)	0.2757(8)	0.5057(3)
C(11)	0.0761(3)	−0.2563(6)	0.6661(2)
C(12)	0.0249(3)	−0.2350(7)	0.7344(3)
C(13)	0.0409(3)	−0.0380(8)	0.7831(3)
C(14)	0.1105(3)	0.1416(7)	0.7658(2)
C(15)	0.1633(3)	0.1250(7)	0.6991(2)
C(16)	0.1444(3)	−0.0719(6)	0.6505(2)
H1(C4)	0.070(3)	−0.137(6)	0.386(2)
H2(C4)	0.116(3)	−0.347(6)	0.450(2)
H1(C9)	0.214(4)	−0.542(8)	0.336(3)
H2(C9)	0.173(3)	−0.334(7)	0.272(3)
H3(C9)	0.301(4)	−0.367(8)	0.300(3)
H1(C10)	0.333(4)	0.374(8)	0.535(3)
H2(C10)	0.410(5)	0.321(9)	0.461(3)
H3(C10)	0.419(5)	0.174(9)	0.538(4)
H1(C11)	0.067(3)	−0.396(7)	0.635(2)
H1(C12)	−0.020(3)	−0.359(6)	0.746(2)
H1(C13)	0.001(3)	−0.021(6)	0.832(2)
H1(C14)	0.122(3)	0.273(6)	0.799(2)
H1(C15)	0.210(3)	0.246(6)	0.685(3)

TABLE 2. Rate constants for hydrolysis in 60% acetonitrile–water at 35°C[a]

Compound	pH[b]	$10^5\ k_{obs}$, s^{-1}
1	4.2	40.0
	5.1	45.0
	6.8	122.0
	6.9	180.0
	7.1	275.0
2	5.1	34.7
	5.2	39.5
	6.2	105.
	6.8	345.
3	4.8	11.9
	6.6	62.0
	7.5	401.

[a]Pseudo first-order conditions. Rate measured by pH-stat by addition of aqueous NaOH.
[b]pH-meter reading from combination electrode.

exclusive cleavage of the exocyclic phenoxy group, while the two alkyl esters, **2** and **3**, cleave between phosphorus and nitrogen to give the ring-opened products of endocyclic cleavage. The exocyclic esters (**4** and **5**) both undergo base-catalyzed hydrolysis to lose the phenoxy group and retain the phosphonyl-urea linkage.

The observed first-order rate constant for base-catalyzed phenoxy cleavage of the cyclic compared to the exocyclic compounds is 10^5 to 10^6. The cleavage of the P—N bond of the

TABLE 3. Rate constants for hydrolysis in acetonitrile–water–NaOH at 35°C[a]

Compound	$[OH^-]$[b]	% Acetonitrile	$10^5\ k_{obs}$, s^{-1}
4	0.08		406.
	0.20		989.
	0.28		1280
5	0.08	60	64.7
	0.10		77.5
	0.20		146.
	0.25		183.
	0.28		188.
4	0.50	23	437.
	1.00	23	7210
	1.00	28	8200
5	0.50	23	1020
	0.50	28	778.
	1.00	23	1740
	1.00	28	1350
4[c]	0.10	60	842.
5[c]	0.10	60	123.

[a]Rates measured by change in uv absorbance.
[b]Concentration of NaOH in water prior to addition of acetonitrile.
[c]In D_2O containing NaOD.

TABLE 4. Second-order rate constants for base-catalyzed hydrolysis in 60% acetonitrile water. From data in Tables 1 and 2[a]

Compound	k_{OH^-}, M^{-1}	k_w, s^{-1}
1	9.0×10^3	4×10^{-4}
2	2.4×10^4	3×10^{-4}
3	1.3×10^3	1.7×10^{-4}
4	4.4×10^{-2}	Not determined
5	6.5×10^{-3}	Not determined

[a]From fit of first-order data to $k_{obs} = k_{OH^-}[OH^-] + k_w$. Values for k_{OH^-} have sd ca. 1%. k_w is approximate.

methyl ester (**2**) is faster than the phenoxy cleavage reaction of **1** while the cleavage of the ethyl ester (**3**) is slower than the phenoxy cleavage of **1**.

Solvent isotope effects

Since the measurement of pH and pD in aqueous acetonitrile and the activity of deuteroxide versus hydroxide under the conditions are not known, the data are not compared in this study.

Crystallographic analysis

The structure of **1** was determined by X-ray crystallography (Fig. 1). The bond lengths and angles that characterize the substituted phospholidine ring are summarized in Fig. 1. The molecule is fully extended with the five- and six-membered rings almost parallel. Analysis of the packing in the crystal structure reveals no apparently unusual interactions. All of the intermolecular associations are best characterized as van der Waals contacts.

The atoms of the phospholidine ring, including the *N*-methyl substituents and carbonyl oxygen, are essentially coplanar; deviations from the least-squares plane calculated through the urea-like atoms are described in Fig. 1. The planarity of this ring arises from resonance structures that require sp^2 hybridization and consequent overlap of the p_z orbitals on the C, N, and O atoms of the ureido moiety; evidence that the carbon and

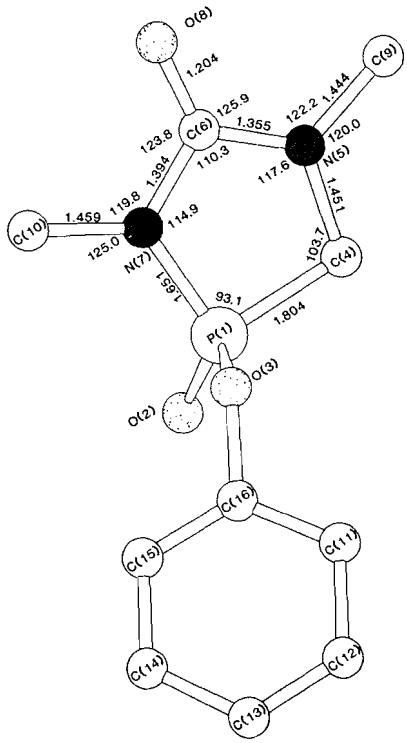

FIG. 1. The structure of **1** as determined by X-ray crystallography. Coordinates can be found in Table 1.

nitrogen atoms of the urea are trigonal is given by noting that, within experimental error, the sum of the valence angles about these atoms is in each case 360°C. The phosphorus and methylene carbon atoms that close the ring, like the carbonyl oxygen and *N*-methyl groups, are therefore coplanar substituents of sp^2 hybridized atoms and all 8 atoms thus adopt a planar arrangement. The P—N(7) bond length of 1.651 Å indicates a bond order greater than unity, and suggests the possibility of π character in this bond. The difference in the C(6)—N bond lengths is in line with this reasoning: if N(7) shares its p_z lone-pair electrons in bonds with phosphorus and the ureido carbonyl carbon, then one would anticipate the observed lengthening of the C(6)—N(7) bond relative to the C(6)—N(5) bond since the N(5) lone pair forms a bond solely with the carbonyl carbon. The present structure is perhaps most directly comparable to that of 1,3-dimethyl-2-methylamino-1,3,2-diazaphospholidine-2,4,5-trione (15) and related compounds (16) where, similarly, the planarity of the five-membered ring is attributed to resonance effects between linked carboxamide moieties.

The coplanarity of the atoms of the phospholidine ring must introduce considerable strain into the molecule. This is manifested most noticeably in the N(7)—P—C(4) (93.4°) and N(7)—C(6)—N(5) (110.3°) angles, but each of the valence angles around the ring is considerably contracted from standard trigonal or tetrahedral values.

Strain calculations

The reactivity of cyclic phosphate derivatives is affected by the strain of the ring system and the nature of the substituents attached to phosphorus (1, 2). The pentacoordinate intermediate generated by addition of a nucleophile to phosphorus is trigonal bipyramidal, and has been shown to be expected to be much less strained (or unstrained) (17). Thus, the effect of ring strain on reactivity can be approximated by comparing the rate of reaction of a strained cyclic compound and an acyclic analogue.

The ring strain in **1** can be approximated using molecular mechanics methodology, following the general procedure described by Westheimer and co-workers (18, 19), which is based on the equations of Shimanouchi *et al.* (20). Holmes has provided a sophisticated force field model that greatly extends the methodology using computer calculations (21). For the purposes of our approximate analysis, the earlier method provides sufficient accuracy. The Westheimer method uses the formula below to calculate the strain energy, E:

$$E = 1/2b^*[\delta\theta]^2$$

The quantity b is the bending force constant for a bond with units of cal mol^{-1} deg^{-2} and the quantity in brackets is the deviation from the equilibrium angle in degrees. The values of the force constant and exponent are uncertain but a value of the force constant of 45 cal mol^{-1} deg^{-2} has given reasonable agreement with experimental determinations, as has the value of the exponent. For the basis of comparison of different compounds, the absolute value is not necessary. While this method cannot generate an optimized structure from first principles, since the structure is known, we can estimate relative strain energies.

Using optimal angles for sp^3 centers as 109.5° and optimal angles for sp^2 centers as 120°, and the bending force constant given above, the strain energy of **1** is calculated to be 8.6 kcal mol^{-1}. Since **1** hydrolyzes at a rate about 10^5 to 10^6 times that of its acyclic analogue, the free energy of activation for **1** is between 7 and 9 kcal/mol^{-1} less than its acyclic analogue. However, unlike the acyclic analogue, **1** must react via a pentacoordinate phosphorus intermediate in which the methylene group of the ring is in an apical position. The electronic barrier to formation of this isomer works against the relief of strain that accompanies its formation. Therefore the acceleration due to ring strain is even larger than is implicit in the differences in free energy of activation from rate constant ratios of cyclic and acyclic compounds.

For comparison, methyl ethylene phosphate is less strained than **1**. We have performed calculations using the same bending force constant, which give a strain energy of 4.6 kcal mol^{-1}, which is about half that of **1**. Yet the acceleration of the rate of hydrolysis relative to an acyclic analogue is the same as it is for **1**. In the case of methyl ethylene phosphate, no electronically unfavourable intermediate is involved in the reaction and the full effect of ring strain can be manifested in the rate constant.

Discussion

The reaction patterns we observe are consistent with the reactions reflecting the stability of the pentacoordinated phosphorus intermediates that are produced. Holmes has summarized preference rules (based on the original rules proposed by Westheimer (2)) for the structure of intermediates in pentacoordinated trigonal bipyramidal phosphorus compounds and ranked these in order of importance (1). Those which apply to our system are as follows:

1. Five-membered cyclic systems preferentially span one apical and one equatorial position.
2. The most electronegative ligands prefer apical sites.
3. π-Bonding ligands prefer equatorial sites.
4. Steric effects are minimized with bulky groups in equatorial positions.

We apply these rules in our analysis.

Enhanced reactivity of cyclic ureaphosphonates

The rate constant for the alkaline hydrolysis of the cyclic phenyl ester (**1**) is about 5×10^5 times as large as that for the

Can. J. Chem. Downloaded from www.nrcresearchpress.com by 118.98.75.50 on 09/07/12
For personal use only.

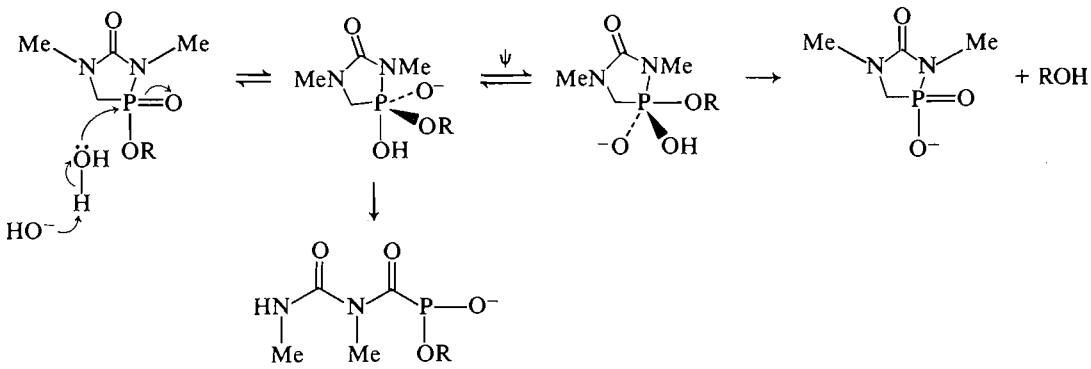

SCHEME 1

base-catalyzed hydrolysis of its acyclic analogue, **4**. The methyl and ethyl esters, **4** and **5**, undergo P—N bond cleavage while acyclic analogues tend to undergo P—O cleavage. Still, the rate of P—N cleavage in the cyclic alkyl esters exceeds the rate of P—O cleavage in the acyclic esters by a large factor. These results agree with those observed by Hudson and co-workers for cyclic phosphoramides (22).

The mechanism of exocyclic cleavage

The tendency for strained cyclic phosphate ester derivatives to undergo rapid hydrolysis reactions has been well documented and has been established as due to reduced strain in the transition state of the rate-determining step. In the case of methyl ethylene phosphate (23–25), the leaving group for exocyclic cleavage is methoxide (pK 15.7) while ring cleavage involves the less basic 2-oxyethyl species (pK ~ 14.7). The transition state probably resembles the high energy intermediate and little development of charge would occur on the leaving group in the transition state. The cyclic phosphonylurea esters with alkoxy leaving groups (**2**, **3**) cleave the phosphorus–urea bond while the phenyl ester (**1**) cleaves at the exocyclic bond. Since phenoxide is a better leaving group than alkoxides, this result is in the expected direction. Based on the low reactivity in alkaline solution of materials analogous to ring-opened material **7** (4), as well as the low reactivity of the ethyl ester of a ureaphosphonate **8** (4), it is reasonable that exocyclic cleavage of the ester is a primary reaction and does not result from recyclization of the endocyclic cleavage product (**7**). Mechanisms based on this analysis are presented in Scheme 1. For the phenyl ester, **1** (R = phenyl), the initially formed intermediate undergoes pseudorotation followed by P—O cleavage to produce the cyclic phosphonylurea, while the alkyl esters (**2** and **3**, R = methyl or ethyl) cleave the ring to produce the methylphosphonylated dimethyl urea derivative. The reaction is shown as involving proton abstraction from water since it is known that reactions of cyclic phosphate triesters may be subject to general base catalysis (26).

The reaction of **1** with hydroxide will produce a trigonal bipyramidal intermediate in which the methylene group of the phosphonylurea ring occupies an equatorial position, while the urea nitrogen adjacent to phosphorus occupies an apical position. Since hydroxide is expected to enter via the apical position, the leaving phenoxy group occupies an equatorial position and pseudorotation of the intermediate is necessary to allow the phenoxy group to occupy an apical position from which it will leave most readily. The pseudorotation places the methylene group of the ring in the apical position. Since the methylene group has low apicophilicity there is a considerable energy barrier to arriving at this intermediate. However, our results suggest that the energy available from relief of strain in forming the five-coordinated intermediate is sufficient to overcome this barrier. Alternatively, phenoxide could leave from the equatorial position of the original trigonal bipyramid. While avoiding the pseudorotation to the higher energy intermediate, the expulsion from the equatorial position must itself be higher in energy than expulsion from an apical position.

Holmes has presented an empirical scale for estimating the apicophilicity of substituents (1). This method gives the difference in free energies between otherwise identical trigonal bipyramidal phosphorus derivatives, in which a pair of apical and equatorial ligands are interchanged, as well as the energy of a square pyramidal transition state. The arbitrary starting free energy is 0.0 for carbon in an equatorial position. Exchange of carbon to an apical position is 7 kcal mol^{-1} endergonic. In general, nitrogen also is at a lower energy in an equatorial position but the difference is much smaller (0.8 kcal) so that the net cost is around 6 kcal mol^{-1}. However, since in the present case the nitrogen atom is also attached to a carbonyl group, its electronegativity is increased. If it is equal in electronegativity to oxygen, then the apical position is preferred by 1.3 kcal mol^{-1} and the interchange of ligands costs about 8 kcal mol^{-1}. Other factors considered by Holmes include changes in steric interactions, but in this case the differences are probably not significant. Thus, the pseudorotation introduces a high cost in terms of electronegativity preferences, which diminishes the apparent acceleration of the cyclic compared to acyclic compounds.

Hall and Inch have reported elegant stereochemical studies of hydrolysis reactions of cyclic phosphoramidic thiones (27). Their results show that retention of stereochemical configuration at phosphorus occurs even when rings are cleaved. These workers explain that thermodynamic apicophilicities, such as those derived by Holmes, cannot account for the reactivity patterns. They propose the concept of apicopotentiality, in which groups that have a thermodynamic preference for the apical position in stable trigonal bipyramids may prefer equatorial positions in transition states. Since these compounds are somewhat similar to those we have studied, the kinetic effects may require further consideration.

To identify the rate-determining step of the reaction, the pseudorotation must be taken into account. Addition of hydroxide to **1** produces the initial intermediate. The barrier to expulsion of hydroxide should normally be higher than that for phenoxide, given the lower basicity of the phenoxide ion. However, since an energetically unfavourable pseudorotation precedes expulsion of phenoxide, the barrier to expulsion of phenoxide must include the energy difference between the pseudorotamers. Thus the rate-determining step is associated with the high energy pseudorotamer. The possibilities for

Can. J. Chem. Downloaded from www.nrcresearchpress.com by 118.98.75.50 on 09/07/12
For personal use only.

reaction of this intermediate are expulsion of phenoxide or pseudorotation back to the lower energy isomer. The heights of the barriers are not known but, since the pseudorotation involves no bond breakage and is in the thermodynamically favoured direction, we are inclined to identify the phenoxide expulsion step as being rate determining.

Effects of antiperiplanar electrons

The addition of hydroxide to **1** does not involve any of the possible postulated special antiperiplanar-oriented interactions between lone pairs of electrons of endocyclic ligands and the entering nucleophile (28, 29) (but see also ref. 24). The importance of such effects in the hydrolysis of acetamidines has recently been shown to be much less significant than originally was proposed (30). The lone pair of electrons on the nitrogen adjacent to phosphorus of **1** is in an orbital synperiplanar to the σ bond that is formed between the adding hydroxide ion and the phosphorus atom. After pseudorotation the lone pair of electrons on nitrogen is still clinal with respect to the σ bond between phosphorus and the leaving group. Since either formation of the intermediate or pseudorotation of the intermediate is rate determining, there is no possibility for stereoelectronic acceleration due to antiperiplanar lone-pair interactions, yet the rate is enhanced to the same degree as in systems in which such assistance has been postulated. However, we have seen that relief of ring strain in arriving at the transition state is the source of considerable acceleration of the rate of reaction of the cyclic ester, as is the case in methyl ethylene phosphate (23). Thus our results indicate that stereoelectronic effects due to antiperiplanar interactions between σ bonds and nonbonding electrons must contribute no more than a very small portion of any acceleration in other systems that show no greater rate enhancement than shown in the cyclic phosphonylurea esters.

Acknowledgements

R.K. thanks the Natural Sciences and Engineering Research Council of Canada for support of this work through an operating grant. W.C.S. thanks the National Institutes of Health for support and Drs. H. L. Carrell and J. P. Glusker for the use of diffraction facilities at the Fox Chase Institute for Cancer Research (Philadelphia, PA, U.S.A.).

1. R. R. HOLMES. Pentacoordinated phosphorus. Vol. I. 1980. American Chemical Society, Washington, DC. 1980.
2. F. H. WESTHEIMER. Acc. Chem. Res. **1**, 70 (1968).
3. G. H. BIRUM. U.S. Patent No. 3 989 727 (1986).
4. R. KLUGER, P. P. DAVIS, and P. D. ADAWADKAR. J. Am. Chem. Soc. **101**, 5995 (1979).
5. R. KLUGER, J. F. CHOW, and J. J. CROKE. J. Am. Chem. Soc. **106**, 4017 (1984).
6. M. F. HERSMAN and L. F. ADRIETH. J. Am. Chem. Soc. **90**, 1959 (1958).
7. F. JORDAN. J. Phys. Chem. **77**, 2681 (1973).
8. C. G. SWAIN, M. S. SWAIN, and L. F. BERG. J. Chem. Inf. Comput. Sci. **20**, 47 (1980).
9. G. GERMAIN, P. MAIN, and M. M. WOOLFSON. Acta Crystallogr. Sect. A: Cryst. Phys. Diffr. Theor. Gen. Crystallogr. **27**, 368 (1971).
10. P. K. GANTZEL, R. A. SPARKS, R. E. LONG, and K. N. TRUEBLOOD. UCLALS4, full-matrix least-squares refinement program in Fortran IV. 1969.
11. H. L. CARRELL. ICRFMLS, modification of UCLALS4, program from the Fox Chase Institute for Cancer Research, Philadelphia, PA. 1975.
12. D. T. CROMER and J. B. MANN. Acta Crystallogr. Sect. A: Cryst. Phys. Diffr. Theor. Gen. Crystallogr. 321 (1968).
13. R. F. STEWART, E. R. DAVIDSON, and W. T. SIMPSON. J. Chem. Phys. **42**, 3175 (1965).
14. H. L. CARRELL. VIEW, Program from the Fox Chase Institute for Cancer Research, Philadelphia, PA. 1977.
15. B. T. HUTTON, T. A. MODRO, M. L. NIVEN, and S. SCAILLET. J. Chem. Soc. Perkin Trans. 2, 17 (1986).
16. J. WEISS and G. HARTMAN. Z. Naturforsch. Teil B, **21**, 891 (1967).
17. F. H. WESTHEIMER. Special Publication No. 8, The Chemical Society, London. 1957. p. 1.
18. D. A. USHER, E. A. DENNIS, and F. H. WESTHEIMER. J. Am. Chem. Soc. **87**, 232 (1965).
19. F. H. WESTHEIMER. *In* Steric effects in organic chemistry. *Edited by* M. S. Newman. Wiley, New York. 1956. pp. 523–555.
20. T. SHIMANOUCHI, M. TSUBOI, and Y. KYOGOKU. Adv. Chem. Phys. **7**, 435 (1964).
21. R. R. HOLMES. J. Am. Chem. Soc. **100**, 433 (1978).
22. C. BROWN, J. A. BOUDREAU, B. HEWITSON, and R. F. HUDSON. J. Chem. Soc. Chem. Commun. 504 (1975).
23. R. KLUGER, F. COVITZ, E. A. DENNIS, L. D. WILLIAMS, and F. H. WESTHEIMER. J. Am. Chem. Soc. **91**, 6066 (1969).
24. R. KLUGER and G. R. J. THATCHER. J. Am. Chem. Soc. **107**, 6006 (1985).
25. R. KLUGER and G. R. J. THATCHER. J. Org. Chem. **51**, 207 (1986).
26. F. COVITZ and F. H. WESTHEIMER. J. Am. Chem. Soc. **85**, 1773 (1963).
27. C. R. HALL and T. D. INCH. J. Chem. Soc. Perkin Trans. 1, 2368 (1981).
28. J. M. LEHN and G. J. WIPFF. J. Chem. Soc. Chem. Commun. 800 (1975).
29. D. G. GORENSTEIN, J. B. FINDLAY, B. A. LUXON, and D. KAR. J. Am. Chem. Soc. **99**, 3473 (1977).
30. C. L. PERRIN and O. NUNEZ. J. Am. Chem. Soc. **109**, 522 (1987).

Can. J. Chem. Downloaded from www.nrcresearchpress.com by 118.98.75.50 on 09/07/12
For personal use only.

The benzylic anomeric effect. Internal rotational potentials of $ArCH_2X$ compounds (X = F, Cl, SH, SCH_3, $S(O)CH_3$, SO_2CH_3)

GLENN H. PENNER, TED SCHAEFER, AND RUDY SEBASTIAN
Department of Chemistry, University of Manitoba, Winnipeg, Man., Canada R3T 2N2

AND

SAUL WOLFE
Department of Chemistry, Queen's University, Kingston, Ont., Canada K7L 3N6

Received December 22, 1986

This paper is dedicated to Professor John T. Edward[1]

GLENN H. PENNER, TED SCHAEFER, RUDY SEBASTIAN, and SAUL WOLFE. Can. J. Chem. **65**, 1845 (1987).

The apparent twofold barriers to rotation about the exocyclic C—C bonds in $ArCH_2X$ (X = SH, SMe, S(O)Me, SO_2Me) compounds have been determined in CS_2 and in benzene-d_6, from the magnitudes of long-range proton–proton coupling constants. The work extends earlier studies of the systems X = F, Cl. Except for X = F, all of the title compounds have a low energy conformation in which the C—X bond is perpendicular to the plane of the benzene ring. The introduction of two *meta*-chlorine substituents leads to a 2 kJ/mol relative destabilization of this structure for X = F, Cl, SH. The trend in the rotational barriers associated with the sulfur substituents is SH, SMe ≪ S(O)Me, SO_2Me. *Ab initio* calculations, with geometry optimization at the STO-3G level for X = F, Cl, SH, reproduce the experimental results, and also the magnitudes of the rotational barriers. Quantitative PMO analyses of these *ab initio* wavefunctions have been employed to distinguish between "steric" and "other" interpretations, and reveal that the preferred conformation of X = F is determined by a first order perturbational effect, manifested in an electrostatic attraction between the heteroatom and a *syn*-periplanar *ortho*-hydrogen. For X = Cl, the PMO analysis suggests that a π_{Ar}–σ^*_{CX} interaction, analogous to the n–σ^*_{CX} interaction postulated as the origin of the anomeric effect in heterocyclohexanes, plays a dominant role. For X = SH, both π_{Ar}–σ^*_{CX} and σ_{CX}–π^*_{Ar} interactions are found; the latter is not possible in the anomeric effect itself. It is concluded that a benzylic anomeric effect exists, and that its magnitude, as a function of X, is S(O)Me, SO_2Me > Cl > SH, SMe > F.

GLENN H. PENNER, TED SCHAEFER, RUDY SEBASTIAN et SAUL WOLFE. Can. J. Chem. **65**, 1845 (1987).

Utilisant les amplitudes des constantes de couplage proton–proton à longue distance, on a déterminé les barrières binaires apparentes à la rotation autour des liaisons exocycliques C—C des composés $ArCH_2X$ (X = SH, SMe, S(O)Me et SO_2Me) dans le CS_2 et dans le benzène-d_6. Ces études sont une extension d'etudes antérieures sur des systèmes dans lesquels X = F et Cl. Excepté pour le cas où X = F, tous les composés mentionnés dans le titre présentent une conformation de basse énergie dans laquelle la liaison C—X est perpendiculaire au plan du noyau benzénique. L'introduction de deux chlores en positions *méta* conduit à une déstabilisation relative de 2 kJ/mol de cette structure pour X = F, Cl et SH. Cette tendance dans les barrières rotationnelles associées avec les substituants contenant du soufre est la suivante : SH, SMe ≪ S(O)Me, SO_2Me. Des calculs *ab initio* impliquant des optimisations de la géométrie au niveau STO-3G ont été réalisés sur les composés contenant X = F, Cl et SH et ils permettent de reproduire les résultats expérimentaux ainsi que les amplitudes des barrières à la rotation. On a utilisé des analyses quantitatives PMO de ces fonctions d'onde *ab initio* pour distinguer entre les interprétations *stériques* et *autres*; ces analyses révèlent que la conformation privilégiée pour X = F est déterminée par un effet de perturbation du premier ordre qui se manifeste par une attraction électrostatique entre l'hétéroatome et un hydrogène *ortho syn* et périplanaire. Pour X = Cl, l'analyse PMO suggère que l'existence d'une interaction π_{Ar}–σ^*_{CX}, semblable à l'interaction n–σ^*_{CX} qui a été suggérée comme étant à l'origine de l'effet anomère dans les hétérocyclohexes, joue un rôle dominant. Pour X = SH, on a trouvé des interactions π_{Ar}–σ^*_{CX} ainsi que σ_{CX}–π^*_{Ar}; ce dernier n'est toutefois possible dans l'effet anomère lui-même. On en conclut qu'un effet anomérique benzylique existe et que son amplitude, en fonction de X, est la suivante : S(O)Me, SO_2Me > Cl > SH, SMe > F.

[Traduit par la revue]

Introduction

The sixfold barrier to internal rotation in toluene is only 0.06 kJ/mol (1) and the preferred conformation is unknown. Semi-empirical INDO-MO computations give results consistent with this low barrier, and suggest that, in the conformation of lowest energy (**1**), the α C—H bond lies in the plane of the benzene ring (2). The same structure is obtained in geometry-optimized STO-3G calculations, but the internal barrier is found to be only 0.015 kJ/mol (3*a*). This is probably below the level of computational significance, as is the barrier computed at the 4-21G level (3*b*). In propylene, the internal barrier to rotation becomes relatively large and threefold. The most stable conformation (**2***a*) has a methyl hydrogen in the plane of the carbon–carbon double bond (4), while in 3-X-substituted propenes either X or H lies in this plane (5). For X = CH_3, the H-in-plane conformation (**3***a*) of ethylbenzene is 3.6 kJ/mol lower[2] in energy than the X-in-plane conformation (**3***b*), and the H-in-plane conformation (**4***a*) of 1-butene is more stable than the X-in-plane conformation (**4***b*) by 0.6–2.2 kJ/mol (6).

It seems reasonable to rationalize these conformational preferences in terms of the concept of "steric effects". In the language of perturbational molecular orbital theory (PMO theory) (7), **2***a* is more stable than **2***b* because the two-orbital four-electron destabilizing interaction between π_{CC} and π_{CH_3} (see **2***a*′ and **2***b*′), which makes the dominant contribution to the HOMO, is minimized in **2***a* (**2***a*′), mainly because of the effect of the secondary overlap depicted by the double-headed arrows. This destabilizing interaction, also known as "overlap

[1]On the occasion of his 65th birthday, and for his pioneering contributions to the study of the anomeric effect.

[2]Unpublished geometry-optimized 6-31G computations by G.H.P.

Can. J. Chem. Downloaded from www.nrcresearchpress.com by 118.98.75.50 on 09/07/12
For personal use only.

Can. J. Chem. Downloaded from www.nrcresearchpress.com by 118.98.75.50 on 09/07/12
For personal use only.

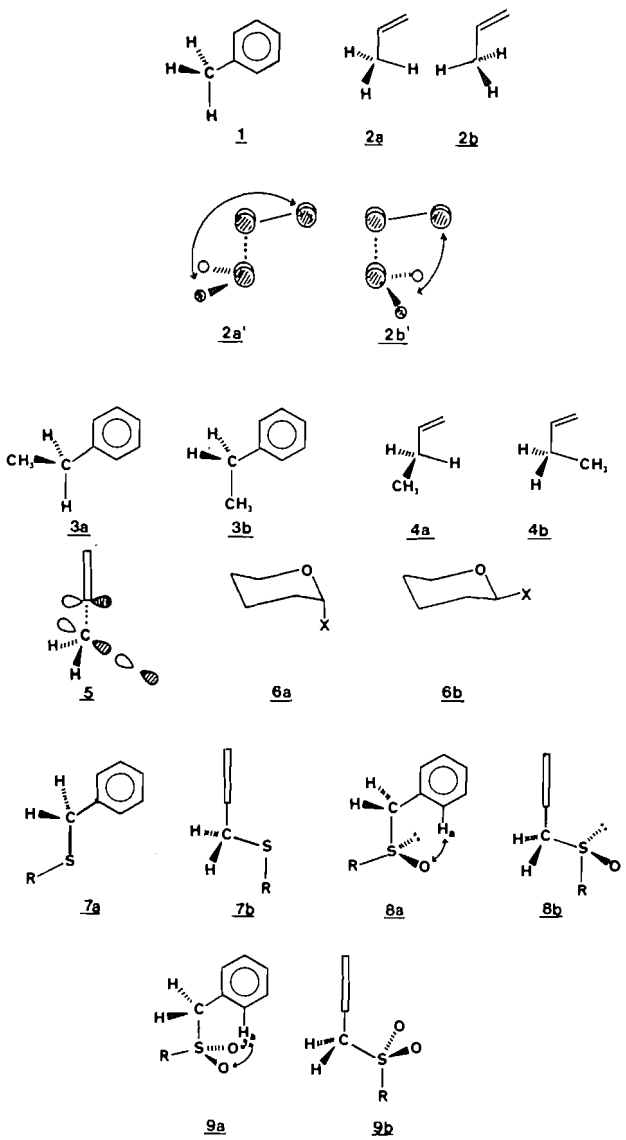

repulsion" (8) or "conjugative destabilization" (9), can be regarded as the MO counterpart of a "steric effect".

The question posed in the present work is whether any additional "conformational effects" (10) have to be invoked to account for the conformational preferences of benzyl-X compounds when X ≠ CH_3. For example, a perpendicular structure such as **5** contains a potential *two*-orbital *two*-electron *stabilizing* interaction between π_{Ar} and σ^*_{C-X}. To the extent that such an anomeric type "effect" (11) exists, it will enhance the conformational preference for this structure.

The magnitude of the anomeric effect, i.e., the conformational preference for **6***a* over **6***b*, is known to be solvent dependent (12), and to decrease for a given electronegative ligand X as the solvent becomes more polar. The conformational behaviour of benzyl fluoride and benzyl chloride is also solvent dependent (3*a*, 3*b*), but the trend is opposite to that observed in the anomeric effect. In CS_2, benzyl fluoride appears to prefer the conformation in which the C—F bond lies in the plane of the benzene ring; as the solvent is changed from CS_2 to DMSO or acetone, the perpendicular structure **5** undergoes relative stabilization by 2 kJ/mol. In benzyl chloride, the low energy conformation is **5**, and the rotational barrier increases from 8.8 kJ/mol in CS_2 to 11.2 kJ/mol in acetone.

Molecular orbital calculations with full geometry optimization at the STO-3G level (3*c*), and the constraint that the benzene ring remain a regular hexagon, reproduce these experimental observations (3*a*, 3*b*). In benzyl fluoride, the calculated low energy conformation has the C—F bond in the plane of the benzene ring, and is 1.6 kJ/mol more stable than **5**. In benzyl chloride, the calculated low energy conformation is **5**, and the rotational barrier is 8.6 kJ/mol. Since benzyl fluoride and benzyl chloride thus exhibit opposite conformational preferences which do not vary with solvent in the same manner as the anomeric effect, this might imply that stabilizing anomeric-type orbital interactions are not important in these compounds. That there is no anomeric effect in benzyl fluoride is evident from its planar conformational preference.

To probe these points further, the *ab initio* wave functions of benzyl fluoride and benzyl chloride were subjected to a quantitative PMO analysis (7). Since the calculated STO-3G dipole moment of planar benzyl fluoride is 1.06 D, and the 3-21G//STO-3G dipole moment is 1.96 D, compared to an experimental value of 1.77 D in benzene at 298 K (13), the analyses of benzyl fluoride were performed on the 3-21G//STO-3G wavefunctions. Extensive experience with quantitative PMO analysis has demonstrated that trends in total energies from conformation to conformation are reproduced by the trends in the orbital interactions that contribute to the HOMO's of these conformations (14), provided that the trend in the HOMO's parallels the trend in the total energies (15). This is the case whenever the properties of the fragment orbitals are dominated by second order perturbational effects (i.e., the familiar in-phase and out-of-phase combinations of interacting orbitals). However, strongly electronegative substituents can cause a lowering (pull-down effect) of the fragment orbital energies and, therefore, a lowering of the energies of the molecular orbitals. This is a first order perturbational effect (16), and it causes the HOMO energy and the total energy to vary in opposite directions for different conformations (17). When this first order effect becomes important the usual PMO analysis will fail, unless the contribution of electronegativity can be taken into account.

Interestingly, benzyl fluoride, which prefers the conformation that apparently maximizes "steric effects", belongs to this latter class of compounds. At the 3-21G//STO-3G level, the planar conformation is 18.5 kJ/mol lower in energy than the perpendicular conformation **5**, but its HOMO lies 24.3 kJ/mol *higher*. In contrast, for benzyl chloride at the STO-3G//STO-3G level, the perpendicular conformation **5** is 8.6 kJ/mol lower in energy than the planar conformation, and its HOMO energy is also lower, by 3.6 kJ/mol. The quantitative PMO analysis was, therefore, expected to reproduce the total energy trend of benzyl chloride, but not that of benzyl fluoride.

The orbital interactions that contribute to the HOMO's of the planar and perpendicular structures of the benzyl halides are depicted in Figs. 1 and 2, respectively. In each case, interactions **1** and **2** are destabilizing, and interactions **3**–**5** are stabilizing. In Fig. 1, π_1 is the in-phase combination of π_{CH_2} with p_X, π_2 is the out-of phase combination of π_{CH_2} with p_X, and π_3 is the out-of-phase combination of $\pi^*_{CH_2}$ with p_X. In Fig. 2, σ_1 is the in-phase combination of the $2a_1$ CH_2 orbital with p_X, σ_2 is the in-phase combination of the $1b_1$ CH_2 orbital with p_X, and σ^* is the out-of-phase combination of $1b_1$ with p_X. The results of the quantitative PMO analyses are summarized in Tables 1 and 2.

For benzyl fluoride, the PMO analysis predicts relative

Can. J. Chem. Downloaded from www.nrcresearchpress.com by 118.98.75.50 on 09/07/12
For personal use only.

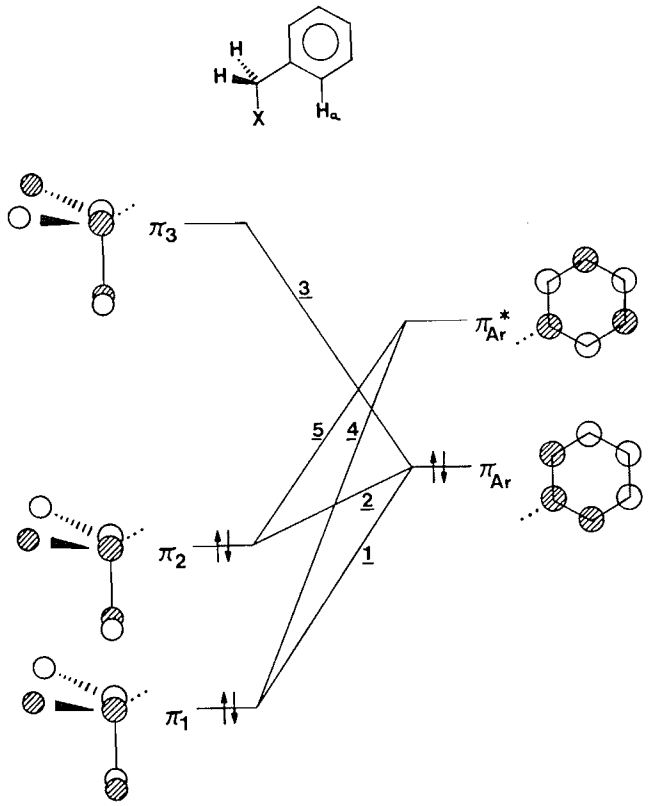

FIG. 1. Frontier orbital interactions between Ph··· and ···CH_2X in planar benzyl halides.

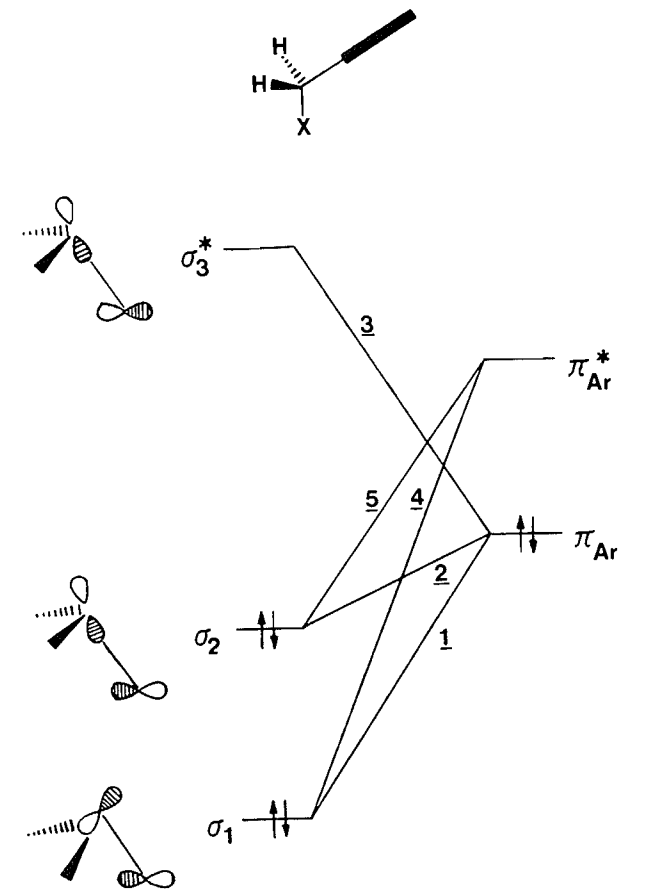

FIG. 2. Frontier orbital interactions between Ph··· and ···CH_2X in perpendicular benzyl halides.

destabilization of the planar conformation by 30.0 kJ/mol, in agreement with the trend in the relative energies of the HOMO's but in disagreement with the trend in the relative total energies. This result was expected, on the basis of the foregoing discussion. In addition, the relative destabilization of the planar conformation is caused almost entirely by the difference in the destabilizing interactions; there is no significant contribution from an anomeric-type interaction in the perpendicular conformation. The PMO analysis thus predicts, ignoring electronegativity, that the conformation of benzyl fluoride is determined by "steric effects", but, as we have seen, this leads to the wrong result.

The electronegativity effect is manifested, in the planar conformation, through an electrostatic interaction between the fluorine atom and H_a, the *ortho*-hydrogen *syn*-periplanar to this fluorine (see Fig. 1). From the net atomic charges on the fluorine (−0.401 electron) and on this hydrogen (+0.267 electron), and their internuclear distance (2.363 Å), the magnitude of the coulombic interaction is calculated to be 62.9 kJ/mol. When this interaction is taken into account in the analysis, the planar conformation now becomes more stable than the perpendicular conformation by 25.7 kJ/mol. This coulombic interaction, and not an anomeric-type effect is, therefore, the origin of the planar conformational preference of benzyl fluoride.

Benzyl chloride differs from benzyl fluoride in several respects. The PMO analysis predicts net stabilization of the perpendicular structure by 22.8 kJ/mol, in agreement with the trend in the relative energies of the HOMO's and also in agreement with the trend in the total energies. The coulombic interaction in the planar conformation is 8.2 kJ/mol; taking this interaction into account reduces the energy difference to 14.6 kJ/mol. Most importantly, the π_{Ar}–σ^* anomeric-type interaction makes a dominant contribution to the relative stabilization of the perpendicular conformation. The conformational preference of benzyl chloride may, therefore, be attributed to the anomeric effect associated with the presence of the Second Row substituent, chlorine.

These considerations lead to an interesting experimental situation for the series of X's SR, S(O)R, SO_2R. Assuming that the R group adopts the staggered orientation shown in **7***a* and **7***b*, the sulfide is expected to prefer the perpendicular conformation **7***b* if there is a benzylic anomeric effect associated with the Second Row substituent, sulfur. However, the sulfoxide and the sulfone may be either planar (**8***a*, **9***a*) or perpendicular (**8***b*, **9***b*), depending on the relative contributions of the electronegativity and benzylic anomeric effects.

The electronegativity effect in **8***a* and **9***a* originates in the O···H_a coulombic interaction. If this dominates, the relative stabilities of the perpendicular conformations will be sulfide > sulfoxide > sulfone.

The magnitude of the benzylic anomeric effect will increase progressively in the series **7***b* > **8***b* ≈ **9***b* because the energies of the σ^*_{C-X} orbitals decrease in this direction. For example, the quantitative PMO analyses of the full optimized 3-21G* structures of $^-CH_2SCH_3$, $^-CH_2S(O)CH_3$, and $^-CH_2SO_2CH_3$ (18) include a stabilizing n_C–σ^*_{C-X} interaction, and the energy of σ^*_{C-X} decreases from 0.350 au in the sulfide to 0.310 au (105.0 kJ/mol) in the sulfoxide and sulfone. Thus, if the benzylic anomeric effect dominates, the relative stabilities of the perpendicular conformations will be sulfide < sulfoxide ≈ sulfone.

The experimental objectives of the present work are, therefore, as follows: (*1*) to synthesize a series of compounds

TABLE 1. Orbital interactions in benzyl fluoride

Conformation	Orbital	Orbital energy (au)	Orbital interaction	Orbital interaction energy (kJ/mol)
Planar	α_{Ar}	−0.355	$\pi_1-\pi_{Ar}$	34.56
	π^*_{Ar}	0.122	$\pi_2-\pi_{Ar}$	31.55
	π_1	−0.689	$\pi_3-\pi_{Ar}$	−1.80
	π_2	−0.521	$\pi_1-\pi^*_{Ar}$	−0.33
	π_3	0.307	$\pi_2-\pi^*_{Ar}$	−4.69
			Total	59.29–62.93[a]
Perpendicular	π_{Ar}	−0.357	$\sigma_1-\pi_{Ar}$	6.40
	π^*_{Ar}	0.122	$\sigma_2-\pi_{Ar}$	27.61
	σ_1	−0.711	$\sigma^*-\pi_{Ar}$	−2.76
	σ_2	−0.648	$\sigma_1-\pi^*_{Ar}$	0.00
	σ^*	0.258	$\sigma_2-\pi^*_{Ar}$	−1.92
			Total	29.33

[a]Refers to the coulombic interaction between F and H_a.

TABLE 2. Orbital interactions in benzyl chloride

Conformation	Orbital	Orbital energy (au)	Orbital interaction	Orbital interaction energy (kJ/mol)
Planar	π_{Ar}	−0.301	$\pi_1-\pi_{Ar}$	39.87
	π^*_{Ar}	0.249	$\pi_2-\pi_{Ar}$	2.13
	π_1	−0.591	$\pi_3-\pi_{Ar}$	−5.82
	π_2	−0.377	$\pi_1-\pi^*_{Ar}$	−6.28
	π_3	0.644	$\pi_2-\pi^*_{Ar}$	−1.05
			Total	28.82–8.16[a]
Perpendicular	π_{Ar}	−0.301	$\sigma_1-\pi_{Ar}$	17.49
	π^*_{Ar}	0.246	$\sigma_2-\pi_{Ar}$	13.35
	σ_1	−0.453	$\sigma^*-\pi_{Ar}$	−14.69
	σ_2	−0.414	$\sigma_1-\pi^*_{Ar}$	−5.06
	σ^*	0.344	$\sigma_2-\pi^*_{Ar}$	−5.06
			Total	6.03

[a]Refers to the coulombic interaction between Cl and H_a.

$ArCH_2SCH_3$, $ArCH_2S(O)CH_3$, $ArCH_2SO_2CH_3$, in which the substitution pattern on Ar allows measurement of long-range coupling constants between ring and benzylic protons; (*2*) to apply this method to the determination of the rotational barriers in solution; (*3*) to determine the effects of Ar substituents upon rotational barriers in $ArCH_2SH$; (*4*) to check some of the conclusions by calculation and PMO analysis of $ArCH_2SH$.

Experimental

3,5-Dichlorobenzyl methyl sulfide

A solution of 3,5-dichlorobenzyl alcohol (1.71 g, 9.6 mmol) in dry pyridine (2.0 mL) was cooled to −40°C and treated dropwise, with stirring under nitrogen, with a solution of *p*-toluenesulfonyl chloride (2.86 g, 15 mmol, freshly recrystallized from petroleum ether (40–60°C)) in dry pyridine (8.0 mL). Stirring was continued at −40°C for 1 h after addition was complete, and the mixture was then poured onto ice–water (200 g), allowed to warm to room temperature, and extracted with ether (4 × 20 mL). The combined ether extracts were washed successively with 10% HCl (2 × 25 mL), 10% sodium carbonate (2 × 25 mL), and water, and dried ($MgSO_4$). Removal of the ether yielded an oil, which crystallized rapidly. This material was dissolved in dry benzene (10 mL) and treated, dropwise at 0°C, with a solution of sodium methylmercaptide, prepared by addition of sodium metal (0.21 g, 9.3 mg-atoms) to absolute methanol (5.0 mL), followed by addition of excess methanethiol and removal of the the excess mercaptan in a stream of nitrogen. When the addition of sodium methyl mercaptide was complete, the milky reaction mixture was stirred for 10 min, poured onto ice-cold 10% NaOH (50 mL), and extracted with ether (4 × 20 mL). The organic extracts were washed with 10% NaOH (1 × 20 mL) and water (3 × 20 mL), dried, and evaporated to yield 1.51 g of crude product. This was purified by chromatography on silica gel. Elution with petroleum ether – ethyl acetate (9:1) afforded 710 mg of colourless oil, R_f 0.57 (petroleum ether – ethyl acetate 9:1).

3,5-Dichlorobenzyl methyl sulfoxide

3,5-Dichlorobenzyl methyl sulfide (100 mg, 0.48 mmol) was dissolved in methylene chloride (3 mL), cooled to 0°C, and an ice-cold solution of *m*-chloroperbenzoic acid (98.1 mg, 0.48 mmol) in methylene chloride (4 mL) was added dropwise during 35 min. The mixture was washed successively with 5% sodium thiosulfate (10 mL), saturated sodium bicarbonate (10 mL) and water, and dried. Removal of the solvent afforded the sulfoxide, 87 mg, mp 83–84°C, R_f 0.11 (20% ethyl acetate – chloroform).

3,5-Dichlorobenzyl methyl sulfone

3,5-Dichlorobenzyl methyl sulfide (100 mg, 0.48 mmol) was dissolved in methylene chloride (3 mL) and a solution of *m*-chloroperbenzoic acid (206 mg, 1.01 mmol) in methylene chloride (4 mL) was added in three portions. The resulting suspension was stirred overnight and then extracted with 5% sodium thiosulfate (2 × 10 mL), saturated sodium bicarbonate (10 mL), brine (10 mL), dried, and

Can. J. Chem. Downloaded from www.nrcresearchpress.com by 118.98.75.50 on 09/07/12
For personal use only.

TABLE 3. ^{1}H nmr spectral parameters for benzylthiol

Parameter	Value	Parameter	Value
ν_{SH}	464.086(1)[a]	$^5J_{25}$	0.583(1)
$\nu(CH_2)$	1091.527(1)[b]	$^4J(H,CH_2)$	−0.559(1)
$\nu_2 = \nu_6$	2159.885(2)	$^5J(H,CH_2)$	0.293(1)
$\nu_3 = \nu_5$	2155.470(2)	$^6J(H,CH_2)$	−0.402(1)
ν_4	2132.416(1)	Calc. transitions	754
$^3J_{23}$	7.715(1)	Peaks observed	72[c]
$^3J_{34}$	7.481(4)	Assigned transitions	583[c]
$^4J_{26}$	1.989(2)	Rms deviation	0.007[c]
$^4J_{24}$	1.215(4)	Largest difference	0.021
$^4J_{35}$	1.430(2)	Temperature	300 K
$^3J(SH,CH_2)$	7.453(1)		

[a]In Hz at 300.135 MHz to high frequency of internal TMS for a 2.8 mol% solution in CS_2, containing also 10 mol% C_6D_{12} and 0.5 mol% TMS.
[b]Numbers in parentheses are standard deviations in the last significant figure.
[c]Although all observed peaks were assigned and the rms error is small, there are large correlations for some parameters, e.g. −0.506 for $^4J(H,CH_2)/^5J(H,CH_2)$; −0.808 for ν_2/ν_3; 0.831 for $\nu_2/^5J_{25}$; −0.817 for $\nu_2/^3J_{34}$; −0.827 for $\nu_3/^5J_{25}$; 0.856 for $\nu_3/^3J_{34}$; −0.952 for $^4J_{24}/^3J_{34}$. They arise because of the small chemical shift between the *ortho* and *meta* protons.

evaporated to give the sulfone, 110 mg, mp 124.5–125.5°C, R_f 0.41 (20% ethyl acetate – chloroform).

The preparation of samples for ^{1}H nmr analysis followed the procedure described previously in detail (19). Concentrations and solvents are given in the following sections. The cw methods were used for all but benzylthiol, again as described previously (20).

A typical procedure for the accumulation of ^{1}H nmr spectra at 300 MHz proceeded as follows. A wide sweepwidth survey spectrum was obtained in order to reference the spectrum with respect to TMS, and to obtain the locations of the aromatic and sidechain regions. Each spectral region was examined in detail, with sweepwidth and data region adjusted to given acquisition times of about 40 s. For example, the ring proton region of benzyl thiol was examined with 32 scans with a sweepwidth of 200 Hz and an acquisition time of 41 s, using 16K of memory. Zero-filling to 32K was followed by resolution enhancement using a Lorentz–Gauss transformation (LB = −0.11, GB = 0.6) to yield a frequency spectrum with linewidths at half-height near 0.05 Hz.

The STO-3G MO computations on benzylthiol employed the program MONSTERGAUSS (21) and were performed on an Amdahl 470 V8 system. Quantitative PMO analyses (7) were performed on the above structures using GAUSSIAN 80 (22).

Results and discussion

Spectral analyses

The ^{1}H nmr spectrum of benzylthiol was analyzed with the computer program NUMARIT (23), yielding the spectral parameters given in Table 3. The program LAME (24, 25) was used for the analysis of the ^{1}H nmr spectra of the compounds whose spectral parameters are listed in Table 4.

The analysis of the ^{1}H nmr spectrum of benzyl thiol (Table 3) gave low standard deviations of the spectral parameters. The peak widths were about 0.05 Hz. However, because the chemical shift between the *ortho* and *meta* protons was only 4.4 Hz and, because of the particular parameter combinations, $^4J(H,CH_2)$ and $^5J(H,CH_2)$ had a correlation coefficient of −0.51. Fortunately, the other important coupling constant, $^6J(H,CH_2)$, did not correlate significantly with other coupling or shift values.

The internal barrier in benzyl thiol

The long-range nuclear spin/spin coupling constants between methyl and ring protons in toluene over four, five, and six formal bonds have been written (19, 26–29) as

TABLE 4. ^{1}H nmr spectral parameters for 3,5-dichlorobenzyl X (X = SCH_3, $S(O)CH_3$, SO_2CH_3)[a]

Parameter	Value		
	SCH_3	$S(O)CH_3$	SO_2CH_3
$\nu(CH_3)$[b]	148.127(2)[c]	166.68	185.13
$\nu(CH_2)$	294.745(1)	301.85	327.35
$\nu_2 = \nu_6$	688.085(2)	683.54(1)	685.85(1)
ν_4	701.187(2)	703.40(1)	700.49(1)
$^4J(CH_2,CH_3)$	±0.144(2)	Very small	±0.73(1)
$^4J_{24}$	1.906(2)	1.90(1)	1.90(1)
$^4J(H,CH_2)$	−0.559(2)	−0.47(1)	−0.49(1)
$^6J(H,CH_2)$	−0.414(2)	−0.33(1)	−0.33(1)
Calc. transitions	416[d]	48[e]	48[e]
Peaks observed	56[e]	18[e]	19[e]
Assigned transitions	37[e]	32[e]	29[e]
Rms deviation	0.006	0.03	0.03

[a]For 3 mol% solutions in benzene-d_6 at a probe temperature of 305 K.
[b]In Hz at 100.001 MHz to high frequency of internal TMS.
[c]Numbers in parentheses are standard deviations in the last significant figure.
[d]Including the transitions of the methyl protons.
[e]For ring and methylene protons only.

$$[1]\quad {}^4J(\text{Hz}) = -1.08\langle\sin^2\theta\rangle - 0.32\langle\cos^2\theta\rangle$$

$$[2]\quad {}^5J(\text{Hz}) = 0.336\langle\sin^2\theta\rangle + 0.322\langle\sin^2(\theta/2)\rangle$$

$$[3]\quad {}^6J(\text{Hz}) = -1.20\langle\sin^2\theta\rangle$$

In eqs. [1] to [3], $\langle\sin^2\theta\rangle$ is the expectation value of $\sin^2\theta$ and θ is the angle by which the α C—H bond twists out of the benzene plane. The coefficients of $\langle\sin^2\theta\rangle$ represent the hyperconjugative or σ–π electron contribution to the couplings, and will here be denoted by ^nJ (n = 4, 5, or 6). The coefficient of $\langle\sin^2(\theta/2)\rangle$ is the σ electron contribution to ^5J and is written as ^5J. For an n-fold internal barrier ($n \geq 2$), $\langle\sin^2(\theta/2)\rangle$ is 0.5. The term in $\langle\cos^2\theta\rangle$ can be regarded as a σ electron component of $^4J(1)$.

In toluene, the internal barrier to rotation is low and sixfold in nature. Consequently, the expectation values in eqs. [1] to [3] are all 0.5. Substitution to yield a benzyl compound leads to a predominantly twofold barrier, possibly with a significant fourfold contribution. The conformation of lowest energy may, in principle, be any of **10**–**12**.

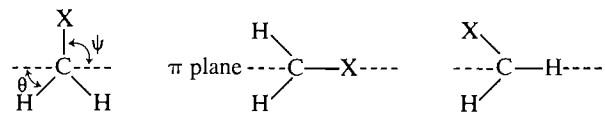

10 θ = 30°, ψ = 90° **11** θ = 60°, ψ = 0° **12** ψ = 60°

The expectation values of $\sin^2\theta$ and $\cos^2\theta$ in eqs. [1] to [3] need no longer be 0.5, unless the internal barrier vanishes. It follows that, if the intrinsic perturbation of J^π and J^σ caused by the substituent, X, can be established, measurements of ^nJ allow determination of the expectation values. These can, in turn, be related to the parameters of a hindered rotor model, viz., the reduced moment of inertia, the temperature, and the internal barrier. Hence ^nJ yields internal barriers to rotation. For example, ^6J has been used in such studies (29) to yield twofold barriers for a variety of benzyl derivatives.

An early study of 3,5-dichlorobenzyl thiol in benzene-d_6 solution led to a barrier of 7.5 ± 0.8 kJ/mol, assumed to be

Can. J. Chem. Downloaded from www.nrcresearchpress.com by 118.98.75.50 on 09/07/12
For personal use only.

TABLE 5. Orbital interactions in benzyl mercaptan[a]

Conformation	Orbital	Orbital energy (au)	Orbital interaction	Orbital interaction energy (kJ/mol)
Planar	π_{Ar}	−0.286	$\pi_1-\pi_{Ar}$	42.21
	π^*_{Ar}	0.261	$\pi_2-\pi_{Ar}$	0.96
	π_1	−0.546	$\pi_3-\pi_{Ar}$	−4.94
	π_2	−0.262	$\pi_1-\pi^*_{Ar}$	−7.70
	π_3	0.682	$\pi_2-\pi^*_{Ar}$	−0.96
			Total	29.67 + 4.18[b]
Perpendicular	π_{Ar}	−0.286	$\sigma_1-\pi_{Ar}$	18.41
	π^*_{Ar}	0.261	$\sigma_2-\pi_{Ar}$	18.45
	σ_1	−0.482	$\sigma^*-\pi_{Ar}$	−3.81
	σ_2	−0.380	$\sigma_1-\pi^*_{Ar}$	−4.94
	σ^*	0.519	$\sigma_2-\pi^*_{Ar}$	−7.87
			Total	20.24

[a]The calculated total energy difference (STO-3G//STO-3G) is 7.75 kJ/mol in favour of the perpendicular structure.
[b]The electrostatic interaction is destabilizing.

twofold, for rotation about the exocyclic C_{sp^2}—C_{sp^3} bond (30). The chlorine substituents were necessary because the available 100 MHz ^{1}H nmr spectrum of benzyl thiol itself was too complex for a reliable spectral analysis.

If ^6J at $\theta = 90°$, $^6J_{90}$, can be determined, then $\langle\sin^2\theta\rangle$ follows immediately from eq. [3] and the observed value of ^6J in benzyl thiol, −0.402(1) Hz (Table 3). From tables of $\langle\sin^2\theta\rangle$ as a function of the internal barrier, the temperature and the reduced moment of inertia, the magnitude of the barrier and the low energy conformation follow directly (29, 31). Recent and detailed studies of benzyl chloride (13*b*), benzyl fluoride (13*a*), and derivatives of benzyl methyl ether (32) yield $^6J_{90}$ as −1.06, −0.95, and −1.02 Hz, respectively, for these compounds. On a scale on which the electronegativities of H, Cl, O—R, and F are 1.78, 3.0, 3.31, and 3.92, respectively, the electronegativity of SH is 2.5 (33–35) and yields $^6J_{90}$ as −1.12 Hz at $\theta = 90°$.

It follows that $\langle\sin^2\theta\rangle$ for benzyl thiol in CS_2 solution at 300 K is 0.359, that the preferred conformer has $\theta = 30°$, as in **10**, and that V_2 is 7.0 kJ/mol. The largest uncertainty in this barrier estimate arises from the uncertainty in $^6J_{90}$. Thus, if $^6J_{90}$ is −1.20 Hz, as in toluene (19), V_2 becomes 9.1 kJ/mol. Accordingly, one may conclude that the barrier to rotation about the C_{sp^2}—C_{sp^3} bond in benzyl thiol in CS_2 solution, *if twofold*, is 8.0 ± 1.0 kJ/mol.

Presumably the ^4J term in eq. [1] will suffer a reduction in magnitude similar to that of $^6J_{90}$, also a π electron transmitted coupling. On this assumption, together with a $\langle\sin^2\theta\rangle$ of 0.359, eq. [1] yields ^4J as −0.567 Hz, compared to the observed value of −0.559 Hz. If the $^4J^\sigma$ term is also reduced by a factor of 1.12/1.20, then ^4J becomes −0.554 Hz. On the other hand, if no reductions occur in $^4J^\pi$ and $^4J^\sigma$ relative to toluene, that is, $^6J^\pi$ is taken to be −1.20 Hz, then ^4J is calculated to be −0.575 Hz. These comparisons could be taken as affirmation of a $^6J_{90}$ near −1.12 Hz, were it not for the substantial correlation between ^4J and ^5J (Table 3). The correlation of −0.51 implies that the sum or difference of these two coupling constants is more reliable than are their individual values.

In fact, agreement between the experimental ^5J of 0.293 Hz and that computed from eq. [2] demands that $^5J^\sigma$ be increased by a factor of 1.12 over its value in toluene. A similar increase has been noted for benzyl chloride (13*b*), and it is known (27) that an electronegative substituent attached to the atoms in the coupling path increases $^5J^\sigma$. However, the correlation between the experimental ^4J and ^5J values casts some doubt upon these considerations.

Computed barrier in benzyl thiol

At the STO-3G level, seven energies, computed at 15° intervals of ψ, can be fit to a potential given by eq. [4]. The

$$[4]\quad V(\psi)/\text{kJ mol}^{-1} = 7.71 \pm 0.04 \sin^2(\psi + 90°) - 0.79 \pm 0.03 \sin^2 2(\psi + 90°)$$

errors are standard deviations at the 95% confidence level. During the computations, all bond lengths and bond angles were optimized, under the constraint that the carbon framework of the phenyl group remain a regular hexagon. The energy at $\psi = 90°$ was −659.644 913 au. The computed twofold component of 7.7 kJ/mol agrees with the apparent twofold barrier deduced from ^6J above.[3]

The theoretical barrier contains a fourfold component of 0.8 kJ/mol. Such a magnitude, ca. 10% of the twofold component, causes a change in $\langle\sin^2\theta\rangle$ of 0.006 at 300 K and, in principle, an error of nearly 0.5 kJ/mol in a twofold barrier of 8 kJ/mol. Evidently the ^6J value is rather insensitive to the presence of a fourfold component of this magnitude.

The computed potential yields a classical $\langle\sin^2\theta\rangle$ of 0.343 at 300 K, as compared to the 0.359 deduced on the basis that $^6J_{90}$ is −1.12 Hz and of 0.335 for $^6J_{90}$ = −1.20 Hz. Of course, the computation refers to an isolated molecule, whereas the coupling data refer to a molecule surrounded by small, nonpolar CS_2 molecules.

The internal barriers in 3,5-dichlorobenzyl-X (X = SH, SCH_3, $S(O)CH_3$, SO_2CH_3)

For X = SH, ^6J is −0.417(4) Hz (30), and for X = SCH_3, ^6J is −0.414(2) Hz, both in benzene-d_6 solution. The internal barrier is thus the same in the two compounds and, if $^6J_{90}$ is −1.12 Hz, the apparent V_2 is 6.1 kJ/mol (the value quoted for the thiol previously assumed the $^6J_{90}$ value for toluene). It has

[3]Similar close agreement between STO-3G barriers and those deduced from coupling constants in CS_2 solutions was found for benzyl chloride (13*b*) and benzyl fluoride (13*a*).

Can. J. Chem. Downloaded from www.nrcresearchpress.com by 118.98.75.50 on 09/07/12
For personal use only.

Can. J. Chem. Downloaded from www.nrcresearchpress.com by 118.98.75.50 on 09/07/12
For personal use only.

previously been found that 3,5-dichloro substitution stabilizes conformation **11** by ca. 2 kJ/mol in both benzyl fluoride (13*a*) and benzyl chloride (13*b*). Apparently, a similar effect is present in benzyl thiol.

In the sulfoxide and the sulfone, ^6J is $-0.33(1)$ Hz. The electronegativities of the $S(O)CH_3$ and SO_2CH_3 groups are rather larger than that of an SCH_3 group. Hence $^6J_{90}$ for these groups should be less than $|1.12|$ Hz (see above). An *upper* limit to an assumed twofold barrier for the sulfoxide and the sulfone follows as 20 kJ/mol because the *lower* limit of $\langle \sin^2 \theta \rangle$ is $-0.32/-1.12 = 0.286$. The electronegativity of SO_2CH_3 is given as 3.1 (36), implying a $^6J_{90}$ of -1.05 Hz. This means that $\langle \sin^2 \theta \rangle$ becomes 0.31(1), corresponding to an apparent V_2 of 12.6 ± 2.5 kJ/mol. An electronegativity of 2.8 for the $S(O)CH_3$ moiety implies a $^6J_{90}$ of -1.09 Hz and hence an apparent V_2 of 13.8 ± 2.5 kJ/mol. In view of the uncertainties in the nature of the barrier, it is best to conclude that the internal barriers in the sulfoxide an sulfone are substantially larger than in the sulfide or thiol.

Quantitative PMO analyses of benzyl mercaptan and the benzylic anomeric effects of benzyl methyl sulfoxide and benzyl methyl sulfone

The PMO analyses were performed on the STO-3G wavefunctions of benzyl mercaptan, and are summarized in Table 5. The planar conformation is seen to be more destabilized, as in the total energy calculations, and as is observed experimentally. Superficially, the perpendicular conformational preference appears to be the result of "steric effects", because the classical $\sigma^*-\pi_{Ar}$ anomeric-type interaction is relatively small. However, closer examination of Table 5 reveals that the $\sigma_1-\pi^*_{Ar}$ and the $\sigma_2-\pi^*_{Ar}$ stabilizing orbital interactions are not negligible in this molecule. This kind of interaction is not possible in the traditional anomeric effect, because the nonbonding heteroatom orbital associated with the $n-\sigma^*$ interaction in the anomeric effect has no antibonding counterpart. Consequently, whether the perpendicular conformational preference of a heteroatom X in benzyl-X can be considered to be the result of a benzylic anomeric effect is less certain in the case of benzyl mercaptan than in the case of benzyl chloride.

Interestingly, in the heterocyclohexanes, the anomeric effect of chlorine is significantly larger than that of SR. For compounds of type **6**, in CCl_4 solvent, the anomeric effect is ≥ 7.5 kJ/mol for X = Cl (37), and 1.46 kJ/mol for X = SCH_3 (38). When the ring heteroatom is sulfur, the anomeric effect is 7.32 kJ/mol for X = Cl, and 1.76 kJ/mol for X = SEt (39).

In view of the borderline benzylic anomeric effect calculated to exist in benzyl mercaptan, and the present experimental findings that $ArCH_2SH$ and $ArCH_2SCH_3$ exhibit similar rotational behaviour, the much greater perpendicular conformational preferences of the sulfoxide and sulfone must be attributed to an enhancement of a benzylic anomeric effect in these latter cases. Unfortunately, such systems are just beyond the current capabilities of reliable *ab initio* computations.

Acknowledgements

The authors thank the Natural Sciences and Engineering Research Council of Canada for support, and Leah Lyubechansky for the preparation of the substrates.

1. H. D. Rudolph, H. Dreizler, A. Jaeschke, and P. Wendling. Z. Naturforsch. **22**, Part A, 940 (1967).
2. R. Wasylishen and T. Schaefer. Can. J. Chem. **50**, 1852 (1972).
3. (*a*) T. Schaefer and G. H. Penner. J. Mol. Struct. (Theochem.) **138**, 305 (1986); (*b*) F. Pang, J. E. Boggs, P. Pulay, and G. Fogarasi. J. Mol. Struct. **66**, 281 (1980); (*c*) W. J. Hehre, R. F. Stewart, and J. A. Pople. J. Chem. Phys. **51**, 2657 (1969); W. J. Hehre, L. Radom, and J. A. Pople. J. Am. Chem. Soc. **94**, 1496 (1972); W. J. Hehre, L. Radom, P. v. R. Schleyer, and J. A. Pople. Ab initio molecular orbital theory. Wiley, New York. 1986.
4. (*a*) D. R. Lide and D. Christensen. J. Chem. Phys. **35**, 1374 (1961); (*b*) E. Hirota and Y. Marino. J. Chem. Phys. **45**, 2326 (1966).
5. H. Schei and Q. Shen. J. Mol. Struct. **81**, 269 (1982); F. Vanhouteghem, W. Pyckhout, C. van Alsenoy, L. van den Ender, and H. J. Geise. J. Mol. Struct. **140**, 33 (1986); J. R. Durig, M. Zhan, and T. S. Little. J. Chem. Phys. **81**, 4259 (1984); Z. Smith, N. Carballo, E. B. Wilson, K.-M. Marstokk, and H. Møllendal. J. Am. Chem. Soc. **107**, 1951 (1985).
6. D. van Hemelrijk, L. van der Enden, H. J. Geise, H. L. Sellers, and L. Schäfer. J. Am. Chem. Soc. **102**, 2189 (1980); K. B. Wiberg and E. Martin. J. Am. Chem. Soc. **107**, 5035 (1985), and references cited therein.
7. M.-H. Whangbo, H. B. Schlegel, and S. Wolfe. J. Am. Chem. Soc. **99**, 1296 (1977); M.-H. Whangbo and S. Wolfe. Isr. J. Chem. **20**, 36 (1980).
8. N. D. Epiotis and R. L. Yates. J. Am. Chem. Soc. **98**, 461 (1976).
9. K. Müller and A. Eschenmoser. Helv. Chim. Acta, **52**, 1823 (1969).
10. N. S. Zefirov. Zh. Org. Khim. **10**, 1131 (1974).
11. S. Wolfe, M.-H. Whangbo, and D. J. Mitchell. Carbohydrate Res. **69**, 1 (1979).
12. J.-P. Praly and R. U. Lemieux. Can. J. Chem. In press.
13. (*a*) T. Schaefer, J. Peeling, and R. Sebastian. Can. J. Chem. **63**, 3219 (1985); (*b*) T. Schaefer, R. Sebastian, and G. H. Penner. Can. J. Chem. **64**, 1372 (1986).
14. A. H. Cowley, D. J. Mitchell, M.-H. Whangbo, and S. Wolfe. J. Am. Chem. Soc. **101**, 5224 (1979).
15. B. M. Deb. J. Am. Chem. Soc. **96**, 2030 (1974); **96**, 2040 (1974).
16. T. A. Albright, J. K. Burdett, and M.-H. Whangbo. Orbital interactions in chemistry. John Wiley, New York. 1985. p. 82.
17. S. Wolfe, D. J. Mitchell, H. B. Schlegel, C. Minot, and O. Eisenstein. Tetrahedron Lett. **23**, 615 (1982); C. Minot, O. Eisenstein, P. C. Hiberty, and Nguyen Trong Anh. Bull. Soc. Chim. II, 119 (1980).
18. S. Wolfe, A. Stolow, and L. A. LaJohn. Tetrahedron Lett. **24**, 4071 (1983).
19. T. Schaefer, R. Sebastian, and G. H. Penner. Can. J. Chem. **63**, 2597 (1985).
20. T. Schaefer and R. Sebastian. J. Magn. Reson. **41**, 395 (1980).
21. M. R. Petersen and R. A. Poirier. MONSTERGAUSS. Department of Chemistry. University of Toronto, Toronto, Ontario. 1981.
22. J. S. Binkley, R. A. Whiteside, R. Krishnan, R. Seeger, D. J. DeFrees, H. B. Schlegel, S. Topiol, L. R. Kahn, and J. A. Pople. GAUSSIAN 80, An ab initio molecular orbital program. QCPE, **13**, 406 (1981).
23. A. R. Quirt and J. S. Martin. J. Magn. Reson. **5**, 318 (1971); J. S. Martin, A. R. Quirt, and K. E. Worvill. The NMR Program Library. Daresbury Laboratory, Daresbury, U.K.
24. S. Castellano and A. A. Bothner-By. J. Chem. Phys. **41**, 3843 (1964).
25. C. W. Haigh. Annu. Rep. NMR Spectrosc. **4**, 311 (1971).
26. M. Barfield, C. J. Fallick, K. Hata, S. Sternhell, and P. W. Westerman. J. Am. Chem. Soc. **105**, 2178 (1983).
27. T. Schaefer and R. Laatikainen. Can. J. Chem. **61**, 2785 (1983).
28. R. Wasylishen and T. Schaefer. Can. J. Chem. **50**, 1852 (1972).

29. W. J. E. PARR and T. SCHAEFER. Acc. Chem. Res. **13**, 400 (1980).
30. T. SCHAEFER and W. J. E. PARR. J. Chem. Soc. Faraday Trans. II, **73**, 1501 (1977).
31. W. DANCHURA. Ph.D. Thesis. University of Manitoba, Winnipeg, Man. 1983.
32. R. LAATIKAINEN. Magn. Reson. Chem. **24**, 588 (1986).
33. B. P. DAILEY and J. N. SHOOLERY. J. Am. Chem. Soc. **77**, 3977 (1956).
34. J. R. CAVANAUGH and B. P. DAILEY. J. Chem. Phys. **34**, 1099 (1961).
35. M. L. HUGGINS. J. Am. Chem. Soc. **75**, 4123 (1953).
36. J. E. HUHEEY. J. Phys. Chem. **70**, 2086 (1966).
37. G. E. BOOTH and R. J. OUELLETTE. J. Org. Chem. **31**, 544 (1966).
38. E. L. ELIEL and C. A. GIZA. J. Org. Chem. **33**, 3754 (1968).
39. A. J. DER HOOG. Ph.D. Thesis. University of Leiden. 1971. p. 42.

Can. J. Chem. Downloaded from www.nrcresearchpress.com by 118.98.75.50 on 09/07/12
For personal use only.

Studies in iridoid chemistry and spruce budworm (*Choristoneura fumiferana*) antifeedants

T. H. CHAN, Y. J. ZHANG, AND F. SAURIOL
Department of Chemistry, McGill University, Montreal, P.Q., Canada H3A 2K6

AND

A. W. THOMAS AND G. M. STRUNZ
Canadian Forestry Service Maritimes, Fredericton, N.B., Canada E3B 5P7

Received December 17, 1986

This paper is dedicated to Professor John T. Edward

T. H. CHAN, Y. J. ZHANG, F. SAURIOL, A. W. THOMAS, and G. M. STRUNZ. Can. J. Chem. **65**, 1853 (1987).

Several compounds derived from aucubin and catalposide were prepared and tested for spruce budworm antifeeding activities. Definite biological activity was observed for compound **11**.

T. H. CHAN, Y. J. ZHANG, F. SAURIOL, A. W. THOMAS et G. M. STRUNZ. Can. J. Chem. **65**, 1853 (1987).

On a préparé plusieurs composés dérivés de l'aucubine et du catalposide et on les a testés pour leurs activités contre la tordeuse d'épinette. On a observé une activité biologique bien définie pour le composé **11**.

[Traduit par la revue]

Can. J. Chem. Downloaded from www.nrcresearchpress.com by 118.98.75.50 on 09/07/12
For personal use only.

Introduction

The spruce budworm, *Choristoneura fumiferana*, is a pest that infests North American fir and spruce forests. In Eastern Canada the larvae of the budworm begin to feed on the buds or the newly opened shoots of the host tree in mid-May, while they consume the greatest amount of foliage during their sixth instar in late June. During a budworm outbreak, this inflicts huge damage to the forest resource, and has devastating consequences for the pulp and paper industry. Efforts to control the spruce budworm up to now have relied on the spraying of insecticides. A strategy that has been suggested for pest control is to employ antifeedants to interfere with the feeding behaviour of insects. The term antifeedant is defined as a chemical that inhibits feeding but does not kill the insect directly, i.e., the insect remains near the treated leaves and dies through starvation (1). The approach is attractive since, in principle, it protects current year foliage while leading indirectly to budworm mortality through use of an agent that may not be generally toxic in the conventional sense. The feeding preferences of spruce budworm larvae have been studied (2). In eastern Canada, balsam fir (*Abies balsamea*) is the most favorable host species, followed by white spruce (*Picea glauca*), red spruce (*Picea rubens*), and black spruce (*Picea mariana*).

In screening programs, a number of natural products have been found to have antifeedant activity against spruce budworm (3, 4). Recently, Chang and Nakanishi reported their studies on extracts of the leaves of 40 different trees that are not attacked by the budworm (4). The extracts were assayed for antifeedant activity using budworm fed on artificial diets with or without the extract. This led to the isolation of the active component from the leaves of *Catalpa speciosa* Warder (Bignoniaceae). They named the compound specionin and proposed its structure to be **1** on the basis of its spectroscopic data (4). However, a chemical synthesis of **1** was recently reported (5) and comparison of spectral data revealed that it was not identical with the natural compound. An alternative structure, **2**, was proposed for specionin and recently synthesized (5).

A common structural feature of many antifeedants known to date, including azadirachtin (6) and clerodin (7), is that they are polyoxygenated compounds. However, there has been little study of structure–activity relationships with respect to antifeedant activity.

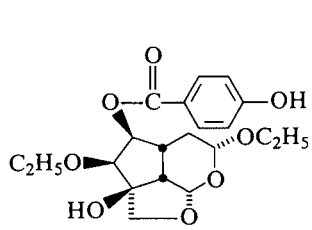

1

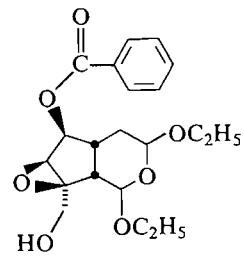

2

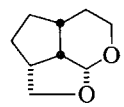

3

The present study led to development of a facile method to obtain the tricyclic structure **3** and several polyoxygenated compounds thereof. At least one of these compounds was found to have definite antifeedant activity against spruce budworm larvae.

While the structures of **1** and **2** are relatively simple so that they are amenable to total synthesis (5), we feel that a totally synthetic approach is not likely to yield compounds in quantities sufficient for large-scale bioassay either in the laboratory or eventually in the field. Our strategy is to effect the syntheses of these compounds starting from iridoid natural products, which are abundant. Furthermore, since the natural antifeedant is likely to be optically active, optical resolution or asymmetric synthesis would be required in a totally synthetic approach. On the other hand, it may be possible to correlate configurationally one of the iridoid natural products with specionin.

As a starting material, we have chosen aucubin (**4**), an iridoid glycoside. It is present to the extent of ~1% of fresh plant weight in *Aucuba japonica* (8, 9) and can be extracted and purified in large quantities (9).[1] In fact, aucubin has been used as starting material for the synthesis of optically active prostaglandinoids (9, 10).

Derivatives from aucubin

The reaction of aucubin with CH_3OH–HCl has been reported

[1]We thank Professor Berkowitz for providing us with the procedure for the extraction of aucubin.

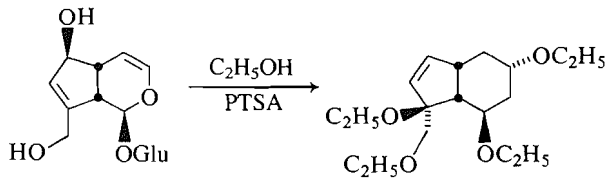

4 5

in the literature (11, 13). Normally, aucubin is degraded extensively under acidic conditions. After trying a number of reaction conditions (BF_3·etherate, HCl, H_2SO_4, etc.), we found that ethanolysis of aucubin with catalytic amounts of *p*-toluenesulfonic acid (PTSA) at room temperature for 11 days gave compound **5** in relatively good yield (~60%). The structure of **5** was based on spectroscopic evidence, in particular, 2D nmr. The absence of the glucose moiety was evident from its tlc mobility and the absence of OH absorption in its ir spectrum. The presence of four ethoxy groups was deduced by its chemical ionization mass spectrum (MH^+ = 315 and base peak at m/z = 269, M − OC_2H_5) and confirmed by the four ethoxy methylene carbons in the ^{13}C nmr spectrum (Table 1). The migration of the double bond is the result of an acid-catalysed allylic rearrangement. In normal allylic rearrangement under acidic conditions, the thermodynamically more stable allylic isomer, which usually is the more substituted double bond isomer, predominates (12). In the present as well as previous cases (11, 13), it is surprising that the less substituted double bond isomer is the only isolable product. The only (speculative) explanation that we can offer at this time is that the ethoxy group, being at C-8 instead of at C-6, can cooperate with the other ethoxy groups in the molecule to form hydrogen bonds more effectively with the solvent or with the acid.

If the ethanolysis of aucubin was carried out with boron trifluoride-etherate as the catalyst, compound **6** was also obtained in addition to **5**. Compound **6** has no hydroxy group according to its ir and ^1H nmr spectra (Table 2). It has only two ethoxy groups, evidenced by its ^{13}C nmr spectrum. The ^1H nmr spectrum of **6** is in agreement with those published for **7***a* and **7***b* (5). Compound **6** could also be prepared from the cyclization of **5**. Thus, when **5** was subjected to *p*-toluenesulfonic acid treatment in methylene chloride instead of ethanol, compound **6** was obtained in moderate yield.

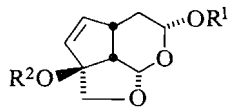

6: $R^1 = R^2 = C_2H_5$
7a: $R^1 = R^2 = H$
7b: $R^1 = C_2H_5$, $R^2 = H$

The double bond of **6** can be further functionalized by hydroxylation or epoxidation to give polyoxygenated derivatives. Oxidation of **6** with osmium tetroxide/pyridine at the less hindered *exo* face gave the diol **8**. Benzoylation of **8** gave the monobenzoate **9** first, then the dibenzoate **10**. Epoxidation of the double bond with *m*-chloroperbenzoic acid gave the epoxide **11**, again from the *exo* face. Treatment of **11** with *p*-toluenesulfonic acid monohydrate gave the tetracyclic alcohol **12**. The structure of **12** was assigned on the basis of spectroscopic data. The alternative structure **12′** was ruled out on the basis of ^1H 2D-HOMO correlation nmr spectrum which showed that H-7 coupled with the hydroxy proton (Fig. 1).

Ethanolysis of catalposide

Both **1** and **2** are structurally similar to catalposide (**13**), the major iridoid compound from the *Catalpa* species. Indeed, Chang and Nakanishi (4) have suggested that specionin could be an artifact derived from catalposide during ethanol extraction.

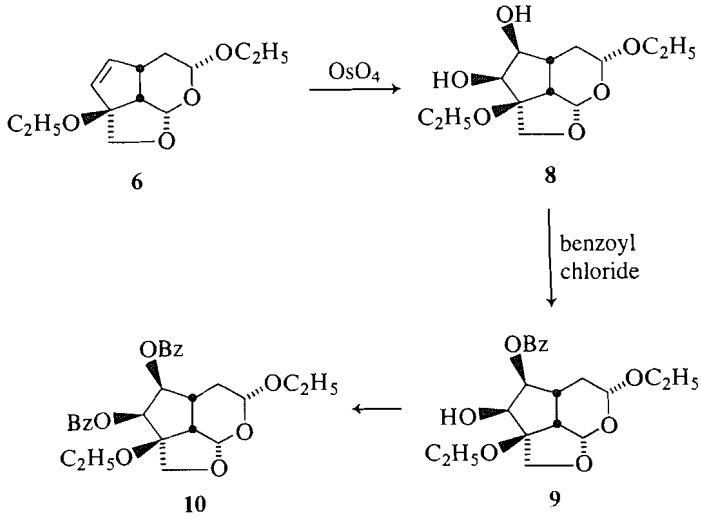

6 8 10 9

In view of the ease of ethanolysis of aucubin, we also attempted the ethanolysis of catalposide. However, in spite of repeated attempts under different conditions, catalposide either resisted ethanolysis or suffered extensive degradation. Using the mildest conditions (catalytic amount of PTSA in ethanol at room

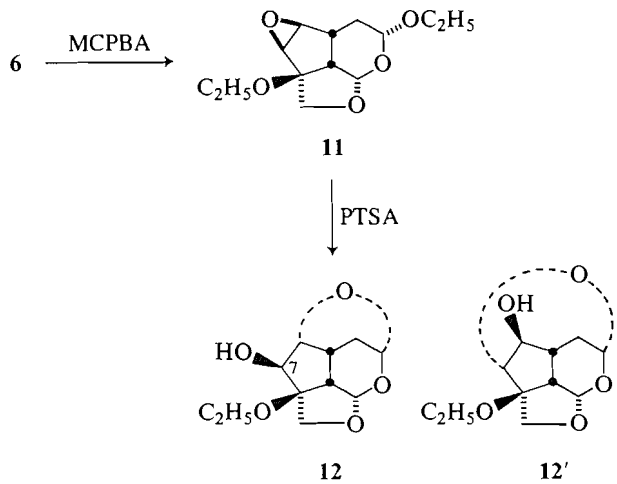

11 12 12′

temperature for 60 days), we were able to isolate compound **14** in very poor yield. Every effort to isolate an intermediate with the epoxide moiety still intact was unsuccessful. It is interesting to note that in the opening of epoxide to give **14**, the ethanol attacked at the more hindered carbon (C-8) with resultant *cis* stereochemistry. The positions of the hydroxyl groups at C-7 and C-10 were assigned by ^1H nmr of **14** in DMSO-d_6, which

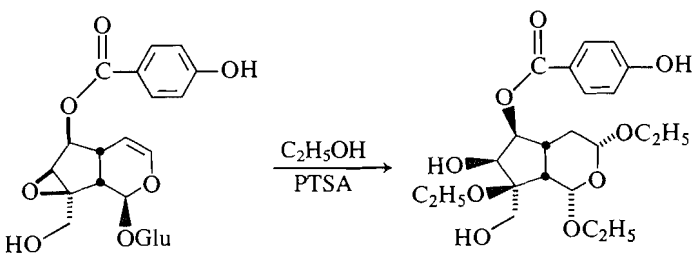

13 14

showed the appropriate coupling between the hydroxyl protons and the adjacent methine (H-7) and methylene (H-10) protons. The relative stereochemistry was determined by nuclear Overhauser effects in that irradiation of H-7 resulted in enhancement of H-6, H-10, and the OH at C-7. Presumably, under the acidic conditions used, epoxide opening proceeded via an S_N1-like

Can. J. Chem. Downloaded from www.nrcresearchpress.com by 118.98.75.50 on 09/07/12
For personal use only.

Can. J. Chem. Downloaded from www.nrcresearchpress.com by 118.98.75.50 on 09/07/12
For personal use only.

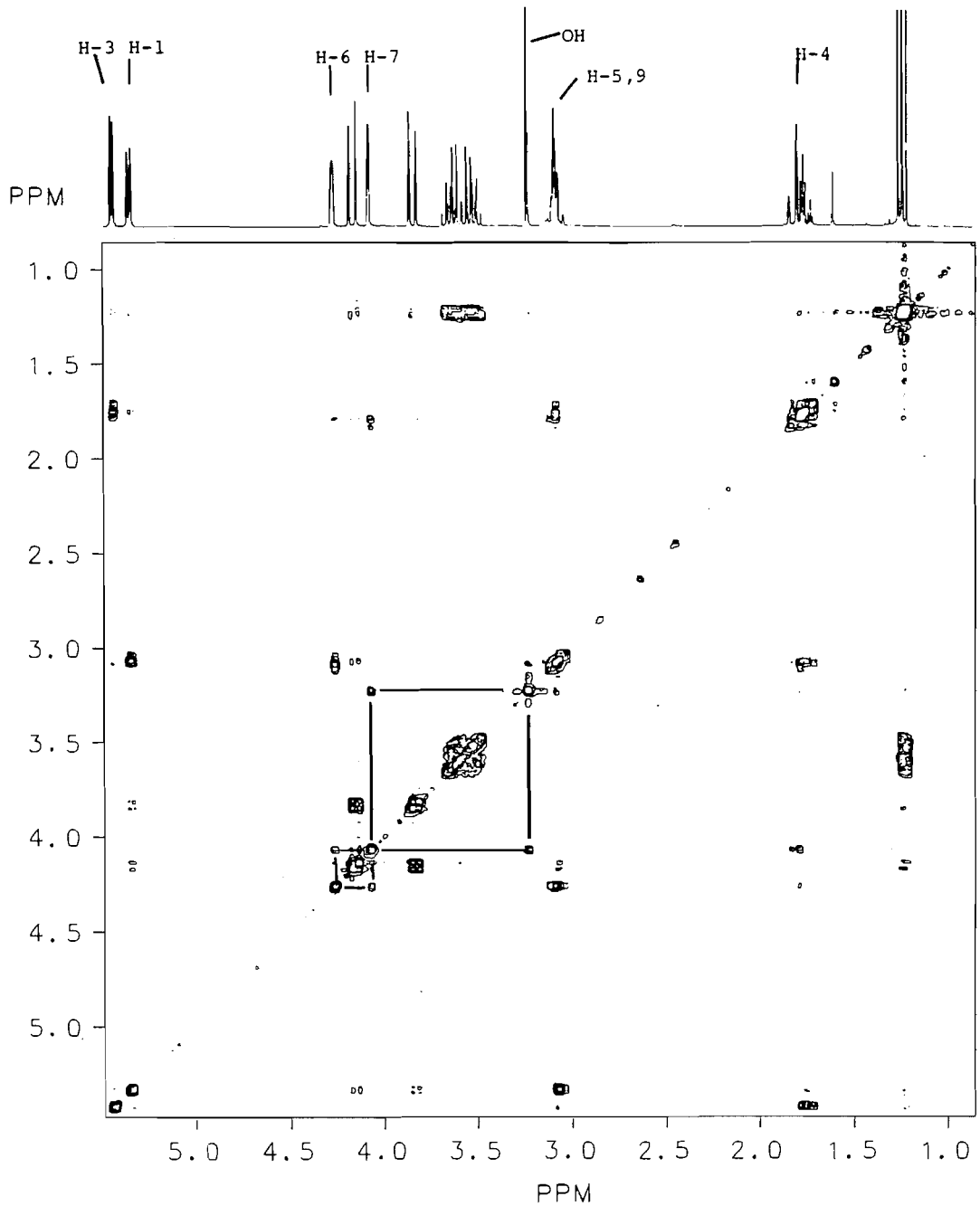

FIG. 1. 2D-HOMO correlation ^{1}H nmr spectrum of **12**. H-7 showed coupling with -OH and H-6.

TABLE 1. ^{13}C nuclear magnetic resonance data[a]

	C-1	C-3	C-4	C-5	C-6	C-7	C-8	C-9	C-10	Others
5	105.53	102.02	34.80	42.41	131.48	139.48	98.30	53.15	73.38	15.28(3C), 15.69, 60.00, 61.08, 61.59, 62.68
6	100.66	94.66	30.43	40.06	132.73	139.84	98.59	44.99	43.95	15.12, 15.64, 59.70, 63.48
9	98.74	95.20	26.84	34.94	77.00	73.09	90.47	46.45	71.40	15.16, 15.59, 60.18, 63.76, 128.42, 129.80, 133.26, 166.36
11	99.00	94.85	27.50	30.09	59.75[b]	61.04[b]	93.96	46.35	71.34	15.12, 15.82, 61.21, 63.23
12	95.42	98.46	31.63	36.51	89.51	74.60	95.52	53.13	71.43	15.58, 60.06
14	94.74	97.62	32.24	37.67	80.85	74.69	85.32	49.06	64.57	14.84, 15.21, 16.01, 58.20, 62.52, 63.41, 115.37(2C), 121.32, 131.97(2C), 160.90, 165.98

[a]Measured in $CDCl_3$.
[b]The assignment may be reversed.

Can. J. Chem. Downloaded from www.nrcresearchpress.com by 118.98.75.50 on 09/07/12
For personal use only.

TABLE 2. ^{1}H nuclear magnetic resonance data

	H-1	H-3	H-4	H-5	H-6	H-7	H-9	H-10	Others
5	5.02 (d, 1.4)	4.58 (t, 6)	1.86 (dt, 6.3, 6.3, 13.8), 1.72 (ddd, 6, 8.8, 13.8)	3.14 (m)	5.61[a] (dd, 2.7, 5.6)	5.97[a] (dd, 1.7, 5.5)	2.61 (dd, 1.2, 8.5)	3.98, 3.82 (AB, 8.8)	1.16 (t, 7.0), 1.21 (t, 7.2), 1.22 (t, 7.1), 3.28–3.80 (m, 9H)
6 ($CDCl_3$)	5.55 (d, 6.1)	4.81 (dd, 3.6, 8.2)	1.95 (dt, 3.8, 3.8, 13.9), 1.79 (ddd, 6.4, 8.4, 1.40)	3.22 (m)	5.72 (dd, 2.8, 5.5)	5.91 (dd, 1.9, 5.5)	2.61 (dd, 6.1, 8.4)	3.95, 3.81 (AB, 9.3)	1.17 (t, 7.0), 1.20 (t, 7.2), 3.28 (m), 3.40 (m), 3.50 (m), 3.89 (m)
7[e]	5.59 (d, 6)	4.80 (dd, 3.7, 8)	1.92 (ddd, 4, 4.1), 1.77 (ddd, 14.8, 6, 5)	3.34 (m)	5.86[b] (dd, 5.5, 2)	5.77[b] (dd, 2.5, 5.5)	—	3.98, 3.78 (AB, 9.5)	1.20 (t, 7), 3.49 (m), 3.88 (m)
9 ($CDCl_3$)	5.54 (d, 5.1)	5.14 (dd, 5.1, 7.3)	2.00 (ddA, 2.9, 5.3, 14.6), 1.64 (ddB, 5.6, 7.3, 14.6)	3.00 (m)	5.25 (dd, (3.6, 10.7)	4.27 (d, 3.6)	2.70 (dd, 5.1, 10.3)	4.14, 3.79 (AB, 11.0)	1.20 (t, 7.1), 1.26 (t, 7.1), 3.55 (m, 3H), 3.90 (m), 7.45–8.11 (m, 5H)
10	5.61 (d, 5.1)	5.20 (dd, 4.8, 7.7)	2.00 (ddA, 2.9, 4.8, 14.5), 1.68 (ddB, 5.6, 7.7, 14.5)	3.08 (m)	5.54 (dd, 3.7, 11.0)	5.80 (d, 3.7)	2.83 (dd, 5.1, 10.2)	4.21 (AB, 10.8), 3.94 (AB, 10.8)	1.05 (t, 6.9), 1.22 (t, 6.8), 3.30 (m), 3.47 (m), 3.54 (m), 3.91 (m), 7.26–8.08 (m, 10H)
11 ($CDCl_3$)	5.44 (d, 5.4)	4.96 (t, 3.1)	1.82, 1.78 (m)	2.80 (dt, 9.2)	3.37[c] (d, 2.5)	3.50[c] (d, 2.5)	2.50 (dd, 5.4, 9.2)	3.89, 3.86 (AB, 10.2)	1.15 (t, 7.1), 1.20 (t, 7.0), 3.46 (m), 3.58 (m), 3.59 (m), 3.76 (m)
12 ($CDCl_3$)	5.33 (d, 4.9)	5.42 (d, 3.5)	1.81 (A, 12.1), 1.75 (Bt, 12.1, 3.5, 3.5)	3.08[d] (m)	4.26 (bs)	4.06 (bs)	3.08[d] (m)	4.15, 3.82 (AB, 10.8)	3.23 (d, 1.7), 1.23 (t, 7.0), 3.51 (m), 3.62 (m)
14 (DMSO-d_6)	5.00 (d, 7.0)	4.79 (dd, 5.3, 8.8)	2.04 (tD, 13.3, 5.3, 5.3), 1.47 (tD, 13.3, 13.3, 8.8)	1.30 (m)	4.96 (dd, 4.5, 5.3)	4.37 (dd, 5.2, 4.5)	2.19 (dd, 6.9, 10.8)	3.79–3.60 (m)	5.08 (d, 5.2, 7-OH), 4.28 (t, 5.2, 10-OH), 1.07–1.16 (m, 9H), 3.46–3.79 (m, 6H), 6.84 (d, 8.8), 7.85 d, 8.8)

[a,b,c,d]Numbers with the same superscript can be exchanged due to uncertain assignment.
[b]Data from ref. 5.

TABLE 3. Mean development stage (instar) of spruce budworm larvae after 15 days at 26°C

Diet	Mean instar[a]
Treated control	5.28
Untreated control	5.12
Compound **13**	5.32
Compound **15**	5.12
Compound **9**	4.40*
Compound **10**	5.32
Compound **11**	4.36*
Compound **12**	4.96
Compound **14**	4.60

[a]Maximum = 6.00 (i.e., all larvae 6th instars).
*Means significantly different from treated control ($P \leq 0.05$, Mann–Whitney U-test).

mechanism with the ethanol molecule attacking the carbonium ion from the *exo* face.

Biological assay

Compounds **9**, **10**, **11**, **12**, and **14** were tested for antifeedant activity against spruce budworm larvae. As control, catalposide **13** was also included. To exclude the possibility that specionin could be an artifact derived from catalposide during ethanol extraction, a sample of catalposide was treated with ethanol for 30 days, and then the solvent was removed. The residue, referred to as ethanol-treated catalposide (sample **15**), was also bioassayed.

Two different bioassays were conducted (see Experimental), both of which involved feeding laboratory-colony spruce budworm larvae on artificial diet (14) containing 0.2% (wet weight) of the test compounds. The first assay showed that the development of larvae reared from second instar on test diets was significantly retarded by compounds **9** and **11**, but not by the other compounds (Table 3). Recognizing that reduction in development rate could be caused by factors other than reduced feeding, a second assay was devised to provide a true reflection of the amount of food ingested by 6th (final) instar larvae. In this test it was found that only compound **11** caused significant reduction in frass produced and moth weight for both male and female insects (although **10** showed significant reductions for males alone) (Table 4).

It is interesting to note that none of the catalposide-derived samples (**13**, **14**, and **15**) showed significant antifeedant activity at the concentration tested. This suggests that specionin is not likely to be an artifact resulting from the ethanolysis of catalopside, since Nakanishi reported that specionin is active at the ca. 50–100 ppm level.

The definite biological activity observed for compound **11** (and possibly compound **10**) provides a lead for further study in the structure–activity relationship of spruce budworm antifeedants.

Experimental

Infrared spectra were obtained on thin films on NaCl plates for liquids and in solution in 0.1-mm cells for solids, using a Perkin–Elmer 297 spectrophotometer. The nmr spectra were recorded on a Varian XL-300 or XL-200 nmr spectrometer. Mass spectra were taken on a Dupont 492B or HP-5980A mass spectrometer. Column chromatography was performed on silica gel 60 (Merck). Elemental analyses were performed by the Institute of Elemento-organic Chemistry, Nankai University, Tianjin, China.

Aucubin and catalposide were isolated according to literature procedure (9).

Ethanolysis of aucubin

A solution of 200 mg of aucubin, 10 mg of *p*-toluenesulfonic acid (PTSA) monohydrate, and 20 mL of C_2H_5OH was stirred at room temperature. Thin-layer chromatography was used to follow the reaction. The colour of the reaction mixture changed from blue to green, brown, and finally yellow. After 11 days, the solution was neutralized with aqueous $NaHCO_3$, filtered, and evaporated under vacuum. Elution on SiO_2 flash chromatography with a mixture of ethyl acetate and hexane (1:2) afforded 0.1 g of compound **5**. (yield 58%); $[\alpha]_D^{22}$ 115.5° (*c* 2.1, $CHCl_3$); ms (CI) (*i*-Bu): 315 (0.3), 314 (0.2), 269 (100), 223 (13). *Anal.* calcd. for $C_{17}H_{30}O_5$: C 64.94, H 9.62; found: C 64.60, H 9.31.

*Cyclization of compound **5** to the tricyclic compound **6***

To 200 mL of CH_2Cl_2 was added 1.2 g of **5** and 0.1 g of PTSA monohydrate. The solution was stirred for 10 h at room temperature. After neutralization with $NaHCO_3$ the mixture was filtered and evaporated under vacuum. Elution of the residue on SiO_2 column flash chromatography with a mixture of ethyl acetate and hexane (1:2) gave 0.60 g of compound **6** as a colorless liquid; $[\alpha]_D^{22}$ 158.4° (*c* 1.9, $CHCl_3$); ms (CI, *i*-Bu): 241 (3), 240 (2), 239 (14), 211 (100), 195 (30). *Anal.* calcd. for $C_{13}H_{20}O_4$: C 64.98, H 8.39; found: C 64.52, H 8.11.

*Epoxidation of compound **6***

To a solution of 0.5 g of **6** in 20 mL of benzene was added 0.2 g of *m*-chloroperbenzoic acid (MCPBA). After stirring for 10 h at room temperature, another 0.2 g of MCPBA was added. Stirring was continued for 5 h at 50–60°C. Additional MCPBA (2 × 0.2 g) was added after each 5 h stirring at 50–60°C. The mixture was washed with aqueous $NaHCO_3$ and dried with $MgSO_4$. It was filtered and evaporated under vacuum. The residue was eluted on SiO_2 column flash chromatography with a mixture of ethyl acetate and hexane to give 0.23 g of **11** as a waxy low-melting white solid; $[\alpha]_D^{22}$ 126.7° (*c* 2.0, $CHCl_3$); ms (CI, *i*-Bu): 257 (14), 256 (2), 255 (14), 211 (100). *Anal.* calcd. for $C_{13}H_{20}O_5$: C 60.92, H 7.87; found: C 60.51, H 7.38.

*Hydroxylation and benzoylation of compound **6***

To 0.11 g of **6** in 10 mL of pyridine was added 0.13 g of OsO_4 in 10 mL pyridine at 5°C. The mixture was kept for 2 h, then at room temperature for 40 h. The mixture was evaporated under vacuum. The residue was eluted on SiO_2 flash chromatography with a mixture of ethyl acetate and hexane (1:1) to give 0.065 g of the diol **8**. The diol was benzoylated without further purification.

To 0.05 g of **8** and 1.0 g of pyridine in 5 mL of $CHCl_3$ was added a solution of 0.03 g benzoyl chloride in 5 mL of $CHCl_3$, dropwise at room temperature. The mixture was stirred at room temperature for 48 h. It was evaporated under vacuum and the residue was purified by silica gel flash chromatography with a mixture of ethyl acetate and hexane (1:1).

Compound **9** (0.03 g) was obtained as the monobenzoate; $[\alpha]_D^{22}$ −18.7° (*c* 1.8 $CHCl_3$); ms (CI, *i*-Bu): 378 (1), 377 (4), 333 (23), 315 (29), 211 (100). *Anal.* calcd. for $C_{20}H_{26}O_7$: C 63.48, H 6.93; found: C 63.71, H 7.23.

If benzoylation was carried out under identical conditions but with excess benzoyl chloride (0.50 g), the dibenzoate **10** was obtained. It had $[\alpha]_D^{22°C}$ −65.05° (*c* 1.5, $CHCl_3$); ms (CI, *i*-Bu): 483 (2), 481 (2), 437 (74), 315 (100). *Anal.* calcd. for $C_{27}H_{30}O_8$: C 67.20, H 6.27; found: C 67.06, H 6.05.

*Acid catalysed reaction of epoxide **11***

To 0.05 g of **11** in 15 mL of ether, 0.01 g of PTSA monohydrate was added. The solution was refluxed for 3 h, then neutralized with aqueous $NaHCO_3$. The ether solution was dried and evaporated under vacuum. The residue was purified on SiO_2 flash chromatography with a mixture of ethyl acetate and hexane to 0.035 g of compound **12**. It had $[\alpha]_D^{22}$ 39.4° (*c* 3.5, $CHCl_3$); ms (EI): 228 (8), 211 (5), 198 (33), 181 (29), 169 (48), 28 (100). *Anal.* calcd. for $C_{11}H_{16}O_5$: C 57.89, H 7.07; found: C 57.99, H 7.37.

Ethanolysis of catalposide

To a solution of 0.5 g of catalposide in 30 mL of C_2H_5OH, 0.05 g of PTSA monohydrate was added. The mixture was stirred at room

Can. J. Chem. Downloaded from www.nrcresearchpress.com by 118.98.75.50 on 09/07/12
For personal use only.

TABLE 4. Frass weights and moth weights resulting from 6th-instar spruce budworm larvae feeding on test diets

Diet	Frass[a] mg dry weight		Moth[a] mg dry weight[b]	
	Males	Females	Males	Females
Treated control	37.5 ± 5.8	50.9 ± 8.2	9.7 ± 1.4	17.7 ± 3.5
Untreated control	32.6 ± 7.4	52.3 ± 12.3	10.1 ± 2.0	18.4 ± 3.5
Compound **13**	37.0 ± 6.2	60.6 ± 12.5	9.9 ± 1.9	19.2 ± 4.6
Compound **15**	36.5 ± 7.1	54.7 ± 13.2	10.6 ± 1.9	18.5 ± 5.0
Compound **9**	35.4 ± 6.5	53.7 ± 8.5	9.8 ± 2.5	18.3 ± 3.9
Compound **10**	29.0 ± 7.0*	49.5 ± 12.6	7.6 ± 2.3*	16.0 ± 5.7
Compound **11**	31.7 ± 7.1*	38.4 ± 10.0*	7.9 ± 1.5*	14.4 ± 4.3*
Compound **12**	35.2 ± 4.6	55.2 ± 18.7	9.9 ± 0.8	21.0 ± 4.5
Compound **14**	38.1 ± 6.1	53.5 ± 22.4	9.9 ± 2.2	18.1 ± 6.9

[a]Mean ± sd.
[b]n = 15–20.
[c]Means significantly different from treated control ($P \leq 0.05$, t-test).

temperature for 60 days. Thin-layer chromatography was used to follow the reaction. The mixture was neutralized with $NaHCO_3$, filtered, and evaporated under vacuum. The residue on elution from Al_2O_3 column by flash chromatography with a mixture of ethyl acetate and hexane (1:2) gave 0.03 g of compound **14**. It had $[\alpha]_D^{22°C}$ −61.6° (c 2.75, $CHCl_3$); ms (CI, i-Bu): 439 (1), 423 (2), 395 (21), 349 (100).

Bioassays

Diet containing 0.2% (wet weight) of the test compounds was prepared by treating lyophilized diet (14) with a solution of the compound, usually in methylene chloride, and then removing the solvent completely at 30°C on a rotary vacuum evaporator. The residual powder was rehydrated to 80% water content with 0.4% aqueous potassium sorbate solution (fungicide). Control diets were treated as above with solvent alone, or were untreated. In the first assay, newly-emerged 2nd-instar larvae were reared individually at 26°C, 17-h photoperiod, 25 replicates per test compound. After 15 days, the larvae were sacrificed and their mean development stage determined (Table 3). In the second assay, newly-moulted 6th-instar larvae were reared under the same conditions. At pupation, the frass were dried (60°C) and weighed. Moths were allowed to emerge and were sacrificed after 24 h, dried, and weighed (Table 4).

Acknowledgement

We thank Professor J. T. Edward for samples of aucubin and catalposide. Financial support from NSERC and FCAC are gratefully acknowledged.

1. K. MUNAKATA. *In* Control of chemical behaviour by natural products. *Edited by* D. L. Wood, R. M. Silverstein, and M. Nakajima. Academic Press, New York. 1970.
2. P. J. ALBERT and P. A. JERRETT. J. Chem. Ecol. **7**, 391 (1981).
3. (*a*) M. D. BENTLEY, D. E. LEONARD, S. LEACH, E. REYNOLDS, W. STODDARD, B. TOMKINSON, D. TOMKINSON, G. STRUNZ, and M. YATAGAI. Effects of some naturally occurring chemicals and extracts of nonhost plants on feeding by spruce budworm larvae (*Choristoneura fumiferana*). Maine Agric. Exp. Stn. Tech. Bull. **107**. 1982; (*b*) M. D. BENTLEY, D. E. LEONARD, W. F. STODDARD, and L. H. ZALKOW. Ann. Entomol. Soc. Am. **77**, 393 (1984); (*c*) G. M. STRUNZ, P. GIGUÈRE, and A. W. THOMAS. J. Chem. Ecol. **12**, 251 (1986).
4. C. C. CHANG and K. NAKANISHI. J. Chem. Soc. Chem. Commun. 605 (1983).
5. E. VAN DE EYCKEN, J. VAN DE EYCKEN, and M. VANDEWALLE. J. Chem. Soc. Chem. Commun. 1719 (1985).
6. P. ZANNO, I. MIURA, K. NAKANISHI, and D. ELDER. J. Am. Chem. Soc. **97** (1975); I. KUBO, A. MATSUMOTO, T. MATSUMOTO, and J. A. KLOCKE. Tetrahedron, 489 (1986); W. KRAUS, M. BOKEL, A. KLENK, and H. POHNL. Tetrahedron Lett. **26**, 6435 (1985); H. B. BROUGHTON, S. V. LEY, A. M. Z. SLAWIN, D. J. WILLIAMS, and E. D. MORGAN. J. Chem. Soc. Chem. Commun. 46 (1986).
7. D. H. R. BARTON, H. T. CHEUNG, A. D. CROSS, L. M. JACKMAN, and M. MARTIN-SMITH. J. Chem. Soc. 5061 (1961).
8. R. B. DUFF, J. S. D. BACON, C. M. MUNDIE, V. C. FARMER, J. D. RUSSELL, and A. R. FORRESTER. Biochem. J. **96**, 1 (1965).
9. (*a*) W. F. BERKOWITZ, I. SASSON, P. S. SAMPATHKUMAN, J. HRABIE, S. CHONDHRY, and D. PIERCE. Tetrahedron Lett. 1641 (1979); (*b*) W. H. LUNN, D. W. EDWARD, and J. T. EDWARD. Can. J. Chem. **40**, 104 (1962).
10. M. MARUTO, K. OHNO, N. NARUSE, and H. TAKEUCHI. Tetrahedron Lett. 251 (1979).
11. M. W. WENDT, W. HAEGELE, E. SIMONITSCH, and H. SCHMID. Helv. Chim. Acta, **43**, 1440 (1960).
12. D. H. DEWOLFE and W. G. YOUNG. Chem. Rev. **56**, 753 (1956); J. H. BABLA and D. O. OLSEN. Tetrahedron Lett. 351 (1974).
13. A. BIANCO, M. GUISO, C. IAVRONE, P. PASSACANTILLI, and C. TROPOLO. Tetrahedron, **40**, 1191 (1984).
14. A. MCMORRAN. Can. Entomol. **97**, 58 (1965).

Can. J. Chem. Downloaded from www.nrcresearchpress.com by 118.98.75.50 on 09/07/12
For personal use only.

Synthesis of carbocycles from ω-substituted α,β-unsaturated esters via radical-induced cyclizations

STEPHEN HANESSIAN,[1] DALJIT S. DHANOA, AND PIERRE L. BEAULIEU
Department of Chemistry, Université de Montréal, Montréal (Qué.), Canada H3C 3J7

Received December 16, 1986

This paper is dedicated to Professor John T. Edward

STEPHEN HANESSIAN, DALJIT S. DHANOA, and PIERRE L. BEAULIEU. Can. J. Chem. **65**, 1859 (1987).

The intramolecular radical cyclization of ω-bromo α,β-unsaturated esters for the synthesis of carbocyclic compounds is described. The effect of carbon chain substituents, the bulk of the ester group, and the olefin geometry were examined. The highest level of stereoselectivity (*trans*/*cis*: 9/1) was achieved with the *Z* ester via an *exo* cyclization. The sequential radical cyclization of a dihalodienoate to give a *cis*-fused bicyclic structure is also described.

STEPHEN HANESSIAN, DALJIT S. DHANOA et PIERRE L. BEAULIEU. Can. J. Chem. **65**, 1859 (1987).

Nous décrivons l'utilisation d'une réaction de cyclisation radicalaire intramoléculaire des esters ω-bromo α,β-insaturés pour la synthèse de composés carbocycliques. Nous avons étudié les paramètres suivants : la substitution de la chaîne, l'encombrement stérique dû à l'ester ainsi que la géométrie de la double liaison des précurseurs radicalaires. Le plus haut degré de stéreosélection (*trans*/*cis*: 9/1) fut obtenu avec l'ester α,β-insaturé *Z*. *exo*. De plus, la cyclisation radicalaire en série d'un dihalogéno dièneoate donne un produit bicyclique.

Can. J. Chem. Downloaded from www.nrcresearchpress.com by 118.98.75.50 on 09/07/12
For personal use only.

The utilization of radical reactions for carbon–carbon bond formation in synthetic organic chemistry has recently attracted considerable interest (1–10). The increasing popularity of radical-based synthetic methods in organic synthesis is attributable to the mild reaction conditions and their compatibility with a number of unprotected functional groups. Despite these recent applications in synthesis (1–10), the formation of carbocycles from α,β-unsaturated esters via intramolecular radical cyclization of esters has received relatively little attention. As part of a program dealing with radical-mediated processes in this laboratory (2, 3), we recently described an efficient use of the intramolecular Michael-type cyclization of a vinyl radical to an α,β-unsaturated ester for the synthesis of the hexahydrobenzofuran subunit of the avermectins (2). We now report our studies on the stereochemical and synthetic aspects of the radical-induced intramolecular cyclization of ω-substituted α,β-unsaturated esters for the production of carbocyclic systems.

Preparation of intermediates

The radical precursors **2** for the intramolecular cyclization were prepared from the corresponding lactones[2] using a three-step reaction sequence outlined in Scheme 1. The lactones were reduced with diisobutylaluminum hydride (DIBALH) to give the corresponding lactols, which were further treated with carboalkoxymethylenetriphenylphosphorane (see, for example, ref. 11) to afford the ω-hydroxy α,β-unsaturated esters **1**. The hydroxyesters **1** were converted to the desired precursors **2** by the action of carbon tetrabromide and triphenylphosphine in dichloromethane (12). Treatment of the hydroxyester **1***a* with sodium hydride, carbon disulfide, and methyl iodide in diethyl ether gave the desired xanthate ester (**2***b*, Table 1) (13). Thiocarbonylimidazolide (**2***d*, Table 1) was obtained by refluxing the corresponding hydroxyester **1***d* with *N*,*N*′-thiocarbonyldiimidazole in dichloromethane (14). The (*R*)-*O*-methylmandelic ester (**2***h*, Table 1) was prepared from the corresponding methyl ester **2***g* by hydrolysis to the corresponding acid derivative, conversion to the acid chloride, and condensation with (*R*)-*O*-methylmandelic alcohol in the presence of pyridine and trace amount of 4-*N*,*N*-dimethylaminopyridine (DMAP).

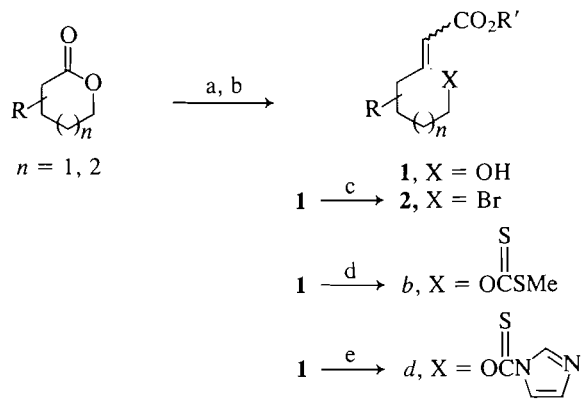

(a) DIBALH, toluene, −78°C; (b) $Ph_3P{=}CHCO_2R'$, cat. $PhCO_2H$, CH_3CN, reflux; (c) Ph_3P, CBr_4, CH_2Cl_2; (d) NaH, CS_2, CH_3I; (e) *N*,*N*′-thiocarbonyldiimidazole, CH_2Cl_2, reflux

SCHEME 1

Haloesters **2***l* and **2***m* were prepared in a straightforward manner. Baeyer–Villiger oxidation of the known 2-(2′-chloroethyl)cyclopentanone (15) with *m*-chloroperbenzoic acid (MCPBA) led to the expected δ-lactone, which was reduced with DIBALH to a mixture of chlorolactols. These halolactols were then heated with carbomethoxymethylenetriphenylphosphorane in acetonitrile to produce the desired α,β-unsaturated ester **2***l*, which in turn was transformed to the bromochloroester **2***m* by treatment with Ph_3P–CBr_4 in dichloromethane (12). Dihalodienoate **2***n* was prepared from ethylacetoacetate according to standard literature methods (see experimental section).

The conjugate radical cyclization of α,β-unsaturated esters to carbocyclics was performed by the slow addition of a benzene or toluene solution of *n*-Bu_3SnH or Ph_3SnH and azobisisobutyronitrile (AIBN) to refluxing solutions of the radical precursors **2** in the same solvent. The corresponding carbocyclic compounds were formed in good to excellent yields (Table 1). The *cis*/*trans* ratios of the cyclized products were determined by high field ^1H and ^{13}C nmr spectroscopic analysis.

Discussion

Several notable features of the intramolecular radical-induced cyclization of ω-halo α,β-unsaturated esters are revealed by

[1]Author to whom correspondence may be addressed.

[2]Lactones were obtained by Baeyer–Villiger oxidation of known ketones.

TABLE 1. Radical-induced cyclization of ω-substituted α,β-unsaturated esters

Entry	Substrate	Products	Isolated yield (%)	Isomeric ratio *cis*:*trans* (%)
1	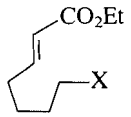 **2***a*, X = Br	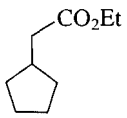 **3***a*	75	
2	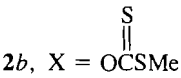 **2***b*, X = OCSMe		68	
3	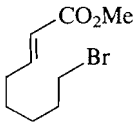 **2***c*	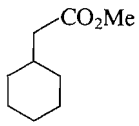 **3***c*	66[a]	
4	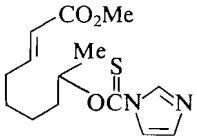 **2***d*	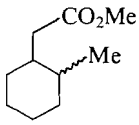 **3***d*	65	
5	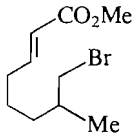 **2***e*	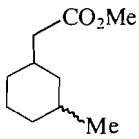 **3***e*	92	43:57
6	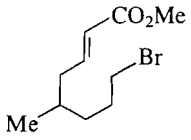 **2***f*	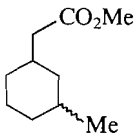 **3***e*	80	37:63
7	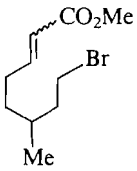 *E*:*Z* = 9:1 **2***g*	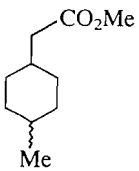 **3***g*	91	35:65
8	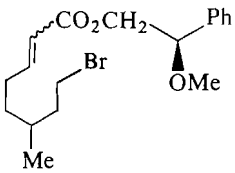 *E*:*Z* = 9:1 **2***h*	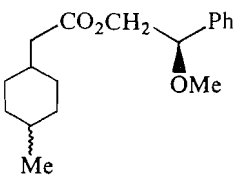 **3***h*	90	35:65

Can. J. Chem. Downloaded from www.nrcresearchpress.com by 118.98.75.50 on 09/07/12
For personal use only.

TABLE 1 (*concluded*)

Entry	Substrate	Products	Isolated yield (%)	Isomeric ratio *cis*:*trans* (%)
9	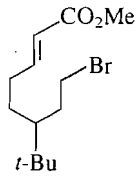 **2*i***	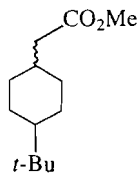 **3*i***	85	35:65
10	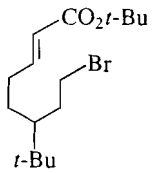 **2*j***	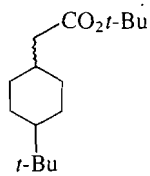 **3*j***	85	25:75
11	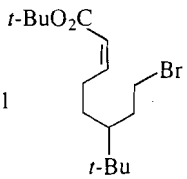 **2*k***	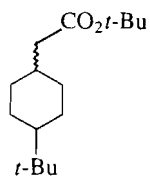 **3*j***	75	10:90
12	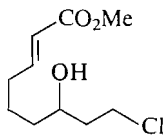 **2*l***	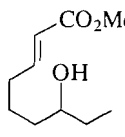 **3*l***	84	
13	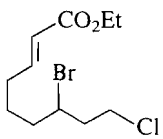 **2*m***	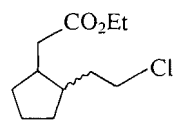 **3*m***	66	70:30[b]
14	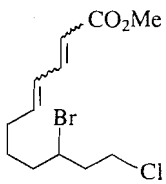 **2*n***	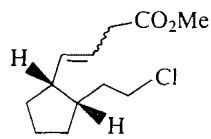 **3*n***	60	95:5
15	**2*n***	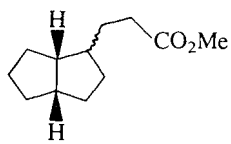 **4**		

[a]Small amount of reduction product, methyl 2-(*E*)-octenoate **3*b***, was obtained.
[b]Stereochemistry unknown.

Can. J. Chem. Downloaded from www.nrcresearchpress.com by 118.98.75.50 on 09/07/12
For personal use only.

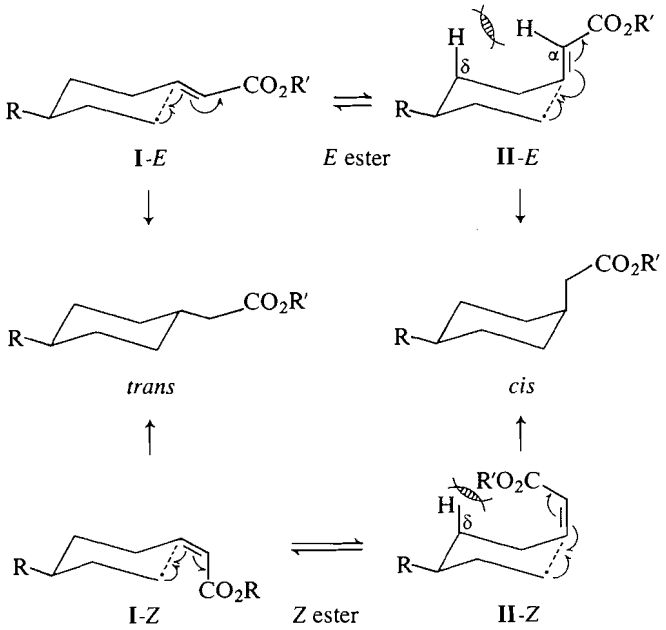

SCHEME 2

the data presented in Table 1. The radical ring closures to carbocycles occurred in 5- or 6-*exo* modes (16) without contamination with the possible *endo* ring closure products to any detectable extent as evidenced by ^{1}H nmr analysis (5, 17). The unsaturated haloester **2***l* failed to cyclize in the 7-*exo*- or 8-*endo* mode, indicating the much slower rate of cyclization compared to the reduction of the C—Cl bond (entry 12). The influence of the position of C-alkyl substituents on the carbon chain of the radical precursors **2** seems to be modest and favours the *trans*-cyclized products (entries 5–7). The stereochemical outcome of the intramolecular radical cyclization appears to be unaffected by the increase in the steric bulk of the carbon chain substituents, as indicated by the unchanged *cis*/*trans* product ratio in going from the C-methyl to the C-*tert*-butyl series (entries 7 and 9). The stereoselectivity can be somewhat improved by increasing the bulk of the ester group of the radical precursors (entries 9 and 10).

Finally, examination of the effect of the C=C geometry of the unsaturated haloesters proved useful in enhancing the stereoselectivity of radical cyclization (7). While the *E*-bromo ester **2***j* gave a 1:3 mixture of *cis*/*trans* products, the *Z*-bromo-ester **2***k* afforded a 1:9 mixture of *cis*/*trans* cyclized *tert*-butylesters (entries 10 and 11). The *trans* stereoselectivity in those cases that produce 1,4-disubstituted cyclohexanes may be rationalized according to the relative stabilities of the respective transition states as shown in Scheme 2.

Of the two chair-like conformations corresponding to the transition states of the *E* and *Z* esters, those derived from **I**-*E* and **I**-*Z* are expected to be of lower energy than their relatively less stable conformers **II**-*E* and **II**-*Z* (Scheme 2). The unfavourable destabilizing nonbonded interactions between the α-vinylic H and the pseudo-axial H at the δ-carbon that are present in **II**-*E* (absent in **I**-*E*) may account for the stereoselectivity observed in favour of the *trans* product. The nonbonding interactions between the bulky ester group and the pseudo-axial H at the δ-carbon of the *Z* ester are more severe in **II**-*Z* (cf. **II**-*E* and **II**-*Z* in Scheme 2), thus giving rise to higher *trans* selectivity in the 6-*exo* cyclization of *Z* esters (entry 11, Table 1). Another noteworthy feature in the cyclizations to form six-membered rings was the apparent absence of intramolecular hydrogen abstraction.[3]

We reasoned that extension of the above radical cyclization method to sequential radical cyclization would constitute an efficient methodology for the construction of bicyclic or tricyclic systems commonly encountered in natural product synthesis (for serial radical cyclizations, see ref. 10). The successful realization of this strategy required chemoselective generation of the radical in substrates such as dihalodienoate (**2***n*, Table 1). The chemoselective radical generation was tested on a simpler system (**2***m*, Table 1). Treatment of **2***m* with Ph_3SnH/AIBN in benzene afforded the expected 5-*exo* cyclized chloroester **3***m* as a 7:3 stereoisomeric mixture (presumably the *cis* isomer as the major product) in 66% yield. Having developed the conditions effective for chemoselective radical generation in the dihaloester **2***m*, the method was applied to the substrate dihalodienoate **2***n* designed for the sequential radical cyclization. When solutions of Ph_3SnH and AIBN in benzene were added to a refluxing benzene solution of **2***n* over 10 h, using a syringe pump, intramolecular radical cyclization (5-*exo*) occurred to give the expected monocyclic chloroester **3***n* as a 19:1 mixture of olefinic esters in 60% yield. Notably, the 5-*exo* ring cyclization led to the deconjugated ester. In the case of sequential cyclization, tratment of **2***n* with Ph_3SnH/AIBN in benzene for 10 h at 90°C, followed by its treatment with Ph_3SnH/AIBN in toluene for 10 h at 120°C, led to the *cis*-fused bicyclic ester **4** in good yield (entry 15).

In summary, the radical-induced intramolecular Michael type cyclization of unsaturated esters, in which the ester group acts as an activating group, constitutes a preparatively useful method for the synthesis of five- and six-membered mono- and bicyclic carbocyclic systems, which are ubiquitous in synthetic organic and natural products chemistry.

Experimental

The ^{1}H nmr spectra were recorded on Varian EM360A and WH-400 nmr spectrometers with TMS as internal standard. The ^{13}C nmr spectra were recorded on WP80 and WH-400 spectrometers. Infrared spectra were recorded on a Perkin–Elmer 781 infrared spectrophotometer. Low resolution mass spectra were recorded on a VG-1212 mass spectrometer and high resolution mass spectra were recorded on a Kratos MS50TCTA instrument. Flash column chromatography was done on silica gel using ethyl acetate – hexane as eluents.

*General procedure for the preparation of ω-hydroxy α,β-unsaturated esters, **1***

A solution of lactol (5 mmol), carboalkoxymethylenetriphenylphosphorane (6 mmol), and a catalytic amount of benzoic acid in acetonitrile (10 mL) (or dimethoxyethane or toluene or methanol) was refluxed (11). Upon completion of the reaction (tlc monitoring) the solvent was removed under reduced pressure and the residue was flash chromatographed (30% EtOAc in hexane) to afford the products **1** in over 60% yield.

*Ethyl 7-hydroxy-2-(*E*)-heptenoate, **1**a*

(Reaction solvent, 1,2-dimethoxyethane); ir: 3420 (OH), 1720, and 1655 cm^{-1}; ^{1}H nmr (60 MHz) δ: 6.875 (dt, 1H, J = 16 Hz, 7 Hz), 5.7 (dt, 1H, J = 16 Hz, 1.5 Hz), 4.1 (q, 2H, J = 7 Hz), 3.7–2.8 (m), 2.50–1.85 (m), 1.75–1.40 (m), 1.25 (t, 3H, J = 7 Hz).

*Methyl 8-hydroxy-2-(*E*)-octenoate, **1**c*

(Reaction solvent, acetonitrile); ^{1}H nmr (60 MHz) δ: 7.07 (dt, 1H, J = 16 Hz, 7 Hz), 5.88 (dt, 1H, J = 16 Hz, 1.5 Hz), 3.77 (s, 3H), 3.64 (t, 2H, J = 6.5 Hz), 3.0 (bs, 1H), 2.50–2.0 (m, 2H), 2.00–1.20 (m, 6H).

[3]We thank one of the referees for pointing out this important feature.

Can. J. Chem. Downloaded from www.nrcresearchpress.com by 118.98.75.50 on 09/07/12
For personal use only.

Can. J. Chem. Downloaded from www.nrcresearchpress.com by 118.98.75.50 on 09/07/12
For personal use only.

*Methyl 8-hydroxy-2-(*E*)-noneonate,* **1**d

(Reaction solvent, acetonitrile); ^{1}H nmr (400 MHz) δ: 7.15–6.92 (m, 1H), 5.82 (dq, 1H, J = 16 Hz, 1.5 Hz), 4.04–3.95 (m, 1H), 3.73 (s, 3H, CO_2CH_3), 2.26–2.16 (m, 2H), 2.10–1.97 (m, 1H), 1.87–1.79 (m), 1.76–1.58 (m), 1.57–1.28 (m), 1.15 (d, 3H, J = 7 Hz).

*Methyl 8-hydroxy-7-methyl-2-(*E*)-octenoate,* **1**e

(Reaction solvent, acetonitrile); ^{1}H nmr (60 MHz) δ: 6.95 (dt, 1H, J = 16 Hz, 7 Hz), 5.75 (dt, 1H, J = 16 Hz, 1.5 Hz), 3.7 (s, 3H), 3.36 (d, 2H, J = 5.5 Hz), 2.7–1.9 (m, 2H), 1.8–1.15 (m, 5H), 0.9 (d, 3H, J = 6.5 Hz).

*Methyl 8-hydroxy-5-methyl-2-(*E*)-octenoate,* **1**f

(Reaction solvent, acetonitrile); ^{1}H (60 MHz) δ: 6.98 (dt, 1H, J = 16 Hz, 7 Hz), 5.83 (dt, 1H, J = 16 Hz, 1.5 Hz), 3.75 (s, 3H), 3.6–3.25 (m, 2H), 2.35 (s, 1H), 2.6–1.95 (m, 2H), 1.9–1.15 (m, 5H), 0.97 (d, 3H, J = 6.5 Hz).

*Methyl 8-hydroxy-6-methyl-2-(*E*)-octenoate,* **1**g

(Reaction solvent, acetonitrile); ^{1}H nmr (60 MHz) δ: 7.10 (dt, 1H, J = 16 Hz, 7 Hz), 5.90 (dt, 1H, J = 16 Hz, 1.7 Hz), 3.80 (s, 3H), 3.73 (t, 2H, J = 7 Hz), 2.5–2.0 (m, 3H), 1.8–1.1 (m, 5H), 0.95 (d, 3H, J = 6.5 Hz).

*Methyl 8-hydroxy-6-*tert*-butyl-2-(*E*)-octenoate,* **1**i

(Reaction solvent, toluene); ir: 3600–3100 (OH), 1725, and 1658 cm^{-1}; ^{1}H nmr (60 MHz) δ: 7.03 (dt, 1H, J = 16 Hz, 7 Hz), 5.85 (dt, 1H, J = 16 Hz, 1.5 Hz), 3.7 (s, 3H), 3.63 (t, 2H, J = 7 Hz), 2.60–1.00 (m, 8H), 0.93 (s, 9H).

tert-*Butyl 8-hydroxy-6-*tert*-butyl-2-(*E*)-octenoate,* **1**j

(Reaction solvent, acetonitrile); ir: 3600–3100 (OH), 1720, and 1650 cm^{-1}; ^{1}H nmr (60 MHz) δ: 6.86 (dt, 1H, J = 16 Hz, 7 Hz), 5.7 (dt, 1H, J = 16 Hz, 1.5 Hz), 4.65 (bs, 1H), 3.6 (t, 2H, J = 7 Hz), 2.75–1.00 (m, 7H), 1.5 (s, 9H), 0.9 (s, 9H).

tert-*Butyl 8-hydroxy-6-*tert*-butyl-2-(*Z*)-octenoate,* **1**k

(Reaction solvent, methanol); ^{1}H nmr (400 MHz) δ: 6.09 (dt, 1H, J = 12 Hz, 8 Hz), 5.69 (dt, 1H, J = 12 Hz, 1.5 Hz), 3.65 (m, 2H), 2.62–2.00 (m, 2H), 1.87 (bs, 1H), 1.85–1.75 (m, 1H), 1.67–1.58 (m, 1H), 1.49 (s, 9H), 1.42–1.295 (m, 1H), 1.24–1.15 (m, 1H), 1.07–1.00 (m, 1H), 0.89 (s, 9H).

General procedure for the preparation of ω-bromo α,β-unsaturated esters, **2**

To a dichloromethane solution of carbon tetrabromide (1.2 equiv.) and triphenylphosphine (1.2 equiv.) (12), was added a dichloromethane solution of the hydroxyester **1**. The resulting solution was stirred for 15 min and then treated with methanol. The volatiles were removed *in vacuo* and the remaining residue was purified by flash chromatography (10% EtOAc in hexane) to afford the corresponding ω-bromo α,β-unsaturated esters.

*Ethyl 7-bromo-2-(*E*)-heptenoate,* **2**a

Yield 61%; ir: 1715 and 1658 cm^{-1}; ^{1}H nmr (60 MHz) δ: 7.025 (dt, 1H, J = 16 Hz, 7 Hz), 5.866 (dt, 1H, J = 16 Hz, 1.5 Hz), 4.22 (q, 2H, J = 7 Hz), 3.425 (t, 2H, J = 7 Hz), 2.60–1.45 (m, 6H), 1.32 (t, 3H, J = 7 Hz); ^{13}C nmr δ: 166.3311, 147.8093, 121.9955, 60.1592, 32.9599, 32.0849, 31.2099, 26.6159, 14.2924; ms m/e: 237 (M^+ + 1, ^{81}Br), 235 (M^+ + 1, ^{79}Br).

*Methyl 8-bromo-2-(*E*)-octenoate,* **2**c

Yield 94%; ^{1}H nmr (60 MHz) δ: 7.03 (dt, 1H, J = 16 Hz, 7 Hz), 5.84 (dt, 1H, J = 7 Hz, 1.5 Hz), 3.75 (s, 3H), 3.43 (t, 2H, J = 7 Hz), 2.50–1.30 (m, 7H), 0.92 (d, 3H, J = 7 Hz); ms m/e: 249 (M^+ + 1, ^{81}Br), 247 (M^+ + 1, ^{79}Br).

*Methyl 8-bromo-7-methyl-2-(*E*)-octenoate,* **2**e

Yield 62%; ir: 1720 and 1658 cm^{-1}; ^{1}H nmr (60 MHz) δ: 6.85 (dt, 1H, J = 16 Hz, 7 Hz), 5.7 (dt, 1H, J = 16 Hz, 1.5 Hz), 3.66 (s, 3H), 3.3 (d, 2H, J = 5.5 Hz), 2.50–2.00 (m, 2H), 2.00–1.20 (m, 5H), 1.03 (d, J = 6.5 Hz); ms m/e: 263 (M^+ + 1, ^{81}Br), 261 (M^+ + 1, ^{79}Br).

*Methyl 8-bromo-5-methyl-2-(*E*)-octenoate,* **2**f

Yield 61%; ir: 1720 and 1655 cm^{-1}; ^{1}H nmr (60 MHz) δ: 6.93 (dt, 1H, J = 16 Hz, 7 Hz), 5.8 (dt, 1H, J = 16 Hz, 1.5 Hz), 3.75 (s, 3H), 3.4 (t, 2H, J = 6 Hz), 2.50–1.10 (m, 7H), 0.96 (d, 3H, J = 6.5 Hz).

*Methyl 8-bromo-6-methyl-2-(*E*)-octenoate,* **2**g

Yield 94%; ^{1}H nmr (60 MHz) δ: 7.03 (dt, 1H, J = 16 Hz, 7 Hz), 5.84 (dt, 1H, J = 7 Hz, 1.5 Hz), 3.75 (s, 3H), 3.43 (t, 2H, J = 7 Hz), 2.50–1.30 (m, 7H), 0.92 (d, 3H, J = 7 Hz); ms m/e: 263 (M^+ + 1, ^{81}Br), 261 (M^+ + 1, ^{79}Br).

*Methyl 8-bromo-6-*tert*-butyl-2-(*E*)-octenoate,* **2**i

Yield 70%; ir: 1725 and 1655 cm^{-1}; ^{1}H nmr (60 MHz) δ: 6.95 (dt, 1H, J = 16 Hz, 7 Hz), 5.8 (dt, 1H, J = 16 Hz, 1.5 Hz), 3.75 (s, 3H), 3.4 (t, 2H, J = 7 Hz), 2.55–1.00 (m, 7H), 0.93 (s, 9H).

tert-*Butyl 8-bromo-6-*tert*-butyl-2-(*E*)-octenoate,* **2**j

Yield 81%; ir: 1725, and 1655 cm^{-1}; ^{1}H nmr (400 MHz) δ: 6.84 (dt, 1H, J = 16 Hz, 7 Hz), 5.757 (dt, 1H, J = 16 Hz, 1.5 Hz), 3.45 (ddd, 1H), 3.405 (m, 1H), 2.33–2.20 (m, 1H), 2.20–2.12 (m, 1H), 2.11–2.00 (m, 1H), 1.71–1.60 (m, 2H), 1.5 (s, 9H), 1.23–1.04 (m, 2H), 0.9 (s, 9H).

tert-*Butyl 8-bromo-6-*tert*-butyl-2-(*Z*)-octenoate,* **2**k

Yield 76%; ^{1}H nmr (400 MHz) δ: 6.08 (dt, 1H, J = 12 Hz, 8 Hz), 5.695 (dt, 1H, J = 12 Hz, 1.5 Hz), 3.52–3.44 (m, 1H), 3.42–3.34 (m, 1H), 2.70–2.61 (m, 2H), 2.11–2.05 (m, 1H), 1.74–1.57 (m, 2H), 1.495 (s, 9H), 1.23–1.13 (m, 1H), 1.12–1.04 (m, 1H), 0.89 (s, 9H).

*Ethyl 7-*S*-methyl dithiocarbonoloxy-2-(*E*)-heptenoate,* **2**b

An ethereal solution of the hydroxyester **1***a* (0.288 g, 1.67 mmol) was refluxed with sodium hydride (1.1 equiv.) and carbon disulfide (1.5 equiv.) for 3 h. To the resulting mixture was added methyl iodide (3 equiv.) and this mixture was refluxed for 3 h (13). Upon completion of the reaction, the mixture was diluted with ether and quenched carefully with water. The aqueous layer was extracted with ether. The ethereal extracts were dried, concentrated, and purified by flash chromatography (10% ethyl acetate in hexane) to give the xanthate ester (**2***b*), (30% yield); ir: 1720, 1660, 1225, and 1065 cm^{-1}; ^{1}H nmr (400 MHz) δ: 6.945 (dt, 1H, J = 15.6 Hz, 6.9 Hz), 5.84 (dt, 1H, J = 15.65 Hz, 1.58 Hz), 4.604 (t, 2H, J = 6.46 Hz), 4.186 (q, 2H, J = 7.1 Hz), 2.57 (s, 3H), 2.230–2.24 (m, 2H), 1.87–1.80 (m, 2H), 1.66–1.57 (m, 2H), 1.29 (t, 3H, J = 7.13 Hz); ms m/e: 263 (M^+ + 1).

*Methyl-8-thiocarbonylimidazolyl-2-(*E*)-nonenoate,* **2**d

A solution of the hydroxyester **1***d* (0.483 g, 2.59 mmol) and *N,N'*-thiocarbonyldiimidazole (0.89 g, 5 mmol) in dichloromethane (20 mL) was refluxed overnight (14). After work-up, the residue was purified by flash chromatography (36% EtOAc in hexane) to give the imidazolide **2***d* (0.59 g, 77%); ^{1}H nmr (60 MHz) δ: 8.4 (bs, 1H), 7.7 (bs, 1H), 7.1 (bs, 1H), 7.20–6.78 (m), 6.05–5.47 (m), 3.73 (s, 3H), 3.15–2.94 (m, 1H), 2.48–1.25 (m), 1.45 (d, 3H, J = 7 Hz).

*(*R*)-O-Methylmandelyl-8-bromo-6-methyl-2-octenoate,* **2**h

To a benzene solution of the 8-bromo-6-methyl-2-octenoic acid (0.112 g, 0.476 mmol in 3 mL of benzene) was added oxalyl chloride (0.07 mL), and the resulting solution was stirred at room temperature for 2 h. The solvent was removed under reduced pressure and to the resulting oil were added (*R*)-*O*-methylmandelic alcohol (0.076 g, 0.5 mmol), pyridine (1 mL), and a catalytic amount of 4-dimethylaminopyridine. The mixture was stirred overnight at room temperature. Removal of the solvent and flash chromatography (10% EtOAc in hexane) of the resulting oil gave **2***h* in 16% yield; ^{1}H nmr δ: 7.4–7.3 (m, 5H), 6.98 (dt, 1H, J = 16 Hz, 7 Hz, *trans* isomer), 6.225 (dt, 1H, J = 11 Hz, 7 Hz, *cis* isomer), 5.875 (dt, 1H, J = 16 Hz, 2 Hz, *trans* isomer), 5.825 (dt, 1H, J = 11 Hz, 2 Hz, *cis* isomer), 4.46 (dd, 1H, CHOMe, *trans* isomer), 4.43 (dd, 1H, CHOMe, *cis* isomer), 4.3–4.185 (m, 2H), 3.63–3.38 (m, 2H), 3.3 (s, 3H, OCH_3), 3.295 (s, 3H, OCH_3, *cis* isomer), 2.32 (m, 2H), 1.94–1.76 (m, 1H), 1.75–1.50 (m, 2H), 1.55–1.45 (m, 1H), 1.36–1.25 (m, 1H), 0.93 (d, 3H, J = 6 Hz, *trans* isomer), 0.927 (d, 3H, J = 6 Hz, *cis* isomer).

*Methyl 9-chloro-7-hydroxy-2-(*E*)-nonenoate,* **2**l

Baeyer–Villiger oxidation of the known 2-(2'-chloroethyl)cyclopentanone (15) with MCPBA in dichloromethane gave the corresponding 5-(2'-chloroethyl)-δ-lactone. DIBALH reduction of the halo-

Can. J. Chem. Downloaded from www.nrcresearchpress.com by 118.98.75.50 on 09/07/12
For personal use only.

lactone in toluene at −78°C afforded the corresponding halolactol, which was then converted to the desired chlorohydroxy ester **2***l* by refluxing with carbomethoxymethylenetriphenylphosphorane in CH_3CN (see general procedure). The product was purified by flash chromatography (20% EtOAc in hexane) to give **2***l* as an oil; ^{1}H nmr (60 MHz) δ: 7.02 (dt, 1H, J = 16 Hz, 6.5 Hz), 5.87 (dq, 1H, J = 16 Hz, 1.5 Hz), 3.90–3.60 (m, 1H), 3.80 (s, 3H), 3.74 (t, 2H, J = 7 Hz), 2.50–1.30 (m, 9H).

*Ethyl 7-bromo-9-chloro-2-(*E*)-nonenoate,* **2***m*

Dihaloenoate **2***m* was prepared from 2-(2′-chloroethyl)cyclopentanone (15) in a straightforward manner as described above for **2***l*. The corresponding chlorohydroxy ester **2***l* was transformed to the bromochloro ester **2***m* by treating with Ph_3P–CBr_4 in CH_2Cl_2 (12) to give an oil; ^{1}H nmr (60 MHz) δ: 7.0 (dt, 1H, J = 16 Hz, 7 Hz), 5.83 (dq, 1H, J = 16 Hz, 1.5 Hz), 4.19 (q, 2H, J = 6.5 Hz), 3.73 (t, 2H, J = 7 Hz), 3.6 (m, 1H), 2.60–1.50 (m, 8H), 1.30 (t, 3H, J = 7.3 Hz).

Ethyl 3-oxo-7-octenoate

Ethyl acetoacetate (7 mL, 55 mmol) was added dropwise to a suspension of sodium hydride (60 mmol) in tetrahydrofuran (130 mL) at 0°C under a nitrogen atmosphere. After 0.25 h, a solution of *n*-BuLi (1.65 *M* in hexane, 60 mmol) was added and the mixture stirred for additional 0.25 h at 0°C to generate the dianion of ethyl acetoacetate (18). To the solution of dianion was added 4-bromo-1-butene (8.17 g, 60.5 mmol) and the stirred mixture was allowed to reach room temperature. After discharge of the orange colouration, the reaction mixture was quenched with 30% aqueous HCl and then concentrated under reduced pressure to give the product as an oil; ^{1}H nmr (60 MHz) δ: 5.80–5.30 (m, 1H), 4.10 (q, 2H, J = 7.0 Hz), 3.23 (s, 2H), 2.50 (t, 2H, J = 7.0 Hz), 2.30–1.20 (m, 4H), 1.20 (t, 3H, J = 7.0 Hz).

Ethyl 3-hydroxy-7-octenoate

An ethanol solution of the above ketoester was added dropwise to a stirring solution of sodium borohydride (0.946 g, 25 mmol) in ethanol containing a drop of aqueous 1 *M* sodium hyroxide. The mixture was stirred for 1 h, then quenched with 10% aqueous HCl solution. After this usual work-up, flash chromatography (10% EtOAc in hexane) of the crude material gave the desired product as an oil (5.06 g, 49% from ethyl acetoacetate); ir: 3700–3200, 1730, and 1645 cm^{-1}; ^{1}H nmr (60 MHz) δ: 6.10–5.40 (m, 1H), 5.15–4.60 (m, 2H), 4.10 (q, 2H, J = 7.0 Hz), 3.80 (m, 1H), 3.15 (bs, 1H), 2.30 (d, 2H, J = 6.0 Hz), 2.0 (m, 2H), 1.7–1.3 (m, 4H), 1.25 (t, 3H, J = 7.0 Hz).

Ethyl 3-bromo-7-octenoate

To a solution of ethyl 3-hydroxy-7-octenoate (1.518 g, 8.15 mmol) and carbon tetrabromide (3.317 g, 10 mmol) in dichloromethane (50 mL) at 0°C was added triphenylphosphine (2.623 g, 10 mmol) in small portions, and the mixture stirred for 6 h at room temperature. After removal of the solvent under reduced pressure, flash chromatography (hexane) of the residue afforded the desired product as a colourless oil (1.305 g, 64%); ir: 1740 and 1642 cm^{-1}; ^{1}H nmr (60 MHz) δ: 6.20–5.40 (m, 1H), 5.30–4.70 (m, 2H), 4.35 (m, 1H), 4.15 (q, 2H, J = 7.0 Hz), 2.80 (d, 2H, J = 7.0 Hz), 2.40–1.50 (m, 6H), 1.30 (t, 3H, J = 7.0 Hz).

3-Bromo-7-octen-1-ol

An ethereal solution of ethyl 3-bromo-7-octenoate (0.854 g, 4.13 mmol) was added to a suspension of lithium aluminum hydride (excess) in ether and the mixture stirred at room temperature. After completion of reduction (tlc monitoring), water was added slowly to the reaction mixture and the crude product extracted with ether. Purification of the crude material by flash chromatography (10% EtOAc in hexane) gave the product as a colourless oil (0.351 g, 49%); ir: 3700–3100 and 1645 cm^{-1}; ^{1}H nmr (60 MHz) δ: 6.10–5.40 (m, 1H), 5.20–4.80 (m, 2H), 4.0 (m, 1H), 3.60 (q, 2H, J = 6.5 Hz), 2.40–1.00 (m, 8H).

6-Bromo-8-chloro-1-octene

3-Bromo-7-octen-1-ol (0.383 g, 1.85 mmol) and carbon tetrachloride (0.57 g, 3.7 mmol) were dissolved in dichloromethane (25 mL). To the ice-cold solution, triphenylphosphine (0.97 g, 3.7 mmol) was added in small portions and the mixture stirred at room temperature until the bromohydrin was consumed. Removal of the solvent under reduced pressure followed by flash chromatography (hexane) of the residue gave the desired bromochloro-octene as an oil; ir: 1650 cm^{-1}; ^{1}H nmr (60 MHz) δ: 6.20–5.50 (m, 1H), 5.30–4.80 (m, 2H), 4.10 (quintet, 1H, J = 6 Hz), 3.70 (t, 2H, J = 6.5 Hz), 2.4–1.0 (m, 8H).

5-Bromo-7-chloro-heptanal

Ozone was bubbled through a dichloromethane (20 mL) solution of the dihalo-olefin (0.417 g, 1.85 mmol) at −78°C until its complete consumption. The reaction mixture was then flushed with argon, quenched with dimethyl sulfide at −78°C, and then allowed to warm to room temperature. After removal of the solvent, flash chromatography (20% EtOAc in hexane) of the residue afforded the bromochloro aldehyde (0.167 g, 40%); ir: 1735 cm^{-1}; ^{1}H nmr (60 MHz) δ: 9.80 (t, 1H, J = 1 Hz), 4.20 (quintet, 1H, J = 6.5 Hz), 3.70 (t, 2H, J = 6.5 Hz), 2.70–1.40 (m, 8H).

*Methyl 9-bromo-11-chloro-2-(*E*)-4-(*E*)-undecenoate,* **2***n*

Sodium hydride (0.024 g, 1 mmol) was added to a stirred suspension of methyl crotonyltriphenylphosphonium bromide (0.441 g, 1 mmol) in THF. To the resulting phosphorane was added a THF solution of 5-bromo-7-chloro-heptanol (0.167 g, 0.73 mmol) and the mixture refluxed for 3 h. The solvent was then removed and the residue was purified by flash chromatography (20% EtOAc in hexane) to give the desired dihalodienoate **2***n* (0.022 g) as an oil; ^{1}H nmr (400 MHz) δ: 6.25–6.06 (m, 3H), 5.81 (d, 1H, J = 15 Hz), 4.22 (m, 1H), 3.77–3.72 (m, 2H), 3.75 (s, 3H, OMe), 2.27–2.16 (m, 2H), 1.85 (m, 2H), 1.81–1.70 (m, 1H), 1.67–1.57 (m, 1H); ms *m/e*: 311 (M^+ + 1).

General procedure for radical cyclization

Benzene or toluene solutions of n-Bu_3SnH or Ph_3SnH (0.07–0.1 *M*, 1.2–1.5 equiv.) and AIBN (0.003 *M*, 0.05 equiv.) were injected, using a syringe pump over 10 h, into a refluxing solution (0.015 *M*) of the unsaturated bromides **2**, or xanthate ester **2***b*, or thiocarbonylimidazolide **2***d*, in the same solvent. Upon completion of the reaction, the solvent was removed *in vacuo* and the residue was purified by flash chromatography (hexane to 5% EtOAc in hexane gradient) to give the cyclized product as homogeneous oils (see Table 1).

Ethyl cyclopentylacetate, **3**a: ir: 1738 cm^{-1}; ^{1}H nmr (400 MHz) δ: 4.12 (q, 2H, J = 7 Hz), 2.33–2.26 (m, 2H), 2.26–2.17 (m, 1H), 1.88–1.78 (m, 2H), 1.69–1.50 (m, 4H), 1.26 (t, 3H, J = 7 Hz), 1.22–1.10 (m, 2H); ^{13}C nmr δ; 173.2585, 60.0133, 40.4707, 36.5330, 32.4495, 25.0116, 14.2924; ms *m/e*: 156 (M^+ + 1).

*Methyl 2-(*E*)-octenoate,* **3**b: ^{1}H nmr (400 MHz) δ: 6.98 (dt, 1H, J = 16 Hz, 8 Hz), 5.82 (dt, 1H, J = 16 Hz, 1.5 Hz), 3.73 (s, 3H, CO_2CH_3); ^{13}C nmr (100.62 MHz) δ: 149.7, 120.7, 32.1, 31.2, 27.6, 23.4; ms *m/e*: 157 (M^+ + 1).

Methyl cyclohexylacetate, **3**c: ^{1}H nmr (400 MHz) δ: 3.66 (s, 3H, CO_2CH_3), 2.19 (d, 2H, J = 8 Hz), 1.85–0.90 (m, 11H); ^{13}C nmr (100.62 MHz) δ: 173.5, 51.2, 41.9, 34.8, 32.9, 26.0, 25.9; ms *m/e*: 157 (M^+ + 1).

Methyl 2-methylcyclohexylacetate, **3**d *(19)*: ^{1}H nmr (400 MHz) δ: 3.68 (s, 3H, CO_2CH_3), 2.575 (d, J = 5 Hz), 2.35 (d, J = 5 Hz), 2.40–2.17 (m), 2.05–1.90 (m), 1.93–1.60 (m), 1.60–1.09 (m), 0.91 (d, 3H, CH_3, J = 7.5 Hz); ^{13}C nmr (100.62 MHz) δ: 174.4192, 174.0936; ms *m/e*: 171 (M^+ + 1).

Methyl 3-methylcyclohexylacetate, **3**e *(19)*: ^{1}H nmr (400 MHz) δ: 3.665 (s, 3H, CO_2CH_3), 2.28 (d, J = 7 Hz), 2.18 (d, J = 7 Hz), 1.86–1.60 (m, 4H), 1.60–1.09 (m, 5H), 0.92 (d, CH_3, J = 7.5 Hz), 0.875 (d, CH_3, J = 7.5 Hz); ^{13}C nmr (100.62 MHz) δ: 173.6987, 173.4372, 51.2368, 41.9799, 41.7191, 39.3563, 38.7897, 34.8296, 34.7189, 33.3538, 32.5334, 32.3675, 32.1847, 31.2638, 29.7933, 27.0799, 25.8969, 22.6628, 22.4247, 20.5754, 20.5256. *Exact Mass*, high resolution mass spectrum, calcd.: 170.1306; found: 170.1310.

Methyl-4-methylcyclohexylacetate, **3**g *(19, 20)*: ir: 1740 cm^{-1}; ^{1}H nmr (400 MHz) δ: 3.67 (s, 3H, CO_2CH_3, *cis* isomer), 3.66 (s, 3H,

CO_2CH_3, *trans* isomer), 2.30 (d, 2H, J = 6 Hz, CH_2CO_2Me, *cis* isomer), 2.19 (d, 2H, J = 6 Hz, CH_2CO_2Me, *trans* isomer), 1.8–1.2 (m, 8H), 1.05–0.90 (m, 5H), 0.91 (d, 3H, CH_3, J = 7 Hz, *cis* isomer), 0.88 (d, 3H, CH_3, J = 7 Hz, *trans* isomer); ^{13}C nmr (100.62 MHz) δ: 173.8 (*cis* isomer), 173.6 (*trans* isomer), 51.3, 41.9, 39.1 (*cis* isomer), 34.9, 34.7, 33.0, 32.4, 30.5, 29.9 (*cis* isomer), 28.6, 22.57, 20.23; ms *m/e*: 171 (M^+ + 1).

(R)-O-Methylmandelyl-4-methylcyclohexylacetate, **3**h: ^{1}H nmr (400 MHz) δ: 7.40–7.30 (m, 5H), 4.415 (dd, 1H, J = 7.5 Hz, 4 Hz), 4.25–4.15 (m, 2H), 3.3 (s, 3H, OCH_3), 2.32 (d, 2H, J = 8 Hz, *cis* isomer), 2.21 (d, 2H, J = 7 Hz, *trans* isomer), 1.73–1.57 (m), 1.53–1.43 (m), 1.41–1.31 (m), 1.30–1.18 (m), 0.96 (bt), 0.9 (d, 3H, J = 7 Hz, *cis* isomer), 0.87 (d, 3H, J = 6 Hz, *trans* isomer); ^{13}C nmr δ: 173.0233 (*cis* isomer), 172.7930 (*trans* isomer), 137.9615, 136.0527, 130.2886, 129.0017, 128.6489, 128.4227, 128.1318, 126.8663, 81.5813, 67.4815, 67.3425, 56.1227, 42.1009, 41.9340, 39.0564, 34.8469, 34.6086, 33.3862, 32.8449, 32.3103, 32.2238, 31.5320, 30.4452, 29.8539, 28.4815, 22.4791 (*trans* isomer), 20.1616 (*cis* isomer); ms *m/e*: 291 (M^+ + 1), 259 (M^+ − OCH_3).

*Methyl 4-*tert*-butylcyclohexylacetate,* **3**i *(20)*: ^{1}H nmr (400 MHz) δ: 3.7 (s, 3H, CO_2CH_3, *cis* isomer), 3.63 (s, 3H, CO_2CH_3, *trans* isomer), 2.36 (d, J = 7 Hz), 2.18 (d, J = 7 Hz), 1.83–1.73 (bt), 1.72–1.46 (m), 1.16–0.85 (m), 0.84 (s, *t*-Bu, *cis* isomer), 0.835 (s, *t*-Bu, *trans* isomer).

tert-*Butyl 4-*tert*-butylcyclohexylacetate,* **3**j *(20)*: ^{1}H nmr (400 MHz) δ: 2.25 (m), 2.07 (d, J = 7 Hz), 1.80–1.70 (bt), 1.68–1.40 (m), 1.44 (CO_2t-Bu), 1.10–0.90 (m), 0.833 (*t*-Bu); ^{13}C nmr (100.62 MHz) δ: 173.0095, 172.5683, 48.3516, 47.8253, 43.9019, 43.3936, 38.3042, 37.7440, 35.7598, 35.2384, 33.9951, 33.3978, 32.9232, 32.5379, 32.3777, 30.8928, 30.5469, 30.0263, 29.8346, 29.6912, 28.1410, 27.5405, 27.4846, 27.0786, 26.4577, 21.6483; ms *m/e*: 255 (M^+ + 1); **3***j* was hydrolyzed (CF_3CO_2H in CH_2Cl_2) to the 4-*tert*-butylcyclohexylacetic acid (20): ^{1}H nmr (400 MHz) δ: 9.7 (bs, 1H, CO_2H), 2.41 (d, J = 7 Hz), 2.22 (d, J = 7 Hz), 1.88–1.81 (m), 1.805–1.74 (m), 1.73–1.64 (m), 1.6–1.48 (m), 1.17–0.9 (m), 0.85 (s, *t*-Bu, *cis* isomer), 0.833 (s, *t*-Bu, *trans* isomer); ^{13}C nmr (100.62 MHz) δ: 179.0674 (*cis* isomer), 178.6325 (*trans* isomer), 48.2376, 47.6876, 41.6553, 36.1315, 34.7817, 33.3593, 32.4700, 32.3119, 30.4616, 29.5141, 29.2679, 27.4642, 27.3925, 26.9638, 26.2055, 21.5611; ms *m/e*: 199 (M^+ + 1).

*Methyl 7-hydroxy-2-(*E*)-octenoate,* **3**l: ^{1}H nmr (400 MHz) δ: 6.97 (ddd, 1H, J = 16 Hz, 8 Hz, 4.2 Hz), 5.85 (dq, 1H, J = 16 Hz, 2 Hz), 3.73 (s, 3H, CO_2CH_3), 3.67 (m, 1H), 2.28–2.2 (m, 2H), 1.92–1.83 (m, 1H), 1.73–1.35 (m, 5H), 0.94 (t, 3H, J = 7 Hz).

Ethyl (2-chloroethyl)cyclopentylacetate, **3**m: ^{1}H nmr (400 MHz) δ: 4.14 (q, 2H, J = 7 Hz, major isomer), 4.13 (q, 2H, J = 7 Hz, minor isomer), 3.65–3.45 (m, 2H), 2.5–2.35 (m, 1H), 2.33 (d, 1H, J = 5 Hz, minor isomer), 2.29 (d, 1H, J = 5 Hz, major isomer), 2.2–1.5 (m, 9H), 1.42–1.35 (m, 1H), 126 (t, 3H, J = 7.0 Hz); ^{13}C nmr (100.62 MHz) δ: major isomer: 173.3, 60.2, 43.9, 39.7, 38.7, 34.9, 33.1, 30.6, 29.3, 22.1, 14.2; minor isomer: 173.0, 42.7, 41.9, 39.4, 37.7, 32.0, 31.4, 23.4.

Methyl 4-[2-(2'-chloroethyl)cyclopentyl]-3-butenoate, **3**n

Benzene solutions of Ph_3SnH (0.102 g, 0.290 mmol in 5 mL) and AIBN (0.005 g, 0.03 mmol in 5 mL) were added to a refluxing solution of **2***n* (0.078 g, 0.252 mmol) in benzene (15 mL) over 6 h using a syringe pump. The mixture was refluxed for an additional 6 h. The solvent was removed under reduced pressure and the residue was purified by flash chromatography to give **3***n* as an oil (0.035 g, 60%); ^{1}H nmr (400 MHz) δ: 5.61–5.4 (m, 2H), 3.7 (s, 3H, CO_2CH_3), 3.81–3.5 (m, 2H), 3.125 (d, minor isomer), 3.05 (d, 2H, major isomer), 2.6 (m, 1H), 2.35 (m), 2.12–1.96 (m), 1.88–1.74 (m), 1.69–1.47 (m), 1.40–1.23 (m); ms *m/e*: 231 (M^+ + 1).

Methyl 2-propanoylbicyclo[3.3.0]octane, **4**

A solution of **2***n* (0.098 g, 0.32 mmol) in benzene (10 mL) was heated in an oil bath maintained at 90°C. Benzene solutions of Ph_3SnH (0.176 g, 0.5 mmol in 5 mL) and AIBN (0.025 g, 0.152 mmol in 5 mL) were added to the stirred solution of **2***n* over 10 h using a syringe pump. Benzene was removed and replaced with toluene (10 mL). The mixture was heated in an oil bath maintained at 120°C. Toluene solutions of Ph_3SnH (0.176 g, 0.5 mmol in 5 mL) and AIBN (0.025 g, 0.152 mmol in 5 mL) were injected into the reaction mixture over 10 h by the use of a syringe pump. The solvent was removed under reduced pressure and the residue was purified by flash chromatography to give the bicyclic ester **4** as an oil; ^{1}H nmr (400 MHz) δ: 3.68 (s, 3H, CO_2CH_3), 2.23 (dd, 1H), 2.13 (dd, 1H), 1.95–1.84 (m, 1H), 1.84–1.73 (m), 1.7–1.6 (m), 1.42–1.13 (m).

Acknowledgements

We wish to acknowledge the financial assistance of the Natural Sciences and Engineering Research Council of Canada, and Le Ministère de l'Education du Québec. We thank M. Evans for recording the mass spectra.

1. B. Giese. Radicals in organic synthesis: formation of carbon–carbon bonds. *Edited by* J. E. Baldwin. Pergamon Press, Oxford, England. 1986; D. J. Hart. Science (Washington, D.C.), **223**, 883 (1984).
2. S. Hanessian, P. Beaulieu, and D. Dubé. Tetrahedron Lett. **27**, 5071 (1986).
3. S. Hanessian and M. Alpegiani. Tetrahedron Lett. **27**, 4857 (1986).
4. G. Stork and R. Mook, Jr. J. Am. Chem. Soc. **105**, 3720 (1983); G. Stork and N. H. Baine. J. Am. Chem. Soc. **104**, 2321 (1982); G. Stork, R. Mook, Jr., S. A. Biller, and S. D. Rychnovsky. J. Am. Chem. Soc. **105**, 3741 (1983); G. Stork and N. H. Baine. Tetrahedron Lett. **26**, 5927 (1985); G. Stork and M. Kahn. J. Am. Chem. Soc. **107**, 500 (1985); G. Stork and P. M. Sher. J. Am. Chem. Soc. **108**, 303 (1986); G. Stork, P. M. Sher, and M.-L. Chen. J. Am. Chem. Soc. **108**, 6384 (1986); G. Stork and M. J. Sofia. J. Am. Chem. Soc. **108**, 6826 (1986); G. Stork and R. Mook, Jr. Tetrahedron Lett. **27**, 4529 (1986).
5. D. L. J. Clive and P. L. Beaulieu. J. Chem. Soc. Chem. Commun. 307 (1983); D. L. J. Clive, P. L. Beaulieu, and L. Set. J. Org. Chem. **49**, 1313 (1984); L. Set, D. R. Cheshire, and D. L. J. Clive. J. Chem. Soc. Chem. Commun. 1205 (1985); S. M. Bennett and D. L. J. Clive. J. Chem. Soc. Chem. Commun. 878 (1986).
6. K. Shankaran, C. P. Sloan, and V. Snieckus. Tetrahedron Lett. **26**, 6001 (1985).
7. C. S. Wilcox and L. H. Thomasco. J. Org. Chem. **50**, 546 (1985); C. S. Wilcox and J. J. Gaudino. J. Am. Chem. Soc. **108**, 3102 (1986).
8. D. J. Hart and C.-P. Chuang. J. Org. Chem. **48**, 1782 (1983); D. A. Burnett, J.-K. Choi, D. J. Hart, and Y.-M. Tsai. J. Am. Chem. Soc. **106**, 8201 (1984); D. J. Hart and Y.-M. Tsai. J. Am. Chem. Soc. **106**, 8209 (1984).
9. A. L. J. Beckwith and D. H. Roberts. J. Am. Chem. Soc. **108**, 5893 (1986); A. L. J. Beckwith and P. E. Pigou. J. Chem. Soc. Chem. Commun. 85 (1986); A. L. J. Beckwith and D. M. O'Shea. Tetrahedron Lett. **27**, 4525 (1986).
10. R. Tsang and B. Fraser-Reid. J. Am. Chem. Soc. **108**, 2116 (1986); A. L. J. Beckwith, D. H. Roberts, C. M. Schiesser, and A. Wallner. Tetrahedron Lett. **26**, 3349 (1985); D. P. Curran and D. M. Rakiewicz. J. Am. Chem. Soc. **107**, 1448 (1985); D. P. Curran, M. H. Chen, and D. Kim. J. Am. Chem. Soc. **108**, 2489 (1986); J. D. Winkler and V. Sridar. J. Am. Chem. Soc. **108**, 1708 (1986).
11. E. J. Corey, D. A. Clark, G. Goto, A. Marfat, C. Mioskowski, B. Samuelsson, and S. Hammarström. J. Am. Chem. Soc. **102**, 1436 (1980).

Can. J. Chem. Downloaded from www.nrcresearchpress.com by 118.98.75.50 on 09/07/12
For personal use only.

12. P. J. KOCIENSKI, G. CERNIGLIARO, and G. FELDSTEIN. J. Org. Chem. **42**, 353 (1977).
13. D. R. HICKS and B. FRASER-REID. Can. J. Chem. **53**, 2017 (1975).
14. D. H. R. BARTON and S. W. MCCOMBIE. J. Chem. Soc. Perkin Trans. 1, 1574 (1975).
15. H. BOOTH, F. E. KING, K. G. MASON, J. PARRICK, and R. L. ST. D. WHITEHEAD. J. Chem. Soc. 1050 (1959); B. M. TROST and L. H. LATIMER. J. Org. Chem. **43**, 1031 (1978).
16. J. E. BALDWIN. J. Chem. Soc. Chem. Commun. 734 (1976).
17. A. L. J. BECKWITH. Tetrahedron, **37**, 3073 (1981).
18. S. HUCKIN and L. WEILER. J. Am. Chem. Soc. **96**, 1082 (1974).
19. Y. IIDA and R. SUGAWARA. Agric. Biol. Chem. **45**, 1553 (1981).
20. P. C. AMSTERDAMSKY, M. MALISSARD, and Z. WELVART. Bull. Soc. Chim. Fr. 635 (1975).

Can. J. Chem. Downloaded from www.nrcresearchpress.com by 118.98.75.50 on 09/07/12
For personal use only.

Direct observation of dienols produced by photochemical enolisation of α,β-unsaturated ketones: rates and activation parameters for dienol reketonisation via a 1,5-hydrogen shift[1]

RANDY M. DUHAIME AND ALAN C. WEEDON[2]

The Photochemistry Unit, Department of Chemistry, University of Western Ontario, London, Ont., Canada N6A 5B7

Received October 28, 1986

This paper is dedicated to Professor John T. Edward

RANDY M. DUHAIME and ALAN C. WEEDON. Can. J. Chem. **65**, 1867 (1987).

The production of stable solutions of *Z*-dienols by ultraviolet light irradiation of α,β-unsaturated ketones at low temperatures (ca. −76°C) in d_4-methanol is reported. The rates of reketonisation of the dienols via a 1,5-sigmatropic hydrogen shift were determined at various temperatures between −43°C and +2°C by monitoring the proton nmr spectra of the dienols. From the data the activation parameters for the reaction were calculated. For the dienol *Z*-2-hydroxy-4-methyl-2,4-pentadiene, **2**, derived from photoenolisation of 4-methyl-3-penten-2-one, **1**, the activation energy from the Arrhenius plot is 62 ± 4 kJ/mol, and the activation entropy and enthalpy from the Eyring plot are −87 ± 15 J/mol K and 60 ± 4 kJ/mol, respectively. For the dienol *Z*-4-*tert*-butyl-2-hydroxy-2,4-pentadiene, **4**, obtained from photoenolisation of 4,5,5-trimethyl-3-hexen-2-one, **3**, the activation energy, entropy, and enthalpy were found to be 47 ± 5 kJ/mol, −135 ± 19 J/mol K, and 45 ± 5 kJ/mol, respectively.

RANDY M. DUHAIME et ALAN C. WEEDON. Can. J. Chem. **65**, 1867 (1987).

On rapporte la production de solutions stables de diènols-*Z* par irradiation ultraviolette de cétones α,β-nonsaturées, à basse température (environ −76°C), dans le méthanol-d_4. Opérant à des températures allant de −43°C à +2°C et utilisant les variations observées dans les spectres rmn du proton des diènols, on a déterminé les vitesses de recétonisation des diènols qui se produisent par le biais d'une transposition sigmatropique-1,5 d'hydrogène. Pour le diènol hydroxy-2 méthyl-4 pentadiène-2,4-(*Z*) (**2**), qui provient de la photoénolisation de la méthyl-4 pentène-3 one-2 (**1**), l'énergie d'activation que l'on peut déduire de la courbe d'Arrhénius est égale à 62 ± 4 kJ/mol et l'enthalpie et l'entropie d'activation que l'on peut déduire de la courbe de Eyring sont respectivement égales à 60 ± 4 kJ/mol et −87 ± 15 J/mol K. Pour le diènol *tert*-butyl-4 hydroxy-2 pentadiène-2,4 (**4**), qui est obtenu par photoénolisation de la triméthyl-4,5,5 hexène-3 one-2 (**3**), on a trouvé que les énergie, entropie et enthalpie d'activation sont respectivement égales à 47 ± 5 kJ/mol, −135 ± 19 J/mol K et 45 ± 5 kJ/mol.

[Traduit par la revue]

Introduction

Ultraviolet light irradiation of β-alkyl-α,β-unsaturated ketones results in efficient *E*–*Z* isomerisation, and less efficient photoenolisation (1) to produce transient dienols, which can be trapped as their silyl ethers (2–4) as is shown in Scheme 1. The dienols are formed from the singlet excited state of the ketones (2, 3) and with a quantum efficiency of approximately 10% (1). They are produced with *Z*-geometry (2) and can reketonise by acidic or basic catalysis to give a β,γ-unsaturated ketone (3, 5), or they can reketonise via a non-catalysed pathway for which a 1,5-sigmatropic hydrogen shift mechanism has been proposed (1–5). Similar results have been obtained with α,β-unsaturated esters (6). The dienols have also been generated by flash photolysis of unsaturated ketones in aqueous base, and the rates of reketonisation of the corresponding dienolates by protonation by water have been measured; in the same experiments the rate of the non-catalysed (1,5-hydrogen shift) reaction was also determined, but rather inaccurately due to limitations in the technique (7). Reported here are the results of experiments in which stable solutions of the dienols **2** and **4** were produced by low temperature irradiation of unsaturated ketones **1** and **3**, respectively, and in which the rate of the non-catalysed reketonisation process was determined for each dienol at a variety of temperatures.

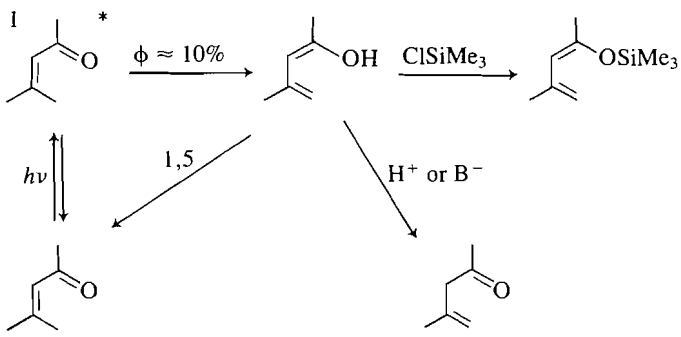

SCHEME 1

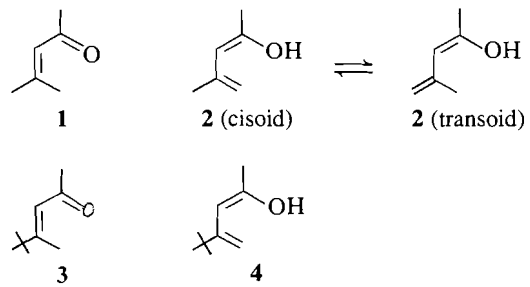

Results

Ketones **1** and **3** were dissolved in d_4-methanol in nmr tubes which were suspended in an acetone/dry ice slurry and irradiated with ultraviolet light. The ^{1}H nmr spectra of the irradiated solutions were recorded at −76°C and indicated that a new set of signals had been formed at the expense of the starting ketones. Disappearance of the ketones was not complete and the rate of their disappearance became slower at higher conversion. This is attributed to overlap of the absorption spectra of the products and those of the starting ketones: as will be discussed below, the photoproducts are assigned structures **2** and **4**, and

[1]Contribution number 376 from the Photochemistry Unit, University of Western Ontario.

[2]Author to whom correspondence may be addressed.

Can. J. Chem. Downloaded from www.nrcresearchpress.com by 118.98.75.50 on 09/07/12
For personal use only.

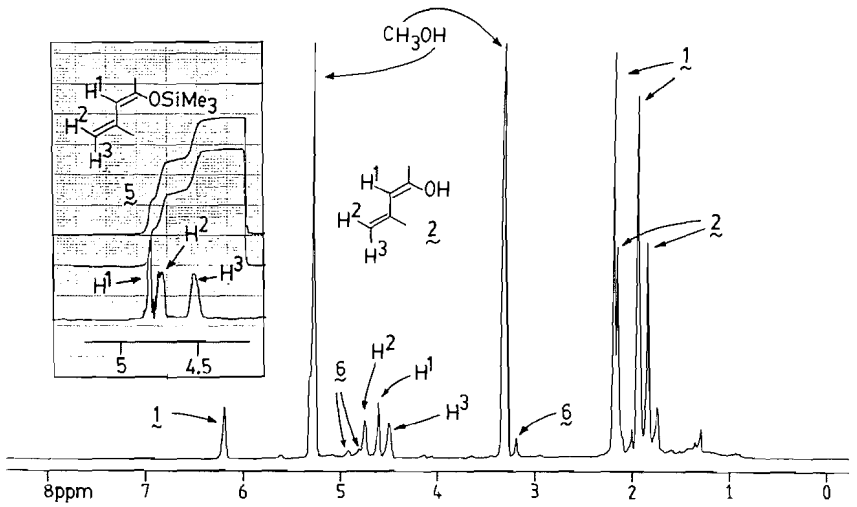

FIG. 1. The ^{1}H nmr spectrum (200 MHz) of dienol **2** in d_4-MeOH at −23°C in the presence of CH_3OH (added for temperature calibration), and ketones **1**, and **6**. Insert: partial ^{1}H nmr spectrum (100 MHz) of siloxydiene **5** recorded at ambient temperature in $CDCl_3$. Assignments for H^2 and H^3 for **2** may be reversed.

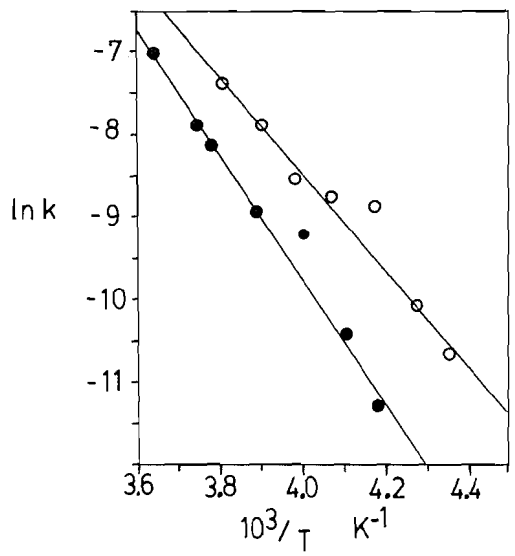

FIG. 2. Arrhenius plot for conversion of dienols **2** and **4** to ketones **1** and **3**, respectively, in d_4-methanol. Upper line, **4**; lower line, **2**.

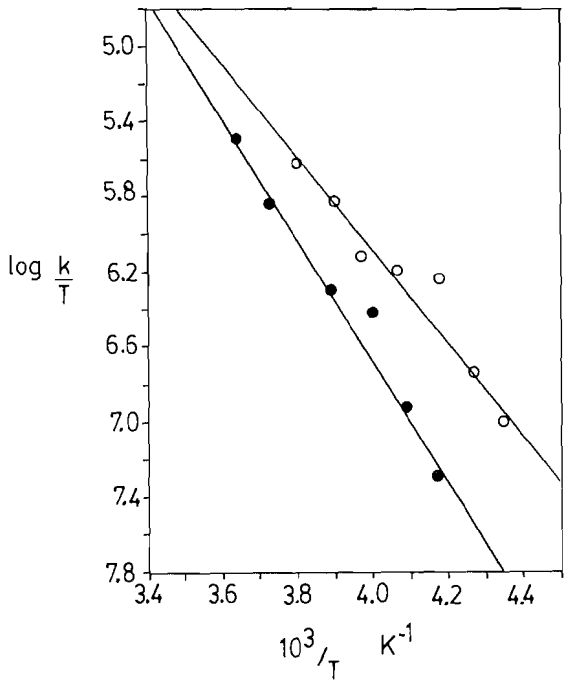

FIG. 3. Eyring plot for conversion of dienols **2** and **4** to ketones **1** and **3**, respectively, in d_4-methanol. Upper line, **4**; lower line, **2**.

the uv absorption spectra of siloxydienes such as **5** (4) indicate that the dienols **2** and **4** should absorb in the same region as the $\pi \rightarrow \pi^*$ absorption band of the ketone. It was found that mixtures of ketone and dienol in which approximately 50% conversion had occurred could be generated before the rate of conversion slowed appreciably, and further conversion was not attempted in order to avoid photochemical *E–Z* isomerisation of the dienol. Such isomerisation has been observed during the preparation of *Z*-siloxydienes such as **5** by trapping of the photochemically produced *Z*-dienols by chlorotrimethylsilane (4). The ^{1}H nmr spectrum recorded at −23°C of the mixture derived from irradiation of ketone **1** is shown in Fig. 1. The solutions appeared to be stable at −76°C, but if they were allowed to warm up to room temperature the new signals disappeared and those of the starting ketones were regenerated. Following their regeneration partial deuteration of the methyl groups of **1** and **3** was apparent. At temperatures intermediate between −76°C and ambient the rate of the reversion process was slow enough to be measured by integration of the peak areas of the signals assigned to the ketones and photoproducts. The rate of the reversion process was measured for the transients from both ketones **1** and **3** at a variety of temperatures. The reversion reaction proceeded with first order kinetics, and the rate constants derived were used to obtain the Arrhenius and Eyring plots shown in Figs. 2 and 3.

Discussion

The photoproducts formed by low temperature irradiation of ketones **1** and **3** are identified as the dienols **2** and **4**, respectively, and the assignment is based upon the similarity of their ^{1}H nmr spectra to that of the siloxydiene **5**, and upon the fact that upon warming they are smoothly converted back into the ketone precursors. The chemical shifts of the protons assigned to **2** recorded in d_4-methanol at −23°C are shown in

Can. J. Chem. Downloaded from www.nrcresearchpress.com by 118.98.75.50 on 09/07/12
For personal use only.

TABLE 1. Proton nmr data for dienols **2** and **4** and siloxydiene **5**[a]

Compound	Solvent	T (°C)	H^1	H^2	H^3	CH_3	R^1
2	d_4-MeOH	−23	4.58	4.74*	4.48*	1.80	1.88
4	d_4-MeOH	−43	4.62	5.28*	4.96*	1.86	1.06
5	$CDCl_3$	35	4.88	4.81	4.59	1.73	1.81

[a]Spectra of **2** and **4** were recorded at 200 MHz, and that of **5** at 100 MHz. Solutions of **2** and **4** contained 5% methanol for temperature calibration (see ref. 17 and Experimental). Chemical shifts for **2** and **4** are given relative to the methanol peak at 3.30 ppm. Data for compound **5** is taken from ref. 4. Assignments for signals marked by an asterisk may be reversed (see Discussion). R′ is the 4-Me or 4-Bu′ substituent in **2** and **4**, respectively.

Table 1 along with those of the corresponding siloxydiene **5** in $CDCl_3$ at ambient temperature. Allowing for solvent and temperature effects upon the chemical shifts, the spectra are sufficiently similar to support strongly the assignment of the dienol structure to the photochemical product, and are in accord with the shifts predicted from calculation using standard chemical shift correlations (8). The signals in the spectrum of **5** have been fully assigned using coupling constant data (4); protons H^2 and H^3 (see Table 1) are geminally coupled (J = 2.7 Hz) as well as coupled allylically (J = 0.8, 0.5 Hz) and therefore their signals are substantially broader in appearance than the signal due to H^3 which is allylically coupled only (J = 0.8 Hz). The signals corresponding to these protons in **5** are shown in the insert in Fig. 1. The olefinic protons in **2** also give broadened signals due to a mixture of allylic and geminal coupling (see Fig. 1). Sufficient resolution could not be obtained at the low temperatures to allow measurement of the coupling constants in the spectrum of **2**. However, the signals at 4.74 ppm and 4.48 ppm were broader than that at 4.58 ppm, and on this basis the latter is assigned to H^1 and the former pair are assigned to protons H^2 and H^3, and their broadness is ascribed to geminal coupling to each other. In the spectrum of the dienol **2**, shown in Fig. 1, small amounts of the deconjugated isomer **6** can also be seen; these were present in the starting ketone and the amount present was unchanged during the experiments, indicating that none was formed photochemically during the irradiation, or during the warming period in which the dienol intermediate was beginning to revert to the starting ketone.

Similar results were obtained when the ketone **3** was irradiated under the same conditions as **1**. In this case, however, the ketone, which was initially present almost exclusively as the *E*-isomer, underwent rapid *E*–*Z* isomerisation during the initial stages of the irradiation, and this was followed by slower conversion to the dienol **4**. In addition, very small amounts of the cyclopropane **7** were formed from irradiation of the *Z*-isomer, as has been reported previously (3, 9). The chemical shifts of the signals seen for **4** in d_4-methanol at −43°C are shown in Table 1. As was the case for **2**, two of the three olefinic protons show evidence of greater broadening due to allylic coupling; thus the signals at 5.28 ppm and 4.96 ppm in the spectrum of **4** are assigned to H^2 and H^3, and that at 4.62 ppm to H^1. Comparison of the chemical shifts of the olefinic protons in **4** with those of **2** and **5** (see Table 1) indicate that protons H^2 and H^3 are to lower field in **4** than in **2** and **5**. This can be rationalised in terms of the preferred conformation of the diene. The dienols would be expected to exist in either a cisoid or transoid planar conformation in order to maximise delocalisation of the π system, and studies have indicated (10) that the transoid conformation is generally preferred in dienes. However, the bulky *tert*-butyl group in **4** might be expected to freeze the diene in a cisoid conformation so as to minimise steric interactions with the enol hydroxyl, whereas dienol **2** is free to adopt the electronically more stable transoid conformation. If this is so, then the protons H^2 and H^3 of **4** will be more deshielded by the OH group of the enol and so appear to lower field than the corresponding hydrogens in **2** and **5**.

When the temperatures of the solutions of the dienols were raised from −76°C to ambient, the new spectra disappeared and the spectra of the conjugated ketones cleanly reappeared. No deconjugated ketones were formed; this supports the proposition that the dienols reketonise via the proposed 1,5-sigmatropic hydrogen shift mechanism and not by an acid or base catalysed sequence, since it has been shown that the main product formed under the latter conditions is the β,γ-unsaturated ketone (1). Since the dienols cleanly reverted to the ketones it was possible to use the relative peak areas of the olefinic protons of each in the ^1H nmr spectra to determine the rate of the reversion reaction at a variety of temperatures. The reversion process followed clean first order kinetics as would be expected for a unimolecular non-catalysed process such as the 1,5-sigmatropic hydrogen shift mechanism. The first order rate constants are shown in Table 2; they indicate that the dienol **2** has a lifetime at 240 K of 23 h while dienol **4** has a lifetime at the same temperature of only 2 h. The greater stability of **2** meant that solutions at temperatures as high as +2°C had a half life of ca. 20 min.

The faster rate of reketonisation of **4** compared with **2** is consistent with the arguments proposed above concerning the preferred conformations of **2** and **4** based upon their ^1H-nmr data. It is also in accord with earlier work reported from this laboratory: using the evidence of steady state kinetic and quantum yield studies of the photochemical deconjugation reaction of α,β-unsaturated esters and ketones it has been suggested (3, 6) that substituents on the dienol can control the conformation of the molecule and freeze it in either the cisoid or transoid conformation, and hence greatly affect the rate of the 1,5-hydrogen shift mechanism for reketonisation. For example, it has been shown that irradiation of the ester **8** results in very efficient photochemical deconjugation towards the isopropyl group to give **9**, unless base is added to the system in which case **10** is also formed. This can be explained if dienols **11** and **12** are formed as transient intermediates in the reaction. In **11** the substituted diene suffers steric interactions between the hydroxyl group of the enol and the methyl substituents which forces the molecule into the transoid conformation. This slows the 1,5-hydrogen shift reaction to the point that acid or base catalysis by the solvent can convert **11** to **9**. In contrast, dienol **12** is held in a cisoid conformation, also for steric reasons, and the 1,5-hydrogen shift is rapid unless a base is added to catalyse its conversion to the deconjugated isomer **10**. Similar arguments can be applied to **2** and **4** to rationalise their relative rates of reketonisation.

The lifetimes of dienols **2** and **4** appear to be shorter than the

Can. J. Chem. Downloaded from www.nrcresearchpress.com by 118.98.75.50 on 09/07/12
For personal use only.

TABLE 2. Rates of reversion and activation parameters for decay of dienols **2** and **4** to ketones **1** and **3**, respectively, in d_4-methanol[a]

Compound	T (K)	$10^5\,k$ (s^{-1})	A (s^{-1})	E_a (kJ/mol)	$\Delta H^{\neq}$ (kJ/mol)	$\Delta S^{\neq}$ (kJ/mol)
Dienol **2**	275	88.2 ± .2	4×10^8	62±4	60±4	−87±15
	268	38.7 ± .3				
	265	29.1 ± .8				
	257.5	12.8 ± .1				
	250	9.77± .54				
	244	2.93± .35				
	240	1.23± .07				
Dienol **4**	230	2.30± .16	1×10^6	47±5	45±5	−135±19
	234	4.14± .26				
	240	13.8 ±1.2				
	246	15.7 ±0.4				
	251.5	18.9 ±0.4				
	257	38.1 ±1.1				
	263	61.5 ±6.9				
Enol **14**[b]	—	—	3×10^{12}	37		

[a]Error limits are standard deviations determined from the least squares fit of the data.
[b]From refs. 14 and 15; A and E_a were measured for **14** by flash photolysis.

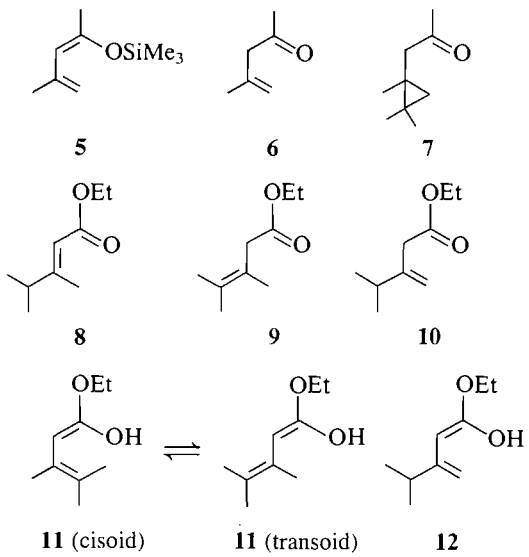

5 **6** **7**

8 **9** **10**

11 (cisoid) **11** (transoid) **12**

lifetimes of simple enols, which are relatively stable in the absence of acidic and basic catalysts, and which have been characterised by a variety of spectroscopic techniques in solution (11). The greater stability of simple enols can be attributed to the fact that in the absence of acidic or basic catalysts the only reasonable mechanism for unimolecular reketonisation of an enol in which orbital symmetry conservation requirements are met is a 1,3-sigmatropic antarafacial hydrogen shift; however, the 4-centre antarafacial transition state, while allowed thermally, is generally unattainable by first row elements. In contrast, for the dienols **2** and **4** the reketonisation via a 1,5-hydrogen shift involves a 6-centre transition state with a suprafacial orbital overlap requirement which can readily be attained.

It is informative to compare the rate of the 1,5-hydrogen shift process in **2** and **4** with that in the enols obtained by irradiation of *ortho*-alkyl aromatic carbonyl compounds such as **13** as shown in Scheme 2. It has been shown (12, 13), that irradiation of ketones such as **13** leads to a mixture of *E*- and *Z*-enols, and that the *E*-enols have lifetimes of seconds and require acid or

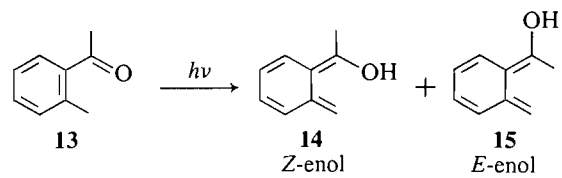

13 **14** *Z*-enol **15** *E*-enol

SCHEME 2

base to catalyse their reketonisation. The *Z*-enols, however, revert to the ketones by a rapid unimolecular process which is assumed to be a 1,5-hydrogen shift. The rate is solvent dependent: in non-polar solvents the lifetime of the enol is ca. 30 ns at ambient temperature whereas in polar solvents the lifetime is ca. 1 μs, and is presumably lengthened because of hydrogen bonding of the solvent to the enol. The much faster rates of reversion in the aromatic systems as compared with those observed for dienols **2** and **4** may reflect the fact that the aromatic system is being reformed, and also that the enol is constrained in the cisoid orientation necessary for the 1,5-shift to occur.

The rates of reversion of the dienols **2** and **4** were also measured at a variety of temperatures and the activation parameters obtained from the Arrhenius and Eyring plots shown in Figs. 2 and 3 are given in Table 2, along with the data reported for the *Z*-enol **14** derived from the aromatic system **13**. The activation energies for **2**, **4**, and **14** are comparable, but a much larger pre-exponential factor is reported for **14** (14, 15); this may reflect the cisoid orientation forced upon the aromatic system as compared with the conformational flexibility of the dienols **2** and **4**.

The errors in the activation parameters shown in Table 2 are considerable. However, if the differences between the values for the dienols **2** and **4** are taken to be real, then they indicate the reverse to what might be expected. Based upon chemical shift data and the arguments put forward to explain the photochemical reactivity of the ester **8** and related systems it was proposed above that the enol **4** is held in a cisoid conformation because of steric interactions between the Bu^t group and the enol hydroxyl, whereas **2** is more able to adopt the electronically more stable transoid conformation. If this is so, it might be

Can. J. Chem. Downloaded from www.nrcresearchpress.com by 118.98.75.50 on 09/07/12
For personal use only.

Can. J. Chem. Downloaded from www.nrcresearchpress.com by 118.98.75.50 on 09/07/12
For personal use only.

expected that the activation entropy for the 1,5 hydrogen shift in **2** would be greater than in **4** since **2** must undergo a conformational change in order to reach the transition state. However, the reverse is indicated by the data, with **2** having a smaller entropy of activation than **4**. In addition, independent of the conformation, the activation enthalpy for both **2** and **4** would be expected to be similar, and yet the activation enthalpy for **4** is less than that for **2**.

To rationalise this anomaly the effects of solvation can be considered. It might be expected that the less efficient delocalisation in **4** (arising from poorer overlap of the π-system because of the adoption of a cisoid conformation) might make the hydroxyl function more basic and so more strongly hydrogen bonded than would be the case for **2**. This will weaken the OH bond and lower the activation enthalpy for a 1,5-hydrogen shift as observed; it would also serve to increase the activation entropy due to the need for greater solvent reorganisation as the transition state is approached.

Alternatively, if the dienol **2** is indeed more stable in the transoid conformation, then the observed rate constant for decay will in fact be the product of the rate constant for reversion to the ketone via the 1,5-hydrogen shift and the equilibrium constant for the conformational equilibrium between the cisoid and transoid forms of **2** (assuming that the rate of conformational interconversion is rapid relative to the rate of the 1,5-shift). Thus the activation parameters determined for **2** are a composite of the temperature dependencies of 1,5-shift rate constant and the equilibrium constant for the cisoid–transoid conformational interconversion, and are therefore not directly comparable with those for **4**, where the observed rate constant is equal to that for the 1,5-shift if this dienol exists preferentially in the cisoid conformation.[3]

In previous work reported from this laboratory approximate values of the rate of the 1,5-hydrogen shift reaction for dienols **2** and **4** were estimated in water at ambient temperatures using the technique of flash photolysis. The value found for **4** was ca. 50 s^{-1} and for **2** the rate was slower and indistinguishable from zero. Extrapolation to room temperature of the values found for **4** and **2** in d_4-methanol at low temperature yields very inaccurate values of the rate which are at least 50 times slower than those observed in water. It has been shown (12) for aromatic enols such as **14** that the lifetimes are little affected by changing solvent from water to methanol (at most a factor of two) but it has been shown that large isotope effects can exist, and that these increase at lower temperatures. Thus for example, the deuterium isotope effect upon the reketonisation rate of **14** is 3 at 298 K and 180 at 140 K (14). Consequently in the case of **2** and **4** the difference between the rates measured at room temperature in water by flash photolysis and those obtained by extrapolation from the results obtained at low temperature in d_4-methanol may be attributed at least in part to a large deuterium isotope effect.

Experimental

A commercially available sample of ketone **1** was used. Ketone **3** was prepared from ethyl 3,4,4-trimethyl-2-pentenoate (6); the ester was hydrolysed to the acid with ethanolic KOH, and the acid was converted to the ketone with methyl lithium using the procedure of Theus *et al.* (16). Both ketones were purified by preparative gas chromatography prior to use.

Procedures for irradiation and kinetic measurements

Solutions of each of the ketones in CD_3OD (0.01–0.05 *M*, ca. 0.5 mL) containing a small quantity (ca. 5%) of non-deuterated methanol were placed in 0.4 mm internal diameter Pyrex nmr tubes which were suspended in a Dewar containing a slurry of dry ice in acetone. The tubes were held in a sleeve similar to that used to hold tubes in nmr probes, and the tube was spun using a jet of compressed air to rotate the sleeve. A quartz rod was placed in the nmr tube so that one end entered the solution of the ketone. The diameter of the quartz rod was optimised so as to minimise the air gap between it and the walls of the nmr tube as much as possible as was consistent with obtaining free rotation of the tube. Pyrex and water filtered light from a 100-W high pressure mercury lamp was focussed into the exterior end of the quartz rod which thereby acted as a light pipe to channel the lamp's output into the ketone solution. The dienols' uv spectra are comparable to those of the ketones (see Discussion). Thus, in order to obtain appreciable conversion of the ketones to the corresponding dienols it was found essential to mix the ketone solutions by rotating the tubes, and also to use solutions with optical densities less than unity so as to ensure that the whole length of the solution was irradiated. Up to 50% conversion to the dienol could be attained after 3–4 hours' irradiation. The irradiated solutions were kept at −76°C until required, and then rapidly transferred to the precooled probe of a Varian XL 200 NMR spectrometer. The probe was then warmed to the desired temperature and the decays of the dienols back to the corresponding ketones were monitored periodically by integration of the olefinic proton signals of both the ketone and the dienol relative to the methyl group of the methanol present. The plots of the areas of the peaks against time at each temperature yielded from their gradients the values of the rate constants shown in Table 2; these were calculated using a least-squares program to fit the data and the error limits indicated in the table are standard deviations calculated from the least-squares fit. The temperatures of the solutions were determined by measuring the separation of the added methanol peaks according to the method of Van Geet (17). The temperature dependent separation of the peaks was not altered by the presence of d_4-methanol, as determined by comparison of the peak separation in pure methanol under identical instrumental conditions.

[3]This argument was suggested by a referee.

1. M. Marjerrison and A. C. Weedon. J. Photochem. **33**, 113 (1986).
2. C. S. K. Wan and A. C. Weedon. J. Chem. Soc. Chem. Commun. 1235 (1981).
3. R. Richard, P. Sauvage, C. S. K. Wan, A. C. Weedon, and D. F. Wong. J. Org. Chem. **51**, 62 (1986).
4. C. S. K. Wan, A. C. Weedon, and D. F. Wong. J. Org. Chem. **51**, 3335 (1986).
5. S. L. Eng, R. Ricard, C. S. K. Wan, and A. C. Weedon. J. Chem. Soc. Chem. Commun. 236 (1983).
6. I. A. Skinner and A. C. Weedon. Tetrahedron Lett. 4299 (1983); A. C. Weedon. Can. J. Chem. **62**, 1933 (1984); R. M. Duhaime, D. A. Lombardo, I. A. Skinner, and A. C. Weedon. J. Org. Chem. **50**, 873 (1985); D. A. Lombardo and A. C. Weedon. Tetrahedron Lett. **27**, 5555 (1986); O. Piva, F. Henin, J. Muzart, and J.-P. Pete. Tetrahedron Lett. **27**, 3001 (1986).
7. R. M. Duhaime and A. C. Weedon. J. Am. Chem. Soc. (*a*) **107**, 6723 (1985); (*b*) In press.
8. E. Pretsch, J. Seibl, W. Simon, and T. Clerc. Spectral data structure determination of organic compounds. Springer, Berlin. 1983.
9. N. C. Yang and M. J. Jorgenson. Tetrahedron Lett. 1203 (1964); M. J. Jorgenson. J. Chem. Soc. Chem. Commun. 137 (1965).
10. H. Suzuki. Electronic absorption spectra and geometry of organic molecules. Academic Press, New York. 1967; P. W. Mui and E. Grunwald. J. Am. Chem. Soc. **104**, 6562 (1982).
11. B. Capon, A. K. Siddhanta, and C. Zucco. J. Org. Chem. **50**, 3580 (1985); A. Henne and H. Fischer. Helv. Chim. Acta, **58**, 1598 (1975); A. Henne and A. Fischer. Angew. Chem. Int. Ed. Engl. **15**, 435 (1976); Y. Chiang, A. J. Kresge, and Y. S. Tang. J. Am. Chem. Soc. **106**, 460 (1984).

12. R. HAAG, J. WIRZ, and P. J. WAGNER. Helv. Chim. Acta, **60**, 2595 (1977); P. J. WAGNER. *In* Rearrangements in ground and excited states. *Edited by* P. de Mayo. Academic Press, New York. 1980. pp. 427–431.
13. P. G. SAMMES. Tetrahedron, **32**, 405 (1976).
14. K.-H. GRELLMAN, H. WELLER, and E. TAUER. Chem. Phys. Lett. **95**, 195 (1983).
15. J. C. SCAIANO. Chem. Phys. Lett. **73**, 319 (1980).
16. V. THEUS, W. SURBER, L. COLOMBI, and H. SCHINZ. Helv. Chim. Acta, **38**, 239 (1955); M. J. JORGENSON. Org. Reactions, **18**, 1 (1970).
17. D. S. RAIFORD, C. L. FISK, and E. D. BECKER. Anal. Chem. **51**, 2050 (1979); A. L. VAN GEET. Anal. Chem. **42**, 679 (1970); **40**, 2227 (1968).

Can. J. Chem. Downloaded from www.nrcresearchpress.com by 118.98.75.50 on 09/07/12
For personal use only.

Nuclear magnetic resonance studies of ionomers. 5. Spectra of poly(methyl methacrylate-*co*-4-vinyl pyridine), poly(methyl methacrylate-*co*-2-methyl-5-vinyl pyridine), and their quaternized derivatives

ALMERIA NATANSOHN[1] AND ADI EISENBERG

Department of Chemistry, McGill University, 801 Sherbrooke St. W., Montreal, P.Q., Canada H3A 2K6

Received November 24, 1986

This paper is dedicated to Professor John T. Edward

ALMERIA NATANSOHN and ADI EISENBERG. Can. J. Chem. **65**, 1873 (1987).

Proton and carbon nuclear magnetic resonance spectra in solution of poly(methyl methacrylate-*co*-4-vinyl pyridine), poly(methyl methacrylate-*co*-2-methyl-5-vinyl pyridine), and of their derivatives obtained by quaternization with methyl iodide are presented. The vinyl pyridine structural units content of the samples is ca. 10%. In different solvents, the spectra provide information about the sequence distribution and configuration of the copolymers. A "coisotactic" alternating addition, defined as the probability of finding a methoxy group and a pyridine ring neighboring each other on the same side of the main chain, can be estimated as about 0.5 in both cases. This information arises from the splitting of the aromatic and of the methoxy signals (both in proton and carbon spectra). As expected, quaternization does not affect the copolymer configuration. Heteronuclear-correlated two-dimensional spectra can help in assigning the spectra.

ALMERIA NATANSOHN et ADI EISENBERG. Can. J. Chem. **65**, 1873 (1987).

On rapporte les spectres rmn du ^{1}H et du ^{13}C, mesurés en solution, du poly(méthacrylate de méthyle-*co*-vinyl-4 pyridine), du poly(méthacrylate de méthyle-*co*-méthyl-2 vinyl-5 pyridine) et de leurs dérivés obtenus par quaternisation avec l'iodure de méthyle. Les unités structurales vinylpyridines forment environ 10% des échantillons. Dans les différents solvants, les spectres fournissent de l'information sur la distribution des séquences ainsi que sur la configuration des copolymères. Dans chacun des cas, on peut évaluer à 0,5 la proportion d'addition « coisotactique » alternante, définie comme la probabilité de trouver un groupement méthoxy et un cycle pyridine côte à côte sur le même coté de la chaîne principale. On peut déduire cette information à partir du dédoublement des signaux dus aux groupements aromatiques et méthoxy (tant en rmn du ^{1}H que du ^{13}C). Comme on pouvait s'y attendre, la quaternisation n'affecte pas la configuration du copolymère. Les spectres bidimensionnels hétéronucléaires peuvent être utiles dans l'attribution des spectres.

[Traduit par la revue]

Introduction

The mechanical properties of a range of ionomers based on various vinyl pyridine units have been studied extensively in this laboratory and compared with those of the non-ionic polymers. Both random and block copolymers were studied. Random copolymers of methyl methacrylate (MMA), ethyl acrylate, butyl acrylate, or styrene with 4-vinyl pyridine (4VP) or 2-methyl-5-vinyl pyridine (2M5VP), respectively, were investigated (1, 2). Studies of ABA block copolymers of styrene (B) with 4VP (A) were performed and the results compared with those of the random copolymers (2). The influence of the chain length of the quaternization agent on the glass transitions was determined (3), and the swelling behavior of the block ionomers was investigated.[2] The random copolymers were also used as components of ionomer blends. When mixed with a proton-donating copolymer, such as poly(styrene-*co*-styrene sulfonic acid), the proton is transferred to the pyridine unit, creating ionic pairs that act as a driving force for compatibilization. This procedure was used to improve the miscibility of poly(ethyl acrylate) with poly(styrene) (4) and with sulfonated poly(phenylene) (5). Recently, blends of poly(MMA-*co*-4VP) with poly(S-*co*-SSA) were proven useful in the study of the process of coil overlap using nmr spectroscopy (6). The kinetics of coil overlap in solution are being thoroughly studied in our laboratory as a function of molecular weight, total solution concentration, ionic group concentration, and temperature.[3] However, since the main utilization for blends is as materials in the solid state, the next step in investigating interactions in this type of material will be CP-MAS ^{13}C nmr spectroscopy, which will give information about coil overlap and its kinetics directly in the solid state.

Before studies in the solid state can be carried out, it is useful to obtain information on the detailed peak assignments and the microstructure of the copolymers. These have to be obtained in solution. This paper therefore presents the ^{13}C nmr spectra of the poly(MMA-*co*-4VP), poly(MMA-*co*-2M5VP), and their quaternized derivatives in solution. To our knowledge, these spectra have not been reported in the literature, and only the proton spectra of poly(MMA-*co*-4VP) were reported earlier by one of us (7). This paper does not intend to elucidate the microstructural mechanism that governs the copolymerization of MMA with 4VP or with 2M5VP.

A survey of the literature showed that ^{13}C nmr spectra of poly(MMA) have been analysed and that signals for the quaternary, carbonyl, and α-methyl carbons are sensitive to configuration, whereas the methoxy signal is not split (8, 9). The methylene signal position also depends on the homopolymer configuration (10). Poly(vinyl pyridines) have also been investigated. The carbon spectrum of poly(4VP), especially the sensitivity of C4 to the polymer configuration, was reported by several authors (11–13). Quaternization of the polymer, using different quaternizing agents, and the influence on the carbon spectra were also reported (14–16). Again, only C4 remained sensitive to configuration. The carbon spectrum of poly(2M5VP) was briefly mentioned in a table in ref. 11. The spectrum was not completely assigned and the configuration sensitivity could not be explained.

Experimental

The copolymers analysed here were prepared by bulk radical copolymerization. Quaternization of the copolymers was performed using methyl iodide. Both copolymerization and quaternization were part of

[1]Author to whom correspondence may be addressed.

[2]J. P. Gouin and A. Eisenberg, to be published.

[3]A. Natansohn and A. Eisenberg, to be published.

Can. J. Chem. Downloaded from www.nrcresearchpress.com by 118.98.75.50 on 09/07/12
For personal use only.

TABLE 1. Triad sequence fractions for two copolymer samples (1 = MMA; 2 = VP) (MMA-4VP: r_1 = 0.57, r_2 = 0.79; MMA-2M5VP: r_1 = 0.52, r_2 = 1.25)

Copolymer	Composition		1-Centered triads			2-Centered triads		
	f_1	f_2	f_{111}	f_{112}	f_{212}	f_{222}	f_{122}	f_{121}
MMA-4VP	0.89	0.11	0.67	0.20	0.02	0.00	0.01	0.10
	Normalized		0.75	0.22	0.02	0.00	0.09	0.91
MMA-2M5VP	0.90	0.10	0.80	0.10	0.00	0.00	0.01	0.09
	Normalized		0.89	0.11	0.00	0.00	0.10	0.90

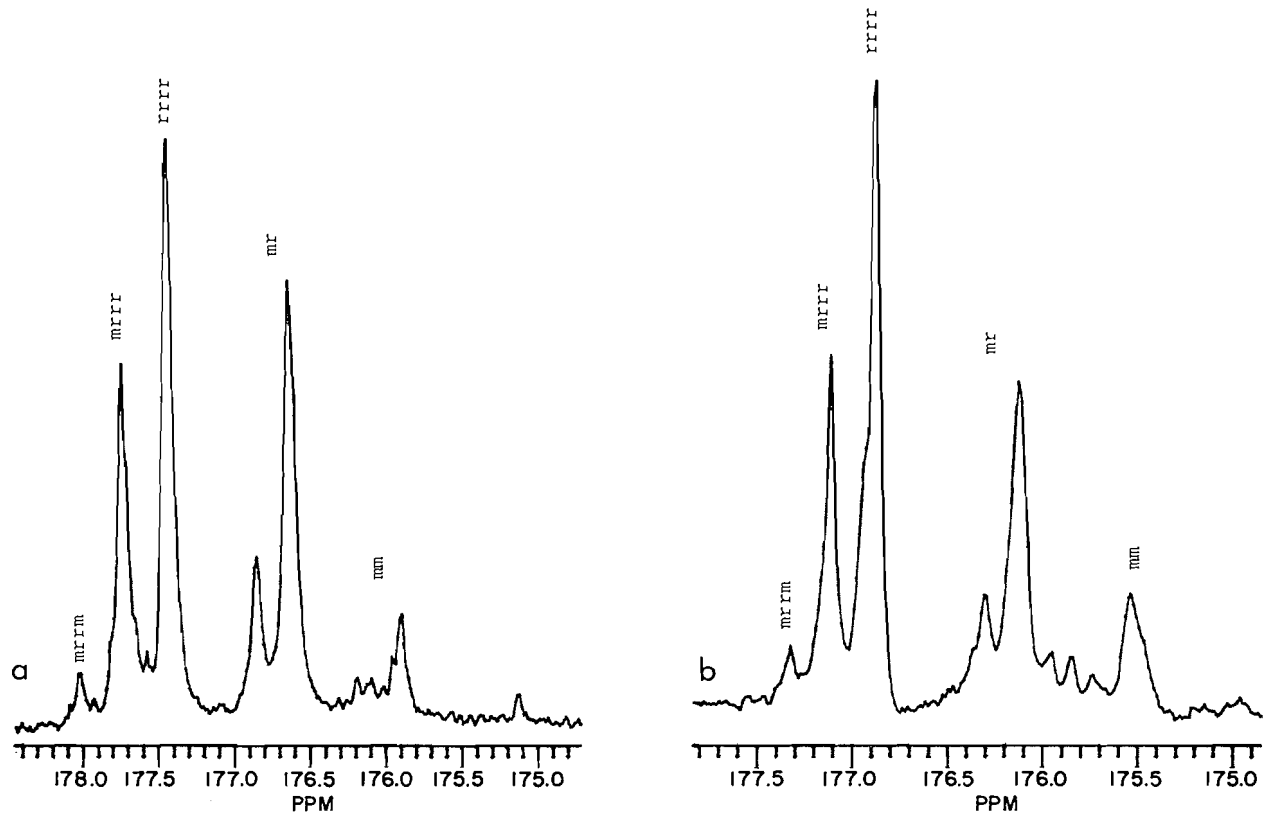

FIG. 1. Carbonyl region of ^{13}C nmr spectra of poly(MMA-*co*-4VP) in C_6D_6 (a) and quaternized poly(MMA-*co*-4VP) in DMSO-d_6 (b).

another project (1). Proton and carbon nmr spectra were obtained on a Varian XL-300 spectrometer in different solvents. Low flip angles (40°) were used to avoid delays between pulses. Two-dimensional heteronuclear-correlated (HETCOR) spectra were recorded on the same spectrometer, using the pulse sequence offered by Varian (17).

Sequence distribution estimation was made using Markov statistics with two parameters, the reactivity ratios of the two comonomers (18). The reactivity ratios were calculated from the copolymerization data and the feed ratio of the two comonomers was used in the calculation (1). There was a systematic error introduced by the fact that copolymerization conversions were higher than 5%, but this error could be neglected at the low fractions obtained. Sequence fractions for samples with the highest content of vinyl pyridine units are presented in Table 1.

Results and discussion

Choosing the right solvent to obtain a good nmr spectrum is very important in this case. The spectra of the normal and quaternized copolymers have to be compared, yet due to their different polarity, the samples have different solubility behavior. At a composition of 10 mol% vinyl pyridine units, the non-ionic copolymers are very soluble in chloroform but only marginally so in the quaternized form. Thus, the spectra of the quaternized copolymers in $CDCl_3$ are of rather poor quality. However, the quaternized samples dissolve very well in DMSO, and their spectra show little difference in peak position when compared with the spectra taken in chloroform. Therefore analysis of microstructural splittings in the quaternized copolymers was performed mainly in DMSO. On the other hand, the solubility of non-quaternized copolymers in DMSO was rather poor, but some spectra were taken and utilized for assignments. Another solvent used was benzene, which was proven very useful by inducing more splittings, due to its aromatic shielding effect (6). This solvent can be used for non-quaternized samples only, for solubility reasons, but it is reasonable to believe that the copolymer configuration is not affected by quaternization. There will be only conformational changes, but these cannot be observed when using different solvents. In the following discussion and presentation of the spectra, only the best spectra obtained will be presented for each sample.

With the exception of the aromatic region, the 4VP and

Can. J. Chem. Downloaded from www.nrcresearchpress.com by 118.98.75.50 on 09/07/12
For personal use only.

TABLE 2. Changes in aromatic chemical shifts with quaternization (ppm) (+ = shift downfield)

Copolymer	Nucleus	Solvent	Proton (carbon) 2	6	3	5	4
MMA-4VP	H	$CDCl_3$		+0.9	+0.9		
	H	DMSO		+0.5	+0.8		
	C	$CDCl_3$		−3.5	+3.0		+10.0
MMA-2M5VP	H	$CDCl_3$		+0.8	+1.3		+0.8
	H	DMSO		+0.8	+0.9		+0.9
	C	$CDCl_3$	+9.0	+6.0	+4.5	+10.0	+8.0

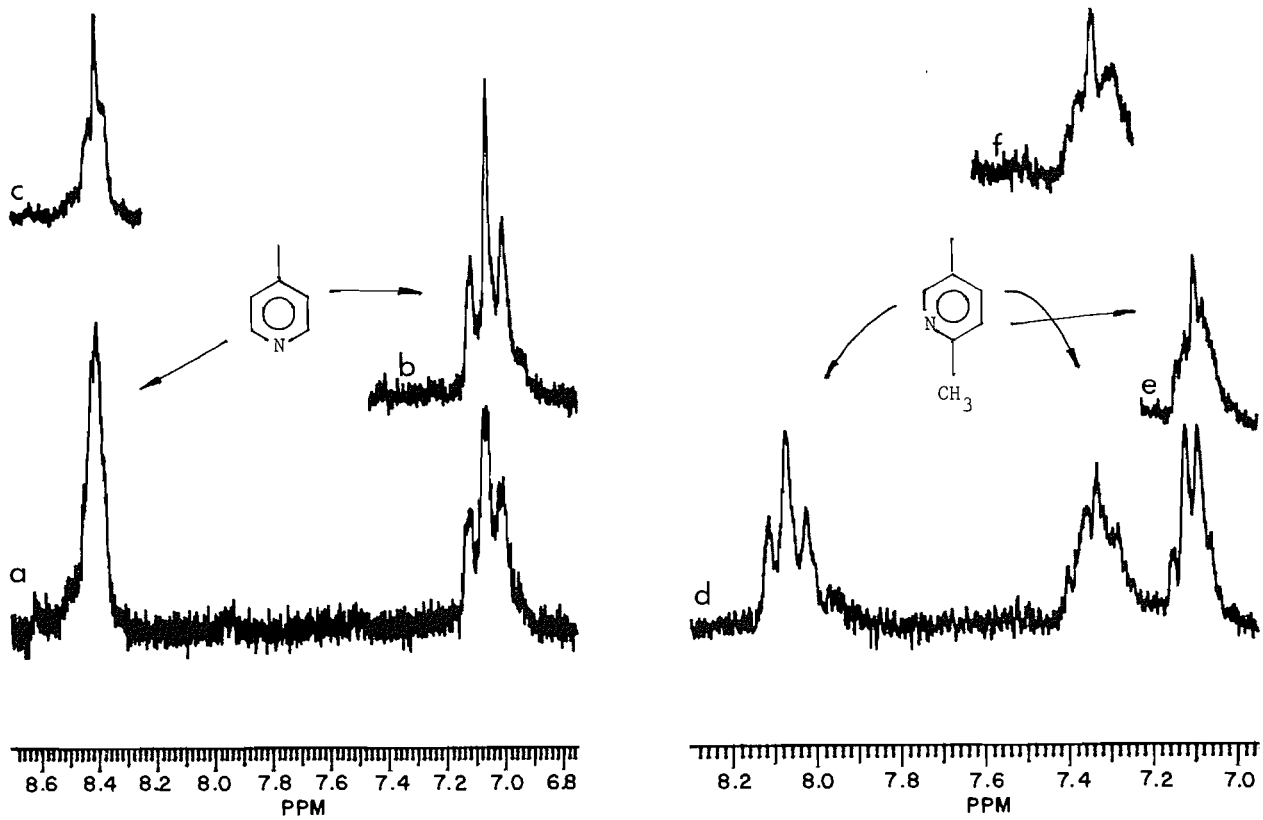

FIG. 2. Aromatic proton spectra of poly(MMA-*co*-4VP) (a), irradiated at 8.40 ppm (b), irradiated at 7.06 ppm (c), and of poly(MMA-*co*-2M5VP) (d), irradiated at 7.33 ppm (e), and irradiated at 7.10 ppm (f) registered in DMSO-d_6 at 70°C.

2M5VP copolymer spectra are rather similar when analysing the main signals and the microstructural splitting. Therefore the spectra will be presented together.

The carbonyl region

The C=O signal of poly(MMA) is split according to pentads and the assignment has been made in the literature (8, 9). It consists mainly in three parts assignable to rr, mr, and mm triads with increasing fields. The rr triad signal, the most intense in radically polymerized MMA, is split in three: mrrm, rrrm, and rrrr pentads, also with increasing field. Figure 1 shows the carbonyl region of the ^{13}C nmr spectra of poly(MMA-*co*-4VP) in C_6D_6 and of quaternized poly(MMA-*co*-4VP) in DMSO-d_6. One can note that, basically, the signal is influenced by MMA configuration only. In the non-ionic copolymer there are at least three signals that appear, probably from the vicinity of a pyridine unit, but they are rather small and their assignment is uncertain. In the quaternized sample, the chemical shifts of these signals probably coincide with the more intense configurational signals. There are some differences here, especially in the iso to hetero region, but again they are difficult to assign properly. Spectra in benzene do not present more splitting than those in chloroform or DMSO in the carbonyl region.

The aromatic region

Figure 2 presents the aromatic spectra of poly(MMA-*co*-4VP) and poly(MMA-*co*-2M5VP) registered in DMSO at 70°C. The solubility of the copolymers in DMSO is not very good, and no carbon spectra were registered in DMSO. For the proton spectra, DMSO is preferable to $CDCl_3$ or C_6D_6, because it lacks interfering signals. The signals belonging to each aromatic proton are split, and the splitting can be either a sequence distribution or a configurational effect. No such splitting is reported for the vinyl pyridine homopolymers. *ortho*-Proton coupling introduces more splitting and can hinder microstructural assignments of the signals. For this reason, Fig. 2 also

Can. J. Chem. Downloaded from www.nrcresearchpress.com by 118.98.75.50 on 09/07/12
For personal use only.

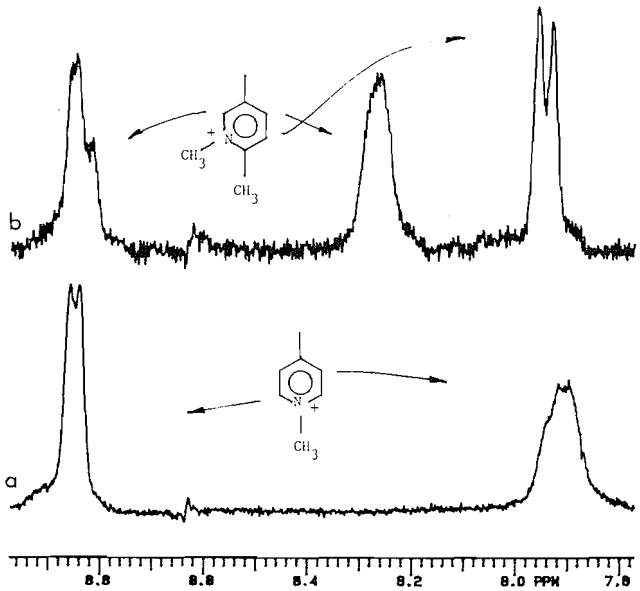

FIG. 3. Aromatic proton spectra of quaternized poly(MMA-*co*-4VP) (a) and quaternized poly(MMA-*co*-2M5VP) (b) registered in DMSO-d_6 at 70°C.

presents the results of decoupling experiments. The only non-coupled signal in these spectra belongs to the aromatic proton 6 in the 2M5VP nucleus (spectrum (d), at 8.07 ppm). This signal is split into three main parts (at 8.11, 8.07, and 8.02 ppm) in a ratio of approximately 1:2:1 and also has a rather small additional signal at 7.95 ppm. The triplet cannot be assigned to sequence splitting, because from Table 2 one can see that 2-centered triads have normalized fractions of 0% (222), 10% (221), and 90% (121). In other words, 90% of the 2M5VP units are isolated between two MMA units, whereas about 10% form blocks of two 2M5VP units. The fraction of a block of three 2M5VP units is practically nil. Consequently, one can tentatively assign the small signal at 7.95 ppm as appearing from a 221 triad, whereas the three main signals of the proton 6 belong to 121 triads and their splitting is due to the configuration of the adjacent MMA unit. At this point, a "coisotactic" addition probability has to be defined as the probability that a MMA unit and a 2M5VP unit neighboring each other will have the methoxy group and the pyridine ring on the same side of the main chain (σ).

The splitting of the main signal belonging to proton 6 can be assigned to 1m2m1, 1m2r1, and 1r2r1 triads (m being previously defined as a methoxy and pyridine ring on the same side of the main chain) or to 1r2r1, 1m2r1, and 1m2m1 triads with the increasing field. The second assignment seems more probable when one considers the shielding induced by the carbonyl groups of the MMA units. In poly(MMA), the α-methyl proton signal is split into three due to this shielding, and the syndiotactic triads resonate at higher fields (19). The shielding introduced by one carbonyl group is ca. 0.17 ppm in DMSO (6). For poly(MMA-*co*-2M5VP) the shielding experienced by the aromatic proton 6 is only 0.05 ppm. The triplet appearance of the signal suggests that σ is approximately 0.5, i.e., there is a random configurational distribution of the alternate sequences. A similar value was obtained for poly(MMA-*co*-4VP) by analysing the methoxy signal in the proton spectra (7). The results of the decoupling experiments show that indeed the triplet pattern is common for all the proton signals but the magnitude of the splittings induced by the carbonyl group is not the same for every signal. This is expected, because the geometry of the molecule allows for the carbonyl group to be closer to some protons than to others. The results of the decoupling experiments are much clearer in poly(MMA-*co*-4VP), where the distance on the chemical shift scale between the coupled protons is much greater.

Quaternization of the copolymers generates an overall shift of the aromatic signals toward lower fields. Figure 3 presents the aromatic region of the proton spectra of quaternized poly(MMA-*co*-4VP) (a) and quaternized poly(MMA-*co*-2M5VP) (b). Similar decoupling experiments were performed on these samples and the results were identical to those obtained in the case of the neutral copolymers. The signals are sensitive to the configuration of the neighboring MMA units and the ratio within a triplet does not change. This indicates an unchanged configuration after quaternization, as expected. The shifts of all signals in the quaternized samples as compared with the neutral ones are summarized in Table 2.

The aromatic carbon spectra obtained in chloroform for the two neutral copolymers are presented in Fig. 4. In this case, there are no scalar couplings to interfere with the configurational and sequence distribution splitting. Carbon 4 of 4VP (155 ppm) does not seem to be split. Carbons 2 and 6 (149 ppm) and 3 and 5 (124 ppm) present the same splittings as the decoupled proton signals. The signals at 149 ppm clearly show the 221 sequence signal (150.3 ppm) and the triplet due to the configuration of the neighbouring MMA units (the chemical shift difference between peaks is ca. 0.4 ppm). The assignment of the signals for poly(MMA-*co*-2M5VP) is somewhat complicated by the lack of literature data. The broad signal at about 136 ppm belongs to carbons 4 and 5 and the triplet at 123 ppm is the resonance of carbon 3 (11). To assign the signals at 156 ppm and 149 ppm to carbons 2 or 6, a two-dimensional HETCOR spectrum is presented in Fig. 5. It clearly shows correlation between signals at 123 ppm (C3) and 6.9 ppm (H3), 136 ppm (C4) and 7.2 ppm (H4), and 149 ppm (C6) and 8.1 ppm (H6). Hence, the signal at 156 ppm is assigned to carbon 2.

Signals belonging to carbons 2, 6, and 3 in Fig. 4 present the characteristic triplet splitting.

Quaternization produces the same shift downfield of most carbon resonances. The chemical shift differences are presented in Table 2 for spectra registered in chloroform. No spectra of the neutral samples were taken in DMSO. Figure 6 shows the spectrum of quaternized poly(MMA-co-4VP) in DMSO. Carbon 4 is shifted downfield to ca. 165 ppm and is probably highly split due to sequence distribution and configuration. Being such a small signal, it appears over a rather broad area and its assignment is very difficult. The other two signals present the triplet configurational splitting.

The aliphatic region

A. Proton spectra

Figure 7 presents the aliphatic region of the proton spectra of poly(MMA-*co*-4VP) and poly(MMA-*co*-2M5VP) registered in benzene at 60°C. Benzene was chosen as a solvent because it maximizes microstructural splitting (6). The main assignments are given in the figure. The methoxy signal consists in a main part, at ca. 3.4 ppm, and a smaller part (ca. 3 ppm) assignable to the methoxy groups that are directly subjected to the screening effect of a neighboring VP ring (i.e., belonging to sequences 2m11 and 2m1r2). This assignment of the splitting of a methoxy

Can. J. Chem. Downloaded from www.nrcresearchpress.com by 118.98.75.50 on 09/07/12
For personal use only.

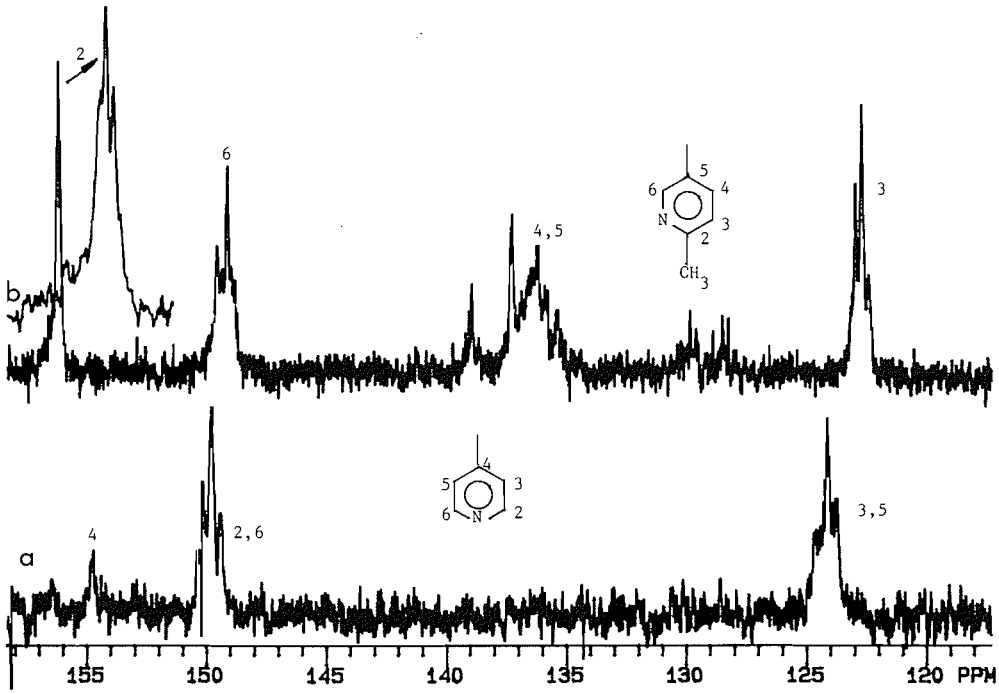

FIG. 4. Aromatic carbon spectra of poly(MMA-*co*-4VP) (a) and poly(MMA-*co*-2M5VP) (b) registered in $CDCl_3$ at room temperature.

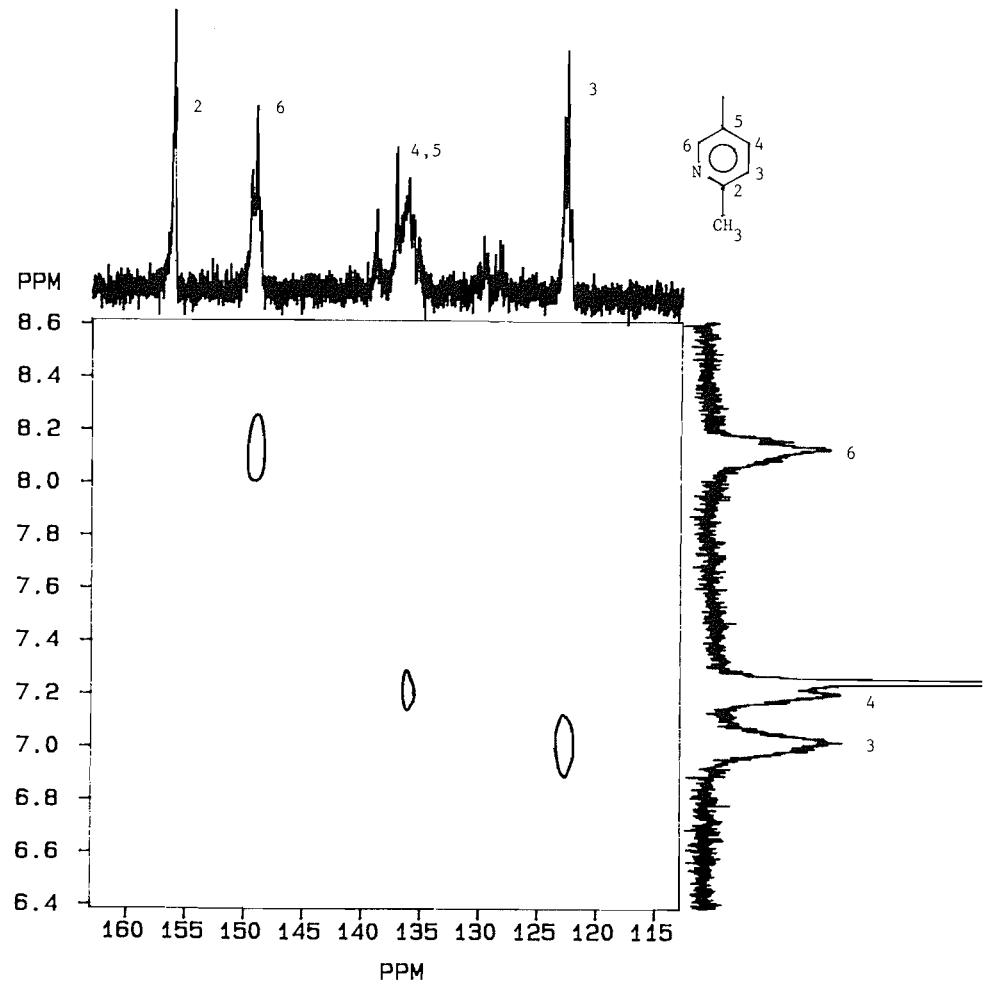

FIG. 5. HETCOR spectrum of the aromatic region of poly(MMA-*co*-2M5VP) in $CDCl_3$ at room temperature.

Can. J. Chem. Downloaded from www.nrcresearchpress.com by 118.98.75.50 on 09/07/12
For personal use only.

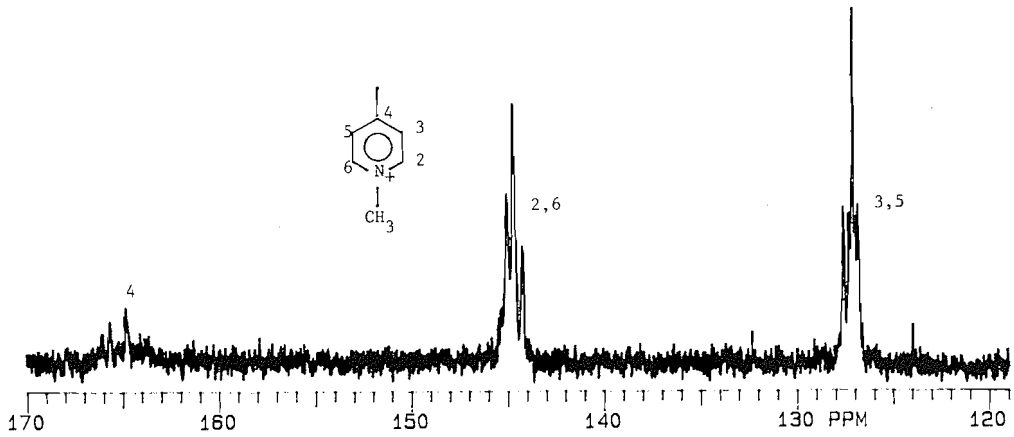

FIG. 6. Aromatic carbon spectrum of quaternized poly(MMA-*co*-4VP) in DMSO-d_6 at 70°C.

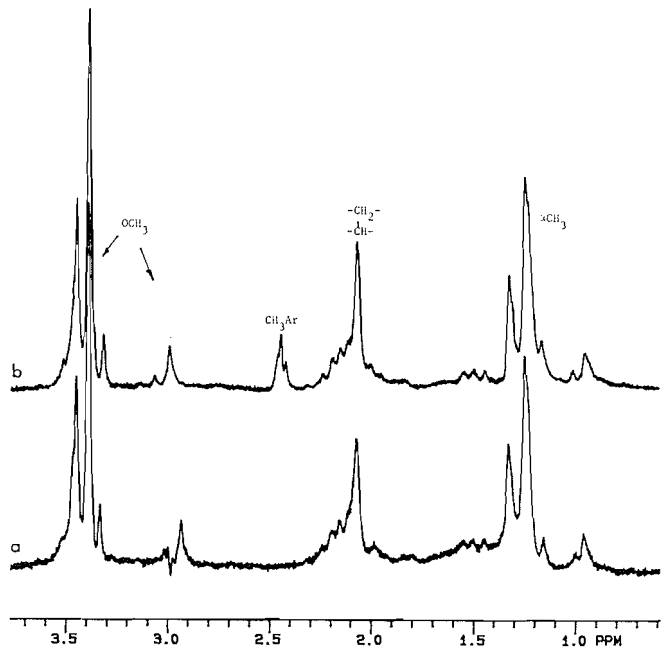

FIG. 7. Aliphatic region of the proton spectra of poly(MMA-*co*-4VP) (a) and poly(MMA-*co*-2M5VP) (b) registered in C_6D_6 at 60°C.

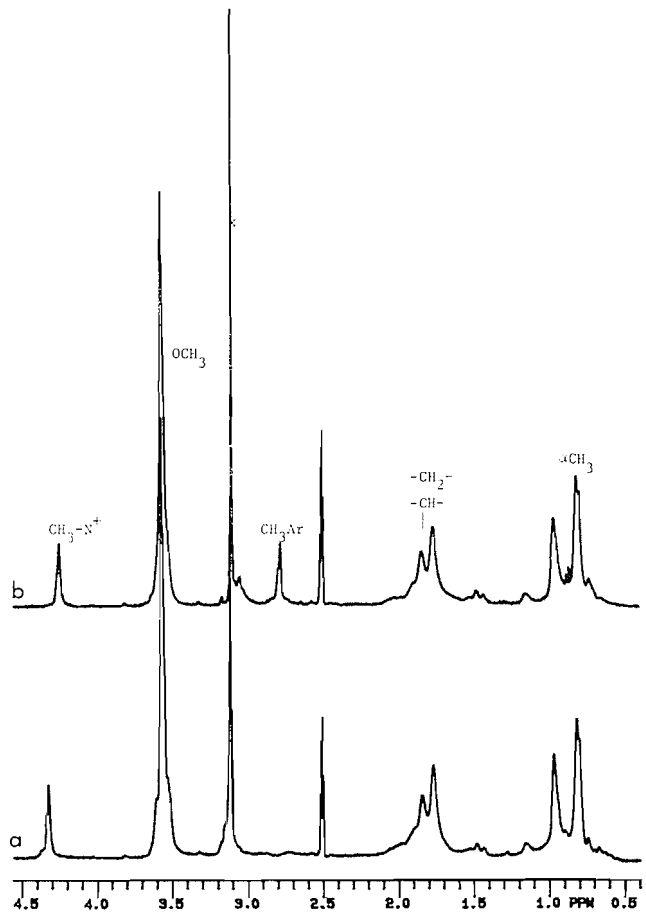

FIG. 8. Aliphatic region of the proton spectra of quaternized poly(MMA-*co*-4VP) (a) and quaternized poly(MMA-*co*-2M5VP) (b) registered in DMSO-d_6 at 70°C.

signal was recently confirmed by two-dimensional nuclear Overhauser enhancement (nOe) correlated spectroscopy (20). From the area of the two main peaks one can calculate the probability of a "coisotactic" addition (σ), using the formula proposed by Ito and Yamashita (21). It has to be emphasized that the value obtained from one single sample is not very reliable. To obtain a more precise value, one has to analyse samples covering most of the possible compositional range. It is not within the scope of our paper to study the microstructural mechanism of synthesis of these copolymers, therefore the value obtained for σ will be used as an approximate one. Values obtained for σ for both copolymers are around 0.5, as previously determined from the splitting of the aromatic signals. They are 0.48 for poly(MMA-*co*-4VP) and 0.49 for poly(MMA-*co*-2M5VP).

There are more signals that appear from different sequences in the copolymers. They can be tentatively assigned using Klesper's hypothesis (22), which postulates that the substitution of a structural unit does not change the configurational splitting. Thus, the two peaks of the "screened" methoxy signal can be assigned to 1r1m2 triads (2.93 ppm in poly(MMA-*co*-4VP) and 2.99 ppm in poly(MMA-*co*-2M5VP)) and 1m1m2 triads (3.00 ppm in poly(MMA-*co*-4VP) and 3.06 ppm in poly(MMA-*co*-2M5VP)). The signals at 3.33 ppm (poly(MMA-*co*-4VP)) and 3.31 ppm (poly(MMA-*co*-2M5VP)) would then be assigned to 1r1r2 triads, with the corresponding 1m1r2 signal being overlapped by the intense signal at 3.39 ppm belonging to the 1r1r1 triads. In a similar manner, the α-methyl signals at 0.96 and 1.00 ppm belong to 1r1r2 and 1m1r2, respectively. In

Can. J. Chem. Downloaded from www.nrcresearchpress.com by 118.98.75.50 on 09/07/12
For personal use only.

Can. J. Chem. Downloaded from www.nrcresearchpress.com by 118.98.75.50 on 09/07/12
For personal use only.

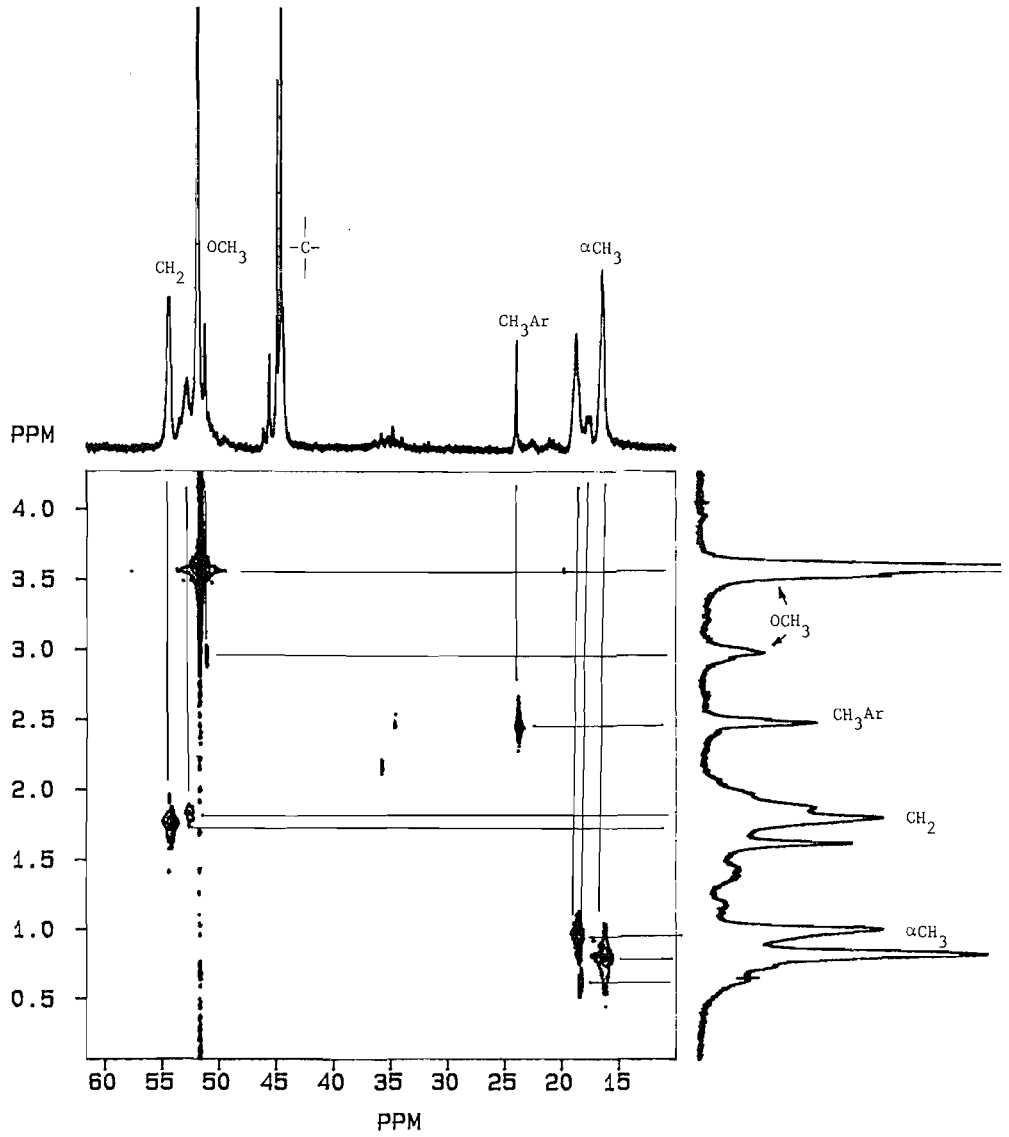

FIG. 9. HETCOR spectrum of poly(MMA-*co*-2M5VP) registered in $CDCl_3$ at room temperature.

this case, a "cosyndiotactic" cross-addition has to be considered, because the "coisotactic" one was defined as the methoxy group and the pyridine ring on the same side of the main chain. The signals at 1.16 ppm are assigned to the 1r1m2 triads. The signal at 2.45 ppm belongs to the methyl group bonded to the pyridine ring. As in the case of the aromatic protons, this signal is split in three by the different configurations of the adjacent MMA units, and the appearance is that of a triplet, confirming the random configuration of the cross-addition (σ = 0.5).

The effect of quaternization on the proton spectra of the copolymers is presented in Fig. 8. To enhance their quality, the spectra presented are taken in DMSO. There are new signals appearing from the methyl groups bonded to the pyridinium nitrogen, appearing at 4.32 ppm for poly(MMA-*co*-4VP) and at 4.26 ppm for poly(MMA-*co*-2M5VP). The fact that these chemical shifts differ slightly can be explained by the differences in the pyridinium rings in the two copolymers. In DMSO, the main methoxy signal is not split according to the configuration of the MMA units, as it is in benzene. The chemical shift of the methyl group directly bonded to the aromatic ring is now 2.8 ppm, due to major changes in the electronic density of the aromatic ring from pyridine to the pyridinium ion. This change can be better observed in spectra registered in chloroform, where it shifts from 2.4 to 3.2 ppm. However, there is another concurrent effect in chloroform solutions, and this can be observed on the shielded methoxy signal. It shifts from 3.00 to ca. 3.4 ppm and it becomes much broader when the ring is quaternized. The only explanation for such a shift is that it is due to a conformational effect of the pyridinium ions in chloroform solutions. Such effects are known for copolymers of styrene with MMA and methyl acrylate, respectively (23). Therefore, the shift of the ring-bonded methyl group in chloroform has to be explained by a combination of electronic density and conformational changes induced by quaternization. In DMSO, the position of the shielded methoxy peak does not change significantly when the copolymer is quaternized, indicating that the copolymer conformation remains basically the same. In Fig. 8 there is some overlapping from the residual water signal, but the chemical shifts of the shielded methoxy peaks can be determined to be 3.15 ppm (poly(MMA-*co*-4VP)) and 3.05 ppm (poly(MMA-*co*-2M5VP)). They were

TABLE 3. Chemical shift differences between the two methoxy carbon signals (ppm)

	Poly(MMA-*co*-4VP)		Poly(MMA-*co*-2M5VP)	
$CDCl_3$	0.84	0.00	0.45	0.00
DMSO	—	0.50	—	0.63
C_6D_6	0.65	—	—	—

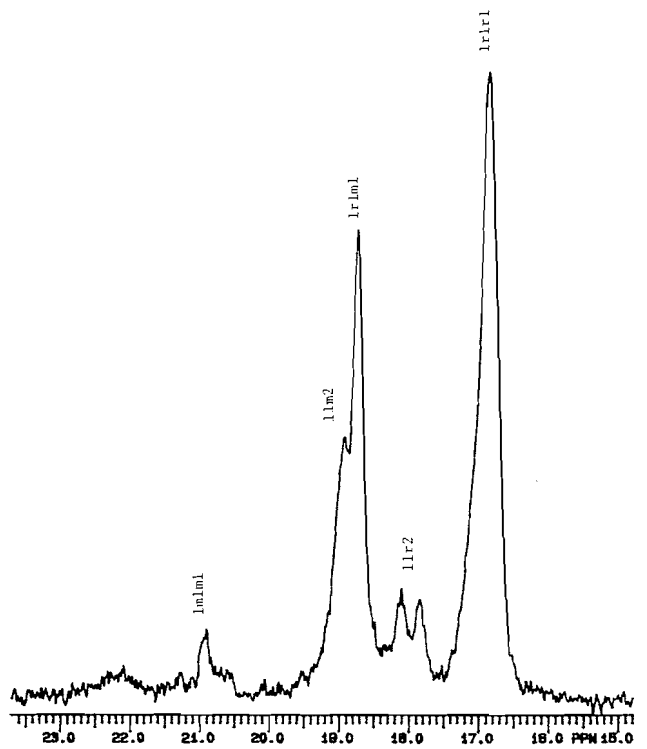

FIG. 10. α-Methyl carbon spectrum of quaternized poly(MMA-*co*-4VP) registered in DMSO-d_6 at 70°C.

different for the neutral samples also (Fig. 7), reflecting small conformational differences induced by the slightly different aromatic rings.

B. Carbon spectra

To facilitate the assignments of the carbon spectra, HETCOR two-dimensional charts were recorded for all the samples in different solvents. Figure 9 presents the HETCOR spectrum of poly(MMA-*co*-2M5VP) as an example of the assignment procedure. The main methoxy signal resonantes at 51.8 ppm (3.6 ppm for protons). The shielded methoxy also gives a separate signal in the carbon spectrum. The difference in chemical shift when compared to the main methoxy signal is 0.45 ppm (as compared with ca. 0.5 ppm for protons, both toward higher fields). This difference varies with the solvent used for spectrum registration. A quaternized sample will present no splitting for the methoxy signal in chloroform, indicating the same conformational change that was observed in the proton spectra. Table 3 summarizes the chemical shift differences observed for different samples in different solvents. The α-methyl group presents mainly three signals arising from the iso (1m1m1), hetero (1m1r1), and syndiotactic (1r1r1) triads with the increasing magnetic field, both in carbon and proton spectra. Cross-peaks can be observed for the syndiotactic signal (16.42 and 0.8 ppm) and for the heterotactic signal (18.66 and 1.0 ppm). The isotactic peak is too small. The 112 sequences, which resonate at higher fields than 1r1r1 in the proton spectra (Fig. 7), present a cross-peak with a signal at 17.66 ppm, situated between the syndiotactic and heterotactic peaks. Finally, the main chain resonances, which present an unresolved multiplet structure in the proton spectrum, are resolved into two, at 52.78 and 54.26 ppm, assignable to the VP main chain resonances and to the MMA methylene main chain, respectively. The only signal in the carbon spectrum without any correlation in the proton spectrum belongs to the quaternary carbons of the MMA units. It is split basically in three parts, 44.53 ppm (syndio), 44.86 ppm (hetero), and 45.53 ppm (isotactic MMA sequences) (10). HETCOR spectra for the other samples show that in chloroform the methyl carbons bonded to the quaternized ring shift to 21.47 ppm (2.47 ppm upfield), and that the methyl bonded to the pyridinium nitrogen resonates at 48.90 ppm (poly(MMA-*co*-4VP)) and 37.26 ppm (poly(MMA-*co*-2M5VP)).

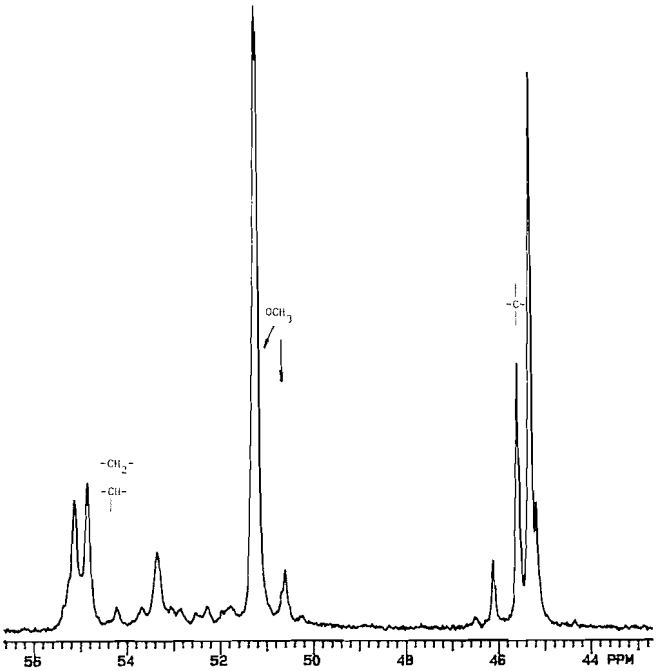

FIG. 11. Main chain carbon spectrum of poly(MMA-*co*-4VP) registered in C_6D_6 at 60°C.

Figure 10 represents the α-methyl signal in the carbon spectrum of the quaternized poly(MMA-*co*-4VP). The spectrum registered in DMSO is better resolved than the spectrum taken in chloroform. The two signals at 17.83 and 18.10 ppm were assigned with the help of the HETCOR spectrum to the 11r2 sequences. The shoulder at 18.93 ppm most likely belongs to the corresponding 11m2 triads. This assignment could not be confirmed by a HETCOR experiment, due to poor resolution. The three main signals belong to the 111 sequences, syndio (16.84 ppm), hetero (18.71 ppm), and isotactic (20.92 ppm).

Figure 11 shows the main chain (including methoxy) carbon spectrum of poly(MMA-*co*-4VP) registered in benzene at 60°C. In the quaternary carbon resonance there is only one signal, the shoulder at 45.21 ppm that can appear from a cross-addition, which can be tentatively assigned to the 112 triads. The main chain resonance is more complicated, with the methylene resonance of the MMA units split into two signals at 55.13 and 54.85 ppm. They can be assigned to the *meso* and racemic diads with increasing field, according to data found in the

Can. J. Chem. Downloaded from www.nrcresearchpress.com by 118.98.75.50 on 09/07/12
For personal use only.

literature (10). The signal at 53.35 ppm belongs to the methylene groups of the 4VP units. Complete assignment of this area could not be accomplished from the few available samples.

Conclusions

Both proton and carbon spectra of poly(MMA-*co*-4VP), of poly(MMA-*co*-2M5VP), and of their quaternized derivatives offer a wealth of information on the copolymer microstructure. There are signals, especially in the aliphatic region, that can be directly assigned to one of the structural units neighboring the other. There are also signals that offer information on the configuration of the cross-addition, especially in the aromatic region of the spectra. It can be estimated that the probability of a "coisotactic" cross-addition is ca. 0.5, indicating a perfectly random nature in such sequences. The MMA sequences have the same configuration as in poly(MMA) obtained by radical polymerization, whereas no information could be obtained about the VP sequences. At copolymer compositions low in VP, the probability of longer VP sequences is nil. This information about the analysed copolymers is needed for the assignments of the solid-state high-resolution nmr spectra.

Acknowledgements

This work was supported in part by a grant from the U.S. Army Research Office. Partial support from the Natural Sciences and Engineering Research Council of Canada is also acknowledged.

1. D. Duchesne. Ph.D. thesis, McGill University, Montreal. 1985.
2. S. Gauthier. Ph.D. thesis, McGill University, Montreal. 1985.
3. D. Wollmann, S. Gauthier, and A. Eisenberg. Polym. Eng. Sci. **26**, 1451 (1986).
4. P. Smith and A. Eisenberg. J. Polym. Sci. Polym. Lett. Ed. **21**, 223 (1983).
5. R. Murali, A. Eisenberg, R. K. Gupta, and F. W. Harris. Polym. Prepr. Am. Chem. Soc. Div. Polym. Chem. **27**(1), 343 (1986).
6. A. Natansohn and A. Eisenberg. Macromolecules, **20**, 323 (1987).
7. A. Natansohn, S. Maxim, and D. Feldman. Eur. Polym. J. **14**, 283 (1978).
8. I. R. Peat and W. F. Reynolds. Tetrahedron Lett. **14**, 1359 (1972).
9. R. C. Ferguson and D. W. Ovenall. Polym. Prepr. Am. Chem. Soc. Div. Polym. Chem. **26**(1), 182 (1985).
10. J. Spevacek. J. Mol. Struct. **129**, 175 (1985).
11. G. M. Lukovkin, O. P. Komarova, V. P. Torchilin, and Yu. E. Kirsch. Polym. Sci. (USSR), **15**, 503 (1973).
12. K. Matsuzaki, T. Matsubara, and T. Kanai. J. Polym. Sci. Polym. Chem. Ed. **15**, 1573 (1977).
13. D. Ghesquiere, B. Ban, and C. Chachaty. Macromolecules, **10**, 743 (1977).
14. C. M. Paleos. J. Polym. Sci. Polym. Lett. Ed. **16**, 540 (1977).
15. D. Ghesquiere and C. Chachaty. Macromolecules, **11**, 246 (1978).
16. D. Ghesquiere, C. Chachaty, and A. Tsutsumi. Macromolecules, **12**, 775 (1979).
17. A. D. Bax and G. A. Morris. J. Magn. Reson. **42**, 51 (1981); A. D. Bax. J. Magn. Reson. **53**, 517 (1983).
18. H. J. Harwood and W. M. Ritchey. J. Polym. Sci. Part B, **2**, 601 (1964).
19. F. C. Schilling, F. A. Bovey, M. D. Bruch, and S. A. Kozlowski. Macromolecules, **18**, 1418 (1985).
20. S. A. Heffner, F. A. Bovey, L. M. Verge, P. A. Mirau, and A. E. Tonelli. Macromolecules, **19**, 1628 (1986).
21. K. Ito and Y. Yamashita. J. Polym. Sci. Part B, **3**, 625 (1965).
22. E. Klesper, W. Gronski, and A. Johnsen. *In* NMR basic principles and progress. Vol. 4. Springer Verlag, New York. 1971. p. 47.
23. T. Tanabe, H. Koinuma, and H. Hirai. Makromol. Chem. **182**, 3237 (1981).

Can. J. Chem. Downloaded from www.nrcresearchpress.com by 118.98.75.50 on 09/07/12
For personal use only.

Catalytic hydrolysis of cAMP

JIK CHIN[1] AND XIANG ZOU
Department of Chemistry, McGill University, Montreal, P.Q., Canada H3A 2K6

Received January 8, 1987

This paper is dedicated to Professor John T. Edward

JIK CHIN and XIANG ZOU. Can. J. Chem. **65**, 1882 (1987).

[Co(trien)(OH_2)(OH)]Cl_2 is highly efficient in catalyzing the hydrolysis of cAMP to adenosine in neutral water (6×10^{-6} $M^{-1}\,s^{-1}$ at 50°C). The cobalt complex promoted hydrolysis of cAMP is estimated to be about a hundred million times faster than the uncatalyzed hydrolysis of cAMP. In the time that [Co(trien)(OH_2)(OH)]Cl_2 produces 50% cleavage of cAMP, [Co$(en)_2(NH_3)$(OH)]Cl_2 or $ZnCl_2$ has no observable effect on the hydrolysis of cAMP. A detailed mechanism is presented for the cobalt complex promoted hydrolysis of the phosphodiester.

JIK CHIN et XIANG ZOU. Can. J. Chem. **65**, 1882 (1987).

Le [Co(trien)(OH_2)(OH)]Cl_2 est très efficace pour catalyser l'hydrolyse de la cAMP en adénosine dans l'eau neutre ($6 \times 10^{-6} M^{-1}\,s^{-1}$ à 50°C). On évalue que l'hydrolyse de la cAMP qui est favorisée par le complexe de cobalt est environ cent million de fois plus rapide que l'hydrolyse non-catalysée de la cAMP. Alors que le [Co(trien)(OH_2)(OH)]Cl_2 provoque 50% de clivage de la cAMP, le [Co$(en)_2(NH_3)$(OH)]Cl_2 ou le $ZnCl_3$ ne provoque aucun effet sur l'hydrolyse de la cAMP. On propose un mécanisme pour l'hydrolyse du phosphodiester qui est favorisée par le complexe de cobalt.

[Traduit par la revue]

Introduction

Adenosine 3′,5′-monophosphate (cAMP) is a key molecule that functions as an intracellular hormone in both bacterial and animal cells (1–3). The level of cAMP in the cell is regulated in part by cAMP phosphodiesterase which catalyzes the hydrolysis of cAMP to adenosine 5′-monophosphate (AMP). cAMP phosphodiesterase is a metalloenzyme as are most other phosphodiesterases that cleave phospholipids or DNA (4). A major problem in studying phosphodiesterase model reactions is that the hydrolysis of phosphodiesters such as dimethyl phosphate and cAMP in neutral water is extremely slow even at elevated temperatures. In contrast, phosphomonoesters such as *p*-nitrophenyl phosphate (5), methyl phosphate (6), and ATP (7, 8) are relatively reactive. Numerous studies have been published on simple catalytic hydrolysis of phosphomonoesters. However, prior to this work, only enzymes had been used to hydrolyze unactivated phosphodiesters such as dimethyl phosphate or cAMP in neutral water. We report here on the non-enzymic hydrolysis of cAMP in neutral water.

Experimental

[Co(trien)(OH_2)(OH)]Cl_2 ("trien": triethylenetetramine) was prepared (9) according to known procedures. In a typical experiment, the hydrolysis of 10 m*M* cAMP in 0.5 mL D_2O buffered at pD 7.0 (0.2 *M* [Co(trien)(OH_2)(OH)]Cl_2/[Co(trien)$(OH_2)_2$]Cl_3) and 50°C was monitored by the ^1H nmr (Varian XL 300) method. During the hydrolysis reaction, the ^1H nmr signal due to the $C_{1'}$-H of cAMP (6.09 s) decreased and the signal due to the $C_{1'}$-H of adenosine (6.01 d, J = 0.03 Hz) increased (Fig. 1). At 10 m*M* cAMP there is negligible stacking of cAMP. The product was confirmed by addition of a genuine sample of adenosine to the reaction mixture. Three other systems were tested as controls (0.2 *M* phosphate; 0.2 *M* [Co$(en)_2(NH_3)$(OH)]Cl_2; 0.1 *M* $ZnCl_2$). The pD values did not drop below 6.5 during any of the hydrolysis reactions.

Results and discussion

The phosphodiester bond of cAMP did not hydrolyze to any observable extent in phosphate buffer even when the reaction solution was heated at 100°C for one month. During the extensive heating of cAMP, some unidentified decomposition reactions occurred, resulting in the formation of some precipitates. In [Co(trien)(OH_2)(OH)]Cl_2/[Co(trien)$(OH_2)_2$]Cl_3 solution, the half-life for hydrolysis of cAMP is 6 days at 50°C (Fig. 1). In [Co$(en)_2(NH_3)$(OH)]Cl_2/[Co$(en)_2(NH_3)(OH_2)$]Cl_3 or $ZnCl_2$ solutions, cAMP did not hydrolyze to any observable extent during 10 days of heating at 50°C. No precipitate formed at 50°C.

[Co(trien)$(OH)_2$(OH)]Cl_2 (0.2 *M*) promotes the hydrolysis of cAMP efficiently at pD 7 and 50°C ($k_{obs} = 1.2 \times 10^{-6}\,s^{-1}$). In order to estimate the rate of the uncatalyzed hydrolysis of cAMP in neutral water, we studied the hydrolysis of sodium ethylene phosphate (10). At pD 7 and 100°C the pseudo first order rate constant for hydrolysis of ethylene phosphate is $3.0 \times 10^{-7}\,s^{-1}$. The rate was reduced to 40% for a temperature decrease of 10°C. Therefore at 50°C the rate constant should be $3.0 \times 10^{-9}\,s^{-1}$. Ethylene phosphate is 10^5 times more reactive than cAMP under basic conditions (11). If we assume that this ratio is maintained in neutral water, the rate constant for the hydrolysis of cAMP in neutral water at 50°C should be $3.0 \times 10^{-14}\,s^{-1}$ (P—O bond cleavage). This corresponds to a half-life for the hydrolysis reaction of about a million years. Therefore we estimate that [Co(trien)(OH_2)(OH)]Cl_2 (0.2 *M*) promoted hydrolysis of cAMP is 10^8 times faster than the uncatalyzed hydrolysis of cAMP.

A variety of interesting phosphodiesterase models have been studied (12–15) Zn^{2+} or Mg^{2+} (0.2 *M*) increases the rate of hydrolysis of catechol cyclic phosphate (14) by a factor of about 10. Various metal ions (Zn^{2+}, Pb^{2+}, La^{3+}, Ba^{2+}) had been used (15, 16) to promote the hydrolysis of RNA. Among the metal ions studied, Zn^{2+} had been found to be highly efficient in cleaving phosphodiesters. It had also been shown that the hydrolysis of adenosine 2′,3′-monophosphate is four times more rapid in the presence of two equivalents of Zn^{2+} than in the absence of the metal ion (16). The present study indicates that [Co(trien)(OH_2)(OH)]Cl_2 is by far the most efficient in promoting the hydrolysis of phosphodiesters.

Phosphatases (ATPase, alkaline phosphatase) are activated by divalent metal ions as are phosphodiesterases (4). There have been many reports on cobalt complex promoted hydrolysis of phosphomonoesters (5–8) but none on that of phosphodiesters. Phosphatase models cannot be used directly as phos-

Can. J. Chem. Downloaded from www.nrcresearchpress.com by 118.98.75.50 on 09/07/12
For personal use only.

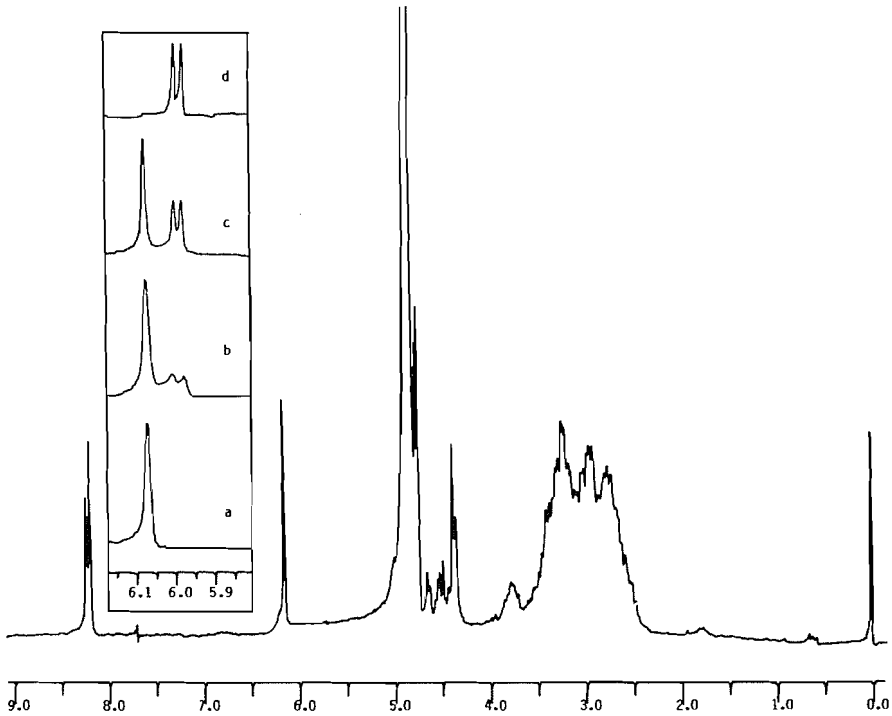

FIG. 1. The ^1H nmr (300 MHz) spectrum of cAMP and $[Co(trien)(OH_2)(OH)]Cl_2$ in D_2O. Inset: time dependence of $C_{1'}$-H signal of cAMP at 50°C: *a*, $t = 0$; *b*, $t = 50$ h; *c*, $t = 120$ h; *d*, pure sample of adenosine.

Can. J. Chem. Downloaded from www.nrcresearchpress.com by 118.98.75.50 on 09/07/12
For personal use only.

phodiesterase models since in neutral water, hydrolysis of phosphomonoesters occurs by the metaphosphate intermediate whereas phosphodiesters are generally hydrolyzed by nucleophilic attack of the water molecule on the phosphoryl group. In an interesting study, Spiro *et al.* (6) showed that $[Co(trien)(OH_2)(OH)]Cl_2$ (0.5 *M*) increases the rate of hydrolysis of methyl phosphate by a factor of 130. Attempts at hydrolyzing dimethyl phosphate with $[Co(trien)(OH_2)(OH)]Cl_2$ (6) or $[Co(NH_3)_5(OH)]Cl_2$ (17) failed. The greater rate enhancement obtained for $[Co(trien)(OH_2)(OH)]^{2+}$-promoted hydrolysis of cAMP over the rate enhancement obtained for the cobalt complex promoted hydrolysis of methyl phosphate can be explained by the fact that the uncatalyzed hydrolysis of the phosphomonoester is rapid in neutral water due to the availability of the metaphosphate mechanism. Since $[Co(trien)(OH_2)(OH)]Cl_2$ greatly increases the rate of hydrolysis of cAMP, it may do the same for dimethyl phosphate. However, dimethyl phosphate is 100 times more stable than cAMP in basic solutions (11). Therefore, even if the cobalt complex increases the rate of hydrolysis of dimethyl phosphate by a factor of 10^8, it should be difficult to detect the hydrolysis reaction.

There are several possible mechanisms for $[Co(trien)(OH_2)(OH)]Cl_2$ promoted hydrolysis of cAMP (Scheme 1). Two cobalt complexes can be involved in the hydrolysis of ATP (7, 8) and *p*-nitrophenyl phosphate (18) since in these cases there are four and two anionic oxygen centers, respectively. Since phosphodiesters have only one anionic oxygen center it is likely that only one cobalt complex is involved. The basicities of the cobalt hydroxides $[Co(trien)(OH_2)(OH)]Cl_2$ and $[Co(en)_2(NH_3)(OH)]Cl_2$ are comparable ($pK_b = 8$). Under our experimental conditions, the Co—O bond of $[Co(en)_2(NH_3)(OH_2)]Cl_3$ is labile (19). The lack of activity of $[Co(en)_2(NH_3)(OH)]Cl_2$ suggests that mechanisms 1 and 2 are not important. Mechanisms 3 and 4 are kinetically indistinguishable. Mechanism 3

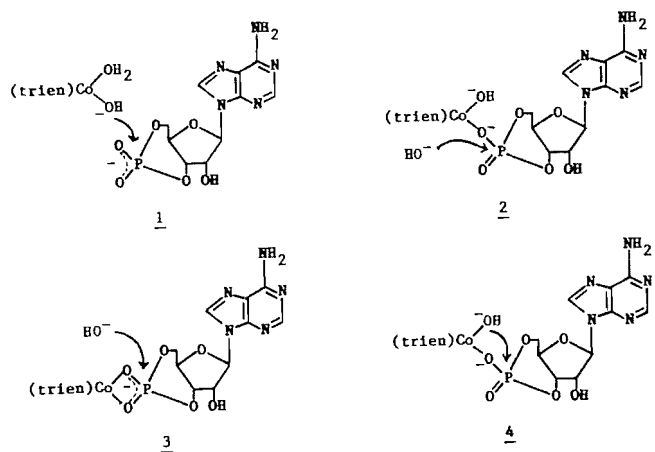

SCHEME 1

is unlikely to occur since binding of phosphoryl oxygen to Co(III) is very weak (17). The most probable mechanism is mechanism 4. Sargeson and co-workers (5) showed that the hydrolysis of a highly activated phosphomonoester, *p*-nitrophenyl phosphate can take place by this last mechanism.

A mechanism for the $[Co(trien)(OH_2)(OH)]Cl_2$-promoted hydrolysis of cAMP is proposed in Scheme 2. Anation (20) of $[Co(trien)(OH_2)(OH)]Cl_2$ (k_1) and its reversion (k_{-1}), hydrolysis of bidentate phosphomonoesters (k_3), and expulsion of phosphate from the cobalt complex (k_4) (20) are fast compared to the overall $[Co(trien)(OH_2)(OH)]Cl_2$ promoted hydrolysis of cAMP. Therefore the rate-determining step for the catalytic cycle should be the k_2 step. For *cis*-$[Co(en)_2(OH)(OH_2)]$-promoted hydrolysis of *p*-nitrophenyl phosphate (5) and $[Co(trien)(OH)(OH_2)]$-promoted hydrolysis of *p*-nitrophenyl methyl phosphonate (21) the rate-determining step is the anation step. The hydrolysis of the phosphodiester bond could result in

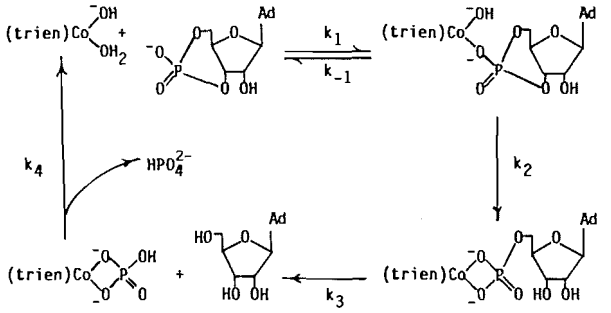

SCHEME 2

either the 3′O—P bond cleavage as shown in Scheme 2 or the 5′O—P bond cleavage. Either of the resulting phosphomonoester should hydrolyze rapidly (6). There is a linear free energy relationship between the equilibrium constant for anation on Co(III) and the basicity of the anionic ligand (22). From this relationship k_1/k_2 can be estimated ($1\,M^{-1}$). Since $k_{obs} = k_1 k_2/k_{-1}$, k_2 is estimated at $6 \times 10^{-6}\,s^{-1}$.

Recently, there has been a lot of progress in designing catalysts that cleave DNA sequence specifically (23). These catalysts are generally based on Fe(II)/O_2 and cleave DNA oxidatively rather than hydrolytically. Although the mechanism of the oxidative cleavage reaction is not clear it is believed that a hydroxyl radical is involved. Since the hydroxyl radical is highly reactive and diffusable, it is practically impossible to control the cleavage reaction with precision (24). Functional groups that promote the hydrolysis of phosphodiesters efficiently will be of great value in developing artificial sequence specific DNase and RNase.

In conclusion, it has been shown for the first time that the highly stable phosphodiester, cAMP can be hydrolyzed efficiently in neutral water with a simple catalyst ([Co(trien)-(OH_2)(OH)]Cl_2). Furthermore, the cobalt complex gives a far greater rate enhancement for the hydrolysis of cAMP ($\sim 10^8$) compared to the rate enhancement for the hydrolysis of methyl phosphate ($\sim 10^2$). We propose that the cobalt(III) ion not only stabilizes the phosphodiester anion but also activates the water molecule. The hydrolysis reaction is effected by an intramolecular nucleophilic attack of the metal hydroxide on the metal bound phosphodiester. Such double activation by a metal ion may play an important role in the enzymatic hydrolysis of cAMP and DNA. Highly efficient catalysts that hydrolyze phosphodiesters will be important in developing artificial restriction enzymes.

Acknowledgment

This work was supported by the Natural Sciences and Engineering Research Council of Canada.

1. L. STRYER. Biochemistry. 2nd ed. Freeman and Co., New York. 1981.
2. M. WATERMAN, G. H. MURDOCH, R. M. EVANS, and M. G. ROSENFELD. Science, **229**, 267 (1985).
3. P. J. MAGISTRETTI and M. SCHORDERET. Nature, **308**, 280 (1984).
4. P. WALSH. Enzymatic reaction mechanisms. Freeman and Co., New York. 1977.
5. D. R. JONES, C. F. LINDOY, and A. M. SARGESON. J. Am. Chem. Soc. **105**, 7327 (1983).
6. T. G. SPIRO, F. J. FARRELL, and W. A. KJELLSTROM. Science, **164**, 320 (1969).
7. R. M. MILBURN, M. GAUTAM-BASAK, R. TRIBOLET, and H. SIGEL. J. Am. Chem. Soc. **107**, 3315 (1985).
8. R. M. MILBURN, S. S. MASSOUD, and F. TAFESSE. Inorg. Chem. **24**, 2593 (1985).
9. A. M. SARGESON and G. H. SEARLE. Inorg. Chem. **6**, 787 (1967).
10. R. KLUGER and P. WASSERSTEIN. Tetrahedron Lett. **38**, 3451 (1974).
11. J. A. GELT, F. H. WESTHEIMER, and J. M. STURTEVANT. J. Biol. Chem. **250**, 5059 (1975).
12. R. BRESLOW *et al.* J. Am. Chem. Soc. **100**, 3227 (1978).
13. R. BRESLOW and M. LABELLE. J. Am. Chem. Soc. **108**, 2655 (1986).
14. P. HAAKE and L. ATWOOD. Bioorg. Chem. **5**, 373 (1976).
15. J. J. BUTZOW and G. L. EICHHORN. Nature, **254**, 358 (1975).
16. J. J. BUTZOW and G. L. EICHHORN. Biochemistry, **10**, 2019 (1971).
17. W. SCHMIDT and H. TAUBE. Inorg. Chem. **2**, 698 (1963).
18. D. R. JONES, L. F. LINDOY, and A. M. SARGESON. J. Am. Chem. Soc. **106**, 7807 (1984).
19. M. L. TOBE. Acc. Chem. Res. **3**, 377 (1970).
20. S. F. LINCOLN and D. R. STRANKS. Aust. J. Chem. **21**, 1733 (1968).
21. R. A. KENLEY, R. H. FLEMING, R. M. LAINE, D. S. TSE, and J. S. WINTERLE. Inorg. Chem. **23**, 1870 (1984).
22. M. L. TOBE. Inorganic reaction mechanisms. Thomas Nelson and Sons Ltd., Great Britain 1972.
23. P. B. DERVAN and R. S. YOUNGQUIST. J. Am. Chem. Soc. **107**, 5528 (1985).
24. L. E. ORGEL and B. C. F. CHU. Proc. Natl. Acad. Sci. USA. **82**, 963 (1985).

Can. J. Chem. Downloaded from www.nrcresearchpress.com by 118.98.75.50 on 09/07/12
For personal use only.

Étude de l'action des organomagnésiens sur les dérivés carboxyliques de la pyridine

P. CANONNE ET M. BELLEY
Département de chimie, Université Laval, Québec (Qué.), Canada

Reçu le 2 décembre 1986

Cet article est dédié au Professeur John T. Edward

P. CANONNE et M. BELLEY. Can. J. Chem. **65**, 1885 (1987).

La réaction de Grignard avec les esters pyridinecarboxyliques **1**, **2**, l'acide pyridinecarboxylique-2 (**3**), et l'anhydride pyridinedicarboxylique-2,3 (**5**) a montré une régiosélectivité au niveau du groupe carbonyle rattaché à la position 2 de l'ester ou de l'anhydride. Ceci nous a permis de développer une nouvelle voie de synthèse des dialkyl-7,7 (7*H*) furo(3,4-*b*) pyridinones-5.

P. CANONNE and M. BELLEY. Can. J. Chem. **65**, 1885 (1987).

Reactions of Grignard reagents with pyridinecarboxylic esters **1**, **2**, pyridine-2-carboxylic acid (**3**), and 2,3-pyridinedicarboxylic acid anhydride (**5**) show regioselectivity at the carbonyl in position 2. This is exemplified by an efficient synthesis of 7,7-dialkylated-7*H*-furo[3,4-*b*]-substituted pyridin-5-ones.

Can. J. Chem. Downloaded from www.nrcresearchpress.com by 118.98.75.50 on 09/07/12
For personal use only.

Dans le cadre général de l'utilisation des anhydrides d'acides dicarboxyliques pour la préparation des lactones dialkylées (1) et monoalkylées (2), nous avons entrepris le présent travail afin de démontrer que la réaction des organomagnésiens constitue une méthode générale qui peut être appliquée pour la synthèse des lactones hétéroaromatiques. Ceci nous a aussi semblé intéressant car l'examen de la littérature a montré qu'aucune étude systématique n'a été effectuée sur les dérivés de la pyridine. De plus, il apparaît que les lactones mono- et bisubstituées sont difficilement accessibles par d'autres méthodes et surtout les (7*H*) furo[3,4-*b*] pyridinones-5 (3).

En effet, récemment (4) il a été observé que l'ortholithiation du *N*,*N*-diisopropylpyridinamide-2 conduit aisément au composé lithié en position 3 lequel à son tour réagit avec un aldéhyde ou cétone pour donner la lactone correspondante. Cependant, l'ortholithiation du *N*,*N*-diisopropylpyridinamide-3 fournit uniquement le composé lithié en position 4 sans aucune trace du composé lithié en position 2. Toute tentative d'introduction, d'une fonction en position 2, n'a pu donné les résultats escomptés. D'autre part, les rendements obtenus lors de l'action des organomagnésiens sur l'ester acide issu de l'anhydride pyridinedicarboxylique-2,3 sont peu concluants et très faibles (5).

Il nous a donc semblé intéressant d'entreprendre l'étude de l'action des organomagnésiens sur les esters pyridinecarboxyliques (**1** et **2**), sur l'acide (**3**) et aussi sur l'anhydride pyrazinedicarboxylique (**4**) et l'anhydride pyridinecarboxylique-2,3 (**5**) afin d'étudier systématiquement leurs réactions avec les organomagnésiens et mettre en évidence l'influence de la position de l'azote sur les rendements réactionnels (6).

En premier lieu, nous avons étudié les facteurs qui influencent les réactions organomagnésiennes (addition, réduction et énolisation). Pour ce faire, nous avons étudié l'action du bromure de propylmagnésium avec les deux esters **1** et **2**, car cet organomagnésien favorise les réactions compétitives (7) à celle de l'addition et notamment lorsque le solvant utilisé est le THF.

Nous avons opéré avec un excès d'organomagnésien[1] aussi bien dans l'éther, dans le THF, et avons trouvé que le produit de la réaction de diaddition n'est le produit principal de la réaction que lorsque le solvant utilisé est l'éther. Nous supposons que la réaction est plus rapide dans le solvant le moins basique. Dans les deux solvants, nous n'avons observé aucune réaction de dimérisation.

En revanche, nous avons observé le propyl-4 pyridinecarboxylate-3 d'éthyle **11** (12%) qui correspond à la réaction d'alkylation du noyau pyridinique. Cependant, ceci n'est obtenu que lorsque la réaction est effectuée dans l'éther diéthylique et à la température ambiante. Il est à noter que cette réaction s'effectue moins facilement que dans le cas de la cyano-3 pyridine (9) et de la cyano-3 quinoline (10).

Les deux esters fournissent les alcools tertiaires correspondants par un processus de diaddition et les deux alcools secondaires par un processus d'addition–réduction. On note également la formation de la (pyridinyl-2)-1 butanone-1 (**6**) qui correspondrait à un processus d'addition–énolisation plutôt qu'à un processus de non réaction de la cétone intermédiaire. Il semble qu'une telle cétone se forme plus difficilement dans le cas de la réaction avec l'ester **2**. On constate généralement que le solvant joue un rôle important dans la distribution des produits de ces réactions. Il est fort probable que cette différence soit due au fait que les organomagnésiens aux concentrations utilisées sont monomères dans le tétrahydrofuranne et dimères dans l'éther diéthylique (11). Cette différence est très grande entre la réaction de diaddition et la réaction d'addition–réduction. Le tétrahydrofuranne favorise la formation de l'alcool secondaire (47% contre 16% dans l'éther). Les résultats obtenus sont rassemblés au tableau 1.

Il en résulte donc de ces expériences que les alcools secondaires ou tertiaires peuvent être obtenus selon le choix du solvant. Une expérience réalisée avec l'acide pyridinecarboxylique-2 dans le tétrahydrofuranne montre que la (pyridinyl-2)-1 butanone-1 peut être obtenue avec un rendement de 55%.

Nous décrivons ainsi une méthode importante de synthèse de cétones sans passer par les chlorures d'acide ou encore les anhydrides en utilisant des organocadmiens (12) ou les composés organiques du manganèse (13).

Les résultats obtenus avec les réactions sur les esters suggèrent que les anhydrides pyrazinedicarboxylique (**4**) et pyridinedicarboxylique (**5**) conduiraient, selon le solvant utilisé, à l'obtention spécifique des lactones monoalkylées et des lactones dialkylées.

Aussi nous avons été intéressés à synthétiser les spirolactones correspondantes en faisant réagir le di(bromomagnésio)-1,4 butane avec les deux anhydrides **4** et **5** afin de démontrer l'influence de l'azote. Nous avons constaté alors que l'anhydride **4**

1. Nous avons observé une grande sensibilité de ces substrats vis-à-vis des organomagnésiens à 25°C se traduisant par la formation d'une quantité importante des composés à haut poids moléculaire.

TABLEAU 1. Réaction du bromure de *n*-propylmagnésium sur les esters **1** et **2** et l'acide **3**

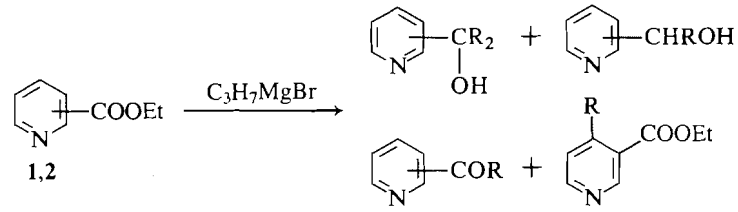

1,2

		Cétone		Alcool II^{aire}		Alcool III^{aire}		Ester alkyle	
Composé	Solvant	N°	Rdt (%)	N°	Rdt (%)	N°	Rdt (%)	N°	Rdt (%)
1	THF	**6**	10	**7**	48	**8**	30		
2	THF	—		**9**	47	**10**	48		
	Ether		>2	**9**	63	**10**	16	**11**	12
3	THF	**6**	55	—	—	—	—		

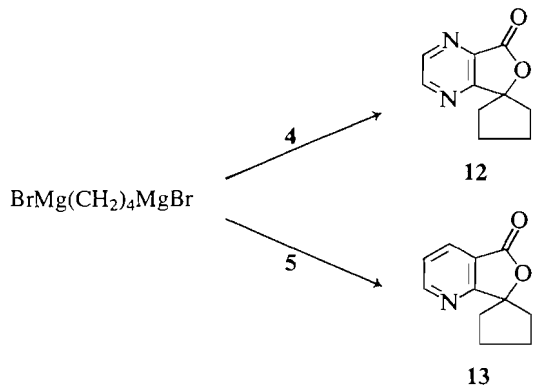

12 **13**

SCHÉMA 1

fournit la lactone correspondante **12** difficilement même à basse température, et que l'anhydride **5** conduit toutefois à la formation de la spiro[cyclopentane-1,7′ (5′*H*) furo[3,4-*b*] pyridin]-one-5′ (**13**) avec un rendement de (45%) (schéma 1). En outre, cette réaction montre une régiosélectivité très marquée. En effet la spiro[cyclopentane-1,5′ (7′*H*) furo[3,4-*b*] pyridin]one-7′ (**14**) isomère n'est obtenue qu'en faible quantité (8%). Nous supposons que cette régiosélectivité peut être attribuée à la proximité de l'atome de l'azote qui forme une liaison de coordination avec l'atome de magnésium, favorisant ainsi l'attaque préférentielle du carbonyle rattaché à la position 2 de l'anhydride **5** (schéma 2). Ainsi, le carboxylate formé réagit à son tour avec une seconde fonction organomagnésienne et conduit après hydrolyse à la lactone **13** (schéma 3).

Nous avons en premier lieu réalisé une étude dans le tétrahydrofuranne à différentes températures et nous avons observé qu'à basse température (−20 à −60°C) le rendement global en lactones est supérieur à celui trouvé à la température ambiante. Ceci peut être attribué à une réactivité plus faible du groupement carboxylate intermédiaire aux températures comprises entre −20 et −60°C. Cette réactivité semble être plus accusée dans le cas du carboxylate rattaché à la position 2 de la pyridine que dans le cas du carboxylate situé en position 3. En effet, les rendements en lactones **21** et **22** ne varient pas avec la température de la réaction alors que le rendement de la lactone **23** passe de 0 à 13%. De plus, on constate une forte augmentation de la propyl-7 (7*H*) furo[3,4-*b*] pyridinone-5 (**22**) (de 10 à 28%). Cette lactone est probablement formée par un processus d'addition–réduction (schéma 4). Comme nous n'avons pas isolé la propyl-5 (5*H*) furo[3,4-*b*] pyridinone-7, nous supposons encore que la formation de lactone **22** peut être attribuée à la présence de l'azote. Enfin une étude réalisée dans le mélange de solvants éther–toluène montre que la formation des lactones **21** et **22** est favorisée au détriment de la lactone **23** (tableau 2). Ces observations sont en accord avec la grande réactivité de l'acide pyridinecarboxylique-2 (**3**) (tableau 1).

De l'ensemble de ces résultats, il apparaît que les réactions secondaires sont favorisées en un moindre degré lorsque les conditions ci-dessous sont respectées :

1. Préparation et réaction des organomagnésiens dans un solvant hydrocarboné en présence de l'éther diéthylique.
2. Utilisation d'une température de réaction comprise entre −20 et −60°C.

Nous constatons ainsi que l'anhydride **5** est un substrat de choix pour la synthèse de (7*H*) furo[3,4-*b*] pyridinones-5 difficilement accessibles par d'autres voies de synthèse.

Partie expérimentale

Les spectres ir ont été enregistrés à l'aide d'un appareil Beckman IR 4250, et les spectres de rmn ^{1}H sur un appareil Bruker (90 MHz) et sur un appareil Varian XL-200 (200 MHz). Les spectres rmn ^{13}C ont été enregistrés sur un appareil Bruker MP-80 (20 MHz). Les spectres de masse ont été effectués sur un appareil Hewlett–Packard 5992 (GS/MG). Les séparations chromatographiques sur colonne ont été effectuées sur gel de silice (Woelms 32–63). Le nicotinate d'éthyle, l'acide picolique, le picolinate d'éthyle et l'acide pyridinedicarboxylique-2,3 sont commercialement accessibles chez Aldrich. Les microanalyses ont été effectuées par Galbraith Laboratories Inc.

Matériel de départ

Le tétrahydrofuranne a été distillé sur sodium et gardé sous atmosphère d'azote, les anhydrides pyridinedicarboxylique-2,3 et pyrazinecarboxylique-2,3 ont été préparés selon la méthode classique en utilisant l'anhydride acétique (14). Les organomagnésiens ont été préparés selon les modes opératoires précédemment décrits (1, 8).

Réaction du bromure de n*-propylmagnésium avec le pyridinecarboxylate-2 d'éthyle ou picolinate d'éthyle (1)*

On prépare dans l'éther un excès de bromure de *n*-propylmagnésium (4 équivalents), et on ajoute l'ester (7,603 g) à 0°C, puis on laisse réagir sous agitation pendant 16 h à la température ambiante. Après hydrolyse et traitement habituel, on sépare les produits par chromatographie sur gel de silice en utilisant le mélange d'éluants acétate d'éthyle – éther de pétrole 1:99 – 20:80. On isole respective-

Can. J. Chem. Downloaded from www.nrcresearchpress.com by 118.98.75.50 on 09/07/12
For personal use only.

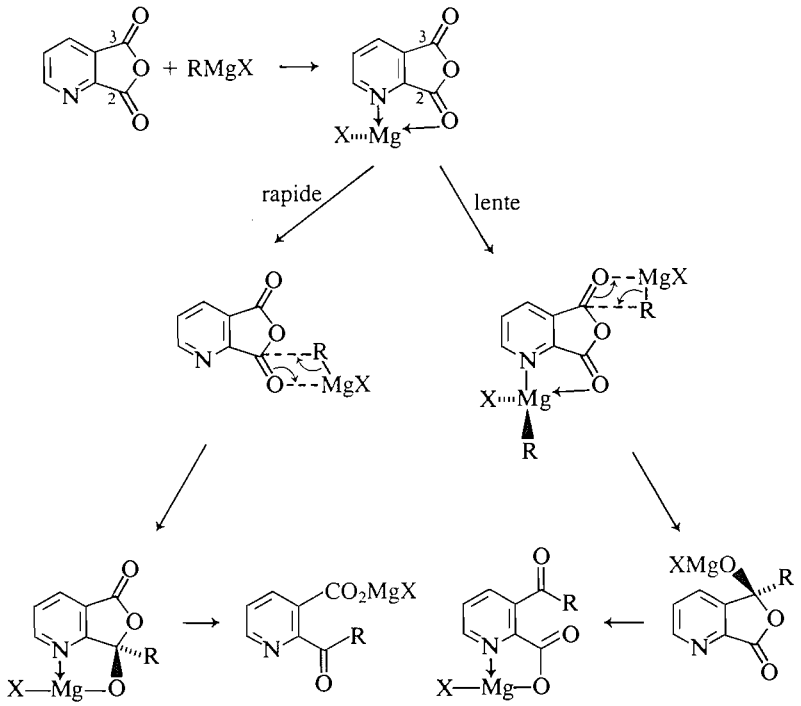

SCHÉMA 2

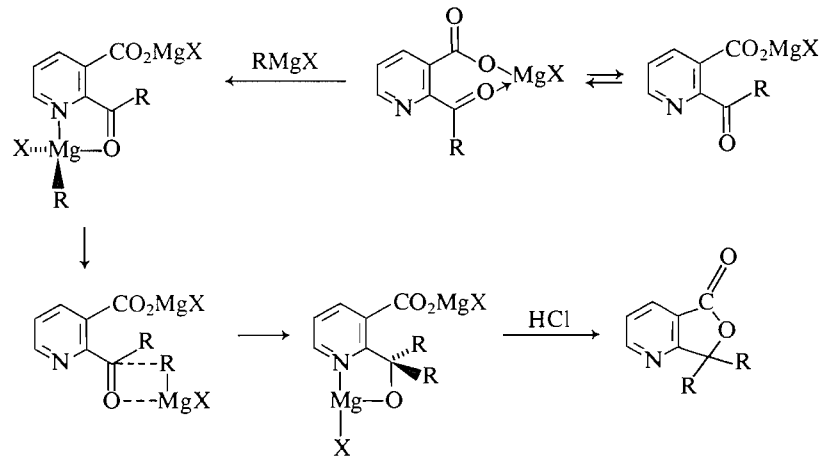

SCHÉMA 3

ment la (pyridinyl-2)-1 butanone-1 (**6**), le (pyridinyl-2)-1 butanol (**7**) et le (pyridinyl-2)-4 heptanol (**8**).

(Pyridinyl-2)-1 butanone-1 (6): Rdt : 10% (0,153 g) liquide; ir ν_{max} : (film) 2960, 2930, 2870, 2851, 2802, 1715, 1455, 1293, 1270, 1160, 1140, 1116, 1008, 871 cm^{-1}; rmn ^1H ($CDCl_3$) δ : 1,02 (3H, *t*, *J* = 7 Hz, CH_3CH_2), 1,78 (2H, q, *J* = 7 Hz, CH_3CH_2), 1,78 (2H, q, *J* = 7 Hz, $CH_3CH_2CH_2$), 3,33 (2H, t, *J* = 7 Hz, CH_2CO), 7,35–8,33 (3H, m), 8,77 (1H, dd) ppm; rmn ^{13}C ($CDCl_3$) δ : 202,1, 154,0, 149,1, 136,9, 127, 121,8, 39,7, 17,6, 13,9 ppm. *Anal.* calc. pour $C_9H_{11}NO$: C 72,46, H 7,43, N 9,38; tr. : C 72,38, H 7,31, N 9,30.

(Pyridinyl-2)-1 butanol-1 (7): Rdt : 48% (0,763 g) liquide; ir ν_{max} (film) : 3380, 2968, 2933, 2871, 1599, 1575, 1468, 1439, 1128, 1069, 1040, 751 cm^{-1}; rmn ^1H ($CDCl_3$) δ : 0,73–2,00 (7H, m), 4,77 (1H, t, *J* = 6 Hz, —C*H*OH), 5,17 (1H, s, OH), 7,03–7,90 (3H, m), 8,53 (1H, dd) ppm; rmn ^{13}C ($CDCl_3$) δ : 163,2, 148,4, 136,8, 122,3, 120,5, 73,1, 40,7, 18,7, 14,0 ppm. *Anal.* calc. pour $C_9H_{13}NO$: C 71,49, H 8,66, N 9,36; tr. : C 71,58, H 8.72, N 9,11.

(Pyridinyl-2)-4 heptanol-4 (8): Rdt : 30% (0,604 g) liquide; ir ν_{max} (film) : 3403, 2958, 2934, 2872, 1599, 1574, 1471, 1440, 1403, 1166, 1031, 798, 756 cm^{-1}; rmn ^1H ($CDCl_3$) δ : 0,67–2,00 (14H, m, $CH_3CH_2CH_2$), 5,40 (1H, s), 7,07–7,90 (3H, m), 8,60 (1H, d, *J* = 5 Hz) ppm; rmn ^{13}C ($CDCl_3$) δ : 164,5, 147,3, 136,8, 121,6, 119,8, 76,2, 44,9, 16,8, 14,5 ppm. *Anal.* calc. pour $C_{12}H_{19}NO$: C 74,57, H 9,91, N 7,24; tr. : C 74,43, H 9,80, N 7,19.

Réactions du bromure de n*-propylmagnésium avec le pyridinecarboxylate d'éthyle ou nicotinate d'éthyle (2)*

1. Dans le THF

On utilise 4 équivalents de réactif de Grignard par équivalent d'ester (**2**) (3,063 g) et on procède comme précédemment. On sépare les composés obtenus par chromatographie sur gel de silice à l'aide du mélange éluant éther de pétrole – acétate d'éthyle.

(Pyridinyl-3)-1 butanol (9): Rdt : 47% (1,421 g) liquide; ir ν_{max} (film) : 3330, 2949, 2862, 1423, 1028, 711 cm^{-1}; rmn ^1H ($CDCl_3$) δ : 0,70–1,90 (7H, m), 4,68 (1H, t, *J* = 6 Hz, C*H*OH), 5,32 (1H, s, OH), 7,23 (1H, dd, *J* = 5 et 8 Hz), 7,77 (1H, dd, *J* = 1,5 et 8 Hz), 8,23–8,50 (2H, m) ppm; rmn ^{13}C ($CDCl_3$) δ : 148,1, 147,7, 141,4, 134,2, 123,6, 71,5, 41,3, 18,9, 13,9 ppm. *Anal.* calc. pour $C_9H_{13}NO$: C 71,49, H 8,66, N 9,26; tr. : C 71,58, H 8,71, N 9,18.

(Pyridinyl-3)-4 heptanol-4 (10): Rdt : 46% (1,775 g) liquide; ir ν_{max} (film) : 3250, 2960, 2932, 2873, 1470, 1420, 718 cm^{-1}; rmn ^1H ($CDCl_3$) δ : 0,60–1,97 (14H, m), 3,97 (1H, s, OH), 7,20 (1H, dd,

Can. J. Chem. Downloaded from www.nrcresearchpress.com by 118.98.75.50 on 09/07/12
For personal use only.

TABLEAU 2. Réactions des organomagnésiens sur l'anhydride pyridinedicarboxylique-2,3 (**5**)

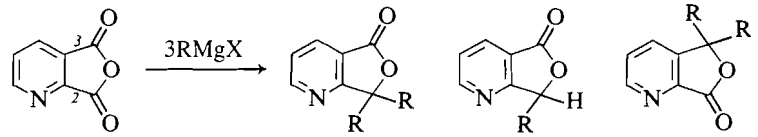

5 I II III

Réactif	Lactone I N°	Lactone I Rdt (%)	Lactone II N°	Lactone II Rdt (%)	Lactone III N°	Lactone III Rdt (%)
$BrMg(CH_2)_4MgBr$ [a]	**13**	50			**14**	8
C_6H_5MgBr [b]	**15**	50			**16**	40
C_6H_5MgBr [a]	**15**	31			—	—
$CH_3C_6H_4MgBr$ [b]	**17**	49			**18**	34
CH_3MgBr [b]	**19**	50			**20**	20
NC_3H_7MgBr [a]	**21**	19	**22**	10	**23**	
NC_3H_7MgBr [c]	**21**	39	**22**	11	**23**	3
NC_3H_7MgBr [b]	**21**	20	**22**	28	**23**	13
NC_6H_{13} [b]	**24**	14	**25**	28	**26**	14

[a]Dans le THF à 25°C.
[b]Dans le THF à −70°C.
[c]Ether–toluène 1:3 à 25°C.

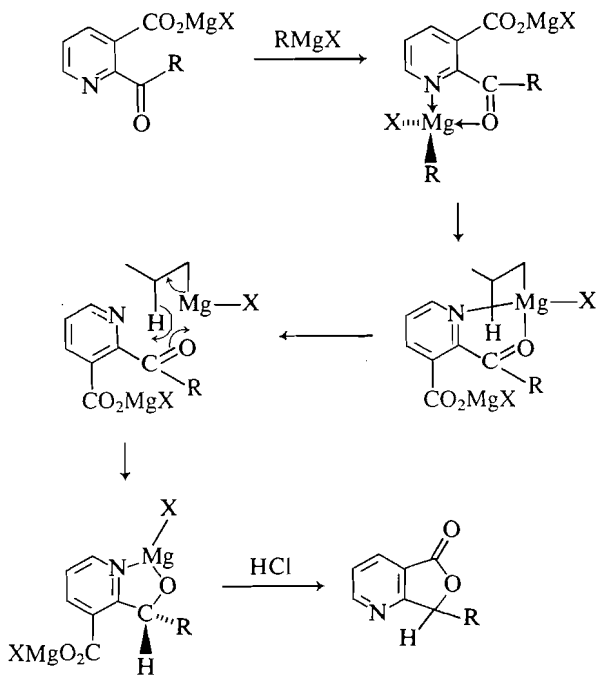

SCHÉMA 4

J = 5 et 8 Hz), 7,80 (1H, dd), 8,40 (1H, dd), 8,61 (1H, d) ppm; rmn ^{13}C ($CDCl_3$) δ: 147,3, 142,7, 133,8, 123,1, 75,7, 45,4, 16,8, 14,4 ppm. *Anal.* calc. pour $C_{12}H_{19}NO$: C 74,57, H 9,91, N 7.24; tr. : C 74,37, H 9,80, N 7,20.

2. *Dans l'éther diéthylique*

À une solution éthérée de bromure de *n*-propylmagnésium (4 équivalents) on ajoute goutte à goutte 1,603 g (10,6 mmol) de nicotinate d'éthyle dilué dans le même solvant et on procède suivant le même mode opératoire que précédemment. Après chromatographie sur colonne de gel de silice on obtient 63% (1,287 g) de (pyridinyl-3)-4 heptanol-4 (**10**), 16% (0,257 g) de (pyridinyl-3)-1 butanol (**9**), 2% (0,033 g) de pyridinyl-3 butanone-1 et 12% (0,250 g) de propyl-4 pyridinylcarboxylate d'éthyle (**11**).

*Propyl-4 pyridinylcarboxylate-3 d'éthyle (**11**)* : Rdt : 12% (0,250 g) liquide; ir ν_{max} (film) : 2951, 2950, 2862, 1861, 1721, 1587, 1271, 1101 cm^{-1}; rmn ^1H ($CDCl_3$) δ : 0,97 (3H, t, J = 7 Hz), 1,40 (3H, t, J = 7 Hz), 1,20–1,90 (2H, m), 2,97 (2H, t, J = 7 Hz), 4,40 (2H, q, J = 7 Hz), 7,20 (1H, d, J = 5 Hz), 8,60 (1H, d, J = 5 Hz), 9,10 (1H, s) ppm; rmn ^{13}C ($CDCl_3$) δ: 166,5, 153,4, 152,2 151,8, 126,4, 125,4, 61,2, 35,8, 24,0, 14,3, 14,0 ppm; sm *m/e*: 194,30 (M + 1, 6,3), 193,20 (M^+, 56,6), 150,2 (35), 148,20 (100%), 135,25 (54), 119,15 (38), 118,15 (36), 91,20 (31), 65,10 (32). *Anal.* calc. pour $C_{11}H_{15}NO_2$: C 68,37, H 7,82, N 7,24; tr. : C 68,30, H 7,75, N 7,20.

*Réaction du bromure de propylmagnésium avec l'acide pyridine-carboxylique-2 ou picolique (**3**)*

À 3,013 g (24,5 mmol) d'acide **3** en suspension dans le THF anhydre, on ajoute goutte à goutte le réactif de Grignard préparé à partir de 18,733 g (152 mmol) de bromopropane et 4,102 g de Mg dans 150 mL de THF, puis on laisse réagir 20 h. Après hydrolyse avec une solution saturée de chlorure d'ammonium, on ramène la phase aqueuse à pH 7, puis on extrait au dichlorométhane. Après chromatographie sur colonne de gel de silice du produit brut de réaction, on isole 2,011 g (55%) de (pyridinyl-2)-1 butanone-1 (**6**).

Réaction des dibromomagnésiens avec les anhydrides

*Réaction du di(bromomagnésio)-1,4 butane avec l'anhydride pyrazinedicarboxylique (**4**)*

À une solution de 64 mL de THF contenant 15,3 mmol de (dibromomagnésio)-1,4 butane (8), on ajoute à −5°C 2,255 g (15,2 mmol) d'anhydride **4** dissous dans 14 mL de THF. Après 10 min d'agitation à −20°C, on hydrolyse le mélange réactionnel. Par chromatographie sur colonne de gel de silice, en utilisant le mélange d'éluants acétate d'éthyle – benzène 3:97, on isole 0,275 g de spirolactone **12** (Rdt 10%). Le dosage par chromatographie en phase gazeuse donne 13% de spiro-[cyclopentane-1,5′ (7′*H*) furo[3,4-*b*] pyrazin]one-7′ (**12**); ir ν_{max} (CH_2Cl_2) : 1777 (C=O) cm^{-1}; rmn ^1H ($CDCl_3$) δ : 1,90–2,35 (8H, s, H), 8,93 (2H, s) ppm. Ce composé semble être sensible à l'air et donc n'a pu être analysé de façon satisfaisante.

*Réactions du di(bromomagnésio)-1,4 butane avec l'anhydride pyridinedicarboxylique-2,3 (**5**)*

À une solution de 29 mmol de di(bromomagnésio)-1,4 butane dans 89 mL de THF maintenue à 0°C, on ajoute 2,88 g (19,3 mmol) d'an-

Can. J. Chem. Downloaded from www.nrcresearchpress.com by 118.98.75.50 on 09/07/12
For personal use only.

Can. J. Chem. Downloaded from www.nrcresearchpress.com by 118.98.75.50 on 09/07/12
For personal use only.

hydride **5** dissous dans 30 mL de THF anhydre, puis on laisse réagir sous agitation pendant 16 h. Après chromatographie sur colonne de gel de silice en utilisant un mélange acétate d'éthyle – éther de pétrole 75:25 comme éluant, on obtient 1,443 g de spirolactone **13**, Rdt 45% (0,252 g), et 8% de la lactone isomère **14**.

*Spiro[cyclopentane-1,7′ (5′*H*)furo[3,4-*b*] pyridin]-one-5 (**13**)* : F = 102,8–103,3°C; ir ν_{max} (CH_2Cl_2) : 1762 (C=O), 1609, 1590, 1108, 1093, 966 cm^{-1}; rmn ^1H ($CDCl_3$) δ : 1,85–2,45 (8H, s), 7,50 (1H, dd, J = 5 et 8 Hz), 8,23 (1H, dd, J = 2 et 8 Hz), 8,93 (1H, dd, J = 2 et 5 Hz) ppm; rmn ^{13}C ($CDCl_3$) δ : 171,4, 168,0, 155,5, 133,8, 123,9, 119,9, 96,4, 38,2, 25,4 ppm; sm *m/e* : 190,10 (M + 1, 4,7%) 189,20 (M^+, 27,5%). *Anal.* calc. pour $C_{11}H_{11}NO_2$: C 76,27, H 6,40, N 8,08; tr. : C 76,40, H 6,51, N 7,98.

*Spiro[cyclopentane-1,5 (7*H*)furo[3,4-*b*] pyridin]-one-7 (**14**)* : F = 84–86°C; ir ν_{max} (CH_2Cl_2) : 2958, 2859, 1770, 1599, 1585, 1470, 1342, 1306, 1102, 988, 959, 801 cm^{-1}; rmn ^1H ($CDCl_3$) δ : 1,93–2,30 (8H, s), 7,67 (1H, dd, J = 5 et 8 Hz), 7,99 (1H, dd, J = 2 et 8 Hz), 8,97 (1H, dd, J = 2 et 5 Hz) ppm; rmn ^{13}C ($CDCl_3$) δ : 167,6, 152,5, 146,8, 144,8, 130,0, 127,6, 93,7, 39,6, 25,0 ppm; sm *m/e* : 190,10 (M + 1, 15), 189,20 (M^+, 100%) 166,15 (140), 160,05, 147,05 (94), 133,10 (42), 132,10 (78), 106,05 (56), 105,05 (84), 104,05 (43), 78,05 (35), 77,05 (67), 51,10 (36). *Anal.* calc. pour $C_{11}H_{11}NO_2$: C 76,27, H 6,40, N 8,08; tr. : C 76,20, H 6,38, N 7,90.

*Réaction du bromure de phénylmagnésium avec l'anhydride pyridinedicarboxylique-2,3 (**5**)*

Une solution de bromure de phénylmagnésium préparée dans le THF (29,5 mmol) est ajoutée à une solution de l'anhydride **5** (13,4 mmol) dans le THF à −70°C et on laisse agiter 20 h à −10°C avant d'hydrolyser. Après chromatographie sur gel de silice du produit brut en utilisant comme éluant le mélange acétate d'éthyle – éther de pétrole 11:89, on recueille 1,910 g de la lactone **15** (Rdt 50%) et 1,862 g de son isomère **16** impur que l'on recristallise pour obtenir 1,456 g (Rdt 40%). À la température ambiante on obtient 31% (1,264 g) de lactone **15**.

*Diphényl-7,7 (7*H*)furo[3,4-*b*] pyridinone-5 (**15**)* : F = 162–163°C; ir ν_{max} (CH_2Cl_2) : 1768, 1600, 1586, 1491, 1160, 1126, 1076, 967, 953 cm^{-1}; rmn ^1H ($CDCl_3$) δ : 7,20–7,70 (11H, m), 8,27 (1H, dd, J = 2 et 8 Hz), 8,97 (1H, dd, J = 2 et 5 Hz) ppm; rmn ^{13}C ($CDCl_3$) δ : 170,8, 167,6, 155,3, 139,9, 134,4, 128,6, 127,0, 124,2, 119,7, 90,7; sm *m/e* : 288,25 (M + 1, 11), 287,15 (M^+, 60,7), 286,15 (21), 243,20 (24), 242,20 (20), 210 (100%), 182,10 (32), 154,25 (22), 105,00 (28), 77,15 (52), 51,10 (25).

*Diphényl-5,5 (5*H*) furo[3,4-*b*] pyridinone-7 (**16**)* : F = 126,2–126,6°C; ir ν_{max} (CH_2Cl_2) : 1780, 1600, 1161, 1125, 1110, 968 cm^{-1}; rmn ^1H ($CDCl_3$) δ : 7,43 (10H, s), 8,13 (1H, dd, J = 2 et 8 Hz), 9,00 (1H, J = 2 et 5 Hz) ppm; rmn ^{13}C ($CDCl_3$) δ : 167,3, 152,9, 146,4, 144,1, 140,2, 132,8, 129,0, 128,9, 127,5, 127,0, 89,9 ppm; sm *m/e* : 288,15 (M + 1, 3,3), 287,15 (M^+, 18,7), 244,20 (18), 243,20 (100%), 242,20 (34), 241,20 (21), 210,05 (48), 182,10 (11), 154,25 (23), 127,10 (31), 120,60 (10), 105 (17), 77,15 (31), 51,10 (22).

Réaction du bromure de p*-tolymagnésium avec l'anhydride pyridinecarboxylique-2,3 (**5**)*

À une solution de 2 g (13,4 mmol) de l'anhydride **5** dans 30 mL de THF, on ajoute goutte à goutte la solution organomagnésienne (4 équivalents) préparée dans le THF à −60°C, puis on laisse agiter pendant 20 h à −10°C, puis on hydrolyse. Après chromatographie flash sur gel de silice en utilisant le mélange acétate d'éthyle – benzène 5:95 et 8:92 on recueille 2,075 g (49%) de di(*p*-tolyl)-7,7 (7*H*) furo-[3,4-*b*] pyridinone-5 (**17**) et 1,439 g (34%) de di(*p*-tolyl)-5,5 (7*H*) furo[3,4-*b*] pyridinone-7 (**18**).

*Di(*p*-tolyl)-7,7 (7*H*)furo[3,4-*b*] pyridinone-5 (**17**)* : F = 112–113°C; ir ν_{max} (CH_2Cl_2) : 1771, 1604, 1511, 1158, 1127, 1121 cm^{-1}; rmn ^1H ($CDCl_3$) δ : 2,33 (6H, s), 7,07–7,64 (9H, m), 8,27 (1H, dd, J = 2 et 8 Hz), 9,00 (1H, dd, J = 2 et 5 Hz) ppm; rmn ^{13}C ($CDCl_3$) δ : 170,7, 167,8, 155,3, 138,4, 137,1, 134,3, 129,2, 127,0, 124,0, 119,7, 91,0, 21,0 ppm; sm *m/e* : 317,20 (M + 2, 2), 316,20 (M + 1, 16,6), 315,20 (M^+, 75,2), 271,30 (70), 256,30 (21), 241,10 (21), 224,15 (100%), 196,20 (25), 167,25 (38), 119,20 (34), 91,15 (42), 77,15 (22), 65,10 (26). *Anal.* calc. pour $C_{21}H_{17}NO_2$: C 79,98, H 5,43, N 4,44; tr. : C 79,91, H 5,38, N 4,32.

*Di(*p*-tolyl)-5,5 (5*H*) furo[3,4-*b*] pyridinone-7 (**18**)* : Rdt : 34% (1,439 g); F = 157–158°C; ir ν_{max} (CH_2Cl_2) : 1777, 1512, 1157, 1128, 1109, 960 cm^{-1}; rmn ^1H ($CDCl_3$) δ : 2,33 (6H, s), 7,23 (8H, s), 7,63 (1H, dd, J = 5 et 8 Hz), 8,07 (1H, dd, J = 2 et 8 Hz), 8,97 (1H, dd, J = 2 et 5 Hz) ppm; rmn ^{13}C ($CDCl_3$) δ : 167,6, 152,9, 146,9, 144,1, 139,0, 137,5, 132,8, 129,5, 127,5, 127,7, 90,1, 21,1 ppm; sm *m/e* : 316,20 (M + 1, 7,4), 315,20 (M^+, 34,5), 272,30 (21), 271,30 (100%), 270,30 (22), 257,20 (22), 256,30 (85), 254,20 (20), 224,15 (47), 167,25 (29), 91,15 (29). *Anal.* calc. pour $C_{21}H_{17}NO_2$: C 79,98, H 5,43, N 4,44; tr. : C 79,80, H 5,45, N 4,38.

*Réaction du bromure de méthylmagnésium avec l'anhydride pyridinedicarboxylique-2,3 (**5**)*

On prépare ce réactif de Grignard en faisant barboter un courant de bromométhane dans le ballon réactionnel refroidi contenant 0,757 g de magnésium et 30 mL de THF anhydre, puis on y ajoute goutte à goutte à −60°C 2,0 g (13,4 mmol) d'anhydride **5** dissous dans 50 mL de THF, et on laisse la réaction se poursuivre sous agitation pendant 16 h à 10°C. Après hydrolyse et traitement habituel, on recueille par chromatographie sur gel de silice, en utilisant comme éluant le mélange de solvants acétate d'éthyle – éther de pétrole 35:65, deux lactones **19** et **20**.

*Diméthyl-7,7 (7*H*)furo[3,4-*b*] pyridinone-5 (**19**)* : Rdt : 50%; F = 85–86°C; ir ν_{max} (CH_2Cl_2) : 1766, 1606, 1589, 1475, 1326, 1200, 1168, 1143, 1092, 1047, 950, 907, 789 cm^{-1}; rmn ^1H ($CDCl_3$) δ : 1,73 (6H, s), 7,53 (1H, dd, J = 5 et 8 Hz), 8,27 (1H, dd, J = 2 et 8 Hz), 8,93 (1H, dd, J = 2 et 5 Hz) ppm; rmn ^{13}C ($CDCl_3$) δ : 1730, 167,8, 155,3, 134,3, 124,1, 119,0, 86,4, 25,7 ppm; sm *m/e* : 163,10 (17), 149,10 (8), 148,20 (100%), 105,05 (9), 92,10 (21), 77,10 (9), 65,15 (10), 51,15 (8).

*Diméthyl-5,5 (5*H*) furo[3,4-*b*] pyridinone-7 (**20**)* : Rdt : 20%; F = 104–104.5°C; ir ν_{max} (CH_2Cl_2) : 1772, 1318, 1206, 1167, 1090, 1050, 949, 900, 801 cm^{-1}; rmn ^1H ($CDCl_3$) δ : 1,73 (6H, s), 7,61 (1H, dd, J = 5 et 8 Hz), 7,98 (1H, dd, J = 2 et 8 Hz), 8,92 (1H, dd, J = 2 et 5 Hz) ppm; rmn ^{13}C ($CDCl_3$) δ : 167,6, 152,6, 149,0, 144,1, 129,9, 127,7, 83,9, 27,3 ppm; sm *m/e* : 164,10 (M + 1, 4,1), 163,20 (M + 37), 148,10 (100%), 120,05 (52), 118,15 (21), 104,05 (15), 92,10 (39), 72,10 (17), 51,15 (22). *Anal.* calc. pour $C_9H_9NO_2$: C 66,25, H 5,56, N 8,58; tr. : C 66,15, H 5,48, N 8,51.

*Réaction du bromure de propylmagnésium avec la furo[3,4-*b*] pyridinedione-5,7 ou l'anhydride pyridinedicarboxylique-2,3 (**5**)*

1. THF à 25°C

À 120 mmol de bromure de propylmagnésium dans le THF on ajoute 34,3 mmol (5,119 g) d'anhydride **5**. Après agitation durant 24 h, on hydrolyse le mélange réactionnel et, par séparation chromatographique, on obtient 1,128 g (Rdt 19%) de dipropyl-7,7 (7*H*) furo[3,4-*b*] pyridinone-5 (**21**) et 0,687 g (Rdt 10%) de propyl-7 (7*H*) furo[3,4-*b*] pyridinone-5 (**22**).

2. Réaction du bromure de propylmagnésium avec l'anhydride pyridinedicarboxylique-2,3 dans un mélange éther diéthylique – toluène 1:3 à 25°C

On prépare le bromure de propylmagnésium à partir de 4,537 g (36,9 mmol) de bromopropane et 0,986 g de magnésium dans 40 mL d'éther diéthylique. À ce réactif refroidi à 0°C, on ajoute goutte à goutte 2,0 g (13,4 mmol) d'anhydride **5** dissous dans 120 mL de toluène anhydre bouillant. On laisse agiter pendant 16 h à la température ambiante avant d'hydrolyser le mélange réactionnel. Après chromatographie sur gel de silice en utilisant comme éluant les mélanges acétate d'éthyle – benzène 5:95 et acétate d'éthyle – benzène 10:90, on isole trois produits dans les proportions citées ci-dessous.

*Dipropyl-7,7 (7*H*) furo[3,4-*b*] pyridinone-5 (**21**)* : 1,150 g (Rdt 39%).

*Propyl-7 (7*H*) furo[3,4-*b*] pyridinone-5 (**22**)* : 0,272 g (Rdt 11%).

*Dipropyl-5,5 (5*H*) furo[3,4-*b*] pyridinone-7 (**23**)* : 0,096 g (Rdt 3%).

Can. J. Chem. Downloaded from www.nrcresearchpress.com by 118.98.75.50 on 09/07/12
For personal use only.

3. À basse température dans le tétrahydrofuranne

On refroidit à −60°C le réactif de Grignard obtenu à partir de 4,124 g (33,5 mmol) de bromopropane et 0,897 g de magnésium dans 28 mL de THF anhydre, puis on y ajoute goutte à goutte 0,986 g (6,61 mmol) d'anhydride **5** dissous dans 25 mL de THF en trois réactions (1–3) à différentes températures : (1) à −60°C, 10 min; (2) à −40°C, 10 min; (3) −20°C, 10 min. Après hydrolyse on dose par chromatographie en phase gazeuse les lactones obtenues en utilisant comme standard interne le phénanthrène. Les rendements correspondants obtenus dans chacune des réactions sont donnés ci-dessous.

(1) À −60°C : dipropyl-7,7 (7*H*) furo[3,4-*b*] pyridinone-5 (**21**) : 21%; propyl-7 (7*H*) furo[3,4-*b*] pyridinone-5 (**22**) : 31%; dipropyl-5,5 (5*H*) furo[3,4-*b*] pyridinone-7 (**23**) : 12%.

(2) À −40°C : dipropyl-7,7 (7*H*) furo[3,4-*b*] pyridinone-5 (**21**) : 20%; propyl-7 (7*H*) furo[3,4-*b*] pyridinone-5 (**22**) : 31%; dipropyl-5,5 (5*H*) furo[3,4-*b*] pyridinone-5 (**23**) : 13%.

(3) À −20°C : dipropyl-7,7 (7*H*) furo[3,4-*b*] pyridinone-5 (**21**) : 19%; propyl-7 (7*H*) furo[3,4-*b*] pyridinone-5 (**22**) : 28%; dipropyl-5,5 (5*H*) furo[3,4-*b*] pyridinone-7 (**23**) : 13%.

*Dipropyl-7,7 (7*H*) furo[3,4-*b*] pyridinone-5 (**21**) :* F = 59–60°C; ir ν_{max} (CCl_4) : 2910, 2876, 2812, 1776, 1612, 1592, 1288, 1184, 1096, 1074, 952 cm^{-1}; rmn ^1H ($CDCl_3$) δ : 0,80–0,90 (6H, m), 0,90–1,55 (4H, m), 1,94–2,20 (4H, m), 7,49 (1H, dd, J = 5 et 8 Hz), 8,20 (1H, dd, J = 2 et 8 Hz), 8,89 (1H, dd, J = 2 et 5 Hz) ppm; rmn ^{13}C ($CDCl_3$) δ : 171,5, 168,4, 155,1, 133,8, 123,8, 121,0, 91,2, 39,7, 16,5, 14,0 ppm; sm *m/e* : 177,10 (71), 176,10 (95), 148,15 (29), 134,10 (100%), 130,10 (17), 106,00 (27), 78,05 (21). *Anal.* calc. pour $C_{13}H_{17}NO_2$: C 71,20, H 7,82, N 6,38; tr. : C 71,02, H 7,91, N 6,46.

*Propyl-7 (7*H*) furo[3,4-*b*] pyridinone-5 (**22**) :* F = 35–35,8°C; ir ν_{max} (CCl_4) : 2915, 2883, 2820, 1781, 1613, 1596, 1161, 1105, 1060, 962 cm^{-1}; rmn ^1H ($CDCl_3$) δ : 1,00 (3H, t, J = 7 Hz), 1,20–2,37 (4H, m), 5,53 (1H, dd, J = 4 et 6 Hz), 7,55 (1H, dd, J = 5 et 8 Hz), 8,27 (1H, dd, J = 2 et 8 Hz), 8,97 (1H, dd, J = 2 et 5 Hz) ppm; rmn ^{13}C ($CDCl_3$) δ : 169,3, 168,8, 155,3, 134,2, 124,2, 120,4, 82,2, 35,1, 18,1, 13,8 ppm; sm *m/e* : 135 (100%), 134,10 (41), 133,20 (16), 107,05 (56), 106,05 (54), 79,10 (16), 78,10 (38), 77,10 (14), 51,15 (25). *Anal.* calc. pour $C_{10}H_{10}NO_2$: C 68,17, H 5,72, N 7,95; tr. : C 68,32, H 5,79, N 8,01.

*Dipropyl-5,5 (5*H*) furo[3,4-*b*] pyridinone-7 (**23**) :* F = 108–109°C; ir ν_{max} (CH_2Cl_2) : 2949, 2920, 2860, 1770, 1593, 1183, 1160, 1101, 1079, 938 cm^{-1}; rmn ^1H ($CDCl_3$) δ : 0,80–1,00 (6H, m), 1,00–1,55 (4H, m), 1,66–2,17 (4H, m), 7,63 (1H, dd, J = 5 et 8 Hz), 7,85 (1H, dd, J = 2 et 8 Hz), 8,90 (1H, dd, J = 2 et 5 Hz) ppm; sm *m/e* : 219,10 (M^+, 5,3), 177,10 (13), 176,20 (100%), 148,15 (9), 134,10 (12), 210,10 (10), 106,16 (53), 78,20 (28), 71,20 (11), 51,15 (9). *Anal.* calc. pour $C_{13}H_{17}NO_2$: C 71,20, H 7,82, N 6,38; tr. : C 71,36, H 7,95, N 6,43.

Réaction du bromure d'hexylmagnésium avec l'anhydride pyridine-carboxylique-2,3 (5)

À une solution de bromure d'hexylmagnésien préparée dans le THF (4 équivalents), on ajoute à −20°C 3,047 g (20,4 mmol) d'anhydride **5** dissous dans 42 mL de THF. On laisse réagir à −20°C pendant 20 min, puis on hydrolyse avec HCl 10%. La chromatographie sur gel de silice avec acétate d'éthyle – benzène 3:97 fournit les trois lactones comme précédemment.

*Dihexyl-7,7 (7*H*) furo[3,4-*b*] pyridinone-5 (**24**) :* Rdt : 14% (0,863 g) ; F = 28–29°C ; ir ν_{max} (CH_2Cl_2) : 2941, 2919, 2827, 1760, 1604, 1588, 1101, 1080 cm^{-1}; rmn ^1H ($CDCl_3$) δ : 0,82 (6H, s), 0,93–1,45 (16H, s), 2,08 (4H, m), 7,48 (1H, dd, J = 5 et 8 Hz), 8,23 (1H, dd, J = 2 et 8 Hz), 8,91 (1H, dd, J = 1 et 5 Hz) ppm; rmn ^{13}C ($CDCl_3$) δ : 171,6, 168,4, 155,0, 133,8, 123,7, 120,9, 91,3, 37,5, 31,5, 29,2, 23,0, 22,5, 13,9 ppm; sm *m/e* : 303,30 (M^+, 0,7), 259,25 (9), 220,10 (15), 219,10 (100%), 218,20 (87), 188,15 (11), 148,10 (39), 134,05 (16), 130,05 (9), 106,05 (27), 105,05 (9), 79,10 (12), 78,10 (9), 77,10 (10), 55,05 (10%). *Anal.* calc. pour $C_{19}H_{29}NO_2$: C 74,71, H 9,57, N 4,58; tr. : C 74,63, H 9,62, N 4,52.

*Hexyl-7 (7*H*) furo[3,4-*b*] pyridinone-5 (**25**) :* Rdt : 28% (1,25 g); F = 54,0–55,0°C; ir ν_{max} (CH_2Cl_2) : 2920, 2852, 1769, 1609, 1590, 1180, 1107, 1069 cm^{-1}; rmn ^1H ($CDCl_3$) δ : 0,87 (3H, s), 1,10–1,67 (8H, s), 1,67–2,30 (2H, m), 5,50 (1H, dd, J = 4 et 6 Hz), 7,50 (1H, dd, J = 5 et 8 Hz), 8,33 (1H, dd, J = 2 et 8 Hz), 8,91 (1H, dd, J = 2 et 5 Hz) ppm; rmn ^{13}C ($CDCl_3$) δ : 169,5, 168,7, 153,3, 134,0, 124,0, 120,1, 82,5, 33,2, 31,6, 29,0, 24,7, 22,5, 14,0 ppm; sm *m/e* : 220,15 (M + 1, 0,8), 219,05 (M^+, 5,4), 148,05 (19), 135,10 (100%), 134,10 (27), 107,00 (43), 106,00 (37), 79,05 (17), 78,05 (25), 51,10 (14).

*Dihexyl-5,5 (5*H*) furo[3,4-*b*] pyridinone-7 (**26**) :* Rdt : 14% (0,865 g); F = 68,8–69,5°C; ir ν_{max} (CH_2Cl_2) : 2950, 2920, 2850, 1772, 1597, 1569, 1091 cm^{-1}; rmn ^1H ($CDCl_3$) δ : 0,83 (6H, s), 0,90–1,40 (16H, m), 1,80–2,18 (4H, m), 7,55 (1H, dd, J = 5 et 8 Hz), 7,84 (1H, dd, J = 2 et 8 Hz), 8,97 (1H, dd, J = 2 et 5 Hz) ppm; rmn ^{13}C ($CDCl_3$) δ : 168,1, 152,4, 146,8, 145,6, 130,2, 127,2, 88,7, 38,7, 31,5, 29,3, 23,3, 22,5, 13,9 ppm; sm *m/e* : 304,30 (M + 1, 0,8), 303,30 (M^+, 4,9), 219,00 (18), 218,10 (100%), 200,15 (25), 148,10 (14), 132,15 (11), 130,05 (13), 106,05 (34), 78,10 (23).

Remerciements

Nous remercions le Conseil de recherches en sciences naturelles et en génie du Canada et les Fonds pour la formation de chercheurs et l'aide à la recherche au Ministère de l'éducation du Québec pour l'aide financière apportée sous forme de subventions et de bourse d'études (M.B.).

1. P. Canonne, M. Akssira et G. Fytas. Tetrahedron, **40**, 1809 (1984).
2. P. Canonne et M. Akssira. Tetrahedron, **41**, 3695 (1985).
3. (*a*) M. Ozutsumi, Y. Miyazawa, S. Ogawa, S. Ishige, A. Watanabe et K. Kaeki. Ger. Offen. 2 412 640 (ct. B41 m) 26 sept 1974; Japan, Apple 7 329 468, 15 mars 1973; Chem. Abstr. **92**, 37353m (1975); (*b*) T. E. Hoover, S. Farber et W. J. Becker. Ger. Offen. 3 008 494 (ct. C07D513/04), 18 sept 1980; U.S. Appl. 17 765 05 mars 1979; Chem. Abstr. **95**, 25057y (1981); (*c*) C. M. Jephcott. J. Am. Chem. Soc. **50**, 1189 (1928).
4. J. Epsztajn, Z. Berski, J. Z. Brzezinski et A. Jozwarak. Tetrahedron Lett. **21**, 4739 (1980).
5. H. Simonis et H. Cohn. Ber. Dtsch. Chem. Ges. **47**, 1238 (1914).
6. J. Barassin, G. Queguiner et H. Lumbroso. Bull. Soc. Chim. Fr. 4707 (1967).
7. P. Canonne, G. B. Foscolos, H. Caron et G. Lemay. Tetrahedron, **38**, 3563 (1982).
8. P. Canonne, D. Bélanger, G. Lemay et G. B. Foscolos. J. Org. Chem. **46**, 3091 (1981).
9. R. L. Frank et C. Weatherbee. J. Am. Chem. Soc. **70**, 3482 (1948).
10. M. Ferles, P. Joncas et O. Kocian. Collect. Czech. Chem. Commun. **44**, 2672 (1972).
11. E. C. Ashby. Pure Appl. Chem. **52**, 545 (1980).
12. J. Michel, E. Henry-Basch et P. Freon. Bull. Soc. Chim. Fr. 4898 (1968).
13. (*a*) G. Friour, A. Alexakis, G. Cahiez et J. F. Normant. Tetrahedron, **40**, 683 (1984); (*b*) G. Friour, G. Cahiez et J. F. Normant. Synthesis, 37 (1984).
14. L. Friedman. Org. Synth. **43**, 80 (1963).

Synthesis and characterization of picryl cellulose

MICHAEL J. STRAUSS,[1] REUBEN TORRES, JOHN PHELAN, ANDY CRAFT, BRUCE PITNER, AND DEANE NASON
Department of Chemistry, University of Vermont, Burlington, VT 05401, U.S.A.

YVON CARIGNAN
U.S. Army Armament Research and Development Command, Dover, NJ 07801, U.S.A.

AND

JULIAN M. DUST AND ERWIN BUNCEL
Chemistry Department, Queen's University, Kingston, Ont., Canada K7L 3N6

Received January 13, 1987

This paper is dedicated to Professor John T. Edward

MICHAEL J. STRAUSS, REUBEN TORRES, JOHN PHELAN, ANDY CRAFT, BRUCE PITNER, DEANE NASON, YVON CARIGNAN, JULIAN M. DUST, and ERWIN BUNCEL. Can. J. Chem. **65**, 1891 (1987).

2,4,6-Trinitrophenyl cellulose (picryl cellulose) was synthesized by S_NAr displacement of chloride from picryl chloride by sodium cellulosate. The cellulosate was prepared *in situ* from microcrystalline cellulose and sodium methoxide. Depending upon the procedure used, two products with different degrees of picrylation resulted; one contained one picryl ring per ca. 6.5 glucosyl units (PC-6), while the other had ca. one picryl ring per 12 (PC-12). These picryl ethers were characterized by several independent methods: 400-MHz ^1H nuclear magnetic resonance spectroscopy of the DMSO-soluble material, temperature-dependent mass spectrometry (ion pyrograms), and differential scanning calorimetry (DSC). The nuclear magnetic resonance spectrum displays peaks in the low field region (8–9.5 ppm) assigned to the picryl rings; these resonances are well separated from those for possible alternative compounds such as unreacted picryl chloride, picric acid, or 2,4,6-trinitroanisole. It is suggested that the various picryl resonances arise primarily from different microenvironments and (or) conformational preferences of the polymer chain rather than from different substitution sites. Substitution at a primary C-6 position of the glucosyl moiety is favoured. DSC shows that while cellulose undergoes an endothermic decomposition between 320 and 350°C, picryl cellulose exhibits an exothermic decomposition at ca. 230°C. This exotherm is accompanied by the liberation of picric acid, as confirmed by nuclear magnetic resonance; mass spectral results indicate concurrent chain cleavage to yield smaller polysaccharides. A mechanism for initiation of pyrolytic decomposition is proposed, in which loss of picric acid is accompanied by rupture of a glycosidic bond with concomitant formation of glucosan and enolic end groups on the remaining fragments.

MICHAEL J. STRAUSS, REUBEN TORRES, JOHN PHELAN, ANDY CRAFT, BRUCE PITNER, DEANE NASON, YVON CARIGNAN, JULIAN M. DUST et ERWIN BUNCEL. Can. J. Chem. **65**, 1891 (1987).

On a réalisé la synthèse de la trinitro-2,4,6 phényl cellulose (picryle de cellulose) en procédant à une substitution S_NAr du chlorure de picryle par le cellulosate de sodium. On a préparé le cellulosate en faisant réagir *in situ* de la cellulose microcristalline avec du méthylate de sodium. Suivant la méthode utilisée, il se forme deux produits comportant des degrés différents de picrylation : un produit qui contient un groupement picryle par 6,5 unités glucosyles (PC-6) et un autre qui contient un groupement picryle par 12 unités glucosyles (PC-12). On a caractérisé ces éthers picryles par plusieurs méthodes indépendantes dont la spectroscopie de résonance magnétique nucléaire du ^1H à 400 MHz du produit soluble dans le DMSO, la spectrométrie de masse à température variable (pyrogrammes ioniques) et la calorimétrie à balayage différentiel (CBD). Les spectres rmn présentent des bandes dans la région des bas champs (8–9,5 ppm) qui ont été attribués aux picryles; ces raies sont bien séparées de celles qui pourraient provenir d'autres composés comme le chlorure de picryle qui n'aurait pas réagi, de l'acide picrique ou du trinitro-2,4,6 anisole. On suggère que les diverses raies dues au picryles proviennent principalement de divers microenvironnements et (ou) de préférences conformationnelles des chaînes de polymères plutôt que de divers sites de substitution. La substitution au niveau du carbone primaire en position C-6 de la portion glucosyle est favorisée. La CBD permet de démontrer que la cellulose subit une décomposition endothermique entre 320 et 350°C et que le picryle de cellulose donne lieu à une décomposition endothermique à environ 230°C. Cette décomposition exothermique est accompagnée d'une libération d'acide picrique et on a confirmé cette conclusion par rmn; le donnée de la spectrométrie de masse indiquent qu'il se produit une clivage concomitant qui fournit des polysaccharides plus petits. On propose un mécanisme pour l'initiation de la décomposition pyrolytique dans lequel la perte d'aide picrique est accompagnée par la rupture d'une liaison glycosidique avec la formation concomitante de glucosane et de groupements énoliques en bout de chaîne sur les fragments qui restent.

[Traduit par la revue]

The interaction of polynitroaromatic and heteroaromatic compounds with electron-rich donors results in the formation of electron donor–acceptor (1) and (or) anionic Meisenheimer type σ-complexes (2). The σ-complexes, particularly the adducts arising from novel electron-deficient substrates, have been the subject of considerable recent interest (3–6). In this context, the reaction of polynitroaryl ether derivatives of cellulose with nucleophiles could form an interesting system of study and part of our ongoing program of research.

During the past few decades there have been several attempts to prepare and characterize the polynitroaryl ethers of cellulose (7, 8). Nitration of cellulose phenyl ether resulted in partial nitration of the hydroxyl as well as the phenyl groups (7). Avny *et al.* attempted the preparation of picryl cellulose (PC) directly from cellulose membrane (cellophane), as well as from cotton fabric, by reacting the corresponding sodium cellulosates with picryl chloride in benzene, but the material obtained was only partially characterized (8). The results of this work were interpreted on the basis of the highly coloured species, assumed to be an adduct formulated as **1**, that was isolated and neutralized with

[1]Author to whom correspondence may be directed.

Printed in Canada / Imprimé au Canada

Can. J. Chem. Downloaded from www.nrcresearchpress.com by 118.98.75.50 on 09/07/12
For personal use only.

acetic acid. Two alternative neutralization routes were proposed, leading either to the cellulose and picryl chloride starting materials or to the desired picryl ether of cellulose. It was suggested that neutralization favoured reversion of adduct **1** to the starting materials, due to steric hindrance between the picryl and glucopyranoside rings in the picryl cellulose (8).

It is known that the kinetically preferred site of attack by nucleophiles on polynitroaromatic substrates such as picryl chloride or 2,4,6-trinitroanisole occurs *meta* to the substituent in the 1-position (9, 10). In the present system such a process would give rise to adduct **2**, which could only regenerate

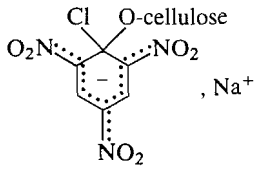

1

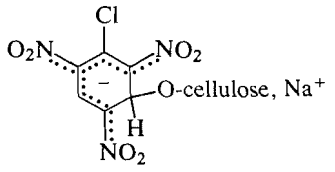

2

starting material upon addition of acid. Intervention of the 1,3 adduct and its subsequent acid decomposition would result in significantly lower yield of picryl cellulose.

Since sodium cellulosate[2] is expected to be more soluble and a better nucleophile in dimethyl sulfoxide (DMSO) than in benzene, the picrylation of cellulose in DMSO should offer advantages (11). We report here our results on the synthesis of picryl cellulose in DMSO and the full characterization of the product.

Results and discussion

Synthesis of picryl celluloses, PC-6 and PC-12

In this work, various procedures were investigated in the preparation of picryl cellulose. Two representative procedures, which led to the successful preparation of products that were subsequently characterized, are described, while one procedure that did not yield desired product is also described.

In all preparations, sodium cellulosate was prepared *in situ* from microcrystalline cellulose by treating a sample of the desiccated cellulose first with DMSO, to swell it thoroughly with the solvent, and then with freshly prepared sodium methoxide. The resulting cellulosate was washed with dry DMSO to remove excess methoxide and, in the first procedure, reacted with a solution of picryl chloride in DMSO to yield PC-12 after work-up. In the second procedure, picryl chloride was added as a powdered solid to the sodium cellulosate in DMSO; this process afforded PC-6, a more highly picrylated material. In either case, the picryl cellulose was well washed with a variety of solvents, followed by Soxhlet extraction of the material for 4 days and drying under vacuum. This extensive washing and extraction procedure militates against the presence of any adsorbed or entrained picryl chloride, or picrate.

In both methods of preparation addition of the picryl chloride, whether in solution or as a solid, was relatively rapid. In one of the attempted preparations, a concentrated solution of picryl chloride in DMSO was allowed to stand for 30 min prior to addition to the cellulosate suspension. The picryl chloride solution became very hot over this period of time and in this preparation no picryl ring was incorporated into the product. These observations are in accord with the known reactivity of picryl chloride in DMSO without added nucleophile (12).

The preferred method for the synthesis of picryl cellulose in terms of yield of product and degree of picrylation (PC-6) involved rapid introduction of finely powdered picryl chloride directly into the stirred solution of sodium cellulosate in DMSO.

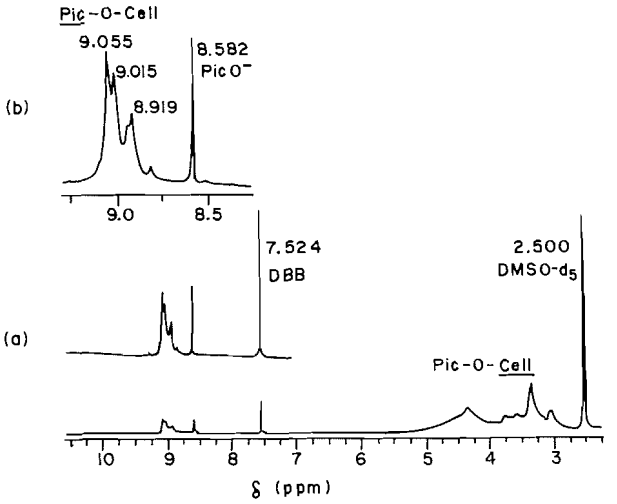

FIG. 1. The ^1H nmr spectrum of picryl cellulose (PC-6) in DMSO-d_6. Inset (a), aromatic region intensified (δ 7–10); inset (b), peaks due to picryl moieties of the picryl cellulose and of picrate ion.

Characterization of picryl celluloses, PC-6 and PC-12

1. Physical properties, elemental analysis, and hydrolytic cleavage

The picryl celluloses synthesized in this work are tan powders when dry. PC-6 and PC-12 are extremely hygroscopic and hydrate rapidly, i.e., the weight of both materials in air increases over time. Hydration is complete within 24 h, at which point the weight increase levels off at 7.3%. The hydrated products are bright yellow in colour, in contrast to the tan anhydrous powder. The process is probably accompanied by some hydrolysis (*vide infra*).

Elemental analysis (C, H, N) clearly differentiates the two picryl cellulose products. The nitrogen content and number of glucosyl units per picryl ring for PC-6 and PC-12 are given in the experimental section. Based on the requirement of 3 nitrogens per picryl ring, the PC-6 contains the larger number of picryl rings per glucosyl residue.

When finely powdered picryl cellulose is rapidly stirred in distilled water, partial dissolution occurs and the pH slowly drops while the solution turns bright yellow. An absorption maximum is noted in the ultraviolet–visible spectrum of the aqueous solution at 352 nm, corresponding to the absorption band for picric acid (13).

Picric acid adsorbed on the surface of cellulose might be expected to be released instantly into aqueous solution. It is, therefore, significant that the absorption assigned to picric acid attained a maximum value only after 30 min at room temperature.

The formation of picric acid is indicative of a hydrolytic cleavage. This hydrolysis could occur either via an S_NAr displacement of the picryl ring (pathway a) or via an S_N2-type attack of water on C-6 (pathway b; Scheme 1).

2. Evidence from ^1H nuclear magnetic resonance

An ^1H nmr spectrum of picryl cellulose in $(CD_3)_2SO$ can be

[2]The exact nature of the sodium cellulosate is not well defined. We consider sodium cellulosate to be the intermediate material derived by treatment of microcrystalline cellulose with base. In this material an equilibrium concentration of oxy-anion or activated hydroxyl sites exists for subsequent reaction with picryl chloride to give the covalently bound picryl cellulose.

Can. J. Chem. Downloaded from www.nrcresearchpress.com by 118.98.75.50 on 09/07/12
For personal use only.

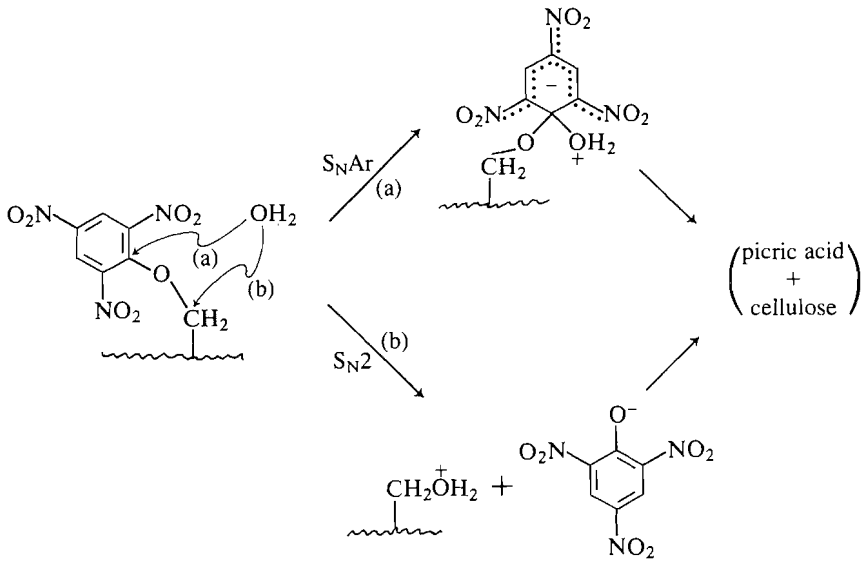

SCHEME 1

obtained using a saturated solution prepared by sonication. The ^{1}H nmr spectrum of PC-12 was identical to that of PC-6, although not as intense. Resonances for the glucosyl residues appear in the upfield region of the spectrum (Fig. 1) from 2.0 to 5.4 ppm; these are broad and not particularly well resolved, presumably due to conformational changes and slow tumbling of the cellulose chains in solution.

Resonances due to the aromatic picryl moieties of picryl cellulose, as well as free picrate, appear in the downfield region of the spectrum. The expanded spectrum of Fig. 1 shows three relatively broad peaks located at 9.055, 9.015, and 8.919 ppm, as well as a very sharp singlet at 8.582 ppm. The sharp singlet at 7.524 ppm is due to *p*-dibromobenzene (DBB), used as an internal standard. The sharp signal at 8.582 ppm results from the two equivalent protons of picrate anion, $PicO^-$. The peaks centered around 9.00 ppm result from picryl ether moieties covalently bonded to the cellulose chain.

It is significant to note that the singlet at 8.582 ppm, which is assigned to picrate anion, appears at exactly the same chemical shift as authentic picric acid in $(CD_3)_2SO$. This compound is known to be fully ionized in DMSO (11). If picrate were adsorbed on the surface of the cellulose or if some free and some adsorbed picrate existed in rapid equilibrium, an averaged signal would be observed at a position different from that for picrate in $(CD_3)_2SO$ alone (14). Similarly, the signals centered at 9.00 ppm are not due to contamination from trace amounts of unreacted picryl chloride or from 2,4,6-trinitroanisole (P-OMe). When picryl chloride or P-OMe was added to the PC sample, the spectra obtained showed sharp singlets for picryl chloride at 9.234 and for P-OMe at 9.101 ppm respectively. These signals do not overlap with those for picryl cellulose. The signals at 9.055–8.919 ppm do not shift from their previously recorded chemical shifts, as would occur if significant equilibration occurred between the free and bound picryl groups. Also, the signals for picryl chloride and P-OMe in $(CD_3)_2SO$ appear at the same chemical shift in the presence or absence of PC.

Clearly, the signals situated at 9.055, 9.015, and 8.919 ppm are assignable to picryl ring(s) covalently bonded to the cellulose polymer. There are three possible sites where bonding of the picryl ring to the glucosyl moiety might occur, namely C-2, C-3, and C-6. It is tempting to assume that the resonances centered around 9.00 ppm result from bonding at these different sites. However, the primary hydroxyl function at C-6 is expected to be the preferred nucleophilic moiety in attack on picryl chloride (15–17), in part because the C-2 and C-3 sites are much more hindered, and also because of the preferential deprotonation of the primary C-6 hydroxyl.

Thus, for reasons of both steric hindrance and relative acidity, it is likely that S_NAr displacement yields picryl moieties bonded to the oxygen on C-6. Conformational preferences in the chain would be expected to produce different microenvironments for a C-6 picryl ether, and this could give rise to the three separate picryl signals that are observed.

The "effective concentration" of the picryl ether moieties is $0.015 \pm 0.005\,M$, as determined by comparison of the integral for the resonances centered around 9.00 ppm with the integral for the protons of the DBB standard at 7.524 ppm. The concentration of picryl ether moieties is much higher than expected from the elemental analysis data.

Two possible explanations can be considered to account for the discrepancy between the "effective concentration" of picryl units as determined by nmr, and the concentration calculated from elemental analysis data and the derived empirical formula. First, it could be argued that a range of lower molecular weight chains has preferentially dissolved in the $(CD_3)_2SO$ solvent and that such lower molecular weight material contains more highly picrylated regions than the bulk material. In this case the ^{1}H nmr spectrum may not be representative of the bulk polymer, which presumably consists of a distribution of various picryl cellulose chain lengths. In short, the process of dissolution has actually been a process of fractionation on the basis of molecular weight. The second possible explanation is that the observed solubility is directly related to the degree of picrylation. In that regard, it has been reported that increased derivatization, by reaction of the hydroxyl groups, leads to increased solubility (17, 18). As well, in the present work we have found that ca. 70 wt.% of PC-6 dissolves in DMSO whereas ca. 39 wt.% of PC-12 is soluble. Thus it is found that the bulk material that is most highly picrylated is also the most soluble in DMSO. It can be concluded that in the case of PC-6 the ^{1}H nmr spectrum obtained on the DMSO-soluble material is certainly representative of the bulk picryl cellulose. The situation in the case of PC-12 is not

Can. J. Chem. Downloaded from www.nrcresearchpress.com by 118.98.75.50 on 09/07/12
For personal use only.

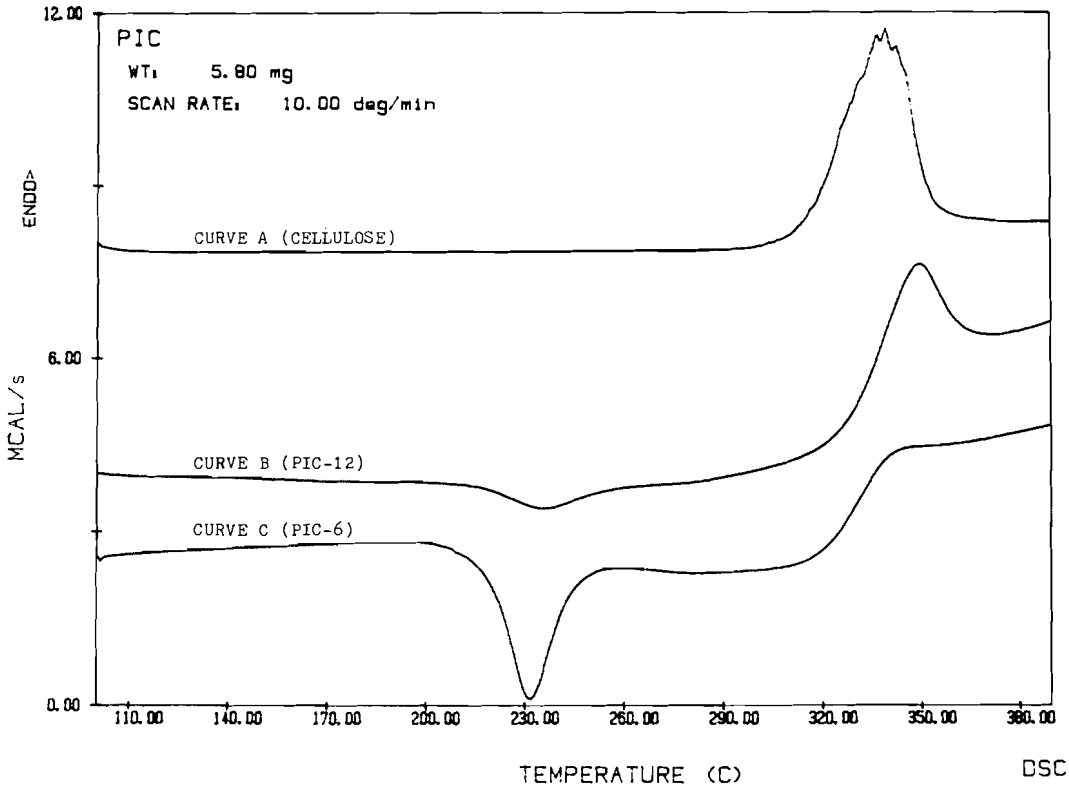

FIG. 2. Differential scanning calorimetry for picryl cellulose (PC-6 and PC-12) and cellulose. The cellulose energy axis has been rescaled to allow comparison of transition temperatures.

as well defined, although it appears that any fractionation that may have occurred on dissolution in DMSO is not extensive.

Also in accord with these observations is the ratio of integrals of the picryl ether absorption to the total glucosyl proton absorption found upfield. Based upon the bulk material, which contained 6.5 glucosyl units per picryl ring (PC-6), this integral ratio is predicted to be ca. 1:29. The measured value is 1:15, a further indication that preferential solubilization of more highly picrylated material in $(CD_3)_2SO$ has occurred.

It should be emphasized that the residual solid material that is insoluble in DMSO still contains picryl groups. Thus the infrared spectrum of the residual solid (PC-6 and PC-12), after removal of DMSO, thorough washing with diethyl ether, removal of the ether, and vacuum drying of the solid, displays ir bands at 1535 and 1340 cm^{-1}, characteristic of the asymmetric and symmetric stretching vibrations of the attached aromatic nitro groups. Clearly, both the DMSO-soluble and insoluble materials are picrylated.

Complementary to the nmr studies described above, further information was sought through differential scanning calorimetry and mass spectral analysis. Since these methods involve heating to high temperatures, it seemed desirable to monitor by ^1H nmr any changes that may occur on heating the picryl cellulose. It is found that in a standard sample (PC-6), the ratio of the integral sum of the picryl ether moieties compared to the picrate anion integral is ca. 9:1. The picrate anion may result from hydrolysis in the DMSO solution caused by small amounts of water bound in the polymer or by adventitious water in the commercial $(CD_3)_2SO$. This ratio was almost reversed (1:7) when the dry picryl cellulose was preheated to 230°C in an argon atmosphere before being dissolved in $(CD_3)_2SO$ for spectral analysis. It is concluded that hydrolysis does not account for this increase in picrate anion concentration but, rather, pyrolytic cleavage occurs in the dry solid. The differential scanning calorimetry and mass spectral studies described below confirm this conclusion.

3. Differential scanning calorimetry (DSC)

The thermal decomposition of cellulose is a complex process, which can be monitored by differential scanning calorimetry. The differential thermal analysis results have been previously found to be dependent on the temperature range studied, the period of heating, and the heating rate, as well as on the physical and chemical properties of the cellulose (19–22). For these reasons, a control DSC curve of the thermal behaviour of the microcrystalline cellulose that was the precursor of both PC-6 and PC-12 was determined (curve A, Fig. 2). The endothermic maximum, which occurs at 340°C, represents an initial depolymerization (which involves cracking and dehydration), closely followed by the competing reactions of decomposition, volatilization, polymerization, and aromatization (19, 20). The large endotherm ($\Delta H = -278$ cal g^{-1}) is indicative of the predominant depolymerization and volatilization processes; at about 350°C these reactions either cease or are masked by the competitive exothermic reactions. The latter subside and little further heat is evolved in the temperature region studied (100–400°C).

While microcrystalline cellulose and picryl cellulose show similarities in their thermal decomposition, it is clear that the latter displays thermal behaviour characteristic of C-6 substituted cellulose ethers. Upon cursory examination both PC-12 and PC-6 exhibit two thermal transitions in their DSC curves (Fig. 2; curves B and C). In the case of PC-12 (curve B), the first is a shallow exotherm that occurs between 230 and 235°C and is not present in the precursor cellulose (curve A). This initial exotherm is the dominant feature of the DSC trace for PC-6 (curve C). Note that the ratio of evolved heats for PC-6 com-

Can. J. Chem. Downloaded from www.nrcresearchpress.com by 118.98.75.50 on 09/07/12
For personal use only.

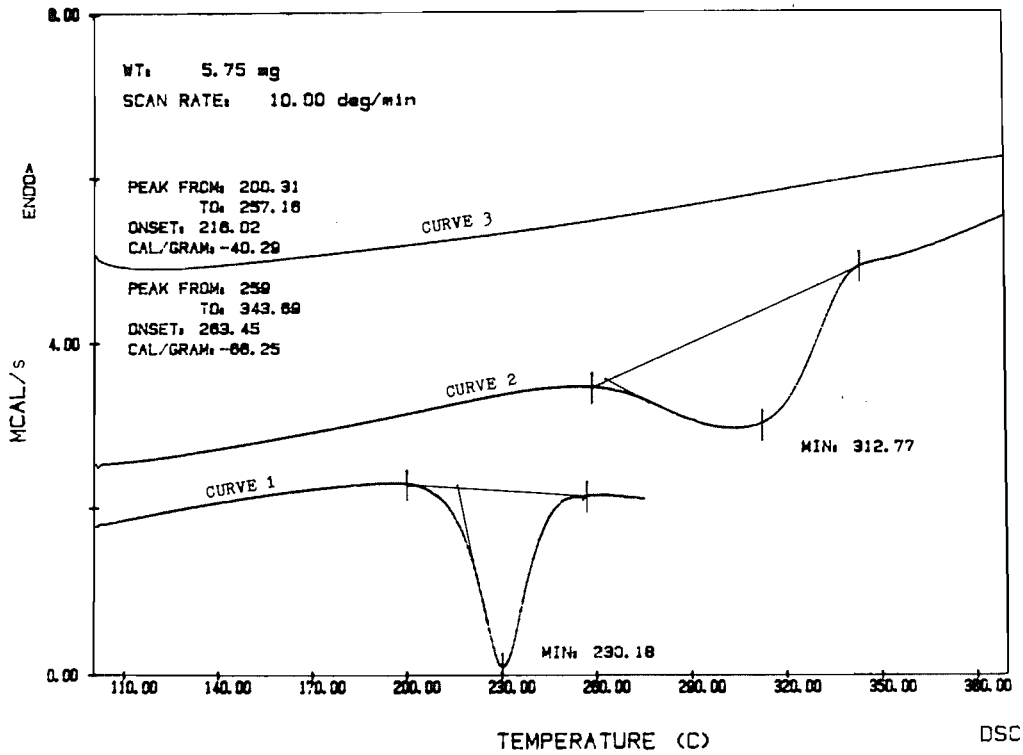

FIG. 3. Differential scanning calorimetry for PC-6. The curves represent cycled heating and recooling: Curve 1, 25–260°C; Curve 2, sample from curve 1 cooled and then heated, 25–380°C; Curve 3, sample from curve 2 cooled and then heated, 25–380°C.

pared to PC-12 ($\Delta H_{PC\text{-}6}/\Delta H_{PC\text{-}12} = -40.3\ cal\ g^{-1}/-9.2\ cal\ g^{-1}$) is 4.4 and parallels the picryl content of the samples. Hence the picryl moiety is directly involved in the exothermic reaction.

The broad and diffuse endotherm with maximum at 350°C (curve B) forms the secondary feature of the DSC plot for PC-12. This endothermic peak corresponds to the same type of decomposition processes that occur in the microcrystalline cellulose sample (curve A). It is significant to note the trend to larger exotherms at 230–235°C and diminished endotherms at 350°C as a function of the increase in the degree of picrylation (cellulose to PC-6).

The interdependence of the endothermic and exothermic features of the DSC trace is clarified in the cycling experiment shown for PC-6 in Fig. 3. First the sample was heated past the point at which the initial exothermic reaction has ceased, i.e., 280°C (curve 1, Fig. 3). The sample was permitted to return to room temperature and was then reheated; the DSC plot (curve 2, Fig. 3) exhibits no exotherm at 230°C, but a significantly broadened exothermic peak commencing at 259°C and centred at 313°C is observed. The diminished endotherms displayed by PC-12, and even more so by PC-6 (Fig. 2), are thus the result of a competing exothermic reaction revealed in this cycling experiment. The heat evolved in this exothermic process is absorbed in the endothermic decomposition of the cellulose chain in PC-6 and PC-12. Note that only in the absence of the 230°C exotherm is the corresponding 313°C exothermic maximum observable.

The disappearance of the 230°C exotherm is indicative of picryl ether bond scission coupled with another process. In this regard, it is important that the sample colour changed markedly at 250°C, in a control experiment conducted in a melting point capillary, going from tan to dark brown. Coincident with the colour change, water and a yellow oil were observed to condense on the unheated upper portions of the capillary. The water no doubt arises from the known loss of adsorbed water that occurs at ca. 80–100°C (20) and from the dehydration processes that accompany depolymerization of the cellulose chain. Thermal decomposition in a sublimation apparatus leads to the isolation of picric acid as crystals on the cold finger and thus identifies the yellow oil noted in the melting point capillary experiment.

Furthermore, in a recent study of the thermal behaviour of the C-6 substituted cellulose ethers, namely cellulose *p*-toluenesulfonate, tritylate, and phosphate, Jain *et al.* found an initial small endotherm for the tritylate and phosphate (157 and 160°C, respectively), which they attributed to cleavage of the ethers (22). In contrast, cellulose tosylate exhibited an exothermic maximum at 175°C (22). The unique behaviour of the C-6 cellulose tosylate was ascribed to a simultaneous endothermic scission of the *p*-toluenesulfonyl group, as the acid, and induced decomposition of the cellulose chain. By analogy, rupture of the C-6 picryl ether bond in PC-12 and PC-6 would be expected to result in the release of picric acid, accompanied by an exothermic cellulose decomposition. In view of these results, the relationship of the large exotherm and the broadened cellulose decomposition endotherm of PC-6 and PC-12 is straightforward. The exotherm (230°C) represents concurrent endothermic picryl ether scission and highly exothermic acid-induced cellulose decomposition. This decomposition pathway may be visualized as in Scheme 2.

4. Mass spectral analysis and ion pyrograms

Further clarification of mechanistic details of the exo- and endothermic pyrolytic reactions of cellulose and picryl cellulose can be obtained by carrying out the pyrolyses directly in the solid probe of a mass spectrometer. Ion pyrograms showing approximate amounts of both primary and secondary products of pyrolysis can be used to identify fragments evolved during the various cleavage processes. While accurate control and

Can. J. Chem. Downloaded from www.nrcresearchpress.com by 118.98.75.50 on 09/07/12
For personal use only.

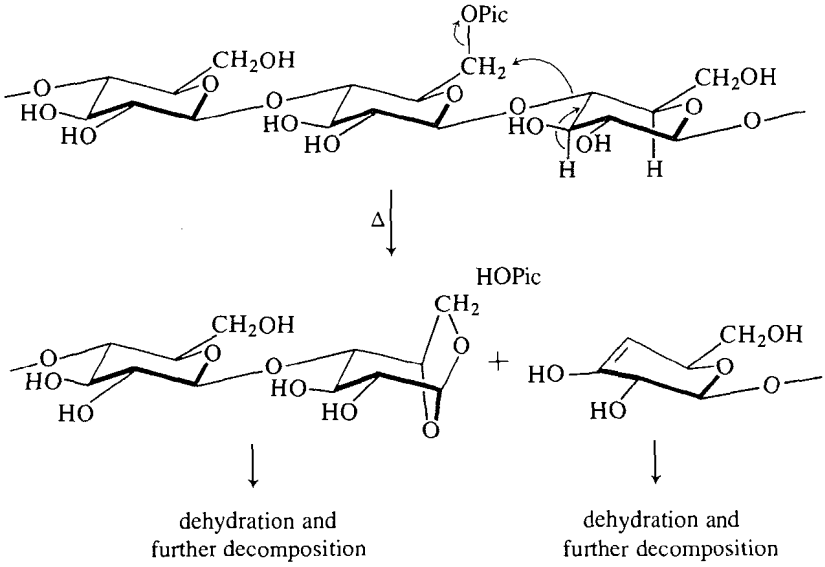

SCHEME 2

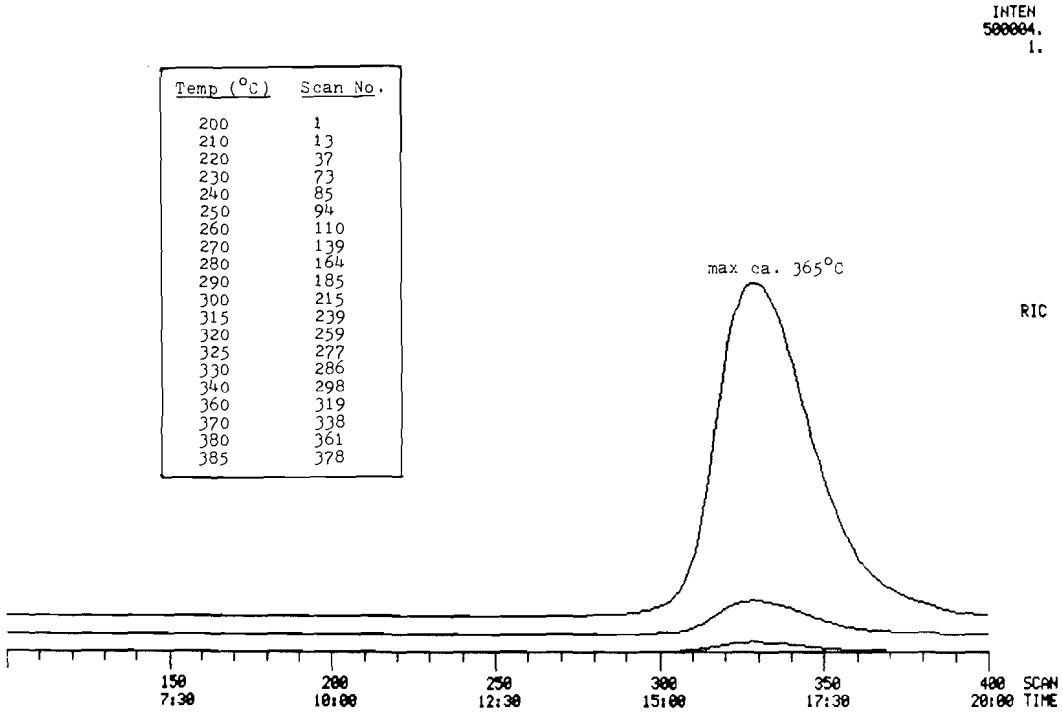

FIG. 4. Electron impact mass spectral map (total ion plot) for microcrystalline cellulose from 200 to 400°C.

measurement of the exact temperature at the point of sample pyrolysis is difficult, the overall qualitative picture is clear and informative.

The total ion spectrum map (ion pyrogram) for microcrystalline cellulose is shown in Fig. 4. Maximum ion intensity is achieved at ca. 365°C, with significant ion production from 350 to 400°C. Based upon the DSC evidence, this behaviour must correspond to the endothermic decomposition processes of cracking and dehydration.

The electron impact (70 eV) mass spectrum, measured at the onset of significant ion production at 350°C, is shown in Fig. 5. The parent ion of 1,4:3,6-dianhydro-β-D-glucopyranose is found at m/e 144. Although this ion is of low relative intensity (1.04%), it is significant in that anhydroglucoses (pyranose or furanose analogs of glucosan, for example) generally do not yield observable ions of m/e larger than 98. Other significant, albeit low intensity, fragments occur at m/e 126 (0.74%) and m/e 98 (5.28%). The former may represent either the ion of 5-hydroxymethyl-2-furfural or of 2-furylhydroxymethyl ketone, whereas the latter arises primarily from fragmentation of the furfural (23–25). The characteristic intense peaks at m/e 73 and 60 derive from anhydroglucose parent ion fragmentation (23).

As in the case of cellulose, the ion pyrogram of PC-6 (Fig. 6) shows maximum ion production at relatively high temperatures (ca. 386°C) but, in contrast, an initial ion-producing process commences at approximately 250°C and reaches a maximum at

Can. J. Chem. Downloaded from www.nrcresearchpress.com by 118.98.75.50 on 09/07/12
For personal use only.

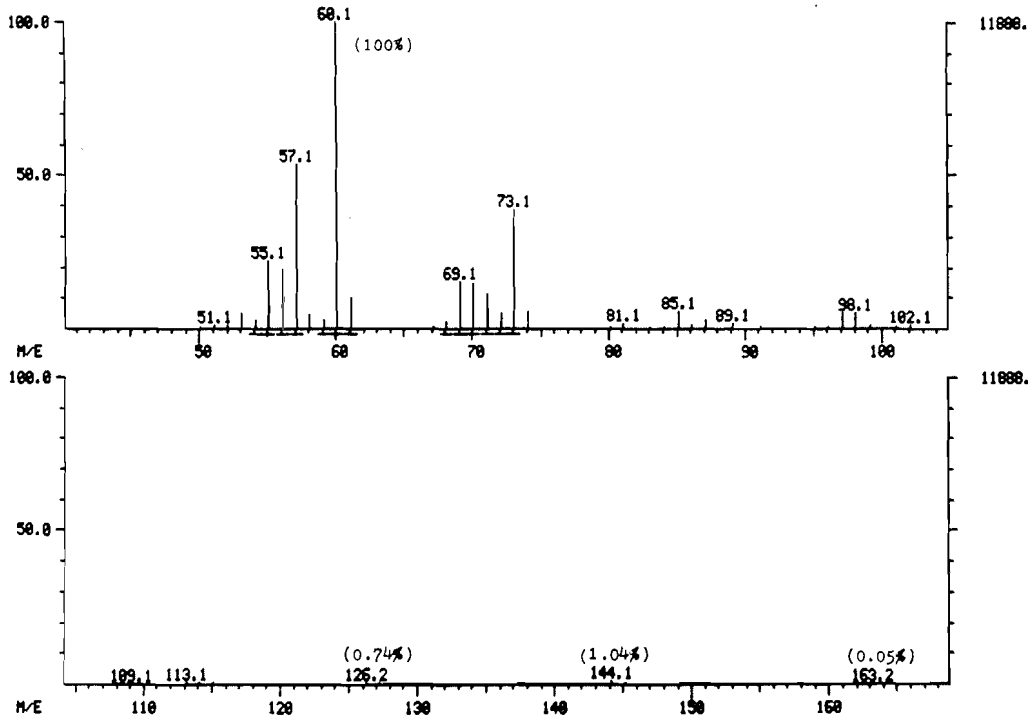

FIG. 5. Electron impact mass spectrum of microcrystalline cellulose at 350°C.

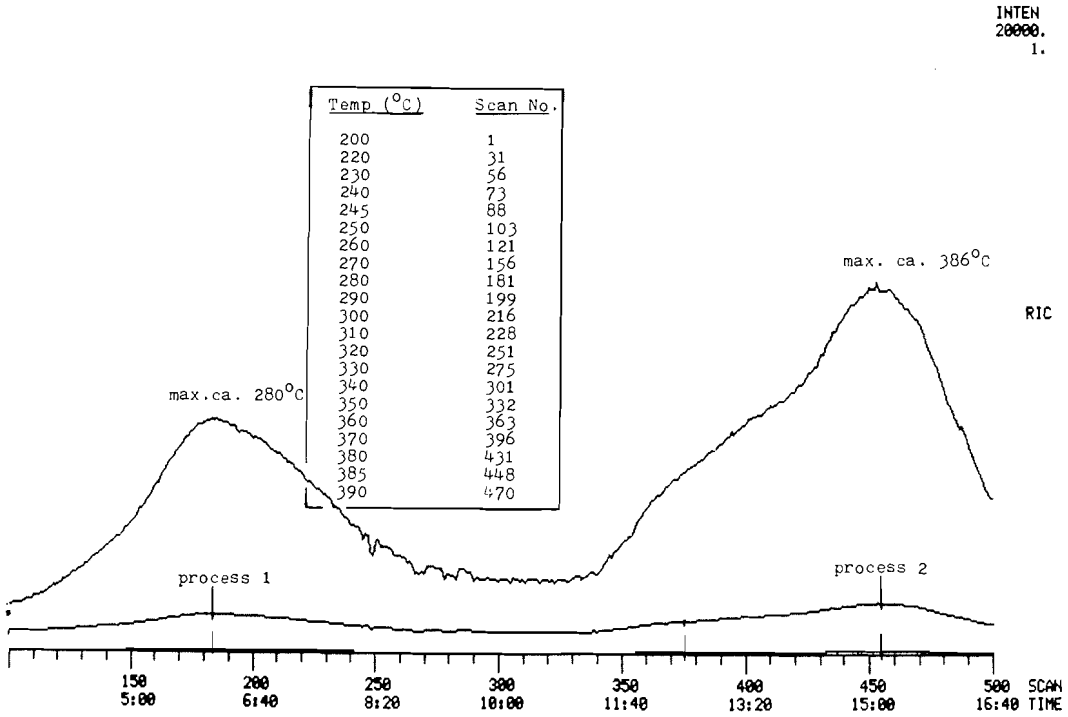

FIG. 6. Electron impact mass spectral map (total ion plot) for picryl cellulose (PC-6).

ca. 280°C. Two temperature-dependent processes appear to exist, each associated with a maximum in ion production (Fig. 6).

A mass spectrum of PC-6 measured at ca. 280°C displays two prominent peaks at m/e 229 (46%) and m/e 199 (4.0%), which are unique to the picrylated product (Fig. 7). The m/e 229 can be readily ascribed to the picric acid radical cation formed by cleavage from the cellulose chain. Loss of NO would give rise to

Can. J. Chem. Downloaded from www.nrcresearchpress.com by 118.98.75.50 on 09/07/12
For personal use only.

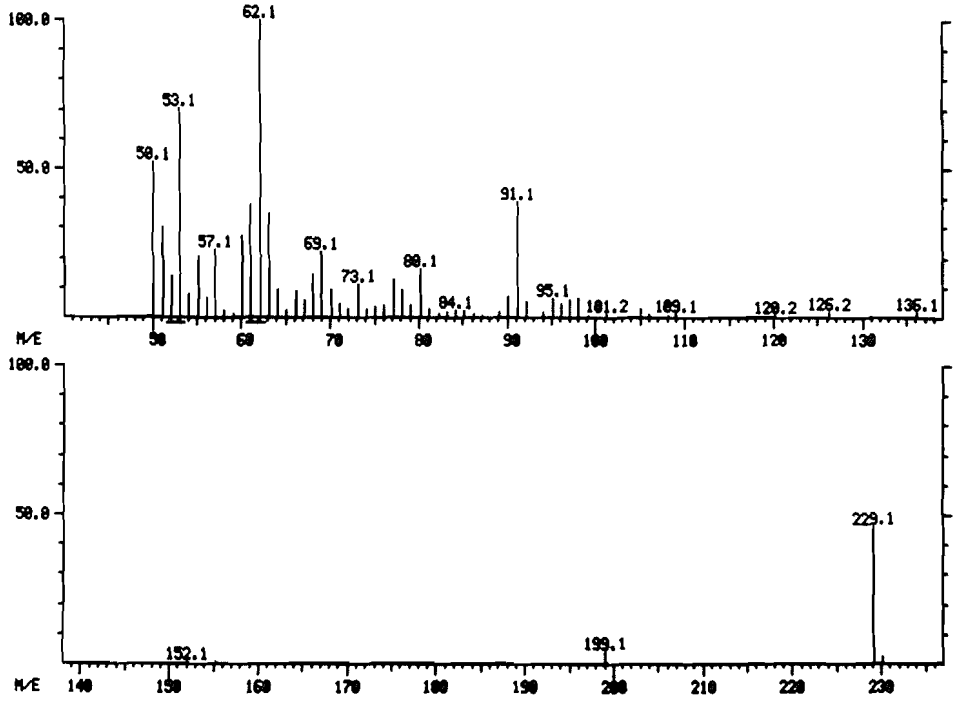

FIG. 7. The electron impact mass spectrum of picryl cellulose (PC-6) at 280°C.

the m/e 199 ion:

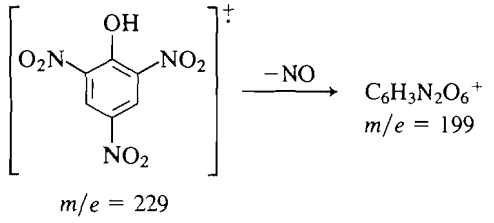

The temperature-dependent behaviour of PC-6 and the pyrolytic product ions of the picryl ether can be correlated. Thus Fig. 8 shows the ion pyrogram of m/e 229, 199, 144, 126, 97, 73, and 60 ions as a function of temperature. As can be seen, maximum intensity of the m/e 229 ion correlates well with ion production at ca. 280°C, as does the intensity of m/e 199, which confirms the relationship between the two peaks. On the other hand, *maximum* intensity for the m/e 144, 126, 97, 73, and 60 ions corresponds to a probe temperature of ca. 386°C. Similar and confirmatory observations can be made from chemical ionization generated mass spectral maps and ion intensities.

Clearly, the decomposition pathways for PC-6 involve the picryl ether moieties. Picric acid is lost from PC-6 at a lower temperature than that at which decomposition is noted in the precursor microcrystalline cellulose. Further, the two temperature/ion production maxima for PC-6 are in accord with the two regions of decomposition detected by DSC.

In fact, the presence of the picryl ring in the cellulose chain promotes the cellulose cleavage, as in the mechanism proposed in Scheme 2. Thus, presuming a relatively random distribution such that approximately one picryl ring is bonded per 6–12 glucosyl residues, fragmentation to release picric acid would lead to smaller oligosaccharides with much greater volatility and mobility. These oligosaccharides would be expected to undergo even more facile pyrolytic rupture than the intact cellulose chain.

Conclusions

Two picryl celluloses were prepared, PC-6 and PC-12, differing only in the number of picryl rings incorporated into the cellulose chain. Elemental analysis, hydrolytic cleavage behaviour, ^{1}H nmr analysis in DMSO-d_6, differential scanning calorimetry, as well as mass spectrometry, identify these products as picryl ethers, distinct from cellulose containing adsorbed picryl chloride, picric acid, or trinitroanisole. The different analytical methods are complementary. Pyrolytic behaviour noted by DSC was confirmed by mass spectrometry. Evolution of picric acid was detected by mass spectrometry, and picric acid was isolated in a control experiment from the thermal decomposition of PC-6 and was also observed in ^{1}H nmr experiments (as picrate anion). The ^{1}H nmr provides evidence that the picryl ether moieties are most likely attached at C-6 of the glucosyl residues. The picryl groups noted in the ^{1}H nmr of the DMSO-soluble material derived from PC-6 or PC-12 are also present, according to ir data, in the DMSO-insoluble residure. It is concluded that the ^{1}H nmr spectral data are representative of the bulk picryl celluloses. The thermal decomposition of the cellulose C-6 tosylate noted in the recent literature (22) is analogous to the thermal behaviour of picryl cellulose and further identifies PC-6 and PC-12 as C-6 cellulose ethers, in accord with the ^{1}H nmr evidence.

Experimental

Preparation of picryl cellulose, PC-6

Microcrystalline cellulose was dried over P_2O_5 at 50°C (2 Torr; 1 Torr = 133.3 Pa) for 5 h. A sample of the desiccated cellulose (9.5 g) was added to 200 mL of dry DMSO and stirred for 20 min. To the stirred mixture was added 140 mL of freshly prepared 4 *M* sodium methoxide in methanol and the mixture was allowed to stir for another 25 min before it was rapidly filtered. The filtered solid was kept covered with dry DMSO and the cake was broken up with a spatula into granular chunks and washed with copious amounts of dry DMSO (5 separate 100 mL washes with dry DMSO). This washing procedure was performed to remove any excess sodium methoxide. The washed material

Can. J. Chem. Downloaded from www.nrcresearchpress.com by 118.98.75.50 on 09/07/12
For personal use only.

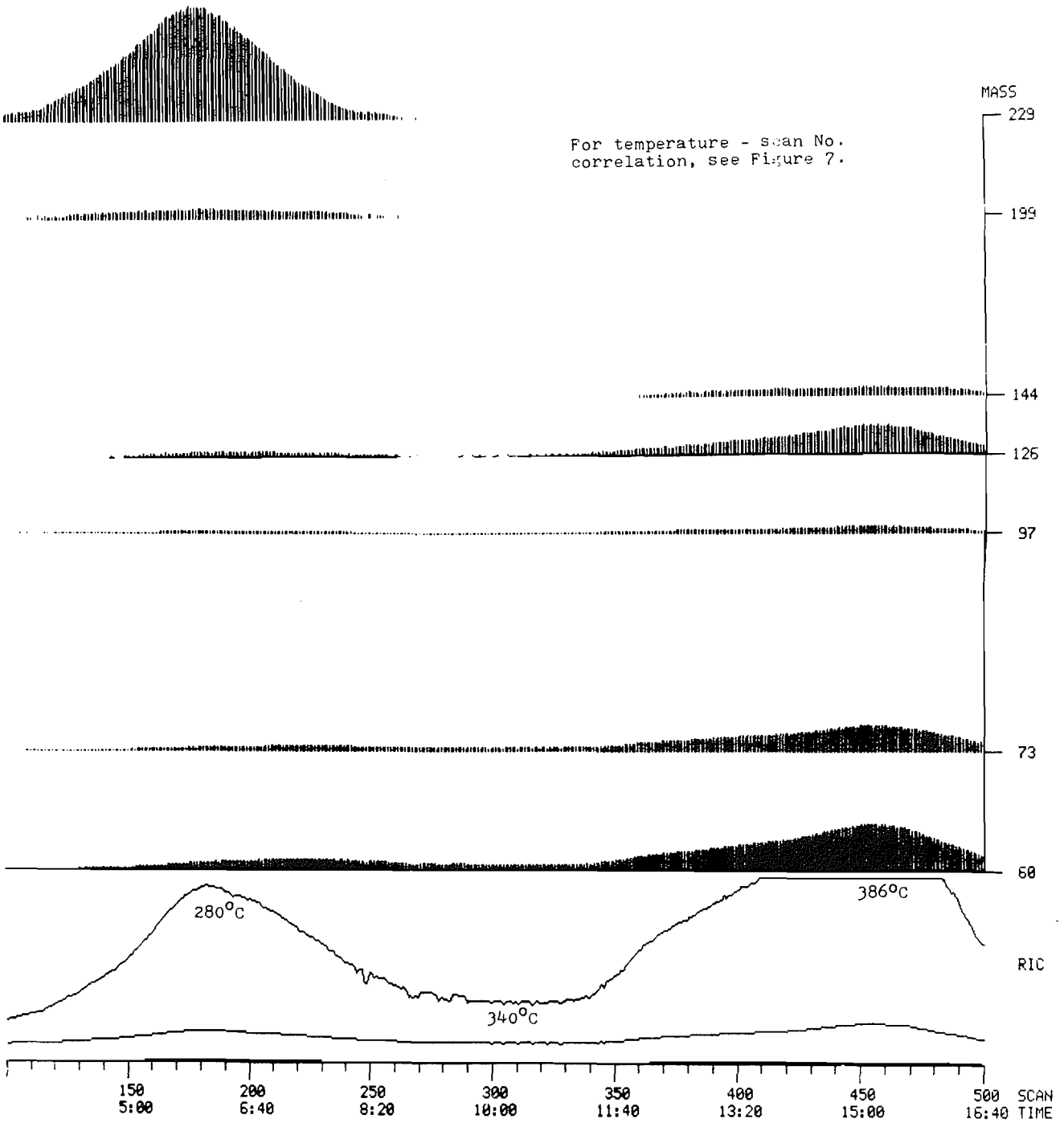

FIG. 8. Electron impact mass spectral map (total ion plot, and masses 60, 73, 97, 126, 144, 199, and 229) for PC-6 from 200 to 400°C.

was added to 300 mL of freshly distilled dry DMSO in a 1-L Erlenmeyer flask and stirred rapidly with a magnetic stirrer until the solid became finely divided. To this rapidly stirred mixture 25 g of dry powdered picryl chloride was added in small portions. During the rapid addition, another 200 mL of dry DMSO was introduced into the flask since the dark red mixture had gelled. After stirring for 7 h at room temperature the gel became less viscous and appeared dark orange-yellow. At this point the reaction was quenched by pouring the mixture into 2 L of anhydrous ether. The yellow precipitate was filtered off and washed with three successive 100 mL portions of dry acetone, followed by two successive 100 mL portions of dry ethanol. At the end of this process the ethanol filtrate was colourless. The resulting yellow powder was extracted with methanol for 4 days using a Soxhlet extractor. The purified solid was transferred to a drying pistol and dried for 2 days over P_2O_5 at 100°C (2 Torr). The total yield of pale tan powder was 7.5 g.

The material obtained is very hygroscopic. It is insoluble in water, methanol, and other organic solvents but slightly soluble in DMSO. Analysis of the tan powder shows C 41.44, H 4.85, and N 3.31%, which, basing calculations on the amount of cellulose bonded to one picryl ring (3 nitrogens), yields an empirical formula of $C_{43}H_{61}N_3O_{39}$. This corresponds to about 6.5 glucosyl moieties per picryl ring.

Preparation of picryl cellulose, PC-12

This preparation was carried out using the same quantities as in the preparation of PC-6, but the picryl chloride was dissolved in DMSO and then added to the stirred sodium cellulosate in DMSO. The product so obtained incorporated less nitrogen. It analyzed for C 42.26, H 5.49,

Can. J. Chem. Downloaded from www.nrcresearchpress.com by 118.98.75.50 on 09/07/12
For personal use only.

N 1.93%, which corresponds to about 12 glucosyl residues per picryl ring.

Solubility studies

Weighed quantities of PC-6 and PC-12 were placed into test tubes fitted with septum caps. The transfer of material was done in an N_2-filled dry box. The sample weights were determined by difference (PC-6: 14.02 mg; PC-12: 93.51 mg). DMSO (800 μL) was injected into each tube. After sonication and centrifugation the supernatant DMSO solution was removed and replaced with diethyl ether by means of a syringe. The samples were repeatedly subjected to ether treatment followed by centrifugation. Finally, the sample was dried at reduced pressure (<1 Torr) in a drying pistol and the dried residues were weighed. Of the PC-6, 4.14 mg remained, while of PC-12, 57.34 mg remained. The weight percent of material that had dissolved is therefore PC-6, 70.5%; PC-12, 38.7%

^1H nuclear magnetic resonance spectroscopy

All nmr spectra were recorded on an AM 400-MHz Bruker spectrometer equipped with a standard $^1H/^{13}C$ probe. Standard Wilmad PP-507 nmr tubes were used. Samples were sonicated using a Bransonic ultrasonic bath. Typically, 10–25 mg of the cellulose derivative was placed in a septum-covered small volumetric flask. $(CD_3)_2SO$ (800 μL) was injected into the nitrogen-flushed vessel and the suspension was sonicated in an ultrasonic bath for 2–3 h. The resultant mixture was allowed to settle and the transparent supernatant solution, usually yellow or orange in colour, was carefully withdrawn through the septum via syringe. (Separate centrifugation of a control sample of the supernatant showed that it contained no visible insoluble material.) The contents of the syringe were injected into a dry, septum-covered, nitrogen-flushed nmr tube containing 2 μL of stock *p*-dibromobenzene (DBB) solution and the spectrum was taken. The DMSO-d_5 resonance centered at 2.500 ppm was used as the internal shift standard. Typically, the instrument was adjusted as follows: spin rate, 25 rps; relaxation delay, 3 s; acquisition time, 2.982 s; pulse width, 5 μs; pulse angle, 45°; temperature, ambient (20 ± 2°C). For most experiments, 128 transients/FID sufficed to obtain the spectra reported herein.

Differential scanning calorimetry

The DSC experiments were performed using a Perkin Elmer DSC-4 instrument equipped with the Thermal Analysis Data Station (TADS). The instrument was calibrated with an indium standard prior to use. Each sample was encapsulated in an aluminum pan. The encapsulated sample was placed in the sample holder and an empty aluminum pan was placed in the reference holder. Samples were heated at a rate of 10°C/min over the ranges shown in the various plots. In all scans nitrogen was used as purge gas. When the scan was completed, onset temperatures and energy changes were determined with the aid of the TADS system. For example, temperature limits for an on-screen peak of interest were input to the TADS. ΔH values and temperatures of maxima or minima were then obtained.

Mass spectroscopy

All spectra were obtained on a Finnegan 4610 quadrupole mass spectrometer at 70 eV and were calibrated with perfluorotributylamine. Scientific Instrument Services S-95A glass capillaries were used for the solid probe. Approximately 100 μg of each sample was placed in the capillary and secured with a plug of clean glass wool. The heating rate was controlled manually and the probe temperature was read directly from the digital display of the instrument. Chemical ionization spectra employed methane.

The heating rate for the electron impact spectra was approximately 10 ± 3°C/min between 200 and 400°C. The scan time was 2.9 s with a 0.05-s hold between scans. CI spectra employed a heating rate of approximately 30°C/min and a scan time of 1.45 s with a 0.05-s hold time.

Acknowledgements

The authors thank the Army Armament Research and Development Command in Dover, New Jersey (M.J.S.), and the Natural Sciences and Engineering Research Council of Canada (E.B.) for support of this research.

1. R. FOSTER. Organic charge transfer complexes. Academic Press, London. 1969.
2. (*a*) E. BUNCEL, M. R. CRAMPTON, M. J. STRAUSS, and F. TERRIER. Electron deficient aromatic– and heteroaromatic–base interactions. Elsevier, Amsterdam. 1984; (*b*) F. TERRIER. Chem. Rev. **82**, 77 (1982); (*c*) E. BUNCEL. The chemistry of amino, nitro and nitroso compounds. Suppl. F, *Edited by* S. Patai, Wiley, London. 1982.
3. R. A. RENFROW, M. J. STRAUSS, S. COHEN, and E. BUNCEL. Aust. J. Chem. **36**, 1843 (1983).
4. F. TERRIER, J. C. HALLE, M. P. SIMONNIN, and M. J. POUET. J. Org. Chem. **49**, 4363 (1984).
5. E. BUNCEL, S. K. MURARKA, and A. R. NORRIS. Can. J. Chem. **62**, 534 (1984).
6. (*a*) M. J. STRAUSS, R. A. RENFROW, and E. BUNCEL. J. Am. Chem. Soc. **105**, 2473 (1983); (*b*) E. BUNCEL, R. A. RENFROW, and M. J. STRAUSS. Can. J. Chem. **61**, 1690 (1983); (*c*) J. Org. Chem. **52**, 488 (1987).
7. Z. A. ROGOVIN. J. Polym. Sci. **30**, 537 (1958).
8. Y. AVNY, R. RAHMAN, and A. ZILKHA. J. Macromol. Sci. Chem. **A6**, 177 (1972).
9. (*a*) B. GIBSON and M. R. CRAMPTON. J. Chem. Soc. Perkin Trans. 2, 648 (1979); (*b*) M. R. CRAMPTON, M. A. EL GHARIANI, and H. A. KHAN. Tetrahedron, **28**, 3299 (1972).
10. (*a*) K. L. SERVIS. J. Am. Chem. Soc. **87**, 5495 (1965); (*b*) J. Am. Chem. Soc. **89**, 1508 (1967).
11. E. BUNCEL and H. WILSON. *In* Advances in physical chemistry. Vol. 14. *Edited by* V. Gold. Academic Press, London. 1977. pp. 133–202.
12. (*a*) J. HIRST and K. U. RAHMAN. J. Chem. Soc. Perkin Trans. 2, 2119 (1973); (*b*) M. E. C. BIFFIN and D. B. PAUL. Aust. J. Chem. **27**, 777 (1974).
13. J. G. GRASSELLI and W. M. RITCHEY (*Editors*). CRC atlas of spectral and physical properties of organic compounds. Vol. IV. 2nd ed. CRC Press, Cleveland, OH. 1980. p. 97.
14. L. ANDO and G. A. WEBB. Theory of NMR parameters. Academic Press, New York. 1983. p. 76.
15. S. K. CHAUDHRY and O. HERNANDEZ. Tetrahedron Lett. **3**, 219 (1978).
16. S. HANESSIAN and P. LAVALLEE. Can. J. Chem. **53**, 2975 (1975).
17. M. D. NICHOLSON and D. C. JOHNSON. Cellul. Chem. Technol. **11**, 349 (1977).
18. T. J. BAKER, L. R. SCHROEDER, and D. C. JOHNSON. Carbohydr. Res. **67**, C4 (1974).
19. R. C. MACKENZIE (*Editor*). Differential thermal analysis. Vol. 2. Academic Press, New York. 1972.
20. M. KILZER and A. BROIDO. Pyrodynamics, **2**, 151 (1965).
21. F. A. WODLEY. J. Appl. Polym. Sci. **15**, 835 (1971).
22. R. K. JAIN, K. LAL, and H. L. BHATNAGAR. Thermochim. Acta, **97**, 99 (1986).
23. W. E. FRANKLIN. Anal. Chem. **51**, 992 (1979).
24. D. GARDNER. J. Chem. Soc. (C), 1473 (1966).
25. F. SHAFIZADEH, R. H. FURNEAUX, T. T. STEVENSON, and T. G. COCHRAN. Carbohydr. Res. **61**, 519 (1978).

Can. J. Chem. Downloaded from www.nrcresearchpress.com by 118.98.75.50 on 09/07/12
For personal use only.

A heuristic formalism for dynamics of spins larger than 1/2 in nuclear magnetic resonance[1]

BYUNG CHAN EU[2]

Department of Chemistry, McGill University, 801 Sherbrooke Street West, Montreal, P.Q., Canada H3A 2K6

Received December 10, 1986

This paper is dedicated to Professor John T. Edward

BYUNG CHAN EU. Can. J. Chem. **65**, 1901 (1987).

A simple heuristic method of constructing tensor operator bases for spins larger than 1/2 is presented which yields the same matrix representations as reported in the literature. By using the basis sets, we discuss the evolution of density matrices which can be put in Sylvester's form for an exponential operator. Use of quaternions is discussed for constructing tensor operator bases for half integer spins.

BYUNG CHAN EU. Can. J. Chem. **65**, 1901 (1987).

On présente une méthode heuristique simple qui permet de construire des bases d'opérateurs de tenseurs pour les spins plus grands que 1/2; cette méthode conduit aux mêmes représentations matricielles que celles rapportées dans la littérature. Utilisant des ensembles de base, on discute de l'évolution des densités matricielles qui peuvent être mises sous la forme de Sylvester pour un opérateur exponentiel. On discute de l'utilisation de quaternions pour la construction de bases d'opérateurs de tenseurs pour les spins fractionnaires.

[Traduit par la revue]

Can. J. Chem. Downloaded from www.nrcresearchpress.com by 118.98.75.50 on 09/07/12
For personal use only.

I. Introduction

In pulsed nmr experiments the evolution of nuclear spins is an interest of study, and it is necessary to have mathematical representations of spin angular momentum operators in order to carry out analysis of their temporal evolution. It is well known in quantum mechanics how to construct such representations in the case of spin 1/2, and we know that spin angular momentum operators are given by the Pauli spin matrices. Textbooks on quantum mechanics do not discuss representations of spin matrices in the case of spins larger than 1/2. In the past attention has been paid to systems of spins larger than 1/2, particularly in connection with pulsed nmr experiments (1–4). For the cases of spins larger than 1/2 Abragam (4) suggests in his classic monograph on nmr spectroscopy to use fictitious spin-1/2 operators to describe such spin systems. If the spin is larger than 1/2, there are more than two energy levels involved, but Abragam's fictitious spin-1/2 operators are constructed by selecting two levels of interest from the whole set of levels and neglecting the rest of them. This procedure creates effectively two-level systems which can then be described by Pauli-spin-like representations for spin angular momentum operators involved. Following Abragam's idea, Vega and Pines (2) introduced fictitious spin-1/2 operators to represent the spin angular momentum and related operators for a spin larger than 1/2. In the case of spin 1 there are nine independent operators acting like Pauli spin operators while in the case of spin 3/2 there are 18 fictitious spin-1/2 operators which one can construct by embedding 2×2 Pauli matrices. However, there are in fact only 16 independent operators required since the operators for spin 3/2 are 4×4 matrices. The overcompleteness is removed by three algebraic relations which hold for the z components of fictitious spin-1/2 operators: $\mathbf{I}_z^{(rs)} + \mathbf{I}_z^{(st)} + \mathbf{I}_z^{(tr)} = 0$ where the notation is that of Vega and Pines (2). One thus obtains 16 independent operators when the unit operator is added to the 15 independent operators so constructed. The result therefore is mathematically correct, but inconvenient in practice for lack of rotation symmetry to which spin operators are generally subject.

However, it is possible to construct 16 independent operators in terms of Pauli spin matrices without using the fictitious spin-1/2 operators if we realize that for spin 3/2 the spin angular momentum operators can be represented by 4×4 matrices and any 4×4 matrix can be thought of as consisting of four 2×2 submatrices which in turn can be written in terms of the 2×2 unit matrix and three Pauli matrices. Since there are 16 elements in the 4×4 spin angular momentum matrix, one requires 16 independent bases in which the matrix can be expanded just as a 2×2 matrix can be expanded in Pauli matrices. As will be shown later, they can be easily constructed and are complete. However, like the fictitious spin-1/2 operators they are mathematical bases which are not easy to associate with readily imaginable physical entities such as the cartesian components of a spin angular momentum. Since such a basis set also is not constructed on the basis of rotational symmetry inherent to spin angular momentum, the equations of motion for spin density operators can be generally more complicated than is in the case of a symmetry-adapted basis set.

A symmetry-adapted basis set should be more suitable and practical for solving physical problems, and such a basis set can be readily constructed if the rotation group theory is applied and in particular the theory of tensor operators is applied. The usefulness of symmetry-adapted basis sets in quantum mechanics is well recognized and exploited widely. In nmr Pyper (1*a*) appears to have used for the first time the symmetry-adapted irreducible tensor operator basis set which was originally developed for nuclear physics. And he has used the tensor operator sets to expand superoperators, Hamiltonians, and the density operator, and has developed a general theory of spin relaxation by means of them. Lynden-Bell (1*b*) and Spiess (1*c*) later have used the tensor operator formalism in nmr, but in their theories it is not shown how the spin matrices can be represented for the cases of $I > 1/2$. By couching the formalism in the language of the theory of Coope *et al.* (5), Sanctuary (3) uses a representation of spherical tensor bases $\mathbf{Y}^{(k)q}(I)$ for spin operators as follows:

$$[1] \qquad \mathbf{Y}^{(k)q}(I) = i^k[(2I+1)(2k+1)]^{1/2} \times \sum_{M,M'} (-)^{I-M} \begin{pmatrix} I & k & I \\ -M & q & M' \end{pmatrix} |IM\rangle\langle IM'|$$

[1]Supported by the Natural Sciences and Engineering Research Council of Canada.

[2]Also affiliated with the Physics Department, McGill University.

Can. J. Chem. Downloaded from www.nrcresearchpress.com by 118.98.75.50 on 09/07/12
For personal use only.

where I is the spin, k and q are integers, and

$$\begin{pmatrix} I & k & I \\ -M & q & M' \end{pmatrix}$$

is the $3 - j$ symbol for a Clebsch–Gordan coefficient (6*a*). He makes extensive use of these bases in his later work (7) on the evolution of isolated spins, e.g., a single spin or two spins interacting with each other through a dipolar interaction, etc. The $\mathbf{Y}^{(k)q}$ is supposedly a tensor of rank k since it is a direct product of k vector components (spin angular momenta more precisely), but its representation as given by [1] is a dyadic since it is basically given by a dyadic $|IM\rangle\langle IM'|$, or in physical terms, the density matrix. Therefore $\mathbf{Y}^{(k)q}$ appears to stand for something other than a tensor of rank k which it is supposedly meant to be. Later on we will be able to interpret it as a matrix representation of a kth rank tensor in the Hilbert space for the spin angular momentum operator. Without this interpretation the mathematical meaning of the right hand side of [1] does not jibe with the terminology "kth rank tensor" associated with the object on the left hand side of [1]. He relates $\mathbf{Y}^{(k)q}$ to spin angular momentum operators, but since the latter are not given by their own representations eq. [1] must be taken as the means for representing spin angular momentum operators. Since there is little physical content in [1], which merely stands for a set of mathematical bases, the physics of the system in hand has become rather opaque and difficult to grasp.

In this paper we present a heuristic method of constructing the spherical basis set in terms of explicitly represented spin angular momentum operators for $I > \frac{1}{2}$. The result is a basis set not only similar to, if not identical with, the one deduced from [1] but also with clear meanings, and the basis is formally uniform for both integer and half-integer spins as is in the formalism by Pyper (1*a*), Lynden-Bell (1*b*), and Spiess (1*c*). We show that the problem in essence boils down to finding representations for spin angular momentum operators $\mathbf{I}_x$, $\mathbf{I}_y$, and $\mathbf{I}_z$ and construct spherical tensor bases with the former by simply following the well established procedure in the theory of angular momentum. It requires a minimum knowledge of rotation group theory and provides a basic and simple mathematical machinery to deal with problems related to spins larger than 1/2. With the basis set so constructed, we consider the evolution of spin density matrix in the cases of $I = 1$ and 3/2 when there is a perturbation turned on by a radiofrequency wave. Calculations can be made facile if the theory of Lie groups is taken advantage of. Some exact results are presented for the density matrices for arbitrary initial conditions. If the Sylvester formula for an exponential operator is made use of for the density matrix, it can be expressed in a rather useful form amenable to facile computation. The usefulness of the Sylvester formula does not appear to be appreciated in nmr.

II. Spherical tensor bases

In quantum mechanics one can construct spherical harmonics in terms of three cartesian components x, y, and z of a vector $\boldsymbol{r}$. In complete analogy to this it is possible to construct spherical tensors in terms of three cartesian components $\mathbf{I}_x$, $\mathbf{I}_y$, and $\mathbf{I}_z$ of spin angular momentum $\mathbf{I}$ which behaves as a vector. We take the z axis as the direction of quantization. These operators obey the well-known commutation relations for angular momentum operators

[2*a*] $[\mathbf{I}_x, \mathbf{I}_y] = \mathrm{i}\mathbf{I}_z$ (cyclical)

[2*b*] $[\mathbf{I}_z, \mathbf{I}_\pm] = \pm\mathbf{I}_\pm$

[2*c*] $[\mathbf{I}_+, \mathbf{I}_-] = 2\mathbf{I}_z$

where $\mathbf{I}_\pm$ are the raising and lowering operators. Fano and Racah (8) define irreducible tensor operators $\mathbf{T}_{lm}$ by the commutation relations

[3] $$[\mathbf{I}_\pm, \mathbf{T}_{lm}] = [(l \mp m)(l \pm m + 1)]^{1/2}\mathbf{T}_{lm\pm1}$$

[4] $$[\mathbf{I}_z, \mathbf{T}_{lm}] = m\mathbf{T}_{lm}$$

That is, if the set $\mathbf{T}_{lm}$ fulfills commutation relations [3] and [4] it is an irreducible tensor set. It is useful to remark at this point that if we define the following operators

$$\mathscr{L}_\pm = [\mathbf{I}_\pm, \ ], \quad \mathscr{L}_z = [\mathbf{I}_z, \ ]$$

the commutation relations [3] and [4] are isomorphic to the well-known relations for the lowering and raising operators of an ordinary angular momentum operator and its z component acting on spherical harmonic Y_l^m. Therefore the tensor operators $\mathbf{T}_{lm}$ may be regarded as eigenoperators for $\mathscr{L}_\pm$ and $\mathscr{L}_z$ which are in fact intimately related to the Liouville operator defined below. This analogy is cogent. Indeed, according to the theory of rotation group, the spherical tensor $\mathbf{T}_{lm}$ corresponding to spherical harmonic $\mathbf{Y}_l^m(\hat{\boldsymbol{r}})$ can be generated by the relation (9)

[5] $$\mathbf{T}_{lm}(\mathbf{I}) = (\mathbf{I}\cdot\nabla)^l Z_l^m(\boldsymbol{r})$$

where Z_l^m is a solid harmonic

$$Z_l^m(\boldsymbol{r}) = r^l Y_l^m(\hat{\boldsymbol{r}})$$

The differential operator ∇ operates on $\boldsymbol{r}$ or one of its components in Z_l^m and replaces it with $\mathbf{I}$ or the component of $\mathbf{I}$ corresponding to the component of $\boldsymbol{r}$ that has been differentiated. An alternative formula for generating spherical tensors is the recurrence relation

[6] $$\mathbf{T}_{lm} = (4\pi/3)^{l/2}[l!(2l+1)!!/4\pi]^{1/2} \times \sum_\mu C(1, l-1, l; -\mu, m+\mu)\mathbf{T}_{l-1,m+\mu}\mathbf{T}_{1,-\mu}$$

where $C(j_1, j_2, j_3; m_1, m_2)$ is another form for the Clebsch–Gordan coefficient (6*a*) and $(2l+1)!! = (2l+1)(2l-1)\ldots 3.1$. The higher order tensors can therefore be constructed with [6] if $\mathbf{T}_{10}$ and $\mathbf{T}_{1,\pm1}$ are given. To construct the higher order tensors it is useful to take advantage of the commutation relations [2*a*]–[2*c*]. The tensor operator $\mathbf{T}_{lm}$ is self-adjoint in the following sense:

[7] $$\mathbf{T}_{lm}^\dagger = (-)^m\mathbf{T}_{l,-m}$$

We also define the unit operator by $\mathbf{I}_0$. It will be 3×3 unit matrix for $I = 1$ and 4×4 unit matrix for $I = 3/2$, etc.

Using [5] for generating irreducible tensors $\mathbf{T}_{lm}$ is not as elegant as using [6], but simple and straightforward. It yields a completely symmetrized set of tensors. We list tensor bases so constructed for $l \leqslant 3$ which are necessary for studying spin 1 and 3/2. The following spherical tensors are renormalized such that $N_{lm} = [\mathrm{Tr}\,(\mathbf{T}_{lm}\mathbf{T}_{lm}^\dagger)]^{-1/2}$:

[8] $$\mathbf{T}_{00} = N_{00}\mathbf{I}_0$$

[9*a*] $$\mathbf{T}_{10} = N_{10}\mathbf{I}_z$$

[9*b*] $$\mathbf{T}_{1,\pm1} = N_{1,\pm1}\mathbf{I}_\pm$$

[10*a*] $$\mathbf{T}_{20} = N_{20}(3\mathbf{I}_z^2 - \mathbf{I}^2)$$

[10*b*] $$\mathbf{T}_{2,\pm1} = \mp N_{2,\pm1}(\mathbf{I}_\pm\mathbf{I}_z + \mathbf{I}_z\mathbf{I}_\pm)$$

[10*c*] $$\mathbf{T}_{2,\pm2} = \mathbf{N}_{2,\pm2}\mathbf{I}_\pm^2$$

[11*a*] $$\mathbf{T}_{30} = N_{30}(5\mathbf{I}_z^2 - 3\mathbf{I}^2 + 1)\mathbf{I}_z$$

Can. J. Chem. Downloaded from www.nrcresearchpress.com by 118.98.75.50 on 09/07/12
For personal use only.

TABLE 1. Normalization constants

N_{lm}/	(l, m)	$I = 1$	$I = \frac{3}{2}$
	$(0, 0)$	$\frac{1}{\sqrt{3}}$	$\frac{1}{2}$
	$(1, 0)$	$\frac{1}{\sqrt{2}}$	$\frac{1}{\sqrt{5}}$
	$(1, \pm 1)$	$\frac{1}{2}$	$\frac{1}{\sqrt{10}}$
	$(2, 0)$	$\frac{1}{\sqrt{6}}$	$\frac{1}{6}$
	$(2, \pm 1)$	$\frac{1}{2\sqrt{3}}$	$\frac{1}{2\sqrt{6}}$
	$(2, \pm 2)$	$\frac{1}{2}$	$\frac{1}{2\sqrt{6}}$
	$(3, 0)$		$\frac{1}{3\sqrt{5}}$
	$(3, \pm 1)$		$\frac{1}{4\sqrt{15}}$
	$(3, \pm 2)$		$\frac{1}{3\sqrt{6}}$
	$(3, \pm 3)$		$\frac{1}{6}$

TABLE 2. Solid harmonics

l, m	Z_l^m
0, 0	$1/(4\pi)^{1/2}$
1, 0	$(3/4\pi)^{1/2}z$
1, $\mp$1	$\pm(3/8\pi)^{1/2}(x \pm iy)$
2, 0	$(5/16\pi)^{1/2}(2z^2 - x^2 - y^2)$
2, $\pm$2	$(15/16\pi)^{1/2}(x \pm iy)^2$
3, 0	$(7/16\pi)^{1/2}(2z^2 - 3x^2 - 3y^2)z$
3, $\pm$1	$\mp(21/64\pi)^{1/2}(4z^2 - x^2 - y^2)(x \pm iy)$
3, $\pm$2	$(105/16\pi)^{1/2}z(x \pm iy)^2$
3, $\pm$3	$\mp(35/64\pi)^{1/2}(x \pm iy)^3$

$$[11b]\quad \mathbf{T}_{3,\pm1} = \mp N_{3,\pm1}[(5\mathbf{I}_z^2 - \mathbf{I}^2 - 1/2)\mathbf{I}_\pm + \mathbf{I}_\pm(5\mathbf{I}_z^2 - \mathbf{I}^2 - 1/2)]$$

$$[11c]\quad \mathbf{T}_{3,\pm2} = N_{3,\pm2}(\mathbf{I}_\pm^2\mathbf{I}_z + \mathbf{I}_z\mathbf{I}_\pm^2 + \mathbf{I}_\pm\mathbf{I}_z\mathbf{I}_\pm)$$

$$[11d]\quad \mathbf{T}_{3,\pm3} = \mp N_{3,\pm3}\mathbf{I}_\pm^3$$

The normalization constants N_{lm} are summarized in Table 1. The above set, apart from the normalization constants, agree with the set by Sanctuary (3) except for $\mathbf{T}_{3,\pm2}$ which is not symmetrized in his set. Pyper and Spiess (1) used a similar set. These irreducible spherical tensor operators may be contrasted with solid harmonics $Z_l^m(\boldsymbol{r})$ list in Table 2.

When appropriate spin angular momentum operators $\mathbf{I}_z$ and $\mathbf{I}_\pm$ are substituted into the tensor bases above, we obtain explicit representations for them in the Hilbert space. When that is done, the irreducible spherical tensors assume basically the same structures as the matrix representations in Sanctuary's table for $\mathbf{Y}^{(k)q}$; see ref. 3. Therefore we are now able to see that the right hand side of [1] is the matrix representation of the kth rank tensor in the Hilbert space where $\mathbf{I}_z$ is diagonal and $\mathbf{I}_\pm$ are given as below. These three operators are the building blocks of the theories for dynamical evolution of isolated spins which are larger than 1/2.

A. $I = 1$

In this case the representations of spin angular momentum operators are exactly the same as those for the ordinary angular momentum operators of magnitude unity. Since the method of finding the representations for the latter is well documented in the literature (8), we will be as brief as possible. The commutation relations [2*a*] suggest that $\mathbf{I}_x$, $\mathbf{I}_y$, and $\mathbf{I}_z$ are traceless. Since we are assuming the z axis as the axis of quantization, in the Hilbert space spanned by eigenvectors $|1\rangle$, $|0\rangle$, and $|-1\rangle$ the z component $\mathbf{I}_z$ must be in the form

$$[12]\quad \mathbf{I}_z = \begin{bmatrix} 1 & 0 & 0 \\ 0 & 0 & 0 \\ 0 & 0 & -1 \end{bmatrix}$$

To obtain the matrix representations for $\mathbf{I}_x$ and $\mathbf{I}_y$ we assume a 3×3 matrix for $\mathbf{I}_+$: $\mathbf{I}_+ = (a_{ij})$. Since $\mathbf{I}_+ = \mathbf{I}_-^\dagger$, we then find $\mathbf{I}_- = (a_{ij}^*)$. If these matrices are substituted into the commutation relations [2*a*]–[2*c*], there follows a set of algebraic equations for matrix elements a_{ij}. Solving the set for a_{ij}, we obtain the matrix elements a_{ij} within the sign. The results are as follows:

$$[13a]\quad \mathbf{I}_x = 2^{-1/2}\begin{bmatrix} 0 & 1 & 0 \\ 1 & 0 & 1 \\ 0 & 1 & 0 \end{bmatrix}$$

$$[13b]\quad \mathbf{I}_y = 2^{-1/2}\begin{bmatrix} 0 & -i & 0 \\ i & 0 & -i \\ 0 & i & 0 \end{bmatrix}$$

As is obvious, $\mathbf{I}_x$, $\mathbf{I}_y$, and $\mathbf{I}_z$ are all traceless. We also find

$$\mathbf{I}^2 = \mathbf{I}_x^2 + \mathbf{I}_y^2 + \mathbf{I}_z^2 = 2\mathbf{I}_0$$

where $\mathbf{I}_0$ is the 3×3 unit matrix. This is an expected result since the eigenvalue of $\mathbf{I}^2$ is 2 in the space spanned by $|1\rangle$, $|0\rangle$, and $|-1\rangle$. If [12], [13*a*], and [13*b*] are substituted into [8] and [9], the matrix representations in the Hilbert space of nine independent, orthogonal spherical tensor operators are obtained for $\mathbf{I} = 1$. It can be easily verified that, apart from the constant multiplication factors, they agree with $\mathbf{Y}^{(k)q}$ for $\mathbf{I} = 1$ given in ref. 3. We therefore see that $\mathbf{Y}^{(k)q}$ in ref. 3 are simply the matrix representations of spherical tensor operators.

B. $I = 3/2$

The procedure for finding the representations of $\mathbf{I}_x$, $\mathbf{I}_y$, and $\mathbf{I}_z$ for $I = 3/2$ is basically the same as for the case of $I = 1$. Again by making use of the fact that $\mathrm{Tr}\,\mathbf{I}_z = 0$ is implied by the commutation relations [2*a*]–[2*c*], we infer that in the Hilbert space spanned by the eigenvectors $|3/2\rangle$, $|1/2\rangle$, $|-1/2\rangle$, and $|-3/2\rangle$ the matrix representation of $\mathbf{I}_z$ is

$$[14a]\quad \mathbf{I}_z = \begin{bmatrix} 3/2 & 0 & 0 & 0 \\ 0 & 1/2 & 0 & 0 \\ 0 & 0 & -1/2 & 0 \\ 0 & 0 & 0 & -3/2 \end{bmatrix}$$

Then by assuming a 4×4 matrix for $\mathbf{I}_+$, $\mathbf{I}_+ = (a_{ij})$, and making use of $\mathbf{I}_+ = \mathbf{I}_-^\dagger$, the commutation relations and [14*a*] we obtain a set of algebraic equations for a_{ij}. Solving these algebraic equations, we find the matrix representations for $\mathbf{I}_x$

and $\mathbf{I}_y$ for $I = 3/2$:

$$[14b] \quad \mathbf{I}_x = \begin{bmatrix} 0 & \sqrt{3}/2 & 0 & 0 \\ \sqrt{3}/2 & 0 & 1 & 0 \\ 0 & 1 & 0 & \sqrt{3}/2 \\ 0 & 0 & \sqrt{3}/2 & 0 \end{bmatrix}$$

$$[14c] \quad \mathbf{I}_y = \begin{bmatrix} 0 & -i\sqrt{3}/2 & 0 & 0 \\ i\sqrt{3}/2 & 0 & -i & 0 \\ 0 & i & 0 & -i\sqrt{3}/2 \\ 0 & 0 & i\sqrt{3}/2 & 0 \end{bmatrix}$$

These matrix representations of $\mathbf{I}_x$, $\mathbf{I}_y$, and $\mathbf{I}_z$ clearly satisfy the commutation relations. They are also traceless. It is easy to show

$$\mathbf{I}^2 = (15/4)\mathbf{I}_0$$

where $\mathbf{I}_0$ is the 4×4 unit matrix. If the representations [14*a*]–[14*c*] are inserted into [8]–[10], there follow the matrix representations of spherical tensor operator basis for $I = 3/2$ in the Hilbert space spanned by $|3/2\rangle$ $|1/2\rangle$, $|-1/2\rangle$, and $|-3/2\rangle$.

III. Quaternions and construction of linearly independent bases

The Pauli spin matrices are quaternions (10–12) and any 2×2 matrix can be expressed in terms of them. The Pauli matrices are written as

$$[15] \quad \sigma_x = \begin{pmatrix} 0 & 1 \\ 1 & 0 \end{pmatrix}, \quad \sigma_y = \begin{pmatrix} 0 & -i \\ i & 0 \end{pmatrix}, \quad \sigma_z = \begin{pmatrix} 1 & 0 \\ 0 & -1 \end{pmatrix}$$

to which the unit matrix σ_0 is added:

$$\sigma_0 = \begin{pmatrix} 1 & 0 \\ 0 & 1 \end{pmatrix}$$

These matrices obey the commutation relations

$$[\sigma_x, \sigma_y] = 2i\sigma_z, \text{ etc. (cyclical)}$$

Now consider a 4×4 matrix

$$\mathbf{S} = \begin{pmatrix} \mathbf{a} & \mathbf{b} \\ \mathbf{c} & \mathbf{d} \end{pmatrix}$$

where **a**, **b**, etc. are 2×2 submatrices. Since the submatrices can be expanded in terms of Pauli matrices (quaternions), e.g.,

$$\mathbf{a} = a_0\sigma_0 + a_x\sigma_x + a_y\sigma_y + a_z\sigma_z$$

where a_x, a_y, etc. are the expansion coefficients, the matrix **S** can be written in terms of Pauli matrices by embedding the latter in the 4×4 array for **S**. This idea motivates us to define the following set of matrices:

$$[16] \quad \begin{aligned} \mathbf{e}_1 &= \begin{pmatrix} \sigma_0 & 0 \\ 0 & \sigma_0 \end{pmatrix}, \quad \mathbf{e}_2 = \begin{pmatrix} 0 & \sigma_0 \\ \sigma_0 & 0 \end{pmatrix}, \quad \mathbf{e}_3 = \begin{pmatrix} 0 & -i\sigma_0 \\ i\sigma_0 & 0 \end{pmatrix}, \quad \mathbf{e}_4 = \begin{pmatrix} \sigma_0 & 0 \\ 0 & -\sigma_0 \end{pmatrix}, \\ \mathbf{e}_5 &= \begin{pmatrix} \sigma_x & 0 \\ 0 & \sigma_x \end{pmatrix}, \quad \mathbf{e}_6 = \begin{pmatrix} 0 & \sigma_x \\ \sigma_x & 0 \end{pmatrix}, \quad \mathbf{e}_7 = \begin{pmatrix} 0 & -i\sigma_x \\ i\sigma_x & 0 \end{pmatrix}, \quad \mathbf{e}_8 = \begin{pmatrix} \sigma_x & 0 \\ 0 & -\sigma_x \end{pmatrix}, \\ \mathbf{e}_9 &= \begin{pmatrix} \sigma_y & 0 \\ 0 & \sigma_y \end{pmatrix}, \quad \mathbf{e}_{10} = \begin{pmatrix} 0 & \sigma_y \\ \sigma_y & 0 \end{pmatrix}, \quad \mathbf{e}_{11} = \begin{pmatrix} 0 & -i\sigma_y \\ i\sigma_y & 0 \end{pmatrix}, \quad \mathbf{e}_{12} = \begin{pmatrix} \sigma_y & 0 \\ 0 & -\sigma_y \end{pmatrix}, \\ \mathbf{e}_{13} &= \begin{pmatrix} \sigma_z & 0 \\ 0 & \sigma_z \end{pmatrix}, \quad \mathbf{e}_{14} = \begin{pmatrix} 0 & \sigma_z \\ \sigma_z & 0 \end{pmatrix}, \quad \mathbf{e}_{15} = \begin{pmatrix} 0 & -i\sigma_z \\ i\sigma_z & 0 \end{pmatrix}, \quad \mathbf{e}_{16} = \begin{pmatrix} \sigma_z & 0 \\ 0 & -\sigma_z \end{pmatrix} \end{aligned}$$

This set is constructed in the following manner: Regard σ_0, σ_x, σ_y, and σ_z as numbers and form Pauli matrices with each one of them. Since there are four Pauli matrices and four super-Pauli matrices are possible to form with each one of the four Pauli matrices, there are 16 elements in all. The result is the set given in [16]. Note that there are four subsets which look like the Pauli matrices. These bases are all hermitean, orthogonal, and linearly independent as can be verified by forming the Gramm determinant which turns out to be non-zero. For the purpose of this and other calculations we define the scalar products by

$$(\mathbf{e}_i, \mathbf{e}_j) = \text{Tr}\,(\mathbf{e}_i\mathbf{e}_j^\dagger)$$

Since the Pauli matrices have the property

$$\sigma_0^2 = \sigma_x^2 = \sigma_y^2 = \sigma_z^2 = 1$$

that is, they are their own inverse (involutional), we easily see that all the elements in the set [16] have the same involution property as the Pauli matrices themselves. The elements in [16] do not generally commute with each other and, when non-commuting, they obey the same commutation relations as the Pauli matrices. To indicate such commutation relations, a commutator table is prepared in Table 3 where a numeral k stands for $2i\mathbf{e}_k$ for the commutator formed with the elements in the column and the row, and in that order.

Since the basis set is linearly independent, any 4×4 matrix can be expressed in terms of the 16 independent orthogonal basis listed above. As in the case of the set constructed with fictitious spin-1/2 operators, this set unfortunately is inconvenient owing to the lack of symmetry. For this reason we will not use it in actual calculations, but since there are some intrinsically interesting features (11, 12) in it which might be useful for study of spin dynamics in another context, it is presented here for completeness and for record.

IV. Dynamics of spins

In pulsed nmr experiments we are interested in the evolution of a spin in interaction with the rest of the system. An appropriate description for the evolution of such a system requires an irreversible relaxation equation such as the Redfield equation as described in ref. 1*a* or the Pauli master equation. In the event that such a relaxation-type equation is not required, the density matrix of a single spin may be described by the von Neumann equation.

Can. J. Chem. Downloaded from www.nrcresearchpress.com by 118.98.75.50 on 09/07/12
For personal use only.

TABLE 3. Commutators[a]
$[\mathbf{e}_j, \mathbf{e}_k] = 2i\mathbf{e}_l$

	$\mathbf{e}_1$	$\mathbf{e}_2$	$\mathbf{e}_3$	$\mathbf{e}_4$	$\mathbf{e}_5$	$\mathbf{e}_6$	$\mathbf{e}_7$	$\mathbf{e}_8$	$\mathbf{e}_9$	$\mathbf{e}_{10}$	$\mathbf{e}_{11}$	$\mathbf{e}_{12}$	$\mathbf{e}_{13}$	$\mathbf{e}_{14}$	$\mathbf{e}_{15}$	$\mathbf{e}_{16}$
$\mathbf{e}_1$	0	0	0	0	0	0	0	0	0	0	0	0	0	0	0	0
$\mathbf{e}_2$	0	0	4	−3	0	0	8	−7	0	0	12	−11	0	0	16	−15
$\mathbf{e}_3$	0	−4	0	2	0	−8	0	6	0	−12	0	10	0	−16	0	14
$\mathbf{e}_4$	0	3	−2	0	0	7	−6	0	0	11	−10	0	0	15	−14	0
$\mathbf{e}_5$	0	0	0	0	0	0	0	0	13	14	15	16	−9	−10	−11	−12
$\mathbf{e}_6$	0	0	8	−7	0	0	4	−3	14	13	0	0	−10	−9	12	0
$\mathbf{e}_7$	0	−8	0	6	0	−4	0	2	15	0	13	0	−11	0	−9	0
$\mathbf{e}_8$	0	7	−6	0	0	3	−2	0	16	0	0	13	−12	0	0	−9
$\mathbf{e}_9$	0	0	0	0	−13	−14	−15	−16	0	0	0	0	5	6	7	8
$\mathbf{e}_{10}$	0	0	12	−11	−14	−13	0	0	0	0	4	−3	6	5	0	0
$\mathbf{e}_{11}$	0	−12	0	10	−15	0	−13	0	0	−4	0	2	7	0	5	0
$\mathbf{e}_{12}$	0	11	−10	0	−16	0	0	−13	0	3	−2	0	8	0	0	5
$\mathbf{e}_{13}$	0	0	0	0	9	10	11	12	−5	−6	−7	−8	0	0	0	0
$\mathbf{e}_{14}$	0	0	16	−15	10	9	0	0	−6	−5	0	0	0	0	4	−3
$\mathbf{e}_{15}$	0	−16	0	14	11	0	9	0	−7	0	−5	0	0	−4	0	2
$\mathbf{e}_{16}$	0	15	−14	0	12	0	0	9	−8	0	0	−5	0	3	−2	0

[a]The commutators are constructed with the column and the row and in that order. The numeral l in the table stands for $2i\mathbf{e}_l = [\mathbf{e}_j, \mathbf{e}_k]$. For example, 4 is for $[\mathbf{e}_2, \mathbf{e}_3] = 2i\mathbf{e}_4$ and its conjugate element in the table is $[\mathbf{e}_3, \mathbf{e}_2] = -2i\mathbf{e}_4$, i.e., −4.

Can. J. Chem. Downloaded from www.nrcresearchpress.com by 118.98.75.50 on 09/07/12
For personal use only.

[17] $i(\partial\rho/\partial t) = [\mathcal{H}, \rho]$

where we have put $\hbar = 1$ and $\mathcal{H}$ is the Hamiltonian. This equation is sometimes called the quantum Liouville equation with the Liouville operator defined by the operator

[18] $\mathcal{L} = [\mathcal{H}, \ ]$

The Liouville equation [17] is considered in ref. 3, but it is solved differently in this paper. We believe the present method is simpler. Equation [17] can be formally solved in the form

[19] $\rho(t) = \exp(-it\mathcal{L})\rho(0)$

if the Hamiltonian is time-independent. Since our aim here is in illustrating an application of the spherical tensor operator set presented, we shall consider the following Hamiltonian studied by others (1–4):

[20] $\mathcal{H} = \omega_0\mathbf{I}_z + \omega_1(\mathbf{I}_x \cos\omega t + \mathbf{I}_y \sin\omega t)$

in the standard notation. The transformation to the rotating frame of reference

[21] $\bar{\rho} = \exp(-i\omega t\mathbf{I}_z)\rho \exp(i\omega t\mathbf{I}_z)$

puts the Hamiltonian in a time-independent form

[22] $\bar{\mathcal{H}} = \exp(-i\omega t\mathbf{I}_z)\mathcal{H} \exp(i\omega t\mathbf{I}_z)$
$= \Delta\omega\mathbf{I}_z + \omega_1\mathbf{I}_x = \Delta\omega\mathbf{I}_z + (1/2)\omega_1(\mathbf{I}_+ + \mathbf{I}_-)$

where $\Delta\omega = \omega_0 - \omega$. The Liouville equation then is

$i(\partial\bar{\rho}/\partial t) = [\bar{\mathcal{H}}, \bar{\rho}] \equiv \bar{\mathcal{L}}\bar{\rho}$

which is formally solved by

[23] $\bar{\rho}(t) = \exp(-it\bar{\mathcal{L}})\bar{\rho}(0)$

This formal solution must be cast in an explicit form so that it can be useful for practical study. This is discussed below.

First, we observe that the initial condition $\bar{\rho}(0)$ is a matrix whose dimension is 3 in the case of $I = 1$ and 4 in the case of $I = 3/2$, etc. Since such a matrix can be expanded in a complete set of tensor bases, we may write

[24] $\bar{\rho}(0) = \sum_{l=0}^{2I} \sum_{m=-l}^{l} \rho_{lm}\mathbf{T}_{lm}$

where ρ_{lm} is the projection of the initial condition onto the base $\mathbf{T}_{lm}$:

[25] $\rho_{lm} = \mathrm{Tr}[\bar{\rho}(0)\mathbf{T}_{lm}^{\dagger}]$

Substituting [24] into [23], we find

[26] $\bar{\rho}(t) = \sum_{l=0}^{2I} \sum_{m=-l}^{l} \rho_{lm} \exp(-it\bar{\mathcal{L}})\mathbf{T}_{lm}$

To calculate the evolution of $\mathbf{T}_{lm}$ in time, we observe the following:

$$[\mathbf{I}_z, \mathbf{T}_{lm}] = m\mathbf{T}_{lm}$$

$$[\mathbf{I}_\pm, \mathbf{T}_{lm}] = [(l \mp m)(l \pm m + 1)]^{1/2}\mathbf{T}_{lm\pm 1}$$

(cf. [3] and [4])

Since the operator $\bar{\mathcal{L}}$ generates a commutator with its operand, in the case of the Hamiltonian [22] we obtain

$$[27]\quad \begin{aligned}\bar{\mathcal{L}}\mathbf{T}_{lm} &= [\bar{\mathcal{H}}, \mathbf{T}_{lm}] \\ &= \Delta\omega[\mathbf{I}_z, \mathbf{T}_{lm}] + \tfrac{1}{2}\omega_1[\mathbf{I}_+, \mathbf{T}_{lm}] + \tfrac{1}{2}\omega_1[\mathbf{I}_-, \mathbf{T}_{lm}] \\ &= m\Delta\omega\mathbf{T}_{lm} + \tfrac{1}{2}\omega_1\{[(l - m)(l + m + 1)]^{1/2}\mathbf{T}_{lm+1} \\ &\quad + [(l + m)(l - m + 1)]^{1/2}\mathbf{T}_{lm-1}\}\end{aligned}$$

The first line is by the definition of $\bar{\mathcal{L}}$, the second line is due to the linearity of the operator $\bar{\mathcal{L}}$, and the last line is due to [3] and [4]. This calculation shows that the operator $\bar{\mathcal{L}}$ maps the subspace spanned by $\{\mathbf{T}_{lm}: m = l, l - 1, \ldots, -l\}$ onto itself. In other words, $\bar{\mathcal{L}}\mathbf{T}_{lm}$ is a linear combination of $\{\mathbf{T}_{ln}\}$ itself. Therefore we may define a matrix $\mathbf{C}^{(l)}$ such that

$$[28]\quad \bar{\mathcal{L}}\mathbf{T}_{lm} = \sum_{p=-l}^{l} C_{mp}^{(l)}\mathbf{T}_{lp}$$

That is,

$$[29]\quad \begin{aligned}C_{mp}^{(l)} &= \mathrm{Tr}\,(\mathbf{T}_{lp}^{\dagger}\bar{\mathcal{L}}\mathbf{T}_{lm}) \\ &= m\Delta\omega\delta_{pm} + \tfrac{1}{2}\omega_1[(l - m)(l + m + 1)]^{1/2}\delta_{pm+1} \\ &\quad + \tfrac{1}{2}\omega_1[(l + m)(l - m + 1)]^{1/2}\delta_{pm-1}\end{aligned}$$

Equation [28] implies the following important result for the present calculation: since the sum over p is over the multiplet of l, the operator $\bar{\mathcal{L}}$ maps $\{\mathbf{T}_{lm}\}$ onto itself. In other words, the new spherical tensor operators generated by $\bar{\mathcal{L}}$ remain within the multiplet corresponding to l. Thus we see that

$$\begin{aligned}\bar{\mathcal{L}}^2\mathbf{T}_{lm} &= \sum_{p=-l}^{l}\sum_{q=-l}^{l} C_{mp}^{(l)}C_{pq}^{(l)}\mathbf{T}_{lq} \\ &= \sum_{q=-l}^{l}(\mathbf{C}^{(l)})_{mq}^2\mathbf{T}_{lq}\end{aligned}$$

Repeating this process, we obtain

$$\bar{\mathcal{L}}^n\mathbf{T}_{lm} = \sum_{q=-l}^{l}(\mathbf{C}^{(l)n})_{mq}\mathbf{T}_{lq}$$

and thus finally the density matrix in the form

$$[30]\quad \begin{aligned}\bar{\rho}(t) &= \sum_{l=0}^{2I}\sum_{m=-l}^{l}\rho_{lm}\exp(-it\bar{\mathcal{L}})\mathbf{T}_{lm} \\ &= \sum_{l=0}^{2I}\sum_{m=-l}^{l}\rho_{lm}\sum_{n=0}^{\infty}\frac{(-it)^n}{n!}\bar{\mathcal{L}}^n\mathbf{T}_{lm} \\ &= \sum_{l=0}^{2I}\sum_{m=-l}^{l}\sum_{q=-l}^{l}\rho_{lm}\sum_{n=0}^{\infty}\frac{(-it)^n}{n!}(\mathbf{C}^{(l)n})_{mq}\mathbf{T}_{lq} \\ &= \sum_{l=0}^{2I}\sum_{m=-l}^{l}\sum_{q=-l}^{l}\rho_{lm}\exp(-it\mathbf{C}^{(l)})_{mq}\mathbf{T}_{lq}\end{aligned}$$

where $\mathbf{C}^{(l)}$ is $(2l + 1) \times (2l + 1)$ tridiagonal matrix and $\mathbf{C}^{(0)} = 0$. There now remains the task of diagonalizing the matrices $\mathbf{C}^{(l)}$ for $l = 1, 2. \ldots$ Obviously, since $\mathbf{C}^{(l)}$ are symmetric, their eigenvalues are real.

If the eigenvalues $\lambda_\alpha^{(l)}$ are all distinct as they will turn out to be in the case of $\bar{\mathcal{L}}$ given by [22], the Sylvester formula (13) puts [30] in a more useful form:

$$[31]\quad \bar{\rho}(t) = \sum_{l=0}^{2I}\sum_{m=-l}^{l}\sum_{q=-l}^{l}\sum_{\alpha\in l}\left[\exp(-it\lambda_\alpha^{(l)})\prod_{\beta\neq\alpha}\frac{(\mathbf{C}^{(l)} - \lambda_\beta^{(l)})}{(\lambda_\alpha^{(l)} - \lambda_\beta^{(l)})}\right]_{mq}\mathbf{T}_{lq}\rho_{lm}$$

where the sum over α runs over all eigenvalues for the lth multiplet. When the eigenvalues are explicitly obtained, the problem is solved and the density matrix is explicitly known for any initial condition that determines ρ_{lm}. We now turn our attention to the eigenvalues.

A. $l = 1$

In this case $\mathbf{C}^{(1)}$ is a 3×3 matrix of the form:

$$[32]\quad \mathbf{C}^{(1)} = \begin{bmatrix}\Delta\omega & \omega_1/\sqrt{2} & 0 \\ \omega_1/\sqrt{2} & 0 & \omega_1/\sqrt{2} \\ 0 & \omega_1/\sqrt{2} & -\Delta\omega\end{bmatrix}$$

The eigenvalues of this matrix are

$$[33]\quad \lambda_0^{(1)} = 0, \quad \lambda_\pm^{(1)} = \pm[\Delta\omega^2 + \omega_1^2]^{1/2}$$

They are all real and distinct. Substitution of this result into the Sylvester form [31] for the density matrix explicitly yields the density matrix for $I = 1/2$.

B. $l = 2$

The matrix $\mathbf{C}^{(2)}$ in this case is a 5×5 matrix of the form:

$$[34]\quad \mathbf{C}^{(2)} = \begin{bmatrix}2\Delta\omega & \omega_1 & 0 & 0 & 0 \\ \omega & \Delta\omega & (\frac{3}{2})^{1/2}\omega_1 & 0 & 0 \\ 0 & (\frac{3}{2})^{1/2}\omega_1 & 0 & (\frac{3}{2})^{1/2}\omega_1 & 0 \\ 0 & 0 & (\frac{3}{2})^{1/2}\omega_1 & -\Delta\omega & \omega_1 \\ 0 & 0 & 0 & \omega_1 & -2\Delta\omega\end{bmatrix}$$

The eigenvalues of this matrix are

$$[35]\quad \begin{aligned}\lambda_0^{(2)} &= 0 \\ \lambda_{\pm\pm}^{(2)} &= \pm[\tfrac{5}{2}(\Delta\omega^2 + \omega_1^2) \pm \tfrac{1}{2}(9\Delta\omega^4 + 18\Delta\omega^2\omega_1^2 \\ &\quad + \omega_1^4)^{1/2}]^{1/2}\end{aligned}$$

which are also real and distinct. These determine the $l = 2$ part of the density matrix. In the case of $I = 1$ the $\mathbf{C}^{(l)}$ up to $l = 2$ are sufficient for determining the density matrix.

C. $l = 3$

In this case the matrix is 7×7:

$$[36]\quad \mathbf{C}^{(3)} = \begin{bmatrix}3\Delta\omega & (\frac{3}{2})^{1/2}\omega_1 & 0 & 0 & 0 & 0 & 0 \\ (\frac{3}{2})^{1/2}\omega_1 & 2\Delta\omega & (\frac{5}{2})^{1/2}\omega_1 & 0 & 0 & 0 & 0 \\ 0 & (\frac{5}{2})^{1/2}\omega_1 & \Delta\omega & \sqrt{3}\omega_1 & 0 & 0 & 0 \\ 0 & 0 & \sqrt{3}\omega_1 & 0 & \sqrt{3}\omega_1 & 0 & 0 \\ 0 & 0 & 0 & \sqrt{3}\omega_1 & -\Delta\omega & (\frac{5}{2})^{1/2}\omega_1 & 0 \\ 0 & 0 & 0 & 0 & (\frac{5}{2})^{1/2}\omega_1 & -2\Delta\omega & (\frac{3}{2})^{1/2}\omega_1 \\ 0 & 0 & 0 & 0 & 0 & (\frac{3}{2})^{1/2}\omega_1 & -3\Delta\omega\end{bmatrix}$$

Can. J. Chem. Downloaded from www.nrcresearchpress.com by 118.98.75.50 on 09/07/12
For personal use only.

The secular determinant of this matrix factorizes to the following form:

$$\det|\mathbf{C}^{(3)} - \lambda\mathbf{1}| = -\lambda f(\lambda^2)$$

where $f(\lambda^2)$ is a cubic polynomial of λ^2, but its coefficients are rather complicated. We present the function $f(\lambda^2)$ for completeness:

$$\begin{aligned} f(\lambda^2) = {} & (\lambda^2 - \Delta\omega^2)\mathbf{D}(\Delta\omega)\mathbf{D}(-\Delta\omega) \\ & - (25/4)\omega_1^2(9\Delta\omega^2 - \lambda^2) \\ & + 6\omega_1^2\mathbf{D}(\Delta\omega)\mathbf{D}(-\Delta\omega) + 225\omega_1^4\Delta\omega^2 \\ & - 15\omega_1^4(6\Delta\omega^2 + \lambda^2 - (3/2)\omega_1^2) \\ & + \tfrac{5}{2}\omega_1^2[(3\Delta\omega - \lambda)(\Delta\omega + \lambda)\mathbf{D}(-\Delta\omega) \\ & \qquad + (3\Delta\omega + \lambda)(\Delta\omega - \lambda)\mathbf{D}(\Delta\omega)] \end{aligned}$$

where

$$\mathbf{D}(x) = \begin{vmatrix} 3x - \lambda & (\frac{3}{2})^{1/2}\omega_1 \\ (\frac{3}{2})^{1/2}\omega_1 & 2x - \lambda \end{vmatrix}$$

and therefore $\mathbf{D}(\Delta\omega)\mathbf{D}(-\Delta\omega)$ is a function of λ^2. The last term, i.e., the term in the square brackets is also a function of λ^2. The roots of the function can be analytically found since it is a cubic function of λ^2. In any case the eigenvalues are also all real and distinct, and there are three pairs of eigenvalues which are not equal to zero, and one which is equal to zero. Since their exact forms are rather devoid of physical insight, we shall not reproduce them here. More useful and insightful solutions can be found by using a perturbation method in the region of small ω_1.

The results for $\mathbf{C}^{(l)}$ above allows to determine the density matrices for spins up to $I = 3/2$. It is useful to note that the dimension of the matrix representations for the tensor operator bases $\mathbf{T}_{lm}$ changes according to the spin values, e.g., 2 for $I = 1/2$, 3 for $I = 1$, and 4 for $I = 3/2$.

V. Concluding remarks

In this paper we have presented a simple pedestrian procedure for constructing spherical tensor operators with which one can expand operators related to spin angular momenta for all values of I. Although it may appear surprising, this simple procedure has not been used in the literature. The procedure reduces to a minimum the use of rotation group theory and complicated algebra associated with it which is difficult to master for one not practicing rotation group theory everyday. The present heuristic method is easy to handle and to apply to other higher spin values. It only takes a rather straightforward algebra. By this formalism the dynamics of one or two isolated spins of $I \geq 1/2$ is reduced to a simple quantum mechanical problem that can be even taught in a quantum mechanics class room. Dynamics of isolated spins is not sufficient for chemical problems, and many-spin problems must be solved for them. The present formalism may be applied to study the latter problems.

1. (*a*) N. C. Pyper. Mol. Phys. **21**, 1, 961, 977 (1971); **22**, 433 (1971); (*b*) R. M. Lynden-Bell. Mol. Phys. **22**, 837 (1971); (*c*) H. W. Spiess. *In* NMR basic principles and progress. *Edited by* P. Diehl, E. Fluck, and R. Kosfeld. Springer, Heidelberg 1978.
2. S. Vega. J. Chem. Phys. **63**, 3769 (1975); S. Vega and A. Pines. J. Chem. Phys. **66**, 5624 (1977).
3. B. C. Sanctuary. Mol. Phys. **48**, 1155 (1983) and references cited therein.
4. A. Abragam. The principles of nuclear magnetism. Clarendon, London. 1961.
5. J. A. R. Coope and R. F. Snider. J. Math. Phys. **11**, 1103 (1970); **11**, 1591 (1970); J. A. R. Coope, R. F. Snider, and F. R. McCourt. J. Chem. Phys. **43**, 2269 (1965).
6. M. E. Rose. Elementary theory of angular momentum. Wiley, New York. 1957; P. Mansfield. *In* Progress in NMR spectroscopy. Vol. 8. Pergamon, Oxford. 1971. Part 1. p. 43.
7. B. C. Sanctuary, T. K. Halstead, and P. A. Osment. Mol. Phys. **49**, 753 (1983).
8. U. Fano and G. Racah. Irreducible tensorial sets. Academic, New York. 1959.
9. M. E. Rose. Elementary theory of angular momentum. Wiley, New York. 1957. pp. 144–149.
10. H. Weyl. The theory of groups and quantum mechanics. Dover, New York.
11. F. Dyson. J. Math. Phys. **3**, 1199 (1962).
12. M. L. Mehta. Random matrices. Academic, New York. 1967.
13. F. B. Hildebrand. Methods of applied mathematics. Prentice-Hall, Englewood Cliffs, NJ. 1952.

Can. J. Chem. Downloaded from www.nrcresearchpress.com by 118.98.75.50 on 09/07/12
For personal use only.

Solvent effects on the photoisomerization of bilirubin

B. M. SAILOFSKY AND G. R. BROWN
Department of Chemistry, McGill University, 801 Sherbrooke St. W., Montreal, P.Q., Canada H3A 2K6

Received January 2, 1987

This paper is dedicated to Professor John T. Edward

B. M. SAILOFSKY and G. R. BROWN. Can. J. Chem. **65**, 1908 (1987).

Studies of the photolysis of bilirubin IX-α by absorbance difference (AD) spectroscopy show that in solvents which do not interfere with the intramolecular hydrogen bonding, e.g., $CHCl_3$, *EZ/ZE* isomers and lumirubins are formed, with the former being predominant. The addition of ethanol to $CHCl_3$, either before or during photolysis, greatly changes the AD spectra, possibly because of a reaction of photoproducts with the ethanol or solvatochromism of the *EZ/ZE* isomers. Solvents which interfere with the intramolecular hydrogen bonding of bilirubin, e.g., DMSO, increase the importance of the photoreaction that forms lumirubins. The kinetics of product formation indicate that the lumirubins result from a photoreaction of *EZ/ZE* isomers. The addition of aqueous buffer to DMSO lowers the extent of photoisomerization and leads to AD spectra that resemble those obtained for the photolysis in $CHCl_3$. The addition of human serum albumin (HSA), using stopped flow techniques, to aqueous buffer solution of bilirubin immediately after photolysis gives evidence that the HSA traps the *EZ/ZE* isomers and prevents their reversion. However, in the presence of HSA the predominant pathway for photoreaction of bilirubin to *EZ/ZE* isomers is by reaction of the bound bilirubin. The AD spectra are similar to those obtained for solvents that interfere with hydrogen bonding.

B. M. SAILOFSKY et G. R. BROWN. Can. J. Chem. **65**, 1908 (1987).

Les études de spectroscopie par absorbance différentielle (AD) ont démontré que la photolyse de la bilirubine-IXα poursuivie en milieux qui ne perturbent pas les liaisons hydrogènes, tel que le chloroforme, produit principalement les isomères *EZ/ZE*, ainsi que des lumirubines. L'addition d'éthanol, par exemple au chloroforme, soit avant ou après la photolyse transforme les spectres AD, peut-être à la suite d'une réaction des photoproduits avec l'éthanol ou en raison du solvatochromisme des isomères *EZ/ZE*. Par contre, la formation des lumirubines par photoréaction est favorisée dans des solvants tel que le sulphoxyde diméthylique, c'est-à-dire dans des solvants qui perturbent les liaisons hydrogènes. Ainsi, les résultats d'études de cinétique démontrent que les lumirubines sont formées par la photoréaction des isomères *EZ/ZE*. L'addition de solutions tampons aqueuses au sulphoxyde diméthylique diminue le degré de photoisomérisation et les spectres AD obtenus ressemblent à ceux obtenus après la photolyse dans le chloroforme. L'addition de la sérum-albumine humaine (SAH), immédiatement après la photolyse, à des solutions tampons aqueuses de bilirubine en utilisant des techniques d'additions simultanées, indique que la SAH capte les isomères *EZ/ZE* et empêche leur inversion. Cependant, la photoréduction de la bilirubine en isomères *EZ/ZE* en présence de la SAH se poursuit principalement par réaction des bilirubines liées. Les spectres AD obtenus sont semblables à ceux obtenus dans des milieux qui perturbent les liaisons hydrogènes.

Can. J. Chem. Downloaded from www.nrcresearchpress.com by 118.98.75.50 on 09/07/12
For personal use only.

Introduction

During the past fifteen years the photochemistry of bilirubin has been studied extensively (1–4), particularly photoisomerization. It is related to phototherapy, used for the treatment of neonatal jaundice (5). Originally it was thought that the major mechanism leading to a lowering in the plasma bilirubin level during phototherapy involves photooxidation of bilirubin (6) but it has subsequently been shown that photoisomerization is a much faster reaction and hence precedes photooxidation (7–9).

Initial evidence suggested that the photoisomerization of bilirubin leads to only one photoproduct, first named "photobilirubin" (8). Further work showed that there are in fact a number of photoproducts, including both structural and geometric isomers (10–13). Furthermore, the photoproduct formed, and in what proportion, seems to be a function of many parameters, including the nature of the solvent and the presence or absence of oxygen or of proteins such as albumin.

The conformation of the bilirubin molecule in solution is highly solvent dependent. In aqueous solution bilirubin is folded into a configuration that has six intramolecular hydrogen bonds (14). This folded, "ridge tile" structure results in the molecule being highly hydrophobic and thus sparingly soluble in aqueous solution. The reported solubility of bilirubin in aqueous solution at physiological pH ranges from 0.007 to 100 μ*M*, with the lower value being favoured according to Brodersen (15). The bilirubin molecule assumes this tight, intramolecularly hydrogen bonded stucture in water and in chloroform (16) but in solvents which interfere with hydrogen bonding, e.g., dimethyl sulfoxide (DMSO), the molecule "opens up" as some of the hydrogen bonds are weakened (10, 17).

Certain conclusions from studies of the photolysis of bilirubin in organic solvents have been extended to phototherapy conditions. Since the ultimate goal of phototherapy is to lower the bilirubin levels in the infant's blood plasma, it is imperative that effect of solvent on the mechanisms of the photoisomerization and photodestruction of bilirubin be understood. Thus, we have studied the photoreaction in various organic and aqueous media, with and without HSA and BSA, and offer some explanation for the photoisomerization results with respect to the environment of the bilirubin.

Experimental

Solutions of bilirubin were prepared daily by dissolving the powder (from bovine gallstones, Sigma) in the appropriate solvent. The purity of the bilirubin was checked using HPLC (18). Chloroform (Spectrograde, Anachemia), triethylamine (Reagent grade, Anachemia) and dimethylsulfoxide (HPLC grade, Anachemia) were used as received, except in experiments for which the ethanol stabilizer in the chloroform was removed immediately prior to use by first distilling over P_2O_5 and then passing the distillate through a column of basic I alumina (Sigma).

Aqueous solutions were made by first dissolving the bilirubin in 0.10 *M* NaOH and adjusting the volume of KH_2PO_4/NaOH buffer to achieve a final pH of 7.8 ± 0.1. Prior to use the solvents were purged with dried nitrogen.

Aliquots of the aqueous solution were added to HSA/buffer solutions to obtain the desired ratio of [HSA]/[BR]. Human serum (Cutter Laboratories) and bovine serum (Sigma, Fraction V) albumin were

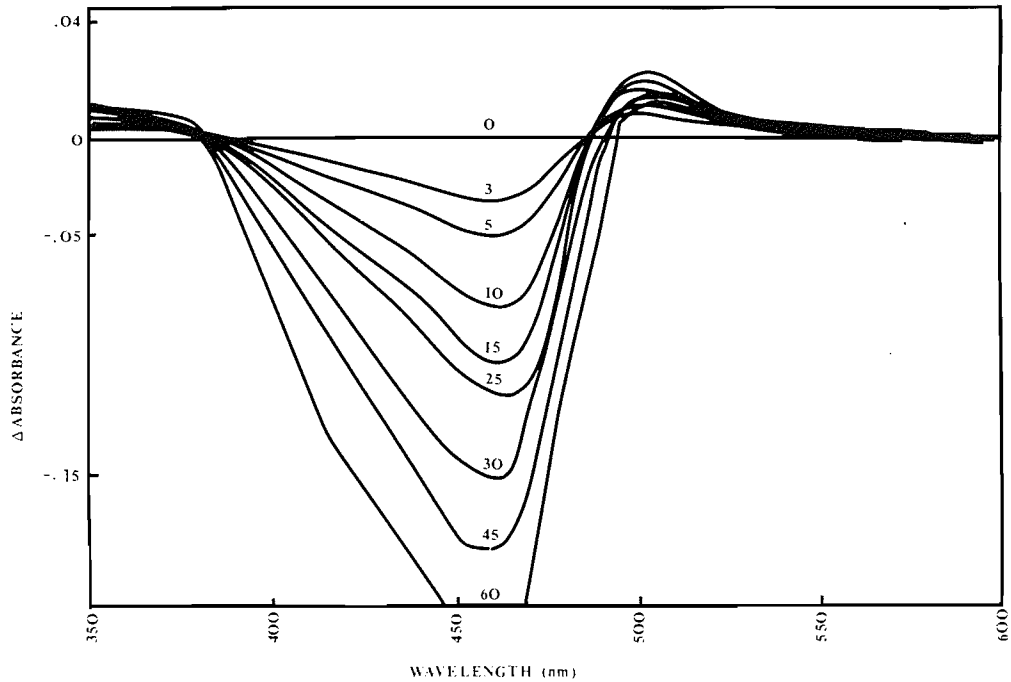

FIG. 1. Absorbance difference spectra for a solution of bilirubin in pure $CHCl_3$ after various times of irradiation. (The numbers refer to the irradiation times, in minutes.)

used as received. For all solutions the final concentration of bilirubin was 1.71×10^{-5} *M*. Studies were done at room temperature, except for those with the pure buffer solutions, which were kept in an ice bath prior to use.

The solutions (< 1 mL), contained in 1.00 cm path length cells, were irradiated directly in the cell holder of the Hewlett Packard Model 8451A Diode Array Spectrophotometer by placing the light source (Cole-Parmer Fiber Optic Illuminator Model 9745-00, fitted with a blue filter with a bandpass of 410–470 nm) over the cell, i.e., by shining the light down through the cell opening (intensity = 0.5 $\mu W/cm^2$). Since the course of bilirubin photochemistry has been shown to depend upon the excitation wavelength (19), the same light source was used throughout this study. The spectrophotometer was capable of recording a spectrum within 1 s *while* the irradiation light source was still on.

The HPLC apparatus and methods, described previously by McCarthy *et al.* (18), used reverse phase methods. The chromatograph consisted of a Waters Associates Model 590 pump, a Rheodyne 7125 injection valve and a Schoeffel Spectraflow (Kratos Analytical Instruments, Ramsay, NJ) Model SF770 variable wavelength detector. The column was a 15.0 × 0.46 cm blank packed in-house with 5 μm Spherisorb (Chromatographic Specialties Company, Town of Mount Royal, Quebec) with a guard column consisting of a 3.5 × 0.46 cm blank packed with a 30–38 μm octyldecyl silica (Whatman Inc., Clinton, NJ). The mobile phase contained 50% phosphate buffer (pH = 7.4), 25% acetonitrile, and 25% dimthylsulfoxide, and 1.5 g/L of tetrabutylammonium chloride (Sigma) as an ion-pairing agent. Prior to sample injection the sample was dissolved in the appropriate amount of phosphate buffer/acetonitrile/dimethylsulfoxide so that the solvent phase matched the mobile phase. All analyses were done at room temperature using a flow rate of 1.0 mL/min with the detector wavelength set at 455 nm.

The stopped flow experiments, made with a Model 1A Stopped-Flow Apparatus (Cantech Scientific Ltd., Winnipeg, Canada), monitored the changes in absorbance, at a fixed wavelength, with a TDI photometer and stored the data with a TDI 1024C transient recorder. The data were transferred to an IBM PC that performed the desired calculations. For these experiments, an aqueous solution of bilirubin was placed into one syringe and of HSA ([HSA]/[BR] = 10) in the second syringe. The syringe containing the bilirubin could be irradiated, using the light source described above, prior to mixing. The two syringes emptied into the observation cell, where the data points (208 points) were collected over a 20 s time span, beginning within 5 ms.

Results and discussion

(A) Photolysis in pure chloroform

When a solution of bilirubin in pure $CHCl_3$ purged with N_2 is irradiated a characteristic absorbance difference (AD) spectrum is obtained (Fig. 1), as reported previously (8, 20). During the first 25 min of irradiation two isosbestic points are obtained. The isosbestic point at 490 nm is not maintained at irradiation times >30 min, but that at 380 nm remains, suggesting two separate photoproducts. The production of *EZ/ZE* isomers of bilirubin leads to the isosbestic point at 490 nm (9). The second isosbestic point results from the formation of a second photoproduct, previously identified as "lumirubins" (12), also referred to as "cyclobilirubin" (9), "unknown pigment" (11), and "pigment 430" (21), that has an absorbance maximum around 430 nm (10). Lumirubin is a configurational isomer of bilirubin formed by an *endo*-vinyl cyclization on one end ring of the molecule (11, 13, 22).

Based on structural arguments obtained by use of molecular models, it seems likely that cyclization to form lumirubins occurs *after* a rotation about the C4—C5 bond of the bilirubin, i.e., by a reaction of *EZ/ZE* isomers. This has been the subject of considerable dispute (11, 22), and is considered more fully later. Although an induction period for the formation of lumirubins would be expected for such a mechanism, it is not detected, probably because the necessary buildup in the concentration of *EZ/ZE* isomers is fairly rapid compared to the frequency at which spectra were taken.

(B) Photolysis in chloroform/ethanol

The photolysis behaviour of bilirubin in $CHCl_3$ containing 1% ethanol stabilizer is similar to that in pure $CHCl_3$ with the exception that, at a given time of irradiation, the resulting gain

Can. J. Chem. Downloaded from www.nrcresearchpress.com by 118.98.75.50 on 09/07/12
For personal use only.

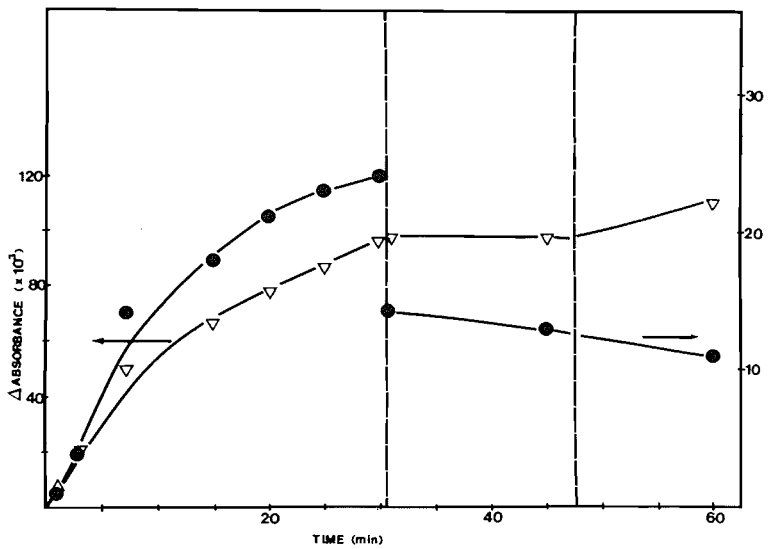

FIG. 2. The absolute values of the absorbance difference of the gain peak (500 nm) and the loss peak (460 nm) for a photolyzed solution of bilirubin in pure $CHCl_3$ as a function of irradiation time. At t = 31 min, irradiation was discontinued and ethanol was added. At t = 47 min, photolysis was continued: ●, gain peak; ▽, loss peak.

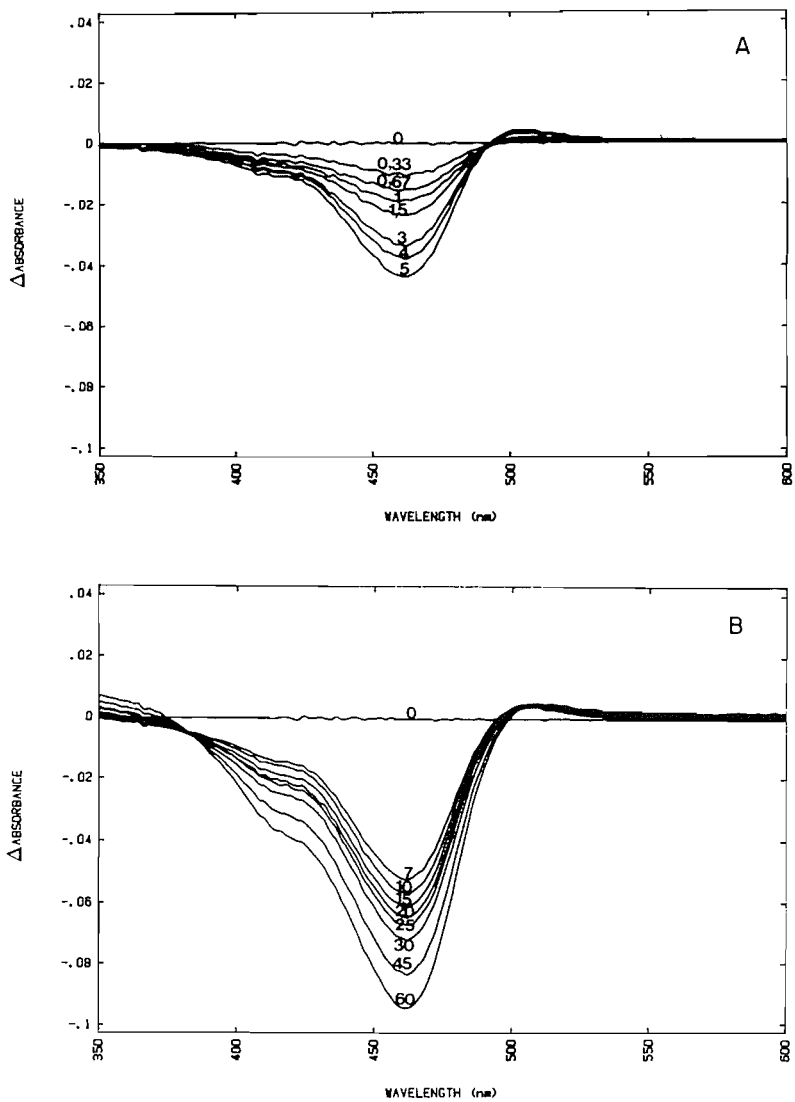

FIG. 3. A/B. Absorbance difference spectra for a solution of bilirubin in DMSO for various irradiation times, in minutes. (The numbers refer to the irradiation times, in minutes.)

Can. J. Chem. Downloaded from www.nrcresearchpress.com by 118.98.75.50 on 09/07/12
For personal use only.

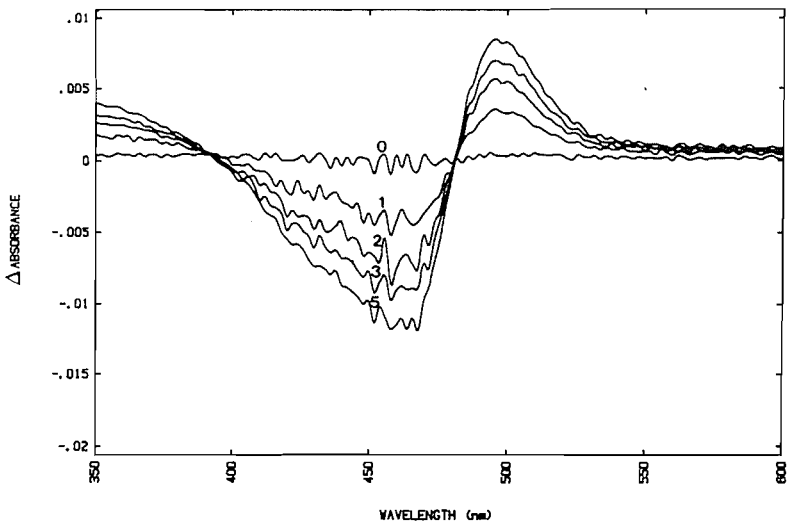

FIG. 4. Absorbance difference spectra for a solution of bilirubin in DMSO/buffer (90:10) for various irradiation times. (The numbers refer to the irradiation times, in minutes.)

peaks are less than one half the size of those using pure $CHCl_3$. However, within experimental uncertainty, the loss peaks remain unchanged. It should be noted that even 1% stabilizer in the solvent corresponds to a molar ethanol concentration that is much greater than the bilirubin concentration.

The following experiment was made to elucidate the role of ethanol: bilirubin in pure $CHCl_3$ purged with N_2 was irradiated for 30 min after which 10 μL of ethanol (1% of the total volume of the solution being irradiated) was added. The cell was gently shaken, the irradiating light was turned off, and additional spectra were taken. Possible side effects due to the addition of ethanol were accounted for by simultaneously adding an equal amount of ethanol to the reference solution. Upon addition of ethanol the height of the gain peak, due to the *EZ/ZE* isomers, immediately decreased substantially while the bilirubin loss peak remained essentially unchanged (Fig. 2). Concomitantly the isosbestic points disappeared. When irradiation of this solution was resumed the gain peak showed a further decrease while the loss peak continued to increase, and the isosbestic point at 380 nm was restored. These observations are consistent with the continued formation of lumirubins, since there is still a loss of bilirubin and an isosbestic point. Meanwhile the peak at 500 nm, corresponding to the *EZ/ZE* isomers, is decreasing slightly such that a new photostationary state is established. Interestingly, the absorbance difference at 500 nm reaches the same final value, 0.011, as in the $CHCl_3$/ethanol system discussed above.

The explanation of these results must account for a rapid decrease in the gain peak due to added ethanol that is not accompanied by any change in the size of the loss peak. A possible explanation is a reaction of ethanol with the *EZ/ZE* isomers. Photochemical addition of alcohols to the *exo*-vinyl group of bilirubin has been reported previously by Garbagnati and Manitto (23). However, the data are not consistent with Manitto's overall mechanism which requires the reaction to be light induced and irreversible. Since the *EZ/ZE* isomers are not entirely consumed, despite a large molar excess of ethanol, the reaction must be an equilibrium process. Furthermore, since the reaction occurs after the light is turned off, it is a reaction with the photoproduct. A reversible reaction of photoproducts with ethanol is consistent with a decrease in the concentration of *EZ/ZE* isomers in $CHCl_3$/EtOH solutions relative to that in pure $CHCl_3$ as well as the immediate decrease in its concentration when ethanol is added after the irradiation.

Alternatively, the changes in the height of the gain peak upon addition of ethanol may indicate solvatochromism of the photoisomers, similar to that exhibited by bilirubin dimethyl ester (24). It is well known that bilirubin dimethyl ester in dilute solution exhibits solvatochromism which has been attributed to the presence of two co-existing conformers with different orientations of the A/B and C/D pyrromethenone moieties with respect to each other (24). It seems likely that the *EZ/ZE* photoisomers can also co-exist in two orientations. Since these photoisomers have less intramolecular H-bonding than bilirubin they are more polar and should have characteristics similar to the bilirubin dimethyl ester so that the relative proportions are likely to be solvent dependent. Thus, while little solvatochromism is expected for bilirubin IX-α in weakly H-bonding solvents, it may well be significant in the case of the *EZ/ZE* photoisomers.

(C) Photolysis in dimethyl sulfoxide

A more dramatic effect on the photoisomerization due to environment can be seen when DMSO is used as solvent rather than $CHCl_3$ (Fig. 3). Similar results were obtained for both DMSO and $CHCl_3/Et_3N$. Comparison with Fig. 1 indicates a difference in shape on the short wavelength side of the loss peak. Specifically, the shoulder at ca. 430 nm seen previously for long irradiation times with $CHCl_3$ is now more distinct such that the loss peak is double humped. Furthermore, the two isosbestic points do not appear simultaneously. The isosbestic point at ca. 490 nm occurs only at short irradiation times (<7 min), while the isosbestic point at 380 nm develops only after longer irradiation times (>7 min).

These data are consistent with the two-step process presented above. The spectra for short times of irradiation indicate that production of *EZ/ZE* isomers predominates (one isosbestic point). An induction period is now evident which could not be seen when bilirubin was irradiated in $CHCl_3$. Since an initial buildup of *EZ/ZE* isomers is required before lumirubins are formed, it is now apparent that the latter results by a reaction of the former. As the time of irradiation is increased, the isosbestic

Can. J. Chem. Downloaded from www.nrcresearchpress.com by 118.98.75.50 on 09/07/12
For personal use only.

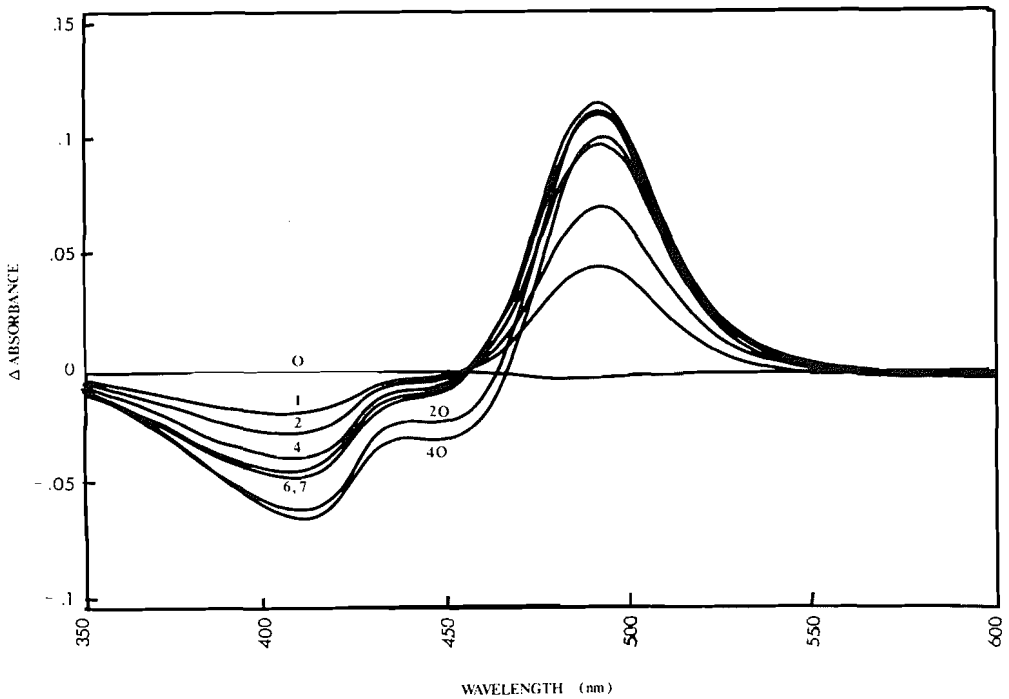

FIG. 5. Absorbance difference spectra for an aqueous buffer solution of bilirubin and human serum albumin for various irradiation times. (The numbers refer to the irradiation times, in minutes.)

point is no longer maintained, indicating that *EZ/ZE* isomers have reached an equilibrium concentration, but another isosbestic point appears at shorter wavelength, indicating that the lumirubins continue to be formed. The increased distortion of the loss peak at 430 nm for DMSO as compared to that with $CHCl_3$ is probably due to an increased concentration of this photoproduct relative to that of *EZ/ZE* isomers. Ostrow and co-workers have shown that in DMSO lumirubins can be produced in sufficient quantities to be isolated (10).

The development of a double-humped loss peak on irradiation of aqueous solutions of bilirubin containing human serum albumin (HSA) has also been attributed, by Davies and Keohane (25), to the presence of a second synthesis peak. To verify that the double-humped loss peaks in the AD spectra result from a superimposed gain peak, experiments were made using HPLC methods described previously by McCarthy *et al.* (18). Chromatograms of the DMSO solution of bilirubin after irradiation confirmed the presence of more than one photoproduct. In fact, McDonagh *et al.* (22), have also reported that irradiation of bilirubin in a $CHCl_3/Et_3N$ system results in a second photoproduct that absorbs at 434 nm. This is consistent with the hypothesis that lumirubins can be formed in solvents which interfere strongly with the intramolecular hydrogen bonding of the bilirubin.

Thus, the mechanism for the formation of photoproducts in DMSO is similar to that in $CHCl_3$ but appears to differ only in the relative quantum yields for the formation of the various photoproducts. It seems that solvents like DMSO and Et_3N permit the *EZ/ZE* isomers to attain certain orientations which favour this internal cyclization. Similar behaviour is seen during photolysis of bilirubin in aqueous solutions containing HSA. As will be shown later, the photoisomers of bilirubin are detected in aqueous solution only when HSA is added. The formation of lumirubins from *EZ/ZE* isomers is consistent with the mechanism proposed previously by Onishi *et al.* (11), rather than that of McDonagh *et al.* (22), who propose that the cyclization process takes place directly from the bilirubin, and not from *EZ/ZE* isomers.

(D) Photolysis in dimethyl sulfoxide/water

To obtain a better understanding of the effect of changes in the polarity a solution of bilirubin in DMSO/buffer (90:10) was irradiated. The AD spectra obtained during the first 5 min of irradiation are analogous to those for the $CHCl_3$ system in that there is only one loss peak with two isosbestic points (Fig. 4). As for photolysis in $CHCl_3$, with increasing time the isosbestic point at 490 nm disappears. Simultaneously, a shoulder begins to form on the loss peak, indicating that the production of *EZ/ZE* isomers has reached a photostationary state but lumirubins are still being formed.

Thus, the relative importance of the different pathways for bilirubin photoisomerization, photodegradation, and photooxidation is highly dependent upon the environment of the bilirubin molecule. The AD spectra resulting from irradiation of bilirubin in DMSO are considerably different from those for bilirubin in $CHCl_3$. Yet, if 10% aqueous phase is added to the DMSO, the spectra become very similar. The addition of water to DMSO causes the bilirubin molecule to adopt a tightly closed, hydrophobic structure, similar to that in $CHCl_3$, and not the more open structure thought to be present in DMSO. The resulting photoprocess in DMSO/buffer becomes more similar to that in the $CHCl_3$/EtOH system rather than that in pure DMSO. In fact, not only are the shapes of the AD spectra very similar, but the absorbance difference is 0.011 in the $CHCl_3$/EtOH system and 0.010 in the DMSO/H_2O.

(E) Photolysis of aqueous solutions containing albumin

The dramatic changes resulting from the addition of water to DMSO suggested that photolysis of bilirubin in aqueous medium should differ considerably from photolysis in organic solvents. Indeed, as reported previously (26), attempts to identify

Can. J. Chem. Downloaded from www.nrcresearchpress.com by 118.98.75.50 on 09/07/12
For personal use only.

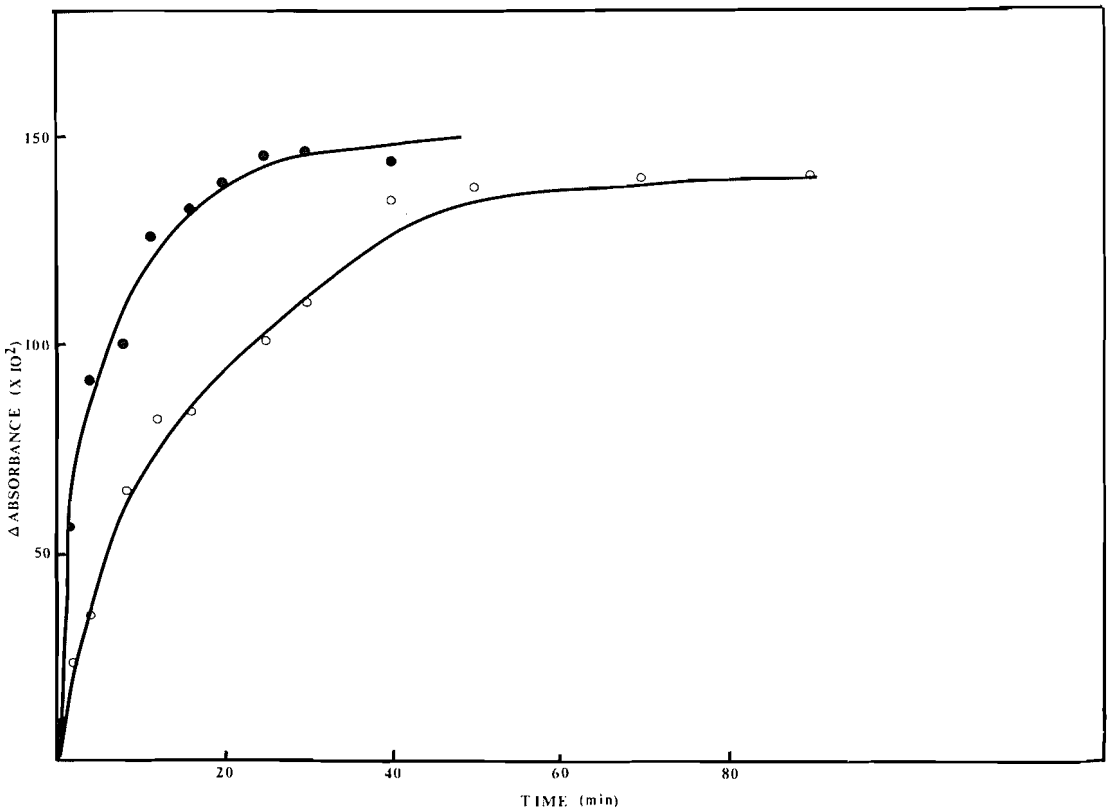

FIG. 6. The absolute values of the absorbance difference of the gain peak (490 nm) for a photolyzed aqueous buffer solution of bilirubin and human serum albumin at different light intensities: ●, high intensity; ○, low intensity.

photoproducts after irradiation of bilirubin in aqueous phosphate buffer were unsuccessful. However, photoproduct formation is readily apparent after the irradiation of the aqueous bilirubin solution containing a small amount of HSA.

When a solution of bilirubin containing HSA with a molar albumin concentration seven times that of the bilirubin is irradiated, the resulting AD spectra (Fig. 5) show three peaks: two loss peaks at 408 and 448 nm, and one large gain peak at 492 nm. In contrast, replacement of HSA with BSA results in one gain peak at ca. 508 nm and a corresponding loss peak at ca. 460 nm (20). These AD spectra show characteristics similar to those for irradiated DMSO solutions of bilirubin. That is, at short irradiation times there is only one isosbestic point, at 460 nm, indicating that initially there is only one product being formed, *EZ/ZE* isomers. As the time of irradiation is increased, this isosbestic point disappears, indicating a disruption in the equilibrium, BR ⇆ *EZ/ZE* isomers, while a second isosbestic point (360 nm) appears, indicating that a second product is now being formed. Thus, the mechanism for photoproduct formation in HSA appears to be the same as in DMSO.

When the height of the gain peak (492 nm) is plotted as a function of the time of irradiation in the presence of HSA a sharp increase is seen initially, followed by the appearance of a photostationary state (Fig. 6). Similar behaviour is seen, but with an increase in initial slope by a factor of 3, so that the photostationary state is reached more rapidly when the intensity of the irradiating light is increased approximately threefold. Thus, a direct relationship is seen between the intensity of the irradiating light and the initial rate of formation of photoproduct. The occurrence of a photostationary state indicates that the formation of *EZ/ZE* isomers from bilirubin is reversible. Furthermore, since the AD spectrum of irradiated bilirubin remains unchanged when it is left in the dark, the reverse process must also be light induced, as proposed by McDonagh and Palma (22).

As mentioned above, it has been suggested previously that the double loss peak is in fact due to the development of a synthesis peak (25). Further evidence is obtained from a plot of peak height after irradiating for 7.0 min, as a function of log {[HSA]/[BR]}, at a fixed bilirubin concentration of $1.71 \times 10^{-5} M$ (Fig. 7). The loss peak at 408 nm behaves identically with the gain peak at 492 nm, while the loss peak at 448 nm behaves differently. (The values have been corrected for the absorbance by HSA at the illuminating wavelength.) The magnitude of the loss peak at 448 nm is, within experimental error, independent of [HSA]/[BR] whereas the other two peaks go through a maximum at a ratio of ca. 1.5/1.0 and then decrease to a plateau. The limit appears to be related to the binding of the bilirubin and/or its photoproducts to the HSA. As the HSA concentration increases, more photoproduct is produced until a [HSA]/[BR] of 1.5 is reached. At higher concentrations of HSA, the amount of photoproduct decreases, perhaps because the binding of bilirubin decreases due to protein aggregation. Such a decrease in binding affinity at high concentrations of HSA has been reported previously (27). When both HSA and bilirubin concentrations are decreased by a factor of 10 a plateau without a "hump" occurs.

The apparent requirement of albumin in aqueous solution of bilirubin to bring about the production of photobilirubin suggests that: (*a*) photoisomerization requires that the albumin bind the bilirubin to facilitate the isomerization, or (*b*) unbound bilirubin can undergo photoisomerization but rapid reversion occurs in the absence of albumin. If the latter were true it should be possible to "trap" photoproducts formed by the

Can. J. Chem. Downloaded from www.nrcresearchpress.com by 118.98.75.50 on 09/07/12
For personal use only.

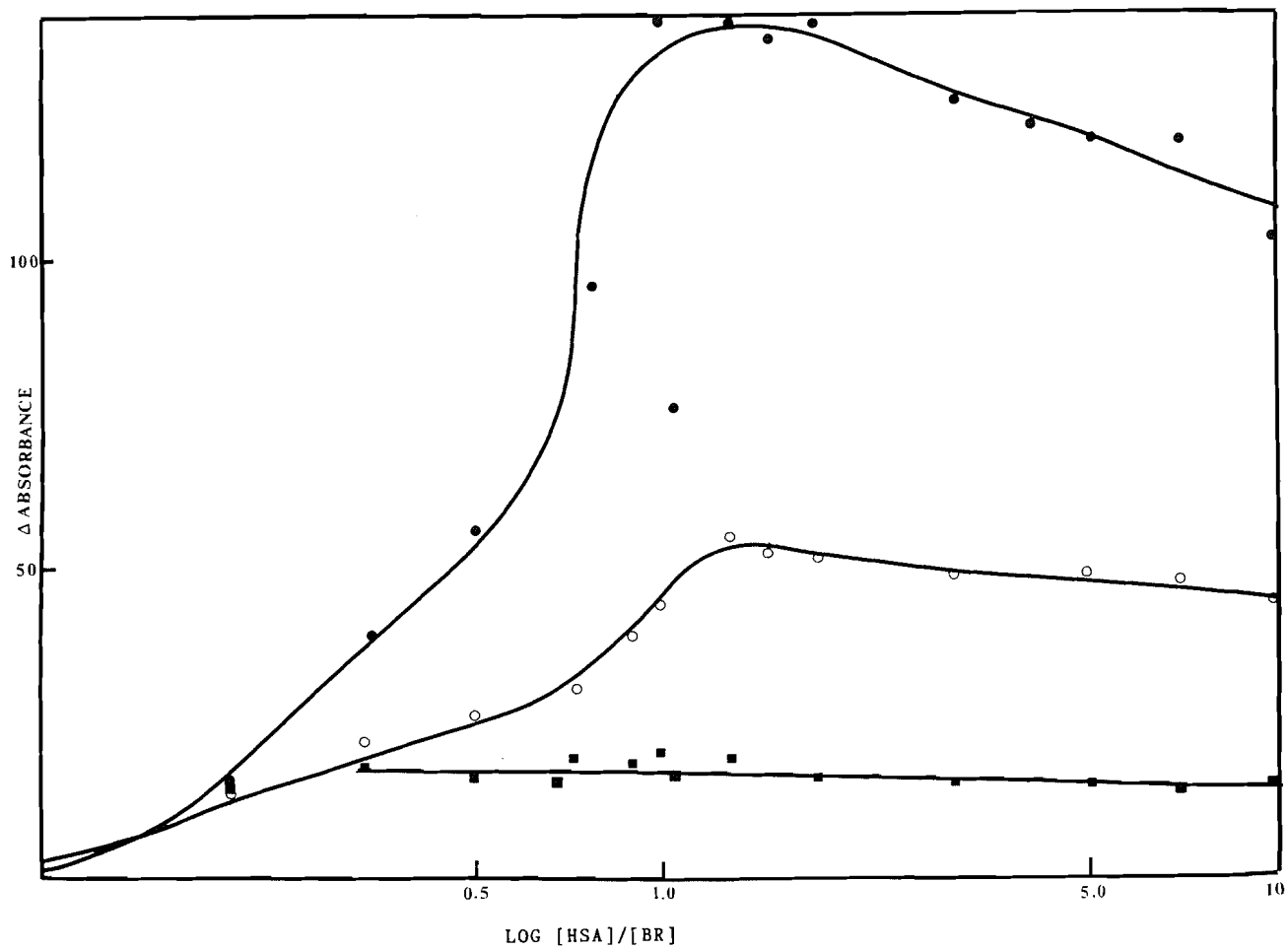

FIG. 7. The absolute values of the absorbance difference, multiplied by 100, of the gain peak (490 nm) and the two loss peaks (448 nm and 408 nm) for a photolyzed aqueous buffer solution of bilirubin and human serum albumin as a function of the log [HSA]/[BR], at 7 min of irradiation: ●, 492 nm; ○, 408 nm; ■, 448 nm.

irradiation of an aqueous solution of bilirubin by adding albumin to bind the photoproducts immediately after irradiation. This was done using the method of stopped flow analysis. The bilirubin buffer solution was irradiated for a given period of time, mixed with a solution of HSA (total mixing time of 20 ms) and the absorbance at the desired wavelength was recorded immediately. A small amount of photoproduct was formed, as evidenced by an increase in absorbance at 490 nm, that increases with time of irradiation (Fig. 8). As expected a concomitant decrease in absorbance was noted at 410 nm while, within experimental error, there was no change in absorbance at 460 nm, which corresponds to an isosbestic point in the AD spectrum of an irradiated solution of bilirubin/HSA. In contrast, no photoproduct formation was detected in an analogous experiment when an irradiated aqueous solution of bilirubin was mixed with buffer, indicating that the presence of HSA is indeed necessary to protect the photoproduct. By comparison, there was approximately a threefold increase in photoproduct formation when the irradiated solution contained both HSA and bilirubin. Thus, it would appear that it is possible for bilirubin to isomerize to form the *EZ*/*ZE* isomers in aqueous solution, but that under these conditions the reversion is too fast to permit their detection. However, when albumin is added to the solution immediately following the irradiation, the *EZ*/*ZE* isomers are bound to the albumin and do not revert to bilirubin.

The fact that more photoproduct is formed when the albumin is present during the irradiation than when it is added just after the irradiation follows from Fig. 7 which shows an increase in photoproduct formation with increasing [HSA]/[BR]. Below the [HSA]/[BR] ratio of 1/1 there is relatively little photoproduct formed. Since the first molecule of bilirubin binds strongly to HSA, with a binding constant of 10^6–10^7 (28), the fraction of free bilirubin is very small at the ratio of [HSA]/[BR] of 1/1, suggesting that it is the irradiation of bound bilirubin that gives rise to the increased formation of photoproducts. Lee and Gillispie (29) have shown that the bilirubin molecule is buried deeply within the HSA. Consequently the HSA can provide a protective environment where the photoproduct is more readily formed. It has been suggested (28) that the HSA molecule maintains the bilirubin in an environment that changes the energies of the transition states leading to the formation of photoproduct. The idea that bilirubin is protected by albumin is also discussed by Rubaltelli and Jori (30).

Summary

It is apparent that the photolysis of bilirubin is a very complex process, involving various photoisomerizations, photodestruction, and photooxidation. Although photoisomerization reactions predominate at short irradiation times under anaerobic conditions, the relative yields of isomers is highly depen-

Can. J. Chem. Downloaded from www.nrcresearchpress.com by 118.98.75.50 on 09/07/12
For personal use only.

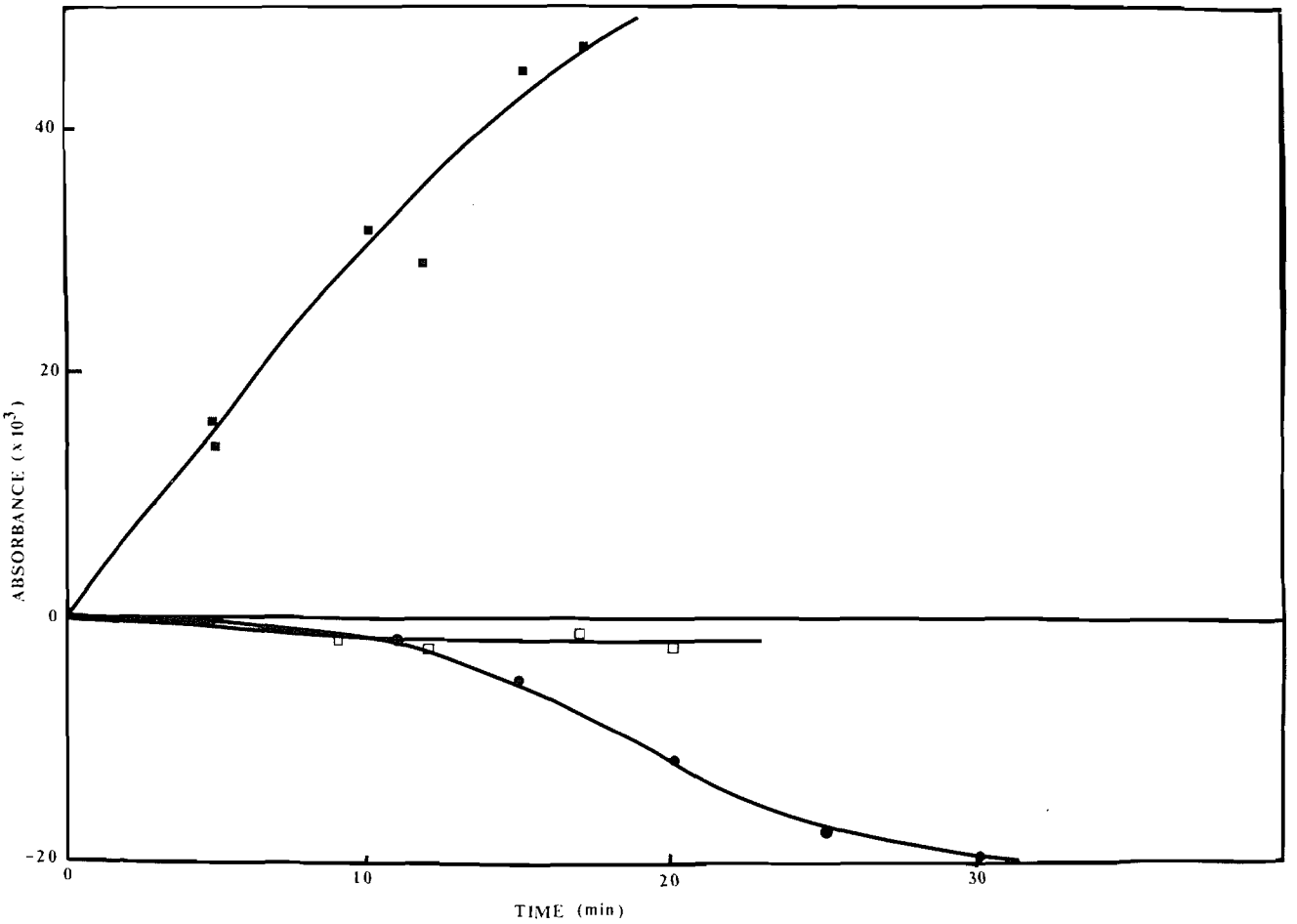

FIG. 8. The absolute values of the absorbance difference at three separate wavelengths (490 nm, 460 nm, and 410 nm) as a function of the irradiation time for a photolyzed aqueous solution of bilirubin after mixing with human serum albumin: ■, 490 nm; □, 460 nm; ●, 410 nm.

dent on the environment of the bilirubin at the time of irradiation. In solvents which interfere weakly with the intramolecular hydrogen bonds of bilirubin, solvents like water or ethanol, formation of lumirubins from *EZ/ZE* isomers is less than in stronger interfering solvents like DMSO and Et_3N. Although small amounts of photoisomers can be "trapped" in irradiated aqueous buffer solutions of bilirubin, substantially greater amounts are formed in the presence of HSA. Indeed, photoisomer production in the presence of HSA is similar to that in DMSO solutions.

Acknowledgements

We wish to thank Professor Jik Chin for the use of his spectrophotometer and for numerous helpful discussions and suggestions. We are particularly indebted to Professor L. E. St-Pierre for his advice, assistance and encouragement. Financial assistance by NSERC and FCAR is gratefully acknowledged.

This paper is submitted to this issue of the Canadian Journal of Chemistry that is dedicated to our colleague Professor J. T. Edward, who never forgets the joys of life.

1. A. N. COHEN and J. D. OSTROW. Pediatrics, **65**, 740 (1980).
2. J. F. LUCEY. Semin. Hematol. **9**, 127 (1972).
3. J. D. OSTROW. Semin. Hematol. **9**, 113 (1972).
4. A. F. MCDONAGH and D. A. LIGHTNER. Pediatrics, **75**, 443 (1985).
5. J. D. OSTROW. Bile pigments and jaundice. Marcel Dekker, Inc., New York. 1986.
6. D. A. LIGHTNER. Photochem. Photobiol. **26**, 427 (1977).
7. D. A. LIGHTNER, A. F. MCDONAGH, and T. A. WOOLDRIDGE. Biochem. Biophys. Res. Commun. **86**, 235 (1979).
8. D. A. LIGHTNER, A. F. MCDONAGH, and T. A. WOOLDRIDGE. Proc. Natl. Acad. Sci. U.S.A. **76**, 29 (1979).
9. A. F. MCDONAGH, D. A. LIGHTNER, and T. A. WOOLDRIDGE. J. Chem. Soc. Chem. Commun. 110 (1979).
10. J. D. OSTROW, M. S. STOLL, E. ZENONE, and J. ZAREMBO. Biochem. J. **183**, 139 (1979).
11. S. ONISHI, I. MIURA, K. ISOBE, S. ITOH, T. OGINO, T. YOKOYAMA, and T. YAMAKAWA. Biochem. J. **218**, 667 (1984).
12. A. F. MCDONAGH and L. A. PALMA. J. Am. Chem. Soc. **104**, 6865 (1982).
13. R. BONNETT, M. S. STOLL, N. VICKER, and C. H. GRAY. Biochem. J. **201**, 179 (1982).
14. R. BONNETT, J. E. DAVIES, and M. B. HURSTHOUSE. Nature, **262**, 326 (1976).
15. R. BRODERSEN. CRC critical review in clinical science. CRC Press, Cleveland. 1980.
16. G. NAVON and D. KAPLAN. J. Chem. Soc. Perkin 2, 1374 (1981).
17. D. KAPLAN and G. NAVON. Biochem. J. **201**, 605 (1982).
18. J. J. MCCARTHY, S. A. MCCLINTOCK, and W. C. PURDY. Anal. Lett. **17**, 1843 (1984).
19. R. PRATESI. Laser photobiology and photomedicine. *Edited by* S. Martellucci and A. N. Chester. Plenum. 1985.
20. R. E. DAVIES and S. J. KEOHANE. Photochem. Photobiol. **17**, 303 (1973).
21. J. KAPITULNIK, N. A. KAUFMAN, K. GOITEIN, G. CIVIDALLI, and S. H. BLONDHEIM. Clin. Chim. Acta, **57**, 231 (1974).

Can. J. Chem. Downloaded from www.nrcresearchpress.com by 118.98.75.50 on 09/07/12
For personal use only.

22. A. F. McDONAGH, D. A. LIGHTNER, and L. A. PALMA. J. Am. Chem. Soc. **104**, 6867 (1982).
23. E. GARBAGNATI and P. MANITTO. J. Paediatrics, **83**, 109 (1973).
24. S. E. BRASLAVSKY, A. R. HOLZWARTH, and K. SCHAFFNER. Angew. Chem. Int. Ed. Engl. **22**, 656 (1983).
25. R. E. DAVIES and S. J. KEOHANE. Boll. Chim. Farm. **109**, 589 (1970).
26. A. F. McDONAGH. Ann. N.Y. Acad. Sci. **244**, 553 (1975).
27. N. THUAUD and B. SEBILLE. J. Chromatogr. **282**, 509 (1983).
28. T. FAERCH and J. JACOBSEN. Arch. Biochem. Biophys. **168**, 351 (1975).
29. J. J. LEE and G. D. GILLISPIE. Photochem. Photobiol. **33**, 757 (1981).
30. F. F. RUBALTELLI and G. JORI. Photochem. Photobiol. **29**, 991 (1979).

Can. J. Chem. Downloaded from www.nrcresearchpress.com by 118.98.75.50 on 09/07/12
For personal use only.

A study of chiral induction in some diene additions catalyzed by chiral alkoxyaluminum dichlorides

COLLEEN J. NORTHCOTT AND ZDENEK VALENTA

Department of Chemistry, University of New Brunswick, Bag Service No. 45222, Fredericton, N.B., Canada E3B 6E2

Received November 4, 1986

This paper is dedicated to Professor John T. Edward

COLLEEN J. NORTHCOTT and ZDENEK VALENTA. Can. J. Chem. **65**, 1917 (1987)

A reliable procedure for the preparation of the chiral Lewis acid catalysts, (−)-menthoxy- ((−)-**1**) and (−)-bornyloxy-aluminum dichloride ((−)-**2**), has been established for the study of diene additions. The geometry of conformationally mobile α,β-unsaturated carbonyl compounds complexed with these catalysts has been probed using the α-methylene ketones **3** and **4** and 2,6-dimethyl-1,4-benzoquinone **5** as dienophiles of fixed geometry. The addition of the first two to cyclopentadiene and (−)-**1** yields *exo* and *endo* adducts that exhibit a range of 28–54% enantiomeric excess (ee); with **5**, only the *endo* isomer, showing 8% ee, is formed. In the corresponding additions catalyzed by (−)-**2**, adducts displaying ee in the range of 3–18% are formed.

COLLEEN J. NORTHCOTT et ZDENEK VALENTA. Can. J. Chem. **65**, 1917 (1987).

Dans le but d'étudier les additions des diènes, on a mis au point une méthode sûre de préparer les catalyseurs chiraux d'acides de Lewis, dichlorures de (−)-menthoxy- ((−)-**1**) et de (−)-bornyloxy-aluminium ((−)-**2**). Utilisant les α-méthylènes cétones **3** et **4** et la diméthyl-2,6 benzoquinone-1,4 (**5**) comme dièenophiles de géométrie définie, on a examiné la géométrie des composés carbonylés α,β-insaturés et conformationnellement mobiles lorsqu'ils sont complexés avec ces catalyseurs. L'addition des deux premiers au cyclopentadiène et au composé (−)-**1** conduit à des adduits *exo* et *endo* dans lesquels on note un excès énantiomérique (ee) allant de 28 à 54%; avec le composé **5**, il ne se forme que de l'isomère *endo* présentant 8% d'ee. Dans les additions correspondantes catalysées par le produit (−)-**2**, les adduits qui se forment présentent des ee qui vont de 3 à 18%.

[Traduit par la revue]

Can. J. Chem. Downloaded from www.nrcresearchpress.com by 118.98.75.50 on 09/07/12
For personal use only.

The Diels–Alder reaction has recently been the subject of many studies aimed at the achievement of high chiral induction (1), not only due to its synthetic usefulness, but also to its well-defined steric features (2). Despite the extensive work carried out on this key cycloaddition with chiral dienophiles (3), chiral dienes (4), and chiral-directing units in the connecting chain of intramolecular systems (5), the search continues for a more general means of inducing asymmetry.

In this regard, the combination of an achiral diene and dienophile with a chiral Lewis acid catalyst is particularly attractive. Independent of the question whether the transition state is "tighter" in catalyzed additions (6), a complexation of the chiral Lewis acid with one of the reaction components would yield an asymmetric reagent with a potential for guiding a selective approach of the remaining component. Also, in addition to the other established advantages of catalysis in the Diels–Alder reaction (7), the use of chiral Lewis acids would be experimentally more convenient, since the necessity for the introduction of a chiral unit into the addend(s) and the subsequent removal from the adduct would be eliminated.

Three important studies have been conducted to probe the feasibility of this combination. Danishefsky and co-workers (8) reported an enantiomeric excess (ee) of 15–58% in the products of additions of various siloxydienes to benzaldehyde in the presence of the chiral lanthanide Eu(hfc)$_3$. Kelly *et al.* (9) obtained a remarkable ee (>98%) in diene additions to juglone (8-hydroxy-1,4-naphthoquinone), which had been made highly chiral by a bidentate attachment of a chiral borate. While this very elegant work with juglone (9) shows that high induction is achievable in diene additions to olefin bonds *provided that a suitably bulky chiral catalyst is essentially fixed in a rigid conformation*, the pioneering work using a chiral lanthanide (8) indicates that, in diene additions to a carbonyl group acting as dienophile, moderate chiral induction can be achieved without a rigidly held catalyst.

This leaves an important question. Is synthetically useful chiral induction achievable in a general case in which neither of the two addends possesses functionality that could provide additional binding to the chiral catalyst and in which the diene is adding to the olefin part of an α,β-unsaturated system? Normally, the Lewis acid catalyst binds to the carbonyl group of the dienophile; in a general case, it can therefore be expected to be further away from the site of bond formation in additions to the olefin bond, rather than the carbonyl group, of the dienophile. Based on the range of ee obtained in additions to the carbonyl group (8), the prospects for high chiral induction in additions to the olefin bond using a conformationally mobile chiral Lewis acid are thus not encouraging.

The work of Koga and co-workers (10) provides useful information and a system for a further study of this question. An encouraging ee of 72% was obtained in the major *exo* adduct from the addition of cyclopentadiene to methacrolein in the presence of (−)-menthoxyaluminum dichloride ((−)-**1**) (Fig. 1). In contrast, the reported selectivity in *exo* Diels–Alder adducts obtained from (nonchiral Lewis acid) catalyzed additions to chiral acrylates is in the range of only 3–45% ee (3). Furthermore, it was noted (10) that the reaction of methyl acrylate and cyclopentadiene, mediated by chiral catalysts (−)-**1** and (+)-**2**, yielded the *endo* adduct in low optical purity (6–9% ee); this is in dramatic contrast to the high chiral induction displayed in the *endo* adducts of (nonchiral Lewis acid) catalyzed additions of chiral acrylates to cyclopentadiene (3).

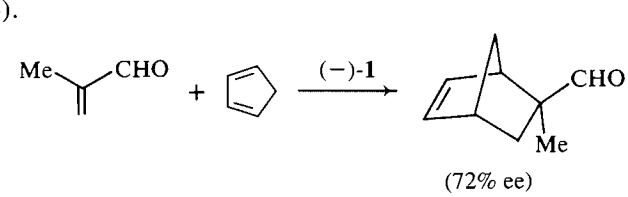

(72% ee)

FIG. 1.

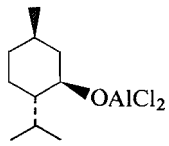

(−)-**1**

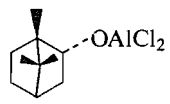

(−)-**2**

These intriguing findings prompted the present investigation into the scope of chiral Lewis acid mediated Diels–Alder reactions. In addition to indicating the chiral induction achievable with conformationally mobile catalysts as discussed above, it was hoped that the study could define at least some aspects of the geometry of the reacting species at the transition state of the Diels–Alder reaction. In the case of conformationally unrestrained α,β-unsaturated carbonyl dienophiles, for example, the *s-trans* and *s-cis* conformations can exist in equilibrium (Fig. 2).[1] Furthermore, catalysts such as **1** and **2** can then bind to one of the two lone pair orbitals of the carbonyl oxygen; this leads to four possible geometries for the reacting complexed dienophile (catalyst attachments a or b in Fig. 2),[1] with further ambiguity arising from possible rotation around the two Al—O bonds and around the O–terpene bond (Fig. 2).

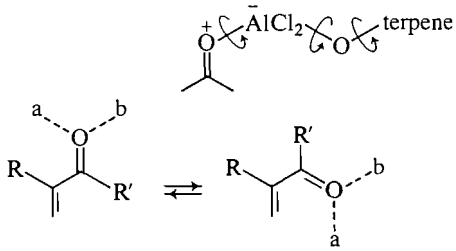

FIG. 2.

An examination of the methacrolein addition (Fig. 1) (10) in this light shows that, in any reasonable conformation of the complexed *s-trans* dienophile (e.g., that shown in Fig. 3), the

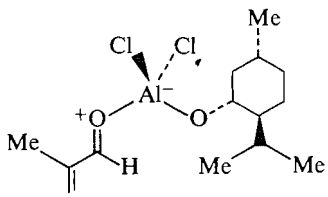

FIG. 3.

chiral moiety is probably located at too great a distance to effect any significant induction. In the case of the *s-cis* conformation of the dienophile, on the other hand, a geometry such as that depicted in Fig. 4 can be visualized in which the isopropyl group of the chiral monoterpene shields one face of the dienophile, and which correctly predicts the observed chirality of the cyclopentadiene adduct (Fig. 1). The *s-cis* conformation of (the reacting complexed) methacrolein is not unreasonable in view of the presence of the α-methyl group (see Discussion and conclusions). Although the attachment of the catalyst to the carbonyl group indicated in Fig. 4 appears sterically unfavorable, it should be noted that a stabilizing electronic interaction between the terpene O-atom and the double bond is possible in this conformation. Furthermore, the geometry of the remaining lone pair orbital of the carbonyl oxygen may well be favored stereoelectronically (11).

[1]For an important recent theoretical study of this equilibrium and many references, see ref. 15.

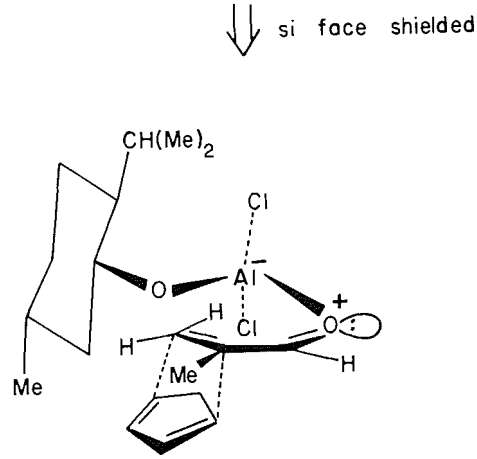

FIG. 4

To test the hypothesis that the *s-cis* conformation of the complexed dienophile is the effective one[2] and to determine whether high chiral induction could be obtained in the more frequently observed *endo* additions, the cyclic cisoid α-methylene carbonyl dienophiles **3** and **4** and the cyclic transoid unsaturated carbonyl compound **5** have been chosen for Diels–Alder reactions with cyclopentadiene in the presence of the chiral alkoxyaluminum dichloride catalysts (−)-**1** and (−)-**2**.

The α-methylene tetralone **3** is not ideal as a model, since the chiral alkoxyaluminum dichlorides can be expected to complex with either of the two lone pair orbitals of the carbonyl oxygen (11), thus placing the chiral moiety in at least one unfavorable (distant) orientation (Fig. 5, formula b). In contrast, the steric hindrance exerted by the methyl groups of **4** should favour complexation with the chiral Lewis acid on the side of the double bond, making it a simpler model (Fig. 6). Finally, the benzoquinone **5** was tested as a check for the

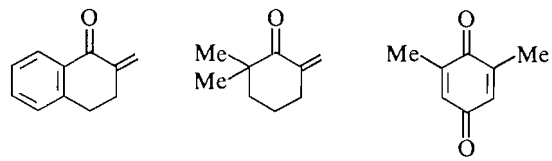

3 **4** **5**

assumption that an *s-trans* conformation of the complexed dienophile is less effective for chiral induction.

The chiral analyst

The combination of chiral monoterpene alcohols with alkylaluminum halides,[3] resulting in alkoxyaluminum dihalides, first reported by Furukawa and co-workers (14), appeared to be a suitable catalytic system (10) for the study. However, when the compounds (−)-**1** and (−)-**2**, formed by the addition of (−)-menthol and (−)-borneol, respectively, to ethylaluminum dichloride, were isolated in our laboratory according to the cited procedure (14), crystalline catalysts giving little or no induction in the addition of methacrolein to cyclopentadiene were obtained.

To prevent a possible hydrolysis of the catalyst, a series of

[2]The concept of a cisoid geometry of the reactive α,β-unsaturated carbonyl dienophile has been proposed to explain results of other asymmetric induction studies (3*a*, 12).

[3]The use of alkylaluminum halides as Lewis acid catalysts has become widespread due to their availability, range of acidity and nucleophilicity of the alkyl group, and mildness (13).

Can. J. Chem. Downloaded from www.nrcresearchpress.com by 118.98.75.50 on 09/07/12
For personal use only.

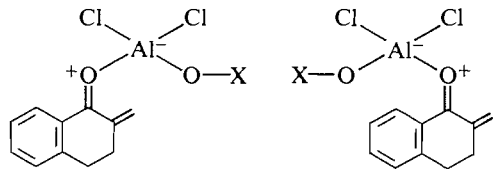

X = (−)-menthyl or (−)-bornyl

FIG. 5.

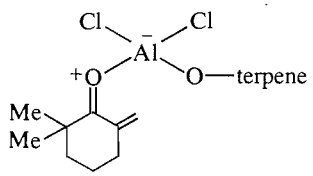

FIG. 6.

in situ preparations of (−)-**1** was run at various temperatures and times. Each of these catalyst solutions was tested in a methacrolein–cyclopentadiene reaction (see Experimental); however, a maximum of only 44% ee (compared to the reported 72% ee) was achieved. Furthermore, the inferiority of all catalysts prepared at temperatures above −15°C, for periods of time longer than 24 h or with fewer recrystallizations than the optimized procedure, suggested that a disproportionation of the catalyst occurs to an equilibrium mixture containing aluminum chloride.

A procedure was finally developed, which included repeated recrystallization of the catalyst from toluene at −78°C under anhydrous conditions and which provided a catalyst of reasonably consistent quality as determined in the methacrolein "test" reaction (Fig. 1).

Results

The relationship between chiral induction and the conformation of the complexed dienophile at the transition state was then investigated by means of the model dienophiles **3**, **4**, and **5**. The additions of these dienophiles to cyclopentadiene catalyzed by (−)-**1** and (−)-**2** were performed in anhydrous toluene at −78°C (Table 1). Chromatographic purification of each of the product mixtures yielded *exo* and *endo* adducts whose geometry was assigned on the basis of ^{1}H nmr spectra and whose optical purity was determined by chiral shift reagent [Eu(hfc)$_3$] ^{1}H nmr analysis. For correlative purposes, the racemic products for each case were obtained from additions catalyzed by boron trifluoride etherate. In addition, a concurrent thermal reaction was run at the low temperature to confirm that no addition took place without the catalyst. A range in quality of the catalysts was observed, even with the optimized preparation, so that the methacrolein–cyclopentadiene addition was also carried out along with every reaction under study (Table 1, last column).

Discussion and conclusions

The results of the investigation are summarized in Table 1. It can be seen that the observed chiral induction using catalyst (−)-**1** and cisoid models **3** and **4** is moderately high in the *exo* and *endo* adducts (entries 2 and 5; 28–54% ee range), and that the value observed with the transoid model **5** is significantly lower (8% ee). The fact that higher ee's have not been obtained indicates the limitations of restricting only the mobility of the dienophile in such systems.

Of particular note is the relatively high induction observed in the *exo* adduct of **4** and cyclopentadiene (entry 5). The catalyst almost certainly is complexed with the carbonyl oxygen orbital projected away from the two methyl groups (Fig. 6), placing the chiral terpene moiety closer to the site of bond formation. The induction obtained in the *exo* adduct, a (normalized) value of 60% ee, corresponds well to the 72% ee observed in the *exo* adduct of methacrolein. This similarity substantiates our proposal of an *s-cis* conformation in the reactive complex of (−)-**1** and methacrolein[4] (Fig. 4).

Furthermore, the benzoquinone **5**, which models the *s-trans* dienophile conformation (Fig. 3), exhibits low chiral induction; this implies that the monoterpene is too distant to effectively shield the olefin in this conformation.

A comparison of chiral inductions achieved with catalyst (−)-**1** and the two cisoid dienophiles in the *exo* and *endo* regions, respectively, shows that the observed ee is significantly higher in the *endo* adduct in the case of **3** (*endo:exo* = 54:38), while the opposite is true for dienophile **4** (*endo:exo* = 28:48)! *A priori*, a higher induction may well have been expected for both the *endo* and the *exo* adduct of **4** (as compared to those of **3**) because of the postulated more favorable attachment of the catalyst to dienophile **4** (compare Figs. 5 and 6). Clearly, other factors come into play; for example, the conformation of the O—Al—O–terpene moiety (see Fig. 2) is no doubt different in the various additions, as influenced by the structure of the dienophile and by different steric influences exerted by the diene in the *exo* and *endo* regions, respectively, during addition. Complicated as this situation may be, the results show that a reasonably useful chiral induction can be achieved in the more commonly encountered *endo* additions, *provided that the olefin bond and the carbonyl group of the dienophile are in the* cis *conformation.*[5]

Houk and co-workers calculated a slight preference for the *s-trans* form of protonated acrolein (0.2 and 1.8 kcal/mol) and a bigger preference for the *s-trans* form of lithium-complexed acrolein (1.9 and 3.2 kcal/mol) (15). If it can be assumed that the H^+ and Li^+ models are reasonable analogies for such carbonyl complexes as those formed with **1** and **2**, their conclusions are in agreement with the experimental results of Koga and co-workers (10) who, as stated above, found very low ee values in the reaction of acrolein and catalysts **1** or **2** with cyclopentadiene in the *endo* region. The carbonyl group points "away" from the cyclopentadiene and the chiral catalysts are thus too far to cause significant induction (see Fig. 3). Our results with quinone **5** (Table 1, entries 7 and 8) complete this consistent picture.

We believe, however, that the results with dienophiles **3** and **4** strongly suggest that complexed methacrolein reacts in the *s-cis* conformation, at least when adding to cyclopentadiene in the *exo* region (10). The calculated energy differences between the *s-cis* and *s-trans* forms of protonated and Li^+-complexed acrolein are sufficiently small (15) to allow a preference for the *s-cis* form when a methyl group is placed in the α position.

[4]The low chemical yield obtained with model **4** is unfortunate, due to polymerization of **4**, but irrelevant to the argument.

[5]It should be remembered, however, that all the above conclusions are strictly relevant to cyclopentadiene only. Useful chiral inductions may well be achievable with transoid dienophiles in additions to dienes that contain the necessary stereo-differentiating features in the appropriate region of space (for example, 1-vinylcyclohexene and larger).

Can. J. Chem. Downloaded from www.nrcresearchpress.com by 118.98.75.50 on 09/07/12
For personal use only.

TABLE 1. Catalyzed Diels–Alder additions with cyclopentadiene[a,b]

Entry	Dienophile	Catalyst (equiv.)	Time (h)	Yield (%)	*exo*:*endo* ratio	$[\alpha]_D$ *exo*	$[\alpha]_D$ *endo*	% ee[c,h] *exo*	% ee[c,h] *endo*	Corresponding methacrolein reaction, % ee
1	**3**	$BF_3 \cdot Et_2O$(1)	3	79	2:1		—		—	—
2	**3**	(−)-**1**(2)	6.5	61	13:1	−14.1	+147	38(49)	54(70)	56[f]
3	**3**	(−)-**2**(1)	8	48	31:1	+11.3	−10.3	18	0–3	32[g]
4	**4**	$BF_3 \cdot Et_2O$(0.6)	20.5	2.6	1.5:1		—		—	—
5	**4**[d]	(−)-**1**(1)	28	1.1	8:1	+39	n.a.[e]	48(60)	28(35)	58[f]
6	**5**	$BF_3 \cdot Et_2O$(0.4)	1	92	0:100		—		—	—
7	**5**	(−)-**1**(0.4)	15	80	0:100	—	+4.6	—	8(9)	66[f]
8	**5**[d]	(−)-**2**(1)	3	53	0:100	—	+5.7	—	6	29[g]

[a]In toluene at −78°C.
[b]With 2 equivalents of cyclopentadiene.
[c]Determined by ^{1}H nmr analysis with Eu(hfc)$_3$.
[d]With 4 equivalents of cyclopentadiene.
[e]n.a., not available.
[f]The reported value (10), for the *exo* adduct is 72% ee.
[g]The reported value (10) for the *exo* adduct is 25% ee.
[h]Numbers in parentheses are normalized to a catalyst giving 72% ee in the methacrolein addition.

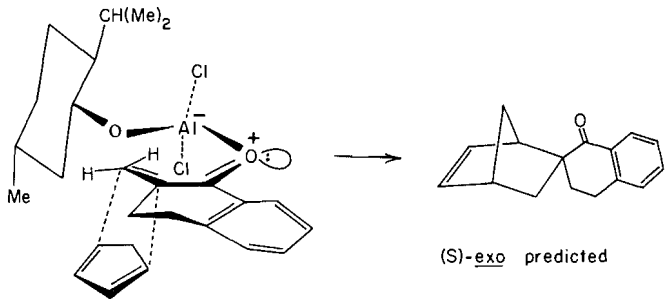

FIG. 7

Clearly, this postulate should be further tested, both by experimental and by computational methods.

Although not included in the table, the reaction of α-methylene γ-butyrolactone with (−)-**1** and cyclopentadiene was carried out in this study as a probe for understanding induction in acrylate additions. *Exo* and *endo* adducts were obtained in a 57:1 ratio. The low yields of the *endo* adduct and the inability to obtain diastereomeric signals for any proton resonance in the ^{1}H nmr analysis made quantification of the induction impossible in this case; for the *exo* product, however, 30% ee was observed. This induction is significantly higher than that observed with methyl acrylate and chiral catalysts (−)-**1** and (+)-**2** (6–9% ee) (10). The ring in α-methylene γ-butyrolactone ensures the *E*-ester–*s-cis* dienophile conformation for this model; this comparison then suggests that a conformation similar to that of α-methylene γ-butyrolactone does not play a significant role in catalyzed additions of the conformationally mobile methyl acrylate.

The Diels–Alder adducts in this study are not easily degraded into compounds of known absolute configuration, nor readily correlated to known configurations; the lack of this information does not detract from the conclusions drawn from this study concerning the magnitude of induction. Furthermore, one can speculate on the probable absolute configurations based on correlation with the defined course of the methacrolein addition as described above (Fig. 4). For example, the *exo* adduct of dienophile **3** and cyclopentadiene formed in a reaction catalyzed by (−)-**1** (Table 1, entry 2) is predicted to have the (*S*) configuration as shown in Fig. 7.

Several comments can be made about the general usefulness of chiral alkoxyaluminum dichlorides for chiral induction. Experimentation with temperatures above −78°C or with an alternate solvent such as methylene chloride, while increasing reaction rate, gave adducts with little or no chiral induction. From our experience, the chiral inducing ability of the catalyst is highly dependent upon the experimental technique in its preparation. The nature of the catalytic species in solution (whether monomeric, polymeric, or a combination) is unknown; increasing the amount of catalyst from 0.4 equivalent to 2 equivalents did not increase ee in the adducts, although amounts lower than 0.4 equivalent gave lower induction. This suggests a possibility of different percentages of the most effective chiral-inducing species with each preparation—a distinct disadvantage of these catalysts.

(−)-**2** exhibited substantially less chiral induction relative to (−)-**1** in all cases. As has been demonstrated in numerous studies with chiral acrylates (3), the diastereo-differentiating moiety may be modified to improve shielding of one face of the reacting species; however, our findings indicate that, despite a possible electronic interaction between the catalyst's oxygen and the dienophile olefin, very high induction is unlikely due to the mobile oxygen–monoterpene bond.

Experimental

The ^{1}H nmr spectra were recorded in $CDCl_3$ on a Varian T60 or Varian XL-200 spectrometer. Anhydrous Eu(hfc)$_3$ (Aldrich) was used in the ^{1}H nmr shift studies. The ir spectra of samples in $CHCl_3$ were obtained on a Perkin–Elmer 727B spectrophotometer with 0.5-mm NaCl cells. Low resolution electron impact (70 eV) mass spectra were recorded with a Hitachi Perkin–Elmer RMU-6D spectrometer. The gas chromatography was carried out on a Varian 6000 capillary gc with flame ionization detector, helium as the carrier gas, and both injection port and detector temperatures at 240°C. A Waters Associates 6000A high pressure liquid chromatograph in combination with a 440 uv absorbance detector at λ_{max} 254 nm and a refractive index detector was employed for analyses by hplc.

Optical rotations of samples in $CHCl_3$ were measured in either 5-mL or 1-mL glass cells at ambient temperature with a Perkin–Elmer 241 polarimeter at λ_{max} 589 nm.

Column chromatography was performed on silica gel (Kieselgel 60G, E. Merck) and preparative thin-layer chromatography was carried out on 0.25-mm silica gel 60F-254 plates (BDH) or on Kieselgel

Can. J. Chem. Downloaded from www.nrcresearchpress.com by 118.98.75.50 on 09/07/12
For personal use only.

Can. J. Chem. Downloaded from www.nrcresearchpress.com by 118.98.75.50 on 09/07/12
For personal use only.

60F-254 plates (E. Merck) of thickness 0.5 mm or 1 mm. Hexane and ethyl acetate were distilled before use in the chromatography.

(−)-Menthol was distilled from sodium at 0.2 Torr (1 Torr = 133.3 Pa) to 99% optical purity and (−)-borneol was sublimed (at 0.2 Torr) to 98% optical purity. Ethylaluminum dichloride (Alfa) was handled as a 25% w/w solution in hexane under argon. All solvents were freshly distilled under an argon atmosphere: toluene and benzene were dried over sodium, heptane over calcium hydride, and tetrahydrofuran with lithium aluminum hydride. Methacrolein and boron trifluoride etherate were distilled before use. Cyclopentadiene was obtained by cracking dicyclopentadiene at 170°C prior to reaction.

Melting points were determined with a Gallenkamp capillary tube apparatus and are uncorrected.

Preparation of (−)-menthoxyaluminum dichloride (−)-1

The procedure given by Furukawa and co-workers (14) was modified as follows.

A flame-dried 100-mL three-neck flask was equipped with a dropping funnel, a rubber septum, a magnetic stirrer, a gas inlet, and a bubbler. The 25% ethylaluminum dichloride solution in hexane (38.3 g, 0.0754 mol) was added via syringe under a slow flow of argon. This was cooled to −78°C and a solution of (−)-menthol (12.0 g, 0.0768 mol) in dry heptane (18 mL) was added dropwise over 25 min. A white precipitate formed. The mixture was carefully allowed to reach 20°C; during this time, a clear solution resulted and ethane was vigorously evolved. After 15 min at 20°C, a white solid formed and was allowed to settle over 15 min. The supernatant liquid (30 mL) was decanted via syringe under positive argon pressure. The remaining white solid was dried under vacuum (0.2 Torr) for 10 min, then was dissolved in anhydrous toluene (28 mL) at room temperature. The clear colorless solution was immediately cooled to −78°C for 24 h to give white crystals. The recrystallization was carried out by decantation as above of the mother liquor at −78°C. The remaining "wet" crystals at −78°C were washed with precooled toluene (5 mL), again followed by removal of the supernatant liquid. The crystals were dissolved in toluene (20 mL) at −10°C, then the solution was again cooled to −78°C for 24 h. This procedure was repeated five times; decreasing volumes of toluene were required to dissolve the crystals at −10°C for the successive recrystallizations. From a total volume of 35 mL of the product (−)-**1** in toluene, a 1-mL aliquot, upon evaporation of the solvent *in vacuo*, yielded white crystals of (−)-**1** (0.284 g, total yield 9.94 g, 52%); mp 87–90°C; ir ν_{max}: 3200 (br), 2950, 1450; ^{1}H nmr δ: 0.8 (3H, d, J = 7 Hz, CH_3), 0.97 (6H, d, J = 7 Hz, $2CH_3$'s), 1.6 (6H, m, —CH_2—), 2.3 (2H, m, —CH—), 4.1 (1H, m, —CH—O$AlCl_2$).

Preparation of (−)-bornyloxyaluminum dichloride, (−)-2

The procedure described for (−)-**1** was carried out, with the following modifications. The solution of (−)-borneol (5.0 g, 0.032 mol) in dry toluene (22 mL) was added dropwise over 10 min to the 25% ethylaluminum dichloride solution in hexane (16 g, 0.032 mol) at −78°C. The mixture was slowly allowed to warm to 15°C when ethane was evolved. After 45 min of stirring at this temperature, a clear solution formed. The solution was concentrated under reduced pressure (1 Torr) to an approximate volume of 20 mL, then was cooled at −78°C for 24 h. The recrystallization procedure for (−)-**1** was followed. From a final volume of 16 mL of product (−)-**2** in toluene, a 1.0-mL aliquot yielded white crystals of (−)-**2** upon evaporation of the solvent *in vacuo* (0.333 g, total yield 5.33 g, 67%); mp 97–98°C; ir ν_{max}: 3400–3100 (br), 2950, 1450; ^{1}H nmr δ: 0.9 (6H, s, $2CH_3$'s), 1.06 (3H, s, CH_3), 1.6 (6H, m, —CH_2—), 2.4 (1H, br m, —CH—), 4.7 (1H, dd, J = 10 and 4 Hz, —CH—O$AlCl_2$).

In situ *preparation of (−)-1*

Dry toluene (2 mL) and a 25% solution of ethylaluminum dichloride in hexane (2.51 g, 0.0049 mol) were added to an apparatus as described for (−)-**1**. After cooling to −78°C, the solution of (−)-menthol (0.80 g, 0.0051 mol) in toluene (3 mL) was added dropwise. The solution was stirred at −15°C for 24 h, and subsequently used as an *in situ* catalyst.

Catalyzed Diels–Alder addition of methacrolein to cyclopentadiene

The procedure cited by Koga and co-workers (10) was used in the methacrolein (0.025 mol) reaction with several modifications. After extraction of the reaction mixture with hexane and drying ($MgSO_4$), the organic phase was concentrated under reduced pressure (95 Torr) with a bath temperature of 35–40°C to one-fifth of its volume. The pale yellow toluene solution contained the aldehyde adducts in a ratio of *exo:endo* 97:3 and in 70% yield as estimated from the ^{1}H nmr spectrum. The aldehyde solution was immediately oxidized with silver oxide and the *endo* acid was removed by iodolactonization (16). The *exo* acid was obtained (0.608 g, 16% overall); mp 34–36°C; $[\alpha]_D$ +48.3° (*c* 6, EtOH, 71.6% ee);[6] ir ν_{max}: 3500–3100 (br), 2700–2500 (br), 1690; ^{1}H nmr δ: 0.90 (1H, dm, J = 12 Hz, *endo* H(3)), 1.20 (3H, s, CH_3), 1.50 (2H, m, apex H_a, H_b), 2.50 (1H, dd, J = 4 and 12 Hz, *exo* (H(3)), 2.87 (1H, m, H(4)), 3.10 (1H, m, H(1)), 6.17 (2H, m, vinylic H(5), H(6)), 11.53 (1H, br m, OH); ms m/e: 152 (M^+).

Preparation of 2-methylene-α-tetralone, 3 and 2,2-dimethyl-6-methylene cyclohexanone, 4

Dienophiles **3** and **4** were prepared from α-tetralone and 2,2-dimethylcyclohexanone (19), respectively, by Gras' method for the formation of α-methylene ketones (18). Due to their ready dimerization at temperatures as low as −15°C, freshly prepared **3** and **4** were immediately used in subsequent Diels–Alder additions without further purification.

3 (91%); tlc in hexane – ethyl acetate (4:1) indicated 80% purity, R_f 0.5; ir ν_{max}: 1670, 1610 (sh), 1600; ^{1}H nmr δ: 3.00 (4H, m, —CH_2—), 5.43 (1H, d, J = 1 Hz, C=CH_2), 6.20 (1H, d, J = 1 Hz, >C=CH_2), 7.00–7.50 (3H, m, aromatic H's), 8.07 (1H, d, J = 6 Hz, aromatic H β to carbonyl).

The product **3** upon sitting at room temperature for 24 h formed its dimer, a bright yellow oil; tlc in hexane – ethyl acetate (4:1), R_f 0.4; ir ν_{max}: 1690, 1665, 1600; uv λ_{max}: 250 (5 200), 282 (6 700); ^{1}H nmr δ: 2.23 (8H, m, —CH_2—), 2.74 (2H, m, —CH_2—aromatic), 3.06 (2H, m, —CH_2—aromatic), 7.00–7.50 (7H, m, aromatic H's), 8.03 (1H, d, J = 6 Hz, aromatic H β to carbonyl); ms m/e: 316 (M^+).

4 (91%); ir ν_{max}: 1700, 1620; ^{1}H nmr δ: 1.10 (6H, s, $2CH_3$'s), 1.73 (4H, m, —CH_2—), 2.60 (2H, br m, —CH_2—C=C), 5.07 (1H, dd, J = 1 and 2 Hz, —C=CH_2), 5.67 (1H, dd, J = 1 and 2 Hz, —C=CH_2).

Diels–Alder additions with cyclopentadiene. General procedure

The apparatus for all of the Diels–Alder reactions comprised a flame-dried 100-mL three-neck flask with a rubber septum, magnetic stirrer, a gas inlet, and a bubbler, and was maintained under an argon atmosphere. In the trials catalyzed by $BF_3 \cdot Et_2O$, the amount of catalyst indicated in Table 1 was added to the dienophile in dry toluene at −78°C, followed by the dropwise addition of two equivalents of cyclopentadiene in toluene (total solvent ratio 28:1), unless otherwise described.

For reactions catalyzed by (−)-**1** or (−)-**2**, a solution of the dienophile in dry toluene was added by syringe to an aliquot of the catalyst in toluene (cf. Table 1 for equivalents) at −78°C. Cyclopentadiene (2 equivalents, unless otherwise stated) in toluene was added dropwise via syringe (total solvent ratio 20:1). The reactions were stirred at −78°C for the times recorded in Table 1. The adducts were isolated by the following extraction procedure. Water (2–5 mL) was added at −78°C, then at ambient temperature the mixture was diluted with water and extracted with hexane. The organic layers were washed with water and brine, dried ($MgSO_4$), and concentrated *in vacuo* to give the crude product mixture. For each reaction catalyzed by (−)-**1** or (−)-**2**, a concurrent methacrolein–cyclopentadiene addition was carried out with the same batch of catalyst and its optical purity was determined by conversion to the *exo* acid as described above. Also, a

[6]The reported rotation of the optically pure *exo* acid is +67.4° (EtOH) and its absolute configuration is reported to be (+)-(2*S*) (17).

Can. J. Chem. Downloaded from www.nrcresearchpress.com by 118.98.75.50 on 09/07/12
For personal use only.

noncatalyzed reaction was performed at −78°C for each dienophile–diene combination.

*Addition of **3** with $BF_3 \cdot Et_2O$*

A crude orange oil (0.30 g) was obtained from the reaction of **3** (0.20 g, 0.0013 mol) with cyclopentadiene (0.16 g, 0.0025 mol) and $BF_3 \cdot Et_2O$ (0.18 g, 0.0013 mol). It was purified by preparative tlc (1-mm plates, hexane – ethyl acetate 9:1) to give the following:

Exo adduct-**3**, yellow oil (0.150 g); tlc, R_f 0.7 (hexane – ethyl acetate 9:1); ir ν_{max}: 1680, 1605; uv λ_{max}: 245 (11 900), 290 (1 200); ^{1}H nmr δ: 0.62 (1H, dd, J = 3 and 11 Hz, *endo* H(3)), 1.30 (1H, d, J = 9 Hz, apex H_a), 1.70 (1H, d, J = 9 Hz, apex H_b), 1.83 (2H, m, —CH_2—), 2.60 (1H, half of dd, J = 4 Hz, *exo* H(3)), 2.80 (4H, m, H(1), H(4), —CH_2—aromatic), 6.20 (2H, m, vinylic H(5), H(6)), 7.30 (3H, m, aromatic), 8.03 (1H, dd, J = 2 and 6 Hz, aromatic H β to carbonyl); ms m/e: 224 (M^+). The addition of Eu(hfc)$_3$ (17 mg) to racemic *exo* adduct-**3** (10 mg) shifted the signal at δ 8.03 to δ 9.5, where the enantiomeric shifts were displayed as two doublets (integration of peak areas 1:1).

Endo adduct-**3**, colorless oil (0.075 g); tlc, R_f 0.63 (hexane – ethyl acetate 9:1); ir ν_{max}: 1680, 1605; uv λ_{max}: 245 (10 000), 287 (2 400); ^{1}H nmr δ: 1.27 (1H, dd, J = 12 and 3 Hz, *exo* H(3)), 1.70 (2H, t, —CH_2—), 2.20 (1H, half of dd, J = 2 Hz, *endo* H(3)), 2.30 (2H, m, apex H_a, H_b), 3.04 (4H, m, —CH_2—aromatic), 5.70 (1H, dd, J = 6 and 3 Hz), and 6.27 (1H, dd, J = 6 and 3 Hz) representing the vinylic H(6) and H(5), 7.30 (3H, m, aromatic), 7.93 (1H, dd, J = 7 and 2 Hz, deshielded aromatic H); ms m/e: 224 (M^+). The signal at δ 7.93 was shifted to δ 8.6, upon addition of Eu(hfc)$_3$ (17 mg) to *endo* adduct-**3** (10 mg), and was exhibited as two doublets of equal density.

*Addition of **3** with (−)-**1***

The addition of **3** (1.10 g, 0.0069 mol) and cyclopentadiene (0.83 g, 0.013 mol) catalyzed by (−)-**1** (3.52 g, 0.014 mol) yielded a crude product mixture as a yellow oil (2.76 g). A portion (0.180 g) was purified by preparative tlc (0.5-mm plates, developed twice in hexane – ethyl acetate 9:1) to yield the following:

Exo adduct-**3**, yellow oil (0.102 g); tlc, R_f 0.7 (hexane – ethyl acetate 9:1, developed twice); $[\alpha]_D$ −14.1° (*c* 10, $CHCl_3$); ir, ^{1}H nmr, uv, and ms confirmed the structure. Addition of Eu(hfc)$_3$ (16 mg) to *exo* adduct-**3** (10 mg) shifted the signal at δ 8.03 (1H, d) to δ 9.25, where two doublets (integration 69:31) were displayed, representing 38% ee.

Endo adduct-**3**, colorless oil (0.008 g); tlc, R_f 0.63 (hexane – ethyl acetate 9:1, developed twice); $[\alpha]_D$ +147° (*c* 0.8, $CHCl_3$); ir, ^{1}H nmr, uv, and ms identified the adduct. Addition of Eu(hfc)$_3$ (20 mg) to *endo* adduct-**3** (10 mg) shifted the signal at δ 7.93 (1H, d) to δ 9.00, where it was exhibited as two doublets (integration 23:77), corresponding to 54% ee.

*Addition of **3** with (−)-**2***

Similarly, the Diels–Alder reaction was carried out, but with 4 equivalents of cyclopentadiene added at 1-, 3-, 5-, and 8-h intervals. Column chromatography (silica gel, hexane – ethyl acetate 9:1), followed by preparative tlc (1-mm plates, developed twice in hexane – ethyl acetate 9:1), yielded the purified adducts, *exo* adduct-**3** and *endo* adduct-**3**, in the chemical and optical yields recorded in Table 1. Spectral data confirmed the structures.

*Addition of **4** with $BF_3 \cdot Et_2O$*

Due to the ready polymerization of **4**, the $BF_3 \cdot Et_2O$ (1.20 mL, 0.0098 mol) was added to the mixture of **4** (3.00 g, estimated 0.017 mol) and cyclopentadiene (4.59 g, 0.069 mol) at −78°C. This temperature was maintained for 6 h, then stirring was continued at −15°C for 14 h. The crude product was partially purified by column chromatography (silica gel, hexane – ethyl acetate 100:3) to yield a yellow oil (0.826 g). A portion (0.226 g) was further purified by preparative tlc (0.5-mm plates, developed twice in hexane – ethyl acetate 100:3) to give:

Exo adduct-**4**, yellow oil (0.054 g); tlc, R_f 0.5 (hexane – ethyl acetate 100:3, developed twice); ir ν_{max}: 1685; ^{1}H nmr δ: 0.90 (1H, dd, J = 12 and 2 Hz, *endo* H(3)), 1.17 (6H, s, 2CH_3's), 1.38 (1H, d, J = 8 Hz, apex H_a), 1.60 (3H, m, apex H_b and —CH_2—), 1.70 (4H, t, —CH_2—), 2.20 (1H, dd, J = 12 and 4 Hz, *exo* H(3)), 2.83 (1H, m, H(4)), 3.00 (1H, m, H(1)), 6.12 (1H, dd, J = 6 and 2 Hz) and 6.22 (1H, dd, J = 6 and 2 Hz) representing vinylic H(5) and H(6); ms m/e: 204 (M^+). When *exo* adduct-**4** (2 mg) was complexed with Eu(hfc)$_3$ (2 mg), the singlet at δ 1.17 of the coincident methyl resonances was split into two singlets at δ 1.24 and δ 1.25, representing the two CH_3 groups; with additional Eu(hfc)$_3$ (3 mg total), the δ 1.25 signal was split into two singlets (integration 1:1) at δ 1.33 and δ 1.34 corresponding to the enantiomers.

Endo adduct-**4**, yellow oil (0.038 g); tlc, R_f 0.45 (hexane – ethyl acetate 100:3, developed twice); ir ν_{max}: 1695; ^{1}H nmr δ: 1.06 (3H, s, CH_3), 1.15 (1H, dd, J = 12 and 4 Hz, *exo* H(3)), 1.20 (3H, s, CH_3), 1.47 (1H, bd, J = 8 Hz, apex H_a), 1.70 (5H, m, apex H_b and —CH_2—), 2.00 (2H, m, —CH_2—), 2.17 (1H, dd, J = 12 and 2 Hz, *endo* H(3)), 2.82 (1H, m, H(4)), 3.16 (1H, m, H(1)), 5.77 (1H, dd, J = 6 and 3 Hz) and 6.20 (1H, dd, J = 6 and 3 Hz) representing vinylic H(6) and H(5); ms m/e: 204 (M^+). The methyl singlet at δ 1.06 of *endo* adduct-**4** (1 mg) appeared as two singlets at δ 1.13 and δ 1.14 of equal intensity, upon addition of Eu(hfc)$_3$ (0.8 mg).

Dimeric **4**, clear crystals (0.055 g); tlc, R_f 0.51 (hexane – ethyl acetate 100:3, developed twice); ir, ^{1}H nmr confirmed its structure; ms m/e: 276 (M^+); glc indicated rt 12.6 min (GSCOT, SP 1000, 44 m, id = 0.5 mm, 160°C, 18 psi (1 psi = 6.9 kPa)).

*Addition of **4** with (−)-**1***

The reverse addition was carried out, with **4** (2.77 g, 0.02 mol) added to the mixture of cyclopentadiene (5.28 g, 0.08 mol) and (−)-**1** (5.06 g, 0.02 mol) in dry toluene. The crude product mixture (3.56 g) was partially purified by column chromatography (silica gel, hexane – ethyl acetate 50:1). The major fraction (1.05 g) was further purified by preparative tlc (0.5-mm plates, developed three times in hexane – ethyl acetate 100:3) to yield *exo* adduct-**4** (0.665 g) and *endo* adduct-**4** (0.079 g). Each of these was prepared for hplc separation by dilution in hexane and passage through Porisil Sep-Packs to remove polar impurities. Then, elution of each with 3% ethyl acetate in hexane on a Porisil M20 column at pressure 1100 psi and flow rate of 5 mL/min, and recycling of the major peaks several times, gave the purified adducts:

Exo adduct-**4**, colorless oil (0.035 g); characterized by tlc, ir, ^{1}H nmr; ms m/e: 204 (M^+); hplc: rt 11.0 min; glc (160°C, 18 psi); rt 4.9 min; $[\alpha]_D$ +39°C (*c* 2, $CHCl_3$). The addition of Eu(hfc)$_3$ (1.8 mg) to *exo* adduct-**4** (1 mg) shifted the signal at δ 1.17 (6H, s) to δ 1.22 (3H, s) and δ 1.23 (3H, s) representing the axial and equatorial methyl resonances. With a total of 5.4 mg of Eu(hfc)$_3$, the δ 1.23 singlet was split into two singlets at δ 1.605 and δ 1.615 (integration 26:74) for one enantiomeric methyl, representing 48% ee.

Endo adduct-**4**, yellow oil (0.009 g); characterized by tlc, ir, ^{1}H nmr; ms m/e: 204 (M^+); hplc: rt 12.0–13.1 min; glc (160°C, 18 psi); rt 5.15 min, also impurities at rt 3.3, 4.4, and 6.0 (~50%); $[\alpha]_D$ not available. The methyl singlet at δ 1.06 of *endo* adduct-**4** (1 mg) appeared as two singlets at δ 1.64 and δ 1.72 (peak area 65:35), upon addition of Eu(hfc)$_3$ (1.6 mg), which corresponded to 30% ee.

*Addition of **5** with $BF_3 \cdot Et_2O$*

The addition of **5** (0.50 g, 0.0037 mol) and cyclopentadiene (0.48 g, 0.0073 mol) catalyzed by $BF_3 \cdot Et_2O$ (0.20 mL, 0.0015 mol) yielded a yellow oil (0.700 g), which was purified by preparative tlc (1-mm plates, hexane – ethyl acetate 4:1) to give the pure *endo* adduct (0.65 g, 92%); tlc R_f 0.5 (hexane – ethyl acetate 4:1); ir ν_{max}: 1660; ^{1}H nmr δ: 1.40 (3H, s, —CH_3), 1.57 (2H, m, apex H_a and H_b), 1.90 (3H, d, J = 1 Hz, C=C—CH_3), 2.80 (1H, d, J = 4 Hz, ring junction H(2)), 3.06 (1H, m, H(4)), 3.37 (1H, m, H(1)), 6.00 (2H, m, vinylic H(5) and H(6)), 6.47 (1H, bs, quinone C=C—H); ms m/e: 202 (M^+). The addition of Eu(hfc)$_3$ (16 mg) to the racemic *endo* adduct (10 mg) caused a diastereomeric shift difference of the quinone vinylic proton at δ 6.47, which was exhibited as two signals of equal intensity at δ 9.2 and δ 9.3.

*Addition of **5** with (−)-**1***

The Diels–Alder reaction of **5** (0.50 g, 0.0037 mol) and cyclopentadiene (0.48 g, 0.0073 mol) catalyzed by (−)-**1** (0.37 g, 0.0015 mol) in anhydrous toluene yielded, after preparative tlc (1-mm plates,

hexane – ethyl acetate 4:1), the pure *endo* adduct (0.65 g, 65%); $[\alpha]_D$ +4.6° (*c* 7, $CHCl_3$); ir, ^1H nmr, ms confirmed the structure. Addition of Eu(hfc)$_3$ (20 mg) to the *endo* adduct (10 mg) gave two diastereomeric quinone vinyl hydrogen signals (peak areas 54:46) at δ 10.0 and δ 10.1, corresponding to 8% ee.

Addition of 5 with (−)-2

The Diels–Alder addition of **5** (0.50 g, 0.0037 mol) and cyclopentadiene (0.48 g, 0.0073 mol) catalyzed by (−)-**2** (0.92 g, 0.0037 mol) was carried out at −78°C for 1 h, then additional cyclopentadiene (0.048 g, 0.0073 mol) was added and stirring was continued for 3 h. The product was purified by preparative tlc (1-mm plates, hexane – ethyl acetate 4:1) to give pure *endo* adduct (0.39 g, 53%); $[\alpha]_D$ +5.7° (*c* 9, $CHCl_3$); ir, ^1H nmr, ms confirmed the structure. Addition of Eu(hfc)$_3$ (20 mg) to the *endo* adduct (10 mg) produced two diastereomeric quinone vinyl hydrogen signals (peak areas 53:47) at δ 9.7 and δ 9.8, representing 6% ee.

Acknowledgements

Financial support by the Natural Sciences and Engineering Research Council of Canada in the form of an operating grant and a graduate fellowship (C.J.N.) is gratefully acknowledged. We thank Dr. S. Wojciech Markowicz, Lodz, Poland, who performed a preliminary study of various chiral Lewis acids during a sabbatical visit in this Department.

1. L. A. PAQUETTE. *In* Asymmetric synthesis. Vol. 3B. *Edited by* J. D. Morrison. Academic Press, Orlando, FL. 1984. p. 455.; W. OPPOLZER. Angew. Chem. Int. Ed. Engl. **23**, 876 (1984); G. HELMCHEN. *In* Modern synthetic methods. Vol. 4. *Edited by* R. Scheffold. Springer Verlag, New York. 1986. p. 262.
2. O. DIELS and K. ALDER. Justus Liebigs Ann. Chem. **460**, 98 (1928); J. SAUER. Angew. Chem. Int. Ed. Engl. **5**, 211 (1966); **6**, 16 (1967); Y. A. TITOV. Russ. Chem. Rev. **31**, 267 (1962); I. I. GUSEINOV and G. S. VASIL'EV. Russ. Chem. Rev. **32**, 20 (1963); J. G. MARTIN and R. K. HILL. Chem. Rev. **61**, 537 (1961).
3. (*a*) H. M. WALBORSKY, L. BARASH, and T. C. DAVIS. J. Org. Chem. **26**, 4778 (1961); Tetrahedron, **19**, 2333 (1963); (*b*) J. SAUER and J. KREDEL. Angew. Chem. Int. Ed. Engl. **4**, 989 (1965); Tetrahedron Lett. 6359 (1966); (*c*) R. F. FARMER and J. HAMER. J. Org. Chem. **31**, 2418 (1966); (*d*) H. E. ENSLEY, C. A. PARNELL, and E. J. COREY. J. Org. Chem. **43**, 1610 (1978); (*e*) D. A. EVANS, K. T. CHAPMAN, and J. BISAHA. J. Am. Chem. Soc. **106**, 4261 (1984); (*f*) W. OPPOLZER and D. DUPUIS. Tetrahedron Lett. 5437 (1985).
4. S. DAVID, A. LUBINEAU, and A. THIEFFRY. Tetrahedron, **34**, 299 (1978); S. DAVID, J. EUSTACHE, and A. LUBINEAU. J. Chem. Soc. Perkin Trans. 1, 1795 (1979); S. DAVID and J. EUSTACHE. J. Chem. Soc. Perkin Trans. 1, 2230 (1979); B. M. TROST, D. O'KRONGLY, and J. L. BELLETIRE. J. Am. Chem. Soc. **102**, 7595 (1980); W. G. DAUBEN and R. A. BUNCE. Tetrahedron Lett. 4875 (1982); W. OPPOLZER and E. FLASKAMP. Helv. Chim. Acta, **60**, 204 (1977).
5. S. G. PYNE, M. J. HENSEL, S. R. BYRN, A. T. MCKENZIE, and P. L. FUCHS. J. Am. Chem. Soc. **102**, 5960 (1980); L.-F. TIETZE and G. V. KIEDROWSKI. Tetrahedron Lett. 219 (1981); T. MUKAIYAMA and N. IWASAWA. Chem. Lett. 29 (1981); Y. ITO, Y. AMINO, M. NAKATSUKA, and T. SAEGUSA. J. Am. Chem. Soc. **105**, 1586 (1983).
6. K. N. HOUK and R. W. STROZIER. J. Am. Chem. Soc. **95**, 4094 (1973); D. J. BURNELL, H. B. GOODBRAND, S. M. KAISER, and Z. VALENTA. Can. J. Chem. **62**, 2398 (1984).
7. I. FLEMING. Frontier orbitals and organic chemical reactions. John Wiley and Sons, Inc., New York. 1976; K. N. HOUK. Acc. Chem. Res. **8**, 361 (1975).
8. M. BEDNARSKI, C. MARING, and S. DANISHEFSKY. Tetrahedron Lett. 3451 (1983); M. BEDNARSKI and S. DANISHEFSKY. J. Am. Chem. Soc. **105**, 3716 (1983).
9. T. R. KELLY, A. WHITING, and N. S. CHANDRAKUMAR. J. Am. Chem. Soc. **108**, 3510 (1986).
10. S. HASHIMOTO, N. KOMESHIMA, and K. KOGA. Chem. Commun. 437 (1979).
11. P. DESLONGCHAMPS. Stereoelectronic effects in organic chemistry. Pergamon Press, London. 1983.
12. J. JURCZAK and A. ZAMOJSKI. Tetrahedron, **28**, 1505 (1972); J. JURCZAK and M. TKACS. J. Org. Chem. **44**, 3347 (1979); W. CHOY, L. A. REED III, and S. MASAMUNE. J. Org. Chem. 1137 (1983); T. POLL, Z. SOBCZAK, H. HARTMANN, and G. HELMCHEN. Tetrahedron lett. 3095 (1985); O. ACHMATOWICZ, JR. and M. PIETRASZKIEWICZ. Polish J. Chem. **56**, 511 (1982).
13. B. B. SNIDER, D. J. RODINI, M. KARRAS, T. C. KIRK, E. A. DEUTSCH, R. CORDOVA, and R. T. PRICE. Tetrahedron, **37**, 3927 (1981); G. GIACOMELLI and L. LARDICCI. J. Org. Chem. **47**, 4335 (1982).
14. Y. HAYAKAWA, R. FUENO, and J. FURUKAWA. J. Polym. Sci. Part A-1, **5**, 2099 (1967).
15. R. J. LONCHARICH, T. R. SCHWARTZ, and K. N. HOUK. J. Am. Chem. Soc. **109**, 14 (1987).
16. J. A. BERSON and A. REMANICK. J. Am. Chem. Soc. **83**, 4947 (1961).
17. J. A. BERSON, J. S. WALLA, A. REMANICK, S. SUZUKI, P. REYNOLDS-WARNHOFF, and D. WILLNER. J. Am. Chem. Soc. **83**, 3986 (1961).
18. J.-L. GRAS. Org. Synth. Vol. **60**, 88 (1980).
19. F. G. FISCHER and K. WUNDERLICH. Chem. Ber. **74**, 1544 (1941).

Can. J. Chem. Downloaded from www.nrcresearchpress.com by 118.98.75.50 on 09/07/12
For personal use only.

Partial molar volumes of phenalkylamines and their physiologically active derivatives in water

FEREIDOON SHAHIDI

Department of Biochemistry, Memorial University of Newfoundland, St. John's, Nfld., Canada A1B 3X9

Received January 10, 1987

This paper is dedicated to Professor John T. Edward

FEREIDOON SHAHIDI. Can. J. Chem. **65**, 1924 (1987).

The partial molar volumes at infinite dilution, V^0, for a number of phenalkylamines, their physiologically active derivatives, and their hydrochloride salts have been measured and related to their van der Waals volumes. Results indicate a value of 13.8 mL mol^{-1} for the electrostriction of water molecules by the terminal $\overset{+}{N}H_3$ group. Volumes of proton ionization in these compounds vary between 2.90 and 6.26 mL mol^{-1}.

FEREIDOON SHAHIDI. Can. J. Chem. **65**, 1924 (1987).

On a mesuré les volumes molaires partiels à dilution infinie, V^0, d'un certain nombre de phénylalkylamines, de leurs dérivés physiologiquement actifs et de leurs chlorhydrates et on a établi une corrélation avec leurs volumes de van der Waals. Les résultats indiquent que l'électrostriction des molécules d'eau par les groupements $\overset{+}{N}H_3$ terminaux est égale à 13,8 mL mol^{-1}. Dans ces composés, les volumes d'ionisation des protons varient de 2,90 à 6,26 mL mol^{-1}.

[Traduit par la revue]

Introduction

One of the most exciting fields in experimental medicine and medicinal chemistry which has advanced over the past thirty years is the work done by neurochemists for the discovery of the chemical messengers or brain chemicals (1–5). The simplest of these neurotransmitters are dopamine, noradrenaline, etc. They are products of enzymatic conversion of tyrosine and are stored in the vesicles of nerve cells. Deficiency of dopamine is found to result in Parkinson's disease and its over-firing causes some forms of paranoid schizophrenia. Dopamine deficiency may be treated with L-dihydroxyphenylalanine (L-DOPA) which appears to indirectly provide dopamine and is over-firing may be treated using dopamine blocking agents such as phenothiazines and other antipsychotic drugs. Although a lot of work has recently been concentrated on the medicinal aspects of these chemicals and their analogues, there has been no attempt to investigate their physicochemical and thermodynamic properties.

In this paper we report on our results for the partial molar volumes for a number of phenalkylamines and their physiologically active derivatives, both as free amines and their hydrochloride salts in water.

Experimental

All the compounds used in this work were reagent-grade commercial products and phenalkylamines were further purified by distillation. Solutions of the corresponding hydrochlorides were prepared just prior to use by titration with stoichiometric amounts of standardized HCl solution.

Density measurements were carried out at 25.00 ± 0.01°C using a Paar digital precision densimeter model DMA 02C. At least eight measurements at concentrations of 0.2–2.0% were carried out for each compound.

The apparent molar volumes, ϕ_v, were obtained from eq. [1] in each case.

$$[1] \quad \phi_v = M(1/d - W_1/d^0)W_2$$

where M is the molecular weight of the solute, W_2 its weight fraction, W_1 the weight fraction of the solvent, and d and d^0 are the densities of the solution and of water, respectively.

The hydrochlorides of the amines studied dissociate in aqueous solution to a very limited extent and the maximum corrections required to account for such processes are <0.1 mL mol^{-1}, thus within the experimental error and were ignored (6).

The partial molar volumes at infinite dilution for phenalkylamines and their derivatives were obtained from least-squares fit of the experimental ϕ_v's against molar concentration ($\phi_v = V^0 + hC$) and the V^0 values and b_v, the deviation constants, for their corresponding hydrochlorides were calculated using equation (2) (7, 8).

$$[2] \quad \phi_v = V^0 + 1.868\sqrt{C} + b_vC$$

The molar concentrations, C, were deduced from weight fraction and density data.

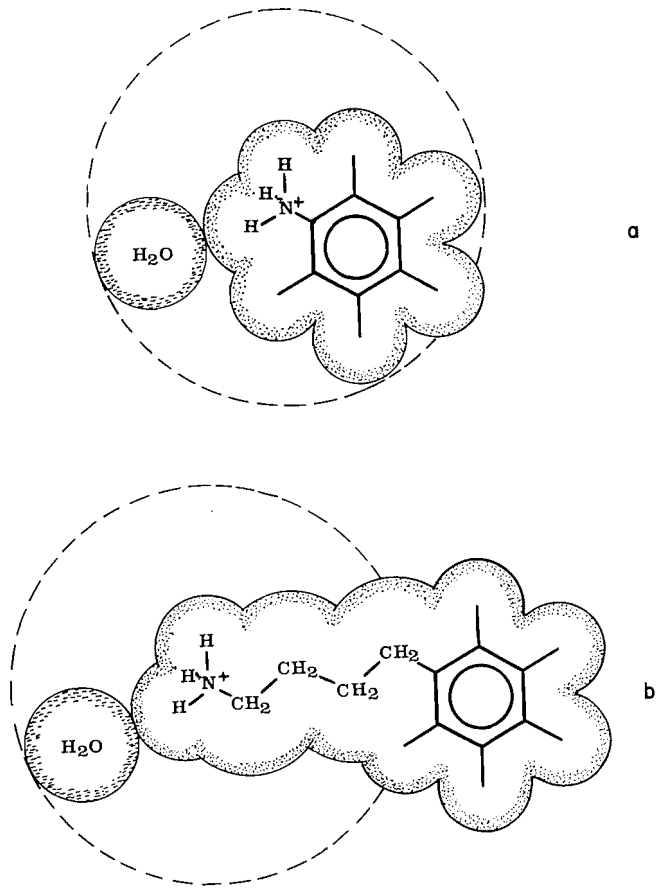

FIG. 1. Scale drawing of *a*, anilinium ion, and *b*, phenbutylammonium ion showing the extent of the first hydration sphere around the $\overset{+}{N}H_3$ group.

Can. J. Chem. Downloaded from www.nrcresearchpress.com by 118.98.75.50 on 09/07/12
For personal use only.

TABLE 1. Partial molar volumes, V^0, of phenalkylamines, Ph—$(CH_2)_n$—NH_2, and their hydrochloride salts in water at 25°C

	V^0/mL mol^{-1}			
n	Expt.	Calcd.[a]	$V^0(CH_2)$/mL mol^{-1}	b_v/mL L mol^{-2}
	Phenalkylamines			
0	89.51 ± 0.16[b]	89.23		—
1	105.11 ± 0.70	105.20	15.60	—
2	120.90 ± 0.30	121.17	15.79	—
3	137.30 ± 0.30	137.13	16.40	—
4	153.30 ± 0.40	153.11	16.00	—
	Phenalkylamine hydrochlorides			
0	101.99 ± 0.08[c]	101.45		−0.66 ± 0.34
1	117.07 ± 0.10	117.42	15.08	−0.40 ± 0.62
2	133.28 ± 0.22	133.39	16.21	−2.37 ± 0.87
3	149.38 ± 0.08	149.36	16.10	−3.67 ± 1.48
4	165.62 ± 0.05	165.34	16.24	−3.75 ± 1.30

[a]Calculated using eq. [3] with a = 15.61, b = 2.13 mL mol^{-1} for phenalkylamines and a = 1.561, b = −11.66 mL mol^{-1} for their corresponding hydrochlorides. The V^0 of chloride ion has not been included in these calculations.
[b]Reference 18 reports 89.30 mL mol^{-1}.
[c]Reference 18 reports 102.74 and ref. 19 reports 101.9 mL mol^{-1}.

TABLE 2. Partial molar volumes, V^0, of physiologically active derivatives of phenethylamine and their hydrochlorides in water at 25°C

Compound	Structure	V^0(B)/mL mol^{-1}	V^0(B.HCl)/mL mol^{-1}	b_v/mL L mol^{-2}
Amphetamine	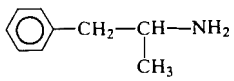	137.54 ± 0.38[a]	151.20 ± 0.12	−1.86 ± 0.64
Tyramine	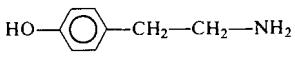	124.35 ± 0.35	135.57 ± 0.04	−3.59 ± 0.33
Dopamine	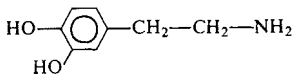	125.68 ± 0.35	136.87 ± 0.15	−1.62 ± 1.50
dl-Adrenaline (norepinephrine)	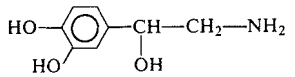	126.88 ± 0.40	138.07 ± 0.13	−5.03 ± 2.30
l-Epinephrine	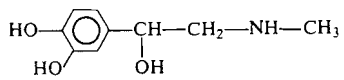	142.51 ± 0.50	156.20 ± 0.10	−1.67 ± 0.40
Ephedrine	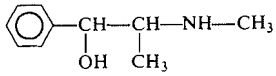	153.96 ± 0.26	168.46 ± 0.39	−1.24 ± 0.93

[a]Average of three determinations at 0.2 to 0.4% concentration.

Results and discussion

Limiting partial molar volumes for phenalkylamines, Ph—$(CH_2)_n$—NH_2, and their hydrochlorides in water are reported in Table 1, together with the deviation constants, b_v, and the calculated V^0 values based on the equation

[3] $V^0 = aV_w + b$

where V_w is the van der Waals volume (9) and a and b are empirical constants derived from the least-squares fit of V^0 against V_w (10), and depend on the type of solute molecules and the nature of the solvent. The calculated values of V^0 are in excellent agreement with the experimental results. From the b values of eq. [3] for phenalkylamines and their hydrochlorides a value of 13.8 mL mol^{-1} may be calculated for the electrostriction of water molecules by the terminal $\overset{+}{N}H_3$ group. This is in accord with values of 12.8–14.5 mL mol^{-1} obtained for $\overset{+}{N}H_3$ in diamines (6), amino acids (11, 12), and their derivatives (13). The b_v values in eq. [2] are all negative for phenalkylamines hydrochlorides and descend with increasing chain length, as observed for other homologous series (6, 13, 14). The h values for phenalkylamines and phenethylamine derivatives were close to zero (in the concentration ranges studied) and did not follow any discernible trends.

The volume increment for methylene groups are all about 16.0 ± 0.4 mL mol^{-1} except for that of benzylamine hydrochloride. The smaller $V^0(CH_2)$ in benzylammonium ion is due to the changes in electrostriction of water molecules by $\overset{+}{N}H_3$ and changes in hydrophobic hydration of the benzene ring. It has been suggested that substitution of a hydrogen atom on $\overset{+}{N}H_3$ or on the carbon atoms adjacent to it by an alkyl group excludes

Can. J. Chem. Downloaded from www.nrcresearchpress.com by 118.98.75.50 on 09/07/12
For personal use only.

TABLE 3. Volumes of proton ionization, V^0_I and pK_a values for phenalkylammonium ions and their derivatives in water at 25°C

Compound	V^0_I/mL mol^{-1}	pK_a[a]
Aniline	5.52 ± 0.33	4.60
Benzylamine	5.79 ± 0.89	9.62
Phenethylamine	5.44 ± 0.61	9.82
3-Phenyl-*n*-propylamine	5.72 ± 0.47	10.16
4-Phenyl-*n*-butylamine	5.48 ± 0.54	10.36
Amphetamine	3.80 ± 0.59	10.03
Tyramine	6.26 ± 0.48	9.22
Dopamine	5.67 ± 0.59	8.93
dl-Adrenaline	6.03 ± 0.62	8.58
l-Epinephrine	4.11 ± 0.69	8.55
Ephedrine	2.90 ± 0.74	9.52

[a] Values from ref. 20.

some of the electrostrictive water molecules surrounding the $\overset{+}{N}H_3$ group (15). Removal of the alkyl substituent further away from the vicinity of the $\overset{+}{N}H_3$ group is therefore responsible for the observed $V^0(CH_2)$ in benzylammonium ion. (There are two β carbon atoms adjacent to $\overset{+}{N}H_3$ group in anilinium ion, whereas only one β carbon atom is present for $\overset{+}{N}H_3$ group in benzylamine.) Similar differences were observed for the V^0 values of isomeric butylamines hydrochlorides (16). The extent of the first hydration shell around $\overset{+}{N}H_3$ group for anilinium and phenbutylammonium ions are shown in Fig. 1, indicating that only small electrostatic changes may be expected in the volumic effects by introduction of intervening methylene groups between the phenyl and $\overset{+}{N}H_3$ groups for phenalkylamines. Partial removal of the fourth intervening methylene group from within the $\overset{+}{N}H_3$ hydration shell of phenbutylamine lends further support to this view.

In Table 2, the V^0 values for phenethylamine derivatives are assembled. From the data presented, an average volume increment, $V^0_{(H\rightarrow OH)}$, of 1.9 ± 0.5 mL mol^{-1} may be calculated for the replacement of a hydrogen atom by an OH group. This agrees well with a value of 2.1 ± 0.4 mL mol^{-1} obtained for hydroxy-containing amino acids (12). Replacement of a hydrogen atom on the α-carbon by a methyl group, $V^0_{(H\rightarrow CH_3)}$, results in a volume increase of 16.3 and 17.3 mL mol^{-1} for phenalkylamines and their hydrochlorides, respectively. A volume change of 18.1 mL mol^{-1} may be obtained when the substitution occurs on a $\overset{+}{N}H_3$ group. These larger volume increments in amine hydrochlorides are caused by the effect of the charge on the orientation of water molecules around the methyl substituent, as well as its effects on reducing the electrostriction of water molecules by the charged group (15, 17). The b_v values for phenethylamine derivatives of Table 2 do not follow any discernible trend.

Volumes of proton ionization, ΔV^0_I, together with the pK_a values for the protonated amines tabulated in Tables 1 and 2 are shown in Table 3. Results indicate that except for epinephrine, ephedrine, and amphetamine, ΔV^0_I values are almost constant for the amines studied in this work. Methylation on α-carbon atom or the nitrogen centre reduces the volumes of proton ionization (epinephrine, ephedrine, and amphetamine), in support of our previous findings for other systems (12, 17) and in agreement with the general expectation that secondary amines have lower ΔV^0_I values than primary amines.

1. S. G. POTKIN, F. KAROUM, L.-W. CHUANG, H. E. CANNON-SPOOR, I. PHILLIPS, and R. J. WYATT. Science, **206**, 470 (1979).
2. S. TURNER. Chem. Brit. **14**, 603 (1978).
3. ANONYMOUS. Chem. Eng. News. 1980. May 26 issue, p. 24.
4. J. FOX. Chem. Eng. News. 1981. Nov. 2 issue, p. 26.
5. J. L. NEUMEYER, S.-I. LAW, R. J. BALESSARINI, and N. S. KULA. J. Med. Chem. **23**, 595 (1980).
6. F. SHAHIDI and P. G. FARRELL. J. Soln. Chem. **7**, 549 (1978).
7. O. REDLICH and D. M. MEYER. Chem. Rev. **64**, 221 (1964).
8. F. J. MILLERO. Chem. Rev. **71**, 147 (1971).
9. J. T. EDWARD. J. Chem. Educ. **47**, 261 (1970); A. BONDI. J. Phys. Chem. **68**, 441 (1964).
10. S. TERASAWA, H. ITSUKI, and S. ARAKAWA. J. Phys. Chem. **79**, 2345 (1975).
11. F. SHAHIDI and P. G. FARRELL. J. Chem. Soc. Faraday Trans. I, **74**, 858 (1978).
12. F. SHAHIDI and P. G. FARRELL. J. Chem. Soc. Faraday Trans. I, **77**, 963 (1981).
13. F. SHAHIDI. J. Chem. Soc. Faraday Trans. I, **76**, 101 (1980).
14. J. E. DESNOYERS and M. AREL. Can. J. Chem. **45**, 359 (1967).
15. R. ZANA. J. Phys. Chem. **81**, 1817 (1977).
16. M. SAKURAI, T. KOMATSU, and T. NAKAGAWA. J. Soln. Chem. **4**, 511 (1975).
17. F. SHAHIDI and P. G. FARRELL. J. Chem. Soc. Faraday Trans. I, **74**, 1268 (1978).
18. R. H. STOKES. Aust. J. Chem. **28**, 2109 (1975).
19. S. D. HAMANN and S. C. LIN. Aust. J. Chem. **7**, 329 (1954).
20. D. D. PERRIN. Dissociation constants of organic bases in aqueous solution. Butterworths, London. 1965; H. A. SOBER. Handbook of biochemistry, selected data for molecular biology. The Chemical Rubber Co., Cleveland. 1968.

Can. J. Chem. Downloaded from www.nrcresearchpress.com by 118.98.75.50 on 09/07/12
For personal use only.

Immobilized replicates of sequence 136–148 of human serum albumin as adsorbents for bilirubin

M. BOUVIER, G. R. BROWN, AND L. E. ST-PIERRE
Department of Chemistry, McGill University, Montreal, P.Q., Canada H3A 2K6

Received January 2, 1987

This paper is dedicated to Professor John T. Edward

M. BOUVIER, G. R. BROWN, and L. E. ST-PIERRE. Can. J. Chem. **65**, 1927 (1987).

Strategic peptide sequences, patterned on the sequence 136–148 of the primary structure of human serum albumin, have been immobilized on a cross-linked polyacrylamide support using the solid phase peptide synthesis technique. Certain of the resulting materials proved to be efficient adsorbents for bilirubin from aqueous phosphate buffer solution. Amino acids such as lysine and arginine favour the binding of the ligand, whereas glutamic acid reduces it markedly. From Scatchard plots, first and second equilibrium binding constants, in the range of $(0.3–9.6) \times 10^4\ M^{-1}$, were obtained using a site treatment. These binding constants are comparable to that for the binding of bilirubin by a larger fragment of bovine serum albumin that contains the synthesized sequence.

M. BOUVIER, G. R. BROWN et L. E. ST-PIERRE. Can. J. Chem. **65**, 1927 (1987).

Des chaînes peptidiques identiques à la séquence 136–148 de la structure primaire de l'albumine humaine ont été immobilisées sur un support de polyacrylamide réticulé en utilisant la synthèse en phase solide des peptides. Certains des polymères à contenu peptidique ainsi obtenus se sont avérés être d'excellents adsorbants pour la bilirubine lorsque testés en milieu tampon. La présence d'acides aminés tels que l'arginine et la lysine dans la séquence peptidique favorisent l'adsorption du ligand tandis que l'acide glutamique la réduit appréciablement. Des constantes d'associations de l'ordre de $(0{,}3–9{,}6) \times 10^4\ M^{-1}$ ont été obtenues pour ces adsorbants directement des courbes de Scatchard à l'aide d'un traitement mathématique basé sur les sites d'adsorption. Ces constantes d'associations sont comparables à celle pour l'association de la bilirubine sur un fragment de l'albumine bovine qui contient la séquence synthétisée.

Can. J. Chem. Downloaded from www.nrcresearchpress.com by 118.98.75.50 on 09/07/12
For personal use only.

Introduction

The tetrapyrrole bile pigment bilirubin (Fig. 1*a*) is a product of the catabolism of hemoglobin from aged red blood cells. It is bound, in the blood, to human serum albumin (HSA) with each protein molecule having a capacity for strong binding of two bilirubin molecules (1). A number of pathologies exist in which the concentration of bilirubin is in excess of that which the HSA can accommodate (2). This results in an elevated free bilirubin concentration that is toxic and can cause a number of disorders, including some that are life threatening.

The removal of excess bilirubin from the blood has been the subject of much research and a number of techniques have been developed to this end. Included in these are certain photoirradiation and hemoperfusion methods.

Hemoperfusion treatments require the use of adsorbents that can bind bilirubin. These include cholestyramine (3, 4), a polymer with quaternary ammonium functional groups, and similar materials (4, 5) that are thought to act as ion-exchange resins by interacting with the two carboxyl groups of bilirubin. However, none of the existing adsorbents is entirely satisfactory for clinical use, their main shortcomings being nonspecificity and low capacity. Indeed, the most selective adsorbent thus far investigated, in terms of plasma components, has been immobilized HSA (6). However, the utility of this material is severely limited because of a low capacity, binding only two bilirubin molecules on a molecule of molecular weight in excess of 66 000.

The ideal adsorbent for bilirubin would exhibit high specificity, biocompatibility, and high capacity. With knowledge of the primary structure of HSA (7, 8) and information available concerning the possible location of the binding sites for bilirubin on that molecule (9–13), it is possible to synthesize onto a suitable polymer support peptide sequences that are replicates of corresponding sections of the primary structure of HSA and to test these materials as adsorbents for bilirubin.

Previous studies from this laboratory have demonstrated that peptide chains consisting of the basic amino acids, arginine or lysine, attached to a cross-linked polyacrylamide support are good adsorbents for bilirubin (14, 15). The binding capacity was shown to depend markedly on the number and arrangement of amino acids in the sequence. This paper describes the synthesis of a series of peptide resins replicating sections of HSA and their properties as adsorbents. A secondary goal was to attempt to shed light on the location of the binding sites for bilirubin on HSA and, to this end, site binding constants have been calculated and compared to those for the binding of bilirubin on the protein.

Experimental

1. Syntheses of peptide resins

The peptide resins were synthesized onto 11% cross-linked polyacrylamide support (Chemalog), which is a copolymer of dimethylacrylamide and *N*-acryl-1,6-diaminohexane reticulated with bisacrylyl-1,2-diaminoethane. The polymer substitution as determined by potentiometric titration with $AgNO_3$ was 0.22 mmol/g. Amino acids were purchased from Vega Biotechnologies as the L form of the Boc-α-amino acids with the side-chain groups protected as follows: Arg(nitro), Glu-(γ-benzyl ester), Tyr(*O*-benzyl), His-(N^{im}-tosyl), Lys-(ε-2-chloro-benzyloxycarbonyl). (Three letter symbols are used for designations of the amino acids as recommended by the Joint Commission on Biochemical Nomenclature of IUPAC-IUB.) Solvents used for synthesis were distilled, except dichloromethane (DCM), which was dried over molecule sieves, Type 4A.

Syntheses were done using a Vega 250 Synthesizer according to a previously published program (14):

"The resin was initially neutralized with 40% diisopropylethylamine (DIEA)/DCM for 20 minutes. Activated amino acids in the form of symmetrical anhydrides were used for coupling reactions. The anhydrides were pre-formed as follows: 6 equivalents of Boc-α-amino acid were dissolved in DCM (dimethylformamide (DMF) for Arg(nitro)) at 0°C. To this solution 3 equivalents of 10% dicyclohexylcarbodiimide (DCC)/DCM (10% DCC/DMF for Arg(nitro)) were slowly added.

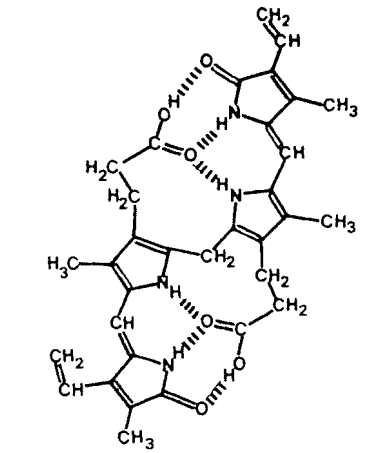

(a)

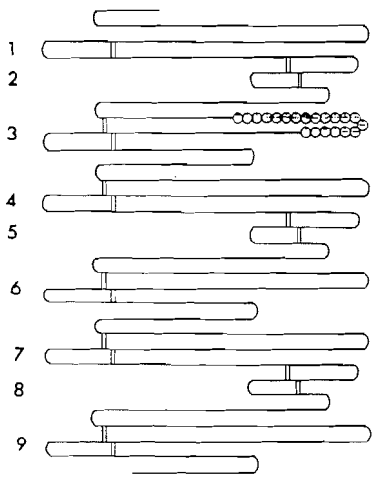

(b)

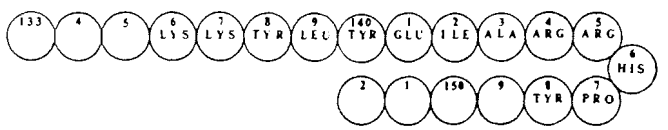

(c)

FIG. 1. (*a*) Structure of bilirubin. (*b*) Illustration of human serum albumin structure displaying the location of the replicated sequence. (*c*) Primary structure of the replicated sequence 136–148, which was immobilized on a polyacrylamide support.

After allowing the mixture to stir for about 30 minutes at 0°C, dicyclohexylurea was filtered off and the filtrate added directly to the flask containing the resin. The reaction was left until satisfactory coupling was obtained, as indicated by a positive ninhydrin test (16). After completion of the coupling step, Boc amino protecting groups were removed using 40% trifluoroacetic acid/DCM followed by neutralization with 5% DIEA/DCM. Deprotection steps were also monitored by the ninhydrin test."

Samples of the peptide resins were removed at strategic points during the course of the synthesis. At the completion of the syntheses, the protecting groups on the side chains of the amino acids were removed by treating the dried peptide resins with anhydrous hydrogen fluoride in the presence of anisole for 60 min at 0°C (30 min at −20°C followed by 30 min at 0°C for peptide resins containing glutamic acid residues). A spacer made of one alanine residue was incorporated at the beginning of the sequence to keep the active portion of the peptide away from the polymer backbone.

2. Amino acid analysis

Peptide resins 10 mg (1–2 μmol of peptide) were hydrolyzed at 110°C for 48 h in a vacuum reaction tube using degassed propionic acid (Gold label, Aldrich), 0.29 mL, and hydrochloric acid 11.90 *M* (Suprapur, BDH), 0.5 mL. After hydrolysis, the acidic solution was filtered and the remaining resin was washed several times with a small portion of water. The filtrate was collected in a test tube and evaporated to dryness under vacuum. The amino acids were then dissolved with sodium citrate dilution buffer pH 2.2, 0.20 *N* (Pierce) in a 10-mL volumetric flask to which 1 mL of 5 m*M* nitrotyrosine solution had been added as an internal standard. Amino acid analyses were performed using a Varian 5500 Analyzer.

3. Adsorption experiments

To determine the times required for equilibrium adsorption data, kinetic studies were done with each of the synthesized peptide resins using a degassed bilirubin (from bovine gallstones, Sigma) solution, 10 mg/dL in a 0.050 *M* KH_2PO_4/NaOH buffer at pH 7.80. An aliquot of 25 mL of that solution was added to 10 mg of a peptide resin and the mixture was stirred at 0°C under nitrogen, as described previously (14). Using a Beckman 25 spectrophotometer, absorbance values for free bilirubin were taken at 438 nm with aliquots withdrawn at 15-min intervals during the first hour and every 30 min thereafter until a constant absorbance was obtained.

Adsorption experiments were then performed with bilirubin solutions of different initial concentrations, up to a maximum of 10 mg/dL in a 0.050 *M* degassed phosphate buffer at pH 7.80. An aliquot of 25 mL of one of the above solutions was added to 10 mg of a peptide resin and the mixture stirred at 0°C under nitrogen for as long as required for the system to reach equilibrium.

Results and discussion

1. Rationalization for choice of sequence

The sequence selected for synthesis is the fragment 136–148 (Fig. 1*c*). Its location in the protein is illustrated in Fig. 1*b*, which exhibits the structure of human serum albumin as determined by Brown and co-workers (7).

The rationale involved in the choice of this fragment is as follows: First, the sequence consists of five basic, five hydrophobic, and three polar amino acid residues, as shown in Table 1. Therefore various types of interactions between bilirubin and these residues are possible. Furthermore, this sequence has an overall basic character at the pH used for the adsorption experiments, with the net charge being +3. This particular feature of the sequence is of interest for the binding of a dianion such as bilirubin. The sequence contains all of the active amino acids, arginine, histidine, tyrosine, and lysine, suggested by Jacobsen to be at or near the strong binding site for bilirubin on HSA (17, 18). Interestingly enough, this fragment also seems to be the only one in the entire protein that, over a short range of amino acids, contains these four residues. It is noteworthy that bovine serum albumin (BSA) and α-fetoprotein, two other proteins which also bind bilirubin, both have very similar primary structures in the region of the selected fragment. Furthermore, the choice of this sequence is based on its particular location in HSA. It forms the tip of loop no. 3 (Fig. 1*b*) and, according to Brown's model for the tertiary structure of albumin (19), the tips of loops form the entrance to narrow channels proposed to be suitable binding locations for bulky ligands like bilirubin. Therefore, the selected sequence within loop no. 3 could very well represent a binding site for bilirubin, owing to its location, and its attachment to a polymer support could produce an efficient adsorbent for bilirubin.

Can. J. Chem. Downloaded from www.nrcresearchpress.com by 118.98.75.50 on 09/07/12
For personal use only.

TABLE 1. Characterization of the amino acids forming the replicate fragment 136–148 of human serum albumin immobilized on a polyacrylamide support

Residues	Amino acids	Resin designation	Classification	Charge (pH 7.80)
		1 2 3 4 5 6		
Spacer	Ala	↑ ↑ ↑ ↑ ↑ ↑	Hydrophobic	
148	Tyr	↓ ↑ ↑ ↑ ↑ ↑	Polar	
147	Pro	↓ ↑ ↑ ↑ ↑ ↑	Hydrophobic	
146	His	↓ ↑ ↑ ↑ ↑ ↑	Basic	
145	Arg	↑ ↓ ↑ ↑ ↑ ↑	Basic	+
144	Arg	↑ ↓ ↑ ↑ ↑ ↑	Basic	+
143	Ala	↑ ↑ ↓ ↑ ↑ ↑	Hydrophobic	
142	Ile	↑ ↑ ↓ ↑ ↑ ↑	Hydrophobic	
141	Glu	↑ ↑ ↑ ↓ ↑ ↑	Acidic	−
140	Tyr	↑ ↑ ↑ ↓ ↑ ↑	Polar	
139	Leu	↑ ↑ ↑ ↓ ↑ ↑	Hydrophobic	
138	Tyr	↑ ↑ ↑ ↑ ↓ ↑	Polar	
137	Lys	↑ ↑ ↑ ↑ ↓ ↑	Basic	+
136	Lys	↑ ↑ ↑ ↑ ↑ ↓	Basic	+

TABLE 2. Amino acid analysis of some peptide resins forming the replicate sequence 136–148 of human serum albumin

^{6}Lys-Lys-^{5}Tyr-Leu-Tyr-^{4}Glu-Ile-^{3}Ala-Arg-^{2}Arg-^{1}His-Pro-Tyr-Ala-polymer	
-(0.8-0.8-0.8-1)-	Resin 1
-(0.8)-	Resin 2
-(0.6-0.6)-	Resin 3
-(0.6-0.6)-	Resin 4
-(0.4-0.4-0.4)-	Resin 5
(0.2-0.2)-	Resin 6

2. Amino acid analysis

Results from peptide resin hydrolysis are given in Table 2 in the form of ratios based on the recovery of the alanine residue of resin 1. The data indicate a loss in the number of growing peptide chains as each succeeding fragment of the sequence is added, with the exceptions of resins 2 and 4. Peptide chain terminations through mechanisms such as resistance of Boc protecting groups to deprotection reagents, amino groups buried in the porous polymer matrix and thus not accessible to the activated amino acids for coupling, can account for failure in the growth of some of the peptide chains (20). The percentage of cross-links in the support used is relatively high and therefore diffusion of the reagents through it is made more difficult than in supports regularly used in solid phase peptide synthesis.

3. Adsorption isotherms

The kinetic studies demonstrated that the peptide resins have saturation times varying between 1 and 2 h. The peptide resins that showed greater binding capacities required between 1.5 and 2 h to reach equilibrium, with the largest change in adsorption occurring within the first hour. Times necessary to obtain equilibrium adsorption isotherms for the peptide resins were based on this information.

Figure 2 shows the equilibrium adsorption isotherms, obtained at 0°C, for the seven synthesized adsorbents that describe in a systematic way the adsorption behaviour of the growing replicate sequence 136–148 of HSA. The parameter r represents the equilibrium molar ratio of bound bilirubin per peptide pendant in the polymer and [A] is the equilibrium concentration of free bilirubin. The curves drawn through the experimental points are derived from a nonlinear iterative computer program, NLIN from SAS (SAS Institute, 1982), using a method described previously (21).

As indicated by the amino acid analyses, a substantial fraction of the pendants terminated at various stages of the synthesis. Consequently, in certain cases the material used for adsorption contained a mixture of pendant lengths. The composition of the mixture can be defined on the basis of the analyses, assuming that a terminated sequence cannot be extended by subsequent syntheses. Adsorption isotherms obtained by normalizing the curves from Fig. 2, in accordance with the hydrolysis data in Table 2, are shown in Fig. 3. This normalization process assumes that the binding behaviour of each type of pendant is not influenced by the presence of other types of pendants. That is, those peptide chains that lacked the amino acids added to form the subsequent peptide resin retain an adsorption capacity that is unaffected by the presence of the other successfully synthesized pendants. Consequently, each normalized isotherm represents the adsorption behaviour of an adsorbent having identical peptide sequences.

The isotherms show that the trend in adsorption, within the range of concentrations used, is not related in a simple manner to the length of the peptide chains. This is in agreement with results obtained previously in this laboratory (15). After the addition of the sequence His-Pro-Tyr-Ala- to the polymer support to form resin 1, the binding capacity remains similar to that of the polymer itself, as shown in Fig. 3. This peptide sequence consists of four different amino acids, of which

Can. J. Chem. Downloaded from www.nrcresearchpress.com by 118.98.75.50 on 09/07/12
For personal use only.

Can. J. Chem. Downloaded from www.nrcresearchpress.com by 118.98.75.50 on 09/07/12
For personal use only.

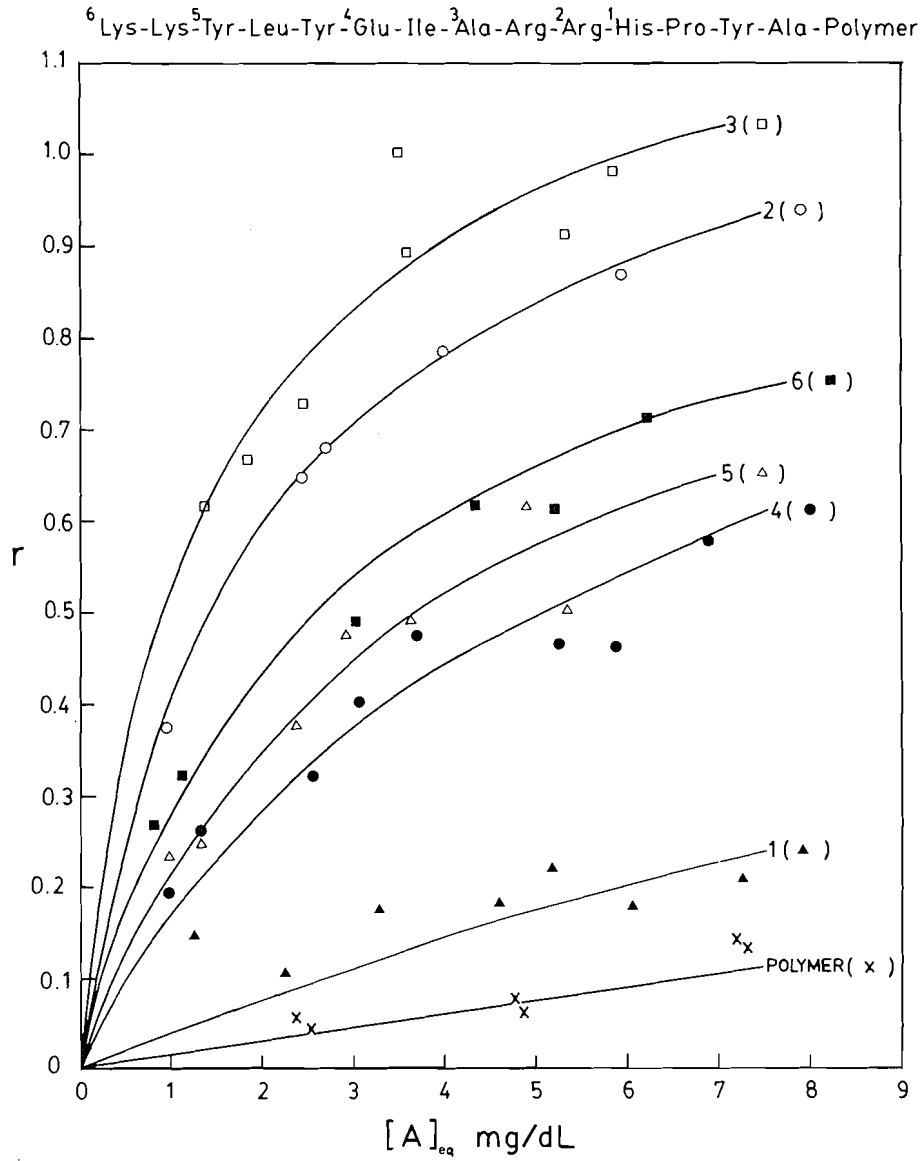

FIG. 2. Experimental equilibrium isotherms for the adsorption of bilirubin on peptide resins that replicate the sequence 136–148 of HSA.

histidine and tyrosine were proposed to be active in the binding of bilirubin on albumin (17). The combination of these two residues with alanine and proline forms an adsorbent that is only moderately active in binding bilirubin.

A large increase in binding capacity occurs following the coupling of one arginine residue to the previous fragment, resin 2. This behaviour reinforces the results of C. Jacobsen regarding the importance of arginine for the binding of bilirubin. The addition of a second arginine, resin 3, has a modest beneficial effect, the increase being much less than that due to the first arginine.

Addition of isoleucine and glutamic acid to form resin 4 results in a sharply diminished binding capacity. This can be attributed to the presence of the negatively charged glutamic acid. The addition of the Tyr-Leu-Tyr- segment, resin 5, causes a small increase in binding capacity over that of the previous peptide resin, probably due to the tyrosine, as indicated by resin 1.

Finally, the replicate sequence 136–148 ends with the addition of two lysine residues, resin 6, resulting in a considerable increase in binding capacity, especially at low bilirubin concentrations. These two basic residues have negated the effect of the glutamic acid residue. However, the adsorption isotherm fails to return to the maximum level exhibited by the sequence containing the first 7 amino acids, i.e., resin 3.

From the adsorption isotherms it is apparent that resins 2 and 3 will exhibit saturation at levels in excess of 1 mole of bound bilirubin per mole of pendant, while resins 1, 4, and 5 saturate at 1 mole, or less, of bound bilirubin per mole of pendant. Within the experimental range of concentration, resin 6 is the only adsorbent that definitely attains saturation (at $r = 1.1$). Thus, resin 6 will be considered similar to resins 1, 4, and 5 in terms of binding capacity, and will hereafter be considered as an adsorbent that has, within experimental error, one binding site per pendant.

These adsorption results support a binding mechanism that involves electrostatic interactions between the positively charged functional groups of the constituent amino acids and the negatively charged carboxyl groups on the bilirubin molecule. Previous results with peptide resins that have arginine and lysine

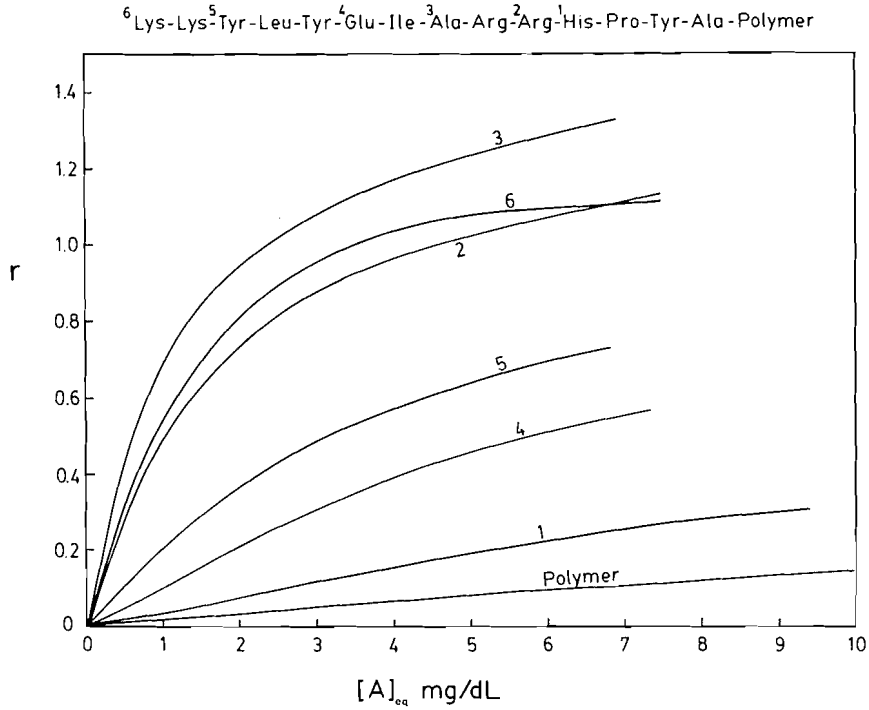

FIG. 3. Normalized equilibrium isotherms for the adsorption of bilirubin.

containing pendants (15) are explicable on the same basis. Furthermore, direct evidence for the interaction of the COOH groups of bilirubin with free NH_2 groups of lysine residues has been obtained from studies of nmr relaxation times (22). However, the results obtained for resins 2 and 3 demonstrate that, as might be expected, there is no simple linear relationship between the number of basic residues in the pendant and its binding capacity. Related factors, such as the length of the resulting sequence, the conformation of the peptide chains, and the position of the basic residues in the sequence, are also expected to influence the adsorption results.

4. Binding constants

The equilibrium isotherms reflect an expression of the binding affinity between bilirubin and the pendants of the peptide resins. Absolute values indicating the strength of these affinities can be expressed in the form of binding constants.

Resin 1 is the classical case of an adsorbent with a single binding site, as shown by a linear Scatchard plot (Fig. 4) that extrapolates to an intercept on the x-axis close to $r = 1$. For an adsorbent with one binding site per pendant, the Scatchard equation (23) has the form

$$[1] \quad r/[A] = k(1 - r)$$

where the parameters r and [A] are as defined previously and k is the binding constant. The binding constant, derived directly from the ordinate intercept, is equal to $0.3 \times 10^4\ M^{-1}$ (Table 3). This binding constant can be viewed as either a stoichiometric or site constant, since for adsorbents with a single site these are equivalent.

The Scatchard plots for resins 2 and 3 are very different than that for resin 1, with both exhibiting similar concave upward behaviour and tending toward an intercept of $r > 1$ (Fig. 4), indicating more than one binding site per pendant but no more than two. Indeed, the size of a molecule of bilirubin, with respect to the length of the peptide pendants considered, precludes a capacity greater than two for these systems. Upward concavity reflects an adsorption isotherm for which r rises rapidly at low [A], after which it increases very slowly so that saturation is reached only at high values of [A]. This behaviour is usually associated with a first binding constant that is larger than the second.

From a molecular point of view, two interpretations are possible for cases when $k_1 > k_2$: (*a*) negative cooperativity is developed between binding sites as a result of the binding of the first bilirubin molecule to a pendant; and (*b*) the binding sites are independent and nonequivalent, with a second binding constant being markedly smaller than the first. From a consideration of binding constant values only, it is not possible to get direct insight into the nature of the binding behaviour. However, due to the relatively short length of the pendants on these peptide resins the two binding sites must be in close proximity. For these particular sequences and placements of amino acids, relatively limited secondary and tertiary structures are expected. This precludes the formation of two classes of sites having different initial affinities. Therefore it seems probable that interactions exist between initially equivalent binding sites, so that the first explanation is more plausible.

For adsorbents with two initially equivalent, interaction sites, binding constants can be derived using a graphical method based on a modified Scatchard equation (21):

$$[2] \quad r/[A] = \frac{k_2 r(2 - r)}{r - 1 + \delta}$$

where

$$\delta = \{1 + 2(\xi - 1)r - (\xi - 1)r^2\}^{1/2}$$

$$\xi = k_2/k_1$$

The constants k_1 and k_2 are first and second *site* binding constants. It can be shown from eq. [2] that as r approaches 0,

Can. J. Chem. Downloaded from www.nrcresearchpress.com by 118.98.75.50 on 09/07/12
For personal use only.

Can. J. Chem. Downloaded from www.nrcresearchpress.com by 118.98.75.50 on 09/07/12
For personal use only.

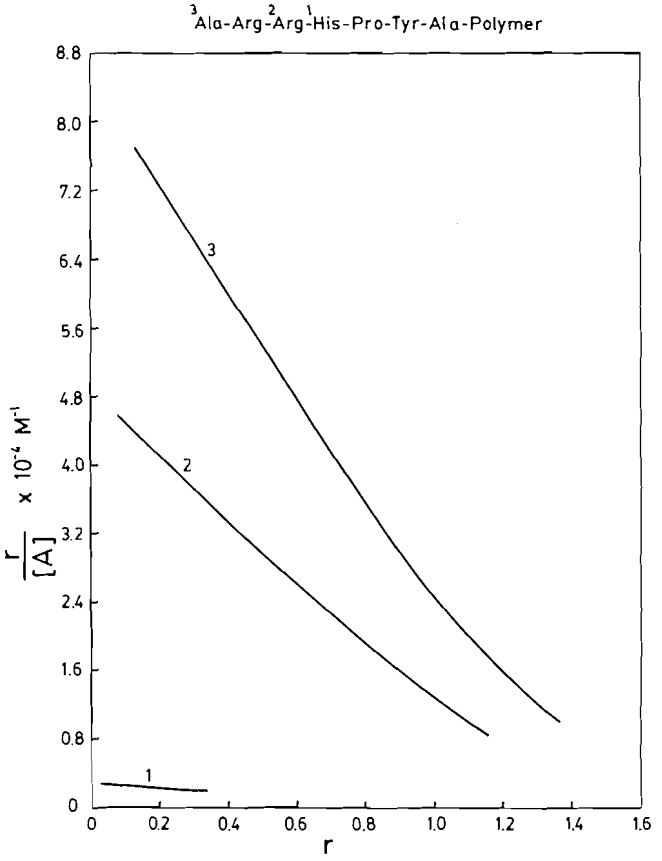

FIG. 4. Scatchard plots for peptide resins representing a portion of the sequence 136–148 of HSA.

TABLE 3. Site equilibrium constants for binding of bilirubin by peptide resins describing the replicate fragment 136–148 of human serum albumin

Peptide resins	Site binding constant $\times 10^{-4} M^{-1}$ k_1	k_2
1 -His-Pro-Tyr-Ala-polymer	0.3	0
2 -Arg-	2.4	0.7
3 -Ala-Arg-	4.3	1.5
4 -Glu-Ile-	0.3	3.3
5 -Tyr-Leu-Tyr-	1.3	2.8
6 Lys-Lys-	4.8	9.6

$r/[A] = 2k_1$, and when $r = 1$, i.e., at half saturation, $r/[A] = (k_1k_2)^{1/2}$.

The intercepts on the ordinate of Fig. 4 are $4.8 \times 10^4\ M^{-1}$ and $8.5 \times 10^4\ M^{-1}$ for resins 2 and 3, respectively, and correspond to k_1 of $2.4 \times 10^4\ M^{-1}$ and $4.3 \times 10^4\ M^{-1}$ (Table 3). The $r/[A]$ values at half saturation are $1.3 \times 10^4\ M^{-1}$ and $2.5 \times 10^4\ M^{-1}$ for resins 2 and 3, respectively, corresponding to values for k_2 of $0.7 \times 10^4\ M^{-1}$ and $1.5 \times 10^4\ M^{-1}$ (Table 3). The importance of arginine in binding bilirubin is clearly demonstrated by the larger value of k_1 for resin 2 as compared to the binding constant for resin 1. Furthermore, k_1 is approximately doubled by the addition of a second arginine to form resin 3. For resin 2 the negative cooperativity is shown by the fact that $k_2/k_1 = 0.29$, so that the binding of the first bilirubin apparently interferes with subsequent binding at the second site. Similarly, $k_2/k_1 = 0.35$ for resin 3, so that the degree of negative cooperativity is decreased somewhat. This might be expected since the increase in length affords more space for the second bilirubin molecule.

The first binding constant of resin 3 is larger than that of resin 2 and reflects the steeper slope of the isotherm at low concentrations. Furthermore, due to the relatively large values of both k_1 and k_2, the adsorption isotherm associated with resin 3 should saturate at a lower concentration, as Fig. 3 indicates.

Scatchard plots with concave downward behaviour (Fig. 5) are obtained as the last three fragments are added to complete the replicate peptide sequence, resins 4, 5, and 6. This pattern is associated with an adsorption isotherm for which, as [A] increases, r rises slowly at low concentration, then increases rapidly, and finally attains saturation, i.e., a sigmoidal isotherm. Such plots manifest positive cooperativity between binding sites, i.e., after filling the first site there is an increase in the affinity of the other binding site. This behaviour is also associated with a second binding constant that is larger than the first.

These three peptide resins are very interesting cases of peptide–ligand interactions in that their Scatchard plots (Fig. 5) manifest positive cooperativity even though r is less than or equal to one. Indeed, as indicated by the adsorption isotherms (Fig. 3), resins 4, 5, and 6 appear to have only one binding site per pendant. Consequently, the cooperative nature of the binding must be between adjacent peptide pendants, each having only one binding site, rather than between two sites on the same pendant, as for resins 2 and 3.

A plausible explanation is obtained from a consideration of the nature of the amino acids making up the peptide pendants of these adsorbents. The introduction of the glutamic acid residue with a negative charge to form resin 4 introduces the possibility of electrostatic interactions with arginine residues on other pendants since, at the pH of these adsorption experiments, both arginine and glutamic acid should be fully ionized. Binding of the first bilirubin molecule could disturb these interactions between pendants and result in the development of a more favourable second binding site on the unoccupied pendant. In terms of binding constants this behaviour would thus be reflected by a larger value of the second binding constant, k_2.

The mathematical treatment required to derive site binding constants for these peptide resins is obtained by extending the model presented previously (21) for adsorbents with two initially equivalent, interacting sites. That model is based on an expression for r in terms of [A] and the site binding constants k_1 and k_2 in the form

$$[3a] \quad r = \frac{2k_1[A] + 2k_1k_2[A]^2}{1 + 2k_1[A] + k_1k_2[A]^2}$$

The binding model for resins 4, 5, and 6 requires that the parameter r, which is the molar ratio of bound bilirubin per pendant, be doubled owing to interactions between two pendants that effectively decrease the substitution on the polymer support by half. Consequently, eq. [3*a*] becomes

$$[3b] \quad r = \frac{k_1[A] + k_1k_2[A]^2}{1 + 2k_1[A] + k_1k_2[A]^2}$$

Equation [3*b*] can be expressed as a quadratic in [A] in the form:

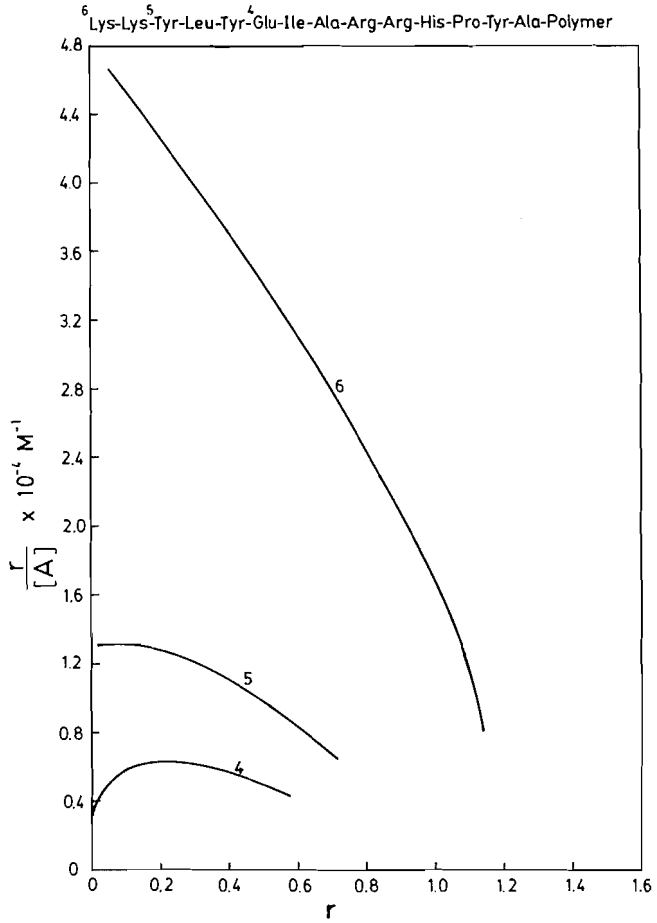

FIG. 5. Scatchard plots for peptide resins describing the sequence 136–148 of HSA.

$$[4a] \quad [A]^2 + [A](1 - 2r)/\{k_2(1 - r)\} - r/\{k_1k_2(1 - r)\} = 0$$

The positive root of eq. [4*a*], which is the only solution that results in positive [A], is

$$[4b] \quad r = \frac{2r - 1 + \delta'}{2k_2(1 - r)}$$

where

$$\delta' = \{1 + 4(\xi - 1)r - 4(\xi - 1)r^2\}^{1/2}$$

$$\xi = k_2/k_1$$

Thus the modified Scatchard equation used for resins 4, 5, and 6 is

$$[5] \quad r/[A] = \frac{2k_2r(1 - r)}{2r - 1 + \delta'}$$

Using the binomial theorem it can be shown that in the limit as r approaches 0, $r/[A] = k_1$, and when $r = 0.5$, or at half saturation, $r/[A] = 1/2(k_1k_2)^{1/2}$. Site binding constants k_1 and k_2 can thus be obtained graphically from a Scatchard plot in a manner analogous to that used for the previous adsorbents.

Binding constants for resins 4, 5, and 6 derived in this manner are given in Table 3. Ordinate intercepts on Fig. 5 yield k_1 equal to $0.3 \times 10^4\ M^{-1}$, $1.3 \times 10^4\ M^{-1}$, and $4.8 \times 10^4\ M^{-1}$ for resins 4, 5, and 6, respectively. The corresponding values of $r/[A]$ at half saturation are $0.5 \times 10^4\ M^{-1}$, $1.0 \times 10^4\ M^{-1}$, and $3.4 \times 10^4\ M^{-1}$, respectively, corresponding to k_2 values of $3.3 \times 10^4\ M^{-1}$, $2.8 \times 10^4\ M^{-1}$, and $9.6 \times 10^4\ M^{-1}$. As expected, second binding constants higher than the first are obtained in all cases. Resin 4 demonstrates the strongest positive cooperativity, having the largest ratio of k_2/k_1, corresponding to an elevenfold enhancement. Resins 5 and 6 have lower, but very similar, ratios of k_2/k_1 (equal to 2.2 and 2, respectively).

These results correlate well with the binding model introduced for these three adsorbents. It is with resin 4 that the glutamic acid was introduced and this adsorbent possesses the largest enhancement. The binding behaviour suggests that the binding of the first bilirubin molecule in some manner either balances or shields the negative charge of the glutamic acid so that the second bilirubin molecule binds more strongly. The introduction of the subsequent amino acids, among which are the strongly basic lysine residues, serve to further attenuate the role of the negative charge and this is reflected by the diminished k_2/k_1 ratio for resins 5 and 6.

As mentioned previously, binding with positive cooperativity is generally reflected by a sigmoidal shape in the adsorption isotherm. In the case of resins 4 and 5, the relatively low slope of the isotherm (Fig. 3) at low adsorbate concentrations is the only sign of such cooperativity. However, the corresponding Scatchard plots (Fig. 5) demonstrate the positive cooperativity binding, in a more obvious way, by the concave downward shape.

The adsorption isotherm of resin 6 (Fig. 3) has a relatively steep slope at low concentrations and also shows saturation, but gives no evidence of a sigmoidal shape. Again, the corresponding Scatchard plot is more appropriate in this regard. The high value for the first binding constant reflects the rapid increase in r at low equilibrium concentrations. Furthermore, combined with this first binding constant is a second binding constant that is twice the first. Consequently, the maximum loading occurs at a relatively low adsorbate concentration.

Resin 6 has several of the characteristics required of a good adsorbent. It has a high binding capacity at low adsorbate concentrations, in part because of positive cooperativity combined with a large first binding constant. At concentrations above 7 mg/dL, resin 2 has a higher binding capacity than does resin 6. It could be concluded that resin 3 would be the best candidate for clinical purposes since it has the highest binding capacity as well as a relatively large k_1. However, this ignores the question of specificity of interactions. The adsorption behaviour of other biological adsorbates will be reported in the near future.

It is of interest to compare the equilibrium binding constants of these peptide resins with those of HSA for the binding of bilirubin. Numerous studies indicate that the first molecule of bilirubin binds to HSA with a binding constant in the region of 10^6–$10^8\ M^{-1}$ (24). The large range in reported values indicates a sensitivity to experimental conditions and methods. Nonetheless, they are larger by a factor of ca. 10^2–10^4 than that for any of the synthesized peptide resins. Similarly, the binding constants for the second site on HSA have been reported to be 10^5–$10^6\ M^{-1}$ (24), i.e., only slightly larger than those of these peptide resins.

It is noteworthy that a binding constant of $1.8 \times 10^5\ M^{-1}$ was obtained by Reed *et al.* (25) for the binding of bilirubin by the fragment 115–184 of BSA. As previously mentioned, HSA and BSA have very similar primary structures in this region, loop no. 3 in Fig. 1*b*, and should therefore have similar binding constants. Reed's value is only slightly higher than the binding

Can. J. Chem. Downloaded from www.nrcresearchpress.com by 118.98.75.50 on 09/07/12
For personal use only.

constants of some of the present peptide resins, which are structurally simpler and consist of shorter sequences composed in this region of HSA.

As postulated previously by many researchers (9–11, 17, 18), bilirubin binding sites on human albumin may be in the amino terminal half of the protein, more specifically in the region of loops no. 3 and no. 4 (Fig. 1*b*). The similarity in binding constants for the peptide resins with that for the BSA fragment offers supporting evidence that the binding location for bilirubin on the protein is in the vicinity of the sequence of the synthesized peptide resins. The existing discrepancy may reflect the flexibility of the albumin, which allows it to adopt conformations that form binding sites that are specifically shaped for a given ligand, as has been suggested by Brodersen (24). Accordingly, a more developed secondary and tertiary structure of HSA, as compared to that of the peptide pendants of the synthesized adsorbents, may contribute to enhance the unique binding character of albumin in terms of affinity, capacity, and specificity.

Conclusion

This work demonstrates that a strategic replicate sequence, patterned after the primary structure of HSA, when immobilized onto a cross-linked polymer support results in a material that can be used as adsorbent for bilirubin. Results show that the introduction of the basic amino acids into the sequence tends to produce adsorbents with a relatively strong binding affinity for bilirubin. Binding constants, comparable to that of a larger fragment of BSA surrounding the replicated sequence, were obtained with these much simpler adsorbents.

Acknowledgements

Financial support in the form of operating grants from the Natural Sciences and Engineering Research Council of Canada and Fonds pour la formation de chercheurs et l'aide à la recherche (Québec) is gratefully acknowledged. We would also like to express our appreciation to Drs. S.-D. Clas and W. C. Galley for helpful discussion.

It gives us great pleasure to submit this paper to this issue of Canadian Journal of Chemistry, which is dedicated to our friend and colleague, J. T. Edward.

1. J. JACOBSEN. FEBS Lett. **5**, 112 (1969).
2. J. D. OSTROW. Bile pigments and jaundice. Molecular, metabolic, and medical aspects. *Edited by* J. D. Ostrow. Marcel Dekker Inc., New York. 1986. pp. 1–6.
3. R. A. WILLSON, K. H. WEBSTER, A. F. HOFMANN, and W. H. J. SUMMERSKILL. Gastroenterology, **62**, 1191 (1972).
4. S. SIDEMAN, L. MOR, and J. M. BRANDES. Trans. Am. Soc. Artif. Intern. Organs, **25**, 497 (1979).
5. Y. IDEZUKI, M. HAMAGUCHI, S. HAMABE, H. MORIYA, T. NAGASHIMA, H. WATANABE, T. SONADA, K. TERAMOTO, T. KIKUCHI, and H. TANZAWA. Trans. Am. Soc. Artif. Intern. Organs **27**, 428 (1981).
6. B. F. SCHARSCHMIDT, P. H. PLOTZ, P. D. BERK, J. G. WAGGONER, and J. VERGALLA. J. Clin. Invest. **53**, 786 (1974).
7. P. Q. BEHRENS, A. M. SPIEKERMAN, and J. R. BROWN. Fed. Proc. **34**, 591 (1975).
8. B. MELOUN, L. MORAVEK, and V. KOSTKA. FEBS Lett. **58**, 134 (1975).
9. N. GITZELMANN-CUMARASAMY, C. C. KUENZLE, and K. J. WILSON. Experientia, **32**, 768 (1976).
10. M. J. GEISOW and G. H. BEAVEN. Biochem. J. **163**, 477 (1977).
11. C. JACOBSEN. Biochem. J. **171**, 453 (1978).
12. T. SJODIN, R. HANSSON, and I. SJOHOLM. Biochim. Biophys. Acta, **494**, 61 (1977).
13. C. C. KUENZLE, N. GITZELMANN-CUMARASAMY, and K. J. WILSON. Experientia, **31**, 722 (1975).
14. D. S. HENNING, G. A. LAJOIE, G. R. BROWN, and L. E. ST-PIERRE. Int. J. Artif. Organs, **7**, 209 (1984).
15. D. S. HENNING, G. R. BROWN, and L. E. ST-PIERRE. Int. J. Artif. Organs, **9**, 33 (1986).
16. E. KAISER, R. L. COLESCOTT, C. D. BOSSINGER, and P. I. COOK. Anal. Biochem. **34**, 595 (1970).
17. C. JACOBSEN. Eur. J. Biochem. **27**, 513 (1972).
18. C. JACOBSEN and J. JACOBSEN. Biochem. J. **181**, 251 (1979).
19. J. R. BROWN and P. SHOCKLEY. Lipid–protein interactions. Vol. 1. *Edited by* P. C. Jost and O. H. Griffith. John Wiley and Sons, New York. 1982. pp. 25–68.
20. J. M. STEWART and J. D. YOUNG. Solid phase peptide synthesis. 2nd ed. Pierce Chemicals Company, Rockford, IL. 1984. p. 41.
21. W. C. GALLEY, M. BOUVIER, S.-D. CLAS, G. R. BROWN, and L. E. ST-PIERRE. Biopolymers. Submitted.
22. X. X. ZHU, G. R. BROWN, and L. E. ST-PIERRE. Can. J. Spectrosc. Submitted.
23. G. SCATCHARD. Ann. N.Y. Acad. Sci. **51**, 660 (1949).
24. R. BRODERSEN. Crit. Rev. Clin. Lab. Sci. **11**, 305 (1980).
25. R. G. REED, R. C. FELDHOFF, O. L. CLUTE, and T. PETERS, JR. Biochemistry, **14**, 4578 (1975).

Can. J. Chem. Downloaded from www.nrcresearchpress.com by 118.98.75.50 on 09/07/12
For personal use only.

Surface adsorption at low coverage of *n*-alkanes on bleached kraft papers using gas chromatography

N. GURNAGUL AND D. G. GRAY

Pulp and Paper Research Institute of Canada, and Department of Chemistry, McGill University, 3420 University St., Montreal, P.Q., Canada H3A 2A7

Received January 13, 1987

This paper is dedicated to Professor John T. Edward

N. GURNAGUL and D. G. GRAY. Can. J. Chem. **65**, 1935 (1987).

The adsorption at low surface coverage of a series of *n*-alkanes on various bleached kraft paper surfaces was measured by gas chromatography. Differences in surface area of the paper samples were readily measured from the gas chromatographic retention volumes. The standard free energy, the enthalpy, and the entropy of adsorption varied linearly with the number of carbon atoms in the *n*-alkanes. The heats of adsorption were close to the heats of liquefaction, indicating the non-specific interactions of the hydrocarbons with the bleached kraft surfaces. The London component of the surface free energy was estimated from the gas chromatographic results to be 47.9 mN/m.

N. GURNAGUL et D. G. GRAY. Can. J. Chem. **65**, 1935 (1987).

Utilisant la chromatographie en phase gazeuse et opérant avec des surfaces qui sont relativement peu couvertes, on a mesuré l'adsorption d'une série de *n*-alcanes sur diverses surfaces de papier kraft blanchi. Grâce aux volumes de rétention en chromatographie en phase gazeuse, on peut facilement mesurer les différences dans les superficies des surfaces des échantillons de papier. L'énergie libre standard, l'enthalpie et l'entropie d'adsorption varient d'une façon linéaire avec le nombre d'atomes de carbone dans les *n*-alcanes. Les chaleurs d'adsorption sont semblables à celles des chaleurs de liquéfation et ce résultat indique que les interactions des hydrocarbures avec les surfaces du papier kraft blanchi ne sont pas spécifiques. En se basant sur les résultats de la chromatographie en phase gazeuse, on a évalué que la composante de London à l'énergie libre de surface est égale à 47,9 mN/m.

[Traduit par la revue]

Introduction

In its simplest form, paper is made from a dilute (0.2–1% by weight) aqueous suspension of wood pulp fibres by draining the water through a fabric mesh which retains the fibres (1). As the water is removed, surface tension forces bring the fibres into intimate contact, resulting after pressing and drying in a fibrous sheet held together primarily by interfibre hydrogen bonds between polysaccharide components on the surface of the wood pulp fibres. Thus paper sheets, unless specially treated, remain sensitive to moisture, changing dimensions with changes in relative humidity and disintegrating when re-immersed in water.

The strength and optical properties of paper sheets depend on many variables in fibre and sheet preparation. In most papermaking processes, the pulp fibres are treated mechanically prior to sheet formation. The operation is known as "beating" or "refining" the pulp. This mechanical treatment of the fibres renders them more flexible and fibrillated. The increase in flexibility was explained by Emerton (2) who suggested that the flexing of the fibres during beating caused the breakdown of the fibre wall into separate lamellae, particularly in the secondary wall layers. This internal fibrillation results in increased amounts of water sorption by the hydrophilic hemicelluloses and the amorphous fraction of cellulose. The water incorporated into the amorphous polysaccharide phase exerts a plasticizing effect on the composite structure which deforms more readily (2). Beating also results in external fibrillation where "fibrils", sometimes aggregated into membranes, extend from, and are attached to, the surfaces of fibres (3). The enhanced flexibility and collapse of fibrillation leads to a denser, stronger, sheet on drying.

The surface area of a paper sheet may be defined as the surface area of the constituent fibres minus the "bonded" area, where fibres are in contact. (This area is of course much larger than the geometric or "purchased" area of a paper sheet because of the porous structure of the sheet.) The surface area is smaller for a beaten sheet than for an unbeaten sheet, because the beaten fibres are more flexible, and they pack together in a denser sheet during drying.

A gas chromatographic (GC) method has been adapted to measure the surface area of pulp fibres and paper (4) and the response of surface area to changes in relative humidity (5). Recently, the responses to changes in relative humidity of a series of paper samples, prepared by beating a sample of bleached kraft wood pulp to different levels, have been followed by this method (6). In essence, (*i*) the gas chromatographic retention of hydrocarbon vapours on a paper stationary phase packed into a column conditioned at a given relative humidity is measured; (*ii*) adsorption isotherms are derived from the GC data (7); (*iii*) surface areas and the thermodynamics of adsorption are determined from the adsorption isotherms. However, measurement of adsorption isotherms by the methods of finite concentration gas chromatography is rather laborious. In favourable situations, a much more rapid indication of vapour–substrate interactions can be derived from gas chromatographic retention data in the infinite dilution or "Henry's law" limit, where the high inherent sensitivity of GC detectors is used to measure the retention of very small concentrations of vapour on the substrate. The retention time is readily related to the slope of the adsorption isotherm if the slope approaches a limiting value at very low surface coverage (7). The gas chromatographic measurements at finite concentration on kraft paper samples prepared from pulp beaten to different degrees (6) are extended in this paper to measurements made at very low coverage. Some indication of the interactions of *n*-alkanes with the paper surface are derived from the measurements, and a facile method for estimating changes in surface area of paper samples is presented. The experimental methods and interpretation follow

Can. J. Chem. Downloaded from www.nrcresearchpress.com by 118.98.75.50 on 09/07/12
For personal use only.

Can. J. Chem. Downloaded from www.nrcresearchpress.com by 118.98.75.50 on 09/07/12
For personal use only.

previous results on cotton filter paper (8). Briefly, the technique of infinite dilution GC involves the introduction of very low probe vapour concentrations in the carrier gas phase. The GC peak shapes in favorable cases are symmetrical and the adsorption isotherms are linear. In this so-called "Henry's law" region, adsorbate–adsorbate interactions are negligible and the net retention volume V_N is independent of the injection size and is related to the limiting slope at zero concentration of the adsorption isotherm (7) by:

$$[1] \quad V_N = A(d\Gamma/dc)_{c\to 0} = AK_s$$

where V_N is the corrected net retention volume at infinite dilution, A is the total surface area of adsorbent in the column, Γ is the concentration of adsorbate on the adsorbent expressed in mol/m^2, c is the gas phase concentration of the adsorbate, and K_s is a surface coefficient. Due to the low adsorbate concentration in the vapour phase and the low column pressure drop, the standard GC corrections (7) are not necessary.

Thermodynamic quantities are derived from the partition coefficients. The standard free energy of adsorption, ΔG_A^0 is given by (9),

$$[2] \quad \Delta G_A^0 = -RT \ln (BK_s)$$

where R is the gas constant, T is the column temperature, and B is a constant that is the ratio of the standard reference states in the gas phase and on the surface:

$$[3] \quad B = p_{s,g}/\pi_s$$

where $p_{s,g}$ is the adsorbate vapour pressure in the gaseous standard state and π_s is the two-dimensional spreading or surface pressure of the adsorbed gas. The values of the standard reference states are taken as $p_{s,g} = 101\ kN/m^2$ (1 atm) and $\pi_s = 0.338\ mN/m$. This value of π_s has been suggested by de Boer such that the standard surface pressure may be defined as the pressure where the average distance of separation between molecules in the adsorbed phase equals that in the standard gas state (9).

At zero surface coverage, the temperature dependence of the partition coefficient, K_s, allows one to calculate the differential heat of adsorption, q_d, which may be identified with $-\Delta\bar{H}_A$ (9), the enthalpy of adsorption,

$$[4] \quad \frac{d(\ln K_s)}{d(1/T)} = \frac{q_d}{R} = \frac{-\Delta\bar{H}_A}{R}$$

The slope of a plot of $\ln K_s$ as a function of T^{-1} will yield the differential heat of adsorption. From the difference between $\Delta\bar{G}_A^0$ and $-q_d$, the standard entropy of adsorption of the probe at zero coverage, $\Delta\bar{S}_A^0$ can be calculated,

$$[5] \quad \Delta\bar{S}_A^0 = -(q_d + \Delta\bar{G}_A^0)/T = \frac{\Delta\bar{H}_A - \Delta\bar{G}_A^0}{T}$$

An empirical method has been proposed to calculate the differential free energy of adsorption from the vapour phase for a —CH_2— segment of an n-alkane chain, at effectively zero surface coverage (8):

$$[6] \quad \Delta\bar{G}_{A(CH_2)}^0 = -RT \ln (K_s^{n+1}/K_s^n)$$

where $\Delta\bar{G}_{A(CH_2)}^0$ is the incremental standard free energy of adsorption per mole of —CH_2— group at zero coverage, R is the gas constant, T is the absolute temperature, and K_s^{n+1}, K_s^n are the partition coefficients for n-alkanes with $n + 1$ and n carbons, respectively. When measurements are made at constant temperature and carrier gas flow rate, assuming gas phase ideality,

$$[7] \quad \frac{K_s^{n+1}}{K_s^n} = \frac{V_R^{n+1}}{V_R^n} = \frac{t_R^{n+1}}{t_R^n}$$

where V_R^{n+1}, V_R^n are the net retention volumes for alkanes with $n + 1$ and n carbon atoms, respectively, and t_R^{n+1}, t_R^n are the corresponding peak retention times (measured from the elution time of a non-interacting vapour). Therefore, it is possible to measure $\Delta\bar{G}_{A(CH_2)}^0$ by simply making an injection of a mixture of a homologous series of n-alkanes and measuring the respective net retention times, without knowledge of the adsorbent surface area or the flow rate of carrier gas.

The adsorption of hydrocarbons on the cellulosic bleached kraft surface is non-specific, and the attractive forces between the adsorbate molecules and the adsorbent surface are essentially dispersive. According to Fowkes, the work of adhesion, W_A, between a nonpolar liquid and surface is given by the geometric mean of the surface tensions of the two components (10),

$$[8] \quad W_A = 2(\gamma_1\gamma_2^L)^{1/2}$$

where γ_1 is the surface tension of the nonpolar liquid and γ_2^L is the London component of the surface tension of the second component.

If the work of adhesion, W_A, is replaced by the free energy of adsorption per mole of CH_2 group (8), then,

$$[9] \quad \frac{-\Delta\bar{G}_{A(CH_2)}^0}{Na_{CH_2}} = 2(\gamma_{CH_2}\gamma_2^L)^{1/2}$$

where $a_{(CH_2)}$ is 0.06 nm^2, the cross-sectional area of a methylene group, $\gamma_{(CH_2)}$ is the surface tension of a surface comprised only of CH_2 groups (from extrapolation of the surface tension of low molecular weight alkanes to infinite chain length). The value of $\gamma_{(CH_2)}$ is about 35 mN/m (11). As stated, γ_2^L is the London component of the surface free energy of the adsorbent and N is the Avogadro number. The GC method provides an alternate route to surface free energies which avoids some of the problems of contact angle measurements on paper.

Experimental

The simple gas chromatographic apparatus with flame ionization detector and thermostatted water-bath has been described in detail previously (5).

Most of the experiments were performed with a commercial bleached kraft pulp (Domtar Q90, 100% black spruce, northern Quebec, 42% yield). The initial pulp samples were in the form of $8\frac{1}{2} \times 11$ dried lap sheets. The edges of the sheets were cut off and the sheets were soaked for 4 h, then disintegrated and beaten to several standard freeness values in a laboratory PFI mill. Five samples were used: the initial unbeaten pulp (Q90) and samples beaten for 3000, 6000, 9000, and 11000 revolutions (Q90-3M, Q90-6M, Q90-9M, and Q90-11M respectively).

Handsheets were prepared from these pulps with a British Standard Handsheet apparatus (12). The handsheets were cut into small (1.8 mm diameter) pieces and packed into 1 m copper columns of 5 mm o.d. previously washed with acetone. All the paper samples had an initial moisture content of about 7–8%, determined by drying small amounts to constant weight. The paper samples were packed directly into the columns without drying, conditioned at 90% RH, then dried overnight at 105°C in a stream of dry nitrogen.

Infinite dilution measurements were made at several temperatures (20°C, 25°C, 30°C, 40°C) on the bleached kraft samples after exposure to 90% relative humidity and drying. The temperatures of the columns

TABLE 1. BET surface areas (*n*-decane adsorbate) at 25°C of the kraft samples dried from 90% RH (6)

Column	Weight (g)	Surface area (m^2/g)
Q90	4.060	0.55
Q90-3M	5.212	0.40
Q90-6M	5.973	0.35
Q90-9M	5.650	0.36
Q90-11M	5.682	0.35

TABLE 2. Partition coefficients for a series of *n*-alkanes on various bleached kraft surfaces at several temperatures

		$K_s \times 10^6$ (m)			
Adsorbents	T (°C)	*n*-C_7	*n*-C_8	*n*-C_9	*n*-C_{10}
Q90	20	6.70	21.8	71.1	231.5
	25	5.00	15.8	50.5	158.3
	30	3.90	12.0	36.8	111.3
	40	2.40	7.0	19.8	56.9
Q90-3M	20	6.40	20.5	67.0	217.9
	25	5.00	15.6	48.7	153.7
	30	3.70	11.5	35.2	106.0
	40	2.30	6.8	19.4	54.8
Q90-6M	20	6.90	23.1	75.8	248.9
	25	5.30	16.7	53.6	169.9
	30	3.90	12.0	37.1	112.7
	40	2.40	7.3	20.8	60.6
Q90-9M	20	6.60	21.8	71.7	239.8
	25	5.10	16.2	51.7	165.1
	30	3.90	12.1	37.1	112.6
	40	2.40	7.0	20.1	58.0
Q90-11M	20	6.80	22.5	74.6	250.8
	25	5.30	17.0	54.8	177.8
	30	4.10	12.8	39.7	122.0
	40	2.50	7.4	21.8	62.1

were maintained to within ±0.05°C by means of a water circulating bath.

The *n*-alkanes (Aldrich gold label) were distilled and passed through a column of activated alumina to remove polar impurities. The *n*-alkanes were injected into the column by drawing in and expelling the vapour over the liquid into Hamilton 10 μL and 1 μL syringes. The vapour remaining in the needle (corresponding to about 10^{-5} mm^3 of liquid hydrocarbon) was expelled when the needle was heated in the injection port. The dead volumes of the columns were determined by simultaneously injecting methane, which was not retained by the bleached kraft stationary phases. The external surface areas of the bleached kraft samples after drying from 90% RH are listed in Table 1. These were measured from finite concentration GC results for *n*-decane (6).

Results and discussion

The peak shapes for all the hydrocarbons on the various bleached kraft papers were symmetrical, with net retention volumes that were independent of sample concentration. This indicates that the Henry's law region was attained.

The partition coefficients at different temperatures, calculated from the net retention volumes and the bleached kraft surface areas (Table 1) according to eq. [1] are listed in Table 2.

TABLE 3. Comparison of chromatographic routes to measure relative surface areas

Sample	$10^3 V_N/w$ (m^3/kg)[a]	Relative surface area (infinite dilution)	Relative surface area (finite GC[b])
Q90	87.1	1	1
Q90-3M	61.4	0.70	0.73
Q90-6M	59.5	0.68	0.64
Q90-9M	60.2	0.69	0.65
Q90-11M	62.1	0.71	0.64

[a]For *n*-decane at 25°C; w is the weight of paper in the column.
[b]From data in Table 1, from ref. 6.

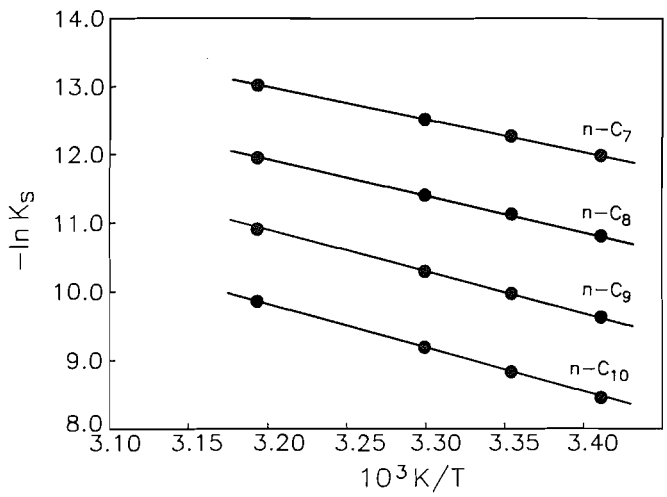

FIG. 1. The variation of the surface partition coefficient with temperature for the *n*-alkanes on Q90 unbeaten bleached kraft at 20°C.

The reproducibility of the coefficients was about 2% for each column. The accuracy of the coefficients depends on the net retention volume and the surface area determined by finite concentration GC. Although the reproducibility in retention volumes for different columns is ~3%, the errors in estimating the surface areas by finite concentration GC are rather large (~5%).

For surfaces with the *same surface composition*, eq. [1] indicates a simple approach for the determination of relative surface areas. The ratio of the specific retention volumes at infinite dilution for two separate columns yields the relative surface areas; these may be compared with relative areas from finite concentration GC (Table 3). The two independent methods give reasonable agreement. Thus the infinite dilution method provides a quick way of determining surface areas with a single injection.

Thermodynamics of adsorption

The temperature dependence of the surface partition coefficient is illustrated for the hydrocarbon probes on the unbeaten Q90 bleached kraft sample in Fig. 1. The differential heats of adsorption, q_d, were obtained from the least-squares determination of the slopes, according to eq. [4]. The standard deviations of the slopes were 2% to 3%.

The standard free energies of adsorption were calculated from eq. [2] using the de Boer standard state for spreading pressure. From the difference in ΔG_A^0 and $-q_d$, standard entropies of adsorption at zero coverage were calculated (eq. [5]). These

Can. J. Chem. Downloaded from www.nrcresearchpress.com by 118.98.75.50 on 09/07/12
For personal use only.

TABLE 4. Standard thermodynamic functions at infinite dilution for *n*-alkanes on bleached kraft papers at 20°C

	Adsorbate	q_d / kJ mol^{-1}	$-\Delta\bar{G}^0_A$ / kJ mol^{-1}	$-\Delta\bar{S}^0_A$ / J K^{-1} mol^{-1}	$-\Delta\bar{H}^{0\,a}_L$ / kJ mol^{-1}
Q90	*n*-Heptane	39.1	18.3	70.9	36.86
	n-Octane	43.1	21.2	74.7	41.82
	n-Nonane	48.6	24.1	83.6	46.81
	n-Decane	53.4	27.0	90.1	51.77
Q90-9M	*n*-Heptane	37.6	18.3	65.8	
	n-Octane	43.0	21.2	74.4	
	n-Nonane	48.6	24.1	83.6	
	n-Decane	54.2	27.0	92.8	

[a]Heats of liquefaction of *n*-alkanes (13, 14).

TABLE 5. Free energies of adsorption per mole of methylene group $\Delta G^0_{A(CH_2)}$ (kJ mol^{-1}) on bleached kraft papers at 20°C

Adsorbent	$\Delta G^0_{A(CH_2)}$ (kJ mol^{-1})
Q90	2.87 ± 0.01
Q90-3M	2.87 ± 0.02
Q90-6M	2.90 ± 0.01
Q90-9M	2.92 ± 0.02
Q90-11M	2.92 ± 0.03

thermodynamic parameters are tabulated in Table 4 for the unbeaten Q90 and the beaten Q90-9M sample at 20°C. The table also includes the heats of liquefaction, ΔH^0_L, for the alkane probes (14). The low heats of adsorption at zero coverage indicate a virtual absence of high-energy sites; the fact that these heats approach the heats of liquefaction indicates the weak physical adsorption of the *n*-alkanes. Thus the bleached kraft surfaces are energetically homogeneous towards saturated alkane adsorption. The values for K_s and the thermodynamic functions on the different paper surfaces are rather scattered, but no significant trend with beating is observed as only the surface area changes and not the chemical composition. The values are similar to those for *n*-alkane adsorption on cellophane (regenerated cellulose) (13) and pure cotton cellulose (8). This is expected as the bleached kraft paper surface is predominantly also almost pure cellulose.

The loss of one translational degree of freedom during the adsorption process results in a decrease in the entropy of the gas molecules. For an ideal gas adsorbate, the magnitude of the entropy loss may be estimated from the simple de Boer model (9). The predicted entropy changes for adsorption of heptane, octane, nonane and decane at 20°C are −52.4, −53.0, −53.5, and −53.9 J K^{-1} mol^{-1}, respectively. The experimental $\Delta\bar{S}_A$ values for Q90 samples are numerically larger than these values. The additional loss of entropy may be attributed to some hindered vibrational and rotational motions of the adsorbed alkanes.

Incremental thermodynamic quantities

The values of the thermodynamic functions (Table 4) vary linearly with the number of carbon atoms. For example, for the Q90-9M sample there is a constant increase of 5.5 ± 0.1 kJ mol^{-1} for the differential heat of adsorption. Constant increments of −2.9 kJ mol^{-1} and −9.0 ± 0.3 J K^{-1} mol^{-1} are observed for $\Delta\bar{G}^0_A$ and $\Delta\bar{S}^0_A$, respectively. The linear variation in $\Delta\bar{G}^0_A$ with

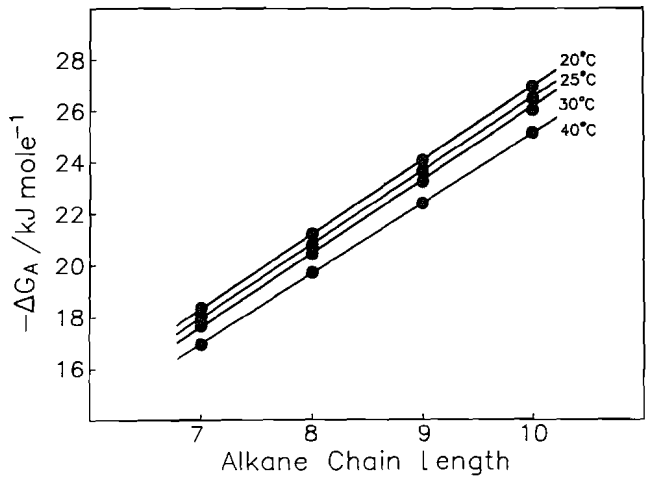

FIG. 2. The standard free energy of adsorption for *n*-alkanes on Q90 unbeaten bleached kraft at four column temperatures as a function of the number of carbon atoms in the hydrocarbon chain.

the number of carbon atoms *n* is illustrated for the unbeaten sample in Fig. 2. This behaviour is analogous to Traube's rule, and the constant increments with carbon number are consistent with a flat orientation on the surface. However, these measurements are made at extremely low surface coverage on dry paper, which has a low surface area (Table 1) and is therefore relatively non-porous. The adsorption process may be quite different at high coverages or on highly porous cellulose surfaces.

The free energies of adsorption per methylene group were calculated according to eq. [6] and are tabulated for the kraft samples at 20°C in Table 5. The values correspond to the constant increments in $\Delta\bar{G}^0_A$ in Table 4.

The London nonpolar component of the surface free energy at 20°C, γ^L_s, was calculated from eq. [9] employing the values of $\Delta\bar{G}^0_{A(CH_2)}$. The average value for all samples was 47.9 ± 2.4 mN m^{-1}. This is close to the value for cotton cellulose (49.9 mN m^{-1}) (8) and somewhat larger than the value for a less dense regenerated cellulose (42.0 mN m^{-1}) (13).

Acknowledgements

The support of the Quebec government (FCAR) is gratefully acknowledged. N.G. thanks the Pulp and Paper Research Institute of Canada for a scholarship.

1. J. P. CASEY (*Editor*). Pulp and paper chemistry and chemical technology. Vol. 2, 3rd ed. Wiley, New York. 1980. p. 965.

Can. J. Chem. Downloaded from www.nrcresearchpress.com by 118.98.75.50 on 09/07/12
For personal use only.

2. H. W. EMERTON. Fundamentals of the beating process. British Paper and Board Industry Research Association, Kenley. 1957.
3. J. D'A. CLARK. Tappi, **52**(2), 335 (1969).
4. U.-B. MOHLIN and D. G. GRAY. J. Colloid Interface Sci. **47**, 747 (1974).
5. G. M. DORRIS and D. G. GRAY. J. Chem. Soc. Faraday Trans. I, **77**, 713 (1981).
6. N. GURNAGUL and D. G. GRAY. J. Pulp Paper Sci. To be published.
7. J. R. CONDER and C. L. YOUNG. Physicochemical measurements by gas chromatography. Wiley, New York. 1979.
8. G. M. DORRIS and D. G. GRAY. J. Colloid Interface Sci. **77**, 353 (1980).
9. J. H. DE BOER. The dynamical character of adsorption. Clarendon Press, Oxford. 1953. pp. 112, 113.
10. F. M. FOWKES. J. Colloid Interface Sci. **28**, 493 (1968).
11. R. J. AVEYARD. J. Colloid Interface Sci. **52**, 621 (1975).
12. CPPA Standard C.4.
13. S. KATZ and D. G. GRAY. J. Colloid Interface Sci. **82**, 318 (1981).
14. Selected properties of hydrocarbons and other related compounds. American Petroleum Institute Project 44. Thermodynamic Research Centre, College Station, TX. 1968.

Can. J. Chem. Downloaded from www.nrcresearchpress.com by 118.98.75.50 on 09/07/12
For personal use only.

Proton spin-lattice relaxation time studies and atom–atom non-bonded potential calculations on ferrocenecarbaldehyde (η^5-C_5H_5)Fe(η^5-C_5H_4CHO)

RICHARD J. PAZUR, D. F. R. GILSON,[1] PIERRE D. HARVEY, AND IAN S. BUTLER
Department of Chemistry, McGill University, 801 Sherbrooke St. W., Montreal, P.Q., Canada H3A 2K6

Received January 2, 1987

This paper is dedicated to Professor John T. Edward

RICHARD J. PAZUR, D. F. R. GILSON, PIERRE D. HARVEY, and IAN S. BUTLER. Can. J. Chem. **65**, 1940 (1987).

The barriers to molecular rotations in the low temperature crystal phase of ferrocenecarbaldehyde, (η^5-C_5H_5)Fe(η^5-C_5H_4CHO), have been measured using proton spin-lattice relaxation methods and assigned to different motions, based on the results of non-bonded atom–atom potential calculations. The principal relaxation is interpreted in terms of a Cole–Davidson distribution of correlation times, and assigned to rotation of the unsubstituted ring, with an activation energy of 15.3 kJ mol^{-1}. Other relaxation processes, observed via T_{1D} measurements, include rotation of the aldehyde group and oscillations of the whole molecule, with barriers of 42.4 and 25.6 kJ mol^{-1}, respectively.

RICHARD J. PAZUR, D. F. R. GILSON, PIERRE D. HARVEY et IAN S. BUTLER. Can. J. Chem. **65**, 1940 (1987).

Utilisant des méthodes de relaxation de réseau spin–proton, on a mesuré les barrières à la rotation moléculaire dans la phase cristalline de basse température du ferrocènecarbaldéhyde, (η^5-C_5H_5)Fe(η^5-C_5H_4CHO), et, en se basant sur les résultats de calculs de potentiels atome–atome non-liés, on les a attribuées aux divers mouvements qui se produisent dans le cristal. On interprète la relaxation principale en fonction d'une distribution de Cole–Davidson des temps de corrélation et on l'attribue à la rotation du noyau qui n'est pas substitué; une énergie d'activation de 15,3 kJ mol^{-1} lui est associée. Parmi les autres processus de relaxation qui ont été observés grâce à des mesures de T_{1D}, on note la rotation du groupement aldéhydique et les oscillations de la molécule dans son ensemble auxquels sont associés des barrières respectives de 42,4 et 25,6 kJ mol^{-1}.

[Traduit par la revue]

Introduction

The bonding and stereochemistry of compounds of unique structure has always been of interest to chemists (1). A particular example is that of ferrocene, where the initial problem of determining the molecular structure (2) has evolved to one of understanding the behaviour of the different crystal forms (3–7). Molecular dynamics are important, since rotation of the cyclopentadienyl rings plays a large role in determining the interactions in the solid phase (8–10). Surprisingly, the introduction of a carbonyl group to give ferrocenecarbaldehyde results in a material that undergoes an order–disorder phase transition at 317 K, with a high entropy of transition of 37.4 J K^{-1} mol^{-1}. Thus the behaviour resembles that of some organic molecular crystals rather than other metallocene derivatives (11). Studies of the crystal structures of both the high- and low-temperature phases have been reported (12–14). According to Leadbetter and co-workers (12, 13), the low-temperature phase is orthorhombic and the high temperature one is face-centered-cubic, but a later study (14) concluded that while the room temperature structure was basically correct, there is a disorder whereby 15% of the molecules are twisted by 36° about the molecular axis. The structure of the high-temperature phase has also been disputed, and Sato and co-workers (14) have claimed that, while the orthorhombic symmetry is maintained, there is an expansion along one crystal axis by 50%.

The molecular dynamics of ferrocenecarbaldehyde have been studied using quasielastic and inelastic neutron scattering methods (15) and interpreted in terms of a hindered rotation of the unsubstituted ring in the ordered phase, and a variety of motions with barriers ranging from less than 6 kJ mol^{-1} to ca. 20 kJ mol^{-1} in the high-temperature phase. However, different treatments of the quasielastic neutron scattering in the ordered phase gave different values for the barrier to rotation: 15 ± 2 kJ mol^{-1} and 22 ± 2 kJ mol^{-1}. By analogy with ferrocene itself, the inelastic neutron scattering peak at 57 cm^{-1} was assigned to the torsional vibration of the ring, leading to a barrier height of 8 kJ mol^{-1}, or, alternatively, if a peak at 80 cm^{-1}, observed in the inelastic scattering spectra at lower temperatures was assigned to this mode, then a barrier of 16 kJ mol^{-1} was obtained.

A determination of the activation energies for molecular motions in ferrocenecarbaldehyde by a different technique seemed appropriate. A study of the behaviour of ferrocenecarbaldehyde by proton spin-lattice relaxation time measurements complements our other studies of ring dynamics in π-arene complexes (16–19) and Raman (20) and XPS (21) studies of a series of ferrocenyl compounds. The properties of substituted ferrocene derivatives are of current interest in the development of chemically derivatised electrodes for photoelectric energy conversion systems (22). At the time that our results were complete, Nakamura and co-workers (23) reported the results of a proton spin-lattice relaxation time study in which they determined activation energies for three different processes in the low-temperature phase. These were assigned to rotation of the unsubstituted ring and to a small angle rotation of the whole molecule. The experimental results are confirmed in the present study, but our interpretation of the results is, however, different.

Experimental

Ferrocenecarbaldehyde was obtained from Aldrich Chemicals and was purified by slow sublimation under reduced pressure (0.1 Torr, 25°C). Proton spin-lattice relaxation times were measured, by the inversion recovery method (180°–t–90°) for T_1 and the Jeener–Broekarts (24, 25) sequence (90°–t_1–45°–t_2–45°) for T_{1D}, using a Spin-Lock CPS2 spectrometer operating at 33 MHz. Sample temperature was controlled by a stream of heated or cooled nitrogen and measured with a digital thermometer. Potential energy calculations were done with the program POTENT, and a SIMPLEX algorithm used to fit the temperature dependence of the spin-lattice relaxation times, both programs were written in TurboPascal.

Results and discussion

Spin-lattice relaxation in the Zeeman field

The temperature dependence of the spin-lattice relaxation

[1]To whom correspondence should be addressed.

Can. J. Chem. Downloaded from www.nrcresearchpress.com by 118.98.75.50 on 09/07/12
For personal use only.

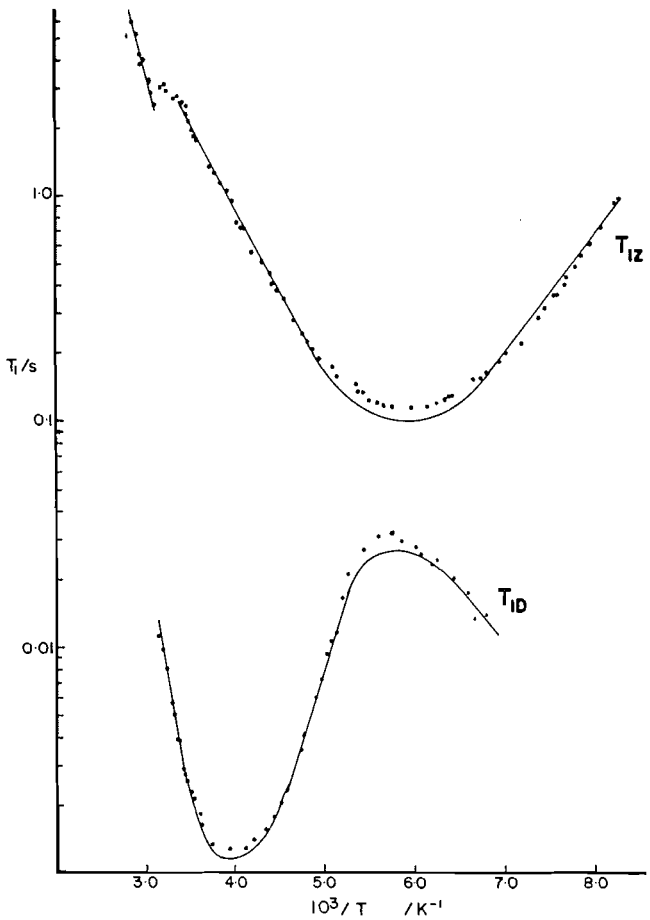

FIG. 1. Temperature dependence of the spin-lattice relaxation times, T_{1Z} and T_{1D}. The solid lines are the theoretical curves based on eqs. [3] and [4].

times is shown in Fig. 1. The phase change at 317 K is shown quite clearly by the discontinuity in T_{1Z}, and there is a change in the slope in the vicinity of 294 K. The results are in good agreement with those reported by Nakamura *et al.* (23), including the proposed second order phase change at 294 K. The existence of this phase change was not reported in two other studies (12, 26).

The usual equation for spin-lattice relaxation by a dipole–dipole mechanism is given by eq. [1];

$$[1] \quad 1/T_{1Z} = (2/3)C\tau\{1/(1 + \omega^2\tau^2) + 4/(1 + 4\omega^2\tau^2)\}$$

where $\tau = \tau_0 \exp(E/RT)$ is the correlation time for molecular reorientation, ω is the measurement frequency, and C is a constant related to the change in second moment resulting from the motion. A plot of $\ln(T_1)$ versus reciprocal temperature should give a V-shaped curve with a minimum value of T_1 occurring at $\omega\tau = 0.6158$. The high temperature limit, $\omega\tau \ll 1$, leads to a straight line with slope $-E/RT$, while the low temperature side, with $\omega\tau \gg 1$, gives a line of slope $+E/RT$. Thus the slopes on either side of the T_1 minimum should be equal. However, in the ferrocenecarbaldehyde case, while the two slopes are linear, they were not the same. This was interpreted by Nakamura and co-workers to be due to two different barriers resulting from cyclopentadienyl rings occupying different sites in the unit cell (23). This implies that different local environments must exist for two distinct sets of molecules, but the two crystallographic structure studies (13, 14) agreed that the space group is $P2_12_12_1$, in which the molecules all occupy equivalent sites. However, Sato *et al.* (14) refined their structure to include two possible molecular orientations (in the ratio 0.85:0.15) with the disordered molecules rotated by 36°. In such a case, there could be a second activation energy, but since a large contribution to the barrier arises from nearest neighbour interactions, the disordering should affect not only the disordered molecules, which, presumably, are random in position in the lattice, but also those surrounding them. Thus, there should be a distribution of barrier heights rather than two discrete barriers.

An alternative approach to the interpretation of the T_1 versus temperature behaviour assumes that a distribution of correlation times exists, $G(\tau)$, such that eq. [1] becomes

$$[2] \quad 1/T_1 = (2/3)C\left\{\int_0^a \tau G(\tau)d\tau/(1 + \omega^2\tau^2) + 4\int_0^a \tau G(\tau)d\tau/(1 + 4\omega^2\tau^2)\right\}$$

The effects of such distributions on the spin-lattice relaxation time have been investigated by Connor (27) and reviewed by Noack (28). Distribution functions such as Gaussian, log-exponential, Fuoss–Kirkwood, and Cole–Cole distributions are symmetric and, therefore, lead to the same slopes on either side of the minimum, although the shape around the minimum is changed. Since an asymmetric function is required in the present case, we have used the empirical Cole–Davidson function

$$G(\tau) = \{\sin(\alpha\pi)/\pi\}(\tau/\tau_0 - \tau) \qquad \tau < \tau_0$$
$$G(\tau) = 0 \qquad \tau > \tau_0$$

where α is a width parameter and τ_0 the mean jump time. With this distribution, T_1 is given by eq. [3]:

$$[3] \quad 1/T_1 = C\alpha\tau\left\{\frac{1}{(1 + \omega^2\tau^2)^{\alpha/2}(1 + \alpha^2\omega^2\tau^2)^{1/2}} + \frac{4}{(1 + 4\omega^2\tau^2)^{\alpha/2}(1 + 4\alpha^2\omega^2\tau^2)^{1/2}}\right\}$$

In the high temperature limit, the slope of the $\ln(T_1)$ plot remains equal to $-E/R$, but for the low temperature side, the slope is $+\alpha E/R$. Thus the value of the width parameter can be obtained from the ratio of the two slopes. Two computer fits to the experimental data were made, using a Simplex algorithm fit to eq. [3]. First, with τ_0, E, and the constant C as variables and the value of α fixed by the ratio of the slopes, and, second, with α as an additional variable parameter. The fit to the slopes is excellent, Fig. 1, with the activation energy being the same in both cases, and reasonable agreement with the two α values (Table 1). The fit to the experimental values of T_1 around the minimum is less satisfactory. The standard deviation in the Simplex fit is the same for eq. [3] and the combination of two spin-lattice relaxation times, even though more variable parameters were used in the latter case. The value of the activation energy, 15.3 kJ mol^{-1}, is in excellent agreement with the values obtained by Leadbetter and co-workers (15) from one set of quasielastic neutron scattering measurements.

In the high-temperature phase a barrier of 26.7 kJ mol^{-1} was determined from a least-squares fit. No T_1 minimum was observed, and, therefore, neither the constant C nor the pre-exponential factor could be evaluated. The barrier is somewhat higher than that determined by the neutron scattering study, and lower than the values given by Nakamura *et al.* (23), who assigned various different barriers to uniaxial rota-

Can. J. Chem. Downloaded from www.nrcresearchpress.com by 118.98.75.50 on 09/07/12
For personal use only.

TABLE 1. Barrier heights for molecular motions in ferrocenecarbaldehyde

E (kJ mol^{-1})	τ_0 (s)	C (rad^2 s^{-2})	α
14.8[a]	1.42×10^{-13}	1.89×10^{9}	0.672
15.0[b]	1.46×10^{-13}	1.81×10^{9}	0.635
13.4[c]	7.94×10^{-14}	1.58×10^{9}	
15.8[c]	1.00×10^{-13}	1.22×10^{9}	
12.9[d]	1.58×10^{-13}	2.22×10^{9}	
15.7[d]	7.94×10^{-14}	1.65×10^{9}	
41[c]	1.26×10^{-14}	(2.15×10^{8})	
26[d]	2.00×10^{-11}	1.07×10^{8}	
41[d]	1.00×10^{-13}	1.15×10^{8}	
42.4[e]	—	—	
25.6[e]	2.22×10^{-11}	3.84×10^{8}	
		4.55×10^{7}	

[a]Using eq. [3] with α fixed.
[b]Using eq. [3] with α allowed to vary.
[c]Reference 11, T_1 studies.
[d]Reference 11, $T_{1\rho}$ studies.
[e]Present work, T_{1D}.

tion (32 kJ mol^{-1}), self-diffusion and/or overall rotation (67 kJ mol^{-1}), and spin-rotation relaxation (11 kJ mol^{-1}).

Spin-lattice relaxation in the dipolar field

The spin-lattice relaxation time in the dipolar field is given by eq. [4];

$$[4]\quad 1/T_{1D} = C_1\tau/(1+\omega^2\tau^2) + C_2\tau/(1+4\omega^2\tau^2) + C_3\tau/(1+\omega_D^2\tau^2)$$

where C_1, C_2, and C_3 are constants and ω_D is the dipolar field (29). The observed temperature dependence shows a change of slope at 294 K (Fig. 1), which is the temperature of the second order phase transition. The T_{1D} temperature dependence between 294 and 317 K was, therefore, treated as a separate process. The activation energy of 42.4 kJ mol^{-1} is in good agreement with a barrier of 41 ± 2 kJ mol^{-1} obtained by Nakamura and co-workers (23) from T_1 measurements and assigned to a small angle reorientation about the molecular axis.

Fitting the remainder of the curve is more complicated since there are two different processes involved and, using eq. [4], a total of twelve different parameters could be varied. The minimum in T_{1D} at about 250 K was assumed to arise from the third term in eq. [3] only and a fit obtained to the experimental points in the temperature range 190 to 290 K. The calculated T_{1D} values were then subtracted from the experimental data for temperatures below 185 K and these points fitted to eq. [4] with the further assumption that $\tau \ll 1$. This fit gave an activation energy of 14.3 kJ mol^{-1} and pre-exponential term of 3.92×10^{-13} s. These values are very close to those obtained from the T_{1Z} fit using the Cole–Davidson distribution and thus the T_{1D} behaviour in the lowest temperature region was identified with the rotation of the unsubstituted cyclopentadienyl ring. Therefore the final fitting procedure involved varying only C_1 and C_3, with the activation energy and pre-exponential term at those values obtained from the T_{1Z} study (14.83 kJ mol^{-1} and 1.42×10^{-13} s, respectively). Thus the number of variable parameters was reduced to six. The values of the various parameters are given in Table 1. The present studies give activation energies for various motions in the low-temperature phase that are in good agreement with the results of Nakamura and co-workers (23). The assignment of the different activation energies to particular molecular motions is not immediately apparent, except for the obvious case of the rotation of the unsubstituted ring.

Non-bonded atom–atom potential energies

In our earlier studies on the barriers to rotation in π-arene metal tricarbonyl complexes (17–19), non-bonded atom–atom potential calculations proved to be very useful in examining the different contributions to the overall barrier. In these cases, the internal barriers are extremely small, and, therefore, the hindrance to ring rotation is due almost entirely to intermolecular contacts. Similar calculations for ferrocenecarbaldehyde seemed appropriate in order to assign the observed barriers in the ordered phase. The known crystal structure (13, 14) was used as the input data for these non-bonded atom–atom potential calculations.

The Buckingham exp-6 potential, eq. [5], was used, with the A, B, and C parameters taken from Mirsky's compilation (30).

$$[5]\quad U(r) = Ar^{-6} - B\exp(-Cr)$$

The energy is calculated as a function of the angle of rotation of a "probe" molecule (or part of a molecule), by summing $U(r)$ over all atom pairs within a given cut-off distance. The difference between the minimum and maximum values gives the barrier height. Since we are not attempting to calculate lattice energies as such, but "potential energy environments" (31), the summation was cut-off at 10 Å, and contributions from the metal atom were omitted, as this atom lies on the molecular (rotational) axis and does not contribute to the angular dependence. The calculation is based upon a single molecule or group rotating in a rigid lattice of surrounding molecules and possible effects of cooperative motions must be examined by considering specific interactions. Furthermore, since the parameters are derived from total lattice energy calculations, heats of sublimation, elastic constants, etc., and not from fitting barriers to rotation, the choice of the parameters for the potential function is quite empirical, with the justification that these terms are considered to be transferable from one system to another (30).

First, we calculate the barrier height for the simplest mode — the rotation of the unsubstituted ring in a rigid lattice. The results are shown in Fig. 2. The contributions to the total energy are shown for ring A – ring A and ring A – ring B contributions (where ring A is the unsubstituted ring and ring B bears the carbonyl substituent). The total calculated barrier height is 14.2 kJ mol^{-1}, with the major contribution, 13.5 kJ mol^{-1}, arising from ring A – ring B interactions. The ring A – ring A contribution is less than 1 kJ mol^{-1}, which means that cooperative rotations between unsubstituted rings are unlikely, but might be important for ring A – ring B motions. The internal barrier is 0.25 kJ mol^{-1} with the minimum at about 36°, i.e. out-of-phase with the total potential. Thus the non-bonded potential minimum for an isolated molecule would be at the staggered conformation, in contrast to the crystal where the rings are nearly eclipsed (12). These calculations do not, of course, include the electronic contribution to the internal barrier. Theoretical calculations (32) showed the eclipsed conformation of ferrocene to be 2.8 kJ mol^{-1} more stable than the staggered form, in reasonable agreement with the value estimated from electron diffraction of 3.8 kJ mol^{-1} (33). The total barrier should be 17 to 18 kJ mol^{-1}, which compares reasonably well with the measured value.

The persistence of the 57 cm^{-1} peak in the inelastic neutron

Can. J. Chem. Downloaded from www.nrcresearchpress.com by 118.98.75.50 on 09/07/12
For personal use only.

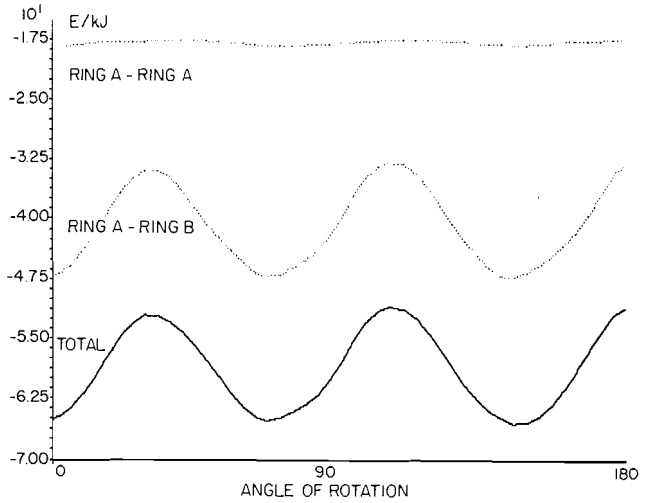

FIG. 2. Potential energy environment as a function of rotation angle of ring A.

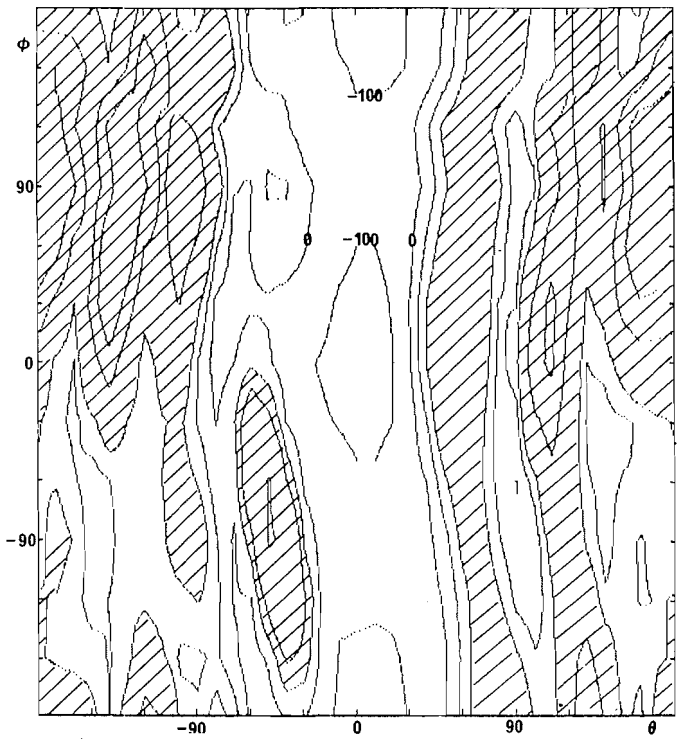

FIG. 3. Contour plot of the potential energy environment for rotations of the whole molecule, angle θ, and the carbaldehyde group, angle ϕ. Positive values of ϕ correspond to a rotation with the hydrogen atom position above the plane of the ring. The contour lines are at −100, 0, 100, 200, 400, and 1000 kJ mol^{-1}. The hatched areas are at potential energies above 200 kJ mol^{-1}.

scattering spectra of both phases led to the conclusion that the observed barrier must arise principally from internal sources (11). However, the present calculations show that the internal barrier is only 16–20% of the total and, therefore, the 57 cm^{-1} peak in the inelastic scattering spectrum should not be assigned to the torsional mode.

The two simplest possibilities for the remaining barriers are (*i*) rotation of the substituent aldehyde group and (*ii*) rotation of the whole molecule. In order to explore the possibility of a cooperative motion between whole molecule and substituent group rotations the potential energy environment was calculated for whole molecule motion at different angles of rotation of the —CHO group. The results are shown in the form of a contour plot in Fig. 3. Rotation of the carbaldehyde group corresponds to variation of the angle ϕ, with θ fixed, and rotation of the whole molecule to ϕ = 0, with θ varied. The non-bonded potential does not include electronic, i.e., bonded, contributions, but the enthalpy for substituent rotation in ferrocenecarbaldehyde in solution has been measured by proton and carbon magnetic resonance to be 31.2 kJ mol^{-1} (34) and this contribution has been added to the non-bonded potential (with the assumption that the internal barrier is a cosine function). Potential minima occur at the crystallographic coordinates and at ϕ = 180°. The latter has a total energy that is 6 kJ mol^{-1} above the true minimum with a barrier of 56 kJ mol^{-1} between the two positions. The calculated barrier to rotation of the carbaldehyde substituent should be somewhat lower since the rest of the molecule can oscillate and the actual equilibrium positions occur at non-zero values of θ. The activation energy of 41 kJ mol^{-1} observed in the T_{1D} measurements above 294 K is, therefore, assigned to the aldehyde group rotation and not to small angle motion of the whole molecule.

For the whole molecule rotation there is a very broad region around the equilibrium position in which the energy increases only slowly over an angle of ±20°. A small angle motion of the whole molecule about a pseudo C_5 axis may be most probable candidate for the small second moment change between 210 and 290° (23) and the motion with an activation energy of 26 kJ mol^{-1}. Also, there are several different minima in the angular dependence at ϕ = 0, with the lowest occurring at −75°. This is actually part of a trough with a negative calculated potential energy environment and a minimum located at θ = −65° and ϕ = 26°. The presence of the second minimum is significant since it can trap the molecule in a second site, and thus provides an alternative molecular orientation in a metastable state. Other minima occur at higher potential energies (the unshaded regions in Fig. 3) and population of these could provide a mechanism whereby the disordering process can occur when ordered crystal is heated and, furthermore, it is possible that molecules could be trapped in these positions if the sample is cooled rapidly from the plastic phase. This may account for the difficulties associated with the Dsc and Dta studies (12, 26).

Acknowledgments

This work was supported by grants from the Natural Sciences and Engineering Research Council of Canada and FCAR (Quebec).

1. A. S. Smith. Chem. Ind. 353 (1955).
2. J. D. Dunitz and L. E. Orgel. Nature, **171**, 121 (1953).
3. J. D. Dunitz, L. E. Orgel, and A. Rich. Acta Crystallogr. **9**, 373 (1956).
4. J. W. Edwards, G. L. Kingston, and R. Mason. Trans. Faraday Soc. **56**, 660 (1960).
5. P. Seiler and J. Dunitz. Acta Crystallogr. Sect. B, **35**, 1068 (1979).
6. P. Seiler and J. Dunitz. Acta Crystallogr. Sect. B, **38**, 1741 (1982).
7. F. Takusagawa and T. F. Koetzle. Acta Crystallogr. Sect. B, **35**, 1074 (1979).
8. A. J. Campbell, C. A. Fyfe, D. Harold-Smith, and K. R. Jeffrey. Mol. Cryst. Liq. Cryst. **36**, 1 (1976).
9. D. C. Levendis and J. C. A. Boeyens. J. Cryst. Spectrosc. Res. **15**, 1 (1985).

Can. J. Chem. Downloaded from www.nrcresearchpress.com by 118.98.75.50 on 09/07/12
For personal use only.

10. A. KUBO, R. IKEDA, and D. NAKAMURA. J. Chem. Soc. Faraday Trans. 2, **82**, 1543 (1986).
11. N. G. PARSONAGE and L. A. K. STAVELEY. Disorder in crystals. Clarendon Press, Oxford. 1978.
12. M. F. DANIEL, A. J. LEADBETTER, R. E. MEADS, and W. G. PARKER. J. Chem. Soc. Faraday Trans. 2, **74**, 456 (1978).
13. M. F. DANIEL, A. J. LEADBETTER, and M. A. MAZID. J. Chem. Soc. Faraday Trans. 2, **77**, 1837 (1981).
14. K. SATO, M. IWAI, H. SANO, and M. KONNO. Bull. Chem. Soc. Jpn. **57**, 634 (1984).
15. M. F. DANIEL, A. J. LEADBETTER, and R. M. RICHARDSON. J. Chem. Soc. Faraday Trans. 2, **77**, 1851 (1981).
16. D. F. R. GILSON and G. GOMEZ. J. Organomet. Chem. **240**, 41 (1982).
17. D. F. R. GILSON, G. GOMEZ, I. S. BUTLER, and P. J. FITZPATRICK. Can. J. Chem. **61**, 737 (1983).
18. P. D. HARVEY, I. S. BUTLER, and D. F. R. GILSON. Inorg. Chem. **25**, 1009 (1986).
19. P. D. HARVEY, I. S. BUTLER, and D. F. R. GILSON. Inorg. Chem. **26**, 32 (1987).
20. I. S. BUTLER, P. D. HARVEY, and G. C. ALLEN. J. Raman Spectrosc. **18**, 1 (1987).
21. G. C. ALLEN, I. S. BUTLER, and C. KIRBY. Inorg. Chim. Acta. To be published.
22. (*a*) M. S. WRIGHTON. J. Chem. Ed. **60**, 335 (1983); (*b*) A. B. FISCHER, J. A. BRUCE, D. R. MCKAY, G. E. MACIEL, and M. S. WRIGHTON. Inorg. Chem. **21**, 1766 (1982).
23. A. KUBO, R. IKEDA, and D. NAKAMURA. Ber. Busenges. Phys. Chem. **90**, 479 (1986).
24. J. JEENER, R. DU BOIS, and P. BROEKART. Phys. Rev. **139**A, 1959 (1965).
25. J. JEENER, H. EISENRATH, and R. VAN STEENWINKEL. Phys. Rev. **133**A, 478 (1964).
26. L. VERBIT and T. R. HALBERT. Mol. Cryst. Liq. Cryst. **30**, 209 (1975).
27. T. M. CONNOR. Trans. Faraday Soc. **60**, 1574 (1964).
28. F. NOACK. NMR basic principles and progress. Vol. 3. *Edited by* P. Diehl, E. Fluck, and R. Kosfeld. Springer Verlag. 1971. p. 83.
29. R. VAN STEENWINKEL. Z. Naturforsch. **24**a, 1526 (1969).
30. K. MIRSKY. *In* Computing in crystallography. Delft University Press, Delft, The Netherlands. 1978.
31. J. C. A. BOEYENS and D. C. LEVENDIS. J. Chem. Phys. **80**, 2681 (1980).
32. S. CARTER and J. N. MURRELL. J. Organomet. Chem. **192**, 399 (1980).
33. A. HAARLAND and J. E. NILSSON. Acta Chem. Scand. **22**, 2653 (1968).
34. J. SANDSTROM and J. SEITA. J. Organomet. Chem. **108**, 371 (1976).

Can. J. Chem. Downloaded from www.nrcresearchpress.com by 118.98.75.50 on 09/07/12
For personal use only.

The products of the reaction of thiiranium ions with competing nucleophiles

GEORGE H. SCHMID,[1] MARK STRUKELJ, AND SNEZANA DALIPI
Department of Chemistry, University of Toronto, Toronto, Ont., Canada M5S 1A1

Received January 15, 1987

This paper is dedicated to Professor John T. Edward

GEORGE H. SCHMID, MARK STRUKELJ, and SNEZANA DALIPI. Can. J. Chem. **65**, 1945 (1987).

The reaction of the stable thiiranium ion, prepared by the reaction of trifluoromethanesulfonic acid and methyl-3-(4-chlorophenylthio)propene with tetraethylammonium chloride in either 3.5 or 36% v/v methanol/dichloromethane with urea as a buffer, forms 2-methoxy-2-methyl-1-propyl 4-chlorophenyl sulfide, 2-chloro-2-methyl-1-propyl 4-chlorophenyl sulfide, and 1-chloro-2-methyl-2-propyl 4-chlorophenyl sulfide as products. While these same products are formed by the addition of 4-chlorobenzenesulfenyl chloride to methylpropene in the same solvents, their proportions differ. This is one of the rare examples in which there is a difference in the product composition of thiiranium ions formed in different ways and allowed to react under identical conditions. One possible explanation for this difference may be that the two thiiranium ions form products by different paths involving different kinds of ion pairs.

GEORGE H. SCHMID, MARK STRUKELJ et SNEZANA DALIPI. Can. J. Chem. **65**, 1945 (1987).

La réaction de l'acide trifluorométhanesulfonique avec le méthyl-3 (chloro-4 phénylthio) propène fournit l'ion thiiranium stable qui, par réaction avec le chlorure de tétraéthylammonium dans un mélange à 3,5 ou à 36% v/v de méthanol dans le dichlorométhane et en présence d'urée comme tampon, conduit à la formation de (chloro-4 phénylthio)-1 méthoxy-2 méthyl-2 propane, de (chloro-4 phénylthio)-1 chloro-2 méthyl-2 propane et de (chloro-4 phénylthio)-2 chloro-1 méthyl-2 propane. L'addition du chlorure de chloro-4 benzènesulfényle au méthylpropène conduit aux mêmes produits; toutefois, leurs proportions diffèrent. Ce cas représente un des rares exemples dans lesquels on note une différence dans la composition des produits qui se forment à partir d'ions thiiranium produits de façons différentes, mais que l'on a fait réagir dans des conditions identiques. Pour expliquer ces différences, on peut imaginer que les deux ions thiiranium forment des produits par des voies différentes impliquant des formes différentes de paires d'ions.

[Traduit par la revue]

Thiiranium ions[2] are postulated as intermediates in the (*i*) solvolysis of β-chloroalkyl aryl sulfides, (*ii*) alkylation of thiiranes, and (*iii*) addition of alkane- or arenesulfenyl derivatives to alkenes (2). They can be prepared and isolated by variations of the reactions in which thiiranium ions are proposed as intermediates (3). The difference is that to form a stable thiiranium ion, the counterion must be a very poor nucleophile to ensure that it will not react with the thiiranium ion. Despite claims to the contrary (4), the products of the reaction of these stable thiiranium ions with nucleophiles are similar in many respects to those formed in the addition reactions of alkane- and arenesulfenyl chlorides to alkenes.

Both are capable of undergoing reactions that involve skeletal rearrangements. For example, the stable thiiranium ion **1** reacts with nucleophiles to form products of 1,5 hydride shift (5). Rearranged products are formed after allowing the stable ion **2** to stand for 1.5 h before it is reacted with chloride ion (6). Rearranged products are also formed by the addition of arenesulfenyl chlorides to alkenes. The reaction of 2,4-dinitrobenzenesulfenyl chloride and norbornene in formic acid forms rearranged solvent-incorporated products (7). Clearly there are examples in the literature where both stable thiiranium ions and intermediates involved in the addition of sulfenyl halides to alkenes form rearranged and (or) solvent-incorporated products.

A second similarity is that nonstereospecific products are formed in both the reaction of stable thiiranium ions with nucleophiles and the addition of arenesulfenyl chlorides to alkenes. The reaction of the isomeric stable ions **4** and **5**

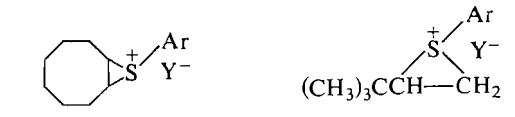

1

Ar = 2,4-di-$NO_2C_6H_3$

2

$Y^- = BF_4^-, SbF_6^-$

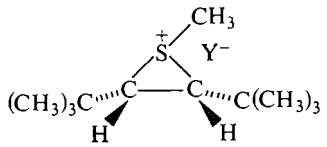

3

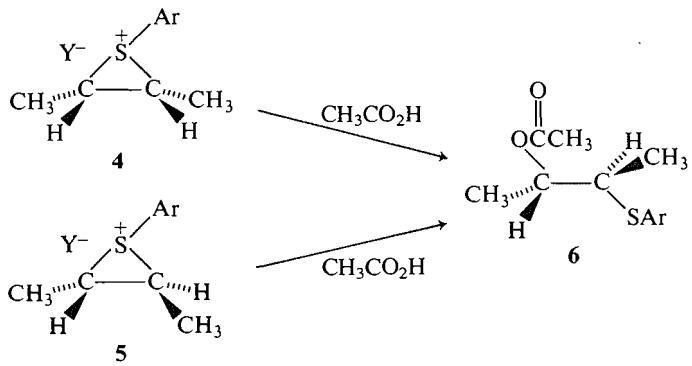

4

5

6

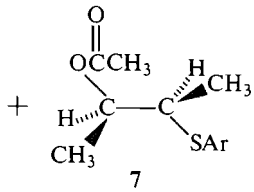

7

[1]Author to whom correspondence may be addressed.

[2]The term "thiiranium ion" has been and is used to designate the positively charged three-member sulfur containing ring irrespective of the location of the counter ion. This is analogous to the original practice of Winstein *et al.* (1) who referred to the carbocation portion of all ion pairs as varieties of carbonium ions.

Can. J. Chem. Downloaded from www.nrcresearchpress.com by 213.166.140.6 on 09/07/12
For personal use only.

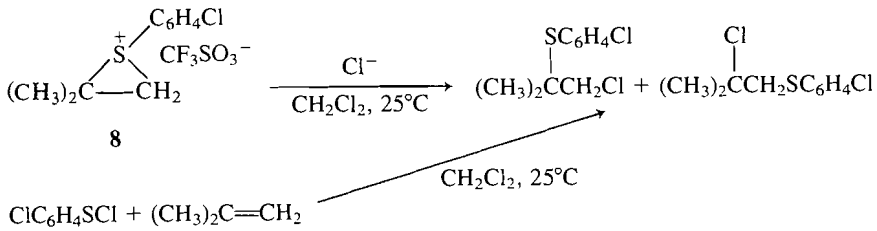

8

with acetic acid at room temperature gives the same mixture of *erythro*-(**6**) and *threo*-(**7**) products (8). Nonstereospecific products are also formed by the addition of 2,4-dinitrobenzenesulfenyl chloride to *E*- and *Z*-anethole (9) and 4-methoxy-β-deutereostyrene (10).

A third similarity is the regiochemistry of the products formed in the two reactions. The stable thiiranium ion **8** forms the same proportion of regioisomers as formed by the addition of 4-chlorobenzenesulfenyl chloride to methylpropene when the two reactions are carried out in the same solvent and at the same temperature (11).

The fourth similarity is the ability of a thiiranium ion, either a stable one or one postulated as an intermediate, to react with chloride ion rather than the solvent. The absence of solvent-incorporated products in the addition of arenesulfenyl chlorides to alkenes has been recognized (4) but the fact that stable thiiranium ions can also discriminate between chloride ion and solvents as nucleophiles seems to have escaped notice. Thus, lithium chloride reacts with the stable thiiranium ion **3** in acetonitrile/dichloromethane to form products of attack by both chloride ion (80%) and acetonitrile (5%) (12). Only products of the reaction of chloride ion are reported for the reaction of the stable ion formed by the reaction of the epoxysulfide **10** with HCl in acetonitrile (13). Thus stable ions, like their counterparts in the addition reaction, react preferentially with the stronger nucleophile.

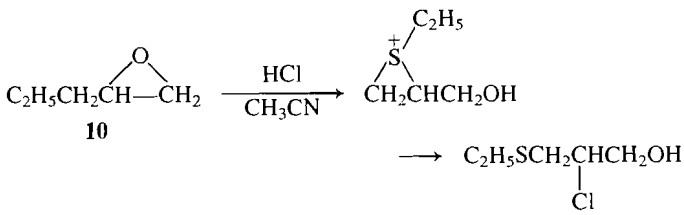

10

However, differences between the reactions of stable thiiranium ions and those proposed as intermediates have been cited (4). It has been stressed that the reaction of 4-chlorobenzenesulfenyl chloride with *E*- and *Z*-2-butene gives different products by *anti*-stereospecific addition (14) while the reaction of stable ions **4** and **5** with acetic acid gives the same product mixture. While this is a clear difference, it must be pointed out in all fairness that the two reactions occur under very different conditions. The addition reaction occurs instantly in 1,1,2,2-tetrachloroethane at 25°C.[3] In contrast, the stable ions **4** and **5** were allowed to stand for 1.5 h at 20°C before reacting them with acetic acid. A thiiranium ion that is allowed to stand for long periods of time in the absence of a good nucleophile has a high kinetic stability (16) and it can undergo reactions that are not available to a thiiranium ion intermediate formed in the presence of a good nucleophile. This has been demonstrated by the reaction of the thiiranium ion **10** (17). The time between formation of **10** and its reaction with added chloride ion has a great effect on the stereochemistry of the product even at −70°C. Thus allowing **10** to stand for a short time before reacting it with chloride ion results in products formed predominantly via a thiiranium ion. When the ion is allowed to stand for longer times before reacting it with chloride ion, products are formed via an open β-chloroalkyl carbocation. Thus the reactions of stable thiiranium ions are not necessarily good models for the intermediates in the addition of arenesulfenyl chlorides to alkenes.

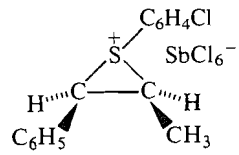

10

The major problem in making comparisons between the reactions of stable thiiranium ions and those proposed as intermediates is the paucity of data available under identical conditions. It is our contention that meaningful conclusions about differences and (or) similarities of the reactions of stable thiiranium ions and thiiranium ion intermediates cannot be reached unless comparisons are made from reactions carried out under identical experimental conditions. The purpose of this paper is to determine if there really is a difference in the product composition of the reaction, *under identical conditions*, of two competing nucleophiles, chloride ion and methanol, with both a stable thiiranium ion and one formed as an intermediate in the addition of arenesulfenyl chlorides to alkenes.

Results and discussion

The thiiranium ion *S*-(4-chlorophenyl)-2,2-dimethylthiiranium trifluoromethanesulfonate, **11**, was prepared by dissolving methyl 3-(4-chlorophenylthio)propene, prepared by the reaction of sodium 4-chlorothiophenoxide and methallyl chloride in methanol, in hexane and adding the resultant solution slowly to trifluoromethanesulfonic acid (11). A solution containing tetramethylammonium chloride, urea, and methanol (3.5 or 36 v/v%) in dichloromethane was added to the stable ion. The product composition of this reaction was compared to that obtained by the addition of 4-chlorobenzenesulfenyl chloride to methylpropene under the same conditions of solvent composition, added urea, and temperature. The data are given in Table 1.

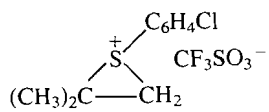

11

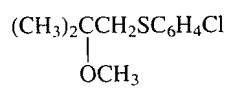

12

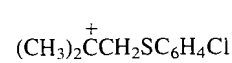

13

[3] k_2(*Z*-2-butene) = 1340 M^{-1} s^{-1}; k_2(*E*-2-butene) = 434 M^{-1} s^{-1}.

Can. J. Chem. Downloaded from www.nrcresearchpress.com by 213.166.140.6 on 09/07/12
For personal use only.

TABLE 1. Product compositions

Reactants	Reaction conditions[a]	Product composition (%)[b] aMCl	MCl	$MOCH_3$
$(CH_3)_2C{=}CH_2$ + 4-ClC_6H_4SCl	3.5% (v/v) CH_3OH/CH_2Cl_2, urea	45.0±0.3	52.0±0.9	3.5±0.8
$(CH_3)_2C{=}CH_2$ + 4-ClC_6H_4SCl	37% (v/v) CH_3OH/CH_2Cl_2, urea	27.7±0.3	47.2±0.5	25.0±0.5
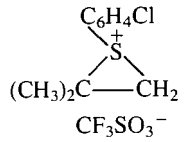	3.5% (v/v) CH_3OH/CH_2Cl_2, $(CH_3)_4NCl$, urea	14.8±0.9	41.9±0.8	43.3±0.8
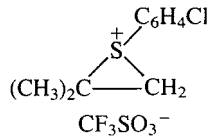	37% (v/v) CH_3OH/CH_2Cl_2, $(CH_3)_4NCl$, urea	16.0±0.8	19.4±0.8	64.6±0.9

[a]At 25°C.
[b]Abbreviations: aMCl = $(CH_3)_2CCH_2Cl$; MCl = $(CH_3)_2CCH_2SC_6H_4Cl$; $MOCH_3$ = $(CH_3)_2CCH_2SC_6H_4Cl$.
| SC_6H_4Cl | Cl | OCH_3

TABLE 2. Methanolysis product composition as a function of time[a]

Time[b] (min)	Product composition (%)[c] aMCl	MCl	$MOCH_3$
5	62±3	32±2	4±2
10	58±3	37±3	4±2
20	48±3	44±3	8±2
40	39±2	43±3	18±3

[a]36% (v/v) CH_3OH/CH_2Cl_2 with added urea at 25°C. Initial composition of aMCl:MCl = 3:1.
[b]Between mixing adducts in solvent and quenching in water.
[c]Abbreviations: aMCl = $(CH_3)_2CCH_2Cl$; MCl = $(CH_3)_2CCH_2SC_6H_4Cl$;
| SC_6H_4Cl | Cl
$MOCH_3$ = $(CH_3)_2CCH_2SC_6H_4Cl$.
| OCH_3

The first point to notice about the data in Table 1 is that the addition of 4-chlorobenzenesulfenyl chloride to methylpropene forms substantial amounts of the solvent-incorporated product 2-methoxy-2-methyl-1-propyl 4-chlorophenyl sulfide (**12**) even at low methanol concentrations. Before concluding that the intermediate thiiranium ion does indeed react with the solvent, it is necessary to consider other possible routes to **12**. One way that **12** could be formed is by methanolysis of the normal chloro adducts. To eliminate this path, it is necessary to know how rapidly methanolysis of the normal adducts occurs. The product compositions of methanolysis of the chloro adducts as a function of time are given in Table 2. After 5 min of methanolysis in 36 v/v% methanol only 4% **12** is formed. Clearly the rate of methanolysis of the adducts is much slower than the rapid addition of 4-chlorobenzenesulfenyl chloride to methylpropene.

Another way that **12** could be formed is by the addition to the double bond of the sulfenate ester ($ArSOCH_3$), known to be formed by the reaction of sulfenyl halides and methanol (18). This seems unlikely for the following reasons. The rate constant for the reaction of 4-chlorobenzenesulfenyl chloride and methanol in dichloromethane at 25°C for concentrations of methanol of 6.4% or lower is $1.48 \pm 1.3 \times 10^{-4}$ s^{-1} (19). This rate constant is much slower than that for the addition of 4-chlorobenzenesulfenyl chloride to methylpropene in dichloromethane at 25°C ($k_2 = 551$ M^{-1} s^{-1}). Therefore under these conditions a carbon–carbon double bond is a much better nucleophile than methanol towards bivalent sulfur (21). Consistent with these rate data is the fact that the reaction of arenesulfenyl chlorides with alkenols occurs only at the double bond (22). Therefore the only logical conclusion is that the intermediate thiiranium ion reacts with methanol to form **12**.

A second point to notice about the addition reaction is that the Markownikoff isomer **12** is the only solvent-incorporated product formed. Rapid acid-catalyzed isomerization of the anti-Markownikoff to the Markownikoff solvent-incorporated product **12** is probably not an explanation of this fact since in our work the addition reaction was carried out in the presence of an excess of urea to capture the HCl generated. It is also known that the reaction of stable thiiranium ion **11** with methoxide ion forms only **12** (23). Thus the Markownikoff isomer seems to be the kinetically controlled product.

It is surprising to find that a thiiranium ion reacts with methanol at only the most substituted carbon. One possible explanation for the formation of only **12** is that different nucleophiles react with thiiranium ions at different sites. Thus hard nucleophiles such as methanol react with the harder, more substituted, carbon while softer nucleophiles react with the softer, less substituted, carbon of **11**. It is also possible that **12** is formed via the open β-arylthio carbocation **13** rather than **11**. The products of addition to methylpropene cannot provide the necessary stereochemical information about the products that would prove the presence of an open ion in the mechanism of

Can. J. Chem. Downloaded from www.nrcresearchpress.com by 213.166.140.6 on 09/07/12
For personal use only.

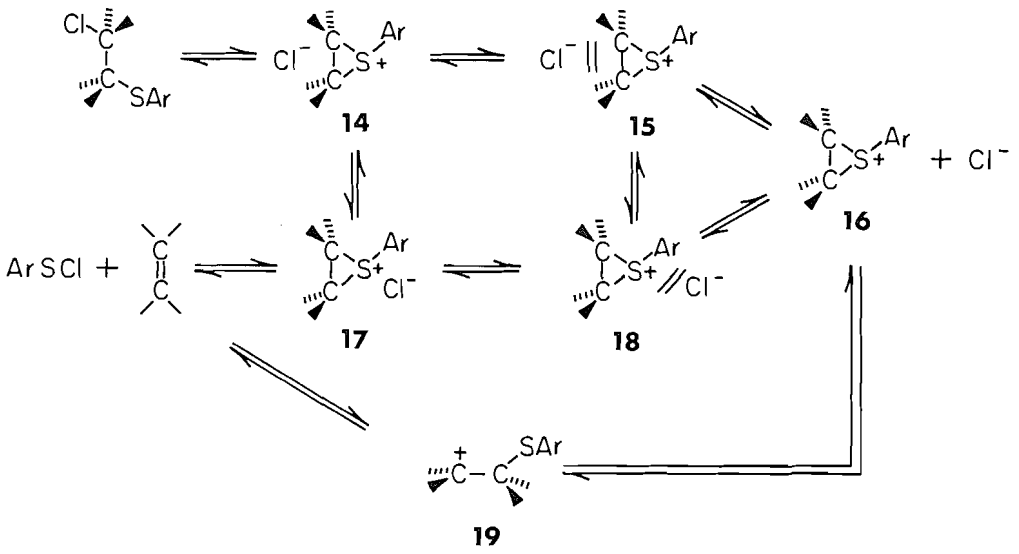

SCHEME 1

this reaction. But whatever the reason, the fact remains that the reaction of methanol with either the stable ion **11** or the intermediate in the addition reaction forms the *same* product.

The product compositions given in Table 1 for the addition of 4-chlorobenzenesulfenyl chloride to methylpropane are those of kinetic control. This was established by carrying out the following experiment. A solution of the alkene in 36 v/v% methanol/dichloromethane containing a fivefold excess of urea was divided into equal halves. To one half was added a 3:1 mixture of the anti-Markownikoff/Markownikoff adducts. An equal quantity of sulfenyl chloride was added to each solution and the products were analyzed by glc. The ratio of anti-Markownikoff/Markownikoff adducts in the solution to which adducts were added was found to be equal within experimental uncertainty to that expected if no isomerization of the added adducts occurred.

While **12** is formed in both reactions, the amount of this product depends on the reaction. The reaction of **11** with 36 v/v% methanol/dichloromethane forms 64.6% **12** while only 25% of **12** is formed in the addition reaction in the same solvent. Similarly, the relative amounts of 1-chloro-2-(4-chlorophenylthio)-2-methylpropane depend on the reaction. Furthermore, the regiochemistry of the chlorine-containing products is predominately Markownikoff in both reactions. This is in contrast to the usual addition of arenesulfenyl chlorides to methylpropene where the kinetically controlled product has the anti-Markownikoff orientation. The data presented here, obtained for both reactions under identical conditions, provide one of the few examples of a difference between the reactions of stable thiiranium ions and those proposed as intermediates.

What is the cause of this difference? One possible explanation may be that different types of ions or ion pairs are involved in the two reactions. The importance of ion pairs in the mechanism of many reactions is well documented (24). Electrophilic additions are no exception. A number of people have proposed that the mechanism of an electrophilic addition reaction could involve ion-pair intermediates (25). Subsequent work by Rolston and Yates (26) and Garnier and Dubois (27) established the importance of ion pairs in the bromination of alkenes. In 1973, Fitzgerald provided evidence that the mechanism of the electrophilic addition of arenesulfenyl chlorides to alkenes and the mechanism of neighboring sulfur participation in the reaction of β-chloroalkyl aryl sulfides both involve the same series of thiiranium ions (28). The major features of the mechanism that we proposed is shown in Scheme 1 (2). The upper sequence of reactions involving ion pairs **14** and **15** and ion **16** is the general solvolysis scheme proposed by Winstein.[4] The lower sequence of ion pairs is similar to that proposed by Poutsma and Kartch (25*c*) and applied to additions of arenesulfenyl chlorides by Zefirov and co-workers (4). The ion pairs **14** and **17** are contact ion pairs and **15** and **18** are solvent-separated ion pairs that differ only in the location of the counterion. Also included in this scheme is the open ion **19**. Our contribution to this mechanism was to provide evidence that these two paths are linked by ion pairs **14** and **17**, **15**, and **18**, and (or) the dissociated ion **16**. We propose in this scheme that electrophilic addition of arenesulfenyl chlorides to alkenes, isomerization of Markownikoff–anti-Markownikoff adducts, and solvolysis of β-chloroalkyl aryl sulfides all occur by means of a common mechanism (2).

While there is evidence in the literature for all of these ion pairs, this does not mean that they are all involved in every reaction. For example, the anti-Markownikoff to Markownikoff isomerization of the adducts of arenesulfenyl chlorides to alkenes is known to occur much faster than their acetolysis (15). A similar conclusion can be reached from the methanolysis data given in Table 2. Similarly, anti-Markownikoff to Markownikoff isomerization occurs faster than the transfer of ArSCl from one alkene to the other in the nonpolar solvent 1,1,2,2-tetrachloroethane (20). From these data we can conclude that internal return from ion pair **14** is faster than formation of **15**. Thus the mechanism of isomerization of the adducts involves ion pair **14** while their solvolysis occurs by means of ion pair **15** and (or) ion **16**. We can also conclude from these data that ion pairs **14** and **17** play an important mechanistic role in the isomerization, exchange, and addition reactions in non-

[4]For a summary and complete references to Winstein's work on ion pairs see ref. 29.

Can. J. Chem. Downloaded from www.nrcresearchpress.com by 213.166.140.6 on 09/07/12
For personal use only.

Can. J. Chem. Downloaded from www.nrcresearchpress.com by 213.166.140.6 on 09/07/12
For personal use only.

hydroxylic nonpolar solvents. Therefore the contact ion pairs **14** and **17** are the important intermediates in the addition of arenesulfenyl chlorides to alkenes in nonpolar solvents such as acetic acid and dichloromethane. The reaction of **11** with chloride ion in dichloromethane forms a similar product mixture to that formed by the addition of 4-chlorobenzenesulfenyl chloride to methylpropene (11). Thus the contact ion pairs **14** and **17** are the important intermediates involved in the mechanism of these two reactions in dichloromethane.

As methanol or other polar solvent is added to dichloromethane, the importance of solvent-separated ion pairs increases in the mechanism of both addition of arenesulfenyl chlorides and the reaction of stable thiiranium ions. It is clear from the data in Table 1 that more of the solvent-incorporated product **12** is formed in the reaction of the stable ion **11** than in the addition reaction. From these data, we can conclude that solvent-separated ion pairs **15** and **18** and (or) ion **16** are the predominant intermediates in the mechanism of the reaction of the stable ion **11** while they play a lesser role in the mechanism of the addition reaction. The data in Table 1, data obtained from the literature, and the mechanism given in Scheme 1 allow us to explain the difference in product composition between the reaction of stable thiiranium ions and those proposed as intermediates in the addition of arenesulfenyl chlorides to alkenes. The addition of arenesulfenyl chloride to alkenes even in 36 v/v% methanol/dichloromethane occurs by a mechanism involving predominantly contact ion pairs **14** and **17**. In contrast, the reaction of stable thiiranium ions such as **11** occurs in methanol/dichloromethane predominantly by means of the solvent-separated ion pair **15**. While both reactions give the same products, their proportions are different because of the differences in their product determining steps.

In conclusion, our data provide a rare example in which there is a clear difference in the product composition of thiiranium ions formed in different ways and allowed to react under identical conditions. This difference is not in the kind but only in the relative amounts of the products, which may be due to their formation by different paths involving different kinds of thiiranium ion pairs.

Experimental

The ^{1}H nmr spectra were recorded on Varian T-60, XL-100, or XL-200 spectrometers. All chemical shifts are relative to TMS. Gas–liquid chromatography was carried out on a Varian 2700 Aerograph equipped with a flame ionization detector using a Varian CDS 111 digital integrator to obtain peak areas. Analysis was carried out using a 5% QF-1 on Chromosorb in a 2 m × 2 mm silanized glass column at 120°C with a flow rate of 24 mL/min.

All solvents used were ACS grade. Dichloromethane was further purified by distillation after refluxing over P_2O_5. Methanol was purified by distilling from magnesium turnings. All solvents were shielded from light and stored over 3 Å molecular sieves that had been activated by heating at 220–300°C for 8–12 h. All reactions were carried out under an atmosphere of argon.

Methyl-3-(4-chlorophenylthio)propene was prepared as previously reported (11).

*S-(4-Chlorophenyl)-2,2-dimethylthiiranium trifluoromethanesulfonate, **11***, was prepared as previously reported (11).

Methanolysis of Markownikoff and anti-Markownikoff adducts

To a solution of 22.5 mL of dry dichloromethane containing 0.0448 g (7.48 mmol) of urea and 0.3515 g (1.50 mmol) of *anti*-Markownikoff and Markownikoff adducts (ratio 3:1) was added 12.5 mL of dry methanol. Each reaction was then stirred at 25°C for the appropriate time before it was quenched by the addition of 35 mL of distilled water. The layers were separated and the organic layer was washed with water (3 × 25 mL). The layers were separated and the organic layer was dried over $MgSO_4$, filtered, and the solvent removed by rotary evaporation. The resulting liquid was analyzed by either nmr (solvent $CDCl_3$) or glc.

*Reaction of thiiranium ion **11** with chloride ion and methanol*

To 30 mL of a methanol/dichloromethane solution containing 36% methanol by volume was added 3.40 g (56.7 mmol) of urea and 0.570 g (3.45 mmol) of tetramethylammonium chloride. This solution was stirred at 25°C for several minutes and then **11**, prepared as previously reported, was added. The reaction was immediately quenched by the addition of 30 mL of water. The layers were separated and the organic layer was washed with water (3 × 20 mL). The organic layer was dried over $MgSO_4$, filtered, and the solvent removed by rotary evaporation. The resulting liquid was analyzed by either nmr (solvent $CDCl_3$) or glc.

Acknowledgment

Financial assistance by the National Sciences and Engineering Research Council of Canada is gratefully acknowledged.

1. S. WINSTEIN, P. E. KLINEDINST, JR., and G. C. ROBINSON. J. Am. Chem. Soc. **83**, 885 (1985).
2. (*a*) G. H. SCHMID. *In* Topics in sulphur chemistry. Vol. 3. *Edited by* A. Senning. G. Thiems, Stuttgart. 1977. p. 100; (*b*) G. H. SCHMID and D. G. GARRATT. *In* The chemistry of double bonded functional groups. Supplement A. Part 2. *Edited by* S. Patai. Wiley, New York. 1977. Chapt. 9.
3. (*a*) G. CAPOZZI, O. DE LUCCHI, V. LUCCHINI, and G. MODENA. Tetrahedron Lett. 2603 (1975); (*b*) A. S. GYBIN, M. Z. KRIMER, V. A. SMIT, V. S. BOGDANOV, and E. A. VOROB'EVA. Izv. Akad. Nauk SSSR, Ser. Khim. 2156 (1978); (*c*) G. K. HELMKAMP, D. C. OWSLEY, W. M. BARNES, and H. N. CASSEY. J. Am. Chem. Soc. **90**, 1635 (1968).
4. (*a*) W. A. SMIT, N. S. ZEFIROV, I. V. BODRIKOV, and M. Z. KRIMER. Acc. Chem. Res. **12**, 282 (1979); (*b*) W. A. SMIT, N. S. ZEFIROV, I. V. BODRIKOV. *In* Org. Sulfur Chem., Invited Lectures, 9th Symposium 1980. *Edited by* R. Kh. Freidlina and A. E. Skora. Pergamon, Oxford. 1981.
5. A. S. GYBIN, W. A. SMIT, M. Z. KRIMER, N. S. ZEFIROV, L. A. NOVGORODTSEVA, and N. K. SADOVAYA. Tetrahedron, **36**, 1361 (1980).
6. N. S. ZEFIROV, N. K. SADOVOYA, A. M. MAGGERRAMOV, I. V. BODRIKOV, and V. R. KASRTASHOV. Tetrahedron, **31**, 2984 (1975).
7. N. S. ZEFIROV, N. K. SADOVAYA, L. A. NOVGORODTSEVA, and I. V. BODRIKOV. Tetrahedron, **34**, 1373 (1978).
8. (*a*) W. A. SMIT, M. Z. KRIMER, and E. A. VOROBIEVA. Tetrahedron Lett. 2451 (1975); (*b*) E. A. VOROBIEVA, M. Z. KRIMER, and W. A. SMIT. Izv. Akad. Nauk SSSR, Ser. Khim. 1318 (1976).
9. G. H. SCHMID and V. J. NOWLAN. J. Org. Chem. **37**, 3086 (1972).
10. I. V. BODRIKOV, A. V. BORISOV, W. A. SMIT, and A. I. LUTSENKO. Tetrahedron Lett. 4983 (1984).
11. G. H. SCHMID, M. STRUKELJ, S. DALIPI, and M. D. RYAN. J. Org. Chem. In press.
12. P. RAYNOLDS, S. ZONNEBELT, S. BAKKER, and R. M. KELLOG. J. Am. Chem. Soc. **96**, 4958 (1974).
13. A. R. DERZHINSKII, L. D. KONYUSHKIN, and A. J. LUTSENKO. Izv. Akad. Nauk SSSR, Ser. Khim. 2652 (1984).
14. G. H. SCHMID and V. M. CSIZMADIA. Can. J. Chem. **44**, 1338 (1966).
15. V. M. CSIZMADIA. Ph.D. Thesis, University of Toronto, 1971.
16. E. M. ARNETT and C. PETRO. J. Am. Chem. Soc. **100**, 5408 (1978).

17. G. H. SCHMID and D. I. MACDONALD. Tetrahedron Lett. 157 (1984).
18. N. KHARASCH. *In* Organic sulfur compounds. Vol. 1. *Edited by* N. Kharasch. Pergamon Press, New York. 1961. p. 375.
19. S. DALIPI. Ph.D. Thesis, University of Toronto, 1987.
20. G. H. SCHMID and P. H. FITZGERALD. J. Am. Chem. Soc. **93**, 2547 (1971).
21. G. H. SCHMID and D. G. GARRATT. Tetrahedron Lett. 5299 (1983).
22. V. R. KARTASHOV, N. A. KARTASHOVA, and E. V. SKOROBOGATOVA. Zh. Org. Khim. **10**, 171 (1974).
23. M. OKI, W. NAKANISHI, and M. FUKUNAGA. Chem. Lett. 1277 (1975).
24. J. E. GORDON. The organic chemistry of electrolyte solutions. Wiley, New York. 1975.
25. (*a*) P. B. D. DE LA MARE, N. V. KLASSEN, and R. KOENIGSBERGER. J. Chem. Soc. 5285 (1961); (*b*) M. C. CABALEIRO and M. D. JOHNSON. J. Chem. Soc. B, 565 (1967); (*c*) M. L. POUTSMA and J. L. KARTCH. J. Am. Chem. Soc. **89**, 6595 (1965).
26. J. H. ROLSTON and K. YATES. J. Am. Chem. Soc. **91**, 1477 (1969).
27. F. GARNIER and J. E. DUBOIS. Bull. Soc. Chim. Fr. 3797 (1968).
28. P. H. FITZGERALD. Ph.D. Thesis, University of Toronto, 1973; Diss. Abstr. **34**, 4855 (1973).
29. P. D. BARTLETT. J. Am. Chem. Soc. **94**, 2161 (1972).

Can. J. Chem. Downloaded from www.nrcresearchpress.com by 213.166.140.6 on 09/07/12
For personal use only.

Hydration of acylimidazoles: tetrahedral intermediates in acylimidazole hydrolysis and nucleophilic attack by imidazole on esters. The question of concerted mechanisms for acyl transfers

J. Peter Guthrie[1] and David C. Pike

Department of Chemistry, University of Western Ontario, London, Ont., Canada N6A 5B7

Received November 17, 1986

This paper is dedicated to Professor John T. Edward

J. Peter Guthrie and David C. Pike. Can. J. Chem. **65**, 1951 (1987).

Heats of hydrolysis have been measured for three acylimidazole acetals. From these results free energies of formation in aqueous solution have been calculated for the acetals and the corresponding tetrahedral intermediates. Having free energies of formation for the tetrahedral intermediates allows a detailed analysis of the energetics of both the unobservable nucleophilic reaction of imidazole with ethyl acetate and also the observable reaction of imidazole with *p*-nitrophenyl acetate. pK_a values of 1-(3-aminopropyl)-imidazole and 1-(2-aminoethyl)-imidazole have been determined to allow calculation of the σ^* value for the imidazolyl substituent. The dependence of imidazole pK_a values on the electron-withdrawing properties of the 1-substituent was also determined. There is a linear free energy relation between the free energy change for replacement of OH in a carbonyl hydrate by imidazolyl and the sum of the σ^* values for the other substituents. The implications of these results for the question of concerted versus stepwise mechanisms for the reactions of imidazole with aryl acetates have been examined. An equilibrium constant has been calculated for the addition of imidazole to *p*-nitrophenyl acetate. A simple extension of Marcus theory allows the free energy surface for a three-dimensional reaction coordinate diagram to be calculated using the energy levels of the tetrahedral intermediate determined in this work, the energy level of the acylium ion derived from literature data, and intrinsic barriers for the edge reactions. It is shown that the reaction of imidazole with *p*-nitrophenyl acetate probably follows a concerted path. General conclusions from this theory of concerted reactions are discussed.

J. Peter Guthrie et David C. Pike. Can. J. Chem. **65**, 1951 (1987).

On a mesuré les chaleurs d'hydrolyse de trois acétals d'acylimidazoles. À partir de ces données, on a calculé les énergies libres de formation, en solutions aqueuses, des acétals et de leurs intermédiaires tétraédriques correspondants. À l'aide des énergies libres de formation des intermédiaires tétraédriques, on peut effectuer une analyse détaillée des énergies impliquées tant dans la réaction nucléophile de l'imidazole avec l'acétate d'éthyle (réaction qui n'est pas observée) que dans la réaction observée de l'imidazole avec l'acétate de *p*-nitrophényle. Afin de permettre le calcul de la valeur σ^* du substituant imidazolyle, on a déterminé les valeurs de pK_a de l'(amino-3 propyl)-1 imidazole et de l'(amino-2 éthyl)-1 imidazole. On a aussi déterminé la relation qui existe entre les valeurs de pK_a de l'imidazole et les propriétés électroaffinitaires du substituant en position 1. Il existe une relation linéaire entre le changement d'énergie libre pour le remplacement d'un OH d'un hydrate de carbonyl par le groupement imidazolyle et la somme des valeurs σ^* des autres substituants. On a examiné les implications de ces résultats sur la question des mécanismes concertés par opposition aux mécanismes par étapes pour les réactions de l'imidazole avec les acétates d'aryles. On a calculé une constante d'équilibre pour l'addition de l'imidazole à l'acétate de *p*-nitrophényle. En se basant sur les niveaux d'énergie des intermédiaires tétraédriques qui ont été déterminés dans ce travail, sur le niveau d'énergie de l'ion acylium que l'on peut dériver des données de la littérature et sur les barrières intrinsèques des réactions se produisant aux arêtes et faisant appel à une extension simple de la théorie de Marcus, on peut calculer le diagramme de coordonnées de la surface d'énergie libre d'une réaction tridimensionnelle. On démontre que la réaction de l'imidazole avec l'acétate de *p*-nitrophényle se produit probablement par une voie concertée. On discute des conclusions générales que l'on peut tirer à partir de cette théorie des réactions concertées.

[Traduit par la revue]

Introduction

Imidazole is well known as a nucleophilic catalyst for the hydrolysis of active esters (1–4); the acylimidazole formed as an intermediate is itself rapidly hydrolyzed (2, 3). We have previously reported a thermochemical approach to determining free energies of formation of tetrahedral intermediates in aqueous solution, as well as of other reactive intermediates (5, 6).

In this paper we wish to report the results of three closely linked investigations aimed at improving understanding of the mechanisms of these reactions. We have studied the thermochemistry of acylimidazole acetals and hence determined free energies of formation in solution of the corresponding tetrahedral intermediates. We developed indirect procedures allowing the estimation of free energies of formation for tetrahedral intermediates involved in reactions of imidazole with some nitrophenyl acetates. Finally, in considering the question of whether the reactions of imidazole with active esters are concerted or stepwise, we have developed a theory of such processes, showing how criteria for "concertion" can be phrased in terms of the characteristics of the limiting stepwise reactions.

We have applied the thermochemical approach, which we previously employed for other systems, to the tetrahedral intermediates involved in hydrolysis of acylimidazoles and the nucleophilic attack of imidazoles on esters. For three acylimidazoles, acetyl, formyl, and benzoyl, we have prepared the acetals, determined the free energies of formation, and then calculated the free energies of formation of the tetrahedral intermediates by means of the hypothetical hydrolysis reaction:

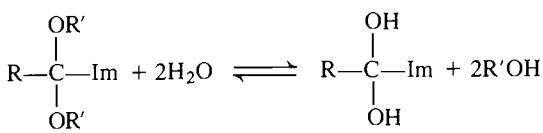

This was accomplished using the previously reported linear free energy relationship (6) for the reaction:

[1]Author to whom correspondence should be addressed.

Can. J. Chem. Downloaded from www.nrcresearchpress.com by 118.98.75.50 on 09/07/12
For personal use only.

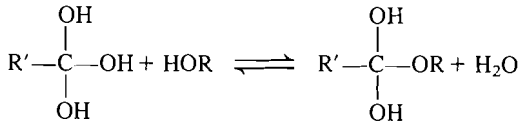

We now find that there is a similar relationship for replacement of OH by imidazolyl:

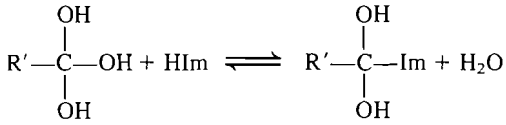

With free energies of formation of the tetrahedral intermediates formed in imidazole-catalyzed hydrolyses now in hand we can investigate the detailed energetics of these reactions. By an extension of our thermochemical calculations we can estimate the free energies of formation of the tetrahedral intermediate formed by the addition of imidazole to *p*-nitrophenyl acetate. This allows us to address the question of the mechanism of this acyl transfer reaction.

Results

Calorimetry

The starting point for the determination of the free energies of formation of tetrahedral intermediates was the determination of the heats of formation of the acylimidazole acetals, based on the calorimetric measurement of the heats of hydrolysis of the acylimidazole acetals.

Heats of reaction were measured with a simple calorimeter using the procedure previously described (7). Stoichiometries were verified by nmr analysis of product solutions and showed that in all cases hydrolysis of acylimidazole acetals in dilute acid led to the ester, one mole of alcohol, and the imidazole in its protonated form.

Our results are summarized in Table 1, which gives both the directly measured heats of reaction and the heats of reaction corrected to pure compound standard states (pure liquid or solid) for all reactants and products. The derived heats of formation are given in Table 2, which includes the other thermodynamic quantities employed in this paper.

Free energies of formation

Calculation of free energies of formation in the gas phase from the heats of formation in condensed phase required heats of vaporization and also standard entropies for the gaseous compounds. Heats of vaporization for the acylimidazole acetals were estimated by a procedure that we developed using the boiling points at reduced pressures (8), in the present case interpolated or extrapolated boiling points at 1 Torr (1 Torr = 133.3 Pa). All of the values of $\Delta H_{\text{vaporization}}$ estimated as just described are found in Table 2. Entropies were estimated by several procedures based on additivity and disproportionation (9). These calculations are found in the Appendix; the entropy values are in Table 2.

Free energies of transfer

The free energy of transfer from the gas phase (at 1 atm; 1 atm = 101.3 kPa) to aqueous solution (1 *M* with an infinitely dilute reference state) could sometimes be measured directly or indirectly and sometimes calculated from the solubility and vapor pressure. For benzoylimidazole dimethyl acetal it was possible to determine the solubility in aqueous sodium hydroxide solution, although there was a slow hydrolysis reaction. Extrapolation to zero time allowed calculation of the actual solubility. From the boiling point data gathered to evaluate the heat of vaporization, the vapor pressure at 25°C could be calculated by a procedure that we recently reported (8). This procedure uses the available vapor pressure data and values of the heat of vaporization and heat capacity of vaporization (estimated using our atomic additivity parameters (10)). The value so obtained was $p_{25°C} = 6.22 \times 10^{-4}$ Torr. We could then calculate the free energy of transfer as -5.73 ± 0.30, with the error limits based on an estimated uncertainty of 50% in the vapor pressure.

For formylimidazole diethyl acetal, the solubility was too high for ideality to be assumed, and was in fact critically dependent on temperature and ionic strength. A solution of 1.54 *M* formylimidazole diethyl acetal in 0.1 *M* NaOH at about 4°C separated into two phases upon warming to room temperature, while at 0.075 *M* NaOH the same proportions of acetal and water gave a homogenous solution from 4 to 25°C. The free energy of transfer for formylimidazole diethyl acetal was estimated indirectly as follows. The solubility was difficult to measure experimentally because of the phase separation behavior with small changes in temperature or salt concentration; this implies that we are dealing with a pair of nearly miscible liquids, with considerable deviations from ideality. To estimate the ideal solubility, we used the relationship reported by Hansch *et al.* (11) between solubility and the partition constant between water and 1-octanol. We have in fact measured the partition constant between water and heptane, but Leo and Hansch have shown (12) that there are linear free energy relations among partition constants for various solvents

TABLE 1. Heats of solution and reaction used in determining heats of formation

Compound	ΔH^a (kcal/mol)	ΔH^b (kcal/mol)
H_2O	-0.06 ± 0.01[c]	
	-0.22 ± 0.01[c,d]	
MeOH	-0.32 ± 0.02[c,d]	
EtOH	-2.43 ± 0.01[e]	
Imidazole	-5.87 ± 0.08[f]	
	-5.41 ± 0.07[d,f]	
HCOOEt	-1.64 ± 0.34[g]	
MeCOOEt	-2.27 ± 0.01[h]	
$HC(OEt)_2$—Im	-18.16 ± 0.02[f]	-8.28 ± 0.42
$MeC(OEt)_2$—Im	-21.19 ± 0.14[f]	-10.68 ± 0.16
PhCOOMe	3.41 ± 0.06[c,d]	
$PhC(OMe)_2$—Im	-15.36 ± 0.14[d,f]	-13.26 ± 0.17

[a]Experimental heats of reaction or solution measured in this work; all at 25°C, in 0.1 *M* aqueous HCl, unless otherwise noted. For water, alcohols, and esters, the quantity measured is the heat of solution (pure liquid to dilute solution). For imidazole the quantity measured is the heat of reaction (pure solid to dilute solution of protonated compound). For the acylimidazole acetals the quantity measured is the heat of reaction (pure compound to dilute solution of stoichiometric amounts of protonated imidazole, alcohol, and ester).

[b]All reactants and products in pure compound standard states, i.e., pure liquid acylimidazole acetal plus pure liquid water going to pure crystalline imidazole, pure liquid alcohol, and pure liquid ester.

[c]Reference 7.

[d]In 50% methanol:water, 0.1 *M* HCl.

[e]Reference 77.

[f]This work.

[g]Reference 14.

[h]Reference 78.

Can. J. Chem. Downloaded from www.nrcresearchpress.com by 118.98.75.50 on 09/07/12
For personal use only.

Can. J. Chem. Downloaded from www.nrcresearchpress.com by 118.98.75.50 on 09/07/12
For personal use only.

TABLE 2. Thermodynamic quantities for compounds discussed in this paper[a]

(*a*) Compounds for which the free energy of formation in aqueous solution has not previously been reported

Compound	ΔH_f^0(g)[b]	S^0(g)[c]	ΔG_f^0(g)[d]	ΔH_v[e]	ΔH_f^0(l)[f]	ΔG_t[g]	ΔG_f^0(aq)[h]
MeCOOEt	-106.34 ± 0.16[i]	86.70 ± 0.10[j]	-78.73 ± 0.16[k]	8.40 ± 0.05[i]	-114.74 ± 0.15[i]	-1.19 ± 0.10[l]	-79.92 ± 0.19[k]
Imidazole	33.29 ± 0.45[k]	67.38 ± 2.00[m]	46.67 ± 0.75[k]	19.31 ± 0.19[n]	13.98 ± 0.41[o,p]	-7.91 ± 0.10[m]	38.76 ± 0.75[k]
$HC(OEt)_2$—Im	-61.02 ± 0.71[k]	126.8 ± 3.1[m]	-2.20 ± 1.16[k]	17.68 ± 0.28[m]	-78.70 ± 0.66[q]	-5.45 ± 0.14[q]	-7.65 ± 1.18[k]
$MeC(OEt)_2$—Im	-70.93 ± 0.55[k]	132.9 ± 3.0[m]	-4.18 ± 1.10[k]	17.25 ± 0.28[m]	-88.18 ± 0.47[q]	-5.49 ± 0.50[m]	-9.71 ± 1.16[k]
$PhC(OMe)_2$—Im	-18.52 ± 0.89[k]	134.0 ± 4.1[m]	39.81 ± 1.51[k]	20.45 ± 0.28[m]	-38.97 ± 0.85[q]	-5.73 ± 0.30[q]	34.08 ± 1.54[k]

(*b*) Compounds for which the free energy of formation in aqueous solution has been reported previously

Compound	ΔG_f^0(aq)
H_2O	-56.69 ± 0.01[r,s]
MeOH	-41.88 ± 0.01[s]
HCOOH	-88.83 ± 0.24[t]
MeCOOH	-94.21 ± 0.23[t]
EtOH	-43.31 ± 0.01[s]
MeCOMe	-38.48 ± 0.19[u]
HCOOEt	-76.36 ± 1.12[v]
PhCOOH	-57.02 ± 0.45[s]
PhCOOMe	-40.95 ± 1.32[s]
$H—C(OH)_3$	-137.35 ± 1.01[m]
$Me—C(OH)_3$	-138.96 ± 0.84[m]
$Ph—C(OH)_3$	-99.44 ± 1.48[x]

(*c*) Compounds for which the free energy of formation in aqueous solution has been calculated in this work

Compound	ΔG_f^0(aq)
H—CO—Im	12.8 ± 3.0[m]
Me—CO—Im	10.73 ± 0.80[y]
HC(OEt)(OH)—Im	-23.65 ± 1.22[m]
$HC(OH)_2$—Im	-38.51 ± 1.27[m]
MeC(OEt)(OH)—Im	-26.09 ± 1.20[m]
$MeC(OH)_2$—Im	-40.87 ± 1.25[m]
Ph—CO—Im	50.90 ± 2.87[m]
PhC(OMe)(OH)—Im	16.40 ± 1.58[m]
$PhC(OH)_2$—Im	-0.02 ± 1.62[m]

(*d*) Compounds for which the heat of formation has been reported previously

Compound	ΔH_f^0(l)
H_2O	-68.32 ± 0.01[i]
MeOH	-57.01 ± 0.05[i]
EtOH	-66.42 ± 0.08[i]
HCOOEt	-102.86 ± 0.30[z]
PhCOOMe	-77.51 ± 0.72[s]

[a]Standard states are pure liquid at 25°C; ideal gas at 25°C and 1 atm, and 1 *M* aqueous solution with an infinitely dilute reference state. Units are kcal mol^{-1} for enthalpies and free energies, and cal deg^{-1} mol^{-1} for entropies.

[b]Heat of formation in the gas phase.

[c]Standard entropy in the gas phase.

[d]Free energy of formation in the gas phase.

[e]Heat of vaporization.

[f]Heat of formation, liquid phase unless otherwise noted.

[g]Free energy of transfer from gas to aqueous solution.

[h]Free energy of formation in aqueous solution.

[i]Reference 76.

[j]Reference 73.

[k]Calculated from other values in this table.

[l]Reference 13.

[m]Estimated as described in the text.

[n]Reference 79. We prefer this value to a lower one reported by Sabbah (80).

[o]Reference 80.

[p]Standard state is the crystalline solid.

[q]Determined in this work.

[r]Standard state is the pure liquid.

[s]Reference 7.

[t]Reference 61.

[u]Reference 81.

[v]Reference 14.

[w]Recalculated from data in refs. 82 and 61.

[x]Calculated from data in ref. 7.

[y]Calculated from the equilibrium constant for its formation in aqueous solutions (45) and other values in this table.

[z]Reference 83.

Can. J. Chem. Downloaded from www.nrcresearchpress.com by 118.98.75.50 on 09/07/12
For personal use only.

and water. Thus we can calculate a partition constant from water to 1-octanol from our measured partition constant from water to heptane, and thence calculate the solubility; the value so obtained was 0.77 *M*. The vapour pressure, determined by extrapolation from our measurements, was 8.38×10^{-3} Torr. These values lead to a free energy of transfer of −6.79 kcal/mol.

We prepared formylimidazole dipropyl acetal and measured its solubility and vapor pressure. The solubility was low enough, 0.062 *M*, to ensure ideality; the vapor pressure, determined by extrapolation, was 2.4×10^{-3} Torr. From these data we obtain a free energy of transfer of −5.86 ± 0.14 kcal/mol. By subtracting twice the $[CH_2(C)_2]$ group contribution (13) we can calculate the free energy of transfer of formylimidazole diethyl acetal as −5.45 ± 0.14 kcal/mol; this value was used for further calculations.

For acetylimidazole diethyl acetal we could neither determine the solubility nor directly determine the free energy of transfer from gas to aqueous solution because of rapid breakdown of the acetal in water even at high pH. However, it was possible to determine an apparent partition coefficient between water and heptane as a function of stirring time and then extrapolate to zero time to correct for the hydrolysis. The value so obtained was $K = c_{water}/c_{heptane} = 0.98$. Estimation of the ideal aqueous solubility, by the same process as for formylimidazole diethyl acetal, led to a value of 0.25 *M*. This value, with the vapor pressure, 6.54×10^{-3} Torr, leads to a free energy of transfer of −5.95 kcal/mol.

In addition, the free energy of transfer from gas to water was estimated by an additivity calculation, assuming that the change in ΔG_t is the same on going from formylimidazole diethyl acetal to acetylimidazole diethyl acetal as from trimethyl orthoformate ($\Delta G_t = -2.52$ (14)) to trimethyl orthoacetate ($\Delta G_t = -2.48$(14)). The estimate so obtained was −5.49 ± 0.50 kcal/mol. This value was used for further calculations.

The free energy of transfer of imidazole itself has recently been reported by Wolfenden *et al.* (15) as −7.91 kcal/mol.

pK_a values and σ values*

To carry out calculations of the free energy changes for hypothetical hydrolyses it was necessary to have a σ* value for imidazole as a substituent. There appeared to be no such value in the literature, so we prepared two ω-aminoalkylimidazoles and determined their pK_a values. The values so obtained were, for *N*-(2-aminoethyl)-imidazole, pK_1 = 5.90 ± 0.02, pK_2 = 8.45 ± 0.02; for *N*-(3-aminopropyl)imidazole, pK_1 = 6.50 ± 0.02, pK_2 = 9.63 ± 0.02. Then, by interpolation from plots of pK_a vs. σ* for suitable sets of substituted alkyl ammonium ions, we could determine σ* values; see Fig. 1. The values that we used for these correlations are found in Table 3. The values so determined for σ* were 2.61 ± 0.07 and 2.84 ± 0.26, for which the weighted average is 2.63 ± 0.06.

These data can also be used to determine the dependence of the pK_a of an N-substituted imidazole on the nature of the substituent; our new pK_1 values give two additional points, which with the available values from the literature are found in Table 3.[2] The best line fitting these points for $X—CH_2—ImH^+$ is pK_a = (6.84 ± 0.13) − (0.302 ± 0.068)σ_x*; see Fig. 1. The fit is less than ideal and in fact there are indications that substituents with and without hydrogen bond donor groups may constitute separate families, but in view of the limited number of values available it seems better to use a general equation fitting all the data and accept larger error limits than to try to develop restricted correlations based on very few points.

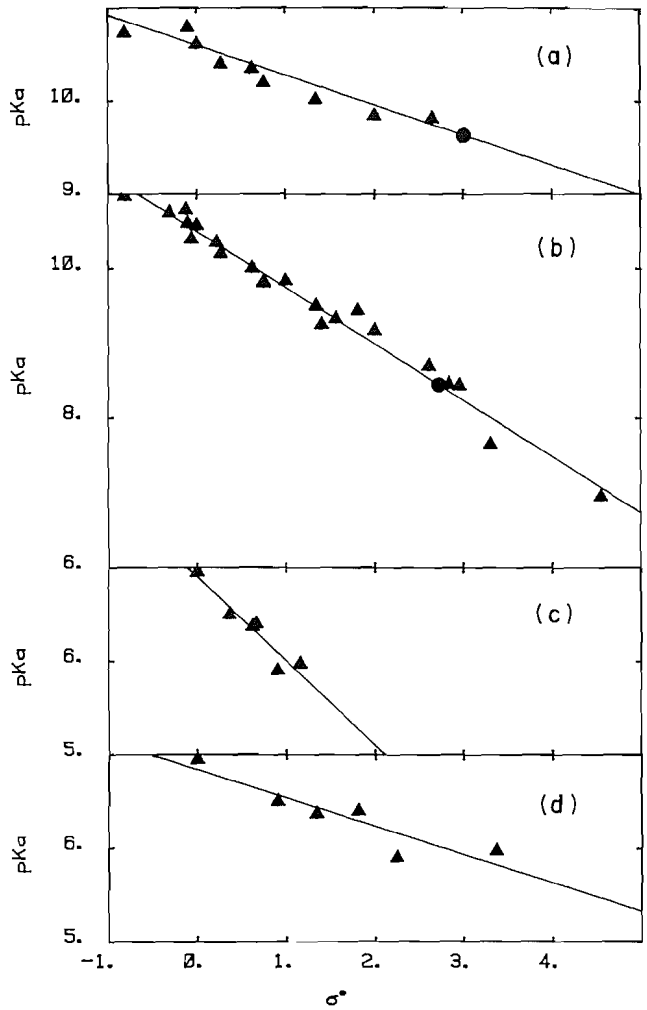

FIG. 1. Relation of pK_a to σ* for ammonium ions. (▲) experimental pK_a and known σ*; (●) experimental pK_a used to define σ* from the correlation line. (*a*) $X—CH_2—CH_2—CH_2—NH_3^+$; (*b*) $X—CH_2—CH_2—NH_3^+$; (*c*) $X—ImH^+$; (*d*) $X—CH_2—ImH^+$.

We also require a value of σ* for imidazolium as a substituent. A value can be calculated from the first pK_a of imidazoleacetic acid (16) by using the equation relating pK_a for RCH_2COOH recommended by Barlin and Perrin (17). The pK_a value of 2.19 leads to a σ* value of 3.84.

Free energies of formation of acylimidazole acetals and tetrahedral intermediates

Now it is possible to calculate the quantities of greatest interest for the rest of this paper, namely the free energies of formation in aqueous solution. The calculation of these values for the acylimidazole acetals is straightforward (5) and leads to the values given in Table 2.

The calculation of the free energies of formation of the tetrahedral intermediates is also straightforward, except for the problem of estimating strain release during the hypothetical hydrolyses. Our approach relies upon fitting the molecule to a diamond lattice and using additive parameters for each interaction, following Pihlaja and Kankare (18). This approach does not work for aryl substituents. Examination of models suggests that there will be only small interactions of the alkyl

[2]We thank Professor R. A. McClelland for kindly communicating a value for the pK_a of 2-imidazolyl-2-methoxypropane prior to publication.

TABLE 3. pK_a values used for linear free energy relations[a]

(*a*) N-substituted imidazolium ions

Compound	pK_a	σ^*[b] X—ImH^+	σ^*[b] X—CH_2—ImH^+
H—Im^+—CH_2—OH	6.37[c]	0.62	1.34
H—Im^+—$(CH_2)_2$—NH_3^+	5.90[d]	0.90[e]	2.24
H—Im^+—$(CH_2)_3$—NH_3^+	6.50[d]	0.36[e]	0.90[e]
H—Im^+—CH_3	6.95[f]	0.00	0.00[g]
H—Im^+—$CH(OEt)_2$	5.97[h]	1.16[i]	3.36[j]
H—Im^+—CH_2OEt	6.4[k]	0.66	1.81

For X—Im—H^+, $pK_a = 6.90 \pm 0.10 - 0.899 \pm 0.143\sigma^*$
For X—CH_2—Im—H^+, $pK_a = 6.84 \pm 0.13 - 0.302 \pm 0.067\sigma^*$

(*b*) β-Substituted ethylammonium ions ($XCH_2CH_2NH_3^+$), pK_a vs. σ^*

Substituent (X)	pK_a[l]	σ^*[b]	Substituent (X)	pK_a[l]	σ^*[b]
CH_3-	10.58	0.00	C_2H_5-	10.61	−0.10
C_6H_5-	9.83	0.75	HO-	9.50	1.34
CH_3CONH-	9.25	1.40	$C_6H_5CH_2CH_2$-	10.40	−0.06
Br-	8.46	2.84	$HOCH_2CH_2$-	10.35	0.25[c]
$(CH_3)_3N^+$-	6.95	4.55	CH_3S-	9.33	1.56
$HOCH_2$-	10.01	0.62	NC-	7.65	3.30
$CH_3O_2CCH_2$-	9.84	1.06	$(CH_3)_3SiCH_2$-	10.73	−0.31
CH_3O-	9.44	1.81	Cl-	8.44	2.96
$(CH_3)_3Si$-	10.97	−0.81	Cl_3CCH_2-	9.81	0.75
CF_3-	8.70	2.61	$C_6H_5CH_2$-	10.20	0.27
C_3H_7-	10.79	−0.12			
CH_3O_2C-	9.17	2.00			

$pK_a = 10.50 \pm 0.05 - 0.752 \pm 0.025\sigma^*$
Imidazolyl $\sigma^* = 2.61 \pm 0.07$

(*c*) γ-Substituted propylammonium ions ($XCH_2CH_2CH_2NH_3^+$), pK_a vs. σ^*

Substituent (X)	pK_a[l]	σ^*[b]
HO-	10.01	1.34
CH_3-	10.61	0.00
CH_3CH_2-	10.79	−0.10
CH_3O_2C-	9.84	2.00
$C_6H_5CH_2$-	10.40	0.27
$HOCH_2$-	10.35	0.62
$(CH_3)_3Si$-	10.73	−0.81
Cl_3C-	9.81	2.65
C_6H_5-	10.20	0.75
H-	10.58	0.00[g]

$pK_a = 10.55 \pm 0.04 - 0.324 \pm 0.035\sigma^*$
Imidazole $\sigma^* = 2.84 \pm 0.26$

[a] In H_2O at 25°C unless otherwise noted.
[b] Reference 86 unless otherwise noted.
[c] Reference 87.
[d] This work.
[e] Estimated using the relationship $\sigma^*_{CH_2R} \cong 0.4 \times \sigma^*_R$ (86).
[f] Reference 84.
[g] Reference 21.
[h] Reference 88.
[i] Estimated (86) as $2 \times \sigma^*_{CH_2OEt}$.
[j] Although this does not fit the pattern, we use $2 \times \sigma^*_{OEt}$.
[k] R. A. McClelland, personal communication.
[l] Reference 89.

Can. J. Chem. Downloaded from www.nrcresearchpress.com by 118.98.75.50 on 09/07/12
For personal use only.

TABLE 4. Equilibrium constants for addition reactions of carbonyl compounds[a]

HCOOEt + H—Im ⇌ HC(OEt)(OH)—Im	13.95 ± 1.82	−10.21 ± 1.33
MeCOOEt + H—Im ⇌ MeC(OEt)(OH)—Im	15.08 ± 1.43	−11.04 ± 1.05
MeCOO*p*NP + H—Im ⇌ MeC(OH)(O*p*NP)—Im	18.29 ± 3.29	−13.39 ± 2.34
MeCOODNP + H—Im ⇌ MeC(OH)(ODNP)—Im	18.15 ± 3.26	−13.29 ± 2.39
MeCOOEt + H—Im ⇌ MeC(O$^-$)(OEt)—ImH$^+$	20.74 ± 1.55	−14.85 ± 1.13
MeCOO*p*NP + HIm ⇌ MeC(O$^-$)(O*p*NP)—ImH$^+$	21.79 ± 3.14	−15.95 ± 2.30
MeCOODNP + HIm ⇌ MeC(O$^-$)(ODNP)—ImH$^+$	21.09 ± 3.21	−15.44 ± 2.35
PhCOOMe + H—Im ⇌ PhC(OMe)(OH)—Im	18.59 ± 2.20	−13.61 ± 1.61
HCOOH + H—Im ⇌ HC(OH)$_2$—Im	11.56 ± 1.85	−8.46 ± 1.36
MeCOOH + H—Im ⇌ MeC(OH)$_2$—Im	14.58 ± 1.47	−10.67 ± 1.08
PhCOOH + H—Im ⇌ PhC(OH)$_2$—Im	18.24 ± 2.22	−13.36 ± 1.63
Me—CO—Me + H—Im ⇌ Me$_2$C(OH)—Im	3.54 ± 0.26[b]	−2.59 ± 0.18[b]
Me—CO—H + H—Im ⇌ MeCH(OH)—Im	−0.25 ± 0.06[c]	0.41 ± 0.04[c]
H—CO—H + H—Im ⇌ CH$_2$(OH)—Im	−6.19 ± 0.06[d]	4.53 ± 0.04[d]
4-py-CHO + H—Im ⇌ 4—pyCH(OH)—Im	>0.71[e]	<−0.52[e]
H—CO—Im + H$_2$O ⇌ HC(OH)$_2$—Im	5.43 ± 2.73[f]	−3.98 ± 2.0[f]
Me—CO—Im + H$_2$O ⇌ MeC(OH)$_2$—Im	5.09 ± 1.48	−3.73 ± 1.08
Ph—CO—Im + H$_2$O ⇌ PhC(OH)$_2$—Im	5.78 ± 1.60[f]	−4.23 ± 1.17[f]
H—CO—Im + OH$^-$ ⇌ HC(OH)(O$^-$)—Im	0.07 ± 2.76[f]	−0.05 ± 2.02[f]
Me—CO—Im + OH$^-$ ⇌ MeC(OH)(O$^-$)—Im	0.61 ± 1.54	−0.44 ± 1.13
Ph—CO—Im + OH$^-$ ⇌ PhC(OH)(O$^-$)—Im	−0.06 ± 1.65[f]	0.04 ± 1.21[f]
H—CO—ImH$^+$ + OH$^-$ ⇌ HC(OH)(O$^-$)ImH$^+$	−5.23 ± 2.81[f]	3.83 ± 2.05[f]
Me—CO—ImH$^+$ + OH$^-$ ⇌ MeC(OH)(O$^-$)ImH$^+$	−4.41 ± 1.59	3.23 ± 1.17
Ph—CO—ImH$^+$ + OH$^-$ ⇌ PhC(OH)(O$^-$)ImH$^+$	−5.13 ± 1.70[f]	3.75 ± 1.25[f]
H—CO—ImH$^+$ + H$_2$O ⇌ HC(OH)$_2$—ImH$^+$	1.84 ± 2.78[f]	−1.35 ± 2.03[f]
Me—CO—ImH$^+$ + H$_2$O ⇌ MeC(OH)$_2$—ImH$^+$	1.77 ± 1.54	−1.30 ± 1.13
Ph—CO—ImH$^+$ + H$_2$O ⇌ PhC(OH)$_2$—Im$^+$	2.41 ± 1.65[f]	−1.76 ± 1.21[f]
H—CO—Im + H$_2$O ⇌ HC(O$^-$)(OH$_2^+$)—Im	19.51 ± 2.76[f,g]	−14.29 ± 2.02[f,g]
Me—CO—Im + H$_2$O ⇌ MeC(O$^-$)(OH$_2^+$)—Im	19.46 ± 1.54[g]	−14.25 ± 1.13[g]
Ph—CO—Im + H$_2$O ⇌ PhC(O$^-$)(OH$_2^+$)—Im	19.70 ± 1.65[f,g]	−14.42 ± 1.21[f]
Me—COOEt + H$_2$O ⇌ MeC(OH)$_2$—OEt	11.20 ± 2.73[h]	−8.2 ± 2.0[h]
Me—CO—O*p*NP + H$_2$O ⇌ MeC(OH)$_2$—O*p*NP	10.73 ± 2.78[f]	−7.86 ± 2.04[f]
Me—CO—ODNP + H$_2$O ⇌ MeC(OH)$_2$—ODNP	9.52 ± 2.73[f]	−6.97 ± 2.05[f]
Me—CO—O*p*NP + *p*NPOH ⇌ MeC(O*p*NP)$_2$OH	24.94 ± 5.07[f]	−18.26 ± 3.71[f]
Me—CO—ODNP + DNPOH ⇌ MeC(ODNP)$_2$OH	28.67 ± 6.33[f]	−20.99 ± 4.64[f]
Me—CO—O*p*NP + *p*NPO$^-$ ⇌ MeC(O$^-$)(O*p*NP)$_2$	27.96 ± 5.08[f]	−20.47 ± 3.72[f]
Me—CO—ODNP + DNPO$^-$ ⇌ MeC(O$^-$)(ODNP)$_2$	34.35 ± 6.35[f]	−25.14 ± 4.65[f]

[a]All in aqueous solution at 25°C; calculated using free energies of formation from Table 2 and pK_a values from Table 5 unless otherwise noted. Abbreviations are Im, 1-imidazolyl; O*p*NP, *p*-nitrophenoxy; ODNP, 2,4-dinitrophenoxy; 4-py, 4-pyridyl.

[b]Experimental value; this work.

[c]Reference 90.

[d]Calculated from data in refs. 87 and 91.

[e]Based on an upper limit placed on the equilibrium constant for imidazole addition (25).

[f]Estimated as described in the text.

[g]Zwitterion content estimated by the method of ref. 20: pK_z = 11.65 − 0.43Σσ*.

substituents on oxygen with imidazolyl or phenyl substituents and that these may be safely ignored.

The free energies of formation for the acylimidazole hemiacetals and hydrates in Table 2 now permit the calculation of the free energy changes for addition of imidazole to the esters or of water to the acylimidazoles. These equilibrium constants are given in Table 4. The latter set of equilibria is more directly related to observable chemistry because the acylimidazoles undergo ready hydrolysis by way of the hydrate while addition of imidazole to esters with poor leaving groups, as in the present cases, does not lead to any net reaction but simply to loss of imidazole and regeneration of starting material.

Equilibrium constant for addition of imidazole to acetone

To extend our calculations to other tetrahedral intermediates, it will be necessary to have as many examples as possible of equilibrium constants for addition of imidazole to carbonyl compounds. One key value, which we realized should be measurable but which had not been reported, is that for addition to acetone. We have measured this equilibrium constant directly by determining the ^{1}H nmr spectrum of a solution 1 *M* in each of imidazole and acetone. No additional peaks could be seen at 60 MHz, but at 200 MHz it was possible to see a new peak, comparable in size to that assigned to acetone hydrate (19). The intensity of this peak was dependent upon the concentration of imidazole for fixed acetone concentration, and became undetectably low when the concentration of acetone was lowered 1000-fold. The position of the new signal was very similar to that of the signal assigned to the *C*-methyl groups in 2-methoxy-2-imidazolylpropane. We conclude that the new peak corresponds to 2-hydroxy-2-imidazolylpropane; the equilibrium constant for addition of imidazole to acetone can be evaluated as 2.6 ± 1.1 × 10^{-3} M^{-1} at 20 ± 3°C. We obtain an equilibrium constant for hydration of acetone of (2.0 ± 0.9) × 10^{-5} M^{-1} at 20 ± 3°C; Hine and Redding reported a value of (2.5 ± 0.7) × 10^{-5} M^{-1} at 33°C (19).

Can. J. Chem. Downloaded from www.nrcresearchpress.com by 118.98.75.50 on 09/07/12
For personal use only.

Can. J. Chem. Downloaded from www.nrcresearchpress.com by 118.98.75.50 on 09/07/12
For personal use only.

pK_a values for tetrahedral intermediates

To include various protonation states of the tetrahedral intermediates, which are important in the actual reaction mechanisms, it was necessary to have values for the various pK_a values of these compounds. These pK_a values were estimated using the procedures previously described (20, 21); the pK_a values that we employ in this paper are found in Table 5. These estimates made use of the σ^* values shown in Table 6.

Discussion

We wish first to test the equilibrium constants that we have derived for hydration of acyl imidazoles, by seeing if they are consistent with other data. One such test is to see if the new points fall on the Marcus curves previously found for hydroxide and water addition to carbonyl groups (20).

Those rate constants for the hydrolysis of the acyl imidazoles that were available from the literature are collected in Table 7. Using these values we can examine the correlation of rate and equilibrium constants: unfortunately only for acetylimidazole is the equilibrium constant for formation of the acylimidazole known. Figure 2 shows that the points for the attack of hydroxide and water on acetylimidazole fall very near the same lines (7) that correlate data for a wide range of acyl compounds (20).

Since, in general, protonation and methylation of imidazole on the remote nitrogen have very similar effects, we can examine the reaction of hydroxide with acetylimidazolium ion by using the observed rate constant for *N*-acetyl-*N'*-methylimidazolium ion and an equilibrium constant calculated for acetylimidazolium ion using estimated pK_a values. This point also falls near the correlation line for other acyl compounds; see Fig. 2.

By inverting the procedure we can estimate the equilibrium constants for addition of water or hydroxide to an acylimidazole from the corresponding rate constants. This is possible for benzoylimidazole, for which the kinetics of hydrolysis have been studied (22). Since all classes of compound fall near a common Marcus correlation line (20), we use the most recent and best-defined line that we have obtained, that for esters (7). This line was derived taking explicit account of diffusion-limited encounter complex formation. From the rate constant for hydroxide attack, we calculate an observable equilibrium constant for addition of hydroxide to give an anionic adduct, $\log K = -1.31$. In the same way we calculate an observable equilibrium constant for addition of hydroxide to *N*-benzoylimidazolium ion (making the assumption that the rate and equilibrium constants for this process will be similar to those for *N*-benzoyl-*N'*-methylimidazolium ion), $\log K = 4.45$. Finally for the reaction of water with benzoylimidazole, which we assume goes through the zwitterion (20, 7), we calculate an equilibrium constant for addition of water to give the zwitterion, and then from the zwitterion content (estimated as previously

TABLE 5. pK_a values for compounds discussed in this paper[a]

(*a*) Experimental pK_a values

Compound	pK_a
HCOOH	3.77[b]
MeCOOH	4.76[b]
PhCOOH	4.17[b]
MeOH	15.49[c]
EtOH	15.90[c]
Imidazole	7.05[b,d]
	14.52[b,e]
N-(2-Aminoethyl)-imidazole	5.90[f]
	8.45[g]
N-(3-Aminopropyl)-imidazole	6.50[f]
	9.63[g]
Imidazole-1-acetic acid	2.19[h,i]
	6.93[h,j]
p-Nitrophenol	7.14[b]
2,4-Dinitrophenol	4.11[b]
Me—CO—ImH^+	3.6[k]
Ph—CO—ImH^+	3.34 ± 0.07[l]

TABLE 5 (*concluded*)

(*b*) Estimated pK_a values

Compound	pK_a	
	NH^+	OH
H—$C(OH)_2$—ImH^+	6.03[m]	8.47[n]
Me—$C(OH)_2$—ImH^+	6.03[m]	9.12[n]
Ph—$C(OH)_2$—ImH^+	5.80[m]	8.13[n]
Me—C(OH)(O*p*NP)—ImH^+	5.56[q]	8.12[n]
Me—C(OH)(ODNP)—ImH^+	5.43[q]	7.58[n]
H—C(OH)(OEt)—ImH^+	5.93[m]	9.10[o]
Me—C(OH)(OEt)—ImH^+	5.93[m]	9.74[o]
Ph—C(OH)(OMe)—ImH^+	5.66[m]	8.58[o]
H—$C(OH)(O^-)$—ImH^+	7.27[m]	14.98[o]
Me—$C(OH)(O^-)$—ImH^+	7.27[m]	15.63[o]
Ph—$C(OH)(O^-)$—ImH^+	7.05[m]	14.64[o]
H—$C(OEt)(O^-)$—ImH^+	7.17[m]	
Me—$C(OEt)(O^-)$—ImH^+	7.17[m]	
Ph—$C(OMe)(O^-)$—ImH^+	6.91[m]	
H—$C(OH)_2$—Im		10.07[n]
Me—$C(OH)_2$—Im		10.72[n]
Ph—$C(OH)_2$—Im		9.73[n]
H—C(OH)(OEt)—Im		10.69[o]
Me—C(OH)(OEt)—Im		11.34[o]
Ph—C(OH)(OMe)—Im		10.18[o]
H—CO—ImH^+	3.4 ± 0.2[p]	
$CH_3C(OH)_2$(O*p*NP)		10.35[n]
$CH_3C(OH)_2$(ODNP)		9.81[n]
$CH_3C(OH)$(O*p*NP)$_2$		9.35[o]
$CH_3C(OH)$(ODNP)$_2$		8.27[o]

[a]All in H_2O at 25°C unless otherwise noted. Abbreviations used are Im, 1-imidazolyl; O*p*NP, *p*-nitrophenoxy; ODNP, 2,4-dinitrophenoxy.

[b]Reference 84.

[c]Reference 85.

[d]Ionization constant for BH^+.

[e]Ionization constant for neutral imidazole.

[f]This work, first ionization constant for BH_2^{2+}.

[g]This work, ionization constant for BH^+.

[h]Reference 16; measured in D_2O. In several cases the pK_a values reported in ref. 16 are in good agreement with literature values for pK_a in water (84).

[i]First apparent ionization constant for BH^+.

[j]Second apparent ionization constant for neutral to anion.

[k]Reference 23.

[l]Reference 22.

[m]Calculated using $pK_a(NH^+) = 6.84 - 0.30\Sigma\sigma^*$.

[n]Calculated using $pK_a(OH) = 14.19 - 1.32\Sigma\sigma^*$ (26).

[o]Calculated using $pK_a(OH) = 17.03 - 1.32\Sigma\sigma^*$ (20).

[p]Estimated assuming that the pK_a of R—CO—ImH^+ is linear in σ_R^*; alternatively one might assume that the pK_a would be the same as for R = Me. The error limits are based on the difference between the results of these assumptions.

described (20)) we calculate the equilibrium constant for formation of the neutral adduct as $\log K = -3.57$.

Now we may compare these values, using pK_a values from Table 5 to relate them. For hydroxide addition, estimates derived from the reactions of hydroxide with benzoylimidazole, water with benzoylimidazole, and hydroxide with benzoylimidazolium are -1.32, 0.70, and 0.74 respectively, for an average of 0.04 ± 1.17. Similarly the estimates for water addition are -5.58, -3.57, and -3.53 respectively, for an average of -4.23 ± 1.17.

$$\text{Ph—CO—OH + HIm} \underset{}{\overset{-14.19\pm1.35}{\rightleftharpoons}} \text{Ph—C(OH)}_2\text{—Im} \overset{4.23\pm1.17}{\rightleftharpoons} \text{Ph—CO—Im + H}_2\text{O}$$

$$\overset{-9.96\pm1.79}{\rightleftharpoons}$$

As a test of this procedure we can ask how it would have worked for acetylimidazole. From the rate data in Table 7 (23) we calculate equilibrium constants for addition of hydroxide to acetylimidazole of -1.25, 0.01, and 1.02 respectively, for an average of -0.08 ± 1.13, and for addition of water of -4.52, -3.29, and -2.27 respectively, for an average of -3.36 ± 1.13. This may be compared to the thermochemical value of -3.73 ± 1.08 for the addition of water to acetylimidazole. The values are in satisfactory agreement.

For formylimidazole no rate or equilibrium data could be found; to obtain an initial estimate we note that $\log K_{hydration}$ is very similar for acetylimidazole (-3.73 ± 1.08) and benzoylimidazole (-4.22 ± 1.19). The values are indistinguishable. Thus we take $\log K_{hydration}$ for formylimidazole as the average of the values for acetylimidazole and benzoylimidazole, -4.0. Rather arbitrarily we assign limits of ± 2.0 to this value. We may now calculate the equilibrium constant for hydrolysis of formylimidazole. From this equilibrium constant it is possible to calculate a free energy of formation in aqueous solution for formylimidazole: see Table 2.

It is now possible to make predictions (necessarily very approximate) of the rate constants for hydrolysis of formylimidazole. For hydroxide plus the acylimidazole we predict $\log k = 3.1 \pm 0.9$; for water plus the acylimidazole, $\log k = -4.4 \pm 1.6$.

We can attempt to estimate the rate of nucleophilic catalysis by imidazole, eq. [1], of the hydrolysis of the methyl or ethyl esters corresponding to our acylimidazole acetals in the following way. We have the equilibrium constants for the addition of imidazole to the esters, calculated from the free energies of formation. We have rate constants for addition of water to the acylimidazoles, and therefore rates for the expulsion of water from the acylimidazole hydrate. If we assume that the rate constants for the analogous steps involving methanol or ethanol would be very similar, we can estimate the overall rates of the nucleophilic catalysis reactions as $k_1k_2/(k_{-1} + k_2) \cong k_1k_2/k_{-1} = K_1k_2$. Using the above assumption and the rate and equilibrium constants for the hydrolysis of acetylimidazole we estimate that $k_2 = 3.9\ s^{-1}$. To support the assumption that k_{-1} is much larger than k_2 we carried out the following

$$\text{H—CO—Im + H}_2\text{O} \underset{}{\overset{-4.0\pm2.0}{\rightleftharpoons}} \text{H—C(OH)}_2\text{—Im} \overset{9.08\pm1.11}{\rightleftharpoons} \text{HCOOH + HIm}$$

$$\overset{5.1\pm2.3}{\rightleftharpoons}$$

estimation of k_{-1} for acetylimidazole. Kirsch and Jencks (2) have shown that there is a linear relation between rates of imidazole- and hydroxide-catalyzed hydrolyses for acetate esters with good leaving groups for which k_1 is the rate-determining step; we extrapolated this relationship to obtain a rate constant for nucleophilic attack of imidazole on ethyl acetate, obtaining an estimated value of $3 \times 10^{-3}\ M^{-1}\ s^{-1}$. This, in combination with the equilibrium constant for addition of imidazole to ethyl acetate, leads to a rate constant for expulsion of imidazole, k_{-1}, of $1.3 \times 10^9\ s^{-1}$. Although there are undoubtedly considerable uncertainties associated with this estimate, there is no doubt that $k_{-1} \gg k_2$. The value estimated for the apparent rate constant for imidazole-catalyzed hydrolysis of ethyl acetate is then $9.1 \times 10^{-12}\ M^{-1}\ s^{-1}$; the reported (24) value for the water rate is $2.5 \times 10^{-10}\ s^{-1}$, so that

$$\text{[1]}\quad \text{CH}_3\text{—CO—OEt + HIm} \underset{k_{-1}}{\overset{k_1}{\rightleftharpoons}} \text{CH}_3\text{—C(OH)(OH)—OEt} \xrightarrow{k_2} \text{CH}_3\text{—CO—Im + HOEt}$$

TABLE 6. σ^* values used in this paper[a]

R	σ^*
H	0,[b] 0.49
Me	0.0
Ph	0.75
OH	1.34
OMe	1.81
OEt	1.68
Im	2.63[c]
ImH^+	3.84[c]
O^-	−2.78
O—pNP[d]	2.91
O—DNP[e]	3.32[f]

[a]All values from ref. 86 unless otherwise noted.
[b]A value of 0 is more appropriate for dissociation of ammonium ions (21), while 0.49 is appropriate for neutral oxyacids.
[c]Determined in this work; see text.
[d]*p*-Nitrophenoxy.
[e]2,4-Dinitrophenoxy.
[f]Estimated from a linear correlation of σ^*_{ArO} vs. σ^*_{Ar} using data from ref. 86.

Can. J. Chem. Downloaded from www.nrcresearchpress.com by 118.98.75.50 on 09/07/12
For personal use only.

TABLE 7. Rates of hydrolysis of acylimidazoles, R—CO—Im, and acylimidazolium ions, R—CO—Im^+—R′ [a]

R,R′	$10^5 k_w$ [b] (s^{-1})	k_{OH} (M^{-1} s^{-1})	k_+ [c] (s^{-1})	pK_a
Me,H	8.33[d]	317.[d]	0.047[d]	3.6[d]
Me,Me		2.08×10^6 [e]	0.047[e]	
Ph,H	9.12 ± 1.54[f]	$292. \pm 22.$[f]	0.0393 ± 0.0036[f]	3.34 ± 0.07[f]
Ph,Me		$(1.19 \pm 0.03) \times 10^5$[f]	0.0388 ± 0.0014[f]	
H,H	2.[f]	700.[g]		

[a]All in aqueous solution at 25°C. R and R′ are defined by

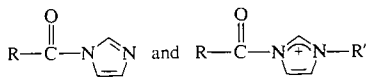

[b]Pseudo-first-order rate constant for water attack on the neutral acylimidazole.
[c]Pseudo-first-order rate constant for water attack on the acylimidazolium ion.
[d]Reference 23.
[e]Reference 92.
[f]Reference 22.
[g]Estimated as described in the text; these values have uncertainties of at least an order of magnitude.

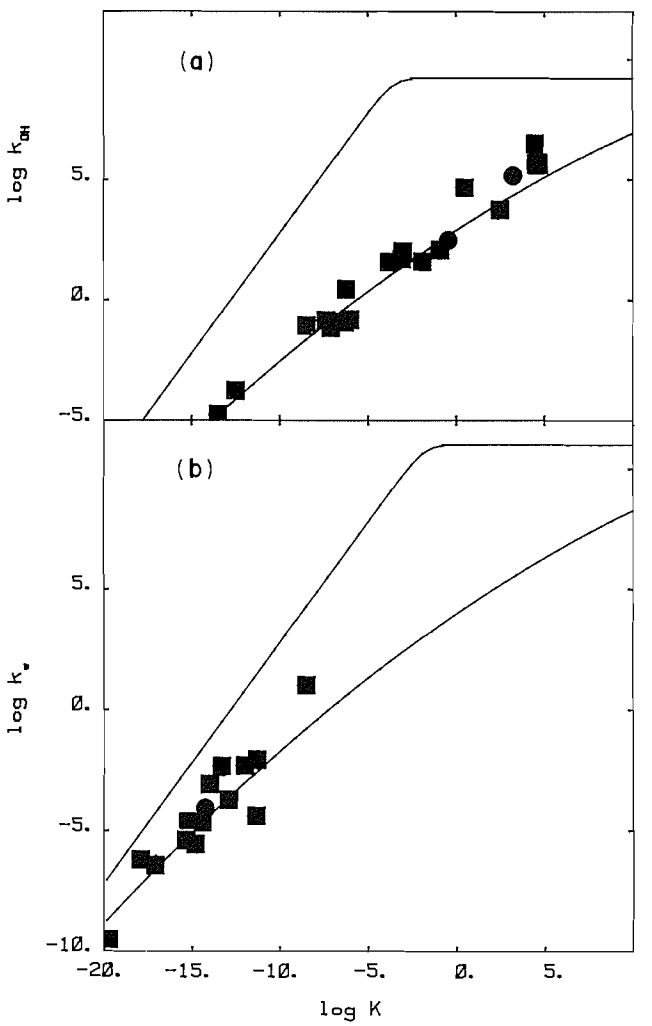

FIG. 2. Marcus curves for addition of hydroxide and water to carbonyl compounds. Lines are calculated as described in ref. 7. (■) Data from refs. 7 and 21; (●) acylimidazoles from this work. (*a*) Hydroxide addition to give the anionic tetrahedral speices, $b = 8.99$. (*b*) Water addition to give the zwitterion, $b = 8.81$.

nucleophilic catalysis could only make a contribution equal to the water rate at 27 *M* imidazole. These calculations are in complete accord with the experimental observation that nucleophilic catalysis by imidazole is not observed for simple alkyl esters, and that only general base catalysis by imidazole is detectable (2).

Free energy changes for replacement of hydroxyl by imidazolyl

In calculating the free energies of formation of the tetrahedral intermediates we used a relationship between the free energy change, corrected for steric and symmetry factors, and the sum of the σ* values for the central carbon, which has been previously established for reaction [2] (6),

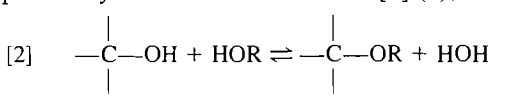

It was of interest to see if a similar relationship would hold for replacement of hydroxyl by imidazolyl, reaction [3],

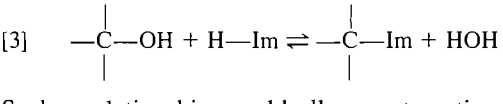

Such a relationship would allow us to estimate free energies of formation for some interesting tetrahedral intermediates for which the corresponding acetals are expected to be very unstable, so that the thermochemical procedures used for the simple acetals described above would be impossible.

Figure 3 shows that there is indeed a relationship but that the number of hydrogens on the central carbon (aldehydic hydrogens on the corresponding carbonyl compound) is an important variable, in addition to the electronic effects of the substituents. The data on which this figure is based are found in Table S1.[3] The results based on thermochemistry are not sufficiently precise to demand different ρ* values for different numbers of hydrogens on the central carbon. The ΔG value for formaldehyde is anomalous because it differs from that for

[3]Tables S1 and S2 may be purchased from the Depository of Unpublished Data, CISTI, National Research Council of Canada, Ottawa, Ont., Canada K1A 0S2.

Can. J. Chem. Downloaded from www.nrcresearchpress.com by 118.98.75.50 on 09/07/12
For personal use only.

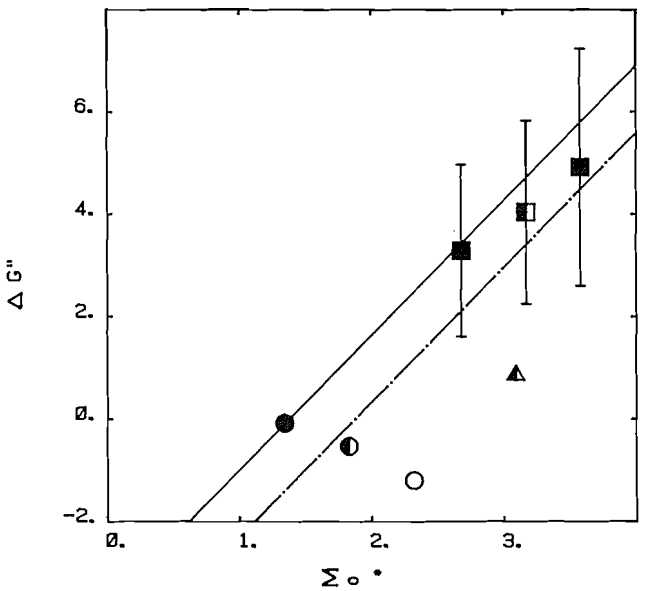

FIG. 3. Free energy change, corrected for symmetry effects, for replacement of OH by imidazolyl, as a function of $\Sigma\sigma^*$ for the remaining substituents on the central carbon, and of the number of hydrogens on the central carbon. Filled symbols, no hydrogens on the central carbon; half-filled symbols, one hydrogen on the central carbon; open symbol, two hydrogens on the central carbon. (○) Equilibrium constants used; (□) thermochemically derived values; (△) pyridine-4-carboxaldehyde adduct, for which only a limit could be placed on the equilibrium constant for addition of imidazole.

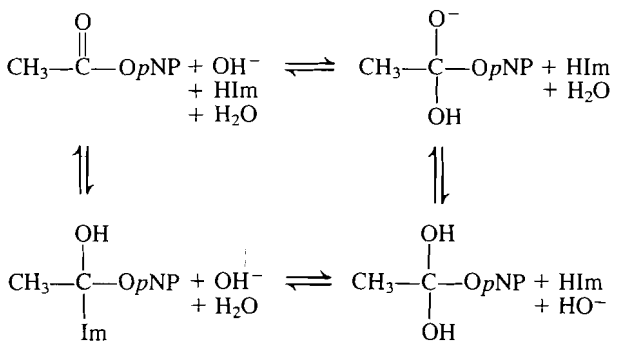

SCHEME 1

acetaldehyde by more than ΔG for acetaldehyde differs from that for acetone. This behavior is puzzling but not unique. Examination of comparable data for replacement of OH by CN, using the equilibrium constants collected in ref. 75, shows a similar anomaly for formaldehyde. Thus the available data for replacement of OH by imidazolyl, excluding the point for formaldehyde, can be fitted by eq. [4], in which Δ is the number of hydrogens on the central carbon:

$$[4] \quad \Delta G = -(3.62 \pm 0.44) + (2.63 \pm 0.30)\Sigma\sigma^* - (1.31 \pm 0.2)\Delta$$

The central feature of this analysis is that electron-withdrawing substituents on the central carbon strongly disfavor the replacement of OH by imidazolyl, i.e., make imidazole less effective relative to water as a nucleophile for equilibrium addition to the corresponding carbonyl compound. There is independent evidence for this proposition in that Sander and Jencks were unable to detect any adduct formation from imidazole and pyridine-4-carboxyaldehyde for which the equilibrium constant for addition of water was readily measured (25). Their detection limits lead to a $\Delta G'' > 0.86$ kcal/mol for replacement of OH by imidazolyl; this is markedly more positive than the value, −0.53, for acetaldehyde.

Equilibrium constants for addition of imidazole to nitrophenyl acetates

Using this relationship we can explore the energetics of the imidazole-catalyzed hydrolysis of *p*-nitrophenyl acetate. If we can calculate the free energy of formation of the covalent hydrate of *p*-nitrophenyl acetate, then we can calculate the free energy change for replacement of one of the hydroxyl groups by an imidazolyl group, and hence the free energy change for addition of imidazole to the ester; see Scheme 1. The free energy change for the addition of water to *p*-nitrophenyl acetate can be estimated from the Marcus curves relating rate and equilibrium for the hydroxide-catalyzed hydrolysis reactions, using the equation previously reported for a variety of esters (7). The calculation involves estimation of the pK_a of the covalent hydrate (20, 26). The equilibrium constant so derived for the addition of water to *p*-nitrophenyl acetate is $\log K_{H_2O} = -7.86 \pm 2.0$. (Most of the equilibrium data for the rate equilibrium correlation were derived from thermochemistry and had uncertainties of ca. ±2.0 in $\log K$, so it is unlikely that interpolated values are better defined.)

The equilibrium constant for replacement of a hydroxyl group in the covalent hydrate of *p*-nitrophenyl acetate by an imidazolyl group may now be calculated as $\log K = -6.64 \pm 1.25$. By combining the equilibrium constants for hydration and for replacement of one hydroxyl by imidazole, we can calculate the equilibrium constant for addition of imidazole to *p*-nitrophenyl acetate as $\log K_{Im} = -13.39 \pm 2.34$. This equilibrium constant is calculated for the addition of neutral imidazole to the neutral ester to give the neutral adduct. Mechanistically it seems clear that the immediate product is the zwitterionic adduct; *N*-methylimidazole is known to be essentially as effective as imidazole as a nucleophilic catalyst for the hydrolysis of active esters (4, 27). The zwitterion content can be calculated from estimates of the pK_a values for the OH and the imidazolium moieties in the cationic form of the tetrahedral intermediate. Using the value of $\sigma^* = 3.84$ for imidazolium estimated above, we calculate the pK_a of the hydroxyl to be 8.12 and the pK_a of the imidazolium to be 5.57; we assume that these estimated pK_a values are uncertain by ±0.3 log units. Then the zwitterion content is given by $\log K_Z = -2.56$, and the equilibrium constant for addition of imidazole to *p*-nitrophenyl acetate to give the zwitterion is -15.95 ± 2.30. The corresponding free energy change, relative to separated reagents, is 21.79 ± 3.14 kcal/mol.

If we assume that the reaction of imidazole with *p*-nitrophenyl acetate to give acetylimidazolium ion and *p*-nitrophenoxide follows a stepwise mechanism, and addition of imidazole is rate limiting with expulsion of *p*-nitrophenoxide a fast second step (2), then we should now be able to calculate the intrinsic barrier for the attack of imidazole. (Jencks and Kirsch did not distinguish between a stepwise mechanism and a one-step mechanism with a skewed transition state, but showed that for *p*-nitrophenyl acetate the rate-determining step involves principally bond formation with little bond breaking (2).) From the equilibrium constant derived above and the rate constant for imidazole attack on *p*-nitrophenyl acetate, $\log k = -0.239$ (2), we may substituent into the Marcus equation (7, 28–30) and attempt to solve for the intrinsic barrier. When we do this we find that no real value can be found because the observed rate is

Can. J. Chem. Downloaded from www.nrcresearchpress.com by 118.98.75.50 on 09/07/12
For personal use only.

Can. J. Chem. Downloaded from www.nrcresearchpress.com by 118.98.75.50 on 09/07/12
For personal use only.

too fast relative to the energy level of the putative intermediate. The free energy of activation, relative to separated reagents, is 17.78 kcal/mol, which is lower than the energy level of the intermediate. This suggests that the reaction may in fact be concerted, and that the tetrahedral species may not be on the reaction coordinate.

This may be compared to the situation for other aminolyses where an intrinsic barrier can be calculated. For the aminolysis of methyl formate, where an equilibrium constant is available for addition of dimethyl amine to give the zwitterion (31), a rate constant may be estimated (31) from the work of Blackburn and Jencks (32). Using $\log K = 7.8 \times 10^{-11}$ (31) and $\log k = 1.60$ (31) we obtain $b = 4.50$ (b is the intrinsic barrier in log k units (33, 7)). From work of Cox and Jencks (34) we obtain rate and equilibrium constants for the addition of methoxyamine to phenyl acetate; their values are $\log k = 2.55$ and $\log K = -7.75$. From these values we obtain $b = 5.26$. This should be larger than the intrinsic barrier for imidazole because methoxyamine has two NH protons that will undergo a major change in solvation as reaction proceeds, while imidazole has only one. Arnett and Wolf have shown that amine NH's are only weakly hydrogen bonded to water, whereas ammonium NH's are strongly hydrogen bonded (35). Thus the available information concerning amine addition to esters requires relatively small intrinsic barriers.

Concerted vs. stepwise reactions

The question of whether a tetrahedral intermediate is on the reaction coordinate or whether a concerted path is preferred is of current interest (36–41) and it seems worthwhile to explore the implications of our thermochemical calculations and of Marcus theory (28–30). A method of presentation frequently used to examine the energetic consequences of structural change is the three-dimensional reaction coordinate diagram first employed by Albery (42–44). We wish to calculate plausible values for all points on the surface and for this purpose need an analytical expression for the energy at any point as well as energies for the four corner points and intrinsic barriers for the four edge reactions. We have three of the corner energies because the equilibrium constants for the overall hydrolysis (45) and addition to give the tetrahedral intermediate are known. The fourth corner is the acylium ion, corresponding to the elimination–addition mechanistic competitor; the energy of this species will be estimated below.

It is quite common to express the reaction coordinate for a single chemical step in terms of two intersecting parabolas (46–49). Kurz (50) has shown that an equivalent representation is a single, inverted parabola, eq. [5]:

$$[5] \quad G = \alpha x + \beta x^2$$

where x is the reaction coordinate, and the free energy at $x = 0$ is defined as 0.0 for convenience. This approximation has been shown to be consistent with Marcus theory (50). We generalize the inverted parabola to three dimensions as eq. [6][4]

$$[6] \quad G = \alpha x + \beta x^2 + \gamma y + \delta y^2 + \epsilon xy$$

where x and y are the reaction coordinates of the "edge reactions" and the free energy at $(x,y) = (0,0)$ has been defined as 0.0, and impose the constraints that the four "edge parabolas" for $x = 0,1$ and $y = 0,1$ must satisfy the Marcus equation for the edge reactions. These constraints and the overall thermodynamics specify all of the parameters in terms of the free energy changes and intrinsic barriers for the edge reactions. When $y = 0$, $G = \alpha x + \beta x^2$. For this reaction, $\Delta G^0 = \alpha + \beta$, where ΔG^0 is the overall free energy change from $x = 0$ to $x = 1$. It is easily seen that $x^{\ddagger} = -\alpha/2\beta$, and hence $\Delta G^{\ddagger} = -\alpha^2/4\beta = \tilde{G}(1 + \Delta G^0/4\tilde{G})^2$, where $\tilde{G}$ is the intrinsic barrier expressed in terms of free energy. These expressions may be solved to give $\alpha = \Delta G^0 + 4\tilde{G}$ and $\beta = -4\tilde{G}$. Similarly, one may express γ and δ in terms of the free energy change and intrinsic barrier for the $x = 0$ edge reaction. It is an unavoidable logical consequence of eq. [6] that the intrinsic barriers for $x = 0$ and $x = 1$, and for $y = 0$ and $y = 1$, must be identical. The final parameter, ϵ, is determined by the thermodynamic requirement that the overall free energy change from starting material to product, $\Delta G_{rxn} = \alpha + \beta + \gamma + \delta + \epsilon$.

The question of whether a reaction is concerted or not can now be phrased in terms of whether there is a path, from starting material to product, that has a maximum free energy less than for either path along two edge parabolas.

We may solve for the coordinates and energy of the transition state in terms of eq. [6] by finding the values of $x^{\ddagger}$ and $y^{\ddagger}$ that make $\partial G/\partial x = 0$ and $\partial G/\partial y = 0$. When this is done we obtain:

$$[7] \quad \begin{aligned} x^{\ddagger} &= (2\alpha\delta - \gamma\epsilon)/(\epsilon^2 - 4\beta\delta) \\ y^{\ddagger} &= (2\beta\gamma - \alpha\epsilon)/(\epsilon^2 - 4\beta\delta) \\ \Delta G^{\ddagger} &= (\alpha^2\delta + \beta\gamma^2 - \alpha\gamma\epsilon)/(\epsilon^2 - 4\beta\delta) \end{aligned}$$

It is also useful to examine the behavior of the energy surface in terms of an alternative pair of coordinates (51), one running from starting material (0) to product (1) ("progress variable" (51), here called p) and the other running from one of the intermediates (0) to the other (1) ("disparity variable" (51), here called q). Following Grunwald (51), we transform and renormalize the coordinates using

$$[8] \quad \begin{aligned} p &= (x + y)/2 & x &= p + q - 1/2 \\ q &= (x - y)/2 + 1/2 & y &= p - q + 1/2 \end{aligned}$$

In terms of p and q we may derive

$$[9] \quad \begin{aligned} G = {} & (\alpha - \beta + \gamma + \delta)p + (\alpha - \beta - \gamma - \delta + \epsilon)q \\ & + (\beta + \delta + \epsilon)p^2 + (\beta + \delta - \epsilon)q^2 + 2(\beta - \delta)pq \\ & + (-2\alpha + \beta + 2\gamma + \delta - \epsilon)/4 \end{aligned}$$

$$p^{\ddagger} = [(\alpha\delta + \beta\gamma) - \epsilon(\alpha + \gamma)/2)]/(\epsilon^2 - 4\beta\delta)$$

$$q^{\ddagger} = 1/2 + [(\alpha\delta - \beta\gamma) + \epsilon(\alpha - \gamma)2]/(\epsilon^2 - 4\beta\delta)$$

A necessary and sufficient condition for a concerted reaction is that the section through the energy surface at $p = 1/2$ be concave upward. Equation [6] defines either a paraboloid or a hyperbolic paraboloid. If a section of $p = 1/2$ is concave downward then the surface is a paraboloid, and there will be an energy mountain in the reaction square; if a section at $p = 1/2$ is concave upward, then the surface is a hyperbolic paraboloid and there is a saddle point, though it may not be at $p = 1/2$.

When we impose the condition that $p = 1/2$, the equation for G as a function of q alone is

$$[10] \quad G = (\gamma + \delta) + (\alpha - \gamma - 2\delta + \epsilon)q + (\beta + \delta - \epsilon)q^2$$

If $(\beta + \delta - \epsilon) > 0$ and $0 < q^{\ddagger} < 1$, then the reaction is concerted.

[4]Throughout our discussion of the three-dimensional reaction surface we will use free energies calculated for the encounter complex, using an equilibrium constant for encounter complex formation assuming no attraction or repulsion, but requiring the nucleophile to be on one or the other face of the planar ester electrophile (7, 33). The reference point is the encounter complex of ester and imidazole.

Can. J. Chem. Downloaded from www.nrcresearchpress.com by 118.98.75.50 on 09/07/12
For personal use only.

A logical consequence of the above analysis is that a reaction is either concerted or stepwise, but that there cannot be coexisting competitive concerted or stepwise paths. This is a consequence of the mathematical simplicity of our model, which does not allow any ridge-like barrier on the surface between a concerted and a stepwise path. If experimental evidence were to demand that concerted and stepwise paths can coexist, then one would have to conclude that our model is, at least, oversimplified. The conclusion, that reactions are either concerted or stepwise but not both, is almost, but not quite, equivalent to saying that concertedness is "enforced", as proposed by Jencks (36), by a lifetime of the intermediate that is less than a single vibration. It is not impossible that one could have a situation such that the kinetic barriers to both breakdown paths of an intermediate (i.e. β and δ) were both large enough in absolute magnitude to correspond to a finite lifetime, while still satisfying the criterion for a concerted process (i.e., $(\beta + \delta - \epsilon) > 0$).

Another interesting case is for the identity reaction where nucleophile and leaving group are the same. In this case $\Delta G^0 = 0$, and $\beta = \delta$ because the intrinsic barriers for addition or expulsion of the nucleophile are necessarily the same. We define Γ_0 to be the energy of the intermediate at $q = 0$, and Γ_1 to be the energy of the intermediate at $q = 1$. Then $\alpha = \Gamma_0 - \beta$, $\gamma = \Gamma_1 - \beta$, $p^{\ddagger} = 1/2$, $q^{\ddagger} = 1/2 + (\Gamma_0 - \Gamma_1)/2(\Gamma_0 + \Gamma_1 + 2\beta)$, and

$$\Delta G^{\ddagger} = \Gamma_1 - (\Gamma_1 + \beta)^2/(\Gamma_1 + \Gamma_0 + 2\beta)$$

and this may be converted into a quadratic in β,

$$[11] \quad \beta^2 + [2\Delta G^{\ddagger}]\beta + [\Delta G^{\ddagger}(\Gamma_1 + \Gamma_0) - \Gamma_1\Gamma_0] = 0$$

which may be solved for β.

Similar ideas have been used by other authors (52–55) but we believe that we have carried the analysis farther than previous workers. Albery and Kreevoy (52) derived expressions relating experimentally determined quantities to positions along the "progress" (51) or "symmetry" (52) (α) and "disparity" (51) or "tightness" (52) (τ) coordinates. Jencks and Jencks (53) used an equation analogous to eq. [6] but did not impose the constraints of Marcus theory (28–30). Gajewski (54) used an analog of eq. [6] with no x^2 or y^2 terms. Dunn (55) explored the implications of two-dimensional reaction surfaces, but had a less satisfactory derivation of the surface.

Acylium ion formation

The equilibrium constant for formation of this ion may be estimated from the nmr studies of Deno *et al.* (56) who found that $[CH_3COOH] = [CH_3COOH_2^+]$ at 77% H_2SO_4 and $[CH_3COOH_2^+] = [CH_3—C{\equiv}O^+]$ at 15% SO_3. 77% H_2SO_4 corresponds to $H_0 = -6.56$ (57) and 15% SO_3 corresponds to $H_0 = -13.23$ (58). To estimate H_R for 15% SO_3 we extrapolated a linear relationship between H_0 and H_R, which holds for aqueous sulfuric acid. Such relationships are general (59) but it is clearly an extrapolation to extend the line into fuming sulfuric acid; this approach leads to an H_R value of -23.92 for 15% SO_3. Now we make the assumption that protonation and dehydration of the acid follow these simple acidity functions and calculate that for $H_0 = -13.23$, $\log([CH_3COOH]/[CH_3COOH_2^+]) = -6.67$; then $pK_R = -17.25$. Assuming that this value can be used in water, we can then calculate the equilibrium constant for reaction [12]

$$[12] \quad CH_3—COOH + p\text{NPOH} \rightleftharpoons CH_3—C{\equiv}O^+ + p\text{NPO}^- + H_2O$$

$$K = \frac{[CH_3—C{\equiv}O^+][p\text{NPO}^-][H^+]}{[CH_3—COOH][H^+][p\text{NPOH}]} = 10^{-17.25} \times 10^{-7.14} = 10^{-24.38}$$

The equilibrium constant for the hydrolysis of *p*-nitrophenyl acetate is $\log K = 6.90$ (45); thus the equilibrium constant for the heterolytic cleavage of *p*-nitrophenyl acetate is $\log K = -17.48$. This value is clearly subject to large uncertainties, because we do not have proper acidity functions for RCOOH in H_2SO_4/SO_3 mixtures either for protonation or protonation/dehydration, and the extrapolations used in the calculation are very long.[5]

Intrinsic barrier for the addition or expulsion of p*-nitrophenoxide*

In addition to an intrinsic barrier for the addition of imidazole to give a tetrahedral intermediate, we need to know the intrinsic barrier for the expulsion of *p*-nitrophenoxide ion from this intermediate. This turns out to be a more difficult problem, because in all of the many studies of *p*-nitrophenoxide replacement, it is the attack of a nucleophile that is rate limiting, and thus the rate of the expulsion is unknown. An estimate may be obtained as follows. We have already estimated the equilibrium constant for the addition of water to *p*-nitrophenyl acetate (*vide supra*); $\log K_{H_2O} = -7.86 \pm 2.0$. Since we have found linear free energy relations for the replacement of OH by OR (6) and by imidazolyl, it seems plausible to postulate that there should be such a relationship for replacement of OH by *p*-nitrophenoxy. Unfortunately there are not sufficient data to test this assumption. From the equilibria for addition of water to acetic acid (61) and to *p*-nitrophenyl acetate and for addition of imidazole to acetic acid and to *p*-nitrophenyl acetate we can determine the slope of a plot of ΔG for replacement of OH by *p*-nitrophenoxy vs. $\Sigma\sigma^*$ for the substituents on the central carbon, and thence calculate the free energy change for the process:

$$[13] \quad CH_3—\underset{\displaystyle OpNP}{\overset{\displaystyle OH}{\overset{|}{\underset{|}{C}}}}—OH + p\text{NPOH} \rightleftharpoons CH_3—\underset{\displaystyle OpNP}{\overset{\displaystyle OH}{\overset{|}{\underset{|}{C}}}}—OpNP + H_2O$$

The uncertainty in this free energy change or in the associated equilibrium constant will be essentially the same as for the replacement of OH by *p*-nitrophenoxy in the imidazole adduct of acetic acid, because $\Sigma\sigma^*$ is very similar. Thus we arrive at $\log K = -10.4 \pm 3.1$ for reaction [13]. Then by estimating the pK_a of this intermediate we can calculate the equilibrium constant for the attack of *p*-nitrophenoxide on *p*-nitrophenyl acetate to give the anionic tetrahedral intermediate; the value we obtain is $\log K = -20.5 \pm 3.7$. The rate constant for this reaction can be estimated by interpolation from data given by Fersht and Jencks (62); the value we obtain is $\log k = -1.15 \pm 0.61$. When we compare the free energy change for addition, 28.0 ± 5.1 kcal/mol, with the free energy of activation for the exchange process, 19.02 ± 0.83 kcal/mol (both calculated with respect to the separated reagents), we find that the free energy

[5] Arnett *et al.* (60) used a similar extrapolation (with similar reservations about the uncertainties involved) to estimate H_R for magic acid.

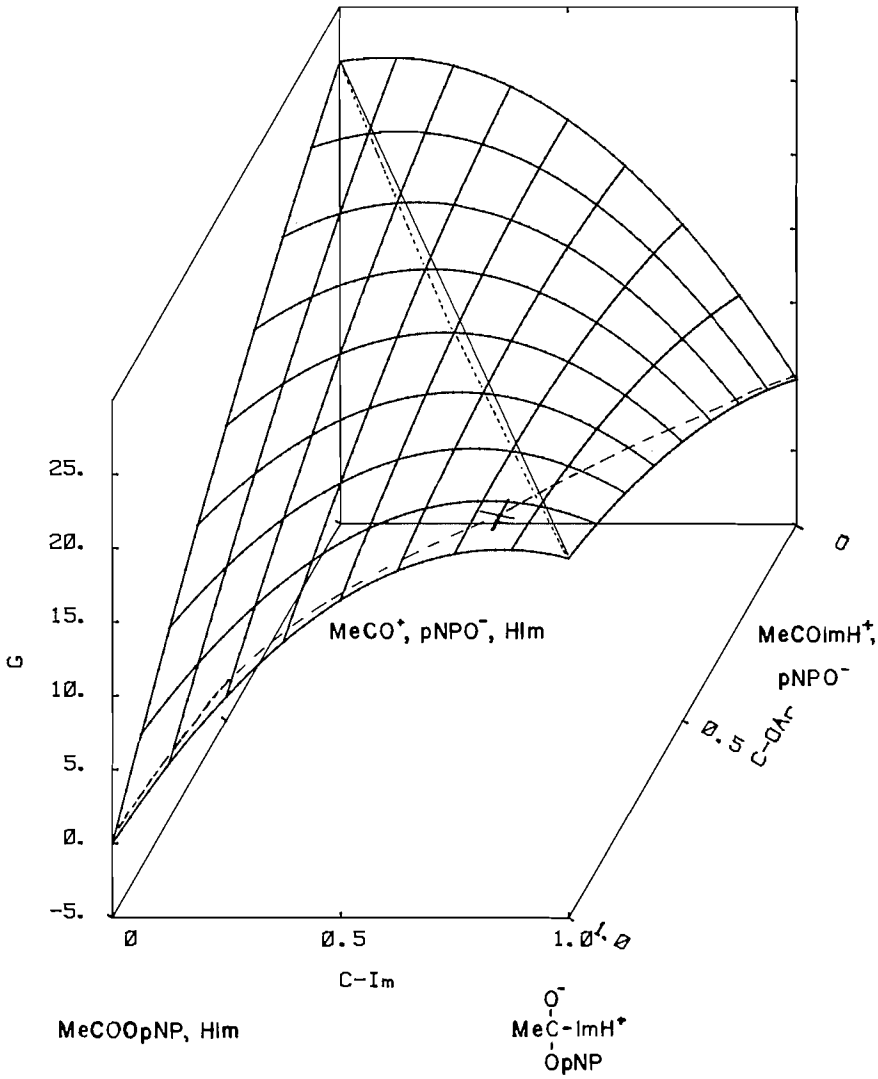

FIG. 4. Three-dimensional reaction coordinate surface for the reaction of imidazole with *p*-nitrophenyl acetate. The surface is calculated using eq. [6], with the thermodynamic and kinetic barriers described in the text. (---) Minimum energy path from starting material to product; (----) section through the energy surface at $p = 1/2$; (—) straight line joining the energies of the two intermediates, for ease of visualization.

of activation is markedly less than the free energy change for forming the intermediate. The difference is large enough that it is outside even the considerable uncertainty of our estimates, so that one must consider the possibility that this reaction is concerted. If we make this assumption, then we may solve eq. [11] and obtain a value of $b = 1.35 \pm 0.38$. (Two roots are obtained but only one corresponds to $0 < q^{\pm} < 1$.)

Reaction surface for imidazole plus p-*nitrophenyl acetate*

The intrinsic barrier for the addition of imidazole to *p*-nitrophenyl acetate will be taken as 5 (*vide supra*). The barrier for the expulsion of *p*-nitrophenoxide is taken as 1.3 (*vide supra*). The thermodynamic barriers for formation of the "corner intermediates" have been calculated above. For use in eq. [6] these values must be corrected to apply to the encounter complexes of starting materials and products. We use the estimate for the equilibrium constant for encounter complex formation suggested by Hine (33). For acylium ion formation there is an unknown contribution from ion pairing. We will assume that this is negligible for the moment; ion pairing is normally not strongly favored for 1:1 electrolytes in water, and in the present case the relevant ion pair, with O^- next to $-C{\equiv}O^+$, has probably lost hydrogen-bonded solvation at O^- relative to the separated ions, with no good compensating interaction. The three-dimensional surface so derived is shown in Fig. 4. The implications of this diagram are that the tetrahedral species is no longer an obligatory intermediate, and that a concerted reaction path is favored. The value of $\Delta G^{\pm}$ implied by Fig. 4 is actually greater than the observed value. If we assume that the errors in the energies of both intermediates are ± 4.3 kcal/mol, then the largest value of b for imidazole addition compatible with the thermodynamics, the observed free energy of activation, and $b = 1.35$ for *p*-nitrophenoxide expulsion is 3.4. This is distinctly smaller than the values established for other aminolyses, although as we argued above there is a basis for expecting a value for imidazole that is smaller than the value for a primary amine. Given the imperfect state of our present knowledge of the thermodynamic and kinetic barriers for the edge reactions, we can only conclude that in terms of the theory given above a concerted reaction is allowed. In fact we may ask what is the upper limit on the intrinsic barrier for *p*-nitrophenoxide expulsion for the overall reaction to be

Can. J. Chem. Downloaded from www.nrcresearchpress.com by 118.98.75.50 on 09/07/12
For personal use only.

Can. J. Chem. Downloaded from www.nrcresearchpress.com by 118.98.75.50 on 09/07/12
For personal use only.

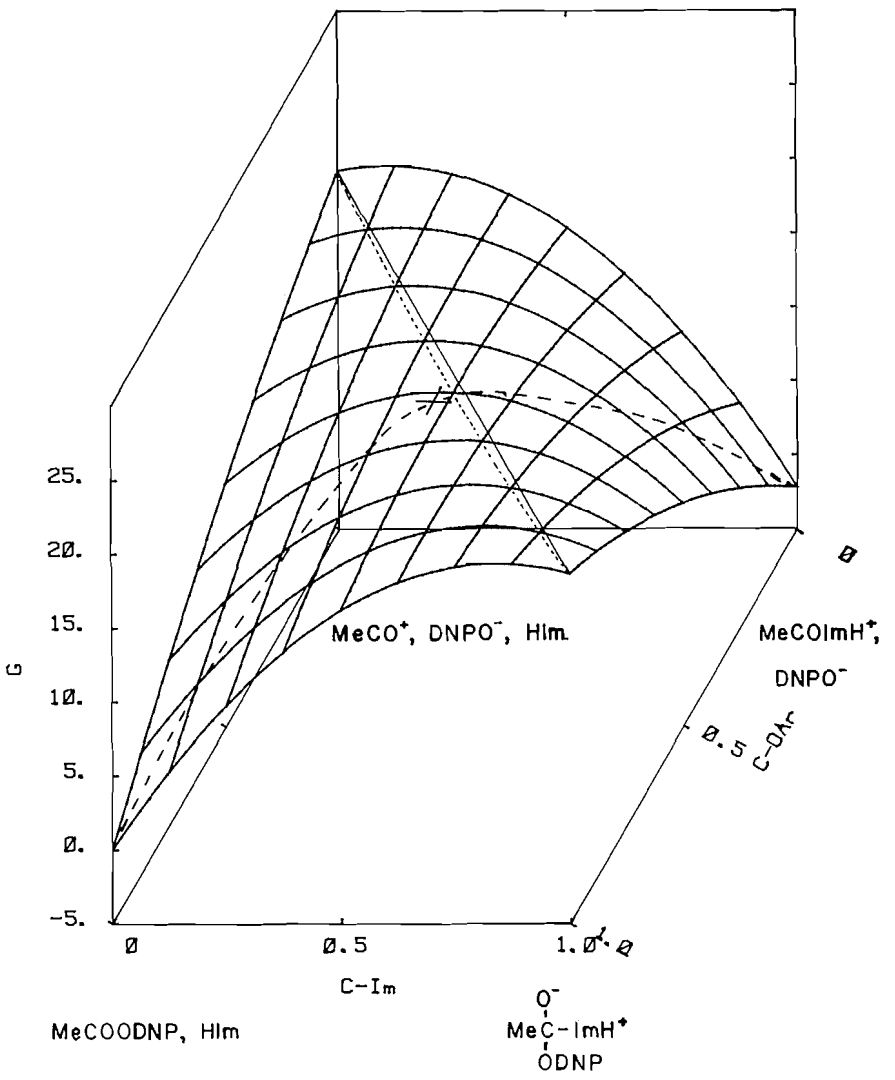

FIG. 5. Three-dimensional reaction coordinate surface for the reaction of imidazole with 2,4-nitrophenyl acetate. The surface is calculated using eq. [6], with the thermodynamic and kinetic barriers described in the text. (---) Minimum energy path from starting material to product; (----) section through the energy surface at $p = 1/2$; (—) straight line joining the energies of the two intermediates, for ease of visualization.

concerted, assuming an intrinsic barrier of 5 for imidazole addition and the energy levels of the intermediates derived above. Using the condition, $(\beta + \delta - \epsilon) > 0$, the answer is that the reaction is concerted if the intrinsic barrier for phenoxide expulsion is $b < 2.5$. Since the observed free energy of activation is less than the free energy change for formation of either of the corner intermediates, our calculations require a concerted mechanism. This in turn says that both intrinsic barriers must be small, which as we have seen is consistent with what is known.

For the corresponding case of 2,4-dinitrophenyl acetate, the overall equilibrium constant for hydrolysis is distinctly more favorable, at $\log K = 9.06$ (63), than for *p*-nitrophenyl acetate; the equilibrium constant for tetrahedral intermediate formation by imidazole addition is estimated in the same way as for *p*-nitrophenyl acetate as $\log K = -13.29 \pm 2.39$. The equilibrium constant for imidazole addition to give the zwitterionic tetrahedral intermediate is estimated to be $\log K = -15.44 \pm 2.35$. The equilibrium constant for cleavage of dinitrophenyl acetate to give acetylium ion and dinitrophenoxide is estimated to be $\log K = -12.3 \pm 3.0$. The equilibrium constant for reaction of dinitrophenyl acetate with imidazole to give acetylimidazolium dinitrophenoxide is $\log K = 1.6$. We have no information allowing estimation of the intrinsic barriers for 2,3-dinitrophenoxide expulsion, so we will use the same intrinsic barriers as for *p*-nitrophenoxide. Figure 5 shows the surface calculated using these values. Once again a concerted reaction is predicted, but once again the prediction is not rigorous. In fact the conditions for a concerted reaction, using the same assumptions as for *p*-nitrophenyl acetate, turn out to be stricter here. The intrinsic barrier for expulsion of 2,4-dinitrophenoxide must be $b < 2.3$ for the reaction to be concerted if the intrinsic barrier for imidazole attack is $b = 5$.

Although it is not possible at this time to give a clear statement of whether or not the theory of concerted reactions outlined above demands a concerted mechanism for the reactions of imidazole with *p*-nitrophenyl acetate and 2,4-dinitrophenyl acetate, it is possible to see why these reactions have become likely candidates for such a mechanism. The intrinsic barriers for leaving group expulsion have become small, and the nucleophile has a small intrinsic barrier for addition. In both cases the demands for new solvation by the attacking or leaving groups are modest and the lone pair basicities are such as to confer high, though not extremely high, reactivity. The energy

Can. J. Chem. Downloaded from www.nrcresearchpress.com by 118.98.75.50 on 09/07/12
For personal use only.

levels of the two corner intermediates have become matched because of the improved leaving group abilities of the nitrophenoxides. Because addition of imidazole becomes relatively less favorable as the substituents on the carbonyl carbon become increasingly more electron withdrawing, we find that the equilibrium constant for addition of imidazole becomes slightly less favorable in the sequence ethyl acetate, *p*-nitrophenyl acetate, 2,4-dinitrophenyl acetate. In the same sequence the equilibrium constant for heterolysis to the acylium ion becomes dramatically more favorable. To our surprise, in the course of asking whether the reaction of imidazole with *p*-nitrophenyl acetate might be concerted, we found not only evidence that this might be so, but that an even stronger case could be made for the virtual reaction of *p*-nitrophenoxide with *p*-nitrophenyl acetate. We can state the assumptions involved in our assertion that the acyl transfer reaction of imidazole with nitrophenyl acetates and the virtual reaction of *p*-nitrophenoxide with *p*-nitrophenyl acetate are concerted:

1. That the energetics of tetrahedral intermediate formation are approximately correct.
2. That the energetics of acylium ion formation are approximately correct.
3. That the assignment of intrinsic barriers is approximately correct.
4. That Marcus theory can be applied to calculate barriers not just at the edges of the diagram, but in the interior as well.
5. That the intrinsic barrier for a given reaction coordinate in a three-dimensional reaction coordinate diagram is independent of the value of the other reaction coordinate.

The value of the picture that we have developed for concerted reactions is that it gives a strong criterion for when a reaction will and will not be concerted. A fully concerted reaction, one where reaction from starting material to product has the disparity variable always close to 1/2, is only possible when the intrinsic barriers for the edge reactions are low and the thermodynamic barriers for formation of the potential intermediates are high.

This new theory of concerted reactions should be quite general. The major impediment to applying it to other reactions is the need for free energies of the two intermediates and for the two intrinsic barriers for the edge reactions. It seems clear that it will be possible, with some effort, to test our ideas on several reactions where there is experimental evidence bearing on the question of a stepwise vs. a concerted path. These investigations are being undertaken, and will be reported in due course.

Experimental

Materials

Acetylimidazole diethyl acetal and formylimidazole diethyl acetal were prepared by distilling off the by-product ethanol from a mixture of imidazole and a catalytic amount of *p*-toluenesulfonic acid in a large excess of triethyl orthoformate or triethyl orthoacetate as solvent over a 2-h period. Excess solvent was removed at room temperature and reduced pressure and the remaining product purified by distillation. Formylimidazole diethyl acetal: bp 82–84°C, 0.3 Torr; lit. (64) bp 52°C, 0.02 Torr; 60-MHz ^{1}H nmr spectrum ($CDCl_3$), δ: 7.8 (s, 1H, imidazole), 7.1 (s, 2H, imidazole), 6.1 (s, 1H, $HC(O)_2(N)$), 3.6 (q, 4H, $CH_2(O)(C)$), 1.2 (t, 6H, CH_3) ppm. Acetylimidazole diethyl acetal: bp 66–69°C, 0.1 Torr; 200-MHz ^{1}H nmr spectrum ($CDCl_3$), δ: 7.44 (s, 1H, imidazole), 7.06, 7.02 (2s, 2H, imidazole), 3.31–3.61 (m, 4H, $CH_2(O)(C)$), 1.74 (s, 3H, $CH_3C(O)_2(N)$), 1.22 (t, 6H, CH_3CH_2) ppm. *Exact Mass* calcd. for $C_9H_{16}N_2O_2$: 184.12116; found: 184.12094.

Formylimidazole dipropyl acetal

Tripropyl orthoformate was prepared by exchange, heating trimethyl orthoformate with excess *n*-propanol in the presence of a catalytic amount of *p*-toluenesulfonic acid. To drive the reaction to completion it was necessary to distill off the propanol and then add and distill off more propanol. Formylimidazole dipropyl acetal was prepared from tripropyl orthoformate by the same procedure used for formylimidazole diethyl acetal; bp 100°C at 0.5 Torr; 200-MHz ^{1}H nmr ($CDCl_3$), δ: 0.99 (t, 6H, CH_3), 1.68 (sextet, 4H, $CH_2(C)_2$), 3.53 (t, 4H, $CH_2(C)(O)$), 6.13 (s, 1H, $HC(O)_2(N)$), 8.1, 8.3, 8.9 (3s, 3H, imidazole) ppm. *Exact Mass* calcd. for $C_{10}H_{18}N_2O_2$: 198.13681; found: 198.13691.

Benzoylimidazole dimethyl acetal was prepared from imidazole with a catalytic amount of *p*-toluenesulfonic acid in trimethyl orthobenzoate as solvent. After heating in a 130°C oil bath for 14.5 h, with periodic addition of more catalyst, an nmr spectrum of the reaction mixture indicated that more than 90% of the imidazole had been consumed. Excess solvent was removed under reduced pressure and the last traces of imidazole were removed from the residue by extracting a diethyl ether solution three times with a 0.05 *M* pH 10.0 sodium carbonate/bicarbonate buffer. After drying, the ether was removed and the residue purified by distillation; bp 108–110°C, 0.1 Torr; 200-MHz ^{1}H nmr spectrum ($CDCl_3$), δ: 7.85 (s, 1H, imidazole), 7.45, 7.31 (2m, 5H, phenyl), 6.98, 6.88 (2s, 2H, imidazole), 3.11 (s, 6H, CH_3O) ppm. *Exact Mass* calcd. for $C_{12}H_{14}N_2O_2$: 218.10551; found: 218.10548.

1-(3'-Aminopropyl)-imidazole dihydrochloride (ref. 65)

N-(3-Bromopropyl)-phthalimide (Aldrich), 25 g (93.2 mmol), and imidazole, 12.7 g (186.5 mmol), were dissolved in acetone (60 mL) and refluxed for 4 h. After evaporation of the solvent under reduced pressure the syrupy yellow residue was redissolved in chloroform (100 mL) and the excess imidazole extracted with aqueous base. The organic layer was dried, the solvent removed, and the solid residue redissolved in ethanol (95%, 100 mL). Hydrazine hydrate (85%, 6 mL) was added and the mixture refluxed for 1.5 h. The solution was then filtered, evaporated, and the syrupy yellow residue dissolved in water, acidified (HCl), and filtered again. It was then made basic (NaOH) and extracted several times with chloroform. The contents of the organic phase were distilled (103–104°C, 500 mTorr), and converted to the dihydrochloride salt by evaporation from aqueous acid. Yield 3.24 g (16.4 mmol, 18%); 60-MHz nmr, free amine in $CDCl_3$ with TMS, δ: 1.3 (br s, NH_2), 1.8 (quintet, —C—CH_2—C—), 2.7 (t, —CH_2—N), 4.0 (t, Im—CH_2—C), 6.9, 7.0, 7.4 (3s, imidazole) ppm.

1-(2'-Aminoethyl)-imidazole dihydrochloride (ref. 65)

N-(2-Bromoethyl)-phthalimide (Aldrich), 25 g (98.4 mmol), and imidazole, 13.4 g (196.8 mmol), were refluxed in acetone (60 mL) for 4 h. Thin-layer chromatography (tlc) (5% methanol in chloroform on silica gel) indicated that the reaction was only about 50% complete so heating was continued for another 4 h. Solvent was then evaporated and excess imidazole was removed by dissolving the residue in chloroform (100 mL) and extracting it with aqueous base. The reaction product, *N*-(2-imidazolylethyl)-phthalimide, was separated from the unreacted *N*-(2-bromoethyl)-phthalimide by crystallizing the contents of the organic phase from acetone. Unreacted starting material was returned, with an excess of imidazole, to acetone solution and refluxed for a further 6 h, resulting in a second crop of product. The combined *N*-(imidazolylethyl)-phthalimide (14.7 g, 60.9 mmol) was dissolved with 4 mL hydrazine hydrate (85%, 183 mmol) in ethanol (95%, 100 mL) and refluxed for 1.5 h. The reaction mixture was then made acidic (HCl), filtered, and solvent removed under reduced presure. Product was recovered from the residue by dissolving it in aqueous base (75 mL), saturating with sodium chloride, and extracting several times with chloroform. The contents of the organic phase were distilled (80–82°C, 200 mTorr) and converted to the dihydrochloride salt by evaporation from aqueous acid. Yield 5.57 g (30.3 mmol, 31%); 60-MHz nmr, free amine in $CDCl_3$ with TMS, δ: 1.2 (br s, NH_2), 3.0 (t, C—CH_2—N), 4.0 (t, Im—CH_2—C), 7.0, 7.1, 7.5 (3s, imidazole) ppm.

TABLE 8. Boiling point measurements

	Boiling point (°C at 1 Torr)	Parameters[b] from least squares		ΔH_{vap}[c]	ΔC_{vap}[d]	$p_{25°C}$[c] (Torr)
		A	B			
Dimethyl phthalate	103.9	21.4 ± 0.92	8.07 ± 0.38			
Benzoylimidazole dimethyl acetal	114.7	26.3 ± 1.19	10.2 ± 0.46	20.45 ± 0.28	−37.2 ± 1.1	8.7×10^{-4}
Formylimidazole diethyl acetal	85.7	24.8 ± 1.23	8.90 ± 0.45	17.70 ± 0.28	−32.8 ± 1.1	8.4×10^{-3}
Acetylimidazole diethyl acetal	79.6	26.8 ± 1.60	9.49 ± 0.58	17.30 ± 0.28	−34.4 ± 1.1	1.4×10^{-2}
Formylimidazole dipropyl acetal	100.3	22.4 ± 0.91	8.37 ± 0.37	19.05 ± 0.28	−36.1 ± 1.1	2.4×10^{-3}

[a]Interpolated using the least-squares line.
[b]For $\ln(p) = A + B(1000/T)$.
[c]Estimated using the procedures of ref. 8.
[d]Estimated using the atomic parameters of ref. 10.

Methods

Heats of hydrolysis

Calorimetry was carried out using the apparatus and procedure previously described (31). The results are summarized in Table 1. For each reaction the stoichiometry was determined by injecting a suitable amount of the compound into the deuterated analog of the calorimetry solvent (using relatively larger amounts of compound to allow nmr analysis), and then recording the ^{1}H nmr spectrum. The acylimidazole acetals invariably gave the corresponding alkyl ester, alcohol, and imidazole as products within the time required to make up the solution and run a spectrum.

Boiling point measurements on dimethyl phthalate, benzoylimidazole dimethyl acetal, formylimidazole diethyl acetal, formylimidazole dipropyl acetal, and acetylimidazole diethyl acetal

The boiling points of these compounds were determined at various pressures using the boiling point apparatus designed by Hoover *et al.* (66). The boiling point at a pressure of 1 Torr was then determined by interpolation, using a least-squares fit of $\ln(p) = A + B(1000/T)$ to the data. The values so obtained are found in Table 8.

The interpolated value for dimethyl phthalate is in good agreement with the accepted value of 100.3°C (67). We require vapor pressures at 25°C for these compounds; the extrapolations were carried out by a method we developed (8), which requires heats and heat capacities of vaporization. The estimated values that we used for this purpose are given in Table 8, as are the estimated vapor pressures.

Pauly assay for imidazole (ref. 68)

A sample, with water added if necessary to give 2 mL, was treated with 1% sulfanilic acid in 1.0 *M* HCl (0.4 mL) and 0.72 *M* $NaNO_2$ (0.4 mL). After 300 s 1.9 *M* sodium carbonate solution (1.2 mL) was added and the volume made up to 10.0 mL with water. At 800–900 s after the addition of $NaNO_2$ solution the absorbance at 498 nm was read. Calibration standards using known amounts of imidazole were run at the same time. The absorbance at 498 nm reaches a maximum and then slowly declines.

Solubility of formylimidazole dipropyl acetal

Portions of formylimidazole dipropyl acetal were stirred at 25°C with 0.1 *M* aqueous sodium hydroxide for 1.5 h in 50-mL centrifuge tubes. The tubes were centrifuged, and 2.0-mL samples were taken and diluted to 25.0 mL with 1.0 *M* HCl and let stand at room temperature. The imidazole content was analyzed by the Pauly procedure, using the absorbance at 498 nm 800–900 s after adding carbonate. The average of four samples was $(60.6 \pm 1.6) \times 10^{-3}$ *M* formylimidazole dipropyl acetal in the original saturated solutions.

Solubility of benzoylimidazole dimethyl acetal

A small quantity of benzoylimidazole dimethylacetal (50–100 μL) was added to 25 mL of a stirred solution of 0.1 *M* NaOH in a large test tube (3 × 20 cm) and the tube placed in a 25°C water bath. The end of the tube was sealed with Parafilm. After one day the mixtures containing 50 μL of benzoylimidazole dimethylacetal appeared homogeneous, while those with 100 μL still contained undissolved material after 3 days. Periodically, over three days, 30-μL aliquots of the supernatant solution from the experiment with 100 μL of benzoylimidazole dimethyl acetal were added to 5 mL 0.1 *M* aqueous HCl and the optical absorbance of this solution measured at 231 nm. The molar extinction coefficient for methylbenzoate in 0.1 *M* aqueous HCl was measured as 11 780 ± 20 M^{-1} cm^{-1}. A plot of the absorbance vs. time (after about 15 h) was best fitted by a straight line of slope 5.022×10^{-3} (absorbance units/h) and an intercept on the absorbance axis of 0.906. Thus the concentration of a saturated solution of benzoylimidazole dimethyl acetal in 0.1 *M* NaOH at 25°C is = 12.9 m*M*. The increase in absorbance at 231 nm with time is interpreted as being due to the slow hydrolysis of benzoylimidazole dimethyl acetal in 0.1 *M* NaOH to methyl benzoate, imidazole, and methanol. This increase of 5.022×10^{-3} absorbance units/h corresponds to a pseudo-first-order rate constant of 1.5×10^{-6} s^{-1} for hydrolysis. In a separate set of fairly crude experiments a small quantity of benzoylimidazole dimethyl dissolved in THF was injected into aqueous phosphate or carbonate buffered solution and the half-life for the hydrolysis of the acetal observed at 254 nm. The results of these experiments as well as the one above are found in Table 9.

TABLE 9. Crude kinetics of hydrolysis for benzoylimidazole dimethyl acetal[a]

	pH	$t_{1/2}$ (s)	log k
	8	28	−1.6
	9.2	400	−2.8
	10	4800	−3.8
0.1 *M* NaOH	13	450000	−5.8

[a]In aqueous solution at 25°C.

The rate observed at pH 13 is about 10 times faster than would have been expected from extrapolation of the data at lower pH; we conclude that there is an uncatalyzed rate of hydrolysis in addition to the acid-catalyzed path that dominates at low pH.

Determination of pK values for aminoethyl- and aminopropyl-imidazole

Solutions for titration of aminoethyl- and aminopropyl-imidazole were prepared by dissolving about 180 mg of the hydrochloride salts, along with sufficient KCl so that the total salt concentration was 0.1 *M*, in 100.0 mL water. This solution was then transferred to a 125-mL

Can. J. Chem. Downloaded from www.nrcresearchpress.com by 118.98.75.50 on 09/07/12
For personal use only.

TABLE 10. Titration of aminoalkyl imidazoles

Wt. of sample (mg)	Conc. of sample (mM)	Wt. of KCl (mg)	C	$10^6 K_1$	$10^9 K_2$
(a) Titration of aminoethylimidazole					
149.85	8.14	624.10	0.813 ± 0.001	1.23 ± 0.02	3.42 ± 0.07
151.15	8.21	623.05	0.818 ± 0.001	1.32 ± 0.02	3.68 ± 0.06
161.30	8.76	614.83	0.867 ± 0.001	1.19 ± 0.01	3.63 ± 0.05
		pK_1 = 5.90 ± 0.20		pK_2 = 8.45 ± 0.02	
(b) Titration of aminopropylimidazole					
185.60	9.37	605.80	0.934 ± 0.001	0.326 ± 0.002	0.240 ± 0.002
186.15	9.40	605.40	0.944 ± 0.001	0.313 ± 0.002	0.235 ± 0.002
187.25	9.45	604.55	0.948 ± 0.001	0.313 ± 0.002	0.234 ± 0.002
		pK_1 = 6.50 ± 0.02		pK_2 = 9.63 ± 0.02	

Erlenmeyer flask with stirring bar and placed in a water bath at 25°C. A pH electrode, which had been calibrated to standard buffers at pH 7.0 and 10.0, was immersed in the solution and it was titrated with 1.0 M NaOH using a Gilmont Ultraprecision micrometer buret, which could be read to 0.0001 mL.

The volume measurements for the background titration of 0.1 M KCl were subtracted from the volume measurements at the corresponding pH for the titration of the samples using a simple computer program. The data were then fitted to the equation

$$X = C(1/(1 + H/K_1) + 1/(1 + H/K_2))$$

where X is the volume of NaOH solution added, C is the volume of NaOH solution required to titrate one equivalent of the sample, H is the hydrogen ion concentration (10^{-pH}), and K_1 and K_2 are acid dissociation constants for the aminoethyl- and aminopropyl-imidazoles, by use of the least-squares program RIGLSQ47. This program takes as input the corrected values of titrant volume and pH, and estimates of C, K_1, and K_2. The results are shown in Table 10.

Equilibrium constant for the addition of imidazole to acetone

Samples were made up in a total volume of 5.0 mL, containing 0.5 mL of D_2O to provide a lock for the nmr spectrometer, 0.37 mL of acetone, 170 or 340 mg imidazole, and 0–0.45 mL 0.98 M HCl to adjust the pH. The 200-MHz nmr spectra showed, in addition to the major peak due to the CH_3 of acetone at 2.04 δ, a ^{13}C satellite signal at 1.72 δ, a signal at 1.26–1.34 δ attributed to the covalent hydrate of acetone (intensity 20.3 ± 8.7% of the ^{13}C satellite), and a peak at 1.44–1.73 δ attributed to the imidazole adduct of acetone (intensity related to imidazole concentration, and absent when no imidazole was present). The data that we obtained are found in Table S2.[3] A least-squares fit of the ratio of imidazole adduct to hydrate signal intensities to the equation $r = a[\text{Imidazole}]_{\text{free base}}$ gave a = 2.33 ± 0.09.

Acknowledgments

We thank the Natural Sciences and Engineering Research Council of Canada for financial support of this work.

1. T. C. BRUICE and S. J. BENKOVIC. Bioorganic mechanisms. Vol. I. W. A. Benjamin, New York. 1966. pp. 46–66.
2. J. F. KIRSCH and W. P. JENCKS. J. Am. Chem. Soc. **86**, 837 (1964).
3. M. L. BENDER and B. W. TURNQUEST. J. Am. Chem. Soc. **79**, 1652 (1957).
4. T. C. BRUICE and G. L. SCHMIR. J. Am. Chem. Soc. **79**, 1663 (1957).
5. J. P. GUTHRIE. Acc. Chem. Res. **16**, 122 (1983).
6. J. P. GUTHRIE. Can. J. Chem. **53**, 898 (1975).
7. J. P. GUTHRIE and P. A. CULLIMORE. Can. J. Chem. **58**, 1281 (1980).
8. J. P. GUTHRIE. Can. J. Chem. **64**, 635 (1986).
9. S. W. BENSON and J. H. BUSS. J. Chem. Phys. **29**, 546 (1958).
10. J. P. GUTHRIE and K. F. TAYLOR. Can. J. Chem. **62**, 363 (1984).
11. C. HANSCH, J. E. QUINLAN, and G. L. LAWRENCE. J. Org. Chem. **33**, 347 (1968).
12. A. LEO and C. HANSCH. J. Org. Chem. **36**, 1539 (1971).
13. J. HINE and P. K. MOOKERJEE. J. Org. Chem. **40**, 292 (1975).
14. J. P. GUTHRIE. Can. J. Chem. **55**, 3562 (1977).
15. R. WOLFENDEN, Y.-L. LIANG, M. MATTHEWS, and R. WILLIAMS. J. Am. Chem. Soc. **109**, 463 (1987).
16. M. TANOKURA. Biochem. Biophys. Acta, **742**, 576 (1983).
17. G. B. BARLIN and D. D. PERRIN. *In* Techniques of chemistry. Vol. IV. *Edited by* K. W. Bentley and G. W. Kirby. Wiley, New York. 1972.
18. K. PIHLAJA and J. KANKARE. Acta Chem. Scand. **23**, 1745 (1969); K. PIHLAJA. Acta Chem. Scand. **25**, 451 (1971).
19. J. HINE and R. W. REDDING. J. Org. Chem. **35**, 2769 (1970).
20. J. P. GUTHRIE. J. Am. Chem. Soc. **100**, 5892 (1978).
21. J. P. GUTHRIE. J. Am. Chem. Soc. **102**, 5286 (1980).
22. J. H. SMITH. J. Am. Chem. Soc. **98**, 3598 (1976).
23. W. P. JENCKS and J. CARRIULO. J. Biol. Chem. **234**, 1272 (1959); **234**, 1280 (1959).
24. A. SKRABAL and A. ZAHORKA. Monatsh. Chem. **53–54**, 562 (1929).
25. E. G. SANDER and W. P. JENCKS. J. Am. Chem. Soc. **90**, 6154 (1968).
26. J. HINE and G. F. KOSER. J. Org. Chem. **36**, 1348 (1971).
27. M. L. BENDER and B. W. TURNQUEST. J. Am. Chem. Soc. **79**, 1656 (1957).
28. A. O. COHEN and R. A. MARCUS. J. Phys. Chem. **72**, 4229 (1968).
29. R. A. MARCUS. J. Am. Chem. Soc. **91**, 7224 (1969).
30. R. A. MARCUS. Annu. Rev. Phys. Chem. **15**, 155 (1964), and references cited therein.
31. J. P. GUTHRIE. J. Am. Chem. Soc. **96**, 3608 (1974).
32. G. M. BLACKBURN and W. P. JENCKS. J. Am. Chem. Soc. **90**, 2638 (1968).
33. J. HINE. J. Am. Chem. Soc. **93**, 3701 (1971).
34. M. M. COX and W. P. JENCKS. J. Am. Chem. Soc. **103**, 572 (1981).
35. E. M. ARNETT and J. F. WOLF. J. Am. Chem. Soc. **95**, 978 (1973).
36. W. P. JENCKS. Acc. Chem. Res. **13**, 161 (1980).
37. R. A. MCCLELLAND. Acc. Chem. Res. **16**, 394 (1983).
38. D. F. DETAR. J. Am. Chem. Soc. **104**, 7205 (1982).
39. T. C. CURRAN, C. R. FARRAR, O. NIAZY, and A. WILLIAMS. J. Am. Chem. Soc. **102**, 6828 (1980).
40. C. D. RITCHIE, J. E. VANVERTH, and P. O. I. VIRTANEN. J. Am. Chem. Soc. **104**, 3491 (1982).

Can. J. Chem. Downloaded from www.nrcresearchpress.com by 118.98.75.50 on 09/07/12
For personal use only.

41. E. CHRYSTIUK, A. JUSOH, D. SANTAFIANOS, and A. WILLIAMS. J. Chem. Soc. Perkin Trans. 2, 163 (1986).
42. W. J. ALBERY. Prog. React. Kinet. **4**, 355 (1967).
43. R. A. MORE O'FERRAL. J. Chem. Soc. (B), 274 (1970).
44. W. P. JENCKS. Chem. Rev. **72**, 705 (1972).
45. J. GERSTEIN and W. P. JENCKS. J. Am. Chem. Soc. **86**, 4655 (1964).
46. R. A. MARCUS. J. Phys. Chem. **72**, 891 (1968).
47. R. A. MARCUS. Disc. Faraday Soc. **29**, 21 (1960).
48. G. W. KOEPPL and A. J. KRESGE. J. Chem. Soc. Chem. Commun. 371 (1973).
49. W. J. ALBERY. Electrode kinetics. Clarendon Press, Oxford. 1975. app. 7.
50. J. KURZ. Chem. Phys. Lett. **57**, 243 (1978).
51. E. GRUNWALD. J. Am. Chem. Soc. **107**, 125 (1985).
52. W. J. ALBERY and M. M. KREEVOY. Adv. Phys. Org. Chem. **16**, 87 (1978).
53. D. A. JENCKS and W. P. JENCKS. J. Am. Chem. Soc. **99**, 7948 (1977).
54. J. J. GAJEWSKI. Acc. Chem. Res. **13**, 142 (1980).
55. B. M. DUNN. Int. J. Chem. Kinet. **6**, 143 (1974).
56. N. C. DENO, C. U. PITTMAN, JR., and M. J. WISOTSKY. J. Am. Chem. Soc. **86**, 4370 (1964).
57. R. H. BOYD. *In* Solute–solvent interactions. *Edited by* J. F. Coetzee and C. D. Ritchie. Marcel Dekker, New York. 1969. p. 98.
58. R. J. GILLESPIE, T. E. PEEL, and E. A. ROBINSON. J. Am. Chem. Soc. **93**, 5083 (1971).
59. K. YATES and R. A. MCCLELLAND. J. Am. Chem. Soc. **89**, 2686 (1967).
60. E. M. ARNETT, J. J. BURKE, J. V. CARTER, and C. F. DOUTY. J. Am. Chem. Soc. **94**, 7837 (1972).
61. J. P. GUTHRIE. J. Am. Chem. Soc. **95**, 6999 (1973).
62. A. R. FERSHT and W. P. JENCKS. J. Am. Chem. Soc. **92**, 5442 (1970).
63. J. P. GUTHRIE. J. Am. Chem. Soc. **99**, 3991 (1977).
64. N. J. CURTIS and R. S. BROWN. J. Org. Chem. **45**, 4038 (1980).
65. R. J. SUNDBERG, D. C. MENTE, I. YILMAZ, and G. GUPTA. J. Heterocycl. Chem. **14**, 1279 (1977).
66. S. R. HOOVER, H. JOHN, and E. F. MELLON. Anal. Chem. **25**, 1940 (1953).
67. R. C. WEAST (*Editor*). Handbook of chemistry and physics. 48th ed. Chemical Rubber Co., Cleveland, OH. 1967.
68. J. P. GREENSTEIN and M. WINITZ. Chemistry of the amino acids. Wiley, New York. 1961. p. 1979; H. PAULY. Z. Physiol. Chem. **42**, 508 (1904).
69. S. E. STEIN and B. D. BARTON. Thermochim. Acta, **44**, 265 (1981).
70. D. W. SCOTT, W. T. BERG, I. A. HOSENLOPP, W. N. HUBBARDD, J. F. MESSERLY, S. S. TODD, D. R. DOUSLIN, J. P. MCCULLOUGH, and G. WADDINGTON. J. Phys. Chem. **71**, 2263 (1967).
71. S. W. BENSON. J. Am. Chem. Soc. **80**, 5151 (1958).
72. S. W. BENSON. Thermochemical kinetics. 2nd ed. Wiley, New York. 1976.
73. D. R. STULL, E. F. WESTRUM, JR., and G. C. SINKE. The chemical thermodynamics of organic compounds. Wiley, New York. 1967.
74. E. MORAWETZ. J. Chem. Thermodyn. **4**, 455 (1972).
75. Beilstein's Handbuch der Organischen Chemie. **5**(4), 1880.
76. J. D. COX and G. PILCHER. Thermochemistry of organic and organometallic compounds. Academic Press, New York. 1970.
77. E. M. ARNETT, W. B. KOVER, and J. V. CARTER. J. Am. Chem. Soc. **91**, 4028 (1969).
78. E. M. ARNETT, J. J. BURKE, J. V. CARTER, and C. F. DOUTY. J. Am. Chem. Soc. **94**, 7837 (1972).
79. H. G. M. DE WITT, J. C. VAN MILTENBURG, and C. G. DE KRUIF. J. Chem. Thermodyn. **15**, 651 (1983).
80. R. SABBAH. Thermochim. Acta, **41**, 33 (1980).
81. J. P. GUTHRIE. Can. J. Chem. **56**, 962 (1978).
82. J. P. GUTHRIE. Can. J. Chem. **54**, 202 (1976).
83. J. HINE and A. W. KLUEPPEL. J. Am. Chem. Soc. **96**, 2924 (1974).
84. W. P. JENCKS and J. REGENSTEIN. C.R.C. Handbook of Biochemistry. 1st ed. *Edited by* H. A. Sober. The Chemical Rubber Co., Cleveland, OH. 1968. pp. J150–J189.
85. P. BALLINGER and F. A. LONG. J. Am. Chem. Soc. **81**, 1050 (1959).
86. D. D. PERRIN, B. DEMPSEY, and E. P. SERJEANT. pK_a prediction for organic acids and bases. Chapman and Hall, London. 1981.
87. R. G. KALLEN and W. P. JENCKS. J. Biol. Chem. **241**, 5864 (1966).
88. R. S. BROWN and J. G. ULAN. J. Am. Chem. Soc. **105**, 2382 (1983).
89. J. FASTREZ. J. Am. Chem. Soc. **99**, 7004 (1977).
90. B. G. COX and P. T. MCTIGUE. Aust. J. Chem. **22**, 1637 (1969).
91. P. LE HENAFF. Bull. Soc. Chim. Fr. 4687 (1968).
92. R. V. WOLFENDEN and W. P. JENCKS. J. Am. Chem. Soc. **83**, 4390 (1961).

Appendix

The standard entropy of imidazole in the ideal gas standard state was estimated starting from the entropy of pyrrole, which is the closest model compound for which an entropy has been reported (69, 70). After suitable correction for the lower symmetry of imidazole, the entropy of pyrrole should be a good estimate for the entropy of imidazole. (The intrinsic[6] entropies of benzene and pyridine are very similar, 69.3 (72) and 69.0 (73) respectively.)

We can estimate entropies for the acylimidazole acetals by a variant on the Atom level method of Benson and Buss (9), with the groups attached to the central atom in the imidazolyl derivatives of interest treated as compound "atoms". For imidazolyl, the entropy contribution, 46.4, is obtained from the intrinsic entropy of imidazole by subtracting the contribution for a hydrogen atom, i.e., 21 (9). For methyl we calculated an average value based on the entropies of ethane, propane, isobutane, and neopentane (73) using suitable atomic parameters from ref. 9; the value was 30.22 ± 0.24. (The group level parameter for methyl is 30.41 (72).) For phenyl we calculated an average value based on the entropies for toluene, fluorobenzene, chlorobenzene, bromobenzene, and iodobenzene (73) using suitable atomic parameters from ref. 9; the value was 47.0 ± 2.0. (The value calculated using group level parameters was 49.96 (72).)

For methoxy and ethoxy, we derived parameters starting from the entropies of dimethyl ether and ethyl methyl ether (73) and the value for methyl derived above; the values so obtained were 39.2 for methoxy (calculated value from group level parameters was 39.09 (72)) and 48.6 for ethoxy (calculated value from group level parameters was 48.89 (72)).

These parameters permit the estimation of intrinsic entropies for the acylimidazole acetals and the 2-alkoxy-2-imidazolylpropanes; the values so calculated are found in Table 11.

We then tried an alternative estimation procedure, starting with the assumption that there is no net change in the intrinsic entropy for the exchange reaction shown:

$$R—C(OR')_2—Ph + H—Im \rightleftharpoons R—C(OR')_2—Im + H—Ph$$

The entropies of R—C(OR′)$_2$—Ph were estimated using Benson's group additivity values (72). No value was available

[6]Intrinsic entropies do not contain the contributions due to symmetry (71).

Can. J. Chem. Downloaded from www.nrcresearchpress.com by 118.98.75.50 on 09/07/12
For personal use only.

TABLE 11. Estimated entropy values for the acylimidazole acetals

Compound	Estimated entropy[a]			
	Atom level calculations	Additivity via hydrocarbons	Additivity via orthoesters	Average
$HC(OEt)_2$—Im	126.6	130.0	123.9	126.8 ± 3.1
$MeC(OEt)_2$—Im	136.0	132.7	130.1	132.9 ± 3.0
$PhC(OMe)_2$—Im	137.1	135.6	129.3	134.0 ± 4.1

[a]Calculated as described in the text.

Can. J. Chem. Downloaded from www.nrcresearchpress.com by 118.98.75.50 on 09/07/12
For personal use only.

for the group $[C(C_B)_2(O)_2]$ needed for R—$C(OR')_2$—Ph with R = Ph or for $[C(C_B)_2(C)_2]$ needed for the analogous hydrocarbon. Accordingly we had to derive a reasonable value for $[C(C_B)_2(C)_2]$ before proceeding. No data allowing direct evaluation could be found, so an indirect approach was necessary. We determined the effect on related group contributions of replacing two tetrahedral carbons by two aromatic carbons and so estimated $[C(C_B)_2(C)_2]$ from $[C(C)_4]$.

We began by determining some of the unknown group contributions from literature data. $[CH_2(C_B)_2]$ was determined from the entropy of diphenylmethane, for which Stull *et al.* (73) report a value of 72.1 for $S^0(l)$. Vapor pressure data (67) lead to $p(25°C) = 0.038$ Torr by a short extrapolation using the Clausius–Clapeyron equation. The heat of vaporization of the liquid has been reported as $\Delta H_v(25°C) = 16.13 \pm 0.07$ (74). From $S^0(l)$, ΔH_{vap}, and $p(25°C)$ we calculate the standard entropy $S^0(g) = 106.52$. When the symmetry contribution is removed, $S^* = 110.66$.[7] Using Benson's values for $[C_BH]$ and $[C_B(C)]$ we can calculate that $[CH_2(C_B)_2] = 10.73$. This value is somewhat larger than the analogous contributions with C in place of C_B: $[CH_2(C)_2] = 9.42$, and $[CH_2(C)(C_B)] = 9.34$.

$[CH(C)(C_B)_2]$ was determined from the entropy of 1,1-diphenylethane for which Stull *et al.* report an $S^0(l) = 80.28$. Using vapor pressure data from Beilstein (75) we could calculate the vapor pressure by a short extrapolation using the Clausius–Clapeyron equation; $p(25°C) = 0.0132$ Torr. From the boiling point at 1 Torr, $\Delta H_v = 17.51 \pm 1.00$ (8). From the vapor pressure at 25°C, ΔH_v, and $S^0(l)$ we can calculate $S^0(g) = 117.22 \pm 3.35$. Removing the symmetry correction, $S^* = 122.17$. Then using Benson's group parameters for $[C_BH]$, $[C_B(C)]$, and $[CH_3(C)]$ we can calculate $[CH(C)(C_B)_2] = -8.16 \pm 3.35$. For comparison, $[CH(C)_3] = -12.07$ and $[CH(C)_2(C_B)] = -12.15$. The vapor pressure data used to estimate ΔH_{vap} and $p(25°C)$ were not of high precision, so that we must assign an uncertainty of 1 kcal/mol to ΔH_{vap}; this leads to an error of 3.35 in $S^0(g)$.

No data could be found for 2,2-diphenylpropane, so an analogous evaluation of $[C(C)_2(C_B)_2]$ was not possible. Instead we estimated the effect of replacing two C's by two C_B's. This effect is seen to be small; on going from $[CH_2(C)_2] = 9.42$ to $[CH_2(C_B)_2] = 10.73$ the change in the group contribution is seen to be 1.31. On going from $[CH(C)_3] = -12.07$ to $[CH(C)(C_B)_2] = -8.16 \pm 3.35$ the change in the group contribution is 3.91 ± 3.35. Thus the second estimate is less precise, but indistinguishable. Consequently we should use the value of 1.31 in estimating the group contribution for $[C(C)_2(C_B)_2]$. Under the circumstances, the best guess for $[C(C)_2(C_B)_2]$ is -35.10 (the value for $[C(C)_4]$ (72)) + 1.31 = -33.79.

We can now estimate the standard entropies for the hydrocarbon analogs of the acylimidazole acetals with $-CH_2-$ in place of -O- and phenyl in place of imidazolyl. From these values we can estimate the standard entropies of the corresponding acetals using the correction from $-CH_2-$ to -O- suggested by Stull *et al.* (73). The values so obtained are, for $(EtO)_2CH$—Ph, $S^*(g) = 133.78$; for $(EtO)_2C(Me)$—Ph, $S^*(g) = 141.17$; for $(MeO)_2C(Ph)_2$, $S^*(g) = 143.27$. Using the disproportionation assumption we may then calculate the entropies of the acylimidazole acetals, obtaining: $(EtO)_2CH$—Im, $S^0(g) = 130.0$; $(EtO)_2C(Me)$—Im, $S^0(g) = 132.7$; $(MeO)_2C(Ph)$—Im, $S^0(g) = 135.62$.

Finally we tried an atomic level calculation starting from the standard entropies of the corresponding orthoesters, and correcting for the difference in contributions between the appropriate alkoxyl group and imidazolyl. It was first necessary to estimate the standard entropies of the orthoesters, because none of these values have been measured. We did this by starting with the closest hydrocarbon analogs for which entropy data were available. For triethyl orthoformate we start with the analogous hydrocarbon, 4-propylheptane, for which $S^0(g) = 125.56$ (73). Correcting for symmetry and replacement of $-C_2-$ and -O-, we get $S^0(g) = 121.78$ for the orthoester and $S^0(g) = 123.9$ for formylimidazole diethyl acetal. For trimethyl orthoacetate the hydrocarbon analog is 4-methyl-4-propylheptane; the standard entropy of this compound has not been reported but a value is available for 3-ethyl-3-methylpentane, $S^0(g) = 103.48$ (73). By adding three times the group contribution for $[CH_2(C)_2]$ we obtain $S^0(g) = 127.96$ for triethyl orthoacetate and $S^0(g) = 130.1$ for acetylimidazole diethyl acetal. For trimethyl orthobenzoate the hydrocarbon analog is 1,1-diethylpropylbenzene. The standard entropy for this compound is unknown, but it can be estimated from that of *tert*-butylbenzene, which can be calculated from the available data: $S^0(l) = 66.6$ (73), $\Delta H_{vap} = 11.50 \pm 0.05$ (76), $p(25°C) = 2.18$ Torr (calculated from data in ref. 67). These values lead to $S^0(g) = 93.53$ for *tert*-butylbenzene, and thence to $S^0(g) = 121.79$ for 1,1-diethylpropylbenzene. Finally we calculate $S^0(g) = 118.01$ for trimethyl orthobenzoate and $S^0(g) = 129.3$ for benzoylimidazole dimethyl acetal.

These values are not in full agreement, but the various estimates are not very different. We use the average of the estimates, with uncertainty limits based on the scatter.

[7]We follow Stull *et al.* (73) and use S^* to mean the entropy not corrected for symmetry, and S^0 to mean the standard entropy, including the symmetry corrections.

Electronegativity in density functional theory: diatomic bond energies and hardness parameters

A. R. ORSKY AND M. A. WHITEHEAD
Department of Chemistry, McGill University, 801 Sherbrooke St. West, Montreal, P.Q., Canada H3A 2K6

Received January 5, 1987

This paper is dedicated to Professor John T. Edward

A. R. ORSKY and M. A. WHITEHEAD. Can. J. Chem. **65**, 1970 (1987).

New definitions of the rate of change of electronegativity with charge, the hardness η, of an atom, are developed for acids A and bases B, where $\eta_A = 1/4(I_{(A^+)} - A_{(A^0)})$ and $\eta_B = 1/4(I_{(B^0)} - A_{(B^-)}) \approx 1/4(I_{(B^0)})$. These definitions reproduce the experimental ordering of hard and soft acids and bases, and produce good trends in diatomic bond energies.

A. R. ORSKY et M. A. WHITEHEAD. Can. J. Chem. **65**, 1970 (1987).

Pour les acides A et les bases B, on a développé de nouvelles définitions du taux de changement de l'électronégativité avec la charge et la dureté η d'un atome; dans cette définition, $\eta_A = 1/4(I_{(A^+)} - A_{(A^0)})$ et $\eta_B = 1/4(I_{(B^0)} - A_{(B^-)}) \approx 1/4(I_{(B^0)})$. Ces définitions permettent de reproduire l'ordre expérimental des acides et des bases durs et mous et elles fournissent de bonnes tendances pour les énergies des liaisons diatomiques.

[Traduit par la revue]

I. Introduction

Pauling postulated the energy of *covalent bonds* to be additive. Thus for two atoms, A and B, the bond energy E_{AB} should be the arithmetic mean of the bond energy E_{A_2} in A_2 and E_{B_2} in B_2,

$$[1] \qquad \frac{E_{A_2} + E_{B_2}}{2} = E_{AB}$$

For a covalent bond with polar character, the *ionic* character of the bond AB reflects the additional stabilization caused by the coulomb energy, and

$$[2] \qquad E^i_{AB} = E_{AB} - 1/2(E_{A_2} + E_{B_2})$$

where E^i_{AB}, the ionic component of the bond energy, increases as the difference in the ability of A and B to attract electrons increases in the *molecule* AB.

This qualitative property of an atom to attract electrons in a molecule is the *chemical electronegativity* (3), $\bar{\chi}$. Mulliken (4) developed an equation to represent $\bar{\chi}$ for an atom, in terms of I and A, the isolated atom ionization energy and electron affinity,

$$[3] \qquad \bar{\chi} = 1/2(I + A)$$

It if is assumed (5, 6) that $\bar{\chi}$ is orbital dependent, then

$$[4] \qquad \bar{\chi}_S = 1/2(I_{jS} + A_{jS})$$

where $\bar{\chi}_S$ is the chemical electronegativity of atom S, I_{jS} is the ionization energy, and A_{jS} is the electron affinity of the jth orbital of S. The chemical electronegativity represents the average binding energy of electrons in an atom and the corresponding negative ion (7),

$$[4a] \qquad X + Y \rightarrow X^+ + Y^- \qquad \Delta E = I_X - A_Y$$

$$[4b] \qquad X + Y \rightarrow X^- + Y^+ \qquad \Delta E = I_Y - A_X$$

because the energy changes of reactions [4*a*] and [4*b*] are equal only if $\bar{\chi}_X = \bar{\chi}_Y$.

The energy of an atom can be expanded as a function of the charge $q = Z - N$, where N is the number of electrons about a nucleus of charge Z. Using a polynomial expansion of q (7),

$$[5] \qquad E(q) = aq + bq^2 + cq^3 + dq^4$$

This function is useful if $E(q)$ is differentiable, leading to *differential electronegativity* (3), $\chi_S(q)$,

$$[6] \qquad \chi_S(q) = \left[\frac{\delta E_S(q)}{\delta q}\right]_q$$

and from [5] and [6] the chemical and differential electronegativities are equal for neutral atoms,

$$[7] \qquad \chi_{q=0} = \bar{\chi}$$

Assuming that $E(q)$ is a differentiable function of q gives a functional definition to χ.

However, this assumption has not been fully proved, and remains a real problem for non-integer q, when $E(q)$ has no clear physical meaning. When the total energy, $E(q)$, is expressed within density functional theory (8), and is assumed differentiable (8),

$$[8] \qquad \chi_S(q) = \left[\frac{\delta E_S(q)}{\delta q}\right]_q = -\mu_S$$

where μ is the *chemical potential* (5).

Consequently when two atoms A and B form a molecule AB, they take on an equilibrium χ-value, $\chi_{AB}(q')$, because of electronegativity equalization (9):

$$[9] \qquad A + B \rightarrow AB$$

and

$$[10] \qquad \chi_A(q_A) + \chi_B(q_B) \rightarrow \chi_{AB}(q_{AB})$$

thus

$$[11] \qquad \chi_{AB}(q_{AB}) = \chi_A(q'_A) = \chi_B(q'_B)$$

and

$$[12] \qquad q'_A - q_A = q_B - q'_B = \Delta q = i$$

where i is the *ionic character* of the bond and primes indicate equilibrium charge values. The initial and equilibrium electron negativities of A and B are given by $\chi_A(q_A)$ and $\chi_A(q'_A)$, and $\chi_B(q_B)$ and $\chi_B(q'_B)$ respectively. In molecular formation, all the valence atomic orbitals determine χ_{AB}, because I, A, and $\chi(q)$ are all functions of the occupancy of all the orbitals in the valence shell.

For the reaction in eq. [9] E_{AB} is given by [13] or [14] where E^c_{AB} and E^i_{AB} are the covalent and ionic components of

Can. J. Chem. Downloaded from www.nrcresearchpress.com by 118.98.75.50 on 09/07/12
For personal use only.

E_{AB}, and $E_{AB}(i)$ is a function of the ionic character

[13] $$E_{AB} = E^c_{AB} + E^i_{AB}$$

and

[14] $$E_{AB} = 1/2(E_{A_2} + E_{B_2}) + E_{AB}(i)$$

which can be rearranged to give covalent and ionic components of the bond energy,

[15] $$E^c_{AB} = 1/2(E_{A_2} + E_{B_2})$$

[16] $$E^i_{AB} = E_{AB}(i)$$

Using the change in energy with respect to the number of electrons in [6] gives

[17] $$E^i_{AB} = E_{AB}(i) \approx \frac{\delta E_{AB}(q)}{\delta q}\Delta q$$

or

[18] $$E^i_{AB} = \chi_{AB}(q)i$$

since $\Delta q = i$ by [12],

[19] $$E^i_{AB} = \chi(q)i = E_{AB} - 1/2(E_{A_2} + E_{B_2})$$

II. Hardness

The second derivative of the energy (10) with respect to charge q was first called the hardness parameter η by Parr and Pearson (2)

[20] $$\eta_S = \left[\frac{\delta^2 E(q)}{\delta q^2}\right]_q = 1/2\left[\frac{\delta \chi}{\delta q}\right]_q$$

and from the finite difference formula that hardness was expressed in terms of the ionization potential and electron affinity as

[21] $$\eta_S = 1/2(I_S - A_S)$$

identical with the c parameter in traditional electronegativity theory (10, 11). The electronegativity is also derivable from the finite difference formula. However, there are two distinct derivations of the electronegativity: one assumes that the dependence of the electronegativity on the charge is linear between A^+ and A^-; the other assumes a distinct discontinuity at A^0 between the $A^+ \rightarrow A^0$ and $A^0 \rightarrow A^-$ lines (8). The present derivation uses the finite difference formula and applies it to a discontinuous electronegativity curve.

The change in energy going from a neutral atom to the positive or negative ion is calculated from the energies of these states:

[22] $$S^- \leftrightarrow S^0 \leftrightarrow S^+$$

$$\textit{Energy:} \quad (E_0 - A_{S^0}) \leftrightarrow E_0 \leftrightarrow (E_0 + I_{S^0})$$

where I_{S^0} and A_{S^0} are the energies necessary to remove an electron from S^0 and S^- respectively. The energy of S in the neutral state is E_0.

To calculate the charge transfer from S^0 to $S^\pm$ it is necessary to calculate the electronegativity at $q = 0$, $\chi_{q=0}$, namely $q'_S = q_S + \Delta q$ ([12]). Combining the electronegativity from [18] with the ionic energy E^i from [17] and the relation of ionic character and change in electronegativity in [12]

[23] $$\chi(q) = \frac{\delta E(q)}{\delta q} \approx \frac{\Delta E}{\Delta q}$$

Therefore

[24] $$\left[\frac{\Delta E}{\Delta q}\right]_{q=0} = \frac{(E_0 + I_{S^0}) - (E_0 - A_{S^0})}{2}$$

where the energies of $S^\pm$ are $E_{S^\pm}$ respectively and $\Delta E = E_{S^+} - E_{S^-}$ with $\Delta q = 2$. Substituting the approximate equality in [23]

[25] $$\left[\frac{\delta E}{\delta q}\right]_{q=0} \approx \frac{(I_{S^0} + A_{S^0})}{2}$$

Therefore

[26] $$\bar{\chi}_{q=0} = 1/2(I_{S^0} + A_{S^0})$$

The equality holds in [23] and [24] in the limit where Δq goes to zero.

This gives a new definition for an acid and a base. Consider an acid–base reaction $A^+ + B^- \rightarrow A^{\delta+}B^{\delta-}$. There will be charge transfer from the base B^- to the acid A^+ until the electronegativity is equalized, giving molecular atoms with charges $A^{\delta+}$ and $B^{\delta-}$. It is assumed that the change in $\chi(q)$ between A^0 and $A^{\delta+}$ is the same as that between A^0 and A^+, so that the change in $\chi(q)$ and charge transfer in the final molecule can be calculated from the covalent state A^0B^0. $\chi(q)$ is defined by the straight line connecting $\chi(A^0)$ and $\chi(A^+)$, and $\chi(B^0)$ and $\chi(B^-)$ for the acid and base, respectively. Therefore $\chi(q)$ is differentiable with respect to charge q and well defined in the region of charge transfer.

The electronegativity of the kth orbital is

[27] $$\chi_k(q_k) = \tfrac{1}{2}(I_k(q_k) + A_k(q_k))$$

where

[28] $$I_k(q_k) = E(q_k) - E(q_k - 1)$$

and

[29] $$A_k(q_k) = E(q_k + 1) - E(q_k)$$

for orbital occupany q_k where A_k and I_k are the electron affinity and ionization potential of the kth orbital respectively, and $E(q_k)$ is the energy of the system as a function of q_k. The finite difference approximation is now applied to the electronegativity line to give the hardness η,

[30] $$\frac{\delta^2 E(q)}{\delta q^2} = \frac{\delta \chi}{\delta q} \approx \frac{1}{2}\left[\frac{\Delta I_k(q_k)}{\Delta q} + \frac{\Delta A_k(q_k)}{\Delta q}\right]$$

For an acid in the reaction $A^+ + B^- \rightarrow A^{\delta+}B^{\delta-}$ the energy changes in going from A^0 to A^+ and B^0 to B^- are used to evaluate the terms in [29], where $q_{A^0} = q_{(A^+)} + \Delta q$, so that

[31] $$\Delta q = 1$$

The change in the ionization potential with charge is

[32] $$\Delta I_k(q_k) = I_k(A^+) - I_k(A^0)$$

In terms of charge this change in ionization potential is

[33] $$\Delta I_k(q_k) = I_k(q_k - 1) - I_k(q_k)$$

and in terms of energies of the atoms and ions is

[34] $$\Delta I_k(q_k) = [(E(q_k - 1) - E(q_k - 2)) - (E(q_k) - E(q_k - 1))]$$

Therefore

[35] $$\Delta I_k(q_k) = -E(q_k) + 2E(q_k - 1) - E(q_k - 2)$$

Can. J. Chem. Downloaded from www.nrcresearchpress.com by 118.98.75.50 on 09/07/12
For personal use only.

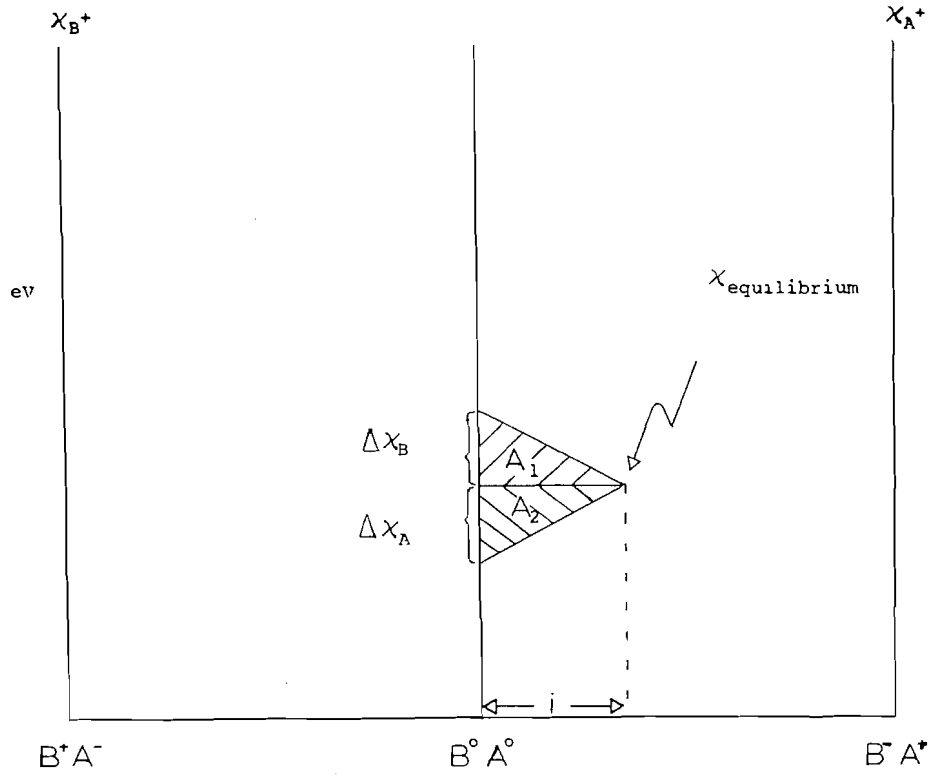

FIG. 1. Graphical intersection of the acid and base electronegativity lines $\chi_A(q)$ and $\chi_B(q)$, the slopes of which are η_A and η_B respectively. The equilibrium electronegativity $\chi_{AB} = \chi_{equilibrium}$ gives the charge transfer i, and the difference in areas $A_2 - A_1$ is the charge transfer energy, ΔE_{ct}.

Similarly the change in the electron affinity with charge, A^0 going to A^+, is

[36] $\Delta A_k(q_k) = A_k(A^+) - A_k(A^0)$

giving

[37] $\Delta A_k(q_k) = A_k(q_k - 1) - A_k(q_k)$

expanding to

[38] $\Delta A_k(q_k) = [(E(q_k) - E(q_k - 1)) - (E(q_k + 1) - E(q_k))]$

and therefore

[39] $\Delta A_k(q_k) = -E(q_k + 1) - 2E(q_k) - E(q_k - 1)$

Using [35] and [39] in [30]

[40] $2\eta_{Acid} = \dfrac{\delta\chi}{\delta q} \approx \frac{1}{2}[E(q_k - 1) - E(q_k - 2) - E(q_k + 1) + E(q_k)]$

reducing to

[41] $2\eta_{Acid} = \dfrac{\delta\chi}{\delta q} \approx -\frac{1}{2}[I_k(q_k - 1) - A_k(q_k)]$

Consequently η_{Acid} is

[42] $\eta_A = \dfrac{1}{2}\dfrac{\delta\chi}{\delta q} \approx \dfrac{1}{4}[I_k(q_k - 1) - A_k(q_k)]$

Similarly the base in the reaction $A^+ + B^- \rightarrow A^{\delta+}B^{\delta-}$ has its terms calculated ([31]) from the transfer B^0 to B^- where $q_{B^0} = q_{(B^-)} - \Delta q$,

[43] $\Delta I_k(q_k) = -E(q_k + 1) + 2E(q_k) - E(q_k - 1)$

and

[44] $\Delta A_k(q_k) = -E(q_k + 2) + 2E(q_k + 1) + E(q_k)$

Using [43] and [44] in [30] gives

[45] $2\eta_{Base} = \dfrac{\delta\chi}{\delta q} \approx \frac{1}{2}[E(q_k) - E(q_k - 1) - E(q_k + 2) + E(q_k + 1)]$

hence

[46] $2\eta_{Base} = \dfrac{\delta\chi}{\delta q} \approx \frac{1}{2}[I_k(q_k) - A_k(q_k + 1)]$

Assuming $A_k(q_k + 1) \approx 0$, which is reasonable because a negative ion has zero or a small negative electron affinity, η_{Base} is

[47] $\eta_B = \dfrac{1}{2}\dfrac{\delta\chi}{\delta q} \approx \dfrac{1}{4}I_k(q_k)$

Within the usual assumptions of electronegativity equalization (8) and the differentiability of the electronegativity with charge, these expressions for the hardness of acids η_{A^+} and bases η_{B^-} are self consistent.

The electronegativity difference of A^+ and B^- indicates which atom in a reaction is the acid and which the base; the hardness shows the rate of change of the electronegativity with charge and governs the charge transfer in the polar covalent bond. The electronegativity variation is that developed by Gopinathan and Whitehead (8) and subsequently discussed by Parr (2), in which there is a discontinuity in the energy as a function of charge at the uncharged atom S^0. This gives rise to two different slopes for η between S^0 and S^+ and between S^0 and S^-.

Can. J. Chem. Downloaded from www.nrcresearchpress.com by 118.98.75.50 on 09/07/12
For personal use only.

Can. J. Chem. Downloaded from www.nrcresearchpress.com by 118.98.75.50 on 09/07/12
For personal use only.

The expression for $E(q)$ can be used to calculate the change in energy in going from the free atom towards the acid A^+ or base B^- (9, 10),

$$[48a] \quad \Delta E_A = E_{(A^{\delta+})} - E_{A^0} = \chi_{A^0}\Delta q + \eta_A \Delta q^2$$

and

$$[48b] \quad \Delta E_B = E_{(B^{\delta-})} - E_{B^0} = -\chi_{B^0}\Delta q + \eta_B \Delta q^2$$

Equalization in the electronegativity gives a total energy change

$$\Delta E = \Delta E_A + \Delta E_B$$

or

$$[49] \quad \Delta E = (\chi_{A^0} - \chi_{B^0})\Delta q + (\eta_A + \eta_B)\Delta q^2$$

where η_A is the slope of the $\chi(q)$ line between $q = 0$ and $q = 1$, and η_B is for $q = 0$ to $q = -1$. Differentiating,

$$[50] \quad \chi_{AB} = \chi'_A = \chi'_B = \chi_{A^0} + 2\eta_A \Delta q = \chi_{B^0} - 2\eta_B \Delta q$$

However, the ionic character is given by the charge transfer

$$[51] \quad i = \Delta q = \frac{(\chi_{B^0} - \chi_{A^0})}{2(\eta_A + \eta_B)}$$

Substituting this expression into the energy expression

$$[52] \quad \Delta E = -\frac{(\chi_{A^0} - \chi_{B^0})^2}{4(\eta_A + \eta_B)}$$

This is the charge transfer energy

$$[53] \quad \Delta E_{ct} = -\frac{(\Delta\chi_i)^2}{4\sum_i \eta_i}$$

This scheme predates any concepts of hardness. The present hardness parameter was simply a constant c in the parabolic expansion of the energy in terms of charge (10, 11, 16),

$$[54] \quad E(q) = a + bq + cq^2$$

$$[55] \quad \chi(q) = b + 2cq$$

where

$$[56] \quad b = 1/2(3I_S - A_S)$$

and

$$[57] \quad c = 1/2(A_S - I_S)$$

which is identical with Parr's definition of hardness (2). Consequently the results in Tables 2 and 3 from Parr are similar to those in Baird and Whitehead (10). The group orbital electronegativities (11) make the Parr and present formulations immediately applicable to large molecules (12), while the wealth of BEEM–π calculations (12, 14, 15) should open the theory to conjugated acids and bases.

The fundamental change in the theory of hardness is caused by the fundamental change in the charge dependence of the electronegativity introduced by Gopinathan and Whitehead (8) within the density functional theory. The present extension of this theory gives the discontinuity of the electronegativity at the unit occupancy of the atom, which insures that the rate of change of the electronegativity is different in going from S^+ to S^0 and from S^0 to S^-, so that two hardness parameters are required.

In Fig. 1, the χ-dependence on q is shown graphically. Where the acid and base lines cross is $\chi_{equilibrium} = \chi_{molecular}$ and this gives the ionic character as the distance from χ^0 in χ–q space.

TABLE 1. Experimental atomic parameters (eV)

Species S	I_S[a]	A_S[b]	I_{S^+}[a]	χ[c]
Li	5.39	0.62	75.6	3.00
Na	5.14	0.55	47.3	2.84
K	4.34	0.50	31.8	2.42
Rb	4.18	0.49	27.3	2.34
Cs	3.89	0.47	25.1	2.18
F	17.42	3.40	35.0	10.41
Cl	13.01	3.62	23.8	8.32
Br	11.84	3.36	21.6	7.60
I	10.45	3.06	19.1	6.76
Cu	7.72	1.23	20.3	4.48

[a]All values from ref. 1.
[b]References 2 and 27.
[c]$\chi_S = 1/2(I_S + A_S)$: eq. [3].

TABLE 2. Calculated atomic parameters (eV)[a]

Species S	η_P[b]	η_A[c]	η_B[d]	$-c$[e]
Li	2.38	18.74	1.35	2.28
Na	2.30	11.69	1.28	2.38
K	1.92	7.83	1.08	
Rb	1.85	6.70	1.04	
Cs	1.71	6.16	0.97	
F	7.01	7.90	4.36	8.68
Cl	4.70	5.04	3.25	5.67
Br	4.24	4.56	2.96	4.70
I	3.70	4.01	2.61	4.57
Cu	3.25	4.77	1.93	

[a]Values taken from Table 1.
[b]$\eta_P = 1/2(I_S - A_S)$: eq. [63] and ref. 2.
[c]$\eta_A = 1/4(I_{S^+} - A_S)$: eq. [42], present theory.
[d]$\eta_B = 1/4I_S$: eq. [47], present theory.
[e]$c = 1/2(A_S - I_S)$: eq. [57] and ref. 9.

The energy stabilization caused by charge transfer is

$$[58] \quad \Delta E = -\int_0^i \chi_B(q_B)dq_B + \int_0^i \chi_A(q_A)dq_A$$

This is the difference in areas $A_2 - A_1$ in Fig. 1.

III. Hard and soft acids and bases

Chemical hardness and softness (17) explained the behaviour of Lewis acids and bases. Depending on the stability of the complex, AB, Lewis acids and Lewis bases were divided into two kinds, hard and soft. The generalized characteristics and behaviour are

Soft base	*Hard base*
low electronegativity	high electronegativity
high polarizability	low polarizability
easily oxidized	hard to oxidize
low energy empty orbitals	high energy empty orbitals
Soft acid	*Hard acid*
low valence	high valence
large size	small size
several easily excited electrons	no easily excited electrons

while the HSAB (17) principle states that hard acids prefer hard bases and soft acids prefer soft bases.

Can. J. Chem. Downloaded from www.nrcresearchpress.com by 118.98.75.50 on 09/07/12
For personal use only.

TABLE 3. Charge transfer i, dipole moment μ, and polarizability α[a]

Compound	$i_{\chi,P}$[b]	i[c]	i_{χ}[d]	i_{exp}[f]	μ[g]	α[l]
LiF	0.39	0.55	0.16	0.852	6.33	1.20
LiCl	0.38	0.52	0.12	0.735	7.13	1.22
LiBr	0.35	0.51	0.11	0.697	7.27	1.15
LiI	0.31	0.48	0.09	0.647	7.43	1.21
NaF	0.41	0.56	0.24	0.923	8.16	1.24
NaCl	0.39	0.55	0.18	0.794	9.00	1.09
NaBr	0.36	0.53	0.16	0.782	9.4[h]	1.04
NaI	0.33	0.51	0.14	—	—	1.17
CuF	0.29	—	0.32	—	—	—
CuCl	0.24	—	0.24	—	—	—
CuBr	0.21	—	0.20	—	—	—
CuI	0.16	—	0.15	—	—	—
KF	0.45	—	0.33	0.841	8.60	0.92
KCl	0.44	—	0.27	0.802	10.27	0.95
KBr	0.42	—	0.24	0.768	10.41	0.98
KI	0.39	—	0.21	—	—	1.01
RbF	0.46	—	0.36	0.786	8.55	0.94
RbCl	0.46	—	0.30	0.792	10.6[h]	0.94
RbBr	0.43	—	0.27	—	—	0.91
RbI	0.40	—	0.24	—	—	1.01
CsF	0.47	—	0.39	0.700	7.88	0.81
CsCl	0.48	—	0.33	0.747	10.42	0.95
CsBr	0.46	—	0.30	—	—	0.91
CsI	0.42	—	0.26	—	—	1.05
LiNa	0.017	—	0.006	0.032	0.45[i]	—
LiK	0.067	—	0.032	0.214	3.41[i]	—
LiRb	0.078	—	0.041	0.242[e]	4.01[i]	—
LiCs	0.100	—	0.054	0.313[e]	5.48[i]	—
NaK	0.050	—	0.023	0.162	2.73[i]	—
NaRb	0.061	—	0.032	0.178	3.05[i]	—
NaCs	0.083	—	0.044	0.247	4.57[i]	—
KRb	0.011	—	0.005	0.033[e]	0.64[j]	—
KCs	0.033	—	0.016	0.094[e]	1.92[j]	—
CsRb	0.022	—	0.011	0.060	1.26[j]	—
FCl	0.09	0.12	0.11	0.113	0.881[k]	—
FBr	0.12	0.18	0.16	0.153	1.29[k]	—
FI	0.17	0.21	0.22	—	—	—
ClBr	0.04	0.06	0.04	0.056	0.57[k]	—
ClI	0.09	0.09	0.11	0.111	1.24[k]	—
BrI	0.05	0.02	0.06	0.101	1.21[k]	—

[a]Values calculated using data of Table 1 and 2; dashes are used where no experimental data are available.

[b]$i_{\chi,P} = \dfrac{\Delta\chi}{2\Sigma\eta_P}$ as in eq. [51] (electrons).

[c]From ref. 10, calculated charge transfer.

[d]$i_{\chi} = \dfrac{\Delta\chi}{2\Sigma\eta_{A,B}}$ as in eq. [51] (electrons).

[e]Using μ/R_e with all R_e from ref. 12 except for alkali alkalides from footnote g (electrons).

[f]Theoretical R_e from footnote g.

[g]Gas phase dipole moments: ref. 28.

[h]Reference 29.

[i]Experimental values: from ref. 30.

[j]Theoretical values: from 30.

[k]Reference 31.

[l]Reference 13.

Without even inventing hardness parameters the sequence above can be easily described in terms of electronegativity (10) of the uncharged atom:

hard acid → soft acid → soft base → hard base

low electronegativity → high electronegativity

Obviously $A^0 \rightarrow A^+$ raises the electronegativity and $B^0 \rightarrow B^-$ lowers the electronegativity; the lower the electronegativity, the higher it becomes, and vice versa. Thus the pattern for the ions is

hard acid → soft acid → soft base → hard base

high electronegativity → low electronegativity

This is obviously true: [52] shows that charge transfer is driven by differences in electronegativity, and inhibited by the sum of hardnesses.

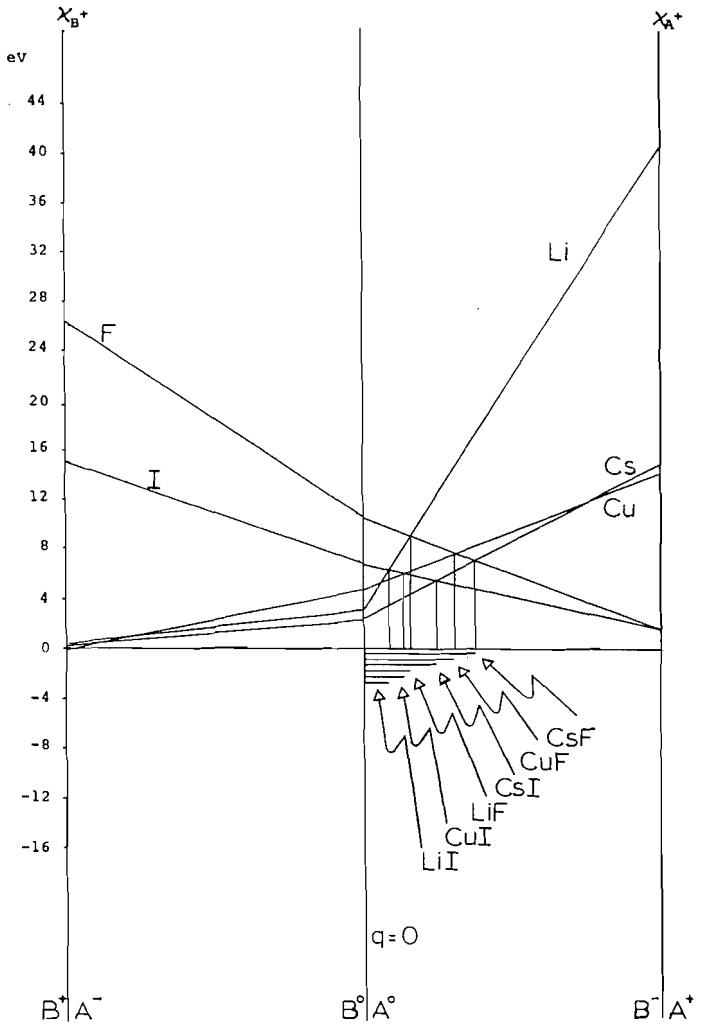

FIG. 2. Illustrative plots of $\chi(q)$ versus $q = Z - N$, which determine the charge transfer and charge transfer energy in the present theory of some typical bases. The discontinuity at $q = 0$ gives two $\chi(q)$ lines: one from $q = 0$ to $q = 1$ and the other from $q = 0$ to $q = -1$ with slopes $\eta_A = 1/4(I_{(A^+)} - A_{(A^0)})$ and $\eta_B = 1/4(I_{(B^0)} - A_{(B^-)})$ corresponding to an acid and base.

IV. Calculated hardness and charge transfer

To compare the present theory with that of Parr (2) the electronegativities χ and hardnesses η were calculated for the same set of alkali and copper halogen compounds. The charge transfer energy ΔE_{ct} and numerical charge transfer, i, were calculated from the data in Tables 1 through 3. The graphs for combining three acids and two bases as selected illustrations are given in Figs. 2 and 3 while the overall trends in Figs. 2 through 6 are discussed in the text.

The new definitions of the hardness η_A and η_B give results whose trend in ΔE_{ct} and i parallel the experimental sequences except for the copper halogenides, which occur between potassium and sodium instead of after lithium, Table 4:

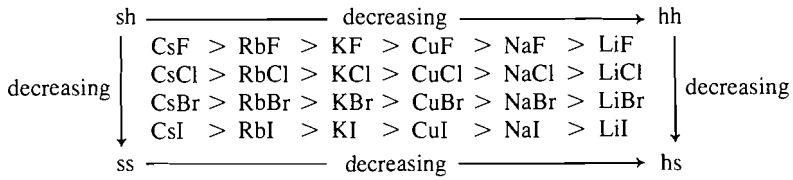

The hardness parameters agree with the sequence expected within the HSAB theory; thus copper is the softest acid,

η_A: acids: Li > Na > K > Rb > Cs > Cu

η_B: bases: F > Cl > Br > I

The hardness of a base behaving as an acid, and vice versa, is well described by the appropriate hardness definition, η_{Acid} or η_{Base}. Thus lithium is a hard acid as Li^+, and a soft base as Li^-. Interhalogen molecules and alkali metal halides are also well described. Figure 2 gives the graphical results.

The calculated charge transfers, Table 3, are quite small and the difference in charge transfer between any pair of compounds is large. The interhalogens are well described. The charge transfer energies, Table 4, are small. The hardness difference is inversely related to the charge transfer,

$$[59] \quad i = \left[\frac{2\chi_{eq} - \Sigma\chi_{A,B}}{2}\right]\frac{1}{\Delta\eta}$$

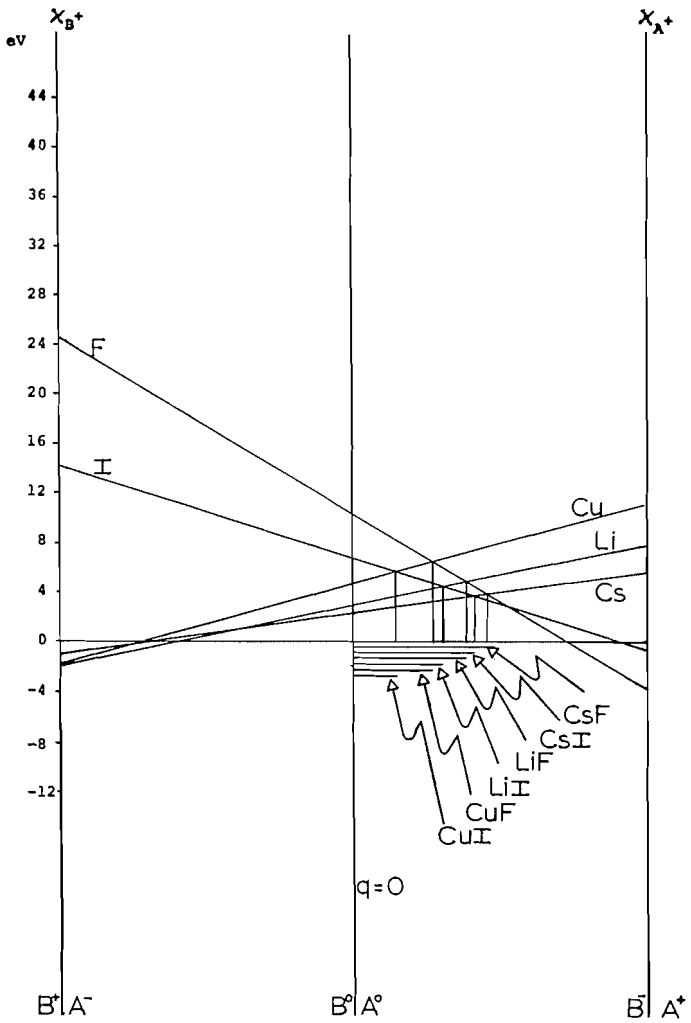

FIG. 3. Illustrative plots of $\chi(q) = Z - N$ using Parr's definition of the hardness, $\eta = 1/2(I - A)$.

and comes from [50]. Therefore the dependence of charge transfer on hardness difference $\Delta\eta$ is the result of [59] and not of

$$[60] \quad I_{B'} - I_{A'} = \eta_B - \eta_A$$

where the primes mean after charge transfer and before bond formation (2). It is dependent on $\Delta\eta$ relative to the sum of the electronegativities of the acid and base, $\Sigma_{AB}\chi$.

The bonding is poorly described quantitatively except for the interhalogens, but the trends are excellent, as shown by the dipole moment μ plot against the calculated charge transfer i, Fig. 4. The plot of hardness sum against the molar polarizability P shows the expected trend: η is proportional to $1/P$ where $P = \frac{4\pi}{3}N(\alpha + \mu^2/3kT)$. The polarizability, α, is the induced moment per molecule from the temporary distortion of the electron orbit by an applied field, Fig. 5.

V. Discussion

From Fig. 2 and the trends above, it can be seen that the new definitions η_A and η_B give different results from the earlier definition. While the earlier definition was also dependent on

TABLE 4. Bond energies — ionic components and experimental[a] data (kJ/mol)

Compound	$E_P^{i\,b}$	$E_{A,B}^{i\,c}$	$E_{exp}^{i\,d}$	$E_{exp}{}^{e}$
LiF	141	57	443 ± 23	573 ± 21
LiCl	96	31	292 ± 13	464 ± 13
LiBr	77	24	270 ± 21	418 ± 21
LiI	56	16	220 ± 13	347 ± 13
NaF	148	86	363 ± 2	477.0
NaCl	103	48	252 ± .4	407.9
NaBr	83	37	232 ± .04	362.8
NaI	62	26	194 ± .04	304.2
CuF	83	93	245 ± 17	~418
CuCl	45	44	146 ± 13	360.7
CuBr	31	30	140 ± 13	330.1
CuI	18	17	−28 ± 13	~142
KF	172	126	388 ± 23	490 ± 21
KCl	126	76	278 ± 8	423 ± 8
KBr	105	60	259 ± 8	378.7 ± 8
KI	80	43	227 ± 13	326 ± 13
RbF	177	142	390 ± 23	490 ± 21
RbCl	131	86	302 ± 21	444 ± 21
RbBr	110	69	267 ± 25	385 ± 25
RbI	85	50	234 ± 13	331 ± 13
CsF	187	155	403 ± 44	502 ± 42
CsCl	141	96	293 ± 21	435 ± 21
CsBr	119	78	299 ± 13	416.3 ± 13
CsI	93	57	239 ± 21	335 ± 21

[a] Values calculated using data from Tables 1 and 2.
[b] Calculated with η_P.
[c] Calculated with $\eta_{A,B}$.
[d] Experimental from eq. [2] with values of ref. 12.
[e] Experimental bond energies from ref. 12.

Can. J. Chem. Downloaded from www.nrcresearchpress.com by 118.98.75.50 on 09/07/12
For personal use only.

Can. J. Chem. Downloaded from www.nrcresearchpress.com by 118.98.75.50 on 09/07/12
For personal use only.

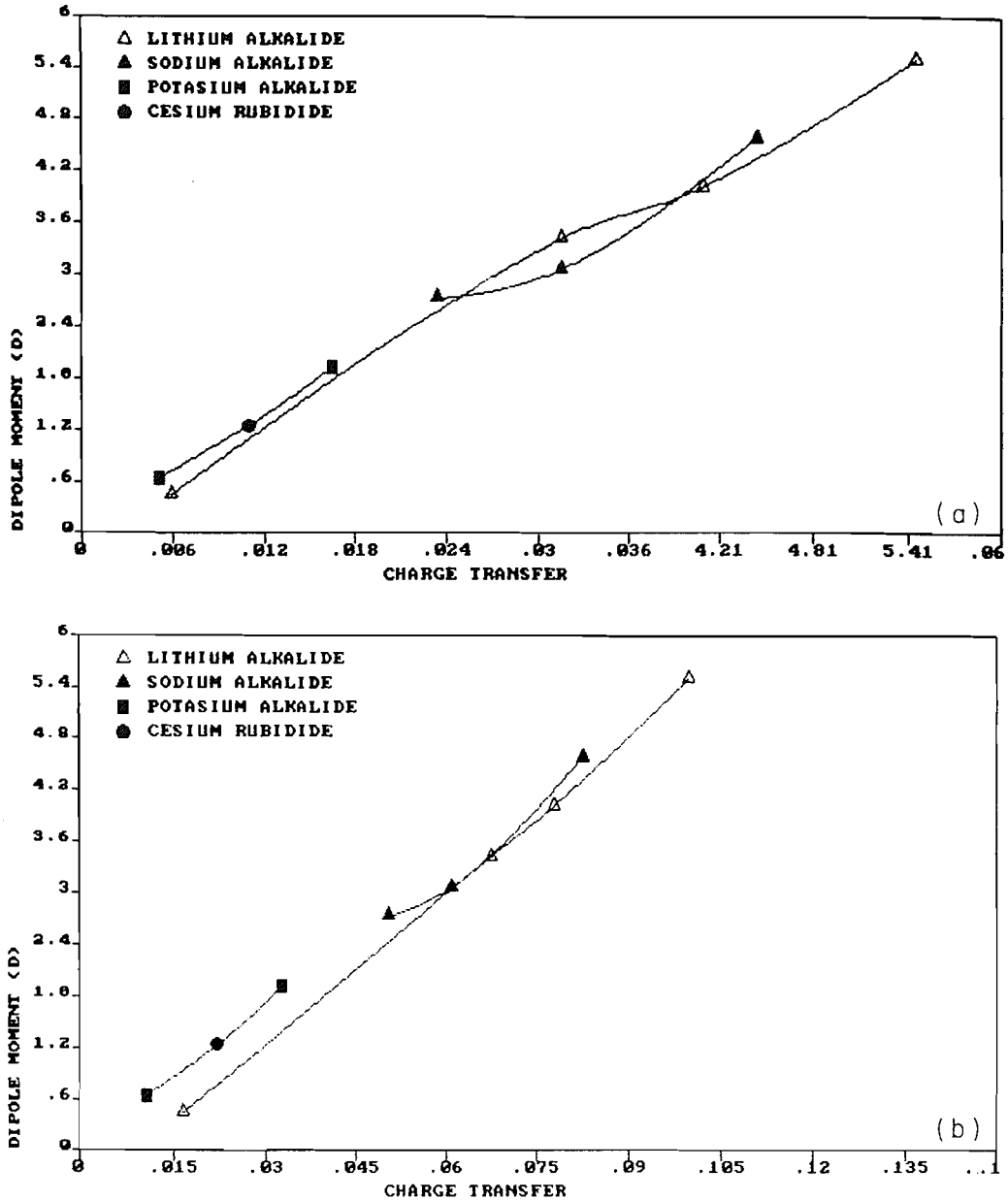

FIG. 4. (*a*) Experimental interalkali dipole moments are related to the calculated charge transfers using the present definitions of hardness $\eta_A = 1/4(I_{(A^+)} - A_{(A^0)})$ and $\eta_B = 1/4(I_{(B^0)} - A_{(B^-)})$ and the charge transfer $i = \dfrac{\Delta\chi_{A,B}}{2\Sigma_{A,B}\eta}$ (from Table 3). (*b*) Experimental interalkali dipole moments are related to the calculated charge transfers using Parr's definition (2) of hardness, $\eta = 1/2(I - A)$ and $i = \dfrac{\Delta\chi_{A,B}}{2\Sigma\eta}$ (Table 3).

whether the hardness was for an acid or base

[61] $\eta_B = \eta(B^+) = 1/2(I_{B^+} - A_{B^+})$

[62] $\eta_B = \eta(B) = 1/2(I_B - A_B)$

and

[63] $\eta_A = \eta(A) = 1/2(I_A - A_A)$

These equations do not fit the definition of η, [20], that hardness is "the resistance of the chemical potential (minus electronegativity) to change in the number of electrons" (2). It would be difficult to imagine that the hardness would not change on adding an electron to a base. Similarly, [6] relates ionization potentials *after charge transfer* to hardnesses *before charge transfer*, which is illogical.

The comparison of the dipole moments and polarizabilities from these equations with the present results, Figs. 4 and 5, shows similar trends although the spread in polarizabilities with the present results are more reasonable.

The trends in the HSAB theory are not predicted by the definitions, [61] through [63]. The hard–soft combination CsF has the most charge transfer, while the hard–hard and soft–soft combinations, LiF and CsI, have moderate charge transfer: they should have the least. Also copper is predicted a harder acid than lithium; HSAB theory requires copper to be a model soft and lithium a model hard acid, Fig. 3 (compare with Fig. 2). The charge transfers, Table 3, are much larger, and the difference in charge transfer is much less by the definitions, [61] through [63]; the alkali halides are, however, better fitted with the new hardness definition. The relations between the

Can. J. Chem. Downloaded from www.nrcresearchpress.com by 118.98.75.50 on 09/07/12
For personal use only.

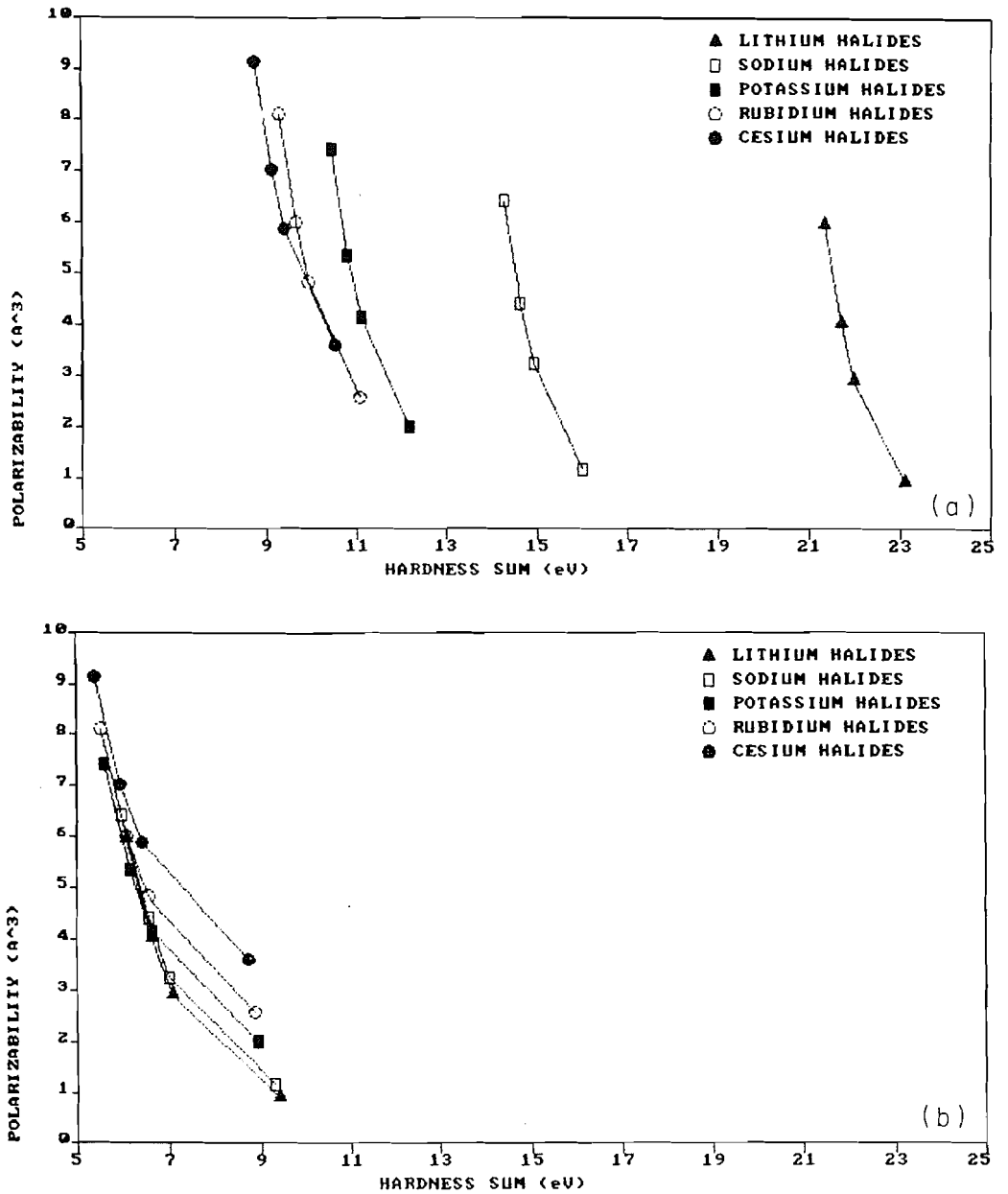

FIG. 5. (*a*) Experimental polarizabilities are related to the sum of the calculated hardness using the definitions of the present theory: $\eta_A = 1/4(I_{(A^+)} - A_{(A^0)})$ and $\eta_B = 1/4(I_{(B^0)} - A_{(B^-)})$ (from Table 3). (*b*) Experimental polarizabilities are plotted against the sum of the calculated hardness using Parr's definition (2), $\eta = 1/2(I - A)$ (from Table 3).

parameters, the experimental results, the charge transfer, and the charge transfer energies are the same for both the old and new definitions.

Equation [51] predicts charge transfer proportional to the difference in electronegativities of the acid and base. The experimental charge transfer, the calculated charge transfer using Parr's hardness, η_P, and the present η_A and η_B for the alkali halogenides are plotted in Fig. 6. There is a linear dependence of the experimental charge transfer in the lithium halogenides on differences in electronegativity, and no consistent trends or relations within or between any other alkali halogenide group. The equations result in a fairly regular dependence of the charge transfer on differences in electronegativity except for the last two points in Parr's results, which have almost constant charge transfer. Hence the calculated trends are not reflected by experimental results except in the lithium halogenides.

To compare the calculated values with other experimental results the ionic component of bond energies was estimated. Using eq. [53], experimental and theoretical bond energies were calculated for the alkali and copper halogenides and are collected in Table 4. Most charge transfer energies are very low compared to the experimental estimates, which is consistent with the low theoretical charge transfers with respect to the experimental ones in Table 3 for this group of compounds. The experimental trends from the results in Table 4 are

$$\begin{aligned}
&\text{LiF} \sim \text{CsF} \sim \text{RbF} \geq \text{KF} > \text{NaF} > \text{CuF}\\
&\text{RbCl} \sim \text{CsCl} \sim \text{LiCl} \sim \text{KCl} > \text{NaCl} > \text{CuCl}\\
&\text{CsBr} \sim \text{LiBr} \sim \text{RbBr} \geq \text{KBr} > \text{NaBr} > \text{CuBr}\\
&\text{CsI} \sim \text{RbI} \sim \text{LiI} > \text{KI} > \text{NaI} > \text{CuI}
\end{aligned}$$

where the bond energies generally decrease moving down the columns. Parr's hardness trends do not match these; the lithium halogenide series is predicted as having a smaller charge

Can. J. Chem. Downloaded from www.nrcresearchpress.com by 118.98.75.50 on 09/07/12
For personal use only.

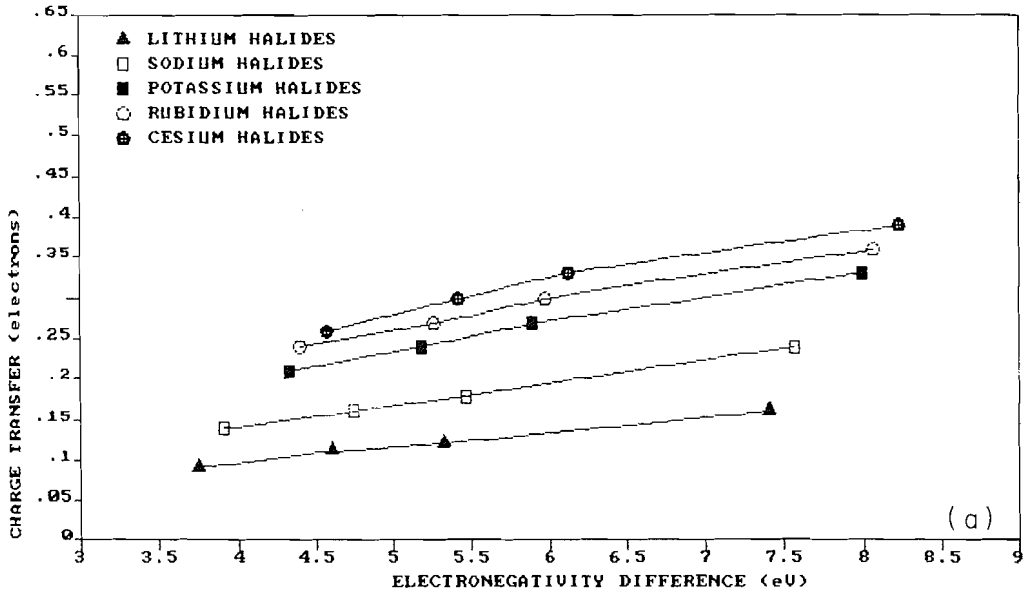

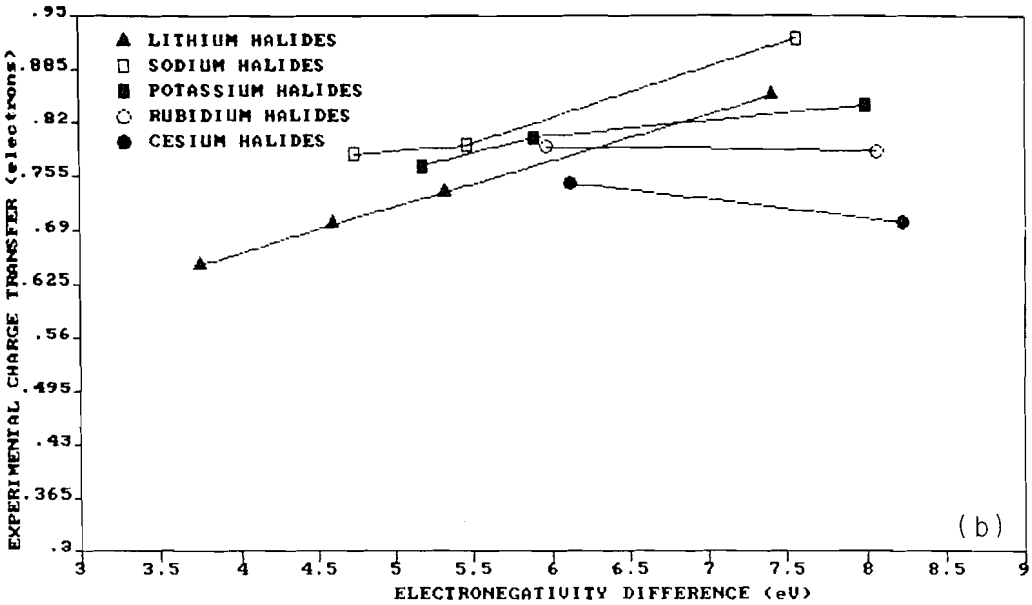

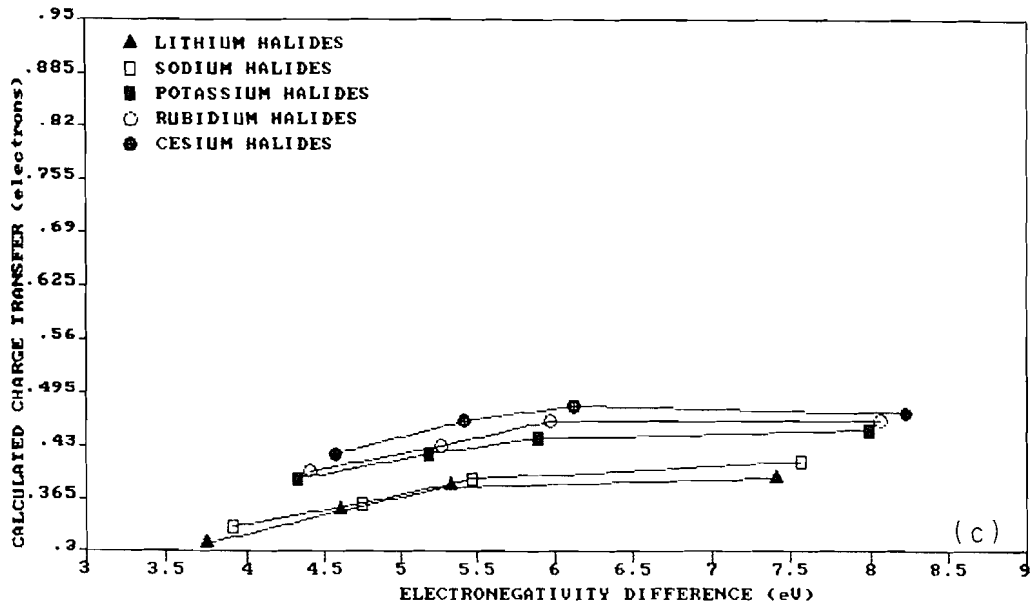

transfer than any other alkali halogenide series, whereas the experimental charge transfer indicates the lithium series has one of the greatest charge transfers.

VI. Conclusions

The new definitions of η, $\eta_A = 1/4(I_{(A^+)} - A_{(A^0)})$ and $\eta = 1/4(I_{(B^0)} - A_{(B^-)})$, in the context of the charge transfer model with equalization of electronegativities, gives a self-consistent theory. Comparing the theoretical charge transfer with experimental and calculated parameters proves Parr's (2) interpretation of bonding in terms of the hardness, $\eta_P = 1/2(I - A)$, to be less than ideal.

The new definitions for hardness, $\eta_A = 1/4(I_{(A^+)} - A_{(A^0)})$ and $\eta_B = 1/4(I_{(B^0)} - A_{(B^-)})$ for an acid and base, improve the continuity and results of this bonding model. Most results correlate qualitatively well with experimental bond energy data, unlike the HSAB. There are still problems in unifying the quantitative hardness theory with the hardness concept in HSAB theory.

The bonding polarity is qualitatively well described, although quantitatively the model breaks down, as illustrated by the small predicted charge transfers. Huheey suggested (18, 19) that this is caused by unequal cancelling of the covalent and electrostatic interactions. However, there are many factors unaccounted for in the model, including the atomic sizes, and the change in nuclear charge, $\Delta Z = |Z_A - Z_B|$, where Z_A and Z_B are the atomic numbers of A and B. This can be accounted for in a full second-order expansion of the energy, $E(N,Z)$. This may correct the anomalous charge transfer predictions for lithium and copper seen in this model, since these two atoms have the highest and lowest field gradients at the nuclei respectively. Many attempts (20–26) have been made to improve the original formulation of $\eta = 1/2(I - A)$. They are not considered here because it is the initial definition of the hardness η which has been changed.

Acknowledgements

This research was supported by the Natural Sciences and Engineering Research Council of Canada.

1. C. E. Moore. Atomic energy levels. Natl. Bur. Stand. (US) Circ. No. 467. Vol. I, 1949; Vol. II, 1952; Vol. III, 1958; NSRDS-NBS-71 1982.
2. R. G. Parr and R. G. Pearson. J. Am. Chem. Soc. **105**, 7512 (1983).
3. L. Komorowski. Chem. Phys. Lett. **103**, 201 (1983).
4. R. S. Mulliken. J. Chem. Phys. **2**, 782 (1934).
5. R. G. Parr, R. A. Donnelly, M. Levy, and W. E. Palke. J. Chem. Phys. **68**, 3801 (1978).
6. T. T. Nguyen-Dang, R. F. W. Bader, and H. Essen. Int. J. Quantum Chem. **22**, 1049 (1982).
7. R. P. Iczkowski and J. L. Margrave. J. Am. Chem. Soc. **83**, 3547 (1961).
8. M. S. Gopinathan and M. A. Whitehead. Isr. J. Chem. **19**, 209 (1980).
9. N. C. Baird, J. M. Sichel, and M. A. Whitehead. Theor. Chim. Acta, **11**, 38 (1968).
10. N. C. Baird and M. A. Whitehead. Theor. Chim. Acta, **2**, 259 (1969).
11. M. A. Whitehead, N. C. Baird, and M. Kaplansky. Theor. Chim. Acta, **3**, 135 (1965).
12. M. Kaplansky and M. A. Whitehead. Mol. Phys. **16**, 481 (1969).
13. H. Coker. J. Phys. Chem. Solids, **40**, 1079 (1979).
14. R. M. Hart and M. A. Whitehead. Trans. Faraday Soc. **67**, 1569 (1971).
15. L. Krause and M. A. Whitehead. Mol. Phys. **26**, 503 (1973).
16. J. Hinze. Ph.D. thesis, University of Cincinnati, Cincinnati, OH. 1962.
17. R. G. Pearson. J. Am. Chem. Soc. **85**, 3533 (1963); Science, **151**, 172 (1966).
18. J. E. Huheey and R. S. Evans. Chem. Commun. 968 (1969).
19. J. H. Huheey. Inorganic chemistry. 3rd ed. Harper & Row, New York. 1970.
20. S. Shankar and R. G. Parr. Proc. Natl. Acad. Sci. U.S.A. **82**, 264 (1985).
21. R. G. Parr. Int. J. Quantum Chem. **26**, 687 (1984).
22. W. Yang, C. Lee, and S. K. Ghosh. J. Phys. Chem. **89**, 5412 (1985).
23. W. Yang and R. G. Parr. Proc. Natl. Acad. Sci. USA, **82**, 6723 (1985).
24. J. L. Gazquez and E. Ortiz. J. Chem. Phys. **81**, 2741 (1984).
25. M. Berkowitz, S. K. Ghosh, and R. G. Parr. J. Am. Chem. Soc. **107**, 6811 (1985), and references therein.
26. J. Robles and J. Bartolotti. J. Am. Chem. Soc. **106**, 3723 (1984).
27. J. Phys. Chem. Ref. Data, **4**, 539 (1975).
28. Natl. Bur. Stand. (US) Circ. No. 537. NBS-10[D].
29. A. L. McClellan. Tables of experimental dipole moments. Freeman, New York. 1963.
30. G. Igel-Mann *et al.* J. Chem. Phys. **84**, 5007 (1986).
31. *In* Comprehensive inorganic chemistry. Vol. 2. Pergamon, New York. 1973. p. 1487.

FIG. 6. (*a*) The difference in electronegativity as a function of the calculated charge transfer using the present hardness definitions: $\eta_A = 1/4(I_{(A^+)} - A_{(A^0)})$ and $\eta_B = 1/4(I_{(B^0)} - A_{(B^-)})$ and the charge transfer $i = \dfrac{\Delta\chi_{A,B}}{2\Sigma_{A,B}\eta}$ (from Table 3). (*b*) The difference in electronegativity as a function of the calculated charge transfer using Parr's definition (2) of hardness, $\eta = 1/2(I - A)$ and $i = \dfrac{\Delta\chi_{A,B}}{2\Sigma\eta}$ (Table 3). (*c*) The difference in electronegativity as a function of experimental charge transfer (Table 3).

Can. J. Chem. Downloaded from www.nrcresearchpress.com by 118.98.75.50 on 09/07/12
For personal use only.

Transient nitronic acid formation in the protonation of the carbanion of 2,2′,4,4′-tetranitrodiphenylmethane in acidic methanol

FRANÇOIS TERRIER,[1] JACQUES LELIÈVRE, ALAIN-PIERRE CHATROUSSE, AND ROBERT SCHAAL

Laboratoire de physicochimie des solutions et Centre national de la recherche scientifique Unité associée n° 403, École nationale supérieure de chimie de Paris, 11 Rue Pierre et Marie Curie, 75231 Paris CEDEX 05 France

AND

PATRICK G. FARRELL[1]

Department of Chemistry, McGill University, 801 Sherbrooke St. W., Montreal, Canada H3A 2K6

Received December 19, 1986

This paper is dedicated to Professor John T. Edward

FRANÇOIS TERRIER, JACQUES LELIÈVRE, ALAIN-PIERRE CHATROUSSE, ROBERT SCHAAL, and PATRICK G. FARRELL. Can. J. Chem. **65**, 1980 (1987).

Rates of deprotonation of 2,2′,4,4′-tetranitrodiphenylmethane (**1**) by a variety of bases B^- and of protonation of the resulting carbanion (**2**) by the conjugated acids BH in methanol have been measured at 20°C. The Brönsted α^{BH} coefficients for protonation of **2** by phenol and carboxylic acid buffers are equal to 0.58 and 0.43, respectively, as compared with α^{BH} values of 0.59 and 0.52 respectively, for the same reactions in 50% H_2O – 50% DMSO. On the other hand, a comparison of the intrinsic rate constants k_0^{BH} (in the Marcus sense) in the two solvents reveals that the effect of going from 50% H_2O – 50% DMSO to methanol is to lower k_0^{ArOH} for the phenol reactions by a factor of 2 but to increase k_0^{RCOOH} for carboxylic acid reactions by a factor of 5. It is shown that the solvent effects on α^{BH} and k_0^{BH} can all be understood in the context of the Principle of Imperfect Synchronisation (PIS) recently proposed by Bernasconi. In addition, a fast equilibrium protonation of the carbanion **2** is found to precede its conversion to **1** at low pH, i.e., pH < 5. The resulting protonated species is suggested to be the nitronic acid **2**,*H* arising from fast protonation of a *para* NO_2 group of **2**. The pK_a' value associated with the ionization of **2**,*H* is ~4.25.

FRANÇOIS TERRIER, JACQUES LELIÈVRE, ALAIN-PIERRE CHATROUSSE, ROBERT SCHAAL et PATRICK G. FARRELL. Can. J. Chem. **65**, 1980 (1987).

Les vitesses de déprotonation du tétranitro-2,2′,4,4′ diphénylméthane (**1**) par diverses bases B^- ainsi que les vitesses de protonation du carbanion correspondant (**2**) par les acides conjugués BH ont été mesurées à t = 20°C dans le méthanol. Les coefficients de Brönsted α^{BH} relatifs à la protonation de **2** par les phénols et les acides carboxyliques sont respectivement égaux à 0,58 et 0,43 alors que des valeurs de α^{BH} de 0,59 et 0,52 ont été trouvées pour ces mêmes réactions dans 50% H_2O – 50% DMSO. Une comparaison des constantes de vitesse intrinsèques k_0^{BH} (définies selon Marcus) mesurées dans les deux solvants montre qu'un transfert du milieu H_2O–DMSO 50:50 au méthanol a pour effet de diminuer la constante k_0^{ArOH} relative aux phénols d'un facteur 2 mais d'augmenter la constante k_0^{RCOOH} relative aux acides carboxyliques d'un facteur 5. Il est montré que les effets de solvants sur α^{BH} et k_0^{BH} sont parfaitement compatibles avec le Principe de Synchronisation Imparfaite (PIS) récemment proposé par Bernasconi. De plus, un équilibre de protonation rapide du carbanion **2** a été observé préalablement à sa conversion en la molécule **1** aux pH < 5. L'espèce acide formée est considérée comme l'acide nitronique **2**,*H* qui résulte d'une protonation de l'un des groupes paranitrés de **2**. Le pK_a' associé à l'ionisation de **2**,*H* est voisin de 4,25 dans le méthanol.

Despite the absence of an electron-withdrawing group directly bonded to the exocyclic ionizable carbon, 2,2′,4,4′-tetranitrodiphenylmethane **1** has a noteworthy acidity in methanol (1). The pK_a^{MeOH} value for formation of the very stable carbanion **2** is 15.30 at 20°C, i.e., **2** is half-formed in a potassium methoxide solution ~0.03 *M*.

We have taken advantage of the stability of **2** to carry out a comprehensive kinetic study of the reactions shown in eq. [1] over the pH range of 3–14.86 at 20°C in methanol. k_p^{MeOH}, k_p^{MeO}, and k_p^B are the rate constants for deprotonation of **1** by methanol, methoxide ion, and any buffer base, respectively, while $k_{-p}^{H^+}$, k_{-p}^{MeOH}, and k_{-p}^{BH} refer to the rates of reprotonation of the carbanion **2** by the solvated proton, methanol, and any buffer acid, respectively. Our results allow the determination of the intrinsic reactivity of **1** in methanol and reveal the existence of a fast equilibrium between **2** and a new species in the most acidic solutions (pH < 5). This species is postulated as a nitronic acid resulting from the protonation of a NO_2 group of **2**. The dependence of the protonation rates of **2** upon the acidity and the nature of the protonating agent is also discussed.

[1] 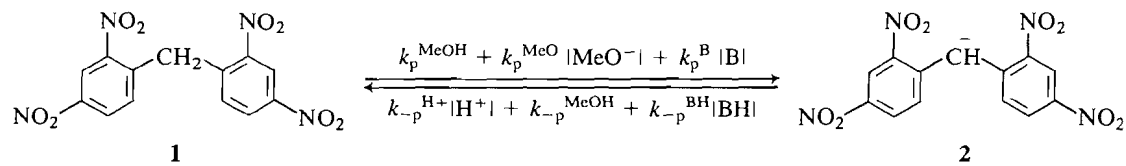

1 **2**

Results

Rates of proton transfer in methanol were measured using buffer solutions or dilute CH_3OK or benzene sulfonic acid solutions, always under pseudo-first-order conditions. The ionic strength was kept constant at 0.01 *M* by adding NaBr as needed. In such conditions, ion pairing effects are negligible and the H^+ concentration of the methanolic solutions can be deduced from the measured pH values ($[H^+] = 10^{-pH}/\gamma^{\pm}$ with $\gamma^{\pm}$ = 0.66 at 20°C) (2, 3). The rates were measured in a

[1] Authors to whom correspondence may be addressed.

Printed in Canada / Imprimé au Canada

Can. J. Chem. Downloaded from www.nrcresearchpress.com by 118.98.75.50 on 09/07/12
For personal use only.

TABLE 1. Variations of k_{obsd} with pH and concentration of the acid form BH of various buffers in methanol[a]

Buffer [BH], mol L^{-1}	k_{obsd}, s^{-1}					
	0.001	0.002	0.004	0.006	0.008	0.01
4-Chlorophenol (pH = 13.05)	0.770	0.782	0.863	0.908	0.975	1.01
4-Cyanophenol (pH = 11.72)	0.842	0.986	1.27	1.53	1.75	1.98
2,6-Dichlorophenol (pH = 11.18)	1.20	1.725	2.705	3.66	4.68	5.59
2,4,6-Trichlorophenol (pH = 10.21)	2.17	3.545	6.42	9.26	12.07	14.95
Benzoic acid (pH = 9.04)	1.60	2.44	4.19	5.89	7.63	9.31
Formic acid (pH = 8.25)	2.36	3.97	7.13	10.21	13.41	14.62
Chloroacetic acid (pH = 7.42)	4.82	8.58	16.10	24	32.2	38

[a] I = 0.01 mol L^{-1}; t = 20°C.

Can. J. Chem. Downloaded from www.nrcresearchpress.com by 118.98.75.50 on 09/07/12
For personal use only.

stopped-flow spectrophotometer by monitoring the appearance or the disappearance of the absorption of the carbanion at or near its λ_{max} (680 nm; ε = 28 000 L mol^{-1} cm^{-1}).

The deprotonation of **1** was first studied using potassium methoxide solutions in the concentration range 0.002–0.01 *M* (I = 0.01 *M*). As expected, the observed rates for the approach to equilibrium [1] fitted nicely eq. [2], allowing a facile determination of the rate constant k_p^{MeO} for deprotonation of **1** by methoxide ion and of the rate constant k_{-p}^{MeOH} for reprotonation of **2** by the solvent: k_p^{MeO} = 24.8 L mol^{-1} s^{-1}; k_{-p}^{MeOH} = 0.75 s^{-1}. These values compare well with those previously determined without maintaining constant ionic strength (k_p^{MeO} = 26.2 L mol^{-1} s^{-1}; k_{-p}^{MeOH} = 0.73 s^{-1}) (1) and confirm the value of the equilibrium constant K_p for the reaction **1** + $MeO^- \rightleftharpoons$ **2** + MeOH: $K_p = k_p^{MeO}/k_{-p}^{MeOH}$ = 33 L mol^{-1}.

$$[2] \quad k_{obsd} = k_p^{MeO}[MeO^-] + k_{-p}^{MeOH}$$

The conversion of **2** to **1** was investigated by carrying out pH-jump experiments. These were performed by mixing a slightly basic solution of **1** with appropriate BH/B^--type buffers made up from various carboxylic acids and phenols. A few experiments were also conducted with benzenesulfonic acid solutions (5×10^{-4} – 8.71×10^{-4} *M* after mixing). Because of the low ionic strength chosen, the concentration of the basic buffer species B^- was varied between 0.001 and 0.01 *M* in the final solutions. Concomitant changes in the BH concentration were between 0.001 and 0.03 *M* since different buffer ratios were used. Although the changes in the buffer concentrations were relatively small, they resulted in appreciable variations in the observed rates of equilibrium at a given pH, as shown in Table 1. The need to work at low B^- concentrations also implied the use of very dilute methoxide solutions of the carbon acid **1** and, depending upon the buffer solution required after the pH jump, only CH_3OK concentrations in the range 0.002–0.02 *M* could be employed. Under such experimental conditions, the concentration of the carbanion **2**, generated from a 10^{-4} *M* solution of **1**, was in the approximate range 5×10^{-6} – 3.7×10^{-5} *M*. However, in view of the high absorbance of **2**, these concentrations made it possible to record reliable kinetic data in all pH-jump experiments.

The general expression for the pseudo-first-order rate constant k_{obsd} associated with the equilibrium between **1** and **2** is given by

$$[3] \quad k_{obsd} = k_p^{MeOH} + k_p^{MeO}[MeO^-] + k_p^{B}[B^-] + k_{-p}^{H^+}[H^+] + k_{-p}^{BH}[BH] + k_{-p}^{MeOH}$$

TABLE 2. Observed rate constants k_{obsd}^0 for protonation of the carbanion **2** at zero buffer concentration and different pH in methanol[a]

pH	$[H^+]^b$	k_{obsd}^0, s^{-1}	pH	$[H^+]^b$	k_{obsd}^0, s^{-1}
3.24	8.71×10^{-4}	363	6.26	8.32×10^{-7}	7.00
4	1.51×10^{-4}	200	6.44	5.5×10^{-7}	4.97
4.16	1.05×10^{-4}	166	7.10	1.20×10^{-7}	1.65
4.48	5×10^{-5}	126	7.42	5.75×10^{-8}	1.18
4.76	2.63×10^{-5}	79.5	7.61	3.71×10^{-8}	1.02
4.96	1.66×10^{-5}	58.5	7.99	1.55×10^{-8}	0.89
5.18	1×10^{-5}	38.5	8.10	1.20×10^{-8}	0.79
5.48	5×10^{-6}	36	8.56	4.37×10^{-9}	0.79
5.66	3.31×10^{-6}	25.1	8.75	2.69×10^{-9}	0.72
5.96	1.66×10^{-6}	12.60	9.04	1.38×10^{-9}	0.75

[a] t = 20°C; I = 0.01 mol L^{-1}.
[b] Calculated from log $[H^+]$ = −pH + 0.18.

but the pH range covered by the buffer and benzenesulfonic acid solutions studied (3–14, 31) lies far below the pK_a value for formation of **2**. Thus, eq. [3] can be safely reduced to

$$[4] \quad k_{obsd} = k_{-p}^{H^+}[H^+] + k_{-p}^{BH}[BH] + k_{-p}^{MeOH}$$

The various rate constants of eq. [4] were evaluated as follows. In carboxylic acid and phenol buffer solutions of pH > 8.5, plots of k_{obsd} vs. [BH] were linear with points determined at different pH falling on the same straight line (Fig. S_1).[2] Results are therefore consistent with the equation:

$$[5] \quad k_{obsd} = k_{-p}^{MeOH} + k_{-p}^{BH}[BH]$$

which is a special case of eq. [4] where $k_{-p}^{H^+}[H^+] \ll k_{-p}^{MeOH}$. The slopes of the k_{obsd} vs. [BH] plots afforded the k_{-p}^{BH} values for the different buffers studied, while the intercepts were all equal to k_{-p}^{MeOH} = 0.73 ± 0.03 s^{-1}, in good agreement with the k_{-p}^{MeOH} value previously determined from eq. [2].

With carboxylic acid buffer solutions in the pH range 5.5–8.5, the contribution of the hydronium ion to the acid catalysis was no longer negligible, as evidenced by the observation that plots of k_{obsd} vs. [BH] were linear with pH-dependent intercepts (Fig. S_2).[2] In this case, eq. [4] applies and determination of k_{-p}^{BH} from the slopes of the buffer plots obtained at constant pH was straightforward. On the other hand, a plot of the intercepts (denoted k_{obsd}^0) of these plots vs. $[H^+]$

[2] Figures S_1–S_4 may be purchased from the Depository of Unpublished Data, CISTI, National Research Council of Canada, Ottawa, Ont., Canada K1A 0S2.

TABLE 3. Rate constants k_{-p}^{BH} and k_p^B for reactions (**1**) in methanol at 20°C[a]

		pK_a^{BH}[b]	k_{-p}^{BH}, L mol^{-1} s^{-1}	k_p^B, L mol^{-1} s^{-1}	$\Delta pK + \log(p/q)$[c]
1	$CH_3OH_2^+$	−1.50	7.12×10^6	1.44×10^{-10}[d]	−16.50
2	Trichloroacetic acid	4.47	4×10^4	5.92×10^{-7}[e]	−11.13
3	Dichloroacetic acid	5.96	1.48×10^4	6.76×10^{-6}[e]	−9.64
4	3,5-Dinitrobenzoic acid	7.20	7940	6.31×10^{-5}[e]	−8.40
5	Chloroacetic acid	7.42	3715	4.90×10^{-5}[e]	−8.18
6	Salicylic acid	7.61	2800	5.72×10^{-5}[e]	−7.99
7	Formic acid	8.25	1580	1.41×10^{-4}[e]	−7.35
8	Benzoic acid	9.04	860	4.73×10^{-4}[e]	−6.56
9	Acetic acid	9.52	500	8.30×10^{-4}[e]	−6.08
10	2,4,6-Trichlorophenol	10.21	1420	1.15×10^{-2}[e]	−5.09
11	2,6-Dichlorophenol	11.18	490	3.72×10^{-2}[e]	−4.12
12	4-Cyanophenol	11.72	130	3.42×10^{-2}[e]	−3.58
13	4-Chlorophenol	13.05	29	0.163[e]	−2.25
14	Phenol	14.32	6.30	0.66[e]	−0.98
15	CH_3OH	18.36	0.029[f]	24.8[g]	3.06

[a] I = 0.01 mol L^{-1}.
[b] pK_a values taken from refs. 4 and 30.
[c] $\Delta pK = pK_a^{BH} - pK_a^{\ddagger}$ with $pK_a^{\ddagger} = 15.30$.
[d] Calculated as $k_p^B/24.7$ with $k_p^B = k_p^{MeOH} = k_{-p}^{H^+}K_a^{\ddagger}$.
[e] $k_p^B = k_{-p}^{BH}K_a^{\ddagger}/K_a^{BH}$.
[f] Calculated as $k_{-p}^{BH} = k_{-p}^{MeOH}/24.7$.
[g] $k_p^B = k_p^{MeO}$.

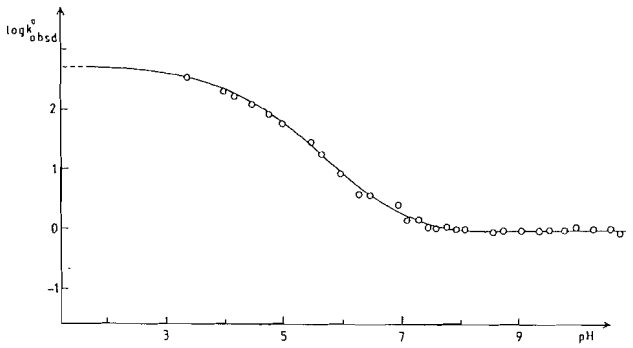

FIG. 1. The pH dependence of the observed rate constant k_{obsd}^0 for protonation of the carbanion **2** at zero buffer concentration in methanol; t = 20°C, I = 0.01 mol L^{-1}.

afforded a straight line (not shown) consistent with eq. [6]. We thus obtain $k_{-p}^{H^+} = 7.12 \times 10^6$ L mol^{-1} s^{-1} and $k_{-p}^{MeOH} = 0.75$ s^{-1}, again in good agreement with previous determinations of k_{-p}^{MeOH}. The experimental k_{obsd}^0 values are summarized in Table 2.

$$[6] \quad k_{obsd}^0 = k_{-p}^{H^+}[H^+] + k_{-p}^{MeOH}$$

In the relatively acidic trichloroacetic acid buffer solutions, very strong catalysis by BH was observed, as expected, but this catalysis cannot be accounted for in terms of eq. [4]. As shown in Fig. S_3,[2] plots of k_{obsd} vs. [BH] at constant pH remain linear but they have slopes that decrease with decreasing pH. This suggests that the decomposition of **2** becomes complicated by another process at pH < 5 (4). The concomitant observation that the k_{obsd}^0 values determined from the intercepts (Table 2) level off at low pH, as shown by the bilogarithmic plot of Fig. 1, confirms this suggestion and indicates in fact that the carbanion **2** is involved in a fast equilibrium protonation prior to its conversion to **1**. As will be discussed later, there is little doubt that the resulting protonated species arises from protonation at a NO_2 group of **2**, most likely at the 4-position, and is therefore the nitronic acid **2**,*H*.

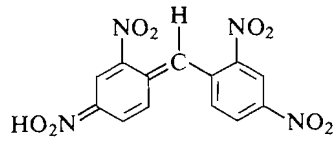

2,*H*

Considering the fast initial formation of **2**,*H*, the conversion of **2** to **1** is now described by eq. [7] where K_a' is the acidity constant of the nitronic acid functionality. Based on this,

$$[7] \quad \mathbf{2},H \rightleftharpoons \mathbf{2} + H^+ \xrightarrow{k_{-p}^{H^+}[H^+] + k_{-p}^{MeOH} + k_{-p}^{BH}[BH]} \mathbf{1}$$

$$[8] \quad k_{obsd} = (k_{-p}^{H^+}[H^+] + k_{-p}^{MeOH})\frac{K_a'}{K_a' + [H^+]} + k_{-p}^{BH}[BH]\frac{K_a'}{K_a' + [H^+]}$$

$$[9] \quad k_{obsd}^0 = (k_{-p}^{H^+}[H^+] + k_{-p}^{MeOH})\frac{K_a'}{K_a' + [H^+]}$$

the values of the observed rate constant k_{obsd} for carbanion protonation should fit eq. [8], accounting for the observed decrease in the slopes of the k_{obsd} vs. [BH] plots with increasing H^+ concentration. Equation [8] simplifies to eq. [9] when no buffer acid is present in the solutions. At pH > 5.5, the formation of **2**,*H* does not occur to significant extent, so that $K_a' \gg [H^+]$ and eq. [9] further reduces to eq. [6]. This situation is consistent with the plateau and the straight line of slope −1 that are observed at pH > 8 ($k_{-p}^{MeOH} \gg k_{-p}^{H^+}[H^+]$) and between pH 5.5 and 6.5 ($k_{-p}^{H^+}[H^+] \gg k_{-p}^{MeOH}$), respectively, in Fig. 1. In contrast, at very low pH where $K_a' \ll [H^+]$, eq. [9] becomes

$$[10] \quad k_{obsd}^0 = k_{-p}^{H^+}K_a'$$

Can. J. Chem. Downloaded from www.nrcresearchpress.com by 118.98.75.50 on 09/07/12
For personal use only.

Can. J. Chem. Downloaded from www.nrcresearchpress.com by 118.98.75.50 on 09/07/12
For personal use only.

giving rise to the second plateau observed in Fig. 1. From measurements in benzenesulfonic acid solutions, one can estimate $k_{-p}^{H^+}K'_a \sim 350\,s^{-1}$ but this value has a large experimental error because rates at low pH are very close to the time resolution of the stopped-flow apparatus. Using this value and the previously determined $k_{-p}^{H^+}$ value (7.12×10^6 L mol^{-1} s^{-1}), one calculates $K'_a = 4.9 \times 10^{-5}$ mol L^{-1} for the acidity constant of **2**,*H*, i.e., $pK'_a \sim 4.30$. Another estimate of K'_a could also be obtained from measurements in the pH range 3.24–5.5. At these pH values, k_{-p}^{MeOH} is negligible in eq. [9], which may be rewritten in the form of eq. [11]. In accordance with this equation, a plot of $1/k^0_{obsd}$ vs. $1/[H^+]$ affords a straight line

$$[11]\quad \frac{1}{k^0_{obsd}} = \frac{1}{k_{-p}^{H^+}[H^+]} + \frac{1}{k_{-p}^{H^+}K'_a}$$

(Fig. S_4),[2] allowing the calculation of $k_{-p}^{H^+}$ and $k_{-p}^{H^+}K'_a$ from the slope and the intercept, respectively: $k_{-p}^{H^+} = 4.27 \times 10^6$ L mol^{-1} s^{-1}, $k_{-p}^{H^+}K'_a = 294\,s^{-1}$. Although the values thus obtained are only in rough agreement with those determined from eq. [6] in the pH range 5.5–8.5 ($k_{-p}^{H^+}$) or at very low pH ($k_{-p}^{H^+}K'_a$), the interesting point is that they confirm the order of magnitude of the acidity of **2**,*H*: $K'_a = 6.88 \times 10^{-5}$ mol L^{-1}; $pK'_a = 4.17$. The knowledge of K'_a allows the calculation of the k_{-p}^{BH} value for trichloroacetic acid buffer from the slopes of the k_{obsd} vs. [BH] plots of eq. [8] (see Fig. S_3).

The various rate parameters associated with the interconversion of **1** and **2** are summarized in Table 3. With the exception of the rate constant associated with the deprotonation of **1** by MeO$^-$ ($k_p^B = k_p^{MeO}$), all k_p^B values were calculated: $k_p^B = k_{-p}^{BH}K_a^1/K_a^{BH}$ (buffer species) or $k_p^B = k_{-p}^{H^+}K_a^1$ (B = MeOH).

Discussion

Nitronic acid formation

The most interesting result of this work is undoubtedly our observation that the carbanion **2** is susceptible to fast reversible protonation in acidic methanol, but our proposal (*vide supra*) that the resulting protonated species is presumably the nitronic acid **2**,*H* needs justification.

We have previously demonstrated that the carbanion **2** is essentially planar and has a highly delocalized negative charge (5). Thus, ^{13}C nmr spectra show that the chemical shift of the exocyclic carbon is strongly shifted to low field on conversion of **1** to **2**: $\delta\ C_\alpha = 35.0$ ppm for **1** and 100.9 ppm for **2** in DMSO. Such values clearly indicate that the bonding to the exocyclic carbon of **2** is essentially olefin-like (6), and that the negative charge is necessarily delocalized over the nitrophenyl rings, as shown in structures **3***a*–**3***d*. A consequence is that the ionization of **1** to give **2** involves an extensive structural–electronic–solvational reorganization, a situation that is typical for many carbon acids and is generally reflected by the finding that the corresponding proton transfer reactions have high intrinsic energy barriers and strongly imbalanced transition states (7–11). Significantly, a kinetic analysis carried out in 50% H_2O – 50% DMSO has revealed that the intrinsic energy barriers for deprotonation of **2** by various bases are among the highest so far measured for carbon acids (5, 11). Similarly, the results obtained have given evidence for a high degree of charge imbalance in the transition states corresponding to the various reactions of eq. [1] (5, 11). The kinetic data therefore support the nmr conclusion that **2** is a planar delocalized carbanion.

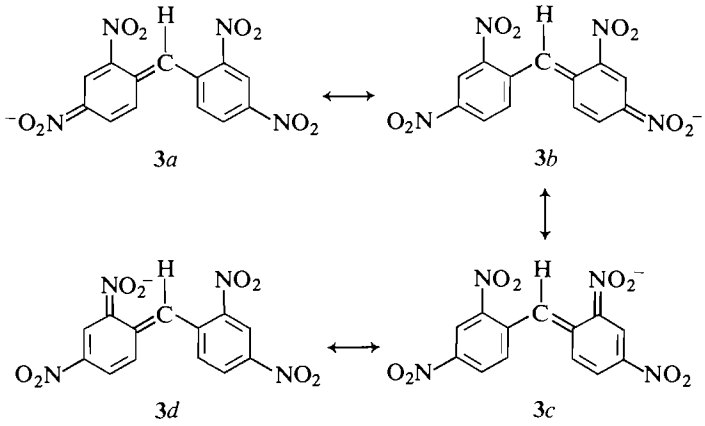

Considering the resonance structures **3***a*–**3***d*, it is clear that the *fast* protonation of **2** in acidic methanol can only occur at a nitro group and hence the protonated species at low pH is a nitronic acid. Furthermore, it is also well known that a *p*-NO_2 group is significantly more effective at resonance stabilization of charge than is an *o*-NO_2 group (12, 13). On this basis, one can reasonably expect that the negative charge of **2** lies preferentially on the 4- and 4′-NO_2 groups, as visualized in structures **3***a* and **3***b*, and that one of these groups will be preferentially protonated to give the nitronic acid **2**,*H*. Some support for this conclusion is provided by our previous observation of a negative transition state imbalance effect for the deprotonation of **1** in 50% DMSO – 50% H_2O (5). As then discussed, this effect is better understood in terms of structures **3***a* and **3***b* rather than in terms of structures **3***c* and **3***d* for the carbanion **2**.

Further support for the identification of the protonated species **2**,*H* as a nitronic acid is that the pK'_a value measured for the ionization of this derivative is in the same range as those reported for nitronic acids resulting from the protonation of a number of nitrocyclohexadienylide rings (13–16). Typical examples are the nitronic acids **4***a*,*H*–**4***d*,*H*, which have been

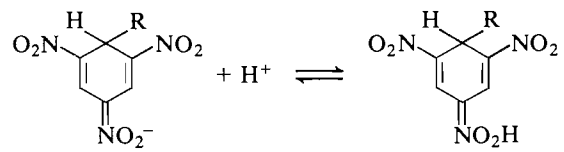

4 **4**,*H*

a, R = 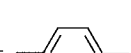 OH; *b*, R = 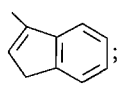 ;

c, R = 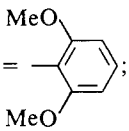 ; *d*, R = H

characterized by nmr and result from the protonation of the trinitrobenzene σ-adducts **4***a*–*d*. Thus, the equilibrium formation of **4***a*,*H* from the parent phenoxide adduct has been spectrophotometrically studied and pK'_a values of −1 and +3 have been derived for the ionization of **4***a*,*H* in aqueous and ethanolic solutions, respectively (16). Since the acidity of oxygen acids usually decreases on going from water to methanol to ethanol (17), these results suggest pK'_a values of ~1–2 for nitronic acids of the type **4**,*H* in methanol. More significantly, we have recently reported pK'_a values in the order of 4.2–4.5 for the ionization of the nitronic acids **5***a*–*d*,*H* resulting from the protonation of the benzofurazan and benzofuroxan adducts **5***a*–*d* in methanol (4). The fact that these values, which refer

to the protonation of a *para*-like NO_2 group, are essentially the same as that found for protonation of **2** under similar experimental conditions lends additional support to our assignment of **2**,*H* as a nitronic acid.[3]

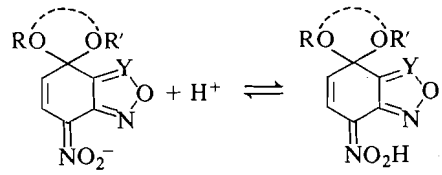

5 **5**,*H*

a, Y = N, R = R′ = CH_3
b, Y = N→O, R = R′ = CH_3
c, Y = N, R = R′ = CH_2—CH_2
d, Y = N→O, R = R′ = CH_2—CH_2

Rate constants for proton transfer

Figure 2 shows that carboxylic acid and phenol buffers obey different Brönsted relationships. For a given $\Delta pK + \log(p/q)$ value ($\Delta pK = pK_a^{BH} - pK_a^1$ and p and q are the usual statistical factors used for Brönsted plots), phenols appear to be more efficient oxygen-acid catalysts than carboxylic acids. This behaviour is qualitatively the same as that found in the study of reactions [1] in 50% H_2O – 50% DMSO (5), and in the study of the ionization of acetylacetone and 1,3-indandione in various H_2O–DMSO mixtures (18, 19).

A noteworthy feature of Fig. 2, however, is that the slopes of the Brönsted lines are markedly different for the two classes of buffers. Thus, the α^{BH} value is equal to 0.58 for the phenols and 0.43 for the carboxylic acids. In this respect, the situation contrasts with that observed in 50% H_2O – 50% DMSO where $\alpha^{ArOH} = 0.59$, a value that is essentially the same as that found in methanol, and $\alpha^{RCOOH} = 0.52$ (5). Using the classical definition of the intrinsic rate constant, i.e., $k_0 = k_{-p}^{BH}/p = k_p^B/q$ where $\Delta pK + \log(p/q) = 0$ (7, 21, 22), the $\log k_0^{RCOOH}$ and $\log k_0^{ArOH}$ values can be readily determined from the Brönsted plots (11). They are equal to 0.15 ± 0.1 and 0.18 ± 0.2, respectively, at 20°C in methanol. These low $\log k_0$ values confirm that high intrinsic energy barriers are associated with reactions [1] (5). The more interesting result, however, is that the intrinsic rate constant for the phenol reactions in methanol is lower by a factor of 2 than that found in 50% H_2O – 50% DMSO solution, while that for the carboxylic acid reactions is greater by a factor of about 5. Since the temperature used in this work (t = 20°C) is lower than that used in 50% H_2O – 50% DMSO (t = 25°C), the observed decrease in k_0^{ArOH} may be the result of a temperature effect rather than of a solvent effect although the temperature difference is extremely small. However, it is clear that this explanation cannot be invoked to account for the increase observed in k_0^{RCOOH} and this latter change must be the reflection of a solvent effect.

Considering the effect of the solvent transfer from 50% H_2O – 50% DMSO (t = 25°C) to methanol (t = 20°C) on the reactions of eq. [1], it is of interest to note that the pK_a's of the buffer carboxylic acids increase by about 3.8 pK units while that for the ionization of **1** increases by 4.40 pK units (5). It thus appears that the protonation of **2** by carboxylic acids is thermodynamically more favorable in the methanolic than in the aqueous DMSO system. The concomitant decrease observed in the α^{RCOOH} value would therefore appear consistent with the reactivity–selectivity principle (RSP) (23). However, the same solvent transfer also increases the pK_a's of the buffer phenols, but to a lesser extent than that of carboxylic acids ($\Delta pK^{ArOH} \sim 3$). As a result, the thermodynamics of the protonation of **2** by phenols is favored to a greater degree than that by carboxylic acids and the RSP would predict a greater decrease in the α^{ArOH} than in the α^{RCOOH} value. This is clearly not the case since α^{ArOH} is essentially the same in the two solvents and thus the reaction is no longer understandable in terms of the RSP.

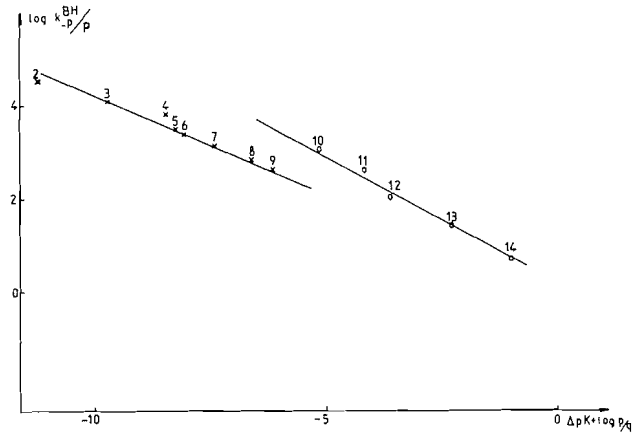

FIG. 2. Brönsted plots for the catalysis of the protonation of the carbanion **2** by carboxylic acids and phenols in methanol; t = 20°C; I = 0.01 mol L^{-1}. The numbering of the catalysts is given in Table 3.

That the RSP fails to account for the situation observed is not surprising since it is now well known that reactions which involve resonance stabilized carbanions, and which are therefore subject to large transition state imbalances, cannot be treated by common formalisms (7, 9, 11, 18, 19, 24). In particular, it has been shown that the effect of a solvent change on the intrinsic rate constant k_0 for the deprotonation of a carbon acid (or reprotonation of the corresponding carbanion) is closely related to specific stabilizing or destabilizing factors of reactants and products (11, 18, 19, 25). For reactions involving an anionic base B^- like those of eq. [1], for example, solvation of the base is a reactant stabilizing factor while solvation of the resulting carbanion C^- is a product stabilizing factor and, to a first approximation, the changes in k_0 can be described by eq. [12] (11, 18, 19). ${}^{S_1}\gamma_B^{S_2}$ and ${}^{S_1}\gamma_C^{S_2}$ are the solvent activity coefficients of the base B^- and the carbanion C^-, respectively, for the transfer from a solvent S_1 to a solvent S_2, $\alpha_d^{B^-}$ and $\alpha_s^{C^-}$ measure the progress of desolvation of B^- and of solvation of C^- at the transition state, respectively, while β is the measured Brönsted β value for deprotonation of the carbon acid by various bases of the B^- type. The presence of the negative sign in front of $\log {}^{S_1}\gamma_C^{S_2}$ but not in front of $\log {}^{S_1}\gamma_B^{S_2}$ is because C^- is a product whereas B^- is a reactant (11). For proton transfer reactions involving carbanions, desolvation of the base B^- is always ahead of proton transfer, i.e., $(\alpha_d^{B^-} - \beta) > 0$, while solvation of C^- is always delayed, i.e., $(\alpha_s^{C^-} - \beta) < 0$ (11, 18,

[12] $$\delta \log {}^{S_1}k_0^{S_2} = (\alpha_d^{B^-} - \beta) \log {}^{S_1}\gamma_B^{S_2} + (\alpha_s^{C^-} - \beta)(-\log {}^{S_1}\gamma_C^{S_2})$$

[3]To obtain an accurate spectrum of the nitronic acid **2**,*H* a concentrated solution of **2** is required. From the pK_a of **1**(15.3 at 20°C in MeOH) it can be calculated that a ca. 0.5 *M* solution of methoxide ion is needed for almost complete conversion to **2**, and reliable pH-jump experiments to produce solutions with final pH ~ 3 cannot be made on such solutions. In spite of numerous attempts, we were unable to overcome the experimental problems and could not obtain a spectrum of **2**,*H*.

Can. J. Chem. Downloaded from www.nrcresearchpress.com by 118.98.75.50 on 09/07/12
For personal use only.

Can. J. Chem. Downloaded from www.nrcresearchpress.com by 118.98.75.50 on 09/07/12
For personal use only.

19).[4] Equation [12] therefore predicts that k_0 will vary, depending upon whether the solvent transfer stabilizes or destabilizes, simultaneously, B^- and C^- or has a different effect on each of these two species. Several situations have been recently discussed and reviewed by Bernasconi, where observed changes in k_0 due to solvent effects were found to agree with the $\delta \log k_0$ values estimated from eq. [12] (11, 18, 19).

In view of the large imbalance effects associated with eq. [1], it is interesting to look at whether the changes in k_0 found for the reactions involving $RCOO^-$ and ArO^- ions on going from 50% H_2O – 50% DMSO (a mixture now denoted as D) to methanol (M) can be understood in terms of eq. [12]. In this respect, let us first note that our studies of eq. [1] have been essentially carried out in the reverse direction so that it is probably more appropriate to discuss our results with reference to the reprotonation of the carbanions **2** by phenols and carboxylic acids and therefore to use eq. [13]. α is the measured Brönsted coefficient for k_{-p}^{BH} while $\alpha_s^{B^-}$ and $\alpha_d^{C^-}$ measure the progress in the solvation of the developing base B^- ($\alpha_s^{B^-} < \alpha$) and of the desolvation of the carbanion C^- ($\alpha_d^{C^-} > \alpha$) at the transition state, respectively. That eq. [13] is equivalent to eq. [12] can be readily seen since we have $\alpha + \beta = 1$ and $\alpha_d + \alpha_s = 1$ (18).

$$[13] \quad \delta \log {}^{D}k_0^{M} = (\alpha_s^{B^-} - \alpha)(-\log {}^{D}\gamma_{B^-}^{M}) + (\alpha_d^{C^-} - \alpha) \log {}^{D}\gamma_{C^-}^{M}$$

Based on eq. [13], the effect of changing solvent from 50% H_2O – 50% DMSO (D) to methanol (M) on the intrinsic rate constant k_0 for reactions [1] with carboxylic acids is given by

$$[14] \quad \delta \log {}^{D}k_0^{M} = (\alpha_s^{RCOO^-} - \alpha)(-\log {}^{D}\gamma_{RCOO^-}^{M}) + (\alpha_d^{C^-} - \alpha) \log {}^{D}\gamma_{C^-}^{M} = 0.70$$

with

$$\alpha = 0.47 \text{ (see footnote 4)}$$

and

$$\log {}^{D}\gamma_{RCOO^-}^{M} = -0.18 \ (\log {}^{D}\gamma_{RCOO^-}^{H_2O} = -3.08 \text{ (ref. 19)}; \ \log {}^{H_2O}\gamma_{RCOO^-}^{M} = 2.9 \text{ (ref. 26)}$$

Since $(-\log {}^{D}\gamma_{RCOO^-}^{M})$ is positive (0.18) and the value of $(\alpha_s^{RCOO^-} - \alpha)$ varies from $-\alpha$ to 0 ($\alpha_s^{RCOO^-} = 0$ corresponds to the hypothetical situation where solvation of the developing carboxylate ion has made no progress in the transition state), we see that the contribution of the first term in eq. [14] is negative, and has values between -0.08 ($\alpha_s^{RCOO^-} = 0$) and zero ($\alpha_s^{RCOO^-} = 0.47$). These values require a positive value between 0.70 and 0.78 for the second term and, since $\alpha_d^{C^-} > \alpha$, a positive value for $\log {}^{D}\gamma_{C^-}^{M}$. Assuming complete desolvation of the carbanion C^- prior to proton transfer, i.e., $\alpha_d^{C^-} \sim 1$, a minimum value of 1.32 can be estimated for $\log {}^{D}\gamma_{C^-}^{M}$. This result suggests that the carbanion **2** is somewhat destabilized on going from the aqueous DMSO mixture to methanol. This conclusion looks quite reasonable since delocalized anionic species are known to be better stabilized in aqueous or alcoholic DMSO mixtures than in protic solvents (13, 26, 27, 28).

Let us now assume that the decrease in k_0^{ArOH} may also be related to the solvent change and not only to the temperature effect. Applying eq. [13] to the phenol reactions gives

$$[15] \quad \delta \log {}^{D}k_0^{M} = (\alpha_s^{ArO^-} - \alpha)(-\log {}^{D}\gamma_{ArO^-}^{M}) + (\alpha_d^{C^-} - \alpha) \log {}^{D}\gamma_{C^-}^{M} = -0.32$$

Qualitatively, we can see that the first term of eq. [15] must be appreciably negative to account for a decrease in k_0. This is because the second term is positive ($\alpha_d^{C^-} - \alpha) > 0$, $\log {}^{D}\gamma_{C^-}^{M} > 0$, *vide supra*) even though the larger α value found for ArOH (0.58) tends to attenuate its contribution compared to that in carboxylic acids. Since, again, we expect that solvation of the developing ArO^- ion is delayed, i.e., $(\alpha_s^{ArO^-} - \alpha) \leqslant 0$, it follows that $\log {}^{D}\gamma_{ArO^-}^{M}$ must be more negative than $\log {}^{D}\gamma_{RCOO^-}^{M}$ and therefore that phenoxide anions are much more stabilized than carboxylate anions on transfer from 50% H_2O – 50% DMSO to methanol. Interestingly, this conclusion is consistent with experimental results obtained by Juillard (29) and Abraham *et al.* (30), who found that changing from water to methanol causes a notable destabilization of carboxylate anions but increases the stabilization of phenoxide anions. It thus appears that both temperature and solvent effects are in accord with the observed decrease in k_0^{ArOH}.

Notwithstanding any possible temperature effect upon k_0 in the case of the phenol reactions, we can conclude from the above discussion that the different behaviour of reactions [1] with carboxylic acids and phenols is qualitatively in agreement with eq. [13]. This further confirms that the ionization of polynitrodiphenylmethanes constitutes a remarkable example of strongly imbalanced proton transfers.

Experimental

Materials

2,2′,4,4′-Tetranitrodiphenylmethane was prepared according to literature procedure and recrystallized in acetic acid; mp 182°C (31). Potassium methoxide solutions were made up as described previously. Buffers were purified commercial products.

Measurements

Kinetic studies were made using a Durrum stopped-flow spectrophotometer with a thermostatted cell compartment (±0.5°C).

pH determinations in methanol were carried out at 20°C using the same procedure as that previously used for other kinetic studies. A Tacussel Isis 20000 electronic pH meter was used.

[4] As noted by Bernasconi and Bunnell (18), a quantitative application of eq. [14] requires α to be solvent independent. For the purposes of a qualitative discussion, an average α value from the two solvents being compared is a satisfactory approximation (11, 18).

1. P. G. Farrell, P. Fogel, A. P. Chatrousse, J. Lelievre, and F. Terrier. J. Chem. Soc. Perkin Trans. 2, 51 (1985).
2. (*a*) F. Terrier, F. Millot, and J. Morel. J. Org. Chem. **41**, 3892 (1976); (*b*) F. Terrier, A. P. Chatrousse, and F. Millot. J. Org. Chem. **45**, 2666 (1980).
3. J. C. Halle, F. Terrier, and R. Schaal. Bull. Soc. Chim. Fr. 37 (1973).
4. F. Terrier, G. Ah-Kow, and A. P. Chatrousse. J. Org. Chem. **50**, 4583 (1985).
5. F. Terrier, J. Lelievre, A. P. Chatrousse, and P. G. Farrell. J. Chem. Soc. Perkin Trans. 2, 1479 (1985).
6. S. E. Browne, S. E. Asher, E. H. Cornwall, J. K. Frisoli, I. I. Harris, E. A. Salot, E. A. Sauter, M. A. Trecoskee, and P. S. Veale. J. Am. Chem. Soc. **106**, 1432 (1984).
7. C. F. Bernasconi. Pure Appl. Chem. **54**, 2335 (1982).
8. A. J. Kresge. *In* Proton transfer reactions. *Edited by* V. Gold and E. F. Caldin. Chapman and Hall, London. 1975. pp. 188–194.
9. (*a*) F. G. Bordwell, J. E. Bartmess, and J. A. Hautala. J. Org. Chem. **43**, 3107 (1978); **43**, 3110 (1978); (*b*) F. G. Bordwell and J. A. Hautala. J. Org. Chem. **43**, 3116 (1978), and references cited.
10. R. P. Bell and S. Grainger. J. Chem. Soc. Perkin Trans. 2, 1370 (1976).

11. C. F. BERNASCONI. Tetrahedron, **41**, 3219 (1985).
12. P. CAVENG, P. B. FISCHER, E. HEILBRONNER, A. L. MILLER, and H. ZOLLINGER. Helv. Chim. Acta, **50**, 848 (1967).
13. F. TERRIER. Chem. Rev. **82**, 77 (1982).
14. O. WENNERSTROM. Acta Chem. Scand. **25**, 2341 (1971).
15. C. MOBERG and O. WENNERSTROM. Acta Chem. Scand. **25**, 2871 (1971).
16. E. BUNCEL and W. EGGIMANN. Can. J. Chem. **54**, 2436 (1976).
17. E. J. KING. *In* Physical chemistry of organic solvent systems. *Edited by* A. K. Covington and T. Dickinson. Plenum Press, London. 1973. p. 344.
18. C. F. BERNASCONI and R. D. BUNNELL. Isr. J. Chem. **26**, 420 (1985).
19. C. F. BERNASCONI and P. PASCHALIS. J. Am. Chem. Soc. **108**, 2969 (1986).
20. A. J. KRESGE. Chem. Soc. Rev. **2**, 475 (1973).
21. R. A. MARCUS. J. Phys. Chem. **72**, 891 (1968).
22. O. COHEN and R. A. MARCUS. J. Phys. Chem. **72**, 4249 (1968).
23. (*a*) C. D. RITCHIE. Acc. Chem. Res. **5**, 348 (1972); (*b*) B. GIESE. Angew. Chem. Int. Ed. Engl. **16**, 125 (1977); (*c*) A. PROSS. Adv. Phys. Org. Chem. **14**, 69 (1977).
24. W. P. JENCKS, S. R. BRANT, J. R. GANDLER, G. FENDRICH, and C. NAKAMURA. J. Am. Chem. Soc. **104**, 7045 (1982).
25. C. F. BERNASCONI, R. A. RENFROW, and P. R. TIA. J. Am. Chem. Soc. **108**, 4541 (1986).
26. A. J. PARKER. Chem. Rev. **69**, 1 (1969).
27. E. BUNCEL and H. WILSON. Adv. Phys. Org. Chem. **14**, 133 (1977).
28. (*a*) J. H. FENDLER and J. W. LARSEN. J. Org. Chem. **37**, 2608 (1972); (*b*) J. W. LARSEN, K. AMIN, and L. L. MAGID. J. Org. Chem. **37**, 3857 (1972).
29. J. JUILLARD. Bull. Soc. Chim. Fr. 1894 (1968).
30. M. H. ABRAHAM, T. HILL, H. C. LENG, R. A. SCHULZ, and R. A. C. WATT. J. Chem. Soc. Faraday Trans. 1, **80**, 489 (1984).
31. G. D. PARKES and R. H. H. MORLEY. J. Chem. Soc. 1478 (1936).

Can. J. Chem. Downloaded from www.nrcresearchpress.com by 118.98.75.50 on 09/07/12
For personal use only.

Particular solution for any consecutive second-order reaction

MARTINO PAVENTI

Department of Chemistry, McGill University, 801 Sherbrooke Street West, Montreal, P.Q., Canada H3A 2K6

Received February 23, 1987

This paper is dedicated to Professor John T. Edward

MARTINO PAVENTI. Can. J. Chem. **65**, 1987 (1987).

Arguments are presented against the accepted notion that multiple rate constants may be obtained from observed singular or pooled kinetic runs. For any competitive consecutive second-order reaction, the particular solution satisfying the total differential equation, derived from $(n + 1)$ simultaneous differential equations, is $S = (aA_0 - S_0)\{(aA_0/S_0)[\exp(aA_0 - S_0)kt] - 1\}^{-1}$, where S is the concentration of reactant common for all the steps, A is the concentration of the substrate with a reactive sites, A_0 and S_0 are the concentration of reactants at zero time, k is the observed rate constant, and t is the time. This equation is shown to reproduce the experimental reported data and yields $k = \min(k(1), \ldots, k(n))$, where $k(i)$ is the rate constant assigned to step i. It is also shown that the initial conditions need not be known. For experiments with the initial condition $(aA_0 = S_0)$, with only species A and S are present at zero time, the expression $(S_0\{\int_0^\infty (S - \alpha)^2 dt\}^{-1})$ may be useful for an approximate evaluation of k when values of S do not approach zero after an infinite time (i.e., $S_\infty = \alpha \neq 0$, where α is the asymptote for the data).

MARTINO PAVENTI. Can. J. Chem. **65**, 1987 (1987).

On présente des arguments contre la notion généralement acceptée que les constantes de vitesse des réactions multiples peuvent être déduites d'études cinétiques uniques ou combinées. Pour toute réaction consécutive et compétitive du deuxième ordre, la solution particulière qui satisfait à l'équation différentielle totale et qui est dérivée de $(n + 1)$ équations différentielles simultanées est la suivante : $S = (aA_0 - S_0)\{(aA_0/S_0)[\exp(aA_0 - S_0)kt] - 1\}^{-1}$ dans laquelle S est la concentration du réactif commun à chacune des étapes, A est la concentration du substrat avec a sites réactifs, A_0 et S_0 sont les concentrations des réactifs au temps zéro, k est la constante de vitesse observée et t est le temps. On démontre que cette équation permet de reproduire les données expérimentales qui ont été rapportées et qu'elle conduit à $k = \min(k(1), \ldots, k(n))$ dans laquelle $k(i)$ est la vitesse attribuée à l'étape i. On démontre aussi qu'il n'est pas nécessaire de connaître les conditions initiales. Pour les expériences particulières dans lesquelles les conditions initiales satisfont à la relation $aA_0 = S_0$ et dans lesquelles seules les espèces A et S sont présentes au temps zéro, on peut utiliser l'expression $(S_0\{\int_0^\infty (S - \alpha)^2 dt\}^{-1})$ pour évaluer k d'une façon approximative, lorsque les valeurs de S ne s'approchent pas de zéro après un temps infini (c'est à dire que $S_\infty = \alpha \neq 0$ lorsque α est une asymptote pour les données).

[Traduit par la revue]

1. Introduction

Exact solutions for nonlinear differential equations are of paramount importance since all natural processes and laws are best described by these equations. For example, the *approximate* solutions of the Schrödinger equation are the backbone of modern chemistry and physics. In recent years, however, the emphasis has shifted from more classical mathematical goal of finding exact (i.e., analytical) solutions to integral equations and differential equations to the more realistic attempts at the quantitative characterization of solutions (1). This change in approach follows necessarily from an increasing preoccupation with nonlinear problems for which exact analytical solutions are unlikely (1). In agreement with Somorjai (1), there is no single best "recipe" for solution (even if a unique solution does exist), and inspired guessing combined with perseverance plays an important role.

Papers have been written advancing the approximate (2), graphical (3–13), and iterative (14–19) methodologies to evaluate *all* the rate constants for a competitive second-order reaction and parasitic papers have resulted as an extension (20, 21) of these concepts. All have irreconcilable mathematical differences between the solutions found and the experimental data. An attempt will be made here to surface some oddities and artifacts of approximate methodologies and to present a clear, simple, particular solution of the total differential equation resulting from the kinetic process. Without recourse to a steady-state treatment, the complete non-linear differential equations, derived below, have been obtained by a process similar to that described by Benson (22).

2. Deduction of the particular solution

Consider the very simple case of a second order irreversible reaction which takes analogy from the one-electron system, of the Schrödinger equation for which an exact solution exists.

$$A + S \xrightarrow{k_1} B$$

SCHEME 1

The differential equations[1] describing this process are:

[1] $A' = -k_1AS$

[2] $S' = -k_1AS$

From formal integration between limits the mass balance is obtained:[2]

[3] $\int_{S_0}^{S} dS = \int_{A_0}^{A} dA$

and therefore

[1]The definition of one operator is helpful for this and other derivations, in writing the equations more succinctly. For a general function f the operator $(')$ defines the derivative of the function with respect to time: $(f)' = (f') = df/dt$ and for the nth derivative with respect to time, the operator is written n times (i.e., $(f''') = d^3f/dt^3$). Also the letters $A, B, \ldots, S$ in the differential equations represent the instantaneous concentrations of species $A, B, \ldots, S$ in the schemes. The subscript 0 relates to the respective concentrations at zero time. The k_i are the individual rate constants described in the schemes.

[2]For more complex schemes, information of the mass-balance equation is also contained in the differential equations.

Can. J. Chem. Downloaded from www.nrcresearchpress.com by 118.98.75.50 on 09/07/12
For personal use only.

Can. J. Chem. Downloaded from www.nrcresearchpress.com by 118.98.75.50 on 09/07/12
For personal use only.

[4] $A = S + A_0 - S_0$

Substitution of eq. [4] into eq. [2] and integrating yields the general solution[3] (23):

[5] $S = (A_0 - S_0)\{(A_0/S_0)[\exp(A_0 - S_0)k_1t] - 1\}^{-1}$

Consider the linear[4] consecutive second-order reaction:

$$A + S \xrightarrow{k_1} B$$

$$B + S \xrightarrow{k_2} C$$

SCHEME 2

This process is mathematically described as:

[6] $A' = -k_1AS$

[7] $B' = k_1AS - k_2BS$

[8] $S' = -k_1AS - k_2BS$

The total differential equation may be derived as follows. Equation [8] is divided by S, differentiated, and A' and B' from eqs. [6] and [7] are substituted to yield:

[9] $$\left(\frac{S'}{S}\right)' = ZAS + (k_2)^2BS$$

where $Z = (k_1^2 - k_1k_2)$. Dividing eq. [9] by k_2 and adding the resultant to eq. [8], one obtains:

[10] $$\left(\frac{1}{k_2}\right)\left(\frac{S'}{S}\right)' + S' = Z_1AS$$

where $Z_1 = (Z/k_2 - k_1)$. Dividing eq. [10] by S, differentiating, and substituting for A' (eq. [6]) gives:

[11] $$\frac{1}{k_2}\left(\frac{1}{S}\left(\frac{S'}{S}\right)'\right)' + \left(\frac{S'}{S}\right)' = -Z_1k_1AS$$

Dividing eq. [11] by k_1 and adding the resultant to eq. [10] yields:

[12] $$\frac{1}{k_1k_2}\left(\frac{1}{S}\left(\frac{S'}{S}\right)'\right)' + \left(\frac{1}{k_1} + \frac{1}{k_2}\right)\left(\frac{S'}{S}\right)' + S' = 0$$

Analogously to the Schrödinger equation for two or more electrons where the hydrogen-like wavefunction is used to solve the Hamiltonian, the equation

[13] $S = (2A_0 - S_0)\{(2A_0/S_0)[\exp(2A_0 - S_0)kt] - 1\}^{-1}$

which is deduced from eq. [5], where k is the observed rate constant, is appropriately differentiated and substituted in eq. [12], giving:

[14] $$\frac{k^2}{k_1k_2} - \left(\frac{1}{k_1} + \frac{1}{k_2}\right)k + 1 = 0$$

[3]This general solution is indicative of all cases: for $S_0 \ll A_0$ (pseudo-first order) eq. [5] reduces to

$$S = S_0 \exp(-A_0k_1t)$$

The case where $A_0 = S_0$ can be shown by application of L'Hôpital's rule (24) to be:

$$S = S_0 \lim_{S_0 \to A_0} A_0(A_0 - S_0)\{(A_0/S_0)[\exp(A_0 - S_0)k_1t] - 1\}^{-1} = S_0(S_0k_1t + 1)^{-1}$$

[4]This is not to be confused with linear differential equations, but meant to illustrate reactions in series (25*a*).

Therefore eq. [12] is satisfied for all the time domain with the condition of eq. [14] that $(k = k_1)$ or $(k = k_2)$ and eq. [13] is a particular solution for the total differential equation [12].

Combination of the mass-balance equation (i.e., $(S_0 - 2A_0) = (S - 2A - B)$ for $B_0 = C_0 = 0$), eqs. [6] and [8] yields:

[15] $$S' + k_2S^2 - k_2(S_0 - 2A_0) = \frac{(2k_2 - k_1)}{-k_1}A'$$

for the case where $(S_0 = 2A_0)$ the limits of integration are known, simplifying eq. [15] to:

[16] $$\int_0^\infty S^2\,dt = S_0\frac{(2k_2 + k_1)}{2k_1k_2}$$

If the function of S is the limiting value[3] (i.e., $S = S_0(S_0kt + 1)^{-1}$) then eq. [16] integrates to:

[17] $$\frac{1}{k} = \frac{2k_2 + k_1}{2k_2k_1}$$

For a realistic solution of the process in Scheme 2, both eq. [14] and eq. [17] must be satisfied simultaneously. Also the reaction will not take place if $(k_1 = 0)$ or stops at species B if $(k_2 = 0)$. Combination of the roots for the two equations give:

[18] if $k = k_1$ (root of eq. [14]) then $k_2 = \infty$ (root of eq. [17])

[19] if $k = k_2$ (root of eq. [14]) then $k_1 = 2k_2$ (root of eq. [17])

and therefore $k = \min(k_1, k_2)$. The question of which of these two cases (roots) applies to the consecutive second order reaction of Scheme 2 may be answered by analysis of the kinetics of the individual steps under pseudo-first-order conditions.

Frost and Schwemer (4) have expressed the essence of eqs. [18] and [19] as the reaction corresponding to simple second order for $(k_2/k_1) = 0, 0.5$, or ∞. But $(k_2/k_1) = 0$ is tantamount to $k_1 = \infty$ (since $k_2 \neq 0$) and $B_0 = A_0$: an imaginary state since $B_0 = 0$ (see condition for deriving eq. [16]). Although k can mathematically equal k_2 for k_1 exactly equal to $2k_2$, this is experimentally improbable. Yet this *must be so* (i.e., $k_1 = 2k_2$) because the data (4) (Table 1) are reproduced by eq. [13], but the numbers obtained for k_1 and k_2 do not reflect this. These two opposing issues may be reconciled if only *one* rate constant is calculated from the data and not two or more.

Consider the parallel consecutive second-order process:

$$A + S \xrightarrow{k_1} B$$

$$A + S \xrightarrow{k_2} C$$

$$B + S \xrightarrow{k_3} D$$

$$C + S \xrightarrow{k_4} D$$

SCHEME 3

The differential equations describing this system are:

[20] $A' = -(k_1 + k_2)AS$

[21] $B' = k_1AS - k_3BS$

[22] $C' = k_2AS - k_4CS$

[23] $S' = -(k_1 + k_2)AS - k_3BS - k_4CS$

Employing the same mathematical manipulation as shown for

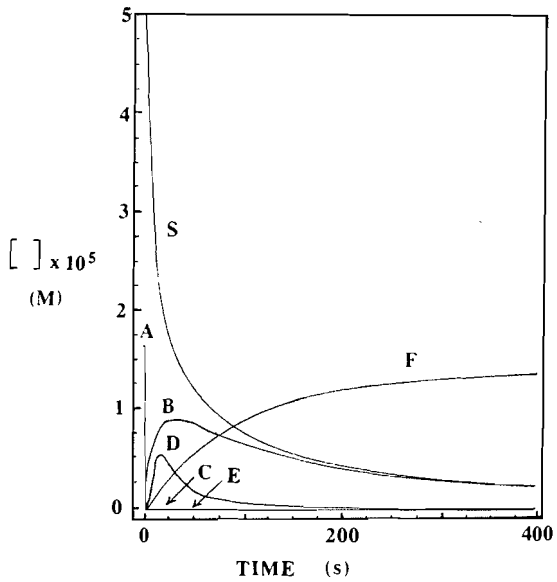

FIG. 1. Concentrations of species (letter symbols: A, B, C, D, E, F, S in Scheme 4) for the simulated tribromination of phenol from RMCHS (27). For the value of rate constants and concentration of the species see text.

the process in Scheme 2 above, we obtain the total differential equation

$$[24]\quad \frac{1}{(k_1+k_2)k_3k_4}\left(\frac{1}{S}\left(\frac{1}{S}\left(\frac{S'}{S}\right)'\right)'\right)' + \left\{\frac{1}{(k_1+k_2)k_3}+\frac{1}{(k_1+k_2)k_4}+\frac{1}{k_3k_4}\right\}\left(\frac{1}{S}\left(\frac{S'}{S}\right)'\right)' + \left\{\frac{1}{(k_1+k_2)}+\frac{1}{k_3}+\frac{1}{k_4}\right\}\left(\frac{S'}{S}\right)' + S' = 0$$

Again appropriate differentiation and substitution of the particular solution (eq. [13]) gives:

$$[25]\quad \frac{k^3}{(k_1+k_2)k_3k_4} - \left\{\frac{1}{(k_1+k_2)k_3}+\frac{1}{(k_1+k_2)k_4}+\frac{1}{k_3k_4}\right\}k^2 + \left\{\frac{1}{(k_1+k_2)}+\frac{1}{k_3}+\frac{1}{k_4}\right\}k - 1 = 0$$

and so $k = (k_1 + k_2)$, k_3, or k_4. Experiments and simulations (see Fig. 1) (26) show that $k = \min((k_1 + k_2), k_3, k_4)$.

The processes of Schemes 2 and 3 may be combined and extended to $(n + 1)$ differential equations. In a similar manner it can be shown that a particular solution[5] is

$$[26]\quad S = (aA_0 - S_0)\{(aA_0/S_0)[\exp(aA_0 - S_0)kt] - 1\}^{-1}$$

where a is the number of reactive sites of species A, k is the observed rate constant, and $k = \min(k(1), \ldots, k(n))$.

To elucidate that this solution is reasonable, computer simulations[6] (27) were done for a more complicated second-order consecutive reaction: tribromination of phenol (26) outlined in Scheme 4.

$$A + S \xrightarrow{k_1} B \qquad S = \text{bromine}$$
$$A + S \xrightarrow{k_2} C \qquad A = \text{phenol}$$
$$B + S \xrightarrow{k_3} D \qquad B = \text{4-bromophenol}$$
$$C + S \xrightarrow{k_4} D \qquad C = \text{2-bromophenol}$$
$$C + S \xrightarrow{k_5} E \qquad D = \text{2,4-dibromophenol}$$
$$D + S \xrightarrow{k_6} F \qquad E = \text{2,6-dibromophenol}$$
$$E + S \xrightarrow{k_7} F \qquad F = \text{2,4,6-tribromophenol}$$

SCHEME 4

Pseudo-first-order kinetics for the aqueous bromination of phenol, object of a different paper,[7] at pH = 1, 25°C in 1 M KBr gave $k(1) = (k_1 + k_2) = 1.33 \times 10^5$, $k(2) = k_3 = 7.74 \times 10^3$, $k(3) = (k_4 + k_5) = 2.24 \times 10^3$, $k(4) = k_6 = 871$, $k(5) = k_7 = 6.02 \times 10^3\ M^{-1}\ s^{-1}$ and assumed that $k_4/k_5 = k_1/k_2 = 50$. The initial conditions for the simulation were $S_0 = 3A_0 = 5 \times 10^{-5}\ M$ and $(B_0 = C_0 = D_0 = E_0 = F_0 = 0)$. When these parameters are input in the program, it generates concentration values for each of the species, by differential solution of the simultaneous equations[8] at different times and these are plotted in Fig. 1. Analysis clearly shows $S = (894t + 2 \times 10^{-4})^{-1}$ correlation coefficient (hereafter denoted as c-c) (0.99994) demonstrating that $k = 894 \simeq k(4) = 871\ M^{-1}\ s^{-1}$: the value of the rate-determining step. The small difference in the magnitude may be attributed, in part, to rounding off errors in the iterations.

Combination of the mass-balance equation (where $(aA_0 = S_0)$, and B_0, C_0,... $= 0$) and the simultaneous differential equations for any consecutive process leads to:

$$[27]\quad k = \frac{S_0}{\int_0^\infty S^2\,dt}$$

identical to eq. [16] but where the expression for k varies with the process.[9]

3. Discussion

3.1. Initial conditions

Initial conditions have been a source of difficulty for all the authors. Frost and Schwemer (4) and Svirbely *et al.* (14–18) dismiss this difficulty by explaining that for $S_0 = aA_0$, where a is the number of reactive sites on species A, the mathematical equations simplify. Wen (20), Khan and Khan (11), and Kubin *et al.* (21) apparently wrote their papers so that the restriction $S_0 = aA_0$ could be lifted. However, these last authors show conflicting arguments within their own papers. Citing (11, 20) the work of Goldfinger *et al.* (28) that stoichiometric concentrations of reactants may be difficult to prepare, particularly when the reactants are gases and the reactions are rapid, they overlook their own analytical solution which requires known initial conditions. If it is difficult to prepare stoichiometric concentra-

[5]The terms $(aA_0 - S_0)$ and (aA_0/S_0) differentiate eq. [5] from eq. [26] where the first term evolves from the mass-balance equation of the reaction scheme. The factor a is justified in eq. [26] because it concatenates earlier observations (4, 14–18) with the shown case[3] that for $(aA_0 = S_0)$ then $S = S_0(S_0kt + 1)^{-1}$.

[6]We acknowledge the guidance of Dr. R. T. Rye to the use and logic of the program: RMCHS (27).

[7]O. S. Tee and M. Paventi, manuscript in preparation.

[8]The differential equations are set up by a subroutine from the input chemical equations.

[9]The expression for k for the process in Scheme 3 is

$$k = \frac{2(k_1 + k_2)k_3k_4}{k_1k_4 + k_2k_3 + 2k_3k_4}$$

Can. J. Chem. Downloaded from www.nrcresearchpress.com by 118.98.75.50 on 09/07/12
For personal use only.

Can. J. Chem. Downloaded from www.nrcresearchpress.com by 118.98.75.50 on 09/07/12
For personal use only.

TABLE 1. Comparison of published rate constants and initial conditions for the alkaline hydrolysis of esters[a] versus those computed from the rate data using eq. [28] or eq. [31]

	Published parameters				Computed parameters[b]				
Compound	(Ref.)	$k(1), \ldots, k(n) \times 10^2$ (M^{-1} s^{-1})	$S_0 \times 10^3$ (M)	$A_0 \times 10^3$ (M)	$k \times 10^2$ (M^{-1} s^{-1})	$S_0 \times 10^3$ (M)	$A_0 \times 10^3$ (M)	$\alpha \times 10^3$ (M)	c-c
Diethyl succinate	(7)[c]	9.33, 6.08	12.417	6.209	4.37	12.419	6.81	0	0.99992
	(2)[d]	20.01, 2.088							
	(4)[e]	19.0, 3.53							
	(17)[f]	8.38, 1.20							
	(12)[g]	10.6, 1.62[h]	8.38	8.91	9.28	8.37	4.99	0	0.99998
Dimethyl glutarate	(2)[d]	12.1, 1.87	1.99	1.99	5.63	1.99	1.99	0	0.99975
	(20)[d]	12.22, 1.845							
	(32)[d]	12.13, 1.87							
	(21)[d]	11.81, 4.138							
Diethyl adipate	(4)[e]	8.57, 3.07	9.96	4.98	3.67	9.67	4.84	0	0.99953
	(2)[d]	5.87, 1.17							
	(13)[i]	9.95, 2.05							
Di-*n*-butyl phthalate	(11)[j]	0.392, 3.57	45.0	25.0	0.393	48.3	26.9	0	0.99962
1,3,5-tri-(4-carbomethoxy-phenyl)-benzene	(6)[k]	8.90, 5.93, 2.97	9.345	3.115	2.47	9.588	3.429	0	0.99986
	(21)[k]	7.213, 5.397, 3.753							
Pentaerithritol tetraacetate	(16)[l]	16.93, 19.87, 17.52, 12.0	20.74	5.184	5.25	21.93	6.29	0	0.99979
Diethyl malate	(17)[m]	72.8, 26.8, 1.77, 14.3	12.14	6.07	11.1[n,o]	—	—	0.941[o]	0.99967[o]
1,3,5-Tricarbomethoxybenzene	(15)[p]	24.52, 2.55, 0.490	20.90	6.966	2.02[n,q]	—	—	1.55[q]	0.99956[q]
	(21)[p]	22.28, 2.707, 0.480							
Triethyl citrate	(18)[m]	82.7, 4.87, 0.82, 1.8 12, 0.23, 0.18	12.14	4.05	8.68[n,r]	—	—	3.13[r]	0.99990[r]

[a]Only type of second-order reaction for which data (i.e., S and t) have been published as revealed by a literature search.
[b]Obtained from regression analysis of eq. [28] unless otherwise indicated.
[c]Dioxane–water 76.30%, dielectric constant (ϵ) = 13.10, 24.93°C.
[d]Water, 20.3°C.
[e]Dioxane–water–KCl, 25.0°C.
[f]Dioxane–water 20%, ϵ = 63.97, 15.07°C.
[g]Water, 15°C.
[h]Determined for sodium ethyl succinate in water at 15°C.
[i]Water, 20°C.
[j]Ethanol–water 80%, 50°C, ionic strength (I) = 0.4 M.
[k]Dioxane–water 82%, ϵ = 9.07, 34.98°C, assumed $k_1:k_2:k_3$ = 3:2:1.
[l]Aqueous barium chloride solution 0.0333 M, I = 0.10, 4.1°C.
[m]Dioxane–water 30%, ϵ = 54.74, 15.07°C.
[n]Obtained from eq. [21] (11).
[o]$\int_0^\infty (S-\alpha)^2 dt = \int_0^{14} (S_1-\alpha)^2 dt + \int_{14}^\infty (S_2-\alpha)^2 dt$; time is in minutes; $S_1 = \{(64.90t + 132.7)^{-1} + 4.053 \times 10^{-3}\}$, c-c = 0.99968; $S_2 = \{(2.784t + 214.7)^{-1} + 9.41 \times 10^{-4}\}$, c-c = 0.99967.
[p]Dioxane–water 60%, ϵ = 28.85, 5.82°C.
[q]$\int_0^\infty (S-\alpha)^2 dt = \int_0^{12.67} (S_1-\alpha)^2 dt + \int_{12.67}^{46.33} (S_2-\alpha)^2 dt + \int_{46.33}^\infty (S_3-\alpha)^2 dt$; time is in minutes; $S_1 = \{(19.23t + 95.19)^{-1} + 0.0104\}$, c-c = 0.99999; $S_2 = \{(2.062t + 83.49)^{-1} + 0.00420\}$, c-c = 0.99969; $S_3 = \{(0.7419t + 89.35)^{-1} + 0.00155$, c-c = 0.99956.
[r]$\int_0^\infty (S-\alpha)^2 dt = \int_0^{4.01} (S_1-\alpha)^2 dt + \int_{4.01}^9 (S_2-\alpha)^2 dt + \int_9^\infty (S_3-\alpha)^2 dt$; time is in minutes; $S_1 = \{(91.94t + 183.3)^{-1} + 0.006689\}$, c-c = 0.99956; $S_2 = \{(282.2t - 286.11)^{-1} + 0.007339\}$, c-c = 0.99976; $S_3 = \{(2.245t + 198.8)^{-1} + 0.00313\}$, c-c = 0.99990.

tions of reactants then it is similarly difficult to know the precise initial conditions. Wen then does not avoid (20), as he claims, the restriction to prepare stoichiometric amounts but merely generalizes the work of Frost and Schwemer (4). It will be shown below that valuable information about initial conditions may be obtained by analysis of the data by eq. [26].

Consider that the experimental data may be reproduced by eq. [26]. The initial conditions need not be known. The pertinent parameters may be found thusly. Equation [26] is rearranged:

$$[28] \quad \ln\left\{\frac{(aA_0 - S_0)}{S} + 1\right\} = (aA_0 - S_0)kt + \ln(aA_0/S_0)$$

To find the individual parameters in Table 1, the left-hand side of eq. [28] is plotted versus t. The unknown constant $(aA_0 - S_0)$ is varied so as to get a maximum correlation coefficient. This task is easily accomplished with a pocket calculator. At maximum correlation, the optimized parameters: $(aA_0 - S_0)$, the slope: $\{(aA_0 - S_0)k\}$, and the intercept: $\{\ln(aA_0/S_0)\}$ are known. Therefore, k is simply the ratio of the slope and $(aA_0 - S_0)$, and A_0 and S_0 can be evaluated from $(aA_0 - S_0)$ and the intercept. These various constants are reported in Table 1 along with the published values. The initial conditions thus calculated compare favourably with the experimental initial conditions. Thus, no prior knowledge of initial conditions or ratio of reactants need be known. The exception to this agreement between the calculated and experimental initial conditions comes from the work of Ritchie (12) on the alkaline hydrolysis of the monoethyl and diethyl succinate, as shown in Table 1. Analysis using eq. [28] leads to a concentration of the diethyl ester approximately half of the initial experimental value. This difference may be explained if the value of a (the "effective" number of reactive sites on A) is one, so that the reaction is not consecutive but stops at the monoester stage. This is plausible since the rate of alkaline hydrolysis of the half-ester of succinic acid would be expected to be much smaller than the rate of hydrolysis of the diester because of the electrostatic effect of the ionized carboxyl group. This electrostatic effect is manifest in the ratio $(k_1/k_2 > 100)$ (12, 13) for diethyl malonate. In the work of Svirbely and Kuchta (7) with diethyl succinate, the electrostatic effect is minimized (so that $k_1/k_2 \approx$ unity) because in the solvent dioxane–water 76.3% (7) ion-association of Na^+ with CO^- will be extensive.

It can be seen from Fig. 1 that immediately after mixing, the original concentration of phenol has totally reacted to form intermediate products. From this simulation it can be deduced that beginning with *any ratio* of reactants it should be possible to obtain the minimum rate constant for the reaction. This statement has a consequence: it is not required for the original reactant to be absolutely pure, as long as the impurities are part of the kinetic scheme. This exposes the futility of the experimental work to obtain very pure substances (6, 16–18). Ingold (2) would seem to have implicitly accepted this fact in obtaining one of the rate constants for the hydrolysis of dimethyl glutarate.

3.2. Closeness of fit

The rate constants are assumed to be a reliable set when the original data are regenerated from the equations employed (2, 14–18, 21) or when a certain shift of a given plot (4) gives coincidence with a calculated family of curves. But degeneracy may occur for certain ratios $(k_2{:}k_1 = 0, 0.5, \infty)$ (4), $(k_1{:}k_2{:}k_3 = 3{:}2{:}1)$ (5, 6), or $(k_1{:}k_2{:}k_3{:}k_4 = 4{:}3{:}2{:}1)$ (16) making the reactions appear simple second order. In cases where the denominator is equal (or close to) zero, extended (16) or quickly-converging (21) power series or differential approximations (14) are used. These particulars and predeterminations of $k(i)$'s (5, 6), make the methodology of solution semi-empirical, confusing, and not as general as claimed.

In fact, closeness of fit cannot be a measure of reliability of the solutions (29) for the rate equations, as has been suggested (11, 16–18, 21). This is illustrated with an example below. Furthermore, the multiple rate constants, however obtained, indicate that a predetermined number of parameters (rate constants) multiplied by a particular function can reproduce the data. But mathematically *any* function can be approximated by *any* number of terms of a power series. Thus, this criterion fails on two counts. Firstly, it forces an arbitrary and finite set of constants to regenerate the function when another more numerous set may improve the "closeness of fit". This is illustrated in section 3.4. Secondly, it fails the test for uniqueness as discussed by Svirbely *et al.* (18) or by inspection of Table 1. For instance the entry for the alkaline hydrolysis of 1,3,5-tri-(4-carbomethoxyphenyl)-benzene reads (k_1, k_2, k_3): 0.0890, 0.0593, 0.0297 $M^{-1}\,s^{-1}$ (6) and 0.0721, 0.0540, 0.0375 $M^{-1}\,s^{-1}$ (21), respectively, for the identical kinetic run.

In one case Kubin *et al.* (21) try to explain the difference in one of their evaluated rate constant versus that reported (see their Fig. 2 (21)), by arguing that it is necessary to measure the reaction course at least up to 70–75% conversion. The deduction was based mainly on their favourable results (graphically represented in their Fig. 1 (21)) using the data of Frost and Schwemer (4) (up to 66% conversion). This explanation cannot be correct because if the function[10] $(\lambda = \int_0^t S\,dt)$ can be determined accurately, then it little matters how its values vary from $t = 0$ to $t = \infty$ (i.e., $\lambda = \int_t^\infty S\,dt$). Regardless of the range of λ: $(\int_0^{t_{30\%}} S\,dt)$ as used in their iteration (21) or $(\int_0^{t_{75\%}} S\,dt)$ as claimed for optimum results, mathematically an identical set of rate constants ought to be produced. In fact, Svirbely *et al.* (14) use values of time very close to zero to avoid the failure of their general eq. [14] when its denominator approaches zero. Likewise it is shown by Radhakrishnamurti *et al.* (9) that in the interval $(0 \leqslant t \leqslant t_{20\%})$ similar values of the rate constants may be obtained as when evaluated over the interval $(0 \leqslant t \leqslant t_{60\%})$. Also application of eq. [27] requires 100% conversion, yet can be solved if the function S is known accurately within a finite time interval.

Although it is not necessary to follow a reaction up to large conversion values, it is a necessary condition that the data for S have zero as their asymptote and no other value no matter how small. Differently stated, it is necessary that the integral (eq. [27]) be finite. For example, consider the smoothed data of Frost and Schwemer (4) (their Table IV (ref. 4) or Table 4 (ref. 25*b*)) where $S = [OH^-]$, $A = [\text{diethyladipate}]$, $S_0 = 2A_0 = 0.00996\,M$. These data may be represented by the two equations below:

$$[29] \quad S = (0.045689t + 107.23)^{-1} + 5.5178 \times 10^{-4} \qquad (\text{c-c} = 0.9999993)$$

where $S_0 = (107.23)^{-1} = 0.009326\,M$, and by

$$[30] \quad S = (0.0365t + 104)^{-1} \qquad (\text{c-c} = 0.9997)$$

[10]Evaluation of such a function was originally introduced by French (3) and then appeared to gain general acceptability with Svirbely *et al.* (14–18), Kubin *et al.* (21), and Saville (30).

Can. J. Chem. Downloaded from www.nrcresearchpress.com by 118.98.75.50 on 09/07/12
For personal use only.

Can. J. Chem. Downloaded from www.nrcresearchpress.com by 118.98.75.50 on 09/07/12
For personal use only.

where $S_0 = (104)^{-1} = 0.00961\ M$.[11] Substituting S from eq. [29] (i.e., the most closely fitting data) in eq. [27], no mathematical solution is obtained because ($\int_0^\infty S^2 dt = \infty$). However, the more poorly correlated data from eq. [30], with a zero asymptote, yield $\int_0^\infty S^2 dt = 0.263\ M^2$. Therefore, from eq. [27], $k = (0.00961/0.263) = 0.0365\ M^{-1}\ s^{-1}$ or $k = (0.00996/0.263) = 0.0379\ M^{-1}\ s^{-1}$ depending on the value of S_0 used. Compare these values with the minimum reported (4): $0.0307\ M^{-1}\ s^{-1}$. The foregoing example then illustrates that a close fit should not necessarily be the aim in deciding the reliability of the equations.

3.3. The nonzero asymptote and variation of initial conditions

Problems of initial conditions arise in eq. [30] if a zero asymptote is forced upon the data which are ultimately reflected in the value of k, but as discussed in section 3.1, initial condition problems are resolved by analysis using eq. [28]. In fact this equation also incorporates the nonzero asymptote, provided it is small, by allowing variations of the terms ($aA_0 - S_0$) and $\ln(aA_0/S_0)$.

Reconsider the smoothed data above (4) and the same data, in its raw form, given in Table III of ref. 4. Analysis of the massaged data via eq. [28] gives the following parameters: $k = 0.0372\ M^{-1}\ s^{-1}$, $S_0 = 0.00973\ M$, $A_0 = 0.00486\ M$, and the optimum c-c = 0.99949. Although the terms ($aA_0 = S_0$) and $\ln(aA_0/S_0)$ are allowed to vary, the calculated values S_0 and A_0 are significantly closer to the experimental values than when evaluated from eq. [29] or eq. [30]. Analysis of the raw data using eq. [28] yields (see Table 1): $k = 0.0367\ M^{-1}\ s^{-1}$, $S_0 = 0.00967\ M$, $A_0 = 0.00480\ M$, and the optimum c-c = 0.99953. From these parameters one immediately concludes that the smoothed data are biased, since the constants do not agree and biased in the wrong direction, since the correlation coefficient from the analysis of the raw data is greater than that evaluated from the smoothed data. Similar bias may exist for pooled data if care is not exercised.

Apparently, no difficulty exists in the analysis of the data if the asymptote is small. However, such compensation via eq. [28] cannot be made if the value of the asymptote is large. Three examples from the literature (15, 17, 18) are shown in Fig. 2. The reason for this experimental abnormality (i.e., high limiting value) may be due, in part, to interferences of intermediate products in the determination of S causing markedly different curvature during the initial stages (see Fig. 2) when intermediate product build-up is fastest. The intersections, shown in Fig. 2, of the apparently bi-phasic plots, numbered **1** and **3**, correspond precisely to the time 8.6 min and 16 min, respectively, at which rate, intermediate product formation has reached a maximum (see Fig. 1 for both refs. 17 and 18). The method for an approximate evaluation of k for these cases is

$$[31] \quad k = \frac{S_0}{\int_0^\infty (S - \alpha)^2 dt}$$

[11]As pointed by a referee, the use of correlation coefficients should not be misconstrued as an adequate (or the only) criterion for goodness of fit. It is offered as a familiar (as opposed to quadratic mean error of fit (17, 18)) one-number quantity that measures the magnitude of the deviation from the data. This number avoids tables of percent differences between calculated and observed values used in earlier papers (15–18), but by itself does not measure the randomness of these differences. To represent a close fit, a correlation coefficient close to unity must be accompanied by such a measure of randomness.

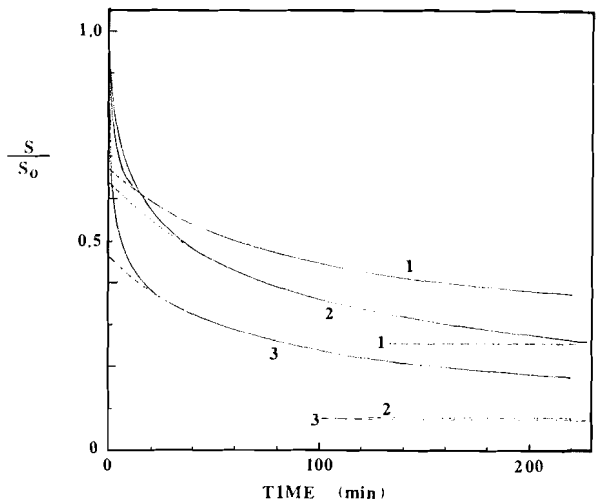

FIG. 2. Ratio of $[HO^-] = S$ to $[HO^-]_0 = S_0$ versus time for the hydrolysis of **1**: triethyl citrate (18), **2**: 1,3,5-tricarbomethoxybenzene (15), and **3**: diethyl malate (17). The numbered dotted segments are the asymptotes (α/S) (see Table 1) for the respective curves. The equations of the dotted lines extrapolating the curves to zero time are given in the footnotes of Table 1. Note that for **2** the data extend to 501 min but the curve was truncated for clarity.

which is deduced from eq. [27] where α is the value of the asymptote.[12] This technique was employed to evaluate the rate constants for the alkaline hydrolysis of 1,3,5-tricarbomethoxybenzene (15), diethyl malate (17), and triethyl citrate (18) shown in Table 1.

3.4. The rate constants

The value of the rate constant calculated from a single set of data must be unique. The wrong assumption made in the literature, cited in this paper, is that two or more rate constants can be evaluated. Firstly, this presupposes a particular mechanism. Secondly, completely false solutions and arguments result. We will point out one.

For the alkaline hydrolysis of diethyl malate, Svirbely and Kundell (17) list the following results (k_i's expressed in $M^{-1}\ s^{-1}$):

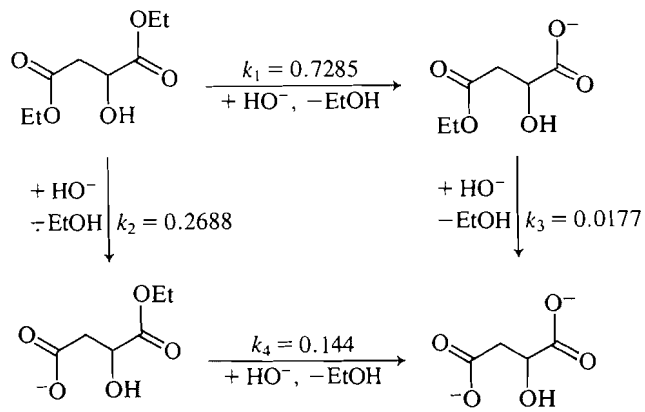

SCHEME 5

[12]The value of α was calculated from analysis of the data via the equation $(S - \alpha)^{-1} = (bt + c)$ where b and c are constants (by analogy to the limiting equation[5] where $\alpha = 0$: b = k and $c = (S_0)^{-1}$. The data for S are analyzed for different time intervals (see footnotes of Table 1). Also the correlation coefficients reported in the footnotes of Table 1 is that resulting from these analyses.

From the Taft reaction constant for the basic hydrolysis of esters (2.48), they calculate that an α-hydroxy substituent should increase the rate of basic hydrolysis of an ester by 25-fold and that for a β-hydroxy substituent by about 3.1-fold, agreeing with their experimental result (17). However, results for the alkaline hydrolysis of triethyl citrate, under the same conditions as for diethyl malate, show different substituent effects. The data of Svirbely *et al.* (18) (k_i's in $M^{-1}\,s^{-1}$) are shown below:

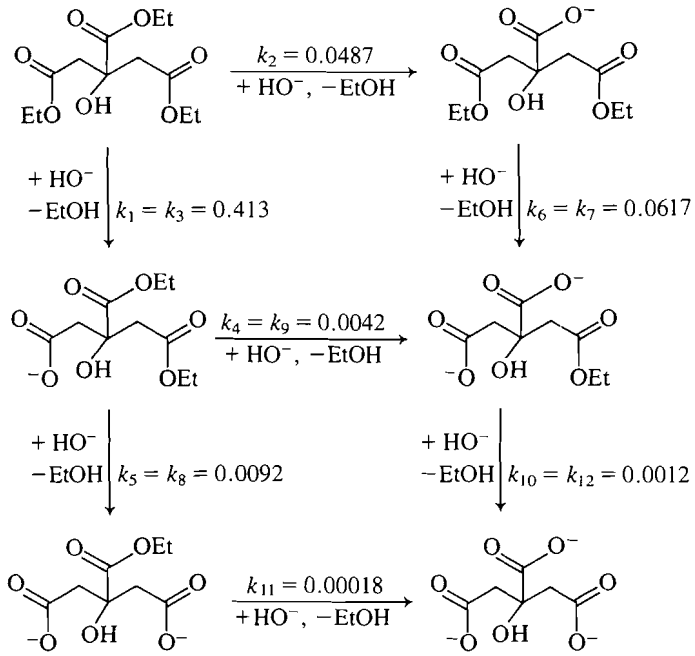

SCHEME 6

This difference is in part dismissed as an effect of steric hindrance (cf. $k_1 = 0.7285\ M^{-1}\,s^{-1}$ for diethyl malate and $k_2 = 0.0487\ M^{-1}\,s^{-1}$ for triethyl citrate) but an opposite effect appears in the second hydrolysis step (cf. $k_3 = 0.0177\ M^{-1}\,s^{-1}$ for diethyl malate and $k_6 = k_7 = 0.0617\ M^{-1}\,s^{-1}$ for triethyl citrate). The answer is that the rate constants for these two reactions are wrong. The apropos mathematical reason for this statement is expounded by Rodriguin and Rodriguina[13] that the assignment of the rate constant to a particular step is haphazard since the rate constants can be interchanged (31*c*). Thus, the literature values reported in Table 1 for a particular step of any reaction cannot be taken seriously!

All the substrates in Table 1, with the exception of 1,3,5-tri-(4-carbomethoxyphenyl)-benzene and 1,3,5-tricarbomethoxy-benzene, may undergo an intramolecular assisted displacement of alkoxide, yet no mention of this is made anywhere. This brings up the second reason why the rate constant must be unique: what if the mechanism also involves a reactive intermediate? The method outlined above by solving eq. [28], independently of the mechanism, gives the rate constant of the rate-limiting step. In combination with pseudo-first-order kinetics, information about a reactive intermediate may be drawn.

[13]The equations shown by Rodriguin and Rodriquina, for instance eq. II.12 (31*a*), are similar to eqs. [2], [3], and [4] reported by Svirbely and Blauer (14) where the values of t, for the case where one component is in large excess (31*b*), is replaced by the value $\lambda = \int_0^t Sdt$. Thus, any argument (31*c*) which is valid for eq. II.12 is also valid for the equations of the papers cited here.

This is illustrated with an example. Let us assume that the processes $A + S \xrightarrow{k_1} B$ and $B + S \xrightarrow{k_2} C$ have been studied independently under pseudo-first-order conditions and the constants k_1 and k_2 are known for different conditions. In particular, it is known that $B + S \xrightarrow{k_2} C$ is the slow step (i.e. $k_2 = \min(k_1, k_2)$). However, analysis of the second-order consecutive reaction, under the same particular conditions, reveals that $k = k_1$. The explanation for such situation may be as follows:

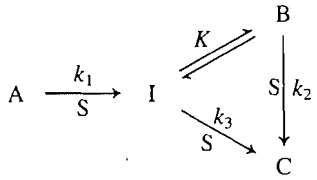

SCHEME 7

where I is an intermediate and K is the tautomeric constant. The applicable equilibrium, mass balance, and differential equations for Scheme 7 are:

[32] $B = KI$

[33] $A_0 = A + (1 + K)I + C$

[34] $A' = -k_1AS$

[35] $C' = (Kk_2 + k_3)IS$

[36] $S' = k_1AS - (Kk_2 + k_3)IS$

By differentiation of eq. [33] and substitution of C' and A' into the resultant equation one obtains:

[37] $$I' = \frac{k_1}{(1 + K)}AS - \frac{(Kk_2 + k_3)}{(1 + K)}IS$$

Assuming that the data are represented by eq. [28], then by the same methodology shown above for Scheme 2, the ultimate equation in k has the form

[38] $$\frac{(1 + K)}{k_1(Kk_2 + k_3)}k^2 - \left(\frac{1}{k_1} + \frac{(1 + K)}{(Kk_2 + k_3)}\right)k + 1 = 0$$

which is satisfied when $k = k_1$ or $k = (Kk_2 + k_3)/(K + 1)$. Now, since it is given that $k = k_1$ and $k_2 < k_1$ then $(Kk_2 + k_3)/(K + 1) > k_1$. Thus, we have a handle in evaluating upper or lower limits of k_3 or K if one of these can be estimated. This example was evident for two kinetic processes studied by the author (26) and are the object of an upcoming paper. These cases can *only* arise from the study of consecutive second-order reactions and explained in conjunction with pseudo-first-order kinetics of the individual processes.

One last point concerning rate constants as determined from the conventional pseudo-first-order analysis and those obtained from eq. [28]. For a substrate A, with a reactive sites, reacting with species S, the second-order rate constant k, for reaction conditions of pseudo-first-order, has been erroneously evaluated from the simple exponential equation: $S = S_0(\exp A_0kt)^{-1}$ or a variant $S = \{S_0(A_0 - S_0)/A_0\}\{\exp\ (A_0 - S_0)kt\}^{-1}$. However, the quaesitum[14] for k must be evaluated from eq. [26] (or eq. [28]) with the pseudo-first-order condition (i.e.,

[14]The Webster dictionary defines quaesitum as the actual value of a quantity.

Can. J. Chem. Downloaded from www.nrcresearchpress.com by 118.98.75.50 on 09/07/12
For personal use only.

$S_0 \ll aA_0$). The limiting functions[3] for eq. [26] are $S = \{S_0(\exp aA_0kt)^{-1}\}$ or $S = \{S_0(aA_0 - S_0)/aA_0\}\{\exp(aA_0 - S_0)kt\}^{-1}$. Thus the conventional second-order rate constant may be up to a times larger than that evaluated from eq. [26].[15] This factor is usually treated as a statistical correction which may be correct if all the reactive sites on species A are symmetrical but obviously wrong if no symmetry exists between the reactive sites.

4. Conclusion

We have shown that experimental data are well reproduced by eq. [26] (or eq. [28]), whose cheaper[16] and faster analysis yields $k = \min(k(1), \ldots, k(n))$ and also the initial conditions (i.e., S_0 and A_0). For data with a large non-zero asymptote eq. [31] may be applied to find the approximation for k. The literature rate constants listed in Table 1 have no scientific significance and appear to be mathematical artifacts[17,18] of the non-linear integral equations used. These constants when introduced into these equations reproduce the data, but because the total number has been predetermined by the chosen mechanism, their significance is on very shaky footing. More pseudo-first-order kinetics need be done with the compounds listed in Table 1 to get a clearer overall picture of the mechanism. Such kinetics should also better demonstrate the validity of eq. [26] as applied to second-order competitive reactions and the significance of k.

5. Acknowledgements

We are grateful to the Natural Sciences and Engineering Research Council of Canada for financial support. Thanks to Dr. J. T. Edward for the literary corrections of the manuscript. Thanks also to Dr. O. S. Tee for the project which provided the inspiration for this paper.

1. R. L. SOMORJAI. *In* Physical chemistry, an advanced treatise. *Edited by* D. Henderson. Academic Press, New York. 1975. Vol. XI B. Chapt. 13, p. 909.
2. C. K. INGOLD. J. Chem. Soc. 2170 (1931).
3. D. FRENCH. J. Am. Chem. Soc. **72**, 4806 (1950).
4. A. A. FROST and W. C. SCHWEMER. J. Am. Chem. Soc. **74**, 1268 (1952).
5. W. J. SVIRBELY. J. Am. Chem. Soc. **81**, 255 (1959).
6. W. J. SVIRBELY and H. E. WEISBERG. J. Am. Chem. Soc. **81**, 257 (1959).
7. W. J. SVIRBELY and A. D. KUCHTA. J. Phys. Chem. **65**, 1333 (1961).
8. W. J. SVIRBELY and P. A. CUNNIFF. Can. J. Chem. **40**, 1862 (1962).
9. P. S. RADHAKRISHNAMURTI and G. P. PANIGRAHI. J. Indian Chem. Soc. **44**, 430 (1967).
10. P. S. RADHAKRISHNAMURTI and G. P. PANIGRAHI. J. Indian Chem. Soc. **46**, 567 (1969).
11. M. N. KHAN and A. KHAN. Indian J. Chem. Sect. A, **15**, 220 (1977).
12. M. RITCHIE. J. Chem. Soc. 3112 (1931).
13. F. H. WESTHEIMER, W. A. JONES, and R. A. LAD. J. Chem. Phys. **10**, 478 (1942).
14. W. J. SVIRBELY and J. A. BLAUER. J. Am. Chem. Soc. **83**, 4115 (1961).
15. W. J. SVIRBELY and J. A. BLAUER. J. Am. Chem. Soc. **83**, 4118 (1961).
16. J. A. BLAUER, L. SCHMID, and W. J. SVIRBELY. J. Am. Chem. Soc. **85**, 2716 (1963).
17. W. J. SVIRBELY and F. A. KUNDELL. J. Am. Chem. Soc. **89**, 5354 (1967).
18. F. A. KUNDELL, D. J. ROBINSON, and W. J. SVIRBELY. J. Phys. Chem. **77**, 1552 (1973).
19. J. ROTGER and M. DERBESY. C.R. Hebd. Seances Acad. Sci. Ser. C (282), 753 (1976).
20. J. ROTGER and M. DERBESY. C.R. Hebd. Seances Acad. Sci. Ser. C (282), 753 (1976).
21. W. J. WEN. J. Phys. Chem. **76**, 704 (1972).
22. K. KUBIN, S. SEVCIK, J. STAMBERG, and P. SPACEK. Coll. Czech. Chem. Commun. **39**, 2591 (1974).
23. S. W. BENSON. The foundations of chemical kinetics. McGraw-Hill Book Company, Toronto. 1960. p. 43.
24. R. C. WEAST (*Editor*). CRC handbook of chemistry and physics. 52nd ed. CRC Press, Cleveland, OH. 1972. p. A114.
25. M. SPIVAK. Calculus. W. A. Benjamin, Menlo Park, CA. 1967. p. 179.
26. A. A. FROST and R. G. PEARSON. Kinetics and mechanism. 2nd ed. Wiley, New York. 1962. Chapt. 8. (*a*) p. 178; (*b*) p. 184.
27. M. PAVENTI. Ph.D. Thesis. Concordia University, Montreal, Quebec. 1984.
27. D. F. DE TAR. *In* Computer programs for chemistry. Vol. II. *Edited by* D. F. De Tar. W. A. Benjamin, New York. 1969. Chapt. 2.
28. P. GOLDFINGER, R. M. NOYES, and W. Y. WEN. J. Am. Chem. Soc. **91**, 4003 (1969).
29. J. L. DYE and V. A. NICELY. J. Chem. Educ. **48**, 443 (1971).
30. B. SAVILLE. J. Phys. Chem. **75**, 2215 (1971).
31. N. M. RODRIGUIN and E. N. RODRIGUINA. *In* Consecutive chemical reactions. *Edited by* R. F. Schnider. D. Van Nostrand Company, Toronto. 1964. Chapt. II. (*a*) p. 11; (*b*) p. 6; (*c*) pp. 17–19.
32. S. WIDEQVIST. Acta Chem. Scand. **4**, 1216 (1950).

[15]This has also been shown to be the case (26) by allowing all the species, derived from A after reaction with S, to account for the disappearance of S. Then assuming the steady state on all these species except that of the rate-determining step, the rate constant works out to be larger than the quaesitum by the number of reactive sites of the species in the rate-determining step.

[16]The acknowledgements of the various papers (14, 16–18) divulge that grants have been required to cover the costs of computer expenses.

[17]Rephrasing the words of Dr. B. C. Eu whose consultation for the nonlinear differential equations is acknowledged, the mathematical iterations can be equated to the chasing of a ghost.

[18]Note that Svirbely *et al.* (14) mention that the guess to the value of the rate constant must be good (close to 100%) for the iteration to converge.

Can. J. Chem. Downloaded from www.nrcresearchpress.com by 118.98.75.50 on 09/07/12
For personal use only.

A theoretical insight into the insertion reaction of singlet methylene to the hydrogen molecule

M. ORTEGA, J. M. LLUCH, A. OLIVA, AND J. BERTRAN
Departamento de Química Física, Universidad Autónoma de Barcelona, Bellaterra, Barcelona, Spain

Received June 20, 1986[1]

M. ORTEGA, J. M. LLUCH, A. OLIVA, and J. BERTRAN. Can. J. Chem. **65**, 1995 (1987).

The least-motion and non-least-motion energy profiles for the insertion reaction of singlet methylene into the hydrogen molecule have been calculated using the 6-31G* basis set and introducing the correlation energy with the Møller–Plesset perturbation theory and with the MC-SCF technique. From the results obtained the effect of geometry optimization including electron correlation on the shape of the energy surface is discussed. The building up of a bidimensional biconfigurational energy surface has permitted one to interpret the opening of the methylene angle during the least-motion process as a direct consequence of the change in the electronic configuration. The TC-SCF/6-31G* second order transition structure for this forbidden process has been directly located using gradient minimization methods.

M. ORTEGA, J. M. LLUCH, A. OLIVA et J. BERTRAN. Can. J. Chem. **65**, 1995 (1987).

En utilisant des ensembles de base 6-31G* et en introduisant l'énergie de corrélation dans la théorie perturbationnelle de Møller–Plesset et dans la technique des OM en champ auto-cohérent, on a calculé les profils d'énergie, impliquant et n'impliquant pas un minimum de mouvement, pour la réaction d'insertion du méthylène singulet dans la molécule d'hydrogène. A partir des résultats obtenus, on discute de l'effet de l'optimisation de la géométrie, y compris de la corrélation électronique, sur la forme de la surface énergétique. En construisant une surface énergétique biconfigurationnelle et bidimentionnelle, on a pu affirmer que l'ouverture de l'angle du méthylène, au cours du processus impliquant un minimum de mouvement, est une conséquence directe du changement dans la configuration électronique. Utilisant des méthodes de minimisation des gradients, on a pu localiser directement la structure de transition du deuxième ordre TC-SCF/6-31G* de ce processus défendu.

[Traduit par la revue]

1. Introduction

It is now well established that Hartree–Fock molecular orbital theory leads to equilibrium structures that show systematic deviations from the experimental results (1). In recent studies of a wide range of molecules, Pople *et al.* (2, 3) have demonstrated that the introduction of electron correlation is essential in order to obtain equilibrium geometries which are in good agreement with experimental data. In spite of these interesting results, most theoretical calculations on chemical reactivity have been done until the present by assuming that the geometries of the critical points of the potential hypersurface remain unchanged when one takes into account electron correlation. So, critical points of a reaction hypersurface are determined at the Hartree–Fock level and the correlation energy is then added, keeping invariant the previously found geometries.

Because of its small size, the insertion of singlet methylene to the hydrogen molecule has been extensively studied at different levels of calculation (4–13). This process is a prototype for reactions where a symmetry-forbidden least-motion path and an allowed non-least-motion path of lower symmetry can compete.

In order to introduce electron correlation in the least-motion path, Bauschlicher *et al.* (9) have calculated a series of contour maps showing several cuts of the potential energy hypersurface which correspond to the initial approach of both reactants, using the configuration interaction method with a double ζ basis set. They have found that the methylene bond angle at the saddle point is much larger than that for either the reactants or products, since it takes a value quite close to 180°. The authors believe that this surprising result can be attributed to the fact that this almost linear arrangement of singlet methylene will substantially decrease the unfavourable interaction between its lone pair and the doubly occupied $1\sigma_g$ orbital of H_2.

In a similar way, the same authors have studied (10) the non-least motion approach. Their CI results lead to no barrier at all for this type of approach. They conclude that the single determinant self-consistent field method does not properly describe several of the main features of the non-least motion pathway, since its results are not only quantitatively, but as well qualitatively different from the CI ones. A different conclusion is reached by Zurawski *et al.* (12). These authors use the reaction coordinate method with complete optimization at the SCF level and then introduce electron correlation in the IEPA, CI, and CEPA schemes, keeping unchanged the SCF geometries. In all cases they find that the minimum energy path does not noticeably change when electron correlation is added. The discrepancy with the results of Bauschlicher is attributed by the authors to the complete geometry optimization carried out by them. However, Schlegel *et al.* (13) have recently studied the same problem with direct location of the stationary points at the HF/3-21G and HF/6-31G* levels and using the Møller–Plesset perturbation theory in order to estimate the effect of the electron correlation energy. They have found a minute energy barrier at the Hartree–Fock level, this barrier disappearing when electron correlation is added. This result seems to show again that electron correlation substantially changes the energy profile of the non-least motion approach.

None of the above mentioned papers have studied the effect of the correlation energy on the geometry optimization process when the reaction coordinate method is used. We believe that it would be very interesting to discuss its effect on the shape of the reaction surface and, therefore, on the reaction path. In order to achieve this aim we have studied the least-motion and the non-least-motion pathways using the reaction coordinate method and optimizing all the geometrical parameters both at the Hartree–Fock level and with inclusion of electron correlation.

This work will also permit discussion on the opening of the methylene angle in the least-motion approach, quite a striking result which, undoubtedly, merits some further consideration.

[1]Revision received February 13, 1987.

Can. J. Chem. Downloaded from www.nrcresearchpress.com by 213.166.140.6 on 09/07/12
For personal use only.

Can. J. Chem. Downloaded from www.nrcresearchpress.com by 213.166.140.6 on 09/07/12
For personal use only.

2. Method of Calculation

Ab initio molecular orbital calculations were performed with the GAUSSIAN 82 (14) and MONSTERGAUSS (15) programs, using the 6-31G* basis set (16), since it is one of the simplest for which the introduction of correlation effects leads to a net improvement in structural predictions (2). Electron correlation energy was estimated by using the Møller–Plesset partition (MP) in the many-body perturbation theory (MBPT) up to second order (17). Multiconfigurational calculations using the ground and the lowest biexcited configurations were also done. These multiconfigurational calculations have been indicated throughout this work with the symbol TC-SCF.

All equilibrium geometries and transition structures were fully optimized with analytical gradient methods (18), both at the Hartree–Fock level and with inclusion of electron correlation.

3. Results and discussion

We will sequentially present the results corresponding to the allowed non-least-motion and the forbidden least-motion pathways. They have been studied with the reaction coordinate method, using the R distance between the carbon atom of methylene and the midpoint of the hydrogen molecule as independent variable. C_{2v} symmetry has been imposed for the study of the least-motion process.

Figure 1 presents the energy profiles obtained at three different levels of calculation for the beginning of the non-least-motion process. At the Hartree–Fock level, one intermediate and one transition state appear, although the resulting energy barrier is quite small. It is interesting to note that the direct location of these stationary points almost does not change the geometry and the energy of them, thus indicating the goodness of the reaction coordinate we have used. The values of R for the intermediate and the transition state are, respectively, 2.50 and 1.84 Å. When electron correlation is added, with the Møller–Plesset perturbation theory, keeping unchanged the Hartree–Fock geometries, an important stabilization of the energy profile can be observed and the energy barrier disappears. These results are in good agreement with those previously obtained by Schlegel (13). Finally, we have recalculated the energy profile with a new geometry optimization which already includes electron correlation. This leads to a new noteworthy stabilization of the energy profile although no important changes in the shape of the energy profile are now produced.

Let us now analyze the effect of electron correlation on the geometry optimization. Table 1 presents the values of the energy and of the different geometrical parameters of the system obtained both at the Hartree–Fock level and with inclusion of electron correlation, for some of the points which we have calculated. These points have been chosen in such a way that the values of R correspond to the Hartree–Fock stationary points. The presented geometrical parameters are defined in Fig. 2. The comparison between HF and MP2 values clearly shows that electron correlation produces only slight changes in the geometry of the system, the most important being the one corresponding to the angle α which measures the inclination of the hydrogen molecule with respect to the plane of methylene. In both levels of calculation the angle θ increases monotonically from its initial value in methylene to the value it has in methane. It is also interesting to note that the angle β is initially very close to 90° in good agreement with the prediction of previous calculations (10, 11, 13). Finally, the energy values of the reactants ($R = \infty$) and of methane ($R = 0.63$ Å) permit the calculation of the exothermicity of the process at both levels of calculation. One obtains 123.0 and 137.4 kcal mol^{-1}, respectively, in satisfactory agreement with the best available value, 122 kcal mol^{-1}, found in the literature (9).

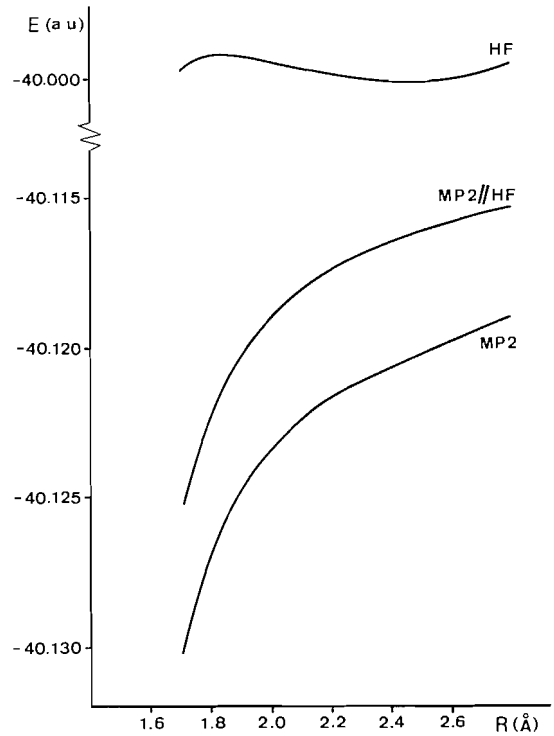

FIG. 1. Energy profiles for the non-least-motion insertion of singlet methylene to the hydrogen molecule.

TABLE 1. Variation of the total energy and of the optimized values of geometrical parameters along the reaction coordinate of the non-least-motion process

R		r	d	θ	α	β	E
∞	HF	0.73	1.10	103.1	—	—	−39.99920
	MP2	0.74	1.11	102.1	—	—	−40.11815
2.50	HF	0.72	1.10	103.3	15.1	95.3	−40.00012
	MP2	0.74	1.11	102.3	22.5	95.4	−40.12033
1.84	HF	0.75	1.10	104.5	14.8	91.8	−39.99917
	MP2	0.77	1.11	103.7	22.0	91.8	−40.12582
0.63	HF	1.77	1.08	109.5	90.0	0.0	−40.19517
	MP2	1.78	1.09	109.5	90.0	0.0	−40.33704

Let us now present the results obtained for the least-motion pathway. Figure 3 shows the energy profiles for this approach corresponding to the same different levels of calculation which have been used for the non-least-motion pathway. One can observe that the 6-31G* Hartree–Fock energy profile presents an important energy barrier, 35.5 kcal^{-1}, whose maximum is situated at about $R = 2.0$ Å. Such a large barrier is consistent with the forbiddenness of the process, our value being something higher than the CI value found by Bauschlicher and co-workers (9). As in the case of the non-least-motion pathway, a great stabilization of the energy profile is obtained when electron correlation is added at the MP2//HF level. However, the position of the maximum along the reaction coordinate scarcely changes and the value of the energy barrier only slightly decreases to the value of 32.9 kcal mol^{-1}. One can also observe that geometry optimization already including electron

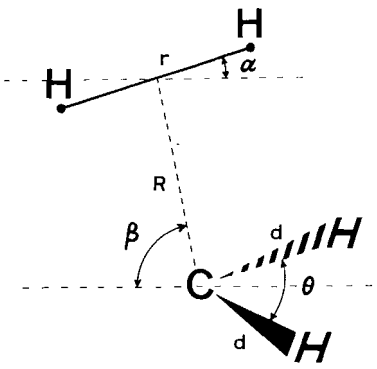

FIG. 2. Geometrical parameters used to describe the reaction system.

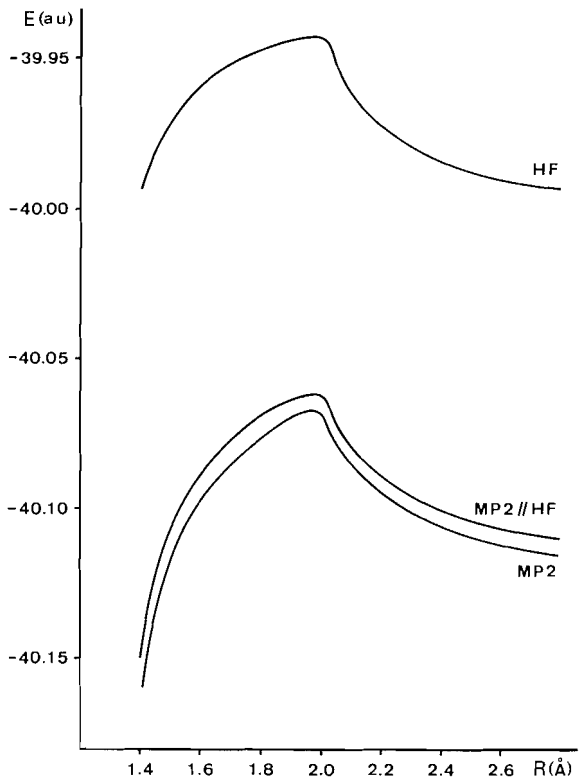

FIG. 3. Energy profiles for the least-motion insertion of singlet methylene to the hydrogen molecule.

TABLE 2. Geometrical parameters corresponding to the maximum point of the least-motion energy profile

Level of calculation	R	r	d	θ
HF	2.02	0.74	1.06	173.9
MP2	2.01	0.76	1.06	172.9

correlation at the MP2 level leads again to a noticeable change of the energy profile, the energy barrier being now 32.6 kcal mol^{-1}. It is also interesting to remark that the three energy profiles have a rather curious shape, the slope of the curve being very much greater before than after the energy maximum. The appearance of these kinks will be discussed later.

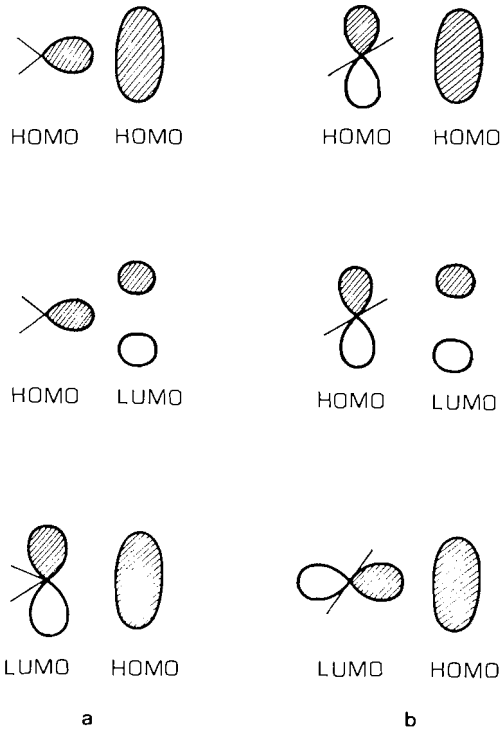

FIG. 4. Schematic representation of the frontier orbital interactions for the insertion of bent (a) and linear (b) singlet methylene to the hydrogen molecule.

The geometries obtained at the HF and MP2 levels of calculation for the structure corresponding to the maximum of the energy profiles are presented in Table 2. Obviously, only four geometrical parameters must now be specified in order to completely determine the geometry of the system, since C_{2v} symmetry has been imposed in the least-motion approach. It has to be emphasized that the values of the methylene angle θ corresponding to the maximum energy point are always rather close to 180°. As mentioned in the introduction, this almost linear arrangement of singlet methylene in the energy maximum was explained by Bauschlicher *et al.* (9) through a decrease of the unfavourable interaction between the lone pair of methylene and the doubly occupied $1\sigma_g$ orbital of the hydrogen molecule. This simple explanation seems reasonable. In the language of the frontier orbital theory, it corresponds to the diminution of the repulsive HOMO–HOMO interaction. This can be easily visualized in Fig. 4 where the different frontier orbital interactions are schematically presented for the bent and linear configurations of methylene. The symmetry of the two frontier orbitals for the linear structure has been deduced by considering the correlation diagram for the least-motion insertion of linear singlet methylene into the hydrogen molecule. Although they are strictly degenerate when the methylene molecule is isolated, the degeneracy is broken down once the process has just begun. The correlation diagram shows that the HOMO and the LUMO of the interacting system have, respectively, b_1 and a_1 symmetries in the point group C_{2v}. One can observe in Fig. 4 that the linear arrangement is not only favoured by the decrease of the repulsive interaction between the lone pair of methylene and the doubly occupied $1\sigma_g$ orbital of H_2, but also by the simultaneous increase of both stabilizing HOMO–LUMO interactions. So, the consideration of HOMO–HOMO and HOMO–LUMO interactions permits an interpretation of the

Can. J. Chem. Downloaded from www.nrcresearchpress.com by 213.166.140.6 on 09/07/12
For personal use only.

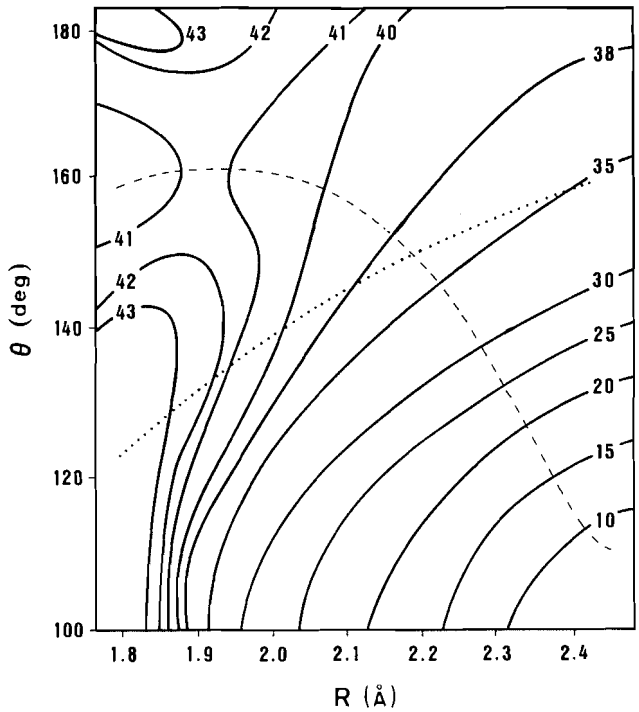

FIG. 5. Bidimensional TC-SCF/6-31G* energy surface for the least-motion path. Contour lines are labeled in kcal mol^{-1} relative to infinitely separated reactants.

TABLE 3. Variation of the geometrical parameters along the reaction coordinate for the least-motion process

	r		*d*		θ	
R	HF	MP2	HF	MP2	HF	MP2
∞	0.73	0.73	1.10	1.11	103.1	102.1
2.8	0.73	0.74	1.10	1.11	102.6	101.5
2.6	0.72	0.73	1.10	1.11	102.4	104.7
2.4	0.72	0.73	1.10	1.12	102.0	101.0
2.2	0.72	0.73	1.10	1.11	101.4	100.3
2.1	0.72	0.73	1.10	1.12	101.1	99.9
2.05	0.72	0.73	1.10	1.12	101.0	99.7
2.0	0.74	0.76	1.06	1.06	173.5	172.6
1.8	0.76	0.78	1.06	1.06	167.8	165.8
1.6	0.81	0.88	1.06	1.06	158.0	153.7
1.4	1.19	1.40	1.06	1.06	137.7	132.6
1.2	1.42	1.42	1.07	1.06	126.2	126.2
1.0	1.49	1.49	1.07	1.08	120.0	120.1
0.8	1.61	1.62	1.08	1.08	114.3	114.4
0.63	1.77	1.78	1.08	1.09	109.5	109.5

opening of the methylene angle which is produced during the process.

Let us now analyze the variation of the geometrical parameters along the reaction coordinate. Table 3 presents this variation at the HF and MP2 levels. In both cases the most important fact to be remarked is the sudden change in geometry which is exactly produced at the energy maximum. Specially interesting is the behaviour of the methylene angle θ. At the energy maximum, this angle suddenly changes from the value it has in the reactants to the value rather close to 180° and, then, it begins to decrease until the tetrahedral value of methane is reached. The sudden change in geometry at the energy

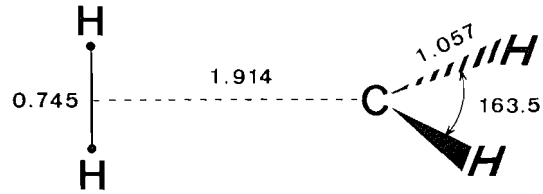

FIG. 6. Geometry of the transition structure of the least-motion path. Bond lengths in Å and angles in deg.

maximum is accompanied by a discontinuous change from the a_1^2 electronic configuration to the b_1^2 one. These results suggest that the angle θ must play an important role in the reaction coordinate and that biconfigurational calculations which take into account the a_1^2 and the b_1^2 configurations have to be done. So the building up of a bidimensional biconfigurational energy surface seems necessary in order to understand the actual mechanism of the least-motion process.

Figure 5 presents this bidimensional energy surface which has been obtained by taking as independent variables of the reaction coordinate the distance *R* and the methylene angle θ. The dotted line represents the points of the surface in which the two configurations have the same weight. Consequently, the a_1^2 configuration predominates for the points situated below the dotted line, while the b_1^2 configuration is dominant for the structures situated above this line. The most interesting fact one can observe in Fig. 5 is the existence of a saddle point situated at about $R = 1.9$ Å and $\theta = 160°$. This saddle point leads to an energy barrier of about 41 kcal mol^{-1}. Given its situation with respect to the dotted line, the dominant configuration at this point is the b_1^2 one, i.e. the change of configuration has already been produced. All these results are consistent with the ones which have been found from the energy profiles of Fig. 3, although the methylene angle and the distance *R* are now smaller and the energy barrier is noticeably higher. However, it has to be reminded that those energy profiles lead to a sudden change of both the methylene angle and the electronic configuration. That this sudden change is a direct consequence of the methodological limitations can now be clearly understood. Starting from the approximate situation of the saddle point we have tentatively drawn, in dashed line, the reaction path which links this point with the valleys of reactants and product. At the beginning of the process, the reaction coordinate is mostly formed by the distance *R* between the two reactants. In a second stage, the methylene angle θ greatly intervenes in the reaction coordinate, since it varies from the value it has in isolated methylene to a value of about 160° at the saddle point. At the same time the weight of the initially dominant a_1^2 configuration monotonically decreases from the reactants to the saddle point, the value of 50% having been reached at about $R = 2.2$ Å where the reaction path crosses the dotted line. The variations of θ and of the electronic configuration are rather fast, but continuous. Figure 5 clearly shows that the above mentioned discontinuity in the energy profiles is essentially due to the use of only the parameter *R* as independent variable of the reaction coordinate.

Starting from the approximate situation of the saddle point in the bidimensional energy surface, we have looked for the actual existence of a stationary point in the biconfigurational hypersurface through analytical gradient minimization. We do have found a stationary point, whose geometry is presented in Fig. 6. The characterization of this stationary point shows that it is a second order saddle point, since its force constant matrix has two negative eigenvalues. This was to be expected, given

Can. J. Chem. Downloaded from www.nrcresearchpress.com by 213.166.140.6 on 09/07/12
For personal use only.

that the least-motion path is not an actual reaction path, the C_{2v} symmetry having been imposed throughout. In fact, the eigenvector corresponding to the most negative eigenvalue corresponds to the breaking of this symmetry, thus leading to the non-least-motion process. On the other side the eigenvector corresponding to the other negative eigenvalue is directly associated to the least-motion approach at the saddle point since its most important components correspond to the shortening of the R distance between the two reactants. The examination of the geometrical parameters R and θ of the located saddle point shows that they are very similar to the ones previously estimated on Fig. 5, thus indicating that the choice of R and θ as the independent variables of the reaction coordinate was very adequate. The energy of the located saddle point leads to a value of 41.1 kcal mol^{-1} for the least-motion energy barrier, this value being again very close to the estimated one.

4. Conclusions

The examination of the effect of electron correlation in geometry has permitted the calculation of the least-motion and of the non-least motion MP2/6-31G* energy profiles. In this way we have found that the non-least-motion approach takes place without any energy barrier, thus confirming the results previously obtained by other authors (10–13) from more restricted studies of the energy surface. In the least-motion pathway we have shown that geometry optimization including electron correlation does not appreciably change the shape of the energy surface at the MP2 level of calculation.

This work has also permitted one to give an interpretation of the sudden opening of the methylene angle which is obtained in all the theoretical calculations carried out until the present on the least-motion path (8, 9). The building up of a bidimensional biconfigurational energy surface has shown that this opening is produced in a continuous, rather than discontinuous, way and that it is intimately related to a simultaneous change in the electronic configuration of the system. The approximate saddle point obtained in this way has permitted the direct location of a second order stationary point for this forbidden process. The results obtained in this work clearly show that the introduction of static correlation is essential in order to give a correct description of the least-motion process.

Acknowledgment

We would like to acknowledge the referees' valuable comments and suggestions which have considerably improved this paper.

1. P. C. Hariharan and J. A. Pople. J. Mol. Phys. **27**, 209 (1974).
2. D. J. DeFrees, B. A. Levi, S. K. Pollack, W. J. Hehre, J. S. Binkley, and J. A. Pople. J. Am. Chem. Soc. **101**, 4085 (1979).
3. D. J. DeFrees, K. Raghavachari, H. B. Schlegel, and J. A. Pople. J. Am. Chem. Soc. **104**, 5576 (1982).
4. R. C. Dobson, D. M. Hayes, and R. Hoffmann. J. Am. Chem. Soc. **93**, 6188 (1971).
5. N. Bodor, M. J. S. Dewar, and J. Wasson. J. Am. Chem. Soc. **94**, 9095 (1972).
6. H. Kollmar. Tetrahedron, **28**, 5893 (1972).
7. J. N. Murrell, J. B. Pedley, and S. Durmaz. J. Chem. Soc. Faraday Trans. II, **69**, 1370 (1973).
8. P. Cremaschi and M. Simonetta. J. Chem. Soc. Faraday Trans. II, **70**, 1801 (1974).
9. C. W. Bauschlicher, Jr., H. F. Schaefer III, and C. F. Bender. J. Am. Chem. Soc. **98**, 1653 (1976).
10. C. W. Bauschlicher, Jr., K. Haber, H. F. Schaefer III, and C. F. Bender. J. Am. Chem. Soc. **99**, 3610 (1977).
11. H. Kollmar and V. Staemmler. Theoret. Chim. Acta, **51**, 207 (1979).
12. D. Jeziorek and B. Zurawski. Int. J. Quant. Chem., **14**, 277 (1979).
13. C. Sosa and H. B. Schlegel. J. Am. Chem. Soc. **106**, 5847 (1984).
14. J. S. Binkley, M. J. Frisch, D. J. DeFrees, R. Krishnan, R. A. Whiteside, H. B. Schlegel, E. M. Fluder, and J. A. Pople. GAUSSIAN-82, Carnegie-Mellon University, Pittsburg, PA.
15. M. Peterson and R. Poirier. MONSTERGAUSS. Department of Chemistry, University of Toronto, Ont., Canada. 1981.
16. P. C. Hariharan and J. A. Pople. Theoret. Chim. Acta, **28**, 213 (1973).
17. J. S. Binkley and J. A. Pople. Intern. J. Quant. Chem. **9**, 229 (1975).
18. H. B. Schlegel. J. Comp. Chem. **3**, 214 (1982).

Can. J. Chem. Downloaded from www.nrcresearchpress.com by 213.166.140.6 on 09/07/12
For personal use only.

Crystal and molecular structure of 8-acetamido-2,4,4,8-tetramethyl-3-azaniumbicyclo[3.3.1]non-2-ene perchlorate

H. R. VITURRO,[1] B. E. RIVERO,[2] AND O. E. PIRO[3]

Laboratorio de Cristalografía, Departamento de Física, Facultad de Ciencias Exactas, Universidad Nacional de La Plata, C.C. 67, 1900 La Plata, Argentina

J. A. CARAM[4] AND M. E. MARTINS[5]

Instituto de Investigaciones Físico Químicas Teóricas y Aplicadas, C.C. 16, Suc. 4, 1900 La Plata, Argentina

AND

C. M. MARSCHOFF[2,5]

Departamento de Ingeniería Química, Facultad de Ingeniería, Universidad de Buenos Aires, Pabellón de Industrias, Ciudad Universitaria, 1428 Buenos Aires, Argentina

Received July 18, 1986[6]

H. R. VITURRO, B. E. RIVERO, O. E. PIRO, J. A. CARAM, M. E. MARTINS, and C. M. MARSCHOFF. Can. J. Chem. **65**, 2000 (1987).

X-ray single crystal analysis sheds further light on the structure of this new iminium salt. ATABNEP crystallizes in the monoclinic system, space group $P2_1$ and shows a very short value for the C—N distance in the iminium group, thus suggesting that the contribution of the carbonium ion form in this particular case is much lower than usual, a fact that can be considered a rationale for the reluctance of ATABNEP to undergo hydrolysis.

H. R. VITURRO, B. E. RIVERO, O. E. PIRO, J. A. CARAM, M. E. MARTINS et C. M. MARSCHOFF. Can. J. Chem. **65**, 2000 (1987).

L'analyse par diffraction des rayons X d'un monocristal de ATABNEP montre que ce nouveau sel d'iminium cristallise dans le système monoclinique et appartient au groupe d'espace $P2_1$. La très courte distance observée pour la liaison C—N dans le group iminium suggère que dans ce cas la contribution de l'ion carbonium est bien moindre que dans la plupart de sels d'iminium connus et, donc, fournit une possible interprétation à la résistance de ce sel à la reaction d'hydrolyse.

Iminium salts have received increasing attention during the last fifteen years because of their potential as reaction intermediates in preparing different organic compounds, both directly (1) and by photochemical excitation (2). Nevertheless, and probably because of the difficulties involved in preparing good single crystals, X-ray diffraction data are not abundant for these compounds (ref. 1, p. 89).

Recently, a new iminium salt, $C_{14}H_{25}N_2O^+.ClO_4^-$ with f.w. = 336.5, whose structure was determined by means of usual spectroscopic techniques to be 8-acetamido-2,4,4,8-tetramethyl-3-azanium-bicyclo[3.3.1]non-2-ene perchlorate (ATABNEP), was prepared by reaction of some terpenes (limonene, β-pinene, and terpinolene) with dilute solutions of perchloric acid in acetonitrile (3). The bicyclic cation of ATABNEP (Fig. 1) shows remarkable properties with respect to the ususal behaviour of iminium salts: thus, it is very stable, as seen from its high melting point (252–252.5°C) and, more important, the solid can be handled and stored without special cares, since it is unaffected by humidity at ambient conditions. This fact gives ATABNEP a particular interest because potential applications of this compound would not require working in controlled environments. It is of interest to note, in this respect, that iminium salts are usually very sensitive to water, undergoing a hydrolysis reaction which yields a ketone and an ammonium salt as products (ref. 1, p. 156), while ATABNEP does not show chemical change when dissolved in water (in fact, it can be recrystallized from aqueous solutions) and, also, does not react when refluxed in 10% H_2SO_4. Reaction with water occurs only in alkaline media but, then, the usual reaction does not take place and an imine that retains the bicyclic structure of the cation is precipitated (4).

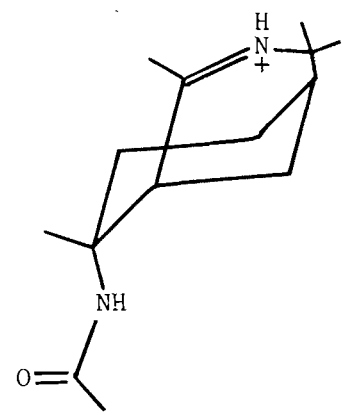

FIG. 1. Schematic drawing of the organic cation in ATABNEP.

Taking all this into account, it was concluded that a complete X-ray study of this compound would be worthwhile.

Experimental

ATABNEP was prepared from (+)limonene and from (−)β-pinene as previously described (3) and recrystallized from ethanol at room temperature. Good colourless crystals were obtained after one month. It has not been possible, up to now, to isolate crystals from the terpinolene-generated ATABNEP adequately to undertake the crystal structure determination of this solid, which has no optical activity. No differences in the diffraction pattern of the salt generated from limonene with respect to samples obtained from pinene were observed.

[1]Supported by a fellowship from the Comisión de Investigaciones Científicas de la Provincia de Buenos Aires (CICPBA).

[2]Member of the Carrera del Investigador, CICPBA.

[3]Member of the Carrera del Investigador Científico of the Consejo Nacional de Investigaciones Científicas y Técnicas (CONICET).

[4]Supported by a fellowship from CONICET.

[5]To whom correspondence should be addressed.

[6]Revision received March 23, 1987.

Can. J. Chem. Downloaded from www.nrcresearchpress.com by 213.166.140.6 on 09/07/12
For personal use only.

Can. J. Chem. Downloaded from www.nrcresearchpress.com by 213.166.140.6 on 09/07/12
For personal use only.

A complete X-ray diffraction data set was obtained from a prismatic crystal of limonene-derived ATABNEP of approximate dimensions $0.45 \times 0.45 \times 0.60$ mm with an Huber four circle diffractometer, used with graphite monochromated MoK_α radiation ($\lambda = 0.7093$ Å). The unit cell dimensions and orientation matrix for data collection were produced from 15 centered reflections by least-squares refinement. The 3543 reflections in the $\pm h, +k, -l$ reciprocal space quadrant having θ in the range 0–25° were measured by the ω-scan technique, working in the constant precision mode. Intensities of two standard reflections were monitored every 180 min and showed to be essentially constant throughout the experiment (within 1%).

For the calculations, the 961 independent reflections having $I > 2.5\sigma(I)$ were used. Data were corrected for Lorentz, polarization, and extinction effects, but not for absorption. The atomic dispersion scattering factors of Cromer and Waber (5) and the anomalous dispersion coefficients of Cromer and Ibers (6) were employed in the calculations. Most of these were performed on a PDP 11/34 computer with the SHELX program (7). The projection shown below was drawn with the program ORTEP (8).

Results

Crystal data are as follows:

Monoclinic, space group $P2_1$, with $a = 7.902(5)$ Å, $b = 8.837(2)$ Å, $c = 12.779(3)$ Å, $\gamma = 110.32(2)°$, $V = 838.1$ Å^3, $Z = 2$, $\rho_c = 1.33$ g/cm^3, $\rho_m = 1.26$ g/cm^3, $\mu(MoK_\alpha) = 2.07$ mm^{-1}, $F(000) = 360$ electrons.

The chlorine atom was readily located from a Patterson map and its position confirmed by the highest peak in the best symbolic addition map for the centrosymmetric projection of the structure along its screw axis (crystal c axis). All other non-hydrogen atoms were subsequently found by alternate difference Fourier synthesis and isotropic least-squares refinement, which converged to an R-factor of 10.7%.

The subsequent difference Fourier synthesis showed peaks corresponding to 17 out of the 25 hydrogen atoms of the molecule. These atoms were positioned at the corresponding positive electron density regions on stereochemical grounds and kept fixed during further isotropic refinement. The eight missing atoms were positioned as follows: two of them, belonging to a methylenic carbon, were also fixed stereochemically, while the remaining six hydrogen atoms, which pertain to two methyl substituents, were refined as rigid groups. The overall vibrational B value for all hydrogen atoms was fixed to be 6.3 Å^2. The final refinement was carried out by anisotropic full-matrix least-square methods keeping all hydrogen atoms fixed at the previously obtained positions. This procedure converged to agreement factors $R = 6.7\%$ and $R_w = 7.1\%$, with the minimization function defined by $M = \Sigma w[|F_0| - |F_c|]$ with weights $w = [\sigma^2(F_0) + 0.0006F_1^2]^{-1}$. At this stage, the number of independent reflections per parameter is 4.8 and the difference Fourier synthesis is essentially flat (maximum and minimum peaks were 0.25 and -0.3 e/Å^3, respectively.)

The difference between the R-factors for both molecular stereoisomers was not statistically significant to afford the determination of the absolute configuration for the limonene-generated ATABNEP. The assignment of the (1S, 5R, 8R) configuration for the employed crystal and (1R, 5S, 8S) for the product obtained from pinene was made on the grounds of chemical path stereospecificity (3).

Final positional parameters and equivalent isotropic temperature factors computed following Hamilton (9) for all non-hydrogen atoms are given in Table 1. An ORTEP projection of the content of one asymmetric unit of the limonene derived ATABNEP, down the a axis, displaying the conformational features of the molecule and atom numbering is shown in Fig. 2. A projection of the crystal packing is presented in Fig. 3.

As it can be readily seen, the obtained structure confirms the previous proposal (3). Bond distances and bond angles for the

TABLE 1. Fractional positional parameters and equivalent isotropic thermal parameter for ATABNEP

Atom	x/a	y/b	z/c	B_{eq} (Å^2)
Cl	0.2189(4)	0.3484(4)	0.0000	5.1
O(I)	0.137(1)	0.211(1)	−0.0592(8)	8.7
O(II)	0.113(2)	0.357(1)	0.0877(9)	9.7
O(III)	0.275(2)	0.488(1)	−0.059(1)	11.7
O(IV)	0.385(1)	0.348(1)	0.038(2)	12.9
C(1)	0.123(1)	0.086(1)	0.6042(7)	3.1
C(2)	0.050(1)	−0.007(1)	0.7040(9)	3.2
N(3)	0.1480(9)	−0.0633(9)	0.7600(7)	3.3
C(4)	0.344(1)	−0.047(1)	0.7392(8)	3.8
C(5)	0.419(1)	0.057(1)	0.6442(9)	3.6
C(6)	0.498(1)	0.238(1)	0.6634(9)	3.9
C(7)	0.358(1)	0.315(1)	0.6963(8)	4.0
C(8)	0.193(1)	0.270(1)	0.6252(8)	3.6
C(9)	0.268(1)	0.027(1)	0.5615(8)	3.5
C(10)	−0.137(1)	−0.042(1)	0.737(1)	4.7
C(11)	0.327(1)	−0.228(1)	0.718(1)	4.9
C(12)	0.440(1)	0.009(1)	0.8416(9)	4.1
C(13)	0.053(1)	0.333(1)	0.6733(8)	4.1
C(14)	0.227(2)	0.467(1)	0.357(1)	6.3
C(15)	0.150(2)	0.345(1)	0.4411(9)	4.5
N(16)	0.256(1)	0.356(1)	0.5243(7)	3.9
O(17)	−0.001(1)	0.2410(8)	0.4316(6)	4.3

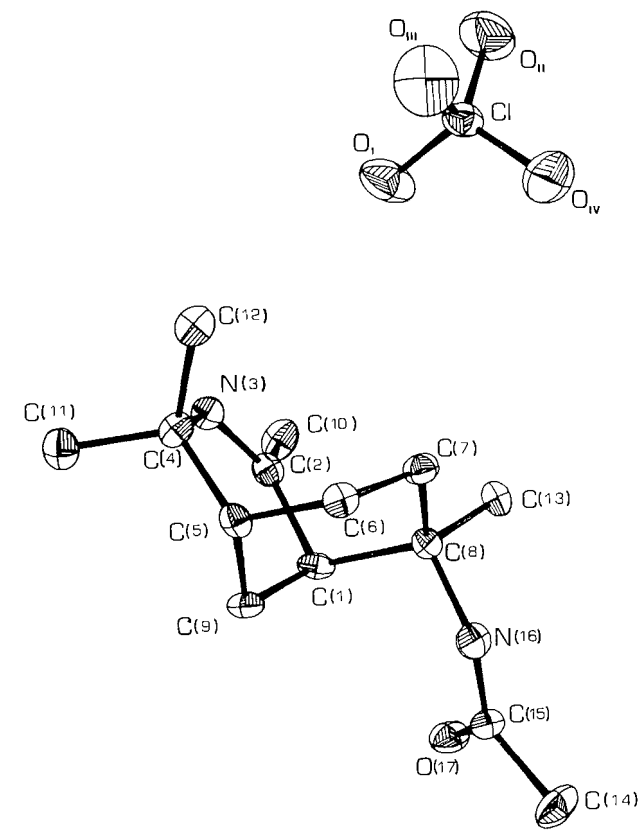

FIG. 2. ORTEP projection of the content of one asymmetric unit of limonene-derived ATABNEP, down the a axis.

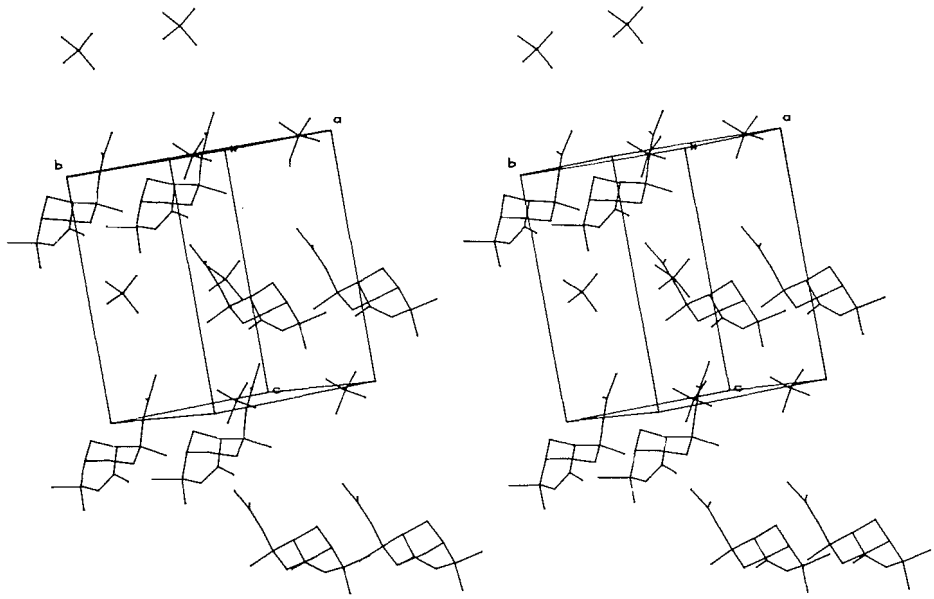

FIG. 3. Stereoscopic projection of the crystal packing of ATABNEP.

TABLE 2. Bond distances (Å) and angles (deg) in the perchlorate anion

Bond	Distance
Cl—O(I)	1.39(1)
Cl—O(II)	1.41(1)
Cl—O(III)	1.39(1)
Cl—O(IV)	1.38(1)

Bonds	Angle
O(I)—Cl—O(II)	112.2(7)
O(I)—Cl—O(III)	112.2(7)
O(I)—Cl—O(IV)	109.8(8)
O(II)—Cl—O(III)	113.6(8)
O(II)—Cl—O(IV)	108.0(8)
O(III)—Cl—O(IV)	100.3(8)

perchlorate anion and the organic cation are listed, respectively, in Tables 2 and 3.[7]

Discussion

In the perchlorate anion the four oxygen atoms form a slightly distorted tetrahedron with mean Cl—O distance 1.39(1) Å and mean O—Cl—O angle 109(4)°, a value that compares well with the perfect tetrahedron (109.5°). The relatively high thermal parameters associated with the oxygen atoms (see Fig. 2 and Table 1) could be due to large rotational dynamic and/or static disorder of the anion around its center.

In the organic cation the six carbon ring has a well defined chair configuration with mean C—C distance equal to 1.54(2) Å and a mean C—C—C angle of 111(3)°, being the largest deviation from perfect sp^3 hybridization 5°. The other ring, which contains the iminium group, has five of its atoms, C(1), C(2), N(3), C(4), and C(5) as well as the substituting atom on the iminium carbon, i.e. C(10), almost in the same plane (within 0.05 Å).

Bond lengths and bond angles in the acetamido residue are in good agreement with data in the literature (10), and the group is in axial position with respect to the chair, as should be expected from the Ritter mechanism (3).

It must also be noticed that the C—N distance in the iminium group, 1.28(1) Å, is shorter than what theoretical arguments would suggest for this particular bond. In this connection, it is to be recalled that, as pointed out by Kollman (ref. 1, chap. 1) iminium ions considered from the point of view of valence bond theory contain significant contributions from the two resonance structures **1** and **2**:

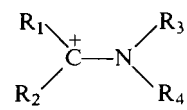

1

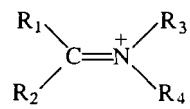

2

their relative importance being dependent on the nature of the substituents. Thus, for the hypothetical $[H_2CNH_2]^+$ ion, the carbon–nitrogen distance has been calculated to be 1.28 Å (ref. 1, chap. 1) while for $[(CH_3)_2CN(CH_3)_2]^+$ the theoretical value is 1.30 Å (ref. 1, chap. 1) which compares well with the experimental datum of 1.302 Å (12). The last figure is theoretically justified because methyl substitution on the carbon stabilizes structure **1** through methyl hyperconjugation with the carbonium center and, thus, leads to longer carbon–nitrogen bonds, while methyl substitution on the nitrogen atom should have an opposite (i.e. iminium stabilizing) though weaker effect, a fact that is confirmed when carbon–nitrogen bond lengths for $[(CH_3)_2NCR_2]^+$ and $[H_2NCR_2]^+$ are compared.

We have, then, that the observed carbon–nitrogen distance in the iminium group of ATABNEP is shorter than what one should expect, particularly if it is considered that there is a methyl substituent on the carbon. This, in turn, suggests that the steric hindrance due to the bicyclic structure enhances the contribution of resonance form **2**, a fact that is confirmed when it is noted that bond angles for C(1)—C(2)—C(10),

[7]Structure factor table, anisotropic thermal parameters, and H-atom coordinates may be purchased from the Depository of Unpublished Data, CISTI, National Research Council of Canada, Ottawa, Ont., Canada K1A 0S2.

Can. J. Chem. Downloaded from www.nrcresearchpress.com by 213.166.140.6 on 09/07/12
For personal use only.

TABLE 3. Bond distances (Å) and angles (deg) in the organic cation of ATABNEP

(*a*) Bond distances

Bond	Distance	Bond	Distance
C(1)—C(2)	1.52(1)	C(5)—C(6)	1.52(1)
C(1)—C(8)	1.55(1)	C(5)—C(9)	1.55(2)
C(1)—C(9)	1.52(1)	C(6)—C(7)	1.54(2)
C(2)—N(3)	1.28(1)	C(7)—C(8)	1.53(2)
C(2)—C(10)	1.46(2)	C(8)—C(13)	1.53(2)
N(3)—C(4)	1.53(1)	C(8)—N(16)	1.49(1)
C(4)—C(5)	1.52(1)	C(14)—C(15)	1.50(2)
C(4)—C(11)	1.58(1)	C(15)—N(16)	1.34(2)
C(4)—C(12)	1.51(2)	C(15)—O(17)	1.23(2)

(*b*) Bond angles

Bonds	Angle	Bonds	Distance
C(2)—C(1)—C(8)	110.6(8)	C(6)—C(5)—C(9)	107.5(8)
C(2)—C(1)—C(9)	107.9(8)	C(5)—C(6)—C(7)	114.3(9)
C(8)—C(1)—C(9)	112.7(8)	C(6)—C(7)—C(8)	113.6(8)
C(1)—C(2)—N(3)	121.0(9)	C(1)—C(8)—C(7)	109.8(8)
C(1)—C(2)—C(10)	121.5(9)	C(1)—C(8)—C(13)	114.3(8)
N(3)—C(2)—C(10)	117.4(9)	C(1)—C(8)—N(16)	108.6(9)
C(2)—N(3)—C(4)	126.7(8)	C(7)—C(8)—C(13)	109.0(9)
N(3)—C(4)—C(5)	111.5(8)	C(7)—C(8)—N(16)	106.2(8)
N(3)—C(4)—C(11)	102.0(8)	C(13)—C(8)—N(16)	108.6(8)
N(3)—C(4)—C(12)	104.9(8)	C(1)—C(9)—C(5)	108.9(8)
C(5)—C(4)—C(11)	110.7(9)	C(14)—C(15)—N(16)	116(1)
C(5)—C(4)—C(12)	116.9(9)	C(14)—C(15)—O(17)	121(1)
C(11)—C(4)—C(12)	109.7(9)	N(16)—C(15)—O(17)	124(1)
C(4)—C(5)—C(6)	116.1(9)	C(8)—N(16)—C(15)	124.2(9)
C(4)—C(5)—C(9)	109.2(8)		

C(1)—C(2)—N(3), and C(10)—C(2)—N(3) are very near the theoretical value for sp^2 hybridization.

This feature affords a rationale for the reluctance of this compound to undergo hydrolysis, since this reaction should occur through the attack of a water molecule on the carbonium ion. The fact that reaction with water in alkali media proceed via direct proton abstraction from the iminium form (7) reinforces this interpretation.

Acknowledgments

This work was supported in part by grants from the Consejo Nacional de Investigaciones Científicas y Técnicas and from the Comisión de Investigaciones Científicas de la Provincia de Buenos Aires.

1. H. BÖHME and H. G. VIEHE (*Editors*). Iminium salts in organic chemistry. Part 1. John Wiley and Sons, New York. 1976.
2. P. S. MARIANO. Tetrahedron, **39**, 3845 (1983).
3. J. A. CARAM, M. E. MARTINS, C. M. MARSCHOFF, L. F. R. CAFFERATA, and E. G. GROS. Z. Naturforsch. **39**b, 972 (1984).
4. J. A. CARAM, B. E. RIVERO, O. E. PIRO, E. G. GROS, and C. M. MARSCHOFF. To be published.
5. D. T. CROMER and J. T. WABER. International tables for X-ray crystallography. Vol. IV. Kynoch Press, Birmingham. 1974. pp. 71–98.
6. D. T. CROMER and J. A. IBERS. International tables for X-ray crystallography. Vol. IV. Kynoch Press, Birmingham. 1974. p. 149.
7. G. M. SHELDRICK. SHELX. A program for crystal structure determination. University of Cambridge, Cambridge, England. 1976.
8. C. K. JOHNSON. ORTEP, Report ORNL-3794. Oak Ridge National Lab., Oak Ridge, TN. 1965.
9. W. C. HAMILTON. Acta Crystallogr. **12**, 609 (1959).
10. O. KENNARD. International tables for X-ray crystallography. Vol. III. Kynoch Press, Birmingham. 1968. p. 276.
11. R. M. CURTIS and R. A. PASTERNAK. Acta Crystallogr. **8**, 675 (1955).
12. L. M. TREFONAS, R. L. FLURRY, JR., R. MAJESTE, E. A. MEYERS, and R. F. COPELAND. J. Am. Chem. Soc. **88**, 2145 (1966).

Can. J. Chem. Downloaded from www.nrcresearchpress.com by 213.166.140.6 on 09/07/12
For personal use only.

Electroionization study of ethane: structures in the ionization and appearance curves[1]

PIERRE PLESSIS AND PAUL MARMET

Herzberg Institute of Astrophysics, National Research Council of Canada, Ottawa, Ont., Canada K1A 0R6

Received January 23, 1987

PIERRE PLESSIS and PAUL MARMET. Can. J. Chem. **65**, 2004 (1987).

Ionization efficiency curves of very high signal-to-noise ratio are presented for ethane and most fragment ions containing at least one carbon atom. These curves, which are produced by monoenergetic electron impact, extend up to 10 eV above the initial onsets. Novel structures are observed in most curves. Certain features appear at the same energy in several of the curves indicating that they belong to a common progenitor, either $C_2H_6^-$ * or $C_2H_6^*$, and not directly to the detected ions. These sets of structure are attributed to negative ion states (Feshbach resonances) and/or to Rydberg autoionizing states.

PIERRE PLESSIS et PAUL MARMET. Can. J. Chem. **65**, 2004 (1987).

Des courbes de section efficace d'ionisation de très grand rapport signal sur bruit sont présentées pour l'éthane et ses fragments ioniques composés d'au moins un atome de carbone. Ces courbes sont produites par impact d'électrons monoénergétiques et s'étendent jusqu'à 10 eV au-dessus des seuils initiaux. De nouvelles structures sont observées dans la plupart des courbes. Certaines structures apparaissent aux mêmes énergies dans plusieurs courbes, ce qui indique qu'elles n'appartiennent pas directement aux ions détectés mais à une particule qui est à l'origine de tous ces ions, soit le $C_2H_6^-$ * ou le $C_2H_6^*$. Ces groupes de structures sont attribués à des états d'ions négatifs (résonances Feshbach) et/ou à des états de Rydberg autoionisants.

1. Introduction

Ethane and its fragment ions have been studied fairly extensively by various methods in the ionization and appearance threshold regions. Our data for these regions have been presented in a recent paper (1). Much less work has been done at energies above the immediate onset regions. Ionization efficiency curves at higher energies are reported by Suzuki and Maeda (2) using a monoenergetic electron beam, Selim (3) using the (pseudo-monoenergetic) electron impact energy distribution difference technique, and Berkowitz (4) using photoionization mass spectrometry. In this paper very high signal-to-noise ratio electroionization efficiency (EIE) data extending up to 10 eV above onset are presented for ethane and all fragment ions containing at least one carbon atom, except CH_4^+. Numerous low intensity features are observed for the first time in most curves. Assignments are proposed for many of these structures.

2. Apparatus and method

More complete descriptions of the apparatus have been given elsewhere (5, 6). It consists of two 127° electrostatic selectors in series producing a monoenergetic electron beam. In this work the full width at half maximum (FWHM) resolution of the beam is approximately 60 meV for a current of 3×10^{-8} A. The molecular beam is bombarded by the electrons; the ions produced are mass analysed by a large quadrupole mass filter and the transmitted ions are detected by a dynode type electron multiplier. Data acquisition is computer controlled. An individual EIE curve takes about 10 s to obtain and the final curves consist of thousands of individual curves summed over periods of about 130 h. The energy scale of the curves is calibrated typically every 24 h using the clear threshold structure of argon (15.760 eV). The energy drift per 24 h period was usually no greater than 20 meV and this was taken into account in adding the data.

Most structures in EIE curves appear as narrow (high frequency) and relatively weak perturbations on an intense, broad (low frequency), and smoothly varying ionization continuum. Filtering out the intense low frequency components allows the high frequency features to be seen much more readily. This is accomplished by a specialized Fourier filtering technique (7–9) whose transmission factor for the mth frequency component is given by

$$[1] \quad T_{m,S} = 1 - \left(\cos\frac{\pi m}{N}\right)^{2S}$$

where S is a parameter controlling the amount of low frequency component that is eliminated and N is the number of channels used. For the special case of $S = 1$ and using the transmission factor $-T_{m,S}$, the result is identical to the second derivative. It has been shown qualitatively that for small values of S ($S \leq 100$) the result is similar to the second derivative but contains a larger amount of low frequency components (10). The vertically inverted filtered curves ($-T_{m,S}$) are presented in this paper in order to have direct resemblance with the second derivative.

3. Results and discussion

The raw data EIE curves of ethane and of the fragments studied in this work are presented in Figs. 1 and 2. The data points, originally taken at an interval of 20 meV per channel, are added 5 by 5 to give 100 meV per channel in order to improve the signal-to-noise ratio and allow weaker features to be detected. Very little structure of detectable intensity narrower than 300 meV could be seen in the curves, so virtually no information was lost by increasing the energy interval. The intensity of the curves of Figs. 1 and 2 increases uniformly with energy and, apart from the initial onset regions that have been analysed previously (1), they show no apparent narrow distinct features. At the vertical scale shown, the general shape of the curves of Fig. 2 differs from that of the Fig. 1 curves in that the intensity of the former increases significantly only several eV above onset. The CH_2^+ curve has an intermediary form to these two groups of curves. From Fig. 2 it is clear that the probability for producing these fragment ions and their respective reaction products with minimal internal and kinetic energy is very small. The relative peak height intensities of the ethane ions are given in Table 1 where it is seen that the most abundant ion at 35 eV is the $C_2H_4^+$ fragment.

Once the low frequency continuum of the Figs. 1 and 2 curves is removed, by using the aforementioned high pass filter, numerous structures can be seen. The filtered curves are presented in Figs. 3 to 5. The data of Fig. 3 are shown at 20 meV per channel. The energies of the indicated structures are given in Table 2. The intensities of these structures are small compared with the ionization continuum, and therefore are not apparent on the original curves. For example, structure E at 13.28 eV of the $C_2H_6^+$ curve and structure H_2 at 18.8 eV of the $C_2H_4^+$ curve have amplitudes of only 0.06% and 0.01% of their respective ionization continuum. Most of the features observed in the

[1]NRCC No. 27662.

Can. J. Chem. Downloaded from www.nrcresearchpress.com by 213.166.140.6 on 09/07/12
For personal use only.

Can. J. Chem. Downloaded from www.nrcresearchpress.com by 213.166.140.6 on 09/07/12
For personal use only.

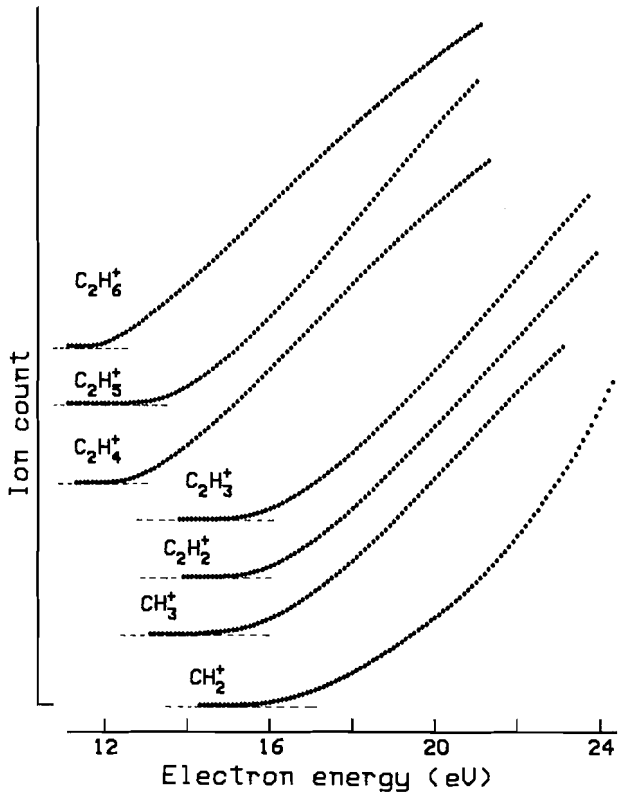

FIG. 1. EIE curves of ethane and of several fragment ions. The zero of the curves have been displaced for clearer presentation. The ion count in the last channel of each curve is given in Table 1 (100 meV per channel).

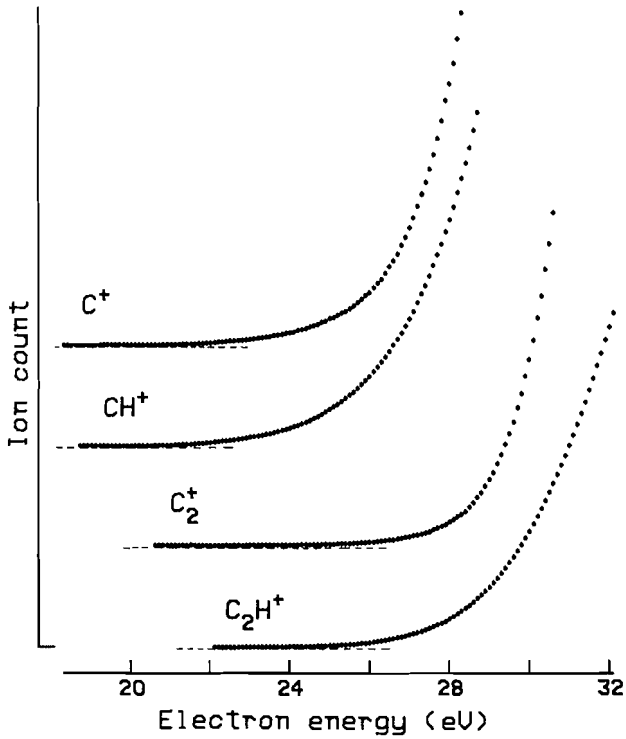

FIG. 2. EIE curves of the weaker intensity ethane fragments. As in Fig. 1.

filtered curves are reported here for the first time. Because of the complexity of the transitions involved and the lack of pertinent experimental and theoretical work on ethane, it is presently not possible to give unequivocal assignments to these features.

TABLE 1. Relative peak height intensities of the ethane ions for 35.0 eV electrons

Ion	Relative intensity	N^a
$C_2H_6^+$	46.33	2.884×10^9
$C_2H_5^+$	28.66	2.225×10^9
$C_2H_4^+$	100.00	1.031×10^{10}
$C_2H_3^+$	29.34	1.913×10^9
$C_2H_2^+$	14.50	6.554×10^8
C_2H^+	0.63	2.727×10^7
C_2^+	0.032	3.841×10^5
CH_3^+	1.93	4.780×10^8
CH_2^+	0.39	6.245×10^6
CH^+	0.070	2.884×10^6
C^+	0.020	4.660×10^5

[a] N is the number of counts in the last channel of the curves of Figs. 1 and 2.

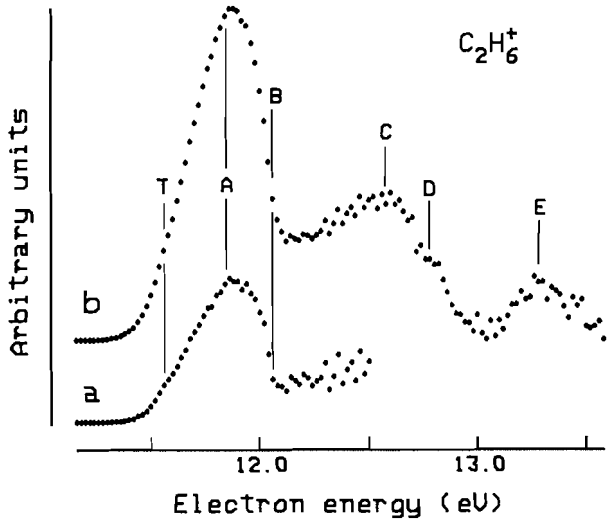

FIG. 3. $C_2H_6^+$ EIE curve high pass filtered using $S = 7$ (curve a) and $S = 30$ (curve b). Energy interval per channel = 20 meV.

However, plausible general interpretations for many of the structures are proposed below. These are summarized in Table 3.

A remarkable aspect of the Figs. 4 and 5 curves is that a number of features having similar profiles appear at the same energy in several of the curves, as listed in Table 3. It is evident that these structures cannot be attributed to states of the detected ions since such series of coincidences are essentially impossible given the great differences in the detected ions. Each set of features must have a common origin. Previous work on methane (11), acetylene (12), and ethylene (13), in which similar sets of structures are observed in the ionization and appearance curves, indicate that negative ion states (Feshbach resonances) and autoionizing states are the major processes responsible for producing these sets of structures as well as most of the features observed in EIE data.

In the present case $C_2H_6^{-*}$ is the source species resulting from the initial collision of an electron on C_2H_6. During the interaction of the electron with the target molecule, quantum transitions take place in which the number of charges is conserved. Thus, at this stage, only negative ion states are involved which correspond to continua, Feshbach resonances or shape resonances. When transitions occur new states of the

TABLE 2. Energies (in eV) of the principal features of the ethane and fragment ion curves

Structure (subscript→)[a]	$C_2H_6^+$	$C_2H_5^+$ (1)	$C_2H_4^+$ (2)	$C_2H_3^+$ (3)	$C_2H_2^+$ (4)	CH_3^+ (5)	CH_2^+ (6)
T	11.57						
A	11.85	13.43	12.09	15.6	15.6	15.5	16.0
B	12.06	14.7	12.70	16.6	16.7	16.6	16.8
C	12.58	15.6	13.50	17.7	19.6	17.9	19.5
D	12.78	16.7	14.9	18.8	20.4	18.8	20.3
E	13.28	17.0	15.5	19.7	21.4	20.1	
F	14.2	17.9	16.7	20.3			
G	15.5	18.9	17.8	21.3			
H	16.6	19.7	18.8				
I	17.6						
J	18.7						

[a]Subscripts are adjoined to the letters as in Figs. 3 to 5.

Can. J. Chem. Downloaded from www.nrcresearchpress.com by 213.166.140.6 on 09/07/12
For personal use only.

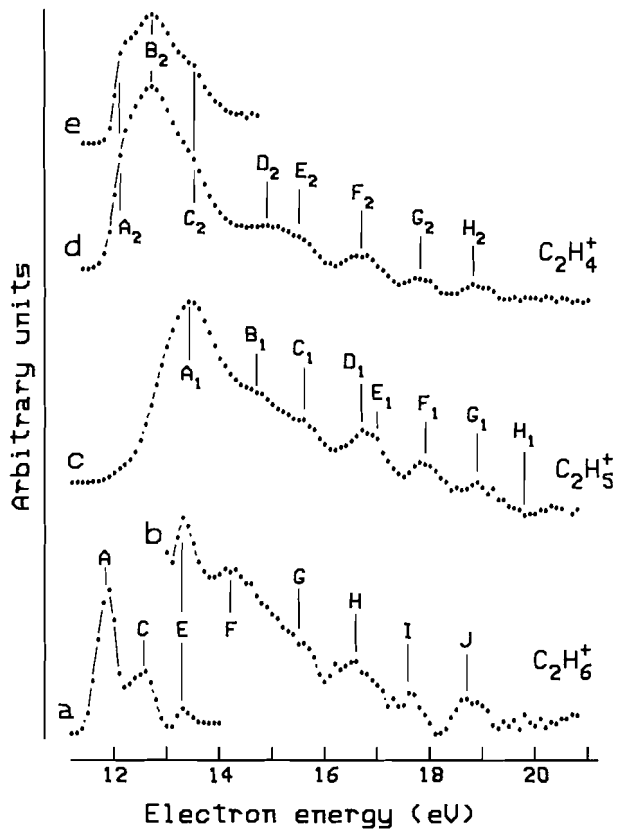

FIG. 4. $C_2H_6^+$ (curves *a* and *b*), $C_2H_5^+$ (curve *c*), and $C_2H_4^+$ (curves *d* and *e*) EIE curves filtered using $S = 2, 10, 10, 7$, and 1, respectively.

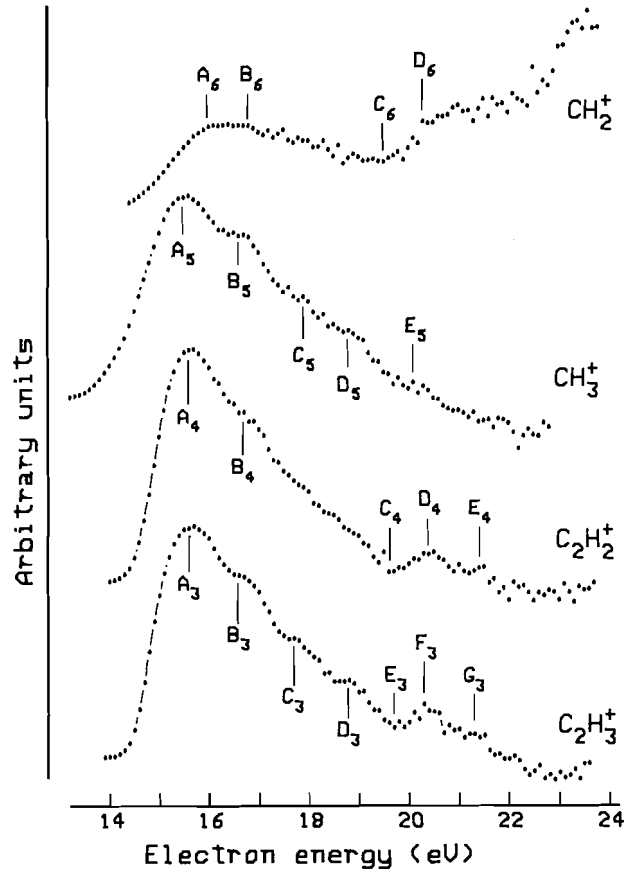

FIG. 5. $C_2H_3^+$, $C_2H_2^+$, CH_3^+, and CH_2^+ EIE curves filtered using $S = 18, 25, 30$, and 100, respectively.

negative ion are formed which can either (directly or indirectly) autoionize, dissociate into fragments, or emit photons. The variations in cross section as a function of energy of the electrons interacting with the ethane molecules to form different states of $C_2H_6^-$* will be reflected in the ionization and various fragment ion cross sections, as seen in the curves of Figs. 4 and 5. It follows that when a structure is common to several ethane ions, it is caused by a configuration of the parent negative ion. Furthermore, the $C_2H_6^-$* cross section can be perturbed by the probability of forming excited neutral states ($C_2H_6^*$ + e^-), consequently the perturbations due to these neutral states will also manifest themselves in the ionization and ionic fragmentation cross sections.

Structures *T*, *A*, and *B* of the $C_2H_6^+$ curve (Fig. 3) have been analysed in detail and at higher resolution in the previous paper on ethane (1). The corresponding interpretations are given in Table 3. All other structures listed in Table 3 are considered to be caused by members of negative ion states series, $^2X\ nl\ n'l'$, or of Rydberg autoionizing states series, $^2X\ nl$, where *X* represents a particular $C_2H_6^+$ state, or to a mixture of these which converge to the different electronic states of the ethane ion. The ethane ground state configuration is generally accepted as being $(1a_{1g})^2(1a_{2u})^2(2a_{1g})^2(2a_{2u})^2(1e_u)^4(3a_{1g})^2(1e_g)^4$, $^1A_{1g}$ (4). The ionization energies for the ethane valence electrons, obtained by photoelectron spectroscopy (14), are

TABLE 3. Interpretation of some structures

Structure	Energy (eV)[a]	Interpretation
T	11.57	Ionization energy $(1e_g)^{-1}$
A	11.85	Due to competition with
B	12.06	$C_2H_4^+ + H_2$ production
D	12.78	
E	13.28	$^2A_{1g}\ nl\ n'l'$ and/or $^2A_{1g}\ nl$
C_2	13.50	
F	14.2	
B_1, D_2	14.8	$^2E_u\ nl\ n'l'$ and/or $^2E_u\ nl$
$G, C_1, E_2, A_3, A_4, A_5$	15.6	
$H, D_1, F_2, B_3, B_4, B_5, B_6$	16.7	
I, F_1, G_2, C_3, C_5	17.8	$^2A_{2u}\ nl\ n'l'$ and/or $A_{2u}\ nl$
J, G_1, H_2, D_3, D_5	18.8	
H_1, E_3, C_4, C_6	19.6	Onset of $^2A_{1g}\ nl\ n'l'$ and/or $^2A_{1g}\ nl$
F_3, D_4, E_5, D_6	20.3	$^2A_{1g}\ nl\ n'l'$ and/or $^2A_{1g}\ nl$
G_3, E_4	21.4	

[a]For the sets of structures the approximate mean energy is given.

TABLE 4. Ionization energies for single electron ejection of ethane (from Bieri and Asbrink (13))

Electron ejected	Adiabatic (eV)	Vertical (eV)
$1e_g$	11.56	12.00[a]
		12.72[a]
$3a_{1g}$		13.5
$1e_u$		15.0[a]
		15.8[a]
$2a_{2u}$	20.16	20.4
$2a_{1g}$		23.9

[a]This state has two maxima due to Jahn–Teller distortion.

reproduced in Table 4. It is assumed in the interpretations given in Table 3, that a series limit can occur in the region starting from the adiabatic ionization energy to just above the vertical ionization energy.

The basic considerations taken into account in assigning the sets of structures listed in Table 3 were the energies of the expected series limits (ethane ion states) and the general shape of the filtered curves. Evidently, a member of a series must appear at an energy below the series limit. From the work on methane (11), members of a series may be found down to about 4 eV below the ionization limit. The interpretation of structures D, E, and C_2 is somewhat ambiguous as these could belong to series converging to either the $^2A_{1g}$ or the ^2E_u state of $C_2H_6^+$. However, since the general shape and intensities of the $C_2H_6^+$ and $C_2H_4^+$ filtered curves above and below 13.5 eV ($^2A_{1g}$ vertical ionization energy) are quite different, this suggests that the structures below 13.5 eV converge to the $^2A_{1g}$ state and not to the ^2E_u state near 15 eV. Structures between 13.5 and 15.8 eV can be confidently assigned to series converging to the ^2E_u state as this is the only energetically plausible limit in this region. Similarly, structures between 16.0 and 19.6 eV are assigned to series which have the $^2A_{2u}$ state as their limit. It is seen in the $C_2H_5^+$, $C_2H_3^+$, $C_2H_2^+$, and CH_2^+ filtered curves that starting from 19.6 eV, the slope of the curves changes and the amplitude of the structures above this energy increases, suggesting the start of a new set of series which must converge to the $^2A_{1g}$ state of the ethane ion.

The C_2H^+, C_2^+, CH^+, and C^+ filtered curves (not shown here) vary gradually with energy and show few distinct features. Little significant information can be drawn from them.

4. Other results

The electron impact works of Suzuki and Maeda (2) and Selim (3) also report structures in the ethane EIE curve and in some of the more intense fragment ion curves. Both detect features in their direct EIE curves. This indicates that the relative intensities of their structures are much larger than those observed in this study. Also, the energies of these structures are not consistent with those reported here. The direct EIE curves of Figs. 1 and 2 show no apparent structures above threshold and it is only when the intense continuum is removed that the weak intensity features are seen. Given that the signal-to-noise ratio of their curves is considerably less than that of our data, it is clear to us that their results are incompatible with ours.

The photoionization mass spectrometric study of ethane by Berkowitz (4) yields little pertinent information in the energy region considered in this work.

5. Conclusion

Numerous clear structures are observed for the first time in the EIE curves of ethane and ethane fragment ions. Several of the features occur at the same energy in these curves and are certainly caused by the common progenitor $C_2H_6^{-}$*. The structures of the Figs. 4 and 5 curves are tentatively assigned to series of negative ion states and/or to autoionizing Rydberg states. Our present knowledge of the $C_2H_6 + e^-$ system is limited. However, we trust that these new results will be helpful in stimulating further experimental and theoretical work on this system.

6. Acknowledgements

The authors wish to thank Drs. M. Proulx and R. Dutil for their contribution to this work. Measurements were carried out at the Laboratoire de physique atomique et moléculaire at Laval University, Québec, and supported by grants from the Natural Sciences and Engineering Research Council of Canada.

Can. J. Chem. Downloaded from www.nrcresearchpress.com by 213.166.140.6 on 09/07/12
For personal use only.

1. P. PLESSIS and P. MARMET. Can. J. Chem. In press.
2. I. H. SUZUKI and K. MAEDA. Int. J. Mass Spectrom. Ion Phys. **24**, 147 (1977).
3. E. T. M. SELIM. Indian J. Pure Appl. Phys. **14**, 547 (1976).
4. J. BERKOWITZ. Photoabsorption, photoionization and photoelectron spectroscopy. Academic Press, New York. 1979. p. 295.
5. P. PLESSIS, P. MARMET, and R. DUTIL. J. Phys. B.:At. Mol. Phys. **16**, 1283 (1983).
6. E. BOLDUC, J. J. QUÉMÉNER, and P. MARMET. J. Chem. Phys. **57**, 1957 (1972).
7. R. CARBONNEAU, E. BOLDUC, and P. MARMET. Can. J. Phys. **51**, 505 (1973).
8. P. MARCHAND and P. VEILLETTE. Can. J. Phys. **54**, 1309 (1976).
9. H. H. ARSENAULT and P. MARMET. Rev. Sci. Instrum. **48**, 512 (1977).
10. M. PROULX and P. MARMET. Int. J. Mass Spectrom. Ion Phys. **50**, 129 (1983).
11. P. MARMET and L. BINETTE. J. Phys. B:At. Mol. Phys. **11**, 3707 (1978).
12. P. PLESSIS and P. MARMET. Int. J. Mass Spectrom. Ion Proc. **70**, 23 (1986).
13. P. PLESSIS and P. MARMET. Can. J. Phys. In press.
14. G. BIERI and L. ASBRINK. J. Elec. Spectrosc. Relat. Phenom. **20**, 149 (1980).

Can. J. Chem. Downloaded from www.nrcresearchpress.com by 213.166.140.6 on 09/07/12
For personal use only.

Concentration profiles in the electrodeposition of copper ferrocyanide by laser interferometry

R. N. O'BRIEN
Department of Chemistry, University of Victoria, Victoria, B.C., Canada V8W 2Y2

AND

K. S. V. SANTHANAM
Tata Institute of Fundamental Research, Bombay 400 005, India

Received November 25, 1986

R. N. O'BRIEN and K. S. V. SANTHANAM. Can. J. Chem. **65**, 2009 (1987).

The electrodeposition of cupric ferrocyanide from a solution of potassium ferrocyanide with the convection-free parallel plane horizontal electrodes with the cathode over the anode was followed by multiple beam laser interferometry as well as the conventional electrochemical instrumentation. It is considered that the cupric ion generated immediately reacts with ferrocyanide ion to form a conducting adhering precipitate layer. The initial resistance of this layer is low. Its resistance is constant with thickness until about 5×10^{-8} C mm^2 has been passed probably representing $\sim 10^5$ molecular layers when the resistance begins to rise. A magnetic field of 0.47 T caused a slight decrease in the resistance of the cell probably due to slow rotation of the inhomogeneous paramagnetic solution. This coating may be useful as an electrode.

R. N. O'BRIEN et K. S. V. SANTHANAM. Can. J. Chem. **65**, 2009 (1987).

Utilisant l'interférométrie à rayons laser multiples ainsi que des méthodes instrumentales électrochimiques conventionnelles, on a étudié l'électrodéposition du ferrocyanure cuivrique à partir d'une solution de ferrocyanure de potassium, à l'aide d'électrodes parralèles, à plan horizontal et sans convection alors que la cathode est au-dessus de l'anode. On considère que l'ion cuivrique qui est généré réagit immédiatement avec l'ion ferrocyanure pour former une couche de précipité qui adhère et qui est conductrice. Jusqu'à environ 5×10^{-8} C mm^2, sa résistance est constante avec l'épaisseur; ceci représente environ 10^5 couches moléculaires avant que la résistance commence à augmenter. Un champ magnétique de 0,47 T provoque une faible diminution dans la résistance de la cellule qui est probablement due à une rotation lente de la solution paramagnétique qui n'est pas homogène. Ce revètement peut s'avérer utile comme électrode.

[Traduit par la revue]

Introduction

A previous paper (1) from our laboratories reported the growth of concentration gradients in the galvanostatic electrodeposition of Cu from a solution of $CuSO_4$ by using two copper disc electrodes (Cu anode and Cu cathode) with parallel, plane working surfaces in the usual interferometric cell arrangement. In the present work early experiments using the electrolyte $K_4Fe(CN)_6$ at vertical electrodes showed that there was a negative refractive index gradient at both electrodes, i.e. decreasing from the bulk solution to the electrode. These gradients increased from the beginning of the electrolysis till a steady state of concentration gradient was reached as convective flow at the electrodes became the limiting factor to growth. The orientation of the electrodes used in the work to avoid convection was the cathode over anode (C/A) position. We have investigated the concentration gradients that are developed using $K_4Fe(CN)_6$ as the electrolyte in the above electrode configuration. The galvanostatic electrolysis produces a reddish brown film of copper ferrocyanide on the anode, and gas on the cathode. Interestingly this anode film shows electronic conduction and changes color upon oxidation and may therefore be useful as an electrode material (2–4). We wish to report here the results of a comparative study of the two types of cells, $Cu|CuSO_4|Cu$ and $Cu|K_4Fe(CN)_6|Cu$ using multiple beam laser interferometry. These results provide insight into the growth of diffusion layers at the two anodes in the two electrolytes.

Experimental

The electrodeposition of copper ferrocyanide was carried out in a cell of 1.39 mm thick with two almost semicircular Cu electrodes, 3 cm long, cut from either side of a disc (Fig. 1) which when the area obscured by the retaining arrangements were subtracted gave a working surface of 30 mm^2. The electrodes were separated by 2.5 mm. The electrodes were cleaned in concentrated HCl for a few minutes and then washed very thoroughly with double distilled water. All sides of the Cu electrodes were coated with an insulating paint (glyptol) except the working sides (parallel to the axis of the disc) now set parallel and horizontal in the cell, leaving only the long side electroactive. The cell (Fig. 1) is similar in design to the one previously employed (1), that is the Teflon body, glass flats, electrolyte, and electrodes could be described as a thin slice of a cylinder of 6 cm outside diameter and the whole electrochemical cell is inside a Fabry-Perot type multiple beam interferometer. The electrical contact to the Cu electrodes was made through a Cu wire inserted through the Teflon holder. The other experimental arrangements consisted of a Spectra physics Model 122, He–Ne laser as light source, a R.C.A. CC030 video camera, a Hitachi VHS portable VTR model VT7A, and a 20″ Hitachi color monitor. The entire experiment has been videotaped for later observations through the viewing optics of a 35 mm Nikon camera and the 35 mm negatives (of pictures taken at desired elapsed times) were projected onto a plotting table. The interferometric cell was mounted on a brass support with three adjustable screws for adjusting the wedge-angle between the 90% reflecting glass flats.

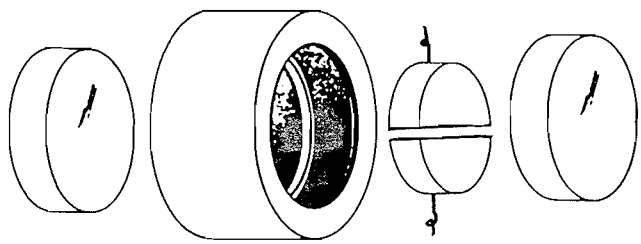

FIG. 1. An exploded isometric view of the interferometer showing the horizontal, plane-parallel electrodes but without the three pointed clamps for closing the cell and adjusting the fringes.

Can. J. Chem. Downloaded from www.nrcresearchpress.com by 213.166.140.6 on 09/07/12
For personal use only.

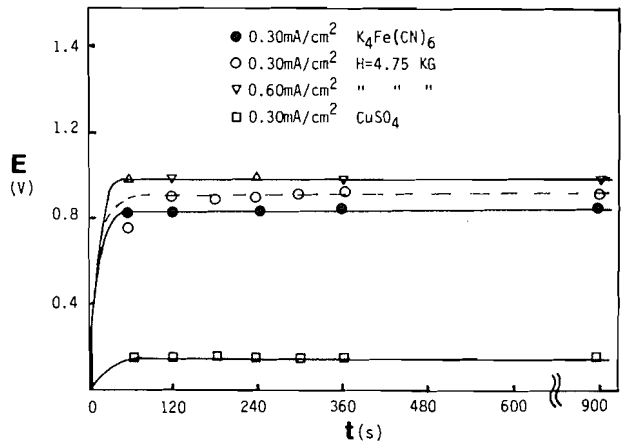

FIG. 2. The impressed voltage vs. time plot in the electrolysis of $K_4Fe(CN)_6$ and $CuSO_4$ at current densities of 0.30 mA cm^{-2} and 0.60 mA cm^{-2}. The effect of magnetic field on the above curve is also shown in the figure.

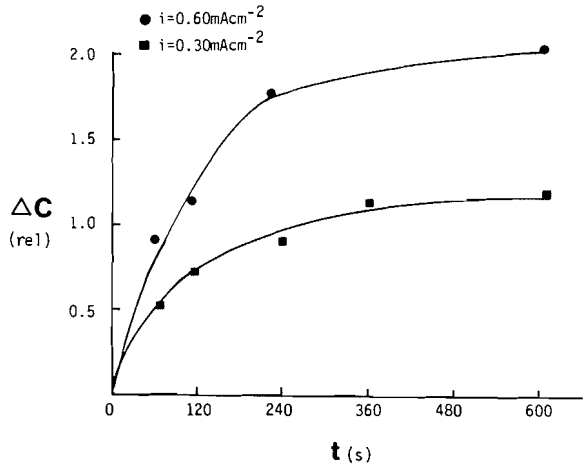

FIG. 3. The plot of ΔC_{max} as a function of the electrolysis time in the electrolysis of $K_4Fe(CN)_6$.

Results and discussion

The galvanostatic electrolysis of 0.1 *M* $K_4Fe(CN)_6$ generated a curve of impressed voltage as a function of the electrolysis duration as did 0.1 *M* $CuSO_4$ as shown in Fig. 2. Due to differences in the conductivities of $K_4Fe(CN)_6$ and $CuSO_4$, and the filming that occurs at the anode by ferrocyanide, the cell voltages in the two cases are significantly different. The other features of the *E*–*t* plots are very similar and the progress of the electrolysis in ferrocyanide was very smooth except for some gas outbursts in the electrolyte adjacent to the cathode which we believe can only be due to the evolution of H_2 gas. It is, however, possible that some ferricyanide ion, if any were present, was also reduced. The effect of current density upon the impressed voltage is also shown in Fig. 2. In $CuSO_4$ electrolysis copper is transferred across the cell by the essentially equivalent dissolution of the Cu anode and the deposition of Cu at the cathode. No difference in electrode efficiencies were detected interferometrically. In the contrasting situation, the electrolysis of $K_4Fe(CN)_6$ results in the deposition of Cu ferrocyanide[1] on the anode and at the cathode evolution of H_2 though as previously mentioned, possibly some reduction to ferrocyanide

[1]A saturated solution of cupric ferrocyanide in water contains 1.0×10^{-5} g-ions of Cu^{2+} per liter (5).

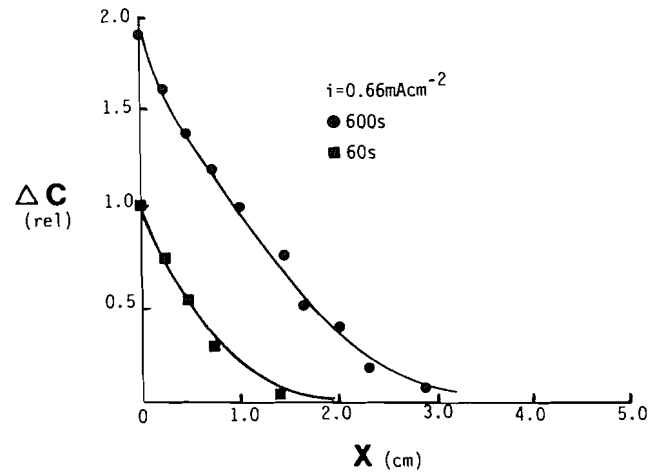

FIG. 4. The concentration–distance profile during the electrolysis of $K_4Fe(CN)_4$ at Cu anode and Cu cathode the X-axis is increased to 50 times the real value.

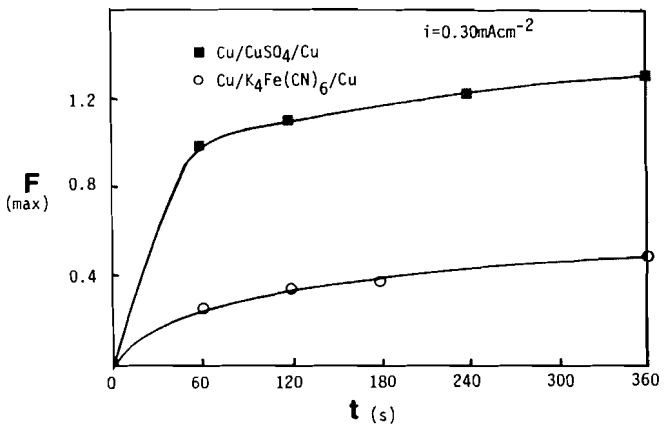

FIG. 5. The fringe shift during the progress of the electrolysis of $CuSO_4$ and $K_4Fe(CN)_6$ at identical current density of 0.30 mA cm^{-2}.

ion. Figure 3 shows the development of the fringe bend (a refractive index increase denoting a concentration change of one or more components) at the Cu anode due to the deposition of the film. The most likely changes in concentration of the solution components to cause this change in refractive index are considered below after introduction of other relevant data. The progressive movement of the fringes during the electrolysis has been followed for over 900 s. Considering the plot of this maximum concentration change (at the anode–electrolyte interface), ΔC_{rel}, vs. elapsed duration of electrolysis, the shape and smoothness of the curves is evidence for the absence of any convection of a magnitude which need be considered during this part of the electrolysis. Figure 4 shows the plot of the concentration profiles at 60 and 600 s (an apparently unlimited growth of the refractive index profile) indicative of diffusion (and the absence of convection) as the dominant transport mode (6, 7). While the above results are similar to those with $CuSO_4$ between the same two electrode materials (1), there were some significant deviations noted relating to the fringe shift or concentration polarization. The calculated fringe shift (*F*) during the electrolysis at the anode is much higher with $K_4Fe(CN)_6$ for an identical current density. In the plot of *F* vs. *t* (Fig. 5) during the electrolysis of $CuSO_4$ and $K_4Fe(CN)_6$; the difference is very obvious between the two electrolytes (see also Fig. 3) and also from the calculated values. The *F* values in

Can. J. Chem. Downloaded from www.nrcresearchpress.com by 213.166.140.6 on 09/07/12
For personal use only.

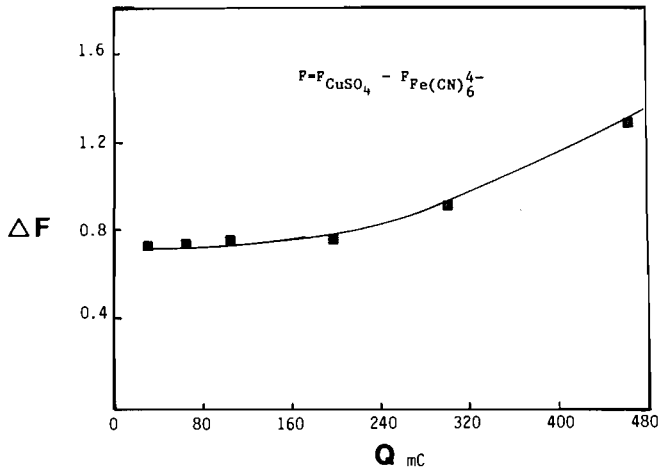

FIG. 6. A plot of fringe shift differences in the electrolysis of $CuSO_4$ and $K_4Fe(CN)_6$ as a function of the charge passed.

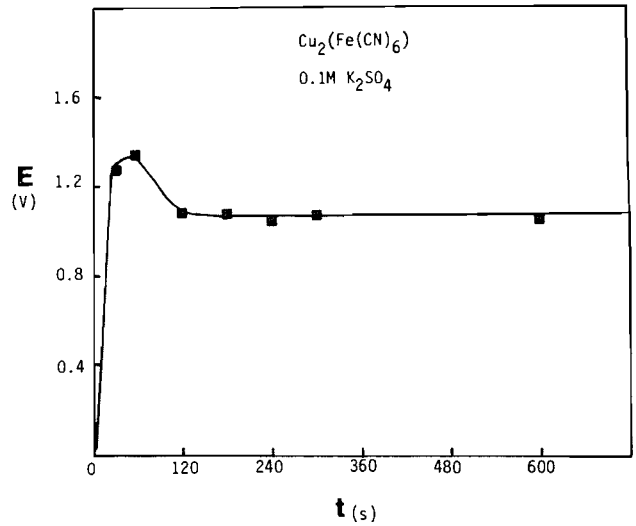

FIG. 7. The impressed voltage vs. time curve in the electrolysis of 0.1 M K_2SO_4 between Cu ferrocyanide anode and Cu cathode.

$K_4Fe(CN)_6$ are always smaller, presumably because four K^+ are in excess as $Fe(CN)_6^{4-}$ is precipitated as $(Cu^{2+})_4[FeCN_6^{4-}]_2$ and a suitable anion such as OH^- diffuses in to maintain electrical neutrality. This KOH has a much lower refractive index in solution than $K_4Fe(CN)_6$. If the difference in fringe shifts ($F_{CuSO_4} - F_{K_4Fe(CN)_6}$) is plotted as a function of the coulombs passed in the electrolysis (Fig. 6), we observe a constancy up to about 200 mC or about 60 $\mu C\ mm^{-2}$ or thicknesses in the range of 10^5 molecular layers. Then a divergence from linearity begins, ΔF rising with a slope of about two fringe shifts per coulomb. Since the oxidation of $Fe(CN)_6^{4-}$ cannot occur at the Cu anode ($E_{Cu_2^{2+}/Cu} = 0.02$ V (in the presence of $Fe(CN)_6^{4-}$) and $E_{Fe(CN)_6^{3-}|Fe(CN)_6^{4-}} = 0.27$ V (5, 7) at the roughly calculated concentrations using the relevant equilibria) the initial reaction can therefore be attributed to the dissolution of the Cu anode. The Cu^{2+} reacts with $Fe(CN)_6^{4-}$ forming a mixed complex (8) via a reaction $4Cu^{2+} + 2Fe(CN)_6^{4-} \rightarrow Cu_4^{2+}[Fe(CN)_6^{4-}]_2$ with perhaps (but unlikely) intermediate formation of $K_2Cu[Fe(CN)_6]$. There may be some incorporation of Cu^+ since the red-brown color of the deposit on the anode is different from the red-brown colour of cupric ferrocyanide or it may reflect the electrochemical mode of formation with the necessary attendant imperfections of a semi-conductor. This deposition results in slowing down the rate of Cu^{2+} escaping to the surface at long times (as the film thickens) but as may be seen from Fig. 5, this film is conducting and the anodic process proceeds. We attribute the anodic fringe shift (where fringe shift is the deviation from the straight fringe condition in the bulk usually measured in fringe separation or fringes for more than one fringe separation distance) observed to the depletion of $Fe(CN)_6^{4-}$ near this electrode. The refractive index (n) measurements on $K_4Fe(CN)_6$ solutions of different concentrations in an Abbé refractometer give a plot of Δn vs. C, and from this a fringe shift is calculated to correspond to $6.7 \times 10^{-3}\ M$ which is greater than for $CuSO_4$ under the same circumstances, or during the electrolysis the refractive index in the anode region should decrease. The possibility of Cu^{2+} escaping into the solution and being involved in an increased fringe shift difference has been considered but was ruled out because of the extremely low solubility of the ferrocyanide product.

Experiments conducted using a mixture of 0.1 M $K_4Fe(CN)_6$ and 0.1 M $K_3Fe(CN)_6$ instead of 0.1 M $K_4Fe(CN)_6$ alone, produce a difference in the cathodic reaction; the H_2 evolution does not occur, otherwise the other results were identical to the simple $K_4Fe(CN)_6$ electrolyte.

Effect of magnetic field

The magnetic field effect was mainly investigated on this system to improve the smoothness of the deposition. The cell was inserted into the cavity of a strong (up to 1.0 T) electromagnet. The laser was removed to 1.2 m to avoid magnetic effects on the plasma. Care was taken to have no Fe or Fe alloys in the field. The impresed voltage vs. time curve in the field deviates from the zero field result in a way shown in Fig. 2. The higher impressed voltages in the field have been attributed to the increased resistances offered by the cell for the same current density as a result of uniform deposition of the Cu ferrocyanide. A more uniform film would be expected to have smaller pores and no pinholes and a generally decreased surface area. With vertical electrodes the magnetic field acts on the hydrodynamic flow and the velocity of the fluid flow increases with increasing magnetic field (1, 9). In the present series of experiments a magnetic field of about 0.5 T has been applied externally. The effect observed was actually a smoother film. This result is similar to that obtained with polycarbazole deposition in a magnetic field (10). Another and expected observation was that the concentration gradients were much more extended at zero field than in the magnetic field; for example at 60 s of electrolysis the diffusion layer extended up to 0.16 mm at B = 0.475 T and up to 0.20 mm at zero field. These results are very similar to those obtained in a 0.1 M $CuSO_4$ solution where the mild convective effects were attributed to differences in the paramagnetism of two concentrations of Cu^{2+} (a $3d^9$ ion) in a strong field (11) causing slow rotation of the electrolyte, which limits the diffusion layer.

Finally, the suitability of electrodeposited Cu ferrocyanide as an electrode was briefly examined by using the filmed electrode as the anode in the electrolysis of 0.1 M K_2SO_4 along with a Cu cathode. This cell was used with current densities ranging from 0.12 mA cm^{-2} to 0.60 mA cm^{-2} and the interference fringes patterns were recorded. Fringe shifts (F_{max}) of 1.1 and 1.4 were noted at 240 s and 360 s in the electrolysis at a current density of 0.12 mA cm^{-2} at the filmed electrode confirming that it is a conducting electrode. The impressed voltage–time curve during this electrolysis is shown in Fig. 7. In view of the

Can. J. Chem. Downloaded from www.nrcresearchpress.com by 213.166.140.6 on 09/07/12
For personal use only.

reported use of $Cu_2Fe(CN)_6$ precipitated into porous pottery in the older chemistry books, e.g., Latimer and Hildebrand (12), to make semi-permeable membranes this material should probably be studied further as an electrode coating.

Acknowledgements

The authors wish to acknowledge the support for this work by the Natural Sciences and Engineering Research Council of Canada and the help of Teddy Gathright of TRIUMF.

1. R. N. O'BRIEN and K. S. V. SANTHANAM. J. Electrochem. Soc. **129**, 1266 (1982).
2. J. BRUININK, C. G. A. KREGTING, and J. J. PORIJEE. J. Electrochem. Soc. **124**, 1854 (1977).
3. B. W. FAUGHAN and R. S. CRANDALL. Display devices. *Edited by* J. I. Pankore. Springer-Verlag, Berlin. 1980.
4. F. B. KAUFMAN, A. H. SCHROEDER, E. M. ENGLER, and V. V. PATEL. Appl. Phys. Lett. **36**, 422 (1980).
5. A. SEIDELL and W. F. LUIKE (*Editors*). Solubilities of inorganic and metal organic compounds. Vol. 1. D. Van Nostrand Company Inc., New York. 1958.
6. R. N. O'BRIEN. (*a*) J. Electrochem. Soc. **119**, 589 (1972); (*b*) Rev. Sci. Instrum. **35**, 803 (1964).
7. R. N. O'BRIEN, W. MICHALIK, B. B. KULKARNI, and K. S. V. SANTHANAM. Can. J. Chem. **59**, 1933 (1981).
8. Handbook of chemistry and physics. 60th ed. C.R.C. Press. 1981.
9. T. Z. FAHIDY. Electrochim. Acta, **18**, 607 (1973).
10. R. N. O'BRIEN and K. S. V. SANTHANAM. J. Electrochem. Soc. **131**, 2028 (1984).
11. R. N. O'BRIEN and K. S. V. SANTHANAM. Electrochem. Acta. To be published.
12. W. M. LATIMER and J. H. HILDEBRAND. Reference book of inorganic chemistry. 3rd ed. McMillan, New York. 1959. p. 112.

Can. J. Chem. Downloaded from www.nrcresearchpress.com by 213.166.140.6 on 09/07/12
For personal use only.

Unusual spectral shifts in the prototropic reactions of 2,7-diaminofluorene

R. MANOHARAN AND SNEH K. DOGRA[1]

Department of Chemistry, Indian Institute of Technology, Kanpur-208016, India

Received July 7, 1986[2]

R. MANOHARAN and SNEH K. DOGRA. Can. J. Chem. **65**, 2013 (1987).

The red shift observed in the absorption spectrum of 2,7-diaminofluorene (DAF) in ether and acetonitrile is either due to the proton-donating capacity of the solute or due to its dispersive interactions with the solvent and a blue shift in methanol and water is due to the proton-accepting nature of DAF. DAF acts as a proton donor in S_1 state in all solvents. The red shift in the fluorescence spectrum of the monocation of DAF relative to that of DAF is not because of the —NH_2 group becoming more basic but because of the large solvent relaxating in aqueous medium. On the other hand, the monocation of DAF in cyclohexane follows the normal blue shift in the fluorescence spectrum. pK_a values for the various prototropic reactions in S_0 and S_1 states are determined and discussed.

R. MANOHARAN et SNEH K. DOGRA. Can. J. Chem. **65**, 2013 (1987).

Lorsqu'on détermine les spectres d'absorption du diamino-2,7 fluorène (DAF) dans l'éther et dans l'acétonitrile, on observe un déplacement vers le rouge; ce résultat est dû soit à la capacité du soluté à donner des protons ou aux interactions dispersives du solvant. Par ailleurs, on observe un déplacement vers le bleu lorsque les spectres sont déterminés dans le méthanol et dans l'eau; ces résultats sont dus à la nature du DAF qui a tendance à accepter des protons. Dans tous les solvants, le DAF agit comme donneur de proton dans l'état S_1. Si on compare le spectre de fluorescence du monocation du DAF avec celui du DAF, on observe un déplacement vers le rouge qui n'est pas dû au fait que le groupement —NH_2 devient plus basique mais plutôt à la relaxation importante du solvant dans le milieu aqueux. Par ailleurs, le spectre de fluorescence du monocation du DAF dans le cyclohexane subit le déplacement normal vers le bleu. On a déterminé et on discute des valeurs de pK_a pour diverses réactions prototropiques dans les états S_0 et S_1.

[Traduit par la revue]

Can. J. Chem. Downloaded from www.nrcresearchpress.com by 213.166.140.6 on 09/07/12
For personal use only.

During electronic transitions, the charge density changes at each atom of the molecule. Depending upon the nature of the transition as well as the nature of the molecule itself, the molecule may become less polar or more polar in the excited state as compared to the ground state. Due to this, the solvent molecules rearrange themselves in the S_1 state, which is different from the ground state. Since the rearrangement of the solvent molecules involves bond breaking or bond formation, the time taken for this phenomenon can be compared with the period of vibrational motion and this is much smaller than the fluorescence lifetime. In other words, the fluorescence always occurs from the thermally equilibrated excited state even though the molecule, to begin with, is in the Franck–Condon state. The equilibrated state is of lower energy than the Franck–Condon state provided the polarity of the molecule changes (increases or decreases) and the solvent is polar (1, 2). Sometimes the stabilisation of the states, called solvent relaxation, is so large that either reversal of states takes place or large Stokes' shifts are observed. For example, if a $\pi \rightarrow \pi^*$ state is the lowest energy transition, a pyridinic-like nitrogen atom becomes more basic upon excitation and protonation in general will lead to red shift in the absorption and fluorescence spectra (3). The absorption spectrum of *O*-phenanthroline (4), which contains two nitrogen atoms at positions 9, 10 is red-shifted upon protonation of both the nitrogen atoms. However, the fluorescence spectrum behaves differently under the above conditions, i.e. a large red shift is observed in the fluorescence spectrum of the neutral molecule on protonation, but upon the second protonation a blue shift is observed. Schulman *et al.* (4) showed that this abnormal spectral shift in the fluorescence spectrum of the monocation is due to a large solvent relaxation in aqueous medium whereas the normal red shift is observed when the fluorescence spectrum of the monocation is taken in hydrocarbon as a solvent.

In the fluorene molecule, electrophilic attack can take place at position 2. If the electron-donating groups are present at positions 2 and 7, the spectral behaviour can be abnormal on protonation. The present study of 2,7-diaminofluorene (DAF) was carried out with the above aim in mind. The absorption and fluorescence spectra are recorded at different pH and in different solvents. The pK_a values have been calculated for the following prototropic reactions both in the ground and excited states.

[1] $DAF \rightleftharpoons DAF^- + H^+$

[2] $DAFH^+ \rightleftharpoons DAF + H^+$

[3] $DAFH_2^{2+} \rightleftharpoons DAFH^+ + H^+$

Experimental

2,7-Diaminofluorene (DAF) was obtained from Aldrich Chemical Co. and recrystallised from benzene. The purity of the compound was checked by noting its melting point, electronic spectrum, and similar fluorescence spectra when excited with different wavelengths. Spectrograde methanol (BDH), analytical grade sulphuric acid, sodium hydroxide, and trifluoroacetic acid (TFA) were used as such. Cyclohexane, ether, and acetonitrile were further purified according to a procedure suggested in the literature (5). Triply distilled water was used for aqueous solutions. Solutions in the pH range of 3 to 10 were prepared by adding appropriate amounts of NaOH and H_3PO_4. A modified Hammett's acidity scale (6) for the H_2SO_4–H_2O mixtures and Yagil's basicity scale (7) for NaOH–H_2O mixtures were used below pH 1 and above pH 13, respectively. Hammett's acidity function (H_0) serves specifically as a measure of the tendency for the solution in question to transfer a proton to an uncharged or charged base molecule, increasingly negative values corresponding to higher acidity.

Absorption spectra were recorded on a Shimadzu 190 UV spectrophotometer, equipped with a U 135 recorder. Fluorescence measurements were carried out on a recording spectrofluorimeter, fabricated in our laboratory and the details are available elsewhere (8). Both monochromators were calibrated from time to time using a low pressure mercury lamp. The excitation source bandwidth was 8 nm. The fluorescence spectra were corrected according to the procedure suggested by Parker (9). The quantum yields were calculated, using quinine sulphate in 0.1 *N* H_2SO_4 as a standard (10) and the wavelength

[1]To whom all correspondence should be addressed.

[2]Revision received February 4, 1987.

Can. J. Chem. Downloaded from www.nrcresearchpress.com by 213.166.140.6 on 09/07/12
For personal use only.

TABLE 1. Absorption maxima, molar extinction coeff, fluorescence maxima, and quantum yields of 2,7-diaminofluorene in different solvents[a].

Compound	λ_{max}(abs) log ϵ_{max}	λ_{max}(flu)	ϕ_f
Cyclohexane	334 299 283 262 212	369	0.25
Ether	340 (3.76) 305 (4.28) 292.5 (4.29) 226 (3.9)	383	0.24
Acetonitrile	338 (3.74) — 296 (4.29) 219 (4.12)	385	0.23
Methanol	337.0 (3.77) — 294 (4.43) 210 (4.48)	388	0.25
Water (pH 8)	328.5 (3.79) — 289.5 (4.38) 207 (4.59)	395	0.03
Monocation (pH 4)	317.5 (3.86) 289.5 (4.26) 202.5 (4.47)	410	0.42
Dication ($H_0 - 4$)	297 (3.93) (s) 290 (3.75) 285.5 (3.81) (s) 275 (3.94) (s) 270 (4.12) 262 (4.29) 257 (4.29) (s) 252.5 (4.25) (s) 217.5 (4.08) 203 (4.59)	300 310	0.072

[a]ϵ is in cubic decimeters per mole per centimeter. s is shoulder.

used for excitation was 313 nm. The concentrations used were in the range of 1.5×10^{-5} *M*. The solutions for absorptiometric and fluorometric titrations were prepared just before taking measurements. The isosbestic wavelengths were used for measuring the fluorescence intensities at any analytical wavelength. The values for dication–monocation, monocation–neutral, and neutral–monoanion couples are 270 nm, 324 nm, and 345 nm, respectively. The pH of the solutions in the range 1–13 were measured on a Toshniwal pH meter, model CL 44A.

Results and Discussion

Effect of solvents

The absorption and fluorescence spectra of DAF were observed in different solvents and the relevant data are compiled in Table 1. The absorption data are depicted in Fig. 1 and the fluorescence data in Fig. 2. When compared to fluorene (11), the absorption maxima of all DAF bands are largely red-shifted in any one solvent. The structures of the ~300 nm and ~200 nm bands of the fluorene molecule are completely destroyed whereas the structure of the middle band (~264 nm) is not affected that much in less polar solvents. All these band maxima are red-shifted (300 to 340 nm, 264 to 290 nm, and 200 to

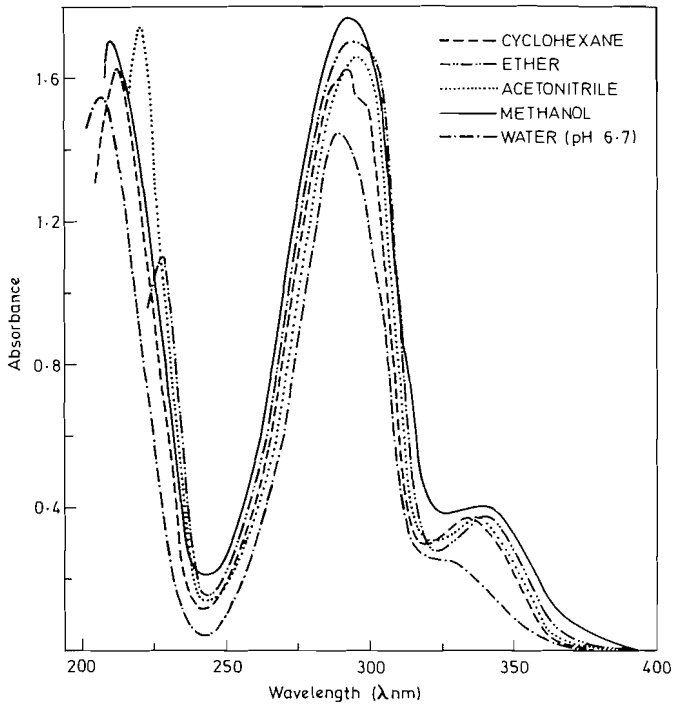

FIG. 1. Absorption spectra of DAF in various solvents at 298 K. Concentration 1×10^{-5} *M*, ----, cyclohexane; ·-·-·-·, ether; ···, acetonitrile; —, methanol; ·····, water (pH 6.7).

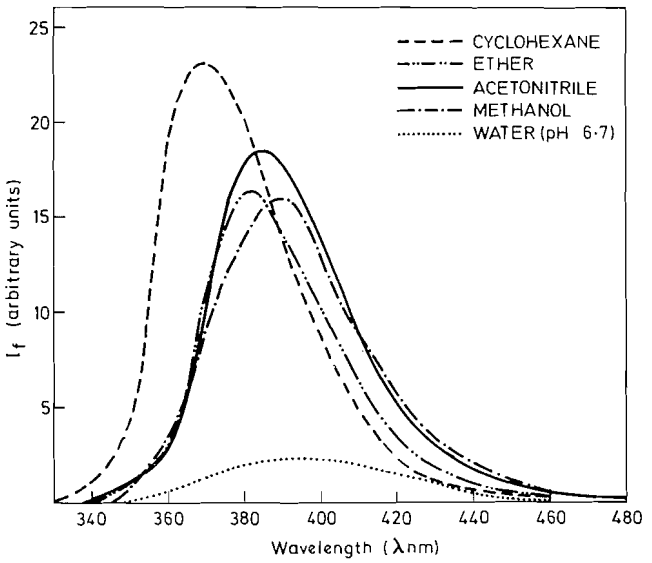

FIG. 2. Fluorescence spectra of DAF in various solvents at 298 K. Concentration 1×10^{-5} *M*, ---, cyclohexane; ·-·-·-·, ether; —, acetonitrile; ·····, methanol; ···, water (pH 6.7).

215 nm) in any one particular solvent. The structure of the middle band is also lost in more polar solvents. The absorption spectrum is red-shifted from cyclohexane to acetonitrile, a more polar solvent and blue-shifted in methanol and water. On the other hand, the fluorescence spectrum is a large red-shifted broad band as compared to the structured fluorescence spectrum of fluorene (11). The fluorescence maximum is regularly red-shifted as the polarity and proton-donor capacity of the solvent increases. Under similar environments the fluorescence quantum yield remains nearly constant except in water, at pH 8.

The structure of the fluorene molecule can be compared with

Can. J. Chem. Downloaded from www.nrcresearchpress.com by 213.166.140.6 on 09/07/12
For personal use only.

O-, O'-condensed biphenyl system (12) and its transitions can be compared with those present in the benzene molecule, although this kind of notation is not applicable to the biphenyl system. Thus, the 300, 260 and 220 nm band systems of fluorene can be assigned to the $^1A_g \rightarrow {}^1L_b$, $^1A_g \rightarrow {}^1L_a$, and $^1A_g \rightarrow {}^1B_b$ transitions, respectively (12). The first and the third transitions are thus long-axis polarised and the second one is short-axis polarised. Since both the amino groups are present on the long axis of fluorene, the interaction is maximum with the ring and the first and the third band will be affected more than the second one. Thus the structure of the long wavelength band of fluorene is completely lost. Though the bathochromic shift is observed in the ~260 nm band system of fluorene, the structure in non-polar solvents is observed. The loss in the structure in more polar solvents is due to the stronger interaction of the solute and solvent molecules. The spectral shifts observed in the absorption spectrum of DAF in more polar or hydrogen bonding solvents are consistent with the characteristic behaviour of amino (13) or hydroxyl groups (14), i.e. it acts as a proton donor to the proton-acceptor solvents but preferably as a proton acceptor if the solvent possesses both proton-donor and proton-acceptor properties in the S_0 state. Ether is acting as a proton acceptor and acetonitrile a dispersive, whereas methanol and water are proton-donor solvents. In the excited singlet state, since the charge migration increases from the $—NH_2$ group to the ring, it will reduce the charge density at the nitrogen atom and thus behave as a proton-donor group. This is further manifested from the increased acidity of the $—NH_2$ group on excitation (*vide infra*). The Stokes shift $[\bar{\nu}_{abs}(max) - \bar{\nu}_{flu}(max)]$ increases with increase in the polarity or hydrogen bonding ability of the solvents, indicating that dipole moment of the molecule increases upon excitation. The decrease in the fluorescence quantum yield of the neutral DAF in water suggests the stronger interactions with water, thereby increasing the rate of radiationless processes.

Effect of pH

The absorption and fluorescence spectra of DAF have been studied in the H_0/pH/H_- range of −10 to 16. The relevant data are compiled in Table 1. Absorption data are shown in Fig. 3 and fluorescence data in Fig. 4. The changes observed in the absorption spectrum of DAF are consistent with the decrease of pH. The absorption spectrum of DAF is blue-shifted around pH 5, indicating the formation of monocation by protonating one of the amino groups and the long wavelength absorption band of this species resembles that of 2-aminofluorene (15). A further blue shift is observed at H_0 −4, suggesting the formation of dication by protonating the second amino group also. This is further confirmed by the resemblance of the absorption spectrum of the latter species to that of fluorene (11), i.e. the band structure of the ~300 nm band system is clearly visible. No further change in absorption spectrum is noticed even at H_0 −10. After pH 12, the maxima of the 329 and 207 nm bands start red shifting and the shift is not complete even at H_- 16; the most strongly basic solution used. The middle band is not much affected until H_- 15 and its intensity is reduced drastically at H_- 16, becoming a flat band, without any change in band maximum. The first change is due to the formation of monoanion, obtained by the deprotonation of one of the $—NH_2$ groups. This is further confirmed by the fact that the major changes in the absorption spectrum are only produced in the long axis polarised bands. The pK_a value for this proton transfer reaction could not be calculated because of the reason

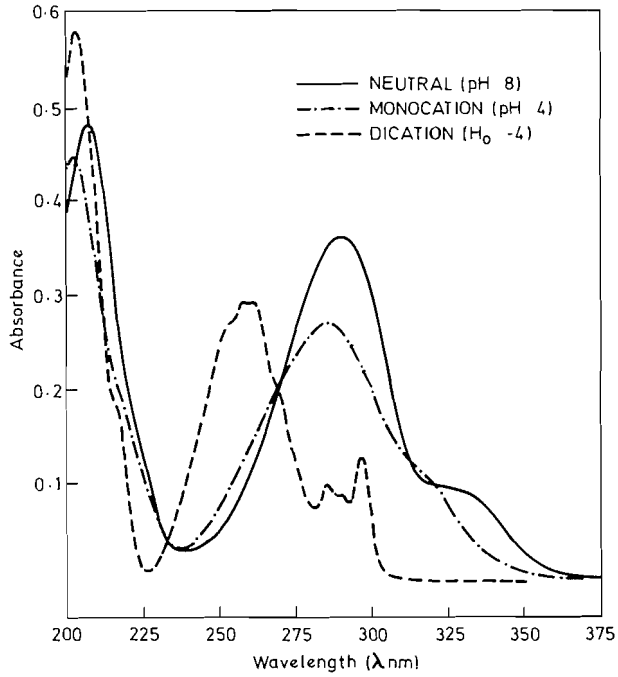

FIG. 3. Absorption spectra of different prototropic species of DAF at 298 K: —, neutral (pH 6.7); ·····, monocation (pH 4); ---, dication (H_0 −4).

mentioned above, but its value will be certainly lower than the pK_a value for other aromatic amines (>16 (13)). This can be explained on the same lines as will be done to explain the high value of pK_a [2].

The effect of pH on the fluorescence spectrum is very different from that of pH on the absorption spectrum. The behaviour of DAF at pH 12 in the excited state is in agreement with the earlier results on similar groups, in the sense that the monoanion formed by the deprotonation of $—NH_2$ group is generally non-fluorescent (16) with few exceptions (17). The pK_a^* calculated from fluorimetric titration curves is 13.9. This is in the same range as the observed pK_a^*'s for other aromatic amines, indicating that the $—NH_2$ group becomes strongly acidic on excitation (16).

The fluorescence characteristics of the cationic species of DAF, with the decrease of pH are different from the absorption characteristics. DAF is weakly fluorescent (395 nm) in basic and nearly neutral solution. In the region near pH 5, the intensity of the weak 395 nm fluorescent band decreases with the decrease of pH while the intensity of the slightly red-shifted (410 nm) fluorescent band increases. The excitation spectra monitored at both wavelengths resemble exactly the absorption spectra of the two species formed in the S_0 state. The intensity of the 410 nm band decreases to nearly 10% of its maximum value at pH 0.5, when a very large blue-shifted, structured fluorescent band (310 nm, 300 nm) starts appearing. The blue-shifted band attains its maximum intensity by H_0 −4. The intensity of the ~310 nm band starts decreasing on increasing the acid concentration without the appearance of any other new fluorescent band and at highest H_0 value, it is 5% of its maximum intensity (I_0). This fluorescence spectrum exactly resembles that of the parent fluorene molecule. The excitation spectrum monitored at the 310 nm band resembles the absorption spectrum of the ground state species as well as that of the fluorene molecule. The excitation spectra, recorded at pH 5, H_0 −1 and below H_0 −1 resemble the absorption spectra of the

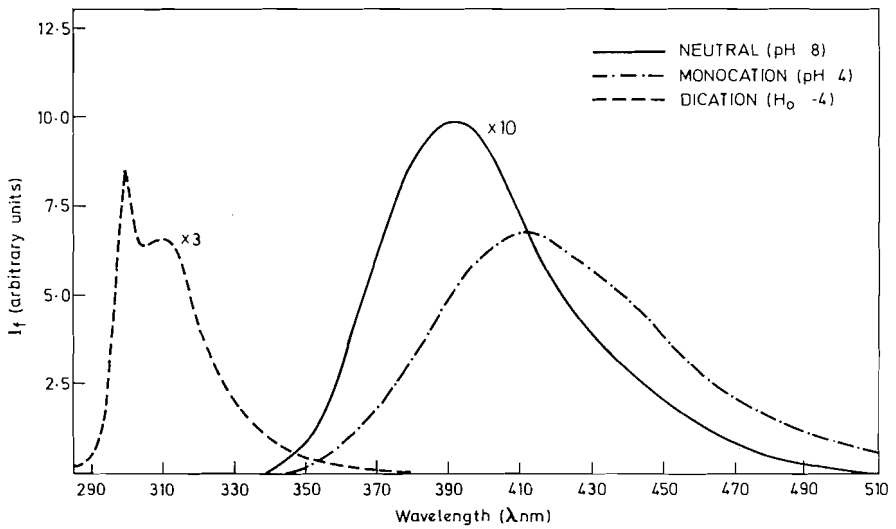

FIG. 4. Fluorescence spectra of different prototropic species of DAF at 298 K: —, neutral; ·····, monocation (pH 4); ---, dication (H_0 −4).

species present in the ground state at these acid concentrations. Thus the species present in the excited singlet state at these conditions are neutral, monocation, and dication, respectively.

As previously mentioned the lowest energy transition in DAF is a $\pi \rightarrow \pi^*$ transition which is long-axis polarised. Since the trend observed in the absorption spectra on addition of protons is similar to that observed in other amines (16), it suggests that the nature of the lowest energy state in these ions remains the same. The mirror image relationship observed between the absorption and fluorescence spectra of the neutral and dication species clearly indicate that fluorescence in these species is taking place from the state polarised along the longer axis. Though the mirror image relationship is not observed in the case of the monocation, it can be concluded that the emitting state is still the same as that observed in other species. This is because the difference between the absorption maxima of the two bands in neutral and monocation remains the same and thus the reverse cannot take place. Also, the proximity of the excitation and fluorescence bands infers that they both arise from the long-axis polarised band.

The ground state pK_a values for the monocation–neutral and dication–monocation equilibria, calculated spectrophotometrically, are 5.8 and 3.6, respectively. These values are listed in Table 2. The pK_a values reported in the literature (18) for the corresponding equilibria are 4.96 and 3.6, respectively. Since the latter values are obtained in 70% ethanol/water (v/v) solutions, these values cannot be compared with our values, which are determined in water. Similarly the pK_a values for these equilibria in the S_1 state are determined from fluorimetric titrations, as well as with the help of the Förster cycle method (17), using absorption, fluorescence, and the average of the absorption and fluorescence maxima. The data are compiled in Table 2. The pK_a [2] value is higher than observed for the aromatic amine protonation reaction (~4.5, ref. 14) and pK_a [3] is lower than ~4.5. This clearly suggests that the charge density at one of the amino group is higher than what is normally present in a monoaromatic amine. This can be explained from the following canonical structure of the fluorene molecule, i.e., it is well known that electrophilic attack in the case of fluorene takes place at position 2, followed by attack at position 7 (1). If the electron-donating group is present at position 7, the charge density at position 2 will increase further. The average charge density at the $—NH_2$ groups will be the same, because of the symmetric nature of DAF. But at any particular instant, one of the $—NH_2$ groups will be a little more basic than the other. This will lead to an increase in the pK_a [2] value for this equilibrium. The opposite is true for the behaviour of the other amino group and the pK_a [3] will be lower than the normal amino group protonation.

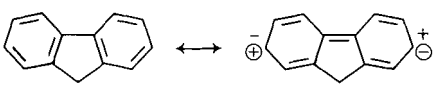

The agreement between the pK_a^* values obtained by various methods is not very good. The value of equilibrium constant for the monocation–neutral equilibrium obtained with the help of fluorimetric titration method has only given the ground-state value. This could be due either to the short lifetimes of the conjugate acid–base pair or the concentration of hydrogen ions are so small that the rate of protonation or deprotonation cannot compete with the rate of emission. The difference between the pK_a^* values for reactions [2] and [3], calculated by the Förster cycle method and using the absorption and fluorescence data, is due to very different solvent relaxation of the various species in these equilibria. The Stokes shift observed for neutral, monocation, and dication in water, i.e., 5120, 7100, 340 cm^{-1}, respectively, further proves the point.

The Förster cycle method, using the fluorescence data, has clearly indicated that the amino group become more basic on excitation, which is completely opposite to the normal behaviour of the aromatic amines. As stated earlier, it is due to the very large solvent relaxation of DAF^+ as compared to that observed for neutral or dication species in water. This can be tested if one records the spectral changes of these three species in a non-polar and non-hydrogen bonding medium. An example is cyclohexane, because in this medium the solvent relaxation effects of three species derived from DAF are expected to be very small compared to those in aqueous or acidic medium. Table 3 depicts the absorption and fluorescence spectrum of neutral DAF, monocation, and dication of DAF. The latter two species were obtained by the addition of different amount of TFA in cyclohexane. The absorption spectra of the ionic species matched with those species derived by the addition of sulphuric acid in aqueous medium but the fluorescence spectra were

Can. J. Chem. Downloaded from www.nrcresearchpress.com by 213.166.140.6 on 09/07/12
For personal use only.

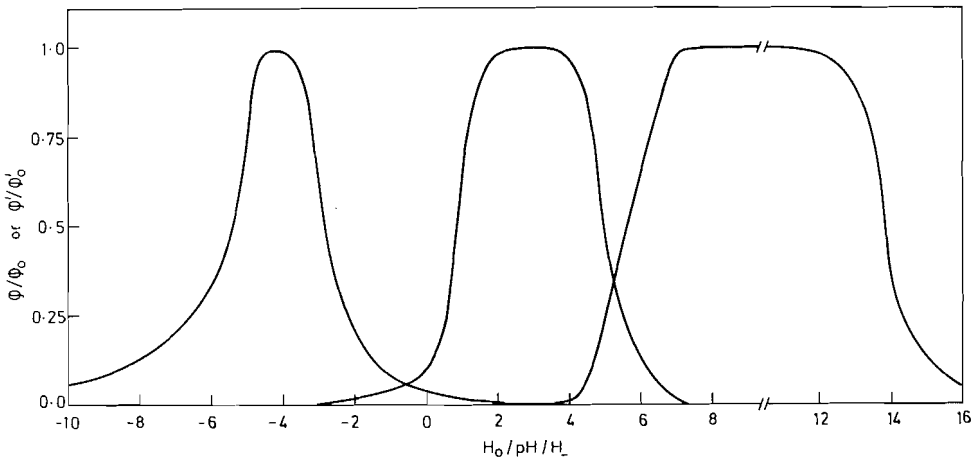

FIG. 5. Plot of ϕ/ϕ_0 versus $H_0/\mathrm{pH}/H_-$ of the various prototropic species of DAF.

TABLE 2. pK values of the prototropic equilibria of DAF in the lowest excited singlet and ground states[a]

Equilibrium	pK_a	p$K_a^{*\,abs}$	p$K_a^{*\,flu}$	p$K_a^{*\,av}$	p$K_a^{*\,ft}$
Neutral ⇌ Monoanion	>16	—	—	—	13.9
Monocation ⇌ Neutral	5.8	3.5	7.9	5.7	5.3
Dication ⇌ Monocation	3.6	−1.0	−15.2	−8.2	−3.0

[a]Förster cycle method using (abs) absorption data (flu) fluorescence data; av, average of absorption and fluorescence maxima; ft, pK_a^* from fluorimetric titrations.

different under the similar environments. The results obtained in fluorescence were similar to the normal behaviour of the aromatic amines, thereby confirming the above explanation i.e. a blue shift (324 nm) is observed in the fluorescence spectrum of DAF. The greater polarity of the monocation can also be noted from the Stokes' shifts observed in non-polar and polar media. For example, in cyclohexane, the Stokes' shifts of the neutral, monocationic, and dicationic species are 2670, 1920, and 770 cm^{-1}, respectively, whereas in water are 5120, 7100, and 340 cm^{-1}, respectively. The large discrepancy between the Stokes' shifts for DAF^+ in cyclohexane and water must be due to solvent relaxation because the change in solvent cannot change the vibrational relaxation or a change in the energy of the excited state by such a large amount. Further, the large Stokes' shift of DAF^+ in water suggests that this species is stabilised in the excited state much more than in the ground state relative to the species with which it is in prototropic equilibrium. Thus, as suggested by Schulman *et al.* (4), the Förster cycle method, using the average of the absorption and fluorescence maxima, will not be useful in these equilibria.

Fluorimetric titrations between dication–monocation indicate that there is no correspondence between the decrease in fluorescence intensity of the monocation and the increase in fluorescence intensity of the dication. This is similar to the normal behaviour observed for the protonation reaction of aromatic amine, i.e., proton-induced fluorescence quenching of the base is observed before it is being protonated (14, 18). In these cases the pK_a^* value is calculated from the formation curve of the dication, rather than from the decrease in intensity of the monocation and the pK_a^*(3) value is −3.0. The agreement between this value and that obtained by the Förster cycle method with absorption data is quite reasonable. The

TABLE 3. Absorption and fluorescence maxima of DAF in the presence of TFA

Compound	λ_{abs} (nm)	λ_{flu} (nm)
Cyclohexane	335	369
	300	
	282.5	
Cyclohexane	305	324
0.001% TFA	292.5	
	266.5	
Cyclohexane	298	
1% TFA	289	
	285	305
	260	

difference may be due to the structured absorption spectrum of dication and the broad band of the monocation. The pK_a^* value obtained using fluorescence maxima cannot be compared with other values due to reasons mentioned earlier. Anyway, the pK_a^*(3) values so obtained do indicate that ammonium ions become more acidic in the excited singlet state.

The proton-induced fluorescence quenching mechanism can be compared with that proposed by Shizuka *et al.* (19) and can be described by the simple Stern–Volmer equation

$$\frac{I_0}{I} = 1 + k_q\tau[H^+]$$

where I and I_0 are the fluorescence intensities of monocation with and without the presence of $[H^+]$, k_q is the proton-induced fluorescence quenching constant, and τ is the lifetime of the

Can. J. Chem. Downloaded from www.nrcresearchpress.com by 213.166.140.6 on 09/07/12
For personal use only.

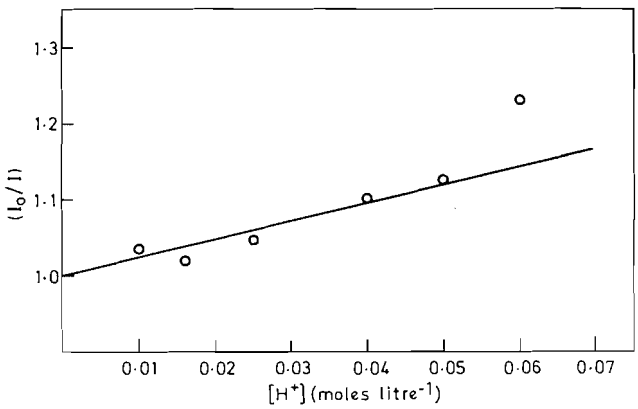

FIG. 6. Plot of I_0/I versus $[H^+]$.

monocation. $k_q\tau$ is calculated from Fig. 6 and is 2.4 dm^3 mol^{-1}. The natural lifetime (τ_{FM}) is calculated by using Strickler-Berg's equation (20), whereas τ is obtained from the relation $\tau = \tau_{FM}\phi_f$. The error involved in the calculation of τ_{FM} is large because the long wavelength absorption band of DAF^+ is not well resolved. This band has been created assuming that the distribution is Gaussian. This assumption is based on the fact that the other absorption bands are Gaussian. The value of k_q thus obtained is 4×10^8 dm^3 mol^{-1} s^{-1} and is less than the value of k_q generally observed for neutral amines (15, 19). This is due to the positive charge already existed on the molecule.

Conclusion

The above study has clearly indicated that the red shift in the fluorescence spectrum of the monocation as compared to the neutral DAF is due to the large solvent relaxation in its excited singlet state. Thus the fluorescence data cannot be used to calculate the pK_a^* values for both prototropic equilibria using the Förster cycle method.

Acknowledgement

We thank the Department of Science and Technology for the financial support to the project "Proton transfer reactions in the excited state".

1. H. H. JAFFE and M. ORCHIN. Theory and applications of ultraviolet spectroscopy. John Wiley. 1962. p. 186.
2. S. G. SCHULMAN. Fluorescence and phosphorescence spectroscopy, physico chemical principles and practice. Pergamon Press, New York. 1977. p. 46.
3. J. F. IRELAND and P. A. H. WYATT. Advances in physical organic chemistry. Vol. 12, *Edited by* V. Gold and D. Bethell. Academic Press, New York. 1976. p. 131.
4. S. G. SCHULMAN, P. T. TIDWELL, J. J. CETORELLI, and J. D. WINEFORDNER. J. Am. Chem. Soc. **93**, 3179 (1971).
5. J. A. RIDDICK and W. B. BUNGER. Techniques of chemistry. Vol. 8. Organic solvents. *Edited by* A. Weissberger. Wiley Interscience, New York. 1970. pp. 592, 644, 695.
6. M. J. JORGENSON and D. R. HARTTER. J. Am. Chem. Soc. **85**, 878 (1963).
7. G. YAGIL. J. Phys. Chem. **71**, 1034 (1967).
8. M. SWAMINATHAN and S. K. DOGRA. Indian J. Chem. **22**A, 853 (1983).
9. C. A. PARKER. Photoluminescence of solutions. Elsevier Publishing Company, New York. 1968. p. 252.
10. G. G. GUILBAULT. Practical fluorescence. Dekker, New York. 1971. p. 13.
11. I. B. BERLMAN. Handbook of fluorescence spectra of aromatic molecules. Academic Press, New York. 1965. p. 119.
12. (*a*) H. SUZUKI. Electronic absorption spectra and geometry of organic molecules. Academic Press, New York. 1967. p. 286; (*b*) J. N. MURRELL. The electronic spectra of organic molecules. Wiley Interscience, New York. 1963. p. 292.
13. (*a*) A. K. MISHRA and S. K. DOGRA. J. Photochem. **23**, 163 (1983); (*b*) M. SWAMINATHAN and S. K. DOGRA. Can. J. Chem. **61**, 1064 (1983); (*c*) M. SWAMINATHAN and S. K. DOGRA. J. Am. Chem. Soc. **105**, 6223 (1983).
14. (*a*) M. SWAMINATHAN and S. K. DOGRA. J. Chem. Soc. Perkin Trans. II, 947 (1984); (*b*) M. KRISHNAMURTHY and S. K. DOGRA. Spectrochim. Acta, **42**A, 793 (1986); (*c*) H. K. SINHA and S. K. DOGRA. J. Photochem. **36**, 149 (1987).
15. H. H. RICHTOL and B. R. FITCH. Anal. Chem. **46**, 1749 (1974).
16. (*a*) H. BOAZ and G. K. ROLLEFSON. J. Am. Chem. Soc. **72**, 3435 (1950); (*b*) A. K. MISHRA and S. K. DOGRA. J. Chem. Soc. Perkin Trans. II, 943 (1984).
17. (*a*) U. PANDE, N. B. JOSHI, and D. D. PANT. CHEM. PHYS. LETT. **72**, 209 (1980); (*b*) TH. FORSTER. Z. Elektrochem. **54**, 531 (1950).
18. P. H. GRANTHAM, E. K. WEISBURGER, and J. H. WEISBURGER. J. Org. Chem. **26**, 1008 (1961).
19. (*a*) K. TSUTSUMI and H. SHIZUKA. Chem. Phys. Lett. **52**, 485 (1977); Z. Phys. Chem. N. F. **111**, 129 (1978); (*b*) H. SHIZUKA, K. TSUTSUMI, H. TAKAUCHI, and I. TANAKA. Chem. Phys. Lett. **62**, 408 (1979); (*c*) H. SHIZUKA and K. TSUTSUMI. J. Photochem. **9**, 334 (1978); (*d*) K. TSUTSUMI and H. SHIZUKA. Z. Phys. Chem. N. F. **122**, 129 (1980); (*e*) K. TSUTSUMI, S. SEKIGUCHI, and H. SHIZUKA. J. Chem. Soc. Faraday Trans. I, **78**, 1087 (1982).
20. S. J. STRICKLER and R. A. BERG. J. Chem. Phys. **37**, 814 (1962).

Can. J. Chem. Downloaded from www.nrcresearchpress.com by 213.166.140.6 on 09/07/12
For personal use only.

A general synthesis of dihydrobenzofurans by intramolecular conjugate addition

GAMINI WEERATUNGA, ALINA JAWORSKA-SOBIESIAK, AND STEPHEN HORNE
Department of Chemistry, University of Waterloo, Waterloo, Ont., Canada, N2L 3G1

AND

RUSSELL RODRIGO[1]
Department of Chemistry, Wilfrid Laurier University, Waterloo, Ont., Canada, N2L 3C5

Received September 9, 1986

GAMINI WEERATUNGA, ALINA JAWORSKA-SOBIESIAK, STEPHEN HORNE, and RUSSELL RODRIGO. Can. J. Chem. **65**, 2019 (1987).

ortho Iodophenoxy crotonates **3***e*–**7***e* cyclize to dihydrobenzo[*b*]furans **1** and **9**–**12** when subjected to lithium–iodine exchange at −100°C. Naphtho[2,1-*b*]furan **13** can be similarly obtained from α-iodonaphthoxy crotonate **8***e*. Methylation of this reaction mixture *in situ* provides a single diastereomer **14**; its relative configuration is assigned by ^{1}H nuclear magnetic resonance, and its formation rationalized by steric arguments. Diastereoselective deuteration is also observed in this case.

GAMINI WEERATUNGA, ALINA JAWORSKA-SOBIESIAK, STEPHEN HORNE et RUSSELL RODRIGO. Can. J. Chem. **65**, 2019 (1987).

Lorsqu'on soumet les crotonates d'*ortho*-iodophénoxyles (**3***e*–**7***e*) à un échange lithium–iode, à 100°C, ils se cyclisent en dihydro benzo[*b*]furannes (**1**, **9**–**12**). De la même manière, le crotonate d'α-iodonaphthoxyle (**8***e*) conduit au naphto[2,1-*b*]furanne (**13**). La méthylation *in situ* de ce mélange réactionnel ne conduit qu'à un seul diastéréoisomère, le composé **14**; on a attribué sa configuration relative en se basant sur son spectre de résonance magnétique nucléaire du ^{1}H et on a rationalisé sa formation en se basant sur des arguments stériques. Dans ce cas, on observe aussi une deutération diastéréosélective.

[Traduit par la revue]

Can. J. Chem. Downloaded from www.nrcresearchpress.com by 213.166.140.6 on 09/07/12
For personal use only.

A current project in natural product synthesis in our laboratory required an efficient method for the preparation of a 4-methyl-7-methoxybenzo[*b*]furan (or the 2,3-dihydro derivative thereof) substituted at C-3 by a functionalized one- or two-carbon unit (e.g. **1** or **2**). Versatile syntheses of such compounds (for a recent review see ref. 1) from easily available starting materials are not commonplace but the subject has attracted some recent attention, and methods of forming the 3–3a bond through anionic (2, 3) or radical (4) intermediates have been employed. Processes involving 1–2 bond formation (5) (from phenols) and the more traditional 2–3 bond formation (6) from phenoxyacetic acids have also been reported. Nevertheless the problem at hand still resisted a satisfactory solution, although a small amount of **2** was prepared by the Bradsher–Parham (3) epoxide cyclialkylation procedure. The main drawback of this synthesis, in our hands, was the sluggish epoxidation of the *O*-allyl phenol, the precursor of the desired epoxide.

In seeking a solution to the problem we attempted to combine the economy of Parham's cyclialkylation with the *ortho*-directing potential of the phenolic hydroxyl group. Thus, after the methoxymethyl ether (**3***b*) of the phenol (**3***a*) was used to effect (7) *ortho*-iodination, an intramolecular 5-*exo*-*trig* Michael addition triggered by lithium–iodine exchange in a subsequent intermediate (**3***e*) was envisaged as depicted. Although the exchange reaction might be very fast, the cyclization still has many obvious pitfalls, the acidity of the γ-hydrogen atoms of the ester for one; we were encouraged to explore it, however, by the recent report of a similar cyclialkylation with some vinyl sulfones (8). We now report the successful realization of these plans, and the development of an efficient, general synthesis of 3-substituted dihydrobenzofurans (e.g. **1** and **9**–**13**).

In these six examples the disposition of the substituents in the benzenoid moiety is controlled by the iodination step. Considerable flexibility is available and can be exercised by judicious choice of starting materials. Phenols **3***a*–**7***a* are converted into their methoxymethyl ethers (**3***b*–**7***b*) in the usual manner (NaH, $ClCH_2OMe$, DMF), deprotonated (7) (*n*-BuLi, ether, O°C), quenched with five equivalents of iodine in dry tetrahydrofuran, and the resultant iodo compounds **3***c*–**7***c* treated with aqueous methanolic hydrochloric acid. The iodophenols **3***d*–**7***d* were produced in overall yields ranging from 50% (**4***d*) to 63% (**7***d*) by this three-step sequence. We note that the iodination sequence with **5***a* produces a contiguously substituted iodophenol (**5***d*) whereas with **6***a* a 1,2,4,5 substitution pattern results (9), a consequence, probably, of differing steric constraints and acidities of the protons in the two benzenoid ring systems. The availability of *ortho* iodophenols from other sources (10) will shorten the synthesis and this is demonstrated here by the direct iodination of 2-naphthol (**8***a*) to provide **8***d* in 90% yield.

Iodophenols **3***d*–**8***d* are then alkylated with ethyl γ-bromocrotonate (acetone – potassium carbonate) and the crotonates **3***e*–**8***e* subjected to metal–halogen exchange at −100°C (in THF–ether–hexane 4:1:1) with *n*-butyl lithium, and quenched with water after 1 h at that temperature. Dihydrobenzofurans **1** and **9**–**12** and dihydronaptho[2,1-*b*]furan **13** produced in the intramolecular Michael addition (cyclialkylation) step were isolated in yields ranging from 60 to 71% and overall yields of 25–44%.

The ^{1}H nmr spectra of the products are summarized in Table 1. Certain features of these spectra provide useful clues for the assignment of the individual A and B components of the two ABX systems (—O—CH_2—CH—CH_2—CO_2Et) and thereby the conformation of the C-3 ethyl acetate side chain. The invariant position of the ethyl ester signals in all six compounds suggests a conformation (Fig. 1), in which the ester is far removed from the structural changes in the aromatic region of the molecule. This is supported by *gauche* (3–5 Hz) and *anti*

[1]Author to whom correspondence may be addressed.

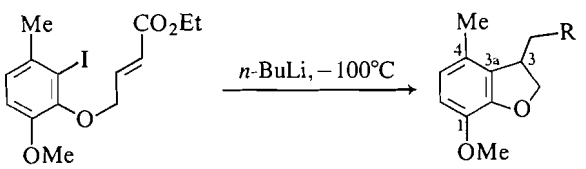

1, R = CO_2Et
2, R = OH

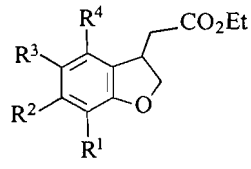

9, R^1 = OMe, R^2 = R^3 = R^4 = H
10, R^1 = R^2 = H, R^3 + R^4 = OCH_2O
11, R^1 = R^4 = H, R^2 = R^3 = Me
12, R^1 = OMe, R^3 = Me, R^2 = R^4 = H

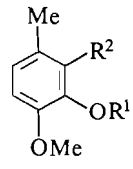

3

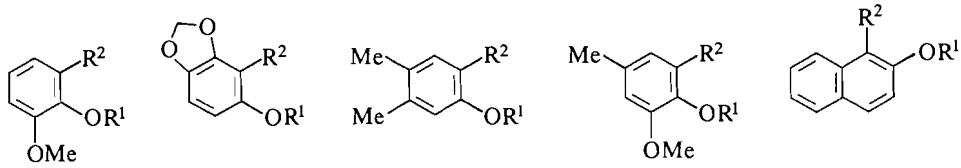

4 **5** **6** **7** **8**

For **3–8**: *a*, R^1 = R^2 = H; *b*, R^1 = CH_2OMe, R^2 = H; *c*, R^1 = CH_2OMe, R^2 = I; *d*, R^1 = H, R^2 = I; *e*, R^1 = $CH_2CH{=}CHCO_2Et$, R^2 = I

TABLE 1. Chemical shifts (δ) and coupling constants (Hz) for dihydrobenzofurans (250 MHz, $CDCl_3$)

	Proton (multiplicity)					
Compound	H-2	H-3	CH_2CO_2Et	CO_2Et	ArH	Aromatic substituent
1	4.46 (q) J_{gem} = 9.4, J_{vic} = 3.3 4.65 (t) $J_{gem} \approx J_{vic} \approx$ 9.0	3.80 (m)	2.48 (q) J_{gem} = 16.5, J_{vic} = 11.1 2.71 (q) J_{gem} = 16.5, J_{vic} = 3.2	1.27 (t) 4.17 (q)	6.61 (s) 6.68 (s)	2.24 (s, Me) 3.84 (s, OMe)
9	4.32 (q) J_{gem} = 9.3, J_{vic} = 6.5 4.81 (t) $J_{gem} \approx J_{vic} \approx$ 9.2	3.92 (m)	2.57 (q) J_{gem} = 16.5, J_{vic} = 9.5 2.78 (q) J_{gem} = 16.5, J_{vic} = 5.2	1.28 (t) 4.18 (q)	6.80 (m)	3.87 (s, OMe)
10	4.24 (q) J_{gem} = 9.3, J_{vic} = 6.7 4.75 (t) $J_{gem} \approx J_{vic} \approx$ 9.1	3.93 (m)	2.53 (q) J_{gem} = 16.6, J_{vic} = 10.4 2.96 (q) J_{gem} = 16.6, J_{vic} = 4.1	1.26 (t) 4.16 (q)	6.21 (d) 6.57 (d) J = 8.3	5.89 (s, OCH_2O)
11	4.20 (q) J_{gem} = 9.1, J_{vic} = 6.3 4.70 (t) $J_{gem} \approx J_{vic} \approx$ 9.0	3.80 (m)	2.53 (q) J_{gem} = 16.4, J_{vic} = 9.4 2.76 (q) J_{gem} = 16.4, J_{vic} = 5.3	1.28 (t) 4.16 (q)	6.61 (s) 6.91 (s)	2.18, 2.20 (2 × s, Me)
12	4.29 (q) J_{gem} = 9.2, J_{vic} = 6.5 4.78 (t) $J_{gem} \approx J_{vic} \approx$ 9.0	3.85 (m)	2.55 (q) J_{gem} = 16.4, J_{vic} = 9.5 2.76 (q) J_{gem} = 16.4, J_{vic} = 5.3	1.28 (t) 4.17 (q)	6.58 (s)	2.29 (s, Me) 3.85 (s, OMe)
13[a]	4.59 (q) J_{gem} = 9.4, J_{vic} = 3.1 4.80 (t) $J_{gem} \approx J_{vic} \approx$ 9.2	4.2 (m)	2.58 (q) J_{gem} = 16.5, J_{vic} = 11 2.99 (q) J_{gem} = 16.5, J_{vic} = 3	1.25 (t) 4.19 (q)	7.1 (d) 7.3 (t) 7.47 (t) 7.67 (d) 7.70 (d) 7.81 (d)	—

[a]Benzofuran numbering used for consistency; aromatic coupling constants ranged from 8 to 8.8 Hz.

(9.5–11 Hz) couplings for the nonequivalent methylene protons of the side chain and by the fact that the more shielded proton is coupled *anti* to H-3. The presence of a carbon substituent at C-4 (as in **1** and **13**) reduces $\Delta\nu$ for the C-2 methylene group from 0.5 to 0.2 ppm and reduces the smaller 2β-3 (*trans*) coupling from about 6.5 to 3 Hz. This is accompanied by a reduction of the *gauche* coupling in the side chain methylene group from ca. 5 Hz to 3 Hz. The changes are satisfactorily rationalized by proposing that steric interaction between the C-4 substituent and the *gauche*-coupled proton of the methylene group enlarges that dihedral angle slightly and thereby brings the *anti*-coupled proton closer to H-2β. Twisting of the C2—C3 bond, which has

Can. J. Chem. Downloaded from www.nrcresearchpress.com by 213.166.140.6 on 09/07/12
For personal use only.

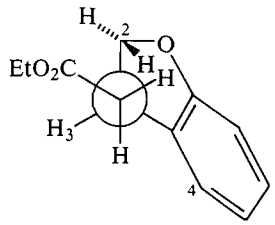

FIG. 1

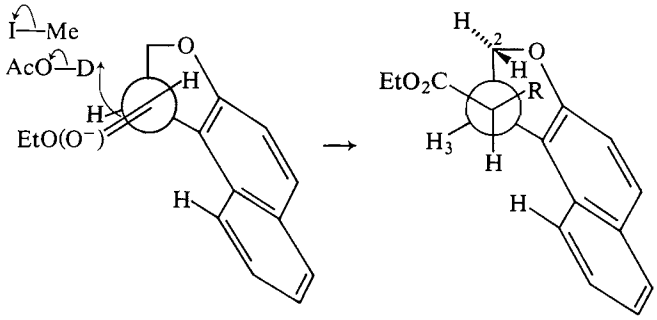

13, R = H
14, R = Me
15, R = D

FIG. 2

been previously observed in dihydrobenzofurans (11), moves H-2β outwards and away in response to this interaction, thus producing the changes in H-2 resonances described above.

Evidence for the ionic character of the cyclialkylation (as opposed to similar radical processes (4)) was sought by *in situ* methylation and deuteration of the enolate (**8***e* → **13**). Quenching this reaction mixture with an excess of the electrophile (methyl iodide or *d*-acetic acid) at −100°C, a mere 30 s after addition of the *n*-butyl lithium, and allowing it to reach room temperature overnight provided satisfactory yields of the desired methylated and deuterated products. The cyclialkylation thus appears to be an extremely rapid process even at −100°C. The methyl derivative **14** so obtained was diastereomerically pure (250-MHz ^{1}H nmr) and its configuration and conformation assigned as in Fig. 2 by interpretation of the spectrum in comparison with that of **13**. The new methyl doublet at 0.93 ppm (J = 7.2 Hz) is at a somewhat higher field than expected,[2] betraying its shielded location *anti* to H-3. The proton remaining appears as an octet at 3.2 δ, *gauche* coupled (J = 3.3 Hz) to H-3, and the ethyl ester resonances are again essentially unchanged (1.29 and 4.20 δ). Very significantly, the usual pattern of H-2 absorptions (Table 1) is reversed in **14**, the quartet for H-2β is now downfield (4.75 δ, J_{gem} = 9.7, $J_{2\beta,3}$ = 3.2 Hz) of the "triplet" for H-2α (4.66 δ, $J_{2\alpha,3}$ = 9.0 Hz), almost certainly because of the increased distortion at C-2 caused by the H2β-methyl interaction. The signal for the central proton H-3 appears at 4.33 and as two triplets with vicinal couplings of 3.2, 3.3, and 9.0 Hz. These assignments and coupling constants are supported by decoupling. The spectra of **13** and **14** are unchanged when run at −20°C. The deuterated product **15** was obtained with similar diastereoselectivity. The ^{1}H and ^{2}H nmr spectra of **15** indicated that, again, the upfield *anti*-coupled proton of **13** is replaced by deuterium with a ca. 7:1 diastereoselectivity (Fig. 2).

[2]The absorption of the *gem*-dimethyl group in methyl 2-methyl propanoate (methyl isobutyrate) is found at 1.2 δ (Aldrich Library of NMR Spectra, Vol. III, spectrum 22D).

The high diastereoselectivity observed in several examples of methylation of acyclic ester enolates has been attributed to the conformation adopted by the enolate and direction of the approaching electrophile by the neighbouring asymmetric substituent antiperiplanar to it for steric (12, 15) or electronic (13) reasons or both (14). In the case at hand a low energy eclipsed (15) conformation and electrophilic attack from the less hindered face of the double bond appears to be reponsible for the exclusive formation of diastereomers **14** and **15** as shown in Fig. 2.

Application of the benzofuran synthesis to natural product chemistry and further investigations of the stereochemistry of the methylation and deuteration are continuing and will be reported in due course.

Experimental

General methods

Melting points were determined on a Fischer Mel Temp apparatus and are uncorrected. Infrared spectra were obtained on a Perkin–Elmer 983 spectrophotometer. Nuclear magnetic resonance spectra were obtained on a Bruker WP-80 or AM 250 spectrometer in deuteriochloroform unless otherwise indicated. Mass spectra were measured on a VG 7070 instrument and are reported in the order m/z (intensity, assignment). Combustion analyses were performed by the Guelph Chemical Laboratories, Guelph, Ontario.

General procedure for the preparation of methoxymethyl esters **3**b–**7**b

The phenol (**3***a*–**7***a*, 40 mmol) was dissolved in dry dimethyl formamide (15 mL) and this solution added dropwise to a suspension of sodium hydride (60 mmol) in dimethyl formamide (25 mL) at 80°C under a nitrogen atmosphere. After 1 h at this temperature the mixture was cooled to 0°C, chloromethyl methyl ether (60 mmol) added, and the solution allowed to reach ambient temperature overnight. Water was added and most of the liquids removed by distillation under reduced pressure. The residue was extracted into ether and the extracts washed successively with 10% aqueous sodium hydroxide and brine and dried (Na_2SO_4). The solvent was removed and the residual oil distilled to provide the desired products.

3*b* (82.5%); bp 60°C (0.1 Torr; 1 Torr = 133.3 Pa); δ (80 MHz): 2.28 (s, 3H, $ArCH_3$), 3.50 (s, 3H, OMe), 3.85 (s, 3H, Ar-OMe), 5.20 (s, 2H, OCH_2O), 6.80, 6.98 (3H, ArH); ms: 182 (100, M^+), 152 (94, $M^+ - CH_2O$), 137 (31, $M^+ - CH_3OCH_2$). *Anal.* calcd. for $C_{10}H_{14}O_3$: C 65.91, H 7.74; found: C 65.68, H 8.10.

4*b* (75%); bp 60–64°C (0.1 Torr).

5*b* (85%); bp 65–70°C (0.05 Torr).

6*b* (81%); bp 44–46°C (0.1 Torr).

7*b* (94%); bp 65–70°C (0.1 Torr).

All compounds had spectroscopic properties consistent with their structures and similar to those reported for **3***b*.

General procedure for preparation of iodophenols **3**d–**7**d

The methoxymethyl derivative (**3***b*–**7***b*) dissolved in anhydrous ether (1 g in 10 mL) was cooled to 0°C and a solution of *n*-butyllithium (1.6 *M* in hexane, 2.2 equiv.) added dropwise, under an atmosphere of nitrogen. After 1 h at this temperature a solution of iodine in dry THF (6 equiv.) was added and the mixture allowed to reach ambient temperature overnight. A saturated aqueous solution of sodium thiosulfate was added, the organic solvents removed under reduced pressure, and the aqueous layer extracted with ether. The extracts were washed and dried (Na_2SO_4) and the solvent removed. The dark residual oil was filtered through a column of silica gel in ethyl acetate – hexane. Iodo compounds **3***c*–**7***c* had the expected spectroscopic properties (nmr, ms) and were used without further purification.

A solution of the above iodo derivative (12.4 mmol) in methanol–THF (20 mL, 1:1) was stirred at room temperature under nitrogen with 2 *M* HCl (8 mL) for 22 h and monitored by tlc. The organic solvents were removed under reduced pressure, the residue extracted with methylene chloride, washed, and dried (Na_2SO_4). The solvent was removed to leave a solid, which was crystallized to provide iodophenols **3***d*–**7***d*.

Can. J. Chem. Downloaded from www.nrcresearchpress.com by 213.166.140.6 on 09/07/12
For personal use only.

Can. J. Chem. Downloaded from www.nrcresearchpress.com by 213.166.140.6 on 09/07/12
For personal use only.

3*d* (62% overall); mp 105–106°C (ethyl acetate – hexane); ir ($CHCl_3$): 3524 cm^{-1}; δ (80 MHz): 2.40 (s, 3H, ArMe), 3.87 (s, 3H, OMe), 6.80 (br s, 2H, ArH); ms: 264 (100, M^+), 249 (57, M^+ – Me). *Anal.* calcd. for $C_8H_9O_2I$: C 36.39, H 3.44; found: C 36.73, H 3.79.

4*d* (67%); mp 58–60°C (hexane–ether); ir (Nujol): 3408 cm^{-1}; δ (80 MHz): 3.87 (s, 3H, OMe), 6.09 (s, 1H, OH), 6.69 (m, 2H, ArH), 7.28 (dd, 1H, J = 7.6, 1.5 Hz, ArH); ms: 250 (100, M^+), 235 (34, M^+ – Me). *Anal.* calcd. for $C_7H_7O_2I$: C 33.62, H 2.82; found: C 33.36, H 2.94.

5*d* (71%); mp 122–123°C (ethyl acetate – hexane); ir (Nujol): 3200 cm^{-1}; δ (80 MHz): 4.98 (s, 1H, OH), 5.99 (s, 2H, OCH_2O), 6.54 (q, 2H, J = 8.2 Hz, ArH); ms: 264 (100, M^+). *Anal.* calcd. for $C_7H_5O_3I$: C 31.84, H 1.91; found: C 31.55, H 2.16.

6*d* (74%); mp 60–61°C (hexane); ir ($CHCl_3$); 3503 cm^{-1}; δ (80 MHz): 2.18 (s, 6H, 2 × ArMe), 5.03 (s, 1H, OH), 6.80, 7.39 (s, 1H each, ArH); ms: 248 (100, M^+), 121 (26, M^+ – I). *Anal.* calcd. for C_8H_9OI: C 38.73, H 3.66; found: C 38.87, H 3.91.

7*d* (67%); mp 54°C (hexane); ir (Nujol): 3547 cm^{-1}; δ (80 MHz): 2.25 (s, 3H, ArMe), 3.85 (s, 3H, OMe), 5.9 (s, 1H, OH), 6.6, 7.1 (s, 1H each, ArH); ms: 264 (100, M^+), 249 (50, M^+ – Me). *Anal.* calcd. for $C_8H_9O_2I$: C 36.39, H 3.44; found: C 36.52, H 3.58.

General procedure for the preparation of γ-phenoxycrotonates ***3****e*–***8****e*

The iodophenol (1 g) was dissolved in dry acetone (15 mL) and ethyl-4-bromocrotonate (1.1 equiv.) added, followed by anhydrous potassium carbonate (1.2 equiv.). The mixture was refluxed for 24 h, the acetone removed, water added, and the aqueous mixture extracted with methylene chloride. The organic extracts were washed, dried (Na_2SO_4), and the solvent removed. The residue was chromatographed on silica gel in the appropriate solvent system (see below).

3*e* (70%), purified by chromatography in ethyl acetate – hexane (1:9). Oil could not be crystallized or distilled without extensive decomposition; ir ($CHCl_3$): 1725, 1664 cm^{-1}; δ (80 MHz): 1.3, 4.2 (t, q, 3H, 2H, CO_2Et), 2.39 (s, 3H, ArMe), 3.80 (s, 3H, OMe), 4.6 (m, 2H, -OCH_2-), 6.32 (br d, 1H, J = 15.6 Hz, =*CH* CO_2Et), 7.11 (dt, 1H, J = 15.6, 4.4 Hz, CH_2—C*H*=), 6.80, 6.95 (q, 2H, J = 8.2 Hz, ArH); ms: 376 (24, M^+), 263 (100, M^+ – CH_2CH=*CH* CO_2Et). *Anal.* calcd. for $C_{14}H_{17}O_4I$: C 44.70, H 4.55; found: C 44.81, H 4.75.

4*e* (98%), purified by chromatography as above. Oil could not be crystallized or distilled; ir (neat): 1719, 1663 cm^{-1}; δ (250 MHz): 1.3, 4.22 (t, q, 3H, 2H, CO_2Et), 3.82 (s, 3H, OMe), 4.64 (m, 2H, -OCH_2-), 6.31 (br d, 1H, J = 15.7 Hz, =*CH* CO_2Et), 7.11 (dt, 1H, J = 15.7, 4.4 Hz, CH_2CH=), 6.83 (m, 2H, ArH), 7.33 (d, 1H, J = 7.7 Hz, ArH); ms: 362 (31, M^+), 249 (100, M^+ – $C_6H_9O_2$). *Anal.* calcd. for $C_{13}H_{15}O_4I$: C 43.11, H 4.17; found: C 42.93, H 4.31.

5*e* (86%), purified by chromatography in ethyl acetate – hexane (1:4) and crystallized from hexane–ether, mp 82–83°C; ir (Nujol): 1712, 1649 cm^{-1}; δ (250 MHz): 1.31, 4.25 (t, q, 3H, 2H, CO_2Et), 4.66 (m, 2H, -OCH_2-), 6.01 (s, 2H, -OCH_2O-), 6.22, 6.66 (q, 2H, J = 8.4 Hz, ArH), 6.35 (br d, 1H, J = 15.7 Hz, =*CH* CO_2Et), 7.06 (dt, 1H, J = 15.7, 3.7 Hz, CH_2CH=); ms: 376 (18, M^+), 263 (100, M^+ – $C_6H_9O_2$). *Anal.* calcd. for $C_{13}H_{13}O_5I$: C 41.51, H 3.48; found: C 41.27, H 3.38.

6*e* (84%), purified by filtering through a silica gel column in hexane–ether (19:1) and crystallized from hexane, mp 68–69°C; ir ($CHCl_3$): 1711, 1664 cm^{-1}; δ (80 MHz): 1.30, 4.22 (t, q, 3H, 2H, CO_2Et), 2.15, 2.19 (s, 3H each, ArMe), 4.69 (m, -OCH_2-), 6.32 (br d, 1H, J = 15.8 Hz, =*CH*CO_2Et), 6.56 (s, 1H, ArH), 7.07 (dt, 1H, J = 15.8, 3.7 Hz, CH_2CH=), 7.51 (s, 1H, ArH); ms: 360 (89, M^+), 247 (100, M^+ – $C_6H_9O_2$). *Anal.* calcd. for $C_{14}H_{17}O_3I$: C 46.68, H 4.76; found: C 46.83, H 4.99.

7*e* (97%), purified by chromatography in ethyl acetate – hexane and crystallized from hexane–ether, mp 46–48°C; ir (Nujol): 1718, 1663 cm^{-1}; δ (250 MHz): 1.30, 4.22 (t, q, 2H, 3H, CO_2Et), 2.27 (s, 3H, ArMe), 3.81 (s, 3H, OMe), 4.60 (m, 2H, -OCH_2-), 6.30 (br d, 1H, J = 15.7 Hz, =*CH*—CO_2Et), 6.68 (s, 1H, ArH), 7.10 (br d, 1H, J = 15.7 Hz, CH_2—*CH*=), 7.16 (s, 1H, ArH); ms: 376 (29, M^+), 263 (100, M^+ – $C_6H_9O_2$). *Anal.* calcd. for $C_{14}H_{17}O_4I$: C 44.69, H 4.56; found: C 44.65, H 4.64.

8*e* (72%), crystallized from ether; mp 34–35°C; ir ($CHCl_3$): 1714, 1664 cm^{-1}; δ (80 MHz): 1.28, 4.23 (t, q, 3H, 2H, CO_2Et), 4.9 (m, 2H, -OCH_2-), 6.44 (dt, 1H, J = 15.6, 2.1 Hz, =$CHCO_2Et$), 7.0–8.3 (m, 7H, aromatic H and CH_2CH=); ms: 382 (56, M^+), 269 (66, M^+ – $C_6H_9O_2$), 142 (100, M^+ – $C_6H_9O_2$-I). *Anal.* calcd. for $C_{16}H_{15}O_3I$: C 50.28, H 3.95; found: C 50.48, H 4.27.

General procedure for cyclialkylation of iodocrotonates; the preparation of ***1*** *and* ***9–13***

The iodocrotonate (0.5 g) dissolved in dry THF–ether–hexane (18 mL, 4:1:1) under a nitrogen atmosphere was cooled to −100°C (liquid nitrogen, ligroin, acetone, isopropanol bath), *n*-BuLi (1.6 *M* in hexane, 1.1 equiv.) was added dropwise, and the mixture maintained at −100°C for 1 h with stirring. Water was added, the solution allowed to reach room temperature, the organic solvents removed, and the aqueous residue extracted with ether, washed, and dried (Na_2SO_4). The ether was removed and the residual oil chromatographed on a silica gel column in the appropriate solvent system (see below).

1 (71%), chromatographed in ethyl acetate – hexane (1:4) and crystallized from hexane; mp 41°C; ir (neat): 1730 cm^{-1}; ms: 250 (62, M^+), 163 (100, M^+ – CH_2CO_2Et). *Anal.* calcd. for $C_{14}H_{18}O_4$: C 67.18, H 7.25; found: C 67.30, H 7.67.

9 (68%), chromatographed in hexane–ether (4:1) and obtained as an oil that resisted crystallization; ir (neat): 1730 cm^{-1}; ms: 236 (64, M^+), 149 (100, M^+ – $C_4H_7O_2$). *Anal.* calcd. for $C_{13}H_{16}O_4$: C 66.08, H 6.83; found: C 65.95, H 7.22.

10 (68%), chromatographed in hexane – ethyl acetate (4:1) and obtained as an oil that resisted crystallization; ir (neat): 1730 cm^{-1}; ms: 250 (100, M^+), 163 (87, M^+ – $C_4H_7O_2$). *Anal.* calcd. for $C_{13}H_{14}O_5$: C 62.39, H 5.64; found: C 62.84, H 6.03.

11 (60%), chromatographed in hexane–ether (4:1) and crystallized from hexane, mp 36–37°C; ir (Nujol): 1739 cm^{-1}; ms: 234 (38, M^+), 147 (100, M^+ – $C_4H_7O_2$). *Anal.* calcd. for $C_{14}H_{18}O_3$: C 71.77, H 7.74; found: C 71.98, H 7.79.

12 (69%), chromatographed in hexane–ether and obtained as an oil that resisted crystallization; ir (neat): 1729 cm^{-1}; ms: 250 (98, M^+), 163 (100, M^+ – $C_4H_7O_2$). Correct analytical figures could not be obtained for this compound in spite of several efforts.

13 (68%), chromatographed in ethyl acetate – hexane (1:4) and crystallized from ether–hexane, mp 48–49°C; ir ($CHCl_3$): 1727 cm^{-1}; ms: 256 (28, M^+), 169 (100, M^+ – $C_4H_7O_2$). *Anal.* calcd. for $C_{16}H_{16}O_3$: C 74.98, H 6.29; found: C 75.24, H 6.74.

*Methylation and deuteration experiments (****14*** *and* ***15****)*

The reactions carried out with **8***e* on a 0.5-mmol scale (191 mg) were quenched with excess methyl iodide or acetic acid-*d* after 0.5 min at −100°C, allowed to reach room temperature overnight, and worked up as described for **13**.

14, ms: 270 (11, M^+), 169 (100, M^+ – $C_5H_9O_2$).

15, ^2H nmr ($CHCl_3$, 38.4 MHz): 2.59, 3.00 in the intensity ratio of 20.005:2.991; ^1H nmr ($CDCl_3$, 250 MHz) shows virtually total disappearance of the quartet at 2.58 δ and broadening (H–C–D coupling) of the quartet at 2.99 δ (Table 1); ms: 257 (24, M^+), 169 (100, M^+ – $C_4H_6O_2D$). A small M − 1 peak at m/z 256 (2.06), not found in the mass spectrum of **13**, represents nondeuterated material. If such an assumption is made and the corresponding M + 1 component is subtracted, the extent of deuteration is calculated to be 92%.

Acknowledgements

We thank the Natural Sciences and Engineering Research Council of Canada for support of this work.

1. D. M. X. Donnelly and M. J. Meegan. *In* Comprehensive heterocyclic chemistry. Vol. 4. *Edited by* C. W. Bird and G. W. H. Cheeseman. Pergamon Press, New York. 1984. p. 657.
2. J. E. Baldwin, W. A. Dupont, and M. F. Ming. J. Chem. Soc. Chem. Commun. 1042 (1980).
3. C. K. Bradsher and D. C. Reames. J. Org. Chem. **43**, 3800

(1978); K. SHANKARAN and V. A. SNIECKUS. J. Org. Chem. **49**, 5022 (1984).
4. A. L. J. BECKWITH and G. F. MEIJS. J. Chem. Soc. Chem. Commun. 136 (1981); 595 (1981); A. N. ABEYWICKREMA and A. L. J. BECKWITH. J. Chem. Soc. Chem. Commun. 464 (1986); Y. UENO, K. CHINO, and M. OKAWARA. Tetrahedron Lett. **23**, 2575 (1982); K. SHANKARAN, C. P. SLOAN, and V. A. SNIECKUS. Tetrahedron Lett. **26**, 6001 (1985).
5. W. HAEFLIGER and D. HAUSER. Synthesis, 236 (1980); P. BRAVO, A. GENTILE, and C. TICOZZI. Gazz. Chim. Ital. **114**, 89 (1984).
6. C. F. CARVALHO and M. V. SARGENT. J. Chem. Soc. Perkin Trans. **1**, 1605 (1984).
7. H. CHRISTENSEN. Synth. Commun. **5**, 65 (1975); R. C. RONALD. Tetrahedron Lett. 3973 (1975).
8. P. R. HAMANN, J. E. TOTH, and P. L. FUCHS. J. Org. Chem. **49**, 3865 (1984); P. L. FUCHS and T. F. BRAISH. Chem. Rev. **86**, 903 (1986).
9. B. A. KEAY and R. RODRIGO. J. Am. Chem. Soc. **104**, 4725 (1982).
10. K. T. POTTS. J. Chem. Soc. 3711 (1953).
11. F. M. DEAN and M. V. SARGENT. *In* Comprehensive heterocyclic chemistry. Vol. 4. *Edited by* C. W. Bird and G. W. H. Cheeseman. Pergamon Press, New York. 1984. p. 570.
12. S. H. AHN, D. KIM, M. W. CHUN, and W.-K. CHUNG. Tetrahedron Lett. **27**, 943 (1986).
13. G. J. MCGARVEY and J. M. WILLIAMS. J. Am. Chem. Soc. **107**, 1435 (1985).
14. W. BERNHARD, I. FLEMING, and D. WATERSON. J. Chem. Soc. Chem. Commun. 28 (1984).
15. K. TOMIOKA, K. YASUDA, H. KAWASAKI, and K. KOGA. Tetrahedron Lett. **27**, 3247 (1986); H. KAWASAKI, K. TOMIOKA, and K. KOGA. Tetrahedron Lett. **26**, 3031 (1985).

Can. J. Chem. Downloaded from www.nrcresearchpress.com by 213.166.140.6 on 09/07/12
For personal use only.

Synthesis and ^{13}C nuclear magnetic resonance spectral analysis of some diterpenoids related to the cleistanthane type hydrocarbon isolated from *Amphibolis antarctica*

TEODORO S. KAUFMAN, MIRTA P. MISCHNE, MANUEL GONZALEZ-SIERRA, AND EDMUNDO A. RUVEDA
Instituto de Quimica Organica de Sintesis (CONICET–UNR), Facultad de Ciencias Bioquimicas y Farmaceuticas, Casilla de Correo 991, 2000 Rosario, Argentina

Received November 26, 1986

TEODORO S. KAUFMAN, MIRTA P. MISCHNE, MANUEL GONZALEZ-SIERRA, and EDMUNDO A. RUVEDA. Can. J. Chem. **65**, 2024 (1987).

The synthesis of the cleistanthane-type diterpene **13** (8-β(H),14-β-ethyl, 13-methylene podocarpane), a dihydro epimer of the natural product **6**, is described. By comparison of the ^{13}C nuclear magnetic resonance spectral data of **13** and related compounds with those reported for **6**, the stereochemistry of the C-14 side chain of the latter was confirmed.

TEODORO S. KAUFMAN, MIRTA P. MISCHNE, MANUEL GONZALEZ-SIERRA et EDMUNDO A. RUVEDA. Can. J. Chem. **65**, 2024 (1987).

On décrit la synthèse du diterpène **13** (l'éthyl-14β méthylène-13 podocarpane-8β(H)) du type cléistanthane, un épimère dihydrogéné du produit naturel **6**. Par comparaison des données spectrales de la résonance magnétique nucléaire du ^{13}C du composé **13** et de celles de composés apparentés au produit **6**, on a pu confirmer la stéréochimie de la chaîne latérale de ce dernier composé.

[Traduit par la revue]

Can. J. Chem. Downloaded from www.nrcresearchpress.com by 213.166.140.6 on 09/07/12
For personal use only.

The cleistanthane type of diterpenoids represents a small group of natural products formally derived from the parent hydrocarbon 14-ethyl-13-methyl podocarpane (**1**), including cleistanthol (**2**) (1), veadeirol (**3**) (2), veaderoic acid (**4**) (2), and the tetracyclic lactone **5** (3), all of them containing an aromatic ring C.

More recently, a new member of this group, the hydrocarbon **6**, was isolated from *Amphibolis antarctica*, one of the major sea grasses of Shark Bay (Western Australia). Structure **6** was established on the basis of its ^1H and ^{13}C nmr spectral data and comparison with those of **7**, **8**, and **9** (4). Interestingly enough, the structure of **6** is reminiscent of that suggested for the cleistanthane framework **12**, biogenetically derived by the pimarane–cleistanthane rearrangement (**10** → **11** → **12**) (5).

A careful analysis of the spectral data reported for **6** showed us that the ^1H nmr coupling constants, from which the stereochemistry of the C-14 side chain was suggested, were not in agreement with the ^{13}C nmr signals assignment. In fact, as the side chain at C-14 is axial, and assuming that the substituent at C-13 will have practically no effect on C-9 in structure **6**, the signal corresponding to C-9 should appear at higher field than those of the same site of **7** and **8**, due to the γ effect imposed by C-15.

To solve this problem and also to obtain spectral information on this type of diterpenoids, we decided to carry out an exhaustive ^{13}C nmr analysis of synthetic compounds related to **6**, such as its dihydro epimer **13** and some of its derivatives.

For the synthesis of **13**, the ketone **14**, readily prepared from manool (6, 7), appeared to be an ideal precursor, since it possesses the required tricyclic skeleton with the necessary functional groups for building up the two-carbon side chain with the required stereochemistry at C-14 and for the transformation of the C-13 carbonyl into the *exo*-methylene group.

Our initial approach to the synthesis of **13** was the lithium in liquid ammonia reduction of **14** with simultaneous trapping of the corresponding enolate with ethyl iodide (8). Unfortunately, under these conditions, compound **8** was obtained as the major product. However, by using the α-alkyation conditions described by Atwater (9), the desired monoethyl-α,β-unsaturated ketone **15** was obtained in 61% yield together with a small amount of the corresponding α,α-diethyl-β,γ-unsaturated ketone **16**. Lithium in liquid ammonia reduction of **15** produced the expected thermodynamically more stable, equatorially substituted, saturated ketone **17** in good yield.

From **17**, by a standard Wittig reaction (triphenylmethylphosphonium bromide, methyl lithium) or thioketalization followed by Raney nickel desulfurization, the desired hydrocarbons **13** and **18** were obtained.

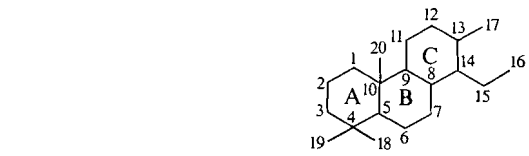

1

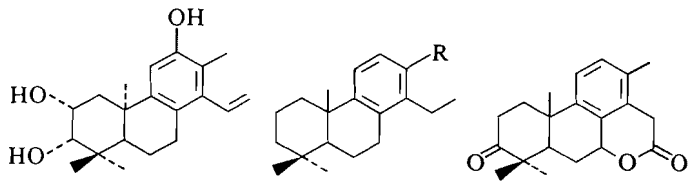

2 **3**, R = CH_2OH; **4**, R = COOH **5**

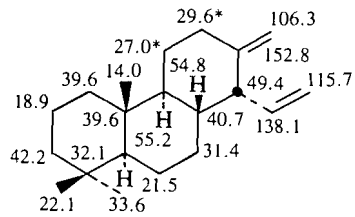

6

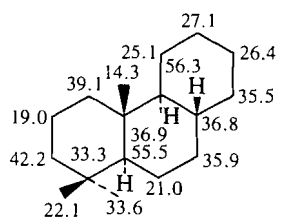

7

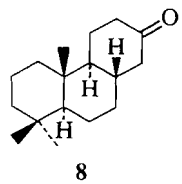

8

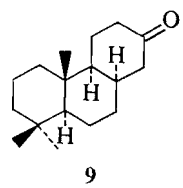

9

TABLE 1. ^{13}C nuclear magnetic resonance chemical shifts of compounds **18**, **17**, **13**, and **6**

Position	**18** (obsd.)	**18** (calcd.)	**17**	**13**	**6** (obsd.)	**6** (calcd.)
1	39.3		39.5	39.3	39.6	
2	18.9		18.2	18.9	18.9	
3	42.1		42.2	42.1	42.2	
4	33.1		33.3	33.1	32.1	
5	55.8		55.1	55.8	55.2	
6	21.6		21.8	20.1	21.5	
7	31.9	31.27	33.5	32.7	31.4	31.27
8	39.9	39.67	41.6	41.0	40.7	40.35
9	55.9	52.47	54.6	55.0	49.4	47.92
10	37.1	37.63	37.4	37.0	39.6	37.63
11	26.5	26.72	26.2	27.1	27.0*	27.40
12	25.1	26.72	42.0	37.0	29.6*	30.58
13	31.1	31.27	212.3	151.2	152.8	
14	45.0	45.37	57.1	49.6	54.8	52.09
15	25.3		19.0	21.8	138.1	
16	10.3		11.5	10.7	115.7	
17				104.3	106.3	
18	33.4		33.7	33.4	33.6	
19	21.9		21.9	21.8	22.1	
20	14.2		14.3	14.2	14.0	

*Assignments may be interchanged.

At this point, a comparative analysis of the ^{13}C nmr spectra obtained for compounds **13**, **17**, and **18**, together with the reported data for compounds **7** and **8** (4) and the calculated chemical shifts obtained by using the substituent parameters proposed by Beierbeck *et al.* (10), allowed the complete shift assignment for **13**, **17**, and **18**.

Comparison of the chemical shifts assigned to **13** and **17** shows that C-12 and C-14, in compound **13**, are shielded, while C-15 is deshielded, as expected for a carbonyl to exocyclic double-bond change (11). The chemical shifts for C-9 in compounds **13**, **17**, and **18** are similar to those observed for the same site in **7** and **8**, and are in agreement with an equatorial orientation of the side chain at C-14.

With this information in hand, together with the data reported by Grover and Stothers (11) on the effects of axial and equatorial methyl groups on their neighboring carbons in methylenecyclohexanes, and assuming that the effect induced by a sp^3 carbon is similar in magnitude to that produced by the C-15 sp^2 of **6**, the reported ^{13}C nmr data for the natural product were reanalyzed. We have found that by reversing the signals previously attributed to C-9 and C-14, an assignment in agreement with the axial position for the C-14 side chain is obtained. Comparison of the C-12 chemical shift for compounds **6** and **13** confirms the above observations. In fact, due to the axial position of the side chain in the natural product, the signal of C-12, suffering a γ effect, resonates at 29.6 ppm, a value very close to the calculated one (30.58 ppm). The upfield shift observed for C-17 in going from **6** to **13** is also in agreement with the different position of the C-14 side chain in both compounds.

In conclusion, the ^{13}C nmr data indicate, in agreement with the ^{1}H nmr coupling constants reported, that the suggested stereochemistry for the side chain in **6** is the correct one (4). The carbon shifts of **18** (observed and calculated), **17**, **13**, and **6** (reported and calculated), with the reassigned signals for C-9 and C-14, are listed in Table 1.

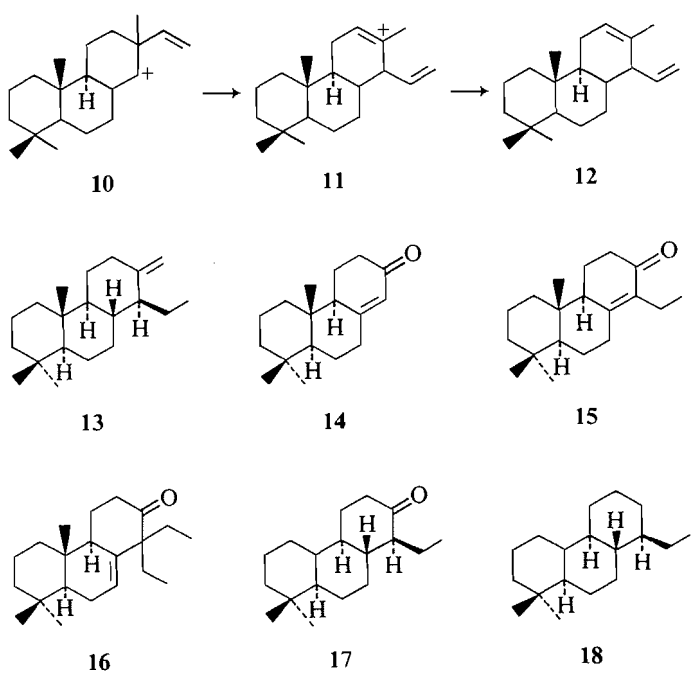

Experimental

Melting points were determined on an Ernst Leitz hot-stage microscope and are uncorrected. Infrared spectra were recorded on a Beckman Acculab 8 spectrometer. The ^{1}H and ^{13}C nmr spectra were recorded at 80.13 and 20.15 MHz on a Bruker WP 80 SY spectrometer in deuteriochloroform, and chemical shifts are expressed in parts per million downfield from internal tetramethylsilane. The carbon shifts of **13**, **17**, and **18** were assigned by comparison with the reported data of **7** (4) and analysis of the generated CH/CH_3 and CH_2/q subspectra by spin-echo sequence utilizing the attached proton test method (APT) (12).

All solvents were purified and dried by standard techniques. All reactions were performed under dry nitrogen atmosphere. Column chromatography was performed on silica gel 60H, slurry packed, run under low pressure of nitrogen, and employing increasing amounts of ethyl ether in hexane as solvent.

14-Ethyl podocarp-8(14)-en-13-one ***15***

To a boiling solution of potassium *tert*-butoxide (prepared from

Can. J. Chem. Downloaded from www.nrcresearchpress.com by 213.166.140.6 on 09/07/12
For personal use only.

Can. J. Chem. Downloaded from www.nrcresearchpress.com by 213.166.140.6 on 09/07/12
For personal use only.

0.6 mg-atom of K) in 1.35 mL of anhydrous *tert*-butyl alcohol was added 100 mg (0.407 mmol) of the enone **14** dissolved in 2.65 mL of hot *tert*-butyl alcohol. After 10 min, 0.052 mL (0.65 mmol) of dry ethyl iodide in 6.75 mL of *tert*-butyl alcohol was added dropwise with stirring, over a 2.5-h period, to the refluxing solution. The mixture was stirred and refluxed for 0.5 h, cooled, and acidified with concentrated hydrochloric acid. After addition of water to dispel the turbidity, *tert*-butyl alcohol was removed under reduced pressure. The organic material was extracted with ether (3 × 50 mL) and dried (Na_2SO_4). Removal of the solvent under reduced pressure gave an oil, which after chromatography afforded 34 mg (28%) of **16** as an oil; ir (film): 2940, 2860, 1715 (C=O), 1460, 1386, 1230, 1200, 1140, 1050, 980, 840 (>C=C—H), and 770 cm^{-1}; ^{1}Hmr ($CDCl_3$): 0.71 (t, 6H, C14 side chain methyl groups J = 8 Hz), 0.84, 0.90, and 0.93 (s, 3H each, C4 and C10 Me), 0.93 (s, 3H), 5.58 (m, $w_{1/2}$ = 8 Hz, 1H, H-C7); mass spectrum *m/e* (relative intensity): 302 (100) M^+, 287(14), 273(62), 255(7), 245(7), 231(8), 215(10), 189(9), 177(10), 166(74), 149(15), 138(20), 123(22), 109(72), 95(23), 85(21), 69(30), 55(26).

Increase in solvent polarity furnished 68 mg (61%) of **15**, which after crystallization from hexane gave crystals, mp 85.0–85.5°C; ir (KBr): 2949, 2860, 1660 (conj. C=O), 1620, 1450, 1320, 1120, 1050, and 960 cm^{-1}; ^{1}Hmr ($CDCl_3$): 0.76, 0.87, and 0.93 (s, 3H each, C4 and C10 Me), 0.91 (t, 3H, H-C16, J = 8 Hz), 2.29–2.42 (m, 2H, H-C15), 2.70–3.25 (m, 1H, H-C9). Irradiation of the triplet at δ 0.91 collapsed the 2.29–2.42 multiplet to a singlet, while irradiation at δ 2.37 simplified the δ 0.91 triplet to a singlet; ms *m/e* (relative intensity): 274(28) M^+, 259(3), 245(2), 205(4), 189(4), 175(5), 163(15), 151(14), 138(100), 137(68), 123(22), 107(12), 95(19), 91(15), 81(23), 69(21), 55(20). *Exact Mass* (M^+) calcd. for $C_{19}H_{30}O$: 274.2385; found: 274.2371.

8-β(H),14-β-Ethyl podocarpan-13-one ***17***

To 20 mL of stirred dry liquid ammonia (distilled from lithium) was added 15 mg (2.16 mg-atom) of lithium wire. After 15 min, a solution of 380 mg (1.387 mmol) of **15** and 0.103 mL (1.387 mmol) of *tert*-butyl alcohol in 5 mL of anhydrous ether was added, and the mixture was refluxed for 50 min. Then an excess of ammonium chloride was added, and the ammonia was removed with a nitrogen stream. Water (20 mL) was added to the remaining solid and then the organic material was extracted with 3 × 40 mL of ether. The combined extracts were washed with brine (1 × 20 mL) and dried over Na_2SO_4. On evaporating the solvent, the residue solidified. After chromatography it gave 340 mg (89%) of **17** as a solid, followed by 11 mg (3%) of **15**. Crystallization of **17** from methanol afforded white crystals, mp 62.5–63.5°C; ir (KBr): 2950, 2880, 1720 (C=O), 1460, and 1380 cm^{-1}; ^{1}Hmr ($CDCl_3$): 0.83 and 0.86 (s, 6 and 3H, C4 and C10 Me), 0.83 (t, 3H, H-C16, J = 8 Hz), 2.28–2.40 (m, 1H, H-C14); ms *m/e* (relative intensity): 276(99) M^+, 261(14), 248(100), 233(11), 215(7), 205(4), 190(7), 177(35), 163(24), 151(19), 136(46), 133(51), 109(34), 95(43), 81(50), 69(58), 67(64), 55(55). *Exact Mass* (M^+) calcd. for $C_{19}H_{32}O$: 276.2453; found: 276.2452.

8-β(H),14-β-Ethyl podocarpane ***18***

1,2-Ethanedithiol (0.15 mL), followed by 0.05 mL of boron trifluoride etherate, was added to 80 mg (0.290 mmol) of **17** dissolved in 5 mL of anhydrous Cl_2CH_2. The mixture was left overnight at room temperature, then 5 mL of 1.5 *M* aqueous NaOH was added. After stirring for 30 min the organic material was extracted with 4 × 30 mL of ether. The ethereal extracts were washed with 2 × 10 mL brine and dried (Na_2SO_4). After removing the solvent under reduced pressure, the remaining solid was crystallized from ether, affording white crystals of the dithioketal derivative in nearly quantitative yield; mp 94.0–96.0°C; ir (KBr): 2900, 2840, 1430, 1370, 1200, 970, 910, 850, 780, and 730 cm^{-1}; ^{1}Hmr ($CDCl_3$): 0.81, and 0.84 (s, 6 and 3H, C4 and C10 Me), 2.07–2.19 (m, 1H, H-C14), 3.22 (s, 4H, $-S(CH_2)_2S-$); ms *m/e* (relative intensity): 352(18) M^+, 324(5), 259(5), 221(6), 177(3), 165(91), 151(11), 137(16), 131(100), 123(24), 118(65), 109(26), 95(34), 81(33), 69(48), 55(32), 41(34).

The above-mentioned compound (100 mg), dissolved in 5 mL of absolute ethanol, was added to 1.5 g of Raney nickel, suspended in 15 mL of anhydrous ethanol. After a 12-h reflux, the catalyst was filtered and washed four times with hot ethanol (10 mL each). After solvent evaporation and chromatography, 52 mg (69% yield from **17**) of **18** as an oil was obtained; ir (film): 2940, 2860, 1460, and 1380 cm^{-1}; ^{1}Hmr ($CDCl_3$): 0.81, and 0.84 (s, 6 and 3H, C4 and C10 Me), 0.68–2.12 (m, 25 H); ms *m/e* (relative intensity): 262(32) M^+, 247(12), 177(72), 165(7), 149(100), 136(35), 123(77), 109(91), 95(69), 81(78), 69(65), 67(67), 55(69). *Exact Mass* (M^+) calcd. for $C_{19}H_{34}$: 262.2661; found: 262.2657.

8-β(H),14-β-Ethyl, 13-methylene podocarpane ***13***

MeLi solution in hexane (0.57 mL of 1.516 *M*) was added dropwise to a stirred suspension of 334 mg (0.93 mmol) of methyltriphenylphosphonium bromide in 2 mL of anhydrous ether. After 2 h at room temperature, 60 mg (0.22 mmol) of ketone **17** in 1 mL of ether was added and the mixture was stirred 24 h; after addition of water (10 mL), the organic material was extracted with 4 × 30 mL of ether, washed with 2 × 10 mL of brine, and dried (Na_2SO_4). The residue was chromatographed and then sublimed to afford 284 mg (85%) of **13**, mp 39.0–39.5°C; ir (KBr): 2940, 2860, 1650 (C=C), 1450, 1390, and 900 ($C=CH_2$) cm^{-1}; ^{1}Hmr ($CDCl_3$): 0.80, 0.82, and 0.85 (s, 3H each, C4 and C10 Me), 0.89 (t, 3H, H-C16, J = 6.4 Hz), 2.41 (m, 1H, H-C14), 4.56 and 4.69 (br s, 1H each, H-C17); ms *m/e* (relative intensity): 274(15) M^+, 259(25), 245(5), 231(4), 218(5), 203(4), 189(8), 177(23), 163(15), 149(22), 136(80), 121(32), 109(43), 107(50), 93(56), 81(80), 69(71), 55(81), 41(100). *Exact Mass* (M^+) calcd. for $C_{20}H_{34}$: 274.2710; found: 274.2695.

NOTE ADDED IN PROOF: While this manuscript was in press, auricularic acid, a cleistanthane diterpene very related to **6**, was isolated from *Pogostemon auricularis* Hassk (Prakash *et al.*, Tetrahedron Lett. **28**, 685 (1987)).

Acknowledgements

We thank Dr. Ferdinand Näf (Firmenich S.A.) for a generous gift of (+)-manool, Dr. O. S. Giordano (Universidad Nacional de San Luis) and Dr. H. Duddeck (Bochum University) for the high-resolution mass spectra determinations, Dr. J. C. Oberti (Universidad Nacional de Cordoba) for the low-resolution mass spectral data, and CONICET (Consejo Nacional de Investigaciones Cientificas y Tecnicas) and UNR for financial support and fellowships (T.S.K. and M.P.M.).

1. E. J. McGarry, K. H. Pegel, L. Phillips, and E. S. Waight. J. Chem. Soc. (C), 904 (1971).
2. R. Pinchin, L. M. U. Mayer, and A. C. Pinto. Phytochemistry, **17**, 1671 (1978).
3. A. C. Pinto. An. Acad. Bras. Cienc. **52**, 473 (1980); Chem. Abstr. **94**, 192482u (1980).
4. R. B. Dunlop. Phytochemistry, **24**, 977 (1985).
5. P. Ceccherelli, M. Curini, R. Cocchia, and N. Cagnoli. J. Chem. Soc. Perkin Trans. 1, 589 (1984).
6. D. D. K. Manh, M. Fetizon, and J. P. Flament. Tetrahedron, **31**, 1897 (1975).
7. P. K. Grant and R. Hodges. J. Chem. Soc. 5274 (1960).
8. G. Stork, P. Rosen, N. Goldman, R. V. Coombs, and J. Tsuji. J. Am. Chem. Soc. **87**, 275 (1965).
9. N. W. Atwater. J. Am. Chem. Soc. **82**, 2847 (1960).
10. H. Beierbeck, J. K. Saunders, and J. W. ApSimon. Can. J. Chem. **55**, 2813 (1977).
11. S. H. Grover and J. B. Stothers. Can. J. Chem. **53**, 589 (1975).
12. M. R. Bandell, D. T. Pegg, D. M. Doddrell, and D. H. J. Williams. J. Org. Chem. **47**, 3023 (1982).

Nouvelle synthèse de chloro-1 méthyl-5 isoquinoléines fusionnées à divers systèmes aromatiques par leur liaison [*g*]

EMILE BISAGNI, MARILYS RAUTUREAU, MARTINE CROISY-DELCEY ET CHRISTIANE HUEL

Unité associée 533, Centre national de la recherche scientifique, Laboratoire de synthèse organique, Institut Curie, Section de biologie, Bât. 110–112, 91405 Orsay, France

Reçu le 16 octobre 1986

EMILE BISAGNI, MARILYS RAUTUREAU, MARTINE CROISY-DELCEY et CHRISTIANE HUEL. Can. J. Chem. **65**, 2027 (1987).

La lithiation de l'acétyl-4 chloro-2 pyridine éthylène glycol acétal, effectuée au moyen du diisopropylamidure de sodium (LDA) fournit le dérivé lithié en 3 correspondant. Celui-ci réagit avec les aldéhydes aromatiques en donnant les alcools secondaires attendus qui sont réduits par le triéthylsilane dans l'acide trifluoroacétique. Les acétyl-4 arylméthyl-3 chloro-2 pyridine éthylène glycol acétals résultants sont directement hydrolysés et cyclisés en milieu acide pour donner les systèmes polycycliques comportant une chloro-1 méthyl-5 isoquinoléine fusionnée par sa liaison [*g*] au noyau aromatique correspondant à l'aldéhyde mis en oeuvre.

EMILE BISAGNI, MARILYS RAUTUREAU, MARTINE CROISY-DELCEY, and CHRISTIANE HUEL. Can. J. Chem. **65**, 2027 (1987).

Lithiation of 4-acetyl 2-chloro pyridine ethylene glycol ketal by exchange with lithium diisopropylamine (LDA) led to 4-acetyl 2-chloro 3-lithio pyridine ethylene glycol ketal. This lithio derivative was reacted with aromatic aldehydes giving the expected alcohols, which were reduced by triethylsilane and trifluoroacetic acid at room temperature. The resulting 4-acetyl 3-arylmethyl 2-chloro pyridine ethylene glycol ketals were hydrolysed and cyclized in acidic medium, leading to polycondensed heterocyclic systems that have a 1-chloro 5-methyl isoquinoline nucleus fused by its [*g*] bond to the starting aromatic aldehyde.

Dans un travail récent (1), nous avons montré que les méthyl-5-2*H*-isoquinolones-1 fusionnées à divers systèmes aromatiques par leur liaison [*g*], puis les dérivés chlorés correspondants, sont accessibles au départ de la [(méthoxy-2 pyridyl)-4]-2 diméthyl-4,4 oxazoline-2 **1**. Ce composé est toutefois préparé en 5 étapes à partir de l'acide chloro-2 isonicotinique et le schéma de synthèse utilisé comporte 5 transformations supplémentaires, ce qui rend la méthode assez laborieuse (schéma 1).

Compte tenu de l'intérêt biologique avéré (2, 3) ou potentiel, des nombreux composés susceptibles d'être obtenus par substitution des chloro-1 méthyl-5 isoquinoléines fusionnées aux systèmes aromatiques hétérocycliques les plus variés, et du fait que la synthèse convergente resumée par le schéma 1 paraissait intéressante malgré certaines limitations pour les composés qui comportent une position facilement échangeable par les lithiens (1), nous avons donc cherché à en appliquer le principe en utilisant des intermédiaires différents, capables de le rendre à la fois plus simple et applicable de manière générale.

Dans le présent article, nous décrivons nos résultats à ce sujet.

Au cours du travail déjà mentionné (1), nous avions constaté qu'à l'exception de certains cas particuliers de la transformations **5** → **6**, toutes les étapes du schéma 1 conduisent aux composés attendus avec de bons rendements. Dans le cas du diméthoxy-2,5 benzaldéhyde nouvellement étudié, le bilan global **1** → **7** s'élève d'ailleurs à 35,5% et le principal problème posé était bien de rendre la synthèse applicable dans tous les cas.

Pour cela, il fallait pouvoir introduire directement le groupement acétyl, en le protégeant pour permettre l'utilisation des lithiens, tout en maintenant par ailleurs une fonction sur le sommet 2 de la pyridine. De préférence, celle-ci devait être inerte vis-à-vis des organo-métalliques et devait limiter le problème de l'éventuelle addition de ces derniers en 1,2 de cet hétérocycle. Enfin, le nouveau composé de départ choisi devait être succeptible d'être lithié en 3, au même titre que l'oxazoline **1**.

L'acetyl-4 chloro-2 pyridine éthylène glycol acétal **8** déjà décrit (4) paraissant réunir les conditions ainsi définies, nous avons étudié sa lithiation par échange au moyen du diisopropylamidure de lithium (LDA), lui-même utilisé dans les conditions précisées par Quéguiner et coll. (5) pour lithier d'autres dérivés de la pyridine.

Après 4 h à −70°C dans le tétrahydrofuranne (THF) l'échange LDA – composé **8** conduit effectivement au lithien attendu **9** dont l'hydrolyse par D_2O fournit le dioxolanne de l'acétyl-4 chloro-2 deuterio-3 pyridine **10** avec un rendement supérieur à 60% (dosage rmn).

Nous avons donc poursuivi notre étude par des essais de condensation du diméthoxy-2,5 benzaldehyde, du β-naphthaldéhyde, du formyl-3 thiophène et du *p*-chlorobenzaldéhyde, pris comme exemples d'aldéhydes aromatiques, sur le dérivé lithié **9**. Cela fournit normalement les dioxolannes des acetyl-4 chloro-2(α-aryl α-hydroxy)méthyl-3 pyridines correspondantes **11***a*, **11***b*, **11***c* et **11***d*, avec des rendements de 72, 73, 61 et 76%, respectivement. Ces alcools secondaires étant apparentés au benzhydrol, ils devaient pouvoir être réduits par le triethylsilane dans l'acide trifluoroacétique, suivant les conditions décrites pour la réduction des alcools benzyliques (6, 7). C'est bien ce que nous avons observé pour **11***a*, **11***b* et **11***c* mais, du fait de la présence du groupement dioxolanne aisément hydrolysable, cette réduction en dérivés arylméthylés **12** s'accompagne toujours de l'apparition des produits cyclisés correspondants, probablement formés par cyclodéshydratation des cétones intermédiaires **13**. L'hydrolyse–cyclisation est toutefois incomplète dans les conditions de la réaction et afin d'améliorer les rendements en produit cyclisé, dont l'obtention dans des conditions aisées constituait le but du travail, nous avons traité directement le mélange réactionnel brut dans l'acide chlorhydrique 6 *M* à 50–60°C pour compléter les transformations. La chloro-1 diméthoxy-6,9 methyl-5 benzo[*g*]isoquinoléine **14** (65%), la chloro-1 methyl-5 naphtho[1,2-*g*]isoquinoléine **15** (40%) et la chloro-1 methyl-5 thiéno[2,3-*g*]isoquinoléine **16** (60%), qui sont bien identiques aux composés que nous avons déjà décrits dans les cas de **15** et de **16** (1), ou à celui formé à partir de **7** pour le composé **14**, ont ainsi été obtenus, avec les rendements indiqués calculés par rapport aux alcools **11** et sans qu'il soit nécessaire d'isoler les intermédiaires **12** et **13** (schéma 2).

Cependant, la suite des transformations décrites ci-dessus

Can. J. Chem. Downloaded from www.nrcresearchpress.com by 213.166.140.6 on 09/07/12
For personal use only.

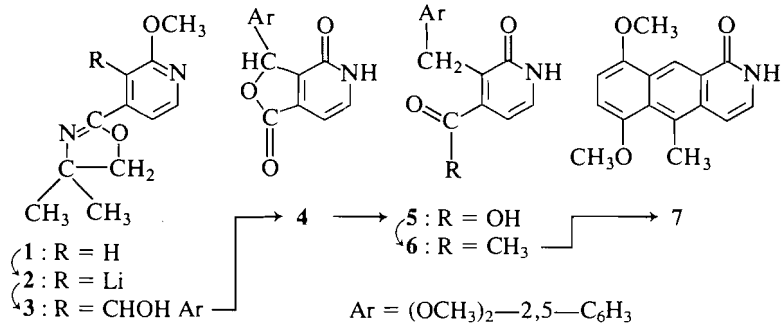

SCHÉMA 1

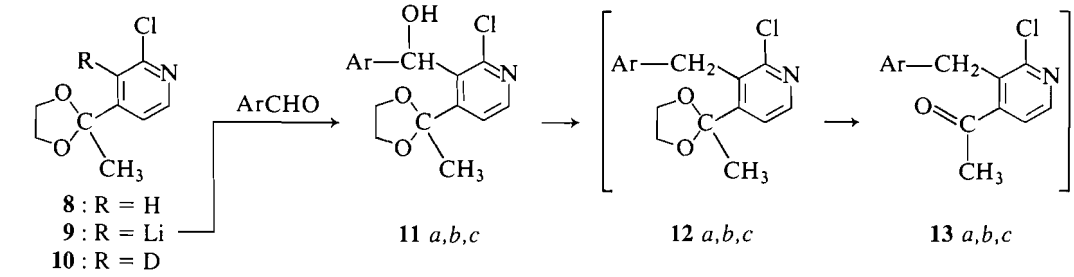

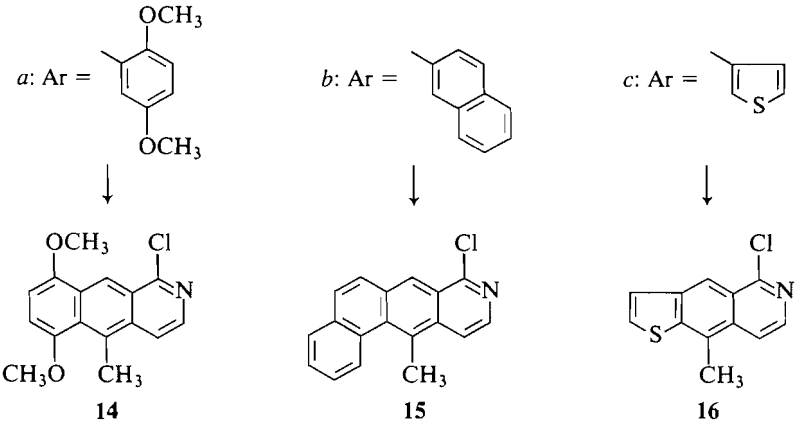

SCHÉMA 2

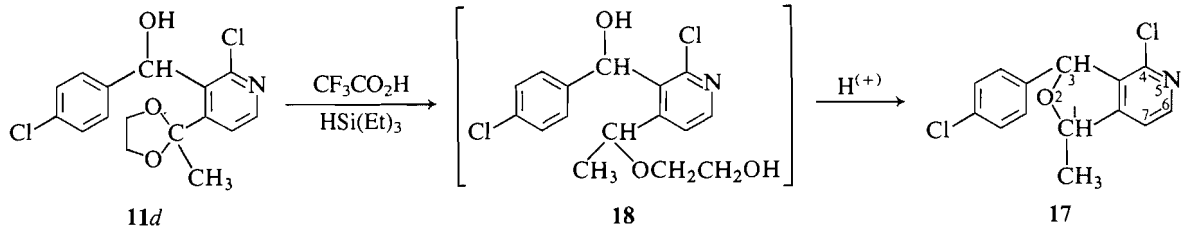

SCHÉMA 3

implique la réduction sélective de la fonction alcool secondaire par le couple triéthylsilane – acide trifluoroacétique alors que la fonction acétal est elle-même réductible dans les conditions utilisées (7).

Lorsque la fonction dioxolanne est affectée en priorité, la réaction suit donc un cours différent, comme nous l'avons observé dans le cas du composé **11***d*. En effet, celui-ci ne conduit pas à la benzoisoquinoléine attendue, mais seulement à la chloro-4 dihydro-1,3 méthyl-1 (*p*-chlorophényl)-3 furo[3,4-*c*]pyridine **17**, très probablement par l'intermédiaire du composé **18**, suivant le schéma 3.

Il est donc évident que tous les alcools de type **11** ne peuvent pas subir la suite des réactions décrites précédemment et que, pour rendre celle-ci applicable dans tous les cas, il sera nécessaire de préciser les conditions pour réduire sélectivement la fonction alcool, au besoin en ajoutant une étape spécifique.

Can. J. Chem. Downloaded from www.nrcresearchpress.com by 213.166.140.6 on 09/07/12
For personal use only.

Can. J. Chem. Downloaded from www.nrcresearchpress.com by 213.166.140.6 on 09/07/12
For personal use only.

Les transformations résumées par le schéma 2 constituent néanmoins une nouvelle méthode de synthèse des chloro-1 méthyl-5 isoquinoléines fusionnées par leur liaison [*g*] à divers systèmes aromatiques.

Le composé de départ utilisé est le dioxolanne de l'acétyl-4 chloro-2 pyridine facile à préparer (4) et bien que cette méthode implique 4 types différents d'intermédiaires, elle s'effectue en réalité en seulement 2 étapes, ce qui la rend facile et rapide. Par ailleurs, le petit nombre de transformations impliquées se traduit naturellement par une amélioration des rendements. C'est ainsi que le bilan global des préparations de **14**, **15** et **16** est de 31,6, 27,5 et 4,7% par la méthode au départ de **1** (1) alors qu'il s'élève à 48,75, 40 et 36,6% au départ du dioxolanne **8**.

Partie expérimentale

(Méthoxy-2' ((α-hydroxy α-(diméthoxy-2",5" phényl)-méthyl))-3' pyridyl-4']-2 diméthyl-4,4 oxazoline-2 **3**

À une solution de l'oxazoline **1** (1) (2,26 g, 11 mmol) dans le THF sec (25 mL), le méthyllithium (9,54 mL d'une solution 1,1 *M* dans l'éther diethylique, 10,5 mmol) est ajouté sous argon, à −5°C. Le mélange se colore rapidement en jaune et après 1 h d'agitation à 0°C, le dimethoxy-2,5 benzaldehyde (1,66 g, 10 mmol) en solution dans le THF (10 mL) est ajouté goutte à goutte. Le mélange est agité à la température ambiante pendant 18 h, décomposé en le versant dans l'eau et extrait au chlorure de méthylène. Le résidu de l'évaporation de ce dernier est repris dans le toluène et recristallisé dans le même solvant pour donner des aiguilles incolores (2,2 g, 68%), F = 161°C; ^{1}H rmn ($(CD_3)_2SO$) δ : 1,31 (s, 2 × 3H, $(CH_3)_2$), 3,43, 3,74, 3,79 (3s, 3 × 3H, OCH_3), 4,08 (q, 2H, CH_2, J_{H-H} = 8,7 Hz), 5,99 (d, 1H, CH—O*H*, J = 8,5 Hz), 6,54 (d, 1H, C*H*—OH), 6,76 (d, 2H, H-3" + H-4" Ar), 7,12 (d, 1H, H-5 py, J_{5-6} = 5 Hz), 7,24 (s élargi, 1H, H-6" Ar), 8,14 (d, 1H, H-6 py). *Anal.* calc. pour $C_{20}H_{24}N_2O_5$: C 64,50, H 6,50, N 7,52; trouvé : C 64,81, H 6,55, N 7,82.

*(Diméthoxy-2',5' phényl)-3-3*H,*5*H*-furo[3,4-*c*]pyridin dione-1,4* **4**

L'oxazoline **3** (4,1 g) est chauffée dans l'acide chlorhydrique 4 *M* (300 mL) au reflux pendant 3 h et le mélange est évaporé à sec, sous pression réduite. Le résidu est recristallisé dans le dioxanne pour donner 2,8 g (89%) de la lactone **4** sous la forme de microcristaux incolores, F = 236°C; ^{1}H rmn ($(CD_3)_2SO$) δ : 3,71 + 3,73 (2s, 2 × 3H, OCH_3), 6,61 (d, 1H, H-7, J_{7-6} = 6,5 Hz), 6,61 (d, 1H, CH), 6,73 (m, 1H, H-6' Ar), 7,04 (m, 2H, H-3' + H-4' Ar), 7,67 (dd, 1H, H-6). *Anal.* calc. pour $C_{15}H_{13}NO_3$: C 62,71, H 4,56, N 4,9; trouvé : C 62,62, H 4,58, N 5,1.

Acide (diméthoxy-2',5' benzyl)-3 hydroxy-2 pyridine carboxylique-4 **5**

La lactone **4** (2,8 g) est réduite en la chauffant pendant 24 h à reflux dans 140 mL d'ammoniaque concentré en présence de 14 g de zinc en poudre, préalablement activé, et de 70 mg de sulfate de cuivre. Le mélange refroidi est filtré, le solide essoré est lavé à l'eau et l'ensemble du filtrat est acidifié par l'acide chlorhydrique. Le précipité obtenu est recristallisé dans l'éthanol pour donner 2,3 g (81%) de microcristaux incolores, F environ 260°C, correspondant à l'acide **5** attendu, légèrement hydraté; ^{1}H rmn ($(CD_3)_2SO$) δ : 3,63 + 3,75 (2s, 2 × 3H, OCH_3), 3,96 (s, 2H, CH_2), 6,35 (d, 1H, H-5 py, J_{5-6} = 6,6 Hz), 6,43 (d, 1H, H-6' Ar, $J_{6'-4'}$ = 2,9 Hz), 6,70 (q, 1H, H-4' Ar), 6,86 (d, 1H, H-3' Ar, $J_{3'-4'}$ = 8,9 Hz), 7,37 (d, 1H, H-6 py). *Anal.* calc. pour $C_{15}H_{15}NO_5$: C 62,28, H 5,23, N 4,83; calc. pour $C_{15}H_{15}NO_5 \cdot 0{,}25H_2O$: C 61,33, H 5,28, N 4,77; trouvé : C 61,48, H 5,07, N 5,09.

*Acétyl-4 (diméthoxy-2,5 benzyl)-3-1*H*-pyridone-2* **6**

À la suspension de l'acide **6** (867 mg, 3 mmol) dans le THF sec (115 mL) «refroidie» à 10°C et maintenue sous agitation, le méthyllithium (27,3 mL d'une solution 0,55 *M* dans l'éther diéthylique, 5 équivalents) est ajouté en une seule fois. Le mélange est agité à la température ambiante pendant 18 h et versé dans 160 mL d'eau. Après évaporation du THF, la solution résiduelle est acidifiée à pH 4 par addition de 2 mL d'acide acétique et saturée par du chlorure de sodium. Le précipité obtenu après 24 h d'abandon à la température ambiante est recristallisé dans le toluène ou l'acétate d'éthyle pour donner 483 mg (56%) de paillettes jaunâtres correspondant à la cétone attendue **6**, F = 141–142°C; ^{1}H rmn ($(CD_3)_2SO$) δ : 2,38 (s, 3H, $COCH_3$), 3,64 (s, 2H, CH_2), 3,74 (s, 2 × 3H, OCH_3), 6,32 (d, 1H, H-5 py, J_{5-6} = 6,6 Hz), 6,51 (d, 1H, H-6' Ar, $J_{6'-4'}$ = 2,6 Hz), 6,72 (q, 1H, H-4' Ar), 6,88 (d, 1H, H-3' Ar, $J_{3'-4'}$ = 8,8 Hz), 7,42 (d, 1H, H-6 py), 11,75 (s large, 1H, NH). *Anal.* calc. pour $C_{16}H_{17}NO_4$: C 66,88, H 5,96, N 4,88; trouvé : C 66,62, H 5,98, N 4,72.

*Méthyl-5 diméthoxy-6,8 benzo[*g*]-2*H*-isoquinolone-1* **7**

Le mélange formé par la cétone précédente **6** (102 mg) dans l'acide chlorhydrique 6 *M* (10 mL) est agité à la température ambiante pendant 1 h et refroidi à 0°C. Le solide formé, filtré et séché, recristallise dans le toluène pour donner 95 mg (91,5%) de microcristaux, F = 256°C, correspondant à l'isoquinolone **7**, hydratée avec 0,25H_2O; ^{1}H rmn ($(CD_3)_2SO$) δ : 3,05 (s, 3H, CH_3), 3,92 + 4,01 (2s, 2 × 3H, OCH_3), 6,84 (d, 1H, H-4, J_{4-3} = 7,7 Hz), 6,88 + 7,03 (2d, 2H, H-7 + H-8, J_{7-8} = 8,9 Hz), 7,16 (dd, 1H, H-3, J_{3-NH} = 5,8 Hz), 9,08 (s, 1H, H-10), 11,04 (s large, 1H, NH). *Anal.* calc. pour $C_{16}H_{15}NO_3 \cdot 0{,}25H_2O$: C 70,20, H 5,66, N 5,11; trouvé : C 69,93, H 5,65, N 5,43.

Remarque : Lorsque la cétone **6** résultant de la transformation de l'acide **5** par le méthyllithium est directement traitée par l'acide chlorhydrique, sans être isolée, le rendement global de la transformation **5** → **7** s'élève à 72,4%.

Dioxolanne de l'acétyl-4 chloro-2 pyridine **8**

Ce composé a été préparé comme indiqué par Lamattina (4) qui le décrit comme un liquide. Distillé à Eb_{10} = 128°C, il cristallise en donnant un solide qui fond aux environs de 30°C.

Acétyl-4 chloro-2 (α-aryl α-hydroxy)méthyl-3 pyridines éthylène glycol acetals **11**a, **11**b, **11**c *et* **11**d

Dans un tricol de 250 mL séché à 120°C et maintenu sous argon, on introduit le tetrahydrofuranne (THF, 50 mL) fraichement distillé sur le mélange benzophénone + sodium. Après avoir refroidi à 0°C, le butyllithium (6,9 mL de la solution commerciale 1,6 *M*, 11 mmol) et la diisopropylamine distillée sur hydrure de calcium (1,54 mL, 11 mmol) sont ajoutés successivement. L'ensemble est agité à 0°C pendant 1 h puis refroidi à −70°C. En continuant à refroidir à cette dernière température, le dioxolanne **8** (1,995 g, 10 mmol) en solution dans le THF (10 mL) est alors ajouté, goutte à goutte. Trente minutes après la fin de l'addition, on observe l'apparition d'un précipité jaune et le mélange hétérogène se transforme progressivement en un gel. Après 4 h à −70°C, l'aldéhyde choisi (10 mmol) en solution dans le THF (10 mL) est ajouté goutte à goutte et le nouveau mélange est agité à la même température pendant 1 h puis abandonné à la température ambiante pendant 15 h. L'ensemble est versé dans l'eau, extrait au chlorure de méthylène, et les phases organiques réunies sont séchées sur sulfate de sodium et évaporées. Le résidu huileux cristallise progressivement dans l'hexane ou le cyclohexane et le solide obtenu est recristallisé dans le même solvant pour fournir le composé attendu, sous la forme de cristaux incolores.

11*a* : Rendement 72%; F : 92°C (cyclohexane); ^{1}H rmn ($CDCl_3$) δ : 1,73 (s, 3H, CH_3), 3,72 (s, 2 × 3H, OCH_3), 3,8–4,6 (m, 4H, CH_2CH_2), 4,29 (d, 1H, OH, J_{CH-OH} = 8,2 Hz), 6,66–6,84 (m, 4H, C*H*OH + 3H-Ar), 7,57 (d, 1H, H-5 py, J_{5-6} = 5 Hz), 8,31 (d, 1H, H-6 py). *Anal.* calc. pour $C_{18}H_{20}ClNO_5$: C 59,10, H 5,51, N 3,83, Cl 9,69; trouvé : C 58,82, H 5,47, N 4,02, Cl 9.67.

11*b* : Rendement 73%; F = 146°C (cyclohexane); ^{1}H rmn ($CDCl_3$) δ : 1,77 (s, 3H, CH_3), 3,58–3,93 (m, 4H, CH_2—CH_2), 4,35 (d, 1H, O*H*, J_{OH-CH} = 11,2 Hz), 6,81 (d, 1H, C*H*—OH), 7,41–7,50 (m, 5H, 5H-Ar), 7,61 (d, 1H, H-5 py, J_{5-6} = 5 Hz), 7,78–7,87 (m, 2H, 2H-Ar), 8,41 (d, 1H, H-6 py). *Anal.* calc. pour $C_{20}H_{18}ClNO_3$: C 67,51, H 5,10, N 3,94, Cl 9,96; trouvé : C 67,71, H 5,16, N 3,96, Cl 9,89.

11*c* : Rendement 61%; F = 105°C (hexane); ^{1}H rmn ($CDCl_3$) δ : 1,75 (s, 3H, CH_3), 3,2–4,02 (m, 4H, CH_2—CH_2), 4,52 (d, 1H, OH, J_{OH-CH} = 11,5 Hz), 6,62 (dd, 1H, C*H*OH, $J_{CH-H\text{-}2\,th}$ = 2 Hz), 6,88–7 (m, 2H, H-2 th + H-4 th), 7,26–7,34 (m, 1H, H-5 th), 7,56 (d, 1H, H-5 py, J_{5-6} = 5 Hz), 8,37 (d, 1H, H-6 py). *Anal.* calc. pour

$C_{14}H_{14}ClNO_3S \cdot 0{,}25H_2O$: C 53,16, H 4,58, N 4,43, S 10,12, Cl 11,23; trouvé : C 53,21, H 4,45, N 4,41, S 10,13, Cl 11,21.

11*d* : Rendement 76%; F = 125°C (cyclohexane); ^{1}H rmn ($CDCl_3$) δ : 1,74 (s, 3H, CH_3), 3,3 (m, 4H, CH_2—CH_2), 4,13 (d, 1H, OH, J_{OH-CH} = 11,7 Hz), 7,13 (d, 2H, H-2′ + H-6′ Ar, $J_{H-3'-H-2'}$ = 8,2 Hz), 7,31 (d, 2H, H-3′ + H-5′ Ar), 7,58 (d, 1H, H-5 py, J_{5-6} = 5 Hz), 8,38 (d, 1H, H-6 py). *Anal.* calc. pour $C_{16}H_{15}Cl_2NO_3$: C 56,49, H 4,44, N 4,12, Cl 20,84; trouvé : C 56,63, H 4,18, N 4,01, Cl 21,07.

*Réduction–hydrolyse–cyclisation des composés **11** : formation des dérivés polycycliques **14**, **15**, **16***

Le composé choisi (**11***a*, **11***b* ou **11***c*, 1 mmol) est ajouté à l'acide trifluoroacétique (2 mL) et à la solution résultante agitée à la température ambiante (20–25°C), le triethylsilane (0,18 mL, 1,1 mmol) est ajouté en une seule fois. L'agitation est poursuivie pendant 18 h à la température ambiante et l'excès d'acide trifluoroacétique est évaporé sous pression reduite. L'acide chlorhydrique 6 *M* (20 mL) est ajouté au résidu et le mélange est agité à 55–60°C pendant 4 h pour former les composés **14** et **15** et seulement pendant 45 min pour préparer la thiénoisoquinoléine **16**. Le mélange refroidi est alcalinisé par l'ammoniaque, extrait au chlorure de méthylène et la phase organique séchée sur sulfate de sodium est filtrée et évaporée. Le résidu obtenu cristallise dans le minimum de méthanol (**14** et **16**) ou dans l'hexane (**15**) et les produits obtenus sont recristallisés dans le même solvant.

14 : F = 170°C; Rdt 65%.

15 : F = 151°C; Rdt 37%.

16 : F = 138°C; Rdt 60%.

Pour les composés **15** et **16**, les points de fusion, les R_f sur plaque de silice, avec plusieurs mélanges de solvants comme éluants, de même que les spectres de ^{1}H rmn sont en tous points identiques à ceux des mêmes produits déja décrits dans la référence 1.

*Chloro-1 dimethoxy-6,9 methyl-5 benzyl[g]isoquinoléine **14***

Méthode A : voir ci-dessus.

Méthode B : le mélange formé par le composé **7** (500 mg) et l'oxychlorure de phosphore (20 mL) est chauffé au reflux pendant 1 h et l'excès d'oxychlorure est évaporé sous pression réduite. Le résidu est décomposé par addition d'eau glacée, alcalinisé par l'ammoniaque et extrait au chlorure de méthylène. La phase organique séchée est filtrée, évaporée, et le résidu est recristallisé dans l'hexane pour fournir 478 mg (89%) d'aiguilles jaunes, F = 170°C, identique au composé formé par la méthode A; ^{1}H rmn ($CDCl_3$) δ : 3,26 (d, 3H, CH_3, $J_{CH_3-H_4}$ = 0,7 Hz), 3,95 + 4,06 (2s, 2 × 3H, OCH_3), 6,7 + 6,84 (2d, 2H, H-7 + H-8, J_{7-8} = 8 Hz), 8,0 (dd, 1H, H-4, J_{4-3} = 6,5 Hz), 8,19 (d, 1H, H-3), 9,3 (s, 1H, H-10). *Anal.* calc. pour $C_{16}H_{14}ClNO_2$: C 66,79, H 4,90, N 4,87, Cl 12,32; trouvé : C 66,52, H 4,75, N 4,97, Cl 12,59.

*Chloro-4 dihydro-1,3 méthyl-1 (p-chlorophenyl)-3 furo[3,4-c]pyridine **17***

Le composé **11***d* (680 mg, 2 mmol) est ajouté à l'acide trifluoroacétique (4 mL) refroidi à 0°C et le triethylsilane (0,64 mL, 4 mmol) est ajouté aussitôt en une seule fois, en maintenant le mélange sous agitation. Après 6 h d'agitation à 0°C et 15 h à la température ambiante, le mélange est versé dans l'eau, aussitôt alcalinisé par l'ammoniaque et extrait au chlorure de méthylène. L'évaporation du solvant fournit un résidu qui est repris dans l'hexane pour donner, après 2 recristallisations dans le même solvant, 190 mg (34%) de microcristaux incolores correspondant au composé **17**, F = 130°C; ^{1}H rmn ($CDCl_3$) δ : 1,63 (d, 3H, CH_3-1, J_{CH_3-H-1} = 6,5 Hz), 5,4 (m, 1H, H-1), 6,1 (d, 1H, H-3, J_{3-1} = 2 Hz), 7,17 (d, 1H, H-7, J_{7-6} = 5 Hz), 7,22 (d, 2H, H-2′ + H-6′ Ar, $J_{2'-3'}$ = 8,3 Hz), 7,35 (d, 2H, H-3′ + H-5′ Ar), 8,4 (d, 1H, H-6). *Anal.* calc. pour $C_{14}H_{11}Cl_2NO$: C 60,01, H 3,96, N 5,00, O 5,71, Cl 25,30; trouvé : C 59,74, H 3,71, N 4,78, O 5,85, Cl 25,26.

Remarque : les eaux mères de la recristallisation du composé précédent, évaporées et traitées par l'acide chlorhydrique (et par l'acide sulfurique) n'ont fourni aucune trace de la benzoisoquinoléine qui aurait pu se former suivant les transformations résumées par le schéma 2.

Remerciements

Les auteurs remercient l'Institut Curie et l'Institut national de la santé et de la recherche médicale (CRE 842001) qui ont partiellement financé ce travail.

1. E. Bisagni et M. Rautureau. Synthesis, 142 (1987).
2. C. Ducrocq, F. Wendling, M. Tourbez-Perrin, C. Rivalle, P. Tambourin, F. Pochon, E. Bisagni et J. C. Chermann. J. Med. Chem. **23**, 1212 (1980).
3. C. Lidereau, J. C. Chermann, J. Gruest, L. Montagnier, C. Rivalle et E. Bisagni. Bull. Cancer, **67**, 1 (1980).
4. J. L. Lamattina. J. Heterocycl. Chem. **20**, 353 (1983).
5. T. Güngör, F. Marsais et G. Queguiner. J. Organomet. Chem. **215**, 139 (1981).
6. M. G. Adlington, M. Orpanopoulos et J. K. Fry. Tetrahedron Lett. 2955 (1976).
7. D. N. Kursanov, S. N. Parnes et N. M. Loim. Synthesis, 633 (1974).

Can. J. Chem. Downloaded from www.nrcresearchpress.com by 213.166.140.6 on 09/07/12
For personal use only.

Réactivité des α-halobutyrolactones à halogènes tertiaires vis-à-vis des nucléophiles faiblement basiques

JOSYANE GHARBI-BENAROUS, MOUNIR M. ESSAYEGH ET GILBERT DANA[1]

Laboratoire de stéréochimie réactionnelle, Bât. F, Université Pierre et Marie Curie, 4 Place Jussieu, 75252 CEDEX 05, France

Reçu le 11 juillet 1986[2]

JOSYANE GHARBI-BENAROUS, MOUNIR M. ESSAYEGH et GILBERT DANA. Can. J. Chem. **65**, 2031 (1987).

Le méthyl-2 phényl-4 buténolide **5** est préparé quantitativement par élimination de HBr à partir des bromolactones correspondantes **3**. La réaction, obtenue par action des ions halogénures à 100°C dans des solvants polaires aprotiques (DMF, DMSO) est accompagnée d'une substitution nucléophile bimoléculaire. Dans ces réactions, le solvant semble jouer un rôle actif. S'il est assez polaire, il provoque une activation du substrat (forte polarisation préalable de la liaison C—Br) nécessaire au déclenchement de la réaction. En l'absence d'ions halogénures une réaction de type solvolytique intervient pour le démarrage de la réaction. Mais dès que la production des ions halogénures par élimination devient notable, les mécanismes bimoléculaires deviennent prépondérants. L'activation des chlorolactones **4** s'avère beaucoup moins aisée que celle des bromolactones **3**, mais dans les deux cas l'élimination est du type E_2ip avec semble-t-il, une approche du type E_2C.

JOSYANE GHARBI-BENAROUS, MOUNIR M. ESSAYEGH, and GILBERT DANA. Can. J. Chem. **65**, 2031 (1987).

2-Methyl-4-phenylbutenolide (**5**) is prepared in a quantitative manner by an elimination of HBr from the corresponding bromolactones **3**. This reaction, induced by halide ions at 100°C in polar aprotic solvents (DMF, DMSO), is accompanied by a bimolecular nucleophilic substitution. In these reactions, the solvent seems able to play an active role. A polar solvent induces the necessary activation of the substrate (by a prior strong polarization of the C—Br bond). In the absence of halide ions, a solvolytic reaction takes place. As soon as the elimination reaction produces enough halide ions, the bimolecular reaction takes over. The activation of the chlorolactones **4** is much more difficult than that of the bromolactones **3**; however, each elimination is of the E_2ip type with some E_2C type.

[Journal translation]

Can. J. Chem. Downloaded from www.nrcresearchpress.com by 213.166.140.6 on 09/07/12
For personal use only.

Dans un précédent mémoire (1), nous avons proposé une nouvelle voie d'accés au méthyl-2 phényl-4 buténolide-2,3. La méthode utilise des dérivés dihydro-2,3 furanniques (2–4) et fait intervenir une réaction d'élimination d'hydracide sur les α-bromobutyrolactones correspondantes. L'intérêt que suscite le motif buténolide pour les nombreuses propriétés physiologiques qui lui sont attachées (5, 6) nous a encouragés à examiner plus en détail ses possibilités de formation à partir des halolactones.

La déshydrohalogénation est effectuée par une base faible en milieu aprotique (LiBr, DMF, 100°C) dans des conditions qui se sont révélées épimérisantes pour le brome (schéma 1).

Cette réaction de substitution peut jouer un rôle important dans la réaction d'élimination, dans la mesure où, entraînant un changement de stéréochimie du brome, elle permet éventuellement de former les stéréoisomères **1** susceptibles de subir l'élimination *anti*.

En fait, deux types de mécanismes reconnus peuvent être envisagés pour ces réactions d'élimination/substitution. Le premier, assez généralement admis, est un *mécanisme bimoléculaire* de type E_2C (en raison de la faible basicité du nucléophile mis en jeu) (7, 8) ou de type E_2ip, mécanisme par paire d'ions (en raison de la forte polarité du solvant) (9, 10). L'autre possibilité est un *mécanisme solvolytique* par formation d'un carbocation en α du carbonyle. Des carbocations de ce type ont été observés et étudiés aussi bien en α d'une cétone (11) que d'un ester (11*d*, 12). Ils sont généralement plus réactifs dans le cas des esters (11*d*). Il nous a semblé intéressant d'envisager le cas d'un substrat lactonique plus propice à l'hypothèse du mécanisme solvolytique que les lactones **1**.

Dans le présent mémoire, nous examinerons le cas des stéréoisomères *a* et *b* des α-méthyl-halolactones **3** et **4**. L'utilisation de tels substrats tertiaires devrait privilégier les mécanismes solvolytique ou par paire d'ions au détriment du mécanisme E_2C. Nous montrerons que des considérations cinétiques de nature semi-quantitative et que des observations stéréochimiques simples permettent, notamment par comparaison du comportement dans divers solvants, de proposer un schéma réactionnel assez détaillé. Nous tiendrons compte également de l'orientation de la réaction vers le buténolide **5** plutôt que vers la méthylène-lactone **6**.

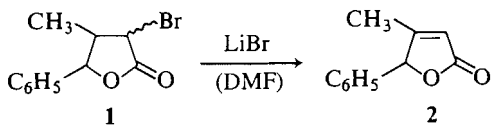

1 **2**

SCHÉMA 1

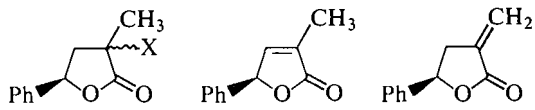

3*a* : X = ''''Br
3*b* : X = ◄Br
4*a* : X = ''''Cl
4*b* : X = ◄Cl

5 **6**

Résultats expérimentaux

Les bromolactones **3***a* et **3***b* sont préparées à partir du composé dihydrofurannique **7** en deux étapes (addition de BrOH par action du *N*-bromosuccinimide dans le DMSO humide suivie d'une oxydation douce) dans des conditions cinétiques (1), avec un rendement global de 97% (voir partir expérimentale).

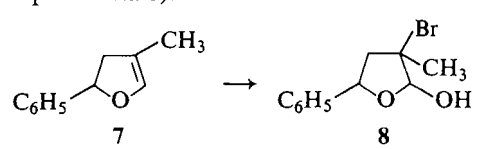

7 **8**

3*a* (85%) + **3***b*(12%)

1. Auteur à qui adresser toute correspondance.
2. Révision reçue le 29 janvier 1987.

TABLEAU 1. Réactivité des bromolactones **3***a* et **3***b* dans le DMF

Expérience	Produits de départ	Conditions	Sel	Produits formés		Lactone résiduelle	(**3***b*)/(**3***a*)[d]
				% E_2 (**5**)	% S_N2		
1	**3***a*	100°C; 1 h[a]	LiBr, 2 équiv.	80	[b]	≈20	
2	**3***a*	60°C; 3 h	LiBr, 2 équiv.	29	10(**3***b*)	61	10/61 = 0,164
3	**3***a*	60°C; 1 h	LiCl, 2 équiv.	65	23(**4***b*)	12	
4	**3***a*	50°C; 30 min	LiCl, 2 équiv.	25	10(**4***b*)	65	
5	**3***a*	50°C; 1 h	LiCl, 1 équiv.	28	10(**4***b*)	62	
6	**3***a*	100°C; 1 h[c]	LiI, 2 équiv.	40	6(**3***b*)	54	6/54 = 0,11
7	**3***a*	60°C; 3 h	LiI, 2 équiv.	6	0	94	
8	**3***b*	60°C; 15 min	LiCl, 2 équiv.	17	53(**4***a*)	30	
9	**3***b*	60°C; 30 min	LiCl, 2 équiv.	25	70(**4***a*)	5	
10	**3***b*	60°C; 3 h	LiBr, 2 équiv.	13	75(**3***a*)	12	12/75 = 0,16
11	**3***b*	60°C; 1 h	LiBr, 2 équiv.	7	72(**3***a*)	21	21/72 = 0,29

[a]Dans les mêmes conditions, mais au bout de 3 h, la transformation en buténolide est totale. Le rendement en buténolide purifié est alors de 94%.
[b]Trace non dosable par rmn.
[c]Au bout de 3 h, on peut également isoler après traitement (lavage à l'eau, extraction à l'éther...) 10% de α-hydroxylactones (13).
[d]Valeur mesurée en fin d'expérience. L'équilibre correspond à une valeur de l'ordre de 0,16 à 60°C.
N.B. Les dosages sont effectués par intégration en rmn et confirmés par ccm préparative. Les expériences ont été répétées (2–3 fois) de façon indépendante avec obtention d'écarts inférieurs à 3%. Les résultats obtenus dans les expériences préliminaires et dans des conditions intermédiaires (ou plus sévères) sont cohérents avec le reste du tableau et ne sont pas mentionnés. La nature de l'halogène présent dans les produits de substitution est confirmée par spectrographie de masse et par analyse centésimale.

TABLEAU 2. Étude de la bromolactone **3***a* dans des solvants de différentes polarités

Expérience	Solvant	Conditions	Sel	Produits formés		Lactone résiduelle	(**3***b*)/(**3***a*)
				% E_2 (**5**)	% S_N2		
1	Toluène	Reflux	[a]	0	0	100	
2	Ether	Reflux	[a]	0	0	100	
3	Acetonitrile	Reflux	[a,b]	0	0	100	
4	Acetone	Reflux	0	0	0	100	
5	Acetone	Reflux, 3 h	LiBr[c]	3	6(**3***b*)	91	6/91 = 0,066
6	Acetone	Reflux, 3 h	LiCl[c]	10	5(**4***b*)	85	
7	DMF	60°C; 3 h	0	0	0	100	
8	DMF	60°C; 7 h	0	5	6(**3***b*)	89	6/89 = 0,067
9	DMF	80°C; 1 h	0	0	0	100	
10	DMF	80°C; 3 h	0	6	7,5(**3***b*)	86,5	7,5/86,5 = 0,087
11	DMF	80°C; 8 h	0	15	11(**3***b*)	74	11/74 = 0,149
12	DMF	80°C; 12 h	0	38	9(**3***b*)	53	9/53 = 0,17
13	DMF	100°C; 1 h	0	13	11(**3***b*)	76	11/76 = 0,145
14	DMF	60°C; 3 h	LiBr[c]	29	10(**3***b*)	61	10/61 = 0,164
15	DMF	50°C; 30 h	LiCl[c]	25	10(**4***b*)	65	
16	DMSO	80°C; 3 h	0	31	10(**3***b*)	59	10/59 = 0,169

[a]Même résultat avec et sans LiBr.
[b]Même résultat avec et sans LiCl.
[c]Deux équivalents de sel (0,8 mmol LiBr ou LiCl) dans 10 mL de solvant pour 1 équivalent (0,4 mmol) de bromolactone **3***a*.
N.B. Voir tableau 1.

L'isomère majoritaire **3***a* correspond à l'attaque électrophile du brome par la face la moins encombrée du dihydrofuranne (face α) (1).

Les chlorolactones **4** sont obtenues de façon analogue en trois étapes. L'isomère **4***a* est alors initialement obtenu pur et son épimère **4***b* est préparé par isomérisation dans la présente étude.

Les quatre lactones sont aisément identifiables par rmn du proton et par chromatographie en couche mince sur silice (ccm). Les dosages réalisés au cours de l'étude qui suit (tableaux 1–4) ont été effectués par intégration en rmn pour la mise au point des conditions expérimentales jusqu'à obtention de résultats reproductibles à 2 ou 3% près. Les dosages sont alors confirmés par ccm préparative et les échantillons purifiés envoyés à l'analyse et à la spectrographie de masse pour vérifier notamment la nature de l'halogène présent (voir partie expérimentale).

D'une façon générale, les halolactones **3** et **4**, à halogène tertiaire, sont moins réactives (en ce qui concerne l'élimination) que les bromolactones **1**. Dans les conditions où ces dernières réagissent totalement pour former le buténolide **2** (isolé avec un rendement de 95% (1)), les taux de transformation des bromolactones **3** et des chlorolactones **4** en buténolide **5** sont seulement de 80 et 24% respectivement (action des sels LiBr ou LiCl, dans le DMF, 1 h à 100°C, tableaux 1 et 3, expériences n° 1). Dans ces conditions, on peut observer l'équilibration des

Can. J. Chem. Downloaded from www.nrcresearchpress.com by 213.166.140.6 on 09/07/12
For personal use only.

TABLEAU 3. Réactivité des chlorolactones **4***a* et **4***b* dans le DMF

Expérience	Produit de départ	Conditions	Sel	Produits formés		Lactone résiduelle	(**4***b*)/(**4***a*)
				% E_2 (**5**)	% S_N2		
1	**4***a*	100°C; 1 h	LiCl, 2 équiv.	24	14(**4***b*)	62	14/62 = 0,23
2	**4***a*	100°C; 3 h	LiCl, 2 équiv.	54	12(**4***b*)	34	12/34 = 0,35
3	**4***a*	80°C; 3 h	LiCl, 2 équiv.	25	12(**4***b*)	63	12/63 = 0,19
4	**4***a*	80°C; 6 h	LiCl, 2 équiv.	40	11(**4***b*)	49	11/49 = 0,23
5	**4***a*	60°C; 1 h	LiCl, 2 équiv.	0	0	100	
6	**4***a*	60°C; 3 h	LiCl, 2 équiv.	5	11(**4***b*)	84	11/84 = 0,13
7	**4***a*	60°C; 6 h	LiCl, 2 équiv.	10	11(**4***b*)	79	11/79 = 0,14
8	**4***a*	60°C; 6 h	LiBr, 2 équiv.	0	0	100	
9	**4***a*	100°C; 1 h	LiBr, 2 équiv.	10	3(**4***b*)	87	3/87 = 0,035
10	**4***a*	100°C; 3 h	LiBr, 2 équiv.	29	9(**4***b*)	62	9/62 = 0,145
11	**4***b*	60°C; 1 h	LiCl, 2 équiv.	0	0	100	
12	**4***b*	60°C; 3 h	LiCl, 2 équiv.	12	16(**4***a*)	72	72/16 = 4,5
13	**4***b*	100°C; 1 h	LiCl, 2 équiv.	19	51(**4***a*)	30	30/51 = 0,59
14	**4***b*	100°C; 3 h	LiCl, 2 équiv.	41	37(**4***a*)	22	22/37 = 0,59

N.B. Voir tableau 1.

TABLEAU 4. Étude de la chlorolactone **4***a* dans des solvants de différentes polarités

Expérience	Solvant	Conditions	Sel	Produits formés		Lactone résiduelle	(**4***b*)/(**4***a*)
				% E_2 (**5**)	% S_N2		
1	Toluène	Reflux	[a]	0	0	100	
2	Ether	Reflux	[a]	0	0	100	
3	Acetonitrile	Reflux	[a]	0	0	100	
4	Acetone	Reflux	[a]	0	0	100	
5	DMF	100°C; 1 h	0	0	0	100	
6	DMF	100°C; 1 h	LiCl[b]	24	14(**4***b*)	62	14/62 = 0,226
7	DMF	100°C; 1 h	LiBr[b]	10	3(**4***b*)	87	3/87 = 0,035
8	DMF	100°C; 3 h	0	10	3(**4***b*)	87	3/87 = 0,035
9	DMF	100°C; 3 h	LiCl[b]	54	12(**4***b*)	34	12/34 = 0,353
10	DMF	100°C; 3 h	LiBr[b]	29	9(**4***b*)	62	9/62 = 0,145
11	DMF	80°C; 16 h	0	0	0	100	
12	DMF	80°C; 3 h	LiCl[b]	25	12(**4***b*)	63	12/63 = 0,19
13	DMSO	100°C; 3 h	0	6	5(**4***b*)	89	5/89 = 0,056
14	DMSO	100°C; 1 h	LiCl[b]	21	15(**4***b*)	64	15/64 = 0,234
15	DMSO	80°C; 3 h	0	0	0	100	
16	DMSO	80°C; 3 h	LiCl[b]	14	14(**4***b*)	72	14/72 = 0,195

[a]Même résultats avec et sans LiCl.

[b]Deux équivalents de sel (0,8 mmol LiBr ou LiCl) dans 10 mL de solvant pour 1 équivalent (0,4 mmol) de chlorolactone **4***a*.

N.B. Voir tableau 1.

stéréoisomères *a* et *b* sur les lactones résiduelles. Contrairement au cas des lactones **1**, l'expérience montre que, pour les lactones à halogène tertiaire, on ne peut pas trouver de conditions d'équilibration (substitution) sans élimination (abaissement de la température, absence de nucléophile, changement de solvant...). Toutefois, par abaissement de température, l'élimination peut être suffisamment ralentie pour que la composition d'équilibre des bromolactones soit approximativement observée (K(**3**) = (**3***b*)/(**3***a*) = 0,162 ± 0,002, expériences n° 2 et 10, tableau 1). Pour les chlorolactones, bien que la vitesse d'élimination soit notablement plus faible que pour les bromolactones, la vitesse d'épimérisation du chlore reste toujours du même ordre de grandeur que la vitesse d'élimination et le rapport (**4***b*)/(**4***a*) stationnaire approximativement atteint (0,4–0,6) ne correspond pas forcément à la constante d'équilibre (expériences n° 2, 13 et 14, tableau 3).

Ces équilibrations sont étudiées sur des solutions de 10 mL de DMF contenant 0,4 mmol d'halolactone et 2 équivalents (0,8 mmol) du nucléophile (LiBr ou LiCl respectivement) à 60°C pour les bromolactones et à 100°C pour les chlorolactones. En l'absence du nucléophile, dans les mêmes conditions, aucune réaction n'est observée (tableau 2, expérience n° 7, et tableau 4, expérience n° 5). Pour développer l'étude de ces réactions, nous avons d'abord modifié la nature et la concentration du nucléophile.

Au point vue préparatif, signalons qu'on peut obtenir de façon optimum le buténolide **5** à partir de la bromolactone **3***a*, en 3 h à 100°C, dans les mêmes conditions (tableau 1, note *a*).

Changement de nucléophile

L'utilisation des ions chlorures (LiCl) au lieu de bromure (LiBr) avec les lactones bromées **3** accélère la réaction d'élimination (tableau 1, expériences n° 2 et 3 et expériences n° 9 et 10). On n'observe plus l'épimérisation du brome et

Can. J. Chem. Downloaded from www.nrcresearchpress.com by 213.166.140.6 on 09/07/12
For personal use only.

Can. J. Chem. Downloaded from www.nrcresearchpress.com by 213.166.140.6 on 09/07/12
For personal use only.

le seul produit de substitution trouvé est la chlorolactone de configuration inverse (**4***b* à partir de **3***a* et **4***a* à partir de **3***b*) comme le montrent la chromatographie en couche mince préparative (ccm), l'analyse centésimale, la rmn du proton et la spectrographie de masse. La comparaison des expériences n° 4 et 5 (tableau 1) montre que la vitesse de formation de la chlorolactone **4***b* à partir de la bromolactone **3***a* est proportionnelle à la concentration des ions chlorures : on obtient autant de chlorolactone **4***b* (10%) en 1 h avec 1 équivalent de Cl^- qu'en 30 min avec 2 équivalents. *Aussi bien par sa stéréochimie que par son ordre, la réaction est du type* S_N2. Notons que les deux chlorolactones **4***a* et **4***b* sont stables dans les conditions de la réaction (tableau 3, expériences n° 5 et 11).

L'utilisation des ions iodures (LiI au lieu de LiBr) ralentit au contraire la réaction d'élimination qui reste tout de même plus rapide qu'en l'absence de sel (tableau 1, expériences n° 6 et 7, et tableau 2, expériences n° 7 et 13). La réaction de substitution principalement observée est une lente épimérisation du brome, sans formation de lactones iodées. On observe en outre l'apparition d'une faible quantité d'α-hydroxylactones (5–10%) (lactols stéréoisomères déjà décrits (13)).

En ce qui concerne les lactones chlorées **4**, elles sont moins réactives que les lactones bromées **3**. En présence de LiCl dans le DMF, il faut attendre plusieurs heures à 100°C, pour approcher d'une composition stationnaire **4***a* ⇄ **4***b*. En présence de LiBr, la formation des lactones bromées ne peut être espérée que dans des conditions où ces dernières perdent rapidement HBr (tableau 3, expériences n° 8, 9 et 10). Dans ces circonstances, on comprend qu'*il n'est possible de changer l'halogène d'une halolactone que pour un halogène plus léger*, l'halolactone à halogène plus lourd étant notablement plus réactive que le produit de départ.

Notons que ce résultat est particulier aux halolactones tertiaires puisque les bromolactones **1**, à brome secondaire, nous ont permis d'accéder par cette méthode aux iodo-lactones correspondantes.[3]

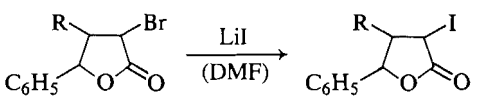

Influence de la polarité du solvant

Dans le DMF pur, lorsqu'on chauffe une solution de bromolactone **3***a* à 80°C ou de chlorolactone **4***a* à 100°C, on observe dans un premier temps une lente apparition du buténolide et de la lactone *b* isomère (tableau 2, expérience n° 10, et tableau 4, expérience n° 8). De la même façon qu'en présence de sel, les deux réactions apparaissent simultanément vers ces températures (tableaux 2 et 4). Toutefois, les vitesses de réactions sont très ralenties par rapport aux résultats observés dans les conditions de réactions bimoléculaires (présence d'ions Br^-, Cl^-, I^-). Nous avons donc entrepris l'étude de l'influence de la polarité du solvant sur le déclenchement de cette réaction de type solvolytique.

L'étude a été effectuée sur les lactones **3***a* et **4***a* dans des solvants purs ou en présence d'un nucléophile (0,4 mmol dans 10 mL de solvant, avec éventuellement 2 équivalents de sel, tableaux 2 et 4).

Dans les solvants peu polaires (toluène, éther, acétonitrile), à reflux, aucune réaction n'est observée, même en présence de sels.

Dans les solvants plus polaires (DMF, DMSO) les réactions d'élimination et de substitution ont lieu, avec ou sans réactifs nucléophiles, à des températures suffisamment élevées. À température ambiante aucune réaction n'est observée. Il existe enfin des températures intermédiaires pour lesquelles les réactions se produisent, mais seulement en présence de sels. C'est le cas par exemple des réactions dans le DMF à 80°C pour la chlorolactone ou à 60°C pour la bromolactone.

L'acétone se classe de ce point de vue parmi les solvants peu polaires pour la chlorolactone (pas de réaction, avec ou sans sel) et comme solvant plus polaires pour la bromolactone (tableau 2, expériences n° 4, 5 et 6), mais en raison de sa basse température d'ébullition, nous n'avons pu observer la réaction en l'absence de sel.

Avec la γ-collidine, solvant basique, le milieu reste exempt d'ions halogènures puisque le bromhydrate et le chlorhydrate de collidine sont insolubles. Dans ces conditions nous avons observé que la chlorolactone **4***a* donne lieu à une élimination lente sans épimérisation (formation de 10% de buténolide **5** en 3 h à 100°C) alors qu'avec la bromolactone **3***a*, l'épimérisation du brome est rapide par rapport à l'élimination (22% d'élimination en 3 h à 100°C, avec un rapport (**3***b*)/(**3***a*) final = 0,15).

Discussion

Il apparaît que les réactions effectuées dans le DMF correspondent à un mécanisme complexe mettant en jeu, suivant les conditions, des réactions de type solvolytique ou (et) des réactions bimoléculaires :

$$[1] \quad v = k_S(RX) + k_2(Y^-)(RX)$$

Pour rendre compte d'une substitution typiquement bimoléculaire sur un substrat tertiaire (15), nous envisageons l'hypothèse de la formation d'une paire d'ions sur laquelle s'effectue l'attaque du nucléophile (16). Dans la paire d'ions, présentant une liaison C—Br (ou C—Cl) activée, fortement polarisée, la stéréochimie de la molécule de départ reste inchangée (10).

En effet, dans les solvants peu polaires (toluène, éther, acétonitrile), aucune réaction n'est observée, même en présence d'un nucléophile. Dans de tels solvants, l'activation du substrat ne se produit pas ($k_1 = 0$, schéma 2). Ni le mécanisme bimoléculaire ni le mécanisme solvolytique ne peuvent être déclenchés.

Dans les solvants plus polaires comme le DMF ou le DMSO, la paire d'ions **3***c* se forme ($k_1 \neq 0$). Selon la température, elle peut réagir selon un mécanisme bimoléculaire (à condition qu'il y ait un sel présent) ou par voie solvolytique. Aux basses températures (vers 50 ou 60°C pour la bromolactone **3***a*) et en l'absence de sel, il n'y a pas de solvolyse, donc $k_S \simeq 0$ et aucune réaction ne se produit malgré l'activation du substrat en paire d'ions **3***c*. À la même température, mais en présence du sel Li^+Y^-, $[Y^-]$ est différent de zéro, et les réactions bimoléculaires apparaissent. Donc k_2 et k'_2 sont différents de zéro à une température où k_S est encore pratiquement nul. Les produits observés dans ces conditions (**3***a* $\xrightarrow{Cl^-}$ **4***b* par exemple), correspondent bien aux critères cinétiques et stéréochimiques d'une réaction bimoléculaire et il faut admettre que le mécanisme bimoléculaire se fait sur la paire d'ions **3***c* et non sur la molécule **3***a* de départ puisqu'il ne se produit pas dans le toluène ou l'acétonitrile.

Toujours dans les solvants polaires, et en l'absence de sel ($[Y^-] = 0$, la voie bimoléculaire est barrée), on peut déclencher les réactions de substitution et d'élimination par la voie solvolytique en augmentant la température (k_S devient alors différent de zéro).

Toutefois la formation du buténolide, à partir de **3***a* par

3. G. Dana et J. Gharbi-Benarous. Travaux non publiés.

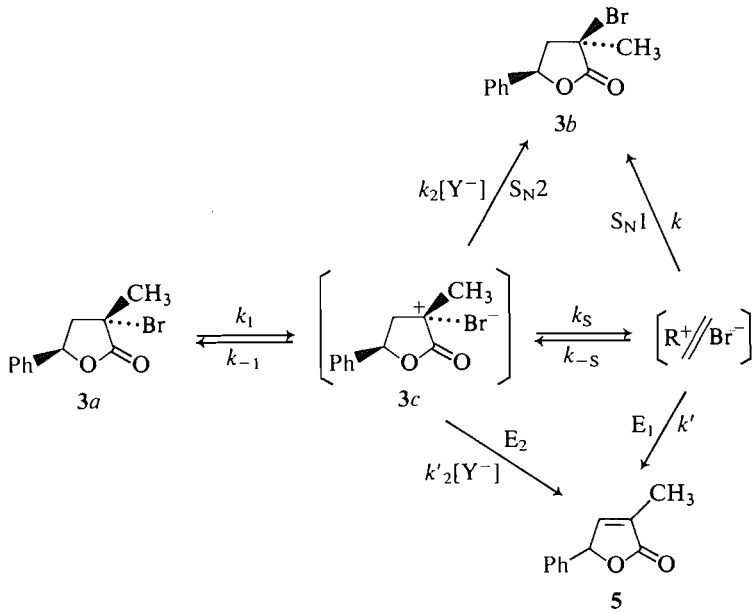

SCHÉMA 2

exemple (schéma 2), entraîne la libération d'une quantité équivalente d'ions bromures, et, très rapidement, les mécanismes bimoléculaires entrent en compétition avec la solvolyse et deviennent prépondérants, $k_2[Br^-] \gg k_S$: la paire d'ions **3***c* réagit beaucoup plus vite avec les réactifs nucléophiles qu'avec le solvant. Il suffit qu'il y ait très peu de base Y^- dans le milieu réactionnel pour que cette constante solvolytique soit masquée par les constantes k_2 et k'_2, plus grandes. Dans les expériences de solvolyse (en l'absence de sel), on observe, en effet, qu'après une période d'induction (au cours de laquelle les produits apparaîssent lentement) l'élimination s'accélère de façon considérable, et la réaction prend une allure autocatalytique (tableau 2, expériences 10, 11 et 12) : il se forme plus de buténolide en 4 h entre la 8^e et la 12^e heure (+23%, expériences 11 et 12) qu'en 5 h, entre la 3^e et 8^e heure (+9%, expériences 10 et 11) dans le DMF à 80°C, malgré la diminution de concentration du substrat. Cette solvolyse ne semble pourtant pas produire de carbocation libre puisque nous n'avons jamais mis en évidence de produits de substitution électrophile sur l'anisole ou le toluène, en ajoutant ces réactifs (avec une concentration de 10%) dans le DMF, dans les conditions de la solvolyse. Dans le schéma 2, nous avons donc représenté l'intermédiaire réactionnel de la solvolyse sous forme d'une paire d'ions intersolvatée $R^+//X^-$ (10).

On voit que malgré la simplicité de l'idée de départ (éq. [1]) une étude cinétique précise du schéma 2 n'est pas aisée d'autant plus que l'isomère **3***b* formé à partir de **3***a* va donner lieu aux mêmes réactions que **3***a*, mais avec des constantes de vitesses propres. Ceci explique le point de vue semi-quantitatif adopté dans cette étude dans laquelle nous avons mis en évidence la participation du solvant dans le processus bimoléculaire, au cours d'une étape préliminaire d'activation réversible des halolactones. Cependant le mécanisme du transfert d'hydrogène dans l'état de transition reste à discuter. Compte tenu du faible caractère basique des réactifs nucléophiles Y^- (Cl^- ou Br^-), on peut a priori envisager une approche de type E_2C sur la paire d'ions préformée **3***c* (schéma 3).

Une telle structure de l'état de transition permet de rendre compte de la grande différence de réactivité entre les ions Cl^-, Br^- et I^- pour des raisons évidentes de difficulté d'approche dûe à la présence du méthyle.

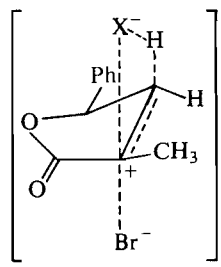

3*c*

SCHÉMA 3

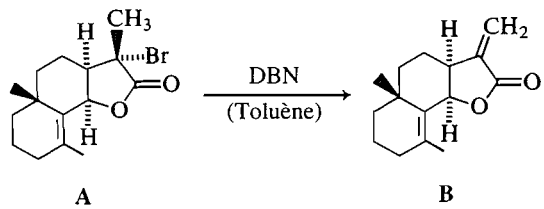

A **B**

SCHÉMA 4

De la même façon, les résultats obtenus suggèrent que les règles de Saitzeff contrôlent l'orientation de l'élimination de HBr. En effet, conduisant de préférence aux oléfines les plus substituées (17), un état de transition E_2C privilégie la formation du buténolide **5** par rapport à la méthylène lactone **6**, dont la double liaison est moins substituée (18).

Une orientation exocyclique de l'élimination sur un substrat analogue a été observé (19) pour la méthyl bromolactone **A**. En utilisant le DBN comme réactif, G. Ourisson et coll. ont obtenu la méthylène-lactone **B** correspondante (schéma 4).

Or, une étude sur la réaction d'élimination avec LiBr dans le DMF ou avec le DBN dans le DMF pour les haloesters de type $ArCH_2—CX(R)—COOEt$ (20) a prouvé que l'état de transition avec le DBN est bien du type E_2C sans variation notable de géométrie par rapport à LiBr. En fait dans le cas de la molécule **A**, on ne pouvait escompter d'élimination antipériplanaire de HBr que du côté du méthyle, conduisant obligatoirement à la lactone insaturée exocyclique **B**. La réaction conduite de façon similaire sur notre substrat **3***a*, a donné en 30 min, à 100°C, 40% de buténolide **5** sans apparition de méthylène-lactone **6**.

Can. J. Chem. Downloaded from www.nrcresearchpress.com by 213.166.140.6 on 09/07/12
For personal use only.

TABLEAU 5. Spectres rmn (^{1}H) des halolactones **3** et **4** effectués à 80 MHz (TMS interne, δ en ppm, J en Hz). Étude des effets de solvants entre $CDCl_3$ et C_6D_6 (cf. fig. 1)[a]

Composé	Solvant	δ H(Me)	δ H3β	δ H3α	δ H4α	δ H(Ph)	J (H3αH3β)	J (H3βH4)	J (H3αH4)
3*a*	C_6D_6	1,42	1,33	2,07	4,94(dd)	6,8	−14,6	10,1	4,9
	$CDCl_3$	1,90	2,17	2,90	5,47(dd)	7,21	−14,5	10,1	4,7
4*a*	C_6D_6	1,15	1,43	2,04	5,01(dd)	6,76	−14	10,4	4,9
	$CDCl_3$	1,7	2,16	2,81	5,47(dd)	7,12	−14	10,9	5,1
3*b*	C_6D_6	1,27	2,11	1,83	4,53(t)	6,75	−14,1	6,0	7,1
	$CDCl_3$	1,91	2,85	2,94	5,40(t)	7,21	−14,1	7,2	7,2
4*b*	C_6D_6	1,28	2,14	1,94	4,6(t)	6,85	−14	7,0	7,0
	$CDCl_3$	1,8	2,67	2,87	5,32(t)	7,21	−13,9	8,5	6,7

[a]Le méthyle en 2 donne un singulet fin. Les trois protons H3 et H4 forment un système ABX. Les déplacements chimiques et les couplages affichés sont les valeurs obtenues par ajustement des paramètres (programme PANIC).

NOTA : La discussion des valeurs de ce tableau et l'étude conformationnelle des lactones sera développée dans un prochain mémoire.

Conclusion

En conclusion, on peut dire, pour ce substrat tertiaire, que l'activation de la liaison C—X en α du carbonyle en paire d'ions peut avoir lieu sous l'effet de solvants suffisamment polaires. Elle rend alors possible (avec des nucléophiles faiblement basiques) des mécanismes bimoléculaires S_N2, normalement peu probables sur des substrats tertiaires, et E_2. En l'absence de nucléophile, le mécanisme solvolytique peut intervenir pour le déclenchement de la réaction qui se poursuit alors selon le processus bimoléculaire de façon autocatalytique. On peut noter qu'avec les lactones bromées, cette activation est favorisée par un meilleur groupe partant (Br^- par rapport à Cl^-) et on observe une grande différence de réactivité entre les deux lactones tertiaires, chlorée et bromée (**3***a* et **4***a*).

Signalons enfin, que les deux substrats **3** et **1** présentent le même intérêt préparatif pour les buténolides **5** ou **2**, la réaction d'élimination conduisant dans les deux cas avec des rendements presque quantitatifs à un buténolide pur à partir d'un mélange de lactones bromées stéréoisomères.

Partie expérimentale

Les études spectroscopiques de ce travail et les microanalyses ont été effectuées au Centre de spectrochimie de Paris-Centre.

Les spectres rmn ^{1}H sont enregistrés sur spectrographe Bruker WP-80, en solution dans $CDCl_3$ ou dans C_6D_6; les déplacements chimiques sont exprimés en δ par rapport au tétraméthylsilane utilisé comme référence interne. Les constantes de couplage sont exprimées en hertz.

Les spectres de masse ont été réalisés avec le spectromètre Kratos MS50 et les spectres ir en film liquide à l'état pur ou en pastille KBr, sur un spectrographe Perkin–Elmer modèle 357. Les points de fusion ont été déterminés sur bloc Kofler.

Les différents produits sont purifiés ou séparés par chromatographie en couche mince (ccm) sur silice (gel de silice, Merck 60 PF 254). Le système de solvant utilisé comme éluant est le mélange éther de pétrole – éther (EP:E), et la visualisation est effectuée par uv.

Préparation des bromolactones 3

Elles sont obtenues en trois étapes.

1. On prépare le *méthyl-4 phényl-2 dihydro-2,3 furanne* selon un procédé déjà décrit, par réduction duplicative de l'aldéhyde benzoïque et de l'α-méthyl acroléine, en présence de magnésium et d'acide acétique (2*c*). La deshydratation de l'hydroxytétrahydrofuranne formé par distillation en présence d'un cristal d'iode conduit au DHF correspondant. L'analyse spectroscopique, en particulier la rmn, est en accord avec la description de ce produit déjà publié (2*b*).

2. *Les bromhydrines* sont obtenues quantitativement à partir du dihydrofuranne selon une méthode précédemment utilisée (1, 21). On traite 500 mg de DHF avec 1,1 g de NBS en solution dans le DMSO (10 mL) humide, à froid (bain de glace). On ajoute une solution d'eau bicarbonatée et on extrait à l'éther. Par évaporation du solvant on obtient 810 mg de bromhydrines cristallisées. Les deux bromhydrines stéréoisomères **8***a* et **8***b* sont séparées par ccm (EP:E = 80:20, 2 élutions), R_f (**8***a*) = 0,36 (88%) et R_f (**8***b*) = 0,23 (12%), et cristallisées dans un mélange EP:E = 90:10.

Hydroxy-2β bromo-3α méthyl-3β phényl-5β tétrahydrofuranne (**8***a*), F = 98°C; ir (KBr) : 3300 cm^{-1}; rmn ^{1}H (C_6D_6) : 5,5 (H2α, s), 1,54 (H(Me), s), 2,17 (H4α), 1,82 (H4β), 5,4 (H5α), 7 (H(Ph)), J (H4αH4β) = −14; J (H5H4α) = 5,8; J (H5H4β) = 10,2. *Anal.* calc. pour $C_{11}H_{13}O_2Br$: C 51,36, H 5,06; tr. : C 51,17, H 5,07%.

Hydroxy-2 bromo-3β méthyl-3α phényl-5β tetrahydrofuranne (**8***b*), F = 81°C; ir (KBr) : 3320 cm^{-1}; rmn ^{1}H (C_6D_6) : la bande de R_f = 0,23 correspond à deux isomères en solution (anomérisation au niveau du carbone C2), 5,46 et 4,52 (H2, s), 1,58 et 1,34 (H(Me), s), 2,12 (H4, m), 5,05 et 4,52 (H5α, t), 7,1 (H(Ph)), J (H5H4α) + J (H5H4β) = 14,5 et 16. Le même dédoublement du spectre apparaît dans le chloroforme. *Anal.* calc. pour $C_{11}H_{13}O_2Br$: C 51,36, H 5,06; tr. : C 51,65, H 5,12%.

3. L'oxydation à l'aide du réactif de Jones du mélange brut des bromhydrines (1) (800 mg dans 20 mL d'acétone), refroidi à 0°C, conduit au mélange des deux lactones bromées **3***a* (88%) et **3***b* (12%) cristallisées (782 mg) (dosées par rmn) : rendement 97% par rapport au dihydrofuranne de départ. Les deux bromolactones **3***a* et **3***b* sont séparables par ccm (EP:E = 80:20; R_f (**3***a*) = 0,49, R_f (**3***b*) = 0,26). Ces deux isomères cristallisent dans un mélange EP:E = 90:10.

Bromo-2α méthyl-2β phényl-4β butyrolactone (**3***a*), F = 63°C; ir (KBr) : 1780 cm^{-1}; rmn ^{1}H (C_6D_6) et ($CDCl_3$) : tableau 5. Cet isomère est facilement dosable en rmn, par son proton H4α à 4,94 ppm dans C_6D_6; mass m/e : 254 et 256 ($M^{\ddagger}$). Ce doublet permet au cours de cette étude de discerner sans ambiguité cet isomère **3***a* de son homologue chloré **4***a*. *Anal.* calc. pour $C_{11}H_{11}O_2Br$: C 51,76, H 4,32; tr. : C 51,72, H 4,52%.

Bromo-2β méthyl-2α phényl-4β butyrolactone (**3***b*), F = 61°C; ir (KBr) : 1780 cm^{-1}; rmn ^{1}H (C_6D_6) et ($CDCl_3$) : tableau 5. Cet isomère est dosable (et aisément discernable de **3***a*) en rmn par la position de son proton H4α à 4,53 ppm dans C_6D_6. La différenciation entre **3***b* et le dérivé chloré correspondant **4***b* s'effectue aisément par effet de solvant.

Notons en effet (tableau 5) que la partie AB du système ABX à même aspect pour **3***b* et **4***b* dans C_6D_6, mais se présente de façon très différente dans $CDCl_3$: $\nu_B - \nu_A$ est très petit pour **3***b* (2,8 Hz à 80 MHz) et grand pour **4***b* (16 Hz). En fait, nous avons indiqué un croisement des déplacements chimiques de H3α et H3β entre ces deux solvants. Ce croisement est observé pour un mélange $CDCl_3$–C_6D_6 = 70:30 pour **3***b* et 50:50 pour **4***b* (fig. 1). Masse m/e : 254 et 256 ($M^{\ddagger}$). Ce doublet confirme la présence du brome dans **3***b* par rapport à son homologue chloré **4***b*. *Anal.* calc. pour $C_{11}H_{11}O_2Br$: C 51,76, H 4,32; tr. : C 51,85, H 4,49%.

Can. J. Chem. Downloaded from www.nrcresearchpress.com by 213.166.140.6 on 09/07/12
For personal use only.

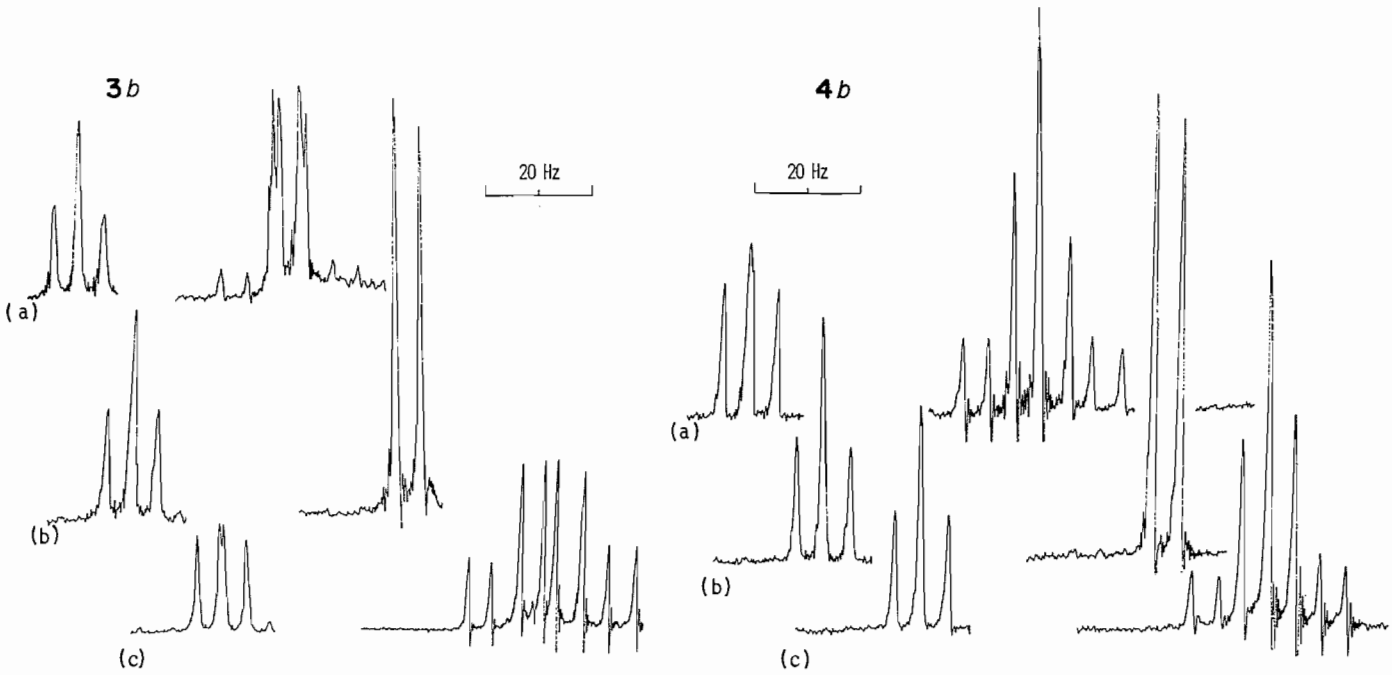

FIG. 1. Croisement des déplacements chimiques des protons H3α et H3β des isomères **3***b* et **4***b* selon le solvant (80 MHz). Aspect du système ABX de **3***b* (a) dans $CDCl_3$: ν_A = 231,10; ν_B = 228,28; ν_X = 432,07 Hz; (b) dans le mélange $CDCl_3$–C_6D_6 = 70:30 : $\nu_{A,B}$ = 211,34; ν_X = 410,12 Hz; (c) dans C_6D_6 : ν_A = 146,69; ν_B = 169,05; ν_X = 362,48 Hz. Aspect du système ABX de **4***b* (a) dans $CDCl_3$: ν_A = 229,65; ν_B = 213,75; ν_X = 426 Hz; (b) dans le mélange $CDCl_3$–C_6D_6 = 50:50 : $\nu_{A,B}$ = 187,75; ν_X = 392 Hz; (c) dans C_6D_6 : ν_A = 156,17; ν_B = 171,83; ν_X = 368 Hz. *N.B.* Le mélange (b) correspond au croisement (système AA′X).

Préparation des chlorolactones **4**

La chloration du phényl-2 méthyl-4 dihydro-2,3 furanne a été effectuée à froid (bain de glace) par le chlore gazeux (22), en atmosphère déchargée d'oxygène par passage préalable d'un courant d'azote. On a utilisé une solution de 1 g du composé dihydrofurannique dilué à 10% dans CCl_4. Le dérivé dichloré formé est directement hydrolysé par simple agitation dans l'eau bicarbonatée pendant 1 h à température ambiante et conduit à l'hémiacétal chloré que l'on extrait à l'éther. L'oxydation du mélange brut (1,26 g) par le réactif de Jones (1) conduit à la chlorolactone **4***a* sous forme d'une huile jaune clair. Une purification par ccm (EP:E = 70:30) nous a permis d'obtenir 706 mg de produit pur : R_f (**4***a*) = 0,46; rendement 54%.

Chloro-2α méthyl-2β phényl-4β butyrolactone (**4***a*), ir : 1775 cm^{-1}; rmn ^1H (C_6D_6) et ($CDCl_3$) : tableau 5. Cet isomère a été dosé au cours de cette étude grâce à son proton H4α (δ = 5,01 ppm, C_6D_6); masse *m/e* : 210 et 212 ($M^{\ddagger}$) (doublet caractéristique d'un produit monochloré). *Anal.* calc. pour $C_{11}H_{11}O_2Cl$: C 62,71, H 5,22; tr. : C 62,83, H 5,32%.

Deshydrohalogénation des halolactones **3** *et* **4**

On opère en milieu anhydre, sous azote, avec 2 équivalents de LiBr (ou LiCl) pour 1 équivalent de bromolactone **3** (ou de chlorolactone **4**). À une solution de 108,5 mg (0,4 mmol) de la bromolactone isomère pur **3***a* (ou 87,5 mg de la chlorolactone **4***a*) dans 8 mL de DMF, on ajoute, sous agitation magnétique, une solution de 72,5 mg de LiBr (0,8 mmol) ou (35,5 mg LiCl) dans 2 mL de DMF. Le mélange est porté à la température de 100 ± 1°C (bain thermostaté) et agité pendant 1 h (3 h pour **4***a*). On laisse alors revenir à température ambiante puis on ajoute 5 mL d'eau avant d'extraire à l'éther. La phase organique est lavée à l'eau puis séchée sur sulfate de sodium. L'éther est alors évaporé sous vide au rotavapor (température du bain : 40°C). Le produit brut est alors analysé par rmn à 80 MHz, puis les différents constituants sont séparés par ccm (EP:E = 60:40), et purifiés. À partir de **3***a*, on obtient 58 mg de buténolide **5**, liquide jaune, R_f (**5**) = 0,35 (rendement 80%), en même temps qu'on récupère 21,5 mg de cristaux de la lactone résiduelle (**3***a*). Signalons que la réaction **3***a* → **5** est totale en 3 h dans les mêmes conditions. Le buténolide **5** est alors isolé pur (68,5 mg) avec un rendement de 94%. À partir de **4***a*, le produit brut obtenu est constitué de trois produits (séparation par ccm, EP:E = 70:30, 2 élutions) : 40 mg de buténolide **5** (rendement 54%), 10 mg de chlorolactone **4***b* (R_f (**4***b*) = 0,23) et 30 mg de l'isomère **4***a* résiduel.

L'étude du comportement de chaque isomère pur **3***a*, **3***b* et **4***a*, **4***b* a été réalisée dans les mêmes conditions (2 équivalents de sels : 35,5 mg de LiCl ou 72,5 mg de LiBr ou 111,5 mg LiI pour 0,4 mmol de lactone), mais à des températures et pour des durées différentes (tableaux 1 et 3).

La proportion des différents constituants des mélanges obtenus est évaluée par un dosage en rmn du proton H4α pour les halolactones isomères : **3***a* ou **4***a*, **3***b* ou **4***b* et du proton H3 pour le buténolide. Leur identification est ensuite confirmée par analyse, par spectrométrie de masse et par effet de solvant en rmn; de même, leur proportion sera confirmée après purification par ccm.

Chloro-2β méthyl-2α phényl-4β butyrolactone **4**b

Cet isomère ne peut être obtenu que par réaction d'isomérisation de la chlorolactone **4***a*; ir (liq.) : 1775 cm^{-1}; rmn ^1H (C_6D_6) et ($CDCl_3$) : tableau 5; dosé dans le mélange réactionnel par la position de H4α (δ = 4,6 ppm, C_6D_6); masse *m/e*: 210 et 212 ($M^{\ddagger}$). *Anal.* calc. pour $C_{11}H_{11}O_2Cl$: C 62,71, H 5,22; tr. : C 62,85, H 5,31%.

Méthyl-2 phényl-4 $\Delta^{2(3)}$ *butyrolactone* (**5**), ir (liq.) : 1775 et 1660 cm^{-1}; rmn ^1H ($CDCl_3$) : 1,90 (H(Me), t), 5,77 (H4, quintuplet), 7,60 (H3, quintuplet), 7,25 (H(Ph)), *J* (H3H(Me)) ≃ *J* (H4H(Me)) ≃ *J* (H3H4) = 1,9 Hz.

Ce produit a déjà été obtenu par d'autres procédés (13, 14). Masse *m/e* : 174 ($M^{\ddagger}$). *Anal.* calc. pour $C_{11}H_{10}O_2$: C 75,86, H 5,74; tr. : C 75,85, H 5,65%.

Elimination par la collidine

On chauffe 100 mg de bromolactone **3***a* (ou chlorolactone **4***a*) dans 10 mL de collidine pendant 3 h (ou 6 h) à 100°C. Le bromhydrate (ou chlorhydrate) de collidine formé est filtré, lavé avec de l'éther anhydre. La collidine restant est diluée dans l'éther et la phase éthérée est très soigneusement lavée par HCl 10% jusqu'à la neutralité (le buténolide est détruit en milieu acide), puis par un peu d'eau. La solution éthérée est séchée sur Na_2SO_4 et évaporée. Le produit brut, dosé par rmn (proton H4α pour les halolactones **3** et **4** et proton H3 pour

Can. J. Chem. Downloaded from www.nrcresearchpress.com by 213.166.140.6 on 09/07/12
For personal use only.

le buténolide **5**) est constitué principalement du substrat de départ et du buténolide, à partir de la chlorolactone **4***a* (10% **5** + 90% **4***a* en 3 h et 24% **5** + 76% **4***a* en 6 h); mais à partir de **3***a*, on isole de plus son isomère **3***b* (22% **5** + 10% **3***b* + 68% **3***a* en 3 h et 44% **5** + 8% **3***b* + 48% **3***a* en 6 h).

Elimination par le DBN

Une solution de 108,5 mg bromolactone **3***a* (0,4 mmol) dans 4 mL de toluène anhydre est traitée avec 300 mL de DBN (diazo-1,5 bicyclononène) et chauffée à 100°C pendant 30 min sous azote. Après addition d'éther la phase organique est lavée avec une solution froide de HCl à 10% saturée en sel. Toutes les phases aqueuses réunies sont ensuite extraites à l'éther. Les phases organiques séchées sur sulfate de sodium, évaporées sous vide, fournissent après séparation sur silice, 30 mg du buténolide **5** (rendement : 40%).

1. J. GHARBI-BENAROUS, M. S. MORALES-RIOS et G. DANA. Can. J. Chem. **63**, 2384 (1985).
2. (*a*) J. WIEMANN. Bull. Soc. Chim. Fr. 2545 (1964); (*b*) P. SCRIBE. C.R. Acad. Sci. Série C, **261**, 160 (1965); (*c*) G. DANA et A. ZYSMAN. Bull. Soc. Chim. Fr. 1951 (1970).
3. (*a*) J. C. PALADINI et J. CHUCHE. Bull. Soc. Chim. Fr. 197 (1974); (*b*) S. HOLLAND et R. EPSZTEIN. Synthesis, 706 (1977).
4. G. DANA, B. FIGADERE et E. TOUBOUL. Tetrahedron Lett. **26**, 5683 (1985).
5. (*a*) D. CAINE et A. S. FROBESE. Tetrahedron Lett. **19**, 5176 (1978); (*b*) E. J. COREY et G. SCHMIDT. Tetrahedron Lett. **21**, 731 (1980).
6. (*a*) Y. S. RAO. Chem. Rev. **76**, 625 (1976); (*b*) E. DEMOLE et D. BERTHET. Helv. Chem. Acta, **55**, 1866 (1972).
7. (*a*) W. T. FORD. Acc. Chem. Res. **6**, 410 (1973); (*b*) D. MCLENNAN. Tetrahedron, **31**, 2999 (1975).
8. (*a*) G. BIALE, D. COOK, D. J. LLOYD, A. J. PARKER, I. D. R. STEVENS, J. TAKAHASHI et S. WINSTEIN. J. Am. Chem. Soc. **93**, 4735 (1971); (*b*) P. BELTRAME, G. BIALE, D. J. LLOYD, A. J. PARKER, M. RUANE et S. WINSTEIN. J. Am. Chem. Soc. **94**, 2240 (1972).
9. F. G. BORDWELL. Acc. Chem. Res. **5**, 374 (1972).
10. R. A. SNEEN. Acc. Chem. Res. **6**, 46 (1973).
11. (*a*) N. H. CROMWELL, R. P. AYER et P. W. FOSTER. J. Am. Chem. Soc. **82**, 130 (1960); N. H. CROMWELL et P. H. HESS. J. Am. Chem. Soc. **83**, 1237 (1961); (*b*) M. CHARPENTIER-MORIZE. Bull. Soc. Chim. Fr. 344 (1974); (*c*) K. TAKEUCHI, T. KITAGAWA et K. OKAMOTO. J. Chem. Soc. Chem. Commun. 7 (1983); (*d*) A. C. HOPKINSON, L. H. DAO, P. DUPERROUZEL, M. MALEKI et E. LEE-RUFF. J. Chem. Soc. Chem. Commun. 727 (1983); (*e*) L. H. DAO, M. MALEKI, A. C. HOPKINSON et E. LEE-RUFF. J. Am. Chem. Soc. **108**, 5237 (1986).
12. (*a*) G. P. NILLES et R. D. SCHUETZ. Tetrahedron Lett. 4313 (1969); (*b*) A. C. HOPKINSON, E. LEE-RUFF et M. MALEKI. Synthesis, 366 (1986).
13. G. LECLERC, C. G. WERMUTH et J. SCHREIBER. Bull. Soc. Chim. Fr. 1302 (1967).
14. S. A. M. T. HUSSAIN, W. D. OLLIS, C. SMITH et J. F. STODDART. J. Chem. Soc. Perkin Trans. 1, 1480 (1975).
15. C. A. GROB, K. SECKINGER, S. W. TAM et R. TRABER. Tetrahedron Lett. 3051 (1973).
16. F. G. BORDWELL et T. G. MECCA. J. Am. Chem. Soc. **94**, 2119 (1972).
17. G. BIALE, A. J. PARKER, I. D. R. STEVENS, J. TAKAHASHI et S. WINSTEIN. J. Am. Chem. Soc. **94**, 2235 (1972).
18. (*a*) J. F. BUNNETT. Angew. Chem. Int. Ed. Engl. **1**, 225 (1962); J. F. BUNNETT. Surv. Progr. Chem. **5**, 53 (1969); (*b*) J. F. BUNNETT et L. D. ECK. J. Am. Chem. Soc. **95**, 1897 (1973); **95**, 1900 (1973).
19. A. E. GREEN, J. C. MULLER et G. OURISSON. J. Org. Chem. **39**, 186 (1974).
20. H. KWART, A. GAFFNEY et K. A. WILK. J. Org. Chem. **48**, 4509 (1983).
21. (*a*) D. R. DALTON, V. P. DUTTA et D. C. JONES. J. Am. Chem. Soc. **90**, 5498 (1968); (*b*) D. R. DALTON et V. P. DUTTA. J. Chem. Soc. (B), 85 (1971).
22. G. DANA et C. ROOS. Bull. Soc. Chem. Fr. 371 (1973).

Can. J. Chem. Downloaded from www.nrcresearchpress.com by 213.166.140.6 on 09/07/12
For personal use only.

Electron transfer reactions. Reaction of nitrones with potassium[1]

KONDA ASHOK AND PALLIKKAPARAMBIL M. SCARIA
Department of Chemistry, Indian Institute of Technology, Kanpur 208016, India

PRASHANT V. KAMAT[2]
Radiation Laboratory, University of Notre Dame, Notre Dame, IN 46556, U.S.A.

AND

MANAPURATHU V. GEORGE[2]
Department of Chemistry, Indian Institute of Technology, Kanpur 208016, India, and Radiation Laboratory and Department of Chemistry, University of Notre Dame, Notre Dame, IN 46556, U.S.A.

Received August 9, 1985[3]

Can. J. Chem. Downloaded from www.nrcresearchpress.com by 213.166.140.6 on 09/07/12
For personal use only.

KONDA ASHOK, PALLIKKAPARAMBIL M. SCARIA, PRASHANT V. KAMAT, and MANAPURATHU V. GEORGE. Can. J. Chem. **65**, 2039 (1987).

Treatment of nitrones (**1***a–d*, **26***a,b*, **34**, **49**) with potassium in tetrahydrofuran (THF) gives rise to radical anion (**2***a–d*, **27***a,b*, **35**, **50**) and dianion intermediates (**3***a–d*, **28***a,b*, **36**) through electron transfer reactions. These intermediates undergo further transformations to give a variety of products. Thus, the aldehydonitrones (**1***a–d*) give the corresponding aldehydes (**10***a–c*), carboxylic acids (**25***a–c*), and azobenzenes (**19***a,d*), whereas the ketonitrones (**26***a,b*) give deoxygenation products (**31***a,b*). The nitrone **34** gave a mixture of products consisting of benzoic acid (**25***a*), dibenzyl (**48**), the dimeric product **38**, and tetraphenylpyrazine (**46**), whereas **49** did not give any isolable product. Cyclic voltammetric studies have been employed to measure the reduction potentials for both one-electron and two-electron transfer processes, leading to the radical anions and dianions respectively. These intermediates have been characterized through their electronic spectra and they were quenched by oxygen. Pulse radiolysis of the nitrones **1***a–d*, **26***a,b*, **34**, and **49** also gave the corresponding radical anions **2***a–d*, **27***a,b*, **35**, and **50**, characterized by their spectra.

KONDA ASHOK, PALLIKKAPARAMBIL M. SCARIA, PRASHANT V. KAMAT et MANAPURATHU V. GEORGE. Can. J. Chem. **65**, 2039 (1987).

La réaction des nitrones **1***a–d*, **26***a,b*, **34** et **49** avec le potassium dans le tétrahydrofuranne (THF) conduit, grâce à des réactions de transfert d'électrons, aux radicaux anions **2***a–d*, **27***a,b*, **35** et **50** et aux intermédiaires dianioniques **3***a–d*, **28***a,b* et **36**. Ces intermédiaires subissent d'autres transformations qui donnent lieu à la formation de plusieurs autres produits. Ainsi, les aldéhydonitrones **1***a,d* conduisent aux aldéhydes **10***a–c*, aux acides carboxyliques **25***a–c* et aux azobenzènes **19***a,d* correspondants; par ailleurs, les cétonitrones **26***a,b* conduisent aux produits de déoxygénation **31***a,b*. La nitrone **34** conduit à un mélange de produits qui est formé d'acide benzoïque (**25***a*), de dibenzyle (**48**), du produit dimère **38** et de tétraphénylpyrazine (**46**); par ailleurs, avec le composé **49**, on ne peut isoler aucune produit. On a utilisé des études de voltammétrie cyclique pour mesurer les potentiels de réduction des processus de transfert, tant à un qu'à deux électrons, qui conduisent respectivement à la formation des radicaux anions et dianions. On a caractérisé ces intermédiares grâce à leurs spectres électroniques et on les a piégés avec de l'oxygène. La radiolyse pulsée des nitrones **1***a–d*, **26***a,b*, **34** et **49** conduit aussi aux radicaux anions correspondants **2***a–d*, **27***a,b*, **35** et **50** que l'on a caractérisé par leurs spectres.

[Traduit par la revue]

Introduction

Alkali metals are known to add to unsaturated organic substrates, giving rise to radical anion and dianion intermediates through electron transfer reactions (for some pertinent reviews, see ref. 1). These intermediates, in turn, can undergo a variety of reactions that include disproportionation, fragmentation, dimerization, oxidation, and rearrangements. Also, these intermediates are very susceptible to air oxidation, which results in a variety of oxidative products.

Of the different organic substrates, nitrones have been of particular interest in view of the deoxygenation reactions, which are reported to occur in presence of metals and other reagents (2–5). Only very few examples of the reaction of alkali metals with nitrones have been reported so far (6–8). The reaction of α,*N*-diphenylnitrone (**1***a*) with sodium in ethanol, for example, has been reported to give *N*-benzylamine, the reduction product. The object of the present investigation has been to examine the potassium-induced transformations of a few representative nitrones, with a view to studying the nature of products formed in these reactions and also to understanding the mechanism of these transformations.

Results and discussion

In the present studies, we have examined the reactions of α,*N*-diphenylnitrone (**1***a*), α,*o*-hydroxyphenyl-*N*-phenylnitrone (**1***b*), *N*-phenyl-α-*p*-tolylnitrone (**1***c*), α-phenyl-*N*-*p*-tolylnitrone (**1***d*), triphenylnitrone (**26***a*), α-diphenylene-*N*-phenylnitrone (**26***b*), *N*-benzyl-α-phenylnitrone (**34**), and 1,1,3-triphenylisoindole-*N*-oxide (**49**) with potassium in THF.

The reaction of **1***a* with potassium in THF, for example, gave a mixture of *trans*-stilbene (**13***a*, 8%), *trans*-azobenzene (**19***a*, 82%), benzaldehyde (**10***a*, 42%), and benzoic acid (**25***a*, 47%). The reaction of **1***b* under analogous conditions gave a mixture of **19***a* (58%), salicylaldehyde (**10***b*, 25%), and salicyclic acid (**25***b*, 30%), along with a 20% recovery of the starting material (**1***b*). When the reaction of **1***b*, however, was carried out in presence of excess of potassium (four equivalents), better yields of **19***a* (69%), **10***b* (37%), and **25***b* (45%) were obtained. Similarly, the reaction of **1***c* with potassium in THF gave a

[1]Document No. NDRL-2656 from Notre Dame Radiation Laboratory.
[2]Authors to whom correspondence may be addressed.
[3]Revision received February 23, 1987.

Can. J. Chem. Downloaded from www.nrcresearchpress.com by 213.166.140.6 on 09/07/12
For personal use only.

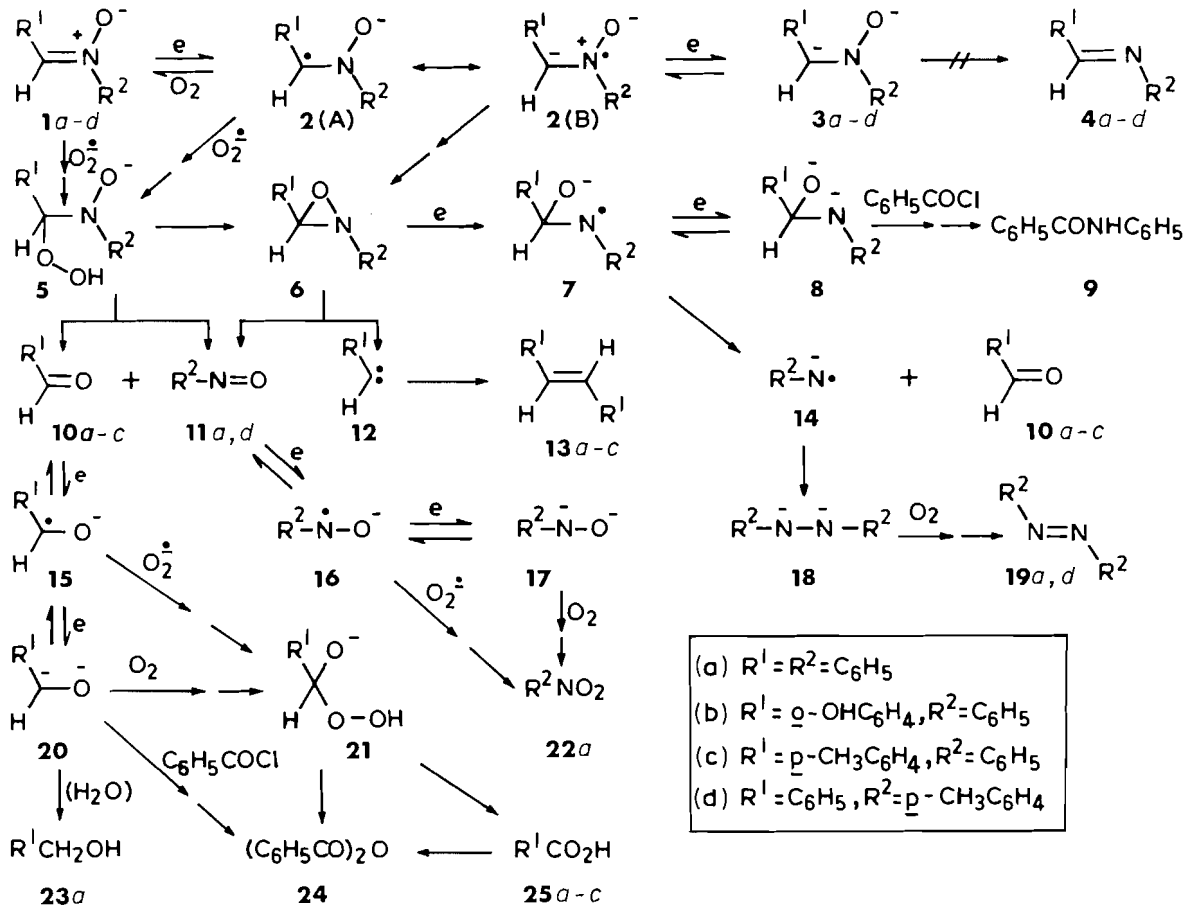

SCHEME 1

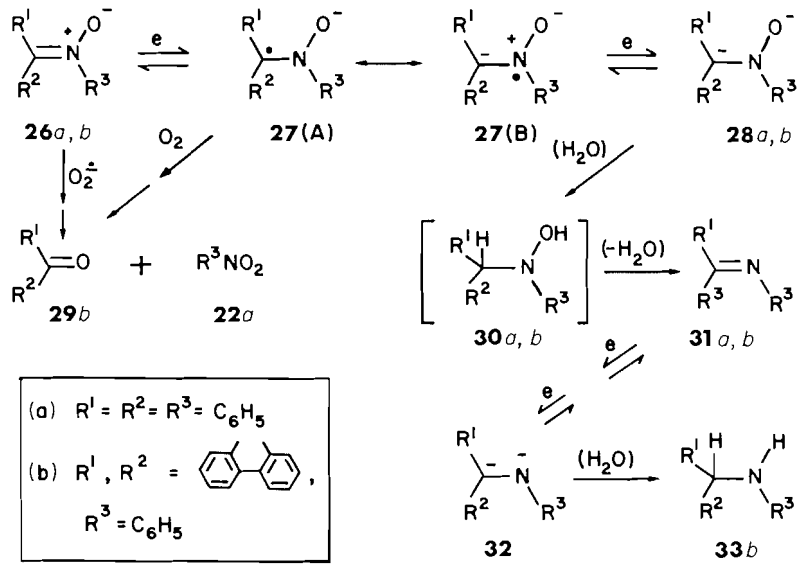

SCHEME 2

mixture of *trans*-1,2-di-*p*-tolylethylene (**13***c*, 6%), **19***a* (80%), *p*-tolualdehyde (**10***c*, 40%), and *p*-toluic acid (**25***c*, 44%), whereas **1***d* under similar conditions gave a mixture of **13***a* (4%), *trans*-*p*-azotoluene (**19***d*, 88%), **10***a* (40%), and **25***a* (49%) (Scheme 1). In contrast to the reactions of **1***a–d*, the reaction of triphenylnitrone (**26***a*) with potassium in THF gave benzhydrylidene aniline (**31***a*, 81%) (Scheme 2). Similarly, the reaction of **26***b* under analogous conditions gave an 81% yield of 9-fluorenylidene aniline (**31***b*). When the reaction of **26***b*, however, was carried out in presence of excess of potassium (four equivalents), a mixture of **31***b* (71%) and 9-anilinofluorene (**33***b*, 8%) was obtained. On the other hand, the reaction of *N*-benzyl-α-phenylnitrone (**34**) with potassium in THF gave a mixture of benzoic acid (**25***a*, 18%), *N*-(2-

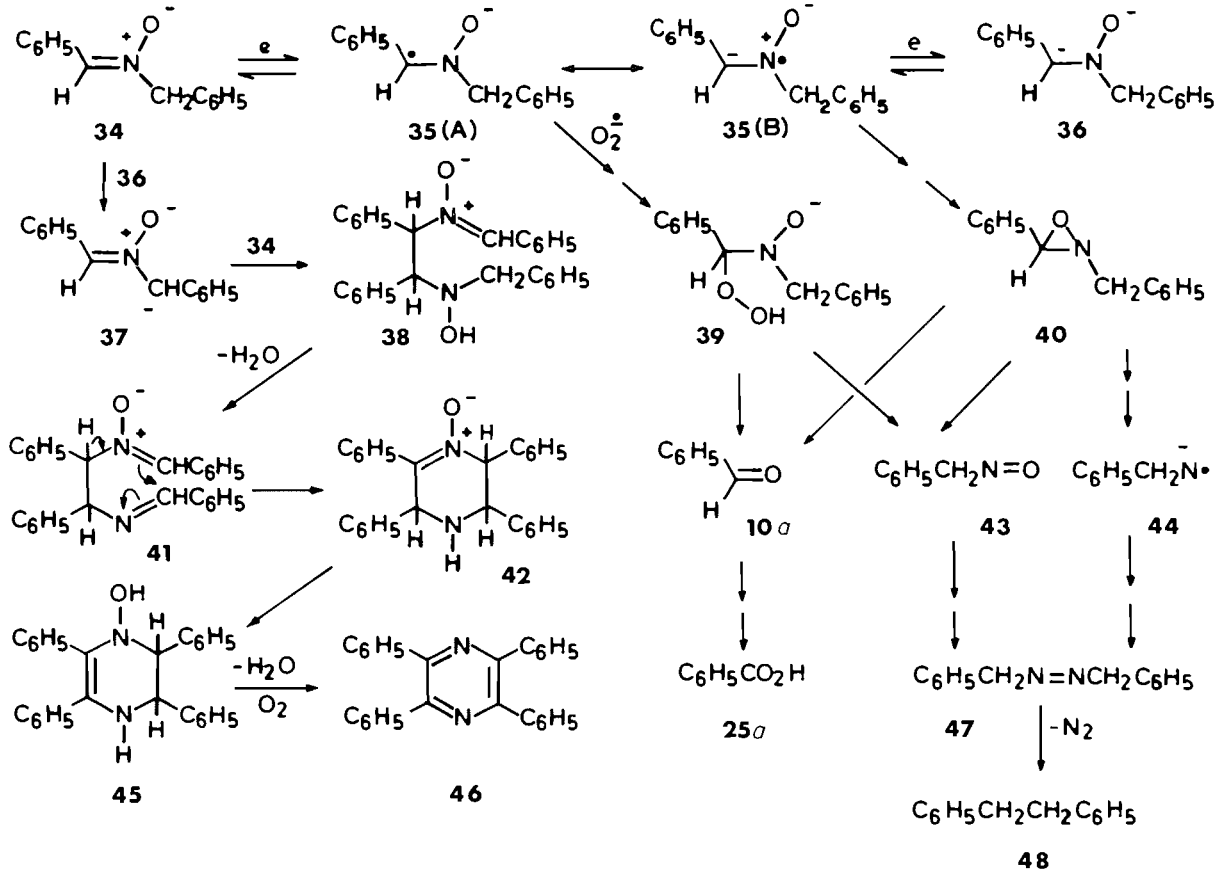

SCHEME 3

benzylhydroxylamino-1,2-diphenylethano)-α-phenylnitrone (**38**, 21%), dibenzyl (**48**, 18%), and 2,3,5,6-tetraphenylpyrazine (**46**, 17%), along with an 8% recovery of the unchanged starting material (**34**) (Scheme 3). The reaction of 1,1,3-triphenylisoindole-*N*-oxide (**49**) with potassium in THF, however, did not lead to any isolable product; most of the starting material (**49**) could be recovered unchanged (69%) (Scheme 4).

The formation of the different products in the reaction of the aldehydonitrones **1***a–d* with potassium can be understood in terms of the reaction pathway shown in Scheme 1.[4] It is assumed that the initial step in the reaction of **1***a–d* with potassium is an electron transfer reaction, leading to the radical anion intermediate **2***a–d*[5] which, in turn, can accept a second electron to give the dianion intermediate **3***a–d*, depending on the ease with which **2** can be converted to **3**. These dianion intermediates (**3***a–d*) could lead to deoxygenated Schiff bases **4***a–d* or products derived from them. To examine the involvement of such Schiff bases **4***a–d* or their further transformation products in these reactions, we have examined the reaction of *N*-benzylideneaniline (**4***a*) with potassium in THF. Treatment of **4***a* with excess of potassium in THF under analogous conditions gave a mixture of benzoic acid (**25***a*, 28%) and *d,l-N,N'*-1,2-tetraphenylethylenediamine (**54**, 55%) (Scheme 4). The fact that we have not been able to isolate the ethylenediamines (**54**) in the reaction of **1***a–d* would indirectly

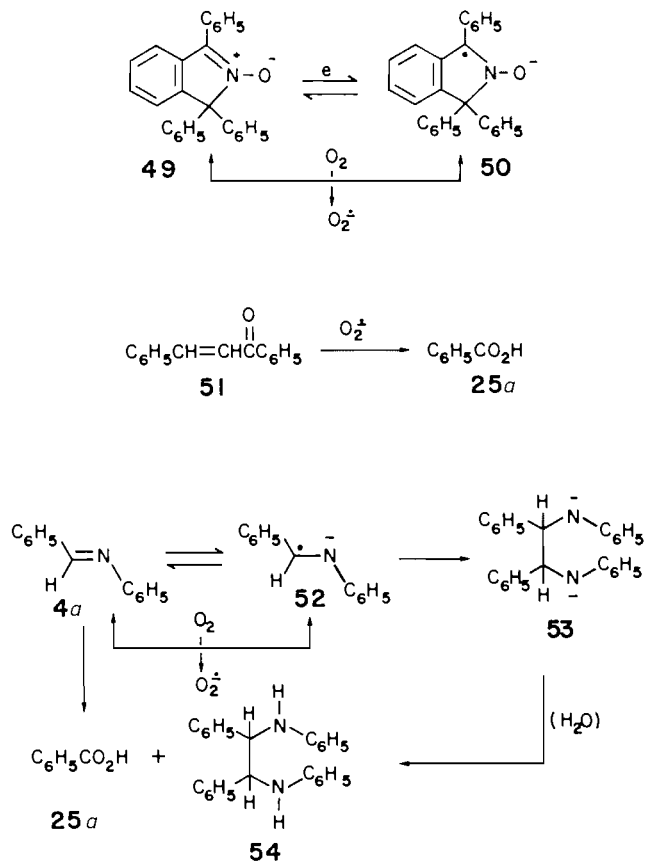

SCHEME 4

[4]The reactions are quite complex and other plausible pathways for the formation of some of the products cannot be excluded.

[5]Several resonance structures can be written for the intermediate radical anion **2**. Two of these structures, **2**(A) and **2**(B) are indicated here.

Can. J. Chem. Downloaded from www.nrcresearchpress.com by 213.166.140.6 on 09/07/12
For personal use only.

Can. J. Chem. Downloaded from www.nrcresearchpress.com by 213.166.140.6 on 09/07/12
For personal use only.

rule out the involvement of the corresponding Schiff bases **4***a–d* in these reactions.

A second possible mode of reaction of **2***a–d*, although not very likely under our reaction conditions, is its interaction with adventitious oxygen[6] to give back the starting nitrone **1***a–d* and potassium superoxide. Several examples of superoxide formation by electron transfer to oxygen from radical anions and also by electrochemical methods are reported in the literature (9). Subsequent reaction of superoxide with **1***a–d* or **2***a–d* will lead to the hydroperoxy intermediate **5**, which can fragment to the aldehyde **10***a–c* and the nitroso compound **11***a,d*. Further reaction of the aldehyde **10***a–c* with potassium will give the radical anion **15** and the dianion **20**, which can ultimately lead to the corresponding carboxylic acid **25***a–c*. The nitroso compound **11***a,d* in the presence of excess of potassium will lead to the azo compound **19***a,d*, or in the presence of excess of oxygen give the corresponding nitro compound **22**. It may be mentioned in this connection that nitrosobenzene, formed as an intermediate in the reaction of nitrobenzene with lithium in THF, is converted to azobenzene in the presence of excess of lithium (10).

A more likely pathway for the reaction of **2***a–d* would be its conversion to the oxaziridine **6**, which can fragment to give the nitroso compound **11***a,d* and the carbene **12**. The formation of small amounts of *trans*-stilbene (**13***a*) from **1***a* and *trans*-1,2-di-*p*-tolylethylene (**13***c*) from **1***c* can be explained in terms of the dimerization of **12**. The oxaziridine **6** can also react further with potassium to give the radical anion **7** and the dianion **8** and ultimately products derived from them. Fragmentation of **7** can lead to the intermediate **14** and the aldehyde **10***a–c*. Further transformations of **14** will ultimately give rise to the azo compound **19***a,d*.

To examine whether or not the involvement of oxygen in the reaction of **2***a–d*, as implicated earlier (Scheme 1), can be justified, we have carried out, in a separate experiment, the reaction of **1***a* with potassium in THF that has been previously saturated with oxygen. The reaction of **1***a*, under these conditions, gave a mixture of *trans*-stilbene (**13***a*, 8%), benzaldehyde (**10***a*, 38%), benzoic acid (**25***a*, 47%), and nitrobenzene (**22***a*, 72%). The fact that there is no appreciable difference in the yields of benzaldehyde (**10***a*) and benzoic acid (**25***a*), when the reaction of **1***a* with potassium is carried out in the absence and in the presence of oxygen, would suggest that the pathway involving the hydroperoxy intermediate **5** in Scheme 1 is not justified. Perhaps the more likely pathway involves the oxaziridine **6**, as stated earlier. The high yield of nitrobenzene (**22***a*) in the reaction of **1***a* with potassium in presence of oxygen would suggest that it is formed from nitrosobenzene (**11***a*) or other precursors such as **7**, **8**, and **14** through their reaction with oxygen.

To examine the type of products encountered in the reaction of the nitrones **1***a–d* with potassium superoxide, we have treated **1***a* with potassium superoxide in benzene containing 18-crown-6 at room temperature, obtaining a mixture of **25***a* (82%) and **22***a* (89%). The formation of both **25***a* and **22***a* in this reaction could be accounted for in terms of the **5** and its subsequent fragmentation to **10***a* and **11***a*. Further reaction of **10***a* and **11***a* with potassium superoxide will give **25***a* and **22***a*, respectively[7] (11). In a separate experiment, we have shown that nitrosobenzene (**11***a*) actually undergoes oxidation to nitrobenzene (**22***a*, 61%) on treatment with potassium superoxide in benzene, justifying our assumption that **11***a*, formed through the fragmentation of **5**, is being converted to **22***a*.

In Scheme 1, we have indicated the involvement of several radical anion and dianion intermediates in the transformation of the nitrones **1***a–d* to the observed products, on treatment with potassium in THF. In an attempt to intercept some of these intermediates, we have treated the reaction mixture from **1***a* and potassium in THF, before work-up, in separate experiments, with moist THF and benzoyl chloride respectively. Treatment of the reaction mixture from **1***a* with moist THF before work-up gave a mixture of **13***a* (7%), **19***a* (78%), **10***a* (32%), **25***a* (25%), and benzyl alcohol (**23***a*, 25%). The formation of **23***a* under these conditions would suggest the involvement of the dianion intermediate **20** in the transformations of **10***a* to **25***a*. Further, it is to be inferred that the dianion **20** is converted to the hydroperoxy anion **21**, a possible precursor of **25***a*, during work-up, through its reaction with oxygen. This fact is further confirmed by the observation that the reaction of **10***a* with potassium in THF, followed by treatment with moist THF, in a separate experiment, gave a mixture of benzyl alcohol (**23***a*, 46%) and benzoic acid (**25***a*, 41%). In contrast, the reaction of **10***a* with potassium in THF, followed by the usual work-up procedure employed in the case of the nitrones **1***a–d*, gave a 75% yield of **25***a*. It is therefore to be inferred that under the conditions of work-up, which involve exposure of the reaction mixture from **10***a* (or **1***a*) to air, most of the dianion **20** is converted to the hydroperoxy intermediate **21** and ultimately to **25***a*. This is further substantiated by the observation that the reaction of **10***a* with potassium in THF, saturated with oxygen, gave a 77% yield of **25***a*.

When the reaction mixture from **1***a* (after treatment with potassium in THF) was treated with benzoyl chloride, a mixture of *trans*-stilbene (**13***a*, 6%), *trans*-azobenzene (**19***a*, 75%), benzaldehyde (**10***a*, 39%), benzoic acid (**25***a*, 5%), benzoic anhydride (**24**, 50%), and benzanilide (**9**, 17%) was obtained. The formation of **24** in this reaction can be explained in terms of the reaction of the intermediates **20** and **21** with benzoyl chloride. In support of this view, it has been observed that treatment of the reaction mixture obtained from the reaction of benzaldehyde (**10***a*) with potassium in THF with benzoyl chloride, in a separate experiment, gave a 81% yield of benzoic anhydride (**24**). The fact that some benzaldehyde (**10***a*) could be isolated from the reaction of **1***a* with potassium in THF, followed by treatment with benzoyl chloride, would suggest that all of **10***a* is not converted to **20** and, ultimately, to other products under our reaction conditions. The formation of small amounts of benzanilide (**9**) in this reaction, however, can be rationalized in terms of the reaction of the dianion intermediate **8** with benzoyl chloride. This would suggest that in the reaction of **1***a* with potassium in THF, at least part of the reaction proceeds through **6** → **7** → **8** (Scheme 1).

In contrast to the reactions of the aldehydonitrones **1***a–d*, the ketonitrones **26***a* and **26***b* with potassium give mostly the deoxygenated products **31***a* and **31***b*, respectively. It is evident that in these cases, the reaction pathway involving the dianion intermediates **28***a,b* becomes important. These dianions, under the conditions of work-up, could be converted to the *N*-hydroxy

[6]Although THF, freshly distilled over sodium, has been employed for these reactions, it has not been possible to completely exclude oxygen under our experimental conditions, which involved shaking the reagents in a stoppered flask for several hours.

[7]For some recent reviews on the chemistry of superoxide, see ref. 11.

Can. J. Chem. Downloaded from www.nrcresearchpress.com by 213.166.140.6 on 09/07/12
For personal use only.

derivatives **30***a*,*b*, which will then undergo dehydration to give the Schiff bases **31***a*,*b* (Scheme 2). This difference in behavior between the aldehydonitrones (**1***a*–*d*) and ketonitrones (**26***a*,*b*) could in part be due to the greater stability of the dianions **28***a*,*b* and also due to the difficulty of forming oxaziridines from the radical anions **27***a*,*b*. It may be pointed out that in the reaction of **26***b* with potassium in oxygen-saturated THF, under conditions analogous to those of the aldehydonitrone **1***a*, only a small amount of fluorenone (**29***b*, 28%) could be isolated; nearly 65% of the unchanged starting material (**26***b*) could be recovered from this reaction. However, when the reaction of **26***b* was carried out in presence of potassium superoxide in benzene containing 18-crown-6, fluorenone (**29***b*) could be obtained in better yields. Thus, the treatment of **26***b* with excess of potassium superoxide in a mixture of benzene and 18-crown-6 for 42 h at room temperature gave a 78% yield of **29***b* and a 24% yield of nitrobenzene (**22***a*), in addition to the recovery of a small amount (19%) of the starting material (**26***b*).

The formation of a small amount of 9-anilinofluorene (**33***b*, 8%), besides the major product **31***b* (71%), in the reaction of **26***b* with excess of potassium could be understood in terms of the further reaction of **31***b* with potassium to give the corresponding dianion intermediate **32***b*, which under the conditions of work-up will lead to **33***b*. In support of this view, it has been observed that treatment of **31***b* with potassium in THF under analogous conditions gave a 73% yield of 9-anilinofluorene (**33***b*), along with a 10% recovery of the starting material, **26***b*.

The formation of the different products such as benzoic acid (**25***a*), dibenzyl (**48**), the nitrone **38**, and the tetraphenylpyrazine **46** in the reaction of **34** with potassium in THF could be understood in terms of the reaction pathway shown in Scheme 3. The oxaziridine **40**, formed from the radical anion intermediate **35**, could fragment to benzaldehyde **10***a* and the nitroso compound **43**. Further reaction of **10***a* will lead to benzoic acid **25***a*, whereas the subsequent reaction of **43** with potassium would give the corresponding azo compound **47**. Nitrogen loss from either **47** or one of its precursors involving intermediates **40** and **44** could give dibenzyl (**48**). The formation of the nitrone **38** and tetraphenylpyrazine (**46**), however, could be rationalized in terms of the anionic intermediate **37**, which may be formed through the abstraction of one of the benzylic protons by superoxide anion or any other base (**36**). This anionic species **37** can combine with the starting nitrone **34** to give **38**. In this connection it may be pointed out that **38** has been reported to be formed in moderate yields, on treatment of **34** with lithium dimsylate (12). Subsequent transformations of **38**, involving the loss of two molecules of water and air oxidation, will ultimately give **46**, as shown in Scheme 3.

In contrast to the reaction of the aldehydonitrones, **1***a*–*d* and ketonitrones, **26***a*,*b*, the reaction of 1,1,3-triphenylisoindole-*N*-oxide (**49**) with potassium in THF did not give rise to any product. It is assumed that **49** initially accepts an electron from potassium to give the radical anion intermediate **50** (as evidenced by color changes), which then reverts to the starting material, on exposure to air, under work-up conditions. To substantiate this view we have, in a separate experiment, bubbled oxygen gas through the reaction mixture obtained by the treatment of **49** with potassium in THF and subsequently treated this mixture with benzalacetophenone (**51**) to give a 70% yield of benzoic acid (**25***a*) and 69% yield of the unchanged starting material (**49**). This clearly shows that the superoxide, generated on reaction of **49** with oxygen, reacts with **51** to give benzoic acid. Mention may be made in this connection that **51** is known to undergo oxidation with potassium superoxide to give benzoic acid (13). The absence of any reaction product, other than the generation of **50**, in the reaction of **49** with potassium would imply the nonreactivity of superoxide with the starting nitrone **49**. This is supported by the observation that the reaction of **49** with potassium superoxide in benzene in presence of 18-crown-6, under conditions analogous to the oxidation of **1***a* and **26***b*, did not give rise to any product; most of the starting material (**49**, 69%) was recovered unchanged.

Cyclic voltammetric studies

It has been reported earlier that aromatic amine *N*-oxides undergo electrochemical reduction to give the corresponding radical anions (14, 15). To examine whether the radical anions **2***a*–*d*, **27***a*,*b*, **35**, and **50** and the dianions **3***a*–*d*, **28***a*,*b*, and **36** are actually involved in the reaction of the starting nitrones **1***a*–*d*, **26***a*,*b*, **34**,and **49** with potassium, an attempt was made to generate these reactive intermediates electrochemically and to characterize them through their reduction potentials and electronic spectra. In this connection, we have recorded the cyclic voltammograms of the nitrones **1***a*–*d*, **26***a*,*b*, **34**, and **49**, and Fig. 1 shows the cyclic voltammograms of three representative nitrones **1***a*, **34**, and **49**. The values for the peak potential for the one-electron (E_p^1) and two-electron (E_p^2) reductions for these quasi-reversible systems were evaluated and are listed in Table 1. It is pertinent to observe that in the cathodic sweep cyclic voltammograms of all the nitrones except **49**, the backward sweep waves, which should correspond to the oxidation of the dianions and radical anions, were not observed. In the case of **49**, however, the backward sweep corresponding to the one-electron redox system could be observed, suggesting thereby that the radical anion **50** and its oxidation are fully reversible.

To characterize the radical anions and dianions generated from the nitrones **1***a*–*d*, **26***a*,*b*, **34**, and **49**, we have electrochemically reduced these substrates in acetonitrile in a specially designed cell, applying the requisite potentials in each case, and have recorded their electronic spectra. The spectral details are summarized in Table 1. Examination of Table 1 reveals that the starting nitrones are characterized by an absorption maximum around 298–353 nm, whereas the corresponding radical anions showed a red shifted absorption maximum around 320–450 nm; the corresponding dianions, however, showed an absorption maximum around 280–295 nm. These observations are in tune with the spectral data reported for the radical anions and dianions derived from azobenzene and nitroaromatics through their reaction with lithium in THF (17–19). An interesting observation was that the radical anions **2***a*–*d*, **27***a*,*b*, **35**, and **50** and the dianions **3***a*–*d*, **28***a*,*b*, and **36** were quenched by oxygen, as evidenced by the disappearance of their absorption bands, on bubbling oxygen gas through their solutions in acetonitrile. It is likely that they react with oxygen to give superoxide anion, as implicated in Schemes 1–4.

Pulse radiolysis studies

Earlier studies from this laboratory have shown that radical anions of unsaturated substrates such as retinal polyenes, for example, can be generated through the attachment of the solvated electron e_{sol}^- in polar solvents such as methanol under pulse radiolysis conditions (16). In the present studies, we have observed that the nitrones **1***a*–*d*, **26***a*,*b*, **34**, and **49** undergo electron attachment in methanol to give the corresponding radical anions **2***a*–*d*, **27***a*,*b*, **35**, and **50**, respectively, characterized through their absorption spectra (Fig. 2). These radical

Can. J. Chem. Downloaded from www.nrcresearchpress.com by 213.166.140.6 on 09/07/12
For personal use only.

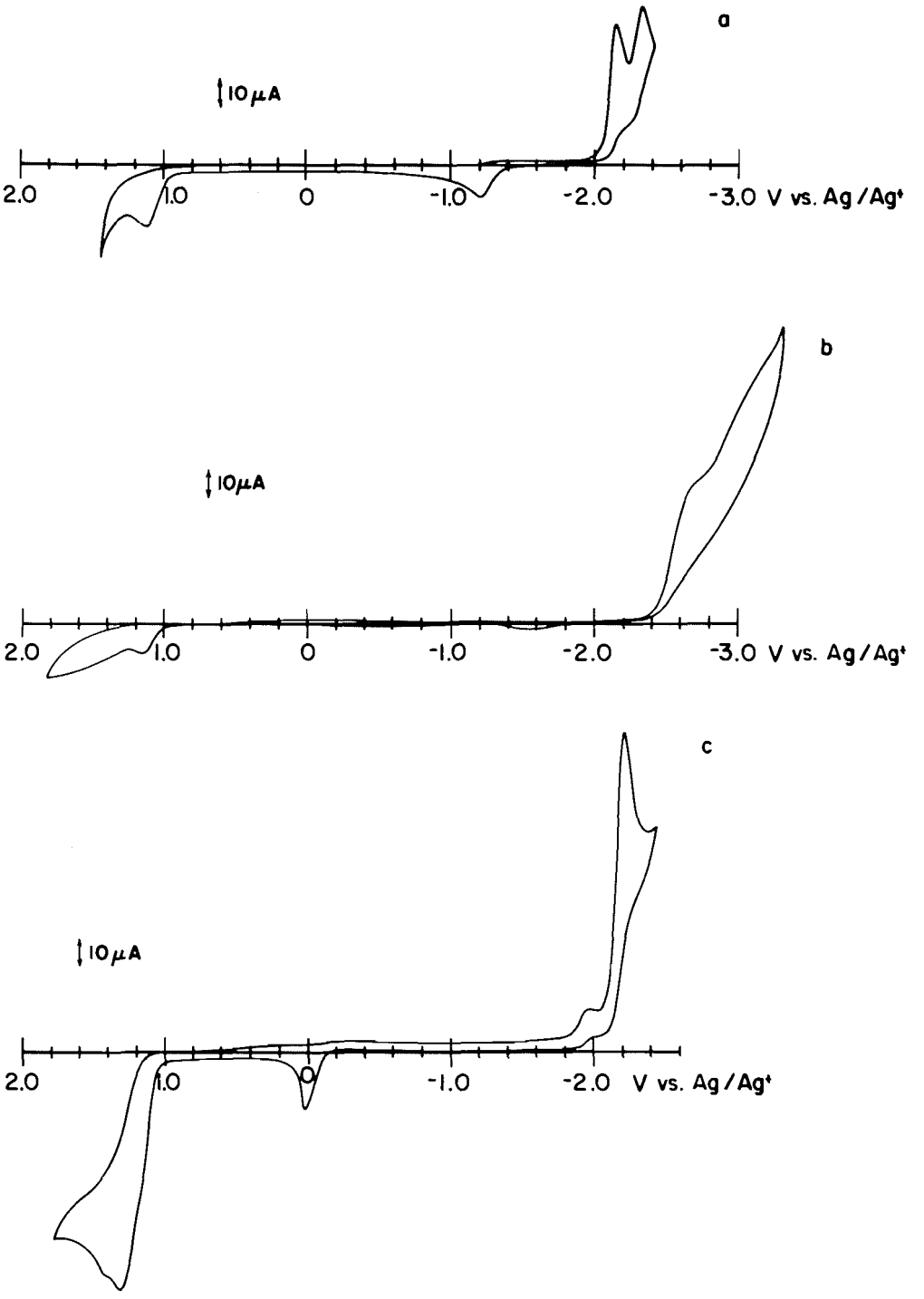

FIG. 1. Cyclic voltammograms of **1***a* (a), **34** (b), and **49** (c) in acetonitrile containing 0.1 *M* tetrabutylammonium perchlorate (TBAP). Sweep rate was 100 mV/s. Working electrode was Pt microelectrode and reference electrode was Ag/Ag^+.

anions showed strong absorption maxima in the 320–450 nm region, similar to the transients formed under electrochemical conditions, and were quenched by oxygen, as evidenced by their enhanced decay at higher concentrations of oxygen. The close similarity in the spectra of the intermediates, generated under both electrochemical and pulse radiolysis conditions, justifies our assumption that radical anions are the primary intermediates formed through electron transfer processes in the reaction of nitrones with potassium.

Experimental

All melting points are uncorrected and were determined on a Mel-Temp melting point apparatus. The ir spectra were recorded on Perkin–Elmer Model 377 or Model 580 infrared spectrophotometers. The electronic spectra were recorded on Cary 17D, Cary 219, or Beckman DB spectrophotometers. The nmr traces were recorded on a Varian EM-390 spectrometer using TMS as internal standard.

Starting materials

α,*N*-Diphenylnitrone (**1***a*) (20), mp 112–113°C; α,*o*-hydroxy-

Can. J. Chem. Downloaded from www.nrcresearchpress.com by 213.166.140.6 on 09/07/12
For personal use only.

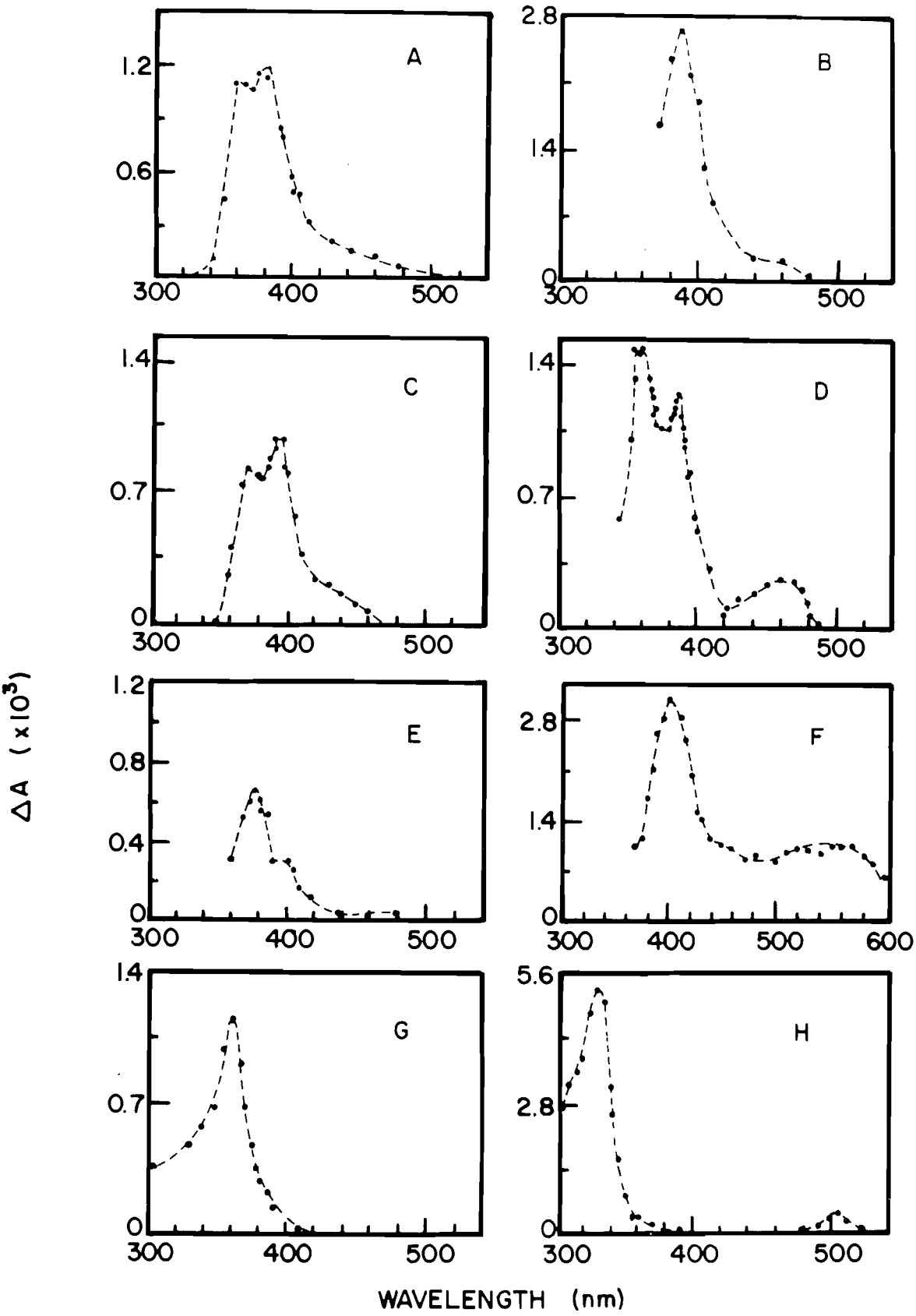

FIG. 2. Absorption spectra of the radical anions **2***a* (A), **2***b* (B), **2***c* (C), **2***d* (D), **27***a* (E), **27***b* (F), **35** (G), and **50** (H) in N_2-saturated methanol, observed at 0.04 μs after the electron pulse.

TABLE 1. Reduction peak potentials and spectral data on nitrones, their radical anions, and dianions

Compound	Reduction		Absorption maxima						
			Nitrone		Radical anion[a]			Dianion[a]	
	E_p^1 (V vs. Ag/Ag^+)	E_p^2 (V vs. Ag/Ag^+)	λ_{max} (nm)	ϵ ($\times 10^3 M^{-1} s^{-1}$)	λ_{max}[b] (nm)	λ_{max}[c] (nm)	ϵ[c,d] ($\times 10^3 M^{-1} s^{-1}$)	λ_{max}[c] (nm)	ϵ[c,d] ($\times 10^3 M^{-1} s^{-1}$)
1*a*	−2.15	−2.35	316	26.5	360, 385	390	4	290	8.6
1*b*	−1.90	−2.68	300	13	390, 450	450	13	290	16.5
1*c*	−2.30	−2.52	320	27	370, 390	380	6.5	280	21
1*d*	−2.28	−2.55	316	20	360, 385	380	4	295	5
26*a*	−2.13	−2.38	312	14.5	376, 400	[e]	[e]	290	14.5
26*b*	−1.75	−1.90	353	30	400, 550	400	60	283	30
34	−2.70	−3.15	298	16	360	380	15	291	30
49	−2.05	−2.30	340	8	330	[e]	[e]	292	8

[a]Both radical anions and dianions were stable under nitrogen atmosphere during the recording of the spectra.
[b]Measured from pulse radiolysis experiments (solvent methanol).
[c]Measured from electrochemical experiments (solvent acetonitrile, 0.1 *M* TBAP).
[d]At the absorption maximum (error ±25%).
[e]Measurements could not be made due to the absorption of the starting nitrone.

phenyl-*N*-phenylnitrone (**1***b*) (21), mp 115°C; *N*-phenyl-α-*p*-tolylnitrone (**1***c*) (22), mp 92–93°C; α-phenyl-*N*-*p*-tolylnitrone (**1***d*) (6), mp 123°C; triphenylnitrone (**26***a*) (3), mp 217–218°C; α-diphenylene-*N*-phenylnitrone (**26***b*) (23), mp 191–192°C; *N*-benzyl-α-phenylnitrone (**34**) (24), mp 82–83°C; 1,1,3-triphenylisoindole-*N*-oxide (**49**) (25), mp 198°C; *N*-benzylideneaniline (**4***a*) (26), mp 89°C; and 9-fluorenylideneaniline (**31***b*) (27), mp 89°C were prepared by reported procedures. Petroleum ether used was the fraction with bp 60–80°C. Gold Label acetonitrile was used for cyclic voltammetric studies.

*Reaction of nitrones (**1**a–d, **26**a,b) with potassium in THF*

A general procedure was to shake a mixture of 3 mmol of the appropriate nitrone (**1***a–d*, **26***a,b*) and finely cut potassium (6 mg-atom) in THF (125 mL) in a stoppered round-bottomed flask for several hours. A few clean, broken glass pieces were added to the mixture to ensure a fresh surface of metal throughout the reaction. In general, the reaction mixture underwent pronounced color changes due to the formation of radical anion and dianion intermediates. On completion of the reaction, the mixture was poured into moist THF (100 mL) to destroy any unchanged potassium and then the solvent was removed under vacuum to give a residual solid. This material was treated with water (10 mL) and extracted with methylene chloride (100 mL). Acidification of the aqueous layer with dilute hydrochloric acid and extraction with methylene chloride (100 mL) gave the carboxylic acid fraction, which was recrystallized from suitable solvents.

Work-up of the nonaqueous fraction (methylene chloride extract), by removal of the solvent under vacuum and fractional crystallization from suitable solvents, gave the nonacidic products.

*Reaction of **1**a*

Treatment of 590 mg (3 mmol) of **1***a* with potassium (235 mg, 6 mg-atom) in THF for 16 h and work-up in the usual manner gave 170 mg (47%) of benzoic acid (**25***a*), mp 121°C (mixture melting point). The non-aqueous fraction (methylene chloride extract) was worked up by removal of the solvent under vacuum and chromatographing over alumina. Elution with petroleum ether gave 20 mg (8%) of *trans*-stilbene (**13***a*), mp 124°C (mixture melting point). Further elution with a mixture (1:4) of benzene and petroleum ether gave 220 mg (82%) of *trans*-azobenzene (**19***a*), mp 68°C (mixture melting point). Subsequent elution with a mixture (1:1) of benzene and petroleum ether gave 130 mg (42%) of benzaldehyde (**10***a*) (superimposable ir spectrum with that of an authentic sample). Treatment of **1***a* (1.77 g, 9 mmol) with potassium (0.7 g, 18 mg-atom) in THF (triply distilled over sodium) for 16 h, under complete exclusion of oxygen (positive nitrogen pressure), and work-up as in the earlier case gave a mixture of **25***a*, **13***a*, **19***a*, and **10***a* in 48, 9, 81, and 40% yields, respectively.

In a repeat run, **1***a* (590 mg, 3 mmol) was treated with potassium (235 mg, 6 mg-atom) in THF (125 mL), saturated with oxygen, for 16 h. Work-up as in the earlier case gave 170 mg (47%) of benzoic acid (**25***a*), mp 121°C (mixture melting point), from the aqueous fraction. The nonaqueous fraction was chromatographed over alumina and eluted with petroleum ether to give 20 mg (8%) of **13***a*, mp 124°C (mixture melting point). Further elution with a mixture (1:9) of benzene and petroleum ether gave 260 mg (70%) of nitrobenzene (**22***a*) (superimposable ir spectrum with that of an authentic sample). Subsequent elution with a mixture (1:1) of benzene and petroleum ether gave 120 mg (38%) of benzaldehyde (**10***a*) (superimposable ir spectrum with that of an authentic sample). In a repeat experiment, the same amount of **1***a* (3 mmol) was treated with potassium (6 mg-atom) in oxygen-saturated THF for 16 h, under identical conditions, and worked up to give a mixture of **25***a*, **13***a*, **22***a*, and **10***a* in 53, 8, 73 and 38% yields, respectively.

In yet another run, **1***a* (590 mg, 3 mmol) was treated with potassium (235 mg, 6 mg-atom) in THF (125 mL) for 16 h. Moist THF (25 mL) was injected into the reaction mixture and the shaking was continued for an additional 5 h. Work-up of the mixture as in the earlier cases gave 90 mg (25%) of benzoic acid (**25***a*), mp 121°C (mixture melting point); 19 mg (7%) of **13***a*, mp 124°C (mixture melting point); 210 mg (78%) of *trans*-azobenzene (**19***a*), mp 68°C (mixture melting point); 80 mg (25%) of benzyl alcohol (**23***a*) (superimposable ir with that of an authentic sample); and 100 mg (32%) of benzaldehyde (**10***a*) (superimposable ir with that of an authentic sample). In a repeat run, **1***a* (3 mmol) was treated with potassium (6 mg-atom) in THF (triply distilled over sodium) for 16 h under the complete exclusion of oxygen (positive nitrogen pressure) and worked up as in the earlier case by treatment with moist THF to give a mixture of **25***a*, **13***a*, **19***a*, **23***a*, and **10***a* in 25, 8, 82, 30, and 29% yields, respectively.

In another run, **1***a* (590 mg, 3 mmol) was treated with potassium (235 mg, 6 mg-atom) in THF (125 mL) for 16 h. A solution of benzoyl chloride (425 mg, 3 mmol) in THF (25 mL) was injected into the reaction vessel and the shaking was continued for an additional 5 h. Work-up of the mixture in the usual manner gave 18 mg (5%) of benzoic acid (**25***a*), mp 121°C (mixture melting point), from the aqueous fraction. The nonaqueous fraction was chromatographed over alumina. Elution with petroleum ether gave 15 mg (6%) of **13***a*, mp 124°C (mixture melting point). Further elution with a mixture (1:9) of benzene and petroleum ether gave 200 mg (75%) of **19***a*, mp 68°C (mixture melting point). Subsequent elution with a mixture (3:7) of

Can. J. Chem. Downloaded from www.nrcresearchpress.com by 213.166.140.6 on 09/07/12
For personal use only.

Can. J. Chem. Downloaded from www.nrcresearchpress.com by 213.166.140.6 on 09/07/12
For personal use only.

benzene and petroleum ether gave 330 mg (50%) of benzoic anhydride (**24**), mp 42°C (mixture melting point). Elution with a mixture (1:1) of benzene and petroleum ether gave 123 mg (39%) of benzaldehyde (**10***a*) and, finally, elution with benzene gave 100 mg (17%) of benzanilide (**9**), mp 163–164°C (mixture melting point).

*Reaction of **10**a*

Treatment of **10***a* (636 mg, 6 mmol) with potassium (235 mg, 6 mg-atom) in THF (125 mL) for 15 h and work-up in the usual manner gave 550 mg (75%) of benzoic acid (**25***a*), mp 121°C (mixture melting point).

In a repeat run, **10***a* (636 mg, 6 mmol) was treated with potassium (235 mg, 6 mg-atom) in THF (125 mL), saturated with oxygen. Work-up of the mixture as in the earlier cases gave 565 mg (77%) of **25***a*, mp 121°C (mixture melting point).

In yet another run, **10***a* (636 mg, 6 mmol) was treated with potassium (235 mg, 6 mg-atom) in THF (125 mL) for 15 h. Moist THF (25 mL) was injected into the reaction vessel and the shaking was continued for an additional 5 h. Work-up of the mixture as in the earlier cases gave 300 mg (41%) of benzoic acid (**25***a*), mp 121°C (mixture melting point), and 300 mg (46%) of benzyl alcohol (**23***a*) (superimposable ir spectrum with that of an authentic sample).

In a repeat run, **10***a* (636 mg, 6 mmol) was treated with potassium (235 mg, 6 mg-atom) in THF (125 mL) for 15 h. A solution of freshly distilled benzoyl chloride (840 mg, 6 mmol) in THF (25 mL) was injected into the reaction flask and the shaking was continued for an additional 5 h. Work-up in the usual manner gave 1.1 g (81%) of benzoic anhydride (**24**), mp 42°C (mixture melting point).

*Reaction of **1**b*

Treatment of 640 mg (3 mmol) of **1***b* with 235 mg (6 mg-atom) of potassium in THF for 10 h and work-up in the usual manner gave 125 mg (30%) of salicylic acid (**25***b*), mp 159°C (mixture melting point), from the aqueous fraction. Work-up of the nonaqueous fraction gave a residual solid, which was chromatographed over alumina. Elution with petroleum ether gave 160 mg (58%) of *trans*-azobenzene (**19***a*), mp 68°C (mixture melting point), after recrystallization from ethanol. Further elution with a mixture (1:1) of benzene and petroleum ether gave 90 mg (25%) of salicylaldehyde (superimposable ir spectrum with that of an authentic sample). Subsequent elution with a mixture (4:3) of benzene and petroleum ether gave 130 mg (20%) of unchanged starting material (**1***b*), mp 118°C (mixture melting point), after recrystallization from benzene.

In a repeat run, 640 mg (3 mmol) of **1***b* was treated with 470 mg (12 mg-atom) of potassium in THF (125 mL) for 15 h and worked up as in the earlier cases to give 185 mg (45%) of **25***b*, mp 159°C (mixture melting point); 190 mg (69%) of **19***a*, mp 68°C (mixture melting point); and 135 mg (37%) of **10***b*.

*Reaction of **1**c*

A solution of **1***c* (640 mg, 3 mmol) in THF (125 mL) was shaken with potassium (235 mg, 6 mg-atom) for 15 h. The colorless solution became yellow at first, later brown, and finally black. Work-up of the mixture as in the earlier cases gave 180 mg (44%) of *p*-toluic acid (**25***c*), mp 182°C (mixture melting point), after recrystallization from benzene. Work-up of the nonaqueous fraction gave a residual solid, which was chromatographed on alumina. Elution with petroleum ether gave 20 mg (6%) of *trans*-1,2-di-*p*-tolylethylene (**13***c*), mp 176°C (mixture melting point). Further elution with a mixture (1:9) of benzene and petroleum ether gave 220 mg (80%) of *trans*-azobenzene (**19***a*), mp 68°C (mixture melting point), after recrystallization from ethanol. Subsequent elution of the column with a mixture (1:1) of benzene and petroleum ether gave 145 mg (40%) of *p*-tolualdehyde (**10***c*) (superimposable ir spectrum with that of an authentic sample).

*Reaction of **1**d*

A solution of **1***d* (640 mg, 3 mmol) in THF (125 mL) was shaken with potassium (235 mg, 6 mg-atom) for 12 h. Work-up of the mixture as in the earlier cases gave 180 mg (49%) of benzoic acid (**25***a*), mp 121°C (mixture melting point). The nonaqueous fraction was chromatographed over alumina and eluted with petroleum ether to give 10 mg (4%) of *trans*-stilbene (**13***a*), mp 124°C (mixture melting point). Further elution with a mixture (1:9) of benzene and petroleum ether gave 280 mg (89%) of **19***d*, mp 144°C (mixture melting point), after recrystallization from ethanol. Subsequent elution with a mixture (1:1) of benzene and petroleum ether gave 130 mg (40%) of benzaldehyde (**10***a*) (superimposable ir spectrum with that of an authentic sample).

*Reaction of **26**a*

Treatment of **26***a* (1.37 g, 5 mmol) with potassium (390 mg, 10 mg-atom) in THF for 3.5 h and work-up as in the earlier cases gave 1.05 g (82%) of benzhydrylideneaniline (**31***a*), mp 113–114°C (mixture melting point), after recrystallization from methanol.

*Reaction of **26**b*

Treatment of **26***b* (1.08 g, 4 mmol) with potassium (315 mg, 8 mg-atom) in THF for 10 h and work-up as in the earlier cases gave 820 mg (81%) of 9-fluorenylideneaniline (**31***b*), mp 89°C (mixture melting point), after recrystallization from a mixture (1:3) of chloroform and ethanol.

In a repeat run, 1.36 g (5 mmol) of **26***b* was treated with excess of potassium (780 mg, 20 mg-atom) in THF for 10 h, under analogous conditions, and worked up to give 100 mg (8%) of 9-anilinofluorene (**33***b*), mp 123–124°C (mixture melting point), and 900 mg (71%) of 9-fluorenylideneaniline (**31***b*), mp 89°C (mixture melting point).

In yet another run, **26***b* (108 mg, 0.37 mmol) was treated with potassium (30 mg, 0.77 mg-atom) for 10 h in THF (125 mL), which was previously saturated with oxygen. Work-up of the reaction mixture as in the earlier cases gave 20 mg (28%) of 9-fluorenone (**29***b*), mp 84°C (mixture melting point), and 70 mg (65%) of the unchanged starting material (**26***b*), mp 191–192°C (mixture melting point).

Reaction of N*-Benzyl-α-phenylnitrone (**34**) with potassium in THF*

A solution of **34** (950 mg, 4.5 mmol) in THF (125 mL) was shaken with potassium (180 mg, 4.5 mg-atom) for 10 h. The solution, which was colorless initially, changed to yellow, red, and finally brown. The reaction mixture was poured into moist THF (100 mL) and then the solvent was removed under vacuum. The residual solid thus obtained was treated with water (10 mL) and extracted with methylene chloride. The aqueous layer, on acidification with dilute hydrochloric acid and extraction with methylene chloride, gave 100 mg (18%) of **25***a*, mp 121°C (mixture melting point). Removal of the solvent from the earlier methylene chloride extract gave a product mixture, which was chromatographed over alumina. Elution with petroleum ether gave 75 mg (18%) of dibenzyl (**48**), mp 52°C (mixture melting point). Further elution with a mixture (1:4) of benzene and petroleum ether gave 150 mg (17%) of 2,3,5,6-tetraphenylpyrazine (**46**), mp 249°C (mixture melting point). Further elution of the column with a mixture (2:3) of benzene and petroleum ether gave 200 mg (21%) of α-phenyl-*N*-(2-benzylhydroxylamino-1,2-diphenylethano)nitrone (**38**), mp 196°C (mixture melting point). Subsequent elution of the column with benzene gave 75 mg (8%) of the unchanged starting material (**34**), mp 82–83°C (mixture melting point).

*Reaction of 1,2,3-triphenylisoindole-*N*-oxide (**49**) with potassium in THF*

A solution of **49** (360 mg, 1 mmol) in THF (125 mL) was shaken with potassium (78 mg, 2 mg-atom) for 12 h. The solution, which was initially colorless, changed to yellow and finally to orange. Exposure of the reaction mixture to air destroyed the color. Work-up of the reaction mixture in the usual manner gave 250 mg (69%) of the unchanged starting material (**49**), mp 198°C (mixture melting point), as the only isolable product.

In a repeat run, 360 mg (1 mmol) of **49** was treated with 78 mg (2 mg-atom) of potassium in THF (125 mL) for 12 h. Oxygen gas was bubbled through the reaction mixture and afterwards a solution of benzalacetophenone (**51**) (210 mg, 1 mmol) in benzene (25 mL) was added and the mixture was shaken for a further period of 2 h. Work-up of the reaction mixture as in the earlier cases gave 250 mg (69%) of the

Can. J. Chem. Downloaded from www.nrcresearchpress.com by 213.166.140.6 on 09/07/12
For personal use only.

unchanged nitrone **49**, mp 198°C (mixture melting point), and 170 mg (70%) of benzoic acid (**25***a*), mp 121°C (mixture melting point).

*Reaction of benzylideneaniline (**4**a) with potassium in THF*

A solution of **4***a* (1.36 g, 7.5 mmol) in THF (125 mL) was shaken with potassium (1.17 g, 30 mg-atom) for 9 h. The solution, which was initially colorless, became yellow, then brown, and finally colorless again. Work-up in the usual manner gave 260 mg (28%) of **25***a*, mp 121°C (mixture melting point), after recrystallization from hot water, and 760 mg (55%) of *d,l-N,N'*,1,2-tetraphenylethylenediamine (**54**), mp 150–151°C (mixture melting point).

*Reaction of 9-fluorenylideneaniline (**31**b) with potassium in THF*

A solution of **31***b* (1.02 g, 4 mmol) in THF (125 mL) was shaken with potassium (315 mg, 8 mg-atom) for 10 h. The reaction mixture was treated with moist THF (10 mL) and the solvent was later removed under vacuum. The residual solid was extracted with ether to give a product mixture that was then triturated with ethanol (2 mL). The ethanol-insoluble product gave 750 mg (73%) of 9-anilinofluorene (**33***b*), mp 124°C (mixture melting point), after recrystallization from ethanol. The ethanol-soluble fraction was evaporated under vacuum to give 100 mg (10%) of the unchanged starting material (**31***b*), mp 89°C (mixture melting point), after recrystallization from a mixture (1:3) of chloroform and ethanol.

*Reaction of α,N-diphenylnitrone (**1**a) with potassium superoxide*

A mixture of **1***a* (390 mg, 1.98 mmol), potassium superoxide (290 mg, 4 mmol), and 18-crown-6 (530 mg, 2 mmol) in benzene (100 mL) was stirred at room temperature for 24 h, protected from sunlight. The reaction mixture became yellow at first and later turned orange and finally red. On completion of the reaction, the mixture was washed several times with aqueous sodium chloride solution. Removal of the solvent from organic layer under vacuum gave 220 mg (89%) of nitrobenzene (superimposable ir with an authentic sample).

The combined aqueous washings were acidified with dilute hydrochloric acid and extracted with benzene. Removal of the solvent from the benzene extract under vacuum gave 200 mg (82%) of benzoic acid, **25***a*, mp 121°C (mixture melting point).

*Reaction of α-diphenylene-N-phenylnitrone (**26**b) with potassium superoxide*

A mixture of the nitrone **26***b* (270 mg, 1 mmol), potassium superoxide (420 mg, 6 mmol), and 18-crown-6 (530 mg, 2 mmol) in benzene (100 mL) was stirred at room temperature for 42 h, protected from sunlight. The reaction mixture became initially yellow and later red. The mixture was washed several times with aqueous sodium chloride solution. Removal of the solvent from the organic layer under vacuum gave a product mixture that was chromatographed over alumina. Elution with petroleum ether gave 30 mg (24%) of nitrobenzene (**22***a*) (superimposable ir spectrum with that of an authentic sample). Elution with a mixture (1:4) of benzene and petroleum ether gave 130 mg (72%) of 9-fluorenone (**29***b*), mp 84°C (mixture melting point). Further elution with a mixture (3:1) of benzene and petroleum ether gave 50 mg (19%) of the unchanged starting material (**26***b*), mp 191–192°C (mixture melting point). Work-up of the aqueous washings by acidification with dilute hydrochloric acid and extraction with benzene, as in the earlier case, did not give rise to any isolable product.

*Attempted reaction of 1,1,3-triphenylisoindole-N-oxide (**49**) with potassium superoxide*

A mixture of **49** (180 mg, 0.5 mmol), potassium superoxide (70 mg, 1 mmol), and 18-crown-6 (135 mg, 0.5 mmol) in benzene (100 mL) was stirred at room temperature for 12 h, protected from sunlight. Work-up of the reaction mixture as in the earlier cases gave 125 mg (69%) of the unchanged starting material (**49**), mp 198°C (mixture melting point), as the only isolable product.

*Reaction of nitrosobenzene (**11**a) with potassium superoxide*

A mixture of **11***a* (428 mg, 4 mmol), potassium superoxide (288 mg, 4 mmol), and 18-crown-6 (530 mg, 2 mmol) in benzene (100 mL) was stirred at room temperature for 6 h. Work-up of the mixture as in the earlier cases gave 300 mg (61%) of nitrobenzene (**22***a*) (superimposable ir spectrum with that of an authentic sample).

Cyclic voltammetry

Cyclic voltammetric measurements were made with a Princeton Applied Research (PAR) Model 173 potentiostat/galvanostat, a PAR Model 175 universal programmer, and a Kipp and Zonen X–Y recorder. Experiments were performed in a standard three-compartment cell equipped with a Pt-disc working electrode, Pt-wire counter electrode, and Ag/Ag^+ reference electrode. For spectroelectrochemical measurements, a specially designed cell was employed, which consists of an extended 10-mm quartz cuvette, equipped with a Pt-gauze working electrode, a Pt-foil counter electrode, and an Ag/Ag^+ reference electrode. The electrolysis was carried out in acetonitrile solutions (~0.05 m*M*) under nitrogen atmosphere at controlled potentials and the absorption spectra of the electrochemically generated radical anions and dianions were recorded directly in a Cary 219 Spectrophotometer. Both one-electron and two-electron reduction processes were monitored directly using a PAR 179 digital coulometer.

Pulse radiolysis

The computer controlled pulse radiolysis apparatus, which allows determination of transient spectra at various times after the pulse, and kinetic measurements of the spectral changes have been described elsewhere (28). The solutions of the nitrones in methanol (~0.5 m*M*) were deaerated before pulse radiolysis by bubbling nitrogen for at least half an hour. The deaeration was continued in the reservoir from which the solution was allowed to flow slowly and continuously through the pulse radiolysis cell. The irradiation was carried out with 5-ns electron pulses from the Notre Dame 7-MeV ARCO LP-7 linear accelerator using dose rates of $\sim 2 \times 10^{16}$ eV/g per pulse.

Acknowledgments

We thank the Department of Science and Technology, Government of India, the Indian Institute of Technology, Kanpur, and the Office of Basic Energy Sciences of the U.S. Department of Energy for financial support of this work.

1. (*a*) A. CARRINGTON. Q. Rev. Chem. Soc. **17**, 67 (1963); (*b*) G. A. RUSSEL. Science, **161**, 423 (1968); (*c*) V. KALYANARAMAN and M. V. GEORGE. J. Organometal. Chem. **47**, 225 (1973); (*d*) G. A. RUSSEL and R. K. NORRIS. *In* Organic reactive intermediates. *Edited by* S. P. McManus. Academic Press, New York. 1973. p. 423.
2. R. BONNETT, R. F. C. BROWN, V. M. CLARK, I. O. SUTHERLAND, and SIR A. TODD. J. Chem. Soc. 2094 (1959).
3. H. STAUDINGER and K. MIESCHER. Helv. Chim. Acta, **2**, 554 (1919).
4. F. AGOLINI and R. BONNETT. Can. J. Chem. **40**, 181 (1962).
5. M. N. SHCHUKINA and G. S. PREDVODITELEVA. Dokl. Akad. Nauk SSSR, **110**, 230 (1956); Chem. Abstr. **51**, 4996c (1957).
6. E. BAMBERGER. Ber. Dtsch. Chem. Ges. B: **57**, 2082 (1924).
7. F. NERDEL and I. HULDSCHINSKY. Chem. Ber. **86**, 1005 (1953).
8. A. R. FORRESTER and R. H. THOMPSON. J. Chem. Soc. 1224 (1965).
9. (*a*) G. A. RUSSELL and A. G. BEMIS. Inorg. Chem. **6**, 403 (1967); (*b*) R. DIETZ, A. E. J. FORNO, B. E. LARCOMBE, and M. E. PEVOR. J. Chem. Soc. (B), 816 (1970); (*c*) J. DIVISEK and B. KASTENING. J. Electroanal. Chem. Interfacial Electrochem. **65**, 603 (1975); Chem. Abstr. **84**, 68861x (1976); (*d*) M. TEZUKA, Y. ONKATSU, and T. OSA. Bull. Chem. Soc. Jpn. **48**, 1471 (1975).
10. V. KALYANARAMAN and M. V. GEORGE. J. Org. Chem. **38**, 507 (1973).
11. (*a*) D. T. SAWYER and J. S. VALENTINE. Acc. Chem. Res. **14**, 393 (1981); (*b*) A. A. FIRMER. *In* The chemistry of functional groups: peroxides. *Edited by* S. Patai. Wiley, Chichester. 1983. p. 429.
12. J. H. HALL and M. R. GISLER. J. Org. Chem. **42**, 1133 (1977).

13. I. ROSENTHAL and A. A. FIRMER. Tetrahedron Lett. 2805 (1976).
14. T. KUBOTA, K. NISHIKIDA, H. MIYAZAKI, K. IWATANI, and Y. OISHI. J. Am. Chem. Soc. **90**, 5080 (1968).
15. H. MIYAZAKI, Y. MATSUHISA, and T. KUBOTA. Bull. Chem. Soc. Jpn. **54**, 3850 (1981).
16. N. V. RAGHAVAN, P. K. DAS, and K. BOBROWSKI. J. Am. Chem. Soc. **103**, 4569 (1981).
17. C. N. R. RAO, V. KALYANARAMAN, and M. V. GEORGE. Appl. Spectrosc. Rev. **3**, 229 (1970).
18. V. KALYANARAMAN, S. S. DUA, C. N. R. RAO, and M. V. GEORGE. Tetrahedron Lett. 235 (1968).
19. V. KALYANARAMAN, C. N. R. RAO, and M. V. GEORGE. Tetrahedron Lett. 4889 (1969).
20. I. BRÜNING, R. GRASHEY, H. HAUCK, R. HUISGEN, and H. SEIDL. Org. Synth. **46**, 127 (1966).
21. J. WIEMANN and CH. GLACET. Bull Soc. Chim. Fr. 176 (1950).
22. A. ANGELI and D. BIGIAIR. Atti Accad. Naz. Lincei Cl. Sci. Fis. Mat. Nat. Rend. **5**, 819 (1927); Chem. Abstr. **21**, 3895 (1927).
23. A. W. JOHNSON. J. Org. Chem. **28**, 252 (1963).
24. A. C. COPE and A. C. HAVEN, JR. J. Am. Chem. Soc. **72**, 4896 (1950).
25. B. SINGH. J. Am. Chem. Soc. **90**, 3893 (1968).
26. L. A. BIGELOW and H. EATOUGH. Org. Synth. Coll. Vol. **1**, 80 (1941).
27. M. E. TAYLOR and T. L. FLETCHER. J. Org. Chem. **21**, 523 (1956).
28. L. K. PATTERSON and J. LILIE. Int. J. Radiat. Phys. Chem. **6**, 129 (1974).

Can. J. Chem. Downloaded from www.nrcresearchpress.com by 213.166.140.6 on 09/07/12
For personal use only.

Orbital control in the 1,3-dipolar cycloaddition of benzonitrile oxide to benzylideneanilines

BENITO ALCAIDE, CARMEN L. MARDOMINGO, AND JOAQUÍN PLUMET[1]
Departamento de Química Orgánica, Facultad de Químicas, Universidad Complutense, Ciudad Universitaria, 28040 Madrid, Spain

AND

CARLOS CATIVIELA AND JOSÉ A. MAYORAL
Instituto de Ciencia de los Materiales de Aragón, Departamento de Química Orgánica, Universidad de Zaragoza, 50009 Zaragoza, Spain

Received December 13, 1985[2]

BENITO ALCAIDE, CARMEN L. MARDOMINGO, JOAQUÍN PLUMET, CARLOS CATIVIELA, and JOSÉ A. MAYORAL. Can. J. Chem. **65**, 2050 (1987).

Twelve *para*-substituted benzylideneanilines selected according to the optimality criteria of experimental matrices were prepared in order to study the influence of the substituents on the cycloaddition rate with benzonitrile oxide. The results obtained indicate that the cycloaddition is a concerted process with a high degree of synchrony.

BENITO ALCAIDE, CARMEN L. MARDOMINGO, JOAQUÍN PLUMET, CARLOS CATIVIELA et JOSÉ A. MAYORAL. Can. J. Chem. **65**, 2050 (1987).

Dans le but de mesurer l'influence des substituants sur leurs vitesses de cycloaddition avec l'oxyde de benzonitrile, on a préparé douze benzylidèneanilines substitués en position *para* qui avaient été choisis d'après des critères d'optimalité de matrices expérimentales. Les résultats obtenus indiquent que la cycloaddition est un processus concerté possédant un degré élevé de synchronisme.

[Traduit par la revue]

Can. J. Chem. Downloaded from www.nrcresearchpress.com by 213.166.140.6 on 09/07/12
For personal use only.

Introduction

Mechanistic studies concerning 1,3-dipolar cycloaddition reactions with all carbon dipolarophiles constitute a well-documented field of research (1). However, the mechanism of 1,3-dipolar cycloaddition processes with heterodipolarophiles has attracted less attention. The reaction between benzonitrile oxide and the azomethinic double bond is a well-known process, and provides an excellent synthetic route to Δ^2-1,2,4-oxadiazolines (2)[3] (Fig. 1).

To the best of our knowledge no systematic study aimed at clarifying the mechanism of this process has been made. The only published antecedent is the measurement of the rate of cycloaddition of benzonitrile oxide (BNO) to benzylidenemethylamine (3) relative to the cycloaddition to ethyl crotonate.

Huisgen (4) has proposed a "concerted but not synchronous" transition state for 1,3-dipolar cycloadditions involving nitrilium betaines and all-carbon dipolarophiles. This is represented by a group of resonance structures that contribute to a different degree to the real structure of the transition state (2).

The study of the influence of different substituents in the aromatic rings of benzylideneanilines on the rate of cycloaddition with BNO represents our contribution to the clarification of the mechanism of this process.

Selection of substrates

The selection of molecules suitable for the kinetic study was effected by an exchange algorithm (5) from a set of 45 4,4′-disubstituted benzylideneanilines (Table 1), assuming a linear model function of the parameters σ_I and σ_R^0 (6), of the type:

$$[1] \quad k_r = a_0 + a_1\sigma_R^0(X) + a_2\sigma_I(X) + a_3\sigma_R^0(Y) + a_4\sigma_I(Y)$$

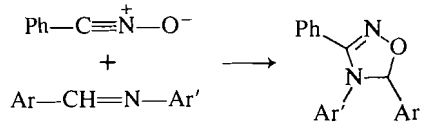

FIG. 1.

The 12 points selected by the optimum *D* criterion (7) (Fig. 2) are also set out in Table 1.

Experimental

(a) Materials and methods

Column chromatography separations were performed on silica gel 60 (Merck) with activity II–IV (Brockmann). Analytical tlc was performed on silica gel 60 F_{254} (Merck).

Gas–liquid chromatographies (competition measurements) were carried out on a Perkin–Elmer Sigma 300 apparatus fitted with a Sigma 10 chromatographic data station using the following conditions: column VCC 10% on Chromosorb W (AW-DCMS, 80–100 mesh); column dimensions, 3 m × 0.32 cm; carrier gas, N_2 (40–45 mL/min); detector temperature (flame ionization), 220°C.

(b) Spectroscopic procedures

The ir spectra were recorded on a Perkin–Elmer 781 spectrophotometer in KBr. The ^{1}H nmr spectra (analytical) were recorded on a Varian T-60 apparatus at 60 MHz. The ^{1}H nmr spectra (competition measurements) were recorded on a Bruker WP 80 spectrometer. The uv spectra were recorded on a Perkin–Elmer Lambda 3 apparatus in $CHCl_3$, at concentrations between 10^{-4} and 10^{-5} *M*.

(c) Melting points were determined in a Büchi 510 apparatus and are not corrected.

(d) Azomethines were prepared using the following general procedure: equimolecular amounts of amine and aldehyde were mixed together in a Dean–Stark device, in benzene, toluene, or xylene as solvent. The system was heated at reflux for 1–2 h and the solvent was then distilled *in vacuo*.

Except for imine no. **22**, the remaining imines have been previously described, e.g., imines **1**, **19**, and **37** by Hall and co-workers (8) and imines **4**, **8**, **9**, **26**, **27**, **37**, **39**, **43**, and **44** by Tokumaru and

[1]Author to whom correspondence may be addressed.

[2]Revision received February 17, 1987.

[3]The observed regioselectivity agrees with that observed in similar cases (2) and may be rationalized by the application of the FMO (Frontier Molecular Orbital) theory.

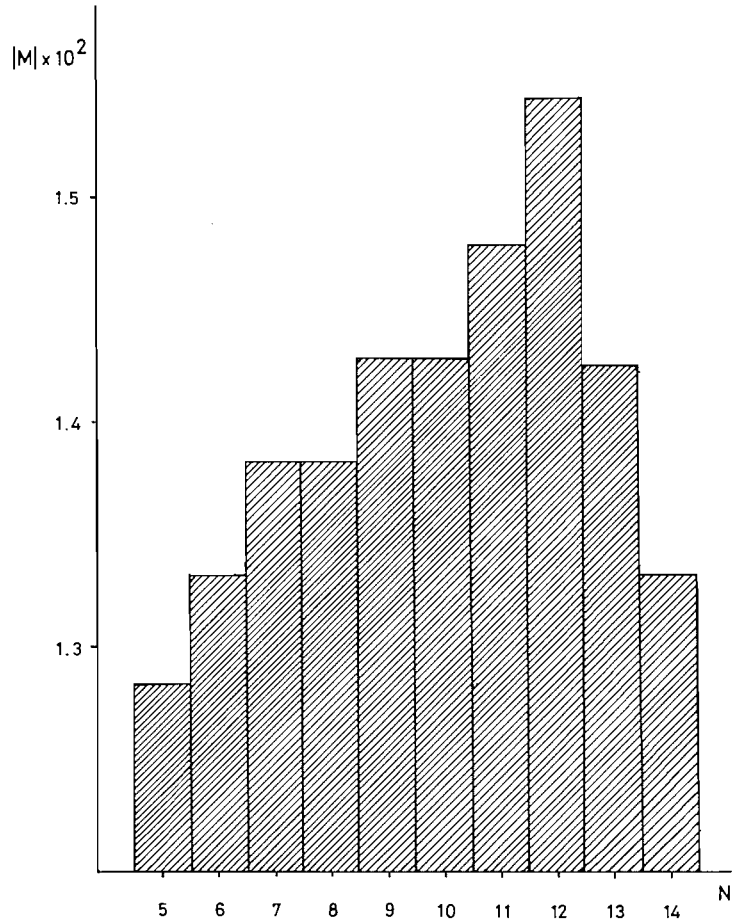

FIG. 2. Value of the determinant $|M|$ as a function of the number of experiments N.

co-workers (9). Contrary to the comments of Hall (8), all imines can be crystallized from ethanol with the exception of the *p*-nitroaniline derivatives (**8**, **26**, and **43**), which afford crystalline ethoxyamino derivatives ArCH(OEt)NHAr′. These azomethines were crystallized from benzene. Yields are expressed as % crystalline product.

p-*Methoxybenzylidene*-p-*fluoraniline* (*22*)

In benzene as solvent, mp 70–72°C; yield, 50%; ν_{max}: 1620 cm^{-1}; ^1H nmr ($CDCl_3$), δ: 3.76 (s, 3H, CH_3—O), 8.27 (s, 1H, CH=N), 6.7–7.9 (m, 8H, aromatics). *Anal.* calcd.: C 73.36, H 5.24, N 6.11; found: C 73.51, H 5.06, N 6.16%.

(e) 3,4-Diaryl-5-phenyl-4,5-dihydro-1,2,4-oxadiazoles

Method A

To a mixture of imine and benzhydroximoyl chloride (10) in chloroform, a solution of freshly distilled triethylamine in chloroform was added. The molar ratio imine:chloride:Et_3N was approximately 1:1.5:1.5. The reaction was stirred at room temperature for between 3 and 7 h. After filtration of triethylamine hydrochloride, the reaction crude was chromatographed on a column (10 g silica gel/1 g crude) using benzene as eluent.

Method B

To a solution of imine in carbon tetrachloride, a solution of benzhydroximoyl chloride and a solution of freshly distilled triethylamine in carbon tetrachloride were simultaneously added. The molar ratio imine:chloride:Et_3N was approximately 1:2.2:2.2. The reaction was continued as in Method A.

3,4,5-Triphenyl-4,5-dihydro-1,2,4-oxadiazol (**1**): 500 mg (2.76 mmol) of **1** was treated with 640 mg (4.11 mmol) of benzhydroximoyl chloride and 420 mg (4.16 mmol) of triethylamine according to Method A. Reaction time, 7 h. Yield, 190 mg (0.63 mmol), 23%; mp 75–76°C (EtOH); ^1H nmr (CCl_4), δ: 6.30 (s, 1H), 6.6–7.5 (m, 15H). *Anal.* calcd.: C 80.00, H 5.33, N 9.33; found: C 79.95, H 5.40, N 9.56%. This product was described by Fabbrini and de Sarlo. (64%) (11), Lauria *et al.* (64%) (12), and Huisgen and co-workers (71%) (13).

*3,5-Diphenyl-4-(*p-*fluorphenyl)-4,5-dihydro-1,2,4-oxadiazol* (**2**): 500 mg (2.51 mmol) of **4** was treated with 570 mg (3.66 mmol) of benzhydroximoyl chloride and 380 mg (3.77 mmol) of triethylamine according to Method A. Reaction time, 7 h. Yield, 160 mg (0.50 mmol), 20%; mp 119–120°C (EtOH); ^1H nmr (CCl_4), δ: 6.30 (s, 1H), 6.6–7.8 (m, 14H). *Anal.* calcd.: C 75.47, H 4.72, N 8.81; found: C 75.52, H 4.78, N 8.80%.

*3,5-Diphenyl-4-(*p-*nitrophenyl)-4,5-dihydro-1,2,4-oxadiazol* (**3**): 340 mg (1.50 mmol) of **8** was treated with 520 mg (3.34 mmol) of benzhydroximoyl chloride and 340 mg (3.37 mmol) of triethylamine according to Method B. Reaction time, 7 h. Yield, 350 mg (1.01 mmol), 67%. The resulting oil (one pot in tlc) could not be crystallized; ^1H nmr (CCl_4), δ: 6.53 (s, 1H), 6.6–8.1 (m, 14H). *Anal.* calcd.: C 69.56, H 4.35, N 12.17; found: C 69.70, H 4.35, N 12.13%.

*3,5-Diphenyl-4-(*p-N,N-*dimethylaminophenyl)-4,5-dihydro-1,2,4-oxadiazol* (**4**): 170 mg (0.76 mmol) of **9** was treated with 180 mg (1.16 mmol) of benzhydroximoyl chloride and 120 mg (1.18 mmol) of triethylamine according to Method A. Reaction time, 2 h. Yield, 140 mg (0.41 mmol), 54%; mp 140–142°C (EtOH); ^1H nmr ($CDCl_3$), δ: 2.83 (s, 6H), 6.33 (s, 1H), 6.5–6.8 (m, 14H). *Anal.* calcd.: C 79.67, H 6.12, N 12.24; found: C 79.62, H 6.05, N 12.21%.

*3,4-Diphenyl-5-(*p-*methoxyphenyl)-4,5-dihydro-1,2,4-oxadiazol* (**5**): 170 mg (0.81 mmol) of **19** was treated with 190 mg (1.22 mmol) of benzhydroximoyl chloride and 120 mg (1.13 mmol) of triethylamine according to Method A. Reaction time, 5 h. Yield, 210 mg (0.64 mmol), 79%. The resulting oil (one pot in tlc) could not be crystallized; ^1H nmr ($CDCl_3$), δ: 3.80 (s, 3H), 6.40 (s, 1H), 6.6–7.8 (m, 15H). *Anal.* calcd.: C 76.36, H 5.45, N 8.48; found: C 76.51, H 5.39, N 8.40%.

Can. J. Chem. Downloaded from www.nrcresearchpress.com by 213.166.140.6 on 09/07/12
For personal use only.

Can. J. Chem. Downloaded from www.nrcresearchpress.com by 213.166.140.6 on 09/07/12
For personal use only.

TABLE 1. Natural and codified variables for the 45 4,4′-disubstituted benzylideneanilines

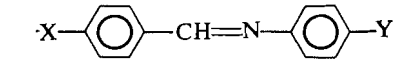

No.	X	Y	$\sigma_R^0(X)$	$\sigma_I(X)$	$\sigma_R^0(Y)$	$\sigma_I(Y)$	Coded variables[a] x_1	x_2	x_3	x_4
1	H-	H-	0.00	0.00	0.00	0.00	0.37	−0.85	0.46	−0.85
2	H-	CH_3-	0.00	0.00	−0.10	−0.05	0.37	−0.85	0.18	−1.00
3	H-	CH_3O-	0.00	0.00	−0.41	0.26	0.37	−0.85	−0.69	−0.10
4	H-	F-	0.00	0.00	−0.34	0.51	0.37	−0.85	−0.49	0.62
5	H-	Cl-	0.00	0.00	−0.20	0.47	0.37	−0.85	−0.10	0.51
6	H-	Br-	0.00	0.00	−0.16	0.45	0.37	−0.85	0.01	0.45
7	H-	I-	0.00	0.00	−0.12	0.39	0.37	−0.85	0.13	0.27
8	H-	$-NO_2$	0.00	0.00	0.19	0.64	0.37	−0.85	1.00	1.00
9	H-	$-N(CH_3)_2$	0.00	0.00	−0.52	0.05	0.37	−0.85	−1.00	−0.71
10	Cl-	H-	−0.20	0.47	0.00	0.00	−0.30	0.51	0.46	−0.85
11	Cl-	CH_3-	−0.20	0.47	−0.10	−0.05	−0.30	0.51	0.18	−1.00
12	Cl-	CH_3O-	−0.20	0.47	−0.41	0.26	−0.30	0.51	−0.69	−0.10
13	Cl-	F-	−0.20	0.47	−0.34	0.51	−0.30	0.51	−0.49	0.62
14	Cl-	Cl-	−0.20	0.47	−0.20	0.47	−0.30	0.51	−0.10	0.51
15	Cl-	Br-	−0.20	0.47	−0.16	0.45	−0.30	0.51	0.01	0.45
16	Cl-	I-	−0.20	0.47	−0.12	0.39	−0.30	0.51	0.13	0.27
17	Cl-	$-NO_2$	−0.20	0.47	0.19	0.64	−0.30	0.51	1.00	1.00
18	Cl-	$-N(CH_3)_2$	−0.20	0.47	−0.52	0.05	−0.30	0.51	−1.00	−0.71
19	CH_3O-	H-	−0.41	0.26	0.00	0.00	−1.00	−0.10	0.46	−0.85
20	CH_3O-	CH_3-	−0.41	0.26	−0.10	−0.05	−1.00	−0.10	0.18	−1.00
21	CH_3O-	CH_3O-	−0.41	0.26	−0.41	0.26	−1.00	−0.10	−0.69	−0.10
22	CH_3O-	F-	−0.41	0.26	−0.34	0.51	−1.00	−0.10	−0.49	0.62
23	CH_3O-	Cl-	−0.41	0.26	−0.20	0.47	−1.00	−0.10	−0.10	0.51
24	CH_3O-	Br-	−0.41	0.26	−0.16	0.45	−1.00	−0.10	0.01	0.45
25	CH_3O-	I-	−0.41	0.26	−0.12	0.39	−1.00	−0.10	0.13	0.27
26	CH_3O-	$-NO_2$	−0.41	0.26	0.19	0.64	−1.00	−0.10	1.00	1.00
27	CH_3O-	$N(CH_3)_2$	−0.41	0.26	−0.52	0.05	−1.00	−0.10	−1.00	−0.71
28	CH_3-	H-	−0.10	−0.05	0.00	0.00	0.03	−1.00	0.46	−0.85
29	CH_3-	CH_3-	−0.10	−0.05	−0.10	−0.05	0.03	−1.00	0.18	−1.00
30	CH_3-	CH_3O-	−0.10	−0.05	−0.41	0.26	0.03	−1.00	−0.69	−0.10
31	CH_3-	F-	−0.10	−0.05	−0.34	0.51	0.03	−1.00	−0.49	0.62
32	CH_3-	Cl-	−0.10	−0.05	−0.20	0.47	0.03	−1.00	−0.10	0.51
33	CH_3-	Br-	−0.10	−0.05	−0.16	0.45	0.03	−1.00	0.01	0.45
34	CH_3-	I-	−0.10	−0.05	−0.12	0.39	0.03	−1.00	0.13	0.27
35	CH_3-	$-NO_2$	−0.10	−0.05	0.19	0.64	0.03	−1.00	1.00	1.00
36	CH_3-	$-N(CH_3)_2$	−0.10	−0.05	−0.52	0.05	0.03	−1.00	−1.00	−0.71
37	$-NO_2$	H-	0.19	0.64	0.00	0.00	1.00	1.00	0.46	−0.85
38	$-NO_2$	$-CH_3$	0.19	0.64	−0.10	0.05	1.00	1.00	0.18	−1.00
39	$-NO_2$	F-	0.19	0.64	−0.34	0.51	1.00	1.00	−0.49	0.62
40	$-NO_2$	Cl-	0.19	0.64	−0.20	0.47	1.00	1.00	−0.10	0.51
41	$-NO_2$	Br-	0.19	0.64	−0.16	0.45	1.00	1.00	0.01	0.45
42	$-NO_2$	-I	0.19	0.64	−0.12	0.39	1.00	1.00	0.13	0.27
43	$-NO_2$	$-NO_2$	0.19	0.64	0.19	0.64	1.00	1.00	1.00	1.00
44	$-NO_2$	$-N(CH_3)_2$	0.19	0.64	−0.52	0.05	1.00	1.00	−1.00	−0.71
45	$-NO_2$	CH_3O-	0.19	0.64	−0.41	0.26	1.00	1.00	−0.69	−0.10

[a]Natural variables (NV) were not standardized in the usual way but following the formula

$$x_{ij} = \frac{NV_{ij} - (\text{center})_i}{(\text{range of variation})_i}$$

where $(\text{centre})_i = (NV_{max} + NV_{min})/2$ and $(\text{range of variation})_i = (NV_{max} - NV_{min})/2$. This method of standardization leads the variables to have values between +1 and −1 (see ref. 7).

*3-Phenyl-4-(*p*-fluorphenyl)-5-(*p*-methoxyphenyl)-4,5-dihydro-1,2,4-oxadiazol* (**6**): 340 mg (1.48 mmol) of **22** was treated with 350 mg (2.25 mmol) of benzhydroximoyl chloride and 220 mg (2.18 mmol) of triethylamine according to Method A. Reaction time, 3 h. Yield, 330 mg (0.95 mmol), 64%. The resulting oil (one pot in tlc) could not be crystallized; ^1H nmr ($CDCl_3$), δ: 3.80 (s, 3H), 6.37 (s, 1H), 6.6–7.7 (m, 13H). *Anal.* calcd.: C 72.41, H 4.89, N 8.05; found: C 72.83, H 4.61, N 8.09%.

*3-Phenyl-5-(*p*-methoxyphenyl)-4-(*p*-nitrophenyl)-4,5-dihydro-1,2,4-oxadiazol* (**7**): 340 mg (1.33 mmol) of **26** was treated with 480 mg (3.10 mmol) of benzhydroximoyl chloride and 310 mg (2.97 mmol) of triethylamine according to Method B. Reaction time, 7 h. Yield, 360 mg (0.96 mmol), 73%. The resulting oil (one pot in tlc) could not be crystallized; ^1H nmr ($CDCl_3$), δ: 380 (s, 3H), 6.4–8.1 (m, 14H). *Anal.* calcd.: C 67.20, H 4.53, N 11.20; found: C 67.09, H 4.40, N 11.81%.

TABLE 2. Experimental conditions for chromatographic measurements

Imine no.	Retention time (min)	Reference imine	Retention time (min)	Internal standard retention time[a] (min)	Temperature program[b]
4	8.0	9[c]	21.0	3.09	185–10/20/230–14
8	11.7	1	8.1	3.12	185–13/20/230–15
9	21.0	1	7.5	3.09	185–10/20/230–14
19	14.1	1	7.5	3.07	185–9/20/225–18
22	12.2	1	7.8	3.13	185–12/20/230–15
37	15.7	1	8.21	3.02	185–13/20/230–15
39	15.9	1	8.06	3.06	185–13/20/230–15

[a]Biphenyl as internal standard in all cases.

[b]Initial temperature – time the initial temperature is maintained/rates of temperature increase of °C/min/final temperature – time the final temperature is maintained.

[c]In this case, considering the similarity of the retention times, the reference imine was **9**; the relative rate measured was subsequently corrected with respect to imine **1**.

*3-Phenyl-4-(*p-N,N-*dimethylaminophenyl)-5-(*p-*methoxyphenyl)-4,5-dihydro-1,2,4-oxadiazol* (**8**): 340 mg (1.33 mmol) of **27** was treated with 350 mg (2.25 mmol) of triethylamine according to Method A. Reaction time, 4 h. Yield, 80 mg (0.21 mmol), 16%; mp 118–120°C (CCl_4); ^1H nmr ($CDCl_3$), δ: 2.70 (s, 6H), 3.63 (s, 3H), 6.10 (s, 1H), 6.2–7.6 (m, 13H). *Anal.* calcd.: C 73.99, H 6.17, N 11.26; found: C 74.11, H 6.21, N 11.24%.

*3,4-Diphenyl-5-(*p-*nitrophenyl)-4,5-dihydro-1,2,4-oxadiazol* (**9**): 170 mg (0.75 mmol) of **37** was treated with 180 mg (1.16 mmol) of benzhydroximoyl chloride and 110 mg (1.09 mmol) of triethylamine according to Method A. Reaction time, 3 h. Yield, 100 mg (0.29 mmol), 39%; mp 104–108°C (EtOH); ^1H nmr ($CDCl_3$), δ: 6.57 (s, 1H), 6.7–8.5 (m, 14H). *Anal.* calcd.: C 69.56, H 4.34, N 12.17; found: C 69.55, H 4.33, N 12.20%.

*3-Phenyl-4-(*p-*fluorphenyl)-5-(*p-*nitrophenyl)-4,5-dihydro-1,2,4-oxadiazol* (**10**): 170 mg (0.70 mmol) of **39** was treated with 160 mg (1.03 mmol) of benzhydroximoyl chloride and 110 mg (1.09 mol) of triethylamine according to Method A. Reaction time, 3 h. Yield, 100 mg (0.28 mmol), 40%; mp 90–92°C (EtOH); ^1H nmr ($CDCl_3$), δ: 6.53 (s, 1H), 6.7–8.5 (m, 13H). *Anal.* calcd.: C 66.12, H 3.86, N 11.57; found: C 66.10, H 3.87, N 11.59%.

*3-Phenyl-4,5-bis(*p-*nitrophenyl)-4,5-dihydro-1,2,4-oxadiazol* (**11**): 340 mg (1.25 mmol) of **43** was treated with 470 mg (3.02 mmol) of benzhydroximoyl chloride and 300 mg (2.97 mmol) of triethylamine according to Method B. Reaction time, 2 h. Yield, 300 mg (0.77 mmol), 62%. The resulting oil (one pot in tlc) could not be crystallized; ^1H nmr ($CDCl_3$), δ: 6.5–8.4 (m, 13H). *Anal.* calcd.: C 61.54, H 3.59, N 14.36; found: C 61.41, H 3.62, N 14.43%.

*3-Phenyl-4-(*p-N,N-*dimethylaminophenyl)-5-(*p-*nitrophenyl)-4,5-dihydro-1,2,4-oxadiazol* (**12**): 340 mg (1.26 mmol) of **44** were treated with 430 mg (2.77 mmol) of benzhydroximoyl chloride and 280 mg (2.77 mmol) of triethylamine according to Method B. Reaction time, 3 h. Yield, 180 mg (0.46 mmol), 37%; mp 170–172°C (EtOH); ^1H nmr ($CDCl_3$), δ: 2.85 (s, 6H), 6.43 (s, 1H), 6.3–8.3 (m, 13H). *Anal.* calcd.: C 68.04, H 5.15, N 14.43; found: C 68.01, H 5.03, N 14.46%.

(f) Competition measurements

Competition measurements corresponding to imines **4**, **8**, **9**, **19**, **22**, **37**, and **39** were carried out by gas–liquid chromatography. The measurements of the areas of the peaks corresponding to the reference imine (**1**) and the internal standard (biphenyl in all cases), both prior to the addition of the reagent ($t = 0$) and when all of the reagent had been consumed (time $t = t$) (14), gave the expression corresponding to the relative cycloaddition rate through the application of eq. [2]:

$$[2] \quad \log \frac{S_{nt}}{S_{n0}} \cdot \frac{S_0}{S_t} = \frac{k_n}{k_1} \log \frac{S_{1t}}{S_{10}} \cdot \frac{S_0}{S_t}$$

where: S_{n0} = area of the peak corresponding to imine n when time $t = 0$; S_{10} = area of the peak corresponding to the reference imine when $t = 0$; S_0 = area of the peak corresponding to biphenyl when time $t = 0$; S_{nt} = area of the peak corresponding to imine n when time $t = t$; S_{1t} = area of the peak corresponding to the reference imine when time $t = t$; S_t = area of the peak corresponding to biphenyl when time $t = t$.

TABLE 3. Experimental conditions for ^1H nmr measurements

Imine no.	δ CH=N	Reference imine	δ CH=N
26	8.32	**9**	8.51
27	8.43	**1**	8.45
43	8.52	**27**	8.43
44	8.62	**27**	8.43

The imine whose relative ratio was to be measured, the reference imine, and the internal standard were dissolved in the minimum, amount of chloroform in a molar ratio of approximately 5:5:1.

Several samples were analyzed by glc and the ratio of the areas relative to the internal standard was determined. Then a chloroform solution of benzhydroximoyl chloride and a solution of freshly distilled triethylamine were added simultaneously. The molar ratio imine:reagent was in all cases 2:1. The reaction mixture was stirred at room temperature for between three and four hours and the samples to be analyzed were then withdrawn. Table 2 shows the retention time for each compound and the optimum temperature programs for each chromatographic analysis.

A typical procedure was the following: benzylideneaniline (**1**) (49.9 mg, 0.276 mmol), *N*-(*p*-*N*,*N*-dimethylaminophenyl)benzylideneamine (**9**) (62.0 mg, 0.277 mmol), and biphenyl (10.2 mg, 0.066 mmol) were mixed together in 8.0 mL of chloroform. Three samples were analyzed by glc under the previously mentioned conditions. The retention times and the areas of **1**, **9**, and biphenyl were the following (see eq. [2]):

Retention times (min)			Areas		
1	**9**	Biphenyl	S_{90}	S_{10}	S_0
7.47	20.95	3.07	6.21	19.84	5.90
7.47	21.09	3.07	6.49	21.36	6.24
7.47	21.00	3.10	8.64	26.39	7.60

A solution of benzhydroximoyl chloride (43.8 mg, 0.282 mmol) in 7.0 mL of chloroform and a solution of triethylamine (30.3 mg, 0.300 mmol) in 7.0 mL of chloroform were simultaneously added to the imine and biphenyl solution. After 3 h 23 min a sample was withdrawn. The chlorhydrate of the amine was removed by filtration and washed with chloroform (3 × 5 mL). The solvent was partially

Can. J. Chem. Downloaded from www.nrcresearchpress.com by 213.166.140.6 on 09/07/12
For personal use only.

TABLE 4. Relative rate constants for the selected benzylideneanilines

Compound no.	**27**	**9**	**22**	**19**	**4**	**1**	**44**	**26**	**37**	**39**	**8**	**43**
k_{rel}	2.3	2.0	1.5	1.4	1.2	1.0	1.4	1.2	1.1	1.0	0.4	0.9

eliminated to a volume of solution of ca. 10 mL and the mixture was analyzed with the following results:

Retention times (min)			Areas		
1	**9**	Biphenyl	S_{9t}	S_{1t}	S_t
7.47	21.12	3.06	5.75	23.92	9.16
7.47	21.12	3.09	6.42	29.76	12.26

Evaluation of three independent experiments by eq. [2] afforded k_9/k_1. Mean value $k_9/k_1 = 2.0$; estimated error ± 0.1.

Competition measurements corresponding to the imines **26**, **27**, **43**, and **44** were carried out by ^{1}H nmr spectroscopy. No internal standard was used. Equimolar amounts of the imine whose relative rate was to be measured and of the reference imine were weighed. Both imines were then dissolved in $CDCl_3$ and the ^{1}H nmr spectrum of the mixture was recorded. The ratio of imines was determined from multiple integration of the signals corresponding to the aldiminic proton on a conveniently expanded spectrum. Subsequently, an equimolar mixture of benzhydroximoyl chloride and triethylamine (ratio imine:reagents approximately 2:1.5) was added and the spectrum was recorded after three hours; the ratio of unreacted imines was then measured. The relative rate was determined by means of a modified eq. [2]. Table 3 shows the experimental conditions used.

A typical procedure was the following: 50.0 mg (0.276 mmol) of imine **1** and 70.2 mg (0.276 mmol) of imine **27** were dissolved in 7.0 mL of $CDCl_3$ and the ^{1}H nmr spectrum of the mixture was then recorded. The integral corresponding to aldiminic protons of each compound was 24.0 mm. To the above solution were added simultaneously a solution of 42.9 mg (0.276 mmol) of benzhydroximoyl chloride in 2 mL of $CDCl_3$ and a solution of 27.9 mg (0.276 mmol) of Et_3N in 2 mL of $CDCl_3$. The reaction was maintained at room temperature for 3 h. The chlorhydrate of the amine was then removed by filtration and washed with $CDCl_3$ (2 × 3 mL). The solution was analyzed by ^{1}H nmr. The areas of the aldiminic protons (multiple integration) were $S_{27t} = 15.1$ mm; $S_1 = 19.5$ mm.

Substitution in eq. [2] yielded

$$k_{27}/k_1 = 2.23$$

The experiment was repeated three times. Mean value $k_{27}/k_1 = 2.3$. Estimated error ± 0.2.

Results and discussion

The competition rate constant values based on 1.0 for X = Y = H (imine **1**) are collected in Table 4.

The total range of k_{rel} covers 5.7 units. The slowest value corresponds to the imine with X = H, Y = NO_2 (**8**), whereas the fastest representative is imine **27**, with X = OCH_3, Y = $N(CH_3)_2$.

The regression obtained with the 12 selected experiments led to the eq. [3]

$$[3] \quad k_r = 1.3 - 0.3(\pm 0.24)x_1 + 0.1(\pm 0.26)x_2 - 0.4(\pm 0.25)x_3 - 0.2(\pm 0.25)x_4$$

$$r^2 = 0.82; \; r_A^2 = 0.72; \; n = 12; \; s = 0.27; \; F_{4,7;0.95} = 4.12$$

This equation is acceptable, though not completely satisfactory from a statistical point of view, if the magnitude of the confidence interval and the small F values are taken into account. The use of more complex models, such as the additive model that takes into account interactions between X and Y through the azomethinic bond, does not improve the results.

TABLE 5. FMO energies for the selected benzylideneanilines

Compound no.	Fully minimized		Planar structure	
	E_{HO}	E_{LU}	E_{HO}	E_{LU}
27	−8.58	−0.07	−8.53	−0.60
9	−8.57	−0.10	−8.58	−0.55
22	−9.19	−0.21	−8.82	−0.82
19	−9.06	−0.08	−8.68	−0.59
4	−9.20	−0.23	−8.98	−0.78
1	−9.05	−0.01	−8.84	−0.54
44	−8.75	−1.15	−8.80	−1.30
26	−9.36	−0.60	−9.21	−1.31
37	−9.39	−0.73	−9.36	−1.31
39	−9.53	−0.83	−9.50	−1.45
8	−9.81	−0.65	−9.55	−1.30
43	−10.43	−0.99	−10.34	−1.76

An examination of the relative rates of cycloadditions (Table 4) indicates a small development of charged species in the transition state. Thus, for the cycloaddition of benzonitrile oxide to substituted styrenes (15) (a concerted process with a high degree of synchrony) the maximum ratio of rates is 2, the fastest representative corresponding to the 4-nitro derivative and the slowest to the unsubstituted one. However, for the cycloaddition of tetracyanoethylene to *p*-substituted styrenes (a typical zwitterionic process) the rate constant presents a variation in the range of 500 from the *p*-methoxy to the *p*-cyclopropyl substituent (16).

Sustmann (17) has collected data for the reactivity of a large number of 1,3-dipolar cycloaddition reactions and the reactivity of the 1,3-dipoles is classified in three groups according to the separation between FMOs of dipoles and dipolarophiles and, therefore, with frontier orbital control for these reactions.

In view of this, we tried to know the electronic configuration of the 1,3-dipole and of the dipolarophiles, to explain the observed reactivity scale by using the FMO theory (18).

The electronic structure for the different benzylideneanilines in their *E* configuration[4] was calculated using an SCF semi-empirical molecular orbital (MO) method MNDO (20). The geometrical features obtained when the azomethinic structures were fully minimized show that both aromatic rings are out of the C=N bond plane, displaying unusually high torsion angles (of between 64° and 83° for both aromatic rings), which are of similar value in every case.

However, it is well known that the aromatic ring attached to the imine carbon is planar or practically planar (21), whereas the ring attached to the nitrogen is twisted in such a way that the loss of π−π conjugation (22) is made up for by the increase in $n-\pi$ conjugation. The lack of planarity may be due to the MNDO

[4]All these benzylideneanilines exist in their more stable *E* configuration; assignments were made in a straightforward way by considering their spectroscopic data and the bibliography on the subject (8, 19).

Can. J. Chem. Downloaded from www.nrcresearchpress.com by 213.166.140.6 on 09/07/12
For personal use only.

TABLE 6. Ultraviolet parameters (λ_{max}, ε), calculated θ, and FMO energies for the benzylideneanilines considered

No.	λ_{max}(nm)	ε	θ_{calc}	E_{HO}(eV)	E_{LU}(eV)	ΔE_I[a]	ΔE_{II}[b]
27	372	9 800	45.8	−8.55	−0.49	7.55	9.51
9	377	16 100	26.8	−8.57	−0.51	7.57	9.49
22	318	9 400	47.0	−8.94	−0.67	7.94	9.33
19	312	9 400	47.0	−8.80	−0.48	7.80	9.52
4	290	2 600	69.0	−9.16	−0.48	8.16	9.52
1	282	3 600	65.0	−9.00	−0.32	8.00	9.68
44	452	20 000	0	−8.80	−1.30	7.80	8.70
26	345	16 000	26.8	−9.24	−1.26	8.24	8.74
37	346	8 900	48.4	−9.36	−1.60	8.36	8.40
39	348	10 000	45.3	−9.50	−1.43	8.50	8.57
8	345	17 400	21.9	−9.58	−1.27	8.58	8.73
43	340	17 200	22.7	−10.36	−1.73	9.36	8.27

[a]Represents E_{HO}(dipolarophile) − E_{LU}(dipole).
[b]Represents E_{HO}(dipole) − E_{LU}(dipolarophile). The values for the FMO of benzonitrile oxide were established by Houk *et al.* (25): $E_{HO} = -10$ eV; $E_{LU} = -1.0$ eV.

tendency to twist groups possessing π-delocalization with phenyl rings (23), a tendency probably due to the overestimation of short nonbonded interactions in this semiempirical method (20).

To test the influence of the geometrical features on the electronic structure of the selected 12 benzylideneanilines the FMO energies were recalculated for a planar structure (Table 5). The values obtained show that this influence is noticeable in particular in the LUMO energy and in the coefficients of both frontier orbitals.

In view of this, it was considered necessary to recalculate the FMO energy levels assuming the aromatic moiety attached to the iminic carbon to be planar; considering a torsion angle, calculated from data, for the aromatic ring attached to the nitrogen atom; and fixing the corresponding dihedral angles.

Equation [4] used by Minkin *et al.* (22*h*) relates the torsion angle θ of a compound to the extinction coefficient (ε) for its conjugation band and the extinction coefficient (ε_0) of a coplanar system.

$$[4] \quad \cos^2\theta = \frac{\varepsilon}{\varepsilon_0}$$

In Table 6 are collected the uv data (λ_{max} and ε of the conjugation band) for the benzylideneanilines considered.

In accordance with Doubt and Vandembert's observations (24), the presence of substituents of complementary electronic demand (attractor–donor) on both rings favours a shift of the azomethinic conjugation band with respect to benzylideneaniline, increasing the system conjugation and therefore the coplanarity. So compound no. **44**, which has a maximum complementary substitution, is taken as the reference system (coplanar, $\theta = 0$) for the evaluation of the torsion angles of the ring attached to the nitrogen atom in our benzylideneanilines. The new values of θ introduced in the molecular geometry for MNDO calculations, as well as the values of E_{HOMO}[5] and E_{LUMO} obtained, are indicated in Table 6.

The ΔE values, set out in Table 6, show that the range studied cannot be satisfied solely by a type of orbital control (HOMO dipole – LUMO dipolarophile or LUMO dipole – HOMO dipolarophile), as was to be expected for a type II dipole (17). This accounts for our difficulty in finding a mathematical model that reproduces the observed rates of cycloaddition for the 12 selected imines. In fact, when the regression is performed with the seven cases with an ΔE value more favourable for the interaction LUMO dipole – HOMO dipolarophile using σ_p(X) and σ_p(Y), an excellent result is obtained (eq. [5]).

$$[5] \quad k_r = 1.19 - 0.88(\pm 0.43)\sigma_p(X) - 1.03(\pm 0.35)\sigma_p(Y)$$
$$r^2 = 0.95;\ r^2_A = 0.92;\ n = 7;\ s = 0.13;\ F_{1,4;0.95} = 4.26$$

The use of σ_p instead of σ^0_R and σ_I is statistically necessary to have an acceptable number of degrees of freedom, and the correlation existing among the variables makes it suitable. When σ_p(X) and σ_p(Y) are used with the 12 imines, r^2 decreases to 0.75.

[5]To our knowledge, the only experimental data in the literature concerning the HOMO of benzylideneaniline (22*i*) agree with the determined value.

Acknowledgements

We would like to express our gratitude to the CAICYT (Ministerio de Educación y Ciencia, Spain) for financial support (Grant no. 320-84).

1. (*a*) A. PADWA. 1,3-Dipolar cycloaddition chemistry. J. Wiley, New York. 1984; (*b*) R. A. FIRESTONE. Tetrahedron, **33**, 3009 (1977); (*c*) R. HUISGEN. J. Org. Chem. **33**, 2291 (1968); (*d*) R. HUISGEN. J. Org. Chem. **41**, 403 (1976).
2. P. CARAMELLA and P. GRUNANGER. *In* 1,3-Dipolar cycloaddition chemistry. *Edited by* A. Padwa. J. Wiley, New York. 1984. Chap. 3. p. 356, and references therein.
3. A. ECKELL, R. HUISGEN, R. SUSTMANN, G. WALLBILICH, and R. SPINDLER. Chem. Ber. **100**, 2192 (1967).
4. G. BIANCHI, R. GANDOLFI, and P. GRUNANGER. *In* The chemistry of triple bonded functional groups. Part 2. *Edited by* S. Patai and Z. Rappoport. J. Wiley, New York. 1983. Chap. 18. p. 752.
5. (*a*) D. MATHIEU and R. PHAN TAN LUU. Logical NEMROD, LPRAI. Université d'Aix-Marseille, France; (*b*) V. V. FEDOROV. Theory of optimal experiments. Appendix IX. Academic Press, New York. 1972. p. 217; (*c*) B. ALCAIDE, C. LOPEZ-MARDOMINGO, R. PEREZ-OSSORIO, J. PLUMET, R. PHAN TAN LUU, and M. SARGENT. Can. J. Chem. **63**, 2241 (1985); (*d*) C. CATIVIELA, E. MELENDEZ, J. ELGUERO, D. MATHIEU, and R. PHAN TAN LUU. Eur. J. Med. Chem. **18**, 359 (1983); (*e*) R. M. CLARAMUNT, J. ELGUERO, D. MATHIEU, and R. PHAN TAN LUU. An. Quim. **80**, 30 (1984); (*f*) D. MATHIEU, R. PHAN TAN LUU, and J. ELGUERO. Bull. Soc. Chim. Belg. **89**, 267 (1980).

Can. J. Chem. Downloaded from www.nrcresearchpress.com by 213.166.140.6 on 09/07/12
For personal use only.

6. D. EXNER. *In* Correlation analysis in chemistry. Recent advances. *Edited by* N. B. Chapman and J. Shorter. Plenum Press, New York. 1978. Chap. 10.
7. R. M. CLARAMUNT, R. GALLO, J. ELGUERO, D. MATHIEU, and R. PHAN TAN LUU. J. Chim. Phys. **78**, 805 (1981).
8. A. S. AL-TAI, D. HALL, and A. R. MEARS. J. Chem. Soc. Perkin Trans. 2, 133 (1976), and references therein.
9. (*a*) R. AKABA, H. SAKURAGI, and K. TOKUMARU. Bull. Chem. Soc. Jpn. **58**, 301 (1985); (*b*) R. AKABA, H. SAKURAGI, and K. TOKUMARU. Bull. Chem. Soc. Jpn. **58**, 1711 (1985).
10. A. WERNER and H. BUSS. Ber. Dtsch. Chem. Ges. **27**, 2193 (1894).
11. L. FABBRINI and F. DE SARLO. Chem. Ind. (Milán), **45**, 242 (1963).
12. F. LAURIA, V. VECCHIETTI, and G. TOSOLINI. Gazz. Chim. Ital **94**, 478 (1964).
13. K. BAST, M. CHRISTL, R. HUISGEN, and W. MACK. Chem. Ber. **105**, 2825 (1972).
14. M. LASPERAS, A. PEREZ RUBALCABA, and M. L. QUIROGA. Tetrahedron, **36**, 3403 (1980).
15. K. BAST, M. CHRISTL, R. HUISGEN, and W. MACK. Chem. Ber. **106**, 3312 (1973).
16. P. D. BARTLETT. Q. Rev. Chem. Soc. **24**, 473 (1970).
17. R. SUSTMANN. Pure Appl. Chem. **40**, 569 (1974).
18. R. HUISGEN. *In* 1,3-Dipolar cycloaddition chemistry. *Edited by* A. Padwa. J. Wiley, New York. 1984. p. 130, and references therein.
19. (*a*) D. WURMB-GERLICH, F. VOGTLE, A. MANNSCHRENCK, and H. A. STABB. Liebigs Ann. Chem. **708**, 35 (1967); (*b*) E. MELENDEZ, R. PEREZ-OSSORIO, and V. SANCHEZ DEL OLMO. An. Quim. Ser. B.: **66**, 87 (1970).
20. (*a*) M. J. S. DEWAR and W. THIEL. J. Am. Chem. Soc. **99**, 4899 (1977); (*b*) J. Am. Chem. Soc. **99**, 4907 (1977).
21. H. B. BURGI and J. D. DUNITZ. Helv. Chem. Acta, **53**, 1747 (1970).
22. (*a*) V. A. IZWAILSKY and E. A. SMIRNOV. J. Gen. Chem. (USSR), **26**, 3389 (1956); (*b*) N. EBARA. Bull. Chem. Soc. Jpn. **34**, 1151 (1961), and references therein; (*c*) P. BROCKELHURST. Tetrahedron, **18**, 229 (1962); (*d*) H. BRODERECH, F. EFFEMBERGER, and H. BOTSCH. Chem. Ber. **97**, 3397 (1964); (*e*) G. FAVINI and A. GAMBA. J. Chem. Phys. **62**, 995 (1965); (*f*) E. HASELBACH and E. HEILBRONNER. Helv. Chim. Acta, **51**, 16 (1968); (*g*) K. TABEI and E. SAITOU. Bull. Chem. Soc. Jpn. **42**, 1440 (1969); (*h*) V. J. MINKIN, Y. A. AHDANOV, E. A. MEDIANTEVA, and V. A. OSTROUMOV. Tetrahedron, **23**, 3651 (1967); (*i*) T. BALLY, E. HASELBACH, S. CANYOVA, F. MARSCHNER, and M. ROSSI. Helv. Chim. Acta, **59**, 486 (1976); (*j*) J. CSASZAR. Acta Phys. Chim. **29**, 133 (1983).
23. (*a*) M. J. S. DEWAR, A. H. PAKIANI, and B. PIERINI. J. Am. Chem. Soc. **104**, 3242 (1982); (*b*) C. CATIVIELA, J. I. GARCIA, C. JAIME, J. A. MAYORAL, and E. MELENDEZ. Heterocycles, **23**, 2685 (1985).
24. (*a*) L. DOUB and J. M. VANDERBELT. J. Am. Chem. Soc. **69**, 2714 (1947); (*b*) J. Am. Chem. Soc. **71**, 2414 (1949).
25. K. N. HOUK, J. SIMS, R. E. DUKE, JR., R. W. STROZIER, and J. K. GEORGE. J. Am. Chem. Soc. **95**, 7287 (1973), and references therein.

Can. J. Chem. Downloaded from www.nrcresearchpress.com by 213.166.140.6 on 09/07/12
For personal use only.

Growing interstellar cyanopolyacetylenes with ion/molecule reactions

DIETHARD K. BOHME, STANISŁAW WŁODEK, AND ASIT B. RAKSIT
Department of Chemistry and Centre for Research in Experimental Space Science, York University, Downsview, Ont., Canada M3J 1P3

Received December 15, 1986

DIETHARD K. BOHME, STANISŁAW WŁODEK, and ASIT B. RAKSIT. Can. J. Chem. **65**, 2057 (1987).

New and recent results of laboratory measurements are presented which allow an assessment of four ion/molecule reaction schemes which have been proposed for the gas-phase synthesis of interstellar cyanopolyacetylenes. The schemes are scrutinized in terms of the manner of growth of the carbon backbone and the manner in which nitrogen is entrained in the formation of ions of the type $H_2C_{2n+1}N^+$ which may neutralize by proton transfer or electron–ion recombination to form cyanopolyacetylenes.

DIETHARD K. BOHME, STANISŁAW WŁODEK et ASIT B. RAKSIT. Can. J. Chem. **65**, 2057 (1987).

On rapporte des résultats nouveaux et récents relatifs à des mesures de laboratoires qui permettent d'évaluer quatre schémas réactionnels ions/molécules qui ont été proposés pour la synthèse en phase gazeuse de cyanopolyacétylènes interstellaires. On a examiné les divers schémas en fonction de la croissance de la chaîne carbonée ainsi que de la façon par laquelle l'azote est entraîné dans la formation d'ions du type $H_2C_{2n+1}N^+$ qui peuvent être neutralisés par un transfert de proton ou par une recombinaison ion/électron conduisant à des cyanopolyacétylènes.

[Traduit par la revue]

Can. J. Chem. Downloaded from www.nrcresearchpress.com by 213.166.140.6 on 09/07/12
For personal use only.

Introduction

Perhaps the most remarkable aspect of the known chemical composition of the interstellar medium is the abundance of the homologous series of cyanopolyacetylene molecules which have been identified by radioastronomers (1). The higher members of this family of chain-like carbon molecules with terminal cyanogen (CN) substituents are not found naturally on earth, but their rotational transitions have been detected at radio frequencies in all types of molecular clouds in interstellar space as well as in circumstellar envelopes. There is now a need to understand the mechanisms of their formation in these environments. Several synthetic pathways have been suggested. These include the fragmentation of grains or very large molecules (2), catalytic surface reactions (3), and homogeneous gas-phase reactions between ions and molecules. Here we examine the various schemes which have been proposed for the latter pathway of gas-phase synthesis by ion chemistry, many elements of which have been included in detailed modelling studies of interstellar clouds. New and recent results of laboratory measurements are presented which advance our understanding of several of these schemes, allow their assessment, and permit some discrimination between them.

Four ion/molecule reaction schemes will be considered. In all of them formation of the cyanopolyacetylene is achieved ultimately by the neutralization of $H_2C_{2n+1}N^+$ through the electron-ion recombination reaction [1].

[1] $H_2C_{2n+1}N^+ + e \rightarrow HC_{2n+1}N + H$

or by a proton-transfer reaction with a molecule having a proton affinity higher than the cyanopolyacetylene. The schemes differ in the manner of growth of the carbon backbone and the manner in which nitrogen is entrained in the formation of $H_2C_{2n+1}N^+$.

The earliest models put forward by Winnewisser and Walmsley (4) and by Schiff and Bohme (5) allow for the buildup of the cyanopolyacetylenes in two ways. In one scheme (Scheme A) the acetylenic chain is conceived to grow two carbon atoms at a time by reactions between acetylene and its ions and then to be substituted by reaction with HCN or CN as indicated in reactions [2] and [3].

[2] $C_{2n}H_{2,3}^+ + HCN \rightarrow H_2C_{2n+1}N^+ + H,H_2$

[3] $C_{2n}H_{2,3}^+ + CN \rightarrow H_2C_{2n+1}N^+ + h\nu,H$

Alternatively (Scheme B), substitution is achieved first, followed by growth of the carbon backbone by reactions with acetylene ions as in reaction [4].

[4] $C_2H_{2,3}^+ + HC_{2n+1}N \rightarrow H_2C_{2n+3}N^+ + H,H_2$

Growth by one carbon atom at a time is the distinguishing feature of the scheme proposed by Woods (6) (Scheme C). The two essential steps in this scheme are given in reactions [5] and [6].

[5] $C^+ + HC_{2n+1}N \rightarrow C_{2n+2}N^+ + H$

[6] $C_{2n+2}N^+ + CH_4 \rightarrow H_2C_{2n+3}N^+ + H_2$

Finally, several authors (7–9) recently have postulated a mechanism (Scheme D) in which build-up of the carbon chain is followed by reactions with N atoms as in reactions [7] and [10]. Depending on the degree of hydrogenation of the carbonaceous reactant ion, secondary hydrogenation reactions may be required as in reactions [8] and [9] before neutralization can yield the cyanopolyacetylene.

[7] $C_{2n+1}H^+ + N \rightarrow C_{2n+1}N^+ + H$

[8] $C_{2n+1}N^+ + H_2 \rightarrow HC_{2n+1}N^+ + H$

[9] $HC_{2n+1}N^+ + H_2 \rightarrow H_2C_{2n+1}N^+ + H$

[10] $C_{2n+1}H_3^+ + N \rightarrow H_2C_{2n+1}N^+ + H$

Reactions with N atoms are attractive in the chemistry of dark interstellar clouds because of the relatively high abundance of these atoms.

Experimental

Several new reactions were measured as part of this more general evaluation of the gas-phase synthesis of cyanopolyacetylenes by ion chemistry. The measurements were performed with the Selected-Ion Flow Tube (SIFT) apparatus in the Ion Chemistry Laboratory (10, 11). Ions were generated in an axial electron impact ionizer (Extranuclear Model 0413) at ca. 50 eV from the pure parent gas or the parent gas diluted with helium: C^+ (cyanogen), C_3^+ (methylacetylene), C_5^+ (*n*-pentane), $C_4H_2^+$ (diacetylene), and C_4N^+ (allyl cyanide). The ions were injected into helium carrier gas at ca. 10 to 50 V. The total pressure was in the range from 0.30 to 0.35 Torr and the ambient temperature was 296 ± 2 K. The reagent gases and helium carrier gas were of high purity (≥99.5 mol%). Hydrogen cyanide was prepared according to the procedure described by Glemser (12). Rate constants and product distributions were derived in the usual manner (13, 14).

Can. J. Chem. Downloaded from www.nrcresearchpress.com by 213.166.140.6 on 09/07/12
For personal use only.

Results and discussion

In this section we provide a detailed and comprehensive assessment of the four ion/molecule reaction schemes which have been advanced for cyanopolyacetylene synthesis. Our new results together with recent results are integrated into the discussion as appropriate. An attempt is made throughout to project the chemistry to higher members of the homologous series for which new measurements are not available.

Series A

Scheme A rests on the likelihood of growing polyacetylene cations. Two obvious routes for the growth of polyacetylene cations involve the sequential addition of C_2 units either directly to the ion as follows:

$$[11]\quad C_2H_{2,3}^+ \xrightarrow{C_2} C_4H_{2,3}^+ \xrightarrow{C_2} C_6H_{2,3}^+ \xrightarrow{C_2} C_8H_{2,3}^+ \xrightarrow{C_2}$$

or indirectly by repeated reaction with the polyacetylene formed through the neutralization of the polyacetylene cations as follows:

$$[12]\quad \begin{array}{ccccccc} C_2H_{2,3}^+ & & C_4H_{2,3}^+ & & C_6H_{2,3}^+ & & C_8H_{2,3}^+ \\ \downarrow & \overset{C_2^+}{\nearrow} & \downarrow & \overset{C_2^+}{\nearrow} & \downarrow & \overset{C_2^+}{\nearrow} & \downarrow \\ C_2H_2 & & C_4H_2 & & C_6H_2 & & C_8H_2 \end{array}$$

Both schemes may also operate with polyatomic carbon units containing an even number of carbon atoms, such as neutral or ionized C_4 or C_6 units. At the low pressures of the interstellar medium the addition of the carbon unit in each step may occur either by radiative association or by condensation as indicated in reactions [13] to [16] for diatomic carbon units:

$$[13]\quad C_{2n}H_{2,3}^+ + C_2 \rightarrow C_{2n+2}H_{2,3}^+ + h\nu$$

$$[14]\quad C_{2n}H_{2,3}^+ + C_2H_{1,2} \rightarrow C_{2n+2}H_{2,3}^+ + H, H_2$$

$$[15]\quad C_{2n}H_2 + C_2H_{0,1}^+ \rightarrow C_{2n+2}H_{2,3}^+ + h\nu$$

$$[16]\quad C_{2n}H_2 + C_2H_{2,3}^+ \rightarrow C_{2n+2}H_{2,3}^+ + H, H_2$$

Only a very few of these reactions have actually been explored in the laboratory. The available measurements provide insight primarily into the kinetics of the initiation steps.

There is no information on the reactions of the acetylenic ions with the molecules C_2 and C_2H, but it is well known that the ions $C_2H_2^+$ and $C_2H_3^+$ react with acetylene to etablish $C_4H_2^+$ and $C_4H_3^+$ (15). Figure 1 displays results of SIFT measurements which show how the reaction of $C_2H_2^+$ with C_2H_2 establishes $C_4H_2^+$ and $C_4H_3^+$ as well as the adduct ion $C_4H_4^+$. The adduct is likely to be collisionally stabilized at the pressures of the SIFT experiments; it is not observed at low pressures in ICR experiments (15). In contrast, the ions $C_4H_2^+$ and $C_4H_3^+$ form adduct ions with acetylene under SIFT conditions (16) as well as at the low pressures of the ICR technique (15, 17). There has been one report of a minor channel at low pressures which leads to $C_6H_3^+$ from $C_4H_2^+$ and C_2H_2 (15). The observation of adducts at low pressures implies the occurrence of radiative association, although both collisional and radiative association have been advanced as the mechanism for the association of $C_4H_2^+$ and $C_4H_3^+$ with C_2H_2 at low pressures (15, 17).

The reactions of acetylene with $C_2H_2^+$ and $C_2H_3^+$ also initiate the reaction sequence [12] and it is known that C_2H^+ reacts rapidly with C_2H_2 to produce $C_4H_2^+$ exclusively (15). SIFT measurements have shown that the chain-lengthening reaction of diacetylene with $C_2H_2^+$ to form $C_6H_3^+$ must compete with a predominant charge transfer channel (16). This may also be the case for reactions of $C_2H_2^+$ with higher polyacetylenes as the ionization energy decreases with chain length. For the reactions with $C_2H_3^+$ proton transfer will be the competitive channel since the proton affinity of C_2H_2 is expected to be lower than that of the polyacetylenes.

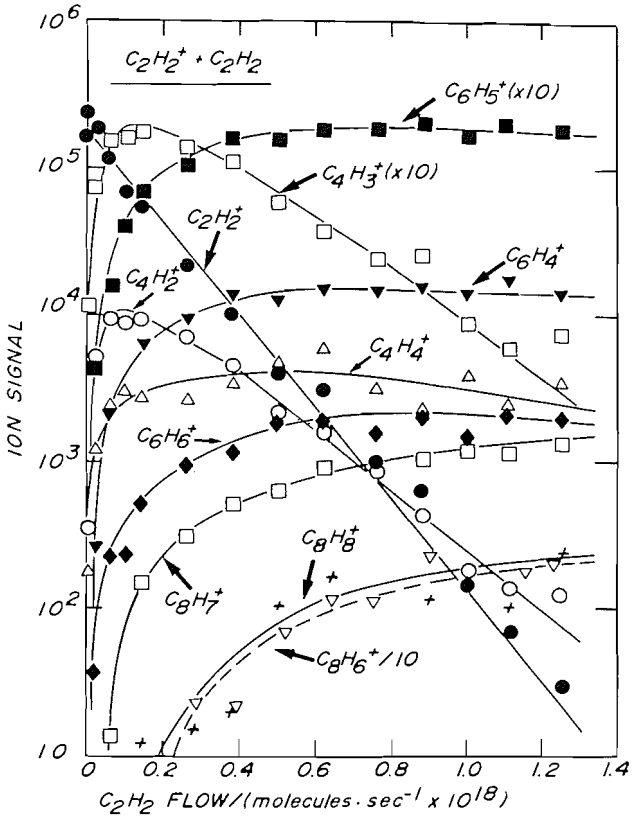

FIG. 1. Observations of the sequential acetylene chemistry initiated by $C_2H_2^+$ in the reaction region of a SIFT apparatus. Three steps are seen to lead to the connection of four C_2 units with overall complete retention of acetylenic hydrogen ($C_8H_8^+$) and with loss of H ($C_8H_7^+$) and H_2 ($C_8H_6^+$). The buffer gas is helium. $P = 0.34$ Torr, $\bar{v} = 7.4 \times 10^3$ cm s^{-1}, $L = 46$ cm, and $T = 296$ K. The $C_2H_2^+$ is derived from acetylene by electron impact at 20 eV.

Some information is also available for reactions between neutral and ionic C_4 units. Recent SIFT measurements have indicated that the reactions of $C_4H_2^+$ and $C_4H_3^+$ with diacetylene can establish $C_6H_2^+$ and $C_6H_3^+$ but that they are dominated by adduct formation, as are the reactions of $C_6H_2^+$ and $C_6H_3^+$ with diacetylene (16). The situation is different at lower pressures where collisional stabilization is less influential. For the reaction of $C_4H_2^+$ with C_4H_2 recent ICR measurements have indicated the formation of the products $C_6H_2^+$ (83%), $C_8H_2^+$ (17%), and $C_8H_3^+$ (1%) (18). Also the reaction of $C_4H_3^+$ with acetylene was observed to produce $C_6H_3^+$ exclusively (18). Other ICR measurements have shown that the $C_6H_2^+$ produced from $C_4H_2^+$ and C_4H_2 reacts with diacetylene to produce $C_8H_2^+$ and $C_{10}H_2^+$ (19). Finally, it has also been shown that C_4H^+ reacts with diacetylene to produce $C_8H_2^+$ exclusively (18).

In summary, the results of laboratory measurements available at this time indicate that polyacetylenic ions are readily generated by sequential reactions involving C_2 or C_4 units. SIFT measurements suggest that collisional association reactions begin to predominate at moderate pressures as the ionic complexity increases, and ICR measurements indicate that ionic

Can. J. Chem. Downloaded from www.nrcresearchpress.com by 213.166.140.6 on 09/07/12
For personal use only.

growth at the low pressures of interstellar environments may proceed by bimolecular condensation reactions, or possibly radiative association reactions.

For Scheme A to succeed in the ultimate formation of cyanopolyacetylenes, the growth of polyacetylene cations must be followed by the entrainment of CN according to reactions of type [2] and [3]. Experimental observations are unavailable for reactions with CN, but some measurements have been reported for reactions with HCN. ICR measurements (15) indicate a fast reaction of $C_2H_2^+$ with HCN to produce two ions as indicated in reaction [17]:

$$[17]\quad C_2H_2^+ + HCN \xrightarrow{0.65} H_2CN^+ + C_2H$$
$$\xrightarrow{0.35} H_2C_3N^+ + H$$

Both product ions have also been observed in SIFT experiments at a branching ratio of 0.05 each, but the predominant product observed at the higher pressures of the SIFT was the ionic adduct (5). $C_2H_3^+$ was observed with both techniques to react with HCN by proton transfer (11, 15). Recent ICR measurements indicate that both $C_4H_2^+$ and $C_4H_3^+$ do not react rapidly with HCN at low pressures, $k < 2 \times 10^{-11}$ cm^3 molecule^{-1} s^{-1} (15). SIFT experiments carried out in this study indicate rapid association in helium at a total pressure of 0.335 Torr and a helium density of 1.1×10^{16} atoms cm^{-3} at 296 ± 2 K. Reaction [18] was observed to have an effective bimolecular

$$[18]\quad C_4H_2^+ + HCN + He \rightarrow H_3C_5N^+ + He$$

rate constant of 2.2×10^{-10} cm^3 molecule^{-1} s^{-1} under these conditions. The structure of the adduct ion is uncertain, but it may be a source for neutral cyanodiacetylene if it loses molecular hydrogen upon recombination with electrons. In the interstellar environment the association must proceed radiatively. The upper limit to the rate constant for this reaction determined with the ICR method does not preclude this possibility, and the high rate of collisional association certainly is suggestive of a relatively efficient radiative association.

Scheme B

Scheme B relies on the build-up of the cyanopolyacetylenes by their repeated reaction with the acetylenic ions $C_2H_2^+$ and $C_2H_3^+$ in which the CN substituent is retained. While experiments have shown that this is achieved for one of the first members of the family of reactions, viz. the reaction of HCN with $C_2H_2^+$, it is not for the next higher member. As indicated earlier, ICR and SIFT measurements have shown that HCN reacts with $C_2H_2^+$ to produce some $H_2C_3N^+$ while the $C_2H_3^+$ ion reacts with HCN only by proton transfer. In contrast, recent SIFT experiments in our laboratory indicate that elimination of HCN and association dominate in the reaction of $C_2H_2^+$ with HC_3N for which $k = 3.2 \times 10^{-9}$ cm^3 molecule^{-1} s^{-1} (20):

$$[19]\quad C_2H_2^+ + HC_3N \xrightarrow{0.5} C_4H_2^+ + HCN$$
$$\xrightarrow{0.5} C_5H_3N^+$$

A similar result has been reported recently by Knight *et al.* (21) who suggest that the ionic adduct which must be formed by radiative association at the low pressures of interstellar clouds may yield some HC_5N by electron/ion recombination. $C_2H_3^+$ is known to react with cyanoacetylene only by proton transfer (20, 21).

Scheme C

The scheme proposed by Woods has as its foundation the atomic carbon ion. Growth is achieved by adding single carbon units through sequential reactions with C^+ and methane. No laboratory data were available for the reactions [5] and [6] involving cyanoacetylenes when this scheme was originally conceived by Woods. However, recent SIFT measurements in our laboratory have shown that this scheme is indeed credible. We have shown that C^+ reacts with the first member of the series of cyanopolyacetylenes extremely rapidly, $k = 6.1 \times 10^{-9}$ cm^3 molecule^{-1} s^{-1}, to produce the C_4N^+ cation 20% of the time as shown in reaction [20] (20):

$$[20]\quad C^+ + HC_3N \xrightarrow{0.8} C_3H^+ + CN$$
$$\xrightarrow{0.2} C_4N^+ + H$$

We report here the results for the subsequent reaction of C_4N^+ with CH_4 which establishes some $H_2C_5N^+$. The latter ion may neutralize to form cyanodiacetylene.

With C^+ as the source ion for C_4N^+, sufficient cyanoacetylene was added into the flow tube of the SIFT apparatus to deplete most of the C^+. The major ion in the flow tube under these conditions was C_3H^+ but addition of methane did provide an assessment of the products of the C_4N^+ reaction since the products of the reaction of C_3H^+ with methane had been characterized previously in our laboratory (10). Experiments performed at low resolution identified product ions at m/z = 51 + 52 ($C_4H_3^+$ or C_3HN^+ and $C_4H_4^+$ or $C_3H_2N^+$), 27 + 28 ($C_2H_3^+$ or CHN^+ and $C_2H_4^+$ or CH_2N^+), and 76 ($C_5H_2N^+$). The rate constant for the decay of C_4N^+ at 296 ± 2 K was determined to be 5.5×10^{-10} cm^3 molecule^{-1} s^{-1}. Further experiments were performed to elucidate the product yields by generating C_4N^+ from allyl cyanide by electron impact (22). The observed product ions with their relative yields were as follows:

$$[21]\quad C_4N^+ + CH_4 \xrightarrow{0.35} C_3H_2N^+ + C_2H_2$$
$$\xrightarrow{0.30} C_4H_3^+ + CHN$$
$$\xrightarrow{0.25} C_2H_3^+ + C_3HN$$
$$\xrightarrow{0.05} CH_2N^+ + C_4H_2$$
$$\xrightarrow{0.05} C_5H_2N^+ + H_2$$

The overall rate constant in this case was 5.7×10^{-10} cm^3 molecule^{-1} s^{-1}. Experiments with CD_4 excluded $C_4H_4^+$, CHN^+, and $C_2H_4^+$ as possible product ions. C_3HN^+ was shown to contribute less than 5% to the total product ions. The results of one experiment with CD_4 are shown in Fig. 2.

Two pairs of the product ions in reaction [21] are related by intramolecular proton transfer. Thus neutral and protonated cyanoacetylene (or isocyanoacetylene) appear to contribute 60% to the total product ions, while neutral and protonated diacetylene appear to contribute 35%. The remaining 5% of the reaction appears to lead to protonated cyanodiacetylene or an isomer of cyanodiacetylene.

Scheme C presumes similar reactions of C^+ with the higher members of the homologous series of cyanopolyacetylenes and similar reactions of the derivative $C_{2n+2}N^+$ ions with CH_4 as indicated by reactions [5] and [6]. Figure 3 projects the

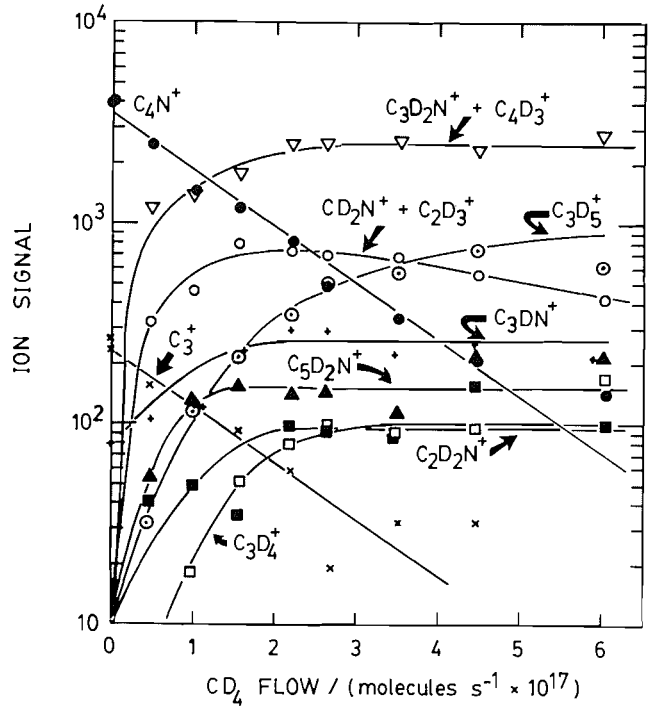

FIG. 2. The variations in ion signals observed for the addition of deuterated methane into the reaction region of the SIFT apparatus in which C_4N^+ is initially established in helium buffer gas. P = 0.35 Torr, $\bar{v} = 6.7 \times 10^3$ cm s^{-1}, L = 46 cm, and T = 294 K. The C_4N^+ is derived from allyl cyanide by electron impact at 55 eV.

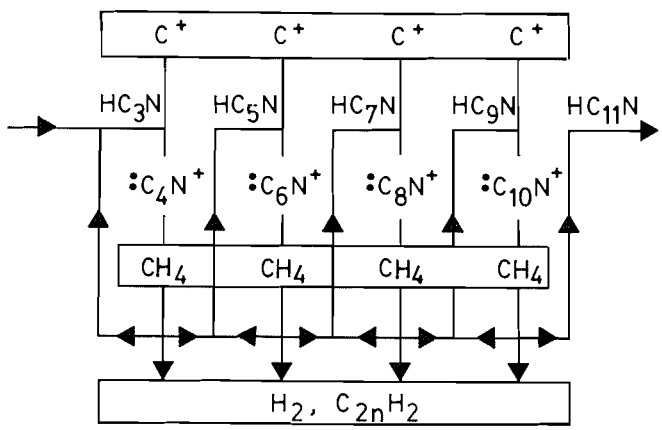

FIG. 3. Hypothetical scheme for the synthesis of cyanopolyacetylenes.

chemistry established in this study for the production of cyanodiacetylene to the production of higher cyanopolyacetylenes. The scheme provides a plausible route to the synthesis of the higher cyanopolyacetylenes. An important feature of this scheme is the chemical feedback of the lower cyanopolyacetylene(s) which may be formed in the reactions of $C_{2n+2}N^+$ with CH_4. In the interstellar chemistry the latter reactions must compete with those involving H_2. In a separate study we have shown that C_4N^+ reacts with H_2 only slowly, $k = 2.2 \times 10^{-11}$ cm^3 molecule^{-1} s^{-1} at 296 K, to produce C_3H^+ (22).

Other reactions of $C_{2n+2}N^+$ which may lead to growth of cyanopolyacetylenes in interstellar chemistry are also possible as is indicated, for example, by reactions [22] and [23]:

[22] $C_{2n+2}N^+ + CH_3 \rightarrow H_2C_{2n+3}N^+ + H$

[23] $C_{2n+2}N^+ + CH_2 \rightarrow H_2C_{2n+3}N^+ + h\nu$

These reactions involve radicals as neutral reactants and would be much more difficult to measure in the laboratory.

Scheme D

The hydrocarbon ions required for reactions [7] and [10] contain an odd number of carbon atoms. There are a number of possible sources for $C_{2n+1}H^+$ ions in the interstellar environment. These include the protonation of odd carbon clusters as illustrated by reaction [24], the hydrogenation of odd carbon ion

[24] $XH^+ + C_{2n+1} \rightarrow C_{2n+1}H^+ + X$

clusters as indicated by reaction [25], or the reactions of C^+

[25] $C^+_{2n+1} + H_2 \rightarrow C^+_{2n+1}H^+ + H$

with polyacetylenes as in reaction [26]. Reactions of type [24]

[26] $C^+ + C_{2n}H_2 \rightarrow C_{2n+1}H^+ + H$

have not yet been observed in the laboratory. Also, the proton affinities of neutral carbon clusters are not known. Nevertheless, these reactions are expected to occur in interstellar clouds because of the presence of likely proton donors such as H_3^+, N_2H^+, and CHO^+. Reactions of type [25] have recently been investigated with the SIFT technique. For the reaction of C_3^+ a rate constant of 3.0×10^{-10} cm^{-3} molecule^{-1} s^{-1} has been reported (23). We can report here new results for our observations of the following two deuteration reactions:

[27] $C_3^+ + D_2 \rightarrow C_3D^+ + D$

[28] $C_5^+ + D_2 \rightarrow C_5D^+ + D$

Reactions [27] and [28] were found to have room temperature rate constants of (1.3 ± 0.4) and $(5 \pm 2) \times 10^{-10}$ cm^3 molecule^{-1} s^{-1}, respectively. Reactions of type [26], important in interstellar clouds because of the relatively high abundance of C^+ ions, have been observed with acetylene and diacetylene for which rate constants of 2.2 and 1.5×10^{-9} cm^3 molecule^{-1} s^{-1}, respectively, have been reported (16, 24).

Still another source of C_nH^+ ions has become apparent in a recent study of the chemistry of C_4N^+. This latter ion was observed to react with acetylene and diacetylene to produce C_5H^+ and C_7H^+ respectively through reactions of type [29] (22):

[29] $C_4N^+ + C_{2n+2}H_2 \rightarrow C_{2n+5}H^+ + HCN$

Possible direct sources of $C_{2n+1}H_3^+$ ions which are likely in dense interstellar clouds involve reactions of CH_3^+ with acetylene and polyacetylenes. The kinetics of the reactions with acetylene and diacetylene have now been characterized in the laboratory. The reaction with acetylene produces $C_3H_3^+$ exclusively according to reaction [30] (5):

[30] $CH_3^+ + C_2H_2 \rightarrow C_3H_3^+ + H_2$

while the reaction with diacetylene produces some $C_5H_3^+$ according to reaction [31] (16).

[31] $CH_3^+ + C_4H_2 \xrightarrow{0.9} C_3H_3^+ + C_2H_2$

$$\xrightarrow{0.1} C_5H_3^+ + H_2$$

There is little experimental information on the reactions of $C_{2n+1}H^+$ and $C_{2n+1}H_3^+$ with N atoms and on the subsequent hydrogenation of the $C_{2n+1}N^+$ ions. Only one member of reactions [7] and [10] has been studied in the laboratory. Recent flow-drift experiments have provided a rate constant of 1.3×10^{-10} cm^{-3} molecule^{-1} s^{-1} for the reaction near thermal ener-

Can. J. Chem. Downloaded from www.nrcresearchpress.com by 213.166.140.6 on 09/07/12
For personal use only.

gies (0.1 to 0.2 eV) of $C_3H_3^+$ derived by electron impact on C_3H_7Br (25):

[32] $C_3H_3^+ + N \rightarrow H_2C_3N^+ + H$

Data for hydrogenation reactions of type [8] is also sparse. SIFT experiments have shown that C_3N^+ rapidly hydrogenates at 300 K according to reaction [33] with a rate constant of 9.1 ×

[33] $C_3N^+ + H_2 \xrightarrow{0.90} HC_3N^+ + H$

$$\xrightarrow{0.10} H_2C_3N^+$$

10^{-10} cm^3 molecule^{-1} s^{-1} at ca. 0.3 Torr in helium buffer gas (21). The further hydrogenation of HC_3N^+ is much slower at 300 K and competes with a dissociative channel in the manner expressed by reaction [34] (21, 26):

[34] $HC_3N^+ + H_2 \xrightarrow{0.5(0.76)} H_2C_3N^+ + H$

$$\xrightarrow{0.5(0.24)} C_2H_2^+ + HCN$$

Rate constants at 300 K of 1.9 and 7 × 10^{-12} cm^3 molecule^{-1} s^{-1} have been reported for this reaction (21, 26). The temperature dependence of this slow reaction is not known but it is conceivable that the rate constant for this reaction increases as the temperature drops in analogy with the reaction of NH_3^+ with H_2 (17).

Conclusions

Some progress has been made in this study and others carried out over the past few years in the characterization of the ion/molecule reactions which constitute the four reaction schemes proposed for the gas-phase synthesis of interstellar cyanopolyacetylenes. Substantial gaps still exist, but there is now sufficient data to allow some discrimination between the four schemes.

The polyacetylenic ions required for Scheme A are readily generated by sequential reactions involving C_2 and C_4 units. But the entrainment of nitrogen through an eventual bimolecular reaction with HCN appears to succeed only with $C_2H_2^+$ and thus only for the formation of cyanoacetylene. The four-carbon ions do not react with HCN in a bimolecular fashion at 300 K; $C_4H_2^+$ was observed to react with HCN in a rapid termolecular association reaction. The success of this scheme must therefore rest on the reactions with CN for which there is no information.

Scheme B relies on the build-up of cyanopolyacetylenes by their repeated reaction with acetylenic ions. However, measurements with cyanoacetylene suggest that this growth may be short-circuited by proton transfer or by elimination of HCN.

Growth by repeated addition of single carbon units to cyanopolyacetylenes through sequential reactions with C^+ ions and CH_n neutrals as described in Scheme C appears to be quite feasible. Results are presented for the critical reaction of C_4N^+ with CH_4 which provides the bridge from cyanoacetylene to cyanodiacetylene. The scheme is projected to higher members of the cyanopolyacetylenes and is attractive especially in view of the chemical feedback that is possible. More information is required for the higher members of the homologous series.

There is still little laboratory evidence for Scheme D in which nitrogen entrainment by slightly hydrogenated hydrocarbon ions occurs through reaction with nitrogen atoms. Nevertheless this route remains an attractive option unless hydrogenation reactions with H_2 are required to build up the hydrogen content before neutralization to form the cyanopolyacetylene. The efficiency of hydrogenation appears variable and unpredictable. New results are presented for the hydrogenation of odd-numbered carbon ions which leads to the slightly hydrogenated hydrocarbon ions which can initiate Scheme D.

Acknowledgment

We thank the Natural Sciences and Engineering Research Council of Canada for financial support.

1. W. M. IRVINE, F. P. SCHLOERB, A. HJALMARSON, and E. HERBST. *In* Protostars and Planets II. *Edited by* D. C. Black and M. S. Mathews. The University of Arizona Press, Tucson, Arizona. 1985. p. 579.
2. C. SAGAN and B. KHARE. Nature, **277**, 102 (1979).
3. R. HAYATSU and E. ANDERS. Top. Curr. Chem. **99**, 1 (1981).
4. G. WINNEWISSER and C. M. WALMSLEY. Astrophys. Space Sci. **65**, 83 (1979).
5. H. I. SCHIFF and D. K. BOHME. Astrophys. J. **232**, 740 (1979).
6. R. C. WOODS. *In* Molecular ions. *Edited by* J. Berkowitz and K. O. Groeneveld. Plenum Publishing Corporation. 1983. p. 511.
7. H. SUZUKI. Astrophys. J. **272**, 579 (1983).
8. E. HERBST. Astrophys. J. Suppl. Ser. **53**, 41 (1983).
9. T. J. MILLAR and A. FREEMAN. Mon. Not. R. astr. Soc. **207**, 405 (1984).
10. A. B. RAKSIT and D. K. BOHME. Int. J. Mass Spectrom. Ion Processes, **55**, 69 (1984).
11. G. I. MACKAY, G. D. VLACHOS, D. K. BOHME, and H. I. SCHIFF. Int. J. Mass Spectrom. Ion Phys. **36**, 259 (1980).
12. O. GLEMSER. *In* The handbook of preparative inorganic chemistry. *Edited by* G. Brauer. Academic Press, New York. 1963. p. 658.
13. A. B. RAKSIT and D. K. BOHME. Int. J. Mass Spectrom. Ion Phys. **49**, 275 (1983).
14. N. G. ADAMS and D. SMITH. J. Phys. B, **9**, 1439 (1976).
15. V. G. ANICICH, W. T. HUNTRESS, and M. J. MCEWAN. J. Phys. Chem. **90**, 2446 (1986).
16. S. DHEANDHANOO, L. FORTE, A. FOX, and D. K. BOHME. Can. J. Chem. **64**, 641 (1986).
17. F. W. BRILL and J. R. EYLER. J. Phys. Chem. **85**, 1091 (1981).
18. V. G. ANICICH, G. A. BLAKE, J. K. KIM, M. J. MCEWAN, and W. T. HUNTRESS. J. Phys. Chem. **88**, 4608 (1984).
19. T. J. BUCKLEY, L. W. SIECK, R. METZ, S. G. LIAS, and J. LIEBMAN. Int. J. Mass Spectrom. Ion Processes, **65**, 181 (1985).
20. A. B. RAKSIT and D. K. BOHME. Can. J. Chem. **63**, 854 (1985).
21. J. S. KNIGHT, C. G. FREEMAN, M. J. MCEWAN, S. C. SMITH, N. G. ADAMS, and D. SMITH. Mon. Not. R. astr. Soc. **219**, 89 (1986).
22. D. K. BOHME, S. WŁODEK, and A. B. RAKSIT. Can. J. Chem. To be published.
23. E. HERBST, N. G. ADAMS, and D. SMITH. Astrophys. J. **269**, 329 (1983).
24. D. K. BOHME, A. B. RAKSIT, and H. I. SCHIFF. Chem. Phys. Lett. **93**, 592 (1982).
25. W. FEDERER, H. VILLINGER, W. LINDINGER, and E. E. FERGUSON. Chem. Phys. Lett. **123**, 12 (1986).
26. A. FOX, A. B. RAKSIT, S. DHEANDHANOO, and D. K. BOHME. Can. J. Chem. **64**, 399 (1986).
27. J. A. LUINE and G. H. DUNN. Astrophys. J. **299**, L67 (1985).

Can. J. Chem. Downloaded from www.nrcresearchpress.com by 213.166.140.6 on 09/07/12
For personal use only.

An electrochemical and spectroelectrochemical study of substituted alkylidenecyclopropabenzenes: 1-(diphenylmethylene)cyclopropabenzene in the first anodic and cathodic voltammetric waves in acetonitrile

KEVIN ASHLEY AND FERESHTEH SARFARAZI
Department of Chemistry, The University of Utah, Salt Lake City, UT 84112, U.S.A.

SIMON J. BUCKLAND
Department of Chemistry, Victoria University of Wellington, Private Bag, Wellington, New Zealand

JOHN K. FOLEY AND QUI MEI
Department of Chemistry, The University of Utah, Salt Lake City, UT 84112, U.S.A.

BRIAN HALTON
Department of Chemistry, Victoria University of Wellington, Private Bag, Wellington, New Zealand

AND

PETER J. STANG AND STANLEY PONS[1]
Department of Chemistry, The University of Utah, Salt Lake City, UT 84112, U.S.A.

Received September 29, 1986[2]

Can. J. Chem. Downloaded from www.nrcresearchpress.com by 213.166.140.6 on 09/07/12
For personal use only.

KEVIN ASHLEY, FERESHTEH SARFARAZI, SIMON J. BUCKLAND, JOHN K. FOLEY, QUI MEI, BRIAN HALTON, PETER J. STANG, and STANLEY PONS. Can. J. Chem. **65**, 2062 (1987).

Electrochemical and modulated specular reflectance spectroelectrochemical (MSRS) investigations were performed on 1-(diphenylmethylene)cyclopropabenzene in nominally dry acetonitrile solution. The results indicate the formation of a stable anion radical (λ_{max} = 587 nm) and a quasi stable cation radical (λ_{max} = 473 nm). The first order homogeneous rate constant for the decay of the cation radical was computed.

KEVIN ASHLEY, FERESHTEH SARFARAZI, SIMON J. BUCKLAND, JOHN K. FOLEY, QUI MEI, BRIAN HALTON, PETER J. STANG et STANLEY PONS. Can. J. Chem. **65**, 2062 (1987).

On a effectué des études électrochimiques et spectroélectrochimiques de réflectance spéculaire modulée (SRSM) sur le diphénylméthylène-1 cyclopropabenzène en solution dans de l'acétonitrile qui est théoriquement sec. Les résultats indiquent qu'il y a formation d'un anion radical complexe (absorption maximale à 587 nm) et d'un cation radical qui est pratiquement stable (absorption maximale à 473 nm). On a évalué la constante de vitesse homogène du premier ordre pour la décomposition du cation radical.

[Traduit par la revue]

Introduction

The unusual properties and reactivity of highly strained molecules have interested chemists for quite some time (1). Presently there is a great deal of interest and research activity in cycloproparene chemistry. Cycloproparenes possess some of the highest strain energies known (2); the parent compound **I** has a strain energy of 68 kcal/mol (3). As a result, the electrochemical oxidation and reduction potentials of the neutral molecules are lower than those of most other electroactive hydrocarbons.

Even more highly strained and unusual alkylidene derivatives of **I** have been reported (4): the diphenylmethylene (**III**) and the 1-phenylethylidene (**IV**) derivatives have been synthesized, as well as the corresponding naphthalene analogs **V** and **VI**.

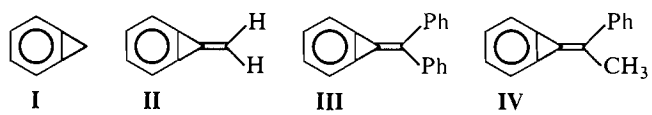

I **II** **III** **IV**

V **VI**

Compounds **III** and **V** are stable in air and in aprotic solvents against rapid oxidation. The methylenecycloproparene parent compound **II** has not been successfully isolated, but attempts to synthesize this species continue.

The possibility of charge separated resonance forms contributing to the stability of the neutral molecule **V** was suggested by an initial spectral characterization. We have recently reported the results of an electrochemical and spectroelectrochemical study of **V** (5), and in an effort to further characterize and understand the nature of the special properties of these molecules we have undertaken an electrochemical and spectroelectrochemical investigation of **III**. One question is how large a role does the aromatic moiety of the cycloproparene ring play in the stability of the ion radicals compared to the substituents on the methylene group. The naphthalene analog in the previous study was shown to form a stable anion radical (on the timescale of the experiment) when electrochemically reduced in oxygen-free acetonitrile solution. When oxygen is present the anion radical reacts rapidly with O_2 at a rate approaching the diffusion limit. Additionally, the compound was shown to form a quasi stable cation radical when electrooxidized. In the present study, compound **III** has been found to behave similarly. In addition, the homogeneous rate constant for the decay of the cation radical in acetonitrile solution has been computed from spectroelectrochemical transient data.

Experimental

Chemicals and reagents

The preparation of **III** has been described in detail (4, 14). A stirred solution of cyclopropabenzene in dry THF was cooled to −70°C under

[1]To whom correspondence should be addressed.
[2]Revision received March 10, 1987.

Can. J. Chem. Downloaded from www.nrcresearchpress.com by 213.166.140.6 on 09/07/12
For personal use only.

oxygen-free nitrogen; *n*-butyllithium in hexane was added slowly, while the bath temperature was allowed to rise to −40°C. After 1.5 h the solution was again cooled to −70°C, and trimethylsilyl chloride was added dropwise until the deep orange solution had become colorless. The reaction mixture was allowed to warm slightly for 1 h and then cooled again to −70°C, at which time the above metallation procedure with *n*-butyllithium was repeated. Quenching of the generated α-silyl carbanion was attained with benzophenone in THF, and the resulting clear yellow solution was allowed to warm to room temperature. After 1.5 h aqueous sodium bicarbonate was added after which the mixture was extracted with dichloromethane. The combined organic extracts were washed with water, dried with magnesium sulfate, and concentrated to an orange oil under reduced pressure. This oil was then passed through a silica gel column (petroleum ether:ethyl acetate, 9:1) and fractions of the most mobile component, 1-(diphenylmethylene)cyclopropabenzene, were collected as a yellow oil which solidified on standing at −20°C. Recrystallization from petroleum ether gave yellow needle-like crystals, mp 89–91°C.

The preparation of tetra-*n*-butylammonium tetrafluoroborate (TBAF) has been described previously (6). This supporting electrolyte was prepared from the metathesis of sodium tetrafluoroborate and tetra-*n*-butylammonium hydrogen sulfate. The crude product was washed with ice water, dissolved in a minimum amount of methylene chloride, and precipitated with cold diethyl ether. After a second recrystallization, the product was air dried and stored in a vacuum oven at 75°C for 24 h before use.

Acetonitrile was hplc grade (Baker Chemicals, 0.001% nominal water content) and was used as received. Deoxygenation of the reaction mixture was accomplished by purging with dry helium gas immediately prior to the experiments.

The reference electrode was a silver wire immersed in 0.01 *M* silver nitrate and 0.10 *M* TBAF in acetonitrile. We report all potentials with respect to this reference.

Electrochemistry and spectroelectrochemistry

A three electrode potentiostat and a waveform generator (JAS Instrument Systems, Inc.) provided the control of electrode potential. Cyclic voltammetry was conducted in a three-electrode kinetic cell wherein a platinum wire working electrode surrounded by a cylindrical platinum foil secondary electrode was mounted. A Luggin capillary reference electrode tip was situated within about 1 mm of the working electrode. Although the geometry of the setup is cylindrical, the experiments were carried out on a timescale where linear diffusion is observed. See ref. 7 for precise details. For spectroelectrochemical experiments, a cell was used that held a 7 mm diameter platinum mirror disk working electrode with a planar Pt foil counter electrode situated opposite, providing good linear diffusion characteristics for up to 10 s. Two quartz windows were mounted to enable passage of incoming and outgoing uv/vis radiation at a 45° angle of incidence and reflectance. A Luggin reference probe was positioned close to the working electrode so as not to obstruct the optical path. Exact details have been described previously (8).

The spectroelectrochemical cell was mounted on an optical bench, and the optical beam from a monochromator (GCA McPherson model 302) was directed onto the electrode surface, and reflected onto a photomultiplier tube (RCA model 31000A). The signal from the PMT was digitized by an oscilloscope (Tektronix model 5223): this datum was transmitted over a GPIB interface to a computer (IBM PC/AT). The computer signal averaged digitized data from single reflectance transients: the background intensity was controlled so that the value of the relative reflectance could be calculated as described in ref. 8. The MSRS technique used in this work was implemented by first maintaining the potential at a value where no electrochemical reaction occurred. The potential was then stepped to a value where electrooxidation or electroreduction was forced into diffusion control, and the spectroelectrochemical reflectance transient response of the electrogenerated species was recorded on the digitizing oscilloscope as a function of time after the potential pulse was applied. Alternately, the potential was also modulated at a high frequency (40 Hz) and the resulting ac reflectance change monitored with a lock-in amplifier: scanning wavelength simultaneously provided uv-vis difference spectra of the reactants, intermediates, and products (8).

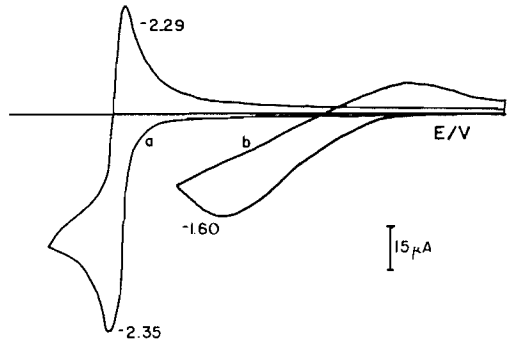

FIG. 1. Cyclic voltammetry for (*a*) 1 m*M* **III** and for (*b*) dioxygen in 0.15 *M* TBAF/acetonitrile solution at a platinum electrode. The sweep rate was 50 mV s^{-1}. Potentials are vs. the Ag/Ag^+ (0.01 *M* $AgNO_3$ in 0.1 *M* TBAF in acetonitrile) reference electrode.

Results and discussion

Voltammetry

A. Anions

At a platinum electrode, the voltammetric reduction of a blank solution containing only supporting electrolyte showed no faradaic current (<0.1 μA cm^{-2}) over the range of potentials studied. Cyclic voltammetry of **III** at negative potentials in oxygen-free acetonitrile solution is shown in Fig. 1*a*. A one-electron wave due to the reduction of the neutral molecule to the anion radical at the platinum working electrode is observed. The voltammetric response indicates electrochemical reversibility at this (50 mV s^{-1}) and faster sweep rates: the voltammetric peak separation is 60 mV, and the ratio of cathodic to anodic peak currents is unity. The half-wave potential is −2.32 V vs. Ag/Ag^+. There is no evidence of anion radical decay on the experimental timescale (ca. 1 min); the anion radical is quite stable, as is that of the naphthyl cycloproparene analog (5).

When only oxygen is present in solution a voltammogram such as that in Fig. 1*b* results. The first cathodic wave at −1.60 V (vs. Ag/Ag^+) corresponds to the reduction of oxygen to superoxide, which is a kinetically slow electron transfer (5). On the return excursion an anodic peak at −0.78 V due to the reoxidation of superoxide is seen. The diffusion-controlled peak for the formation of superoxide is thus 750 mV less negative than the peak potential for the formation of the anion radical of **III** at a sweep rate of 50 mV/s. (At glassy carbon the reduction of oxygen is kinetically more reversible: the separation between the cathodic peak due to the formation of superoxide and the corresponding oxidation peak is reduced from about 820 mV at platinum at 240 mV on carbon at these sweep rates.)

Plots of cathodic peak current versus square root of sweep rate for both dioxygen and isolated **III** are linear for sweep rates of up to 500 mV/s; the plots intersect the origin. This is the expected result for an electrochemical reaction where there are no complicating side reactions involving reactants or products, and where there are no complications due to adsorption of species undergoing electron transfer. Uncomplicated electrochemical formation of the anion radical of **III** and of superoxide is thus consistent with observations; both reductions are simple one-electron transfers.

However, solutions containing both **III** and oxygen demonstrate more complicated voltammetry than that of the individual systems described above (Fig. 2). As in Fig. 1, the first reduction wave at −1.60 V corresponds to the formation of

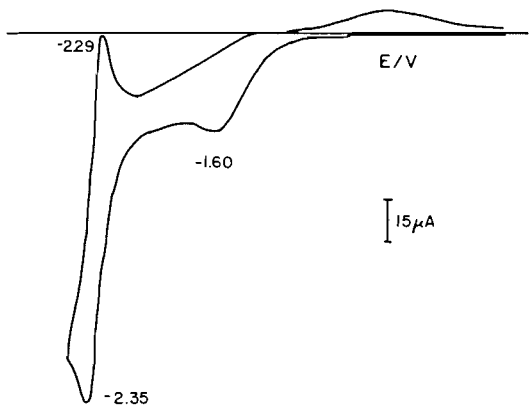

FIG. 2. Cyclic voltammetry of the mixed system of the components in Fig. 1. Parameters the same as in Fig. 1.

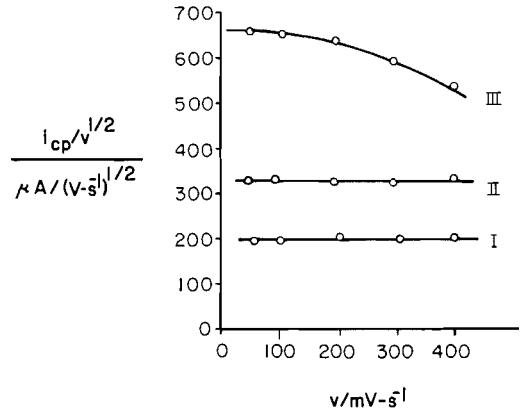

FIG. 3. Plots of the normalized peak current vs. sweep rate for the data in Figs. 1 and 2. (I) is that for the reduction peak in Fig. 1*b*; (II) is that for the reduction peak in Fig. 1*a*; (III) is for the reduction peak at −2.35 V in Fig. 2. Except for the sweep rate, the parameters are the same as those in Fig. 1.

superoxide. We observe, however, that the magnitude of the current in the second wave at −2.35 V, due to the formation of the anion radical of **III** is larger than that for the simple one electron transfer as was observed in the single component **III** system. There are several possible explanations for this behavior.

One possibility is the case where an electroactive product is formed whose reduction potential is less negative than that of **III**. In the present case, this would most likely be due to the reaction of the anion radical of **III** with diffusing oxygen or superoxide:

$$\mathbf{III}^{\cdot -} + O_2 \rightarrow W$$

$$W + ne^- \rightarrow X$$

or

$$\mathbf{III} + O_2^- \rightarrow Y$$

$$Y + ne^- \rightarrow Z$$

(The second reaction is unlikely, as it is unfavorable energetically.) However, bulk electrolysis of **III** at potentials up to and less negative than −2.35 V yielded no evidence of the expected products of either of the proposed reaction schemes. Additionally, if such an electron transfer — chemical step — electron transfer scheme were indeed occurring, the height of the second cathodic wave would imply the involvement of more than one electron in the reduction of W or Y which, though possible, is unlikely.

Voltammetric experiments revealed no evidence of the reaction of unreduced **III** with oxygen. Upon deoxygenation with helium purging of the mixed (both **III** and O_2 present) solution, the uncomplicated electrochemical behavior shown in Fig. 1*a* could be reproduced. Also, if in the mixed system, a cyclic voltammogram was run to a switching potential past the peak for oxygen reduction but prior to the cathodic wave corresponding to reduction of **III**, the reverse sweep yielded an oxidation peak for superoxide which was uncomplicated, as per Fig. 1*b*. This is evidence that superoxide does not react chemically to any appreciable extent with **III**, although Fig. 2 shows a depletion of available total radical anion of **III** in the diffusion layer; the oxidation peak at −2.29 V is reduced in magnitude when O_2 is present. All of the above possibilities suggest that a product of the addition of **III** and oxygen should be observed, but exhaustive electrolyses at or beyond the second reduction wave gave no significant yields of any product of **III** except the anion radical.

Another possible explanation for the unusually high current seen in the second reduction wave (in the mixed system) is the catalytic regeneration of **III** by reaction of oxygen with the anion radical to form **III** and superoxide:

$$\mathbf{III}^{\cdot -} + O_2 \rightleftharpoons \mathbf{III} + O_2^-$$

In turn, superoxide reacts with the anion radical to form **III** and peroxide in the presence of a proton donor:

$$HS + \mathbf{III}^{\cdot -} + O_2^- \rightleftharpoons S^- + \mathbf{III} + HO_2^-$$

Whereas O_2^- is not a strong enough base to react with HS in dry acetonitrile (O_2^- is stable in dry acetonitrile for about 40 min), electron transfer from $\mathbf{III}^{+\cdot}$ to O_2^- would form a base (5) such as O_2^{2-} that is now strong enough to react with HS (the solvent). These results imply that electrochemical reduction of superoxide to peroxide is thermodynamically feasible at potentials where **III** is reduced, but that the electrode reaction is very slow. The formation of peroxide in acetonitrile has been previously observed (9), where superoxide in the presence of any available proton donor was reported to disproportionate to peroxide and oxygen. Bulk electrolysis of the mixed system at a potential of −2.40 V did indeed give rise to solutions which were found to contain peroxide ion, as evidenced by testing with Fenton's reagent. Thus, if **III** is regenerated continuously in the presence of oxygen, the cathodic current at the electrode, which is diffusion limited, will be expected to increase as observed, without the production of any other organic product of **III** (except the anion radical).

Figure 3 shows a plot of the normalized (to the square root of the sweep rate) current magnitude as a function of the sweep rate for the aromatic hydrocarbon–oxygen system. The lowest plot (I) is that for the oxygen reduction peak. Plot II is that for the uncomplicated one electron reduction peak of **III** to its anion radical in the absence of oxygen. Plot III is for the cathodic peak at −2.35 V when both **III** and oxygen are present in comparable amounts. The reduction peak in plot III is the sum of the currents for the reduction of **III** to its anion radical and the reduction of electroactive products formed from the reaction of the anion radical with oxygen and superoxide, which the data suggest to be more regenerated **III** as proposed in the preceding paragraph.

It should be noted that in the mixed system, a subsequent cathodic excursion following cyclic voltammetry from 0 to −2.5 V vs. Ag/Ag^+ gave rise to no additional reduction waves

Can. J. Chem. Downloaded from www.nrcresearchpress.com by 213.166.140.6 on 09/07/12
For personal use only.

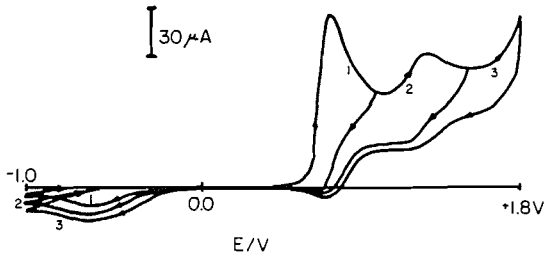

FIG. 4. Cyclic voltammetry of 1 m*M* **III** in acetonitrile. Potential program was 0.0 V to positive potentials, then reversing to negative potentials, then returning to zero. Parameters the same as in Fig. 1.

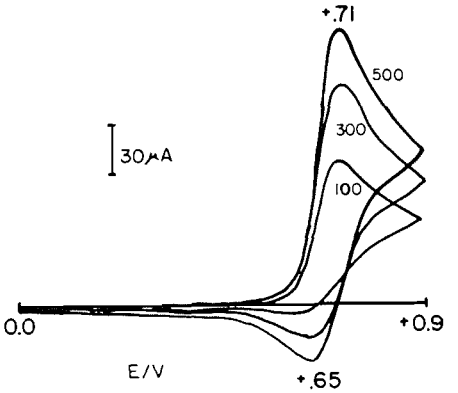

FIG. 5. Cyclic voltammetry of 1 m*M* **III** in acetonitrile as a function of sweep rate. Parameters the same as in Fig. 1.

at lower potentials than that for **III** reduction. This is further evidence that no long-lived organic products of the reaction of the anion radical with O_2 and superoxide other than **III** are generated. Though short-lived products of this reaction cannot be ruled out, the fact that the cathodic peak at −2.35 V grows in comparison with the anodic peak at −2.29 V is certainly consistent with regeneration of additional **III**.

The half wave potential for the reduction of **III** is 400 mV more negative than that for the reduction of **V** (5). This is the expected result in view of the greater delocalization of the extra electron possible in the larger π orbital system: the stability of the naphthyl anion is greater than that of the benzyl analog, just as it is known to be in naphthalene and benzene. We have performed simple Hückel calculations on **III** and **V** and find that this assumption is in line with the results of those calculations.

B. Cations

In deoxygenated acetonitrile solution, a voltammetric sweep to positive potentials gives rise to single electron oxidations of **III** to its radical cation and of its radical cation to dication (Fig. 4). The second reduction is irreversible: the lifetime of the dication is very short on the experimental timescale. On the other hand, the anodic and cathodic peak potential separation (corresponding to oxidation of **III** and reduction of $\mathbf{III}^{+\cdot}$, respectively), approach 60 mV when sweep rates are increased to 500 mV s^{-1}, suggesting electrochemical reversibility at this sweep rate; the half-wave potential there is +0.68 V. However, up to 500 mV s^{-1}, the anodic peak current (oxidation of **III**) is greater than the cathodic peak current (reduction of $\mathbf{III}^{+\cdot}$), and the ratio of cathodic to anodic peak current increases with sweep rate (Fig. 5). These observations are consistent with a reversible electron transfer followed by kinetic decomposition of the resulting cation radical (5). If the potential is swept immediately to more negative values following the oxidation of **III** to its cation radical, a new peak appears at about −0.7 V (Fig. 4); this peak is due to the reduction of protons formed in the decomposition of the cation radical. If the potential is swept positive enough to form the dication, and then immediately swept negative to potentials where the anion radical is formed, no peak for the reduction of the dication is observed; only the reduction due to the protrons is evident.

At a glassy carbon electrode, virtually identical behavior was observed for **III** at all applied potentials except the cathodic peak at −0.7 V disappeared, which confirms that this wave corresponds to the reduction of protons formed in the first anodic wave. Also, oxygen had no effect on the electrochemistry of the cation radical or dication; the very same voltammetry as described above was observed even if oxygen was present in solution.

It is interesting to note that the half wave potential for the oxidation of the benzyl derivative **III** is about 130 mV *less* positive than the half wave potential for the oxidation of the naphthyl derivative **V** (5). This surprising result is not explained by simply considering the stabilities of the ions as was possible in the case of the reduction of these two compounds. The result can be explained for both oxidation and reduction if one assumes that there is a large difference in the ground state energies of the two neutral compounds **III** and **V**, and lesser differences in the electronic energies of their respective cation radicals. If neutral **V** is energetically more stable than **III**, it will be more difficult to oxidize than **III**, given that the cations of each are closer in energy than are the neutral species. This trend was indeed indicated in the Hückel calculations; the overall stabilization energy of **V** was predicted to be greater than that of **III**, whereas the electronic energy difference between the cation radicals is less than the energy difference between the neutral species.

C. Structural considerations

The consideration of the possible structures of the electrochemically formed ion radicals is of interest. The reversible behavior of **III** upon oxidation and reduction indicates that no opening of the three-membered ring occurs when either the cation radical or the anion radical is formed. The compound is reduced at slightly less negative potentials than many other aromatic hydrocarbons in acetonitrile. The half-wave potential for the reduction of **III** was seen to be −2.32 V vs. Ag/Ag^+. This value compares with half-wave potentials of −2.9 V for naphthalene, −2.5 V for tetraphenylethylene, −2.5 V for pyrene, −2.4 V for diphenylanthracene, and −1.93 V for diphenylmethylenecyclopropa[*b*]naphthalene. Compound **III** is oxidized at somewhat less positive potentials than many other aromatic hydrocarbons in this solvent. It has a half-wave potential of +0.68 V for oxidation to the cation radical. For naphthalene this value is +1.40 V, for pyrene +1.06 V, for tetraphenylethylene +1.0 V, for diphenylanthracene +0.92 V, for anthracene +0.91 V, for diphenylmethylenecyclopropa[*b*]-naphthalene +0.81 V, and for perylene +0.66 V.[3]

On formation of the radical ions, it is most likely that the olefinic double bond is broken. This release of strain would yield a reduced free energy of ion formation. The anion would be then formed at less negative potentials and the cation formed

[3]These half-wave potentials were obtained from refs. 5, 10, and 11, assuming where necessary that the potential of the Ag/Ag^+ reference electrode is 0.3 V more positive than that of the saturated calomel electrode.

Can. J. Chem. Downloaded from www.nrcresearchpress.com by 213.166.140.6 on 09/07/12
For personal use only.

at less positive potentials than what might be predicted from half-wave potentials of other aromatic hydrocarbons. Proposed structures for the anion radical are:

while possible structures for the radical cation might be:

It is not possible from our voltammetric data to conclude for either species which resonance structure contributes most to the lowest overall energy state.

Spectroelectrochemistry

A. The anion radical

Modulated specular reflectance spectroscopy (MSRS) in the visible range was performed on solutions containing **III** (1 m*M*) in acetonitrile in the absence of oxygen. The potential was stepped from 0 to −2.50 V and the frequency of modulation was 40 Hz. The MSRS technique is described more explicitly in refs. 8 and 12. A single peak (λ_{max} = 587 nm) due to absorption by the radical anion was observed. Reflection spectroelectrochemical transients for the formation of the anion radical were then obtained at this wavelength using the same potentials. Figure 6 shows the transient for radical anion formation of **III** at the platinum mirror electrode in the absence of oxygen. Composite transient data from 100, 200, 400, and 1000 ms transients were combined to examine the linearity of the optical response with the square root of time over an extended period. Linearity indicates anion radical stability over the examined timescale, if the amplitude of $\Delta R/R$ is kept small. The plots of $-\Delta R/R$ vs. $t^{1/2}$ were indeed linear with a correlation coefficient of 0.99885, showing the radical anion to be very stable for times of at least 1 s. This also demonstrates the reproducibility and accuracy of this transient technique.

Figure 7 shows the transient that results when oxygen is present in solution together with **III**. MSRS data data of this system at the same potentials of modulation still revealed a single peak at the same wavelength as that for the oxygen-free system, demonstrating that superoxide does not absorb at this or at any nearby frequency. We still observe the formation of the radical anion during the forward potential step although the reflectance is somewhat less. When the potential is reversed to its base value, however, to where only neutral **III** and O_2 are stable, the reflectance, which is proportional to absorbance at low values of $\Delta R/R$, is observed to decay rapidly to zero. Clearly, the anion radical of **III** reacts rapidly with oxygen.

Regeneration of **III** is suggested by the observed reflectance–time profile during the forward applied potential pulse; the shape of the transient is still a linear function of the square root of time. $\mathbf{III}^+$ diffuses from the electrode surface into the oxygen and superoxide rich solution, neutral **III** is formed and can therefore diffuse back to the electrode and undergo another reduction.

The results are consistent with the following proposed mechanism for the cathodic reduction of **III**:

IN THE ABSENCE OF OXYGEN

$$\mathbf{III} + e^- \rightleftharpoons \mathbf{III}^{\cdot-} \qquad E^{\circ} = -2.32 \text{ V}$$

In oxygen-free solution a simple electron transfer occurs reversibly to form the anion radical from neutral **III**.

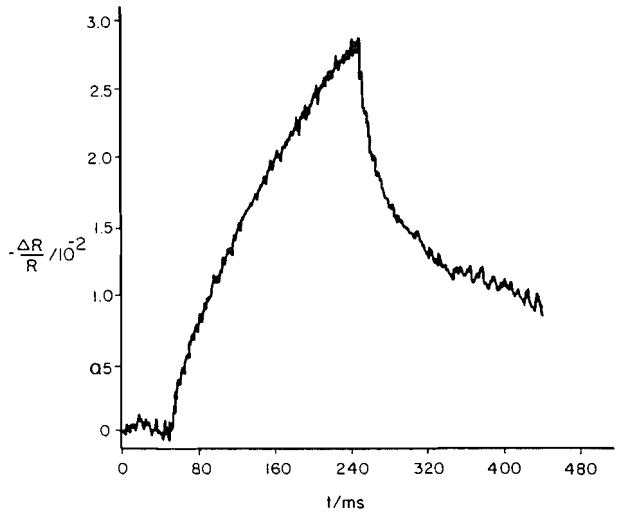

FIG. 6. Reflectance spectroelectrochemical transient at 587 nm for the anion radical of **III** in the solution described in Fig. 1*a*. (The solution is oxygen-free.)

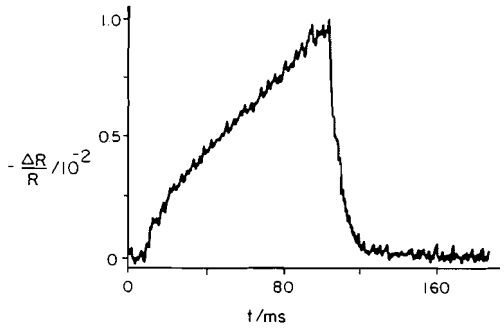

FIG. 7. Reflectance spectroelectrochemical transient at 587 nm for the anion radical of **III** in the solution described in Fig. 2. (The solution contains oxygen.)

IN THE PRESENCE OF OXYGEN

$$O_2 + e^- \rightleftharpoons O_2^{\cdot-} \qquad E^{\circ} = -1.18 \text{ V}$$

$$\mathbf{III} + e^- \rightleftharpoons \mathbf{III}^{\cdot-} \qquad E^{\circ} = -2.32 \text{ V}$$

$$O_2 + \mathbf{III}^{\cdot-} \rightleftharpoons O_2^- + \mathbf{III}$$

$$HS + O_2^{\cdot-} + \mathbf{III}^{\cdot-} \rightleftharpoons S^- + HO_2^- + \mathbf{III}$$

Here the mean of the oxidation and reduction peak potentials for dioxygen have been taken to be the standard potential. During the forward potential step, the rate of production of the anion at the electrode is limited by the diffusion of the neutral species to the surface. Reaction of anion with oxygen and superoxide regenerates the neutral molecule, so more of **III** is available to diffuse to the interface. Because of this, the absorbance of the radical anion in oxygen-containing solution is not much lower than it is in the solution in which oxygen is not present. During the reverse potential pulse, however, the oxygen consumes the anion while the regenerated starting material cannot react electrochemically to form more anion to replace that which is consumed. The reflectance therefore fails rapidly in comparison to the case in an oxygen-free environment.

The supporting electrolyte cation, TBA^+, probably acts as a proton donor in the proposed scheme. The peroxide dianion most likely abstracts a proton from the background electrolyte.

Can. J. Chem. Downloaded from www.nrcresearchpress.com by 213.166.140.6 on 09/07/12
For personal use only.

Can. J. Chem. Downloaded from www.nrcresearchpress.com by 213.166.140.6 on 09/07/12
For personal use only.

Further studies on this possibility are underway and will appear elsewhere.

Evidence for the greater stability of the anion radical of **V** than that of **III** is apparent from the MSRS experiment. The wavelength of maximum absorption for the anion radical of **III** appears at 587 nm, while that for the anion radical of **V** is observed at 529 nm (5); the energy of the electronic transition for the naphthyl derivative anion radical is higher than that for the benzyl derivative anion radical. Energy levels predicted from the Hückel calculations appeared at relative energies which are consistent with these data.

B. The cation radical

A reflectance transient spectrum was obtained as before for the cation radical formation from **III**, by stepping the electrode potential (chronoamperometric experiment) from 0 to +0.9 V, which causes diffusion-controlled mass transport of neutral **III** to the electrode. The current response indicated a simple one-electron transfer. The wavelength of maximum $\Delta R/R$ was found at 473 nm for the formation of the radical cation. Identical spectra resulted whether O_2 was present or absent in the solution. Spectroelectrochemical transients for the anodic oxidation of **III** to its radical cation were then taken at the above λ_{max} for pulse lengths of 20, 40, 100, 200, and 400 ms duration; a typical transient is shown in Fig. 8. Such transients were identical whether O_2 existed in solution or did not, suggesting no cation radical reaction with oxygen. The composite data from the above transients of different length were plotted as before ($\Delta R/R$ vs. $t^{1/2}$) (Fig. 9). The plot is linear up to times of about 100 ms, and thereafter we see a fall-off region; the cation radical is stable for a short period before it undergoes decay.

Whether this decay involves an electron transfer or not, a chemical step is certainly involved; it is the product of this decay which appears at cathodic potentials upon reverse sweep to negative values in the cyclic voltammetry described earlier. Assuming first or pseudo first order kinetic behavior, we can compute the homogeneous rate constant for the decay of the radical cation from the spectroelectrochemical data utilizing the technique described in refs. 12 and 13, where the rate constant

$$k = \frac{\left[-\frac{\Delta R}{R}\right]_0 - \left[-\frac{\Delta R}{R}\right]}{\int_0^t \left[-\frac{\Delta R}{R}\right]_k dt}$$

Here $[-\Delta R/R]_0$ is the change in reflectance which would be obtained at time t if the absorbing species does not decay, and $[-\Delta R/R]_k$ is the change in reflectance where decay occurs with a first order rate constant k. Computation of this k value was performed from data from various transients in excess of 100 ms length, and a mean homogeneous first order rate constant of 1.99 s^{-1} was determined for the degradation of the cation radical.

The data are consistent with the following mechanism for the oxidation of **III**, either in the presence or absence of oxygen:

$$\mathbf{III} \rightleftharpoons \mathbf{III}^{+\cdot} + e^-$$

$$\mathbf{III}^{+\cdot} \xrightarrow{k} P$$

$$(P + ne^- \rightleftharpoons Q)$$

It was not possible from the spectroelectrochemical data to determine between an EC or an ECE mechanism where the second electron transfer could not be observed (*vide infra*).

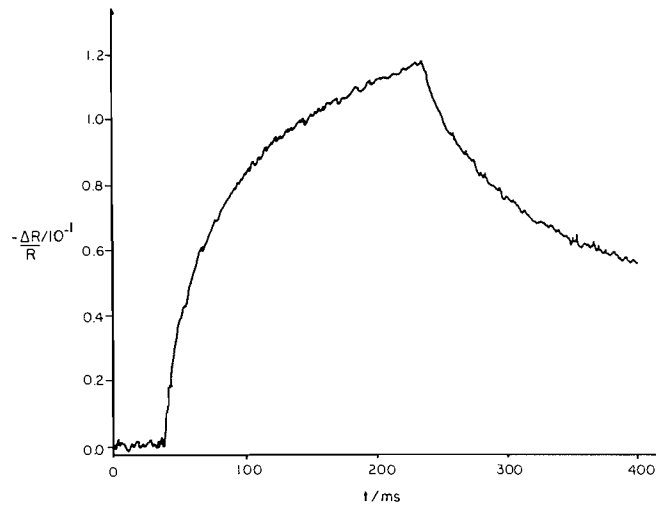

FIG. 8. Reflectance spectroelectrochemical transient at 473 nm for the cation radical of **III** in the solution described in Fig. 4.

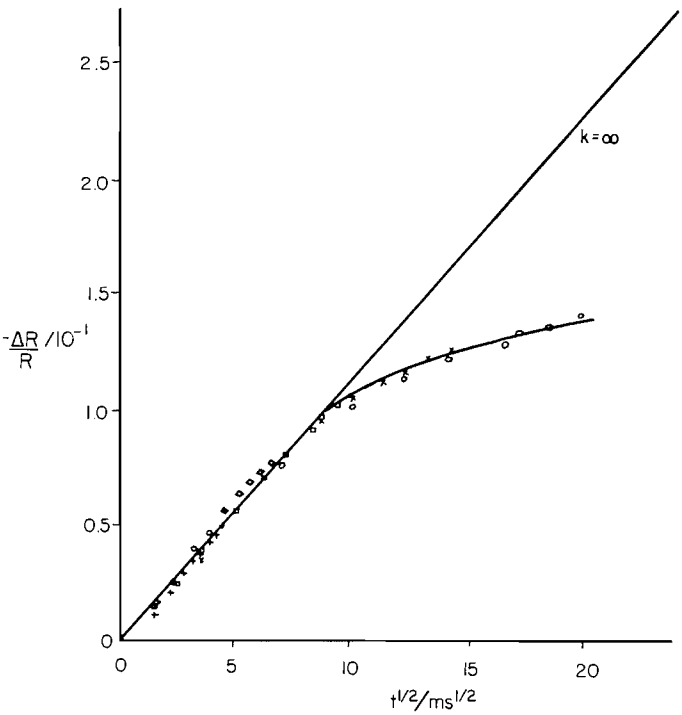

FIG. 9. Reflectance vs. square root of time plot for the formation of the cation radical from transients of duration: +, 20 ms; □, 40 ms; ◇, 100 ms; ×, 200 ms; ○, 400 ms. Solution is that described in Fig. 4.

The electrochemical and spectroelectrochemical (*vide infra*) evidence is for an EC type of reaction mechanism: subsequent electron transfer reactions are not indicated after the initial chemical reaction product is formed. If the concentration of the hydrocarbon is increased, the rate constant for reaction of the cation radical does not increase when the solution is very dry, indicating that in this solvent of low nucleophilicity, dehydrodimerization reactions to form the biphenyl or other dimer products with starting material or other cation radicals is not the major chemical reaction of the cation radical. The reaction also is not dependent on the nature or concentration of supporting electrolyte as long as the solutions are of sufficient conductivity to allow for reliable electrochemical measurements; lithium perchlorate, tetrabutylammonium tetrafluoro-

borate, and tetraethylammonium perchlorate all gave similar results at 0.05, 0.10, and 0.25 *M* concentrations. Water addition at the 1–20 m*M* level in all of these solutions did not lead to changes in the rate of cation radical reaction.

Other possible pathways (13, 15) for hydrocarbon cation radical reactions are well known. They proceed generally by an ECE type reaction, such as loss of proton to give the free radical with subsequent loss of another electron to give the carbenium species, which reacts with any nucleophile to give stable products. Disproportionation reactions occur much less frequently, and these are also overall two electron transfer reactions. The most plausible reaction is that there is a proton loss (*vide supra*) to form the free radical of **III**, which is (*a*) either electrochemically more difficult to oxidize than the starting material (this is indicated by the Hückel calculation), and/or (*b*) because of the slow rate of production from the cation the free radical species will be concentrated at a distance far from the electrode compared to the size of the reaction layer of the radical. The radical reacts away (probably by radical–radical dimerization) before it can be transported back to the electrode to undergo another electron transfer (cf. (*a*)).

MSRS spectra for the cation radicals of **III** and **V** gave similar wavelengths of maximum absorption: 473 and 480 nm, respectively. This indicates that the cation radicals have similar ground state electronic energies. The HOMO–LUMO electronic transition energies calculated with the Hückel programs were also consistent with these observations.

Conclusion

The voltammetric and spectroelectrochemical studies of the title compound suggest significant electronic differences in both **III** and **V** as well as their respective anion radicals, while indicating that the cation radicals of the two species are energetically similar. Studies on neutral alkylidene cyclopropabenzenes (14) have shown the stability of the cyclopropabenzene derivatives to be less than that of their naphthyl homologs. Simple Hückel molecular orbital calculations gave results which were consistent with these observations.

Acknowledgements

S.P. thanks the Office of Naval Research for support of part of this work, and John Mellor for valuable discussions regarding the electrochemical results. P.J.S. acknowledges the support of the National Science Foundation (CHE84-19099). K.A. thanks Carol Korzeniewski for the use of her Hückel programs. S.J.B. thanks the NZUGC for a postdoctoral fellowship.

1. A. GREENBERG and J. I. LIEBERMAN. Strained organic molecules. Academic Press, New York. 1978.
2. W. E. BILLUPS. Acc. Chem. Res. **11**, 245 (1978).
3. B. HALTON. Ind. Eng. Chem. Prod. Res. Dev. **19**, 349 (1980).
4. B. HALTON, C. J. RANDALL, and P. J. STANG. J. Am. Chem. Soc. **106**, 6108 (1984).
5. K. ASHLEY, J. K. FOLEY, Q. MEI, J. GHOROGHCHIAN, F. SARFARAZI, J. CASSIDY, B. HALTON, P. J. STANG, and S. PONS. J. Org. Chem. **51**, 2089 (1986).
6. D. B. CLARK, M. FLEISCHMANN, and D. PLETCHER. J. Chem. Soc. Perkin II, 1578 (1973).
7. J. CASSIDY. Ph.D. Thesis, University of Utah. 1985.
8. S. PONS and S. B. KHOO. J. Am. Chem. Soc. **104**, 3845 (1982).
9. T. A. LORENZOLA, B. A. LOPEZ, and M. C. GIORDANA. J. Electrochem. Soc. **130**, 1359 (1983).
10. H. SIEGERMAN. *In* Technique of electroorganic synthesis. Part II. *Edited by* N. L. Weinberg. Wiley, New York. 1975.
11. A. J. BARD and H. LUND (*Editors*). Encyclopedia of electrochemistry of the elements. Vol. XI-1. Marcel Dekker, New York. 1978.
12. S. B. KHOO. Ph.D. Thesis, University of Alberta. 1984.
13. A. BEWICK, J. M. MELLOR, and B. S. PONS. Electrochem. Acta, **25**, 931 (1980).
14. B. HALTON, C. J. RANDALL, G. J. GAINSFORD, and P. J. STANG. J. Am. Chem. Soc. In press.
15. L. EBERSON and J. H. P. UTLEY. *In* Organic electrochemistry. *Edited by* M. Baizer. Marcel Dekker, New York. 1983.

Can. J. Chem. Downloaded from www.nrcresearchpress.com by 213.166.140.6 on 09/07/12
For personal use only.

The hex-5-enose degradation: cleavage of glycosiduronic acid linkages in modified methylated *Sterculia* gums[1,2]

GERALD OLIVER ASPINALL,[3] LEV KHONDO, AND BRUCE ALAN WILLIAMS
Department of Chemistry, York University, North York, Toronto, Ont., Canada M3J 1P3

Received October 17, 1986

GERALD OLIVER ASPINALL, LEV KHONDO, and BRUCE ALAN WILLIAMS. Can. J. Chem. **65**, 2069 (1987).

Reduction of uronic acid residues in permethylated polysaccharides from *Sterculia urens* and *S. caudata* gums, followed by transformation of the resulting hexose into 6-deoxy-6-iodohexose residues, affords modified polysaccharides that undergo depolymerization on treatment with zinc dust. The main products after reduction with sodium borohydride are hexenitol-terminated oligosaccharides. Their structures have been assigned as members of a series of *O*-[α-L-rhamnopyranosyl]-(1→3)-1,2-dideoxyhex-1-enitol derivatives, with and without attendant β-D-galactopyranosyl substituents, on the basis of nuclear magnetic resonance and mass spectral data and compositional analysis of trideuteriomethylated derivatives. The structures of the polysaccharides have been reassessed in the light of these and other experiments, and may now be formulated as containing a backbone of alternating 4-linked α-D-galacturonic acid and 2-linked α-L-rhamnopyranose residues bearing a minimum of three types of side chains attached at specific sites. Characterization of some of the degradation products provides evidence that limited degradation had occurred during methylation of the glycuronans.

GERALD OLIVER ASPINALL, LEV KHONDO et BRUCE ALAN WILLIAMS. Can. J. Chem. **65**, 2069 (1987).

La réduction de résidus d'acide uronique de polysaccharides perméthylés provenant de gommes de *Sterculia urens* et de *S. caudata*, suivie d'une transformation de l'hexose qui en résulte en résidus déoxy-6 iodo-6 hexose, fournit des polysaccharides modifiés qui subissent une dépolymérisation lorsqu'on les traite par de la poudre de zinc. Les produits principaux provenant d'une réduction par le borohydrure de sodium sont des oligosaccharides se terminant par un hexènitol. En se basant sur des données de résonance magnétique nucléaire et de spectre de masse ainsi que sur des analyses de composition des dérivés trideutérométhylés, on a attribué leurs structures aux membres d'une série de dérivés *O*-[α-L-rhamnopyrannosyl]-(1→3)-didéoxy-1,2 hexène-1 itols qui pouvaient aussi porter des groupements β-D-galactopyrannosyles. On a réévalué les structures des polysaccharides à la lumière de ces expériences ainsi que d'autres et on peut maintenant affirmer qu'elles contiennent une unité de base formée d'acide α-D-galacturonique lié par la position 4 qui alterne avec un résidu du α-L-rhamnopyrannose lié par la position 2; cette unité répétitive porte un minimum de trois types de chaînes latérales qui sont attachées à des sites spécifiques. La caractérisation de quelques produits de dégradation fournit des données permettant d'affirmer qu'il s'est produit une dégradation limitée au cours de la méthylation des glycuronanes.

[Traduit par la revue]

Exudate gums from the *Sterculia* genus contain structurally similar, partially acetylated polysaccharides with residues of D-glucuronic acid, D-galacturonic acid, D-galactose, and L-rhamnose (1–5). The most detailed studies have been carried out on *S. urens* gum and led to the formulation of two structural regions: (A) repetitive 4-linked *O*-α-D-galactopyranosyluronic acid-(1→2)-L-rhamnopyranose units bearing β-D-glucopyranosyluronic acid residues at O-3 of galacturonic acid and undefined side chains at O-4 of rhamnose residues; and (B) branched trisaccharide units that are probably not present in repetitive sequences. Indirect evidence suggested that these latter units were continuous with and interrupted the rhamnogalacturonan regions at intervals (**1**). Other neutral sugar residues were not placed with certainty. Acid hydrolysis or acetolysis was used for partial fragmentation and took advantage of the relative resistance to acid-catalyzed cleavage of glycosiduronic acid linkages. A reversal of these preferences was effected by partial acetolysis of the carboxyl-reduced polysaccharide, which permitted the isolation of a more random selection of oligosaccharides, but it was not always possible to distinguish between galactose residues originally present and those formed from the reduction of galacturonic acid units. The recently developed hex-5-enose degradation (6, 7) provides an alternative fragmentation procedure in which selective cleavage takes place at former glycosiduronic acid linkages with the formation of hexenose-terminated oligosaccharides containing unaltered neutral glycosyl substituents. We describe here the application of this degradation to permethylated derivatives of *S. caudata* and *S. urens* gums with the formation of oligosaccharides that throw fresh light on the detailed structures of these polysaccharides.

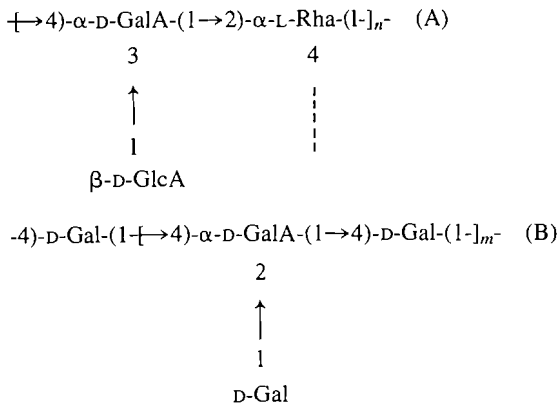

1: previously formulated structural regions in *Sterculia urens* gum

The hex-5-enose degradation as applied to glycuronans (Scheme 1, **I**) involves methylation (**I** → **II**), followed by reduction (**II** → **III**) of hexuronic acid residues, iodination (**III** → **IV**), analysis by reductive deiodination (**IV** → **V**), and zinc dust degradation (**IV** → **VI**) to generate hexenoses

[1]Dedicated to Professor D. E. Ryan on the occasion of his 65th birthday.

[2]Presented in part at the 13th International Carbohydrate Symposium, Cornell University, Ithaca, New York, U.S.A., August 10–16, 1986.

[3]Author to whom correspondence should be addressed.

Can. J. Chem. Downloaded from www.nrcresearchpress.com by 213.166.140.6 on 09/07/12
For personal use only.

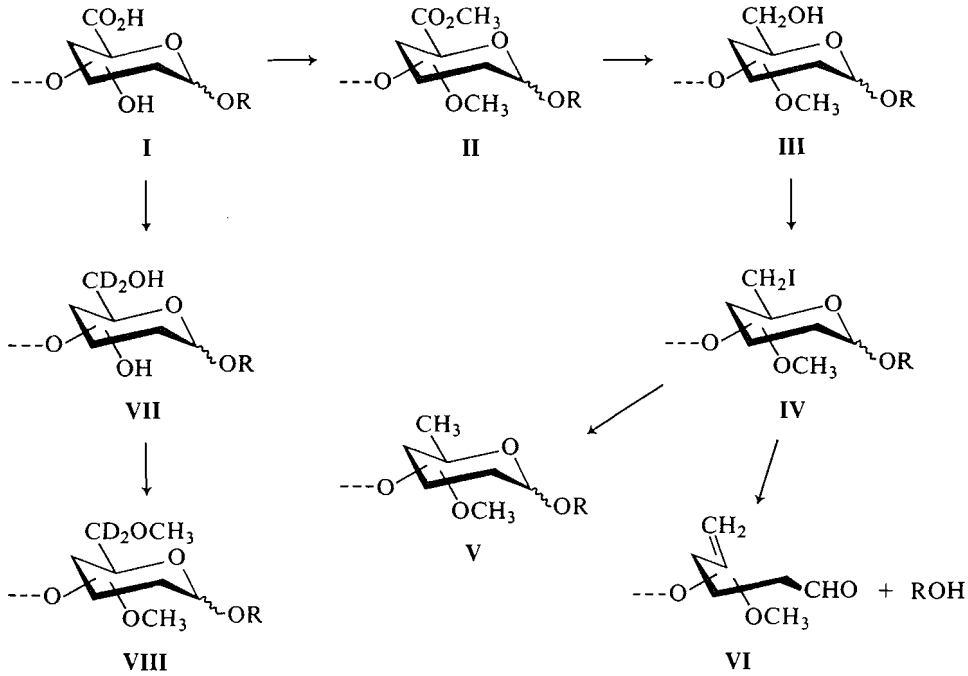

SCHEME 1. Modifications of *Sterculia* gums showing generalized structures for glycosiduronic acid residues undergoing change as described in the text.

with liberation of aglycons. Reduction of the methylated gum samples prepared in earlier investigations (1, 2) with lithium aluminum hydride afforded some material that was mobile on tlc plates, and the material of higher molecular weight that was required was separated by gel permeation chromatography on Sephadex LH-20. The methylated glycans after carboxyl reduction (**III**) were treated with *N*-iodosuccinimide and triphenylphosphine (8) to give iodinated derivatives. Since previous studies had established the presence of at least three types of uronic acid residues it was necessary to demonstrate completeness of reaction at each type of unit. This was achieved by treatment of samples of the iodinated glycans (**IV**) with tributylstannane (9) followed by hydrolysis and normal methylated sugar analysis by glc–ms of the derived partially methylated alditol acetates (10). In this manner newly formed 6-deoxyhexose residues (in **V**) were recognized as originating from the corresponding methylated uronic acid residues (in **II**). The results for both gums (Table 1) showed that a satisfactory degree of structural modification had occurred in the iodination step through disappearance of hexose (in **III**) and appearance of the related 6-deoxyhexose derivatives. Table 1 also presents the results of a different analysis of uronic acid residues in which deuterium-labelled carboxyl-reduced polysaccharides (**VII**), formed by treatment of polysaccharide 2-hydroxyethyl esters (1) with sodium borodeuteride, were converted into their methylated derivatives (**VIII**). Although reduction was not complete after two esterification–reduction cycles, a sufficiently high degree of modification had been achieved for methylation to be performed with the retention of potentially base-sensitive residues (*vide infra*). The glc–ms analysis of deuterium-labelled methylated sugar devivatives (Table 1) confirmed the presence of terminal glucuronic acid and two types of galacturonic acid residues as branch points, as required in the previously formulated structure (**1**). In addition, the results showed that *S. urens* gum contained some unbranched 4-linked galacturonic acid residues, as did *S. caudata* gum together with some galacturonic acid end groups.

Iodinated methylated *S. caudata* gum (**IV***a*) was heated with zinc dust in 95% ethanol and the whole reaction mixture was reduced with sodium borohydride. That a high degree of depolymerization had occurred was indicated by trideuteriomethylation of exposed hydroxyl groups in otherwise unaltered neutral sugar components, in which process most of the 3-*O*-methylrhamnose was alkylated at O-2, some of the 2,3,6-tri-*O*-methylgalactose was alkylated at O-4, but the highly volatile derivatives of alkylated alditol and hexenitol terminal units were not detected. Direct analysis of the peralkylated degradation products by glc–ms showed the presence of five separable oligosaccharide derivatives (**2**–**6**) for which partial structural assignments could be made. With minor exceptions, fragment ions from individual glycosyl units showed that these were uniformly substituted with respect to isotopic labels.

For preparative purposes the mixture of products formed

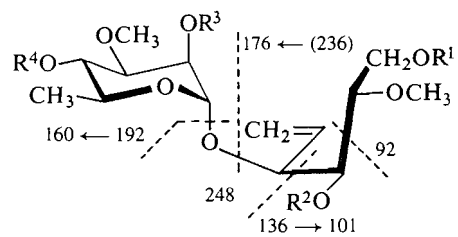

2 (α-L-Rha-(1→4)-D-GalA)[≠]
2*a* $R^1 = R^3 = H$, $R^2 = R^4 = CH_3$
2*b* $R^1 = R^3 = CD_3$, $R^2 = R^4 = CH_3$ (fragment ions shown with parent ions of the *J* series in parenthesis)
2*c* $R^1 = R^2 = R^3 = R^4 = H$
2*d* $R^1 = R^2 = R^3 = R^4 = CD_3$
2*e* $R^1 = H$, $R^2 = R^3 = R^4 = CH_3$
2*f* $R^1 = CD_3$, $R^2 = R^3 = R^4 = CH_3$

[≠]The shorthand designation of hexenitol-terminated oligosaccharides indicates the nature and linkage site of the uronic acid from which the unit originates.

Can. J. Chem. Downloaded from www.nrcresearchpress.com by 213.166.140.6 on 09/07/12
For personal use only.

TABLE 1. Sugar analyses of methylated *Sterculia* gum derivatives[a]

Sugars[b]	Relative proportions					
	S. caudata			*S. urens*		
	III*a*	**V***a*	**VIII***a*	**III***b*	**V***b*	**VIII***b*
From uronic acids						
2,3,4-Me_3Glc	14.2[e]			7.1[e]		
2,3,4-Me_3 6-*d* Glc		15.2[c]			6.9[c]	
2,3,4,6-Me_4Glc			15.2*			8.6*
2,3,4-Me_3Gal	3.0					
2,3,4-Me_3Fuc		2.2				
2,3,4,6-Me_4Gal			2.0**			
2,3-Me_2Gal	4.7			1.7		
2,3-Me_2Fuc		5.1[d]			2.0[d]	
2,3,6-Me_3Gal			4.7**			1.7**
2-MeGal	10.8			8.5		
2-MeFuc		12.7			8.1	
2,6-Me_2Gal			12.8*			11.0*
3-MeGal	6.5			18.2		
3-MeFuc		6.3			17.2	
3,6-Me_2Gal			8.2*			16.3*
From neutral sugars						
2,3,4-Me_3Rha	1.0	1.0[c]	1.0	8.5	8.5[c]	7.8
3,4-Me_2Rha	8.4	8.1	10.5	10.3	11.0	10.1
3-MeRha	17.2	15.4	15.3	10.4	9.5	11.3
2,3,4,6-Me_4Gal	5.5	6.8[d]	6.0**	15.8	16.8[d]	15.4
2,3,6-Me_3Gal	17.3[e]	17.3	13.9**	12.0[e]	12.0	10.9**
2,6-Me_2Gal	3.0	2.1	3.0*			

[a]**III***a*, methylated *S. caudata* gum after carboxyl reduction; **V***a*, iodinated methylated *S. caudata* gum after treatment with tributylstannane; **VIII***a*, carboxyl-reduced ($NaBD_4$) *S. caudata* gum after methylation. **III***b*, **V***b*, and **VIII***b* are the corresponding derivatives of *S. urens* gum.

[b]Sugars characterized by conversion into partially methylated alditol acetates for analysis by glc–ms.

[c]It is assumed that the proportions of inseparable derivatives of 2,3,4-Me_3Rha and 2,3,4-Me_3 6-*d*Glc in **V***a* and **V***b* are unchanged from those in **III***a* and **III***b*.

[d]Since derivatives of 2,3-Me_2Fuc and 2,3,4,6-Me_4Gal were not separated it is assumed that the relative proportions of these two sugars in **V***a* and **V***b* are the same as those of 2,3-Me_2Gal and 2,3,4,6-Me_4Gal in **III***a* and **III***b*.

[e]Since derivatives of 2,3,4-Me_3Glc and 2,3,6-Me_3Gal were not separated it is assumed that the proportions of the latter in **III***a* and **III***b* were the same as those in **V***a* and **V***b*.

*The glc–ms showed at least 80% incorporation of label in $-CD_2OCH_3$ groups in relevant fragment ions. Allowance is made for nonlabelled components where there is evidence for their formation from neutral sugars.

**The glc–ms showed 20–25% incorporation of label in $-CD_2OCH_3$ groups. These are apportioned between neutral and uronic acid-derived sugars.

from modified methylated *S. caudata* gum on zinc degradation followed by reduction was chromatographed on silica gel plates to give 1,2-dideoxy-3,4,5-tri-*O*-methyl-L-*xylo*-hex-1-enitol[4] and fractions containing oligosaccharides, mainly as 2- or 3-component mixtures. Each fraction was converted into trideuteriomethylated derivatives, and the identities and relative proportions of the components were determined by glc–ms (Table 2) so that the configurations of glycosidic linkages, even for compounds in admixture, could be unambiguously assigned from the anomeric signals of corresponding intensity in the nmr spectra (Table 3). Substitution patterns of terminal 1,2-dideoxyhex-1-enitol or alditol residues were evident from simple fragment ions in the ms and, where necessary, the positions of trideuteriomethyl substituents in glycosyl residues were confirmed by conversion of the hydrolysis products into partially methylated alditol acetates for glc–ms analysis. The results established the presence of six oligosaccharides (**2***a*–**6***a* and **2***c*) in the original mixture, and the structures of the corresponding trideuteriomethylated derivatives (**2***b*–**6***b* and **2***d*) are shown with *m/z* values for significant fragment ions in their mass spectra.

Four of the oligosaccharides contain 1,2-dideoxyhex-1-enitol termini. Since acid residues in internal chains are those of D-galacturonic acid only, it is assumed without further proof that all glycosylated hexenitols have the L-*lyxo* configuration. The disaccharide derivatives **2***a* and **2***c* differ only in the degree of methylation and, after trideuteriomethylation, give chromatographically indistinguishable compounds. The nature of the two different glycosyl substituents of the hexenitol residue in the branched trisaccharide **5***b* is apparent from the mass spectral fragment ions at *m/z* 192 and 219 together with those of the corresponding aglycons at *m/z* 380 and 353, and the location of the hexopyranosyl substituent at O-5 of the hexenitol (O-2 of the parent galacturonic acid) is shown from the fragment

[4]Systematic nomenclature requires that reduction of 5,6-dideoxyhex-5-enoses gives 1,2-dideoxyhex-1-enitols with consequent changes in configurational prefixes and the numbering of substituents.

Can. J. Chem. Downloaded from www.nrcresearchpress.com by 213.166.140.6 on 09/07/12
For personal use only.

TABLE 2. Reduced oligosaccharides formed by the hex-5-enose degradation from iodinated methylated *Sterculia* gums

Oligosaccharides (*i*) Initially formed	Oligosaccharides (*ii*) After trideuteriomethylation	Retention times (*ii*)[a]	Major fragment ions (*m/z*)	Relative proportions[b] *S. caudata*	Relative proportions[b] *S. urens*
2*a*	**2***b*	4.0	192, 176	19	7
2*c*	**2***d*	4.0	195, 179	2	1
2*e*	**2***f*	4.0	189, 176		2
2*a*	**3***b*	7.9	222, 214	6	2
4*a*	**4***b*	9.0	222, 192	9	5
5*a*	**5***b*	18.7	192, 219	25	39
5*c*	**5***d*	18.7	189, 219		27
6*a*	**6***b*	21.6	222, 179	35	11

[a]Retention times (min) are for column C (180°C, 4°/min → 250°C, hold).
[b]The relative proportions of compounds whose trideuteriomethylated derivatives differed only in isotopic labelling are based on the abundances of relevant fragment ions.

TABLE 3. Nuclear magnetic resonance data of oligosaccharides from iodinated methylated *S. caudata* gum (**IV***a*) on zinc degradation followed by reduction

Fraction	Weight (mg)	Compounds formed on trideuteriomethylation (% in fraction[a])	^{1}H nmr data for anomeric centres[b] δ[$J_{1,2}$(Hz)]	Assignment (methylation[c])
2	5.0	**4***b*† (58)	4.73[1.80]	α-Rha(2*,3)
			4.59[7.58]	β-Gal(2,3,4*,6)
		5*b* (34)		
		2*b* (5)		
3	4.0	**2***b*† (88)	4.99[1.60]	α-Rha(2*,3,4)
		5*b* (10)		
4	2.5	**5***b*† (70)	5.04[1.30]	α-Rha(2*,3,4)
			4.26[7.67]	β-Gal(2,3,4,6)
		2*b* (15)		
		6*b* (10)		
5	3.0	**5***b* (70)		
		2*b* (16)		
		6*b* (29)		
6	6.5	**6***b*† (78)	5.00[1.60]	α-Rha(2*,3)
			4.58[7.59]	β-Gal(2,3,4*,6)
		3*b* (16)[d]	4.26[7.72]	β-Gal(2,3,4*,6)
7[e]	6.0	**6***b* (37)		
		3*b* (13)		
		2*d* (10)		
8[e]	2.0	**2***d* (42)		
		6*b* (17)		
		3*b* (8)		

[a]Determined by glc as in Table 2.
[b]Consistent data were obtained for the same compounds in different fractions but are reported only where the designated (†) compound is the major component of the mixture. All spectra of relevant compounds showed signals at δ 1.27 (d, 3H, $J_{1,2}$ = 6.22 Hz, H-6 of α-L-Rha), 5.21–5.35 (m, 2H, -CH=CH_2), and 5.84–5.96 (m, 1H, -CH=CH$_2$).
[c]Glycosyl (but not hexenitol/alditol) substituents in designated (†) compounds were characterized on hydrolysis and methylated sugar analysis.
[d]Although a minor component, the anomeric signal was unambiguously assigned in the two-component mixture. The methylation pattern was inferred from ms data.
[e]These fractions also contained some chromatographically mobile material, which would not be estimated by glc analysis of fully alkylated derivatives.

ions at *m/z* 340 and 305. The presence in the mass spectrum of a **V** ion (11) at *m/z* 190 supports the branched structure, and the relatively low abundance of this ion suggests that the glycosyl substituents are not vicinal. Mass spectral data likewise define the second trisaccharide **6***b* as having a linear structure in which locations of trideuteriomethyl groups indicate former points of attachment of glycosyl substituents. The rhamnitol-terminated disaccharide **3***b* is related to the linear trisaccharide **6***b*, and evidence that it is the product of inadvertent breakdown was obtained from deuterium incorporation into the rhamnitol

Can. J. Chem. Downloaded from www.nrcresearchpress.com by 213.166.140.6 on 09/07/12
For personal use only.

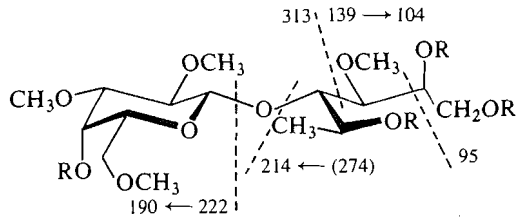

3 (β-D-Gal-(1→4)-L-Rhamnitol)
3*a* R = H; **3***b* R = CD_3 (fragment ions shown)

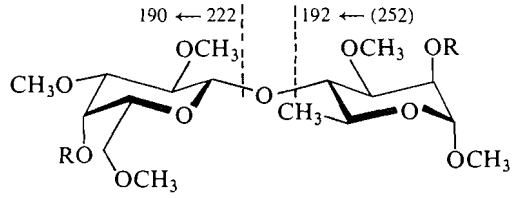

4 (β-D-Gal-(1→4)-α-L-Rha as methyl glycoside)
4*a* R = H; **4***b* R = CD_3 (fragment ions shown)

moiety when the products of zinc degradation were treated with sodium borodeuteride. Acid lability of 4-*O*-glycosylhex-5-enoses under the conditions of the zinc degradation was observed previously (6). The disaccharide derivative **4***a* was characterized as a methyl glycoside in which the fragment ion at *m/z* 311 (**7**) from the trideuteriomethylated derivative **4***b* is characteristic of a (1→4)-linked disaccharide, a conclusion supported by the identities of the hydrolysis products, 2,3,4*,6-

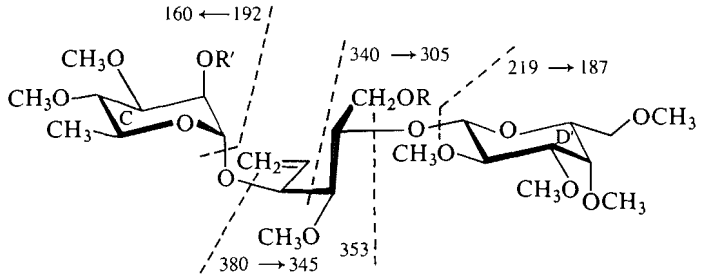

5 (α-L-Rha-(1→4)-D-GalA-(2←1)-β-D-Gal)
5*a* R = R¹ = H; **5***b* R = R¹ = CD_3 (fragment ions shown)
5*c* R = H, R¹ = CH_3; **5***d* R = CD_3, R¹ = CH_3

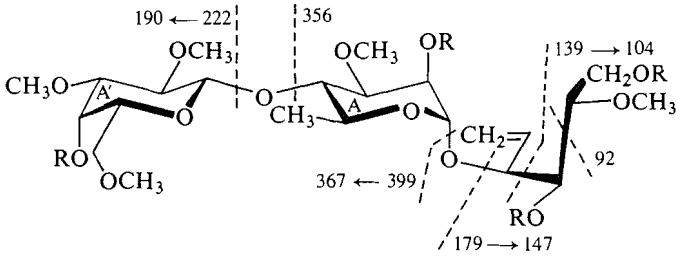

6 (α-D-Gal-(1→4)-L-Rha-(1←4)-D-GalA)≠
6*a* R = H; **6***b* R = CD_3 (fragment ions shown)

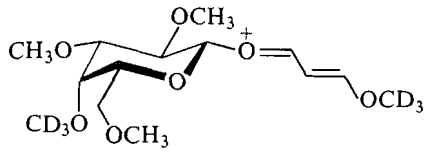

7

tetra-*O*-methylgalactose[5] and 2*,3-di-*O*-methylrhamnose. The nmr data showed that all the neutral glycosyl residues in the oligosaccharides were those of β-D-galactopyranose and α-L-rhamnopyranose.

Modified methylated *S. urens* gum (**IV***b*) was degraded in the same way and reduction of products from the zinc treatment gave oligosaccharides that were shown by glc–ms of the trideuteriomethylated derivatives to be qualitatively similar to those formed from *S. caudata* gum. The relatively large excess of fully alkylated trisaccharide **5***b* over other components in the mixture may reflect incomplete reaction during the zinc degradation, and is probably not representative of the parent methylated polysaccharide since compositional analyses of methylated polysaccharides (e.g. **III***a* and *b*, and **VIII***a* and *b*) from the two gums showed smaller differences (Table 1). However, the mass spectrum of fully alkylated trisaccharide **5** from *S. urens* gum showed that the rhamnose residues were not uniformly labelled with trideuteriomethyl groups. Although an attempt to separate chromatographically the oligosaccharide mixture, **2***a*, **3***a*, etc., was only partly successful, samples of differently labelled trisaccharides **5***a* and **5***c* were isolated and these were converted into the corresponding fully alkylated derivatives **5***b* and **5***d* for individual examination.

Revised by still incomplete structures for the two closely related polysaccharides from *S. urens* and *S. caudata* gums may be considered in the light of the oligosaccharides isolated from partial acid hydrolysis or acetolysis in earlier studies (1, 2), the new degradation products, and the compositional analyses of modified methylated polysaccharides (Table 1). The results show that the backbone consists exclusively of chains of 4-linked α-D-galacturonic acid and 2-linked L-rhamnopyranose residues with all other sugar residues present in side chains. Oligosaccharides **2***a*, **5***a*, and **6***a*, isolated as degradation products from both gums, are derivatives of 1,2-dideoxy-3-*O*-α-L-rhamnopyranosyl-L-*lyxo*-hex-1-enitol, and confirm earlier conclusions from the acetolysis of carboxyl-reduced *S. urens* gum (1) that residues of the two sugars are in alternating sequence, and also provide evidence for the anomeric configuration of rhamnose residues. In the case of *S. urens* gum, independent evidence for this assignment has now been obtained from the degraded rhamnogalactan, formed on Smith degradation of the carboxyl-reduced gum (1), whose Cmr spectrum shows two main resonances in the anomeric region at δ_C 99.3 ($^1J_{^{13}C_1,^1H_1}$ = 174.5 Hz, α-Gal) and 97.5 ($^1J_{^{13}C_1,^1H_1}$ = 170.4 Hz, α-Rha). Trideuteriomethylation at O-4 of 1,2-dideoxyhex-1-enitol residues in **6***b* (corresponding to O-3 of galacturonic acid residues in the parent glycan) indicates the site of former attachment of β-D-glucuronic acid residues. Oligosaccharides **5***b* and **6***b* contain β-D-galactopyranose residues of different types, nonreducing end groups linked (1→2) to galacturonic acid and 4-linked residues attached (1→4) to rhamnose residues. The disaccharide **2***b* arises from an unbranched segment of the rhamnogalacturonan chain. The conclusions so far necessitate a revision of the earlier formulation (**1**) in that the 4-linked galactose residues must now be accommodated in side chains rather than as part of the sequences interrupting the regular backbone, and the following partial structure **8** may be proposed. The only contiguous neutral sugar residues are those giving rise to the two glycosyl residues in trisaccharide **6**. Support for this aspect of the structure was obtained when the only oligosaccharide product

[5]The asterisk (*) designates trideuteriomethyl substituents.

Can. J. Chem. Downloaded from www.nrcresearchpress.com by 213.166.140.6 on 09/07/12
For personal use only.

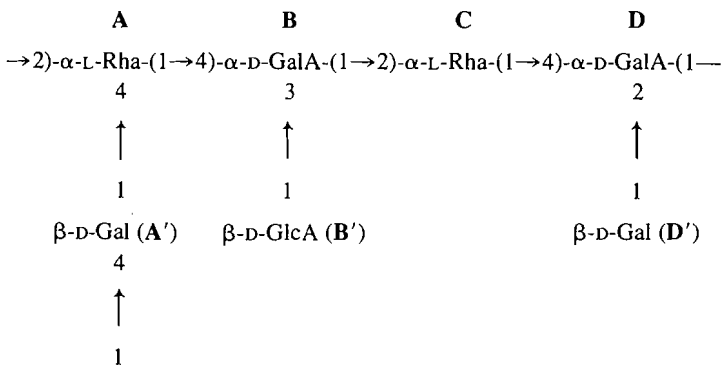

8: rhamnogalacturonan backbone (**A–D**) in *Sterculia* gums showing side-chain attachments of β-D-galactopyranose residues (not necessarily in sequence), based on the characterization of oligosaccharides **5***b* (with glycosyl residues corresponding to **C** and **D**′) and **6***b* (with glycosyl residues corresponding to **A** and **A**′).

detected on treatment of *S. urens* gum with lithium in 1,2-diaminoethane (12) was characterized as 4-*O*-β-D-galactopyranosyl-L-rhamnitol. Although not fully understood, this degradation results in destruction of uronic acid residues by base-catalyzed β-elimination with exposure of reducing sugar residues, which, during this treatment or on subsequent reaction with sodium borohydride, are reduced to alditols (13).

Structure **8** contains two types of galacturonic acid residues as branch points. Although a high degree of accuracy should not be placed on the compositional analyses of these complex methylated polysaccharide derivatives, there is a reasonable correspondence in both methylated glycans after carboxyl reduction (**III***a* and **III***b*) between the proportions of 2- and 3-*O*-methylgalactoses formed from these branch points and those of 2,3,4-tri-*O*-methylglucose and 2,3,4,6-tetra-*O*-methylgalactose respectively, which are attached as side chains. It is therefore no longer possible to associate these branched galacturonic acid residues with the 4-linked galactose residues now located in side chains. On the other hand, the proportion of 2,3,4-tri-*O*-methylgalactose formed on hydrolysis of methylated glycan derivatives (**III**), and originating from galacturonic acid end groups, is insufficient to account for all of the units of the aldobiouronic acid, 4-*O*-α-D-galactopyranosyluronic acid-D-galactose, which is a significant partial acid hydrolysis product (1–4) from each of the *Sterculia* gums so far examined. A possible explanation for this discrepancy is that a substantial proportion of side-chain galacturonic acid residues was lost by base-catalyzed β-elimination during methylation by the classical Haworth and Purdie procedures. Assuming that the base-catalyzed β-elimination of 4-*O*-substituents from uronic esters has some E2 character and occurs more readily with, but is not restricted to, galacturonates with leaving groups in the anti-periplanar orientation, loss of outer chain galacturonic acid residues at a late stage in the alkylation process could expose new terminal 2,3,6-tri-*O*-methylgalactose residues. With reagent largely spent, further alkylation at the axially oriented hydroxyl group might not occur. A second observation that is consistent with the susceptibility of galacturonate esters to base degradation is the isolation of the disaccharide glycoside **2***a*, which can only represent reducing termini of the rhamnogalacturonan chain. The formation of such a disaccharide accounting for ~10% of the degradation products would suggest a degree of polymerization in the region of 20–30 residues for the supposedly least degraded and chromatographically immobile fraction of the methylated gums after carboxyl reduction (**III**). We have no information on the molecular weight of our sample(s) of *Sterculia* gums, but a value 9×10^6 for *S. urens* gum has been reported from ultracentrifuge data (14). We regard it as highly probable that most of the units of disaccharide **2** originate from the glycosidation of reducing rhamnose residues inadvertently exposed with accompanying chain scission by β-elimination under the basic conditions necessarily used during the methylation. McNeil *et al.* (15) have reported the formation of methyl glycosides from the partial depolymerization of a methylated rhamnogalacturonan. A recent paper by Sømme reports degradation of a glucuronan during methylation using dimsyl base (16).

Analyses (Table 1) performed on methylated derivatives (**VIII**) of deuterium-labelled carboxyl-reduced polysaccharides confirmed the presence of the known uronic acid components in structure **8**, and showed in addition that *S. urens* gum contained some unbranched 4-linked galacturonic acid residues, as did *S. caudata* gum, together with some galacturonic acid end groups. These observations do not fully account quantitatively for side-chain galacturonic acid residues or define their complete structural environments. In *S. caudata* gum some galacturonic acid end groups were also indicated by the detection of 2,3,4-tri-*O*-methylfucose in the analysis of the iodinated methylated glycan after treatment with tributylstannane (**V***a*), but there is no evidence yet for the identity of residues external to the 4-linked uronic acid units. In *S. urens* gum the presence of rhamnopyranose end groups, together with the detection of some rhamnose-terminated disaccharide **2***f* from the hexenose degradation, points to some α-L-Rha*p*-(1→4)-α-D-Gal*p*A-(1→4)-β-D-Gal*p*- sequences. However, rhamnopyranose end groups in disaccharide **2***f* could also, as presumably do those in the branched trisaccharide **5***f*, arise from main chain nonreducing termini resulting from depolymerization during methylation.

Revision of the previously proposed structure (**1**) for *Sterculia* gums requires exclusively a rhamnogalacturonan backbone with residues of other sugar constituents attached in side chains. Tomoda *et al.* (17) have carried out a series of studies on plant mucilages of the Malvaceae family and have shown that these polysaccharides are of a closely related type in which rhamnogalacturonan chains carry β-D-glucuronic acid residues linked in the same manner as in the *Sterculia* gums. Some of these glycans also contain β-D-galactopyranose residues whose attachment (1→4) to rhamnose is inferred rather than directly proven. However, the absence of the aldobiouronic acid,

Can. J. Chem. Downloaded from www.nrcresearchpress.com by 213.166.140.6 on 09/07/12
For personal use only.

Can. J. Chem. Downloaded from www.nrcresearchpress.com by 213.166.140.6 on 09/07/12
For personal use only.

4-*O*-α-D-galactopyranosyluronic acid-D-galactose, from the products of partial acid hydrolysis suggests that side-chain galacturonic acid residues do not occur in these mucilages. Rhamnogalacturonans of great complexity occur widely as cell wall constituents of dicots (13, 18). Since they are liberated by the action of *endo*-α-D-galacturonanase, it has yet to be ascertained whether they occur as independent molecular species or originate from the excision of rhamnogalacturonan domains from more extended structures in which galacturonan regions are also present.

Our results show that the hex-5-enose degradation may be used to probe aspects of structure through the isolation of oligosaccharide derivatives from otherwise inaccessible structural regions. The differentiation of residues of the same sugar, e.g. D-galactose, in different locations is only possible when the degradation is performed on a polysaccharide containing stable methyl ether substituents. However, the results point to an inherent limitation of the methylation procedure when applied to glycuronans, often suspected but rarely documented, that the basic conditions necessarily used may be accompanied by degradation. For many purposes, limited depolymerization with retention of the essential repetitive structure may be of little consequence. It is a much more substantial matter if loss of certain sugar residues gives rise to methylated glycans whose structures are no longer representative of the parent polysaccharides.

Experimental

Samples of *Sterculia urens* and *S. caudata* gums and the derived methylated polysaccharides were those used in the earlier series of investigations (1–5). The ^1H and ^{13}C nmr spectra were recorded on a Bruker AM 300 spectrometer in deuteriochloroform with tetramethylsilane as internal standard. Gas–liquid chromatography was performed on a Perkin–Elmer Sigma 3B chromatograph using (A) a packed column of 3% of silicone gum Silar 10 CP on Chromosorb W-HP (100/200 mesh), (B) a capillary column of DB-225, or (C) a capillary column of DB-17. For glc – mass spectrometry, columns (B) or (C) were attached by a jet separator to a VG Micromass 16F mass spectrometer operated with an inlet temperature of 250°C, an ionization potential of 70 eV, and an ion source temperature of ~250°C.

Unsubstituted polysaccharides and their methylated derivatives were hydrolysed by the methods of Albersheim *et al.* (19) and the resulting sugars were converted into alditol acetates for glc analysis (20). Iodinated methylated polysaccharides (**IV**) were boiled in dry oxolane for 1 h with tributylstannane in the presence of a trace quantity of 2,2′-azobis(2-methylpropionitrile) as radical initiator (9, 21), to furnish the corresponding 6-deoxy-methylated polysaccharides (**V**). Uronic acid determinations were by the method of Blumenkrantz and Asboe-Hansen (22). Zinc dust was activated by the method of Frank and Smith (23). Preparative tlc was conducted on a Chromatotron (Model 7924, Harrison Research, Palo Alto, CA, U.S.A.).

Iodination of carboxyl-reduced methylated S. caudata *gum (**III**)*

Carboxyl-reduced methylated *S. caudata* gum (**III***a*) was prepared as described for the corresponding derivative of methylated *S. urens* gum (5) by reduction of methylated gum (**II***a*) with lithium aluminum hydride in oxolane. Chromatographically mobile (tlc in benzene–methanol, 6:1) material, which presumably contained severely degraded products, was separated by gel filtration on Sephadex LH-20 in dichloromethane–methanol (2:1) and a sample of the immobile fraction, which contained no uronic acid and was used in further experiments, was hydrolysed for methylated sugar analysis (Table 1). Carboxyl-reduced methylated polysaccharide (192 mg) in dry pyridine (30 mL) containing *N*-iodosuccinimide (666 mg) and triphenylphosphine (778 mg) was heated at 60°C for 16 h. Methanol (1 mL) was added to quench the reaction, the mixture was concentrated, the residue was dissolved in dichloromethane, and the solution was washed with aqueous sodium thiosulfate, dried, and concentrated. Residual material was twice fractionated by passage through a column (450 × 40 mm) of Sephadex LH-20, using dichloromethane–methanol (2:1) as eluant to ensure the complete removal of triphenylphosphine oxide, and afforded iodinated methylated polysaccharide (**IV***a*) (173 mg). A sample of the modified polysaccharide was deiodinated and hydrolysed for sugar analysis (Table 1).

Zinc degradation of iodinated methylated S. caudata *gum (**IV**a)*

Iodinated methylated polysaccharide (**IV***a*) (170 mg) was heated in boiling ethanol–water (19:1, 10 mL) with freshly activated zinc dust for 6 h. Thin-layer chromatography in benzene–methanol (6:1) showed the formation of mobile oligosaccharides together with a substance with the mobility of 5,6-dideoxy-2,3,4-tri-*O*-methyl-D-*xylo*-hex-5-enose. The cooled reaction mixture was filtered, and the filtrate was diluted with water, reduced with sodium borohydride, and processed to give the corresponding alditol/hexenitol-terminated derivatives (165 mg). Completeness of deiodination was confirmed by (*i*) analysis of sugars formed on direct hydrolysis and (*ii*) analysis of sugars formed on hydrolysis after treatment with tributylstannane, which showed no products that could have arisen from unchanged 6-deoxy-6-iodohexose constituents. A further quantity of the oligosaccharide mixture was trideuteriomethylated and hydrolysis of the product showed that 2,3,6-tri-*O*-methylgalactose had been largely replaced by 2,3,4*,6-tetra-*O*-methylgalactose, and 3-*O*-methylrhamnose by 2*,3-di-*O*-methylrhamnose. Direct examination of the fully alkylated oligosaccharide mixture by glc–ms showed the presence of five components in only one of which was there appreciable nonuniformity of isotopic labelling (Table 2). Reduction of the zinc degradation products with sodium borodeuteride, followed by trideuteriomethylation and glc–ms analysis, showed deuterium incorporation into all derivatives except **4***b*.

The oligosaccharide alditol/hexenitol mixture (33 mg) was separated by preparative tlc on a 1-mm silica gel plate preequilibrated with benzene, and elution with mixtures of benzene and methanol (1–10%) gave 8 fractions. Fraction 1 (5 mg) was indistinguishable (glc, tlc, and ^1H nmr) from 1,2-dideoxy-3,4,6-tri-*O*-methyl-L-*xylo*-hex-1-enitol prepared from methyl 6-deoxy-6-iodo-2,3,4-tri-*O*-methyl-α-D-glucopyranoside by treatment with zinc dust followed by reduction with sodium borohydride. Oligosaccharide fractions 2–8 contained mixtures of components and were individually trideuteriomethylated; the fully alkylated products were examined by glc (Table 2 for conditions) to determine the proportions of components and, by their relative intensities, to assign signals of anomeric protons in the ^1H nmr spectra (Table 3). From another preparative tlc separation a chromatographically homogeneous sample of disaccharide methyl glycoside **4***a* was isolated and converted into the trideuteriomethylated derivative **4***b*, which was hydrolyzed to give 2,3,4*,6-tetra-*O*-methylgalactose and 2*,3-di-*O*-methylrhamnose.

Zinc degradation of iodinated methylated S. urens *gum (**IV**b)*

Iodinated methylated *S. urens* gum was prepared from the methylated gum via the carboxyl-reduced methylated polysaccharide in the same way as the corresponding derivative of *S. caudata* gum, and compositional analyses are given in Table 1. Degradation with zinc was carried out as described previously and, after treatment with sodium borohydride, a sample of the mixture of alditol/hexenitol-terminated oligosaccharides was trideuteriomethylated and analyzed by glc–ms (Table 2). Attempted preparative separation of the oligosaccharide mixture was only partially successful, but chromatographically pure samples of oligosaccharides **5***a* and **5***c* were isolated, and these were converted into the corresponding fully alkylated derivatives **5***b* and **5***d*, which differed only in the proportion of OCD_3 substituents. Anomeric configurations in **5***b* were assigned from ^{13}C resonances at δ_C 105.1 ($^1J_{^{13}C_1,^1H_1}$ = 157 Hz, β-Gal) and 96.7 ($^1J_{^{13}C_1,^1H_1}$ = 168 Hz, α-Rha), and in both **5***b* and **5***d* from ^1H nmr resonances at δ 5.07 (br s) and 4.27 ($J_{1,2}$ = 7.7 Hz). Hydrolysis of both oligosaccharides gave 2,3,4,6-tetra-*O*-methylgalactose with 2*,3,4-tri- and 2,3,4-tri-*O*-methylrhamnose from **5***b* and **5***d* respectively.

Deuterium-labelled carboxyl-reduced Sterculia *gums (VII)*

Deacetylated *S. caudata* gum (900 mg, as ammonium salt) in water (60 mL) was treated with Dowex 50(H^+) resin and ethylene oxide was passed through the solution to give a concentration of ~20% (w/w). The solution was kept for 5 days with a pH change from 2.9 to 6, and the addition of ethanol (2 vol) in the presence of a small amount of potassium acetate to effect coagulation of the precipitate afforded polysaccharide glycol ester (700 mg), which was redissolved in water and freeze-dried. A suspension of the glycol ester (680 mg) in aqueous 2 *M* sodium borodeuteride (40 mL) was stirred gently and the resulting viscous solution was left overnight. Polysaccharide (590 mg) isolated by precipitation with an equal volume of ethanol contained 22% of uronic acid residues. Repetition of the esterification–reduction sequence (24) gave deuterium-labelled carboxyl-reduced *S. caudata* gum (**VII***a*) (400 mg) containing 10% of uronic acid residues, and giving on hydrolysis rhamnose (27%), galactose (48%), and glucose (15%). A similarly prepared sample of deuterium-labelled carboxyl-reduced *S. urens* gum (**VII***b*) contained 7% of uronic acid residues and gave on hydrolysis rhamnose (30%), galactose (51%), and glucose (7%). Samples of both carboxyl-reduced polysaccharides were methylated (10) and methylated sugar derivatives were analyzed by glc–ms (Table 1).

Degradation of S. urens *gum with lithium in 1,2-diaminoethane*

Dry deacetylated *S. urens* gum (500 mg, as ammonium salt) was stirred under argon in dry 1,2-diaminoethane for 30 min. Lithium was added in portions until the suspension became blue, and further lithium was added for 5 h until most of the suspended polysaccharide had dissolved. When complete reaction of lithium had taken place, ice was added in portions during 30 min, the solution was concentrated with repeated additions of toluene, and the residue in water was passed through Dowex 50(H^+) resin to remove lithium ions and the remaining diaminoethane, and concentrated to a residue (190 mg). To ensure complete conversion of reducing sugars to alditols the residue was treated with sodium borohydride and the resulting solution was applied to a column of charcoal–Celite (1:1). Elution of the column with water gave rhamnitol as the sole product detected by tlc, and elution with water containing 0.5% of butanone gave a fraction (50 mg) containing a single disaccharide (tlc in ethyl acetate – acetic acid – formic acid – water, 18:3:1:4). The disaccharide was converted into the fully methylated derivative **3***c*, nmr δ: 4.26 (d, 1H, $J_{1,2}$ = 7.72 Hz, H-1′), 3.31–3.57 (8s, 8 × OMe), 1.26 (d, 3H, $J_{5,6}$ = 6.22 Hz, H-6); δ_C: 104.6 (C-1′), 55.6–61.2 (8 × OCH_3), 16.0 (C-6). The glc–ms gave a single peak and showed fragment ions at m/z 395 (M − CH_2OCH_3), 307, 305, 275, 265, 219, 205, 187, 173, 155, 133. No other chromatographically mobile oligosaccharides were detected on elution of the charcoal–Celite column with water containing up to 5% of butanone.

Smith degradation of carboxyl-reduced S. urens *gum*

Carboxyl-reduced *S. urens* gum with a residual uronic acid content of ~3% was prepared by the method of Taylor and Conrad (25) and modified polysaccharide from the Smith degradation was isolated as described previously (1). Methylation analysis confirmed the identity of the glycan by the formation of derivatives of 2,3,6-tri-*O*-methylgalactose and 3,4-di-*O*-methylrhamnose as the major products.

Acknowledgements

The authors are grateful to the Natural Sciences and Engineering Research Council for Canada for financial support (to G.O.A.) and for Summer Studentships (to B.A.W. in 1982 and 1983). They also thank Dr. B. H. Khouw for recording mass spectra.

1. G. O. Aspinall and G. R. Sanderson. J. Chem. Soc. C, 2259 (1970).
2. G. O. Aspinall and G. R. Sanderson. J. Chem. Soc. C, 2256 (1965).
3. G. O. Aspinall, R. N. Fraser, and G. R. Sanderson. J. Chem. Soc. 4325 (1965).
4. G. O. Aspinall and R. N. Fraser. J. Chem. Soc. 4318 (1965).
5. G. O. Aspinall and Nasir-ud-din. J. Chem. Soc. 2710 (1965).
6. G. O. Aspinall, D. Chatterjee, and L. Khondo. Can. J. Chem. **62**, 2728 (1984).
7. G. O. Aspinall and V. Puvanesarajah. Can. J. Chem. **62**, 2736 (1984).
8. S. Hanessian, M. M. Ponpipom, and P. Lavalee. Carbohydr. Res. **24**, 45 (1972).
9. A. Klemer, B. Brandt, U. Hofmeister, and E. R. Ruter. Justus Liebigs Ann. Chem. 1920 (1983).
10. P.-E. Jansson, L. Kenne, H. Liedgren, B. Lindberg, and J. Lönngren. Chem. Commun. Univ. Stockholm, **8**, 1 (1976).
11. B. Fournet, J.-M. Dhalluin, G. Strecker, J. Montreuil, C. Bosso, and J. Defaye. Anal. Biochem. **108**, 35 (1980).
12. A. J. Mort and W. D. Bauer. J. Biol. Chem. **257**, 1870 (1982).
13. A. G. Darvill, P. Albersheim, M. McNeil, J. M. Lau, W. S. York, T. T. Stevenson, J. Thomas, S. Doares, D. J. Gollin, P. Chelf, and K. Davis. *In* New developments in industrial polysaccharides. *Edited by* V. Crescenzi, I. C. M. Dea, and S. S. Stivala. Gordon and Breach, New York. 1985. pp. 57–80.
14. J. V. Kubal and N. Gralen. J. Colloid Sci. **3**, 457 (1948).
15. M. McNeil, A. G. Darvill, and P. Albersheim. Plant Physiol. **70**, 1586 (1982).
16. R. Sømme. Carbohydr. Res. **152**, 237 (1986).
17. M. Tomoda, R. Gonda, N. Shimuzu, S. Akiyama, and H. Arai. Chem. Pharm. Bull. **33**, 4320 (1985), and papers cited therein.
18. L. D. Melton, M. McNeil, A. G. Darvill, P. Albersheim, and A. Dell. Carbohydr. Res. **146**, 279 (1986).
19. P. Albersheim, D. J. Nevins, P. D. English, and A. Karr. Carbohydr. Res. **5**, 340 (1967).
20. J. H. Sloneker. Methods Carbohydr. Chem. **6**, 20 (1972).
21. G. O. Aspinall, R. C. Carpenter, and L. Khondo. Carbohydr. Res. Submitted.
22. N. Blumenkrantz and G. Asboe-Hansen. Anal. Biochem. **54**, 184 (1973).
23. R. L. Frank and P. V. Smith. Org. Synth. Coll. Vol. **3**, 410 (1955).
24. G. O. Aspinall and A. Cañas-Rodriguez. J. Chem. Soc. 4020 (1958).
25. R. L. Taylor, J. E. Shively, and H. E. Conrad. Methods Carbohydr. Chem. **8**, 149 (1976).

Can. J. Chem. Downloaded from www.nrcresearchpress.com by 213.166.140.6 on 09/07/12
For personal use only.

A nuclear magnetic resonance relaxation study of liquid hydrogen cyanide

RODERICK E. WASYLISHEN
Department of Chemistry, Dalhousie University, Halifax, N.S., Canada B3H 4J3

Received December 15, 1986

RODERICK E. WASYLISHEN. Can. J. Chem. **65**, 2077 (1987).

The rates of ^2H, ^{13}C, and ^{14}N spin-lattice relaxation for liquid deuterium cyanide have been studied as a function of temperature. The quadrupolar nuclei relax exclusively by the quadrupolar relaxation mechanism while the rate of ^{13}C and ^{15}N relaxation is completely dominated by the spin-rotation mechanism. The apparent activation energy that describes the temperature dependence of spin-lattice relaxation for all nuclei studied is approximately 1.6 kcal mol^{-1}. The temperature dependence of the rate of ^{13}C relaxation in liquid HCN was also investigated. Although the determination of very accurate rotational and angular momentum correlation times is hampered by intermolecular effects on the nuclear quadrupolar coupling constants and the appropriately averaged C—H bond separation, the derived correlation times for DCN and HCN are in reasonable agreement (± 15%).

RODERICK E. WASYLISHEN. Can. J. Chem. **65**, 2077 (1987).

On a étudié les vitesses de relaxation spin-réseau ^2H, ^{13}C et ^{14}N du cyanure de deutérium liquide, à diverses températures. Le mécanisme de relaxation du noyau quadrupolaire n'implique qu'une relaxation quadrupolaire alors que la vitesse de relaxation du ^{13}C et du ^{14}N est complètement dominée par un mécanisme spin-rotation. L'énergie d'activation apparente qui décrit la relation entre la température et la relaxation spin-réseau de chacun des noyaux étudiés est d'environ 1,6 kcal mol^{-1}. On a aussi étudié la relation entre la température et la vitesse de relaxation du ^{13}C, dans le HCN liquide. Même si la détermination de valeurs très précises pour les temps de corrélation des moments rotationnel et angulaire est rendue difficile par les effets intermoléculaires sur les constantes de couplages nucléaires quadrupolaires et par la séparation de la liaison C—H qui est approximativement moyenne, on obtient un accord raisonnable (± 15%) pour les temps de corrélation que l'on a dérivé pour le DCN et le HCN.
[Traduit par la revue]

Can. J. Chem. Downloaded from www.nrcresearchpress.com by 213.166.140.6 on 09/07/12
For personal use only.

Introduction

At atmospheric pressure hydrogen cyanide, HCN, exists as a liquid over a relatively narrow temperature range, 39 degrees between 259.8 and 298.8 K (1). Many of the liquid state properties of HCN such as its unusually high dielectric constant are best interpreted in terms of the formation of linear polymeric hydrogen-bonded chains (2). Indeed, such one-dimensional hydrogen-bonded chains are the dominant structural feature of the solid (3–6). In the gas phase, the linear dimer is known to exist and its structure has recently been investigated using rotational microwave spectroscopy (7–10).

The objective of this study is to probe the rotational motion of HCN in the liquid phase using the results of nmr relaxation measurements (11–21). Hydrogen cyanide is a particularly attractive molecule for nmr study because there are potentially five different stable nmr active isotopes: ^1H, ^2H, ^{13}C, ^{14}N, and ^{15}N. Another advantage of HCN is that its structure is accurately known (3, 22–26) and, as well, a number of spectroscopic constants such as nuclear quadrupolar couplings (8, 9, 22–29), nuclear spin rotation constants (22, 24, 26, 30), and chemical shielding anisotropies (31–35) are available. These constants are essential in the interpretation of the nmr relaxation data.

Previous nmr studies on HCN include a comprehensive study of the temperature dependence of the ^1H, ^{13}C, and ^{15}N nuclear magnetic shielding by Jameson *et al.* (36). The only nmr relaxation measurement on HCN of which we are aware is a ^{13}C measurement of HCN in chloroform, which led the authors to suggest that the ^1H,^{13}C dipole–dipole, spin-rotation, and chemical shielding anisotropy mechanisms all contribute to ^{13}C relaxation (37). No attempt was made to analyze the data to obtain information about the rotational dynamics of HCN. In fact, we have been unable to find any reports of rotational correlation times for HCN in the liquid phase. In contrast, considerable information is available for molecules such as water (13, 17, 38–41), ammonia (17, 42–44), and acetonitrile (12, 20, 45–53). In the present study we obtain rotational correlation times, τ_2, and angular momentum correlation times, τ_J, for hydrogen cyanide as a function of temperature.

Theory

In this section a brief summary of the relationships between ^2H, ^{14}N, ^{13}C, and ^{15}N nmr relaxation times and the rotational and angular momentum correlation times, τ_2 and τ_J respectively, is presented.

Deuterium and nitrogen-14 are both quadrupolar nuclei with spin $I = 1$, which almost always relax by the quadrupolar mechanism. For a small molecule such as HCN, the extreme narrowing condition applies and the rate of quadrupolar relaxation, R_1^Q, is given eq. [1], where T_1 is the spin-lattice

$$[1] \quad R_1^Q = 1/T_1 = 1.5\pi^2\chi^2(1 + \eta^2/3)\tau_2$$

relaxation time, χ is the nuclear quadrupolar coupling constant, e^2qQ/h, in Hz, η is the asymmetry parameter, and τ_2 is the rotational correlation time.

The relaxation of a first row spin 1/2 nucleus such as ^{13}C or ^{15}N is generally governed by the dipole–dipole interaction with neighbouring protons. In general, the rate of I-spin relaxation due to I,S dipole–dipole relaxation is given by eq. [2], where

$$[2] \quad R_1^{DD}(I,S) = 1/T_1 = (4/3)\gamma_I^2\gamma_S^2 r_{IS}^{-6}\hbar^2 S(S + 1)\tau_2$$

γ_I and γ_S are the gyromagnetic ratio of I and S respectively, r_{IS} is the I-nucleus, S-nucleus separation, and S is the spin of nucleus S.

In small molecules where τ_2 is of the order of 10^{-12} s or less, the spin-rotation relaxation mechanism often dominates the relaxation of a spin 1/2 nucleus. For a linear molecule, where I is the moment of inertia, k is the Boltzmann constant, T is the absolute temperature, $C_\perp$ is the spin-rotation constant in Hz, and τ_J is the angular momentum correlation time, eq. [3] applies.

$$[3] \quad R_1^{SR} = 1/T_1 = (16\pi^2/3)(IkT/h^2)(2\pi C_\perp)^2\tau_J$$

TABLE 1. Nitrogen-14 T_1's and τ_2 values for liquid deuterium cyanide. The τ_2 values are calculated assuming $\chi(^{14}N) = 4707.9$ kHz (24, 26)

Temperature (K)	T_1 (ms)[a]	τ_2 (ps)
295	9.29	0.328
288	8.81	0.346
280	8.06	0.378
272	7.35	0.415
266	7.00	0.435
261	6.39	0.477

[a]Estimated error is less than 5%.

TABLE 2. Deuterium T_1's and τ_2 values for liquid deuterium cyanide. The τ_2 values are calculated assuming $\chi(^2H) = 202.23$ kHz (24, 26)[a]

Temperature (K)	T_1 (s)[a]	τ_2 (ps)
297	5.38	0.307
290	5.01	0.330
275	4.35	0.380
270	4.14	0.399
265	3.87	0.427
260	3.65	0.453

[a]Estimated error is less than 5%.

For a molecule undergoing small-step diffusion, τ_2 and τ_J are related by the Hubbard relationship (14–21, 54), eq. [4], where

$$[4] \quad \tau_2^*\tau_J^* = 1/6$$

$\tau_2^* = \tau_2(kT/I)^{1/2}$ and $\tau_J^* = \tau_J(kT/I)^{1/2}$ are dimensionless.

Experimental

A mixture of $D^{13}CN/D^{12}CN$ (45:45) and $H^{13}CN/H^{12}CN$ (5:5) was prepared by adding an aqueous NaCN (50% ^{13}C enriched) solution to a sulfuric acid solution (55); 90% of all the hydrogen was deuterium. The evolved hydrogen cyanide was passed through a series of $CaCl_2$ drying tubes and condensed directly into an nmr tube designed to restrict liquid vapor interchange (56). Deuterium, ^{13}C, and ^{14}N nmr relaxation measurements were performed on this sample. A second sample of hydrogen cyanide in which 20% of all nitrogens present were ^{15}N and 20% of all hydrogens present were ^2H was prepared, as described above, for ^{15}N measurements. All labelled compounds were obtained from Merck Sharp & Dohme, Canada, Limited. Finally, an unlabelled sample of HCN was prepared from a cylinder of HCN and helium supplied by Matheson. All samples were degassed and sealed under vacuum.

The nmr spectra were recorded at 9.40 and at 5.875 T on Bruker WH-400 and WM-250 spectrometers, respectively. All nmr measurements on hydrogen cyanide were carried out at 8.48 T on a Nicolet 360 nmr spectrometer. Spin-lattice relaxation times were measured using the inversion–recovery technique (56) and calculated using a 3-parameter fitting procedure (57, 58).

Results and discussion

1. Deuterium cyanide

Measured ^{14}N, ^2H, and ^{13}C spin-latice relaxation times for deuterium cyanide are summarized in Tables 1–3, respectively.

(a) Nitrogen-14 relaxation

The temperature dependence of the ^{14}N spin-lattice relaxation times in liquid deuterium cyanide are represented by eq. [5]; the slope indicates an Arrhenius activation energy, E_a,

$$[5] \quad \ln T_1 = -0.8182(10^3/T) - 1.896$$

of 1.62 kcal mol^{-1}. This value for E_a is much smaller than the value reported for water, which varies from about 5 kcal mol^{-1} at 0°C to approximately 3.5 kcal mol^{-1} in the temperature range 40–100°C (13). The E_a value observed here for DCN is comparable to the value of 1.9 kcal mol^{-1} observed for ammonia (42) and the value of 1.7 kcal mol^{-1} reported for rotations of the CN axis in acetonitrile (12).

To calculate the rotational correlation times, τ_2 values, from the data in Table 1 one requires a value of the ^{14}N quadrupolar coupling constant. In molecules such as HCN there is considerable variation in $\chi(^{14}N)$ depending on the intermolecular interactions (41, 59). In the gas-phase monomer the value is 4707.9 kHz (22, 24, 26), while in the solid state a value of 4018.3 kHz (28) has been reported. In the gas-phase dimer, **1**,

$$H_1—C\equiv N_1\cdots H_2—C\equiv N_2$$

1

Buxton *et al.* (9) recently found the two nitrogens N_1 and N_2 have χ values of 4097.3 kHz and 4440 kHz, respectively. In a detailed study of liquid acetonitrile, Böhm *et al.* (45) have found that τ_2 values from ^{14}N nmr relaxation data are consistent with those from Raman experiments only if the gas-phase nuclear quadrupolar coupling constant is used. In the present study further evidence is presented for using the value obtained for the gas-phase monomer (see discussion on HCN that follows). The τ_2 values given for DCN in Table 1 were calculated using $\chi(^{14}N) = 4707.9$ kHz and thus represent a lower limit on τ_2 at any given temperature. Rotational correlation times calculated using the χ value obtained in the solid state would result in τ_2 values that are longer by a factor of 1.37.

(b) Deuterium relaxation

The temperature dependence of the ^2H relaxation times is indicated in Table 2; the best linear fit is given by eq. [6]. The

$$[6] \quad \ln T_1 = -0.8081(10^3/T) + 4.400$$

value of E_a, 1.61 kcal mol^{-1}, is in excellent agreement with the value obtained from the temperature dependence of the ^{14}N data.

For the gas-phase monomer the ^2H nuclear quadrupolar coupling constant in DCN is 202.23 kHz (22, 24, 26). In the gas-phase hydrogen-bonded dimer $\chi(^2H_1) = 182.9$ kHz and $\chi(^2H_2) = 175.6$ kHz (8). The value of the deuterium nuclear quadrupolar coupling constant in the solid state has not been reported but is probably between 170 and 175 kHz. Reduction of nuclear quadrupole coupling constants on hydrogen bonding is well known (41, 59); for example, in water the gas-phase monomer values are $\chi(^2H) = 318.6$ kHz and $\chi(^{17}O) = 10.17$ MHz while in ice the values are $\chi(^2H) = 215$ kHz and $\chi(^{17}O) = 6.41$ MHz (38–41). The problems associated with obtaining accurate single-molecule reorientational correlation times in these systems have been previously discussed (40, 41, 59).

The τ_2 values in Table 2 were calculated using the $\chi(^2H)$ value obtained for the gas-phase monomer; at any given temperature τ_2 is within experimental error of the value obtained from the ^{14}N T_1 data.

Can. J. Chem. Downloaded from www.nrcresearchpress.com by 213.166.140.6 on 09/07/12
For personal use only.

TABLE 3. Carbon-13 relaxation data and angular momentum and rotation correlation times for deuterium cyanide

Temperature (K)	T_1^{obs} (s)[a]	R_1^{obs} (10^3 s^{-1})	R_1^{other} (10^3 s^{-1})[b]	R_1^{SR} (10^3 s^{-1})	τ_J (ps)	τ_J^*	τ_2 (ps)[c]	τ_2^*	$\tau_2^*\tau_J^*$
300	28.5	35.09	2.33	32.76	0.0316	0.133	0.305	1.28	0.170
290	28.6	34.97	2.56	32.41	0.0323	0.133	0.335	1.38	0.184
280	33.9	29.50	2.82	26.68	0.0276	0.112	0.370	1.50	0.168
275	33.0	30.30	2.98	27.32	0.0288	0.116	0.390	1.57	0.182
270	35.0	28.57	3.14	25.43	0.0273	0.109	0.412	1.64	0.179
260	38.0	26.32	3.53	22.79	0.0253	0.991	0.463	1.81	0.179

[a]Measurements carried out at 9.4 T; estimated error in T_1 is 5%.
[b]R_1^{other} represents the total contribution that mechanisms other than the spin-rotation mechanism make to the observed rate of relaxation. See text.
[c]Average values, calculated from the ^{14}N and ^{2}H T_1 data.

TABLE 4. Carbon-13 relaxation data and rotational and angular momentum correlation times for hydrogen cyanide[a]

Temperature (K)	T_1^{obs} (s)	η^b	R_1^{DD} (10^3 s^{-1})	τ_2 (ps)	R_1^{other} (10^3 s^{-1})[c]	R_1^{SR} (10^3 s^{-1})	τ_J (ps)	τ_2^*	τ_J^*	$\tau_2^*\tau_J^*$
300	21.6	0.28	6.52	0.265[d]	1.34	38.44	0.0305	1.23	0.141	0.17
295	21.8	0.31	7.15	0.290	1.47	37.25	0.0313	1.33	0.144	0.19
290	22.6	0.34	7.57	0.308	1.56	35.12	0.0288	1.40	0.131	0.18
280	22.8	0.39	8.60	0.350[d]	1.77	33.49	0.0285	1.56	0.127	0.20
270	24.8	0.48	9.73	0.394	1.99	28.60	0.0252	1.73	0.111	0.19
260	24.2	0.56	11.64	0.473[d]	2.39	27.29	0.0250	2.04	0.108	0.22

[a]All measurements were carried out at 8.48 T; the error in the observed T_1's is less than 5% while the error in η is ± 0.05.
[b]$\eta_{max} = \gamma(^1H)/2\gamma(^{13}C) = 1.988$.
[c]In this case $R_1^{other} = R_1^{CSA} + R_1^{DD}(^{13}C,^{14}N)$.
[d]τ_2 values of 0.291, 0.356, and 0.450 ps were obtained from ^{14}N nmr measurements on this same sample at 300, 279, and 260 K respectively.

(c) Carbon-13 relaxation

The variations in carbon-13 T_1 values with temperature for $^2H^{13}C^{14}N$ are given in Table 3. The observed increase in the ^{13}C T_1 values with decreasing temperature is an indication that the spin-rotation mechanism dominates. Other mechanisms that may make a contribution to the observed rate of carbon relaxation include the chemical shielding anisotropy mechanism (11, 16, 17, 19, 21) and the dipole–dipole mechanism with the directly bonded ^{2}H and ^{14}N nuclei. The efficiency of each of these mechanisms was evaluated using eqs. [7] and [2], respectively.

$$[7] \quad R_1^{CSA} = 1/T_1 = (2/15)\omega_C^2(\Delta\sigma)^2\tau_2$$

In eq. [7] ω_C is the carbon resonance frequency in angular units and $\Delta\sigma = \sigma_\parallel - \sigma_\perp$ is the ^{13}C chemical shielding anisotropy, 334 ppm (32). At any given temperature the value of τ_2 was taken to be the average of the values obtained from the ^{14}N and ^{2}H nmr data given in Tables 1 and 2. The r_{CN} and r_{CD} bond lengths required to evaluate the efficiency of the dipole–dipole mechanism were taken as 1.1532 and 1.0655 Å, respectively (22). Even at 9.4 T the chemical shielding anisotropy mechanism contributes less than 12% to the total rate of carbon relaxation. The ^{14}N,^{13}C and ^{2}H,^{13}C dipole–dipole mechanisms are much less efficient. The results in Table 3 indicate that the spin-rotation mechanism accounts for about 93% of the total rate of carbon spin-lattice relaxation at 300 K, and about 86% at 260 K. A plot of $\ln R_1^{SR}$ vs. $1/T$ results in a straight line with a slope corresponding to $E_a = 1.5 \pm 0.3$ kcal mol^{-1}.

From the rate of spin-rotation relaxation, one can use the experimental spin-rotation constant, $C_\perp = 15.0 \pm 1.0$ kHz (22, 30), to obtain the τ_J values listed in Table 3. Because of the uncertainty in $C_\perp$ the error in the τ_J values is about ±15%. The final values of τ_2 and τ_J for DCN are summarized in Table 3. At any given temperature the product $\tau_2^*\tau_J^*$ is within experimental error of the value expected for small-step rotational diffusion, 0.167.

2. Hydrogen cyanide

Carbon-13 spin-lattice relaxation times and nuclear Overhauser enhancement factors for a sample of hydrogen cyanide are given in Table 4. All isotopes are present in natural abundance. Measurement of the nOe permits one to obtain the rate of ^{13}C,^{1}H dipole–dipole relaxation, from which it is possible to calculate τ_2 (eq. [8]). In calculating the τ_2 values

$$[8] \quad R_1^{DD}(^{13}C,^1H) = (\eta_{obs}/\eta_{max})R_1^{obs}$$

in column 5 of Table 4 we have substituted the equilibrium carbon–hydrogen bond length, 1.0655 Å, in eq. [2]. The values obtained for τ_2 from the ^{13}C nmr measurements are within experimental error of those obtained from ^{14}N T_1's on this same sample (see footnote *d* of Table 4). The rates of CSA and ^{14}N,^{13}C dipole–dipole relaxation were evaluated using eqs. [7] and [2] as already described for DCN; however, the τ_2 values in Table 4 were used.

Plots of $\ln R_1^{DD}(^{13}C,H)$ and $\ln R_1^{SR}(^{13}C)$ as a function of $10^3/T$ have slopes of $+2.1 \pm 0.5$ kcal mol^{-1} and -1.4 ± 0.3 kcal mol^{-1}, respectively. The slope of the ^{13}C,^{1}H dipolar contribution is within experimental error of the slope obtained for an analogous plot involving the relaxation of the quadrupolar nuclei (^{14}N and ^{2}H). The values of E_a obtained from the temperature dependence of T_1^{SR} in DCN and HCN are in excellent agreement.

The τ_J values in Table 4 were calculated assuming the value of the product $C_\perp I_\perp$ for $^2H^{13}C^{14}N$ is equal to this same product

Can. J. Chem. Downloaded from www.nrcresearchpress.com by 213.166.140.6 on 09/07/12
For personal use only.

Can. J. Chem. Downloaded from www.nrcresearchpress.com by 213.166.140.6 on 09/07/12
For personal use only.

in $^1H^{13}C^{14}N$. The resulting τ_2 and τ_J values for hydrogen cyanide are summarized in Table 4. In general, the τ_2 values for HCN appear to be slightly less than those for DCN, as one would intuitively expect, since $[I(DCN)/I(HCN)]^{1/2} = 1.10$. At any given temperature, the τ_2^* and τ_J^* values obtained for DCN and HCN are within 15% of one another.

There has been considerable debate in the literature concerning the value of r that one should substitute into eq. [2] to calculate accurate rotational correlation times from dipolar relaxation data (60–62). Harris and Newman (60) argue that one should use r_{-3} where

$$[9] \quad r_k = \langle r^k \rangle^{1/k} = r_1 + (k-1)\mu^2/2r_1$$

and r_1 is the mean bond length (vibrational average) and μ the root-mean-square amplitude of the ground state vibration (63). Using this notation, r_{-1} and r_{-2} are the averages generally obtained from diffraction and rotational spectroscopy, respectively (60). If one applies eq. [9] to any given molecule, r_{-3} is usually about 1% less than r_1 and this results in a 6% change in τ_2. However, in the case of a hydrogen-bonded liquid such as hydrogen cyanide there is no guarantee that the mean bond length in the liquid state will be the same as it is in the gas-phase monomer. Qualitatively one would expect the average C—H bond length to increase when the hydrogen is involved in intermolecular hydrogen bonding.

The above mentioned problems of vibrational averaging and molecular structure in a hydrogen-bonded system lead to considerable uncertainty (perhaps, ±15%) in the rotational correlational times derived here.

3. Nitrogen-15 relaxation

Nitrogen-15 nmr measurements were performed on a sample of hydrogen cyanide that contained 20% deuterium. Because of a two-bond isotope effect the ^{15}N resonance of $^2HC^{15}N$ was 0.960 ppm to low frequency of the corresponding resonance in $^1HC^{15}N$, permitting the measurement of separate T_1 values for each isotopomer.

For HCN the ^{15}N T_1 was 50.0 ± 5 s at 5.875 T and 52.9 ± 3 s at 9.4 T. For DCN the ^{15}N T_1 at 9.4 T was 55.0 ± 5 s. All measurements were carried out at 297 ± 2 K. The ^2H T_1 for this same sample was 5.15 ± 0.3 s, in good agreement with the value obtained for $^2HC^{14}N$ (Table 2).

The similar ^{15}N T_1's observed for HCN at the two different applied fields indicate that the CSA mechanism makes a negligible contribution to the rate of ^{15}N relaxation. Also, the similar $T_1(^{15}N)$ values observed for HCN and DCN indicate that the $^1H,^{15}N$ dipole–dipole mechanism plays a minor role. The spin-rotation mechanism completely dominates the rate of ^{15}N relaxation and, following the procedure previously outlined for ^{13}C relaxation, one finds that T_1^{SR} is 52.9 s for HCN and 57.7 s for DCN. The value of the nitrogen-14 spin rotation constant in HCN is 10.13 kHz (23, 24, 26) and, using eq. [10]

$$[10] \quad (C_\perp I_\perp)/\gamma_N = (C'_\perp I'_\perp)/\gamma'_N$$

for two isotopomers of hydrogen cyanide, one finds that $C_\perp(^{15}N)$ is 13.80 and 11.21 kHz in $HC^{15}N$ and $^2HC^{15}N$ respectively. Substitution into eq. [3] results in τ_J^* values of 0.116 and 0.124 for HCN and DCN, respectively. For HCN the τ_J^* values obtained from the ^{15}N relaxation data are about 20% shorter than the value obtained from the ^{13}C measurements (at 300 K); however, considering the errors in our measurements, the errors associated with the spin-rotation constants, and the assumptions made, we consider this agreement satisfactory. The agreement of τ_J^* values from ^{13}C and ^{15}N relaxation measurements on DCN is much better, approximately 7%.

Conclusions

The most important mechanism for ^{13}C and ^{15}N spin-lattice relaxation in liquid hydrogen cyanide is the spin-rotation mechanism. At 300 K, analyses of ^2H, ^{14}N, ^{13}C, and ^{15}N spin-lattice relaxation times indicate $\tau_2^* = 1.3 \pm 0.2$ and $\tau_J^* = 0.13 \pm 0.02$. For $\tau_2^* = 1.3$, the J-diffusion model (15) predicts $\tau_J^* = 0.15$, while for small-step rotational diffusion $\tau_J^* = 0.13$. It is hoped this investigation of HCN will stimulate investigation by other techniques.

Acknowledgements

I would like to thank Drs. Robert Lenkinski and Charles Rodger for making spectrometer time available at the Southwestern Ontario NMR Centre (9.40 T) and at Bruker Spectrospin Canada (5.875 T), respectively. The nmr measurements on HCN (8.48 T) were carried out at the Atlantic Regional NMR Centre, Dalhousie University. I wish to thank NSERC for financial support in establishing and maintaining the regional centre, and also for operating grants. Finally I would like to thank Kenneth J. Friesen for his assistance in preparing some of the samples and Professors Cynthia Jameson and Brian Pettitt for several stimulating discussions.

1. (*a*) F. A. COTTON and G. WILKINSON. Advanced inorganic chemistry—a comprehensive text. 4th ed. John Wiley and Sons, New York. 1980. p. 364 and pp. 368–369; (*b*) J. JANDER and C. LAFRENZ. Ionizing solvents. John Wiley and Sons Ltd., New York. 1970. p. 101; (*c*) H. H. SISLER. Chemistry in non-aqueous solvents. Reinhold Publishing Corporation, New York. 1961. p. 107.
2. L. PAULING. The nature of the chemical bond. 3rd ed. Cornell University Press, Ithaca, NY. 1959. p. 458.
3. W. J. DULMAGE and W. N. LIPSCOMB. Acta Crystallogr. **4**, 330 (1951).
4. M. PÉZOLET and R. SAVOIE. Can. J. Chem. **47**, 3041 (1969).
5. F. G. BAGLIN, G. L. COULTER, and J. R. DURIG. Mol. Cryst. Liq. Cryst. **10**, 47 (1970).
6. A. KARPFEN. Chem. Phys. **79**, 211 (1983).
7. K. GEORGIOU, A. C. LEGON, D. J. MILLEN, and P. J. MJÖBERG. Proc. R. Soc. London, A: **399**, 377 (1985).
8. A. J. FILLERY-TRAVIS, A. C. LEGON, L. C. WILLOUGHBY, and A. D. BUCKINGHAM. Chem. Phys. Lett. **102**, 126 (1983).
9. L. W. BUXTON, E. J. CAMPBELL, and W. H. FLYGARE. Chem. Phys. Lett. **56**, 399 (1981).
10. A. C. LEGON, D. L. MILLEN, and P. J. MJÖBERG. Chem. Phys. Lett. **47**, 589 (1977).
11. A. ABRAHAM. The principles of nuclear magnetism. Oxford University Press, Oxford. 1961.
12. W. T. HUNTRESS. Adv. Magn. Reson. **4**, 1 (1970).
13. H. G. HERTZ and M. D. ZEIDLER. *In* The hydrogen bond — recent developments in theory and experiments. Vol. 3. *Edited by* P. Schuster, G. Zundel, and C. Sandorfy. North-Holland Publishing Comp., New York. 1976. p. 1027.
14. W. A. STEELE. Adv. Chem. Phys. **34**, 1 (1976).
15. R. E. D. MCCLUNG. Adv. Mol. Relaxation Interact. Processes, **10**, 83 (1977).
16. H. W. SPIESS. NMR Basic Principles and Progress, **15**, 59 (1978).
17. R. T. BOERÉ and R. G. KIDD. Annu. Rep. NMR Spectrosc. **13**, 319 (1982).
18. W. G. ROTHSCHILD. Dynamics of molecular liquids. J. Wiley and Son, New York. 1984.
19. H. VERSMOLD. *In* Molecular liquids — dynamics and interactions. *Edited by* A. J. Barns, W. J. Orville-Thomas, and

J. Yarwood. D. Reidel Publishing Company, Boston. 1984. p. 309.
20. M. W. EVANS and G. J. EVANS. Adv. Chem. Phys. **63**, 377 (1985).
21. R. E. WASYLISHEN. *In* NMR spectroscopy techniques. *Edited by* C. R. Dybowski and R. L. Lichter. Marcel Dekker, Inc., New York. 1986. p. 45.
22. A. G. MAKI. J. Phys. Chem. Ref. Data, **3**, 221 (1974).
23. B. M. CHADWICK and H. G. M. EDWARDS. *In* Molecular spectroscopy — specialist periodical reports. Vol. 1. The Chemical Society, London. 1973. p. 446.
24. G. R. TOMASEVICH. Ph.D. thesis, Harvard University, 1970.
25. K. KARAKIDA, T. FUKUYAMA, and K. KUCHITSU. Bull. Chem. Soc. Jpn. **47**, 299 (1974).
26. W. L. EBENSTEIN and J. S. MUENTEN. J. Chem. Phys. **80**, 3989 (1984).
27. G. CAZZOLI, C. DEGLI ESPOSTI, and P. G. FAVERO. J. Phys. Chem. **84**, 1756 (1980).
28. H. NEGITA, P. A. CASABELLA, and P. J. BRAY. J. Chem. Phys. **32**, 314 (1960).
29. E. FLIEGE, H. DREIZLER, A. P. COX, and S. D. HUBBARD. Z. Naturforsch. A: Phys. Phys. Chem. Kosmophys. **39**, 1104 (1984).
30. R. M. GARVEY and F. C. DELUCIA. J. Mol. Spectrosc. **50**, 38 (1974).
31. F. S. MILLETT and B. P. DAILEY. J. Chem. Phys. **54**, 5434 (1971).
32. G. DOMBI, P. DIEHL, J. LOUNILA, and R. WASSER. Org. Magn. Reson. **22**, 573 (1984).
33. M. SCHINDLER and W. KUTZELNIGG. Mol. Phys. **48**, 781 (1983).
34. J. S. TSE. Chem. Phys. Lett. **92**, 144 (1982).
35. T. D. GIERKE and W. H. FLYGARE. J. Am. Chem. Soc. **94**, 7177 (1972).
36. C. J. JAMESON, A. K. JAMESON, D. OPPUSUNGGU, and S. WILLE. J. Chem. Phys. **76**, 152 (1982).
37. P. LOFTUS, W. H. BEARDEN, and J. D. ROBERTS. Nouv. J. Chim. **1**, 283 (1977).
38. E. W. LANG and H.-D. LÜDEMANN. Ber. Bunsenges. Phys. Chem. **85**, 603 (1981); **85**, 1016 (1981).
39. (*a*) D. LANKHORST, J. SCHRIEVER, and J. C. LEYTE. Ber. Bunsenges. Phys. Chem. **86**, 215 (1982); (*b*) C. W. R. MULDER, J. SCHRIEVER, and J. C. LEYTE. J. Phys. Chem. **87**, 2336 (1983).
40. J. R. C. VAN DER MAAREL, D. LANKHORST, J. DE BLEIJSER, and J. C. LEYTE. Chem. Phys. Lett. **122**, 541 (1985).
41. P. L. CUMMINS, G. B. BACSKAY, N. S. HUSH, B. HALLE, and S. ENGSTRÖM. J. Chem. Phys. **82**, 2002 (1985).
42. P. W. ATKINS, A. LOEWENSTEIN, and Y. MARGOLIT. Mol. Phys. **17**, 329 (1969).
43. W. M. LITCHMAN and M. ALEI. J. Chem. Phys. **56**, 5818 (1972).
44. H. HAUER, E. LANG, and H.-D. LÜDEMANN. Ber. Bunsenges. Phys. Chem. **83**, 1262 (1979).
45. H. J. BÖHM, R. M. LYNDEN-BELL, P. A. MADDEN, and I. R. MCDONALD. Mol. Phys. **51**, 761 (1984).
46. T. T. BOPP. J. Chem. Phys. **47**, 3621 (1967).
47. D. E. WOESSNER, B. S. SNOWDEN, and E. THOMAS STROM. Mol. Phys. **14**, 265 (1968).
48. T. K. LEIPERT, J. H. NOGGLE, and K. T. GILLEN. J. Magn. Reson. **13**, 158 (1974).
49. E. VON GOLDAMMER, H.-D. LÜDEMAN, and A. MÜLLER. J. Chem. Phys. **60**, 4590 (1974); Erratum: J. Chem. Phys. **61**, 3493 (1974).
50. T. E. BULL and J. JONAS. J. Chem. Phys. **53**, 3315 (1970).
51. H. VERSMOLD. Ber. Bunsenges. Phys. Chem. **82**, 451 (1978).
52. J. R. LYERLA, D. M. GRANT, and C. H. WANG. J. Chem. Phys. **55**, 4676 (1971).
53. A. KRATOCHWILL. Ber. Bunsenges. Phys. Chem. **82**, 783 (1978).
54. P. S. HUBBARD. Phys. Rev. **131**, 1155 (1963).
55. K. ZIEGLER. Organic syntheses. Vol. 1. John Wiley and Sons, Inc., New York. 1932. p. 307.
56. T. C. FARRAR and E. D. BECKER. Pulse and Fourier transform NMR — introduction to theory and methods. Academic Press, New York. 1971.
57. (*a*) G. C. LEVY and I. R. PEAT. J. Magn. Reson. **18**, 500 (1975); (*b*) D. J. CRAIK and G. C. LEVY. *In* Topics in carbon-13 NMR spectroscopy. Vol. 4. *Edited by* G. C. Levy. Wiley–Interscience, New York. 1984. p. 241.
58. J. C. MACDONALD. J. Magn. Reson. **38**, 381 (1980).
59. B. A. PETTITT, R. J. BOYD, and K. E. EDGECOMBE. Chem. Phys. Lett. **89**, 478 (1982).
60. R. K. HARRIS and R. H. NEWMAN. Mol. Phys. **38**, 1315 (1979).
61. N. C. PYPER. Mol. Phys. **45**, 441 (1982).
62. E. R. HENRY and A. SZABO. J. Chem. Phys. **82**, 4753 (1985).
63. E. MEISINGSETH and S. J. CYVIN. Acta Chem. Scand. **16**, 1321 (1962).

Can. J. Chem. Downloaded from www.nrcresearchpress.com by 213.166.140.6 on 09/07/12
For personal use only.

Structures of the pyrazolones formed by oxidative coupling of phenols with 4-aminoantipyrine

RICHARD J. BARTON, KEITH E. JOHNSON, BEVERLY E. ROBERTSON, AND F. WAYNE YERHOFF
Department of Chemistry, University of Regina, Regina, Sask., Canada S4S 0A2

AND

SHENGZHI HU
Department of Chemistry, University of Xiamen, Xiamen, Peoples' Republic of China

Received October 28, 1986

RICHARD J. BARTON, KEITH E. JOHNSON, BEVERLY E. ROBERTSON, F. WAYNE YERHOFF and SHENGZHI HU. Can. J. Chem. **65**, 2082 (1987).

The structures of reaction products between 4-amino-2,3-dimethyl-1-phenyl-3-pyrazolin-5-one and *o*-cresol, *p*-cresol, and *p*-ethylphenol are reported. The reaction of the former compound with phenols is used to estimate the concentration of phenol in potable water supplies. The reaction products are 2,3-dimethyl-4-[4-oxo-2,5-cyclohexadien-1-ylidene)amino]-1-phenyl-3-pyrazolin-5-one (monoclinic, $P2_1/c$, red, $Z = 4$, $a = 7.092(1)$, $b = 26.616(2)$, $c = 8.644(2)$ Å, $\beta = 79.17(3)°$, 1432 reflections, $R = 0.083$, $R_w = 0.040$), 1,9*a*-dihydro-1,6,9*a*-trimethyl-2-phenylpyrazolo[3,4-*b*][1,4]benzoxazin-3(2*H*)-one (orthorhombic, *Pbca*, yellow, $Z = 8$, $a = 18.943(3)$, $b = 12.749(5)$, $c = 13.223(2)$ Å, 2122 reflections, $R = 0.067$, $R_w = 0.038$), and 6-ethyl-1,9a-dihydro-1,9a-dimethyl-2-phenylpyrazolo[3,4-*b*][1,4]benzoxazin-3(2*H*)-one (orthorhombic, *Pbca*, yellow, $a = 18.895(11)$, $b = 12.737(5)$, $c = 14.041(6)$ Å, $Z = 8$, 1126 reflections, $R = 0.068$, $R_w = 0.061$), respectively. The latter two compounds rearrange to form 1,2,4,10-tetrahydro-1,6-dimethyl-2-phenyl-3*H*-pyrazolo[3,4-*c*][1,5]benzoxazepin-3-one (monoclinic, $P2_1/c$, white, $Z = 8$, $a = 15.072(4)$, $b = 14.491(4)$, $c = 15.505(3)$ Å, $\beta = 111.15(1)°$, 3416 reflections, $R = 0.101$, $R_w = 0.046$) and 6-ethyl-1,2,4,10-tetrahydro-1-methyl-2-phenyl-3*H*-pyrazolo[3,4-*c*][1,5]benzoxazepin-3-one (monoclinic, $C2/c$, white, $Z = 8$, $a = 33.768(3)$, $b = 6.678(1)$, $c = 15.836(2)$ Å, $\beta = 115.41(1)$, 2805 reflections, $R = 0.076$, $R_w = 0.043$), respectively. The rearrangement is consistent with the observation that the pyrazolone rings of benzoxazinones are strained, as manifested by enlarged perimeters.

RICHARD J. BARTON, KEITH E. JOHNSON, BEVERLY E. ROBERTSON, F. WAYNE YERHOFF et SHENGZHI HU. Can. J. Chem. **65**, 2082 (1987).

On a déterminé les structures des produits de la réaction de l'amino-4 diméthyl-2,3 phényl-1 pyrazoline-3 one-5 avec l'*o*-crésol, le *p*-crésol et le *p*-éthylphénol. On utilise la réaction de ce produit hétérocyclique avec les phénols pour déterminer la concentration des phénols dans les sources d'eau potable. Les produits de la réaction sont respectivement la diméthyl-2,3 [(oxo-4 cyclohexadiène-2,5 ylidène-1)-1 amino]-4 phényl-1 pyrazoline-3 one-5 (monoclinique, $P2_1/c_0$ rouge, $Z = 4$, $a = 7{,}092(1)$, $b = 26{,}616(2)$ et $c = 8{,}644(2)$ Å, $\beta = 79{,}17(3)°$, 1432 réflexions, $R = 0{,}083$ et $R_w = 0{,}040$), la dihydro-1,9a triméthyl-1,6,9a phényl-2 2*H*-pyrazolo[3,4-*b*][1,4]benzoxazinone-3 (orthorhombique, *Pbca*, jaune, $Z = 8$, $a = 18{,}943(3)$, $b = 12{,}749(5)$ et $c = 13{,}223(2)$ Å, 2122 réflexions, $R = 0{,}067$ et $R_w = 0{,}038$) et l'éthyl-6 dihydro-1,9a diméthyl-1,9a phényl-2 2*H*-pyrazolo[3,4-*b*][1,4]benzoxazinone-3 (orthorhombique, *Pbca*, jaune, $a = 18{,}895(11)$, $b = 12{,}737(5)$ et $c = 14{,}041$ Å, $Z = 8$, 1126 réflexions, $R = 0{,}068$ et $R_w = 0{,}061$). Les deux derniers composés se transposent pour former respectivement la tétrahydro-1,2,4,10 diméthyl-1,6 phényl-2 3*H*-pyrazolo[3,4-*c*][1,5]benzoxazépinone-3 (monoclinique, $P2_1/c$, blanc, $Z = 8$, $a = 15{,}072(4)$, $b = 14{,}491(4)$ et $c = 15{,}505(3)$ Å, $\beta = 111{,}15(1)°$, 3416 réflexions, $R = 0{,}101$, $R_w = 0{,}046$) et l'éthyl-6 tétrahydro-1,2,4,10 méthyl-1 phényl-2 3*H*-pyrazolo[3,4-*c*][1,5]benzoxazépinone-3 (monoclinique, $C2/c$, blanc, $Z = 8$, $a = 33{,}768(3)$, $b = 6{,}678(1)$ et $c = 15{,}836(2)$ Å, $\beta = 115{,}41(1)°$, 2805 réflexions, $R = 0{,}076$ et $R_w = 0{,}043$). La transposition est en accord avec l'observation qui a été faite, par le biais de leurs périmètres agrandis, que les cycles pyrazolones des benzoxazinones sont tendus.

[Traduit par la revue]

Introduction

A standard procedure (1) for the estimation of phenols at low (ng/mL) concentrations in potable water supplies consists of measuring the intensity of the red colour formed when the phenol is oxidized in the presence of excess 4-aminoantipyrine (4-amino-2,3-dimethyl-1-phenyl-3-pyrazolin-5-one). Several papers (2–7) suggested that the reaction product was a *p*-quinoneimide and that the reaction could not proceed when the position *para*- to OH was occupied by alkyl, aryl, nitroso, nitro, benzoyl, ester, or aldehyde groups but would take place when that position was substituted by halo, carbonyl, alkoxyl, and sulfonic acid groups. It was reported (6) that although the colour reaction did not occur with certain *p*-substituted phenols, a white reaction product could be isolated and this material was purported to be the result of an *ortho* coupling process.

Investigations in this laboratory by ^{1}H nmr spectroscopy (8, 9) confirmed the formation of *p*-quinoneimides. *p*-Alkylphenols gave an orange solution from which a yellow product, assigned the structure of an *o*-quinoneimide, was isolated. The yellow product underwent thermal and base-catalysed rearrangement to a white benzodihydrooxazepine. ^{13}C nuclear magnetic resonance spectroscopy subsequently indicated the yellow product was a benzoxazinone (10).

In this paper we report on the X-ray crystallographic structures of the red product obtained from *o*-cresol, the yellow products obtained from *p*-cresol and *p*-ethylphenol, and the white rearrangement products from the latter two.

Experimental

The compounds were prepared as described previously (9). Methyl and ethyl benzoxazinone were recrystallized thrice by dissolving in a minimum of boiling *n*-pentane, filtering, and cooling slowly to 5°C. Methyl and ethyl benzoxazepinone were recrystallized thrice by dissolving in boiling 95% ethanol and cooling slowly to 5°C. Densities

Can. J. Chem. Downloaded from www.nrcresearchpress.com by 213.166.140.6 on 09/07/12
For personal use only.

TABLE 1. Crystal data, cell dimensions, and refinement parameters

Crystal data	*p*-Quinoneimide	Methyl benzoxazinone	Ethyl benzoxazinone	Methyl benzoxazepinone	Ethyl benzoxazepinone
Formula	$C_{18}H_{17}N_3O_2$	$C_{18}H_{17}N_3O_2$	$C_{19}H_{19}N_3O_2$	$C_{18}H_{17}N_3O_2$	$C_{19}H_{19}N_3O_2$
Molecular weight	307.4	307.4	321.4	307.4	321.4
Crystal system	Monoclinic	Orthorhombic	Orthorhombic	Monoclinic	Monoclinic
Space group	$P2_1/c$	*Pbca*	*Pbca*	$P2_1/c$	$C2/c$
Colour	Red	Yellow	Yellow	White	White
Crystal dimensions (mm)	$0.6 \times 0.1 \times 0.2$	$0.7 \times 0.5 \times 0.1$	$0.5 \times 0.3 \times 0.15$	$0.1 \times 0.5 \times 0.5$	$0.5 \times 0.2 \times 0.3$
μ(MoKα) (cm^{-1})	0.924	0.926	0.908	0.936	0.922
D_x (g cm^{-3})	1.274	1.277	1.262	1.291	1.322
D_m (g cm^{-3})	1.27	1.28	1.26	1.29	1.32
Z	4	8	8	8	8
Cell dimensions					
a (Å)	7.092(1)	18.943(3)	18.895(11)	15.072(4)	33.768(3)
b (Å)	26.616(2)	12.749(5)	12.737(5)	14.491(4)	6.678(1)
c (Å)	8.644(2)	13.223(2)	14.041(6)	15.505(3)	15.836(2)
β (deg)	79.17(3)	—	—	111.15(1)	115.41(1)
V (Å^3)	1602.6(6)	3193(2)	3379(3)	3158(2)	3225.6(6)
Number of reflections	90	184	148	94	200
2θ range (deg)	35–39	6–37	7–38	34–40	32–45
Intensity data					
2θ range (deg)	4–45	4–50	4–40	4–50	4–55
Number of reflections measured	2111	2809	1575	5500	3714
$I/\sigma(I)_{limit}$	0.8	0.8	0.8	0.8	0.8
Number of reflections in refinement	1432	2122	1126	3416	2805
Number of variables in refinement	276	276	293	551	293
$\Sigma\|\Delta F\|/\Sigma\|F_o\|$	0.083	0.067	0.068	0.101	0.076
$(\Sigma w\Delta^2\|F\|/\Sigma wF^2)^{1/2}$	0.040	0.038	0.061	0.046	0.043
Maximum shift/error[a]	0.29	0.18	0.35	0.19	0.14
Maximum $\Delta\rho$ (e Å^{-3})	0.33	0.32	0.24	0.36	0.26

[a]For atomic coordinates and thermal parameters of non-hydrogen atoms.

Can. J. Chem. Downloaded from www.nrcresearchpress.com by 213.166.140.6 on 09/07/12
For personal use only.

were measured by flotation. Crystal data and refinement parameters for the five compounds are given in Table 1. Data were collected using MoKα radiation, $\lambda = 0.70926$ Å, in the θ–2θ scan mode and a graphite monochromator on a modified Picker diffractometer at 291 K. The intensities of three standard reflections were monitored after every 47 reflections were recorded. In all cases their intensities did not change significantly. Standard deviations of the intensities of the reflections were calculated from counting statistics with an additional contribution from the excess scatter in the intensities of the standard reflections. Data were reduced to structure amplitudes in the usual manner. Corrections for absorption and extinction were not applied. Structures were solved by direct methods and Fourier methods using the National Research Council of Canada program package (11) and the XRAY-76 system of programs (12). There are two independent molecules in the asymmetric unit of the rearrangement product of *p*-ethylphenol. All structures were refined with anisotropic non-hydrogen atoms and isotropic hydrogen atoms by full-matrix least squares, using $\sigma^{-2}(F)$ weights. Scattering factors for all atoms were taken from the XRAY-76 system (12).

Results

The red product obtained from *o*-cresol is 2,3-dimethyl-4-[4-oxo-2,5-cyclohexadien-1-ylidene)amino]-1-phenyl-3-pyrazolin-5-one (*p*-quinoneimide). The yellow products obtained from *p*-cresol and *p*-ethylphenol are 1,9a-dihydro-1,6,9a-trimethyl-2-phenylpyrazalo[3,4-*b*][1,4]benzoxazin-3(2*H*)-one (methyl benzoxazinone) and 6-ethyl-1,9a-dihydro-1,9a-dimethyl-2-phenylpyrazolo[3,4-*b*][1,4]benzoxazin-3(2*H*)-one (ethyl benzoxazinone), respectively. Their rearrangement products are 1,2,4,10-tetrahydro-1,6-dimethyl-2-phenyl-3*H*-pyrazolo-[3,4-*c*][1,5]benzoxazepin-3-one (methyl benzoxazepinone) and 6-ethyl-1,2,4,10-tetrahydro-1-methyl-2-phenyl-3*H*-pyrazolo[3,4-*c*][1,5]benzoxazepin-3-one (ethyl benzoxazepinone).

Figure 1 shows the structures of the three product types. Figure 2 contains stereoscopic views of the *p*-quinoneimide molecule, the methyl benzoxazinone molecule, and one of the methyl benzoxazepinone molecules. The labelling of the atoms for the *p*-quinoneimide molecule is given in Fig. 3.[1] In the ethyl benzoxazinone and ethyl benzoxazepinone molecules C(19) replaces H(7,3). In both benzoxazinone molecules O(1) bridges atoms C(5) and C(9). In the three benzoxazepinone molecules, O(1) bridges atoms C(5) and C(11). In methyl benzoxazinone, the atoms belonging to the two independent molecules in the asymmetric unit are labelled 1 and 2.

Bond lengths and angles not involving hydrogen atoms for all

[1]Structure amplitude tables, tables of atomic parameters, isotropic temperature factors for hydrogen atoms, and anisotropic temperature factors for non-hydrogen atoms are available, at a nominal charge, from the Depository of Unpublished Data, CISTI, National Research Council of Canada, Ottawa, Ont., Canada K1A 0S2.

TABLE 2. Bond lengths (Å) and angles (deg), with estimated standard deviations

	Length					
				Methyl benzoxazepinone		
Bond	*p*-Quinoneimide	Methyl benzoxazinone	Ethyl benzoxazinone	Mol. 1	Mol. 2	Ethyl benzoxazepinone
C(1)—C(2)	1.338(7)	1.378(4)	1.389(9)	1.379(7)	1.379(7)	1.389(4)
C(2)—C(3)	1.455(8)	1.379(4)	1.378(11)	1.394(5)	1.401(6)	1.387(4)
C(3)—C(4)	1.458(7)	1.380(4)	1.397(9)	1.371(7)	1.372(8)	1.372(4)
C(4)—C(5)	1.332(7)	1.379(3)	1.369(9)	1.377(7)	1.382(7)	1.388(4)
C(5)—C(6)	1.452(6)	1.392(3)	1.392(9)	1.402(5)	1.402(5)	1.395(4)
C(6)—C(1)	1.460(6)	1.397(4)	1.382(9)	1.399(7)	1.392(7)	1.398(3)
C(2)—C(7)	1.516(7)	1.515(4)	1.518(10)	1.502(8)	1.511(8)	1.523(4)
C(7)—C(19)	—	—	1.485(12)	—	—	1.506(5)
C(3)—O(1)	1.235(6)	—	—	—	—	—
C(6)—N(1)	1.300(6)	1.426(3)	1.436(7)	1.399(5)	1.394(5)	1.394(3)
N(1)—C(8)	1.362(6)	1.263(3)	1.266(7)	1.385(6)	1.389(5)	1.388(3)
C(8)—C(9)	1.387(7)	1.504(3)	1.482(9)	1.336(5)	1.345(5)	1.338(4)
C(9)—C(11)	1.492(6)	1.547(4)	1.581(10)	1.480(5)	1.483(5)	1.488(4)
C(11)—O(1)	—	—	—	1.429(5)	1.440(5)	1.434(3)
O(1)—C(5)	—	1.392(3)	1.386(7)	1.394(6)	1.397(6)	1.392(3)
C(9)—O(1)	—	1.402(3)	1.387(7)	—	—	—
C(8)—C(10)	1.474(6)	1.498(3)	1.478(8)	1.445(6)	1.435(5)	1.447(3)
C(10)—O(2)	1.227(6)	1.219(3)	1.237(7)	1.235(4)	1.229(4)	1.226(3)
C(10)—N(3)	1.412(6)	1.367(3)	1.357(7)	1.386(6)	1.389(5)	1.383(3)
N(3)—N(2)	1.401(5)	1.448(3)	1.449(6)	1.420(4)	1.409(4)	1.414(3)
N(2)—C(9)	1.328(6)	1.462(3)	1.432(8)	1.403(6)	1.403(6)	1.404(3)
N(2)—C(12)	1.483(6)	1.512(3)	1.584(8)	1.486(5)	1.484(5)	1.472(3)
N(3)—C(13)	1.426(5)	1.423(3)	1.395(7)	1.402(6)	1.418(5)	1.430(3)
C(13)—C(14)	1.380(7)	1.377(4)	1.378(9)	1.372(6)	1.376(6)	1.377(4)
C(14)—C(15)	1.380(6)	1.384(4)	1.383(10)	1.386(9)	1.366(7)	1.379(4)
C(15)—C(16)	1.362(8)	1.374(4)	1.355(12)	1.399(12)	1.374(7)	1.374(5)
C(16)—C(17)	1.375(8)	1.377(4)	1.370(12)	1.362(9)	1.370(6)	1.368(5)
C(17)—C(18)	1.379(7)	1.373(4)	1.370(10)	1.367(11)	1.377(7)	1.384(4)
C(18)—C(13)	1.373(7)	1.390(4)	1.386(9)	1.393(8)	1.394(6)	1.378(4)

	Angle					
				Methyl benzoxazepinone		
Bonds	*p*-Quinoneimide	Methyl benzoxazinone	Ethyl benzoxazinone	Mol. 1	Mol. 2	Ethyl benzoxazepinone
C(6)—C(1)—C(2)	124.5(4)	121.8(2)	122.1(6)	122.9(3)	122.2(4)	121.7(2)
C(1)—C(2)—C(3)	118.5(4)	117.9(2)	117.6(6)	118.3(4)	118.4(5)	118.4(2)
C(2)—C(3)—C(4)	117.8(4)	122.0(2)	121.9(6)	119.9(4)	120.5(4)	120.7(3)
C(3)—C(4)—C(5)	122.5(5)	119.3(2)	118.9(6)	121.6(3)	120.4(4)	120.9(3)
C(4)—C(5)—C(6)	120.9(46)	120.4(2)	121.0(6)	120.1(4)	120.4(4)	119.7(3)
C(5)—C(6)—C(1)	115.7(4)	118.5(2)	118.5(6)	117.1(4)	117.4(4)	118.4(2)
C(1)—C(2)—C(7)	123.1(5)	121.4(2)	122.0(6)	120.4(3)	121.0(4)	120.3(2)
C(3)—C(2)—C(7)	118.5(4)	120.7(2)	120.3(6)	121.2(4)	120.6(4)	121.3(2)
C(2)—C(7)—C(19)	—	—	112.8(7)	—	—	112.7(2)
C(2)—C(3)—O(1)	121.6(4)	—	—	—	—	—
C(4)—C(3)—O(1)	120.6(5)	—	—	—	—	—
C(1)—C(6)—N(1)	115.4(4)	120.0(2)	119.1(5)	120.4(3)	118.5(3)	118.8(2)
C(5)—C(6)—N(1)	128.9(4)	121.4(2)	122.3(5)	122.4(4)	123.5(4)	122.8(2)
C(4)—C(5)—O(1)	—	118.6(2)	118.9(6)	117.7(3)	116.3(3)	116.8(2)
C(6)—C(5)—O(1)	—	120.9(2)	120.0(5)	122.1(4)	123.0(4)	123.1(2)
N(1)—C(8)—C(9)	118.5(4)	126.5(2)	126.7(5)	129.6(4)	130.2(3)	130.9(2)
C(8)—C(9)—C(11)	127.7(4)	112.6(2)	112.8(5)	129.5(4)	128.4(4)	129.5(2)
C(8)—C(9)—O(1)	—	111.2(2)	112.9(5)	—	—	—
C(9)—O(1)—C(5)	—	113.4(2)	115.1(4)	—	—	—
C(9)—C(1)—O(1)	—	—	—	108.8(3)	109.3(3)	110.6(2)
C(11)—C(1)—C(5)	—	—	—	115.1(3)	116.7(3)	117.8(2)
N(1)—C(8)—C(10)	135.3(4)	127.3(2)	127.5(5)	120.9(3)	120.2(3)	120.3(2)
C(9)—C(8)—C(10)	106.2(4)	106.2(2)	105.8(5)	109.4(4)	109.4(4)	108.8(2)

Can. J. Chem. Downloaded from www.nrcresearchpress.com by 213.166.140.6 on 09/07/12
For personal use only.

TABLE 2 (*concluded*)

Bonds	Angle					
	p-Quinoneimide	Methyl benzoxazinone	Ethyl benzoxazinone	Methyl benzoxazepinone		Ethyl benzoxazepinone
				Mol. 1	Mol. 2	
C(8)—C(10)—N(3)	104.7(4)	103.8(2)	104.8(5)	104.5(3)	104.5(3)	104.4(2)
C(10)—N(3)—N(2)	108.9(3)	115.0(2)	113.2(4)	110.5(3)	110.6(3)	111.1(2)
N(3)—N(2)—C(9)	108.8(4)	102.0(2)	102.9(4)	105.0(3)	105.0(3)	104.2(2)
N(2)—C(9)—C(8)	111.3(4)	104.6(2)	104.8(5)	110.4(3)	109.9(3)	110.9(2)
C(8)—C(10)—O(2)	133.7(4)	128.6(2)	128.0(5)	130.4(4)	130.5(4)	130.1(2)
N(3)—C(10)—O(2)	121.5(4)	127.5(2)	127.2(5)	125.0(4)	124.9(4)	125.5(2)
C(10)—N(3)—C(13)	122.2(3)	128.0(2)	128.2(5)	127.9(3)	126.5(3)	125.6(2)
N(2)—N(3)—C(13)	120.4(3)	117.0(2)	118.5(4)	119.2(3)	119.9(3)	119.1(2)
N(3)—N(2)—C(12)	119.8(3)	107.7(2)	106.5(4)	111.5(3)	112.4(3)	113.6(2)
C(9)—N(2)—C(12)	127.6(4)	110.6(2)	108.5(5)	116.1(4)	117.2(3)	117.3(2)
N(2)—C(9)—C(11)	121.0(4)	107.2(2)	103.0(5)	119.9(4)	121.4(3)	119.6(2)
C(11)—C(9)—O(1)	—	109.9(2)	109.3(5)	—	—	—
N(2)—C(9)—O(1)	—	111.2(2)	113.5(5)	—	—	—
N(3)—C(13)—C(14)	119.7(4)	120.2(2)	121.5(5)	120.2(5)	119.8(4)	120.8(2)
N(3)—C(13)—C(18)	120.1(4)	119.2(2)	120.5(5)	119.2(4)	120.5(3)	118.7(2)
C(18)—C(13)—C(14)	120.2(4)	120.6(2)	117.9(6)	120.6(5)	119.7(4)	120.4(2)
C(13)—C(14)—C(15)	118.3(4)	119.3(2)	121.3(6)	120.5(6)	120.0(4)	119.6(3)
C(14)—C(15)—C(16)	121.3(5)	120.6(2)	119.2(7)	118.5(5)	120.9(4)	120.5(3)
C(15)—C(16)—C(17)	120.6(4)	119.5(3)	120.8(7)	120.0(7)	119.5(5)	119.6(3)
C(16)—C(17)—C(18)	118.5(5)	121.1(2)	119.9(7)	122.0(8)	120.7(4)	120.8(3)
C(17)—C(18)—C(13)	121.1(4)	118.9(2)	120.7(6)	118.4(5)	119.3(4)	119.1(3)

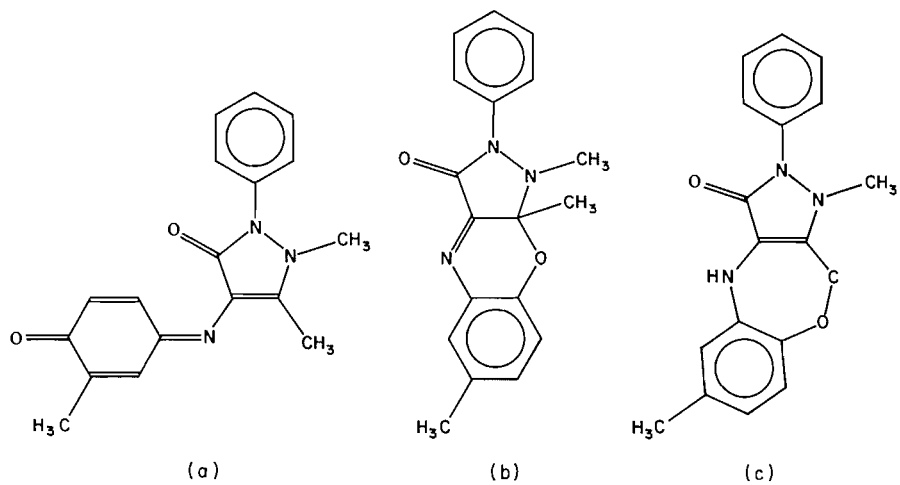

FIG. 1. The structure of (*a*) the *p*-quinoneimide molecule derived from *o*-cresol, (*b*) the methyl benzoxazinone molecule, (*c*) the methyl benzoxazepinone molecule.

compounds are given in Table 2. The angles between the planar rings of the molecules, as defined in Fig. 4, are given in Table 3. The torsional angles in the antipyrine ring and the torsional angles in the rings involving N(1) are given in Table 4. Hydrogen bond parameters for the benzoxazepinone structures are given in Table 5.

Discussion

The bond lengths in *p*-quinoneimide are consistent with its formula; in particular, [C(1)—C(2)], [C(4)—C(5)], and [C(6)—N(1)] are short in this molecule, consistent with the assignment of the quinonoid group. Within the pyrazolone ring in *p*-quinoneimide [C(10)—N(3)] is long, [N(3)—N(2)] short, and [N(2)—C(9)] very short, compared to their lengths in the other five molecules. The [N(1)—C(8)] distance in this molecule is also short (1.362(6) Å), supporting the notion of some delocalization through the C(8)—N(1)—C(6) group. If the bond distances in *p*-quinoneimide are compared with those in antipyrine (13), in the former the bonds from C(8) to C(9) and to C(10) are longer by 0.04(1) Å and that from C(9) to N(2) is shorter by 0.05(1) Å. The C(8)—N(1) bond length is reduced by 0.07(1) Å compared to that in amidopyrone (14). The N(2)—N(3)—C(10) linkage changes little but [N(2)—C(12)] is longer in the *p*-quinoneimide than in the antipyrine and amidopyrone molecules.

The benzoxazinones are conceptually the intramolecular Michael condensation products of *o*-quinoneimides. So far we have not isolated the latter from the *p*-alkylphenol–amino-

Can. J. Chem. Downloaded from www.nrcresearchpress.com by 213.166.140.6 on 09/07/12
For personal use only.

Can. J. Chem. Downloaded from www.nrcresearchpress.com by 213.166.140.6 on 09/07/12
For personal use only.

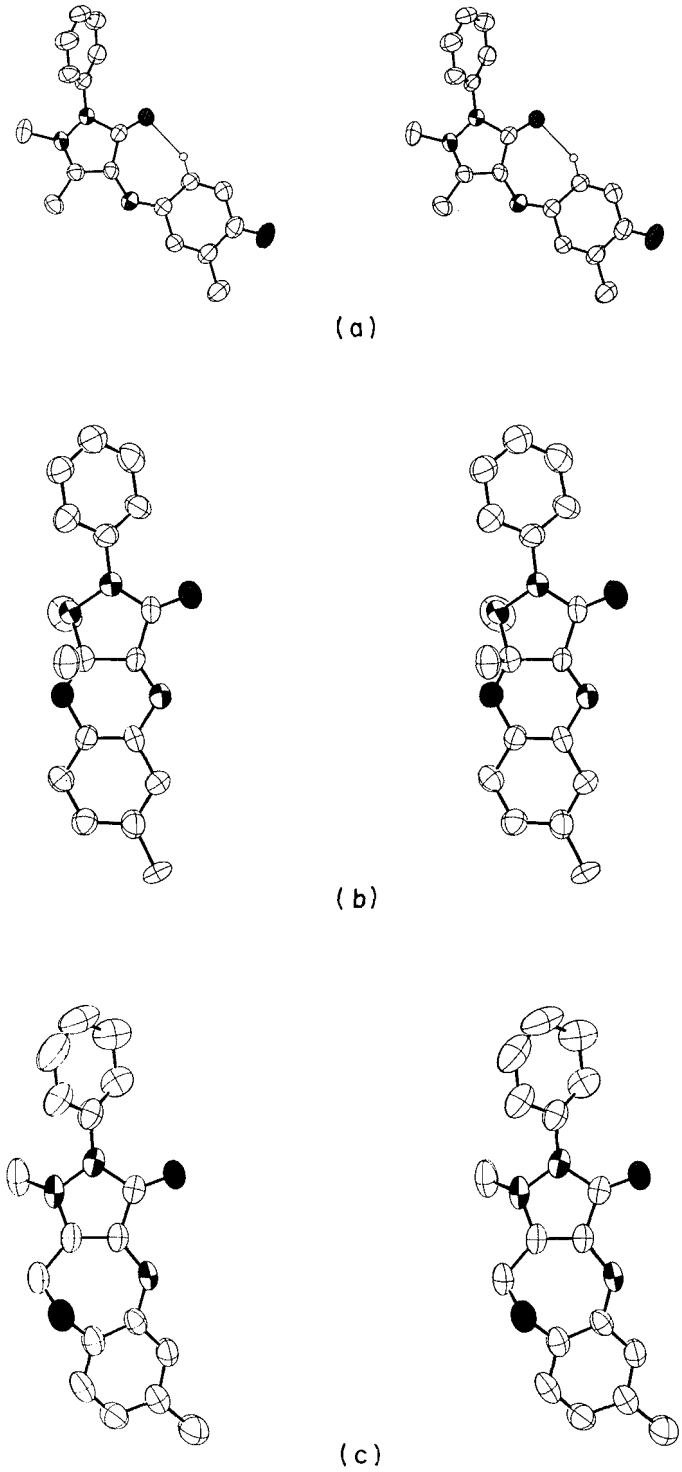

FIG. 2. Stereoscopic views of (*a*) the *p*-quinoneimide molecule, (*b*) the methyl benzoxazinone molecule, (*c*) a methyl benzoxazepinone molecule. The oxygen atoms are filled, the nitrogen atoms partially filled.

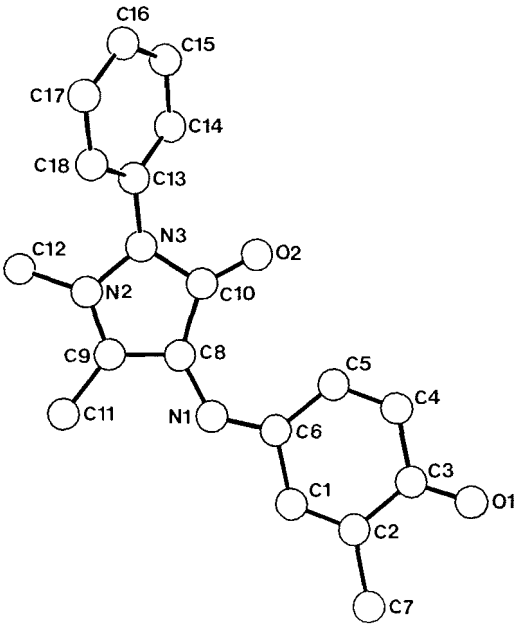

FIG. 3. Labelling of the atoms in the *p*-quinoneimide molecule. See text for labelling of the other compounds.

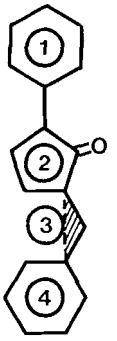

FIG. 4. Definition of the molecular planes.

antipyrine–ferricyanide mixtures. Within the benzoxazinone molecules we find [N(1)—C(8)] to be even shorter than [N(1)—C(6)] in *p*-quinoneimide while [N(1)—C(6)] in the former is the distance of a single bond; conjugation in the C(8)—N(1)—C(6) linkage is reduced and the shift in λ_{max} from 455 to 335 nm and reduction in ϵ_{max} corroborate this. In the pyrazolone rings [C(8)—C(9)], [C(9)—C(11)], [N(2)—C(9)], and [N(2)—N(3)] are lengthened while [C(10)—N(3)] is shortened. Since C(9) is common to two rings and bonded to a methyl group the distances of other atoms from it are long merely because of the congestion.

The benzoxazepinones possess the appropriate bond lengths relative to the benzoxazines: [C(8)—C(10)], [C(8)—C(9)], [C(9)—C(11)], [C(9)—N(2)], [N(2)—C(12)], and [N(2)—N(3)] are shorter while [C(10)—N(3)] is longer. The C(8)—N(1)—C(6) group is different in that the nitrogen atom carries a hydrogen atom: [N(1)—C(6)] is close to a single bond distance although it is shorter than that in the benzoxazinones and [N(1)—C(8)] is shorter than that in amidopyrone. The new seven-membered rings are decidedly puckered.

In the *p*-quinoneimide molecule, the hydrogen atom H(5) on C(5) is only 2.06(3) Å removed from the oxygen atom O(2) and the possibility that carbon atoms in quinone rings may act as donors of hydrogen bonds cannot be *a priori* eliminated. Therefore, the possibility that the H(5)...O(2) interaction has some hydrogen bond character must be considered. Other relevant parameters are the [C(5)—O(2)] distance at 2.973(5) Å, the [C(5)—H(5)] distance at 1.01(3) Å and the C(5)—H(5)—O(2) angle at 148(3)°.

As is clear from Table 5, the three atoms labelled O(2) in the two benzoxazepinone structures are hydrogen bonded, but the atoms O(2) in the two benzoxazinone molecules are not.

TABLE 3. Interplanar angles (deg)[a]

Planes	*p*-Quinoneimide	Methyl benzoxazinone	Ethyl benzoxazinone	Methyl benzoxazepinone Mol. 1	Methyl benzoxazepinone Mol. 2	Ethyl benzoxazepinone
1,2	55.7(2)	40.9(1)	34.5(2)	41.6(2)	45.8(2)	40.2(1)
2,3	2.2(3)	14.8(1)	14.0(4)	14.1(4)	9.7(4)	21.6(2)
3,4	185.1(4)	13.1(3)	8.7(5)	31.8(4)	24.4(5)	28.2(2)

[a]See Fig. 3 for the labelling of the planes.

TABLE 4. Torsional angles (deg) in the antipyrene ring and in the ring containing N(1)

Bonds	Torsional angle: *p*-Quinoneimide	Methyl benzoxazinone	Ethyl benzoxazinone	Methyl benzoxazepinone Mol. 1	Methyl benzoxazepinone Mol. 2	Ethyl benzoxazepinone
N(2)—N(3)—C(10)—C(8)	−3.5(4)	−7.5(2)	−5.1(7)	−5.4(6)	−6.8(5)	−5.7(3)
N(3)—C(10)—C(8)—C(9)	1.5(4)	−11.5(3)	−13.3(8)	3.3(6)	2.5(6)	0.8(3)
C(10)—C(8)—C(9)—N(2)	1.1(5)	25.6(3)	26.7(8)	0.0(6)	2.8(6)	4.4(3)
C(8)—C(9)—N(2)—N(3)	−3.3(4)	−28.4(2)	−28.6(7)	−3.2(6)	−6.8(5)	−7.6(3)
C(9)—N(2)—N(3)—C(10)	4.3(4)	23.5(3)	21.9(7)	5.4(6)	8.5(6)	8.2(3)
C(9)—C(8)—N(1)—C(6)	—	4.6(4)	6.5(1.0)	14.8(8)	10.8(8)	21.2(4)
C(8)—N(1)—C(6)—C(5)	—	14.4(4)	9.0(9)	−33.9(7)	−26.4(8)	−28.8(4)
N(1)—C(6)—C(5)—O(1)	—	−3.7(5)	0.0(1.2)	−3.9(8)	−5.8(9)	−13.2(5)
C(6)—C(5)—O(1)—C(9)	—	−25.8(3)	24.1(9)	—	—	—
C(5)—O(1)—C(9)—C(8)	—	40.4(3)	36.2(8)	—	—	—
O(1)—C(9)—C(8)—N(1)	—	−33.0(4)	−29.9(1.0)	—	—	—
C(6)—C(5)—O(1)—C(11)	—	—	—	70.8(9)	66.9(9)	72.0(5)
C(5)—O(1)—O(11)—C(9)	—	—	—	−77.2(9)	−76.6(9)	−69.7(5)
O(1)—C(11)—C(9)—C(8)	—	—	—	29.4(8)	35.2(9)	26.6(4)
C(11)—C(9)—C(8)—N(1)	—	—	—	2.6(9)	−2.4(9)	−4.6(5)

TABLE 5. Hydrogen bond distances (Å) and angles (deg)

Compound	A—H.....B		[A—H]	[H...B]	[A...B]	∠AHB
Methyl benzoxazepinone(1)	N(1,1)	O(2,2)	0.81(2)	2.26(3)	3.034(4)	160(7)
Methyl benzoxazepinone(2)	N(2,1)	O(1,2)	0.83(3)	2.19(3)	2.998(4)	161(7)
Ethyl benzoxazepinone	N(1)	O(2)	0.89(2)	2.05(2)	2.875(3)	154(5)

TABLE 6. Perimeters of the pyrazolone rings (Å)

Compound	Perimeter
Antipyrine (14)	6.97
Amidopyrone (15)	7.03
p-Quinoneimide	7.00
Methyl benzoxazinone	7.28
Ethyl benzoxazinone	7.20
Methyl benzoxazepinone, mol. 1	6.99
Methyl benzoxazepinone, mol. 2	6.98
Ethyl benzoxazepinone	6.99
Several metal complexes (21, 22)	6.89–7.06

Nevertheless, the average [C(10)—O(2)] distances are very similar for the hydrogen bonded and non-hydrogen bonded O(2) atoms and are similar to the [C(10)—O(2)] distance of 1.227(6) Å in *p*-quinoneimide. The closure of the seven-membered heterocyclic ring in the former case and closure of the six-membered ring in the latter case lead to variations in the bonding of the antipyrine ring which change the environment of the C(10)—O(2) bond. In the antipyrine (13) and amidopyrone (14) molecules, the equivalent atom O(2) is not hydrogen bonded and the [C(10)—O(2)] length is 1.237(6) Å. The average [C(10)—O(2)] distance in complexes of amidopyrone with barbital (15) and cyclobarbital (16), in which the O(2) atoms is hydrogen bonded, is 1.244(3) Å. In view of the similarity of these molecules to the *p*-quinoneimide molecule, the [C(10—O(2)] distance here is short, even for the non-hydrogen bonded case. A further indication that the O(2)...H(5) interaction is essentially repulsive is that the ring O(2), H(5), C(5), C(6), N(1), C(8), C(10) is not planar. The torsional angles C(8)—C(10)—O(2)—H(5), C(10)—O(2)—H(5)—C(5), and O(2)—H(5)—C(5)—C(6) are 8(4)°, −19(3)°, and 16(3)°, respectively. Finally, the quinone ring is bent at the bridge-head carbon atom, C(6), 6.8(4)° away from O(2) with respect to the position that would leave the angles N(1)—C(6)—C(5) and N(1)—C(6)—C(1) equal. Therefore we conclude that O(2) is not the acceptor of a hydrogen bond from C(5).

The perimeters of the pyrazolone rings in the various

Can. J. Chem. Downloaded from www.nrcresearchpress.com by 213.166.140.6 on 09/07/12
For personal use only.

structures are listed in Table 6. The distortion in the benzoxazinones shows as the enlarged "perimeters" for these molecules, where the atoms are not coplanar. Otherwise, the perimeter of a pyrazolone ring appears to be 7.00 ± 0.02 Å, giving an average bond length of 1.40 Å. Pyrazolones as a class are considered to be π-excessive aromatics, intermediate between benzene and pyridine in degree of aromaticity (17). In benzene the average bond length is 1.40 Å; in a selection of pyridine compounds and complexes the average bond length is 1.37 ± 0.01 Å (18). Pyrazole, the parent of pyrazolones, has a perimeter of 6.77 Å (19), giving an average bond length of 1.354 Å and the complex $Ni(pyrazole)_4Cl_2$ (20) has pyrazole perimeters of 6.74 and 6.80 Å. In pyrazolone complexes we find a range of perimeters from 6.89 to 7.06 Å (21, 22). It appears then that the perimeter of a potentially aromatic molecule can act as a measure of its aromaticity; experimental errors and alterations in bond lengths due to local short range effects involving the position of a single atom will have a minimal effect on the value of the perimeter in such a system.

Acknowledgements

The authors thank the Natural Sciences and Engineering Research Council of Canada for an Operating Grant to R.J.B. and B.E.R., the University of Regina for computing time, and the Visiting Chinese Scholars Program for the support of S.H.

1. Standard methods for the examination of water and wastewater. 13th ed. American Public Health Association, Washington. 1971. p. 504.
2. E. EMERSON. J. Org. Chem. **8**, 417 (1943).
3. E. EMERSON and J. SAGAL. J. Org. Chem. **13**, 535 (1948).
4. K. H. MULLER, B. CHRIST, and M. SCHNEIDER. Arch. Pharm. **293**, 567 (1960).
5. D. SVOBODOVA and J. GASPARIC. Collect. Czech. Chem. Commun. **33**, 42 (1968).
6. D. SVOBODOVA and J. GASPARIC. Collect. Czech. Chem. Commun. **35**, 1567 (1970).
7. D. SVOBODOVA, J. GASPARIC, and L. NOVAKOVA. Collect. Czech. Chem. Commun. **35**, 31 (1970).
8. P. F. JONES and K. E. JOHNSON. Can. J. Chem. **51**, 2860 (1973).
9. P. F. JONES and K. E. JOHNSON. Can. J. Chem. **51**, 3733 (1973).
10. V. DAVE, J. B. STOTHERS, and E. W. WARNHOFF. Can. J. Chem. **52**, 2932 (1974).
11. A. C. LARSON and E. J. GABE. Computing in crystallography. *Edited by* H. Shenk, R. Olthof-Hazekamp, H. Van Konigsveld, and G. C. Bassi. Delft University Press. 1978. p. 81.
12. J. M. STEWART (*Editor*). The X-ray system of crystallographic programs-XRAY76. Tech Rep. TR-446. Computer Science Center, University of Maryland, College Park, MD. March, 1976.
13. T. P. SINGH and M. VIJAYAN. Acta Crystallogr. **B29**, 714 (1973).
14. T. P. SINGH and M. VIJAYAN. Acta Crystallogr. **B32**, 2432 (1976).
15. S. KIRYU. J. Pharm. Sci. **60**, 699 (1971).
16. S. KIRYU, F. HIRAYAMA, and S. IGUCHI. Chem. Pharm. Bull. **22**, 1588 (1974).
17. J. ELGUERO. Comprehensive heterocyclic chemistry. *Edited by* A. R. Katritzky and C. W. Rees. Vol. 5. Pergamon, Oxford. 1984. Chap. 4.4.
18. P. J. WHEATLEY. Physical methods in heterocyclic chemistry. *Edited by* A. R. Katritzky. Vol. V. Academic Press, New York. 1972.
19. H. W. W. EHRLICH. Acta Crystallogr. **13**, 946 (1960).
20. C. W. REIMANN, A. D. MIGHELL, and F. A. MAUER. Acta Crystallogr. **23**, 135 (1967).
21. M. VIJAYAN and M. A. VISWAMITRA. Acta Crystallogr. **21**, 522 (1966); **23**, 1000 (1967); **B24**, 1067 (1968).
22. H. JAGGI. Helv. Chim. Acta, **51**, 580 (1968).

Can. J. Chem. Downloaded from www.nrcresearchpress.com by 213.166.140.6 on 09/07/12
For personal use only.

Structural properties of modified deoxyadenosine structures in solution. Impact of the *gauche* and anomeric effects on the furanose conformation

LEO H. KOOLE[1] AND HENK M. BUCK
Department of Organic Chemistry, Eindhoven University of Technology, P.O. Box 513, 5600 MB Eindhoven, The Netherlands

AND

AGNES NYILAS AND JYOTI CHATTOPADHYAYA
Department of Bioorganic Chemistry, Biomedical Center, Uppsala University, Uppsala, Sweden

Received January 6, 1987

LEO H. KOOLE, HENK M. BUCK, AGNES NYILAS, and JYOTI CHATTOPADHYAYA. Can. J. Chem. **65**, 2089 (1987).

A variable temperature high resolution ^{1}H nuclear magnetic resonance study (at 300 or 500 MHz) of the two modified nucleosides 9-(2′-deoxy-β-D-*threo*-ribofuranosyl)-adenine (**1**) and 9-(3′-deoxy-β-D-*threo*-ribofuranosyl)-adenine (**2**) has been performed. It was found that the furanose conformation in **1** and **2** can be best described as a rapid North (N) ⇄ South (S) equilibrium that is biased toward the N-form. For **1**, a marked temperature dependence of the N ⇄ S equilibrium was found, whereas the furanose conformation in **2** is virtually insensitive to temperature changes. Comparison of these results with the well-known conformational properties of the natural nucleosides 2′-deoxyadenosine (2′-dA) and 3′-deoxyadenosine (3′-dA) revealed that the net result of the *gauche* effect and the anomeric effect is of major importance in determining the furanose conformation. A brief discussion in terms of the thermodynamic parameters that govern the N ⇄ S equilibria in the investigated nucleosides is given.

LEO H. KOOLE, HENK M. BUCK, AGNES NYILAS et JYOTI CHATTOPADHYAYA. Can. J. Chem. **65**, 2089 (1987).

On a effectué une étude de résonance magnétique nucléaire à haute résolution (à 300 ou 500 MHz) et à température variable de deux nucléosides modifiés, soit la (déoxy-2 β-D-*thréo*-ribofurannosyl)-9 adénine (**1**) et la (déoxy-3 β-D-*thréo*-ribofurannosyl)-9 adénine (**2**). On a trouvé que la meilleure façon de décrire la conformation du furannose des composés **1** et **2** fait appel à un équilibre rapide nord (N) ⇄ sud (S) dans lequel la forme N est favorisée. Dans le cas du composé **1**, on a observé que l'équilibre (N) ⇄ (S) est soumis à une dépendance marquée sur la température; par ailleurs, la conformation du furannose de la molécule **2** est virtuellement insensible aux changements de température. Une comparaison de ces résultats avec les propriétés conformationnelles bien connues des nucléosides naturels déoxy-2′ adénosine (d-2′ A) et déoxy-3′ adénoside (d-3′ A) révèle que le résultat net de l'effet *gauche* et de l'effet anomérique est important dans la détermination de la conformation du furannose. On présente une brève discussion en fonction des paramètres thermodynamiques qui influencent l'équilibre (N) ⇄ (S) dans les nucléosides étudiés.

[Traduit par la revue]

Introduction[2]

Naturally occurring nucleic acids display a marked structural versatility, which is essential to their function of storing and transmitting genetic information in the living cell (1). In particular, the backbone chain, in which negatively charged phosphate groups alternate with furanose sugar units (ribose in RNAs, 2′-deoxyribose in DNAs), is capable of adopting a variety of distinct conformations. It has been shown that the overall structural flexibility of DNA and RNA is largely determined by the furanose rings in the backbone, and this insight has stimulated extensive experimental (2–4) and theoretical (5–13) research on furanose puckering in nucleosides and nucleotides. We report herein a detailed ^{1}H nmr conformational study on the modified deoxyadenosine systems (14, 15) 9-(2′-deoxy-β-D-*threo*-ribofuranosyl)-adenine (**1**) and 9-(3′-deoxy-β-D-*threo*-ribofuranosyl)-adenine (**2**). Both structures (Fig. 1) have the hydroxyl group on the furanose ring in the unnatural *endo* position.

It should be noted that Mengel and Wiedner (14), as well as Lüdemann *et al.* (16), have previously reported ^{1}H nmr studies on **1** and **2**. However, the work of Mengel and Wiedner does not mention a conformational analysis of the furanose moieties in **1** and **2**. The conformational studies as reported by Lüdemann *et al.* refer exclusively to the solvent ND_3 and a sample temperature of 213 K. In the present work, we determined the conformational properties of **1** and **2** as a function of the sample temperature in the solvents D_2O or dimethyl formamide-d_6. Comparison with the natural nucleosides 2′-deoxyadenosine (2′-dA) and 3′-deoxyadenosine (3′-dA), also called cordycepin, provided new details on the nature of furanose puckering. It is found that the net effect of two stereoelectronic factors (i.e., the *gauche* effect and the anomeric effect) is of major importance in determining the conformational preferences of the sugar unit in solution.

Experimental

Preparation

The preparation of the modified nucleosides **1** and **2** has been described previously (14, 15). The essential step in the synthesis route for both compounds involves the $LiAlH_4$ reduction of a (6*N*,5′) doubly protected 2′,3′-*lyxo*-anhydroadenosine structure. Using $LiAlD_4$ in the reduction step, the synthesis route can be used to introduce deuterium in a stereospecific way (15). After this reaction, one obtains **1** with a deuterium in the *exo* position at $C_{2'}$ ($C_{2'}$(*R*) configuration), and **2** with a deuterium in the *exo* position at $C_{3'}$ ($C_{3'}$(*S*) configuration). The natural nucleosides 2′-dA and 3′-dA were purchased from Sigma.

Nuclear magnetic resonance spectroscopy

The ^{1}H nmr spectra were recorded at different sample temperatures on a Bruker CXP 300 nmr spectrometer[3] (^{1}H frequency: 300.13 MHz),

[1]Author to whom correspondence may be addressed.

[2]Nomenclature in this work follows recent IUPAC–IUB recommendations on nucleotide conformational nomenclature. See D. B. Davies and H. B. E. Dixon, IUPAC–IUB Discussion Draft on abbreviations and symbols for the description of polynucleotide chains. Document J.C.B.N. 14.2 (1980).

[3]NMR facility at the Eindhoven University of Technology.

Printed in Canada / Imprimé au Canada

Can. J. Chem. Downloaded from www.nrcresearchpress.com by 213.166.140.6 on 09/07/12
For personal use only.

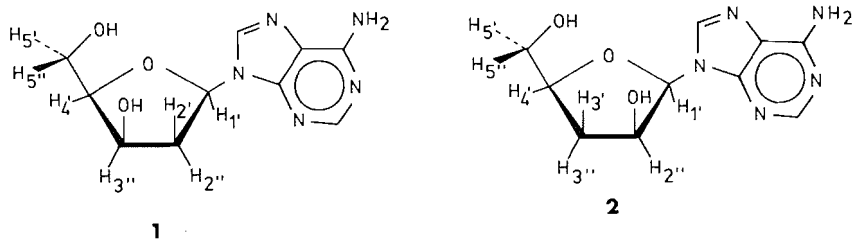

1 2

FIG. 1. Structural formulas of the model compounds **1** and **2**. The numbering of the furanose hydrogens is indicated.

Can. J. Chem. Downloaded from www.nrcresearchpress.com by 213.166.140.6 on 09/07/12
For personal use only.

or on a Bruker AM 500 nmr spectrometer[4] (^{1}H frequency: 500.1 MHz). In all cases, the field-frequency lock was provided by the solvent (D_2O or dimethyl formamide-d_6). At 300 MHz, we used a spectral window of 3000 Hz; at 500 MHz this was 5000 Hz. Before Fourier transformation, the spectra were zero-filled to 32 or 64 K, and resolution enhanced by an appropriate Gaussian multiplication. In some cases, a standard computer simulation–iteration procedure was employed to obtain accurate values for spin–spin couplings and chemical shifts.

Furanose conformation

The description of the puckered conformation in furanose rings is greatly facilitated by the pseudorotation concept (5, 17), in which the conformations of the five ring torsions are mathematically related to a puckering amplitude (ν_m), and a phase angle of pseudorotation (P). The puckering amplitude identifies the deviation from planarity of the furanose ring. From the large number of X-ray crystallographic studies of nucleosides and nucleotides (18) it is known that ν_m is confined to a narrow range around $\nu_m = 39°$. Potential energy calculations have clearly shown that the stability of the furanose systems decreases sharply when ν_m is varied (2). The phase angle of pseudorotation actually indicates which part of the ring is bent. P lies in the range 0–360°, thus encompassing an entire pseudorotation cycle. Also from crystallographic studies, it is known that P values occur in two distinct and relatively narrow ranges (18). The first range is centered around $P = 18°$ ($C_{3'}$-*endo* ring conformation), and is designated as N (North). The N pucker is characteristic for all RNAs and, for example, the A form of DNA (4). The second range is centered around $P = 162°$ ($C_{2'}$-*endo* ring conformation), and is called S (South). This pucker is found, for example, in B DNA. Conformational studies on nucleosides and nucleotides in solution have shown that the furanose ring is generally involved in a rapid N ⇄ S equilibrium, which is an approximate 1:1 blend for ribose rings, and clearly biased toward the S form for 2′-deoxyribose rings (2, 19–21).

A rationale for this different conformational behavior of ribose vs. 2′-deoxyribose has been given by Olson (2). She stated that the preferred conformation in solution is determined by the so-called *gauche* effect, i.e., the tendency of vicinal oxygen atoms to adopt a *gauche* rotational arrangement (12, 22, 23). For furanose units, this means that the oxygens $O_{2'}$ and $O_{3'}$ are preferentially located in an axial position.

Looking at the N and S forms of ribose, it is seen that the N form corresponds with $O_{2'}$ axial and $O_{3'}$ equatorial, whereas the reverse situation occurs in the S form. Consequently, ribose shows a 1:1 distribution over N and S in solution. 2′-Deoxyribose, on the other hand, has $O_{3'}$ axial in the S form, and $O_{3'}$ equatorial in the N form, which leads to a preference for S in solution. The theory also correctly predicts the experimentally observed preference of 3′-deoxy nucleosides (e.g. cordycepin) for the N pucker (24–26). At first sight, the *gauche* effect theory seems to account for all experimental data that have been obtained on nucleosides and nucleotides in solution. However, a substantial shortcoming is obvious, since the theory does not explain why the N ⇄ S conformational equilibrium in 2′-deoxy nucleosides is virtually temperature independent (25). This experimental fact indicates that the free energy difference between the N and S states is in fact solely determined by entropy factors. Apparently, the entropy is 1–2 eu larger in the S form than in the N form. In contrast, the N ⇄ S equilibrium for 3′-deoxy nucleosides is clearly temperature sensitive (*vide infra*). In this case, raising the temperature leads to increased populations of the S pucker, i.e., the N form is associated with the lowest enthalpy.

In the present work, we have specifically focused on the temperature dependence of the conformational equilibria of **1**, **2**, 2′-dA, and 3′-dA. A brief discussion of the thermodynamic parameters governing the N ⇄ S equilibria is given. It appears to be necessary to account explicitly for the so-called anomeric effect (27), i.e. the preference of the nucleobase to be axially located on the furanose unit.

Results

We have recorded 300- and 500-MHz ^{1}H nmr spectra of **1**, **2**, 2′-dA, and 3′-dA in the temperature range of −40 to 95°C. In the experiments at sample temperatures higher than 0°C, we used D_2O as the medium; all other experiments refer to the solvent dimethyl formamide-d_6. Table 1 summarizes the ^{1}H nmr parameters that were obtained on **1** and **2** at 25°C. The data obtained at other sample temperatures are listed as supplementary material.[5]

*9-(2′-Deoxy-β-D-*threo*-ribofuranosyl)-adenine (**1**)*

The conformation of the furanose ring in **1** was determined from the relationship between the coupling constants of the vicinal ring protons (i.e., $J_{1'2'}$, $J_{1'2''}$, $J_{2'3''}$, $J_{2''3''}$, and $J_{3''4'}$) and the pseudorotational parameters of the ring. The assignment of the protons $H_{2'}$ and $H_{2''}$ was based on a comparison with the analogue of **1**, in which $H_{2''}$ was substituted by deuterium (15). From this, it follows that $\delta(2'') > \delta(2')$. Using the generalized Karplus equation of Altona and co-workers (28), we calculated the variation of the five ring-coupling constants over the full pseudorotation circuit.[6] A convenient qualitative representation of the conformational equilibrium of the furanose ring in **1** is

[4]Dutch National 500/200 hf NMR facility at Nijmegen, The Netherlands.

[5]Tables of nmr spectral parameters obtained on **1**, **2**, 2′-dA, and 3′-dA may be purchased from the Depository of Unpublished Data, CISTI, National Research Council of Canada, Ottawa, Ont., Canada K1A 0S2.

[6]Analogous calculations have recently been performed for 5-methoxymethyl-1-(2′-deoxy-β-D-*lyxo*-furanosyl uracil). See Fig. 3 in ref. 29.

TABLE 1. Nuclear magnetic resonance spectral data, obtained on **1** and **2** in D_2O, at 25°C

	J			δ^a	
Protons	**1**	**2**	Proton	**1**	**2**
1′2′	2.6	—	1′	6.27	6.14
1′2″	8.7	5.1	2′	2.44	—
2′3″	1.0	—	2″	2.91	4.60
2″3′	—	6.8	3′	—	1.93
2″3″	5.8	6.8	3″	4.52	2.43
3′4′	—	8.3	4′	4.14	4.25
3″4′	3.5	6.8	5′	3.94	3.80
4′5′	4.2	3.0	5″	3.83	3.70
4′5″	7.3	5.2	2	8.26	8.15
			8	8.14	8.08

[a]Referenced against the HDO residual peak (δ 4.68).

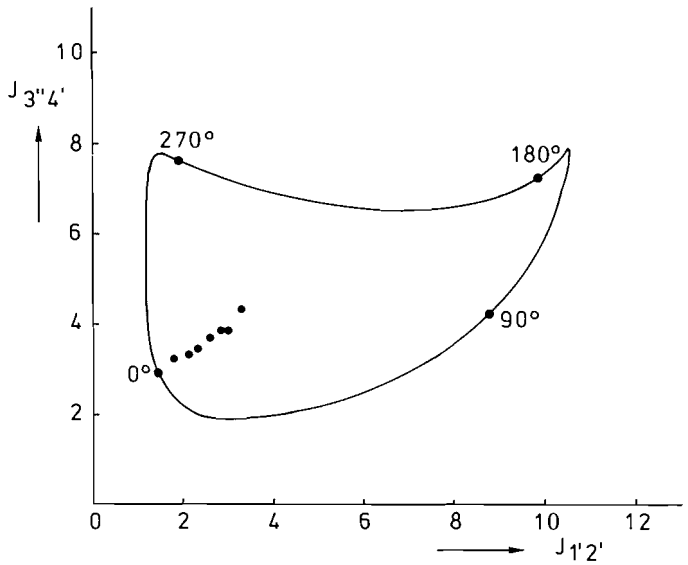

FIG. 2. Calculated variation of the proton–proton coupling constants $J_{1'2'}$ and $J_{3''4'}$ in **1** with the phase angle of pseudorotation (P). The experimental data points are found in the lower left region of the graph.

given in Fig. 2, which shows the variation of $J_{1'2'}$ and $J_{3''4'}$ with P. Note that $J_{1'2'}$ is a transoidal coupling, showing a large variation of 9.4 Hz (from 1.2 to 10.6 Hz) over the pseudorotation cycle. The cisoidal coupling $J_{3''4'}$, on the other hand, shows a much smaller variation of 5.9 Hz (from 1.9 to 7.8 Hz). The experimental data points are found in the lower left part of the cycle, close to $P = 0°$. From the plot, it is evident that the conformation of the furanose ring is strongly biased toward the N form. Also, it is seen that the ring conformation varies with the sample temperature in such a way that increasing the temperature results in an enhanced population of an S form, which is found in the upper right region of the graph. A quantitative picture of the furanose conformation could be obtained by application of the PSEUROT method (30), after correct parametrization for the *endo* orientation of the 3′-OH group on the ring.

The PSEUROT algorithm calculates the best fit of P_N, P_S (the phase angles of pseudorotation in the N and S forms), $\nu_{m,N}$, $\nu_{m,S}$ (the puckering amplitudes in the N and S forms), and the mol fraction of the participating conformers, to the experimental spin–spin couplings between the ring protons.

TABLE 2. Calculated population of the N conformer in **1** as a function of the sample temperature (see text)

T	x_N
233	1.00
255	0.98
276	0.97
286	0.96
300	0.94
322	0.91
345	0.89
365	0.86

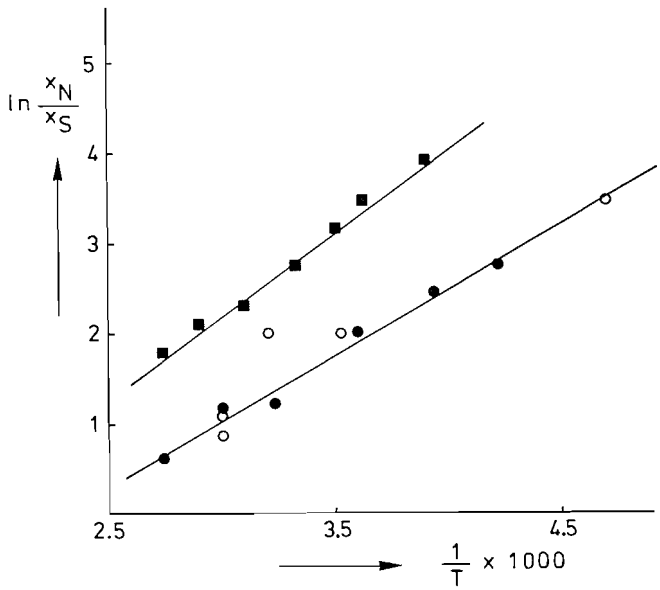

FIG. 3. Van't Hoff plot, based on the experimental data on **1** (black squares) and 3′-dA (black circles). The open circles refer to nmr measurements on 3′-dA, described in ref. 25.

The program was run under the reasonable assumption that the N and S forms have the same puckering amplitude. Based on our data, it was found that the furanose conformation in **1** is best described by a dominant N form with $P = 0°$, $\nu_m = 33°$, and a minor S form with $P = 208°$, $\nu_m = 33°$. Table 2 lists the calculated populations of the N form (x_N) as a function of the sample temperature. Interestingly, these data can be used to estimate the thermodynamic parameters of the N ⇄ S conformational equilibrium in **1**. In the van't Hoff plot ($\ln x_N/x_S$ vs. $1/T$) of Fig. 3, the data on **1** correspond with the black squares. From the slope of the best-fit line through the data points, it follows that the conversion from N toward S is associated with an increase of the standard enthalpy of 17 kJ/mol. The estimated inaccuracy in this number is ±3 kJ/mol. The intercept with the vertical axis reveals that the standard entropies of the N and S forms differ by approximately 1.5 eu, in favor of S. In addition, the conformation of the exocyclic $C_{4'}$—$C_{5'}$ bond in **1** was analyzed on the basis of the vicinal proton–proton coupling constants $J_{4'5'}$ and $J_{4'5''}$ (28, 31, 32). At a sample temperature of 25°C, it was found that $J_{4'5'}$ = 4.2 Hz, and $J_{4'5''}$ = 7.3 Hz. From this, it was calculated that the populations of γ^+, γ^t, and γ^- are 0.20, 0.60, and 0.20, respectively. Thus, γ^t is the preferred $C_{4'}$—$C_{5'}$ conformation in

Can. J. Chem. Downloaded from www.nrcresearchpress.com by 213.166.140.6 on 09/07/12
For personal use only.

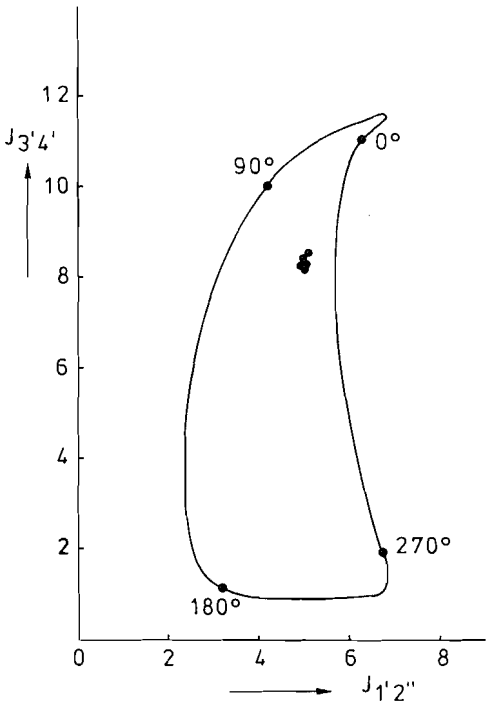

FIG. 4. Calculated variation of $J_{1'2''}$ and $J_{3'4'}$ in **2** with the phase angle of pseudorotation (P). The experimental data obtained on **2** at different sample temperatures are clustered in the midregion of the graph (see text).

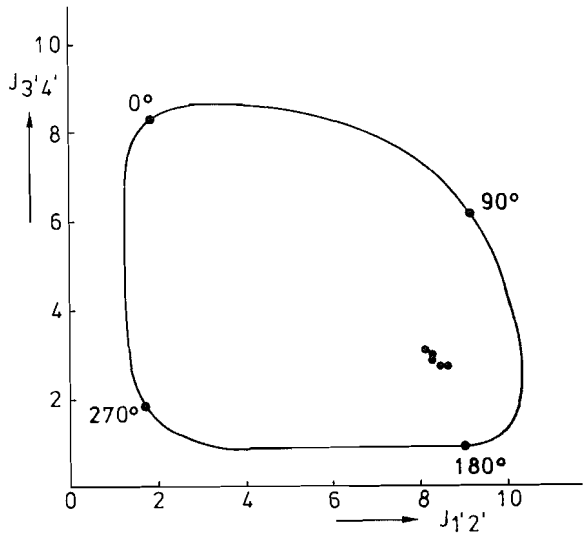

FIG. 5. Calculated variation of $J_{1'2'}$ and $J_{3'4'}$ in 2′-dA with the phase angle of pseudorotation (P).

1, whereas γ^+ always dominates in unmodified nucleosides. Most likely, the cisoidal orientation of the 3′- and 5′-hydroxyl groups in **1** strongly destabilizes γ^+ because of unfavorable electrostatic and (or) steric interactions. Therefore the $C_{4'}$—$C_{5'}$ conformation is strongly biased toward γ^t. We also observed a marked temperature dependency of the $C_{4'}$—$C_{5'}$ conformational equilibrium. Lowering the temperature results in a more pronounced preference for γ^t. Details are given in the supplementary material.

*9-(3′-Deoxy-β-D-*threo*-ribofuranosyl)adenine (2)*

For this compound, the furanose conformation was determined from the vicinal coupling constants $J_{1'2''}$, $J_{2''3'}$, $J_{2''3''}$, $J_{3'4'}$, and $J_{3''4'}$. The assignment of the protons $H_{3'}$ and $H_{3''}$ was based on a comparison with the analogue structure of **2** in which $H_{3''}$ was replaced by deuterium (15). It is found in this way that $\delta(3'') > \delta(3')$. After calculating the dependence of the ring-coupling constants on the phase angle of pseudorotation (28), we could construct Fig. 4, showing the variation of $J_{1'2''}$ and $J_{3'4'}$ with P. Note that $J_{1'2''}$ is a cisoidal coupling with a variation of only 4.5 Hz (from 2.3 to 6.8 Hz) over the entire pseudorotation cycle. A much greater variation of 10.8 Hz (from 0.8 to 11.6 Hz) was calculated for the transoidal coupling $J_{3'4'}$. The experimental data are clustered in the upper region of the graph, close to the line that connects the calculated points for $P = 0°$ and $P = 180°$. Figure 4 immediately shows that the N ⇄ S equilibrium in **2** is virtually temperature independent. Therefore it can be concluded that the enthalpy difference between the N and S forms in **2** is close to zero. Also, it is seen that the distribution over N and S is biased toward N, i.e., the entropy of the N form slightly exceeds that of the S form. In the case of **2**, we confined ourselves to the qualitative description of the furanose conformation as given above. This is due to the fact that the five ring couplings are practically constant over the temperature range of −45 to 95°C. With respect to the $C_{4'}$—$C_{5'}$ conformation it was found that $J_{4'5'} = 3.0$ Hz, and $J_{4'5''} = 5.2$ Hz. From this, we calculated that γ^+, γ^t, and γ^- have the relative populations of 0.53, 0.41, and 0.06, respectively at a sample temperature of 25°C. Lowering the temperature results in a pronounced preference for the γ^+ rotamer. All relevant data are given in the supplementary material.

2′-Deoxyadenosine (2′-dA)

The conformational properties of 2′-dA, an essential building block of DNA, have been studied extensively by means of X-ray crystallography (33) and nmr spectroscopy (25, 34–36). In the crystal structure, 2′-dA shows an N-type furanose ring ($P = 14°$, $\nu_m = 35.5°$). The conformations around the $C_{1'}$—N_9 and $C_{4'}$—$C_{5'}$ bonds are *anti* and γ^+, respectively. From the nmr data, it was concluded that the conformation of the furanose ring in 2′-dA is best described as a rapid N ⇄ S equilibrium. The best-fit pseudorotational parameters for the N form are $P = 10°$, $\nu_m = 35.5°$; for the S form, $P = 167°$, $\nu_m = 35.5°$ (30). In Fig. 5, we have plotted both $J_{1'2'}$ and $J_{3'4'}$ as a function of P (*vide supra*). The calculations were performed for a puckering amplitude of 35.5°. The data points in the graph refer to literature data (25), as well as to our own experiments in D_2O in deuterated dimethyl formamide (see supplementary material). Clearly, the data points are clustered in the lower right region of the plot, indicating that the S form of the furanose ring is slightly preferred in solution. Remarkably, the N ⇄ S equilibrium is virtually insensitive to temperature changes, i.e., the enthalpy difference between the N and S forms is close to zero.

3′-Deoxyadenosine (3′-dA)

The conformation of 3′-dA in the solid state and in solution has also received considerable attention (25, 26). The interest in 3′-dA stems from its pronounced antibiotic properties (37). The X-ray structure shows an N-type furanose ring with $P = 12.7°$, and $\nu_m = 32°$. Westhof *et al.* (25) have recorded nmr spectra of 3′-dA at different temperatures (ranging from −60 to 80°C), and in different solvents (e.g., D_2O, ND_3, and deuterated pyridine). They have shown that the furanose conformation in 3′-dA is heavily biased toward N, and also that the N ⇄ S equilibrium is strongly temperature dependent. Raising the temperature results in an enhanced population of the S form. In

Can. J. Chem. Downloaded from www.nrcresearchpress.com by 213.166.140.6 on 09/07/12
For personal use only.

TABLE 3. Calculated population of the N conformer in 3′-dA as a function of the sample temperature (see text)

T	x_N
213[a]	0.97
235	0.94
254	0.92
278	0.88
283[a]	0.75
300	0.77
313[a]	0.88
333[a]	0.75
333[a]	0.70
336	0.76
365	0.62

[a]Abstracted from ref. 25.

this work, we have estimated the thermodynamic parameters governing the N ⇄ S equilibrium in 3′-dA on the basis of our own data (which were obtained in D_2O or in deuterated dimethyl formamide), as well as on Westhof's data. Application of the PSEUROT method revealed that the conformation of the furanose moiety is best described as a rapid equilibrium between a dominant N form with $P = 13°$, $\nu_m = 32°$, and an S form with $P = 169°$, $\nu_m = 32°$. Table 3 summarizes the calculated population of the N form as a function of the temperature. From the van't Hoff plot in Fig. 3 it was calculated that the N ⇄ S transition in 3′-dA is associated with an increase of the standard enthalpy by approximately 14 kJ/mol. The estimated inaccuracy of this number is again 3 kJ/mol. The entropy change of the N → S transition is again approximately +1.5 eu.

Discussion

From the results, it is evident that **1** and 3′-dA have highly similar conformational properties with respect to the furanose rings. In both cases, a pronounced preference for the N form is found. Also, the N ⇄ S equilibria in **1** and 3′-dA show a highly comparable variation with the sample temperature, since the enthalpy differences between N and S (17 ± 3 kJ/mol for **1**; 14 ± 3 kJ/mol for 3′-dA) are essentially similar. A tentative explanation for these findings is derived on the basis of Fig. 6, which shows the N and S forms for both structures. In both cases, the N form is associated with a favorable axial orientation of the adenine base (anomeric effect), as well as a favorable axial orientation of the hydroxyl group on the furanose ring (3′-OH in **1**, or 2′-OH in 3′-dA). The conversion from N toward S results in undesirable equatorial locations of the base and the hydroxyl group in either case. Clearly, the anomeric effect and the *gauche* effect are cooperative, since both effects drive the N ⇄ S equilibrium toward the N form. Logically, the N form has the lower enthalpy, which explains the experimentally observed temperature dependence of the N ⇄ S equilibria in both structures.

For model compound **2** and 2′-dA it holds that the sugar ring is involved in an N ⇄ S equilibrium that is insensitive to temperature changes. Figure 7 offers a tentative explanation for these results. The N conformation for **2** and 2′-dA has a favorable axial location of the base, combined with unfavorable equatorial furanose OH groups, whereas the reverse situation (equatorial base and axial furanose hydroxyl) is found in the corresponding S form. Evidently, the anomeric effect and the *gauche* effect are counteractive in these cases, which apparently results in cancelling of the enthalpy differences between the N and S forms. For 2′-dA, this reasoning is further substantiated by the experimental finding that structure **3**, in which the base is in fact replaced by hydrogen, shows a temperature-dependent N ⇄ S equilibrium with a preference for S.[7] The anomeric effect is eliminated in this case, i.e., the furanose conformation in **3** is solely determined by the *gauche* effect. Variable temperature measurements on **3** have shown that the enthalpy is approximately 8 kJ/mol lower in the S form than in the N form.[7]

The results show that both the *gauche* effect and the anomeric effect should be taken into account for the description of the conformation of the furanose ring in nucleosides and nucleotides. It goes without saying that other factors, such as chemical

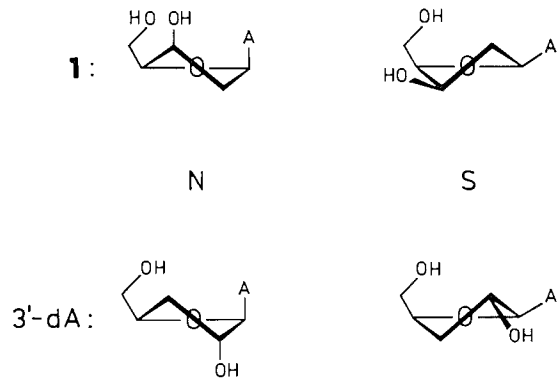

FIG. 6. N and S forms of **1** and 3′-dA. Clearly, the N forms have axial orientation of the adenine base, and axial orientation of the furanose OH. In the corresponding S forms, both the base and the OH group are equatorial.

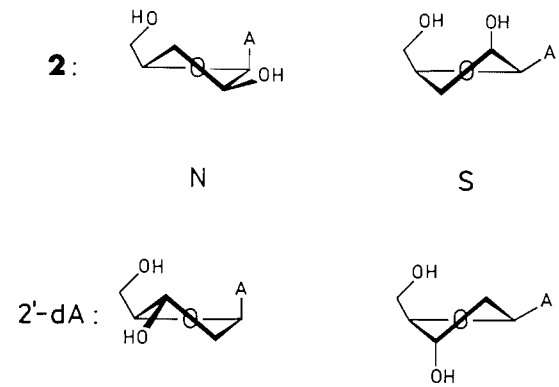

FIG. 7. N and S forms of **2** and 2′-dA. The N forms have axial orientation of the adenine base, combined with an equatorial OH group. The corresponding S forms have an equatorial base, and an axial OH group.

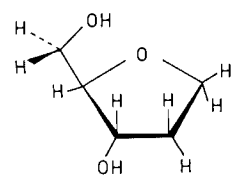

3

FIG. 8. Structural formula of **3**.

[7]L. H. Koole, unpublished results.

Can. J. Chem. Downloaded from www.nrcresearchpress.com by 213.166.140.6 on 09/07/12
For personal use only.

modifications of the base or the introduction of bulky groups on the furanose ring, may also have an important impact on the conformation. However, the present theory may offer an explanation for the well-known polymorphism of oligomeric and polymeric DNA structures, since it is clear that the individual 2′-deoxyribose units may occur in N or S without substantially affecting the enthalpy content of the structure. On the other hand, RNA structures are uniform with N-type conformations of the ribose rings. This is consistent with the fact that the anomeric effect actually determines the enthalpy preference for the N form of ribose.

Acknowledgements

H.M.B. thanks the Netherlands Foundation for Chemical Research (SON) and the Netherlands Organization for the Advancement of Pure Research (ZWO) for financial support of this research. J.C. thanks the Swedish Board for Technical Development (STU) and the Swedish Science Research Council (NFR) for financial aid.

1. S. Arnott, R. Chandrasekaran, P. J. Bond, D. L. Birdsall, A. G. W. Leslie, and L. Puigjaner. Proceedings of the Seventh Aharon Katzir-Katchalski Conference on Structural Aspects of Recognition and Assembly in Biological Macromolecules, Nof Ginossar, Israel. 1980.
2. W. K. Olson and J. L. Sussman. J. Am. Chem. Soc. **104**, 270 (1982).
3. C. Altona. Recl. Trav. Chim. Pays-Bas, **101**, 413 (1982).
4. W. Saenger. Principles of nucleic acid structure. Springer, New York. 1984.
5. C. Altona and M. Sundaralingam. J. Am. Chem. Soc. **94**, 8205 (1972).
6. D. Cremer and J. A. Pople. J. Am. Chem. Soc. **97**, 1354 (1975).
7. S. T. Rao, E. Westhof, and M. Sundaralingam. Acta Crystallogr. Sect. A: Found. Crystallogr. **37**, 421 (1981).
8. M. Levitt and A. Warshell. J. Am. Chem. Soc. **100**, 2607 (1978).
9. E. Westhof and M. Sundaralingam. J. Am. Chem. Soc. **102**, 1493 (1980).
10. H.-D. Lüdemann and E. Westhof. *In* Nuclear magnetic resonance in molecular biology. *Edited by* B. Pullman. D. Reidel, Dordrecht, Holland. 1978. p. 1141.
11. O. Roder, H.-D. Lüdemann, and E. von Goldammer. Eur. J. Biochem. **53**, 517 (1975).
12. W. K. Olson. J. Am. Chem. Soc. **104**, 278 (1982).
13. S. J. Weiner, P. A. Kollman, D. A. Case, U. C. Singh, C. Ghio, G. Alagona, S. Profeta, and P. Weiner. J. Am. Chem. Soc. **106**, 765 (1984).
14. R. Mengel and H. Wiedner. Chem. Ber. **109**, 1395 (1976).
15. A. Nyilas and J. Chattopadhyaya. Synthesis, 196 (1986).
16. H.-D. Lüdemann, G. Knopp, F. Hansske, and M. J. Robins. Nucleic acids: the vectors of life. *Edited by* B. Pullman and J. Jortner. D. Reidel Publishing Co., Dordrecht, Holland. 1984.
17. J. E. Kilpatrick, K. S. Pitzer, and R. Spitzer. J. Am. Chem. Soc. **69**, 2483 (1947).
18. H. P. M. de Leeuw, C. A. G. Haasnoot, and C. Altona. Isr. J. Chem. **20**, 108 (1980).
19. D. B. Davies and S. S. Danyluk. Biochemistry, **13**, 4417 (1974).
20. D. B. Davies and S. S. Danyluk. Biochemistry, **14**, 543 (1975).
21. F. E. Evans and R. H. Sarma. Nature (London), **263**, 567 (1976).
22. S. Wolfe. Acc. Chem. Res. **5**, 102 (1972).
23. T. K. Brunck and F. Weinhold. J. Am. Chem. Soc. **101**, 1700 (1979).
24. P. O. P. Ts'o. *In* Basic principles in nucleic acid chemistry. Vol. 1. *Edited by* P. O. P. Ts'o. Academic Press, New York. 1974. p. 453.
25. E. Westhof, H. Plach, I. Cuno, and H.-D. Lüdemann. Nucleic Acids Res. **4**, 939 (1977).
26. M. M. Radwan and H. R. Wilson. Acta Crystallogr. Sect. B: Struct. Crystallogr. Cryst. Chem. **36**, 2185 (1980).
27. A. J. Kirby. The anomeric effect and related stereoelectronic effects at oxygen. Springer Verlag, Berlin. 1983.
28. C. A. G. Haasnoot, F. A. A. M. de Leeuw, H. P. M. De Leeuw, and C. Altona. Recl. Trav. Chim. Pays-Bas, **98**, 576 (1979).
29. J. W. Quail, I. Ekiel, O. A. L. El-Kabbani, G. Tourigny, L. T. J. Delbaere, A. L. Stuart, and S. V. Gupta. Can. J. Chem. **64**, 1355 (1986).
30. F. A. A. M. de Leeuw and C. Altona. J. Chem. Soc. Perkin Trans. 2, 375 (1982); Quantum Chemistry Program Exchange No. 463.
31. L. H. Koole, R. J. L. van Kooyk, and H. M. Buck. J. Am. Chem. Soc. **107**, 4032 (1985).
32. L. H. Koole, H. M. Buck, J. A. Kanters, and A. Schouten. Can. J. Chem. **65**, 326 (1987).
33. D. G. Watson, D. J. Sutor, and P. Tollin. Acta Crystallogr. **19**, 111 (1965).
34. K. N. Slessor and A. S. Tracey. Carbohydr. Res. **27**, 407 (1973).
35. F. E. Hruska, D. J. Wood, and K. K. Ogilvie. Can. J. Chem. **52**, 3353 (1974).
36. D. B. Davies and S. S. Danyluk. Biopolymers, **13**, 4417 (1974).
37. R. J. Suhadolnik. Nucleoside antibiotics. Wiley–Interscience, New York. 1970.

Can. J. Chem. Downloaded from www.nrcresearchpress.com by 213.166.140.6 on 09/07/12
For personal use only.

Kinetics of the thermolysis of *para*-substituted benzylcobalamins and derivatives

FARUK NOME, MARCOS CAROLI REZENDE, CLAUDIA MARIA SABÓIA, AND ARLINDO CLEMENTE DA SILVA
Departamento de Química, Universidade Federal de Santa Catarina, 88.001-Florianópolis, S.C.-Brasil

Received October 17, 1986

FARUK NOME, MARCOS CAROLI REZENDE, CLAUDIA MARIA SABÓIA, and ARLINDO CLEMENTE DA SILVA. Can. J. Chem. **65**, 2095 (1987).

The thermolysis of five *para*-substituted benzylcobalamins was studied at different temperatures. In the presence of KCN the observed rates increase with the cyanide concentration until a constant value is attained at high [CN^-]. In both series the homolytic cleavage of the Co—C bond is slightly dependent on the *para*-substituent of the benzyl moiety, with ρ values of −0.1 and −0.2 when 5,6-dimethylbenzimidazole (Bzm) and cyanide are the axial ligands respectively. The Co—C bond is weakened by electron-donating axial ligands and the homolytic cleavage rates increase in the order H_2O < Bzm < CN.

FARUK NOME, MARCOS CAROLI REZENDE, CLAUDIA MARIA SABÓIA et ARLINDO CLEMENTE DA SILVA. Can. J. Chem. **65**, 2095 (1987).

La thermolyse de cinq benzylcobalamines *para*-substituées a été étudiée à diverses températures. Les constantes de vitesse observées augmentent avec la concentration de cyanure jusqu'à une valeur constante à haute [CN^-]. Dans les deux séries, la rupture homolytique de la liaison Co—C dépend légèrement du *para*-substituant de la moitié benzylique, les valeurs de ρ étant respectivement −0,1 et −0,2 pour les ligands axiaux 5,6-dimethylbenzimidazole (Bzm) et cyanure. Les ligands axiaux affaiblissent la liaison Co—C et les constantes de vitesse de rupture homolytique augmentent dans l'ordre H_2O < Bzm < CN.

Can. J. Chem. Downloaded from www.nrcresearchpress.com by 213.166.140.6 on 09/07/12
For personal use only.

Introduction

The chemistry of the Co(III)—C bond plays a central role in the biochemistry of vitamin B_{12} (1, 2). As a consequence, the formation and cleavage of the Co—C bond of alkylcobalamins and cobinamides in various chemical processes have been topics of continuous interest in the vitamin B_{12} chemistry (1–14). Examples are found of homolytic and heterolytic cleavages and it is not always an easy task to decide which is the preferred pathway in many thermal decompositions. Even when a homolytic pathway is firmly established, the charge distribution in the transition state remains a subject of speculation. Although large kinetic effects arising from electronic factors are not to be expected in these homolytic processes, such effects do exist and can shed more light on the nature of the transition state of these cleavages. Changes in the ease of the Co—C bond breaking may be observed by either changing the charge of the Co atom, or of the alkyl moiety. Schrauzer and Grate (10) studied the thermolysis of benzylcobalamin and showed, on the basis of the products formed under aerobic and anaerobic conditions, that this is a homolytic process. We decided to study other substituted benzylcobalamins and evaluate the effect of these substituents on the rate of the Co—C bond cleavage. We were also interested in the effects of axial ligands on the cobalt atom, and how they might affect this thermolysis process. Such a *trans* effect should be larger than the result of altering the benzyl moiety, as the ligand is directly attached to the cobalt atom.

Experimental

Vitamin B_{12a} (aquocobalamin) and vitamin B_{12} (cyanocobalamin) were purchased from Merck, Sharp and Dohme. Diaquocobinamide was obtained from vitamin B_{12} following the procedures reported by Pratt and co-workers (14) and Friedrich and Bernhauer (15). The benzyl- and *p*-methylbenzylcobinamide and the various substituted benzylcobalamins **1** employed were prepared following Schrauzer's procedure (9). The products obtained were spectroscopically identical with those reported in the literature.

The spectroscopic characterization of all cobalamins and cobinamides prepared and the kinetic measurements were performed with a Shimadzu UV-210A spectrophotometer equipped with thermostatted water-jacketted cell compartments. The analysis of the organic products of the reactions was carried out with a gas chromatograph CG 370, equipped with an OV-17 column, retention times being identical with those of authentic samples.

The aerobic decomposition of benzylcobalamins and cobinamides was studied in aqueous buffered solution at pH 7.0 by following the change of absorbance at 350 and 425 nm respectively. The spectral changes observed were identical with those reported by Schrauzer and Grate (10) with isobestic points at 370 and 480 nm. The decomposition of benzylcobalamins **1** in the presence of KCN was studied in aqueous buffered solution at pH 11, by monitoring the formation of the products at 367 nm. The spectral changes observed were similar to those described by Jencks and co-workers (11) for the thermolysis of (methoxycarbonyl)methylcobalamin in the presence of excess cyanide, which yields a mixture of cyano- and dicyanocobalamins (λ_{max}: 575, 540, and 370 nm).

Rate constants were obtained from linear plots of $\ln(A_\infty - A_t)$ vs. time. All plots were linear for at least 90% of the reaction, with correlation coefficients greater than 0.99. The activation parameters were calculated from Arrhenius plots of the rate constants at different temperatures.

Results and discussion

Benzylcobalamin decomposes in the presence of oxygen to form benzaldehyde and vitamin B_{12a} (9). The reaction is much slower under nitrogen because of recombination of the benzyl radical and the Co(II) species formed by the homolytic cleavage of the Co—C bond.

We have studied the thermolysis of five *p*-substituted benzylcobalamins **1** at pH 7.0 and different temperatures.

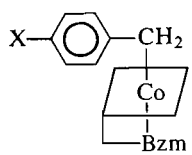

X = H, Me, MeO, Br, CO_2^-

1

The observed rate constants are given in Table 1. The activation parameters for the thermolysis process for each benzylcobalamin were calculated from the observed pseudo-first-order rate constants and are given in Table 2. For the sake of comparison and the discussion below, activation parameters for the benzyl- and *p*-methylbenzylcobinamide are also included in Table 2.

We have also followed the decomposition of cobalamins **1** in the presence of cyanide anion. As with the experiments in the absence of CN^-, the thermolysis is considerably slower

TABLE 1. Observed rate constants for the thermolysis of *p*-substituted benzylcobalamins at pH 7 and various temperatures

Temperature (°C)	$10^3\ k_{obs}\ (s^{-1})$				
	X = H	X = Me	X = OMe	X = Br	X = CO_2^-
15	0.65	0.64	0.51	0.56	0.36
20	1.28	1.23	1.08	1.11	0.77
25	2.40	2.45	2.08	2.26	1.63
30	4.50	4.55	4.14	4.45	3.36
35	8.20	8.51	7.81	8.47	6.65

under nitrogen. Similarly to the reaction in the absence of CN^- the products were the corresponding benzaldehyde and 1,2-diarylethane in aerobic and anaerobic conditions respectively. Toluene, a product that could be formed by homolysis of the Co—C bond followed by electron transfer, was not detected under our experimental conditions. However, in this case, the spectral analysis of the products revealed the formation of a mixture of cyano- and dicyanocobalamin, both under aerobic and anaerobic conditions. The formation of a cobalt(III) species in a homolytic process can be explained by the disproportionation of the Co(II) species initially formed in the presence of excess cyanide, the Co(I) species being consumed by trace oxygen (16).

[1] $2Co(II) + 2CN^- \overset{K_D = 0.28}{\rightleftharpoons} Co(III)(CN^-)_2 + Co(I)$

As shown by Savéant and co-workers, this disproportionation is not as important when the axial ligand is water, hydroxide, or benzimidazole (16).

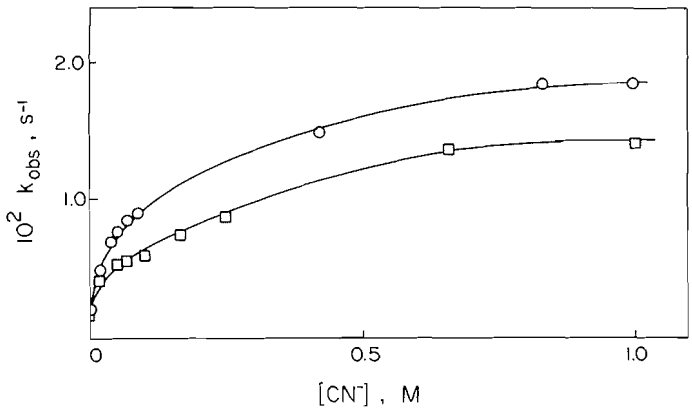

FIG. 1. Variation of k_{obs} as a function of the concentration of cyanide ion for the thermolysis of *p*-methoxybenzylcobalamin (○) and benzylcobalamin (□) at 25.0°C.

Table 3 lists the observed rate values for the decomposition of cobalamins **1** at 25°C, pH 11, and increasing concentrations of cyanide anion. The thermolysis rate is found to increase with $[CN^-]$ until a constant value is reached. Such behaviour is illustrated for the benzyl- and the *p*-methoxybenzylcobalamin in Fig. 1, and has been described by Jencks and co-workers (11) in the decomposition of (methoxycarbonyl)methylcobalamin in the presence of cyanide. Our data can be rationalized by a mechanism that involves a preequilibrium between two cobalt species with different axial ligands, -CN and 5,6-dimethylbenzimidazole (Bzm), which undergo thermolysis at different rates.

[2]

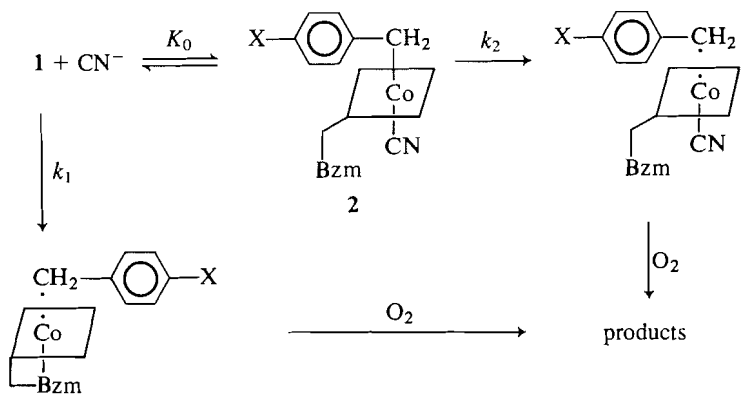

At high cyanide concentrations the benzimidazole ligand is completely displaced by CN^-, the observed rate becoming constant and equal to k_2. Equation [3] relates the observed rate constant to the cyanide concentration.

[3] $k_{obs} = (k_1 + k_2 \cdot K_0[CN^-])/(1 + K_0 \cdot [CN^-])$

Since $k_{obs} = k_1$ when $[CN^-] = 0$, and $k_{obs} = k_2$ for sufficiently high concentrations of cyanide, the preequilibrium constant K_0 can be estimated by proper adjustment of eq. [3] to the experimental values. For the five cobalamins studied, the average K_0 value was $12 \pm 6\ M^{-1}$, not very different from the value of $22.7\ M^{-1}$ for a similar equilibrium involving the (methoxycarbonyl)methylcobalamin (11).

The observed rate values for the thermolysis of the five cobalamins in the presence of a high concentration of cyanide ($[CN^-] = 0.83\ M$) at various temperatures are given in Table 4. Under these conditions, these rates are equal to the rate values k_2, and the activation parameters derived from them (Table 5) correspond to the homolytic cleavage of the Co—C bond when -CN is the axial ligand. We can thus compare the two homolytic processes that differ in the nature of the axial ligand. Figure 2 is a Hammett plot of the thermolysis rate constants for all *p*-substituted benzylcobalamins. The ρ values are −0.1 and −0.2, in the absence and presence of cyanide respectively. The small values were expected for a homolytic process, but the negative sign in both cases is an indication of a slight nucleophilic character of the incipient benzyl radical in the transition state.

Can. J. Chem. Downloaded from www.nrcresearchpress.com by 213.166.140.6 on 09/07/12
For personal use only.

TABLE 2. Activation parameters and calculated rate values at 25°C for the thermolysis of *p*-substituted benzylcobalamins and cobinamides

Substituent X	Axial ligand	$\Delta H^{\ddagger}$ (kcal mol^{-1})	$\Delta S^{\ddagger}$ (cal mol^{-1} deg^{-1})	$\Delta G^{\ddagger}$ kcal mol^{-1}	$10^3 k_2^{25}$ (s^{-1})
H	Bzm	21.7±0.3	2.4±1.0	21.02	2.41
Me	Bzm	22.3±0.5	4.3±1.7	21.01	2.42
MeO	Bzm	23.4±0.6	7.7±1.9	21.10	2.11
Br	Bzm	23.5±0.5	8.1±1.6	21.06	2.26
CO_2^-	Bzm	25.0±0.5	12.8±1.6	21.22	1.72
H[a]	H_2O	28.6±1.3	14.4±4.1	24.30	0.0093
Me[b]	H_2O	27.2±1.4	10.1±4.7	24.20	0.011

[a]Parameters and rate values calculated from the following observed rate constants, k_{obs}: 9.4×10^{-5} (40°C), 1.95×10^{-4} (45°C), 3.98×10^{-4} (50°C), 7.80×10^{-4} (55°C), and 1.55×10^{-3} s^{-1} (60°C).
[b]Observed rate constants, k_{obs}: 1.05×10^{-4} (40°C), 2.12×10^{-4} (45°C), 4.3×10^{-4} (50°C), 8.22×10^{-4} (55°C), and 1.60×10^{-3} s^{-1} (60°C).

TABLE 3. Observed rate constants for the thermolysis of *p*-substituted benzylcobalamins at 25°C and pH 11 in the presence of potassium cyanide

	$10^2 k_{obs}$ (s^{-1})				
10[KCN] (*M*)	X = H	X = Me	X = MeO	X = Br	X = CO_2^-
0	0.21	0.23	0.18	0.20	0.13
0.17	0.42	0.61	0.49	0.36	0.76
0.33	0.51	0.81	0.70	0.44	—
0.50	0.54	1.02	0.76	0.49	—
0.66	0.56	1.10	0.85	—	—
0.83	—	1.14	0.88	—	—
1.00	0.59	1.16	—	0.52	0.96
1.67	0.74	1.21	—	0.59	—
2.50	0.87	1.28	—	—	1.11
3.33	—	1.31	—	0.88	—
4.17	—	1.32	1.45	0.97	1.34
6.67	1.24	1.45	—	1.19	—
8.33	1.22	1.49	1.89	1.20	1.56
10.00	1.23	1.53	1.83	—	1.54

TABLE 4. Pseudo-first-order rate constants for the thermolysis of *p*-substituted benzylcobalamins at various temperatures and pH 11, in the presence of 0.83 *M* KCN

Temperature (°C)	$10^2 k_{obs}$ (s^{-1})				
	X = H	X = Me	X = MeO	X = Br	X = CO_2^-
15	0.598	0.687	0.750	0.537	0.790
20	0.876	1.03	1.18	0.826	1.12
25	1.22	1.49	1.89	1.20	1.56
30	1.69	2.09	2.91	1.80	2.23
35	2.33	3.01	4.45	2.60	3.04

The nature of the axial ligand was expected to play an important role in the homolytic cleavage of the Co—C bond. In fact, for the reaction in which water was the axial ligand (Table 2), the values of $\Delta H^{\ddagger}$ and $\Delta S^{\ddagger}$ for the compounds studied are in the range of 27.2–28.6 kcal mol^{-1} and 10.1 – 14.4 eu respectively. When benzimidazole is the axial ligand, a slight decrease in $\Delta H^{\ddagger}$ (21.7–25.0 kcal mol^{-1}) is observed (Table 2). This trend is maintained when cyanide is the ligand, the range of $\Delta H^{\ddagger}$ values being 15.1–11.3 kcal mol^{-1}, but in this case a strong decrease in $\Delta S^{\ddagger}$ (−15.6 to −29.3 eu) is also observed (Table 5).

The changes observed in both enthalpy and entropy of activation are noteworthy and, as should be expected for reactions occurring through the same mechanism, a linear dependence of $\Delta H^{\ddagger}$ on $\Delta S^{\ddagger}$ is observed (graph not shown), implying a partial compensation of both factors. It is clear from Table 2 that the variations of $\Delta H^{\ddagger}$ predominate in the overall changes of $\Delta G^{\ddagger}$ for the reaction series.

It may be argued in the case of cobalamins that these activation parameters do not correspond solely to the homolytic cleavage of the Co—C bond. In fact, as pointed out by Schrauzer and Grate (10), the activation parameters for the thermolysis of the organocobalamins include a contribution from the base-on/base-off benzimidazole coordination equilibria. A comparison between benzylcobalamins and other related systems where these contributions are absent should be valid only if the benzimidazole coordination equilibria for all benzylcobalamins studied do not vary with the temperature, being cancelled in the calculation of the activation parameters. This was in fact observed by us with the *p*-substituted benzylcobalamins studied in this work. As was the case of benzylcobalamin itself (10), our cobalamins showed very small spectral changes in the temperature range of our experiments, indicating that variations of coordination equilibria with temperature are negligible.

The pronounced entropic change from positive (benzimida-

Can. J. Chem. Downloaded from www.nrcresearchpress.com by 213.166.140.6 on 09/07/12
For personal use only.

TABLE 5. Activation parameters and calculated rate values at 25°C for the thermolysis of *p*-substituted benzylcobalamins in the presence of excess cyanide

Substituent X	E_a (kcal mol^{-1})	$\Delta H^{\neq}$ (kcal mol^{-1})	$\Delta S^{\neq}$ (cal mol^{-1} deg^{-1})	$\Delta G^{\neq}$ (kcal mol^{-1})	$10^2\, k_2^{25}$ (s^{-1})
H	11.9±0.4	11.3±0.4	−29.3±1.3	20.06	1.21
Me	12.9±0.4	12.3±0.4	−25.5±1.4	19.95	1.48
MeO	15.7±0.3	15.1±0.3	−15.6±1.0	19.80	1.87
Br	13.9±0.4	13.3±0.4	−22.7±1.3	20.05	1.22
CO_2^-	11.9±0.4	11.3±0.4	−28.7±1.2	19.91	1.58

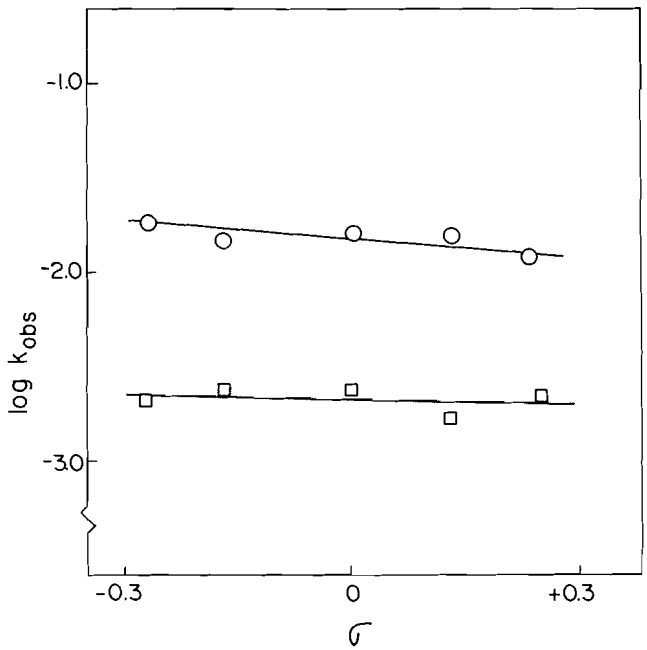

FIG. 2. Variation of log k_{obs} as a function of the substituent constant for the decomposition of **1** in the presence (○) and absence (□) of cyanide ion at 25.0°C.

TABLE 6. Co—C bond dissociation energies and rate constants for the Co—C cleavage of benzylcobinamides, cobalamins **1**, and the cyanoderivatives **2**

	Benzyl substituent			
	Benzyl		*p*-Methylbenzyl	
Axial ligand	D_{Co-C}[a] (kcal mol^{-1})	k_2^{25} (s^{-1})	D_{Co-C}[a] (kcal mol^{-1})	k_2^{25} (s^{-1})
H_2O	26.6±1.3	9.3×10^{-6}	25.2±1.4	1.10×10^{-5}
Bzm	19.7±0.3	2.41×10^{-3}	20.3±0.5	2.42×10^{-3}
CN	9.3±0.4	1.21×10^{-2}	10.3±0.4	1.48×10^{-2}

[a]Value calculated as $D_{Co-C} = \Delta H^{\neq} - 2.0$ kcal mol^{-1} (see ref. 12).

zole and water as axial ligands) to negative values when cyanide is coordinated to the cobalt(III) atom is, to the best of our knowledge, unprecedented. Following Schrauzer's tentative arguments (10), we may regard such an entropic change as the result of two opposing trends, an entropic gain due to the departure of the benzyl groups, and an entropy loss, when -CN is the axial ligand. Thus, the order imposed on the benzylcobalamin and benzylcobinamide by the benzyl group is lost in the transition state, which should be very nearly cobalt(II) in nature. When CN^- is the axial ligand, the order imposed by axial cyanide coordination is increased in going from the Co(III) to the Co(II) species and more than compensates the entropy gain due to the benzyl group departure. The overall result is then a net entropy decrease of the cyanide coordinated system.

Table 6 lists the rate constants at 25°C for the Co—C bond cleavage reaction of the benzyl and *p*-methylbenzylcobalamins in the presence and absence of cyanide ion, and the dissociation energies of the corresponding Co—C bond, estimated, according to Halpern (12), to be 2.0 kcal mol^{-1} less than the homolysis activation enthalpies. For the sake of comparison we also include the Co—C bond dissociation energies estimated from the thermolysis of the benzyl- and *p*-methylbenzylcobinamide at 25°C. Inspection of this table shows that the homolysis is facilitated by the increasing electron-donating ability of the axial ligand. By reducing the charge of the cobalt atom, the electron-donating axial cyanide weakens the Co—C bond considerably, as compared to the more stable cobalamin and cobinamide systems. This ground-state effect is much more important than an eventual transition state destabilization by the cyanide ligand, which renders more difficult the transition from Co(III) to Co(II) by increasing the electron density around the cobalt atom.

In conclusion, the present work extends Schrauzer's original studies on the homolytic cleavage of benzylcobalamin (10) by varying both the benzyl moiety and the substituent in the fifth coordination position. As anticipated, the homolytic fission is only slightly dependent on the nature of the *para* substituent of the benzyl moiety, but the negative values obtained argue for some small degree of nucleophilic character of the incipient benzyl radical in the transition state. Changing the axial substituent results in considerable changes in the rates of homolytic Co—C cleavage, such rates increasing in the order H_2O < Bzm < CN. It is noteworthy that, in spite of the large changes brought about by the replacement of the 5,6-dimethylbenzimidazole ligand by water or cyanide, the reaction mechanism and the mode of cleavage of the Co—C bond are essentially the same.

It is important to emphasize that, because of the particular steric and electronic labilization of the Co—C bond in benzylcobalamins, any mechanistic extension of our results to other organocobalamins should be made with caution.

Acknowledgements

We are grateful to the Conselho Nacional de Pesquisa Científica e Tecnológica (CNPq) for financial support of this work.

1. D. Dolphin (*Editor*). B_{12}. Vol. 2. Wiley, New York. 1982.
2. J. M. PRATT. Inorganic chemistry of vitamin B_{12}. Academic Press, London. 1972.

Can. J. Chem. Downloaded from www.nrcresearchpress.com by 213.166.140.6 on 09/07/12
For personal use only.

3. D. ZANETTE and F. NOME. Can. J. Chem. **58**, 2402 (1980).
4. F. NOME and D. ZANETTE. J. Org. Chem. **44**, 2308 (1979).
5. D. A. BALDWIN, E. A. BETTERTON, S. M. CHEMALY, and J. M. PRATT. J. Chem. Soc. Dalton Trans. 1613 (1985).
6. G. N. SCHRAUZER, J. W. SIBERT, and R. J. WINDGASSEN. J. Am. Chem. Soc. **90**, 6681 (1968).
7. G. N. SCHRAUZER. Pure Appl. Chem. **33**, 545 (1973).
8. J. HALPERN, F. T. T. NG, and G. L. REMPEL. J. Am. Chem. Soc. **101**, 7124 (1979).
9. G. N. SCHRAUZER and J. H. GRATE. J. Am. Chem. Soc. **101**, 4601 (1979).
10. G. N. SCHRAUZER and J. H. GRATE. J. Am. Chem. Soc. **103**, 541 (1981).
11. W. E. REENSTRA, R. H. ABELES, and W. P. JENCKS. J. Am. Chem. Soc. **104**, 1016 (1982).
12. J. HALPERN. Acc. Chem. Res. **15**, 238 (1982).
13. F. NOME, A. NEVES, and L. G. IONESCU. *In* Solution behavior of surfactants. Theoretical and applied aspects. *Edited by* E. J. Fendler and K. Mittal. Plenum Press, New York. 1982.
14. R. A. FIRTH, H. A. O. HILL, J. M. PRATT, and R. G. THORP. J. Chem. Soc. A, 453 (1968).
15. W. FRIEDRICH and K. BERNHAUER. Chem. Ber. **90**, 465 (1957).
16. D. LEXA, J. M. SAVÉANT, and J. ZICLER. J. Am. Chem. Soc. **102**, 2654 (1980).

Can. J. Chem. Downloaded from www.nrcresearchpress.com by 213.166.140.6 on 09/07/12
For personal use only.

Thioamide spectroscopy: long path length absorption and quantum chemical studies of thioformamide vapour, $CHSNH_2/CHSND_2$

R. H. JUDGE[1] AND D. C. MOULE
Department of Chemistry, Brock University, St. Catharines, Ont., Canada L2S 3A1

AND

J. D. GODDARD
Department of Chemistry and Biochemistry, University of Guelph, Guelph, Ont., Canada N1G 2W1

Received December 9, 1986

R. H. JUDGE, D. C. MOULE, and J. D. GODDARD. Can. J. Chem. **65**, 2100 (1987).

The 270 nm absorption spectra of thioformamide, $CHSNH_2$ and $CHSND_2$, have been photographically recorded under conditions of long path length (88 m) and moderate resolution (7.5 Å/mm). The absorption was assigned to the electron promotion, $n_S \rightarrow \pi^*$ (CS), and to the electronic transition, $\tilde{A}\,^1A'' \leftarrow \tilde{X}\,^1A'$. The spectra proved to be complex, highly congested and somewhat diffuse which limited the extent of the vibrational assignments. Progressions in five members were observed in both $CHSNH_2/CHSND_2$ in intervals of 516/496 cm^{-1} which were assigned to ν_{10}, the out-of-plane aldehyde wagging mode. It was concluded on Franck–Condon grounds that the $\tilde{A}\,^1A''$ molecule was non-planar at the aldehyde center. Structures and vibrational frequencies were calculated for the $\tilde{X}\,^1A'$ and the $\tilde{a}\,^3A''$ electronic states at the 3-21G* SCF level. The calculations confirmed that the lower state was strictly planar and predicted that both the aldehyde and amino groups were pyramidal in the upper electronic state.

R. H. JUDGE, D. C. MOULE et J. D. GODDARD. Can. J. Chem. **65**, 2100 (1987).

Utilisant des conditions de grandes longueurs de passage (88 m) et de résolutions modérée (7,5 Å/mm), on a procédé à un enregistrement photographique des spectres d'absorption à 270 nm du thiformamide, du $CHSNH_2$ et du $CHSND_2$. On a attribué l'absorption à une promotion électronique $n_S \rightarrow \pi^*$ (CS) et à une transition électronique $\tilde{A}\,^1A'' \leftarrow \tilde{X}\,^1A'$. Il s'avère que le spectre est complexe, qu'il est très congestionné et assez diffus; ceci limite le degré des attributions vibrationnelles. Tant dans le $CHSNH_2$ que dans le $CHSND_2$, on a observé des progressions dans cinq membres, à des intervalles de 516/496 cm^{-1}, que l'on a attribué à la vibration ν_{10}, le mode d'oscillation hors-plan du groupement aldéhyde. En se basant sur la théorie de Franck–Condon, on en conclut que la molécule $\tilde{A}\,^1A''$ n'est pas planaire au niveau du carbone aldéhydique. On a calculé les structures et les fréquences vibrationnelles des états électroniques $\tilde{X}\,^1A'$ et $\tilde{a}\,^3A''$ au niveau de champ auto-cohérent 3-21G*. Les calculs ont permis de confirmer que l'état d'énergie le plus bas est strictement plan et de prédire que le groupement aldéhyde ainsi que le groupement amino sont de nature pyramidale à l'état électronique élevé.

[Traduit par la revue]

Introduction

The electronic spectra which result from excitations within the amide chromophore have been extensively studied (1). A disappointing feature of these spectra is that the band systems lie in the far and vacuum uv regions. Moreover, they are diffuse and thus not amenable to detailed vibronic analyses. When the oxygen is replaced by sulphur, the situation improves considerably. In the case of thioformamide, Tsuboi *et al.* (2) found three absorption systems in the accessible region of the spectrum. The first absorption which they observed at 190 nm was assigned as a $\pi(C{=}S) + n_N \rightarrow \pi^*(C{=}S)$ electron promotion. A second system at 230 nm which contained discrete vibrational fine structure was analyzed in some detail and assigned to n_N-$\pi(C{=}S) \rightarrow \pi^*(C{=}S)$ excitation. The third system at 270 nm was described as weak and very broad and was given the assignment $n_S \rightarrow \pi^*(C{=}S)$. When the thioformamide molecule is considered from the viewpoint that it represents an extension in a series of thiocarbonyl molecules, which begins with the prototype CH_2S, an immediate complication to the electronic configuration is the presence of an a'' electron pair formally on the nitrogen atom. In the simplest of localized orbital pictures, these electrons would be contained in a second nonbonding orbital, in this case, n_N-$\pi(C{=}S)$. The photoelectron spectrum (2) of thioformamide shows that the ease of ionization of the two nonbonding pairs n_S and n_N-$\pi(C{=}S)$ is nearly the same, 8.70 and 9.30 eV, respectively. The lack of extensive Franck–Condon activity associated with the first photoelectron transition shows that n_S is essentially nonbonding. Promotion of an electron from either of the orbitals to the $\pi^*(C{=}S)$ orbital would give rise to two $n \rightarrow \pi^*(C{=}S)$ transitions. The first of these would be the $\tilde{A}\,^1A''$ (n_S, $\pi^*(C{=}S)$) $\leftarrow \tilde{X}\,^1A'$ transition which occurs at 270 nm, the second $\tilde{B}\,^1A'$ (n_N-$\pi(C{=}S)$, $\pi^*(C{=}S)$) $\leftarrow \tilde{X}\,^1A'$ at 230 nm. We decided to make a study of the system at 270 nm since the $n_S \rightarrow \pi^*$ transitions in thiocarbonyl molecules often generate spectra which are vibrationally discrete. As the compound is a solid at room temperature, its vapour pressure is relatively low and long path lengths of the vapour are required. In order to obtain a better understanding of the electronic assignments and particularly as an aid to the assignments of the vibronic intervals, the geometries of the $\tilde{X}\,^1A'$ and $\tilde{a}\,^3A''$ states (Fig. 1) and the vibrational frequencies were evaluated by *ab initio* techniques at the 3-21G* SCF level.

The molecular structure of thioformamide has been fully determined in the lower $\tilde{X}\,^1A'$ state by microwave spectroscopy. From a study of seven isotopic species, Sugisaki *et al.* (3) demonstrated that the thioformamide molecule is planar. Vibrational frequencies for the NCS bending and amino wagging modes were also established from relative intensity measurements of the satellite microwave lines. Infrared measurements

[1]Present address: Department of Chemistry, University of Wisconsin–Parkside, Kenosha, WI 53141–2000, U.S.A.

Can. J. Chem. Downloaded from www.nrcresearchpress.com by 213.166.140.6 on 09/07/12
For personal use only.

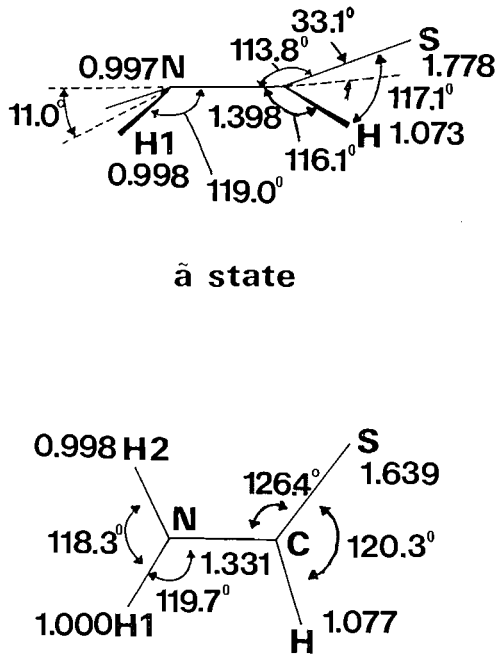

FIG. 1. The structures of $CHSNH_2$ in the $\tilde{X}$ ground electronic state and the $\tilde{a}$ first triplet excited state.

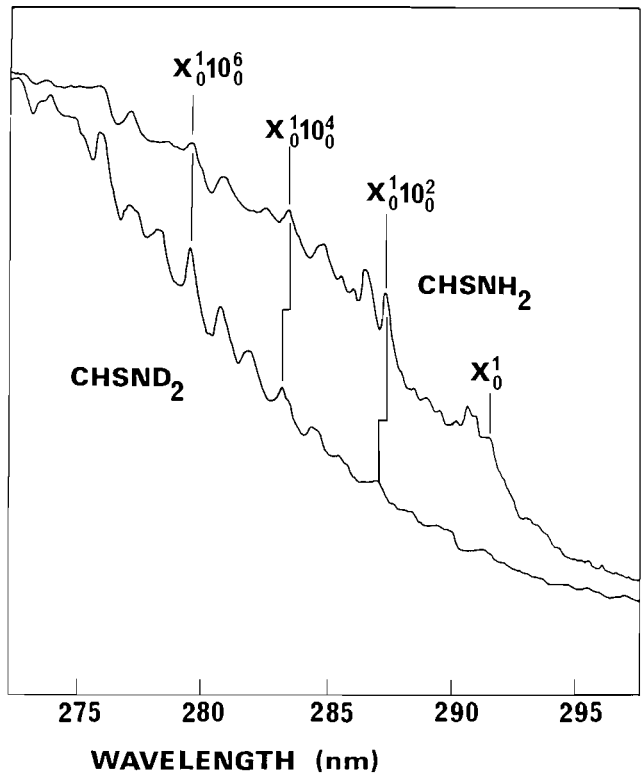

FIG. 2. Microdensitometer traces of the spectra of (*a*) $CHSNH_2$ and (*b*) $CHSND_2$.

have been made on crystal samples of $CHSNH_2$ and $CHSND_2$ by Susuki (4). The complete assignment of the twelve normal modes of vibration was aided by a normal coordinate analysis in which the Urey–Bradley force constants were transferred from similar molecules.

Experimental methods

Thioformamide was prepared by the method of Willstäter and Werth (9). To 100 g of formamide in an ice–salt bath, 50 g of powdered P_2S_5 was added slowly with vigorous stirring over a 2 h period. At the end of this time, 500 mL of absolute ether was added and the mass stirred for an additional 24 h at room temperature. The ethereal solution was decanted and the sticky residue repeatedly washed with ether. The extracts were combined and the solvent was stripped off under reduced pressure (water aspirator). The thioformamide remained as a red–orange oil.

The raw thioformamide was dissolved in H_2O (thus forming the hydrate) and any suspended sulphur removed by filtration. Ether was added and the hydrated thioformamide salted out by saturating the water layer with $(NH_4)_2SO_4$. Addition of P_2O_5 to the ether solution converted the hydrated thioformamide to free thioformamide, the solution was filtered, concentrated, and then cooled to −25°C. When cold petroleum ether (−25°C) was added, white crystals precipitated from solution. These crystals were filtered, washed with cold solvent, and dried in a vacuum desiccator for 30 min. The yield was 10 g of pure thioformamide, mp 26–27°C. The product was stored at −20°C until required.

A small amount of solid thioformamide was placed in a 2 m glass multiple reflection cell set to 44 traversals. The cell was evacuated and then allowed to reach saturation vapour pressure of the solid at 20°C. Spectra were recorded on Kodak Spectrum Analysis No. 1 film using a 1.5 m Bausch & Lomb Spectrograph with a dispersion of 15Å mm. A 1000 W Xe arc supplied the continuum and lines from a Fe/Ne hollow cathode tube were used for calibration. A Joyce–Lobel microdensitometer was used to obtain the tracings displayed in Fig. 2. Frequencies were obtained from the tenfold enlargements of the photographic films.

The deuterated thioformamide was obtained by the lyophilization of thioformamide in D_2O. The spectrum of $CHSND_2$ was obtained by conditioning the absorption cell with D_2O before introducing the sample of $CHSND_2$.

Computational methods

All computations were performed with the GAUSSIAN82 program system (10). Geometries for the ground and lowest excited triplet electronic states were optimized at the SCF level (UHF for the triplet state) using analytic gradient methods and the 3-21G* basis set (11, 12). Although it is the singlet $n_S \rightarrow \pi^*(C{=}S)$ state which has been observed in the experiments, the calculations focussed on the companion triplet principally due to the computational ease of an UHF approach. The modelling of the structures and vibrational frequencies of a $^1n\pi^*$ state by the $^3n\pi^*$ companion cannot produce results of extraordinarily high accuracy. However, the conclusion that such a model is certainly a very reasonable one is supported by experimentally based comparisons of the $^1n\pi^*$ and $^3n\pi^*$ states of formaldehyde or thioformaldehyde (13). For example, the structural parameters for H_2CO ($^1n\pi^*//^3n\pi^*$) are r(CO) 1.323//1.307, r(CH) 1.098//1.084, ∝(HCH) 118.4°//121.8° and ρ(oop) 34.0°//41.1°. For H_2CS the vibrational frequencies (cm^{-1}) in the $\tilde{A}\,^1A_2$ state in comparison with the $\tilde{a}^3A_2$ state are ($^1n\pi^*//^3n\pi^*$) (13): $\nu_2(a_1)$ 1316//1320, $\nu_3(a_1)$ 861.6//820, and $\nu_6(b_2)$ 799//762.3. Harmonic vibrational frequencies were computed using analytical second derivatives (14*a*) and then scaled by 0.90 (to approximately correct for both the SCF method and anharmonicity (14*b*)) prior to comparisons with experiment. The vertical excitation energies to the lowest $^3A'$ and $^3A''$ states at the ground state geometry as well as the

Can. J. Chem. Downloaded from www.nrcresearchpress.com by 213.166.140.6 on 09/07/12
For personal use only.

TABLE 1. The observed and calculated structure of thioformamide in the $\tilde{X}\,^1A'$ electronic state (in Å and degrees)

	Microwave[a] r_s	3-21G* SCF r_e
CS	$1.626_2 \pm 0.002$	1.639
C—N	$1.358_2 \pm 0.003$	1.331
C—H	$1.09_6 \pm 0.08$	1.077
N—H_1	$1.001_8 \pm 0.006$	1.000
N—H_2	$1.006_5 \pm 0.003$	0.998
NCS	126.65 ±5	126.44
NCH	108.08 ±5	113.27
CNH_1	117.92 ±0.67	119.71
CNH_2	120.37 ±0.50	121.96
H_1NH_2	121.70 ±0.67	118.33
μ_{tot}(D)	4.01 ±0.03	5.025

[a]From ref. 3.

adiabatic energy difference to the nonplanar ^3A state derived from the $^3A''$ one were computed using the 6-31G* basis set (12, 15) and including electron correlation effects by full fourth order Moller–Plesset perturbation theory (MP4SDTQ) (16).

Results and assignments

The equilibrium structure and vibrational frequencies of ground state $CHSNH_2$ and $CHSND_2$ were calculated by *ab initio* methods at the 3-21G* SCF level. Table 1 presents the results of the structural calculations for the $\tilde{X}\,^1A'$ state along with the bond lengths and bond angles derived from microwave analyses (3). The calculated values are strictly r_e quantities where each of the nuclei are at the bottoms of their potential wells while the results of the microwave analyses are r_s substitution quantities (20) and usually $r_e < r_s$. The agreement is satisfactory with the largest difference in a bond length being 0.027 Å for C—N. At this level of computation, thioformamide was found to be strictly planar at the nitrogen centre. The computed total dipole moment is ~25% greater than experiment as is often the case with such calculations (e.g. ref. 17).

Table 2 gives the calculated vibrational frequencies for $CHSNH_2$ and $CHSND_2$ and makes a comparison to the observed crystal phase ir data and the vibrational frequencies derived from microwave intensities (3, 4). When the calculated SCF harmonic vibrational frequencies are scaled by 0.90 to approximately correct for the SCF method and for anharmonicity, the agreement with the observed data is reasonable for the small amplitude vibrations. For 21 comparisons the average absolute deviation is 47 cm^{-1}. As would be expected the torsional frequencies, ν''_{12} = 551 cm^{-1} $CHSNH_2$ or 410 cm^{-1} $CHSND_2$, are too high relative to the observed frequencies (393/293 cm^{-1}) since the torsional functions should be highly anharmonic and not adequately described by the harmonic oscillator approximation.

The weak absorption system observed at 270 nm proved to have a complex vibrational fine structure and could not be assigned without some assistance from theory. Clearly, it would be most desirable to have a knowledge of the $\tilde{A}\,^1A''$ excited state geometry. The vibrational modes active in the spectrum would be those which have coordinates (bond lengths and bond angles) undergoing the greatest changes upon electronic excitation. In order to employ the UHF method, the properties of the companion state $\tilde{a}^3A''$ were calculated rather than those of the $\tilde{A}\,^1A''$ state. These states are expected to be close in energy and should be rather similar in their structure and dynamics. At the geometry of the ground state molecule, restricted open shell SCF calculations indicated that the $^1n\pi^*$–$^3n\pi^*$ splitting was only about 1300 cm^{-1}.

A number of higher level calculations were carried out at the 3-21G* SCF geometries to determine the vertical and adiabatic excitation energies to the lowest triplet state. The best calculations involved the 6-31G* basis set and included electron correlation effects (MP4SDTQ). The vertical excitation energy to the $\tilde{a}^3A''$ state was calculated to be 28183 cm^{-1} and the adiabatic energy gap 23596 cm^{-1}. Thus relaxation of the geometry in the triplet state lowers the energy by 4587 cm^{-1} or 13.1 kcal mol^{-1}.

TABLE 2. Observed and calculated vibrational frequencies (cm^{-1}) and rotational constants (GHz) of the $\tilde{X}\,^1A'$ electronic state of thioformamide

		$CHSNH_2$				$CHSND_2$		
Mode	Description	Unscaled	Scaled	Obs.[a]	Description	Unscaled	Scaled	Obs.[a]
a' 1	NH_2 asym. stretch	3867	3480	3287	CH_x stretch	3298	2968	2905
2	NH_2 sym. stretch	3472	3368	3165	ND_2 asym. stretch	2864	2578	—
3	CH_x stretch	3297	2967	2905	ND_2 sym. stretch	2703	2433	2290
4	NH_2 bend	1828	1647	1612	CH_x bend	1588	1429	1470
5	CH_x bend	1606	1445	1443	ND_2 bend	1451	1306	1328
6		1397	1257	1325		1258	1132	1128
7		1274	1147	1125		1130	1017	994
8	CS stretch	930	837	843	CS stretch	838	754	760
9	NCS bend	476	428	457[b]	NCS bend	429	386	400[b]
a'' 10	CH_x bend	1112	1001	985	CH_x bend	1098	988	959
11	NH_2 wag	805	725	670	ND_2 wag	641	577	552
12	NH_2 torsion	612	551	393[b]	NH_2 torsion	455	410	293[b]
	A_e	64.14587				53.67054		
	B_e	6.08227				5.51520		
	C_e	5.55551				5.00126		

[a]From ref. 4.
[b]From ref. 3.

Can. J. Chem. Downloaded from www.nrcresearchpress.com by 213.166.140.6 on 09/07/12
For personal use only.

Can. J. Chem. Downloaded from www.nrcresearchpress.com by 213.166.140.6 on 09/07/12
For personal use only.

TABLE 3. The calculated structure of thioformamide in the $\tilde{a}^3A''$ electronic state (in Å and degrees)

	3-21G* SCF r_e
C—S	1.778
C—N	1.398
C—H	1.073
N—H_1	0.998
N—H_2	0.997
NCS	113.80
NCH	116.07
SCH	117.14
CNH_1	119.04
CNH_2	119.71
HNHoop	11.0
CSoop	33.10
μ_{tot}(D)	2.336 D

Table 3 gives the equilibrium geometry for the upper state and Table 4, the vibrational frequencies. In the $\tilde{a}^3A$ state derived from the lowest $^3A''$ state, thioformamide is predicted to be nonplanar at both the nitrogen and carbon centres. The angle formed between the CHN frame and the CS bond is calculated to be 33.10°. For comparison, the calculated CS out-of-plane angle in triplet HFCS is 35.2° (18). (The structures of $CHSNH_2$ in the two combining states are illustrated in Fig. 1.) In thioformamide, inversion motion in the ν_{10} wag between the two nonplanar equilibrium configurations should be possible. The calculated height of the potential barrier at the 6-31G* MP3 level (with planarity imposed at C but other geometrical parameters relaxed at the 3-21G* SCF level) relative to the equilibrium structure of Table 3 is calculated to be 992 cm^{-1}. On Franck–Condon grounds ν'_{10} should be very active in forming strong progressions in the spectrum. Tables 2 and 4 predict that the frequency of this mode should drop from 1001 to 599 cm^{-1} upon electronic excitation of $CHSNH_2$. In $CHSND_2$, the decrease is from 988 to 596 cm^{-1}. The dynamics of the nitrogen centre are also of interest. Upon excitation, the two low-lying out-of-plane vibrational modes described as nitrogen wagging, ν''_{11} = 725 cm^{-1}, and NH_2 torsion, ν''_{12} = 551 cm^{-1} decrease to ν'_{11} = 280 cm^{-1} and ν'_{12} = 257 cm^{-1}. These changes could be the result of a broadening and flattening of these potentials in the upper state perhaps to the extent that they can no longer be described well in the harmonic approximation. Both ν'_{11} and ν'_{12} would be better treated as coupled large amplitude motions and would be expected to be active. The other significant structural change is the elongation of the CS bond. The calculation indicates that the CS bond in the excited triplet state is longer than that in the ground state by 0.139 Å. The magnitude of this lengthening is probably somewhat overestimated (19). However, the thiocarbonyl stretch, ν'_8, also should be active in the spectrum.

Microdensitometer traces of the many banded spectra of $CHSNH_2$ and $CHSND_2$ are given in Fig. 1. The observed bandheads are collected together in Table 5. It is clear that the spectra are highly congested and that the $CHSNH_2$ traces are more complex than those of $CHSND_2$. For this reason we turn first to the $CHSND_2$ spectra. The foregoing theoretical discussion indicates that the major change in structure occurs at the thiocarbonyl end of the molecule where the thiocarbonyl bond is distorted by 33.1° from the molecular plane. This is accompanied by a reduction in frequency of ν'_{10} from 988 to 596 cm^{-1}. The most prominent feature in the spectrum should be a progression in a frequency of about 600 cm^{-1}. This is precisely what is observed in the $CHSND_2$ spectra: namely, a progression of bands which form intervals of 496, 497, 490, and 496 cm^{-1}. These bands can immediately be assigned to the activity of the out-of-plane sulphur wagging mode. The assignment of the lower vibrational quantum number $v'' = 0$ follows from the large value of ν''_{10} (hot bands in this mode can be excluded.) The assignment for the numbering of ν' is more difficult. At this time only a provisional assignment is possible and this comes from the value of the origin isotope shift calculated from the theoretical vibrational frequencies (of the triplet) and from a comparison of the spectra of the two isotopes.

TABLE 4. Calculated vibrational frequencies (cm^{-1}) and rotational constants (GHz) of the $\tilde{a}^3A''$ electronic state of thioformamide[a]

		$CHSNH_2$			$CHSND_2$	
Mode	Description	Unscaled	Scaled	Description	Unscaled	Scaled
a' 1	NH_2 asym. stretch	3875	3488	CH_α stretch	3335	3002
2	NH_2 sym. stretch	3754	3379	ND_2 asym. stretch	2867	2580
3	CH_α stretch	3334	3001	ND_2 sym. stretch	2708	2437
4	NH_2 bend	1820	1638	CH_α bend	1438	1294
5	CH_α bend	1469	1322	ND_2 bend	1370	1233
6		1242	1118		1161	1045
7		1171	1054		991	892
8	CS stretch	760	684	CS stretch	711	640
9	NCS bend	443	399	NCS bend	361	325
a' 10	CH_α bend	665	599	CH_α bend	662	596
11	NH_2 wag	311	280	ND_2 wag	271	244
12	NH_2 torsion	286	257	ND_2 torsion	217	195
	A_e	47.03836			40.65406	
	B_e	5.89469			5.33405	
	C_e	5.32804			4.82978	

[a]Thioformamide in the $\tilde{a}$ state is treated as a nonrigid molecule which is characterized by the point group $G(2)$ which is isomorphous with C_s.

Can. J. Chem. Downloaded from www.nrcresearchpress.com by 213.166.140.6 on 09/07/12
For personal use only.

TABLE 5. Observed bandheads and some assignments of the vibronic transitions in the 270 nm absorption system of $CHSNH_2$ and $CNSND_2$ (cm^{-1})

	$CHSNH_2$		$CHSND_2$
$X_0^1 0_0^0$	34222	$X_0^1 10_0^2$	34779
	34313		34830
	34367		34893
	34454		34983
$X_0^1 10_0^2$	34738		35128
	34836	$X_0^1 10_0^4$	35276
	34895		35486
	34956		35623
	35036	$X_0^1 10_0^6$	35773
	35081		35910
$X_0^1 10_0^4$	35256		35938
	35350		36043
	35396		36106
	35597	$X_0^1 10_0^8$	36264
$X_0^1 10_0^6$	35771		36379
	36052		36541
	36216		36599
$X_0^1 10_0^8$	36273		36759
	36398		

A set of bands in the spectrum of the other isotope, $CHSNH_2$, can be grouped into a progression in intervals of 516, 518, 514, and 503 cm^{-1}. These bands show a small but uniformly decreasing shift of 41, 19, 2.1, and -10.3 cm^{-1} with respect to the bands of the major progression in $CHSND_2$. The calculated origin isotope effect from Tables 2 and 4 is 69.5 cm^{-1} which places the X_0^1 suborigin one further quantum of ν'_{10} to lower energies. In $CHSNH_2$ this band is clearly observed at 34222 cm^{-1}. The assignments given to the two main progressions are shown in Table 5. The remaining bands in the two spectra are more difficult to assign. Part of the reason for this is that the band patterns in $CHSNH_2$ and $CHSND_2$ are so different that vibrational correlations cannot be easily made. As the effect of deuterating at the nitrogen end of the molecule grossly changes the vibrational fine structure it follows that the ν_{11} and ν_{12} wagging and torsional modes must be active in the spectrum. On Franck–Condon grounds this would be a consequence of a non-planar distortion of thioformamide at the nitrogen centre. Indeed, the calculations show that while the ground state is strictly planar, the nitrogen is pyramidal in the $\tilde{a}$ state. The angle between the plane defined by the CSN and the line bisecting the HNH angle is calculated to be 11.0°. The calculated vibrational frequencies also demonstrate that a distortion occurs at the nitrogen centre. For example, $\nu'_{12}/\nu''_{12} =$ 551/257 cm^{-1} is calculated for $CHSNH_2$ and 410/195 cm^{-1} for $CHSND_2$. Since the excited state potential for this mode undoubtedly contains a double minimum it follows that the harmonic approximation used in the calculations is not particularly reliable. For this reason the complex structure which was attributed to out-of-plane wagging or torsion was not assigned.

The underlying continuum absorption results from several factors. The output of the Xe arc source decreases rapidly with decreasing wavelength as does the response of the film. In addition, the calculations suggest that the gross structural changes lead to long Franck–Condon induced progressions. Such progressions are expected to be complex and highly conjested and could create a quickly rising background continuum.

Discussion

Three absorption systems are observed in the vapour phase spectra of $CHSNH_2/CHSND_2$: a weak system at 270 nm, a moderately intense and structured system at 230 nm and a very strong continuum at 190 nm. Tsuboi *et al.* (2) assigned these spectra, respectively to the electronic promotions $n_S \rightarrow \pi^*$ (CS), $n_N \rightarrow \pi^*$ (CS), and π (CS) $\rightarrow \pi^*$ (CS). Their analyses of the vibrational structure which is contained in the 230 nm system are consistent with the assignment $n_N \rightarrow \pi^*$ (CS). This system is found to have a strong O_0^0 origin band, and only moderate activity in the in-plane stretching and bending modes. In particular, the spectrum does not display bands which can be attributed to conformational distortion. That is, the symmetry of the $\tilde{B}\,^1A'$ state is that of the $\tilde{X}\,^1A'$ ground state and the molecule is strictly planar in both equilibrium configurations. This is to be expected for a transition which involves the removal of an electron from the n_N (a'') orbital and its insertion into a π^* (a'') orbital. The electron configuration for the excited state could be described as $H_2N^+CHS^-$. The positive charge stabilizes the nitrogen center in the planar form.

Experimental difficulties prevented us from obtaining a definitive assignment of the vibrational fine structure in the $n_S \rightarrow \pi^*$ (CS) system. The major problem was a lack of (pressure × path length) and as a consequence the weak bands at longer wavelengths were poorly defined. This is partly because the sample is unstable in the vapour phase. Moreover, $CHSNH_2$ is a solid at room temperature and must be observed at its sublimation vapour pressure. The other difficulty is the spectrum. While the transition is allowed by electric dipole selection rules (out-of-plane polarized), it is forbidden by the local symmetry of the molecule. The excitation process may be considered to be a rotational displacement of the electron from the n_S to the π^* (CS) orbital rather than a translation. While this gives the transition a high magnetic dipole strength, the electric dipole strength is low. The other factor which complicates the analysis is that the origin is expected to be weak. This is a consequence of the formation of long progressions in the out-of-plane vibrational modes. Indeed, the bands which lie in the region of the vertical transition could be several orders of magnitude stronger than the 0_0^0 origin band. The 6-31G* MP4SDTQ calculations predict that the electronic origin in the $\tilde{a}^3A$ state is some 4587 cm^{-1} below the position of the vertical transition.

The bands in the thioformamide–H_2 spectra can be grouped into intervals of 516 cm^{-1} which drop to 496 cm^{-1} in the D_2 compound. The assignment to ν'_{10}, the hydrogen out-of-plane wagging mode follows from the calculated values for the two species 599/596. Activity in an out-of-plane wagging mode is only possible if the CHS group in the upper state is nonplanar. As a consequence, the potential function governing out-of-plane motion would contain double minima. Quanta of ν_{10} would be arranged into a state of +, − inversion doublet levels which are degenerate for energies well below the top of the barrier. As the intervals in $CHSNH_2$ are grouped into a progression of 516, 518, 514, 503 cm^{-1} which does not display any gross effects of inversion doubling, it follows that the height of the barrier governing aldehyde wagging is large. A high barrier height is not unexpected. In the series of molecules (5–8) $CHOCl/CHOF/CCl_2O$ and CF_2O the barrier heights to molecular inversion are 1609/2550/3170/8200 cm^{-1}, respectively. The variation in the barrier heights has been attributed to the inductive effect of the attached halogen atom. The NH_2 group is electronegative and would pull electron density onto the carbon atom, thereby destabilizing the planar form of the $\tilde{A}\,^1A''$ molecule.

Detailed experimental information about the dynamics and structure of the NH_2 group was limited by the diffuse and congested nature of the spectrum. Both the microwave and the *ab initio* calculations demonstrate that the $\tilde{X}\,A'$ ground state is rigidly planar. The calculated values of the ν_{11} and ν_{12} NH_2 wagging and torsional frequencies are 725 and 551 cm^{-1}. In the excited state $\tilde{A}\,^1A''$ state, the hydrogen atoms are predicted to be distorted from the plane of the molecule by 11°. As a result, the ν_{11} hydrogen wagging mode would be a molecular inversion. The barrier height for NH_2 inversion (6-31G* MP3), other variables relaxed at the 3-21G* SCF level, is calculated to be 792 cm^{-1}. That the spectra of $CHSNH_2$ and $CHSND_2$ are very different is an indication that NH_2 wagging and torsion are active in the spectrum. The calculated values for these modes are 280 and 257 cm^{-1} respectively.

Acknowledgement

Financial support of this work by the Natural Sciences and Engineering Research Council of Canada is acknowledged.

1. H. Basch, M. B. Robin, and N. A. Kuebler. J. Chem. Phys. **47**, 1201 (1967).
2. M. Tsuboi, A. Y. Hirakawa, T. Hoshino, T. Ishiguro, K. Kimura, and S. Katsumata. J. Mol. Spectrosc. **63**, 80 (1976).
3. R. Sugisaki, T. Tanaka, and E. Hirota. J. Mol. Spectrosc. **49**, 241 (1974).
4. I. Susuki. Bull. Chem. Soc. Jpn. **35**, 1286 (1962).
5. R. H. Judge and D. C. Moule. J. Mol. Spectrosc. **113**, 302 (1985).
6. G. Fisher and Y. Soreki. J. Mol. Spectrosc. **74**, 136 (1979).
7. D. C. Moule and P. D. Foo. J. Chem. Phys. **55**, 1262 (1971).
8. R. H. Judge and D. C. Moule. J. Chem. Phys. **78**, 4806 (1983).
9. R. Willstäter and T. Werth. Ber. Deut. Chem. Ges. **42**, 1908 (1909).
10. J. S. Binkley, M. Frisch, K. Raghavachari, D. DeFrees, H. B. Schlegel, R. Whiteside, E. Fluder, R. Seeger, and J. A. Pople. GAUSSIAN82. Department of Chemistry, Carnegie-Mellon University, Pittsburgh, PA. 1983.
11. J. S. Binkley, J. A. Pople, and W. J. Hehre. J. Am. Chem. Soc. **102**, 939 (1980).
12. (*a*) M. S. Gordon, J. S. Binkley, J. A. Pople, W. J. Pietro, and W. J. Hehre. J. Am. Chem. Soc. **104**, 2797 (1982); (*b*) M. M. Francl, W. J. Pietro, W. J. Hehre, J. S. Binkley, M. S. Gordon, D. DeFrees, and J. A. Pople. J. Chem. Phys. **77**, 3654 (1982).
13. (*a*) D. J. Clouthier and D. A. Ramsay. Ann. Rev. Phys. Chem. **34**, 31 (1983); (*b*) T. Suzuki, S. Saito, and E. Hirota. J. Chem. Phys. **79**, 1641 (1983).
14. (*a*) J. A. Pople, R. Krishnan, H. B. Schlegel, and J. S. Binkley. Int. J. Quantum Chem. **13S**, 225 (1979); (*b*) J. A. Pople, H. B. Schlegel, R. Krishnan, D. J. DeFrees, J. S. Binkley, M. J. Frisch, R. A. Whiteside, R. F. Hout, and W. J. Hehre. Int. J. Quantum Chem. **15S**, 269 (1981).
15. P. C. Hariharan and J. A. Pople. Theoret. Chim. Acta, **28**, 213 (1973).
16. R. Krishnan, M. J. Frisch, and J. A. Pople. J. Chem. Phys. **72**, 650 (1980) and references therein.
17. S. Green. Adv. Chem. Phys. **25**, 179 (1974).
18. A. Kapur, R. P. Steer, and P. G. Mezey. J. Chem. Phys. **70**, 745 (1979).
19. J. D. Goddard. Can. J. Chem. **63**, 1910 (1985).
20. C. C. Costain. J. Chem. Phys. **29**, 864 (1958).

Can. J. Chem. Downloaded from www.nrcresearchpress.com by 213.166.140.6 on 09/07/12
For personal use only.

Effets de solvant sur les complexes par transfert de charge iode – composés thiocarbonylés

GEORGES GUIHENEUF,[1] JOSÉ-LUIS M. ABBOUD[2] ET WIDDED BOUAB
Laboratoire de chimie physique organique, Université Cadi Ayyad, BP S 15, Marrakech, Maroc

Reçu le 25 août 1986[3]

GEORGES GUIHENEUF, JOSÉ-LUIS M. ABBOUD et WIDDED BOUAB. Can. J. Chem. **65**, 2106 (1987).

Les effets de solvant sur divers complexes par transfert de charge iode – bases thiocarbonylées de stabilité variable ont été déterminés et sont comparés aux effets de solvant sur les complexes iode – composés carbonylés. L'inversion de l'effet des solvants donneurs de liaison hydrogène en passant d'une série à l'autre résulte du caractère dur des bases carbonylées et mou des bases thiocarbonylées.

GEORGES GUIHENEUF, JOSÉ-LUIS M. ABBOUD, and WIDDED BOUAB. Can. J. Chem. **65**, 2106 (1987).

The effects of solvents on different iodine – thiocarbonyl base charge-transfer complexes of variable stability have been examined and these are compared with the effects of solvents of the iodine – carbonyl compound complexes. There is an inversion of the effect of those solvents that can form hydrogen bonds on going from one series to the other, which is attributed to the fact that the carbonyl compounds are hard bases while the thiocarbonyl compounds are soft bases.

[Journal translation]

Introduction

Parmi les multiples facteurs qui gouvernent la stabilité des complexes par transfert de charge, le milieu : phase gazeuse ou solution exerce une influence déterminante (1). La nature du solvant, elle-même, modifie notablement les constantes de complexation. En général, ces valeurs diminuent lorsque la polarité du solvant augmente; c'est le cas, par exemple, pour les complexes entre un donneur d'électron et un accepteur π (2). Lorsque l'accepteur d'électron est la molécule d'iode, un changement de solvant peut, selon le donneur considéré, conduire aussi bien à un accroissement (3–7) qu'à une diminution (8–11) des constantes K_c de complexation. Ainsi pour le complexe entre l'iode et la *N,N* diméthylacétamide, K_c diminue de 15 $dm^3\ mol^{-1}$ (12) lorsque le solvant est l'heptane, à 1,4 $dm^3\ mol^{-1}$ avec le dichlorométhane (8). Au contraire, si l'on considère la complexation de l'iode avec la tétraméthylthiourée, la constante subit une forte augmentation de 13 000 $dm^3\ mol^{-1}$ dans l'heptane (3) à 49 000 $dm^3\ mol^{-1}$ dans CH_2Cl_2 (3).

Pour expliquer ces divergences dans les variations de K_c avec le solvant, Augdahl et coll. (3) ont émis l'hypothèse que le sens de l'effet de solvant dépend du pourcentage de transfert de charge dans l'état fondamental et donc de la grandeur de la constante de formation du complexe. Si le transfert de charge est faible (*N,N* diméthylacétamide par exemple) la constante décroît lorsque la polarité du solvant augmente (11). À l'inverse, si le complexe correspond à un transfert de charge élevé (tétraméthylthiourée) un solvant polaire stabilise le complexe et entraîne une forte augmentation de la constante d'équilibre. Le sens de variation de K_c avec la polarité du solvant dépendrait donc uniquement de la stabilité du complexe et par conséquence, pour un accepteur donné, de la basicité du donneur d'électron. Il est possible de tester la validité de ce modèle en étudiant l'effet des solvants sur les complexes de l'iode avec des composés thiocarbonylés dont la basicité est voisine de celle de la diméthylacétamide. Si l'hypothèse d'Augdahl et coll. est justifiée, on doit alors observer le même sens d'effet de solvant pour les bases carbonylées et thiocarbonylées.

1. Adresse pour la correspondance : Institut Universitaire de Technologie, B.P. 420, 44606 Saint-Nazaire CEDEX, France.
2. Adresse pour la correspondance : Instituto de Quimica Fisica «Rocasolano», C.S.I.C. Serrano, 119, 28006 Madrid, Espagne.
3. Révision reçue le 3 avril 1987.

TABLEAU 1. Constantes de formation K_c des complexes de l'iode avec le dithioester $C_4H_9CSSCH_3$ et le thiocamphre

Solvants	ε	K_c[a] ($C_4H_9CSSCH_3$)	K_c[a] (thiocamphre)
nC_7H_{16}	1,92	13,2 ± 1	141 ± 9
CCl_4	2,24	12,6 ± 0,4	152 ± 13
$CHCl_3$	4,80	17,7 ± 0,9	231 ± 8
C_6H_5Cl	5,62	20 ± 1	270 ± 12
CH_3CCl_3	7,53	20 ± 1	315 ± 20
CH_2Cl_2	8,93	24 ± 1	370 ± 36
o-$C_6H_4Cl_2$	9,93	31 ± 2	—
CH_2ClCH_2Cl	10,36	29 ± 1	474 ± 50

[a]En $dm^3\ mol^{-1}$, à 25°C, la reproductibilité correspond à un degré de confiance de 95%.

Résultats

Deux bases thiocarbonylées ont été retenues : le thiocamphre et le dithioester $C_4H_9CSSCH_3$. Les constantes de complexation du tableau 1 ont été calculées à partir des absorbances des bandes de l'iode libre et complexé qui se trouvent entre 400 et 520 nm. Les deux bases absorbent également dans ce domaine de longueur d'onde; une correction a été effectuée pour chaque solution. La méthode de calcul est celle de Rose et Drago ou une méthode dérivée (13).

Nous avons vérifié qu'il n'y avait pas précipitation du complexe dans les solvants apolaires et que les spectres n'évoluaient pas pendant la durée de l'expérience. Nous nous sommes également assurés de l'absence des ions I_3^- qui apparaissent fréquemment dans les milieux polaires et entraînent des erreurs importantes sur les valeurs des constantes.

Discussion

Parmi les solvants, aucun ne possède un caractère basique suffisant pour entrer en compétition avec les bases thiocarbonylées. La présence d'un ou deux atomes de chlore sur le noyau abaisse sensiblement la basicité du cycle aromatique du chloro ou de l'*ortho*-dichlorobenzène. Les constantes mesurées dans ces deux solvants ne révèlent pas une présence significative de complexe iode–solvant analogue au complexe iode–benzène (8).

Avec les bases thiocarbonylées étudiées nous constatons, comme pour les thioamides et les thiourées, une augmentation des valeurs de K_c avec la polarité du solvant, caractérisée par sa

Can. J. Chem. Downloaded from www.nrcresearchpress.com by 213.166.140.6 on 09/07/12
For personal use only.

TABLEAU 2. Constantes de complexation de I_2 avec $CH_3CON(CH_3)_2$ (DMA) et $HCON(CH_3)_2$ (DMF)

	Solvants					
	nC_7H_{16}	CCl_4	CH_2Cl_2	$CHCl_3$	C_6H_5Cl	o-$C_6H_4Cl_2$
K_c[a] (DMA...I_2) :	15[b]	6,9[c]	1,4[c]	0,6±0,3	7,3±1	8,7±1
K_c[a] (DMF...I_2) :	6,45[b]	2,9[d]	0,9$_5$±0,2	—	2,7±0,5	5,3±0,7

[a] K_c en $dm^3\ mol^{-1}$, à 25°C. La reproductibilité, indiquée uniquement pour les valeurs déterminées au cours de cette étude, correspond à un degré de confiance de 95%.
[b] Référence 12.
[c] Référence 8.
[d] Référence 21.

constante diélectrique. Nous pouvons donc immédiatement en conclure que le modèle d'Augdahl et coll. n'est pas satisfaisant : «*le sens de l'effet de solvant, diminution ou augmentation de la constante de complexation, n'est pas lié uniquement au pourcentage de transfert de charge dans l'état fondamental et à la grandeur de la constante d'équilibre*». Il apparaît au contraire comme une propriété qui dépend de la nature chimique du site donneur d'électron. Pour tous les donneurs d'électrons thiocarbonylés le sens de l'effet de solvant est identique, quel que soit la valeur de la constante d'association avec l'iode. Il faut donc rechercher ailleurs les raisons de l'inversion des effets de solvant entre les bases carbonylées et thiocarbonylées.

Il est indispensable, auparavant, de préciser la notion, souvent ambigüe, de polarité des solvants. Nous distinguerons les effets liés réellement à la polarité–polarisabilité de ceux qui dépendent des interactions spécifiques (14). Ces interactions, par liaison hydrogène ou transfert de charge, sont fonction de la basicité (ou de l'acidité) du solvant d'une part, de l'acidité (ou de la basicité) de l'accepteur et du donneur d'électron, d'autre part. Or les basicités relatives d'une série de donneurs d'électron dépendent de l'acide choisi comme référence; il est impossible de caractériser la basicité par un paramètre unique qui établirait une échelle intrinsèque des basicités (15, 16). Pour pallier cette difficulté, Pearson a proposé de distinguer entre acidité et basicité dures et molles (17). Ce modèle permet de prévoir les interactions privilégiées entre acides et bases possédant des caractères durs ou mous semblables. Nous avons pu expliquer, de cette façon, que les constantes d'association de l'iode (acide mou) avec les bases thiocarbonylées (bases molles) sont beaucoup plus grandes que les constantes d'association avec les bases carbonylées (bases plus dures) (18). L'inverse est observé avec les donneurs de liaison hydrogène (acides relativement durs) : par exemple, à 20°C, dans CCl_4, la constante d'association du phénol avec la diméthylacétamide est de 152 $dm^3\ mol^{-1}$ alors qu'elle n'est que de 12 $dm^3\ mol^{-1}$ avec la diméthylthioacétamide (19).

Jusqu'à présent, ces paramètres de dureté, ou de mollesse, n'ont pas été pris en considération lors de la comparaison des effets des solvants étudiés bien que ceux-ci soient donneurs de liaison hydrogène (CH_2Cl_2, $CHCl_3$) ou accepteur d'électron (CCl_4) (20). Compte tenu des observations précédentes nous prévoyons, dans le cadre de ce modèle, que les interactions par liaison hydrogène de CH_2Cl_2 et $CHCl_3$ sont privilégiées avec les bases les plus dures, c'est-à-dire les composés carbonylés. Elles sont, en revanche, faibles avec les bases thiocarbonylées. En conséquence, la composante prédominante de l'effet de CH_2Cl_2 ou $CHCl_3$ sur la stabilité des complexes iode – bases carbonylées est l'interaction par liaison hydrogène du solvant avec la base. Il en résulte, par rapport à l'heptane, une diminution de la constante de complexation avec l'iode. Au contraire, dans le cas des bases thiocarbonylées, l'incidence des liaisons hydrogène est négligeable; ce sont les effets de polarité–polarisabilité qui vont déterminer le sens de variation de la constante. Or le complexe avec l'iode possède, en raison du transfert de charge, un moment dipolaire plus important que celui du donneur libre ce qui conduit, puisque la polarité du solvant s'accroît de l'heptane à CH_2Cl_2 ou $CHCl_3$, à un terme énergétique favorable qui stabilise le complexe et augmente la constante. L'inversion du sens des effets de solvant est donc une conséquence de la dualité du caractère basique, mou et dur, des donneurs d'électron.

Plusieurs résultats confirment cette interprétation et la validité du modèle :

(*i*) Le chloroforme est un donneur de liaison hydrogène plus fort que le dichlorométhane, l'abaissement de la constante d'association iode – base carbonylée doit être plus importante avec le chloroforme. Conformément à cette précision, la constante de formation du complexe iode–diméthylacétamide est de 1,4 $dm^3\ mol^{-1}$ dans le dichlorométhane (8) et seulement de 0,6 $dm^3\ mol^{-1}$ dans le chloroforme (tableau 2).

(*ii*) CH_2Cl_2 ($\varepsilon = 8{,}93$) est plus polaire que $CHCl_3$ ($\varepsilon = 4{,}8$); la stabilisation des complexes iode–diméthylthioacétamide et iode–thiocamphre doit donc être plus forte dans CH_2Cl_2. Les valeurs expérimentales vérifient cet ordre : les constantes sont plus élevées dans CH_2Cl_2 que dans $CHCl_3$.

(*iii*) Les abaissements des constantes en passant de l'heptane au tétrachlorure de carbone sont importants avec les bases carbonylées; dans le cas des bases thiocarbonylées, les valeurs diffèrent peut entre les deux solvants. Ici encore, les résultats corroborent pleinement le modèle proposé. Le chlore, atome accepteur du CCl_4, est un site relativement dur, les complexes carbonyle–CCl_4 sont donc plus stables que les complexes thiocarbonyle–CCl_4. La compétition entre les deux complexes base–I_2 et base–CCl_4 est plus marquée dans le cas des bases carbonylées d'où les variations plus importantes qu'avec les bases thiocarbonylées.

(*iv*) Avec les solvants non donneurs de liaison hydrogène (CH_3CCl_3, ClC_6H_5, o-$Cl_2C_6H_4$, ...) les interactions polaires sont seules présentes, quel que soit la base. Elles conduisent à des augmentations des constantes de formation avec la polarité du milieu, indépendantes de la stabilité des complexes iode–thiocarbonyles.

Dans le cadre de ce modèle des effets de solvant et en se limitant aux solvants non donneurs de liaison hydrogène, nous attendons également une augmentation des constantes de complexation de l'iode avec la diméthylacétamide et la diméthylformamide lorsque la polarité du solvant s'accroît. Nous avons, pour ces deux amides, élargi la gamme de polarité

Can. J. Chem. Downloaded from www.nrcresearchpress.com by 213.166.140.6 on 09/07/12
For personal use only.

des solvants aux chloro et *ortho*-dichlorobenzène (tableau 2). Nous observons effectivement un accroissement régulier des valeurs K_c en passant de CCl_4 à ClC_6H_5 et o-$Cl_2C_6H_4$. Cependant, même dans ce dernier solvant, la valeur K_c est inférieure à celle de l'heptane. Il faudrait, pour retrouver une valeur identique, accroître encore la polarité du solvant, ce qui est difficile à réaliser expérimentalement : les ions I_3^- se forment alors très rapidement et interdisent une détermination significative de la constante. Lors de la formation du complexe, une molécule d'iode se substitue à une molécule de solvant dans la couche de solvatation, ce qui introduit sur le plan énergétique un terme de déstabilisation du complexe. Pour avoir une augmentation de la constante, il faut que la stabilisation due à l'interaction dipolaire du solvant avec le complexe compense le terme défavorable. Le pourcentage de transfert de charge peut alors intervenir; il doit être suffisant pour que l'interaction supplémentaire complexe–solvant l'emporte sur l'effet résultant de l'approche de l'iode. Ces deux facteurs antagonistes peuvent expliquer les variations observées dans le cas des bases carbonylées : diminution puis augmentation des constantes lorsque la polarité des solvants s'accroît. En l'absence de modèle autorisant une évaluation quantitative des diverses contributions nous devons nous limiter à l'interprétation qualitative fondée sur la dualité des caractères acides et basiques.

Nous retiendrons que les solvants polaires non donneurs de liaison hydrogène (*o*-dichlorobenzène, par exemple) stabilisent, en règle générale, les complexes par transfert de charge avec l'iode. Les solvants polaires donneurs de liaison hydrogène ($CHCl_3$), qui sont des acides durs au sens de Pearson, stabilisent également les complexes par transfert de charge de l'iode avec les bases molles (thiocarbonylées) car ils interviennent quasi exclusivement par leurs effets non spécifiques de polarité. En revanche, ces solvants déstabilisent les complexes de iode avec les bases dures (carbonylées) puisqu'ils entrent en compétition avec l'iode pour se complexer avec la base.

Partie expérimentale

Les mesures d'absorbance ont été réalisées sur un spectromètre Cary 219 équipé de cellules quartz de 1 cm. La température était maintenue constante, à 25°C, par une circulation d'eau à partir d'un cryostat Lauda K2R.

Le thiocamphre, préparé par action de P_4S_{10} sur le camphre (22) a été recristallisé dans un mélange eau–alcool puis chromatographié sur colonne de gel de silice (éluant : hexane). Il a ensuite été séché sous vide sur P_2O_5. Le dithioester $C_4H_9CSSCH_3$, obtenu par la méthode de Meijer *et al.* (23), a été purifié par distillations répétées.

Tous les solvants ont été purifiés avant usage (24) et séchés sur tamis moléculaires 4 Å.

1. K. M. C. Davis. *Dans* Molecular association. Vol. 1. *Edité par* R. Foster. Academic Press, New York. 1975.
2. J. P. Mouchet et Y. Rousset. J. Chim. Phys. **77**, 529 (1980).
3. H. Mollendal, J. Grundnes et E. Augdahl. Acta Chem. Scand. **23**, 3525 (1969).
4. E. Augdahl, J. Grundnes et P. Klaboe. Inorg. Chem. **4**, 1475 (1965).
5. F. A. Devillanova et G. Verani. Tetrahedron, **35**, 511 (1979).
6. I. Uruska. Spectrochim. Acta Part A : **36**, 639 (1980).
7. A. Suszka. J. Chem. Soc. Perkin Trans. 2, 531 (1985).
8. R. S. Drago, T. F. Bolles et R. J. Niedzielski. J. Am. Chem. Soc. **88**, 2717 (1966).
9. J. D'Hondt, C. Dorval et T. Zeeger-Huyskens. J. Chim. Phys. **69**, 516 (1972).
10. B. B. Bhowmik et S. P. Chattopadhyay. Spectrochim. Acta Part A : **36**, 543 (1980).
11. C. Dorval-Burnotte et T. Zeeger-Huyskens. Ann. Soc. Chim. Belg. **89**, 559 (1975).
12. C. Laurence, G. Guiheneuf et B. Wojtkowiak. J. Am. Chem. Soc. **101**, 4793 (1979).
13. R. Foster. Organic charge-transfer complexes. Academic Press, New York. 1969.
14. J. L. M. Abboud, R. W. Taft et M. J. Kamlet. J. Chem. Soc. Perkin Trans. 2, 815 (1985).
15. R. S. Drago, G. C. Vogel et T. E. Needham. J. Am. Chem. Soc. **93**, 6014 (1971).
16. C. Laurence, M. Queignec-Cabanetos, T. Dziembowska, R. Queignec et B. Wojtkowiak. J. Am. Chem. Soc. **103**, 2567 (1981).
17. R. G. Pearson. J. Am. Chem. Soc. **85**, 3533 (1963).
18. G. Guiheneuf, W. Bouab, J. L. M. Abboud et A. Boussaoud. Can. J. Chem. À paraître.
19. T. Gramstad et J. Sandstrom. Spectrochim. Acta Part A : **25**, 31 (1969).
20. J. M. Dumas, H. Peurichard et M. Gomel. J. Chem. Res. (S), 54 (1978).
21. R. S. Drago, D. A. Wenz et D. A. Carlson. J. Am. Chem. Soc. **84**, 1106 (1962).
22. J. W. Sheeren, P. H. J. Ooms et R. J. F. Nivard. Synthesis, 149 (1973).
23. J. Meijer, P. Vermeer et L. Brandsma. Recl. Trav. Chim. Pays-Bas, **92**, 601 (1973).
24. J. A. Riddick et W. B. Bunger. Organic solvents. Wiley–Interscience, New York. 1970.

Can. J. Chem. Downloaded from www.nrcresearchpress.com by 213.166.140.6 on 09/07/12
For personal use only.

La dissolution anodique du cuivre en présence d'ions F^- dans des solutions aqueuses acides

E. POTVIN, M. DROGOWSKA ET H. MÉNARD

Département de chimie, Université de Sherbrooke, 2500, Boul. Université, Sherbrooke (Québec), Canada J1K 2R1

ET

L. BROSSARD

Institut de Recherche de l'Hydro-Québec, P.O. Box 100, Varennes (Québec), Canada J0L 2P0

Reçu le 21 novembre 1986

E. POTVIN, M. DROGOWSKA, H. MÉNARD et L. BROSSARD. Can. J. Chem. **65**, 2109 (1987).

Nous avons étudié l'influence de l'ion F^- sur la dissolution anodique du cuivre dans des solutions aqueuses acides (pH 1,6–6), principalement à pH 5, en présence de KF 0,1 *M*. La nature des changements se produisant sur l'électrode durant l'oxydation a été mise en évidence par la voltampérométrie cyclique ainsi que par différentes techniques d'analyse de surface (SEM, XPS, AES). Afin d'établir le mécanisme d'oxydation électrochimique du cuivre à pH 5, des études avec l'électrode tournante à disque ont été menées dans des conditions où la dissolution du cuivre est généralisée. Aux pH 1,6–6, l'électrode de cuivre se dissout uniformément i.e. sans qu'il y ait de zones préférentielles sur la surface lorsqu'elle subit une polarisation potentiodynamique (10 mV s^{-1}) à des potentiels supérieurs à 0 V_{ECS}. À pH faiblement acide (pH 5, KF 0,1 *M*), lorsque le balayage du potentiel va jusqu'à +0,5 V, l'oxydation du cuivre débute par la corrosion généralisée de l'électrode suivi de la formation d'un film de Cu_2O non passivant; au fur et à mesure que le temps d'oxydation augmente, le courant diminue et l'électrode devient passivée. Un modèle de dissolution anodique est présenté pour les résultats obtenus à pH 5. Lorsqu'il y a corrosion uniforme de l'électrode tournante, le cuivre s'oxyde en ions Cu^{2+}. Lorsque $\omega \rightarrow 0$, la vitesse de dissolution de l'électrode est limitée par la diffusion de l'ion Cu^{2+} de l'électrode vers le coeur de la solution alors que lorsque $\omega \rightarrow \infty$, le processus de transfert de charge limite la cinétique de la dissolution.

E. POTVIN, M. DROGOWSKA, H. MÉNARD, and L. BROSSARD. Can. J. Chem. **65**, 2109 (1987).

The influence of F^- ions on the anodic dissolution of copper in aqueous acidic solutions (pH 1.6–6), mainly at pH 5 with 0.1 *M* KF, has been studied. The nature of the changes that occur on the electrode during the oxidation has been examined by cyclic voltamperometry as well as by different techniques of surface analysis (SEM, XPS, AES). To determine the mechanism of the electrochemical oxidation of copper at pH 5, studies with rotating disk electrodes have been carried out under conditions giving rise to a general dissolution of copper. At pH 1.6–6, the copper electrode dissolves uniformly, i.e., without preferential zones on the surface, when it is submitted to a potentiodynamic polarization (10 mV s^{-1}) at potentials above 0 V_{ECS}. At slightly acidic pH (pH 5, KF 0.1 *M*), with a sweep of potential up to +0.5 V, the oxidation of copper begins with a generalized corrosion of the electrode and it is followed by the formation of a film of Cu_2O that is not passivating; as the oxidation proceeds, the current drops and the electrode becomes passivated. One model for the anodic dissolution is presented for the results obtained at pH 5. When a uniform corrosion develops on the rotating electrode, the copper is oxidized to Cu^{2+} ions. When $\omega \rightarrow 0$, the rate of dissolution of the electrode is limited by the diffusion of the Cu^{2+} ions from the electrode to the solution, whereas when $\omega \rightarrow \infty$ the process of charge transfer is the limiting factor to the kinetics of the dissolution.

[Journal translation]

Introduction

Les travaux rapportés dans la littérature concernant la dissolution anodique du cuivre en solution aqueuse acide ont surtout été réalisés en présence des anions Cl^- (1–7) et SO_4^{2-} (8–16). Ces études ont démontré l'influence déterminante de l'anion en solution ainsi que la rôle clé joué par les complexes du cuivre dans les procédés d'oxydation de ce métal.

En ce qui concerne les ions fluorures, l'oxydation électrochimique du cuivre a été étudiée dans le HF anhydre (17). L'oxydation se produit en deux étapes soient la dissolution du cuivre en ion Cu^{2+} et la précipitation du CuF_2 sur l'électrode. À notre connaissance, la dissolution anodique du cuivre dans des solutions aqueuses légèrement acides contenant des ions F^- n'a pas été abordée dans la littérature.

De façon plus générale, la forme stable du cuivre dissous dans des solutions non complexantes comme les sulfates, les nitrates et les perchlorates est le Cu(II) alors que les espèces du Cu(I) sont stables dans des solutions complexantes comme les Cl^-, Br^-, I^- et l'ammoniaque (18). La dismutation de l'espèce Cu^+ est largement favorisée lorsque l'ion n'est pas stabilisé par la formation d'un complexe.

L'ion fluorure est peu complexant pour le cuivre. À la différence des autres halogénures, la thermodynamique prévoit que les composés et complexes du fluor avec le cuivre bivalent seront favorisés par rapport à ceux du cuivre monovalent (19–22).

Au cours de ce travail, nous avons étudié le comportement anodique du cuivre en solutions aqueuses acides (pH 1,6–6) en présence de KF 0,1 *M*, principalement à pH 5. La nature des changements se produisant sur l'électrode durant l'oxydation a été mise en évidence par la voltampérométrie cyclique, ainsi que par différentes méthodes d'analyse de surface (SEM, XPS et AES). Des essais avec l'électrode tournante à disque ont été menés à pH 5 dans des conditions où la dissolution du cuivre est généralisée afin d'établir le mécanisme d'oxydation électrochimique du cuivre.

Partie expérimentale

Une cellule électrochimique conventionnelle de verre, à trois compartiments, a été utilisée pour les pH 5 et 6 et une cellule de matériaux inertes au HF, à deux compartiments, pour les pH allant de 1,6 à 5.

L'électrode de travail est constituée d'un cylindre de cuivre (diamètre ~ 0,56 cm) coupé à partir d'une tige de cuivre polycristallin (Alpha-Ventron Corporation 99,99%) et scellé dans un tube de verre avec de la colle époxy ou dans une gaine de Kel F (pour l'électrode tournante). De cette manière une surface circulaire en position horizontale (~0,25 cm^2) est en contact avec la solution. La surface de l'électrode de cuivre a été polie mécaniquement sur une polisseuse

Can. J. Chem. Downloaded from www.nrcresearchpress.com by 213.166.140.6 on 09/07/12
For personal use only.

Can. J. Chem. Downloaded from www.nrcresearchpress.com by 213.166.140.6 on 09/07/12
For personal use only.

Leco avec une suspension de particules d'alumine de 5 à 0,3 μm puis nettoyée abondamment avec de l'eau triplement distillée.

Avant chaque essai, l'électrode est plongée en solution à un potentiel de −0,4 V pour réduire les oxydes se trouvant sur la surface; lorsque le courant atteint −0,4 μA cm^{-2}, l'électrode est jugée prête pour l'essai proprement dit.

L'électrode de référence est l'électrode au calomel saturé Hg/HgCl/KCl (sat) (E = 0,24 V_{ESH}); elle est séparée du compartiment principal par un pont qui est relié à un capillaire de Luggin. Aux pH inférieurs à 5, l'électrode de référence a été séparée du compartiment principal par un capillaire de Lugin de matériau inerte au HF. Les potentiels sont indiqués par rapport à cette électrode. L'électrode auxiliaire est une tige de carbone ou une grille de platine placée dans un 2e compartiment.

Pour les analyses de surface, les échantillons de cuivre ont été lavés après l'essai avec de l'eau tridistillée et du méthanol distillé puis scellés dans un tube de verre sous atmosphère d'azote pour être analysés. La pression résiduelle durant les analyses était de 5 × 10^{-8} Torr (1 Torr = 133,3 Pa). Les analyses par XPS ont été faites avec une source de Mg Kα de 480 W de puissance. Un canon à électrons de 10 kV a servi aux analyses par AES; le courant était de 4 nA.

Les solutions acides ont été préparées par un mélange de KF et de HF. Avant chaque essai, la solution a été désaérée par un barbottage d'azote. Les expériences ont été menées à 25°C.

Les essais en balayage linéaire de la tension ont été réalisés avec un potentiostat PAR modèle 173, contrôlé par un programmeur universel PAR modèle 175. Les charges ont été mesurées avec un coulomètre intégré PAR modèle 179 et le courant avec un ampèremètre Keithley modèle 177.

Résultats et discussion

La figure 1 montre un voltampérogramme réalisé dans une solution de HF 1 M (pH = 1,6) à une vitesse de balayage en tension de 10 mV s^{-1}. Le courant d'oxydation du cuivre est négligeable de −0,8 V jusqu'à ~0 V où la dissolution généralisée du cuivre est observée. En balayage inversé, le processus de réduction commence à un potentiel de ~0 V et un pic cathodique est formé. La charge anodique, Q_{ox} (~300 mC cm^{-2}), est beaucoup plus grande que la charge cathodique, Q_{red} (~20 mC cm^{-2}), ce qui est compatible avec la dissolution du cuivre en solution. Au cours de l'oxydation, la surface de l'électrode passe d'un éclat brillant à mat. La microscopie optique a révélé que ce changement est dû à une augmentation de la rugosité de la surface.

Un essai dans une solution de KF 0,1 M additionnée de HF (pH = 5), à une vitesse de balayage de 10 mV s^{-1}, est effectué sur une échelle de potentiel allant du dégagement de H_2 (~ −1,8 V) jusqu'à +2,8 V sans qu'il y ait formation apparente de O_2 (fig. 2). Le courant d'oxydation est négligeable jusqu'à ~0 V puis la dissolution généralisée commence. Au cours du balayage anodique, on voit apparaître un film sur l'électrode sans constater une baisse significative du courant d'oxydation. On observe la présence de deux zones de réduction distinctes; la première débute à ~ −0,1 V et la seconde à ~ −0,9 V.

Lorsque l'électrode est polarisée jusqu'à +0,5 V dans les mêmes conditions (fig. 3, ligne pleine), on voit à l'oeil nu qu'un film anodique se forme et un pic de réduction est présent; il débute autour de −0,8 V.

Dans une solution de KF 0,1 M (pH = 5) tamponnée avec le phtalate de potassium (P.P.) (fig. 3, ligne pointillée), un pic anodique est présent autour de +0,2 V; au-delà de ce potentiel, la dissolution généralisée de l'électrode a lieu. Aucun produit visible à l'oeil nu n'est observé sur le cuivre et l'électrode qui avait initialement un éclat métallique est devenue terne. Aucun pic cathodique n'est présent en balayage de retour avant le dégagement d'hydrogène. Ces courbes montrent une différence significative du comportement de l'anode de cuivre en solution

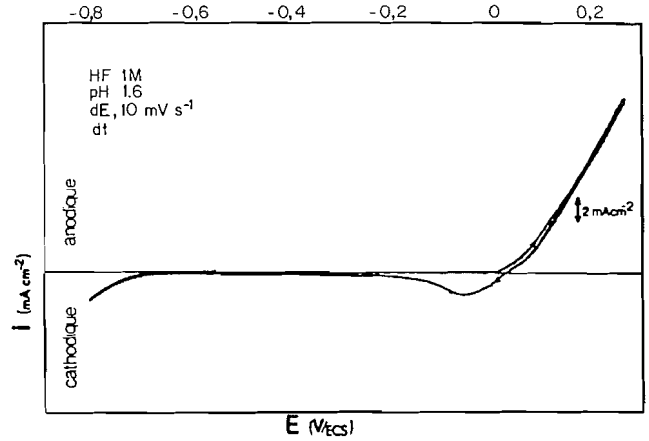

FIG. 1. Voltampérogramme dans une solution de HF 1 M, pH 1,6. dE/dt = 10 mV s^{-1}.

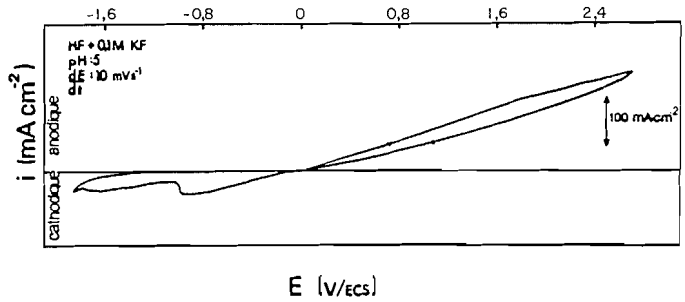

FIG. 2. Voltampérogramme dans une solution de KF 0,1 M à pH 5. dE/dt = 10 mV s^{-1}.

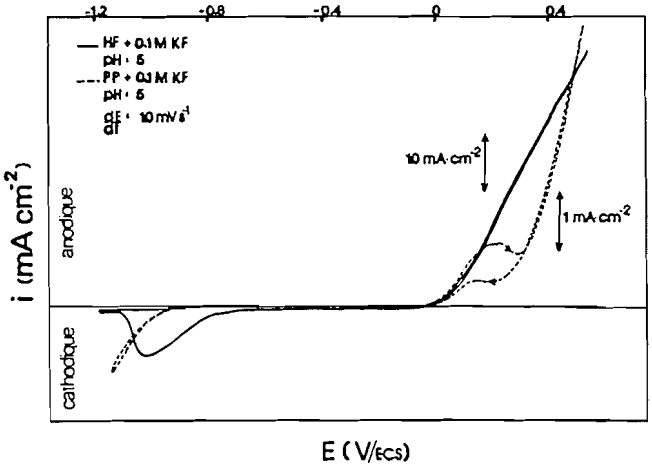

FIG. 3. Voltampérogrammes à pH 5, dans une solution de KF 0,1 M (—) et dans une solution de KF 0,1 M additionnée du tampon phtalate de potassium (---).

fluorurée selon qu'il y ait ou non du phtalate de potassium dissous. Il est en effet admis que le pouvoir complexant de l'ion phtalate par rapport au cuivre est supérieur à celui de l'ion fluorure (22). Pour cette raison, les analyses ont été effectuées dans des solutions de KF 0,1 M titrées avec HF aux pH désirés.

Dans une solution de KF 0,1 M (pH = 5), l'électrode a subi un balayage en tension de −0,8 à +0,5 V à une vitesse de 10 mV s^{-1}, suivi d'un arrêt du potentiel à +0,5 V durant plusieurs minutes. L'électrode de cuivre se recouvre peu à peu d'un film. En prolongeant l'oxydation au-delà d'une heure, la

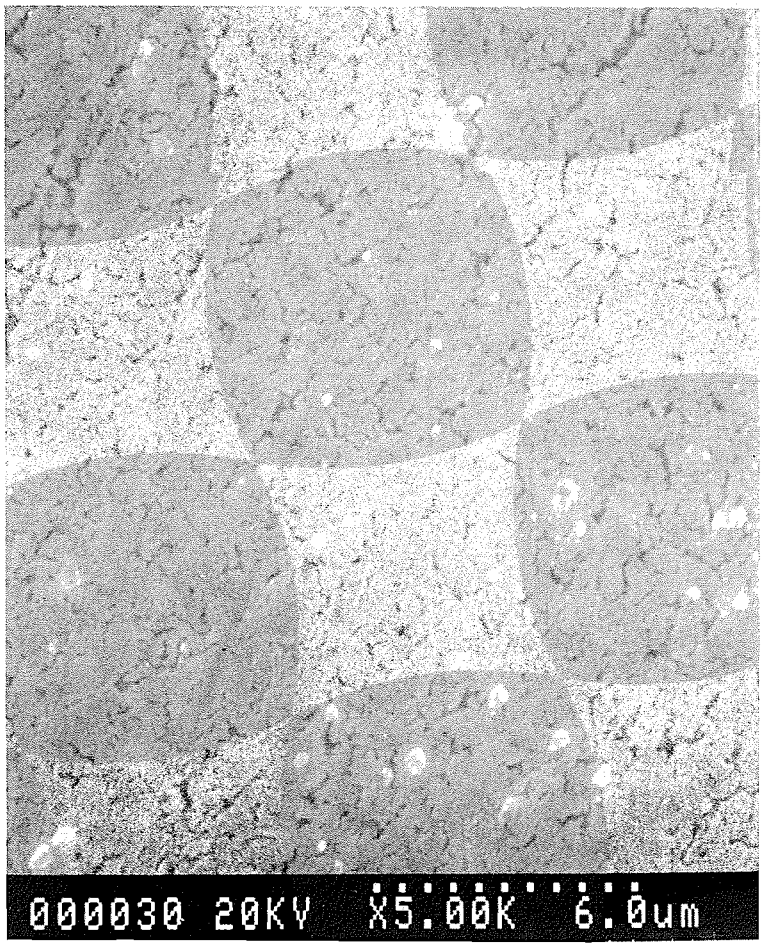

FIG. 4. Photographie par microscopie électronique à balayage du film anodique formé sur l'électrode de cuivre dans une solution de KF 0,1 *M* à pH 5. $dE/dt = 10\,mV\,s^{-1}$. Balayage de −800 à +580 mV; arrêt à +580 mV, 10 min.

surface est entièrement recouverte et la vitesse de dissolution du cuivre devient considérablement réduite.

La microscopie électronique à balayage (SEM) a été utilisée pour étudier la morphologie du film anodique généré sur une électrode qui a subi un balayage (10 mV s^{-1}) de −800 à +580 mV, avec un arrêt à ce dernier potentiel durant 10 min, dans une solution de KF 0,1 *M* à pH 5. Le film est poreux et il est composé d'un produit qui conduit mal le courant (fig. 4). Une analyse en spectroscopie des photoélectrons X (XPS) et en spectroscopie des électrons Auger (AES) a révélé que le film se compose de Cu_2O mais ne contient pas le composé fluoruré qui peut exister dans ces conditions à pH 5, i.e. le $3CuF_2 \cdot Cu(OH)_2$ (23).

Afin d'établir le mécanisme d'oxydation électrochimique du cuivre à pH 5, des études avec l'électrode tournante à disque ont été menées dans des conditions où la dissolution du cuivre est généralisée.

L'électrode est plongée dans une solution de KF (a_{F^-} = 0,074) ayant un pH de 5, avec un potentiel imposé de −0,4 V. Le courant est lu pour chaque vitesse de rotation allant de 81 à 4 rotations par seconde (rps). Une plage de potentiel de −0,05 à +0,05 V est couverte en effectuant des sauts de potentiel de +0,01 V. Les courbes i vs. $\omega^{1/2}$ (ω, vitesse de rotation angulaire de l'électrode en s^{-1}) sont montrées à la figure 5. Les courbes s'écartent d'une droite et ne passent pas par l'origine, ce qui indique que l'oxydation du cuivre est quasi réversible (24), i.e. limitée à la fois par le transfert de masse et par une réaction de surface.

Dans ce cas où le système est quasi réversible, il est possible de décomposer le courant total en deux termes associés à chaque processus lent comme suit :

$$[1] \quad i^{-1} = i_\infty^{-1} + i_{d,a}^{-1}$$

i_∞ : composante du courant indépendante de $\omega^{1/2}$-réaction de surface; et $i_{d,a}$: courant de diffusion-convective anodique qui obéit à l'équation de Levich, [2] :

$$[2] \quad i_{d,a} = 0{,}62nFAD^{2/3}\omega^{1/2}\gamma^{-1/6}(C^s - C^*) = B\omega^{1/2}$$

(réf. 24)

n : nombre d'électron; F : constante de Faraday; A : aire géométrique de l'électrode; D : coefficient de diffusion de l'espèce oxydée ($cm^2\,s^{-1}$); γ : viscosité cinématique ($cm^2\,s^{-1}$); ω : vitesse de rotation angulaire de l'électrode (s^{-1}); C^* : concentration de l'espèce qui diffuse dans la solution ($mol\,cm^{-3}$); C^s : concentration de l'espèce qui diffuse à la surface de l'électrode ($mol\,cm^{-3}$).

Les relations [1] et [2] conduisent à

$$[3] \quad i^{-1} = i_\infty^{-1} + B^{-1}\omega^{-1/2}$$

Les courbes i^{-1} en fonction de $\omega^{-1/2}$ doivent donner une droite pour chaque potentiel appliqué (fig. 6), dont les valeurs B^{-1} et i_∞^{-1} sont déterminables à partir de la pente et de l'ordonnée

Can. J. Chem. Downloaded from www.nrcresearchpress.com by 213.166.140.6 on 09/07/12
For personal use only.

Can. J. Chem. Downloaded from www.nrcresearchpress.com by 213.166.140.6 on 09/07/12
For personal use only.

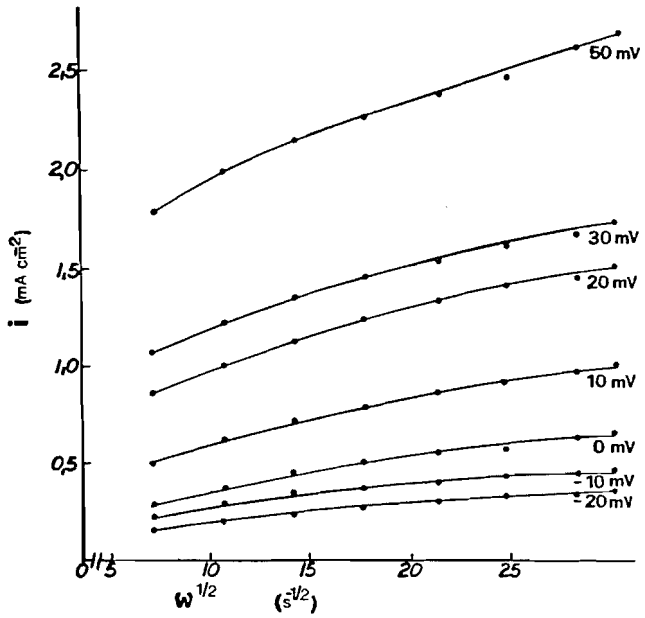

FIG. 5. Courbes $i = f(\omega^{1/2})$ pour différents potentiels appliqués. Solution KF–HF: $a_{F^-} = 0{,}074$, pH = 5.

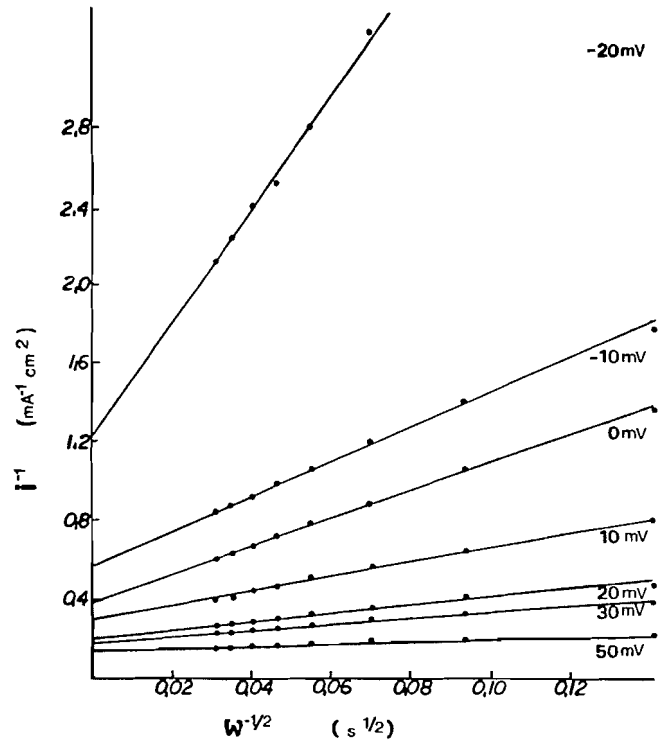

FIG. 6. Courbes $i^{-1} = f(\omega^{-1/2})$ pour différents potentiels appliqués. Solution KF–HF: $a_{F^-} = 0{,}074$, pH = 5.

à l'origine respectivement. L'inverse de la pente du graphique i^{-1} en fonction de $\omega^{-1/2}$ correspond à B, c'est-à-dire au produit, $i_{d,a}\omega^{-1/2}$ alors que i_∞^{-1} est obtenu par extrapolation de la droite jusqu'à $\omega^{-1/2}$ égale zéro. Les valeurs de B ou $i_{d,a}\omega^{-1/2}$ ont été déterminées pour différents potentiels. La relation log $i_{d,a}\omega^{-1/2}$ vs. E est linéaire (fig. 7, ligne pleine) et la pente moyenne obtenue pour plusieurs essais dans une solution de KF ($a_F = 0{,}074$) à pH 5 est de 29,2 ± 0,5 mV. La relation log i_∞ vs. E est linéaire ce qui indique que la réaction de surface

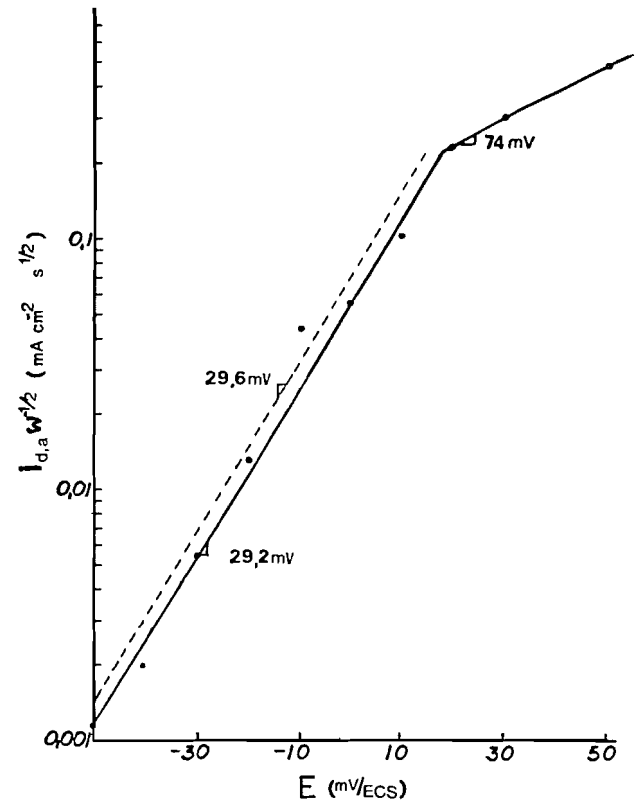

FIG. 7. Courbes log $i_{d,a}\omega^{-1/2} = f(E)$. Solution KF–HF: $a_{F^-} = 0{,}074$, pH = 5. (—) courbe expérimentale; (---) courbe calculée.

est une réaction de transfert d'électron. Nous obtenons avec la relation log i_∞ vs. E une courbe de Tafel dont la pente moyenne est de 32 ± 6 mV.

Le pouvoir peu complexant de l'ion fluorure favorise la formation de l'ion Cu^{2+} (18). Considérons le cas où le cuivre se dissout sous forme de Cu^{2+} et où le transfert de masse fait intervenir la diffusion du Cu^{2+} formé à l'électrode. Nous pouvons résumer la réaction globale d'oxydation du cuivre en deux étapes : (1) l'étape globale de transfert d'électron conduisant à la formation de Cu^{2+}, i.e. $Cu = Cu^{2+} + 2e^-$; (2) la diffusion du Cu^{2+} de l'électrode vers la solution.

Lorsque $\omega \to 0$, l'étape (2) est lente et l'étape (1) rapide; le terme $B^{-1}\omega^{-1/2}$ de l'équation [3] devient le terme dominant et $i \sim i_{d,a}$.

Le courant de diffusion de l'ion Cu^{2+} est donné par l'équation de Levich :

$$[4] \quad i_{d,a} = 0{,}62nFAD_{Cu^{2+}}^{2/3}\omega^{1/2}\gamma^{-1/6}(C^s_{Cu^{2+}} - C^*_{Cu^{+}})$$

où $C^s_{Cu^{2+}}$: concentration de Cu^{2+} à la surface de l'électrode et $C^*_{Cu^{2+}}$: concentration de Cu^{2+} en solution.

Puisque la vitesse de transfert de masse est lente par rapport à la vitesse de transfert d'électron lorsque $\omega \to 0$, l'équation de Nernst s'applique ce qui nous permet de calculer la concentration de Cu^{2+} à la surface de l'électrode :

$$[5] \quad E = E^0_{Cu/Cu^{2+}} + \frac{RT}{nF} \ln C^s_{Cu^{2+}} \cdot f_{Cu^{2+}}$$

$f_{Cu^{2+}}$: coefficient d'activité du Cu^{2+}.

En combinant les équations [4] et [5] et en tenant compte du fait que $C^*_{Cu^{2+}} \lessapprox C^s_{Cu^{2+}}$, on obtient la relation du courant de diffusion :

[6] $$i_{d,a} = 0{,}62nFAD^{2/3}_{Cu^{2+}}\omega^{1/2}\gamma^{-1/6}(1/f_{Cu^{2+}}) \times \exp\left[\frac{nF}{RT}(E - E^0_{Cu/Cu^{2+}})\right]$$

Pour une réaction procédant d'un échange de 2 électrons comme l'oxydation du cuivre sous forme de Cu^{2+}, la relation $\log i_{d,a}\omega^{-1/2}$ vs. E tirée de l'équation [6] donne une pente de 29,6 mV (25°C). La courbe expérimentale représentée à la figure 7 (ligne pleine) a deux pentes différentes, 29,2 mV et 74 mV. La cassure des droites a lieu à $\sim +15$ mV. Nous considérons dans l'analyse des résultats uniquement la partie de la courbe allant de -50 à $+15$ mV parce que la cassure apparaît près du potentiel pour lequel un dépôt noir commence à se former sur l'électrode. Les composés prévus à partir de la thermodynamique dans ces conditions expérimentales sont le Cu_2O et le $3CuF_2 \cdot Cu(OH)_2$ (23). Nous avons obtenu à partir de nos mesures une pente moyenne de 29,2 ± 0,5 mV. Les résultats expérimentaux concordent très bien avec la réaction d'oxydation du cuivre sous forme Cu^{2+}.

À partir de l'équation [6], on a tracé la courbe calculée de la relation $\log i_{d,a}\omega^{1/2}$ en fonction de E (fig. 7, ligne pointillée), en utilisant les valeurs suivantes : $E^0_{Cu/Cu^{2+}} = 0{,}105\ V_{ECS}$ (18), $f_{Cu^{2+}} = -0{,}40$ (25), $D_{Cu^{2+}} = 0{,}83 \times 10^{-5}\ cm^2\ s^{-1}$ (26), $\gamma = 0{,}01\ cm^2\ s^{-1}$ (24), $A = 0{,}20\ cm^2$.

Les droites expérimentale et calculée (fig. 7) sont séparées par un faible écart; il y a donc harmonie entre les résultats expérimentaux obtenus à pH 5 et le modèle proposé pour l'oxydation du cuivre. On explique l'écart par la différence entre les valeurs $D_{Cu^{2+}}$, $f_{Cu^{2+}}$, $E^0_{Cu/Cu^{2+}}$ utilisées pour le calcul et les valeurs réelles du système expérimental et possiblement par une faible différence de potentiel dans la jonction liquide.

La réaction de transfert d'électron peut être déterminée par l'analyse de la courbe de Tafel, $\log i_\infty$ vs. E. Lorsque $\omega \rightarrow \infty$, le terme i^{-1} de l'équation [3] devient dominant et $i \sim i_\infty$, c'est-à-dire que le transfert d'électron est l'étape déterminante.

Un mécanisme conduisant à la formation de Cu^{2+} peut être envisagé (12). Il fait intervenir deux étapes d'oxydation électrochimique successives pour lesquelles la deuxième étape est déterminante (l'espèce Cu^+ reste adsorbée sur l'électrode) :

[7] $Cu \rightleftarrows Cu^+ + 1e$ rapide

[8] $Cu^+ \rightleftarrows Cu^{2+} + 1e$ lente

Pour un tel mécanisme, la pente de la courbe de Tafel a une valeur théorique de 40 mV. Étant donné que la pente expérimentale de la relation $\log i_\infty$ vs. E est comprise entre 26 et 38 mV, le mécanisme procédant des étapes [7] et [8] est envisageable. Par ailleurs, la dismutation de l'espèce intermédiaire Cu^+ est aussi probable (27), ce qui conduit dans ce cas à une valeur pour la pente de Tafel de 30 mV.

Conclusion

Cette étude nous a permis de mettre en évidence l'influence de l'ion F^- sur la dissolution anodique du cuivre dans des solutions aqueuses acides (pH 1,6–6), principalement à pH 5, en présence de KF 0,1 *M*. Aux pH 1,6–6, l'électrode de cuivre se dissout uniformément, i.e. sans qu'il y ait de zones préférentielles sur la surface lorsqu'elle subit une polarisation potentiodynamique (10 mV s^{-1}) à des potentiels supérieurs à $0\ V_{ECS}$. À pH faiblement acide (pH 5, KF 0,1 *M*), lorsque le balayage du potentiel va jusqu'à +0,5 V, l'oxydation du cuivre débute par la dissolution généralisée de l'électrode suivi de la formation d'un film de Cu_2O non passivant; au fur et à mesure que le temps d'oxydation augmente, le courant diminue et l'électrode devient passivée. À pH 5, dans les conditions où la dissolution de l'électrode tournante est généralisée, les courbes $i = f(\omega^{1/2})$ sont caractéristiques d'un système quasi réversible. Lorsque $\omega \rightarrow 0$, l'oxydation est limitée par l'étape de diffusion du Cu^{2+} de l'électrode jusqu'au coeur de la solution, alors que lorsque $\omega \rightarrow \infty$, l'oxydation du cuivre est limitée par le processus de transfert de charge conduisant à la formation de Cu^{2+}.

Remerciements

Ce travail a été supporté par l'Institut de recherche de l'Hydro-Québec (IREQ) et par le Conseil de recherches en sciences naturelles et en génie du Canada (CRSNG). Nous tenons à remercier Monsieur A. Adnot du «Laboratoire d'analyse de surface du GRAPS» (Université Laval) pour les analyses de XPS et AES.

1. K. KINOSHITA, D. HANDOLT et T. MULLER. J. Electrochem. Soc. **117**, 1248 (1970).
2. V. K. ALTUKOV et T. A. MORGUNOVA. Zashch. Met. **17**, 444 (1981).
3. A. MOREAU. Electrochim. Acta, **26**, 1281 (1981).
4. T. HURLEN. Acta Chem. Scand. **15**, 1231 (1961).
5. L. BROSSARD. Can. J. Chem. **61**, 2022 (1983).
6. A. L. BACARELLA et J. C. GRIESS. J. Electrochem. Soc. **120**, 459 (1973).
7. M. BRAUN et K. NOBE. J. Electrochem. Soc. **126**, 10 (1979).
8. R. ASTAKHOVA, J. SZALMA, J. FARKAS et L. KISS. Magy. Kem. Foly. **85**, 315 (1979).
9. A. HICKLING et D. TAYLOR. Trans. Faraday Soc. **44**, 262 (1948).
10. H. P. LECKIE. J. Electrochem. Soc. **117**, 1478 (1970).
11. L. KISS, A. BOSQUEZ et M. L. VARSANYI. Acta Chim. Acad. Sci. Hung. **108**, 369 (1981).
12. E. MATTSON et J. O'M. BOCKRIS. Trans. Faraday Soc. **55**, 1586 (1959).
13. G. W. TINDALL et S. BRUCKENSTEIN. Anal. Chem. **40**, 1402 (1968).
14. W. H. SMYRL. *Dans* Comprehensive treatise of electrochemistry. Vol. 4. *Edité par* J. O'M. Bockris, B. E. Conway, E. Yeager et R. E. White. Plenum Press, New York, NY. 1981.
15. C. P. KIM et K. NOBE. Corrosion, **27**, 382 (1971).
16. T. HURLEN. Acta Chem. Scand. **15**, 630 (1961).
17. B. BURROWS et R. JASINSKI. J. Electrochem. Soc. **115**, 348 (1968).
18. U. BERTOCCI et D. R. TURNER. *Dans* Encyclopedia of electrochemistry of the elements. Vol. II. *Edité par* A. J. Bard. Marcel Dekker Inc., New York, NY. 1973.
19. I. LEDEN. J. Chem. Soc. 2936 (1955).
20. S. ARHLAND et K. ROSENGREN. Acta Chem. Scand. **10**, 727 (1956).
21. R. E. CONNICK et A. D. PAUL. J. Am. Chem. Soc. **80**, 2069 (1958).
22. A. RINGBOM. Les complexes en chimie analytique. Dunod, Paris, France. 1967. p. 302.
23. P. DUBY. The thermodynamic properties of aqueous inorganic copper systems. International Copper Research Association INCRA. 1977.
24. A. J. BARD. Electrochimie. Principes, méthodes et applications. Masson, New York, NY. 1983. Chap. 8.
25. D. A. SKOOG. Principles of instrumental analysis. 3e éd. Saunders College Publishing, Montréal. 1985. p. 900.
26. P. W. WEST, J. DEAN et E. J. BREDA. Collect. Czech. Chem. Commun. **13**, 1 (1948).
27. S. A. AWARD, KH. M. KAMEL, Z. ABD EL-HADI et H. A. BAYUMI. J. Electroanal. Chem. **199**, 341 (1986).

Can. J. Chem. Downloaded from www.nrcresearchpress.com by 213.166.140.6 on 09/07/12
For personal use only.

Assisted hydrolysis of the nitrile group of 2-aminoadamantane-2-carbonitrile

MARTINO PAVENTI, FRANCIS L. CHUBB, AND JOHN T. EDWARD
Department of Chemistry, McGill University, 801 Sherbrooke Street West, Montreal, P.Q., Canada H3A 2K6

Received February 10, 1987

MARTINO PAVENTI, FRANCIS L. CHUBB, and JOHN T. EDWARD. Can. J. Chem. **65**, 2114 (1987).

Attempts to hydrolyse the nitrile group of 2-aminoadamantane-2-carbonitrile by mineral acid or alkali have been unsuccessful. However, treatment of the aminonitrile with benzaldehyde in alkaline solution gives the benzal derivative of the α-aminoamide, readily hydrolysed to the α-aminoamide. Alternatively, benzoylation of the amino group followed by acid hydrolysis gives successively the α-benzamido acid and the α-amino acid. Possible mechanisms for these facilitated hydrolyses are advanced.

MARTINO PAVENTI, FRANCIS L. CHUBB et JOHN T. EDWARD. Can. J. Chem. **65**, 2114 (1987).

Des essais menés en vue d'hydrolyser le groupement nitrile de l'amino-2 adamantanecarbonitrile-2 par les acides minéraux ou par les hydroxydes alcalins se sont avérés infructueux. Toutefois, si on traité l'aminonitrile par du benzaldéhyde en solution alcaline, on obtient un dérivé benzal de l'α-aminoamide qui peut facilement être hydrolysé en α-aminoamide. Une méthode alternative implique une benzoylation du groupement aminé qui est suivie d'une hydrolyse acide pour conduire avec succès à l'acide α-benzamido et à l'acide α-aminé. On propose des mécanismes possibles pour ces hydrolyses rendues faciles.

[Traduit par la revue]

Can. J. Chem. Downloaded from www.nrcresearchpress.com by 213.166.140.6 on 09/07/12
For personal use only.

2-Aminoadamantane-2-carbonitrile **2** is readily prepared from adamantanone **1** (1), but attempts to hydrolyse it to the amino acid **5** have been unsuccessful (2). This is not totally surprising, since the nitrile group of **2** is constrained into an axial position, in which it is known to resist hydrolysis (3). The amino acid **5** was eventually obtained by Nagasawa *et al.* (2) by preparing first the hydantoin **4** by reaction of the ketone **1** with cyanide and ammonium carbonate (the Bucherer–Bergs reaction) in a pressure vessel at 120°C and 170 psi (1 psi = 6.9 kPa), and then hydrolysing the hydantoin to the amino acid by heating it with 1.25 *M* aqueous sodium hydroxide in a pressure vessel at 195°C and 250 psi (Scheme 1).

The severity of these conditions challenged us to devise an easier preparation. The most obvious was the aldehyde- or ketone-assisted hydrolysis of the α-aminonitrile in alkaline solution to give the Schiff base (e.g. **8**) of the α-aminoamide (4–12); this is usually hydrolysed with extreme ease to the α-aminoamide (e.g. **9**) and then, with more difficulty, to the α-amino acid (e.g. **5**). The mechanism of this reaction has been studied by Commeyras and co-workers (4–6); in the present instance the reaction steps would be **2** → **6** → **7** → **8**. However, the procedure of Commeyras (who worked with simple α-aminonitriles in aqueous solution) was judged unsuitable for our water-insoluble compound **2**, and so we used the earlier procedure of Cook *et al.* (7–12) in which the α-aminonitrile was treated with sodium methoxide in neat ketone (e.g. acetone). This reaction yielded only adamantanone, from the base-catalysed decomposition of **2** (13). However, reaction of **2** with benzaldehyde and KOH in aqueous ethanol[1] gave the Schiff base **8** (R^1 = Ph, R^2 = H), although reaction with cyclohexanone under these conditions gave nothing. Evidently steric hindrance to the formation of the five-membered ring intermediate **7** becomes excessive if R^2 is larger than hydrogen.

The aminoamide **9** was readily obtained from the benzal derivative **8** (R^1 = Ph, R^2 = H) by treatment with dilute acid or with phenylhydrazine in benzene containing a trace of acetic acid. However, its further hydrolysis to **5** by strong acid or alkali was extremely slow, and so other routes were investigated.

One of these was the ketone-assisted thiohydrolysis of the nitrile group (9, 15) with cyclohexanone as the ketone. This would be expected to yield the imidazolidine-4-thione **10** by the mechanism shown in Scheme 2 (15). In fact, this compound was obtained, but in small yield, along with the compounds **11** and **13** (15). Evidently steric hindrance at the cyclization step leading to **10** is sufficient to allow the competing hydrolysis of the intermediate to yield **11**, and steric hindrance at an earlier stage causes **2** to react so slowly that the competing breakdown of **2** to adamantanone, NH_3, and HCN (13) can result in the formation of significant amounts of **12** and thence of **13**.[2]

In the end of the most practical route to the amino acid **5** was found to start with the α-benzamidonitrile **14** (Scheme 3). Our previous experience with α-benzamidonitriles[3] led us to expect a rapid hydrolysis of the nitrile **14** to the amide **16** in concentrated hydrochloric acid, probably by way of the oxazoline intermediate **15** (16), followed by a slower hydrolysis of the amide **16** to the acid **17**. In fact, both stages of the acid hydrolysis seem to be accelerated by the benzamido group, the nitrile **14** readily giving the acid **17**. More prolonged acid treatment is required to hydrolyse the benzamido group of **17** to give the hydrochloride of the amino acid **5**. This last hydrolysis, which contrasts with the resistance of the amido group of **9** to aqueous acid, probably takes place because of the greater distance of the amido carbonyl of **17** from the crowding adamantane moiety.

It may be noted that the anchimerically assisted attacks on the nitrile group in the four routes depicted in Schemes 1–3 are all basically similar, but that the route via the hydantoin **4** suffers from the disadvantage of the excessive stability of this intermediate. Anchimeric assistance by the α-benzamido group to the hydrolysis of nitriles seems not to have been recognized previously, and is under active investigation in this laboratory.

[1]We had previously found that this reaction converted α-amino-α-phenylacetonitrile to the Schiff base of α-amino-α-phenylacetamide. The experiment was suggested by the observation of Clarke and Francis (14) that treatment of benzaldehyde cyanohydrin with ammonia and benzaldehyde in aqueous ethanol containing KOH gave the Schiff base of α-amino-α-phenylacetamide.

[2]This experiment was repeated with the addition of varying amounts of aqueous ammonia, and the crude product analysed by thin-layer chromatography. A rough estimate of the relative amounts of **10**, **11**, and **13**, based on the intensity of the spots, was 20:15:65; this ratio was not appreciably affected by the amount of ammonia present.

[3]M. Paventi and J. T. Edward, unpublished research.

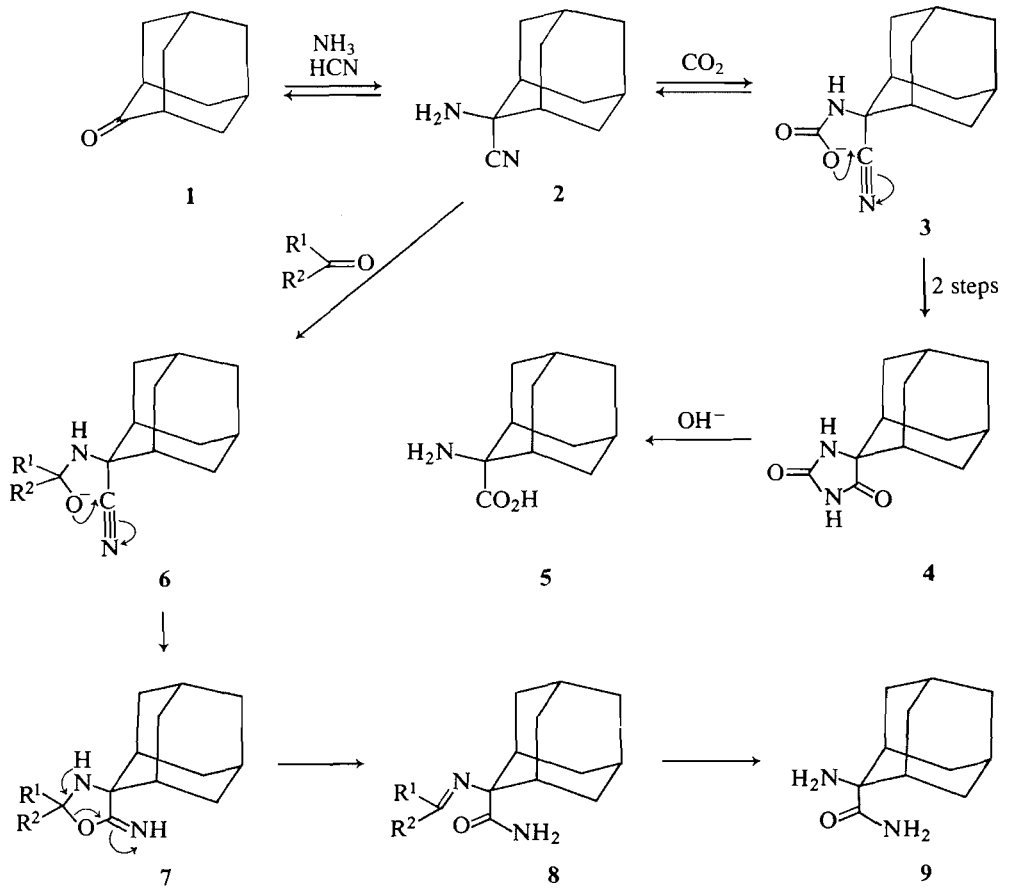

SCHEME 1

Experimental

α-Benzylideneamino-α-phenylacetamide

α-Amino-α-phenylacetonitrile (10 g) in ethanol (20 mL) was added dropwise to a stirred mixture of benzaldehyde (7 g), 15% aqueous potassium hydroxide (10 mL), concentrated aqueous ammonia (10 mL), and ethanol (4 mL). A first crop (12.5 g) of crystalline solid was removed by filtration after 1 h, and a second crop (1.5 g) from the filtrate after it had stood overnight. The combined crops were recrystallized from ethyl acetate – light petroleum (1:1 v/v) to yield α-benzylideneamino-α-phenylacetamide (13 g, 72%), mp 125–127°C (lit. (14) mp 126°C); ν_{max} (Nujol): 3380, 3290, 3180, 1660, 1640 cm^{-1}; ^1H nmr ($CDCl_3$) δ: 4.92 (1H, S, =NC*H*Ph—CO—), 6.33 (1H, s, NH), 6.90 (1H, s, NH), 7.07–7.90 (10H, m, aromatic), 8.18 (1H, s, PhC*H*=N—).

2-Aminoadamantane-2-carbonitrile (2) hydrochloride

The reaction of adamantanone with sodium cyanide, ammonium chloride, and aqueous ammonia in ethanol–water was carried out following ref. 1, after which the reaction mixture was extracted with ether (200 mL). The extract was dried, and HCl gas was passed through the solution. The precipitated hydrochloride was filtered, washed with water (68% yield), and recrystallized from acetonitrile, charring above 300°C.

2-Benzylideneaminoadamantane-2-carboxamide (8; R^1 = Ph, R^2 = H)

A solution of 2-aminoadamantane-2-carbonitrile (6.0 g) and benzaldehyde (3.6 g) in ethanol (13 mL), concentrated aqueous ammonia (4.6 mL), and 15% aqueous potassium hydroxide (4.6 mL), stirred at room temperature, deposited a white solid. After 2.5 h, filtration removed 3.85 g, mp 185–186°C, and after standing overnight, 1.1 g, mp 186–187°C (total yield 52%); ν_{max} (KBr): 3390, 3350, 3310, 3210 (NH), 3030 (aromatic CH), 2940–2850 (aliphatic CH), 1685, 1655 (amide), 1630 (C=N) cm^{-1}; ^1H nmr (DMSO-d_6) δ: 1.33–2.20 (12H, m, adamantane), 2.37 (2H, m, adamantane), 5.80 (2H, s, $CONH_2$, removed by D_2O), 7.20–7.53 (3H, m, aromatic), 7.53–7.87 (2H, m, aromatic), 8.40 (1H, s, PhC*H*=N—).

2-Aminoadamantane-2-carboxamide (9)

A solution of 2-benzylideneaminoadamantane-2-carboxamide (2.0 g) and phenylhydrazine (0.8 g) in benzene (60 mL) containing two drops of acetic acid was heated under reflux for 1.5 h. The solution after concentration and cooling deposited colourless platelets (1.2 g, 88%), mp 184–186°C; ν_{max} (KBr): 3350, 3270, 3100 (NH), 2900, 2820 (aliphatic CH), 1670 (amide) cm^{-1}; ^1Hmr (DMSO-d_6) δ: 1.3–2.5 (14H, m), 1.87 (2H, s, NH_2, removed by D_2O), 6.73 (2H, br s, $CONH_2$, removed by D_2O). *Anal.* calcd. for $C_{11}H_{18}N_2O$: C 68.01, H 9.34, N 14.42; found: C 67.89, H 8.75, N 14.37.

2-Benzamidoadamantane-2-carboxamide (16)

Benzoyl chloride (0.52 g) was added gradually to a stirred solution of 2-aminoadamantane-2-carboxamide (0.60 g) and potassium carbonate (0.64 g) in water (10 mL) – tetrahydrofuran (10 mL). The mixture was left overnight and the insoluble product then removed and recrystallized from ethyl acetate: prisms (0.80 g, 87%), mp 232–234°C; ν_{max} (KBr): 3463, 3328, 3207, 3243 (NH), 3168, 3055 (aromatic CH), 2928, 2903, 2853 (aliphatic CH), 1686, 1659, 1636 (amide); ^1Hmr (DMSO-d_6) δ: 1.66 (12H, m), 2.43 (1H, m, amide), 2.66 (2H, m), 6.55 (2H, br d, amide), 7.00–7.50 (5H, m, aromatic). *Anal.* calcd. for $C_{18}H_{22}N_2O_2$: C 72.46, H 7.43, N 9.39; found: C 72.62, H 7.61, N 8.80.

Adamantane-2-spiro-5'-imidazolidin-4'-thione-2'-spirocyclohexane (10)

Hydrogen sulfide was bubbled for 1.5 h into an ethanolic solution (20 mL) at 0°C containing 2-aminoadamantane-2-carbonitrile hydro-

Can. J. Chem. Downloaded from www.nrcresearchpress.com by 213.166.140.6 on 09/07/12
For personal use only.

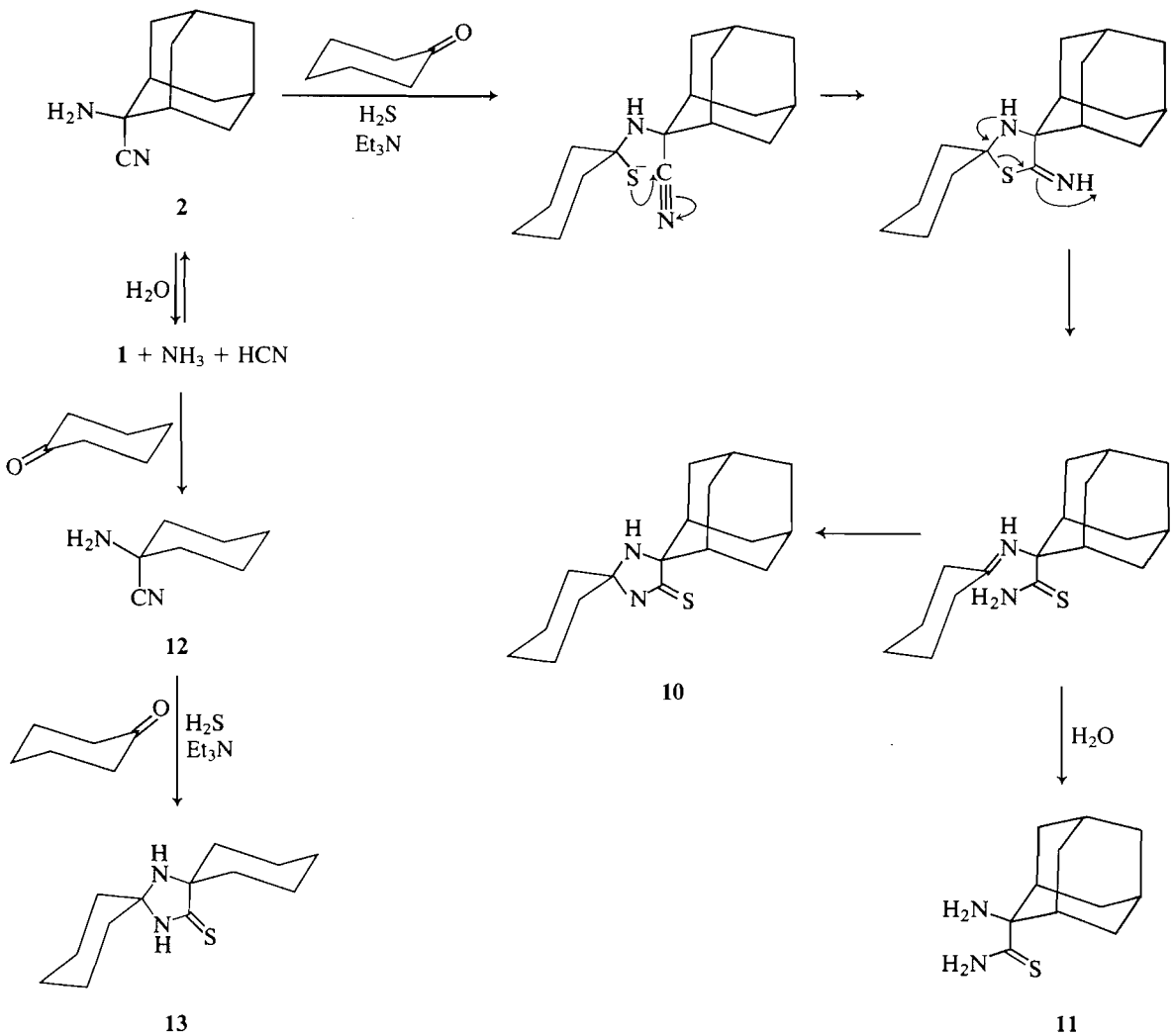

SCHEME 2

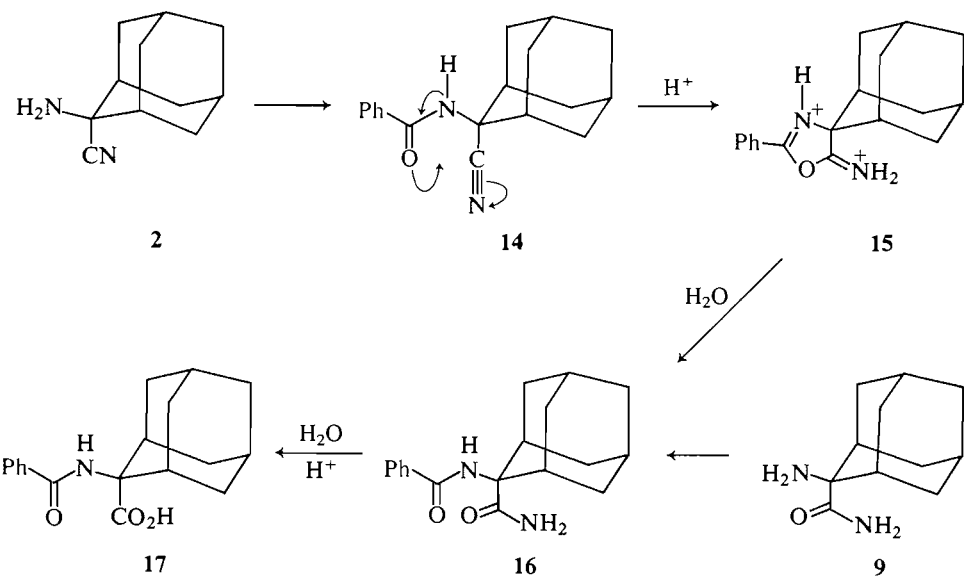

SCHEME 3

Can. J. Chem. Downloaded from www.nrcresearchpress.com by 213.166.140.6 on 09/07/12
For personal use only.

Can. J. Chem. Downloaded from www.nrcresearchpress.com by 213.166.140.6 on 09/07/12
For personal use only.

chloride (2.12 g, 0.010 mol), triethylamine (1.03 g, 0.010 mol), and cyclohexanone (1.0 g, 0.010 mol), and the reaction vessel was then stoppered and left at room temperature for 2 h. The solution was then purged of excess H_2S by a stream of N_2 for 1.5 h at room temperature, and left at room temperature for 48 h. Slender yellow needles were removed by filtration and washed with ethanol. The dried product (0.12 g, 4%) was recrystallized from acetonitrile to give needles, mp 235–237°C, shown by thin-layer chromatography to be contaminated with a small amount of the compound **13**. This was removed by chromatography on Florisil and elution with chloroform, the less polar **10** being removed first. It was recrystallized from acetonitrile: needles, mp 236–238°C; ν_{max}: 3285 (N—H), 3145 (thioamide N—H), 2915, 2895, 2850, 1495, 1458, 1443 cm^{-1}; uv (95% ethanol) λ_{max}: 274 nm (ε 13 500); uv (0.9 *M* ethanolic KOH) λ_{max}: 258 nm (ε 10 200; uv (3.6 *M* ethanolic HCl) λ_{max}: 277 nm (ε 13 000); ^{1}Hmr (DMSO-d_6) δ: 1.67–1.93 (22H, m), 2.30 (2H, m), 3.47 and 3.67 (1H, NH),[4] 10.67 (1H, s, thioamide); electron impact ms *m/z* (formula, intensity, fragment): 290 ($C_{17}H_{26}N_2S$, 27, M^+), 256 ($C_{17}H_{24}N_2$, 22, M − H_2S), 231 ($C_{16}H_{25}N$, 97, M − HNCS), 149 ($C_{10}H_{15}N$, 92), 134 ($C_{10}H_{14}$, 31). *Anal.* calcd. for $C_{17}H_{26}N_2S$: C 70.30, H 9.02, S 11.04; found: C 70.63, H 9.14, S 11.33.

*2-Aminoadamantane-2-thionamide (**11**)*

2-Aminoadamantane-2-carbonitrile hydrochloride (1.06 g) was allowed to react with H_2S and cyclohexanone in ethanol according to the procedure above, and the crude product was chromatographed on Florisil. Elution with chloroform removed the less polar materials **1**, **10**, and **13**; elution with chloroform–methanol 9:1 (v/v) removed 2-aminoadamantane-2-thionamide, which crystallized from chloroform was white plates, mp 164–166°C; ν_{max} (KBr): 3381, 3335, 3263, 3171, 2931, 2897, 2847, 2323 (w br), 1620, 1571, 1560, 1418 cm^{-1}; uv (water) λ_{max}: 273 nm (ε 8350); ^{1}Hmr (DMSO-d_6) δ: 1.82 (10H, m), 2.40 (6H, m, CH + NH_2), 7.8 (~2H, br s, $CSNH_2$); ms *m/z* (formula, intensity, fragment): 176 ($C_{11}H_{16}N_2$, 32, M^+ − H_2S), 151 ($C_{10}H_{17}N$, 250, M^+ − HNCS), 150 ($C_{10}H_{16}N$, 922, M^+ − H_2NCS), 149 ($C_{10}H_{15}N$, 1000, M^+ − H_2NCSH). *Anal.* calcd. for $C_{11}H_{18}N_2S$: C 62.81, H 8.62, N 13.32; found: C 62.78, H 8.68, N 13.25.

The nitrate salt was prepared by adding 70% nitric acid to a chloroform solution of the free base, and was recrystallized from water: yellow needles, mp 225–226°C; ν_{max}: 3305, 3285, 3135, 2985, 2910, 2855, 1640, 1630, 1587, 1525, 1495, 1475, 1465 cm^{-1}; ^{1}Hmr (DMSO-d_6) δ: 2.0 (10H, m), 2.77 (4H, s), 8.20 (3H, br s, $—\overset{+}{N}H_3$), 10.9 (2H, br s, thioamide).

*2-Benzamidoadamantane-2-carbonitrile (**14**)*

Benzoyl chloride (1.70 g) was added slowly with stirring to a solution of 2-aminoadamantane-2-carbonitrile hydrochloride (2.13 g) and potassium carbonate (2.10 g) in water (30 mL) – tetrahydrofuran (20 mL). After 1 h the precipitated solid was removed by filtration and recrystallized from ethyl acetate: slender needles (2.4 g, 86% yield), mp 241–243°C; ν_{max} (KBr): 3365 (N—H), 2227 (C≡N), 1650 (NHCO) cm^{-1}; ^{1}Hmr (DMSO-d_6) δ: 0.87–2.20 (12H), 2.73 (2H, s), 7.42–7.92 (5H, m, Ph), 8.53 (1H, br s, amide). *Anal.* calcd. for $C_{18}H_{20}N_2O$: C 77.11, H 7.19, N 9.99; found: C 77.05, H 7.85, N 10.37.

*2-Benzamidoadamantane-2-carboxylic acid (**17**)*

2-Benzamidoadamantane-2-carbonitrile (0.10 g) in tetrahydrofuran (4 mL) and concentrated aqueous hydrochloric acid (10 mL) was kept overnight at room temperature[5] and then diluted with water (40 mL), giving the acid **17** (0.10 g, 93%), mp 240–241°C after recrystallization from chloroform; ν_{max} (KBr): 3495 (N—H), 1738 (CO_2H), 1625 (amide) cm^{-1}; ^{1}H nmr (DMSO-d_6) δ: 1.47–2.41 (14H, m), 2.63 (2H, m), 7.42–7.91 (5H, m, Ph), 8.08 (1H, s, amide). *Anal.* calcd. for $C_{18}H_{21}NO_3$: C 72.22, H 7.07, N 4.68; found: C 72.12, H 6.98, N 4.65.

*2-Aminoadamantane-2-carboxylic acid (**5**)*

A solution of 2-benzamidoadamantane-2-carboxylic acid (0.50 g) in acetic acid (200 mL), concentrated aqueous hydrochloric acid (8.0 mL), and water (8.0 mL) was boiled under reflux for 30 h and then concentrated under reduced pressure. The solid residue was extracted with hot diethyl ether (2 × 50 mL) and with hot acetonitrile (2 × 50 mL), and then dissolved in methanol (5 mL) and filtered. Addition of diethyl ether (100 mL) to the filtrate, and scratching, induced crystallization of the hydrochloride (0.25 g, 65%), mp 269–270°C (lit. (2) mp ≥280°C); ν_{max} (KBr): 3230, 3180 (NH_3^+), 1722 (CO_2H) cm^{-1}; ^{1}Hmr (DMSO-d_6) δ: 1.83 (10H, m), 2.27 (4H, br, m), 7.97–9.97 (3H, NH_3^+). An aqueous solution of the hydrochloride was filtered, and the pH of the filtrate adjusted to ca. 5 with sodium bicarbonate. Fine white plates crystallized out, mp 303–305°C, raised to 308–311°C (lit. (2) mp 308–310°C) on recrystallization from water; ν_{max} (KBr): 3470, 3360, 3260 (NH_3^+), 1642 (CO_2^-) cm^{-1}. *Anal.* calcd. for $C_{11}H_{17}NO_2$: C 67.66, H 8.77, N 7.17; found: C 67.65, H 8.94, N 7.35.

Acknowledgment

Grateful acknowledgment is made to the Natural Sciences and Engineering Research Council of Canada for financial support.

1. F. L. CHUBB, J. T. EDWARD, and S. C. WONG. J. Org. Chem. **45**, 2315 (1980).
2. H. T. NAGASAWA, J. A. ELBERLING, and F. N. SHIROTA. J. Med. Chem. **16**, 823 (1973).
3. L. MUNDAY. J. Chem. Soc. 4372 (1961).
4. R. PASCAL, J. TAILLADES, and A. COMMEYRAS. Bull. Soc. Chim. Fr. II, 177 (1978).
5. R. PASCAL, J. TAILLADES, and A. COMMEYRAS. Tetrahedron, **34**, 2275 (1978).
6. R. PASCAL, J. TAILLADES, and A. COMMEYRAS. Tetrahedron, **36**, 2999 (1980).
7. J. T. EDWARD and F. L. CHUBB. Proc. R. Ir. Acad. Sect. B: **83B**, 57 (1983).
8. A. H. COOK, I. HEILBRON, and A. L. LEVY. J. Chem. Soc. 201 (1948).
9. A. H. COOK, I. HEILBRON, and A. P. MAHADEVAN. J. Chem. Soc. 1061 (1949).
10. A. H. COOK and S. F. FOX. J. Chem. Soc. 2337 (1949).
11. A. H. COOK and A. L. LEVY. J. Chem. Soc. 642 (1950).
12. A. C. DAVIS and A. L. LEVY. J. Chem. Soc. 3479 (1951).
13. M. BEJAUD, L. MION, and A. COMMEYRAS. Bull. Soc. Chim. Fr. II, 233 (1976).
14. C. H. CLARKE and F. FRANCIS. J. Chem. Soc. 319 (1911).
15. M. PAVENTI and J. T. EDWARD. Can. J. Chem. **65**, 282 (1987).
16. J. LICHTENBERGER and L. P. FLEURY. Bull. Soc. Chim. Fr. [5] 1185 (1956).

[4]The two broad peaks for N(1′)—H, each of equal area and adding up to one proton, are puzzling. A referee has suggested that the peaks are singlets from axial and equatorial NH. The ^{1}Hmr spectrum of cyclohexane-spiro-5′-imidazolin-4′-thione-2′-spirocyclohexane shows only one singlet for this NH (15), but possibly the more rigid spiroadamantane raises the barrier to axial–equatorial interconversion of the spirocyclohexane.

[5]Later experiments showed this time to be unnecessarily long; in fact, thin-layer chromatography showed that hydrolysis of **14** to **17** was complete in about 5 min, with no appreciable amount of the intermediate **16** present.

Topsentins, new toxic bis-indole alkaloids from the marine sponge *Topsentia genitrix*[1]

KRISTIN BARTIK, JEAN-CLAUDE BRAEKMAN, DÉSIRÉ DALOZE, AND CATHERINE STOLLER
Unité de chimie bio-organique, Faculté des sciences, Université Libre de Bruxelles, 50 Av. F. D. Roosevelt, 1050 Brussels, Belgium

JOËLLE HUYSECOM AND GYSÈLE VANDEVYVER
Laboratoire de biologie animale et cellulaire, Faculté des sciences, Université Libre de Bruxelles, 50 Av. F. D. Roosevelt, 1050 Brussels, Belgium

AND

ROBERT OTTINGER
Service de chimie organique, Faculté des sciences appliquées, Université Libre de Bruxelles, 50 Av. F. D. Roosevelt, 1050 Brussels, Belgium

Received February 11, 1987

KRISTIN BARTIK, JEAN-CLAUDE BRAEKMAN, DÉSIRÉ DALOZE, CATHERINE STOLLER, JOËLLE HUYSECOM, GYSÈLE VANDEVYVER, and ROBERT OTTINGER. Can. J. Chem. **65**, 2118 (1987).

Three new bis-indole alkaloids, topsentin-A (**1**), -B1 (**2**), and -B2 (**3**) have been isolated from the Mediterranean sponge *Topsentia genitrix* and their structure determined by spectroscopic methods. These compounds are weakly toxic for fish and for dissociated cells of the freshwater sponge *Ephydatia fluviatilis* and thus might be partially responsible for the chemical defense of the sponge.

KRISTIN BARTIK, JEAN-CLAUDE BRAEKMAN, DÉSIRÉ DALOZE, CATHERINE STOLLER, JOËLLE HUYSECOM, GYSÈLE VANDEVYVER et ROBERT OTTINGER. Can. J. Chem. **65**, 2118 (1987).

Trois alcaloïdes bis-indoliques nouveaux, les topsentines-A (**1**), -B1 (**2**) et -B2 (**3**), ont été isolés de l'éponge méditerranéenne *Topsentia genitrix*, et leurs structures déterminées par des méthodes spectroscopiques. Ces composés, qui sont faiblement toxiques vis-à-vis des poissons et des cellules dissociées de l'éponge d'eau douce *Ephydatia fluviatilis*, sont donc probablement responsables de la défense chimique de cette éponge.

[Traduit par la revue]

Introduction

Among marine organisms, sponges appear to be one of the richest phylum in toxicogenic species. They are also remarkable for their ability to synthesize a wide variety of secondary metabolites (1, 2) that, in several cases, have been demonstrated to be responsible for the observed toxicity (3, 4). It is now generally admitted that these noxious compounds may act to minimize predation by mobile animals and (or) to reduce settlement and overgrowth of fouling organisms (5).

In the course of our search for compounds involved in the defense mechanism of sponges, we observed that the methanolic extract of the sponge *Topsentia genitrix* (Halichondriidae) is weakly toxic to the fish *Lebistes reticulatus* (LD: <50 mg/L) and to mice (LD_{50}: 10 mg/kg), kills dissociated cells of the freshwater sponge *Ephydatia fluviatilis* before early aggregation (<100 mg/L) (6), and shows antibacterial activities. We wish to report here on the isolation and structure determination of three new bis-indole alkaloids partially responsible for these activities.

Results and discussion

A large specimen of *Topsentia genitrix*, a rarely encountered Mediterranean sponge, was collected near Banyuls (France) by scuba diving. The three major compounds of the active fraction, named topsentin-A (**1**), topsentin-B1 (**2**), and topsentin-B2 (**3**), were separated by droplet counter current chromatography (DCCC: $CHCl_3$, CH_3OH, H_2O, 13:7:8) and further purified by flash chromatography on silica gel ($CHCl_3$, CH_3OH, NH_3 25%, 19:0.5:1 or 9:1:1).

Topsentin-A (1)

The pattern of the uv (CH_3OH, λ_{max} at 209 (43 000) sh 228, 253 (21 200) sh 270, 373 nm (17 930)) and ir spectra (KBr, no aliphatic ν C—H, aromatic out-of-plane bending band at 735 cm^{-1}), together with the absence in the ^1H nmr spectrum of topsentin-A of signals between 0 and 7 ppm, are indicative of an aromatic skeleton. The EI mass spectrum shows an intense molecular ion at m/z 326 and high resolution measurements provide the molecular formula $C_{20}H_{14}N_4O$ (*Exact Mass* calculated: 326.1168; measured: 326.1169). Although the behaviour of topsentin-A, both in tlc and hplc, suggests that it is a pure compound, its ^1H nmr spectrum, recorded in CD_3COCD_3, shows signals ($2 \times 14H$) attributable to a mixture of two closely related derivatives in a ratio 60:40. Four peaks amounting to a total of 6 protons (3H per derivative) disappear on treatment with D_2O and the addition of a few drops of CF_3COOD induces a dramatic simplification of the spectrum, which under these conditions shows signals integrating for 11 protons only. Such behaviour is reminiscent of the existence of two slowly interconverting compounds whose protonated forms are identical.

The ^{13}C nmr spectra of **1** (CD_3COCD_3–D_2O–CF_3COOD; BBD and DEPT) ascertain the presence of 20 carbon atoms (9 quaternary and 11 tertiary). The $^1H/^1H$ correlated 2D nmr spectrum of the protonated form of **1** shows that the four protons absorbing at 8.35, 7.65, 7.36, and 7.35 ppm and the four protons absorbing at 7.96, 7.60, 7.28, and 7.25 ppm form two separated 4-spin systems attributable to two 1,2-disubstituted benzene rings. The simulation of the two 4-spin systems using the PANIC program (7) confirms this attribution and allows accurate determination of the chemical shifts and coupling constants. The assignment of the carbon–proton connectivities of these protons was deduced from the $^1H/^{13}C$ correlated 2D nmr spectrum. SPI experiments (8) showed that the 1H singlet at δ 8.72 undergoes long range heteronuclear coupling

[1]This paper is dedicated to the memory of Dr. N. Defay.

Printed in Canada / Imprimé au Canada

Can. J. Chem. Downloaded from www.nrcresearchpress.com by 213.166.140.6 on 09/07/12
For personal use only.

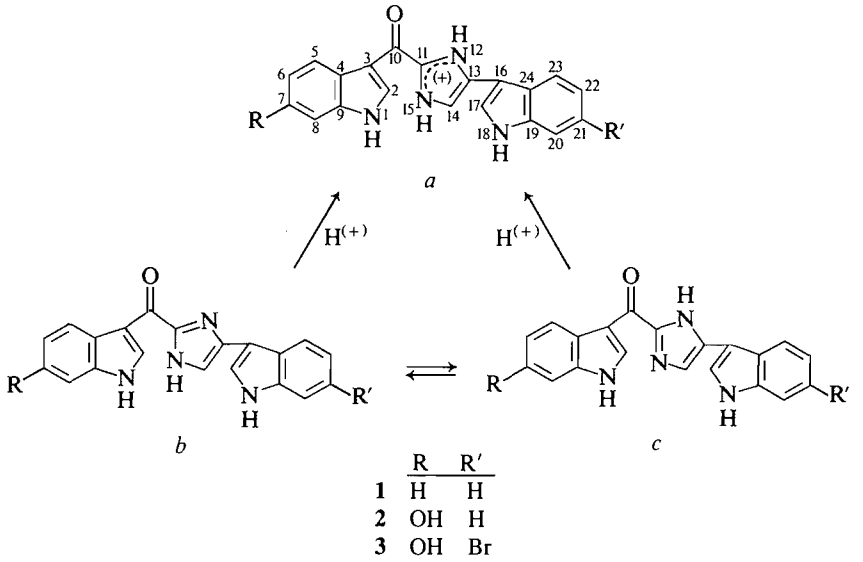

	R	R′
1	H	H
2	OH	H
3	OH	Br

with the ^{13}C signals at δ 114.8, 126.9, and 138.0, while the 1H singlet at δ 8.15 is long-range coupled with the ^{13}C signals at δ 125.4, 137.6, and 103.1. All these data, together with the presence of a deshielded carbon atom at δ 172.1, are consistent with the presence in topsentin-A of both a 3-ketoindole and a 3-substituted indole chromophore. The comparison of the ^1H and ^{13}C chemical shifts with those of model compounds (9–15) strongly supports this hypothesis. Thus, all signals in the ^1H and ^{13}C nmr spectra of **1** have been assigned, except for a 1H singlet at 8.08 ppm and 3 peaks corresponding to 1 tertiary (116.6) and two quaternary (141.5 and 132.5) carbon atoms in the ^{13}C nmr spectra. That these signals are attributable to a C-disubstituted imidazole ring follows from comparison with reported values (16) and from SPI experiments, which showed that the proton at δ 8.08 is long-range coupled with the ^{13}C signal at δ 141.5 and 132.5. The presence of an imidazole ring explains the modifications observed in the ^1H nmr spectrum of topsentin-A on addition of CF_3COOD. In neutral solution, asymmetrically C-disubstituted imidazoles exist as mixtures of slowly interconverting tautomers, and protonation yields a symmetrical imidazolium cation (17). It is known that, of the three carbon atoms of imidazole derivatives, the C-2 (imidazole numbering) is the most deshielded (δ ~ 140) (16). Since in topsentin-A this signal (δ 141.5) corresponds to a quaternary carbon atom, the imidazole ring is necessarily substituted at the carbon bearing the two nitrogen atoms. Moreover, further SPI experiments indicated that the signal at δ 8.15, attributable to the proton H-17 α to the nitrogen atom of the indole chromophore, is coupled (^3J) with the C-4 (or C-5) of the imidazole ring (δ 132.5). It follows from all these data that the protonated form of topsentin-A may be represented by structure **1***a*.

A careful analysis of the ^1H nmr spectrum of topsentin-A measured in CD_3COCD_3 permits us to assign the signals of both tautomers. Interestingly, the two signals at 7.62 and 7.70 ppm attributable to H-14 show different NH/CH coupling constants (2.2 and 1.5 Hz respectively). Since it is reasonable to assume that the larger *J* infers coupling between adjacent protons (17), the signal at 7.7 ppm may be assigned to tautomer **1***b*, which is thus the most abundant. The mass spectrum of topsentin-A entirely corroborates the proposed structure. It shows characteristic fragments corresponding to cleavages α to the carbonyl group. Cleavage of the C10—C11 bond gives rise to fragments *a* (*m/z* 144), *a* + H• (*m/z* 145), and *d* + H• (*m/z* 183), while cleavage of the C3—C10 bond gives rise to fragments *c* (*m/z* 210) and *c* − H• (*m/z* 209). Subsequent loss of a molecule of carbon monoxide leads to fragments *b* (*m/z* 116; *a* − CO), *b* + H• (*m/z* 117; *a* + H• − CO), and *d* − H• (*m/z* 181; *c* − H• − CO) respectively. The composition of all these fragments was confirmed by high resolution measurements. The parent–daughter relationships $M^{+\bullet} \rightarrow c - H^\bullet \rightarrow d - H^\bullet$ and $a \rightarrow b$ are ascertained by the presence of metastable peaks at *m/z* 134, 157, and 94 respectively.

Topsentin-B1 (2)

The spectroscopic properties of topsentin-B1 are closely related to those of topsentin-A. The EI mass spectrum shows an intense molecular ion at *m/z* 342 and high resolution measurements provide the molecular formula $C_{20}H_{14}N_4O_2$ (*Exact Mass* calculated: 342.1117; measured: 342.1129). Thus, topsentin-B1 possesses one more oxygen atom than topsentin-A. Moreover, in the ms of **2**, the peaks corresponding to fragments *a*, *a* + H•, *b*, and *b* + H• in the ms of **1** are shifted to *m/z* 160 (*a*′), *m/z* 161 (*a*′ + H•), *m/z* 132 (*b*′), and *m/z* 133 (*b*′ + H•), respectively, while those corresponding to fragments *c*, *c* − H•, *d* − H•, and *d* + H• are unchanged. This suggests that the extra oxygen atom is located on the 3-ketoindole moiety of the molecule. The presence in the ^1H nmr of 4 exchangeable protons implies that this oxygen atom is involved in an hydroxyl group. Further examination of the ^1H nmr data shows that the 4-spin system attributable to protons H-5 to H-8 in topsentin-A

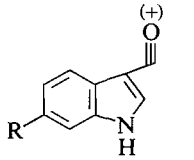

a R = H *m/z* 144
a′ R = OH *m/z* 160

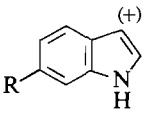

b R = H *m/z* 116
b′ R = OH *m/z* 132

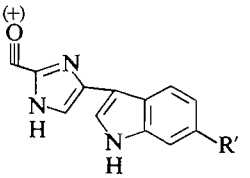

c R′ = H *m/z* 210
c′ R′ = Br *m/z* 288/290

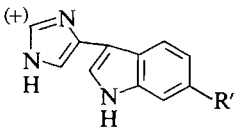

d R′ = H *m/z* 182
d′ R′ = Br *m/z* 260/262

Can. J. Chem. Downloaded from www.nrcresearchpress.com by 213.166.140.6 on 09/07/12
For personal use only.

Can. J. Chem. Downloaded from www.nrcresearchpress.com by 213.166.140.6 on 09/07/12
For personal use only.

is replaced, in the spectrum of topsentin-B1, by a 3-spin system whose pattern indicates a 1,2,4-benzene substitution. The positioning of the hydroxyl group at C-6 follows from comparison of the chemical shifts of these three protons and their adjacent carbon atom in the ^1H and ^{13}C nmr spectra of topsentin-B1 with the chemical shifts calculated from the shielding effects[2] induced by the introduction of an hydroxyl group at C-6 or C-7 in topsentin-A, taken as reference compound. It follows that topsentin-B1 is 6-hydroxytopsentin-A. This structure is fully confirmed by the $^1H/^1H$ and $^1H/^{13}C$ correlated 2D nmr spectra.

In CD_3COCD_3, topsentin-B1 behaves as topsentin-A, existing as a mixture of two tautomeric forms (55:45) in slow interconversion. Again the *b* tautomer is the most abundant.

*Topsentin-B2 (**3**)*

Topsentin-B2 has the same R_f as topsentin-B1 in tlc and the two compounds can only be separated by DCCC. Their spectroscopic properties are closely related and suggest that topsentin-B2 is a monobromo derivative of topsentin-B1. The EI mass spectrum of **3** shows an intense molecular ion cluster at *m/z* 420–422 (50:50) which analyzes for $C_{20}H_{13}N_4O_2Br$ (measured: 420.0237/422.0215; calculated: 420.0222/422.0203) by high resolution mass spectrometry. Moreover, the peaks corresponding to fragments *c*, $c - H^\cdot$, and $d + H^\cdot$ in **1** and **2** are shifted 78–80 daltons to the high masses in the mass spectrum of **3** while those corresponding to fragments *a'* and *b'* are unchanged. These data demonstrate that the bromine atom is attached to the indole moiety of the molecule. Additional support for this hypothesis is provided by the ^1H nmr spectrum, which shows two 3-spin systems characteristic of the presence of two 1,2,4-trisubstituted benzene rings. The locations of the OH and Br substituents in **3** are based, as discussed above, on calculations of the ^1H and ^{13}C shielding effects taking **1** and **2** as reference compounds. Thus, topsentin-B2 is 21-bromotopsentin-B1. The $^1H/^1H$ and $^1H/^{13}C$ correlated 2D nmr spectra are in complete agreement with the proposed structure. As **1** and **2**, topsentin-B2 exists in neutral solution as a mixture of two tautomeric forms (67:33) in slow interconversion, with tautomer *b* being preponderant.

The LD of these three bis-indole alkaloids, for the fish *Lebistes reticulatus*, is between 15 and 20 mg/L, indicating that they are, at least in part, responsible for the toxicity of the methanolic extract of the sponge *Topsentia genitrix*. From a biogenetic point of view, the topsentins most probably derive from the combination of 2 tryptamine (or tryptophane) units.

Until now, only a few tryptamine-derived indole compounds have been isolated from marine invertebrates in general, and from sponges in particular (1, 2, 19, 20). Most of the marine indoles are rather simple compounds, presumably representing small deviations or sidelines in tryptophane metabolism. The topsentins fit nicely into this scheme and reinforce the idea that the complex indole alkaloid metabolic pathways that have appeared in higher plants probably have no counterpart in the marine environment.

Experimental

Thin-layer chromatographic analyses (tlc) were realized on SilG UV_{254} (Macherey Nagel) and visualized by using uv light at 254 nm. Silica gel column chromatographies were performed by the flash technique (21) on MN-Kieselgel 60 (0.04–0.063 mm) and droplet counter current chromatographies (DCCC) on a Büchi B670 (288 tubes, l = 40 cm, i.d. = 2.7 mm).

The ^1H and ^{13}C nmr spectra were recorded at 250 and 62.8 MHz respectively, using a Bruker WM 250 spectrometer. Chemical shifts are quoted in δ values downfield from TMS as internal standard. The 2D experiments were performed using the Bruker microprograms. EI hrms were recorded on a Micromass 7070 F mass spectrometer.

Extraction and purification procedures

The fresh animal, collected by scuba diving near Banyuls (France), was preserved in MeOH and transported to the laboratory in Brussels. The sponge was cut into small pieces and exhaustively extracted with MeOH. Evaporation of the organic solvent under reduced pressure led to an aqueous solution that was extracted with dichloromethane (fraction A: 1.5 g) and dichloromethane–ethanol 3:2 (fraction B: 8.1 g) respectively. The residual aqueous solution was evaporated to dryness and the resulting solid was treated with ethanol (fraction D: 18 g). This latter fraction was percolated on silica gel (eluent:hexane–acetone 6:4 to 0:10).

The less polar fraction (3.1 g) contained mainly topsentin-A, -B1, and -B2, which were separated by DCCC (descending mode; solvent: $CHCl_3$–CH_3OH–H_2O, 13:7:8; flow 7 mL/h; fractions of 10 mL). Fractions 4–11 yielded crude topsentin-A (~500 mg), fractions 35–52 crude topsentin-B1 (~350 mg), and fractions 65–85 crude topsentin-B2 (~100 mg). All three derivatives were purified by silica gel flash chromatography ($CHCl_3$–CH_3OH–NH_3 25%, 19:0.5:1). They were found to be homogenous by hplc (CH_3OH–H_2O, 1:1; RP-18 5μm).

Topsentin-A: mp 290–292°C; uv (CH_3OH) λ_{max}: 209 (43 000), 253 (21 200), 373 nm (17 930) shoulders at 228 and 270 nm; ir (film): characteristic bands at 3250 (br), 1700, 1230, 845, and 735 cm^{-1}; EI ms: 326 (M^+, 100), 210 (13), 209 (78), 183 (23), 181 (7), 163 (15), 154 (13), 144 (56), 117 (16), 116 (21), 89 (15). *Exact Mass* calcd. for $C_{20}H_{14}N_4O$: 326.1168; found (hrms): 326.1169.

Topsentin-B1: mp 270°C; uv (CH_3OH) λ_{max}: 209 (34 900), 237 (23 600), 278 (13 350), 375 nm (13 000) shoulders at 254 nm; ir (film): characteristic bands at 3300 (br), 1710, 1525, 870, and 745 cm^{-1}; EI ms: 342 (M^+, 100), 210 (11), 209 (37), 183 (30), 182 (5), 181 (5), 171 (17), 161 (6), 160 (44), 155 (11), 133 (57), 132 (14), 105 (14). *Exact Mass* calcd. for $C_{20}H_{14}N_4O_2$: 342.112; found (hrms): 342.113.

Topsentin-B2: mp 260°C; uv (CH_3OH) λ_{max}: 285 (17 270), 375 nm (15 870) shoulders at 236 and 256 nm; ir (film): characteristic bands at 3300 (br), 1705, 1590, 1520, 1160, 870 cm^{-1}; EI ms: 422/420 (M^+, 24), 290/288 (3), 289/287 (9), 263/261 (7), 161 (14), 160 (72), 134 (17), 133 (100), 132 (22). *Exact Mass* calcd. for $C_{20}H_{13}N_4O_2Br$: 420.022/420.020; found (hrms): 420.024/422.020.

^1H nuclear magnetic resonance spectra: *: Assignments may be reversed. [a]: Becomes singlet after D_2O treatment; [b]: Disappears after D_2O treatment; s = singlet; bs = broad singlet; d = doublet; dd = double doublet; m = multiplet.

1*a* (CD_3COCD_3, D_2O, CF_3COOD): 8.72 (s, H-2), 8.35 (m, H-5), 8.15 (s, H-17), 8.08 (s, H-14), 7.96 (m, H-23), 7.65 (m, H-8), 7.60 (m, H-20), 7.36 (m, H-7), 7.35 (m, H-6), 7.28 (m, H-21), 7.25 (m, H-22).

1*b* (CD_3COCD_3): 12.05*[b] (bs, H-1), 11.12*[b] (bs, H-18), 10.34[b] (bs, H-15), 9.63 (d,[a] H-2, J = 3 Hz), 8.52 (m, H-5), 8.22 (m, H-23), 7.84 (d,[a] H-17, J = 3 Hz), 7.70 (d,[a] H-14, J = 2.2 Hz), 7.57 (m, H-8), 7.47 (m, H-20), 7.24 (m, H-6 + H-7), 7.15 (m, H-21 + H-22).

1*c* (CD_3COCD_3): 12.05*[b] (bs, H-1), 11.12*[b] (bs, H-18), 10.60[b] (bs, H-12), 9.41 (d,[a] H-2, J = 3 Hz), 8.52 (m, H-5), 8.07 (d,[a] H-17, J = 3 Hz), 7.96 (m, H-23), 7.62 (d,[a] H-14, J = 1.5 Hz), 7.57 (m, H-8), 7.47 (m, H-20), 7.24 (m, H-6 + H-7), 7.15 (m, H-21 + H-22).

2*a* (CD_3COCD_3, D_2O, CF_3COOD): 8.42 (s, H-2), 8.13 (s, H-17), 8.08 (d, H-5, J = 8.6 Hz), 8.04 (s, H-14), 7.90 (m, H-23), 7.56 (m, H-20), 7.25 (m, H-21 + H-22), 7.07 (d, H-8, J = 2 Hz), 6.91 (dd, H-6, J = 8.6 and 2 Hz).

2*b* (CD_3COCD_3): 11.93*[b] (bs, H-1), 10.82*[b] (bs, H-18), 10.33*[b] (bs, H-15), 9.44 (d,[a] H-2, J = 3 Hz), 8.29 (d, H-5, J = 8.6 Hz), 8.21 (m, H-23), 8.14[b] (s, OH), 7.81 (d,[a] H-17, J = 2.6 Hz), 7.67

[2]The shielding effects utilized are those reported for monosubstituted benzene (18).

(d,[a] H-14, J = 2.2 Hz), 7.46 (m, H-20), 7.16 (m, H-21 + H-22), 7.00 (d, H-8, J = 2.2 Hz), 6.82 (dd, H-6, J = 8.6 and 2.2 Hz).

2*c* (CD_3COCD_3): 11.93*[b] (bs, H-1), 10.82*[b] (bs, H-18), 10.77*[b] (bs, H-12), 9.22 (d,[a] H-2, J = 3 Hz), 8.27 (d, H-5, J = 8.6 Hz), 8.11[b] (s, OH), 8.05 (d,[a] H-17, J = 2.6 Hz), 7.94 (m, H-23), 7.55 (d,[a] H-14, J = 1.6 Hz), 7.51 (m, H-20), 7.21 (m, H-21 + H-22), 6.99 (d, H-8, J = 2.2 Hz), 6.80 (dd, H-6, J = 8.6 and 2.2 Hz).

3*a* (CD_3COCD_3, D_2O, CF_3COOD): 8.43 (s, H-2), 8.14 (s, H-17), 8.09 (s, H-14), 8.08 (d, H-5, J = 8.6 Hz), 7.84 (d, H-23, J = 8.5 Hz), 7.78 (d, H-20, J = 1.7 Hz), 7.33 (dd, H-22, J = 8.5 and 1.7 Hz), 7.08 (d, H-8, J = 2.2 Hz), 6.93 (dd, H-6, J = 8.6 and 2.2 Hz).

3*b* (CD_3COCD_3): 12.03*[b] (bs, H-1), 10.8*[b] (bs, H-15), 10.5*[b] (bs, H-18), 9.41 (d,[a] H-2, J = 3 Hz), 8.28 (d, H-5, J = 8.6 Hz), 8.19 (d, H-23, J = 8.5 Hz), 8.11[b] (s, OH), 7.83 (d,[a] H-17, J = 2.5 Hz), 7.69 (d,[a] H-14, J = 2.1 Hz), 7.67 (d, H-20, J = 1.7 Hz), 7.23 (dd, H-22, J = 8.5 and 1.7 Hz), 7.00 (d, H-8, J = 2.2 Hz), 6.83 (dd, H-6, J = 8.6 and 2.2 Hz).

3*c* (CD_3COCD_3): 12.03*[b] (bs, H-1), 10.8*[b] (bs, H-12 and H-18), 9.22 (d,[a] H-2, J = 3 Hz), 8.27 (d, H-5, J = 8.6 Hz), 8.10[b] (s, OH), 8.07 (d,[a] H-17, J = 2.6 Hz), 7.88 (d, H-23, J = 8.5 Hz), 7.72 (d,[a] H-14, J = 1.6 Hz), 7.57 (d, H-20, J = 1.7 Hz), 7.30 (dd, H-22, J = 8.5 and 1.7 Hz), 6.99 (d, H-8, J = 2.2 Hz), 6.82 (dd, H-6, J = 8.6 and 2.2 Hz).

^{13}C nuclear magnetic resonance spectra: *$^{\Phi}$: Assignments may be reversed. The multiplicity of the carbon atom signals have been assigned by using the DEPT pulse sequence. d = CH and s = C.

1*a* (CD_3COCD_3, D_2O, CF_3COOD): 172.1 (C-10, s), 141.5 (C-11, s), 138.5 (C-2, d), 138.0 (C-9, s), 137.6 (C-19, s), 132.5 (C-13, s), 126.9 (C-4, s), 126.4 (C-17, d), 125.4 (C-24, s), 125.3 (C-6*, d), 124.0 (C-7*, d), 123.5 (C-21$^{\Phi}$, d), 122.5 (C-5, d), 121.7 (C-22$^{\Phi}$, d), 119.7 (C-23, d), 116.6 (C-14, d), 114.8 (C-3, s), 113.7 (C-8, d), 113.2 (C-20, d), 103.1 (C-16, s).

2*a* (CD_3COCD_3, D_2O, CF_3COOD): 171.4 (C-10, s), 156.2 (C-7, s), 141.3 (C-11, s), 139.5 (C-9, s), 137.9 (C-2, d), 137.7 (C-19, s), 132.2 (C-13, s), 126.6 (C-17, d), 125.4 (C-24, s), 123.7* (C-21, d), 123.2 (C-5, d), 121.7* (C-22, d), 120.0 (C-4, s), 119.7 (C-23, d), 116.1 (C-14, d), 115.2 (C-3, s), 114.2 (C-6, d), 113.3 (C-20, d), 102.7 (C-16, s), 99.2 (C-8, d).

3*a* (CD_3COCD_3, D_2O, CF_3COOD): 171.3 (C-10, s), 156.3 (C-7, s), 141.6 (C-11, s), 139.5 (C-9, s), 138.5 (C-19, s), 137.8 (C-2, d), 131.5 (C-13, s), 127.5 (C-17, d), 124.8 (C-24, s), 124.5 (C-22, d), 123.3 (C-5, d), 121.4 (C-23, d), 120.0 (C-4, s), 116.7 (C-21, s), 116.5 (C-14, d), 116.1 (C-20, d), 115.2 (C-3, s), 114.1 (C-6, d), 103.2 (C-16, s), 99.1 (C-8, d).

Can. J. Chem. Downloaded from www.nrcresearchpress.com by 213.166.140.6 on 09/07/12
For personal use only.

Acknowledgements

The authors are indebted to the Fonds National de la Recherche Scientifique (Belgium) for financial support (grant no. 2.4515.85).

1. D. J. FAULKNER. Nat. Prod. Rep. **1**, 513 (1984).
2. D. J. FAULKNER. Nat. Prod. Rep. **3**, 1 (1986).
3. J. C. BRAEKMAN and D. DALOZE. Pure Appl. Chem. **58**, 357 (1986).
4. R. P. WALKER, J. E. THOMPSON, and D. J. FAULKNER. Mar. Biol. **88**, 27 (1985).
5. J. E. THOMPSON, R. P. WALKER, and D. J. FAULKNER. Mar. Biol. **88**, 11 (1985).
6. J. HUYSECOM, G. VANDEVYVER, J. C. BRAEKMAN, and D. DALOZE. In preparation.
7. PANIC (Parameter Adjustment in NMR by Iteration Calculation). Bruker Aspect 2000 NMR software. 1981.
8. R. BENN and H. GÜNTHER. Angew. Chem. Int. Ed. Engl. **22**, 350 (1983).
9. Y. GOPICHAND and F. J. SCHMITZ. J. Org. Chem. **44**, 4995 (1979).
10. S. HEITZ, M. DURGEAT, C. BRASSY, B. BACHET, and M. GUYOT. Tetrahedron Lett. **21**, 1457 (1980).
11. I. T. HOGAN and M. SAINSBURY. Tetrahedron, **40**, 681 (1984).
12. A. JOSSANG, H. JACQUEMIN, J. L. POUSSET, A. CAVE, M. DAMAK, and C. RICHE. Tetrahedron Lett. 1219 (1977).
13. P. WULFF, J. S. CARLE, and C. CHRISTOPHERSEN. J. Chem. Soc. Perkin Trans. 1, 2895 (1981).
14. M. P. KIRKUP and R. E. MOORE. Tetrahedron Lett. **24**, 2087 (1983).
15. E. WENKERT, J. S. BINDRA, C. CHANG, D. W. COCHRAN, and F. M. SCHELL. Acc. Chem. Res. **7**, 46 (1974).
16. A. R. KATRITZKY and C. W. REES (*Editors*). Comprehensive heterocyclic chemistry. Vol. 5. Pergamon Press, Oxford. 1984.
17. D. H. R. BARTON and W. D. OLLIS (*Editors*). Comprehensive organic chemistry. Vol. 4. Pergamon Press, Oxford. 1979.
18. E. PRETSCH, J. SEIBL, W. SIMON, and T. CLERC. Tables of spectral data for structure determination of organic compounds. Springer Verlag, Berlin. 1981.
19. C. CHRISTOPHERSEN. *In* The alkaloids. Vol. XXIV. *Edited by* A. Brossi. Academic Press, New York. 1985.
20. C. CHRISTOPHERSEN. *In* Marine natural products. Vol. V. *Edited by* P. J. Scheuer. Academic Press, New York. 1983.
21. W. C. STILL, M. KAHN, and A. MITRA. J. Org. Chem. **43**, 2923 (1978).

Phonon spectra of *ortho*-dinitrotetramethylbenzene crystals

PAOLO SGARABOTTO
Centro per la strutturistica diffrattometrica del C.N.R., Università di Parma, Parma, Italy

MARIO BRAGHETTI
Dipartimento di Chimica, Università di Camerino, Camerino, Italy

AND

ROSARIO SERGIO CATALIOTTI,[1] GIULIO PALIANI, SALVATORE SORRISO, VINCENZO CAIA, AND SERGIO SANTINI
Dipartimento di Chimica, Laboratorio di Chimica fisica dell'Università, Via Elce di Sotto, 8, 06100 Perugia, Italy

Received January 22, 1987

PAOLO SGARABOTTO, MARIO BRAGHETTI, ROSARIO SERGIO CATALIOTTI, GIULIO PALIANI, SALVATORE SORRISO, VINCENZO CAIA, and SERGIO SANTINI. Can. J. Chem. **65**, 2122 (1987).

We have studied the vibrational spectra and thermal behaviour of *ortho*-dinitrotetramethylbenzene (*o*-DNTMB) to learn more about its molecular and lattice dynamics. The molecule undergoes two solid–solid phase transitions, close to the melting point, which could be explained by the relaxation of forces hindering the methyl-group and nitro-group free rotations. We have deduced the nature of the solid state vibrational motions, particularly those of lattice phonons, using group theory.

PAOLO SGARABOTTO, MARIO BRAGHETTI, ROSARIO SERGIO CATALIOTTI, GIULIO PALIANI, SALVATORE SORRISO, VINCENZO CAIA et SERGIO SANTINI. Can. J. Chem. **65**, 2122 (1987).

Dans le but d'obtenir de l'information sur ses dynamiques moléculaire et de réseau, on a étudié les spectres vibrationnels et le comportement thermique de l-*o*-dinitrotétraméthylbenzène (*o*-DNTMB). Près du point de fusion, la molécule subit deux transitions de phase solide–solide; on peut les expliquer par la relaxation des forces qui empêchent respectivement les rotations libres du groupement méthyle et celle du groupement nitro. On a déduit la nature des mouvements vibrationnels à l'état solide, spécialement en ce qui a trait aux phonons.

[Traduit par la revue]

1. Introduction

In this paper we report the results of a study of the vibrational spectra of *ortho*-dinitrotetramethylbenzene (*o*-DNTMB) in the crystalline state. The analysis of the spectroscopic properties of this type of crystal is interesting in that recent report shows that (1) similar molecules have a centre of inversion in the Bravais cell, in spite of the absence of this symmetry element in the molecule itself (2–5).

Studies of the dielectric relaxation properties of similar compounds (6, 7) and of the calorimetric behaviour of *o*-DNTMB (8), have been performed in our laboratory, but the information derived needs to be confirmed by spectroscopic technique where symmetry characteristics of molecules and crystals determine decisively the validity of certain selection rules.

With this in mind, we studied the vibrational spectra of the title molecule using one-phonon ir absorption and Raman scattering. We paid special attention to the low frequency region of the crystal spectra, as from the results we could be able to determine with certainty if the propagated or scattered photons originated from lattice phonons.

2. The model

Crystals of *o*-DNTMB are triclinic at room temperature and belong to the centrosymmetric $P\bar{1}$ (C_i^1) space group, as established by X-ray diffractometry in our laboratory (9). There are two molecular units in the Bravais cell, they couple appreciably, probably through strong dipolar interactions to produce the separation of the doubly degenerate molecular vibrational states of the lattice. Since the molecules have low symmetry, at the most planar C_s, all the fundamental molecular vibrations are active both in the infrared as well in the Raman spectra. The molecular vibrations give rise to Davidov's doublets, through coupling of the quasi degenerate vibrational states of the two interacting molecules of the unit cell. However, with a centrosymmetric crystal, one component (a_u) of the crystal splitting should be active in the infrared spectrum only and the other one (a_g) in the Raman only. This is well featured in the whole mid-frequency region (see Table 1), and also in the region of the lattice vibrations as per Table 2. The centrosymmetric C_i unit cell will give 12 lattice phonons distributed into three acoustical branches and nine optical branches having nine non-zero frequencies at the γ point of the first Brillouin zone. These will involve both translational and librational components to the eigenvectors and, at zero value of the wavevector $\boldsymbol{K}$, those motions having a high translational component can be of LO or TO character.

3. Experimental part

o-DNTMB was prepared in our laboratory following standard procedures, and was purified by a series of crystallization from $C_2H_5OH/CHCl_3$ mixtures. It was finally obtained from $CHCl_3$.

The mid-ir spectra were measured by a Perkin-Elmer, model 983 grating spectrometer, and the far-ir spectra (250–20 cm^{-1}) with a Bruker FT-IR spectrometer, with a resolution in this range of 2 cm^{-1}. Raman spectra were obtained with a Jobin-Yvon RAMANOR HG 2S grating double monochromator. The scattered photons were detected by a thermoelectrically cooled RCA C31034A phototube, coupled with a photon counting chain by Strumentazioni Elettroniche Avanzate (S.E.A., Rome). The exciting source was a Spectra-Physics argon ion laser, model 164-O9, of 5W (all lines power), the power collimated on the samples being at 514.5 nm, ca. 400 mW for the solutions in $CHCl_3$ and ca. 250 mW for the powders. The spectral slit width was 3 cm^{-1} for the solutions and 2 cm^{-1} for the solid samples. Depolarization ratios on the solution spectra were measured with conventional half-wave polarization rotors, standardised on the Raman lines of CCl_4.

4. Results

The results of our vibrational measurements are collected in Tables 1 and 2. The most important crystallographic data are reported in Table 3. Molecular bond distances are shown in

[1]Author to whom correspondence should be addressed.

Printed in Canada / Imprimé au Canada

Can. J. Chem. Downloaded from www.nrcresearchpress.com by 213.166.140.6 on 09/07/12
For personal use only.

TABLE 1. Observed ir and Raman frequencies of *o*-DNTMB in the mid-frequency region

Infrared crystal		Raman crystal		Raman solution[a]		
Frequency, cm^{-1}	Int.	Frequency, cm^{-1}	Int.	Frequency, cm^{-1}	s	Assignment
169	mw	164	mw	—		$t(NO_2)$
225	m	231	w	—		
288	m	292	m	—		zone for
311	ms	315	mw	302		tentative
319	sh	324	w	—		assignment
388	mw	393	mw	—		of o.o.p.
—		419	mw	402		motions of
478	mw	—		—		ring and
488	m	492	s	480	0.14	X-groups
532	mw	—		—		$r(NO_2)$
550	w	546	vw	—		
—		619	w	603		γ(ring)?
642	m	639	vw	—		
690	m	—		—		$w(NO_2)$
722	s	727	m	740	0.84	
762	mw	766	mw	—		δ(ring) +
779	vs	782	w	—		ν(C—X)
858	vs	854	w	838	0.09	$\delta(NO_2)$
883	ms	—				
1001	mw	983	w	—		$r(CH_3)$
1019	w	1023	mw			
1054	m	1048	vw	—		ν(C—N)
1228	mw	—		1224	0.45	ν(ring) +
1265	m	1269	m	1258	0.38	$\nu(C—CH_3)$
1294	mw	1299	m	1286	0.76	
1356	vvs	1360	vs	1350	0.24	$\nu_s(NO_2)$
1389	vs	1395	ms	1380	0.28	$\delta_s(CH_3)$
1446	sh	—		1450	0.33	$\delta_a(CH_3)$ +
1458	ms	1442	w			ν(ring)
1542	vvs	1537	m	1510	0.77	$\nu_a(NO_2)$
1562	s	1570	m	1552	0.75	ν(ring)
2881	mw	2897	mw	—		
2934	w	2938	ms	2910	0.22	$\nu(CH_3)$
2982	mw	2978	w	2995	0.15	
3001	mw	3007	w	—		

[a]Frequency values below 300 cm^{-1} are covered by strong scattering of the Rayleigh line. ν = stretch; δ = in-plane bend; r = rock; w = wag; t = twist.

TABLE 2. Lattice vibrational parameters of *o*-DNTMB as a function of the temperature

	273 K				200 K				77 K			
Mode[a]	Frequency (cm^{-1})	$I/I_{(165)}$	$\Delta\nu_{1/2}$	Area	Frequency (cm^{-1})	$I/I_{(165)}$	$\Delta\nu_{1/2}$	Area	Frequency (cm^{-1})	$I/I_{(165)}$	$\Delta\nu_{1/2}$	Area
ω_1	28	9.08	3.5	31.78	31	5.39	4.0	21.56	33	3.77	5.25	19.79
ω_2	37	10.23	4.0	40.92	42	7.86	4.5	35.37	44	5.28	5.0	26.40
ω_3	45											
ω_4	58	5.15	6.0	30.90	61	4.69	5.0	23.45	63	3.99	5.75	22.94
ω_5	72											
ω_6	80	—	—	—	85	—	—	—	88	—	—	—
ω_7	87	5.54	12.0	66.48	90	4.33	10.0	43.30	92	4.10	10.5	43.05
ω_8	95											
ω_9	108	5.69	10.0	56.90	114	6.80	7.5	51.0	117	6.20	8.5	52.70

[a]ω_3, ω_5, and ω_8 are taken from the far infrared spectrum (Fig. 3).

Fig. 1. Figure 2 shows the one-phonon Raman scattering at low frequency of the crystals at room temperature. The corresponding region of the infrared absorption is shown in Fig. 3.

Thermal behaviour of solid *o*-DNTMB was followed with scanning calorimetry in a temperature range from 298 K to the solid–liquid transition (451.5 K), to confirm that the solid phase that is stable from 77 to 298 K, remains the only form stable above room temperature, or if phase transitions are possible before fusion occurs.

In Table 4 we have collected the results of the calorimetric

Can. J. Chem. Downloaded from www.nrcresearchpress.com by 213.166.140.6 on 09/07/12
For personal use only.

TABLE 3. Crystallographic data of *o*-DNTMB at 298 K

Space group	$P\bar{1}$	(C_i^1)	$Z = 2$
A = 8.3270 (0.0030) Å			α = 63.60 (0.10) deg
B = 8.7340 (0.0030) Å			β = 97.00 (0.10) deg
C = 8.4530 (0.0030) Å			γ = 100.40 (0.10) deg
V = 541.01 (0.59) Å^3			D = 1.3764 g/cm^3

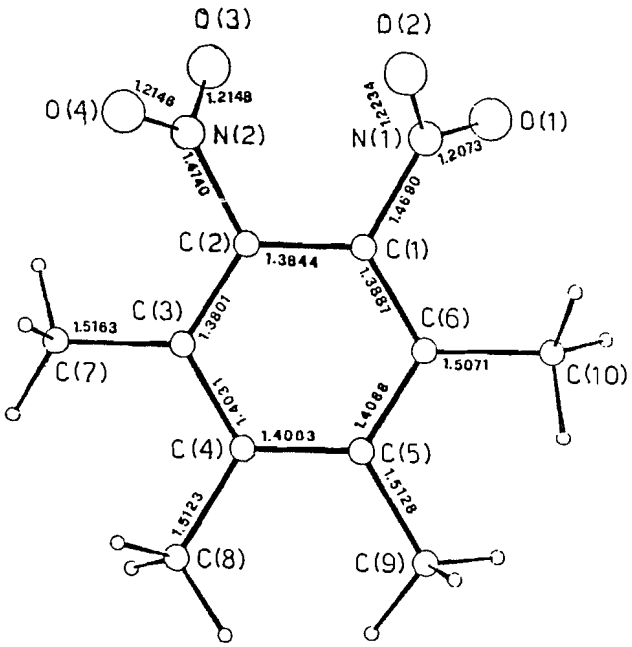

FIG. 1. Schematic drawing and bond distances in *o*-DNTMB crystals at room temperature; average values as follows: C_7—H, 1.0822; C_8—H, 1.0809; C_9—H, 1.0834; C_{10}—H, 1.0812.

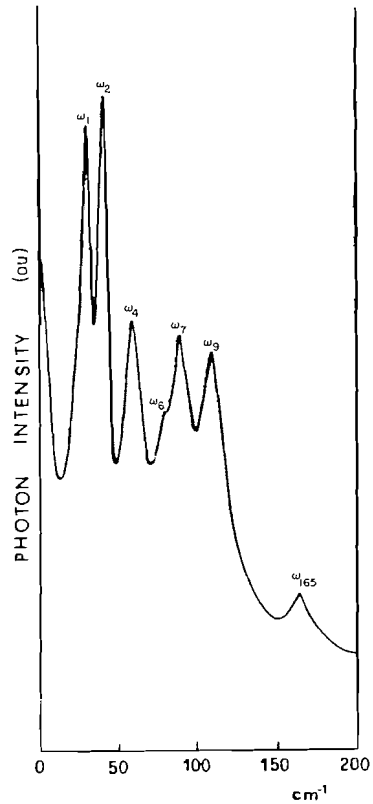

FIG. 2. Low-frequency Raman scattering in *o*-DNTMB crystals at room temperature.

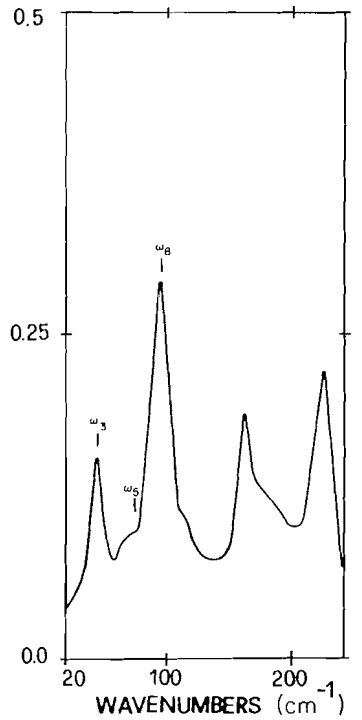

FIG. 3. Low-frequency FTIR spectrum of *o*-DNTMB crystals (polyethylene matrix) at room temperature.

measurements. The data show that two solid–solid phase transitions are present in a restricted temperature range near the melting point. The broadening of the ir and Raman peaks and the temperature dependence of the thermodynamic functions allows us (8) to establish the nature of these phase transitions in the solid state, which, on these grounds, seem to be first-order transitions (10). These might be due to the relaxation, by effect of temperature, of the forces which prevent the free rotation of the methyl- and nitro-groups. The interaction energy among the two different types of substituents should, in fact, be quite different and one could confidently assume that, in the case of the strongly polar NO_2 groups, only very close to the solid–liquid transition the dipole–dipole forces may be overcome.

As appears from Table 1, frequency values of molecular motions are higher in solid state spectra than in solution, except for a few modes. This fact is somewhat surprising, especially because, for stretching vibrations, the intermolecular coupling in the solid state always produces frequency lowering, due to the intramolecular force field variation caused by anharmonicity factors of the crystal field. We shall discuss this point in the following section.

5. Discussion

The vibrational assignment of the fundamental vibrations of *o*-DNTMB was made following previous studies on *ortho*-dinitrobenzene (*o*-DNB) (11), and disubstituted hexamethylbenzenes (1). It is not difficult to attribute the intense infrared peak at 1542 cm^{-1} (the corresponding Raman line is at 1537 cm^{-1}, of medium intensity), to the antisymmetric N—O stretching mode of the —NO_2 groups. The symmetric N—O stretching mode is at 1356 cm^{-1} in the infrared and the depolarization ratio of the Raman line in solution supports

Can. J. Chem. Downloaded from www.nrcresearchpress.com by 213.166.140.6 on 09/07/12
For personal use only.

TABLE 4. Thermal data[a] of crystalline *o*-DNTMB

Type of translation	T (K)	ΔH (J mol^{-1})	ΔS (J mol^{-1} K^{-1})
S—S (1)	423.7 ± 0.5	1727 ± 17	4.88
S—S (2)	445.5 ± 0.5	1323 ± 13	2.97
S—L	451.5 ± 0.5	13483 ± 81	29.86

[a]Obtained from scanning calorimetry.

this assignment. The remaining vibrations of the NO_2 group (scissor, rock, wag, and twist modes) are found at frequencies near those of *o*-DNB (11). Each of these modes gives rise to four ir frequencies, because there are two nitro groups per molecule and two molecules per unit cell.

Methyl group vibrations are assigned in a straightforward manner, since their frequency values are found in the regions expected according to classic group frequency correlations. Thus, besides the C—H stretchings around 2900 cm^{-1}, there are the well-known internal CH_3 bending vibrations δ_a at 1458 and 1446 cm^{-1} (this mode is probably strongly coupled with the ν_{19} mode of the benzenic ring) and δ_s at 1389 cm^{-1}. The rocking modes of the CH_3 groups fall in the region around 1000 cm^{-1} (12, 13). For assignment of the ring modes we have studied extensive literature (1, 11–13) and found many frequencies near those of relevant similar molecules. However, it should be noted that some frequencies have not been assigned with certainty, since we have not performed a normal coordinate calculation.

One peculiar aspect of the lattice properties of *o*-DNTMB in its internal phonon spectrum is the anomalous shift of its vibrational frequencies to the red in going from crystal to solution phase. We can explain this by assuming that the interactions of the solute and solvent molecules to be very strong. This can be true since both the solvent ($CHCl_3$) and the solute are highly polar. Thus, an intimate contact between solute and solvent molecules — as it happens in solution phase — can produce frequency lowerings of dipolar nature much more effectively than the crystalline field acting on the dipoles of the two *o*-DNTMB molecules alone. This interpretation could be supported by the fact that the amount of the crystal splitting, i.e. the frequency difference between a_g and a_u components of the Davidov's doublets is never more than 6–7 wavenumbers.

Table 2 lists some vibrational data for the lattice phonons at three temperatures. It shows a systematic trend towards higher frequencies in all these motions on going from room to liquid nitrogen temperature. Since it is known (14, 15) that cooling changes the molecular packing in crystals, because of the contraction of the unit cell constants, such a systematic increase in frequency at the lower temperatures is attributed to anharmonicity factors on the effective force constants and to an increase of the interaction force constants among the molecules in the lattice potential energy function.

The nine lattice motions having nonzero frequencies at the centre of the first Brillouin zone are, of course, mixed modes. Three of these have the character of nonpure translations of the two molecules out-of-phase (those in-phase constitute the three acoustical branches), and six are nonpure librations due to factor group coupling. The Raman modes have gerade representations and thus, with $Z = 2$, can have translation components with change of polarizability of the unit cell. The three molecular nonpure librations are separated into three a_g (Raman active) and three a_u (infrared active) representations, leading to the tentative pairing of the relevant frequencies: ω_2 with ω_3, ω_5 with ω_6, and ω_7 with ω_8. The frequency separation between infrared and Raman modes is, for all three pairs, of 8 wavenumbers, in quite good agreement with the average frequency separation of motions observed in the mid-frequency region.

The last point we wish to discuss is that connected with parameters such as intensities and half-band widths of these modes. We must expect this latter parameter to decrease systematically from room to liquid nitrogen temperature, as a result of a better definition of the energy values of the excited vibrational states (uncertainty principle). However, we do not observe a regular decrease of the half-band widths, whereas the variation with temperature of the peak intensities seems to be quite regular, being proportional to $(v + 1)$ and increases with temperature. This behaviour might be connected to the systematic variations of the band areas. The freezing, in this case, of the lattice type motions will produce a decrease in the mode amplitudes and consequently in the polarizability variations. This can provide a good explanation of the systematic reduction of the band areas of the Raman lines.

Acknowledgement

The authors are much indebted to the Italian Consiglio Nazionale delle Ricerche, Rome, for having partly sponsored the present research.

1. B. M. BUSSIAN and H. H. EYSEL. Spectrochim. Acta, Part A, **41**, 1149 (1985).
2. L. O. BROCKWAY and J. M. ROBERTSON. J. Chem. Soc. A, 1324 (1939).
3. G. CHARBONNEAU, M. SANQUER, and J. MEINNEL. J. Chim. Phys. **64**, 273 (1967).
4. R. FOURME and M. RENAUD. Mol. Cryst. Liq. Cryst. **17**, 223 (1972).
5. A. TULINSKI and J. G. WHITE. Acta Crystallogr. **11**, 7 (1958).
6. S. SORRISO and S. SANTINI. Z. Phys. Chem. N.F. **129**, 161 (1982).
7. S. SORRISO. Z. Phys. Chem. N.F. **131**, 37 (1982).
8. M. BRAGHETTI and S. SORRISO. To be published.
9. P. SGARABOTTO. Unpublished results.
10. C. N. R. RAO and K. J. RAO. Phase transitions in solids. McGraw-Hill. 1978.
11. J. H. S. GREEN and H. A. LAUWERS. Spectrochim. Acta, Part A, **27**, 817 (1971).
12. J. H. S. GREEN, D. J. HARRISON, and W. KYNASTON. Spectrochim. Acta, Part A, **27**, 793 (1971).
13. G. VARSANYI. Vibrational spectra of benzene derivatives. Academic Press, New York. 1974.
14. G. CARERI, U. BUONTEMPO, F. GALLUZZI, A. C. SCOTT, E. GRATTON, and E. SHYAMSUNDER. Phys. Rev. B, **30**, 4689 (1984).
15. B. MOROSIN. Acta Crystallogr. B, **28**, 1899 (1972).

Can. J. Chem. Downloaded from www.nrcresearchpress.com by 213.166.140.6 on 09/07/12
For personal use only.

The constitution and properties of a pyochelin–zinc complex[1]

DIANE A. CUPPELS, ROBERT D. STIPANOVIC,[2] ALBERT STOESSL, AND J. B. STOTHERS
London Research Centre, Agriculture Canada, and the Department of Chemistry, The University of Western Ontario, University Sub-Post Office, London, Ont., Canada N6A 5B7

Received March 6, 1987

DIANE A. CUPPELS, ROBERT D. STIPANOVIC, ALBERT STOESSL, and J. B. STOTHERS. Can. J. Chem. **65**, 2126 (1987).

The siderophore pyochelin, identified for the first time as a metabolite of *Pseudomonas fluorescens*, was isolated in highly pure form as a dimeric complex with two zinc atoms. The ^{1}H and ^{13}C magnetic resonance data for the two pyochelin moieties of the complex differ significantly from each other and from those of free pyochelin. The complex also exhibits unusual solubility and stability properties. Since it is easily isolable and can be readily converted into highly pure, free pyochelin, it offers an excellent entry to further biological studies on this important metabolite.

DIANE A. CUPPELS, ROBERT D. STIPANOVIC, ALBERT STOESSL et J. B. STOTHERS. Can. J. Chem. **65**, 2126 (1987).

La pyochéline sidérophore a été identifiée pour la première fois comme un métabolite du *Pseudomonas fluorescens*; on l'a isolée à l'état pur sous la forme d'un complexe dimère contenant deux atomes de zinc. Les données de la résonance magnétique nucléaire du ^{1}H et du ^{13}C pour chacune des deux portions du complexe de la pyochéline ainsi que pour la pyochéline libre diffèrent beaucoup entre elles. Le complexe présente aussi des propriétés inhabituelles tant au point de vue de la solubilité que de la stabilité. Puisqu'on peut facilement l'isoler et qu'on peut facilement le retransformer en pyochéline très pure, ce complexe offre une excellente porte d'entrée vers d'autres études biologiques de ce métabolite important.

[Traduit par la revue]

Can. J. Chem. Downloaded from www.nrcresearchpress.com by 213.166.140.6 on 09/07/12
For personal use only.

During the course of a recent biosynthetic study (1) of the antibiotic and phytotoxic pyoluteorin (**1**) from a culture of *Pseudomonas fluorescens*, we obtained another highly fluorescent substance in microcrystalline form and in relatively substantial yield. After extensive ^{1}H and ^{13}Cmr studies of this material, the various carbon–hydrogen part structures were identified and, with additional evidence concerning functional groups, it became apparent that the substance was a metal complex of pyochelin (**2***a*), a recently reported siderophore from *Pseudomonas aeruginosa* (2, 3). This conclusion was confirmed by the ready conversion of the complex into **2***a* and its methyl ester **2***b*. The complex itself, however, is inherently interesting and we wish to describe its properties and our structural studies in some detail in this paper.[3]

The complex separated as a granular powder on concentration of vividly fluorescent fractions eluted after **1**, from a column of TLC grade silica by MeOH–$CHCl_3$–HOAc (10:90:1). After trituration with MeOH, the product was essentially pure as judged by comparison of its ir and nmr spectra with those obtained for a more extensively purified analytical sample. The latter gave combustion results that were in excellent agreement with the values for C, H, and N calculated for $C_{28}H_{28}N_4O_6S_4M_x$ or $C_{28}H_{30}N_4O_6S_4M_x$; values for O and S were within acceptable limits. By difference, these figures also indicated an approximate value for M_x as 17%; ashing, determination of the equivalent weight by titration with 0.1 *M* HCl, paper chromatography, and the volatility of the resulting chloride at red heat tentatively identified M_x as Zn_2. Atomic absorption spectrometry of the complex confirmed this conclusion both qualitatively and quantitatively.

The ^{1}Hmr spectrum of the complex contained separately resolved patterns for 15 protons, two multiplets arising from three and four protons, respectively, and two methyl singlets, δ 2.62, 2.64, ascribable to N-Me groups. The ^{13}C spectrum

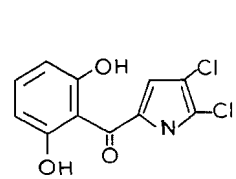

1

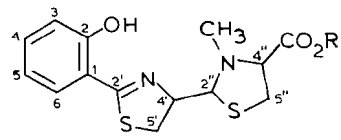

2*a* R=H
b R=Me

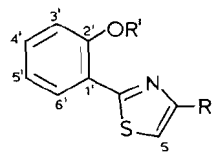

3*a* R=CHO, R'=H
b R=CO_2H, R'=H
c R=CH_2OAc, R'=Ac

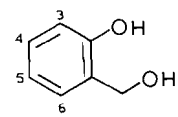

4

exhibited signals for 28 nonequivalent carbons and the number of protons bonded to each was revealed by a DEPT spectrum (5), which also clearly revealed the two methine signals, δ_C 77.6, 77.9, partially obscured by the solvent absorption in the normal spectrum. A ^{1}H–^{1}H correlation (COSY) spectrum (6) permitted a complete analysis of the proton patterns and a ^{13}C–^{1}H correlation spectrum (7) led directly to six part structures. These consist of two aryl fragments **A** and **B** and four saturated units **C**–**F** with the N-Me carbons at δ_C 45.8 and 46.1 and four additional fully substituted carbons at δ_C 174.1, 176.2, 177.6, and 178.4.

Attempted methylation of the complex with CH_2N_2 gave an intractable product but treatment with methanolic HCl under mild conditions afforded two crystalline compounds. One, obtained in high yield (ca. 2 mol based on a molecular weight of 774 for the complex), was an amino acid hydrochloride, identified as either *N*-methylcysteine methyl ester hydrochloride or its autoxidation product, *N*,*N*′-dimethylcystine dimethyl ester hydrochloride, from its ^{1}Hmr spectrum (see Experimental). This substance decomposed before it could be studied further and a second attempt to isolate it failed, for

[1]Part 132 of ^{13}Cmr studies; Part 131 see ref. 13.

[2]Permanent address: USDA Agricultural Research Service, Cotton and Small Grains Research Laboratory, College Station, Texas 77841.

[3]A preliminary account in the published proceedings of a recent symposium (4) contains reproductions of the ^{1}H and ^{13}Cmr spectra.

TABLE 1. ^1H and ^{13}C magnetic resonance data[a] for **2***a* and **2***b*

	2*a*				**2***b*			
	^1H		^{13}C		^1H		^{13}C	
Position	A	B	A	B	A	B	A	B
1	—		116.5	116.0	—	—	116.3	116.2
2	—		158.8	159.0	—	—	159.2	159.0
3	6.85	6.98 [8.0, 1.3]	117.4	117.2	6.91 [8, 2]	6.96 [8.1, 1.2]	117.1	117.0
4		7.37 [8.0, 7.5, 1.7]	133.5	133.6	7.28 [8, 2]	7.30 [8.1, 7.2]	133.1	133.1
5	7.42	6.88 [8.0, 7.5, 1.3]	119.2	119.1	6.80 [8, 2]	6.85 [8.0, 7.2, 1.2]	118.7	118.8
6		7.39 [8.0, 1.7]	131.0	130.7	7.34 [8, 2]	7.36 [8.0]	130.6	130.6
2′	—	—	(173.2)	172.1	—		(172.9)	172.8
4′	4.93	4.85 [7.7, 8.0, 8.6]	(74.3)	80.1	5.01 [8.9, 5.9]	5.06 [9.1, 8.6, 5.1]	(72.4)	79.4
5′	3.40	3.25 [11.3, 8.0]	33.6	33.3	3.39 [11.2, 8.5]	3.38 [11.3, 9.1]	(32.4)	32.5
		3.45 [11.3, 8.6]			3.33 [11.2, 9.0]	3.45 [11.3, 8.6]		
2″	4.42	4.34 [7.7]	(77.7)	77.9	4.45 [5.2]	4.50 [5.1]	(76.1)	76.1
4″	3.78	3.83 [6.4, 6.8]	(76.3)	73.6	3.58 [9.0, 6.3]	3.63 [8.7, 6.7]	[b]	72.4
5″	3.29	3.30 [11.6, 6.8]	33.6	33.9	3.03 [10.7, 9.0]	3.09 [10.5, 6.7]	(32.9)	33.0
		3.36 [11.6, 6.4]			3.10 [10.7, 6.3]	3.15 [10.5, 8.7]		
N-Me	2.65	2.69	43.4	44.0	2.51	2.56	41.2	41.3
COOR	—	—	(174.2)	173.8	3.69	3.74	(171.4)	171.3
							52.3	52.5

[a]Shieldings in ppm from internal TMS for $CDCl_3$ solutions: columns A from ref. 3, columns B this work; similar values in parentheses may be interchanged. ^1H–^1H couplings in Hz listed in square brackets.
[b]Signal masked by $CDCl_3$ absorption.

reasons that are unclear. Unfortunately this precluded determination of its configuration. As models, L-*N*,*N*′-dimethylcystine and L-*N*-methylcysteine were prepared according to literature procedures (8) and their proton data strongly favored formulation of the degradation product as the monomer. However, attempts to convert the authentic compounds into their methyl ester hydrochlorides by treatment with methanolic HCl gave only ill-defined products. In the meantime, other evidence had rendered a rigorous identification of the degradation product unnecessary and these problems were not pursued further.

The second methanolysis product, obtained in only small quantity, had the constitution $C_{10}H_7NO_2S$ according to precise mass measurements and its structure was readily shown to be that of aeruginaldehyde (**3***a*) from its uv, ^1H, and ^{13}C spectra. The uv and proton data were in close agreement with those for aeruginoic acid (**3***b*), which has been described as a metabolite of *P. aeruginosa* (9). In further confirmation of structure **3***a*, the compound gave an intensely yellow spot on tlc with 2,4-dinitrophenylhydrazine as spray reagent and was readily reduced by sodium borohydride to furnish, upon acetylation, the diacetate **3***c* with the requisite ^1Hmr spectrum (see Experimental).

When a solution of the complex in $CHCl_3$ was briefly shaken with 0.01 *M* HCl, the organic phase furnished a syrup with the uv, ^1H, and ^{13}C spectra corresponding to those reported for pyochelin (2, 3). Methylation of this product with CH_2N_2 gave a methyl ester whose ^1H and ^{13}Cmr parameters agreed closely with those reported for **2***b* (3). Our nmr data are collected in Table 1 together with those reported previously for **2***a* and **2***b*. In the earlier report, no ^1H–^1H coupling constants were given for **2***a*, which also contained an unidentified contaminant. However, we found that the components of the various multiplets could be clearly resolved and the coupling constants readily determined; the coupling interactions were confirmed with a ^1H–^1H COSY spectrum and a decoupling experiment. With a complete analysis of the ^1H spectrum, the ^{13}C assignments listed in Table 1 were definitively determined from a ^{13}C–^1H heteronuclear correlation spectrum. A complete analysis of the proton spectrum of **2***b* was straightforward and a ^{13}C–^1H correlation spectrum led to the unequivocal ^{13}C assignments listed in Table 1.

A sample of the zinc-free product obtained by treatment of the complex with dilute HCl was passed through a column of silica as in the original isolation of the complex and found to yield the original complex as judged by the ^1H spectrum of the eluted material. In a supplementary experiment, a small amount of the complex in chloroform was shaken with a 1% solution of HOAc in water. The product from the organic phase was a 2:5 mixture of the complex and free **2***a*, as estimated from the proton spectrum. The constitution of the complex as $(pyochelin)_2Zn_2$ was therefore established beyond doubt but several additional points merit discussion.

The ready conversion of pyochelin into the complex on SiO_2 indicated that the original isolate was probably an artifact of chromatography. This was confirmed by extracting a fresh batch of bacterial cultures with EtOAc both before and after acidification. Both extracts exhibited uv spectra characteristic of a mixture of **1** (λ_{max} 255, 310 nm) and free **2***a* (λ_{max} 250, 310 nm) without detectable peaks or shoulders ascribable to the complex (λ_{max} 264, 359 nm), but the latter was obtained upon chromatography of the combined extracts over SiO_2. The source of the zinc is almost certainly a zinc salt, the supposedly inert but otherwise unspecified phosphor, incorporated into the silica by the manufacturers. Elution of a sample of the silica with a volume of solvent approximately equivalent to that used in the isolation of the complex furnished only about 20% of the zinc eluted as the pyochelin complex in the main experiment, thereby implying a high affinity of pyochelin for this metal.

A more difficult question is the manner in which the part structures **A**–**F** are combined to form two pyochelin moieties since no long-range proton interactions were resolved in the

Can. J. Chem. Downloaded from www.nrcresearchpress.com by 213.166.140.6 on 09/07/12
For personal use only.

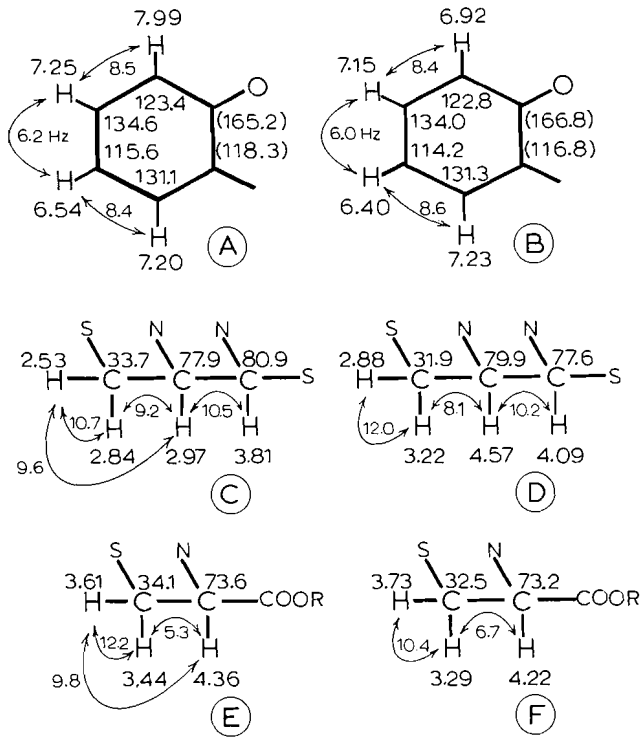

^{1}H spectrum. However, the COSY spectrum of the complex revealed weak cross-peaks (off-diagonal elements) for the pair of protons at δ 3.81 and 4.36 and for those at δ 4.09 and 4.22 signalling weak long-range interactions between H-2″ and H-4″ in each of the thiazolidine rings, thereby correlating part structure **C** with **E**, **D** with **F**, and identifying the linked pairs of thiazolidine and thiazoline rings in the two moieties; but no evidence was available through which we could assign **A** or **B** to the **C**–**E** or **D**–**F** fragments.

Thirdly, it remained to determine the nature of the binding of zinc to the pyochelin units. At this stage, only a partial answer to this question can be presented. The ir spectrum of the complex, in $CHCl_3$, shows no strong absorption in the 1650–1800 cm^{-1} region that could be attributed to free carboxyl or ester. On the other hand, strong absorption at 1592 cm^{-1} indicated that both carboxyl groups are present in ionized form. This does not necessarily imply that the zinc atoms are in close proximity thereto. In the uv spectrum, the band at 359 nm undergoes a hypochromic shift on acidification, clearly because of liberation of pyochelin, but no significant bathochromic shift is observed on addition of alkali.[4] This implies that at least one of the phenolic hydroxyls is ionized while the other is either ionized or coordinately bonded to zinc. The ^{1}Hmr spectrum does not resolve this question. The proton *ortho* to oxygen in the aryl fragment **A** absorbs at anomalously low field, δ 7.99, which is 1 ppm downfield from the corresponding protons in **2***a*, **2***b*, **3***a*, and the second pyochelin moiety of the complex. Direct comparison with a model phenol and its phenolate was not possible with the $CDCl_3$ solvent used. The only readily available information from the literature indicated that ionization of phenols produces a small upfield shift of the *ortho* protons (10). In a model experiment, we found pronounced upfield shifts for all aryl protons of salicyl alcohol in DMSO-d_6 – 1 *M* NaOH (4:1) relative to its equimolar solution in DMSO-d_6–H_2O (4:1) (see Experimental). A direct comparison with the complex and pyochelin in these solvents was not possible because of apparent decomposition of the complex, even in DMSO-d_6–H_2O alone. Fortunately, the ^{13}C spectrum was more informative. The shieldings of both oxygen bearing carbons of the complex are similar (δ_C 165.2, 166.8), and both absorb distinctly downfield from the corresponding signals for **2***a* (δ_C 159.0) and **2***b* (159.0). Similar differences are found for the protonated aryl carbon *ortho* to oxygen (C-3) while the C-5 signals, *para* to oxygen, are shielded by 3–5 ppm in the complex relative to **2***a* and **2***b*. These trends are similar to those recently reported for the *ipso*, *ortho*, and *para* carbons in a series of phenols upon deprotonation (11). It is interesting that only one of the substituted carbons *ortho* to oxygen in the complex exhibits an appreciable downfield shift relative to the shielding of this carbon (C-1) in **2***a*. Furthermore, the imino and carboxyl carbons in the complex, δ_C 174.0, 176.1, 177.4, and 178.4, are downfield from the corresponding signals in **2***a*, δ_C 172.1, 173.8. The most probable explanation of the sum of these data is that the hydroxyl and carboxyl groups are ionized and the *ortho* hydrogen of part structure **A** is strongly and differentially shielded by spatial proximity to zinc or other functional group. It may be noted that the relative orientations of the thiazolidine and thiazoline rings in the two pyochelin moieties in the complex must differ from that in pyochelin itself since the vicinal couplings between H-2″ and H-4′ are 10.2 and 10.5 Hz in the complex but only 7.7 Hz in **2***a* (5.1 Hz in **2***b*). It seems curious that no vicinal coupling was resolved for one of the methylene protons in each of the rings containing fragments **D** and **F** while significant vicinal interactions were apparent for each of the corresponding methylene protons in **C** and **E** as well as **2***a* and **2***b*.

During the final stages of preparation of this manuscript, a report appeared (12) describing the formation, upon SiO_2 chromatography, of an aluminum complex of 2-hydroxy-4-methoxy-5-methylpyridine-*N*-oxide, a siderophore of *Pseudomonas cepacia*. The authors comment, as we have (4), that the binding of siderophores to cations other than Fe^{3+} may have biological significance.

Experimental

Mass spectra were obtained with a Varian MAT 311A system, uv spectra on EtOH solutions with a Shimadzu 240 uv, and ir spectra on $CHCl_3$ solutions with a Pye–Unicam PU9516 spectrophotometer. The ^{1}Hmr spectra were recorded with Varian XL-200 and -300 systems on $CDCl_3$ solutions with TMS as internal reference while ^{13}C spectra were determined with the XL-300 system employing $CDCl_3$ solutions. The number of protons on individual carbons was assessed using the DEPT sequence (5) whereby the signals for methylene carbons are 180° out of phase with the methine and methyl peaks and those for fully substituted carbons are nulled. The ^{1}H and ^{13}C nmr spectra were independent of concentration over a 5-fold range, 5–25 mg/0.4 mL. Homonuclear ^{1}H–^{1}H correlation spectra were obtained using the HOMCOR sequence of the XL software with a 1024 × 512 data point matrix transforming 1024 points in both domains using a spectral width of 1 kHz (**2***a*, XL-200) and 1.8 kHz (Zn complex, XL-300) in both domains. The heteronuclear ^{13}C–^{1}H correlation spectra were recorded with the XL-300 utilizing the HETCOR sequence of the XL software using a 2048 × 128 data matrix, transforming 2048 and 512 points across spectral widths of 8.2 kHz for ^{13}C and 1.8 kHz for ^{1}H, respectively.

Unless otherwise indicated, all solvents were redistilled before use; EtOH was the 95% product. Macherey–Nagel Polygram Sil G/UV_{254} 0.25-mm sheets were used for tlc and SiO_2 (Camag DFO) for column chromatography, with MeOH–$CHCl_3$–HOAc (10:90:1) as solvent.

[4]However, a significant bathochromic shift was observed on rendering the acidified solution alkaline.

Can. J. Chem. Downloaded from www.nrcresearchpress.com by 213.166.140.6 on 09/07/12
For personal use only.

Can. J. Chem. Downloaded from www.nrcresearchpress.com by 213.166.140.6 on 09/07/12
For personal use only.

Evaporations were done at water aspirator pressures. Melting points were determined on a Kofler apparatus and are uncorrected. Microanalyses were carried out by Guelph Chemical Laboratories Ltd.

Isolation and properties of the pyochelin–zinc complex

Pseudomonas fluorescens Pf5 was grown for two days on King's B broth (16 × 40 mL) and harvested as described previously (1) except that the cultures were not amended with sodium acetate. The EtOAc extracts obtained from four batches of the centrifuged and acidified culture media were combined (800 mg) and chromatographed (25-mL fractions) over SiO_2 (500 g) that had been packed from ca. 1 L and then prewashed with another 4 L of the standard solvent. Pyoluteorin (**1**) was eluted in fractions 40–45 and the pyochelin–zinc complex in fractions 58–72 (tlc). The latter were combined, the solvent evaporated, and the solid residue triturated with MeOH (10 mL). The product was removed by filtration and washed with several small portions of MeOH to give practically pure complex (117 mg), identical by ^{1}H and ^{13}Cmr with material initially isolated in the biosynthetic experiments (1).[5]

An analytical specimen was prepared by washing the above material (34 mg) in $CHCl_3$ (10 mL) with water (2 × 2 mL) and reextracting the aqueous phase with $CHCl_3$ (10 mL). The material obtained from the combined filtered $CHCl_3$ layers by evaporation was precipitated from $CHCl_3$ (0.2 mL) by dropwise addition of MeOH (2 mL) to give pure complex (26 mg after drying *in vacuo* at room temperature for 24 h).

Ultraviolet spectrum, λ_{max} (ϵ): 359 (13 800), 264 (19 800), and 244 (44 600) nm; λ_{max} (EtOH/$^+$H): 311 (10 200), 250 (22 900), and 210 (46 200); λ_{max} (EtOH/$^-$OH): 361 (12 900), 262 (19 700), and 221 (46 200) when determined immediately but after 1 h, following the addition of alkali, λ_{max}: 354 (12 000), 252 (19 700), and 220 (sh) (40 900). Similar values were obtained for the alkaline solution after 3.5 h but very extensive decomposition was apparent when the spectrum was examined 3 days later. After treatment of the acidified solution (1 drop of 0.1 *M* HCl) with a small excess of 0.1 *M* NaOH (2 drops), λ_{max}: 368 (10 900), 255 (18 200), and 220 (40 200). Infrared spectrum ($CHCl_3$): 2840 (w), 2700–2800 (vw), 1670 (m), 1657 (sh), 1608, 1592 (vs), 1573, 1463, 1440, 1402, 1400, 1361, 1331, 1310, 1152, 1143, 1134, 1090, 1035, 976, 964, and 952 cm^{-1}. *Anal.* calcd. for $C_{28}H_{28}N_4O_6S_4Zn_2$: C 43.36, H 3.64, N 7.22, O 12.38, S 16.53, ash (as ZnO) 20.99, Zn 16.86; calcd. for $C_{28}H_{30}N_4O_6S_4Zn_2$: C 43.25, H 3.89, N 7.21, O 12.35, S 16.49, ash 20.93, Zn 16.81; found: C 42.98, H 3.83, N 7.23, O 13.75, S 15.13, ash 18.3, Zn (atomic absorption) 16.67.

The complex was readily soluble in $CHCl_3$ when obtained by evaporation of a water-washed solution but, when dry, required a small drop of MeOH for complete solution. It was precipitated on addition of more MeOH and was practically insoluble in EtOH, Me_2CO, and C_6H_6. Dilute solutions for uv measurements were effected only by prolonged heating. The complex dissolved in hot EtOAc but, on cooling, separated in amorphous form that was not further investigated.

Methanolysis of the complex

A solution of the complex (16 mg, 0.02 mmol) in MeOH (5 mL) containing HCl (3.8%) was evaporated after standing at room temperature for 1 day. After repeated reevaporation from MeOH–$CHCl_3$, the product was dissolved in $CHCl_3$ (ca. 2 mL) on addition of just sufficient MeOH. After standing in an open flask for ca. 2 h, a crystalline substance separated (product **A**, 7.8 mg). The residue obtained by evaporation of the mother liquors was dissolved in $CHCl_3$, washed with water, reevaporated, and chromatographed over SiO_2 (15 g) with $CHCl_3$ (2-mL fractions). Fraction 18 (2.8 mg) crystallized from MeOH upon addition of water to turbidity and refrigeration (product **B**, 2 mg, mp 60–63.5°C).

Product A

After washing with $CHCl_3$, this methyl ester (see text) had mp 174–175°C; R_f 0.34 on Whatman No. 1 paper in *n*-BuOH–H_2O–HOAc (4:5:1) (weak purple to ninhydrin); only end absorption in the uv spectrum; ^{1}Hmr (D_2O) δ: 4.37 (t, $J \sim 5$ Hz, 1H), 3.75 (s, 3H, OMe), 3.44 (dd, $J = 4.6$, 15.6 Hz, 1H), 3.26 (dd, $J = 5.5$, 15.6 Hz, 1H), and 2.68 (s, 3H, N-Me). On standing three days in D_2O the substance had decomposed to several products (deposition of solid, paper chromatography). A portion of the residue obtained upon evaporation of the solvent was ignited with sodium, the product giving strongly positive reactions in the standard tests for N, S, and Cl^-.

L-*N*,*N*′-Dimethylcystine, prepared from L-thiazolidine carboxylic acid (1.66 g) as described in the literature (8), had mp 221°C (dec.) (capillary inserted at 210°C, lit. (8) mp 217–219°C); ^{1}Hmr (D_2O) δ: 3.80 (t, $J \sim 6$ Hz, 1H), 3.19 (d, $J = 6$ Hz, 2H), 2.61 (s, 3H).

L-*N*-Methylcysteine, prepared from the cystine derivative (8), had mp 233–233.5°C (dec.) (capillary inserted at 220°C, lit. (8), mp 228–229°C); ^{1}Hmr (D_2O) δ: 4.11 (dd, $J = 4.4$, 6.1 Hz, 1H), 3.43 (dd, $J = 4.4$, 15.4 Hz, 1H), 3.34 (dd, $J = 6.1$, 15.4 Hz, 1H), 2.65 (s, 3H).

Product B

Recrystallization from cyclohexane gave aeruginaldehyde, mp 135–135.5°C; ir ($CHCl_3$): 3120, 3050, 3020, 2050, 1701 (s), 1622, 1582, 1481 (s), 1270, 1160, 1138, 1012, 946 cm^{-1}; λ_{max} (EtOH): 321 (7 800), 280 (8 500), 212 sh (13 000), and 203 (14 300); (EtOH/$^-$OH): 367 (10 300), 278 (10 600), 237 (22 500), 206 (75 000); ^{1}Hmr ($CDCl_3$) δ: 10.03 (s, 1H, -CHO), 8.12 (s, H-5), 7.62 (dd, $J = 1.5$, 7.9 Hz, H-6), 7.37 (ddd, $J = 1.5$, 7.4, 8.4 Hz, H-4′), 7.09 (dd, $J = 1.2$, 8.4 Hz, H-3′), 6.94 (ddd, $J = 1.2$, 7.4, 7.9 Hz, H-5′; ^{13}Cmr ($CDCl_3$) δ_C: 183.3 (CHO), 118.2, 119.8, 125.1, 127.6, 132.9 (5 × aryl CH), 116.0, 153.5, 156.8, 163.0 (4 × aryl C). *Exact Mass* calcd. for $C_{10}H_7NO_2S$: 205.0197; found: 205.0192.

The compound (0.5 mg) in MeOH (0.5 mL) was treated with a few crystals of $NaBH_4$ at room temperature and reaction was complete almost immediately (tlc). After the addition of water and a drop of HOAc, the product was extracted into $CHCl_3$, the solvent evaporated, and the residue acetylated with a few drops of Ac_2O–C_5H_5N (2:3) overnight. Preparative tlc (precoated plate, Baker 1007-4) in MeOH–$CHCl_3$–HOAc (5:95:1) gave the diacetate of the reduction product as an oil, homogeneous on tlc; ^{1}Hmr ($CDCl_3$) δ: 8.22 (dd, $J = 1.8$, 7.5 Hz, H-3′), 7.46 (dt, $J = 1.8$, 7.5 Hz, H-5′), 7.38 (t, $J = 0.8$ Hz, H-5), 7.35 (dt, $J = 1.5$, 7.5 Hz, H-4′), 7.22 (dd, $J = 1.5$, 7.5 Hz, H-6′), 5.30 (d, $J = 0.8$ Hz, -CH_2O-), 2.44 (s, 3H, ArOAc), 2.15 (s, 3H, OAc). Assignments were confirmed by irradiation at δ 8.22, which produced doublets of doublets at δ 7.46 ($J = 7.5$, 7.8 Hz), 7.35 ($J = 1.5$, 7.5 Hz), and 7.22 ($J = 1.5$, 7.8 Hz).

Interconversions of the complex and pyochelin

The complex (10.9 mg) in $CHCl_3$ (10 mL) was shaken for 2 min with 0.01 *M* HCl (10 mL). The aqueous layer was extracted with more $CHCl_3$ (2 × 4 mL), and the organic phases were washed in turn with water (2 × 2 mL), combined, and evaporated to furnish a fluorescent syrup (9.6 mg) identified as pyochelin (**2***a*) by the spectral data; ir ($CHCl_3$): 1767 (vs), 1725 (sh), 1620, 1590, 1564, 1490, 1452, 1355, 1295, 1152, 1118, 949, 904 cm^{-1}; λ_{max} (EtOH): 312 (9 900), 250 (22 200), 210 (48 100); λ_{max} (EtOH/$^-$OH): 348 (14 600), 250 (26 700), 220 (55 500); ^{1}Hmr and ^{13}Cmr (see Table 1).

Methylation of the product (4.8 mg) as reported (3) gave **2***b*, the ^{1}H and ^{13}Cmr data for which are collected in Table 1.

Another portion (2.9 mg) of **2***a* obtained above was chromatographed in 5-mL fractions over SiO_2 (4 g) packed in 20 mL and prewashed with 25 mL of the standard solvent. The material (~3 mg) eluted in fractions 4 and 5 was substantially pure complex as judged by its ^{1}Hmr spectrum. In a second experiment, the centrifugate obtained from a fresh batch of cultures (16 × 40 mL) was divided into two equal portions; one (pH 7.2) was extracted with EtOAc (3 × 300 mL) while the second was acidified with 2 *M* HCl (40 mL) before extraction. After evaporation, dissolution in EtOH, and dilution to 1 L, the two extracts exhibited λ_{max} 310 (d 0.205), 250 (0.335), and 222 (0.78) and λ_{max} 310, 290 (sh), 250, 211 (d 0.63, 0.56, 1.20, 2.92), respectively. The extracted centrifugate, pH 7.2, was then acidified with HOAc and reextracted similarly, to give a solution (1 L) with λ_{max} 310, 250, 209 (d 0.092, 0.68, 1.92). Further acidification with 2 *M* HCl and extraction gave material with only ill-defined absorption bands. The

[5]Both in the biosynthetic and several other runs, the highly pure complex separated directly on concentration of the appropriate fractions.

first pair of extracts were combined and chromatographed over SiO_2 (100 g) in the usual way to furnish the complex (8.8 mg after washing in, and precipitation from, $CHCl_3$), identified by the ^{1}Hmr spectrum.

A solution of pure complex (3.6 mg) in $CHCl_3$ (4 mL) was shaken for 2 min with 0.1 *M* Na_2CO_3 (2 mL) and then water (2 × 2 mL) and the aqueous layers were extracted in sequence with $CHCl_3$ (3 × 2 mL). The material obtained upon evaporation of the solvent from the combined $CHCl_3$ layers exhibited the ^{1}Hmr spectrum of the complex.

Another sample of the pure complex (3.5 mg) was shaken with 1% HOAc (2 mL) and worked up as described above. The proton spectrum of the product (3.1 mg) corresponded to that of a mixture of complex and free **2***a* in a 2:5 ratio.

In a control experiment, a column of SiO_2 (50 g) was packed in, and washed with, the standard solvent until 400 mL had been collected. Another 200 mL of solvent was then percolated through the column and collected separately. The first eluate, after washing and reevaporation from 2 *M* HCl, contained only a barely detectable trace of zinc (paper chromatography). The material (ca. 5 mg) similarly obtained from the second eluate contained 0.35 mg of Zn (atomic absorption).

Formation of ferripyochelin

The complex (1 mg) was distributed between EtOAc (3 × 5 mL) and aqueous $FeCl_3$ (0.1%, 3 × 5 mL). The EtOAc layers were washed with water (3 × 0.8 mL), combined, and evaporated to give free **2***a* (0.16 mg) as estimated from the uv spectrum. The extracted $FeCl_3$ layers and washings were combined, strongly acidified (0.8 mL, 2 *M* HCl), and extracted with EtOAc (4 × 10 mL). On attempted washing with water (2 × 0.8 mL), much of the red color of the extracts passed into the water but was reextracted on acidification (0.05 mL, 2 *M* HCl) of the combined washings. After washing with another portion of HCl (1 mL, 0.1 *M*), the EtOAc extracts were combined, diluted with EtOH, and evaporated. The product exhibited an uv spectrum (λ_{max} 520, 420 sh, 320, 255, 232, and 213 nm) very similar to that reported for ferripyochelin (λ_{max} 520, 425, 325, 255, and 237 nm), in an amount corresponding to 0.38 mg as estimated from the published data (2).

Alkali-induced ^{1}Hmr shifts in salicyl alcohol

Salicyl alcohol (**4**) (12.4 mg, 1.0 mmol) exhibited a spectrum in DMSO-d_6 (0.4 mL)/H_2O (0.1 mL) solution containing signals at δ 8.28 (dd, J = 1.7, 7.2 Hz, H-6), 8.09 (dt, J = 1.7, 7.5 Hz, H-4), 7.82 (dt, J = 1.1, 7.5 Hz, H-5), 7.79 (dd, J = 1.1, 7.8 Hz, H-3), and 5.28 (s, 2H, CH_2O) and, in DMSO-d_6 (0.4 mL)/NaOH (0.1 mL, 1 *M*), these signals appeared at δ 7.76 (m, 2H, H-4, -6), 7.30 (dd, J = 1.2, 8.4 Hz, H-3), 7.14 (dt, J = 1.2, 7.2 Hz, H-5), and 5.35 (s, 2H, -CH_2O-).

The proton spectrum of the complex (3 mg) in DMSO-d_6–H_2O showed only a few broad absorption bands that bore little, if any, resemblance to the features of the $CDCl_3$ spectrum.

Acknowledgements

We are grateful to G. L. Rock and F. Smith for experimental assistance, D. Hairsine for mass measurements, S. Wilson for ^{1}Hmr spectra, and for the financial support of the Natural Sciences and Engineering Research Council of Canada.

1. D. A. Cuppels, C. R. Howell, R. D. Stipanovic, A. Stoessl, and J. B. Stothers. Z. Naturforsch. C: Biosci. **41**, 532 (1986).
2. C. D. Cox and R. Graham. J. Bacteriol. **137**, 357 (1979).
3. C. D. Cox, K. L. Rinehart, M. L. Moore, and J. C. Cook. Proc. Natl. Acad. Sci. U.S.A. **78**, 4256 (1981).
4. A. Stoessl and J. B. Stothers. *In* Ann. Proc. Phytochem. Soc. Europe. *Edited by* K. Hostettman. Oxford University Press. In press.
5. D. M. Doddrell, D. T. Pegg, and M. R. Bendall. J. Magn. Reson. **48**, 323 (1982).
6. A. Bax, R. Freeman, and G. A. Morris. J. Magn. Reson. **42**, 169 (1981).
7. G. A. Morris and I. D. Hall. J. Am. Chem. Soc. **103**, 4703 (1981).
8. W. Keller-Schierlein, M. L. Mihailovic, and V. Prelog. Helv. Chim. Acta, **42**, 305 (1959); S. Ratner and H. T. Clarke. J. Am. Chem. Soc. **59**, 200 (1937).
9. Y. Yamada, N. Seki, T. Kitahara, M. Takahashi, and M. Matsui. Agric. Biol. Chem. **34**, 780 (1970).
10. L. M. Jackman and S. Sternhell. Applications of nuclear magnetic resonance spectroscopy in organic chemistry. 2nd ed. Pergamon Press, Oxford. 1969. p. 204.
11. P. K. Agrawal and H.-J. Schneider. Tetrahedron Lett. **24**, 177 (1983).
12. S. Winkler, W. Ockels, H. Budzikiewicz, H. Kort, and G. Pulverer. Z. Naturforsch. C: Biosci. **41**, 807 (1986).
13. G. A. Antoniadis, M. T. M. Clements, S. Peiris, and J. B. Stothers. Can. J. Chem. **65**, 1557 (1987).

Can. J. Chem. Downloaded from www.nrcresearchpress.com by 213.166.140.6 on 09/07/12
For personal use only.

Photochemistry of dibenzylketone in Nafion membranes[1]

V. WINTGENS AND J. C. SCAIANO

Division of Chemistry, National Research Council of Canada, Ottawa, Ont., Canada K1A 0R6

Received January 14, 1987

V. WINTGENS and J. C. SCAIANO. Can. J. Chem. **65**, 2131 (1987).

Photolysis of dibenzyl ketone in vacuum-dried Nafion membranes leads to the detection of fluorescence from the protonated ketone and formation of modest yields of benzyl cations characterized using laser photolysis techniques. Exchange of the acid sites in Nafion by cationic surfactants leads to decreased environmental polarity and a change in mechanism towards the benzyl radical chemistry which is common in organic solvents. The decay of benzyl radicals in Nafion membranes shows magnetic field dependence which indicates that geminate processes play an important role.

V. WINTGENS et J. C. SCAIANO. Can. J. Chem. **65**, 2131 (1987).

La photolyse de la dibenzyl cétone, adsorbée sur membranes Nafion déshydratées sous vide, conduit à la détection de la fluorescence de la cétone protonée et à la formation en faible quantité de cations benzyliques, caractérisés par l'intermédiaire de techniques de photolyse laser. Lorsque les sites acides de la membrane Nafion sont échangés avec des surfactants cationiques, la polarité du milieu diminue, et le mécanisme change pour la chimie du radical benzylique, habituellement observée dans les solvants organiques. La décroissance du radical benzylique dans les membranes Nafion dépend du champ magnétique appliqué, indiquant que les processus géminés jouent un rôle important.

Can. J. Chem. Downloaded from www.nrcresearchpress.com by 213.166.140.6 on 09/07/12
For personal use only.

Introduction

The photochemistry of dibenzylketone (DBK) has been examined in several solvents (1) and leads to the efficient formation of 1,2-diphenylethane as the only major product. The product is formed by reaction of the benzyl radicals, which are generated in two ways, in the Norrish type I reaction from the triplet state of DBK, and in the decarbonylation of the phenylacetyl radicals, i.e.:

[1] $PhCH_2COCH_2Ph \xrightarrow{h\nu} {}^3PhCH_2COCH_2Ph^*$

[2] ${}^3PhCH_2COCH_2Ph^* \rightarrow PhCH_2^{\cdot} + PhCH_2CO^{\cdot}$

[3] $PhCH_2CO^{\cdot} \rightarrow PhCH_2^{\cdot} + CO$

[4] $PhCH_2^{\cdot} + PhCH_2^{\cdot} \rightarrow PhCH_2CH_2Ph$

The decarbonylation reaction is a very fast process (2, 3); the lifetime of $PhCH_2CO^{\cdot}$ is 190 ns at 300 K in methanol (3). In homogeneous solution, this reaction is usually quantitative, but instances of intermolecular reactions of the phenylacetyl radical are common in micellar and zeolite systems (4–6) where the geminate radical pairs tend to be relatively long lived. These reactions have also been used to study the influence of a solid matrix on the photochemistry of DBK (5, 7).

In a recent paper, two ketones, benzophenone and xanthone (8), have been used as probes for polarity and acidity of Nafion membranes. We report here the results of a study of the DBK photochemistry in Nafion membranes in their acid form and in membranes exchanged with cationic surfactants.

Nafion membranes provide a very peculiar type of environment. They consist of a perfluorinated carbon backbone with pendant chains terminated in sulfonate head groups which are responsible for their ion exchange and swelling properties. The photochemistry of several other systems has been reported in Nafion membranes, including pyrene (9), $Ru(bpy)_3^{2+}$ (10), semiconductors (11), and other organic substrates (12).

This work on the photochemistry of DBK incorporated into Nafion membranes clearly shows that the process leads to chemical consequences quite different from those observed in homogeneous or micellar solution, or in zeolite systems (1–7).

[1]NRC No. 27493.

Experimental

Nafion 117 membranes (0.007 in.) and Nafion powder (10–35 mesh) were purchased from Aldrich. They were washed by refluxing with methanol, and then dried at room temperature under vacuum.

The membranes were swollen with 5×10^{-2} *M* DBK in water–methanol (1:1) solution, or with 0.01 *M* DBK in a 0.1 *M* aqueous solution of surfactant. Several hours are necessary to get enough adsorption by DBK in the Nafion membranes. Then, they were washed with methanol, dried in air, and positioned in 7×7 mm^2 Suprasil cells. The samples were deaerated by a nitrogen stream, or under vacuum.

Ultraviolet–visible and fluorescence spectra were recorded using an HP-8451-A diode array spectrometer and a Perkin-Elmer LS-5 spectrofluorimeter, respectively.

The laser flash photolysis experiments were carried out using the pulses (308 nm, ~4 ns, ≤60 mJ/pulse) from a Lumonics TE-860-2 excimer laser filled with Xe–HCl–He mixtures; the samples were positioned at 45° with respect to both the excitation and monitoring beams. Further details on the experimental set-up have been reported elsewhere (13). Transient spectra were recorded using an E.G.&G. gated intensified optical multichannel analyzer equipped with a model 1420 detector.

The preparative experiments were carried out using both the Nafion membrane (prepared as described before) and Nafion powder. The pellets were swollen with only the necessary volume of 5×10^{-3} *M* DBK solution in methanol to get a gel-like material. They were gently outgassed by a nitrogen stream, or under vacuum. The excitation light used was centered around 300 nm (RPR-300 lamps). After desorption by methanol the products were detected by GC using a Perkin-Elmer 8320 capillary instrument. We noted in all cases a small percentage of products with short retention time, but high molecular weight, probably due to perfluorinated fragments released by the photo-irradiated membrane.

Pyrene was used as a probe to study the surfactant exchanged membrane Nafion. The ration (I_3/I_1) for the fluorescence bands depends on the medium polarity, and can give interesting information about the microenvironment (9). The detailed description of this well-known technique is beyond the scope of this paper.

The membranes were swollen in saturated pyrene–water solution, or in 5×10^{-6} *M* pyrene in surfactant solution (1×10^{-2} *M* dodecyltrimethylammonium chloride = DTAC). They were then rinsed with methanol, dried in air, and positioned in 7×7 mm^2 Suprasil cells. The fluorescence spectra were recorded before and after the samples were degassed under vacuum.

For the pyrene–Nafion membranes, the I_3/I_1 ratios are of the order of 0.85 and 1.2 for wet and dried samples, respectively; these values

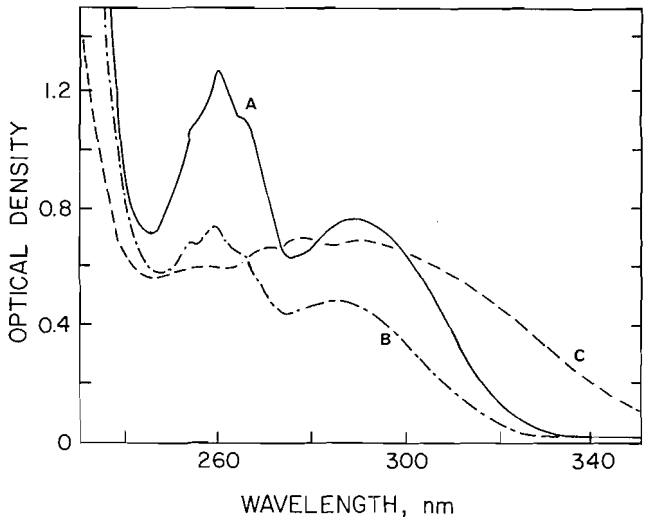

FIG. 1. Ground state absorption of DBK in methanol (*A*), H-Nafion (*B*), and H_2SO_4 (*C*).

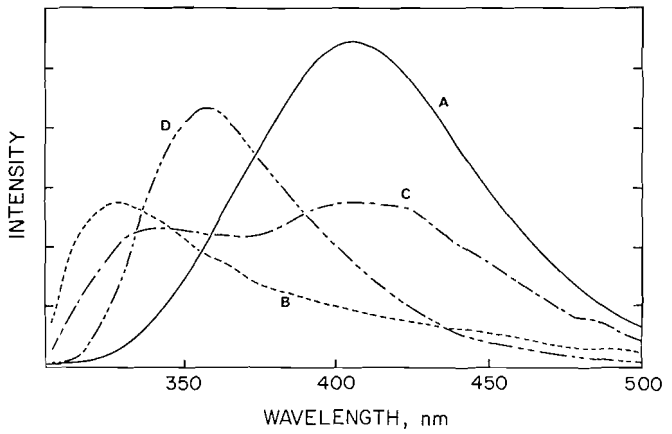

FIG. 2. Fluorescence spectra of DBK in methanol (*A*), H-Nafion (*B*), DTAC exchanged Nafion (*C*), and H_2SO_4 (*D*).

are close to those reported in the literature (9). The I_3/I_1 increase reflects the decrease of the microenvironment polarity after the loss of water. However, in the case of the system pyrene–DTAC–Nafion, the ratio remains constant at 0.9, even after several hours under vacuum. The probe does not see any change in its microenvironment; it seems that it is "protected" by the surfactant, which acts as a "shelter". Interestingly, the I_3/I_1 value compares well with that obtained independently in DTAC micelles.

Results and discussion

Absorption spectra

The absorption spectrum of DBK on the acid form of Nafion (H-Nafion) is very similar of those recorded in organic solvents; a red shift is observed in sulfuric acid (see Fig. 1). This result is similar to those for xanthone and benzophenone (8), where the acidity of the membrane is not enough to protonate the ground state of the ketone.

Fluorescence spectroscopy

The weak fluorescence emission from DBK in H-Nafion is quite different from that typically observed in homogeneous solution. This is a clear indication of protonation of the DBK excited singlet state; similarly, xanthone and benzophenone are also protonated (and fluoresce) under these conditions (8). Figure 2 shows a comparison of the fluorescence from DBK in

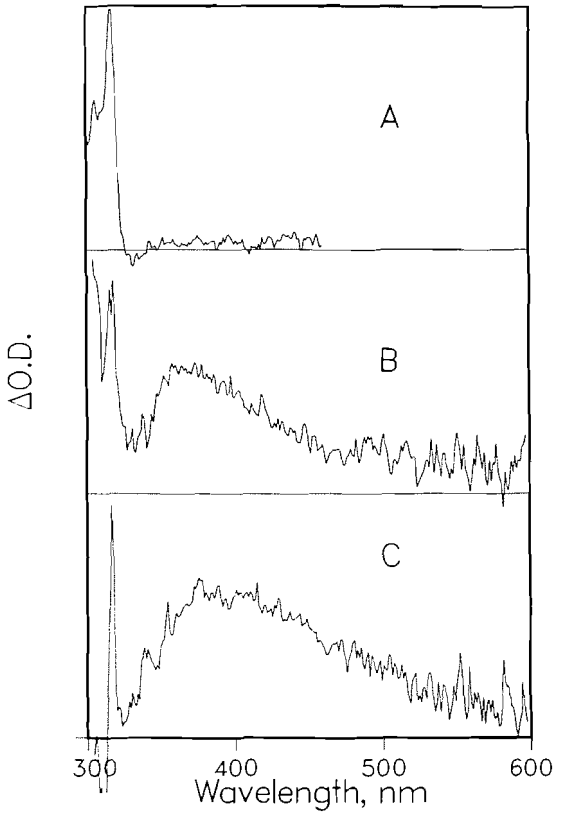

FIG. 3. Transient absorption from DBK in methanol solution (delay: 1 μs) (*A*) and from DBK on DTAB/Nafion 1 μs (*B*) or 10 μs (*C*) after 308 nm laser excitation.

H-Nafion (protonated singlet) and in methanol (unprotonated singlet). The maximum in H-Nafion is 330 nm and can be compared with solution values of 355 nm in sulfuric acid (protonated) and 405 nm in methanol (unprotonated).

It is now well established that the properties of polyelectrolytes as media for photochemical reactions can be significantly modified by addition of surfactants (14, 15). We have tried a similar approach in the case of Nafion membranes, by partially exchanging the protons with cationic surfactants. By using dodecyltrimethylammonium halides (DTAC = chloride, DTAB = bromide) the organic substrates can be "protected" from the acidic environment. Indeed, in the case of DBK–surfactant–Nafion system, we observe the fluorescence from both forms, protonated at ~340 nm, and unprotonated at ~400 nm (see Fig. 2). This property of the surfactant to provide a "shelter" from the polar and acidic H-Nafion medium has also been confirmed using pyrene as a fluorescent probe (see Experimental).

Laser flash photolysis

Pulsed laser excitation (308 nm) of DBK in homogeneous solution leads to strong and readily characterized transient absorption signals due to benzyl radicals (λ_{max} = 317 nm) (16). On short time scales the production of the radical by two separate processes (i.e. reactions [2] and [3]) can be easily identified (2, 3).

The photochemical behaviour of DBK in H-Nafion and in surfactant-exchanged membranes is quite different from that observed in homogeneous solution. Thus, in H-Nafion, no signal at or around 317 nm was detected; the only observable

Can. J. Chem. Downloaded from www.nrcresearchpress.com by 213.166.140.6 on 09/07/12
For personal use only.

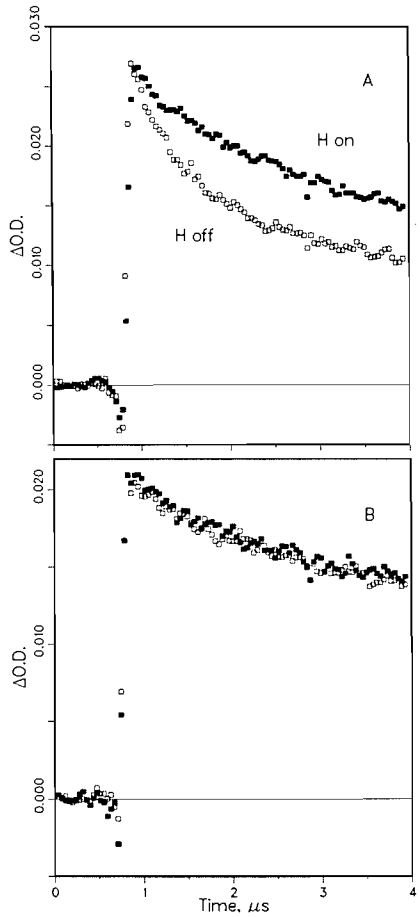

FIG. 4. Magnetic field effect for DBK on DTAB/Nafion monitored at 317 nm (*A*) and 370 nm (*B*). Filled points correspond to data under a 4000 G field.

transient was a very weak and long-lived broad absorption band centered around 370 nm (complex decay kinetics, $t_{1/2} \sim 3$ μs).

In surfactant-exchanged Nafion, two bands at 317 and 370 nm were observed. The corresponding transient spectra are illustrated in Fig. 3. The sharp 317 nm band can be readily assigned to the benzyl radical (compare with Fig. 3, spectrum *A*). The broad 370 nm is tentatively assigned to the benzyl cation by analogy with the reported spectrum for this species (17, 18). The decay of both bands followed complex kinetics, a feature which is not uncommon in solid heterogeneous systems (19). The decay at 317 nm could be adequately fitted by a biexponential function and led to lifetimes of ~0.6 μs and ~7 μs. The 370 nm band was longer-lived than the 317 nm band ($\tau \simeq 9$ μs).

Magnetic field effects

Several studies in the last few years have clearly demonstrated that triplet radical-pairs in organized media frequently show substantial magnetic field dependence (6, 20, 21). The effect at moderate fields is due to Zeeman splitting of the triplet sublevels which leads to the slow down, or eventually the shut-off of some intersystem crossing channels.

In order to test the radical-pair behaviour, we examined the photolysis of DBK in the surfactant exchanged membrane at fields of around 4000 G. The effect is illustrated in Fig. 4; the decay of the 317 nm band clearly depends on the magnetic field, which further supports the assignment of this transient to the benzyl radical, and suggests that the geminate radical-pair is held in close proximity for a considerable time. The magnitude of this effect is, however, smaller than those typically observed in micellar systems. (The effect is outside the experimental uncertainty at ~900 G.) On the other hand, the 370 nm band does not show magnetic field dependence (see Fig. 4). This observation provides strong support for our assignment of this band to the benzyl cation, rather than to a radical species, since no magnetic field effect is expected for a closed shell species.

Preparative experiments

Preparative experiments were carried out on H-Nafion films, surfactant exchanged Nafion films, and H-Nafion pellets.

In the case of samples deaerated by a stream of nitrogen, the only significant product is 1,2-diphenylethane, produced very slowly by comparison with homogeneous systems. The quantum yield for photodecomposition must be extremely small, as could be anticipated from the failure to detect benzyl radicals in the laser photolysis experiment. It is apparent that small residual amounts of solvent (water or methanol) affect the polarity of the membrane and lead to the slow formation of 1,2-diphenylethane. In the case of vacuum-dried samples no photoproducts were detected following extraction of the irradiated samples.

The behaviour of the DBK–surfactant–Nafion membranes under irradiation is quite different. Even with vacuum-dried samples, the formation of 1,2-diphenylethane can be readily observed. For example, under the same conditions that the H-Nafion system leads to no photoproducts, a conversion of ~50% is observed in the surfactant-exchanged membrane. This result is in good agreement with the observation of both radical and cation species in the laser photolysis experiments. Comparison of the exchanged membrane with homogeneous solution (methanol) led to slightly smaller (75%) conversion to diphenylethane in the membrane, although problems in matching the irradiation dose of solid and liquid samples cast some doubts on the significance of this small difference.

After exhaustive extraction of the irradiated Nafion film with refluxing methanol, a new ground state absorption was detected ($\lambda_{max} \sim 260$ nm) in the usually transparent Nafion films. Since the absorption is produced in the same conditions under which the benzyl cation is detectable it is probably due to an aromatic chromophore covalently bonded to the membrane. The most likely bonding site in the membrane is the SO_3^- group, thus leading to $—SO_3CH_2Ph$.

Thus, our results suggest that protonation of the excited state of DBK leads to the photogeneration of benzyl cations and that the Nafion membrane behaves as a chemical scavenger for these cations. Of course, trapping of the benzyl cation leaves unanswered the question of the fate of the rest of the molecule. An obvious candidate would be phenylacetaldehyde. Unfortunately, our attempts to detect it were unsuccessful. On the other hand, when in a separate experiment phenylacetaldehyde was adsorbed on H-Nafion, the uv–visible spectra recorded before and after irradiation showed that the sample was not stable under these conditions, and led to a new absorption at 260 nm, which also did not disappear completely after desorption. We suggest that the aldehyde undergoes polymerization and/or oligomerization and that, in the case of DBK–H–Nafion (where the phenylacetaldehyde would be generated in situ) this process is responsible for the failure to extract and/or detect this product.

No $PhCH_2OCH_3$ (the expected methanol scavenging product) was detected among the products even when the membrane

Can. J. Chem. Downloaded from www.nrcresearchpress.com by 213.166.140.6 on 09/07/12
For personal use only.

contained some residual methanol. This may indicate that only benzyl radicals are produced at the methanol-containing sites, with the benzyl cations being the preferred products in the "dry" or methanol-deficient sites.

Conclusion

The photolysis of DBK on vacuum dried membranes leads to a transient absorption at 370 nm that has been tentatively assigned to the benzyl cation. Under these conditions no benzyl radicals are formed, and fluorescence studies indicate that the only important excited intermediate is the protonated singlet state.

In air-dried samples, deaerated by a steam of nitrogen, the residual amount of solvent (water or methanol) is enough to affect the polarity of the membrane and to lead to the formation of 1,2-diphenylethane in small amounts.

The Nafion environment can be further modified by exchange with cationic surfactants. Thus, in the DBK–DTAB–Nafion system, both absorptions, attributed to benzyl radicals (317 nm) and benzyl cations (370 nm) have been detected in laser photolysis experiments. Quite clearly, decreased acidity leads to a transition from the cationic mechanism toward the typical "organic media" behaviour with benzyl radical formation. Magnetic field effects show that benzyl radicals are distributed in local cages, a requirement for the observation of magnetic field effects on the geminate radical-pair. The 370 nm transient did not show any effect with fields of up to 5000 G, as expected for the benzyl cation.

Product studies indicate that while benzyl radicals lead to easily extractable 1,2-diphenylethane, the benzyl cations appear to be efficiently scavengered within the Nafion matrix, leading to permanent incorporation of aromatic moieties.

Acknowledgements

Thanks are due to Dr. D. Weir for his advice on the handling of Nafion membranes. The support from a NATO fellowship (to V.W.) and from C.N.R.S. (France) is gratefully acknowledged.

1. P. S. Engel. J. Am. Chem. Soc. **92**, 6074 (1970) and references therein.
2. N. J. Turro, I. R. Gould, and B. H. Baretz. J. Phys. Chem. **87**, 531 (1983).
3. L. Lunazzi, K. U. Ingold, and J. C. Scaiano. J. Phys. Chem. **87**, 529 (1983).
4. G. F. Lehr and N. J. Turro. Tetrahedron, **37**, 3411 (1981).
5. N. J. Turro, C.-C. Cheng, X.-G. Lei, and E. M. Flanigen. J. Am. Chem. Soc. **107**, 3740 (1985).
6. H. Hayashi, Y. Sakaguchi, and S. Nagakura. Chem. Lett. 1149 (1980).
7. N. J. Turro. Pure Appl. Chem. **58**, 1219 (1986).
8. D. Weir and J. C. Scaiano. Tetrahedron. **43**, 1617 (1987).
9. (*a*) D. C. Dong and M. A. Winnik. Can. J. Chem. **62**, 2560 (1984); (*b*) P. C. Lee and D. Meisel. Photochem. Photobiol. **41**, 21 (1985); (*c*) M. N. Szentirmay, N. E. Prieto, and C. R. Martin. J. Phys. Chem. **89**, 3017 (1985).
10. (*a*) P. C. Lee and D. Meisel. J. Am. Chem. Soc. **102**, 5477 (1980); (*b*) I. Rubinstein, J. Rishpon, and S. Gottesfeld. J. El. Soc. Electrochem. Sci. Tech. **133**, 730 (1986).
11. (*a*) A. W.-H. Mau, G.-B. Huang, N. Kakuta, A. J. Bard, A. Campion, M. A. Fox, J. M. White, and S. E. Webber. J. Am. Chem. Soc. **106**, 6537 (1984); (*b*) N. Kakuta, K. H. Park, M. F. Finlayson, A. Veno, A. J. Bard, A. Campion, M. A. Fox, S. E. Webber, and J. M. White. J. Phys. Chem. **89**, 732 (1985); (*c*) M. Krishnan, J. R. White, M. A. Fox, and A. J. Bard. J. Am. Chem. Soc. **105**, 7002 (1983).
12. (*a*) R. F. Childs, B. Duffey, and A. Mika-Gibala. J. Org. Chem. **49**, 4352 (1984); (*b*) R. F. Childs and A. Mika-Gibala. J. Org. Chem. **49**, 4204 (1982); (*c*) G. A. Olah, P. S. Iyer, and G. K. S. Prakash. Synthesis, 513 (1986).
13. J. C. Scaiano. J. Am. Chem. Soc. **102**, 7747 (1980).
14. E. B. Abuin and J. C. Scaiano. J. Am. Chem. Soc. **106**, 6274 (1986).
15. E. G. Goddard. Colloids Surf. **19**, 301 (1986).
16. J. C. Scaiano, W. J. Leigh, and G. Ferraudi. Can. J. Chem. **62**, 2355 (1984).
17. L. M. Dorfman, R. J. Sujdak, and B. Bockrath. Acc. Chem. Res. 352 (1976).
18. R. L. Jones and L. M. Dorfman. J. Am. Chem. Soc. **96**, 5715 (1974).
19. F. Wilkinson, C. J. Willsher, H. L. Casal, L. J. Johnston, and J. C. Scaiano. Can. J. Chem. **64**, 539 (1986).
20. J. C. Scaiano, E. B. Abuin, and L. C. Stewart. J. Am. Chem. Soc. **104**, 5673 (1982).
21. N. J. Turro. Proc. Natl. Acad. Sci. U.S.A. **80**, 609 (1983).

Can. J. Chem. Downloaded from www.nrcresearchpress.com by 213.166.140.6 on 09/07/12
For personal use only.

Structure and conformation of 3′-azido-3′-deoxythymidine (AZT), an inhibitor of the HIV (AIDS) virus[1]

GEORGE I. BIRNBAUM[2] and JERZY GIZIEWICZ
Division of Biological Sciences, National Research Council of Canada, Ottawa, Ont., Canada K1A 0R6

ERIC J. GABE
Division of Chemistry, National Research Council of Canada, Ottawa, Ont., Canada K1A 0R9

AND

TAI-SHUN LIN AND WILLIAM H. PRUSOFF
Department of Pharmacology, Yale University School of Medicine, New Haven, CT 06510, U.S.A.

Received February 4, 1987

GEORGE I. BIRNBAUM, JERZY GIZIEWICZ, ERIC J. GABE, TAI-SHUN LIN, and WILLIAM H. PRUSOFF. Can. J. Chem. **65**, 2135 (1987).

3′-Azido-3′-deoxythymidine (AZT), an inhibitor of HIV (human immunodeficiency virus) replication, was recently found to improve the condition of patients suffering from AIDS (acquired immunodeficiency syndrome) or ARC (AIDS-related complex). An X-ray analysis of AZT was undertaken in order to determine the three-dimensional structure of this thymidine analogue. The crystals belong to the monoclinic space group $P2_1$ and the cell dimensions are a = 5.6282(4), b = 12.0130(7), c = 17.5072(10) Å, β = 95.946(5)°. The structure was determined by direct methods and refined to R = 0.028 for 2029 observed reflections. Two crystallographically independent molecules were found in the asymmetric unit. One of them, molecule A, adopts a conformation which is fairly common in nucleosides, viz. a C2′ *endo*/C3′ *exo* pucker of the furanose ring and a glycosidic torsion angle χ_{CN} = 53.4°. However, the conformation of molecule B is highly unusual. The sugar ring pucker is C3′ *exo*/C4′ *endo* and χ_{CN} = 2.3°. This high-energy conformation may represent the biologically active form of AZT. Its determination may therefore assist in the design of other inhibitors of HIV.

GEORGE I. BIRNBAUM, JERZY GIZIEWICZ, ERIC J. GABE, TAI-SHUN LIN et WILLIAM H. PRUSOFF. Can. J. Chem. **65**, 2135 (1987).

Il a été récemment découvert que l'azido-3′ déoxy-3′ thymidine (AZT), un inhibiteur de la réplication du VIH (virus immunodéficitaire humain), améliore la condition des patients soufrant du SIDA (syndrome de l'immuno-déficience acquise) ou du SAS (syndrome associé au SIDA). On a entrepris une étude par diffraction des rayons-X du AZT dans le but de déterminer la structure tridimensionnelle de cet analogue de la thymidine. Les cristaux appartiennent au groupe d'espace monoclinique $P2_1$ et les dimensions de la maille sont a = 5,6282(4), b = 12,0130(7) et c = 17,5072(10) Å et β = 95,946(5)°. On a déterminé la structure par des méthodes directes et on l'a affinée jusqu'à une valeur de R = 0,028 pour 2029 réflexions observées. On a trouvé que l'unité asymétrique contient deux molécules qui sont indépendantes d'un point de vue cristallographique. L'une d'elles, la molécule A, adopte une conformation qui est assez commune dans les nucléosides, soit un plissement C2′ *endo*/C3′ *exo* du noyau furannose et un angle de torsion glycosidique χ_{CN} = 53,4°. Toutefois, la conformation de la molécule B est assez inusitée. Le noyau de sucre subit un plissement C3′ *exo*/C4′ *endo* et χ_{CN} = 2,3°. Cette conformation de haute énergie pourrait s'avérer être la forme biologiquement active de l'AZT. La détermination de la configuration de l'AZT peut donc aider au développement d'autres inhibiteurs du VIH.

[Traduit par la revue]

Introduction

3′-Azido-3′-deoxythymidine (AZT, BW A509U) was first synthesized by Horwitz *et al.* (1) and later, by a modification of this procedure, by Lin and Prusoff (2). The antiviral activity of AZT was first reported by Ostertag *et al.* (3) and Dube *et al.* (4) who found a dramatic decrease of Friend virus (FV) in murine erythroleukemia cells previously transformed by the FV complex, whereas AZT had only a minimal effect on the replication of the host cell. They suggested that AZT could possibly be used to inhibit viral DNA replication by interfering with DNA chain elongation, without significantly affecting cellular viability. Krieg *et al.* (5) also reported the inhibition of Friend virus by AZT. More recently Mitsuya *et al.* (6) reported the inhibitory effect of AZT on the infectivity and cytopathic effect of HIV *in vitro*. This virus is considered to be responsible in humans for the development of acquired immunodeficiency syndrome (AIDS) or AIDS-related complex (ARC). Mitsuya *et al.* found that the triphosphate of AZT competitively inhibits

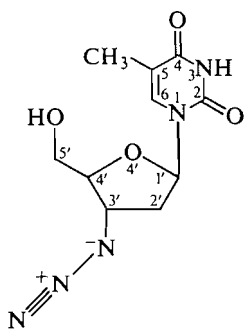

reverse transcriptase encoded by the HIV virus. Infected H9 cells exposed to AZT were prevented, in a dose-dependent fashion, from expressing reverse transcriptase as well as the viral p24 *gag* protein (6). AZT behaves like an analog of thymidine, since the inhibitory effect of AZT is prevented in a dose-dependent manner by thymidine.

Since 1981, about 52 000 individuals have been diagnosed as having AIDS and about 5 to 10 million are believed to be infected with HIV. Of those who developed AIDS, about half

[1]NRC No. 27717.

[2]To whom correspondence should be addressed.

Can. J. Chem. Downloaded from www.nrcresearchpress.com by 213.166.140.6 on 09/07/12
For personal use only.

TABLE 1. Final atomic parameters and their standard deviations[a]

	Molecule A				Molecule B			
Atom	x	y	z	B_{eq}	x	y	z	B_{eq}
N1	4408(4)	4085	88675(13)	1.4	1688(4)	5440(3)	61496(13)	1.5
C2	5963(5)	4383(3)	83468(15)	1.4	306(5)	5161(3)	67176(15)	1.5
O2	7675(3)	5010(3)	85044(10)	1.7	−1309(3)	4468(3)	66108(10)	1.8
N3	5466(4)	3927(3)	76318(14)	1.4	855(4)	5694(3)	74047(14)	1.5
C4	3670(5)	3178(3)	73897(15)	1.4	2666(5)	6479(3)	75801(16)	1.6
O4	3489(4)	2813(3)	67296(11)	1.9	2955(4)	6883(3)	82270(11)	2.1
C5	2112(5)	2897(3)	79675(16)	1.5	4033(5)	6733(3)	69470(16)	1.6
C6	2535(5)	3353(3)	86647(16)	1.5	3514(5)	6206(3)	62746(16)	1.5
C7	90(6)	2092(4)	77758(18)	1.8	6007(6)	7572(4)	70651(19)	2.0
C1′	4769(5)	4494(3)	96610(15)	1.6	1176(5)	4813(3)	54070(16)	1.5
C2′	2701(6)	5202(3)	98869(16)	1.7	−1288(5)	5092(4)	49989(17)	1.9
C3′	2663(5)	4921(3)	107322(16)	1.7	−777(5)	5307(3)	41778(16)	1.8
C4′	3493(5)	3710(3)	107948(16)	1.6	1775(5)	5759(3)	42814(15)	1.6
O4′	4918(4)	3552(3)	101565(10)	1.7	2891(3)	5117(3)	49170(10)	1.6
C5′	1491(5)	2857(4)	107652(17)	1.8	1899(6)	7001(4)	44480(17)	1.9
O5′	−225(4)	3041(3)	101222(12)	2.3	4310(4)	7358(3)	46188(12)	2.3
N3′α	4417(5)	5687(3)	111775(14)	2.2	−905(4)	4207(3)	37612(14)	1.9
N3′β	4503(4)	5562(3)	118787(14)	1.9	−673(4)	4248(3)	30819(14)	1.9
N3′γ	4720(5)	5532(3)	125301(14)	2.3	−498(5)	4184(3)	24388(16)	2.4

[a]The x and y coordinates were multiplied by 10^4 and the z coordinates by 10^5.

are now dead, and the number who will develop AIDS is expected in the next four years to increase to 400 000 in the United States alone. Yarchoan *et al.* (7), in a Phase I clinical trial of several regimes of AZT in 19 patients with AIDS or ARC, found it to be well absorbed from the gastrointestinal tract, to cross the blood brain barrier, to produce some immunological improvement and — most important — it appeared that some of the patients improved. These encouraging findings have resulted in its current licensing for treatment of AIDS patients in the United Kingdom and the United States.

In view of the strong interest in this useful drug for the therapy of AIDS and ARC, we consider it important to learn more about its physical and chemical properties. In this report we describe the three-dimensional structure of AZT determined by an X-ray analysis.

Experimental

Crystalline clusters of AZT were grown from a mixture of ethanol and acetone. A wedge-shaped fragment, measuring 0.3 × 0.5 × 0.6 mm, was cut off and mounted on a Picker diffractometer equipped with a copper tube and a graphite monochromator. The following data were obtained:

$C_{10}H_{13}N_5O_4$ fw = 267.15

Monoclinic, a = 5.6282(4), b = 12.0130(7), c = 17.5072(10) Å, β = 95.946(5)°, V = 1177.3 Å^3, ρ_c = 1.51 g cm^{-3}, Z = 4 (150 K; CuKα_1, λ = 1.54056 Å); $F(000)$ = 560, μ(CuKα) = 9.7 cm^{-1}.

The crystal was cooled to 150 K and the intensity data were measured with $\theta/2\theta$ scans and profile analysis (8). Of the 2037 unique reflections accessible to the diffractometer ($2\theta \leqq 127°$), only 8 had $I < 3\sigma(I)$ and were considered unobserved.

The intensities were corrected for Lorentz and polarization factors; absorption corrections were considered unnecessary. The crystal structure was determined by direct methods (9). All hydrogen atoms were located on difference Fourier maps. Atomic parameters were refined by full-matrix least squares with anisotropic temperature parameters for nonhydrogen atoms and isotropic parameters for hydrogens. After the final least-squares cycle the largest parameter shift equalled 0.25σ. The refinement converged at R = 0.028 and R_w = 0.035. All calculations were performed with the NRCVAX system of programs (10). The coordinates and equivalent isotropic temperature parameters of nonhydrogen atoms are listed in Table 1. Their anisotropic temperature parameters as well as lists of hydrogen atom parameters and of observed and calculated structure factors are available.[3]

Results and discussion

Molecular geometry

The conformations of the two independent molecules in the asymmetric unit are quite different (Fig. 1). In molecule A, the glycosidic torsion angle χ_{CN} [C6—N1—C1′—O4′] is 53.4(3)°, the pucker of the furanose ring is C2′ *endo*/C3′ *exo* (^2_3T, P = 175.2°, τ_m = 32.3°) and the side chain is *gauche*$^+$. In molecule B, χ_{CN} = 2.3(4)°, the ring pucker is C3′ *exo*/C4′ *endo* (^4_3T, P = 214.5°, τ_m = 36.6°) and the side chain is *trans*. Stereoscopic views of the two molecules are shown in Fig. 2. The conformation of molecule A is quite normal for a 2′-deoxynucleoside (11). The ring pucker is dictated by the *gauche* effect (12): the ^2_3T conformation places the polar C3′—N3′ bond approximately *gauche* to C4′—O4′. The χ_{CN} value is within the range usually associated with such a ring pucker (11) and the *gauche*$^+$ conformation of the side chain is stabilized by an intramolecular C6—H···O5′ hydrogen bond, a fairly common phenomenon (13).

On the other hand, the conformation of molecule B is highly unusual. The most recent Cambridge Crystallographic Database (14), containing almost 600 nucleosides and nucleotides, lists only two structures with a furanose ring in a similar conformation (P = 215 ± 9°). In deoxycytidine 5′-phosphate, 5′-dCMP (15), and in 5′-methylthioadenosine, TMA (16), the ring pucker is also ^4_3T, the phase angles of pseudorotation, 213° and 216°, respectively, being almost identical to that in molecule B in AZT. Interestingly, a low value of χ_{CN} (−6.0°) was found in 5′-dCMP as well. The small torsion angle χ_{CN} means that

[3]These tables may be purchased from the Depository of Unpublished Data, CISTI, National Research Council of Canada, Ottawa, Ont., Canada K1A 0S2.

Can. J. Chem. Downloaded from www.nrcresearchpress.com by 213.166.140.6 on 09/07/12
For personal use only.

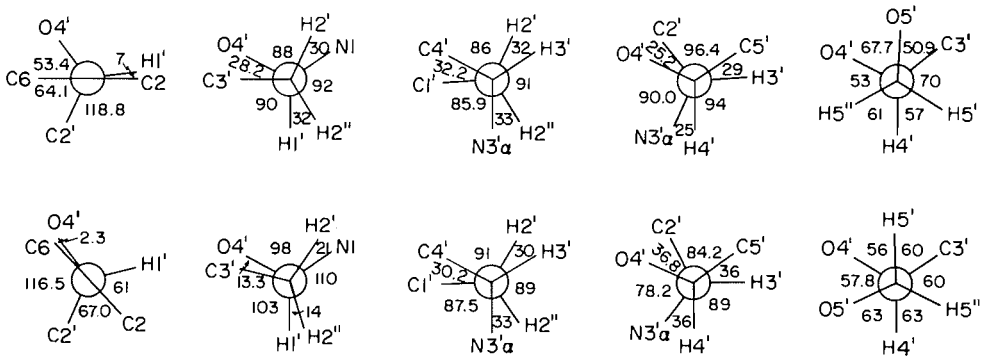

FIG. 1. Newman projections along (left to right) N1—C1′, C1′—C2′, C2′—C3′, C3′—C4′, and C4′—C5′, in molecules A (top) and B (bottom).

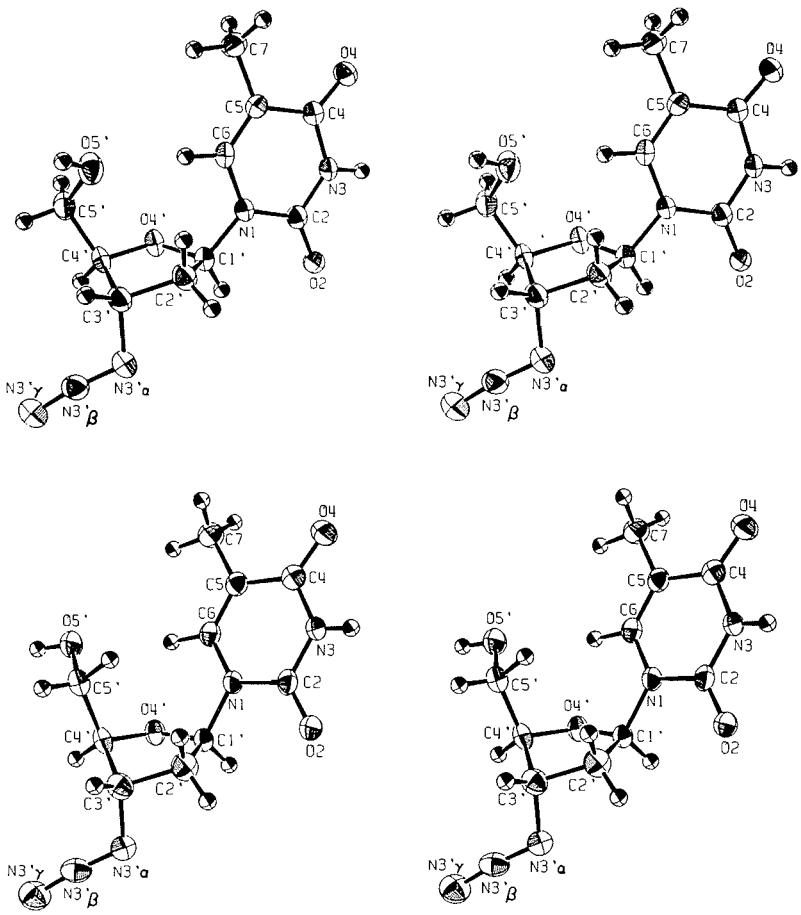

FIG. 2. Stereoscopic views of molecule A (top) and molecule B (bottom); the thermal ellipsoids correspond to 70% probability.

the N1—C6 bond eclipses C1′—O4′. This, in turn, imposes significant changes in the geometry of molecule B. Thus, the glycosidic bond N1—C1′ (1.505(4) Å) is much longer than the one in molecule A (1.468(4) Å). The strain also causes an increase of the bond angle C6—N1—C1′ to 123.0(2)°, as compared to 118.7(2)° in molecule A. Bond lengths and bond angles are listed in Tables 2 and 3, respectively.

The conformation of the azido group is similar in molecules A and B, the torsion angles C2′—C3′—N3′α—N3′β being 178.1(3) and 175.8(3)°, respectively. This places the terminal nitrogen atom N3′γ as far away from the aglycon as possible. The C—N and N—N bond lengths indicate that the C—$\overset{+}{N}$—$\overset{+}{N}$≡N resonance form predominates and that there is also some contribution of the C—N=$\overset{+}{N}$=$\overset{-}{N}$ resonance form.

Hydrogen bonding and packing

As mentioned above, there is an intramolecular hydrogen bond involving H6 in molecule A. After normalizing the C6—H6 distance to the nominal value of 1.09 Å, we obtained a corrected H6···O5′ distance of 2.06 Å (Table 4). This distance corresponds to a relatively strong C—H···O hydrogen bond (13*c*). In molecule B, H6 also participates in intramolecular hydrogen bonding, being donated to both O4′ and O5′. The distances and angles, while less favorable than those in molecule A, are well within the range of such interactions tabulated by Taylor and Kennard (13*c*). The O—H and N—H distances in the intermolecular hydrogen bonds listed in Table 4 were normalized to 0.97 and 1.04 Å, respectively.

The packing of the molecules in the crystal is shown in Fig. 3.

Can. J. Chem. Downloaded from www.nrcresearchpress.com by 213.166.140.6 on 09/07/12
For personal use only.

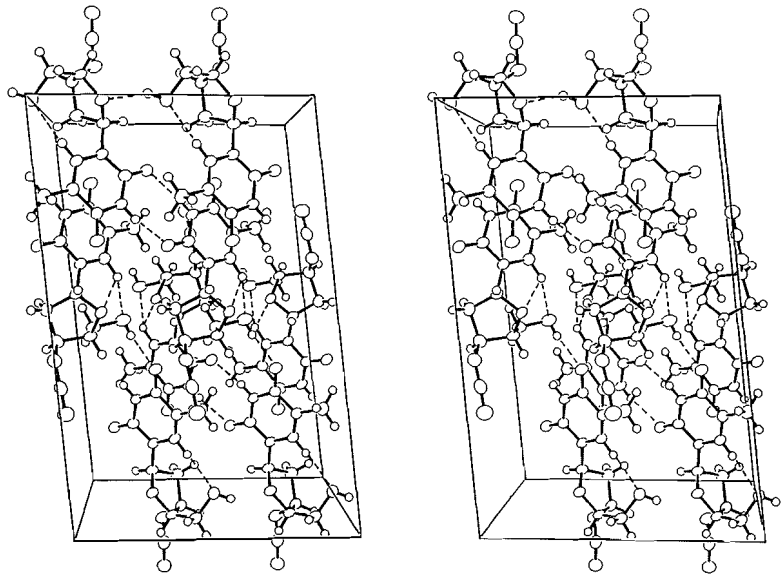

FIG. 3. Stereoscopic view of molecular packing in two unit cells. Some hydrogen bonds are indicated by dashed lines. The directions of the axes are $x\rightarrow$ ($-a$ to $+a$), y down, and $z\uparrow$.

TABLE 2. Bond lengths (Å)

Bond	Length	
	Molecule A	Molecule B
N1—C2	1.375(4)	1.366(4)
N1—C6	1.390(4)	1.380(4)
N1—C1′	1.468(4)	1.505(4)
C2—O2	1.232(4)	1.232(4)
C2—N3	1.368(4)	1.369(4)
N3—C4	1.386(4)	1.399(5)
C4—O4	1.230(4)	1.228(4)
C4—C5	1.446(4)	1.446(4)
C5—C6	1.337(4)	1.342(4)
C5—C7	1.504(5)	1.498(5)
C1′—C2′	1.526(5)	1.530(4)
C1′—O4′	1.424(5)	1.405(3)
C2′—C3′	1.520(4)	1.517(4)
C3′—C4′	1.528(6)	1.528(4)
C3′—N3′α	1.507(5)	1.508(5)
C4′—O4′	1.454(3)	1.443(4)
C4′—C5′	1.520(5)	1.521(6)
C5′—O5′	1.422(4)	1.425(4)
N3′α—N3′β	1.233(3)	1.211(4)
N3′β—N3′γ	1.135(4)	1.143(4)

TABLE 3. Bond angles (deg)

Angle	Bond angle (deg)	
	Molecule A	Molecule B
C2—N1—C6	120.9(2)	121.3(3)
C2—N1—C1′	120.4(2)	115.7(3)
C6—N1—C1′	118.7(2)	123.0(2)
N1—C2—O2	123.2(3)	121.4(3)
N1—C2—N3	114.8(3)	115.5(3)
O2—C2—N3	122.0(3)	123.0(3)
C2—N3—C4	127.8(3)	126.9(3)
N3—C4—O4	120.3(3)	119.5(3)
N3—C4—C5	114.4(3)	114.1(3)
O4—C4—C5	125.2(3)	126.4(3)
C4—C5—C6	118.7(3)	119.2(3)
C4—C5—C7	119.6(3)	118.8(3)
C6—C5—C7	121.8(3)	122.0(3)
N1—C6—C5	123.5(3)	123.0(3)
N1—C1′—C2′	113.4(2)	112.1(3)
N1—C1′—O4′	107.7(3)	108.4(3)
C2′—C1′—O4′	106.5(2)	107.8(2)
C1′—C2′—C3′	102.5(3)	103.2(2)
C2′—C3′—C4′	104.2(3)	102.5(2)
C2′—C3′—N3′α	107.1(3)	107.8(3)
C4′—C3′—N3′α	111.4(3)	111.5(3)
C3′—C4′—O4′	105.0(3)	103.3(3)
C3′—C4′—C5′	114.8(3)	113.3(3)
O4′—C4′—C5′	110.6(3)	111.6(3)
C1′—O4′—C4′	111.2(3)	109.8(2)
C4′—C5′—O5′	111.2(3)	111.1(3)
C3′—N3′α—N3′β	113.4(3)	115.8(3)
N3′α—N3′β—N3′γ	173.5(4)	173.7(4)

One of the interesting features is the base pairing of molecules A and B via N3—H···O2 hydrogen bonds. There are also some stacking interactions between molecules A and B. The C2—O2 bond in molecule B and the N3—C4 bond in molecule A are almost superimposed, thus being stabilized by a dipole–dipole interaction. Some short inter-stack distances are C4(A)···C2(B) 3.191(5) Å, C4(A)···O2(B) 3.365 (4) Å. There is also a short inter-stack distance of 3.327(5) Å between two carbonyl carbon atoms C2(A) and C4(B).

Biological considerations

The rare occurrence of the ${}^{4}_{3}T$ sugar ring pucker, found in molecule B of AZT, reflects the potential energy of this conformation which is approximately 1.7 kcal/mol higher than the global minimum corresponding to a C2′ *endo* (${}^{2}E$) pucker (17). This energy difference is similar to the 1.8 kcal/mol energy barrier which hinders free pseudorotation of 2′-deoxyribose along the ${}^{2}E$—${}^{0}E$—${}^{3}E$ pathway. In fact, very few nucleosides have been found with an O4′ *endo* (${}^{0}E$) conformation of the sugar ring in the solid state, although this pucker may contribute to the equilibrium population in solution (18). The eclipsing of N1—C6 and C1′—O4′ bonds, as evidenced by

Can. J. Chem. Downloaded from www.nrcresearchpress.com by 213.166.140.6 on 09/07/12
For personal use only.

TABLE 4. Distances and angles for hydrogen bonds[a]

			Distances (Å)			Angles (deg)
D	*A*	*A* at	*D*···*A*	H···*A*	H···A_{corr}	*D*—H···*A*
C6(A)—H···O5′(A)	*x*, *y*, *z*		3.144	2.20	2.06	175
O5′(A)—H···O4′(A)	−1 + *x*, *y*, *z*		2.808	2.03	1.93	150
N3(A)—H···O2(B)	1 + *x*, *y*, *z*		2.754	1.87	1.72	171
N3(B)—H···O2(A)	−1 + *x*, *y*, *z*		2.881	2.07	1.85	171
C6(B)—H···O4′(B)	*x*, *y*, *z*		2.704	2.21	2.19	106
C6(B)—H···O5′(B)	*x*, *y*, *z*		3.285	2.38	2.34	144
O5′(B)—H···O4(A)	1 − *x*, ½ + *y*, 1 − *z*		2.830	1.99	1.88	167

[a]The esd's are 0.003–0.004 Å and 0.03–0.06 Å for *D*···*A* and H···*A* distances, respectively, and 3° for *D*—H···*A* angles.

the low value of χ_{CN}, further increases the potential energy of molecule B. Since substrates often adopt a high-energy transition state upon binding to an enzyme or receptor, it is possible that the conformation of molecule B represents the biologically active form of AZT. In this conformation, the binding of AZT—triphosphate to its target enzyme may be enhanced by a more favorable geometry of hydrogen bonds involving O2 and N3, resulting from the 51° rotation of the base about the glycosidic bond. The azido group is most likely responsible for the antiviral properties of AZT, and it is reasonable to assume that its terminal nitrogen atom Nγ, with its partial negative charge, is involved in the binding of AZT—triphosphate to the retroviral DNA polymerase. The following intramolecular distances were calculated in molecule B: N′γ···O2 7.373(3) Å, N′γ···N3 8.836(4) Å, N′γ···O4 10.625(4) Å. Such geometrical considerations may assist in the design of new and more effective drugs.[4]

Can. J. Chem. Downloaded from www.nrcresearchpress.com by 213.166.140.6 on 09/07/12
For personal use only.

Acknowledgements

T.S.L. and W.H.P. acknowledge support by USPHS grant CA05262 from the National Institutes of Health. Figures 2 and 3 were drawn with the ORTEP program of Johnson (19).

1. J. P. HORWITZ, J. CHUA, and M. NOEL. J. Org. Chem. **29**, 2076 (1964).
2. T. S. LIN and W. H. PRUSOFF. J. Med. Chem. **21**, 109 (1978).
3. W. OSTERTAG, G. ROESLER, C. J. KRIEG, T. COLE, T. CROZIER, G. GAEDICKE, G. STEINHEIDER, N. KLUGE, and S. K. DUBE. Proc. Natl. Acad. Sci. U.S.A. **71**, 4980 (1974).
4. S. K. DUBE, I. B. PRAGNELL, N. KLUGE, G. GAEDICKE, G. STEINHEIDER, and W. OSTERTAG. Proc. Natl. Acad. Sci. U.S.A. **72**, 1863 (1975).
5. C. J. KRIEG, W. OSTERTAG, U. CLAUSS, I. B. PRAGNELL, P. SWETTY, G. ROESLER, and B. J. WEIMANN. Exptl. Cell Res. **116**, 21 (1978).
6. H. MITSUYA, K. J. WEINHOLD, P. A. FURMAN, M. H. ST. CLAIR, S. NUSINOFF LEHRMAN, R. C. GALLO, D. BOLOGNESI, D. W. BARRY, and S. BRODER. Proc. Natl. Acad. Sci. U.S.A. **82**, 7096 (1985).
7. R. YARCHOAN, K. J. WEINHOLD, H. K. LYERLY, E. GELMANN, R. M. BLUM, G. M. SHEARER, H. MITSUYA, J. M. COLLINS, C. E. MYERS, R. W. KLECKER, P. D. MARKHAM, D. T. DURACK, S. NUSINOFF LEHRMAN, D. W. BARRY, M. A. FISCHL, R. C. GALLO, D. P. BOLOGNESI, and S. BRODER. Lancet i, 575 (1986).
8. D. F. GRANT and E. J. GABE. J. Appl. Crystallogr. **11**, 114 (1978).
9. P. MAIN, S. E. HULL, L. LESSINGER, G. GERMAIN, J.-P. DECLERCQ, and M. M. WOOLFSON. MULTAN78, University of York, England, and University of Louvain, Belgium, 1978.
10. E. J. GABE, F. L. LEE, and Y. LE PAGE. *In* Crystallographic computing 3. *Edited by* G. M. Sheldrick, C. Kruger, and R. Goddard. Clarendon Press, Oxford. 1985. p. 167.
11. H. P. M. DELEEUW, C. A. G. HAASNOOT, and C. ALTONA. Isr. J. Chem. **20**, 108 (1980).
12. G. I. BIRNBAUM and D. SHUGAR. *In* Topics in nucleic acid structure. Part 3. *Edited by* S. Neidle. Macmillan, London. In press.
13. (*a*) G. I. BIRNBAUM, W. J. P. BLONSKI, and F. E. HRUSKA. Can. J. Chem. **61**, 2299 (1983); (*b*) G. I. BIRNBAUM, K. L. SADANA, W. J. P. BLONSKI, and F. E. HRUSKA. J. Am. Chem. Soc. **108**, 1671 (1986); (*c*) R. TAYLOR and O. KENNARD. J. Am. Chem. Soc. **104**, 5063 (1982).
14. F. H. ALLEN, O. KENNARD, and R. TAYLOR. Acc. Chem. Res. **16**, 146 (1983).
15. M. A. VISWAMITRA, B. S. REDDY, G. H.-Y. LIN, and M. SUNDARALINGAM. J. Am. Chem. Soc. **93**, 4565 (1971).
16. F. GHIASSY, J. N. LOW, and H. R. WILSON. Acta Crystallogr. Sect. B, **37**, 1921 (1981).
17. W. K. OLSON. J. Am. Chem. Soc. **104**, 278 (1982).
18. G. I. BIRNBAUM, T.-S. LIN, G. T. SHIAU, and W. H. PRUSOFF. J. Am. Chem. Soc. **101**, 3353 (1979).
19. C. K. JOHNSON. "ORTEP-II", Report ORNL-5138, Oak Ridge National Laboratory, Oak Ridge, TN. 1976.
20. G. V. GURSKAYA, E. N. TSAPKINA, N. V. SKAPTSOVA, A. A. KRAEVSKII, S. V. LINDEMAN, and YU. T. STRUCHKOV. Dokl. Akad. Nauk SSSR, **291**, 854 (1986); Chem. Abstr. **106**, 111695g (1987).

[4]NOTE ADDED IN PROOF: It has just come to our attention that an X-ray analysis of AZT was published by Gurskaya *et al.* (20).

Syntheses of chiral intermediates of 1-β-methylcarbapenems: (3*S*,4*R*)-3-[1(*R*)-*tert*-butyldimethylsilyloxyethyl]-4-chloroazetidin-2-one and (3*S*,4*S*)-3-[1(*R*)-*tert*-butyldimethylsilyloxyethyl]-4-[1(*R*)-*tert*-butylthiocarbonylethyl]azetidin-2-one

MASAKI ENDO

Chemical Process Development, Bristol-Myers Pharmaceutical Research and Development Division, 100 Industrial Blvd., Candiac, P.Q., Canada J5R 1J1

Received March 30, 1987

MASAKI ENDO. Can. J. Chem. **65**, 2140 (1987).

The 4-chloroazetidinone **10**, a very reactive chiral intermediate for 1-β-methylcarbapenems (**1***b*), was easily prepared and isolated as a solid crystalline compound from the corresponding sulfide **5**. Another chiral intermediate (**16***d*) bearing the 1-β-methyl moiety was prepared by stereoselective aldol type condensation of either azetidinone **4** or **10** with metal enolates **14** (R = S—Bu^t, M = $ZrCp_2Cl$, 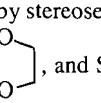 , and SnBr). The β/α ratios were 9:1, 3:1, and 2:1 respectively.

MASAKI ENDO. Can. J. Chem. **65**, 2140 (1987).

On a préparé facilement la chloro-4 azétidinone (**10**), un intermédiaire chiral très réactif dans la synthèse des méthyl-1β carbapénèmes (**1***b*); on l'a isolé sous la forme d'un composé cristallin solide à partir du sulfure **5** correspondant. On a aussi préparé un autre intermédiaire chiral (**16***d*) qui porte une portion méthyle-1β; pour ce faire, on a utilisé une condensation de type aldolique stéréosélective des azétidinones **4** ou **10** avec les énolates métalliques **14** (R = S—*tert*-Bu, M = $ZrCp_2Cl$, $B(OCH_2)_2$ ou SnBr). Les rapports β/α sont respectivement de 9:1, de 3:1 et de 2:1.

[Traduit par la revue]

Can. J. Chem. Downloaded from www.nrcresearchpress.com by 213.166.140.6 on 09/07/12
For personal use only.

Since the discoveries of the highly active β-lactam antibiotics, carbapenem (**1***a*) (R = 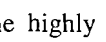 , thienamycin) (1) and 1-β-methylcarbapenem (**1***b*) (2), and the synthesis of penems (**2**) by Woodward (3), much attention has been directed toward the syntheses of these compounds and their analogs (4).

The most commonly used chiral intermediates for both penem and carbapenem syntheses are azetidinones **3**, where

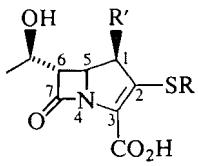

1 *a*: R′ = H
b: R′ = CH_3

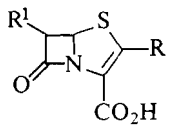

2

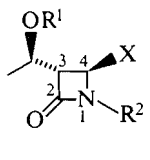

3

particularly 4-acetoxyazetidinone **4** has been widely used as an important intermediate (6). Although compound **4** is a stable solid easily available both from well-described procedures (5, 7) and from a commercial source,[1] its reactivity is limited, particularly at low temperature. It is such low temperature reaction conditions that are required for kinetic control, for example to control the stereochemistry in the syntheses of 1-β-methylcarbapenems (**1***b*). Thus, the more reactive 4-chloroazetidinone **10** might better serve as the substrate for such kinetically controlled reactions.

Karady *et al.* (8) reported the *N*-protected 4-chloroazetidinone **3** ($R^1 = R^2 = Si\!\!\leftarrow\!\!\rightarrow$; X = Cl), and demonstrated it to be a useful intermediate. However, because the nitrogen was protected with a *tert*-butyldimethylsilyl group, the reactivity of **3** ($R^1 = R^2 = Si\!\!\leftarrow\!\!\rightarrow$; X = Cl) at the C-4 position is dramatically

[1]Kanegafuchi Chemical Industry Company, Osaka, Japan.

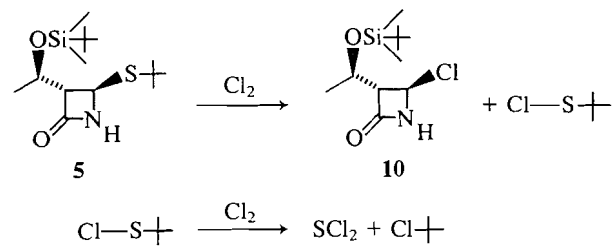

SCHEME 1

reduced compared to that of **10** without nitrogen protection.[2] Synthesis of the 4-chloroazetidinone **10** has been briefly reported by Perrone and co-workers (9), but these workers do not describe its isolation.

Herein is reported an easy preparation of the title compound **10**. Compound **10** was prepared by chlorinolysis of sulfide **5** with two equivalents of chlorine at −15°C (Scheme 1). Although one equivalent of chlorine is theoretically enough to produce **10**, a nonvolatile by-product produced with one equivalent of chlorine contaminates the product. The by-product, *tert*-butylsulfenyl chloride, reacts with an additional equivalent of chlorine to give volatile products. The crude

[2]It has been proven that the displacement reactions of 2-azetidinone **3** ($R^1 = Si\!\!\leftarrow\!\!\rightarrow$; R^2 = H; X = OAc) at the C-4 position go via a reactive intermediate

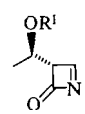

(10). It is more difficult to form the corresponding iminium salt of the *N*-protected azetidinone.

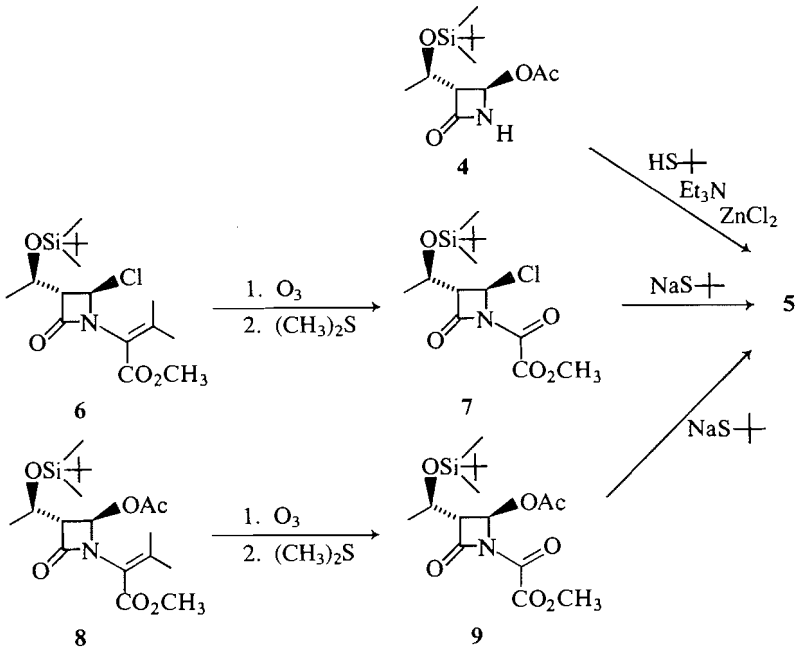

SCHEME 2

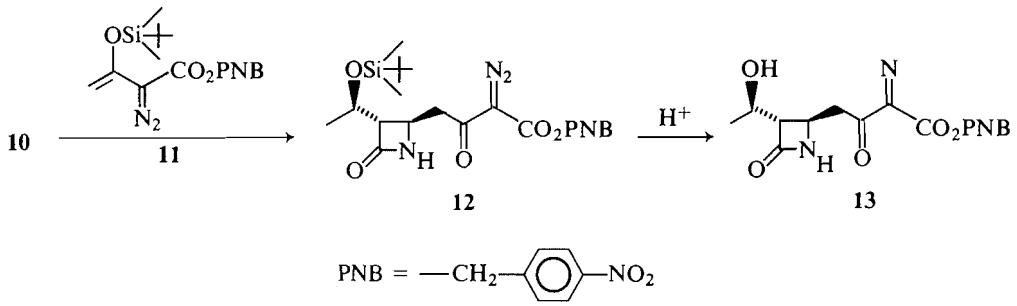

SCHEME 3

product was easily recrystallized from cold pentane, affording white crystalline solid **10** in 76% yield (Scheme 1). This product is rather unstable at room temperature but reasonably stable at −20°C. Compound **5**, the precursor of **10**, may be prepared from three different starting materials (Scheme 2). Treatment of 4-acetoxyazetidinone **4** (5) with *tert*-butylmercaptan, triethylamine, and zinc chloride gave compound **5** in 70% yield. The other two starting materials **7** (11) and **9** (11) (prepared quantitatively from the corresponding secopenams **6** (11) and **8** (11) by ozonolysis) reacted with sodium *tert*-butylmercaptide in ethanol, affording the sulfide **5** in good yields.

Chiral 4-chloroazetidinone **10** was converted to a known intermediate **13** (6*c*) for carbapenem syntheses (Scheme 3). Compound **10**, as expected, demonstrated its high reactivity, undergoing reaction with the *tert*-butyldimethylsilylenol ether **11** (6*c*) at low temperature to afford azetidinone **12** (6*c*). Deprotection of the hydroxy moiety (6*c*) was carried out by treating **12** with 1 *M* aqueous hydrochloric acid in methanol to give **13** in 64% overall yield.

Compound **10** also showed its usefulness for kinetically controlled reactions in 1-β-methylcarbapenem synthesis by reacting with metal enolates **14** at −78°C to give compound **16** (described below).

1-β-Methylcarbapenems (**1***b*) have been shown to be chemically and metabolically more stable than 1-unsubstituted carbapenems (**1***a*), and also to retain high antimicrobial activity (2). However, a stereoselective introduction of the β-methyl group into the carbapenem precursors has been a major problem (2, 12). Recently, several research groups have discovered means to overcome the problem. Fuentes *et al.* (13) reported that Evans type enolates **14***a* (14) undergo stereoselective aldol type condensation with 4-acetoxyazetidinone **4** in the presence of Lewis acid to afford **16***a* in good yields with predominantly the β-isomer. Similar results on **16***b*, using tin(II) enolates of thiazolidine-2-thiones and oxazolidine-2-thiones, have been reported by other groups (15, 16). As well, Iimori and Shibasaki (17) reported a stereoselective introduction of the β-methyl group by reducing an olefinic ester **15***a* with L-Selectride (β/α 8:1, 77% yield). Kim *et al.* (18) similarly achieved a stereoselective hydrogenation of **15***b* to give **16** (R = OCH_3, β/α 3:1) (Scheme 4).

In the search for a new way to introduce the β-methyl group, we conducted a series of coupling reactions of azetidinones **4** or **10** with the metal enolates **14** (R = OBz and S—Bu^t).

The enolates **14** were prepared by three known methods (19–21) depending on the reagent used (Scheme 5).

As mentioned earlier, 4-chloroazetidinone **10** has an advantage over 4-acetoxyazetidinone **4** in dealing with unstable metal enolates **14** that require low reaction temperature. The required low reaction temperature, as well, fulfils the kinetic condition to

Can. J. Chem. Downloaded from www.nrcresearchpress.com by 213.166.140.6 on 09/07/12
For personal use only.

TABLE 1. Results of coupling reaction

	R	Parameters	$AlEt_2$	$Sn\phi_3$	SnBr	$ZrCp_2Cl$		$B(n\text{-}Bu)_2$	$TiCp_2Cl$
16*c*	OBz	β/α[a]	52:48	42:58		33:67	45:55	38:62	33:67
		Yield (%)	73	37	—	20	20	29	71
		Method[b]	C	C		A	C	C	C
		Amount used (equiv.)	1.9	3.1		2.5	2.0	2.0	2.0
		Reaction temperature (°C)	−10	23		0	0	23	0
		Reaction time (h)	1	1		1	3	1	1
16*d*	S-Bu^t	β/α	25:75	20:80	69:31	94:6	77:23	20:80	16:84
		Yield (%)	68	24	66	15	30	57	51
		Method	C	C	C[c]	A[d]	B	C	C
		Amount used (equiv.)	1.9	2.0	3.0	2.5	2.0	2.0	2.0
		Reaction temperature (°C)	0	−5 to 0	23	−78	23	−5 to 0	−10 to −5
		Reaction time (h)	1/3	2	72	2	48	2/3	5/6

[a]The ratio was determined by hplc (column: Hypersil, column length: 200 × 2.1 mm, solvent: 10–20% EtOAc/hexane, detection: uv 260 nm).
[b]**4** was used for all cases except the one indicated.
[c]Tin powder (3 equiv.) was used instead of zinc dust and $AgBF_4$ (10 mol%) was added to activate metal tin.
[d]**10** was used. This gives slightly better yield than **4**.

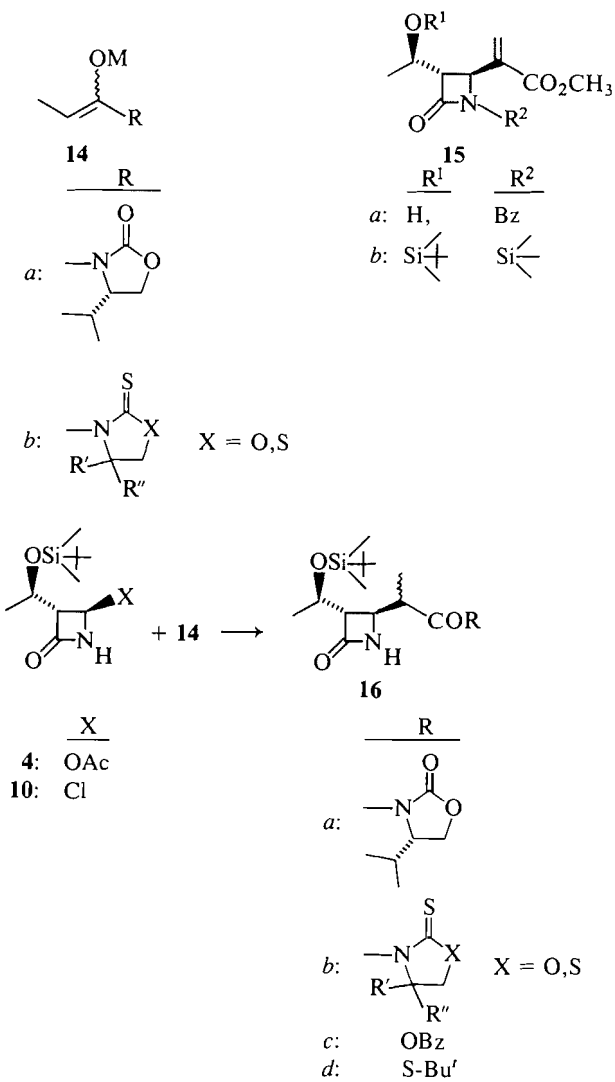

SCHEME 4

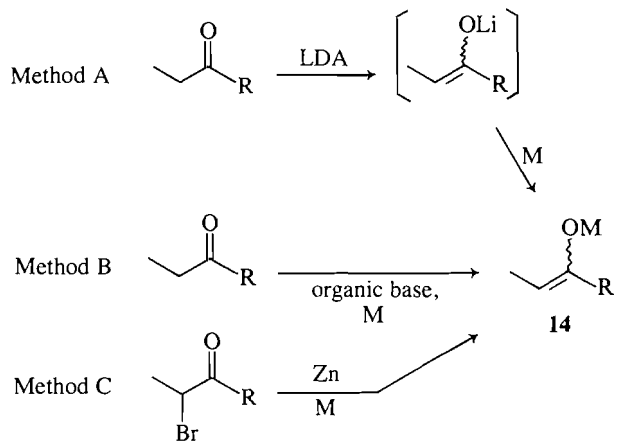

SCHEME 5

control the stereochemistry. The 4-chloroazetidinone **10** reacts at temperatures as low as −78°C, while 4-acetoxyazetidinone **4** does not react at a significant rate below −10°C.

The results are shown in Table 1. When R = OBz, product **16***c* was obtained, for which there was little stereoselectivity observed favoring the β-isomer regardless of the metal enolate used. The β/α ratio was more or less in a range of 1:1, or weighted towards the α-isomer. On the other hand, *tert*-butyl thiopropionate (R = S—Bu^t), giving product **16***d*, showed greater stereoselectivity, either favoring the α-isomer or the β-isomer. Thus, zirconium, boronyl, and tin(II) enolates were found to be good reagents to introduce the β-methyl group stereoselectivity.

It is not yet known which factors determine the stereochemical outcome in the coupling reaction with azetidinones **4** or **10**. Therefore it is rather difficult to predict the result, while the stereochemistry of analogous aldol condensations is generally well predicted (22).

One of the causes of the low yields in the series of *tert*-butyl thio(bromo)propionate reactions seems to be ketene formation,

Can. J. Chem. Downloaded from www.nrcresearchpress.com by 213.166.140.6 on 09/07/12
For personal use only.

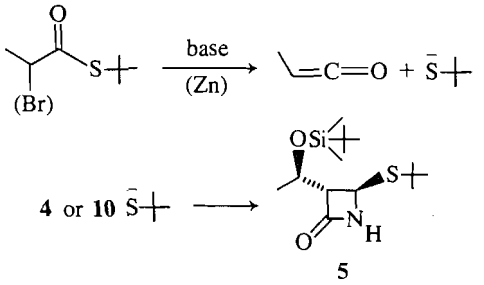

particularly under strongly basic conditions where more by-product **5** was isolated.

The structures **16***c* and **16***d* were confirmed by converting them to the known acid **17** (2*a*). Thus, the benzyl ester **16***c* was subjected to hydrogenolysis to give crystalline **17** as a β/α mixture in 76% yield. The α-isomer crystallized out from an ethyl acetate solution and was isolated pure. The thioester **16***d*

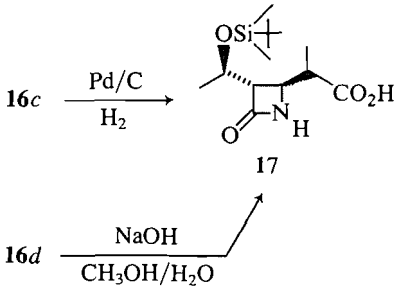

(β/α 94:6) was hydrolyzed under basic conditions to **17** (90%). However, the ^{1}H nmr spectrum indicated partial epimerization of the β-methyl group (β/α 70:30). Intermediate **17** has been converted to 1-β-methylcarbapenems (2*a*).

Experimental

*(3S,4R)-3-[1(R)-*tert*-Butyldimethylsilyloxyethyl]-4-chloro-1-(1-methoxycarbonyl-2-methyl-1-propenyl)azetidin-2-one (6)*

Compound **6** was prepared as described in ref. 11 except that the *tert*-butyldimethylsilyl function served to protect the hydroxy group instead of the trichloroethyl carbonate group. The crude solid (100% yield) was used without further purification; ^{1}H nmr (60 MHz, $CDCl_3$) δ: 0.03 (s, 6H, CH_3), 0.83 (s, 9H, CH_3CSi), 1.23 (d, J = 6 Hz, 3H, CH_3CHO), 1.93, 2.22 (2s, 6H, $=C(CH_3)_2$), 3.32 (dd, J = 1.5 Hz, 1H, H-3), 3.71 (s, 3H, CO_2CH_3), 4.18 (m, 1H, CH_3CHO), 5.86 (d, J = 1.5 Hz, H-4).

*(3S,4R)-4-Acetoxy-3-[1(R)-*tert*-butyldimethylsilyloxyethyl]-1-(2-methoxy-1,2-dioxyethyl)azetidine-2-one (9)*

A solution of compound **8** (5) (7.98 g, 0.02 mol) in dichloromethane (80 mL) was cooled to −78°C and ozone gas was bubbled in until a blue color persisted. The cooling bath was removed and the excess ozone was expelled by bubbling nitrogen gas. The ozonide solution was treated at room temperature with dimethyl sulfide (3 mL) for 1.5 h. The clear, colorless solution was washed with water (3×), dried over anhydrous magnesium sulfate, and concentrated *in vacuo* to give the white crystalline title compound (7.7 g, 98%), which was recrystallized from ether/petroleum ether (1:1), mp 54–55°C; ir (Nujol): 1700, 1760, 1828 cm^{-1}; ^{1}H nmr (200 MHz, $CDCl_3$) δ: 0.01, 0.06 (2s, 6H, CH_3Si), 0.81 (s, 9H, CH_3CSi), 1.29 (d, J = 6.4 Hz, 3H, CH_3CHO), 2.11 (s, 3H, $OCOCH_3$), 3.26 (dd, J = 1.9 and 2.0 Hz, 1H, H-3), 3.90 (s, 3H, CO_2CH_3), 4.31 (m, 1H, CH_3CHO), 6.73 (d, J = 2.0 Hz, 1H, H-4). *Anal.* calcd. for $C_{16}H_{27}NO_7Si$ (373.447): C 51.46, H 7.29, N 3.75; found: C 51.44, H 7.37, N 3.71.

*(3S,4R)-3-[1(R)-*tert*-Butyldimethylsilyloxyethyl]-4-chloro-1-(2-methoxy-1,2-dioxyethyl)azetidin-2-one (7)*

Compound **7** was prepared in 97% yield as described in ref. 11 except that the *tert*-butyldimethylsilyl group served as protection for the hydroxy group instead of the trichloroethyl carbonate group. The crystalline solid was pure enough to be used in the next step without further purification; mp 69–71°C (recrystallized from petroleum ether); ir (Nujol): 1715, 1760, 1825 cm^{-1}; ^{1}H nmr (200 MHz, $CDCl_3$) δ: 0.01, 0.06 (2s, 6H, CH_3Si), 0.81 (s, 9H, CH_3CSi), 1.28 (d, J = 6.3 Hz, 3H, CH_3CHO), 3.53 (overlapping dd, 1H, H-3), 3.92 (s, 3H, CO_2CH_3), 4.32 (m, 1H, CH_3CHO), 6.01 (d, J = 1.9 Hz, 1H, H-4). *Anal.* calcd. for $C_{14}H_{24}ClNO_5Si$ (349.856): C 48.06, H 6.91, N 4.00, Cl 10.13; found: C 47.94, H 7.03, N 3.95, Cl 9.89.

*(3S,4R)-3-[1(R)-*tert*-Butyldimethylsilyloxyethyl]-4-*tert*-butylthioazetidin-2-one (5)*

Method A: via 4-acetoxyazetidinone 4

To a solution of compound **4** (57.4 g, 0.2 mol) in dichloromethane (600 mL) under nitrogen atmosphere was added *tert*-butylmercaptan (24.6 mL, 0.22 mol) followed by addition of triethylamine (30.6 mL, 0.2 mol). The solution was cooled to 0°C and zinc chloride (27.2 g, 0.2 mol) was added. The resulting milky solution was stirred at room temperature for 2 days. The reaction mixture was successively washed with 1 *M* aqueous hydrochloric acid (500 mL), saturated sodium bicarbonate (500 mL), and water (500 mL), dried over anhydrous magnesium sulfate, and concentrated to give a wet crystalline solid (70 g). The crude product was triturated in isopropyl alcohol (150 mL) and then diluted with water (150 mL). The slurry was cooled to 5°C and the solid was collected by filtration. The cake was washed with cold (5°C) isopropyl alcohol – water (1:2, 100 mL) and dried *in vacuo* to give the title compound **5**. Yield 44.3 g (70%); mp 152–154°C; $[\alpha]_D^{23}$ +85.0° (*c* 0.57, $CHCl_3$); ir (Nujol): 1715, 1762 cm^{-1}; ^{1}H nmr (200 MHz, $CDCl_3$) δ: 0.06, 0.07 (2s, 6H, CH_3Si), 0.87 (s, 9H, CH_3CSi), 1.20 (d, J = 6.3 Hz, 3H, CH_3CHO), 1.36 (s, 9H, $S(CH_3)_3$), 3.03 (m, 1H, H-3), 4.25 (m, 1H, CH_3CHO), 5.00 (d, J = 2.6 Hz, 1H, H-4), 6.06 (br s, 1H, NH). *Anal.* calcd. for $C_{15}H_{31}NO_2SSi$ (317.563): C 56.73, H 9.84, N 4.41, S 10.10; found: C 56.74, H 9.91, N 4.37, S 10.09.

Method B: via 4-chlorooxamate (7)

To an ice-cooled solution of compound **7** (0.349 g, 1 mmol) in ethanol (5 mL) under nitrogen atmosphere was added dropwise sodium *tert*-butylmercaptide (1.1 mL of 1 *M* solution in ethanol–water 6:1). The resulting solution was stirred at 5–10°C for 15 min. The reaction mixture was diluted with diethyl ether (70 mL), washed with brine (4×), dried over anhydrous magnesium sulfate, and concentrated to give crystalline **5** (0.31 g, 98%).

Method C: via 4-acetoxyoxamate (9)

To a solution of compound **9** (0.389 g, 1.04 mmol) in ethanol (6 mL) under nitrogen atmosphere was added sodium *tert*-butylmercaptide (1.1 mL of 1 *M* solution in ethanol–water 6:1). The hazy solution was stirred at room temperature for 2 h. The reaction mixture was diluted with diethyl ether (70 mL), washed with brine (4×), dried over anhydrous magnesium sulfate, and concentrated to dryness, affording the white crystalline product **5** (0.32 g, 96%).

Compound **5** produced by methods B and C showed identical spectral values to compound **5** produced by method A.

*(3S,4R)-3-[1(R)-*tert*-Butyldimethylsilyloxyethyl]-4-chloroazetidin-2-one (10)*

Chlorine gas (2.24 g, 31.54 mmol) was gently bubbled into a solution of compound **5** (5.0 g, 15.77 mmol) in dichloromethane (50 mL) while maintaining the temperature at −5 to −15°C. The yellow solution was concentrated (*in vacuo*, <20°C) to give a crystalline solid, which was recrystallized from cold (−70°C) pentane to give the title compound **10**. Yield 3.12 g (76%), white crystals; mp 84–85°C; $[\alpha]_D^{23}$ +23.5° (*c* 0.49, $CHCl_3$); ir (Nujol): 1736, 1775 cm^{-1}; ^{1}H nmr (200 MHz, $CDCl_3$) δ: 0.03, 0.05 (2s, 6H, CH_3Si), 0.84 (s, 9H, CH_3CSi), 1.26 (d, J = 6.4 Hz, 3H, CH_3CHO), 3.41 (m, 1H, H-3), 4.21 (m, 1H, CH_3CHO), 5.67 (d, J = 1.3 Hz, 1H, H-4), 6.25 (br s, 1H, NH). *Anal.* calcd. for $C_{11}H_{22}ClNO_2Si$ (263.810): C 50.08, H 8.41, N 5.30, Cl 13.43; found: C 50.11, H 8.50, N 5.22, Cl 13.24.

Can. J. Chem. Downloaded from www.nrcresearchpress.com by 213.166.140.6 on 09/07/12
For personal use only.

Can. J. Chem. Downloaded from www.nrcresearchpress.com by 213.166.140.6 on 09/07/12
For personal use only.

*(3S,4R)-3-[1(R)-*tert*-Butyldimethylsilyloxyethyl]-4-(3-*p*-nitrobenzyloxycarbonyl-2-oxo-3-diazopropan-1-yl]-azetidin-2-one (**12**) and (3S,4R)-3-[1(R)-hydroxyethyl]-4-(3-*p*-nitrobenzyloxycarbonyl-2-oxo-3-diazopropan-1-yl]-azetidin-2-one (**13**)*

To a solution of compound **10** (0.264 g, 1 mmol) in dichloromethane (6 mL) at −40°C under nitrogen atmosphere was added silver tetrafluoroborate (0.195 g, 1 mmol), followed by addition of a solution of enol ether **11** (0.57 g, 1.5 mmol) (6*c*) in dichloromethane (6 mL) over 20 min. The resulting solution was stirred at −30 to −40°C for 2 h. The reaction mixture was diluted with ethyl acetate (40 mL), then washed successively with saturated sodium bicarbonate (30 mL) and brine (2 × 40 mL). Concentration of the organic phase gave a mixture of oil and solid that was dissolved in methanol (10 mL). Insoluble solids were filtered off and washed with methanol (5 mL). The combined filtrate (containing compound **12**) was treated at room temperature with 1 *M* aqueous hydrochloric acid (2.5 mL) for 18 h. The reaction mixture was diluted with water (30 mL), then extracted with ethyl acetate (60 mL and 40 mL respectively). The organic phase was washed successively with saturated sodium bicarbonate (40 mL) and brine (2 × 50 mL), dried over anhydrous magnesium sulfate, and concentrated to give a wet solid. The product (**13**) was isolated by triturating in ether (10 mL). Yield 0.24 g (64%), mp 149–150°C (lit. (6*c*) mp 151–152°C). The ^{1}H nmr spectrum was identical to that reported (6*c*).

Metal enolate/azetidinone coupling reactions

A typical procedure for each method is described.

Method A (ref. 19)

To a lithium diisopropylamine (2.5 mmol) solution in dry tetrahydrofuran (6 mL) at −78°C was added a solution of *tert*-butyl thiopropionate (0.365 g, 2.5 mmol) in tetrahydrofuran (2 mL) over 10 min. The resulting lithium enolate solution was stirred at −78°C for 0.5 h. Then, a solution of zirconocene dichloride (0.73 g, 2.5 mmol) in tetrahydrofuran (10 mL) was added dropwise over 15 min and the mixture was stirred for 0.5 h. To this was added all at once 4-chloroazetidinone **10** (0.264 g, 1 mmol). The resulting solution was stirred at −78°C for 2 h. The reaction mixture was diluted with ether (60 mL), washed successively with 1 *M* hydrochloric acid (20 mL), saturated sodium bicarbonate (20 mL), and brine (2 × 30 mL), dried over anhydrous magnesium sulfate, and concentrated to give an oil (0.248 g), which was chromatographed on silica gel (ether – petroleum ether 1:1), yielding 56 mg (15%) of **16***d* with a β/α ratio of 94:6; mp 109–113°C (recrystallized from petroleum ether); ^{1}H nmr (200 MHz, $CDCl_3$) δ: 0.04, 0.05 (2s, CH_3—Si, αβ), 0.84, 0.85 (2s, CH_3—C—Si, αβ), 1.14, 1.24 (2d, J = 6.4 and 7.0 Hz, CH_3—CH—OSi and CH_3—CH—C=O, β), 1.20 (2 overlapping d, J = 6.2 and 7.2 Hz, CH_3—CH—OSi and CH_3—CH—C=O, α), 1.43 (s, *t*-BuS, β), 1.44 (s, *t*-BuS, α), 2.61 (m, CH_3—*CH*—C=O, α), 2.73 (m, overlapping, H-3, α, and CH_3—*CH*—C=O, β), 2.94 (dd, J = 2.2 and 3.5 Hz, H-3, β), 3.68 (dd, J = 2.1 and 9.5 Hz, H-4, α), 3.82 (dd, J = 2.2 and 6.2 Hz, H-4, β), 4.15 (m, CH_3—*CH*—OSi, αβ), 5.86 (br s, NH, β), 5.93 (br s, NH, α). *Anal.* calcd. for $C_{18}H_{35}NO_3SSi$ (373.601): C 57.87, H 9.44, N 3.75, S 8.58; found: C 58.11, H 9.50, N 3.70, S 8.42.

Method B (ref. 20)

To an ice-cooled solution of *tert*-butylthiopropionate (0.584 g, 4 mmol) in dry methylene chloride (10 mL) was added diisopropylethylamine (0.75 mL, 4.3 mmol), followed by dropwise addition of a solution of ethylenechloroboronate (4 mmol) in methylene chloride (3 mL). The resulting solution was stirred at room temperature for 3.5 h. To this solution was added **4** (5) (0.574 g, 2 mmol) and it was stirred at room temperature for 2 days. The reaction mixture was washed successively with 1 *M* hydrochloric acid, saturated sodium bicarbonate, and water, dried over anhydrous magnesium sulfate, concentrated, and chromatographed on silica gel (ether – petroleum ether 1:1), giving 0.23 g of **16***d* (30%, β/α 77:23). The ^{1}H nmr spectrum was identical to that of compound **16***d* produced by method A.

Method C (ref. 21)

To a slurry of activated zinc dust (0.5 g, 7.7 mmol) in dry tetrahydrofuran (10 mL) at −10°C was added diethylaluminum chloride (3.8 mmol, in hexane). A solution of **4** (0.574 g, 2 mmol) and benzyl 2-bromopropionate (1.46 g, 6 mmol) in tetrahydrofuran (10 mL) was added dropwise over 0.5 h. The resulting slurry was stirred at −10°C for 1 h. The reaction mixture was filtered on Celite and the filtrate was diluted with ether (70 mL), washed successively with 1 *M* hydrochloric acid (25 mL), saturated sodium bicarbonate (25 mL), and brine (2 × 30 mL), dried over anhydrous magnesium sulfate, and concentrated to give an oil, which was chromatographed on silica gel (ether – petroleum ether 1:1), yielding 0.57 g of **16***c* (73%, β/α 52:48); mp 61–62°C (recrystallized from petroleum ether); ^{1}H nmr (200 MHz, $CDCl_3$) δ: 0.04, 0.06 (2s, CH_3—Si, αβ), 0.84, 0.85 (2s, CH_3—C—Si, αβ), 1.12, 1.23 (2d, J = 6.3 and 7.0 Hz, CH_3—CH—OSi and CH_3—CHC=O, β), 1.22 (2 overlapping d, J = 6.2 and 7.2 Hz, CH_3—CH—OSi and CH_3—CH—C=O, α), 2.55 (m, CH_3—*CH*—C=O, α), 2.71 (m, overlapping H-3, α, and CH_3—*CH*—C=O, β), 2.96 (dd, J = 2.2 and 4.3 Hz, H-3, β), 3.69 (dd, J = 2.0 and 9.4 Hz, H-4, α), 3.90 (dd, J = 2.2 and 5.4 Hz, H-4, β), 4.42 (m, CH_3—*CH*—OSi, αβ), 5.11 (CH_2Ph, β), 5.13 (s, CH_2Ph, α), 5.82 (br s, NH, β), 5.92 (br s, NH, α), 7.33 (s, Ph, αβ). *Anal.* calcd. for $C_{21}H_{33}NO_4Si$ (391.553): C 64.42, H 8.50, N 3.58; found: C 64.65, H 8.83, N 3.54.

*Hydrogenolysis of **16**c*

Compound **16***c* (β/α 52:48, 0.41 g, 1.05 mmol) was dissolved in methanol (30 mL). To this were added 10% Pd/C (200 mg), water (1.5 mL), and pH 7 phosphate buffer (3 mL). This mixture was placed in an hydrogenation bottle that was shaken at room temperature under 7 psi/H_2 (1 psi = 6.9 kPa) for 1.5 h. The reaction mixture was filtered on Celite and the Celite was washed with methanol (10 mL). The filtrate was concentrated to give a white solid (0.33 g), which was dissolved in a mixture of saturated sodium bicarbonate (8 mL) and water (8 mL), and washed with ether (2 × 10 mL). The aqueous phase was acidified with 2 *M* hydrochloric acid and extracted with ether (2 × 15 mL). The ether extract was washed with brine (20 mL), dried over anhydrous magnesium sulfate, and concentrated to give crystalline **17** as a β/α mixture (0.24 g, 76%, β/α 1:1, mp 130–134°C). The pure α-isomer was isolated by crystallization from ethyl acetate; mp 160–162°C, $[\alpha]_D^{23}$ −2.7° (*c* 0.11, CH_3OH); ir (Nujol): 2190, 2800–2400 (br), and 1712 (br) cm^{-1}; ^{1}H nmr (200 MHz, $CDCl_3$) δ: 0.06, 0.07 (2s, 6H, CH_3—Si), 0.87 (s, 9H, CH_3—C—Si), 1.24, 1.27 (2 overlapping d, J = 5.7 and 7.0 Hz, 6H, CH_3—CH—OSi and CH_3—CH—C=O), 2.55 (m, 1H, CH_3—CH—C=O), 2.78 (dd, J = 1.0 and 5.2 Hz, 1H, H-3), 3.68 (dd, J = 1.9 and 9.8 Hz, 1H, H-4), 4.18 (m, 1H, CH_3—CH—OSi), 6.59 (br s, NH). *Anal.* calcd. for $C_{14}H_{27}NO_4Si$ (301.428): C 55.78, H 9.03, N 4.65; found: C 55.63, H 9.20, N 4.61. The reported ^{1}H nmr spectrum of the β-isomer (2*a*) supports the structure as well.

*Hydrolysis of **16**d*

Compound **16***d* (β/α 94:6, 31 mg, 0.083 mmol) was dissolved in methanol (1.7 mL). To this were added water (0.25 mL) and 2.5 *M* sodium hydroxide (0.1 mL). The resulting solution was stirred at room temperature for 2 days. The reaction mixture was diluted with water (20 mL) and washed with ether (2 × 20 mL). The aqueous phase was then acidified with concentrated hydrochloric acid (0.5 mL) and extracted with ethyl acetate (2 × 25 mL). The organic phase was washed with brine (2 × 25 mL), dried over anhydrous magnesium sulfate, and concentrated to give crystalline **17** as a white solid (23 mg, 90%). Although the ^{1}H nmr spectrum showed the expected product, it indicated partial epimerization of the methyl group (β/α 70:30).

Acknowledgement

The author would like to thank Drs. J. L. Douglas and Y. G. Perron for advice during the course of this work.

1. (*a*) H. Kropp, J. S. Kahan, J. Sundelof, G. Darland, and J. Birnbaum. 16th Interscience Conference Antimicrobial Agents and Chemotherapy, Chicago (1976); (*b*) G. Albers-Schonberg, B. H. Arison, O. D. Hensens, J. Hirshfield, K. Hoogsteen,

E. A. KACZKA, R. E. RHODES, J. S. KAHAN, F. M. KAHAN, R. W. RATCLIFFE, E. WALTON, L. J. RUSWINKLE, R. B. MORIN, and B. G. CHRISTENSEN. J. Am. Chem. Soc. **100**, 6491 (1978).
2. (*a*) D. H. SHIH, L. BAKER, I. CAMA, and B. G. CHRISTENSEN. Heterocycles, 1, 29 (1984); (*b*) D. H. SHIH, J. A. FAYTER, L. D. CAMA, B. G. CHRISTENSEN, and J. HIRSHFIELD. Tetrahedron Lett. **26**, 583 (1985); **26**, 89 (1985).
3. R. B. WOODWARD. *In* Recent advances in the chemistry of β-lactam antibiotics. *Edited by* J. Elks. Chem. Soc. Spec. Publ. No. 28. 1977.
4. (*a*) T. KAMETANI. Heterocycles, **17**, 463 (1982); (*b*) Recent advances in the chemistry of β-lactam antibiotics. *Edited by* A. G. Brown and S. W. Roberts. The Royal Society of Chemistry, London. 1984; (*c*) W. DURCKHEIMER, J. BLUMBACH, R. LATTRELL, and K. H. SCHEUNEMANN. Angew. Chem. Int. Ed. Engl. **24**, 180 (1985).
5. A. YOSHIDA, T. HAYASHI, N. TAKEDA, S. OIDA, and E. OHKI. Chem. Pharm. Bull. **29**, 2899 (1981).
6. (*a*) K. FUJIMOTO, Y. IWANO, and K. HIRAI. Tetrahedron Lett. **26**, 89 (1985); (*b*) W. J. LEANZA, F. DININNO, D. A. MUTHARD, R. R. WILKENING, K. J. WILDONGER, R. W. RATCLIFFE, and B. G. CHRISTENSEN. Tetrahedron, **39**, 2505 (1983); (*c*) Y. UEDA, G. ROBERGE, and V. VINET. Can. J. Chem. **62**, 2936 (1984).
7. (*a*) A. MARTEL and J. P. DARIS. U.S. Patent No. 4,596,677 (1986); (*b*) M. ENDO. Synth. Commun. In press.
8. S. KARADY, J. S. AMATO, R. A. REAMER, and L. M. WEINSTOCK. J. Am. Chem. Soc. **103**, 6765 (1981).
9. A. ALPEGIANI, A. BEDESCHI, M. FOGLIO, F. GIUDICI, and E. PERRONE. Tetrahedron Lett. **24**, 1627 (1983).
10. Y. UEDA and S. C. MAYNARD. Tetrahedron Lett. **26**, 6309 (1985).
11. V. M. GIRIJAVALLABHAN, A. K. GANGULY, S. W. MCCOMBIE, P. PINTO, and R. RIZVI. Tetrahedron Lett. **22**, 3485 (1981).
12. K. FUJIMOTO, Y. IWANO, and K. HIRAI. Tetrahedron Lett. **26**, 89 (1985).
13. L. M. FUENTES, I. SHINKAI, and T. N. SALZMANN. J. Am. Chem. Soc. **108**, 4675 (1986).
14. D. A. EVANS, J. BATTROLI, and T. L. SHIH. J. Am. Chem. Soc. **103**, 2127 (1984).
15. Y. NAGAO, T. KUMAGAI, S. TAMAI, T. ABE, Y. KURAMOTO, T. TAGA, S. AOYAGI, Y. NAGASE, M. OCHIAI, Y. INOUE, and E. FUJITA. J. Am. Chem. Soc. **108**, 4673 (1986).
16. R. DEZIEL and D. FAVREAU. Tetrahedron Lett. **27**, 5687 (1986).
17. T. IIMORI and M. SHIBASAKI. Tetrahedron Lett. **27**, 2149 (1986).
18. C. U. KIM, B. LUH, and R. A. PARTYKA. Tetrahedron Lett. **28**, 507 (1987).
19. (*a*) D. A. EVANS and L. R. MCGEE. Tetrahedron Lett. **21**, 3975 (1980); (*b*) Y. YAMAMOTO and K. MURAYAMA. Tetrahedron Lett. **21**, 4107 (1980); (*c*) T. MUKAIYAMA, H. SUZUKI, and T. YAMADA. Chem. Lett. 915 (1986).
20. (*a*) C. GENNARI, L. COLOMBO, and G. POLI. Tetrahedron Lett. **25**, 2279 (1983); (*b*) **26**, 797 (1985).
21. K. MARUOKA, S. HASHIMOTO, Y. KITAGAWA, H. YAMAMOTO, and H. NOZAKI. J. Am. Chem. Soc. **99**, 7705 (1977).
22. D. A. EVANS, J. V. NELSON, and T. R. TABER. *In* Topics in stereochemistry. Vol. 13. *Edited by* N. L. Allinger, E. L. Eliel, and S. H. Wilen. John Wiley and Sons, New York. 1982. pp. 1–115.

Can. J. Chem. Downloaded from www.nrcresearchpress.com by 213.166.140.6 on 09/07/12
For personal use only.

The binding energies of trialkylgermanium cations to water molecules studied by high pressure mass spectrometry

JOHN ALFRED STONE AND WILHELMUS JOHANNES WYTENBURG
Chemistry Department, Queen's University, Kingston, Ont., Canada K7L 3N6

Received February 5, 1987

JOHN ALFRED STONE and WILHELMUS JOHANNES WYTENBURG. Can. J. Chem. **65**, 2146 (1987).

The binding energies of H_2O to R_3Ge^+ have been measured using pulsed electron beam, high pressure mass spectrometry. van't Hoff plots have yielded thermodynamic data (ΔH^0, ΔS^0) for the reactions, [5], $R_3Ge^+ + H_2O \rightleftharpoons R_3GeOH_2^+$ (R = CH_3, C_2H_5, C_3H_7, C_4H_9) and [7], $R_3GeOH_2^+ + H_2O \rightleftharpoons R_3Ge(OH_2)_2^+$ (R = CH_3, C_2H_5). ΔH_5^0 decreases with increasing size of R (CH_3 28.6 ± 0.5 kcal mol^{-1}, C_4H_9 20.6 ± 1.2 kcal mol^{-1}) while ΔS_5^0 shows much less change (34.4 ± 0.9 to 30.3 ± 2.8 cal K^{-1} mol^{-1}). Comparison with data for $(CH_3)_3M^+$ (M = Si, Sn) shows that binding energy decreases with increasing size of M.

JOHN ALFRED STONE et WILHELMUS JOHANNES WYTENBURG. Can. J. Chem. **65**, 2146 (1987).

On a mesuré les énergies de liaison du H_2O au R_3Ge^+ en faisant appel à la spectrométrie de masse à haute pression et à faisceau d'électrons pulsés. Les courbes de van't Hoff ont permis d'obtenir les données thermodynamiques (ΔH^0 et ΔS^0) pour les réactions $R_3Ge^+ + H_2O \rightleftharpoons R_3GeOH_2^+$ (5) (R = CH_3, C_2H_5, C_3H_7 et C_4H_9) et $R_3GeOH_2^+ + H_2O \rightleftharpoons R_3Ge(OH_2)^+$ (7) (R = CH_3 et C_2H_5). Le ΔH_5^0 diminue avec une augmentation de la taille du groupement R (CH_2, 28,6 ± 0,5 kcal mol^{-1}, C_4H_9, 20,6 ± 1,2 kcal mol^{-1}) alors que le ΔS_5^0 varie beaucoup moins (34,4 ± 0,9 à 30,3 ± 2,8 cal K^{-1} mol^{-1}). Une comparaison des données pour $(CH_3)_3M^+$ (M = Si, Sn) démontre que l'énergie de liaison diminue avec une augmentation de la taille de M.

[Traduit par la revue]

Introduction

The adducts formed between trimethylgermylium ($(CH_3)_3Ge^+$) and Lewis bases are reported to be considerably more stable than those formed between trimethylsilylium ($(CH_3)_3Si^+$) and the same bases. For example at low pressure ($\sim 10^{-4}$ Torr (1 Torr = 133 Pa)) under ion cyclotron resonance (ICR) conditions the adducts formed by the addition of $(CH_3)_3Ge^+$ to a wide variety of N, O, or S containing bases (alcohols, amines, esters etc.) generally do not decompose. By contrast the adducts formed by the addition of $(CH_3)_3Si^+$ to the same bases decompose to a very great extent under the same experimental conditions. The only $(CH_3)_3Ge^+$ adducts which decompose to a considerable extent are those of carboxylates and thio-esters and even these show much less fragmentation than the analogous $(CH_3)_3Si^+$ adducts (1). This increased stability of the germanium adducts cannot be ascribed to a greater Lewis acid–base interaction since under ICR conditions the increased reaction exothermicity would lead to enhanced decomposition. The explanation must lie in a much reduced exothermicity of adduct formation and/or to the larger germanium centre closing off decomposition channels which are readily accessible in the silicon complexes. A first determination of the thermochemistry of adduct formation by $(CH_3)_3Ge^+$ is the subject of this study.

We have previously reported the enthalpies of binding of $(CH_3)_3Si^+$ to a variety of aromatic and oxygen-containing bases (2, 3). The enthalpy values are based on an absolute measurement obtained from the temperature coefficient of the equilibrium constant for reaction [1].

[1] $(CH_3)_3Si^+ + H_2O \rightleftharpoons (CH_3)_3SiOH_2^+$

In this paper we report a similar measurement for the analogous reaction [2]

[2] $(CH_3)_3Ge^+ + H_2O \rightleftharpoons (CH_3)_3GeOH_2^+$

In addition, the ready availability of other germanium tetraalkyl compounds allowed the measurement of the enthalpy of binding of water to other R_3Ge^+ ions (R = C_2H_5, n–C_3H_7, butyl).

Experimental

The pulsed electron beam mass spectrometer with ion source operable at pressures up to 5 Torr, and the method of obtaining equilibrium data have been described previously (4). Premixed samples are made up in a heated 5 L flask from which they are bled into the ion source via a heated leak valve. A typical sample contained <0.3 mol% R_4Ge (R = CH_3, C_2H_5, n-C_3H_7, butyl), 0.02 mol% sulfur hexafluoride, >99 mol% methane, and water vapour whose amount was always small and optimized to give best precision for each equilibrium measurement.

All the tetraalkyl germanium compounds were from Morton Thiokol Inc., Alfa Products, and were used as received except for $(CH_3)_4Ge$. This compound was found to be contaminated with more than 1 mol% tetrahydrofuran which forms a much more strongly bonded complex with $(CH_3)_3Ge^+$ than does water and hence prevents the study of reaction [2]. Gas liquid chromatography was used to remove this impurity. The tetrapropylgermanium contained n-propyl groups but the tetrabutylgermanium, with butyl groups whose structure was not identified by the manufacturer, was found to contain a mixture of butyl isomers. Its nmr spectrum was complex and no attempt was made to characterize it further.

The sulfur hexafluoride was present in each sample to capture electrons and decrease the rate of positive ion diffusion to the ion source walls and hence increase the ion residence times in the source (4).

Results and discussion

The ion chemistry of $R_4Ge/SF_6/CH_4$ (0.002/0.0002/0.99) mixtures was studied briefly at ion source pressures in the range 2–4 Torr and temperatures in the range 350–600 K. The reactions observed are analogous to those reported for $(CH_3)_4Si/SF_6/CH_4$ mixtures under similar ion source conditions (3).

R_3Ge^+ is the only initial ion resulting from the reaction of R_4Ge with the major reagent ions CH_5^+ and $C_2H_5^+$ present in methane under chemical ionization (CI) conditions. R_3Ge^+ then reacts with R_4Ge giving $R_7Ge_2^+$.

[3] $CH_5^+(C_2H_5)^+ + R_4Ge \rightarrow R_3Ge^+ + RH + CH_4(C_2H_4)$

[4] $R_3Ge^+ + R_4Ge \rightleftharpoons R_7Ge_2^+$

Can. J. Chem. Downloaded from www.nrcresearchpress.com by 213.166.140.6 on 09/07/12
For personal use only.

Can. J. Chem. Downloaded from www.nrcresearchpress.com by 213.166.140.6 on 09/07/12
For personal use only.

Reaction [4] is assumed to be, and is written as, an equilibrium although this was not ascertained. The assumption is justifiable since $(CH_3)_7Si_2^+$ and $(CH_3)_3Si^+$ are found to participate in the analogous equilibrium in $(CH_3)_4Si/CH_4$ mixtures (2). The formation of $(CH_3)_7M_2^+$ seems to be a common characteristic for all members M except carbon of Group IV A; the formation of $(CH_3)_7Sn_2^+$ in $(CH_3)_4Sn/CH_4$ mixtures has been previously reported (5).

The addition of small amounts of water to the $R_4Ge/CH_4/SF_6$ system results in the appearance of three new ions, a drastic reduction in the abundance of $R_7Ge_2^+$, and a significant reduction in R_3Ge^+. Two of the new ions are the water adducts $R_3GeOH_2^+$ and $R_3Ge(OH_2)_2^+$. $R_3GeOH_2^+$ is formed by addition of water to R_3Ge^+ and probably also by displacement of R_4Ge from $R_7Ge_2^+$.

[5] $R_3Ge^+ + H_2O \rightleftharpoons R_3GeOH_2^+$

[6] $R_7Ge_2^+ + H_2O \rightleftharpoons R_3GeOH_2^+ + R_4Ge$

$R_3GeOH_2^+$ is further solvated by water

[7] $R_3GeOH_2^+ + H_2O \rightleftharpoons R_3Ge(OH_2)_2^+$

Reactions [5], [6], and [7] are written as equilibrium reactions; [5] and [6] were examined in detail and proved to be so. No such study was made for reaction [6] but if reactions [4] and [5] are equilibrium reactions then reaction [6], if it occurs, must also be.

The third new ion which was formed upon addition of water to the sample had an isotopic pattern showing the presence of two germanium atoms and six R groups, leading to the formula $R_6Ge_2OH^+$. We suggest that this is a protonated germoxane which is analogous to protonated hexamethyl disiloxane observed in $(CH_3)_4Si/CH_4/H_2O$ mixtures (2).

[8] $R_3GeOH_2^+ + R_4Ge \rightarrow R_3GeO(H)GeR_3^+ + RH$

The formation of this ion is an irreversible process and at long reaction times under suitable conditions, it can become the dominant ion. However, equilibria [5] and [7] are set up very rapidly and the measured equilibrium constants are not perturbed by the much slower reaction [8].

The equilibrium constants K_5 and K_7 for reactions [5] and [7] are defined as

$$K_5 = \frac{i_{R_3GeOH_2^+}}{i_{R_3Ge^+}(P_{H_2O}/P^0)} \qquad K_7 = \frac{i_{R_3Ge(OH_2)^+}}{i_{R_3GeOH_2^+}(P_{H_2O}/P^0)}$$

where i is an ion current at long ion residence time when equilibrium has been attained, P_{H_2O} is the pressure (Torr) of water vapour in the ion source, and P^0 is standard pressure (760 Torr). K_5 was measured over a range of temperatures for R = CH_3, C_2H_5, C_3H_7, and C_4H_9 while K_7 was measured under similar conditions only for R = CH_3 and C_2H_5. The van't Hoff plots are shown in Figs. 1 and 2 while the ΔH^0 and ΔS^0 values obtained from the slopes of these plots are given in Table 1. Also shown in this table are data for some analogous reactions of $(CH_3)_3M^+$ (M = C, Si, Sn).

The data for the addition of one molecule of water to R_3Ge^+ show that the binding energy decreases as the size of R increases i.e. in the order $CH_3 > C_2H_5 > n\text{-}C_5H_7 > C_4H_9$. The decrease from CH_3 to C_4H_9 is 8 kcal mol^{-1}, a 30% change. This is understandable in terms of an increasing stabilization of R_3Ge^+ due to electron transfer from R to Ge with increasing size of R. As the electron density on Ge increases the interaction energy with H_2O correspondingly decreases. The decrease in enthalpy

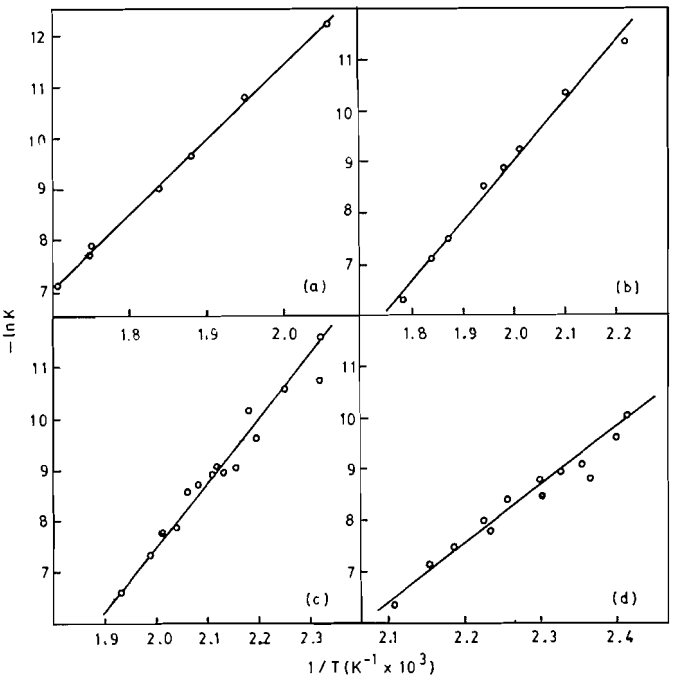

FIG. 1. van't Hoff plots for the reaction $R_3Ge^+ + H_2O \rightleftharpoons R_3GeOH_2^+$: (*a*) R = CH_3, (*b*) R = C_2H_5, (*c*) R = n-C_3H_7, (*d*) R = C_4H_9.

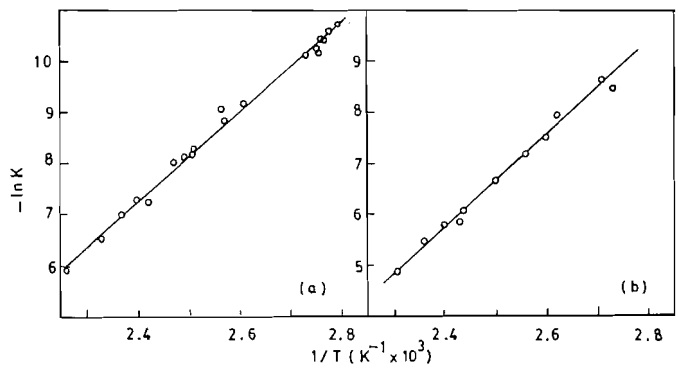

FIG. 2. van't Hoff plots for the reaction $R_3GeOH_2^+ + H_2O \rightleftharpoons R_3Ge(OH_2)_2^+$: (*a*) R = CH_3, (*b*) R = C_2H_5.

of binding from R = CH_3 to R = C_2H_5 (3.7 kcal mol^{-1}) is considerably greater than that from R = C_2H_5 to R = n-C_3H_7 (~1.5 kcal mol^{-1}) in line with the rapid attenuation of electron-releasing ability with length of an alkyl chain (6). The significantly larger increase from R = n-C_3H_7 to R = C_4H_9 (~2.8 kcal mol^{-1}) is consistent with the presence of branched, isomeric butyl groups in $(C_4H_9)_3R^+$.

The decreases in entropy shown in Table 1 for reaction [6] are large and show only small changes with change of R. These values imply the formation of products by condensation, i.e., covalent bond formation, rather than the formation of cluster ions for which entropies of formation are usually considerably smaller (7). The reaction products are therefore equivalent to those obtained by protonation of the germanols R_3GeOH. The absence of appropriate thermodynamic data for such compounds prevents the calculation of their proton affinities from the enthalpies of binding as was done for trimethylsilanol (3). The additions of the second water molecule to $(CH_3)_3GeOH_2^+$ and to $(C_2H_5)_3GeOH_2^+$ are much less exothermic processes

TABLE 1. Thermodynamic data for reactions [3] ($R_3M^+ + H_2O \rightleftharpoons R_3MOH_2^+$) and [4] ($R_3MOH_2^+ + H_2O \rightleftharpoons R_3M(OH_2)_2^+$)

M	R	$-\Delta H_5^0$ (kcal mol^{-1})	$-\Delta S_5^0$ (cal K^{-1} mol^{-1})	$-\Delta H_7^0$ (kcal mol^{-1})	$-\Delta S_7^0$ (cal K^{-1} mol^{-1})
Ge	CH_3	28.6 ± 0.5	34.4 ± 0.9	17.2 ± 0.3	26.7 ± 0.8
Ge	C_2H_5	24.9 ± 0.5	31.6 ± 1.0	18.4 ± 0.2	32.8 ± 0.5
Ge	n-C_3H_7	23.4 ± 1.3	31.8 ± 2.7	—[a]	—
Ge	C_4H_9	20.6 ± 1.2	30.3 ± 2.8	—	—
Si	CH_3	30.1 ± 1.9[b]	27.0 ± 3.2[b]	19.9 ± 0.4	28.1 ± 0.9
Sn[c]	CH_3	25.7 ± 2.0	31.7 ± 3.0	—	—
C[d]	CH_3	11.7		~20	

[a]Not determined.
[b]Data from ref. 3.
[c]Data from ref. 5.
[d]Data from ref. 8. ΔH_5^0 was measured experimentally and ΔH_7^0 was estimated.

than the addition of the first molecules. The exothermicity is slightly greater for the latter ion than for the former while the entropy change is much more negative for latter. These changes suggest a lessening influence of the alkyl groups as the number of water molecules increases in line with the suggestion of Hiraoka and Kebarle (8) who studied $(CH_3)_3C(OH_2)_2^+$ that the positive charge becomes largely located on the hydroxyl hydrogens and the thermochemistry approaches that for $H(H_2O)_2^+$. For example, for reaction [9], $-\Delta H^0$ is ~21 kcal mol^{-1} and $-\Delta S^0$ has values between 20 and 28 cal K^{-1} mol^{-1} (9), values very similar to those for $(CH_3)_3MOH_2^+$.

[9] $H^+(H_2O)_2 + H_2O \rightleftharpoons H(H_3O)_3^+$

This argument is strengthened by the enthalpy and entropy changes shown in Table 1 for hydration of $(CH_3)_3SiOH_2^+$, the values being closely similar to those for the germanium compounds.

Stabilization of $(CH_3)_3X^+$ by hyperconjugation appears to be much more important for X = C than for X = Si, Ge, or Sn (10). This can be associated with the very small size of C and is in line with its higher electronegativity. The assigned electronegativities of the other elements have very similar values (11) and Table 1 shows that their enthalpies of binding for $(CH_3)_3X^+$ to one molecule of water are grouped together but are very different from the value for carbon. The order of decrease in binding energy, Si > Ge > Sn, presumably reflects the normal decrease in binding energy with increasing atomic weight in a column of the periodic table which is usually associated with the size of the atom.

We have previously shown that the H_2O in $(CH_3)_3SiOH_2^+$ is readily displaced in exothermic reactions by oxygen bases such as alcohols, ethers, esters, etc. (2). We determined that such reactions also occur with $(CH_3)_3GeOH_2^+$. The only quantitative data obtained in this study are for reaction [10].

[10] $(CH_3)_3GeOH_2^+ + CH_3OH \rightleftharpoons (CH_3)_3GeO(H)CH_3^+ + H_2O$

Here $\Delta H^0 = -6.4 \pm 0.1$ kcal mol^{-1} and $\Delta S^0 = -1.6 \pm 0.1$ cal K^{-1} mol^{-1} while ΔH^0 for the silicon compound was -9.1 kcal mol^{-1} (2). The latter was obtained from a standard free energy measurement at 468 K and a calculated entropy. The binding energies of alcohols to $(CH_3)_3Ge^+$ are therefore in line with those for water in being significantly lower than the binding energies to $(CH_3)_3Si^+$.

Acknowledgements

The authors thank the Natural Sciences and Engineering Research Council of Canada for financial assistance.

1. V. C. TRENERRY and J. H. BOWIE. Org. Mass Spectrom. **16**, 344 (1981).
2. A. C. M. WOJTYNIAK and J. A. STONE. Int. J. Mass. Spectrom. Ion. Proc. In press.
3. J. A. STONE, A. C. M. WOJTYNIAK, and W. WYTENBURG. Can. J. Chem. **64**, 575 (1986).
4. J. A. STONE and D. E. SPLINTER. Can. J. Chem. **59**, 1779 (1981).
5. J. A. STONE and D. E. SPLINTER. Int. J. Mass. Spec. Ion Proc. **59**, 169 (1984).
6. R. W. TAFT. *In* Progress in physical organic chemistry. Vol. 14. John Wiley and Sons, New York. 1983. p. 247.
7. M. MEOT-NER, M. M. ROSS, and J. E. CAMPANA. J. Am. Chem. Soc. **107**, 4839 (1985).
8. K. HIRAOKA and P. KEBARLE. J. Am. Chem. Soc. **99**, 360 (1977).
9. R. G. KEESEE and A. W. CASTLEMAN. J. Phys. Chem. Ref. Data, **15**, 1011 (1986).
10. M. F. LAPPERT, J. B. PEDLEY, J. SIMPSON, and T. R. SPALDING. J. Organomet. Chem. **29**, 195 (1971).
11. A. L. ALFRED. J. Inorg. Nucl. Chem. **17**, 215 (1961).

Can. J. Chem. Downloaded from www.nrcresearchpress.com by 213.166.140.6 on 09/07/12
For personal use only.

Secondary α hydrogen–deuterium kinetic isotope effects in the *syn*-elimination reaction of 2-phenylethyldimethylamine oxide

PETER JAMES SMITH
Department of Chemistry, University of Saskatchewan, Saskatoon, Sask., Canada S7N 0W0

AND

KENNETH CHARLES WESTAWAY
Department of Chemistry, Laurentian University, Sudbury, Ont., Canada P3E 2B6

Received December 8, 1986

PETER JAMES SMITH and KENNETH CHARLES WESTAWAY. Can. J. Chem. **65**, 2149 (1987).

The secondary α-deuterium kinetic isotope effect has been measured for the thermal reaction of 2-phenylethyldimethylamine oxide in 90 mol% DMSO–H_2O at 60.0°C. A large secondary α-deuterium isotope effect of 1.158 per α-D was found, which indicates significant C—$\overset{+}{N}$ bond rupture and very little double bond formation at the transition state for this concerted *syn*-elimination process. The observed large normal value for $(k_H/k_D)_\alpha$ is discussed in terms of the use of secondary α-D isotope effects for the determination of stereochemistry for a concerted elimination process. Various isotope effects found for the *syn* elimination of the above amine oxide and those for the *anti* elimination of 2-arylethyltrimethylammonium salts with ethoxide are considered with respect to the relative transition state structures for *syn*- and *anti*-elimination reactions.

PETER JAMES SMITH et KENNETH CHARLES WESTAWAY. Can. J. Chem. **65**, 2149 (1987).

Opérant à 60,0°C, dans un mélange à 90 mol% de DMSO–H_2O, on a mesuré l'effet isotopique cinétique secondaire du deutérium en α sur la réaction thermique de l'oxyde de la phényl-2 éthyl diméthyl amine. On a observé un effet isotopique secondaire élevé (1,158) pour le deutérium en α et ce résultat indique que, dans l'état de transition de cette élimination *syn* concertée, il se produit beaucoup de rupture de la liaison C—$\overset{+}{N}$ et très peu de formation de double liaison. On discute de cette valeur normale, mais élevée, qui a été observée pour le $(k_H/k_D)_\alpha$ en fonction de l'utilisation des effets isotopiques secondaires des deutérium en α pour la détermination de la stéréochimie d'un processus concerté d'élimination. Divers effets isotopiques qui ont été observés pour l'élimination *syn* de l'oxyde d'amine mentionnée plus haut et d'autres effets rapportés pour l'élimination *anti* des sels d'aryl-2 éthyl triméthyl ammonium par l'éthylate ont été considérés en relation avec les structures relatives des états de transition des réactions d'éliminations *syn* et *anti*.

[Traduit par la revue]

Introduction

In a recent study (1, 2) on the E2 reaction of the 2-phenylethyl halides with *tert*-butoxide in *tert*-butyl alcohol it was found that the magnitude of the secondary α-deuterium kinetic isotope effect was dependent on the concentration of the abstracting base when chlorine and fluorine were the leaving groups. The secondary isotope effect, $(k_H/k_D)_\alpha$, was inverse at "low" base concentrations and normal at "high" base concentrations. These and other results were discussed in terms of both *syn*- and *anti*-elimination pathways promoted by various associated and dissociated base species. It was suggested that the $(k_H/k_D)_\alpha$ effect may be useful as a criterion for determining the stereochemistry of E2 elimination reactions.

At low *tert*-butoxide concentrations, it was suggested that the reaction of both the chloro and fluoro substrates proceed via a *syn*-elimination pathway where the loss of the leaving group and the β-hydrogen is assisted by the *t*-BuOK ion pair. For such a transition state, **1**, which is expected to have considerable carbanionic character (3), it was considered that sufficient negative charge could develop on the β carbon so that inversion occurs at both C_β and C_α. It was proposed that attack of the incipient lone pair of electrons from the backside of C_α would increase the $\overset{H}{C}$—X out-of-plane bending frequencies at the transition state and lead to an inverse isotope effect (4–7).

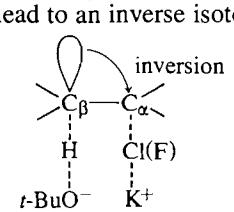

1

To investigate whether the observation of inverse secondary α hydrogen–deuterium kinetic isotope effects for reactions via the concerted one-step elimination pathway can be used as a test for *syn* stereochemistry we decided in the present study to examine the thermolysis reaction of 2-phenylethyldimethylamine oxide in 90 mol% dimethyl sulfoxide in water at 60°C, eq. [1], by determining the secondary α-deuterium kinetic isotope effect. The thermal decomposition of amine oxides has been established to be a concerted intramolecular *syn*-elimination process (8–12).

[1] $PhCH_2CH_2\overset{+}{N}(CH_3)_2$ (with O^-) $\xrightarrow[60°C]{90\ mol\%\ DMSO\text{–}H_2O}$ $PhCH{=}CH_2 + N(CH_3)_2$ (with OH)

The nature of the transition state for the thermal decomposition of amine oxides has been recently investigated. Chiao and Saunders (13) determined the primary hydrogen–deuterium kinetic isotope effect for reaction of 2-phenylethyldimethylamine and 2-phenylpropyldimethylamine oxides in various binary solvent mixtures. They found that the $(k_H/k_D)_\beta$ values varied very little with changes in solvent composition and were small in magnitude (14), between 2 and 3.[1] Their results were interpreted in terms of a nonlinear proton transfer, as required for the intramolecular *syn* elimination of amine oxides, transition state **2**, to avoid strain.

On the other hand, Kwart and Brechbiel (15) measured the primary β-deuterium kinetic isotope effect over a 70°C temperature

[1]The small kinetic hydrogen isotope effects are consistent with theoretical predictions (14).

Can. J. Chem. Downloaded from www.nrcresearchpress.com by 213.166.140.6 on 09/07/12
For personal use only.

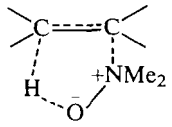

2

range for the thermolysis reaction of n-$C_6H_{11}CHDCH_2\overset{+}{N}Me_2$ with O^-

in dimethyl sulfoxide and found a significant temperature dependence. They interpreted their results in terms of a linear proton transfer to the oxygen of the dimethyl sulfoxide in a seven-membered ring via a product-like transition state where Me_2SO is coordinated to the amine oxide oxygen, transition state **3**. However, it has been recently pointed out (16) that the temperature dependence of the primary β-deuterium kinetic isotope effect should not be used as a mechanistic tool in differentiating between linear and bent transition states.

Carbon-14 kinetic isotope effects and a ρ value for the reaction of several ring substituted 2-phenylethyldimethylamine oxides in 10% water – 90% Me_2SO at 65°C have recently been determined (17). The large carbon isotope effects at both the α and β carbons, $(k_{12}/k_{14})_\alpha = 1.061 \pm 0.006$ and $(k_{12}/k_{14})_\beta = 1.036 \pm 0.005$, respectively, together with the calculated ρ value of +2.11 led the authors to conclude that there was some buildup of negative charge at C_β and extensive rupture of both the C_β—N and C_β—H bonds with relatively little double bond formation at the transition state.

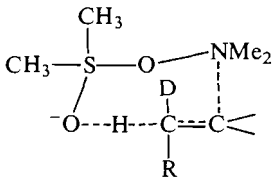

3

The results of the present study will be considered in terms of the use of the magnitude of secondary α-deuterium isotope effects as a criterion for the determination of the stereochemistry of concerted one-step elimination processes. As well, our results and those of other workers (13, 17) will be used to shed light on the transition state structure for the thermal *syn*-elimination reaction of amine oxides.

Results and discussion

The thermal elimination reaction of 2-phenylethyldimethylamine oxide was investigated in the present study in 90 mol% DMSO–H_2O solution to compare our results with those of previous workers (13, 17). Rate measurements were carried out spectrophotometrically using amine oxide samples containing some water, as the anhydrous form is unstable (13). The rate constants for reaction of a pair of undeuterated and α-dideuterated substrates were determined simultaneously to minimize possible effects due to temperature fluctuations in the constant temperature bath. The rate constants determined for each of the four pairs of kinetic runs are given in Table 1, as well as the calculated secondary α-deuterium kinetic isotope effects, $(k_H/k_D)_\alpha$.

The rate constants determined for reaction of the undeuterated amine oxide at 60.0°C, k_H(ave.) = 15.40 s^{-1}, are in good agreement with the literature value (13) of 13.0 s^{-1} determined in the same solvent conditions at 59.8°C. The small discrepancy between the rate constants could be due to the temperature difference and (or) to a slight solvent effect, as it has been shown (13) that the presence of water sharply decreases the rate, presumably due to a decrease in the basicity of the oxide oxygen through increased hydrogen bonding with water.

TABLE 1. The rate constants and secondary α-deuterium kinetic isotope effects for the *syn*-elimination reaction of 2-phenylethyldimethylamine oxide and its α-d_2 analogue in 90 mol% DMSO–water at 60.0°C

Run no.	$k_H \times 10^5$ s^{-1}	$k_D \times 10^5$ s^{-1}	$(k_H/k_D)_\alpha$
1	14.34[a] ±0.04[b]	10.53[a] ±0.03[b]	1.362[a]
2	15.72 ±0.02	11.66 ±0.04	1.348
3	15.03 ±0.02	11.35 ±0.04	1.324
4	15.46 ±0.02	11.65 ±0.03	1.327
		Average	1.340±0.018[c] (1.158 per α-D)

[a]Measured at a lower temperature of 59.9°C.
[b]Standard deviation within a kinetic run.
[c]Standard deviation.

The average of the four α-deuterium kinetic isotope effect determinations, $(k_H/k_D)_\alpha$ (ave.) = 1.340 ± 0.018 ($(k_H/k_D)_{\alpha\text{-D}}$ = 1.158 per α-D), is large and normal, indicating a significant decrease in the out-of-plane bending vibration involving the α C—H bonds at the transition state (6). The conclusion is reached from the results of the present study, where *syn* elimination in amine oxide pyrolysis did not give rise to an inverse secondary α-deuterium kinetic isotope effect, that the magnitude of $(k_H/k_D)_\alpha$ cannot be used as a criterion for the determination of the stereochemistry of a one-step elimination process (1, 2).[2] The large kinetic isotope effect of 1.34 may be compared with the small value of $(k_H/k_D)_\alpha$ = 1.02 found for the E2 reaction of 2-phenylethyltrimethylammonium ion with ethoxide at 40°C, which has been shown to proceed via an *anti*-elimination pathway (18) with a carbanionic transition state where C_β—H bond rupture has progressed to a greater degree than C—$\overset{+}{N}$ bond weakening (19). As well, the S_N2 reaction of thiophenoxide ion with benzyldimethylanilinium ion in *N*,*N*-dimethylformamide at 0°C gave a secondary α-deuterium isotope effect of 1.18 (20).

Although the magnitude of the secondary α-deuterium isotope effect is dependent on the nature of the leaving group, it is reasonable to qualitatively compare the magnitude of the secondary isotope effects above since in all cases the leaving group is a tertiary amine. Clearly the isotope effect found in the present study is much larger than those found for the E2 and S_N2 processes and is close to the theoretical maximum predicted for carbocation formation.[3] To our knowledge, $(k_H/k_D)_\alpha$ = 1.340 is the largest value found for a one-step concerted elimination process. Such a large value must arise due to an extensive decrease in the C_α—H out-of-plane bending vibrations at the transition state. This suggests that there is considerable C—$\overset{+}{N}$ bond rupture and very little carbon–carbon double bond formation at the activated complex.

The observation of the large normal secondary α-deuterium isotope effect, therefore, indicates that the transition state for the intramolecular *syn* elimination of the amine oxide cannot have significant S_N2 character, as illustrated in transition state **1**. Interaction of the developing electron density at C_β with C_α

[2]This conclusion will be considered in a full paper currently in preparation, concerning the reaction of *tert*-butoxide in *tert*-butyl alcohol with the 2-phenylethyl halides.

[3]Hartshorn and Skiher (21) found a value of $(k_H/k_D)_\alpha$ = 1.19 per α-D for the reaction, $CH_3\overset{+}{N}H_3 \rightarrow \overset{+}{C}H_3 + NH_3$.

Can. J. Chem. Downloaded from www.nrcresearchpress.com by 213.166.140.6 on 09/07/12
For personal use only.

TABLE 2. Isotope effects for the elimination reactions of 2-phenylethyltrimethylammonium ion with ethoxide in ethanol at 40°C and 2-phenylethyldimethylamine oxide thermolysis in 90 mol% DMSO–H_2O at 65°C

Substrates	$(k_H/k_D)_\beta$	$(k_H/k_D)_\alpha$	$(k_{12}/k_{14})_\alpha$	$(k_{12}/k_{14})_\beta$	$[(k_{14}/k_{15}) - 1]100$
$PhCH_2CH_2\overset{+}{N}Me_3$	3.23(19)	1.02(19)	1.044(17)	1.040(17)	1.33
$PhCH_2CH_2\overset{+}{N}Me_2$ $\vert$ ^-O	2.91(59.8°C)(13)	1.34(60°C)	1.061(17)	1.036(17)	—

would be expected to give rise to a small or inverse secondary α-deuterium isotope effect (6).

Accordingly, it is proposed that the transition state for the amine oxide decomposition has extensive C_β—H and C_α—N bond rupture but negligible interaction between the orbital developing at C_β with the α carbon (very little double bond formation), **4**, and a nonlinear proton transfer (13). Such a transition state could be described as carbanionic since there is significant charge buildup at C_β that can be stabilized by delocalization into the aromatic ring. This is consistent with the observed ρ value of +2.1 found for the reactions of the 2-arylethyldimethylamine oxides (17).

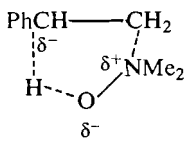

4

Substantial negative charge buildup at C_β at the transition state is expected for *syn* eliminations, particularly when the leaving group is a poor nucleofuge like dimethylhydroxylamine (23). For reactions involving competing *syn*- and *anti*-elimination pathways, ρ_{syn} was found to be significantly greater than ρ_{anti}, indicating greater carbanionic character at the transition state for *syn* as compared with *anti* elimination. This conclusion receives support from the molecular orbital approach of Bach *et al.* (24) who considered that the S_N2-like reaction, as illustrated in **1**, can be viewed as interaction of the C_β—H bonding electrons with the vacant σ* orbital of the C—$\overset{+}{N}$ bond. For this to occur effectively, considerable electron density at C_β must be generated *anti* to the C—$\overset{+}{N}$ bond, **1**.

The conclusion that there is significant C—N bond rupture at the transition state, based on the observation of the large normal α-D isotope effect, receives support from the study on the pyrolysis reaction of several 1-arylethyldimethylamine oxides (9) where a ρ value of +0.77 was found, which indicates a decrease in the induced positive charge at C_α in the activated complex.

Reaction proceeding by way of a true carbanion intermediate, either short or long lived, can be ruled out. For a long lived carbanion intermediate, inversion and rotation prior to the loss of the leaving group would lead to both *syn* and *anti* elimination, contrary to observation (12). The large secondary α-deuterium isotope effect and the large carbon isotope effect, $(k_{12}/k_{14})_\alpha$, which both indicate considerable C—$\overset{+}{N}$ bond weakening at the transition state, are not in accord with rate limiting carbon–hydrogen bond rupture to form a high energy carbanion intermediate.

It is interesting to compare the transition state structure for the reaction of 2-phenylethyltrimethylammonium ion with ethoxide, a concerted *anti* elimination, with the transition state geometry for reaction of 2-phenylethyldimethylamine oxide, a concerted *syn* elimination, since the structure of the two substrates is similar. Isotope effects determined for the two reactions are given in Table 2.

A comparison of the primary hydrogen–deuterium isotope effects, $(k_H/k_D)_\beta$, obtained for the two reactions is difficult since they were determined under different reaction conditions via transition states of different geometry (linear vs. nonlinear proton transfer). The comparison is further complicated by the possibility of different tunneling contributions for the two reactions.

A comparison of the carbon isotope effects (17) determined at both C_β and C_α, $(k_{12}/k_{14})_\beta$ and $(k_{12}/k_{14})_\alpha$, respectively, for the two reactions indicates that both transition states, *syn* and *anti*, have extensive C—H and C—$\overset{+}{N}$ bond rupture. The nitrogen isotope effect, $[(k_{14}/k_{15}) - 1]100 = 1.33$, determined for the ammonium salt reaction confirms that there is significant C—$\overset{+}{N}$ bond weakening at the transition state.

It appears, however, that C—$\overset{+}{N}$ bond rupture is *more* advanced at the transition state for the *syn* elimination of the amine oxide, $(k_{12}/k_{14})_\alpha = 1.061$, as compared with the *anti* elimination of the ammonium salt, $(k_{12}/k_{14})_\alpha = 1.044$. This receives support from the relative magnitude of the secondary α-deuterium isotope effects determined for the two systems, $(k_H/k_D)_\alpha = 1.34$ and 1.02 for the amine oxide and ammonium salt reactions, respectively.

In conclusion, it appears that the transition state for both the *anti* and *syn* processes has considerable C—H and C—$\overset{+}{N}$ bond weakening. They differ significantly, however, in the degree of double bond formation. While the *anti* process has considerable π bond formation at the transition state, as indicated by the small $(k_H/k_D)_\alpha$ value, the activated complex for the *syn* reaction has very little double bond character. This conclusion is reasonable in the light of the theoretical treatments of Bach *et al.* (24) and More O'Ferrall (25) since *anti* elimination is the more favoured process for stereochemical reasons.

Experimental

Melting points are uncorrected. The proton nmr spectra were determined on a Varian T-60 spectrometer. All reagents and solvents were reagent grade and were dried and purified by the usual procedures. The dimethyl sulfoxide solvent (Baker Analyzed) was refluxed over calcium hydride for 6 h and distilled.

Methyl phenylacetate

After a mixture of 55 g (0.40 mol) of phenylacetic acid, 125 mL (3.1 mol) of methanol, and 5 mL of concentrated sulfuric acid had refluxed overnight, the methanol was removed on a rotary evaporator. The residue was mixed with 250 mL of water and 10 mL of carbon tetrachloride in a separatory funnel. The organic layer was separated and washed with water, a 20% sodium hydrogen carbonate solution, and finally with water. The organic layer was dried with 5 g of anhydrous magnesium sulfate and the carbon tetrachloride was removed under reduced pressure. Distillation gave 39.9 g (66.5%) of methyl phenylacetate, bp 68–70°C/2 Torr (1 Torr = 133.3 Pa) (lit. (26) bp 218°C).

Can. J. Chem. Downloaded from www.nrcresearchpress.com by 213.166.140.6 on 09/07/12
For personal use only.

Can. J. Chem. Downloaded from www.nrcresearchpress.com by 213.166.140.6 on 09/07/12
For personal use only.

2-Phenylethyl-1,1-d_2*-alcohol*

This compound was synthesized by the procedure described by Westaway and Ali (27). A mixture of 24 g (0.16 mol) of methyl phenylacetate in 25 mL of dry (distilled from lithium aluminum hydride) ether was added dropwise to a solution prepared by dissolving 4 g (0.095 mol) of lithium aluminum deuteride (Merck) in 600 mL of dry ether in a 3-L three-necked flask. When the addition was complete, the mixture was refluxed overnight. Then the excess lithium aluminum deuteride was destroyed by carefully adding 150 mL of 10% sulfuric acid. The ether layer was removed and the aqueous layer was washed three times with 100-mL aliquots of ether. The ether layers were combined and washed with a 5% sodium hydrogen carbonate solution until all the acid had been removed. Finally the ether layer was washed with 100 mL of water and dried over anhydrous magnesium sulfate. Removal of the ether on the rotary evaporator and distillation gave 17.6 g (87.5%) of 2-phenylethyl-1,1-d_2-alcohol, bp 100°C/6 Torr (lit. (28) bp 110°C/20 Torr). An nmr analysis indicated that the product was at least 99% deuterated at the one position.

2-Phenylethyl-1,1-d_2*-p-toluenesulfonate*

The tosylate was prepared by the method developed by Tipson (29). 2-Phenylethyl-1,1-d_2-alcohol, 18.0 g (0.145 mol) was dissolved in 175 mL of pyridine and cooled to 0°C in an ice–salt bath. Then, 30 g of purified[4] *p*-toluenesulfonyl chloride was added and the mixture was stirred at 0°C for 2.5 h. Then, 3-, 3-, 6-, and 15-mL portions of cold water were added at 5-min intervals so that the temperature did not rise. Then, 150 mL of cold water was added and the product was extracted with five 75-mL portions of chloroform. The pyridine was removed from the product by extraction with several 100-mL portions of 10% sulfuric acid and one 250-mL portion of water. Most of the chloroform was removed on the rotary evaporator and the remaining solution was dried over anhydrous sodium sulfate. Removal of the chloroform left 33.6 g of an orange liquid that eventually crystallized to give white needles. These needles were recrystallized from ether–pentane to give 30.3 g (74.4%) of 2-phenylethyl-1,1-d_2-*p*-toluenesulfonate, mp 37–38°C (lit. (22) mp 37.5–38.2°C).

2-Phenylethyldimethylamine-1,1-d_2

This substance was prepared by the method described by Saunders and Edison (28). Twelve grams (0.27 mol) of anhydrous dimethylamine (Matheson) was bubbled into a solution prepared from 30.3 g (0.109 mol) of 2-phenylethyl-1,1-d_2-*p*-toluenesulfonate and 225 mL of ether. After the mixture had stirred overnight, the reaction mixture was diluted with 150 mL of water. The ether layer was separated and the remaining product was extracted with five 50-mL portions of ether. The amine was purified by extracting it with four 50-mL portions of 10% HCl. The acid extracts were made basic with 40% sodium hydroxide and the amine was extracted with five 50-mL portions of ether. The ether solution was reduced to 50 mL on the rotary evaporator, dried over anhydrous sodium sulfate, and distilled to give 7.8 g (47%) of 2-phenylethyldimethylamine-1,1-d_2, bp 62–64°C/4.5 Torr (lit. (13) bp 50–51°C/0.8 Torr). An nmr analysis indicated that the compound was at least 99% deuterated at the one position.

2-Phenylethyldimethylamine-1,1-d_2 *oxide*

The amine oxide was prepared by the method described by Dohner and Saunders (12). Approximately 1.6 mL of a 30% hydrogen peroxide solution was added to a mixture of 73.0 mg (4.83 mmol) of 2-phenylethyldimethylamine-1,1-d_2 in 95 mL of methanol that had been cooled in an ice bath. Then, 50.4 mg of 10% platinum on activated carbon (Aldrich) was weighed accurately into a 250-mL round-bottomed flask and the flask was flushed with dry nitrogen for 2 min. The hydrogen peroxide – amine solution was poured rapidly onto the activated carbon and the resulting mixture was stirred for 3.5 h at room temperature. The carbon particles were removed by filtering the reaction mixture through a fine sintered glass filter. Removing the methanol on the rotary evaporator left a pale yellow solution that contained a small amount of water (13). The nmr spectrum was consistent with the expected product and indicated that the compound was at least 99% deuterated at the α carbon.

2-Phenylethyldimethylamine oxide

The undeuterated analogue of 2-phenylethyldimethylamine-1,1-d_2 oxide was prepared using the procedures described above. Comparable yields and physical properties were found for the deuterated and undeuterated products.

Kinetic measurements

All but one set of the kinetic experiments were carried out at 60.0 ± 0.1°C. In one experiment, the kinetic isotope effect was measured at a slightly lower temperature. In all cases, however, the kinetic isotope effects were calculated from rate constants determined for reaction of the deuterated and undeuterated substrates, which were measured simultaneously. This procedure eliminated the effect of any possible fluctuations in temperature that occurred in the constant temperature bath.

Each kinetic run was initiated by weighing approximately 20 mg of the amine oxide accurately in a small Erlenmeyer flask fitted with a serum cap. The 90 mol% DMSO–water solvent used in these experiments was prepared from purified DMSO (*vide supra*) and distilled water. Each run was begun by pipetting 15 mL of the 90 mol% DMSO–water solution, which had been temperature equilibrated for at least 1 h, into the Erlenmeyer flask containing the amine oxide. The serum cap was replaced and 100-μL aliquots were withdrawn from the reaction flask at appropriate times with a Hamilton gas-tight fixed needle syringe. Each sample was diluted to 5.00 mL with 95% ethanol and the absorbance at 248 nm was recorded against a blank prepared by diluting 100 μL of 90 mol% DMSO–water to 5.00 mL with 95% ethanol on a Hewlett–Packard Model HP 8451A diode array uv–vis spectrophotometer. This removed the small absorbance due to the solvent at 248 nm. Each absorbance was the average of at least three separate readings on the spectrophotometer. The rate constant was determined from the slope of the least-squares line of the plot of $\ln (OD_\infty - OD_t)$ against time. The correlation coefficient for each kinetic run was at least 0.999. The kinetic isotope effect was calculated from rate constants for a pair of deuterated and undeuterated substrates that were determined simultaneously.

[4]*p*-Toluenesulfonyl chloride, 50 g, was dissolved in 125 mL of chloroform and 375 mL of petroleum ether (bp 35–55°C). Decolourizing carbon was added and the solution was filtered via a suction filtration. The filtrate was heated to boiling, sufficient chloroform was added to dissolve any precipitated product, and the solution was allowed to cool. Filtration gave 43 g of pure *p*-toluenesulfonyl chloride.

Acknowledgements

The authors gratefully acknowledge the financial support provided by the Natural Sciences and Engineering Research Council of Canada. The authors also acknowledge Mrs. L. Baldisera's assistance in the syntheses.

1. K. C. Westaway, Z. Waszczylo, P. J. Smith, and K. S. Rangappa. Tetrahedron Lett. 25 (1985).
2. P. J. Smith, K. S. Rangappa, and K. C. Westaway. Can. J. Chem. **63**, 100 (1985).
3. C. H. DePuy, D. L. Storm, J. T. Frey, and C. G. Naylor. J. Org. Chem. **35**, 2746 (1970).
4. M. Wolfsberg and M. J. Stern. Pure Appl. Chem. (*a*) **8**, 225 (1964); (*b*) **8**, 325 (1964).
5. V. J. Shiner, Jr., M. W. Rapp, E. A. Halevi, and M. Wolfsberg. J. Am. Chem. Soc. **90**, 7171 (1968).
6. V. J. Shiner, Jr. *In* Isotope effects in chemical reactions. *Edited by* C. J. Collins and N. S. Bowman. ACS Monograph 167, Van Nostrand Reinhold Co., New York, NY. 1970. Chap. 2.
7. L. Melander and W. H. Saunders, Jr. Reaction rates of isotopic molecules. Wiley–Interscience, New York. 1980.
8. M. J. V. Sahyun and D. J. Cram. J. Am. Chem. Soc. **85**, 1263 (1963).
9. J. Zavada, M. Pankova, and M. Svoboda. Collect. Czech. Chem. Commun. **38**, 2102 (1973).

10. D. J. CRAM and J. E. MCCARTY. J. Am. Chem. Soc. **76**, 5740 (1954).
11. A. C. COPE and N. A. LEBEL. J. Am. Chem. Soc. **82**, 4656 (1960).
12. B. R. DOHNER and W. H. SAUNDERS, JR. Can. J. Chem. **64**, 1026 (1986).
13. W.-T. CHIAO and W. H. SAUNDERS, JR. J. Am. Chem. Soc. **100**, 2802 (1978).
14. (*a*) W. H. SAUNDERS, JR. Chem. Scr. **8**, 27 (1975); (*b*) R. A. MORE O'FERRALL. J. Chem. Soc. B, 785 (1970).
15. H. KWART and M. BRECHBIEL. J. Am. Chem. Soc. **103**, 4650 (1981).
16. B. ANHEDE and N.-A. BERGMAN. J. Am. Chem. Soc. **106**, 7634 (1984).
17. D. R. WRIGHT, L. B. SIMS, and A. FRY. J. Am. Chem. Soc. **105**, 3714 (1983).
18. A. N. BOURNS and A. C. FROSST. Can. J. Chem. **48**, 133 (1970).
19. P. J. SMITH and A. N. BOURNS. Can. J. Chem. **52**, 749 (1974).
20. K. C. WESTAWAY and S. F. ALI. Can. J. Chem. **57**, 1354 (1979).
21. S. R. HARTSHORN and V. J. SHINER, JR. J. Am. Chem. Soc. **94**, 9002 (1972).
22. W. H. SAUNDERS, JR., S. ASPERGER, and D. H. EDISON. J. Am. Chem. Soc. **80**, 2421 (1958).
23. B. R. DOHNER and W. H. SAUNDERS, JR. J. Am. Chem. Soc. **108**, 245 (1986).
24. R. D. BACH, R. C. BADGER, and T. J. LANG. J. Am. Chem. Soc. **101**, 2845 (1979).
25. R. A. MORE O'FERRALL. J. Chem. Soc. B, 274 (1970).
26. R. C. WEAST (*Editor*). Handbook of physics and chem. 61st ed. CRC Publishing, Cleveland, OH. 1980.
27. K. C. WESTAWAY and S. F. ALI. Can. J. Chem. **57**, 1089 (1979).
28. W. H. SAUNDERS, JR., and D. H. EDISON. J. Am. Chem. Soc. **82**, 138 (1960).
29. R. S. TIPSON. J. Org. Chem. **9**, 235 (1944).

Can. J. Chem. Downloaded from www.nrcresearchpress.com by 213.166.140.6 on 09/07/12
For personal use only.

pK_a values for substituted acetophenones: values determined by study of rates of halogenation

J. Peter Guthrie,[1] John Cossar, and Alex Klym

Department of Chemistry, University of Western Ontario, London, Ont., Canada N6A 5B7

Received November 11, 1986

J. Peter Guthrie, John Cossar, and Alex Klym. Can. J. Chem. **65**, 2154 (1987).

pK_a values in aqueous solution have been determined for seven *p*-substituted acetophenones. The determinations are based on the diffusion-controlled reaction of an enolate with hypochlorous acid. The values determined for the acetophenones are as follows: substituent, value; H, 18.4; *p*-MeO, 19.0; *p*-F, 18.5; *p*-Cl, 18.1; *p*-Br, 18.0; *p*-NO_2, 16.7; *p*-Me_3N^+, 17.1. ρ for these pK_a values is −1.95. Using literature values for the enol content we show that most of this ρ value reflects substituent effects upon enolization. With relatively high hydroxide and low hypochlorite concentrations the major products from chlorination of acetophenones are the corresponding mandelic acids. Under similar conditions bromination of acetophenone gives benzoic acid.

J. Peter Guthrie, John Cossar et Alex Klym. Can. J. Chem. **65**, 2154 (1987).

Opérant dans des solutions aqueuses, on a déterminé les valeurs de pK_a de sept acétophénones substituées en para. Ces déterminations sont basées sur la réaction, contrôlée par la diffusion, d'un énolate avec l'acide hypochloreux. Pour les diverses acétophénones, les valeurs déterminées sont (substituants, valeurs) : H, 18,4; *p*-MeO, 19,0; *p*-F, 18,5; *p*-Cl, 18,1; *p*-Br, 18,0; *p*-NO_2, 16,7; *p*-Me_3N^+, 17,1. La valeur de ρ pour ces valeurs de pK_a est de −1,95. Utilisant les valeurs trouvées dans la littérature pour la quantité d'énol présente dans ces systèmes, on démontre que cette valeur de ρ est un reflet des effets des substituants sur l'énolisation. Avec des concentrations relativement élevées d'hydroxyde de sodium et relativement basses d'hypochlorite, les produits majeurs de la chloration des acétophénones sont les acides mandéliques correspondants. Dans des conditions semblables, la bromation de l'acétophénone conduit à de l'acide benzoïque.

[Traduit par la revue]

Can. J. Chem. Downloaded from www.nrcresearchpress.com by 213.166.140.6 on 09/07/12
For personal use only.

Introduction

We have developed a method for determining pK_a values of simple ketones (1, 2). Such pK_a values are useful in our investigations of the aldol condensation (3–9). Some of the simple aldol reactions which we have been investigating involve acetophenone as reactant; examples are the retroaldol cleavages of chalcone (7) and dypnone. For detailed analysis of these reactions it would be useful to have a pK_a value for acetophenone itself. With a method for determining pK_a's in hand it seemed worthwhile to investigate a series of substituted acetophenones, as a convenient series for mapping out the effects of substituents upon the equilibrium constant for enolate formation. Accordingly we wish to report the results of our investigations on a set of *p*-substituted acetophenones.

We have already reported (10) the results of a detailed investigation of the path of halogenation of acetone, which with hypochlorite at low concentrations at room temperature leads not to acetic acid as textbooks might suggest, but to lactic acid as major product. Various *p*-substituted acetophenones lead to the corresponding substituted mandelic acids; we have not performed detailed studies of the analogous intermediates, but presume that the qualitative pattern of the reaction is the same for these derivatives. A simplified form of the mechanism is shown in Scheme 1. Bromination gives the textbook product in the expected fashion.

Results and discussion

Product studies

We have shown that for *p*-methoxy-, *p*-fluoro-, *p*-chloro-, *p*-bromo-, and *p*-nitroacetophenone the corresponding mandelic acids can be prepared by hypochlorite oxidation. In the case of *p*-nitroacetophenone the conditions are critical because further slow oxidation to nitrobenzoic acid takes place. Even with only a slight excess of hypochlorite over the amount required by stoichiometry, and slow addition of hypochlorite to keep the instantaneous concentration low, we obtained only a 1:1 mixture of *p*-nitromandelic acid and *p*-nitrobenzoic acid. Although we doubt that this reaction will be of practical significance as a preparative route to mandelic acids, it does demonstrate very clearly that with low hypochlorite and high hydroxide concentrations the haloform reaction does not occur because competing hydrolysis diverts the reaction path. At this time we have not established whether the diversion takes place at the monochloroketone stage, as was found for acetone (10), or at the dichloroketone stage. Experiments to settle this point are in progress.

Kinetics

The results of our kinetics investigations on *p*-substituted acetophenones are found in Tables 1–7. Except for a few experiments with acetophenone all of these kinetics were carried out using hypochlorite in excess. All kinetics were carried out under pseudo-first order conditions. With hypochlorite in excess,

$$v = k_{obs}[\text{ketone}]$$

$$k_{obs} = k_{II}[OCl^-]_{total}$$

$$k_{II} = k_{II}^0 + k_{II}^-[OH^-]$$

The k_{II}^0 term represents reaction of the enolate ion with hypochlorous acid; thus it depends only on the rate constant for a diffusion-controlled reaction and the pK_a of the ketone and of hypochlorous acid (2). The k_{II}^- term represents reaction of the enolate ion with hypochlorite ion (2). The dependence of the apparent second order rate constants, k_{II}, upon the hydroxide concentration is shown in Fig. 1. These experiments were done at a constant ionic strength of 1 *M*, maintained with KCl. However, we found that for $[OH^-] > 0.5$ *M* these plots of k_ψ vs. $[OH^-]$ showed upward curvature. We attribute these deviations from linearity to imperfect matching of solvent properties between aqueous KCl and NaOH, and used only experiments with $[OH^-] \leq 0.5$ *M* for the final least-squares fits. From

[1]Author to whom correspondence should be addressed.

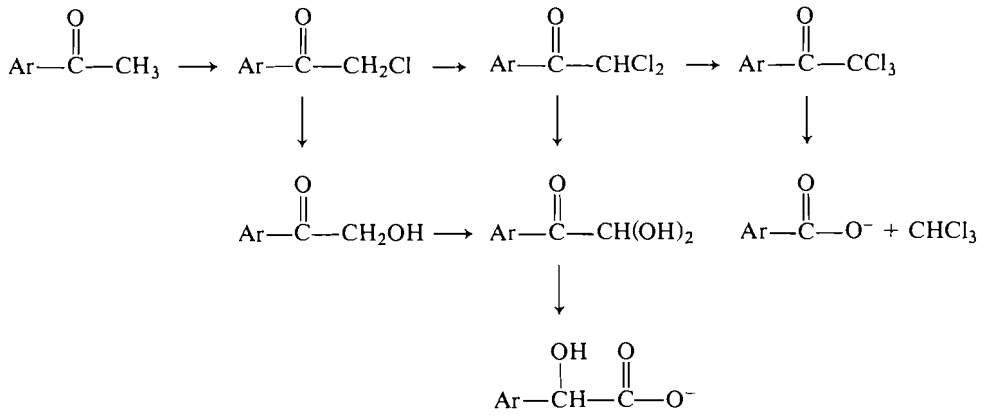

SCHEME 1

TABLE 1. Kinetics of chlorination of acetophenone[a]

[Ketone] $10^3\ M$	[OCl^-] $10^3\ M$	[OH^-] M	k_ψ[b] $10^4\ s^{-1}$	k_{II}[c] $10^2\ M^{-1}\ s^{-1}$
2.62	0.794	0.01	2.45(0.018)	3.12(0.02)[d]
2.62	0.796	0.05	3.32(0.029)	4.22(0.04)[d]
2.62	0.774	0.10	4.29(0.027)	5.46(0.03)[d]
2.62	0.796	0.20	7.06(0.056)	8.98(0.07)[d]
2.62	0.796	0.30	9.19(0.083)	11.69(0.11)[d]
2.62	0.796	0.40	13.33(0.057)	16.96(0.07)[d]
2.62	0.796	0.50	12.45(0.18)	15.84(0.23)[d]
0.282	0.0723	0.50	1.594(0.086)	18.84(1.02)[d]
0.282	0.0723	0.30	0.971(0.034)	11.48(0.40)[d]
0.331	5.57	0.01	1.67(0.013)	3.00(0.02)
0.331	5.57	0.10	3.40(0.024)	6.10(0.04)
0.331	5.57	0.50	12.26(0.20)	22.01(0.36)
0.271	5.32	0.301	6.86(0.032)	12.89(0.06)
0.271	5.38	0.0996	3.57(0.0096)	6.63(0.02)
0.271	5.43	0.0505	2.66(0.0056)	4.90(0.01)
0.271	5.80	0.0108	2.15(0.0065)	3.70(0.01)
0.271	5.65	0.543	15.93(0.069)	28.2(0.12)[e]
0.271	5.54	0.486	14.18(0.057)	25.6(0.10)
0.271	5.46	0.383	11.15(0.050)	20.4(0.09)
0.271	5.42	0.383	11.05(0.060)	20.3(0.11)
0.271	5.43	0.381	11.58(0.087)	21.33(0.16)
0.220	5.08	0.486	12.88(0.078)	25.4(0.15)
0.220	5.10	0.215	6.18(0.034)	12.1(0.07)

[a]In water at 25°C, ionic strength = 1.00 (KCl).
[b]Observed pseudo-first order rate constant.
[c]Apparent second order rate constant: $k_{II} = k_\psi/[OCl^-]$.
[d]Calculated using an assumed stoichiometry of 3 hypochlorites per ketone. This stoichiometry is required by the classical mechanism, but is clearly incorrect; see Fig. 1 and the text.
[e]Not included in the least-squares fit; see text.

TABLE 2. Kinetics of chlorination of *p*-methoxyacetophenone[a]

[Ketone] $10^3\ M$	[OCl^-] $10^3\ M$	[OH^-] M	k_ψ[b] $10^4\ s^{-1}$	k_{II}[c] $10^2\ M^{-1}\ s^{-1}$
0.0155	0.72	0.2	0.233(0.0012)	3.22(0.02)
0.0155	0.72	0.4	0.445(0.0021)	6.29(0.03)
0.0155	0.72	0.6	0.620(0.0053)	8.98(0.07)[d]
0.0155	0.72	0.8	0.803(0.0053)	11.5(0.07)[d]
0.0044	0.267	0.713	0.3036(0.00066)	11.4(0.02)[d]
0.010	0.258	0.197	0.0789(0.0022)	3.06(0.09)
0.1	4.08	0.481	2.711(0.0037)	6.65(0.01)
0.1	4.00	0.481	2.768(0.0033)	6.83(0.01)
0.12	3.93	0.104	0.741(0.0046)	1.88(0.01)
0.12	3.88	0.0127	0.2699(0.0020)	0.696(0.005)

[a]In water at 25°C, ionic strength = 1.00 (KCl).
[b]Observed pseudo-first order rate constant.
[c]Apparent second order rate constant: $k_{II} = k_\psi/[OCl^-]$.
[d]Not included in the least-squares fit; see text.

TABLE 3. Kinetics of chlorination of *p*-fluoroacetophenone[a]

[Ketone] $10^3\ M$	[OCl^-] $10^3\ M$	[OH^-] M	k_ψ[b] $10^4\ s^{-1}$	k_{II}[c] $M^{-1}\ s^{-1}$
0.02	0.604	0.497	1.32(0.015)	0.218(0.002)
0.0205	0.613	0.997	3.097(0.0033)	0.505(0.0005)[d]
0.0205	0.912	0.996	4.727(0.0036)	0.518(0.0004)[d]
0.0205	1.215	0.995	6.117(0.0062)	0.504(0.0005)[d]
0.0205	0.597	0.798	2.312(0.0035)	0.387(0.0006)[d]
0.0205	0.895	0.798	3.372(0.0035)	0.377(0.0004)[d]
0.0205	0.602	0.499	1.399(0.0016)	0.232(0.0003)
0.0205	0.903	0.499	2.051(0.0031)	0.227(0.0003)
0.0205	0.607	0.200	0.653(0.0028)	0.108(0.0005)
0.0205	0.910	0.200	1.016(0.0055)	0.112(0.0006)
0.0196	0.555	0.499	1.323(0.0042)	0.238(0.0008)
0.0196	0.555	0.998	2.755(0.0086)	0.466(0.0015)[d]
0.100	1.96	0.099	1.227(0.0076)	0.0626(0.0004)
0.390	7.86	0.096	4.414(0.0025)	0.0562(0.00003)
0.107	0.842	0.10	0.472(0.0047)	0.0555(0.0006)
0.107	0.842	0.90	3.615(0.037)	0.429(0.0044)[d]
0.107	0.842	0.30	1.212(0.0045)	0.144(0.0005)
0.107	0.842	0.50	1.931(0.0083)	0.229(0.0010)
0.230	6.00	0.026	1.921(0.0059)	0.0320(0.0001)

[a]In water at 25°C, ionic strength = 1.00 (KCl).
[b]Observed pseudo-first order rate constant.
[c]Apparent second order rate constant: $k_{II} = k_\psi/[OCl^-]$.
[d]Not included in the least squares fit; see text.

the intercepts, k_{II}^0 of these plots, the pK_a values found in Table 8 could be calculated, using relationship [1]; we use $\log k_{diffusion} = 9.23 \pm 0.5$ (2),[2] and $pK_a^{HOCl} = 7.53$ (11),

[1] $\quad pK_a = \log k_{diffusion} + pK_{diffusion} + pK_a^{HOX} - \log k_{II}^0$

When pseudo-first order kinetics are carried out with ketone in excess, it may be shown that the pseudo-first order rate constant depends on the stoichiometry number for the reaction,

[2]The rate constant for a diffusion-controlled reaction is insensitive to the exact nature of the reactants (12); the difficulty in choosing an appropriate value is in making proper allowance for the non-spherical nature of the reactants (2).

Can. J. Chem. Downloaded from www.nrcresearchpress.com by 213.166.140.6 on 09/07/12
For personal use only.

Can. J. Chem. Downloaded from www.nrcresearchpress.com by 213.166.140.6 on 09/07/12
For personal use only.

TABLE 4. Kinetics and chlorination of *p*-chloroacetophenone[a]

[Ketone] 10^3 *M*	[OCl^-] 10^3 *M*	[OH^-] *M*	k_ψ[b] 10^4 s^{-1}	k_{II}[c] M^{-1} s^{-1}
0.0105	0.210	1.0	2.022(0.0040)	0.963(0.002)[d]
0.0105	0.210	1.0	1.995(0.011)	0.951(0.005)[d]
0.208	5.21	0.024	3.487(0.0077)	0.0669(0.0001)
0.160	6.57	0.091	7.476(0.010)	0.114(0.0002)
0.0313	0.816	0.097	1.125(0.0044)	0.138(0.0005)
0.028	0.687	0.204	1.556(0.011)	0.227(0.0016)
0.0210	0.807	0.505	3.722(0.011)	0.462(0.001)
0.0210	0.807	0.505	3.821(0.0086)	0.474(0.001)
0.021	0.626	0.795	4.589(0.0082)	0.732(0.001)[d]
0.021	0.722	0.338	2.202(0.0075)	0.306(0.001)

[a]In water at 25°C, ionic strength = 1.00 (KCl).
[b]Observed pseudo-first order rate constant.
[c]Apparent second order rate constant: $k_{II} = k_\psi/[OCl^-]$.
[d]Not included in the least squares fit; see text.

TABLE 5. Kinetics of chlorination of *p*-bromoacetophenone[a]

[Ketone] 10^3 *M*	[OCl^-] 10^3 *M*	[OH^-] *M*	k_ψ[b] 10^4 s^{-1}	k_{II}[c] M^{-1} s^{-1}
0.0154	0.461	0.996	4.718(0.0095)	1.023[d]
0.0154	0.461	0.200	1.014(0.0024)	0.220
0.0154	0.461	0.400	1.910(0.0027)	0.414
0.0154	0.456	0.600	2.795(0.0026)	0.612[d]
0.0154	0.456	0.797	3.762(0.0042)	0.825[d]
0.0154	0.453	0.102	0.620(0.0019)	0.137
0.0153	0.904	0.103	1.262(0.0059)	0.1395
0.0800	0.0404	0.018	3.282(0.011)	0.0812
0.0154	0.600	0.050	0.668(0.0048)	0.1113
0.0154	0.461	0.797	4.005(0.0070)	0.869[d]

[a]In water at 25°C, ionic strength = 1.00 (KCl).
[b]Observed pseudo-first order rate constant.
[c]Apparent second order rate constant: $k_{II} = k_\psi/[OCl^-]$.
[d]Not included in the least squares fit; see text.

TABLE 6. Kinetics of chlorination of *p*-nitroacetophenone[a]

[Ketone] 10^3 *M*	[OCl^-] 10^3 *M*	[OH^-] *M*	k_ψ[b] 10^4 s^{-1}	k_{II}[c] M^{-1} s^{-1}
0.011	0.715	0.340	49.1(0.29)	6.87
0.011	0.662	0.0975	17.8(0.11)	2.70
0.010	0.222	0.047	4.67(0.0047)	2.10
0.010	0.309	0.0193	5.30(0.0075)	1.71

[a]In water at 25°C, ionic strength = 1.00 (KCl).
[b]Observed pseudo-first order rate constant.
[c]Apparent second order rate constant: $k_{II} = k_\psi/[OCl^-]$.

while the pseudo-first order rate constant for kinetics with hypochlorite in excess is independent of the stoichiometry.

[2] $k_{pseudo} = nk_{II}[ketone]$ ketone in excess

$k_{pseudo} = k_{II}[OCl^-]$ hypochlorite in excess

Thus we must know the actual stoichiometry of the reaction under the conditions employed if k_{II} is to be calculated from the observed pseudo-first order rate constant. However, since the hypochlorite concentration is changing and the stoichiometry depends on the hypochlorite concentration, one must expect that the ratio of k_{pseudo} to k_{II} will change during a reaction. It is in fact surprising that one observes apparently good first order kinetics; it is quite possible that an average, effective, value of n is required.

TABLE 7. Kinetics of chlorination of *p*-trimethylammonioacetophenone[a]

[Ketone] 10^3 *M*	[OCl^-] 10^3 *M*	[OH^-] *M*	k_ψ[b] 10^4 s^{-1}	k_{II}[c] M^{-1} s^{-1}
0.018	1.114	0.1006	10.27(0.038)	0.9219
0.0176	0.717	0.341	13.87(0.017)	1.934
0.021	0.781	0.510	20.28(0.013)	2.60
0.021	0.663	0.098	5.32(0.010)	0.802
0.035	1.11	0.1004	8.47(0.13)	0.763
0.021	0.606	0.802	27.43(0.033)	4.526[d]
0.012	0.368	0.0464	2.641(0.0022)	0.718

[a]In water at 25°C, ionic strength = 1.00 (KCl).
[b]Observed pseudo-first order rate constant.
[c]Apparent second order rate constant: $k_{II} = k_\psi/[OCl^-]$.
[d]Not included in the least squares fit; see text.

Figure 2 shows a Hammett plot for the pK_a values of the substituted acetophenones; the slope of this plot is -1.95 ± 0.19. This is distinctly more negative than the value of -1.0 which might have been anticipated by analogy with the corresponding benzoic acids. However, the process for which we might expect an analogy with ionization of benzoic acids is not really ionization of the acetophenones, but ionization of the acetophenone enols, since ionization of acetophenones involves a tautomerization as well. The equilibrium constants for enolization of acetophenones (13, 14) give a ρ value of -1.39 ± 0.11 when log K is plotted against σ (Table 9). Thus we are left with the surprising finding that the actual ionization of the enols is in fact quite *insensitive* to substituents.

$$\rho_{pK_a}^{Keto} = \rho_{enolization} + \rho_{pK_a}^{Enol}$$

$$\rho_{pK_a}^{Enol} = -0.56 \pm 0.22$$

Given the sizeable uncertainties in pK_a values determined by assumption of a value for the rate constant of a diffusion-controlled reaction (2) this is not a strong conclusion. Nonetheless it seems likely that ionization of the enols is less sensitive to substituents than ionization of the corresponding benzoic acids.

There is also the interesting question of why there is a large ρ for enolization. A possible rationalization is that tautomerization from the keto to the enol is accompanied by a significant decrease in the partial positive character of the carbon bonded to the aromatic ring because of the change from sp^3 carbon and sp^2 oxygen as substituents on this carbon to sp^2 carbon and sp^3 oxygen. The decrease in electronegativity on going from sp^2 to sp^3 oxygen is much larger than the increase on going from sp^3 to sp^2 carbon; using the values suggested by Gasteiger (15) the decrease for oxygen is -2.89 and the increase for carbon is $+0.81$ (electronegativities, on the Mulliken scale, for the neutral atoms (15)). Thus the central atom sees a decrease in electron-withdrawing power of the atoms to which it is bonded, and becomes less positive itself.

Kresge and Wirz have recently (16) reported a pK_a value for acetophenone. Their value, 18.24 ± 0.03, is in good agreement with ours, 18.38 ± 0.52. The method of Kresge and Wirz is inherently precise, but requires synthesis of a suitable precursor which will give the desired enol on flash photolysis. Our method is inherently imprecise, but requires neither preparation of precursors nor the use of specialized apparatus.

Can. J. Chem. Downloaded from www.nrcresearchpress.com by 213.166.140.6 on 09/07/12
For personal use only.

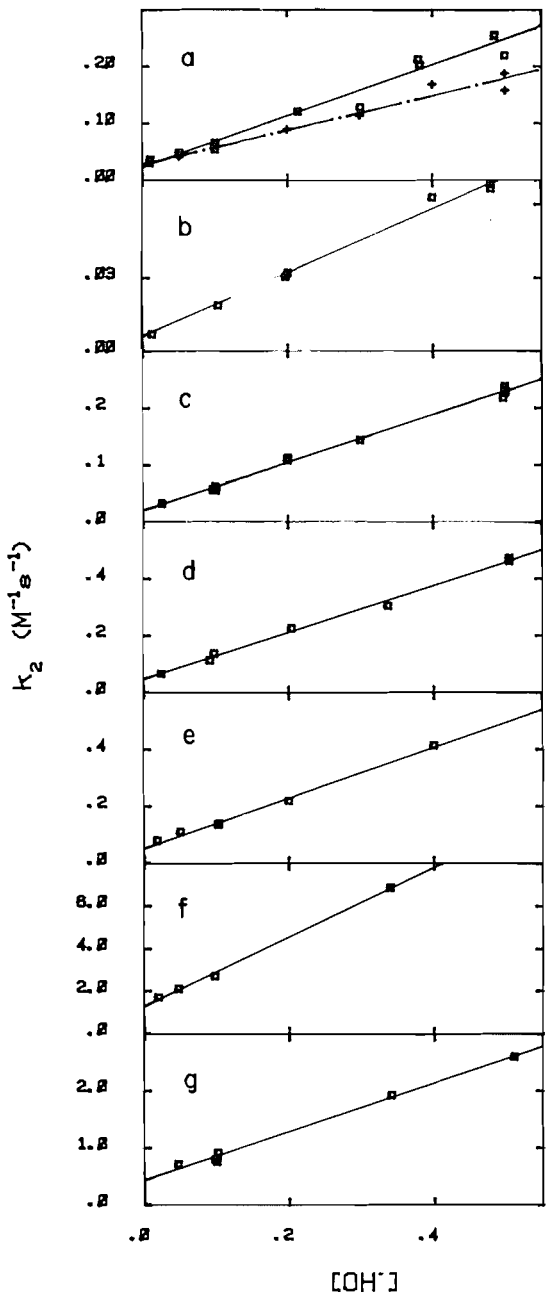

FIG. 1. Chlorination of substituted acetophenones; $k_{obs}/[OCl^-]$ (hypochlorite excess) or $k_{obs}/3$[ketone] (ketone excess) as a function of $[OH^-]$. (□, ---) Data and least-squares lines for runs with hypochlorite excess; (+, ···) data and least-squares line for runs with ketone excess (unsubstituted acetophenone only). (*a*) Acetophenone; (*b*) *p*-methoxyacetophenone; (*c*) *p*-fluoroacetophenone; (*d*) *p*-chloroacetophenone; (*e*) *p*-bromoacetophenone; (*f*) *p*-nitroacetophenone; (*g*) *p*-trimethylammonioacetophenone.

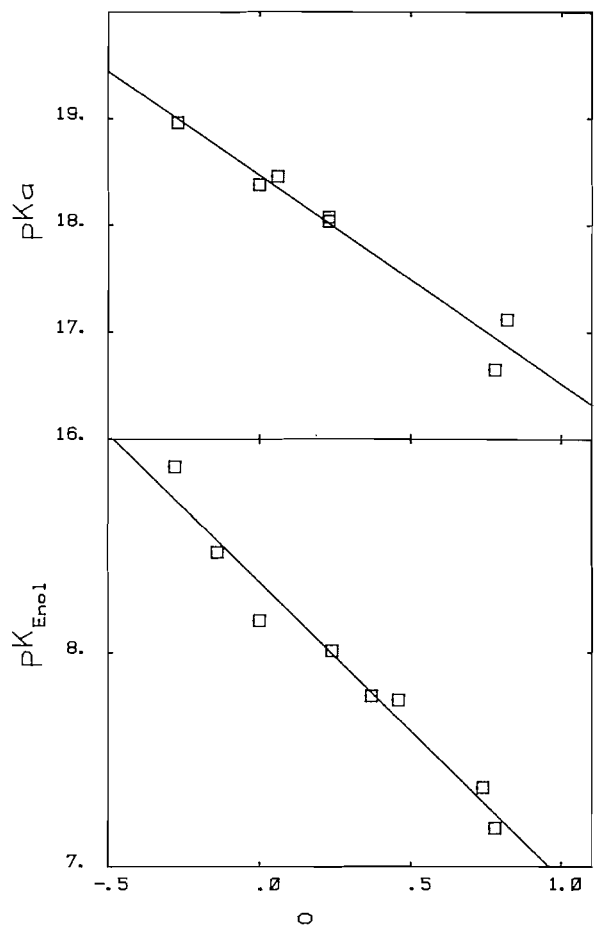

FIG. 2. pK_a values (this work) and enol contents (13, 14) for *m*- and *p*-substituted acetophenones as a function of Hammett σ values.

Experimental

Materials

All of the ketones used for kinetics were purified before use and purity was checked by running 200 MHz nmr spectra. In all cases negligible amounts of impurities were detectable except for traces of water in the liquid ketones.

Acetophenone, BDH "99%", was freshly distilled; bp 102–103°C (30 Torr), mp 20°C, lit. 20.5°C (17). p-*Bromoacetophenone*, Aldrich "98%", was purified by Kugelrohr distillation; mp 50–52°C, lit. 50–51°C (17). p-*Chloroactophenone*, Aldrich "97%", was purified by sublimation, 45°C at 0.02 Torr; mp 19°C, lit. 20°C (17). p-*Chloromandelic acid* was prepared by way of the intermediate α,α-dibromoacetophenone (18); mp 119–120°C; lit. (19) 120–121°C. p-*Fluoroacetophenone*, Aldrich "99%", was purified by gas chromatography on SE30 at 150°C; purity was confirmed by analytical gas chromatography (same conditions); only one peak was observed. p-*Fluoromandelic acid* was prepared by hydrolysis of the cyanohydrin derived from *p*-fluorobenzaldehyde (20), mp 135–136°C; lit. 137°C (20). p-*Methoxyacetophenone*, Aldrich "98%", was purified by Kugelrohr distillation; mp 37–38°C, lit. 38–39°C (17). p-*Nitroacetophenone*, Aldrich "97%", was purified by Kugelrohr distillation; mp 78–80°C, lit. 80–81°C (17).

p-*Nitromandelonitrile* was prepared from *p*-nitrobenzaldehyde and sodium cyanide (21). The literature procedure was modified by using a volume of dioxane equal to that of acetic acid to dissolve the *p*-nitrobenzaldehyde before the reaction. *p*-Nitrobenzaldehyde (2.0 g) yielded 0.91 g of a mixture which by ^{1}H-nmr appeared to be 25% *p*-nitrobenzoic acid and 75% *p*-nitromandelonitrile (35% crude yield). The α-proton appeared at δ = 5.77 ppm in 50:50 $CDCl_3/CD_3OD$. Crystallization, first from 80:20 CCl_4:$CHCl_3$, and then from toluene, gave 319 mg (13.5%) of purified material, mp 112–113°C; lit. mp (21) 114–116°C with decomposition. Exact mass calculated for $C_8H_6N_2O_3$: 178.03782; found: 178.0377 ± 0.0001. 200 MHz ^{1}H-nmr (1:1 $CDCl_3$:CD_3OD); δ = 4.80 (s, 1H) O*H*; 5.77 (s, 1H) C*H*(OH)(CN), 7.75, 7.79, 8.27, and 8.31 (1H multiplets), aromatic C*H*.

p-*Nitromandelic acid* was prepared by hydrolysis of the nitrile in 6 *M* HCl (21). The reaction mixture was extracted with ether, and the residue after evaporation was purified by column chromatography on silica gel, eluting with EtOAc:hexanes:acetone:formic acid 25:64:10:1.

TABLE 8. pK_a values for substituted acetophenones[a]

Ketone	σ_p[b]	k_{II}^0[c]	k_{II}^-[d]	pK_a^{Ketone}[e]	k_{OCl}[f]
H	0.00	0.0239 ± 0.0075	0.450 ± 0.024	18.38 ± 0.52	4.03 ± 0.52
p-MeO	−0.27	0.00626 ± 0.00141	0.130 ± 0.005	18.96 ± 0.51	4.08 ± 0.51
p-F	0.06	0.0201 ± 0.0031	0.419 ± 0.009	18.46 ± 0.50	4.08 ± 0.50
p-Cl	0.23	0.0480 ± 0.0082	0.823 ± 0.026	18.08 ± 0.51	3.99 ± 0.51
p-Br	0.23	0.0523 ± 0.0059	0.887 ± 0.030	18.04 ± 0.50	3.99 ± 0.50
p-NO_2	0.78	1.29 ± 0.11	16.3 ± 0.60	16.65 ± 0.50	3.86 ± 0.50
p-Me_3N^+	0.82	0.440 ± 0.049	4.26 ± 0.19	17.12 ± 0.50	3.75 ± 0.50

[a]In water at 25°C, ionic strength = 1.00 (KCl).
[b]σ_p values from ref. (26).
[c]Intercept of a plot of $k_{obs}/[OCl^-]$ vs. $[OH^-]$ for the acetophenones.
[d]Slope of a plot of $k_{obs}/[OCl^-]$ vs. $[OH^-]$ for the acetophenones.
[e]$pK_a^{ketone} = \log k_{diff} + pK_a^{HOCl} - \log k_{II}^0 = 16.76 - \log k_{II}^0$.
[f]$\log k_{OCl} = \log k_{II}^- - pK_w + pK_a^{ketone}$.

TABLE 9. Keto–enol equilibrium constants for acetophenones[a]

Ketone	σ[b]	pK_{Enol}[c]
H	0.00	8.15
p-MeO	−0.28	8.87
p-Me	−0.14	8.47
p-Cl	0.24	8.01
m-Cl	0.37	7.80
m-CF_3	0.46	7.78
m-NO_2	0.74	7.37
p-NO_2	0.78	7.18

[a]In water at 25°C. For the substituted acetophenones, least squares gives $pK_{Enol} = 8.33 \pm 0.49 - (1.39 \pm 0.11)\sigma$.
[b]Reference 27.
[c]References 13, 14.

Chromatographically purified material was crystallized once from toluene and once again from $CHCl_3$:CCl_4 to yield 105 mg of needle-like crystals, mp 128–130°C, lit. (21) mp 131–132°C. 200 MHz ^{1}H-nmr (80:20 $CDCl_3$:CD_3OD): δ = 4.65 (b, 2H) O*H*; 5.30 (s, 1H) C*H*(OH)(COOH); 7.70, 7.75, 8.20, and 8.25, (1H multiplets) aromatic C*H*. Exact mass calculated for $C_8H_7NO_5$: 197.0334; found: 197.0326. Ultraviolet (water): λ_{max} = 280 nm, ε = 9300; shoulder at 214, ε = 6300; also ϵ_{292} = 8300, ϵ_{274} = 9100. There was little or no change upon addition of NaOH.

p-*Dimethylaminoacetophenone*. *p*-Aminoacetophenone (Aldrich), 2.3 g (0.017 mol); 98% formic acid, 5.3 mL (0.14 mol); and 37% formalin, 3.4 mL (0.037 mol HCHO) were heated on a steam bath for 2.5 h. Reaction progress was followed by TLC using 20% ethanol in hexanes. The reaction mixture was partitioned between 100 mL 1 *M* NaOH and 100 mL ether, and the aqueous phase was then extracted with ether (2 × 100 mL). The pooled ether solutions were dried (Na_2CO_3) and evaporated to yield a yellow, partially crystalline mixture. This was dissolved in boiling petroleum ether (100–110°C) containing 10% 1-propanol. On cooling in dry ice, darker impurities settled out; the solution was filtered, evaporated, and purified by Kugelrohr distillation to give material containing about 10% mono-*N*-methylaminoacetophenone and 90% di-*N*-methylacetophenone. This material was further purified by column chromatography on silica gel, eluting with 10% ethyl acetate in hexanes to give 180 mg *p*-di-*N*-methylaminoacetophenone, mp 103-105°C; lit. (17) mp 105.5°C.

p-*Trimethylammonioacetophenone*. *p*-Dimethylaminoacetophenone, 180 mg (1.1 mmol), was dissolved in benzene, 5 mL, treated with 0.34 mL (4.4 mmol) of dimethyl sulphate and allowed to stand at room temperature for 10 days. Crystals, 250 mg, were collected and washed with CCl_4; mp 128–131°C. This material was used without further purification. ^{1}H-nmr, 200 MHz (D_2O, DSS as reference) δ = 2.74 (3H, s) C*H*$_3$—CO; 3.77 (s) C*H*$_3$—OSO_3^- and 3.79 (s) $(CH_3)_3N^+$, (combined integral 12H); 8.16, (4H, AB pattern) aromatic C*H*. Lit. (22) δ 3.68 for $(CH_3)_3N^+$ at infinite dilution in D_2O containing 1% DSS. A sample of our material gave δ 3.69 for a 0.0012 *M* solution in D_2O containing 1% DSS.

Product studies were carried out by preparing aqueous solutions containing hydroxide, hypochlorite, and ketone at known concentration, allowing reaction at room temperature for a period approximately equal to that for a kinetics run, then destroying excess hypochlorite by adding sodium bisulphite, extracting the basic solution with three equal volumes of ether, acidifying (concentrated HCl) and extracting with three equal volumes of ether to obtain the organic acids. In some cases, repeated additions of small amounts of hypochlorite were used to simulate kinetics concentrations. Products were identified by 60 MHz ^{1}H-nmr and, where possible, by melting point and TLC comparison with authentic compounds.

p-*Methoxyacetophenone*, 0.0027 *M*; OH^-, 0.53 *M*; and OCl^-, 0.027 *M*, were allowed to react for 1 h. Workup gave *p*-anisic acid in 94% yield, mp 181–183°C; lit. (17) 185°C, mixture mp with an authentic sample (Matheson, Coleman and Bell) 181–183°C. *p*-Methoxyacetophenone, 0.0007 *M*; OH^-, 0.25 *M*; and OCl^-, 0.00025 *M*, in a volume of 2 L, were allowed to react over a period of 20 days; the hypochlorite concentration was maintained by seven additions at one day intervals of 0.5 *M* stock hypochlorite, 1 mL. The first five additions of hypochlorite were fully consumed within 1 day. *p*-Anisic acid (30%), and *p*-anisaldehyde (10%) were identified by TLC and nmr comparison with authentic standards: *p*-methoxymandelic acid, (60%) by nmr analysis, was isolated by preparative TLC. Two Kugelrohr distillations gave material of mp 103–105°C; lit. (23) 108°C. The mass balance based on the product ratio was 92%.

We suspect that the anisaldehyde was generated by oxidation of the mandelic acid by chlorine generated from chlorate plus chloride during and after extraction from acid. Chlorate is produced by disproportionation of hypochlorite (24). Bromine is known to bring about oxidative decarboxylation of mandelic acid (25) so it seems likely that chlorine could do so.

p-*Fluoroacetophenone*, 0.0013 *M*; OH^-, 0.2 *M*; and OCl^-, 0.005 *M*, were allowed to react for 20 h. Workup and crystallization from water gave *p*-fluorobenzoic acid, mp 183°C, lit. (17) 185°C, mixture mp with authentic sample 183°C. ^{1}H-nmr analysis of the initial extract showed that the product mixture contained 5% *p*-fluoromandelic acid as well as *p*-fluorobenzoic acid. When *p*-fluoroacetophenone, 0.00018 *M*; OH^-, 0.25 *M*; and OCl^-, 0.0002 *M* in a volume of 1 L were allowed to react for 3 days, with the hypochlorite concentration maintained by three additions of 0.5 *M* stock hypochlorite, 0.4 mL; final concentration was 0.0001 *M*. The extract of the acidified product mixture gave a spectrum almost identical to that of *p*-fluoromandelic

Can. J. Chem. Downloaded from www.nrcresearchpress.com by 213.166.140.6 on 09/07/12
For personal use only.

acid. Spectrum integrals indicated 5–10% *p*-fluorobenzoic acid and 90–95% *p*-fluoromandelic acid as products.

p-*Bromoacetophenone*, 0.00025 *M*; OH^-, 0.50 *M*; and OCl^-, 0.0005 *M* were allowed to react for 3 days, with the hypochlorite concentration maintained by three additions of stock hypochlorite. ^{1}H-nmr analysis of the extract from the acidified product mixture showed 90% *p*-bromomandelic acid and 10% *p*-bromobenzoic acid with 94% mass recovery.

p-*Chloroacetophenone*, 0.001 *M*; OH^-, 1.0 *M*; and OCl^-, $\leq$0.003 *M*, were allowed to react over a 3-h period with slow addition of hypochlorite, and then for a further 3 days. Workup gave a mixture identified by ^{1}H-nmr analysis as 10% *p*-chlorobenzoic and 90% *p*-chloromandelic acid. Crystallization from CH_2Cl_2 gave *p*-chloromandelic acid mp 120–121°C; lit. (19) 120–121°C.

p-*Nitroacetophenone*, 0.002 *M*; OH^-, 1.0 *M*; and OCl^-, 0.007 *M*, were allowed to react for 2 h. Workup gave *p*-nitrobenzoic acid in 76% yield as the only acidic product found: mp 240–241°C, lit. (17) 242°C.

p-*Nitroacetophenone*, 0.0005 *M*; OH^-, 0.4 *M*; and OCl^-, 0.002 *M*, were allowed to react for 24 h, and samples were taken at intervals and analyzed by HPLC. At 11 min after the start of the reaction, no more starting material could be detected, and the product ratio, *p*-nitrobenzoic acid:*p*-nitromandelic acid, was 1:1. After 24 h, only *p*-nitrobenzoic acid could be detected.

p-*Nitroacetophenone*, 0.0013 *M*; OH^-, 1.0 *M*; and OCl^-, 0.005 *M*, were allowed to react for 20 h, and samples were taken at intervals and analyzed by HPLC. At 6 min after the start of the reaction, no more starting material could be detected, and the product ratio, *p*-nitrobenzoic acid:*p*-nitromandelic acid, was 1.4:1. After 20 h, this ratio had become 5.5:1.

p-*Nitromandelic acid by hypochlorite oxidation of* p-*nitroacetophenone*. *p*-Nitroacetophenone, 165 mg (1.00 mmol), was dissolved in 1 L of boiling water and allowed to cool before dissolving NaOH, 20 g (0.5 mol). Sodium hypochlorite, 27.5 mL of 0.08 *M* solution (2.2 mmol), was added slowly over a period of 90 min with vigorous stirring at room temperature. After an additional 30 min, sodium bisulphite, 200 mg, was added to stop the reaction. The basic solution was extracted with ether (3 × 100 mL), acidified cautiously with 6 *M* H_2SO_4, 44 mL, and extracted again with ether (3 × 100 mL). The acid extract yielded 84 mg of yellow solid. Analysis of this material by ^{1}H-nmr revealed both *p*-nitrobenzoic and *p*-nitromandelic acids in almost equal amounts. TLC showed only two uv-active spots.

Bromination of acetophenone

Acetophenone, 0.00030 *M*; OH^-, 0.30 *M*; and OBr^-, 0.005 *M*, were allowed to react in aqueous solution 0.70 *M* in KBr (total volume 100 mL) at room temperature for 15 min. The reaction was quenched with 10 mL of a solution 0.05 *M* in bisulfite and 0.3 *M* in phosphoric acid, and adjusted to pH 7 with 6 *M* HCl (ca. 4 mL). The solution was analyzed by HPLC, with a Waters radial-PAK C8 reverse phase column, eluting with 24% methanol:76% aqueous 0.001 *M* H_3PO_4, 0.0001 *M* NH_3. Peaks were detected by uv absorption at 225 nm. The products, identified by comparison of retention times with authentic standards were mandelic acid, 2.6 ± 1%, and benzoic acid 97 ± 5%.

Methods

For ^{1}H-nmr spectra, all chemical shifts are relative to TMS as internal standard unless otherwise stated.

HPLC analyses were carried out using C8 or C18 reverse phase columns, with mixtures of aqueous buffers and methanol as eluting solvent and uv detection.

Kinetics procedures

All reactions were studied in aqueous solution at 25°C and ionic strength 1.0 *M* (KCl) using apparatus and procedures previously described (10). Hydroxide and hypochlorite solutions were titrated against standards as before (10). With acetophenone, *p*-chloro-, *p*-methoxy-, *p*-nitro-, *p*-trimethylammonio-, reactions were initiated as before (10) by injection of aqueous ketone solution. With *p*-fluoro- and *p*-bromoacetophenone, reactions were initiated by injection (Hamilton syringe) of aqueous hypochlorite, titrated just before use, into ketone solutions containing known hydroxide concentrations at 1 *M* ionic strength (KCl). All kinetics reactions were run with hypochlorite in large (ca. 20-fold) excess.

Acknowledgments

We thank the Natural Sciences and Engineering Research Council of Canada, and the Academic Development Fund of the University of Western Ontario for financial support of this work.

1. J. P. GUTHRIE, J. COSSAR, and A. KLYM. J. Am. Chem. Soc. **104**, 895 (1982).
2. J. P. GUTHRIE, J. COSSAR, and A. KLYM. J. Am. Chem. Soc. **106**, 1351 (1984).
3. J. P. GUTHRIE. Can. J. Chem. **52**, 2037 (1974).
4. J. P. GUTHRIE. Can. J. Chem. **56**, 962 (1978).
5. J. P. GUTHRIE. Can. J. Chem. **59**, 45 (1981).
6. J. P. GUTHRIE and B. A. DAWSON. Can. J. Chem. **61**, 171 (1983).
7. J. P. GUTHRIE, J. COSSAR, P. A. CULLIMORE, N. M. KAMKAR, and K. F. TAYLOR. Can. J. Chem. **61**, 2621 (1983).
8. J. P. GUTHRIE, K. J. COOPER, J. COSSAR, B. A. DAWSON, and K. F. TAYLOR. Can. J. Chem. **62**, 1441 (1984).
9. J. P. GUTHRIE, J. COSSAR, and K. F. TAYLOR. Can. J. Chem. **62**, 1958 (1984).
10. J. P. GUTHRIE and J. COSSAR. Can. J. Chem. **64**, 1250 (1986).
11. W. P. JENCKS and J. REGENSTEIN. *In* Handbook of biochemistry. 1st ed. *Edited by* H. A. Sober. Chemical Rubber Publishing Co., Cleveland. 1968.
12. J. H. RIDD. Adv. Phys. Org. Chem. **16**, 1 (1978).
13. J. TOULLEC. Adv. Phys. Org. Chem. **18**, 1 (1982).
14. J. E. DUBOIS, J. TOULLEC, and M. EL-ALAOUI. J. Am. Chem. Soc. **103**, 5393 (1981).
15. J. GASTEIGER and M. MARSILI. Tetrahedron, **36**, 3219 (1980).
16. Y. CHIANG, A. J. KRESGE, and J. WIRZ. J. Am. Chem. Soc. **106**, 6392 (1984).
17. R. C. WEAST (*Editor*). Handbook of chemistry and physics. 48th ed. Chemical Rubber Co., Cleveland, OH. 1967.
18. J. J. KLINGENBERG. Org. Synth. **35**, 11 (1955).
19. S. S. JENKINS. J. Am. Chem. Soc. **53**, 2341 (1931).
20. G. P. HAGER and E. B. STARKEY. J. Am. Pharm. Assoc. **32**, 44 (1943).
21. G. CARRARA, F. FAVA, C. MARTINUZZI, and A. VECCHI. Gazz. Chim. Ital. **82**, 674 (1952).
22. G. R. WILEY and S. I. MILLER. J. Org. Chem. **37**, 767 (1972).
23. W. F. BARTHEL, J. LEON, and S. A. HALL. J. Org. Chem. **19**, 485 (1954).
24. F. A. COTTON and G. WILKINSON. Advanced inorganic chemistry. 4th ed. Wiley, New York. 1980. p. 558.
25. J. M. PINK and R. STEWART. Can. J. Chem. **49**, 649 (1971).
26. C. G. SWAIN and E. C. LUPTON. J. Am. Chem. Soc. **90**, 4328 (1968).
27. D. D. PERRIN, B. DEMPSEY, and E. P. SERJEANT. pK_a prediction for organic acids and bases. Chapman and Hall, London. 1981.

Can. J. Chem. Downloaded from www.nrcresearchpress.com by 213.166.140.6 on 09/07/12
For personal use only.

Influence of steric hindrance in molecules of substituted 2-phenyl-1,1,3,3-tetramethylguanidines on the kinetics and isotope effects of their proton transfer reactions with 4-nitrophenylnitromethane in acetonitrile solvent

PRZEMYSLAW PRUSZYNSKI[1]

Department of Chemistry, A. Mickiewicz University, Poznan, Poland

Received January 17, 1987

PRZEMYSLAW PRUSZYNSKI. Can. J. Chem. **65**, 2160 (1987).

Rate constants have been determined for the proton and deuteron transfer reactions of 4-nitrophenylnitromethane, $NO_2C_6H_4CH_2NO_2$, with three phenyl substituted derivatives of 2-phenyl-1,1,3,3-tetramethylguanidine, $X—C_6H_4—N=C[N(CH_3)_2]_2$, where X = 4-Cl, 2-Cl, and 2-Br, in the temperature range 278–308 K in acetonitrile solvent. In the concentration ranges used, the reaction to form an ion-paired product is first order in acid and first order in base. The reaction was followed spectrophotometrically using the stopped-flow technique. The reaction is fastest for the 4-Cl substituted base and slowest for the 2-Br analogue. The observed deuterium kinetic isotope effects show a clear dependence on the position and the size of the substituent in the base molecule. Kinetic isotope effects at 25°C, $k_H/k_D = 9.7 \pm 0.3$, 12.5 ± 0.3, and 15.6 ± 0.3, were observed for 4-Cl, 2-Cl, and 2-Br substituted bases respectively. The appropriate ratios of Arrhenius preexponential factors, $A_H/A_D = 0.98 \pm 0.10$, 0.87 ± 0.10, and 0.77 ± 0.10, may indicate increasing importance of tunnelling of the proton when the substituent is moved from the *para* to the *ortho* position or when the size of *ortho* substituent increases. Values of tunnelling correction factors were calculated using Bell's equation by means of the Caldor and Saunders method.

PRZEMYSLAW PRUSZYNSKI. Can. J. Chem. **65**, 2160 (1987).

Opérant dans l'acétonitrile comme solvant et à des températures allant de 278 à 308 K, on a déterminé les constantes de vitesse des réactions de transfert de proton et de deutéron du nitro-4 phénylnitrométhane, $NO_2C_6H_4CH_2NO_2$, vers trois dérivés, portant des groupements phényles substitués, de la phényl-2 tétraméthyl-1,1,3,3 guanidine, $X—C_6H_4—N=C[N(CH_3)_2]_2$ dans lequel X = les substituants Cl-4, Cl-2 et Br-2. Aux concentrations utilisées, la réaction conduisant à la formation d'une paire d'ions est du premier ordre en acide et du premier ordre en base. On a suivi la réaction en faisant appel à la spectrophotométrie et à la technique du flux stoppé. La vitesse de réaction de la base substituée par un Cl-4 est la plus rapide alors que celle de la base substituée par un Br-4 est la plus lente. Les effets isotopiques cinétiques du deutérium qui ont été observés démontrent clairement qu'il existe une relation avec la position et la taille du substituant dans la molécule basique. Pour les bases portant les substituants Cl-4, Cl-2 et Br-2, les effets isotopiques cinétiques à 25°C, k_H/k_D, sont respectivement de $9,7 \pm 0,3$, $12,5 \pm 0,3$ et $15,6 \pm 0,3$. Les rapports appropriés des facteurs préexponentiels d'Arrhénius, $A_H/A_D = 0,98 \pm 0,10$, $0,87 \pm 0,10$ et $0,77 \pm 0,10$, pourraient éventuellement indiquer que l'effet tunnel du proton augmente lorsqu'on déplace le substituant de la position *para* à la position *ortho* ou lorsqu'on augmente la taille du substituant *ortho*. On a calculé les facteurs de correction pour l'effet tunnel en faisant appel à l'équation de Bell et en appliquant la méthode de Caldor et Saunders.

[Traduit par la revue]

Introduction

The kinetics of the reaction between 4-nitrophenylnitromethane (4-NPNM) and 1,1,3,3-tetramethylguanidine (TMG) have been studied in several aprotic solvents by Caldin and Mateo (1). The large kinetic isotope effect values and anomalous Arrhenius parameters found for nonpolar solvents were explained in terms of participation of tunnelling to the reaction pathway (2–6). The strong solvent dependance of the kinetic isotope effect and the manifestation of the tunnelling effect were interpreted in terms of increase of effective mass of the transferred proton in polar solvents, when changes in solvation during the course of the reaction accompanied the translational movement of solvent molecules. The change in steric structure of tertiary amines caused by their protonation could also be considered as a factor increasing the effective mass of the transferred proton. Caldin and co-workers (7–10) compared the isotope effect for the reaction of 4-NPNM with tertiary amines (NEt_3 and NBu_3) with that measured for the more rigid quinuclidine. Their results were consistent with that for solvent dependance in the case of TMG, but the isotope effect was much smaller for tertiary amines than for TMG. These differences were explained in the terms of a greater curvature of the energy barrier in the case of imine bases. They suggested that the sp^2 nitrogen lone pair in TMG is more spherical, because of the greater contribution of the *s* orbital, than the lone pair of sp^3 hybridized nitrogen in amines, demanding closer approach of the reacting acid and base in the reaction complex. The values of volume of activation $\Delta V^{\neq}$ for the reaction of 4-NPNM and TMG in several solvents of low polarity were also measured (11). Other reactions of 4-NPNM with bases containing sp^2 hybridized nitrogen were then examined. Alkylimidamides (10), cyclic imidamide-DBU (12), and pentamethylguanidine (13) gave results confirming the need for a tunnelling correction; however, the values of the isotope effects were much lower than in the case of TMG as a base (1). Hubbard *et al.* (14) in a later paper reported k_H/k_D = 20–30 for the reaction of 4-NPNM with dialkylbenzamidamides in a series of solvents of low polarity. Rogne and co-workers (15–17), in a series of papers, discussed the influence of exchangeable hydrogen present in the TMG molecule on the kinetics of the deuteron transfer reaction. The "isotopic scrambling" effect, more important when the equilibrium constant is small, i.e., in the case of the reaction studied in solvents of low polarity, creates spurious values of the kinetic isotope effect. TMG and other imine bases are very difficult to dry, so the influence of residual water on the kinetics of the deuteron transfer reaction was also examined (18–20). This residual water can especially affect the deuteron transfer reaction when the concentration of the TMG solution is high (18), the condition used for reactions with low equilibrium constants. The influence of extraneous water was studied in the reaction of 4-NPNM with pentamethylguanidine (19) and with TMG in toluene (20). In both cases no such influence was observed, which must not be in contrast with the calculated

[1]Address for correspondence: Department of Chemistry, Dalhousie University, Halifax, N.S., Canada B3H 4J3.

Can. J. Chem. Downloaded from www.nrcresearchpress.com by 213.166.140.6 on 09/07/12
For personal use only.

Can. J. Chem. Downloaded from www.nrcresearchpress.com by 213.166.140.6 on 09/07/12
For personal use only.

influence of TMG residual water as there were no data for water-free systems (18).

This work adds some further data to the widely studied kinetics and isotope effects of 4-NPNM. The synthesis of various phenyl substituted derivatives of 2-phenyl-1,1,3,3-tetramethylguanidine (21) was also accomplished earlier by Kessler and Leibfritz (22) and Oszczapowicz and Osek (23). Bases used in these studies, 2-(4′-chlorophenyl)-1,1,3,3-tetramethylguanidine, 2-(2′-chlorophenyl)-1,1,3,3-tetramethylguanidine, and 2-(2′-bromophenyl)-1,1,3,3-tetramethylguanidine, do not have the exchangeable hydrogens and are much less hygroscopic than TMG, so the measurements should not be affected either by isotopic scrambling or by water brought into the reaction mixture with the solution of base. These bases are also weaker than most of the imidine bases used before (21, 23), so one can expect a more symmetrical energy barrier and therefore a higher isotope effect arising from bigger loss of the zero-point energy difference between initial and transition states and from higher probability of tunnelling (4, 5). Results of Lewis and Funderberk (24, 25) and our previous measurements (26, 27) showed the strong dependance of the observed isotope effects on the presence of the substituent group close to the acidic or basic sites in the reactants. Changing the position and the size of the substituent on the phenyl ring creates the possibility of further observing the relation between the structure of the reactants and the isotope effects.

Experimental

Materials

4-Nitrophenylnitromethane and its deuterated analogue were prepared as previously reported (1). 2-(4′-Chlorophenyl)-1,1,3,3-tetramethylguanidine, 2-(2′-chlorophenyl)-1,1,3,3-tetramethylguanidine, and 2-(2′-bromophenyl)-1,1,3,3-tetramethylguanidine were synthesized using the condensation reaction of an appropriate derivative of aniline with 1,1,3,3-tetramethylurea in the presence of $POCl_3$ (21). The purity of these bases was checked by means of spectroscopic methods as described in ref. 21. The elemental analyses of these compounds, in good agreement with the calculated elemental content (21), confirm that they are not very hygroscopic. Acetonitrile was purified by the method of O'Donnell *et al.* (28), distilled through the 1.5-m column from P_2O_5, and only the middle fraction (about 60%) was collected. Its purity was checked by means of uv spectroscopy.

Measurements

The equilibrium measurements were performed using the Specord M-40 spectrophotometer equipped with a thermostating device by the method described in ref. 29. Values of the absorbance for solutions of 4-NPNM and base, with known initial concentration, were determined. Two millilitres of both acid and base solution were placed in the cuvette and thermostated for about 5 min in the spectrophotometer. The particular absorbance measurements could be affected by a slow decolorizing process, which might be a reason for some discrepancy between the equilibrium constants found from these measurements and those from the kinetic data. The decolorization is slow (half-life time of about 1 h or more) but it may lead to some errors in the equilibrium measurements. This effect cannot affect the kinetic runs, which are completed within seconds, especially as the Guggenheim method of calculation of the observed rate constant was used (30). The kinetic measurements were done spectrophotometrically using a stopped-flow apparatus. The kinetic runs were performed under pseudo-first-order conditions with base always in large excess. The kinetic curves were exactly exponential in the case of the proton transfer reaction. In the case of the deuteron transfer reaction the early part of the kinetic curve (about 10%) showed some contribution of the proton transfer reaction. This part showed a tendency to increase with time. Fresh solutions of deuterated 4-nitrophenylnitromethane were always used. After neglecting the beginning part of the curve (usually about 30%) the remainder was exactly exponential, giving a Guggenheim plot with a correlation coefficient similar to that for the proton transfer reaction. The observed rate constants k_{obs} for five base concentrations (b) were determined at each temperature. Then the least-squares method was used to fit the k_{obs} values against the base concentration, and the second-order rate constant for forward reaction k_2 and rate constant for backward reaction k_b were determined from the slope and the intercept of eq. [1]:

$$[1] \quad k_{obs} = (k_2 \times b) + k_b$$

The temperature dependance of the second-order rate constants in the temperature range 278–308 K allowed the activation parameters to be calculated. Calculations of the tunnelling correction factors were done using Bell's equation (4, 5) and the program of Kaldor and Saunders (31).

Results and discussion

The reaction of 4-nitrophenylnitromethane with three phenyl substituted derivatives of 2-phenyl-1,1,3,3-tetramethylguanidine: 2-(4′-chlorophenyl)-1,1,3,3-tetramethylguanidine, (**1**, 4-ClPhTMG), 2-(2′-chlorophenyl)-1,1,3,3-tetramethylguanidine (**2**, 2-ClPhTMG), 2-(2′-bromophenyl)-1,1,3,3-tetramethylguanidine (**3**, 2-BrPhTMG), in acetonitrile gives the red product, $\lambda_{max} = 500$ nm.

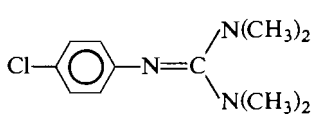

1

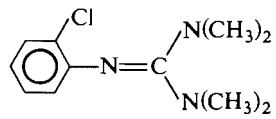

2

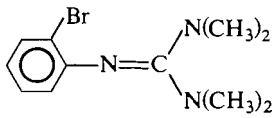

3

The equilibrium measurements gave a linear plot of a/A (a, the initial concentration of acid; A, the equilibrium absorbance of the reaction mixture) with $1/b$ (b, initial concentration of base), a relation expected for products existing in the form of ion pairs (29). The relation of a/A against A/b, expected to be linear when the product is in the form of separate ions (29), shows a distinct upward curvature so that the form of product is certain and in agreement with previous measurements (1, 29). A molecular extinction coefficient of the order of magnitude 2×10^4 dm^3 mol^{-1} cm^{-1} and equilibrium constants 600 ± 200, 400 ± 200, and 300 ± 140 dm^3 mol^{-1} for 4-ClPhTMG, 2-ClPhTMG, and 2-BrPhTMG respectively were calculated. The pK_a values measured in water at 25°C at ionic strength 0.1 mol dm^{-3} (21) are 11.70 ± 0.02 for 4-ClPhTMG, 11.16 ± 0.10 for 2-ClPhTMG, and 10.97 ± 0.04 for 2-BrPhTMG. The pK_a of 4-NPNM in water is 6.49 ± 0.01 (32). Kolthoff *et al.* (33) measured the pK_a values for various types of acids in acetonitrile. For tetramethylguanidine pK_a values of 23.3 in acetonitrile and 13.6 in water were found ($\Delta pK_{a(W-AN)} = 9.7$) (33). For uncharged acids, which during the dissociation process form an anion strongly solvated by water, the $\Delta pK_{a(W-AN)}$ value changes between 10.7 for picric acid and 17.5 for acetic acid (33). This value is lower when the extent of the delocalization of the negative charge in the anion increases. The anion of 4-NPNM resembles the picric acid anion much more than the acetic acid anion with negative charge localized at the oxygen. The difference in the pK_a for 4-NPNM and derivatives of Ph-TMG, 4–5 in water, decreases to about 2–3 when the system is transferred to acetonitrile, which is in

Can. J. Chem. Downloaded from www.nrcresearchpress.com by 213.166.140.6 on 09/07/12
For personal use only.

TABLE 1. Observed and second-order rate constants for the proton and deuteron transfer reactions from 4-NPNM to 4-ClPhTMG, 2-ClPhTMG, and 2-BrPhTMG in acetonitrile

	Proton transfer			Deuteron transfer		
Temperature (°C)	10^3 [B] (M)	k_{obs} (s^{-1})	k_2 ($M^{-1} s^{-1}$)	10^3 [B] (M)	k_{obs} (s^{-1})	k_2 ($M^{-1} s^{-1}$)
2-(4′-Chlorophenyl)-1,1,3,3-tetramethylguanidine						
5	0.92–4.58	0.56–1.86	346 ± 12	1.83–9.16	0.10–0.32	30.0 ± 0.7
10		0.64–2.32	436 ± 27		0.12–0.41	39.5 ± 0.8
15		0.87–2.94	559 ± 6		0.16–0.54	51.3 ± 0.6
20		1.10–3.44	631 ± 16		0.20–0.68	65.5 ± 0.6
25		1.32–4.37	810 ± 28		0.26–0.87	83.5 ± 0.5
30		1.60–5.17	953 ± 46		0.32–1.10	107.2 ± 0.8
35		1.89–6.66	1263 ± 51		0.40–1.36	132.2 ± 0.8
2-(2′-Chlorophenyl)-1,1,3,3-tetramethylguanidine						
5	1.23–6.10	0.26–0.65	80 ± 2	3.66–14.65	0.026–0.082	5.2 ± 0.1
10		0.32–0.83	101 ± 2		0.037–0.118	7.3 ± 0.4
15		0.43–1.06	130 ± 4		0.049–0.156	9.7 ± 0.6
20		0.53–1.32	160 ± 4		0.064–0.204	12.7 ± 0.8
25		0.67–1.69	202 ± 9		0.081–0.259	16.2 ± 0.6
30		0.84–2.02	240 ± 6		0.105–0.333	20.7 ± 1
35		1.01–2.55	312 ± 5		0.131–0.427	26.8 ± 1
2-(2′-Bromophenyl)-1,1,3,3-tetramethylguanidine						
5	1.07–5.36	0.17–0.46	69 ± 4	2.14–10.72	0.012–0.043	3.7 ± 0.1
10		0.20–0.59	92 ± 2		0.014–0.058	5.0 ± 0.1
15		0.26–0.75	115 ± 2		0.019–0.077	6.7 ± 0.1
20		0.34–0.93	140 ± 2		0.025–0.099	8.7 ± 0.1
25		0.44–1.18	176 ± 3		0.032–0.129	11.3 ± 0.1
30		0.54–1.46	216 ± 2		0.040–0.162	14.3 ± 0.1
35		0.70–1.80	260 ± 3		0.051–0.217	19.2 ± 0.1

TABLE 2. Activation parameters for the proton and deuteron transfer reactions from 4-NPNM to 4-ClPhTMG, 2-ClPhTMG, and 2-BrPhTMG in acetonitrile solvent

Parameter	4-ClPhTMG	2-ClPhTMG	2-BrPhTMG
$\Delta H_H^{\ddagger}$ (kJ mol^{-1})	27.2 ± 1.1	29.3 ± 0.5	28.5 ± 0.5
$\Delta H_D^{\ddagger}$ (kJ mol^{-1})	32.8 ± 0.2	35.9 ± 0.7	35.9 ± 0.5
$\Delta S_H^{\ddagger}$ (J mol^{-1} deg^{-1})	−97.8 ± 4.0	−102.4 ± 1.7	−105.7 ± 1.7
$\Delta S_D^{\ddagger}$ (J mol^{-1} deg^{-1})	−97.8 ± 0.8	−101.2 ± 2.1	−103.7 ± 3.3
A_H (dm^3 mol^{-1} s^{-1})	(1.26 ± 0.59) × 10^8	(7.43 ± 1.59) × 10^7	(4.75 ± 0.99) × 10^7
A_D (dm^3 mol^{-1} s^{-1})	(1.29 ± 0.10) × 10^8	(8.50 ± 2.31) × 10^7	(6.11 ± 0.12) × 10^7

good agreement with the equilibrium constants observed for the reactions studied.

The value of the molecular extinction coefficient, about 2 × 10^4 dm^3 mol^{-1} cm^{-1}, is in good agreement with values found in previous measurements for reactions with 4-NPNM as an acid (1).

Table 1 presents the rate constants measured for the reactions studied. The second-order rate constants k_{2H} for 4-ClPhTMG, 2-ClPhTMG, and 2-BrPhTMG at 25°C are 810 ± 28, 202 ± 9, and 176 ± 3 dm^3 mol^{-1} s^{-1} respectively. The respective backward rate constants at 25°C are 0.7 ± 0.1, 0.4 ± 0.1, and 0.3 ± 0.1. The ratio of forward and backward rate constants gives the equilibrium constants 1100 ± 200, 500 ± 50, and 550 ± 100 for 4-Cl, 2-Cl, and 2-Br derivatives respectively. These values are in satisfactory agreement with those found from equilibrium measurements in the light of problems explained in the experimental section.

This reaction is fastest for the strongest base 4-ClPhTMG and is much slower for both *ortho*-substituted bases. Table 2 gives the activation parameters for the reactions studied.

These values show that the enthalpy of activation increases in the order 4-ClPhTMG, 2-BrPhTMG, and 2-ClPhTMG showing that the bond-forming–bond-breaking process on the way to the transition state is becoming more endoergic in this sequence. This is not in full agreement with the pK_a values in the case of 2-Cl and 2-Br derivatives. Nevertheless the difference of the pK_a in water for these two bases is small, and might be easily reversed in acetonitrile. The activation parameters in the case of 2-BrPhTMG and 2-ClPhTMG are comparable within the experimental error but, if their mean values are considered, it is the entropy of activation that makes reaction of 2-BrPhTMG slower. The more negative value of the entropy of activation and the lower value of the Arrhenius preexponential factor for 2-BrPhTMG than for 2-ClPhTMG may be explained in terms of greater steric inhibition in forming the transition state for reaction when larger bromine is present in the position *ortho* to the basic site of the reactant. Such a case is an interesting model for studying the influence of steric hindrance on the values of kinetic isotope effects. The strength of the bases used differs so slightly that, especially in the case of carbon acids, it should not

TABLE 3. Isotope effects for the proton transfer reactions from 4-NPNM to 4-ClPhTMG, 2-ClPhTMG, and 2-BrPhTMG in acetonitrile

	4-ClPhTMG	2-ClPhTMG	2-BrPhTMG
k_{2H}/k_{2D} at 5 (°C)	11.5 ± 0.5	15.4 ± 0.5	18.6 ± 1.2
10	11.0 ± 0.7	13.8 ± 0.8	18.4 ± 0.5
15	10.9 ± 0.2	13.4 ± 0.9	17.2 ± 0.4
20	9.6 ± 0.3	12.6 ± 0.8	16.1 ± 0.3
25	9.7 ± 0.3	12.5 ± 0.7	15.6 ± 0.3
30	8.9 ± 0.4	11.6 ± 0.6	15.1 ± 0.2
35	9.5 ± 0.4	11.6 ± 0.5	13.5 ± 0.2
$\Delta\Delta H^*$ (kJ mol^{-1})	5.7 ± 1.6	6.6 ± 0.8	7.4 ± 0.7
$\Delta\Delta S^*$ (J mol^{-1} deg^{-1})	0.0 ± 3.8	1.3 ± 2.7	2.1 ± 3.8
A_H/A_D	0.98 ± 0.46	0.87 ± 0.19	0.77 ± 0.16
$Q_{t,H}/Q_{t,D}$	—	1.12 ± 0.12	1.22 ± 0.19

affect the symmetry of the transition state, and the variation in the isotope effects can be entirely attributed to the steric conditions of the reactions.

Table 3 presents the values of kinetic isotope effects k_{2H}/k_{2D}, differences in the activation parameters, and the calculated tunnelling correction factors. The kinetic isotope effect increases when the Cl substituent is moved from the *para* to the *ortho* position and increases further when Cl is replaced by the larger Br substituent (Table 3). In the case of 4-ClPhTMG the observed isotope effects, both on the rate constants and on the activation parameters, are within the range predicted from the zero-point energy difference for C—H and C—D bonds. The A_H/A_D value is often used as an indicator of the occurrence of a tunnelling effect in proton transfer reactions (4–6). In the present results a part of the increase in the isotope effect can be attributed to the increasing importance of proton tunnelling. The value $A_H/A_D = 0.98 \pm 0.46$ for 4-ClPhTMG is close to the classical value $A_H/A_D = 1$, and decreases smoothly to $A_H/A_D = 0.87 \pm 0.19$ for 2-ClPhTMG and to 0.77 ± 0.16 for 2-BrPhTMG, although the mean values are still within the so-called "classical" range (4, 5). Also, the standard deviation values indicate that the tunnelling effect explanation should be treated as an alternative. For the last two bases the tunnelling correction factors were calculated using Bell's equation (4, 5) and the Kaldor and Saunders computing procedure (31). The values of the ratio of tunnelling correction factors for the proton and deuteron transfer reactions, $Q_H/Q_D = 1.12 \pm 0.12$ for the 2-ClPhTMG and 1.22 ± 0.19 for 2-BrPhTMG, indicate a small participation of tunnelling in these reactions that increases smoothly with steric crowding around the basic site. These results are in good agreement with those of Lewis and Funderburk for the reaction of 2-nitropropane with pyridine bases (24, 25) and with our previous results (26, 27).

Can. J. Chem. Downloaded from www.nrcresearchpress.com by 213.166.140.6 on 09/07/12
For personal use only.

Acknowledgements

I would like to express my gratitude to Professor A. Jarczewski, A. Mickiewicz University, Poznan, Poland, for his help and encouragement. The financial assistance of the Polish Academy of Sciences is also gratefully acknowledged.

1. E. F. CALDIN and S. MATEO. J. Chem. Soc. Faraday Trans. 1, 1876 (1975).
2. E. WIGNER. Z. Phys. Chem. Abt. B: **19**, 203 (1932).
3. R. B. BELL. Proc. R. Soc. London, A: **139**, 466 (1933).
4. R. P. BELL. The proton in chemistry. 2nd ed. Chapman and Hall, London. 1973. Chap. 12.
5. R. P. BELL. The tunnel effect in chemistry. Chapman and Hall, London. 1980.
6. L. MELANDER and W. H. SAUNDERS. Reaction rates of isotopic molecules. Wiley, New York. 1980. pp. 36, 75, 140 et *seq.*
7. E. F. CALDIN and S. MATEO. J. Chem. Soc. Faraday Trans. 1, 112 (1976).
8. E. F. CALDIN and C. J. WILSON. Faraday Symp. Chem. Soc. **10**, 121 (1976).
9. E. F. CALDIN, D. M. PARBOO, F. A. WALKER, and C. J. WILSON. J. Chem. Soc. Faraday Trans. 1, 1856 (1976).
10. E. F. CALDIN, D. M. PARBOO, and C. J. WILSON. J. Chem. Soc. Faraday Trans. 1, 2645 (1976).
11. C. D. HUBBARD, C. J. WILSON, and E. F. CALDIN. J. Am. Chem. Soc. **98**, 1870 (1976).
12. E. F. CALDIN, O. ROGNE, and C. J. WILSON. J. Chem. Soc. Faraday Trans. 1, 1796 (1978).
13. E. F. CALDIN and O. ROGNE. J. Chem. Soc. Faraday Trans. 1, 2065 (1978).
14. C. D. HUBBARD, D. L. HARRIS III, D. W. HOOPER, and A. F. TUCCI. J. Chem. Soc. Faraday Trans. 1, 3619 (1982).
15. I. HEGGEN, J. LINDSTROM, and O. ROGNE. J. Chem. Soc. Faraday Trans. 1, 1263 (1978).
16. O. ROGNE. Acta Chem. Scand. Ser. A: **32**, 559 (1978).
17. J. H. BLANCH and O. ROGNE. J. Chem. Soc. Faraday Trans. 1, 1263 (1978).
18. E. F. CALDIN, S. MATEO, and P. WARRICK. J. Am. Chem. Soc. **103**, 202 (1981).
19. J. H. BLANCH, O. ROGNE, and L. I. ROSSEMYR. J. Chem. Soc. Faraday Trans. 1, 1905 (1980).
20. A. J. KRESGE and M. F. POWELL. J. Am. Chem. Soc. **103**, 201 (1981).
21. P. PRUSZYNSKI. Can. J. Chem. **65**, 626 (1987).
22. H. KESSLER and D. LEIBFRITZ. Tetrahedron, **26**, 1805 (1970).
23. J. OSZCZAPOWICZ and J. OSEK. Pol. J. Chem. **57**, 93 (1983).
24. E. S. LEWIS and L. H. FUNDERBURK. J. Am. Chem. Soc. **89**, 2322 (1967).
25. L. FUNDERBURK and E. S. LEWIS. J. Am. Chem. Soc. **86**, 2531 (1964).
26. A. JARCZEWSKI and PRUSZYNSKI. Pol. J. Chem. **58**, 1175 (1984).
27. P. PRUSZYNSKI and A. JARCZEWSKI. J. Chem. Soc. Perkin Trans. 2, 1117 (1986).
28. J. F. O'DONNELL, J. T. AYERS, and C. K. MANN. Anal. Chem. **37**, 1161 (1965).
29. E. F. CALDIN, A. JARCZEWSKI, and K. T. LEFFEK. Trans. Faraday Soc. **67**, 110 (1971).
30. E. A. GUGGENHEIM. Philos. Mag. **2**, 538 (1926).
31. S. B. KALDOR and W. H. SAUNDERS, JR. J. Am. Chem. Soc. **101**, 7954 (1979).
32. F. G. BORDWELL and W. J. BOYLE, JR. J. Am. Chem. Soc. **94**, 3907 (1972).
33. I. M. KOLTHOFF, M. K. CHANTOONI, JR., and S. BHOWMIK. J. Am. Chem. Soc. **90**, 23 (1968).

(±)-4-Oxo-9-deoxy-9-azaprostaglandin I_2 derivatives. Very stable prostacyclin analogs[1]

ANGEL GUZMÁN, ELFIDA MARTINEZ, AND ESPERANZA VELARDE
Syntex, S.A., División, Apartado Postal 10-820, 11000 Mexico, D.F.

AND

MICHAEL L. MADDOX AND JOSEPH M. MUCHOWSKI[2]
Syntex Research, Institute of Organic Chemistry, 3401 Hillview Avenue, Palo Alto, CA 94304, U.S.A.

Received February 5, 1987

ANGEL GUZMÁN, ELFIDA MARTINEZ, ESPERANZA VELARDE, MICHAEL L. MADDOX, and JOSEPH M. MUCHOWSKI. Can. J. Chem. **65**, 2164 (1987).

The synthesis of 4-oxo-9-deoxy-9-azaprostaglandin I_2 (**23***a*) and two ω-chain analogues thereof (**23***c* and **23***e*) is described. The most salient features of the synthetic process used were (*a*) introduction of the nitrogen functionality at C-9 by [3,3] sigmatropic rearrangement of the trichloroacetamidate **5***b* to the trichloroacetamide **6**, (*b*) transformation of **6** into the bicyclic lactam **7** with sodium borohydride, (*c*) stereospecific introduction of the 11α-hydroxyl group via the bromohydrin **8***a*, and (*d*) attachment of the α chain by extrusion of sulfur from the thioimidates **20** by the Eschenmoser sulfide contraction process.

ANGEL GUZMÁN, ELFIDA MARTINEZ, ESPERANZA VELARDE, MICHAEL L. MADDOX et JOSEPH M. MUCHOWSKI. Can. J. Chem. **65**, 2164 (1987).

On décrit la synthèse de l'oxo-4 déoxy-9 aza-9 prostaglandine I_2 (**23***a*) et de deux de ses analogues avec une chaîne ω (**23***c* et **23***e*). Les caractéristiques principales du processus de synthèse utilisé sont (*a*) l'introduction d'une fonction azotée en C-9 par une transposition sigmatropique [3,3] du trichloroacétamidate **5***b* en trichloroacétamide **6**, (*b*) l'utilisation du borohydrure de sodium pour transformer le composé **6** en la lactame bicyclique **7**, (*c*) l'introduction stéréospécifique du groupement hydroxyle en 11α par le biais de la bromohydrine **8***a* et (*d*) l'attache de la chaîne α par une extrusion de soufre à partir des thioimidates **20** en faisant appel au processus d'Eschenmoser pour la contraction des sulfures.

[Traduit par la revue]

Can. J. Chem. Downloaded from www.nrcresearchpress.com by 213.166.140.6 on 09/07/12
For personal use only.

Prostacyclin (PGI_2, **1**) is the most powerful endogenous inhibitor of platelet aggregation discovered to date (1, 2). The endocyclic enol ether moiety present in this molecule renders it exceedingly sensitive to acidic conditions and even at physiological pH its half-life is only ca. 3 min. It is thus ineffective orally and when it is administered by intravenous infusion its physiological effects disappear rapidly after termination of the infusion. Considerable effort has been devoted to the synthesis of prostacyclin analogues with reduced acid sensitivity and improved metabolic stability. The acid sensitivity problem has been solved by stratagems such as replacement of the enol ether oxygen by other atoms (e.g., sulfur, nitrogen, or carbon), resonance stabilization in the vinylogous sense (for example, with an oxo group at C-4 (3) or a nitrile moiety at C-5 (4)), inductive stabilization by suitably placed electron attracting substituents (e.g. fluorine at C-7 (5) or C-10 (6)), etc. (for reviews on this subject, see refs. 7–9). Metabolic stability has been conferred upon prostacyclin derivatives by the incorporation of a wide variety of structural modifications into the upper (α) and lower (ω) side chains (7–9). It occurred to us that the prostacyclin analogue **2** was a particularly attractive synthetic target because of the minimal acid sensitivity, good chemical stability, and marked preference for the hydrogen bonded *Z* isomeric form associated with the vinylogous amide functionality (10, 11).

It was our intention of effect the introduction of the vinylogous amide moiety of **2** by the Eschenmoser sulfide contraction reaction (10) and thus the lactam **3** was an obvious starting material. One such compound (**3**, R^1 = Ac, R^2 = OTHP) had already been synthesized by Bartmann *et al.* (12) in seven steps from the Corey lactone **4** (13). In our hands,

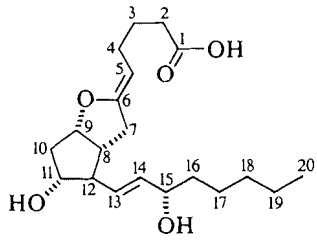

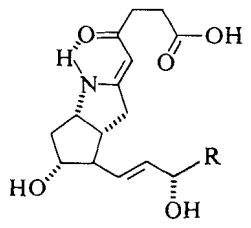

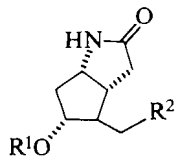

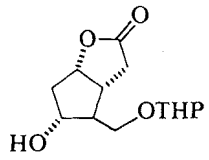

this reaction sequence was not easily reproducible and therefore another synthetic route to lactams of this class was devised. Thus, the readily available unsaturated ester **5***a* (ref. 14, Scheme 1) was converted into the trichloroacetamidate **5***b*, which underwent [3,3] sigmatropic rearrangement (15) to the allylic trichloroacetamide **6** (54% yield from **5***a*) in boiling xylene (133°C in Mexico City!). This compound was transformed directly into the unsaturated bicyclic lactam **7** (80%) on reductive deacylation with ethanolic sodium borohydride at 60°C (16). The structure on this compound is fully supported by the 300-MHz nmr spectrum (Table 1). *N*-Bromosuccinimide in wet dimethylsulfoxide (17) effected the conversion of **7** into a single bromohydrin **8***a* in 72% yield. The stereo- and regiochemistry shown in **8***a* was originally assigned by analogy to that observed for the products obtained from the very closely related bicyclic unsaturated systems **10**, **11**, and **12** with *N*-bromoacetamide in aqueous acetone (18), iodine acetate in

[1]Contribution No. 700 from the Syntex Institute of Organic Chemistry.

[2]Author to whom correspondence may be addressed.

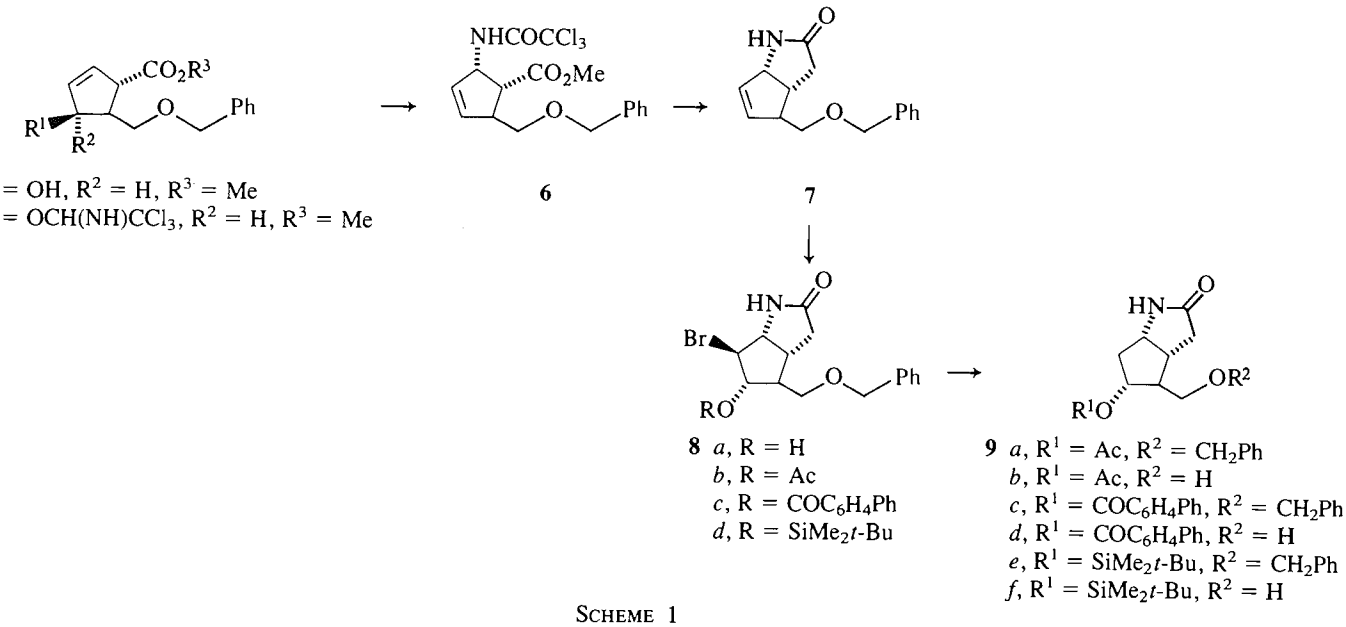

5 *a*, R^1 = OH, R^2 = H, R^3 = Me
b, R^1 = $OCH(NH)CCl_3$, R^2 = H, R^3 = Me

6

7

8 *a*, R = H
b, R = Ac
c, R = COC_6H_4Ph
d, R = $SiMe_2t$-Bu

9 *a*, R^1 = Ac, R^2 = CH_2Ph
b, R^1 = Ac, R^2 = H
c, R^1 = COC_6H_4Ph, R^2 = CH_2Ph
d, R^1 = COC_6H_4Ph, R^2 = H
e, R^1 = $SiMe_2t$-Bu, R^2 = CH_2Ph
f, R^1 = $SiMe_2t$-Bu, R^2 = H

SCHEME 1

dry acetic acid (19), and *N*-bromosuccinimide in wet dimethylsulfoxide (14), respectively. In addition, the proton coupling constants (Table 1) were similar to those reported for a closely related model system (20). The structure of **8***a* was verified by reductive debromination of the derived acetate **8***b* with tri-*n*-butyltin hydride followed by hydrogenolytic debenzylation (Pd–C) of **9***a*, thus obtained, to the known (12) diol monoacetate **9***b*.[3]

For the synthesis of the desired prostacyclin derivatives, the bromohydrin **8***a* was converted into the *p*-phenylbenzoate ester **8***c* or the *tert*-butyldimethylsilyl ether **8***d*, which, on reductive debromination (to **9***c* and **9***e*) and subsequent catalytic hydrogenolysis, as described above, gave the primary alcohols **9***d* and **9***f*. Oxidation of these alcohols with Collins reagent (21) and immediate condensation of the crude, unstable aldehydes **13***a* and **13***b* (Scheme 2) with the sodium salts of the appropriate ketophosphonates provided the enones **14***a–d*. In general, considerably better overall yields of the enones **16** were

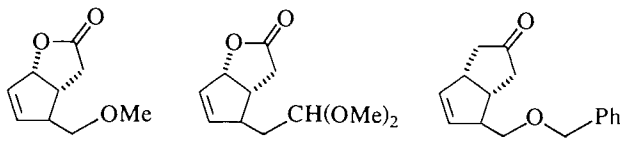

10 **11** **12**

obtained when the silylated alcohol **9***f* was used as the aldehyde precursor for the Wadsworth–Emmons (22) reaction. Reduction of the enones with methanolic sodium borohydride containing cerous chloride (23) produced mixtures of epimeric alcohols, the ratios of which depended on the nature of the alcohol protecting group at C-11 (prostaglandin numbering). The *p*-phenyl benzoate esters **14***a* and **14***c* gave rise to nearly equal amounts of the 15α and 15β isomers[4] **15***a,c* and **15***b,d* whereas a 2:1 ratio of epimers **17***a,c* and **17***b,d* was formed from the silyl ethers **14***b,d*. These alcohols (separable by flash chromatography or preparative tlc on silica gel) were then transformed into the bis-*tert*-butyldimethylsilyl ethers **18***a–f*, either directly, in the case of **17***a–d*, or after conversion into the diols **16***a–d*. Reaction of **18** with Lawesson's reagent (24) in hot benzene provided the thiolactams **19** (Scheme 3) in ca. 70–80% yield. The stage was now set for the introduction of the upper (α) side chain by the sulfide contraction process. Alkylation of the sodium salts of the thiolactams with methyl 5-bromolevulinate gave the unstable thiaimino compounds **20**, which, without purification, were heated with potassium-*tert*-butoxide in a xylene–*tert*-butanol mixture containing triphenylphosphine. The silylated vinylogous amides (**21***a–f*), formed in 55–70% yield, showed the expected infrared absorptions at 3280, 1625, and 1545 cm^{-1} and, in the case of **21***f*, the broad band at 3280 cm^{-1} did not shift on dilution (0.1–0.01 *M*). In addition, the compounds had a singlet nmr absorption at ca. δ 5.0 for the lone olefinic hydrogen atom (at C-5), a broad peak for a strongly H-bonded NH at δ 9.9 ± 0.2, and an intense uv absorption near 306 nm (ε ~ 19 000) for the vinylogous amide chromophore. These spectroscopic properties are virtually identical to those reported (10) for the monocyclic vinylogous amide **24**. Desilylation of **21** was effected with tetra-*n*-butylammonium fluoride in tetrahydrofuran (25) at 40°C and the methyl esters **22**, so produced, were hydrolysed with potassium carbonate in methanol–water solution. Both the methyl esters **22** and the carboxylic acids **23** could be kept for long periods of time at ambient temperature without appreciable decomposition. The carboxylic acids exhibit considerable stability under acidic conditions. Indeed, tlc purification thereof was carried out using an acetic acid containing solvent system.

The carboxylic acids were tested as inhibitors of ADP induced aggregation of human platelet rich plasma in vitro by a modification of the method of Born (26). The 15-cyclopentyl compound **23***e* was the most active member of this series of compounds (see Table 2) with a potency ca. one-quarter that of PGE_1. This low level of activity (~0.01 × prostacyclin sodium salt) was surprising in view of the fact that, where comparisons were possible, the nmr spectral parameters of **23***b* (Table 1), and by implication **23***a*, and prostacyclin (27) showed considerable

[3]We thank Dr. W. Bartmann, Hoechst, A. G. Frankfurt am Main, for providing us with a copy of the nmr spectrum of **9***b*, which was identical to that obtained by us (see Table 1).

[4]The α stereochemistry was assigned to the less polar 15-hydroxy compounds **15***a,c* and **17***a,c* (see Table 3) because, in each case, these gave rise to the azaprostacyclin epimer, which was the more potent inhibitor of adenosine diphosphate (ADP) induced aggregation of human platelet rich plasma (HPRP; see below).

Can. J. Chem. Downloaded from www.nrcresearchpress.com by 213.166.140.6 on 09/07/12
For personal use only.

Can. J. Chem. Downloaded from www.nrcresearchpress.com by 213.166.140.6 on 09/07/12
For personal use only.

TABLE 1. Chemical shifts and coupling constants of 15-epi-3-oxo-9-deoxy-9-aza PGI_2 and precursors thereof[a]

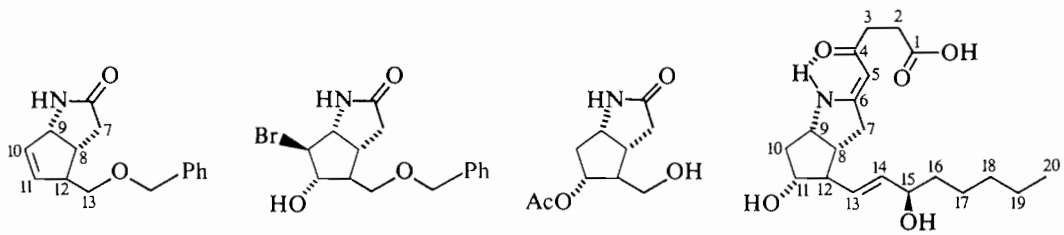

7 **8***a* **9***b* **23***b*

Proton	δ (ppm)	*J* values (Hz)	Proton	δ (ppm)	*J* values (Hz)	Proton	δ (ppm)	*J* values (Hz)	Proton	δ (ppm)	*J* values (Hz)
7α	2.19	$J(7\alpha-7\beta) = 17.4$	7α	2.23	$J(7\alpha-7\beta) = 17.5$	7α	2.23	$J(7\alpha-7\beta) = -17.1$	2	2.57[b,e]	
		$J(7\alpha-8) = 5.2$			$J(7\alpha-8) = 4.1$			$J(7\alpha-8) = 2.1$	3	2.57[b,e]	
7β	2.65	$J(7\alpha-7\beta) = 17.4$	7β	2.60	$J(7\alpha-8) = 17.5$	7β	2.64	$J(7\alpha-7\beta) = -17.1$	5	5.08[f]	
		$J(7\beta-8) = 10.0$			$J(7\beta-8) = 10.4$			$J(7\beta-8) = 9.6$	7α	2.57[b,e]	
8	2.85[b,c]		8	2.74	$J(7\alpha-8) = 4.1$	8	2.74	$J(7\alpha-8) = 2.1$	7β	2.87	$J(7\alpha-7\beta) = 17.7$
9	4.61	$J(8-9) = 7.8$			$J(7\beta-8) = 10.4$			$J(7\beta-8) = 9.6$			$J(7\beta-8) = 9.3$
10	5.78[d]	$J(10-11) = 5.7$			$J(8-9) = 9.3$			$J(8-9) = 7.6$			$J(5-7\beta) = 0.5$
		$J(9-10) \simeq 1.7$			$J(8-12) = 9.4$			$J(8-12) = 6.9$	8	2.57[b,e]	
		$J(10-12) \simeq 1.7$	9	4.11	$J(8-9) = 9.3$	9	4.10	$J(8-9) = 7.6$	9	4.33	$J(8-9) = 7.5$
11	5.85[d]	$J(10-11) = 5.7$			$J(9-10) = 6.3$			$J(9-10\alpha) = 3.6$			$J(9-10\alpha) = 4.5$
		$J(9-11) \simeq 1.4$	10	3.82	$J(9-10) = 6.3$			$J(9-10\beta) = 7.0$			$J(9-10\beta) = 7.5$
12	2.85[b,c]				$J(10-11) = 9.4$	10α	1.84	$J(9-10\alpha) = 3.6$	10α	1.73	$J(9-10\alpha) = 4.5$
13	3.35	$J(13-13') = 9.05$	11	4.04	$J(10-11) = 9.4$			$J(10\alpha-10\beta) = -14.1$			$J(10\alpha-10\beta) = 3.8$
		$J(12-13) = 6.7$			$J(11-12) = 9.6$			$J(10\alpha-11) = 6.6$			$J(10\alpha-11) = 8.8$
13′	3.45	$J(13-13') = 9.05$			$J(11-OH) = 3.3$	10β	2.38	$J(9-10\beta) = 7.0$	10β	1.57[b,e]	
		$J(12-13') = 5.4$	12	1.97	$J(11-12) = 9.6$			$J(10\alpha-10\beta) = -14.1$	11	3.96	$J(10\alpha-11) = 8.8$
OCH_2	4.52				$J(12-13) = 5.8$			$J(10\beta-11) = 6.6$			$J(10\beta-11) = 7.2$
NH	6.72				$J(12-13') = 5.1$	11	5.06	$J(10\alpha-11) = 6.6$			$J(11-12) = 8.0$
Ph	7.3[b]				$J(8-12) = 9.4$			$J(10\beta-11) = 6.6$	12	2.17	$J(8-12) = 10.0$
			13	3.58	$J(12-13) = 5.8$			$J(11-12) = 6.6$			$J(11-12) = 8.0$
					$J(13-13') = 9.3$	12	2.03	$J(8-12) = 6.9$			$J(12-13) = 8.0$
			13′	3.67	$J(12-13') = 5.1$			$J(11-12) = 6.6$	13	5.58	$J(13-14) = 15.5$
					$J(13-13') = 9.3$			$J(12-13) = 4.9$			$J(12-13) = 8.0$
			OH	3.17	$J(11-OH) = 3.3$			$J(12-13') = 4.7$			$J(13-15) = 0.8$
			OCH_2	4.55		13	3.58	$J(12-13) = 4.9$	14	5.66	$J(13-14) = 15.5$
			Ph	7.3[b]				$J(13-13') = 11.6$			$J(14-15) = 5.7$
						13	3.65	$J(12-13') = 4.7$	15	4.13	$J(15-16) = 6.2$
								$J(13-13') = 11.6$			$J(14-15) = 5.7$
						OH	2.54	$J(13-OH) = 4.5$			$J(13-15) = 0.8$
								$J(13'-OH) = 4.5$	16	1.52	
									17	1.29[b,g]	
									18	1.29[b,g]	
									19	1.29[b,g]	
									20	0.90	$J(19-20) = 6.7$
									NH	10.00	

[a]Spectra measured at 300 MHz. Coupling constants measured to first order.
[b]Centre of multiplet.
[c]H-8 and H-12 overlap.
[d]This assignment could be reversed.
[e]H-2, H-3, H-7α, H-8, and H-10β overlap.
[f]Broad singlet.
[g]H-17, H-18, and H-19 overlap.

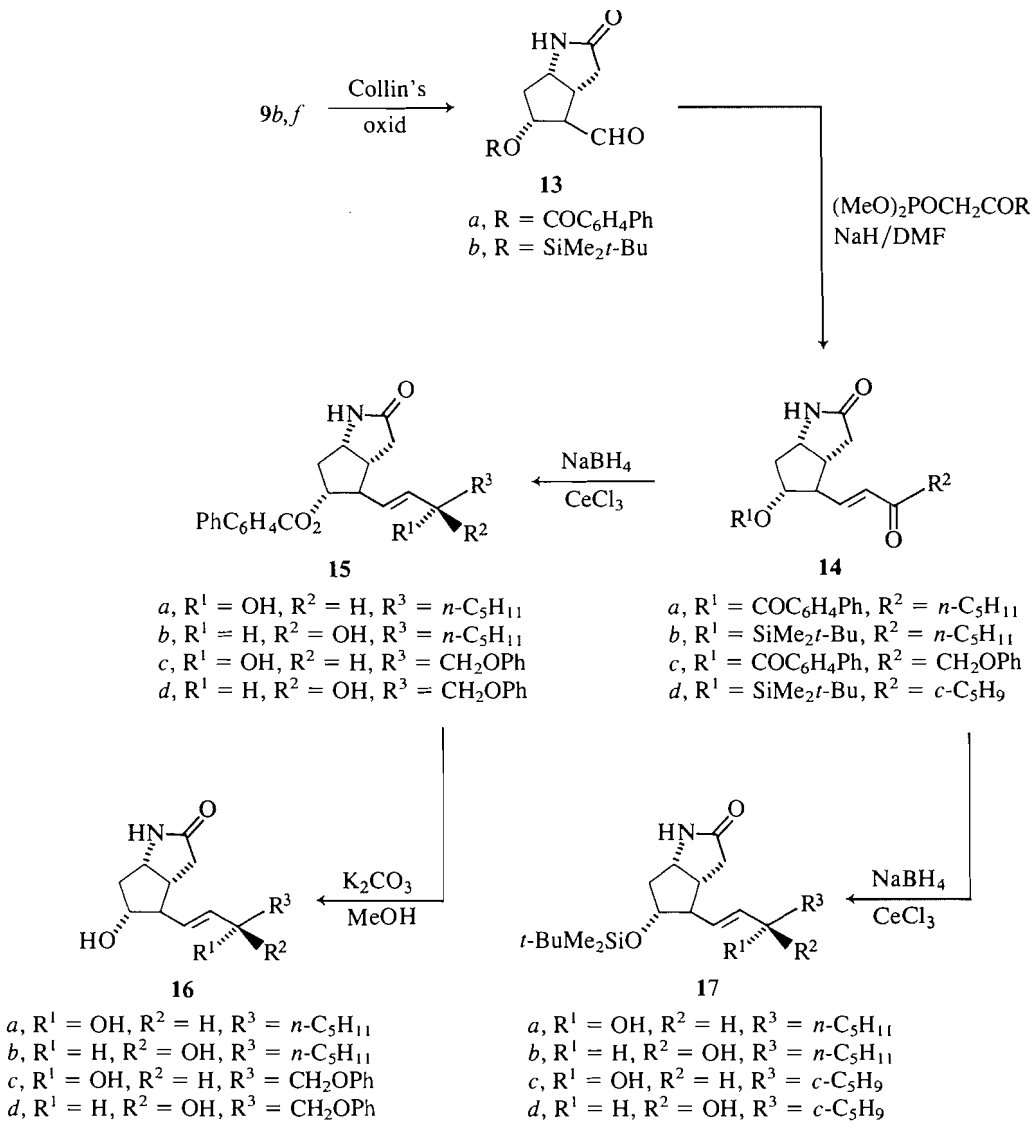

SCHEME 2

similarity, indicating a significant conformational congruence between these compounds. It is conceivable that the weak activity of these compounds is a consequence of the rigidity of the vinylogous amide system, which may not permit the carboxyl group to reach the required PGI_2 receptor binding site,[5] but other explanations are possible.

Experimental

The melting points were determined in a Mel-Temp melting point apparatus and are not corrected. The infrared spectra were measured in chloroform solution, unless specified otherwise, with a Perkin–Elmer Model 237 grating spectrophotometer. The ultraviolet spectra were recorded in methanol solution with a Perkin–Elmer Model 402 ultraviolet visible spectrometer. The nmr spectra were obtained with a Varian EM-390 or a Bruker WM 300 nmr spectrometer and are expressed as parts per million (δ) from internal tetramethylsilane. The high resolution mass spectra were measured with a Varian-MAT 311A mass spectrometer.

The terms "worked up in the usual manner" or "the usual work-up" signify that the extract was washed successively with water and saturated sodium chloride solution, then it was dried over magnesium sulfate, and the solvent was removed *in vacuo*.

[5]We thank a referee for this suggestion.

TABLE 2. Inhibition, in vitro, of ADP induced aggregation of HPRP by 3-oxo-9-deoxy-9-azaprostaglandin I_2 derivatives

Compound	Relative potency
PGE_1	1[a]
*23*a	0.032
*23*b	0.0008
*23*c	0.0047
*23*d	0.0007
*23*e	0.24
*23*f	0.0044

[a]$IC_{50} = 5.5 \pm 3.9 \times 10^{-8}$ *M*.

Methyl ω-bromolevulinate

Monomethyl succinate (87 g, 724 mmol) and thionyl chloride (103 mL) were heated together at 40°C for 2 h. The excess thionyl chloride was removed *in vacuo* and the residual oil was distilled at 77–80°C/4 Torr (1 Torr = 133.3 Pa) (95% yield). The acid chloride (6 g) was added dropwise at 0°C to ethereal diazomethane (2.5 equiv. in ether (58 mL)). One half hour after the addition was completed a stream of argon was passed through the solution to remove the excess diazomethane. The solvent was then removed *in vacuo* at room

Can. J. Chem. Downloaded from www.nrcresearchpress.com by 213.166.140.6 on 09/07/12
For personal use only.

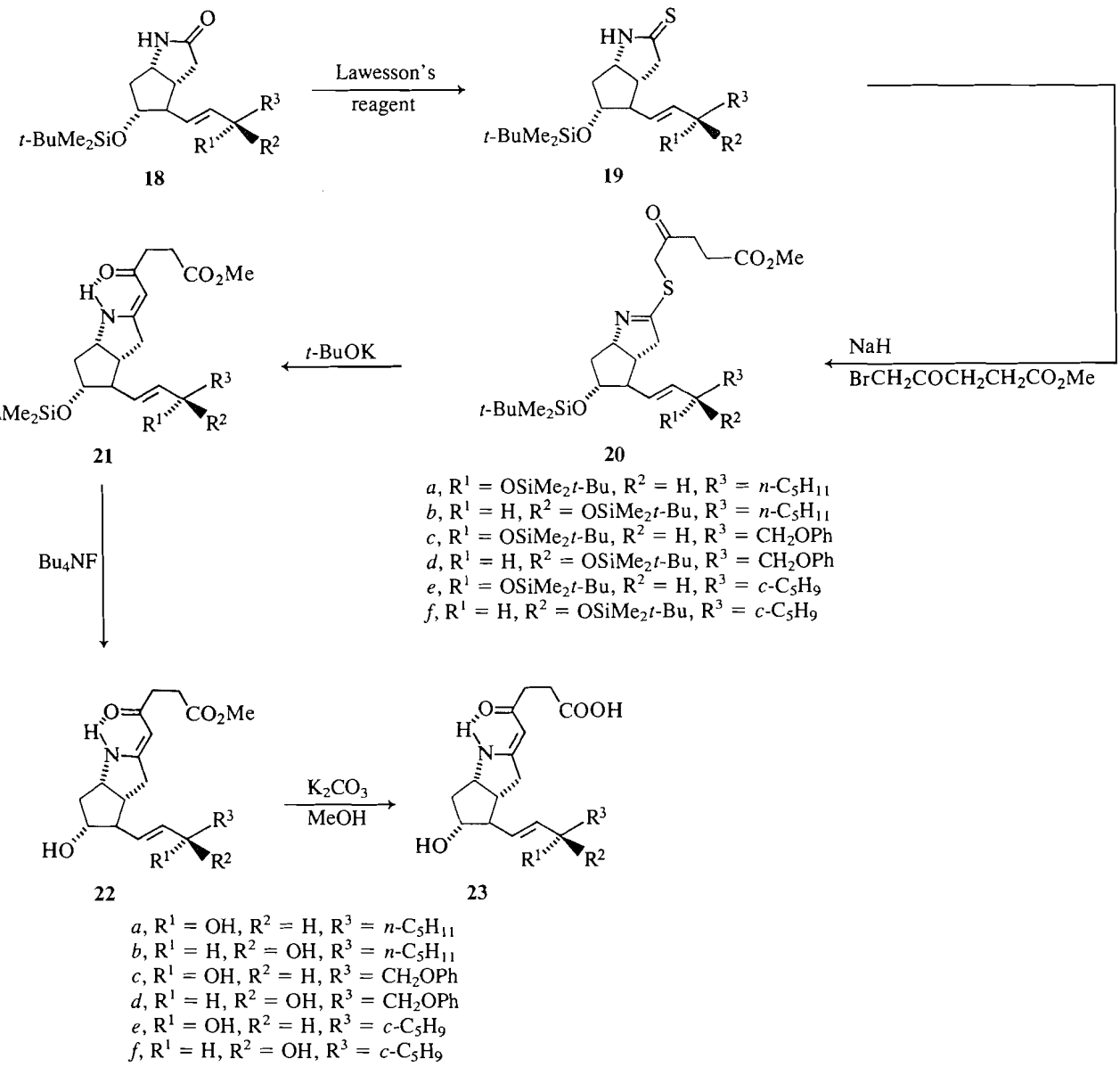

SCHEME 3

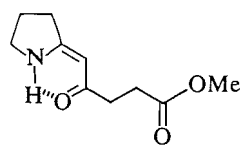

24

temperature and the residue was dissolved in ether (85 mL) and cooled to 0°C. An ethereal solution of 1.17 *M* hydrogen bromide (14.2 mL) was added and stirring was maintained for 1 h. The ether was washed with saturated sodium carbonate solution and then worked up as usual. The crude product was distilled at 66–70°C/0.3 Torr (85% yield). This oil solidifies (lit. (10) mp 4°C) in the refrigerator.

Synthesis of the trichloroacetamide **6**

A solution of the unsaturated alcoholic ester **5***a* (12.8 g, 82.6 mmol) in anhydrous ether (100 mL) was added at room temperature to a stirred suspension of sodium hydride (0.328 g, 8.2 mmol; 60% dispersion in mineral oil) in anhydrous ether (90 mL). When hydrogen evolution had terminated (20 min), the solution was cooled to −30°C and a solution of trichloroacetonitrile (8.3 mL, 11.9 g, 82 mmol) in dry ether (15 mL) was added slowly to the stirred solution. The reaction temperature was allowed to reach −10°C and after 25 min at this temperature methanol (1.5 mL) and pentane (750 mL) were added, the mixture was filtered to remove a small amount of a solid, and the filtrate was evaporated *in vacuo*. The crude[6] trichloroacetamidate **5***b* was dissolved in xylene

[6]If the crude trichloroacetamidate was subjected to flash chromatography on silica gel (50 g/g mixture) using hexane – ethyl acetate (4:1) as the eluting solvent, a sample of the pure imidate **5***b* could be isolated, in about 30% yield, as an oil; ir: 3350, 1735, 1665 cm^{-1}; nmr δ: 2.32 (m, 1H, H-12), 2.47 (dd, 1H, $J_{7A,8}$ = 8.0 Hz, $J_{7A,7B}$ = 20.4 Hz, H-7A), 2.57 (dd, 1H, $J_{7B,8}$ = 7.0 Hz, $J_{7A,7B}$ = 20.4 Hz, H-7B), 2.93 (m, 1H, H-8), 3.61 (d, 2H, *J* = 7.5 Hz, 13-CH_2), 3.66 (s, 3H, OMe), 4.54 (s, 2H, OCH_2), 5.66 (m, 1H, H-11), 5.95 (m, 1H, H-10), 6.08 (m, 1H, H-9), 7.32 (m, 5H, C_6H_5), 8.28 (s, 1H, NH); ms *m/e* (CI NH_3): 439, 437 (MNH_4^+), 420 (MH^+), 386 (MH^+ − Cl + H), 352 (386 − Cl + H). This material was not characterized further. Continued elution of the column gave an apparent mixture (3:1) as judged by tlc and nmr (ca. one-half, in weight terms, of the pure imidate), as an oil; ir: 3350, 1735, 1665 cm^{-1}; nmr δ: 2.14, 2.33, 2.46 (multiplets, total 3H), 2.89 (m, 1H), 3.55 (d, 1.5H, *J* = 6.3 Hz), 3.59 (d, 0.5H, *J* = 6.4 Hz), 3.64 (s, 1H, OCH_3), 4.51, 4.53 (singlets, total 2H, OCH_2), 5.54 (bs, 0.75H), 5.66 (bs, 0.25H), 5.75 (m, 0.75H), 5.94 (m, 1H), 6.06 (m, 0.25H), 7.29 (m, 5H, C_6H_5), 8.27

Can. J. Chem. Downloaded from www.nrcresearchpress.com by 213.166.140.6 on 09/07/12
For personal use only.

Can. J. Chem. Downloaded from www.nrcresearchpress.com by 213.166.140.6 on 09/07/12
For personal use only.

(250 mL) and the solution was heated at reflux temperature (133°C in Mexico City) for 6 h. The solvent was removed *in vacuo* and the residue was dissolved in anhydrous methanol (328 mL) and anhydrous potassium carbonate (18.7 g, 135 mmol) was added thereto. The mixture was stirred at room temperature for 2.5 h, it was then cooled to 0°C and 1 *M* hydrochloric acid was added until a neutral solution was obtained. The methanol was removed *in vacuo* and the aqueous phase was extracted with ethyl acetate. After the usual work-up the crude product was subjected to column chromatography on silica gel. Elution with hexane – ethyl acetate (9:1) gave the crystalline trichloroacetamide **6** (18.7 g). Elution with hexane – ethyl acetate (85:15) gave the starting ester **5***a* (7.1 g, 33%). The yield of the trichloroacetamide, based on trichloroacetonitrile, was 54%. After crystallization from dichloromethane–hexane the amide **6** had mp 81–82°C; ir: 3460, 1730 cm^{-1}; nmr δ: 2.40–3.15 (m, 4H, 7-CH_2, H-8,12[7]), 3.43 (d, 2H, J = 6 Hz, 13-CH_2), 3.63 (s, 3H, OMe), 4.50 (s, 2H, OCH_2), 5.13 (m, 1H, H-9), 5.70 (m, 1H, H-10), 5.98 (m, 1H, H-11), 7.05 (bs, 1H, NH), 7.30 (s, 5H, C_6H_5). *Anal.* calcd. for $C_{18}H_{20}Cl_3NO_4$: C 51.38, H 4.79, Cl 25.28, N 3.33; found: C 51.65, H 4.72, Cl 25.13, N 3.30.

Sodium borohydride induced reductive cyclization of **6** *to bicyclic lactam* **7**

A solution of sodium borohydride (3.39 g, 95 mmol) in anhydrous ethanol (118 mL) was added to a stirred solution of **6** (10.0 g, 23.7 mmol) in ethanol (115 mL) maintained in a heating bath at 60°C in an argon atmosphere. The rate of addition was controlled so that the reaction temperature did not exceed 70°C. When the addition was completed, stirring was continued for a further 0.5 h and then the mixture was cooled to 0°C. Acetone (225 mL) was added and after stirring for 15 min the mixture was evaporated to dryness and the residue was extracted with ethyl acetate. The extract was worked up as usual and the crude product was purified by preparative tlc on silica gel using dichloromethane–ether (1:1) as the developing solvent. The crystalline bicyclic lactam **7** (4.6 g, 80%) was obtained, which after crystallization from ether had mp 56–57°C; ir: 3450, 1690 cm^{-1}; nmr (see Table 1). *Anal.* calcd. for $C_{15}H_{17}NO_4 \cdot 0.33H_2O$: C 72.26, H 7.14, N 5.62; found: C 71.84, H 6.84, N 5.58.

Synthesis of the bromohydrin **8**a

N-Bromosuccinimide (13.2 g, 74 mmol) was added to a cooled (10°C) stirred solution of the unsaturated lactam (9.0 g, 36.9 mmol) in dimethylsulfoxide (162 mL) containing water (18 mL). The reaction mixture was stirred at 20°C for 1 h, the dimethylsulfoxide was removed *in vacuo* (40°/0.4 Torr), and the residue was diluted with saturated aqueous sodium potassium tartarate solution (40 mL). The product was extracted into a 1:1 ether – ethyl acetate solution, the extract was worked up as usual, and the product was purified by tlc on silica gel using ethyl acetate – dichloromethane (9:1) as the developing solvent. The bromohydrin **8***a* was obtained as a solid (5.2 g, 72%) that, after crystallization from ether–hexane, had mp 89–90°C; ir: 3450, 3300, 1700 cm^{-1}; nmr (see Table 1). *Anal.* calcd. for $C_{15}H_{18}BrNO_3 \cdot 0.5H_2O$: C 51.78, H 5.48, Br 22.88, N 4.01; found: C 51.71, H 5.38, Br 22.58, N 4.07.

Conversion of the bromohydrin **8**a *to the diol monoacetate* **9**b

A solution of the bromohydrin **8***a* (0.750 g, 2.2 mmol) in pyridine (1.8 mL) and acetic anhydride (0.8 mL) was stirred at room temperature for 2 h. The solution was diluted with water, the product was extracted into ethyl acetate, and the extract was washed with 2% aqueous sodium bicarbonate solution, dried, and evaporated *in vacuo*. The residue was purified by preparative tlc on silica gel using ethyl acetate – dichloromethane (1:1) as the developing solvent. The acetate **8***b* (0.600 g, 72%) was obtained as an oil; ir: 3430, 1745, 1710 cm^{-1}; nmr δ: 1.90–3.15 (m, 4H), 2.06 (s, 3H, CH_3), 3.36–3.73 (m, 2H, CH_2O), 3.86–4.30 (m, 2H), 4.50 (s, 2H, OCH_2Ph), 5.37 (m, 1H, H-11), 6.80 (bs, 1H, NH), 7.33 (s, 5H, Ph). This material was used without further characterization as follows. A solution of the acetate **8***b* (0.600 g, 1.6 mmol) in toluene (15 mL) containing tri-*n*-butyltin hydride (0.727 g, 2.5 mmol) and azobisisobutyronitrile (0.003 g) was heated at 60°C for 1 h. The solvent was removed *in vacuo*, the residue was dissolved in acetonitrile and this solution was extracted with hexane. The acetonitrile phase was evaporated *in vacuo* and the residue was purified by tlc on silica gel using ethyl acetate as the developing solvent. The debrominated acetate **9***a* (0.370 g, 78%) was isolated as an oil; ir: 3440, 1730, 1690 cm^{-1}; nmr δ: 1.60–2.83 (m, 6H), 2.00 (s, 3H, CH_3), 3.50 (d, 2H, J = 4.5 Hz, CH_2O), 4.50 (s, 2H, OCH_2Ph), 5.03 (m, 1H, H-11), 6.53 (bs, 1H, NH), 7.33 (s, 5H, Ph). This compound was used without further characterization. A solution of **9***a* (0.350 g, 1.15 mmol) in ethyl acetate (20 mL) containing suspended 10% palladium on charcoal catalyst (0.070 g) was stirred under hydrogen at atmospheric pressure until 1 equivalent of hydrogen was absorbed (2.5 h). The mixture was filtered through Celite, the filtrate was evaporated *in vacuo*, and the residue was purified by tlc on silica gel using ethyl acetate – methanol (9:1) as the developing solvent. After crystallization from hexane–dichloromethane the diol monoacetate **9***b* (0.200 g, 82%) had mp 74–76°C; ir: 3400, 1730, 1700 cm^{-1}; nmr δ (see Table 1); *m/e*: 213.1001 (calcd. for $C_{10}H_{15}NO_4$: 213.1000).

Synthesis of the p*-phenylbenzoate* **8**c

4-Phenylbenzoyl chloride (6.65 g, 30.6 mmol) was added to a solution of the bromohydrin **8***a* (8.7 g, 25.6 mmol) in dry pyridine (31 mL). After stirring for 2 h at room temperature water (3 mL) was added and the mixture was stirred for a further 1 h. The pyridine was removed *in vacuo*, dichloromethane was added to the residue, and the mixture was filtered through a pad of Celite. The filtrate was washed with 10% hydrochloric acid and then worked up in the usual way. The crude product was subjected to column chromatography on neutral alumina (Fluka, Act. II) using dichloromethane as the eluant. The pure material (9.5 g, 71%) was obtained as a solid that, after crystallization from dichloromethane, had mp 131–133°C; ir: 3420, 1710 cm^{-1}; nmr δ: 2.10–3.16 (m, 4H, H-8,12), 3.60 (m, 2H, 13-CH_2), 4.00–4.33 (m, 2H, H-9,10), 4.47 (s, 2H, OCH_2Ph), 5.60 (t, 1H, J = 6 Hz, H-11), 6.80 (s, 1H, NH), 7.30 (s, 5H, Ph), 7.33–8.26 (m, 9H, C_6H_4–C_6H_5). *Anal.* calcd. for $C_{28}H_{26}BrNO_4$: C 64.61, H 5.03, Br 15.35, N 2.69, found: C 64.53, H 5.05, Br 15.38, N 2.60.

Synthesis of the tert*-butyldimethylsilyl ether* **8**d

tert-Butyldimethylsilyl chloride (1.60 g, 10.6 mmol) and imidazole (1.86 g, 27.4 mmol) were added to a stirred solution of the bromohydrin (1.00 g, 2.94 mmol) in dry dimethylformamide (14 mL). After 3 h at room temperature the solution was diluted with water and extracted with ethyl acetate. After the usual work-up the crude material was purified by tlc on silica gel using dichloromethane – ethyl acetate (1:1) as the developing solvent. The product (0.866 g, 65%) was obtained as a solid that, after crystallization from dichloromethane–hexane, had mp 106–108°C; ir: 3450, 1700 cm^{-1}; nmr δ: 0.07 (s, 3H, MeSi), 0.16 (s, 3H, MeSi), 0.86 (s, 9H, Me_3CSi), 1.70–3.06 (m, 4H, 7-CH_2, H-8,12), 3.55 (d, 2H, J = 4.5 Hz, 13-CH_2), 3.78 (m, 1H, H-11), 3.96–4.26 (m, 2H, H-9,10), 4.48 (s, 2H, OCH_2Ph), 6.60 (s, 1H, NH), 7.30 (s, 5H, Ph). *Anal.* calcd. for $C_{21}H_{32}BrNO_3Si$: C 55.49, H 7.19, Br 17.58, N 3.08; found: C 55.58, H 7.39, Br 17.69, N 3.06.

Reductive debromination of the p*-phenylbenzoate* **8**c *to* **9**c

A solution of the bromo compound **8***c* (8.50 g, 16.3 mmol) in dry benzene (140 mL) containing tri-*n*-butyltin hydride (5.82 g, 20 mmol) and azobisisobutyronitrile (0.028 g) was heated at 60°C for 4 h. The solvent was removed *in vacuo* and the residue was dissolved in acetonitrile (400 mL). The solution was washed several times with hexane (discarded) and then evaporated *in vacuo*. The residue was subjected to column chromatography on neutral aluminia (Fluka, Act

(s, 0.25H, NH). Meaningful mass spectra could not be obtained for this material. It was not characterized further.

When the pure imidate **5***b* was heated in dry xylene as described in the body of the experimental section, the pure trichloroacetamide **6** was obtained directly in 80% yield. When the above mixture was subjected to the same conditions, it was transformed into the trichloroacetamide **6** (40%) and the starting ester **5***a* (30%), but only after treatment with methanolic potassium carbonate.

[7]Prostaglandin numbering system.

Can. J. Chem. Downloaded from www.nrcresearchpress.com by 213.166.140.6 on 09/07/12
For personal use only.

TABLE 3. Purification conditions, yields, and physical constants of 9-azaprostacyclins and precursors thereof

Compd. no.	Purification process[a]	R_f	Yield (%)	Melting point (°C)	Cryst. solvent	Molecular formula	Calcd. C	Calcd. H	Calcd. N	Found C	Found H	Found N
14*a*	tlc;[b] CH_2Cl_2–A[c] (1:1)	0.52	29	150–151	CH_2Cl_2–MeOH	$C_{28}H_{31}NO_4$	73.98	7.09	3.14[d]	74.09	6.80	3.10
14*b*	tlc; CH_2Cl_2–A (7:3)	0.46	59	100–102	CH_2Cl_2–hexane	$C_{21}H_{37}NO_3Si$	66.44	9.82	3.68	66.20	9.87	3.63
14*c*	tlc; EtOAc	0.16	19	166–168	CH_2Cl_2–MeOH	$C_{30}H_{27}NO_5$	73.45	5.75	2.86[d]	73.36	5.72	2.75
14*d*	tlc; CH_2Cl_2–A (3:1)	0.42	68	146–148	CH_2Cl_2–hexane	$C_{21}H_{35}NO_3Si$	66.79	9.34	3.70	66.50	9.40	3.50
15*a*	tlc; CH_2Cl_2–A (1:1)	0.50	38	151–152	Ether–hexane	$C_{28}H_{33}NO_4$	75.13	7.43	3.13	74.97	7.35	3.10
15*b*	tlc; CH_2Cl_2–A (1:1)	0.34	34	181–182	Ether–hexane	$C_{28}H_{33}NO_4$	75.13	7.43	3.13	74.90	7.36	3.10
15*c*	tlc; CH_2Cl_2–A (4:1)	0.54	37	154–156	CH_2Cl_2–hexane	$C_{30}H_{29}NO_5$	73.60	6.11	2.88[e]	73.79	6.35	2.84
15*d*	tlc; CH_2Cl_2–A (4:1)	0.40	32	158–160	CH_2Cl_2–hexane	$C_{30}H_{29}NO_5$	72.71	6.17	2.83[f]	72.87	6.17	3.19
16*a*	tlc; CH_2Cl_2–A (1:1)	0.29	83	146–148	Ether–MeOH	$C_{15}H_{25}NO_3$	67.38	9.42	5.24	67.14	9.20	4.96
16*b*	tlc; A	0.23	83	138–140	Ether–MeOH	$C_{15}H_{25}NO_3$	67.38	9.42	5.24	67.21	9.31	4.98
16*c*	tlc; A	0.38	85	123–125	Ether–hexane	$C_{17}H_{21}NO_4$	67.30	6.98	4.62	66.99	6.98	4.31
16*d*	tlc; A	0.30	83	146–148	CH_2Cl_2–hexane	$C_{17}H_{21}NO_4$	67.30	6.98	4.62	67.00	7.04	4.76
17*a*	tlc; CH_2Cl_2–A (7:3)	0.52	60	86–87	CH_2Cl_2–hexane	$C_{21}H_{39}NO_3Si$	66.09	10.30	3.66	66.15	9.96	3.62
17*b*	tlc; CH_2Cl_2–A (7:3)	0.41	23	146–147	CH_2Cl_2–hexane	$C_{21}H_{39}NO_3Si$	66.09	10.30	3.66	66.14	10.22	3.88
17*c*	fc;[g] EtOAc–hexane (1:1)		68	98–99	Ether–hexane	$C_{21}H_{37}NO_3Si$	66.44	9.82	3.68	66.18	9.66	3.68
17*d*	fc; EtOAc–hexane (1:1)		23	147–148	Ether–hexane	$C_{21}H_{37}NO_3Si$	66.44	9.82	3.68	66.34	9.74	3.59
18*a*	tlc; CH_2Cl_2–EtOAc (95:5)	0.48	72	82–83	Ether–hexane	$C_{27}H_{53}NO_3Si_2$	65.52	10.99	2.82	65.42	11.01	2.72
18*b*	tlc; EtOAc	0.32	68	98–99	Ether–hexane	$C_{27}H_{53}NO_3Si_2$	65.52	10.99	2.82	65.21	10.85	2.69
18*c*	tlc; EtOAc	0.34	76	130–132	CH_2Cl_2–hexane	$C_{29}H_{49}NO_4Si_2$[h]						
18*d*	tlc; EtOAc–CH_2Cl_2 (7:3)	0.21	78	Oil		$C_{29}H_{49}NO_4Si_2$[i]						
18*e*	cc; CH_2Cl_2–EtOAc (9:1)		87	127–128	CH_2Cl_2–hexane	$C_{27}H_{51}NO_3Si_2$	65.66	10.40	2.83	65.61	10.37	2.63
18*f*	cc; CH_2Cl_2–EtOAc (9:1)		88	159–160	CH_2Cl_2–hexane	$C_{27}H_{51}NO_3Si_2$	65.66	10.40	2.83	65.54	10.23	2.63
19*a*	tlc; CH_2Cl_2	0.20	70	Oil		$C_{27}H_{53}NO_2SSi_2$	63.35	10.43	2.73	63.45	10.40	2.57
19*b*	tlc; CH_2Cl_2	0.18	72	85–86	CH_2Cl_2	$C_{27}H_{53}NO_2SSi_2$	63.35	10.43	2.73	63.49	10.49	2.62
19*c*	tlc; CH_2Cl_2–EtOAc (95:5)	0.54	80	Oil		$C_{29}H_{49}NO_3SSi_2$[j]						
19*d*	tlc; CH_2Cl_2–EtOAc (95:5)	0.50	82	Oil		$C_{29}H_{49}NO_3SSi_2$[k]						
19*e*	tlc; hexane–EtOAc (7:3)	0.31	71	146–147	CH_2Cl_2–hexane	$C_{27}H_{51}NO_2SSi_2$	63.59	10.08	2.74	63.41	9.90	2.65
19*f*	tlc; hexane–EtOAc (7:3)	0.31	67	141–142	Ether–hexane	$C_{27}H_{51}NO_2SSi_2$	63.59	10.08	2.74	63.40	9.92	2.85
21*a*	tlc; CH_2Cl_2–ether (95:5)	0.27	64	Oil		$C_{33}H_{61}NO_5Si_2$	65.17	10.11	2.03	65.25	9.82	1.91
21*b*	tlc; CH_2Cl_2–ether (95:5)	0.24	56	Oil		$C_{33}H_{61}NO_5Si_2$	65.17	10.11	2.03	65.16	9.83	2.04
21*c*	tlc; CH_2Cl_2–ether (9:1)	0.26	68	Oil		$C_{35}H_{57}NO_6Si_2$[l]						
21*d*	tlc; CH_2Cl_2–ether (9:1)	0.16	73	Oil		$C_{35}H_{57}NO_6Si_2$	65.27	8.92	2.19	65.20	8.87	2.10
21*e*	cc; CH_2Cl_2–ether (95:5)		66	Oil		$C_{33}H_{59}NO_5Si_2$	65.40	9.81	2.31	65.19	9.60	2.10
21*f*	cc; CH_2Cl_2–ether (95:5)		68	Oil		$C_{33}H_{59}NO_5Si_2$	65.40	9.81	2.31	65.08	9.56	1.71

Can. J. Chem. Downloaded from www.nrcresearchpress.com by 213.166.140.6 on 09/07/12
For personal use only.

TABLE 3 (*concluded*)

Compd. no.	Purification process[a]	R_f	Yield (%)	Melting point (°C)	Cryst. solvent	Molecular formula	Calcd. C	Calcd. H	Calcd. N	Found C	Found H	Found N
22*a*	tlc; CH_2Cl_2–A (1:1)	0.34	82	72–73	Ether	$C_{21}H_{33}NO_5$	66.46	8.76	3.68	66.25	8.53	3.61
22*b*	tlc; CH_2Cl_2–A (1:1)	0.30	73	Oil		$C_{21}H_{33}NO_5$[m]						
22*c*	tlc; CH_2Cl_2–A (1:1)	0.26	78	Oil		$C_{23}H_{29}NO_6$[n]						
22*d*	tlc; CH_2Cl_2–A (1:1)	0.16	77	Foam		$C_{23}H_{29}NO_6$[o]						
22*e*	tlc; CH_2Cl_2–A (1:1)	0.30	95	Oil		$C_{21}H_{31}NO_5$	66.81	8.28	3.71	66.91	8.17	3.53
22*f*	tlc; CH_2Cl_2–A (1:1)	0.30	91	Oil		$C_{21}H_{31}NO_5$	66.81	8.28	3.71	66.83	8.11	3.56
23*a*	catlc; B		74	Oil		$C_{20}H_{31}NO_5$[p]	65.73	8.55	3.83			
23*b*	Crystallization		76	118–120	Ether–hexane	$C_{20}H_{31}NO_5$	65.73	8.55	3.83	65.56	8.40	3.64
23*c*	catlc; B		92	Oil		$C_{22}H_{27}NO_6$	65.82	6.78	3.49	65.60	6.78	3.38
23*d*	catlc; B		90	69–70	Ether–hexane	$C_{22}H_{27}NO_6$	65.82	6.78	3.49	65.58	6.63	3.40
23*e*	tlc; B	0.16	60	112–114	Ether–hexane	$C_{20}H_{29}NO_5$	66.09	8.04	3.81	65.90	7.89	3.70
23*f*	tlc; B	0.16	45	Oil		$C_{20}H_{29}NO_5$	66.09	8.04	3.81	66.19	7.90	3.90

[a]Chromatographic separations using silica gel as stationary phase.
[b]tlc = thin-layer chromatography, cc = column chromatography; fc = flash chromatography, catlc = centrifically accelerated tlc.
[c]A = CH_2Cl_2–MeOH – conc. NH_4OH (60:10:1); B = CH_2Cl_2–MeOH–HOAc (60:10:1). The R_f values were measured on 2.5 × 10 cm plates coated with silica gel GF-254 (0.2 mm).
[d]*Anal.* calcd. for hemihydrate.
[e]*Anal.* calcd. for 1/3 H_2O.
[f]*Anal.* calcd. for 2/3 H_2O.
[g]Silica gel, Merck no. 9385.
[h]*m/e* 516.2965 (calcd. for $C_{29}H_{49}NO_4Si_2 - CH_3$: 516.2962).
[i]*m/e* 516.2967 (calcd. for $C_{29}H_{49}NO_4Si_2 - CH_3$: 516.2962).
[j]*m/e* 490.2278 (calcd. for $C_{29}H_{49}NO_3SSi_2 - C_4H_9$: 490.2267).
[k]*m/e* 490.2287 (calcd. for $C_{29}H_{49}NO_3SSi_2 - C_4H_9$: 490.2267).
[l]*m/e* 643.3724 (calcd. for $C_{35}H_{57}NO_6Si_2$: 643.3717).
[m]*m/e* 379.2358 (calcd. for $C_{21}H_{33}NO_5$: 379.2358).
[n]*m/e* 415.1993 (calcd. for $C_{23}H_{29}NO_6$: 415.1995).
[o]*m/e* 415.1997 (calcd. for $C_{23}H_{29}NO_6$: 415.1995).
[p]*m/e* 365.2200 (calcd. for $C_{20}H_{31}NO_5$: 365.2202).

Can. J. Chem. Downloaded from www.nrcresearchpress.com by 213.166.140.6 on 09/07/12
For personal use only.

II) using dichloromethane as the eluant. The product **9***c* was isolated as a solid (6.10 g, 85%) that on crystallization from dichloromethane–hexane, had mp 145–146°C; ir: 3460, 1695 cm^{-1}; nmr δ: 2.10–2.86 (m, 4H, 7-CH_2, H-8,12), 3.51 (d, 2H, J = 6 Hz, 13-CH_2), 4.13 (m, 1H, H-9), 4.50 (s, 2H, OCH_2Ph), 5.35 (dd, 1H, $J \simeq 4.5$ Hz, H-11), 6.50 (s, 1H, NH), 7.28 (s, 5H, Ph), 7.20–8.50 (m, 9H, $C_6H_4C_6H_5$). *Anal.* calcd. for $C_{28}H_{27}NO_4$: C 76.06, H 6.16, N 3.17; found: C 75.88, H 6.17, N 3.08.

Reductive debromination of the tert*-butyldimethylsilyl ether 8*d *to 9*e

The debromination of **8***d* was effected in the same manner as described for **8***c* except that the reaction was carried out at 70°C for 2 h and the product, obtained in 95% yield, was purified by crystallization from dichloromethane–hexane. It had mp 108–110°C; ir: 3460, 1695 cm^{-1}; nmr δ: 0.10 (s, 6H, Me_2Si), 0.86 (s, 9H, Me_3CSi), 1.20–2.73 (m, 4H, 7-CH_2, H-8,12), 3.44 (d, 2H, J = 4.5 Hz, 13-CH_2), 3.80–4.20 (m, 2H, H-9,11), 4.46 (s, 2H, OCH_2Ph), 5.53 (s, 1H, NH), 7.30 (s, 5H, Ph). *Anal.* calcd. for $C_{21}H_{33}NO_3Si$: C 67.15, H 8.85, N 3.72; found: C 67.03, H 8.71, N 3.60.

*Hydrogenolysis of 9*c *to 9*d

A stirred solution of the benzyl ether **9***c* (8.70 g, 19.7 mmol) in dimethyoxyethane (75 mL) containing 70% perchloric acid (1.3 mL) and suspended 10% palladium on charcoal catalyst (3.1 g) was hydrogenated at room temperature and atmospheric pressure until hydrogen absorption ceased (10 h). The mixture was filtered through Celite, the filtrate was evaporated *in vacuo*, and the residue was dissolved in dichloromethane. This solution was worked up in the usual way to give the alcohol **9***d* as a solid (6.50 g, 94%) that, on crystallization from ethyl acetate – methanol, had mp 175–178°C; ir: 3480, 1695 cm^{-1}; nmr δ: 2.00–2.96 (m, 6H), 3.60 (m, 2H, 13-CH_2), 4.20 (m, 1H, H-9), 5.36 (q, $J \simeq 6$ Hz, H-11), 5.80 (s, 1H, NH), 7.33–7.66 (m, 5H, Ph), 7.89 (q, 4H, J_o = 7.5 Hz, C_6H_4). *Anal.* calcd. for $C_{21}H_{21}NO_4 \cdot 0.5H_2O$: C 69.98, H 6.15, N 3.89; found: C 70.00, H 5.87, N 3.89.

*Hydrogenolysis of 9*e *to 9*f

A stirred solution of the benzyl ether **9***e* (0.750 g, 2 mmol) in ethyl acetate (40 mL) containing suspended 10% palladium on carbon catalyst (0.15 g) was hydrogenated as described for the synthesis of **9***d* (18 h). After filtration of the mixture through Celite and evaporation of the filtrate *in vacuo*, the residue was purified by tlc on silica gel using ethyl acetate – methanol (98:2) as the developing solvent. The solid product (0.432 g, 76%), on crystallization from dichloromethane–hexane, had mp 80–82°C; ir: 3440, 3250, 1690 cm^{-1}; nmr δ: 0.07 (s, 6H, Me_2Si), 0.86 (s, 9H, Me_3CSi), 1.20–2.73 (m, 4H), 3.55 (d, 2H, J = 6 Hz, 13-CH_2), 3.80–4.20 (m, 2H, H-9,11). *Anal.* calcd. for $C_{14}H_{27}NO_3Si$: C 58.90, H 9.53, N 4.90; found: C 58.65, H 9.86, N 4.72.

Synthesis of the enones 14

(a) n*-Amyl enone 14*a

Collins reagent (22.7 g) and a suspension of the alcohol **9***d* (3.50 g, 10 mmol) in dry dichloromethane (100 mL) were added successively to a stirred suspension of Celite (45.4 g, dried at 125°C for 24 h) in anhydrous dichloromethane (300 mL) at 0°C. The reaction mixture was stirred at 5°C for 15 min, sodium bisulfate dihydrate (45.4 g) was added, and agitation was continued for a further 10 min at 5°C. The mixture was filtered through a pad of anhydrous magnesium sulfate, the filtrate was evaporated *in vacuo*, and the residual aldehyde **13***a* (~3.5 g) was used directly as follows. Dimethyl 2-oxoheptylphosphonate (2.09 g, 9.4 mmol) dissolved in dry dimethoxyethane (47 mL) was added to a stirred suspension of sodium hydride (obtained from a 60% dispersion in mineral oil (0.378 g, 9.4 mmol) washed with dry hexane) in anhydrous dimethoxyethane (112 mL). After 0.5 h at room temperature a solution of the above aldehyde (3.5 g) in dry dimethoxyethane (50 mL) was added and the mixture was stirred at room temperature for 2.5 h. Acetic acid (0.54 mL) was added, the solvent was removed *in vacuo*, and ethyl acetate was added to the residue. The mixture was filtered through Celite, the filtrate was dried, and the solvent was removed *in vacuo*. The residue was purified by the process indicated in Table 3. The yield, mp, solvent of crystallization, and elemental analysis are also found in this table.

*(b) Silylated enone 14*b

The synthesis of this compound was carried out as described for **14***a* except that the quantities of the phosphonate (0.490 g, 1.9 mmol), 60% sodium hydride (0.070 g, 1.75 mmol), and the crude aldehyde **13***b* (derived from 1.4 mmol (0.400 g) of the alcohol **9***f*) were slightly different and the reaction time was 1 h. See Table 3 for purification and physical constants; uv: 236 (10 700) nm; ir: 3460, 1700, 1670 cm^{-1}; nmr δ: 0.03 (s, 6H, Me_2Si), 0.73–1.03 (m, 12H), 1.16–2.80 (m, 14H), 3.77–4.20 (m, 2H, H-9,11), 6.15 (d, 1H, $J_{13,14}$ = 16 Hz, H-14), 6.63 (dd, 1H, $J_{12,13}$ = 7.5 Hz, $J_{13,14}$ = 16 Hz, H-13), 6.80 (s, 1H, NH).

*(c) 16-Phenoxy enone 14*c

The synthesis of this enone was carried out as described for **14***b* except that the phosphonate was dimethyl-2-oxo-3-phenoxypropylphosphonate and the reaction time was 3 h.

*(d) Cyclopentyl enone 14*d

This enone was prepared in the same manner as described for **14***b* except that dimethyl 2-oxo-2-cyclopentylethylphosphonate was used and the reaction time was 1.5 h.

Sodium borohydride reduction of the enones 14

*(a) Synthesis of 15*a *and 15*b

Methanolic cerous chloride hexahydrate (1.35 mL of a 0.4 *M* solution; 0.54 mmol) was added, at 0°C, to a stirred solution of the enone **14***a* (1.30 g, 2.9 mmol) in tetrahydrofuran (25 mL). Immediately thereafter, sodium borohydride (0.133 g, 3.5 mmol) was added in four equal portions at 1-min intervals. Stirring was continued for 7 min and then water (15 mL) was added and the reaction mixture was extracted with ethyl acetate. After the usual work-up, the crude product was purified as indicated in Table 3. The physical constants of the less polar 15α alcohol **15***a* and the more polar **15**β alcohol **15***b* are also found in Table 3.

*(b) Synthesis of 17*a *and 17*b *from 14*b

This reduction was effected as described above for **14***a* except that the enone (0.300 g, 0.79 mmol) was dissolved in methanol (28 mL) and was reacted with 0.4 *M* methanolic cerous chloride hexahydrate (0.3 mL) and sodium borohydride (0.030 g, 0.79 mmol). The mixture was separated by tlc as indicated in Table 3 to give the 15α (less polar) and 15β (more polar) alcohols **17***a* and **17***b*. Compound **17***a* had the following spectroscopic properties: ir: 3610, 3460, 1695 cm^{-1}; nmr δ: 0.03 (s, 6H, Me_2Si), 0.73–1.00 (m, 12H), 1.13–2.66 (m, 14H), 3.66–4.23 (m, 3H, H-9,11,15), 5.40–5.63 (m, 2H, H-13,14), 6.73 (bs, 1H, NH).

*(c) Synthesis of 15*c *and 15*d *from 14*c

This reduction was carried out as described for **14***a* except that the enone was dissolved in a tetrahydrofuran (30 mL/g enone) – methanol (10 mL/g enone) solvent mixture. The mixture of alcohols produced was separated by tlc on silica gel using the solvent system indicated in Table 3.

*(d) Reduction of 14*d *to 17*c *and 17*d

This reduction was carried out as described for **14***c* except that the enone **14***d* (3.6 g, 9.65 mmol) in methanol (100 mL) was reacted with 0.4 *M* methanolic cerous chloride hexahydrate (25 mL, 10 mmol) and sodium borohydride (0.377 g, 9.9 mmol). The mixture of alcohols obtained was separated by flash chromatography on silica gel (Merck, no. 9385) using hexane – ethyl acetate (1:1) as the eluting solvent.

Hydrolysis of the esters 15 to the diols 16

The conversion of **15***a* to **16***a* was typical. A solution of the *p*-phenylbenzoate **15***a* (0.500 g, 1.12 mmol) in absolute methanol (10 mL) containing anhydrous potassium carbonate (0.154 g, 1.12 mmol) was stirred at room temperature for 3 h. The solution was cooled

Can. J. Chem. Downloaded from www.nrcresearchpress.com by 213.166.140.6 on 09/07/12
For personal use only.

to 0°C, neutralized with 1 *M* hydrochloric acid (2.2 mL), and the methanol was removed *in vacuo*. The residue was mixed with ethyl acetate, and the organic phase was washed with 10% sodium bicarbonate solution and then worked up in the usual way. The crude diol was purified as indicated in Table 3. After crystallization, the less polar diol **16***a* had the following spectroscopic properties: ir: 3620, 3450, 1680 cm^{-1}; nmr δ: 0.88 (t, 3H, J = 6 Hz, 20-CH_3), 1.03–2.66 (m, 14H), 3.97 (m, 3H, H-9,11,15), 5.53 (m, 2H, H-13,14), 7.04 (bs, 1H, NH).

The diols **16***b*, **16***c*, and **16***d* were prepared as described above for **16***a* except that a mixture of methanol (10 mL) and tetrahydrofuran (2 mL) was used as the solvent for a reaction carried out on a 1-mmol scale.

*Synthesis of the bis-*tert*-butyldimethylsilyl compounds **18***

Imidazole (10 mmol) and *tert*-butyldimethylsilyl chloride (5 mmol) were added to a stirred solution of the diol **16** or monosilylated diol **17** (1 mmol) in anhydrous DMF (25–35 mL/g alcohol). After reaction for 1–3 h, the solution was diluted with water and the product was extracted with ethyl acetate or a 1:1 benzene – ethyl acetate mixture (for **18***e* and **18***f*). After the usual work-up, the crude products were purified as indicated in Table 2. Compound **18***a* had the following spectroscopic properties: ir: 3450, 1698 cm^{-1}; nmr δ: 0.03 (s, 12H, Me_2Si), 0.86 (m, 21H, Me_3CSi, 20-CH_3), 1.13–2.60 (m, 14H), 3.93 (m, 3H, H-19,11,15), 5.43 (m, 2H, H-13,14), 6.50 (s, 1H, NH).

*Synthesis of the thiolactams **19***

A solution of the lactam (2 mmol) and Lawesson's reagent (1–1.4 mmol); 2,4-bis(4-methoxyphenyl)-1,3-dithia-2,4-diphosphetane-2,4-disulfide, Aldrich Chem. Co.) in anhydrous benzene (25–50 mL/g of lactam) was heated at reflux temperature for 0.5–1 h. The solvent was removed *in vacuo*, the residue was mixed with dichloromethane, and the mixture was filtered. The filtrate was evaporated *in vacuo* and the residue was purified by preparative tlc on silica gel using the solvent system indicated in Table 3. The tlc pure 15α compound **19***a* had the following spectroscopic properties: ir: 3420, 1500 cm^{-1}; nmr δ: 0.03 (s, 12H, Me_2Si), 0.88 (m, 21H, 20-Me, Me_3CSi), 1.06–3.26 (m, 14H), 4.05 (m, 3H, H-9,11,15), 5.43 (m, 2H, H-13,14), 8.72 (s, 1H, NH).

*Synthesis of the bis-*tert*-butyldimethylsilyl vinylogous amides **21***

Sodium hydride in mineral oil (50% suspension, 1 mmol) was washed with dry hexane, layered with anhydrous tetrahydrofuran (10–20 mL), and the thiolactam (1 mmol) dissolved in dry tetrahydrofuran (10–20 mL) was added thereto with stirring. After 1 h at room temperature the mixture was cooled to 0°C and a solution of methyl 5-bromolevulinate (1.1 mmol) in dry tetrahydrofuran (10–20 mL) was added slowly and then the reaction mixture was stirred for 0.25–0.5 h. Ethyl acetate, or ethyl acetate – ether (1:1) in the case of **20***e* and **20***f*, and water were added and the reaction was then worked up as usual to give the thioimidates **20**. The crude thioimidates (ir absorption of 1740–1750 cm^{-1}) were used immediately in the next step.

*(a) Synthesis of **21***a–d

Triphenylphosphine (1.5 mmol) and potassium-*tert*-butoxide (0.2 mmol) were added to the crude thioimidate dissolved in 1:1 xylene–*tert*-butanol solution (7 mL, anhydrous) and the mixture was heated at reflux temperature for 2–3 h. The mixture was diluted with water and worked up in the usual way. The crude products were purified in the manner described in Table 3. The tlc-pure, oily **21***a* had the following spectroscopic properties: uv: 270 (1590), 308 (20 000) nm; ir: 3260, 1740, 1625, 1540 cm^{-1}; nmr δ: 0.03 (s, 12H, Me_2Si), 0.66 (m, 21H, 20-Me_3CSi), 1.03–3.00 (m, 14H), 2.56 (s, 4H, 2-CH_2, 3-CH_2), 3.93 (m, 3H, H-9,11,15), 3.63 (s, 3H, OMe), 4.96 (s, 1H, H-5), 5.24 (m, 2H, H-13,14), 9.88 (bs, 1H, NH).

*(b) Synthesis of **21***e,f

Triphenylphosphine (0.16 mmol) and potassium-*tert*-butoxide (0.2 mmol) were added to the crude thioimidate from above dissolved in 10:1 xylene–*tert*-butanol (10 mL) and the reaction was effected as described for **21***a–d*.

*Hydrolysis of the bis-*tert*-butyldimethylsilyl ethers **21** to the 11,15-diols **22***

A solution of tetra-*n*-butylammonium fluoride (4 mmol) in anhydrous tetrahydrofuran (5 mL) was added to a stirred solution of the disilyl ether (1 mmol) in the same solvent (10–25 mL). The resulting solution was heated at 40°C for 18–24 h and the solvent was then removed *in vacuo*. The residue was partitioned between water and ethyl acetate and worked up in the usual way. The product was purified in the manner described in Table 3. Pure **22***a* had the following spectroscopic properties: uv: 215 (1660), 317 (19 600) nm; ir: 3620, 3390 (br) 1740, 1625, 1540 cm^{-1}; nmr δ: 0.88 (m, 3H, 20-CH_3), 1.16–3.33 (m, 18H), 3.95 (m, 3H, H-9,11,15), 5.01 (s, 1H, H-5), 5.46 (m, 2H, H-13,14), 9.77 (bs, 1H, NH).

*Hydrolysis of the azaprostacyclin methyl esters **22** to the carboxylic acids **23***

A solution of the ester (1 mmol) in methanol (15 mL) containing water (1 mL) and potassium carbonate (3 mmol) was stirred at room temperature for 38–64 h. The methanol was removed *in vacuo*, water was added to the residue, and the solution was extracted with dichloromethane. The aqueous phase was cooled to 0°C and brought to pH 4 by the addition of a saturated aqueous oxalic acid solution. The product was extracted into ethyl acetate and worked up in the usual way.

1. S. Moncada. J. Pharmacol. (Paris), **16**, suppl. I, 71 (1985).
2. S. Moncada and J. R. Vane. J. Med. Chem. **23**, 591 (1980).
3. G. Galambos, V. Simonidesz, J. Ivanics, K. Horvath, and G. Kovacs. Tetrahedron Lett. **24**, 1281 (1983).
4. H. Vorbrüggen, W. Skuballa, B. Radüchel, W. Losert, O. Loge, B. Müller, and G. Mannesmann. German Offen. 2,753,244 (1979); Chem. Abstr. **91**, 91250z (1979).
5. K. Bannai, T. Toru, T. Oba, T. Tanaka, N. Okamura, K. Watanabe, A. Hazato, and S. Kurozumi. Tetrahedron, **39**, 3907 (1983).
6. J. Fried, D. K. Mitra, M. Nagarajan, and M. M. Mehrotra. J. Med. Chem. **23**, 234 (1980).
7. W. Bartmann and G. Beck. Angew. Chem. Int. Ed. Engl. **21**, 751 (1982).
8. R. J. K. Taylor. *In* New synthetic routes to prostaglandins and thromboxanes. *Edited by* S. M. Roberts and F. Scheinmann. Academic Press, New York. 1982. pp. 181–241.
9. R. C. Nickolson, M. H. Town, and H. Vorbrüggen. Med. Res. Rev. **5**, 1 (1985).
10. M. Roth, P. Dubs, E. Götschi, and A. Eschenmoser. Helv. Chim. Acta, **54**, 710 (1971).
11. W. Ried and L. Kaiser. Synthesis, 535 (1976); G. J. Martin and M. L. Martin. *In* Progress in nuclear magnetic resonance spectroscopy. Vol. 8. *Edited by* J. W. Emsley, J. Feeney, and L. H. Sutcliffe. Pergamon Press, Oxford. 1972. pp. 177–178.
12. W. Bartmann, G. Beck, J. Knolle, and R. H. Rapp. Angew. Chem. Int. Ed. Engl. **19**, 819 (1980).
13. E. J. Corey, N. M. Weinshenker, T. K. Schaaf, and W. Huber. J. Am. Chem. Soc. **91**, 5675 (1969); E. J. Corey, K. B. Becker, and R. K. Varma. J. Am. Chem. Soc. **94**, 8616 (1972).
14. Y. Konishi, M. Kawamura, Y. Iguchi, Y. Arai, and M. Hayashi. Tetrahedron, **37**, 4391 (1981).
15. L. E. Overman. Acc. Chem. Res. **13**, 218 (1980).
16. F. Weygand and E. Frauendorfer. Chem. Ber. **103**, 2437 (1970).
17. D. R. Dalton, V. P. Dutta, and D. C. Jones. J. Am. Chem. Soc. **90**, 5498 (1968).
18. S. Ranganathan, D. Ranganathan, and A. K. Mehrotra. Tetrahedron Lett. 1215 (1976).
19. L. A. Paquette and G. D. Crouse. Tetrahedron, **37**, Suppl. 1, 281 (1981).
20. P. De Clercq, D. Van Haver, D. Tavernier, and M. Vandewalle. Tetrahedron, **30**, 55 (1974).

21. J. C. COLLINS, W. W. HESS, and F. J. FRANK. Tetrahedron Lett. 3363 (1968).
22. J. BOUTAGY and R. THOMAS. CHEM. REV. **74**, 87 (1974).
23. J. L. LUCHE, L. RODRIGUEZ-HAHN, and P. CRABBÉ. J. Chem. Soc. Chem. Commun. 601 (1978).
24. R. A. CHERKASOW, G. A. KUTYREV, and A. N. PUDOVIK. Tetrahedron, **41**, 2567 (1985), and refs. therein.
25. E. J. COREY and B. B. SNIDER. J. Am. Chem. Soc. **94**, 2549 (1972); E. J. COREY and A. VENKATESWARLU. J. Am. Chem. Soc. **94**, 6190 (1972).
26. G. V. R. BORN. Nature, **194**, 927 (1962).
27. G. KOTOVYCH, G. H. M. AARTS, T. T. NAKASHIMA, and G. BIGAM. Can. J. Chem. **58**, 974 (1980).

Can. J. Chem. Downloaded from www.nrcresearchpress.com by 213.166.140.6 on 09/07/12
For personal use only.

The conformational properties of some phenyl esters. Molecular orbital and nuclear magnetic resonance studies

TED SCHAEFER AND GLENN H. PENNER
Department of Chemistry, University of Manitoba, Winnipeg, Man., Canada R3T 2N2

Received January 13, 1987

TED SCHAEFER and GLENN H. PENNER. Can. J. Chem. **65**, 2175 (1987).

Extensive, geometry-optimized, STO-3G MO computations on phenyl formate imply a strongly nonplanar *Z* conformer (C=O bond *cis* to the phenyl group) at ambient temperatures. The internal barrier to rotation about the C(1)—O bond in this conformer is computed as $V/\text{kJ mol}^{-1} = (-5.17 \pm 0.27) \sin^2\theta - (2.42 \pm 0.27) \sin^2 2\theta$, θ being zero for the planar conformer; the twofold is nearly twice as large as the fourfold component. The expectation value of θ is 58° at 300 K. The spin–spin coupling constants over six bonds between ^{13}C and ^{19}F nuclei in 4-fluorophenyl formate, acetate, propionate, and isobutyrate, as well as in the 2,6-dichloro-4-fluorophenyl acetate, are adduced as evidence for nonplanar conformers of these molecules. The magnitudes of these six-bond coupling constants are consistent with internal barriers to rotation about the C(1)—O bonds, which are similar in magnitude to those given by the computations on the *Z* conformer of phenyl formate. The energies of the planar and nonplanar *E* conformers, as well as the interconversion energies for $E \rightleftharpoons Z$ isomerization, are computed. Small amounts of the nonplanar *E* conformer are predicted at ambient temperatures. The ^{13}C chemical shifts and the one-bond ^{13}C, ^{19}F coupling constants are consistent, respectively, with only minor variations in the conformational behavior of the ester moieties caused by the fluorine substituent and by changes in the structures of these moieties themselves.

TED SCHAEFER et GLENN H. PENNER. Can. J. Chem. **65**, 2175 (1987).

Des calculs étendus d'OM effectués au niveau STO-3G sur du formate de phényle optimisé pour la géométrie laissent fortement supposer que le conformère *Z* non-plan (la liaison C=O est *cis* par rapport au groupement phényle) est privilégié à la température ambiante. On a calculé que la barrière interne à la rotation autour de la liaison C(1)—O de ce conformère peut être exprimée par l'équation $V/\text{kJ mol}^{-1} = (-5{,}17 \pm 0{,}27) \sin^2\theta - (2{,}42 \pm 0{,}27) \sin^2 2\theta$ dans laquelle θ est égal à zéro pour le conformère plan; la composante binaire est deux fois plus importante que la composante quaternaire. À 300 K, la valeur attendue pour θ est de 58°. On a aussi utilisé les constantes de couplage spin–spin à travers six liaisons entre les noyaux de ^{13}C et de ^{19}F des formate, acétate, propionate et isobutyrate de fluoro-4 phényle de même que de l'acétate du dichloro-2,6 fluoro-4 phényle comme preuve de l'existence des conformères non-plans de ces molécules. Les amplitudes de ces constantes de couplage à travers six liaisons sont en accord avec des barrières à la rotation autour des liaisons C(1)—O qui sont semblables en amplitude à celles obtenues par calculs sur la conformère *Z* du formate de phényle. On a aussi calculé les énergies des conformères *E* plan et non-plan ainsi que les énergies d'interconversion pour l'isomérisation $E \rightleftharpoons Z$. À la température ambiante, on prédit que de faibles proportions du conformère *E* non-plan existeront. Le déplacements chimiques en résonance magnétique nucléaire du ^{13}C et les constantes de couplage ^{13}C–^{19}F sont respectivement en accord uniquement avec des variations mineures dans le comportement conformationnel des portions esters qui sont causées par le substituant fluor et par des changements dans les structures de ces portions elle-mêmes.

[Traduit par la revue]

Introduction

Alkyl esters are usually discussed in terms of planar or nearly planar *Z* and *E* conformers (1–7). In the formates (R = H), small amounts of *E* have been detected at low temperatures when R′ = CH_3, C_2H_5, and $CH(CH_3)_2$ (6). Rather larger populations of *E* occur for R′ = $C(CH_3)_3$ (4–6). The free energy barriers to interconversion of *E* and *Z* are available from dynamic nmr measurements (4–6).

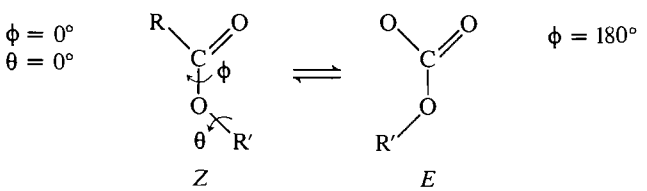

Z *E*

A combination of diffraction and spectroscopic data for vinyl formate in the gas phase, supplemented by 4-21G MO and molecular mechanics computations, indicate the planar *Z* conformer at room temperature (8). It is at least 9.6 kJ/mol more stable than the *E* form.

It has been suggested that phenyl formate exists in the *Z* form, nearly planar because of conjugation involving the aromatic π electrons (3). Phenyl thiolformate, however, displays almost equal stabilities of the *Z* and *E* conformers at 193 K in solution (9). There is some evidence that the phenyl group in the latter molecule is not coplanar with the S—C(H)=O moiety, that is, θ ≠ 0° and is perhaps as large as 90° in structures analogous to those above (9).

In this paper, MO calculations and long-range ^{13}C, ^{19}F spin–spin coupling constants are found to be consistent with severely nonplanar *Z* conformations of phenyl formate and 4-fluorophenyl—O—C(=O)R (R = H, CH_3, C_2H_5, and $CH(CH_3)_2$). Appreciable populations of planar forms at 300 K are unlikely.

Experimental

The 4-fluorophenyl formate was made by the Vilsmeier reaction from 4-fluorophenol exactly as described (10). The other esters were prepared in the usual way by reaction of 4-fluorophenol with the appropriate acid anhydrides in the presence of some pyridine. Samples for nmr spectra were prepared as solutions in acetone-d_6, concentrations being given in Table 1 below, which also contained some tetramethyl silane (TMS). The solutions were transferred to 10-mm od nmr sample tubes and were degassed by the freeze–pump–thaw procedure prior to flame-sealing of the tubes. The $^{13}C\{^1H\}$ nmr spectra were accumulated on an AM300 Bruker spectrometer at a probe temperature of 300 K in a manner described before (11). Peak widths at half height were typically 0.1 Hz, so that splittings due to coupling with ^{19}F nuclei could be determined with satisfactory precision (Table 1).

STO-3G MO computations employed the computer program MONSTERGAUSS (12) on an Amdahl V7 system. Rather extensive geometry optimization was demanded during the computations, with, how-

Can. J. Chem. Downloaded from www.nrcresearchpress.com by 213.166.140.6 on 09/07/12
For personal use only.

TABLE 1. ^{13}C chemical shifts[a] and $^{n}J(^{13}C, ^{19}F)$ for 4-fluorophenyl—O—C(=O)R at 300 K

Parameter	R = H	R = H	R = CH_3[c]	R = CH_2CH_3[d]	R = $CH(CH_3)_2$[d]
δ(C=O)[e]	160.50[b]	157.44[i]	169.62	173.13	175.68
δ_1	147.22	146.19	147.94	148.01	148.05
δ_2	123.97	122.80	124.23	124.21	124.14
δ_3	117.00	116.13	116.54	116.53	116.54
δ_4	161.29	160.64	160.90	160.88	160.89
^1J[f]	−242.56[j]	−245.96	−241.85	−241.86	−241.83
^2J	23.72	23.41	23.75	23.55	23.57
^3J	8.68	8.27	8.58	8.46	8.62
^4J	2.82	3.02	2.11	2.74	2.78
^6J[g,h]	0.91	0.85	0.88	0.84	0.83

[a]At a spectrometer frequency of 75.477 MHz.
[b]2.6 mol% in acetone-d_6, containing TMS.
[c]10 mol% in acetone-d_6.
[d]7 mol% in acetone-d_6.
[e]In ppm relative to internal TMS with a precision of 0.01 ppm.
[f]Reproducible to ±0.01 Hz.
[g]^7J is less than 0.05 Hz in magnitude for R = CH_3, CH_2CH_3, and $CH(CH_3)_2$. δ(CH_3) is 290.80 ppm for R = CH_3; δ(CH_2) and δ(CH_3) are 27.82 and 9.19, respectively, for R = CH_2CH_3; δ(CH) and δ(CH_3) are 34.55 and 19.08, respectively, for R = $CH(CH_3)_2$.
[h]For a 14 mol% solution of 2,6-dichloro-4-fluorophenyl acetate in acetone-d_6 solution, δ(CH_3) is 19.62 ppm while δ(C=O), δ_1, δ_2, δ_3, and δ_4 are 167.44, 141.78, 130.16, 117.00, and 160.08, respectively. ^1J, ^2J, ^3J, ^4J, and ^6J are −249.6, 26.8, 12.0, 4.3, and 1.19$_4$ Hz, respectively.
[i]7.0 mol% in CS_2, containing also 15 mol% C_6D_{12} and 0.5 mol% TMS.
[j]^1J is −244.9 Hz in 4-fluorotoluene in CS_2 solution and is −241.9 Hz in acetone solution.

ever, the constraint that the aromatic carbon atoms remain in a plane. INDO MO FPT calculations (13) were also performed on the Amdahl.

Results and discussion

STO-3G MO structure of phenyl formate

The planar *Z* form has φ = 0° (see structure above) and θ = 0°, where the latter angle gives the angle of twist about the C(1)—O bond; C(1) is an aromatic carbon atom. As θ increases, the total energy decreases. The relative energies, computed at 15° intervals in θ, are reproduced by eq. [1]. The quoted

$$[1]\quad V/\text{kJ mol}^{-1} = -(5.17 \pm 0.27)\sin^2\theta - (2.42 \pm 0.27)\sin^2 2\theta = V_2\sin^2\theta + V_4\sin^2 2\theta$$

errors are calculated at the 95% confidence level. Figure 1 displays the computed energies and the twofold and fourfold components as θ goes from 0 to 180°, φ being 0° (C=O *cis* to the benzene plane). At 300 K the expectation or average value of θ is 58.1° and that of $\sin^2\theta$ is 0.685. The minimum energy occurs for θ near 60° and for φ = 0°, the total energy being −412.974 198 au. Figure 2 displays the computed geometry for phenyl formate at θ = 60°, where the energy is 0.4 kJ/mol higher.

Table 2 presents the energies at 15° intervals in θ between 0° and 90° and at 30° intervals in φ between 0° and 180°. Symmetry arguments then yield the energies for θ and φ values lying in other quadrants. Direct conversion of the most stable, nonplanar, *Z* conformer to the *E* conformer requires about 31 kJ/mol, although there are other pathways somewhat less energetically demanding. At 300 K the most stable *E* conformer would be present to the extent of less than 3% on the assumption of similar entropies for the various conformers. Dynamic nmr experiments are contraindicated by these computations because, even if the interconversion barriers are large enough to observe, the required low temperatures would reduce the *E* populations

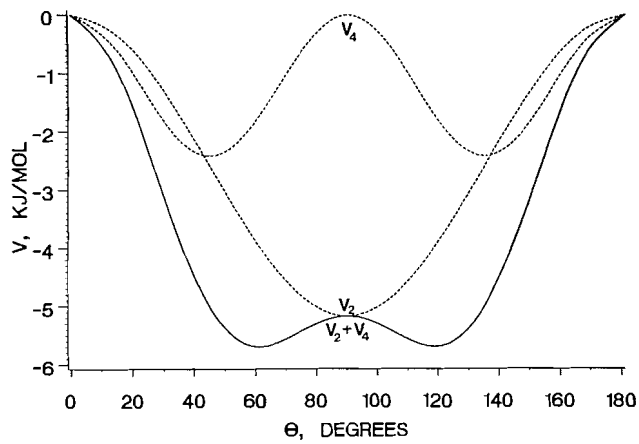

FIG. 1. The solid line represents the geometry-optimized STO-3G MO relative energies for the *Z* conformer of phenyl formate (C=O bond pointing towards the phenyl group) as a function of the twist angle, θ, about the C(1)—O bond. When θ is 0°, the molecule is planar; that is, the C=O bond lies in the benzene plane. The dashed lines represent the twofold and fourfold components of the computer barrier about the C(1)—O bond. The relative energies are given by $V/\text{kJ mol}^{-1} = (-5.17 \pm 0.27)\sin^2\theta - (2.42 \pm 0.27)\sin^2 2\theta$. See the text for a fuller discussion and Fig. 2 for the computed geometry at θ = 60°.

even further. To our knowledge such experiments have not been reported for phenyl esters.

In summary, the nonplanar *Z* form of phenyl formate, the C=O bond pointing towards the phenyl group, is computed as much the most stable at ambient temperatures. These predictions for the isolated molecule are compared below with long-range coupling constants for some derivatives of phenyl formate. These yield information about θ preferences but not about φ values.

Can. J. Chem. Downloaded from www.nrcresearchpress.com by 213.166.140.6 on 09/07/12
For personal use only.

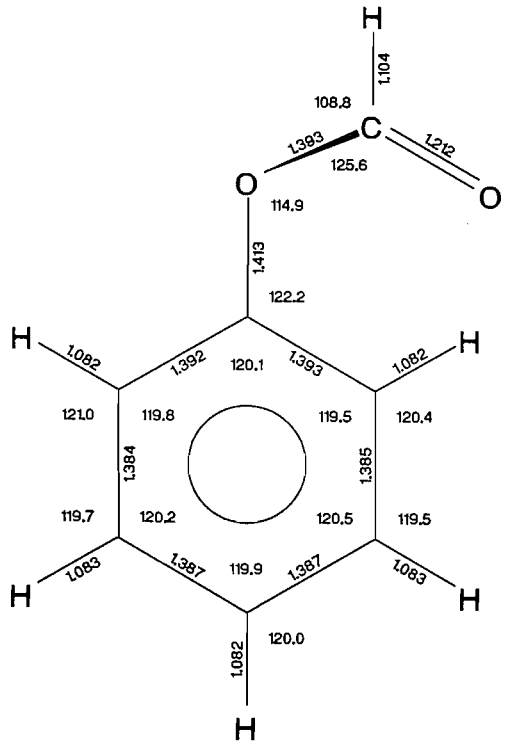

FIG. 2. The geometry-optimized STO-3G structure of phenyl formate. It has the *Z* conformation (see text) and is nonplanar. The side chain is twisted out of the benzene plane by 60°, that is, about the C(1)—O bond. The computed energy is −412.974 027 au and is 5.9 kJ/mol lower than that for the planar *Z* conformer (see text for energies of other conformations). In the planar form the C(1)—O—C angle is computed as 121.0°, indicating a reason for its instability. The O—C=O angle in this figure is computed as 0.7° larger than in vinyl formate (8) using 4-21G. The present geometry provides a starting point for higher level MO computations.

Conformational indications from $^6J(^{13}C, ^{19}F) \equiv {}^6J$

In previous work on 4-fluorophenyl derivatives of methane, ethene, and cyclohexane, $^6J(^{13}C, ^{19}F) \equiv {}^6J$ was established as a σ–π coupling. Such a coupling constant is proportional to $\sin^2\theta$ and is therefore a valuable indicator of the conformational behaviour of the side chain (14). Again, in anisole derivatives (15), ^6J also appears as σ–π coupling constant. In both instances, INDO MO FPT computations appear to confirm the $\sin^2\theta$ dependence of ^6J, although they underestimate the magnitude of $^6J_{90}$, the maximum value of ^6J. Similar behaviour was found here for 4-fluorophenyl formate. The previous work also implied (14) that ^6J is not very sensitive to the hybridization state of the carbon atom containing the coupled ^{13}C nucleus.

$^6J_{90}$ in 4-fluoroanisole was assessed as 1.48 Hz, from its value in the 2,6-dibromo derivative (15), and as 1.42 Hz in 4-fluorophenyl acetic acid (14). In 2,6-dichloro-4-fluorophenyl acetate (Table 1), ^6J is 1.19 Hz. For a hypothetical rigid conformation of this molecule, that is, for $\theta = 90°$, this number would represent $^6J_{90}$. Of course, the molecule is not rigid, so that 1.19 Hz represents a lower limit of $^6J_{90}$ in 4-fluorophenyl acetate. An upper limit will be taken as 1.42 Hz, implying $^6J_{90}$ as 1.30 ± 0.12 Hz. In 4-fluorophenyl acetate, $^6J_{90}$ is 0.88(1) Hz, and $\langle\sin^2\theta\rangle$ follows as 0.88(1)/1.30(12) or 0.68 ± 0.07, perhaps in accidental agreement with the value of 0.685 implied by the STO-3G MO energies for phenyl formate.

The ^6J values in Table 1 do not vary drastically from compound to compound. This behavior is expected if the *Z* conformer is predominant (R pointing away from the phenyl plane). ^6J in the formate is 0.08 ± 0.02 Hz larger than in the isopropyl derivative. One possible reason is that $^6J_{90}$ varies from molecule to molecule, substitution of the aldehydic hydrogen atom in the formate by an alkyl group causing a reduction in $^6J_{90}$. An indirect and supportive piece of evidence for such a reduction comes from the ^6J of 1.37(2) Hz in 2,6-dibromo-4-fluoro phenyl ethyl ether (unpublished work in this laboratory). Replacement of a hydrogen atom by a methyl group in the corresponding anisole therefore leads to a reduction of nearly 0.1 Hz in ^6J. However, it is also conceivable that, in the esters, the alkyl groups aid conjugation with the aromatic π electrons, thereby causing somewhat lower values of $\langle\sin^2\theta\rangle$; in the planar form the latter vanishes.

TABLE 2. The STO 3G MO relative energies[a] of phenyl formate

	φ						
θ	0	30	60	90	120	150	180
0	0.00[b]	4.81	15.35	20.05	15.91	12.41	11.91[c]
15	−0.67	3.35	14.91	21.13	19.04	14.78	10.27
30	−2.89	1.69	15.26	23.05	21.21	14.28	6.40
45	−5.10	8.51	16.72	24.85	21.43	11.56	3.15
60	−5.88	2.00	18.69	25.75	20.23	9.12	2.99
75	−5.43	3.60	20.08	25.88	19.25	9.02	4.84
90	−4.93[d]	4.44	20.14	25.42	19.08	9.86	5.99[e]

[a]Energies in kJ/mol and angles in degrees.
[b]The relative energy of the planar *Z* conformer (see structures in the text).
[c]The relative energy of the planar *E* conformer.
[d]The relative energy of the perpendicular *Z* conformer.
[e]The relative energy of the perpendicular *E* conformer.

Furthermore, the fluorine substituent is a weak π electron donor. Its presence will favor somewhat the nonplanar *Z* conformers for the esters in Table 1 (see below). Hence the ^6J values and the $\langle\sin^2\theta\rangle$ values derived from them cannot be rigorously compared with $\langle\sin^2\theta\rangle$ given by the MO calculations. Additionally, the latter refer to the free molecule and the measurements in Table 1 were made in acetone-d_6 solution. However, the computed moment of phenyl formate varies by only 0.02 D as θ goes from zero to 90°. To a first approximation, therefore, the influence of the solvent on the stability of the conformers is expected to be small. Indeed, in CS_2 solution, ^6J in 4-fluorophenyl formate is 0.85 Hz, 0.06 Hz smaller than in acetone-d_6 solution. This decrease implies a reduction of 0.05 in $\langle\sin^2\theta\rangle$ and therefore one of less than 3° in arc sin $\langle\sin^2\theta\rangle^{1/2}$ for the nonpolar solution.

The ^6J values are sensitive to the conformational angle θ but their dependence on φ is not known. The MO computations imply negligible populations of the *E* conformers at 300 K. Furthermore, the computed energies imply that dynamic nmr measurements would be uninformative. It is concluded that the ^6J values in solution are consistent with nonplanar conformers having $\langle\theta\rangle \sim 55°$. However, the *J* values cannot exclude the presence of *E* conformers at these θ values.

The ^{13}C chemical shifts

The ^{13}C chemical shifts in Table 1 are consistent with the idea that the *para* fluorine substituent does not alter substantially the conformational behaviour of the ester groupings. Using the chemical shifts known for fluorobenzene and phenyl acetate (16) and assuming additivity, the aromatic ^{13}C chemical shifts predicted for 4-fluorophenyl acetate deviate by an

Can. J. Chem. Downloaded from www.nrcresearchpress.com by 213.166.140.6 on 09/07/12
For personal use only.

average of only 0.4 ppm from those in Table 1. By way of contrast, in the 2,6-dichloro derivative, an additive scheme yields chemical shifts deviating by about 4 ppm at C-4, for example. In this compound, of course, there must exist a much stronger preference for a perpendicular conformation of the ester moiety than in 4-fluorophenyl acetate.

Conformational evidence from $^1J(^{13}C, ^{19}F) \equiv {}^1J$

The $OCOCH_3$ group causes increased shielding at the *para* position (16), but to a much smaller extent than a methoxy group, of course, and, in fact, to an extent similar to alkyl groups. Because ^1J is proportional to the mesomeric properties of the *para* substituent in fluorobenzene derivatives (17, 18), it is therefore reasonable that ^1J in 4-fluorotoluene is -241.4 Hz (14) and is -241.9 Hz in 4-fluorophenyl acetate (Table 1), both measured in acetone solution (^1J ranges from -233 Hz in the 4-amino compound to -257 Hz in the 4-nitro derivative (18)). The ^1J values in Table 1 appear consistent with only minor changes in the side-chain conformation from compound to compound. ^1J in fluorobenzene derivatives is known to vary by as much as 10 Hz in various solvents (18). In a recent study of ^{13}C chemical shifts of 1,4-disubstituted benzenes (19), it was concluded that the $OCOCH_3$ group may be characterized as a noninteracting substituent, that is, interacting very weakly with a *para* substituent. This conclusion is consistent with the results of the present study.

Acknowledgments

We are grateful to the Natural Sciences and Engineering Research Council of Canada for financial assistance. A referee is thanked for thoughtful criticism.

1. R. F. CURL, JR. J. Chem. Phys. **30**, 1529 (1959).
2. G. I. L. JONES and N. L. OWEN. J. Mol. Struct. **18**, 1 (1973).
3. M. ŌKI and H. NAKANISHI. Bull. Chem. Soc. Jpn. **43**, 2558 (1970).
4. T. DRAKENBERG and S. FORSEN. J. Phys. Chem. **76**, 3582 (1972).
5. H. NAKANISHI, H. FUJITA, and O. YAMAMOTO. Bull. Chem. Soc. Jpn. **51**, 214 (1978).
6. T. B. GRINDLEY. Tetrahedron Lett. **23**, 1757 (1982).
7. J. R. LARSON, N. D. EPIOTIS, and F. BERNARDI. J. Am. Chem. Soc. **100**, 5713 (1978).
8. W. PYCKHOUT, C. VAN ALSENOY, H. J. GEISE, V. VAN DER VEKEN, P. COPPENS, and M. TRAETTEBERG. J. Mol. Struct. **147**, 85 (1986).
9. E. A. NOE, T. SANDERS, M. GARAHI, H. HOSSEINI, and R. YOUNG. J. Am. Chem. Soc. **107**, 4785 (1985).
10. S. MORIMURA, H. HORIUCHI, and K. MURAYAMA. Bull. Chem. Soc. Jpn. **50**, 2189 (1977).
11. T. SCHAEFER, J. PEELING, and R. SEBASTIAN. Can. J. Chem. **63**, 3219 (1985).
12. M. R. PETERSEN and R. A. POIRIER. MONSTERGAUSS. Department of Chemistry, University of Toronto, Toronto, Ontario. 1981.
13. P. DOBOSH and N. S. OSTLUND. QCPE, **11**, 281 (1975).
14. T. SCHAEFER, J. PEELING, G. H. PENNER, A. LEMIRE, and R. SEBASTIAN. Can. J. Chem. **63**, 24 (1985).
15. T. SCHAEFER, R. LAATIKAINEN, T. A. WILDMAN, J. PEELING, G. H. PENNER, J. BALEJA, and K. MARAT. Can. J. Chem. **62**, 1592 (1984).
16. J. D. MEMORY and N. K. WILSON. NMR of aromatic compounds. Wiley, New York. 1982. p. 117.
17. M. M. DHINGRA, G. GOVIL, and C. L. KHETRAPA. Proc. Indian Acad. Sci. Part A, **64**, 91 (1966).
18. J. B. STOTHERS. Carbon-13 nmr spectroscopy. Academic Press, New York. 1972. p. 364.
19. R. T. C. BROWNLEE and M. SADEK. Aust. J. Chem. **34**, 1593 (1981).

Can. J. Chem. Downloaded from www.nrcresearchpress.com by 213.166.140.6 on 09/07/12
For personal use only.

Anhydropenicillin: a key intermediate for the stereocontrolled introduction of the 6-*R*-hydroxyethyl side chain of the penem and carbapenem antibiotics

ALAIN MARTEL,[1] JEAN-PAUL DARIS, CAROL BACHAND, AND MARCEL MENARD
Groupe Pharmaceutique Bristol-Myers, 100 Boulevard de l'Industrie, Candiac (Que.), Canada J5R 1J1

Received March 23, 1987

ALAIN MARTEL, JEAN-PAUL DARIS, CAROL BACHAND, and MARCEL MENARD. Can. J. Chem. **65**, 2179 (1987).

Aldol condensation of the magnesium enolate derived from anhydro-6,6-dibromopenicillin with acetaldehyde allows for the stereospecific introduction of a 1-*R*-hydroxyethyl substituent at C-6. Protection of the hydroxy group followed by reductive dehalogenation provides anhydro-6(α)-[(1-*R*)-(*tert*-butyldimethylsilyloxy)-ethyl]-penicillin, an intermediate in the synthesis of thienamycin. A high yield conversion of this anhydro derivative to (4-*R*)-acetoxy-(3-*S*)-[(1-*R*)-(*tert*-butyldimethylsilyloxy-ethyl]-azetidin-2-one (**5**) is also reported.

ALAIN MARTEL, JEAN-PAUL DARIS, CAROL BACHAND et MARCEL MENARD. Can. J. Chem. **65**, 2179 (1987).

La condensation aldolique de l'acétaldéhyde avec l'énolate magnésien dérivé de l'anhydro dibromo-6,6 pénicilline permet d'introduire d'une façon stéréospécifique un substituant hydroxyéthyle-1(*R*) au niveau du carbone-6. La protection du groupement hydroxyle, suivie d'une déshalogénation réductrice, conduit à l'anhydro [(*tert*-butyldiméthylsilyloxy)-1(*R*) éthyl]-6α pénicilline, un intermédiaire dans la synthèse de la thiénamycine. On rapporte aussi une méthode de transformer ce dérivé anhydro en acétoxy-4(*R*) [(*tert*-butyldiméthylsilyloxy-1(*R*) éthyl]-3(*S*) azétidinone-2 (**5**), avec un excellent rendement.

[Traduit par la revue]

Can. J. Chem. Downloaded from www.nrcresearchpress.com by 213.166.140.6 on 09/07/12
For personal use only.

Penems **1** (1) and carbapenems **2** (2) are highly potent β-lactam antibiotics whose structural features differ considerably from the classical β-lactams (i.e., penicillins and cephalosporins). The most notable difference is the presence of a 6-*R*-hydroxyethyl side chain, which confers chemical as well as enzymatic stability to these molecules (3). The synthesis of chiral azetidinones that possess a hydroxyethyl side chain having the proper configuration, and which can be readily transformed into either penems or carbapenems, has been the subject of numerous reports (4). We have previously described the synthesis of key intermediates such as (4*R*)-(tritylthio)azetidinone and the corresponding silver mercaptide (5) as well as (3*S*)-bromo-(4*R*)-chloro-2-azetidinone (6), and their conversion to penems or to carbapenem precursors. This paper describes the stereoselective introduction of the *trans*-*R*-hydroxyethyl side chain onto anhydro-6,6-dibromopenicillin[2] and the subsequent conversion of this adduct to the very useful carbapenem precursor 4-acetoxyazetidinone **5** (7).

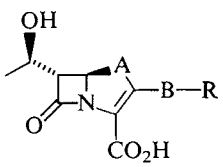

1: A = S, B = CH_2
2: A = CH_2, B = S

Since the initial report of DiNinno *et al.* (8) on the regiospecific hydroxyethylation of the C-6 position of penicillinates, many research groups have used this approach to prepare penem and carbapenem precursors (7). This method proved to be very useful even though the aldol condensation suffered from a lack of stereospecificity. Subsequent work by Kellogg and co-workers (9*a*, *b*) suggested that complete stereoselectivity in the aldol reaction could be achieved if a metal enolate of the penicillin nucleus could chelate with β-face selectivity, and if the steric effect of the 2-β-methyl group was eliminated.[3]

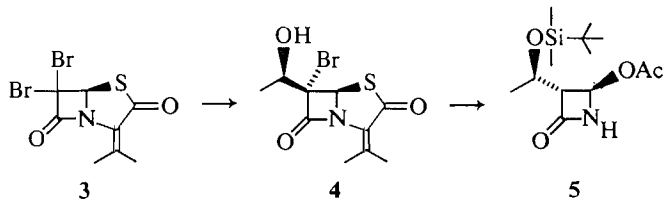

3 **4** **5**

SCHEME 1

Indeed, we have found that an anhydropenicillin (10) ring fulfilled these requirements, since the aldol condensation of the enolate derived from anhydro-6,6-dibromopenicillin **3** with acetaldehyde proceeded with 100% stereoselectivity and only the *cis* 6-*R* derivative **4** was obtained.

Anhydro-6,6-dibromopenicillin **3** (Scheme 2) was prepared by the treatment of an activated ester of dibromopenicillin **6** with base. Specifically, treatment of the triethylamine salt of 6,6-dibromopenicillin with trifluoroacetic anhydride gave a mixed anhydride that, on standing in pyridine, rearranged to give the anhydro ring (85% yield). The physical and spectral characteristics of **3** were identical to those reported by Clayton (11).

The magnesium enolate (8) of derivative **3** (Scheme 2) was reacted with acetaldehyde to give a single aldol adduct, presumably the *cis* *R*-hydroxyethyl derivative **4**, in essentially a quantitative yield (see Table 1). However, the structural assignment of **4** was unambiguously confirmed by the single crystal X-ray analysis of its *tert*-butyldimethylsilyl ether derivative **7** (see Fig. 1).

Reduction of **4** with zinc–silver couple at −15°C (12) gave a mixture of the two expected isomers from which crystalline **8** (R = H) was isolated in 42% yield. This was not unexpected since it has been shown (7) that the α/β ratio of 6-hydroxyethyl isomers that are obtained by reduction of such 6-α-bromo derivatives is influenced by both the temperature of the reduction and the steric bulk of the hydroxyethyl protecting group. When the reduction of **4** was carried out at −50°C the yield of crystalline **8** (R = H) was increased to 57%. Almost complete stereoselection was achieved when the TBDMS ether **7** (80.6%) of **4** was reduced at −45°C; the 6-α-hydroxyethyl derivative **8** was formed in 96.8% yield, contaminated only with starting material (0.7%) and the undesired β isomer (2.5%).

Further manipulation of derivative **8** gives a precursor that is

[1]Author to whom correspondence may be addressed.

[2]This work is part of a Bristol-Myers U.S. patent No. 4,596,677 filed on April 6, 1984 and issued on June 24, 1986.

[3]Although Kim *et al.* reported on a stereospecific C_6-hydroxyethylation of penicillin (9*c*), this result could not be reproduced by B. B. Brown and R. A. Volkmann (9*b*).

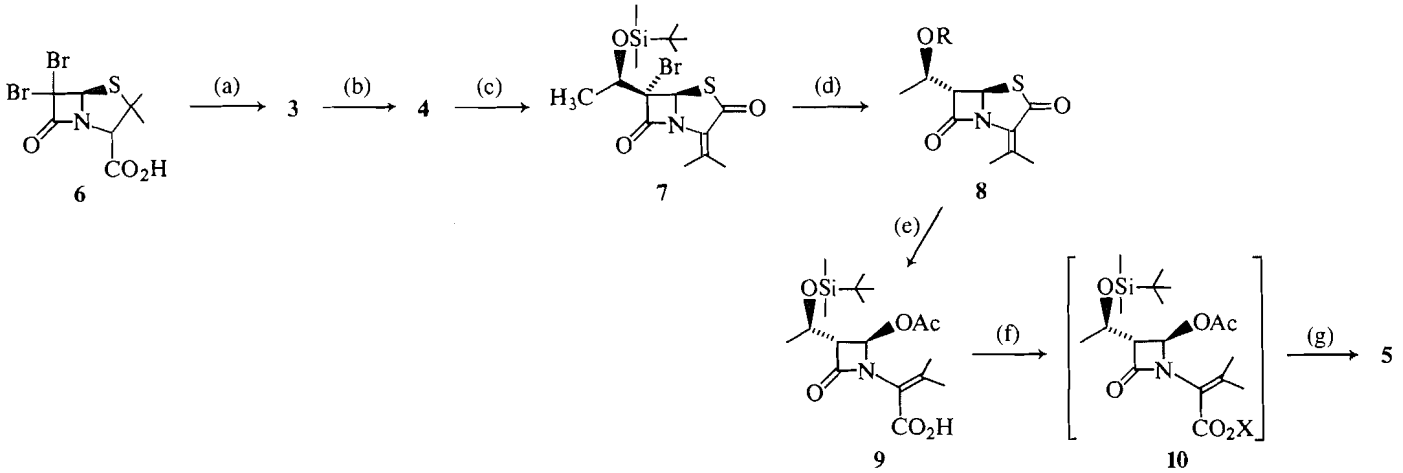

(a) Triethylamine, trifluoroacetic anhydride, −15°C, 30 min; pyridine, CH_2Cl_2, 18 h, 5°C; mp 102–103°C; (b) MeMgBr, THR, −78°C, CH_3CHO, 20 min; (c) TBDMS triflate, 2,6-lutidine, CH_2Cl_2, 5°C, 1 h; (d) 25% THF–MeOH, Zn(Ag), −45°C with R = Si+, mp 56–57.5°C, with R = H, mp 173–174°C; (e) $Hg(OAc)_2$ 5 equiv. CH_3CO_2H, r.t., 48 h, mp 119–120°C; (f) EEDQ, CH_2Cl_2, 18 h, for X = CO_2Et; $(CH_3O)_2SO_2$, K_2CO_3, $(CH_3)_2CO$, 3 h, for X = Me; (g) O_3, CH_2Cl_2, Me_2S, MeOH, 2,6-lutidine when X = CO_2Et; O_3, MeOH, SiO_2, 18 h, when X = H; $KMnO_4$ 1.5 equiv., $(CH_3)_2CO$, 15 h, r.t., when X = CH_3.

SCHEME 2

TABLE 1. ^1H magnetic resonance spectral data*

Compound	H-5(4)	H-6(3)	CH_3	H-1′	Vinylic CH_3	Others
3	5.80 (s)				2.21 (s) 2.15 (s)	
4	5.61 (s)		1.31 (d) J = 6.0	4.28 (q) J = 6.0	2.21 (s) 2.16 (s)	1.64 (OH)
7	5.53 (s)		1.28 (d) J = 6.1	4.27 (q) J = 6.1	2.20 (s) 2.13 (s)	0.9 (s, 9H, *t*-Bu) 0.09 (s, 3H, CH_3) 0.07 (s, 3H, CH_3)
8(α) R = Si+	5.29 (d) J = 1.8	3.52 (dd) J = 3.5 J = 1.8	1.25 (d) J = 6.3	4.34 (dq) J = 6.3 J = 3.5	2.17 (s) 2.08 (s)	0.89 (s, 9H, *t*-Bu) 0.09 (s, 6H, CH_3)
8(β) R = Si+	5.35 (d) J = 4.6	3.86 (dd) J = 4.6 J = 9.4	1.23 (d) J = 6.0	4.31 (dq) J = 6.0 J = 9.4	2.18 (s) 2.08 (s)	0.89 (s, 9H, *t*-Bu) 0.10 (s, 3H, CH_3) 0.06 (s, 3H, CH_3)
9	6.32 (d) J = 1.4	3.20 (dd) J = 1.4 J = 5.8	1.29 (d) J = 6.3	4.24 (m) J = 6.0	2.24 (s) 1.97 (s)	2.05 (s, 3H, CH_3) 0.86 (s, 9H, *t*-Bu) 0.08 (s, 3H, CH_3) 0.05 (s, 3H, CH_3)
10 X = CO_2Et	6.23 (d) J = 1.4	3.23 (dd) J = 1.4 J = 6.1	1.29 (d) J = 6.1	4.17 (m) J = 6.1	2.25 (s) 1.17 (s)	4.32 (q, 2H, J = 7.1) 2.06 (s, 3H, CH_3) 1.35 (t, 3H, J = 7.1) 0.86 (s, 9H, *t*-Bu) 0.08 (s, 3H, CH_3) 0.05 (s, 3H, CH_3)
5	5.84 (d) J = 1.1	3.18 (dd) J = 1.1 J = 3.4	1.25 (d) J = 6.3	4.22 (dq) J = 6.3 J = 3.4		6.42 (bs, 1H, NH) 2.10 (s, 3H, CH_3) 0.86 (s, 9H, *t*-Bu) 0.07 (s, 6H, CH_3)
8(α) R = H	5.28 (d) J = 1.7	3.57 (dd) J = 1.7 J = 6.2	1.40 (d) J = 6.3	4.35 (q) J = 6.2	2.19 (s) 2.11 (s)	1.72 (bs, 1H, OH)
8(β) R = H	5.40 (d) J = 4.6	3.74 (dd) J = 4.6 J = 9.0	1.27 (d) J = 6.0	4.36 (dq) J = 6.1 J = 9.0	2.19 (s) 2.09 (s)	2.07 (bs, 1H, OH)

*Recorded at 80 MHz in $CDCl_3$ using tetramethylsilane as internal standard. The chemical shifts are recorded in δ (ppm) and the J's in Hz.

Can. J. Chem. Downloaded from www.nrcresearchpress.com by 213.166.140.6 on 09/07/12
For personal use only.

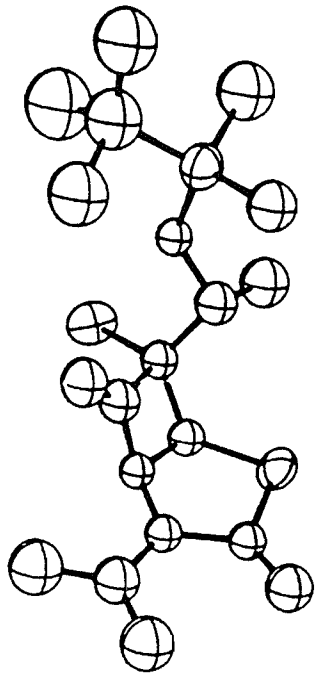

FIG. 1. ORTEP stereoview of compound **7**.

common to both the penems[4] and the carbapenems. This is illustrated by the conversion of **8** to the 4-acetoxyazetidinone **5** via a two-step process that is modeled after one which has been used (*7b,c*) to degrade the penicillin molecule to an azetidinone. Thus treatment of **8** with excess $Hg(OAc)_2$ in CH_3CO_2H (Scheme 2) afforded the crystalline *N*-substituted 4-acetoxyazetidinone **9** in excellent yield (95%).

Oxidative cleavage of the *N*-β-methylcrotonic acid portion was carried out either by treatment with ozone or permanganate. To avoid side reactions ($KMnO_4$ oxidation) or to facilitate the base catalyzed solvolysis of the intermediate oxamate (ozonolysis), the carboxylic acid **9** was first protected. Thus, reaction of **9** with EEDQ gave the anhydride **10** (X = CO_2Et), which was then treated with ozone. Reduction of the ozonide (Me_2S) and methanolysis of the resulting oxamate yielded the desired 4-acetoxyazetidinone **5** (95%), for which physical and spectral data were identical to those previously reported (7). It was subsequently found that ozonolysis of **9** in MeOH followed by silica gel treatment of the resulting oxamic acid gave the free 4-acetoxyazetidinone **5** directly (75%).

[4]The thiolactone **8** can be transformed easily to a silver mercaptide **11** in an alcoholic solvent. Acylation of the latter gave an intermediate **12** already reported for the preparation of penems (see ref. 13).

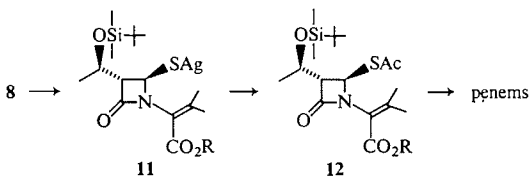

Similarly, permanganate oxidation of the methyl ester **10** (X = Me) gave the acetoxyazetidinone **5** in good yield (85%).

Acknowledgments

We would like to thank Professor B. Belleau, McGill University, and Drs. H. Mastalerz, R. Vanga, and E. Ruediger for helpful discussions. We would like also to thank Professor A. Michel, Université de Sherbrooke, for the X-ray structure determination.

1. R. B. WOODWARD. Acta Pharm. Suec. **14** (Suppl.), 23 (1977).
2. H. KROPP, J. S. KAHAN, J. SUNDELOF, G. DARLAND, and J. BIRMBAUM. Abstract 228, 16th Intersci. Conf. Antimicr. Agents and Chemotherapy, Chicago. 1976.
3. H. R. PFAENDLER, J. GOSTELI, and R. B. WOODWARD. J. Am. Chem. Soc. **102**, 2039 (1980), and refs. cited therein.
4. (*a*) A. G. BROWN and S. M. ROBERTS (*Editors*). Recent advances in the chemistry of β-lactam antibiotics. Third International Symposium, Royal Society of Chemistry. 1984; (*b*) I. ERNEST. *In* Chemistry and biology of β-lactam antibiotics. Vol. 2. *Edited by* R. B. Morin and M. Gorman. Academic Press, New York. 1982; (*c*) G. I. GREGORY (*Editor*). Recent advances in the chemistry of β-lactam antibiotics. Second International Symposium, Royal Society of Chemistry. 1980; (*d*) A. MARTEL, J. COLLERETTE, J. BANVILLE, J. P. DARIS, P. LAPOINTE, B. BELLEAU, and M. MENARD. Can. J. Chem. **61**, 613 (1983).
5. A. MARTEL, P. DEXTRAZE, J. P. DARIS, R. SAINTONGE, P. LAPOINTE, T. CONWAY, I. MONKOVIC, G. KAVADIAS, Y. UEDA, P. ELIE, S. PATIL, G. CARON, J. L. DOUGLAS, M. MENARD, and B. BELLEAU. Can. J. Chem. **60**, 942 (1982).
6. A. MARTEL, J. P. DARIS, C. BACHAND, M. MENARD, T. DURST, and B. BELLEAU. Can. J. Chem. **61**, 1899 (1983).
7. (*a*) V. M. GIRIJAVALLABHAN, A. K. GANGULY, S. W. MCCOMBIE, P. PINTO, and R. RIZVI. Tetrahedron Lett. **22**, 3485 (1981); (*b*) K. HIRAI, Y. IWANO, and K. FUJIMOTO. Tetrahedron Lett. **22**, 4021 (1981); (*c*) A. YOSHIDA, T. HAYASHI, N. TAKEDA, S. OIDA, and E. OHKI. Chem. Pharm. Bull. **29**, 2899 (1981); (*d*) M. LANG, P. SCHNEIDER, W. TOSCH, R. SCARTAZZINI, and O. ZAK. J. Antibiot. **39**, 525 (1986), and refs. cited therein.
8. F. DININNO, T. R. BEATTIE, and B. G. CHRISTENSEN. J. Org. Chem. **42**, 2960 (1977).
9. (*a*) J. A. AIMETTI and M. S. KELLOGG. Tetrahedron Lett. 3805 (1979); (*b*) B. B. BROWN and R. A. VOLKMANN. Tetrahedron Lett. **27**, 1545 (1986); (*c*) W. J. KIM, G. S. LEE, and S. C. SHIM. J. Antibiot. **37**, 1276 (1984).
10. S. WOLFE, J. C. GODFREY, C. T. HOLDREGE, and Y. G. PERRON. Can. J. Chem. **46**, 2549 (1968); J. Am. Chem. Soc. **85**, 643 (1963).
11. (*a*) J. P. CLAYTON. J. Chem. Soc. C, 2123 (1969); (*b*) R. A. VOLKMANN, R. D. CARROLL, R. B. DROLET, M. L. ELLIOT, and B. S. MOORE. J. Org. Chem. **47**, 3344 (1982).
12. (*a*) J. M. DENIS, C. GIRARD, and J. M. CONIA. Synthesis, 549 (1972); (*b*) R. D. CLARK and C. H. HEATHCOCK. J. Org. Chem. **38**, 3658 (1973).
13. M. ALPEGIANI, A. BEDESCHI, F. GIUDICI, E. PERRONE, and G. FRANCHESCHI. J. Am. Chem. Soc. **107**, 6398 (1985), and refs. cited therein.

Can. J. Chem. Downloaded from www.nrcresearchpress.com by 213.166.140.6 on 09/07/12
For personal use only.

Diels–Alder reactions of methyl-*N*-acyl-α,β-dehydroalaninates with cyclopentadiene

M. P. Bueno, C. Cativiela,[1] C. Finol, and J. A. Mayoral
Instituto de Ciencia de los Materiales de Aragón, Departamento de Química Orgánica, Universidad de Zaragoza, 50009 Zaragoza, Spain

and

C. Jaime
Departamento de Química, Unidad de Química Orgánica, Facultad de Ciencias, Universidad Autónoma de Barcelona, 08193 Bellaterra, Spain

Received November 26, 1986

M. P. Bueno, C. Cativiela, C. Finol, J. A. Mayoral, and C. Jaime. Can. J. Chem. **65**, 2182 (1987).

A study has been made of the Diels–Alder reaction of methyl-*N*-acetyl (and benzoyl)-α,β-dehydroalaninates with cyclopentadiene. In the reaction of methyl-*N*-acetyl-α,β-dehydroalaninate total conversion is obtained under several conditions, while the *N*-benzoyl derivative shows a lower reactivity. The stereoselectivity of the reaction is determined by ^{1}H nuclear magnetic resonance spectroscopy. Perturbation MO calculations, using wave functions generated by the MNDO method, are used to rationalize the relative reactivity of the dienophiles and the stereoselectivity observed.

M. P. Bueno, C. Cativiela, C. Finol, J. A. Mayoral et C. Jaime. Can. J. Chem. **65**, 2182 (1987).

On a réalisé une étude sur la réaction de Diels–Alder entre les *N*-acétyl (et benzoyl) α,β-déhydroalaninates de méthyle et le cyclopentadiène. Utilisant diverses conditions, la réaction du *N*-acétyl α,β-déhydroalaninate de méthyle conduit toujours à une conversion totale alors que la réactivité du dérivé *N*-benzoylé est beaucoup plus faible. On a déterminé la stéréosélectivité de la réaction par résonance magnétique nucléaire du ^{1}H. On a utilisé des calculs d'OM, faisant appel à des fonctions d'ondes générées par la méthode MNDO, pour rationaliser la réactivité relative des dièndophiles ainsi que la stéréosélectivité observée.

[Traduit par la revue]

Can. J. Chem. Downloaded from www.nrcresearchpress.com by 213.166.140.6 on 09/07/12
For personal use only.

Cycloaliphatic amino acids such as those having a norbornane skeleton are known to possess interesting biological properties that affect the transport of ions through biological membranes (1). These amino acids have usually been synthesized from the corresponding carbonyl compounds by Strecker or Bucherer synthesis. To the best of our knowledge there is only one reference dealing with their preparation from *N*-acyl-α,β-dehydroalaninates by means of Diels–Alder reactions (2). In conjunction with the biological interest of these amino acids we have studied the Diels–Alder reaction between methyl-*N*-acetyl (or benzoyl)-α,β-dehydroalaninates (Fig. 1) and cyclopentadiene. The results obtained encouraged us to make a theoretical study by means of the MNDO method (3). There is a good correlation between the calculations and the experimental results.

Synthesis of dienophiles and Diels–Alder reactions

Methyl *N*-acetyl (and benzoyl)-α,β-dehydroalaninates (**1***a*,*b*) were prepared by methylation with methyl iodide of the corresponding acids, which were obtained by condensation of pyruvic acid and acetamide or benzamide (4). While methyl *N*-acetyl-α,β-dehydroalaninate (**1***a*) is a stable product, the *N*-benzoyl derivative (**1***b*) is a rather oily unstable one (5) and a pure sample could only be obtained by means of column chromatography.

Methyl *N*-acetyl-α,β-dehydroalaninate (**1***a*) was allowed to react with cyclopentadiene under several conditions. The results (Table 1) show that total conversion can be obtained by using a moderate excess of cyclopentadiene, $TiCl_4$ as a catalyst, or high reaction temperatures. The adducts were separated by column chromatography and the structural assignments were made on the basis of the ^{1}H nmr signals of the substituents at C-2. The shielding of the double bond of 2-substituted-5-norbornene derivatives leads the signals of the protons in the *endo* substituents to a higher field than those in the *exo* substituents (2); thus the *exo*/*endo* ratio could be directly estimated from the ^{1}H nmr spectrum of the mixture. The *exo*/*endo* ratio does not change noticeably according to the conditions of reaction. Methyl *N*-benzoyl-α,β-dehydrolaninate (**1***b*) shows a lower reactivity (Fig. 1).

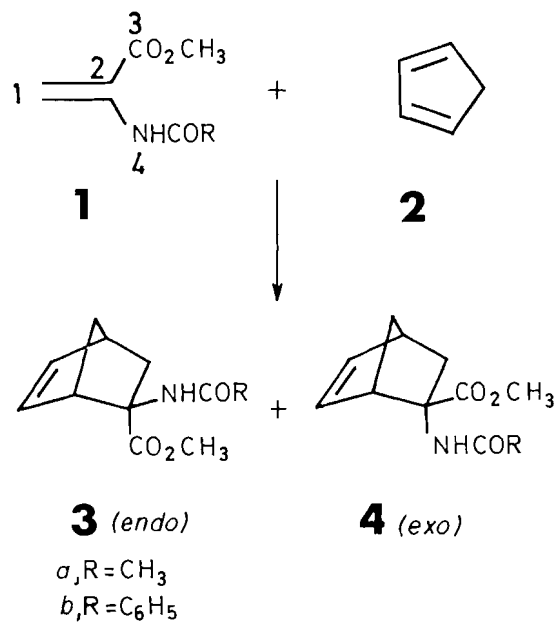

FIG. 1. Reaction between cyclopentadiene and methyl-*N*-acyl-α,β-dehydroalaninates.

Study of the reactivity and stereochemistry of the Diels–Alder reactions

The perturbational treatment leads to three different types of Diels–Alder reactions (6): normal, inverse, and neutral,

[1]Author to whom correspondence may be addressed.

Printed in Canada / Imprimé au Canada

TABLE 1. Diels–Alder reactions of *N*-acyl-α,β-dehydroalaninates with cyclopentadiene

Substrate	Temperature (°C)	Time (h)	Solvent	Lewis acid	Reagents ratio dienophile/diene	Yield (%)[a]	Adducts ratio[a] *exo*:*endo*
1*a*	90–100	5	Toluene	—	1:6	100	6.9:3.1
1*a*	90–100	5	Toluene	—	1:9	100	7.1:2.9
1*a*	130–140	5	Xylene	—	1:3	100	7.2:2.8
1*a*	80–90	5	EtOH	—	1:3	78	6.4:3.6
1*a*	25–30	5	CH_2Cl_2	$TiCl_4$	1:3	100	5.7:4.3
1*a*	−10	5	CH_2Cl_2	$TiCl_4$	1:6	No reaction	—
1*b*	130–140	5	Xylene	—	1:9	25	—

[a]Determined by ^{1}H nmr analysis of crude products integrating on methyl ester signals.

TABLE 2. Frontier molecular orbital coefficients and energies of methyl-*N*-acyl-α,β-dehydroalaninates

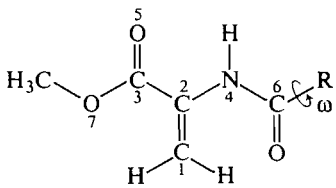

Compound	Orbital	*E* (eV)	C1	C2	C3	N4	O5	C6	O7
1*a*	HOMO	−9.42	−0.602	−0.462	−0.020	0.569	0.135	0.065	0.041
1*a*	LUMO	−0.057	−0.610	0.432	0.456	−0.075	−0.353	−0.207	−0.158
1*b*[a]	HOMO	−9.33	0.597	0.455	0.028	−0.573	−0.133	−0.061	−0.040
1*b*[a]	LUMO	−0.437	−0.190	0.115	0.079	0.078	−0.066	−0.272	−0.029
1*b*[a]	HOMO	−9.38	−0.602	−0.456	−0.019	0.573	0.134	0.064	0.040
1*b*[b]	LUMO	−0.198	0.031	−0.021	−0.018	−0.003	0.015	0.024	0.006

[a]$\omega = 0°$.
[b]$\omega = 90°$.

depending on which HOMO–LUMO interaction is the dominant stabilizing factor.

To evaluate the different interactions, the electronic structures of dienophiles **1***a* and **1***b* and cyclopentadiene (**2**) were calculated by the MNDO method (3). Compounds **1***a* and **1***b* show a considerable mobility around their σ bonds, but fortunately Ajò *et al.* (7) have studied the structure of several α,β-unsaturated acetylamino acid ethyl esters, and found that dehydroalanine derivatives are planar or quasiplanar. Thus, we have only considered planar conformations for **1***a* and **1***b* (8).

Only conformations *s-cis* and *s-trans* regarding the C2—C3 bond in **1***a* were considered. Calculations showed conformer *s-trans* to be more stable than *s-cis* by 0.6 kcal/mol, consequently only the results of the calculations for the *s-trans* conformer were taken into account (Table 2). A schematic representation of the MNDO calculated HOMO and LUMO for *s-trans* **1***a* and **2** is shown in Fig. 2 together with their atomic electron densities (Σc^2).

The reaction occurs between C1 and C4 of cyclopentadiene (**2**), and C1 and C2 of the dienophile **1**, respectively. The following simplified equation expresses the main orbital interactions (9).

$$[1]\quad E = \frac{2[(c_1^{HO})^2(c_1^{LU})^2 + (c_4^{HO})^2(c_2^{LU})^2 + (c_3^{HO})^2(c_3^{LU})^2]\beta_{C-C}^2}{E_{diene}^{HO} - E_{dienophile}^{LU}} + \frac{2[(c_1^{LU})^2(c_1^{HO})^2 + (c_4^{LU})^2(c_2^{HO})^2]\beta_{C-C}^2 + [(c_3^{LU})^2(c_4^{HO})^2]\beta_{C-N}^2}{E_{dienophile}^{HO} - E_{diene}^{LU}}$$

According to the energy gaps between HOMO's and LUMO's, the reaction between **1***a* and **2** can be classified as normal, although nearly neutral ($E_2^{HOMO} - E_{1a}^{LUMO} = -8.985$ eV, $E_{1a}^{HOMO} - E_2^{LUMO} = -9.724$ eV).

The *endo*/*exo* selectivity of Diels–Alder reactions is generally explained by additional overlap between orbitals of atoms not directly intervening in bond formation, secondary interactions. In our case, we must focus attention on the N atom in the acylamino group and on the carbonyl carbon in the ester moiety (Fig. 2).

If the $HOMO_{diene}$–$LUMO_{dienophile}$ pair is considered, the only relevant secondary interaction occurs between C3 of both diene and dienophile, leading to a preference for the *endo* stereoisomer. However, in the $LUMO_{diene}$–$HOMO_{dienophile}$ pair the only relevant secondary interaction occurs between C3–diene and N4–dienophile, so this orbital pair favours the formation of the *exo* adduct (Fig. 3).

Introducing the atomic coefficients and MO energies for **1***a* and **2**, and taking the resonance integrals, β_{C-X}, as the geometric average of individual β values (9), we obtain a

Can. J. Chem. Downloaded from www.nrcresearchpress.com by 213.166.140.6 on 09/07/12
For personal use only.

TABLE 3. Frontier molecular orbital coefficients and energies of methyl-*N*-acetyl-α,β-dehydroalaninate protonated on the acetamido oxygen

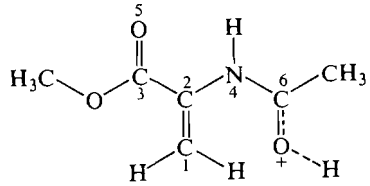

Orbital	*E* (eV)	C1	C2	C3	N4	O5	C6	O7
HOMO	−14.54	−0.584	−0.630	0.048	0.287	0.275	0.245	−0.028
LUMO	−5.81	0.331	−0.083	−0.018	−0.417	0.025	0.765	0.012
LUMO + 1	−4.01	−0.663	0.523	0.310	−0.230	−0.268	0.198	−0.129

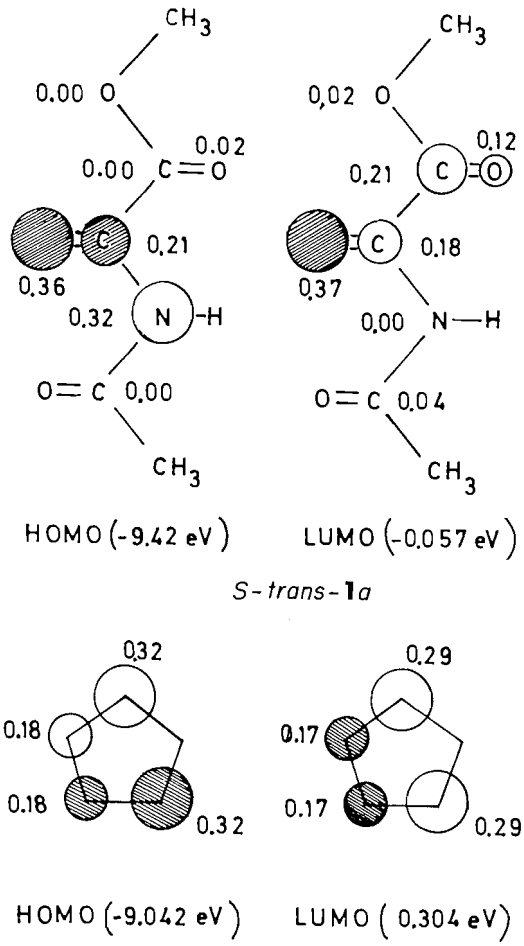

FIG. 2. Schematic representation of MNDO calculated HOMO and LUMO for **1***a* and **2**. Figures denote electron densities on each atom.

$\Delta E_{endo} = -0.082\beta_C^2$ and a $\Delta E_{exo} = -0.089\beta_C^2$. From these values we can infer that the *exo* isomer is slightly favoured over the *endo*, being in qualitative agreement with the experimentally observed preference for the *exo* over the *endo* isomer (Table 1).

With regard to compound **1***b*, the only relevant torsion angle to be determined in the MNDO calculations is the one formed by the phenyl ring plane and the amido unit plane, "ω", whose calculated value under geometry optimization is ω = 90°. This lack of planarity may, however, be due to the MNDO tendency to twist groups with π-systems conjugated to phenyl rings (10), a tendency probably due to the overestimation of short nonbonded contacts in this semiempirical method (3). This situation can affect the electronic structure of **1***b*, and the calculation was repeated fixing ω = 0°.

The electronic structures of planar (ω = 0°) and perpendicular (ω = 90°) **1***b* show no difference in their atomic orbital contributions from those of $C1^{LUMO}$ and $C2^{LUMO}$, because the LUMO of the perpendicular conformation is aromatic-like, while that of the planar structure is ethylenic-like (Table 2). Consequently only the planar conformation will be considered.

The HOMO − LUMO energy gaps are $E_{diene}^{HOMO} - E_{dienophile}^{LUMO} = -8.605$ eV and $E_{dienophile}^{HOMO} - E_{diene}^{LUMO} = -9.634$ eV. Again the reaction can be classified as normal or neutral. The only important secondary interactions are those coming from the N atom of the benzamido group, since the carbonyl carbon of the ester moiety has no significant coefficients at all (Table 2). The application of eq. [1] to the present case allows us to obtain $\Delta E_{endo} = -0.040\beta_C^2$ and $\Delta E_{exo} = -0.054\beta_C^2$, so the *exo* stereoisomer must be favoured again.

It is remarkable that although several approximations have been made in the calculation of ΔE's, the results agree qualitatively with the experiments. Moreover, the low reactivity of **1***b* can be explained by considering the lower values for its calculated ΔE's compared to those of **1***a*, or by a possible contribution of the nonplanar conformation leading to steric hindrance in the transition state.

The lower *exo*/*endo* ratio obtained when $TiCl_4$ is used as a catalyst is difficult to account for. The catalyst can coordinate at several sites within **1***a*. To simulate this coordination in the simplest possible way, a proton was attached to the carbonyl oxygen of the ester and acetamido units of **1***a*. Calculations show that coordination at the acetamido group is more favoured, by 10.9 kcal/mol, so only this possibility is considered. The LUMO of this protonated species has no significant coefficients at C1 and C2, the effective LUMO then being LUMO + 1 (Table 3). The energy gap between frontier orbitals of the reactants is now clearly shifted to the $HOMO_{diene}$ – $(LUMO + 1)_{dienophile}$ pair, and the reaction can be classified as normal. Figure 4 shows a schematic representation of this interaction.

In this simple model for $TiCl_4$ coordination, only the *endo* adduct is favoured by secondary interactions, so it is reasonable to expect a lower experimental *exo*/*endo* ratio.

Can. J. Chem. Downloaded from www.nrcresearchpress.com by 213.166.140.6 on 09/07/12
For personal use only.

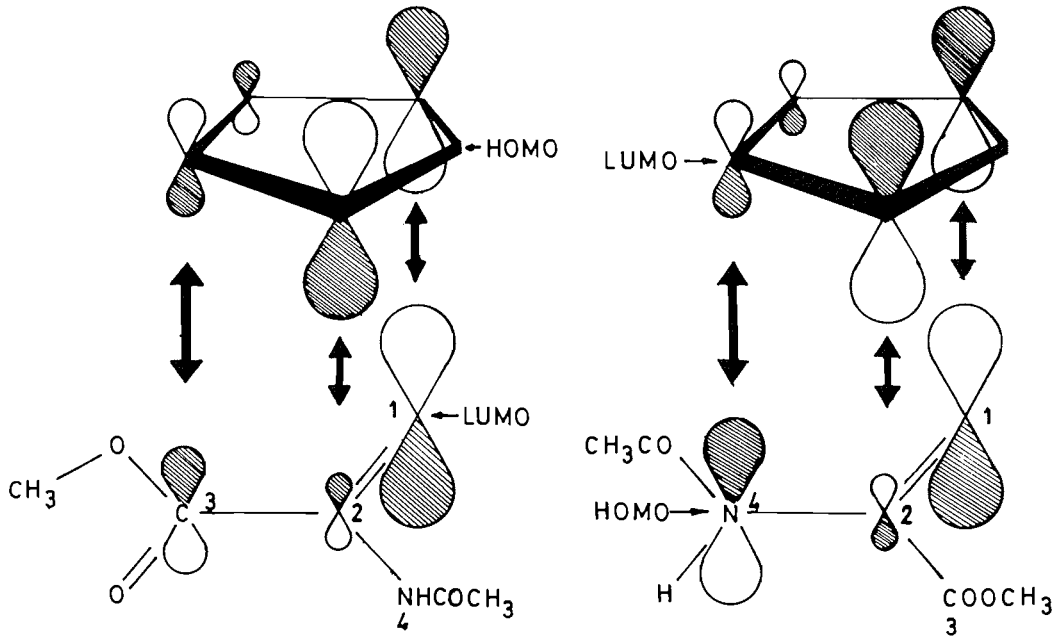

FIG. 3. Orbital interactions between **1***a* and **2**.

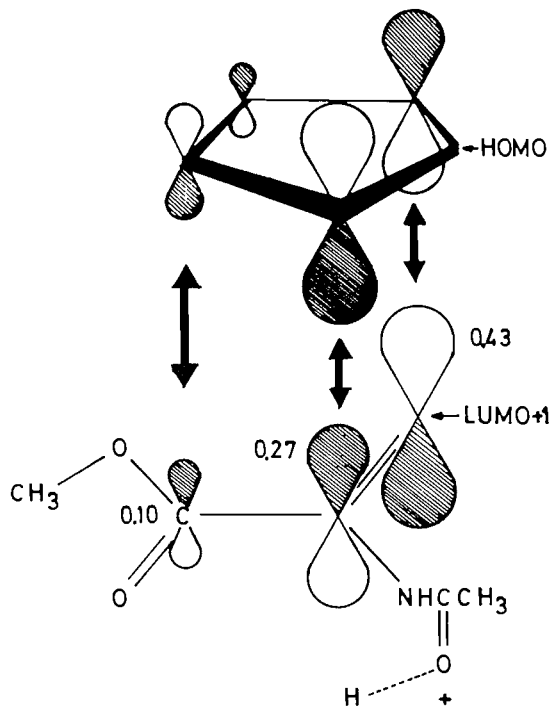

FIG. 4. LUMO + 1 of protonated **1***a* interacting with HOMO of **2** in *endo* approach. Numbers represent Σc^2 for each atom.

Discussion

While methylacrylate reacts with cyclopentadiene giving an *endo/exo* ratio of about 70:30 (11), the reverse is found with **1***a* (*exo/endo* ratio of about 70:30) (Table 1). Formally, the reason for this is the replacement of an H atom by an acetamido group. Methylacrylate has ethylene π-type frontier orbitals with contribution of the carbonyl carbon atom; consequently only the *endo* approach shows stabilizing secondary interactions in the $HOMO_{diene}$–$LUMO_{dienophile}$ pair. Compound **1***a* also has ethylene π-type frontier orbitals, but the presence of the acetamido group gives rise to the existence of a new secondary interaction, which favours the obtention of the *exo* isomer. The application of eq. [1] shows the importance of secondary interaction in this particular case.

The replacement of the acetamido group in **1***a* by a methyl group, leading to methyl methacrylate, does not change the observed *exo/endo* ratio, 68:32 (11). In this case secondary interaction cannot be invoked, and the reason for this remains controversial, to say the least. While some authors propose destabilizing van der Waals interactions (12), others suggest attractive van der Waals interactions (11).

Although a simple model enables us to rationalize the lower *exo/endo* ratio obtained when $TiCl_4$ is used, we cannot explain the experimental result. Seven-membered chelate complexes where $TiCl_4$ is coordinated to two carbonyl oxygens are known, which suggests that species with the catalyst coordinated to both carbonyl oxygen atoms may exist in our case.

In summary, we can conclude that in the Diels–Alder reaction between **1** and **2**, in the absence of a catalyst, the secondary interactions play an important role in determining the experimental *exo/endo* ratios.

Experimental

Melting points were determined on a Büchi apparatus and are uncorrected; ir spectra were registered on a Perkin–Elmer 283 spectrophotometer, and ^1H nmr spectra on a Bruker WP 80 CW apparatus.

Synthesis of methyl N*-acetyl-α,β-dehydroalaninate (**1**a)*

CH_3I (11.36 g, 80 mmol) and 12.15 g (88 mmol) of anhydrous K_2CO_3 were added to a solution of 5.16 g (40 mmol) of *N*-acetyl-α,β-dehydroalanine in dry acetone. The mixture was refluxed for 3 h and then an additional 5.68 g (40 mmol) of CH_3I was added and the reflux was maintained for another 3 h. The solution was then cooled and the solid was separated by filtration and washed with acetone. The acetone was removed by distillation under reduced pressure and the oily residue was extracted with chloroform. The removal of the chloroform by

Can. J. Chem. Downloaded from www.nrcresearchpress.com by 213.166.140.6 on 09/07/12
For personal use only.

distillation under reduced pressure afforded 4.60 g (80%) of methyl *N*-acetyl-α,β-dehydroalaninate (**1***a*), which can be recrystallized from *n*-pentane. The mp and the ^{1}H nmr spectrum were in accordance with those given in the literature; mp 50–52°C (lit. (13) mp 50–52°C).

Synthesis of methyl N-*benzoyl-α,β-dehydroalaninate (1*b*)*

CH_3I (11.36 g, 80 mmol) and 12.15 g (88 mmol) of anhydrous K_2CO_3 were added to a solution of 7.64 g (40 mmol) of *N*-benzoyl-α,β-dehydroalanine in dry acetone and the mixture was refluxed for 3.5 h. The solution was then cooled and the solid was separated by filtration and washed with acetone. The removal of the acetone by distillation under reduced pressure afforded 7.0 g (85%) of crude material whose main component is the methyl *N*-benzoyl-α,β-dehydroalaninate (**1***b*). A pure oily sample was prepared by column chromatography on silica gel using CCl_4/AcOEt = 15:1 as eluent. The ir and ^{1}H nmr spectra were in accordance with those given in ref. 4.

Diels–Alder reactions

Without a catalyst

To a solution of 2 mmol of the corresponding methyl *N*-acyl-α,β-dehydroalaninate and a little hydroquinone in the appropriate dry solvent, the amount of freshly distilled cyclopentadiene previously chosen was added, and the solution was refluxed for 5 h. The solvent was then removed by distillation under reduced pressure and the residue analyzed by ^{1}H nmr.

The adducts were separated by means of column chromatography using Et_2O/Me_2CO = 9:1 as eluent.

Methyl 2-*exo*-acetylamino-5-norboren-2-*endo*-carboxylate (**3***a*): mp 131–133°C (lit. (2) mp 132–133°C); ir (Nujol) ν: 3270 (NH), 1755 (CO), 1650 (CO) cm^{-1}; ^{1}H nmr ($CDCl_3$) δ: 6.75 (m, 1H), 6.29 (m, 1H), 5.84 (m, 1H), 3.63 (s, 3H), 2.93 (m, 3H), 2.69–2.13 (m, 2H), 1.98 (s, 3H), 1.88–1.39 (m, 2H).

Methyl 2-*endo*-acetylamino-5-norboren-2-*exo*-carboxylate (**4***a*): mp 148–150°C (lit. (2) mp 148–149°C); ir (Nujol) ν: 3290 (NH), 1740 (CO), 1650 (CO) cm^{-1}; ^{1}H nmr ($CDCl_3$) δ: 6.38 (m, 2H), 6.07 (m, 1H), 3.75 (s, 3H), 3.31 (m, 1H), 2.89 (m, 1H), 2.75–2.48 (m, 1H), 1.91 (s, 3H), 1.72–1.10 (m, 3H).

With a catalyst

Under nitrogen, 2.2 mmol of $TiCl_4$ in dry CH_2Cl_2 was added at the appropriate temperature to a stirred solution of **1***a* (2 mmol) in dry CH_2Cl_2. Then a solution of the amount of cyclopentadiene previously chosen in dry CH_2Cl_2 at the same temperature was added. The mixture was stirred for 5 h, treated with a saturated solution of aqueous Na_2CO_3, and washed with a saturated solution of aqueous NaCl. Evaporation of the organic phase yielded a residue that was analyzed by ^{1}H nmr.

MNDO calculations

The dienophiles were considered planar and to have the conformation represented in Fig. 3. In two different calculations the planarity of the phenyl ring and carbonyl group of the amide in **1***b* was fixed, or the dihedral angle "ω" (Fig. 4) was optimized. The other geometrical parameters were optimized, except those of the phenyl ring, which were fixed as follows: C—C = 1.3970 Å, C—H = 1.048 Å, C—C—C = 120.0°, C—C—H = 120.0°; endocyclic C—C—C—C = 0.0° and H—C—C—H = 0.0°.

Acknowledgements

This research was made possible by the generous financial support of the Comisión Asesora de Investigación Científica y Técnica. M. P. Bueno would like to express her gratitude to the Diputación General de Aragón for a grant.

1. (*a*) H. N. Christensen, M. E. Handlogten, I. Lam, H. S. Tager, and R. Zand. J. Biol. Chem. **244**, 1510 (1969); (*b*) H. N. Christensen and A. M. Cullen. J. Biol. Chem. **244**, 1521 (1969); (*c*) H. S. Tager and H. N. Christensen. J. Am. Chem. Soc. **94**, 968 (1972).
2. H. Horikawa, T. Nishitani, T. Iwasaki, Y. Mushika, I. Inoue, and M. Miyoshi. Tetrahedron Lett. **21**, 4101 (1980).
3. M. J. S. Dewar and W. H. Thiel. J. Am. Chem. Soc. **99**, 4917 (1977).
4. T. Wieland, G. Ohnacker, and W. Ziegler. Chem. Ber. **90**, 194 (1957).
5. M. L. Graziano, M. R. Iesce, A. Carotenuto, and R. Scarpati. J. Heterocycl. Chem. **14**, 261 (1977).
6. R. Sustmann. Tetrahedron Lett. 2721 (1971).
7. D. Ajò, M. Casarin, G. Granozzi, H. C. J. Ottenheijm, and R. Plate. Recl. Trav. Chim. Pays-Bas, **103**, 365 (1984).
8. D. Ajò, G. Granozzi, E. Tondello, A. Del Prà, and G. Zanotti. J. Chem. Soc. Perkin Trans. 2, 927 (1979).
9. G. Klopman. J. Am. Chem. Soc. **90**, 223 (1968).
10. (*a*) M. J. S. Dewar, A. H. Pakiari, and A. B. Pierini. J. Am. Chem. Soc. **104**, 3242 (1982); (*b*) C. Cativiela, J. I. Garcia, J. A. Mayoral, E. Melendez, and C. Jaime. Heterocycles, **23**, 2685 (1985).
11. (*a*) Y. Kobuke, T. Fueno, and J. Furukawa. J. Am. Chem. Soc. **92**, 6548 (1970); (*b*) Y. Kobuke, T. Sugimoto, J. Furukawa, and T. Fueno. J. Am. Chem. Soc. **94**, 3633 (1972).
12. K. N. Houk and L. J. Luskus. J. Am. Chem. Soc. **93**, 4606 (1971).
13. A. J. Kolar and R. K. Olsen. Synthesis, 457 (1977).

Can. J. Chem. Downloaded from www.nrcresearchpress.com by 213.166.140.6 on 09/07/12
For personal use only.

The crystal structure of $Sn_6O_2(CF_3CO_2)_8.CF_3CO_2H$

R. J. BATCHELOR, T. BIRCHALL,[1] AND J. P. JOHNSON

Department of Chemistry and Institute for Materials Research, McMaster University, 1280 Main Street West, Hamilton, Ont., Canada L8S 4M1

Received February 24, 1987

R. J. BATCHELOR, T. BIRCHALL, and J. P. JOHNSON. Can. J. Chem. **65**, 2187 (1987).

The X-ray crystal structure of $Sn_6O_2(CF_3CO_2)_8.CF_3CO_2H$ has been determined: $R_1 = 0.0519$. The crystals were orthorhombic, space group $Pna2_1$, $a = 18.327(4)$ Å, $b = 12.209(3)$ Å, $c = 19.218(3)$ Å, $f_w = 1762.29$, and $Z = 4$. The structure consists of two sets of three tin(II) atoms, each set linked by a μ_3-oxo bridge. The tin atoms are further linked by trifluoroacetate groups to form an extended structure in which the tin atoms can be described as having either SnX_4E or SnX_5E coordination.

R. J. BATCHELOR, T. BIRCHALL et J. P. JOHNSON. Can. J. Chem. **65**, 2187 (1987).

On a déterminé la structure cristalline du $Sn_6O_2(CF_3CO_2)_8.CF_3CO_2H$ par diffraction des rayons-X : $R_1 = 0{,}0519$. Les cristaux sont orthorhombiques, groupe d'espace $Pna2_1$, $a = 18{,}327(4)$, $b = 12{,}209(3)$ et $c = 19{,}218(3)$ Å, masse = 1762,29 et $Z = 4$. La structure comporte deux ensembles de trois atomes d'étain(II), chacun des ensembles étant relié par un pont oxo-μ_3. Les atomes d'étain sont de plus reliés par les groupements trifluoroacétates pour former une structure importante dans laquelle la coordination des atomes d'étain peut être décrite comme étant soit SnX_4E ou SnX_5E.

[Traduit par la revue]

Introduction

A number of tin(II) carboxylates have been prepared, studied by a variety of spectroscopic techniques and were inferred to have trigonal-pyramidal stereochemistry about tin (1, 2). However, relatively few of these carboxylates have been obtained in a pure form. Recently we were able to isolate tin(II) trifluoroacetate and characterize it spectroscopically (3). Our spectroscopic results seemed to indicate that the tin environment was unlikely to be that of a trigonal pyramid. These spectroscopic data were more consistent with the trigonal-bipyramidal tin environment found in tin(II) formate (4). In an attempt to obtain crystals of tin(II) trifluoroacetate, suitable for analysis by X-ray crystallography, we sublimed some of the original compound in a sealed tube and obtained crystals of $Sn_6O_2(CF_3CO_2)_8.CF_3CO_2H$ whose crystal structure we now report.

Experimental

Preparation

A sample of $Sn(CF_3CO_2)_2$ was prepared according to the literature method (3). Since none of this material was suitable for X-ray crystallographic analysis, some of the material was placed in a dry 6 mm diameter Pyrex tube, evacuated, sealed and the tube laid horizontally on top of a 150°C oven so that a temperature gradient was set up across the diameter of the tube. After several days small crystals had formed on the coolest side of the tube. These were removed in a dry atmosphere box and a crystal suitable for X-ray analysis was mounted in a capillary tube which was then sealed and the analysis performed on a Nicolet P3 diffractometer. The methods of selection of scan rates and initial data treatment have been described (5, 6). Details of the crystal data, acquisition and structure refinement are summarized in Table 1.

Computations were carried out on a Cyber 17/730 computer. Data reduction employed programs from the XRAY 76 package (7). Lorentz, polarization and empirical absorption corrections were applied (8–10). The intensity-weighted reciprocal lattice indicated the space groups *Pnma* or $Pna2_1$. The eventual choice of $Pna2_1$ was justified by the successfully refined structure. The coordinates of the tin atoms were obtained using the program MULTAN (11) and a series of full-matrix least-squares refinements, followed by three-dimensional electron density difference syntheses, using the program SHELX 76 (12), revealed all of the C, O, and F atoms. Because of the large number

[1]To whom all correspondence should be addressed.

TABLE 1. Crystal and diffraction data acquisition parameters for $Sn_6O_2(CF_3CO_2)_8.CF_3CO_2H$

Crystal parameters	
$a = 18.327(4)$ Å	Orthorhombic
$b = 12.209(3)$ Å	Space group: $Pna2_1$
$c = 19.218(3)$ Å	$Z = 4$
$U = 4300(3)$ Å^3	$f_w = 1762.29$
$(Mo K_\alpha) = 33.36$ cm^{-1}	$\rho_{calcd} = 2.722(2)$ g cm^{-3}
Conditions: 0 k l : $k + 1 = 2n$	
h 0 l : $h = 2n$	
Crystal dimensions: 0.26 mm × 0.23 mm × 0.19 mm	
Intensity measurements	
Radiation: Mo K_α (wavelength = 0.71069 Å; graphite monochrometer)	
Scan mode: θ: 2θ	
Scan range: ($K_{\alpha1}$ − 1.0°) to ($K_{\alpha2}$ + 1.0°)	
Scan rates[a]: 5.86 to 29.3° min^{-1}	
Reflections measured: h, k, $\pm l$	
Maximum 2θ: 55°	
Standard reflections: 3 2 −4 (e.s.d. 1.2%)	
3 2 2 (e.s.d. 1.4%)	
Details of refinement	
Unique observed reflections: 4577	$I > 3\sigma(I)$
Unobserved reflections: 4072	$3\sigma(I) > I > 0$[b]
1705	$I \leq 0$[c]
10354	
R factors[d,e]: $R_1 = 0.0519$, $R_2 = 0.0478$	
Weighting scheme: $w = [\sigma F^2 + 0.0002F^2]^{-1}$	
"Secondary extinction": $F^* = F(1 - gF^2/\sin\theta)$	
$g = 4 \times 10^{-9}$	
Final | shift/error: maximum 0.089	
average 0.020	
Highest peak in final difference map: 2.67 e Å^{-3} at 0.360, 0.309, 0.343	
Lowest trough in final difference map: −2.64 e Å^{-3}	
$F(000) = 3244$	

[a]Dependent upon the intensity of a preliminary count.

[b]Suppressed in the refinement.

[c]Not included.

[d]$R_1 = \Sigma(|F_o| - |F_c|)/\Sigma(|F_o|)$. $R_2 = [\Sigma(w \times (|F_o| - |F_c|)^2)/\Sigma(w \times F_o^2)]^{1/2}$.

[e]When unobserved reflections are not suppressed in the calculation of R_1 and R_2: $R_1 = 0.1125$, $R_2 = 0.0644$.

Can. J. Chem. Downloaded from www.nrcresearchpress.com by 213.166.140.6 on 09/07/12
For personal use only.

TABLE 2. Final atomic positional fractional coordinates × 10^3 and equivalent isotropic thermal parameters for $Sn_6O_2(CF_2CO_2)_8.CF_3CO_2H$

Atom	x	y	z	U_{eq} (Å^2 × 10^{-3})[b]
Sn(1)	273.8(1)	426.6(1)	895.4[c]	40.2(8)
Sn(2)	416.3(1)	633.3(1)	892.1(1)	38.9(8)
Sn(3)	275.6(1)	146.9(1)	762.2(1)	37.3(7)
Sn(4)	404.9(1)	433.3(1)	1029.3(1)	43.2(8)
Sn(5)	266.8(1)	−99.6(1)	869.4(1)	40.6(8)
Sn(6)	128.2(1)	−42.5(1)	744.7(1)	39.2(8)
O(1)	363.8(7)	502.7(8)	938.8(6)	36(7)
O(2)	224.4(6)	−0.3(9)	788.7(6)	39(7)
O(3)	279.4(7)	626.0(9)	840.6(6)	46(8)
O(4)	219.4(7)	−230.3(9)	798.5(6)	47(8)
O(5)	285.6(6)	409.1(11)	1041.5(7)	54(8)
O(6)	278.2(8)	381.7(11)	1154.9(7)	67(10)
O(7)	344.4(7)	270.9(9)	933.6(6)	43(8)
O(8)	318.6(6)	119.6(9)	876.0(6)	41(7)
O(9)	162.1(7)	110.9(10)	671.3(6)	46(8)
O(10)	388.7(7)	605.3(10)	1067.2(6)	56(9)
O(11)	344.5(6)	397.3(10)	801.6(6)	46(8)
O(12)	431.2(6)	531.2(9)	796.0(6)	45(8)
O(13)	507.0(7)	540.3(11)	940.6(6)	53(9)
O(14)	392.7(6)	408.0(9)	1381.0(6)	48(8)
O(15)	366.7(7)	−129.7(11)	808.3(7)	62(9)
O(16)	388.6(7)	15.5(10)	740.4(8)	63(9)
O(17)	176.1(6)	1230.2(10)	816.1(6)	47(8)
O(18)	83.3(6)	115.7(9)	801.9(6)	42(8)
O(19)	315.3(10)	107.6(15)	618.4(9)	93(15)
O(20)	434.2(9)	94.1(14)	583.0(12)	83(13)
F(1)	158.9(9)	656.1(10)	700.0(8)	90(9)
F(2)	179.3(8)	511.5(11)	761.7(9)	89(12)
F(3)	259.3(10)	577.0(15)	695.9(8)	123(14)
F(4)	146.4(12)	309(3)	1135.0(14)	221(27)
F(5)	145.5(11)	365(2)	1040.1(13)	177(20)
F(6)	197.0(12)	223(2)	1061.2(15)	197(25)
F(7)	338.3(10)	65(2)	1022.7(10)	163(18)
F(8)	419.8(13)	28.6(15)	957.3(12)	161(18)
F(9)	430.5(12)	157.6(12)	1016.0(10)	174(20)
F(10)	204.2(12)	310.1(12)	640.0(12)	145(17)
F(11)	164(2)	298(2)	547.4(9)	183(24)
F(12)	99.1(12)	327.2(12)	620(2)	214(31)
F(13)	366.0(8)	391(2)	661.6(6)	111(14)
F(14)	471.2(11)	462(2)	674.0(8)	150(17)
F(15)	449.0(11)	306.4(15)	709.6(9)	137(16)
F(16)	669.2(8)	419.5(13)	951.3(8)	97(11)
F(17)	585.5(8)	428(2)	1026.8(10)	163(17)
F(18)	663.5(10)	550(2)	1018.4(8)	144(17)
F(19)	506.6(9)	−79(2)	695.4(9)	136(15)
F(20)	475.0(8)	−229.3(11)	737.5(9)	110(13)
F(21)	522.7(9)	−116(2)	803.7(10)	146(19)
F(22)	3.9(13)	242(2)	876(2)	245(29)
F(23)	31.2(15)	339(2)	808(2)	251(32)
F(24)	84.8(8)	350(2)	893.2(13)	160(17)
F(25)	433(2)	87(2)	475.1(11)	233(30)
F(26)	340.0(13)	181(2)	472.7(10)	192(24)
F(27)	436.3(12)	244(2)	508.7(13)	197(25)
C(1)	273.2(10)	673.1(14)	798.6(9)	34(5)
C(2)	209.2(12)	603.(2)	739.9(12)	50(6)
C(3)	258.7(10)	372.8(14)	1095.4(9)	40(5)
C(4)	187(2)	317(3)	1086(2)	78(8)
C(5)	347.4(10)	173.1(15)	925.2(9)	37(5)
C(6)	381.9(13)	110(2)	979.4(12)	51(6)
C(7)	142.8(11)	151.0(15)	616.9(9)	42(5)
C(8)	151.1(15)	275(2)	610.4(12)	53(6)
C(9)	394.2(10)	447(2)	777.2(10)	47(6)
C(10)	422(2)	404(2)	701.9(14)	76(8)
C(11)	574.6(11)	546.0(15)	931.3(9)	42(5)
C(12)	621.5(15)	478(2)	982.8(14)	67(7)
C(13)	401.1(12)	−73(2)	767.4(12)	62(6)
C(14)	477.8(13)	−125(2)	748.5(12)	56(6)
C(15)	111.8(11)	199(2)	817.6(10)	48(6)
C(16)	61.5(15)	281(2)	853.0(13)	64(7)
C(17)	378(2)	115(2)	583.0(12)	57(6)
C(18)	396(2)	158(3)	509(2)	106(11)

[a]Equivalent positions: $x, y, z; \bar{x}, \bar{y}, \frac{1}{2}+z; \frac{1}{2}-x, \frac{1}{2}+y, \frac{1}{2}+z; \frac{1}{2}+x, \frac{1}{2}-y, z$.
[b]$U_{eq} = (1/3)\sum_i\sum_j U_{ij} a_i^* a_j^* \boldsymbol{a}_i \boldsymbol{a}_j$; U_{iso} for carbon atoms.
[c]Coordinate arbitrarily fixed to define unit cell origin.

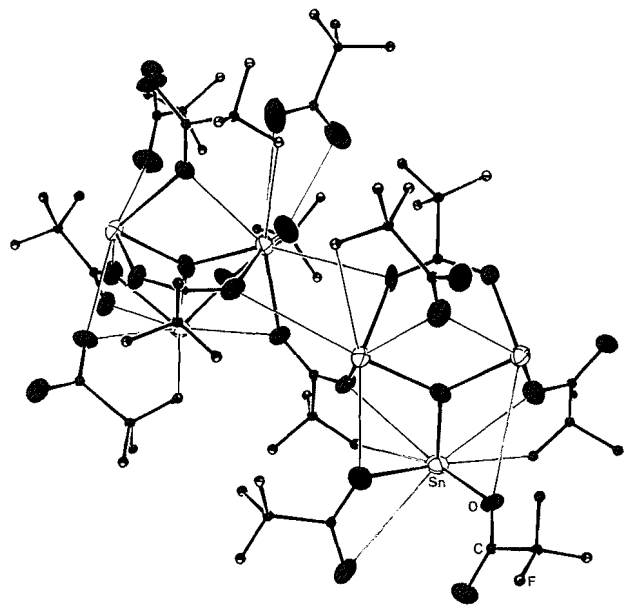

FIG. 1. The structure of $Sn_6O_2(CF_3CO_2)_8.CF_3CO_2H$ showing all interatomic distances smaller than the sum of van der Waals radii.

of atoms in this structure it was necessary to refine it using a large block approximation to the normal matrix. Two blocks were refined alternately. The first included all parameters for the tin atoms as well as for O(1) to O(18) inclusive. The second included the parameters for the remaining atoms. The scale, and in the final stages the "extinction" parameter (see Table 1) were included as variables in each cycle. Using this method, final refinement of a total of 391 variables, including anisotropic atomic temperature factors for Sn, O, and F, minimized $\Sigma_w(|F_o|-|F_c|)^2$ for the 4577 observed reflections, yielding a final residual of $R_1 = 0.0519$. The H atom was not located in the final difference Fourier map.

The final atomic positional coordinates are given in Table 2, interatomic distances (Sn—O) and bond angles (O—Sn—O) in Table 3(*a*). Other bond distances and angles (Table 3(*b*)), anisotropic temperature factors for the Sn, O, and F atoms (Table 4) and the observed and calculated structure factors (Table 5) have been deposited as Supplementary Information and are available on request.[2] Plots were generated using ORTEP II (13).

[2]Complete set of data may be purchased from the Depository of Unpublished Data, CISTI, National Research Council of Canada, Ottawa, Ont., Canada K1A 0S2.

Can. J. Chem. Downloaded from www.nrcresearchpress.com by 213.166.140.6 on 09/07/12
For personal use only.

Can. J. Chem. Downloaded from www.nrcresearchpress.com by 213.166.140.6 on 09/07/12
For personal use only.

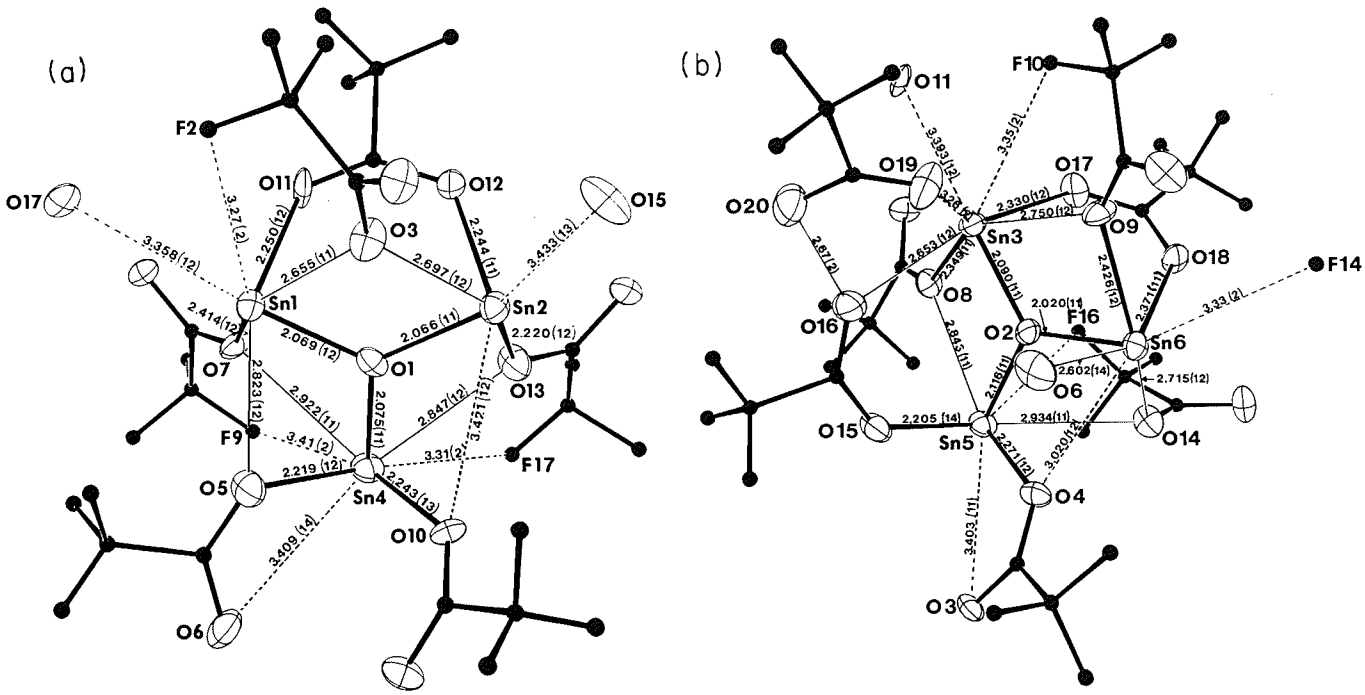

FIG. 2. The two Sn_3O units, *a* and *b*, together with their most closely associated carboxylate ligands. Thick lines represent strong bonds, thin lines represent weak but significant interactions, while hatched lines represent very weak interactions, or non-bonding contacts.

Results and discussion

Preliminary spectroscopic data obtained on the sublimed material revealed that the compound could not be the expected $Sn(CF_3CO_2)_2$. The X-ray solution shows that the structure consists of two sets of three tin(II) atoms, each set being linked by a μ_3-oxo bridge. Two crystallographically independent Sn_3O units are linked by trifluoroacetate groups to form an extended structure. The two Sn_3O units and their surrounding trifluoroacetate groups are shown in Fig. 1. In addition to the trifluoroacetate ligands which link the Sn_3O units, there are trifluoroacetate groups which are bonded to each tin in order to satisfy its charge and coordination requirements. One trifluoroacetic acid molecule completes the asymmetric unit. This results in there being six different tin environments in the structure. Although each of the trifluoroacetate groups is crystallographically different, there are three basic types. These are, monodentate with one strong O—Sn bond, bidentate-chelating two different tin atoms in a symmetric fashion, and bidentate-chelating two different tin atoms in an asymmetric fashion. The trifluoroacetic acid molecule is hydrogen bonded to an oxygen of one of the trifluoroacetate ligands, O(20)—O(16), 2.67(2) Å and has a long contact O(19)—Sn(3), 3.26(2) Å. Not one of the carboxylate ligands forms a bidentate chelating link to a single tin atom.

For convenience the two Sn_3O units together with their most closely associated carboxylate ligands have been represented in Fig. 2*a* and *b* with all interatomic distances less than the sum of the Van der Waals radii being indicated. A number of these distances which are close to the Van der Waals separations are almost certainly non-bonding interactions, however they are included for completeness. Nevertheless, the Sn—O distances displayed range from 2.02 Å out to the Van der Waals separation of 3.45 Å and it is difficult to draw a clear distinction between bonding and non-bonding interactions. Each of the Sn_3O units is almost planar, with plane *1*, (Sn(1), Sn(2), Sn(4), O(1)) defined by $0.5840x - 0.6179y - 0.5265z + 9.3489 = 0$, while plane 2 (Sn(3), Sn(5), Sn(6), O(2)) is defined by $0.5167x - 0.5024y - 0.6933z + 8.4461 = 0$. The deviation of O(1) from plane *1* is −0.05(1) Å while O(2) is +0.06(1) Å out of plane 2: the dihedral angle between these two planes is 12.3°.

The unit containing Sn(1), Sn(2), Sn(4), O(1), shown in Fig. 2(*a*), is the more symmetric of the two, the tin—μ_3O distances being essentially equal, with the Sn—O—Sn angles close to 120° (Table 3). There is a variation in Sn—O bond lengths in the second unit ranging from O(2)—Sn(6), 2.020(11) Å through O(2)—Sn(3), 2.090(11) Å to 0(2)—Sn(5), 2.116(11) Å, though the Sn—O—Sn angles again remain close to 120°. These μ_3 oxo—tin bonds are shorter than those found recently in mixed valence tin caboxylates (3, 14, 15) and are among the shortest Sn(II)—O bond lengths measured to date (16), with O(2)—Sn(6) at 2.020(11) Å being the shortest known. Each tin has two relatively short Sn—O interactions in addition to the short bond to the μ_3 oxygen atom giving a pyramidal arrangement at the tin atoms. This arrangement, however, is not a trigonal one since the Sn—Oμ_3 bond is always significantly shorter than the other tin–oxygen interactions and furthermore the O—Sn—O angles vary from 74.3 to 90.6° (Table 3), presumably to accommodate the other longer tin—oxygen interactions and the non-bonding electron pair.

In the Sn(1)Sn(2)Sn(4)O(1) unit tin atoms (1) and (2) are symmetrically bridged by one trifluoroacetate group through O(11) and O(12) and these are strong interactions. These two tin atoms also are weakly μ-bridged via O(3) of a trifluoroacetate whose other oxygen O(4) forms a strong bond to Sn(5) of another Sn_3O unit. The Sn(1)—O(3) and Sn(2)—O(3) distances are 2.655(11) and 2.697(12) Å, respectively, clearly interactions of a weaker type but still significant being only

Can. J. Chem. Downloaded from www.nrcresearchpress.com by 213.166.140.6 on 09/07/12
For personal use only.

TABLE 3. Interatomic distances (Sn—O) and bond angles (O—Sn—O) for $Sn_6O_2(CF_3CO_2)_8.CF_3CO_2H$

(*a*) Bond distances (Å)

Bond	Distance	Bond	Distance
Sn(1)—O(1)	2.069(12)	Sn(3)—O(2)	2.090(11)
Sn(1)—O(11)	2.250(12)	Sn(3)—O(17)	2.330(12)
Sn(1)—O(7)	2.414(12)	Sn(3)—O(8)	2.349(11)
Sn(1)—O(3)	2.655(11)	Sn(3)—O(16)	2.653(12)
Sn(1)—O(5)	2.823(12)	Sn(3)—O(9)	2.750(12)
Sn(1)—O(17)	3.358(12)	Sn(3)—O(11)	3.393(12)
Sn(1)—F(2)	3.27(2)	Sn(3)—O(19)	3.26(2)
		Sn(3)—F(10)	3.35(2)
Sn(2)—O(1)	2.066(11)		
Sn(2)—O(13)	2.220(12)	Sn(5)—O(2)	2.116(11)
Sn(2)—O(12)	2.244(11)	Sn(5)—O(15)	2.205(14)
Sn(2)—O(3)	2.697(12)	Sn(5)—O(4)	2.271(12)
Sn(2)—O(10)	3.421(12)	Sn(5)—O(8)	2.843(11)
Sn(2)—O(15)	3.433(13)	Sn(5)—O(14)	2.934(11)
		Sn(5)—O(3)	3.403(11)
Sn(4)—O(1)	2.075(11)	Sn(5)—F(16)	3.24(2)
Sn(4)—O(5)	2.219(12)		
Sn(4)—O(10)	2.243(13)	Sn(6)—O(2)	2.022(11)
Sn(4)—O(13)	2.847(12)	Sn(6)—O(18)	2.371(11)
Sn(4)—O(7)	2.922(11)	Sn(6)—O(9)	2.426(12)
Sn(4)—O(6)	3.409(14)	Sn(6)—O(6)	2.602(14)
Sn(4)—F(17)	3.31(2)	Sn(6)—O(14)	2.715(12)
Sn(4)—F(9)	3.41(2)	Sn(6)—O(4)	3.020(12)
		Sn(6)—F(14)	3.33(2)

(*b*) Bond angles (deg)

Atoms	Angle	Atoms	Angle
Sn(1)—O(1)—Sn(2)	122.8(5)	Sn(3)—O(2)—Sn(5)	120.5(5)
Sn(1)—O(1)—Sn(4)	116.3(5)	Sn(3)—O(2)—Sn(6)	120.6(5)
Sn(2)—O(1)—Sn(4)	120.7(6)	Sn(5)—O(2)—Sn(6)	118.7(5)
O(1)—Sn(1)—O(11)	86.3(4)	O(2)—Sn(3)—O(17)	85.2(4)
O(1)—Sn(1)—O(7)	78.7(4)	O(2)—Sn(3)—O(8)	78.6(4)
O(1)—Sn(1)—O(3)	73.6(4)	O(2)—Sn(3)—O(16)	82.4(4)
O(1)—Sn(1)—O(5)	64.7(4)	O(2)—Sn(3)—O(9)	71.3(4)
O(1)—Sn(1)—F(2)	126.7(4)	O(2)—Sn(3)—O(11)	152.5(4)
O(1)—Sn(1)—O(17)	158.2(4)	O(2)—Sn(3)—O(19)	102.0(3)
O(11)—Sn(1)—O(7)	79.0(4)	O(2)—Sn(3)—F(10)	120.5(5)
O(11)—Sn(1)—O(3)	78.8(4)	O(17)—Sn(3)—O(8)	84.9(4)
O(11)—Sn(1)—O(5)	137.8(4)	O(17)—Sn(3)—O(16)	160.9(4)
O(11)—Sn(1)—F(2)	74.0(4)	O(17)—Sn(3)—O(9)	76.2(4)
O(11)—Sn(1)—O(17)	80.2(4)	O(17)—Sn(3)—O(11)	78.4(4)
O(7)—Sn(1)—O(3)	145.3(4)	O(17)—Sn(3)—O(19)	131.9(3)
O(7)—Sn(1)—O(5)	66.3(4)	O(17)—Sn(3)—F(10)	75.3(5)
O(7)—Sn(1)—F(2)	140.6(4)	O(8)—Sn(3)—O(16)	78.4(4)
O(7)—Sn(1)—O(17)	82.0(4)	O(8)—Sn(3)—O(9)	145.3(4)
O(3)—Sn(1)—O(5)	117.5(4)	O(8)—Sn(3)—O(11)	78.2(3)
O(3)—Sn(1)—F(2)	54.4(4)	O(8)—Sn(3)—O(19)	143.3(3)
O(3)—Sn(1)—O(17)	119.7(3)	O(8)—Sn(3)—F(10)	150.4(4)
O(5)—Sn(1)—F(2)	147.9(4)	O(16)—Sn(3)—O(9)	113.1(4)
O(5)—Sn(1)—O(17)	116.0(3)	O(16)—Sn(3)—O(11)	106.8(3)
F(2)—Sn(1)—O(17)	65.7(3)	O(16)—Sn(3)—O(19)	65.4(3)
		O(16)—Sn(3)—F(10)	123.7(5)
		O(9)—Sn(3)—O(11)	124.5(3)
O(1)—Sn(2)—O(13)	76.8(5)	O(9)—Sn(3)—O(19)	62.2(3)
O(1)—Sn(2)—O(12)	89.2(4)	O(9)—Sn(3)—F(10)	49.8(4)
O(1)—Sn(2)—O(3)	72.6(4)	O(11)—Sn(3)—O(19)	105.3(2)
O(1)—Sn(2)—O(10)	55.0(4)	O(11)—Sn(3)—F(10)	76.5(4)
O(1)—Sn(2)—O(15)	137.0(4)	O(19)—Sn(3)—F(10)	59.9(4)
O(13)—Sn(2)—O(12)	88.3(4)		
O(13)—Sn(2)—O(3)	146.5(4)		

TABLE 3 (*concluded*)

Atoms	Angle	Atoms	Angle
O(13)—Sn(2)—O(10)	69.3(4)	O(2)—Sn(5)—O(15)	90.6(5)
O(13)—Sn(2)—O(15)	145.7(4)	O(2)—Sn(5)—O(4)	79.8(4)
O(12)—Sn(2)—O(3)	78.1(4)	O(2)—Sn(5)—O(8)	67.4(4)
O(12)—Sn(2)—O(10)	140.5(4)	O(2)—Sn(5)—O(14)	70.8(4)
O(12)—Sn(2)—O(15)	96.6(4)	O(2)—Sn(5)—O(3)	118.0(4)
O(3)—Sn(2)—O(10)	102.7(3)	O(2)—Sn(5)—F(16)	76.4(4)
O(3)—Sn(2)—O(15)	67.0(3)	O(15)—Sn(5)—O(4)	83.2(5)
O(10)—Sn(2)—O(15)	120.6(3)	O(15)—Sn(5)—O(8)	84.5(4)
		O(15)—Sn(5)—O(14)	150.8(4)
		O(15)—Sn(5)—O(3)	72.1(4)
O(1)—Sn(4)—O(5)	77.6(5)	O(15)—Sn(5)—F(16)	146.1(4)
O(1)—Sn(4)—O(10)	80.9(4)	O(4)—Sn(5)—O(8)	144.7(4)
O(1)—Sn(4)—O(13)	63.3(4)	O(4)—Sn(5)—O(14)	71.7(4)
O(1)—Sn(4)—O(7)	67.2(4)	O(4)—Sn(5)—O(3)	40.2(4)
O(1)—Sn(4)—O(6)	115.0(4)	O(4)—Sn(5)—F(16)	123.8(4)
O(1)—Sn(4)—F(17)	111.0(5)	O(8)—Sn(5)—O(14)	107.4(3)
O(1)—Sn(4)—F(9)	113.0(5)	O(8)—Sn(5)—O(3)	155.7(3)
O(5)—Sn(4)—O(10)	87.7(5)	O(8)—Sn(5)—F(16)	61.6(4)
O(5)—Sn(4)—O(13)	140.6(4)	O(14)—Sn(5)—O(3)	96.4(3)
O(5)—Sn(4)—O(7)	66.6(4)	O(14)—Sn(5)—F(16)	52.5(4)
O(5)—Sn(4)—O(6)	39.6(4)	O(3)—Sn(5)—F(16)	141.6(4)
O(5)—Sn(4)—F(17)	169.8(5)		
O(5)—Sn(4)—F(9)	90.7(5)		
O(10)—Sn(4)—O(13)	81.5(4)	O(2)—Sn(6)—O(18)	84.3(4)
O(10)—Sn(4)—O(7)	142.2(4)	O(2)—Sn(6)—O(9)	79.8(4)
O(10)—Sn(4)—O(6)	81.5(4)	O(2)—Sn(6)—O(6)	78.1(4)
O(10)—Sn(4)—F(17)	98.9(5)	O(2)—Sn(6)—O(14)	77.1(4)
O(10)—Sn(4)—F(9)	165.3(5)	O(2)—Sn(6)—O(4)	64.4(4)
O(13)—Sn(4)—O(7)	100.6(3)	O(2)—Sn(6)—F(14)	148.1(5)
O(13)—Sn(4)—O(6)	163.0(4)	O(18)—Sn(6)—O(9)	74.3(4)
O(13)—Sn(4)—F(17)	48.9(4)	O(18)—Sn(6)—O(6)	145.7(4)
O(13)—Sn(4)—F(9)	108.6(4)	O(18)—Sn(6)—O(14)	71.6(4)
O(7)—Sn(4)—O(6)	93.6(3)	O(18)—Sn(6)—O(4)	130.7(4)
O(7)—Sn(4)—F(17)	111.0(5)	O(18)—Sn(6)—F(14)	69.5(4)
O(7)—Sn(4)—F(9)	48.3(4)	O(9)—Sn(6)—O(6)	73.8(4)
O(6)—Sn(4)—F(17)	133.4(4)	O(9)—Sn(6)—O(14)	140.2(4)
O(6)—Sn(4)—F(9)	87.9(4)	O(9)—Sn(6)—O(4)	130.1(4)
F(17)—Sn(4)—F(9)	81.0(5)	O(9)—Sn(6)—F(14)	75.9(5)
		O(6)—Sn(6)—O(14)	130.8(4)
		O(6)—Sn(6)—O(4)	66.0(4)
		O(6)—Sn(6)—F(14)	113.8(4)
		O(14)—Sn(6)—O(4)	65.1(3)
		O(14)—Sn(6)—F(14)	109.7(4)
		O(4)—Sn(6)—F(14)	147.3(4)

0.25 Å longer than the sum of the ionic radii (16). This bridging interaction gives these two tin atoms a coordination represented as SnX_4E rather than as SnX_3E, where E represents the non bonding electron pair (17). The situation at Sn(4) is slightly different in that there are two longer secondary interactions at 2.847(12) and 2.922(11) Å, giving it a SnX_5E coordination. There are longer Sn—O,F interactions also listed in Table 3 and shown in the figures but these are obviously of marginal significance. Of the six trifluoroacetate ligands bonded to the tin atoms in this unit, only one forms an essentially symmetric bidentate bridge (see O(11)—Sn(1), O(12)—Sn(2)). The other five trifluoroacetates interact to varying degrees with both Sn_3O units or symmetry related ones.

As indicated earlier the second unit is not as symmetric as the one just described. Figure 2(*b*) shows all the interactions to Sn less than Van der Waals separations. There is again one trifluoroacetate which symmetrically bridges Sn(3) and Sn(6). The atom O(9) forms a μ-oxo bridge between these tin atoms but this is quite asymmetric, unlike the O(3) bridging Sn(1) and Sn(2). The coordination about each tin in this unit can be represented as SnX_5E, if the very long interactions are discounted. There are six trifluoroacetate groups associated with this unit, as in the previous case, but in addition a trifluoroacetic acid molecule is hydrogen bonded to O(16) and weakly coordinating to Sn(3), O(20)—O(16) and O(19)—Sn(3), respectively. This may be one reason for the more distorted geometry of this unit compared to the other, pushing O(9) away from Sn(3) towards Sn(6) to give distances of 2.759(12) and 2.426(12) Å compared to 2.655(11) and 2.697(12) Å for Sn(1)—O(3) and Sn(2)—O(3), respectively.

Figure 3 summarizes the bonding interactions for each trifluoroacetate group. No two are identical though in the broadest sense there are three types, monodentate, bidentate (symmetrically bridged), and bidentate (asymmetrically bridged), with the trifluoroacetic acid molecule, of course, being unique. Little can be said about the internal geometry of the carboxylate

Can. J. Chem. Downloaded from www.nrcresearchpress.com by 213.166.140.6 on 09/07/12
For personal use only.

Can. J. Chem. Downloaded from www.nrcresearchpress.com by 213.166.140.6 on 09/07/12
For personal use only.

TABLE 4. Anisotropic temperature factors for the Sn, O, and F atoms in $Sn_6O_2(CF_3CO_2)_8.CF_3CO_2H$ ($Å^2 \times 10^{-3}$)

Atom	U_{11}	U_{22}	U_{33}	U_{12}	U_{13}	I_{23}
Sn(1)	34.4(8)	45.2(7)	41.0(8)	−7.3(7)	−1.2(7)	−3.5(7)
Sn(2)	43.6(8)	31.4(7)	41.7(8)	−2.9(6)	−5.0(7)	3.1(7)
Sn(3)	39.4(8)	32.0(6)	40.5(7)	−3.7(7)	3.9(7)	2.6(6)
Sn(4)	46.2(9)	48.4(8)	35.1(7)	0.9(7)	−5.2(7)	9.1(7)
Sn(5)	45.1(9)	42.3(7)	34.3(7)	3.8(7)	−3.8(7)	9.0(7)
Sn(6)	34.8(8)	40.8(7)	42.1(8)	−3.7(7)	−9.3(7)	−3.2(7)
O(1)	44(8)	27(6)	37(7)	5(6)	15(6)	−1(5)
O(2)	32(7)	32(7)	54(8)	1(6)	12(7)	−3(6)
O(3)	35(8)	36(7)	68(9)	12(7)	−16(7)	3(6)
O(4)	49(9)	27(7)	66(9)	8(7)	−3(8)	−5(6)
O(5)	35(8)	75(9)	51(8)	−3(7)	−5(7)	11(7)
O(6)	75(11)	72(10)	55(10)	−26(9)	−25(9)	−5(8)
O(7)	60(9)	34(7)	36(7)	−6(7)	−12(7)	−9(6)
O(8)	39(7)	48(7)	36(7)	0(6)	−11(6)	−4(6)
O(9)	57(9)	45(8)	36(7)	−16(7)	−4(7)	16(6)
O(10)	75(11)	61(9)	32(7)	−18(8)	8(7)	−24(7)
O(11)	25(7)	43(8)	69(9)	−19(6)	10(7)	−16(7)
O(12)	51(9)	46(8)	37(7)	−16(7)	−10(6)	9(6)
O(13)	31(8)	72(9)	56(9)	−5(7)	−5(6)	17(8)
O(14)	49(9)	61(8)	34(7)	−9(6)	−9(6)	2(7)
O(15)	54(9)	60(9)	72(10)	26(8)	29(8)	33(8)
O(16)	60(10)	49(8)	81(10)	9(7)	23(8)	9(8)
O(17)	43(9)	51(9)	47(8)	9(7)	2(7)	−27(7)
O(18)	38(8)	32(7)	57(8)	−6(6)	−3(7)	−18(6)
O(19)	50(12)	101(15)	128(17)	−26(11)	9(12)	4(12)
O(20)	52(12)	109(15)	87(13)	−2(10)	12(10)	37(11)
F(1)	108(13)	59(9)	102(11)	2(9)	−52(10)	−1(8)
F(2)	117(12)	77(9)	140(15)	−55(9)	−76(12)	49(11)
F(3)	121(14)	178(17)	70(10)	35(13)	3(10)	−65(11)
F(4)	116(20)	370(36)	178(20)	−166(23)	67(17)	−71(26)
F(5)	117(16)	201(22)	215(22)	−117(16)	−75(17)	113(19)
F(6)	171(22)	95(14)	325(34)	−64(14)	5(21)	−94(18)
F(7)	140(16)	226(22)	125(15)	12(17)	−6(14)	147(16)
F(8)	207(22)	100(13)	175(18)	75(15)	−88(18)	19(13)
F(9)	262(26)	79(11)	181(20)	−42(13)	−194(20)	54(12)
F(10)	182(22)	72(11)	181(18)	−71(12)	−106(17)	41(12)
F(11)	340(36)	118(15)	91(14)	−97(20)	−33(18)	53(12)
F(12)	101(19)	39(11)	501(50)	17(11)	12(22)	−13(18)
F(13)	78(11)	218(19)	37(8)	−11(12)	−15(8)	−12(10)
F(14)	158(18)	210(20)	82(11)	−131(16)	65(11)	−73(12)
F(15)	173(19)	137(16)	101(13)	74(15)	7(13)	−53(12)
F(16)	80(11)	116(12)	94(11)	49(10)	23(9)	17(10)
F(17)	75(11)	252(23)	163(17)	53(14)	38(13)	169(18)
F(18)	141(16)	219(22)	70(11)	0(16)	−37(12)	21(14)
F(19)	102(13)	190(18)	114(14)	51(13)	66(11)	97(13)
F(20)	111(13)	81(11)	137(14)	44(10)	37(12)	−8(11)
F(21)	43(9)	243(25)	151(18)	6(13)	−17(11)	−4(17)
F(22)	208(26)	100(14)	427(42)	−41(15)	263(30)	−87(22)
F(23)	191(27)	252(32)	309(36)	196(26)	−117(26)	−127(27)
F(24)	58(9)	177(17)	244(23)	13(11)	−4(13)	−179(18)
F(25)	371(41)	235(29)	94(15)	162(30)	96(21)	65(18)
F(26)	184(22)	314(33)	77(13)	0(23)	−17(14)	97(18)
F(27)	151(20)	238(28)	200(25)	−83(19)	24(18)	92(22)

units in these trifluoroacetate ligands since the errors on the C—O bonds are rather high.

Conclusions

Sublimation of $Sn(CF_3CO_2)_2$ results in the production of $Sn_6O_2(CF_3CO_2)_8.CF_3CO_2H$. This has two groups of three tin(II) atoms each connected by a μ_3-oxo bridge. The tin atoms are further coordinated by trifluoroacetate ions and one trifluoroacetic acid molecule. This latter presumably arises from the presence of small quantities of water adsorbed on the surface of the glass tube used for the sublimation, or picked up when the original $Sn(CF_3CO_2)_2$ was introduced into the tube, although this was carried out in a dry atmosphere glove box. The oxo-bridges arise either from surface moisture or by the

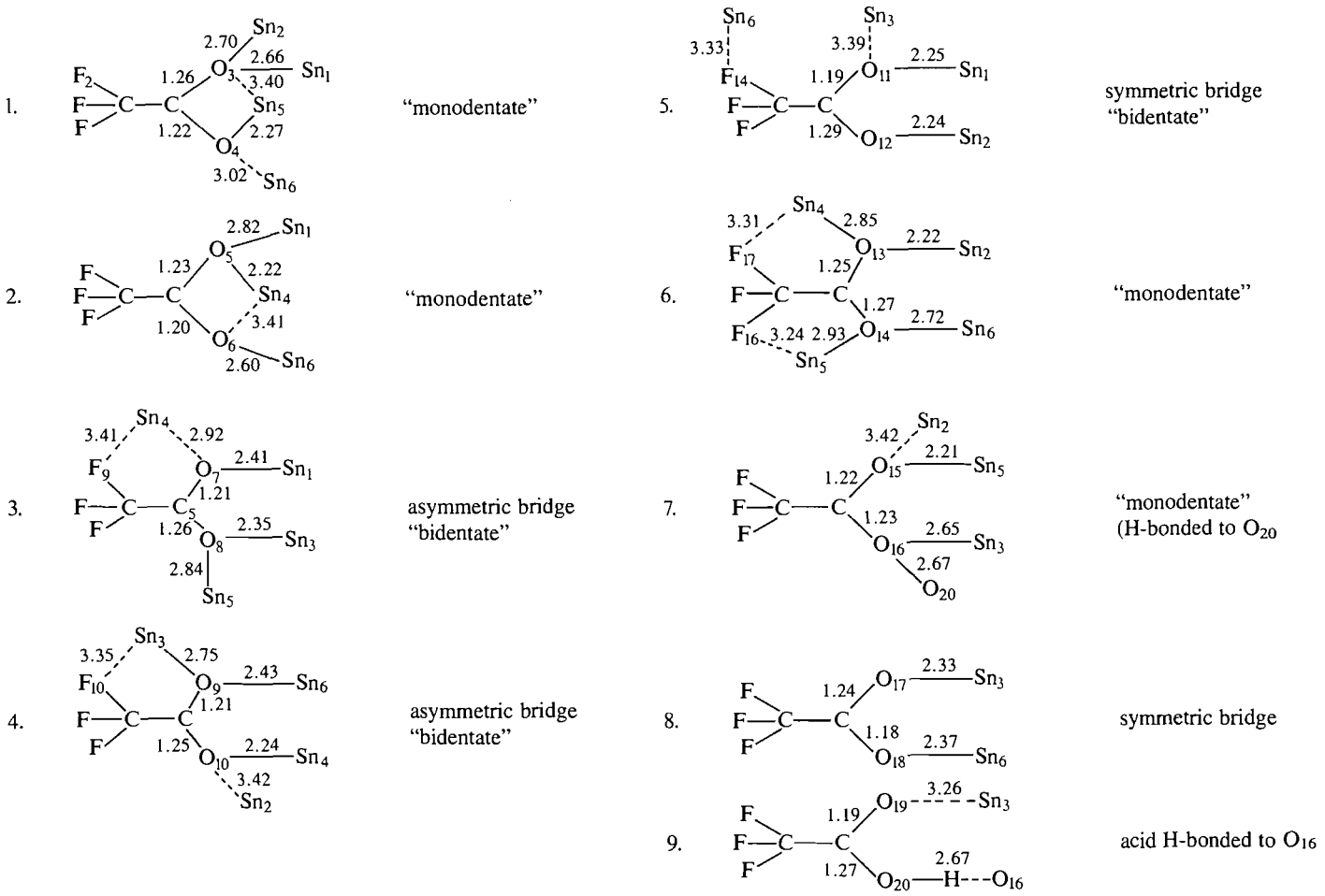

FIG. 3. Bonding interactions for each trifluoroacetate group.

elimination of O^{2-} from two trifluoroacetate ligands.

We are continuing our efforts to obtain crystals of $Sn(CF_3CO_2)_2$ suitable for X-ray crystallographic analysis.

Acknowledgements

We wish to thank Mr. R. Faggiani for help with the data collection and the Natural Sciences and Engineering Research Council of Canada for financial support.

1. J. D. DONALDSON and A. JELEN. J. Chem. Soc. A, 224 (1960) and references therein.
2. J. D. DONALDSON and A. JELEN. J. Chem. Soc. A, 1448 (1968).
3. T. BIRCHALL, R. FAGGIANI, C. J. L. LOCK, and V. MANIVANNAN. J. Chem. Soc. Dalton Trans. In press.
4. P. G. HARRISON and E. W. THORNTON. J. Chem. Soc. Dalton Trans. 1274 (1978).
5. R. P. HUGHES, N. KRISHNAMACHARI, C. J. L. LOCK, J. POWEL, and G. TURNER. Inorg. Chem. **16**, 314 (1977).
6. B. LIPPERT, C. J. L. LOCK, B. ROSENBERG, and M. ZVAGULIS. Inorg. Chem. **16**, 1525 (1977).
7. J. M. STEWART. The XRAY 76 System, Technical Report TR-446; Computer Science Centre, University of Maryland; College Park, MD. 1976.
8. W. L. BOND. International tables for X-ray crystallography. Vol. II. *Edited by* J. A. Ibers and W. L. Hamilton. Kynoch Press, Birmingham, England. 1974. pp. 292–300.
9. A. C. T. NORTH, D. C. PHILLIPS, and F. S. MATHEWS. Acta Crystallogr. A**24**, 351 (1968) (reference for Psi Scan).
10. N. WALKER and D. STUART. Acta Crystallogr. A**39**, 158 (1983) (reference for DIFABS).
11. P. MAIN. MULTAN-80. University of York, York, England. 1980.
12. G. M. SHELDRICK. SHELX-76. Program for crystal structure determination. University of Cambridge. 1975.
13. C. K. JOHNSON. Report ORNL-5138, Oak Ridge National Laboratory; Oak Ridge, TN. 1976.
14. P. R. EWINGS, P. G. HARRISON, A. MORRIS, and T. J. KING. J. Chem. Soc. Dalton Trans. 1602 (1976).
15. T. BIRCHALL and J. P. JOHNSON. J. Chem. Soc. Dalton Trans. 69 (1981).
16. J. D. DONALDSON and S. M. GRIMES. Reviews on Si, Ge, Sn and Pb Compounds. Vol. VIII. 1984. p.1.
17. R. J. GILLESPIE. Molecular geometry. Van Nostrand Reinhold Co., London. 1972.

Can. J. Chem. Downloaded from www.nrcresearchpress.com by 213.166.140.6 on 09/07/12
For personal use only.

Radical reactions of *N*-haloamides with olefins. XIII.[1] Quantum yields for the photochemical addition of *N*-halo-*N*-hydroamides and *N*-chlorosuccinimide to 3,3-dimethyl-1-butene

JACQUES TUAILLON,[2] YVON COUTURE, AND JEAN LESSARD[3]

Département de chimie, Université de Sherbrooke, Sherbrooke (Qué.), Canada J1K 2R1

Received October 20, 1986

JACQUES TUAILLON, YVON COUTURE, and JEAN LESSARD. Can. J. Chem. **65**, 2194 (1987).

The quantum yield of the photochemically initiated radical chain addition of ZCONHX to 3,3-dimethyl-1-butene increases with Z in the order $CH_3 < ClCH_2 < C_2H_5O < CCl_3 < CF_3$ and is governed by the transfer step. The quantum yields are similar for *N*-chloroacetamide and *N*-chlorosuccinimide but the yield of addition is lower with the latter due to photodecomposition of the 1,2-adduct.

JACQUES TUAILLON, YVON COUTURE et JEAN LESSARD. Can. J. Chem. **65**, 2194 (1987).

Le rendement quantique de l'addition radicalaire en chaîne de ZCONHX au diméthyl-3,3 butène-1, initiée par dissociation photochimique, augmente avec Z dans l'ordre $CH_3 < ClCH_2 < C_2H_5O < CCl_3 < CF_3$ et dépend essentiellement de l'efficacité de l'étape de transfert. Le *N*-chloroacétamide et le *N*-chlorosuccinimide donnent des rendements quantiques semblables, mais le rendement d'addition est plus faible avec le dernier dû à la photodécomposition de l'adduit-1,2.

Introduction

We reported that in the photochemically initiated radical chain addition of *N*-chloro-*N*-hydroamides (ZCONHCl, **1**) to cyclohexene, the yield of 1,2-addition increases with the electron-withdrawing power of Z (2): CH_3 (53%) < C_2H_5O (84%) < $ClCH_2$ (89%) < Cl_2CH (94%) < CCl_3 (99%) ≃ CF_3 (100%). Thus, as the ZCO moiety becomes more electronegative, the 1,2-addition chain (steps [2] and [3]) competes more effectively with other processes such as halogenation (hydrogen abstraction).

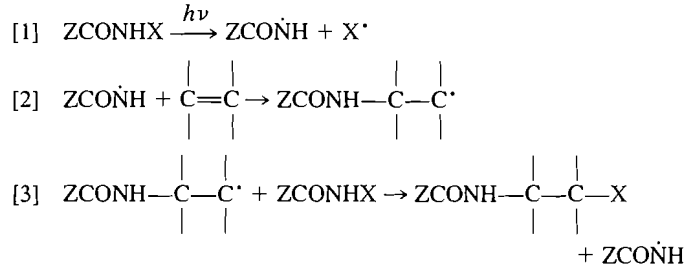

By studying the addition of ZCONHCl to 1,6-heptadiene (**2**), we have shown that the **3**-to-**4** ratio (*tr*ansfer-to-*cy*clization ratio) (Scheme 1), and hence the reactivity of ZCONHCl as chlorine atom donor towards a carbon radical (transfer step [3], X = Cl), increases with the electron-withdrawing power of Z (3): $CH_3 < ClCH_2 < C_2H_5O < CCl_3 \simeq CF_3$.

We now report the quantum yields for the photochemical addition of *N*-haloamides **1** and *N*-chlorosuccinimide (NCS) (**7**) to 3,3-dimethyl-1-butene (**5**) (Schemes 2 and 3), chosen as olefin to minimize the importance of hydrogen abstraction (no allylic hydrogen), and compare them with the transfer-to-cyclization ratios (**3**/**4**) for the addition to 1,6-heptadiene (**2**) (Scheme 1).

Results and discussion

The irradiations were carried out at 254 nm in a Vycor cell under conditions similar to those used in ref. 2 (see footnote *a* of Table 1). Cyclohepta-1,3-diene in ethanol was used as actinometer (4). The quantum yields for the addition process and the yields of addition are recorded in Table 1 and were measured at 15–20%, 30–35%, and 50–55% conversion (determined by iodometry) for each *N*-haloamide; no significant differences were noted with the extent of conversion up to 55% conversion. The material balance based on the amide moiety of **1** and **7** (1,2-adduct plus parent amide) was better than 95% in all cases. The identification and characterization of the 1,2-adducts **6** and **8** have already been described (5). The transfer-to-cyclization (*tr*/*cy*) (**3**/**4**) ratios for the additions of *N*-haloamides **1** to 1,6-heptadiene (**2**) taken from ref. 3 are also included in Table 1.

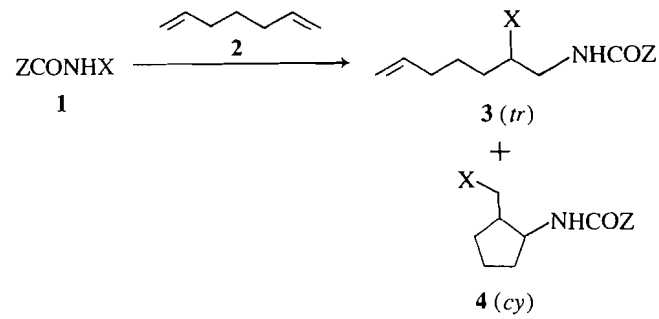

SCHEME 1

The 1,2-adducts **6***c* and **8** underwent photodecomposition, to the extent of 10 and 30% respectively, when irradiated over the time required for complete conversion of the *N*-haloamide. The other 1,2-adducts **6** showed no sign of photodecomposition. The photodecomposition of **6** and **8**[4] did not result in any significant change in the yield of addition or in the material balance based on the amide moiety up to 55% conversion.

With NCS (**7**), we studied the effect of the NCS-to-olefin (**7**/**5**) molar ratio and the effect of the number of photons per unit of time on the chemical and quantum yield of addition up

[1]For part XII, see ref. 1.

[2]NATO Visiting Scientist (1980–1981) from the Faculté des Sciences et des techniques de Besançon, 25030 Besançon CEDEX, France.

[3]Author to whom correspondence may be addressed.

[4]The photodecomposition of **8** gives succinimide. No attempt was made to detect and identify other products from the photodecomposition of **8** or any product from the photodecomposition of **6***c*. The literature contains reports on the photochemical addition of NCS (6) and *N*-bromosuccinimide (6–8) to 3,3-dimethyl-1-butene (**5**) but no mention is made that **8** or its bromo analogue were photolabile under the reaction conditions.

Can. J. Chem. Downloaded from www.nrcresearchpress.com by 213.166.140.6 on 09/07/12
For personal use only.

TABLE 1. Quantum yields and yields of addition for the photochemical addition of *N*-haloamides **1** and NCS (**7**) to 3,3-dimethyl-1-butene (**5**)[a]

Entry	*N*-Haloamide (**1**)	Yield of addition[b] (%)	Φ[c] (mol einstein^{-1})	Relative Φ	*tr*/*cy*[d] Addition to ⩘	Relative *tr*/*cy*
1	$CH_3CONHCl$ (**1***a*)	76–80	3.5–4.5	1.0	0.06	1.0
2	$ClCH_2CONHCl$ (**1***b*)	88–92	8–11	2.4	0.18	3.0
3	$C_2H_5OCONHCl$ (**1***c*)	⩾81–85[e]	⩾9.5–12.5[e]	⩾2.8[e]	0.45	7.5
4	$CCl_3CONHCl$ (**1***d*)	100	12–16	3.5	0.49	8.2
5	$CF_3CONHCl$ (**1***e*)	100	27–34	7.6	>0.42	>7
6	NCS (**7**)	>58–64[e,f]	>3.5–4.5[e]	>1.0[e]	—	—
7	$CCl_3CONHBr$ (**1***f*)[f,g]	100	245–265	64 (18[h])	9.6	160 (19[h])

[a]Reaction conditions: 25–30°C; CH_2Cl_2 (distilled over P_2O_5) as solvent; solutions 0.2 *M* in *N*-haloamide, 1.5–1.7 mol of **5** per mol of *N*-haloamide; argon atmosphere; deoxygenated solutions; irradiations carried out in an RPR-100 Rayonnet apparatus with a merry-go-round using four 254-nm lamps (1.8×10^{-7} einstein s^{-1}) and Vycor cells.

[b]Yields of isolated product (preparative layer chromatography) based on the *N*-haloamide and measured at 15–20%, 30–35%, and 55–60% conversion (followed by iodometry). Range of values from three runs. The material balance (**6** or **8** + parent amide) was nearly 100% in each case.

[c]Measured from cyclohepta-1,3-diene actinometry (see ref. 4) and based on the amount of 1,2-adduct formed. Range of values from three runs.

[d]*tr* = transfer, *cy* = cyclization (Scheme 1). Taken from ref. 3.

[e]Minimum value since the 1,2-adduct is photolabile (see text).

[f]Yield determined by vapor phase chromatography.

[g]Two 254-nm lamps were used (1×10^{-8} einstein s^{-1}).

[h]Relative to **1***d* (entry 4).

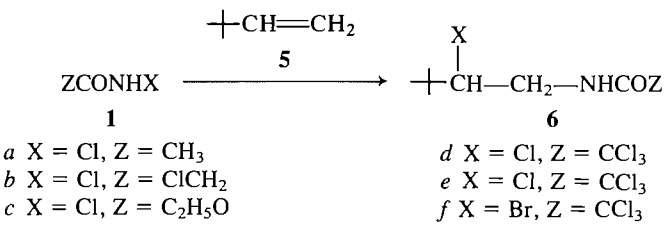

1 **6**

a X = Cl, Z = CH_3
b X = Cl, Z = $ClCH_2$
c X = Cl, Z = C_2H_5O
d X = Cl, Z = CCl_3
e X = Cl, Z = CCl_3
f X = Br, Z = CCl_3

SCHEME 2

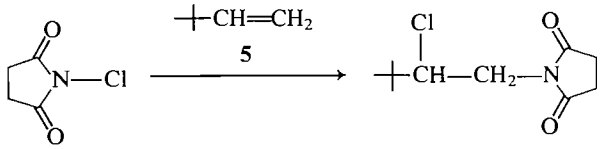

7 **8**

SCHEME 3

to 55% loss of NCS. Both yields increase (*i*) as the **7**/**5** molar ratio decreases: from 20%, Φ = 0.4 mol einstein^{-1} (Φ for loss of NCS = 1.9), for a molar ratio of 3, to 61%, Φ = 4 mol einstein^{-1} (Φ for loss of NCS = 6.5), for a molar ratio of 0.67 (case reported in Table 1, entry 6); (*ii*) as the number of photons decreases: from 38%, Φ = 1.7 mol einstein^{-1} (Φ for loss of NCS = 4.5) with 7×10^{-7} einstein s^{-1}, to 61%, Φ = 4 mol einstein^{-1} (Table 1, entry 6) (Φ for loss of NCS = 6.5) with $(0.5–1.8) \times 10^{-7}$ einstein s^{-1}. The irradiations of Table 1 were consequently carried out with 1.8×10^{-7} einstein s^{-1} or less, using an *N*-haloamide-to-olefin molar ratio of 0.59 to 0.67.

We determined the material balance based on chlorine for the addition of NCS (**7**), which gave the lowest yields of addition. The chlorine balance consists of 1,2-adduct **8** and 1,2-dichloro-3,3-dimethylbutane. The yield of the latter was determined by vpc: 33% (chlorine balance ≃ 53%) for a **7**/**5** molar ratio of 3; 6% (chlorine balance ≃ 61–70%) for a **7**/**5** molar ratio of 0.67 (Table 1, entry 6). No 4-chloro-3,2-dimethyl-1-butene, resulting from hydrogen abstraction on **5**, was detected in the 250-MHz ^{1}Hmr spectrum of the crude reaction mixture (no singlet at 3.30 ppm (9)) and only a trace amount of chloroform resulting from hydrogen abstraction on methylene chloride was detected (≃1% by vpc). This is surprising since in the radical photochlorination of **5**, 4-chloro-3,2-dimethyl-1-butene represents 12–13% of the chlorinated products and since the photolysis of NCS in methylene chloride in the presence of neopentane and ethylene was reported to give neopentyl chloride (81%) and chloroform (15%) plus a small amount (5%) of 1,2-adduct (**8**). Thus, hydrogen abstraction does not appear to be an important process under the conditions we used unless 4-chloro-3,3-dimethyl-1-butene underwent photodecomposition (e.g. dehydrochlorination). Two to three other products were present in small amounts in the crude reaction mixture according to the ^{1}Hmr spectrum and vpc analysis. They are fairly volatile and could result from dehydrochlorination of chlorinated products but they were not identified.

When NCS (**7**) is in excess with respect to the olefin (**7**/**5** = 3), 1,2-dichloro-3,3-dimethylbutane is a major product together with the 1,2-adduct **8**. Considering the low material balance based on chlorine (53%), any discussion concerning the process(es) responsible for the formation of the dichloro adduct would be highly speculative. The photodecomposition of 1,2-adduct **8** can be partly responsible for the relatively low chlorine balance (the dichloro adduct is stable under the photolysis conditions).

It is interesting to compare the photolysis of NCS (**7**) and *N*-bromosuccinimide (NBS) in the presence of 3,3-dimethyl-1-butene (**5**). Skell and co-workers (8) reported that, for a NBS/**5** molar ratio of 3.5, the quantum yield for the loss of NBS in methylene chloride is 67 mol einstein^{-1} for a 82% conversion. The main products are β-bromopropylisocyanate and the 1,2-adduct, and the bromine balance is quite good. The different product distribution and the longer chain of the NBS reaction result from the fact that NBS is a better halogen atom donor (better transfer agent) than NCS, an N—Br bond being weaker than an N—Cl bond (10).

The results of Table 1 show that the yield of addition increases as Φ increases, that is, as the 1,2-addition chain

Can. J. Chem. Downloaded from www.nrcresearchpress.com by 213.166.140.6 on 09/07/12
For personal use only.

Can. J. Chem. Downloaded from www.nrcresearchpress.com by 213.166.140.6 on 09/07/12
For personal use only.

becomes longer and thus competes more and more effectively with other processes. When comparing an *N*-bromoamide with its *N*-chloro analogue, the relative chain lengths for the addition, and hence the relative quantum yields, depend solely on the relative rates of the transfer step [3] since the same amidyl radical is involved in the addition step [2]. The transfer step [3] should be faster with the *N*-bromoamide because an N—Br bond is weaker than an N—Cl bond (10) as stated above. Indeed, the entries 6 and 4 of Table 1 show that the quantum yield is 18 times larger for *N*-bromotrichloroacetamide (**1***f*) than for the *N*-chloro analogue **1***d*. The agreement between this figure and the relative rate of the transfer step [3] (19 times faster with **1***f* than with **1***d*) obtained from the addition to 1,6-heptadiene (**2**) (3) is excellent.

As shown in entries 1 to 5 of Table 1, the increase of the quantum yield of addition, and hence of the 1,2-addition chain length with the electron-withdrawing power of Z, parallels the reactivity of ZCONHCl as chlorine atom donor towards a carbon radical (transfer step [3])[5] as determined by the *tr* (**3**)/*cy* (**4**) ratio for addition to 1,6-heptadiene (**2**) (Scheme 1) (3). Thus, the chain length of the 1,2-addition process is governed by the transfer step [3], which implies that chain termination involves the adduct radical, and *N*-chloramides are good transfer agents resulting in high yields of addition.

NCS (**7**), with two acyl (electron-attracting) groups attached to the nitrogen, should be a better chlorine atom donor than *N*-chloroacetamide (NCA (**1***a*) (LUMO = σ* (N—Cl) lower in energy or more polar transition state for NCS than for NCA).[5] Therefore Φ(NCS) (addition of NCS: Table 1, entry 6) should be larger (longer 1,2-addition chain) than Φ(NCA) (entry 1). The 1,2-adduct **8** being photolabile, the value of Φ in entry 6 is a minimum value and the true Φ(NCS) is probably larger than Φ(NCA).

If we compare the yields of 1,2-addition of *N*-haloamides to 3,3-dimethyl-1-butene (**5**) and to cyclohexene, they are usually higher with **5**. For instance, the yield of addition of NCA (**1***a*) to **5** is 72% after complete conversion of NCA (5) and that to cyclohexene is 55% (1). This is due to the fact that in the case of cyclohexene, which possesses reactive allylic hydrogens, hydrogen abstraction, a chain process competing with 1,2-addition (2, 13),[6] is more effective than the process(es) competing with 1,2-addition in the case of **5**. With NCS, the yield of addition to **5** (48%) (5) is somewhat lower than that to cyclohexene (54%) (1) due to the photodecomposition of the 1,2-adduct **8**. No such photodecomposition of the 1,2-adduct of NCS to cyclohexene was observed (1). When 1,2-addition accounts for 90% or more of the reaction, there is no difference in the yields of addition to cyclohexene and to **5** (2, 5) as expected. As for the chlorine balance, the situation is much better in the case of cyclohexene where the chlorinated products could be clearly identified (2, 13). The chlorine balance (1,2-adduct + dichlorocyclohexane + 3-chloro- and 4-chlorocyclohexene) is better than 90% in most cases (13).[6]

Conclusion

The close parallel between the variation of the quantum yield in the photochemical addition of ZCONHX (**1**) to 3,3-dimethyl-1-butene (**5**) and the variation of the rate of halogen atom transfer (eq. [3]) as evaluated from the addition of ZCONHX to 1,6-heptadiene (**2**) (3) with the electronegativity of Z, shows that the transfer step [3] is governing the 1,2-addition chain length. Thus *N*-haloamides are good transfer agents and good to excellent yields of 1,2-addition are obtained. The implication of this on the competition between 1,2-addition and hydrogen abstraction and on the mechanism of hydrogen abstraction in the case of cyclohexene will be discussed in a forthcoming paper, together with the results of a study of the halogenated products.[6]

In the case of 3,3-dimethyl-1-butene (**5**), which has no reactive allylic hydrogen, hydrogen abstraction, even from the solvent, does not appear to be an important process competing with 1,2-addition, and the nature of the main competing process(es) is unknown at present.

Experimental

Vapor phase chromatographic (vpc) analyses were performed with a Hewlett Packard chromatograph model 5710A equipped with a flame ionization detector on a DB-5 (95% dimethyl – 5% diphenylpolysiloxane) fused silica capillary column 30 m long using an internal standard (phthalimide or methyl benzoate). Merck silica gel $60F_{254}$ was used for preparative layer chromatography (CH_2Cl_2 or ether–hexane 50:50 containing 4% CH_3OH saturated with NH_3 as eluent). Ultraviolet spectrophotometric determinations were carried out on a Varian Techtron spectrophotometer model 635 or a Beckman uv spectrophotometer model 5230. The ^{1}Hmr spectra were recorded on a Bruker WM-250 spectrometer.

The preparation of the *N*-haloamides (2) and the isolation and characterization of the 1,2-adducts **6** and **8** from preparative photolyses (5) have been described. *1,2-Dichloro-3,3-dimethylbutane* was prepared by chlorination of a CCl_4 solution of 3,3-dimethyl-1-butene in the dark at 0°C (14). The product was purified by fractional distillation and its purity checked by vpc and ^{1}Hmr: bp 60–61°C/21 Torr (lit. (15) bp 63.5°C/20 Torr) (1 Torr = 133.3 Pa).

Quantum yield determinations

The irradiations were carried out at 254 nm in a Rayonnet RPR reactor equipped with a merry-go-round using 14 × 170 mm Vycor test tubes fitted with a 19/40 ground quartz female joint and, as stopper, a two-way Teflon stopcock on a 19/40 ground glass male joint. A test tube (A) containing the solution of the *N*-haloamide and the olefin was followed by a test tube (B) containing the actinometer in succession: $A^1B^1A^2B^2$... At a given time, the merry-go-round was stopped and a test tube A and a test tube B were quickly removed together. Concentrations were chosen to ensure that all the light hitting the cell was absorbed by the actinometer and by the *N*-haloamide (up to 80% conversion). Cyclohepta-1,3-diene (CHD) in 95% ethanol (10 mL of a 30 m*M* solution) was used as actinometer (4). The quantum yield for the disappearance of CHD was determined to be 0.50 ± 0.05 (lit. (4) 0.48 ± 0.01) with ferrioxalate actinometry (16). The CHD solution was diluted (1 mL to 250 mL with 95% ethanol) and the absorbance was measured at 250 nm; the concentration of remaining CHD was obtained from an absorbance vs. concentration graph (ε = 7835). The solution of *N*-haloamide and 3,3-dimethyl-1-butene (passed through alumina)

[5]The increase of the reactivity of ZCONHCl in the transfer step [3] with the electronegativity of Z has been explained in terms of a polar effect stabilizing the transition state (3) (a polar transition state has been proposed for the attack of carbon radicals on carbon–halogen bonds (11)):

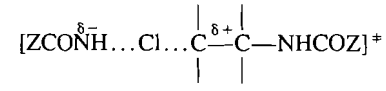

In terms of frontier orbital (12) ([3] is an exothermic reaction), such a polar effect corresponds to a dominant SOMO (carbon radical)–LUMO (the σ* (N—Cl) orbital of ZCONHCl) interaction: as the electron-attracting power of Z increases, the energy of σ* (N—Cl) diminishes (12) and the perturbation energy (the reactivity) should increase accordingly.

[6]D. Touchard, Y. Couture, M. Mondon, and J. Lessard. Unpublished results.

(10 mL of a 200 m*M* solution in *N*-haloamide containing the required amount of olefin) in CH_2Cl_2 (freshly distilled over P_2O_5) was freed from oxygen (three successive freeze–thaw cycles under argon). After irradiation, the amount of *N*-haloamide consumed was determined by iodometry from a 3-mL aliquot. To the remaining solution, solid sodium bisulfite (~200 mg) and water (~0.2 mL) were added. After a few minutes (negative starch–iodide paper test), the solution was dried over $MgSO_4$, filtered, then transferred into a 25-mL volumetric flask with CH_2Cl_2 for quantification by vpc and (or) preparative layer chromatography. The results are recorded in Table 1.

In the experiments with NCS, the reaction solution from 25–30% conversion of NCS was distilled through a Vigreux column to remove CH_2Cl_2 and 3,3-dimethyl-1-butene. The residue and the liquid remaining in the Vigreux column were analyzed by ^{1}Hmr. *Excess of olefin*: *residue*: two singlets of very low intensity at 1.57 and 2.17 ppm besides the absorptions due to 1,2-adduct **8** and succinimide, and no absorptions corresponding to 1,2-dichloro-3,3-dimethylbutane (formed in 6% yield according to vpc analysis); *liquid in the column*: three singlets at 1.24, 1.57, and 2.17 ppm besides the absorptions due to 3,3-dimethyl-1-butene and CH_2Cl_2. *Excess of NCS*: *residue*: two singlets of low intensity at 1.59 and 2.17 ppm besides the absorptions due to 1,2-adduct **8**, succinimide, and 1,2-dichloro-3,3-dimethylbutane; *liquid in the column*: two singlets at 1.57 and 2.17 ppm besides the absorptions due to 3,3-dimethyl-1-butene and CH_2Cl_2.

The products in the liquid from the Vigreux column contained no chlorine according to the mass spectrum. They were not investigated further. In none of the above ^{1}Hmr spectra was singlet at 3.30 ppm detectable, due to the presence of 4-chloro-3,3-dimethyl-1-butene.

Acknowledgements

We are grateful to the Natural Sciences and Engineering Council of Canada and to the "Fonds pour la formation de chercheurs et l'aide à la recherche du Québec" for their financial support, and to Mrs. Ginette Roy for typing the manuscript.

1. J. LESSARD, Y. COUTURE, M. MONDON, and D. TOUCHARD. Can. J. Chem. **62**, 105 (1984).
2. J. LESSARD, M. MONDON, and D. TOUCHARD. Can. J. Chem. **59**, 431 (1981); D. TOUCHARD and J. LESSARD. Tetrahedron Lett. 4425 (1971).
3. M. MONDON and J. LESSARD. Can. J. Chem. **56**, 2590 (1978).
4. N. NUMAO, T. HAMADA, and O. YONEMITSU. Tetrahedron Lett. 1661 (1977).
5. J. LESSARD and J. TUAILLON. J. Org. Chem. **47**, 5013 (1982).
6. J. C. DAY, M. G. KATSAROS, W. D. KOCHER, A. E. SCOTT, and P. S. SKELL. J. Am. Chem. Soc. **100**, 1950 (1978).
7. F. L. LU, Y. M. A. NAGUIB, M. KITADANI, and Y. L. CHOW. Can. J. Chem. **57**, 1967 (1979).
8. R. L. TLUMAK, J. C. DAY, J. P. SLANGA, and P. S. SKELL. J. Am. Chem. Soc. **104**, 7257 (1982).
9. M. L. POUTSMA. J. Am. Chem. Soc. **87**, 4285 (1965).
10. T. L. COTTRELL. The strengths of chemical bonds. 2nd ed. Butterworths, London. 1958.
11. C. WALLING. Free radicals in solution. John Wiley and Sons Ltd., New York, NY. 1957. p. 158; P. I. ABELL. *In* Free radicals. Vol. 2. *Edited by* J. K. Kochi. John Wiley and Sons Ltd., New York, NY. 1973. p. 86.
12. J. FOSSEY. Thèse de doctorat d'état, Université de Paris-Sud (Centre d'Orsay), 1974. pp. 50–125; I. FLEMING. Frontier orbitals and organic reactions. John Wiley and Sons, New York, NY. 1978.
113. D. TOUCHARD. Ph.D. thesis, Université de Sherbrooke, Sherbrooke, Québec. 1974.
114. D. A. DAWSON and W. F. REYNOLDS. Can. J. Chem. **49**, 3498 (1971).
115. L. M. JACKMAN and D. P. KELLY. J. Chem. Soc. (B), 110 (1970).
116. C. G. HATCHARD and C. A. PARKER. Proc. R. Soc. A, **235**, 518 (1956).

Can. J. Chem. Downloaded from www.nrcresearchpress.com by 213.166.140.6 on 09/07/12
For personal use only.

Solubility of non-polar gases in cyclohexanone between 273.15 and 303.15 K at 101.32 kPa partial pressure of gas

MARÍA ASUNCIÓN GALLARDO, JOSÉ MARÍA MELENDO, JOSÉ SANTIAGO URIETA, AND CELSO GUTIERREZ LOSA
Departamento de Química Física, Facultad de Ciencias, Universidad de Zaragoza, 50009-Zaragoza, Spain

Received September 18, 1986[1]

MARÍA ASUNCIÓN GALLARDO, JOSÉ MARÍA MELENDO, JOSÉ SANTIAGO URIETA, and CELSO GUTIERREZ LOSA. Can. J. Chem. **65**, 2198 (1987).

Solubility measurements of several non-polar gases (He, Ne, Ar, Kr, Xe, H_2, D_2, N_2, O_2, C_2H_4, C_2H_6, CF_4, SF_6, and CO_2) in cyclohexanone at 273.15 to 303.15 K and a partial pressure of gas of 101.32 kPa, are reported. Gibbs energy, enthalpy, and entropy of solution at 298.15 K and 101.32 kPa partial pressure of gas were evaluated. Effective hard-sphere diameter temperature dependence has been studied and its effect on the calculated SPT (Scaled Particle Theory) solubilities, and enthalpies and entropies of solution was also examined.

MARÍA ASUNCIÓN GALLARDO, JOSÉ MARÍA MELENDO, JOSÉ SANTIAGO URIETA et CELSO GUTIERREZ LOSA. Can. J. Chem. **65**, 2198 (1987).

Opérant à des températures allant de 273,15 à 303,15 K et à des pressions partielles de gaz de 101,32 kPa, on a mesuré les solubilités de plusieurs gaz non polaires (He, Ne, Ar, Kr, Xe, H_2, D_2, N_2, O_2, C_2H_4, C_2H_6, CF_4, SF_6 et CO_2) dans la cyclohexanone. On a évalué l'énergie libre de Gibbs, l'enthalpie ainsi que l'entropie de solution à 298,15 K et à une pression partielle de gaz de 101,32 kPa. On a étudié la relation entre le diamètre effectif des sphères solides et la température et on a aussi étudié son effet sur les solubilités calculées sur la base de la théorie de la particule graduée; de plus, on a aussi examiné les enthalpies et les entropies de solution.

[Traduit par la revue]

Can. J. Chem. Downloaded from www.nrcresearchpress.com by 213.166.140.6 on 09/07/12
For personal use only.

Introduction

Apart from their practical usefulness, solubility measurements of non-polar gases in liquids are of great interest in the theoretical study of liquids.

In spite of the various approaches proposed up to now, no general method exists for rigorous gas solubility predictions. While it is true that some successful calculations of solubility and of thermodynamic properties for simple systems, using either perturbation or variation methods, were performed (1–8) when more complex molecules are involved, a strict explanation of solubility at molecular level is unattainable, specially when anisotropy effects are important.

While lacking the strictness of the above-mentioned methods, Pierotti's "Scaled Particle Theory" (SPT) (1963) (9) shows an outstanding consistency and was extensively used for estimating molecular pair-potential parameters of liquids from gas solubility data. The main simplifications introduced into the original cavity theory for solutions are as follows: (*a*) solutions are made up of "hard-sphere" molecules; (*b*) the radial distribution function is independent of temperature and therefore $G_i = E_i$; and (*c*) solvent molecules are uniformly distributed around each solute molecule, that is to say, the radial distribution function, $g(\sigma,r)$, is unity.

In the first steps of the development of the cavity theory the effect of temperature on the "effective hard-sphere diameter" of solvent molecules was ignored. However, more recent works (10–15) have revealed that a hard-sphere temperature dependence must be taken into account if an adequate theoretical explanation of solubility results is to be given. In 1981, Cosgrove analysed in depth the effect of the effective hard-sphere diameter temperature dependence on solution enthalpies of rare gases in some non-polar organic solvents (benzene, cyclohexane, tetrachloromethane, and *n*-hexane) and in water, too (15).

In the present paper, the effect of temperature on effective hard-sphere diameter, a_1, is studied for a polar molecule, cyclohexanone ($\mu = 9.34 \times 10^{-30}$ m C), and solubility data of fourteen gases in this solvent, between 273.15 and 303.15 K and at a gas pressure of 101.32 kPa, are given.

Experimental

The equipment used for solubility measurements and the associated experimental technique were similar to those described in previous papers (16, 17).

The purity of the gases (all from Sociedad Española de Oxígeno except Ne and CF_4 which were from Baker) was He 99.995%, Ne 99.9%, Ar 99.9990%, Kr 99.95%, Xe 99.995%, H_2 99.99%, D_2 99.4%, N_2 99.998%, O_2 99.98%, C_2H_4 99.90%, C_2H_6 99.0%, CF_4 99%, SF_6 99.5%, and CO_2 99.998%. Cyclohexanone (Carlo Erba: ≧99%) was used as solvent; its purity was checked by GLC and by refractive index measurement (experimental value, n_D (293.15 K) = 1.45071; literature, 1.4507 (18)). Vapour pressure data of the solvent were taken from the literature (18).

The uncertainty on about the reported solubilities is estimated in ±0.7%, or less, except for gases with low solubilities (He and Ne) for which it is approximately ±2.0%.

Results

In Table 1, the experimental results for the solubilities of He, Ar, Kr, Xe, H_2, D_2, N_2, O_2, C_2H_4, C_2H_6, CF_4, SF_6, and CO_2 in cyclohexanone in terms of the equilibrium mole fraction, x_2, are given at temperatures ranging from 273.15 to 303.15 K, and at 101.32 kPa partial pressure of gas. The results were fitted by least squares to an equation of the form:

$$[1] \quad -\ln x_2 = a \ln T + b$$

In Table 1 the values of a and b for each system are set out together with the standard deviations

$$\sigma = \left\{ \sum_{i=1}^{n} (\ln x_{2,1} + a \ln T_i + b)^2/(n-2) \right\}^{1/2}$$

Table 2 shows the values of partial molar Gibbs energy, $\Delta G^0_{m,2}$, partial molar enthalpy, $\Delta H^0_{m,2}$, partial molar entropy, $\Delta S^0_{m,2}$, and partial molar Hildebrand entropy, ΔS^0_H, for the

[1]Revision received April 3, 1987.

TABLE 1. Solubility of gases ($x_2 \times 10^4$) in cyclohexanone, at 101.32 kPa partial pressure of gas between 273.15 and 303.15 K, coefficients of the equation $-\ln x_2 = a \ln T + b$, and standard deviations as defined in the text

	T/K							
Gas	273.15	283.15	293.15	298.15[a]	303.15	a	b	$\sigma \times 10^4$ (st. dev.)
He	0.447	0.529	0.621	0.665	0.669	−4.3682	34.541	0.008
Ne	0.667	0.787	0.897	0.942	0.973	−3.5518	29.513	0.019
Ar	7.11	7.17	7.23	7.26	7.33	−0.2711	8.770	0.017
Kr	25.6	24.3	23.2	22.6	22.2	1.3667	−1.698	0.021
Xe	130.6	114.8	101.9	96.4	91.3	3.4340	−14.922	0.355
H_2	1.80	1.95	2.13	2.20	2.30	−2.3330	21.711	0.006
D_2	1.89	2.05	2.22	2.30	2.37	−2.1982	20.904	0.009
N_2	3.39	3.54	3.66	3.74	3.80	−1.0981	14.149	0.006
O_2	6.06	6.19	6.29	6.31	6.35	−0.4394	9.871	0.020
C_2H_4	150	131.5	114.5	106.9	100.5	3.8489	−17.393	0.594
C_2H_6	146	126.9	110.3	103.5	97.2	3.9250	−17.790	0.258
CF_4	3.77	3.83	3.90	3.96	3.97	−0.5278	10.845	0.013
SF_6	20.5	19.3	18.2	17.7	17.2	1.6511	−3.072	0.014
CO_2		216	176	160	147	5.6368	−27.986	0.882

[a]From ref. 19.

TABLE 2. Gibbs energies, enthalpies, entropies of solution, and SPT calculated enthalpies and entropies in cyclohexanone at 298.15 K and 101.32 kPa partial pressure of gas, both when $l_1 = 0$, and $l_1 = 1.87 \times 10^{-4}$ K^{-1}

Gases	$\Delta G^0_{m,2}$ / kJ mol^{-1}	$\Delta H^0_{m,2}$ / kJ mol^{-1}	$\Delta S^0_{m,2}$ / kJ K^{-1} mol^{-1}	ΔS^0_H / kJ K^{-1} mol^{-1}	$\Delta H^0_{m,2}$ ($l_1 = 0$) / kJ mol^{-1}	$\Delta H^0_{m,2}$ ($l_1 \neq 0$) / kJ mol^{-1}	$\Delta S^0_{m,2}$ ($l_1 = 0$) / kJ K^{-1} mol^{-1}	$\Delta S^0_{m,2}$ ($l1 \neq 0$) / kJ K^{-1} mol^{-1}
He	23.86	10.8	−0.044	0.036	4.98	10.34	−0.060	−0.042
Ne	23.00	8.8	−0.048	0.030	2.28	8.13	−0.060	−0.041
Ar	17.91	0.67	−0.057	0.003	−1.64	6.42	−0.061	−0.034
Kr	15.10	−3.39	−0.062	−0.011	−3.28	5.56	−0.062	−0.032
Xe	11.51	−8.51	−0.067	−0.029	−6.47	4.32	−0.062	−0.026
H_2	20.87	5.78	−0.051	0.019	3.04	9.18	−0.060	−0.040
D_2	20.77	5.45	−0.051	0.018	2.87	9.01	−0.060	−0.040
N_2	19.56	2.72	−0.056	0.009	0.69	9.95	−0.062	−0.031
O_2	18.26	1.09	−0.058	0.004	−1.39	6.88	−0.061	−0.034
C_2H_4	11.24	−9.54	−0.070	−0.032	−6.43	4.41	−0.062	−0.026
C_2H_6	11.34	−9.73	−0.071	−0.033	−6.66	5.62	−0.063	−0.022
CF_4	19.43	1.31	−0.061	0.004	0.37	14.05	−0.063	−0.017
SF_6	15.70	−4.09	−0.066	−0.014	−3.17	15.15	−0.064	−0.003
CO_2	10.24	−14.0	−0.081	−0.047				

solution process calculated from our experimental results, and using the adequate relations (20).

Discussion

The scaled particle theory formalism of gas solubility has been explained so many times that we consider unnecessary to do it again; we will just summarize the pertinent equations instead. The changes in Gibbs energy and enthalpy for the solution process are given by equations (9, 12):

$$[2]\quad \Delta G^0_{m,2} = -RT \ln K_H = G_c + G_i + RT \ln (RT/v^0_1)$$

$$[3]\quad \Delta H^0_{m,2} = |\partial(\Delta G^0/T)/\partial(1/T)|_p = H_c + H_i - RT + \alpha_p RT^2$$

where R is the gas constant, T is the absolute temperature, $K_H = p_2/x_2$ is the Henry's law constant, p_2 is the partial pressure of the gas, x_2 is the gas mole fraction in the solution, v^0_1 is the molar volume of the solvent, α_p is the thermal expansion coefficient of the solvent; the subscripts 1 and 2 refer to the solvent and the solute, respectively, and c and i refer to cavity formation and interaction steps, respectively.

In the present paper we are interested in the temperature dependence of the effective hard-sphere diameter. It can be seen (Fig. 1) that Henry's law constant decreases regularly with the polarizability of the rare gases; from this plot, the extrapolated value of ln K_H to zero polarizability leads to the solubility of a hard sphere of 0.258 nm diameter. This diameter is obtained from the extrapolation to zero polarizability of the plot of diameter of the rare gases against the corresponding polarizabilities. Introducing such a value in eq. [2] with $\alpha_2 = 0$, the effective hard-sphere diameter of the solvent, a_1, can be calculated (9). As solubility data of rare gases were available for several temperatures, we were able to evaluate the linear coefficient of expansion of a_1, at 298.15 K and 101.32 kPa, namely:

$$l_1 = (1/a_1)(\partial a_1/\partial T)_p = -2.07 \times 10^{-4}\ \text{K}^{-1}$$

The necessary data used in the calculations are given in Table 3.

Can. J. Chem. Downloaded from www.nrcresearchpress.com by 213.166.140.6 on 09/07/12
For personal use only.

Can. J. Chem. Downloaded from www.nrcresearchpress.com by 213.166.140.6 on 09/07/12
For personal use only.

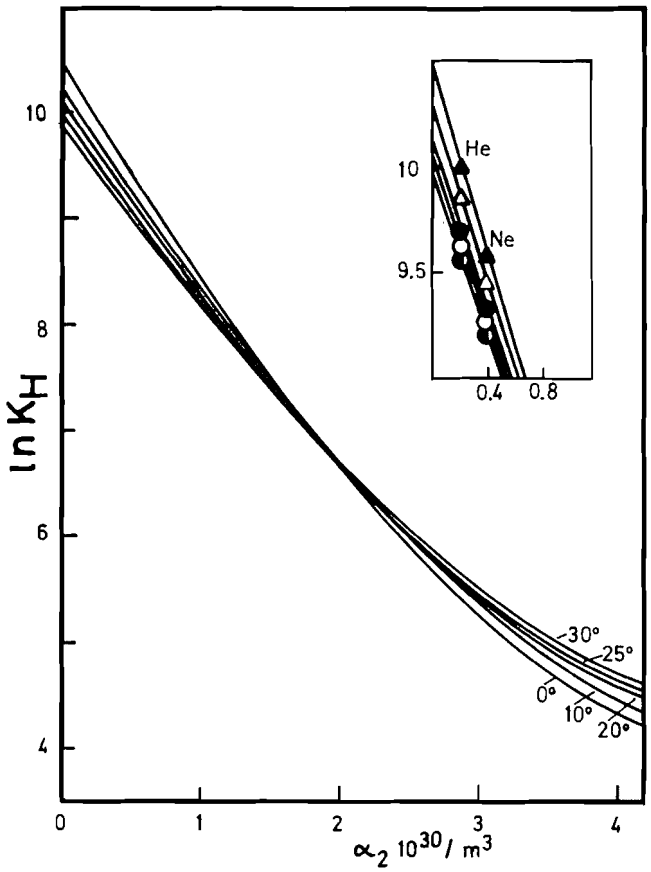

FIG. 1. Experimental ln K_H versus α_2 for the rare gases in cyclohexanone at different temperatures.

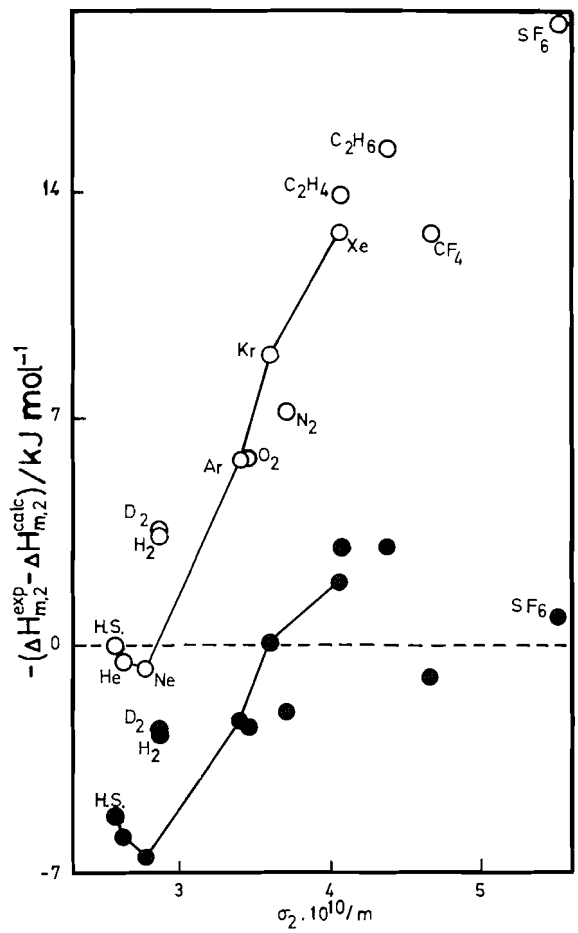

FIG. 2. Difference between experimental and calculated (SPT) values of the partial molar enthalpy of solution, $-(\Delta H^{exp}_{m,2} - \Delta H^{calcd}_{m,2})$, of gases dissolved in cyclohexanone at 298.15 K, versus the effective hard sphere diameter of solutes: ○, values calculated with $l_1 \neq 0$; ●, values calculated with $l_1 = 0$.

TABLE 3. Parameters and properties used in calculations

Gases	$10^{30}\,\alpha_2{}^a$ / m^3	$10^{10}\,\sigma_2{}^a$ / m	ϵ_2/k^a / K
He	0.204	2.63	6.03
Ne	0.393	2.78	34.9
Ar	1.63	3.40	122
Kr	2.46	3.60	158
Xe	4.00	4.06	229
H_2	0.802	2.87	29.2
D_2	0.79	2.87	31.1
N_2	1.73	3.70	95
O_2	1.56	3.46	118
C_2H_4	3.19	4.07	230
C_2H_6	4.33	4.38	236
CF_4	2.86	4.66	134
SF_6	4.48	5.51	201
Hard sphere	0	2.58	—

Liquid	$10^{30}\,\mu_1{}^b$ / C m	$10^4\,\alpha_p$ / K^{-1}	10^{-3} density$^{25°}$ / kg m^{-3}	$10^9\,a_1{}^c$ / m	ϵ_1/k^c / K
$C_6H_{10}O$	9.34	9.446	0.9433	0.5651	584

[a]Reference 21.
[b]Reference 22.
[c]Reference 19.

Recently, Cosgrove and Walkley have proposed a method for calculating l_1 from enthalpy of solution data (15). If the enthalpies of solution of rare gases in a given solvent are available, the enthalpy of solution of a hard sphere (a_2 = 0.258 nm), $\Delta H_{2,0}$, can be obtained from extrapolation of $\Delta H^0_{m,2}$ vs. α_2 to zero polarizability; then l_1 can be calculated by means of eq. [3] and also the corresponding expression for H_c which depends on the linear coefficient of expansion of a_1. The value of $\Delta H_{2,0}$ found for cyclohexanone was 12.24 kJ mol^{-1}. Likewise, the value of l_1 obtained for cyclohexanone at 298.15 K and 101.32 kPa was -1.87×10^{-4} K^{-1}, in good agreement with that calculated from ln K_H at several temperatures.

In order to study the effect of the effective hard-sphere diameter temperature dependence, solubility and thermodynamic functions associated to the solution process were calculated by means of the scaled particle theory either assuming a constant a_1 ($l_1 = 0$) or admitting its temperature dependence ($l_1 \neq 0$).

Table 2 contains also the theoretical values for $\Delta H^0_{m,2}$ and $\Delta S^0_{m,2}$, both when $l_1 = 0$ or $l_1 \neq 0$. In Figs. 2 and 3 the differences between experimental and calculated values are plotted against the effective hard-sphere diameter of the solute. The following observations are worth making: (*i*) for He and Ne (that is to say, the gases with the shallowest energy well)

Can. J. Chem. Downloaded from www.nrcresearchpress.com by 213.166.140.6 on 09/07/12
For personal use only.

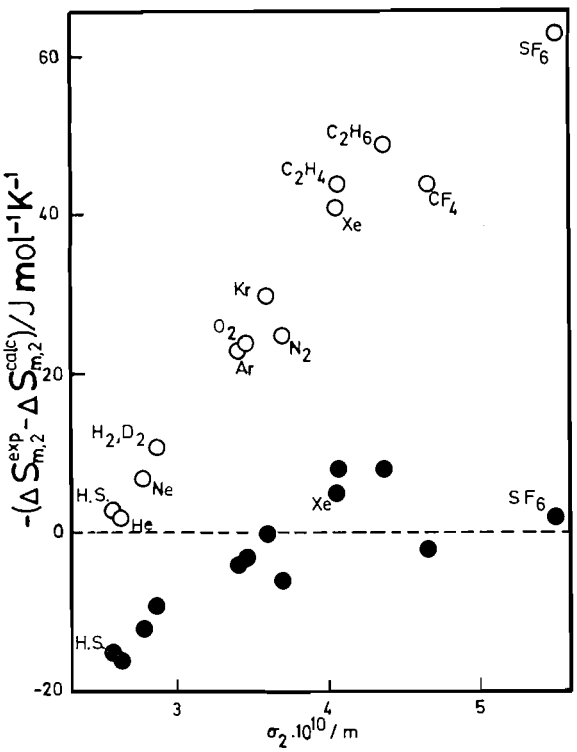

FIG. 3. Difference between experimental and calculated (SPT) values of the partial molar entropy of solution, $-(\Delta S^{exp}_{m,2} - \Delta S^{calcd}_{m,2})$, of gases dissolved in cyclohexanone at 298.15 K, versus the effective hard sphere diameter of solutes: ○, values calculated with $l_1 \neq 0$; ●, values calculated with $l_1 = 0$.

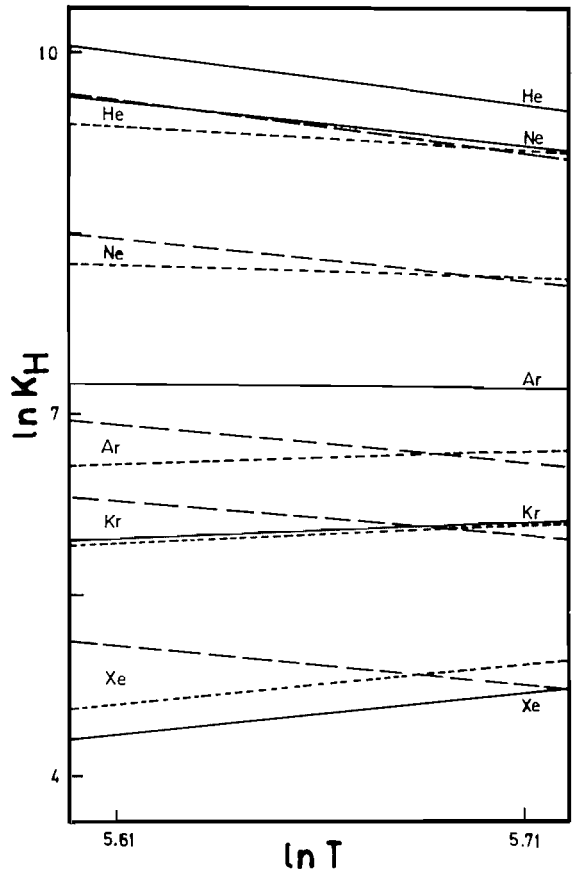

FIG. 4. ln K_H of inert gases in cyclohexanone as a function of ln T: the unbroken line are experimental values; the broken lines are calculated (SPT) values using G_i temperature independent, – – – with $l_1 = -2.07 \times 10^{-4}\,K^{-1}$ and - - - with $l_1 = 0$.

experimental and calculated $\Delta H^0_{m,2}$ and $\Delta S^0_{m,2}$ are in good agreement when $l_1 = -1.87 \times 10^{-4}\,K^{-1}$ is used; with $l_1 = 0$ the calculated values differ greatly from the experimental ones; (*ii*) for gases whose potential energy curves are similar in depth to that of Kr, only the values of $\Delta H^0_{m,2}$ and $\Delta S^0_{m,2}$ obtained with $l_1 = 0$ agree with the experimental ones. Cosgrove and Walkley found similar concordance pattern for the calculated enthalpies of solution for other solvents (15).

When the values of solution enthalpy obtained from eq. [3] (Table 2) are compared with those deduced from the slope of the plot of the theoretical ln K_H against ln T, one can observe that the two ways only agree when G_i is temperature independent. This is because the theory assumes the entropy of interaction to be equal to zero. However, the predicted values of ln K_H are better if G_i is assumed to be temperature dependent in eq. [2]. Figure 4 shows the plot of ln K_H against ln T for the rare gases with G_i = constant.

Following Cosgrove and Walkley (15), we have checked the thermodynamic consistency of equations [2] and [3] for a hypothetical solute of hard-sphere molecules for which $G_i = H_i = 0$. The diameters used were the hard-sphere effective diameters for the rare gases (see Table 3). Enthalpy of solution at 298.15 K was calculated from [3], either with $l_1 = 0$ or with $l_1 = 1.87 \times 10^{-4}\,K^{-1}$. Once the values of ln K_H were obtained from eq. [2] at 293.15 and 303.15 K, the enthalpy of solution was calculated by means of:

$$[4] \quad \Delta H^0_{m,2}(\ln K_H) = -RT^2[\ln K_H(303) - \ln K_H(293)]/10$$

both supposing a_1 = constant = $a_1(298.15)$, $\Delta H^P(\ln K_H)$, and $a_1 = a_1(T)$, $\Delta H^1(\ln K_H)$. The results obtained (Table 4) show

TABLE 4. Enthalpies of solution of rare gases as hard spheres ($G_i = H_i = 0$)

Gases	ΔH^P / kJ mol^{-1}	ΔH^1 / kJ mol^{-1}	$\Delta H^P(\ln K_H)$ / kJ mol^{-1}	$\Delta H^1(\ln K_H)$ / kJ mol^{-1}
He	7.3	12.6	7.6	12.6
Ne	8.1	13.9	8.5	14.1
Ar	11.8	19.9	12.2	19.9
Kr	13.1	21.9	13.5	22.0
Xe	16.4	27.2	17.2	27.2

that [2] and [3] lead to similar values when the same criterion about hard-sphere temperature dependence is used in both cases (either with $l_1 = 0$ or with $l_1 \neq 0$). This confirms that the disagreement between the values for $\Delta H^0_{m,2}$ calculated using both ways should be ascribed to the interaction term, G_i.

Acknowledgements

Authors are grateful for financial assistance of Comisión Asesora de Investigación Científica y Técnica (Madrid) (Proyecto 1788/82). One of the authors (M.A.G.) thanks P.F.P.I. (Plan de Formación del Personal Investigador) for a grant.

1. R. O. NEFF and D. A. MC. QUARRIE. J. Chem. Phys. **77**, 413 (1973).
2. S. GOLDMAN. J. Phys. Chem. **81**, 608 (1977).

3. S. GOLDMAN. J. Solution Chem. **6**, 461 (1977).
4. S. GOLDMAN. J. Chem. Phys. **67**, 727 (1977).
5. S. GOLDMAN. J. Phys. Chem. **81**, 1428 (1977).
6. T. BOUBLIK and B. C.-Y. LU. J. Phys. Chem. **82**, 2801 (1978).
7. S. GOLDMAN. J. Chem. Phys. **69**, 3775 (1978).
8. S. GOLDMAN. J. Chem. Phys. **75**, 4064 (1981).
9. R. A. PIEROTTI. J. Phys. Chem. **67**, 1840 (1963).
10. A. BEN-NAIM and H. L. FRIEDMAN. J. Phys. Chem. **71**, 448 (1967).
11. E. WILHELM. J. Chem. Phys. **58**, 3558 (1973).
12. R. A. PIEROTTI. Chem. Rev. **76**, 717 (1976).
13. J. P. MONFORT and J. L. PEREZ. Chem. Eng. J. **16**, 205 (1978).
14. J. I. KIM and N. BRÜCKL. Z. Phys. Chem. Neue Folge (Wiesbaden), **110**, 197 (1978).
15. B. A. COSGROVE and J. WALKLEY. Can. J. Chem. **60**, 1896 (1982).
16. M. A. GALLARDO, J. S. URIETA, and C. GUTIERREZ LOSA. J. Chim. Phys. **80**, 621 (1983).
17. J. CARNICER, F. GIBANEL, J. S. URIETA, and C. GUTIERREZ LOSA. Rev Acad. Ciencias Zaragoza **34**, 115 (1979).
18. Handbook of Chemistry and Physics. 59th ed. 1978–1979. The Chemical Rubber Company.
19. J. M. MELENDO, M. A. GALLARDO, J. S. URIETA, and C. GUTIERREZ LOSA. Acta Cient. Compostelana, **XXII**, 269 (1985).
20. E. WILHELM and R. BATTINO. Chem. Rev. **73**, 1 (1973).
21. E. WILHELM and R. BATTINO. J. Chem. Phys. **55**, 4012 (1971).
22. A. WIESSBERGER, E. S. PROSKAUER, J. A. RIDDICK, and E. E. TOOPS, JR. Organic solvents. Physical properties and methods of purification. 2nd ed. Interscience Publishers, Inc. 1955.

Can. J. Chem. Downloaded from www.nrcresearchpress.com by 213.166.140.6 on 09/07/12
For personal use only.

Studies of the synthesis of 5-hydroxy 6-keto steroids and related 6-keto steroids

PETER YATES AND SHIRLEY STIVER
Lash Miller Chemical Laboratories, University of Toronto, Toronto, Ont., Canada M5S 1A1

Received March 17, 1987

PETER YATES and SHIRLEY STIVER. Can. J. Chem. **65**, 2203 (1987).

Syntheses of 5-hydroxy-5α- and 5β-cholestan-6-one (**11** and **13**) and their 3β-acetoxy (**10** and **21**) and 3β-benzyloxy derivatives (**12** and **19**) are described, as are syntheses of the 7α-deutero derivatives of **10** and **21**. Related investigations of the syntheses of the 5-methoxy and 5-methyl analogues of these compounds are also discussed. Treatment of **12** with potassium *tert*-butoxide has been shown to give 5-hydroxy-5β-cholest-3-en-6-one (**14**) and its Δ^2 isomer **15**. Reaction of 6-nitrocholesteryl acetate (**50**) with lithium dimethylcuprate gives 3α,5-cyclo-5α-cholestan-6-one (*E*)-oxime (**51**) as the major product.

PETER YATES et SHIRLEY STIVER. Can. J. Chem. **65**, 2203 (1987).

On décrit la synthèse des hydroxy-5 5α- et 5β-cholestanones-6 (**11** et **13**) et de leurs dérivés acétoxy-3β (**10** et **21**) et benzyloxy-3β (**12** et **19**) ainsi que celle des dérivés deutéro-7α des composés **10** et **21**. On discute aussi des études apparentées orientées vers la synthèse des analogues méthoxy-5 et méthyl-5 de ces composés. On a démontré que la réaction du composé **12** avec le *tert*-butylate de potassium conduit à l'hydroxy-5 5β-cholestène-3 one-6 (**14**) et à son isomère Δ^2 (**15**). Le produit principal de la réaction de l'acétate de nitro-6 cholestéryle (**50**) avec le diméthylcuprate de lithium est l'oxime-(*E*) de la cyclo-3α,5 5α-cholestanone (**51**).

[Traduit par la revue]

Can. J. Chem. Downloaded from www.nrcresearchpress.com by 213.166.140.6 on 09/07/12
For personal use only.

In the course of our work on the photochemistry of cyclic α-hydroxy ketones (1), we have had occasion to investigate the synthesis of a number of 5-hydroxy 6-keto steroids and their 7-deutero derivatives together with related 6-keto steroids with other C-5 substituents. Since these studies were extensive and gave results of intrinsic interest, we discuss them separately here and plan to give a detailed account of the photochemical results separately.

Synthesis of steroidal ketols

5α-Hydroxy 6-keto steroids **10–12** were synthesized by the general sequence shown in Scheme 1. Treatment of cholest-5-enes **1–3** with *m*-chloroperoxybenzoic acid gave in each case a mixture of α- and β-epoxides **4–6** that was not separated, since the mixtures gave solely the 5α,6β-diols **7–9** upon treatment with aqueous acid. *p*-Toluenesulfonic acid in aqueous dioxane proved particularly useful for this transformation. Preferential *trans* diaxial ring opening accounts for the observed stereoselectivity (2). Oxidation of the 5α,6β-diols to the 5α-ketols **10–12** was achieved with several reagents; pyridinium chlorochromate is favored as the most reliable and easiest to use. *N*-Bromosuccinimide, the work-horse reagent in these systems (3), gave in our hands variable results.

Spectral data for the compounds in Scheme 1 are in accord with expectation. In the ^{1}H nmr spectra of the ketols **10–12** a triplet (J = 13 Hz) at δ 2.7–2.8 is assigned to the 7α proton. Deshielding of protons situated in a 1,3-diaxial relationship to electronegative substituents such as hydroxyl has been documented (9).

5α-Hydroxy 6-keto steroids have long been recognized to equilibrate under basic conditions with their 5β counterparts (10). Preponderance of the 5β epimer in these equilibria has been attributed to intramolecular hydrogen bonding between the hydroxyl and carbonyl groups in the 5β-ketols where it is geometrically favored. Epimerization of 5-hydroxy-5α-cholestan-6-one (**11**) with methanolic 10% potassium hydroxide (10) gave a ~9:1 mixture of the 5β-ketol **13** and **11**, which were separated chromatographically. The 5β-ketol **13** was also obtained from hydrogenation of the Δ^3-5β-ketol **14** (*vide infra*).

Treatment of the 3β-benzyloxy-5α-ketol **12** with methanolic potassium hydroxide as above did not effect epimerization; largely unconsumed starting material was recovered even after 56 h. Attempted epimerization of **12** with potassium *tert*-butoxide in *tert*-butyl alcohol resulted instead in a facile synthesis of 5-hydroxy-5β-cholest-3-en-6-one (**14**) (Scheme 2). In the ^{1}H nmr spectrum of **14** the hydroxyl proton signal appears as a sharp singlet at δ 4.20, indicative of intramolecular hydrogen bonding (11) and strongly suggesting the 5β configuration. This was confirmed by hydrogenation of **14** to the 5β-ketol **13**. The ^{1}H nmr spectrum of **14** displays two one-proton multiplets at δ 5.42 (width = 13 Hz) and 6.00 (width = 17 Hz), consistent with the Δ^3 position assigned to the olefinic bond. Based on observed correlations between the vicinal coupling constant in H—C—C—H systems and the allylic coupling constant in H—C=C—C—H systems with dihedral angles (12, 13), the multiplet at δ 6.00 is assigned to the C-3 vinyl proton and that at δ 5.42 to the C-4 vinyl proton.

Treatment of **12** with potassium *tert*-butoxide in *tert*-butyl alcohol also gave rise to a minor product, considered to be 5-hydroxy-5-cholest-2-en-6-one (**15**) (Scheme 2). The Δ^2- and Δ^3-5β-ketols **14** and **15** were separated by flash chromatography on a silver nitrate impregnated silica gel column. A sharp singlet at δ 4.05 in the ^{1}H nmr spectrum of **15** again signaled the 5β configuration. A narrow two-proton multiplet ($W_{1/2}$ = 4 Hz) at δ 5.67 arising from the vinyl protons (14) and a peak in its mass spectrum at m/z 346 (80) (M − C_4H_6), considered to originate from a retro Diels–Alder fragmentation, distinguished the Δ^2-5β-ketol **15** from the Δ^3-5β-ketol **14**.

The Δ^3-ketol **14** is postulated to arise by elimination of benzyloxy anion from the enolate of the *A*-homo *B*-nor ketol **16** to give **17** (Scheme 3). Mazur and Nussim (10) have provided evidence to support their postulate that such an *A*-homo *B*-nor ketol is an intermediate in the epimerization of 5-hydroxy-5α-cholestan-6-one (**11**) to its 5β epimer **13**. The presence, under the basic reaction conditions, of a small amount of the Δ^2-ketol **18** in equilibrium with its Δ^3 isomer **17** accounts for the formation of the Δ^2-ketol **15**.

In continuing pursuit of the conversion of **12** to its 5β epimer we next investigated its reaction with Grignard reagents, which can induce rearrangements of α-hydroxy ketones, albeit with the complication of addition to the carbonyl group (15, 16). We found that the very sterically congested 2-mesitylmagnesium

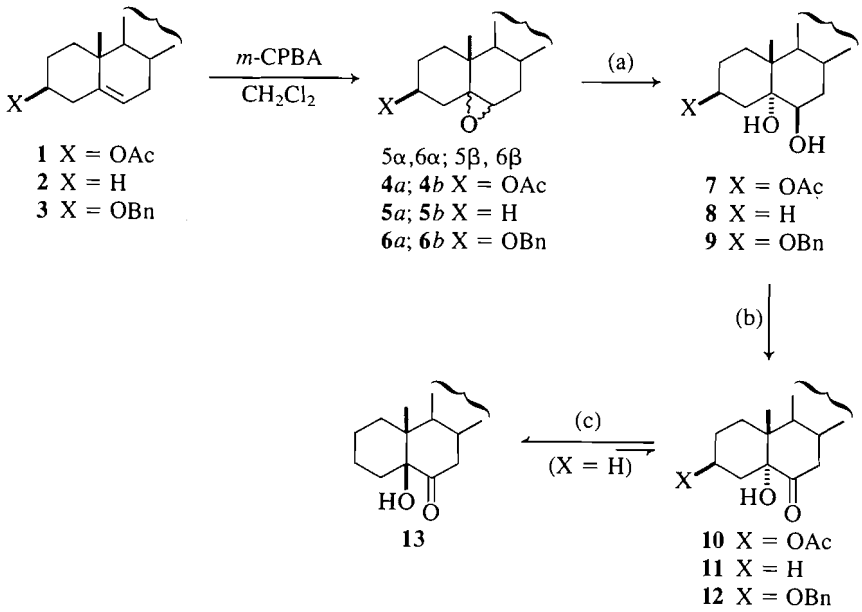

(a) **4**: 70% $HClO_4$/aq. acetone (4); **5**, **6**; *p*-TSA/aq. dioxane, 1.5 h
(b) **7**: $PCC/Al_2O_3/CH_2Cl_2$ (5) or Ag_2CO_3 on Celite/C_6H_6, 96 h (6);
8: NBS/aq. dioxane (7); **9** PCC/3 Å molecular sieves/Al_2O_3/CH_2Cl_2 (8)
(c) **11**: 10% of KOH/CH_3OH, Δ, 8 h (10)

SCHEME 1

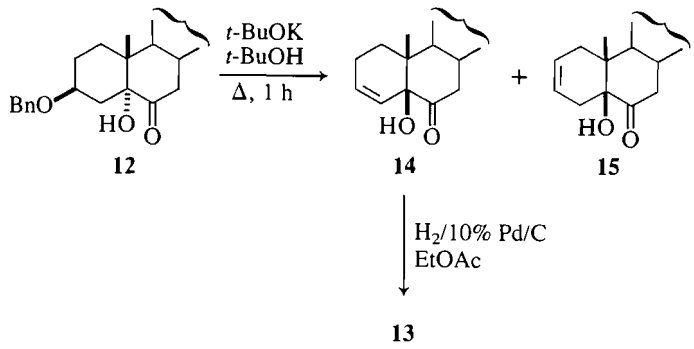

SCHEME 2

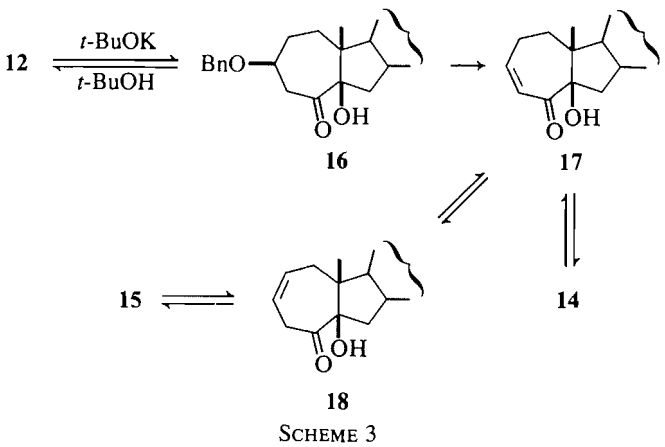

SCHEME 3

bromide cleanly epimerized the 3β-benzyloxy-5α-ketol **12** to its 5β epimer **19**, the only other component of the reaction product being unconsumed **12** (~30%) (Scheme 4). Care in the preparation of the Grignard reagent was critical to the success of this reaction. We found that it was important that Grignard reagent formation be initiated as early as possible during addition of 2-bromomesitylene to magnesium. Failure to ensure this often resulted in a delayed, exothermic reaction between the magnesium and halide, which was detrimental to the capability of the reagent to effect epimerization. We thus found it advantageous to ensure smooth formation of the reagent by entrainment of the magnesium with 1,2-dibromoethane.

Hydrogenolysis of **19** gave 3β,5-dihydroxy-5β-cholestan-6-one (**20**), which on acetylation afforded 3β-acetoxy-5-hydroxy-5β-cholestan-6-one (**21**) in high yield. Interestingly, the mass spectra of the 3-acetoxy- and 3-deoxy-5β-ketols **21** and **13** each exhibit a base peak at m/z 318, which is an ion of low relative abundance in the spectra of the corresponding 5α epimers **10** and **11**. This fragment, assigned the composition $C_{22}H_{38}O$ on the basis of an accurate mass measurement, can be envisioned to arise as depicted in Scheme 5.[1] The reason for the divergent fragmentation behaviour observed for the 5α- and 5β-ketols is not apparent.

Synthesis of 7α-deutero steroidal ketols

The reaction sequence used for the synthesis of the 7α-deutero-3β-acetoxy 5α- and 5β-ketols **23** and **25** is shown in Scheme 6. Bromination of **10** with bromine in acetic acid and chloroform, according to the method of Rodewald *et al.* (18), gave the 7α-bromo-5α-ketol **22** in high yield. Application of this procedure to **21** proved equally successful, yielding solely the 7α-bromo-5β-ketol **24**. The stereochemistry at C-7 in **22** and **24** was witnessed by the narrow multiplets observed for the C*H*Br proton signals at δ 4.18 and 4.42, respectively, in their ^1H nmr spectra (19).

Reduction of **22** and **24** with zinc and *O*-deuteroacetic acid (19, 20) provided an excellent method for the stereoselective

[1]A similar fragmentation pattern has been suggested to account for the intense m/z 318 ions observed in the mass spectra of a number of 3-substituted 6-oxa-*B*-homo-5a-cholestan-7-ones (17).

Can. J. Chem. Downloaded from www.nrcresearchpress.com by 213.166.140.6 on 09/07/12
For personal use only.

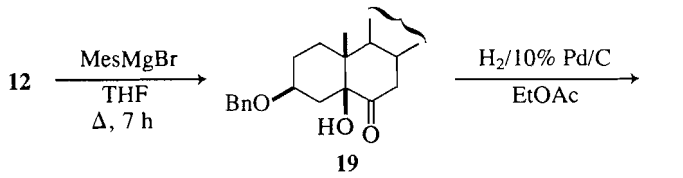

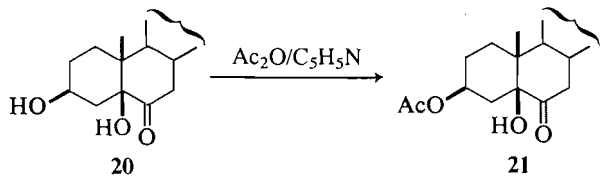

SCHEME 4

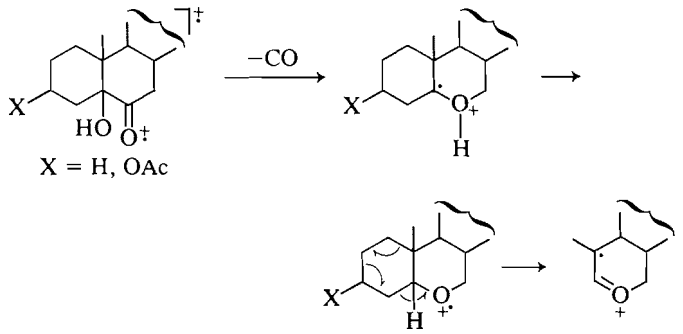

SCHEME 5

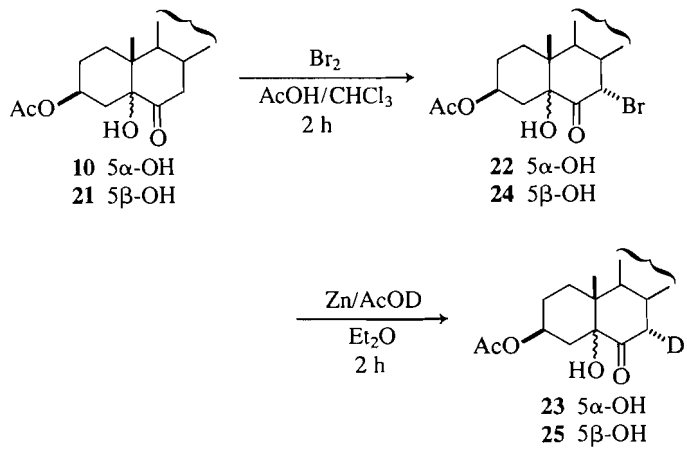

SCHEME 6

introduction of deuterium into the 7α site. The deuterated ketols **23** and **25** were thus obtained in high chemical yield as well as with good incorporation of deuterium label. The deuterium content, d_0, d_1, and d_2, was calculated from the mass spectra according to the method of Budzikiewicz, Djerassi, and Williams (21). The intensities of the molecular ions were relatively weak, and the low signal-to-noise ratios that resulted led to wide scatter in the values calculated for the deuterium content. Therefore, calculations of the deuterium content were based on the more abundant (M − AcOH) fragments. These calculations, which are considered to be valid since the loss of acetic acid from the molecular ions is not expected to involve the C-7 methylene group, gave d_0 15%, d_1 80%, and d_2 5% for **23**.

The deuterium content of **23** and **25** was also calculated from their ^{1}H nmr spectrum. In the spectrum of the undeuterated 3β-acetoxy-5α-ketol **10**, the axial 5-hydroxyl group deshields the 7α proton, whose signal appears at δ 2.76, downfield of the steroidal envelope. Upon deuteration, this signal almost completely disappeared; the weak intensity residual signal for **23** had an area that was 12% of that observed for the C*H*OAc proton at δ 5.03 and thus established that the deuterium content at the 7α site was 88%. Calculations based on the mass spectrum gave a d_1 value of 80% and a maximum deuterium content of 85%. Both of these values were lower than that obtained from the ^{1}H nmr analysis, showing that all of the deuterium label in **23** resided in the 7α site. In the light of the margins of error accompanying deuterium content calculations from the mass and ^{1}H nmr spectra (22 (also pp. 218–221), 23, 24), differences between the two of 5–10% were routinely observed and are considered acceptable.

The situation for **25** is somewhat more complex. The ^{1}H nmr spectrum of the undeuterated ketol **21** exhibits a two-proton multiplet at δ 2.17–2.30 and a one-proton doublet of doublets at δ 2.42 (J = 14, 4 Hz). The latter signal is readily assignable to the 7β proton on the basis of the coupling constants. Upon deuteration, the signal at δ 2.42 collapsed to a doublet (J = 3 Hz) showing that the 14-Hz coupling is attributable to a geminal interaction, as expected. In addition, a doublet of doublets at δ 2.24 (J = 15, 4 Hz) was revealed, thereby demonstrating that the multiplet at δ 2.17–2.30 in the spectrum of **21** is composed of two doublets of doublets, one at δ 2.23 (J = 14, 12 Hz) and the other at δ 2.24 (J = 15, 4 Hz). The former is assigned on the basis of the 12-Hz coupling constant, indicative of an axial–axial interaction, to the 7α proton, while the latter is tentatively ascribed to either the 4α or the 4β proton. In the spectrum of **25** the areas of the δ 2.24 doublet of doublets and of the doublet at δ 2.42 assigned to the 7β proton were observed to be equal. This established that the 7β site was completely protonated and that all the deuterium label again was present in the 7α configuration. From the mass spectrum of **25**, the deuterium content was calculated to be 80–85%.

Studies of the synthesis of 5-methoxy 6-keto steroids

Despite the seeming simplicity of the approach, *O*-methylation of the 3β-acetoxy-5α- and 5β-ketols **10** and **21** under a variety of conditions did not provide a useful synthesis of the corresponding 5-methoxy 6-keto steroids. In the 5α series, a route from the 5β,6β-epoxide **4*b*** to the methoxy ketone **32** was therefore devised (Scheme 7). Since the 5α,6α-epoxide **4*a*** is known to afford the 5-hydroxy 6-methoxy regiochemistry upon acid-catalyzed addition of methanol (25), the mixture of α- and β-epoxides **4*a*** and **4*b*** described previously could not be used in the synthesis of **32**. The required stereoselective synthesis of the β-epoxide **4*b*** was achieved via the 5α-bromo-6β-acetate **26**. This was formed as the major product, together with its stereoisomer **27**, from the reaction of cholesteryl acetate (**1**) with *N*-bromoacetamide and lithium acetate in acetic acid (cf. ref. 26). The structural assignments for **26** and **27** were based on comparison of their ^{1}H nmr spectra with the spectrum of 5-bromo-5α-cholestane-3β,6β-diol 3-acetate **28**, prepared by bromination of cholesteryl acetate (**1**) in aqueous medium (27).

The 5β-bromo-6α-acetate **27** can be conjectured to arise via attack of bromine on the β face of olefin **1** followed by attack of acetate ion at C-6 in the intermediate bromonium ion, thus avoiding an unfavorable 1,3-diaxial bromine–methyl interaction that would have resulted from addition in the opposite regiochemical sense.

Treatment of the 5α-bromo 6β-acetoxy isomer **26** with ethanolic sodium ethoxide at room temperature gave the

Can. J. Chem. Downloaded from www.nrcresearchpress.com by 213.166.140.6 on 09/07/12
For personal use only.

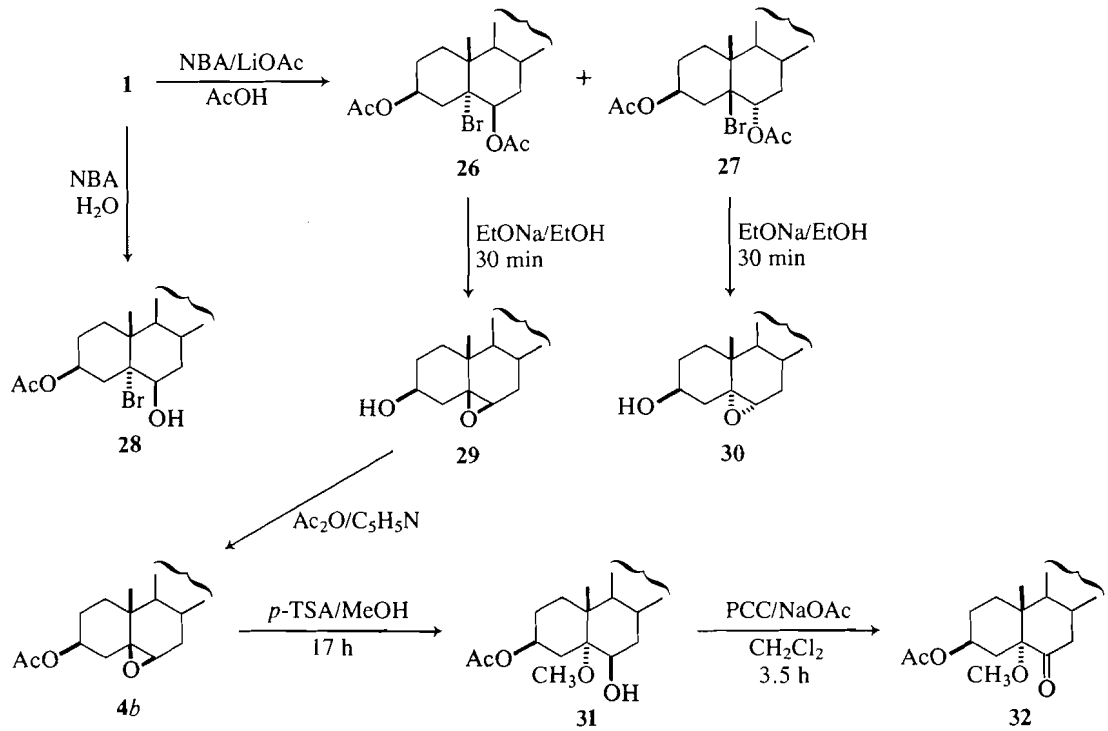

SCHEME 7

3-hydroxy-5β,6β-epoxide **29**. Similar reaction with a mixture of **26** and **27** gave both **29** and the α-epoxide **30**, demonstrating the necessity for separation of **26** and **27** for a stereoselective synthesis of the β-epoxide. The structures of the α- and β-epoxides **30** and **29** were assigned on the basis of the higher field chemical shift of the C-19 methyl signal and the smaller coupling constant for the C-6 methine proton in the ^{1}H nmr spectrum of the β- relative to the α-epoxide (28). The α-epoxide appears to originate from the 5β-bromo 6α-acetate **27**, although the substituents are not aligned for an *anti*-periplanar displacement of bromide by the alkoxide formed from attack of ethoxide on the 6α-acetoxy group. However, participation of a boat form of ring B would permit an *anti*-periplanar transition state for displacement.

Epoxide **29** was also prepared by treatment of the triacetate **35** (29), obtained from cholesterol (**33**) via the triol **34** (30), with

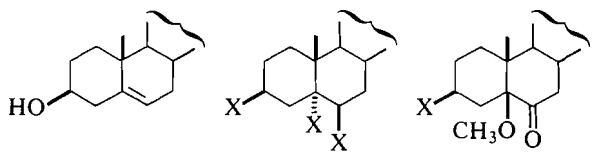

33 **34** X = OH, **35** X = OAc, **36** X = OBn, **37** X = OH

ethanolic sodium ethoxide. Acetylation of **29** gave the acetoxy β-epoxide **4*b***. Acid-catalyzed, regioselective opening of the epoxide ring of **4*b*** with methanol and oxidation of the resulting 5α-methoxy 6β-alcohol **31**, gave the desired 5α-methoxy ketone **32**.

It was envisioned that synthesis of the 5β-methoxy ketone **37** could be accomplished by *O*-methylation of the 3β-benzyloxy-5β-ketol **19** to give the ether **36** followed by hydrogenolysis and acetylation. In the event, methylation of **19** gave a dimethylation product. The presence in its ^{1}H nmr spectrum of a doublet (J = 7 Hz) at δ 1.06 (CH_3CH) and a doublet of quartets (J = 7,

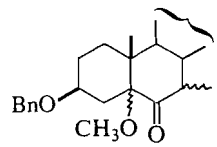

38 5α-OCH_3
39 5β-OCH_3

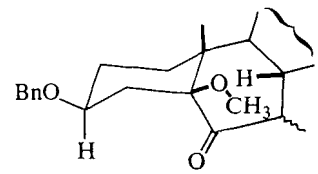

39*A*

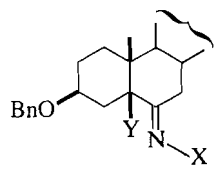

40 X = Y = OH
41 X = OCH_3, Y = OH
42 X = Y = OCH_3

7 Hz) at δ 2.32 (CH_3CHCH) in addition to an *O*-methyl signal at δ 3.60 indicated that both *O*-alkylation and *C*-alkylation α to the carbonyl group had occurred. The 5α configuration as in **38** was initially suggested by the appearance of the C*H*OBn proton signal at δ 3.60 as a broad multiplet. However, other features of the ^{1}H nmr spectrum of the methylation product were not readily accommodated by the 5α-methoxy assignment **38**.[2]

This circumstance and results from methylation of the C-5 hydroxyl group in systems in which the C-6 carbonyl group was protected (*vide infra*) led us to consider the possibility that the product from methylation of **19** had the 5β stereochemistry as in **39** and that the broad multiplet assigned to the C*H*OBn proton

[2]The possibility that methylation had occurred at C-4 via an *A*-homo *B*-nor intermediate was excluded by the observation that the C*H*OBn signal at δ 3.60 was unaffected by irradiation at δ 2.32, the chemical shift of the signal assigned to the C*H*CH_3 proton.

Can. J. Chem. Downloaded from www.nrcresearchpress.com by 213.166.140.6 on 09/07/12
For personal use only.

Can. J. Chem. Downloaded from www.nrcresearchpress.com by 213.166.140.6 on 09/07/12
For personal use only.

arose from an axial conformation of this proton resulting from the preference of either ring A or B in **39** to exist in a boat-like conformation. A conformation with ring A in a chair and ring B in a boat form as in **39***A* appears to be the most favorable conformation available to **39** consistent with an axial disposition of the C-3 methine proton. This conformation also reconciles the unusual chemical shifts observed in the ^{1}H nmr spectrum of the methylation product. In this conformer, the C-19 methyl group (δ 1.04) resides in a completely different environment from that in the 3β-benzyloxy-5β-ketol **19** (C-19 Me at δ 0.83), and a large difference in their chemical shifts is not unexpected. The unusually deshielded resonance at δ 2.67 for the C-8 methine proton is consistent with the propinquity of this proton to the methoxyl substituent (ref. 11, pp. 71, 72; ref. 31), as in **39***A*. Models demonstrate that the 4α proton is situated in the deshielding cone of the C-6 carbonyl group, and the unusually low field resonance for this proton at δ 2.60 provides further evidence for the existence of **39** in the ring B boat conformation and its assignment to the methylation product. The coupling of 7 Hz between the C-7 and C-8 methine protons did not permit an unambiguous assignment of the configuration at C-7 (ref. 9, p. 51; ref. 32).

We proceeded to protect the 6-keto group in **19** to inhibit *C*-methylation. The oxime **40** and oxime methyl ether **41** were prepared following standard procedures. In their ^{1}H nmr spectra they both exhibited broad doublets (J = 12 Hz) at δ 3.3, assigned to the 7β proton and indicative of the *E* geometry (33–36). Methylation of either **40** or **41** gave the 5β-methoxy 6-oxime methyl ether **42**. The ^{1}H nmr spectrum of **42** exhibited two three-proton singlets at δ 3.10 and 3.87. The former was assigned to the C-5 methoxyl protons and the latter to the oxime methyl ether protons, based on reported chemical shifts of oxime methyl ether signals (35). Since both **40** and **41** would be extremely unlikely to undergo epimerization under the mild methylation conditions employed, the 5-methoxy 6-oxime methyl ether **42** was assigned the 5β configuration. As in the case of the analogous 5β-methoxy ketone **39**, the ^{1}H nmr spectrum of **42** was consistent with the 5β stereochemistry with ring B existing in a boat conformation, resulting in an axial disposition of the C*H*OBn proton and a broad multiplet for its proton signal. The chemical shift of the C-19 methyl singlet of the oxime **42** at δ 1.03 reflects its similarity to that of **39**. Compound **42** was assigned the *E* configuration since oximes with an α quaternary center are known to prefer this geometry (37). The *E* geometry in **42**, unlike that in **40** and **41**, was not evident from its ^{1}H nmr spectrum: neither of the C-7 methylene protons was shifted downfield from the steroidal envelope. The deshielding for α protons *syn* to an oxime group has been attributed to the anisotropy of the lone pairs on oxygen (38), and has been observed to decrease as the dihedral angle between the relevant C—H bond and the C=N—OH plane increases (36). Since in the ring B boat conformer of **42** both of the C-7 methylene protons are out of the C=N—OMe plane, the fact that they do not give rise to signals usually associated with the *E* geometry of the oxime derivative is readily explicable.

Attempted hydrolysis of the oxime methyl ether group in **42** with aqueous perchloric acid and methyl pyruvate (39) gave, following chromatography, a major fraction comprising a ~70:30 mixture of two compounds containing a single methoxyl group. The ir and ^{1}H nmr spectra of this mixture indicated that the C-5 methoxyl group had been removed while the oxime methyl ether moiety had remained intact. With this result, the synthesis of the 5β-methoxy ketone **37** was not pursued further.

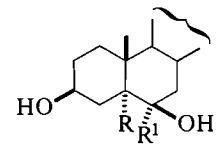

43 R = CH_3, R′ = H
44 R = H, R′ = CH_3

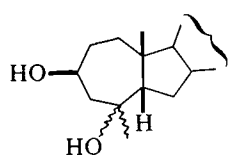

45

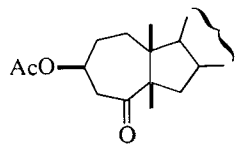

47

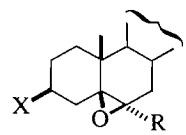

46 X = OAc, R = CH_3
49 X = $OCOCH_2COCH_3$, R = H

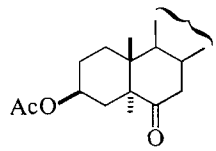

48

Approaches to the synthesis of 5-methyl 6-keto steroids

Direct methylation of 6-keto steroids has been reported to require vigorous reaction conditions, under which 5-methyl 6-keto steroids were obtained in poor yield (40). Addition of methylmagnesium iodide to the β-epoxide **29** has been claimed to give the 5α-methyl 6β-alcohol **43** (41), but Julia *et al.* (42) concluded that the product had structure **44**, and was formed via rearrangement of **29** (43). Our own investigation of the reaction has confirmed this conclusion (see Experimental) and also led to the isolation of a minor product to which we assign the structure **45**. It is considered to originate from initial isomerization of **29** to the *A*-homo *B*-nor 4a-ketone and subsequent Grignard addition. The 5β configuration was assigned based on analogy to the boron trifluoride catalyzed rearrangement of the 6α-methyl 5β,6β-epoxide **46**, which is reported to give the *A*-homo *B*-nor 5β-methyl 4a-ketone **47** together with the ketone **48** (44).

Lithium dialkylcuprate reagents also react with epoxides to give alkyl alcohols and have the advantage that they do not, in general, induce epoxide-to-ketone isomerizations; furthermore, reactions of cuprate reagents with epoxy esters have been observed to occur with chemoselective attack at the oxirane ring (45). However, reaction of the 3β-acetoxy β-epoxide **4***b* with lithium dimethylcuprate gave none of the desired 5-methyl 6-alcohol, but two other products—the 3-hydroxy β-epoxide **29** and its acetoacetic ester **49**. Bands at 5.73 and 5.81 μm in its ir spectrum and a broad two-proton singlet in its ^{1}H nmr spectrum at δ 3.42, which slowly disappeared upon treatment with deuterium oxide, indicated that the acetoacetic ester **49** exists largely as the keto ester tautomer, in accord with expectation (46). Abstraction of a proton α to the carbonyl moiety of the acetoxy group and acylation of the resulting enolate by another molecule of **46** accounts for the formation of both products.

In another approach to the synthesis of 5-methyl 6-keto steroids, we investigated the conjugate addition of lithium dimethylcuprate to 6-nitrocholesteryl acetate (**50**).[3] We hoped that this might provide a method for regioselective introduction of a methyl substituent at the C-5 site. Subsequent Nef reaction of the resulting 5-methyl 6-nitrocholestane would then afford a route to 5-methyl 6-keto steroids. Although reports of reactions between lithium dialkylcuprates and α,β-unsaturated nitro compounds are rare, conjugate addition has been observed in the reactions of 1-(4-chlorophenyl)-2-nitropropene with both lithium dimethyl- and diphenylcuprate (48). However, the reaction between **50**, prepared by nitration of cholesteryl acetate (**1**) (49), and lithium dimethylcuprate followed a different

[3]This study has been the subject of a preliminary communication (47).

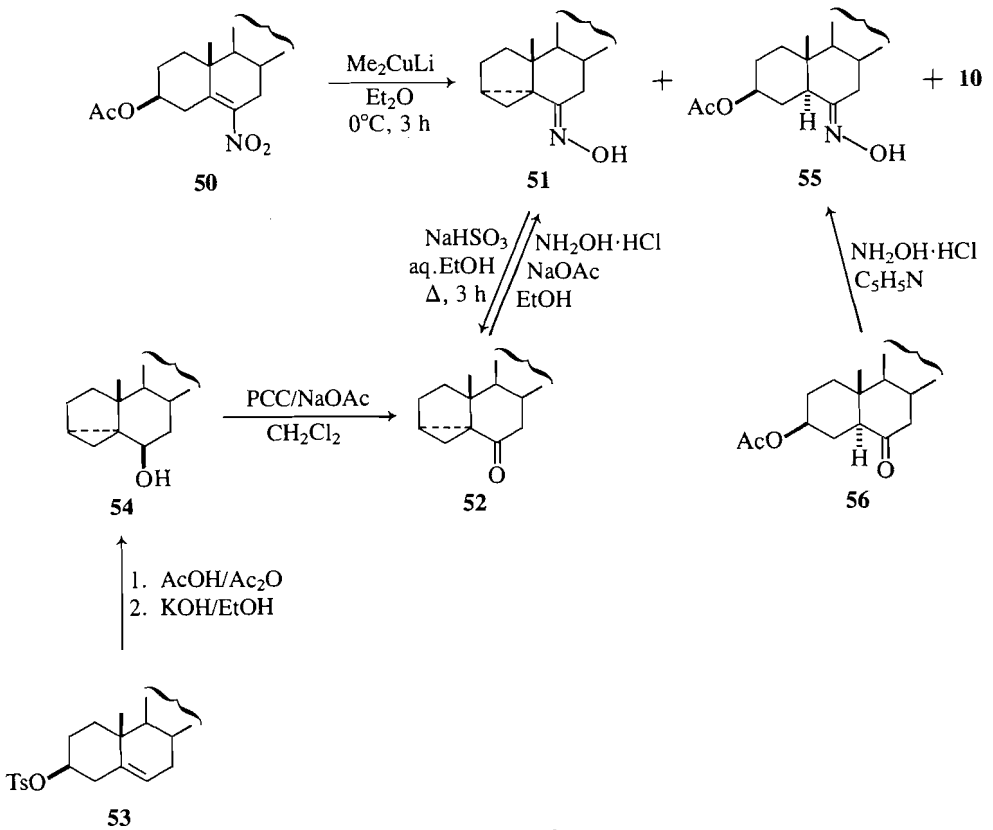

SCHEME 8

course, giving 3α,5-cyclo-5α-cholestan-6-one (*E*)-oxime (**51**) in 65% yield (Scheme 8). In the single frequency off-resonance decoupled ^{13}C nmr spectrum of **51**, a triplet at δ 8.0 and a singlet at δ 160.5 signaled cyclopropyl and oximino functions, respectively. The presence in its ^1H nmr spectrum of a broad doublet at δ 3.30 (J = 11 Hz) evidenced the *E* geometry about the C=N bond (33, 34, 36) and a high field multiplet at δ 0.49 is ascribed to the C-4 methylene protons of the cyclopropane ring. In the mass spectrum of **51**, a relatively abundant ion (40%) at m/z 383 is assigned to an ion formed by loss of an oxygen atom from the molecular ion. This type of fragmentation has been observed in the mass spectrum of cyclohexanone oxime (50). The structural assignment **51** was confirmed by treatment of the product with sodium bisulfite in aqueous ethanol to give the 3α,5α-cyclo ketone **52** (51).

The structural assignment was further verified by an independent synthesis. 3α,5-Cyclo-5α-cholestan-6β-ol (**54**) formed by solvolysis of cholesteryl tosylate (**53**) (ref. 2*a*, pp. 236–248; ref. 52) was oxidized with pyridinium chlorochromate (PCC) in the presence of sodium acetate (2 equiv./mol PCC) to give the cyclopropyl ketone **52**. The amount of sodium acetate employed was critical to the success of this oxidation, since the product obtained following the recommended conditions (0.2 equiv. NaOAc/mol PCC) (53) contained olefinic and aldehydic side products presumed to arise from acid-initiated opening of the cyclopropyl ring. Oximination of ketone **52** gave the *E* oxime; the formation of the *E* geometrical isomer is considered to be due to the presence of the quaternary center at C-5 (37). A number of minor products were formed in the reaction between lithium dimethylcuprate and **50** (Scheme 8). We have identified 3β-acetoxy-5α-cholestan-6-one (*E*)-oxime (**55**), isolated in a mixture with the acetoxy 5α-ketol **10**, by direct comparison with a sample prepared by oximination of the parent ketone **56** (54).

A possible mechanism for the formation of oxime **51** from the reaction of lithium dimethylcuprate with **50** is detailed in Scheme 9. Introduction of an electron into the α,β-unsaturated nitro system would lead to a radical anion **57**. House and Umen (55) have reported that unsaturated systems with reduction potentials less negative than −2.4 V (in *N*,*N*-dimethylformamide) will accept an electron from lithium dimethylcuprate, and Sato *et al.* (56) have reported that the reduction potential of the nitro olefin **50** lies in the range −1.35 to −1.37 V (in *N*,*N*-dimethylformamide). Intramolecular nucleophilic displacement of the acetoxy group in **57** would generate the cyclopropane ring with the 3α,5α geometry.[4] The ability of anions at C-5 to displace good leaving groups in the β orientation at C-3 leading to 3α,5α-cyclo steroids is well documented (54), although this may be the first example in which an acetoxy group has been so displaced. Sato *et al.* (56) have observed that while electrolysis of the tosylate **61** gave a 43% yield of the cyclo nitro compound **62**, no evidence of any 3,5-cyclo products derived from internal displacement of the acetoxy group could be detected from similar electrolysis of the analogous acetate **50**, which gave the bimolecular product **63**. In the case of the cuprate reaction of **50**, displacement of the acetoxy group may be facilitated by complexation with lithium or copper species. To account for further reduction of **58** to oxime **51** (Scheme 9), complex **59** is postulated to form and undergo methyl insertion (55) to give the nitronate ester **60**.

[4]While a two-electron transfer mechanism cannot be excluded, related studies lead us to favor internal displacement from a radical anion formed by a one-electron process (56, 57).

Can. J. Chem. Downloaded from www.nrcresearchpress.com by 213.166.140.6 on 09/07/12
For personal use only.

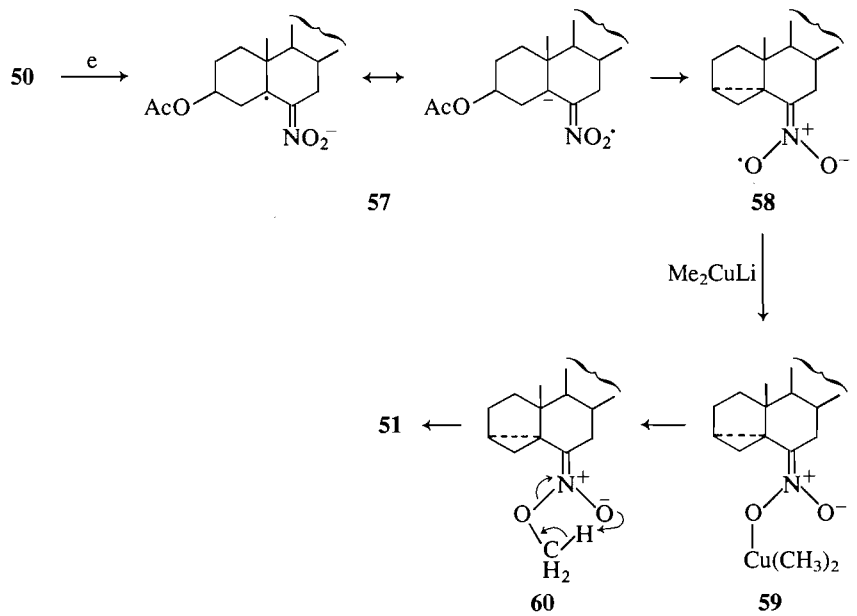

SCHEME 9

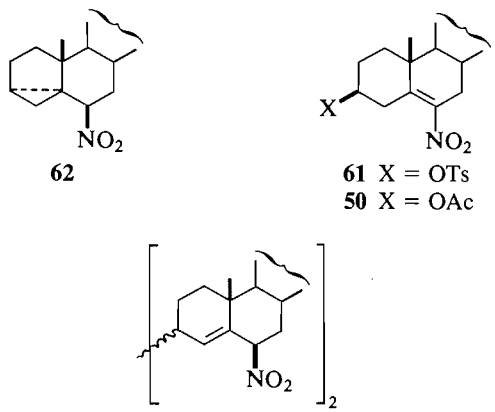

This postulate is not without precedent, for in the reduction of nitroalkanes to oximes by carbon monoxide and copper salts Knifton (58) has suggested that carbon monoxide insertion into a copper–oxygen bond occurs in a related copper-bound nitronate anion. Decomposition of the nitronate ester **60** to afford the oxime **51**, as depicted, is well documented (58, 59). The stereochemical consequences for the oxime generated by the mechanism outlined in Scheme 9 are undefined; however, equilibration of the *Z* to the *E* isomer during work-up would account for isolation of only the latter from the reaction mixture. Oxime **51** was recovered unchanged following resubjection to lithium dimethylcuprate treatment.

Experimental[5]

Melting points were recorded on a Fisher–Johns melting point apparatus and are uncorrected. The ir spectra were recorded in chloroform and the ^{1}H nmr spectra at 60 MHz in deuterochloroform unless otherwise specified. For symmetrical multiplets in the latter the width at half-height ($W_{1/2}$) is recorded while for unsymmetrical multiplets the total width is given. Low resolution mass spectra were recorded with a Bell and Howell CEC 21-490 mass spectrometer. For the deuterium content calculations, 10–20 scans of the region of the spectrum containing the isotopic cluster associated with the molecular ion or, where appropriate, of the (M − CH_3CO_2H) fragment were obtained at a high signal-to-noise ratio and averaged. Accurate mass measurements were made with an AEI MS-3074 spectrometer with a DS-50 data system.

Organic solutions were concentrated on a rotary evaporator under water aspirator pressure. Column chromatography was carried out on silica gel (Grace Davison, grade 923, 100–200 mesh), neutral alumina (Merck, activity 1, 70–230 mesh, 90 Å mean pore diameter), or Florisil (Aldrich, 100–200 mesh). Flash chromatography was performed on 40–60 μm silica gel (Merck, grade 60, 230–400 mesh, 60 Å mean pore diameter) under air, nitrogen, or argon pressure so that the drop in solvent height was 5 cm/min.

Several compounds described here have been obtained previously. Full experimental details for their preparation in the present work are given only when a new method or a significant variation of an earlier method has been used.

*5,6α-Epoxy-5α- and 5,6β-epoxy-5β-cholestan-3β-yl acetate (**4**a and **4**b)*

Oxidation of cholesteryl acetate (**1**) (60) with *m*-chloroperoxybenzoic acid in dichloromethane gave a mixture of **4***a* and **4***b* (99%) as a white solid. Crystallization from aqueous 90% acetone gave a 50:50 mixture of **4***a* and **4***b* as white crystals, mp 103–109°C; ir λ_{max}: 5.78 μm; ^{1}H nmr δ: 0.62 (s, C-18 Me α-epoxide), 0.65 (s, C-18 Me β-epoxide), 1.03 (s, C-19 Me β-epoxide), 1.10 (s, C-19 Me β-epoxide), 2.03 (s), 2.83 (d, J = 4 Hz, α-epoxide) and 3.07 (d, J = 3 Hz, β-epoxide) (1H), 4.83 (br m, $W_{1/2}$ = 24 Hz, 1H); ms m/z: 444 (6), 384 (100).

*5,6α-Cholestane-3β,5,6β-triol 3-acetate (**7**)*

Perchloric acid (70%; 0.35 mL) was added dropwise to a solution of a 50:50 mixture of **4***a* and **4***b* (1.14 g, 2.57 mmol) in acetone (50 mL) and water (3 mL), and after the solution was stirred at room temperature for 5 h, water was added to precipitate the product. The collected product was washed with water and crystallized from aqueous 90% acetone to give **7** (1.02 g, 86%) as white crystals, mp 206.5–208.5°C (lit. (61) mp 207–208°C); ir λ_{max}: 3.02 (sh, w), 3.14 (br, w), 5.79 μm; ^{1}H nmr δ: 0.68 (s, C-18 Me), 1.20 (s, C-19 Me), 1.93 (br s, OH, absent after treatment with deuterium oxide), 2.03 (s), 3.53 (nar m, $W_{1/2}$ = 8 Hz, 1H), 5.13 (br m, $W_{1/2}$ = 20 Hz, 1H); ms m/z: 462 (20), 384 (100).

[5]For additional details of experimental procedures, see ref. 1*b*.

Can. J. Chem. Downloaded from www.nrcresearchpress.com by 213.166.140.6 on 09/07/12
For personal use only.

Can. J. Chem. Downloaded from www.nrcresearchpress.com by 213.166.140.6 on 09/07/12
For personal use only.

*3β-Acetoxy-5-hydroxy-5α-cholestan-6-one (**10**)*

*(i) Oxidation of **7** with pyridinium chlorochromate*

A solution of **7** (0.984 g, 2.13 mmol) in dichloromethane (55 mL) was added all at once to a stirred suspension of pyridinium chlorochromate (Aldrich; 1.15 g, 5.33 mmol) and neutral, activity I, 70–230 mesh alumina (Merck; 4.45 g) in dichloromethane (30 mL) under an argon atmosphere. The reaction mixture was stirred at room temperature for 2 h, and ether (25 mL) was added to the resulting brown suspension. The mixture was filtered through a Florisil column (2 × 12 cm) and the column was eluted with ether (100 mL). The combined organic solutions were concentrated to give **10** (0.86 g, 88%) as a white solid. Crystallization from methanol gave **10** as white needles, mp 231.5–233.5°C. Flash chromatography of the product on silica gel (2 × 14 cm) with chloroform – ethyl acetate (9:1 v/v) as eluent gave **10** (0.78 g, 79%), which crystallized from methanol as white needles, mp 235.5–238°C (lit. (30) mp 232–233°C); ir λ_{max}: 2.81 (sh, w), 2.95 (br, w), 5.83 μm; ^{1}H nmr (400 MHz) δ: 0.64 (s, C-18 Me), 0.81 (s, C-19 Me), 0.86 (d, J = 6 Hz, C-26,27 Me), 0.91 (d, J = 7 Hz, C-21 Me), 2.01 (s), 2.10 (dd, J = 13, 4 Hz), 2.76 (dd, J = 13, 13 Hz, 1H), 3.11 (br s, OH, 1H), 5.03 (br m, $W_{1/2}$ = 24 Hz, 1H); ms m/z: 460 (20), 400 (100).

*(ii) Oxidation of **7** with silver carbonate on Celite*

Silver carbonate precipitated on Celite was prepared following the method of Balogh, Fetizon, and Golfier (6). The Ag_2CO_3/Celite reagent was assumed to contain approximately 1 mmol of silver carbonate for every 0.57 g of reagent (6). A stirred suspension of **7** (216 mg, 0.47 mmol) and Ag_2CO_3/Celite (2.85 g, ~5 mmol) in anhydrous benzene (25 mL) under a nitrogen atmosphere was heated under reflux for 96 h with azeotropic removal of water by means of a Dean–Stark apparatus. The resultant dark green reaction mixture was filtered and concentrated to give a brownish colored solid. This was dissolved in chloroform, and the solution was filtered through Celite. The filtrate was concentrated to give **10** (210 mg, 98%) as a white solid, which on crystallization from methanol gave **10** as white needles, mp 233–235°C.

*5,6α-Epoxy-5α- and 5,6β-epoxy-5β-cholestane (**5**a and **5**b)*

Oxidation of 5-cholestene (**2**) (62) with *m*-chloroperoxybenzoic acid in dichloromethane gave a ~70:30 mixture of **5***a* and **5***b* (2.95 g) in quantitative yield as a pale yellow solid; ir λ_{max}: 3.47 μm; ^{1}H nmr δ: 0.60 (s, C-18 Me α-epoxide), 0.63 (s, C-18 Me β-epoxide), 1.00 (s, C-19 Me β-epoxide), 1.05 (s, C-19 Me α-epoxide), 2.83 (d, J = 4 Hz, α-epoxide) and 2.97 (d, J = 3 Hz, β-epoxide) (1H); ms m/z: 386 (90), 55 (100).

*5α-Cholestane-5,6β-diol (**8**)*

A solution of a 70:30 mixture of **5***a* and **5***b* (2.38 g, 6.17 mmol) and *p*-toluenesulfonic acid monohydrate (65 mg, 0.34 mmol) in dioxane–water (9:1 v/v; 43 mL) was stirred and heated under reflux for 1.5 h. The solution was allowed to cool to room temperature and poured into aqueous 10% Na_2CO_3 (20 mL). The dioxane was removed under water aspirator pressure on a rotary evaporator equipped with a cold trap condenser. The residue was extracted with ether (4 × 25 mL), and the combined ethereal extracts were washed with water (4 × 25 mL), dried (Na_2SO_4), and concentrated to give **8** (2.17 g, 87%) as a yellow oil that partially crystallized on standing; ir λ_{max}: 2.75 (sh, w), 2.88 (br, w) μm; ^{1}H nmr δ: 0.70 (s, C-18 Me), 1.17 (s, C-19 Me), 1.50 (m, OH, absent after treatment with D_2O), 3.48 (nar m, $W_{1/2}$ = 6 Hz, 1H); ms m/z: 404 (10), 386 (100).

*5-Hydroxy-5α-cholestan-6-one (**11**)*

Oxidation of **8** in dioxane–water with purified (63) *N*-bromosuccinimide gave **11** as a white solid (61%), which exhibited a ^{1}H nmr spectrum in accord with expectation. However, thin-layer chromatography indicated the presence of a very small amount of impurity, and a solution of the compound became darker yellow in color during attempted crystallization from methanol. The methanolic solution was concentrated, and flash chromatography of the yellow solid on silica gel (2 × 15 cm) with hexanes – ethyl acetate (9:1 v/v) gave **11** (284 mg, 44%). Crystallization from methanol gave **11** as fine white needles, mp 150–153°C (lit. (7) mp 152–153°C); ir λ_{max}: 2.75 (sh, w), 2.96 (br, w), 5.82 μm; ^{1}H nmr δ: 0.65 (s, C-18 Me), 0.78 (s, C-19 Me), 1.77 (br s, OH), 2.77 (dd, J = 12 Hz, 12 Hz); ms m/z: 402 (100).

*Cholesteryl benzyl ether (**3**)*

Benzylation of cholesterol (**33**) (64) in anhydrous benzene and anhydrous dimethyl sulfoxide with NaH (50% dispersion in oil) followed by purified benzyl bromide (65) gave a yellow solid, which on crystallization from acetone gave **3** (76%) as white needles, mp 115–116°C. The melt solidified on cooling, and the solid remelted at 119–121.5°C (lit. (66) mp 118.5°C). Compound **3**: ir λ_{max}: 6.19 (vw) μm; ^{1}H nmr δ: 0.70 (s, C-18 Me), 1.03 (s, C-19 Me), 3.25 (br m, $W_{1/2}$ = 20 Hz, 1H), 4.57 (s, 2H), 5.33 (nar m, $W_{1/2}$ = 8 Hz, 1H), 7.33 (s, 5H); ms m/z: 476 (2), 370 (100), 91 (98).

*5,6α-Epoxy-5α- and 5,6β-epoxy-5β-cholestan-3β-yl benzyl ether (**6**a and **6**b)*

Oxidation of **3** with *m*-chloroperoxybenzoic acid in dichloromethane gave an 80:20 mixture of **6***a* and **6***b* (94%) as a white solid, mp 102–113°C; ir λ_{max}: 3.55 μm; ^{1}H nmr δ: 0.60 (s, C-18 Me), 1.00 (s, C-19 β-epoxide), 1.07 (s, C-19 Me α-epoxide), 2.87 (d, J = 4 Hz, α-epoxide) and 3.00 (d, J = 3 Hz, β-epoxide) (1H), 3.60 (br m, $W_{1/2}$ = 24 Hz, 1H), 4.50 (s, 2H), 7.30 (s, 5H); ms m/z: 492 (5), 91 (100).

*5α-Cholestane-3β,5,6β-triol 3-benzyl ether (**9**)*

A suspension of an 80:20 mixture of **6***a* and **6***b* (79.7 g, 0.162 mol) and *p*-toluenesulfonic acid monohydrate (1.65 g, 0.009 mol) in dioxane (1 L) and water (100 mL) was stirred and heated under reflux under an argon atmosphere for 1.5 h. The resulting solution was allowed to cool to room temperature and was added to aqueous 10% Na_2CO_3 (500 mL). The dioxane was removed under water aspirator pressure on a rotary evaporator equipped with a cold trap condenser. The residue was dissolved by adding ether (550 mL), dichloromethane (200 mL), and water (150 mL), and the aqueous layer was extracted with ether (2 × 100 mL) and ether–dichloromethane (70:30 v/v; 1 × 100 mL). The combined organic phases were washed with water (300 mL, 5 × 50 mL), dried ($MgSO_4$), and concentrated to give **9** (77 g, 93%) as a white solid. Crystallization from hexanes–acetone (75:25 v/v; 650 mL) gave white needles, mp 185–187°C; (lit. (67) mp 185–186°C); ir λ_{max}: 2.88 (sh, w), 3.01 (br, w) μm; ^{1}H nmr δ: 0.67 (s, C-18 Me), 1.18 (s, C-19 Me), 1.57 (m, OH, absent after treatment with D_2O), 3.43 (nar m, $W_{1/2}$ = 5 Hz, 1H), 3.78 (br m, $W_{1/2}$ = 20 Hz, 1H), 4.53 (s, 2H), 7.30 (s, 5H); ms m/z: 510 (0), 91 (100).

*3β-Benzyloxy-5-hydroxy-5α-cholestan-6-one (**12**)*

*(i) Oxidation of **9** with pyridinium chlorochromate in the presence of molecular sieves and alumina*

A solution of **9** (20.0 g, 39.2 mmol) in anhydrous dichloromethane (100 mL) was added over a period of 5 min to a mechanically stirred mixture of pyridinium chlorochromate (Aldrich; 16.1 g, 74.6 mmol), 3 Å molecular sieves (BDH; 60 g), activated by crushing the $\frac{1}{8}$-in. pellets with a mortar and pestle and heating over a flame under a flow of argon for 2 h, and neutral, activity I, 70–230 mesh alumina (Merck; 57 g) in anhydrous dichloromethane (35 mL) under an argon atmosphere. Initially, the brown reaction mixture became warm, causing the dichloromethane to boil gently. After the mixture was stirred for 1 h, ether (100 mL) was added, and the mixture was filtered through a Florisil column (54 g, 4 × 10 cm). The column was eluted with ether (800 mL), and the combined organic solutions were concentrated to give a brown solid. A solution of the solid in ether (600 mL) was filtered through an alumina column (65 g, 4 × 8 cm), and the column was eluted with ether (800 mL). The combined ethereal solutions were concentrated to give **12** (13.9 g, 70%) as a white solid, mp 180.5–184°C. Crystallization from cyclohexane gave **12** as white needles, mp 189.5–190°C (lit. (68) mp 186–188°C); ir λ_{max}: 2.84 (sh, w), 3.00 (br, w), 5.82 μm; ^{1}H nmr δ: 0.65 (s, C-18 Me), 0.83 (s, C-19 Me), 2.13 (br s, OH, absent after treatment with D_2O), 2.70 (dd, J = 12, 12 Hz, 1H), 3.72 (br m, $W_{1/2}$ = 20 Hz, 1H), 4.53 (s, 2H), 7.32 (s, 5H); ms m/z: 508 (14), 91 (100).

Can. J. Chem. Downloaded from www.nrcresearchpress.com by 213.166.140.6 on 09/07/12
For personal use only.

(ii) Oxidation of ***9*** *with pyridinium chlorochromate in the presence of alumina*

A solution of **9** (6.10 g, 12.0 mmol) in anhydrous dichloromethane (310 mL) was added to a stirred suspension of pyridinium chlorochromate (Aldrich; 6.50 g, 30.2 mmol) and neutral, activity I, 70–230 mesh alumina (Merck; 25 g) in anhydrous dichloromethane (170 mL) under an argon atmosphere. The mixture was stirred at room temperature for 1.5 h, and ether (140 mL) was added to the resulting brown mixture. The mixture was filtered through a Florisil column (57 g, 4 × 14 cm), and the column was eluted with ether (300 mL); the organic solutions were concentrated to give a yellow solid. A solution of the solid in ether (200 mL) was passed through an alumina column (30 g, 2 × 12 cm), and the column was eluted with ether (50 mL). The combined ethereal solutions were concentrated to give **12** (5.76 g, 95%). Crystallization from cyclohexane gave **12** (5.05 g, 83%) as white needles, mp 179–181.5°C.

Treatment of ***12*** *with potassium* tert*-butoxide. Formation of 5-hydroxy-5β-cholest-3-en-6-one (****14****) and 5-hydroxy-5β-cholest-2-en-6-one (****15****)*

Compound **12** (3.01 g, 5.93 mmol) was added to a solution of potassium *tert*-butoxide (Aldrich; 13.9 g, 124 mmol) in anhydrous *tert*-butyl alcohol (75 mL), and the suspension was heated to give a red solution. The solution was boiled under reflux for 1 h, allowed to cool to room temperature, and poured into water (50 mL). The *tert*-butyl alcohol was removed under water aspirator pressure on a rotary evaporator equipped with a cold trap condenser, and the residue was extracted with ether (3 × 50 mL, 1 × 25 mL). The combined ethereal extracts were washed with saturated aqueous NaCl and water, dried ($MgSO_4$), and concentrated. Medium pressure liquid chromatography of the residual orange oil (2.73 g), in three portions, on a size B (3 × 25 cm) silica gel column (Merck) with hexanes – ethyl acetate (95:5 v/v) gave the Δ^3-ketol **14** as a white solid (1.55 g, 65%). The ^{13}C nmr spectrum suggested that the product contained a small amount of the Δ^2-ketol **15**. The mixture (1.30 g) of the two olefinic isomers was separated in 350-mg portions by flash chromatography with hexanes – ethyl acetate (95:5 v/v) on a column (2.5 × 14 cm) of silica gel containing 7% (w/w) $AgNO_3$. This was prepared by shaking 40–60 μm silica gel (Merck; 60 g) with a solution of $AgNO_3$ (4.3 g) in water (20 mL) and drying the adsorbent in an oven at 140°C overnight. Compound **15** (61 mg, 3%) was eluted first as a white solid that was crystallized from methanol to give white needles, mp 125–126.5°C (lit. (14, 69)[6] mp 122–124.5°C); ir λ_{max}: 2.96 (br, w), 5.85, 5.99 (w) μm; ^1H nmr δ: 0.67 (s, C-18 Me), 0.76 (s, C-19 Me), 4.05 (s, OH, 1H), 5.67 (nar m, $W_{1/2}$ = 4 Hz, 2H); ms *m/z*: 400 (38), 55 (100). *Accurate Mass* calcd. for $C_{27}H_{44}O_2$: 400.3341; found: 400.3349.

Further elution gave **14** (1.2 g, 58%) as a white solid. Crystallization from methanol gave **14** as white needles, mp 92–93.5°C; the melt was cooled, and the solid was remelted, mp 95–96.5°C. Compound **14**: ir λ_{max}: 2.95 (sh, w), 5.86 μm; ir λ_{max}(KBr): 2.89 (sh, m), 5.86, 6.05 (v w), 14.59 (w) μm; uv λ_{max} (ε) (ethanol): 283 (83); ^1H nmr (200 MHz) δ: 0.65 (s, C-18 Me), 0.77 (s, C-19 Me), 0.86 (d, *J* = 6 Hz, C-26,27 Me), 0.91 (d, *J* = 7 Hz, C-21 Me), 4.20 (s, OH, absent after treatment with D_2O, 1H), 5.42 (dt, *J* = 10, 2 Hz, 1H), 6.00 (dt, *J* = 10, 3.5 Hz, 1H); ms *m/z*: 400 (21), 55 (100). *Accurate Mass* calcd. for $C_{27}H_{44}O_2$: 400.3341; found: 400.3351. *Anal.* calcd. for $C_{27}H_{44}O_2$: C 80.86, H 11.02; found: C 80.94, H 11.07.

*5-Hydroxy-5β-cholestan-6-one (****13****)*

(i) Hydrogenation of ***14***

A solution of **14** (86 mg, 0.22 mmol) in ethyl acetate (3 mL) was stirred with 10% palladium on carbon (11 mg) in a Morton flask under an atmosphere of hydrogen for 48 h. The reaction mixture was filtered through anhydrous $MgSO_4$, and the solution was concentrated to give **13** (80 mg, 93%) as a white solid. Crystallization from methanol gave white needles, mp 104–105°C (lit. (69) mp 103–104°C); ir λ_{max}: 2.84 (w), 5.86 μm; ^1H nmr δ: 0.65 (s, C-18 Me), 0.70 (s, C-19 Me), 3.83 (s, OH, absent after treatment with D_2O, 1H); ms *m/z*: 402 (22), 318 (100).

(ii) Epimerization of ***11***

A solution of **11** (108 mg, 0.27 mmol) in methanolic 10% KOH (3 mL) was heated under reflux for 8 h. The solution was allowed to cool, and the methanol was removed. The residue was added to water (10 mL), and the mixture was extracted with ether (30 mL, 2 × 10 mL). The combined ethereal extracts were washed with saturated aqueous NaCl (4 × 10 mL), dried (Na_2SO_4), and concentrated. The resulting yellow oil (110 mg) was flash chromatographed on silica gel with hexanes – ethyl acetate (95:5 v/v) as eluent to afford **13** (83 mg, 77%) as a white solid that was crystallized from methanol as white needles, mp 103–104.5°C. Further elution gave **11** (9 mg, 8%) as a white solid.

Epimerization of ***12****. Formation of 3β-benzyloxy-5-hydroxy-5β-cholestan-6-one (****19****)*

1,2-Dibromoethane (0.17 mL, 1.97 mmol) was added dropwise to a stirred mixture of magnesium turnings (1.67 g, 68.9 mmol) in anhydrous tetrahydrofuran (11 mL) under an argon atmosphere. The reaction mixture warmed to approximately 40°C, and the edges of the magnesium turnings became tinged with black. After 10 min the mixture had cooled to room temperature, and a solution of a mixture of 2-bromomesitylene (5.92 mL, 38.7 mmol) and 1,2-dibromoethane (3.17 mL, 36.8 mmol) in anhydrous tetrahydrofuran (44 mL) was added dropwise over a period of 6 h. With this slow addition the temperature of the reaction mixture did not increase during the addition. After the addition, the mixture was stirred for an additional 30 min to ensure complete consumption of the magnesium. The resulting grey solution, containing a white precipitate, was devoid of any yellow color.[7] It was treated dropwise over a period of 30 min with a solution of **12** (5.00 g, 9.84 mmol) in anhydrous tetrahydrofuran (65 mL). The resulting grey solution, which contained less white precipitate than before the addition of **12**, was heated under reflux for 7 h. A gold-colored solution containing a very small amount of white precipitate resulted. This was poured into cold (0°C) water (40 mL), and the tetrahydrofuran was removed. Benzene (100 mL) and 2 *M* aqueous HCl (25 mL) were added to the residue and the mixture was filtered through Celite. The Celite was washed with benzene (2 × 25 mL), and the washings were combined with the filtrate. The benzene layer was separated and washed with saturated aqueous $NaHCO_3$ (25 mL) and water (3 × 15 mL), dried, and concentrated. The ^1H nmr spectrum of the residue suggested that it contained mesitylene or 2-bromomesitylene, and it was pumped under high vacuum (0.25 Torr; 1 Torr = 133.3 Pa) in a water bath at 80°C to give an oil. Preparative high performance liquid chromatography of the oil was performed on a PrePak-500 silica gel column (Waters Associates; 5.7 × 30 cm) with chloroform–hexanes – ethyl acetate (65:34:1 v/v/v) as eluent. Compound **19** was eluted first as a white solid (3.50 g, 70%). Crystallization from aqueous methanol gave white crystals, mp 113–114°C; the melt solidified on cooling, and the solid remelted at 124–125°C; ir λ_{max}: 2.98 (m), 5.83, 8.57 (m) μm; ir λ_{max} (KBr): 2.87 (sh, m), 5.84, 6.68 (w), 8.56 (sh, m), 13.68 (br, m), 14.40 (m) μm; ^1H nmr δ: 0.67 (s, C-18 Me), 0.83 (s, C-19 Me), 3.83 (nar m, $W_{1/2}$ = 8 Hz, 1H), 4.35 (s, OH, 1H), 4.53 (s, 2H), 7.28 (s, 5H); ms *m/z*: 508 (1), 402 (100). *Anal.* calcd. for $C_{34}H_{52}O_3$: C 80.26, H 10.30; found: C 80.29, H 10.37.

Further elution gave **12** (1.5 g, 30%) as a white solid.

Hydrogenolysis of ***19****. Formation of 3β,5-dihydroxy-5β-cholestan-6-one (****20****)*

A solution of **19** (1.54 g, 3.03 mmol) in ethyl acetate (65 mL) was stirred with 10% palladium on carbon (160 mg) under hydrogen at atmospheric pressure for 5 h. The reaction mixture was filtered through anhydrous $MgSO_4$, and the filtrate was concentrated to give **20** (1.27 g) in quantitative yield as a colorless oil; ^1H nmr δ: 0.67 (s, C-18 Me),

[6]Compound **15** was originally structure **14** (69).

[7]Grignard solutions that developed a yellow color did not effect epimerization.

Can. J. Chem. Downloaded from www.nrcresearchpress.com by 213.166.140.6 on 09/07/12
For personal use only.

0.77 (s, C-19 Me), 4.03 (m), 4.43 (br s, OH). It was not purified further, but was acetylated directly.

3β-Acetoxy-5-hydroxy-5β-cholestan-6-one (21)

A solution containing **20** (1.21 g, 2.90 mmol), anhydrous pyridine (6.8 mL, 84 mmol), and freshly distilled acetic anhydride (5.6 mL, 59 mmol) was allowed to stand under an argon atmosphere for 68 h. The resulting orange solution was added to ice-water (50 mL), and the yellow solid that precipitated was filtered, washed with water (25 mL), and dissolved in ether (125 mL). The ethereal solution was washed with 2 *M* aqueous HCl (2 × 5 mL), saturated aqueous $NaHCO_3$ (25 mL), and water (3 × 10 mL), dried (Na_2SO_4), and concentrated. The yellow solid obtained (1.22 g) was flash chromatographed on silica gel (2.5 × 17 cm) with chloroform as eluent to give **21** (1.18 g, 89%) as a white solid. Crystallization from methanol gave white needles, mp 143.5–145°C (lit. (70) mp 142.5–144.5°C); ir λ_{max}: 2.95 (br, w), 5.78, 5.84, 7.26 (m), 8.58 (m) μm; ir λ_{max} (KBr): 2.90 (sh, m), 5.80, 5.89, 8.74 (w), 8.98 (m) μm; ^{1}H nmr (200 MHz) δ: 0.66 (s, C-18 Me), 0.76 (s, C-19 Me), 0.87 (d, J = 6 Hz, C-26,27 Me), 0.92 (d, J = 6 Hz, C-21 Me), 2.07 (s), 2.17–2.30 (m, 2H), 2.42 (dd, J = 14, 4 Hz, 1H), 3.92 (s, OH, 1H), 5.07 (nar m, $W_{1/2}$ = 8 Hz, 1H); ms m/z: 460 (2), 318 (100). *Accurate Mass* calcd. for $C_{22}H_{38}O$ (M − $C_7H_{10}O_3$): 318.2923; found: 318.2921.

3β-Acetoxy-7α-bromo-5-hydroxy-5α-cholestan-6-one (22)

Compound **22** was prepared from **10** by the method (procedure d) of Rodewald *et al.* (18). The crude product was flash chromatographed on silica gel with chloroform – ethyl acetate (97:3 v/v) as eluent to give **22** in 84% yield as a colorless oil that solidified on standing. Crystallization from methanol gave **22** as a white powder, mp 172.5–174.5°C (lit. (18) mp 170–172°C); ir λ_{max}: 2.78 (sh, w), 2.98 (br, w), 5.79, 5.83 μm; ir λ_{max} (CCl_4): 2.72 (sh, w), 2.98 (br, w), 5.74, 5.82 μm; ^{1}H nmr δ: 0.68 (s, C-18 Me), 0.83 (s, C-19 Me), 2.02 (s), 3.08 (s, OH, 1H), 4.18 (nar m, $W_{1/2}$ = 5 Hz, 1H), 5.12 (br m, $W_{1/2}$ = 20 Hz, 1H); ms m/z: 400 (42), 43 (100).

3β-Acetoxy-7α-deutero-5-hydroxy-5α-cholestan-6-one (23)

In a separatory funnel, a solution of **22** (110 mg, 0.20 mmol) in ether (10 mL) was treated with D_2O (99.8%, Aldrich; 4 × 1 mL), and the organic phase was added via cannula to zinc dust (307 mg, 4.69 mmol) in a D_2O-pretreated flask under argon. The mixture was stirred, and (*O*-D) acetic acid (98%, Aldrich; 550 μL, 9.45 mmol) was added dropwise over a period of 1 min. The suspension was stirred at room temperature for 2 h, and solid Na_2CO_3 (~8 g) was added. The mixture was filtered, and the zinc and Na_2CO_3 solids were washed with ether (7 × 10 mL). The combined filtrate and washings were washed with a solution of 5% $NaHCO_3$ in D_2O (1 mL) and saturated aqueous NaCl (2 × 10 mL), dried (Na_2SO_4), and concentrated to give **23** (76 mg, 81%) as a white solid. Crystallization from methanol gave white needles, mp 231–233°C; ir λ_{max}: 3.08 (br, w), 5.83 μm; ^{1}H nmr (200 MHz) δ: 0.64 (s, C-18 Me), 0.81 (s, C-19 Me), 0.86 (d, J = 7 Hz, C-26,27 Me), 0.91 (d, J = 7 Hz, C-21 Me), 2.00 (s), 2.76 (dd, J = 12, 12 Hz, 0.12H), 3.20 (br s, OH, 1H), 5.03 (br m, $W_{1/2}$ = 19 Hz, 1H); ms m/z: d_0 15%, d_1 80%, d_2 5% (based on M − AcOH); d_0 15%, d_1 82%, d_2 3% (based on M).

3β-Acetoxy-7α-bromo-5-hydroxy-5β-cholestan-6-one (24)

A solution of **21** (215 mg, 0.47 mmol) in chloroform (3.3 mL) was treated with 1.42 mL of a solution of bromine (0.40 mL) and acetic acid (1.0 mL) in chloroform (20 mL). The red solution was allowed to stand at room temperature for 2 h, and the resulting yellow solution was poured into aqueous 10% Na_2SO_3 (5 mL). The mixture was extracted with benzene (25 mL, 2 × 10 mL), and the combined organic extracts were washed with saturated aqueous $NaHCO_3$ (5 mL) and water (3 × 5 mL), dried (Na_2SO_4), and concentrated to give **24** as a pale yellow solid (256 mg) in quantitative yield. Flash chromatography on silica gel (2.5 × 17 cm) with dichloromethane–ether (98:2 v/v) gave **24** (230 mg, 91%) as a white solid. Crystallization from methanol gave white needles, mp 139–139.5°C (lit. (71) mp 137–138°C); ir λ_{max} (KBr): 2.89 (m), 5.76, 5.85 μm; ^{1}H nmr δ: 0.70 (s, C-18 Me), 0.80 (s, C-19 Me), 2.07 (s), 3.07 (dd, J = 16, 4 Hz, 1H), 3.65 (s, OH, 1H), 4.42 (nar m, $W_{1/2}$ = 5 Hz, 1H), 5.07 (nar m, $W_{1/2}$ = 8 Hz, 1H); ms m/z: 400 (30), 318 (100).

3β-Acetoxy-7α-deutero-5-hydroxy-5β-cholestan-6-one (25)

A solution of **24** (120 mg, 0.22 mmol) in ether (11 mL) was reduced with zinc dust (333 mg, 5.09 mmol) and (*O*-D) acetic acid (600 μL, 10.2 mmol) at room temperature for 2.5 h following the procedure for **23** (*vide supra*). The reaction mixture was neutralized with solid Na_2CO_3 (12 g), and work-up as for **23** gave **25** (79 mg, 77%) as a white solid. Crystallization from methanol gave transparent square plates, mp 143.5–144.5°C; ir λ_{max} (KBr): 2.90 (sh, w), 5.81, 5.88, 8.91 (w) μm; ^{1}H nmr (200 MHz) δ: 0.66 (s, C-18 Me), 0.76 (s, C-19 Me), 0.87 (d, J = 7 Hz, C-26,27 Me), 0.92 (d, J = 6 Hz, C-21 Me), 2.07 (s), 2.24 (dd, J = 15, 4 Hz, 1H), 2.40 (d, J = 3 Hz, 1H), 3.92 (s, OH, 1H), 5.07 (nar m, $W_{1/2}$ = 8 Hz, 1H); ms m/z: 461 (2), 319 (100); d_0 16%, d_1 78%, d_2 6% (based on M − AcOH).

Bromination of cholesteryl acetate (1) in acetic acid. Formation of 5-bromo-5α-cholestane-3β,6β-diol diacetate (26) and 5-bromo-5β-cholestane-3β,6α-diol diacetate (27)

Cholesteryl acetate (**1**) was treated with *N*-bromoacetamide in a solution of lithium acetate in acetic acid to give **26** accompanied by ~10–20% of **27**. The crude product was crystallized from methanol to give **26** (34%) as white needles, mp 91.5–93°C (lit. (72) mp 89–91°C). A second crop of crystals, found to be a mixture of **26** and **27**, was recrystallized from methanol to give a further amount of **26** (total 39%). The crystallized **26** was chromatographed on silica gel with cyclohexane–ether (9:1 v/v) as eluent; recrystallization from methanol raised the melting point to 95.5–96°C. Compound **26**: ir λ_{max}: 5.76 μm; ^{1}H nmr δ: 0.70 (s, C-18 Me), 1.30 (s, C-19 Me), 2.03 (s), 2.10 (s), 5.35 (nar m) and 5.47 (br m) (2H); ms m/z: 384 (82), 368 (95), 43 (100).

A portion of the mother liquor from the first crystallization was applied to a silica gel preparative thin-layer chromatography plate, and the plate was eluted twice with hexanes – ethyl acetate (4:1 v/v). The upper band (R_f 0.65) gave **27**; ir λ_{max}: 5.77 μm; ^{1}H nmr (100 MHz) δ: 0.70 (s, C-18 Me), 0.85 (d, J = 6 Hz, C-26,27 Me), 0.94 (d, J = 6 Hz, C-21 Me), 1.37 (s, C-19 Me), 2.00 (s), 2.06 (s), 2.86 (br dd, J = 14, 5 Hz, 1H), 4.66 (br m, $W_{1/2}$ = 20 Hz, 1H), 5.24 (nar m, $W_{1/2}$ = 8 Hz, 1H); ms m/z: 384 (80), 368 (80), 43 (100). The lower band (R_f 0.57) gave **26**.

Bromination of 1 in aqueous medium. Formation of 28

Cholesteryl acetate (**1**) in acetone, ether, and water was treated with *N*-bromoacetamide to give a yellow solid, shown by ^{1}H nmr spectroscopy to contain at least two major products. Crystallization from hexanes gave **28** (15%) as a white powder, mp 167–170°C (lit. (73) mp 168–170°C); ir λ_{max}: 2.76 (sh, w), 2.90 (br, w), 5.78 μm; ^{1}H nmr δ: 0.67 (s, C-18 Me), 1.30 (s, C-19 Me), 1.77 (m, OH, absent after treatment with D_2O), 2.02 (s), 4.18 (nar m, $W_{1/2}$ = 7 Hz, 1H), 5.47 (br m, $W_{1/2}$ = 20 Hz, 1H); ms m/z: 384 (100).

5α-Cholestane-3β,5,6β-triol (34)

Compound **34** was prepared from cholesterol (**33**) according to the method of Fieser and Rajagopalan (30). Crystallization from methanol gave **34** in 79% yield as white needles, mp 229–232°C (lit. (30) mp 237–239°C); ir λ_{max}: 2.94 (sh, w), 3.07 (br, w) μm; ^{1}H nmr (dimethyl sulfoxide-d_6) δ: 0.63 (s, C-18 Me), 1.03 (s, C-19 Me), 3.50–4.40 (m), 3.57 (s, OH, absent after treatment with D_2O, 1H), 4.12 (d, J = 5 Hz, OH, absent after treatment with D_2O, 1H), 4.32 (d, J = 4 Hz, OH, absent after treatment with D_2O, 1H); ms m/z: 420 (2), 384 (100).

5α-Cholestane-3β,5,6β-triol triacetate (35)

Compound **35** was prepared in 98% yield by acetylation of **34** with acetic anhydride and *p*-toluenesulfonic acid monohydrate in acetic acid (28). Crystallization from methanol gave **35** (78%) as white needles, mp 149.5–151.5°C (lit. (28) mp 151.2–151.8°C); ir λ_{max}: 5.76 μm; ^{1}H nmr δ: 0.70 (s, C-18 Me), 1.20 (s, C-19 Me), 1.97 (s, one Ac), 2.07 (s, two Ac), 2.83 (br dd, J = 13, 5 Hz, 1H), 4.73 (br m, $W_{1/2}$ = 18 Hz, 1H), 5.83 (nar m, $W_{1/2}$ = 6 Hz, 1H); ^{1}H nmr (benzene) δ:

Can. J. Chem. Downloaded from www.nrcresearchpress.com by 213.166.140.6 on 09/07/12
For personal use only.

0.65 (s, C-18 Me), 1.17 (s, C-19 Me), 1.62 (s), 1.68 (s), 1.73 (s), 3.17 (dd, J = 14, 5 Hz), 5.08 (br m), 6.28 (nar m); ms m/z: 384 (100).

*5,6β-Epoxy-5β-cholestan-3β-ol (**29**)*

*(i) From **26** and ethanolic sodium ethoxide*

To a solution of sodium ethoxide in ethanol, prepared by the addition of sodium (5.90 g, 0.256 mol) to absolute ethanol (300 mL), **26** (7.50 g, 0.013 mol) was added, and the colorless solution was stirred at room temperature under nitrogen for 0.5 h. Water (30 mL) was added to the resulting pale yellow solution and the ethanol was removed on the rotary evaporator under water aspirator pressure. The residue was extracted with ether, and the combined organic extracts were washed with water, dried ($MgSO_4$), and concentrated to give **29** (6.33 g) as a white solid in quantitative yield. Two crystallizations from methanol gave **29** (4.1 g, 77%) as white needles, mp 139–140°C (lit. (28) mp 130–133.5°C (from acetone–methanol); ir λ_{max}: 2.72 (sh, w), 2.85 (br, w) μm; ^{1}H nmr δ: 0.65 (s, C-18 Me), 1.00 (s, C-19 Me), 1.83 (br s, OH, absent after treatment with D_2O), 3.03 (d, J = 3 Hz, 1H), 3.63 (br m, $W_{1/2}$ = 18 Hz, 1H).

*(ii) From **35** and ethanolic sodium ethoxide*

Treatment of **35** with sodium ethoxide in refluxing ethanol following the method of Rowland and Nace (29) gave **29** in 84% yield.

*5,6β-Epoxy-5β-cholestan-3β-yl acetate (**4**b) from **29***

Compound **29** was acetylated with acetic anhydride and pyridine (28) to give **4***b* in 70% yield; ir λ_{max}: 5.78 μm; ^{1}H nmr δ: 0.65 (s, C-18 Me), 1.02 (s, C-19 Me), 2.02 (s), 3.05 (d, J = 3 Hz, 1H), 4.73 (br m, $W_{1/2}$ = 22 Hz, 1H).

*5-Methoxy-5α-cholestane-3β,6β-diol 3-acetate (**31**)*

A solution of **4***b* (1.00 g, 2.25 mmol) and *p*-toluenesulfonic acid monohydrate (36 mg, 0.19 mmol) in methanol (250 mL) was allowed to stand at room temperature for 17 h. The solution was poured into saturated aqueous $NaHCO_3$ (100 mL) and the methanol was removed. The residue was extracted with ether (100 mL, 2 × 25 mL), and the combined organic extracts were washed with water (3 × 10 mL), dried (Na_2SO_4), and concentrated to give **31** (1.01 g, 94%) as a white solid. Crystallization from methanol gave white needles, mp 161–162°C (lit. (74) mp 152.5–154°C); ir λ_{max}: 2.83 (sh, w), 2.94 (br, w), 5.79 μm; ^{1}H nmr δ: 0.68 (s, C-18 Me), 1.18 (s, C-19 Me), 1.45 (m, OH, absent after treatment with D_2O), 2.02 (s), 3.18 (s, 3H), 3.85 (nar m, $W_{1/2}$ = 8 Hz, 1H), 4.85 (br m, $W_{1/2}$ = 20 Hz, 1H); ms m/z: 476 (3), 366 (100).

*3β-Acetoxy-5-methoxy-5α-cholestan-6-one (**32**)*

A solution of **31** (678 mg, 1.42 mmol) in dichloromethane (5 mL) was added to a stirred suspension of pyridinium chlorochromate (Aldrich; 503 mg, 2.34 mmol) and anhydrous sodium acetate (29 mg, 0.36 mmol) in dichloromethane (5 mL) under a nitrogen atmosphere, and the mixture was stirred at room temperature for 3.5 h. Ether (5 mL) was added, and the brown mixture was applied to a Florisil column (18 g, 2 × 10 cm). The column was eluted with ether (40 mL), and the combined eluents were concentrated to give **32** (678 mg) as a white solid in quantitative yield. Crystallization from methanol gave white needles, mp 152–153°C (lit. (74) mp 149–150°C); ir λ_{max}: 5.78, 5.82 μm; ^{1}H nmr δ: 0.63 (s, C-18 Me), 0.80 (s, C-19 Me), 2.00 (s), 3.13 (s, 3H), 4.80 (br m, $W_{1/2}$ = 20 Hz, 1H); ms m/z: 474 (42), 414 (100). *Accurate Mass* calcd. for $C_{30}H_{50}O_4$: 474.3709; found: 474.3723.

*3β-Benzyloxy-5-methoxy-7α-methyl-5β-cholestan-6-one (**39**)*

Sodium hydride (80% dispersion in oil; 42.0 mg, 1.40 mmol) was added in three portions over a period of 30 min to a stirred solution of **19** (32.8 mg, 0.064 mmol) and iodomethane (1.0 mL, 16 mmol) in anhydrous tetrahydrofuran (5 mL) under argon. The reaction mixture was stirred at room temperature for a further 3.5 h and added cautiously to water (5 mL). The mixture was extracted with ether, and the combined ethereal extracts were washed with aqueous 10% Na_2SO_3 and water, dried (Na_2SO_4), and concentrated to give a colorless oil (42 mg). Flash chromatography of the oil on silica gel (1.5 × 12 cm) with chloroform–hexanes (4:1 v/v) as eluent gave **39** (25 mg, 73%) as a white solid. Crystallization from methanol gave white crystals shaped like fir trees, mp 107.5–109°C; ir λ_{max}: 5.85 μm; ^{1}H nmr (200 MHz) δ: 0.71 (s, C-18 Me), 0.87 (d, J = 7 Hz, C-26,27 Me), 0.91 (d, J = 7 Hz, C-21 Me), 1.04 (s, C-19 Me), 1.06 (d, J = 7 Hz), 2.32 (dq, J = 7, 7 Hz, 1H), 2.60 (dd, J = 12, 5 Hz, 1H), 2.67 (br m, $W_{1/2}$ = 20 Hz, 1H), 3.16 (s, 3H), 3.60 (br m, $W_{1/2}$ = 20 Hz, 1H), 4.58 (s, 2H), 7.33–7.36 (m, 5H); ms m/z: 536 (6), 91 (100). *Anal.* calcd. for $C_{36}H_{56}O_3$: C 80.55, H 10.52; found: C 80.38, H 10.51.

3β-Benzyloxy-5-hydroxy-5β-cholestan-6-one (E)*-oxime (**40**)*

Compound **19** was treated with hydroxylamine hydrochloride in 95% ethanol and pyridine to give **40** as a colorless oil (61 mg, 88%). Crystallization from methanol–hexanes gave **40** as colorless needles, mp 157.5–159°C; ir λ_{max}: 2.78 (sh, w), 2.88 (br, w), 6.12 (v w) μm; ^{1}H nmr δ: 0.67 (s, C-18 Me), 0.93 (s, C-19 Me), 3.37 (br d, J = 12 Hz, 1H), 3.80 (nar m, $W_{1/2}$ = 8 Hz, 1H), 4.50 (m, OH, absent after treatment with D_2O, 1H), 4.52 (s, 2H), 7.30 (s, 5H); ms m/z: 523 (1), 91 (100).

3β-Benzyloxy-5-hydroxy-5β-cholestan-6-one (E)*-oxime methyl ether (**41**)*

Compound **19** was treated with methoxylamine hydrochloride in anhydrous pyridine to give a pale yellow oil, which was flash chromatographed on silica gel (2 × 19 cm) with dichloromethane–ether (99:1 v/v) as eluent to give **41** (478 mg, 85%) as a colorless oil that resisted crystallization; ir λ_{max}: 2.99 (sh, m), 6.24 (w), 8.58 (m) μm; ^{1}H nmr δ: 0.67 (s, C-18 Me), 0.90 (s, C-19 Me), 3.27 (d, J = 12 Hz, 1H), 3.83 (nar m) and 3.93 (s) (4H), 4.43 (s, OH, 1H), 4.53 (s, 2H), 7.33 (s, 5H); ms m/z: 537 (<1), 91 (100). *Anal.* calcd. for $C_{35}H_{55}O_3N$: C 78.16, H 10.31, N 2.60; found: C 77.72, H 10.11, N 2.61.

3β-Benzyloxy-5-methoxy-5β-cholestan-6-one (E)*-oxime methyl ether (**42**)*

*(i) From methylation of **41***

Sodium hydride (80% dispersion in oil; 159 mg, 5.29 mmol) was added in portions to a stirred solution of **41** (452 mg, 0.84 mmol) and iodomethane (1.5 mL, 24 mmol) in anhydrous tetrahydrofuran (25 mL) under an argon atmosphere. The mixture was stirred at room temperature overnight and added cautiously to water (25 mL). The tetrahydrofuran was removed and the residue was extracted with ether (50 mL, 2 × 25 mL). The combined ethereal layers were washed with water (2 × 15 mL), dried (Na_2SO_4), and concentrated. The residual oil (488 mg) was flash chromatographed on silica gel (2 × 13 cm) with chloroform–hexanes (85:15 v/v) as eluent to give **42** (412 mg, 89%) as a colorless oil that resisted crystallization; ir λ_{max}: 6.12 (w) μm; ^{1}H nmr δ: 0.73 (s, C-18 Me), 1.03 (s, C-19 Me), 2.70 (dd, J = 12, 4 Hz, 1H), 3.10 (s, 3H), 3.73 (br m) and 3.87 (s) (4H), 4.60 (s, 2H), 7.37 (m, 5H); ms m/z: 551 (1), 460 (95), 91 (100). *Anal.* calcd. for $C_{36}H_{57}O_3N$: C 78.35, H 10.41, N 2.54; found: C 78.30, H 10.27, N 2.55.

*(ii) From methylation of **40***

Treatment of **40** (31 mg, 0.06 mmol) with NaH (80% dispersion in oil; 25 mg, 0.83 mmol) and iodomethane (0.20 mL, 3.2 mmol) in anhydrous tetrahydrofuran (3 mL) for 12 h and work-up as in (*i*) gave a colorless oil (32 mg), shown by ^{1}H nmr spectroscopy to be **42**.

*Reaction of **29** with methylmagnesium iodide. Formation of 6α-methyl-5α-cholestane-3β,6β-diol (**44**) and 4aξ-methyl-*A*-homo-*B*-nor-5β-cholestane-3β,4aξ-diol (**45**)*

An ethereal solution of methylmagnesium iodide was prepared by the addition of a solution of freshly distilled iodomethane (10.1 mL, 162 mmol) in anhydrous ether (4 mL) to a stirred mixture of purified magnesium turnings[8] (0.802 g, 33.0 mmol) in anhydrous ether (1 mL) under a nitrogen atmosphere. Grignard formation was self-initiated and the mixture was stirred at room temperature for 3 h. Anhydrous ether

[8]Magnesium turnings were washed with aqueous 2 *M* HCl (25 mL), water (×5), ethanol (×10), and anhydrous ether (×5), and pumped under high vacuum overnight.

Can. J. Chem. Downloaded from www.nrcresearchpress.com by 213.166.140.6 on 09/07/12
For personal use only.

(10 mL) was added, and the resulting slightly cloudy, grey mixture was transferred via cannula to an addition funnel, added dropwise over a period of 1 h to a stirred solution of **29** (2.48 g, 6.17 mmol) in a mixture of anhydrous benzene (25 mL) and ether (15 mL) under a nitrogen atmosphere, and heated at reflux. Following the addition, solvent (20 mL) was removed by distillation at atmospheric pressure, bp 40–51°C, and the residual solution was heated under reflux for a further 9 h. The resulting colorless, slightly cloudy reaction mixture was poured into ice, and saturated aqueous NH_4Cl was added. The organic phase was separated and washed with aqueous 5% $Na_2S_2O_3$, saturated aqueous $NaHCO_3$, and water, dried ($MgSO_4$), and concentrated to give a white solid (2.56 g). The ^1H nmr spectrum of the product indicated the presence of two major components, **44** and **45**, in a ~60:40 ratio. The solid was triturated with acetone, and **44** was obtained as the residual white powder, mp 184–186°C (lit. (42) mp 194°C); ir λ_{max}: 2.82 (sh, w), 2.95 (br, w) μm; ^1H nmr δ: 0.67 (s, C-18 Me), 1.02 (s, C-19 Me), 1.15 (s), 1.57 (m, OH, absent after treatment with D_2O), 3.53 (br m, $W_{1/2}$ = 20 Hz, 1H); ms *m/z*: 418 (3), 403 (100), 400 (68). *Accurate Mass* calcd. for $C_{27}H_{47}O_2$ (M − CH_3), $C_{28}H_{48}O$ (M − H_2O): 403.3576, 400.3705; found: 403.3563, 400.3698.

The acetone solution from the trituration was concentrated, and the residual solid was crystallized from ethyl acetate to give **45** (0.14 g, 5%) as white crystals, mp 86.5–88.5°C; ir λ_{max}: 2.83 (sh, w), 2.93 (br, w) μm; ^1H nmr δ: 0.67 (s, C-18 Me), 0.98 (s, C-19 Me), 1.22 (s), 1.90 (m, OH, absent after treatment with D_2O), 3.98 (nar m, $W_{1/2}$ = 12 Hz, 1H); ms *m/z*: 418 (5), 87 (100). *Accurate Mass* calcd. for $C_{28}H_{50}O_2$: 418.3811; found: 418.3787.

Reaction of ***4b*** *with lithium dimethylcuprate. Formation of 5,6β-epoxy-5β-cholestan-3β-yl 3-oxobutyrate (**49**) and 5,6β-epoxy-5β-cholestan-3β-ol (**29**)*

A stirred suspension of CuI (147 mg, 0.77 mmol) in anhydrous ether (10 mL) under a nitrogen atmosphere and cooled in an ice–salt bath was treated dropwise with a solution of methyllithium–LiBr complex in ether (1.2 *M*; 1.25 mL, 1.50 mmol). To the ethereal solution of lithium dimethylcuprate, a solution of **4*b*** (172 mg, 0.39 mmol) in anhydrous ether (5 mL) was added dropwise over a period of 15 min. A yellow precipitate slowly began to fall from solution, and the mixture was stirred in the ice–salt bath for 3 h. The resulting yellow suspension was treated with saturated aqueous NH_4Cl (10 mL), and the two-phase mixture was stirred at room temperature overnight. The ethereal layer was separated, washed with saturated aqueous $Na_2S_2O_3$ and water, dried ($MgSO_4$), and concentrated to give a white solid (130 mg). The ^1H nmr spectrum of the product evidenced a ~40:60 mixture of **49** and **29**. An ethereal solution of the solid was applied to a 1-mm silica gel plate, and the plate was eluted with ether. The upper band (R_f 0.66) gave **49** (40 mg, 21%) as a white solid; ir λ_{max}: 5.73, 5.81 μm; ^1H nmr (100 MHz) δ: 0.64 (s, C-18 Me), 1.00 (s, C-19 Me), 2.25 (s, 3H), 3.07 (d, *J* = 3 Hz, 1H), 3.42 (br s, exchanges slowly with D_2O, 2H), 4.84 (br m, $W_{1/2}$ = 24 Hz, 1H); ms *m/z*: 486 (2), 384 (100). The lower band (R_f 0.41) gave **29** (65 mg, 42%) as a white solid.

*6-Nitrocholesteryl acetate (**50**)*

Nitration of cholesteryl acetate (**1**) (49) gave **50** in 68% yield as white needles, mp 103.5°C–105°C (from methanol) (lit. (49) mp 102.5–103°C); ir λ_{max}: 5.75, 6.62 (m) μm; ^1H nmr δ: 0.70 (s, C-18 Me), 1.15 (s, C-19 Me), 2.02 (s), 4.60 (br m, $W_{1/2}$ = 18 Hz, 1H); ms *m/z*: 473 (6), 413 (100).

Reaction of ***50*** *with lithium dimethylcuprate. Formation of 3α,5-cyclo-5α-cholestan-6-one (*E*)-oxime (**51**), 3β-acetoxy-5α-cholestan-6-one (*E*)-oxime (**55**), and 3β-acetoxy-5-hydroxy-5α-cholestan-6-one (**10**)*

An ethereal solution of lithium dimethylcuprate was prepared by the dropwise addition of a solution of methyllithium–LiBr complex in ether (1.7 *M*; 17.4 mL, 29.6 mmol) to a stirred suspension of purified (75) CuI (2.93 g, 15.4 mmol) in anhydrous ether (125 mL) under an argon atmosphere and cooled in an ice bath. A solution of **50** (1.39 g, 2.94 mmol) in anhydrous ether (15 mL) was added dropwise over a period of 30 min, and the resulting yellow suspension was stirred at 0°C for 3 h and subsequently added via cannula to a stirred solution of saturated aqueous NH_4Cl (250 mL) buffered to pH 8 with aqueous 28% NH_3. The two-phase mixture was stirred overnight, and the blue aqueous layer was extracted with ether (3 × 50 mL). The combined ethereal layer and extracts were washed with saturated aqueous NaCl (4 × 10 mL), dried (Na_2SO_4), and concentrated to give a yellow oil (1.32 g). Preparative thin-layer chromatography of the oil (134 mg) on silica gel with hexanes – ethyl acetate (4:1 v/v) gave **51** (77 mg, 65%) as a white solid. Crystallization from aqueous ethanol gave white crystals, mp 126–126.5°C (lit. (76) mp 125–126°C). A mixture mp taken with a sample of **51**, mp 124.5–125.5°C, prepared by oximination of ketone **52** (*vide infra*) was 125–126°C. Compound **51**: ir λ_{max}: 2.78 (sh, m), 3.06 (br, m), 6.07 (w) μm; ^1H nmr δ: 0.49 (m, 1H), 0.68 (s, C-18 Me), 0.91(s, C-19 Me), 3.30 (br d, *J* = 11 Hz, 1H), 8.67 (v br m, OH, 1H); ms *m/z*: 399 (12), 135 (100). *Accurate Mass* calcd. for $C_{27}H_{45}ON$: 399.3501; found: 399.3505. *Anal.* calcd. for $C_{27}H_{45}ON$: C 81.14, H 11.35, N 3.50; found: C 80.79, H 11.31, N 3.55.

A portion (411 mg) of the crude oil was purified by medium pressure liquid chromatography on a 3 × 25-cm silica gel column (Merck) with hexanes – ethyl acetate (85:15 v/v) as eluent. Compound **51** (176 mg, 48%) was eluted first, and further elution gave a white solid (46 mg) and a colorless oil (22 mg). Flash silica gel chromatography of the solid with dichloromethane – ethyl acetate (9:1 v/v) gave a mixture (30 mg) of **55** and **10** as a white solid; ir λ_{max}: 2.88 (sh, w), 3.06 (br, w), 5.79, 6.20 (w) μm; ^1H nmr δ: 0.63 (s, C-18 Me), 0.75 (s, C-19 Me, **55**), 0.80 (s, C-19 Me, **10**), 2.00 (s), 3.33 (br d, *J* = 11 Hz, **55** 7β-H), 4.67 (br m, **55** C*H*OAc), 5.05 (br m, **10** C*H*OAc); ^{13}C nmr (δ > 60 ppm) δ: 70.8, 73.4, 80.3, 159.8, 170.6, 171.0, 212.2; ms *m/z*: 460 (10), 459 (5), 43 (100).

Hydrolysis of ***51***. *Formation of 3α,5-cyclo-5α-cholestan-6-one (**52**)*

A mixture of **51** (58 mg, 0.15 mmol) and $NaHSO_3$ (311 mg) in absolute ethanol (14 mL) and water (2.7 mL) was stirred and heated under reflux for 3 h. The mixture was allowed to cool and the ethanol was removed. The residue was extracted with ether (25 mL, 3 × 10 mL), and the ethereal extract was washed with saturated aqueous $NaHCO_3$ (10 mL) and water, dried (Na_2SO_4), and concentrated to give **52** (49 mg, 87%) as a white solid. Crystallization from methanol gave white crystals, mp 97–98°C (lit. (77) mp 97.2–97.6°C). A mixture mp taken with a sample of **52**, mp 99–99.5°C, prepared by oxidation of **54** (*vide infra*) was 97.5–99.5°C. Ketone **52**: ir λ_{max}: 5.94 μm; ^1H nmr δ: 0.70 (s, C-18 Me), 1.00 (s, C-19 Me); ms *m/z*: 384 (100). *Accurate Mass* calcd. for $C_{27}H_{44}O$: 384.3392; found: 384.3398.

*3α,5-Cyclo-5α-cholestan-6β-ol (**54**)*

Cholesteryl *p*-toluenesulfonate (**53**) was treated with a mixture of potassium acetate and acetic anhydride, and the resulting mixture of acetates was hydrolyzed with ethanolic KOH (78) to give **54** (62%) as a white solid, mp 64.5–68°C (lit. (78) 74–75°C); ir λ_{max}: 2.77 (sh, w), 2.90 (br, w) μm; ^1H nmr δ: 0.17–0.57 (m), 0.72 (s, C-18 Me), 1.07 (s, C-19 Me), 1.50 (m, OH, absent after treatment with D_2O), 3.22 (nar m, $W_{1/2}$ = 6 Hz, 1H); ms *m/z*: 386 (1), 368 (100).

Oxidation of ***54***. *Formation of 52*

A stirred suspension of pyridinium chlorochromate (Aldrich: 97 mg, 0.45 mmol) and anhydrous sodium acetate (69 mg, 0.84 mmol) in dichloromethane (1 mL) under a nitrogen atmosphere was treated with a solution of **54** (112 mg, 0.29 mmol) in dichloromethane (1 mL). The mixture was stirred at room temperature for 25 h, and ether (2 mL) was added to the resulting olive-colored suspension. The reaction mixture was applied to a Florisil column (5 g, 2 × 4 cm), and the column was eluted with ether (100 mL). The eluent was concentrated to give **52** (105 mg, 94%) as a white solid. Crystallization from methanol gave white crystals, mp 99–99.5°C (lit. (77) mp 97.2–97.6°C). The spectra of this product were identical to those of **52** prepared by hydrolysis of **51**.

Oximation of ***52***. *Formation of 51*

Compound **52** was treated with hydroxylamine hydrochloride and anhydrous sodium acetate in ethanol to give **51** (91%) as a colorless oil.

Crystallization from aqueous ethanol gave white crystals, mp 124.5–125.5°C (lit. (78) mp 125–126°C). The ir, ^{1}H nmr, ^{13}C nmr, and mass spectra were identical to those of **51** obtained by reaction of **50** with lithium dimethylcuprate.

3β-Acetoxy-5α-cholestan-6-one (56)

Reduction of 6-nitrocholesteryl acetate (**50**) with zinc and acetic acid (54) gave **56** in 88% yield as white needles, mp 128–131.5°C (lit. (54) mp 127–128°C); ir λ_{max}: 5.77, 5.82 μm; ^{1}H nmr δ: 0.68 (s, C-18 Me), 0.80 (s, C-19 Me), 2.03 (s), 4.67 (br m, $W_{1/2}$ = 20 Hz, 1H).

3β-Acetoxy-5α-cholestan-6-one (E)*-oxime (55)*

Compound **56** was treated with hydroxylamine hydrochloride and sodium acetate in ethanol to give **55** (83%) as a white solid. Crystallization from methanol–hexanes gave colorless plates, mp 198–199°C (lit. (79) mp 206–208°C (from methanol)); ir λ_{max}: 2.90 (sh, w), 3.11 (br, w) 5.77, 6.00 (w) μm; ^{1}H nmr δ: 0.67 (s, C-18 Me), 0.75 (s, C-19 Me), 2.00 (s), 3.32 (br d, J = 11 Hz, 1H), 4.65 (br m, $W_{1/2}$ = 22 Hz, 1H), 9.33 (v br m, OH, 1H); ms m/z: 459 (15), 399 (100).

Acknowledgments

We thank the Natural Sciences and Engineering Research Council of Canada for support of this work and Imperial Oil Limited for the award of a Graduate Research Fellowship to S.S.

1. (*a*) S. Stiver and P. Yates. Tetrahedron Lett. **25**, 3289 (1984); **26**, 5501 (1985); **27**, 2215 (1986); (*b*) S. Stiver. Ph.D. thesis, University of Toronto. 1985.
2. (*a*) D. N. Kirk and M. P. Hartshorn. Steroid reaction mechanisms. Elsevier, New York. 1968. pp. 112–114; (*b*) J. G. Buchanan and H. Z. Sable. *In* Selective organic transformations. Vol. 2. *Edited by* B. S. Thyagarajan. Wiley–Interscience, New York. 1972. pp. 11–13.
3. L. F. Fieser and M. Fieser. Reagents for organic synthesis. Wiley, New York. 1967. p. 79.
4. L. N. Nysted and R. Pappo. Brit. Patent No. 1,152,128; Chem. Abstr. **71**, 50392R (1969).
5. Y. Cheng, W. Liu, and S. Chen. Synthesis, 223 (1980).
6. V. Balogh, M. Fetizon, and M. Golfier. Angew. Chem. Int. Ed. Engl. **8**, 444 (1969).
7. K. T. Alston, P. M. Bebbington, S. E. Green, E. D. Morgan, and C. F. Poole. Steroids, **27**, 609 (1976).
8. J. Herscovici and K. Antonakis. J. Chem. Soc. Chem. Commun. 561 (1980).
9. N. S. Bhacca and D. H. Williams. Applications of NMR spectroscopy in organic chemistry. Holden–Day, London. 1964. pp. 186–190.
10. Y. Mazur and M. Nussim. Tetrahedron Lett. 817 (1961).
11. L. M. Jackman and S. Sternhell. Applications of nuclear magnetic resonance spectroscopy in organic chemistry. 2nd ed. Pergamon, New York. 1969. p. 103.
12. E. W. Garbisch, Jr. J. Am. Chem. Soc. **86**, 5561 (1964).
13. D. J. Collins, J. J. Hobbs, and S. Sternhell. Tetrahedron Lett. 197 (1963); D. J. Collins, J. J. Hobbs, and S. Sternhell. Aust. J. Chem. **16**, 1030 (1963).
14. A. T. Rowland, A. F. Kriner, Jr., and K. P. Long. J. Org. Chem. **34**, 2768 (1969).
15. I. Elphimoff-Felkin. Bull. Soc. Chim. Fr. 1845 (1956).
16. I. Elphimoff-Felkin, G. Le Ny, and B. Tchoubar. Bull. Soc. Chim. Fr. 522 (1958).
17. M. S. Ahmad, G. Moinuddin, and I. A. Khan. Org. Mass. Spectrom. **13**, 382 (1978); M. S. Ahmad, M. Mushfiq, M. Asif, and G. A. S. Ansari. J. Prakt. Chem. **317**, 1049 (1975).
18. W. J. Rodewald, W. J. Szczepek, and J. Gumulka. Pol. J. Chem. **53**, 797 (1979).
19. E. J. Corey. J. Am. Chem. Soc. **76**, 175 (1954); E. J. Corey and R. A. Sneen. J. Am. Chem. Soc. **78**, 6269 (1956).
20. E. J. Corey and G. A. Gregoriou. J. Am. Chem. Soc. **81**, 3127 (1959).
21. H. Budzikiewicz, C. Djerassi, and D. H. Williams. Structure elucidation of natural products by mass spectrometry. Vol. 1. Holden–Day, London. 1964. pp. 34–36.
22. K. Biemann. Mass spectrometry, organic chemical applications. McGraw–Hill, Toronto. 1962. pp. 212–223.
23. C. Djerassi, R. H. Shapiro, and M. Vandewalle. J. Am. Chem. Soc. **87**, 4892 (1965).
24. E. Lund, H. Budzikiewicz, J. M. Wilson, and C. Djerassi. J. Am. Chem. Soc. **85**, 1528 (1963).
25. A. Bowers, E. Denot, R. Urquiza, and L. M. Sanchez-Hidalgo. Tetrahedron, **8**, 116 (1960).
26. C. H. Robinson, L. Finckenor, M. Kirtley, D. Gould, and E. P. Oliveto. J. Am. Chem. Soc. **81**, 2195 (1959).
27. A. Lardon and T. Reichstein. Helv. Chim. Acta, **26**, 747 (1943).
28. A. D. Cross. J. Am. Chem. Soc. **84**, 3206 (1962).
29. A. T. Rowland and H. R. Nace. J. Am. Chem. Soc. **82**, 2833 (1960).
30. L. F. Fieser and S. Rajogapalan. J. Am. Chem. Soc. **71**, 3938 (1949).
31. D. H. Williams and I. Fleming. Spectroscopic methods in organic chemistry. 2nd ed. McGraw–Hill, London. 1973. p. 82.
32. K. L. Williamson and W. S. Johnson. J. Am. Chem. Soc. **83**, 4623 (1961).
33. W. F. Trager and A. C. Huitric. Tetrahedron Lett. 825 (1966).
34. G. J. Karabatsos and R. A. Taller. Tetrahedron, **24**, 3347 (1968).
35. G. J. Karabatsos and N. Hsi. Tetrahedron, **23**, 1079 (1967).
36. R. Durand, P. Geneste, C. Moreau, and A. A. Pavia. Org. Magn. Reson. **6**, 73 (1974).
37. G. E. Hawkes, K. Herwig, and J. D. Roberts. J. Org. Chem. **39**, 1017 (1974).
38. G. J. Karabatsos and R. A. Taller. Tetrahedron, **24**, 3923 (1968).
39. N. Finch and J. J. Fitt. Tetrahedron Lett. 4639 (1969).
40. J. H. Fried, A. N. Nuttle, and G. E. Arth. J. Am. Chem. Soc. **82**, 5704 (1960); J. H. Fried, G. E. Arth, and L. H. Sarett. J. Am. Chem. Soc. **82**, 1684 (1960).
41. Y. Urushibara and M. Chuman. Bull. Chem. Soc. Jpn. **22**, 69 (1949); M. Chuman. J. Chem. Soc. Jpn. **70**, 253 (1949); Chem. Abstr. **45**, 6651c (1951).
42. S. Julia, C. Neuville, and R. Kévorkian. C.R. Hebd. Seances Acad. Sci. **258**, 5900 (1964).
43. N. D. Hall and R. B. Just. Steroids, **6**, 111 (1965).
44. J. W. Blunt, M. P. Hartshorn, and D. N. Kirk. Tetrahedron, 559 (1965).
45. R. Herr, D. Wieland, and C. Johnson. J. Am. Chem. Soc. **92**, 3813 (1970); B. Hartman, T. Livinghouse, and B. Rickborn. J. Org. Chem. **38**, 4346 (1973).
46. J. March. Advanced organic chemistry. 2nd ed. McGraw–Hill, New York. 1977. p. 72.
47. S. Stiver and P. Yates. J. Chem. Soc. Chem. Commun. 50 (1983).
48. S. B. Bowlus. Tetrahedron Lett. 3591 (1975).
49. A. T. Rowland. Steroids, **26**, 251 (1975).
50. D. Goldsmith, D. Becher, S. Sample, and C. Djerassi. Tetrahedron Suppl. **7**, 145 (1966).
51. S. H. Pines, J. M. Chemerda, and M. A. Kozlowski. J. Org. Chem. **31**, 3446 (1966).
52. G. H. Whitham and J. A. F. Wickramasinghe. J. Chem. Soc. 1655 (1964).
53. E. J. Corey and J. W. Suggs. Tetrahedron Lett. 2647 (1975).
54. R. M. Dodson and B. Riegel. J. Org. Chem. **13**, 424 (1948).
55. H. O. House and M. J. Umen. J. Am. Chem. Soc. **94**, 5495 (1972); H. O. House. Acc. Chem. Res. **9**, 59 (1976).
56. T. Sato, Y. Komeichi, S. Kobayashi, and A. Omura. Bull. Chem. Soc. Jpn. **55**, 520 (1982).

Can. J. Chem. Downloaded from www.nrcresearchpress.com by 213.166.140.6 on 09/07/12
For personal use only.

57. R. A. J. SMITH and D. J. HANNAH. Tetrahedron Lett. **21**, 1081 (1980); Tetrahedron, **35**, 1183 (1979); R. A. RUDEN and W. E. LITTERER. Tetrahedron Lett. 2043 (1975).
58. J. F. KNIFTON. J. Org. Chem. **38**, 3296 (1973).
59. P. A. S. SMITH. Open chain nitrogen compounds. Vol. 2. Benjamin, New York. 1966. p. 413.
60. W. F. BRUCE and J. O. RALLS. Org. Synth. Coll. Vol. 2, 191 (1943).
61. Y. KAMANO. Chem. Pharm. Bull. **17**, 1711 (1969).
62. P. KŐCOVSKÝ and V. ČERNÝ. Collect. Czech. Chem. Commun. **44**, 246 (1979).
63. L. F. FIESER and M. FIESER. Reagents for organic synthesis. Vol. 1. Wiley, New York. 1967. p. 78.
64. C. H. HEATHCOCK and R. RATCLIFFE. J. Am. Chem. Soc. **93**, 1746 (1971).
65. D. D. PERRIN, W. L. F. ARMAREGO, and D. R. PERRIN. Purification of laboratory chemicals. 2nd ed. Pergamon, New York. 1980. p. 126.
66. J. H. BEYNON, I. M. HEILBRON, and F. S. SPRING. J. Chem. Soc. 907 (1936).
67. I. G. GUEST, J. G. L. JONES, B. A. MARPLES, and M. J. HARRINGTON. J. Chem. Soc. (C), 2360 (1969).
68. L. KNOF. Justus Liebigs Ann. Chem. **656**, 183 (1962).
69. B. W. SANDS and A. T. ROWLAND. Steroids, **4**, 175 (1964).
70. A. T. ROWLAND. J. Org. Chem. **27**, 1135 (1962).
71. M. J. THOMPSON, W. E. ROBBINS, C. F. COHEN, J. N. KAPLANIS, S. R. DUTKY, and R. F. N. HUTCHINS. Steroids, **17**, 399 (1971).
72. S. G. LEVINE and M. E. WALL. J. Am. Chem. Soc. **81**, 2826 (1959).
73. M. STEFANOVIĆ, A. JOKIĆ, and M. L. J. MIHAILOVIĆ. Glas. Hem. Drus. **31**, 139 (1966).
74. P. MORAND and M. KAUFMAN. J. Org. Chem. **34**, 2175 (1969).
75. G. B. KAUFFMAN and L. A. TETER. Inorg. Synth. **7**, 9 (1963).
76. H. SUGINOME, H. TAKAHASHI, and T. MASAMUNE. Bull. Chem. Soc. Jpn. **45**, 1836 (1972).
77. I. A. KAYE, U. WEISS, and R. J. HIGHET. Steroids, **8**, 1 (1966).
78. E. S. WALLIS, E. FERNHOLZ, and F. T. GEPHART. J. Am. Chem. Soc. **59**, 137 (1937).
79. M. ONDA and K. TAKEUCHI. Chem. Pharm. Bull. **23**, 677 (1975).

Can. J. Chem. Downloaded from www.nrcresearchpress.com by 213.166.140.6 on 09/07/12
For personal use only.

Étude radiocristallographique comparée de quelques Δ-2 imidazolines substituées

PIERRE BROUANT ET JACQUES BARBE[1]

Groupe d'études et de recherches en chimie thérapeutique organique et physique, Faculté de pharmacie, 27 boul. Jean-Moulin, 13385 Marseille CEDEX 5, France

ET

ALAIN MARSURA, CATHERINE SOULA ET CUONG LUU-DUC

Groupe de pharmacochimie, Faculté de pharmacie, Domaine de la Merci, 38700 La Tronche, France

Reçu le 7 janvier 1987

PIERRE BROUANT, JACQUES BARBE, ALAIN MARSURA, CATHERINE SOULA et CUONG LUU-DUC. Can. J. Chem. **65**, 2217 (1987).

La comparaison des configurations de trois composés de la série des Δ-2 imidazolines fonctionnalisées, montre une géométrie spatiale constante. Tous les substituants sont en position *trans* les uns par rapport aux autres et contribuent ainsi à une minimisation des gênes stériques. D'apprès cette étude, il semble également que la nature du substituant à l'azote N(3) influe de manière importante sur la position du carbonyle. Les résultats confortent ceux d'une étude en résonance magnétique nucléaire antérieure.

PIERRE BROUANT, JACQUES BARBE, ALAIN MARSURA, CATHERINE SOULA, and CUONG LUU-DUC. Can. J. Chem. **65**, 2217 (1987).

The solid state structures of three compounds belonging to the Δ-2 imidazoline series have been compared. X-ray data and molecular parameters are given. It is noteworthy to point out that substituents are *trans* to one another in these structures. Moreover, the spatial orientation of the carbonyl group attached to C(4) depends on the nature of the substituent attached to nitrogen N(3). In addition, results are in close agreement with those of nuclear magnetic resonance spectroscopy.

Can. J. Chem. Downloaded from www.nrcresearchpress.com by 213.166.140.6 on 09/07/12
For personal use only.

Introduction

Les Δ-2 imidazolines sont des substances dont l'intérêt thérapeutique déjà ancien s'est encore affirmé récemment. En effet, ce sont des antidépresseurs (1), des antiparasitaires (2), des bactériostatiques (3), mais ces composés possèdent aussi des propriétés hypotensives dont exemple est donné par la clonidine et ses homologues (4). Cependant, à ce jour, peu de dérivés fonctionnalisés ont été décrits. Le travail présenté concerne l'analyse structurale par radiocristallographie de molécules nouvelles dont la formule générale est donnés sur la figure 1 et qui ont été obtenues par action de cétones α-bromées α,β-éthyléniques avec des amidines N-substituées (5). Il s'agit plus particulièrement de la benzyl-1 diphényl-2,4 acétyl-5 Δ-2 imidazoline (**2**) et de l'isopropyl-1 diphényl-2,4 benzoyl-5 Δ-2 imidazoline (**3**) qui ont été choisies comme témoins. Les résultats, discutés en se référant à ceux d'une étude préliminaire (6) consacrée à l'isopropyl-1 diphényl-2,4 pivaloyl-5 Δ-2 imidazoline (**1**), permettent une discussion comparative des configurations.

Partie expérimentale

Les données cristallines comparées pour les deux composés sont rapportées dans le tableau 1.

Les monocristaux des deux composés ont été obtenus par simple évaporation à température ambiante de leurs solutions saturées dans le chloroforme (**2**) ou dans un mélange équimolaire d'acétate d'éthyle et d'ether éthylique (**3**). Les densités ont été mesurées par flottaison.

La détermination des mailles et l'enregistrement des intensités diffractées ont été effectués sur un diffractomètre automatique 4 cercles CAD-4 Enraf Nonius à monochromateur de graphite : $\lambda(\text{Mo K}\bar{\alpha}) = 0{,}7107$ Å. Les paramètres des mailles ont été obtenus par moindres carrés à partir des positions angulaires de 25 réflexions pour les deux composés.

Les conditions expérimentales d'enregistrement des intensités peuvent être considérées comme identiques (T = 293 K) pour les deux composés. La technique de balayage en $\theta-2\theta$ a été utilisée. On a réalisé des contrôles d'orientation toutes les 300 mesures et des contrôles d'intensité toutes les 10 000 secondes. La déviation angulaire maximum acceptée était de 0,12 et les variations d'intensité ont toujours été inférieures à 3% (**2**) ou 2% (**3**).

Aucune correction particulière d'absorption n'a été effectuée. Les structures ont été déterminées par les méthodes directes (7). Elles ont été ensuite précisées par une succession de synthèses de différences-Fourier et de cycles d'affinements par moindres carrés.

Les atomes d'hydrogène, en partie localisés sur les cartes de densités-différences et construits géométriquement pour les autres, ont été inclus mais non affinés dans les deux derniers cycles d'affinement qui ont eu lieu en matrice entière. Tous les atomes ont été affectés d'un facteur d'agitation thermique anisotrope sauf les atomes d'hydrogène affectés d'un facteur d'agitation fixé à 5 Å^2 pour les deux composés. La fonction à minimiser était $\Sigma w(|F_o| - |F_c|)^2$ avec $w = 1$. Les facteurs de diffusion atomique proviennent de la réf. 8. Tous les calculs ont été effectués sur ordinateur DEC PDP 11/44 sous logiciel SDP (9).

L'enregistrement et les calculs ont été réalisés dans le Service de cristallochimie de l'Université d'Aix-Marseille III, rue Henri Poincaré 13397 Marseille Cedex 13.

Les tableaux 2 et 3 donnent les coordonnées atomiques.[2] Dans les tableaux 4 et 5 sont portés les paramètres angulaires et de liaison. Les valeurs des angles de torsion les plus significatives sont présentées dans le tableau 6.

On doit noter ici que la présence dans chacune des molécules considérées de centres asymétriques implique l'existence d'images non superposables. Les structures ont été résolues dans des groupes d'espace centrosymétriques. Cependant, les coordonnées atomiques ont été transformées pour se rapporter toutes au même conformère.

Les représentations géométriques de ces conformères sont données sur la figure 2.

1. Auteur à qui toute correspondance doit être adressée.

2. Les tableaux des amplitudes des facteurs de structure, des facteurs d'agitation thermique, des paramètres positionnels et des équations des principaux plans des moindres carrés sont disponibles. On peut les acheter en s'adressant au Dépôt de données non publiées, ICIST, Conseil national de recherches du Canada, Ottawa (Ont.), Canada K1A 0S2.

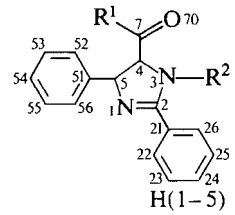

	R^1	R^2
1	H(14–16) C(73) C(74)—C(71)—C(72) (17–19)H H(11–13)	H(22) C(62)—C(6)—C(61) (26–28)H H(23–25)
2	H(11–13) C(71)	(62)C—C(63) (16–18)H C(6)—C(61) C(64) (66)C—C(65) H (18–22)
3	C(74) (75)C C(73) H(11–15) (76)C C(72) C(71)	H(18) C(62)—C(6)—C(61) (22–24)H H(19–22)

FIG. 1. Formule générale et numérotation des composés étudiés.

TABLEAU 1. Données cristallines

Paramètre	Composé **2**	Composé **3**
Formule brute :	$C_{25}H_{22}N_2O$	$C_{25}H_{24}N_2O$
Dimensions des cristaux en mm :	0,2 × 0,4 × 0,6	0,3 × 0,3 × 0,5
Densités mesurées, D_m :	1,20(2)	1,20(2)
Densités calculées en mg mm^{-3}, D_c :	1,223	1,193
Masse moléculaire relative M_r :	354,46	368,48
Système :	Monoclinique	Monoclinique
Groupe :	$P2\ 1/c$	$P2\ 1/n$
Maille en Å et °, a :	13,612(3)	8,272(1)
b :	14,667(3)	16,138(4)
c :	9,644(2)	15,403(4)
β :	90,80(5)	94,02(5)
Volume de la maille en Å^3, V :	1925,2(7)	2051,1(7)
Nombre de molécules par maille, Z :	4	4
μ en mm^{-1} :	0,6	0,6
$F(000)$:	752	784
Limites angulaires en θ :	1 et 25	0 et 20
Nombre total de mesures :	3648	3495
Nombres de mesures avec $I > \sigma(I)$:	Sans objet	2141
Nombre de mesures utilisées pour la résolution :	3444	2055
Facteur d'accord sur toutes les intensités mesurées, R_{sym} :	0,024	0,028
Nombre de mesures avec $I > 3\sigma(I)$ utilisées pour les affinements :	1849	1754
Limite de rejet en Fourier-différence, $(\Delta e)_{max}$ en e Å^{-3} :	0,330	0,299
Résidus R :	0,045	0,044
R_w :	0,044	0,042
Variation sur erreur maximum, $(\Delta/\sigma)_{max}$:	0,76	0,03
Erreur sur une observation de poids unitaire :	0,90	0,91

Can. J. Chem. Downloaded from www.nrcresearchpress.com by 213.166.140.6 on 09/07/12
For personal use only.

TABLEAU 2. Coordonnées atomiques et déviations standards de **2**

Atome	x	y	z	B (Å^2)*
O(70)	−0,3830(2)	−0,3983(2)	0,4831(3)	7,8
N(1)	−0,1365(2)	−0,4700(2)	0,2396(3)	3,6
N(3)	−0,3022(2)	−0,4501(2)	0,2326(2)	3,0
C(2)	−0,2112(2)	−0,4430(2)	0,1690(3)	3,0
C(4)	−0,2863(2)	−0,5042(2)	0,3582(3)	3,1
C(5)	−0,1724(2)	−0,5074(2)	0,3721(3)	3,4
C(6)	−0,3950(2)	−0,4646(2)	0,1561(3)	3,5
C(7)	−0,3358(2)	−0,4672(3)	0,4844(3)	4,3
C(21)	−0,1989(2)	−0,4031(2)	0,0291(3)	3,2
C(22)	−0,2495(2)	−0,3264(2)	−0,0146(3)	3,8
C(23)	−0,2311(3)	−0,2893(3)	−0,1445(4)	4,7
C(24)	−0,1631(3)	−0,3291(3)	−0,2290(4)	5,3
C(25)	−0,1126(3)	−0,4055(3)	−0,1863(4)	5,0
C(26)	−0,1309(2)	−0,4427(2)	−0,0571(3)	3,9
C(51)	−0,1310(2)	−0,6005(2)	0,3990(3)	3,9
C(52)	−0,0634(3)	−0,6146(3)	0,5058(4)	5,7
C(53)	−0,0234(3)	−0,7002(4)	0,5241(5)	9,4
C(54)	−0,0490(4)	−0,7709(3)	0,4436(6)	10,5
C(55)	−0,1157(4)	−0,7579(3)	0,3389(6)	8,0
C(56)	−0,1558(3)	−0,6726(3)	0,3157(4)	5,5
C(61)	−0,4114(2)	−0,5613(2)	0,1084(3)	3,2
C(62)	−0,3629(3)	−0,5944(3)	−0,0058(4)	4,7
C(63)	−0,3785(3)	−0,6824(3)	−0,0514(4)	6,1
C(64)	−0,4425(3)	−0,7382(3)	0,0166(4)	5,8
C(65)	−0,4906(3)	−0,7072(3)	0,1301(4)	5,1
C(66)	−0,4752(2)	−0,6188(2)	0,1762(3)	4,1
C(71)	−0,3231(3)	−0,5227(3)	0,6137(4)	5,4

*Les atomes affinés anisotropiquement sont donnés sous la forme d'équivalents isotropiques définis ainsi au moyen des paramètres de la maille :

$$B_{eq} = 4/3[a^2B(1,1) + b^2B(2,2) + c^2B(3,3) + ab(\cos\gamma)B(1,2) + ac(\cos\beta)B(1,3) + bc(\cos\alpha)B(2,3)]$$

TABLEAU 3. Coordonnées atomiques et déviations standards de **3**

Atome	x	y	z	B (Å^2)*
O(70)	0,1664(7)	0,4222(3)	1,1207(3)	7,6
N(1)	0,1154(6)	0,2229(3)	1,0046(3)	4,7
C(2)	0,0316(8)	0,2789(4)	0,9630(4)	4,1
N(3)	−0,0502(6)	0,3349(3)	1,0110(3)	4,2
C(4)	−0,0256(8)	0,3100(4)	1,1033(4)	4,1
C(5)	0,0934(8)	0,2332(4)	1,0983(3)	4,3
C(6)	−0,2068(8)	0,3738(4)	0,9785(4)	4,4
C(7)	0,0707(8)	0,3783(4)	1,1558(4)	4,5
C(21)	0,0253(7)	0,2848(4)	0,8669(4)	4,0
C(22)	−0,0074(8)	0,2140(4)	0,8175(4)	4,6
C(23)	−0,0102(8)	0,2169(4)	0,7276(4)	5,2
C(24)	0,0179(9)	0,2910(5)	0,6870(4)	5,5
C(25)	0,0510(9)	0,3609(5)	0,7349(4)	5,8
C(26)	0,0536(9)	0,3581(4)	0,8243(4)	5,6
C(51)	0,0255(7)	0,1552(4)	1,1363(4)	4,0
C(52)	0,0537(8)	0,1386(4)	1,2241(4)	4,8
C(53)	−0,0080(9)	0,0680(5)	1,2610(4)	5,7
C(54)	−0,0983(9)	0,0125(4)	1,2096(5)	5,5
C(55)	−0,1244(9)	0,0275(5)	1,1222(5)	6,0
C(56)	−0,0644(9)	0,0978(4)	1,0863(4)	5,2
C(61)	−0,3431(9)	0,3092(5)	0,9738(5)	6,4
C(62)	−0,2411(10)	0,4499(5)	1,0358(5)	6,3
C(71)	0,0502(7)	0,3858(4)	1,2512(4)	3,6
C(72)	0,1529(8)	0,4401(4)	1,2986(4)	4,7
C(73)	0,1434(9)	0,4506(4)	1,3866(4)	5,3
C(74)	0,0307(9)	0,4081(4)	1,4280(4)	5,3
C(75)	−0,0761(8)	0,3542(4)	1,3834(4)	4,9
C(76)	−0,0643(9)	0,3430(4)	1,2947(4)	4,0

*Les atomes affinés anisotropiquement sont donnés sous la forme d'équivalents isotropiques définis ainsi au moyen des paramètres de la maille :

$$B_{eq} = 4/3[a^2B(1,1) + b^2B(2,2) + c^2B(3,3) + ab(\cos\gamma)B(1,2) + ac(\cos\beta)B(1,3) + bc(\cos\alpha)B(2,3)]$$

Discussion

Les trois composés adoptent une conformation du cycle imidazoline en forme d'enveloppe. Cela ressort du tableau 7, qui donne les distances des atomes du cycle et celles du premier atome de chaque substituant au plan moyen défini par les atomes coplanaires N(1), C(2), N(3) et C(5). La position de C(4) est nettement hors du plan moyen chez **1** et **2** mais, les cotes étant opposées par rapport à ce plan, les conformations sont inversées. En revanche, le composé **3** est à ce niveau plus plan que les précédents, la tendance au pliage ayant lieu, dans ce cas, de part et d'autre d'un axe imaginaire C(2)–C(4) avec un atome N(3) qui ne s'élève qu'à 0,05 Å au dessus d'un plan formé par C(4), C(5), N(1) et C(2). Quant aux substituants, leurs cotes sont de même signe pour les trois composés et ils conservent ainsi une même orientation *trans*, ce qui s'accorde avec les mesures antérieures des constantes de couplage ^3J(H4–H5) (10). On peut également évaluer la planéité du cycle en s'intéressant aux plans des moindres carrés formés par N(1), C(2), N(3), C(4) et C(5). Il apparaît alors que les distances maximales au plan moyen sont de 0,089 Å (**1**), 0,069 Å (**2**) et 0,021 Å (**3**).

En ce qui concerne les différences dans les longueurs de liaison, elles sont relativement faibles entre liaisons de nature identique : 0,018 Å en moyenne, avec un maximum de 0,053 Å pour la liaison C(4)—C(7). La liaison N(1)—C(2) est en moyenne de 1,28 Å, les liaisons N(3)—C(4), C(3)—C(6) et N(1)—C(5) sont de 1,48 Å, celle entre C(2)—N(3) étant de 1,38 Å. Ces valeurs peuvent être comparées aux valeurs théoriques d'une double liaison carbone–azote (1,29 Å) ou d'une simple liaison carbone–azote (1,48 Å). On en déduit que si la liaison N(1)—C(2) est bien une liaison double N_{sp^2}—C_{sp^2}, si les liaisons N(3)—C(4), N(3)—C(6) et N(1)—C(5) sont bien des liaisons simples N_{sp^3}—C_{sp^3}, la liaison C(2)—N(3), en revanche, présente un caractère partiel de double liaison N_{sp^3}—C_{sp^2}. On notera, en outre, que ces valeurs concordent avec celles de 1,27(1) et 1,33(1) données pour la dihydro-7,8 diphényl-2,5 imidazo [1,2-*f*] [1,3,4,6] triazépine (11) ou avec celles de 1,28(3) et 1,37(2) données pour la (dihydro-4,5 imidazolyl-2)-2 benzophénone (12) ou encore avec celles de 1,28(7) et 1,38(2) données pour les *N*,*N*-diméthylamidoximes (13).

D'autre part, la moyenne des variations des angles n'est que de 2,04°. L'angle C(2)—N(3)—C(4) a une valeur moyenne de 106,8°. Ce résultat s'accorde avec ceux de Beagley *et al.* (11) et ceux de MacKechnie et Paul (12) qui, dans le cas des composés déjà cités, donnent la valeur 105,8°. De plus le substituant C(6) porté par l'azote N(3) est situé nettement hors du plan comme cela apparait dans le tableau 7. Tout ceci, compte tenu par ailleurs du caractère partiel de double liaison pour la liaison C(2)—N(3), est en faveur d'un état intermédiaire d'hybridation de l'azote N(3).

Pour ce qui est des substituants portés par le cycle en position 2, 3, 4 et 5, on peut relever les observations suivantes liées aux

Can. J. Chem. Downloaded from www.nrcresearchpress.com by 213.166.140.6 on 09/07/12
For personal use only.

Can. J. Chem. Downloaded from www.nrcresearchpress.com by 213.166.140.6 on 09/07/12
For personal use only.

TABLEAU 4. Longueurs de liaisons et leur déviation standard en Å

Atomes	Composé **1**	Composé **2**	Composé **3**
O(70)—C(7)	1,214(7)	1,197(4)	1,216(8)
N(1)—C(2)	1,285(7)	1,280(4)	1,282(8)
N(1)—C(5)	1,473(7)	1,480(4)	1,477(8)
N(3)—C(2)	1,387(7)	1,393(4)	1,375(8)
N(3)—C(4)	1,480(7)	1,462(4)	1,477(7)
N(3)—C(6)	1,483(7)	1,470(4)	1,493(8)
C(2)—C(21)	1,496(8)	1,482(4)	1,481(8)
C(4)—C(5)	1,575(8)	1,555(4)	1,587(9)
C(4)—C(7)	1,528(8)	1,501(5)	1,554(9)
C(5)—C(51)	1,516(8)	1,499(5)	1,514(9)
C(6)—C(61)	1,534(9)	1,508(5)	1,534(10)
C(6)—C(62)	1,531(9)		1,550(10)
C(7)—C(71)	1,556(8)	1,497(5)	1,497(8)
C(21)—C(22)	1,392(8)	1,382(5)	1,289(9)
C(21)—C(26)	1,380(7)	1,382(5)	1,380(9)
C(22)—C(23)	1,397(8)	1,391(5)	1,385(9)
C(23)—C(24)	1,356(9)	1,372(6)	1,375(10)
C(24)—C(25)	1,371(9)	1,376(6)	1,365(10)
C(25)—C(26)	1,389(9)	1,385(5)	1,377(9)
C(51)—C(52)	1,374(8)	1,387(5)	1,382(8)
C(51)—C(56)	1,387(9)	1,367(6)	1,387(9)
C(52)—C(53)	1,378(10)	1,378(8)	1,386(10)
C(53)—C(54)	1,359(11)	1,340(10)	1,380(10)
C(54)—C(55)	1,383(10)	1,361(9)	1,369(10)
C(55)—C(56)	1,384(9)	1,382(6)	1,370(10)
C(61)—C(62)		1,379(5)	
C(61)—C(66)		1,380(5)	
C(62)—C(63)		1,380(6)	
C(63)—C(64)		1,369(6)	
C(64)—C(65)		1,361(6)	
C(65)—C(66)		1,386(5)	
C(71)—C(711)	1,536(10)		
C(71)—C(712)	1,555(10)		
C(71)—C(713)	1,525(9)		
C(71)—C(72)			1,391(8)
C(71)—C(76)			1,382(8)
C(72)—C(73)			1,373(9)
C(73)—C(74)			1,352(10)
C(74)—C(75)			1,387(9)
C(75)—C(76)			1,388(9)

TABLEAU 5. Angles de liaisons et leur déviation standard en °

Atomes	Composé **1**	Composé **2**	Composé **3**
C(2)—N(1)—C(5)	106,9(5)	107,7(3)	108,0(5)
C(2)—N(3)—C(4)	106,8(5)	106,5(2)	107,3(5)
C(2)—N(3)—C(6)	128,3(5)	123,6(3)	122,9(5)
N(1)—C(2)—N(3)	117,3(5)	116,6(3)	117,6(5)
N(1)—C(2)—C(21)	120,4(5)	120,5(3)	121,6(6)
N(3)—C(4)—C(5)	101,2(5)	102,9(3)	102,2(5)
N(3)—C(4)—C(7)	110,8(5)	114,3(3)	109,7(5)
C(5)—C(4)—C(7)	109,4(5)	113,6(3)	106,4(5)
N(1)—C(5)—C(4)	105,4(5)	104,8(2)	104,7(5)
N(1)—C(5)—C(51)	110,3(5)	111,0(3)	111,0(5)
C(4)—C(5)—C(51)	114,6(5)	114,4(3)	112,5(5)
N(3)—C(6)—C(61)	112,3(5)	114,3(3)	110,4(5)
N(3)—C(6)—C(62)	110,9(6)		109,4(5)
C(61)—C(6)—C(62)	113,3(6)		113,7(6)
O(70)—C(7)—C(4)	120,1(6)	123,0(3)	120,6(5)
O(70)—C(7)—C(71)	120,3(6)	121,6(4)	120,7(6)
C(4)—C(7)—C(71)	119,6(5)	115,4(3)	118,6(5)
C(2)—C(21)—C(22)	121,6(6)	122,5(3)	119,1(6)
C(2)—C(21)—C(26)	118,1(6)	122,5(3)	122,3(6)
C(22)—C(21)—C(26)	120,0(6)	119,6(3)	118,5(6)
C(21)—C(22)—C(23)	119,0(6)	119,8(4)	120,6(6)
C(22)—C(23)—C(24)	120,3(6)	120,0(4)	119,5(6)
C(23)—C(24)—C(25)	121,0(6)	120,5(4)	120,4(6)
C(24)—C(25)—C(26)	119,7(6)	119,7(4)	120,1(7)
C(21)—C(26)—C(25)	119,9(6)	120,4(4)	120,9(6)
C(5)—C(51)—C(52)	121,5(6)	120,5(4)	119,8(5)
C(5)—C(51)—C(56)	119,7(6)	120,9(3)	122,7(5)
C(52)—C(51)—C(56)	118,8(6)	118,5(4)	117,5(6)
C(51)—C(52)—C(53)	120,9(7)	119,2(5)	121,2(6)
C(52)—C(53)—C(54)	120,8(7)	122,1(6)	119,9(6)
C(53)—C(54)—C(55)	118,8(7)	119,1(6)	119,4(7)
C(54)—C(55)—C(56)	121,0(7)	120,3(6)	120,4(7)
C(51)—C(56)—C(55)	119,6(7)	120,8(5)	121,6(6)
C(6)—C(61)—C(62)		120,3(3)	
C(6)—C(61)—C(66)		121,4(3)	
C(61)—C(62)—C(63)		120,7(4)	
C(62)—C(63)—C(64)		120,2(4)	
C(63)—C(64)—C(65)		120,1(4)	
C(64)—C(65)—C(66)		119,9(4)	
C(61)—C(66)—C(65)		120,8(4)	
C(7)—C(71)—C(711)	107,9(6)		
C(7)—C(71)—C(712)	109,6(6)		
C(7)—C(71)—C(713)	110,1(7)		
C(711)—C(71)—C(712)	108,0(7)		
C(711)—C(71)—C(713)	110,9(7)		
C(712)—C(71)—C(713)	110,2(7)		
C(7)—C(71)—C(72)			117,3(5)
C(7)—C(71)—C(76)			124,4(5)
C(72)—C(71)—C(76)			118,3(5)
C(71)—C(72)—C(73)			121,3(6)
C(72)—C(73)—C(74)			119,5(6)
C(73)—C(74)—C(75)			121,3(6)
C(74)—C(75)—C(76)			118,9(6)
C(71)—C(76)—C(75)			120,6(6)

valeurs des angles de torsion présentées dans le tableau 6 :

(*i*) Le phényle en 2 prend chez les trois composés une angulation voisine afin de s'éloigner au maximum du substituant greffé en N(3). Donc il n'y pas de conjugaison entre ce groupement et la liaison imine intracyclique comme en témoigne la valeur moyenne de l'angulation qui est égale à 41,5°.

(*ii*) On note également une angulation assez voisine pour les substituants isopropyle ou benzyle greffés en N(3). Le cycle phényle du substituant benzyle dans le composé **2** prend la place d'un des groupements méthyles de **1** ou **3**. Les angulations de **2** et **3** autour de la liaison N(3)—C(6) sont très proche de 60° et donc de la valeur théorique pour une conformation décalée. D'autre part dans le cas de **3** le calcul des distances entre l'hydrogène porté par C(4) et les hydrogènes respectivement portés par C(61) et C(62) : 2,37 Å et 2,42 Å, révèle une proximité entre ces atomes conforme aux résultats observés en rmn par effet Overhauser (10) et s'accorde avec l'état d'hybridation de N(3) mentionné précédement. De même, la distance de 2,55 Å entre l'hydrogène porté par C(6) et l'hydrogène porté par C(22) confirme aussi les résultats de rmn (10).

(*iii*) La projection de l'angle C(4)—N(3)—C(2) dans un plan perpendiculaire à la liaison N(3)—C(6), qui serait de 180° pour un azote N(3) purement sp^2 ou de 120° pour un azote purement sp^3, vaut respectivement 156,2(9)° pour **1**, 136,0(5)° pour **2** et 131,1(5)° pour **3**. On en déduit 40% de caractère sp^3 pour **1**, 73% pour **2** et 81% pour **3**.

(*iv*) La liaison C(7)—O(70) est, dans les trois cas, située dans le même quadrant que la liaison C(4)—N(3) ce qui correspond à une forme cisoide, **3** ayant en outre même

TABLEAU 6. Principaux angles de torsion et leur déviation standard en °

Atomes	Composé **1**	Composé **2**	Composé **3**
C(5)—N(1)—C(2)—N(3)	4,6(9)	3,2(5)	2,4(5)
C(2)—N(1)—C(5)—C(4)	−12,5(9)	4,9(5)	0,1(5)
N(1)—C(2)—N(3)—C(4)	5,9(9)	−10,4(5)	−3,8(5)
C(2)—N(3)—C(4)—C(5)	−12,6(9)	12,1(5)	3,3(5)
N(3)—C(4)—C(5)—N(1)	−15,1(9)	10,4(5)	2,1(5)
N(1)—C(2)—C(21)—C(26)	35,0(9)	40,2(5)	49,4(5)
N(3)—C(2)—C(21)—C(22)	39,1(9)	40,6(5)	49,2(5)
C(2)—N(3)—C(6)—C(61)	100,0(9)	77,6(5)	69,7(5)
C(2)—N(3)—C(6)—C(62)	−132,1(9)	—	−164,5(5)
C(4)—N(3)—C(6)—C(61)	−56,2(9)	−58,4(5)	−71,4(5)
C(4)—N(3)—C(6)—C(62)	71,7(9)	—	54,4(5)
C(5)—C(4)—C(7)—C(71)	−97,9(9)	−64,0(5)	−96,0(5)
N(3)—C(4)—C(7)—O(70)	−30,4(9)	−1,2(5)	−29,3(5)
N(1)—C(5)—C(51)—C(56)	−44,6(9)	−66,1(5)	−24,7(5)
C(4)—C(5)—C(51)—C(52)	−108,4(9)	−130,4(5)	−88,3(5)

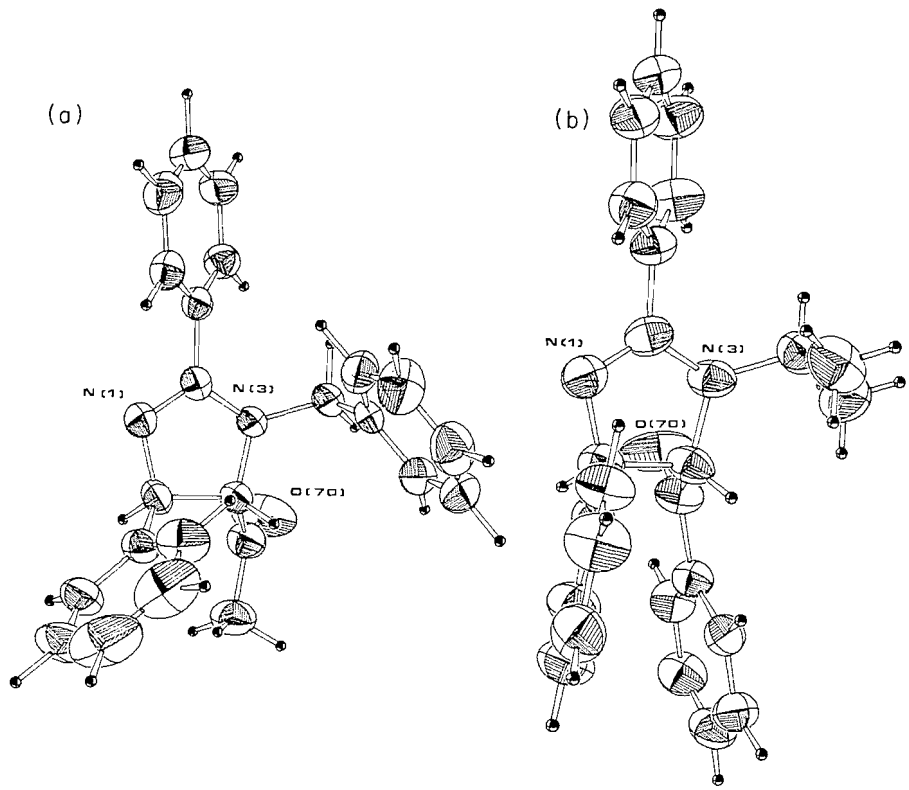

FIG. 2. Représentations géométriques des composés **2** (*a*) et **3** (*b*) rapportées au même référentiel.

TABLEAU 7. Distances au plan moyen défini par les atomes C(5)—N(1)—C(2)—N(3)

Atomes	Composé **1**	Composé **2**	Composé **3**
N(1)	−0,021(7)	−0,019(3)	−0,011(5)
C(2)	0,023(8)	0,016(3)	0,012(7)
N(3)	−0,013(7)	−0,009(3)	−0,006(5)
C(4)	−0,243(8)	0,188(3)	0,045(7)
C(5)	0,011(9)	0,008(3)	0,006(7)
C(21)	0,059(8)	0,023(3)	0,025(6)
C(6)	0,546(9)	0,622(3)	0,658(7)
C(7)	−1,694(9)	−0,732(4)	−1,267(7)
C(51)	1,320(8)	1,076(3)	1,198(6)
χ^2	22,694	74,478	10,458

conformation que **1**. On doit souligner, à ce propos, que par nOe-différence entre les atomes d'hydrogène portés par C(5) et C(72) on avait abouti à la même conclusion (10).

(*v*) Enfin, le phényle greffé en 5 est toujours presque quasiment perpendiculaire au plan du cycle imidazoline comme le montre la distance entre l'atome d'hydrogène porté par C(5) et celui porté par C(52). Cette valeur (2,36 Å) est proche du minimum observable par simulation de rotation autour de la liaison C(5)—C(51) (2,13 Å). Ce résultat concorde avec l'interaction notée par nOe-différence (10).

Conclusion

La différence structurale essentielle relevée dans cette étude tient à une inversion d'enveloppe chez **2**. Néanmoins, la similitude conformationnelle est particulièrement marquée entre

Can. J. Chem. Downloaded from www.nrcresearchpress.com by 213.166.140.6 on 09/07/12
For personal use only.

1 et **3**. Il semblerait donc que les substituants greffés sur N(3) influencent de manière prépondérante la conformation du carbonyle dans ces espèces fonctionnalisées. L'ensemble de ces résultats est en stricte conformité avec ceux observés en solution. Il reste à savoir désormais si cette particularité intervient dans une corrélation avec les activités biologiques.

1. H. DABIRE, P. MOUILLE, M. ANDREJAK, B. FOURNIER et H. SCHMITT. Arch. Int. Pharmacodyn. Ther. **254**, 252 (1981).
2. (*a*) F. GAEDCKE et F. ZYMALKOWSKI. Arch. Pharm. **312**, 812 (1979); (*b*) F. GAEDCKE, R. KNORR et F. ZYMALKOWSKI. Arch. Pharm. **313**, 166 (1980).
3. H. FOKS et M. HANOWIEC. Acta Pol. Pharm. **39**, 79 (1982).
4. (*a*) W. HOEFKE et W. KOBINGER. Arzneim. Forsch. **16**, 1038 (1966); (*b*) P. B. TIMMERMANS, A. DE JONGE, J. VAN MEEL, F. SLOTHORST-GRISDIJK, E. LAM et P. VAN ZWIETEN. J. Med. Chem. **24**, 502 (1981); (*c*) D. CAMBRIDGE. Eur. J. Pharmacol. **72**, 413 (1981).
5. A. MARSURA, C. LUU-DUC et G. GELLON. Synthesis, 537 (1985).
6. P. BROUANT, J. BARBE, A. MARSURA et C. LUU-DUC. Acta Crystallogr. Sect. C: Cryst. Struct. Commun. **41**, 1369 (1985).
7. P. MAIN, S. J. FISKE, S. E. HULL, L. LESSINGER, G. GERMAIN, J. P. DECLERCQ et M. M. WOOLFSON. MULTAN 80. A system of computer programs for the automatic solution of crystal structures from X-ray diffraction data. Univ. York. (Angleterre) et Louvain (Belgique), 1980.
8. International tables for X-ray crystallography. Tome IV. Kynoch Press, Birmingham. 1974; distribué par D. Reidel, Dordrecht.
9. B. A. FRENZ. Computing in crystallography. *Edité par* H. Schenk, R. Olthof-Hazekamp, H. van Koningsveld et G. C. Bassi. Delft Univ. Press, Pays-Bas. 1978. pp. 44–71.
10. A. MARSURA, C. LUU-DUC et R. NARDIN. Magn. Reson. Chem. **23**, 639 (1985).
11. B. BEAGLEY, S. F. MOSS, R. G. PRITCHARD et R. D. TAYLOR. Acta Crystallogr. Sect. B: Struct. Crystallogr. Cryst. Chem. **37**, 486 (1981).
12. J. S. MACKECHNIE et L. C. PAUL. J. Chem. Soc. B, 984 (1968).
13. H. GOZLAN, R. MICHELOT, C. RICHE et R. RIPS. Tetrahedron, **33**, 2535 (1977).

Can. J. Chem. Downloaded from www.nrcresearchpress.com by 213.166.140.6 on 09/07/12
For personal use only.

Photochemistry of halogenated benzene derivatives. Part VIII.[1] Photoformation of 2-methyl-4,5,6,7-tetrachlorobenzoxazole from pentachlorophenol in water–acetonitrile

GHULAM GHAUS CHOUDHRY,[2] NORMA JEAN GRAHAM, AND G. R. BARRIE WEBSTER
Pesticide Research Laboratory, Department of Soil Science, University of Manitoba, Winnipeg, Man., Canada R3T 2N2

Received September 3, 1986[3]

GHULAM GHAUS CHOUDHRY, NORMA JEAN GRAHAM, and G. R. BARRIE WEBSTER. Can. J. Chem. **65**, 2223 (1987).

Photolysis of a solution of pentachlorophenol (**1**) in H_2O–CH_3CN (2:3 v/v) was conducted on a synthetic scale using wavelengths ≥ 290 nm. After changing the pH of the photolyzate of **1** to ≥ 12, the photoproduct 2-methyl-4,5,6,7-tetrachlorobenzoxazole (**2**) was extracted with *n*-hexane. The product **2** was crystallized from methanolic solution. Ultraviolet, IR, FT-^{1}H-NMR, proton-decoupled normal FT-^{13}C-NMR, and proton-decoupled DEPT (distortionless enhancement by polarization transfer) sequence FT-^{13}C-NMR spectroscopy were used to identify photoproduct **2** as 2-methyl-4,5,6,7-tetrachlorobenzoxazole. A mechanism for the photoformation of benzoxazole **2** from **1** is proposed. 3,4,5,6-Tetrachlorocyclohexa-3,5-diene-1,2-ketocarbene formed from 2-hydroxy-3,4,5,6-tetrachlorophenyl radical is suggested as key intermediate involved in the generation of oxazole **2** from phenol **1**. The chemical yield of **2** on the basis of **1** was ca. 1%. A mechanism is proposed to explain the mass spectral fragmentation of **2** via the losses of Ċl, :C=O, Cl—Ċ=O, CH_3—Ċ=O, CH_3CN, and $\dot{C}_3H_3ClNO$ species from the parent molecular ion.

GHULAM GHAUS CHOUDHRY, NORMA JEAN GRAHAM et G. R. BARRIE WEBSTER. Can. J. Chem. **65**, 2223 (1987).

Utilisant des longueurs d'onde ≥ 290 nm et opérant à une échelle synthétique, on a procédé à une photolyse d'une solution de pentachlorophénol (**1**) dans le H_2O/CH_3CN (2/3 v/v). Après avoir ajusté le pH de la solution à une valeur supérieure à 12, on a extrait le photoproduit, le méthyl-2 tétrachloro-4,5,6,7 benzoxazole (**2**), par de l'hexane. On a recristallisé le produit **2** à partir du méthanol. L'identification du produit **2** comme le méthyl-2 tétrachloro-4,5,6,7 benzoxazole a été réalisée grâce aux spectres UV et IR, aux spectres rmn ^{1}H par transformation de Fourier et à une séquence de spectres rmn du ^{13}C normalement découplés du proton et découplés des protons grâce à un rehaussement sans distorsion effectué par transfert de polarisation (RDTP). On propose un mécanisme pour la photoformation du benzoxazole **2** à partir du composé **1**. Dans la génération de l'oxazole **2** à partir du phénol **1**, on suggère que l'intermédiaire clé est le tétrachloro-3,4,5,6 cyclohexadiène-3,5 céto-1 carbène-2, qui se forme à partir du radical hydroxy-2 tétrachloro-3,4,5,6 phényle. Le rendement chimique du composé **2**, sur la base de la quantité de **1** mise en jeu, est de 1%. On propose un mécanisme pour expliquer pourquoi la fragmentation du composé **2** en spectrométrie de masse se produit avec des pertes de .Cl, :C=O, Cl—Ċ=O, CH_3CN et .C_3H_3ClNO à partir de l'ion moléculaire de base.
[Traduit par la revue]

Introduction

The contamination of soil and aquatic environments by chlorinated aromatic pollutants (CAPs) such as polychlorophenols (PCPs) is well known. PCPs includingg several other chloroorganics have been recently identified in the flue gas and fly ash emitted from some municipal and industrial incinerators located in Canada, Japan, Switzerland, and the Netherlands (2–4). Likewise, PCPs have been widely found in surface waters and in wastewaters, in particular, in pulp mill effluents (5–7). In the environment, PCPs originate from pulp bleaching and the disinfection of waters, but are also contaminants and degradation products of pesticides (8). Furthermore, pentachlorophenol (P_5CP) (**1**) itself has been widely used in agriculture and industry as a fungicide, bactericide, herbicide, molluscicide, algicide, and insecticide (9, 10). Presently, CAP **1** is utilized mainly as a wood preservative, which has led to its widespread presence in the environment (9).

Photochemical transformation caused by sunlight is an important environmental process for chemicals present in air, water, and soils (11). Several authors have reported solution phase as well as solid phase environmental photochemistry of P_5CP (**1**) (12–21). Recently, we (22) have reported our investigations on the environmental photochemistry of several PCPs, namely tetra- and pentachlorophenols in H_2O–CH_3CN (2:3 v/v) at λ ≥ 290 nm concluding that the process of reductive dechlorination is dependent not only upon the position of the OH group but also upon the relative positions of the Cl substituents on the benzene nucleus. In aqueous acetonitrile, for instance, **1** also gave rise to the generation of a photoproduct of molecular formula $C_8H_3Cl_4NO$ (22).

In view of our continuing interest in the environmental photolytic fate of pollutants, viz., halogenated benzene derivatives (see ref. 1; and the preceding articles of this series cited therein), we decided to further investigate the photochemistry of **1** dissolved in water-acetonitrile (2:3 v/v) at λ ≥ 290 nm. This paper presents the structural elucidation of the photoproduct $C_8H_3Cl_4NO$ (**2**) arising from pentachlorophenol (**1**) in aqueous acetonitrile along with the proposed mechanisms for the formation and mass fragmentation pattern of compound **2**.

Experimental

(a) Substrates and solvents

Pentachlorophenol (P_5CP) (**1**) and 1,2,3,4-tetrachlorobenzene (internal standard) were supplied by Aldrich Chemical Co., Inc. Solvents such as methanol and *n*-hexane were purchased from Caledon Laboratories Ltd., Ont., Canada, while spectrograde acetonitrile was supplied by Aldrich Chem. Co., Inc. The source of water was same as previously described (23).

(b) Preparation of solution of P_5CP (1) in water-acetonitrile (2:3)

A stock solution of P_5CP (**1**) was prepared by heating 0.7 g **1** in 250 mL CH_3CN at 45°C and filtering through a medium porosity sintered glass filter. To 50 mL of the stock solution in a 500 mL volumetric flask, 250 mL acetonitrile were added. With continuous manual shaking, 200 mL water was then added to this diluted acetonitrile solution of **1**. The concentration of P_5CP (**1**) in H_2O–CH_3CN

[1]For Part VII, see ref. 1.
[2]To whom all correspondence should be addressed.
[3]Revision received April 29, 1987.

Can. J. Chem. Downloaded from www.nrcresearchpress.com by 213.166.140.6 on 09/07/12
For personal use only.

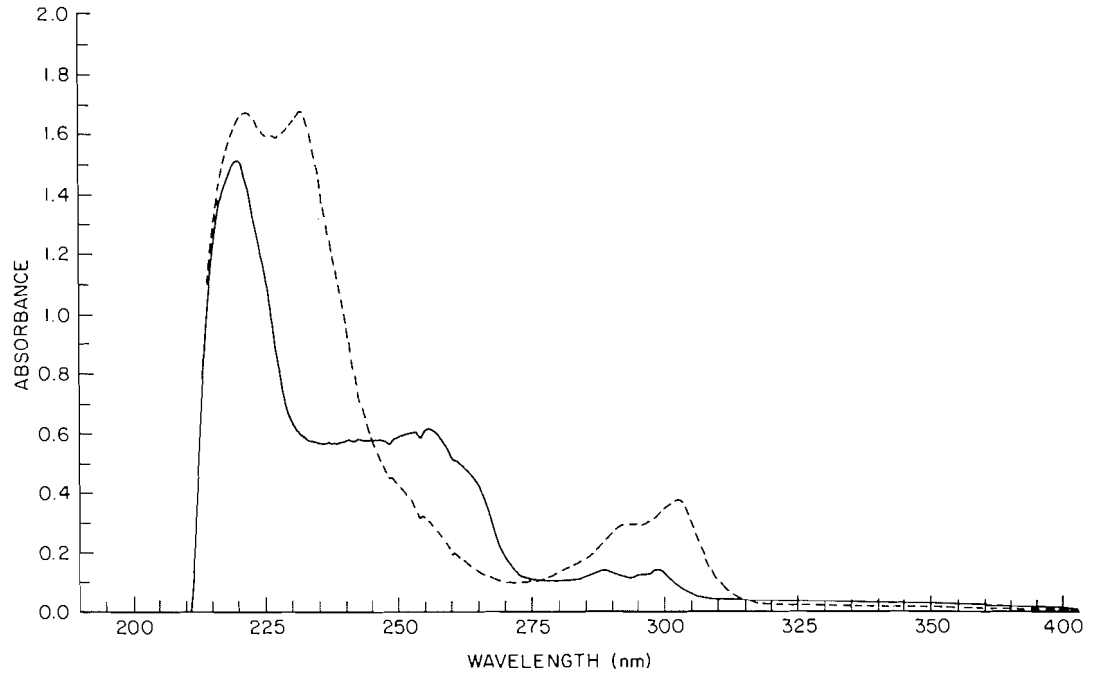

FIG. 1. UV absorption spectra of solutions of 0.25×10^{-3} *M* pentachlorophenol (**1**) (---) and 0.62×10^{-4} *M* 2-methyl-4,5,6,7-tetrachlorobenzoxazole (**2**) (—) in *n*-hexane.

(2:3 v/v) was determined by HPLC to be 1.000 m*M*; utilizing a 1.124 m*M* solution of **1** in methanol as an analytical standard. In this manner, 6.5 L of 1.00 m*M* solution of the starting material **1** was prepared in H_2O–CH_3CN (2:3 v/v).

(c) Irradiation experiments

The solution-phase photoreactions of pentachlorophenol in water–acetonitrile (2:3 v/v) were carried out using previously reported (22–25) Rayonet Photochemical Reactor (The Southern New England Ultra Violet Company) equipped with 16 RPR-3000 Å lamps having an energy output of 90% in the wavelength range 290 to 310 nm. In order to determine the optimum UV light photolytic exposure time as well as the retention time of the desired photoproduct $C_8H_4Cl_3NO$ (**2**) from **1**, analytical scale photolysis experiments were conducted in Pyrex glass tubes containing 2 mL sample solution each. On synthetic scale, 6.5 L of 1.000 m*M* solution of P_5CP (**1**) were photolyzed in 250 mL aliquots contained in a 1-litre Pyrex glass conical flask, photoreaction time for each aliquot being 30 h.

(d) High performance liquid chromatography (HPLC) analysis

The formation of the photoproduct **2** was monitored using a Waters Model 4000 HPLC equipped with Model 6000A pump, U6K injector, and an M440 UV absorbance detector. Separations were obtained with a 30 cm × 3.9 mm μBondapak C_{18} column (reverse phase). The UV detector wavelength used for these analyses was 254 nm. The photolyzates of P_5CP (**1**) were analyzed with the eluting solvent system CH_3CN–H_2O (3:2 v/v) at a flow rate of 1 mL/min. Under these conditions, the retention times of P_5CP (**1**), photoproduct $C_8H_3Cl_4NO$ (**2**), and 1,2,3,4-tetrachlorobenzene (internal standard) were 1.98, 15.30, and 18.65 min, respectively.

(e) Extraction and crystallization of the photoproduct $C_8H_3Cl_4NO$ (2)

The synthetic scale photolyzate (250 mL) of PCP **1** in H_2O–CH_3CN (2:3 v/v) was equally divided into two portions. Each portion was treated with 62.5 mL of 0.590 *M* aqueous solution of NaOH (the resultant pH being ≥12) and was subsequently extracted with 125 mL *n*-hexane. The *n*-hexane extracts of both portions of the photolyzate of **1** which contained the photoproduct $C_8H_3Cl_4NO$ (**2**) were evaporated to a few mL with a rotary evaporator and were then transferred to a 15 mL centrifuge tube. To this tube, similar *n*-hexane extracts of four additional 250 mL photolyzates of **1** were also added and the solvent was evaporated to dryness with nitrogen gas. The compound **2** was redissolved in the minimal amount of methanol by heating the centrifuge tube in a hot water bath maintained at 35°C. The conventional procedures were unsuccessful for crystallizing the product **2**. The technique and apparatus consisting of Teacup, sintered glass filter tubes, recrystallization Craig tubes, and centrifuge tubes, previously described by Martin-Smith (26) for the small scale crystallization of biological organic compounds, were utilized for crystallizing the photoproduct **2** from its methanolic solution.

The remaining 5250 mL of the photolyzate of PCP **1** in H_2O–CH_3CN (2:3 v/v) was also subjected to the above cited methods for the isolation and crystallization of the photoproduct $C_8H_3Cl_4NO$ (**2**). Total amount of the pure crystallin compound **2** synthesized photochemically from 6.5 L solution of P_5CP (**1**) (1.000 m*M*) was 0.01175 g thereby indicating that the chemical yield of **2** from phenol **1** was 0.667%.

(f) Melting point determination

Melting points for P_5CP (**1**) and $C_8H_3Cl_4NO$ (**2**) were 185–188 and 133°C; where as the literature values of such data were 188–191 (27) and 140.5–141.5°C (28) for **1** and 2-methyl-4,5,6,7-tetrachlorobenzoxazole (**2**) (designation of this structure to the compound $C_8H_3Cl_4NO$ **2** is discussed below), respectively.

(g) Spectroscopy

The spectroscopic instrumentations and techniques utilized for the elucidation of structure of the photolytic product $C_8H_3Cl_4NO$ (**2**), which was isolated in the crystalline form as cited above, are as follows:

(i) UV light absorbing

Light absorption spectra (Fig. 1) of the starting material **1** and the desired photoproduct **2** dissolved in *n*-hexane were recorded using Unicam Spectrophotometer. Quartz glass cuvets used were of 1-cm pathlength.

(ii) Infrared (IR)

Infrared spectrum (Fig. 2) of the product **2** in KBr was recorded on a Perkin Elmer 457 Grating IR Spectrophotometer.

(iii) Nuclear magnetic resonance (NMR)

All the NMR spectra of the compound **2** shown in Figs.3–5 were recorded on a Bruker AM-300 Spectrophotometer using tetramethylsilane (TMS) as an internal standard and $CDCl_3$ as a solvent. Chemical

Can. J. Chem. Downloaded from www.nrcresearchpress.com by 213.166.140.6 on 09/07/12
For personal use only.

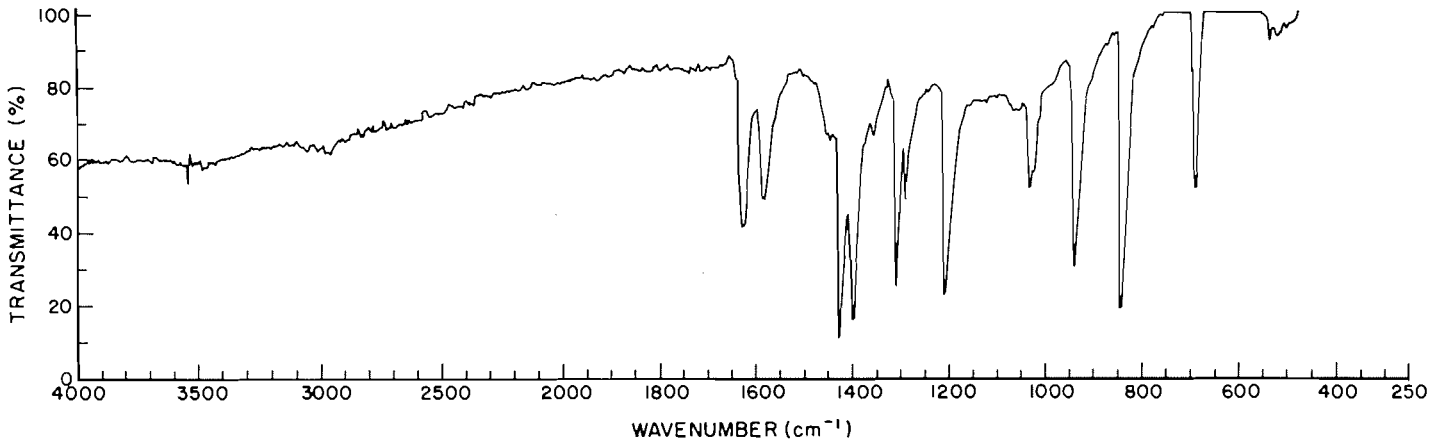

FIG. 2. IR spectrum of 2-methyl-4,5,6,7-tetrachlorobenzoxazole (**2**) in KBr.

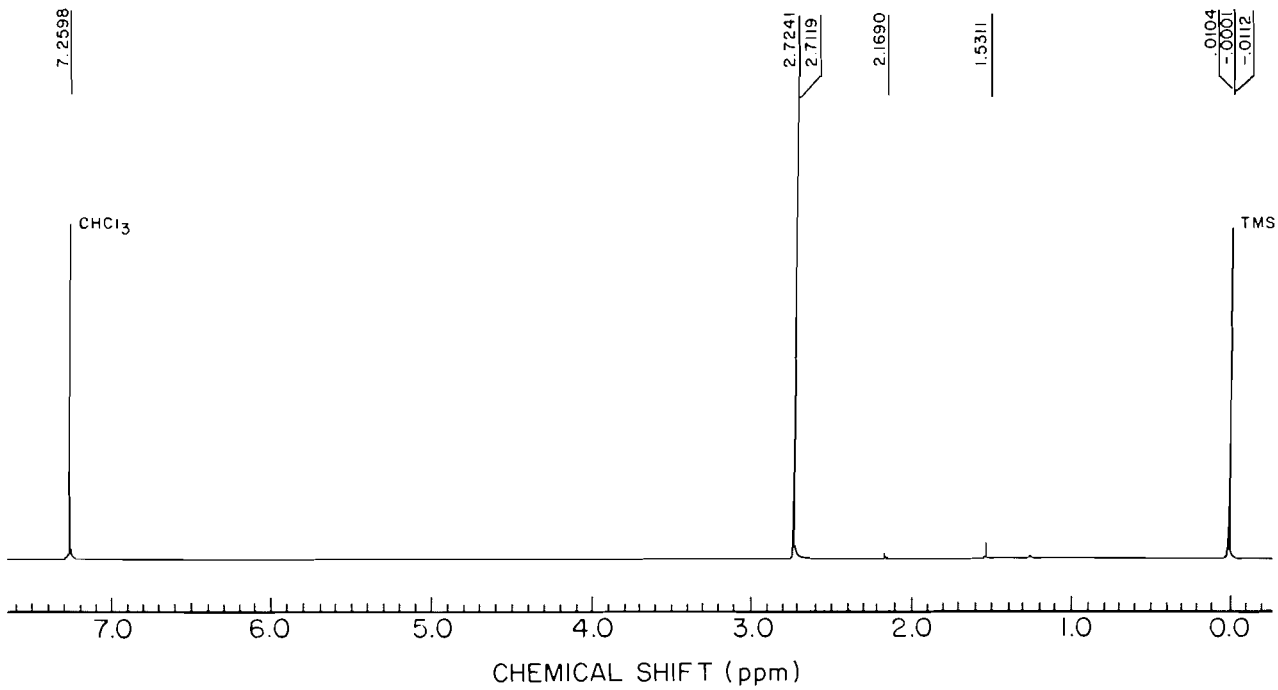

FIG. 3. ^{1}H-NMR spectrum (300.13 MHz) of 2-methyl-4,5,6,7-tetrachlorobenzoxazole (**2**) in deuterated chloroform.

shifts, quoted as δ values (units being ppm), were measured in relation to TMS.

The ^{1}H-NMR (Fig. 3) and ^{13}C-NMR (Figs. 4 and 5) spectra of **2** were run at 300.13 and 75.40 MHz, respectively. Due to the limited amount of **2** available, all NMR spectra were obtained by averaging multiscan runs; the total number of scans were 32, 2718, and 2048 in the case of ^{1}H-NMR (Fig. 3), proton-decoupled normal ^{13}C-NMR (Fig. 4), and proton-decoupled distortionless enhancement by polarization transfer (DEPT) sequence ^{13}C-NMR (Fig. 5), respectively.

The DEPT spectra of **2** (Fig. 5) were recorded by the techniques recently published by Doddrell and co-workers (29). The spectra (*a*), (*b*), and (*c*) (see Fig. 5) were determined with pulse (θ) of values $\pi/4$, $\pi/2$, and $3\pi/4$, respectively. In these DEPT spectra, which are the consequence of the transfer of polarization of protons to C, signals from non-protonated carbon atoms did not appear. It should be pointed out that in the context of polarization transfer ^{13}C-NMR spectroscopy, the DEPT sequence overcomes several important limitations of the INEPT (insensitive nuclear enhanced polarization transfer) pulse sequence (29). The technique of INEPT was originally developed by Morris and Freeman (30), and later was modified and used by several investigators (cf. refs. 31, 32).

(h) Gas chromatography – mass spectrometry

A Hewlett-Packard 5894 A gas chromatograph mass spectrometer (GC–MS) operating in the electron-impact mode at 70 eV was utilized for recording the mass spectrum (MS) of $C_8H_3Cl_4NO$ compound (**2**) (Fig. 6). Other conditions for the operation of this GC–MS were the same as previously described by Choudhry *et al.* (22).

Results and discussion

Spectroscopic analysis of the product $C_8H_3Cl_4NO$ (2)

The pure crystalline 2-methyl-4,5,6,7-tetrachlorobenzoxazole (**2**) (structure assigned to the compound $C_8H_3Cl_4NO$ **2** as discussed below), synthesized on large scale by photolyzing P_5CP (**1**) in water-acetonitrile (2:3 v/v), viz., reaction [1] was subjected to several analytical methodologies. Figures 1–5 record UV absorption, IR, FT 300 MHz ^{1}H-NMR, normal proton decoupled FT 75 MHz ^{13}C-NMR, and DEPT sequence proton decoupled FT 75 MHz ^{13}C-NMR spectra of benzoxazole **2**, respectively. Previously reported electron impact mode MS of compound **2** is reproduced in Fig. 6.

Can. J. Chem. Downloaded from www.nrcresearchpress.com by 213.166.140.6 on 09/07/12
For personal use only.

Can. J. Chem. Downloaded from www.nrcresearchpress.com by 213.166.140.6 on 09/07/12
For personal use only.

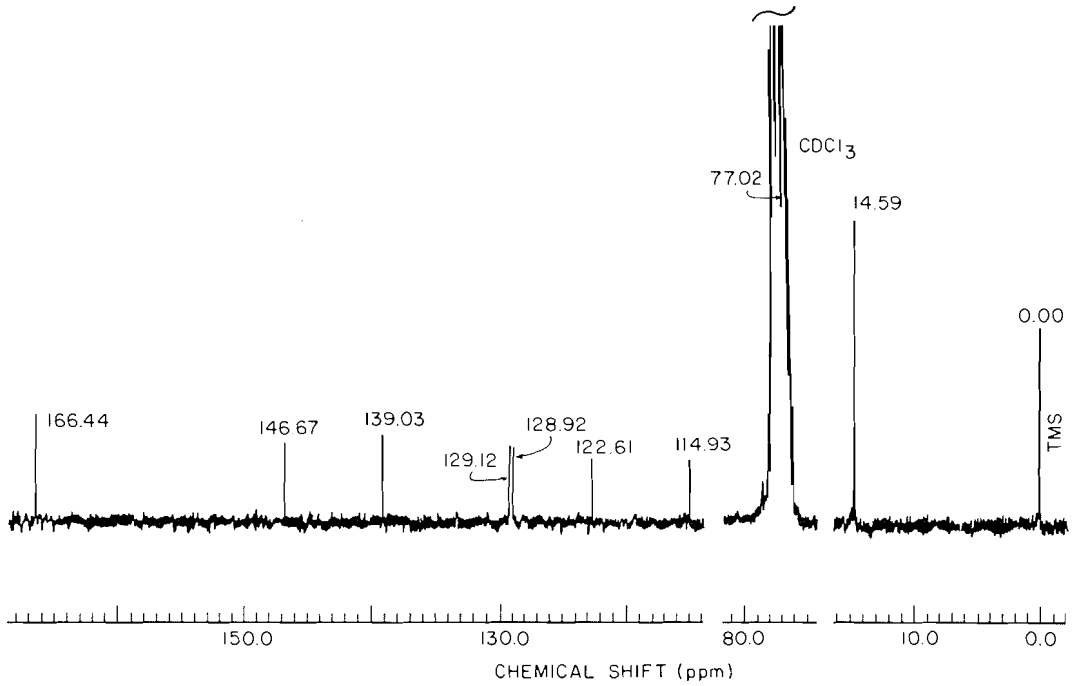

FIG. 4. Proton-decoupled 75.4 MHz ^{13}C-NMR spectrum of 2-methyl-4,5,6,7-tetrachlorobenzoxazole (**2**) in deuterated chloroform.

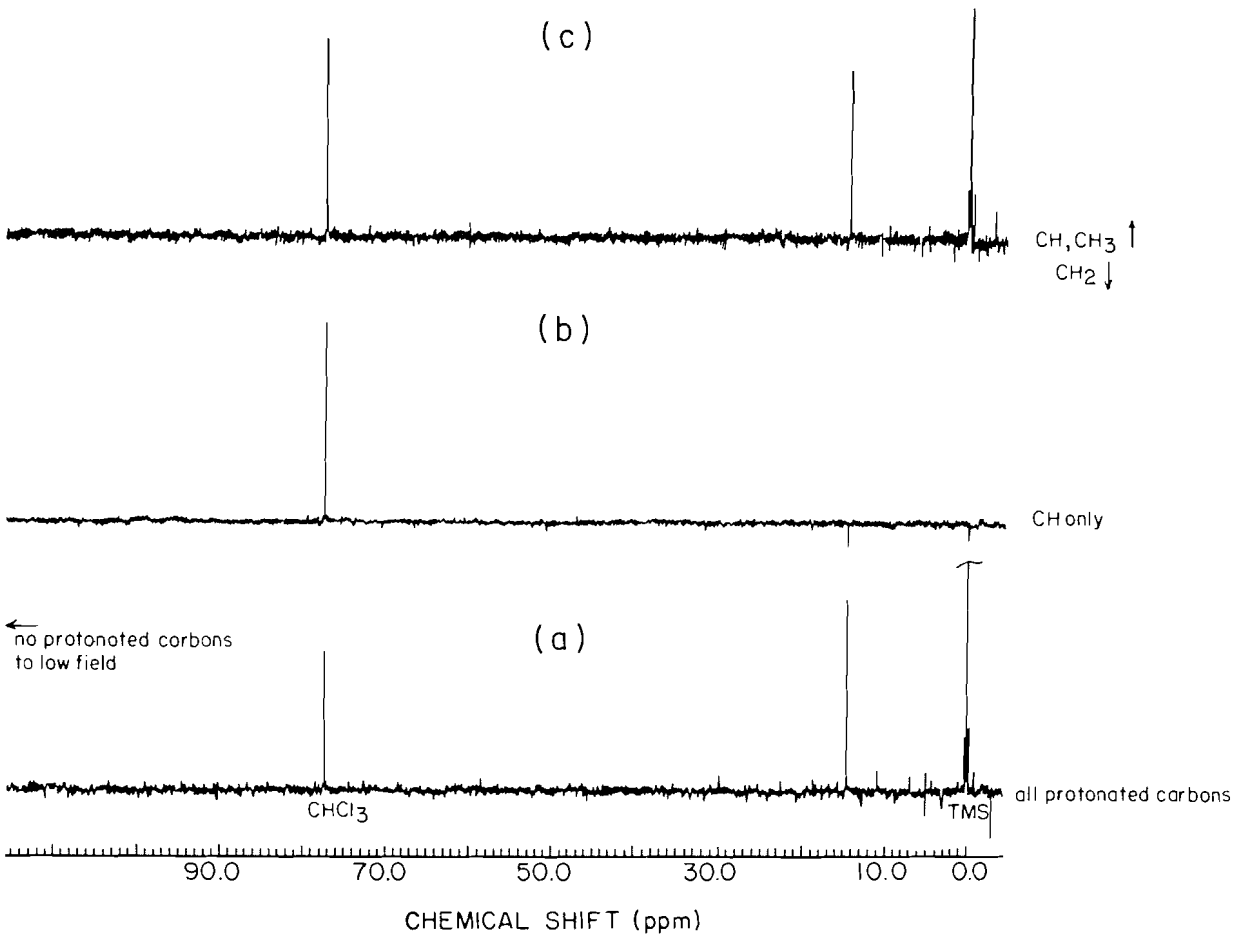

FIG. 5. Proton-decoupled distortionless enhancement by polarization transfer (DEPT) sequence 75.4 MHz ^{13}C-NMR spectra of 2-methyl-4,5,6,7-tetrachlorobenzoxazole (**2**) in deuterated chloroform. All protonated carbons' signals (*a*), CH signals only (*b*), and CH(↑), CH_3(↑), and CH_2(↓) signals (*c*) (see also the related text.).

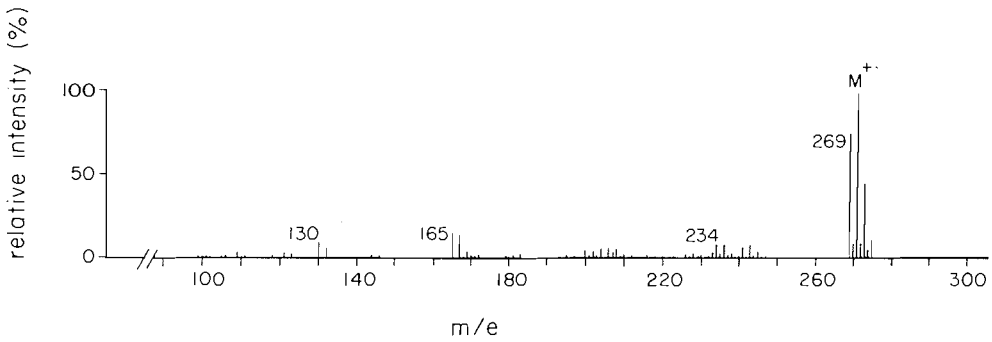

FIG. 6. Mass spectrum of 2-methyl-4,5,6,7-tetrachlorobenzoxazole (**2**) (reproduced from Choudhry et al. (22)).

Can. J. Chem. Downloaded from www.nrcresearchpress.com by 213.166.140.6 on 09/07/12
For personal use only.

[1] 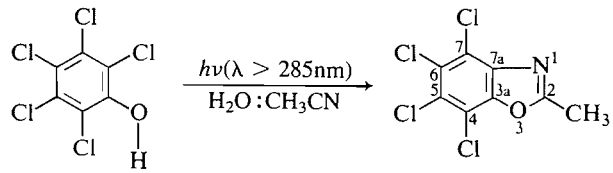

1 **2** ~1%

The comparison of UV spectrum of oxazole **2** with phenol **1** shows that the photoproduct **2** has acquired absorption maxima (λ_{max}) at 219, 253, 255.5, 261, 288.5, 295, and 298.5 nm, the values of molar extinction coefficients (ϵ_λ) being 24516, 9839, 9919, 8145, 2177, 1936, and 2258 l mol^{-1} cm^{-1}, respectively. The IR spectral data of **2** in KBr (see Fig. 2) provide the evidence for the possible presence of CH_3 (absorption at 2980 cm^{-1} (w)), aromatic C=C and C=N (1630 (m), 1590 (m) cm^{-1}), conjugated C—O (1310 (s), 1290 (m), 1210 (vs), 1034 (m), 1025 (m) cm^{-1}), and aromatic C—Cl (692 cm^{-1} (m)) groups in the product **2**. The symbols such as w, m, s, and vs shown in the parentheses indicate weak, medium, strong, and very strong intensity of the peaks, respectively.

The interpretations of ^{1}H- and ^{13}C-NMR spectra of tetrachlorobenzoxazole **2** are documented in Table 1. The presence of CH_3 group is also evident from the ^{1}H-NMR spectrum of the product **2** (see Fig. 3), which possesses a peak with δ = 2.17 ppm. In this proton NMR, the other peaks at 0.00, 1.53, 2.72, and 7.26 ppm are attributable to the protons of TMS (added to the sample solution as an internal standard), water, acetone, and chloroform, respectively; the latter three chemicals being present as impurities in $CDCl_3$ used as dissolving solvent (Table 1, Section I).

The normal proton decoupled ^{13}C-NMR spectrum of benzoxazole **2** (Fig. 4) displays, in addition to the resonance absorptions at 0.00 and 77.02 ppm due to the carbons of TMS and $CDCl_3$, respectively, eight carbon resonance absorptions arising from compound **2**. The interpretation of this spectrum, conducted with the aid of inductive effect theory and possible resonance structures of **2** (not shown herein), is included in Table 1 (Section II).

The proton decoupled DEPT sequence ^{13}C-NMR of **2**, which were recorded at 45°, 90°, and 135° pulse, are documented in Fig. 5. According to Doddrell and co-workers (29), the enhancement by polarization transfer in the case of methine (CH), methylene (CH_2), and methyl (CH_3) carbon will depend upon mathematical relations, viz. sin θ, sin 2θ, and sin θ + sin 3θ, respectively; whereby indicating that at $\theta = \pi/4$, methine, methylene, and methyl resonances should appear as positive (↑) signals. At $\theta = \pi/2$, only methine C resonance as positive signal should appear, and at $\theta = 3\pi/4$, methine and methyl C resonances should appear as positive signal, whereas methylene C resonance should appear as negative (↓) signal. Thus following these investigators (29), Fig. 5(*a*) records all protonated carbons, i.e., CH, CH_2 (if it is present), and CH_3 groups, while Fig. 5(*b*) provides only absorption due to CH group. Likewise, Fig. 5(*c*) is expected to display a negative absorption arising from the CH_2 carbon resonance (if it is present); whereas CH and CH_3 resonances have appeared as positive peaks. In conclusion, it is apparent from the DEPT sequence ^{13}C-NMR (Fig. 5) as well as from the Section III in Table 1, that only one sort of proton absorption is seen in Fig. 3, and that this absorption indicates the presence of methyl group in **2**.

Structural elucidation of the photoproduct $C_8H_3Cl_4NO$ (2)

Mass spectrum of the photoproduct **2** (Fig. 6) suggests that the molecular weight of this compound is 269 (calculated on the basis of fragments containing ^{35}Cl only), which is an odd number, thereby indicating that **2** contains an odd number of nitrogen atoms. Furthermore, in this MS, the ion clusters for the parent molecular ion ($M^{+\cdot}$) possess relative abundances characteristic of 4 Cl atoms (33). Thus a likely molecular formula for the compound **2** is $C_8H_3Cl_4NO$. Among several structures attributable to **2** of molecular formula $C_8H_3Cl_4NO$, the following ones are attractive to consider.

Structure **A**, namely hydroxytetrachlorophenylacetonitrile(s)

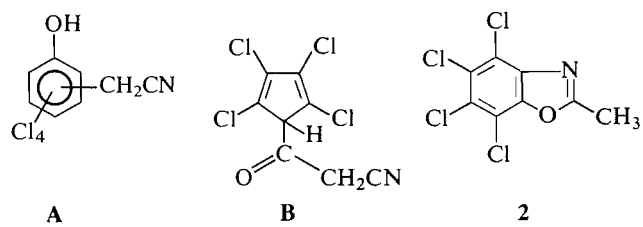

A **B** **2**

is (are) expected to be formed through the combination of the photolytically generated hydroxytetrachlorophenyl radicals from P_5CP (**1**) with $^{\cdot}CH_2$-CN species (which may have been generated via abstraction of H atoms from the cosolvent acetonitrile by intermediate free radical species). Structure **A** has been ruled out as described elsewhere (22). In addition this structure can also be rejected on the basis of its IR, ^{1}H-NMR, and ^{13}C-NMR spectral data (see Figs. 2–5 and Table 1) described above. In particular, DEPT sequence ^{13}C-NMR spectrum (Fig. 5) clearly provides evidence that CH_2 and CH units are absent.

TABLE 1. Proton and carbon-13 NMR spectral data of 2-methyl-4,5,6,7-tetrachlorobenzoxazole (**2**) in deuterated chloroform

I. 300 MHz ^{1}H-NMR spectral data[a]

Chemical shift, δ_H (ppm)	Protons
0.00	Protons of the CH_3 groups of tetramethylsilane (TMS) used as a reference compound
1.53	Protons of H_2O present as an impurity
2.17	Protons of the CH_3 groups of acetone present as an impurity
2.72	Protons of the CH_3 group of oxazole **2**
7.26	Proton of $CHCl_3$ present as an impurity in deuterated chloroform used as a solvent

II. 75 MHz ^{13}C-NMR spectral data[b]

Chemical shift, δ_C (ppm)	Carbon-13 atoms
0.00	Carbons of TMS used as a reference compound
14.59	Carbon of the methyl group of oxazole **2**
77.02	Carbon of the solvent $CDCl_3$
114.93	7-C of oxazole **2**
122.61	4-C of oxazole **2**
128.92	5-C of oxazole **2**
129.12	6-C of oxazole **2**
139.03	7a-C of oxazole **2**
146.67	3a-C of oxazole **2**
166.44	2-C of oxazole **2**

III. DEPT sequence 75 MHz ^{13}C-NMR spectral data[c]

Figure No. (type of carbons observed)	Chemical shift, δ_C (ppm)	Remarks
5a (All protonated carbons)	0.0	Signal from the protonated C of the TMS
	14.6	Signal from the protonated C of oxazole **2**
	77.4	Signal from the protonated C of the chloroform (an impurity in $CDCl_3$) (see below also)
5b (CH units only)	77.4	Signal from the CH unit of the chloroform present as an impurity in $CDCl_3$
5c (CH, CH_3 and CH_2 units)	0.0	The absence of a negative peak expected to originate from the CH_2 group indicates that the peak centered at 14.6 ppm δ_C is due to the protonated C of the methyl group of the oxazole **2** (compare these data with those of Figs. 5*a* and 5*b*)
	14.6	
	77.4	

[a]Spectrum is plotted in Fig. 3.
[b]Spectrum is mentioned in Fig. 4.
[c]Spectra are shown in Fig. 5.

Similarly, structure **B** (cyanomethyl 2,3,4,5-tetrachloro-2,4-cyclopentadien-1-yl ketone) for **2**, a product anticipated to be yielded through the pathways shown in reaction [2], can be ruled out due to the following reasons: (*a*) IR spectrum (Fig. 2) does not show any evidence for the presence of a carbonyl group, (*b*) ^{1}H-NMR spectrum (Fig. 3) displays only one type of protons, (*c*) DEPT sequence ^{13}C-NMR spectrum (Fig. 5) provides evidence for the absence of methine and methylene carbon atoms, and (*d*) MS does not show the expected losses of $^{\bullet}CH_2$—CN and O=Ċ—CH_2CN species from $M^{+\bullet}$. The rejection of the structure (**B**) evidently reflects that the ring contraction process,

$$\mathbf{4} \not\longrightarrow \mathbf{C}$$

does not occur in the present circumstances. However, it should be mentioned that previously Lemaire and his associates (16, 34, 35) during their photochemical investigations on 2-chlorophenol (in anionic form) have invoked the concept of 1,2-ketocarbene **4** (non-chlorinated) and its contraction to a five member ring, i.e. ketene (C) (non-chlorinated).

Can. J. Chem. Downloaded from www.nrcresearchpress.com by 213.166.140.6 on 09/07/12
For personal use only.

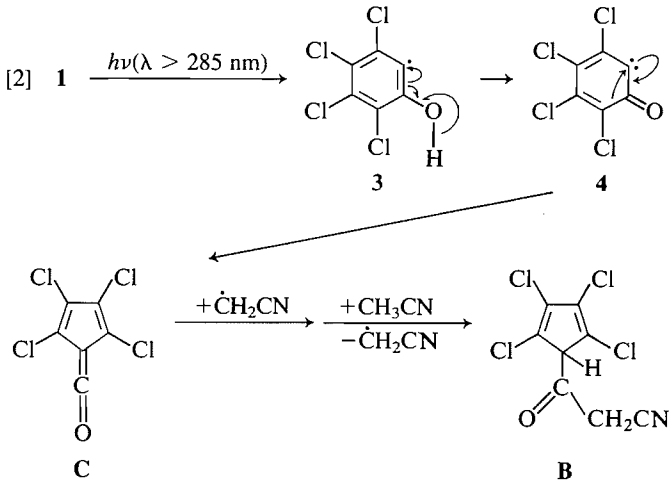

After discarding structures **A** and **B**, the most appropriate and logical structure, which can be assigned to the product $C_8H_3Cl_4NO$ is 2-methyl-4,5,6,7-tetrachlorobenzoxazole (**2**). As discussed above, the supporting facts from the spectral analysis are following: (*a*) IR spectrum (Fig. 2) shows absorption due to aromatic C—O, C=C, and C=N groups, (*b*) ^{1}H-NMR spectrum (Fig. 3) indicates resonance from only one type of proton CH_3 group, (*c*) Normal ^{13}C-NMR spectrum (Fig. 4) displays resonances from one aliphatic carbon and seven aromatic carbons, (*d*) DEPT pulse ^{13}C-NMR spectrum (Fig. 5) yields conclusive evidence for the presence of methyl carbon and the absence of methylene and methine carbons, and (*e*) MS (Fig. 6) reveals fragmentation pattern (discussed below) favoring structure **2**.

Mechanism for the photogeneration of 2-methyl-4,5,6,7-tetrachlorobenzoxazole (2)

The photoformation of 2-methyl-4,5,6,7-tetrachlorobenzoxazole (**2**) from pentachlorophenol (**1**) in water–acetonitrile (2:3 v/v) solution wavelength ~ 300 nm can be explained by the proposed Scheme 1. Accordingly, absorption of UV light by molecules of **1** would result in the production of 2-hydroxy-3,4,5,6-tetrachlorophenyl radicals (**3**) through the homolytic cleavage of the C—Cl bond at position 2 of compound **1** (step *i*), which subsequently would lose H atoms to yield 3,4,5,6-tetrachlorocyclohexa-3,5-diene-1,2-ketocarbene (**4**) (step *ii*). Another mechanism for the formation of carbenes **4** is discussed below (see reaction [6]). Nucleophilic attack of the cosolvent acetonitrile at position 1 of carbenes **4** accompanied by ring closure would then take place (step *iii*), thereby producing benzoxazole **2**. In addition, ketocarbenes **4** could yield the 1,3-dipolar species **4***a*, which could react with CH_3CN to give rise to oxazole **2** (step *iv*).

Evidence for the production of the intermediate 2-hydroxyphenyl radical **3** is provided by the appearance of the photoproduct 2,3,4,5-tetrachlorophenol (2,3,4,5-T_4CP) which is formed as the result of the abstraction of H atoms from the cosolvent and from other hydrogen donors by species **3** (22). Likewise, the intermediate involvement of the radical species **3** in the production of chlorinated 1,2-ketocarbenes **4** is supported by the fact that in H_2O–CH_3CN (2:3 v/v) the photolysis of 2,3,4,5-T_4CP did not yield product of the type **2**, i.e. $C_8H_4Cl_3NO$, while the other two tetrachlorophenols provided such products (22). It is noteworthy that the former CAP also did not yield 3,4,5-T_3CP anticipated to be formed through the photohomolysis of the C—Cl bond at position 2 and the subsequent abstraction of H atoms from the hydrogen donors (22). However, 1,2,4,5- and 1,3,4,5-T_4CP produced trichlorophenols via such photoprocesses, thereby revealing that 2-hydroxypolychlorophenyl radicals are key intermediates for the generation of 1,2-ketocarbenes and eventually of the benzoxazole type products. It should be mentioned that 1,3-dipolar cycloaddition of intermediate **4** and **4***a* species generated photochemically and thermally from 3,4,5,6-tetrachlorobenzene-2-diazo-1-oxide (**D**) (reaction [3]) to several nitriles

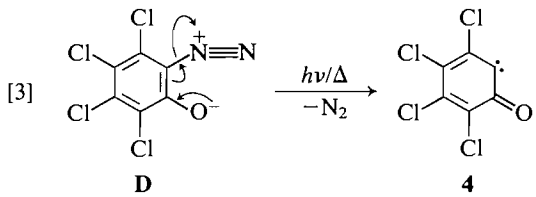

such as acetonitrile, benzonitrile, etc. is a well known phenomenon (28). When the photoreaction of **D** was carried out in CH_3CN, oxazole **2** was produced (28); these investigators analyzed **2** with the support of elemental analysis, melting point determination, and IR spectroscopy.

Moreover, Husigen and co-workers (28) reported that 2-methoxy-3,4,5,6-tetrachlorophenol is formed, when chemical D is subjected to photolysis in CH_3OH; the final product being the consequence of the nucleophilic attack of the solvent on the intermediates **4** (see reaction [3]). Thus in our present studies 3,4,5,6-tetrachlorocatechol is expected to be yielded via the chemical reactions of intermediate species **4** and **4***a* with water. However, as reported earlier (22), among the photoproducts of **1** in H_2O–CH_3CN (2:3 v/v), tetrachlorocatechol as well as lower chlorinated catechols were not observed. The reason for the failure to detect such catechol(s) on GC–MS may be that these compounds face deep secondary photodegradation on the benzene nucleus (e.g. ref. 20). In the case of the pyrolytic reactions of the sodium salt of *o*-halogenophenoxides at 260°C leading to the generation of substituted dibenzo-*p*-dioxins, trapping of the intermediary substituted 1,2-ketocarbenes using sodium salts of phenol and benzene thioalcohol as well as benzamide is well known (see pp. 78–80 of ref. 3).

Furthermore, the likelihood that the molecules of **1** in the photoexcited state are converted into radical pairs, i.e. [(**3**) Ċl], which may be responsible for the formation of the ultimate photoproducts, is not ruled out. Such radical pairs may be generated within the solvent cage. Those which escape the solvent cage would yield reductively dechlorinated phenol as the primary product; whereas in the case of those pairs staying within the cage, conversion of radicals **3** into 1,2-ketocarbenes **4** would occur (see step *ii* in Scheme 1), the loss of H atoms from **3** being facilitated by the chlorine radicals present in the cage.

It is interesting to mention that in the past several authors have reported nucleophilic photosubstitution reactions of unsubstituted (36–39) and substituted (40–47) aromatic hydrocarbons in aqueous and non-aqueous organic solvents at $\lambda < 266$ nm. For example, Lemmetyinen *et al.* (40) and Liu and Weiss (41) have demonstrated the intermediate involvement of radical cations (formed from the starting aromatic hydrocarbons) in the photohydrolysis and photocyanation of 4-chloro- and 4-fluoroanisole and 2-fluoroanisole, respectively. Likewise, Previtali and Ebbesen (42) observed the photo-ionization of chlorobenzene in polar solvents leading to the intermediate formation

Can. J. Chem. Downloaded from www.nrcresearchpress.com by 213.166.140.6 on 09/07/12
For personal use only.

TABLE 2. Interpretation of mass spectrum of 2-methyl-4,5,6,7-tetrachlorobenzoxazole (**2**) shown in Fig. 6

Peak No.	*m/e* value[a]	Molecular formula	Proposed structures[b]	Sources of the fragments
a	269	$C_8H_3Cl_4NO$	**5**, **6**, **7**, **8**, **15**, **16**, **18**, **19**, **27**, **28**, **29**	$M \rightarrow M^{\cdot +} + e$
b	241	$C_7H_3Cl_4N$	**10**	a-28 (a-CO)
c	234	$C_8H_3Cl_3NO$	**14**, **25**, **26**	a-35 (a-Cl)
d	228	C_6Cl_4O	**17**, **23**, **24**	a-41 (a-CH_3CN)
e	226	C_6Cl_4N	**30**, **31**, **32**	a-43 (a-CH_3CO)
f	206	$C_7H_3Cl_3N$	**11**, **13**	a-63 (a-COCl); b-35 (b-Cl); c-28 (c-CO)
g	200	C_5Cl_4	**9**	a-69 (a-CO, CH_3CN); b-41 (b-CH_3CN)
h	165	C_5Cl_3	**12**, **21**	a-104 (a-C_3H_3ClNO); f-41 (f-CH_3CN)
i	130	C_5Cl_2	**22**	h-35 (h-Cl)

[a]Calculations based upon fragments containing ^{35}Cl only.
[b]For structures, see Scheme 2.

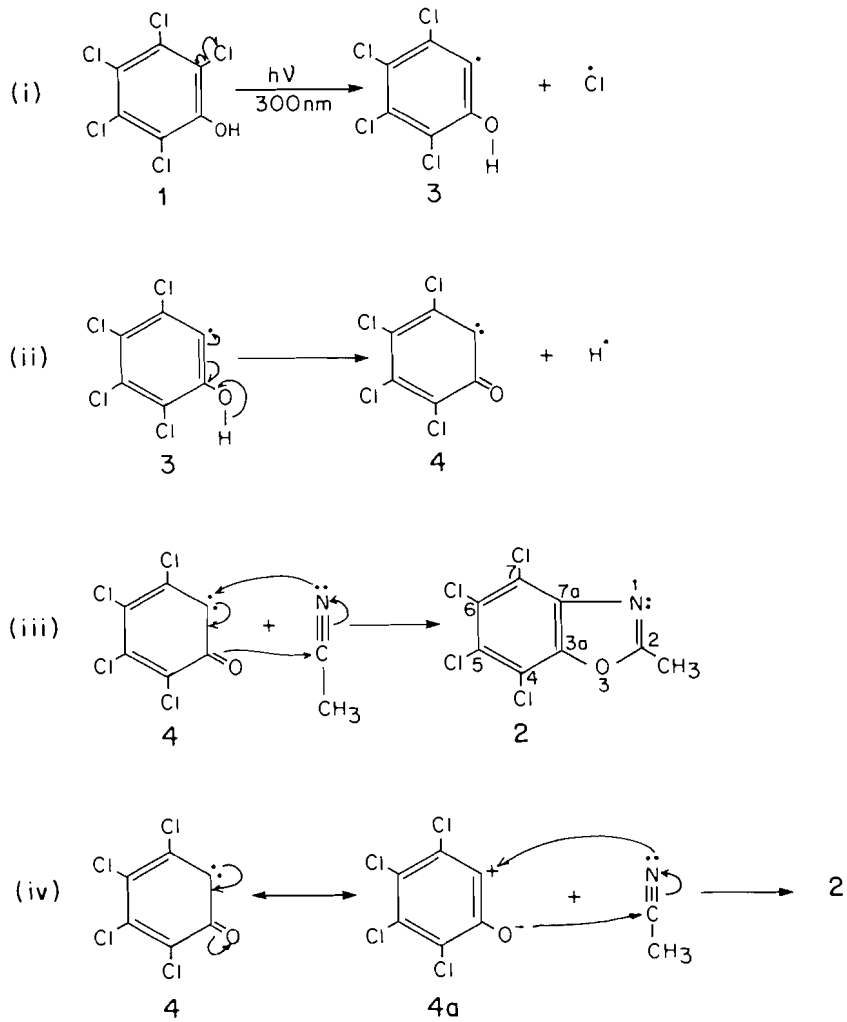

SCHEME 1

Can. J. Chem. Downloaded from www.nrcresearchpress.com by 213.166.140.6 on 09/07/12
For personal use only.

Can. J. Chem. Downloaded from www.nrcresearchpress.com by 213.166.140.6 on 09/07/12
For personal use only.

of radical cations during laser flash photolysis studies. Furthermore, Bunce and co-workers (36) have recently reported the mechanism of the photohydroxynitration of biphenyl by nitrate ions involving radical cation species. Thus, in the present studies, one may consider to invoke the intermediate involvement of tetrachloro radical cations, e.g., species **E** which might have undergone the nucleophilic attack of acetonitrile to yield the tetrachlorobenzoxazole **2** via the intermediates **F**, **G**, and **H** (see reaction [4]). However, this pathway for the photo-

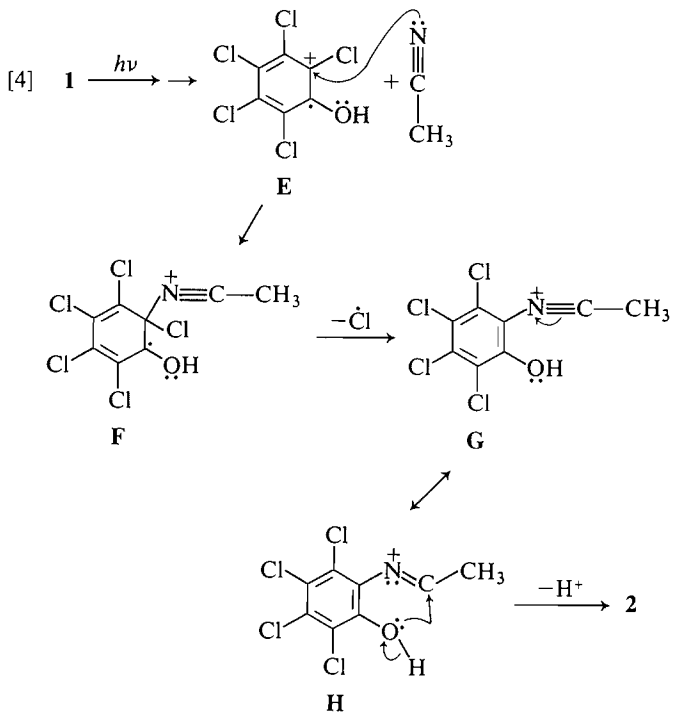

generation of the oxazole **2** can be discarded due to the facts that the intermediate cation species **H** did not produce other photoproducts such as phenols **I** and **J** and **K** expected to be formed through the loss of H^+ ions from **H** and nucleophilic attack of water on **H**, respectively (reaction [5]).

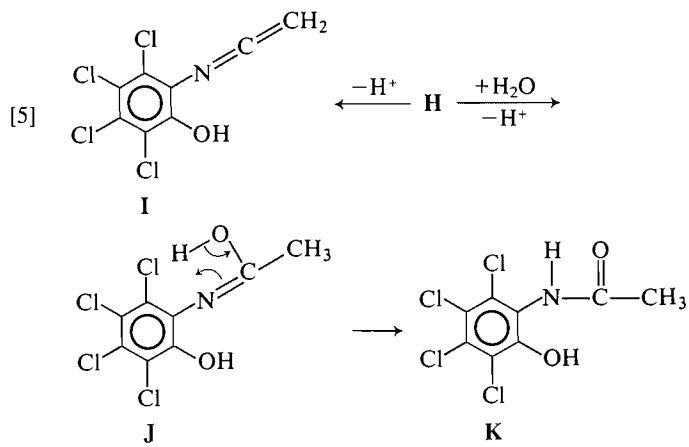

Previously, Siegman and Houser (43) explained the photoproduction of 1,4-dimethoxybenzene from 4-chloroanisole in methanol by invoking the concept of the formation of radical anions from the substrate and radical cations from the solvents molecules as intermediates. Following these authors' (43) concept, an alternative plausible mechanism involving intermediary anion species, viz. **L** could be considered for the

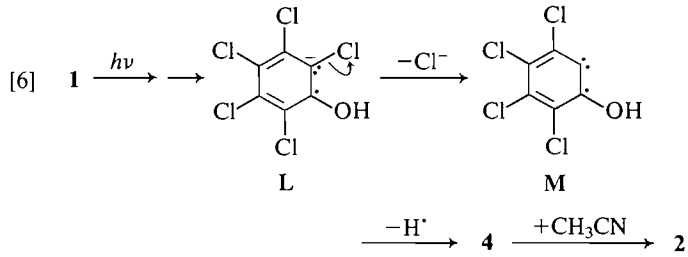

photogeneration of the oxazole **2** from phenol **1** (reaction [6]). In reaction [6], the anions **L** may lose Cl^- ions to give species **M** which subsequently yield 1,2-ketocarbene **4** via the loss of H atoms and eventually producing **2**. Species **M** may also abstract H atoms from the solvent system to yield 2,3,4,5-tetrachlorophenol. Contrary to reaction [4], the anticipated reaction [6] would proceed via the ejection of Cl substituent prior to the introduction of the acetonitrile molecule (see discussion described above). We do not have any apparent argument to reject the mechanism shown in reaction [6].

Mechanistic interpretation of the MS of the benzoxazole 2

Table 2 records the *m/e* values of the fragments seen in the MS of the benzoxazole **2** along with their corresponding molecular formulae and sources. The mechanism given in Scheme 2 is proposed to explain the fragmentation pattern for the oxazole **2** upon electron impact. Loss of an electron from **1** would result in formation of carbonium radical ions **5** and **27**. Carbonium species **5** would lead to the oxonium radical ions **6**, which subsequently would undergo simultaneous ring contraction and expansion of the benzene and oxazole nuclei of **6**, respectively; whereby oxonium radical ions **7** would be produced. Alternatively, species **6** could be generated via the ejection of an electron from the non-bonding lone pair of electrons on the oxygen atom of **2** and the conversion of the resulting radical ions into **6** (not shown in Scheme 2). The oxonium radical ions **7** would then undergo scission of the appropriate C—C, C—O, C—N, and C—Cl bonds as well as 1,2-shift of chlorine substituents on the cation species leading to the generation of positively charged species **8**–**22** with the losses of molecular acetonitrile and radicals, viz. $^{\bullet}Cl$, Cl—$\dot{C}$=O, and $\ddot{C}$=O. In addition, positively charged species **23** and **24** together with **25** and **26** are yielded from carbonium radicals **5** through the respective loss of CH_3CN and chlorine radicals. Similarly, azonium radical species **29** are produced from carbonium radicals **27** via the intermediate species **28**; which then lose acetyl radicals to give rise to the formation of azonium carbenes **30**. Species **30** can be transformed into cations **31** and **32**. The processes depicted in Scheme 2 are supported by the fragmentation pattern in the mass spectrum of product **2**, although in this spectrum some fragments are of rather low relative intensity (Fig. 6).

Miscellaneous

Choudhry and Hutzinger (24) have also reported the photogeneration of compounds with empirical formulae $C_8H_5Cl_2NO$ and $C_8H_4Cl_3NO$ (two isomers of each) in the case of the UV irradiation of 1,2,3,4-tetrachlorobenzene and pentachlorobenzene in water–acetonitrile mixtures, respectively. Likewise, compounds $C_8H_5Cl_2NO$ (three isomers) and C_8H_6ClNO were also seen in the acetone-sensitized photolysis of 1,2,3,4-tetrachlorobenzene in aqueous acetonitrile; whereas, such photoreaction of 1,2,3,5-tetrachlorobenzene provided one isomer of $C_8H_5Cl_2NO$ (24). It can be speculated with the support of discussions given above that all these products are 2-methyl-

Can. J. Chem. Downloaded from www.nrcresearchpress.com by 213.166.140.6 on 09/07/12
For personal use only.

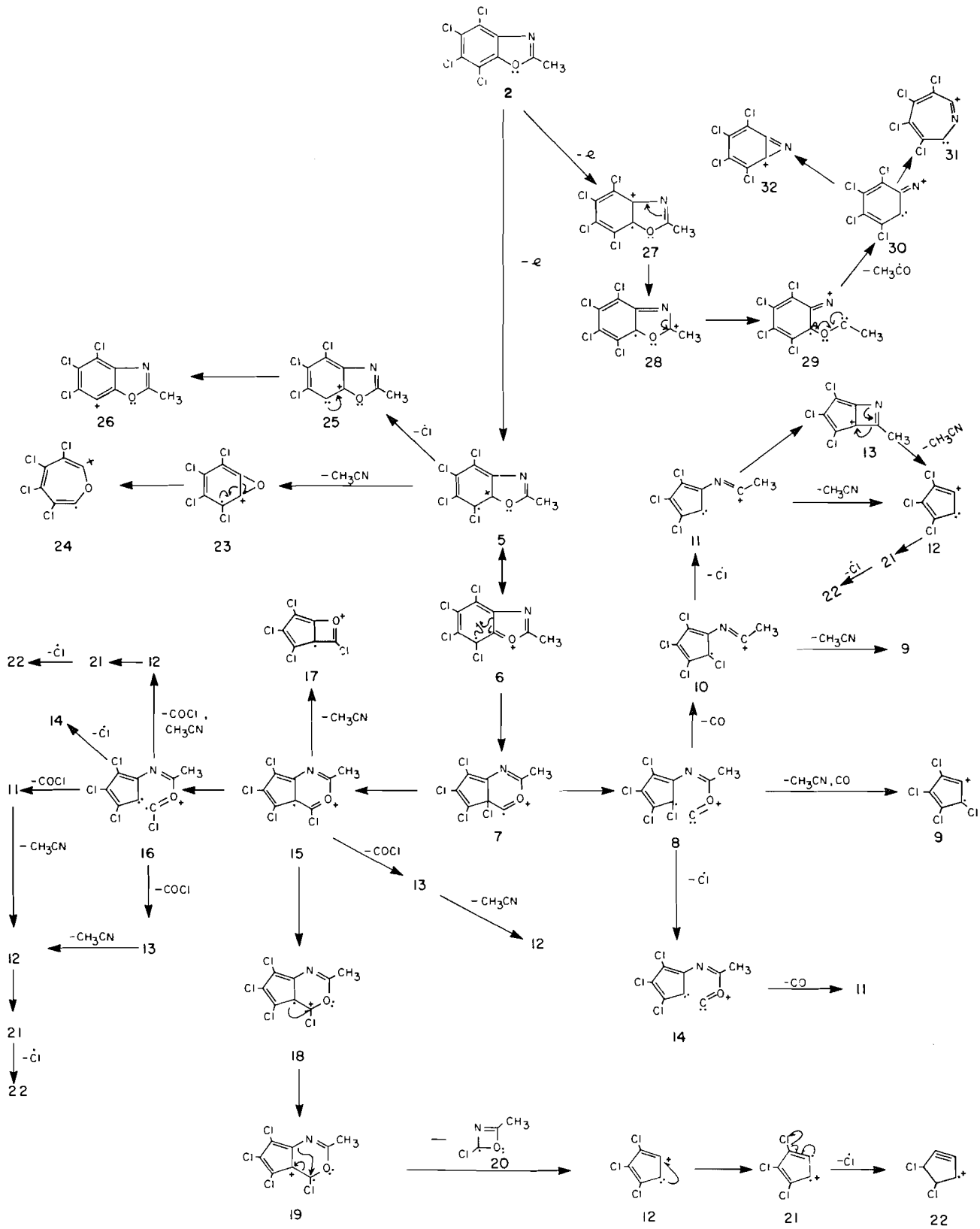

SCHEME 2

benzoxazoles having various numbers of chlorine substituents at the benzene nucleus presumably yielded via the secondary photoreactions of the appropriate polychlorophenols, which may be the photoproducts of the polychlorobenzenes.

The synthetic yield of photoproduct benzoxazole **2** from pentachlorophenol (**1**) was ca. 1% (see reaction [1]), thereby indicating that this photochemical process is undoubtedly of little synthetic applicability. However, it is notable that the analytical yield of oxazole **2**, calculated from the amount of photoconverted starting material **1**, was 11%, when 4.11 m*M*

solution of **1** in CH_3CN–H_2O (2:3 v/v) was exposed to UV light of $\lambda \geq 290$ nm for 6 h (22). Although natural water bodies contaminated with phenol **1** are not expected to contain acetonitrile which could result in the sunlight photolytic generation of oxazole **2**, the results of present and previous (22) investigations clearly reflect that other natural organics of similar or greater nucleophilicity to that of CH_3CN are likely to react with the intermediate species **4** and **4***a* produced from the sunlight photolysis of **1** in natural aquatic systems.

Finally, acetonitrile is strongly recommended and is therefore frequently utilized as cosolvent for investigations aiming for the determination of aquatic (photo)chemical fate of pesticides and other pollutants. Our results presenting the photoincorporation of cosolvent acetonitrile into pentachlorophenol (**1**) are of significant importance, which are anticipated to assist the investigators to interpret their experimental photolytic data in the context of photoproducts identifications.

Conclusions

Spectral data, especially NMR and MS, lead us to conclude that the compound $C_8H_3Cl_4NO$ (**2**) synthesized through the photolysis of pentachlorophenol (**1**) in H_2O–CH_3CN (2:3 v/v) at $\lambda \geq 290$ nm is 2-methyl-4,5,6,7-tetrachlorobenzoxazole. This photoproduct can only be yielded *if* the homolysis of the C—Cl bond at the *ortho* position with respect to hydroxy group on **1** has occurred; the resulting *o*-hydroxytetrachlorophenyl radicals play a key role of utmost importance for the reaction leading to the eventual generation of benzoxazole **2**. In the environment, natural water bodies may contain several other nucleophiles which may react with the sunlight photolytically generated intermediate 1,2-ketocarbens (cf. structure **4**) and 1,3-dipolar species (cf. structure **4***a*) from CAPs, viz. polychlorophenols.

Acknowledgements

We are grateful to Mr. R. K. Marat, Department of Chemistry, University of Manitoba, Winnipeg, for running the NMR spectra and for his expert scientific advice. Also we thank Professor K. J. Friesen, Department of Chemistry, University of Winnipeg, for generating the IR spectral data.

1. G. G. Choudhry, J. A. Van Den Broecke, G. R. B. Webster, and O. Hutzinger. Environ. Toxicol. Chem. **5**, 625 (1986).
2. G. G. Choudhry, K. Olie, and O. Hutzinger. Pergamon Ser. Environ. Sci. **5**, 275 (1982).
3. G. G. Choudhry and O. Hutzinger. Mechanistic aspects of the thermal formation of halogenated organic compounds including polychlorinated dibenzo-*p*-dioxins. Gordon and Breach Science Publishers, New York. 1983. pp. 1–194.
4. G. A. Eiceman, R. E. Clement, and F. W. Karasek. Anal. Chem. **51**, 2343 (1979).
5. R. C. C. Wegmann and A. W. M. Hofstee. Water Res. **13**, 651 (1979).
6. C. Leuenberger, R. Coney, J. W. Graydon, E. Molnar-Kubica, and W. Giger. Chimia **37**, 345 (1983).
7. W. Giger and C. Schaffner. *In* Advances in the identification and analysis of organic pollutants in water. Vol. 1. *Edited by* L. H. Keith. Ann Arbor, MI. 1981. p. 41.
8. M. T. Virtanen and M.-L. Hattula. Chemosphere, **11**, 641 (1982).
9. U. M. Weiss, P. Mosa, I. Scheunert, A.-Ul Haque, and F. Korte. J. Agric. Food Chem. **30**, 1186 (1982).
10. U. M. Weiss, I. Scheunert, W. Klein, and F. Korte. J. Agric. Food Chem. **30**, 1191 (1982).
11. G. G. Choudhry and G. R. B. Webster. Residue Rev. **96**, 79 (1985).
12. R. H. Stehl, R. R. Papenfuss, R. A. Bredeweg, and R. W. Roberts. Adv. Chem. Ser. **120**, 119 (1973).
13. M. Kuwahara, N. Kato, and K. Munakata. Agric. Biol. Chem. **30**, 239 (1966).
14. M. Kuwahara, N. Shindo, N. Kato, and K. Munakata. Agric. Biol. Chem. **33**, 892 (1969).
15. M. Kuwahara, N. Kato, and K. Munakata. Agric. Biol. Chem. **30**, 232 (1966).
16. J. Lemaire, J. A. Guth, O. Klais, J. Leahey, W. Merz, J. Philp, R. Wilmas, and C. J. M. Wolf. Chemosphere, **14**, 53 (1985).
17. C. W. Hiatt, W. T. Hoskins, and L. Olivier. Am. J. Trop. Med. Hygiene, **9**, 527 (1960).
18. A. S. Wong and D. G. Crosby. J. Agric. Food Chem. **29**, 125 (1981).
19. L. L. Lamparski, R. H. Stehl, and R. L. Johnson. Environ. Sci. Technol. **14**, 196 (1980).
20. M. J. Miile and D. G. Crosby. Mar. Chem. **14**, 111 (1983).
21. M. Barbeni, E. Pramuaura, and E. Pelizzetti. Chemosphere, **14**, 195 (1985).
22. G. G. Choudhry, F. W. M. Van Der Wielen, G. R. B. Webster, and O. Hutzinger. Can. J. Chem. **63**, 469 (1985).
23. G. G. Choudhry and G. R. B. Webster. Chemosphere, **14**, 9 (1985).
24. G. G. Choudhry and O. Hutzinger. Environ. Sci. Technol. **18**, 235 (1984).
25. G. G. Choudhry, A. A. M. Roof, and O. Hutzinger. J. Chem. Soc. Perkin Trans. I, 2957 (1982).
26. M. Martin-Smith. Laboratory Practice **7**, 572 (1958).
27. Aldrich-Chimie S.A./N.V., Catalogue, B-1030 Brussels, Belgium, p. 851 (1985/86).
28. R. Huisgen, G. Binsch, and H. Konig. Chem. Ber. **97**, 2868 (1964).
29. D. M. Doddrell, D. T. Pegg, and M. R. Bendall. J. Magn. Reson. **48**, 323 (1982).
30. G. A. Morris and R. Freeman. J. Am. Chem. Soc. **101**, 760 (1979).
31. D. P. Burum and R. R. Ernst. J. Magn. Res. **39**, 163 (1980).
32. D. M. Doddrell and D. T. Pegg. J. Am. Chem. Soc. **102**, 6388 (1980).
33. O. Hutzinger, S. Safe and V. Zitko. The chemistry of PCB's. CRR Press, Cleveland, OH, U.S.A. 1974. pp. 151–170.
34. P. Boule, C. Guyon, and J. Lemaire. Chemosphere, **11**, 1179 (1982).
35. C. Guyon, P. Boule, and J. Lemaire. Tetrahedron Lett. **23**, 1581 (1982).
36. N. J. Bunce, S. R. Cater, and J. M. Willson. J. Chem. Soc. Perkin Trans. II, 2013 (1985).
37. N. J. Bunce, J. Bergsma, and J. Schmidt. J. Chem. Soc. Perkin Trans. II, 713 (1981).
38. H. Lemmetyinen. J. Chem. Soc. Perkin Trans. II, 1269 (1983).
39. H. Lemmetyinen, J. Koskikallio, J. Niiranen, and J. Lilie. Acta Chem. Scand. Ser. A, **38**, 765 (1984).
40. H. Lemmetyinen, J. Konijnenberg, J. Cornelisse, and C. A. G. O. Varma. J. Photochem. **30**, 315 (1985).
41. J. H. Liu and R. G. Weiss. J. Photochem. **30**, 303 (1985).
42. C. M. Previtali and T. W. Ebbesen. J. Photochem. **30**, 259 (1985).
43. Y. Y. Kulis, I. Y. Poltaeva, and M. G. Kuzmin. Zh. Org. Khim. **6**, 1214 (1973).
44. J. R. Siegman and J. J. Houser. J. Org. Chem. **47**, 2773 (1982).
45. J. T. Pinhey and R. D. G. Rigby. Tetrahedron Lett. 1271 (1969).
46. E. Havinga and J. Cornelisse. Pure Appl. Chem. **47**, 1 (1976).
47. J. den Heijer, O. Shadid, J. Cornelisse, and E. Havinga. Tetrahedron, **33**, 779 (1977).

Can. J. Chem. Downloaded from www.nrcresearchpress.com by 213.166.140.6 on 09/07/12
For personal use only.

Determination of the intercarbonyl dihedral angle of 1,2-diketones by ^{17}O nmr

HANS CERFONTAIN,[1] COR KRUK, ROEL REXWINKEL, AND FRANK STUNNENBERG
Laboratory for Organic Chemistry, The University of Amsterdam, Nieuwe Achtergracht 129, 1018 WS Amsterdam, The Netherlands

Received March 5, 1987

HANS CERFONTAIN, COR KRUK, ROEL REXWINKEL, and FRANK STUNNENBERG. Can. J. Chem. **65**, 2234 (1987).

This study describes a method using ^{17}O nmr to determine the intercarbonyl dihedral angle in a homologous series of seven 1,2-diketones. It is shown that the ^{17}O nmr shifts of the 1,2-diketones are linearly dependent on both the electron density at the oxygen atoms and the $n \rightarrow \pi^*$ excitation energy of the 1,2-diketo chromophore. Reduction of the overlap in the π system of the 1,2-diketo moiety leads to a gradual upfield shift of the ^{17}O nmr signal, due to the increase in both the π-electron density at the oxygen atoms q_O^π and the mean transition energy ΔE.

HANS CERFONTAIN, COR KRUK, ROEL REXWINKEL et FRANK STUNNENBERG. Can. J. Chem. **65**, 2234 (1987).

Cette étude décrit une méthode qui fait appel à la rmn du ^{17}O pour déterminer l'angle dièdre intercarbonyles dans un série homologue de sept dicétones-1,2. On démontre que les déplacements des dicétones-1,2 en rmn du ^{17}O dépendent d'une façon linéaire à la fois sur la densité électronique des atomes d'oxygène que sur l'énergie d'excitation $n \rightarrow \pi^*$ du chromophore dicéto-1,2. La réduction dans le recouvrement du système-π de la portion dicéto-1,2 conduit à un déplacement graduel vers les hauts champs du spectre rmn du ^{17}O; ce résultat provient d'une augmentation tant de la densité des électrons-π au niveau des atomes d'oxygène (q_O^π) que de l'énergie de transition moyenne (ΔE).

[Traduit par la revue]

Introduction

Since the first detection of the ^{17}O isotope in 1951 (1), there has not been much research towards direct application of ^{17}O in chemistry, compared to other nuclei like ^1H, ^{13}C, ^{31}P, and ^{19}F. This is partly caused by the very much lower natural abundance of the ^{17}O nucleus (0.037%) (2) but also by the more limited importance of ^{17}O in elucidation of chemical structures as compared with ^1H and ^{13}C. In the 35 years following its first nmr detection the techniques of measuring ^{17}O have improved enormously. Nowadays ^{17}O spectra are easily obtained, even of natural, i.e. ^{17}O non-enriched, compounds and the very large ^{17}O chemical shift range (800 ppm) compensates sufficiently for the inevitable line-broadening.

In this study we have used ^{17}O nmr measurements as a method for the conformational analysis of the 1,2-dicarbonyl chromophore in 1,2-diketones, with special reference to the intercarbonyl dihedral angle θ, i.e. the angle of twist around the C—C bond between the two carbonyl groups, defined in the Newman Projection of Fig. 1. So far the dihedral angles of 1,2-diketones were determined by time-consuming dipole-moment measurements (3) and very occasionally by crystallographic X-ray determination (4).

The origin of our interest in the 1,2-diketo chromophore stems from our photochemical studies of 1,2-diketones (5, 6), in particular by the observation that the photochemical behaviour of (cyclic) 1,2-diketones depends on the size of the dihedral angle of the 1,2-diketo chromophore.

^{17}O nmr chemical shifts

The local magnetic field B at a nucleus N is not the same as the applied magnetic field. As a result of electronic movements the nucleus is shielded and senses a magnetic field B, which differs from the applied field B^0 according to eq. [1] in which

$$[1] \quad B = B^0(1 - \sigma_N)$$

σ_N is the shielding constant for nucleus N. According to Pople (7) σ_N is the sum of three intramolecular contributions, viz. the local diamagnetic electron ring current term (σ_N^d), the term due to the paramagnetic anisotropic local electron effects (σ_N^p),

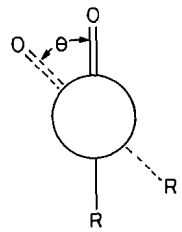

FIG. 1. Newman projection of the 1,2-diketo chromophore along the central C—C bond.

and the term accounting for the shielding effects caused by the neighbouring groups ($\Sigma\sigma_{NB}$):[2]

$$[2] \quad \sigma_N = \sigma_N^d + \sigma_N^p + \Sigma\sigma_{NB}$$

σ_N^d is always positive and works against the applied field, σ_N^p is negative and contributes to the applied field, while the other term can be positive or negative in sign. It has been established that the main term of σ_N for ^{17}O nmr is σ_N^p (8, 9). In the present series of symmetric 1,2-diketones θ covers the full range from 0 to 180°. Given the similarity of the environment of the 1,2-diketo moiety in the 1,2-diketones of the present study, the shielding effect $\Sigma\sigma_{NB}$ will be constant.[3] Accordingly, the first and third contribution to σ_N (cf. eq. [2]) will, in first approximation, be constant and the changes in the ^{17}O chemical shift will depend only on changes in the paramagnetic contribution σ_N^p as a result of variations in the dihedral angle θ. According to Karplus and Pople σ_N^p is determined by eq. [3]

$$[3] \quad \sigma_N^p = k(\Delta E^{-1})\langle r^{-3}\rangle_{2p_N}\{Q_{NN} + \Sigma Q_{NB}\}$$

(10, 11) in which k is a constant and $\langle r^{-3}\rangle_{2p_N}$ stands for the observable of the reciprocal cube of the mean radius of the $2p$ orbital on atom N which depends upon the actual charge on that

[1]Author to whom correspondence may be addressed.

[2]For the sake of simplicity the external contributions from solvents and other intermolecular interactions are neglected. The dependence of the ^{17}O chemical shift on the solvent was obviated by performing all the nmr experiments in the same solvent and at the same temperature.

[3]Camphorquinone (**8**) does not fit in this series. The asymmetrical methyl substituent in this molecule renders the two oxygens non-equivalent, as illustrated by two ^{17}O nmr signals.

Printed in Canada / Imprimé au Canada

Can. J. Chem. Downloaded from www.nrcresearchpress.com by 213.166.140.6 on 09/07/12
For personal use only.

TABLE 1. ^{17}O chemical shifts ($\delta\ ^{17}O$) in dry acetonitrile at 70°C, line width (time averaged), intercarbonyl dihedral angle ($\bar{\theta}$), and $\Delta E(n\rightarrow\pi^*)$ data calculated from the λ_{max} (cyclohexane) data of the 1,2-diketones **1–8**

1,2-Diketone		$\delta\ ^{17}O$ (ppm, ±1.0)	$w_{1/2}$ (Hz)	$\bar{\theta}$ (°)[a]	n→π* excitation[b] λ_{max} (nm)	n→π* excitation[b] ΔE (eV)
3,3,5,5-Tetramethylcyclopentane-1,2-dione	**1**	572.9	140	0	510	2.43
3,3,6,6-Tetramethylcyclohexane-1,2-dione	**2**	563.9	83	42	371	3.34
3,3,7,7-Tetramethylcycloheptane-1,2-dione	**3**	556.9	130	82	337	3.67
2,2,5,5-Tetramethylhexane-3,4-dione	**4**	557.7	83	122	376	3.29
Butane-2,3-dione	**5**	568.9	100	158	422	2.93
Cyclododecane-1,2-dione	**6**	576.1	120	180	435	2.84
Homoadamantane-4,5-dione	**7**	571.6	70	12	424	2.92
Camphorquinone	**8**	538.2	160	14		
		546.5	160			

[a]Data estimated by Verheijdt *et al.* (3) from dipole moment measurements.
[b]Data taken from ref. 3.

atom. The terms Q_{NN} and ΣQ_{NB} contain the bond orders of the *p* orbitals at atom N and the bond orders between the *p* orbitals of the atom in question and its neighbours B, respectively. For the homologous series of the present structurally related 1,2-diketones the term in parentheses is taken to be constant.[4] The most problematic factor in eq. [3] is the mean excitation energy ΔE. This arbitrary term is generally replaced by an average excitation energy and is in first approximation equal to the lowest excitation energy (12). For 1,2-diketones that transition is of $n\rightarrow\pi^*$ character and its energy varies strongly with variations in θ (3); the factor ΔE^{-1} can therefore not be taken to be constant (see also Discussion).

Results and discussion

The ^{17}O chemical shift data of the 1,2-diketones **1–7** have

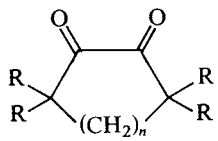

1 *n* = 1, R = Me
2 *n* = 2, R = Me
3 *n* = 3, R = Me
6 *n* = 8, R = H

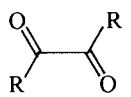

4 R = *t*-Bu
5 R = Me
9 R = H

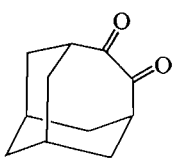

7

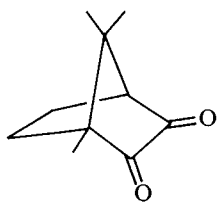

8

been determined in dry acetonitrile as solvent at 70°C at natural abundance. The results are collected in Table 1. The ^{17}O signal shifts to higher field upon increasing θ from 0 to 90° to decrease again upon further increasing θ from 90 to 180° (Fig. 2A). Twisting of the π system of the 1,2-diketo chromophore away from coplanarity (θ = 0 or 180°) leads to a reduction of

[4]MNDO studies on glyoxal (**9**) as model compound showed that the terms Q_{NN} and ΣQ_{NB} are both independent of the dihedral angle θ. Upon varying θ (the selected values being 12, 42, 82, 122, and 158°), the charge at the oxygen atom changes, but the terms Q_{NN} and ΣQ_{NB} remain constant at values of 1.69 (sd 0.01) and 0.449 (sd 0.001), respectively.

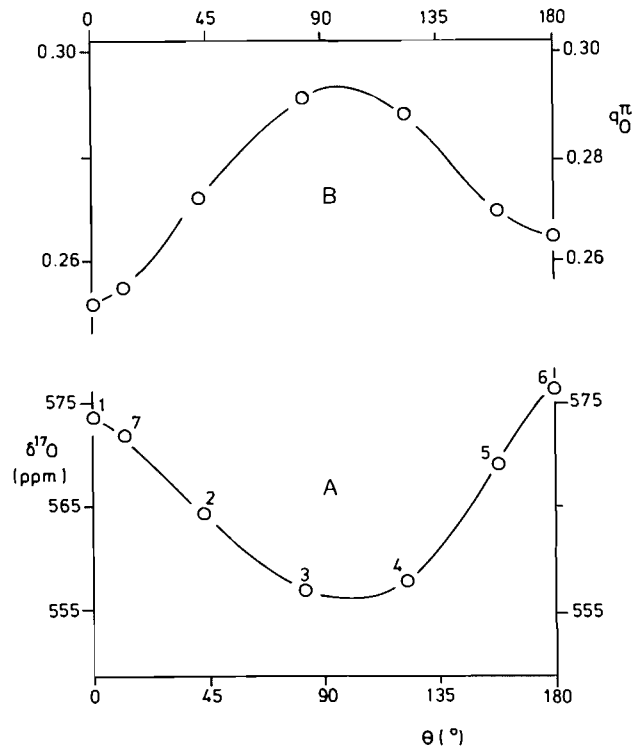

FIG. 2. Variation of $\delta\ ^{17}O$ of a series of 1,2-diketones (A) and of the MNDO calculated π-electron densities at the oxygen atoms of glyoxal (**9**) (B) with the dihedral angle θ of the O=C—C=O moiety.

the overlap integral S_{ij} of the central C—C bond and since —according to Mulliken's approximation (13)—the resonance integral H_{ij} is proportional to the overlap integral (eq. [4]),

[4] $S_{ij} = \langle\Psi_i|\Psi_j\rangle \sim \langle\Psi_i|H|\Psi_j\rangle = H_{ij}$

also to a reduction of the resonance integral. This is illustrated qualitatively in a simplified MO-scheme for the 1,2-diketo moiety (Fig. 3). The overlap integral S_{ij} is proportional to cos θ and, using (second order) perturbation theory, the resonance integral H_{ij} follows a $\cos^2\theta$ dependence (14). Thus at θ = 90° there is no interaction between the two C=O chromophores: they are degenerate.

[5] $S_{ij}(\theta) = S^0_{ij}\cos\theta$

[6] $H_{ij}(\theta) \simeq H^0_{ij}\cos^2\theta$

Can. J. Chem. Downloaded from www.nrcresearchpress.com by 213.166.140.6 on 09/07/12
For personal use only.

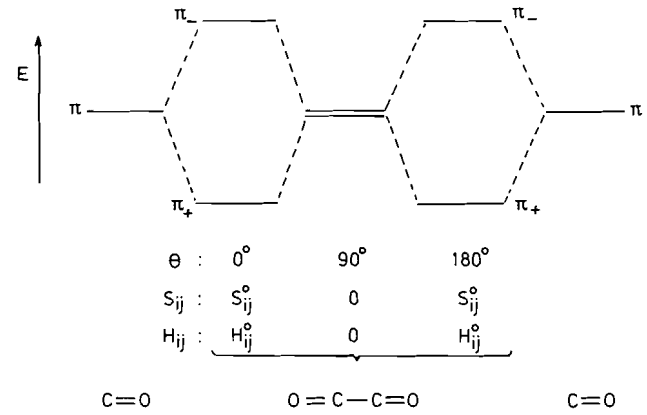

FIG. 3. Simplified MO-scheme for the π-MO's of the C=O and O=C—C=O chromophores: $\pi = \pi[\Psi_{CO}]$; $\pi_+ = \pi + \pi$; $\pi_- = \pi - \pi$.

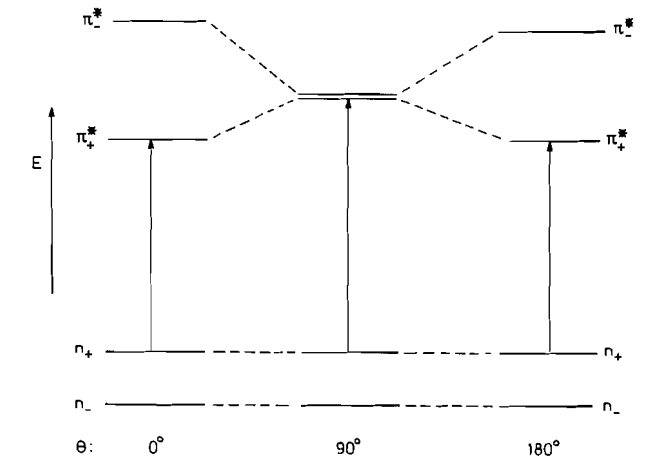

FIG. 4. Simplified MO-scheme of the 1,2-diketo chromophore at varying dihedral angles, illustrating the increase of $\Delta E(n \rightarrow \pi^*)$ upon twisting.

Changes in θ, and thus in both S_{ij} and H_{ij}, lead to a change in the electron density on the oxygen atoms q^{π}_{O}. This change has a dramatic effect on the chemical shift of the ^{17}O nucleus (15). An increase of the electron density on oxygen results in a spatial expansion of the 2*p* orbitals and this to a reduction of the term $\langle r^{-3} \rangle_{2p_N}$ in eq. [3]. A reduction in this term implies a reduction in the paramagnetic contribution to the shielding constant σ^{P}_{N} and thus an upfield shift of the ^{17}O resonance signal.

In order to obtain information on the effect of the π-electron density at the oxygen atom (q^{π}_{O}), the charge densities were calculated for glyoxal (**9**) as model compound, using semi-empirical SCF-MO calculations (the MNDO semi-empirical SCF-MO theory was developed by Dewar and Thiel (16)). The thus calculated π-electron densities at the oxygen atoms are shown in Fig. 2B as a function of θ. Clearly, the π-electron density at oxygen increases as the overlap in the π system decreases and *vice versa*. However, not only the term $\langle r^{-3} \rangle_{2p_N}$ in eq. [3] changes upon varying θ, but also the mean excitation energy ΔE is liable to depend on θ. For the series of the presently studied 1,2-diketones ΔE is not constant, as was sometimes assumed (for a discussion on the contribution of ΔE to the ^{17}O chemical shifts, see ref. 17), but varies considerably. Again, upon varying θ from both 0 and 180° to 90° the integral S_{ij} decreases to become zero at θ = 90°. The lowest vacant MO of the 1,2-diketo chromophore, which is a π* level (cf. Fig. 4),

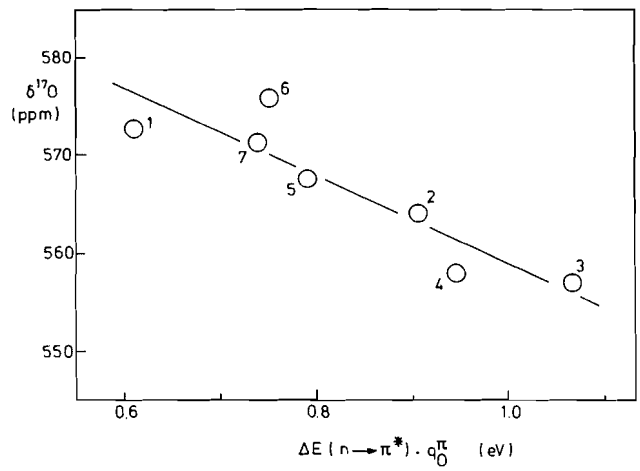

FIG. 5. Relationship between δ ^{17}O and $\Delta E(n \rightarrow \pi^*).q^{\pi}_{O}$ (n = 7, coefficient of correlation, $r = -0.90$).

increases in energy, while the highest occupied n-orbital is not affected.

The values of ΔE, calculated from the uv band maxima are compiled in Table 1. The effects of ΔE and q^{π}_{O} on σ^{P}_{N} (cf. eq. [3]) work in the same direction, both leading to an upfield shift due to the reduction in the overlap of the π system in the O=C—C=O chromophore. So, the relation between the product $\Delta E.q^{\pi}_{O}$ and the ^{17}O chemical shift should be linear, as is in fact observed (Fig. 5). The deviations from linearity are thought to be due in part to the use of uv-band maxima instead of the O–O transitions.

Performing least-square curve fitting methods on the data of the Figs. 2A and B give the best fits for a $\cos^4 \theta$ dependence for δ ^{17}O and a $\cos^2 \theta$ dependence for the π-electron density at the oxygen atoms with coefficients of correlation of 0.99 and −0.94, respectively. These results closely agree with the $\cos^2 \theta$ dependence for $\Delta E(n \rightarrow \pi^*)$, found theoretically (14), and support the linear relationship between δ ^{17}O and $\Delta E(n \rightarrow \pi^*).q^{\pi}_{O}$.

Experimental

The preparation of the 1,2-diketones was described before (5, 19). Homoadamantane-4,5-dione (**12**) was a gift from Philips Duphar B.V. The ^{17}O nmr spectra were recorded on a Bruker WM 250 spectrometer, operating at 33.905 MHz with a 10 mm broad band probe. The spectra were obtained at natural abundance on about 0.5 *M* solutions at 343 K in dry acetonitrile. The ^{17}O chemical shifts are relative to the absorption signal of water as external reference. The instrument settings are as follows: 25 kHz spectral width, 4K data points, 15 μs pulse width, corresponding to a 30° pulse angle, 82 ms acquisition time and no relaxation delay. The signal-to-noise ratio (s/n) was improved by a 25 Hz exponential broadening factor. Number of scans = 25 000. Data point resolution was improved by zero filling to 8K data points.

The dihedral angle of dodecane-1,2-dione (**6**) was obtained from Stuart molecular model studies (this method was described in ref. 18); the other values for θ were taken from ref. 3. The semi-empirical MNDO calculations (16) were performed on a DEC VAX 11/785 computer of the K. U. Nijmegen CAOS/CAMM calculating facility, using the QCPE Nr. 455 MOPAC program (20). The calculations were performed on glyoxal (**9**) as model compound for chosen fixed dihedral angles, using full geometry optimization.

1. F. ALDER and F. C. YU. Phys. Rev. **81**, 1067 (1951).
2. W. G. KLEMPERER. Angew. Chem. **90**, 258 (1978).
3. P. L. VERHEIJDT and H. CERFONTAIN. J. Chem. Soc. Perkin Trans. II, 1541 (1982).

Can. J. Chem. Downloaded from www.nrcresearchpress.com by 213.166.140.6 on 09/07/12
For personal use only.

4. L. C. G. GOAMAN and D. F. GRANT. Tetrahedron, **19**, 1531 (1963).
5. P. L. VERHEIJDT, C. KRUK, and H. CERFONTAIN. Recl. Trav. Chim. Pays-Bas, **101**, 85 (1982); L. A. SARPHATI, P. L. VERHEIJDT, and H. CERFONTAIN. Recl. Trav. Chim. Pays-Bas, **102**, 9 (1983).
6. P. L. VERHEIJDT and H. CERFONTAIN. Recl. Trav. Chim. Pays-Bas, **102**, 173 (1983).
7. J. A. POPLE. J. Chem. Phys. **37**, 53 (1962).
8. H. A. CHRIST and P. DIEHL. Helv. Phys. Acta, **36**, 170 (1963).
9. B. N. FIGGIS, R. G. KIDD, and R. S. NYHOLM. Proc. R. Soc. London, Ser. A, **269**, 469 (1962).
10. M. KARPLUS and T. P. DAS. J. Chem. Phys. **34**, 1683 (1961).
11. M. KARPLUS and J. A. POPLE. J. Chem. Phys. **38**, 2803 (1963).
12. W. S. JUNG, H. TOMIYASU, and H. FUKUTOMI. Bull. Chem. Soc. Jpn. **58**, 938 (1985).
13. R. S. MULLIKEN, C. A. RIEKE, and W. G. BROWN. J. Am. Chem. Soc. **63**, 41 (1941).
14. H. H. JAFFÉ and M. ORCHIN. Theory and application of ultraviolet spectroscopy. John Wiley Inc., New York. 1962. p. 389.
15. M. T. BERALDIN, E. VAUTHIER, and S. FLISZAR. Can. J. Chem. **60**, 106 (1982).
16. M. J. S. DEWAR and W. THIEL. J. Am. Chem. Soc. **99**, 4899 (1977); **99**, 4907 (1977).
17. R. T. C. BROWNLEE, M. SADEK, and D. J. CRAIK. Org. Magn. Reson. **21**, 616 (1983).
18. T. S. V. BUYS, H. CERFONTAIN, F. STUNNENBERG, and J. N. LOUWEN. Recl. Trav. Chim. Pays-Bas, **105**, 54 (1986).
19. J. STRATING, S. REIFFERS, and H. WIJNBERG. Synthesis, 209 (1971).
20. J. J. P. STEWART. QCPE Bulletin, **3**, 45 (1983).

Can. J. Chem. Downloaded from www.nrcresearchpress.com by 213.166.140.6 on 09/07/12
For personal use only.

Deuterium isotope effects on nuclear shielding constants and spin–spin coupling constants in the ammonium ion, ammonia, and water

RODERICK E. WASYLISHEN[1] AND JAN O. FRIEDRICH
Department of Chemistry, Dalhousie University, Halifax, N.S., Canada B3H 4J3

Received April 1, 1987

RODERICK E. WASYLISHEN and JAN O. FRIEDRICH. Can. J. Chem. **65**, 2238 (1987).

Deuterium isotope effects on ^{15}N chemical shifts have been investigated for the ammonium ion, ammonia, and aniline; $^1\Delta^{15}N(^{2/1}H)$ equals −293.3, −622.9, and −714.6 ppb respectively. Deviations from additivity are noted for $NH_{4-n}D_n^+$ and $NH_{3-n}D_n$; these deviations follow the predictions of Jameson and Osten. For ammonia, examination of the proton nuclear magnetic resonance spectrum yields $^1\Delta^1H(^{15/14}N) = -2.0 \pm 0.4$ ppb and $^2\Delta^1H(^{2/1}H) \simeq -28.6$ ppb. An accurate value of -1545 ± 5 ppb was obtained for $^1\Delta^{17}O(^{2/1}H)$ in water. Derivatives of the heavy atom shielding constants with respect to extensions in the equilibrium bond length have been estimated for NH_4^+, NH_3, and H_2O; these derivatives are compared with the recent calculations of Chesnut. Deuterium isotope effects on $^1J(^{15}N,H)$ in ammonia and aniline have been measured for the first time. For the ammonium ion, deuterium isotope effects on $^1J(^{15}N,H)$ are in good agreement with the less accurate values we previously observed on $^1J(^{14}N,H)$. In the case of water, both primary and secondary deuterium isotope effects on $^1J(^{17}O,H)$ are less than 2%. The isotope effects on the spin–spin coupling constants observed here are compared with those previously reported for other hydrides in the literature.

RODERICK E. WASYLISHEN et JAN O. FRIEDRICH. Can. J. Chem. **65**, 2238 (1987).

On a étudié les effets isotopiques du deutérium sur les déplacements chimiques du ^{15}N dans l'ion ammonium, dans l'ammoniac et dans l'aniline; les valeurs des $^1\Delta^{15}N(^{2/1}H)$ sont respectivement égales à −293,3, −622,9 et −714,6 ppb. On a noté des déviations de l'additivité pour les antités $NH_{4-n}D_n^+$ et $NH_{3-n}D_n$; ces déviations suivent les prédictions de Jameson et Osten. Pour l'ammoniac, l'examen du spectre en résonance magnétique nucléaire du proton permet de déduire les valeurs suivantes; $^1\Delta(^{15/14}N) = -2{,}0 \pm 0{,}4$ ppb et $^2\Delta^1H(^{2/1}H) \simeq -28{,}6$ ppb. Dans l'eau, on a déterminé que la valeur précise de $^1\Delta^{17}O(^{2/1}H)$ est égale à -1545 ± 5 ppb. Pour le NH_4^+, le NH_3 et le H_2O, on a évalué les dérivés des constantes de blindage de l'atome lourd par rapport aux extensions de la longueur de la liaison à l'équilibre; on a comparé ces dérivés avec les calculs récents de Chesnut. On a aussi mesuré pour la première fois les effets isotopiques du deutérium sur les constantes $^1J(^{15}N,H)$ de l'ammoniac et de l'aniline. Dans le cas de l'ion ammonium, les effets isotopiques du deutérium sur la constante $^1J(^{15}N,H)$ sont en bon accord avec les valeurs beaucoup moins précises que nous avons observées sur la constante $^1J(^{14}N,H)$. Dans le cas de l'eau, les effets isotopiques du deutérium, tant primaire que secondaire, sur la constante $^1J(^{17}O,H)$ sont plus faibles que 2%. On a comparé les effets isotopiques sur les constantes de couplage spin–spin observées dans ce travail avec celles rapportées antérieurement dans la littérature pour d'autres hydrures.

[Traduit par la revue]

Introduction

Deuterium isotope effects on nuclear shielding constants have been actively investigated for more than 20 years. The results of this work have been summarized in three recent reviews (1–3). The following are some general observations pertinent to the present study.

1. Replacement of hydrogen by deuterium results in greater shielding of a neighbouring nucleus; the magnitude of this isotope shift depends on the remoteness of the nucleus from the site of isotopic substitution and the chemical shift range of the nucleus under observation.

2. To a very good approximation, isotope shifts are additive; that is, the magnitude of observed isotope shifts is generally directly proportional to the number of equivalent protons that have been replaced by deuterium.

One object of the present study was to determine whether $^{2/1}H$ isotope effects on ^{15}N and ^{17}O nuclear shielding constants in ammonia and water are strictly additive. Deuterium isotope effects in these molecules have been previously reported (4, 5); however, for ammonia the deviations from additivity were zero within experimental error. In the case of water only the value of $\sigma(H_2O) - \sigma(D_2O)$ is available (5).

The replacement of hydrogen by deuterium has provided a means of measuring spin–spin coupling constants between equivalent protons. For example, in ammonia, $^2J(H,D) = -1.54 \pm 0.12$ Hz (6); hence the value quoted for $^2J(H,H)$ is (γ_H/γ_D) (−1.54 Hz) or -10.0 ± 0.8 Hz. This procedure has recently been questioned by Raynes and co-workers (7–9), who argue that vibrational effects on J due to isotopic substitution may be significant. Recently Jameson and Osten (10) have summarized isotope effects on spin–spin coupling constants and provided an explanation for some of the observed effects. Unlike isotope effects on shielding constants, which are invariably of the same sign, isotope effects on J can be of either sign. For example, the primary isotope effect on J (defined by eq. [1]) is only positive in molecules where A has an electron lone pair.

$$[1] \quad {}^1\Delta_p{}^nJ(A,{}^{2/1}H) \equiv |{}^nJ(A,D)|(\gamma_H/\gamma_D) - |{}^nJ(A,H)|$$

Secondary deuterium isotope effects on J (defined by eq. [2])

$$[2] \quad \Delta_s{}^nJ(A,B) \equiv |{}^nJ(A,B)_D| - |{}^nJ(A,B)_H|$$

are also of either sign and at this time there appears to be no simple criterion for predicting the sign of Δ_s in a particular molecule. A second objective of the present study was to provide further accurate experimental data of isotope effects on J in a few relatively simple molecules and determine if the reuslts are consistent with the general trends recently summarized in ref. 10.

Theory

Here we will use the notation introduced by Gombler (11) and used extensively by Jameson and Osten (3). The isotope shift observed for a nucleus A upon substitution of a hydrogen by

[1]Author to whom correspondence may be addressed.

Can. J. Chem. Downloaded from www.nrcresearchpress.com by 213.166.140.6 on 09/07/12
For personal use only.

Can. J. Chem. Downloaded from www.nrcresearchpress.com by 213.166.140.6 on 09/07/12
For personal use only.

deuterium is expressed by eq. [3],

$$[3]\quad {}^{n}\Delta A(^{2/1}H) = \sigma^{A}(A—{}^{1}H) - \sigma^{A}(A—{}^{2}H)$$

where n is the number of bonds between A and the position of substitution. Jameson and Osten (12–14) have shown that one-bond isotope shifts can be estimated using eq. [4],

$$[4]\quad {}^{1}\Delta A(^{2/1}H) \simeq (\partial\sigma^{A}/\partial\Delta r_{AH})_{e}\Delta_{H}$$

where $(\partial\sigma^{A}/\partial\Delta r_{AH})_{e}$ is the shielding derivative of A with respect to bond extension at the site of substitution. This derivative is generally negative (3, 15, 16) and independent of mass. The last term in eq. [4] is the *difference* in the mean bond displacement between the light isotopomer and the heavy isotopomer and is often referred to as the dynamic factor (12). For a single substitution of an end hydrogen the dynamic factor is given by eq. [5] (13),

$$[5]\quad \Delta_{H} = [\langle\Delta r_{AH}\rangle - \langle\Delta r_{AD}\rangle] \simeq \langle\Delta r_{AH}\rangle\tfrac{1}{2}((m_{D} - m_{H})/m_{D})(m_{A}/(m_{A} + m_{H})) \simeq \tfrac{1}{4}\langle\Delta r_{AH}\rangle$$

For hydrides the mean bond displacement, $\langle\Delta r_{AH}\rangle$, will depend on A but is in the range of 15–21 $\times 10^{-3}$ Å (14). A more complete analysis of isotope shifts is generally difficult because one must consider differences in mean bond angle deformations $\langle\Delta\alpha\rangle$ and terms such as $\langle(\Delta\alpha)^2\rangle$ and $\langle(\Delta r)^2\rangle$ (3, 17, 18).

In the special case of highly symmetrical molecules such as a simple tetrahedral molecule or ion, AH_4, Jameson and Osten (3, 13) have shown that the isotope shift is given by eq. [6],

$$[6]\quad \sigma^{A}(AH_{4-n}D_{n}) - \sigma^{A}(AH_{4-n'}D_{n'}) = (\partial\sigma^{A}/\partial\Delta r_{AH})_{e}[(n' - n)\Delta_{H} + \delta(n) - \delta(n')]$$

where δ is a secondary effect related to the extent a bond is perturbed by isotopic substitution in an adjacent bond. Because the difference, $\delta(n) - \delta(n')$, is much less than Δ_{H}, isotope shifts generally show small deviations from additivity. Detailed analysis indicates that for the series AH_4, AH_3D, AH_2D_2, AHD_3, and AD_4 deviations from additivity should be in the ratios 0:3:4:3:0 (13). In the case of A ≡ carbon, Bigeleisen and Goldstein (19) have shown that deviations in the zero-point energies vs. n are also in the ratios 0:3:4:3:0.

Isotope effects on spin–spin coupling constants can also be interpreted in terms of differences in dynamical averaging upon isotopic substitution (10). The primary isotope effect on the one-bond coupling constant is given by eq. [7],

$$[7]\quad \Delta_{p}{}^{1}K(A,^{2/1}H) = (\partial K/\partial\Delta r_{AH})_{e}[\langle\Delta r_{AD}\rangle - \langle\Delta r_{AH}\rangle] + \ldots$$

where ${}^{1}K$ is the reduced spin–spin coupling constant defined by eq. [8],

$$[8]\quad K(A,B) = 4\pi^{2}J(A,B)/h\gamma_{A}\gamma_{B}$$

and all other terms have been defined. Note that, as written, the dynamical factor in eq. [7] is negative.

Secondary isotope effects on spin–spin coupling constants are more complex and the interested reader should consult ref. 10.

Experimental

Nuclear magnetic resonance spectra were obtained at 20°C on a Nicolet 360 operating at a proton frequency of 361.05 MHz. All isotopically labelled compounds used in this study were obtained from Merck, Sharp and Dohme.

A 4 *M* aqueous solution of $NH_{4-n}D_{n}{}^{+}NO_{3}{}^{-}$ in 2 *M* HCl was prepared for ^{15}N nmr measurements; approximately 55% of the ammonium ions were ^{15}N labelled.

A sample of $NH_{3-n}D_{n}$ was prepared by mixing $^{15}NH_3$ and ND_3. The resulting mixture was dried over Na metal, distilled into a thick walled 10-mm o.d. nmr tube, and then sealed under vacuum.

Approximately 35% of the amino hydrogens of aniline-^{15}N were replaced by deuterium by adding a precalculated amount of D_2O to aniline-^{15}N. The solution was dried over solid KOH, and dissolved in chloroform-*d* containing 4A molecular sieves. The final concentration of aniline in chloroform was approximately 1 *M*; the sample was degassed and sealed in a 10-mm o.d. nmr tube.

A sample containing oxygen-17 labelled H_2O, HDO, and D_2O was prepared by mixing approximately 3 parts H_2O (20% ^{17}O) with 2 parts D_2O. A small quantity of this mixture was added to cyclohexane-d_{12}.

TABLE 1. Nitrogen-15 chemical shifts in $NH_{4-n}D_{n}{}^{+}$ ($n \leq 4$)[a]

Molecule	${}^{1}\Delta^{15}N(^{2/1}H)_{obs}$	${}^{1}\Delta^{15}N(^{2/1}H)_{additivity}$	Δ	Δ′
$NH_4{}^{+}$	0.0	0.0	0.0	0
NH_3D^{+}	−307.7	−293.3	14.4	3.1
$NH_2D_2{}^{+}$	−604.8	−586.5	18.3	4.0
$NHD_3{}^{+}$	−893.7	−879.8	13.9	3.0
$ND_4{}^{+}$	−1173.0	−1173.0	0.0	0

[a]In parts per billion (±0.5) relative to $^{15}NH_4{}^{+}$.

TABLE 2. Nitrogen-15 chemical shifts in $NH_{3-n}D_{n}$ ($n \leq 3$)[a]

Molecule	${}^{1}\Delta^{15}N(^{2/1}H)_{obs}$	${}^{1}\Delta^{15}N(^{2/1}H)_{additivity}$	Δ
NH_3	0.0	0.0	0.0
NH_2D	−626.4	−622.9	3.5
NHD_2	−1249.1	−1245.8	3.3
ND_3	−1868.7	−1868.7	0.0

[a]In parts per billion (±0.5) relative to $^{15}NH_3$.

TABLE 3. $^{2/1}H$ isotope effects on ^{15}N chemical shifts in aniline[a]

Molecule	${}^{1}\Delta^{15}N(^{2/1}H)_{obs}$	${}^{1}\Delta^{15}N(^{2/1}H)_{additivity}$	Δ
ϕ-NH_2	0	0	0
ϕ-NHD	−714.6±0.8	−714.3	0.3
ϕ-ND_2	−1428.6±1.0	−1428.6	0

[a]In parts per billion.

Results and discussion

1. $^{2/1}H$ isotope effects on ^{15}N and ^{17}O shielding constants

(a) ${}^{1}\Delta^{15}N(^{2/1}H)$ in the ammonium ion, ammonia, and aniline

Deuterium/proton isotope effects on the ^{15}N chemical shifts in the ammonium ion, ammonia, and aniline are summarized in Tables 1–3 respectively. The ^{15}N nmr spectrum of $NH_{3-n}D_{n}$ is shown in Fig. 1. The isotope shifts, ${}^{1}\Delta^{15}N(^{2/1}H)$ in ammonia and aniline, −623 and −715 ppb/D, respectively, are more than twice the magnitude of the corresponding value (−293 ppb/D) in the ammonium ion. The relatively small isotope shift observed for the ammonium ion compared to that in ammonia apparently arises primarily because of the reduced electron density about the nitrogen nucleus of $NH_4{}^{+}$. If one assumes that eqs. [4] and [5] apply we obtain $\partial\sigma(N)/\partial\Delta r_{NH}$ values of −60 and −124 ppm/Å for $NH_4{}^{+}$ and NH_3, respectively. These values are in excellent agreement with theoretical values of −67.9 and −130.3 ppm/Å recently reported by Chesnut (15). In the above calculations we have used Δr_{NH}

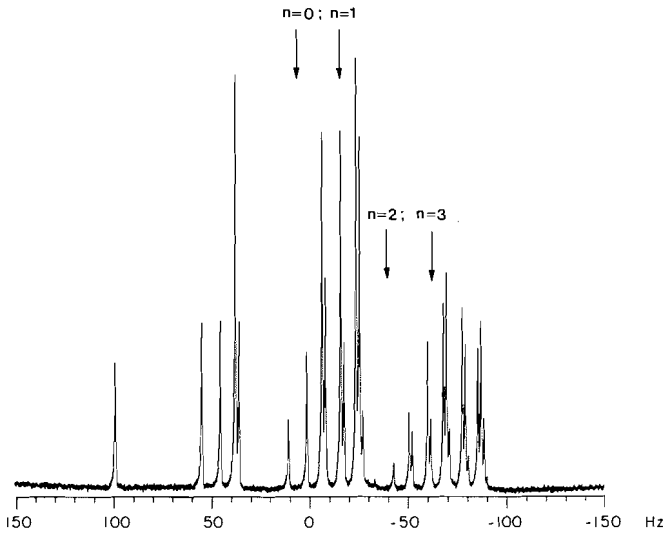

FIG. 1. Nitrogen-15 nmr spectrum of neat $NH_{3-n}D_n$ at 36.585 MHz.

values of 20.34×10^{-3} Å (12) and 20.2×10^{-3} Å (18) for the ammonium ion and ammonia. The good agreement in the experimental and theoretical shielding derivatives suggests that terms involving partial derivatives of σ with respect to changes in bond angle, such as $\partial\sigma/\partial\alpha$, must make a small contribution to $^1\Delta^{15}N(^{2/1}H)$. Recently calculations of Chesnut and Foley (16) also indicate that the bond angle derivatives in ammonia are relatively small.

The second point evident from the data in Tables 1–3 is that the isotope shifts in the ammonium ion and ammonia are *not* perfectly additive. Although we previously observed non-additivity in the ^{14}N chemical shifts of the ammonium ion (20) the ^{15}N results in Tables 1 are slightly more accurate. Deuterium isotope shifts on nitrogen shielding in the ammonium ion have been previously reported by numerous workers (21–24); however, due to the experimental errors, deviations from strict additivity were not observed. As mentioned in the theoretical section, Jameson and Osten (13) predict that the deviations from perfect additivity in $AH_{4-n}D_n$ should be in the ratio 0:3:4:3:0, in excellent agreement with our experimental results. For stannane, $SnH_{4-n}D_n$, we recently found that the deviations from strict additivity are also in the ratio 0:3:4:3:0 (25). Deviations from perfect additivity have not been observed in an earlier ^{15}N nmr study of ammonia (4). Following the arguments of Jameson and Osten (13) the ratio of the deviations in $AH_{3-n}D_n$ should be 0:1:1:0, in excellent agreement with the observations in Table 2. Any deviations from strict additivity in aniline are too small to be observed. We would like to point out that in the case of aniline we observed all three species, ϕNH_2, ϕNHD, and ϕND_2, in the same solution under conditions of slow exchange; previous workers (24) have utilized coaxial tubes to observe separate resonance signals for ϕNH_2 and ϕND_2.

(b) $^1\Delta^{17}O(^{2/1}H)$ in water and the hydronium ion

A part of the ^{17}O nmr spectrum of the various isotopomers of water immersed in cyclohexane-d_{12} is shown in Fig. 2. This portion of the spectrum is attributed to cyclohexane-solvated water molecules. If water clusters (e.g., dimers or trimers) are responsible for this part of the ^{17}O nmr spectrum it is clear that O—H and O—D exchange is relatively slow since $\nu_{1/2}(^{17}O) <$ 4 Hz. At about 14.8 ppm to high frequency of the $H_2{}^{17}O$ resonance shown in Fig. 2 we observed a broad intense peak

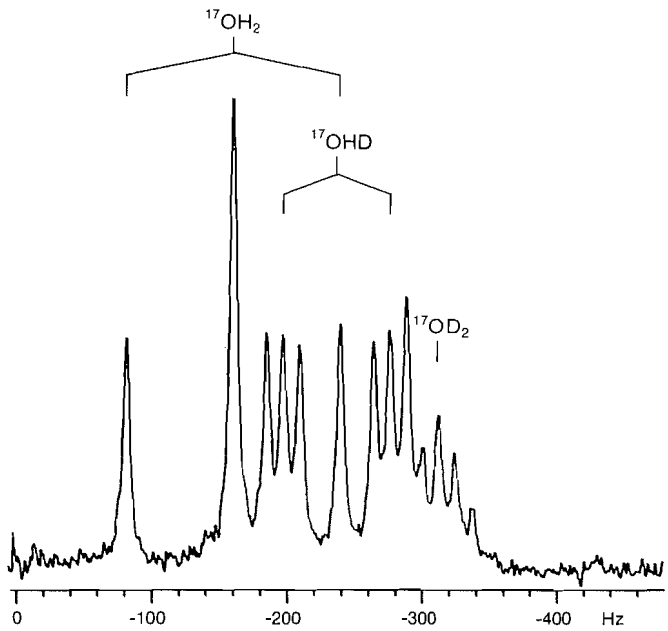

FIG. 2. Oxygen-17 nmr spectrum of $H_{2-n}D_nO$ dissolved in cyclohexane-d_{12} at 48.946 MHz.

TABLE 4. Oxygen-17 chemical shifts for $H_{2-n}D_nO$ ($n \leq 2$) in cyclohexane

Molecule	$^1\Delta^{17}O(^{2/1}H)_{obs}$[a]	$^1\Delta^{17}O(^{2/1}H)_{additivity}$	Δ
H_2O	0	0	0
HDO	−1550	−1545	5
D_2O	−3090	−3090	0

[a] In parts per billion (±5). Temperature 20°C.

TABLE 5. Proton chemical shifts in $^{15}NH_{3-n}D_n$ and spin–spin coupling constants from ^1H nmr[a]

Molecule	$^2\Delta^1H(^{2/1}H)^b$	$^1J(^{15}N,H)^c$	$^2J(H,D)^c$
NH_3	0.00	−61.47	—
NH_2D	−28.61	−61.42	−1.47[5] (−9.61)
NHD_2	−56.28	−61.33	−1.43 (−9.35)

[a] The protons of $^{14}NH_3$ resonante at 2.0 ± 0.4 parts per billion to high frequency of those in $^{15}NH_3$; i.e., $^1\Delta^1H(^{15/14}N) = -2.0 \pm 0.4$ ppb.

[b] In parts per billion (±0.05) relative to NH_3; negative shifts are to low frequency (high field).

[c] In Hz (±0.02), values in brackets are $^2J(H,H) = 6.51440\ ^2J(H,D)$.

($\nu_{1/2} \simeq 140$ Hz), not shown, which is attributed to suspended drops of water (water-solvated water). A similar observation for water immersed in CCl_4 has been reported by Mateescu and Benedikt (26). The downfield shift (high frequency) with increased association is consistent with the direction of the gas to liquid shift observed for H_2O, but is only about half this value, +36 ppm (5*b*, 27).

The total isotope shift that we observe for water, −3.090 ± 0.005 ppm (i.e., $^1\Delta^{17}O(^{2/1}H) = 1.550$ ppm/D, see Table 4) is in excellent agreement with the early value of Lutz and Oehler (5*a*), −3.08 ± 0.2 ppm, and the recent value of −2.9 ppm of S. Aime *et al.* (28). The value of Lutz and Oehler (5*a*) was obtained by measuring the ^{17}O resonance of various D_2O/H_2O mixtures, while the value of S. Aime *et al.* (28) was determined

Can. J. Chem. Downloaded from www.nrcresearchpress.com by 213.166.140.6 on 09/07/12
For personal use only.

TABLE 6. Isotope effects on spin–spin coupling constants in the ammonium ion

Molecule	$^1J(^{15}N,H)^a$	$^1J(^{15}N,D)^b$	$(\gamma_H/\gamma_D)^1J(^{15}N,D)^c$	$\Delta_p{}^1J(^{15}N,H)$
NH_4^+	−73.62	—	—	
NH_3D^+	−73.51	−11.33	−73.81	+0.30
$NH_2D_2^+$	−73.43	−11.33	−73.81	+0.38
NHD_3^+	−73.40	−11.29	−73.55	+0.15
ND_4^+	—	−11.25	−73.29	

[a]Estimated error ±0.02 Hz; $\Delta_s{}^1J(^{15}N,H)[^{2/1}H] = -0.07 \pm 0.03$ Hz.
[b]Estimated error ±0.03 Hz except for ND_4^+ (±0.05).
[c]Estimated error ±0.02 Hz; $\gamma_H/\gamma_D = 6.51440$.

TABLE 7. Isotope effects on spin–spin coupling constants in ammonia

Molecule	$^1J(^{15}N,H)^a$	$^1J(^{15}N,D)^a$	$(\gamma_H/\gamma_D)^1J(^{15}N,D)^b$	$\Delta_p{}^1J(^{15}N,H)$
NH_3	−61.45[3]		—	—
NH_2D	−61.38[7]	−9.49[5]	−61.85[4]	0.46[7]
NHD_2	−61.31[4]	−9.48[3]	−61.77[6]	0.46[2]
ND_3	—	−9.47	−61.69[1]	—

[a]Error is less than ±0.02 Hz; $\Delta_s{}^1J(^{15}N,H)[^{2/1}H] = -0.07 \pm 0.02$ Hz.
[b]$\gamma_H/\gamma_D = 6.51440$; error in the calculated values of $^1J(^{15}N,H)$ is ±0.13 Hz.

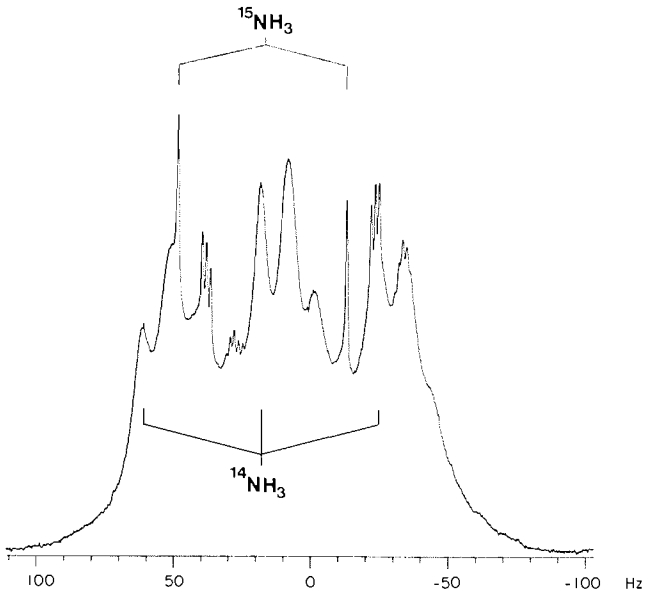

FIG. 3. Proton nmr spectrum of neat $^{15/14}NH_{3-n}D_n$ at 361.050 MHz.

by simultaneously measuring the ^{17}O resonance of D_2O and H_2O in concentric 5- and 10-mm nmr tubes. Interestingly, the isotope shift we measured in cyclohexane is within experimental error of the values reported in aqueous solution but substantially smaller than the gas-phase value of 4.04 ± 0.35 ppm (5*b*).

Mateescu *et al.* have apparently measured $^1\Delta^{17}O(^{2/1}H)$ values for H_2O and H_3O^+; however, only their value for the hydronium ion has been reported in the literature (29), $^1\Delta^{17}O(^{2/1}H) = -0.3$ ppm/D. Using $\langle \Delta r_{OH} \rangle = 20.0 \times 10^{-3}$ Å for both H_2O (18) and H_3O^+ we calculate $\partial\sigma(O)/\partial\Delta r$ values of −296 and −60 ppm/Å, respectively. The value of $\partial\sigma(O)/\partial\Delta r$ obtained for water is essentially the same value obtained by Osten and Jameson (18) and is in good agreement with values of −270.9 ppm/Å (30) and −267 ppm/Å (15, 16) calculated using molecular orbital theory. Qualitatively, the smaller magnitude of the isotope shift and of $\partial\sigma(O)/\partial\Delta r$ observed for H_3O^+ compared to H_2O can be accounted for in terms of the charge density argument used to account for differences between NH_4^+ and NH_3 (15). It is of interest to point out that we also observed very small isotope shifts in the stannonium cation, $^1\Delta Sn(^{2/1}H) = -0.05$ ppm/D compared to a value of $^1\Delta Sn(^{2/1}H) = -0.403$ ppm/D for stannane (25).

Finally, the much larger negative value of $^1\Delta O(^{2/1}H)$ observed for water compared to the value of $^1\Delta N(^{2/1}H)$ observed for ammonia is part of a general trend for all hydrides, AH_n. As one moves across any row of the periodic table the isotope effect, $^1\Delta A(^{2/1}H)$, becomes more negative because of the behaviour of $\partial\sigma(A)/\partial\Delta r$ (15).

2. *The ^1H nmr spectrum of $^{15/14}NH_{3-n}D_n$*

The proton nmr spectrum of $^{15/14}NH_{3-n}D_n$ is rather complex (Fig. 3) because it arises from the overlapping spectrum of six different isotopomers. For the three isotopomers containing ^{14}N ($^{14}NH_3$, $^{14}NH_2D$, and $^{14}NHD_2$) the main feature in each of their ^1H nmr spectra is a broad 1:1:1 triplet due to spin–spin coupling ($J \simeq 43.8$ Hz) with a rapidly relaxing ^{14}N ($I = 1$). This is a classic example of ^1H scalar relaxation (T_2) of the second kind (31). The principal feature in the ^1H nmr spectra of the three other isotopomers is of course a doublet due to $^1J(^{15}N,H)$. All isotope shifts and spin–spin coupling constants are summarized in Table 5.

We observed a very small isotope shift, $^1\Delta^1H(^{15/14}N) = -2.0 \pm 0.4$ ppb; this is within experimental error of the value recently observed in NH_4^+ (32), and is comparable to the value of $^1\Delta^1H(^{13/12}C)$, −2.4 ± 0.2 ppb (33), in methane. The value of $^1\Delta^1H(^{18/16}O)$ in water is approximately −12 ± 3 ppb (34); however, the fractional change in mass here is also larger. As well, $\partial\sigma(^1H)/\partial\Delta r$ shows increasing negative values on going from methane to water (15, 16).

The two-bond isotope shift, $^2\Delta^1H(^{2/1}H)$ shows small deviations from strict additivity; this was not evident in an earlier study (6).

The value of $^2J(H,D)$ in $^{15}NH_2D$, −1.475 ± 0.02 Hz, leads to a more accurate value of $^2J(H,H)$, −9.6 ± 0.2 Hz, compared

Can. J. Chem. Downloaded from www.nrcresearchpress.com by 213.166.140.6 on 09/07/12
For personal use only.

TABLE 8. $^{2/1}$H isotope effects on spin–spin coupling constants in aniline

Molecule	$^1J(^{15}N,H)^a$	$^1J(^{15}N,D)$	$(\gamma_H/\gamma_D)^1J(^{15}N,D)$	$\Delta_p{}^1J(^{15}N,H)$
ϕ-NH_2	−78.03[5]	—	—	—
ϕ-NHD	−77.91[5]	−12.00[b]	−78.17	+0.26 ± 0.2
ϕ-ND_2	—	−11.96[c]	−77.91 ± 0.26	—

[a]Error ±0.02 Hz; $\Delta_s{}^1J(^{15}N,H)$ [$^{2/1}$H] = −0.12 ± 0.02 Hz.
[b]Error ±0.03 Hz.
[c]Error ±0.04 Hz.

TABLE 9. Isotope effects on spin–spin coupling constants in water

Molecule	$^1J(^{17}O,H)^a$	$^1J(^{17}O,D)^a$	$(\gamma_H/\gamma_D)^1J(^{17}O,D)^b$	$\Delta_p{}^1J(^{17}O,H)$
H_2O	−78.70	—	—	—
HDO	−78.78	−12.14	−79.08	0.3 ± 1.3
D_2O	—	−11.96	−77.91	—

[a]Estimated error is ±0.02 Hz. Sign of J(O,H) is negative (35).
[b]Error in the calculated value of $^1J(^{17}O,H)$ is ±1.3 Hz.

TABLE 10. Calculated spin–spin coupling constants for the ammonium ion

Number of atoms 1.03 Å from N	$^1J(^{15}N,H)^a$, Hz	Number of atoms 1.02 Å from N	$^1J(^{15}N,H)^b$, Hz
4	−73.52	0	—
3	−73.43	1	−72.24
2	−73.33	2	−72.15
1	−73.23	3	−72.07
0	—	4	−71.97

[a]These values of J are between ^{15}N and a hydrogen that is 1.03 Å from the central nitrogen atom.
[b]These values of J involve ^{15}N and a hydrogen that is 1.02 Å from the central nitrogen atom. These values would correspond to J(N,D) γ_H/γ_D.

to the earlier result, −10.0 ± 0.8 Hz (6). The values of $^1J(^{15}N,H)$ obtained from the ^{1}H nmr spectrum are within experimental error of those measured in the ^{15}N nmr spectrum (see discussion to follow).

3. Isotope effects on J

Isotope effects on spin–spin coupling constants are generally difficult to measure because typically they are less than 0.5 Hz (10). Spin–spin coupling constants in the various isotopomers of the ammonium ion, ammonia, aniline, and water are summarized in Tables 6–9, respectively. Both primary and secondary isotope effects on $^1J(^{15}N,H)$ are apparent for the ammonium ion, ammonia, and aniline; however, for water Δ_p $^1J(^{17}O,^{2/1}H)$ and Δ_s $^1J(^{17}O,H)$ [$^{2/1}$H] are both less than the experimental error. In the case of hydrogen selenide, the primary and secondary deuterium isotope effects on $^1J(^{77}Se,H)$ are approximately 2.5 Hz (4%) and 1.0 Hz (1.6%), respectively (36); thus it is not surprising that isotope effects on J in water are not observed (*vide infra*).

For ammonia Δ_p $^1J(^{15}N,^{2/1}H)$ and Δ_s $^1J(^{15}N,H)$ [$^{2/1}$H] are 0.46 ± 0.13 Hz (0.75%) and −0.07 ± 0.02 Hz (0.11%), respectively. These primary and secondary isotope effects are of the same sign as those observed for phosphine (37); however, the values for ammonia are approximately an order of magnitude smaller than those observed for phosphine. Interestingly, the relative magnitudes of the $^{2/1}$H induced one-bond isotope effect on the ^{15}N and ^{31}P chemical shifts in these two molecules are comparable (37). The primary and secondary isotope effects on J(N,H) in aniline are within experimental error of those measured for ammonia.

Jameson and Osten found primary isotope effects to be positive in molecules where one of the coupled nuclei had one or more lone pairs; otherwise the primary isotope effect was negative (10). Thus for the ammonium ion one would expect Δ_p $^1J(^{15}N,^{2/1}H)$ to be negative; the observed value, however, appears to be positive, +0.28 ± 0.2 Hz. To determine whether or not a positive value is consistent with theory, we carried out semiempirical MO calculations at the INDO level of approximation (38). We assumed a tetrahedral geometry for NH_4^+ and carried out the finite perturbation calculations of $J(^{15}N,H)$ for five different combinations of N—H bond lengths. To simulate the effect of deuterium substitution we used an N—H bond length of 1.02 Å as opposed to 1.03 Å for a regular N—H bond. The results (Table 10) predict $^1\Delta_p$ $^1J(^{15}N,^{2/1}H)$ to be negative (−1.2 Hz) and the secondary isotope effect to also be negative (≃ −0.10 Hz) as observed (−0.07 ± 0.03 Hz). Although the actual values of these calculated isotope effects are not accurate we believe their calculated signs and relative magnitudes are relevant. The results of analogous semiempirical calculations for methane (39) agree with experimental (10). The ammonium ion also exhibits an unusual positive isotope shift $^2\Delta^1H(^{2/1}H)$ (32, 40), which has been attributed to intermolecular effects (32); also see ref. 24. It is likely that these effects are also responsible for the unexpected sign of Δ_p $^1J(^{15}N,H)$ in the ammonium ion.

In summary, our results indicate that in the first row hydrides,

Can. J. Chem. Downloaded from www.nrcresearchpress.com by 213.166.140.6 on 09/07/12
For personal use only.

NH_4^+, NH_3, and H_2O substitution of hydrogen by deuterium results in a very small change in the average value of the various spin–spin coupling constants investigated in this study. Nevertheless, in comparing theoretical calculations of J with experiment it is important to consider the influence of vibrational averaging (see refs. 7–10, 41–43).

Acknowledgements

We wish to thank the Natural Sciences and Engineering Research Council of Canada for financial support, Professor C. J. Jameson for a preprint of ref. 32, and A. M. Salsman for typing this manuscript.

1. P. E. Hansen. *In* Annual reports on NMR spectroscopy. Vol. 15. *Edited by* G. A. Webb. Academic Press, London. 1983. p. 105.
2. D. A. Forsyth. *In* Isotopes of organic chemistry. Vol. 6. *Edited by* E. Buncel and C. C. Lee. Elsevier, Amsterdam. 1984. p. 1.
3. C. J. Jameson and H. J. Osten. *In* Annual reports on NMR spectroscopy. Vol. 17. *Edited by* G. A. Webb. Academic Press, London. 1986. p. 1.
4. W. M. Litchman, M. Alei, and A. E. Florin. J. Chem. Phys. **50**, 1897 (1969).
5. (*a*) O. Lutz and H. Oehler. Z. Naturforsch. A: Phys. Phys. Chem. Kosmophys. **32**, 131 (1977); (*b*) W. T. Raynes. Mol. Phys. **49**, 443 (1983).
6. R. A. Bernheim and H. Batiz-Hernandez. J. Chem. Phys. **40**, 3446 (1964).
7. W. T. Raynes, P. Lazzeretti, R. Zanasi, and P. W. Fowler. J. Chem. Soc. Chem. Commun. 1538 (1985).
8. P. Lazzeretti, R. Zanasi, and W. T. Raynes. J. Chem. Soc. Chem. Commun. 57 (1986).
9. W. T. Raynes, P. Lazzeretti, and R. Zanasi. Chem. Phys. Lett. **132**, 173 (1986).
10. C. J. Jameson and H. J. Osten. J. Am. Chem. Soc. **108**, 2497 (1986).
11. W. Gombler. J. Am. Chem. Soc. **104**, 6616 (1982).
12. C. J. Jameson and H. J. Osten. J. Chem. Phys. **81**, 4300 (1984).
13. C. J. Jameson and H. J. Osten. J. Chem. Phys. **81**, 4293 (1984).
14. C. J. Jameson and H. J. Osten. J. Am. Chem. Soc. **107**, 4158 (1985).
15. D. B. Chesnut. Chem. Phys. **110**, 415 (1986).
16. D. B. Chesnut and C. K. Foley. J. Chem. Phys. **85**, 2814 (1986).
17. P. W. Fowler and W. T. Raynes. Mol. Phys. **43**, 65 (1981).
18. H. J. Osten and C. J. Jameson. J. Chem. Phys. **82**, 4595 (1985).
19. J. Bigeleisen and P. Goldstein. Z. Naturforsch. A: **18**, 205 (1963).
20. R. E. Wasylishen and J. O. Friedrich. J. Chem. Phys. **80**, 585 (1984).
21. R. B. Johannesen. J. Chem. Phys. **48**, 1444 (1968).
22. W. McFarlane and R. R. Dean. J. Chem. Soc. A, 1535 (1968).
23. V. P. Tarasov, V. I. Privalov, Y. A. Buslaev, and U. Eichhoff. Z. Naturforsch. B: Anorg. Chem. Org. Chem. **39**, 1230 (1984).
24. A. Lyčka and P. E. Hansen. Magn. Reson. Chem. **23**, 973 (1985).
25. K. Leighton and R. E. Wasylishen. Can. J. Chem. **65**, 1469 (1987).
26. G. D. Mateescu and G. M. Benedikt. J. Am. Chem. Soc. **101**, 3959 (1979).
27. A. R. Florin and M. Alei. J. Chem. Phys. **47**, 4268 (1967).
28. S. Aime, E. Santucci, and R. Fruttero. Magn. Reson. Chem. **24**, 919 (1986).
29. G. D. Mateescu, G. M. Benedikt, and M. P. Kelly. *In* Synthesis and applications of isotopically labelled compounds. *Edited by* W. P. Duncan and A. B. Susàn. Elsevier Scientific Publishing Company, Amsterdam, The Netherlands. 1983.
30. P. W. Fowler, G. Riley, and W. T. Raynes. Mol. Phys. **42**, 1463 (1981).
31. A. Abragam. The principles of nuclear magnetism. Oxford University Press, Oxford. 1961. p. 309.
32. J. K. M. Sanders, B. K. Hunter, C. J. Jameson, and G. Romeo. Chem. Phys. Lett. In press.
33. H. J. Osten and C. J. Jameson. J. Chem. Phys. **81**, 4288 (1984).
34. B. Sredni and S. Pinchas. J. Magn. Reson. **7**, 289 (1972).
35. W. B. Jenkins and W. McFarlane. J. Chem. Soc. Chem. Commun. 922 (1977).
36. H. J. Jakobsen, A. J. Zozulin, P. D. Ellis, and J. D. Odom. J. Magn. Reson. **38**, 219 (1980).
37. A. K. Jameson and C. J. Jameson. J. Magn. Reson. **32**, 455 (1978).
38. J. A. Pople and D. L. Beveridge. Approximate molecular orbital theory. McGraw–Hill, New York. 1970.
39. N. M. Sergeyev and V. N. Solkan. J. Chem. Soc. Chem. Commun. 12 (1975).
40. G. Fraenkel, Y. Asaki, H. Batiz-Hernandez, and R. A. Bernheim. J. Chem. Phys. **44**, 4647 (1966).
41. J. Kowalewski and B. Roos. Chem. Phys. **11**, 123 (1975).
42. P. Solomon and J. M. Schulman. J. Am. Chem. Soc. **99**, 7776 (1976).
43. J. Geerten and J. Oddershede. Chem. Phys. **90**, 301 (1984).

Can. J. Chem. Downloaded from www.nrcresearchpress.com by 213.166.140.6 on 09/07/12
For personal use only.

Terpenoid metabolites from skin extracts of the dendronotid nudibranch *Tochuina tetraquetra*

DAVID E. WILLIAMS AND RAYMOND J. ANDERSEN[1]

Departments of Chemistry and Oceanography, University of British Columbia, Vancouver, B.C., Canada V6T 1W5

Received March 10, 1987

DAVID E. WILLIAMS and RAYMOND J. ANDERSEN. Can. J. Chem. **65**, 2244 (1987).

The skin chemistry of specimens of the dendronotid nudibranch *Tochuina tetraquetra* collected at Port Hardy and Bamfield, British Columbia, has been examined. Port Hardy animals yielded tochuinyl acetate (**1**) and dihydrotochuinyl acetate (**2**), two new cuparane sesquiterpenoids, as well as rubifolide (**3**) and pukalide (**4**), two previously known cembrane diterpenoids. Bamfield animals yielded the known briarein-type diterpenoid ptilosarcenone (**5**) and the previously unreported butanoate analogue **6**. The *T. tetraquetra* metabolites are sequestered from coelenterates in the nudibranch's diet.

DAVID E. WILLIAMS et RAYMOND J. ANDERSEN. Can. J. Chem. **65**, 2244 (1987).

On a étudié la chimie de la peau de spécimens de dendronotides nudibranches *Tochuina tetraquetra* recueillis à Port Hardy et Bamfield, Columbie britannique. Les animaux de Port Hardy fournissent de l'acétate de tochuinyle (**1**) et de l'acétate de dihydrotochuinyle (**2**), deux nouveaux sesquiterpénoïdes du cuparane, ainsi que du rubifolide (**3**) et du pukalide (**4**), deux diterpénoïdes antérieurement connus du cembrane. Les animaux de Bamfield fournissent la ptilosarcénone (**5**), un diterpénoïde connu du type de la briaréine, et l'analogue buténoate **6** qui était antérieurement inconnu. Les métabolites du *T. tetraquetra* sont séquestrés des coélentérates dans la diète de la nudibranche.

[Traduit par la revue]

Can. J. Chem. Downloaded from www.nrcresearchpress.com by 213.166.140.6 on 09/07/12
For personal use only.

The cold temperate waters of coastal British Columbia are inhabited by more than 100 species of subtidal and intertidal nudibranchs (1). Many of these species are abundant and easily collected by SCUBA. We have found that the skin extracts of a number of British Columbia nudibranchs contain interesting secondary metabolites (2). The majority of the compounds isolated to date have been sesquiterpenoids or diterpenoids. We have also found that many of the metabolites are of dietary origin (3). A variation in skin chemistry from one collecting site to the next, reflecting a change in the nudibranch's diet, provides strong evidence for a dietary origin (3, 4). It has been shown by us and others that nudibranchs can sequester secondary metabolites, sometimes selectively, from dietary sponges (4), bryozoans (5), soft corals (6), and hydroids (7).

Tochuina tetraquetra is a large (up to 30 cm) orange-yellow dendronotid nudibranch that is commonly found from the Kuril Islands, USSR, to the Santa Cruz Islands, California (8). We have made collections of *T. tetraquetra* from two British Columbia sites and we wish to report the isolation of tochuinyl acetate (**1**), dihydrotochuinyl acetate (**2**), rubifolide (**3**), and pukalide (**4**) from Port Hardy animals, and the isolation of ptilosarcenone (**5**) and its butanoate analogue **6** from Barkley Sound animals.

Specimens of *T. tetraquetra* were collected by hand using SCUBA at depths of −3 to −15 m. Freshly collected whole animals were immersed in methanol as soon as they were brought to the surface. After extraction at room temperature for at least 48 h, the methanol was decanted, concentrated *in vacuo*, and partitioned between brine and ethyl acetate. The ethyl acetate soluble materials were fractionated by silica gel preparative tlc and reverse phase hplc to give pure metabolites.

Port Hardy animals

Tochuinyl acetate (**1**) was obtained as a colorless oil that gave a parent ion at m/z 260.1777 daltons in the EIMS, appropriate for a molecular formula of $C_{17}H_{24}O_2$ (deviation 0.0 mmu). A carbonyl stretching band at 1735 cm^{-1} in the ir, in combination with a methyl singlet resonance at 1.94 ppm in the ^1H nmr and a carbonyl resonance at 171.2 ppm in the ^{13}C nmr, identified an acetate residue. Additional methyl singlets at 1.13, 1.33, and 2.30 ppm in the ^1H nmr suggested that the remaining 15 carbon atoms of tochuinyl acetate were part of a sesquiterpenoid fragment.

The ^1H nmr resonances at 2.30 (s, 3H), 7.08 (d, J = 8 Hz, 1H), and 7.22 (d, J = 8 Hz, 1H) ppm, ^{13}C nmr resonances at 20.8 (CH_3), 126.7 (2CH), 128.6 (2CH), 135.3 (C), and 142.9 (C) ppm, and a ms fragment at m/z 91 (C_7H_7) were assigned to a 4-methylphenyl moiety. A pair of ^1H nmr signals at 3.36 (d, J = 11 Hz, 1H) and 3.59 (d, J = 11 Hz, 1H) ppm were assigned to the geminal protons of a tertiary acetoxymethyl group. The molecular formula of tochuinyl acetate required six degrees of unsaturation, which could be satisfied by the phenyl ring, the acetate carbonyl, and an additional carbocyclic ring.

Structure **1**, based on a cuparene sesquiterpenoid skeleton, effectively accounted for all the spectral features of tochuinyl acetate. Two SINEPT (9) experiments, optimized for polarization transfer through 7-Hz coupling, confirmed the proposed constitution. Irradiation of the methyl resonance at 1.13 ppm (Me15) showed transfer to carbon resonances at 34.8 (C10), 47.4 (C7 or C11), 49.8 (C7 or C11), and 70.6 (C14) ppm; irradiation of the methyl resonance at 1.33 (Me13) ppm showed transfer to carbon resonances at 37.6 (C8), 47.4 (C7 or C11), 49.8 (C7 or C11), and 142.9 (C6) ppm. A series of difference nOe (nuclear Overhauser enhancement) experiments established that the relative stereochemistry about the cyclopentane ring was as shown in **1**. Irradiation of the methyl resonance at 1.13 ppm (Me15) induced nOe's into the methyl resonance at 1.33 (Me13), the geminal methylene protons at 3.36 and 3.59 (H14 and H14a), and into the aromatic protons at 7.22 (H1 and H5) ppm. Irradiation of the methyl resonance at 1.33 (Me13) ppm induced nOe's into the methyl resonance at 1.13 (Me15) and the aromatic resonance at 7.22 (H1 and H5) ppm.

Dihydrotochuinyl acetate (**2**) was also obtained as a colorless oil that gave a parent ion at m/z 262.1926 daltons in the EIMS, appropriate for a molecular formula of $C_{17}H_{26}O_2$ (deviation −0.7 mmu). A fragment ion at m/z 260 in the ms of **2** indicated a facile loss of H_2 from the parent ion, and the ^1H and ^{13}C nmr

[1]Author to whom correspondence may be addressed.

Can. J. Chem. Downloaded from www.nrcresearchpress.com by 213.166.140.6 on 09/07/12
For personal use only.

TABLE 1. ^{1}H nuclear magnetic resonance assignments for tochuinyl acetate (**1**) and dihydrotochuinyl acetate (**2**). Spectra were run in $CDCl_3$ and chemical shifts are reported in ppm from internal TMS

Carbon no.	Tochuinyl acetate (**1**)	Dihydrotochuinyl acetate (**2**)
1	7.22 (d, J = 8 Hz, 1H)	2.70 (m, 2H)
2	7.08 (d, J = 8 Hz, 1H)	5.39 (m, 1H)
4	7.08 (d, J = 8 Hz, 1H)	2.61 (m, 2H)
5	7.22 (d, J = 8 Hz, 1H)	5.53 (bs, 1H)
8	1.75–1.88 (m)	2.20 (m, 1H)
	2.48 (m, 1H)	1.65–1.80 (m)[a]
9	1.75–1.88 (m)	1.42–1.55 (m)[a]
		1.65–1.80 (m)[a]
10	1.58 (m, 1H)	1.42–1.55 (m)[a]
	1.75–1.88 (m)	1.65–1.80 (m)[a]
12	2.30 (s, 3H)	1.65 (s, 3H)
13	1.33 (s, 3H)	1.07 (s, 3H)[b]
14	3.36 (d, J = 11 Hz, 1H)	3.74 (d, J = 11 Hz, 1H)
	3.59 (d, J = 11 Hz, 1H)	3.81 (d, J = 11 Hz, 1H)
15	1.13 (s, 3H)	1.04 (s, 3H)[b]
17	1.94 (s, 3H)	2.02 (s, 3H)

[a–b]Signals within a column may be reversed.

TABLE 2. ^{13}C nuclear magnetic resonance assignments for tochuinyl acetate (**1**) and dihydrotochuinyl acetate (**2**). Spectra were run in $CDCl_3$

Carbon no.	Tochuinyl acetate (**1**)[a]	Dihydrotochuinyl acetate (**2**)[b]
1	126.7 (CH)	31.9[x]
2	128.6 (CH)	119.0[w]
3	135.3 (C)	130.5[y]
4	128.6 (CH)	28.4[x]
5	126.7 (CH)	119.1[w]
6	142.9 (C)	138.5[y]
7	49.8 (C)[v]	50.3
8	37.6 (CH_2)	37.0[z]
9	20.2 (CH_2)	20.1
10	34.8 (CH_2)	35.3[z]
11	47.4 (C)[v]	46.9
12	20.8 (CH_3)	22.7[v]
13	25.0 (CH_3)	22.8[v]
14	70.6 (CH_2)	70.1
15	19.5 (CH_3)	19.5[v]
16	171.2 (C)	171.4
17	20.9 (CH_3)	21.0

[a]Hydrogen attachments were determined using a gated decoupled ^{13}C and 2D-HETCOR spectrum.

[b]Assignments based on chemical shifts, a gated decoupled ^{13}C spectrum, 2D-HETCOR, and SINEPT experiments.

[v–z]Signals within a column may be reversed.

spectra of **2** suggested that it was the 1,4-dihydro derivative of **1**. Thus, the ^{1}H and ^{13}C resonances assigned to the 4-methylphenyl fragment in the nmr spectra of **1** (Tables 1 and 2), were replaced in the nmr spectra of **2** with ^{1}H resonances at 1.65 (s, 3H), 2.61 (m, 2H), 2.70 (m, 2H), 5.39 (bs, 1H), and 5.53 (bs, 1H) ppm, and ^{13}C resonances at 28.4 (CH_2), 31.9 (CH_2), 119.0 (CH), 119.1 (CH), 130.5 (C), and 138.5 (C) ppm, which could be assigned to a 1-alkyl-4-methyl-1,4-cyclohexadiene residue. Dihydrotochuinyl acetate (**2**) was quantitatively converted to tochuinyl acetate (**1**) by dehydrogenation with palladium on charcoal in refluxing ethanol in accordance with the proposed structure.

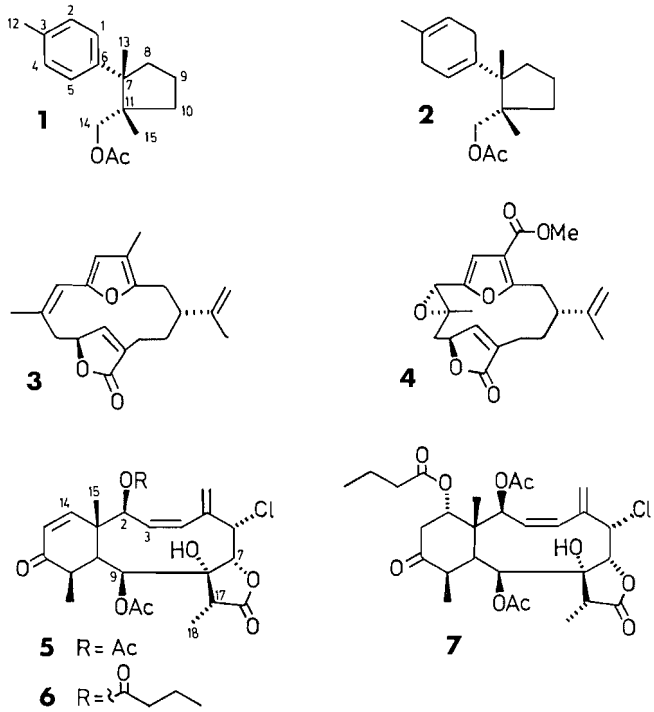

We subsequently isolated tochuinyl acetate (**1**) and dihydrotochuinyl acetate (**2**) as minor constituents from extracts of the soft coral *Gersemia rubiformis*. *Tochuina tetraquetra* is often found feeding on *G. rubiformis*. To the best of our knowledge, **1** and **2** represent the first examples of cuparane sesquiterpenoids isolated from a soft coral.

The two final components of the Port Hardy *T. tetraquetra* extracts were the known diterpenoids rubifolide (**3**) (10) and pukalide (**4**) (11). Rubifolide was shown to be identical to an authentic sample by spectroscopic and tlc comparison. Pukalide was identified by comparison of its spectral data to literature values.

Bamfield animals

Skin extracts of the Bamfield specimens of *T. tetraquetra* contained only the known diterpenoid ptilosarcenone (**5**) (12) and its butanoate analogue **6**, which has not been previously reported. Ptilosarcenone was identified by comparing its ^{1}H nmr spectrum to the ^{1}H nmr spectrum of authentic material.

Butanoate **6** was obtained as a colorless oil that showed a weak parent ion in the EIMS at 508.1873 daltons, corresponding to a molecular formula of $C_{26}H_{33}ClO_8$. The ^{1}H nmr spectrum indicated that **6** was closely related to ptilosarcenone (**5**); however, one of the acetate resonances in the spectrum of **5** was replaced in the spectrum of **6** by resonances at 0.99 (t, J = 7 Hz, 3H), 1.71 (m, 2H), 2.38 (t, J = 7 Hz, 2H) ppm assigned to a butanoate ester. A series of difference nOe experiments demonstrated that the butanoate ester in **6** was attached to C2, while the acetate ester was attached to C9. Irradiation of the acetate methyl resonance at 2.20 ppm induced nOe's into Me15 (1.17), H3 (5.60), and H7 (4.98), while simultaneous irradiation of the butanoate α-methylene (H24 and H24a) proton resonance and the H17 resonance, which both occur at 2.38 ppm, induced nOe's into H7 (4.98, from H17), H9 (5.46, from H17), Me18 (1.20, from H17), and H14 (6.58, from butanoate α-CH_2).

Ptilosarcenone was reported to be generated by facile elimination of butanoic acid from ptilosarcone (**7**) (12). To

TABLE 3. ^{1}H nuclear magnetic resonance assignments for the butanoate (**6**) and ptilosarcenone (**5**) (12). Spectra were run in $CDCl_3$ and chemical shifts are reported in ppm from internal TMS

Carbon no.	Butanoate (**6**)	Ptilosarcenone (**5**)
2	5.79 (d, J = 9 Hz, 1H)	5.72 (d, J = 9 Hz, 1H)
3	5.60 (dd, J = 12, 9 Hz, 1H)	5.63 (dd, J = 12, 9 Hz, 1H)
4	5.93–5.96 (m)[a]	5.99 (d, J = 12 Hz, 1H)
6	5.23 (dm, J = 4 Hz, 1H)	5.26 (ddd, J = 4, 2, 1 Hz, 1H)
7	4.98 (d, J = 4 Hz, 1H)	5.01 (d, J = 4 Hz, 1H)
9	5.46 (d, J = 8 Hz, 1H)	5.49 (d, J = 7 Hz, 1H)
10	2.73 (m, 1H)	2.82 (m, 1H)
11	2.79 (m, 1H)	2.82 (m, 1H)
13	5.87 (d, J = 11 Hz, 1H)	5.90 (d, J = 11 Hz, 1H)
14	6.58 (d, J = 11 Hz, 1H)	6.61 (d, J = 11 Hz, 1H)
15	1.17 (s, 3H)	1.18 (s, 3H)
16	5.93–5.96 (m)[a]	5.96 (dd, J = 2, 1 Hz, 1H)
	6.12 (dm, J = 1 Hz, 1H)	6.12 (dd, J = 1, 1H, 1H)
17	2.36 (q, J = 7 Hz, 1H)	2.41 (q, J = 7 Hz, 1H)
18	1.20 (d, J = 7 Hz, 3H)	1.21 (d, J = 7 Hz, 3H)
20	1.30 (d, J = 7 Hz, 3H)	1.30 (d, J = 7 Hz, 3H)
22	2.20 (s, 3H)	
24	2.38 (t, J = 7 Hz, 2H)	
25	1.71 (6, J = 7 Hz, 2H)	
26	0.99 (t, J = 7 Hz, 3H)	

[a]Signals lie partially on top of one another.

discount the possibility that **5** and **6** were isolation artifacts, we carried out a rapid work-up of a $CHCl_3$ extract of freshly collected *T. tetraquetra* specimens. We found only diterpenes **5** and **6** with no trace of the putative parent compounds, for example ptilosarcone (**7**). It appears that ptilosarcenone (**5**) and its butanoate analogue **6** are the metabolites actually present in the skin extracts of *T. tetraquetra*.

Discussion

All of the metabolites present in the skin extracts of *T. tetraquetra*, with the exception of pukalide, can be directly traced to the coelenterates that make up its diet. Tochuinyl acetate (**1**), dihydrotochuinyl acetate (**2**), and rubifolide (**3**) are all metabolites of the soft coral *Gersemia rubiformis*, which is one of the major dietary organisms of Port Hardy animals (10). Pukalide has been reported as a metabolite of the tropical soft coral *Sinularia abrupta* (11*a*) and the tropical gorgonian *Lophogorgia rigida* (11*b*); however, *G. rubiformis* is the only species of soft coral or gorgonian reported to grow in the same habitat as *T. tetraquetra* (1) and we have not been able to find pukalide in *G. rubiformis* extracts. Thus, the exact origin of pukalide remains unknown. It could be an extremely minor metabolite of *G. rubiformis* that has eluded us thus far, it could be a metabolite of an as yet unreported soft coral, or it could result from chemical transformations carried out by the nudibranch on some *G. rubiformis* metabolite. Ptilosarcenone (**5**) has been reported as one of the major metabolites of the sea pen *Ptilosarcus gurneyi* (12), which is a component of the diet of Bamfield specimens of *T. tetraquetra*. An exhaustive study of the metabolites of *P. gurneyi* collected at Seattle, Washington, and Sidney, B.C, failed to uncover the butanoate analogue **6** or any metabolite that could be viewed as a precursor to it (13). Probably the chemistry of the Bamfield population of *P. gurneyi* differs slightly from the Strait of Georgia and Puget Sound populations.

Experimental

The ^{1}H nmr spectra were recorded on Varian XL-300 and Bruker WH-400 spectrometers. The ^{13}C nmr spectra were recorded on a Varian XL-300 spectrometer. TMS was used as an internal standard. Low resolution mass spectra were recorded on an AEI MS902 spectrometer and high resolution mass spectra on an AIE MS50 spectrometer. The ir spectra were recorded on a Perkin–Elmer 1710 Fourier Transform spectrometer. Ultraviolet–visible spectra were recorded on a Bausch and Lomb Spectronic-2000 instrument. Optical rotation measurements were recorded on a Perkin–Elmer 141 polarimeter.

Merck silica gel 230–400 mesh was used for flash and preparative thin-layer chromatography and a Whatman Magnum-9 Partisil-10 column was used for preparative hplc.

Specimens of *Tochuina tetraquetra* were collected by hand using SCUBA in several exposed rocky channels (−5 to −15 m) located within the Gordon Group of Islands, Port Hardy, British Columbia (found feeding on or sitting nearby *Gersemia rubiformis*—two animals were collected), and within the Deer Group of Islands, Barkley Sound, British Columbia ("Bamfield animals"—three animals were collected).

Freshly collected animals were immediately immersed in methanol and extracted at room temperature for 2–3 days before decanting the methanol to give a first skin extract. Fresh methanol was added to the animals and they were left for a further 2 days. The second methanol extract was decanted and the two skin extracts were combined.

Port Hardy animals

The methanol extract (1000 mL) was concentrated *in vacuo* to 50 mL and partitioned between brine (100 mL) and ethyl acetate (4 × 150 mL). The combined ethyl acetate layers were dried over sodium sulphate for 2 h and then reduced *in vacuo* to yield 0.5 g of an orange oil.

The oil was fractionated by preparative thin-layer silica gel chromatography (2% methanol/98% methylene chloride) to yield two short wave uv active bands. The least polar band contained 10.7 mg of a mixture of rubifolide (**3**), tochuinyl acetate (**1**), dihydrotochuinyl acetate (**2**), and fats (R_f 0.66). The more polar band contained pukalide

Can. J. Chem. Downloaded from www.nrcresearchpress.com by 213.166.140.6 on 09/07/12
For personal use only.

(**4**) and fats (R_f 0.28). The polar band was further purified via reverse phase hplc (70% methanol/30% water) to yield 15.7 mg of pukalide (**4**) as a white solid (powdery).

The less polar band was further fractionated on reverse phase hplc (80%/15%/5% methanol/water/methylene chloride) to yield crude samples of rubifolide (**3**), tochuinyl acetate (**1**), and dihydrotochuinyl acetate (**2**). Repetitive reverse phase hplc purifications (80%/15%/5% methanol/water/methylene chloride) on these crude samples yielded pure rubifolide (**3**) as a white crystalline solid (4.2 mg), and pure samples of tochuinyl acetate (**1**) (1.4 mg) and dihydrotochuinyl acetate (**2**) (0.7 mg), both as clear oils.

Bamfield animals

The methanol extract (1000 mL) was worked up as described above to yield 0.6 g of an orange oil.

The oil was fractionated by preparative thin-layer silica gel chromatography (2% methanol/98% methylene chloride) to yield a uv active (254 nm) band (R_f 0.25). This band was further purified on reverse phase hplc (70% methanol/30% water) to yield ptilosarcenone (**5**) (7.2 mg) as an amorphous solid, and its butanoate analogue (**6**) (5.1 mg) as a glass.

In the rapid work-up, freshly collected animals were immediately immersed in chloroform and left standing at room temperature for 1 day. The chloroform (600 mL) was decanted off and reduced *in vacuo* to 200 mL before being partitioned between brine (200 mL) and ethyl acetate (4 × 200 mL). The combined ethyl acetate layers were dried over sodium sulphate and reduced to dryness *in vacuo* to give an orange oil. The oil was fractionated by preparative thin-layer chromatography using nonactivated silica gel (i.e., cured at room temperature) (eluent 8% ethyl acetate/92% methylene chloride). A uv active band (R_f 0.23) was further fractionated on normal phase hplc (15% ethyl acetate/85% methylene chloride) to yield only ptilosarcenone (**5**) and its butanoate analogue **6**. Total work-up took less than 3 days.

*Tochuinyl acetate (**1**)*: $[\alpha]_D^{25}$ −42.5° (*c* 1.09, CH_2Cl_2); R_f 0.80 (5% MeOH/95% CH_2Cl_2); ir (CH_2Cl_2): 2963, 2882, 1734, 1516, 1480, 1466, 1379, 1245, and 1034 cm^{-1}; ^1H nmr (Table 1); ^{13}C nmr (Table 2); ms, *m/z* (rel. intensity): 260 (23), 217 (3), 200 (12), 185 (13), 171 (9), 158 (51), 143 (61), 132 (100), 119 (77), 105 (48), 91 (39), 77 (13), 65 (10), 55 (12). *Exact Mass* calcd. for $C_{17}H_{24}O_2$: 260.1777; found (hrms): 260.1777.

*Dihydrotochuinyl acetate (**2**)*: $[\alpha]_D^{25}$ −29.3° (*c* 1.11, CH_2Cl_2); R_f 0.84 (5% MeOH/95% CH_2Cl_2); ir (CH_2Cl_2): 2963, 2882, 2820, 1731, 1653 (very weak), 1468, 1379, 1238, 1034, 985, and 952 cm^{-1}; ^1H nmr (Table 1); ^{13}C nmr (Table 2); ms, *m/z* (rel. intensity): 262 (24), 260 (7), 219 (2), 217 (1), 202 (21), 200 (10), 187 (26), 185 (11), 173 (17), 171 (6), 159 (31), 145 (55), 132 (85), 119 (100), 105 (78), 91 (70), 77 (39), 67 (33), 61 (41), 55 (42). *Exact Mass* calcd. for $C_{17}H_{26}O_2$: 262.1934; found (hrms): 262.1926.

*Oxidation of dihydrotochuinyl acetate (**2**)*

Dihydrotochuinyl acetate (**2**) (3.8 mg) was refluxed for 18 h in 95% ethanol (3 mL) containing a catalytic amount of palladium on activated charcoal. The palladium catalyst was filtered off (on fine sintered glass) and the ethanol filtrate was reduced to dryness to yield 3.5 mg of **1**.

*Butanoate **6***: $[\alpha]_D^{25}$ −49.2° (*c* 0.41, CH_2Cl_2); R_f 0.71 (5% MeOH/95% CH_2Cl_2); uv (MeOH) λ_{max}: 220 nm (4857); ir (CH_2Cl_2) 3590, 2940, 2880, 1790, 1735, 1689, and 1371 cm^{-1}; ^1H nmr (Table 3); ms, *m/z* (rel. intensity): 508 (0.2), 438 (5), 422 (3), 402 (3), 378 (4), 360 (4), 342 (4), 324 (4), 307 (4), 297 (4), 287 (4), 279 (5), 271 (4), 269 (7), 255 (5), 253 (5), 251 (7), 231 (14), 219 (12), 203 (10), 191 (18), 175 (15), 147 (17), 135 (32), 123 (72), 107 (27), 95 (17), 81 (14), 71 (95), 55 (13), 43 (100). *Exact Mass* calcd. for $C_{26}H_{33}ClO_8$: 508.1865; found (hrms): 508.1873.

Acknowledgements

The authors wish to thank Mike LeBlanc and the staff of the Bamfield Marine Station for assistance with collecting the invertebrates. Financial support was provided by grants to R.J.A. from the Natural Sciences and Engineering Research Council of Canada and Rohm and Haas Co. D.W. was supported by a UBC graduate fellowship. The authors wish to thank Dr. D. J. Faulkner for supplying an ^1H nmr spectrum of authentic ptilosarcenone, and Dr. P. J. Scheuer for supplying an ^1H nmr spectrum of authentic pukalide.

1. W. C. Austin. An annotated checklist of marine invertebrates in the cold temperate Northeast Pacific, Khoyatan Marine Laboratory, Cowichin Bay, B.C. 1985.
2. K. Gustafson and R. J. Andersen. Tetrahedron, **41**, 1101 (1985).
3. D. W. Williams, S. W. Ayer, and R. J. Andersen. Can. J. Chem. **64**, 1527 (1986).
4. (*a*) J. Hellou, R. J. Andersen, and J. Thompson. Tetrahedron, **38**, 1875 (1982); (*b*) J. E. Thompson, R. P. Walker, S. J. Wratten, and D. J. Faulkner. Tetrahedron, **38**, 1865 (1982).
5. B. Carte and D. J. Faulkner. J. Org. Chem. **48**, 2314 (1983).
6. J. C. Coll, B. F. Bowden, D. M. Tapiolas, R. H. Willis, P. Djura, M. Streamer, and L. Trott. Tetrahedron, **41**, 1085 (1985).
7. G. Cimino, S. De Rosa, S. De Stephano, and G. Sodano. Tetrahedron Lett. **21**, 3303 (1980).
8. D. W. Behrens. *In* Pacific Coast nudibranchs. Sea Challengers, Los Osos, CA. 1980.
9. A. Bax. J. Magn. Reson. **57**, 314 (1984).
10. D. Williams, R. J. Andersen, G. Van Duyne, and J. Clardy. J. Org. Chem. **52**, 332 (1987).
11. (*a*) M. G. Missakian, B. J. Burreson, and P. J. Scheuer. Tetrahedron, **31**, 2513 (1975); (*b*) M. M. Bandurraga. Ph.D. thesis, University of California, San Diego. 1982.
12. S. J. Wratten, W. Fenical, D. J. Faulkner, and J. C. Wekell. Tetrahedron Lett. 1559 (1977).
13. R. L. Hendrickson and J. H. Cardellina II. Tetrahedron, **42**, 6565 (1986).

Can. J. Chem. Downloaded from www.nrcresearchpress.com by 213.166.140.6 on 09/07/12
For personal use only.

Additivity of the partial molar volumes of organic compounds

NORIO NISHIMURA, TOHRU TANAKA, AND TAKUSHI MOTOYAMA
Department of Chemistry, Faculty of Science, Okayama University, Tsushima, Okayama 700, Japan

Received December 5, 1986

NORIO NISHIMURA, TOHRU TANAKA, and TAKUSHI MOTOYAMA. Can. J. Chem. **65**, 2248 (1987).

A critical test of additivity for partial molar volume has been made at 25°C in CCl_4 with polyethylene glycol dimethyl ethers, crown ethers, cycloalkanes, *n*-alkanes, and others. Plots of partial molar volume at infinite dilution ($\bar{V}^0$) against the properly chosen number of repeating unit (n) are linear except for small cyclic molecules, and the slopes of homologous straight chain and ring compounds are the same. The values of $\bar{V}^0$ extrapolated to $n = 0$ for cycloalkanes and crown ethers support the validity of the contribution due to the translational kinetic energy that has been predicted recently on a theoretical basis. The importance of packing efficiencies around the solute molecules has been examined by means of simple models.

NORIO NISHIMURA, TOHRU TANAKA et TAKUSHI MOTOYAMA. Can. J. Chem. **65**, 2248 (1987).

Opérant à 25°C, dans des solutions de CCl_4, on a effectué une évaluation critique de l'additivité des volumes molaires partiels pour des éthers diméthyliques du polyéthylène glycol, des éthers couronnes, des cycloalcanes, des *n*-alcanes et d'autres composés. A l'exception des molécules contenant des petits cycles, on a trouvé qu'il existe une relation linéaire entre les volumes molaires partiels à dilution infinie ($\bar{V}^0$) et le nombre choisi approprié d'unités periodiques (n); de plus, les pentes des courbes pour les composés homologues aliphatiques sont les mêmes que celles pour les composés cycliques. Pour les cycloalcanes et pour les éthers couronnes, les valeurs de ($\bar{V}^0$) extrapolées à $n = 0$ sont en accord avec la prédiction qui a récemment été faite sur une base théorique et selon laquelle on prévoit une contribution de la part de l'énergie cinétique de translation. Utilisant des modèles simples, on a étudié l'importance des efficacités d'empilement autour des molécules de solutés.

[Traduit par la revue]

Introduction

Volume additivity has been assumed since the end of the 19th century. For example, Traube (1) considered the molar volume as consisting of a covolume (ϕ) that corresponds to the free volume term in the van der Waals equation, and the sum of atomic volumes based on the constituent atoms:

$$[1] \quad V = \phi + \Sigma n^i V^i$$

Here n^i is the number of, and V^i is the volume associated with, atoms of type i. A similar equation that does not involve the ϕ terms was proposed by Exner (2).

Recently, Edward and co-workers (3–5) measured a vast number of compounds in various solvents. They concluded that the partial molar volume of alkanes at infinite dilution ($\bar{V}^0$) can be expressed by

$$[2] \quad \bar{V}^0 = V_c + n^k I^k + Z_g^l \delta^l + C$$

where the first term is a constant covolume; n^k is the number of, and I^k the volume increment associated with, atomic groups of type k; Z_g^l is the average number of *gauche* interactions of type l and δ^l the volume change associated with the interaction; C is a cyclization parameter the magnitude of which depends on the number of skeletal atoms in the ring. Using eq. [2], they estimated the value of V_c and I^k by means of a least-squares fitting of their experimental data. Citing Stillinger's theory (6), they advocated that the estimated V_c of 11.61 cm^3/mol (in CCl_4 at 25°C) is the volume increase that would result even for a point particle on account of its kinetic contribution (5). However, the kinetic contribution predicted by Stillinger on the basis of the scaled-particle theory is $\kappa_T RT$ (2–3 cm^3/mol for most solvents). It is curious that they made no comment on this large discrepancy.

Another important contribution has been made by Teresawa and co-workers (7) who showed that the partial molar volume of a series of homologous compounds can be related to their van der Waals volume:

$$[3] \quad \bar{V}^0 = aV_w + b$$

where a and b are constants for the series of interest at constant temperature and pressure. At first sight, one might think that the b term corresponds to the covolume V_c, since b is the volume at $V_w = 0$. However, it is not the case, as will be shown later.

Very recently, Yoshimura and Nakahara (8) derived expressions for the volume change accompanying contact-complex formation in hard-sphere fluids. They pointed out that the volume change is composed of two terms related to (*i*) molecular packing and (*ii*) thermal motion of molecules. Their ideas are of great significance for high pressure kineticists since they have not been taken into account for the activation volume ($\Delta V^{\ddagger}$) and reaction volume (ΔV). They further developed the additivity rule of the partial molar volume (9, 10). Based on the virial theorem, they have derived the following equation:

$$[4] \quad \bar{V}^0 = \bar{V}^0_{conf} + \kappa_T RT$$

where $\bar{V}^0_{conf}$ denotes the volume contribution due to the configurational interaction between solute and solvent molecules, and κ_T the isothermal compressibility of the solvent used. The second term arises from the translational motion of a solute in solution. This term is completely in accord with the one derived by Stillinger. They have shown that the additivity rule for *n*-alkanes consisting n methylene units can be expressed as

$$[5] \quad \bar{V}^0_{conf} = \alpha n + \beta$$

and that this equation is obeyed quite accurately.

Their work has motivated us to examine the additivity scheme for a series of compounds in various solvents. In this work, we have estimated the translational contribution by using large ring compounds composed of the same repeating unit. The aspects of the volume additivity were examined by comparing ring compounds with similar chain compounds. In order to understand the essential feature of the volume additivity, branched alkanes for which vicinal steric effects may exist were avoided. The packing efficiencies around atomic groups having different size and shape have also been examined.

Can. J. Chem. Downloaded from www.nrcresearchpress.com by 213.166.140.6 on 09/07/12
For personal use only.

TABLE 1. Partial molar volumes (cm^3/mol) of various series of compounds in CCl_4 at 25°C (probable errors in parentheses)

Substance	$\bar{V}^0$	Substance	$\bar{V}^0$
1,2-Dimethoxyethane	104.85 (0.03)	CCl_4	97.09 (0.00)
Diethene glycol – dimethyl ether	143.20 (0.04)	Hexachloroethane	132.06 (0.18)
		Octachloropropane	163.83 (0.25)
Triethylene glycol – dimethyl ether	181.83 (0.03)	Cyclohexane	109.63 (0.03)
		Cyclooctane	135.22 (0.11)
Tetraethylene glycol – dimethyl ether	220.18 (0.12)	Cyclodecane	165.32 (0.22)
		Cyclododecane	197.38 (0.30)
Dioxane	85.02 (0.04)	Cyclopentadecane	248.37 (1.70)
12-Crown-4	157.59 (0.02)	Cyclohexadecane	262.46 (0.62)
15-Crown-5	196.28 (0.07)	Octane	166.26 (0.38)
18-Crown-6	234.75 (0.17)	Nonane	182.82 (0.52)
21-Crown-7	273.68 (0.72)	Undecane	216.29 (0.34)
24-Crown-8	311.85 (0.50)	Tridecane	248.78 (0.30)
Benzene	89.90 (0.02)	Tetradecane	265.33 (0.44)
Naphthalene	124.57 (0.14)	Pentadecane	283.29 (0.22)
Anthracene	158.17 (0.42)		

Can. J. Chem. Downloaded from www.nrcresearchpress.com by 213.166.140.6 on 09/07/12
For personal use only.

Experimental

Materials

Cycloalkanes $C_{15}H_{30}$ and $C_{16}H_{32}$ were prepared by reducing the corresponding cycloketones according to the modified Wolff–Kishner method (11). For $C_{15}H_{30}$: mp 65.8–66.0°C, lit. 62.3–63.5°C (12); for $C_{16}H_{32}$: mp 62.8–63°C, lit. 60–61°C (12).

Reagent grade *n*-alkanes were used as received, and the purity checked by VPC. Pure 21-crown-7 and 24-crown-8 were kindly supplied by Professor T. Iwachido. Other substances were purified either by recrystallization, distillation, or sublimation, and dried in the usual manner.

Density measurements

A Kyoto Denshi digital precision density meter DA-101B placed in an air-thermostated box was used. Solutions of different molalities were prepared and deaerated with an ultrasonic cleaner. The solution was transferred into a measurement cell by means of an air-baffle. After measurement, the solution was purged by replacing in the measurement cell the next, more concentrated solution. This process was repeated until the end. From the relationship between molality and specific volume, the partial molar volume at infinite dilution were estimated in the usual manner.

Results

The partial molar volumes of polyethylene glycol dimethyl ethers (PEGDE), crown ethers (CE), *n*-alkanes (NA), cycloalkanes (CA), and other kinds of compounds in CCl_4 at 25°C are given in Table 1. Figure 1 shows the relationship between $\bar{V}^0$ and n, the number of repeating units properly chosen (for example, $n = 8$ for decane). The linear regression equations for these series of compounds are

[6] $\bar{V}^0/\text{cm}^3\ \text{mol}^{-1} = (16.6 \pm 0.1)n + (66.5 \pm 0.6)$

for *n*-alkanes ($n = 6, 7, 9, 11, 12, 13$; $r = 0.999943$).

[7] $\bar{V}^0/\text{cm}^3\ \text{mol}^{-1} = (16.4 \pm 0.2)n + (1.5 \pm 2.3)$

for cycloalkanes ($n = 10, 12, 15, 16$; $r = 0.99976$).

[8] $\bar{V}^0/\text{cm}^3\ \text{mol}^{-1} = (38.5 \pm 0.0)n + (66.4 \pm 0.1)$

for PEGDE (repeating unit = —O—CH_2—CH_2—; $n = 1, 2, 3, 4$; $r = 0.99999$).

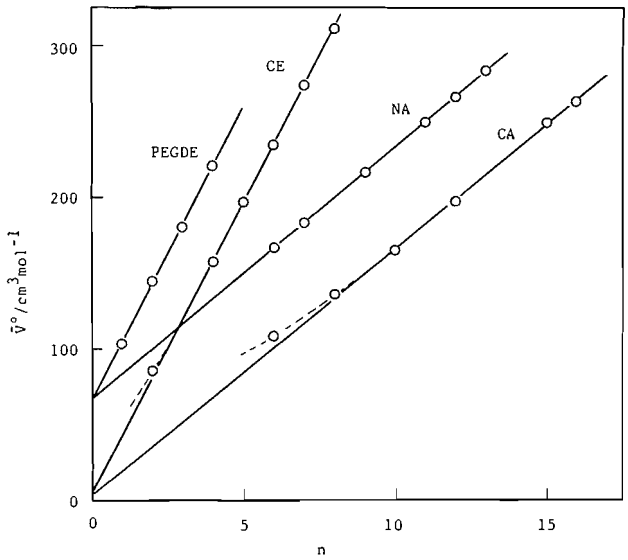

FIG. 1. Plots of the partial molar volume against the number of repeating unit for polyethylene glycol dimethyl ethers (PEGDE), crown ethers (CE), *n*-alkanes (NA), and cycloalkanes (CA).

[9] $\bar{V}^0/\text{cm}^3\ \text{mol}^{-1} = (38.6 \pm 0.4)n + (3.3 \pm 0.3)$

for crown ethers ($n = 4, 5, 6, 7, 8$; $r = 0.999996$).

A similar but modified treatment can be done by using eq. [3]. For example,

[10] $\bar{V}^0/\text{cm}^3\ \text{mol}^{-1} = (1.33 \pm 0.01)V_w + (25.5 \pm 0.6)$

for aromatics ($r = 0.99996$), and

[11] $\bar{V}^0/\text{cm}^3\ \text{mol}^{-1} = (1.25 \pm 0.02)V_w + (35.2 \pm 1.9)$

for chloroalkanes ($r = 0.9996$). This is shown in Fig. 2. The van der Waals volumes were estimated by using Bondi's data (13).

Discussion

Contribution of translational motion to $\bar{V}^0$ and the validity of additivity rule

On the basis of the scaled-particle theory, Stillinger (6)

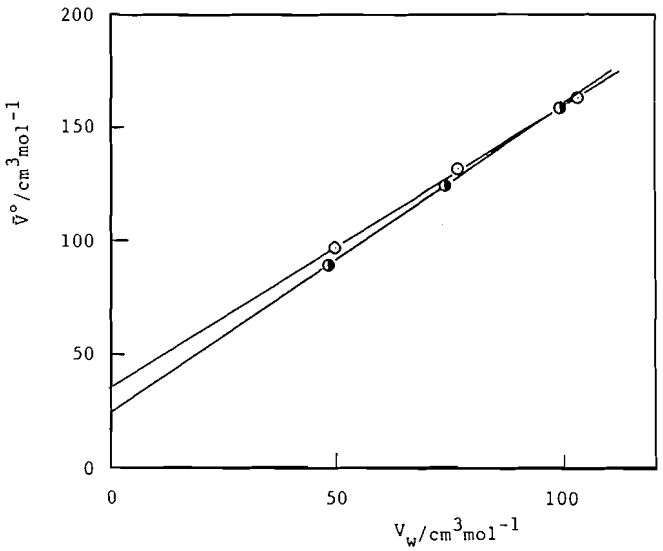

FIG. 2. $\bar{V}^0$ versus V_w plots for aromatics (—●—) and chloroalkanes (—○—).

pointed out that one of the distinct contributions to $\bar{V}^0$ is the volume increase ($= \kappa_T RT$) that would result even for a point particle on account of its kinetic contribution to pressure. The same expression has been derived by Yoshimura *et al.* (8, 9) on the basis of the virial theorem for classical fluids. However, the experimental verification of this term is difficult. As far as we are aware, no such trial has yet been made. We have undertaken to tackle the problem by using large ring compounds consisting of the same repeating unit. The reason is as follows: for normal alkanes, $\bar{V}^0_{conf}$ in eq. [5] can be written as (10)

$$[12]\quad \bar{V}^0_{conf} = n\bar{V}^0(\text{—}CH_2\text{—}) + 2\bar{V}^0(CH_3\text{—})$$

$$[13]\quad = na_1V_w(\text{—}CH_2\text{—}) + 2a_2V_w(CH_3\text{—})$$

where $\bar{V}^0(\text{—}CH_2\text{—})$ and $\bar{V}^0(CH_3\text{—})$ denote the contributions of the methylene and methyl groups to $\bar{V}^0_{conf}$, respectively; a_1 and a_2 denote the ratios $\bar{V}^0(\text{—}CH_2\text{—})/V_w(\text{—}CH_2\text{—})$ and $\bar{V}^0(CH_3\text{—})/V_w(CH_3\text{—})$, respectively, and are the partial molar volumes normalized to their van der Waals volumes. The a terms measure how loosely the molecular moiety (or molecule) in question is packed. From eqs. [4] and [12], we have

$$[14]\quad \bar{V}^0 = n\bar{V}^0(\text{—}CH_2\text{—}) + 2\bar{V}^0(CH_3\text{—}) + \kappa_T RT$$

For cycloalkanes we have

$$[15]\quad \bar{V}^0 = n\bar{V}^0(\text{—}CH_2\text{—}) + \kappa_T RT$$

In this case, if we plot $\bar{V}^0$ against n, and extrapolate to $n = 0$, the intercept should be $\kappa_T RT$. This equation can be applied to any cyclocompounds consisting of the same repeating unit. The intercepts for CA and CE are (1.5 ± 2.3) cm^3/mol and (3.3 ± 0.3) cm^3/mol, respectively (eqs. [7] and [9]). These values may be compared with the reported values of $\kappa_T RT/cm^3\ mol^{-1}$ = 2.64 (14), 2.62 (15), and 2.67 (16) for CCl_4 at 25°C and 1 atm. If the number of measurement points, experimental accuracy for estimating $\bar{V}^0$, and inevitable uncertainties involved in the estimation of the intercept are taken into account, the intercepts of such compounds could be regarded as the $\kappa_T RT$ term. Indeed, if $\kappa_T RT$ = 2.64 cm^3/mol is fixed, the average slopes of the $\bar{V}^0$ vs. n plot only change from 16.4 (eq. [7]) to 16.3 for CA, and from 38.6 (eq. [9]) to 38.7 for CE. It is noted that the covolume of 11.61 cm^3/mol proposed by Edward *et al.* (3–5) has no theoretical background in spite of that the arbitrariness of the value of covolume appeared in the literature was discussed by them.

The second remarkable point in Fig. 1 is that the strictly linear relationship between $\bar{V}^0$ and n holds for each series of compounds and that, if we eliminate the data for small-membered ring compounds (*vide infra*), the slopes of the plots for NA and CA, and PEGDE and CE are virtually the same (eqs. [6]–[9]). The above findings means that all the repeating units, irrespective of their positions, contribute equally to $\bar{V}^0$. In other words, the solvent CCl_4 as a probe for tracing volumes cannot distinguish the position and/or conformations with respect to neighbours (*trans* and *gauche*) of these repeating groups.

The third notable point is that for small-membered ring compounds, deviations from linearity can be observed. According to Edward *et al.*, an additional cyclization parameter C (eq. [2]) which varies with the number n of ring atoms for alkanes, from C = 5.3 cm^3/mol (n = 3) to C = −21.0 cm^3/mol (n = 10). Judging from features in Fig. 1, it is clear that this way of correction is upside down. The reason for the upward deviations for small-membered ring compounds has been discussed (10) using and comparing cylindrical and torus models for the linear alkanes and cycloalkanes, respectively.

Generalized form of the additivity rule

Let us consider a chain molecule of the type A—(B)$_n$—A. Equation [14] can be generalized as

$$[16]\quad \bar{V}^0 = n\bar{V}^0(\text{—}B\text{—}) + 2\bar{V}^0(A\text{—}) + \kappa_T RT$$

$$[17]\quad = na_1V_w(\text{—}B\text{—}) + 2V_wa_2(A\text{—}) + \kappa_T RT$$

The van der Waals volume can be written as

$$[18]\quad V_w = nV_w(\text{—}B\text{—}) + 2V_w(A\text{—})$$

From eqs. [17] and [18], it is deduced that if we plot $\bar{V}^0$ against V_w for a series of the A—(B)$_n$—A type of molecules, then the trajectory of $P(\bar{V}^0, V_w)$ on the V_w–V^0 vector plane constitutes two straight lines as shown in Fig. 3. It is clear that the point b (see eq. [3]) has no physical meaning. Alternatively, such aspects can be explained in terms of two kinds of operations: addition and substitution. An increase in the chain number for n-alkanes, for example, is a kind of addition operation. Introduction of C in place of A for A—(B)$_n$—A type of molecules is a kind of substitution operation. Generally, the volume change $\Delta\bar{V}^0$ upon substitution of an atomic group or an atom Y— in place of X— can be expressed as

$$[19]\quad \Delta\bar{V}^0 = \bar{V}^0(Y\text{—}) - \bar{V}^0(X\text{—})$$

Repetition of these operations constitutes a network. An example is shown in Fig. 4. It must be noted that the above additivity rule would hold strictly only when mesomeric and vicinal steric effects or special interactions such as hydrogen bonding can be neglected. If it is not so, corrections would be necessary as in the case of van der Waals volume calculations (13).

Significance of molecular packing around atomic groups of different sizes and shapes

By using the data in Table 1 and eqs. [6]–[12] and [14], we can allot the partial molar volumes for any atomic groups. For example, $\bar{V}^0(\text{—}CH_2\text{—})$ = 16.5 cm^3/mol (average of the

Can. J. Chem. Downloaded from www.nrcresearchpress.com by 213.166.140.6 on 09/07/12
For personal use only.

Can. J. Chem. Downloaded from www.nrcresearchpress.com by 213.166.140.6 on 09/07/12
For personal use only.

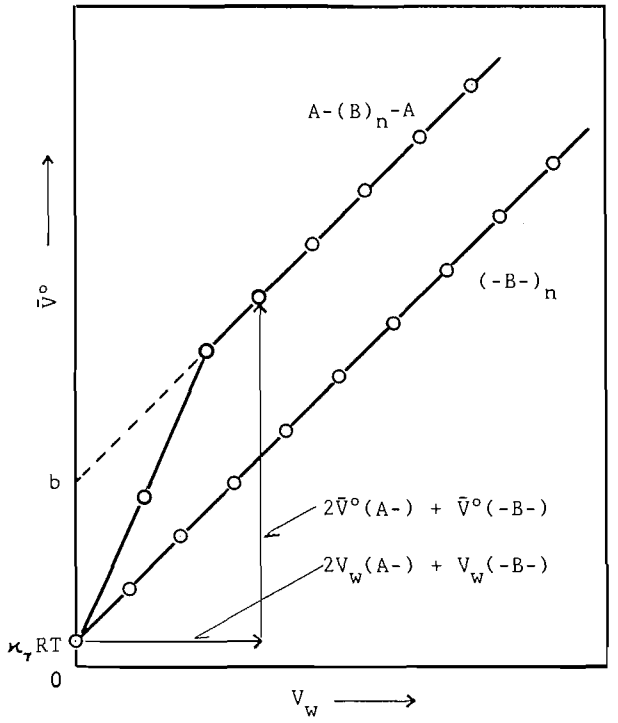

FIG. 3. Schematic representation of the relationship between $\bar{V}^0$ and V_w for a series of compounds of the type A—(B)$_n$—A and (—B—)$_n$.

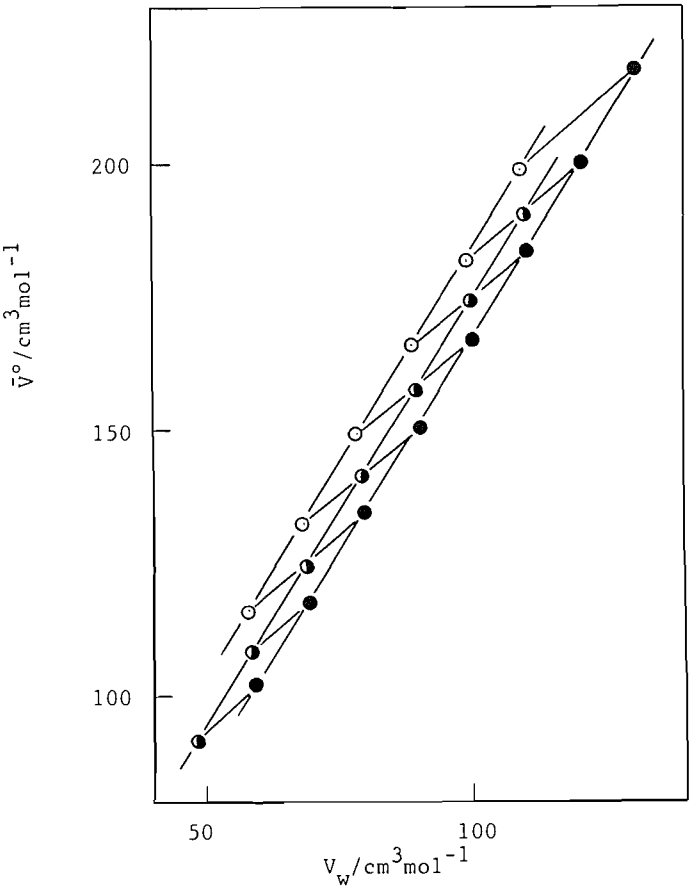

FIG. 4. Example of a network as a result of addition and substitution operation. (—○—): CH_3—$(CH_2)_n$—CH_3; (—◑—): $BrCH_2$—$(CH_2)_n$—CH_3; (—●—): $BrCH_2$—$(CH_2)_n$—CH_2Br. Data cited from ref. 4.

slopes of the straight lines in eqs. [6] and [7]). Once it is fixed, then $\bar{V}^0(CH_3—) = 32.0\,cm^3/mol$ can be estimated by using eqs. [6] and [14], and so on. The partial molar volumes allotted for several atomic groups are given in Table 2, together with their van der Waals volumes calculated by using Bondi's data (13). The *a* term in the table denotes the partial molar volumes reduced to their van der Waals volumes, and the value measures how loosely the atomic group in question is packed. The data for benzene, naphthalene, anthracene, carbon tetrachloride, and adamantane are also given for the sake of discussion in this section.

Inspection of the data in Table 2 reveals some interesting points. First of all, the partial molar volume allotted for atomic groups is not always proportional to their van der Waals volume. For example, $\bar{V}^0(H—)$ is as large as $\bar{V}^0(—CH_2—)$. Further, $\bar{V}^0(\text{—}\underset{|}{C}\text{—})$ has a negative volume of $-14.5\,cm^3/mol$. It was pointed out (3) that Exner's scheme has no covolume term, which leads to a very large $\bar{V}^0(H—)$ (14.90 cm^3/mol) and a negative increment ($-13.22\,cm^3/mol$) for carbon. These values are very near to those in Table 2. Edward *et al.* do not object to a negative increment since the additive scheme works fairly well, but this is hard to comprehend intuitively. In our opinion, the partial molar volumes in Table 2 are calculated using the empirical equations and as long as we use these values we have no problems. One must keep in mind that the "carbon" is never faced to solvents. Since $\bar{V}^0$ is determined by the interaction of a solute with the surrounding solvent molecules, the formally negative value of $\bar{V}^0(\text{—}\underset{|}{C}\text{—})$ itself bears no physical meaning.

Secondly, the reduced partial molar volume clearly reflects

TABLE 2. Partial molar volumes, van der Waals volumes allotted for atomic groups or molecules (cm^3/mol), and reduced partial molar volumes

Atomic group	$\bar{V}^0$	V_w	$a\,(=\bar{V}^0/V_w)$
$\text{—}\underset{|}{C}\text{—}$ (alkanes)	−14.5	3.33	
—CH_2—	16.5	10.2	1.62
CH_3—	32.0	13.7	2.34
H— (alkanes)	15.5	3.45	4.50
—O—CH_2—CH_2—	38.5	24.1	1.60
—CCl_2—	31.8	26.6	1.20
CCl_3—	64.7	38.2	1.69
Cl—	32.7	11.6	2.82
Benzene	89.9	48.4	1.86
Naphthalene	124.6	74.0	1.68
Anthracene	158.2	99.6	1.59
=CH—CH=CH—[a]	45.0	24.2	1.86
=CH—C=C—CH—[b]	34.5	25.6	1.35
Adamantane[c]	140.2	84.0	1.67
CCl_4	97.1	49.8	1.95
CH_4[d]	50.1	17.2	2.92

[a]Half of benzene.
[b]Inner part of naphthalene and anthracene.
[c]Data cited from ref. 5.
[d]Calcd by $\bar{V}^0(CH_4) = \bar{V}^0(CH_3—) + \bar{V}^0(H—) + \kappa_T RT$.

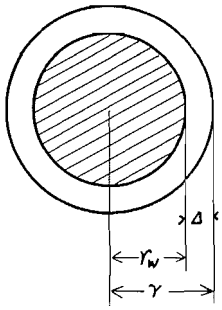

FIG. 5. A sphere-in-continuum model proposed by Edward and Farrell (17).

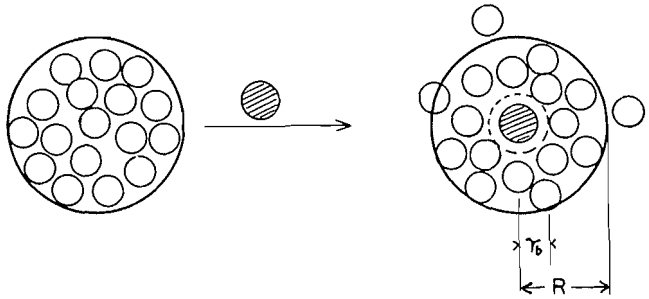

FIG. 6. Schematic representation of the physical meaning of the partial molar volume at infinite dilution ($\bar{V}^0$).

the size and shape of molecular moieties. On the molecular basis, the following sets of atomic groups or molecules having different van der Waals volumes could be regarded as similar in shape to each other: (—CH_2—, —CCl_2—), (CH_3—, CCl_3—), (H—, Cl—), and (CH_4, CCl_4, adamantane). Within these sets, the a value is always larger for the atomic group which has a smaller van der Waals volume. Thirdly, if we compare $\bar{V}^0$(CH_3—) with $\bar{V}^0$(—CH_2—), the former is unexpectedly larger than the latter. The same is true for $\bar{V}^0$(CCl_3—) and $\bar{V}^0$(—CCl_2—). We could say that the geometrical differences between "hemispherical" CH_3— and "cylindrical" —CH_2— moieties are responsible for the above findings.

Interpretation of the partial molar volume

We have seen that the size as well as shape of the atomic groups are the important factors in determining the a term. On the assumption that solute molecules are spherical, Edward and Farrell (17) have given an expression for the partial molar volume of the solute molecule of effective van der Waals radius r_w.

$$[20] \quad \bar{V}^0 = (4/3)\pi L(r_w + \Delta)^3$$

where L is the Avogadro number and Δ denotes a parameter adjusting for the void where solvent molecules are excluded (Fig. 5). By using the volume data of aliphatic and aromatic hydrocarbons in water, they examined eq. [20], and found that the average separation of the solute molecules from the solvent as a continuum is 5.3 nm.

Recently, Lee (18) developed a theory for the partial molar volume of the solute in infinitely dilute hard-sphere binary mixtures. The expression for $\bar{V}^0$ is formally the same as eq. [20]. However, Δ is not constant but a slowly varying function of r_w and depends primarily on the size of solvent molecule and the packing density of the pure solvent. According to his calculation, Δ gradually increases as the solute-to-solvent radius ratio decreases. Therefore, this theory predicts that if we measure $\bar{V}^0$ for a series of spherical solutes of varying r_w in a fixed solvent, the thickness Δ will become larger the smaller the solute molecule is. This must be kept in mind for the sake of later discussion.

Let us consider a space enveloped by a spherical surface of radius R, centered by a solute molecule. The number of solvent molecules N within the sphere is given by

$$[21] \quad N = \int_0^R 4\pi r^2 \rho_0 g(r) \mathrm{d}r$$

where ρ_0 is the number density of the pure solvent molecule and $g(r)$ is the radial distribution function at the distance r from the solute molecule. In the absence of the solute molecule, the number of solvent molecule N_0 is given by

$$[22] \quad N_0 = \int_0^R 4\pi \rho_0 r^2 \mathrm{d}r$$

If R is large enough compared with molecular dimensions, and the solution is sufficiently dilute, the partial molar volume of the solute in question at infinite dilution can be given by

$$[23] \quad \bar{V}^0 = (N_0 - N)V_0 = 4\pi L \int_0^R r^2\{1 - g(r)\}\mathrm{d}r$$

where V_0 is the molar volume of the solvent. Therefore, $\bar{V}^0$ is interpreted as the number of "solvent" molecules excluded from the space, multiplied by the solvent molar volume, as depicted in Fig. 6.

In real solutions, it is difficult to estimate the radial distribution function. In the simplest case, we assume that $g(r) = 0$ in the region $r < r_b$, and $g(r) = 1$ in the region $r > r_b$. Then it follows from eq. [23],

$$[24] \quad \bar{V}^0 = (4/3)\pi L r_b^3$$

If we set $r_w + \Delta = r_b$, eq. [24] becomes identical to eq. [20]. Therefore, this oversimplified model calculation is virtually the same as that of Edward and Farrell (Fig. 5), based on the sphere-in-continuum model. The success of their treatment for comparatively small molecules suggests that the proposed model is reasonable. Since the shapes of most of real molecules and atomic groups are far from spherical, more realistic models will be needed. We have seen that the a term depends on the size and shape of the atomic groups concerned. As the simplest models, we could regard CH_3—, CCl_3—, H—, and Cl— as hemispherical, —CH_2— and —CCl_2— as cylindrical with a height of 12.6 nm (estimated from the C—C bond length and C—C—C bond angle). Based on these models, the radius r and r_w of the sphere, hemisphere, and cylinder models can be estimated from the data in Table 2. If Δ is defined as

$$[25] \quad \Delta = r - r_w$$

as in the case of the sphere model (18), then Δ can be regarded as the thickness of the zone where the solvent molecules are excluded. In Table 3, r, r_w, and Δ are given. If a liquid consists of hard spheres and has a randomly closest packing structure (19), the radius of the sphere r could be calculated by using the following equation:

$$[26] \quad 1.56(4/3)\pi r^3 L = V - \kappa_T RT$$

where V is the molar volume of the liquid. Based on this

Can. J. Chem. Downloaded from www.nrcresearchpress.com by 213.166.140.6 on 09/07/12
For personal use only.

TABLE 3. Model calculation of r, r_w, and Δ (nm) for atomic groups and molecules

Atomic group	r	r_w	Δ	Assumed model
Adamantane	38.2	32.2	6.0	Spherical
CCl_4	33.8	27.0	6.8	
CH_4	27.1	19.0	8.1	
CCl_3—	37.2	31.2	6.0	Hemispherical
CH_3—	29.4	22.1	7.3	
Cl—	29.6	21.0	8.6	
H—	23.1	13.9	9.2	
—CCl_2—	36.5	33.4	3.1	Cylindrical
—CH_2—	26.3	20.7	5.6	

equation, r is calculated to be 28.8 nm for CCl_4, which agrees fairly well with $r_w = 27.0$ nm in Table 3.

If the data in Table 3 are inspected, we notice that the Δ values also depend on the molecular size and shape. One might think the Δ should be independent of the size and shape, since these have already been taken into account. According to our view, this dependency of the Δ value on the molecular size and shape reflects the significance of the molecular packing. In the above treatment, the solvent molecules have been regarded as continuum medium. In fact, it is not the case. In principle, if an explicit expression for $g(r)$ in eq. [23] is given for a specified system, $\bar{V}^0$ could be estimated.

A new framework for the understanding of the partial molar volume on the molecular level has also been put forward by Yoshimura and Nakahara (8). Their conclusion is essentially the same as that of Lee (18); it involves the solute to solvent size ratio, and this involvement overwhelms the classical picture of the sphere-in-continuum model. According to both theories, the solvent molecules can be packed more closely on a flat surface than on a surface of large curvature. Indeed, we can see in Table 3 that the Δ value increases in the order of increasing curvature of the surface of solute molecules or moieties. The above findings support the validity of their prediction, at least on the CPK model level.

Concluding remarks

The additive scheme we have put forward indicates the significance of molecular packing in solution. So far, however, the intrinsic volume changes ($\Delta V^{\ddagger}_{int}$, $\Delta \bar{V}^{0}_{int}$) accompanying chemical reactions have often been discussed and interpreted in terms of van der Waals volume changes. Therefore, it seems necessary to make a new framework for the intrinsic volume change for various types of chemical reactions. In this respect, the additivity rule seem to have a potential importance for the prediction of volume profile for chemical reactions, though in a limited scope for the time being. We also suggest that the contribution of translational motion to volume change will become very important, for instance, for aggregation reactions for which a great number of solute molecules aggregate to form a micelle.

Acknowledgements

The authors wish to thank Professor W. le Noble, Chemistry Department, State University of New York at Stony Brook, for his valuable suggestions and for polishing the manuscript. We also wish to thank Professor T. Iwachido, School of General Education, Okayama University, for kindly supplying crown ethers.

1. J. TRAUBE. Sammul. Chem. Vortr. **4**, 255 (1899).
2. O. EXNER. Coll. Czech. Chem. Commun. **32**, 1 (1967).
3. J. T. EDWARD, P. G. FARRELL, and F. SHAHIDI. J. Phys. Chem. **82**, 2310 (1978).
4. F. SHAHIDI, P. G. FARRELL, and J. T. EDWARD. J. Phys. Chem. **83**, 419 (1979).
5. J. T. EDWARD, P. G. FARRELL, and F. SHAHIDI. Can. J. Chem. **57**, 2585 (1979); **57**, 2887 (1979); **57**, 2892 (1979).
6. F. H. STILLINGER. J. Solution Chem. **2**, 141 (1973).
7. S. TERASAWA, H. ITSUKI, and S. ARAKAWA. J. Phys. Chem. **79**, 2345 (1975).
8. Y. YOSHIMURA and M. NAKAHARA. J. Chem. Phys. **81**, 4080 (1984).
9. Y. YOSHIMURA, J. OSUGI, and M. NAKAHARA. Ber. Bunsenges. Phys. Chem. **89**, 25 (1985).
10. Y. YOSHIMURA and M. NAKAHARA. Ber. Bunsenges. Phys. Chem. **89**, 426 (1985); **89**, 1004 (1985).
11. F. MUKAWA and W. NAGATA. Bull. Chem. Soc. Jpn. **45**, 574 (1972).
12. H. FRITZ, E. LOGEMANN, G. SCHILL, and T. WINKLER. Chem. Ber. **109**, 1258 (1976).
13. A. BONDI. J. Phys. Chem. **68**, 441 (1964).
14. R. E. GIBSON and O. H. LOEFFLER. J. Am. Chem. Soc. **63**, 898 (1941).
15. M. DIAZ PENA and M. L. MCGLASHAN. Trans. Faraday Soc. **57**, 1511 (1961).
16. G. A. HOLDER and E. WHALLEY. Trans. Faraday Soc. **58**, 2095 (1962).
17. J. T. EDWARD and P. G. FARRELL. Can. J. Chem. **53**, 2965 (1975).
18. B. LEE. J. Phys. Chem. **87**, 112 (1983).
19. Y. MARCUS. Introduction to liquid state chemistry. John Wiley and Sons. 1977.

Can. J. Chem. Downloaded from www.nrcresearchpress.com by 213.166.140.6 on 09/07/12
For personal use only.

An ^{1}H nuclear magnetic resonance study of derivatives of 3-hydroxy-12,13-epoxytrichothec-9-enes[1]

MARC E. SAVARD, BARBARA A. BLACKWELL, AND ROY GREENHALGH[2]
Plant Research Centre, Agriculture Canada, Ottawa, Ont., Canada K1A 0C6

Received March 18, 1987

MARC E. SAVARD, BARBARA A. BLACKWELL, and ROY GREENHALGH. Can. J. Chem. **65**, 2254 (1987).

The 250-MHz ^{1}H nuclear magnetic resonance spectra of 36 natural and synthetic trichothecenes have been analyzed and the chemical shifts as well as the vicinal and long-range coupling constants determined. Knowledge of the 16-CH_3 chemical shift enables the substitution pattern of the A ring to be defined. Similarly, oxygenation in the C ring results in easily identifiable resonances. The $J_{2,3}$ and $J_{3,4}$ values define the configuration of substituents at C-3 and C-4, while the configuration at C-7 and C-8 can be defined by the $J_{7,8}$, $J_{7\alpha,11}$, and $J_{7\beta,15}$ values. The trichothecene ring system adopts the most stable A-half-chair, B-chair conformation in solution. The correlations obtained allow easy structural determination of unknown trichothecenes.

MARC E. SAVARD, BARBARA A. BLACKWELL et ROY GREENHALGH. Can. J. Chem. **65**, 2254 (1987).

On a déterminé les spectres en résonance magnétique nucléaire du ^{1}H à 250 MHz de 36 trichothécènes naturels et de synthèse et on a déterminé les déplacements chimiques ainsi que les constantes de couplage tant vicinales qu'à longue distance. La connaissance du déplacement chimique du CH_3 en position 16 permet de définir le patron de substitution du cycle A. De la même manière, l'oxygénation du cycle C conduit à des résonances qui sont facilement identifiables. Les valeurs des constantes $J_{2,3}$ et $J_{3,4}$ permettent de définir la configuration des substituants dans les positions C-3 et C-4 alors que les configurations dans les positions C-7 et C-8 peuvent être définies par les valeurs des constantes $J_{7,8}$, $J_{7\alpha,11}$ et $J_{7\beta,15}$. En solution, le système de cycles des trichothécènes adopte la conformation la plus stable, impliquant un cycle A en demi-chaise et un cycle B en forme chaise. Les corrélations obtenues permettent d'attribuer facilement des structures à des trichothécènes inconnus.

[Traduit par la revue]

Can. J. Chem. Downloaded from www.nrcresearchpress.com by 213.166.140.6 on 09/07/12
For personal use only.

Introduction

Mycotoxins are common contaminants of grains in temperate climates, and result in significant economic losses in the agro-food sector. In Canada, an epidemic infestation of *Fusarium* in wheat and corn in recent years resulted in high levels of mycotoxin-contaminated grains, which, when used for feed, produced emesis in pigs (1). The causative factor was identified as 3α,7α,15-trihydroxy-12,13-epoxytrichothec-9-en-8-one (4-deoxynivalenol, DON, vomitoxin, **24**) (see Fig. 1 for the basic skeleton and numbering system of trichothecenes). A process was developed for the large-scale production of DON (2), which was required for toxicological testing and feeding trials. In addition to DON, a large number of other trichothecenes were isolated in trace amounts (2–7). These compounds are of interest because of the diverse antifungal, cytotoxic, and phytotoxic properties they exhibit.

The first trichothecene was reported by Freeman *et al.* in 1959 (8), and was followed by the characterization of several other trichothecenes (9–11). In these studies, an incorrect structure was proposed in that a reactive oxygen was misinterpreted as being part of an oxetane ring instead of an epoxide (12, 13). Most trichothecenes contain a double bond at C-9 and an epoxide ring at C-12, and are oxygenated at one or more positions. These oxygen functions can occur as esterified or free hydroxyl groups or as ketones.

Some ^{1}H nmr characteristics of the trichothecene skeleton have been reported (14–16). However, the substitution patterns of these compounds are not always readily discerned. As a result of the large number of trichothecenes isolated in our laboratory (2–7), an extensive nmr data base has been developed. The present study attempts to correlate structural features with chemical shift, and the coupling constants with the conformation of the substituents. This knowledge will facilitate the characterization of new trichothecenes.

[1]PRC Contribution No. 1044.

[2]Author to whom correspondence may be addressed.

Experimental

Instruments

The ^{1}H nmr spectra were recorded at 250 MHz on a Bruker WM 250 spectrometer. Spectra were acquired with 16K data points, a 2200-Hz spectral window, 60° pulses, and an 8-s repetition rate. Chemical shifts were referenced to deuterochloroform at 7.24 ppm and reported (ppm) relative to tetramethylsilane (Me_4Si). Confirmation of ^{1}H chemical shift assignments was made for several compounds by ^{1}H homonuclear correlation spectroscopy. The (90–t_1–45 FID) pulse sequence (COSY-45) was accumulated by using 512 × 1K FID's of 16 scans each. Sine bell windows (shifted $\pi/4$ in F_1) were employed in data processing. The spectral resolution was 1.4 Hz/point. These 2D spectra were especially useful in resolving overlapping AB systems.

Melting points were determined on a Fisher–Johns heating stage apparatus and are uncorrected. Mass spectra were obtained on either a Finnigan MAT 312 mass spectrometer or a Finnigan MAT 4500 gc/ms system. Accurate mass measurements were determined by peak matching with an ion in the spectrum of perfluorokerosene.

Chemicals

Most trichothecenes were isolated from fermentations of *Fusarium sporotrichioides* (5), *F. roseum* (3), *F. graminearum* (4), *F. culmorum* (2), or *F. crookwellense* (6). The synthesis of the T-2 analogues **16**, **17**, **18**, and **19** has been reported elsewhere (17). Other trichothecenes synthesized include:

*7,15-Diacetyl-4-deoxynivalenol (**29**) and 7-acetyl-4-DON (**26**)*

Triacetyl-DON (**30**) (7) (500 mg) was dissolved in a 100:1 solution (50 mL) of methanol and concentrated HCl and stirred overnight at room temperature. The reaction was neutralized with sodium methoxide (325 mg), concentrated, and the residue partitioned between water and ethyl acetate. The organic phase was washed with brine, dried over sodium sulfate, concentrated, and chromatographed on silica gel (50 g) with 25:75 EtOAc/hexane (200 mL) followed by 50:50 EtOAc/hexane (300 mL). Three compounds were isolated: (*a*) the starting material **30** (114 mg); (*b*) 7,15-diacetyl-4-deoxynivalenol (**29**) (230 mg, 51%), mp 142–144°C; ^{1}H nmr: see Table 2; ms: 380 (5), 338 (13), 320 (10), 278 (33), 260 (38), 248 (52), 136 (90), 108 (80), 98 (100), 79 (91), 55 (85). *Exact Mass* (ms) calcd. for $C_{19}H_{24}O_8$: 380.1471; found: 380.1481 (M^+); and (*c*) 7-acetyl-4-deoxynivalenol (**26**) (64 mg, 16%), mp: 218–220°C; ^{1}H nmr: see Table 2; ms: 338 (4),

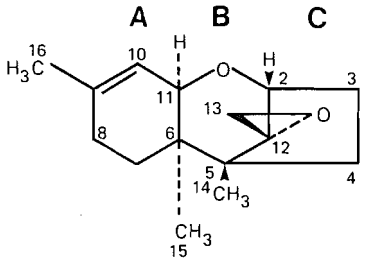

No.	Substituents						Name
	3α	4β	7α	8α	8β	15	
1	OAc	H	H	H	H	H	isotrichodermin
2	OAc	H	H	H	H	OAc	calonectrin
3	OAC	H	H	H	H	OH	15-deacylcalonectrin
4	OH	OAc	H	H	H	OAc	diacetoxyscirpenol
5	OAc	H	OH	H	H	OAc	7-hydroxycalonectrin
6	OAc	H	OH	H	H	H	7-hydroxyisotrichodermin
7	OAc	H	OH	OH	H	H	7,8-dihydroxyisotrichodermin
8	OAc	H	OH	OH	H	OAc	7,8-dihydroxycalonectrin
9	OAc	H	BOR	BOR	H	OAc	7,8-dihydroxycalonectrin-boronate
10	OAc	H	H	OH	H	H	8-hydroxyisotrichodermin
11	OAc	H	H	OH	H	OAc	8-hydroxycalonectrin
12	OH	OAc	H	OH	H	OAc	neosolaniol
13	OH	OAc	H	OH	H	OH	15-deacylneosolaniol
14	OH	OAc	H	H	OH	OH	8-β-OH-deacylneosolaniol
15	OH	OAc	H	iVal	H	OAc	T-2 toxin
16	OH	OAc	H	Prop	H	OAc	8-propionyl-neosolaniol
17	OH	OAc	H	iBut	H	OAc	8-isobutyryl-neosolaniol
18	OH	OAc	H	But	H	OAc	8-butyryl-neosolaniol
19	OH	OAc	H	OAc	H	OAc	8-acetyl-neosolaniol
20	OAc	H	H	=O		H	8-ketoisotrichodermin
21	OH	OAc	H	=O		OAc	4,15-diacetyl-7-deoxynivalenol
22	OAc	H	H	=O		OH	3-acetyl-7-deoxy-4-deoxynivalenol
23	OH	OAc	OH	=O		OAc	4,15-diacetyl-nivalenol
24	OH	H	OH	=O		OH	4-deoxynivalenol
25	OAc	H	OH	=O		OH	3-acetyl-4-deoxynivalenol
26	OH	H	OAc	=O		OH	7-acetyl-4-deoxynivalenol
27	OH	H	OH	=O		OAc	15-acetyl-4-deoxynivalenol
28	OAc	H	OH	=O		OAc	3,15-diacetyl-4-deoxynivalenol
29	OH	H	OAc	=O		OAc	7,15-diacetyl-4-deoxynivalenol
30	OAc	H	OAc	=O		OAc	triacetyl-4-deoxynivalenol
31	=O	H	OH	=O		OH	3-keto-4-deoxynivalenol
32	OH	H	OH	=O		=O	15-keto-4-deoxynivalenol
33	=O	H	OH	=O		=O	3,15-diketo-4-deoxynivalenol
34	OH	H	BOR	=O		BOR	4-deoxynivalenol-boronate
35	OAc	H	BOR	=O		BOR	3-acetyl-4-deoxynivalenol-boronate
36	=O	H	BOR	=O		BOR	3-keto-4-deoxynivalenol-boronate

FIG. 1. Structure and numbering system of trichothecenes.

278 (11), 249 (40), 137 (49), 107 (56), 98 (100), 79 (88), 55 (87). *Exact Mass* (ms) calcd. for $C_{17}H_{22}O_7$: 338.1365; found: 338.1317 (M^+). The yield of compound **26** was not maximized.

*3-Keto-4-deoxynivalenol (**31**), 3,15-diketo-4-DON (**33**), and 15-keto-4-DON (**32**)*

Oxalyl chloride (30 μL, 0.32 mmol) in freshly distilled dichloromethane (2 mL) was cooled to −60°C. DMSO (50 μL) in CH_2Cl_2 (2 mL) was slowly added, under N_2 (18). DON (**24**) (85 mg, 0.29 mmol) in CH_2Cl_2 (2 mL) and DMSO (100 μL) were added over 5 min. The resulting solution was stirred at −60°C for 15 min and triethylamine (0.2 mL) was added. After a further 5 min, the solution was warmed to room temperature, water (10 mL) added, and the mixture extracted with CH_2Cl_2 (3 × 10 mL). The organic fractions were combined, washed with water, then with brine, dried over Na_2SO_4, concentrated, and chromatographed on silica gel (3 g) with 50:50 EtOAc/hexane to yield three compounds: (*a*) 3,15-diketo-4-deoxynivalenol (**33**) (52 mg, 62%); ^{1}H nmr: see Table 2; ms: 292 (4), 277 (1), 263 (5), 245 (23), 231 (56), 221 (49), 204 (84), 175 (40), 124 (91), 123 (96), 43 (100). *Exact Mass* (ms) calcd. for $C_{15}H_{16}O_6$: 292.0947; found: 292.0935 (M^+); (*b*) 3-keto-4-deoxynivalenol (**31**) (7 mg, 8.3%); ^{1}H nmr: see Table 2; ms: 294 (4), 279 (2), 276 (3), 264 (2), 246 (29), 231 (39), 204 (94), 175 (37), 136 (70), 124 (100), 108 (91), 77 (62), 55 (55), 43 (90). *Exact Mass* (ms) calcd. for $C_{15}H_{18}O_6$: 294.1103; found: 294.1111 (M^+); and (*c*) 15-keto-4-deoxynivalenol (**32**) (12 mg, 14.2%); ^{1}H nmr: see Table 2; ms: 294 (9), 279 (2), 276 (2), 265 (45), 248 (41), 208 (22), 179 (22), 167 (29), 151 (23), 137 (32), 123 (41), 105 (32), 98 (45), 95 (45), 77 (47), 55 (49), 43 (100). *Exact Mass* (ms) calcd. for $C_{15}H_{18}O_6$: 294.1103; found: 294.1083 (M^+).

*7,8-Dihydroxycalonectrin 7,8-boronate ester (**9**)*

7,8-Dihydroxycalonectrin (**8**) (50 mg, 0.13 mmol) and phenylboronic acid (23 mg, 0.19 mmol) in dry acetone were refluxed for 4 h, then cooled and concentrated to give a white oily solid. When washed with hexane, it yielded a white crystalline solid (60 mg, 98%), mp 119–120°C. ^{1}H nmr: see Table 1; ms: 468 (26), 426 (6), 408 (10), 395 (28), 304 (50), 262 (100), 223 (74). *Exact Mass* (ms) calcd. for $C_{25}H_{29}O_8B$: 468.1955; found: 468.1923 (M^+).

*3-Acetyl-4-deoxynivalenol 7,15-boronate ester (**35**)*

The same procedure as above with 3-acetyl-4-DON (**25**) gave a

Can. J. Chem. Downloaded from www.nrcresearchpress.com by 213.166.140.6 on 09/07/12
For personal use only.

Can. J. Chem. Downloaded from www.nrcresearchpress.com by 213.166.140.6 on 09/07/12
For personal use only.

TABLE 1. ^{1}H nuclear magnetic resonance data (250 MHz) for trichothecenes **1–19** (chemical shifts, multiplicity, (*J* in Hz))

	Position															
No.	2	3	4α	4β	7α	7β	8α	8β	10	11	13a	13b	14	15a	15b	16
1	3.73d (4.6)	5.15dt (10, 5)	2.1m		1.0–2.0m		1.0–2.0m		5.44dq (5.5, 1.5)	3.96d (5.5)	2.84d (4.0)	3.07d (4.0)	0.80s	0.74s		1.71bs
2	3.74d (4.6)	5.15dt (9.6, 5)	2.1–2.19m		1.78–2.19m		1.78–2.19m		5.45dq (5.4, 1.3)	4.00d (5.6)	2.84d (4.0)	3.08d (4.0)	0.81s	3.82d (12.2)	4.06d (12.2)	1.70bs
3	3.72d (4.7)	5.13dt (10, 5)	2.1–2.30m		1.73–2.30m		1.73–2.30m		5.46dq (5.3, 1.6)	3.96d (5.3)	2.84d (4.0)	3.07d (4.0)	0.90s	3.47dd (11.6, 4.5)	3.66dd (11.6, 3.2)	1.71bs
4	3.61d (4.9)	4.10dd (4.9, 2.9)	5.11d (2.9)		1.67m (AB = 11)	2.00m (AB = 11)	1.93m		5.45d (5.3)	4.02d (5.3)	2.70d (4.9)	2.99d (4.9)	0.74s	3.90d (12.3)	4.10d (12.3)	1.65bs
5	3.78d (4.4)	5.17m (10, 8, 4.5)	1.97–2.18m			4.55td (11.2, 5.9)	2.41dd (17.6, 5.9)	1.95m	5.38dq (5.4, 1.3)	4.11d (5.4)	3.09d (4.4)	3.23d (4.4)	1.14s	4.05d (12.2)	4.31d (12.2)	1.72bs
6	3.76d (4.5)	5.16m (9.2, 6.7, 4.5)	2.06m			4.46dt (10.1, 6.0)	2.19dd (17.2, 5.9)	1.90m	5.40dq (5.5, 1.2)	4.10d (5.5)	3.08d (4.4)	3.14d (4.4)	0.82s	1.04s		1.70bs
7	3.76d (4.5)	5.17m (8.8, 6.9, 4.5)	2.05d (6.9)	2.05d (8.8)		4.41dd (9.7, 5.5)		3.98bt (6)	5.59dq (5.9, 1.6)	4.16d (5.9)	3.10d (4.3)	3.17d (4.3)	1.06s	0.89s		1.87bs
8	3.77d (4.4)	5.15dt (11.1, 4.4)	2.34dd (15, 4.6)	2.13dd (15, 11.2)		4.50dd (9.6, 5.4)		3.99bt (5.8–7.5)	5.58dq (5.8, 0.9)	4.32d (5.8)	3.09d (4.3)	3.20d (4.3)	1.12s	4.14d (12.3)	4.44d (12.3)	1.86bs
9	3.81d (4.6)	5.22dt (10.8, 4.3)	2.37dd (15, 4.1)	2.19dd (15, 11.0)		5.40d (8.8)		4.94bd (8.7)	5.74dp (6.5, 1.5)	4.58d (6.5)	3.22s	3.22s	1.19s	4.11d (11.8)	4.35d (11.8)	2.01bs
10	3.72d (4.6)	5.16dt (9.8, 5)	2.07–2.11m		1.69dt (14.3, 1.4)	2.21dd (14.3, 6)		4.11t (5.4)	5.59dq (5.9, 1.1)	4.04d (5.7)	2.87d (4.3)	3.07d (4.3)	0.77s	0.98s		1.86bs
11	3.73d (4.6)	5.15m (10, 5)	1.90–2.30m		1.90–2.30m			4.14m	5.58dq (5.7, 1.1)	4.14m	2.89d (4)	3.08d (4)	0.83s	4.13d (12.5)	4.15d (12.5)	1.85bs
12	3.67d (4.9)	4.15dd (4.9, 2.8)	5.25d (2.8)		1.88dt (14.5, 1.5)	2.32dd (14.5, 5.5)		4.11bd (5.5)	5.67dq (6, 1)	4.25d (5.7)	2.80d (4)	3.05d (4)	0.85s	4.11d (12.5)	4.25d (12.5)	1.86bs
13	3.64d (4.9)	4.17dt (5, 3)	4.94d (3)		2.06dt (14.3, 1.6)	2.19dd (14.3, 5.2)		4.12m	5.65dq (5.8, 1.5)	3.88d (5.8)	2.79d (4)	3.02d (4)	0.89s	3.48d (12.6)	3.76d (12.6)	1.85bs
14	3.68d (4.9)	4.25dt (4.9, 3.4)	5.42d (3.2)		2.02ddd (12, 6, 1.8)	1.90dd (12, 10.2)	4.17bd (6)		5.62dp (5.9, 1.8)	4.17d (5.9)	2.80d (4)	3.06d (4)	0.84s	3.59dd (12.5, 6)	3.77dd (12.5, 4.5)	1.82bs
15	3.68d (4.9)	4.14dd (4.9, 3)	5.28d (3)		1.89dd (15, 1.5)	2.38dd (15, 5.5)		5.26bd (5.5)	5.78dp (6, 1.5)	4.32d (6)	2.78d (4)	3.04d (4)	0.79s	4.03d (12.5)	4.27d (12.5)	1.73bs
16	3.68d (4.9)	4.14dd (4.9, 3)	5.25d (3)		1.92dd (15, 1.5)	2.37dd (15, 5.5)		5.26bd (5.5)	5.78dp (6, 1.5)	4.30d (6)	2.78d (4)	3.04d (4)	0.79s	4.03d (12.5)	4.27d (12.5)	1.72bs
17	3.68d (4.9)	4.14dd (4.9, 3)	5.36d (3)		1.82dd (15, 1.5)	2.41dd (15, 5.5)		5.26bd (5.5)	5.78dp (6, 1.5)	4.38d (6)	2.78d (4)	3.04d (4)	0.79s	4.02d (12.5)	4.31d (12.5)	1.72bs
18	3.68d (4.9)	4.14dd (4.9, 3)	5.26d (3)		1.90dd (15, 1.5)	2.37dd (15, 5.5)		5.26bd (5.5)	5.78dp (6, 1.5)	4.31d (6)	2.78d (4)	3.04d (4)	0.79s	4.03d (12.5)	4.27d (12.5)	1.72bs
19	3.66d (4.9)	4.13dd (4.9, 3)	5.19d (3)		1.9–2.0m	2.32dd (15, 5.5)		5.22bd (5.5)	5.78dp (6, 1.5)	4.25d (6)	2.77d (4)	3.02d (4)	0.79s	4.03d (12.5)	4.24d (12.5)	1.71bs

Can. J. Chem. Downloaded from www.nrcresearchpress.com by 213.166.140.6 on 09/07/12
For personal use only.

TABLE 2. ^{1}H nuclear magnetic resonance data (250 MHz) for trichothecenes **20–36** (chemical shifts, multiplicity, (*J* in Hz))

	Position													
No.	2	3	4α	4β	7α	7β	10	11	13a	13b	14	15a	15b	16
20	3.83d (4.6)	5.22dt (10.9, 4.6)	2.03dd (14.8, 4.6)	2.17dd (14.8, 10.6)	2.26dd (15.3, 1.5)	2.87dq (15.3, 1.2)	6.51dq (5.7, 1.5)	4.32d (5.7)	2.86d (3.9)	3.10d (3.9)	0.75s	0.92d (1.2)		1.81bs
21	3.77d (4.9)	4.21dd (4.9, 2.9, 2.6)	5.06d (2.9)		2.46dd (15.9, 1.6)	2.92d (15.9)	6.59dq (5.9, 1.5)	4.51d (5.9)	2.79d (3.9)	3.07d (3.9)	0.80s	4.12d (12.4)	4.15d (12.4)	1.82bs
22	3.81d (4.6)	5.18dt (10.2, 4.4)	2.40dd (14.7, 4.1)	2.17dd (14.7, 11.2)	2.42d (16.8)	2.80d (16.8)	6.55dq (5.7, 1.4)	4.52d (5.7)	2.86d (5.9)	3.09d (5.9)	0.83s	3.64s		1.80bs
23	3.82d (4.7)	4.22dt (4.8, 3)	5.16d (3.1)			4.86d (2)	6.63dq (5.9, 1.6)	4.72d (5.9)	3.06d (4.3)	3.09d (4.3)	1.09s	4.19d (12.3)	4.32d (12.3)	1.88bs
24	3.62d (4.5)	4.53dt (10.7, 4.5)	2.21dd (14.8, 4.5)	2.07dd (14.8, 10.7)		4.83d (2)	6.61dq (5.9, 1.5)	4.80d (5.9)	3.07d (4.3)	3.15d (4.3)	1.13s	3.73d (11.7)	3.89d (11.7)	1.86bs
25	3.87d (4.5)	5.18dt (11.2, 4.5)	2.35dd (15.1, 4.5)	2.12dd (15.1, 11.2)		4.79d (2.1)	6.56dq (5.9, 1.5)	4.66d (5.9)	3.08d (4.3)	3.14d (4.3)	1.12s	3.75d (11.7)	3.81d (11.7)	1.85bs
26	3.62d (4.5)	4.52dt (10.9, 4.5)	2.39dd (14.9, 3.7)	2.07dd (14.9, 11)		6.07s	6.59m	4.98d (5.8)	2.77d (3.5)	3.09d (3.5)	0.96s	3.89d (12)	3.92d (12)	1.84bs
27	3.60d (4.4)	4.50dt (10.6, 4.5)	2.20dd (14.8, 4.5)	2.07dd (14.8, 10.6)		4.81d (1.9)	6.58dq (5.8, 1.5)	4.87d (5.8)	3.06d (4.2)	3.11d (4.2)	1.04s	4.21s		1.86bs
28	3.91d (4.5)	5.22dt (10.9, 4.6)	2.30dd (15, 4.7)	2.18dd (15, 11)		4.81d (2)	6.57dq (5.8, 1.6)	4.70d (5.8)	3.10d (4.3)	3.15d (4.3)	1.09s	4.23d	4.27d	1.89bs
29	3.61d (4.5)	4.51dt (11, 4.5)	2.28dd (15, 4.3)	2.11dd (15, 10.7)		6.07s	6.58dq (5.8, 1.5)	4.94d (5.8)	2.78d (3.5)	3.09d (3.5)	0.93s	4.30d (12.2)	4.34d (12.2)	1.85bs
30	3.89d (4.5)	5.21dt (11.1, 4.5)	2.34dd (15, 4.5)	2.18dd (15, 11.1)		6.04s	6.54dq (5.8, 1.5)	4.73d (5.8)	2.80d (3.5)	3.12d (3.5)	0.94s	4.28d (12.2)	4.36d (12.2)	1.84bs
31	3.50s		2.26dd (19.5, 1.0)	3.11s (19.6)		4.88s (1.7)	6.52dq (5.9, 1.5)	4.54d (5.9)	3.21d (4.2)	3.33d (4.2)	1.31s	3.73d (12.3)	3.90d (12.3)	1.88bs
32	3.66d (4.5)	4.60dt (10.9, 4.3)	2.39dd (15.1, 4.3)	2.15dd (15.1, 10.8)		4.88d (2.4)	6.56dq (5.9, 1.5)	5.16d (5.9)	3.09d (4.2)	3.21d (4.2)	1.16s	9.66s		1.86bs
33	3.52s		2.28dd (19.5, 1.0)	2.97d (19.5)		5.01d (1.9)	6.50dq (5.9, 1.5)	4.66d (5.9)	3.23d (4.1)	3.39d (4.1)	1.33s	9.67s		1.86bs
34	3.67d (4.4)	4.62m (10.8, 4.4, 3.8)	2.05dd (14.9, 3.8)	2.20dd (14.9, 10.8)		5.23d (2.2)	6.56dq (5.7, 1.5)	4.56d (5.8)	3.19d (4.4)	3.17d (4.4)	1.09s	3.91d (12.6)	4.11dd (12.6, 2.2)	1.90bs
35	3.95d (3.2)	5.29dt (11.0, 4.7)	2.09dd (15.3, 4.8)	2.28dd (15.2, 11.1)		5.22d (2.2)	6.54dq (5.6, 1.5)	4.36d (5.6)	3.20s		1.11s	3.92d (12.4)	4.10dd (12.4, 2.3)	1.90bs
36	3.57s		2.37d (19.5)	2.67d (19.5)		5.26d (2.2)	6.45dq (5.8, 1.5)	4.05d (5.8)	3.29d (4)	3.36d (4)	1.24s	3.92d (12.7)	4.07dd (12.7, 2.2)	1.89bs

quantitative yield; mp 209–210°C; ^{1}H nmr: see Table 2; ms: 424 (12), 327 (6), 267 (22), 163 (32), 98 (100), 79 (54). *Exact Mass* (ms) calcd. for $C_{23}H_{25}O_7B$: 424.1693; found: 424.1710 (M^+).

4-Deoxynivalenol 7,15-boronate ester (34)

The same procedure as above with 4-DON (**24**) gave a quantitative yield; mp 221–223°C; ^{1}H nmr: see Table 2; ms: 382 (29), 241 (55), 98 (100), 79 (49). *Exact Mass* (ms) calcd. for $C_{21}H_{23}O_6B$: 382.1587; found: 382.1592 (M^+).

3-Keto-4-deoxynivalenol 7,15-boronate ester (36)

The same oxidation conditions used for **31**, **32**, and **33** were followed with 4-DON boronate ester (**34**) as a substrate. The product consisted of a 50:50 mixture of the desired **36** and 3-keto-DON (**31**). This mixture was then boronated as above to yield the product **36** in 97% yield; mp 174–176°C; ^{1}H nmr: see Table 2; ms: 380 (100), 281 (16), 241 (24), 173 (50), 108 (93), 97 (89), 79 (70). *Exact Mass* (ms) calcd. for $C_{21}H_{21}O_6B$: 380.1430; found: 380.1414 (M^+).

Results and discussion

The most recognizable feature in the ^{1}H nmr spectrum of 12,13-epoxytrichothec-9-enes is a quartet for the C-13 methylene protons of the epoxy moiety. This AB system occurs between 2.70 and 3.40 ppm, with a coupling constant of 3.5–4.5 Hz, $\Delta\delta$ = 0.05–0.32 ppm. In some derivatized trichothecenes, this AB system collapses to a singlet. Other spectral characteristics are a sharp singlet for the C-14 methyl protons and a broad singlet for the C-16 methyl protons.

(A) C-13 methylene protons

The epoxide moiety projects upwards from the middle of the β face of the trichothecene molecule, hence it would be expected that its resonance would be affected by any structural variation. However, oxygenation at C-3, C-4, C-8, or C-15 has essentially no effect (Tables 1 and 2). The basic chemical shifts for the C-13 AB system are 2.80 and 3.05 ppm. For trichothecenes hydroxylated at C-7, these resonances are shifted downfield to 3.06–3.10 and 3.09–3.23 ppm, respectively. All the 7-OH trichothecenes reported to date have an α orientation.

That the H-13 chemical shifts are affected by substitution on the opposite face of the molecule can be rationalized using 3-dimensional models. In the most stable conformation of the trichothecene molecule (3*a*, 13, 19, 20), the A ring assumes a half-chair and the B ring a chair conformation (Fig. 2A). It can be clearly seen that C-13 is closer to the 7α-OH than other hetero substituents. In other possible conformations of the trichothecene molecule (i.e., A half-chair, B boat (Fig. 2B) and A boat, B boat), the 7α-OH group will be farther from the H-13 protons, resulting in minimal effect on their chemical shift.

(B) 16-Methyl group

These protons appear as a broad singlet in the range 1.65–1.89 ppm. Although this range is small, it is indicative of the substitution pattern of the A ring. Thus, for trichothecenes not substituted in the A ring, the 16-CH_3 chemical shift ranges from 1.65 to 1.71 ppm (**1–4**). The range is similar for compounds with a 7-OH (**5**, **6**); however, an 8-OH induces a downfield shift to 1.82–1.86 ppm (**10–14**). As expected, hydroxylation at both C-7 and C-8 induces no further shift (**7**, **8**). Acylation of the 8-OH returns the chemical shift upfield to 1.71–1.73 ppm (**15–19**) while oxidation of 8-OH to a ketone results in a slight upfield shift to 1.80–1.82 ppm (**20–22**). Hydroxyl or acetyl moieties at C-7 of the 8-ketotrichothecenes result in an even further downfield shift to 1.84–1.89 ppm (**23–33**).

(C) 14-Methyl group

The basic chemical shift for the 14-CH_3 is 0.80 ± 0.05 ppm (**1**). Hydroxylation of C-7 causes no significant change, and

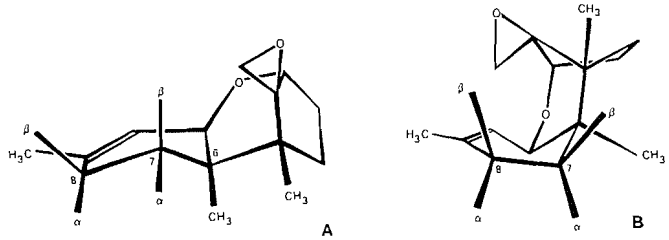

FIG. 2. Conformations of trichothecene ring system. (A) A half-chair, B chair; (B) A half chair, B boat.

hydroxylation of C-8 or C-15 results only in a minor downfield shift (0.01–0.1 ppm) (**3**, **13**, **14**, **22**). However, if both C-7 and either C-8 or C-15 are hydroxylated, the 14-CH_3 resonance is shifted downfield to 1.04–1.14 ppm (**7**, **24**, **25**). Acylation of the 15-OH has little effect (**5**, **8**, **23**, **27**, **28**), while acylation of the 7-OH produces an upfield shift to ~0.95 ppm (**26**, **29**, **30**). Oxidation of the 15-OH to an aldehyde or the 8-OH to a ketone, such as in **32**, **33** and **23**, **27**, **28**, has no effect on the 14-CH_3 chemical shift.

This dependence on C-8 or C-15 for an effect of C-7 substitution on the chemical shift of 14-CH_3 may be due more to steric than electronic factors as hydroxylation of C-8 or C-15 forces the 7-OH closer to the 14-CH_3.

An alternative explanation for the change in the 14-CH_3 chemical shift would invoke the less stable conformation in which ring A is in a half-chair and ring B in a boat conformation (Fig. 2B). This conformation would relieve the strain involved with both the 8-OH and the 15-CH_2OH being in axial positions (Fig. 2A). However, this implies a downfield effect on the chemical shift of H-14 for compounds hydroxylated at C-8 and C-15 but not at C-7, as in **13** (0.89 ppm), which is not observed.

(D) A ring

(a) C-7

When the A ring is not substituted, the H-7α resonance occurs at 1.7–1.8 ppm, and H-7β is at approximately 2.00 ppm (**2**, **4**). Hydroxylation at C-8 shifts these resonances slightly downfield to 1.7–2.1 ppm and 2.2–2.3 ppm (**10**, **13**), respectively, while acetylation of the 8-OH shifts the H-7β signal further to 2.3–2.4 ppm (**15–19**). No significant change is observed for the H-7α resonance. A ketone at C-8 results in an H-7β chemical shift of 2.85 ± 0.05 ppm, and H-7α resonance in the range 2.26–2.46 ppm.

Hydroxylation of C-7 (α position) shifts the H-7β resonance downfield to 4.5 ± 0.05 ppm (**5**, **6**). Hydroxylation of C-8 to give a dihydroxy compound has no further effect (**7**, **8**). Oxidation of C-8 to a ketone results in a chemical shift for H-7β of 4.8–4.9 ppm (**23**, **24**, **25**, **27**, **28**, **31**, **32**) and acetylation of the 7-OH of the resulting compounds shifts H-7β downfield to 6.05 ppm (**26**, **29**, **30**).

The H-7α and H-7β assignments are based on the $J_{7\alpha,8\beta}$ and $J_{7\beta,8\beta}$ coupling constants for the 8α-OH compounds. A value of $J_{7\alpha,8\beta}$ = 1.4–1.8 Hz is typical of an equatorial–equatorial dihedral angle $\Phi_{e,e}$ of 80°–90°, while $J_{7\beta,8\beta}$ = 5–6 Hz is typical for a $\Phi_{a,e}$ of 30°–40°. The lower field position of H-7β as compared to H-7α can be ascribed to its proximity to the oxygens at position 1 and in the epoxide moiety (16). Assignment of the higher field resonance to H-7α is aided by its coupling to H-11 observable in compounds **10–14**, **20**, and **21** ($J_{7\alpha,11}$ = 1.4–1.8 Hz). Only H-7α can achieve a "W" relationship with H-11 to show this long-range coupling (see Fig. 5). This necessitates an A half-chair, B chair conformation (Fig. 2A) for trichothecenes.

Can. J. Chem. Downloaded from www.nrcresearchpress.com by 213.166.140.6 on 09/07/12
For personal use only.

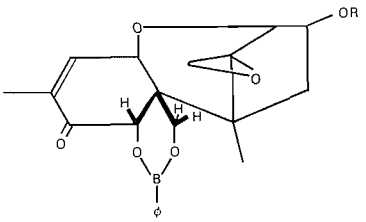

FIG. 3. Conformation of DON-boronate showing the 7,15-pro-*R* "W" relationship.

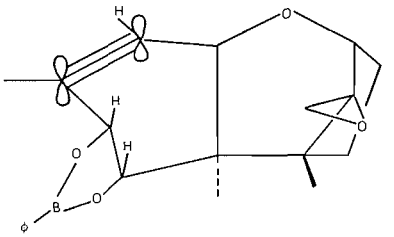

FIG. 4. Conformation of 7,8-dihydroxycalonectrin-boronate showing the steric relationship between the axial 8-H and the 9,10 π electron system.

W coupling is also observed in COSY spectra between H-7β and one of the H-15 protons but is measurable only for 8-keto-isotrichodermin (**20**) ($J_{7\beta,15}$ = 1.2 Hz) and some trichothecene derivatives such as the 7,15-boronates of DON (**34**) and 3-AcDON (**35**), where the H-7β and pro-*R*-H-15 are locked in a W conformation (Fig. 3). This rigid structure causes the H-7β signal to be a doublet (5.22–5.23 ppm) coupling with one H-15 ($J_{7\beta,15}$ = 2.2 Hz).

(b) C-8

The chemical shifts of the methylene protons at C-8 range from 1.7 to 2.4 ppm and exhibit small AB character. In addition to coupling to the H-7 methylene protons, the H-8 protons show long-range coupling with the 16-CH_3 and H-10 methine protons, which broadens the H-8 resonances, occasionally resulting in the dispersion of the H-8 signal beneath other peaks.

Hydroxylation at C-8 induces a downfield shift to 4–4.15 ppm (**7**, **8**, **10**–**14**), and acetylation of the resulting alcohols shifts the H-8 resonance further downfield to 5.2–5.3 ppm (**15**–**19**). These shifts permit easier assignment of the H-8 resonance, which appears as a broadened doublet (triplet when C*H*—O*H* coupling is present).

The 8-OH moiety in naturally occurring trichothecenes normally has the α configuration, which the exception of the 8β-hydroxytrichothecene isolated by Corley *et al.* (21) and two synthetic compounds, **14** (17) and its 15-Ac analogue (22). The *cis* coupling constant $J_{7\beta,8\beta}$ of 8α-OH trichothecenes is ~5 Hz, while the *trans* $J_{7\alpha,8\beta}$ is only 0–1.8 Hz. This result is consistent with the Karplus relationship for the stable conformation of the A ring (Fig. 2A and ref. 1). The *J* values of the synthetic 8β-OH epimer of 15-deacylneosolaniol (**14**) are 6 Hz (*cis*) and 10.2 Hz (*trans*), in agreement with the other reported values (21, 22). This sharp distinction in *J* values facilitates the assignment of the proper configuration at C-8.

(c) C-10

The H-10 resonance is also very characteristic of trichothecenes. It is usually a multiplet at 5.4–5.8 ppm but high field analysis with resolution enhancement shows this resonance to be a doublet of quartets, as originally postulated (23), which may be complicated by long-range coupling to the H-8. If $J_{10,8}$ is of the same order as $J_{10,16}$ (1.5 Hz), H-10 appears as a doublet of pentets as for compound **14**, which has an 8β-OH. In this case the axial C8—H bond is coplanar with the C9—C10 π orbital system thus maximizing the long-range coupling between H-8 and H-10.

The H-8β may also be forced into an axial position by acylation (**15**–**19**) or by boronation of 7,8-dihydroxycalonectrin (**8**) yielding the boronate **9**. In this derivative, $J_{7\beta,8\beta}$ has increased from the usual 5.5 Hz to 8.8 Hz as the C7—Hβ and C8—Hβ bonds are almost parallel. This reduction of the dihedral angle (Fig. 4) forces the H-8β into a pseudo-axial position parallel to the C9—C10 π-system, thus increasing the $J_{8\beta,10}$ to 1.5 Hz.

The H-10 chemical shift is significantly affected only by substitution at C-8 and C-3. Hydroxylation at C-8 moves the H-10 resonance from 5.4 to 5.6 ppm; acetylation of this alcohol moves it further downfield to 5.78 ppm, and oxidation to a ketone shifts it to 6.5–6.6 ppm. Since all compounds studied were oxygenated at C-3, the value of 5.27 ppm reported for 8β-hydroxytrichothecene may be used as a reference (21). The corresponding 3-hydroxylated compound, **14**, shows an increase in the H-10 chemical shift to 5.62 ppm as compared to 5.65 ppm for the 8α-OH isomer **13**, and acetylation of the 3-OH shifts it slightly to just under 5.6 ppm. Similar considerations about the effects of C-3 substitution are applicable to the 8-ketotrichothecenes.

(d) C-11

The H-11 resonance may be confused with that of H-8 when C-8 is hydroxylated since both are broad doublets in the same spectral region. The H-11 chemical shift ranges from 3.9 to 4.4 ppm and from 4.3 to 5.0 ppm for 8-ketotrichothecenes. The chemical shift is affected by oxidation at all ring positions and is therefore unsuitable for structure determination.

The broadness of this signal is due to long-range coupling to the 16-CH_3 and occasionally H-7α (see section *D* (*a*)), as shown by COSY experiments.

(E) C ring

(a) C-2

The H-2 resonance is a simple doublet due to coupling to H-3 and is observed at 3.6–3.9 ppm. The H-2 resonance occurs at a slightly lower field with a C-3 acetoxy group (3.72–3.75 ppm) than with a C-3 hydroxyl moiety (3.60–3.67 ppm). A C-8 keto group also affects the H-2 chemical shift of the 3-acetoxy compounds appreciably (3.8–3.9 ppm) but has apparently little effect in the case of 3-hydroxytrichothecenes.

(b) C-3

In this study, all compounds are oxygenated at C-3. The H-3 chemical shifts can be classified into three groups based on three structural variations: 3-OH-4-OAc-trichothecenes (4.15 ± 0.05 ppm), 3-OAc-trichothecenes (5.15 ± 0.05 ppm), and 3-OH-8-ketotrichothecenes (4.5 ± 0.1 ppm). Substitution at C-15, C-7, and C-8 has little effect (0.2 ppm) on the H-3 chemical shift.

All C-3 hydroxy or acetoxy trichothecenes isolated have in common the α configuration as deduced from $J_{2,3}$ = 4.4–5 Hz, typical of a Φ = 20°–30°. The $J_{3\beta,4\alpha}$ of trichothecenes is dependent on whether C-4 is oxygenated or not; if not substituted, $J_{3\beta,4\alpha}$ ranges from 4.5 to 8 Hz and is approximately 3 Hz if C-4 is substituted, as steric crowding appreciably reduces the 120° dihedral angle.

(c) C-4

If C-4 is not substituted, H-4α and H-4β range from 2.0 to 2.4 ppm, with H-4β usually at the higher field. The H-4

Can. J. Chem. Downloaded from www.nrcresearchpress.com by 213.166.140.6 on 09/07/12
For personal use only.

Can. J. Chem. Downloaded from www.nrcresearchpress.com by 213.166.140.6 on 09/07/12
For personal use only.

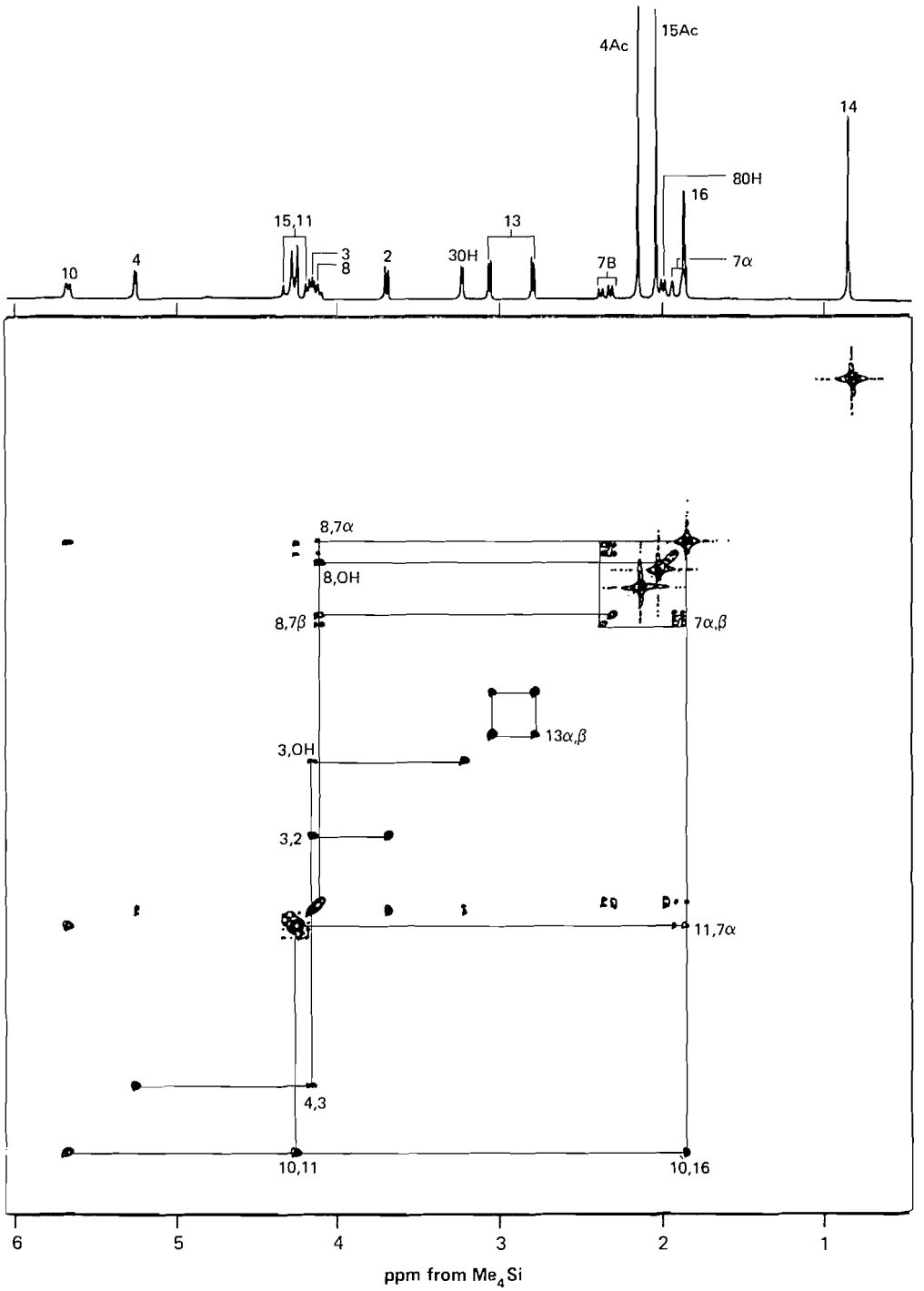

FIG. 5. $^1H/^1H$ correlation spectrum of neosolaniol (**12**), illustrating the first-order and long-range coupling typical for trichothecenes. The single pulse spectrum is shown at the top of the figure.

resonances are not resolved from H-7 and H-8 when these positions are unsubstituted. When resolved, the H-4 resonances can be easily identified by their $J_{3,4}$ coupling. Their geminal coupling constant $J_{4\alpha,4\beta}$ is approximately 15 Hz, while $J_{3\beta,4\beta}$ is about 10 Hz ($\Phi \sim 0°$) and $J_{3\beta,4\alpha}$ can vary from 4.5 to 8 Hz ($\Phi \sim 120°$) (20, 24). The large variation in the latter is due to the sensitivity of J to small changes in Φ at this angle as predicted by the Karplus relationship.

Acetylation of 4-OH gives H-4 resonances ranging from 5.0 to 5.4 ppm. The small values of $J_{3,4}$ (2.8–3.4 Hz) indicate a *trans* relationship (3α,4β) between the C-3 and C-4 substituents for all naturally occurring trichothecenes.

The H-4α resonance is affected by the acetylation of the C-3, C-7, C-8, and C-15 hydroxyl groups, all of which cause a slight downfield shift of the H-4α resonance but have a minimal effect on H-4β. Acetylation of the 3-OH has the greatest effect, as can be more clearly seen in synthetic derivatives (17). Compounds **15–19** provide another interesting series since the only variation is in the size of the C-8 substituent. The H-4 resonance occurs at 5.19 ppm when a C-8 acetoxy group is present, whereas a propionoxy group moves it to 5.25 ppm. Further increases in the straight-chain length of the C-8 substituent have no effect on H-4; however, branching at C-2′ (**17**) produces a further downfield shift of H-4 to 5.36 ppm (17).

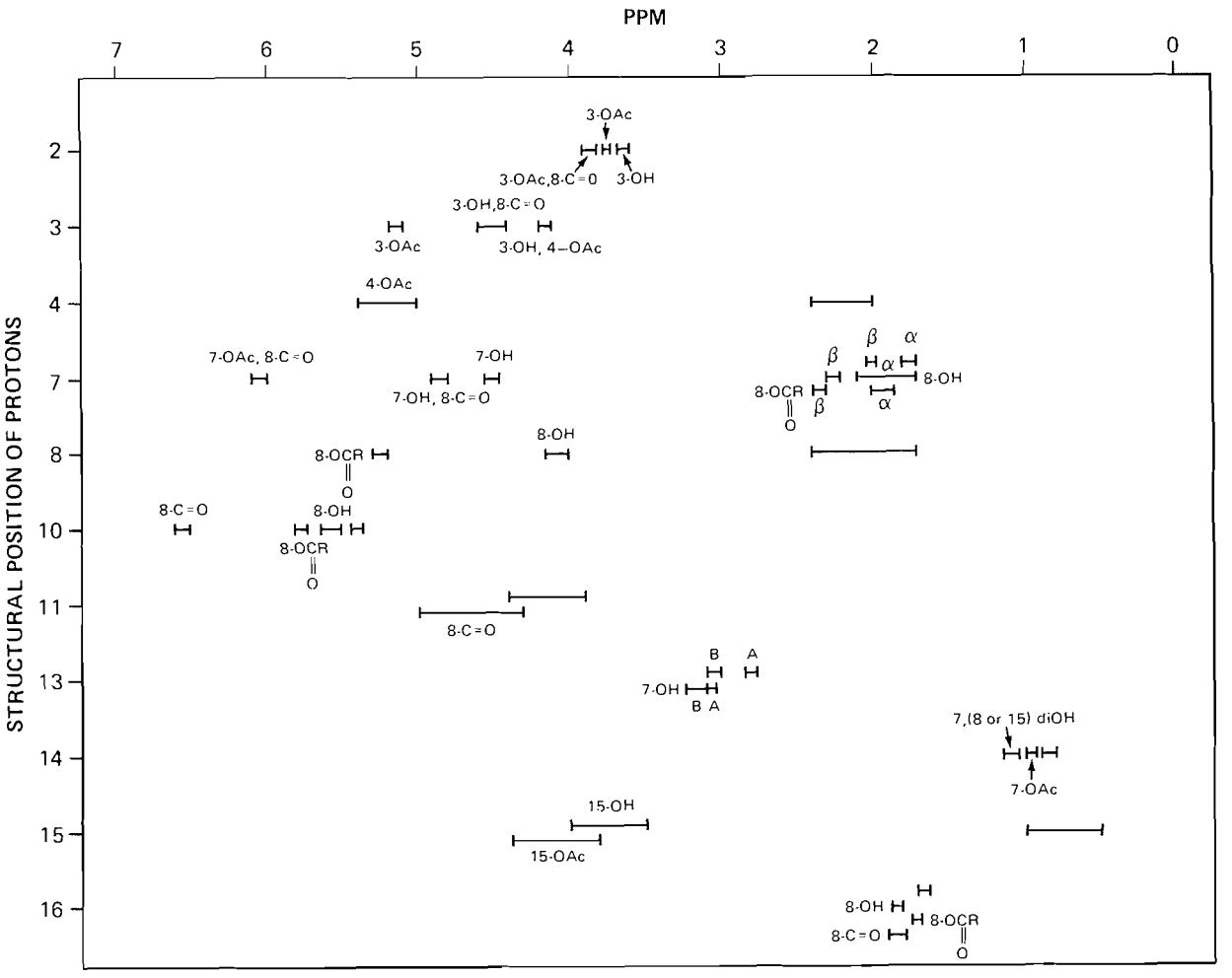

FIG. 6. Characteristic chemical shifts for trichothecene protons.

(F) C-15

For the isotrichodermin-type compounds (**1**, **6**, **7**, **10**, **20**), the 15-CH_3 resonance occurs as a singlet between 0.74 and 1.0 ppm. This resonance can be differentiated from the 14-CH_3 singlet by its long-range coupling to H-7β as observed in COSY spectra. When C-15 is oxygenated, the H-15 methylenic protons appear as an AB system ($\Delta\delta$ = 0–0.3 ppm) centered between 3.5 and 4.0 ppm for the free OH and between 3.9 and 4.4 ppm for the C-15 acetylated compounds. Occasionally further coupling to the 15-OH is observed.

The chemical shift of both methyl and methylenic H-15 protons is moved downfield by hydroxylation at either C-7 or C-8, the shift being greater for the 7-OH. Further downfield shift is induced by acetylation of the 7-OH, but acetylation or oxidation of the 8-OH to a ketone shows little effect.

Conclusion

Knowledge of the effect of the bonded and nonbonded interactions of trichothecenes on their nmr spectra facilitates the characterization of unknown compounds. The chemical shifts of the 16-CH_3, H-10, 14-CH_3, and H-15 protons provide information on the degree and type of oxygenation in ring A. The vicinal coupling constants $J_{7,8}$ and $J_{3,4}$ provide information on the orientation (α or β) for the various substituents. Long-range coupling observed between H-7 and H-15, between H-8 and H-16, and between H-8 and H-10 also offers specific information on the conformation of the trichothecene ring system. All these data are consistent with the stable conformation in solution having the A ring in a half-chair and the B ring in a chair conformation. The data are summarized in Fig. 6.

Acknowledgements

The authors wish to thank W. Adams, D. Levandier, and R.-M. Meier for their diligent efforts in the isolation and characterization of the various *Fusarium* secondary metabolites, also J. D. Miller and A. Taylor for their efforts in carrying out the various fermentations of the *Fusarium* fungi.

1. H. L. TRENHOLM, W. COCHRANE, H. COHEN, J. I. ELLIOT, E. R. FARNSWORTH, D. W. FRIEND, R. M. G. HAMILTON, J. F. STANDISH, and B. K. THOMPSON. J. Assoc. Off. Anal. Chem. **66**, 92 (1983).
2. R. GREENHALGH, D. LEVANDIER, W. ADAMS, J. D. MILLER, B. A. BLACKWELL, A. J. MCALEES, and A. TAYLOR. J. Agric. Food Chem. **34**, 98 (1986).
3. (*a*) R. GREENHALGH, A. W. HANSON, J. D. MILLER, and A. TAYLOR. J. Agric. Food Chem. **32**, 945 (1984); (*b*) R. GREENHALGH, R. M. MEIER, B. A. BLACKWELL, J. D. MILLER, A. TAYLOR, and J. W. APSIMON. J. Agric. Food Chem. **32**, 1261 (1984); (*c*) J. Agric. Food Chem. **34**, 115 (1986).
4. J. D. MILLER, A. TAYLOR, and R. GREENHALGH. Can. J. Microbiol. **29**, 1171 (1983).
5. R. GREENHALGH, B. A. BLACKWELL, M. SAVARD, J. D. MILLER, and A. TAYLOR. J. Agric. Food Chem. In press.
6. D. R. LAUREN, A. ASHLEY, B. A. BLACKWELL, R. GREENHALGH, J. D. MILLER, and G. A. NEISH. J. Agric. Food Chem. In press.

Can. J. Chem. Downloaded from www.nrcresearchpress.com by 213.166.140.6 on 09/07/12
For personal use only.

7. R. R. KING and R. GREENHALGH. Can. J. Chem. **63**, 1089 (1985).
8. G. G. FREEMAN, J. J. GILL, and W. S. WARING. J. Chem. Soc. 1105 (1959).
9. J. FISHMAN, E. R. H. JONES, G. LOWE, and M. C. WHITING. J. Chem. Soc. 3948 (1960).
10. P. W. BRIAN, A. W. DAWKINS, J. F. GROVE, H. G. HEMMING, D. LOWE, and G. L. F. NORRIS. J. Exp. Bot. **12**, 1 (1961).
11. (*a*) C. TAMM and J. GUTZWILLER. Helv. Chim. Acta, **45**, 1726 (1962); (*b*) J. GUTZWILLER and C. TAMM. Helv. Chim. Acta, **46**, 1786 (1963).
12. W. O. GODTFREDSEN and S. VANGEDAL. Proc. Chem. Soc. 188 (1964).
13. (*a*) S. ABRAHAMSSON and B. NILSSON. Proc. Chem. Soc. 188 (1964); (*b*) Acta Chem. Scand. **20**, 1044 (1966).
14. R. J. COLE and R. H. COX. *In* Handbook of toxic fungal metabolites. Academic Press, New York. 1981. Chap. 5.
15. B. A. BLACKWELL, R. GREENHALGH, and A. D. BAIN. J. Agric. Food Chem. **32**, 1078 (1984).
16. C. TAMM and M. TORI. *In* Mycotoxins, production, isolation, separation and purification. *Edited by* V. Betina. Elsevier Science Publishers, Amsterdam, Netherlands. 1984. Chap. 8.
17. M. E. SAVARD and R. GREENHALGH. J. Nat. Prod. In press.
18. A. J. MANCUSO, S.-L. HUANG, and D. SWERN. J. Org. Chem. **43**, 2480 (1978).
19. J. F. GROVE. J. Chem. Soc. Perkin Trans. 1, 647 (1986).
20. B. K. TIDD. J. Chem. Soc. C, 218 (1967)
21. D. G. CORLEY, G. E. ROTTINGHAUS, J. K. TRACY, and M. S. TEMPESTA. Tetrahedron Lett. **27**, 4133 (1986).
22. T. KANEKO, H. SCHMITZ, J. M. ESSERY, W. ROSE, H. G. HOWELL, F. A. O'HERRON, S. NACHFOLGER, J. HUFTALEN, W. T. BRADNER, R. A. PARTYKA, T. W. DOYLE, J. DAVIES, and E. CUNDLIFFE. J. Med. Chem. **25**, 579 (1982).
23. J. R. BAMBURG, N. V. RIGGS, and F. M. STRONG. Tetrahedron, **24**, 3329 (1968).
24. J. GUTZWILLER, R. MAULI, H. P. SIGG, and C. TAMM. Helv. Chim. Acta, **48**, 962 (1965).

Can. J. Chem. Downloaded from www.nrcresearchpress.com by 213.166.140.6 on 09/07/12
For personal use only.

Kinetics of hydrolysis of aromatic mono- and disulfonyl chlorides

PRZEMYSLAW SANECKI AND EDWARD ROKASZEWSKI
Faculty of Chemistry, I. Lukasiewicz Technical University, 35-959 Rzeszów, Poland

Received October 29, 1986[1]

PRZEMYSLAW SANECKI and EDWARD ROKASZEWSKI. Can. J. Chem. **65**, 2263 (1987).

A continuous polarographic method of recording instantaneous concentrations of —SO_2Cl groups in an aqueous acetic acid system containing CH_3CO_2Na has been elaborated. Ten model monosulfonyl chlorides underwent hydrolysis according to pseudo-first order kinetics (20% H_2O, 80% v.v. CH_3CO_2H, 0.5 mol × dm^{-3} CH_3CO_2Na). Plots of hydrolysis for seven disulfonyl dichlorides with different number of —CH_3 groups have been determined. Pseudo-first order rate constants for two consecutive reactions of hydrolysis (k_1 and k_2) have been computed and the influence of —SO_2Cl and —SO_3^- groups on the reactivity of the second group —SO_2Cl has been discussed. The mechanism of nucleophilic substitution has also been discussed.

PRZEMYSLAW SANECKI et EDWARD ROKASZEWSKI. Can. J. Chem. **65**, 2263 (1987).

On a développé une méthode polarographique continue qui permet d'enregistrer instantanément la présence de groupements —SO_2Cl dans des systèmes aqueux d'acide acétique contenant du CH_3CO_2Na. Dix chlorures modèles de monosulfonyles ont subi une hydrolyse suivant une cinétique de pseudo-premier ordre (20% H_2O, 80% v/v de CH_3CO_2H et 0,5 mol × dm^{-3} de CH_3CO_2Na). On a déterminé les courbes d'hydrolyse de sept dichlorures de disulfonyles qui diffèrent par le nombre de groupements CH_3. On a calculé les constantes de pseudo-premier ordre pour les deux réactions d'hydrolyse consécutives (k_1 et k_2) et on discute de l'influence des groupements —SO_2Cl et —SO_3^- sur la réactivité du deuxième groupement —SO_2Cl. On discute aussi du mécanisme de la substitution nucléophile.

[Traduit par la revue]

Introduction

The solvolysis and hydrolysis of sulfonyl halogenides are subject of many papers (refs. 1–23 and references therein). The character of the investigations is closely linked with advances in knowledge on reaction mechanism as reported by Arrhenius, Bodenstein, Ingold, Winstein, Brønsted, and Hammett and co-workers. The titrimetric or conductometric methods were used in the determination of instantaneous concentrations of reagents or products, and spectral uv was used only in two cases.

It has been found that monosulfonyl chlorides hydrolyze according to the S_N2 mechanism (e.g. refs. 9, 10):

$$(R)Ar—SO_2Cl + H_2O \rightarrow (R)Ar—SO_3H + HCl$$

At a constant concentration of the nucleophilic agent such as H_2O (2, 8, 12, 14, 16, 17), OH^- (8, 22), $CH_3CO_2^-$ (12, 19, 22), the reaction is described by a pseudo-first order kinetic equation.

Only one paper (6) on the hydrolysis of bifunctional sulfonyl chlorides has been published so far but it does not attempt to determine separate rate constants (k_1 and k_2). The hydrolysis was investigated in a dioxane–water (30% by vol.) medium at an initial concentration of sulfonyl chloride 0.006–0.0125 mol dm^{-3} and temperatures of 303, 313, and 323 K. Five monofunctional sulfonyl chlorides were investigated: X—C_6H_4—SO_2Cl, X— = H—, C_6H_5—, C_6H_5—CH_2—, C_6H_5—O—, C_6H_5—CO—, and seven bifunctional derivatives: 4,4′-ClO_2S—Ar—X—Ar—SO_2Cl X = (—, good, biphenyl), CH_2, $(CH_2)_2$, O, CO, SO_2 (2,2′), and *m*-$C_6H_4(SO_2Cl)_2$. It was found that most bifunctional derivatives hydrolyze according to the first order kinetics (6). For *m*-benzenedisulfochloride we observed a continuous decrease in the rate constant as the reaction progressed (6).

This paper is, therefore, to determine the hydrolysis rate constant for each group of disulfonyl chlorides and to discuss some possible changes in the hydrolysis mechanism. The polarographic method enables us to register the instantaneous concentration of the —SO_2Cl groups in a detailed and continuous (or semi-continuous) manner.

Experimental

Chemicals

Seventeen sulfonyl and disulfonyl chlorides were used. The compounds were synthesized and purified by classical methods (24–26). The other substances used here (CH_3COOH, CH_3COONa) were p.p.a. Acetic acid was further purified by distillation over $KMnO_4$. Twice distilled water was used.

Apparatus

LP-60 polarograph with EZ-2 recorder and MLW-U-7^c ultrathermostat (±0.05 K) were used.

Rate measurements

The rate of hydrolysis in CH_3CO_2H containing H_2O medium in the presence of CH_3CO_2Na was determined by a polarographic method in a cell of 7 cm^3 capacity. The cell was connected to an external reference electrode (the saturated aqueous acetate electrode) by a reservoir filled with the same solution as that used for dissolving the substrates. The reservoir was separated from the reaction mixture and the reference electrode by a glass sinter G-5. Deaerated solution of the substrate in glacial acetic acid was introduced into deaerated solution of the other components in the polarographic cell and stirred with a stream of nitrogen at 298 ± 0.05 K for 3 s. Then, the polarographic circuit was closed and current intensity as a function of time was recorded, the nitrogen or argon atmosphere over the reaction mixture being continuously maintained. The current intensity ($i_{l,obs}$) − time (t) was continuously recorded at a constant potential corresponding to the potential of the limiting current. The latter was determined earlier for each compound from the polarographic wave. Initially, the concentration of —SO_2Cl was always 1.7×10^{-3} mol dm^{-3}. Paper feed rate was 8.0 cm h^{-1} (1 cm = 450 s), for *p*-$N(CH_3)_2C_6H_4SO_2Cl$ 4.0 cm min^{-1} (1 cm = 15 s). The measurement was terminated when ratio i_l/i_{l0} was smaller than or equal to 0.1. A slight adjustment (less than 0.3%) was made for residual current (i_{res}) using $i_l = i_{l,obs} - i_{res}$. The value of i_{res} did not change after all compound had reacted.

Kinetics

Compounds containing two —SO_2Cl groups should under-

[1]Revision received April 13, 1987.

Can. J. Chem. Downloaded from www.nrcresearchpress.com by 213.166.140.6 on 09/07/12
For personal use only.

go two consecutive irreversible reactions of hydrolysis in accordance with the scheme

$$\underset{\text{A}}{\text{ClO}_2\text{S—Ar—SO}_2\text{Cl}} + \text{H}_2\text{O} \xrightarrow{k_1} \underset{\text{A}_1}{\text{ClO}_2\text{S—Ar—SO}_3\text{H}} + \text{HCl}$$

$$\underset{\text{A}_1}{\text{ClO}_2\text{S—Ar—SO}_2\text{H}} + \text{H}_2\text{O} \xrightarrow{k_2} \underset{\text{A}_2}{\text{HO}_3\text{S—Ar—SO}_3\text{H}} + \text{HCl}$$

It follows from statistical data that at identical reactivities of $—SO_2Cl$ groups in A and A_1 the ratio of constants $k_2/k_1 = r$ should be 0.5.

A system of two irreversible consecutive first order reactions

$$[1] \quad \text{A} \xrightarrow{k_1} \text{A}_1 \xrightarrow{k_2} \text{A}_2$$

is described by the known set of differential equations (27)

$$[2] \quad -\frac{da}{dt} = k_1 a$$

$$[3] \quad \frac{da_1}{dt} = k_1 a - k_2 a_1$$

$$[4] \quad \frac{da_2}{dt} = k_2 a_1$$

where $a = c_A/c_{0A}$, $a_1 = c_{A_1}/c_{0A}$, $a_2 = c_{A_2}/c_{0A}$; c_A, c_{A_1}, c_{A_2} are the instantaneous concentrations of compounds A, A_1, A_2, and c_{0A} is the initial concentration of substrate A. A solution to this problem is the following set of equations:

$$[5] \quad a = \exp(-k_1 t)$$

$$[6] \quad a_1 = (a - a^r)/(r - 1)$$

$$[7] \quad a_2 = 1 + ra/(1 - r) - a^r/(1 - r)$$

where $r = k_2/k_1$ and $a + a_1 + a_2 = 1.0$. An exact determination of constants k_1 or k_2 is possible by means of recording instantaneous concentrations of A, A_1, or A_2. It is also possible to record instantaneous concentrations of functional groups such as c_{SO_2Cl}.

In accordance with the reaction scheme, during hydrolysis we may expect two polarographically active compounds, A and A_1. The limiting current (i_l) measured at a given moment must be the sum of limiting currents of both forms A and A_1 which, in accordance with Ilkovič's equation, may be written as

$$[8] \quad i_l = \text{constant} \times n_A D_A c_A + \text{constant} \times n_{A_1} D_{A_1} c_{A_1}$$

where n is the number of electrons transferred during the reduction, D is diffusion coefficient, and c is concentration in mol dm^{-3}. For the reduction of both forms A and A_1 the numbers of transferred electrons are 4 and 2, respectively. A polarographic method does not produce a noticeable decrease in the concentration of $—SO_2Cl$ groups. We can assume that $D_A = D_{A_1}$. Hence from eq. [8] we get

$$[9] \quad i_l = 2\,\text{constant}_1 \times c_A + \text{constant}_1 \times c_{A_1}$$

For $t = 0$ eq. [9] takes the form

$$[10] \quad i_{l,0} = 2\,\text{constant}_1 \cdot c_{0A}$$

Dividing the members of eqs. [9] by [10] we get

$$[11] \quad i_l/i_{l,0} = c_A/c_{0A} + c_{A_1}/(2c_{0A})$$

or, having taken into consideration formulas for a, a_1, and a_2

$$[12] \quad i_l/i_{l,0} = a + a_1/2$$

From [5], [6], and [12] we get [13]:

$$[13] \quad p = i_l/i_{l,0} = \exp(-k_1 t) + \frac{\exp(-k_1 t) - \exp(-k_2 t)}{2(k_2/k_1 - 1)}$$

Rate constants were computed from the final non-linear equation [13] in which k_1 and k_2 are unknown. Equation [13] were utilized here for computing constants k_1 and k_2 on the basis of continuous recording of instantaneous concentrations of $—SO_2Cl$ groups, i.e., $p = f(t)$. We used a polarographic method which makes this recording possible.

The method of least squares was used in accordance with the condition

$$[14] \quad S = \sum_{j=1}^{n} \left[1 - \frac{p_j}{(i_l/i_{l,0})_j}\right]^2 = \text{minimum}$$

where p_j was a value computed on the basis of an assumed pair of values k_1 and k_2, but $(i_l/i_{l0})_j$ was measured at time t_j. From the continuous course $i_l = f(t)$ values $(i_l)_j$, differing by a constant step, at $n \geqslant 20$, were chosen.

Results and discussion

The suitability of the polarographic method was tested for the model compound $C_6H_5—SO_2Cl$ and for nine substituted derivatives $X—C_6H_4—SO_2Cl$ for which the following dependence was expected:

$$[15] \quad i_l/i_{l0} = \exp(-kt)$$

The results showed that in media presented in Fig. 1 and in Table 1 $\ln(i_l/i_{l0})$ is a linear function of time and that the rate constants of a pseudo-first order reaction do not change up to the reaction degree of 95 ± 5%.

The rate of hydrolysis of $C_6H_5SO_2Cl$ is a complex function of the electrolyte concentration (CH_3CO_2Na) and of the used solvents (H_2O, CH_3CO_2H), Fig. 1. With a constant concentration of solvents (80% CH_3CO_2H, 20% v.v. H_2O) an increase in acetate concentration from 0.1 to 0.3 mol dm^{-3} causes a slight increase in the hydrolysis rate-constant, curve *1*. This medium is characterized by an approximately equimolar ratio of the acid to water ($c_{CH_3CO_2H}/c_{H_2O} = 1.15/1.0$) and the hydrolysis reactions in it run more slowly than those in aqueous solutions (2, 8, 12). Probably the active concentration of water is lower than its computed value because of its co-association with acetic acid molecules. From extrapolation it follows that in the case of electrolyte shortage $k = 1.4 \times 10^{-5}$ s^{-1}; however, experimental determination of the constant by means of polarographic method cannot be done.

Simple nucleophiles such as H_2O, OH^-, $CH_3CO_2^-$ and complex nucleophiles such as hydrated ions, ion pairs, and larger aggregates may be present in the medium. However, we consider the participation of free OH^- groups improbable. When the acetate concentration increases in the range 0.1 to 0.3 mol dm^{-3}, a mixed hydrolysis involving water and a form of acetic anion may take place. When the acetate concentration increases in the range 0.3 to 0.5 mol dm^{-3} (Fig. 1, curve 1), an approximately linear increase in the hydrolysis rate is observed. This suggests the participation of acetic anions or the anions in complex nucleophiles.

Further increase in acetate concentration no longer causes a

Can. J. Chem. Downloaded from www.nrcresearchpress.com by 213.166.140.6 on 09/07/12
For personal use only.

Can. J. Chem. Downloaded from www.nrcresearchpress.com by 213.166.140.6 on 09/07/12
For personal use only.

TABLE 1. Pseudo-first order hydrolysis rate constants (k) of monobenzenesulfonylchlorides in 20% H_2O, 80% v.v. CH_3CO_2H, $c_{CH_3CO_2Na}$ = 0.5 mol dm^{-3}, $c_{X-C_6H_4-SO_2Cl}$ = 1.7 × 10^{-3} mol dm^{-3}, T = 298.15K

No.	X—	σ_X (28)	(k_X ± sd) 10^5 (s^{-1})	log (k_X/k_H)
1	H—	0.00	3.54± 0.02	0.000
2	*p*-CH_3—	−0.17	2.25± 0.05	−0.197
3	*p*-CH_3—CO—NH—	0.00	2.48± 0.04	−0.155
4	*p*-F—	0.06	3.11± 0.03	−0.056
5	*p*-Cl—	0.23	4.33± 0.04	0.087
6	*p*-Br—	0.23	5.26± 0.03	0.172
7	*p*-I—	0.28	6.71± 0.14	0.278
8	*m*-NO_2—	0.71	23.5 ± 0.64	0.822
9	*p*-NO_2—	0.78	42.7 ± 0.39	1.081
10	*p*-$(CH_3)_2N$—	(−0.83)	495 ±10	2.146

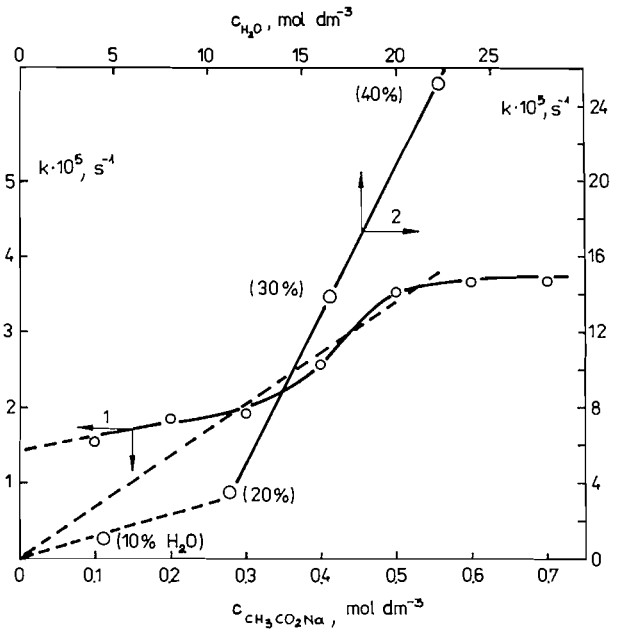

FIG. 1. Influence of sodium acetate concentration (curve *1*) at constant concentration of the solvents (80% CH_3CO_2H, 20% v.v. H_2O), and of water concentration (curve 2) at constant concentration of sodium acetate (0.5 mol × dm^{-3}) on the rate of hydrolysis of $C_6H_5SO_2Cl$ (c_0 = 1.7 × 10^{-3} mol × dm^{-3}), T = 298.15 K.

visible increase in the hydrolysis rate (Fig. 1, curve 1). In solutions with more water (20–40% v.v. H_2O, Fig. 1, curve 2), the investigated reaction is very sensitive to water concentration and the relationship $k = f(c_{H_2O})$ is linear. The increase in water concentration is accompanied by an increase in the concentration of acetate ions and within this range of water concentrations the hydrolysis probably involves "free" $CH_3CO_2^-$ ions as mentioned in refs. 12 and 19.

For comparison a solution 20% H_2O, 80% v.v. CH_3CO_2H, 0.5 mol dm^{-3} CH_3CO_2Na was used as a model medium. The results of hydrolysis of ten monosulfonylchlorides X—C_6H_4—SO_2Cl have been presented in Table 1.

Using the nine values of constants k (compounds **1** to **9**) a Hammett correlation [16] was determined:

$$[16]\quad \log (k_X/k_H) = \rho\sigma_X + \delta$$

ρ = 1.34 ± 0.25; δ = −0.091 ± 0.097, n = 9, r = 0.9788, s_0 = 0.097, for $t_{0.05,7}$. The probable reaction scheme is

$$[17]\quad Ar—SO_2Cl + CH_3CO_2^- \xrightarrow{k} Ar—SO_2—O—COCH_3 + Cl^-$$

$$[18]\quad Ar—SO_2—O—COCH_3 + CH_3CO_2^- + H_2O \xrightarrow{\text{fast}} Ar—SO_3^- + 2CH_3CO_2H$$

Of the ten investigated derivatives *p-N,N*-dimethylaminebenzenesulfonylchloride hydrolyzes exceptionally fast. One observes here a change in the character of the substituent from a donor to a strong acceptor and the estimated value of σ_X from [16] is as high as 1.66, greater than the value for *p*-$(CH_3)_2NH^+$ (32). The possible explanation is an elimination–additive mechanism such as those described in refs. 19, 22, 23:

$$[19]\quad (CH_3)_2N—C_6H_4—SO_2Cl \rightarrow (CH_3)_2\overset{+}{N}=\langle\bigcirc\rangle=SO_2 + Cl^-$$

This reaction is confirmed since the hydrolysis rate is independent of acetate concentration: $c_{CH_3CO_2Na}$ = 0.1; 0.3; 0.5 mol dm^{-3}, k = (4.67; 5.11; 4.95 ± 0.1) × 10^{-3} s^{-1}, respectively.

Using hyperchloric acid instead of sodium acetate (c_{HClO_4} = 0.5 mol × dm^{-3}) gives k = (1.38 ± 0.12) 10^{-3} s^{-1}. This medium allows the equilibrium —$N(CH_3)_2$ + H^+ ⇌ —$NH(CH_3)_2H^+$ to occur. The 3.6-fold rate reduction (from 4.95 × 10^{-3} to 1.38 × 10^{-3} s^{-1}) suggests a significant decrease in —$N(CH_3)_2$ concentration.

Our procedure enables us to study the hydrolysis kinetics of seven disulfonyl compounds $C_6H_{4-n}(CH_3)_n(SO_2Cl)_2$ where n = 0, 1, 2, 3, to determine their k_1 and k_2 values. Our results are presented in Table 2.

The rate constant ratio $r = k_2/k_1$ suggests a change in the reactivity of the second —SO_2Cl group after the charged SO_3^- group has appeared. Despite the negative charge, the group shows an acceptor character and the rate constants of the investigated derivatives are greater than the hydrolysis rate constant of the model compound $C_6H_5SO_2Cl$. For *meta* and *para* disulfonyldichlorides they are, on average, one order lower than the corresponding values of k_1 ($r = k_2/k_1$ = 0.066 ÷ 0.28).

On the other hand, for two compounds (11, 14) with —SO_2Cl groups in the *ortho position* $k_2 \cong k_1$. Here there is probably a change in the reaction mechanism from S_N2 to S_Ni for the second reaction [21]:

$$[20]\quad o\text{-}(ClO_2S)_2C_6H_4 + CH_3CO_2^- + H_2O \xrightarrow{k_1} 4\text{-}HO_3S—C_6H_4—SO_2Cl + CH_3CO_2H + Cl^-$$

$$[21]\quad C_6H_4(SO_2Cl)SO_3H \xrightarrow{k_2 \cong k_1} C_6H_4\langle{}^{SO_2}_{SO_2}\rangle O + H^+ + Cl^-$$

$$[22]\quad C_6H_4(SO_2)_2O + CH_3CO_2^- + H_2O \xrightarrow{\text{fast}} C_6H_4(SO_3H)SO_3^- + CH_3CO_2H$$

In the hydrolysis reaction of the second —SO_2Cl group (S_Ni mechanism) —OH group from SO_3H or —O^- from SO_3^- becomes an internal nucleophilic agent. From a statistical viewpoint, the second reaction is two times faster than the first one.

We have gathered below some σ_X constants for —SO_2Cl and —SO_3^- substituents calculated from eq. [16] and the data

TABLE 2. Pseudo-first order rate constants of consecutive hydrolysis (k_1, k_2) of benzenedisulfonylchlorides $C_6H_{4-n}(CH_3)_n(SO_2Cl)_2$, $c_{SO_2Cl} = 1.7 \times 10^{-3}$ mol dm^{-3}, $T = 298.15$K

No.	Compound	$k_1 \times 10^5$ (s^{-1})	$k_2 \times 10^5$ (s^{-1})	$r = k_2/k_1$	sd 100%*
11	*o*-ClO_2S—C_6H_4—SO_2Cl	21.5±0.1	22.6 ±0.34	1.05	0.76
12	*m*-ClO_2S—C_6H_4—SO_2Cl	85.0±1	8.90±0.30	0.105	1.4
13	*p*-ClO_2S—C_6H_4—SO_2Cl	180 ±2	11.9 ±0.33	0.066	1.3
14	2-ClO_2S-4-$CH_3C_6H_3$—SO_2Cl	16.6±0.1	17.1 ±0.44	1.03	2.5
15	5-ClO_2S-2-CH_3—C_6H_3—SO_2Cl	56.3±0.3	8.16±0.22	0.145	1.9
16	5-ClO_2S-2,4-$(CH_3)_2$—C_6H_2—SO_2Cl	32.7±0.1	9.16±0.36	0.28	1.4
17	3-ClO_2S-2,4,6-$(CH_3)_3$—C_6H_1—SO_2Cl	135 ±2	13.2 ±0.50	0.098	3.4

*sd = $[S/(n-1)]^{1/2}$, eq. [14].

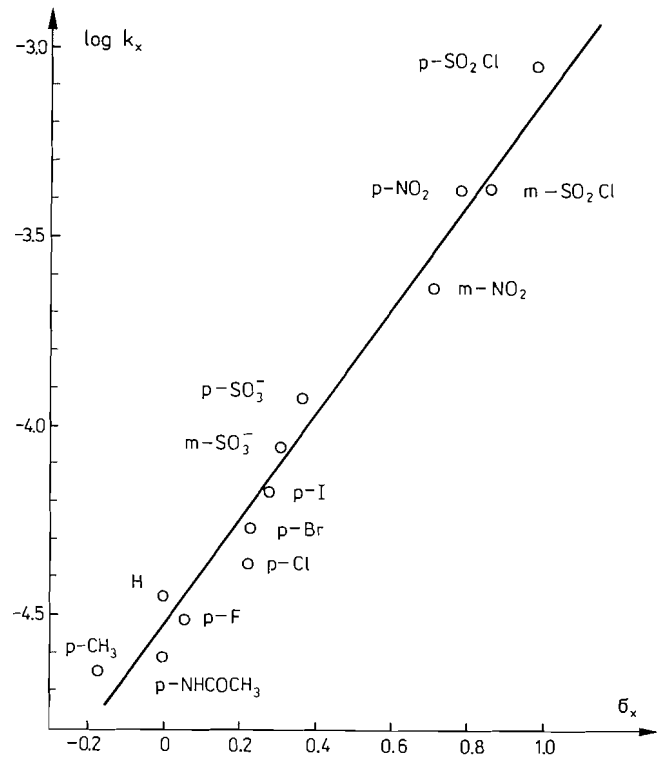

FIG. 2. Hammett correlation for the hydrolysis of substituted benzenesulfonylchlorides in the solution 80% CH_3CO_2H, 20% v.v. H_2O; $c_{CH_3CO_2Na} = 0.5$ mol × dm^{-3}, $c_{0,SO_2Cl} = 1.7 \times 10^{-3}$ mol × dm^{-3}, $T = 298.15$ K.

in Table 2, after taking the statistical data into account: $k_{SO_2Cl} = k_1/2$, $k_{SO_3^-} = k_2$.

o-SO_2Cl	*m*-SO_2Cl	*p*-SO_2Cl
0.43	0.87	1.11
o-SO_3^-*	*m*-SO_3^-	*p*-SO_3^-
0.66	0.37	0.46

*indicates a change in hydrolysis mechanism

For *meta* and *para* substituents these values are within the range given in the literature (28–34).

Compound **14** (Table 2) may undergo a parallel two step hydrolysis since it contains two unidentical groups —SO_2Cl. The actual summary hydrolysis rate should thus be described by four constants. The same is true for compound **15**. The other compounds (**16** and **17**) contain —SO_2Cl groups which are identical because of their symmetrical structures and it is of no significance which of these hydrolyzes first. The presence of methyl groups in *ortho* position increases the hydrolysis rate.

By adding four points for hydrolysis *m*- and *p*-disulfonyldichlorides and their intermediates ($k_1/2$ and k_2, Table 2) to correlation [16] we get a more general and accurate Hammett correlation (Fig. 2):

$$\log (k_X/k_H) = (1.42 \pm 0.16)\sigma_X - (0.087 \pm 0.082)$$

$$n = 13,\ r = 0.9852,\ s_0 = 0.094, \quad \text{for } t_{0.05,11}$$

The literature substituent constants were taken into account: $\sigma^m_{SO_3^-} = 0.31$, $\sigma^p_{SO_3^-} = 0.37$ (35), $\sigma^m_{SO_2Cl} = 0.86$ (36, 37), and $\sigma^p_{SO_2Cl} = 0.98$ (38). The value $\sigma^p_{SO_2Cl} = 0.98$ was also computed from Exner's equation (39). The value 1.11 determined from the correlation [16] is close to the value computed from the data given by Taft *et al.* (36, 37): $\sigma^p_{SO_2Cl} = 1.14$ ($\sigma_I = 0.86$, $\sigma_R = 0.28$) as well as to the value given by Bray and Barnes (29): $\sigma^p_{SO_2Cl} = 1.114$.

Acknowledgements

The authors would like to thank a referee for pointing out that our present results show a good correlation with Rogne's k_{OH^-} values (8), indicating the ionic character of the reaction.

1. Z. G. LINETSKAYA and N. V. SAPOZNIKOVA. J. Appl. Chem. USSR, Engl. Trans. **21**, 876 (1948).
2. H. K. HALL, JR. J. Am. Chem. Soc. **78**, 1450 (1956).
3. E. F. JENKINS and A. N. HAMBLY. Aust. J. Chem. **14**, 190 (1961).
4. F. E. JENKINS and A. N. HAMBLY. Aust. J. Chem. **14**, 205 (1961).
5. R. V. VIZGERT. Usp. Khim. **32**, 3 (1963).
6. R. V. VIZGERT, I. E. KACHANKO, and V. E. YAVOROVSKAYA. Reakts. Sposobn. Org. Soedin. **3**, 16 (1966).
7. I. E. KACHANKO and R. V. VIZGERT. Reakts. Sposobn. Org. Soedin. **3**, 170 (1966).
8. O. ROGNE. J. Chem. Soc. B, 1294 (1968).
9. R. E. ROBERTSON, B. ROSSALL, S. E. SUGAMORI, and L. TREINDL. Can. J. Chem. **47**, 4199 (1969).
10. R. E. ROBERTSON and B. ROSSALL. Can. J. Chem. **49**, 1441 (1971).
11. O. ROGNE. J. Chem. Soc. B, 727 (1970).
12. O. ROGNE. J. Chem. Soc. B, 1056 (1970).
13. O. ROGNE. J. Chem. Soc. B, 1334 (1971).
14. M. L. TONNET and A. N. HAMBLY. Aust. J. Chem. **24**, 703 (1971).
15. R. FOON and A. N. HAMBLY. Aust. J. Chem. **24**, 713 (1971).

Can. J. Chem. Downloaded from www.nrcresearchpress.com by 213.166.140.6 on 09/07/12
For personal use only.

16. R. V. VIZGERT, I. M. TUCHAPSKI, and Y. G. SKRYPNIK. Reakts. Sposobn. Org. Soedin. **11**, 21 (1974).
17. B. G. GNEBIN, S. N. IVANOV, and A. A. SPRYSKOV. Zhurn. Org. Khim. **12**, 1939 (1976).
18. B. G. GNEDIN, S. N. IVANOV, and A. A. SPRYSKOV. Vopr. Kinet. Katal. (3), 3 (1976); Ref. Zh. Khim. Abs. 12B992 (1977).
19. L. O. FARNG and J. L. KICE. J. Am. Chem. Soc. **103**, 1137 (1981).
20. R. V. VIZGERT, I. M. OZDROVSKAYA, S. G. SHEIKO, E. S. MITCHENKO. Strukt. Reakts. Sposobn. Org. Soedin. Kiev, 104 (1981); Ref. Zh. Khim. Abs. 11Zh35 (1982).
21. J. F. KING, J. H. HILLHOUSE, and S. SKONIECZNY. Can. J. Chem. **62**, 1977 (1984).
22. T. DEACON, C. B. FARRAR, B. J. SIKKEL, and A. J. WILLIAMS. J. Am. Chem. Soc. **100**, 2525 (1978).
23. S. THED and G. GUANTI. J. Am. Chem. Soc. **104**, 1128 (1982).
24. C. M. SUTER. Chemistry of sulfur. John Wiley and Sons, New York. 1948.
25. HOUBEN-WEYL. Methoden der organischem Chemie. Bd. 9, G. Thieme Verlag, Stuttgart, 1955.
26. G. MALEWSKI and H. J. WEIGMAN. Spectrochim. Acta, **18**, 725 (1962).
27. G. NATTA and E. MANTICA. J. Am. Chem. Soc. **74**, 3152 (1952).
28. C. HANSCH and A. LEO. Substituent constants for correlation analysis in chemistry and biology. J. Wiley, New York. 1979.
29. P. J. BRAY and R. G. BARNES. J. Chem. Phys. **27**, 551 (1957).
30. B. J. LINDBERG. Arkiv Kemi **32**, 317 (1970).
31. C. G. SWAIN and E. G. LUPTON, JR. J. Am. Chem. Soc. **90**, 4328 (1968).
32. A. J. HOEFNAGEL, M. A. HOEFNAGEL, and B. M. WEPSTER. J. Org. Chem. **43**, 4720 (1978).
33. C. G. SWAIN, S. H. UNGER, N. R. ROSENQUIST, and M. S. SWAIN. J. Am. Chem. Soc. **105**, 492 (1983).
34. C. G. SWAIN, M. S. SWAIN, A. L. POWELL, and S. ALUNI. J. Am. Chem. Soc. **105**, 502 (1983).
35. H. ZOLLINGER, W. BÜCHLER, and C. WITTWER. Helv. Chim. Acta, **36**, 1711 (1953).
36. R. W. TAFT, E. PRICE, I. R. FOX, I. C. LEWIS, K. K. ANDERSON, and G. T. DAVIS. J. Am. Chem. Soc. **85**, 709 (1963).
37. R. W. TAFT, E. PRICE, I. R. FOX, I. C. LEWIS, K. K. ANDERSON, and G. T. DAVIS. J. Am. Chem. Soc. **85**, 3146 (1963).
38. H. S. GUTOWSKY, D. W. MCCALL, B. R. MCGARWEY, and L. M. MEYER. J. Am. Chem. Soc. **74**, 4809 (1952).
39. O. EXNER. Chem. Listy **59**, 1047 (1965).

Can. J. Chem. Downloaded from www.nrcresearchpress.com by 213.166.140.6 on 09/07/12
For personal use only.

The phosphorylation of chrysotile asbestos fibers with phosphorus oxychloride ($POCl_3$): mechanism of reaction and chemical composition of the external coating

JALEH KHORAMI AND ALAIN LEMIEUX

Programme de recherche sur l'amiante de l'Université de Sherbrooke (PRAUS), Département de chimie, Faculté des sciences, Université de Sherbrooke, Sherbrooke (Qué.), Canada J1K 2R1

AND

DENIS NADEAU

Programme de recherche sur l'amiante de l'Université de Sherbrooke (PRAUS), Département de biologie, Faculté des sciences, Université de Sherbrooke, Sherbrooke (Qué.), Canada J1K 2R1

Received January 26, 1987

JALEH KHORAMI, ALAIN LEMIEUX, and DENIS NADEAU. Can. J. Chem. **65**, 2268 (1987).

Magnesium hydroxide and silica, which are at the base of the chemical composition of chrysotile asbestos fibers, have been treated with phosphorus oxychloride vapors and compared to chrysotile asbestos treated similarly. Thermogravimetric, evolved gas analyses, and Fourier Transform infrared spectroscopy techniques were used to identify the compounds formed and (or) adsorbed on the surface of the minerals phosphorylated at room temperature and after a heat post-treatment at 300°C. The results obtained show that the reaction of silica with phosphorus oxychloride can be considered negligible. However, the modifications induced on magnesium hydroxide and chrysotile asbestos fibers are similar. After the chemical treatment at room temperature, it was possible to identify the presence of hydrochloric acid, phosphorus oxychloride, magnesium chloride (nH_2O), and acid orthophosphate salts. In comparison, the compounds formed after the 300°C heat post-treatment were only hydrated polyphosphate salts and magnesium chloride (nH_2O). It is postulated that a polyphosphorus coating is formed at the surface of the chrysotile asbestos fibers when these are treated with phosphorus oxychloride at room temperature and then treated at 300°C after the phosphorylation process.

JALEH KHORAMI, ALAIN LEMIEUX et DENIS NADEAU. Can. J. Chem. **65**, 2268 (1987).

L'hydroxyde de magnésium et la silice, qui constituent la base de la composition chimique de l'amiante chrysotile, ont été traitées avec des vapeurs d'oxychlorure de phosphore pour être ensuite comparées avec des fibres d'amiante chrysotile traitées de façon similaire. Des techniques telles que les analyses thermogravimétriques, les gaz dégagés et la spectroscopie infrarouge ont été utilisées pour identifier les composés formés et (ou) adsorbés sur la surface des minéraux phosphorylés à la température ambiante, et après un post-traitement à la chaleur (300°C). Les résultats obtenus montrent que la réaction de la silice avec l'oxychlorure de phosphore peut être considérée comme négligeable. Cependant, les modifications induites sur l'hydroxyde de magnésium et les fibres d'amiante chrysotile sont similaires. Après traitement chimique à la température ambiante, on a pu identifier la présence d'acide chlorhydrique, d'oxychlorure de phosphore, de chlorure de magnésium (nH_2O) et des sels d'orthophosphates acides. Comparativement, les composés retrouvés après le post-traitement à 300°C sont uniquement des sels hydratés de polyphosphate et le chlorure de magnésium. Il est postulé que, lorsque la réaction de l'amiante chrysotile avec l'oxychlorure de phosphore à la température de la pièce est suivie d'un post-traitement à 300°C, le traitement chimique conduit à la formation d'un revêtement de polyphosphate sur la surface des fibres.

Introduction

It has been repeatedly demonstrated that one of the factors responsible for the biological activity of chrysotile asbestos fibers is related to its chemical structure, particularly in relation to the surface reactivity of the mineral (1, 2). Several methods have been devised to study the effect of a chemical modification on the biological reactivity of chrysotile asbestos. These methods include acid leaching (3, 4) and metal deposition (5). One of the methods selected by Lalancette and co-workers (6, 7) for inducing a chemical modification of this mineral was phosphorylation with phosphorus oxychloride ($POCl_3$). Chrysotile fibers thus treated showed successful reduction of biological activity without losing their main industrial properties.

Previously we characterized these chemically modified fibers using thermogravimetric methods (TG/DTG), infrared spectroscopy (IR), surface charge or zeta potential (ZP), and specific surface area (SSA) measurements (8, 9). From these studies it was concluded that, after the treatment with $POCl_3$ vapours and a post-treatment at 300°C, the chrysotile fibers were coated with phosphorus compounds. Nevertheless, none of these previous methodologies could clearly establish the chemical composition of the phosphorus compounds deposited at the surface of the chrysotile fibers. For example, IR spectra of the treated fibers revealed several modifications, but it was concluded that the vibration bands of the phosphorus compounds were overlaying the Si—O bands of the crystalline structure of chrysotile (9).

Chrysotile asbestos fibers belong to the serpentine family. The basic structure of this mineral group is a sheet of silica

TABLE 1. Physicochemical properties of the minerals before and after the $POCl_3$ treatment

Sample	ZP (mV)	SSA (m^2/g)	Percentage phosphorus retained
SiO_2	−51	1.0	0
SiO_2 + $POCl_3$ (room temp.)	−51	1.0	0.1
SiO_2 + $POCl_3$ + Δ 300°C	−51	1.0	0.1
$Mg(OH)_2$	+9	20.0	0
$Mg(OH)_2$ + $POCl_3$ (room temp.)	−10	*	1.5
$Mg(OH)_2$ + $POCl_3$ + Δ 300°C	−15	14.0	1.9
Chrysotile very short fibers (VSF)	+40	38.0	0
VSF + $POCl_3$ (room temp.)	−20	*	3.2
VSF + $POCl_3$ + Δ 300°C	−26	24.0	3.6

*The presence of volatile materials in these products did not allow us to determine the exact SSA for these samples.

Can. J. Chem. Downloaded from www.nrcresearchpress.com by 213.166.140.6 on 09/07/12
For personal use only.

TABLE 2. Thermogravimetric profiles of the magnesium hydroxide sample before and after the phosphorylation process

Compound	Percentage of weight loss between 30 and 300°C	Percentage of weight loss between 300 and 600°C	Total percentage of weight loss up to 1000°C
$Mg(OH)_2$	1.7	25.5	30.4
$Mg(OH)_2 + POCl_3$ (room temp).	15.6	25.2	43.1
$Mg(OH)_2 + POCl_3 + \Delta$ 300°C	1.5	31.0	33.8

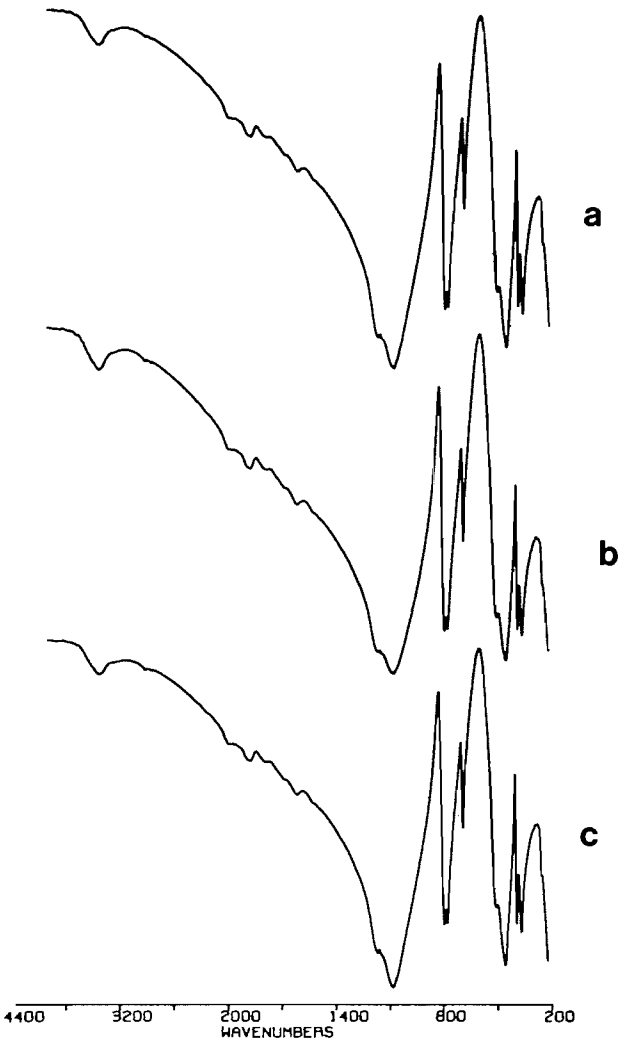

FIG. 1. FTIR spectra of SiO_2 before and after the $POCl_3$ treatment. (*a*) SiO_2; (*b*) $SiO_2 + POCl_3$; $SiO_2 + POCl_3 + \Delta$ 300°C.

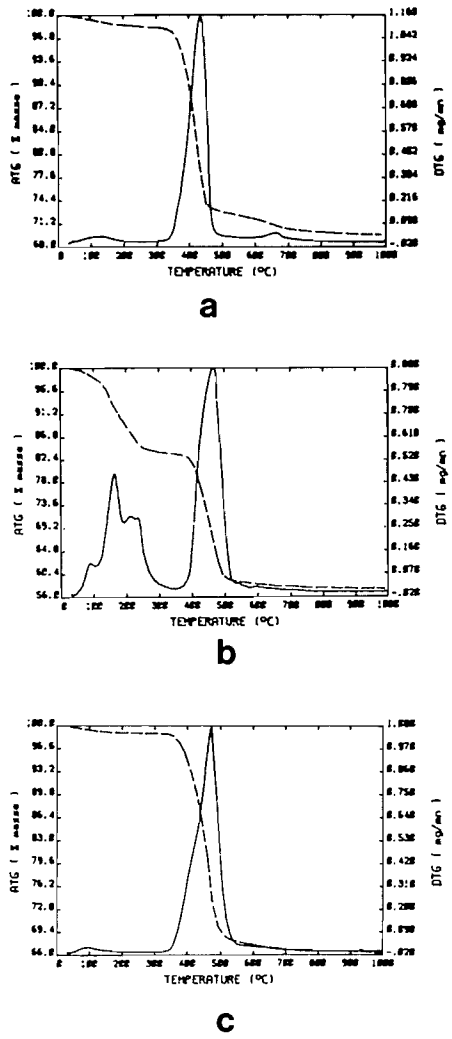

FIG. 2. TG/DTG profiles of magnesium hydroxide before and after the $POCl_3$ treatment. (*a*) $Mg(OH)_2$; (*b*) $Mg(OH)_2 + POCl_3$; (*c*) $Mg(OH)_2 + POCl_3 + \Delta$ 300°C.

tetrahedra, overlaid with a sheet of magnesium hydroxide (Mg—OH). With chrysotile, the differences in the lattice parameters of the silica and magnesium hydroxide layers induce the composite to adopt a curvature, with the Mg—OH groups on the external surface (10).

In this study two compounds, magnesium hydroxide ($Mg(OH)_2$) and silica (SiO_2), which are the basis of the chemical composition of chrysotile asbestos, have been phosphorylated in the same manner as the chrysotile fibers. These two composites were selected mainly to determine which of the hydroxyl (O—H) groups, situated on the surface, or the silica sheet, from the inner layer of the chrysotile structure, show the strongest reactivity with $POCl_3$.

From the IR spectra of $Mg(OH)_2$ before and after treatment with $POCl_3$, we could identify the chemical composition of the phosphorus compounds that were formed during reaction at room temperature and after the post-treatment at 300°C. Finally, from the comparison of the IR spectra of the powders, the thermal curves, the IR spectra of the evolved gases from the thermal decompositions, and from the ZP and SSA measurements on $Mg(OH)_2$, SiO_2, and chrysotile asbestos before and after the

Can. J. Chem. Downloaded from www.nrcresearchpress.com by 213.166.140.6 on 09/07/12
For personal use only.

Can. J. Chem. Downloaded from www.nrcresearchpress.com by 213.166.140.6 on 09/07/12
For personal use only.

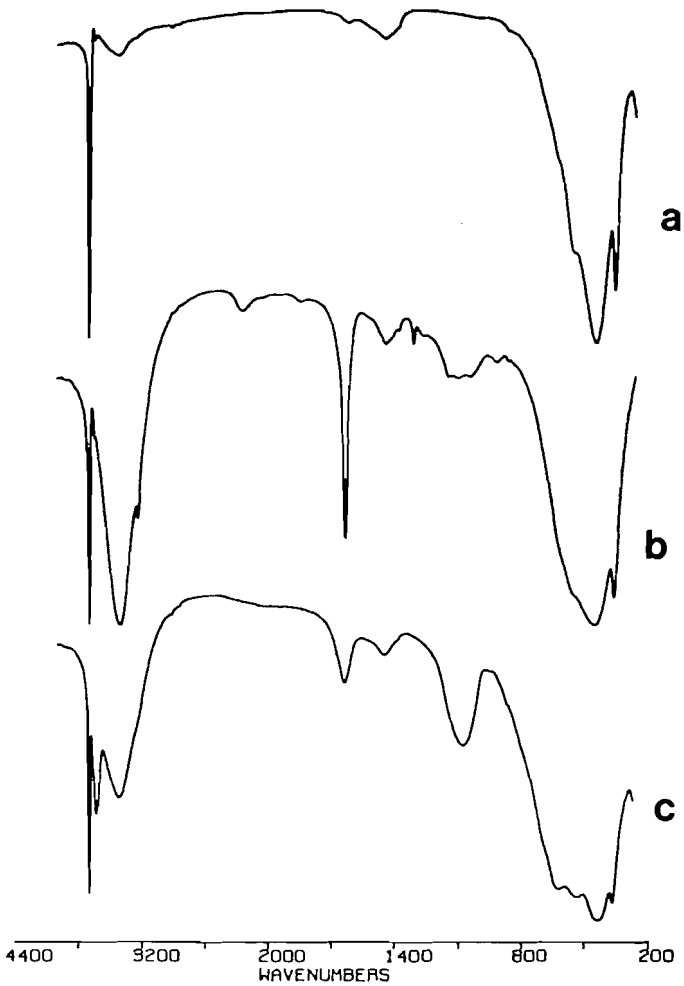

FIG. 3. FTIR spectra of magnesium hydroxide before and after the $POCl_3$ treatment. (*a*) $Mg(OH)_2$; (*b*) $Mg(OH)_2$ + $POCl_3$; (*c*) $Mg(OH)_2$ + $POCl_3$ + Δ 300°C.

$POCl_3$ treatment, we were able to elucidate the nature of the phosphorus compounds retained on the surface of the chrysotile fibers.

Experimental

The chemicals used in this study are as follows: (*a*) $POCl_3$ (from BDH Chemicals code No. B29536); (*b*) $Mg(OH)_2$ (from Fluka AG, BUCHS SG purum p.a. code no. 63078); (*c*) SiO_2 (from Fisher No. S-153 Floated powders 240 mesh); (*d*) chrysotile asbestos. (Very short fibers from the commercial grade 4T30 were isolated by a method based on the procedure of Jolicoeur *et al.* (11).)

Each sample was characterized before and after the $POCl_3$ treatment, with the following methods:

(a) Fourier Transform Infrared (FTIR) spectroscopy (Model MX-1, Nicolet Instrument Corp., Madison, WI).

(b) TG/DTG (Model TGS-2, Perkin–Elmer Canada Ltd, Montréal, Québec, Canada).

(c) ZP in 1 m*M* KCl, pH 7.0 (Zeta-reader, model ZR-11, Komline–Sanderson, Noram, Pointe Claire, Québec).

(d) SSA by nitrogen (N_2) adsorption (Quantasorb, model QS-10, Quantachrome Corp., Syosset, NY).

Twenty-four hours before the treatment with $POCl_3$, a known amount of each sample was dried at 110°C. The dried samples were then treated according to the procedure outlined by Lalancette and Dunnigan (7), by circulating N_2 gas saturated with $POCl_3$ vapors at 14°C through a reaction vessel held at ambient temperature. Finally, the $POCl_3$-treated samples were withdrawn and heated in an oven at 300°C for 2.5 h (8).

Results and discussion

In this study we will examine the SiO_2, $Mg(OH)_2$, and chrysotile asbestos before the chemical treatment, after treatment in the gas phase with $POCl_3$ at room temperature, and after the heat post-treatment at 300°C. The physicochemical analyses performed on these samples are summarized in Table 1.

Reaction of $POCl_3$ with SiO_2

Silicates are known to have a high thermal stability; the thermal trace TG/DTG (not illustrated) of untreated SiO_2 and $POCl_3$-treated SiO_2 did not show any significant thermal decomposition between 30 and 1000°C. Infrared spectra of SiO_2 treated with $POCl_3$ at room temperature and heated are compared with those of untreated SiO_2 (Fig. 1). No striking changes occurred during treatment of SiO_2 with $POCl_3$ either at room temperature or after the 300°C post-treatment. In Table 1 it is shown that, for SiO_2, ZP and SSA measurements are comparable before and after the treatments. Nevertheless, a small percentage of phosphorus is retained on the surface of the mineral (0.1%).

Reaction of $POCl_3$ with $Mg(OH)_2$

The thermal curves TG/DTG as well as the IR spectra of $Mg(OH)_2$, before and after the treatment with $POCl_3$, are given in Figs. 2 and 3. The thermogravimetric results (weight losses) are given in Table 2 and the physicochemical properties before and after the chemical treatment are presented in Table 1. From these results, one can see that $Mg(OH)_2$ has reacted more strongly with $POCl_3$ than has SiO_2 and that the composition of the phosphorus compounds formed during the treatment at room temperature and after the 300°C heat treatment are different.

(a) Treatment of $Mg(OH)_2$ with $POCl_3$ at room temperature

The thermogravimetric analyses show a 15.6% total weight loss between 30 and 300°C. The weight losses in this temperature range indicate the existence of volatile compounds absorbed, and (or) the presence of physisorbed and crystallization water.

From the FTIR spectra of gases evolved between 30 and 300°C and 300 and 600°C (Figs. 4 and 5), one can characterize these volatile compounds by evolved gas analyses (EGA). Gases like H_2O, HCl, CO_2, and $POCl_3$ evolved between 30 and 300°C. Between 300 and 600°C, TG/DTG and EGA data indicate a decomposition of the $Mg(OH)_2$. However, we cannot rule out the possible formation of $MgCl_2 \cdot nH_2O$ during the reaction. Todor (12) showed that a partial hydrolysis of the type shown in eq. [1], as well as some decomposition of $Mg(OH)_2$, can occur in this range of temperature.

[1] $MgCl_2 + H_2O \rightarrow MgO + 2HCl$

The spectra of the gases evolved between 300 and 600°C, showing traces of HCl, confirm the overlapping of the decomposition of $Mg(OH)_2$ and the partial hydrolysis of $MgCl_2 \cdot nH_2O$ occurring in this temperature range. The FTIR analyses of $Mg(OH)_2$ treated with $POCl_3$ at ambient temperature are given in Table 3 and Fig. 3. From these results, it is believed that the major phosphorus compounds formed during the phosphorylation at ambient temperature are acid orthophosphate salts.

In summary, from the TG/DTG, EGA, and FTIR analyses, it was possible to identify the presence of the following compounds formed and (or) adsorbed during the reaction: HCl, $POCl_3$, $MgCl_2 \cdot nH_2O$, and acid orthophosphate salts.

(b) Treatment of the phosphorylated $Mg(OH)_2$ sample at 300°C

The TG/DTG curves of $Mg(OH)_2$ treated with $POCl_3$ and

Can. J. Chem. Downloaded from www.nrcresearchpress.com by 213.166.140.6 on 09/07/12
For personal use only.

TABLE 3. FTIR vibration bands of the magnesium hydroxide and chrysotile asbestos samples before and after the phosphorylation process

$Mg(OH)_2$ (cm^{-1})	$Mg(OH)_2 + POCl_3$ ambient temp. (cm^{-1})	$Mg(OH)_2 + POCl_3$ + Δ 300°C (cm^{-1})	Chrysotile VSF (cm^{-1})	VSF + $POCl_3$ ambient temp. (cm^{-1})	VSF + $POCl_3$ + Δ 300°C (cm^{-1})	Vibration assignment	Reference
3697	3696	3697				OH^- of $Mg(OH)_2$	13
			3690	3690	3690	OH^- stretching of asbestos	14, 15
			3645	3645	3645	OH^- stretching of asbestos	14, 15
		3626			Hidden by the peak at 3645 cm^{-1}	OH^- of cryst. water	16
3408	3408	3408	3400	3412	3410	OH^- stretching of free or cryst. water	16
	2257			2260		$(OH)^-\ldots Cl^-$ due to hydrogen bending between HCl and MgOH	17
	1860			1864		$\ldots Cl^- {}^+HO\ldots$	17
1630	1635	1640	1640	1635	1640	OH free bending	16
1445	1440	1445				CO_3^{2-} in carbonates	16
	1386			1386		P—O stretching in acid salts	18, 19
	1317			1317		P—O stretching in $POCl_3$	18, 19
	1277			1277		P—OH deformation	18, 19
			1080	1080	1080	Si—O—Si stretching of chrysotile	14, 15
		1078			Hidden by Si—O—Si bands	P—O—P stretching	18, 20
	1155			1156		PO_4^{3-} in acid salts	18, 19
	1113			Hidden by Si—O—Si bands		PO_4^{3-} in acid salts	18, 19
	1055			Hidden by Si—O—Si bands		PO_4^{3-} in acid salts	18, 19
			1020	1024	1030	Si—O—Mg of chrysotile	14, 15
			956	956	960	Si—O^- stretching of chrysotile	14, 15
	926			Hidden by Si—O bands		P—OH bending	18, 19
875	875	Hidden by broad band in this region			Hidden by the Si—O—Si bands in this region	CO_3^{2-} in carbonates	16
			650–620	650–620	650–620	Si—O—Si of chrysotile	14, 15
		627			Hidden by the Si—O—Si bands	P—O—P bending	18, 20
			560	560	560	Si—O—Si Si—O—Mg of chrysotile	14, 15
565	565					Mg—O in Mg $(OH)_2$	13
		533			Hidden by Si—O—Si bands	P—O—P bending	18, 20
458	457	457				Superimposition of Mg—O and P—Cl stretching	13, 19
			440	440	440	Of deformation SiO^-	14, 15
						Mg—O in chrysotile	14, 15
368	367	370				Mg—O—Mg in $Mg(OH)_2$	12

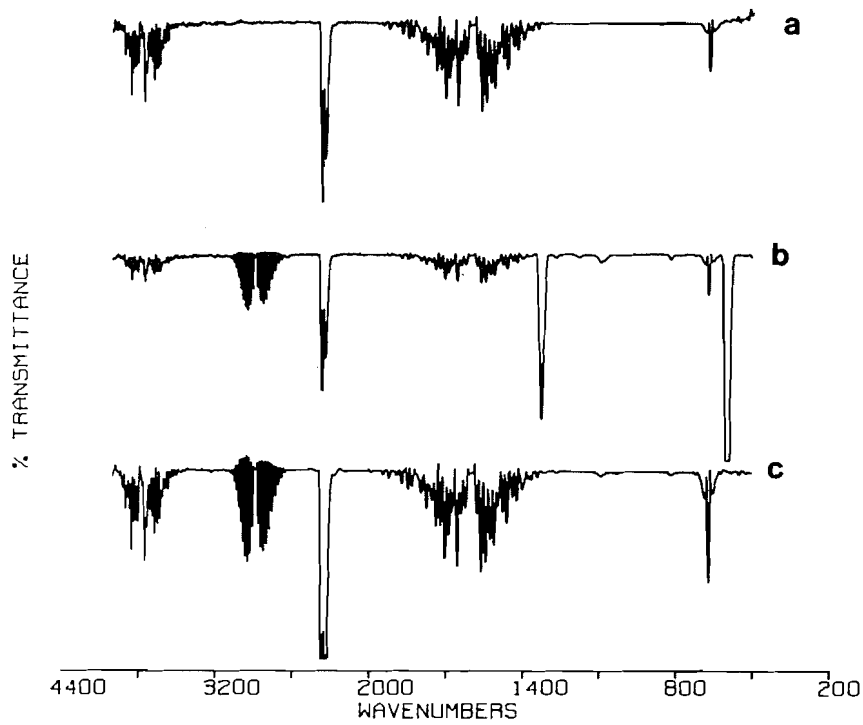

FIG. 4. FTIR analyses of the gases evolved between 30 and 300°C before and after the $POCl_3$ treatment at room temperature for $Mg(OH)_2$. EGA (30–300°C): (*a*) $Mg(OH)_2$; (*b*) $Mg(OH)_2$ + $POCl_3$; (*c*) $Mg(OH)_2$ + $POCl_3$ + Δ 300°C.

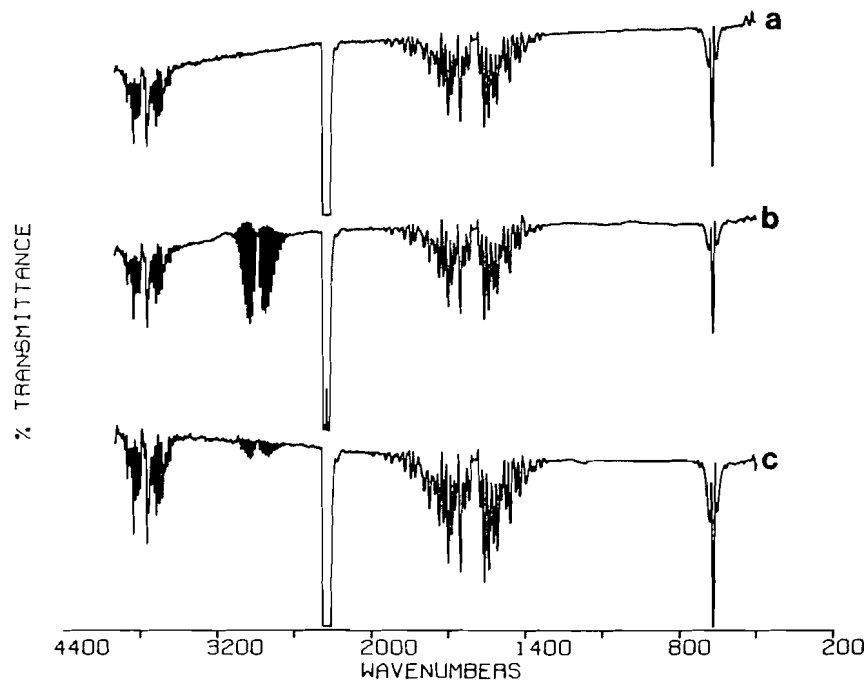

FIG. 5. FTIR analyses of the evolved gases between 300 and 600°C for $Mg(OH)_2$ before and after the 300°C heat post-treatment. EGA (300–600°C): (*a*) $Mg(OH)_2$; (*b*) $Mg(OH)_2$ + $POCl_3$; (*c*) $Mg(OH)_2$ + $POCl_3$ + Δ 300°C.

Can. J. Chem. Downloaded from www.nrcresearchpress.com by 213.166.140.6 on 09/07/12
For personal use only.

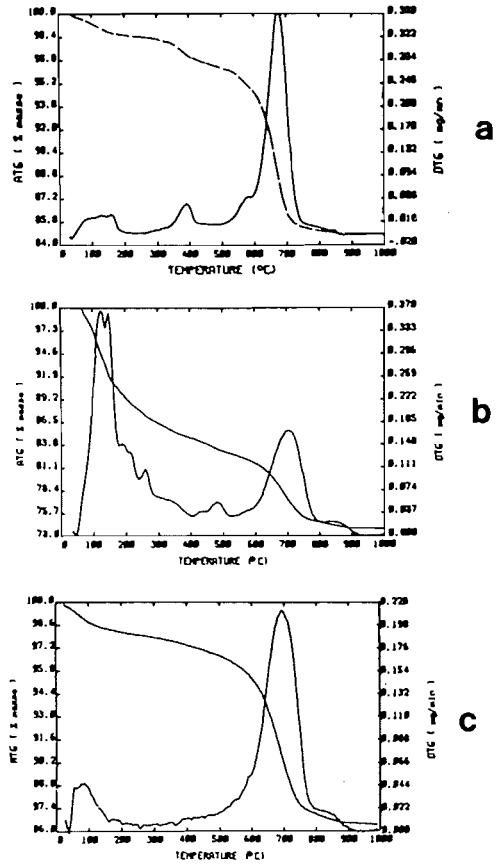

FIG. 6. TG/DTG profiles of chrysotile before and after the $POCl_3$ treatment. (*a*) Chrysotile (VSF); (*b*) VSF + $POCl_3$; (*c*) VSF + $POCl_3$ + Δ 300°C.

heated at 300°C (Fig. 2 and Table 2) indicate a slight percentage of weight loss between 30 and 300°C. Nevertheless, as judged by the percentage of weight loss and the DTG curve profile in the range 300–600°C, we can predict the superimposition of several decomposition products (Fig.2 and Table 2). The IR spectra of the gases evolving between 300 and 600°C (Fig. 5) show the presence of H_2O, CO_2, and HCl. From these results we can conclude that the following decompositions are overlapping in this range of temperature:

[2] $Mg(OH)_2 \rightarrow H_2O + MgO$

[3] $MgCl_2 + H_2O \rightarrow MgO + 2HCl$

The IR spectra of the phosphorylated $Mg(OH)_2$ sample after the 300°C heat treatment (Fig. 3 and Table 3) show significant changes when compared to the $Mg(OH)_2$ treated only with $POCl_3$ at room temperature. We observe the disappearance of absorption bands related to the presence of acid orthophosphate salts and the appearance of a broad band between 1200 and 980 cm^{-1}, with a maximum at 1080 cm^{-1}. This is interpreted as P—O—P stretching bands, while the P—O—P bending band is observed as a shoulder at 630 cm^{-1}. We also notice the absence of bands due to HCl vibrations (linked to the $Mg(OH)_2$ by H-bonds) at 2260 and 1860 cm^{-1}. The presence of the bands at 3625 and 3408 cm^{-1} (O—H stretching) indicates the presence of more than one type of water of crystallization and (or) free water (physisorbed water).

The appearance of CO_2 vibrations in the spectra of evolved gases from $Mg(OH)_2$ can be due to CO_2 impurities in the gas cell and (or) the atmosphere, as well as to traces of CO_2 adsorbed on the surface of the mineral.

Reaction of $POCl_3$ with chrysotile asbestos

The TG/DTG curve and data for the native chrysotile fibers

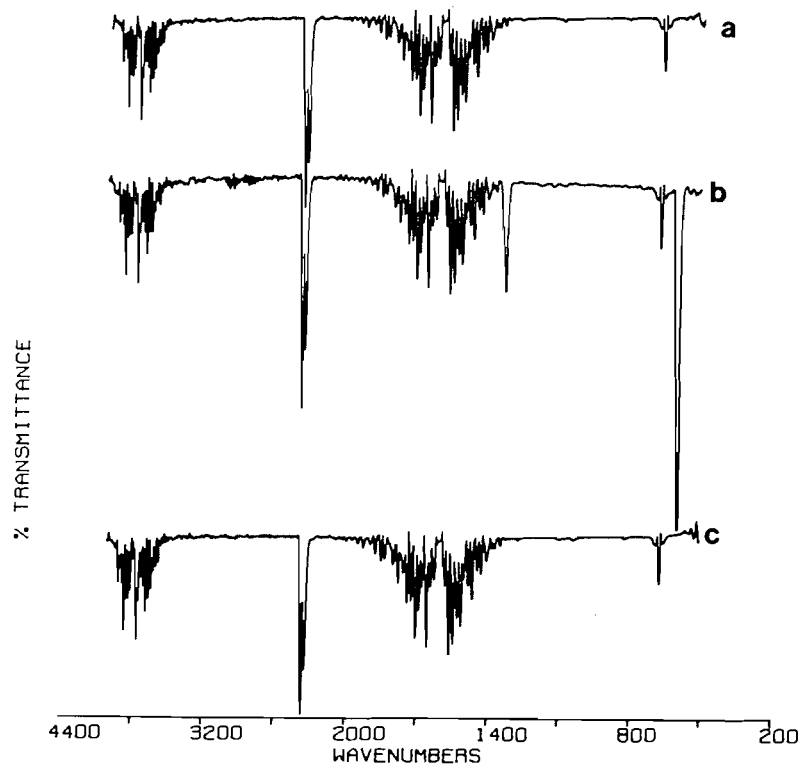

FIG. 7. FTIR analyses of the evolved gases between 30 and 300°C for chrysotile, and for chrysotile treated with $POCl_3$ at room temperature before and after the 300°C heat post-treatment. EGA (30–300°C): (*a*) VSF; (*b*) VSF + $POCl_3$; (*c*) VSF + $POCl_3$ + Δ 300°C.

Can. J. Chem. Downloaded from www.nrcresearchpress.com by 213.166.140.6 on 09/07/12
For personal use only.

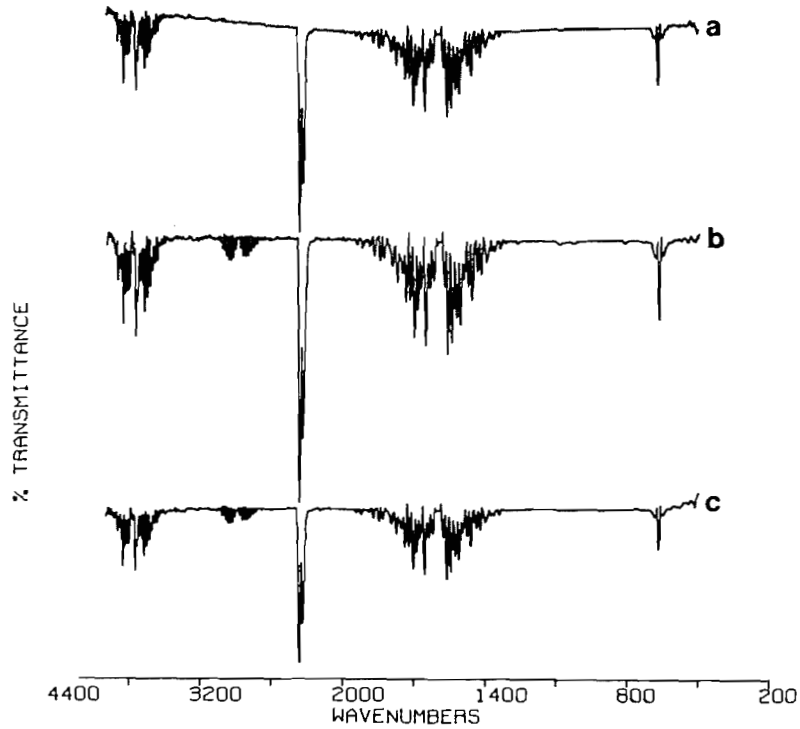

FIG. 8. FTIR analyses of the evolved gases between 300 and 550°C for chrysotile, chrysotile treated with $POCl_3$ at room temperature, and after the 300°C heat post-treatment. EGA (300–550°C): (*a*) VSF; (*b*) VSF + $POCl_3$; (*c*) VSF + $POCl_3$ + Δ 300°C.

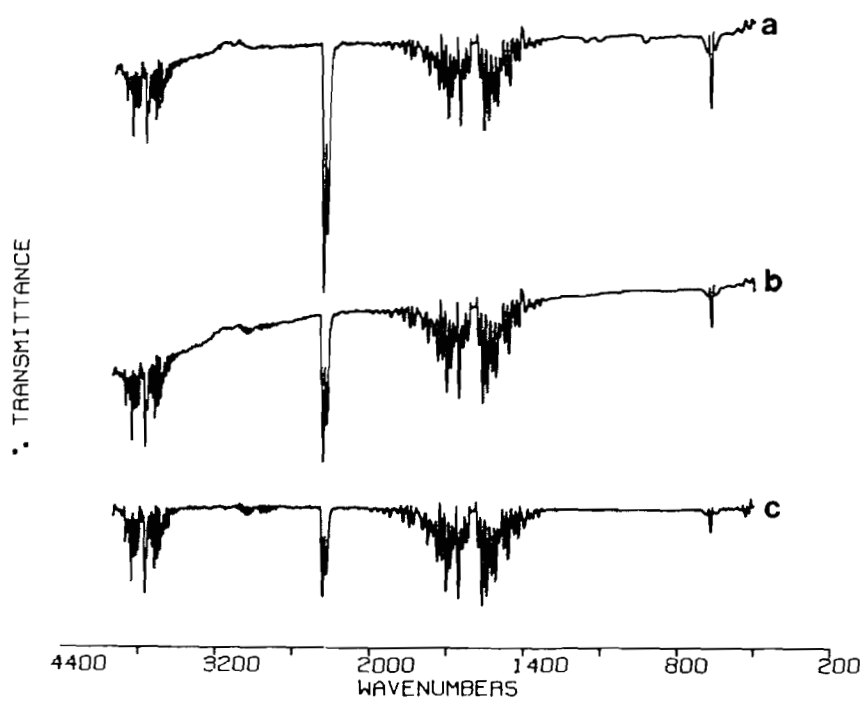

FIG. 9. FTIR analyses of the evolved gases between 550 and 1000°C for chrysotile, chrysotile treated with $POCl_3$ at room temperature, and after the 300°C heat post-treatment. EGA (550–1000°C): (*a*) VSF; (*b*) VSF + $POCl_3$; (*c*) VSF + $POCl_3$ + Δ 300°C.

Can. J. Chem. Downloaded from www.nrcresearchpress.com by 213.166.140.6 on 09/07/12
For personal use only.

TABLE 4. Thermogravimetric profiles of the chrysotile asbestos fibers before and after the phosphorylation process

Compound	Percentage of weight loss between 30 and 300°C	Percentage of weight loss between 300 and 600°C	Percentage of weight loss between 600 and 1000°C	Total percentage of weight loss up to 1000°C
Chrysotile VSF	1.8	3.6	9.9	15.3
VSF + $POCl_3$ (room temp.)	13.6	4.8	7.7	26.5
VSF + $POCl_3$ + Δ 300°C	2.0	2.2	9.3	13.5

before and after treatment with $POCl_3$ at room temperature and after the 300°C heat post-treatment, respectively, are presented in Fig. 6 and Table 4. The EGA for the thermal decomposition of the three samples of chrysotile in the temperature ranges 30–300°C, 300–550°C, and 550–1000°C are respectively illustrated in Figs. 7, 8, and 9. While the IR results are reported in Fig. 10 and Table 3, in Fig. 11 is found the comparison between the IR spectra of chrysotile asbestos and of $Mg(OH)_2$ treated with $POCl_3$ at room temperature and after the 300°C heat post-treatment.

One can observe the similarity of the compounds formed during the treatment with $POCl_3$ at room temperature and after the heat post-treatment of the two minerals. As can be seen from Fig. 11, the silicate vibrations of the chrysotile fibers overlap those of the phosphate compounds (between 1200 and 800 cm^{-1}; also between 800 and 400 cm^{-1}). Due to the superimposition of these bands, it was not possible to clearly identify by IR the characteristic bands of the different phosphorus compounds formed during the phosphorylation of chrysotile asbestos. However, as schematized in Fig. 12, it is strongly suspected that the

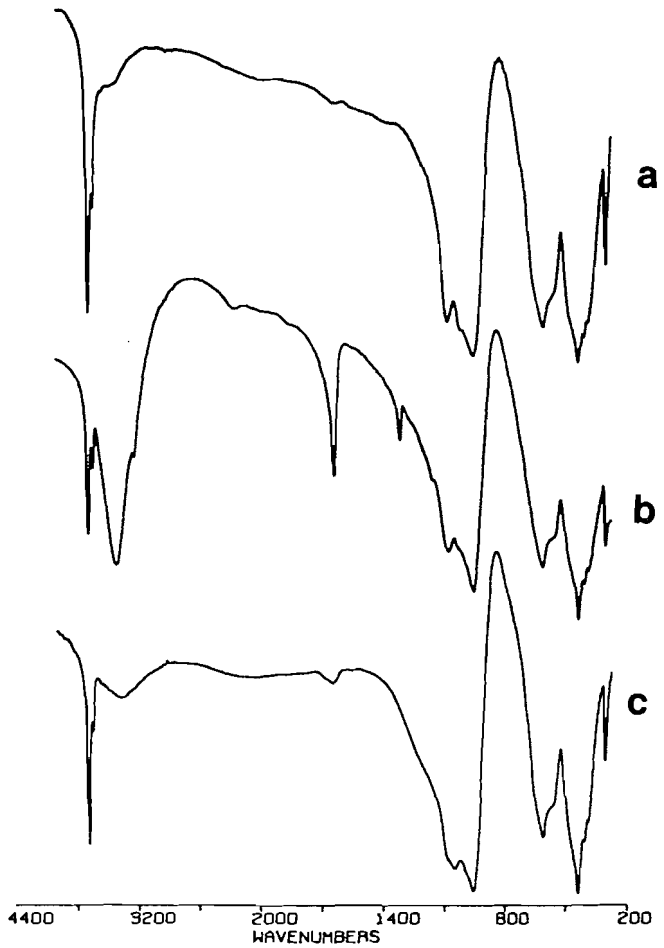

FIG. 10. FTIR spectra of chrysotile, and for chrysotile treated with $POCl_3$ at room temperature before and after the 300°C heat post-treatment. (*a*) VSF; (*b*) VSF + $POCl_3$; (*c*) VSF + $POCl_3$ + Δ 300°C.

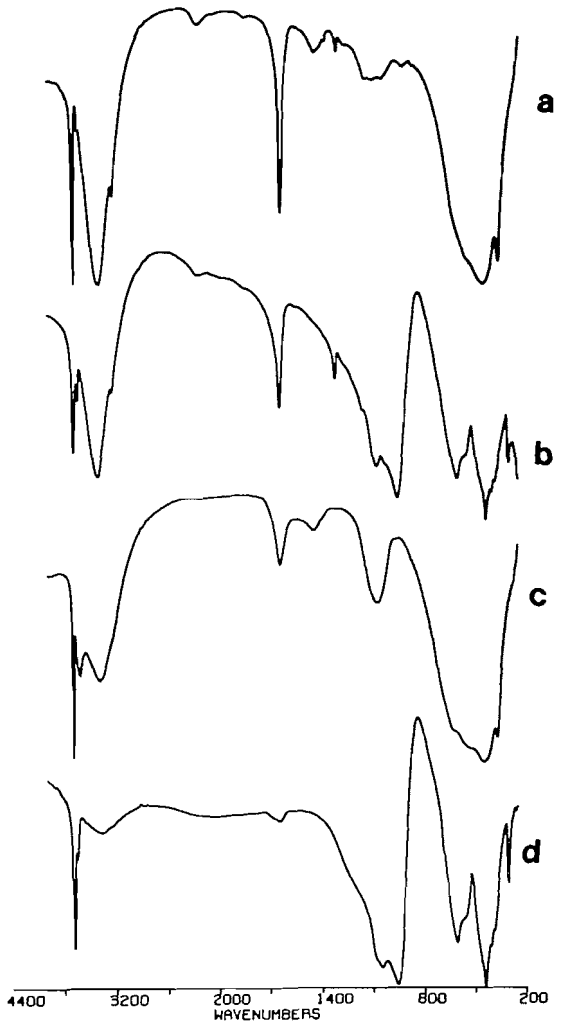

FIG. 11. FTIR spectra of the magnesium hydroxide and chrysotile asbestos samples treated with $POCl_3$. (*a*) $Mg(OH)_2$ + $POCl_3$; (*b*) VSF + $POCl_3$; (*c*) $Mg(OH)_2$ + $POCl_3$ + Δ 300°C; (*d*) VSF + $POCl_3$ + Δ 300°C.

Can. J. Chem. Downloaded from www.nrcresearchpress.com by 213.166.140.6 on 09/07/12
For personal use only.

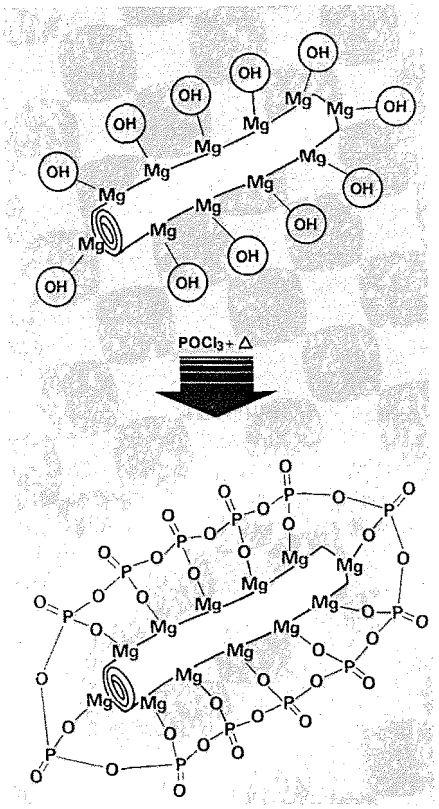

FIG. 12. Schematic representation of a chrysotile asbestos monofibril before and after the $POCl_3$ process and post-treatment at 300°C.

modification of chrysotile asbestos fibers by $POCl_3$ involved a coating of the fibers with polyphosphate compounds, implicating the structural O—H groups at the surface of the mineral fibers.

Conclusion

From the data of this study, one can summarize the following points:

(*a*) The results obtained with SiO_2 and $Mg(OH)_2$ after the treatment with $POCl_3$ at ambient temperature and after the 300°C heat post-treatment show that the reaction of $POCl_3$ with silica can be considered negligible.

(*b*) The modifications induced by the $POCl_3$ treatment on $Mg(OH)_2$ and chrysotile asbestos fibers are similar.

(*c*) The phosphate compounds formed during the chemical treatment at room temperature are mostly hydrated acid orthophosphate salts, while those formed after the 300°C heat post-treatment are hydrated polyphosphate salts.

(*d*) $MgCl_2 \cdot nH_2O$ salts are formed either during the $POCl_3$ treatment at room temperature or after the heat post-treatment, while the presence of $POCl_3$, HCl, and H_2O adsorbed on the surface were only observed after the $POCl_3$ treatment at room temperature.

Therefore one can conclude that between the silica and the magnesium sheets of the structure of chrysotile asbestos fibers, the magnesium sheet and, more especially, the O—H layer on the external surface of the fibers possess the strongest reactivity with $POCl_3$ vapors.

1. V. BOLIS, B. FUBINI, and G. VENTURELLO. J. Therm. Anal. **28**, 249 (1983).
2. W. G. LIGHT and E. T. WEI. Nature, **265**, 537 (1977).
3. J. GONI, J. H. THOMASSIN, M. C. JAURAND, and J. C. TOURAY. Phys. Chem. Earth, **11**, 807 (1979).
4. M. C. JAURAND, L. MAGNE, J. L. BOULNER, and J. BIGNON. Toxicology, **21**, 323 (1981).
5. P. A. PEZZOLI. U.S. Patent No. 4,171,405 (1979).
6. J. DUNNIGAN, D. NADEAU, D. PARADIS, J. P. PELE, R. CALVERT, J.-M. LALANCETTE, and M. COSSETTE. Proceedings 4th Int. Conf. on Asbestos, Torino, Italy. May 26–30, 1980. Vol. II. pp. 747–772.
7. J.-M. LALANCETTE and J. DUNNIGAN. U.S. Patent No. 4,356,057 (1982).
8. F. M. KIMMERLE, J. KHORAMI, and D. CHOQUETTE. Proceedings 7th Int. Conf. on Thermal Analysis. Vol. 1. 1982. pp. 614–620.
9. J. KHORAMI and D. NADEAU. Thermochim. Acta, **108**, 279 (1986).
10. A. A. HODSON. Fibrous silicate. Lecture Series of the Royal Institute of Chemistry. Vol. 4. European Printing Co., London. 1965. p. 1.
11. C. JOLICOEUR, P. ROBERGE, and J. L. FORTIER. Can. J. Chem. **59**, 1140 (1981).
12. D. N. TODOR. Thermal analysis of minerals. Abacus Press, England. 1976. pp. 118–119.
13. R. M. HEXTER. J. Opt. Soc. Am. **48**, 770 (1958).
14. V. C. FARMER and J. D. RUSSEL. Spectrochim. Acta, **20**, 1149 (1964).
15. W. R. LUCE. U.S. Geol. Survey. Prof. Paper 750-B 3199–3201 (1971).
16. C. ALEXANIAN, P. MOREL, and L. LE BOUFFANT. Bull. Soc. Fr. Ceram. **72**, 3 (1966).
17. J. C. LASSEGUES, J. C. CARNUT, and P. V. HUONG. Liaison Hydrogène et protonation dans les systèmes halogénures d'hydrogène ether en phase solide. Spectrochim. Acta, Part A: **27**, 73 (1971).
18. D. E. C. CARBRIDGE and E. J. LOWE. J. Chem. Soc. Part I, 493 (1954).
19. D. E. C. CARBRIDGE. J. Appl. Chem. **6**, 456 (1956).
20. B. O. MYSEN, F. J. RYERSON, and D. VIRGO. Am. Mineral. **66**, 106 (1981).

Can. J. Chem. Downloaded from www.nrcresearchpress.com by 213.166.140.6 on 09/07/12
For personal use only.

Reactivity and photophysical behavior of chromone triplet. A laser flash photolysis study

S. RAJADURAI AND P. K. DAS[1]

Radiation Laboratory, University of Notre Dame, Notre Dame, IN 46556, U.S.A.

Received February 9, 1987

S. RAJADURAI and P. K. DAS. Can. J. Chem. **65**, 2277 (1987).

The chromone triplet (λ^T_{max} = 620 nm, $\varepsilon^T_{max} = 2.5 \times 10^3 M^{-1}\,cm^{-1}$ in acetonitrile) is produced in quantitative yields upon 308- or 337.1-nm laser pulse excitation and is characterized by submicrosecond lifetimes in solutions at room temperature. The short-lived nature of the triplet is attributable to intrinsically fast $T_1 \rightsquigarrow S_0$ intersystem crossing, nearly diffusion-limited self-quenching, and facile interactions with solvents in the form of charge and hydrogen-atom transfer. The unusually high self-quenching rate constants, $(0.9–4.0) \times 10^9 M^{-1}\,s^{-1}$, are related in a major part to the presence of the ene double bond at which the photocycloaddition of the triplet may occur; this is supported by large bimolecular rate constants (k_q^T) observed for chromone triplet quenching by various alkene derivatives. Although, based on low-temperature photophysical behaviors, the lowest triplet state of chromone in polar solvents is expected to be of reduced n,π^* character, the reactivity of the triplet toward hydrogen donors is very pronounced in acetonitrile (for example, $k_q^T = 1.7 \times 10^9$ and $7.4 \times 10^6 M^{-1}\,s^{-1}$ for tri-*n*-butylstannane and 2-propanol, respectively). Carbon tetrachloride and benzene prove to be facile quenchers of chromone triplet; the quenching interactions probably involve charge transfer, the carbonyl triplet acting as a donor and an acceptor, respectively. The electrophilic role of chromone triplet in the quenching by benzene derivatives is supported by a good correlation between k_q^T and quencher oxidation potential.

S. RAJADURAI et P. K. DAS. Can. J. Chem. **65**, 2277 (1987).

Utilisant une excitation par laser pulsé à 308 ou 337,1 nm, on a produit le triplet de la chromone (λ^T_{max} = 620 nm; $\varepsilon^T_{max} = 2{,}5 \times 10^3 M^{-1}\,cm^{-1}$, dans l'acétonitrile) et on l'a caractérisé, en solutions, à la température ambiante, en faisant appel à des temps de demi-vie plus courts que les microsecondes. On attribue les temps de demi-vie très courts du triplet à un passage intersystème $T_1 \rightsquigarrow S_0$ qui est intrinsèquement rapide, à un auto-piégeage qui est pratiquement limité par la diffusion ainsi qu'à des interactions faciles avec les solvants sous la forme de transfert de charges et d'atomes d'hydrogènes. On a établi que les constantes de vitesses d'auto-piégeage qui sont inhabituellement élevées, $(0{,}9–4{,}0) \times 10^9 M^{-1}\,s^{-1}$, sont principalement reliées à la présence de la double liaison ène à partir de laquelle la photocycloaddition du triplet peut se produire; cette conclusion est supportée par les constantes de vitesses bimoléculaires élevées (k_q^T) qui ont été observée pour le piégeage du triplet de la chromone par divers dérivés des alcènes. Même si, sur la base des comportements photophysiques à basses températures, on s'attend à ce que le caractère n,π^* de l'état triplet le plus bas de la chromone soit réduit dans les solvants polaires, la réactivité du triplet vis-à-vis des donneurs d'hydrogène est très prononcée dans l'acétonitrile (par exemple, $k_q^T = 1{,}7 \times 10^9$ et $7{,}4 \times 10^6 M^{-1}\,s^{-1}$ respectivement pour le tri-*n*-butylstannane et le propanol-2). Le tétrachlorure de carbone et le benzène s'avèrent de bons pièges pour le triplet de la chromone; les interactions de piégeage impliquent probablement des transferts de charges dans lesquels le triplet du carbonyle agissant suivant le cas soit comme donneur soit comme accepteur. Le rôle électrophile du triplet de la chromone dans le piégeage des dérivés du benzène est supporté par une bonne corrélation entre les valeurs de k_q^T et les potentiels d'oxydation des pièges.

[Traduit par la revue]

Introduction

Interactions of proximate n,π^* and π,π^* states in both singlet and triplet manifolds of heteroatom-containing π-systems have long been topics of interest to spectroscopists, photochemists, and photophysicists. Vibronic mixing and occasional inversion of the relative location of these two states, when lying close to each other as the lowermost singlet excited states, are easily affected by variation of substituent, solvent, and temperature, and result in dramatic changes in the fluorescence properties of a molecule (1–3). Quite often such a molecule serves as a useful probe for micropolarity in multiphase systems. Vibronic interactions and (or) thermal equilibria involving lowest-lying n,π^* and π,π^* triplet states determine the radical-like behavior of carbonyl compounds in hydrogen-abstraction photoreactions (4–6). Finally, the rate of intersystem crossing between two electronic states of different multiplicity depends strongly on whether or not these two states are of the same orbital origin (7–9).

For several reasons we have been interested in a laser flash photolysis study of chromone (**1**) in solutions at room temperature. First, several studies (10–12) based on EPR (electron paramagnetic resonance) and phosphorescence spectra in low temperature matrices have shown the low-lying n,π^* and π,π^* triplet states of chromone to be essentially isoenergetic. It is of interest to know if a similar situation prevails at room temperature and manifests itself in the photophysical and photochemical behavior of the triplet in fluid solutions. Second, chromone has been shown to undergo facile photoaddition reactions in which olefins or acetylenes are added along the ene double bond and, in some cases, at the carbonyl group (13, 14). The products of coupling of radicals derived from hydrogen abstraction are also observed (14). The sustained interest in the photocycloaddition of chromone is borne out by the fact that it has formed the subject of a recent theoretical study (15). Although the triplet has been implicated as the photoexcited species participating in chromone photochemistry, very little is known about the kinetics of its decay and bimolecular interactions under reaction conditions. To the best of our knowledge, all the time-resolved studies of chromone photophysics have so far focused only on the decay of triplet absorption or phosphorescene over milliseconds in grassy matrices at 77 K (10, 11, 16) or the picosecond buildup of triplet absorption giving intersystem crossing rates over picoseconds at room temperature (16). Third, in a recent report (17) based on evidence from triplet quenching behavior we have suggested that in fluid solutions 2,3-diphenylchromone (**2**) undergoes considerable structural relaxation in the triplet state, probably in the form of twisting about the ene double bond (to relieve the steric hindrance between the neighboring phenyl

[1]Author to whom correspondence may be addressed.

Printed in Canada / Imprimé au Canada

Can. J. Chem. Downloaded from www.nrcresearchpress.com by 213.166.140.6 on 09/07/12
For personal use only.

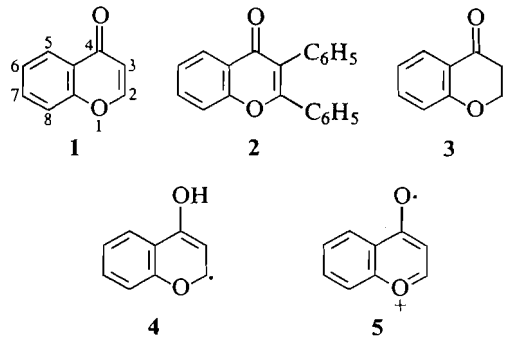

groups). Obviously, it is important to establish if such a relaxation occurs in the triplet state of the parent molecule in the absence of the steric crowding.

Experimental

Chromone (**1**) and 4-chromanone (**3**) were supplied by Aldrich. The former was recrystallized from aqueous ethanol while the latter was used as received. Since the authenticity of the chromone sample was not guaranteed by the vendor, this was checked by mass and ^{1}H nmr spectra (18) recorded in a Finnigan–Mat Model 8430 mass spectrometer and a Nicolet NB-300 nmr spectrometer, respectively. Acetonitrile and chloroform, both of spectral grade from Aldrich, were distilled before use. The other solvents were also of spectral grade and were used as received from commercial sources (mostly Fisher and Aldrich). For some experiments, benzene and CCl_4 were purified in the following manner (19). The solvent (400 mL) containing 5 g benzophenone in a Pyrex flask was photolyzed for 12 h under argon saturation in a Rayonet reactor fitted with 16 RPR-3500 lamps and was then fractionally distilled. The procedure was repeated once with the distillate. The reagents used in the quenching studies were of best grades commercially available and were subjected to standard purification procedures (recrystallization, vacuum sublimation, or fractional distillation under reduced pressure). Toluene-d_8 (Aldrich, 100.0 at.% D) was used as received.

Most of the laser flash photolysis experiments were performed with 308-nm laser pulses (~20 ns, 10–100 mJ/pulse) from a Lambda-Physik EMG-100 MSC excimer unit (filled with Xe/HCl gas mixture). For some experiments use was also made of 248-nm laser pulses (~20 ns, 10–100 mJ/pulse) from the same excimer laser unit (filled with Kr/F_2 mixture) and 337.1-nm nitrogen laser pulses (~8 ns, 2–3 mJ/pulse) from a Molectron UV-400 source. The kinetic spectrophotometer and the data collection system have been described in previous publications (20, 21) from the Radiation Laboratory. Except for triplet self-quenching studies, a front-face configuration was used for laser excitation, the direction of the latter being at 20°–30° with respect to that of the analyzing light. The path lengths of the quartz cells were 1–3 mm; those used in experiments involving comparisons of transient absorbances for yield measurements were of optically flat surfaces and 2-mm path lengths. The kinetics of chromone triplet quenching by its ground state were studied in 1 cm × 1 cm square cells with a right angle geometry between the laser excitation pulse (308 nm) and the monitoring light. The intensity of the laser pulse in these experiments was so attenuated that the end-of-pulse triplet concentration was less than 5% of the ground-state concentration in each kinetic measurement. The deoxygenation of solutions was effected by saturation with high-purity argon.

Results

Triplet state photophysical properties

The preliminary flash photolysis experiments on chromone were carried out with nitrogen laser pulses at 337.1 nm. At this wavelength, the light absorption occurs into the lowest-lying weak $^1(n,\pi^*)$ band system ($\varepsilon = 22 M^{-1}\,cm^{-1}$ at 337 nm in acetonitrile). For sufficient absorbance (~0.1 in a 2-mm cell) at the laser excitation wavelength, the solutions of chromone have

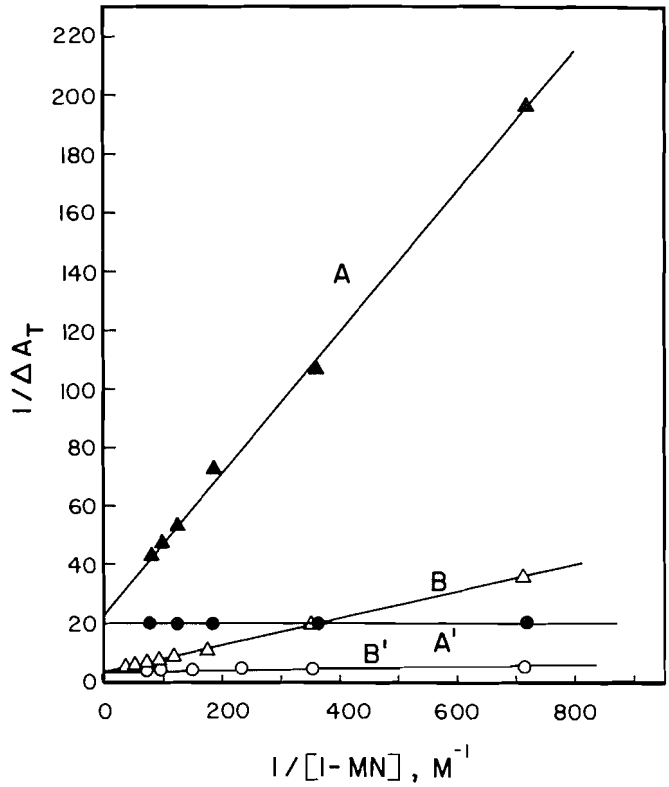

FIG. 1. Double reciprocal plots based on eq. [3], with 1-methylnaphthalene as the quencher in (A,A′) benzene and (B,B′) acetonitrile. The solutions of (A,B) chromone and (A′,B′) benzophenone were optically matched at the laser excitation wavelength, 337.1 nm (absorbance = 0.2 in 2-mm cells).

to be concentrated (40–60 m*M*). Upon laser pulse excitation, chromone solutions at these high concentrations in various solvents, namely, benzene, acetonitrile, methanol, 2-propanol, *tert*-butanol, and carbon tetrachloride, give a fast-decaying transient ($\tau \leq 30$ ns) characterized by absorption maxima at 620–640 nm. The short lifetimes of the transient preclude any study of its diagnostic quenching behaviors. However, that a short-lived triplet is produced in high yields under 337.1-nm laser excitation is shown by experiments in the presence of 1-methylnaphthalene and biphenyl. The triplets of the latter with characteristic transient absorption spectra (λ^T_{max} = 420–425 and 355–360 nm, respectively) are produced, presumably as a result of energy transfer from the flash-photolytic chromone triplet. With 1-methylnaphthalene in benzene and acetonitrile and biphenyl in benzene, the absorbance changes due to their triplets monitored at the respective maxima were measured as functions of the acceptor concentrations. Based on triplet excitation transfer from chromone triplet (^{3}CH*) in competition with its decay (eq. [1] and [2]), a double-reciprocal relationship is expected between the acceptor triplet absorbance (ΔA_T) and its ground-state concentration, [A], see eq. [3]. In this equation ϕ_T represents the triplet yield of chromone.

$$[1] \quad {}^3CH^* \xrightarrow{1/\tau_T} {}^1CH \text{ or products}$$

$$[2] \quad {}^3CH^* + {}^1A \xrightarrow{k_q^T} {}^1CH + {}^3A^*$$

$$[3] \quad \frac{1}{\Delta A_T} = \text{Const.}\,\frac{1}{\phi_T}\left[1 + \frac{1}{k_q^T \tau_T [A]}\right]$$

Figure 1 shows the plots based on eq. [3] for 1-methylnaphthalene in benzene and acetonitrile. The intercept-to-slope ratios of

Can. J. Chem. Downloaded from www.nrcresearchpress.com by 213.166.140.6 on 09/07/12
For personal use only.

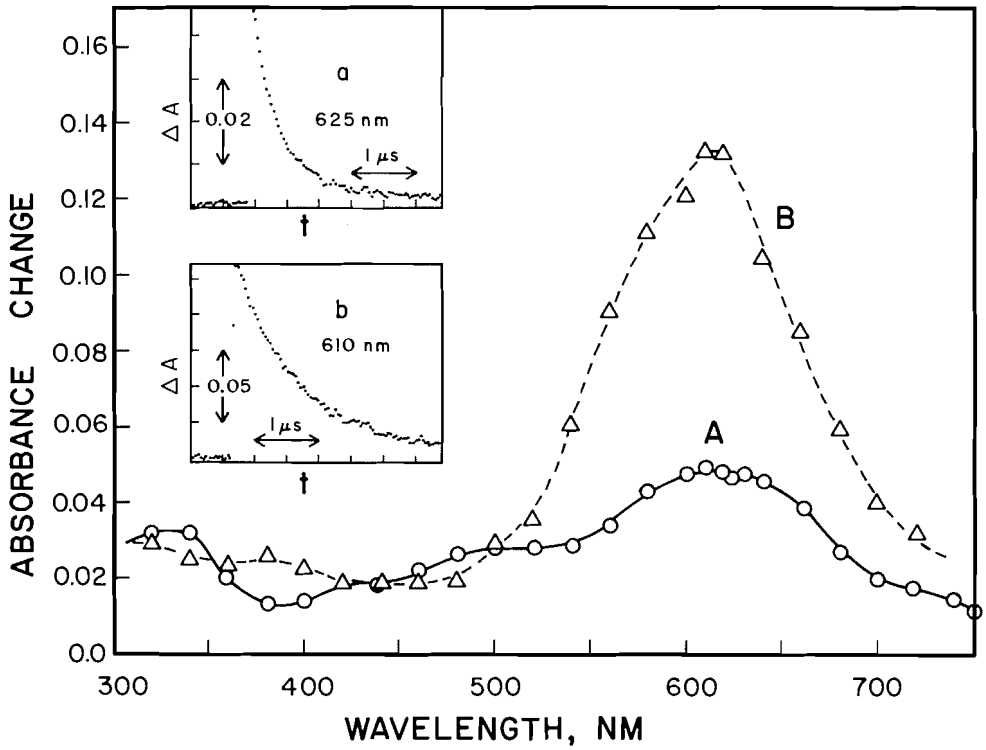

FIG. 2. Triplet–triplet absorption spectra of chromone observed at 0.1 μs following 308-nm laser excitation in (A) acetonitrile and (B) 2,2,2-trifluoroethanol. Insets: representative kinetic traces for chromone triplet decay in (a) acetonitrile and (b) 2,2,2-trifluoroethanol containing 0.19 and 0.84 m*M* chromone, respectively.

these plots gave 20 and 16 M^{-1} for $k_q^T\tau_T$ values in the two solvents, respectively. A similar value, i.e., 17 M^{-1} was obtained for biphenyl as acceptor in benzene. Assuming a value of $5 \times 10^9 M^{-1} s^{-1}$ for k_q^T under diffusion control (see later), we estimate lifetimes (τ_T) of 3–4 ns for chromone triplet under the conditions of the measurements. It will be shown later that the short triplet lifetimes are due to efficient self-quenching and interactions with solvent.

Also in Fig. 1 are shown the plots based on eq. [3] for 1-methylnaphthalene as acceptor of energy from benzophenone triplet in benzene and acetonitrile. The benzophenone solutions were optically matched with those of chromone at the laser excitation wavelength (337.1 nm). The comparison of the reciprocal of the intercept for chromone with that for benzophenone under the same condition led to the determination of ϕ_T. We obtained values of 0.86 ± 0.15 and 1.0 ± 0.15 for ϕ_T of chromone in benzene and acetonitrile, respectively.

The use of 308- and 248-nm laser pulses enabled us to conduct flash photolysis experiments on chromone solutions of submillimolar concentrations. In Fig. 2 is shown the transient absorption spectrum upon 308-nm laser pulse excitation of 0.19 m*M* chromone in acetonitrile. As evident from the kinetic trace in the inset, the transient (λ_{max} = 620 nm) observed in this dilute solution is relatively long-lived (τ = 0.6 μs). Quenching behaviors (*vide infra*) combined with sensitization of triplets of typical acceptors of lower energy, e.g., 1-methylnaphthalene and biphenyl, establish the identity of the 620-nm transient as chromone triplet (^{3}CH*). A comparison of end-of-pulse transient absorbance at 620 nm due to ^{3}CH*, observed in acetonitrile in the absence of biphenyl, with that at 360 nm due to biphenyl triplet, produced in the chromone solution containing ~10 m*M* biphenyl, suggests that the maximum extinction coefficient (ε_{max}^T) of ^{3}CH* is 1/16 of that of biphenyl triplet. Assuming that ε_{max}^T of biphenyl in acetonitrile is not very different from that in cyclohexane ($\varepsilon_{max}^T = 4.3 \times 10^4 M^{-1} cm^{-1}$ at 361 nm (22)), we estimate ε_{max}^T of ^{3}CH* to be (3 ± 1) × $10^3 M^{-1} cm^{-1}$ (at 620 nm). A similar value, (2.5 ± 0.3) × $10^3 M^{-1} cm^{-1}$, is obtained through a comparison of end-of-pulse triplet absorbances (at respective maxima) observed upon 308-nm laser excitation of optically matched solutions of chromone and benzophenone ($\varepsilon_{max}^T = 6.5 \times 10^3 M^{-1} cm^{-1}$ at 520 nm (23) in acetonitrile). The comparative measurements were carried out in the linear region over a tenfold change in laser pulse intensity (ca. 1–10 mJ/pulse) and ϕ_T's were taken to be unity for both ketones in acetonitrile.

The rate constant (k_{obs}^T) for the decay of chromone triplet is found to be strongly dependent on the ground state concentration, [CH]. In several solvents, the intrinsic triplet lifetime (τ_T^0), determined by the $S_0 \leftrightsquigarrow T_1$ process as well as interactions with solvent (eqs. [4*a*,*b*]), and the self-quenching rate constant (k_{SQ}^T, eq. [5]) were obtained from the intercept and slope of the linear plots of k_{obs}^T vs. [CH] (see eq. [6]).

$$[4a] \quad {}^3CH^* \xrightarrow{1/\tau_T^0} {}^1CH$$

$$[4b] \quad {}^3CH^* + S \rightarrow {}^1CH \text{ or products}$$

$$[5] \quad {}^3CH^* + {}^1CH \xrightarrow{k_{SQ}^T} 2\,{}^1CH \text{ or products}$$

$$[6] \quad k_{obs}^T = 1/\tau_T^0 + k_{SQ}^T[CH]$$

Some representative plots based on eq. [6] are shown in Fig. 3. The data concerning τ_T^0 and k_{SQ}^T are presented in Table 1.

From the location of the 0–0 band of the phosphorescence spectrum of chromone in 2-methyltetrahydrofuran glass at 77 K, its triplet energy (E_T) is measured to be 75.1 kcal/mol (14). Thus chromone is not expected to be an efficient quencher of the triplets of benzophenone (E_T = 69 kcal/mol (24)) or *p*-methoxyacetophenone (E_T = 72 kcal/mol (24)). Employing chro-

Can. J. Chem. Downloaded from www.nrcresearchpress.com by 213.166.140.6 on 09/07/12
For personal use only.

TABLE 1. Lifetimes and self-quenching rate constants of chromone triplet in various solvents at 295 K

Solvent	Chromone concentration range, mM [a]	τ_T^0, μs [b]	k_{SQ}^T, $10^9 M^{-1} s^{-1}$ [b]
Acetonitrile	0.075–1.1	1.8	4.1
Acetonitrile + water (1:1)	0.075–1.1	8.3	4.0
Chloroform	0.11 –0.99	0.26	2.2
Ethyl acetate	0.15 –1.5	0.36	3.3
Methanol	0.38 –1.5	0.18	3.1
tert-Butanol	0.30 –1.2	0.86	1.6
2,2,2-Trifluoroethanol	0.075–0.45	13.	0.85
Acetic acid	0.15 –1.2	0.10	2.1

[a]Used for plots, based on eq. [5], to determine τ_T^0 and k_{SQ}^T.
[b]±15%.

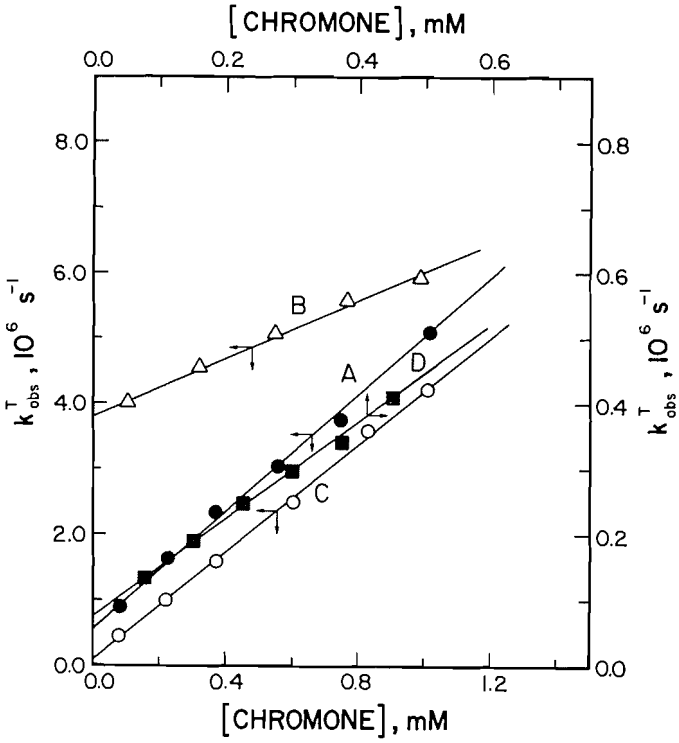

FIG. 3. Representative plots for self-quenching based on eq. [6]: (A) acetonitrile, (B) chloroform, (C) acetonitrile + water (1:1), and (D) 2,2,2-trifluoroethanol.

mone at 0–5 mM in benzene, its effect on the decay of benzophenone and *p*-methoxyacetophenone triplet was studied. The quenchee triplets were monitored at 532 and 375 nm, respectively. In these experiments (λ_{ex} = 337.1 nm), the absorption of laser photons by chromone at its highest concentration was negligible and, because of short lifetime in benzene (see later), chromone triplet (if any) formed as a result of endothermic energy transfer did not interfere with the measurement of the decay rate constant (k_{obs}^T) of the triplets of the two aromatic ketones. From the dependence of k_{obs}^T on [CH], we obtained 8.7×10^7 and $1.6 \times 10^8 M^{-1} s^{-1}$ for the bimolecular rate constants for the quenching of benzophenone and *p*-methoxyacetophenone triplet, respectively. This result establishes the triplet energy (E_T) of chromone at room temperature to be higher than that of *p*-methoxyacetophenone (E_T = 72 kcal/mol). It should be noted that the quenching of the two ketone triplets can occur

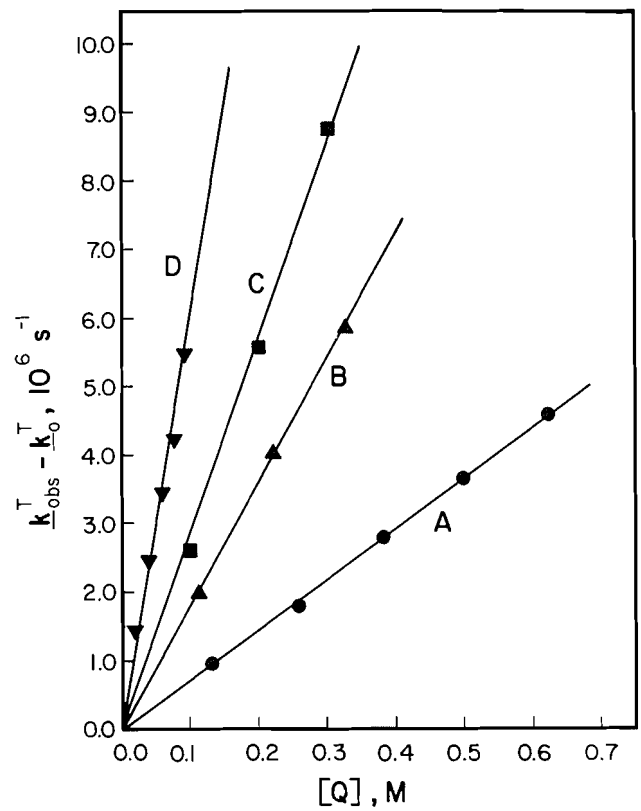

FIG. 4. Linear plots, based on eq. [7], for the quenching of chromone triplet in acetonitrile by (A) 2-propanol, (B) benzene, (C) carbon tetrachloride, and (D) toluene.

not only by energy transfer (endothermic but essentially irreversible because of short chromone triplet lifetime in benzene), but also via oxetane formation with the ene double bond of chromone.

Triplet quenching studies

The kinetics of the quenching of chromone triplet by a variety of quenchers capable of interacting with the triplet by chemical as well as physical mechanisms were studied in detail. Dilute solutions of chromone (0.15–0.25 mM) in acetonitrile were used and the triplet, produced by 308-nm laser excitation, was monitored at 600–620 nm. In all cases, the pseudo-first-order rate constant (k_{obs}^T) for the triplet decay was measured as a function of quencher concentration, [Q], and the quenching rate constant (k_Q^T) was obtained from the slope of the linear plot of k_{obs}^T against [Q], based on eq. [7].

$$[7] \quad k_{obs}^T = 1/\tau_T + k_Q^T[Q]$$

Some representative plots are presented in Fig. 4 and the k_q^T data are compiled in Table 2.

Though non-hydrogen-donating, benzene and carbon tetrachloride proved to be "reactive" solvents for chromone triplet. Although in benzene no residual absorption could be observed following the rapid triplet decay, this was not the case with carbon tetrachloride. In the later solvent, a broad long-lived transient absorption at 350–700 nm ($\lambda_{max} \sim$ 550 nm) was noted on the microsecond time scale and the decay of this absorption was found to be oxygen insensitive. We have also examined benzene and carbon tetrachloride as specific quenchers for chromone triplet in acetonitrile, and k_q^T's were found to be significantly high (1.8×10^7 and $3.0 \times 10^7 M^{-1} s^{-1}$, respectively). Since the observed quenching could be due to

Can. J. Chem. Downloaded from www.nrcresearchpress.com by 213.166.140.6 on 09/07/12
For personal use only.

TABLE 2. Bimolecular rate constants for chromone triplet quenching and efficiencies of hydrogen abstraction in acetonitrile at 295 K

Quencher	Maximum quencher conc., mM [a]	k_q^T, $10^8 M^{-1} s^{-1}$		ϕ_{ketyl} [c]
		Chromone	4-Chromanone	
Oxygen	2.7	53.	57.	
DTBN	1.2	64.	51.	
Ferrocene	0.46	167.	155.	
Biphenyl	1.3	90.		
1-Methylnaphthalene	0.56	115.		
2,5-Dimethyl-2,4-hexadiene	0.70	83.	97.	0.09
Cyclohexene	1.4	38.	0.51	0.15
2,3-Dimethyl-2-butene	7.6	5.5	0.63	0.28
Methyl acrylate	1.1	55.	15.	
Acrylonitrile	2.2	44.		
Maleic anhydride	0.8	113.	89.	
2,5-Dimethoxydihydrofuran	6.2	6.0		
2-Butyne	64.	1.4		
Triethylamine	0.71	77.	16.	0.90
DABCO	0.95	31.		1.
Tri-*n*-butylstannane	4.4	17.	3.7	0.69
1,4-Cyclohexadiene	1.3	41.	1.1	0.20
Diphenylmethanol	78.	1.0	0.02	0.38
2-Propanol	624.	0.074	<0.01	1.
Tetrahydrofuran	473.	0.27	~0.01	1.
Carbon tetrachloride	500.	0.30	≤0.001 [d]	

[a] Used in k_q^T measurements.
[b] ±15%.
[c] For chromone; ±20%.
[d] From τ_T^0 in neat solvent.

TABLE 3. Bimolecular rate constants for chromone triplet quenching by benzene and methylated benzenes in acetonitrile at 295 K

Quencher	$E_{1/2}^{ox}$, V [a]	Maximum quencher conc., M [b]	k_q^T, $10^8 M^{-1} s^{-1}$ [c]	ϕ_{ketyl} [d]
Benzene (1)	2.08	0.33	0.18	
Toluene (2)	1.98	0.094	0.55	
o-Xylene (3)	1.58	0.062	1.7	
m-Xylene (4)	1.58	0.082	1.5	
p-Xylene (5)	1.56	0.041	2.1	
Mesitylene (6)	1.55	0.018	5.8	
1,2,4-Trimethylbenzene (7)	1.41	0.019	7.1	
1,2,3,5-Tetramethylbenzene (8)	1.43	0.015	14.	
Durene (9)	1.29	0.0037	30.	0.14
Pentamethylbenzene (10)	1.28	0.0016	57.	0.14
Hexamethylbenzene (11)	1.16	0.0011	73.	0.13

[a] Versus Ag/0.1N Ag^+ in acetonitrile, taken from ref. 28.
[b] Used in k_q^T measurement.
[c] ±20%.

impurities (namely, olefin derivatives) in the two solvents, the experiments were repeated with samples of benzene and carbon tetrachloride that were subjected to special purification procedures (see the experimental section). k_q^T's obtained with purified samples were essentially the same as those with untreated samples.

To ascertain the direction of charge transfer, if any, in the interaction of chromone triplet with benzene, k_q^T's were measured for a series of methylated benzenes (Table 3). It is noted that k_q^T's increase progressively as the electron-donating nature of the benzene derivatives increases. Furthermore, the rate constant for quenching by toluene-d_8 ($k_q^T = 5.6 \times 10^7 M^{-1} s^{-1}$) is found to be practically identical to that for toluene ($k_q^T = 5.5 \times 10^7 M^{-1} s^{-1}$).

Transient photoproduct spectra and efficiencies of hydrogen abstraction

In hydrogen-donating solvents (e.g., 2-propanol) as well as in the presence of hydrogen donors (e.g., tri-*n*-butylstannane) as quenchers, the decay of chromone triplet leads to a long-

Can. J. Chem. Downloaded from www.nrcresearchpress.com by 213.166.140.6 on 09/07/12
For personal use only.

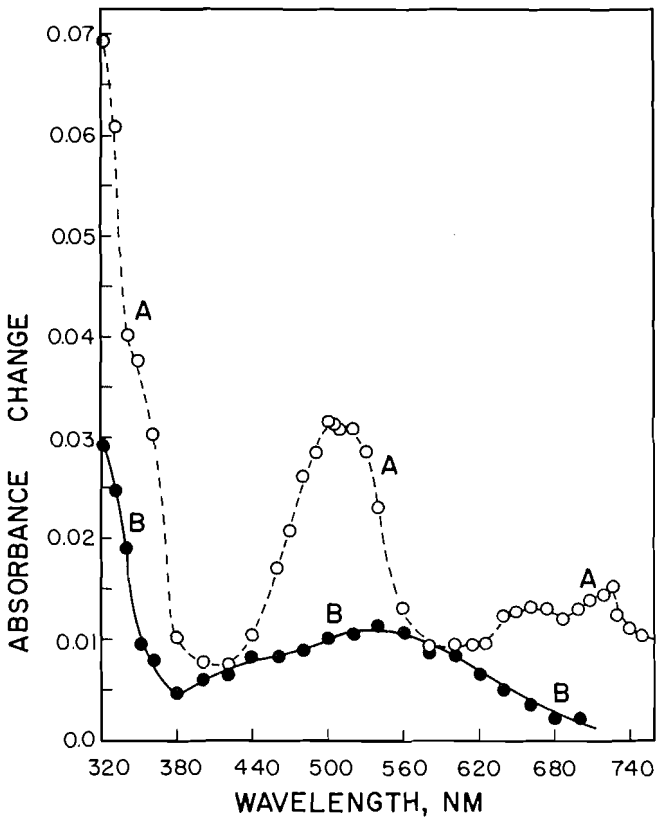

FIG. 5. The transient absorption spectra of (A) ketyl radical from chromone in neat 2-propanol and (B) product(s) of the quenching of chromone triplet by carbon tetrachloride (1.0 *M*) in acetonitrile (observed at 3.2 and 0.50 μs, respectively, following 308-nm laser pulse excitation). [Chromone] = 0.21 m*M* in both cases.

lived residual absorption (λ_{max} = 520 nm) attributable to the ketyl radical (**4**) formed as a result of hydrogen atom transfer (eq. [8]). The transient spectrum in neat 2-propanol is shown in Fig. 5A. Note that the longest-wavelength band system (600–750 nm) is unusual for a ketyl radical and may be due to its deprotonated form (radical anion). However, we found the spectrum of the long-lived transient in 2-propanol containing 13 m*M* trifluoroacetic acid to be identical to that in the absence of the acid. Based on this, the assignment of the long-wavelength band to the radical anion seems unlikely (unless the ketyl radical has an abnormally low pK_a value). The decay of the transient is very oxygen sensitive; from the observed lifetime (128 ± 5 ns) in air-saturated 2-propanol, the rate constant for oxygen quenching is calculated to be $3.5 \times 10^9 M^{-1} s^{-1}$. The similarity of decay kinetics at various wavelength maxima suggests that the observed band systems belong to either one single species, or more than one species in fast equilibrium. Assuming that the quenching of chromone triplet by 2-propanol or tetrahydrofuran in acetonitrile occurs solely by hydrogen abstraction, we determined the extinction coefficient of the radical to be $2.1 \times 10^3 M^{-1} cm^{-1}$ (at 510 nm). This was based on the comparison of the end-of-pulse absorbance due to ^{3}CH* in acetonitrile (λ_{ex} = 308 nm) in the absence of a quencher with the maximum transient absorbance due to the ketyl radical produced under extensive triplet quenching (≥80%) by 2-propanol and tetrahydrofuran.

Practically no residual absorbance changes are noted at 320–700 nm following the quenching of chromone triplet (in acetonitrile) by its ground state and by the olefin derivatives (Table 2) having no easily abstractable H atom. As noted earlier for the neat solvent, ^{3}CH* quenching by CCl_4 added to an acetonitrile solution leads to the formation of an oxygen-insensitive transient species, the spectrum of which is shown in Fig. 5B. Very probably, this is the radical cation (**5**) of chromone formed as a result of electron transfer from the triplet to CCl_4 (eq. [9]).[2]

[8] $^3\mathbf{1}^* + SH \rightarrow \mathbf{4} + S\cdot$

[9] $^3\mathbf{1}^* + CCl_4 \rightarrow \mathbf{5} + \cdot CCl_3 + Cl^-$

For many of the reagents under consideration (Tables 2 and 3), hydrogen atom transfer is feasible in competition with other modes of quenching. The efficiencies of hydrogen abstraction in the course of the quenching processes have been determined in acetonitrile in terms of yields (ϕ_{ketyl}) of the ketyl radical (**4**) monitored at 520 nm. The transient absorbances due to the radical, kinetically corrected to values corresponding to the total quenching of ^{3}CH*, were compared with those observed with 2-propanol or tetrahydrofuran as the quencher. The relative ϕ_{ketyl} values obtained in this manner in several cases are given in Tables 2 and 3.

Photophysical and quenching behaviors of 4-chromanone triplet

For comparison, 4-chromanone (**3**) was also subjected to a limited number of laser flash photolysis experiments. The triplet and ketyl radical absorption spectra, obtained upon 308-nm laser pulse excitation in acetonitrile and 2-propanol respectively, are presented in Fig. 6. The long-wavelength maximum at 430 nm in the triplet–triplet spectrum agrees with the maxima reported by Hamanoue *et al.* (16). From the concentration dependence of triplet decay rate constant in acetonitrile, benzene, and carbon tetrachloride, k_{SQ}^T's are estimated to be smaller than $2 \times 10^8 M^{-1} s^{-1}$ in these solvents and τ_T^0's are measured to be 5.0, 1.2, and 1.3 μs, respectively. Employing techniques similar to those in the case of chromone (*vide supra*), we obtained values of unity for ϕ_T and of $3.7 \times 10^3 M^{-1} cm^{-1}$ for ε_T^{max} at 430 nm (in acetonitrile, λ_{ex} = 337.1 nm). 1-Methylnaphthalene was used as the triplet energy acceptor in these experiments.

The kinetics of the quenching of 4-chromanone triplet (monitored at 430 nm) were studied in acetonitrile using a number of selected reagents. The k_q^T data obtained from linear plots based on eq. [7] are included in Table 2. The most notable difference in the quenching behavior of chromone and 4-chromanone triplets lies in that toward alkenes and hydrogen donors, chromone triplet being much more reactive. The relative inefficiency of 4-chromanone triplet to abstract hydrogen atoms is also evident from the fact that the triplet is quite long-lived in neat 2-propanol (observed τ_T = 520 ns for 0.34 m*M* 4-chromanone).

[2]A similar transient spectrum ascribable to **5** formed as a result of charge transfer from solvent-derived radical cation is also observed upon pulse radiolysis of **1** in 1,2-dichloroethane. Furthermore, the aqueous extract from a carbon tetrachloride solution of chromone (1.3 m*M*) that has been subjected to continued photolysis by repetitive 308 nm laser pulses slowly forms a white precipitate upon addition of an $AgNO_3$ solution. This test proves negative with similarly photolyzed carbon tetrachloride (alone) and with unphotolyzed chromone solution. These qualitative results suggest that the cleavage of CCl_4 is sensitized by chromone, leading to product(s) capable of forming AgCl upon reaction with $AgNO_3$ in the aqueous medium. The fact that the precipitation is not instantaneous indicates that Cl^- or HCl does not accumulate as an initial photoproduct.

Can. J. Chem. Downloaded from www.nrcresearchpress.com by 213.166.140.6 on 09/07/12
For personal use only.

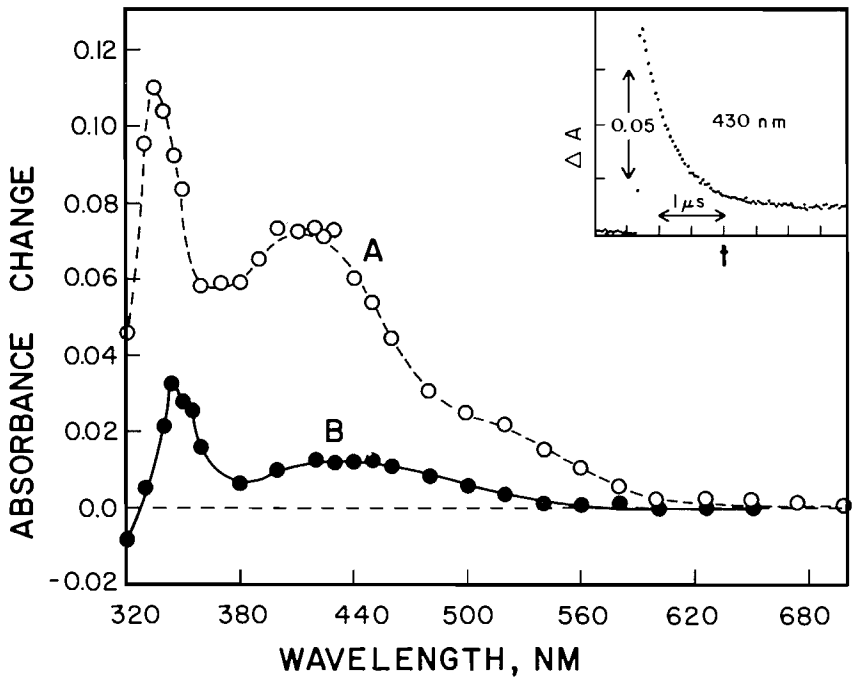

FIG. 6. The transient absorption spectra of (A) 4-chromanone triplet in acetonitrile and (B) ketyl radical from 4-chromanone in neat 2-propanol (λ_{ex} = 308 nm and [4-chromanone] = 0.60 mM in both cases). The spectra were observed at (A) 0.5 and (B) 3.2 μs following laser pulse excitation. Inset: kinetic trace of decay of 4-chromanone triplet in neat 2-propanol.

Discussion

As noted in the Introduction, the excited-state properties of chromone and 4-chromanone have been examined (10–12) by various spectroscopic methods including phosphorescence emission/excitation spectra, phosphorescence polarization/lifetimes, oxygen and heavy-atom perturbed singlet–triplet absorption, and triplet-state esr (electron spin resonance). Both of these carbonyl compounds have weak lowest-lying singlet states with properties consistent with an n,π^* orbital character (10). For chromone, the low-temperature spectroscopic data indicate that the low-lying n,π^* and π,π^* triplet states are nearly isoenergetic, strongly mixed, and subject to reordering upon changing the nature of solvent (11). In comparison, for 4-chromanone, a greater energy gap is suggested between the lowest-lying n,π^* and the proximate π,π^* triplet states (11). These state orders in chromone and 4-chromanone have been claimed to be consistent with the picosecond intersystem crossing rates at room temperature (16). Interestingly, for chromone at 77 K, the appearance of multiple components in phosphorescence decay curves (e.g., in 2-methyltetrahydrofuran glass) and the concentration dependence of phosphorescence spectra in nonpolar solvents (e.g., 3-methylpentane glass) have been explained in terms of involvement of several different lowest triplet conformations of chromone and conglomeration of solute molecules, respectively (10).

Since the environmental effect on an electronic transition resulting from dispersive interaction is determined by the oscillator strength of the transition, the lowering of density and refractive index of the medium upon going from glassy matrices at 77 K to room-temperature solutions is not expected to bring about dramatic changes in the state order in the triplet manifold of chromone and 4-chromanone. Thus, to begin with, it is reasonable to assume that in solutions at room temperature chromone possesses low-lying n,π^* and π,π^* triplet states, close to each other, with relative location sensitive to the polarity and hydrogen-bonding nature of the medium, and the 4-chromanone has the lowest triplet state of predominantly n,π^* character. It is of interest to examine whether and to what extent the photophysical and photochemical behaviors of the two aromatic carbonyl systems at room temperature reflect these state orders.

Perhaps the best photochemical criterion of an n,π^* carbonyl triplet is its radical-like behavior in hydrogen abstraction reactions. As the k_q^T data for the quenching of chromone triplet by tri-n-butyl stannane, 2-propanol, and tetrahydroguran (Table 2) suggest, even in the polar solvent (acetonitrile) this carbonyl triplet is an efficient hydrogen abstractor. In particular, the reactivity of chromone triplet toward tri-n-butylstannane in acetonitrile ($k_q^T = 1.7 \times 10^9 M^{-1} s^{-1}$) is as high as that of xanthone triplet in carbon tetrachloride ($k_q^T = 1.5 \times 10^9 M^{-1} s^{-1}$ (6)). The triplet of xanthone is recognized to be of predominantly n,π^* character in nonpolar solvents and the bimolecular rate constant for its reaction with 2-propanol exhibits a dramatic decreasing trend, attributable to $^3(n,\pi^*)$–$^3(\pi,\pi^*)$ inversion, upon going from a nonpolar solvent to a polar one (e.g., $k_q^T = 1.1 \times 10^8 M^{-1} s^{-1}$ in carbon tetrachloride vs. $2.2 \times 10^5 M^{-1} s^{-1}$ in neat propanol (6)). Since the triplet energy of xanthone (E_T = 74 kcal/mol (24)) is similar to that of chromone (E_T = 75 kcal/mol), it is tempting to make an attempt to determine the n,π^* character of chromone triplet by consideration of its hydrogen abstraction reactivity relative to that of xanthone triplet. However, this would be misleading because of the fact that the resonance stabilization (25) of the ketyl radical and the enthalpy change in the course of hydrogen atom transfer are different in the two cases. Unfortunately, we could not find a suitable unreactive nonpolar solvent for use to determine an upper limit of the hydrogen abstraction reactivity of chromone triplet in a predominantly n,π^* configuration. Nevertheless, the facts that the k_q^T's for various hydrogen donors in acetonitrile are relatively high and that in neat 2-propanol the hydrogen abstrac-

Can. J. Chem. Downloaded from www.nrcresearchpress.com by 213.166.140.6 on 09/07/12
For personal use only.

Can. J. Chem. Downloaded from www.nrcresearchpress.com by 213.166.140.6 on 09/07/12
For personal use only.

tion rate is higher, by one order of magnitude, for chromone ($k_q^T > 3 \times 10^6 M^{-1} s^{-1}$, based on $\tau_T < 25$ ns) than for xanthone triplet ($k_q^T = 2.2 \times 10^5 M^{-1} s^{-1}$) suggest that even in polar solvents the lowest triplet state of chromone has a substantial contribution from the n,π^* configuration (either through vibronic mixing or in thermal equilibrium). This conclusion suggests that the theoretical treatment of the cycloaddition reactivity of chromone triplet would be more relevant in terms of an n,π^* configuration than a π,π^* configuration (as considered in the recent study (15)).

At low temperature (77 K) the lowermost triplet state of 4-chromanone is recognized to be of n,π^* nature; the $^3(\pi,\pi^*)$ state is located at an energy too high for its contribution to the lowest-energy state to be significantly influenced by solvent (10–12). Thus, compared to chromone in a given solvent at room temperature, 4-chromanone is expected to have a higher n,π^* character and hence a greater hydrogen abstraction reactivity in its lowest triplet state. Surprisingly, however, as the data in Table 2 show, the rate constants for the quenching of 4-chromanone triplet by various hydrogen donors are considerably smaller than those for the chromone triplet. This is explainable by the facts that the triplet energy (E_T) of the former is lower than that of the latter by about 2 kcal/mol (10, 11) and that the resonance stabilization of the ketyl radical is higher in the case of chromone (because of participation of the double bond in delocalizing the unpaired electron). Thus, the enthalpy change associated with hydrogen abstraction would be more favorable for chromone triplet.

The high rate constants for chromone triplet quenching by many of the molecules containing multiple bonds (Table 2) are explainable in terms of cycloaddition at the ene double bond. In several cases, namely, cyclohexene, 2,3-dimethyl-2-butene, and methyl acrylate, this is supported by the fact that the quenching of 4-chromanone triplet by these molecules is much less efficient. The photocycloaddition reaction of chromone involving the ene double bond is established as its major photoreaction under steady-state irradiation in the presence of alkene/alkyne derivative (13, 14). As a matter of fact, the order of k_q^T for cyclohexane, 2,3-dimethyl-2-butene, and 2-butyne is in agreement with that of the reactivity of cyclopentene, 2,3-dimethyl-2-butene, and 2-butyne observed in the steady-state study (14). Chromone triplet has been considered to be an electrophile in its photocycloaddition reactions (14). Interestingly, however, the k_q^T's for electron-poor olefins, namely, maleic anhydride, methyl acrylate, and acrylonitrile, are found to be higher than the electron-rich ones, namely, 2,5-dimethoxydihydrofuran, 2,3-dimethyl-2-butene, and cyclohexene (Table 2). It would, however, be premature to take this as evidence against the electrophilic character of chromone triplet because the observed k_q^T's contain contributions of the various processes, namely, cycloaddition at the ene double bond, oxetane formation, energy transfer, and hydrogen abstraction. The relative importance of these contributions has to be sorted out before a meaningful conclusion can be drawn regarding the trend of a given type of photoreaction.

The behavior of chromone triplet as an electrophile is, however, evident in its quenching by benzene and methylated benzenes (Table 3). Figure 7 shows the logarithmic plot of k_q^T vs. oxidation potential of the benzene derivatives. Evidently there is a good correlation between the quenching rate constant and the electron-donating capability of these quenchers. The fact that the k_q^T for benzene fits well into the correlation can be taken to mean that its interaction with chromone triplet involves

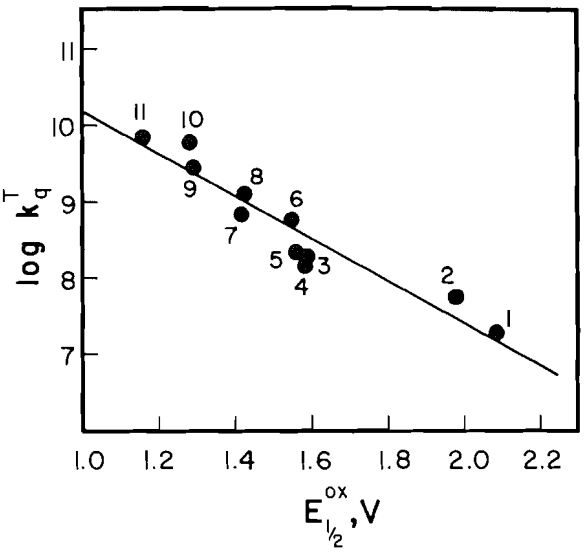

FIG. 7. The logarithmic plot of bimolecular rate constant for chromone triplet quenching vs. oxidation potential of benzene and methylated benzenes. For the numbers identifying the quenchers, see Table 3. The least-squares best-fit straight line (correlation coefficient = 0.948) is given by: $\log(k_q^T) = -2.79\,(E^{ox}_{1/2}) + 12.98$.

charge transfer. Interestingly, the rate constant for chromone triplet quenching by diphenylmethanol ($1.0 \times 10^8 M^{-1} s^{-1}$) is almost what is expected from k_q^T for the toluene ($5.5 \times 10^7 M^{-1} s^{-1}$), after taking into account the presence of two phenyl groups in the former. This suggests that the quenching by the aromatic alcohol is dominated by charge transfer interaction at the aromatic nucleus, rather than by direct hydrogen abstraction. This is also supported by less than quantitative yield (0.38) of ketyl radical formation and by the absence of isotope effect in the quenching by toluene and toluene-d_8. It should be noted that the ketyl radical in the case of diphenylmethanol may originate from intra-ion-pair proton transfer following the charge transfer interaction, rather than from direct hydrogen atom transfer (26).

The most plausible mechanism for the facile quenching of chromone triplet by CCl_4 appears to be the one involving charge transfer in which the triplet acts as a donor. The formation of oxygen-insensitive transient product, most probably chromone radical cation, as a result of the quenching shows that the charge transfer is not totally reversible (as in the case of benzene). Lissi and Encina (27) have observed the reaction of acetone and 2-pentanone triplets with CCl_4, the rate constant for 2-pentanone triplet being $1.2 \times 10^7 M^{-1} s^{-1}$ (in *n*-hexane). Chromone appears to be the rare example of an aromatic carbonyl system the triplet of which shows high reactivity toward CCl_4. The enhanced reactivity is attributable to the relatively high triplet energy and the structural feature of chromone (i.e., ether linkage) giving rise to a favorable oxidation potential.

The self-quenching rate constants (k_{SQ}^T) of chromone triplet in different solvents (Table 1) are all close to the limit of diffusion control. As far as we know, among aromatic carbonyl triplets, chromone is characterized by the highest k_{SQ}^T's in polar solvents. For xanthone, k_{SQ}^T's have been found to range from $4.2 \times 10^7 M^{-1} s^{-1}$ in 1:1 water:acetonitrile to $4 \times 10^9 M^{-1} s^{-1}$ in *n*-heptane. The solvent dependence of the self-quenching in the case of xanthone triplet has been attributed to interaction at the oxygen bridge. While a similar interaction is

also possible in the case of chromone, it is more likely that chromone in the ground state acts as an olefin, leading to photocycloaddition with the triplet (i.e., dimerization). The difference in the mechanism of the self-quenching of xanthone and chromone triplets becomes apparent when one considers the fact that, on going from neat acetonitrile to 1:1 water:acetonitrile, k_{SQ}^{T} for xanthone drops by a factor of ten (6) while that for chromone remains practically unchanged (Table 1).

Finally, it should be pointed out that with quenchers such as ferrocene, biphenyl, 1-methylnaphthalene, and 2,5-dimethyl-2,4-hexadiene having triplet energies lower than E_T of chromone by at least 10 kcal/mol, k_q^T's are all in the limit of diffusion control (Table 2). In particular, with ferrocene ($E_T \cong$ 40 kcal/mol), for which both energy and electron transfer are feasible, the value of $1.7 \times 10^{10} M^{-1} s^{-1}$ for k_q^T in acetonitrile is very close to the theoretical diffusion rate (k_{diff}). Also, as expected for the energy transfer quenching of a triplet by a radical, the spin-statistically limited maximum value of $1/3k_{diff}$ is achieved in the case of quenching by DTBN. These large rate constants for energy transfer quenching are evidence against any extensive structural relaxation in the lowest triplet state of chromone (for example, in the form of twisting about the ene double bond). On the contrary, in the case of 2,3-diphenylchromone (**2**), the triplet quenching by 1-methylnaphthalene, 2,5-dimethyl-2,4-hexadiene, ferrocene, and DTBN occurs at considerably slower rates (17) suggesting extensive triplet state relaxation in **2** (possibly in the form of partial twisting about the double bond to relieve the steric hindrance between the two adjacent phenyl substituents).

Acknowledgement

The work described herein was supported by the Office of Basic Energy Sciences, Department of Energy (U.S.). This is Document No. NDRL-2937 from the Notre Dame Radiation Laboratory.

1. R. S. Becker. Theory and interpretation of fluorescence and photophorescence. Wiley, New York. 1969. Chap. 10.
2. K. Bredereck, T. Förster, and H. G. Oesterlin. *In* Luminescence of organic and inorganic materials. *Edited by* H. P. Kallman and G. M. Spruch. Wiley, New York. 1962. p. 161.
3. P. K. Das and R. S. Becker. J. Phys. Chem. **82**, 2093 (1978).
4. P. J. Wagner, A. E. Kemppainen, and H. N. Schott. J. Am. Chem. Soc. **95**, 5604 (1973).
5. N. C. Yang, D. S. McClure, S. L. Murov, J. J. Houser, and R. Dusenbery. J. Am. Chem. Soc. **89**, 5466 (1967).
6. J. C. Scaiano. J. Am. Chem. Soc. **102**, 7747 (1980).
7. M. A. El-Sayed. J. Chem. Phys. **36**, 573 (1962); **38**, 2834 (1963); **41**, 2462 (1964).
8. S. K. Lower and M. A. El-Sayed. Chem. Rev. **66**, 199 (1966).
9. C. V. Kumar, S. K. Chattopadhyay, and P. K. Das. Photochem. Photobiol. **38**, 141 (1983).
10. J. B. Gallivan. Can. J. Chem. **48**, 3928 (1970).
11. J. B. Gallivan and J. S. Brinen. Chem. Phys. Lett. **10**, 455 (1971).
12. J. B. Gallivan. Can. J. Chem. **50**, 3601 (1972).
13. J. W. Hanifin and E. Cohen. Tetrahedron Lett. 1419 (1966).
14. J. W. Hanifin and E. Cohen. J. Am. Chem. Soc. **91**, 4494 (1969).
15. R. Chadha and N. K. Ray. Indian J. Chem. Sect. A, **25**, 111 (1986).
16. K. Hamanoue, T. Nakayama, T. Miyake, and H. Teranishi. Chem. Lett. 39 (1981).
17. K. Bhattacharyya, D. Ramaiah, P. K. Das, and M. V. George. J. Phys. Chem. **90**, 5984 (1986).
18. M. M. Badawi and M. B. E. Fayez. Indian J. Chem. **5**, 93 (1967).
19. D. I. Schuster and T. M. Weil. Mol. Photochem. **4**, 447 (1972).
20. P. K. Das, M. V. Encinas, R. D. Small, Jr., and J. C. Scaiano. J. Am. Chem. Soc. **101**, 6965 (1979), and references to earlier work therein.
21. V. Nagarajan and R. W. Fessenden. J. Phys. Chem. **89**, 2330 (1985).
22. R. Bensasson and E. J. Land. Photochem. Photobiol. Rev. **3**, 163 (1978).
23. R. V. Bensasson and J.-C. Gramain. J. Chem. Soc. Faraday Trans. 1, **76**, 1801 (1980).
24. S. L. Murov. Handbook of photochemistry. Marcel–Dekker, New York. 1973.
25. L. Giering, M. Berger, and C. Steel. J. Am. Chem. Soc. **96**, 953 (1974).
26. P. J. Wagner, M. J. Thomas, and A. E. Puchalski. J. Am. Chem. Soc. **108**, 7739 (1986).
27. E. A. Lissi and M. V. Encina. J. Photochem. **3**, 237 (1974).
28. H. Siegerman. *In* Techniques of chemistry. Vol. V. part II. *Edited by* W. L. Weinberg. Wiley, New York. 1975. p. 667.

Can. J. Chem. Downloaded from www.nrcresearchpress.com by 213.166.140.6 on 09/07/12
For personal use only.

Interaction between bromothymol blue and antipyrine in dichloromethane

ALBERTO HERNANDEZ GAINZA AND LUISA PUERTA JIMENEZ
Departamento de Quimica Fisica, Facultad de Farmacia, Universidad de Granada, 18001 Granada, España

Received June 11, 1986[1]

ALBERTO HERNANDEZ GAINZA and LUISA PUERTA JIMENEZ. Can. J. Chem. **65**, 2286 (1987).

Antipyrine (AT) reacts with bromothymol blue (BTB) in dichloromethane (DCM), forming an ion pair of 1:1 stoichiometry. Chemical equilibrium has been demonstrated and the formation constants of the ion pair at various temperatures have been calculated spectrophotometrically. The thermodynamic parameters of the reaction are $\Delta H^0 = -6994$ cal/mol, $\Delta S^0 = -11.05$ cal/K mol, and $\Delta G^0_{25°C} = -3703$ cal/mol.

ALBERTO HERNANDEZ GAINZA et LUISA PUERTA JIMENEZ. Can. J. Chem. **65**, 2286 (1987).

La antipyrine (AT) réactionne avec le bleu de bromothymol (BTB) dans chlorure de méthylène formant une paire d'ions d'estequiométrie 1:1. C'est évident une équilibre chimique et on a calculé les constantes de formation de la paire d'ions à différentes températures et le coefficient d'extinction molaire à partir de mésures spectrophotométriques. Les parametres thermodynamiques de la réaction sont $\Delta H^0 = -6994$ cal/mol, $\Delta S^0 = -11{,}05$ cal/K mol et $\Delta G^0_{25°C} = -3703$ cal/mol.

Can. J. Chem. Downloaded from www.nrcresearchpress.com by 84.22.46.98 on 09/08/12
For personal use only.

Introduction

Bromothymol blue is the most widely used dye for the determination of amines of pharmaceutical interest by photometric titration in two phases (1–7). The amine – bromothymol blue reaction has been described as a non-specific acid–base process in one non-polar phase (8, 9), and in two non-miscible phases (1–7). However, the reaction is not totally non-specific because some amines give practically no reaction either in one or two phases, such as the benzodiazepines medazepam and bromazepam (9, 10). There are many other amines, for which the reaction has not been described, and in view of the great deal of work published on this topic, it is easy to conclude that most amines give no reaction with bromothymol blue (BTB), or that the reaction is so weak that it can not be studied with conventional methodology.

In this work the reaction of bromothymol blue (free acid) with an analgesic derivative of pyrazolone, antipyrine (free base), has been studied. Conventional methods of study and quantification of this interaction in dichloromethane can not, because of its weak character, be studied by the classic methods described for strong associations. Therefore the methods of Benesi–Hildebrand (11, 12) and Rosseinsky (13) have been used to calculate equilibrium constants and molar absorptivity. The values of the thermodynamic quantities ΔG^0, ΔH^0, and ΔS^0, which are not known for the strong complexes of bromothymol blue, have been evaluated. This work also presents a comparison between strong and weak types of associations and of the interaction that generates them. It suggests that the one-phase interaction has the same chemical nature for amines that form strong associates (8, 9) as that for antipyrine (AT), the only amine known that forms both a weak associate with BTB and a quantifiable reaction.

In previous studies (9) it has been demonstrated that an identical BTB – amine ion pair is obtained from extraction in two-phase systems (water/chloroform) as from direct reaction between BTB (free acid) and the amine (free base) in chloroform. In this study the properties of the BTB–AT ion pair are investigated only for the reaction of BTB (free acid) with AT (free base) in a one-phase dichloromethane system. In two-phase systems the identical BTB–AT ion pair obtained by extraction is difficult to study, given its low stability in organic solvents, and that its pK_a value is inadequate ($pK_a = 1.5$) for extraction as an ion pair with BTB (1, 2).

[1]Revision received May 11, 1987.

Experimental

Apparatus

The spectrophotometer used was a Perkin-Elmer Lambda 5 with B. Braun Melsungen AG models Frigomix 1.495 and Thermomix 1.441 (±0.2°C) thermostats. Quartz cells of 1-cm path length were employed. Other apparatus included a Hewlett-Packard 9825 A microcomputer and a Radiometer model CDM 83 conductimeter.

Reagents

1,2-Dihydro-1,5-dimethyl-2-phenyl-3*H*-pyrazol-3-one (antipyrine) Merck, analytical grade, was stored in desiccator over phosphorus pentoxide. Dichloromethane, DCM (Carlo Erba, spectrophometric grade), with water content less than 0.02% and bromothymol blue (Merck, analytical grade) were used without further purification.

Results

Spectrophotometry and conductimetry of antipyrine and bromothymol blue solutions

Upon mixing of solutions of antipyrine (free base) with bromothymol blue (free acid) a new band of absorption appears with a maximum at 410 nm that is not observed in separate spectra of the reagents. In Fig. 1 a spectrum of an antipyrine – bromothymol blue mixture is shown, along with spectra of the reagents separately. Job's method (14) of continuous variation was used to determine the stoichiometric ratio of bromothymol blue to antipyrine. For this method, solutions of amine and dye whose concentration sum is constant were prepared at mole ratios between 0.01 and 0.99 (dye–amine), and the absorbances of the resulting solutions were recorded at 410 nm against pure dichloromethane. A Job's representation is shown in Fig. 2.

A series of experiments were carried out to determine the formation constant, K, and molar absorptivity, ε, of the dye–amine product. In all the experiments, solutions of dye and amine whose molar ratio had been held constant were used to simplify the experimental methodology and the treatment of data. Measurements of absorbance of the solutions were always carried out with an excess of amine at temperatures from 15 to 40°C and at 410 nm, the wavelength of the absorption maximum of the association compound. Experimental data for the antipyrine – bromothymol blue associated species are presented in Table 1. The absorption spectra and the absorbance

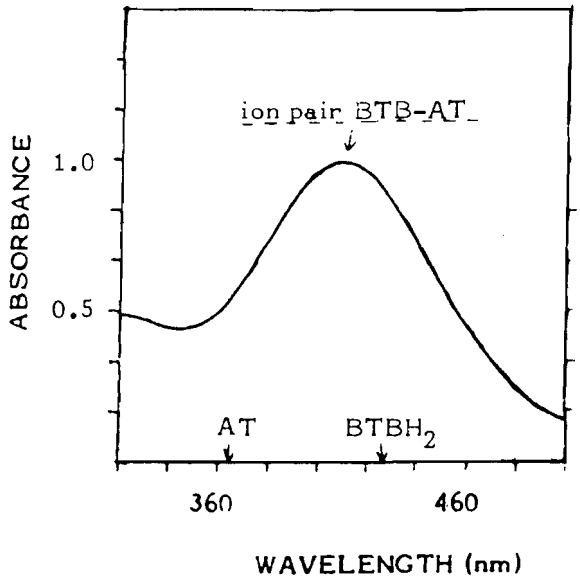

FIG. 1. Absorption spectra of dichloromethane solutions of antipyrine – bromothymol blue ion pair ($4 \times 10^{-4} M$ antipyrine, $4 \times 10^{-4} M$ bromothymol blue), antipyrine ($4 \times 10^{-4} M$), and bromothymol blue ($4 \times 10^{-4} M$), $T = 20°C$.

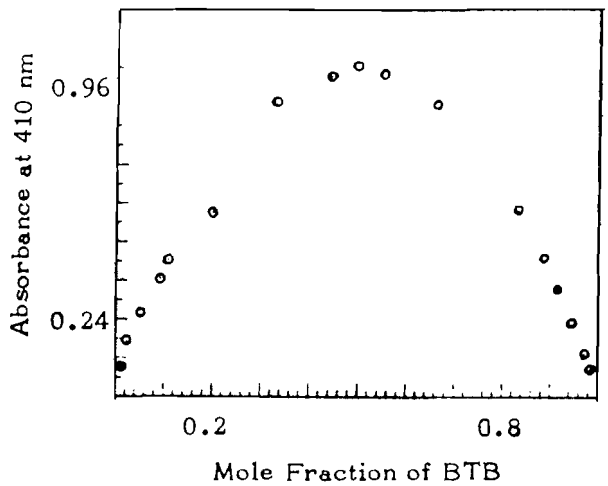

FIG. 2. Job's plot of absorbance values at 410 nm against mole fraction of BTB for antipyrine–dye complex; $C^0_{BTB} + C^0_{AT} = 8 \times 10^{-4} M$.

values at 410 nm of bromothymol blue – antipyrine mixtures remain constant for at least 48 h.

The conductivity in dichloromethane of solutions of bromothymol blue, antipyrine, and mixtures of the two were measured at 20°C. The results are presented in Table 2.

Discussion

The reaction of antipyrine (free base) with bromothymol blue (free acid) gives in dichloromethane solution an ion pair with an absorption maximum at 410 nm, a wavelength where absorption is not present for either the antipyrine of the dye (Fig. 1). Evidence for formation of this new compound only occurs at high concentrations of both reagents, which is in contrast to the associations that have been described for other amines (1, 8, 9). This suggests the weak character of the reaction. The stoichiometric balance of the product, using the method of continuous variations, is 1:1 given that the graphic representation in Fig. 2 shows a maximum at 0.5 molar fraction. On the other hand, the absence of inflections as well as the presence of a finite gradient, at zero and at unit mole fraction indicate that the complex formed is 1:1 and not 2:2 or 3:3 (15).

The absorption spectrum of the new compound is the same in shape and in wavelength at maximum absorption (410 nm) as those presented by other amines which are strongly associated with BTB (1, 8, 9). This suggests an interaction of the same chemical nature as that of amines which give strong reaction. Consequently, the reaction can be considered an acid–base process in which the antipyrine neutralizes the first proton of the dye and, in view of the low dielectric constant of the solvent, probably an antipyrine–dye ion pair is formed. The reaction can be shown by the equation:

[1] $BTBH_2 + AT \rightleftharpoons \{BTBH^-, ATH^+\}$

for which the equilibrium constant is

TABLE 1. Absorbance values at 410 nm of solutions with different concentrations of bromothymol blue, C^0_{BTB}, and antipyrine C^0_{AT}, at various temperatures

$10^5 C^0_{BTB}$	$10^3 C^0_{AT}$	Absorbance at 410 nm					
		15°C	20°C	25°C	30°C	35°C	40°C
1.0	1.0	0.093	0.081	0.072	0.067	0.058	0.051
1.5	1.5	0.175	0.153	0.138	0.126	0.111	0.102
2.0	2.0	0.267	0.235	0.225	0.202	0.181	0.166
2.5	2.5	0.362	0.323	0.308	0.280	0.254	0.235
3.0	3.0	0.457	0.411	0.374	0.353	0.322	0.299
3.5	3.5	0.558	0.507	0.466	0.441	0.406	0.379
4.0	4.0	0.664	0.612	0.571	0.538	0.517	0.482
4.5	4.5	0.768	0.712	0.667	0.632	0.608	0.569
5.0	5.0	0.888	0.824	0.777	0.732	0.660	0.640
5.5	5.5	0.993	0.927	0.876	0.830	0.756	0.731
6.0	6.0	1.094	1.014	0.967	0.907	0.865	0.843
6.5	6.5	1.200	1.118	1.068	1.008	0.965	0.937
7.0	7.0	1.306	1.212	1.163	1.112	1.073	1.032
7.5	7.5	1.412	1.317	1.265	1.215	1.175	1.128
8.0	8.0	1.510	1.435	1.368	1.310	1.285	1.208
8.5	8.5	1.617	1.541	1.471	1.414	1.389	1.306
9.0	9.0	1.723	1.660	1.585	1.570	1.498	1.417
9.5	9.5	1.830	1.766	1.689	1.675	1.604	1.516

TABLE 2. Specific conductivity values, χ, ($\mu S\ cm^{-1}$) of dichloromethane solutions of antipyrine and bromothymol blue at different concentrations, $T = 20°C$

$C^0_{BTB}\ 10^3$	$C^0_B\ 10^3$	χ
10.00	0	0.01
0	10.00	0.00
9.87	2.63	1.40
9.74	5.19	3.03
9.61	7.69	4.83
9.49	10.01	6.67
9.37	12.50	8.70
9.26	14.81	10.52
9.15	17.07	12.16
9.04	19.28	13.90
8.93	21.43	15.40
8.82	23.53	16.80

Can. J. Chem. Downloaded from www.nrcresearchpress.com by 84.22.46.98 on 09/08/12
For personal use only.

$$[2] \quad K = \frac{(\{BTBH^-, ATH^+\})}{(BTBH_2)(AT)}$$

where $BTBH_2$ is bromothymol blue (free acid), AT antipyrine (free base), and $\{BTBH^-, ATH^+\}$ the product formed and stabilized as a 1:1 ion pair.

Determination of the equilibrium constant, K, of process [1] requires the use of a calculation method suitable for weak associations, since the molar absorptivity of the 1:1 ion pair can not be determined directly.

It is easy to prove that the equation which relates the experimental absorbance at 410 nm, A, the initial concentrations of bromothymol blue and antipyrine, C^0_{BTB} and C^0_{AT}, the equilibrium constant, K, and the molar absorptivity, ε, of the product, $\{BTBH^-, ATH^+\}$, is (16, 17)

$$[3] \quad A = A_0 + \tfrac{1}{2}\varepsilon\{C^0_{BTB} + C^0_{AT} + K^{-1} - [(C^0_{BTB} + C^0_{AT} - K^{-1})^2 - 4C^0_{BTB}C^0_{AT}]^{1/2}\}$$

where A_0 is a correction factor for the experimental absorbance.

To resolve this equation in a general way Rosseinsky's iterative method can be applied, since the product formed is of 1:1 stoichiometry and the reagents do not absorb at 410 nm, the wavelength of maximum absorbance for the product. It is also assumed that the ion pair obeys Beer's law. The iterative procedure also supplies a criterion for eliminating data that present higher experimental error than the average. The chosen parameters are K^{-1}, $\sigma_{K^{-1}}$, ε, σ_ε and r.m.s.d., where $\sigma_{K^{-1}}$ and σ_ε are the standard deviations of K^{-1} and ε and r.m.s.d. is the mean square deviation of the experimental absorbance values.

The cycle of iterations is continued until $\Delta\varepsilon < 10^{-3}$ and $\Delta K^{-1} < 10^{-8}$. The estimation of K and ε with their confidence intervals is carried out by using Tchevicheff's equation (18*a*), which needs no assumptions about the type of distribution of errors, for the probability level 0.95. Application of this iteration method requires that an approximate first value of K and ε (K_1 and ε_1) be known. To obtain these values the Benesi–Hildebrand method was used since in all of the experiments the concentration of antipyrine was much higher than that of bromothymol blue. The Benesi–Hildebrand equation as applied to this reaction is

$$[4] \quad \frac{C^0_{BTB}}{A} = \frac{1}{K_1\varepsilon_1} \cdot \frac{1}{C^0_{AT}} + \frac{1}{\varepsilon_1}$$

Figure 3 shows that eq. [4] is satisfied over the range of concentrations used for all temperatures studied. The values of K_1 and ε_1, and the coefficient of determination r^2 were obtained by least squares.

The values of K and ε along with their statistical uncertainties obtained by Rosseinsky's method, and the coefficient of determination r^2 of the Benesi–Hildebrand approximation are listed in Table 3. Because the values of r^2 are close to 1 and the r.m.s.d. is less than 0.01 in most cases (the spectrophotometric error is 0.005) it is possible to conclude that the experimental data agree quantitatively with the proposed equations. Another important result is that the ε values for $\{BTBH^-, ATH^+\}$ are constant at different temperatures.

The absorption spectrum of the BTB–antipyrine associate in DCM (Fig. 1) is very similar to that of the strong associates in dichloromethane and chloroform (1, 8, 9). Moreover, the molar absorption value of the $\{BTBH^-, ATH^+\}$ ion pair is also equal to that of the strong associates (1, 8, 9), which suggests that for both strong and weak associates the reaction is of the same chemical nature. The only difference between the strong and weak associates is the extension of the acid–base reaction, which is governed by the pK_a value of the amine. Thus antipyrine gives a weak reaction with BTB since its pK_a value is 1.5, although atropine, atropamine, strychnine, tropine, quinine, etc. give strong associates since their pK_a values range from 8 to 11.

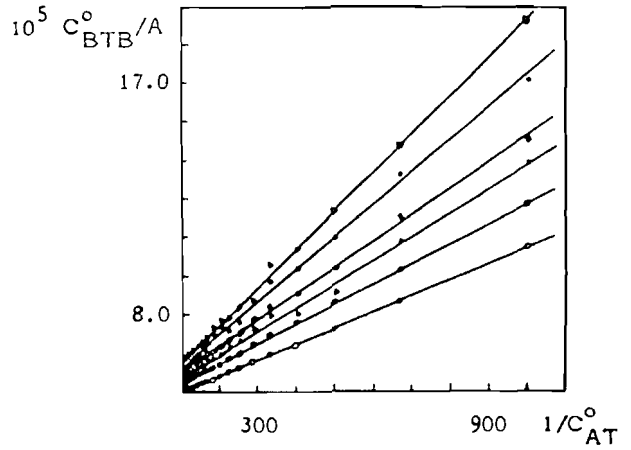

FIG. 3. Benesi–Hildebrand plot at 15, 20, 25, 30, 35, and 40°C of data from Table 1.

TABLE 3. Formation constants, K, and molar absorptivities, ε at various temperatures, calculated by Rosseinsky's method; confidence intervals are at a probability of 0.95, and r^2 values are from the Benesi–Hildebrand approximation for the antipyrine – bromothymol blue compound

T (°C)	K (L/mol)	ε (L/mol cm)	r.m.s.d.	r^2
15	832±130	21867± 531	0.006	0.999
20	592± 99	21907± 742	0.008	0.999
25	518± 81	21449± 747	0.007	0.996
30	417±131	22220±1908	0.015	0.997
35	321± 80	22716±1794	0.012	0.996
40	322± 55	21365±1140	0.008	0.999

Gupta (8) has suggested that moderately high values for the formation constants can mean a complex character for the 1:1 addition products between bromothymol blue and those amines with pK_a's between 8–11 which give a quantitative reaction with BTB in chloroform (but not one of salts). By analogy the magnitude of the obtained constants reveals a complex character for the 1:1 compound given that the value of K is very small and oscillates widely with temperature. However, the reaction is apparently an acid–base process in which the magnitude of the equilibrium constants depends on the basic properties of the amine under consideration.

The conductivity data of dye and antipyrine solutions in dichloromethane reinforce the previous interpretation, since they suggest both the presence of ions in the organic phase and the ionic nature of the product formed. The specific conductivity of separate dye or antipyrine solutions in dichloromethane is next to zero, while solutions containing mixtures of both reagents show an increase in specific conductivity (Table 2). Although the specific conductivities increase with the concentrations of dye and amine taken, the specific conductivity values of BTB–AT solutions in dichloromethane are very low,

Can. J. Chem. Downloaded from www.nrcresearchpress.com by 84.22.46.98 on 09/08/12
For personal use only.

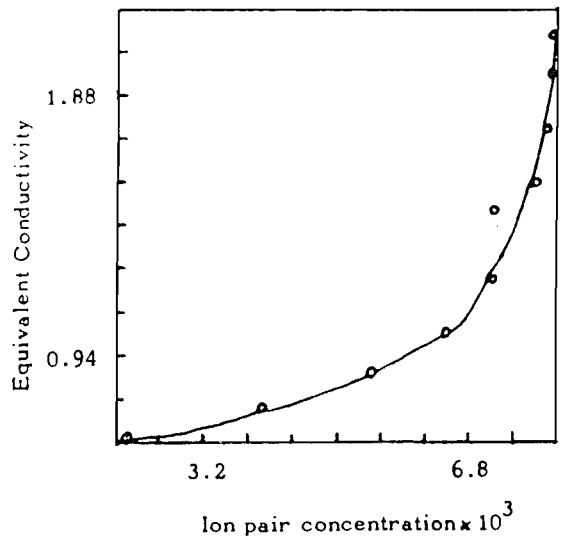

FIG. 4. Plot of equivalent conductivity values ($\mu S\,cm^2\,equiv.^{-1}$), against concentration (mol/L) of BTB–AT ion pair, T = 20°C.

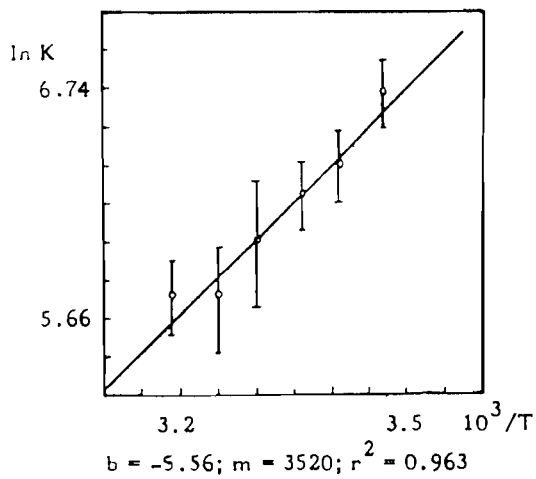

FIG. 5. Van't Hoff plot of antipyrine – bromothymol blue reaction. Formation constants plotted with confidence intervals. Intercept value b, slope m, and determination coefficient r^2 obtained by least squares method.

which shows that only a small fraction of the BTB–AT ion pair is dissociated in nonpolar solvents.

In Fig. 4 values of equivalent conductivity ($\mu S\,cm^2\,equiv^{-1}$) have been plotted against the ion pair concentration of BTB–AT. These have been calculated from K = 592 L/mol at 20°C. The specific and equivalent conductivity increases with ion pair concentration, probably owing to the presence of increasing concentrations of ions.

Calculations of changes in the thermodynamic quantities ΔG^0, ΔH^0, and ΔS^0 were carried out starting with the expressions (19)

$$[5] \quad \ln K = \frac{\Delta S^0}{R} - \frac{\Delta H^0}{RT}$$

and

$$[6] \quad \Delta G^0 = -RT \ln K$$

The calculated constants fall within the respective confidence intervals of the linear regression of eq. [5] (Fig. 5). The calculated thermodynamic parameters were $\Delta S^0 = -11.05 \pm 6.37$ cal/mol; $\Delta H^0 = -6994 \pm 1912$ cal/mol for the range 15 to 40°C; and $\Delta G^0 = -3534$ to -3850 cal/mol over these temperatures. These data are shown in Table 4. The 95% confidence intervals of ΔS^0 and ΔH^0 were calculated by Student's method (18*b*) and the confidence interval of ΔG^0 was calculated from the confidence interval of K.

TABLE 4. Thermodynamic parameters ΔH^0, ΔS^0, and ΔG^0 for AT–BTB system in dichloromethane, with 95% confidence intervals; values obtained from van't Hoff plot

T (°C)	ΔH^0 (cal/mol)	ΔS^0 (cal/K mol)	ΔG^0 (cal/mol)
15	−6994±1912	−11.05±6.37	−3850± 97
20	−6994±1912	−11.05±6.37	−3718±107
25	−6994±1912	−11.05±6.37	−3703±101
30	−6994±1912	−11.05±6.37	−3634±227
35	−6994±1912	−11.05±6.37	−3534±175
40	−6994±1912	−11.05±6.37	−3593±116

Values of ΔH^0 are negative, which suggests that formation of the ion pair is exothermic. The change in ΔS^0 is also negative, which points to a high degree of order in the complex; ΔG^0 is also less than zero since the process is spontaneous.

The study was repeated for diazepam, dipyrone, and ampyrone (analytical grade) for which the reaction with BTB has not been described. Apparently the reaction is very weak, and it was not possible to obtain values for ion pairs with satisfactory small statistical uncertainties.

Similar experiments to those carried out with antipyrine were performed with these amines. Solutions of BTB were mixed with each amine in dichloromethane and an absorbance at 410 nm (yellow) was shown. The experimental results were not, however, in agreement with the previous theoretical model proposed for antipyrine. The reason for the different behaviour of diazepam, dipyrone, and ampyrone in contrast to antipyrine could be due to their particular molecular structure, their insolubility in dichloromethane (which makes their study difficult), or dislocation factors of the charge over the nitrogens (the reactive element of the amine); as well, these amines have nitrogen more suitable to give both a weak and overlapped reaction. Thus in the absence of these factors, it is only the pK which is responsible for the greater or lesser extension of the amine–BTB reaction in DCM. For this reason atropine, atropamine, strychnine, tropine, quinine, belladonna, imipramine, etc., with pK_a's between 8 and 11, give a quantitative reaction with BTB in chloroform (8, 9), in contrast with antipyrine (pK_a = 1.5) which gives a weak reaction.

Conclusions

Antipyrine reacts with bromothymol blue in dichloromethane in an acid–base process forming a 1:1 ion pair (antipyrine–bromothymol blue). Conductivity and spectral data clearly indicate that the associated species with visible absorption are ion pairs. Formation constants for ion pair association are low, suggesting that the associated species are more complex in nature than the simple salts. The formation process is spontaneous, exothermic, and gives rise to a structured complex. Some of these conclusions could be extended to strongly associated species involving amines and bromothymol blue, for which the present study can not be repeated owing to the large formation constants for the reactions.

Can. J. Chem. Downloaded from www.nrcresearchpress.com by 84.22.46.98 on 09/08/12
For personal use only.

1. G. SCHILL and M. MARSCH. Sven. Farm. Tidskr. **67**, 385 (1963).
2. G. SCHILL. Acta Pharm. Suec. **2**, 13 (1965).
3. V. D. GUPTA and D. E. CADWALLADER. J. Pharm. Sci. **57**, 112 (1968).
4. F. MATSUI and W. N. FRENCH. J. Pharm. Sci. **60**, 287 (1971).
5. L. G. CHATTEN and K. O. OKAMURA. J. Pharm. Sci. **62**, 1328 (1973).
6. A. HERNÁNDEZ, P. GUTIÉRREZ, and J. THOMAS. An. Real Acad. Farm. **51**, 79 (1985).
7. A. HERNÁNDEZ, P. GUTIÉRREZ, and J. THOMAS. Il Fármaco, **40**, 63 (1985).
8. V. D. GUPTA. J. Pharm. Sci. **60**, 1585 (1971).
9. A. HERNÁNDEZ, P. GUTIÉRREZ, and J. THOMAS. An. Real Acad. Farm. **49**, 483 (1983).
10. A. HERNÁNDEZ, P. GUTIÉRREZ, and J. THOMAS. Il Fármaco, **9**, 300 (1986).
11. H. A. BENESI and J. H. HILDEBRAND. J. Am. Chem. Soc. **70**, 2832 (1948).
12. H. A. BENESI and J. H. HILDEBRAND. J. Am. Chem. Soc. **71**, 2703 (1949).
13. D. R. ROSSEINSKY and H. KELAWI. J. Chem. Soc. A, 1207 (1969).
14. P. JOB. Ann. Chem. **9**, 113 (1928).
15. K. S. KLAUSEN and F. J. LANGMYHR. Anal. Chim. Acta, **28**, 335 (1963).
16. J. R. MASAGUER, A. SOUSA-ALONSO, J. SUEIRAS, and J. A. GARCÍA. An. Quím. **71**, 384 (1977).
17. N. J. ROSE and R. S. DRAGO. J. Am. Chem. Soc. **81**, 6138 (1959).
18. V. K. ROHATGI. An introduction to probability theory and mathematical statistics. Chap. 2, p. 100; (*b*) Chap. 12, p. 506.
19. W. E. WENTWORTH, W. HIRSCH, and E. CHEN. J. Phys. Chem. **71**, 218 (1967).

Can. J. Chem. Downloaded from www.nrcresearchpress.com by 84.22.46.98 on 09/08/12
For personal use only.

Model compounds for poly(oligomethylene glycol-4,4′-biphenyl dicarboxylates). An X-ray diffraction study

SUZANNE DEGUIRE, JOHANNE GAGNÉ, HERMANN DUGAS, AND FRANÇOIS BRISSE

Département de chimie, Université de Montréal, C.P. 6128, Succ. A, Montréal (Qué.), Canada H3C 3J7

Received March 4, 1987

SUZANNE DEGUIRE, JOHANNE GAGNÉ, HERMANN DUGAS, and FRANÇOIS BRISSE. Can. J. Chem. **65**, 2291 (1987).

To provide the necessary parameters required for the conformational analysis of poly(oligomethylene glycol-4,4′-biphenyl dicarboxylates), two model compounds related to the above polyesters have been synthesized and their structures established by X-ray diffraction. The crystal structures of ethylene glycol di-*para*-phenylbenzoate (2DPPB) and 1,4-butylene glycol di-*para*-phenylbenzoate (4DPPB) have been solved by direct methods. 2DPPB is monoclinic with a = 7.174(2) Å, b = 8.101(2) Å, c = 19.183(4) Å, β = 102.48(2)°, Z = 2, space group $P2_1/c$. 4DPPB is triclinic with a = 9.978(2) Å, b = 11.172(3) Å, c = 11.437(2) Å, α = 85.46(2)°, β = 79.40(2)°, γ = 71.03(2)°, Z = 2, space group $P\bar{1}$. The weighted least-squares refinements converged to R_w = 0.054 (2DPPB) and R_w = 0.057 (4DPPB). The values of ε, the tilt angle of the carboxylate group with respect to the phenylene ring, are 3.5° for 2DPPB and 1.5° and 1.4° for 4DPPB. A systematic study of this dihedral angle showed that the values of ε remain in the vicinity of 0°–10° and the value observed most frequently is 5°. The values of Φ, the dihedral angle between the two six-membered rings, are 36.2° in 2DPPB and 14.7° and 31.0° for 4DPPB. A systematic study with 71 biphenyl molecular fragments showed that distribution of Φ presents two maxima: one around 30°–40° and the other in the range of 0°–10°. The conformation of the methylenic sequence is all-*trans* for 2BPPB and gtttt for 4DPPB.

SUZANNE DEGUIRE, JOHANNE GAGNÉ, HERMANN DUGAS et FRANÇOIS BRISSE. Can. J. Chem. **65**, 2291 (1987).

Dans le but d'obtenir les paramètres requis pour l'analyse conformationnelle des poly(carboxylates d'oligométhylèneglycol-biphényles-4,4′), on a synthétisé deux composés modèles apparentés à ces polyesters et on a déterminé leur structure par diffraction des rayons X. On a fait appel aux méthodes directes pour déterminer les structures cristallines des di-*para*-phénylbenzoates d'éthylèneglycol (2DPPB) et de butylèneglycol (4DPPB). Le 2DPPB est monoclinique avec a = 7,174(2), b = 8,101(2) et c = 19,183(4) Å, β = 102,48(2)°, Z = 2, et groupe d'espace $P2_1/c$. Le 4DPPB est triclinique avec a = 9,978(2), b = 11,172(3) et c = 11,437(2) Å, α = 85,46(2)°, β = 79,40(2)° et γ = 71,03(2)°, Z = 2 et groupe d'espace $P\bar{1}$. Un affinement par le méthode des moindres carrés converge à R_w = 0,054 (2DPPB) et R_w = 0,057 (4DPPB). Les valeurs de ε, l'angle de torsion du groupement carboxylate par rapport au noyau phénylène, est de 3,5° pour le 2DPPB et de 1,5° et 1,4° pour le 4DPPB. Une étude systématique de cet angle dièdre démontre que les valeurs de ε se maintiennent entre 0° et 10° et que la valeur observée le plus fréquemment est 5°. Les valeurs de Φ, l'angle dièdre entre les deux cycles à six chaînons, sont de 36,2° dans le 2DPPB et de 14,7° et 31,0° dans le 4DPPB. Une étude systématique de 71 fragments moléculaires biphénylés montre que la distribution de Φ présente deux maxima : l'un autour de 30°–40° et l'autre entre 0° et 10°. La conformation de la séquence des méthylènes est complètement *trans* pour le 2DPPB et gtttt pour le 4DPPB.

[Traduit par la revue]

Can. J. Chem. Downloaded from www.nrcresearchpress.com by 213.166.140.6 on 09/07/12
For personal use only.

Introduction

The study of a new class of thermotropic polyesters, the poly(oligomethylene glycol biphenyl dicarboxylates) has recently been undertaken (1). These polyesters, which incorporate in their backbone a flexible aliphatic segment and a slightly more rigid biphenyl dicarboxylate group, melt to an ordered liquid. It is important to know the manner in which the macromolecules pack because it provides additional information regarding the identification and the structure of the liquid crystal phase. Since the crystal structures of the polyesters have not yet been established, we have chosen to tackle this problem by the model compound approach.

This approach, although it has its problems, has been quite successful in helping to solve the structure of the related polyester. The structure of poly(trimethylene terephthalate) or poly(3GT) was established using geometrical information obtained from the crystal structures of two related model compounds: trimethylene glycol dibenzoate and trimethylene glycol di-*para*-chlorobenzoate (2). It was not only the bond distances and angles but also the conformational angles of the model compounds that helped significantly in solving the parent polyester's structure. The torsion angles describing the conformation of the trimethylene sequence in the model compounds were found to be within 2° of those adopted for the most reasonable structure of poly(3GT). In the case of poly(1,4-*trans*-cyclohexanediyldimethylene succinate), the bond distances, bond angles, and torsion angles found in *trans*-1,4-cyclohexanedimethyl-3,3′-bis(methoxy carbonyl) dipropionate, the related model compound, allowed for the calculation of the fiber repeat of the above polyester to within 0.06 Å of its experimental fiber repeat (3, 4).

Two model compounds, ethylene glycol di-*para*-phenylben-

TABLE 1. Crystal data of interest

Parameter	Compound	
	2DPPB	4DPPB
Molecular formula	$C_{28}H_{22}O_4$	$C_{30}H_{26}O_4$
Molecular weight	422.49	450.54
F(000)	444	476
Melting point (K)	458	426
Unit cell	Monoclinic	Triclinic
a (Å)	7.174(2)	9.978(2)
b (Å)	8.101(2)	11.172(3)
c (Å)	19.183(4)	11.437(2)
α (deg)	90	85.46(2)
β (deg)	102.48(2)	79.40(2)
γ (deg)	90	71.03(2)
V (Å^3)	1088.5	1184.9
d_o (g cm^{-3})	1.31	1.28
d_c (g cm^{-3})	1.289	1.262
Z	2	2
Space group	$P2_1/c$	$P\bar{1}$
μ (Kα) (cm^{-1})	6.51	6.27
T (K)	293	293
Crystal size (mm)	0.14 × 0.30 × 0.40	0.20 × 0.30 × 0.50

TABLE 2. Summary of data collection and refinement

Parameters	Compound 2DPPB	Compound 4DPPB
Scan range (deg)	$(1.0 + 0.14 \tan \theta)$	$(1.0 + 0.14 \tan \theta)$
Scan rate (deg min^{-1})	1.5–10.0	1.0–10.0
$2\theta_{max}$ (deg)	150.0	140.0
h, k, l ranges	$0 \leq h \leq 8$	$0 \leq k \leq 12$
	$0 \leq k \leq 10$	$-13 \leq k \leq 13$
	$-24 \leq l \leq 24$	$-13 \leq l \leq 13$
Max. fluctuations of standard reflections (%)	1.0	1.1
Number of reflections measured	2241	4488
Number of reflections observed	1413	3605
if $I \geq k\sigma(I)$, $k =$	1.96	1.96
$R = \Sigma\|\Delta F\|/\Sigma\|F_o\|$	0.047	0.040
$R_w = [\Sigma w \Delta F^2/\Sigma w F_o^2]^{1/2}$	0.054	0.057
$S = [\Sigma w \Delta F^2/(m - n)]^{1/2}$	1.70	2.56
$(\text{Displacement}/\sigma)_{max}$	0.05	0.15
$(\text{Displacement}/\sigma)_{average}$	0.01	0.04
Extreme fluctuations of residual electron density (e $Å^{-3}$)	−0.25, 0.17	−0.19, 0.15

zoate (2DPPB) and 1,4-butylene glycol di-*para*-phenylbenzoate (4DPPB), have been synthesized and their structures have been determined by X-ray diffraction to compare the equivalent fiber repeat of the model compounds to the experimental values in the parent polyesters. The parameters of interest in this study are (*i*) the value of ε, the tilt angle of the carboxylate group with respect to the phenylene ring; (*ii*) the value of Φ, the dihedral angle between the two six-membered rings; and (*iii*) τ, the conformation of the methylenic sequence.

Experimental

The model compounds were synthesized by reacting *para*-phenylbenzoyl chloride with either ethylene glycol or 1,4-butanediol in the presence of pyridine for 30 min at room temperature (5). After decantation and washing with water the light yellow powders were purified by recrystallization in ethanol. In another slow crystallization in CCl_4 (2DPPB) or in $CHCl_3$ (4DPPB), clear prismatic crystals suitable for X-ray diffraction were obtained. The densities were measured by flotation in $ZnCl_2$ solutions. The unit cell dimensions and the crystal orientations were obtained by accurate centering of 25 reflections on the Nonius CAD-4 automatic diffractometer. The unit cell dimensions are listed with other crystal data of interest in Table 1. The integrated intensities were measured by the $\omega/2\theta$ technique using graphite monochromatized CuKᾱ radiation. The orientation of the crystal was verified after every 100 measurements. The intensities of 3 reference reflections were monitored every hour to assess the stability of the system.

Structure factors were obtained after scaling of the intensity data, and Lorentz and polarization corrections were applied.[1] No absorption correction was judged necessary due to the small value of the absorption coefficients. The details of the data collection are summarized in Table 2. The density of 2DPPB implies that there is only half a molecule per asymmetric unit. Thus 2DPPB possesses a crystallographic center of symmetry. The structure of 2DPPB was solved by direct methods (MULTAN 80) with some difficulty and only when the non-centrosymmetric space group $P2_1$ was assumed. Even then only the phenylbenzoate fragments could be recognized. The complete molecule was eventually revealed by the use of the DFOUR option. After a few cycles of full-matrix least-squares refinement, the correlation matrix indicated strong correlations between the coordinates of chemically equivalent atoms of 2DPPB. The refinement progressed smoothly in the centrosymmetric $P2_1/c$ space group. The various steps of the refinement, anisotropic for O and C, isotropic for H atoms, are given in Table 2. In the case of 4DPPB there is one molecule per asymmetric unit if the space group is $P\bar{1}$. Here again the symmetry had to be lowered to $P1$. Two nearly centrosymmetrically related molecules of 4DPPB were found. The coordinates of corresponding atoms turned out to be strongly correlated. Using the coordinates of one molecule in the $P\bar{1}$ space group, the refinement proceeded normally. In both cases the H atoms were found in difference Fourier syntheses. The weighted least-squares refinements of the atomic coordinates, minimizing $\Sigma w(|F_o| - |F_c|)^2$, were conducted with anisotropic temperature factors for O and C and isotropically for H atoms. The weights were derived from the counting statistics of the intensities. The details of the least-squares refinements are given in Table 2 for both compounds. The scattering curves for non-hydrogen atoms were taken from ref. 10 and those for H atoms from ref. 11. The tables of observed and calculated structure factors are part of the Supplementary Material.[2]

Results and discussion

The positional and equivalent thermal parameters and their standard deviations are presented in Tables 3*a* and *b*. The atomic numbering is shown in Fig. 1 and the molecular structures are presented as stereopairs in Fig. 2. The final bond distances and angles of the *para*-phenyl benzoate groups in 2DPPB and 4DPPB are compared in Table 4, while the geometries and conformations in the ethylene glycol and 1,4-butylene glycol segments are compared in Table 5 to those in other related compounds.

[1]The programs used here are modified versions of NRC-2, data reduction; NRC-10, bond distance and angles; NRC-22, mean planes; FORDAP, Fourier and Patterson maps (A. Zalkin); MULTAN, multisolution program; NUCLS, least-squares refinement; and ORTEP, stereodrawings (6–9).

[2]Structure factor tables, hydrogen atom coordinates, anisotropic temperature factor tables, and details of the least-squares planes calculations have been deposited. Copies may be purchased from the Depository of Unpublished Data, CISTI, National Research Council of Canada, Ottawa, Ont., Canada K1A 0S2.

Can. J. Chem. Downloaded from www.nrcresearchpress.com by 213.166.140.6 on 09/07/12
For personal use only.

TABLE 3. (*a*) Fractional atomic coordinates for 2DPPB ($\times 10^4$ for O and C) and U_{eq} (Å^2, $\times 10^4$)

Atom	*x*	*y*	*z*	U_{eq}^*
O(1)	8322(2)	2983(2)	5133(1)	798
O(2)	6964(2)	664(2)	4633(1)	614
C(1)	9472(3)	1745(2)	4176(1)	512
C(2)	9247(3)	476(2)	3680(1)	586
C(3)	10351(3)	437(2)	3168(1)	582
C(4)	11707(3)	1647(2)	3144(1)	514
C(5)	11954(3)	2892(2)	3658(1)	582
C(6)	10845(3)	2948(2)	4166(1)	593
C(7)	8238(3)	1889(2)	4704(1)	559
C(8)	5654(3)	716(2)	5108(1)	588
C(11)	12831(3)	1639(2)	2576(1)	547
C(12)	11997(3)	1129(3)	1889(1)	681
C(13)	13055(4)	1112(3)	1359(1)	818
C(14)	14912(4)	1605(3)	1506(1)	834
C(15)	15746(3)	2134(3)	2183(1)	847
C(16)	14716(3)	2158(3)	2716(1)	704

$$^*U_{eq} = \frac{1}{3}\sum_i \sum_j U_{ij} a_i^* a_j^* a_i \cdot a_j$$

(*b*) Fractional atomic coordinates for 4DPPB ($\times 10^4$ for O and C) and U_{eq} (Å^2, $\times 10^4$)

Atom	*x*	*y*	*z*	U_{eq}
O(1)	1772(2)	6559(1)	−59(1)	796
O(2)	2114(1)	7603(1)	1391(1)	550
O(11)	8035(1)	2896(1)	4104(1)	634
O(12)	5707(1)	3177(1)	4153(1)	678
C(1)	1801(2)	8679(2)	−429(1)	411
C(2)	1972(2)	9730(2)	−4(1)	474
C(3)	1915(2)	10795(2)	−713(2)	479
C(4)	1681(2)	10856(1)	−1885(1)	385
C(5)	1510(2)	9785(2)	−2297(1)	487
C(6)	1561(2)	8728(2)	−1586(2)	506
C(7)	1887(2)	7500(2)	293(2)	494
C(8)	2305(2)	6498(2)	2185(2)	556
C(9)	3867(2)	5865(2)	2220(2)	545
C(11)	6927(2)	1555(2)	5359(1)	446
C(12)	5700(2)	1223(2)	5748(2)	621
C(13)	5710(2)	233(2)	6553(2)	627
C(14)	6943(2)	−453(2)	7008(1)	440
C(15)	8174(2)	−117(2)	6602(2)	481
C(16)	8163(2)	877(2)	5798(2)	471
C(17)	6974(2)	2603(2)	4484(2)	504
C(18)	5626(2)	4225(2)	3285(2)	683
C(19)	4091(2)	4772(2)	3137(2)	572
C(21)	1619(2)	12005(2)	−2650(1)	407
C(22)	1460(2)	13160(2)	−2174(2)	538
C(23)	1400(2)	14230(2)	−2888(2)	605
C(24)	1464(2)	14184(2)	−4092(2)	624
C(25)	1626(3)	13062(2)	−4577(2)	729
C(26)	1714(2)	11978(2)	−3875(2)	592
C(31)	6947(2)	−1501(2)	7894(1)	465
C(32)	5722(2)	−1464(2)	8711(2)	637
C(33)	5709(2)	−2420(2)	9552(2)	693
C(34)	6919(2)	−3438(2)	9599(2)	598
C(35)	8155(2)	−3489(2)	8812(2)	567
C(36)	8175(2)	−2533(2)	7967(2)	508

$$^*U_{eq} = \frac{1}{3}\sum_i \sum_j U_{ij} a_i^* a_j^* a_i \cdot a_j$$

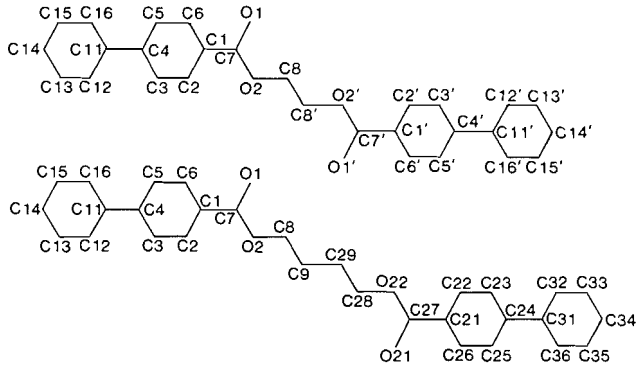

FIG. 1. Atomic numbering adopted for 2DPPB and 4DPPB.

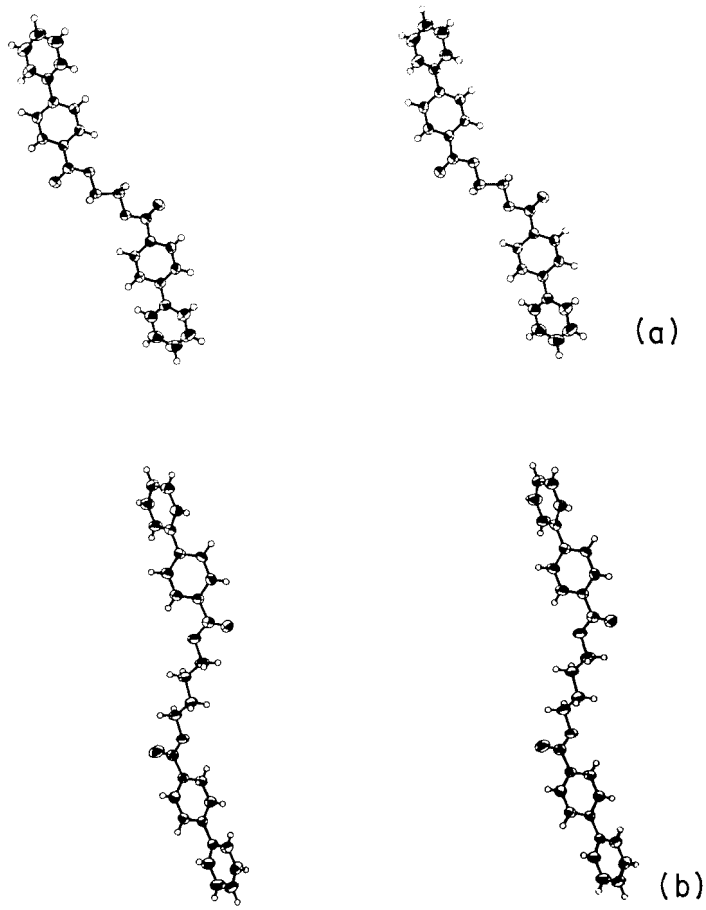

FIG. 2. Stereopairs showing the molecular conformation of (*a*) 2DPPB and (*b*) 4DPPB.

The para*-phenylbenzoate group*

The least-squares plane calculations for the aromatic rings and the carboxylic groups reveal that the atoms in each of these groups are coplanar.

The carboxylic groups have bond lengths in excellent agreement with the average geometry computed from the distances and angles of several dibenzoates and terephthalates. The average values of the C—O and C=O bonds are 1.334(3) and 1.204(3) Å while the O—C=O, C—C=O, and C—C—O bond angles have averages of 123.0(3)°, 124.6(2)°, and 112.4(2)° respectively (12). The carboxylic planes of atoms are only slightly tilted from the aromatic plane. The tilt angle, ε, has values of 3.5° for the 2DPPB and 1.5° and 1.4° in the case of

Can. J. Chem. Downloaded from www.nrcresearchpress.com by 213.166.140.6 on 09/07/12
For personal use only.

TABLE 4. Comparison of bond distances (Å), bond angles (deg), and torsion angles (deg) in the di-*para*-phenylbenzoate region of 2DPPB and 4DPPB

	2DPPB		4DPPB			
Distances (Å)	$x = 0$	$x = 1$	$x = 0$	$x = 1$	$x = 2$	$x = 3$
C(x1)—C(x2)	1.386(3)	1.387(3)	1.377(2)	1.390(2)	1.380(3)	1.386(3)
C(x2)—C(x3)	1.389(3)	1.394(3)	1.377(2)	1.384(3)	1.381(3)	1.381(3)
C(x3)—C(x4)	1.389(3)	1.361(4)	1.395(2)	1.371(3)	1.390(3)	1.369(3)
C(x4)—C(x5)	1.395(3)	1.376(4)	1.391(2)	1.360(3)	1.388(3)	1.374(3)
C(x5)—C(x6)	1.386(3)	1.385(4)	1.372(3)	1.386(3)	1.383(3)	1.385(3)
C(x6)—C(x1)	1.389(3)	1.386(3)	1.381(3)	1.389(2)	1.381(3)	1.393(3)
C($x + 1$, 1)—C(x4)	1.489(3)		1.486(2)		1.486(2)	
C(x7)—C(x1)	1.487(3)		1.485(2)		1.486(2)	
C(x7)—O(x1)	1.202(2)		1.201(2)		1.204(2)	
C(x7)—O(x2)	1.336(2)		1.336(2)		1.328(2)	
Angles (deg)						
C(x1)—C(x2)—C(x3)	120.2(2)	120.3(2)	121.0(2)	121.5(2)	120.8(2)	121.5(2)
C(x2)—C(x3)—C(x4)	121.2(2)	120.6(2)	121.6(6)	120.5(2)	121.5(2)	120.5(2)
C(x3)—C(x4)—C(x5)	118.0(2)	119.6(2)	116.4(2)	118.9(2)	117.2(2)	119.3(2)
C(x4)—C(x5)—C(x6)	121.1(2)	120.6(2)	121.7(2)	121.2(2)	121.3(2)	120.5(2)
C(x5)—C(x6)—C(x1)	120.2(2)	120.4(2)	121.2(2)	121.1(2)	120.8(2)	120.9(2)
C(x6)—C(x1)—C(x2)	119.3(2)	118.5(2)	118.0(2)	116.8(2)	118.4(2)	117.3(2)
C(x6)—C(x1)—C(x7)	118.9(2)		119.1(2)		118.8(2)	
C(x2)—C(x1)—C(x7)	121.8(2)		122.9(2)		122.8(2)	
C(x1)—C(x7)—O(x1)	125.1(2)		124.6(2)		124.4(2)	
C(x1)—C(x7)—O(x2)	111.5(2)		112.0(2)		112.1(2)	
O(x1)—C(x7)—O(x2)	123.3(2)		123.5(2)		123.5(2)	
C(x7)—O(x2)—C(x8)	116.0(2)		118.4(1)		117.0(2)	
C($x + 1$, 2)—C($x + 1$, 1)—C(x4)	120.4(2)		121.6(2)		120.6(2)	
C($x + 1$, 6)—C($x + 1$, 1)—C(x4)	121.1(2)		121.6(2)		122.1(2)	
C($x + 1$, 1)—C(x4)—C(x5)	121.0(2)		121.7(2)		121.5(2)	
C($x + 1$, 1)—C(x4)—C(x3)	121.0(2)		121.9(2)		121.3(2)	

	2DPPB	4DPPB	
Torsion angles (deg)	$x = 0$	$x = 0$	$x = 2$
C($x + 1$, 2)—C($x + 1$, 1)—C(x4)—C(x3)	35.7(3)	−15.0(3)	−31.8(3)
C($x + 1$, 6)—C($x + 1$, 1)—C(x4)—C(x3)	−145.2(2)	165.2(2)	150.2(2)
C($x + 1$, 2)—C($x + 1$, 1)—C(x4)—C(x5)	−142.8(2)	165.1(2)	148.1(2)
C($x + 1$, 6)—C($x + 1$, 1)—C(x4)—C(x5)	36.3(3)	−14.8(3)	−29.9(3)
O(x1)—C(x7)—C(x1)—C(x2)	−177.7(2)	−178.4(2)	−178.1(2)
O(x1)—C(x7)—C(x1)—C(x6)	0.2(3)	0.6(3)	1.5(3)
O(x2)—C(x7)—C(x1)—C(x2)	0.6(3)	1.4(2)	1.2(3)
O(x2)—C(x7)—C(x1)—C(x6)	178.4(2)	−179.6(2)	−179.3(2)
C(x1)—C(x7)—C(x2)—C(x8)	−178.2(2)	−176.6(1)	−179.7(2)

4DPPB. The distribution of the values taken by the dihedral angle, ε, in 221 molecular fragments found in the Cambridge Data File, is represented in Fig. 3*a*. The dihedral angle values remain in the vicinity of 0°–10°, and the value observed most frequently is 5°.

In 2DPPB, the dihedral angle Φ between the two six-membered rings has a value of 36.2°, while in 4DPPB the two values are 14.7° and 31.0°.

It is very interesting to note that if the two symmetrically related torsion angles ϕ_1 and ϕ_5 ($= \phi_1'$) have the values of ±177.1(2)° in 2DPPB, they take the values of $\phi_1 = 100.3(2)°$ and $\phi_5 = -175.5(2)°$ in 4DPPB. In all the *para*-substituted benzoates studied, ϕ and the chemically equivalent ϕ_5 were always nearly 180°. However, this observation should be combined with the fact that the two rings in the diphenyl groups are at $\Phi = \pm 36°$ from one another in 2DPPB, while they take different tilt values, i.e., 15° and 31° in 4DPPB. These two effects (differences in ϕ_1 and differences in Φ) are attributed to packing interaction.

The Cambridge Data File revealed the existence of 71 biphenyl molecular fragments. The distribution of the dihedral angle, Φ, between the two phenylene rings is shown on Fig. 3*b*. The distribution of Φ, in the range of 0°–90°, presents two maxima: one around 30°–40° and the other in the range of 0°–10°. The larger values of Φ, in the interval of 30°–40°, are observed when the hydrogen atom on the *ortho* carbon is replaced by a larger atom such as chlorine (13).

The aromatic C—C distances observed average 1.385 Å for 2DPPB and 1.382 Å for 4DPPB. They are comparable to the mean bond length of 1.378 Å reported in ref. 14. The average

Can. J. Chem. Downloaded from www.nrcresearchpress.com by 213.166.140.6 on 09/07/12
For personal use only.

TABLE 5. Comparison of the methylenic region in (*a*) ethylene glycol and (*b*) 1,4-butylene glycol dibenzoates variously substituted in *para*

(*a*) Ethylene glycol di-*para*-X-benzoate

Parameter	X						
	H		CH_3†	OCH_3*		C_6H_5*	Cl†
O(2)—C(8)	1.442(3) Å	1.441(3) Å	1.446(2) Å	1.443(3) Å	1.439(3) Å	1.444(2) Å	1.452(2) Å
C(8)—C(8′)	1.499(3)		1.495(3)	1.471(3)	1.488(3)	1.493(3)	1.493(2)
O(2)—C(8)—C(8′)	104.7(2)°	105.2(2)°	106.6(2)°	105.1(2)°	104.6(2)°	104.9(2)°	107.3(2)°
ϕ_1 = C(7)—O(2)—C(8)—C(8′)	175.6(5)°		177.1(2)°	−163.3(2)°	174.7(2)°	177.1(2)°	−175.7(1)°
ϕ_2 = O(2)—C(8)—C(8′)—O(2′)	−172.8(5)		67.7(2)	180	180	180	74.5(1)
ϕ_3 = C(8)—C(8′)—O(2′)—C(7′)	+176.1(4)		ϕ_1	$-\phi_1$	$-\phi_1$	$-\phi_1$	ϕ_1
Conformation	ttt		tgt	ttt	ttt	ttt	tgt

*This compound has a crystallographic center of symmetry at the midpoint of the methylenic sequence.
†This compound has a crystallographic twofold axis of rotation at the midpoint of the methylenic sequence.

(*b*) 1,4-Butylene glycol di-*para*-X-benzoate

Parameter	X					
	H		NO_2*	Cl*	C_6H_5	
O(2)—C(8)	1.457(2) Å	1.451(2) Å	1.452(3) Å	1.455(5)	1.455(2)	1.465(2)
C(8)—C(9)	1.505(2)	1.511(2)	1.529(3)	1.499(6)	1.494(3)	1.489(3)
C(9)—C(9′)	1.529(2)		1.470(3)	1.523(5)	1.532(3)	
O(2)—C(8)—C(9′)	107.1(1)°	107.1(1)°	106.0(4)°	107.6(3)°	110.0(2)	106.7(2)
C(8)—C(9)—C(9′)	110.5(1)	112.3(2)	113.0(4)	110.3(3)	111.1(2)	111.8(2)
ϕ_1 = C(7)—O(2)—C(8)—C(9)	170.9(2)°		172.7(6)°	168.1(3)°	100.3(2)	
ϕ_2 = O(2)—C(8)—C(9)—C(9′)	59.6(2)		−65.4(8)	178.3(3)	174.7(2)	
ϕ_3 = C(8)—C(9)—C(9′)—C(8′)	−175.1(1)		180*	180*	−173.4(2)	
ϕ_4 = C(9)—C(9′)—C(8′)—O(2′)	−176.0(1)		$-\phi_1$	$-\phi_1$	−178.6(2)	
ϕ_5 = C(9′)—C(8′)—O(2′)—C(7′)	−171.5(1)		$-\phi_2$	$-\phi_2$	−175.5(2)	
Conformation	tgttt		tg^-tg^+t	ttttt	stttt	

*This compound has a crystallographic center of symmetry at the midpoint of the methylenic sequence.
†t = *trans* ≃ 180°, $g^{\pm}$ = *gauche*$^{\pm}$ ≃ ±60°, s = skew ≃ ±120°.

angle in each of the six-membered ring is 120°. However, the angles, α, at the junction of the two phenyl groups deviate the most from the mean value. If we retain (from the systematic study) only the structures refined to an *R*-value lower than 5% and exclude structures not containing hydrogen atoms in the *ortho* position, we see that a trend seems to appear between the values of the α angles and Φ, the dihedral angle between the two rings (see Fig. 4*a*). The closer the two phenylene rings are to being coplanar, the smaller these α angles will be, to minimize the steric repulsions between the pairs of *ortho* hydrogen atoms. Conversely, when Φ is large, the angle α tends to get larger again, to minimize the interactions of the *ortho* H atoms.

At the same time, the inter-ring bond distance, *d*, is influenced by the repulsions between the hydrogen atoms in the *ortho* position (see Fig. 4*b*). Combining our observations with other published data yields another apparent relationship between the C—C distance, *d*, and the dihedral angle between the two rings (Fig. 4). The smaller the dihedral angle, the larger is the C—C distance. This is so to minimize the hydrogen–hydrogen interactions.

The methylenic sequence

In our two models and other related compounds, the methylenic sequence is quite flexible. The observed torsion angles take values near 180° or ±60°. A torsional angle of 180° corresponds to a *trans* (t) conformation while values of ±60° correspond to *gauche*$^+$ (g^+) or *gauche*$^-$ (g^-). The CH_2—CH_2 bond length in 2DPPB is 1.493(3) Å and those adjacent to oxygen atoms in 4DPPB are 1.494(3) and 1.489(3) Å. These values are significantly shorter than the expected C(sp^3)—C(sp^3) distance of 1.541(3) Å (15). Note also that the angles O—C—C involving these CH_2—CH_2 bonds have values of 104.9(2)° for 2DPPB and 110.0(2)° and 106.7(2)° for 4DPPB. The two lower angles are also strikingly smaller than is usually accepted for a molecule with no apparent strain.

Packing of the molecules

The shortest nonbonded intermolecular C...O distance is 3.561(3) Å for 2DPPB and 3.338(2) Å for 4DPPB. The C...C distances are all larger than 3.55 Å. Therefore, the molecules are held in the crystal by van der Waals forces only. The packing of the molecules is shown by the stereopairs in Figs. 5*a* and *b*. In 2DPPB, the molecules are packed in a herringbone manner, while in 4DPPB the molecules place themselves parallel to each other.

Extension to the parent polyesters

The 2DPPB molecule has a nearly fully extended conformation so that the distance between the midpoints of the central

Can. J. Chem. Downloaded from www.nrcresearchpress.com by 213.166.140.6 on 09/07/12
For personal use only.

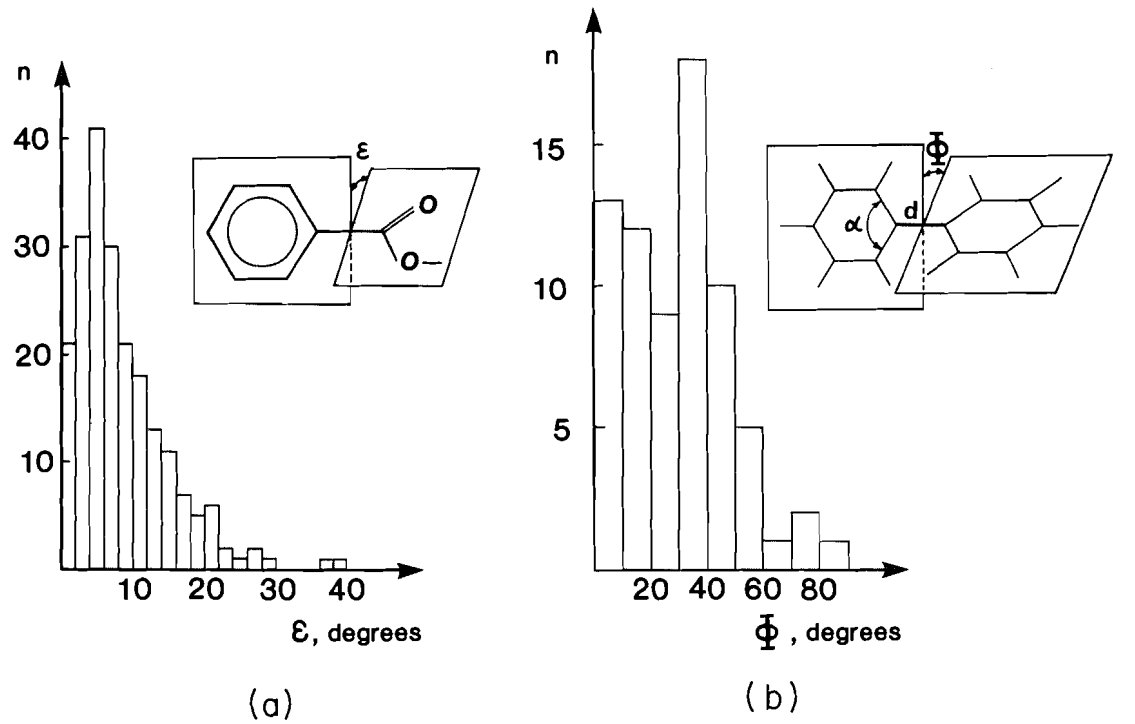

FIG. 3. (*a*) Histogram of the distribution of ε, the dihedral angle between the phenyl and carboxylate groups. (*b*) Histogram of the distribution of Φ, the dihedral angle between the two six-membered rings.

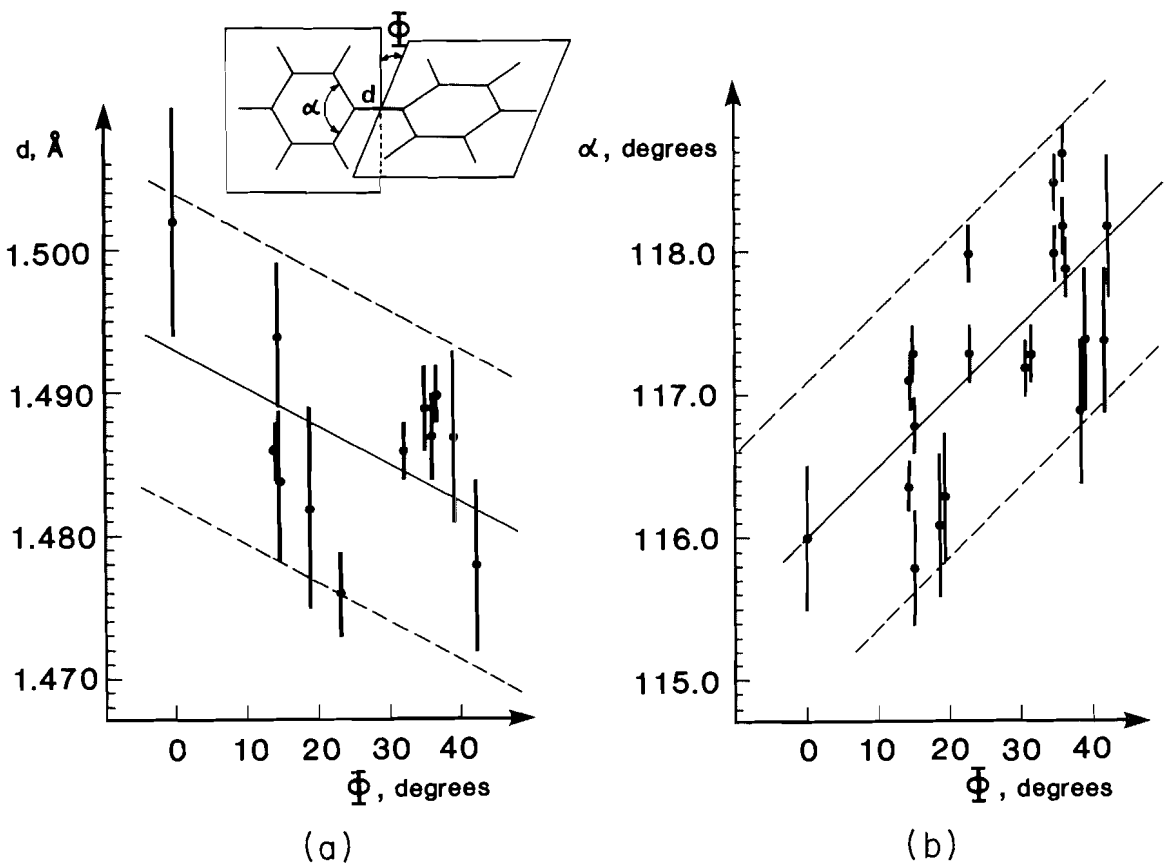

FIG. 4. Variation of *d* (*a*) and α (*b*) in biphenyl groups as a function of the dihedral angle between the two six-membered rings.

Can. J. Chem. Downloaded from www.nrcresearchpress.com by 213.166.140.6 on 09/07/12
For personal use only.

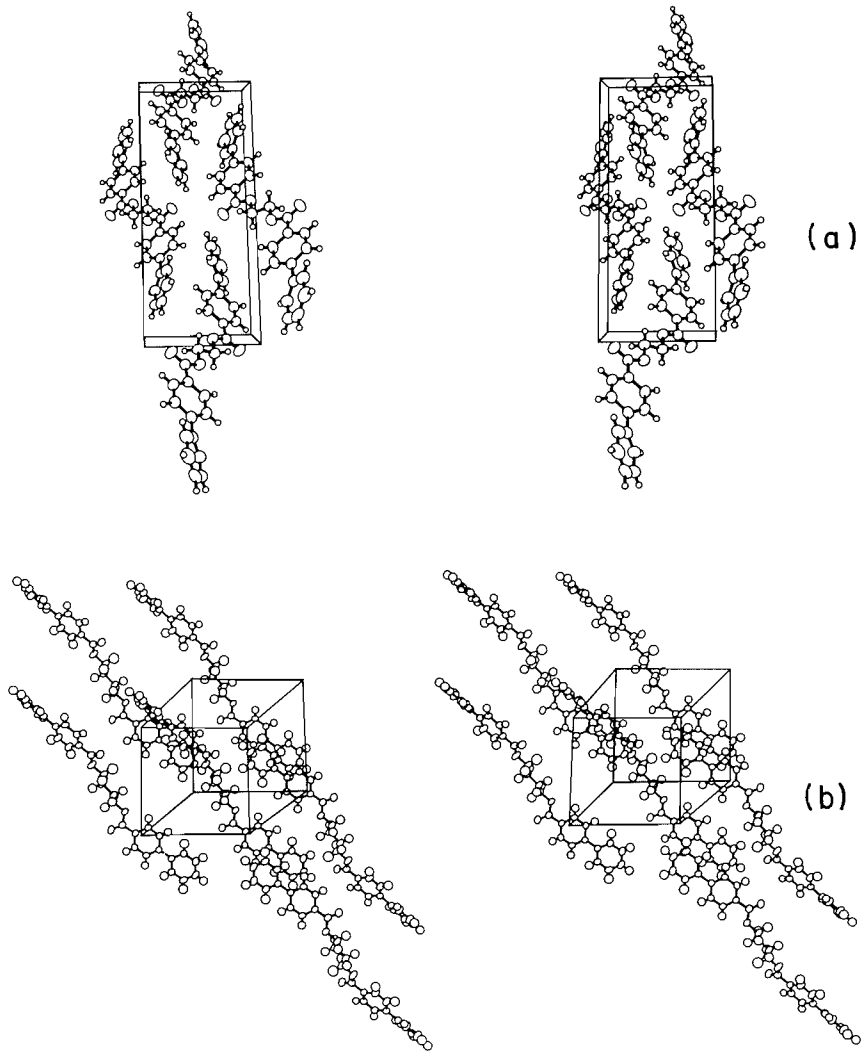

FIG. 5. Stereopairs showing the crystal packing of (*a*) 2DPPB and (*b*) 4DPPB.

C—C bond of the two biphenyl groups is 14.84 Å. This distance, which is defined as the equivalent fiber repeat of the polyester, would be 14.85 Å if all the torsion angles were exactly 180°.

In the case of 4DPPB the equivalent fiber repeat is only 15.78 Å. For a fully extended conformation this value would increase to 17.24 Å.

It is worth noting that, in both cases, the fiber repeat is not affected by the value taken by the dihedral angle Φ.

Poly(ethylene glycol-4,4′-biphenyldicarboxylate) and poly-(1,4-butylene-4,4′-diphenyldicarboxylate) have been synthesized by interfacial polycondensation according to the general method given by Eareckson (16). These syntheses proceeded normally but with yields of only 20%. That the polyesters have been thus produced was confirmed by infrared spectroscopy and X-ray powder diffraction. The two polymers are crystalline, but because the quantities produced were small, no film or fiber of the polyesters could be obtained to check on the value of their fiber repeats.

Conclusion

There are three types of information required to describe the structure of the poly(oligomethylene glycol-4,4′-biphenyl dicarboxylates).

In the biphenyl region, the Φ angle ranges from −60° to 60°, but is most likely to have a value of 30°. Furthermore, once this angle has been chosen, the inter-ring distance, *d*, as well as the α angles are defined.

The carboxylate tilt angle is restricted to around ±5°.

The methylenic sequence is flexible; torsion angles may take any value near 180°, 60°, or −60°. Care should be taken to select appropriate C—C bond length and O—C—C angle.

Acknowledgements

We thank the Natural Sciences and Engineering Research Council of Canada for its financial support. We also thank Mr. M. J. Olivier for collecting the X-ray data.

1. P. MEURISSE, C. NOËL, L. MONNERIE, and B. FAYOLLE. Br. Polym. J. **13**, 55 (1981).
2. S. POULIN-DANDURAND, S. PÉREZ, J.-F. REVOL, and F. BRISSE. Polymer, **20**, 419 (1979).
3. F. BRISSE and B. RÉMILLARD. Acta Crystallogr. Sect. B: Struct. Crystallogr. Cryst. Chem. **38**, 825 (1982).
4. F. BRISSE, B. RÉMILLARD, and H. CHANZY. Macromolecules, **17**, 1980 (1984).
5. H. C. HEIM and C. F. POE. J. Org. Chem. **9**, 299 (1944).
6. F. R. AHMED, S. R. HALL, M. E. PIPPY, and C. P. HUBER. J. Appl. Crystallogr. **6**, 309 (1973).

Can. J. Chem. Downloaded from www.nrcresearchpress.com by 213.166.140.6 on 09/07/12
For personal use only.

7. P. MAIN, S. J. FISKE, S. E. HULL, L. LESSINGER, G. GERMAIN, J. P. DECLERCQ, and M. M. WOOLFSON. MULTAN 80. A system of computer programs for the automatic solution of crystal structures from X-ray diffraction data. Universities of York, England, and Louvain, Belgium. 1980.
8. R. J. DOEDENS and J. A. IBERS. Inorg. Chem. **6**, 204 (1967).
9. C. K. JOHNSON. ORTEP, Report ORNL-3794. Oak Ridge National Laboratory, Oak Ridge, TN. 1965.
10. D. T. CROMER and J. B. MANN. Acta Crystallogr. Sect. A: Cryst. Phys. Diffr. Theor. Gen. Crystallogr. **24**, 321 (1968).
11. R. F. STEWART, E. R. DAVIDSON, and W. T. SIMPSON. J. Chem. Phys. **42**, 3175 (1965).
12. F. BRISSE and S. PÉREZ. Acta Crystallogr. Sect. B: Struct. Crystallogr. Cryst. Chem. **32**, 2110 (1976).
13. J. J. DYNES, F. L. BAUDAIS, and R. K. BOYD. Can. J. Chem. **63**, 1292 (1985).
14. F. BRISSE and J. SYGUSCH. Acta Crystallogr. Sect. B: Struct. Crystallogr. Cryst. Chem. **30**, 480 (1974).
15. Molecular structures and dimensions. International Union of Crystallography, Cambridge, England. 1972.
16. W. M. EARECKSON. J. Polym. Sci. **40**, 399 (1959).

Can. J. Chem. Downloaded from www.nrcresearchpress.com by 213.166.140.6 on 09/07/12
For personal use only.

Thermodynamic properties and structure of the water–ethanol silicone oil interface

DOMINIQUE SOHOUNHLOUE, LOUIS TENEBRE, MIREILLE PRIVAT, JEAN-MARC DOUILLARD, RENÉ BENNES, AND EMMANUEL TRONEL-PEYROZ

Unité associée 330, « Physicochimie des systèmes polyphasés », Route de Mende, B.P. 5051, 34033 Montpellier CEDEX, France

Received July 15, 1986[1]

DOMINIQUE SOHOUNHLOUE, LOUIS TENEBRE, MIREILLE PRIVAT, JEAN-MARC DOUILLARD, RENÉ BENNES, and EMMANUEL TRONET-PEYROZ. Can. J. Chem. **65**, 2299 (1987).

The interface between the water (1) – ethanol (2) system and silicone oil was studied over the whole composition range of the aqueous mixtures by means of adsorption and ellipticity measurements. The adsorbed layer was treated as a phase and, after derelativization of the relative surface excess, the adsorption isotherm (in term of molar fractions) as well as the activity coefficients of water and ethanol were calculated. From the above results and by analysing the ellipticity coefficient, we calculated the contribution to this latter due to the anisotropy of the adsorbed layer; the resulting "polynomial of anisotropy" was analyzed as a consequence of water and ethanol reorientations as the surface composition is changed.

DOMINIQUE SOHOUNHLOUE, LOUIS TENEBRE, MIREILLE PRIVAT, JEAN-MARC DOUILLARD, RENÉ BENNES et EMMANUEL TRONET-PEYROZ. Can. J. Chem. **65**, 2299 (1987).

L'interface entre le système eau–éthanol et l'huile de silicone a été étudiée dans tout le domaine de composition du mélange aqueux au moyen de mesures d'adsorption et de coefficient d'ellipticité. La couche adsorbée a été traitée comme une phase et, après dérelativisation de l'excès superficiel relatif, l'isotherme d'adsorption (exprimée en fractions molaires) ainsi que les coefficients d'activité de l'eau et de l'éthanol ont été calculés. À partir des résultats précédents et de l'analyse du coefficient d'ellipticité, nous avons calculé la contribution à celui-ci due à l'anisotropie de la couche adsorbée; le « polynôme de polarisabilité » qui en résulte a été interprété comme la conséquence des réorientations de l'eau et de l'éthanol quand la composition de la phase de surface change.

Can. J. Chem. Downloaded from www.nrcresearchpress.com by 213.166.140.6 on 09/07/12
For personal use only.

I. Introduction

The study of interfaces considered as autonomous phases in equilibrium with contiguous bulk phases from a thermodynamical point of view has been extensively developed in the past (1–7). Its aim is to calculate the activity coefficients of the constituents of these layers (1, 5, 6), so as to explain the interactions between the molecules as well as to propose a plausible structure of the surface phase (9).

This procedure tends to give more vigour to adsorption studies, as has been noted in the study of other types of surface phase (8).

This kind of study is also of industrial interest, where many applications depend on the state of the surface, e.g., adhesion, wetting, corrosion, nucleation.

In our previous work (9) we considered the liquid–vapor interface of such simple binary systems as water–ethanol and water–*tert*-butanol. We tried to link the results of adsorption measurements, i.e., the relative excess Γ_{21}, to the ellipticity coefficient measured at the Brewster angle. This last parameter contains a contribution due to the heterogeneity along the perpendicular direction to the surface (Drude's theory (10)), as well as an anisotropic term due to the polarizability of molecules (11) and a contribution coming from the thermal fluctuations of the surface location (12).

As we have shown previously (9), the "Drude part" of the ellipticity coefficient can be related to the surface excesses; in turn, the anisotropic contributions may be calculated if the thermal fluctuations of the surface area are neglected. The anisotropic part of the ellipticity coefficient contains information concerning the orientations of surface molecules and their change with the composition.

Thus, this work is concerned with two kinds of results: the first involves the composition of the surface phase, the activities of the constituents, and other related thermodynamic properties (excess free energy), and the second concerns the structural meaning, such as an indication of molecular orientation.

In the present work, we extend our previous treatment on the liquid–vapor interphase to the oil – aqueous solution interface. The oil is a silicone oil of type 604 V 50 from Rhône–Poulenc Industry. We expect that this oil will have a strong influence on the water structure.

II. Theoretical part

For the system studied, we will demonstrate in the paragraph entitled "chemicals" that water and ethanol do not dissolve into the oil used in this work, and conversely. Thus in the following theoretical part we consider the oil to be a wall.

1. Determination of the adsorption isotherm: x_2^σ vs. x_2^α

We call σ the surface phase and α the aqueous bulk phase. Water is denoted by the subscript 1 and ethanol by 2. The first aim is to determine the mole fraction of constituent 2 in the surface phase, i.e., x_2^σ; the adsorption isotherm will be the relation between the mole fraction in the surface x_2^σ and in the bulk x_2^α. The aqueous mixture is the binary water (1) – ethanol (2) system.

The surface mole fraction is obtained after the resolution of the set of relations:

$$[1a] \quad \Gamma_{21} = \Gamma_2 - \Gamma_1 \frac{x_2^\alpha}{x_1^\alpha}$$

$$[1b] \quad 1 = A_1^\sigma \Gamma_1 + A_2^\sigma \Gamma_2$$

where

$$\Gamma_{21} = \text{Gibbs surface excess} = -\left(\frac{\partial \gamma}{\partial \mu_2^\alpha}\right)_T$$

In fact, the oil is composed of several polymer oils; however, water and alcohol being unsoluble in this mixed oil (Sect. IIIA), the chemical potentials of every component of the oil are

[1]Revision received April 10, 1987.

Can. J. Chem. Downloaded from www.nrcresearchpress.com by 213.166.140.6 on 09/07/12
For personal use only.

constant as the composition of the water–ethanol mixture varies. So the terms in the Gibbs equation due to the components of the oil vanish:

$$\Sigma \Gamma_i^0 \, d\mu_i^0 = 0 \; (\mu_i^0 = C^t)$$

where

Γ_i ($i = 1, 2$) = total excess (4) in the absorbed layer

A_i^σ ($i = 1, 2$) = partial molar area of $i = \left(\frac{\partial A}{\partial ni}\right)_{TP\gamma n_{j\neq i}}$

A = area of the surface

γ = interfacial tension

So

$$[2] \quad x_2^\sigma = \Gamma_2/(\Gamma_2 + \Gamma_1)$$

Equation [1*b*] is a result of the molar area surface definition:

$$A^\sigma = \frac{1}{\Gamma_1 + \Gamma_2}$$

and also of its property of being a homogeneous function, of first degree, of the composition of the surface phase. This is expressed by the relation

$$[3a] \quad A^\sigma = x_1^\sigma A_1^\sigma + x_2^\sigma A_2^\sigma$$

where A_i^σ has the same meaning as in eq. [1*b*] and x_i^σ is defined by eq. [2].

There exists a similar property for the surface molar volume:

$$[3b] \quad v^\sigma = x_1^\sigma v_1^\sigma + x_2^\sigma v_2^\sigma$$

which is a copy of the ordinary property of the volumes to be a homogeneous function, of first degree, of the phase composition. The v_i^σ are the surface molar partial volumes for the i species.

Incidentally, the ratio between v^σ and A^σ gives the thickness of the surface phase (see below).

It is clear that, for solving the set of eqs. [1] or for calculating the interfacial thickness d, values of v_i^σ and A_i^σ are needed. These v_i^σ and A_i^σ values being a priori unknown, we assign them respectively the values of the molar volume, $v_i^{\sigma 0}$, and molar area, $A_i^{\sigma 0}$, for the pure components, in accord with a currently used hypothesis (1):

$$[4] \quad A_i^\sigma = A_i^{\sigma 0}; \; v_i^\sigma = v_i^{\sigma 0}$$

We suppose $A_i^{\sigma 0}$ and $v_i^{\sigma 0}$ to have the same value as these relative to the liquid vapor interface (9*b*).

The approximation $v_i^\sigma \simeq v_i^{\sigma 0}$ is based on the fact that within the bulk, even for mixtures showing strong volumic contractions (for example, water (1) – *tert*-butanol (2)), the volume versus the molar fraction x_2^α is practically linear from $v_1^{\alpha 0}$ to $v_2^{\alpha 0}$. We can imagine that the same behavior exists for the surface, and hence $v_i^\sigma \simeq v_i^\sigma$. In our opinion this simplification does not introduce an error of more than a few percent to the molar volume of the mixture. By analogy, the same assumption was made for the partial molar areas: $A_i^\sigma \simeq A_i^{\sigma 0}$. This kind of approximation is often made a priori (1, 3) in the literature since the volume and areas cannot be measured directly as in a bulk phase.

Now the mole fraction in the surface phase σ can be calculated for each corresponding bulk mole fraction.

2. Anisotropic part of the ellipticity coefficient

Once x_2^σ is known, the contribution of the heterogeneity along a normal direction with respect to the surface (due to a composition profile and thus to a dielectric constant profile) to the ellipticity coefficient can be calculated by means of Drude's theory, in the case, for instance, with the light incident from the oil phase (10):

$$[5] \quad \bar{\rho}_D = \frac{\pi}{\lambda} \frac{\sqrt{\varepsilon_H + \bar{\varepsilon}}}{\varepsilon_H - \bar{\varepsilon}} \left[\varepsilon_H + \bar{\varepsilon} - \frac{\varepsilon_H \bar{\varepsilon}}{\varepsilon^\sigma} - \varepsilon^\sigma \right] d$$

where ε_H = dielectric constant of the oil from which the light comes, $\bar{\varepsilon}$ = dielectric constant of water–ethanol mixture, ε^σ = mean dielectric constant of the surface layer, λ = wave length of the incident light, and d = thickness of the interfacial zone.

As is shown in ref. 9:

$$[6] \quad \varepsilon^\sigma = \frac{1}{d} \int_0^d \varepsilon(z) \, dz = 1 + \frac{4\pi N}{d} (\alpha_1 \Gamma_1 + \alpha_2 \Gamma_2)$$

$$= 1 + \frac{4\pi N}{v^\sigma} (\alpha_1 x_1^\sigma + \alpha_2 x_2^\sigma)$$

α_1, α_2 = polarizabilities of components 1 and 2.

Thus ε^σ can be calculated in terms of $v_i^{\sigma 0}$, $A_i^{\sigma 0}$, x_i^σ; the interfacial thickness d is defined as $d = v^\sigma/A^\sigma$.

Because the surface tension in our systems generally has a significant value (1–40 mN m^{-1}), we neglect the contribution due to thermically excited waves (14, 15). If the surface layer is anisotropic, i.e., if its dielectric constant in the direction parallel to the interfacial plane, ε_x, is different from the dielectric constant in a direction perpendicular to this same plane, ε_z, the ellipsometric coefficient is written as (11):

$$[7] \quad \bar{\rho} = \frac{\pi}{\lambda} \frac{\sqrt{\varepsilon_H + \bar{\varepsilon}}}{\varepsilon_H - \varepsilon} \left\{ \int_0^d \frac{[\bar{\varepsilon} - \varepsilon_z(z)][\varepsilon_z(z) - \varepsilon_H)]}{\varepsilon_z(z)} \, dz + \int_0^d [\varepsilon_z(z) - \varepsilon_x(z)] \, dz \right\}$$

The first term is the Drude term describing a heterogeneity perpendicular to the surface ($\bar{\rho}_D$); the second term corresponds to the anisotropic contribution of the layer ($\bar{\rho}_A$).

By writing:

$$\int_0^d [\varepsilon_z(z) - 1] \, dz = 4\pi N(\alpha_1^z \Gamma_1 + \alpha_2^z \Gamma_2)$$

and

$$\int_0^d [\varepsilon_x(z) - 1] \, dz = 4\pi N(\alpha_1^x \Gamma_1 + \alpha_2^x \Gamma_2)$$

where N is the Avogadro Number and $A^\sigma = 1/(\Gamma_1 + \Gamma_2)$, $\bar{\rho}_A$ is written as

$$[9] \quad \bar{\rho}_A = -\frac{4\pi^2}{\lambda} \frac{\sqrt{\varepsilon_H + \bar{\varepsilon}}}{\varepsilon_H - \bar{\varepsilon}} \frac{d}{v^\sigma} P(x_2^\sigma)$$

where $P(x_2^\sigma)$ is an anisotropic polynomial defined as

$$[10] \quad P(x_2^\sigma) = (\alpha_1^x - \alpha_1^z) x_1^\sigma + (\alpha_2^x - \alpha_2^z) x_2^\sigma$$

with α_i^x and α_i^z = polarizability along the parallel (x) and the perpendicular (z) directions with respect to the (horizontal) surface ($i = 1, 2$). $P(x_2^\sigma)$ will be treated as a homogeneous function of first degree in composition x_1^σ and x_2^σ. One can ob-

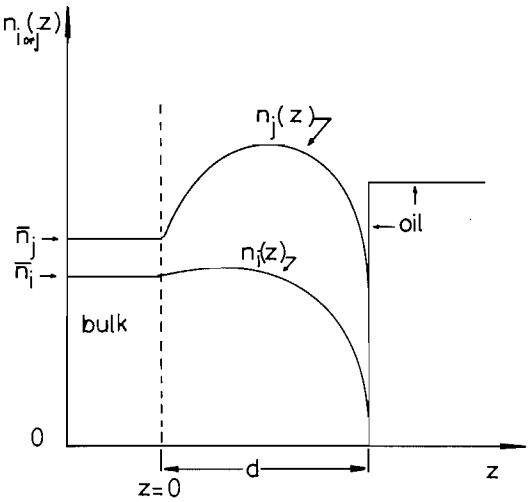

FIG. 1. An example of profiles in the interfacial region; the $z = 0$ and $z = d$ surfaces are chosen to take into account the totality of the molecules i and j in the interface. The oil is considered as a step, since water and ethanol are not soluble in this type of oil.

tain an idea of the structural changes occurring in the adsorbed layer, when the composition varies, by calculation of the $(\alpha_i^x - \alpha_i^{\bar{x}})$ terms.

Thus the total difference between the experimental ellipticity coefficient ($\bar{\rho}_E$) and the part calculated by Drude's law ($\bar{\rho}_D$) can be assigned to the anisotropic part of the ellipticity coefficient ($\bar{\rho}_A$):

$$[11] \quad \bar{\rho}_A = \bar{\rho}_E - \bar{\rho}_D$$

3. The choice of the dividing surfaces

As shown in the experimental part, the water and ethanol used in this study being insoluble in the oil, we consider this latter as a wall for water and ethanol (see Fig. 1). The interface considered goes from the dividing surface chosen as the origin ($z = 0$) (for which the bulk compositions are at negative values of z) to the oil surface. The oil profile is considered as a step at this point ($z = 0$). The excesses Γ_i and Γ_j are defined classically as being the surfaces under the curves $n_i(z)$ and $n_j(z)$, from $z = 0$ to $z = d$. This choice of surface permits us to take into account all the i and j molecules present in the interfacial zone (5).

At this stage, the thermodynamic and the ellipsometric reasoning (eqs. [5] and [9]) are in agreement in the sense that both apply to mean quantities (dielectric constant, molar volume, and areas of mixtures) or total quantities (Γ_i and Γ_j), the thickness of the layer being the distance characterizing the whole heterogeneous zone taken into account by the ellipsometry.

III. Experimental conditions and results

A. Chemicals

The water–ethanol/silicone oil (604 V 50) system at 25°C has been chosen because of its simplicity and the knowledge of thermodynamic values or properties: bulk activities for the water–ethanol binary system, insolubility of the ethanol in this oil, and known properties of the liquid–vapor interface (9) in terms of adsorption and the ellipticity coefficient.

Water–ethanol solutions from 0 to 100% were shaken with the oil and equilibrated for 3 days. Then the refractive indexes of the solutions and of the oil were measured with an Abbe refractometer; no change was detected for the concentration used, and so we considered the water and the ethanol as totally insoluble in the oil, and vice versa. In addition, the interfacial tension and the ellipticity coefficient do not change during the measurements (several hours), indicating no dissolution of water and ethanol in the oil.

Silicone oils are used extensively in industry (paper, textile, ...) often for emulsion conditioning. For such purposes, their stability is ensured by a tensioactive molecule coating the oil droplets to hinder their coalescence; the properties and structure of the adsorbed film that exists between the water solution and the oil are hence very important (16). Other interesting properties, for example, the viscoelasticity of the film, are not studied in this paper, but we shall see that a rudimentary property like the density of the phases may be important.

The oil used was a mixture of fully substituted polymethylsiloxanes ($R_3SiO(R_2SiO)_n$—$SiOR_3$ with R = methyl). Hence there are no reactive sites of the type SiOH on the molecules. The polydispersity ratio (equal to 2.15) was determinated by gpc (gel permeation chromatography), the mean distribution being 7605 and the number distribution 3530. The silicone oil was supplied by Rhône–Poulenc Silicone.

The water used was distilled on potassium permanganate in sulfuric acid medium. The ethanol was 100% from Carlo et Erba chemicals.

B. Techniques

All the measurements were made at a temperature of 25.0 ± 0.1°C.

1. The interfacial tension was measured by the determination of the maximum force acting on a horizontal straight platinum wire and a balance built in the laboratory, with a precision of $\pm 0.1\ \text{mN m}^{-1}$ (see results, Fig. 2).

Some care was necessary to make reproducible measurements. We started with the platinum wire immersed in the water–ethanol mixture. The oil was added to this phase (or conversely, depending on the relative densities) very gently to avoid the formation of an emulsion in the neighborhood of the interface. The platinum wire was located at the interface and the meniscus stretched toward the oil phase until it was broken. The measurement of the force was made at that very moment. Then, the measurements of the tension γ can be reproduced to a few tenths of mN m^{-1}. The contact angle on the platinum wire is nearly zero at the breaking of the film.

2. The activities of water and ethanol in the bulk aqueous solution, a_i^α at 25°C, were obtained from the literature (17).

From γ and a_2^α the relative surface excess is evaluated as:

$$[12] \quad \Gamma_{21} = -\left(\frac{\partial \gamma}{\partial \mu_2^\alpha}\right)_T$$

3. For the ellipsometric measurements a beam of light (laser He–Ne; 6328 Å), linearly polarized, was reflected on the surface studied. The reflected beam is elliptically polarized. The ratio between the minor and major axis of the ellipse at the Brewster incident angle is called $\bar{\rho}_E$, the ellipsometric coefficient (13). The apparatus was a homemade one (18).

The refractive indexes of the bulk phases, n, were measured with an Abbe refractometer; the necessary dielectric constants ε are known by the relation $\varepsilon = n^2$.

4. The contact angle θ was measured at the silica–solution–oil interfaces by the determination of the meniscus height h. The capillary ascension h of the interface along the silica plate is related to the contact angle through this equation (19):

$$[13] \quad \sin\theta = 1 - \frac{\Delta\rho g h^2}{2\gamma}$$

where $\Delta\rho$ = density difference between the two bulk phases, g = the acceleration of gravity, γ = interfacial tension measured independently (see above), and h = meniscus height.

The system studied shows an embarrassing peculiarity for each of the interfacial techniques: the binary aqueous phase has a decreasing density when increasing the ethanol composition; the density difference between the oil and water–ethanol bulk phases, $\Delta\rho$, becomes zero between 22 and 30% by weight of ethanol in water. The interfacial tension, ellipticity coefficient, and contact angle are of course

Can. J. Chem. Downloaded from www.nrcresearchpress.com by 213.166.140.6 on 09/07/12
For personal use only.

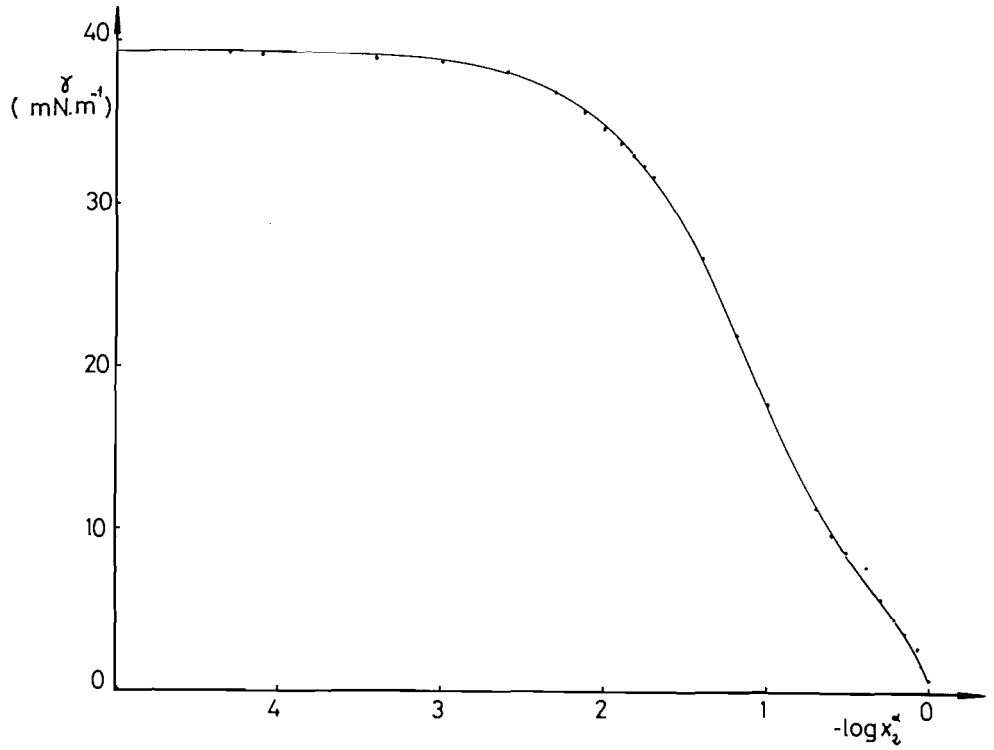

FIG. 2. Variation of the interfacial tension at the water + ethanol/silicone oil interface versus the logarithm of the ethanol molar fraction in the aqueous phase.

undeterminable in this domain with the methods used here, which are applicable only to flat and horizontal interfaces.

The experimental results are shown in Table 1.

IV. Discussion

A. Thermodynamics

The mole fraction of species 2 in the interfacial phase was calculated as indicated above (Fig. 3). The adsorption isotherm, x_2^σ vs. x_2^α, shows a classical shape similar to the corresponding one at the liquid–vapor interface.

The activities of water and ethanol (a_1^σ and a_2^σ respectively) are calculated from the equation giving the identity of the chemical potentials in the bulk and in the surface phase, namely $\mu_i^\alpha = \mu_i^\sigma$ or $RT \ln a_i^\alpha = A_i^{\sigma 0}(\gamma_i^0 - \gamma) + RT \ln a_i^\sigma$, with γ_i^0 the interfacial tension between water or ethanol and the silicone oil. The values of a_2^σ are in the neighborhood of the first bisector (Fig. 4). This indicates small deviations from ideal behavior. The shape of the curve is very close to that found at the liquid–vapor interface for the same aqueous system. The part of the curve corresponding to $x_2^\sigma < 0.275$ remains inferior to the first bisector, which corresponds to Raoult's Law. McGlashan (20) points out that such types of systems contain associated species like $(H_2O)_x(\text{ethanol})_y$.

From these activities, the activity coefficients can be calculated ($f_i^\sigma = a_i^\sigma / x_i^\sigma$), as well as the excess of Gibbs free energy in the surface (Fig. 5):

$$[14] \quad g^{E\sigma}/RT = x_1^\sigma \ln f_1^\sigma + x_2^\sigma \ln f_2^\sigma$$

$g^{E\sigma}/RT$ has a minimal value of -0.14; the deviations from ideality of the mixture are always negative.

B. Structural terms

The anisotropic polynomial, $P(x_2^\sigma)$ is shown in Fig. 6. Its peculiarity is to take into account all the anisotropic contributions in the adsorbed phase σ.

TABLE 1. Bulk activities, surface tension, relative excess, bulk dielectric constant, ellipticity coefficient, and contact angle for the water–ethanol/silicone oil interface at different bulk molar ratios

x_2^α	a_2^α	γ mN/m	Γ_{21} ($\times 10^{10}$)	$\bar{\varepsilon}$	$\bar{\rho}_E$ ($\times 10^4$)	θ (°)
0	0	39.50	0.0	1.774	1.50	
$4.89\ 10^{-5}$	$1.61\ 10^{-4}$	39.35	0.1	1.774	2.85	
$7.82\ 10^{-5}$	$2.58\ 10^{-4}$	39.15	0.12	1.774	3.39	
$3.91\ 10^{-4}$	$1.29\ 10^{-3}$	39.0	0.23	1.774	4.20	
10^{-3}	$3.3\ 10^{-3}$	38.8	0.43	1.774	4.20	
$2.5\ 10^{-3}$	$8.25\ 10^{-3}$	38.2	0.71	1.771	3.90	5
$5.0\ 10^{-3}$	$1.65\ 10^{-2}$	36.9	1.13	1.776	3.55	22
$7.5\ 10^{-3}$	$2.48\ 10^{-2}$	35.7	1.29	1.777	3.35	52
0.01	$3.3\ 10^{-2}$	34.7	1.45	1.7775	3.20	55
0.0125	0.0412	33.8	1.70	1.7787	3.00	57
0.015	0.495	33.1	1.70	1.7795	2.85	
0.0175	0.0577	32.4	2.10	1.781	2.68	
0.02	0.066	31.7	2.30	1.7825	2.50	
0.04	0.132	26.7	3.43	1.791	0.35	70
0.064	0.208	22.0	4.32	1.8005	−2.00	76
0.1	0.305	17.8	5.05	1.8135	−2.35	81
0.12	0.347	16.2*	6.02*	1.82		
0.15	0.397	14.2*	6.58*	1.828		
0.2	0.454	11.4	7.28	1.8375	−2.05	62
0.25	0.497	9.8	7.71	1.844	−2.05	47
0.3	0.525	8.7	7.71	1.8485	−2.05	
0.4	0.575	7.8	7.67	1.8545	−2.05	26
0.5	0.622	5.7	5.77	1.857	−2.00	
0.6	0.676	4.6	4.64	1.858	−1.65	12
0.7	0.741	3.6	4.12	1.8575	−1.30	
0.8	0.817	2.8	3.76	1.8555	5.00	
0.9	0.902	1.7	3.39	1.8515	3.20	
1.0	1.0	0.8	3.26	1.8463	5.55	5

*Interpolated values.
$\varepsilon_H = 1.9712$.

Can. J. Chem. Downloaded from www.nrcresearchpress.com by 213.166.140.6 on 09/07/12
For personal use only.

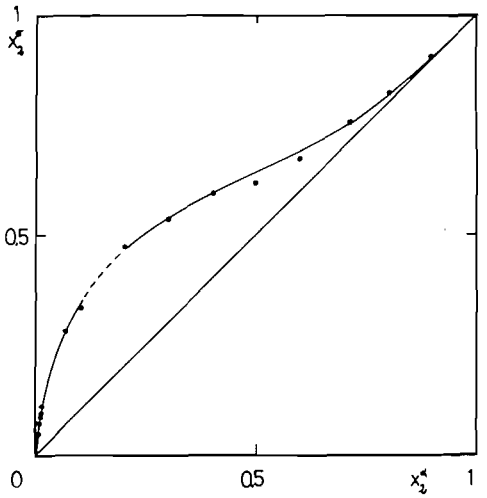

FIG. 3. Adsorption isotherm, 25°C. x_2^σ is the surface mole fraction and x_2^σ the bulk mole fraction.

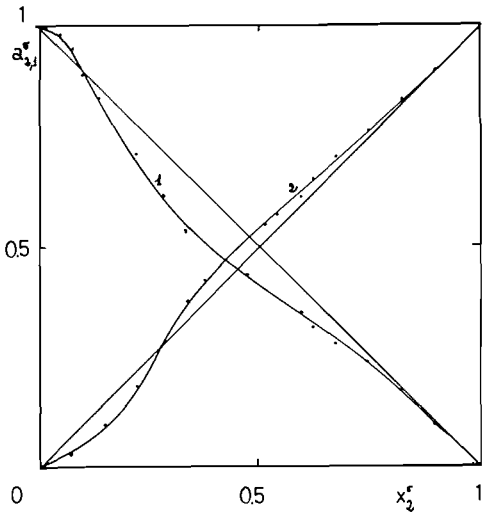

FIG. 4. Surface activities of the two constituents water (1) and ethanol (2) versus the mole fraction of the bulk.

The different changes in the slope of the curves $P(x_2^\sigma)$ vs. x_2^σ are linked to the different structures of the water and ethanol molecules in the surface mixture. $P(x_2^\sigma)$ can be interpreted as a homogeneous function of first degree of the mole fraction, as is done for a volume or an area. The behavior shown in Fig. 6 comes from the shape of the ellipticity coefficient curve, $\bar{\rho} = f(x_2^\sigma)$, and the isotherms; $\bar{\rho}$ vs. x_2^σ presents a maximum in the range of the dilute solutions of ethanol and a plateau in the range of the concentrated solutions with negative values of the ellipticity $\bar{\rho}_E$.

The curve of Fig. 6 shows the orientation of water and ethanol molecules to hardly vary with the composition.

First, for $x_2^\sigma = 0$, i.e., for pure water in contact with silicone oil, $P(x_2^\sigma = 0)$ has a negative value: $\alpha_1^x - \alpha_1^z = -0.12 \times 10^{-24}\,\text{cm}^3$; this value stays the same until $x_2^\sigma = 0.1$ where $\alpha_1^x - \alpha_1^z = -0.13 \times 10^{-24}\,\text{cm}^3$. This parameter reaches a value of $-0.05 \times 10^{-24}\,\text{cm}^3$ for $0.2 < x_2^\sigma < 0.3$ and slows down to $-0.17 \times 10^{-24}\,\text{cm}^3$ at $x_2^\sigma = 0.3$. For $x_2^\sigma > 0.55$ it reaches a constant value of $-0.116 \times 10^{-24}\,\text{cm}^3$.

The above description shows how much the water orientation is changing with the alcohol quantity present in the σ phase. The value $\alpha_1^x - \alpha_1^z = -0.06 \times 10^{-24}\,\text{cm}^3$ can be

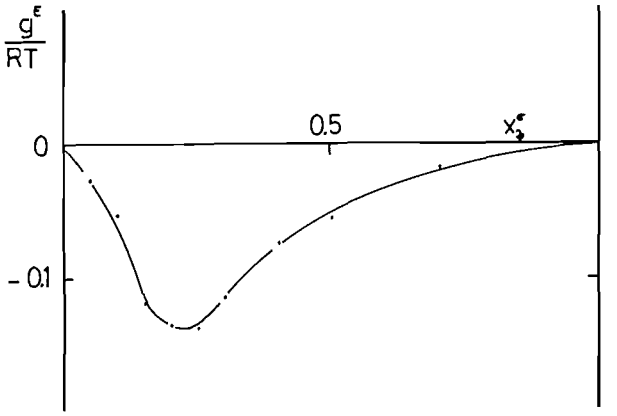

FIG. 5. Excess of the Gibbs free energy for the surface phase versus x_2^σ.

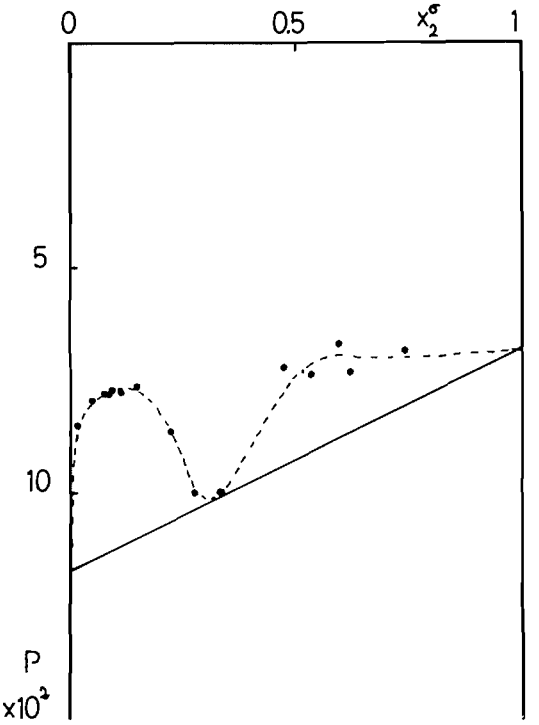

FIG. 6. Anisotropy polynomial P versus x_2^σ.

considered as characteristic of the "new water" invoked by one of us (21) in the case of aliphatic alcohols or acids adsorbed at the liquid–vapor interface.

This water, of a different structure than that of the pure water in contact with silicone oil, is certainly structured both by the alcohol polar group, —OH, and by the aliphatic chain, $-C_2H_5$.

A similar analysis concerning the ethanol can be made.

From the above discussion it seems the silicone oil influences the pure components in a marked way. The molecules of the interfacial mixture reorient themselves when the composition varies. The reorientations are different than those occurring at the liquid–vapor interface for the ethanol–water system. Thus the silicone oil induces a peculiar structure of the interface.

C. Correlation between these results and an interesting experimental fact

The structure change shown by the ellipticity results is closely correlated with the strong variation of surface tension and contact angle with the composition of the system.

Can. J. Chem. Downloaded from www.nrcresearchpress.com by 213.166.140.6 on 09/07/12
For personal use only.

It is a remarkable fact that the water–ethanol mixture has a density very near to the density of the silicone oil in the same region of composition. There, the contact angle on a silica plate is nearly 90°.

The meeting of such properties of both surface phase and volume densities is certainly the cause of a very surprising ability of the system to emulsify. By shaking the two liquid phases in a turbine at 1500 rpm we produce an "oil in water" emulsion with a stability of a few hours; the diameters of the oil droplets are about 12 μm. It seems that, in this case, it is not very difficult to build a relatively stable film of ethanol and water between the oil droplets of the emulsion. The relative emulsion stability is due to the difficulty of the oil droplets to meet and coalesce, because the gravitational forces do not drive them upward or downward.

V. Conclusion

The water–ethanol/silicone oil interface at 25°C shows several reorientations of water and ethanol molecules when the composition is changed. The adsorption isotherm and the activities of the two constituents of the aqueous phase are not noticeably different from those calculated at the liquid–vapor interface.

Finally, the composition domain, where the densities of the two liquid phases are practically the same, corresponds to a zone of possible emulsion, partial or total, which is surprising when taking into account the short alkyl chain of the ethanol.

Acknowledgements

This work was supported by Rhône–Poulenc Silicone in the framework of the "Groupement Scientifique Silicone" in association with the Centre national de la recherche scientifique.

1. J. C. Eriksson. Ark. Kemi, **25**, 331 (1965); **25**, 342 (1965); **26**, 49 (1966).
2. D. H. Everett. Trans. Faraday Soc. **60**, 1803 (1964); **61**, 2478 (1965).
3. J. E. B. Randles and B. Behr. J. Electroanal. Chem. **35**, 389 (1972).
4. R. Defay, I. Prigogine, A. Bellemans, and D. H. Everett. Surface tensions and adsorption. Longmans, London. 1966.
5. D. M. Mohilner, H. Nakadomari, and P. R. Mohilner. J. Phys. Chem. **81**, 244 (1977).
6. G. Schay. *In* Surface and colloid science. Vol. 2. *Edited by* Matijevic. Wiley Science. 1969. p. 155.
7. B. E. Conway and H. P. Dhar. Surf. Sci. **44**, 261 (1974).
8. N. R. Pallas and B. A. Pethica. Langmuir, **1**, 509 (1985).
9. (*a*) E. Tronel-Peyroz, R. Bennes, J. M. Douillard, and M. Privat. C.R. Acad. Sci. Paris. Sér. II, **299**, 1313 (1984); **299**, 1379 (1984); (*b*) J. M. Douillard. Thèse, Montpellier. 1985.
10. P. Drude. Ann. Phys. Chem. **36**, 532 (1889).
11. F. Abeles. J. Phys. Colloq. C5, 67 (1977).
12. L. Mandelstam. Ann. Phys. **41**, 609 (1913).
13. B. E. Conway. *In* Techniques of electrochemistry. Vol. 1. *Edited by* E. Yeager and A. J. Salkind. Wiley Interscience, New York. 1972. p. 389.
14. J. Meunier. *In* Colloids and interfaces. École d'Été 1983. *Edited by* A. M. Cazabat and M. Veyssie. Éditions de Physique, Les Ulis, France. 1984. p. 191.
15. M. A. Bouchiat, J. Meunier, and J. Brossel. C.R. Acad. Sci. Paris. Sér. B, **266**, 255 (1968).
16. P. Becher. Emulsions theory and practice. 2nd ed. Reinhold Publishing Corp. New York. 1965; J. T. Davies and E. K. Rideal. Interfacial phenomena. Academic Press, New York. 1961.
17. D. Dobson. J. Chem. Soc. **121**, 2866 (1925).
18. L. Tenebre. Thèse, Montpellier. 1971.
19. A. W. Neumann. Adv. Colloid Interface Sci. **4**, 105 (1974).
20. M. L. McGlashan. J. Chem. Educ. **10**, 516 (1963).
21. L. Tenebre. J. Phys. Colloq. C5, 123 (1977).

Can. J. Chem. Downloaded from www.nrcresearchpress.com by 213.166.140.6 on 09/07/12
For personal use only.

Synthesis and characterization of Hg(II) complexes of Me_3MCH_2SeMe, (M = Si, Ge). Crystal structures of $[HgX_2(Me_3SiCH_2SeMe)]_2$, X = Cl, Br, I

RAJ K. CHADHA, JOHN E. DRAKE, NEIL T. MCMANUS, AND ANIL MISLANKAR
Department of Chemistry and Biochemistry, University of Windsor, Windsor, Ont., Canada N9B 3P4

Received December 10, 1986

RAJ K. CHADHA, JOHN E. DRAKE, NEIL T. MCMANUS, and ANIL MISLANKAR. Can. J. Chem. **65**, 2305 (1987).

Complexes of the general formula $[HgX_2(Me_3MCH_2SeMe)]_2$, where M = Si, Ge; X = Cl, Br, I, have been prepared and characterized by ^1H nuclear magnetic resonance and Raman spectroscopy. Crystal structures of $[HgX_2(Me_3SiCH_2SeMe)]_2$, where X = Cl, Br, and I (**1**, **2**, and **3** respectively), show that they have centrosymmetric dinuclear structures. The crystals of **1** and **2** are monoclinic, while those of **3** are triclinic. For **1**: $P2_1/c$, a = 14.235(11), b = 6.551(6), c = 14.211(9) Å, β = 117.33(5)°, Z = 2, and R = 0.0560. For **2**: $P2_1/c$, a = 14.329(6), b = 6.695(2), c = 14.819(4) Å, β = 118.47(2)°, Z = 2, and R = 0.0540. For **3**: $P\bar{1}$, a = 7.651(2), b = 8.387(2), c = 12.321(4) Å, α = 90.07(2), β = 91.80(2), γ = 116.02(2)°, Z = 1, and R = 0.0565. All three complexes show the expected pseudotetrahedral geometry about mercury. The stereochemical differences arise in the arrangement of the bulky trimethylsilylmethyl groups, which in the HgI_2 adduct are rotated away from the centre of the molecule but which in the $HgCl_2$ and $HgBr_2$ adducts are turned towards the centre. These are the first dinuclear structures reported of $HgBr_2$ and HgI_2 adducts since it was demonstrated 46 years ago by Evans *et al.* that $[HgBr_2(AsBu_3)]_2$ was present in $[HgBr_2(AsBu_3)_2 \cdot HgBr_2]$.

RAJ K. CHADHA, JOHN E. DRAKE, NEIL T. MCMANUS et ANIL MISLANKAR. Can. J. Chem. **65**, 2305 (1987).

On a préparé les complexes de la formule générale $[HgX_2(Me_3MCH_2SeMe)]_2$ dans lesquels M = Si et Ge; X = Cl, Br et I; de plus, on les a caractérisés par la résonance magnétique nucléaire du ^1H et par spectroscopie Raman. Les structures cristallines des complexes $[HgX_2(Me_3SiCH_2SeMe)]_3$ dans lesquels X = Cl, Br et I (respectivement **1**, **2** et **3**) démontrent qu'ils possèdent des structures dinucléaires centrosymétriques. Les cristaux des composés **1** et **2** sont monocliniques alors que ceux du composé **3** sont tricliniques. Pour **1**: $P2_1/c$, a = 14,235(11), b = 6,551(6) et c = 14,211(9) Å, β = 117,33(5)°, Z = 2 et R = 0,0560. Pour **2**: $P2_1/c$, a = 14,329(6), b = 6,695(2) et c = 14,819(4) Å, β = 118,47(2)°, Z = 2 et R = 0,0540. Pour **3**: $P\bar{1}$, a = 7,651(2), b = 8,387(2) et c = 12,321(4) Å, α = 90,07(2), β = 91,80(2) et γ = 116.02(2)°, Z = 1 et R = 0,0565. Ces trois complexes présentent tous, autour du mercure, la géométrie pseudotétraédrique qui est attendue. Les différences stéréochimiques proviennent d'un arrangement des groupements triméthylsilylméthyles qui sont volumineux et qui, dans l'adduit avec le HgI_2, sa retrouent en s'éloignant du centre de la molécule; toutefois, dans les adduits avec le $HgCl_2$ et le $HgBr_2$, ils se retournent vers le centre de la molécule. Ces produits correspondent aux premières structures dinucléaires à être rapportées pour des adduits de $HgBr_2$ et de HgI_3 depuis qu'il a été démontré par Evans *et al.* il y a 46 ans que du $[HgBr_2(AsBu_3)]_2$ est présent dans le $[HgBr_2(AsBu_3)_2 \cdot HgBr_2]$.

[Traduit par la revue]

Introduction

There have been extensive studies of metal–selenoether complexes with respect to the study of pyramidal inversion barriers at Se (2–7). However, there are few examples of crystallographic studies of such complexes. Apart from our recent description of the structures of *trans*-$(Me_3SiCH_2SeMe)_2PdCl_2$ and *trans*-$(Me_3SiCH_2SeMe)_2PtCl_2$ (8), there are three other reports of selenoether–metal complexes; *trans*-$(Et_2Se)_2PdCl_2$ (9), $(MeSeCHCH_3)_2PdCl_2$ (10), and *trans*-$(O(CH_2)_4Se)_2PtBr_2$ (11).

There are a number of reports of structures of mercuric halide adducts with phosphorus donors (12–16) and there have been a few reports of structures of adducts with chalcogen donor molecules, largely of sulfur-containing ligands (17–20). There has been a single report of a mercuric halide adduct with a selenium donor, that of $[HgCl_2(Ph_3P{=}Se]$ (21), and several structural reports of sulfur-containing mercuric chloride adducts (22).

In this paper we report on the preparation and crystal structures of the compounds $[HgX_2(Me_3SiCH_2SeMe)]_2$ (X = Cl, Br, I) as well as the preparation of the germanium analogues $[HgX_2(Me_3GeCH_2SeMe)]_2$ (X = Cl, Br).

Experimental

Materials

Mercuric halide salts were obtained from Mallinkrodt Chemical Co. Me_3MCH_2SeMe (M = Si, Ge) were prepared by the literature method (23).

Preparation of $[HgX_2(Me_3SiMCH_2SeMe)]_2$, where M = Si, Ge; X = Cl, Br)

Me_3MCH_2SeMe (1 mmol) in ethanol (1 mL) was added to an ethanol (5 mL) solution of HgX_2 (1 mmol). The solution was stirred for 1 h before the product was separated by filtration. Recrystallization from refluxing ethanol gave the pure product in ca. 80% yield.

Crystals of $[HgX_2(Me_3SiCH_2SeMe)]_2$, where X = Cl and Br, suitable for X-ray diffraction were obtained by slow evaporation of a saturated solution of the compounds in 50% methanol/acetone.

Preparation $[HgI_2(Me_3SiCH_2SeMe)]_2$

$MeSiCH_2SeMe$ (0.1 g; 0.55 mmol) in ethanol (1 mL) was added to a stirred slurry of HgI_2 (0.21 g; 0.44 mmol) in ethanol (5 mL). The mixture was stirred until the orange slurry had turned to an almost colorless solution (ca. 0.5 h). The volume of solvent was reduced to ca. 3 mL under vacuum and then the solution was stored at 4°C for 20 h, yielding yellow crystals (0.23 g; 82%). Crystals suitable for X-ray studies were obtained by slow evaporation of an acetone solution. The crystals were hygroscopic and decomposed on prolonged exposure to the atmosphere.

Attempted isolation of $[HgI_2(Me_3GeCH_2SeMe)]_2$

A procedure analogous to that just described for the preparation of $[HgI_2(Me_3SiCH_2SeMe)]_2$ was carried out starting with Me_3GeCH_2SeMe. However, whenever attempts were made to remove the solvent under vacuum, the pale yellow solid reverted to the orange red of HgI_2 and a suitable sample for analysis was not obtained.

Instrumentation

The ^1H nmr spectra were recorded on a Varian EM360 spectrometer in acetone-d_6 and $CDCl_3$ using TMS as internal standard. Raman

Can. J. Chem. Downloaded from www.nrcresearchpress.com by 213.166.140.6 on 09/07/12
For personal use only.

TABLE 1. Summary of crystal data, intensity collection, and structural refinement for **1**, **2**, and **3**

Parameters	**1**	**2**	**3**
Cell constants	14.235(11), 6.551(6), 14.211(9) Å; 117.33(5)°	14.329(6), 6.695(2) 14.819(4) Å; 118.47(2)°	7.651(2), 8.387(2), 12.321(4) Å; 90.07(2), 91.80(2), 116.02(2)°
Cell volume (Å^3)	1177.2(15)	1249.7(6)	710.1(3)
Crystal system	Monoclinic	Monoclinic	Triclinic
Space group	$P2_1/c$	$P2_1/c$	$P\bar{1}$
Mol. wt.	452.3	541.4	1271
Z, F (000)	2 (dimers), 824	2 (dimers), 968	1 (dimer), 556
ρ_c (g cm^{-3})	2.55	2.87	2.97
Cryst. dimensions (mm)	0.19 × 0.23 × 0.42	0.15 × 0.19 × 0.31	0.20 × 0.40 × 0.45
Abs. coeff., μ (cm^{-1})	158.43	208.03	171.2
Min. abs. corr.	9.060	9.630	14.586
Max. abs. corr.	34.550	27.343	74.323
Radiation		MoKα, λ = 0.71069 Å	
Monochromator		Highly oriented graphite	
Temp. (°C)		20 ± 2	
2θ angle (°)		45	
Scan type		Coupled θ (crystal)/2θ (counter)	
Scan width		$K_{\alpha 1}$ −1° to $K_{\alpha 2}$ +1°	
Scan speed (° min^{-1})		Variable, 2.02–4.88	
Bkgd. time/scan time		0.5	
Total reflcns. measd.	2472(+h, +k, ±l)	2647(+h, +k, ±l)	2657(+h, ±k, ±l)
Unique data used	1091[$I > 3\sigma(I)$]	1265[$I > 3\sigma(I)$]	1561[$I > 3\sigma(I)$]
No. of parameters (NP)	92	92	92
$R = (\Sigma\|\|F_o\| - \|F_c\|\|/\Sigma\|F_o\|)$	0.0560	0.0540	0.0565
$R_w = [\Sigma\omega(\|F_o\| - \|F_c\|)^2/\Sigma\omega\|F_o\|^2]^{1/2}$	0.0580	0.0580	0.0601
$\Delta\rho_{max}$(e Å^{-3})	1.9(0.043, 0.307, 0.129)	1.2(−0.035, −0.005, −0.121)	2.25(0.325, −0.115, 0.309)
Shift error (max)	0.01	0.11	0.07

spectra were obtained of solid samples in glass capillaries on a Spex 1403 double monochromator using the 488-nm argon line for excitation.

Crystal structure determination

In each determination, a prismatic crystal sealed in a capillary tube was mounted along the largest dimension and the data were collected with a Syntex $P2_1$ diffractometer following the procedure described earlier (24). The intensities of three monitor reflections changed only by approximately ±2% during the entire period of data collection (69–72 h). The least-squares refinement of the setting angle of 15 high angle reflections ($15 < 2\theta < 30°$) yielded the cell constants given in Table 1. The systematic absences of $0k0$ and $h0l$ were noted for odd k and l in **1** and **2**, indicating the space group $P2_1/c$. For **3**, the space group $P\bar{1}$ was used and later assumed correct because of successful refinement. The data were corrected for Lorentz and polarization effects, and analytical absorption corrections were applied.

The structures of **1** was solved by using the conventional sharpened Patterson synthesis. Since **1** is isomorphous with **2**, the same set of atomic coordinates were used for **2**. The structure of **3** was solved by direct methods using the program SHELX.

The structure of **1** was solved by using the conventional sharpened minimizing the function $(|F_o| - |F_c|)^2$ with all non-hydrogen atoms being treated anisotropically. Hydrogen atoms were included at the idealized positions (C—H = 0.95 Å, HCH = 109.5°) with isotropic U's set at 0.01 Å^2 greater than that of the corresponding carbon atom. Convergence was achieved at R = 0.0560, 0.0540, and 0.0565 and $R_{\omega F}$ = 0.0580, 0.0580, 0.0601 for **1**, **2**, and **3** respectively. A weighting scheme of the form $\omega = [\Sigma\sigma^2(F) + \rho F^2]^{-1}$ was employed, with final ρ values of 0.00035, 0.00078, and 0.00040 in **1**, **2**, and **3** respectively. For **2** and **3**, a few low angle reflections were found to be affected by secondary extinctions. An empirical isotropic extinction parameter, x, was used employing the equation $F_c = F[1 - 0.0001x(F^2/\sin\theta)]$ and refined to the values of 0.00422 and 0.00400 respectively. The final difference map had a few peaks with intensities between 1 and 2 e Å^{-3}, which were without any chemically feasible connectivity.

Sources of scattering factors and computer programs are given elsewhere (24). The final atomic coordinates are given in Table 2 and important distances and angles in Table 3. The structure factor tables and unit cell diagrams have been deposited.[1]

Results and discussion

The adducts $[HgX_2(Me_3MCH_2SeMe)]_2$ (X = Cl, Br, I; M = Si, Ge) are prepared by mixing equimolar amounts of the appropriate mercuric halide and the selenoether in ethanol at room temperature; for X = Cl or Br the adducts precipitate from ethanol at room temperature whereas the adduct of mercuric iodide crystallizes out on cooling the solution to −4°C.

$$HgX_2 + Me_3MCH_2SeMe \rightarrow [HgX_2(Me_3MCH_2SeMe)]_2$$

(X = Cl, Br, I; M = Si)

(X = Cl, Br, M = Ge)

The analytical results, melting points, and ^{1}H nmr chemical shifts are given in Table 4. We had some difficulty in finding suitable solvents in which to record the ^{1}H nmr spectrum of the adducts because of their lack of solubility. In $CDCl_3$, the $CHCl_3$ peak was considerably stronger than any of the peaks attributable to the adduct. In acetone-d_6, the CD_3OCD_2H peak was also much in evidence but it was clear that the adducts were more soluble in this medium. There was no indication that acetone had displaced the selenium-containing ligand so this became the medium of choice. The lack of additional peaks in acetone-d_6 solution and the expected integration ratios indicate that there are no other proton-containing species present. Because of the lack of solubility we did not undertake any studies to establish if there was rapid exchange between complex and free ligand, and so the ^{1}H nmr spectra only serve to

[1]A complete set of these data may be purchased from the Depository of Unpublished Data, CISTI, National Research Council of Canada, Ottawa, Ont., Canada K1A 0S2.

Can. J. Chem. Downloaded from www.nrcresearchpress.com by 213.166.140.6 on 09/07/12
For personal use only.

Can. J. Chem. Downloaded from www.nrcresearchpress.com by 213.166.140.6 on 09/07/12
For personal use only.

TABLE 2. Final fractional coordinates and isotropic thermal parameters for non-hydrogen atoms of **1**, **2**, and **3** with standard deviations in parentheses

Atom	*x*	*y*	*z*	U_{eq} [a] ($Å^2 \times 10^3$)
Compound **1**				
Hg	0.0509(1)	0.1533(1)	0.1318(1)	43.6(6)
Se	−0.1120(2)	0.3193(3)	0.1259(1)	37(1)
Cl(1)	0.2352(4)	0.1105(10)	0.2280(4)	55(3)
Cl(2)	0.0271(4)	0.2256(8)	−0.0649(4)	46(3)
Si	−0.3431(5)	0.4113(9)	−0.0751(4)	43(3)
C(1)	−0.1695(17)	0.0955(38)	0.1723(17)	55(14)
C(2)	−0.2082(16)	0.2944(33)	−0.0271(12)	41(12)
C(3)	−0.3327(18)	0.6810(30)	−0.0354(15)	46(13)
C(4)	−0.4023(20)	0.3891(44)	−0.2220(17)	69(17)
C(5)	−0.4254(18)	0.2641(34)	−0.0278(20)	57(15)
Compound **2**				
Hg	0.04951(6)	0.14817(13)	0.13062(6)	48.1(5)
Br(1)	0.2443(2)	0.1210(4)	0.2377(2)	40(1)
Br(2)	0.0264(2)	0.2396(3)	−0.0651(1)	58(1)
Se	−0.1165(2)	0.3073(3)	0.1226(1)	46(1)
Si	−0.3485(4)	0.3953(9)	−0.0764(4)	44(3)
C(1)	−0.1707(15)	0.0850(29)	0.1685(14)	46(11)
C(2)	−0.2114(14)	0.2856(31)	−0.0258(12)	42(10
C(3)	−0.3366(19)	0.6597(29)	−0.0387(15)	54(13)
C(4)	−0.4094(17)	0.3738(35)	−0.2147(17)	65(14)
C(5)	−0.4299(18)	0.2576(41)	−0.0305(22)	79(12)
Compound **3**				
Hg	0.3912(1)	−0.0058(1)	0.3558(1)	64.0(5)
I(1)	0.4725(2)	−0.0568(2)	0.1538(1)	62(1)
I(2)	0.3377(2)	−0.2782(1)	0.5092(1)	62(1)
Se	0.0576(2)	0.0278(2)	0.3527(1)	51(1)
Si	0.1650(7)	0.3188(6)	0.1646(4)	52(3)
C(1)	−0.1244(28)	−0.2245(27)	0.3491(18)	74(12)
C(2)	0.0442(23)	0.0766(20)	0.1970(13)	51(9)
C(3)	0.4224(27)	0.4220(29)	0.2236(19)	90(13)
C(4)	0.1710(43)	0.3299(34)	0.0154(18)	107(18)
C(5)	0.0237(27)	0.4281(25)	0.2251(18)	73(12)

[a] U_{eq} is calculated from the refined anisotropic thermal parameters ($U_{eq} = 1/3\ \Sigma_i \Sigma_j U_{ij} a_i^* a_j^* a_i \cdot a_j$).

TABLE 3. Interatomic distances (Å) and angles (68)

	Compound				Compound		
Distance	**1**	**2**	**3**	Angle	**1**	**2**	**3**
Hg—Se	2.528(2)	2.558(2)	2.687(2)	Se—Hg—X(1)	146.3(2)	143.2(1)	109.3(1)
Hg—X(1)	2.354(5)	2.473(2)	2.663(1)	Se—Hg—X(2)	102.3(1)	102.2(1)	105.3(1)
Hg—X(2)	2.698(5)	2.826(2)	2.863(1)	Se—Hg—X(2)′	99.3(2)	99.8(1)	106.2(1)
Hg—X(2)′	2.707(5)	2.803(2)	2.861(1)	X(1)—Hg—X(2)	101.5(2)	102.6(1)	117.4(1)
Se—C(1)	1.94(2)	1.95(2)	1.96(2)	X(1)—Hg—X(2)′	105.2(2)	106.7(1)	121.6(1)
Se—C(2)	1.98(2)	1.96(2)	1.97(2)	X(2)—Hg—X(2)′	87.8(2)	90.5(1)	95.2(1)
Si—C(2)	1.88(2)	1.89(2)	1.86(2)	Hg—X(2)—Hg′	92.2(2)	89.5(2)	84.8(1)
Si—C(3)	1.84(2)	1.84(2)	1.89(2)	Hg—Se—C(1)	100.8(8)	100.5(6)	98.3(6)
Si—C(4)	1.86(2)	1.81(2)	1.84(2)	Hg—Se—C(2)	99.4(6)	98.8(5)	98.3(5)
Si—C(5)	1.87(2)	1.85(2)	1.87(2)	C(1)—Se—C(2)	97.1(9)	99.0(8)	98.5(8)
				Si—C(2)—Se	116.3(9)	116.8(9)	113.7(8)
X(2)---H(11)	2.875	2.952		C(2)—Si—C(3)	111(1)	109(1)	109.5(8)
X(2)---H(12)	2.915	2.989		C(2)—Si—C(4)	104(1)	106(1)	106(1)
Hg---Se″	3.827	4.020		C(2)—Si—C(5)	111(1)	112(1)	108.7(9)
Hg---Hg′	3.896	3.962		C(3)—Si—C(4)	111(1)	110(1)	109(1)
Hg---Hg‴			3.859(2)	C(3)—Si—C(5)	111(1)	111(1)	110(1)
Hg---Se*			4.994(2)	C(4)—Si—C(5)	109(1)	109(1)	114(1)
I(2)---I(2)‴			4.723(2)	Se″---Hg—X(2)	154.3	156.6	

Symmetry equivalent position: ′ is $-x, -y, -z$; ″ is $-x, 0.5 + y, 0.5 + z$; ‴ is $1 - x, -y, 1 - z$; * is $-x, -y, 1 - z$.

TABLE 4. Analytical and ^{1}H nuclear magnetic resonance data for $[HgX_2((CH_3)_3MCH_2SeCH_3)]_2$[a]

Compound	X	M	Calculated C	Calculated H	Found C	Found H	Melting point (°C)	^{1}H nmr[b] $\delta_{(CH_3)_3}$	$\delta_{CH_3\text{-}Se}$	δ_{CH_2}
1	Cl	Si	13.28	3.09	12.89	3.26	155	0.22	2.22	2.12
2	Br	Si	11.09	2.59	10.95	2.49	121	0.20	2.43	2.27
3	I	Si	9.45	2.20	9.18	2.11	79	0.22	2.37	2.16
4	Cl	Ge	12.08	2.81	11.65	2.74	132	0.31	2.36	2.28
5	Br	Ge	10.24	2.39	10.07	2.26	117	0.30	2.34	2.29

[a]All compounds are white except **3**, which is yellow.
[b]Recorded in acetone-d_6.

indicate that the adducts do exist in solution because the chemical shifts are different from those of free ligands and differ from adduct to adduct.

All three Me_3SiCH_2SeMe adducts, **1**, **2**, and **3**, have the same basic structure, in the solid state, of centrosymmetric, dinuclear, halogen-bridged units. Similar structures have been observed for $[HgCl_2(Ph_3P{=}Se)]_2$ (21), $[HgCl_2(PPh_3)_2]_2$ (14), $[HgCl_2(1,1,5\text{-triphenylphosphate})]_2$ (14), $[HgCl_2(PBu_3)]_2$ (16), and $[HgCl_2(\text{methylpyrolidine 1-carbodithioate})]_2$ (17), but these are by no means the only possible structures for mercuric halide adducts, mononuclear complexes having been isolated such as $[HgCl_2(S(CH_2CH_2)O)_2]$ (19) as well as polymeric structures such as $[HgCl_2(PMe_3)]$ (13). Mononuclear and polymeric structures seem to be preferred when the donor ligand is strongly electron releasing, such as PMe_3 and PEt_3. However, **2** and **3** have dinuclear structures that are closely related to the structure of $[(HgBr_2)_3(AsBu_3)_2]$ in which there are units of $[HgBr_2(AsBu_3)]_2$ linked to $HgBr_2$ units by bromine bridges (1). Apart from this related compound, they are the first dinuclear structures reported for $HgBr_2$ and HgI_2 adducts.

All three adducts, **1**, **2**, and **3**, contain mercury atoms surrounded by a pseudotetrahedral arrangement. However, the distortion from all-tetrahedral angles is considerably larger in **1** and **2** than in **3**. Also, although the terminal Hg—X bonds, as expected, are significantly shorter than the bridging Hg—X bonds, the difference is once again much more marked for HgCl and HgBr (13 and 12% respectively), than for HgI (only 7%). Further, in **1** and **2**, the position of the selenoether group is such that the methylene group sits over the central bridging group so that the bulkier Me_3SiCH_2 moiety is essentially sitting on top of the bridge system (Figs. 1 and 2). By contrast, in **3**, the Me_3SiCH_2 moiety is positioned away from the central bridging system (Fig. 3). In all of the complexes the two selenoether groups are mutually *trans*.

The large distortion from tetrahedral angles in **1** and **2** is particularly evident for the terminal X(1)—Hg—Se angle (146.312°) for X = Cl and 143.2(1°) for X = Br), which thus displays a tendency towards a linear bonding system. This phenomenon has also been observed in $[HgCl_2(Ph_3P{=}Se)]_2$ (21) (Cl—Hg—Se = 136.3(2)°) and β$[HgCl_2(PBu_3)]_2$ (12) (Cl—Hg—P = 150.6(3)°) and has been ascribed to the strong donor–acceptor bond between mercury and the donor atom, which confers a high degree of *s*-character in the X—Hg—L bonding system. Such a postulate is supported by the fact that the X—Hg—X′ angles for the bridging halides, i.e., Cl(2)—Hg—Cl(2′) = 87.8(2)° and Br(2)—Hg—Br(2′) = 90.5(1)°, are close to 90°C, as they are in $[HgCl_2(Ph_3P{=}Se)]$ and β$[HgCl_2(PBu_3)]_2$, which would be expected if these bonds essentially use orbitals of *p*-character on mercury in forming the bridge. By contrast, in **3**, the

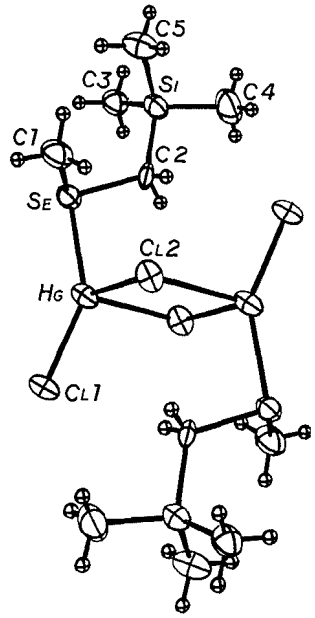

FIG. 1. ORTEP drawing of $[Me_3SiCH_2SeMe]HgCl_2$. The thermal parameters are drawn at 50% probability except for H atoms, which are at an arbitrary level. Unlabeled atoms are related to the labeled ones by a centre of inversion.

TABLE 5. Selected Raman spectroscopy data for $[HgX_2(Me_3MCH_2\text{-}SeMe)]_2$

X	M	ν(Hg—X_t) (terminal)	ν(Hg—X_b) (bridge)	ν(Hg—Se)	δ(Hg—X_t)
Cl	Si	301 (100)	169 (20)	205 (45)	119 (90)
Br	Si	213 (30)	131 (30)	176 (60)	74 (60)
I	Si	124 (90)	90 (20)	162 (80)	35 (100)
Cl	Ge	299 (100)	157 (39)	199 (60)	102 (80)
Br	Ge	211 (40)	130 (30)	188 (50)	71 (80)

Numbers in parentheses indicate relative intensities of peaks below 400 cm^{-1}.

I(1)—Hg—Se angle is essentially tetrahedral, (109.3(1)°, with the I(2)—Hg—I2′) angle at 95.3(1)°. These trends are consistent with a weaker Hg—Se interaction, presumably because HgI_2 is the weakest Lewis acid of the three mercuric halides.

This assumption is supported by the fact that the Hg—Se bond of **3** is considerably longer, 2.687(2) Å, than in **1** and **2**, 2.528(2) and 2.558(2) Å respectively. The distance observed for **1** is virtually identical to that of $[HgCl(Ph_3P{=}Se)]$, 2.527 Å. In both **1** and **2** the distances are significantly shorter than that

Can. J. Chem. Downloaded from www.nrcresearchpress.com by 213.166.140.6 on 09/07/12
For personal use only.

TABLE 6. Anisotropic thermal parameters[a] (Å^2 × 10^3) for **1**, **2**, and **3**

Atom	U_{11}	U_{22}	U_{33}	U_{12}	U_{13}	U_{23}
Compound **1**						
Hg	25.6(5)	54.5(6)	43.4(6)	−2.1(4)	6.6(4)	0.1(4)
Se	30(1)	42(1)	36(1)	1(1)	9(1)	−3(1)
Cl(2)	28(3)	82(4)	46(3)	3(3)	6(2)	−4(3)
Cl(2)	46(3)	44(3)	39(3)	−(2)	12(2)	1(2)
Si	31(3)	50(4)	39(3)	3(3)	7(3)	−1(3)
C(1)	32(12)	75(17)	57(13)	−26(11)	13(11)	−5(12)
C(2)	42(12)	67(15)	15(9)	11(11)	9(9)	−11(9)
C(3)	50(13)	54(15)	39(11)	−6(11)	22(10)	4(10)
C(4)	51(16)	89(20)	57(15)	8(14)	8(12)	−16(13)
C(5)	45(14)	51(14)	86(17)	3(11)	37(13)	17(12)
Compound **2**						
Hg	42.2(5)	49.7(6)	45.4(6)	−1.3(4)	15.2(4)	−1.0(4)
Br(1)	46(1)	72(2)	49(1)	−4(1)	18(1)	−4(1)
Br(2)	60(1)	35(1)	41(1)	−5(1)	23(1)	2(1)
Se	48(1)	34(1)	37(1)	1(1)	19(1)	−2(1)
Si	39(3)	48(3)	39(3)	0(2)	15(2)	−2(2)
C(1)	55(12)	41(11)	37(11)	−20(10)	18(9)	−7(9)
C(2)	41(10)	49(12)	13(8)	14(9)	−5(7)	−5(8)
C(3)	82(16)	41(12)	31(11)	2(11)	20(11)	3(9)
C(4)	54(13)	63(15)	66(15)	19(11)	19(12)	−16(12)
C(5)	57(14)	85(18)	118(22)	−25(14)	61(16)	−17(17)
Compound **3**						
Hg	59.5(5)	94.1(6)	41.9(5)	37.6(4)	−5.9(3)	12.2(4)
I(1)	61(1)	80(1)	51(1)	35(1)	5(0)	7(1)
I(2)	68(1)	47(1)	54(1)	11(1)	−14(1)	15(0)
Se	49(1)	44(1)	58(1)	19(1)	4(1)	3(1)
Si	52(3)	53(3)	52(3)	25(2)	−6(2)	5(2)
C(1)	58(11)	74(12)	85(14)	23(9)	17(10)	24(10)
C(2)	47(9)	45(9)	57(10)	19(7)	−16(8)	−14(7)
C(3)	72(13)	93(15)	89(15)	24(12)	−23(11)	37(12)
C(4)	158(26)	100(17)	64(14)	58(17)	5(15)	18(13)
C(5)	75(13)	57(11)	91(15)	34(10)	7(11)	4(10)

[a]Anisotropic temperature factors are of the form

$$\exp[-2\pi^2(U_{11}h^2a^{*2} + U_{22}k^2b^{*2} + U_{33}l^2c^{*2} + 2U_{12}hka^*b^* - 2U_{13}hla^*C^* + 2U_{23}klb^*C^*)].$$

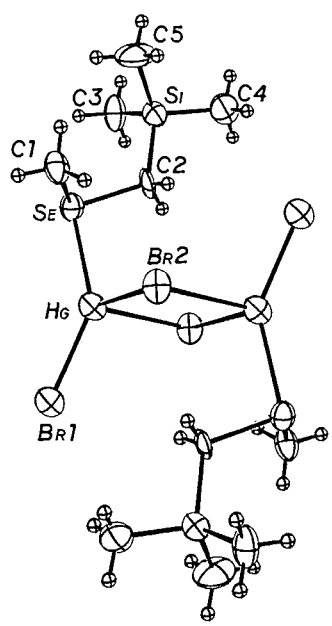

FIG. 2. Perspective view of $[Me_3SiCH_2SeMe]HgBr_2$.

predicted by summing the covalent radii of Se and tetrahedral Hg (2.63 Å) (25). The Hg—Se bond is markedly longer and the weakness of the Se—HgI_2 bond may be related to the ease with which the complex decomposes in moist air. The adduct between Me_3GeCH_2SeMe and HgI_2 was too weak to withstand attempts at isolation.

The bond angles around Se should also reflect the strength of the donor bond. With increased donation there should be an increase toward all tetrahedral angles, as has been illustrated well for trimethylarsine derivatives (26). The C(1)—Se—Hg angle is indeed slightly larger in **1** and **2** (100.8(9) and 100.5(6)° respectively) than in **3** (98.3(6)°). All are considerably smaller than the equivalent C—Pd—Se bond in $(Me_3SiCH_2SeMe)_2$-$PdCl_2$, which is 108.0(2)° (8). In the latter compound the Pd—Se bond is relatively short, suggesting that $PdCl_2$ is a better Lewis acid than $HgCl_2$. It has been observed for a number of $HgCl_2$ adducts that the terminal Hg—Cl distance reflects the donor action of the attached ligand in such a manner that longer Hg—Cl distances are obtained with stronger donors (27), e.g., for $\beta[HgCl_2(PBu_3)]_2$, Hg—Cl = 2.348(6) and for $[HgCl_2$-$(PPh_3)]_2$, Hg—Cl = 2.370(7). The Hg—Cl distance for **1** of 2.354(5) Å implies a donor strength intermediate between PBu_3 and PPh_3. The bridging Hg—Cl distances for **1** (2.698(5) and

Can. J. Chem. Downloaded from www.nrcresearchpress.com by 213.166.140.6 on 09/07/12
For personal use only.

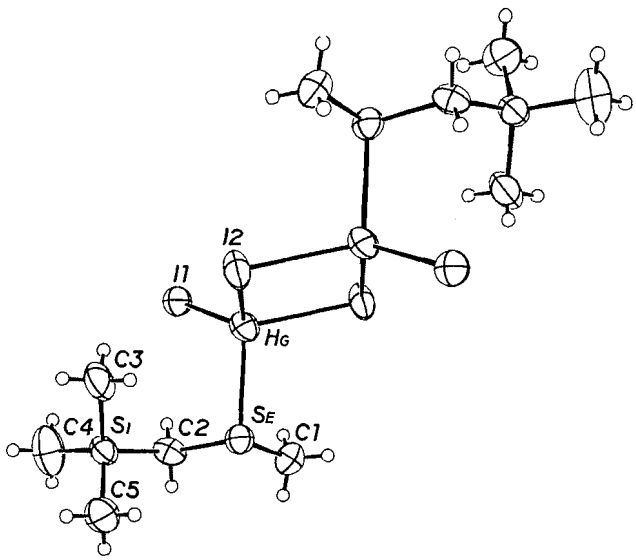

FIG. 3. Perspective view of $[Me_3SiCH_2SeMe]HgI_2$.

2.707(5) Å) also fall between those of the PPh_3 and PBu_3 adducts (2.623(8) and 2.658(8), and 2.718(6) and 2.737(6) Å, respectively). The Hg—Br distance for **2** of 2.473(2) Å is very close to that reported for the $[HgBr_2(AsBu_3)]_2$ unit in $[(HgBr_2)_3(AsBu_3)_2]$, while the Hg—Br bridging distances of 2.803(2) and 2.826(2) Å in **2** bracket the values of 2.6 and 2.9 Å reported for $[HgBr_2(AsBu_3)]_2$ (1). There has been a structural report of a Cd—Hg iodo-bridged species, $I_2Cd\mu(I)_2Hg(PPc_3)_2$ (28), and the monomeric species $HgI_2(PPh_3)_2$ (29). The bridging Hg—I distances in $I_2Cd\mu(I)_2Hg(PPr_3)_2$ of 3.077(1) and 3.056(1) Å are rather longer than those for **3** (2.863(1) and 2.861(1) Å). This is probably a reflection of electron-donating effects of the PPr_3 groups in the former complex.

Selected low frequency vibrational bands in the solid-state Raman spectra are shown with their assignments in Table 5. The far infrared region showed very broad bands from which it was impossible to identify individual features. The values of the bridging and terminal Hg—X bands are consistent with those reported for various HgX_2 phosphine adducts (30). It is clear that the bands in the Me_3GeCH_2SeMe adducts are in general similar in shape, position, and relative intensity to those of Me_3SiCH_2SeMe, suggesting that they probably also have a similar dimeric structure. Unfortunately, it was not possible to obtain crystals of sufficient quality to obtain their structures by X-ray diffraction.

The assignments of the Hg—X (terminal) stretching vibrations, $\nu(Hg—X_t)$, can also be readily made by comparison with the assignment of ν_1 in $HgCl_2$ (313), $HgBr_2$ (195) (31), and HgI_2 (137 cm^{-1} (32). Similarly the Hg—X_t bending mode, $\delta(Hg—X_t)$, can be assigned by comparison with ν_2 in $HgCl_2$ (126) (33), $HgBr_2$ (66) (34), and HgI_2 (26 cm^{-1} (32). The stretching vibrations are assigned in the spectrum of $[HgBr_2(Me_3SiCH_2SeMe)]_2$ as $\nu(Hg—Br_t)$, 213; $\nu(Hg—Se)$, 176; and $\nu(Hg—Br_b)$, 131 cm^{-1}. Given the different environments but at the same time recognizing that the masses of Br and Se are essentially the same, this successive lowering of the wave number fits well with the increasing bond lengths of Hg—Br_t, 2.473(2); Hg—Se, 2.558(2); and Hg—Br_b, 2.81(2) Å. Similar sequential shifts are noted in the assignments of the spectrum of $[HgBr_2(Me_3GeCH_2SeMe)]_2$. The assignment of $\nu(Hg—Se)$ in the chloride, bromide, and iodide adducts, $[HgX_2(Me_3SiCH_2SeMe)]_2$, of 205, 176, and 162 cm^{-1} respectively also match the increase in the bond lengths of Hg—Se along the series, i.e., 2.70(1), 2.81(2), and 2.862(2) Å. In species such as Al_2X_6, Ga_2X_6, and In_2I_6, where there are both bridging and terminal halogen bonds, the ratio of the assigned frequencies, $\nu(M—X_b)$, varies from approximately 1:2 (e.g., in Al_2I_6) (35) to 3:4 (e.g., Ga_2Cl_6) (36). The assignments in the $[HgX_2(Me_3MCH_2SeMe)]_2$ adducts fall in this range, with the biggest difference being noted for the chloride, where there is the largest difference between the Hg—Cl_t, 2.354(5), and Hg—Cl_b, 2.70(1) Å, bond lengths. In summation, the Raman spectra totally reflect the findings from the X-ray diffraction data.

TABLE 7. Final fraction coordinates and thermal parameters for hydrogen atoms of **1**, **2**, and **3**

Hydrogen atom	x	y	z	U
Compound **1**				
H11	−0.1316	0.0833	0.2471	50
H12	−0.1632	0.0277	0.1404	50
H13	−0.2420	0.1212	0.1521	50
H21	−0.2175	0.1531	−0.0440	50
H22	−0.1751	0.3579	−0.0642	50
H31	−0.3024	0.6897	0.0396	50
H32	−0.4012	0.7407	−0.0662	50
H33	−0.2892	0.7518	−0.0590	50
H41	−0.4715	0.4452	−0.2533	60
H42	−0.4057	0.2493	−0.2411	60
H43	−0.3598	0.4613	−0.2464	60
H51	−0.3956	0.2749	−0.0471	70
H52	−0.4274	0.1247	−0.0471	70
H53	−0.4952	0.3178	−0.0593	70
Compound **2**				
H(11)	−0.1317	0.0751	0.2411	40
H(12)	−0.1632	−0.0354	0.1386	40
H(13)	−0.2436	0.1068	0.1481	40
H(21)	−0.2193	0.1478	−0.0430	40
H(22)	−0.1779	0.3512	−0.0596	40
H(31)	−0.3046	0.6692	0.0339	50
H(32)	−0.4052	0.7187	−0.0686	50
H(33)	−0.2939	0.7276	−0.0621	50
H(41)	−0.4792	0.4270	−0.2449	60
H(42)	−0.4123	0.2371	−0.2332	60
H(43)	−0.3684	0.4459	−0.2387	60
H(51)	−0.3983	0.2685	0.0421	80
H(52)	−0.4339	0.1209	−0.0491	80
H(53)	−0.4994	0.3128	−0.0608	80
Compound **3**				
H(11)	−0.1353	−0.2704	0.4203	60
H(12)	−0.0779	−0.2867	0.3026	60
H(13)	−0.2485	−0.2388	0.3226	60
H(21)	−0.0888	0.0298	0.1738	60
H(22)	0.1060	0.0188	0.1581	60
H(31)	0.4199	0.4164	0.3006	80
H(32)	0.4866	0.5424	0.2025	80
H(33)	0.4901	0.3591	0.1974	80
H(41)	0.2311	0.4506	−0.0057	100
H(42)	0.0419	0.2742	−0.0146	100
H(43)	0.2430	0.2708	−0.0105	100
H(51)	0.0836	0.5510	0.2093	80
H(52)	0.0213	0.4135	0.3016	80
H(53)	−0.1056	0.3754	0.1953	80

Can. J. Chem. Downloaded from www.nrcresearchpress.com by 213.166.140.6 on 09/07/12
For personal use only.

Acknowledgements

We wish to thank the Natural Sciences and Engineering Research Council of Canada for financial support.

1. R. C. Evans, F. G. Mann, H. S. Peiser, and D. Purdie. J. Chem. Soc. 1209 (1940).
2. E. W. Abel, G. W. Farrow, K. G. Orrell, and V. Sik. J. Chem. Soc. Dalton Trans. 42 (1977).
3. E. W. Abel, A. K. S. Ahmed, G. W. Farrow, K. G. Orrell, and V. Sik. J. Chem. Soc. Dalton Trans. 47 (1977).
4. E. W. Abel, S. K. Bhargava, K. Kite, K. G. Orrell, V. Sik, and B. L. Williams. Polyhedron, **1**, 289 (1982).
5. E. W. Abel, S. K. Bhargava, M. M. Bhatti, K. Kite, M. A. Mazid, K. G. Orrell, V. Sik, B. L. Williams, M. B. Hursthouse, K. M. Malik, and J. Abdul. J. Chem. Soc. Dalton Trans. 2065 (1982).
6. E. W. Abel, S. K. Bhargava, M. M. Bhatti, K. Kite, M. A. Mazid, V. Sik, M. B. Hursthouse, K. M. Malik, and J. Abdul. J. Organomet. Chem. **250**, 373 (1983).
7. E. W. Abel, S. K. Bhargava, K. Kite, K. G. Orrell, V. Sik, and B. L. Williams. J. Chem. Soc. Dalton Trans. 365 (1984).
8. R. K. Chadha, J. M. Chehayber, and J. E. Drake. Inorg. Chem. **25**, 611 (1986).
9. P. E. Skakke and S. E. Rasmussen. Acta Chem. Scand. **24**, 2634 (1970).
10. H. J. Whitfield. J. Chem. Soc. (A), 113 (1970).
11. J. C. Barnes, G. Hunter, and M. W. Lown. J. Chem. Soc. Dalton Trans. 458 (1977).
12. N. A. Bell, M. Goldstein, T. Jones, L. A. March, and I. W. Nowell. Inorg. Chim. Acta, **61**, 83 (1982).
13. N. A. Bell, M. Goldstein, T. Jones, and I. W. Nowell. Inorg. Chim. Acta, **48**, 185 (1981).
14. N. A. Bell, M. Goldstein, T. Jones, and I. W. Nowell. Inorg. Chim. Acta, **43**, 87 (1980).
15. N. A. Bell, M. Goldstein, L. A. March, and I. W. Nowell. J. Chem. Soc. Dalton Trans. 1621 (1984).
16. D. W. Allen, N. A. Bell, S. T. Fong, L. A. March, and I. W. Nowell. Inorg. Chim. Acta, **99**, 157 (1985).
17. P. O. Brotherton, J. M. Epstein, A. H. White, and A. C. Willis. J. Chem. Soc. Dalton Trans. 2341 (1974).
18. K. K. Cheung and G. A. Sim. J. Chem. Soc. 5988 (1965).
19. R. S. McEwen and G. A. Sim. J. Chem. Soc. (A), 271 (1967).
20. N. W. Alcock, N. Herron, and P. Moore. J. Chem. Soc. Dalton Trans. 394 (1978).
21. L. S. Dent Glasser, L. Ingram, M. G. King, and G. P. McQuillan. J. Chem. Soc. (A), 2501 (1969).
22. C. I. Braüden. Ark. Kemi, **22**, 83 (1964); **22**, 495 (1964); **22**, 501 (1964).
23. J. Chehayber and J. E. Drake. Inorg. Chim. Acta, **111**, 51 (1986).
24. R. K. Chadha, J. E. Drake, and A. B. Sarkar. Inorg. Chem. **25**, 2201 (1986).
25. L. Pauling. The nature of the chemical bond. 3rd ed. University Press, Cornell University, Ithaca, NY. 1960.
26. R. K. Chadha, J. Chehayber, and J. E. Drake. J. Crystallogr. Spectrosc. Res. **15**, 53 (1985).
27. N. A. Bell, T. D. Dee, M. Goldstein, P. J. McKenna, and I. W. Nowell. Inorg. Chim. Acta, **71**, 135 (1983).
28. N. A. Bell, M. Goldstein, L. A. March, and I. W. Nowell. Inorg. Chim. Acta, **83**, 75 (1984).
29. L. Fälth. Chem. Scr. **9**, 71 (1976).
30. N. A. Bell, M. Goldstein, T. Jones, and I. W. Nowell. Inorg. Chim. Acta, **69**, 155 (1983).
31. G. J. Janz and D. W. James. J. Chem. Phys. **38**, 905 (1963).
32. R. P. J. Cooney, J. R. Hall, and M. A. Hooper. Aust. J. Chem. **21**, 2145 (1968).
33. H. Poulet and J.-P. Mathieu. J. Chim. Phys. 442 (1963).
34. G. Randi and F. Gesmundo. Atti. Accad. Naz. Lincei, Cl. Sci. Fis. Mat. Nat. Rend. **41**, 200 (1966).
35. I. R. Beattie, T. Gilson, and G. A. Ozin. J. Chem. Soc. A, 813 (1968).
36. I. R. Beattie, T. Gilson, and G. A. Ozin. J. Chem. Soc. A, 702 (1967).

Can. J. Chem. Downloaded from www.nrcresearchpress.com by 213.166.140.6 on 09/07/12
For personal use only.

Radical ions in photochemistry. 18. The photosensitized (electron transfer) tautomerization of alkenes; the 1,1-diphenyl alkene system

DONALD R. ARNOLD[1] AND SHELLEY A. MINES
Department of Chemistry, Dalhousie University, Halifax, N.S., Canada B3H 4J3

Received March 12, 1987

This paper is dedicated to Professor Douglas E. Ryan

DONALD R. ARNOLD and SHELLEY A. MINES. Can. J. Chem. **65**, 2312 (1987).

The photosensitized (electron transfer) irradiation of several conjugated 1,1-diphenyl alkenes, in acetonitrile with 1,4-dicyanobenzene or 1-cyanonapthalene as electron accepting sensitizer and 2,6-lutidine as base, leads essentially quantitatively to tautomerization to the less stable unconjugated isomer(s). The proposed mechanism for this reaction involves formation of the alkene radical cation and sensitizer radical anion followed by deprotonation of the radical cation, reduction of the resulting radical to the ambident anion by back electron transfer from the radical anion, and reprotonation. There are several steps in this mechanism that could control the ratio of isomers. Evidence is provided that, at least in some cases, it is the relative rate of deprotonation from the isomeric radical cations that is the determining factor. This rate is influenced by the conformation of the radical cation; the carbon–hydrogen bond involved in the deprotonation step must overlap with the singly occupied molecular orbital.

DONALD R. ARNOLD et SHELLEY A. MINES. Can. J. Chem. **65**, 2312 (1987).

L'irradiation photosensibilisée (transfert d'électron) de plusieurs diphényl-1,1 alcènes conjugués, effectuée dans l'acétonitrile avec du dicyano-1,4 benzène ou du cyano-1 naphtalène comme sensibilisateur acceptant les électrons et de la lutidine-2,6 comme base, conduit essentiellement et avec un rendement quantitatif à une tautomérisation vers le (ou les) isomère(s) le(s) moins stable(s). Le mécanisme proposé pour cette réaction implique (*a*) la formation du cation radical de l'alcène et de l'anion radical du sensibilisateur, (*b*) une déprotonation du cation radical, (*c*) une réduction du radical qui en résulte, par un retransfert d'électron de la part du radical anion, conduisant à l'anion ambidentate et (*d*) une reprotonation. Plusieurs étapes de ce mécanisme pourraient contrôler le rapport des isomères. On présente des données qui suggèrent, au moins dans quelques cas, que c'est la vitesse relative de déprotonation des cations radicaux isomères qui est le facteur déterminant. Cette vitesse est influencée par la conformation du cation radical; il doit y avoir un recouvrement de la liaison carbone–hydrogène impliquée dans l'étape de déprotonation avec l'orbitale moléculaire qui est occupée d'une façon célibataire.

[Traduit par la revue]

The tautomerization of alkenes, by either acid or base catalysis, is an old and relatively well-understood process (1). The composition of the equilibrium mixture reflects the thermodynamic stability of the isomers. Conjugation of a double bond with an aryl group has a profound effect on stability; for example, at equilibrium β-methyl styrene dominates over allylbenzene by three to four orders of magnitude (2). Until now there has been no direct way to counteract the thermodynamic driving force of this equilibrium, that is, to convert a conjugated aryl alkene into a less stable unconjugated isomer. Such a process would have significant synthetic utility because the more stable isomer is usually much more readily prepared by classical methods. We can now describe the first examples of this process, the photosensitized (electron transfer) tautomerization of alkenes.

A solution of 1,1-diphenyl-2-methylpropene (**1**) in acetonitrile, with 1,4-dicyanobenzene or 1-cyanonapthalene as electron accepting sensitizer and 2,6-lutidine as base, was irradiated with a medium-pressure Hg vapor lamp through Pyrex. Progress of the reaction was followed by capillary column gas chromatography with a mass selective detector (gc/ms). The tautomer, 3,3-diphenyl-2-methylpropene (**2**), was the only volatile product detected. Irradiation was continued until the reaction was complete, when chromatography of the crude photolysate gave **2** in excellent yield. The photosensitizer was largely recovered.

Several related conjugated 1,1-diphenyl alkenes are likewise converted into less stable tautomers by irradiation under these conditions. Table 1 provides a summary of these results. In every case the isomerization went to completion and the isolated yield of the tautomer(s) was excellent.

All of the starting alkenes and most of the tautomers were known compounds; *E*-**4**, *Z*-**4**, **5**, **7**, and **12** have not, to our knowledge, been described previously. Structural assignments rest firmly on a thorough analysis of the ^{1}H and ^{13}C nmr spectra. The assignment of configuration of the isomers *E*-**4** and *Z*-**4** was made on the basis of the ^{1}H–^{13}C coupling constants observed in the ^{13}C nmr spectra.[2]

The proposed mechanism is shown (simplified) in Scheme 1. If we consider the process in general, there are several key steps ([2], [3], [4], and [7]) that could direct the product ratio toward the less thermodynamically stable tautomer.[3] The rates of steps [2*a*] and [2*b*] depend upon the oxidation potentials of the tautomers in relation to the reduction potential of the excited state of the photosensitizer. These rates can be estimated by use of the Weller equation (5). Since the oxidation potentials of the tautomers may be significantly different, it will be possible in some cases to choose a sensitizer that will accept an electron

[1]Author to whom correspondence may be addressed.

[2]Coupling of the vicinal vinyl proton to the carbon of the allylic methyl should be greater for the *Z*-**4** than for the *E*-**4**; the observed coupling constants are 7.1 and 2.9 Hz.

[3]A similar mechanism was recently proposed for the tautomerization of an acetylene to an allene (3). There are some other less closely related photochemical tautomerization reactions (4).

Can. J. Chem. Downloaded from www.nrcresearchpress.com by 213.166.140.6 on 09/07/12
For personal use only.

TABLE 1. The photosensitized (electron transfer) tautomerization of 1,1-diphenyl alkenes[a]

Starting alkene	Product
1,1-Diphenyl-2-methylpropene (**1**)	3,3-Diphenyl-2-methylpropene (**2**)
1,1-Diphenyl-2-methylbutene (**3**)	(*E*)-1,1-Diphenyl-2-methyl-2-butene (*E*-**4**)[b]
	(*Z*)-1,1-Diphenyl-2-methyl-2-butene (*Z*-**4**)
	3,3-Diphenyl-2-ethylpropene (**5**)
1,1-Diphenyl-2,3-dimethylbutene (**6**)	3-Methyl-2-(diphenylmethyl)-1-butene (**7**)[c]
	1,1-Diphenyl-2,3-dimethyl-2-butene (**8**)
1,1-Diphenylmethylenecyclohexane (**9**)	1-(Diphenylmethyl)cyclohexene (**10**)
1,1-Diphenylmethylenenorbornane (**11**)	2-(Diphenylmethyl)norbornene (**12**)
1-Phenyl-3,4-dihydronaphthalene (**13**)	1-Phenyl-1,4-dihydronaphthalene (**14**)[d]
	1-Phenylnaphthalene (**15**)

[a]A solution in acetonitrile of 2,6-lutidine (0.1 *M*), 1,4-dicyanobenzene or 1-cyanonaphthalene (0.1 *M*), and the starting alkene (0.15 *M*) was irradiated at 10°C with a 1-kW medium-pressure Hg vapor lamp until reaction was complete. The product(s) was (were) isolated, in high yield (>85%), by column chromatography on silica gel. Both sensitizers work well; both are largely recovered. The greater solubility and extended long-wavelength absorption of 1-cyanonaphthalene make it the sensitizer of choice.

[b]The initial ratio of *E*-**4**:*Z*-**4**:**5** was 80:10:1. This ratio was dependent upon extent of conversion; when the reaction was complete the ratio was 8:4:1.

[c]**7**:**8** > 200:1 (**8** was not detected (gc/ms, ^{1}Hmr).

[d]**14**:**15**, 7:1. Disproportionation of the intermediate radical may account for the formation of **15**; driven by aromatization.

from the more easily oxidized tautomer at a significantly faster rate. The rates of the back electron transfer process, steps [3*a*] and [3*b*], will also depend upon the oxidation potentials of the two tautomers. Back electron transfer may be so energetically favourable that the rates are in the "inverted Marcus region"; that is, the more exothermic the process, the slower the rate (6). If the alkene radical cations can equilibrate (steps [7*a*] and [7*b*]), the tautomer with the lower oxidation potential will be favoured. Competition at all of these steps tends to favour the ultimate formation of the tautomer with the higher oxidation potential.

Steps [4*a*] and [4*b*] represent the deprotonation of the two radical cations. The tautomer with the higher oxidation potential will have the greater acidity and it may be possible to choose a base that will deprotonate it selectively (7). This would shift the product ratio in favour of the conjugated tautomer. However, it is the relative rates of steps [4*a*] and [4*b*] that are important and the relationship between the thermodynamic and kinetic acidity of radical cations is still poorly understood.

Relevant to the discussion of the specific mechanism involved in the case of these 1,1-diphenyl alkenes are the reactions of the series: 1,1-diphenyl-2-methylpropene (**1**), 1,1-diphenyl-2-methylbutene (**3**), and 1,1-diphenyl-2,3-dimethylbutene (**6**). While both [2*a*] and [2*b*] should be diffusion controlled when 1,4-dicyanobenzene is the acceptor, [2*a*] should be significantly faster than [2*b*] when 1-cyanonapthalene is used (8). Because the unconjugated tautomer(s) is (are) the exclusive product(s) with both sensitizers, the relative rates of these initial electron transfer processes cannot be the only factor influencing the product ratio.

The tautomerization of **1** indicates that deprotonation from a methyl group and subsequent isomerization to a terminal alkene (**2**) is possible. However, the predominant formation of *E*-**4** and *Z*-**4** from **3** indicates that deprotonation from the ethyl group is kinetically favoured over deprotonation from the methyl group. This is consistent with the relative thermodynamic acidity at these two positions since deprotonation from the ethyl group gives the more heavily substituted, and therefore more stable, allylic radical (7). In contrast, **7** is formed exclusively upon

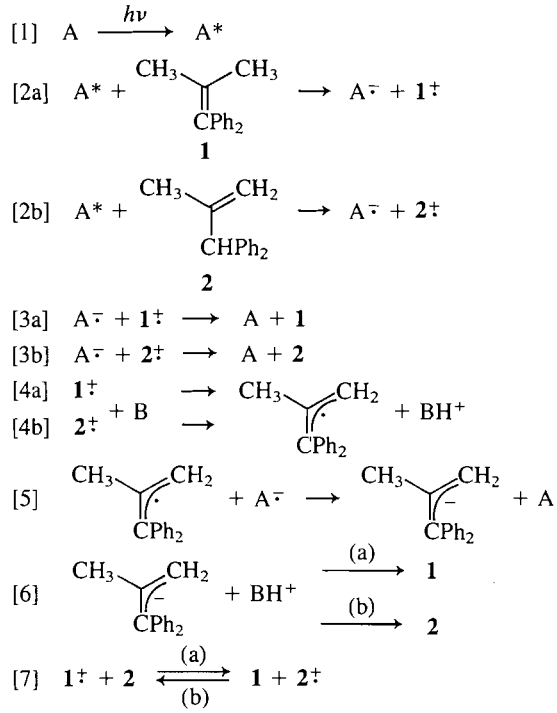

SCHEME 1

tautomerization of **6**. In this case, deprotonation occurs preferentially from the methyl group rather than from the isopropyl group.

For deprotonation to occur, the radical cation must adapt a conformation that allows overlap of the allylic carbon–hydrogen bond with the singly occupied molecular orbital (SOMO). This is possible with the methyl groups of **1** and with the ethyl group of **3**, but the two methyls of the isopropyl group of **6** prefer the out-of-plane staggered orientation. In this conformation the allylic isopropyl hydrogen is orthogonal to the SOMO.[4] Therefore, we conclude that the ratio of product

[4]This line of reasoning has been used before (9).

Can. J. Chem. Downloaded from www.nrcresearchpress.com by 213.166.140.6 on 09/07/12
For personal use only.

tautomers is dependent upon the relative rates of deprotonation of the radical cation from the allylic positions (steps [4*a*] and [4*b*]).

A thorough study of the scope and mechanism of this reaction is now in progress.

Acknowledgments

Acknowledgment is made to the Donors of the Petroleum Research Fund, administered by the American Chemical Society, and to the Natural Sciences and Engineering Research Council of Canada for partial support of this research. We also thank D. L. Hooper and the Atlantic Regional Magnetic Resonance Centre at Dalhousie University for the 360 MHz nmr spectra.

1. (*a*) C. K. INGOLD. Structure and mechanism in organic chemistry. Cornell University Press, Ithaca, NY. 1953. Chap. 10; (*b*) D. J. CRAM. Fundamentals of carbanion chemistry. Academic Press, New York. 1965. Chap. 5.
2. (*a*) A. G. CATCHPOLE, E. D. HUGHES, and C. K. INGOLD. J. Chem. Soc. 8 (1948); (*b*) S. W. ELA and D. J. CRAM. J. Am. Chem. Soc. **88**, 5791 (1966).
3. M. W. KLETT and R. P. JOHNSON. J. Am. Chem. Soc. **107**, 6615 (1985).
4. (*a*) P. DEMAYO and G. WENSKA. J. Chem. Soc. Chem. Commun. 1626 (1986); (*b*) H. MORRISON and C. KOVIAK. Tetrahedron Lett. **27**, 2711 (1986); (*c*) R. M. DUCHAIME, D. A. LOMBARDO, I. A. SKINNER, and A. C. WEEDON. J. Org. Chem. **50**, 873 (1985); (*d*) R. RICARD, P. SAUVAGE, C. S. K. WAN, A. C. WEEDON, and D. F. WONG. J. Org. Chem. **51**, 62 (1986).
5. (*a*) D. REHM and A. WELLER. Isr. J. Chem. **8**, 259 (1970); (*b*) Ber. Bunsenges. Phys. Chem. **73**, 834 (1969).
6. (*a*) G. L. CLOSS, L. T. CALCATERRA, N. J. GREEN, K. W. PENFIELD, and J. R. MILLER. J. Phys. Chem. **90**, 3673 (1986); (*b*) C. J. SCHESENER, C. AMATORE, and J. K. KOCHI. J. Phys. Chem. **90**, 3747 (1986).
7. A. M. DE P. NICHOLAS and D. R. ARNOLD. Can. J. Chem. **60**, 2165 (1982).
8. D. R. ARNOLD and A. J. MAROULIS. J. Am. Chem. Soc. **98**, 5932 (1976).
9. (*a*) F. D. LEWIS. Acc. Chem. Res. **19**, 401 (1986); (*b*) T. SHONE and Y. MATSUMURA. J. Org. Chem. **35**, 4157 (1970); (*c*) P. J. WAGNER, R. J. TRUMAN, A. E. PUCHALSKI, and R. WAKE. J. Am. Chem. Soc. **108**, 7727 (1986).

Can. J. Chem. Downloaded from www.nrcresearchpress.com by 213.166.140.6 on 09/07/12
For personal use only.

The stereoselective alkylation and conformational analysis of 14-membered lactones

J. TERCIO B. FERREIRA,[1] EDWARD G. NEELAND, JAMES P. OUNSWORTH, AND LARRY WEILER[2]

Department of Chemistry, University of British Columbia, Vancouver, B.C., Canada V6T 1Y6

Received April 2, 1987

J. TERCIO B. FERREIRA, EDWARD G. NEELAND, JAMES P. OUNSWORTH, and LARRY WEILER. Can. J. Chem. **65**, 2314 (1987).

The 14-membered lactone, 13-tetradecanolide, can be alkylated to give mainly the 2*R**,13*S**-dimethyltridecanolide. A second alkylation gives the 2,2-dimethyl lactone. The conformation of the starting material and alkylation products exist in the regular [3434] conformation. This model is used to rationalize the stereochemical outcome of the reaction and suggest the conformation of the intermediate enolate.

J. TERCIO B. FERREIRA, EDWARD G. NEELAND, JAMES P. OUNSWORTH et LARRY WEILER. Can. J. Chem. **65**, 2314 (1987).

On peut alkyler la lactone à 14 chaînons, tétradécanolide-13, et l'on obtient principalement le diméthyl-2*R**,13*S** tridécanolide. Une seconde alkylation conduit à la lactone diméthylée en position 2,2. Les conformations du produit de départ ainsi que des produits d'alkylation sont les conformations régulières [3434]. On a utilisé ce modèle pour rationaliser l'évolution stéréochimique de la réaction et pour suggérer une conformation pour l'intermédiaire énolique.

[Traduit par la revue]

In 1981 Still and Galynker, in a seminal paper, reported the stereoselective alkylation of a number of monosubstituted 8- to 12-membered ring ketones and lactones (1). Invariably these reactions proceeded with high selectivity to yield one of the two possible diastereomeric products. This high diastereoselectivity was rationalized in terms of the conformational energies of the enolate intermediates, which were obtained from molecular mechanics calculations. The model that evolved from these studies was that of a relatively rigid enolate that was attacked by an electrophile from the more open face (1). Subsequent studies, particularly by Still's group, illustrated this conformational control of stereochemistry in other reactions of medium and large rings (2). Molecular mechanics calculations were required to rationalize the observed stereoselectivity because of the irregular conformations of many medium and large ring systems (3). However, the 14-membered ring is known to often exist in a well-defined diamond lattice, which can be considered to be composed of portions of a chair cyclohexane as illustrated in **1**. We were interested in studying the reactivity of the 14-membered lactone to see if the stereoelectronic properties of cyclohexane and other 6-membered rings might be extended to these systems. This communication reports our results on the alkylation and conformational properties of tridecanolides.

Treatment of lactone **2** with lithium 2,2,6,6-tetramethylpiperidide in THF at −78°C followed by alkylation of the resulting enolate with methyl iodide gave a mixture of two

[1]On leave from the Departamento de Quimica, Universidade Federal de Sao Carlos, Sao Carlos, Brazil.

[2]Author to whom correspondence may be addressed.

tautomers is dependent upon the relative rates of deprotonation of the radical cation from the allylic positions (steps [4*a*] and [4*b*]).

A thorough study of the scope and mechanism of this reaction is now in progress.

Acknowledgments

Acknowledgment is made to the Donors of the Petroleum Research Fund, administered by the American Chemical Society, and to the Natural Sciences and Engineering Research Council of Canada for partial support of this research. We also thank D. L. Hooper and the Atlantic Regional Magnetic Resonance Centre at Dalhousie University for the 360 MHz nmr spectra.

1. (*a*) C. K. INGOLD. Structure and mechanism in organic chemistry. Cornell University Press, Ithaca, NY. 1953. Chap. 10; (*b*) D. J. CRAM. Fundamentals of carbanion chemistry. Academic Press, New York. 1965. Chap. 5.
2. (*a*) A. G. CATCHPOLE, E. D. HUGHES, and C. K. INGOLD. J. Chem. Soc. 8 (1948); (*b*) S. W. ELA and D. J. CRAM. J. Am. Chem. Soc. **88**, 5791 (1966).
3. M. W. KLETT and R. P. JOHNSON. J. Am. Chem. Soc. **107**, 6615 (1985).
4. (*a*) P. DEMAYO and G. WENSKA. J. Chem. Soc. Chem. Commun. 1626 (1986); (*b*) H. MORRISON and C. KOVIAK. Tetrahedron Lett. **27**, 2711 (1986); (*c*) R. M. DUCHAIME, D. A. LOMBARDO, I. A. SKINNER, and A. C. WEEDON. J. Org. Chem. **50**, 873 (1985); (*d*) R. RICARD, P. SAUVAGE, C. S. K. WAN, A. C. WEEDON, and D. F. WONG. J. Org. Chem. **51**, 62 (1986).
5. (*a*) D. REHM and A. WELLER. Isr. J. Chem. **8**, 259 (1970); (*b*) Ber. Bunsenges. Phys. Chem. **73**, 834 (1969).
6. (*a*) G. L. CLOSS, L. T. CALCATERRA, N. J. GREEN, K. W. PENFIELD, and J. R. MILLER. J. Phys. Chem. **90**, 3673 (1986); (*b*) C. J. SCHESENER, C. AMATORE, and J. K. KOCHI. J. Phys. Chem. **90**, 3747 (1986).
7. A. M. DE P. NICHOLAS and D. R. ARNOLD. Can. J. Chem. **60**, 2165 (1982).
8. D. R. ARNOLD and A. J. MAROULIS. J. Am. Chem. Soc. **98**, 5932 (1976).
9. (*a*) F. D. LEWIS. Acc. Chem. Res. **19**, 401 (1986); (*b*) T. SHONE and Y. MATSUMURA. J. Org. Chem. **35**, 4157 (1970); (*c*) P. J. WAGNER, R. J. TRUMAN, A. E. PUCHALSKI, and R. WAKE. J. Am. Chem. Soc. **108**, 7727 (1986).

Can. J. Chem. Downloaded from www.nrcresearchpress.com by 213.166.140.6 on 09/07/12
For personal use only.

The stereoselective alkylation and conformational analysis of 14-membered lactones

J. TERCIO B. FERREIRA,[1] EDWARD G. NEELAND, JAMES P. OUNSWORTH, AND LARRY WEILER[2]

Department of Chemistry, University of British Columbia, Vancouver, B.C., Canada V6T 1Y6

Received April 2, 1987

J. TERCIO B. FERREIRA, EDWARD G. NEELAND, JAMES P. OUNSWORTH, and LARRY WEILER. Can. J. Chem. **65**, 2314 (1987).

The 14-membered lactone, 13-tetradecanolide, can be alkylated to give mainly the 2*R**,13*S**-dimethyltridecanolide. A second alkylation gives the 2,2-dimethyl lactone. The conformation of the starting material and alkylation products exist in the regular [3434] conformation. This model is used to rationalize the stereochemical outcome of the reaction and suggest the conformation of the intermediate enolate.

J. TERCIO B. FERREIRA, EDWARD G. NEELAND, JAMES P. OUNSWORTH et LARRY WEILER. Can. J. Chem. **65**, 2314 (1987).

On peut alkyler la lactone à 14 chaînons, tétradécanolide-13, et l'on obtient principalement le diméthyl-2*R**,13*S** tridécanolide. Une seconde alkylation conduit à la lactone diméthylée en position 2,2. Les conformations du produit de départ ainsi que des produits d'alkylation sont les conformations régulières [3434]. On a utilisé ce modèle pour rationaliser l'évolution stéréochimique de la réaction et pour suggérer une conformation pour l'intermédiaire énolique.

[Traduit par la revue]

In 1981 Still and Galynker, in a seminal paper, reported the stereoselective alkylation of a number of monosubstituted 8- to 12-membered ring ketones and lactones (1). Invariably these reactions proceeded with high selectivity to yield one of the two possible diastereomeric products. This high diastereoselectivity was rationalized in terms of the conformational energies of the enolate intermediates, which were obtained from molecular mechanics calculations. The model that evolved from these studies was that of a relatively rigid enolate that was attacked by an electrophile from the more open face (1). Subsequent studies, particularly by Still's group, illustrated this conformational control of stereochemistry in other reactions of medium and large rings (2). Molecular mechanics calculations were required to rationalize the observed stereoselectivity because of the irregular conformations of many medium and large ring systems (3). However, the 14-membered ring is known to often exist in a well-defined diamond lattice, which can be considered to be composed of portions of a chair cyclohexane as illustrated in **1**. We were interested in studying the reactivity of the 14-membered lactone to see if the stereoelectronic properties of cyclohexane and other 6-membered rings might be extended to these systems. This communication reports our results on the alkylation and conformational properties of tridecanolides.

Treatment of lactone **2** with lithium 2,2,6,6-tetramethylpiperidide in THF at −78°C followed by alkylation of the resulting enolate with methyl iodide gave a mixture of two

[1]On leave from the Departamento de Quimica, Universidade Federal de Sao Carlos, Sao Carlos, Brazil.

[2]Author to whom correspondence may be addressed.

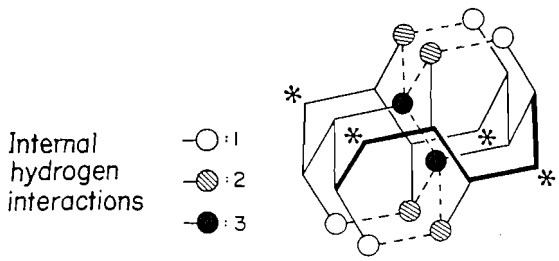

isomeric monoalkylated products, **3** and **4**, in 80–85% yield, and the ratio of isomers was 13:1. Surprisingly, the two isomers were easily separated by tlc or flash chromatography (4). The spectroscopic data of the two isomers, although clearly differ-

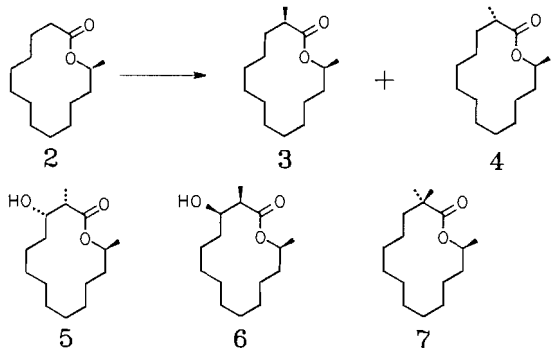

ent, did not allow us to readily assign the stereochemistry to each diastereomer.

We have prepared the substituted 14-membered lactones **5** and **6** (5), and determined their structures by X-ray crystallography[3] and spectroscopic methods. Treatment of the alcohol **5** with LDA, CS_2, and MeI gave the xanthate, which was deoxygenated with tri-*n*-butyltin hydride to give the 2*S**,13*S**-dimethyltridecanolide in 41% yield (6). This compound was identical in all respects to the minor isomer **4** in the alkylation. Similarly **6** was deoxygenated to the 2*R**,13*S** isomer, which was identical to the major alkylation product **3**.

Treatment of **3** or **4** with LDA and MeI gave the *gem*-dimethyl product **7**. The nmr spectrum of **7** contained a symmetric 11-line signal at δ 4.92 (J = 3, 6, 9 Hz) due to the C-13 methine. Dale has shown that a *gem*-dialkyl substituent will prefer a "corner" position in the conformations of large rings (7). The corner positions of the [3434] conformation of the 14-membered rings are shown with an asterisk (*) in **1**. From the coupling constants between the proton on C-13 and the protons on C-12 (J = 3 and 9 Hz), we conclude that **7a** is the preferred conformation.[4]

From an analysis of the ^{1}H nmr spectra of **3** and **4**, we concluded that the major dimethyl lactone **3** must exist mainly in

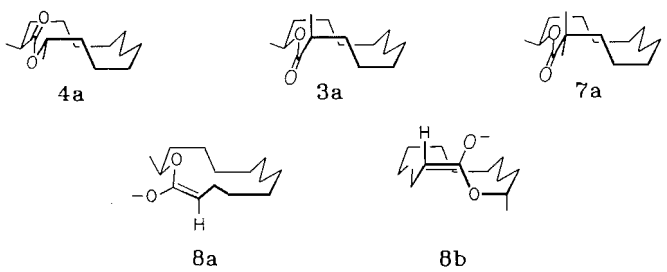

conformation **3a**.[5] The C-2 methine in **3** is an 11-line multiplet at δ 2.41 with J = 2.5, 6.8, and 10.9 Hz, and the C-13 methine is an 11-line multiplet at δ 4.93 with J = 2.7, 6.1, and 9.0 Hz. The C-2 methine in the minor isomer **4** is a symmetric 12-line multiplet at δ 2.53 with J = 3.5, 6.8, and 9.2 Hz, and the C-13 methine is a symmetric 6-line multiplet at δ 5.00 with J = 4.9, 6.3, and 6.7 Hz. This is consistent with conformation **4a** predominating for the minor isomer.[5] At present, we cannot offer an explanation for the fact that **3** and **4** adopt similar conformations, but with different positions for the lactone group.

The stereoselectivity in the alkylation of **2** can be rationalized as follows. The enolate of **2** was generated with LDA and trapped with trimethylsilyl chloride to give the *E*-enol ether. The geometry about the double bond in the silyl enol ether was determined by ^{1}H nmr nuclear Overhauser enhancements (9). Alkylation of this enol ether with chloromethyl phenyl sulfide and zinc bromide followed by Raney nickel desulphurization (10) gave a 3:1 mixture of **3**:**4**. Deprotonation of **2** should involve loss of the C-2 hydrogen, which is closest to being parallel to the *p* orbitals of the π bond of the carbonyl group (11). This would lead to **8a** or **8b** as possible conformations for the enolate or enol ether. Alkylation of **8a** or **8b** from the same direction as deprotonation would lead to the 2*R**,13*S** isomer as the major product. Thus the same stereoelectronic factors as found in small rings might be operative in this system (12). However, it should also be noted that **3** would be the expected product from attack of **8a** or **8b** from the more open face of the enolate.

Acknowledgments

We are grateful to the Natural Sciences and Engineering Research Council of Canada for financial support and the award of a postgraduate fellowship to J.P.O., and to CNPq (Brazil) for the award of a fellowship to J.T.B.F.

1. W. C. Still and I. Galynker. Tetrahedron, **37**, 3981 (1981).
2. (*a*) I. Paterson and M. M. Mansuri. Tetrahedron, **41**, 3569 (1985); (*b*) S. L. Schreiber and R. C. Hawley. Tetrahedron Lett. **26**, 5971 (1985); (*c*) J. E. McMurry and G. K. Bosch. Tetrahedron Lett. **26**, 2167 (1985); (*d*) W. C. Still and V. J. Novack. J. Am. Chem. Soc. **106**, 1148 (1984).
3. J. Dale. Top. Stereochem. **9**, 199 (1976).
4. W. C. Still, M. Kahn, and A. Mitra. J. Org. Chem. **43**, 2923 (1978).
5. E. Neeland, J. P. Ounsworth, R. J. Sims, and L. Weiler. Tetrahedron Lett. **28**, 35 (1987).
6. D. H. R. Barton and W. B. Motherwell. Pure Appl. Chem. **53**, 15 (1981).
7. J. Dale. Acta Chem. Scand. **27**, 1149 (1973).
8. W. B. Schweizer and J. D. Dunitz. Helv. Chim. Acta, **65**, 1547 (1982).
9. T. H. Keller, E. G. Neeland, and L. Weiler. J. Org. Chem. **52**, 1870 (1987).
10. I. Paterson and I. Fleming. Tetrahedron Lett. **20**, 993 (1979).
11. (*a*) E. J. Corey. J. Am. Chem. Soc. **76**, 175 (1954); (*b*) R. E. Ireland, R. H. Mueller, and A. K. Willard. J. Am. Chem. Soc. **98**, 2868 (1976).
12. P. Deslongchamps. *In* Stereoelectronic effects in organic chemistry. *Edited by* J. E. Baldwin. Pergamon Press, Oxford. 1983.

[3]S. Rettig and J. Trotter, to be published.

[4]In secondary esters or lactones, one of the alkyl groups prefers to be *trans* coplanar to the ester C—O bond, ref. 8.

[5]Analysis of the coupling constants and the possible conformations of these compounds suggest that some may be rapidly equilibrating mixtures of two or three conformations, with one conformation predominating.

Can. J. Chem. Downloaded from www.nrcresearchpress.com by 213.166.140.6 on 09/07/12
For personal use only.

S. Valverde, B. Herradón, R. M. Rabanal, and M. Martín-Lomas. Can. J. Chem. **65**, 332 (1987). Preparation of (4*R*,5*S*)-5-methyl-2,2-dimethyl-1,3-dioxolane-4-ylmethyl)-phosphonium iodide. A synthetic approach to olguine: further model studies.

Page 332. The title should read: "Preparation of (4*R*,5*S*)-(2,2,5-trimethyl-1,3-dioxolane-4-ylmethyl)triphenylphosphonium iodide. A synthetic approach to olguine: further model studies."

Can. J. Chem. Downloaded from www.nrcresearchpress.com by 213.166.140.6 on 09/07/12
For personal use only.

Glycosides from *Muscari comosum*. 7.[1] Structure of three novel muscarosides

MATTEO ADINOLFI,[2] GASPARE BARONE, MARIA MICHELA CORSARO, ROSA LANZETTA, AND LORENZO MANGONI
Dipartimento di Chimica Organica e Biologica della Università di Napoli, Via Mezzocannone 16, 80134 Napoli, Italy

AND

MICHELANGELO PARRILLI
Istituto di Chimica della Università della Basilicata, Via Nazario Sauro 85, 85100 Potenza, Italy

Received January 26, 1987

MATTEO ADINOLFI, GASPARE BARONE, MARIA MICHELA CORSARO, ROSA LANZETTA, LORENZO MANGONI, and MICHELANGELO PARRILLI. Can. J. Chem. **65**, 2317 (1987).

Muscarosides D, E, and F, three new 27-norlanostane tetra-, penta-, and hexasaccharides, respectively, isolated from the bulbs of *Muscari comosum*, were respectively shown to be (23*S*,24*S*)-3-*O*-{α-L-arabinopyranosyl(1→3)[β-D-apio-D-furanosyl(1→2)]-β-D-glucopyranosyl(1→2)-α-L-arabinopyranosyl(1→6)-β-D-glucopyranosyl}-17,23-epoxy-3β,24,30,31-tetrahydroxy-27-nor-5α-lanost-8-ene **4**, (23*R*)-3-*O*-{α-L-arabinofuranosyl(1→2)-α-L-arabinopyranosyl(1→3)[α-L-rhamnopyranosyl(1→2)]-β-D-glucopyranosyl(1→2)-α-L-arabinopyranosyl(1→6)-β-D-glucopyranosyl}-17,23-epoxy-3β,31-dihydroxy-27-nor-5α-lanost-8-en-15,24-dione **5**, and (23*S*)-3-*O*-[β-D-apio-D-furanosyl(1→2)-β-D-glucopyranosyl(1→2)-α-L-arabinopyranosyl(1→6)-β-D-glucopyranosyl]-17,23-epoxy-3β,31-dihydroxy-27-nor-5α-lanost-8-en-15,24-dione **6**. The structural details were elucidated by a combination of fast-atom-bombardment mass spectroscopy, one- and two-dimensional nuclear magnatic resonance spectroscopy, and comparison to model compounds expressly synthesized.

MATTEO ADINOLFI, GASPARE BARONE, MARIA MICHELA CORSARO, ROSA LANZETTA, LORENZO MANGONI et MICHELANGELO PARRILLI. Can. J. Chem. **65**, 2317 (1987).

Les muscarosides D, E et F sont respectivement de nouveaux tétra-, penta- et hexasaccharides du nor-27 lanostane qui ont été isolés des bulbes du *Muscari comosum* et pour lesquels il a été établi que les structures sont respectivement les suivantes : {α-L-arabinopyrannosyl(1→3) [β-D-apio-D-furannosyl(1→2)]-β-D-glucopyrannosyl(1→2)-α-L-arabinopyrannosyl(1→6)-β-D-glucopyrannosyl}-3-*O* époxy-17,23 tétrahydroxy-3β,24,30,31 nor-27 5α-lanostène-8-(23*S*,24*S*) (**4**), {α-L-arabinofuranosyl(1→2)-α-L-arabinopyrannosyl(1→3)-[α-L-rhamnopyrannosyl(1→2)]-β-D-glucopyrannosyl(1→2)-α-L-arabinopyrannosyl(1→6)-β-D-glucopyrannosyl}-3-*O* époxy-17,23 dihydroxy-3β,31 nor-27 5α-lanostène-8 dione-15,24-(23*R*) (**5**) et [β-D-apio-D-furannosyl(1→2)-β-D-glucopyrannosyl(1→2)-α-L-arabinopyrannosyl(1→6)-β-D-glucopyrannosyl]-3*O* époxy-17,23 dihydroxy-3β,31 nor-27 5α-lanostène-8 dione-15,24-(23*S*) (**6**). On a établi les détails de ces structures en faisant appel à une combinaison de spectroscopie de masse par bombardement avec des atomes rapides, de spectroscopie en résonance magnétique nucléaire à une et à deux dimensions et par comparaison avec des composés modèles qui ont été synthétisés expressément dans ce but.

[Traduit par la revue]

Previous papers (1–3) have described the isolation and the structure determination of three main components (muscarosides A **1**, B **2**, and C **3** (see Chart 1)) of the glycoside mixture isolated from the bulbs of *Muscari comosum* Miller. The aglycone moieties of these glycosides possess a 27-norlanostane skeleton and their structures are characterized by a spiro-fused tetrahydrofuran ring at the C-17 position. They are structurally related to a series of free nortriterpenes that we have isolated from the same source (4–7). The accumulation of knowledge on the isolation and the structure of both these glycosides and these nortriterpenes has enabled us to thoroughly examine the glycoside mixture. Thus we have isolated three further glycosides, muscarosides D–F, and have assigned them structures **4**–**6**, respectively, mainly by nmr spectroscopy and FAB (free atom bombardment) ms. Whereas the aglycone moieties **8** and **14** of **5** and **6**, respectively, were known compounds, that of muscaroside D **4** is the novel nortriterpene **7**.

Muscarosides E and F were isolated by hplc (C-18 reverse phase column) of the mother liquors from the crystallization of muscaroside B (2). Muscaroside D was isolated by hplc (C-18 reverse phase column) and dry column chromatography (silica gel) of the fractions *c* of the crude glycoside mixture obtained from the bulbs. Muscarosides D–F were all homogeneous (tlc, ^{1}H and ^{13}C nmr spectroscopy) powder solids.

The negative-ion FAB mass spectrum of muscaroside D **4** (Fig. 1*a*) exhibited an ion peak at *m/z* 1195 $(M - H)^-$, which, together with ^{13}C and ^{1}H nmr data, suggested the molecular formula $C_{56}H_{92}O_{27}$. The corresponding molecular weight of 1196 daltons was confirmed by the presence of the peaks at *m/z* 1219 and 1197, formed by cationization of the molecule with Na^+ and H^+ respectively, in the positive-ion spectrum (Fig. 1*b*).

The appearance of the ^{1}H nmr signals of the aglycone moiety in the upfield part of the spectrum of muscaroside D in Py-d_5 at 500 MHz (Table 1, Fig. 2) was reminiscent of that of the 27-norlanostane triterpenes found in the bulbs of *Muscari comosum*. However, in the spectra of these latter the signals corresponding to the presence of the (24)C=O group ((25)CH_2 quartet at δ ca. 2.5) and (or) those corresponding to the presence of the (15)C=O group ((16)CH_2 ABq in the δ 2.3–3.1 zone) are clearly discerned (4–9). On the contrary, both these features are lacking in the spectrum of muscaroside D and, accordingly, no carbonyl-carbon signal was displayed in the ^{13}C spectrum. The novel structure **7** for the aglycone moiety of muscaroside D was mainly deduced from a 2D-COSY spectrum (Fig. 3), which allowed us to establish the scalar connectivity of the resonances of all the side-chain protons (positions 20–26), and from the comparison (Table 1) of the ^{13}C data of muscaroside D with those of known 27-norlanostanes **9** (8) and **10** (4) for the carbons 1–19 and 30–32 and for the carbons 20–26 respectively.

[1]Part 6: ref. 3.

[2]Author to whom correspondence may be addressed.

Can. J. Chem. Downloaded from www.nrcresearchpress.com by 213.166.140.6 on 09/07/12
For personal use only.

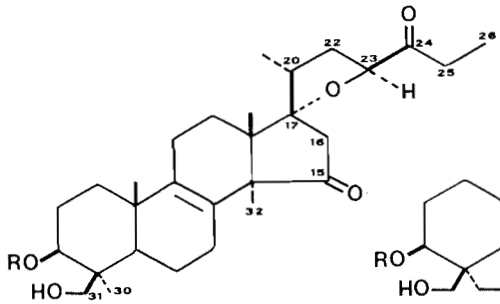

1 R = Ch1

2 R = Ch2

6 R = Ch3

14 R = H

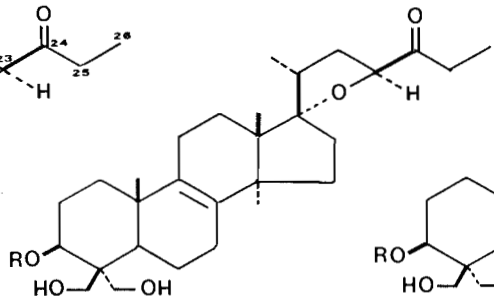

3 R = Ch3

9 R = H

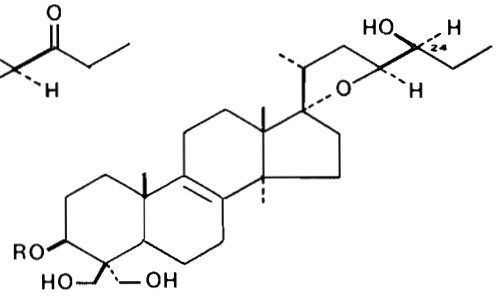

4 R = Ch4

7 R = H

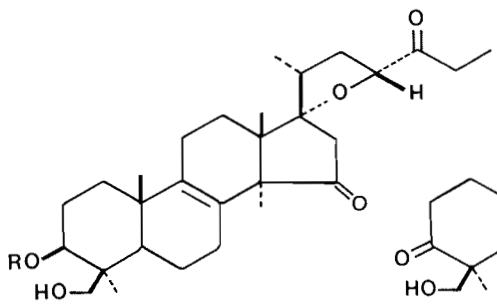

5 R = Ch2

8 R = H

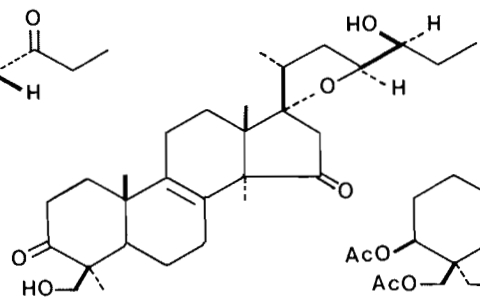

10

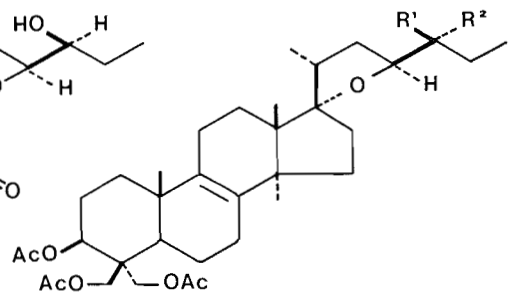

11 R', R² = O

12 R' = OH , R² = H

13 R' = H , R² = OH

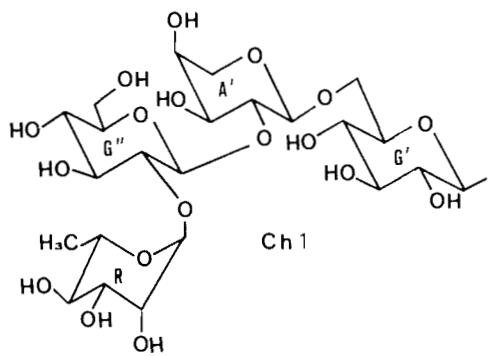

Ch 1

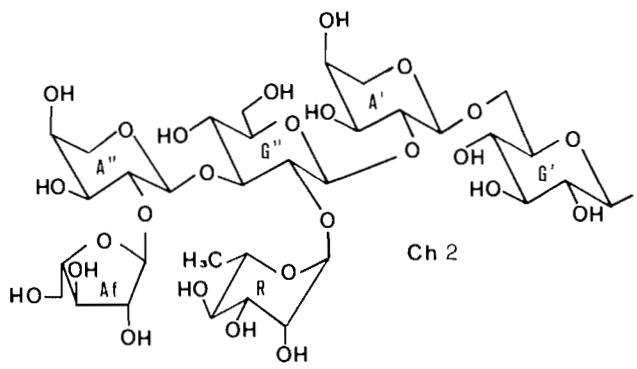

Ch 2

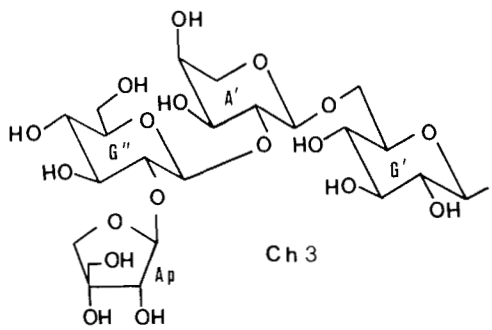

Ch 3

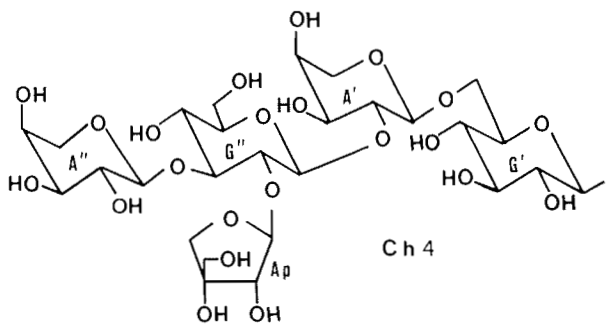

Ch 4

Can. J. Chem. Downloaded from www.nrcresearchpress.com by 213.166.140.6 on 09/07/12
For personal use only.

Can. J. Chem. Downloaded from www.nrcresearchpress.com by 213.166.140.6 on 09/07/12
For personal use only.

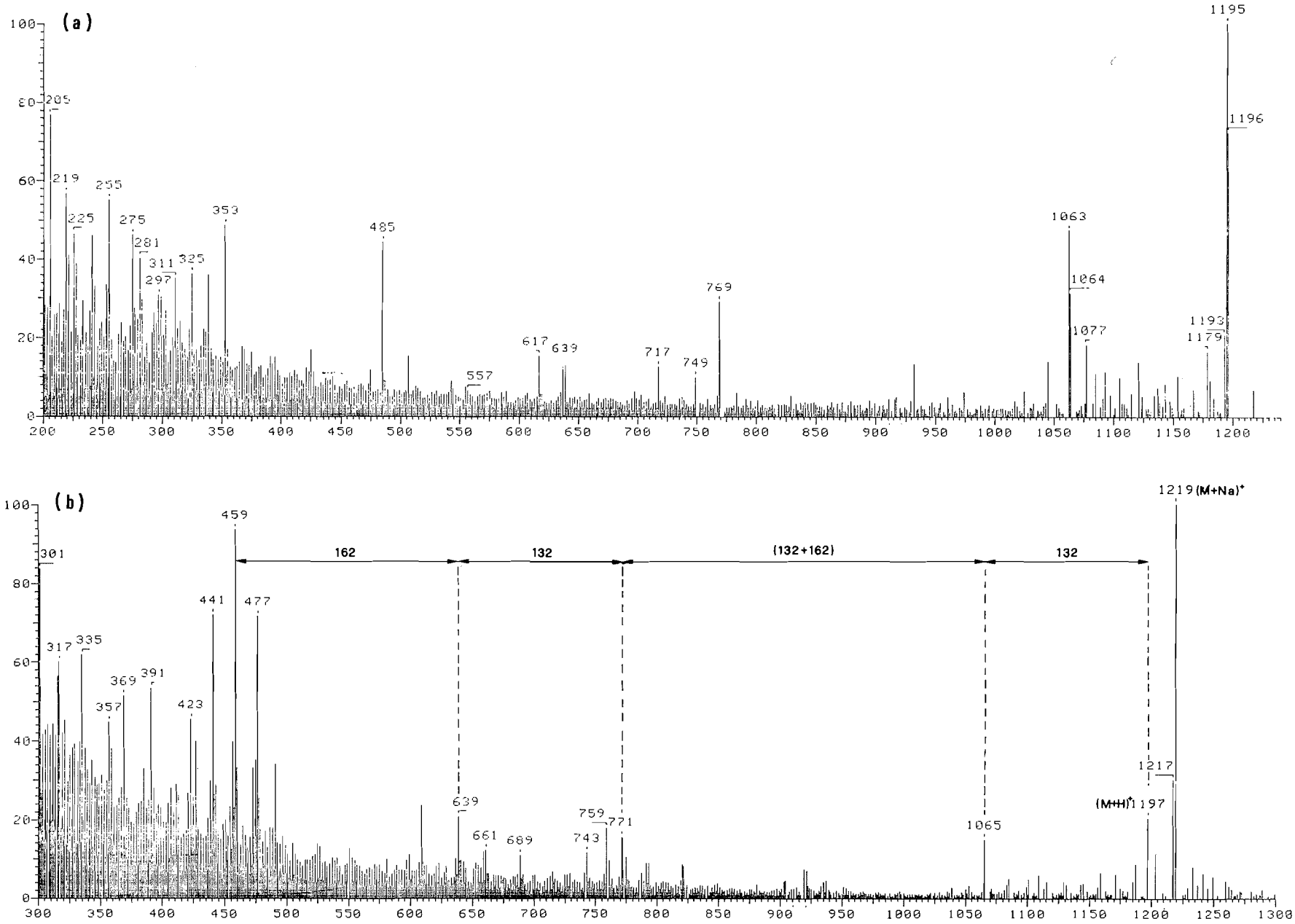

FIG. 1. Negative (*a*) and positive (*b*) ion FAB mass spectra of **4** (molecular weight = 1096 daltons). In (*b*) the losses of pentose (132 mass units) and hexose (162 mass units) residues are indicated.

TABLE 1. ^1H and ^{13}C data of muscaroside D **4** from one- and two-dimensional experiments and ^{13}C chemical shifts of reference substances

Carbon	Reference substances		**4**[a]	Glycosylation shift	Proton	δ[a,b]	Carbon	Reference substances[e]		**4**[a]	Glycosylation shift	Proton	2D-COSY[a]
							1	A[a]	105.4	G′ 105.5		1	5.12 (7.9)[f]
1	**9**[c]	35.5	Agl. 35.8		1a, 1b	1.72, 1.26	2		74.8	75.4		2	4.01
							3		78.1	78.4		3	4.05
2		27.5	27.2		2a, 2b	2.38, 2.12	4		71.4	72.4		4	4.15
							5		78.1	75.7	−2.4	5	3.86
3		77.9	82.3	+4.4	3	4.48	6		62.5	69.0	+6.5	6a, 6b	4.45, 4.22
4		46.0	48.1		—	—							
5		47.3	43.6	−3.7	5	[d]	1	B[a]	105.9	A′ 101.8	−4.1	1	5.05 (4.8)[f]
6		18.7	18.7		6a, 6b	[d]	2		72.2	80.8	+8.6	2	4.46
7		26.2	27.1		7a, 7b	[d]	3		74.4	72.4	−2.0	3	4.44
8		134.1	135.0		—	—	4		69.1	67.2		4	4.47
9		135.5	136.2		—	—	5		66.6	64.2		5a, 5b	4.28, 3.74
10		36.5	36.7		—	—							
11		20.8	21.2		11a, 11b	[d]	1	A[a]	105.4	G″ 103.7	−1.7	1	5.05 (7.9)[f]
12		24.9	25.4		12a, 12b	[d]	2		74.8	81.5	+6.7	2	3.95
13		48.7	49.0		—	—	3		78.1	87.0	+8.9	3	4.03
14		50.6	50.8		—	—	4		71.4	68.9	−2.5	4	4.01
15		31.7	32.2		15a, 15b	2.00, 1.48	5		78.1	77.7		5	3.66
							6		62.5	61.7		6a, 6b	4.33, 4.20
16		39.7	41.3		16a, 16b	2.42, 2.16							
17		97.2	95.4		—	—	1	B[a]	105.9	A″ 105.1		1	4.91 (7.2)[f]
18		19.5	19.5		18-H_3	0.93	2		72.2	72.6		2	4.35
19		19.2	19.6		19-H_3	1.04	3		74.4	74.4		3	4.42
							4		69.1	69.5		4	4.10
20	**10**[c]	44.4	44.2		20	2.05	5		66.6	67.7		5a, 5b	4.25, 3.78
21		17.7	17.2		21-H_3	1.02							
22		36.4	36.4		22a, 22b	1.90, 1.40	1	C[a]	111.2	Ap 111.1		1	6.24 (4.3)[f]
							2		78.1	77.7		2	4.74
23		82.0	81.5		23	4.10	3		80.4	79.5		—	—
24		77.9	76.9		24	3.52	4		75.3	74.7		4a, 4b	4.82, 4.32
25		30.0	29.9		25a, 25b	1.55	5		65.5	64.8		5a, 5b	4.17
26		10.2	10.7		26-H_3	1.12							
30	**9**[c]	71.3	61.2	−10.1	30a, 30b	4.90, 3.98							
31		63.8	62.4		31a, 31b	4.61, 3.96							
32		25.9	26.5		32-H_3	1.34							

[a]Measured in pyridine-d_5.
[b]Chemical shifts of the aglycone moiety protons were assigned mainly from two-dimensional carbon–proton shift correlation. Correlations clearly recognizable in the 2D-COSY are indicated by solid lines.
[c]Measured in $CDCl_3$.
[d]Not identified.
[e]Reference substances: A = methyl β-D-glucopyranoside (10); B = methyl α-L-arabinopyranoside (10); C = methyl β-D-apio-D-furanoside (11).
[f]$^3J_{H\text{-}1,H\text{-}2}$ (Hz).

Comparison with the nmr carbon lines of **10** suggested the *S* configuration for the chiral 24-position of muscaroside D. This was strengthened by comparison of the chemical shift of the 23- and 24-protons with those of model compounds. 27-Norlanostane **9** was transformed with acetic anhydride/pyridine into triacetate **11** and this latter was reduced with sodium borohydride to the 24-epimeric alcohols **12** and **13**, whose configuration at C-24, *S* and *R* respectively, was established by the glc modification of the Horeau method (12). Owing to the close similarity of the chemical shifts of the 23- and 24-protons of **4** (δ 4.10 and δ 3.52, respectively; Table 1) with those of **12** (δ 4.13 and δ 3.57, respectively) rather than with those of **13** (δ 4.20 and δ 3.78, respectively), *S* configuration may be confidently assigned to the chiral centre at C-24 of muscaroside D.

The 2D-COSY spectrum also allowed the identification of the proton signals of each monose unit of the sugar chain and then the assignment of the ^{13}C signals by tracing out the one-bond proton–carbon connectivities through the use of heteronuclear carbon–proton shift correlation. In addition to the nature of each monose unit, comparison of the ^{13}C chemical shifts with those of reference methyl glycosides also revealed the attachment positions in the sugar chain (through the glycosylation shifts) and the configuration at the anomeric centres. These data showed that muscaroside D possessed one terminal β-apiose unit, one terminal α-arabinopyranose unit, one nodal β-glucopyranose unit linked at its positions 2 and 3, one inner β-glucopyranose unit linked at its 6-position, and one inner arabinopyranose unit linked at its 2-position. The attachment of the sugar chain at the 3-position of the aglycone **7** was evident from the downfield shift (+4.4) observed for the 3-carbon of muscaroside D. The upfield shifts of the C-30 and C-5 signals were in agreement with this conclusion (13).

Can. J. Chem. Downloaded from www.nrcresearchpress.com by 213.166.140.6 on 09/07/12
For personal use only.

Can. J. Chem. Downloaded from www.nrcresearchpress.com by 213.166.140.6 on 09/07/12
For personal use only.

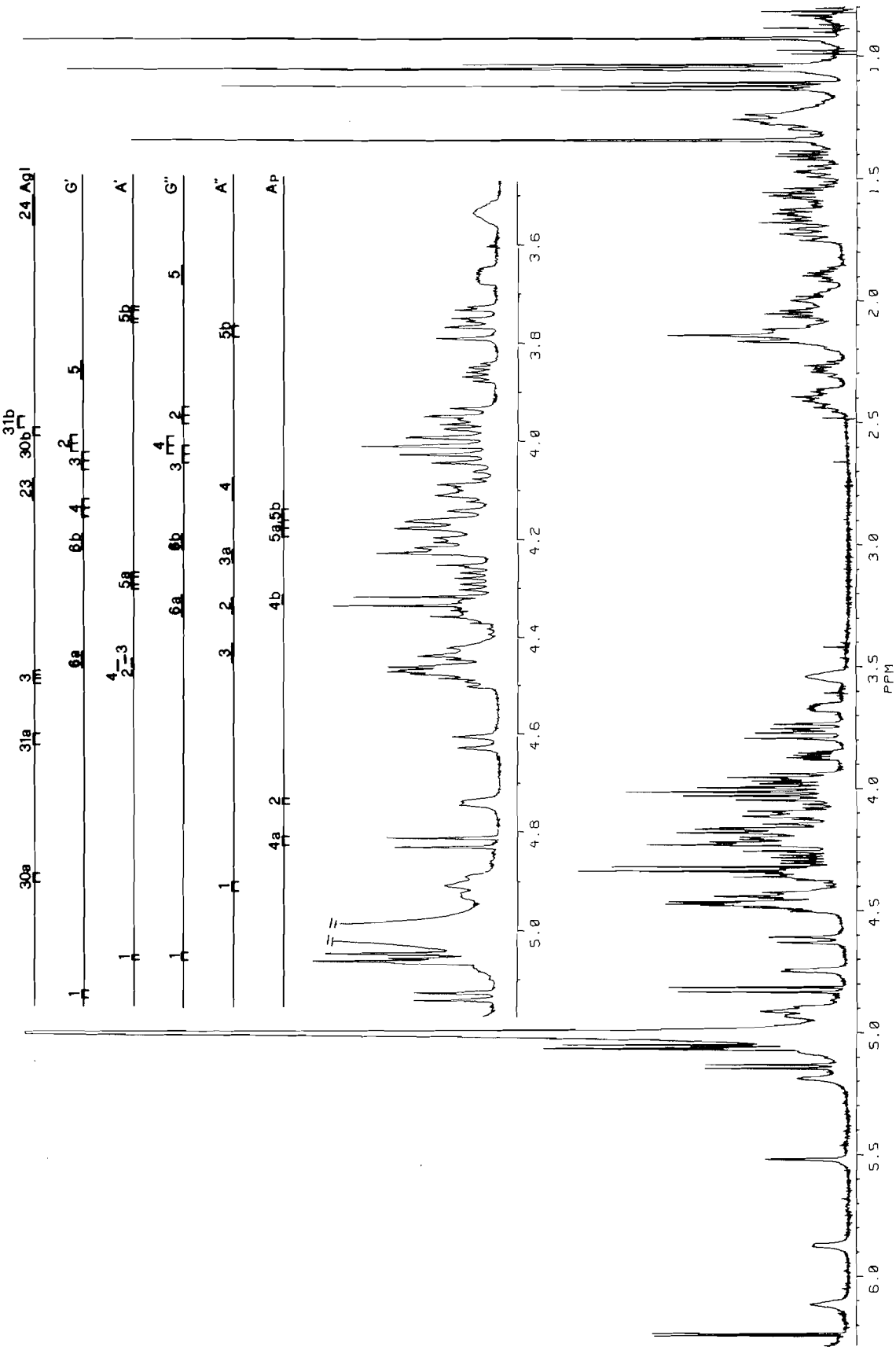

FIG. 2. The 500-MHz ^{1}H nmr spectrum of **4** in pyridine-d_5. The signals between δ 5.15 and δ 6.15 disappear upon addition of D_2O. In the insert, expansion of the sugar proton region is shown. Signal assignment derived from COSY (see Fig. 3) and C—H correlation experiments is indicated. Agl = aglycone; G′, G″, A′, A″, Ap = monose units as indicated in formula **4**.

Can. J. Chem. Downloaded from www.nrcresearchpress.com by 213.166.140.6 on 09/07/12
For personal use only.

The values of the coupling constants $^3J_{H\text{-}1,H\text{-}2}$ listed in Table 1 were consistent with the configuration of the anomeric centres determined from the ^{13}C data, the inner arabinopyranose unit excluded, owing to its high conformational mobility (1, 2, 14–16). However, the close similarity between the ^{13}C data of this monose unit of muscaroside D and those found for the α-arabinopyranosyl residues identically located in muscarosides A **1** and B **2** (Table 3) strongly supports the α-configuration for the relevant anomeric centre. The value of $^3J_{H\text{-}1,H\text{-}2}$ (4.8 Hz) observed for this monose unit, as compared to the value (7.9 Hz) displayed by the terminal arabinopyranose residue, would indicate that in the former a $^1C_4$ conformer is in considerable excess over the $^4C_1$ conformer.

A significant Overhauser effect measured for the nmr signal at δ 3.95 of the 2-proton of the nodal glucopyranose upon irradiation of the anomeric proton (δ 6.24) of the apiose terminal residue indicated that this latter is directly linked to the 2-proton of the nodal glucopyranose. The determination of the glycone sequence was completed on the basis of the positive-ion FAB-ms data. The peak at m/z 639 $[(M + H) - (132 + 132 + 132 + 162)]^+$ due to the loss of a fragment constituted by three pentose and one hexose indicated that the inner glucopyranose is directly linked to the aglycone. Thus the m/z 771 (= 639 + 132) peak indicated that the inner arabinopyranose is located between the nodal glucopyranose and the inner glucopyranose and, consequently, that also the terminal arabinopyranose is directly linked to the nodal residue. This latter point is also confirmed by the lack in the spectrum of a peak corresponding to the loss of a disaccharide. The sugar sequence, therefore, is that depicted in formula **4**.

Owing to the small amount of **4** available, chemical degradative methods could be applied to the structure determination of the compound only after the spectral data were collected. Acid hydrolysis (7% H_2SO_4) of **4** confirmed apiose, glucose, and arabinose to be the monose units of the sugar chain by tlc and hplc of the water-soluble fraction of the hydrolysate through comparison with authentic samples of the monosaccharides. A 1:2:2 molar ratio of the monoses was established on calibration of the hplc peak integrated areas against known concentrations. The monose-containing water-soluble fraction of the hydrolysate was perbenzoylated with benzoyl chloride and pyridine and the pure perbenzoates (α-anomers (17)) of glucose and arabinose were isolated by hplc. Identity in chirality and amplitude of their cd (circular dichroism) curves with those of the perbenzoates (α-anomers) obtained from authentic samples of D-glucose and L-arabinose established the absolute configuration D of both glucopyranose units and the absolute configuration L of both arabinopyranose units in the sugar chain of muscaroside D. The absolute configuration of the apiose unit was assumed to be the same as in muscaroside C **3** (3).

The positive-ion FAB mass spectrum of muscaroside E showed a pseudomolecular ion peak at m/z 1361 $[M + Na]^+$, which, together with ^{13}C data (Table 3), suggested the molecular formula $C_{62}H_{96}O_{31}$.

In the upfield part of the ^1H spectrum (Table 2) of muscaroside E the signals of four tertiary (δ 0.93 s, δ 0.96 s, δ 1.54 s, δ 1.55 s), one secondary (δ 0.87 d), and one primary (δ 1.13 t) methyl group are observed. In addition, the signals of one methylene group appear centered at δ 2.7 and δ 2.8 as 16 lines of the AB part of an ABX_3 system, correlated by scalar coupling with the primary methyl group, and the signals of a second methylene group appear centered at δ 2.37 and δ 2.78 as an AB quartet. The close similarity between these ^1H nmr

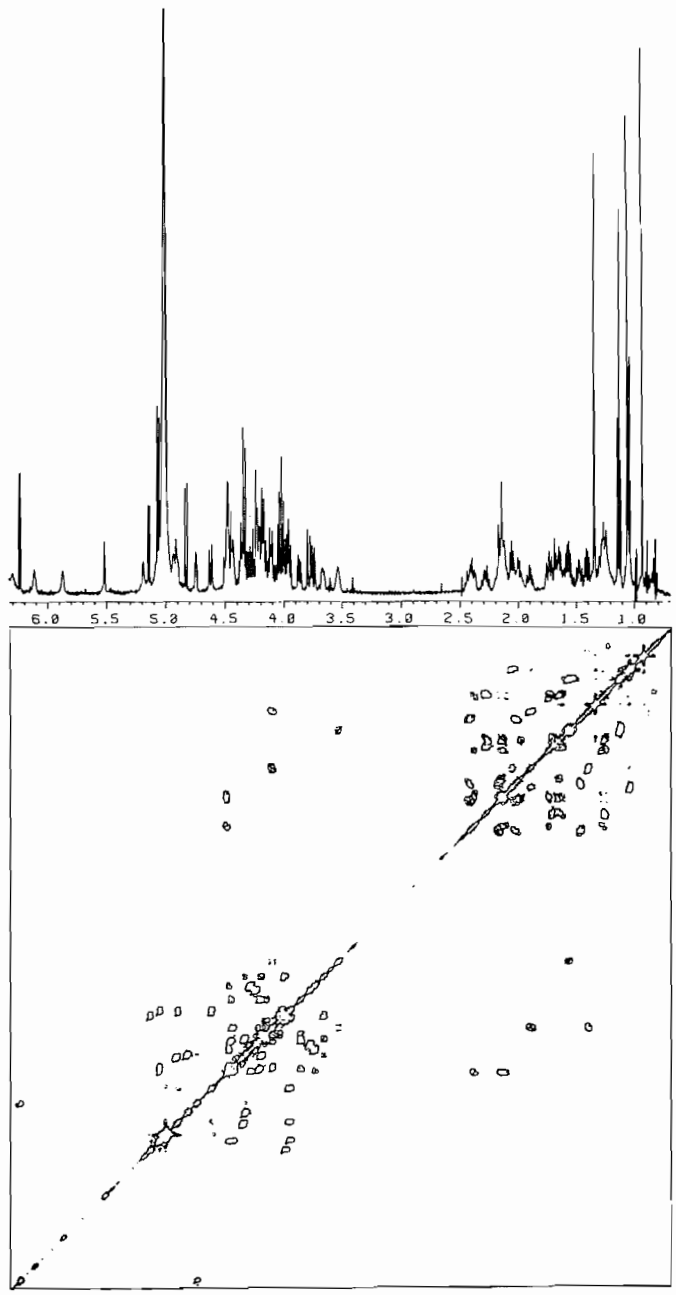

FIG. 3. Contour plot of COSY of **4** (500 MHz, pyridine-d_5).

data and the ^{13}C nmr data for the aglycone carbons of muscaroside E with the relevant nmr data obtained for (23*R*)-17,23-epoxy-3β,31-dihydroxy-27-nor-5α-lanost-8-ene-15,24-dione **8** (5) indicated that this latter constitutes the aglycone moiety of muscaroside E.

Upon the application of the chemical procedure used for **4**, the sugar chain of muscaroside E was confirmed to be constituted by one rhamnose, three arabinose, and two glucose units, whose absolute configuration was established to be L, L, and D, respectively, by the cd method already applied to **4**.

Comparison of the nmr data of muscaroside E with the ^{13}C (Table 3) and ^1H (Table 2) data of muscaroside B **2**, whose sugar chain has the same monose composition, showed the *quasi*-identity of the sugar-carbon chemical shifts in the two compounds and therefore indicated that the sequence of the

TABLE 2. ^{1}H nuclear magnetic resonance chemical shifts (δ) of **2**, **5**, **6**, and **8** in pyridine-d_5

Proton	**8** [a,b]	**5**	**2** [c]	**6**
18-H_3	0.938 s	0.93 s [d]	0.93 s [d]	0.90 s [c]
19-H_3	0.958 s	0.96 s [d]	0.95 s [d]	0.94 s [c]
21-H_3	0.903 d	0.87 d	1.05 d	1.05 d
	J = 6.99	J = 6.8	J = 6.6	J = 7.0
30-H_3	1.260 s	1.54 s [e]	1.55 s	1.54 s [e]
32-H_3	1.343 s	1.55 s [e]	1.70 s	1.69 s [e]
25-H_2	2.667, 2.754 [f]	2.7, 2.8 [g]	2.46 q	2.46 q
			J = 7.3	J = 7.4
26-H_3	1.087 t	1.13 t	1.03 t	1.03 t
		J = 7	J = 7.3	J = 7.4
16-H_2	2.244, 2.658	2.37, 2.78	2.38, 3.06	2.31, 3.03
	ABq, J = 19.12	ABq, J = 19.4	ABq, J = 19.0	ABq, J = 19.4
R-6-H_3		1.74 d	1.75 d	
		J = 6.2	J = 6.1	
G′-1-H		4.96 d	4.98 d	4.98 d
		J = 7.5	J = 7.7	J = 7.9
A′-1-H		5.27 d	5.29 d [e]	5.23 d
		J = 3.9	J = 4.4	J = 3.9
G″-1-H		5.20 d	5.21 d	5.09 d
		J = 6.6	J = 7.2	J = 7.3
A″-1-H		5.17 d	5.18 d [e]	
		J = 6.1	J = 6.1	
A_f-1-H		6.04 d	6.05 d	
		J = 1.3	J = 1.5	
R-1-H		5.97 d	5.98 d	
		J = 1.8	J = 1.8	
Ap-1-H				6.37 bs

[a] Measured in $CDCl_3$.
[b] Reference 5.
[c] Reference 2.
[d,e] Interchangeable values.
[f] Sixteen lines of the AB part of a nearly first-order ABX_3 spectrum (X_3 = 26-H_3); J_{AB} = 18.02, J_{AX} = 7.35, J_{BX} = 7.35.
[g] Sixteen lines of the AB part of a nearly first-order ABX_3 spectrum (X_3 = 26-H_3).

monose units, the configuration at the anomeric centres, the position of the interglycosidic linkages, and the monose-ring size were the same in both muscarosides. Therefore, muscaroside E possesses structure **5**.

On acid hydrolysis, muscaroside F afforded glucose, arabinose, and apiose (molar ratio 2:1:1) as sugar components. This result suggested that muscaroside F possessed a sugar chain identical with that of known muscaroside C **3**. This was confirmed by comparison of the ^{13}C signals. The aglycone portion was identified to be eucosterol **14** (9) as in muscaroside A **1** and muscaroside B **2** by analysis of the ^{13}C and ^{1}H spectra (Tables 2 and 3). Muscaroside F was consequently identified as eucosterol 3-*O*-β-D-apio-D-furanosyl(1→2)-β-D-glucopyranosyl-(1→2)-α-L-arabinopyranosyl(1→6)-β-D-glucopyranoside **6**. Structure **6** was confirmed by the negative-ion FAB mass spectrum, which displayed peaks at m/z 1059 (pseudomolecular ion, $(M - H)^-$) and at m/z 927, 765, and 633, corresponding to the losses of the apiosyl, apiosyl-glucosyl, and apiosyl-glucosyl-arabinosyl fragments, respectively.

Experimental

General

The ^{1}H (270 MHz) and ^{13}C (67.88 MHz) spectra were taken on a Fourier transform Bruker instrument WH 270 (TMS as internal reference) with an Aspect 2000 computer with 48 K memory (32 K data). Mass spectra were recorded with a VG ZAB HF or a Kratos MS 50 instrument equipped with an FAB source. The hplc was performed with a Varian 5060 instrument using a differential refractometer Waters R 401 as the detector. The tlc was carried out on precoated silica gel layers (0.25 mm, Merck F_{254}). Silica gel 0.05–0.20 (Merck) was used for column chromatography.

*Proton and carbon nuclear magnetic resonance spectra of **4***

Spectra were obtained at 500/125.77 MHz (^{1}H/^{13}C) on a Fourier transform Bruker WM 500 spectrometer equipped with a dual probe and with an Aspect 2000 computer.

One-dimensional spectra were obtained with 5000 Hz (0–10 ppm) and 27 500 Hz (0–220 ppm) spectral widths for proton and carbon respectively.

Nuclear Overhauser enhancements were obtained in the difference mode as reported in ref. 1.

Two-dimensional correlated spectroscopy (COSY-45) was executed with 90°–45° pulses separated by an incrementable evolution time t_1. Each spectrum required a total of 32 pulses in a 512 × 2048 data set, which took approximately 10 h to acquire. Quadrature detection was applied in both directions using a 16-step phase cycling for N-type peak selection. Data were multiplied with a sine-bell shaping function, zero filled, Fourier transformed, and symmetrized. Processing and plotting time for the spectrum was approximately 2 h.

Two-dimensional carbon–proton shift correlations were performed by choosing polarization transfer delays equal to average one-bond couplings of J(CH) = 140 Hz. Exponential multiplication in the ^{13}C domain and Gaussian resolution enhancement in the ^{1}H were applied to a 256 × 1024 data matrix prior to Fourier transformation.

Isolation of muscarosides D, E, and F

Fraction *c* (ref. 1) was subjected to hplc (Lichrosorb RP-18 (7 μm),

Can. J. Chem. Downloaded from www.nrcresearchpress.com by 213.166.140.6 on 09/07/12
For personal use only.

TABLE 3. ^{13}C nuclear magnetic resonance shifts of **1**, **2**, **3**, **5**, **6**, and reference substances (glycosylation shifts)

Carbon	Reference substances[a,b]			**1**[b,c]	**2**[b,d]	**3**[b,e]	**5**[b]	**6**[b]
G′-1	A	105.4		106.1	106.2	105.5	106.1	106.1
G′-2		74.8		75.4	75.3	75.5	75.3	75.4
G′-3		78.1		78.2	78.2	78.3	78.2	78.4
G′-4		71.4		71.5	71.8	72.6	71.7	72.7
G′-5		78.1		75.5 (−2.6)	75.6 (−2.5)	75.5 (−2.6)	75.6 (−2.5)	75.8 (−2.3)
G′-6		62.5		68.7 (+6.2)	68.8 (+6.3)	68.8 (+6.3)	68.8 (+6.3)	69.0 (+6.5)
A′-1	B	105.9		101.2 (−4.7)	101.4[h]	101.3 (−4.6)	101.4[h]	101.5 (−4.4)
A′-2		72.2		79.3 (+7.1)	79.4 (+7.2)	79.6 (+7.4)	79.4 (+7.2)	79.7 (+7.5)
A′-3		74.4		72.3 (−2.1)	72.3 (−2.1)	72.1 (−2.3)	72.3 (−2.1)	72.2 (−2.4)
A′-4		69.1		66.5	67.0	66.9	67.0	67.1
A′-5		66.6		64.2	63.2	63.2	63.1	63.5
G″-1	A	105.4		103.1 (−2.3)	102.8[h]	103.7 (−1.7)	102.8[h]	103.7 (−1.7)
G″-2		74.8		78.3 (+3.5)	76.2 (+1.4)	79.8 (+5.0)	76.2 (+1.4)	80.0 (+5.2)
G″-3		78.1		77.7 (−0.4)	87.3 (+9.2)	77.6 (−0.5)	87.3 (+9.2)	77.8 (−0.3)
G″-4		71.4		71.5	68.9 (−2.5)	71.2	68.9 (−2.5)	71.3
G″-5		78.1		78.3	77.7	78.2	77.7	78.5
G″-6		62.5		62.7	61.8	63.2	61.8	63.2
R-1	C	102.4		102.2	102.4		102.5	
R-2		71.9		72.7	71.9		71.9	
R-3		72.5		72.7	72.9		72.9	
R-4		73.6		74.3	73.9		74.0	
R-5		69.4		69.5	70.2		70.2	
R-6		18.4		18.7	18.7		19.7	
A″-1	B	105.9			102.6[h]		102.5[h]	
A″-2		72.2			77.8 (+5.6)		77.7 (+5.5)	
A″-3		74.4			72.5 (−1.9)		72.5 (−1.9)	
A″-4		69.1			68.1		68.0	
A″-5		66.6			65.7		65.6	
A_f-1	D	110.4			110.0		110.0	
A_f-2		83.0			81.8		81.8	
A_f-3		78.5			78.7		78.7	
A_f-4		85.5			85.3		85.3	
A_f-5		62.7			62.5		62.5	
Ap-1	E	111.2				111.2		111.2
Ap-2		78.1				77.9		78.2
Ap-3		80.4				80.4		80.3
Ap-4		75.3				75.4		75.4
Ap-5		65.5				66.0		66.0
1	**8**[f,g]	35.7	**14**[b,c] 35.9	35.7	35.63	35.8	35.7	35.6
2		28.5	29.0	27.4	27.34	27.3	27.5	27.3
3		80.7	80.0	89.0	88.85	82.2	88.9 (+8.2)	88.9 (+8.9)
4		43.1	43.2	44.4	44.35	48.2[h]	43.4	44.3
5		49.5	51.3	51.4	51.25	43.6	49.4	51.3
6		18.4	18.9	18.7	18.73	18.8	18.7	18.6
7		27.0	27.3	27.4	27.34	26.6	27.5	27.5
8		133.4	133.1	133.2	132.83	134.8	133.1	133.0
9		135.9	136.4	136.6	136.18	135.8	136.5	136.4
10		37.5	37.7	37.3	37.19	36.8	37.3	37.2
11		20.7	20.9	20.8	20.76	21.2	20.7	20.7
12		23.3	23.3	23.3	23.14	25.4	23.3	23.1
13		47.4	47.6	47.7	47.65	49.0[h]	47.4	47.7
14		58.0	58.0	58.0	57.98	50.9	58.0	58.0
15		215.5	215.2	215.2	215.10	32.2	215.1	215.2
16		51.1	52.0	52.0	51.91	39.8	51.4	51.9
17		90.9	91.3	91.3	91.22	97.2	91.1	91.2
18		20.5	20.4	20.5	20.44	19.4	20.4	20.4
19		20.0	20.0	19.4	19.37	19.7	19.3	19.3
20		41.3	43.4	43.4	43.33	43.8	41.0	43.3
21		18.4	17.2	17.1	17.13	17.3	18.4	17.1
22		36.1	36.9	36.9	36.87	36.9	36.0	36.8

Can. J. Chem. Downloaded from www.nrcresearchpress.com by 213.166.140.6 on 09/07/12
For personal use only.

TABLE 3. (*concluded*)

Carbon	Reference substances[a,b]		**1**[b,c]	**2**[b,d]	**3**[b,e]	**5**[b]	**6**[b]
23	81.0	81.9	81.9	81.80	81.7	80.3	82.0
24	213.0	211.9	211.7	211.31	212.5	212.2	211.4
25	32.1	32.4	32.3	32.29	32.4	32.1	32.2
26	7.7	7.6	7.6	7.61	7.7	7.8	7.5
30	22.4	23.4	23.2	23.14	61.2	23.2	23.1
31	64.6	64.4	62.3	63.11	62.7	63.1	62.1
32	24.7	24.1	24.1	24.14	26.3	24.5	24.1

[a]Reference substances: A = methyl β-D-glucopyranoside (10); B = methyl α-L-arabinopyranoside (10); C = methyl α-L-rhamnopyranoside (10); D = methyl α-L-arabinofuranoside (18); E = methyl β-D-apio-D-furanoside (11).
[b]Measured in pyridine-d_5.
[c]Reference 1.
[d]Reference 2.
[e]Reference 3.
[f]Reference 5.
[g]Measured in $CDCl_3$.
[h]Interchangeable values.

70:30 methanol–water, 5 mL min^{-1}) and subsequent dry column chromatography (silica gel, 14:6:1 chloroform–methanol–water) to give muscaroside D **4** (6 mg). Positive-ion FAB ms (Fig. 1*b*): 1219 (M + Na)$^+$, 1197 (M + H)$^+$, 1065 (M + H − 132)$^+$, 771 (M + H − 132 − 132 − 162)$^+$, 639 (M + H − 132 − 132 − 162 − 132)$^+$, 477 (M + H − 132 − 132 − 162 − 132 − 162)$^+$ *m/z*. Negative-ion FAB ms (Fig. 1*a*): 1195 (M − H)$^-$, 1063 (M − H − 132)$^-$, 769 (M − H − 132 − 132 − 162)$^-$, 637 (M − H − 132 − 132 − 162 − 132)$^-$ *m/z*. The ^{1}H and ^{13}C nmr data are given in Table 1 and Figs. 2 and 3.

The mother liquors from the crystallization (ethanol) of crude muscaroside B (ref. 2) were subjected to hplc (Lichrosorb RP-18 (7 μm), 80:20 methanol–water, 5 mL min^{-1}) to give pure muscaroside E **5** (30 mg) and pure muscaroside F **6** (10 mg). Negative-ion FAB ms of **5**: 1337 (M − H)$^-$, 1205 (M − H − 132)$^-$, 1191 (M − H − 146)$^-$, 1073 (M − H − 132 − 132)$^-$, 1059 (M − H − 132 − 146)$^-$, 927 (M − H − 132 − 132 − 146)$^-$, 765 (M − H − 132 − 132 − 146 − 162)$^-$, 633 (M − H − 132 − 132 − 146 − 162 − 132)$^-$ *m/z*. Negative-ion FAB ms of **6**: 1059 (M − H)$^-$, 927 (M − H − 132)$^-$, 765 (M − H − 132 − 162)$^-$, 633 (M − H − 132 − 162 − 132)$^-$ *m/z*. The ^{1}H and ^{13}C nmr data of **5** and **6** are given in Tables 2 and 3.

Acid hydrolysis of muscarosides D, E, and F

Acid hydrolysis of muscarosides D, E, and F was performed with 7% H_2SO_4 as for muscaroside A (1). The water-soluble fraction of each hydrolysate was analyzed by tlc (silica gel layers, 14:6:1 chloroform–methanol–water) and by hplc ((Lichrosorb RP-18 (10 μm), 4:1 acetonitrile–water, 0.5 mL min^{-1}). The presence of apiose, arabinose, and glucose in the 1:2:2 molar ratio in the hydrolysate from muscaroside D; of rhamnose, arabinose, and glucose in the 1:3:2 molar ratio in the hydrolysate from muscaroside E; and of apiose, arabinose, and glucose in the 1:1:2 molar ratio in the hydrolysate from muscaroside F was established by tlc and hplc comparison with authentic samples of the monoses and by integration of the hplc peaks (1).

Perbenzoylation of the hydrolysates from muscarosides D and E

The water-soluble fraction obtained from the hydrolysis of **4** was perbenzoylated with benzoyl chloride in dry pyridine at room temperature for 12 h. The reaction mixture was diluted with methanol and toluene and the excess solvent was evaporated. The residue was filtered through a short silica gel column with chloroform and then submitted to hplc (μ Porasil, 9:1 hexane – ethyl ether, 2 mL min^{-1}). The two fractions containing the perbenzoates of glucose and of arabinose, respectively, were evaporated and the residues were dissolved in methanol. The amplitudes +16 and +72, respectively, of the split cd curves (19) were measured for the two samples by deducing concentration from uv absorbance.

Upon application of the same procedure to the hydrolysate obtained from muscaroside E, perbenzoates of glucose, arabinose, and rhamnose were obtained. The amplitudes +14, +69, and −10, respectively, were calculated from the split cd curves in methanol.

Authentic samples of D-glucose, L-arabinose, and L-rhamnose were equilibrated in acidic water and then perbenzoylated under the same conditions as the above hydrolysates to give α-D-1,2,3,4,6-pentabenzoylglucopyranose, α-L-1,2,3,4-tetrabenzoylarabinofuranose, and α-L-1,2,3,4-tetrabenzoylrhamnopyranose. The amplitudes of their split cd curves in methanol were +15, +74, and −11, respectively.

*Alcohols **12** and **13***

A sample of **9** (8) (4 mg) was acetylated (acetic anhydride and pyridine, 24 h, room temperature) to give crude triacetate **11** (6 mg), which was dissolved in methanol (1 mL) and treated with sodium borohydride (5 mg) at 5°C for 30 min. Usual work-up and subsequent tlc (silica gel layer, 4:1 hexane – ethyl acetate, 4 runs) gave pure alcohols **12** (2 mg) and **13** (2 mg).

The ^{1}H nmr data of **12**, δ: 0.94 and 1.09 (3H, s each, 18-H_3 and 19-H_3), 1.08 (3H, d, $J_{20,21}$ = 6.6 Hz, 21-H_3), 1.14 (3H, t, $J_{25,26}$ = 7.3 Hz, 26-H_3), 1.39 (3H, s, 32-H_3), 3.57 (1H, m, 24-H), 4.13 (1H, m, 23-H), 4.42 and 4.51 (2H, ABq, J_{AB} = 11.6 Hz, 30-H_2 or 31-H_2), 4.46 and 4.72 (2H, ABq, J_{AB} = 12.2 Hz, 31-H_2 or 30-H_2), 5.16 (1H, X of ABX, J_{AX} + J_{BX} = 17.2 Hz, 3-H).

The ^{1}H nmr data of **13**, δ: 0.95 and 1.10 (3H, s each, 18-H_3 and 19-H_3), 1.11 (3H, d, $J_{20,21}$ = 6.6 Hz, 21-H_3), 1.18 (3H, t, $J_{25,26}$ = 7.3 Hz, 26-H_3), 1.40 (3H, s, 32-H_3), 3.78 (1H, m, 24-H), 4.20 (1H, m, 23-H), 4.42 and 4.51 (2H, ABq, J_{AB} = 11.8 Hz, 30-H_2 or 31-H_2), 4.47 and 4.72 (2H, ABq, J_{AB} = 12.1 Hz, 31-H_2 or 30-H_2), 5.17 (1H, X of ABX, J_{AX} + J_{BX} = 17.2 Hz, 3-H).

24-Alcohols **12** and **13** were separately treated with (±)-α-phenylbutyric anhydride, and the excess of anhydride was analyzed by glc at 200°C on a 25-m glass capillary column coated with OV-101 as (+)-*R*-α-phenylethylamides of (−)*R*- and (+)*S*-phenylbutyric acid, following the procedure described in ref. 12. A peak increment of +8% for the *R*-acid was calculated in the experiment for the alcohol **12**, indicating *S* configuration of C-24 in **12**. A peak increment of +5% for the *S*-acid was calculated in the experiment for the alcohol **13**, indicating *R* configuration of C-24 in **13**.

Acknowledgments

We thank Prof. H. Egge, Institut für Physiologische Chemie, Bonn, for the FAB mass spectra of **5** and **6**; the IMIB-CNR, Napoli, for the FAB mass and the 500/125.77 MHz nmr spectra of **4**; the Centro Interdipartimentale di Metodologie Chimico-Fisiche, Università di Napoli, for the 270/67.88 MHz nmr

Can. J. Chem. Downloaded from www.nrcresearchpress.com by 213.166.140.6 on 09/07/12
For personal use only.

spectra; and the Ministero della Pubblica Istruzione, Roma, for financial support of this work.

1. M. ADINOLFI, G. BARONE, R. LANZETTA, G. LAONIGRO, L. MANGONI, and M. PARRILLI. Can. J. Chem. **61**, 2633 (1983).
2. M. ADINOLFI, G. BARONE, R. LANZETTA, G. LAONIGRO, L. MANGONI, and M. PARRILLI. Can. J. Chem. **62**, 1223 (1984).
3. R. LANZETTA, G. LAONIGRO, M. PARRILLI, and E. BREITMAIER. Can. J. Chem. **62**, 2874 (1984).
4. M. ADINOLFI, G. BARONE, R. LANZETTA, G. LAONIGRO, L. MANGONI, and M. PARRILLI. J. Nat. Prod. **46**, 559 (1983).
5. M. ADINOLFI, G. BARONE, R. LANZETTA, G. LAONIGRO, L. MANGONI, and M. PARRILLI. J. Nat. Prod. **47**, 100 (1984).
6. M. ADINOLFI, G. BARONE, R. LANZETTA, G. LAONIGRO, L. MANGONI, and M. PARRILLI. J. Nat. Prod. **47**, 541 (1984).
7. M. ADINOLFI, G. BARONE, R. LANZETTA, G. LAONIGRO, L. MANGONI, and M. PARRILLI. J. Nat. Prod. **47**, 721 (1984).
8. M. PARRILLI, R. LANZETTA, M. ADINOLFI, and L. MANGONI. Tetrahedron, **36**, 3591 (1980).
9. M. PARRILLI, M. ADINOLFI, and L. MANGONI. Gazz. Chim. Ital. **109**, 611 (1979).
10. S. SEO, Y. TOMITA, K. TORI, and Y. YOSHIMURA. J. Am. Chem. Soc. **100**, 3331 (1978).
11. H. ISHII, K. TORI, T. TOZIO, and Y. YOSHIMURA. Chem. Pharm. Bull. **26**, 674 (1978).
12. C. J. BROOKS and J. D. GILBERT. J. Chem. Commun. 194 (1973).
13. K. TORI, Y. YOSHIMURA, S. SEO, K. SAKURWI, Y. TOMITA, and I. ISHII. Tetrahedron, 4167 (1976).
14. K. MIZUTANI, R. KASAI, and O. TANAKA. Carbohydr. Res. **87**, 19 (1980).
15. H. ISHII, I. KITAGAWA, K. MATSUSHITA, K. SHIRAKAWA, K. TORI, T. TOZIO, M. YOSHIKAWA, and Y. YOSHIMURA. Tetrahedron Lett. 1529 (1981).
16. K. MIZUTANI, A. HAYASHI, R. KASAI, and O. TANAKA. Carbohydr. Res. **126**, 177 (1984).
17. H. LIU and K. NAKANISHI. Tetrahedron, **38**, 513 (1982).
18. R. ENCARNATION, L. KENNE, G. SAMUELSSON, and F. SANDBERG. Phytochemistry, **20**, 1939 (1981).
19. N. HARADA and K. NAKANISHI. Circular dichroic spectroscopy—Exciton coupling in organic stereochemistry. Oxford University Press. 1983.

Can. J. Chem. Downloaded from www.nrcresearchpress.com by 213.166.140.6 on 09/07/12
For personal use only.

Acetyl transfer reactions on $AlPO_4$–Al_2O_3

ANTONIO COSTA AND JUAN MARTIN RIEGO
Department of Chemistry, Universitat de les Illes Balears, E-07071 Palma de Mallorca, Spain

Received March 10, 1987

ANTONIO COSTA and JUAN MARTIN RIEGO. Can. J. Chem. **65**, 2327 (1987).

An efficient acetylation of alcohols and aliphatic amines promoted by the $AlPO_4$–Al_2O_3/ethyl acetate system is described. The solid catalyst acts, at least in part, as the acetyl carrier.

ANTONIO COSTA et JUAN MARTIN RIEGO. Can. J. Chem. **65**, 2327 (1987).

On décrit une méthode efficace d'acétyler les alcools et les amines aliphatiques qui est catalysée par le système $AlPO_4$–Al_2O_3/acétate d'éthyle. Le catalyseur solide agit, au moins en partie, comme porteur de groupements acétyles.

[Traduit par la revue]

Can. J. Chem. Downloaded from www.nrcresearchpress.com by 213.166.140.6 on 09/07/12
For personal use only.

Introduction

Derivatization of hydroxy and amino groups to the corresponding acetates and acetamides is a very common transformation in organic chemistry. Among the plethora of published methods, one of the most convenient is that of Posner *et al.* (1), which allows the chemoselective acetylation of primary alcohols under heterogeneous conditions, i.e., with ethyl acetate over commercial Al_2O_3 at room temperature.[1]

Continuing our work on solid acids (for a general discussion, see ref. 3), we would here like to report the use of synthetic $AlPO_4$–Al_2O_3 for the mild and efficient acetylation not only of aliphatic primary and (or) secondary alcohols but also of aliphatic amines.[2]

Experimental

The typical experimental procedure involves stirring a solution of the substrate (10 mmol) in dry ethyl acetate (150 mL) over 10 g of $AlPO_4$–Al_2O_3.[3] After 24 h at room temperature (or reflux in the case of secondary alcohols or aliphatic amines) work-up is simply carried out by filtration, solvent evaporation, and final distillation or recrystallization.

Results and discussion

As shown in Table 1, room temperature acetylation works well for primary monoalcohols and diols (entries 1–5). Refluxing is, however, required to drive the reaction of secondary alcohols to completion (entries 6–8). This difference in reactivity may be of utility for the chemoselective acetylation of primary alcohols. In accordance with this, in a competitive experiment carried out with an equimolar mixture of 1- and 2-pentanol under standard conditions (room temperature) only 1-pentyl acetate[4] was isolated in 75% yield (based on 1-pentanol). Not unexpectedly, however, 1,2- and 1,4-diols gave the corresponding diacetates (entries 9 and 10), probably because of the easy intramolecular migration of the acetate group.

Mild acetylation of labile molecules such as allylic and homoallylic alcohols (entries 12 and 13) was also successful, as it was with MOM (methyl-oxy-methyl) protected hydroxyalkyl phenol ethers (entry 14).

TABLE 1. $AlPO_4$–Al_2O_3 promoted acetylation of alcohols

Entry	Alcohol	Temperature (°C)	Yield (%)[a]
1	n-$C_6H_{13}OH$	25	85
2	n-$C_{16}H_{33}OH$	25	95
3	$PhCH_2OH$	25	95
4	$HO(CH_2)_2O(CH_2)_2OH$	25	75[b]
5	$HO(CH_2)_4OH$	25	90[b]
6	Cyclohexanol	77	60
7	Cholesterol	25	0
8	Cholesterol	77	96
9	$CH_3CH(OH)CH_2OH$	77	85[b]
10	$CH_3CH(OH)CH_2CH_2CH_2OH$	25	90[b]
11	$CH_3CH(OH)CH_2CH_2CH(OH)CH_3$	77	85[b]
12	(Z)-$CH_3CH_2CH{=}CHCH_2CH_2OH$	25	85
13	Geraniol	25	90
14	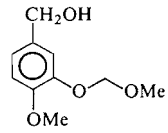	25	60[c]
15	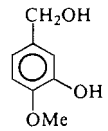	25	52[c,d]
16	$H_2N(CH_2)_2OH$	25	60[b]
17	$H_2N(CH_2)_5OH$	25	75[b]
18	n-$C_4H_9NH_2$	77	75
19	$PhNH_2$	77	0
20	p-MeO—$PhNH_2$	77	0

[a]Isolated yields of spectroscopically pure acetates.
[b]The product was the corresponding diacetate.
[c]After column chromatography of crude product.
[d]The product was 3-hydroxy-4-methoxy-benzyl acetate.

On the other hand, whilst our catalyst does not promote the acetylation of phenols (entry 15) and aromatic amines (entries 19 and 20), it did facilitate, however, the conversion of aliphatic amines and aminoalcohols (6) to the corresponding acetyl derivatives (entries 16–18).

These results are in sharp contrast with those reported by Posner (1), who describes Al_2O_3 as being capable of acylating aromatic amines but inefficient for aliphatic amines.

Although the understanding of the mechanism of acetyl transfer is restricted by lack of information about the nature of the actual acetylating agent (7), we felt that acyl transfer might

[1]For an excellent review covering organic reactions at alumina surfaces, see refs. 2 and 8.

[2]For recent applications of the $AlPO_4$–Al_2O_3 system, see ref. 4*a*; for synthesis and applications of other aluminophosphates, see ref. 4*b*.

[3]$AlPO_4$–Al_2O_3 can be handled in open atmosphere without appreciable loss of activity. See directions for preparation in ref. 5.

[4]2-Pentyl acetate could not be detected by gc or ^1H nmr analysis of the crude mixture.

Printed in Canada / Imprimé au Canada

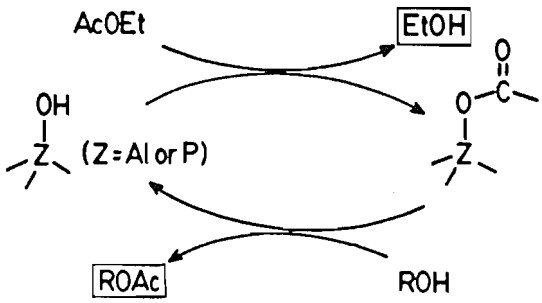

FIG. 1. Suggested mechanism for transesterification over $AlPO_4$–Al_2O_3.

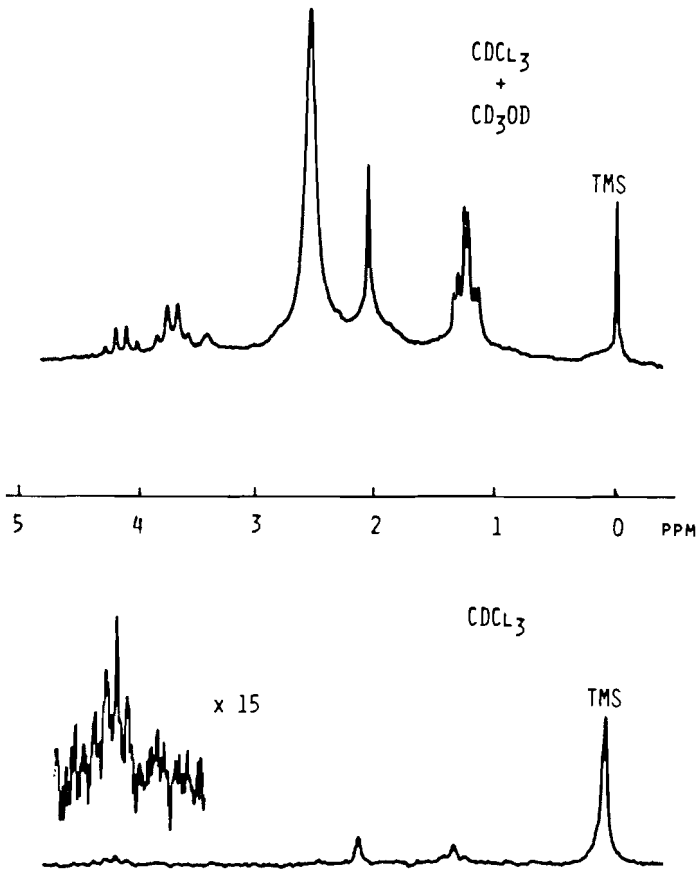

FIG. 2. The ^1H nmr spectrum of supernatant $CDCl_3$ over an acetylated catalyst before and after addition of CD_3OD.

take place first on the hydroxyl groups of the catalyst surface (8), thus generating a mixed anhydride-like structure that would eventually transfer the acetyl group to incoming nucleophiles (see Fig. 1).

Evidence in support of this mechanistic hypothesis was obtained by examining (gc, ^1H nmr) the behaviour of a sample of "acetylated catalyst" before and after the addition of alcohols. Thus treatment of a sample of $AlPO_4$–Al_2O_3 with *n*-butyl acetate (12 h, reflux) allowed us to unambiguously demonstrate (gc, ^1H nmr) the presence of *n*-butanol in the supernatant. Furthermore, filtration of the mixture followed by thorough drying of the solid under high vacuum (0.003 Torr, 10 h; 1 Torr = 133.3 Pa) yielded an acetylated catalyst that reacted with benzyl alcohol in toluene (room temperature, 24 h) providing the expected benzyl acetate (gc, ^1H nmr, ir). The presence of some *n*-butanol was also observed in the reaction mixture.

In a further experiment a sample of thoroughly dried acetylated catalyst (obtained as above by treatment of the solid catalyst with ethyl acetate) was suspended in $CDCl_3$. Its ^1H nmr spectrum (bottom, Fig. 2) indicated the presence of only trace amounts of ethyl acetate. After addition of CD_3OD to the mixture, the spectrum (top, Fig. 2) clearly showed signals corresponding to residual ethanol[5] and ethyl acetate. It therefore appears that acetylations promoted by $AlPO_4$–Al_2O_3 take place, at least to some extent, by a mechanism of acetyl transfer mediated by the solid catalyst acting as a carrier.

In summary, acetylation of alcohols and aliphatic amines can be carried out efficiently by the mild $AlPO_4$–Al_2O_3/ethyl acetate heterogeneous system, thus complementing the acylating capacity of alumina (1).

1. G. H. POSNER, S. S. OKADA, K. A. BABIAK, K. MIURA, and R. K. ROSE. Synthesis, 789 (1986); G. H. POSNER and M. ODA. Tetrahedron Lett. **22**, 5003 (1981).
2. G. H. POSNER. Angew. Chem. Int. Ed. Engl. **17**, 487 (1978).
3. K. TANABE. Solid acids and bases. Their catalytic properties. Academic Press, New York. 1970.
4. (*a*) J. M. CABELLO, J. M. CAMPELO, A. GARCÍA, D. LUNA, and J. M. MARINAS. J. Org. Chem. **49**, 5195 (1984); J. RIEGO, A. COSTA, and J. M. SAÁ. Chem. Lett. 1565 (1986). (*b*) S. T. WILSON, B. M. LOK, C. A. MESSINA, and E. M. FLANIGEN. J. Am. Chem. Soc. **104**, 1146 (1982).
5. A. COSTA, P. M. DEYÁ, J. V. SINISTERRA, and J. M. MARINAS. Can. J. Chem. **58**, 1266 (1980).
6. R. B. MARTIN and A. PARCEL. J. Am. Chem. Soc. **83**, 4835 (1961); G. H. PORTER, H. M. RYDON, and J. A. SCHOFIELD. J. Am. Chem. Soc. **82**, 2686 (1960); A. P. PHILLIPS and R. BALTZLY. J. Am. Chem. Soc. **69**, 200 (1947).
7. J. C. BUCHHOLZ and G. A. SOMORJAI. Acc. Chem. Res. **9**, 333 (1976).
8. A. MCKILLOP and D. W. YOUNG. Synthesis, 481 (1979), and references cited therein.

[5]Unambiguous evidence for the presence of residual ethanol adsorbed on the surface of the catalyst has been obtained by examining the ^1H nmr spectrum (before and after addition of CD_3OD) of a sample of thoroughly dried catalyst previously treated with ethanol.

Can. J. Chem. Downloaded from www.nrcresearchpress.com by 213.166.140.6 on 09/07/12
For personal use only.

Permanganate oxidation of glycine: Kinetics, catalytic effects, and mechanisms

JOAQUIN F. PEREZ-BENITO,[1] FERNANDO MATA-PEREZ, AND ENRIQUE BRILLAS
Departamento de Quimica Fisica, Facultad de Quimica, Universidad de Barcelona, Avenida Diagonal, 647, 08028 Barcelona, Spain

Received January 27, 1987

JOAQUIN F. PEREZ-BENITO, FERNANDO MATA-PEREZ, and ENRIQUE BRILLAS. Can. J. Chem. **65**, 2329 (1987).

The oxidation of glycine by permanganate ion in aqueous phosphate buffers is autocatalyzed by the soluble form of colloidal manganese dioxide formed as a reaction product. Both the noncatalytic and the catalytic reaction pathways are first order in permanganate, the noncatalytic pathway is also first order in glycine, whereas the catalytic pathway has a kinetic order unity for the autocatalytic agent and a non-integral order (1.31) for glycine. Both reaction pathways are accelerated by an increase in the pH of the medium, whereas an increase in the buffer concentration at constant pH results in an increase in the rate of the noncatalytic pathway and a decrease in the rate of the catalytic one. Additions of potassium chloride to the solutions have no kinetic effect on the reaction. The apparent activation energies of the noncatalytic and catalytic reaction pathways are 64.5 and 62.0 kJ mol^{-1}, respectively. On the other hand, manganese(II), thiosulfate, and hexacyanoferrate(II) ions, as well as benzyltriethylammonium chloride and arabic gum, have all been found to increase the initial reaction rate. Mechanisms in concordance with the experimental findings are proposed.

JOAQUIN F. PEREZ-BENITO, FERNANDO MATA-PEREZ et ENRIQUE BRILLAS. Can. J. Chem. **65**, 2329 (1987).

L'oxydation de la glycine par l'ion permanganate dans des tampons de phosphates aqueux est autocatalysée par la forme soluble du bioxyde de manganèse colloïdal qui se forme comme produit de la réaction. Les voies réactionnelles tant de la réaction catalysée que de la réaction qui n'est pas catalysée sont toutes les deux du premier ordre en permanganate; par ailleurs, la réaction qui n'est pas catalysée est aussi du premier ordre en glycine alors que la réaction catalysée est du premier ordre pour l'agent autocatalytique et d'un ordre qui n'est pas entier (1,31) pour la glycine. Les deux voies réactionnelles sont accélérées par une augmentation du pH du milieu alors qu'une augmentation de la concentration du tampon à pH constant provoque une augmentation de la vitesse de la voie qui n'est pas catalysée et une diminution dans la vitesse de la réaction catalysé. Des additions de chlorure de potassium aux solutions n'ont aucun effet cinétique sur la réaction. Les énergies d'activation apparentes pour les réactions catalysée et non catalysée sont respectivement de 62,0 et 64,5 kJ mol^{-1}. Par ailleurs, on a trouvé que le manganèse(II), les ions thiosulfate et hexacyanoferrate(II) ainsi que le chlorure de benzyltriéthylammonium et la gomme arabique augmentent tous la vitesse initiale de la réaction. On propose des mécanismes qui sont en accord avec les données expérimentales.

[Traduit par la revue]

Can. J. Chem. Downloaded from www.nrcresearchpress.com by 213.166.140.6 on 09/07/12
For personal use only.

Introduction

The permanganate oxidation of the components of large biological molecules such as nucleic acids and proteins has received considerable attention. For instance, kinetic studies of the permanganate oxidation of thymine (1), uracils (2), and several amino acids (3–5) have already been undertaken. In this paper, the results concerning the kinetic and mechanistic aspects of the reaction between glycine and potassium permanganate in neutral aqueous solutions will be presented and discussed in detail. It will be shown that it is in fact autocatalytic. Although a kinetic study concerning the same reaction has already been reported (6), it deals exclusively with very acid media and does not provide thorough information as far as the catalytic reaction pathway is concerned.

The occurrence of autocatalysis in permanganate reactions appears to be extensive (7–21). In particular, the permanganate oxidation of amines (22–25) deserves special mention among the autocatalytic reactions, due to the close relation that can be established between amines and amino acids. Because of the extensive occurrence of this phenomenon, one might think that kinetic and mechanistic information concerning the catalytic pathway is also abundant; however, the truth is that few rigorous kinetic data are available for the catalytic pathway, not only in permanganate reactions but also in all kinds of autocatalytic processes. A small contribution to fill this gap will be made in this paper.

[1]Author to whom correspondence may be addressed.

Experimental

The solvent used in the kinetic runs was twice-distilled water. The oxidizing agent was potassium permanganate and the reducing agent, glycine, was used in great excess with respect to the former. A KH_2PO_4–K_2HPO_4 buffer mixture was used with the double purpose of keeping the pH of the medium constant and of stabilizing manganese dioxide as a soluble colloid while the experiments were being performed. The possible effect of increasing ionic strength on the rate of reaction was analysed with the help of potassium chloride additions to the solutions. The effects of manganese(II) sulfate, sodium thiosulfate, potassium hexacyanoferrate(II), arabic gum, and benzyltriethylammonium chloride on the reaction were also studied.

The development of the reactions was monitored by following both the decrease in absorbance at 526 nm (reactant + product) and the increase in absorbance at 418 nm (product) by means of a Varian Cary 219 spectrophotometer. The permanganate concentrations were obtained according to the following equation:

$$[1] \qquad c = (A^{526} - \varepsilon_P^{526} A^{418}/\varepsilon_P^{418})/\varepsilon_R^{526} l$$

where the superscripts indicate wavelengths of the corresponding absorbances or extinction coefficients, and the subscripts R and P stand for reactant (permanganate ion) and product (colloidal manganese dioxide), respectively, whereas l is the cuvette pathlength (1 cm).

The pH of the solutions was measured by a conventional pH-meter provided with a combination electrode, and the temperature was kept constant by means of a thermostated bath with water continuously circulating through the cuvette holder of the spectrophotometer.

Results

The visible spectrum of the soluble form of colloidal manga-

Printed in Canada / Imprimé au Canada

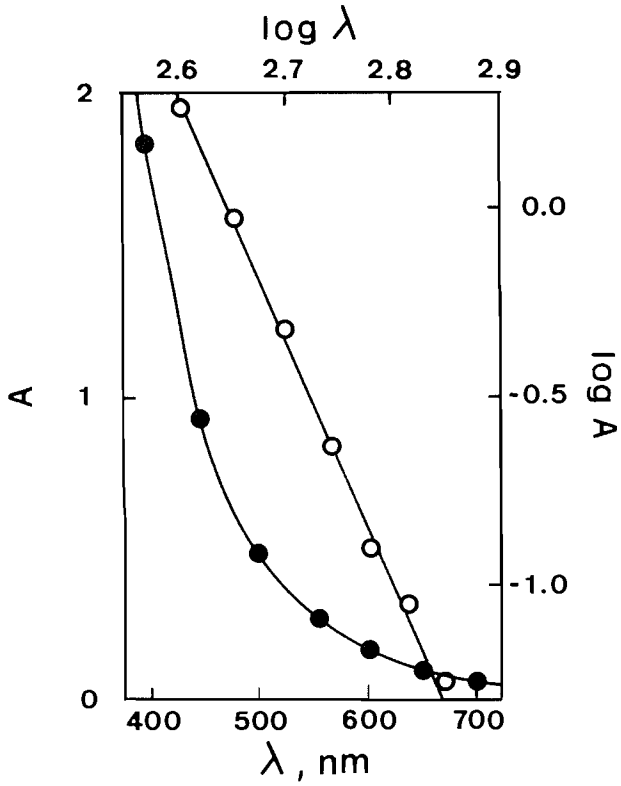

FIG. 1. Visible spectrum and log A vs. log λ linear plot for the product solution from the oxidation of glycine (0.01 M) by potassium permanganate (0.01 M) in aqueous KH_2PO_4 (0.04 M) – K_2HPO_4 (0.04 M) buffer at ionic strength 0.17 M, pH 6.78, and 25.0°C. The product solution was diluted 25 times before recording the spectrum (r = 0.998 for the linear plot).

nese dioxide generated as a reactant product is shown in Fig. 1. Since this spectrum overlaps the permanganate band at 526 nm, the absorbances at this wavelength must be corrected to obtain the permanganate concentrations. Taking into account that permanganate is transparent to radiation at 418 nm (26), eq. [1] can be used for that purpose.

We can see in Fig. 1 that a plot of log A vs. log λ is linear. This seems to be a reflection of the colloidal nature of the manganese reaction product (27), although the experimental slope (−6.48) is somehow different from the theoretical value (−4.00) expected from Rayleigh's Law (28). This deviation appears to be typical of colloidal manganese dioxide solutions, for which the absolute value of the slope of a log A vs. log λ linear plot is usually slightly higher than 4 (29, 30). Spectra similar to that in Fig. 1 were recorded for the products obtained from the reduction of permanganate by a great variety of reducing agents in both aqueous and methylene chloride solutions (31–40).

As shown in Fig. 2 for a typical kinetic run, all the experiments displayed a bell-shaped profile when the reaction rate was plotted against time. The rate values were determined from the experimental data as minus the derivative of the permanganate concentration with respect to time. It is clear that, if the rate presents both an acceleration and a decay period, a product concentration against time plot is necessarily S-shaped; i.e., the reaction is autocatalytic (41).

A differential rate law that can be tried for autocatalytic reactions is as follows:

$$[2] \quad -dc/dt = k_1 c + k_2 c(c_0 - c)$$

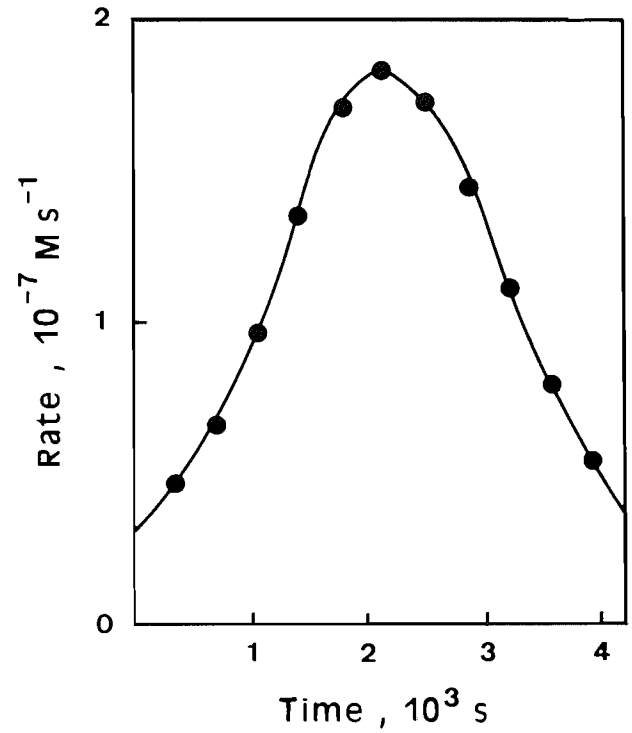

FIG. 2. Reaction rate vs. time plot for the oxidation of glycine (0.20 M) by potassium permanganate (5×10^{-4} M) in aqueous KH_2PO_4 (0.04 M) – K_2HPO_4 (0.04 M) buffer at ionic strength 0.16 M, pH 6.78, and 25.0°C.

its associated integral rate law being

$$[3] \quad \ln [(k_1 + k_2 c_0 - k_2 c)/c] = \ln (k_1/c_0) + (k_1 + k_2 c_0)t$$

In eqs. [2] and [3], c and c_0 are the concentrations of permanganate ion at time t and at the beginning of the reaction, while k_1 and k_2 are the pseudo rate constants of the noncatalytic and catalytic pathways, respectively. Owing to the fact that k_1 and k_2 appear not only in the intercept and the slope but also on the left-hand side of eq. [3], this equation must be used in an iterative way, starting with some trial values of the rate constants to fit the left-hand side of eq. [3] against time by the least-squares method, which allows new values of k_1 and k_2 to be derived from the intercept and the slope of that fit, and repeating the cycle till convergence is achieved.

Equation [3] was fulfilled in all the experiments performed, the linear correlation coefficients being between 0.9994 and 0.999997; a typical example is shown in Fig. 3. Reproducibility of the rate constants was assured within an acceptable error interval (4%). Since the experiments confirm the fulfilment of eq. [3], the differential form of the same law also holds (see eq. [2]). Therefore, it can be concluded that the rate of the noncatalytic pathway is first-order dependent on the permanganate concentration, whereas the rate of the catalytic pathway is first-order dependent on the concentrations of both permanganate ion and the autocatalytic agent, for in eq. [2] ($c_0 - c$) represents the autocatalytic agent concentration at time t.

The values of the rate constants corresponding to several initial permanganate concentrations have been compiled in Table 1; we can see that k_1 is independent of the initial permanganate concentration, but k_2 decreases as the initial permanganate concentration increases. The dependence of the rate constants on the glycine concentration is shown in Fig. 4; we can see that both log k_1 and log k_2 are linear when plotted

Can. J. Chem. Downloaded from www.nrcresearchpress.com by 213.166.140.6 on 09/07/12
For personal use only.

Can. J. Chem. Downloaded from www.nrcresearchpress.com by 213.166.140.6 on 09/07/12
For personal use only.

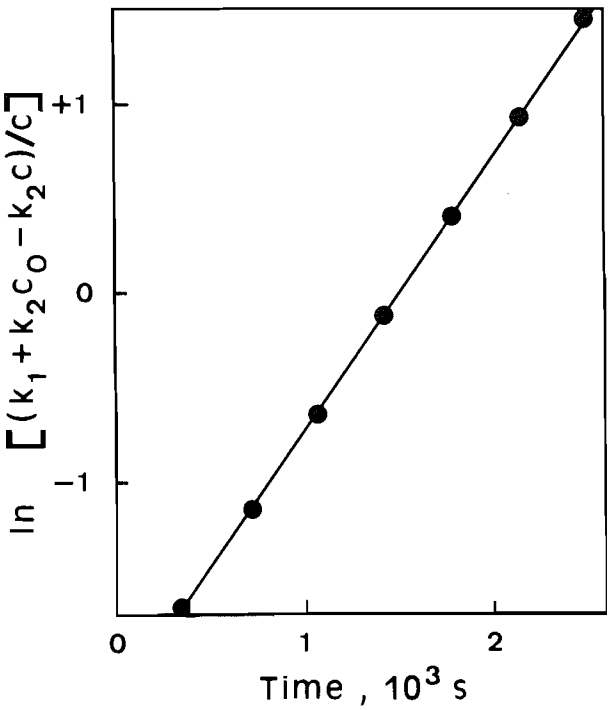

FIG. 3. Integral rate-law plot for the oxidation of glycine (0.20 M) by potassium permanganate (5×10^{-4} M) in aqueous KH_2PO_4 (0.04 M) – K_2HPO_4 (0.04 M) buffer at ionic strength 0.16 M, pH 6.78, and 25.0°C ($r = 0.99996$).

TABLE 1. Rate constants at several initial permanganate concentrations[a]

10^4 $[MnO_4^-]_0$ (M)	10^5 k_1 (s^{-1})	k_2 (M^{-1} s^{-1})[b]
5.01	4.79	1.92
6.51	5.26	1.75
7.83	5.21	1.62
9.07	5.00	1.57
10.26	5.15	1.48

[a][glycine] = 0.15 M; $[KH_2PO_4] = [K_2HPO_4] = 0.04$ M; ionic strength = 0.16 M; pH = 6.78; temperature = 25.0°C.
[b]$\log k_2 = -0.89 - 0.36 \log [MnO_4^-]_0$ ($r = 0.997$).

against log [glycine] but, although the slope corresponding to k_1 is fairly near unity (0.99), the slope corresponding to k_2 is higher than unity (1.31). As a result, only k_1 increases linearly with the glycine concentration, the corresponding intercept (5.12×10^{-7} s^{-1}) being negligible compared to the rate constant values involved in the plot (2.24×10^{-5} s^{-1} or higher); the slope and the linear correlation coefficient of the k_1 vs. [glycine] plot are 2.76×10^{-4} M^{-1} s^{-1} and 0.9998, respectively. Hence, the noncatalytic pathway is first order with respect to the reducing agent.

The concentrations of the components of the buffer mixture (KH_2PO_4 and K_2HPO_4) have been changed in two different ways, changing the concentrations of KH_2PO_4 and K_2HPO_4 so that the total phosphate concentration remains constant and the pH varies (as in Fig. 5), or changing the concentrations of KH_2PO_4 and K_2HPO_4 so that both are in equimolar amount and the pH of the solutions remains constant (as in Table 2). It can be seen in Fig. 5 that log k_1 increases in a nonlinear way as the pH increases, whereas log k_2 increases linearly with the pH (slope = 0.28). On the other hand, Table 2 indicates that when

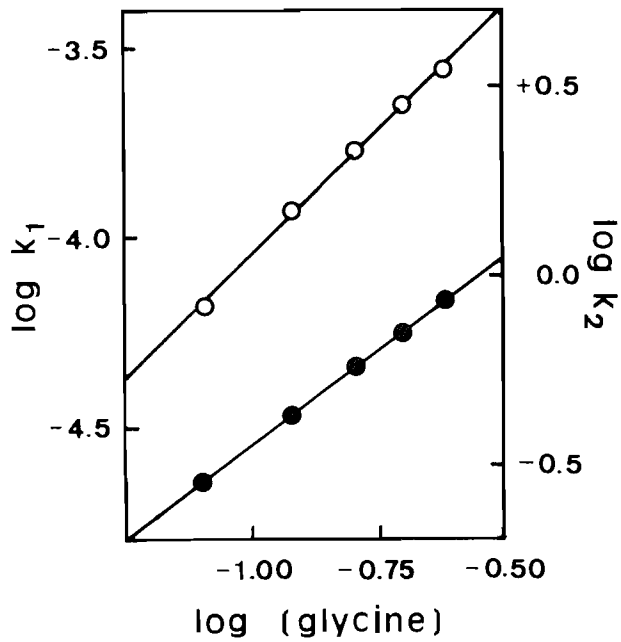

FIG. 4. Dependence of the rate constants on the reductant concentration for the oxidation of glycine by potassium permanganate (5×10^{-4} M) in aqueous KH_2PO_4 (0.04 M) – K_2HPO_4 (0.04 M) buffer at ionic strength 0.16 M, pH 6.78, and 25.0°C. Closed circles: k_1 in s^{-1} ($r = 0.9999$); open circles: k_2 in M^{-1} s^{-1} ($r = 0.9991$).

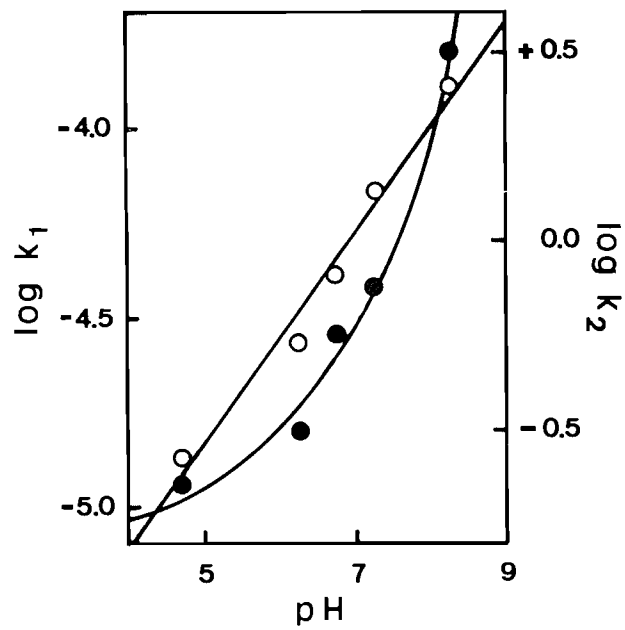

FIG. 5. Dependence of the rate constants on the pH for the oxidation of glycine (0.08 M) by potassium permanganate (5×10^{-4} M) in aqueous KH_2PO_4–K_2HPO_4 buffer ($[KH_2PO_4] + [K_2HPO_4] = 0.06$ M) at ionic strength 0.19 M (KCl) and 25.0°C. Closed circles: k_1 in s^{-1}; open circles: k_2 in M^{-1} s^{-1} ($r = 0.989$).

the buffer concentration increases at constant pH a slight increase in k_1 and a decrease in k_2 are observed.

Additions of potassium chloride to the solutions do not significantly affect the rate constants (see Table 3), so both k_1 and k_2 are independent of the ionic strength of the medium. The dependence of both k_1 and k_2 on temperature follows the Arrhenius equation (see Fig. 6), the corresponding activation energies being 64.5 and 62.0 kJ mol^{-1}.

Can. J. Chem. Downloaded from www.nrcresearchpress.com by 213.166.140.6 on 09/07/12
For personal use only.

TABLE 2. Rate constants at several buffer concentrations[a]

10^2 [K_2HPO_4] (M)[b]	10^5 k_1 (s^{-1})	k_2 (M^{-1} s^{-1})
1.6	4.75	2.34
3.2	4.93	1.98
4.8	5.01	1.86
6.4	5.28	1.80
8.0	5.55	1.75

[a] $[MnO_4^-]_0 = 5 \times 10^{-4} M$; [glycine] = $0.16 M$; ionic strength = $0.32 M$ (KCl); pH = 6.78; temperature = 25.0°C. [b] An equimolar amount of KH_2PO_4 was also used.

TABLE 3. Rate constants at several potassium chloride concentrations[a]

[KCl] (M)	10^5 k_1 (s^{-1})	k_2 (M^{-1} s^{-1})
0.00	6.94	2.72
0.08	6.89	2.76
0.16	7.30	2.73
0.24	7.04	2.69
0.32	6.97	2.69

[a] $[MnO_4^-]_0 = 5 \times 10^{-4} M$; [glycine] = $0.20 M$; [KH_2PO_4] = [K_2HPO_4] = $0.04 M$; ionic strength = 0.16 + [KCl] (M); pH = 6.78; temperature = 25.0°C.

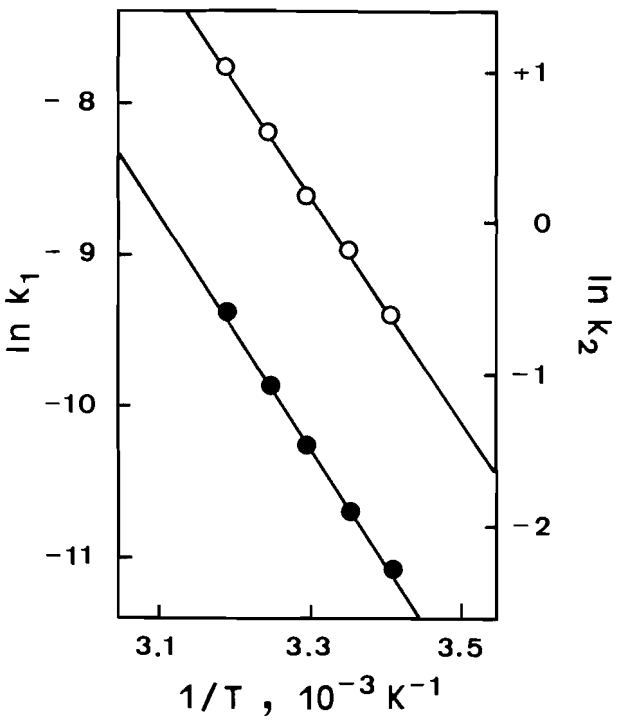

FIG. 6. Arrhenius plots for the oxidation of glycine ($0.08 M$) by potassium permanganate ($5 \times 10^{-4} M$) in aqueous KH_2PO_4 ($0.04 M$) – K_2HPO_4 ($0.04 M$) buffer at ionic strength $0.16 M$ and pH 6.78. Closed circles: k_1 in s^{-1} ($r = 0.9994$); open circles: k_2 in M^{-1} s^{-1} ($r = 0.9996$).

The effect of additives other than potassium chloride on the reaction was also studied. Upon stirring, the solutions immediately became red when manganese(II), thiosulfate, or hexacyanoferrate(II) ions were present; afterward, the colour slowly changed from red to yellow. When arabic gum or benzyltriethylammonium chloride was present, the transition of colour

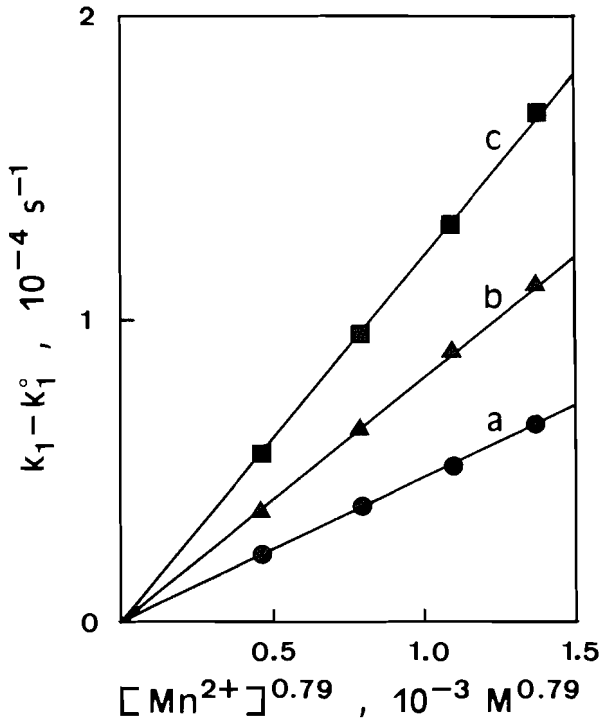

FIG. 7. $(k_1 - k_1^0)$ vs. $[Mn^{2+}]^{0.79}$ plots for the oxidation of glycine by permanganate ion ($5 \times 10^{-4} M$) at pH 6.78 and 25.0°C. [glycine] = $0.12 M$ (a); $0.16 M$ (b); and $0.20 M$ (c).

from purple to red, and also that from red to yellow, was slow. Moreover, the spectrophotometer showed that the initial absorbance at 526 nm decreased and the initial absorbance at 418 nm increased with increasing additive concentration when the additive was Mn^{2+}, $S_2O_3^{2-}$, or $Fe(CN)_6^{4-}$. On the contrary, neither arabic gum nor $BzEt_3NCl$ changed the initial absorbance values.

None of these additives seems to affect the value of k_2 to an important extent. However, the five of them have a definite increasing effect on k_1, as can be seen in Figs. 7–11 where k_1^0 stands for the rate constant of the noncatalytic pathway in the absence of any additive. Whilst $(k_1 - k_1^0)$ increases linearly with both the arabic gum and benzyltriethylammonium chloride concentrations, to get linear plots in the case of manganese(II), thiosulfate, and hexacyanoferrate(II) ions it is necessary to raise their concentrations to a certain power lower than unity (0.79, 0.89, and 0.70, respectively). The slopes and linear correlation coefficients corresponding to those plots are compiled in Tables 4–8. We observe that the slope associated with each additive also increases as the glycine concentration increases, and can thus conclude that the catalytic effect of each additive is a function of the concentration of amino acid present in the solutions.

Discussion

In the pH range used (4.70–8.25), the amino acid is present chiefly in the zwitterionic form, given the closeness of that range to the isoelectric point of glycine (6.06). The oxidation of the zwitterionic form of the amino acid through the noncatalytic pathway might happen according to the following mechanism:

[4] $^+H_3NCH_2CO_2^- + MnO_4^- \xrightarrow{\text{slow}} {}^+H_3NCH_2CO_2^{\bullet} + MnO_4^{2-}$

[5] $^+H_3NCH_2CO_2^{\bullet} \rightarrow {}^+H_3NCH_2^{\bullet} + CO_2$

[6] $^+H_3NCH_2^{\bullet} \rightarrow H_2NCH_2^{\bullet} + H^+$

Can. J. Chem. Downloaded from www.nrcresearchpress.com by 213.166.140.6 on 09/07/12
For personal use only.

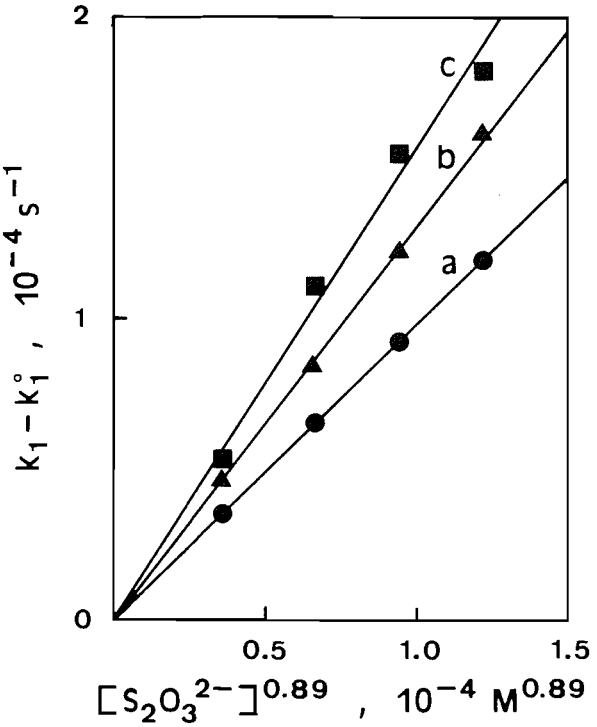

FIG. 8. $(k_1 - k_1^0)$ vs. $[S_2O_3^{2-}]^{0.89}$ plots for the oxidation of glycine by permanganate ion ($5 \times 10^{-4} M$) at pH 6.78 and 25.0°C. [glycine] = 0.12 M (a); 0.16 M (b); and 0.20 M (c).

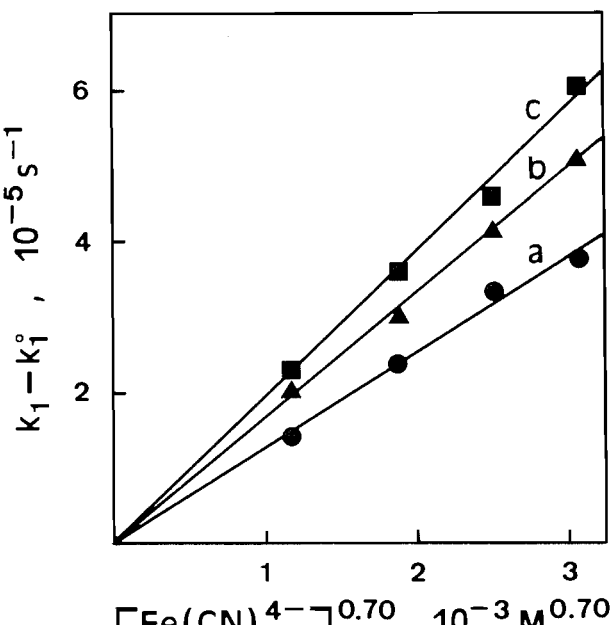

FIG. 9. $(k_1 - k_1^0)$ vs. $[Fe(CN)_6^{4-}]^{0.70}$ plots for the oxidation of glycine by permanganate ion ($5 \times 10^{-4} M$) at pH 6.78 and 25.0°C. [glycine] = 0.12 M (a); 0.16 M (b); and 0.20 M (c).

[7] $H_2NCH_2^\bullet + MnO_4^- \rightarrow CH_2{=}NH_2^+ + MnO_4^{2-}$

[8] $CH_2{=}NH_2^+ + H_2O \rightarrow CH_2O + NH_4^+$

[9] $3MnO_4^{2-} + 2H_2O \rightarrow 2MnO_4^- + MnO_2 + 4OH^-$

Although that mechanism probably accounts for a considerable proportion of the reaction, Fig. 5 suggests that the anionic form of the amino acid is also involved in the oxidation

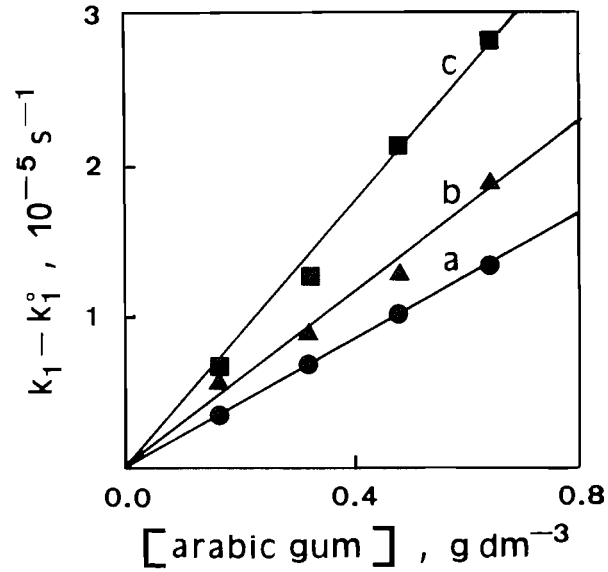

FIG. 10. $(k_1 - k_1^0)$ vs. [arabic gum] plots for the oxidation of glycine by permanganate ion ($5 \times 10^{-4} M$) at pH 6.78 and 25.0°C. [glycine] = 0.08 M (a); 0.12 M (b); and 0.20 M (c).

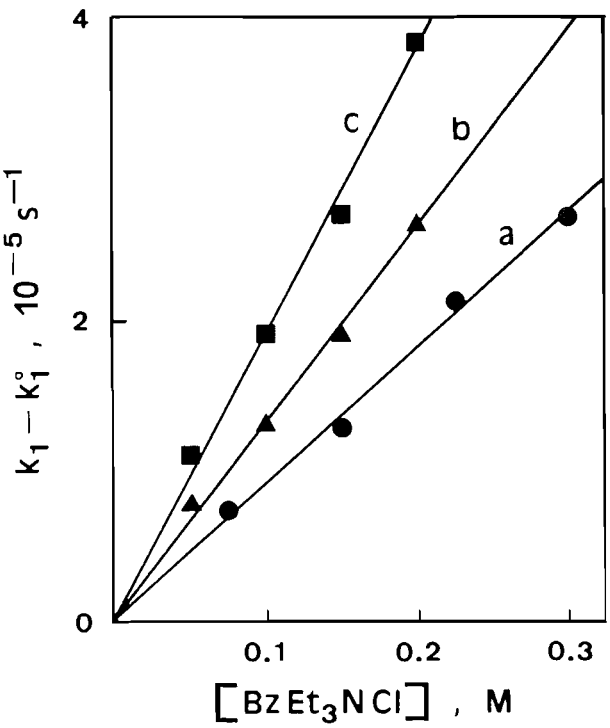

FIG. 11. $(k_1 - k_1^0)$ vs. $[BzEt_3NCl]$ plots for the oxidation of glycine by permanganate ion ($5 \times 10^{-4} M$) at pH 6.78 and 25.0°C. [glycine] = 0.08 M (a); 0.12 M (b); and 0.20 M (c).

process, for only then will rate constant k_1 increase with the pH of the medium. This oxidation will be similar to that of the zwitterionic form, as eqs. [10] and [11] show:

[10] $H_2NCH_2CO_2^- + MnO_4^- \xrightarrow{\text{slow}} H_2NCH_2CO_2^\bullet + MnO_4^{2-}$

[11] $H_2NCH_2CO_2^\bullet \rightarrow H_2NCH_2^\bullet + CO_2$

Once free radical $H_2NCH_2^\bullet$ is formed, its oxidation will take place as in eqs. [7] and [8].

The two mechanisms proposed for the noncatalytic pathway are indeed in agreement with the experimental results pre-

TABLE 4. Effect of manganese(II) ion. Parameters from Fig. 7[a]

[glycine] (M)	Slope $\times 10^2$ ($M^{-0.79}$ s^{-1})[b,c]	r[d]
0.12	4.78	0.9995
0.16	8.14	0.9998
0.20	12.14	0.9998

[a]The experimental conditions are given in Fig. 7.
[b]Slopes for plots in Fig. 7.
[c]log (slope) = 0.36 + 1.83 log [glycine] (r = 0.99996).
[d]Linear correlation coefficients for plots in Fig. 7.

TABLE 5. Effect of thiosulfate ion. Parameters from Fig. 8[a]

[glycine] (M)	Slope ($M^{-0.89}$ s^{-1})[b,c]	r[d]
0.12	0.97	0.9998
0.16	1.30	0.9996
0.20	1.56	0.9950

[a]The experimental conditions are given in Fig. 8.
[b]Slopes for plots in Fig. 8.
[c]log (slope) = 0.85 + 0.93 log [glycine] (r = 0.998).
[d]Linear correlation coefficients for plots in Fig. 8.

TABLE 6. Effect of hexacyanoferrate(II) ion. Parameters from Fig. 9[a]

[glycine] (M)	Slope $\times 10^2$ ($M^{-0.70}$ s^{-1})[b,c]	r[d]
0.12	1.26	0.997
0.16	1.64	0.999
0.20	1.92	0.998

[a]The experimental conditions are given in Fig. 9.
[b]Slopes for plots in Fig. 9.
[c]log (slope) = −1.13 + 0.83 log [glycine] (r = 0.997).
[d]Linear correlation coefficients for plots in Fig. 9.

TABLE 7. Effect of arabic gum. Parameters from Fig. 10[a]

[glycine] (M)	Slope $\times 10^5$ (g^{-1} dm^3 s^{-1})[b,c]	r[d]
0.08	2.09	0.999
0.12	2.86	0.993
0.20	4.33	0.997

[a]The experimental conditions are given in Fig. 10.
[b]Slopes for plots in Fig. 10.
[c]log (slope) = −3.81 + 0.80 log [glycine] (r = 0.99991).
[d]Linear correlation coefficients for plots in Fig. 10.

TABLE 8. Effect of benzyltriethylammonium chloride. Parameters from Fig. 11[a]

[glycine] (M)	Slope $\times 10^4$ (M^{-1} s^{-1})[b,c]	r[d]
0.08	0.90	0.997
0.12	1.30	0.997
0.20	1.89	0.997

[a]The experimental conditions are given in Fig. 11.
[b]Slopes for plots in Fig. 11.
[c]log (slope) = −3.15 + 0.81 log [glycine] (r = 0.998).
[d]Linear correlation coefficients for plots in Fig. 11.

sented in this paper, for according to those mechanisms the rate of disappearance of permanganate ion through the noncatalytic pathway is

$$[12] \quad r_1 = k_1[MnO_4^-]$$

where k_1 is

$$[13] \quad k_1 = k_4[^+H_3NCH_2CO_2^-] + k_{10}[H_2NCH_2CO_2^-]$$

k_4 and k_{10} being the rate constants corresponding to eqs. [4] and [10], respectively. According to eqs. [12] and [13] the kinetic orders of the noncatalytic pathway with respect to permanganate and glycine are both unity. On the other hand, the different ionic forms of the amino acid are in equilibrium:

$$[14] \quad ^+H_3NCH_2CO_2H \rightleftharpoons ^+H_3NCH_2CO_2^- + H^+$$

$$[15] \quad ^+H_3NCH_2CO_2^- \rightleftharpoons H_2NCH_2CO_2^- + H^+$$

the respective pK_a's corresponding to eqs. [14] and [15] being 2.35 and 9.78 at 25.0°C (42). Thus, application of eq. [13] for the k_1 data measured at several pH values allows the obtention of the rate constants of the rate-controlling steps, these being $k_4 = 2.28 \times 10^{-4} M^{-1}$ s^{-1} and $k_{10} = 6.16 \times 10^{-2} M^{-1}$ s^{-1}. Hence, the anionic amino acid form is more reactive toward permanganate than the zwitterionic one, probably due to the higher electron density of $H_2NCH_2CO_2^-$ compared to that of $^+H_3NCH_2CO_2^-$, because an increase in the electron density results in a promotion of the reducing power.

Table 2 shows a slight increase in k_1 as the total phosphate concentration increases. Although this suggests that there might be a small contribution of general base catalysis due to HPO_4^{2-} ion, the minor importance of that dependence indicates that it might be due to a systematic error in the measurement of the rate constants instead.

The k_1 value at pH 6.78 is independent of the ionic strength of the medium (see Table 3); thus, we can infer that, at that pH, the oxidation of the zwitterionic form of the amino acid is predominant over the oxidation of the anionic form, since eq. [4] is a reaction between an ion and a neutral molecule, whereas eq. [10] is a reaction between two ions with like charges. This is consistent with the values found for rate constants k_4 and k_{10} (see above), for according to them at pH 6.78 eq. [4] accounts for most of the total reaction (80%). It should be noticed that the activation energy found for k_1 (64.5 kJ mol^{-1}) is an apparent value, in which the effects of temperature on rate constants k_4 and k_{10} and on the equilibrium constants associated with eqs. [14] and [15] are all included.

Although the kinetic data collected for the noncatalytic pathway give information only as far as the rate-controlling steps are concerned (eqs. [4] and [10]), there are some bibliographic references that support the noncontrolling steps proposed. In the first place, eq. [6] is analogous to the deprotonation of cation radicals formulated for the permanganate oxidation of amines (43), for which imines are also proposed as intermediary species (see eq. [7]). On the other hand, it is well known that hydrolysis of imines (or of methyliminium ion, as in eq. [8]) results in aldehydes and ammonia (or ammonium ion) formation, while dismutation of manganate ion into permanganate and manganese dioxide (see eq. [9]) is very fast in all but very alkaline solutions (44). The mechanisms proposed for the oxidations of the zwitterionic and anionic forms of glycine are similar to the one proposed for the permanganate oxidation of the cationic form of amino acids in very acid media (6).

As far as the reaction products are concerned, colloidal man-

Can. J. Chem. Downloaded from www.nrcresearchpress.com by 213.166.140.6 on 09/07/12
For personal use only.

Can. J. Chem. Downloaded from www.nrcresearchpress.com by 213.166.140.6 on 09/07/12
For personal use only.

ganese dioxide has been identified as the species responsible for the spectrum shown in Fig. 1. Moreover, it has been reported that carbon dioxide (45), aldehydes (46), and ammonia (47) are all obtained from the permanganate oxidation of amino acids. Under the experimental conditions of the present work, formaldehyde (generated as a reaction product in eq. [8]) is expected to behave as an intermediate since it will be readily oxidized by permanganate ion to formic acid and, further, to carbon dioxide (48).

In relation to the catalytic pathway, the following mechanism is proposed:

[16] MnO_2 + glycine $\rightleftharpoons$ adsorbate

[17] Adsorbate + MnO_4^- $\xrightarrow{\text{slow}}$ products

In eq. [16] glycine is adsorbed on the surface of colloidal manganese dioxide, since the capacity of that colloid to strongly adsorb organic substrates is known (49). Then the adsorbed species may suffer an oxidative attack by permanganate ion from the solution surrounding the colloidal particles (eq. [17]).

According to eqs. [16] and [17], the rate of disappearance of permanganate ion through the catalytic pathway is

[18] $r_2 = k_2[MnO_4^-][MnO_2]$

where k_2 is

[19] $k_2 = k_{17}a[\text{glycine}]^b$

k_{17} being the rate constant associated with eq. [17], whereas a and b are the parameters of the Freundlich isotherm for adsorption of glycine on the surface of the colloidal particles of manganese dioxide (see eq. [16]).

Equation [18] is indeed in agreement with the differential rate law (eq. [2]) whose integral form (eq. [3]) was experimentally confirmed, as shown in Fig. 3. It has been observed that k_2 decreases as the initial permanganate concentration increases (see Table 1); this may be due to the increase in the size of the colloidal particles as a consequence of an increasing manganese dioxide concentration. Moreover, eq. [19] is in agreement with the log k_2 vs. log [glycine] linear plot found in Fig. 4; the fact that the slope of this plot is higher than unity (1.31) indicates that the catalytic power of manganese dioxide increases with the glycine concentration, since the density of active sites on the colloid surface depends on its rate of formation as well as on the experimental conditions of the medium where it is formed.

It is convenient to mention that, although manganese dioxide is formed in eq. [9] of the noncatalytic pathway as a discrete species, prior to its participation in the catalytic pathway it must flocculate to generate colloidal particles on whose surface the autocatalytic reaction takes place. As a result, the size of these particles is a function of the flocculation rate and so it also depends on the experimental conditions that might affect the flocculation process. Hence, both the oxidant and reductant concentrations have some influence on the catalytic power of colloidal manganese dioxide. Since the number of molecules that are actually forming each colloidal particle is not known, in the differential rate law (eq. [2]) the autocatalytic agent concentration was taken as equal to $(c_0 - c)$; in fact, no problem arises with this assumption other than k_2 being expressed per manganese dioxide molecule instead of per colloidal particle.

We can see in Fig. 5 that log k_2 also increases linearly as the pH of the solution increases. Although a common explanation might be given for the variations of both k_1 and k_2 with the pH, the fact that the log k_2 vs. pH plot is linear whereas the other is not suggests that the dependence of k_2 on pH is due to a different reason. This dependence might be a reflection of the fact that hydroxyl ions linked to colloidal manganese dioxide (50–52) are the active sites for adsorption of glycine on its surface.

On the other hand, Table 2 shows a decrease in k_2 as the total phosphate concentration increases at constant pH. Retardation of permanganate reactions taking place on the surface of colloidal manganese dioxide as a consequence of an increasing phosphate concentration has previously been reported (53). Since phosphate ions are known to be strongly adsorbed on colloidal manganese dioxide generated as a product from the reduction of permanganate ion in aqueous phosphate buffers (54), that retardation might be due to the electrostatic repulsion between the phosphate ions linked to the colloid surface and the permanganate ion that must approach the surface so that the reaction depicted by eq. [17] can take place.

One is not entitled to infer conclusions from the independence of k_2 with respect to the ionic strength of the medium (see Table 3), at least as far as the Debye–Hückel theory is concerned, for that theory does not apply to reactions taking place on the surface of colloidal particles such as those of manganese dioxide. It should also be mentioned that the activation energy found for k_2 (62.0 kJ mol^{-1}) is not properly a true activation energy but only an apparent value in which the effects of temperature on both eqs. [16] and [17] (an adsorption enthalpy and an activation energy, respectively) are included.

As far as the effect of additives on the reaction is concerned, it is necessary to take into consideration that manganese(II), thiosulfate, and hexacyanoferrate(II) are all inorganic ions with a common property, that of reducing permanganate ion almost instantaneously in neutral aqueous solutions according to the following stoichiometries:

[20] $2MnO_4^- + 3Mn^{2+} + 2H_2O \rightarrow 5MnO_2 + 4H^+$

[21] $8MnO_4^- + 3S_2O_3^{2-} + 2H^+ \rightarrow 8MnO_2 + 6SO_4^{2-} + H_2O$

[22] $MnO_4^- + 3Fe(CN)_6^{4-} + 4H^+ \rightarrow MnO_2 + 3Fe(CN)_6^{3-} + 2H_2O$

Hence the red colour whose appearance was observed right after the solutions containing the reactants came in contact was due to a mixture of permanganate ion (purple), which was used in excess with respect to the additive, and colloidal manganese dioxide (yellow) formed according to eqs. [20]–[22]. This colloid was stabilized in aqueous solutions owing to the adsorption of phosphate ions on its surface (54). Since manganese dioxide is formed during the process of stirring the mixtures, the initial absorbances at 418 and 526 nm given by the spectrophotometer will depend on the Mn^{2+}, $S_2O_3^{2-}$, and $Fe(CN)_6^{4-}$ concentrations, for the higher the concentration of additive the lower the initial absorbance at 526 nm and the higher the initial absorbance at 418 nm will be, because more permanganate and more manganese dioxide will have been consumed and formed, respectively.

It is necessary to notice that the reaction monitored with the aid of the spectrophotometer was that of glycine with permanganate ion, but the MnO_4^-/Mn^{2+}, $MnO_4^-/S_2O_3^{2-}$, and $MnO_4^-/Fe(CN)_6^{4-}$ reactions cannot be followed with a conventional spectrophotometer due to their being extremely fast; other methods, such as the stopped-flow technique, would be needed for that purpose.

Can. J. Chem. Downloaded from www.nrcresearchpress.com by 213.166.140.6 on 09/07/12
For personal use only.

Therefore when the kinetic data were determined, manganese(II), thiosulfate, and hexacyanoferrate(II) ions were no longer in the solutions, their presence being replaced by that of colloidal manganese dioxide. Furthermore, we can see that the behavior of Mn^{2+} is similar to that of other inorganic species capable of instantaneously reducing permanganate ion in neutral solutions, such as $S_2O_3^{2-}$ and $Fe(CN)_6^{4-}$. Thus there is no reason to think that manganese(II) ion is the true autocatalytic agent for the permanganate oxidation of amino acids, as sometimes proposed (3, 5, 6, 55). In fact, such an explanation cannot account for the autocatalytic effect found for those reactions when they are performed in neutral solutions (in which the product is MnO_2) and would only apply (in principle) to very acid media (in which the product is Mn^{2+}). On the contrary, the catalytic effect of colloidal manganese dioxide is capable of explaining the autocatalysis found both in neutral solutions and in acid media, for at very low pH values manganese dioxide may form as a colloidal intermediate (56).

We can thus conclude that the increase in rate constant k_1 caused by addition of manganese(II) ion to the solution (see Fig. 7) is not due to the formation of a glycine–manganese(II) complex but to the obtention of colloidal manganese dioxide according to Guyard's reaction (57), as depicted in eq. [20]. Therefore, manganese(II) ion is not actually the catalytic agent but only a precursor of the true catalyst, colloidal manganese dioxide, and the same can be stated as far as thiosulfate and hexacyanoferrate(II) ions are concerned. Hence, this is a phenomenon of heterogeneous autocatalysis in which the colloid offers its surface for the encounter of the reactants.

Figures 7–9 show that the increases in k_1 due to additions of Mn^{2+}, $S_2O_3^{2-}$, and $Fe(CN)_6^{4-}$ are not directly proportional to the additive concentration, the function relating $(k_1 - k_1^0)$ with that concentration being different for each additive. On the other hand, Tables 4–6 show that the effect of the three additives on the rate of reaction depends on the glycine concentration, but the dependence in the case of manganese(II) ion is much stronger than in the other two cases. These differences are probably due to the colloidal nature of manganese dioxide, for its catalytic power is a function of the experimental conditions of the medium where it is formed. Consequently, it is not easy to establish a quantitative relationship between the kinetic effects of the additives and the stoichiometries given in eqs. [20]–[22], owing to the fact that the catalytic properties of colloidal manganese dioxide strongly depend on the nature of the species used to reduce permanganate.

On the other hand, arabic gum is a water-soluble colloid whose resistance to oxidation by permanganate ion has made it useful in kinetic studies of permanganate reactions (8). It seems clear that the catalytic effect of this colloid is totally similar to that of manganese dioxide, both colloids acting as heterogeneous catalysts on whose surface the reaction between the amino acid and permanganate ion can take place.

The effect of benzyltriethylammonium chloride on the reaction, however, requires a different explanation. Since potassium chloride additions had no effect on the reaction rate (see Table 3), the possibility of a salt effect due to an increase in the ionic strength of the medium has also to be excluded.

It has been reported (58) that quaternary ammonium salts are used as phase-transfer agents in permanganate reactions due to their tendency to form quaternary ammonium permanganate. Thus a small concentration of benzyltriethylammonium permanganate might be present in the solutions (in concentration too small to precipitate), and this new variety of permanganate might react with glycine to generate the reaction products according to the following scheme:

$$[23] \quad BzEt_3N^+ + MnO_4^- \rightleftharpoons BzEt_3NMnO_4$$

$$[24] \quad BzEt_3NMnO_4 + \text{glycine} \xrightarrow{\text{slow}} \text{products}$$

The rate law corresponding to that mechanism is

$$[25] \quad r = K_{23}k_{24}[MnO_4^-][\text{glycine}][BzEt_3N^+]$$

where K_{23} and k_{24} are the equilibrium and rate constants associated with eqs. [23] and [24], respectively. Hence, the increase in rate constant k_1 will be directly proportional to both the quaternary ammonium chloride and glycine concentrations, in reasonably good agreement with the results found in Fig. 11 and Table 8, respectively.

In conclusion, it can be stated that the reaction between glycine and permanganate ion in aqueous phosphate buffers is catalyzed by soluble colloids, such as arabic gum and colloidal manganese dioxide. Those species capable of instantaneously reducing permanganate to colloidal manganese dioxide have an increasing effect on the reaction rate. Quaternary ammonium salts also catalyze the reaction due to the formation of quaternary ammonium permanganate.

Acknowledgment

One of the authors (J.F.P.B.) wishes to thank the Spanish Ministry of Education and Science for a grant that made possible his participation in this work.

1. F. Freeman, C. O. Fuselier, and E. M. Karchefski. Tetrahedron Lett. 2133 (1975).
2. F. Freeman, C. O. Fuselier, C. R. Armstead, C. E. Dalton, P. A. Davidson, E. M. Karchefski, D. E. Krochman, M. N. Johnson, and N. K. Jones. J. Am. Chem. Soc. **103**, 1154 (1981).
3. O. G. Pokrovskaya. Izv. Sib. Otd. Akad. Nauk SSSR Ser. Khim. **8**, 50 (1959).
4. U. D. Mudaliar, V. R. Chourey, R. S. Verma, and V. R. Shastry. J. Indian Chem. Soc. **60**, 561 (1983).
5. F. J. Andres, A. Arrizabalaga, and J. I. Martinez. An. Quim. Ser. A, **80**, 531 (1984).
6. R. S. Verma, M. J. Reddy, and V. R. Shastry. J. Chem. Soc. Perkin Trans. 2, 469 (1976).
7. J. Bradley and G. Van Praagh. J. Chem. Soc. 1624 (1938).
8. F. C. Tompkins. Trans. Faraday Soc. **38**, 131 (1942).
9. F. Fouinat and M. Magat. J. Chim. Phys. **47**, 514 (1950).
10. J. M. Malcolm and R. M. Noyes. J. Am. Chem. Soc. **74**, 2769 (1952).
11. C. F. Cullis and J. W. Ladbury. J. Chem. Soc. 4186 (1955).
12. K. B. Wiberg and R. Stewart. J. Am. Chem. Soc. **77**, 1786 (1955).
13. R. Stewart. *In* Oxidation in organic chemistry. Part A. *Edited by* K. B. Wiberg. Academic Press, New York. 1965. p. 20.
14. D. A. Skoog and D. M. West. Fundamentals of analytical chemistry. 2nd ed. Holt, Rinehart and Winston, Toronto. 1969. p. 422.
15. M. Wronska and T. Ernst. Z. Phys. Chem. (Leipzig), **244**, 144 (1970).
16. K. K. Banerji. J. Chem. Soc. Perkin Trans. 2, 435 (1973).
17. E. G. Prout and C. M. Lownds. Inorg. Nucl. Chem. Lett. **9**, 617 (1973).
18. J. S. Booth, D. Dollimore, and G. R. Heal. Thermochim. Acta, **39**, 293 (1980).
19. J. S. Reckley and K. Showalter. J. Am. Chem. Soc. **103**, 7012 (1981).
20. A. Z. Moghaddam and G. J. Rees. Fuel, **63**, 653 (1984).

21. D. G. LEE and J. F. PEREZ-BENITO. Can. J. Chem. **63**, 1275 (1985).
22. M. M. WEI and R. STEWART. J. Am. Chem. Soc. **88**, 1974 (1966).
23. F. MATA-PEREZ, J. F. PEREZ-BENITO, and A. ARRANZ. Z. Phys. Chem. (Neue Folge), **135**, 141 (1983).
24. F. MATA-PEREZ and J. F. PEREZ-BENITO. Z. Phys. Chem. (Neue Folge), **141**, 213 (1984).
25. F. MATA-PEREZ and J. F. PEREZ-BENITO. An. Quim. Ser. A, **81**, 79 (1985).
26. D. G. LEE and J. R. BROWNRIDGE. J. Am. Chem. Soc. **95**, 3033 (1973).
27. F. MATA-PEREZ and J. F. PEREZ-BENITO. Z. Phys. Chem. (Leipzig), **267**, 120 (1986).
28. G. M. BARROW. Physical chemistry. 2nd ed. McGraw–Hill, New York. 1966. p. 803.
29. J. F. PEREZ-BENITO and D. G. LEE. Can. J. Chem. **63**, 3545 (1985).
30. F. FREEMAN and J. C. KAPPOS. J. Am. Chem. Soc. **107**, 6628 (1985).
31. S. SENENT and L. MARTIN. An. Quim. Ser. B, **56**, 123 (1959).
32. B. JEZOWSKA-TRZEBIATOWSKA and J. KALECINSKI. Bull. Acad. Polon. Sci., Ser. Sci. Chim. **9**, 791 (1961).
33. K. B. WIBERG, C. J. DEUTSCH, and J. ROCEK. J. Am. Chem. Soc. **95**, 3034 (1973).
34. M. JAKY and L. I. SIMANDI. React. Kinet. Catal. Lett. **3**, 397 (1975).
35. F. FREEMAN and E. M. KARCHEFSKI. Biochim. Biophys. Acta, **447**, 238 (1976).
36. N. T. SON, M. JAKY, and L. I. SIMANDI. Inorg. Nucl. Chem. Lett. **12**, 291 (1976).
37. M. JAKY and L. I. SIMANDI. Magy. Kem. Foly. **86**, 136 (1980).
38. N. T. SON, M. JAKY, and L. I. SIMANDI. Magy. Kem. Foly. **86**, 139 (1980).
39. T. OGINO. Tetrahedron Lett. **21**, 177 (1980).
40. D. G. LEE and K. C. BROWN. J. Am. Chem. Soc. **104**, 5076 (1982).
41. J. W. MOORE and R. G. PEARSON. Kinetics and mechanism. 3rd ed. Wiley, New York. 1981. p. 26.
42. B. B. OWEN. J. Am. Chem. Soc. **56**, 24 (1934).
43. D. H. ROSENBLATT, G. T. DAVIS, L. A. HULL, and G. D. FORBERG. J. Org. Chem. **33**, 1649 (1968).
44. F. FREEMAN. Rev. React. Species Chem. React. **1**, 179 (1976).
45. A. M. UNRAU and M. L. FAN. Can. J. Chem. **44**, 2090 (1966).
46. F. FEIGL. Spot tests in organic chemistry. Elsevier, Amsterdam. 1956. p. 331.
47. T. HAKE. Lab. Invest. **14**, 1208 (1965).
48. J. HOLLUTA and A. MUTSCHIN. Z. Phys. Chem. **150**, 381 (1930).
49. M. FIESER and L. F. FIESER. Reagents for organic synthesis. Vol. 1. Wiley, New York. 1967. p. 943.
50. J. J. MORGAN and W. STUMM. J. Colloid Sci. **19**, 347 (1964).
51. J. P. GABANO, P. ETIENNE, and J. F. LAURENT. Electrochim. Acta, **10**, 947 (1965).
52. V. V. VOL'KHIN and G. V. LEONT'EVA. Izv. Akad. Nauk SSR, Neorg. Mater. **5**, 1224 (1969).
53. E. NARITA and T. OKABE. Ind. Eng. Chem. Prod. Res. Dev. **21**, 662 (1982).
54. F. MATA-PEREZ and J. F. PEREZ-BENITO. Can. J. Chem. **63**, 988 (1985).
55. F. J. ANDRES and A. ARRIZABALAGA. An. Quim. Ser. A, **81**, 431 (1985).
56. E. ABEL. Monatsh. Chem. **86**, 952 (1955).
57. G. GUYARD. Soc. Chim. Paris, **1**, 89 (1864).
58. D. G. LEE. *In* Oxidation in organic chemistry. Part D. *Edited by* W. S. Trahanovsky. Academic Press, New York. 1982. p. 147.

Can. J. Chem. Downloaded from www.nrcresearchpress.com by 213.166.140.6 on 09/07/12
For personal use only.

Formation of oxy radicals by oxygen reduction arising from the surface activity of asbestos

ROGER ZALMA, LIONEL BONNEAU, JOËLLE GUIGNARD, AND HENRI PEZERAT[1]

Laboratoire de réactivité de surface et structure, Unité associée 1106, Centre national de la recherche scientifique, Université Pierre et Marie Curie, 4, Place Jussieu, 75252-Paris CÉDEX 05, France

AND

MARIE-CLAUDE JAURAND

Institut national de la santé et de la recherche médicale, Unité 139, Centre hospitalier universitaire Henri Mondor, 94010-Creteil CÉDEX, France

Received March 3, 1987

ROGER ZALMA, LIONEL BONNEAU, JOËLLE GUIGNARD, HENRI PEZERAT, and MARIE-CLAUDE JAURAND. Can. J. Chem. **65**, 2338 (1987).

Formation of hydroxyl radicals, in relatively large quantities, by oxygen reduction due to the surface activity of asbestos in a cell-free system is demonstrated, using electron spin resonance and a spin trapping agent. The quantity of OH• produced (in general, above 10^{14} mg^{-1} for a Canadian chrysotile) is a function of activation or passivation of the electron donor surface sites of the minerals. The role of these radicals in oxidative stress in relation to the toxic properties of these minerals is discussed.

ROGER ZALMA, LIONEL BONNEAU, JOËLLE GUIGNARD, HENRI PEZERAT et MARIE-CLAUDE JAURAND. Can. J. Chem. **65**, 2338 (1987).

En utilisant la technique des piégeurs de radicaux et la spectroscopie en résonance paramagnétique électronique on peut montrer que la réactivité de surface des amiantes permet, en milieu tampon, la réduction de l'oxygène en radicaux hydroxyles (OH•). La quantité de radicaux formés (en général supérieure à 10^{14} mg^{-1} pour le chrysotile canadien) est fonction de l'activation ou de la passivation des sites de surface à caractère électro-donneur. Le rôle de ces radicaux dans les phénomènes de «stress oxydant» est discuté en relation avec les propriétés toxiques des amiantes.

Can. J. Chem. Downloaded from www.nrcresearchpress.com by 213.166.140.6 on 09/07/12
For personal use only.

It is known that asbestos fibres induce chromosome damage, which might be implicated in the sequential steps of carcinogenesis. This phenomenon might be related to the formation of oxy radicals in the presence of asbestos, this formation being postulated from biochemical data concerning asbestos-induced damage to cells and lipid peroxidation (1–4), and in relation to redox properties as shown up by electron spin resonance (esr) (5, 6).

Weitzman and Graceffa (7) and Eberhart and Romano-Franco (8) demonstrated that asbestos catalyzes the generation of hydroxyl (OH•) and superoxide (O_2^{-}•) radicals from hydrogen peroxide (H_2O_2) in a cell-free system. But all iron-containing minerals (with Fe^{2+} or Fe^{3+}) have approximately the same activity in such a system (9, 10), and the bioavailability of H_2O_2 is low. In our model system, with techniques similar to that of Weitzman and Graceffa (7) (esr and spin trapping agent), but taking into account the phenomenon of activation or passivation of the surface active sites of asbestos, we are able to demonstrate the formation of a high level of OH• from the reduction of oxygen, which is completely bioavailable. Our model system differs from the one employing H_2O_2 in that only part of the iron-containing minerals is active in the reduction of O_2, according to the following reactions:

$$[1]\quad O_2 \xrightarrow{+e^-} O_2^{-}\cdot$$

$$[2]\quad O_2^{-}\cdot \xrightarrow{+e^- + 2H^+} H_2O_2$$

$$[3]\quad H_2O_2 \xrightarrow{+e^-} OH\cdot + OH^-$$

$$[4]\quad OH\cdot \xrightarrow{+e^- + H^+} H_2O$$

Morever, if we have some organic molecules (RH) in the reactor, then we obtain:

$$[5]\quad OH\cdot + RH \rightarrow R\cdot + H_2O$$

[1]Author to whom correspondence may be addressed.

Methods

We used 5,5′-dimethyl-1-pyrroline-*N*-oxide (DMPO) as a spin trapping agent to produce adducts with OH•, or more generally with a radical R•, sufficiently stable to be detected in esr (11, 12). The reaction medium in our study is a suspension of fibres or particles (45 mg) in aqueous buffer solution (potassium phosphate, pH = 7.4) at 37°C in a dark reactor. All reactions were duplicated in the presence of a probe anion $HCOO^-$ (cf. reaction [5]) to obtain, from OH•, the radical CO_2^{-}•, and consequently the (DMPO, CO_2)$^{-}$• adduct. This procedure was used to take into account the possible artefact in the formation of (DMPO, OH)• by an oxidative pathway without intervention of OH• (13), and also to reduce the importance of reaction [4], i.e., destruction of OH• in contact with active sites of the solid. Therefore we used 1 mL of 1 *M* sodium formate solution in the buffer, to which we added the solid and 1 mL of 100 m*M* DMPO solution, prepared according to Buettner and Oberley (14); time was counted from this moment. Aliquots of the suspension were withdrawn at the indicated times without modification of the relative concentrations and then filtered through 0.65 μm porosity filters. Controls contained no solid particles.

Detection of radical adducts was performed by epr (electron paramagnetic resonance) spectroscopy, 2 min after withdrawal of aliquots. Spectral data of radical adducts accorded well with those reported by Kirino *et al.* (15) and Makino *et al.* (13). Ethanol, acetone, or DMSO were also used instead of formate, and examples of esr spectra of DMPO-radical adducts, formed in our model system, are given in Fig. 1. In this publication, all the results are reported from the measuring of the intensity of the (DMPO, CO_2)$^{-}$• signal after the addition of formate. To ascertain mechanisms we added 250 μL of catalase (1 g L^{-1}) or 200 μL of superoxide dismutase (SOD, 2.5 g L^{-1}) to the reaction medium, which had a final volume of 2 mL for 45 mg of solid.

Materials

Asbestos samples

We used the following:

Rhodesian and Canadian chrysotile (A and B); crocidolite and amosite obtained from the Union Internationale contre le Cancer (UICC), the respective surface areas (BET) being 19, 27, 8, and 6 m^2 g^{-1}; and also two commercial asbestos samples.

Printed in Canada / Imprimé au Canada

Can. J. Chem. Downloaded from www.nrcresearchpress.com by 213.166.140.6 on 09/07/12
For personal use only.

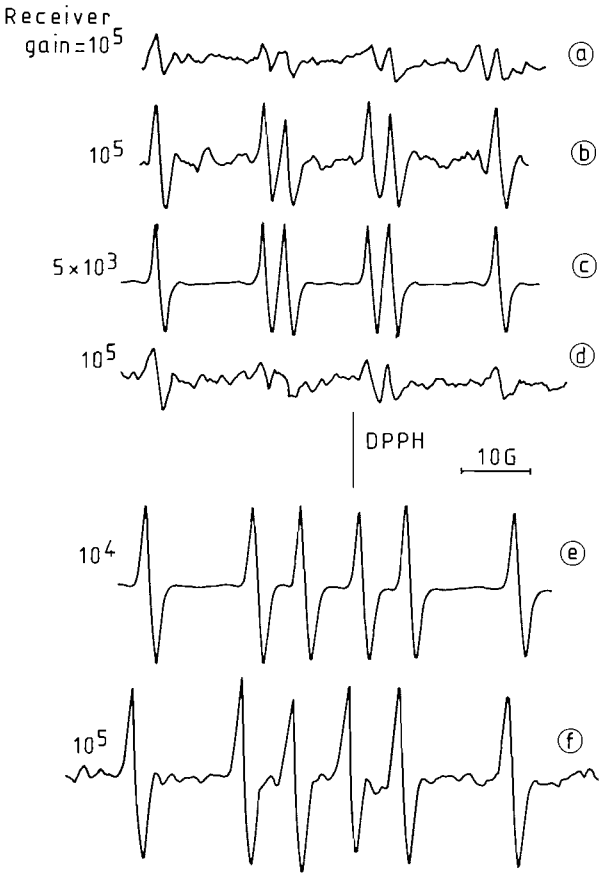

FIG. 1. Examples of spectra of DMPO-radical adducts, after 25 min of incubation of fibres in buffer, with DMPO and formate solution or ethanol or acetone. (a) Control in presence of formate anion. (b) Case of UICC crocidolite in presence of formate (Table 1). (c) Same sample but 5 min after grinding (Table 3). (d) Same sample, ground, then 2 h in buffer and 1 h with ultrasonic treatment (Table 4). (e) Case of commercial amosite, ground, in presence of ethanol. (f) Same sample, in presence of acetone. Varian CSE instrument, field set 3380 G, scan range 100 G, microwave power level 10 mW, time constant 1 s. Constants for (DMPO, OH)$^{\cdot}$: $g = 2.0054$, $a_N = a_H = 14.9$ G; for (DMPO, CO_2)$^{\cdot-}$: $g = 2.0055$, $a_N = 15.6$ G, $a_H = 19.0$ G; for (DMPO, CH_3CHOH)$^{\cdot}$: $g = 2.0052$, $a_N = 15.8$ G, $a_H = 23.2$ G.

Six samples of Canadian chrysotile, supplied by C. Jolicoeur (Asbestos research programme, Sherbrooke, Québec), from Bell asbestos mines (Ltd 7D-700 no. 6781), J. M. Asbestos Inc. (6D-12), Lac d'amiante Ltée (no. 85-530 7D-3), Carey Canada Inc. (7TS-3 O.S. 7021), Asbestos corporation Ltd. (BC-753-7m), J. M. Asbestos (gr 7).

Two samples of "short fiber" chrysotile, one of them after treatment with $POCl_3$ to obtain a "chrysophosphate" (supplied also by C. Jolicoeur). The short fibers were obtained by sedimentation from a sample of J. M. Asbestos mine.

Mineralogical samples

Magnetite (from Norway) and nemalite (from Asbestos, Quebec) are classical contaminants of chrysotile, but we have verified the absence of nemalite in Rhodesian chrysotile UICC. Nemalite is a fibrous brucite ($Mg(OH)_2$) where 8% of Mg^{2+} is substituted by Fe^{2+}. These substitutions led to slight modifications of the crystallographic parameters, which we have verified.

Reagents

Catalase, SOD, and DMPO were from Sigma, the last having been purified by filtering through activated charcoal.

Results

In Tables 1, 2, and 3 we present the results as the intensity of the (DMPO, CO_2)$^{\cdot-}$ signals (arbitrary scale) obtained with different materials. These radical adducts arise from:

$$OH^{\cdot} + HCO_2^- \rightarrow H_2O + CO_2^{\cdot-} \xrightarrow{\text{DMPO}} (\text{DMPO}, CO_2)^{\cdot-}$$

For purposes of comparison, we also added H_2O_2 (0.3%) to the reactor, following Weitzman and Graceffa (7). In this case the intensities of the same signals, after 30 min, are 2200 for magnetite, 720 for Canadian (UICC) chrysotile, 1000 for UICC crocidolite, and 800 for commercial chrysotile. Thus we

TABLE 1. Intensity of the esr signals of (DMPO, CO_2)$^{\cdot-}$. All values are given to ±20%

Nature of materials	(DMPO, CO_2)$^{\cdot-}$ signal intensity	
	After 25 min	After 60 min
Magnetite	40	30
Chrysotile UICC Rhod. (A)	25	30
Crocidolite UICC	25	40
Amosite UICC	30	50
Chrysotile (commercial)	1800	1500
Chrysotile UICC Can. (B)	1200	600
Nemalite	200	3000
Controls	10	15

TABLE 2. Results of "activation" treatments. Because of differences in grinding, the intensities of the (DMPO, CO_2)$^{\cdot-}$ signals may differ by ±30%. The controls are the same as in Table 1

Materials and treatment	(DMPO, CO_2)$^{\cdot-}$ signal intensity	
	After 25 min	After 60 min
Crocidolite (commercial) 5 min after grinding	690	1030
Crocidolite (UICC) 5 min after grinding	640	600
Amosite (UICC) 5 min after grinding	850	1000

TABLE 3. Results of "passivation" treatments. The controls are the same as in Table 1

Materials	(DMPO, CO_2)$^{\cdot-}$ signal intensity	
	After 25 min	After 60 min
Chrysotile (UICC) Can. after 16 h in buffer	20	15
Crocidolite (UICC) ground, then 2 h in buffer and 1h with ultrasonic treatment	15	15
Crocidolite (UICC) ground, then exposed to air, during 1 day	220	180
during 20 days	230	170
Chrysotile (short fibers)	490	225
Chrysotile (phosphated fibers)	135	75

observed that in some cases the intensities have the same order of magnitude, irrespective of the addition of H_2O_2.

The spin number was calculated using as a reference the signal of DPPH in benzene at different concentrations, in the same esr cell. The conversion of the signal intensity to radical concentrations is obtained by means of double integration of the area under the peaks for DPPH and (DMPO, CO_2)$^{\cdot}$ solutions. The tests were made rapidly to avoid problems with the stability of DPPH solutions. We may consider that a (DMPO, CO_2)$^{\cdot}$ signal of intensity 1000 implies presence of approximately 8×10^{15} R$^{\cdot}$ in our reactor, for 45 mg of solid. Consequently, for an active chrysotile giving a signal of 1000, we may consider that a fibre of 5 μm length and 0.1 μm diameter might lead to the formation of a minimum of 10^4 OH$^{\cdot}$ in such a model system.

Table 1 shows that some minerals are very active while others are poorly active in the reduction of oxygen. On the other hand, all the samples of Canadian chrysotile—UICC sample and the six samples supplied by C. Jolicoeur from different mines—are active. For the last six samples the intensity of the (DMPO, CO_2)$^{\cdot}$ signal varies from 940–1000, in the case of the less active one, to 2200–2700 for the most active one.

Table 2 reveals that poorly active amphibole fibres can become very active after moderate grinding without significant increase of their surface area (BET). The activation in this case implies merely the emergence of fresh surfaces (not oxidized).

On the contrary, Table 3 presents evidence of a considerable alteration of surface properties of chrysotile after some hours in the buffer, and illustrates a lower passivation of crocidolite surface in air. In other respects the short fibres of chrysotile prepared in aqueous phase are less active than the fibers of Canadian chrysotile (Table 1) and the activity of phosphated fibers is clearly weaker.

Figure 1 (spectra b, c, d) illustrates the phenomena of activation and passivation with the UICC crocidolite.

Moreover, we confirm by addition of SOD and catalase that the reactions concerned are [1], [2], and [3]: SOD does not inhibit the reactivity but slightly enhances it, and catalase reduces the (DMPO, OH)$^{\cdot}$ signals to the control level. Finally, we have evidence that the activity is a surface activity, as shown by adding the DMPO to the filtrate at variable time, instead of adding DMPO to the suspension. In this case we do not observe the formation of the radical adducts.

Discussion

The reduction of O_2 in OH$^{\cdot}$ is realized by transfer of electrons from the electron donor surface sites of the solid. The initial step [1] can be schematized as below, where the active site is OH_2, in low coordination and linked to a Fe^{2+}:

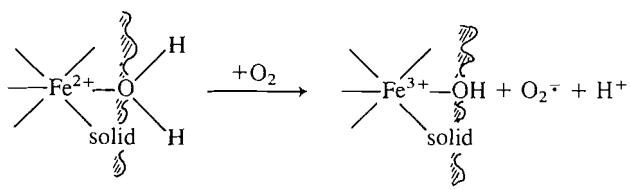

Thus an active material may, for example, be a divalent iron-containing material, but this condition is not sufficient if there is easy reconstruction of the solid surface to an oxidized sheet, impermeable to air even in aqueous medium (case of the magnetite).

In amphiboles, Fe^{2+} is present in an octahedral sheet of the I-beams and Bonneau *et al.* have published studies on the surface sites (5, 16). The oxidation of these sites—which is relatively easy—indicates the need to use freshly ground fibres for in vitro experiments to test the redox activity of the surface of the fibers.

Examination of chrysotile samples leads to the consideration that the iron is found essentially in the contaminants (magnetite and nemalite), the reason being the steric constraints that hinder the insertion of iron in the brucitic sheets of the chrysotile.

The presence of magnetite in the samples studied is demonstrated either by electron microscopy and electron diffraction patterns or by X-ray diffraction from the fraction adhering to a magnetic stirring bar during the stirring of a suspension of chrysotile in benzene.

Nemalite is revealed from the X-ray diffraction of samples from Quebec. Mg^{2+} is partially substituted by Fe^{2+} in the brucite structure in a relatively homogeneous manner, as shown by the measurement of crystalline parameters and by electron diffraction spectroscopy. The weak solubility of this material probably allows a permanent creation of new active sites, explaining the high activity of this mineral, specially in potassium phosphate buffer, where the solubility increases because of the precipitation of $KMgPO_4 \cdot 6H_2O$ (verified by X-ray).

In addition, we can consider the presence of a coating containing Fe^{2+}, between the fibrils of chrysotile or in a closed porosity, becoming accessible to oxygen in aqueous medium. But for the time being it is not possible either to confirm or to exclude this hypothesis.

The redox activity of a mineral sample is a function of the density of surface active sites accessible to O_2 in the buffer medium, of the redox potential of these sites (related to their configuration), and of the surface area of the sample.

In biological media other phenomena may occur, as part of activation or passivation of surface activity of mineral dusts. For example, the leaching of mineral particles, the splitting of the amphiboles (17), or the "opening" of the bundles of chrysotile can lead to the emergence of new active sites. On the contrary, a coating by some biological molecules may "poison" these surface sites. The observed formation of OH$^{\cdot}$ and R$^{\cdot}$ in biological medium from the surface activity of fibres and other nonfibrous minerals, encountered for example in some metallic mine ores (10, 18), may give these dusts an important role in oxidative stress (19) and so explain their role in fibrogenesis (20) and in the steps of bronchopulmonary carcinogenesis.

Acknowledgment

The authors thank B. Morin for technical help, and C. Jolicoeur for the samples of Canadian chrysotile.

1. B. T. Mossman, J. P. Marsh, and M. A. Shatos. Lab. Invest. **54**, 204 (1986).
2. S. A. Weitzman and A. B. Weitberg. Biochem. J. **225**, 259 (1985).
3. M. Gulumian, F. Sardianos, T. Kilroe-Smith, and G. Ockerse. Chem. Biol. Interact. **44**, 111 (1983).
4. C. J. Turver, A. Poole, and R. C. Brown. In vitro effects of mineral dusts. *Edited by* E. G. Beck and J. Bignon. NATO ASI Series Vol. G3, Springer-Verlag, Berlin. 1985. pp. 267–273.
5. L. Bonneau and H. Pezerat. J. Chim. Phys. **80**, 275 (1983).
6. A. M. Langer, A. N. Wolf, and I. J. Selikoff. J. Toxic. Environ. Health, **4**, 173 (1978).
7. S. A. Weitzman and P. Graceffa. Arch. Biochem. Biophys. **228**, 373 (1984).
8. M. K. Eberhardt and A. A. Romano-Franco. Environ. Res. **37**, 287 (1985).
9. B. Halliwel and J. M. C. Gutteridge. Biochem. J. **219**, 1 (1984).

Can. J. Chem. Downloaded from www.nrcresearchpress.com by 213.166.140.6 on 09/07/12
For personal use only.

10. R. ZALMA, L. BONNEAU, J. GUIGNARD, H. PEZERAT, and M. C. JAURAND. Toxicol. Environ. Chem. **13**, 171 (1987).
11. E. G. JANZEN. Acc. Chem. Res. **4**, 31 (1971).
12. E. FINKELSTEIN, G. M. ROSEN, and E. J. RAUCKMAN. Mol. Pharmacol. **16**, 676 (1979).
13. K. MAKINO, M. M. MOSSOBA, and P. RIESZ. J. Phys. Chem. **87**, 1369 (1983).
14. G. R. BUETTNER and L. W. OBERLEY. Biochem. Biophys. Res. Commun. **83**, 69 (1978).
15. Y. KIRINO, T. OHKUMA, and T. KWAN. Chem. Pharm. Bull. **29**, 29 (1981).
16. L. BONNEAU, H. SUQUET, C. MALARD, and H. PEZERAT. Environ. Res. **41**, 251 (1986).
17. P. M. COOK, L. D. PALEKAR, and D. L. COFFIN. Toxicol. Lett. **13**, 151 (1982).
18. O. AXELSON. Prevention of occupational cancer. International Symposium, ILO Geneva no. 46. 1982. pp. 135–149.
19. H. SIES. Oxidative stress. Academic Press, London. 1985.
20. B. W. CASES, M. P. C. IP, M. PADILLA, and J. KLEINERMAN. J. Environ. Res. **39**, 299 (1986).

Can. J. Chem. Downloaded from www.nrcresearchpress.com by 213.166.140.6 on 09/07/12
For personal use only.

Transient intermediates in the photolysis of iodonium cations

R. J. DEVOE AND M. R. V. SAHYUN[1]
3M Corporate Research Laboratories, 3M Center, St. Paul, MN 55144, U.S.A.

AND

N. SERPONE AND D. K. SHARMA
Canadian Centre for Picosecond Laser Flash Photolysis, Concordia University, Montreal, P.Q., Canada H3G 1M8

Received February 20, 1987

R. J. DEVOE, M. R. V. SAHYUN, N. SERPONE, and D. K. SHARMA. Can. J. Chem. **65**, 2342 (1987).

Pulsed picosecond laser photolysis of the diphenyliodonium cation indicates that excitation of the allowed transition is followed by rapid (ps) deactivation to a homolytically dissociative state, presumably T_1. Steady-state photolysis yields iodobenzene and biphenyl from the primary radical products. Iodobiphenyl is also observed. We infer in-cage recombination of these radical products, with intervention of a carbocationic intermediate. Laser flash photolysis of diphenyliodonium iodide in its charge transfer band yields an initial transient with a lifetime of ca. 200 ps. A strongly absorbing secondary transient is observed on the nanosecond time scale. Iodobenzene is the exclusive reaction product. We infer that it is not formed directly from the primary photoproduct, but through in-cage recombination of phenyl cation with iodide anion, as in benzenediazonium iodide.

R. J. DEVOE, M. R. V. SAHYUN, N. SERPONE et D. K. SHARMA. Can. J. Chem. **65**, 2342 (1987).

La photolyse laser pulsée au picoseconde du cation diphényliodonium indique que l'excitation de la transition permise est suivie par une désactivation rapide (ps) conduisant à un état dissocié homolytique, probablement T_1. La photolyse à l'état dissocié homolytique, probablement T_1. La photolyse à l'état stationnaire conduit à la formation d'iodobenzène et de biphényle à partir des produits radicalaires primaires. On observe aussi la formation d'iodobiphényle. On en conclut qu'il se produit une recombinaison en cage de ces produits radicalaires, avec une intervention d'un intermédiare carbocationique. La photolyse laser flash de l'iodure de diphényliodonium dans sa bande de transfert de charge conduit initialement à la formation d'une espèce transitoire dont le temps de demi-vie est d'environ 200 ps. On observe aussi la formation d'une espèce transitoire secondaire qui absorbe fortement et dont le temps de demi-vie est de l'ordre de la nanoseconde. L'iodobenzène est le seul produit de la réaction. On en déduit qu'il ne se forme pas directement à partir du photoproduit primaire, mais plutôt par une recombinaison en cage du cation phényle avec un anion iodure, comme dans le cas de l'iodure de benzènediazonium.

[Traduit par la revue]

Introduction

Photolabile 'onium salts, particularly those of aryldiazonium, diaryliodonium, and triarylsulfonium cations, have found application in imaging media and in radiation curable coatings (1). The mechanism of photolysis of diphenyliodonium cations was probed by following the absorption spectroscopy of light absorbing transient intermediates on the nanosecond time scale by Klemm *et al.* (2) and by Pappas *et al.* (3). These workers observed iodobenzene radical cation and, in the former instance, phenyl radical, both of which had been formed on a time scale fast compared to the resolution capabilities of their experiments. Accordingly, we decided to probe this chemistry with picosecond time-resolved absorption spectroscopy.

Results

We flash photolyzed diphenyliodonium hexafluorophosphate (6×10^{-4} *M* in acetonitrile) with 30-ps (FWHM) pulses of 266-nm radiation from a mode-locked, frequency quadrupled Nd-YAG laser. Representative transient absorption spectra are shown as absorbance change, ΔA, vs. wavelength, in Fig. 1. The principal transient absorbance occurs at 650 nm; it is formed during the light pulse ($\leq$30 ps), hence in an essentially unactivated process. This transient barely begins to decay during the lifetime of the experiment (10 ns); it corresponds to the iodobenzene radical cation (4), observed by Klemm (2) to survive ca. 500 ns in the same medium.

The rising absorbance at the short wavelength limit of the probe continuum suggests the presence of phenyl cation, also found by Klemm. Although the changes in ΔA with time are small, they nevertheless suggest growth over the period of time from 1 to 5 ns of some broad transient centered at ca. 460 nm (see below), perhaps at the expense of the 650-nm species.

We complemented the spectroscopic observations with steady-state photolysis product studies, using the 254-nm line from a medium pressure mercury source, followed by glc. Within experimental error there was no difference in the product distribution from nitrogen-purged samples and that from air-equilibrated samples. The results of these analyses are reported in Table 1. The iodobiphenyl product comprised two isomers, distinguishable in the glc analysis. By comparison of the retention times with those of authentic samples we identify these isomers as *para*- and *ortho*-iodobiphenyl, obtained, typically, in 80:20 ratio.

It also appeared instructive to carry out a sensitized photolysis of the diphenyliodonium hexafluorophosphate. Although sensitizations with both acetophenone (1, 3) and benzophenone (5) have been reported, the mechanism of sensitization is ambiguous in these cases inasmuch as both electron transfer and triplet energy transfer (see below) are energetically feasible. We chose *m*-trifluoromethylacetophenone (0.05 *M* in acetonitrile) as sensitizer, insofar as its triplet energy (3.17 eV) is equal to that of acetophenone itself; however, it is 0.20 V less reducing (6), and hence energetically incapable of electron transfer from its triplet excited state to the diphenyliodonium cation (3). The quantum yield for iodobenzene formation (by glc) in this sensitized photolysis at 313 nm was 0.04. The same products were observed for the sensitized and the direct photolyses, though with altered distribution (Table 1). On the other hand,

[1]Author to whom correspondence should be addressed. This is Contribution no. 1446a from the Corporate Research Laboratories, 3M.

Printed in Canada / Imprimé au Canada

Can. J. Chem. Downloaded from www.nrcresearchpress.com by 213.166.140.6 on 09/07/12
For personal use only.

TABLE 1. Product distributions for diphenyliodonium cation photolyses

Product	in:	$Ar_2I^+PF_6^-$ AN	$Ar_2I^+PF_6^-$ AN[a,b]	$Ar_2I^+PF_6^-$ H_2O[c]	$Ar_2I^+Cl^-$ H_2O	$Ar_2I^+I^-$[a] H_2O
Chlorobenzene		—	—	—	1.2	—
Acetanilide		10.7%	31.0	—	—	—
Iodobenzene		47.8	63.9	55.0	79.5	100[d]
Biphenyl		23.5	3.3	26.5	0.6	0
Hydroxybiphenyl		—	—	—	10.2	—
Iodobiphenyl		18	0.5	18.5	7.9	0
Other products		0	1.3	0	0.6	0[d]
Phenyl/I		2.15	1.59	1.97	1.35	1.0

[a]Irradiation at 313 nm.
[b]Sensitized with 0.05 *M* *m*-trifluoromethylacetophenone.
[c]Including 1% AN to effect solubility of the iodonium salt.
[d]Iodobenzene was the only product reproducibly obtained; other unidentified volatile products were occasionally observed in trace amounts.

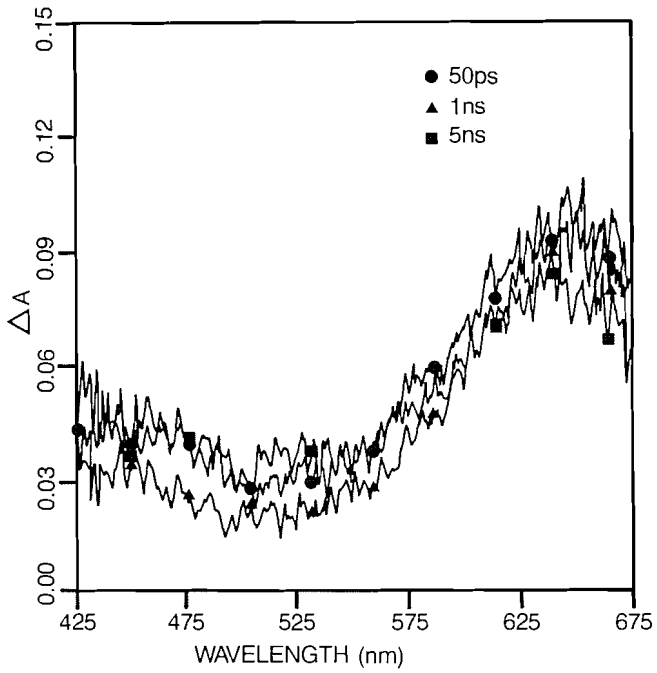

FIG. 1. Light absorbing transients observed on laser flash photolysis (266 nm) of diphenyliodonium hexafluorophosphate in acetonitrile.

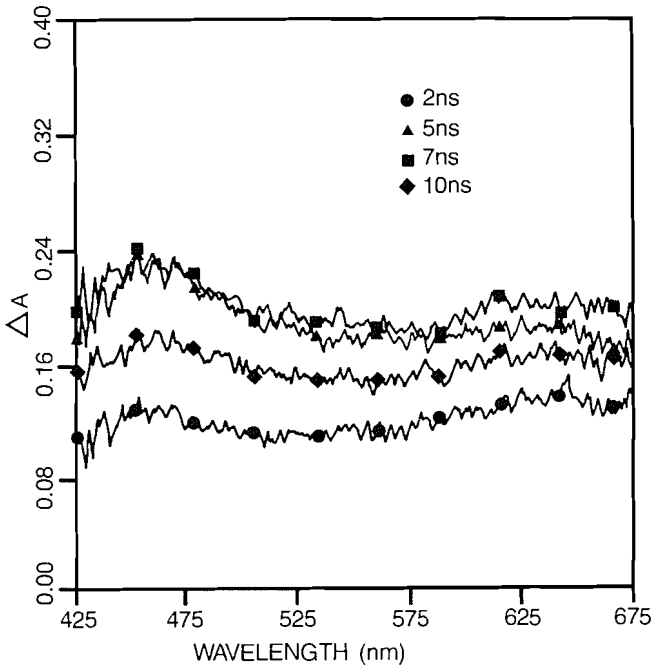

FIG. 2. As Fig. 1, for photolysis of diphenyliodonium hexafluorophosphate in water.

with chloranil (triplet energy 2.7 eV) as sensitizer, no decomposition of the iodonium cation was obtained on irradiation into the chloranil absorption band.

Photolysis of both the iodonium hexafluorophosphate and chloride salts in water was complicated by insolubility of the products. Although the product distribution (Table 1) indicated no change in mechanism, in the case of the hexafluorophosphate salt, changing the solvent (acetonitrile to water), led to dramatic differences in the transient absorption spectra. The greatly enhanced absorption centered on 460 nm grew in on the time scale of the laser flash photolysis experiment, but not at the expense of the iodobenzene radical cation (see Fig. 2). The absorption bands are broader than in acetonitrile, probably an artifact resulting from light scattering by the insoluble photoproduct. In addition, broad absorption across the visible, arising from solvated electrons, a usual side-product observed in 266-nm aqueous photolyses, may contribute to the observed transient absorption. This species lives for at least tens of nanoseconds in neutral aqueous environment (7). Laser flash photolysis of the chloride salt in water yielded, in fact, only the broad transients associated with solvated electrons.

As a result of these complications, absolute values of ΔA for the photolysis of the hexafluorophosphate salt in water were reproducible only to $\pm 25\%$. From the time dependence of the 460-nm absorbance intensity, normalized to the 650-nm absorption, shown in Fig. 3, we infer a half-life of ca. 1 ns for its formation, consistent with an in-cage reaction.

Steady-state photolysis of the diphenyliodonium chloride in water generates new products (Table 1), principally at the expense of biphenyl and iodobiphenyl. The isomer distribution of the hydroxybiphenyl was unresolvable by glc. The overall product distribution was unaltered, within experimental error, when the photolysis was carried out in the presence of 0.017 *M* additional chloride ion (in 17-fold excess, as sodium chloride).

In the direct photolyses of the hexafluorophosphate salt, the ratio of phenyl moieties to iodine atoms in the isolated products

Can. J. Chem. Downloaded from www.nrcresearchpress.com by 213.166.140.6 on 09/07/12
For personal use only.

TABLE 2. Optical absorption characteristics of diphenyliodonium iodide

Solvent	λ_{max} (nm)	hc/λ_{max} (eV)	E_T 30 (eV)	K_{diss} (M)
Water	320	3.91	2.74	0.6
Ethanol	307	4.07	2.26	0.015
90% acetonitrile – 10% water	314	3.98	2.09	0.009
Acetonitrile	324	3.86	2.00	≤0.001
DMF	328	3.81	1.91	—
1,2-DCE[a]	352	3.55	1.78	—
THF	347	3.60	1.62	—

[a]1,2-Dichloroethane.

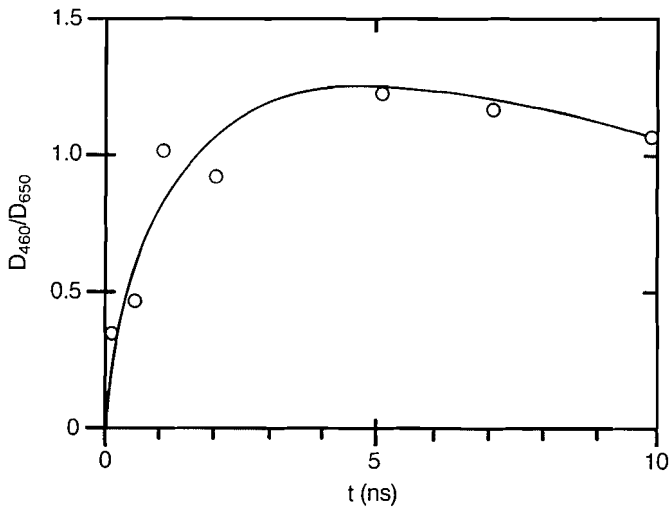

FIG. 3. Time dependence of relative intensities of transient absorbances at 460 and 650 nm in the experiment of Fig. 2. Solid line corresponds to a computer model of reaction [6].

reflects the stoichiometry of the starting materials, suggesting complete recovery of products. An expected reaction product, benzene, could not be resolved from the extraction solvent, cyclohexane, by chromatographic methods. The low yield of biphenyl in the photolysis of the chloride salt, combined with the low phenyl-to-iodine ratio, suggests that the phenyl radicals have been diverted to benzene in this case; formation of benzene was confirmed by nmr. The low phenyl-to-iodine ratio for the sensitized photolysis lends itself to a similar interpretation. In addition, the high resolution mass spectrometric analyses of the reaction mixtures all indicated the presence of trace quantities of polyphenyls.

Formation of iodobenzene from the homolysis products has been rationalized by McEwen and co-workers (8); biphenyl results by in-cage recombination of the phenyl radicals. The higher polyphenyls are also typical products of radical reaction. The acetanilide may be formed by attack of either phenyl radical or phenyl cation on acetonitrile solvent. The origin of the *p*-iodobiphenyl will be discussed below.

Diphenyliodonium iodide, **5**, was prepared *in situ* from the hexafluorophosphate salt (6×10^{-4} M) and tetrabutylammonium iodide (0.045 M) in water, as direct dissolution of the pure iodonium iodide proved difficult to effect. The solubility product, K_{sp} of **1** was determined to be 3×10^{-5} M^{-1} in water. Solutions of this salt exhibited λ_{max} beyond 300 nm, which we assign to an iodide–iodonium (σ^*) charge transfer (CT) absorption, in keeping with the charge transfer absorption observed in *N*-alkylpyridinium iodides (9) and in triphenylsulfonium iodide (10). Other charge transfer complexes of the diaryliodonium cations have been reported (11). The identification of this electronic transition was confirmed by a study of its solvent dependence; as shown by the data of Table 2, in organic solvents the transition energy, hc/λ_{max}, varies systematically with the polarity index, E_T 30 (12), of the solvent. (The correlation coefficient for the regression of hc/λ_{max} on E_T 30 is 0.925 and the slope is 0.84; the data point obtained in pure water does not fit the correlation.)

Absorption in the CT band did not follow Beer's Law in water; in acetonitrile, in which the iodonium iodide is more soluble, Beer's Law is followed for concentrations below 10^{-4} M, and $\varepsilon = 1.2 \times 10^4$ L mol^{-1} cm^{-1} at 324 nm. These observations suggest the following scheme:

[1]

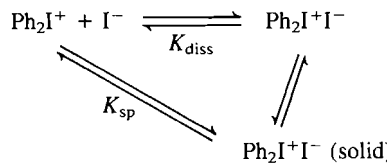

where the 324-nm absorption is associated with the ion-paired species. The Beer's Law behaviour suggests that only the ion-paired species obtains in acetonitrile. Based on the extinction coefficient from acetonitrile solution, the maximum *observed* concentration of **1** in water is 5×10^{-5} M, from which we infer a dissociation constant, K_{diss}, of ca. 0.6 M. We similarly estimate dissociation constants of 0.015 M in ethanol and 0.009 M in 90% acetonitrile – 10% water. There thus seems to be a trend for dissociation constant to increase with the polarity of the solvent (Table 2).

Excitation at 355 nm of the long wavelength tail of the charge transfer band was expected to lead to the diphenyliodo radical, **2**, plus iodine atom, by analogy to the photochemistry of the triphenylsulfonium iodide (10). The radical has been proposed as an intermediate in the sensitized photolysis of iodonium cations (1) and the mode and dynamics of its decomposition were accordingly of particular interest.

[2] $Ph_2I^+ I^- \xrightarrow{h\nu} [Ph_2I^{\cdot}\ I^{\cdot}] \longrightarrow 2\,PhI$

2

We carried out the laser flash photolysis of the iodonium–iodide ion pair with frequency tripled 355-nm Nd-YAG emission. The transients are shown in Figs. 4*a* and *b*. The initial broadly absorbing transient centered on 560 nm decays within 200 ps. Bands centered on 430 and at >670 nm grow in with first-order kinetics as shown in Fig. 5; $k = (7.1 \pm 0.4) \times$

Can. J. Chem. Downloaded from www.nrcresearchpress.com by 213.166.140.6 on 09/07/12
For personal use only.

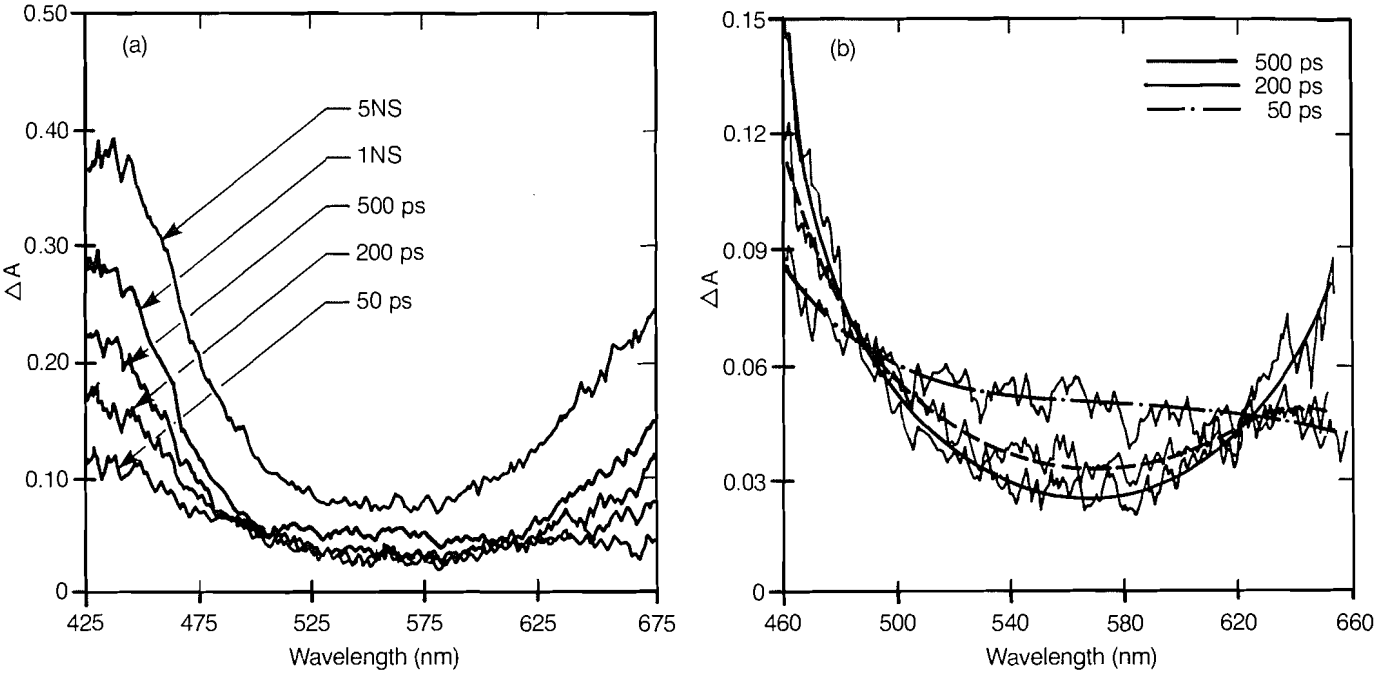

FIG. 4. (a) Spectra of light absorbing transients observed at various times following 355-nm laser flash photolysis of diphenyliodonium iodide in water; (b) detail of (a) for times 500 ps and shorter to show transient centered on 560 nm.

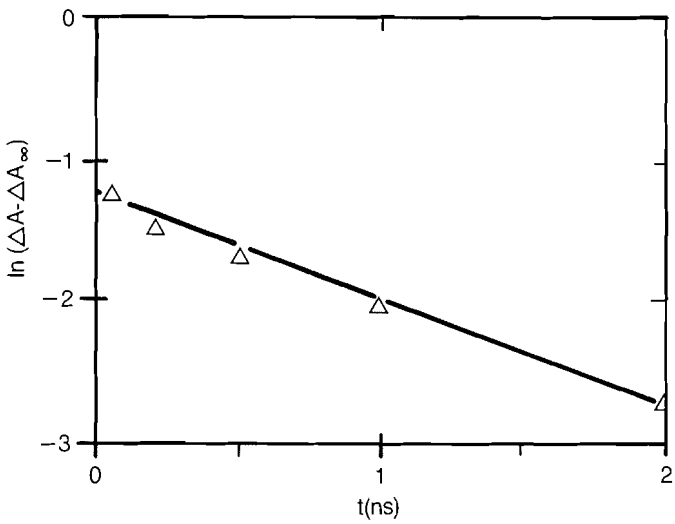

FIG. 5. First-order kinetics of rise of the 430-nm transient in laser flash photolysis of aqueous **1** at 355 nm, as ln $(\Delta A_\infty - \Delta A)$ vs. time where ΔA_∞ is taken as the value observed at 10-ns delay.

$10^8\ s^{-1}$. The latter two transitions thus appear to belong to the same species.

The only reproducibly isolable organic product of the steady-state photolysis of **1** is iodobenzene (Table 1). In this respect our results differ from the observation of a more complex mixture of products from solution irradiation into the CT band of triphenylsulfonium iodide (10) and from those of Irving and Reid (13) who, however, studied the photolysis of a suspension of **1** in chloroform, using a broad spectrum light source. These authors noted that the course of the photolysis was solvent dependent; in addition, the use of a broad spectrum source can lead to secondary photoreactions, e.g., of iodobenzene. Clean thermolyses of **1** and other iodonium iodides have been reported (14). In this context, it is important to note that photolysis of **1**, unlike that of other iodonium cations (e.g., from the hexafluorophosphate salt), does not initiate polymerization of vinyl monomers (15); this indicates either that the phenyl radical expected from the disproportionation of **2** (16) does not form, or that it is trapped rapidly in-cage.

Based on the formation of iodobenzene, the quantum yield for the photolysis of **1**, in aqueous solution of similar composition to that used for flash photolysis, is 0.05 ± 0.01. Steady-state photolysis of an acetonitrile solution of comparable optical density at 313 nm (6×10^{-5} *M* in iodonium cation) indicated a quantum yield for the disappearance of **1** (spectrophotometric) of 0.6 in this solvent; in 90% acetonitrile – 10% water the quantum yield is 0.25 ± 0.03. The only persistent absorption observed in the near-uv or visible, subsequent to photolysis in either pure solvent, occurred at 360 nm, outside the continuum used to probe the flash photolyses. This absorption was also observed on photolysis of the tetrabutylammonium iodide alone; the spectrum corresponds to that of triiodide ion (17). Absorption spectroscopy also indicated that I_3^- is formed in ca. 15% yield relative to that for iodobenzene; the quantum yield is thus <0.01 and also appears to be wavelength dependent.

Given the absence of typical radical products, the possible intervention of phenyl cation in the photolysis of **1**, as originally proposed for its thermolysis (14), had to be considered. The only reliable, independent means for generating phenyl cations appears to be the photolysis of benzenediazonium cation (18, 19). The fate of this hypothetical intermediate in the reaction environment was accordingly probed by photolyzing 1×10^{-3} *M* benzenediazonium tetrafluoroborate at 313 nm under similar conditions. The aqueous solution exhibits a pH of ca. 4 and the loss of the diazonium salt occurs with a (spectrophotometric) quantum yield of 0.20; the photolysis yields no products extractable with nonpolar organic solvents.

Can. J. Chem. Downloaded from www.nrcresearchpress.com by 213.166.140.6 on 09/07/12
For personal use only.

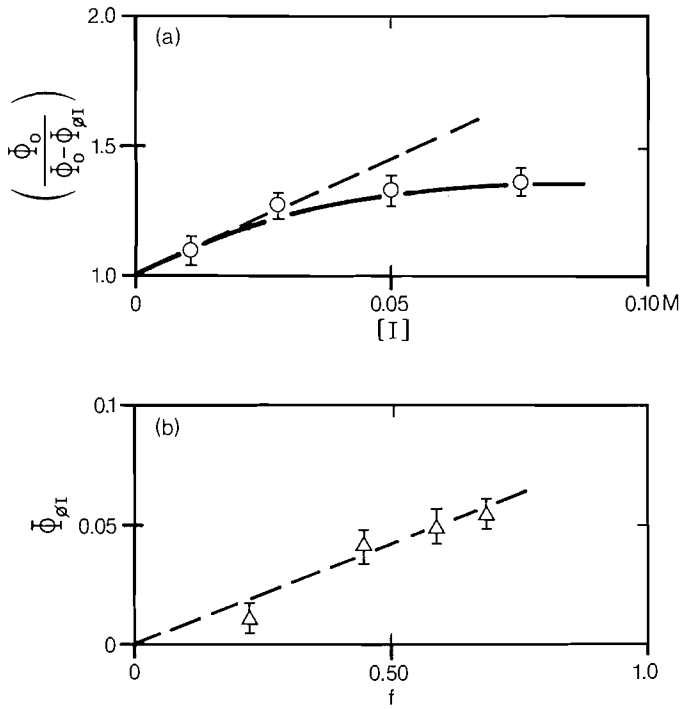

FIG. 6. Dependence of the quantum yield for iodobenzene formation from benzenediazonium cation photolysis on: (a) iodide ion concentration; (b) fraction, f, of the diazonium cation complexed by iodide ion.

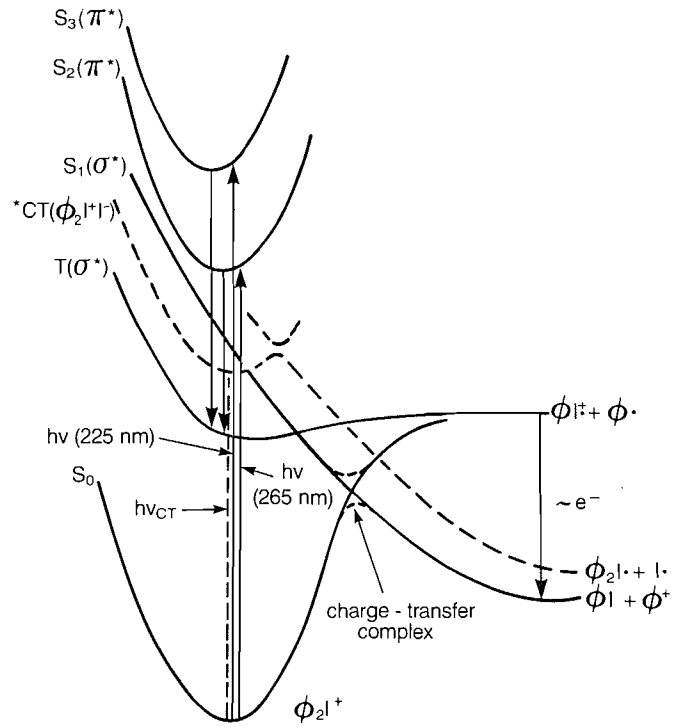

FIG. 7. Schematic diagram of potential energy levels for the diphenyliodonium cation (solid lines) and its charge transfer complex with iodide counterion (dashed lines). The reorganization coordinate (abscissa) for the latter is different from that for the former, insofar as the CT state dissociates primarily with increasing I—I bond length, while the cation, itself, dissociates by extension of a C—I bond.

When tetrabutylammonium iodide was added to the diazonium salt photolysis solution, a new optical absorption centered on 346 nm was observed, which we attribute to a charge transfer complex between iodide anion and the diazonium cation, i.e., "specific solvation" (20). A Benesi–Hildebrand treatment yielded $K_{diss} = 0.029 \pm 0.07\,M$ and $\varepsilon = (3.8 \pm 0.4) \times 10^2\,L\,mol^{-1}\,cm^{-1}$ at 346 nm.

Photolysis at 313 nm (free diazonium cation absorption band) in the presence of tetrabutylammonium iodide allowed isolation of iodobenzene. The quantum yield for its formation did not exhibit a Stern–Volmer type dependence on iodide concentration (Fig. 6*a*), indicative of diffusional capture of the primary photoproduct (19); instead it was reasonably linear with the fraction, f, of the iodonium salt in the iodide complexed form, as calculated from K_{diss}, and shown in Fig. 6*b*. We infer exclusive in-cage capture of the primary photoproduct, involving either direct reaction between phenyl cation and iodide anion, or an electron transfer from iodide anion to phenyl cation followed by radical recombination (18). Observation of the characteristic absorption of I_3^- after irradiation (formed with a quantum yield of ca. 0.01 with 0.05 M iodide ion) supports the latter interpretation. In either case, iodobenzene forms rapidly, in ca. 1 ns, compared to cage escape that occurs in ca. 2–5 ns (21) and presumably results in the triiodide product.

[3] $\mathrm{Ph{-}N{=}N^+\ I^-} \xrightarrow{h\nu} \mathrm{N_2 + [Ph^+\ I^-]}$

$\mathrm{[Ph^{\cdot}\ I^{\cdot}]} \xrightarrow[5\ ns]{1\ ns} \mathrm{PhI}$ or $\mathrm{Ph^{\cdot} + I^{\cdot}}$

Laser flash photolysis of benzenediazonium iodide at 352 nm (CT band) yielded no detectable light absorbing transients. We infer that intermediates in scheme [3] do not absorb in the continuum probed under our experimental conditions.

Discussion

A potential energy diagram correlating the various excited states of the diphenyliodonium cation with the photolysis products is shown in Fig. 7. The spectroscopically accessible levels are as assigned by Jaffe and Orchin (22); the ground state level is correlated with the electrochemical energy scale according to the procedure of Miller *et al.* (23). E_{red} was determined by cyclic voltammetry[2] to be −0.7 V vs. SCE, somewhat less oxidizing than reported earlier (16) from polarography. This level, which correlates with *CT of **1**, would be located on the diagram midway between the spectroscopically inaccessible singlet and triplet σ* states, for which a singlet–triplet splitting of 1 eV is assumed. The energy of the lowest triplet state of the diphenyliodonium cation is then 2.8 eV, consistent with its sensitizability by *m*-trifluoromethylacetophenone but not by chloranil.

The S_0 and S_1 surfaces cross at the top of the energy barrier for thermolysis of the cation; $\Delta H^* = 1.26$ eV for diphenyliodonium chloride in DMF (14). Using this experimental value in the Marcus equation, with $\Delta G^* \leq \Delta H^*$, as demonstrated by Beringer *et al.* (14), we estimate that the heterolysis (see below) of the diphenyliodonium cation is endergonic by ≤0.6 eV.

By analogy to other iodoaromatics (25), intersystem crossing in the free diphenyliodonium cation, from S_n ($n > 1$) to T_1, is rapid compared to the time scale of the experiment, so that

[2]M. C. Palazzotto, unpublished results.

Can. J. Chem. Downloaded from www.nrcresearchpress.com by 213.166.140.6 on 09/07/12
For personal use only.

Can. J. Chem. Downloaded from www.nrcresearchpress.com by 213.166.140.6 on 09/07/12
For personal use only.

photolysis occurs in accord with the Bersohn mechanism (26):

[4] $S_0 \xrightarrow{h\nu} S_2 \longrightarrow [S_1\ ?] \longrightarrow T_1 \longrightarrow$ products

This interpretation has been disputed by Pappas *et al.* (3) as they did not observe triplet sensitized photolysis of diaryliodonium cations. Baumann and Timpe (5) have, however, observed a substantially higher quantum yield, ca. 0.06, for the benzophenone sensitized photolysis of diphenyliodonium hexafluorophosphate, than that reported by Pappas. The photolysis sensitized with *m*-trifluoromethylacetophenone is furthermore unequivocal, as electron transfer sensitization is not energetically feasible; it confirms that a triplet pathway can lead to the same photolysis products observed on direct irradiation. The photochemistry of the diphenyliodonium cation is, in this respect, different from that of the benzenediazonium cation, for which the triplet pathway has been excluded (27).

From spin conservation only C—I bond *homolysis* to phenyl radical (undetected) and iodobenzene radical cation can occur (scheme [5]) from the σ^* triplet state (7). This triplet state should be directly dissociative; in *p*-diiodobenzene the lowest triplet dissociates in a few hundred femtoseconds (28). As with

[5] $Ph_2I^+ \xrightarrow{h\nu} [PhI^+ + Ph^\cdot] \rightleftharpoons [PhI + Ph^+] \longrightarrow$ products

$PhI^+ + Ph^\cdot \longrightarrow$ products

diazonium salts (17) the heterolysis products correlate with the S_1 state and, accordingly, may also result along an "avoided crossing" pathway on thermolysis of the cation (Fig. 7), consistent with the observations that diaryliodonium salts thermally arylate nucleophiles (29) and that their hydrolysis proceeds by an S_N1-type mechanism (13, 30).

The transient absorption observed at 460 nm in the aqueous photolysis of diphenyliodonium hexafluorophosphate must correspond to an intermediate in iodobiphenyl formation, as the other observable products all form from the primary photoproducts by simple electron or hydrogen atom transfers (see above). The intermediate is more visible in water, compared to acetonitrile, owing to changes in solvation and (or) rate constants subsequent to the product-determining step.

The iodobiphenyl may, in principle, result from in-cage recombination of either the homolytic or heterolytic primary products, followed by deprotonation. The former possibility has been suggested by Pappas *et al.* (3). We accordingly assign

[6] $PhI^\ddagger + Ph^\cdot \xrightarrow{k_c}$ 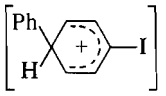 (**3**)

$PhI^\ddagger + Ph^\cdot$ (k_x)

$Ph—C_6H_4—I + H^+$ (k_h)

the 460-nm absorbance to intermediate **3**, as proposed by Pappas (3). Since it is formed in ca. 500 ps, its origin in homolytic primary photoproducts is reasonable; phenyl cation would be expected to react with water on this time scale (18). Deprotonation of **3** accounts, in part, for the differences observed in quantum yields of iodobenzene and proton formation in diaryliodonium cation photolyses (1, 3). The solid line in Fig. 3 corresponds to a computer model of the mechanism of scheme [6] with $k_c = 4 \times 10^8\ s^{-1}$, $k_x = 6 \times 10^8\ s^{-1}$, and $k_h = 3 \times 10^7\ s^{-1}$; the lifetime of **3** in aqueous medium is thus ca. 30 ns, and the cage escape efficiency is ca. 0.6.

The diversion of iodobiphenyl to hydroxybiphenyl in the photolysis of the chloride salt is additional evidence for the participation of **3**, insofar as the capture of **3** by water readily explains the formation of the hydroxy product:

[7] **3** $\longrightarrow$ 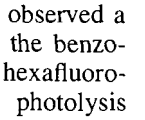 (**4**) $\longrightarrow H_2O + Ph—C_6H_4—I$ / $\longrightarrow HI + Ph—C_6H_4—OH$

Observation of the hydroxy product from the readily soluble chloride salt, but not from the sparingly soluble hexafluorophosphate salt, suggests significant differences in solvation not only of the two salts, but of the intermediates in their photolyses, as well. The significant yield of biphenyl from the direct photolyses of the hexafluorophosphate salt suggests that it is present in either solvent in aggregated form.

The chloride ion concentration independence of the low yield of chlorobenzene in the photolysis of the chloride salt indicates that chloride ion does not diffusionally capture phenyl cation. Thus, if phenyl cation were formed by the process of eq. [4], it would not live as long as ca. 5 ns, the half-life expected for its diffusion controlled scavenging by 0.02 *M* chloride ion, let alone the 2 μs claimed by Klemm *et al.* (2). The inference is consistent with the observations of Scaiano and Kim-Thuan (19).

The transient absorption spectra obtained in the photolysis of diphenyliodonium iodide (Figs. 4*a* and *b*) provide evidence for two intermediates but do not provide clear evidence for their assignment. Since the decay time of the first does not correspond to the rise time of the second, it is not certain that they obtain sequentially. The involvement of a CT excited state under the conditions of irradiation is established both by analogy to the photolysis of the sulfonium iodide (9) and from the spectroscopic observations, above; i.e., the CT state is populated directly on irradiation. The initial 560-nm transient may thus be this CT state of the iodonium–iodide complex, with which the decay lifetime of ca. 200 ps is consistent. However, the transient may also arise from an adventitious impurity or along a minor photolysis pathway, not detected by the chemical analysis.

The following considerations bear on the identity of the species absorbing at 430 and >670 nm. The exclusive reaction product, iodobenzene, can result by two routes: (*a*) that of eq. [2], in which **2** decomposes to iodobenzene and phenyl radical (15), which then combines with iodine atom; and (*b*) that corresponding to heterolysis of the iodonium cation, to yield phenyl cation, which is captured in-cage by the iodide ion. The lifetime of this second transient (>10 ns) is, however, too long for either phenyl cation (18) or **2**.[3] *We therefore exclude the mechanism of eq. [2].* The diazonium salt experiment, on the other hand, demonstrates that *if formed in intimate association with iodide ion*, the phenyl cation can react to yield iodobenzene on the sub-ns time scale, without, however, producing any light absorbing transients in the process.

Intermediacy of the phenyl cation (13) thus remains consistent with all the experimental results, even though, on spectral (2) as well as kinetic grounds, it cannot be the observed

[3]We have recently generated **2** independently by electron-transfer sensitized photolysis of a diphenyliodonium salt, and shown that the upper limit to its lifetime in solution, under our conditions, is ca. 200 ps. A manuscript describing this work is in preparation for submission to this journal.

intermediate, itself. It correlates with the S_1 excited state of the iodonium cation, above. The iodonium–iodide charge transfer complexation mixes this directly inaccessible S_1 state with the ground S_0 state, so that the crossing of the potential surfaces of these states will be avoided (Fig. 7). (Since the activation energy for thermolysis of the iodonium cation is lowered by 0.15 eV on pairing with iodide ion (13), the splitting between the surfaces at the crossing must be 0.3 eV.) The dissociation products from the charge transfer excited state, **2** and iodine atom, would be formed endergonically, by $q[E_{ox}(I^-) - E_{red}(Ph_2I^+)]$, 0.98 eV, relative to the ground state, more endergonic than the products of heterolysis of **1**. The potential surfaces for dissociation of the CT and of the S_1 states must therefore cross, as shown in Fig. 7.

We hypothesize that the charge transfer excited state undergoes internal conversion to S_1 *at its conformational potential energy minimum*, i.e., at the crossing point with S_0. Thence it decays to S_0 on the potential energy surface for heterolytic dissociation of the cation. These considerations allow us to write the mechanism of scheme [8], which incorporates both the excitation of the CT state of **1** and the intermediacy of phenyl cation. There is precedent for decay of a CT excited state to a donor (or acceptor) localized excited state; for example, the CT excited state of the anthracene–TCNE complex decays to a triplet anthracene containing complex, which then dissociates to liberate triplet excited anthracene (32). Within this scheme we

$$Ph_2I^+\ I^- \xrightarrow{h\nu} CT^*\ [Ph_2I^+\ I^-] \longrightarrow [^1(Ph_2^+)^*\ I^-] \longrightarrow PhI + [Ph^+\ I^-] \longrightarrow PhI \quad [8]$$

are tempted to assign the 430 and >670 nm absorptions to the metastable S_1 state of the diphenyliodonium salt in its minimum potential energy conformation, although chemical intuition suggests that excited states trapped at such a "funnel" might also be shorter lived than the intermediate we have observed.

Experimental

Diphenyliodonium hexafluorophosphate (33), mp 136°C, was purified by recrystallization from isopropyl alcohol. Diphenyliodonium chloride, mp 233–235°C, was obtained from Aldrich Chemical Co., U.S.A. The *m*-trifluoromethylacetophone was also obtained from Aldrich and used without further purification when glc analysis showed it to be 99.4% pure. Glass distilled, deionized water and spectral quality acetonitrile were used to prepare solutions.

Laser flash photolyses were carried out in closed 2-mm quartz cuvettes. The frequency tripled or quadrupled Nd-YAG laser system delivered ca. 2 mJ per pulse to a 2-mm diameter spot of the sample cuvette; pulse width was typically of the order of 30 ps (FWHM). The optical arrangement for these photolyses and the data collection and processing procedures were as previously described (24). The design of the experiment allows detection of transients absorbing in the region 425–675 nm. Except as noted above, photolyses were conducted on samples in equilibrium with the ambient atmosphere; the reaction mixture for the photolysis sensitized by *m*-trifluoromethylacetophenone was, for example, purged of dissolved oxygen by passage of dry argon for 10 min.

Photolyses for product analysis were carried out on 3-mL samples, 0.001 *M* in the iodonium salt; the solutions in 13-mm quartz test tubes were irradiated by a 450-watt medium pressure mercury arc lamp, usually for 1 h with appropriate filters as necessary, in a "merry-go-round" apparatus. Shorter reaction times, as required for ca. 10% conversion, were used for quantum yield determinations. The products were separated by programmed temperature glc, identified by comparison with authentic samples, and confirmed by high resolution mass spectrometry. Product distributions were corrected for the relative sensitivity of the flame ionization detector to the various substances, as calculated from the signals obtained for known concentrations thereof, relative to dodecane as an internal standard.

In the preparative scale photolyses in water, the aqueous reaction mixtures were extracted with analytically pure (to glc) cyclohexane (1 mL) containing the dodecane internal standard (0.0010 *M*) and the extract chromatographed; control experiments indicated quantitative recovery of the major products, e.g., iodobenzene, by this technique. For quantum yield determination, the mercury source was calibrated by means of stilbene actinometry in toluene (31); whole sample irradiances of 5×10^{15} photons s^{-1} at 313 nm were typical.

Acknowledgments

We thank Ms. Judy Allbutt, 3M Corporate Research Laboratories, and Mr. Reza Danesh, Concordia University, for their expert technical assistance. This work was supported in part by 3M Canada, Ltd., and in part by a grant from the Natural Sciences and Engineering Research Council of Canada. Dr. Bradford B. Wright, 3M Corporate Research, provided the purified sample of benzenediazonium tetrafluoroborate. We also acknowledge helpful discussion with Dr. Ranjana C. Patel, Minnesota 3M Research, Ltd., Harlow, U.K., and with Dr. Alfred Marchetti, Research Laboratories, Eastman Kodak Co., Rochester, NY, U.S.A. The high resolution mass spectrometric analyses were carried out by Dr. Joseph Schroepfer of the 3M Corporate Research Laboratories.

1. S. P. PAPPAS. J. Imaging Technol. **11**, 146 (1985), and references cited therein; S. P. PAPPAS, L. R. GATECHAIR, and J. H. JILEK. J. Polym. Sci. Polym. Chem. Ed. **22**, 77 (1984).
2. E. KLEMM, E. RIESENBERG, and A. GRANESS. Z. Chem. **23**, 222 (1983).
3. S. P. PAPPAS, B. C. PAPPAS, L. R. GATECHAIR, and W. SCHNABEL. J. Polym. Sci. Polym. Chem. Ed. **22**, 69 (1984).
4. R. C. DUNBAR, H. H.-I. ING, and E. W. FU. J. Am. Chem. Soc. **101**, 6506 (1979).
5. H. BAUMANN and H.-J. TIMPE. Acta Polym. **37**, 309 (1986).
6. P. J. WAGNER and E. J. SIEBERT. J. Am. Chem. Soc. **103**, 7329 (1981).
7. N. SERPONE and M. Z. HOFFMAN. J. Phys. Chem. **91**, 1737 (1987).
8. J. W. KNAPCZYK, J. J. LUBINKOWSKI, and W. E. MCEWEN. Tetrahedron Lett. 3739 (1972).
9. E. M. KOSOWER. J. Am. Chem. Soc. **80**, 3253 (1958); E. M. KOSOWER and L. LINDQVIST. Tetrahedron Lett. 4481 (1965).
10. S. L. NICKOL and J. A. KAMPMEIER. J. Am. Chem. Soc. **95**, 1908 (1973).
11. O. A. PTITSYNA, O. A. REUTOV, and G. G. LYATIEV. Zh. Org. Khim. **5**, 401 (1969).
12. K. DIMROTH, C. REICHARDT, T. SIEPMANN, and F. BOHLMANN. Justus Liebigs Ann. Chem. **661**, 1 (1963).
13. H. IRVING and W. R. REID. J. Chem. Soc. 2078 (1960).
14. H. J. LUCAS, E. R. KENNEDY, and C. A. WILMOT. J. Am. Chem. Soc. **58**, 157 (1936); F. M. BERINGER, E. J. GEERING, I. KUNTZ, and M. MCCREADY. J. Phys. Chem. **60**, 141 (1956).
15. G. H. SMITH and P. M. OLOFSON. U.S. Patent No. 4,173,476 (1979), and references cited therein.
16. H. E. BACHOFNER, F. M. BERINGER, and L. MEITES. J. Am. Chem. Soc. **80**, 4269 (1958).
17. E. L. GILBERT, R. R. GOLDSTEIN, and T. M. LOWREY. J. Chem. Soc. 1092 (1931).
18. J. G. CALVERT and J. N. PITTS, JR. Photochemistry. John Wiley, New York. 1966. pp. 471–473; H. B. AMBROZ and T. J. KEMP. J. Chem. Soc. Faraday Trans. 1, **78**, 1269 (1982); P. HABERFIELD, C. CARDONA, and M. BELL. J. Org. Chem. **49**, 78 (1984).
19. J. C. SCAIANO and N. KIM-THUAN. J. Photochem. **23**, 269 (1983).

Can. J. Chem. Downloaded from www.nrcresearchpress.com by 213.166.140.6 on 09/07/12
For personal use only.

20. H. ZOLLINGER. Angew. Chem. **90**, 151 (1978).
21. S. L. MATTES and S. FARID. J. Am. Chem. Soc. **108**, 7356 (1986).
22. H. H. JAFFE and M. ORCHIN. Theory and applications of ultraviolet spectroscopy. John Wiley, New York. 1962.
23. L. L. MILLER, D. G. NORDBLOM, and E. A. MAYEDA. J. Org. Chem. **37**, 916 (1972).
24. G. PONTERINI, N. SERPONE, M. A. BERGKAMP, and T. L. NETZEL. J. Am. Chem. Soc. **105**, 4639 (1983); N. SERPONE, T. L. NETZEL, and M. GOUTERMAN. J. Am. Chem. Soc. **104**, 246 (1982); N. SERPONE, D. K. SHARMA, J. MOSER, and M. GRAETZEL. Chem. Phys. Lett. In press.
25. J. B. HOPKINS and P. RENTZEPIS. Chem. Br. **22**, 236 (1986); E. F. HILLINSKI, D. HUPPERT, D. F. KELLEY, S. V. MILTON, and P. RENTZEPIS. J. Am. Chem. Soc. **106**, 1951 (1984).
26. A. FRIEDMAN, S. C. YANG, M. KAWASAKI, and R. BERSOHN. Chem. Phys. **22**, 1028 (1980).
27. H. BAUMANN, H. G. O. BECKER, K. P. KRONFELD, D. PFEIFER, and H.-J. TIMPE. J. Photochem. **28**, 393 (1985).
28. A. MARCHETTI and D. R. KEARNS. J. Am. Chem. Soc. **89**, 5335 (1967).
29. F. M. BERINGER, A. BRIERLEY, M. DREXLER, E. M. GINDER, and C. C. LUMPKIN. J. Am. Chem. Soc. **75**, 2708 (1953).
30. M. C. CASERIO, D. L. GLUSKER, and J. D. ROBERTS. J. Am. Chem. Soc. **81**, 336 (1959).
31. B. S. GREEN, M. RETJO, D. E. JOHNSON, C. E. HOYLE, J. T. SIMPSON, P. E. CORREA, T.-I. HO, F. MCCOY, and F. D. LEWIS. J. Am. Chem. Soc. **101**, 3325 (1979).
32. J. M. MASNOVI, J. K. KOCHI, E. F. HILINSKI, and P. M. RENTZEPIS. J. Am. Chem. Soc. **108**, 1126 (1986).
33. J. V. CRIVELLO and J. H. W. LAM. Macromolecules, **10**, 1307 (1977).

Can. J. Chem. Downloaded from www.nrcresearchpress.com by 213.166.140.6 on 09/07/12
For personal use only.

Bis(dimethoxymethyl) peroxide and bis(1,1-dimethoxyethyl) peroxide[1]

KARL R. KOPECKY AND JOSÉ MOLINA[2]
Department of Chemistry, University of Alberta, Edmonton, Alta., Canada T6G 2G2

Received January 20, 1987

KARL R. KOPECKY and JOSÉ MOLINA. Can. J. Chem. **65**, 2350 (1987).

The title compounds **1** and **2**, the first examples of peroxides polysubstituted at the α and α′ positions by alkoxy groups, are formed by benzophenone sensitized photooxygenation of trimethoxymethane and 1,1,1-trimethoxyethane, respectively. No peroxide was formed from tetramethoxymethane. Allowing 98% hydrogen peroxide and trimethoxymethane to stand results in an 80% yield of **1**, so that **1** and **2** are probably formed by such a disproportionation reaction during photooxygenation. Compound **1** is converted quantitatively to methanol, methyl formate, and dimethyl carbonate in pyridine solution at 60°C. In acidic methanol both **1** and **2** undergo solvolysis rapidly with exclusive cleavage of the carbon – peroxy oxygen bond. Signals for the ether and peroxy oxygens of **1** appear at 34 and 263 ppm and those of **2** appear at 40 and 264 ppm in the ^{17}O nuclear magnetic resonance spectrum. Luminescence results when **1** and **2** are heated to 150°C.

KARL R. KOPECKY et JOSÉ MOLINA. Can. J. Chem. **65**, 2350 (1987).

Les composés **1** et **2** mentionnés dans le titre, qui sont les premiers exemples de peroxydes polysubstitués par des groupements alcoolates dans les positions α et α′, se forment respectivement par la photooxygénation, sensibilisée par la benzophénone, du triméthoxyméthane et du triméthoxy-1,1,1 éthane. Il ne se forme pas de peroxyde à partir du tétraméthoxyméthane. Lorsqu'on place du peroxyde d'hydrogène à 98% en présence de triméthoxyméthane, le composé **1** se forme avec un rendement de 80%; on en déduit que les composés **1** et **2** se forment probablement par une réaction de disproportionation qui accompagne la photooxygénation. En solution dans la pyridine, à 60°C, le composé **1** se transforme quantitativement en méthanol, en formate de méthyle et en carbonate de diméthyle. Dans le méthanol, en milieu acide, les composés **1** ainsi que **2** subissent une solvolyse rapide qui est uniquement accompagnée d'un clivage de la liaison carbone – oxygène du peroxyde. Dans le spectre en résonance magnétique nucléaire du ^{17}O, les signaux des oxygènes de l'éther et du peroxyde du composé **1** apparaissent respectivement à 34 et 263 ppm alors que ceux du composé **2** apparaissent respectivement à 40 et 264 ppm. Il se produit de la luminescence lorsqu'on chauffe les composés **1** ou **2** à 150°C.

[Traduit par la revue]

Introduction

The present study grew out of a desire to learn about the properties of trimethoxymethyl hydroperoxide and bis(trimethoxymethyl) peroxide in connection with another problem. A possible route to these compounds might be the benzophenone-sensitized photooxygenation of trimethoxymethane. Cyclic acetal derivatives of some aldehydes have been oxidized to hydroperoxides and peroxides with oxygen (1) but trimethoxymethane does not appear to have been converted to such products, although the central C—H bond ought to be relatively reactive with a bond dissociation energy (BDE) of about 89 kcal/mol. This value is estimated as follows. Replacement of an alkyl group by a methoxy group on a hydrocarbon lowers the C—H BDE by an amount that decreases with decreasing C—H BDE of the corresponding hydrocarbon (2). The BDE of the central C—H bond in isobutane is 93.3 kcal/mol (3) and substitution of a methyl group by a methoxy group should lower the BDE by about 3 kcal/mol (2). Replacement of the two remaining methyl groups by methoxy groups would lower the BDE more, but by decreasing amounts estimated to be 1 and 0.5 kcal/mol. Although attack on the central C—H hydrogen should be relatively easy, none of the desired peroxide or hydroperoxide was formed in the reaction.

Results and discussion

Isolation and characterization

The benzophenone-sensitized photooxidation of trimethoxymethane, neat or in benzene solution, results in formation of bis(dimethoxymethyl) peroxide **1**, which appears to be the first example of a peroxide polysubstituted in the α and α′ positions by alkoxy groups. This product was obtained nearly pure in 2% yield by simple vacuum distillation after removal of starting material and solvent from the reaction mixture. There is no evidence for the formation of either of the desired molecules trimethoxymethyl hydroperoxide or bis(trimethoxymethyl) peroxide. The structure of **1** is readily apparent. It gives an intense positive test with iodide ion and the ^1H nmr spectrum has only two signals at δ 3.50 (12H) and 5.50 (2H).

At 60°C in pyridine solution **1** is converted quantitatively to methanol, methyl formate, and dimethyl carbonate (Scheme 1), the result of an elimination reaction characteristic of peroxides that bear an α hydrogen atom (4, 5).

The ready formation of **1** suggested that replacement of a methoxy group by a peroxy group might be a general reaction with appropriate substrates under these conditions. No peroxidic material was formed from tetramethoxymethane but oxidation of the homologous molecule 1,1,1-trimethoxyethane did proceed in an analogous manner, Scheme 2. Bis(1,1-dimethoxyethyl) peroxide **2** was easily isolated in 1% yield but the crude product was contaminated with about 10% of another product, presumed to be the mixed peroxide 1,1-dimethoxyethyl 2,2,2-trimethoxyethyl peroxide **3**, from which it could not be separated by distillation. The ^1H nmr spectrum of the product mixture exhibited strong signals at δ 1.59 (6H) and 3.393 (12H) for **2** and weaker signals at δ 1.56 (3H), 3.27 (2H), and 3.385 (9H), which were assigned to **3**. The signal of the *gem* dimethoxy group of **3** is presumably under that of the methoxy groups of **2**. It was easy to destroy **3** preferentially by warming the product mixture with pyridine, thus allowing a pure sample of **2** to be isolated. No attempt was made to identify the products formed from **3**.

The ^{17}O nmr signals of the peroxy groups of both **1**, δ 263,

[1]Supported by a grant from the Natural Sciences and Engineering Research Council of Canada.

[2]Recipient of a travel grant from the Consejeria de Education y Ciencia, Junta de Andalucia. Present address: Departamento de Quimica Organica, Universidad de Granada, Granada, Spain.

Can. J. Chem. Downloaded from www.nrcresearchpress.com by 213.166.140.6 on 09/07/12
For personal use only.

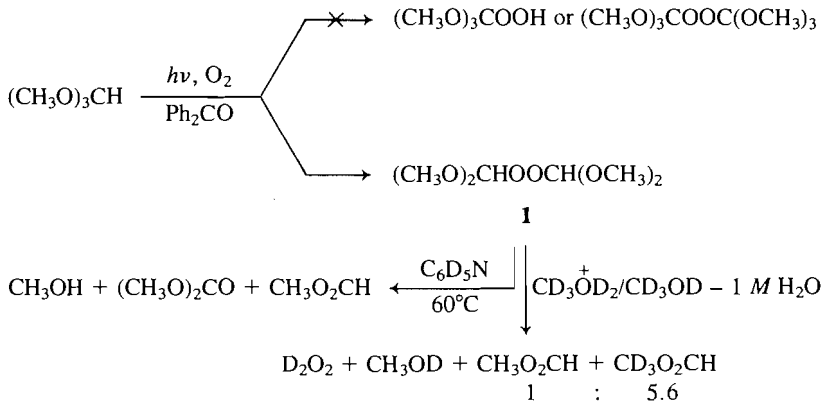

SCHEME 1

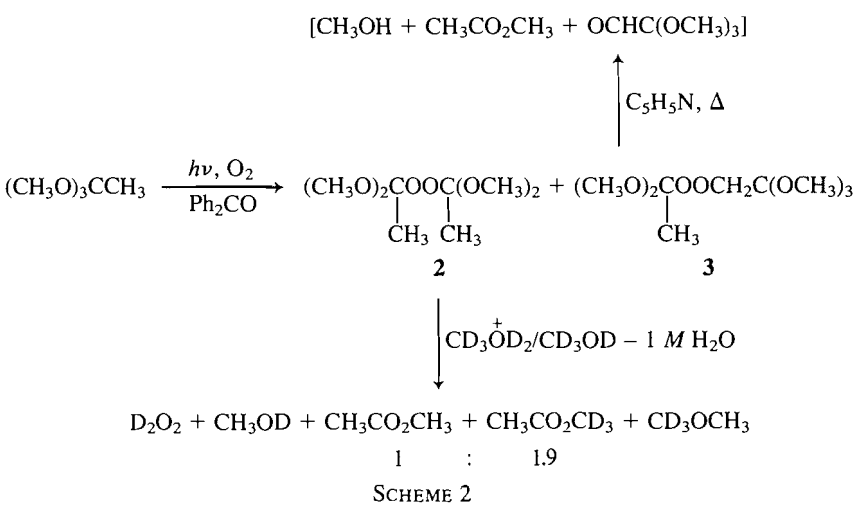

SCHEME 2

and **2**, δ 264, are near that of di-*tert*-butyl peroxide, δ 273. The ^{13}C nmr spectra of **1** and **2** are also consistent with their structures.

The O–O bond stretching frequency of **1** is 845 cm^{-1}, which is, as expected (6), appreciably higher than those of acyclic dialkyl peroxides without electronegative substituents.

Acid catalyzed solvolysis of 1 and 2

It was of interest to study the behaviour of **1** and **2** toward acid. In CD_3OD three reactions are possible, Scheme 3.

Protonation of the ether oxygen and subsequent reversible loss of methanol, path A, would lead to exchange of the methoxy groups in the starting material. Such a reaction appears to occur when (1-methoxy)methylethyl hydroperoxide is treated with acid in methanol, eq. [1] (7).

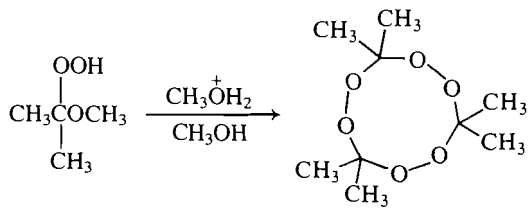

Reaction by path B, protonation of the peroxy group followed by ionization of the peroxy–carbon bond, would lead eventually to the trimethyl ortho esters (which would undergo methoxy group exchange).

Path C involves a rearrangement reaction, or loss of the α-proton when R = H, which would lead to different types of products from **1** and **2**. From **1** there would be formed dimethyl carbonate, methyl formate (both undeuterated), and methanol, while **2** would be converted to tetramethoxymethane, methyl acetate (undeuterated), and methanol. There are numerous examples of peroxide reactions following either path B or C (4). A recent relevant example of a reaction proceeding by path C is given by eq. [2] (7).

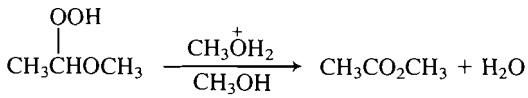

Solutions containing ~0.15 *M* of **1** or **2** in CD_3OD were treated with a trace of *p*-toluenesulfonic acid and the reactions monitored by ^1H nmr. The reactions proceeded at convenient rates at −30°C with **1** and at −70°C with **2**, having half-lives of ~30 min and ~10 min, respectively. Both **1** and **2** are consumed exclusively according to path B. Actually, the CD_3OD used was found to contain ~1 *M* of water and the proposed ortho ester products were immediately hydrolyzed. No signals attributable to these esters could be detected in the nmr spectra taken during the reaction. In a control experiment the methoxy groups of 1,1,1-trimethoxyethane were found to be completely exchanged within 5 min at −80°C in CD_3OD containing a trace of both *p*-toluenesulfonic acid and water. At this point ~15% of the ortho ester had been converted to methyl acetate. The $CH_3CO_2CH_3$:$CH_3CO_2CD_3$ ratio was 1:2.1. The ortho ester is thus much more reactive than is **2** and is also converted to a mixture of deuterated and undeuterated acetate. The observed final products were 2.0 moles of methyl formate from **1** and 2.0 moles of methyl acetate from **2**, together with the

Can. J. Chem. Downloaded from www.nrcresearchpress.com by 213.166.140.6 on 09/07/12
For personal use only.

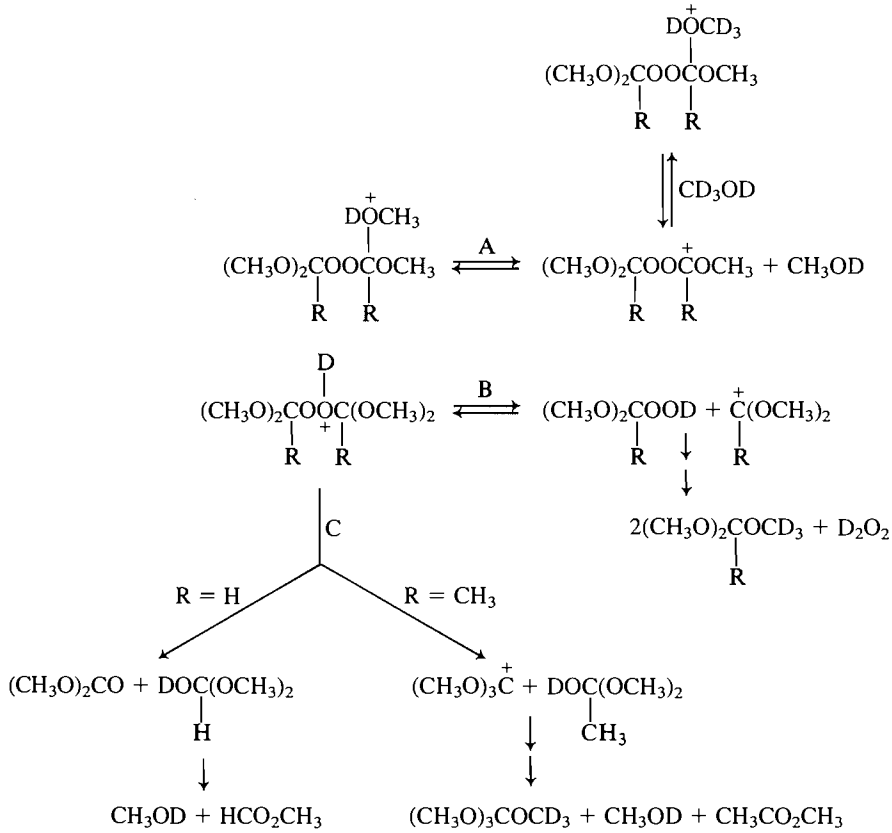

SCHEME 3

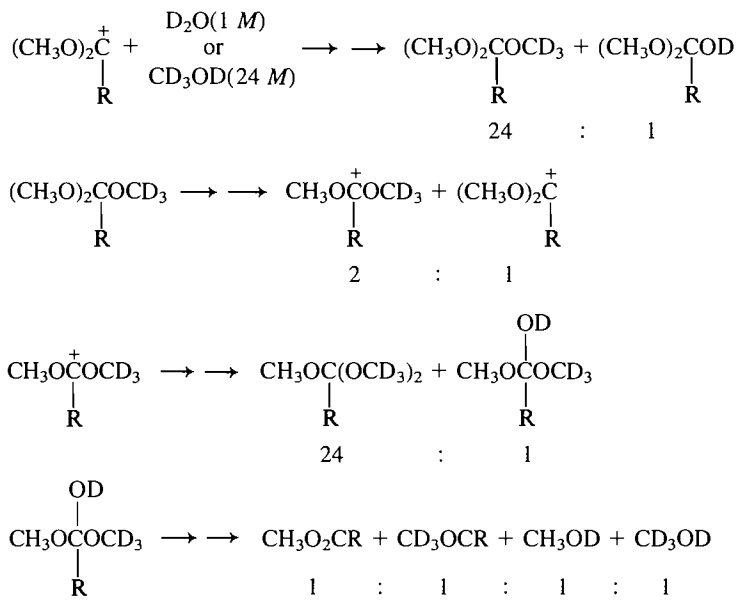

SCHEME 4

corresponding amounts of methanol. The deuterium content of the esters will be discussed later. The presence of hydrogen peroxide in the solutions was confirmed by an intense positive test with iodide ion.

There was no detectable methoxy interchange in either **1** or **2** during the reaction. The signal of CH_3OD grew in 15 and 7 Hz upfield from the signals of the methoxy groups of **1** and **2**, respectively, at the same rate as the signals of the C-H or C-CH_3 groups of the starting materials disappeared.

No signals for dimethyl carbonate, a primary product of **1** and the hydrolysis product of orthocarbonate from **2**, which would result from any reaction via path C, could be detected in the nmr spectra. A control experiment showed that there was no methoxy group interchange in dimethyl carbonate under the reaction conditions.

Signals attributed to the C-H and C-CH_3 groups of the hydroperoxides, which are the initial products of reaction via path B, appeared in the nmr spectra taken during the reaction at δ 5.23 and 1.50, respectively, slightly upfield from the corresponding signals of the starting materials. The hydro-

Can. J. Chem. Downloaded from www.nrcresearchpress.com by 213.166.140.6 on 09/07/12
For personal use only.

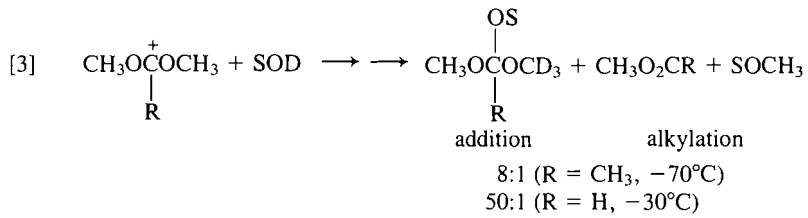

peroxides would be expected to undergo solvolysis at rates similar to those of the starting materials. The concentration of the hydroperoxides built up to a maximum of about 10% of the initial concentration of the starting material.

The exclusive carbon – peroxy oxygen bond cleavage observed for **1** and **2** is a completely different type of reaction from those shown in eqs. [1] and [2] for hydroperoxides containing one α methoxy group. However, it may be that the products shown in eqs. [1] and [2] are not the initially formed products. Rapid solvolysis corresponding to that observed in the present study would be reversible in the absence of water, and the observed final products might be formed in slower side reactions.

The deuterated esters produced in the solvolysis of **1** and **2** should predominate by a ratio of about 8:1 under the reaction conditions (24 *M* CD_3OD and 1 *M* water) if there is no discrimination by the dimethoxy carbocations between CD_3OD and water to give tetrahedral intermediates. This ratio is obtained by an iterative calculation using the cascade of reactions, shown in part in Scheme 4, which the initial dimethoxy carbocation would undergo if only addition of solvent molecules occurred. Addition of D_2O would result in a product that would form undeuterated ester. Addition of CD_3OD would give partially exchanged ortho ester. This in turn would form both half-deuterated and undeuterated dimethoxy carbocation. The fraction of half-deuterated cation that would be captured by D_2O would result in the formation of equal amounts of deuterated and undeuterated esters, and so on. However, the observed ratios of deuterated:undeuterated esters, Schemes 1 and 2, are significantly different from 8:1 in such a way that would require water to be more nucleophilic than CD_3OD. There must be another reaction of the dimethoxy carbocations that occurs in competition with formation of a tetrahedral intermediate: alkylation of solvent. This would result in the formation of more undeuterated ester. The relative rates of addition and alkylation given in eq. [3] are required to reproduce the observed product distributions. These values were obtained from iterative calculations with the assumption that water and CD_3OD add to or are alkylated by the dimethoxy carbocation in a statistical manner, depending on their relative concentrations and without taking into account any possible isotope effects in the alkylation reactions or in the cascade of exchange reactions with CD_3OD. Alkylation of alcohol by dimethoxy carbocations has long been known and becomes more important as the stability of the carbocation increases (8).

Considering the reaction conditions under which **1** and **2** are formed, it is tempting to postulate that these compounds result by way of radical intermediates. However, this is unlikely as there are several difficulties with possible radical pathways. The pathways that would have to be considered if one tried to devise a radical route to **1** will be discussed. The conclusions reached should also apply to the formation of **2**.

Mechanism of formation of 1 and 2

The structures of some of the many radicals and compounds that might be formed from trimethoxymethane under the reaction conditions, along with the structures of some compounds needed to calculate the heats of formation of some radicals, are given below. The heats of formation, in kcal/mol at 298 K (1 atm; 1 atm = 101.3 kPa), are given under the structures. The number(s) below the heat of formation is the BDE of the relevant C—H or OH bond that is broken to derive a given radical. The values of the heats of formation and BDEs were calculated using known methods and approximations (9) where not already available (2, 3, 9, 10).

The ultimate product-forming step in a radical pathway would presumably be the coupling of two oxy radicals. These would have to couple in the solvent cage in which they were

$(CH_3O)_3CH$	$(CH_3O)_2CHOCH_2\cdot$	$(CH_3O)_2CH\cdot$	CH_2O
4		**5**	
−127.7 93.3 89	−86.5	−45.0	−26.0
$(CH_3O)_2CH_2$	$(CH_3O)_2CHOH$	$(CH_3O)_2CHO\cdot$	$CH_3\cdot$
	6		
−82.9 90	−133.7	−81.8	34.3
$(CH_3O)_2CHOCH_2OH$	$(CH_3O)_2CHOCH_2O\cdot$	$CH_3O\cdot$	CH_3O_2CH
7			
−172.5 104	−120.6	5.1	−83.6
$(CH_3O)_3C\cdot$	$(CH_3O)_2CO$		
8			
−90.8	−136.3		

Can. J. Chem. Downloaded from www.nrcresearchpress.com by 213.166.140.6 on 09/07/12
For personal use only.

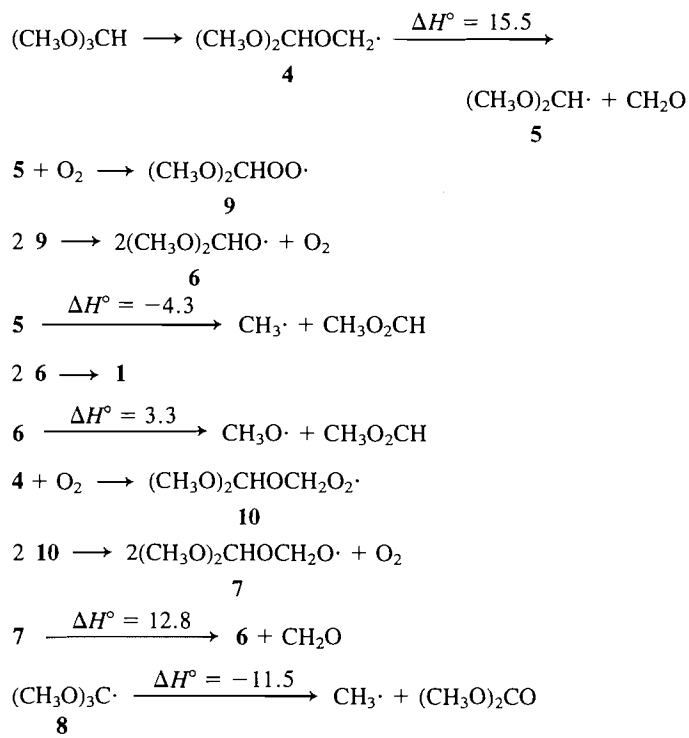

SCHEME 5[3]

formed. There would be two different possible routes to the caged oxy radicals **6**, Scheme 5. Each includes a rather endothermic step, which could result in diversion of reactants from a route to **6**. The most direct route involves fragmentation of the initially formed radical **4** to the radical **5** and formaldehyde, followed by reaction of **5** with oxygen to give the peroxy radical **9**. The oxy radical **6** would then be formed from **9**. The formation of oxy radicals from peroxy radicals with α hydrogen atoms was long thought to be impossible but there is growing evidence that this can occur (11). However, the fragmentation of **4** is endothermic by 15.5 kcal/mol and **4** should be trapped efficiently by oxygen in an oxygen-saturated solution before fragmentation can occur. Even if fragmentation occurred, the resulting radical **5** can fragment by an exothermic pathway, 4.3 kcal/mol, and may be too short-lived to react with oxygen. The trapping of **4** by oxygen could provide an alternate route to the oxy radical **6**. The product of **4** and oxygen is the peroxy radical **10**. In this route to **6**, conversion of **10** to the oxy radical **7** would be followed by fragmentation to formaldehyde and **6**. However, this fragmentation is also quite endothermic, 12.8 kcal/mol, and **7** should be long-lived enough so that no **6** would be formed in the original solvent cage. Any **6** formed without a caged radical partner would never undergo coupling with another radical **6** (12). Hydrogen abstraction and fragmentation reactions would intervene. In addition to the difficulty in finding a plausible route to a caged radical pair of **6**, there is an even more fundamental problem with a radical pathway to **1** (but not necessarily to **2**). Oxy radicals with α hydrogen atoms do not couple (11, 13). There is one apparent exception (14), which has been widely cited, but an alternative explanation for the observations will be proposed below. Clearly a different type of reaction must occur.

[3]Many more reactions than shown undoubtedly occur. Only those that might contribute to the formation or lack of formation of **1** are given here.

A simple route to **1** that avoids the above difficulties is the exchange reaction, eq. [4], between trimethoxymethane and

[4] $2(CH_3O)_3CH + H_2O_2 \rightarrow \mathbf{1} + 2CH_3OH$

hydrogen peroxide. It is easy to envisage the formation of hydrogen peroxide under the reaction conditions. The reaction of eq. [4] would be an ionic reaction catalyzed by adventitious acid. Indeed, an 80% yield of **1** could be isolated after a mixture of trimethoxymethane and 98% hydrogen peroxide was allowed to stand overnight. The analogous reaction to form **2** was not carried out, but it is likely that **2** was formed in the same way in the photosensitized oxidation reaction.

The apparent exception (14) to the conclusion that oxy (and peroxy) radicals bearing α hydrogen atoms do not form peroxides results from a study of the reaction between 1-*tert*-butoxy-1-hydroperoxynonane **11** and ceric ion, eq. [5]. A 50%

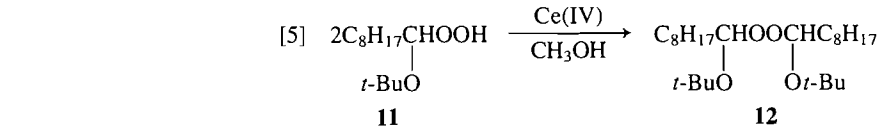

yield of the peroxide **12** was isolated. It was suggested that **12** was formed by coupling of oxy radicals generated from **11** by ceric ion, but an acid-catalyzed disproportionation reaction to give **12** seems to be a quite plausible alternative.

Abstraction of the methine hydrogen atom from trimethoxymethane should occur readily under the photosensitized oxidation conditions and would form the trimethoxymethyl radical **8**. This can undergo a fragmentation reaction to methyl radical and dimethyl carbonate that is exothermic by 11.5 kcal/mol. Thus **8** is probably too short-lived to react with oxygen, and the peroxide or hydroperoxide initially sought is not formed.

Thermolysis of 1 and 2

The concerted decompositions of **1** and **2** to dimethyl carbonate and hydrogen or ethane are calculated to be exothermic by over 70 kcal/mol. This is about as exothermic as is the decomposition of tetramethyl-1,2-dioxetane (15). These compounds might thus have enhanced rates of thermolysis (16) and be luminescent. Preliminary experiments have given ambiguous results. Solutions of **1** and **2** both emit clearly visible long-lived luminescence at 150°C, but not at 105°C, in the presence of a mixture of 9,10-dibromoanthracene and 9,10-bis(phenylethynyl)anthracene. Heating solutions of **1** and **2** in C_6D_6 at 77°C in neutralized glassware does result in the formation of dimethyl carbonate. However, there are ionic routes to this compound, and corresponding amounts of hydrogen or ethane were not formed (small amounts, <5%, would not have been detected). Methanol and the esters methyl formate or methyl acetate were the major products and the corresponding ortho esters were also formed. Obviously, acid-catalyzed reactions are predominating and conditions have not yet been found to suppress them with these very sensitive materials. In one run, 20% of **1** was left after 160 h at 77°C, which corresponds to a half-life of about 80 h. This compares with a calculated half-life of about 70 h at this temperature for bis(diphenylmethyl) peroxide, which undergoes concerted decomposition exclusively (16). In fact, the half-life of **1** is likely much greater than 80 h because the majority of **1** was probably consumed by acid-catalyzed reactions. The rate of thermolysis of **1** is not nearly as much enhanced as is that of bis(diphenylmethyl) peroxide.

Can. J. Chem. Downloaded from www.nrcresearchpress.com by 213.166.140.6 on 09/07/12
For personal use only.

Experimental

Boiling points are uncorrected. The nmr spectra were measured on Brucker WH 200 (^{1}H and ^{13}C) and WH 400 spectrometers (^{17}O), the latter operating at 54.244 MHz; sweepwidth 50,000 Hz; pulse width 350.0 μs (90°); acquisition time 0.041 s; data points 4,000; scans 70,000 (**1**) and 108,000 (**2**). The ^{17}O chemical shifts are reported relative to internal acetone. Raman spectra were recorded on a Beckman Model 700 laser Raman spectrometer using the 488.0-nm exciting line from a Coherent Radiation Model 52 argon laser using neat **1** in a capillary tube. Infrared spectra were recorded on a Perkin–Elmer Model 457 spectrometer.

Bis(dimethoxymethyl) peroxide 1

A. A solution of 150 g trimethoxymethane and 1.5 g benzophenone was irradiated for 20 h with a 200-watt medium pressure Hanovia lamp, which was in an immersion well, at 10°C through a Pyrex filter in a reaction vessel fitted with a Dry Ice condenser. A stream of oxygen was passed continuously through the solution. The resulting solution was concentrated under 20 Torr (1 Torr = 133.3 Pa) and the product was distilled from the residual oil through a short Vigreux column to give 2.5 g (2%) of a colorless oil; bp 66–69°C/4 Torr; ir (film): 3004, 2956, 2854, 1465, 1452, 1330, 1202, 1170, 1105, 1002, 950, 920 cm^{-1}; Raman (neat) (parallel polarization): 2970 (s), 2870 (s); 1465 (s), 1005 (m), 920 (m), 845 (m) cm^{-1}; (perpendicular polarization): 2970 (vw), 2870 (vw), 1465 (s), 1005 (w), 920 (w), 900 (m), 845 (w) cm^{-1}; ^{1}H nmr ($CDCl_3$) δ: 3.50 (s, 12H) and 5.50 (s, 2H); ^{13}C nmr ($CDCl_3$) δ: 52.95 and 117.10; ^{17}O nmr (CH_2Cl_2) δ: 34 and 263. *Anal.* calcd. for $C_6H_{14}O_6$: C 39.56, H 7.75; found: C 39.72, H 7.70.

B. A solution of 25 mL trimethoxymethane and 1 mL of 98% hydrogen peroxide was allowed to stand at 22°C for 9 h and then concentrated. Distillation of the residual oil gave 4.1 g (80%) of **1** whose ^{1}H nmr spectrum was identical with that of the product obtained in A.

Bis(1,1-dimethoxyethyl) peroxide 2

Using the procedure for the preparation of **1** by method A, there was isolated from 200 mL of 1,1,1-trimethoxyethane 1.7 g (1%) of **2** as a colorless oil, bp 54–56°C/0.3 Torr. This material was contaminated with another compound, as described in the text. Redistillation gave a product with an identical nmr spectrum. It was taken up in 5 mL pyridine and warmed to 60°C for several min. Distillation gave a product with no extraneous signals in the ^{1}H nmr spectrum, ^{1}H nmr ($CDCl_3$) δ: 1.59 (s, 6H) and 3.39 (s, 12H); ^{13}C nmr ($CDCl_3$) δ: 19.16, 50.56, and 117.83; ^{17}O nmr (CH_2Cl_2) δ: 40 and 264. *Anal.* calcd. for $C_8H_{18}O_6$: C 45.70, H 8.63; found: C 45.02, H 8.41. Redistillation did not improve the analysis. An intense iodine color developed immediately upon addition of **2** to KI in acetic acid.

Methanolysis of 1 and 2

Solutions ~0.15 *M* of peroxide in CD_3OD in nmr tubes were cooled to −80°C and a tiny crystal of *p*-toluenesulfonic acid was added. The solutions were slowly warmed until reaction was observed to occur at a rate that could be conveniently monitored by ^{1}H nmr. It was found (^{1}H nmr) that the CD_3OD contained ~1 *M* water. The results have been described in the "Results and discussion" section.

1. (*a*) R. CRIEGEE. *In* Methoden der Organischen Chemie. Vol. 8. *Edited by* E. Mueller. Thieme, Stuttgart, 1952. p 23; (*b*) A. RIECHE, E. SCHMITZ, and E. BEYER. Chem. Ber. **91**, 1935 (1958); (*c*) A. RIECHE, E. SCHMITZ, W. SCHADE, and E. BEYER. Chem. Ber. **94**, 2926 (1961); (*d*) A. RIECHE, H. E. SEYFARTH, and A. HESSE. Angew. Chem. Int. Ed. Engl. **5**, 253 (1965); (*e*) H. E. SEYFARTH and A. HESSE. Chem. Ber. **100**, 2491 (1967); (*f*) H. E. SEYFARTH, A. HESSE, and A. RIECHE. Chem. Ber. **101**, 623 (1968); (*g*) H. E. SEYFARTH, A. RIECHE, and A. HESSE. Chem. Ber. **100**, 624 (1967).
2. O. KONDO and S. W. BENSON. Int. J. Chem. Kinet. **16**, 949 (1984).
3. T. S. A. ISLAM and S. W. BENSON. Int. J. Chem. Kinet. **16**, 995 (1984).
4. B. PLESNICAR. *In* The chemistry of peroxides. *Edited by* S. Patai. John Wiley and Sons, New York. 1983. Chap. 17.
5. N. KORNBLUM and H. E. DE LA MARE. J. Am. Chem. Soc. **73**, 880 (1951).
6. K. R. KOPECKY and R. RICO. Can. J. Chem. **62**, 277 (1984).
7. H. KEUL and K. GRIESBAUM. Can. J. Chem. **58**, 2049 (1980).
8. S. M. MCELVAIN and C. L. STEVENS. J. Am. Chem. Soc. **69**, 2663 (1947).
9. (*a*) S. W. BENSON. Thermochemical kinetics. John Wiley and Sons, New York. 1976; (*b*) P. S. NANGIA and S. W. BENSON. J. Am. Chem. Soc. **102**, 3105 (1980).
10. J. HINE and A. W. KLUEPPEL. J. Am. Chem. Soc. **96**, 2924 (1974).
11. G. D. MENDENHALL and E. M. Y. QUINGA. Int. J. Chem. Kinet. **17**, 1187 (1985).
12. R. HIATT and T. G. TRAYLOR. J. Am. Chem. Soc. **87**, 3766 (1965).
13. R. HIATT and L. ZIGMUND. Can. J. Chem. **48**, 3967 (1970).
14. D. G. M. DIAPER. Can. J. Chem. **48**, 3967 (1970).
15. (*a*) H. E. O'NEAL and W. H. RICHARDSON. J. Am. Chem. Soc. **92**, 6553 (1970); (*b*) J. Am. Chem. Soc. **93**, 1828 (1971).
16. R. HIATT, D. J. LEBLANC, and C. THANKACHAN. Can. J. Chem. **52**, 4090 (1974).

Can. J. Chem. Downloaded from www.nrcresearchpress.com by 213.166.140.6 on 09/07/12
For personal use only.

Enantioselective synthesis of isoquinoline alkaloids: phenylethylisoquinoline and aporphine alkaloids[1]

ZBIGNIEW CZARNOCKI AND DAVID B. MACLEAN[2]
Department of Chemistry, McMaster University, Hamilton, Ont., Canada L8S 4M1

AND

WALTER A. SZAREK[2]
Department of Chemistry, Queen's University, Kingston, Ont., Canada K7L 3N6

Received March 10, 1987

ZBIGNIEW CZARNOCKI, DAVID B. MACLEAN, and WALTER A. SZAREK. Can. J. Chem. **65**, 2356 (1987).

A new and improved procedure for the preparation of (*R*)-2-alkoxycarbonyl-1-formyl-1,2,3,4-tetrahydro-6,7-dimethoxyisoquinolines has been developed beginning from D-(−)-tartaric acid. The utility of these aldehydes in the asymmetric synthesis of isoquinoline alkaloids of high enantiomeric purity has been extended to the synthesis of phenylethylisoquinolines, which have been further transformed in straightforward steps into the homoprotoberberine and homoaporphine ring systems. In this manner, (*S*)-homolaudanosine, (*S*)-5′-methoxyhomolaudanosine, (*S*)-2,3,9,10,11-pentamethoxyhomoprotoberberine, and (*S*)-*O*-methylkreysigine have been synthesized. The conversion of (*S*)-laudanosine to (*S*)-glaucine, an aporphine alkaloid, has also been realized.

ZBIGNIEW CZARNOCKI, DAVID B. MACLEAN et WALTER A. SZAREK. Can. J. Chem. **65**, 2356 (1987).

Utilisant l'acide D-(−)-tartrique comme produit de départ, on a développé une nouvelle méthode améliorée pour la préparation des alkoxycarbonyl-2(*R*) formyl-1 tétrahydro-1,2,3,4 diméthoxy-6,7 isoquinoléines. L'utilité de ces aldéhydes dans les synthèses asymétriques de haute pureté énantiomérique des alcaloïdes de l'isoquinoléine a déjà été démontrée et on l'a étendue aux synthèses des phényléthylisoquinoléines qui ont été transformées par la suite, par des étapes ne créant pas d'ambiguités, en systèmes cycliques homoprotoberbérine et homoaporphine. De cette façon, on a synthétisé l'homolaudanosine-(*S*), la méthoxy-5′ homolaudanosine-(*S*), la pentaméthoxy-2,3,9,10,11 homoprotoberbérine-(*S*) et la *O*-méthylkreysigine-(*S*). On a aussi réalisé la transformation de la laudanosine-(*S*) en glaucine-(*S*), un alcaloïde aporphine.

[Traduit par la revue]

The asymmetric synthesis of several classes of isoquinoline alkaloids from (*R*)- and (*S*)-2-ethoxycarbonyl-1-formyl-1,2,3,4-tetrahydro-6,7-dimethoxyisoquinolines, (*R*)-**1** and (*S*)-**1**, has been reported by us in several publications (1*a*–*c*). These publications include a review of previous approaches to the asymmetric synthesis of isoquinoline alkaloids; in the interim, Noyori *et al.* (2) have described a new method, and Meyers and Bailey (3) have extended the chiral amidine approach to the synthesis of morphinans. Two methods were used by us to generate the enantiomeric aldehydes. The first was based upon the induction of asymmetry at C-1 of the tetrahydroisoquinoline system through a Pictet–Spengler reaction of dopamine hydrochloride with (*R*)-glyceraldehyde (1*a*,*b*) followed by subsequent transformation of the condensation product. In the second method, optically pure (*R*)- and (*S*)-calycotomine (see **2**) were prepared by resolution and converted to *N*-ethoxycarbonyl derivatives, which were then oxidized to the aldehydes (1*c*). In this article we report a third and improved procedure for the formation of the (*R*)-aldehyde, which is based upon the use of D-(−)-tartaric acid as a means of inducing asymmetry at C-1 of the isoquinoline system. The enantiomeric aldehyde would be equally accessible from L-(+)-tartaric acid. We also show that aldehydes (*R*)-**1** and the 2-methoxycarbonyl analogue (*R*)-**5** may be used as starting materials for the asymmetric synthesis of phenylethylisoquinolines and report the transformation of the latter into the homoprotoberberine (4) and the homoaporphine (4) ring systems. The conversion of the previously prepared (1*b*) (*S*)-laudanosine (**3**) into (*S*)-glaucine (**4**) (4) has also been achieved.

The new and improved procedure for the preparation of (*R*)-**1** and its *N*-methoxycarbonyl analogue (*R*)-**5** is partially outlined in Scheme 1. The starting material, methyl [(2*S*,3*R*)-dihydroxy-3-(6′,7′-dimethoxy-1′,2′,3′,4′-tetrahydroisoquinolin-1′ (*R*)-yl)] propanoate hydrochloride (**6**), was prepared by the method employed by Dörnyei and Szántay (5) for the preparation of the enantiomer. Treatment of **6** with an excess of ethyl chloroformate or an excess of methyl chloroformate provided the *N*,*O*-acylated compounds, **7** and **8**, respectively. The *O*-acyl groups were selectively removed from **7** and **8** by methanolysis affording the *N*-alkoxycarbonyldihydroxy compounds **9** and **10**, which, on periodate oxidation, yielded the aldehydes **1** and **5**, respectively. Both aldehydes are prone to racemization and should be used immediately in subsequent steps.

This method of preparation of (*R*)-**1** has several advantages over the preparation from glyceraldehyde (1*b*). Fewer steps are involved in formation of the immediate precursor to the aldehyde and the reaction leading to generation of asymmetry at C-1 is for all practical purposes stereospecific; none of the diastereomer of **6** was detected, confirming the previous report (5). The periodate cleavage of the glycol unit of **9** and **10** proceeds in nearly quantitative yield, as does glycol cleavage in the first method. However, the tartaric acid route has the potential advantage that it may be used to prepare 1-formylisoquinolines, with substituents other than *O*-methyl on the aromatic ring; such preparations are not practicable beginning from glyceraldehyde. In comparison with the route from (±)-calycotomine (1*c*), the present method is superior in terms of yield (33% from tartaric acid vs. 22% from (±)-calycotomine for (*R*)-**1**) and roughly similar in terms of convenience.

The asymmetric synthesis of a variety of alkaloids belonging to the 1-benzylisoquinoline family beginning from (*R*)-**1** has been reported previously by us (1*b*,*c*). We demonstrate here

[1]For a preliminary account of a part of this work, see ref. 15.
[2]Authors to whom correspondence may be addressed.

Can. J. Chem. Downloaded from www.nrcresearchpress.com by 213.166.140.6 on 09/07/12
For personal use only.

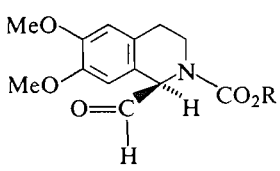

(*R*)-**1** R = Et
(*R*)-**5** R = Me

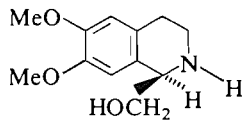

(*R*)-**2**

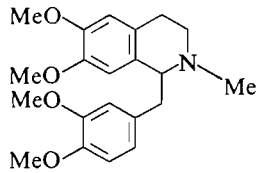

(*S*)-**3**

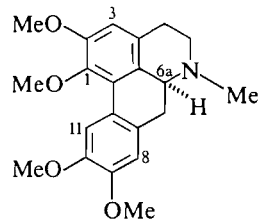

(*S*)-**4**

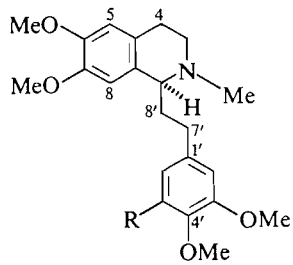

11 R = H
12 R = OMe

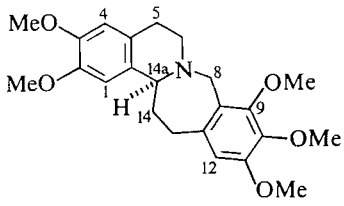

13

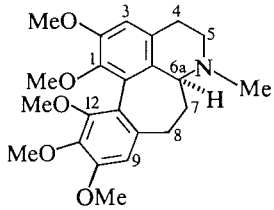

14

that (*R*)-**1** (or (*R*)-**5**) is an equally valuable starting material for the synthesis of several alkaloids and related compounds belonging to the 1-phenylethylisoquinoline group. Specifically, we have prepared (*S*)-homolaudanosine (**11**) (6, 7), (*S*)-5′-methoxyhomolaudanosine (**12**) (8, 9), (*S*)-2,3,9,10,11-pentamethoxyhomoprotoberberine (**13**) (10), and (*S*)-*O*-methylkreysigine (**14**) (8, 11).

The synthesis of (*S*)-homolaudanosine (**11**) is outlined in Scheme 2. The ylid **15** was prepared from 3,4-dimethoxybenzylphosphonium chloride by treatment with *n*-butyllithium in THF, first at −78°C and then at −20°C. The mixture was then cooled to −78°C and treated with a solution of **1** in THF. The product (**16**) was a *trans*-alkene as evidenced by ^{1}H nmr ($J_{7',8'} \approx 16$ Hz). Catalytic reduction of **16** afforded the carbamate **17**, which was reduced with lithium aluminium hydride (LAH) to (*S*)-homolaudanosine (**11**). The alkaloid was isolated as an oil in an overall chemical yield from (*R*)-**1** of 47% and in 78% ee (enantiomeric excess).

The synthesis of phenylethylisoquinoline **12**, homoprotoberberine **13**, and homoaporphine **14** is outlined in Scheme 3. Aldehyde **5** was used as starting material in these syntheses because the removal of the alkoxycarbonyl group is an essential step in the synthesis of **13** and it was thought that the methyl carbamate might be converted more readily into a secondary amine than the ethyl carbamate. Accordingly, aldehyde (*R*)-**5** was treated with 3,4,5-trimethoxybenzyltriphenylphosphonium ylid **18** under conditions similar to those used for the conversion of **1** to **16**. The product (**19**) of this reaction, also a *trans*-alkene ($J_{7',8'} \approx 15$ Hz), was reduced catalytically to the carbamate **20**. The conversion of **20** to the secondary amine proved to be difficult. Alkaline hydrolysis of the carbamate function of **20** proceeded slowly and was accompanied by racemization. Treatment with trimethylsilyl chloride and sodium iodide in refluxing acetonitrile yielded the secondary amine but there was extensive racemization and the reaction was therefore of little value in the context of this research. However, when **20** was treated with an excess of methyllithium in THF at room temperature, the reaction proceeded in acceptable chemical yield and without loss of optical purity. The conversion of **21** into homoprotoberberine **13** was accomplished by treatment of the hydrobromide of **21** with formaldehyde using a literature procedure (10). The spectroscopic properties of **13** were the same as those already reported (10) and the optical purity was 81.9% based on published data.

The synthesis of (*S*)-*O*-methylkreysigine (**14**) (11) was achieved by oxidative cyclization of **12** using the procedure of Taylor *et al.* (8). Compound **12**, prepared by reduction of **20** with LAH, was treated with thallium(III) trifluoroacetate. *O*-Methylkreysigine was isolated as an oil in 27% chemical yield based on **12** and in 84% ee. The spectroscopic properties of **12** and **14** were in accord with those reported (8, 11).

Finally, the procedure of Taylor *et al.* (8) was applied to the synthesis of (*S*)-glaucine (**4**). To this end, (*S*)-laudanosine (**3**) in 82% ee, prepared in the manner previously described (1*b*), was treated with thallium(III) trifluoroacetate. Oxidative coupling occurred in the expected fashion affording (+)-

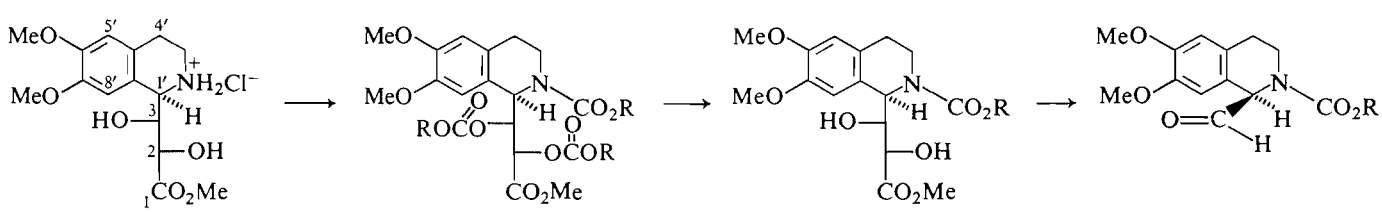

6

7 R = Et
8 R = Me

9 R = Et
10 R = Me

1 R = Et
5 R = Me

SCHEME 1

Can. J. Chem. Downloaded from www.nrcresearchpress.com by 213.166.140.6 on 09/07/12
For personal use only.

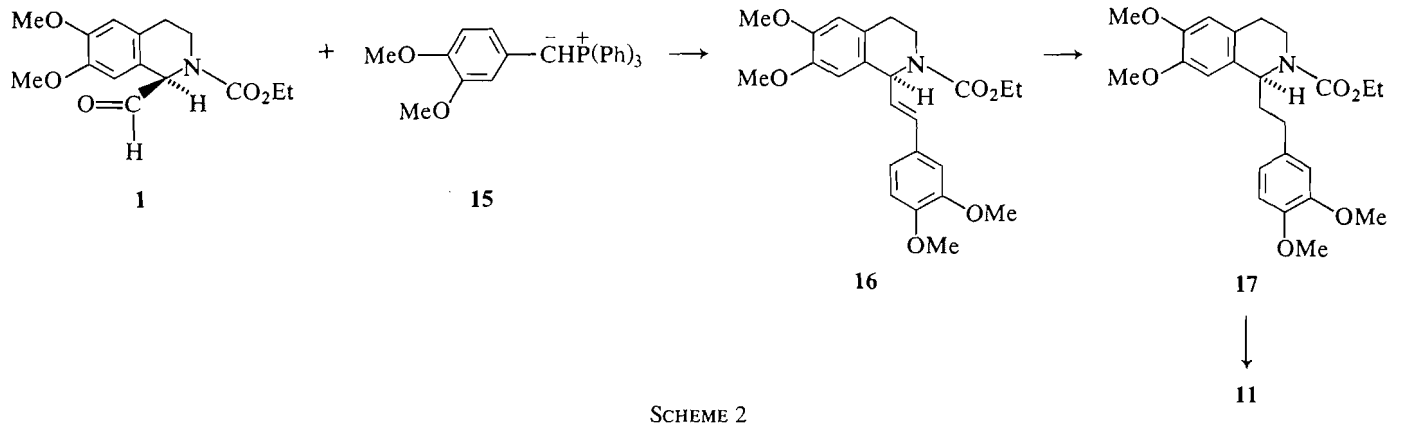

SCHEME 2

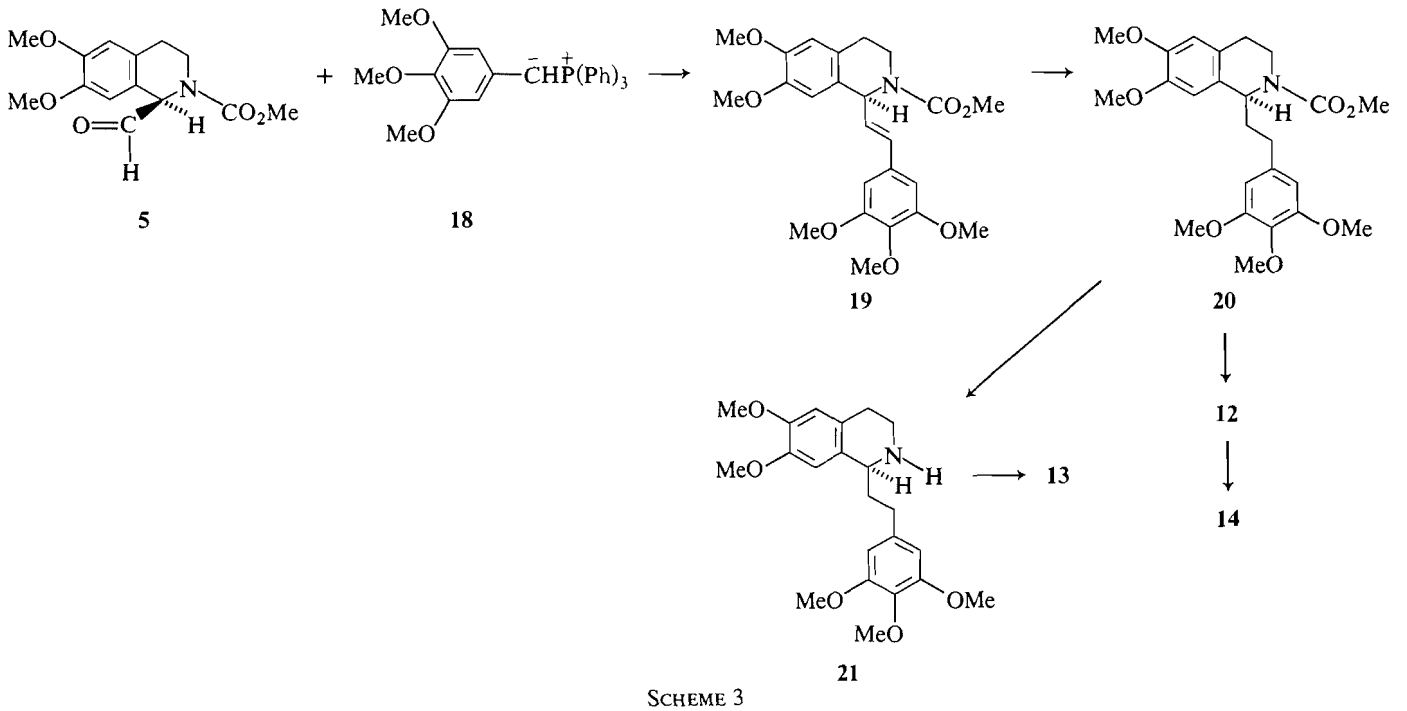

SCHEME 3

glaucine in 47% chemical yield and in 83% ee. Thus, the coupling reaction proceeded without racemization at the asymmetric centre.

The work described in this article is a further demonstration of the utility of 2-alkoxycarbonyl-1-formyl-1,2,3,4-tetrahydro-6,7-dimethoxyisoquinolines in the synthesis of a wide variety of isoquinoline alkaloids of high enantiomeric purity. Of the three routes developed by us for the preparation of the (*R*)-aldehydes, the one described in this article, namely that from D-(−)-tartaric acid, is the method of choice.

Experimental

The ^{1}H nmr spectra were recorded on a Bruker AM500 spectrometer at 500 MHz or a Varian EM390 spectrometer at 90 MHz; $CDCl_3$ was the solvent and, unless otherwise stated, tetramethylsilane (TMS) was used as the internal standard. Chemical shifts are reported in ppm (δ) downfield from the signal of TMS. The symbols, s (singlet), d (doublet), t (triplet), q (quartet), m (multiplet), and br (broadened), are used to report the multiplicity and shape of signals. EI mass spectra were recorded on a VG Micromass 7070F mass spectrometer at an ionizing voltage of 70 eV or on a VG Analytical ZAB-E mass spectrometer, and CI spectra were recorded using NH_3 at ~1 Torr (1 Torr = 133.3 Pa) as reagent gas; data are given as *m*/*z* (% relative intensity).

Melting points were determined using a Gallenkamp apparatus and are uncorrected. Optical rotations were measured using a Perkin–Elmer 247MC polarimeter in a 1-mL microcell that is 1 dm in length. The values for ee were calculated as described by Andersen *et al.* (12). Flash chromatography was performed on Kieselgel 60 (230–400 mesh).

The homogeneity of the products was established on the basis of chromatographic and spectroscopic (^{1}H nmr and mass spectral) examination.

*Methyl [(2S,3R)-dihydroxy-3-(6′,7′-dimethoxy-1′,2′,3′,4′-tetrahydroisoquinolin-1′(R)-yl)]propanoate hydrochloride (**6**)*

The compound was prepared by the procedure of Dörnyei and Szántay (5) except that D-tartaric acid (2*S*,3*S*) was used in place of the enantiomer employed in the earlier study.[3] The hydrochloride was obtained as colorless crystals from methanol in 57% overall yield from D-tartaric acid; mp 184–186°C (lit. (5) mp 186–187°C for the enantiomer); $[\alpha]_D^{25}$ −82.2° (*c* 1.31, H_2O); ^{1}H nmr (500 MHz, DMSO-d_6) δ: 2.84 (1H, m, C-3′ H_{ax}), 2.99 (2H, m, C-4′ H's), 3.05 (2H, m, disappeared in D_2O, 2 × OH), 3.33 (2H, br s, disappeared in D_2O, NH_2), 3.54 (1H, m, C-3′ H_{eq}), 3.67 (3H, s, CO_2CH_3), 3.75 and

[3]The previous authors have inadvertently designated the acid employed by them as D-tartaric acid; however, their stereostructures clearly show that the L-isomer, (2*R*,3*R*), was used.

Can. J. Chem. Downloaded from www.nrcresearchpress.com by 213.166.140.6 on 09/07/12
For personal use only.

Can. J. Chem. Downloaded from www.nrcresearchpress.com by 213.166.140.6 on 09/07/12
For personal use only.

3.76 (3H each, s's, 2 × OCH_3), 3.98 (1H, d, J = 1.1 Hz, C-1′ H), 4.45–4.65 (2H, br m, C-2 H and C-3′ H, collapses to br s at 4.64 on addition of D_2O), 6.85 and 6.89 (1H each, s's, C-5′ and C-8′ H's).

Preparation of carbamate 7 by treatment of 6 with ethyl chloroformate

Ethyl chloroformate (12 mL) was added dropwise over a period of 30 min to a vigorously stirred solution of **6** (10.77 g) in pyridine (100 mL). The temperature was maintained in the range 5–10°C during the addition and the mixture was stirred an additional 45 min at 5°C. The pyridine was then removed under reduced pressure and the residue taken up in $CHCl_3$. The $CHCl_3$ solution was washed first with water, then with 2% HCl(aq), and again with water before drying over $MgSO_4$. Evaporation of the solvent yielded a residue that crystallized from CH_3OH–Et_2O. The product **7** (13.99 g, 86% based on **1**) melted at 159–161°C; $[\alpha]_D^{25}$ +112.8° (*c* 1.66, $CHCl_3$); ^1H nmr (90 MHz, $CDCl_3$) δ: 1.11, 1.23, 1.38 (3H each, t's, J = 7.1, 7.3 and 6.7 Hz, resp., 3 × CH_2CH_3), 2.73–2.95 (2H, m, C-4′ H's), 3.30–3.57 (2H, m, C-3′ H's), 3.78 (3H, s, CO_2CH_3), 3.87 (6H, s, 2 × OCH_3), 3.93–4.37 (6H, m, 3 × CH_2CH_3), 5.27–5.40 (3H, m, C-1′ H, C-3 H, and C-2 H), 6.65 and 6.83 (1H each, s's, C-5′ H and C-8′ H); ms (CI, NH_3) *m/z* (%): 528 (M + 1, 100), 264 (85), 192 (10). *Anal.* calcd. for $C_{24}H_{33}NO_{12}$: C 54.64, H 6.31, N 2.65; found: C 54.83, H 6.63, N 2.40.

Preparation of carbamate 8 by treatment of 6 with methyl chloroformate

Methyl chloroformate (17.8 mL) was added to a solution of **6** (14.4 g) in pyridine (150 mL) under conditions identical with those described for the preparation of **7**. The reaction mixture was processed similarly affording **8** (17.7 g, 88% from **1**) as white crystals from $CHCl_3$–MeOH–Et_2O; mp 178–180°C; $[\alpha]_D^{25}$ +114.8° (*c* 1.97, $CHCl_3$); ^1H nmr (90 MHz, $CDCl_3$) δ: 2.73–2.97 (2H, m, C-4′ H's), 3.26–3.50 (2H, m, C-3′ H's), 3.57 (3H, s, CO_2CH_3), 3.70, 3.85, 3.88, 3.89, 3.90 (3H each, 5s, 5 × OCH_3), 5.27–5.38 (3H, m, C-1′ H, C-2 H, C-3 H), 6.65 and 6.95 (1H each, s's, C-5′ and C-8′ H's); ms (CI, NH_3) *m/z* (%): 486 (M + 1, 50), 250 (100).

Methyl [(2S,3R)-dihydroxy-3-(N-ethoxycarbonyl-6′,7′-dimethoxy-1′,2′,3′,4′-tetrahydroisoquinolin-1′-(R)-yl)]propanoate (9): methanolysis of 7

A solution of **7** (1.095 g) and NaOMe (200 mg) in dry MeOH (100 mL) was stirred at room temperature under nitrogen for 4 h or until the reaction was complete. The reaction was monitored by tlc (solvent system, 5% MeOH in $CHCl_3$). The solution was neutralized with acetic acid and evaporated to dryness. The residue was treated with H_2O (50 mL) and $CHCl_3$ (50 mL), the $CHCl_3$ layer separated and washed with saturated $NaHCO_3$(aq). The $CHCl_3$ solution was dried over $MgSO_4$ and evaporated, and the residue was taken up in $CHCl_3$ and chromatographed on a column of silica gel. The nonpolar impurities were eluted with $CHCl_3$ and compound **9** with 5% MeOH in $CHCl_3$. The product (640 mg, 80.4%) was obtained as an unstable oil; $[\alpha]_D^{25}$ +29.3° (*c* 1.28, $CHCl_3$); ^1H nmr (90 MHz, $CDCl_3$) δ: 1.27 (3H, t, J = 7.5 Hz, CH_2CH_3), 2.83 (2H, apparent t, J = 6.4 Hz, C-4′ H's), 3.30–3.67 (2H, m, C-3′ H's), 3.20 (2H, m, disappeared in D_2O, 2 × OH), 3.75 (3H, s, CO_2CH_3), 3.85 (6H, s, 2 × OCH_3), 4.02 (1H, m, sharpens on addition of D_2O to a broad doublet, J = 9.0 Hz, C-3 H), 4.20 (2H, q, J = 7.5 Hz, CH_2CH_3), 4.38 (1H, m, sharpens on addition of D_2O to doublet, J = 1.5 Hz, C-2 H), 4.98 (1H, d, J = 9.0 Hz, C-1′ H), 6.66 and 6.97 (1H each, s's, C-5′ H and C-8′ H); ms (CI, NH_3) *m/z* (%): 384 (M + 1, 25), 338 (28), 294 (85), 264 (80), 236 (60), 192 (100), 176 (40).

Methyl [(2S,3R)-dihydroxy-3-(N-methoxycarbonyl-6′,7′-dimethoxy-1′,2′,3′,4′-tetrahydroisoquinolin-1′-(R)-yl)]propanoate (10): methanolysis of 8

A solution of **8** (1.148 g) and NaOMe (238 mg) in dry MeOH (100 mL) was treated under the same conditions as those described above for the methanolysis of **7**. Compound **10** was isolated as an unstable oil (609 mg, 69.8%); $[\alpha]_D^{25}$ +27.3° (*c* 1.63, $CHCl_3$); ^1H nmr (90 MHz, $CDCl_3$) δ: 2.83 (2H apparent t, J = 7.5 Hz, C-4′ H's), 3.40–3.61 (2H, m, C-3′ H's), 3.50 (2H, m, disappeared in D_2O, 2 × OH), 3.78 and 3.88 (6H each, s's, 4 × OCH_3), 4.05 (1H, m, on addition of D_2O becomes dd, J = 1.5 and 9.0 Hz, C-3 H), 4.43 (1H, d, J = 1.5 Hz, C-2 H), 5.12 (1H, d, J = 9.0 Hz, C-1′ H); 6.68 and 7.00 (1H each, s's, C-5′ and C-8′ H); ms (CI, NH_3) *m/z* (%): 370 (M + 1, 100), 250 (100).

(R)-2-Ethoxycarbonyl-1-formyl-6,7-dimethoxy-1,2,3,4-tetrahydroisoquinoline (1)

A solution of $NaIO_4$ (852 mg) in H_2O (30 mL) was added over a period of 5 min to a stirred solution of **9** (762 mg) in MeOH (100 mL) at 5°C. The resulting mixture was stirred at the same temperature for 1 h and then filtered to remove inorganic precipitates. The methanol was then evaporated, benzene (100 mL) was added to the residue, and the organic layer was washed three times with water (50 mL each) before drying over $MgSO_4$. Evaporation of the solvent yielded **1** as a colorless oil (554 mg, 95%), which was used immediately. The analytical properties of **1** were identical with those already described (*1b,c*).

(R)-2-Methoxycarbonyl-1-formyl-6,7-dimethoxy-1,2,3,4-tetrahydroisoquinoline (5)

Compound **5** was prepared from **10** using a procedure identical with that described for the conversion of **9** to **1**. Thus, **10** (2.435 g) in MeOH (220 mL) was treated with $NaIO_4$ (2.72 g) in H_2O (50 mL). The product **5** isolated in similar fashion to **1** was an oil (1.84 g, 90%), which rapidly racemizes and must be used immediately in subsequent steps; ^1H nmr (90 MHz, $CDCl_3$) δ: 2.76–2.87 (2H, m, C-4 H's), 3.23–3.57 (2H, m, C-3 H's), 3.82 (3H, s, CO_2CH_3), 3.90 and 3.93 (3H each, s's, 2 × OCH_3), 5.36 (1H, br s, C-1 H), 6.72 and 6.88 (1H each, s's, C-5 H and C-8 H), 9.60 (1H, s, CH=O); ms (CI, NH_3) *m/z* (%): 280 (M + 1, 100), 250 (14). *Mol. Wt.* calcd. for $C_{14}H_{17}NO_5$: 279.1107; found (hrms): 279.1111.

Preparation of homolaudanosine (11)

(a) Preparation of the Wittig reagent 15

3,4-Dimethoxybenzyltriphenylphosphonium chloride was prepared by heating on the steam bath for 1 h a mixture of 3,4-dimethoxybenzyl chloride (2.98 g) and triphenylphosphine (4.21 g). The crystalline product (6.33 g, 88%) obtained from EtOH melted at 235–237°C. A suspension of the salt (908 mg) in dry THF (50 mL) was treated under nitrogen at −78°C over a 5-min period with *n*-butyllithium (0.93 mL of 2.4 *M* *n*-BuLi in hexane). The orange-colored mixture was stirred for another 0.5 h at the same temperature and then slowly warmed to −20°C at which temperature it was maintained for another 0.5 h. The solution containing the ylid **15** was cooled to −78°C before proceeding to the next step.

(b) Preparation of 16 by treatment of 1 with the Wittig reagent 15

To the solution prepared in (*a*) above was added all at once a solution of freshly prepared **1** (590 mg) in THF (10 mL). The reaction mixture was stirred vigorously during the addition and for another 2 h at −78 to −60°C. The mixture was stored in a freezer overnight at −30°C before removing the solvent. The residue was thoroughly extracted with dry Et_2O (6 × 30 mL each), and the extract dried and evaporated. The residue was taken up in 5% EtOAc in C_6H_6 and chromatographed on a column of silica gel with the same solvent system. Compound **16** was isolated as a colorless oil (596 mg, 69%); $[\alpha]_D^{25}$ +135.5° (*c* 0.90, $CHCl_3$); ^1H nmr (90 MHz, $CDCl_3$) δ: 1.32 (3H, t, J = 7.5 Hz, CH_2CH_3), 2.66–2.93 (2H, m, C-4 H's), 3.10–3.50 (2H, m, C-3 H's), 3.85 (3H, s, OCH_3), 3.88 (3H, s, OCH_3), 3.92 (6H, s, 2 × OCH_3), 4.23 (2H, q, J = 7.5 Hz, CH_2CH_3), 5.73 (1H, d, J = 4.5 Hz, C-1 H), 6.06–6.51 (2H, m, $J \approx$ 16.0 Hz, C-7′ H and C-8′ H),[4] 6.72 (2H, apparent s, C-5 and C-8 H's), 6.86 (1H, br s, C-2′ H), 6.93 (2H, m, C-5′ and C-6′ H's); ms (CI, NH_3) *m/z* (%): 428 (M + 1, 60), 354 (15), 264 (100).

(c) Preparation of 17 by catalytic reduction of 16

Compound **16** (224 mg) prepared above was dissolved in EtOH (50 mL) and treated with H_2 over Adams' catalyst for 4 h at 1 atm (1 atm = 101.3 kPa). The catalyst was separated by filtration and the solvent evaporated, affording **17** as a colorless oil (218 mg, 97%);

[4]The C-8′ proton is coupled to the C-1 proton but the signal is poorly resolved even at 50°C presumably because of restricted rotation of the carbamate function.

Can. J. Chem. Downloaded from www.nrcresearchpress.com by 213.166.140.6 on 09/07/12
For personal use only.

$[\alpha]_D^{25}$ +64.9° (*c* 1.68, $CHCl_3$); ^1H nmr (90 MHz, $CDCl_3$) δ: 1.30 (3H, t, *J* = 7.2 Hz, CH_2CH_3), 1.92–2.25 (2H, m, C-8′ H's), 2.55–2.93 (4H, m, C-4 H's and C-7′ H's), 3.05–3.48 (2H, m, C-3 H's), 3.85 (9H, apparent s, 3 × OCH_3), 3.88 (3H, s, OCH_3), 4.22 (2H, q, *J* = 7.2 Hz, CH_2CH_3), 5.17 (1H, apparent t, *J* = 7.5 Hz, C-1 H), 6.60 and 6.63 (1H each, s's, C-5 and C-8 H's), 6.82 (3H, br s, C-2′, C-5′, and C-6′ H's); ms (CI, NH_3) *m/z* (%): 430 (M + 1, 20), 358 (10), 328 (5), 296 (11), 264 (100). *Mol. Wt.* calcd. for $C_{24}H_{31}NO_6$: 429.2151; found (hrms): 429.2149.

*(d) Preparation of **11** by reduction of **17** with lithium aluminium hydride*

Compound **17** (417 mg), dissolved in THF (75 mL), was treated with LAH (400 mg). The mixture was then heated under reflux for 1.5 h, cooled, and the excess of hydride decomposed by addition of saturated NaCl(aq). Chloroform (30 mL) and $MgSO_4$ (ca. 2 g) were added and the mixture was heated under reflux for 15 min. The cooled mixture was filtered free of inorganic salts, the solids were washed twice with boiling $CHCl_3$, and the combined filtrate evaporated to dryness. The residue was taken up in $CHCl_3$, adsorbed on a column of silica gel, and eluted with 2% MeOH in $CHCl_3$. Homolaudanosine (**11**) was obtained as a colorless oil (254 mg, 70.1%); $[\alpha]_D^{25}$ +8.61° (*c* 0.85, EtOH) (lit. (6) $[\alpha]_D^{25}$ +11.0° (*c* 0.21, EtOH)]; ^1H nmr (500 MHz, $CDCl_3$) δ: 2.02 (2H, m, C-8′ H's), 2.45 (3H, s, NCH_3), 2.51 (1H, m, C-3 H_{ax}), 2.70 (4H, m, C-4 H's and C-7′ H's), 3.13 (1H, m, C-3 H_{eq}), 3.40 (1H, t, *J* = 5.4 Hz, C-1 H), 3.78, 3.79, 3.80, 3.82 (3H each, s's, 4 × OCH_3), 6.51 and 6.54 (1H each, s's, C-5 and C-8 H's), 6.69 (1H, d, *J* = 1.8 Hz, C-2′ H), 6.70 (1H, dd, *J* = 1.8 and 8.4 Hz, C-6′ H), 6.75 (1H, d, *J* = 8.4 Hz, C-5′ H) (lit. spectrum (6)); ms (CI, NH_3) *m/z* (%): 372 (M + 1, 100), 342 (7). *Mol. Wt.* calcd. for $C_{22}H_{29}NO_4$: 371.2097; found (hrms): 371.2099.

*Preparation of homoprotoberberine **13***

*(a) Preparation of the Wittig reagent **18***

3,4,5-Trimethoxybenzyltriphenylphosphonium chloride was prepared by heating on the steam bath for 1 h a mixture of triphenylphosphine (1.65 g) and 3,4,5-trimethoxybenzyl chloride (1.37 g). The product was recrystallized from EtOH, affording colorless crystals (2.53 g, 84%), mp 234–236°C. A suspension of the product chloride (1.42 g) in THF (200 mL) was treated under nitrogen at −78°C over a period of 5 min with *n*-butyllithium (1.38 mL of 2.4 *M* *n*-BuLi in hexane). The orange solution containing the ylid **18** was kept at this temperature for 0.5 h and then warmed to −20°C for another 0.5 h.

*(b) Preparation of **19** by treatment of **5** with the Wittig reagent **18***

The Wittig reagent prepared above was cooled to −78°C and treated all at once with a solution of freshly prepared **5** (820 mg) in THF (10 mL). The reaction mixture was processed in the same manner as that described above for the preparation of **16**, affording **19** as a colorless oil (865 mg, 66%); $[\alpha]_D^{25}$ +129.4° (*c* 0.935, $CHCl_3$); ^1H nmr (90 MHz, $CDCl_3$) δ: 2.68–2.93 (2H, m, C-4 H's), 3.10–3.48 (2H, m, C-3 H's), 3.80 (3H, s, CO_2Me), 3.88 (15H, br s, 5 × OCH_3), 5.77 (1H, d, *J* ≈ 1.0 Hz, C-1 H), 5.97–6.40 (2H, AB m, *J* ≈ 15 Hz, C-7′ and C-8′ H's), 6.65 and 6.73 (2H each, apparent s's, C-2′ H, C-6′ H, C-5 H, and C-8 H); ms (CI, NH_3) *m/z* (%): 444 (M + 1, 45), 250 (100). *Mol. Wt.* calcd. for $C_{24}H_{29}NO_7$: 443.1944; found (hrms): 443.1955.

*(c) Preparation of **20** by catalytic reduction of **19***

Compound **19** (758 mg) was treated with H_2 over Adams' catalyst (140 mg) in methanol in the manner described for the conversion of **16** to **17**. The product **20** was obtained as a colorless oil (746 mg, 98%); $[\alpha]_D^{25}$ +66.2° (*c* 1.12, $CHCl_3$); ^1H nmr (90 MHz, $CDCl_3$) δ: 1.97–2.23 (2H, m, C-8′ H's), 2.58–2.88 (4H, m, C-4 H's and C-7′ H's), 3.05–3.47 (2H, m, C-3 H's), 3.78 (3H, s, CO_2CH_3), 3.88 (15H, apparent s, 5 × OCH_3), 5.18 (1H, br s, C-1 H), 6.48 (2H, apparent s, C-2′ and C-6′ H's), 6.62 and 6.65 (1H each, s's, C-5 and C-8 H's); ms (CI, NH_3) *m/z* (%): 446 (M + 1, 7), 392 (10), 362 (15), 280 (10), 250 (100). *Mol. Wt.* calcd. for $C_{24}H_{31}NO_7$: 445.2101; found (hrms): 445.2115.

*(d) Preparation of **21** by treatment of **20** with methyllithium*

A solution of **20** (255 mg) in THF (5 mL) was added dropwise to a vigorously stirred solution of methyllithium (2.67 mL of 1.5 *M* MeLi in Et_2O) in THF (25 mL) at room temperature. The mixture was stirred for a further 1 h and then the excess of methyllithium was decomposed by the addition of MeOH (1 mL). The solvents were evaporated and a saturated solution of NaCl and enough NH_3(aq) to make the solution strongly basic were added to the residue before extraction with benzene (4 × 20 mL). Evaporation of the dried extract yielded a residue from which compound **21** was obtained as a colorless oil (117 mg, 53%) after purification by column chromatography on silica gel; $[\alpha]_D^{25}$ −12.3° (*c* 1.71, $CHCl_3$); ^1H nmr (90 MHz, $CDCl_3$) δ: 1.83 (1H, br s, disappeared in D_2O, NH), 2.00–2.33 (2H, m, C-8′ H's), 2.60–2.86 (4H, m, C-4 H's and C-7′ H's), 2.98–3.40 (3H, C-1 H and C-3 H's), 3.87 (15H, br s, 5 × OCH_3), 6.48 (2H, apparent s, H-2′ and H-6′), 6.61 and 6.63 (1H each, s's, C-5 and C-8 H's); ms (CI, NH_3) *m/z* (%): 388 (M + 1, 100), 192 (10).

*(e) Preparation of **13** by treatment of **21** with formaldehyde*

A solution of the hydrobromide of **21** (109.0 mg) in H_2O (8 mL) and formaldehyde (5 mL, 37%) was heated under reflux in a nitrogen atmosphere for 3 h. The mixture was cooled, made strongly alkaline by addition of solid NaOH, and extracted 4 times with benzene (15 mL each). The extract was washed with saturated NaCl, dried, and evaporated. The residue was purified by chromatography on silica gel, eluting with 1% MeOH in $CHCl_3$. Compound **13** (54 mg, 58%) was obtained as a glass. The base was converted to the hydrochloride (for measurement of optical rotation), which was isolated also as a glassy solid; $[\alpha]_D^{25}$ −97.8° (*c* 1.07, MeOH) (lit. (10) $[\alpha]_D$ −112.5° (MeOH)); ^1H nmr (90 MHz, $CDCl_3$), free base, δ: 1.80–2.00 (2H, m, C-14 H's), 2.57–2.83 (4H, m, C-5 H's and C-13 H's), 2.97–3.40 (3H, m, C-14a H and C-6 H's), 3.79, 3.81, 3.82, 3.83, 3.84 (3H each, s's, 5 × OCH_3), 3.89 and 3.46 (1H each, ABq, *J* = 17 Hz, C-8 H's), 6.50, 6.57, 6.59 (1H each, s's, C-1 H, C-4 H, and C-12 H) (lit. spectrum (10)); ms (CI, NH_3) *m/z* (%): 400 (M + 1, 100), 208 (52). *Mol. Wt.* calcd. for $C_{23}H_{29}NO_5$: 399.2019; found (hrms): 399.2045.

*Preparation of **12** by treatment of **20** with lithium aluminium hydride*

To a solution of **20** (120 mg) in THF (50 mL) was added LAH (150 mg). The mixture was heated under reflux in a nitrogen atmosphere for 2 h, cooled, and the excess of hydride decomposed by careful addition of a saturated solution of sodium sulfate. Solid $MgSO_4$ and $CHCl_3$ were added to the system, which was then heated under reflux for 5 min. The suspension was filtered, the solid residue washed three times with boiling chloroform, and the combined filtrates evaporated to dryness. The residue was taken up in $CHCl_3$ and adsorbed on a column of silica gel. Elution of the column with 2% MeOH in $CHCl_3$ yielded **12** (78 mg, 72%) as a colorless oil, as the main fraction; $[\alpha]_D^{25}$ +4.51° (*c* 0.96, MeOH) (lit. (9) $[\alpha]_D^{25}$ 4.8° (MeOH)); ^1H nmr (90 MHz, $CDCl_3$) δ: 1.95–2.23 (2H, m, C-8′ H's), 2.50 (3H, s, NCH_3), 2.58–2.83 (4H, m, C-4 H's and C-7′ H's), 3.08–3.53 (3H, m, C-1 H and C-3 H's), 3.87 (15H, br s, 5 × OCH_3), 6.45 (2H, apparent s, H-2′ and H-6′), 6.60 and 6.62 (1H each, s, C-5 H and C-8 H) (lit. spectrum (8, 9)); ms (CI, NH_3) *m/z* (%): 402 (M + 1, 100), 318 (17), 206 (16). *Mol. Wt.* calcd. for $C_{23}H_{31}NO_5$: 401.2202; found (hrms): 401.2204.

*(S)-O-Methylkreysigine (**14**)*

A solution of **12** (150 mg) in freshly distilled and deoxygenated trifluoroacetic acid (100 mL) was treated at 0°C under a nitrogen atmosphere, first with thallium(III) trifluoroacetate (260 mg) and then with boron trifluoride etherate (1 mL). The mixture was stirred for 8 h at 0°C and for an additional 20 h at room temperature. The mixture was then taken to dryness under reduced pressure and the residue treated with H_2O (30 mL). The resulting solution was made strongly alkaline with NH_3 and extracted with $CHCl_3$ (4 × 20 mL). The combined extract was dried over K_2CO_3 and then evaporated. The residual brown oil was purified by preparative layer chromatography on silica plates; 10% MeOH in $CHCl_3$ was used as developing agent. The main fraction eluted from the plates was **14**, obtained as a yellow oil (41 mg, 27%); $[\alpha]_D^{25}$ +68.1° (*c* 0.84, $CHCl_3$) (lit. (11) $[\alpha]_D^{21}$ +81° (*c* 0.43, $CHCl_3$)); ^1H nmr (90 MHz, $CDCl_3$) δ: 1.97–2.33 (2H, m, C-7 H's), 2.43 (3H, s, NCH_3), 2.60–3.40 (7H, m, C-4 H's, C-5 H's, C-6a H, C-8 H's), 3.55, 3.65, 3.84, 3.88, 3.92 (15H, 5s, 5 × OMe), 6.57, 6.70 (each 1H, s, C-3 H and C-9 H) (lit. spectrum (8, 11));

ms (EI) m/z (%): 399 (30), 384 (20), 368 (100). *Mol. Wt.* calcd. for $C_{23}H_{29}NO_5$: 399.2045; found (hrms): 399.2019.

(S)-Glaucine (4)

A solution of (*S*)-laudanosine (1*b*) (76 mg) (82% ee) in freshly distilled and deoxygenated trifluoroacetic acid (70 mL) was treated at 0°C under a nitrogen atmosphere with thallium(III) trifluoroacetate (117 mg) followed by $BF_3 \cdot Et_2O$ (0.6 mL). The temperature was maintained at 0°C for 3 h and the mixture, which was stirred throughout, was allowed to warm slowly to room temperature. The mixture was taken to dryness, the residue taken up in water (30 mL), the resulting solution made strongly alkaline with ammonia and then extracted with $CHCl_3$ (4 × 20 mL). The combined extract was dried over K_2CO_3, evaporated to dryness, and the residual oil chromatographed on a column of silica gel using 2% MeOH in $CHCl_3$. The oily residue (35.4 mg, 47%), obtained on evaporation of the eluant, crystallized on addition of ethyl acetate yielding (+)-glaucine as a colorless crystalline solid; mp 117–118°C; $[\alpha]_D^{25}$ +99.6° (*c* 0.89, $CHCl_3$) (lit. (13) mp 119–120°C (EtOAc); $[\alpha]_D$ +120° ($CHCl_3$)); ^1H nmr (90 MHz, $CDCl_3$) δ: 2.37–3.12 (7H, m, C-4 H's, C-5 H's, C-7 H's, C-6a H), 2.57 (3H, s, N—CH_3), 3.68, 3.90, 3.90, 3.98 (12H each, s's, 4 × OCH_3), 6.63, 6.81 (1H each, s's, C-3 H and C-8 H), 8.16 (1H, s, C-11 H) (lit. spectrum (14)); ms (EI) m/z (%): 355 (80), 354 (100), 340 (50), 324 (23), 206 (34). *Mol. Wt.* calcd. for $C_{21}H_{23}NO_4$: 355.1772; found (hrms): 355.1773.

Acknowledgements

We thank the Natural Sciences and Engineering Research Council of Canada for financial support in the form of research grants to D. B. MacLean and W. A. Szarek.

1. (*a*) Z. Czarnocki, D. B. MacLean, and W. A. Szarek. J. Chem. Soc. Chem. Commun. 1318 (1985); (*b*) Z. Czarnocki, D. B. MacLean, and W. A. Szarek. Can. J. Chem. **64**, 2205 (1986); (*c*) Z. Czarnocki, D. B. MacLean, and W. A. Szarek. Bull. Soc. Chim. Belg. **95**, 749 (1986).
2. R. Noyori, M. Ohta, Y. Hsiao, M. Kitamura, T. Ohta, and H. Takaya. J. Am. Chem. Soc. **108**, 7117 (1986).
3. A. I. Meyers and T. R. Bailey. J. Org. Chem. **51**, 872 (1986).
4. M. Shamma. The isoquinoline alkaloids, chemistry and pharmacology. Academic Press, New York. 1972; M. Shamma and J. L. Moniot. Isoquinoline alkaloid research 1972–1977. Plenum Press, New York. 1978.
5. G. Dörnyei and Cs. Szántay. Acta Chim. Acad. Sci. Hung. **89**, 161 (1976).
6. A. J. Aladesanmi, C. J. Kelley, and J. D. Leary. J. Nat. Prod. **46**, 127 (1983).
7. A. I. Meyers, M. Boes, and D. A. Dickman. Angew. Chem. Int. Ed. Engl. **23**, 458 (1984).
8. E. C. Taylor, J. G. Andrade, G. J. H. Rall, and A. McKillop. J. Am. Chem. Soc. **102**, 6513 (1980).
9. A. Brossi, J. O'Brien, and S. Teitel. Helv. Chim. Acta, **52**, 678 (1969).
10. A. Brossi and S. Teitel. Helv. Chim. Acta, **52**, 1228 (1969).
11. M. K. Yusupov, D. T. B. Nqo, and Kh. A. Aslanov. Khim. Prir. Soedin. 526 (1975); Chem. Nat. Compd. (Engl. Transl.) 555 (1976).
12. K. K. Andersen, D. M. Gash, and J. D. Robertson. *In* Asymmetric synthesis. Vol. 1. *Edited by* J. D. Morrison. Academic Press, Inc., New York. 1983. p. 45.
13. T. Kametani. The chemistry of isoquinoline alkaloids. Elsevier, Amsterdam. 1969. p. 90.
14. O. Hoshino, M. Ohtani, and B. Umezawa. Chem. Pharm. Bull. **27**, 3101 (1979).
15. Z. Czarnocki, D. B. MacLean, and W. A. Szarek. J. Chem. Soc. Chem. Commun. 493 (1987).

Can. J. Chem. Downloaded from www.nrcresearchpress.com by 213.166.140.6 on 09/07/12
For personal use only.

8*H*-Isoquino[2,1-*b*][2,7]naphthyridin-8-ones: synthesis of the *Alangium* alkaloids, alangimaridine and alangimarine[1]

JAHANGIR, MICHAEL A. BROOK, AND DAVID B. MACLEAN[2]
Department of Chemistry, McMaster University, Hamilton, Ont., Canada L8S 4M1

AND

HERBERT L. HOLLAND
Department of Chemistry, Brock University, St. Catharines, Ont., Canada L2S 3A1

Received March 31, 1987

JAHANGIR, MICHAEL A. BROOK, DAVID B. MACLEAN, and HERBERT L. HOLLAND. Can. J. Chem. **65**, 2362 (1987).

It is shown that 3,4-dihydroisoquinolines are activated toward nucleophilic attack by reaction with trimethylsilyl trifluoromethanesulfonate. The complex so formed reacts readily with the lithio derivative of 3-cyano-4-methyl-5-vinylpyridine, affording in a single step a tetracyclic amidine from which a lactam is obtained by hydrolysis. These reactions have been applied to the synthesis of the *Alangium* alkaloids, (±)-alangimaridine and alangimarine.

JAHANGIR, MICHAEL A. BROOK, DAVID B. MACLEAN et HERBERT L. HOLLAND. Can. J. Chem. **65**, 2362 (1987).

On démontre que les dihydro-3,4 isoquinoléines sont activées par rapport aux réactions nucléophiles avec le trifluorométhanesulfonate de triméthylsilyle. Le complexe qui se forme ainsi réagit facilement avec le dérivé lithien de la cyano-3 méthyl-4 vinyl-5 pyridine pour conduire en une seule étape à une amidine tétracyclique à partir de laquelle on peut obtenir une lactame par hydrolyse. On a appliqué ces réactions à la synthèse des alcaloïdes suivants de l'*Alangium* (±)-alangimaridine et alangimarine.

[Traduit par la revue]

Introduction

Alangium lamarckii Thw. has been used in Indian medicine for many years (2–4) and it has been claimed that the extracts of the plant are useful in the treatment of a large number of human disorders. Extensive investigation has resulted in the isolation of several biologically active alkaloids including emetine, cephaetine, and psychotrine (5). Recently, Pakrashi *et al.* (6–8) have isolated several new alkaloids from the seeds of *A. lamarckii*, namely, alangimaridine **1**, alangimarine **2**, isoalangimarine **3**, alamarine **4**, isoalamarine **5**, dihydroalamarine **6**, dihydroisoalamarine **7**, alangimarinone **8**, and alamaridine **9** (Fig. 1). These alkaloids are tetracyclic like the protoberberines but have a pyridine ring instead of the benzenoid D ring in the protoberberines; they possess the 8*H*-isoquino[2,1-*b*][2,7]naphthyridine ring system, an unusual ring system in natural products chemistry.

Ninomiya and co-workers (9) reported the first total synthesis in this class of alkaloids in their synthesis of alamarine **4** via a route involving enamide cyclization under both thermal and photochemical conditions. The enamide **10** when heated produced a mixture of two lactams, **11** (43%) and **12** (10%). On the other hand, irradiation of **10** gave the lactams **11** and **12** in 25 and 13% yields, respectively. Debenzylation and sodium borohydride reduction of the major product **11** gave (±)-alamarine **4** as shown in Scheme 1. Alamarine had previously been dehydrated to alangimarine **2** (6). In the past year two synthetic routes to (±)-alamaridine **9** have been reported (10, 11) but neither is applicable, without modification, to the preparation of alkaloids substituted at C-12.

The *Alangium* alkaloids bearing a substituent at C-12 may be considered to be related biogenetically to deacetylipecoside **15**, which in turn is derived from secologanin **13** and dopamine **14** (12–16). Deacetylipecoside **15**, through cyclization to alangiside **16** followed by hydrolysis, amination, and other unexceptional transformations, may be imagined to produce these alkaloids, as shown in Scheme 2. The *R* configuration is shown in the diagram but the absolute configuration of the alkaloids has not been established. It is also possible that alamaridine **9** is derived from deacetylipecoside **15** by ring closure between the isoquinoline nitrogen and the methine carbon of the vinyl group via the postulated intermediate **17**, followed by other transformations (Scheme 2). Biosynthetic studies have not been conducted on this new class of protoberberine analogues.

Here we report a new approach to the synthesis of those *Alangium* alkaloids bearing a vinyl substituent at C-12, which uses two readily available starting materials, namely, 3-cyano-4-methyl-5-vinyl pyridine **18** (17, 18) as its lithio derivative **18***a*, and substituted 3,4-dihydroisoquinolines.

Results and discussion

It has been shown (19) by us that the 8*H*-isoquino[2,1-*b*][2,7]naphthyridine ring system is formed in high yield by interaction of 3,4-dihydroisoquinolines **20** and the lithio derivative **19***b* of azaphthalide **19***a* (Scheme 3). This strategy was used to synthesize the ring system of alamaridine **9** with the methyl group of **9** being introduced in a subsequent step (11). The same approach was investigated for the synthesis of alkaloids **1–8** bearing substituents at C-12 but was abandoned because the azaphthalide **19***c* could not be prepared by us in good yield. In another approach, attempts to introduce a two-carbon unit at C-12 in **21** were also unsuccessful. Next, our attention was focussed on 3-cyano-4-methyl-5-vinylpyridine **18** as a potential precursor of rings C and D of the alkaloids **1–8** of Fig. 1. The compound readily formed an anion **18***a* in the presence of strong bases and it was considered that this anion might react with 3,4-dihydroisoquinolines in the same manner as the azaphthalide anion **19***b*, leading to formation of the appropriately substituted tetracyclic system. However, starting materials were recovered virtually quantitatively when the lithium derivative **18***a* and imine **20***a* were allowed to interact under a variety of reaction conditions. In other experiments (20) it was found that **18***a* added readily to iminium salts such as **22** but we were

[1]A preliminary account of a part of this work has appeared (1).
[2]Author to whom correspondence may be addressed.

Can. J. Chem. Downloaded from www.nrcresearchpress.com by 213.166.140.6 on 09/07/12
For personal use only.

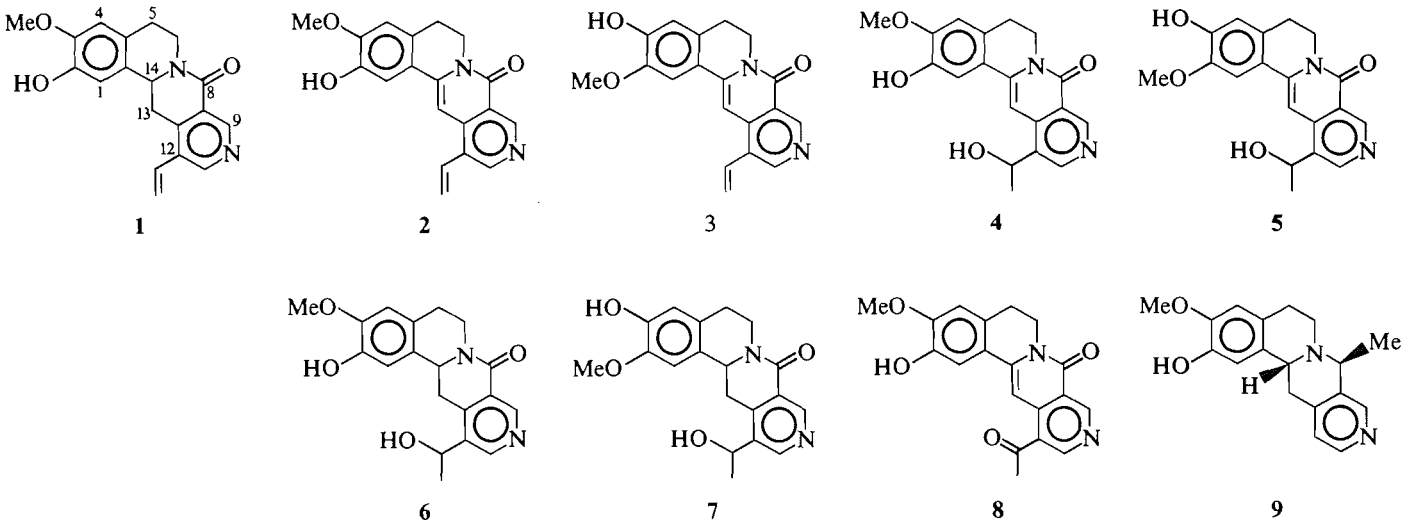

FIG. 1. Benzopyridoquinolizidine alkaloids of *Alanguim lamarckii*.

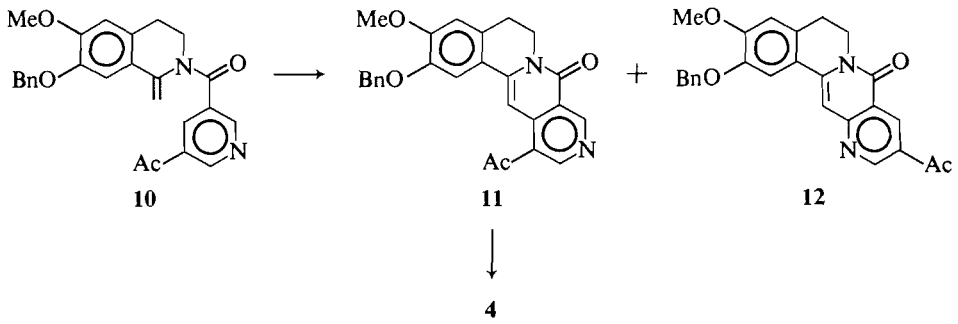

SCHEME 1

unable to find an alkyl group that could be removed from the resulting tertiary amines **23**. Had it been possible to convert the tertiary amines **23** to the corresponding secondary amines **24**, the latter would have been expected to react readily with the cyano function on the pyridine ring to yield the desired tetracyclic ring system (see Scheme 4).

It was apparent that a reagent was required that would activate an imine to nucleophilic attack and would be readily removed after the nucleophile had added. Eventually, we found that treatment of imines with trimethylsilyl trifluoromethanesulfonate (TMSOTf) prior to addition of the nucleophile achieved our purpose. A reaction occurred between the nucleophile and the imine–triflate complex that yielded a tetracyclic product without isolation of a tricyclic intermediate. Trimethylsilyl trifluoromethanesulfonate has been used previously as a powerful silylating agent for a wide range of active hydrogen compounds (21) and also for converting imines to the corresponding enamines (22, 23) in the presence of alkylamine bases. To our knowledge, its use to activate an imine toward nucleophilic addition has not been reported prior to its use by us (1, 11).

Treatment of 3,4-dihydroisoquinoline **20***a* with TMSOTf afforded a complex formulated as **25***a* (Scheme 5) to which the lithio derivative **18***a* was added dropwise at −78°C. When the addition was complete the mixture was stirred at −40°C for 4 h and then at 20°C for 12 h. The product of the reaction was a polar crystalline compound isolated in 87% yield. Its infrared spectrum displayed an absorption band at 1610 cm^{-1} indicative of an amidine function (>N—C=NH). The EI mass spectrum showed a molecular ion at m/z 335 of composition $C_{20}H_{21}N_3O_2$, as determined by high resolution mass spectroscopy. All the spectral evidence indicated that the product was a tetracyclic amidine of structure **26***a* (Scheme 5). The mode of cyclization is probably similar to that described elsewhere (19) for the reactions between lithium azaphthalide **19***b* and imines **20***a* and **20***b*. The exact role of the trimethylsilyl group in this reaction, except for activating the imine, has not been clarified but the reactions reported here did not proceed in the absence of this reagent. However, it seems likely that the trimethylsilyl group resides eventually on the amidine nitrogen atom and is lost on work-up. Hydrolysis of amidine **26***a* with 20% KOH solution (aqueous) in dioxane afforded (±)-*O*-methylalangimaridine **27***a* in 99% yield. The ^1H nmr spectrum of lactam **27***a*, except for the extra methoxyl signal, closely resembled that reported for alangimaridine **1** (7). Oxidation of **27***a* with iodine in refluxing methanol gave *O*-methylalangimarine **28** in 81% yield, whose spectral data were consistent with the proposed structure.

The synthesis of the *Alangium* alkaloids themselves was accomplished beginning with imine **20***b*, in which C-7 carries an *O*-benzyl group, and 3-cyano-4-methyl-5-vinylpyridine **18** as its lithio derivative. Condensation of the lithium salt **18***a* with the complex **25***b* afforded amidine **26***b* in 98% yield, which was then hydrolysed to the lactam **27***b* in 98% yield. Debenzylation of the protected phenol in **27***b* was readily achieved by heating it in ethanolic hydrochloric acid; racemic alangimaridine **1** was

Can. J. Chem. Downloaded from www.nrcresearchpress.com by 213.166.140.6 on 09/07/12
For personal use only.

Can. J. Chem. Downloaded from www.nrcresearchpress.com by 213.166.140.6 on 09/07/12
For personal use only.

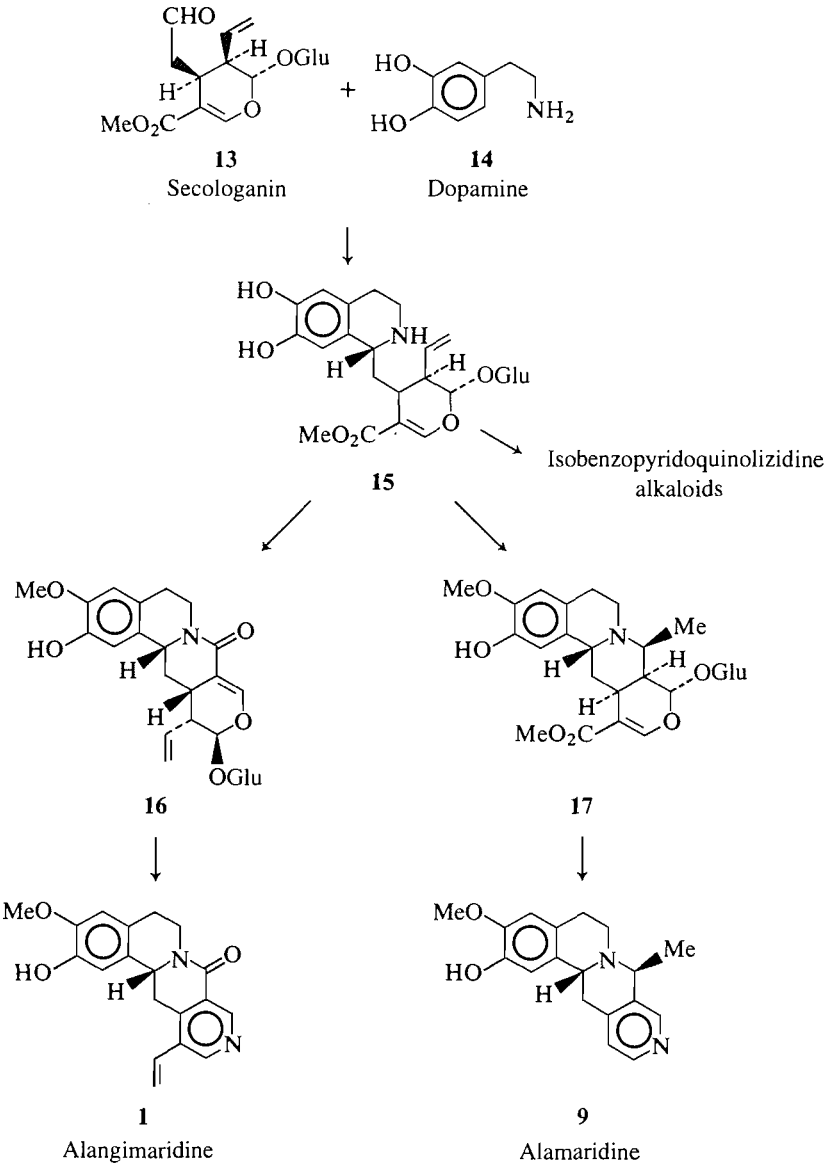

SCHEME 2

obtained in 97% yield (Scheme 5). The spectroscopic properties in solution of (±)-alangimaridine, prepared in this study, agree with those reported (7) for the natural product. The chemical shifts of the aliphatic protons in the ^{1}H nmr spectrum of **1**, assigned previously (7) in analogy with the ^{1}H nmr data reported for 8-oxotetrahydroberberines (24), were reconfirmed by high field (500 MHz) 2D ^{1}H nmr (COSY) spectroscopy. Dehydrogenation of **1** with iodine in methanol afforded alangimarine **2** in 80% yield. The ^{1}H nmr and infrared spectral data of the synthetic alangimarine were in agreement with those reported (7) for the natural alkaloid. (±)-*O*-Methylalangimaridine **27***a* and (±)-alangimaridine **1** on catalytic hydrogenation over 10% Pd–C afforded the corresponding 12-ethyl derivatives, **29***a* and **29***b*, respectively, in almost quantitative yields. Compound **29***b* has been prepared previously (7) and the spectroscopic properties of our sample agree with those previously reported (Scheme 6).

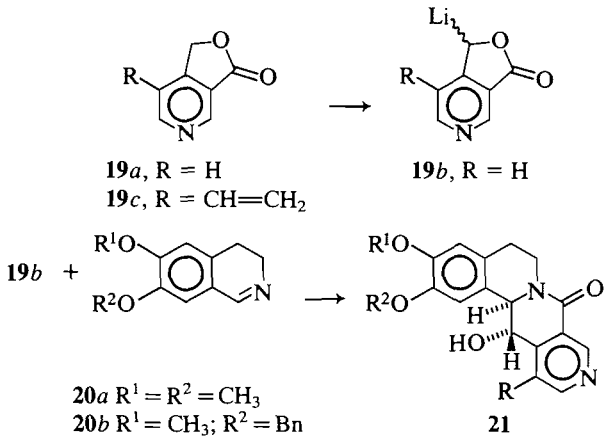

SCHEME 3

Examination of the ^{1}H nmr spectra of lactams **27***a*, **1**, **29***a*, and **29***b* revealed that the angular proton at C-14 was deshielded and appeared at or below δ 4.80, in comparison to the amidines **26***a* and **26***b* in which the chemical shifts of the protons at C-14 were at δ 4.49 and 4.56, respectively. Both in the lactams and amidines the C-6 axial proton was the most shielded among the aliphatic protons of the ring system. The large coupling constant for the C-14 proton ($J_{13ax,14} \approx 13$ Hz) in the lactams and the amidines clearly indicated that this proton has a *trans* diaxial relationship with an axial proton at C-13; thus the junction

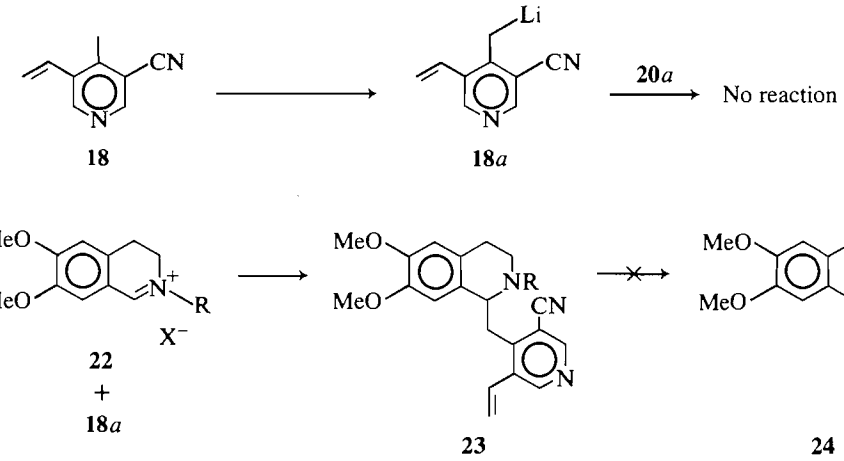

SCHEME 4

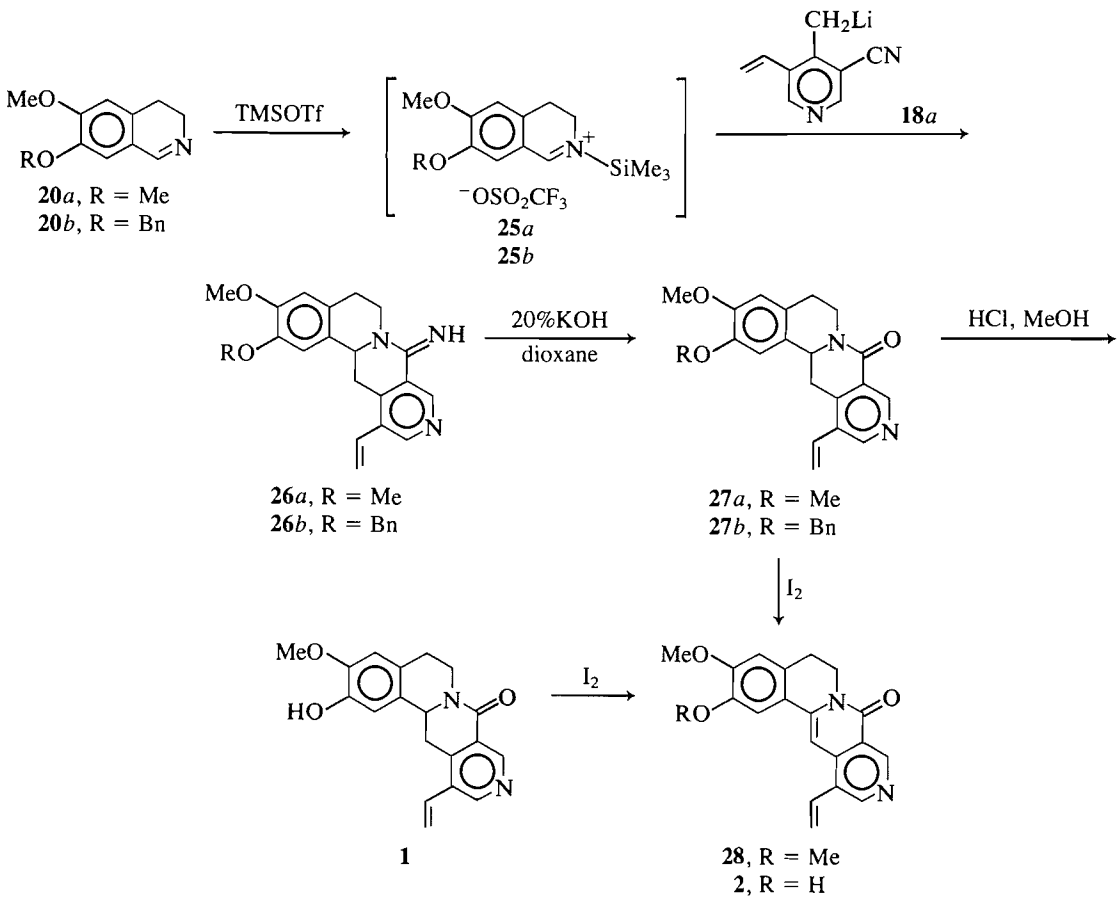

SCHEME 5

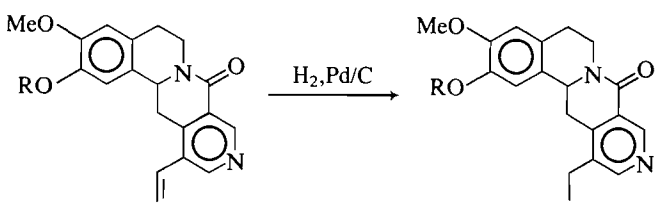

SCHEME 6

of rings B and C approximates that of *trans*-quinolizidine. A comparison of the chemical shifts of C-9 H in the tetrahydrolactams with that in the corresponding 13,14-dehydrolactams **2** and **28** showed that C-9 H underwent deshielding by ca. 0.3 ppm with the oxidation of the C(13)—C(14) bond.

Under electron ionization conditions the molecular ion of amidine **26***a* was the base peak in the mass spectrum, while amidine **26***b* with an *O*-benzyl group had its base peak at m/z 91. The compounds showed strong $M - 1$ peaks arising presumably by loss of a hydrogen atom at C-14. Other major ions in the spectra probably result from a retro-Diels–Alder

Can. J. Chem. Downloaded from www.nrcresearchpress.com by 213.166.140.6 on 09/07/12
For personal use only.

Can. J. Chem. Downloaded from www.nrcresearchpress.com by 213.166.140.6 on 09/07/12
For personal use only.

opening of ring C. Ions at m/z 192 and 191 in **26***a* and at m/z 178 and 177 in **26***b* are derived from the isoquinoline moiety. Ions derived from ring C and D were also observed in both compounds; they appear in each case at m/z 144 and undergo further fragmentation through loss of HCN, affording ions at m/z 117.

The mass spectral fragmentation of the lactams **27***a*, **27***b*, **29***a*, and **29***b*, prepared in this study, resembles that of tetrahydroberberines (25). All lactams, except **27***b* with an *O*-benzyl group, had the molecular ions as the base peak and strong $M - 1$ ions. Other important fragment ions in the mass spectra may be attributed to the retro-Diels–Alder opening of ring C. Ions corresponding to the isoquinoline moiety and fragment ions derived from rings C and D were present in all five compounds. The latter fragment ions lose the elements of carbon monoxide to give further daughter ions. The mass spectra of the 13,14-dehydrolactams **2** and **28** did not exhibit significant fragmentation, in keeping with their aromatic character.

In this paper we have described a new approach to the synthesis of (±)-alangimaridine and alangamarine that should be adaptable with minor modification to the synthesis of the related alkaloids shown in Fig. 1. A key feature of the synthetic method is the activation of the imines **20** toward nucleophilic attack through formation of a complex between the imine and trimethylsilyl trifluoromethanesulfonate. The product of nucleophilic attack at the imine carbon atom undergoes reaction (without isolation of an intermediate) with the suitably disposed electrophilic centre (the CN group) present in the attacking nucleophile. Reactions of this type have potential in the synthesis of other nitrogen heterocycles. The scope of the reaction is currently under investigation.

Experimental

Apparatus, materials, and methods

The continuous wave ^{1}H nmr spectra were recorded on a Varian EM 390 spectrometer and the Fourier transform spectra on either a Bruker WP 80 (80 MHz), WM 250 (250 MHz), or WM 500 (500 MHz) spectrometer. Unless otherwise specified, the samples were dissolved in chloroform-*d* using tetramethylsilane (TMS) as internal standard. Chemical shifts, quoted as δ values, were measured in relation to TMS. The symbols s, singlet, d, doublet, t, triplet, q, quartet, br, broad, and m, multiplet, are used in reporting spectra. The ^{13}C nmr spectra were recorded at 62.9 MHz on a Bruker WM 250 FT or at 125.76 MHz on a WM 500 FT spectrometer at ambient temperature.

EI mass spectra were recorded at 70 eV with a source temperature of ca. 200°C either on a VG Micromass 7070 F mass spectrometer equipped with a data system comprised of a PDP 8A with VG 2000 software or a VG analytical ZAB E mass spectrometer equipped with a VG 11-250 data system. High resolution mass spectra (hrms) were recorded on either of the above instruments. CI mass spectra were recorded on a VG Micromass 7070 F mass spectrometer using NH_3 at ca. 1 Torr (1 Torr = 133.3 Pa) as reagent gas and DCI mass spectra were recorded under similar conditions on a VG analytical ZAB E mass spectrometer. Infrared spectra were run on a Perkin–Elmer 283 spectrometer in $CHCl_3$ solution or $CHCl_3$ film. Melting points were determined using a Gallenkamp apparatus and are uncorrected. Thin-layer chromatography (tlc) was performed using Polygram Sil G/UV_{254} and Polygram Alox N/UV_{254} plates. For flash column chromatography Kieselgel 60 (230–400 mesh) was used.

All reactions involving lithiation steps were carried out in flame-dried apparatus under a blanket of argon, using septa and syringes for transfer of reagents. Diisopropylamine and 1,1,1,3,3,3-hexamethyldisilazane were heated under reflux over calcium hydride and distilled onto activated molecular sieves (4A) for storage. THF was dried by distillation from Na/benzophenone under a nitrogen atmosphere just prior to use.

The following compounds were prepared using literature procedures, sometimes with minor modifications: 3,4-dihydro-6,7-dimethoxyisoquinoline (19), 7-benzyloxy-3,4-dihydro-6-methoxyisoquinoline (19), 3-cyano-4-methyl-5-vinylpyridine (17, 18). Trimethylsilyl trifluoromethanesulfonate was obtained commercially.

Condensation of 3,4-dihydroisoquinolines activated with trimethylsilyl trifluoromethanesulfonate with the lithium salt of 3-cyano-4-methyl-5-vinylpyridine ***18***a

*(a) 12-Ethenyl-5,6,13,14-tetrahydro-2,3-dimethoxy-8*H*-isoquino[2,1-*b*][2,7]naphthyridin-8-imine* ***26***a

A solution of 3,4-dihydro-6,7-dimethoxyisoquinoline **20***a* (0.61 g, 3.19 mmol) in dry THF (4 mL) was treated dropwise with TMSOTf (0.75 mL, 3.83 mmol), at −78°C under an argon atmosphere. The resulting cloudy suspension was stirred first at −78°C for 1 h, then at 0°C for an additional 2 h. Meanwhile a solution of *n*-BuLi (2.33 mL of a 1.55 *M* solution in hexane, 3.6 mmol) was added dropwise to a stirred solution of 1,1,1,3,3,3-hexamethyldisilazane (0.76 mL, 3.6 mmol) in THF (3 mL) at −78°C. The lithium derivative of hexamethyldisilazane (LHS) so generated was stirred for an additional 10 min at −20°C and then cooled to −78°C. A solution of 3-cyano-4-methyl-5-vinylpyridine **18** (0.432 g, 3.0 mmol) in THF (2 mL) was added dropwise to the above LHS solution at −78°C, and the red solution so generated was stirred for a further 20 min at −78°C.

The red anion solution was then added dropwise at −78°C to the imine–TMSOTf complex and, when the addition was complete, the mixture was stirred at −40°C for 4 h. The mixture was allowed to warm to room temperature and stirred for ca. 12 h. The reaction mixture was quenched with saturated NH_4Cl solution (1 mL, aq.) and the resulting mixture was evaporated, water added, and the contents extracted with $CHCl_3$; the $CHCl_3$ extract was dried (Na_2SO_4, anhydrous) and evaporated to dryness *in vacuo*. The crude product was filtered through a short neutral alumina column, eluting with CH_2Cl_2 to remove any starting materials, then with $CHCl_3$–MeOH (3:1), yielding **26***a* (0.87 g, 87%); mp 189–191°C (EtOAc); ir ($CHCl_3$, film), ν_{max}: 1610 cm^{-1}; ^{1}H nmr (500 MHz), δ: 2.76–2.82 (2H, complex m, C-6 H_{ax} and C-13 H_{ax} H's), 2.99–3.04 (2H, complex m, C-5 H's), 3.29 (1H, dd, J = 16.4 and 3.0 Hz, C-13 H_{eq}), 3.89 (3H, s, —OCH_3), 3.90 (3H, s, —OCH_3), 4.56 (1H, dd, J = 12.2 and 3.0 Hz, C-14 H), 4.81 (1H, m, C-6 H_{eq}), 5.54 (1H, d, J = 11.2 Hz, —CH=CH_2), 5.77 (1H, d, J = 17.6 Hz, —CH=CH_2), 6.66 (1H, s, C-4 H), 6.70 (1H, s, C-1 H), 6.83 (1H, dd, J = 17.6 and 11.2 Hz, —CH=CH_2), 8.71 (1H, s, C-11 H), and 9.03 (1H, s, C-9 H); ^{13}C nmr (125.76 MHz), δ: 29.2 (C-5), 35.9 (C-13), 39.8 (C-6), 54.1 (C-14), 56.1 (—OCH_3), 56.5 (—OCH_3), 119.8 (—CH=CH_2), 130.7 (—CH=CH_2), 109.4, 111.7, 147.0, and 148.6 (4 × ArCH's), 125.2, 127.5, 127.6, 131.2, 141.8, 148.2, and 148.3 (7 × ArC's), and 159.6 (>C=NH); ms (EI), m/z (%): 335 (100) $M^{+\cdot}$, 334 (24), 320 (41), 318 (5), 192 (24), 191 (13), 190 (14), 176 (37), 144 (10), 143 (39), 117 (13), and 90 (11). *Exact mass* calcd. for $C_{20}H_{21}N_3O_2$: 335.163; found (hrms): 335.163; calcd. for fragment ion $C_{19}H_{18}N_3O_2$ ($M - CH_3$): 320.140; found: 320.140; calcd. for fragment ion $C_9H_7N_2$: 143.061; found: 143.061.

*(b) 2-Benzyloxy-12-ethenyl-5,6,13,14-tetrahydro-3-methoxy-8*H*-isoquino[2,1-*b*][2,7]naphthyridin-8-imine* ***26***b

This condensation was carried out in a manner similar to that described previously for the conversion of **20***a* to **26***a*, using imine **20***b* (0.804 g, 3.03 mmol). The reaction mixture was processed in the usual manner and the crude product chromatographed on neutral alumina, eluting first with CH_2Cl_2 and then with increasing concentrations of MeOH, affording the amidine **26***b* (1.023 g, 83%); mp 218–221°C (dec.) (EtOH–EtOAc); ir ($CHCl_3$), ν_{max}: 1615 cm^{-1}; ^{1}H nmr (500 MHz), MeOH-d_4, δ: 2.90–3.04 (1H, m, C-6 H_{ax}), 3.17–3.44 (3H, complex m, C-5 and C-13 H_{ax} H's), 3.65–3.67 (1H, m, C-13 H_{eq}), 4.06 (3H, s, —OCH_3), 4.49 (1H, m, C-14 H), 4.96 (1H, m, C-6 H_{eq}), 5.30 and 5.34 (2H, ABq, J = 12.3 Hz, —OCH_2Ar), 5.37 (1H, d, J = 11.1 Hz, —CH=CH_2), 5.55 (1H, d, J = 17.3 Hz, —CH=CH_2), 6.90 (1H, s, C-4 H), 6.97 (1H, dd, J = 17.3 and 11.1 Hz, —CH=CH_2), 7.04 (1H, s, C-1 H), 7.45–7.72 (5H, complex m, aromatic H's), 9.06 (1H, s, C-11 H), and 9.18 (1H, s, C-9 H); ms (EI), m/z (%): 411 (7) $M^{+\cdot}$, 410 (2), 320 (95), 268 (1), 178 (2),

Can. J. Chem. Downloaded from www.nrcresearchpress.com by 213.166.140.6 on 09/07/12
For personal use only.

177 (4), 176 (6), 144 (2), 143 (5), 117 (3), 91 (100), and 90 (4). *Exact mass* calcd. for $C_{26}H_{25}N_3O_2$: 411.195; found (hrms): 411.194.

Hydrolysis of amidines ***26***a *and* ***26***b *to lactams* ***27***a *and* ***27***b

*(a) 12-Ethenyl-5,6,13,14-tetrahydro-2,3-dimethoxy-8*H*-isoquino-[2,1-*b*][2,7]naphthyridin-8-one* ***27***a

Amidine ***26****a* (250 mg) was dissolved in a mixture of dioxane (15 mL) and 20% KOH solution (10 mL, aq.) and the mixture was gently heated under reflux for 2 days. The solution was then evaporated to dryness *in vacuo*, acidified with concentrated HCl (aq.), and heated under reflux for an additional 30 min. Evaporation of the acidified solution was followed by basification with saturated Na_2CO_3 solution (aq.) and extraction with $CHCl_3$. The combined $CHCl_3$ extracts were washed with brine and dried over $MgSO_4$ (anhyd.). Removal of the solvent *in vacuo* and crystallization from EtOAc gave lactam ***27****a* (249 mg, 99.3%) as cubic crystals; mp 181–182°C; R_f 0.46 (alumina, 2% MeOH in $CHCl_3$), 0.14 (silica, 5% MeOH in $CHCl_3$); ir ($CHCl_3$, film), ν_{max}: 1650 cm^{-1}; ^1H nmr (500 MHz), δ: 2.76–2.82 (2H, complex m, C-6 H_{ax} and C-13 H_{ax} H's), 2.84–2.99 (2H, complex m, C-5 H's), 3.40 (1H, dd, J = 16.5 and 3.6 Hz, C-13 H_{eq}), 3.90 (3H, s, —OCH_3), 3.91 (3H, s, —OCH_3), 4.84 (1H, dd, J = 13.1 and 3.6 Hz, C-14 H), 4.97 (1H, m, C-6 H_{eq}), 5.56 (1H, d, J = 11.2 Hz, —CH=CH_2), 5.79 (1H, d, J = 17.6 Hz, —CH=CH_2), 6.71 (1H, s, C-4 or C-1 H), 6.72 (1H, s, C-1 or C-4 H), 6.86 (1H, dd, J = 17.6 and 11.2 Hz, —CH=CH_2), 8.77 (1H, s, C-11 H), and 9.19 (1H, s, C-9 H); ^{13}C nmr (125.76 MHz), δ: 29.1 (C-5), 34.5 (C-13), 38.7 (C-6), 54.2 (C-14), 56.1 (OCH_3), 56.5 (OCH_3), 119.8 (—CH=CH_2), 130.5 (—CH=CH_2), 109.1, 111.8, 149.3, and 150.1 (4 × ArCH's), 124.4, 126.9, 127.5, 130.5, 142.4, 148.3, and 148.4 (7 × ArC's), and 165.6 (>C=O); ms (EI), m/z (%): 336 (100) $M^{+\cdot}$, 335 (52), 321 (30), 307 (11), 305 (23), 192 (9), 191 (14), 190 (21), 176 (20), 145 (19), 117 (57), and 90 (22). *Exact Mass* calcd. for $C_{20}H_{20}N_2O_3$: 336.147; found (hrms): 336.149; calcd. for fragment ion $C_{11}H_{12}NO_2$: 190.087; found: 190.087; calcd. for fragment ion C_9H_7NO: 145.053; found: 145.052.

*(b) 2-Benzyloxy-12-ethenyl-5,6,13,14-tetrahydro-3-methoxy-8*H*-isoquino[2,1-*b*][2,7]naphthyridin-8-one* ***27***b

Hydrolysis of the amidine ***26****b* (250 mg) was achieved with 20% KOH solution (15 mL, aq.) in dioxane (25 mL) under the conditions described previously for the preparation of ***27****a* from ***26****a* with slight modification. The reaction mixture was heated under reflux for 2 days, the dioxane removed *in vacuo*, and the mixture diluted with water (50 mL). The product was extracted thoroughly with CH_2Cl_2 and, after successively washing the extract with water and brine, it was dried over $MgSO_4$ (anhyd.). Evaporation of the solvent *in vacuo* gave the lactam ***27****b* (246 mg, 98%); mp 175–177°C (EtOAc); R_f 0.53 (alumina, EtOAc); ir ($CHCl_3$, film), ν_{max}: 1655 cm^{-1}; ^1H nmr (500 MHz), $CDCl_3$ + MeOH-d_4, δ: 2.65–2.71 (1H, m, C-6 H_{ax}), 2.81–3.00 (3H, complex m, C-5 and C-13 H_{ax} H's), 3.17 (1H, dd, J = 16.7 and 3.8 Hz, C-13 H_{eq}), 3.93 (3H, s, —OCH_3), 4.80 (1H, dd, J = 13.1 and 3.8 Hz, C-14 H), 4.86–4.90 (1H, m, C-6 H_{eq}), 5.16 and 5.25 (2H, AB q, J = 12.5 Hz, —OCH_2Ar), 5.61 (1H, d, J = 11.7 Hz, —CH=CH_2), 5.81 (1H, d, J = 17.0 Hz, —CH=CH_2), 6.69 (1H, s, C-4 or C-1 H), 6.77 (1H, dd, J = 17.0 and 11.7 Hz, —CH=CH_2), 7.26 (1H, s, C-1 or C-4 H), 7.34–7.47 (5H, complex m, aromatic H's), 8.72 (1H, s, C-11 H), and 9.06 (1H, s, C-9 H); ms (EI), m/z (%): 412 (33) $M^{+\cdot}$, 411 (6), 321 (12), 176 (3), 145 (2), 117 (7), 91 (100), and 90 (6). *Exact Mass* calcd. for $C_{26}H_{24}N_2O_3$: 412.179; found (hrms): 412.178.

*(±)-Alangimaridine(12-ethenyl-5,6,13,14-tetrahydro-2-hydroxy-3-methoxy-8-isoquino[2,1-*b*][2,7]naphthyridin-8-one)* ***1***

A solution of *O*-benzyl lactam ***27****b* (50 mg) in EtOH (5 mL) and concentrated HCl solution (5 mL) was heated under reflux gently for 3 h under a nitrogen atmosphere. The solvent was removed *in vacuo*, the residue treated with water (10 mL), and the mixture basified with saturated $NaHCO_3$ solution (aq.). The resulting mixture was extracted with $CHCl_3$, and the $CHCl_3$ extract washed with brine and dried over Na_2SO_4 (anhyd.). Removal of the solvent and crystallization from MeOH–$CHCl_3$ gave colourless crystals of (±)-alangimaridine **1** (38 mg, 97.2%), mp 242–245°C; R_f 0.20 (silica, 10% MeOH in $CHCl_3$); ir ($CHCl_3$, film), ν_{max}: 1650 cm^{-1}; ^1H nmr (500 MHz), δ: 2.76–2.82 (2H, complex m, C-6 H_{ax} and C-13 H_{ax} H's), 2.94–3.00 (2H, complex m, C-5 H's), 3.40 (1H, dd, J = 16.5 and 3.8 Hz, C-13 H_{eq}), 3.92 (3H, s, —OCH_3), 4.81 (1H, dd, J = 13.1 and 3.8 Hz, C-14 H), 4.95 (1H, m, C-6 H_{eq}), 5.55 (1H, d, J = 11.1 Hz, —CH=CH_2), 5.73 (1H, s, exchanges with D_2O, phenolic OH), 5.77 (1H, d, J = 17.5 Hz, —CH=CH_2), 6.69 (1H, s, C-4 H), 6.81 (1H, s, C-1 H), 6.85 (1H, dd, J = 17.5 and 11.1 Hz, —CH=CH_2), 8.77 (1H, s, C-11 H), and 9.20 (1H, s, C-9 H); ^{13}C nmr (125.76 MHz), δ: 29.0 (C-5), 34.1 (C-13), 38.8 (C-6), 53.8 (C-14), 56.0 (—OCH_3), 119.8 (—CH=CH_2), 130.6 (—CH=CH_2), 111.0, 111.7, 149.1, and 149.9 (4 × ArCH's), 124.3, 126.6, 127.6, 130.3, 142.7, 144.8, and 145.8 (7 × ArC's), and 163.5 (>C=O); ms (EI), m/z (%): 322 (100) $M^{+\cdot}$, 321 (53), 307 (23), 305 (12), 291 (7), 293 (12), 178 (7), 177 (7), 176 (13), 162 (16), 145 (18), 117 (46), and 90 (28). *Exact Mass* calcd. for $C_{19}H_{18}N_2O_3$: 322.132; found (hrms): 322.131.

Oxidation of lactams ***27***a *and* ***1*** *to dehydrolactams* ***28*** *and* ***2***

*(a) 5,6-Dihydro-2,3-dimethoxy-8*H*-isoquino[2,1-*b*][2,7]naphthyridin-8-one* ***28***

A solution of lactam ***27****a* (50 mg) and iodine (100 mg) in EtOH (10 mL) was gently heated under reflux on a steam bath for 6 h. The progress of the reaction was monitored by tlc. When the reaction was complete, the solvent was evaporated *in vacuo* and 10% $Na_2S_2O_3$ solution (5 mL, aq.) was added to decompose excess iodine. The mixture was basified with saturated Na_2CO_3 solution (aq.) and the product was thoroughly extracted into $CHCl_3$. The combined $CHCl_3$ extracts were washed successively with 10% $Na_2S_2O_3$ solution and brine, and dried over Na_2SO_4 (anhyd.). Evaporation of the solvent gave dehydrolactam **28** (41 mg, 81%) as an amorphous solid, mp 145–150°C (dec.) ($CHCl_3$–MeOH); R_f 0.26 (alumina, 5% MeOH in $CHCl_3$); 0.60 (alumina, EtOAc); ir ($CHCl_3$, film), ν_{max}: 1650 cm^{-1}; ^1H nmr (500 MHz), δ: 2.97 (2H, t, J = 5.9 Hz, C-5 H's), 3.96 (3H, s, —OCH_3), 4.01 (3H, s, —OCH_3), 4.35 (2H, t, J = 5.9 Hz, C-6 H's), 5.59 (1H, d, J = 11.9 Hz, —CH=CH_2), 5.87 (1H, d, J = 17.5 Hz, —CH=CH_2), 6.77 (1H, s, C-4 H), 6.94 (1H, s, C-1 H); 7.15 (1H, dd, J = 17.5 and 11.9 Hz, —CH=CH_2), 7.27 (1H, s, C-13 H), 8.98 (1H, s, C-11 H), and 9.52 (1H, s, C-9 H); ms (EI), m/z (%): 334 (100) $M^{+\cdot}$ and 319 (55). *Exact Mass* calcd. for $C_{20}H_{18}N_2O_3$: 334.132; found (hrms): 334.132.

*(b) Alangimarine (12-ethenyl-5,6-dihydro-2-hydroxy-3-methoxy-8*H*-isoquino[2,1-*b*][2,7]naphthyridin-8-one)* ***2***

Oxidation of the lactam **1** (20 mg) with iodine (50 mg) in EtOH (20 mL) by the method described previously for the oxidation of ***27****a* to **28** gave the crude product, which was purified by flash column chromatography on silica gel eluting with 5% MeOH in $CHCl_3$. Crystallization from MeOH afforded yellow needles of **2** (17 mg, 86%); mp 245–247°C (dec.) (lit. (7) mp 247°C ($CHCl_3$–MeOH); R_f 0.35 (silica, 10% MeOH in $CHCl_3$); ^1H nmr (500 MHz), δ: 2.96 (2H, t, J = 6.3 Hz, C-5 H's), 3.98 (3H, s, —OCH_3), 4.35 (2H, t, J = 6.3 Hz, C-6 H's), 5.58 (1H, d, J = 11.1 Hz, —CH=CH_2), 5.84 (1H, d, J = 17.4 Hz, —CH=CH_2), 5.84 (1H, s, exchanges with D_2O, phenolic OH), 6.75 (1H, s, C-4 H), 6.98 (1H, s, C-1 H), 7.12 (1H, dd, J = 17.4 and 11.1 Hz, CH=CH_2), 7.42 (1H, s, C-13 H), 8.76 (1H, s, C-11 H), and 9.50 (1H, s, C-9H); ^{13}C nmr (125.76 MHz), δ: 28.1 (C-5), 39.8 (C-6), 56.3 (—OCH_3), 96.4, 110.1, 111.7, 119.1, 119.6, 122.6, 127.9, 129.0, 130.7, 139.5, 145.4, 148.2, 148.9, 150.9, and 150.9 (vinylic and aromatic carbons), 162.0 (>C=O); ms (EI), m/z (%): 320 (100) $M^{+\cdot}$ and 305 (66). *Exact Mass* calcd. for $C_{19}H_{16}N_2O_3$: 320.116; found (hrms): 320.115.

Hydrogenation of lactams ***27***a *and* ***1*** *to dihydro compounds* ***29***a *and* ***29***b

*(a) 12-Ethyl-5,6,13,14-tetrahydro-2,3-dimethoxy-8*H*-isoquino-[2,1-*b*][2,7]naphthyridin-8-one* ***29***a

A solution of lactam ***27****a* (100 mg) in EtOH (15 mL) containing 10% Pd–C (50 mg) was treated with H_2 in a Parr hydrogenator at ca. 25 psig at room temperature for 3 h. The reaction mixture was filtered through Celite to remove catalyst and the Celite thoroughly washed with $CHCl_3$. The filtrate and washings were evaporated to dryness *in vacuo*

and the residue crystallized from EtOH, yielding white cubic crystals of **29***a* (100 mg, 99%); mp 185–187°C; R_f 0.45 (alumina, EtOAc), 0.26 (silica, EtOAc); ir ($CHCl_3$, film), ν_{max}: 1650 cm^{-1}; ^1H nmr (500 MHz), δ: 1.26 (3H, t, J = 7.6 Hz, —CH_2CH_3), 2.73–2.81 (4H, complex m, C-6 H_{ax}, —CH_2—CH_3, and C-5 H_{ax} H's), 2.93–2.97 (2H, m, C-5 H_{ax} and C-13 H_{ax}), 3.31 (1H, dd, J = 16.4 and 3.5 Hz, C-13 H_{eq}), 3.91 (3H, s, —OCH_3), 3.92 (3H, s, —OCH_3), 4.84 (1H, dd, J = 13.1 and 3.5 Hz, C-14 H), 4.98 (1H, m, C-6 H_{eq}), 6.69 (1H, s, C-4 H), 6.72 (1H, s, C-1 H), 8.54 (1H, s, C-11 H), and 9.16 (1H, s, C-9 H); ^{13}C nmr (125.76 MHz), δ: 14.6 (—CH_2CH_3), 23.1 (—CH_2CH_3), 29.1 (C-5), 34.0 (C-13), 38.6 (C-6), 54.2 (C-14), 56.0 (2 × OCH_3), 109.2, 111.8, 148.2, and 152.1 (4 × ArCH's), 124.4, 126.9, 127.6, 135.0, 143.6, and 148.4 (ArC's),[3] and 163.6 (>C=O); ms (EI), m/z (%): 338 (100) $M^{+\cdot}$, 337 (76), 323 (61), 309 (37), 307 (50), 192 (8), 191 (27), 190 (37), 147 (34), 119 (63), 92 (24), and 91 (82). *Exact Mass* calcd. for $C_{20}H_{22}N_2O_3$: 338.163; found (hrms): 338.161.

*(b) 12-Ethyl-5,6,13,14-tetrahydro-2-hydroxy-3-methoxy-8*H*-isoquino[2,1-*b*][2,7]naphthyridin-8-one **29***b*

Hydrogenation of lactam **1** (10 mg) with 10% Pd–C (10 mg) in EtOH (15 mL) by the method described above for the hydrogenation of **27***a* gave compound **29***b* (10 mg, 99%), which crystallized as colorless crystals from MeOH; mp 228°C (lit. (7) mp 232°C (EtOH)); R_f 0.44 (silica, 10% MeOH in $CHCl_3$); ir ($CHCl_3$, film), ν_{max}: 1655 cm^{-1}; ^1H nmr (500 MHz), δ: 1.24 (3H, t, J = 7.7 Hz, —CH_2—CH_3), 2.71–2.79 (4H, complex m, —CH_2CH_3, C-5 H_{ax} and C-6 H_{ax} H's), 2.94–2.98 (2H, m, C-5 H_{eq} and C-13 H_{ax} H's), 3.33 (1H, dd, J = 16.4 and 3.6 Hz, C-13 H_{eq}), 3.92 (3H, s, —OCH_3), 4.80 (1H, dd, J = 13.3 and 3.6 Hz, C-14 H), 4.95–4.98 (1H, m, C-6 H_{aq}), 5.75 (1H, s, exchanges with D_2O, phenolic OH), 6.69 (1H, s, C-4 H), 6.81 (1H, s, C-1 H), 8.54 (1H, s, C-11 H), and 9.15 (1H, s, C-9 H); ^{13}C nmr (125.76 MHz), δ: 14.9 (—CH_2CH_3), 23.3 (—CH_2CH_3), 29.3 (C-5), 34.0 (C-13), 38.9 (C-6), 54.2 (C-14), 56.2 (—OCH_3), 111.1, 111.8, 126.7, 127.8, 130.6, 135.3, 142.8, 143.8, 148.4, 150.2, and 152.3 (aromatic carbons), and 163.5 (>C=O); ms (EI), m/z (%): 324 (100) $M^{+\cdot}$, 323 (68), 309 (31), 307 (14), 295 (19), 178 (3), 177 (11), 176 (15), 162 (26), 147 (23), 119 (30), 92 (8), and 91 (32). *Exact Mass* calcd. for $C_{19}H_{20}N_2O_3$: 324.147; found (hrms): 324.147.

Acknowledgements

We thank the Natural Sciences and Engineering Research Council of Canada for financial support of this investigation. We thank Dr. S. C. Pakrashi for authentic samples of alangimarine and (±)-alangimaridine.

1. JAHANGIR, M. A. BROOK, D. B. MACLEAN, and H. L. HOLLAND. J. Chem. Soc. Chem. Commun. 1608 (1986).
2. K. R. KIRTIKAR and D. B. BASU. Indian Medicinal Plants. 2nd ed. Vol. II. L. M. Basu, Allahabad, India. 1933. p. 1236.
3. R. N. CHOPRA, K. L. HANDA, and L. D. KAPUR. Indigenous drugs of India. 2nd ed. U. N. Dhar and Sons, Calcutta. 1958. p. 270.
4. B. DASGUPTA. J. Pharm. Sci. **54**, 481 (1965).
5. H. BUDZIKIEWICZ, S. C. PAKRASKI, and H. VORBÜEGGEN. Tetrahedron, **20**, 399 (1964).
6. S. C. PAKRASHI, B. ACHARI, E. ALI, P. P. GHOSH DASTIDAR, and R. R. SINHA. Tetrahedron Lett. 2667 (1980).
7. S. C. PAKRASHI, R. MUKHOPADHYAY, R. R. SINHA, P. P. GHOSH DASTIDAR, B. ACHARI, and E. ALI. Ind. J. Chem. **24**B, 19 (1985).
8. S. C. PAKRASHI, R. R. SINHA, A. BHATTACHARJYA, R. MUKHOPADHYAY, and E. ALI. Heterocycles, **21**, 557 (1984).
9. T. NAITO, O. MIYATA, I. NINOMIYA, and S. C. PAKRASHI. Heterocycles, **16**, 725 (1981).
10. A. BHATTACHARJYA, R. MUKHOPADHYAY, and S. C. PAKRASHI. Tetrahedron Lett. 1215 (1986).
11. JAHANGIR, D. B. MACLEAN, and H. L. HOLLAND. Can. J. Chem. **65**, 727 (1987).
12. A. R. BATTERSBY, A. R. BURNETT, and P. G. PARSONS. J. Chem. Soc. Chem. Commun. 1280 (1968); J. Chem. Soc. C, 1187 (1969).
13. A. R. BATTERSBY and R. J. PARRY. J. Chem. Soc. Chem. Commun. 901 (1971).
14. N. NAGAKURA, G. HÖFLE, and M. H. ZENK. J. Chem. Soc. Chem. Commun. 896 (1978).
15. N. NAGAKURA, G. HÖFLE, D. COGGIOLA, and M. H. ZENK. Planta Med. **34**, 381 (1978).
16. A. R. BATTERSBY, N. G. LEWIS, and J. M. TIPPETT. Tetrahedron Lett. 4849 (1978).
17. T. KAMETANI, M. TAKEASHITA, M. IHARA, and K. FUKUMOTO. J. Org. Chem. **41**, 2542 (1976).
18. T. R. GOVINDACHARI, K. NAGARAJAN, and S. RAJAPPA. J. Chem. Soc. 2725 (1957).
19. JAHANGIR, D. B. MACLEAN, and H. L. HOLLAND. Can. J. Chem. **64**, 1031 (1986).
20. JAHANGIR. Ph.D. thesis, McMaster University, May 1987.
21. R. NOYORI, S. MURATA, and M. SUZUKI. Tetrahedron, **37**, 3899 (1981).
22. H. AHLBRECHT and E.-O. DÜBER. Synthesis, 273 (1982).
23. H. EMDE, D. DOMSCH, H. FEGER, U. FRICK, A. GÖTZ, H. H. HERGOTT, K. HOFMANN, W. KOBER, K. KRÄGELOH, T. OSTERLE, W. STEPPAN, W. WEST, and G. SIMCHEN. Synthesis, 1 (1982).
24. G. R. LENZ. J. Org. Chem. **39**, 2846 (1974); **41**, 2201 (1976).
25. C.-Y. CHEN and D. B. MACLEAN. Can. J. Chem. **46**, 2501 (1968).

[3]Six signals observed for 7 aromatic carbons (ArC).

Can. J. Chem. Downloaded from www.nrcresearchpress.com by 213.166.140.6 on 09/07/12
For personal use only.

Previously unreported *p*-terphenyl derivatives with antibiotic properties from the fruiting bodies of *Sarcodon leucopus* (Basidiomycetes). A two-dimensional nuclear magnetic resonance study

C. TRINGALI[1] AND M. PIATTELLI
Dipartimento di Scienze Chimiche, Viale A. Doria 6, I-95125 Catania, Italy

AND

C. GERACI, G. NICOLOSI, AND C. ROCCO
Istituto del CNR per lo Studio delle Sostanze Naturali di Interesse Alimentare e Chimico-farmaceutico, Viale A. Doria 6, I-95125 Catania, Italy

Received March 13, 1987

C. TRINGALI, M. PIATTELLI, C. GERACI, G. NICOLOSI, and C. ROCCO. Can. J. Chem. **65**, 2369 (1987).

Two previously unreported antibiotic metabolites, 2′,3′,4″-triacetoxy-3,4,5′,6′-tetrahydroxy-*p*-terphenyl (**10**) and 2′,3′-diacetoxy-3,4,5′,6′,4″-pentahydroxy-*p*-terphenyl (**11**), have been isolated from the basidiomycete *Sarcodon leucopus*. Their structures have been determined by chemical transformations and spectral analysis, including heteronuclear two-dimensional nuclear magnetic resonance methods.

C. TRINGALI, M. PIATTELLI, C. GERACI, G. NICOLOSI et C. ROCCO. Can. J. Chem. **65**, 2369 (1987).

On a isolé deux nouveaux métabolites d'antibiotiques du basidiomycète *Sarcodon leucopus*; il s'agit du triacétoxy-2′,3′,4″ tétrahydroxy-3,4,5′,6′ *p*-terphényle (**10**) et du diacétoxy-2′,3′ pentahydroxy-3,4,5′,6′,4″ *p*-terphényle (**11**). On a déterminé leurs structures en faisant appel à des transformations chimiques et à des analyses spectrales, y compris des méthodes de résonance magnétique nucléaire hétéronucléaire en 2D.

[Traduit par la revue]

Introduction

Natural *p*-terphenyl derivatives occur in fungi mostly as 2,5-diphenyl-1,4-benzoquinones (1, 2). Fully aromatic *p*-terphenyl compounds from Basidiomycetes are less common and include protoleucomelone **1** from *Polyporus leucomelas* (3), the first to be isolated, dibenzoylleucoaurantiacin **2** from *Hydnum aurantiacum* (4), and 2′,3′,5′-trimethoxy-*p*-terphenyl **3** from *Peniophora gigantea* (5). *Aspergillus candidus*, a member of the Ascomycetes, has yielded terphenyllin **4** (6–8), deoxyterphenyllin **5** (9), 3-hydroxyterphenyllin **6** (10), 3,3″-dihydroxyterphenyllin **7** (11), and candidusin A (**8**) and B (**9**) (12, 13). Compounds **4** and **5** are reported to be active against HeLa cells, while **6–9** are effective inhibitors of sea urchin embryonic development.

The present paper describes the structure determination of two previously unreported bioactive *p*-terphenyl derivatives isolated from *Sarcodon leucopus* (Pers.) (Basidiomycetes).

The crude aqueous acetone extract from the fruiting bodies of *S. leucopus* possesses antimicrobic activity against both Gram-positive and Gram-negative bacteria. Activity-guided separation of the crude extract resulted in the isolation of two compounds, **10** and **11**, which accounted for most of the bioactivity. They gave phenolic reactions (ferric chloride and diazonium salts) and showed aromatic absorption in the uv spectrum. The ir spectrum displayed, in addition to benzenoid bands, absorptions associated with hydroxy (3420 cm^{-1}) and acetate (1760 cm^{-1}) groups. The empirical formulae, as established by exact mass measurement and nmr data, were found to be $C_{24}H_{20}O_{10}$ for **10** and $C_{22}H_{18}O_9$ for **11**. It is to be noted that in the mass spectrum of both compounds an ion was clearly discernible at 42 amu higher than the parent ion, which was explained as the result of an intermolecular transacetylation occurring in the mass spectrometer. Acetylation of both metabolites gave the same heptaacetate $C_{32}H_{28}O_{14}$. This result and considerations of the ^1H and ^{13}C nmr spectra (Tables 1, 2) allowed expansion of the molecular formulae to $C_{18}H_7(OH)_4(OAc)_3$ and $C_{18}H_7(OH)_5(OAc)_2$, respectively, and indicated a terphenyl as the parent hydrocarbon. The observation that the melting point of the heptaacetate closely compares to that reported for protoleucomelone **1** was suggestive of the identity of the two compounds and this, if confirmed, would have defined the carbon skeleton and, in addition, the oxygenation pattern in both **10** and **11**. Unfortunately, lack of spectral data about protoleucomelone as well as unavailability of a reference sample prevented us from clarifying this point. Formation of *p*-terphenyl by zinc-dust distillation of **10** settled the nature of the carbon skeleton, while as concerns further structural aspects of **10** and **11** we decided to rely mainly on their spectral properties.

The ^1H nmr spectrum of **10** displays, in addition to the resonances of the acetates, signals in the aromatic region due to strongly coupled spin systems. Two resonances centered at δ 7.38 and 7.12, respectively (2H each, N = 8.5 Hz), form an AA′BB′ system arising from the protons of a 1,4-disubstituted benzene ring; by comparison with the pertinent data for related compounds (**4** and **5**) (6–9), the former was assigned to the isochronous protons at the 2″ and 6″ positions, and the latter to the protons at the 3″ and 5″ positions. The rest of the spectrum was a three-spin system due to protons in a 1,4,5-trisubstituted aromatic ring.

The ^{13}C nmr spectrum of **10** contains 21 distinct resonances. Signals at 20.2 (2C), 21.1, 169.7, 169.8, and 170.7 ppm were readily assigned to three acetate groups. Based on a DEPT sequence, five of the remaining resonances could be associated with hydrogen-bearing carbons, four with quaternary carbons, and seven with O-substituted sp^2 carbons. One-bond H,C correlations were identified with signals at 121.7 (2C, C-3″ and C-5″) and 131.8 ppm (2C, C-2″ and C-6″), while chemical shift substituent effects allowed assignment of the remaining resonances arising from hydrogenated carbons (117.5 (C-2),

[1]Author to whom correspondence may be addressed.

Printed in Canada / Imprimé au Canada

Can. J. Chem. Downloaded from www.nrcresearchpress.com by 213.166.140.6 on 09/07/12
For personal use only.

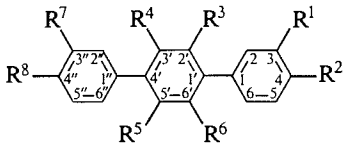

1 $R^1 = R^2 = R^3 = R^4 = R^5 = R^6 = R^8 = OAc$, $R^7 = H$
2 $R^1 = R^7 = H$, $R^2 = R^8 = OH$, $R^3 = R^4 = R^5 = R^6 = OCOC_6H_5$
3 $R^1 = R^2 = R^6 = R^7 = R^8 = H$, $R^3 = R^4 = R^5 = OMe$
4 $R^1 = R^4 = R^7 = H$, $R^2 = R^6 = R^8 = OH$, $R^3 = R^5 = OMe$
5 $R^1 = R^4 = R^7 = R^8 = H$, $R^2 = R^6 = OH$, $R^3 = R^5 = OMe$
6 $R^1 = R^2 = R^6 = R^8 = OH$, $R^3 = R^5 = OMe$, $R^4 = R^7 = H$
7 $R^1 = R^2 = R^6 = R^7 = R^8 = OH$, $R^3 = R^5 = OMe$, $R^4 = H$
10 $R^1 = R^2 = R^5 = R^6 = OH$, $R^3 = R^4 = R^8 = OAc$, $R^7 = H$
11 $R^1 = R^2 = R^5 = R^6 = R^8 = OH$, $R^3 = R^4 = OAc$, $R^7 = H$

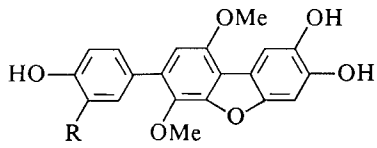

8 R = H
9 R = OH

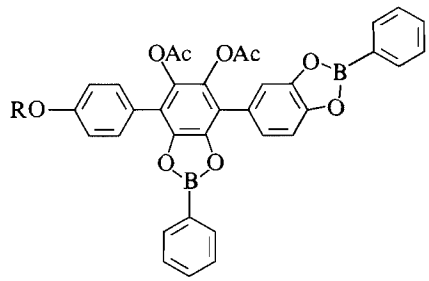

12 R = Ac
13 R = H

TABLE 1. ^1H nuclear magnetic resonance data for compounds **10** and **11**

	Compound					
	10			**11**		
Proton	δ_H[a]	*m*	*J*[b]	δ_H[a]	*m*	*J*[b]
2	6.83	d	2.0	6.82	d	2.0
5	6.85	d	8.5	6.84	d	8.5
6	6.73	dd	8.5, 2.0	6.70	dd	8.5, 2.0
2″,6″	7.38	AA′BB′	$N^c = 8.5$	7.18	AA′BB′	$N^c = 8.5$
3″,5″	7.12			6.84		
2′-OAc	1.93[d]	s		1.92[d]	s	
3′-OAc	1.95[d]	s		1.94[d]	s	
4″-OAc	2.30	s				

[a]Measured in $CDCl_3$–CD_3OD (7:3); chemical shifts (δ) are relative to CH_3OD at δ 3.30.
[b]*J* values are expressed in Hz.
[c]$N = J_{AB} + J_{AB'}$, with $J_{AB'} < 0.5$ Hz.
[d]Values with identical superscript within each column may be interchanged.

115.8 (C-5), and 122.4 (C-6) ppm. Confirmation was obtained from gated decoupled and H,C-COLOC spectra, as well as literature data for terphenyllin triacetate and 3-hydroxyterphenyllin (10). Assignment of the signals at 144.9 (C-3), 145.1 (C-4), and 150.5 (C-4″) ppm essentially followed from three-bond carbon–proton couplings. Resonances at 133.7, 133.8, 141.1, and 141.2 ppm, which appear as sharp singlets in the gated decoupled spectra, are due to oxygen-bonded carbons in the central ring. Finally, assignment of signals at 121.6 (C-4′), 123.1 (C-1′), 123.9 (C-1), and 130.8 (C-1″) ppm was based on J_{CH} values and carbon–proton shift correlations via two- and three-bond coupling.

The oxygenation pattern having been determined, the last point to be assessed was the location of the acetate groups. In the ^1H nmr spectrum of **10**, two of these groups resonate at higher field (δ 1.93 and 1.95) and, on the basis of literature data (14–16), must be located on the central ring, while the third appears at decidedly lower field (δ 2.30), indicating its location on an outer ring. When compound **10** was reacted with phenylboronic acid and the reaction mixture examined directly by mass spectrometry (attempts towards isolation of individual product(s) resulted in extensive hydrolytic removal of phenylboronate groups), a parent ion was observed at *m/z* 640, indicating the formation of a bis-phenylboronate (**12**). Therefore the novel fungal metabolite must have structure **10**.

The second compound, **11**, isolated from *S. leucopus*, possesses spectral properties very similar to those of **10**, the only obvious differences being associated with the presence of only two acetate groups, both resonating at high field (δ 1.92 and 1.94). Also in this case, reaction with phenylboronic acid yielded a bis-phenylboronate **13**, *m/z* 598 (as observed in the parent compound, in the mass spectrum of the reaction mixture a peak was discernible at 42 amu higher than the parent ion). Therefore the novel fungal metabolite was formulated as **11**.

The results obtained in the agar dilution test of compounds **10** and **11** against several Gram-positive and Gram-negative bacteria are reported in Table 3.

Experimental

Melting points were determined on a Kofler block and are uncorrected. Mass spectra were obtained at 70 eV with a Kratos MS-50S spectrometer. The ir and uv spectra were recorded with Perkin–Elmer

Can. J. Chem. Downloaded from www.nrcresearchpress.com by 213.166.140.6 on 09/07/12
For personal use only.

TABLE 2. ^{13}C nuclear magnetic resonance data and $^{1}H-^{13}C$ 2D correlations for compounds **10** and **11**

		10						**11**					
Carbon	DEPT	δ_C[a]	m[b]	^1J[b]	^2J[b]	^3J[b]	Long-range correlations[c]	δ_C[a]	m[b]	^1J[b]	^2J[b]	^3J[b]	Long-range correlations[c]
1	C	123.9	d			8.0	H-5	124.2	d			7.6	
2	CH	117.5	dd	158.0		7.8	H-6	117.7	dd	158.8		7.4	
3	C	144.9	dd		2.5	7.2	H-2	145.0	d			7.3	H-5
4	C	145.1	dt		2.0	9.0	H-6, H-2	145.0	t			9.3	
5	CH	115.8	d	158.0				115.7	d	159.0			
6	CH	122.4	dd	162.0		8.0	H-2	122.5	dd	161.4	7.4		
1′	C	123.1	t			3.5	H-2	122.6	bs				
2′	C	141.1[d]	s					141.0[d]	s				
3′	C	141.2[d]	s					141.1[d]	s				
4′	C	121.6	t			3.5	H-2″, H-6″	122.6	bs				H-2″, H-6″
5′	C	133.7[e]	s					133.9[e]	s				
6′	C	133.8[e]	s					134.0[e]	s				
1″	C	130.8	t			7.5	H-3″, H-5″	123.9	t			7.4	H-3″, H-5″
2″	CH	131.8	dd	163.0		7.5	H-6″	131.8	dd	161.0		7.4	
6″	CH					7.5	H-2″					7.4	
3″	CH	121.7	dd	164.0		4.5	H-5″	115.6	d	159.0		6.9	
5″	CH					4.5	H-3″					6.9	
4″	C	150.5	tt		3.0	9.5	H-2″, H-6″	157.0	t			9.5	
$COCH_3$	C	169.7	q		6.5		2′-, 3′-OAc	169.9	q		6.5		2′-, 3′-OAc
$COCH_3$	C	169.8	q		6.5			170.0	q		6.5		
$COCH_3$	C	170.7	q		6.5		4″-OAc						
$2 \times COCH_3$	CH_3	20.2	q	128.0				20.2	q	130.4			
$COCH_3$	CH_3	21.1	q	128.0									

[a]Measured in $CDCl_3-CD_3OD$ (7:3); chemical shifts (ppm) are relative to CD_3OD at 49.00 ppm.
[b]Multiplicities and ^1J, ^2J, ^3J values as obtained from gated decoupling experiments. J values are expressed in Hz.
[c]^1H,^{13}C long-range shift correlations observed in 2D nmr spectrum.
[d,e]Values with identical superscript within each column may be interchanged.

TABLE 3. Antibacterial spectrum of compounds **10** and **11**

Bacterial strains	MIC (μg/mL) **10**	**11**
Eubacteriales, Gram-negative		
Proteus mirabilis	75	50
Escherichia coli	>100	>100
Hafnia alvei	>100	50
Aeromonas hydrophila	>100	>100
Eubacteriales, Gram-positive		
Staphylococcus aureus	75	50
Streptococcus faecalis	>100	>100
Micrococcus luteus	>100	>100

684 and Perkin–Elmer 330 spectrometers, respectively. Fruiting bodies of *Sarcodon leucopus* were collected on Mount Etna in November 1985.

*Isolation of compounds **10** and **11***

Fresh plant material (3.5 kg) was extracted three times with acetone–water (final concentration 70%). Bulk extracts were evaporated under reduced pressure to remove acetone and the residual aqueous suspension extracted five times with ether. The ether extracts were pooled, dried over Na_2SO_4, and taken to dryness to give a crude extract (11 g) that was chromatographed on an open column of silica gel (5 × 100 cm; a gradient of Et_2O in hexane followed by a gradient of MeOH in Et_2O as the eluents). Fractions of 50 mL were collected and pooled according to their tlc profiles. Compound **10** was eluted in fractions 39–43 and further purified by successive chromatographies on silica gel, using as solvent MeOH–CH_2Cl_2 1:24 vol/vol and then acetone–hexane 1:1 vol/vol, to give 70 mg of pure compound. Further chromatographic purification (silica gel, MeOH–CH_2Cl_2 1:12 vol/vol as the eluent) of fractions 45–55 gave pure **11** (185 mg).

2′,3′,4″-Triacetoxy-3,4,5′,6′-tetrahydroxy-p-*terphenyl (**10**)*: uv (EtOH) λ_{max} (ε): 204 (33 800), 270 (28 350) nm; ir (KBr): 3420, 3050, 2930, 1750, 1730, 1610, 1525, 1455, 1370, 1210, 1095, 1020, 980 cm^{-1}; hrms, m/z calcd. for $C_{24}H_{20}O_{10}$: 468.1056 (M^+); found: 468.1049 (15%), 510 ($M^+ + CH_2CO$, 5%), 426 ($M^+ - CH_2CO$, 66%), 384 ($M^+ - CH_2CO \times 2$, 100%), 342 ($M^+ - CH_2CO \times 3$, 46%), 326 (11%), 323 (11%), 57 (15%), 43 (48%). ^1H and ^{13}C data are given in Tables 1 and 2.

2′,3′-Diacetoxy-3,4,5′,6′,4″-pentahydroxy-p-*terphenyl (**11**)*: uv (EtOH) λ_{max} (ε): 205 (46 200), 265 (15 300) nm; ir (KBr): 3420, 3050, 2935, 1750, 1730, 1620, 1520, 1460, 1435, 1370, 1230, 1090, 1020, 980 cm^{-1}; hrms, m/z calcd. for $C_{22}H_{18}O_9$: 426.0951 (M^+); found: 426.0957 (6%), 468 ($M^+ + CH_2CO$, 15%), 385 (10%), 384 ($M^+ - CH_2CO$, 27%), 344 (6%), 343 (14%), 342 ($M^+ - CH_2CO \times 2$, 100%), 341 (10%), 340 (12%), 326 (12%), 324 ($M^+ - CH_2CO \times 2 - H_2O$, 5%), 323 (8%), 43 (35%). ^1H and ^{13}C data are given in Tables 1 and 2.

*Acetylation of compounds **10** and **11***

A solution of **10** (25 mg) in pyridine (0.5 mL) and acetic anhydride (1 mL) was stirred at room temperature for 1 h. Conventional work-up and flash chromatography (silica gel, acetone–hexane 3:7 vol/vol as the eluent) of the crude product provided the heptaacetate **1** (30 mg), mp 205–207°C (from acetone) (lit. (3) mp for protoleucomelone 204–205°C); uv (EtOH) λ_{max} (ε): 204 (52 600), 249 (19 100) nm; ir (KBr): 3020, 2400, 1780, 1520, 1460, 1440, 1375, 1215, 1100, 1030, 910 cm^{-1}; ^1H nmr (200 MHz, $CDCl_3-CD_3OD$ 7:3) δ: 7.19, 7.24, 7.26 (H-2, H-5, H-6, ABC system), 7.37, 7.17 (H-2″, H-3″, H-5″, H-6″, AA′BB′ system, N = 8.5 Hz), 2.02, 2.07 (2s, 2′-, 6′-OAc and 3′-, 5′-OAc), 2.31, 2.33, 2.34 (3s, 3-, 4-, 4″-OAc); ^{13}C nmr (50.2 MHz, $CDCl_3-CD_3OD$ 7:3) δ: 130.0 (C-1), 125.6 (C-2), 142.4

Can. J. Chem. Downloaded from www.nrcresearchpress.com by 213.166.140.6 on 09/07/12
For personal use only.

(C-3), 142.8 (C-4), 123.7 (C-5), 128.2 (C-6), 129.7 (C-1′), 139.6 and 139.7 (C-2′, C-3′, C-5′, C-6′), 130.9 (C-4′), 129.1 (C-1″), 131.1 (C-2″, C-6″), 122.0 (C-3″, C-5″), 151.4 (C-4″), 168.5 (2 × $COCH_3$), 168.6 (2 × $COCH_3$), 169.0 (2 × $COCH_3$), 170.1 ($COCH_3$), 20.0 (4 × $COCH_3$), 20.5 ($COCH_3$), 20.6 ($COCH_3$), 21.1 ($COCH_3$) ppm; ms, *m/z*: 636 (M^+, 0.5%), 594 ($M^+ - CH_2CO$, 4%), 552 ($M^+ - CH_2CO \times 2$, 58%), 510 ($M^+ - CH_2CO \times 3$, 85%), 470 (73%), 468 ($M^+ - CH_2CO \times 4$, 100%), 428 (44%), 427 (84%), 426 ($M^+ - CH_2CO \times 5$, 58%), 386 (78%), 384 ($M^+ - CH_2CO \times 6$, 49%), 366 (17%), 344 (61%), 343 (29%), 342 (27%), 326 (12%), 325 (36%), 315 (17%), 46 (75%). Under the same experimental conditions **11** gave a compound indistinguishable (ms, uv, ir, nmr) from **1**.

*Zinc dust distillation of **10***

An intimate mixture of compound **10** (20 mg) and zinc dust (800 mg) was distilled in an open test tube. The sublimate was dissolved in hexane and purified by hplc (Whatman Partisil PXS 10/25 silica gel, hexane), to give *p*-terphenyl (2 mg), mp 210–211°C, undepressed on admixture with an authentic sample; uv (EtOH) λ_{max} (ε): 277 (26 900) nm; ms, *m/z*: 230 (100%), 228 (10%), 115 (12%), 101 (4%), 57 (11%), 43 (15%).

*Reaction of **10** and **11** with phenylboronic acid*

A solution of **10** (5 mg) and phenylboronic acid (3 mg) in acetone (0.5 mL) was refluxed for 4 h. After removal of the solvent, the residue was examined by mass spectrometry without any further purification. A parent ion at *m/z* 640 indicated the formation of a bis-phenylboronate; major fragments were observed at *m/z* 598 ($M^+ - CH_2CO$, 15%), 556 ($M^+ - CH_2CO \times 2$, 100%), 555 (53%), 514 ($M^+ - CH_2CO \times 3$, 75%), 513 (47%), 470 (50%), 469 (18%), 428 (22%), 427 (12%), 78 (19%), 44 (56%).

When **11** was reacted with phenylboronic acid under the same experimental conditions as above, mass spectral examination of the crude product gave evidence of a parent ion at *m/z* 598, indicating the formation of bis-phenylboronate also in this case; major ions were observed at *m/z* 640 ($M^+ + CH_2CO$, 16%), 556 ($M^+ - CH_2CO$, 60%), 555 (30%), 514 ($M^+ - CH_2CO \times 2$, 64%), 513 (36%), 78 (100%), 44 (76%), 43 (80%).

Proton and carbon nuclear magnetic resonance spectra

The nmr spectra were recorded at 200 MHz (^1H) and 50 MHz (^{13}C), respectively, using a Bruker AC-200 instrument equipped with a carbon-13–proton dual probehead, an Aspect 3000 data system, and a 160 MByte Disk cartridge. One-dimensional proton and carbon-13 Fourier transform nmr spectra with sweep widths and transmitter frequencies optimized for the lowest possible digital resolution (Hz/data point) were obtained from 32 K free induction decay signals. Gaussian resolution enhancements for proton nmr and exponential multiplication for carbon-13 nmr were applied before performing Fourier transformations; LB (line broadening) constants were adapted to the digital resolution. Coupled carbon-13 nmr spectra were obtained using the gated decoupling technique. Two-dimensional carbon-13–proton shift correlation was performed by polarization transfer via J_{CH}. Relaxation delays were 0.8 s; incremented delays of 1/8 W were adapted to the individual proton chemical shift ranges optimized as described previously. Polarization transfer delays ($1/2J_{CH}$ = 0.35 s and $1/^{2,3}J_{CH}$ = 0.1 s) were adapted to the expected averages of one-bond couplings (J_{CH} = 150 Hz) for CH correlations and two- or three-bond couplings ($^{2,3}J_{CH}$ = 5 Hz) for long-range CH correlations. The commercially available microprogram XHCORR for X–H shift correlation was used throughout, and 1024 × 256 data matrices were applied for the carbon and proton chemical shift domains. Shifted ($\pi/4$) sine squared shaping functions were applied before performing Fourier transformation in both domains.

Antibacterial activity

In the course of fractionation, antibacterial activity was followed by the paper disc – agar diffusion assay using *Staphylococcus aureus* as test organism. The minimum inhibitory concentrations (MICs) were determined by the conventional agar dilution method. All test strains were grown in Mueller Hinton medium incubated at 37°C for 18 h. Data of antibacterial activity are reported in Table 3.

Acknowledgements

Thanks are due to NATO Scientific Affairs Division (Brussels) and Ministero della Pubblica Istruzione (Roma) for financial support. The authors express their sincere thanks to Professor Breitmaier (Institut für Organische Chemie und Biochemie, Universität Bonn) for the nmr spectra and for helpful discussions during this study. We are grateful to Dr. F. Eckhardt (Institut für Organische Chemie und Biochemie, Universität Bonn) for the mass spectra, and to the "Gruppo Micologico Bresadola" (Catania) for classification of the mushroom and the generous gift of several samples.

1. W. B. Turner. Fungal metabolites. Academic Press, London. 1971.
2. W. B. Turner and D. C. Aldridge. Fungal metabolites II. Academic Press, London. 1983.
3. M. Akagi. J. Pharm. Soc. Jpn. **62**, 129 (1942).
4. J. Gripenberg. Acta Chem. Scand. **12**, 1411 (1958).
5. L. H. Briggs, R. C. Cambie, I. C. Dean, S. H. Dromgoole, B. J. Fergus, W. B. Ingram, K. G. Lewis, C. W. Small, R. Thomas, and D. A. Walker. N.Z. J. Sci. **18**, 565 (1975).
6. C. Takahashi, K. Yoshihira, S. Natori, M. Umeda, K. Ohtsubo, and M. Saito. Experientia, **30**, 529 (1974).
7. G. D. Andreetti, G. Bocelli, and P. Sgarabotto. Cryst. Struct. Commun. **3**, 145 (1974).
8. R. Marchelli and L. C. Vining. J. Antibiot. **28**, 328 (1975).
9. C. Takahashi, K. Yoshihira, S. Natori, and M. Umeda. Chem. Pharm. Bull. **24**, 613 (1976).
10. I. Kurobane, L. C. Vining, A. G. McInnes, and D. G. Smith. J. Antibiot. **32**, 559 (1979).
11. A. Kobayashi, A. Takemoto, K. Koshimizu, and K. Kawazu. Agric. Biol. Chem. **49**, 867 (1985).
12. A. Kobayashi and K. Koscimizu. Agric. Biol. Chem. **44**, 393 (1980).
13. A. Kobayashi, A. Takemura, K. Koshimizu, H. Nagano, and K. Kawazu. Agric. Biol. Chem. **46**, 585 (1982).
14. T. C. McMorris and M. Anchel. Tetrahedron, **23**, 3985 (1967).
15. R. Herrmann. Dissertation, Bonn (1980).
16. W. Quack, H. Scholl, and H. Budzikiewicz. Phytochemistry, **21**, 2921 (1982).

Can. J. Chem. Downloaded from www.nrcresearchpress.com by 213.166.140.6 on 09/07/12
For personal use only.

Kinetics and mechanisms of oxidation of methylamine by permanganate ion

FERNANDO MATA-PEREZ AND JOAQUIN F. PEREZ-BENITO[1]

Departamento de Quimica Fisica, Facultad de Quimica, Universidad Central de Barcelona, Avenida Diagonal, 647, 08028 Barcelona, Spain

Received October 31, 1986[2]

FERNANDO MATA-PEREZ and JOAQUIN F. PEREZ-BENITO. Can. J. Chem. **65**, 2373 (1987).

The oxidation of methylamine by permanganate ion in aqueous phosphate buffers is autocatalyzed by a soluble form of colloidal manganese dioxide temporarily stabilized in solution by adsorption of phosphate ions on its surface. The dependence of the rate constants of both the noncatalytic and catalytic mechanisms on the concentrations of both methylammonium and hydroxyl ions and on temperature has been determined. The activation parameters have been obtained. Mechanisms in agreement with the experimental data are proposed.

FERNANDO MATA-PEREZ et JOAQUIN F. PEREZ-BENITO. Can. J. Chem. **65**, 2373 (1987).

L'oxydation de la méthylamine par l'ion permanganate, en solution dans des tampons de phosphates, est autocatalysée par une forme soluble du bioxyde de manganèse colloïdal qui est temporairement stabilisée en solution par adsorption des ions phosphates sur sa surface. On a déterminé les relations qui existent entre les constantes de vitesse, tant des mécanismes catalysés que ceux des mécanismes non-catalysés, et soit les concentrations tant des ions méthylammonium que des ions hydroxyles soit la température. On a obtenu les paramètres d'activation. On propose des mécanismes qui sont en accord avec les données expérimentales.

[Traduit par la revue]

Can. J. Chem. Downloaded from www.nrcresearchpress.com by 213.166.140.6 on 09/07/12
For personal use only.

Introduction

Although some kinetic studies on the permanganate ion oxidation of tertiary (1, 2) and secondary (3) amines have been reported, little attention has been paid to the kinetic aspects of the oxidation of primary amines by permanganate ion, save for the case of benzylamine (4). On the other hand, the products from the oxidation of a wide variety of amines by permanganate ion are known (5–7).

We have now undertaken the kinetic study of the permanganate ion oxidation of methylamine in aqueous phosphate buffers. This reaction is clearly of the autocatalytic type.

Autocatalysis seems to be a rather general phenomenon for the oxidation of amines by permanganate ion (2–4, 8), but is by no means limited to amines, for many permanganate reactions have been found to be autocatalytic (9–27).

Despite the extensive occurrence of autocatalysis in permanganate reactions, there is not much information on the autocatalytic mechanism, since for the sake of simplicity the kinetic parameters of the autocatalytic pathway are, more often than not, ignored.

To compensate for that lack of information, in the work reported here a great deal of emphasis has been placed on the comprehension of both the noncatalytic and catalytic processes involved in the oxidation of methylamine by permanganate ion.

Experimental

The solvent used in all the experiments was triply-distilled water. The oxidant was potassium permanganate and the reductant (in great excess with respect to the oxidant) was methylamine in the chlorhydrate form.

A KH_2PO_4–NaOH buffer mixture was used with a double purpose: to stabilize temporarily in solution the Mn(IV) species generated as a reaction product, thus avoiding the appearance of a MnO_2 precipitate while the kinetic measurements were being taken (28), and to keep the pH of the medium constant. In the pH range 6–8 allowed by the buffer, the amine was present chiefly in the protonated form, since the pK_a corresponding to methylammonium ion is 10.62 (29).

In the experiments where the reductant concentration or the pH were changed, the ionic strength was held constant by addition of proper amounts of potassium chloride. The same electrolyte was used when the ionic strength of the medium was the factor to be changed.

The kinetic runs were followed by monitoring the disappearance of permanganate ion at 525 nm by means of a PE Coleman-55 spectrophotometer provided with a thermostated cell. The contribution from the reaction product to the total absorbance was discounted (30).

The pH's of the solutions were measured by means of a Radiometer pH-meter 51, and the temperature was controlled using a conventional thermostat.

In a typical experiment, two flasks, one of them containing 100 mL of a solution 10^{-3} *M* in potassium permanganate and the other containing the same volume of a solution 2.40 *M* in methylammonium chloride, were kept in a thermostatic bath at 25.0°C long enough to reach the thermic equilibrium. Both solutions were buffered at pH 8.0. Then the solution containing the organic substrate was added to the permanganate solution, the mixture was vigorously stirred, and an aliquot was extracted with the aid of a syringe and then injected into the thermostated cell. The absorbances at 525 nm were periodically taken until total permanganate consumption.

Results

A decrease in the absorbance at 525 nm and an increase at 420 nm (wavelength at which permanganate is transparent) were observed in all the experiments. The solutions passed successively through the following colours: purple (reactant), red (reactant + product), and brown-yellow (product). The spectrum recorded for the product solution when all the permanganate had been consumed showed a broad band with the absorbance continuously decreasing with increasing wavelength. Similar spectra were obtained in many permanganate reactions (2, 3, 27, 31–42). The solutions remained totally clear throughout the reaction, and a brown precipitate of managanese dioxide was observed the day after.

As illustrated by Fig. 1, all the reaction rate vs. time plots showed a definite bell-shaped profile, the rate having been calculated point by point from the experimental data as minus the derivative of the permanganate concentration with respect to time; i.e., the reaction is autocatalytic. Therefore two mechanisms have to be involved in the total process to account for both the acceleration and decay periods of the reaction

[1]Author to whom correspondence may be addressed.

[2]Revision received May 26, 1987.

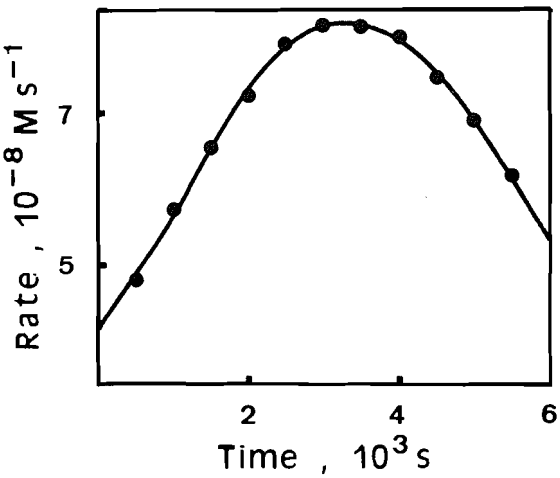

FIG. 1. Reaction rate vs. time plot. Initial permanganate concentration, 5×10^{-4} *M*; methylammonium ion concentration, 1.20 *M*; ionic strength, 1.35 *M*; pH, 8.0; temperature, 25.0°C.

rate (43). This duality of mechanism must be reflected in the differential rate equation.

If we assume that the noncatalytic mechanism is first order in one of the reactants (permanganate ion), and the catalytic mechanism first order in both reactant and autocatalytic product since the kinetics were performed in great excess of the other reactant (methylamine), the differential rate law can be written as follows:

$$[1] \quad r = k_1[\mathrm{R}] + k_2[\mathrm{R}][\mathrm{P}]$$

where k_1 and k_2 are the pseudo rate constants corresponding to the noncatalytic and catalytic mechanisms, respectively.

Equation [1] can also be expressed in the following manner:

$$[2] \quad -\mathrm{d}c/\mathrm{d}t = k_1 c + k_2 c(c_0 - c)$$

c and c_0 being the permanganate concentrations at time t and at the beginning of the reaction, respectively.

The integral form of eq. [2] is

$$[3] \quad \ln [k_1 + k_2 c_0 - k_2 c)/c] = \ln (k_1/c_0) + (k_1 + k_2 c_0)t$$

This equation was successfully used for the kinetic study of the permanganate ion oxidation of dimethylamine (3) and trimethylamine (2) and was also proposed for the acid-catalyzed hydrolysis of esters (44).

By fitting the left-hand side of eq. [3] against time by the least-squares method a linear correlation is obtained, and from the intercept and the slope of that straight line the values of the rate constants can be derived. However, it is clear that the values of both k_1 and k_2 must first be known, to make that fit possible. This paradoxical situation has been resolved by means of an iterative procedure. The left-hand side of eq. [3] is fitted against time by the help of some trial values of the rate constants; from the intercept and the slope thus obtained, new values of k_1 and k_2 are inferred and the cycle is repeated until convergence is achieved.

Figure 2 shows an excellent agreement between eq. [3] and the experimental data for a typical kinetic run. The linear correlation coefficient associated with eq. [3] remained in all the cases within the limits 0.9992 and 0.99997.

Since the integral rate law (eq. [3]) is fulfilled, it follows that the kinetic order of permanganate ion in both mechanisms and that of the autocatalytic agent in the catalytic pathway are unity (see eqs. [1] and [2]).

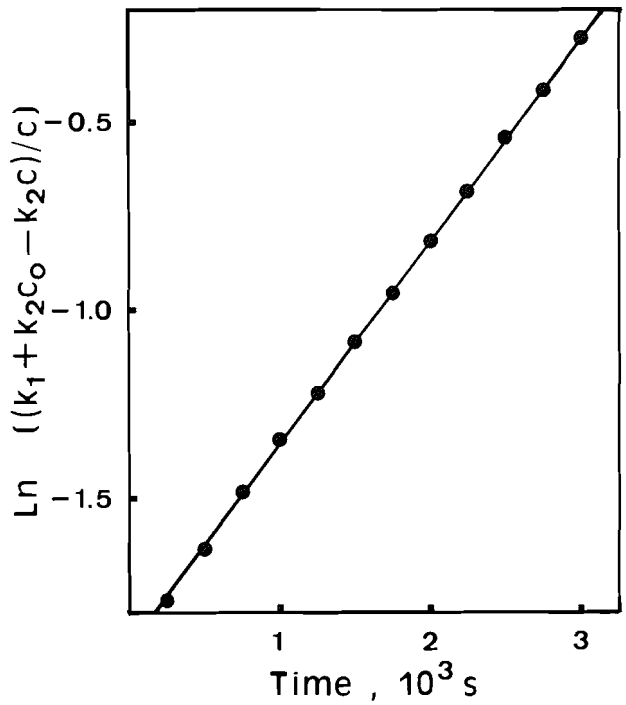

FIG. 2. Rate-law plot. Initial permanganate concentration, 5×10^{-4} *M*; methylammonium ion concentration, 1.20 *M*; ionic strength, 1.35 *M*; pH, 8.0; temperature, 25.0°C (r = 0.9999).

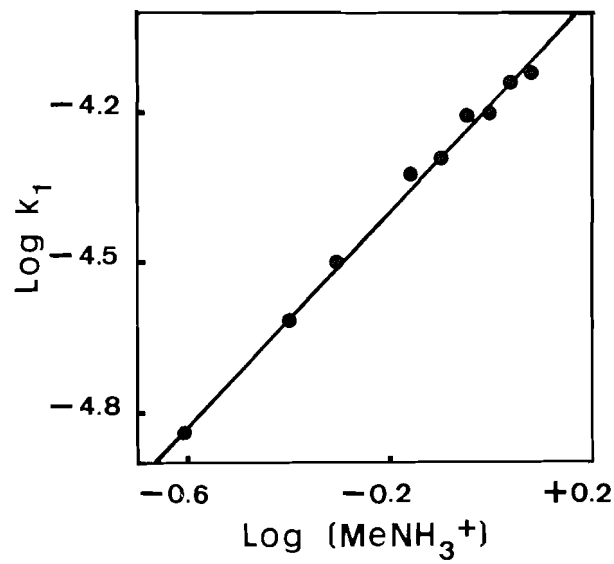

FIG. 3. Dependence of the rate constant of the noncatalytic mechanism on the methylammonium ion concentration. Initial permanganate concentration, 5×10^{-4} *M*; ionic strength, 1.35 *M* (KCl); pH, 8.0; temperature, 25.0°C (slope = 1.07, r = 0.998).

The values of the rate constants corresponding to different methylammonium ion concentrations have been determined. We can see in Fig. 3 that a log k_1 vs. log $[MeNH_3^+]$ plot is linear, the slope of that correlation being 1.07. Thus, the noncatalytic mechanism is first-order dependent on the substrate concentration. On the other hand, Fig. 4 indicates that there exists a linear relationship between $1/k_2$ and $1/[MeNH_3^+]$.

A plot of k_1 vs. $[OH^-]$ is also linear (see Fig. 5); since the intercept is different from zero, it follows that a log k_1 vs. log $[OH^-]$ plot is not linear. In the case of the catalytic

Can. J. Chem. Downloaded from www.nrcresearchpress.com by 213.166.140.6 on 09/07/12
For personal use only.

Can. J. Chem. Downloaded from www.nrcresearchpress.com by 213.166.140.6 on 09/07/12
For personal use only.

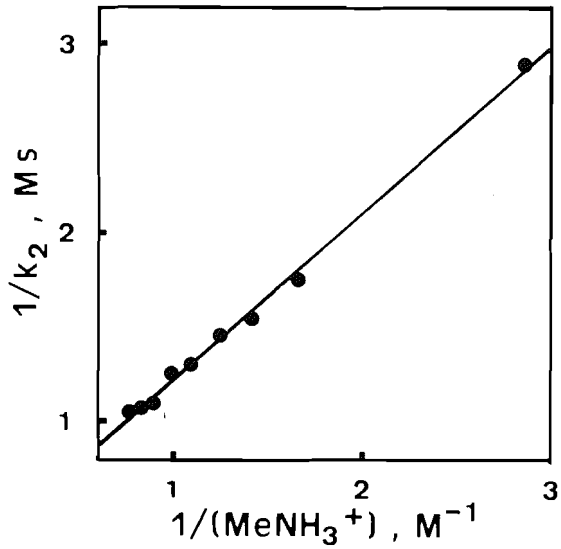

FIG. 4. Dependence of the rate constant of the catalytic mechanism on the methylammonium ion concentration. Initial permanganate concentration, 5×10^{-4} M; ionic strength, 1.35 M (KCl); pH, 8.0; temperature, 25.0°C ($r = 0.997$).

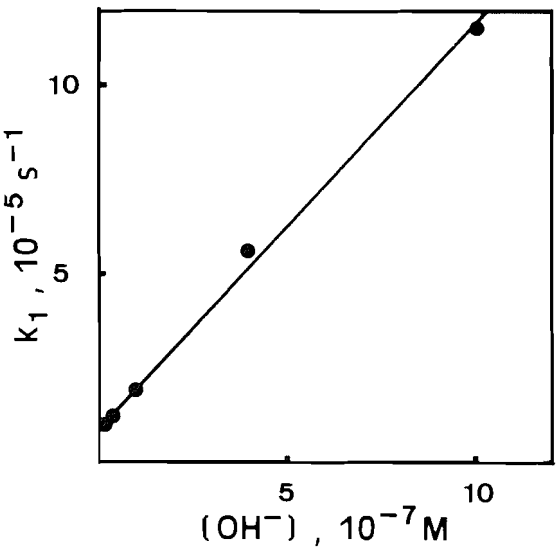

FIG. 5. Dependence of the rate constant of the noncatalytic mechanism on the hydroxyl ion concentration. Initial permanganate concentration, 5×10^{-4} M; methylammonium ion concentration, 0.30 M; ionic strength, 0.45 M (KCl); temperature, 50.0°C ($r = 0.999$).

mechanism linearity is found, however, in a correlation of the type $\log k_2$ vs. $\log [OH^-]$ (see Fig. 6).

The rate constants at several potassium chloride concentrations are given in Table 1. We can see that both k_1 and k_2 decrease as the ionic strength of the medium increases.

The values of k_1 and k_2 at different temperatures were also determined and are listed in Table 2. Both rate constants fulfill the Arrhenius equation, and the corresponding energies of activation are compiled in Table 3.

Discussion

As far as the noncatalytic mechanism is concerned, the following two rate-determining steps can be proposed:

[4] $CH_3NH_3^+ + OH^- \overset{\text{fast}}{\rightleftharpoons} CH_3NH_2 + H_2O$

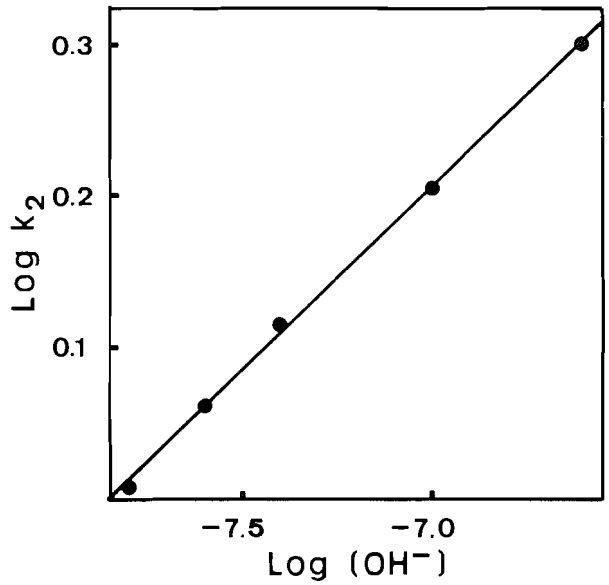

FIG. 6. Dependence of the rate constant of the catalytic mechanism on the hydroxyl ion concentration. Initial permanganate concentration, 5×10^{-4} M; methylammonium ion concentration, 0.30 M; ionic strength, 0.45 M (KCl); temperature, 50.0°C (slope = 0.24, $r = 0.999$).

TABLE 1. Dependence of the rate constants on the ionic strength[a]

Ionic strength (M)[b]	$10^5 k_1$ (s^{-1})	k_2 ($M^{-1} s^{-1}$)
0.65[c]	1.50	0.235
0.75	1.43	0.219
0.85	1.40	0.197
0.95	1.38	0.191
1.05	1.35	0.177

[a]Initial permanganate concentration, 5×10^{-4} M; methylammonium ion concentration, 0.50 M; pH, 8.0; temperature, 25.0°C.
[b]Potassium chloride as background electrolyte.
[c]Ionic strength due to the buffer and reactant concentrations.

TABLE 2. Dependence of the rate constants on temperature[a]

T (°C)	$10^5 k_1$ (s^{-1})	k_2 ($M^{-1} s^{-1}$)
31.0	2.73	0.430
33.0	3.32	0.463
35.1	4.23	0.624
37.5	4.88	0.765
40.0	6.31	0.945
42.5	8.39	1.168
45.1	10.26	1.447

[a]Initial permanganate concentration, 5×10^{-4} M; methylammonium ion concentration, 0.50 M; ionic strength, 0.65 M; pH, 8.0.

[5] $CH_3NH_2 + MnO_4^- \overset{\text{slow}}{\longrightarrow} CH_3NH_2^{+\bullet} + MnO_4^{2-}$

Accordingly, the noncatalytic portion of the total rate is

[6] $r_1 = k_5[MnO_4^-][MeNH_2]$

where k_5 is the rate constant associated with eq. [5]. Now, if the free and protonated forms of the amine are in equilibrium, we

TABLE 3. Activation energies for both mechanisms of reaction[a]

Mechanism	E_a (kJ mol^{-1})	r^b
Noncatalytic	75.6	0.998
Catalytic	71.8	0.997

[a]From data in Table 1.
[b]Linear correlation coefficient for each Arrhenius plot.

TABLE 4. Obtention of the activation parameters for the electron-transfer step in the noncatalytic mechanism

Constant	ΔH^0 (kJ mol^{-1})	ΔS^0 (J K^{-1} mol^{-1})
k_1	73.1[a]	−240[a]
K_a	54.8[b]	−20[b]
k_5	18.3[c]	−220[c]

[a]Activation parameters associated with rate constant k_1. From a ln $(k_1[H^+]/[MeNH_3^+]T)$ vs. $1/T$ plot of data in Table 1.
[b]Thermodynamic parameters associated with equilibrium constant K_a (49).
[c]Activation parameters associated with rate constant k_5. From eqs. [12] and [13].

can also write:

[7] $r_1 = K_4k_5[MnO_4^-][MeNH_3^+][OH^-]$

K_4 being the equilibrium constant corresponding to eq. [4].

Equation [7] is in full agreement with the kinetic orders found for the oxidizing and reducing agents in the noncatalytic pathway (see eq. [2] and Fig. 3).

Moreover, Fig. 5 shows that the noncatalytic mechanism is first-order dependent on the hydroxyl ion concentration, as required by eq. [7]. Although the existence of an intercept different from zero suggests that the protonated form of the amine also has some reactivity toward permanganate ion, the small magnitude of that intercept indicates that this other modality of reaction is of very minor importance, the predominant oxidation being that of free methylamine by permanganate ion (see eq. [5]).

The experimental rate law found for the noncatalytic pathway in the permanganate ion oxidation of methylamine (see eq. [7]) is quite similar to those reported for the oxidation of dimethylamine (3) and of trimethylamine (2) by permanganate.

It has been observed that electrolyte additions slow down the reaction; this behavior is probably due to a decrease in equilibrium constant K_4 as the ionic strength of the medium increases, for eq. [4] implies the encounter of two ions with unlike charges.

We can easily see that eqs. [4] and [5] fully agree with the experimental results. However, it has been much discussed whether the oxidation of amines occurs through transfer of an electron, of a hydrogen atom, or of a hydride ion (45, 46). Obviously, from the kinetic data found for the reaction, the type of particle transferred to permanganate ion from methylamine does not directly follow, since the three kinds of transfer would lead to the same rate law (see eq. [7]).

The study of deuterium isotope effects reported in the literature indicates that the permanganate oxidation of benzylamine shows a primary isotope effect (4) and that of trimethylamine a secondary one (47). Therefore, one must conclude that in the first case the predominant oxidation mechanism is one of hydrogen-atom or hydride transfer, while in the second case the predominant oxidation mechanism is one of electron transfer. Consequently, it seems that oxidation of the amine by transfer of a hydrogen atom or a hydride ion from the α position in the substrate to permanganate ion is reserved for those amines (such as benzylamine) that would lead to a free radical (for hydrogen-atom transfer) or to a carbocation (for hydride transfer) highly stabilized by resonance. For those substrates (such as trimethylamine and methylamine) that do not lead to resonance stabilized products, electron transfer seems to be the main oxidation mechanism.

Moreover, a comparison of the rate constants given in the literature for the oxidation of dimethylamine (3) and trimethylamine (2) by permanganate ion in aqueous phosphate buffers with the data reported in this paper for the oxidation of methylamine reveals that the sequence of reactivity toward permanganate ion is

[8] trimethylamine > dimethylamine > methylamine

that is, the reactivity decreases as the ionization potential of the amine increases (48). Thus it does not seem unreasonable to assume that electron transfer is most likely the process involved (see eq. [5]).

From eqs. [2] ane [7] it follows that the pseudo rate constant of the noncatalytic mechanism is

[9] $k_1 = K_4k_5[MeNH_3^+][OH^-]$

By taking into consideration the identity:

[10] $K_4 = K_a/[H^+][OH^-]$

where K_a is the equilibrium constant for dissociation of methylammonium ion, eq. [9] can also be written as follows:

[11] $k_5 = k_1[H^+]/K_a[MeNH_3^+]$

Therefore, although the experimental activation parameters associated with k_1 are only apparent, the true activation parameters corresponding to eq. [5] can be derived from them by means of eq. [11].

If $\Delta H^1_{\ddagger}$ and $\Delta S^1_{\ddagger}$ stand for the activation parameters obtained from a plot of the data compiled in Table 1 according to the function $\ln(k_1[H^+]/[MeNH_3^+]T)$ vs. $1/T$, while ΔH^0 and ΔS^0 are the thermodynamic magnitudes corresponding to the methylammonium dissociation constant K_a (data available in the literature (49)), it follows from eq. [11] that the activation parameters associated with the electron-transfer step (eq. [5]) are given by the expressions:

[12] $\Delta H^5_{\ddagger} = \Delta H^1_{\ddagger} - \Delta H^0$

[13] $\Delta S^5_{\ddagger} = \Delta S^1_{\ddagger} - \Delta S^0$

The true values of the activation parameters derived from eqs. [12] and [13], as well as those necessary for their obtention, are listed in Table 4. We can see that the electron-transfer step (eq. [5]) only accounts for a small part of the experimental activation enthalpy found for k_1, but the same step accounts for a large portion of the experimental activation entropy.

Though no information concerning the noncontrolling steps can be inferred from the kinetic results, we can propose a reasonable scheme for the obtention of the reaction products from the intermediary species generated in eq. [5].

By analogy with the mechanism proposed for the permanga-

Can. J. Chem. Downloaded from www.nrcresearchpress.com by 213.166.140.6 on 09/07/12
For personal use only.

Can. J. Chem. Downloaded from www.nrcresearchpress.com by 213.166.140.6 on 09/07/12
For personal use only.

nate ion oxidation of trimethylamine (47), the noncontrolling steps of the reaction could be the following:

[14] $CH_3NH_2^{+\cdot} \rightarrow {}^{\cdot}CH_2NH_2 + H^+$

[15] ${}^{\cdot}CH_2NH_2 + MnO_4^- \rightarrow CH_2{=}NH_2^+ + MnO_4^{2-}$

[16] $CH_2{=}NH_2^+ + H_2O \rightarrow CH_2O + NH_4^+$

[17] $3MnO_4^{2-} + 2H_2O \rightarrow 2MnO_4^- + MnO_2 + 4OH^-$

According to this mechanism, it is supposed that the cation radical generated in eq. [5] first suffers the loss of a proton (eq. [14]) to be then oxidized by permanganate ion (eq. [15]), so that methyliminium ion is formed. By hydrolysis of the latter (eq. [16]) formaldehyde and ammonium ion are formed, while manganese dioxide comes from dismutation of manganate ion (eq. [17]).

A number of reasons supporting this mechanism can be outlined. In the first place, imines are thought to be likely intermediates in the permanganate oxidation of amines (4).

On the other hand, ammonia is one of the products obtained from the permanganate degradation of primary amines, while aldehydes are obtained as reaction products from the oxidation of primary, secondary, and tertiary amines by aqueous potassium permanganate (5–7); in particular, formaldehyde was obtained from the permanganate oxidation of dimethylamine when this volatile product was rapidly distilled from the product mixture into 2,4-dinitrophenylhydrazine reagent (7), whereas under the experimental conditions of this work formaldehyde is expected to be readily oxidized by permanganate to formic acid and, further, to carbon dioxide (50).

Finally, manganate ion is known to disproportionate into permanganate ion and manganese dioxide in all but very basic aqueous media, the disproportionation being instantaneous in acid and neutral solutions (45), thus explaining the spectrophotometric detection of colloidal manganese dioxide at the end of the reaction between permanganate ion and methylamine. The same product was detected in many permanganate reactions carried out in aqueous media (42, 51) and in methylene chloride solutions (52).

As far as the catalytic pathway is concerned, it has been reported that a soluble form of colloidal manganese dioxide, temporarily stabilized in aqueous solution by adsorption of phosphate ions on its surface (42), is the actual autocatalytic agent for the permanganate ion oxidation of amines in aqueous phosphate buffers (3, 8). This soluble colloid is also responsible for the spectra recorded at the end of many permanganate oxidations (2, 3, 27, 31–42), and the recording of the same spectrum after completion of the permanganate–methylamine reaction allows its identification in our system as well. Therefore, once manganese dioxide has been formed through the noncatalytic mechanism (eq. [17]), the catalytic mechanism taking place on the colloid surface can be determined by the following equations:

[18] $MnO_2 + CH_3NH_3^+ \overset{\text{fast}}{\rightleftharpoons}$ adsorbate

[19] Adsorbate + $MnO_4^- \overset{\text{slow}}{\longrightarrow}$ products

In eq. [18] a fast equilibrium for adsorption of methylammonium ion on colloidal manganese dioxide has been assumed. In fact, manganese dioxide is known to strongly adsorb cations on its surface (53). Then, methylammonium ion thus adsorbed may suffer an oxidative attack by a permanganate ion from the double layer surrounding the colloidal particles (eq. [19]). As a result, the reaction products are formed.

Hence, the rate equation associated with the catalytic pathway is

[20] $r_2 = k_{19}[MnO_4^-][\text{adsorbate}]$

where k_{19} is the rate constant corresponding to eq. [19].

If the ratio between the adsorbate and manganese dioxide concentrations is given by the Langmuir equation (54) as a function of the concentration of methylammonium ion in solution:

[21] $[\text{adsorbate}]/[MnO_2] = a[MeNH_3^+]/(1 + b[MeNH_3^+])$

we can also write eq. [20] as follows:

[22] $r_2 = ak_{19}[MnO_4^-][MnO_2][MeNH_3^+]/(1 + b[MeNH_3^+])$

and, by comparing eqs. [2] and [22], the pseudo rate constant of the catalytic mechanism is

[23] $k_2 = ak_{19}[MeNH_3^+]/(1 + b(MeNH_3^+])$

Equation [23] is in agreement with the relationship between k_2 and $[MeNH_3^+]$ found in Fig. 4.

On the other hand, correlations similar to the one shown in Fig. 6 have been found for adsorption of cations on colloidal manganese dioxide, since it has been established that the logarithm of the ratio between the concentrations of cation adsorbed and manganese dioxide increases linearly with the pH of the medium (55, 56). From eqs. [21] and [23] it follows that the logarithm of k_2 must increase linearly with the pH of the solution or, in other words, with the logarithm of the hydroxyl concentration (see Fig. 6).

There are several possibilities to explain this behavior. In the first place, hydrated manganese dioxide may be regarded as an ion exchanger (57, 58), according to the equilibrium:

[24] $MnO_2{-}H_2O + CH_3NH_3^+ \rightleftharpoons MnO_2{-}OH^-{-}CH_3NH_3^+ + H^+$

whose equilibrium constant is

[25] $K_{24} = [\text{adsorbate}][H^+]/[MnO_2][MeNH_3^+]$

leading to the following expression for the rate constant (from eqs. [2], [20], and [25]):

[26] $k_2 = k_{19}K_{24}[MeNH_3^+]/[H^+]$

or, by using the definition of the water ionic product (K_w):

[27] $k_2 = k_{19}K_{24}[MeNH_3^+][OH^-]/K_w$

Equation [27] can indeed explain the log k_2 vs. log $[OH^-]$ linear relationship found in Fig. 6. However, the experimental value of the slope (0.24) is much lower than the kinetic order unity expected from eq. [27] for hydroxyl ion in the catalytic mechanism. Moreover, eq. [27] requires that k_2 be directly proportional to $[MeNH_3^+]$, in open disagreement with the experimental situation (see Fig. 4).

A second alternative might be given by the following equilibrium:

[28] $MnO_2 + nOH^- \rightleftharpoons MnO_2{-}(OH^-)_n$

where n is the number of hydroxyl ions linked to the colloid per manganese dioxide molecule. Hydroxyl ions are actually known to be bonded to colloidal manganese dioxide (59). Hence hydroxyl ions, instead of molecules of water (see eq. [24]), might be the real active points for adsorption of methylammonium ion on the surface of the colloidal particles:

[29] $MnO_2{-}(OH^-)_n + CH_3NH_3^+ \rightleftharpoons$ adsorbate

Accordingly, eq. [21] can be rewritten as

[30] $$[\text{adsorbate}]/[MnO_2{-}(OH^-)_n] = a[MeNH_3^+]/(1 + b[MeNH_3^+])$$

and, if the equilibrium constant associated with eq. [28] is called K_{28}:

[31] $$[MnO_2{-}(OH^-)_n] = K_{28}[MnO_2][OH^-]^n$$

Froms eqs. [2], [20], [30], and [31]:

[32] $$k_2 = ak_{19}K_{28}[OH^-]^n[MeNH_3^+]/(1 + b[MeNH_3^+])$$

This equation represents an improvement with respect to eq. [23], since eq. [32] takes into account the dependence of k_2 on the hydroxyl ion concentration. According to eq. [32], log k_2 must be linear when plotted against log $[OH^-]$ (see Fig. 6), the slope being the number of hydroxyl ions fixed on the colloid surface per MnO_2 molecule (see eq. [28]). The experimental fractionary value for that slope (0.24) is indeed logical, for only those molecules of manganese dioxide belonging to the colloid surface are available for complexation with hydroxyl ions.

Unfortunately, it has been reported that the number of OH^- ions linked to each MnO_2 molecule increases with the pH of the medium (55); thus n is at best an average value for the pH range used.

Finally, as a third alternative, Figs. 4 and 6 might be the result of consecutive adsorption equilibrium of hydroxyl and methylammonium ions on the surface of colloidal manganese dioxide. If adsorption of hydroxyl ion is best described by an isotherm of the Freundlich type (60), while adsorption of methylammonium ion is best accounted for by an isotherm of the Langmuir type (54), and if hydroxyl ions previously adsorbed are the active points for adsorption of methylammonium ion on the colloid surface, a situation such as the one made evident by Figs. 4 and 6 is perfectly consistent with theoretical considerations.

In conclusion, the experimental results seem to indicate that the catalytic pathway takes place by reaction between a permanganate ion from the solution and a methylammonium ion previously adsorbed on the surface of colloidal manganese dioxide, hydroxyl ions linked to the colloid surface being the active points for adsorption of the protonated form of the amine. This explanation is consistent with previous reports found in the literature (2, 3, 8).

1. S. Senent, F. Mata-Perez, and M. A. De La Peña. Rev. Roum. Chim. **23**, 841 (1978).
2. F. Mata-Perez and J. F. Perez-Benito. An. Quim. Ser. A, **81**, 79 (1985).
3. F. Mata-Perez, J. F. Perez-Benito, and A. Arranz. Z. Phys. Chem. (Neue Folge), **135**, 141 (1983).
4. M. M. Wei and R. Stewart. J. Am. Chem. Soc. **88**, 1974 (1966).
5. H. Shechter, S. S. Rawalay, and M. Tubis. J. Am. Chem. Soc. **86**, 1701 (1964).
6. H. Shechter and S. S. Rawalay. J. Am. Chem. Soc. **86**, 1706 (1964).
7. S. S. Rawalay and H. Shechter. J. Org. Chem. **32**, 3129 (1967).
8. F. Mata-Perez and J. F. Perez-Benito. Z. Phys. Chem. (Neue Folge), **141**, 213 (1984).
9. J. Bradley and G. Van Praagh. J. Chem. Soc. 1624 (1938).
10. F. C. Tompkins. Trans. Faraday Soc. **38**, 131 (1942).
11. F. Fouinat and M. Magat. J. Chim. Phys. **47**, 514 (1950).
12. J. M. Malcolm and R. M. Noyes. J. Am. Chem. Soc. **74**, 2769 (1952).
13. C. F. Cullis and J. W. Ladbury. J. Chem. Soc. 4186 (1955).
14. K. B. Wiberg and R. Stewart. J. Am. Chem. Soc. **77**, 1786 (1955).
15. O. G. Pokrovskaya. Izvest. Sibir. Otdel. Akad. Nauk SSSR, **8**, 50 (1959).
16. R. Stewart. *In* Oxidation in organic chemistry. Part A. *Edited by* K. B. Wiberg. Academic Press, New York. 1965. p. 20.
17. D. A. Skoog and D. M. West. Fundamentals of analytical chemistry. 2nd ed. Holt, Rinehart and Winston, Toronto. 1969. p. 422.
18. M. Wronska and T. Ernst. Z. Phys. Chem. (Leipzig), **244**, 144 (1970).
19. K. K. Banerji. J. Chem. Soc. Perkin Trans. 2, 435 (1973).
20. E. G. Prout and C. M. Lownds. Inorg. Nucl. Chem. Lett. **9**, 617 (1973).
21. Marigangaiah, P. Nath, and K. K. Banerji. Aust. J. Chem. **29**, 1939 (1976).
22. J. S. Booth, D. Dollimore, and G. R. Heal. Thermochim. Acta, **39**, 293 (1980).
23. J. S. Reckley and K. Showalter. J. Am. Chem. Soc. **103**, 7012 (1981).
24. E. Narita and T. Okabe. Ind. Eng. Chem. Prod. Res. Dev. **21**, 662 (1982).
25. F. J. Andres, A. Arrizabalaga, and J. I. Martinez. An. Quim. Ser. A, **80**, 531 (1984).
26. A. Z. Moghaddam and G. J. Rees. Fuel, **63**, 653 (1984).
27. D. G. Lee and J. F. Perez-Benito. Can. J. Chem. **63**, 1275 (1985).
28. R. Stewart. Oxidation mechanisms: applications to organic chemistry. Benjamin, New York. 1964. p. 60.
29. H. K. Hall. J. Am. Chem. Soc. **79**, 5441 (1957).
30. K. B. Wiberg. Physical organic chemistry. Wiley, New York. 1964. p. 312.
31. S. Senent and L. Martin. An. Quim. Ser. B, **56**, 123 (1959).
32. B. Jezowska-Trzebiatowska and J. Kalecinski. Bull. Acad. Polon. Sci., Ser. Sci. Chim. **9**, 791 (1961).
33. K. B. Wiberg, C. J. Deutsch, and J. Rocek. J. Am. Chem. Soc. **95**, 3034 (1973).
34. M. Jaky and L. I. Simandi. React. Kinet. Catal. Lett. **3**, 397 (1975).
35. F. Freeman and E. M. Karchefski. Biochim. Biophys. Acta, **447**, 238 (1976).
36. N. T. Son, M. Jaky, and L. I. Simandi. Inorg. Nucl. Chem. Lett. **12**, 291 (1976).
37. M. Jaky and L. Simandi. Magy. Kem. Foly. **86**, 136 (1980).
38. N. T. Son, M. Jaky, and L. Simandi. Magy. Kem. Foly. **86**, 139 (1980).
39. T. Ogino. Tetrahedron Lett. **21**, 177 (1980).
40. F. Freeman, C. O. Fuselier, C. R. Armstead, C. E. Dalton, P. A. Davidson, E. M. Karchefski, D. E. Krochman, M. N. Johnson, and N. K. Jones. J. Am. Chem. Soc. **103**, 1154 (1981).
41. D. G. Lee and K. C. Brown. J. Am. Chem. Soc. **104**, 5076 (1982).
42. F. Mata-Perez and J. F. Perez-Benito. Can. J. Chem. **63**, 988 (1985).
43. J. W. Moore and R. G. Pearson. Kinetics and mechanism. 3rd ed. Wiley, New York. 1981. p. 26.
44. C. Capellos and B. H. J. Bielski. Kinetic systems. Wiley, New York. 1972. p. 63.
45. F. Freeman. Rev. React. Species Chem. React, **1**, 179 (1976).
46. I. P. Gragerov, L. K. Skrunts, and B. A. Geller. Russ. Chem. Rev. **51**, 68 (1982).
47. D. H. Rosenblatt, G. T. Davis, L. A. Hull, and G. D. Forberg. J. Org. Chem. **33**, 1649 (1968).
48. K. Watanabe and J. R. Mottl. J. Chem. Phys. **26**, 1773 (1957).

Can. J. Chem. Downloaded from www.nrcresearchpress.com by 213.166.140.6 on 09/07/12
For personal use only.

49. J. F. COETZEE and C. D. RITCHIE. Solute–solvent interactions. Dekker, New York. 1969. p. 15.
50. J. HOLLUTA and A. MUTSCHIN. Z. Phys. Chem. **150**, 381 (1930).
51. F. MATA-PEREZ and J. F. PEREZ-BENITO. Z. Phys. Chem. (Leipzig), **267**, 120 (1986).
52. J. F. PEREZ-BENITO and D. G. LEE. Can. J. Chem. **63**, 3545 (1985).
53. H. S. POSSELT, F. J. ANDERSON, and W. J. WATER. Environ. Sci. Technol. **2**, 1087 (1968).
54. S. VOYUTSKY. Colloid chemistry. Mir Publishers, Moscow. 1978. p. 139.
55. J. J. MORGAN and W. STUMM. J. Colloid Sci. **19**, 347 (1964).
56. P. GABANO, P. ETIENNE, and J. F. LAURENT. Electrochim. Acta, **10**, 947 (1965).
57. M. H. KURBATOV, G. B. WOOD, and J. D. KURBATOV. J. Chem. Phys. **19**, 258 (1951).
58. M. H. KURBATOV, G. B. WOOD, and J. D. KURBATOV. J. Phys. Colloid Chem. **55**, 1170 (1951).
59. V. V. VOL'KHIN and G. V. LEONT'EVA. Izv. Akad. Nauk SSSR, Neorg. Mater. **5**, 1224 (1969).
60. G. M. BARROW. Physical chemistry. 2nd ed. McGraw–Hill, New York. 1966. p. 766.

Can. J. Chem. Downloaded from www.nrcresearchpress.com by 213.166.140.6 on 09/07/12
For personal use only.

Synthetic studies on cyathins. Synthesis of the ring system

DALE E. WARD
Department of Chemistry, University of Saskatchewan, Saskatoon, Sask., Canada S7N 0W0

Received April 3, 1987

DALE E. WARD. Can. J. Chem. **65**, 2380 (1987).

The tricyclic intermediate **4** has been converted into **2**, a compound that possesses the ring system and stereochemistry of the cyathins. The transformation was accomplished by the preparation of **11**, which underwent efficient base catalysed epimerization to give **12**. Functional group manipulation and selective oxidation provided keto-aldehyde **16**. Upon treatment with acid, **16** undergoes stereoselective aldol cyclization, transacylation, and hemiacetal formation to give **18**. Methylation under basic conditions provides **4**.

DALE E. WARD. Can. J. Chem. **65**, 2380 (1987).

On a transformé l'intermédiaire tricyclique en composé **2** qui possède le système cyclique et la stéréochimie des cyathines. On a effectué cette transformation en procédant à la préparation du composé **11** qui, sous l'influence des bases, subit ensuite une épimérisation efficace conduisant au produit **12**. La manipulation du groupement fonctionnel et une oxydation sélective conduisent au céto-aldéhyde **16**. Par traitement avec de l'acide, le composé **16** subit une cyclisation aldolique stéréosélective, une transacylation et la formation d'un hémiacétal conduisant au produit **18**. Sa méthylation, utilisant des conditions basiques, fournit le composé **4**.

[Traduit par la revue]

Can. J. Chem. Downloaded from www.nrcresearchpress.com by 213.166.140.6 on 09/07/12
For personal use only.

The cyathins (cf. cyathin A_3, **1***a*) are a unique family of diterpenoids produced by bird's nest fungi of the genus *Cyathus* (1). We have previously reported (2) on the preparation of the tricyclic compound **4** as an intermediate in our synthetic studies on cyathins. In this paper we describe the transformation of **4** into **2**, a compound that possesses the ring system and stereochemistry of the cyathins.

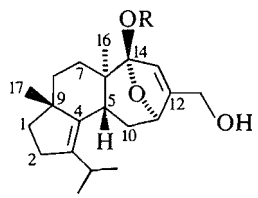

1*a* R = H, cyathin A_3
1*b* R = CH_3

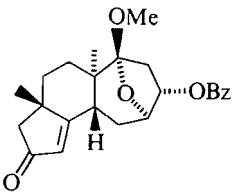

2

The procedure for the preparation of **4** has been improved. Thus the 4:1 mixture of **3***a* and **3***b*, obtained as before (2), was oxidized with *m*-chloroperbenzoic acid in dichloromethane. The resulting mixture of epoxides was dissolved in tetrahydrofuran (THF) and the unsaturated ketone selectively reduced (3) with 9-borabicyclo[3.3.1]nonane (9-BBN). Excess borane was quenched by addition of methanol. After treatment with benzenethiol and base to induce epoxide ring opening, the resulting solution was refluxed with excess base to effect cyclization. Aqueous work-up provided an oil, which upon trituration with ether gave pure crystalline **4**. In this way, the mixture of photoadducts **3***a*,*b* could be converted into **4** in essentially "one pot" in 75% overall yield without the need of chromatography.

The cyathins possess a *trans* BC ring junction and thus we wished to epimerize the *cis*-6,6 ring junction in **4** to *trans*. We have previously (2) shown that **4** is the thermodynamically favored isomer. The major factor disfavoring the *trans* form is $A^{1,3}$ strain between the thiophenyl group and the C-13 methylene hydrogens. Thus the desulfurized derivative **5** (2) gives a 1:1.2 equilibrium mixture of *cis* and *trans* isomers after treatment with sodium methoxide in methanol. In an effort to improve on this ratio, we reasoned that if the C-8 carbonyl could be reduced to give the axial alcohol, the resulting 1,3 diaxial interaction between the C-8 -OH group and the C-13 methylene would further destabilize the *cis* form. To prevent any possible hydrogen bonding between a C-8 axial -OH group and the C-12 allylic alcohol, we sought to protect the latter.

Treatment of **4** with benzoic acid in the presence of triphenylphosphine and diethyl azodicarboxylate (4) gave the benzoate **6** with the desired (cf. C-11 in cyathin A_3) configuration at C-12. That inversion of configuration had indeed occurred in this reaction was readily demonstrated by direct benzoylation (benzoyl chloride, pyridine) of **4** to obtain a different benzoate. Reduction of **6** with sodium borohydride in methanol provided the mixture of alcohols **7**, which could be selectively oxidized by manganese dioxide to produce **8**. The presence of dichloromethane markedly reduced the rate of reduction of the unsaturated ketone with respect to the saturated one. Thus treatment of **6** with sodium borohydride in methanol–dichloromethane (1:1) at −78°C led exclusively to **8** in quantitative yield. The stereochemistry at C-8 was readily assigned by ^{1}H nmr spectroscopy; the C-8 hydrogen appears at δ 4.06 with equatorial–equatorial and equatorial–axial couplings (J = 2.5, 3 Hz). The attempted desulfurization of **8** with Raney nickel under a variety of conditions gave several products of which the desired **9** was, at best, a minor component. Alternatively, hydrolysis of **8** (NaOH, methanol) followed by treatment of the

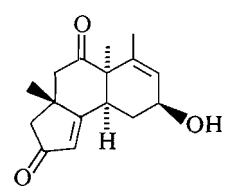

5

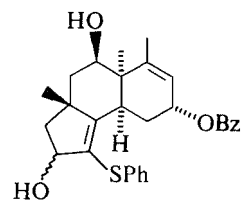

7

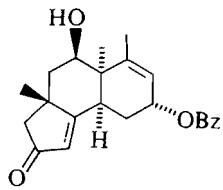

9

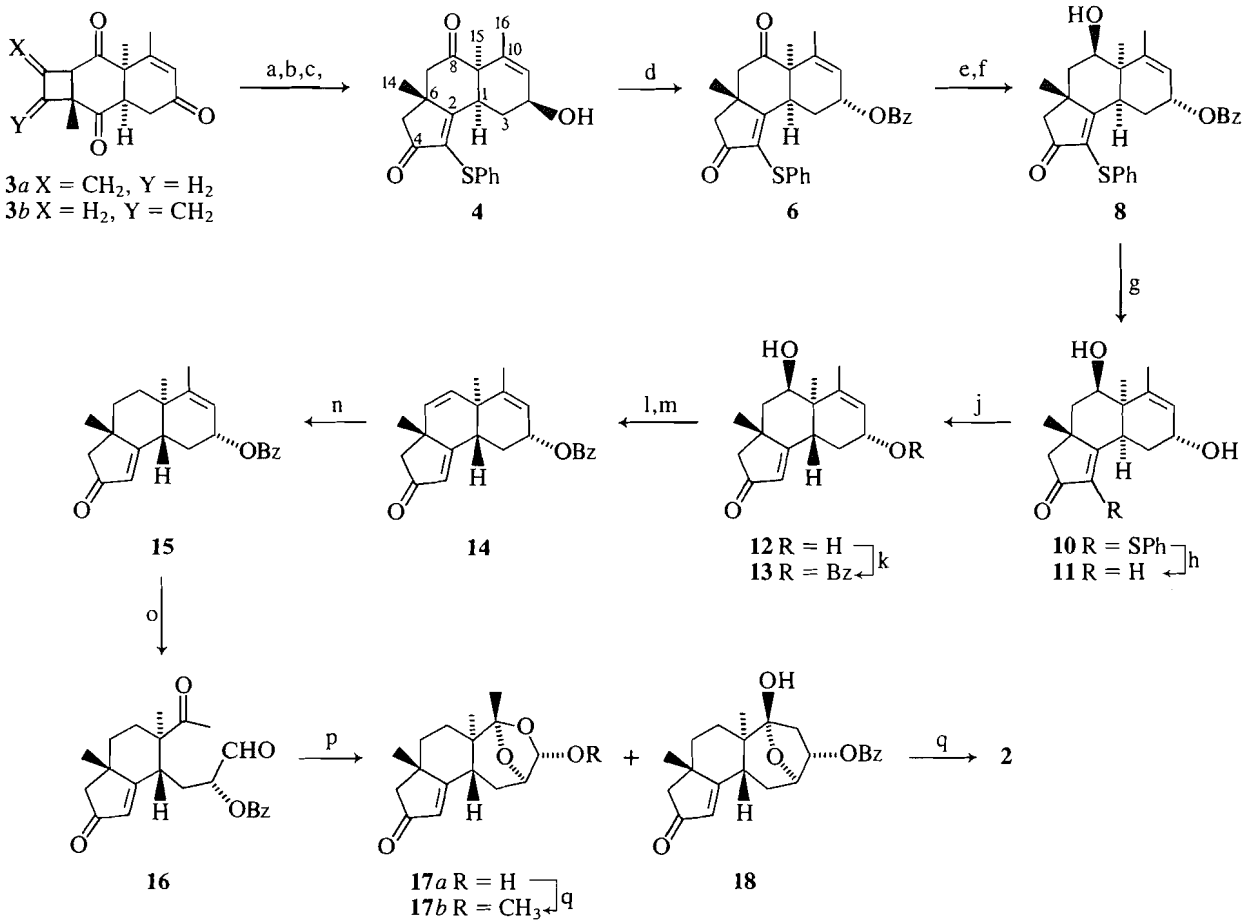

(a) mCPBA, CH_2Cl_2, r.t.; (b) 9-BBN, THF, 15°C–r.t.; (c) PhSH, NaOH, MeOH, THF, 0°C–reflux; (d) PhCOOH, Ph_3P, DEAD, THF, 15°C; (e) $NaBH_4$, MeOH, CH_2Cl_2, −78°C; (f) HOAc, −78°C–r.t.; (g) NaOH, MeOH, H_2O, 50°C; (h) RaNi, MeOH, r.t.; (j) NaOH, MeOH, reflux; (k) PhCOCl, Et_3N, DMAP, CH_2Cl_2, 3°C; (l) MsCl, pyridine, 50°C; (m) DBU, toluene, reflux; (n) H_2, $(Ph_3P)_3RhCl$, benzene; (o) O_3, Sudan III, CH_2Cl_2, −78°C, DMS, pyridine; (p) *p*-TsOH, benzene, r.t.; (q) CH_3I, NaH, THF, r.t.

SCHEME 1

resulting alcohol **10** with Raney nickel in methanol provided **11** in excellent yield. The role of the benzoate group in this reaction is unclear.

We were delighted to find that treatment of **11** with sodium hydroxide in refluxing methanol for 5 days led to a 95:5 (^{1}H nmr) mixture of **12** and **11** respectively. The stereochemistry was readily assigned by ^{1}H nmr. For **12**, the C-3 hydrogen appears at δ 5.82 and is coupled to the C-1 hydrogen (J = 1.5 Hz) whereas for **11**, the C-3 hydrogen appears at δ 6.0 as a singlet (2). While the rate of epimerization of **11** under these conditions is rather slow ($t_{1/2} \approx 24$ h), deuterium incorporation (NaOH, CH_3OD) at C-1 in **11** is complete within 4 h. The equilibrium ratio of **12** to **11** must be greater than 95:5 since a sample of pure **12** does not show epimerization (^{1}H nmr) after the same (NaOH, CH_3OH, reflux, 5 days) treatment. The separation of **12** from **11** is easily accomplished by trituration with ether, providing **12** in 65% overall yield from **4**.

With the four stereocenters of the cyathins in place in **12**, the next stage of our synthetic plan required deoxygenation at C-8 and cyclohexene ring expansion to produce the cyathin ring system.

The sterically hindered nature of the C-8 -OH group allowed the ready preparation (C_6H_5COCl, $(C_2H_5)_3N$, dimethylaminopyridine, 94%) of the monobenzoate **13**. Mesylation (CH_3SO_2Cl, C_5H_5N, 50°C), followed by elimination (DBU, toluene, 110°C) provided the triene **14**. The yield for the two steps was 76%. The disubstituted olefin could be selectively reduced using Wilkinson's catalyst under H_2 (50 psi; 1 psi = 6.9 kPa) for 48 h to give **15** in 92% yield.

The stage was set for ring expansion and towards this end a solution of **15** in 10% methanol in dichloromethane was "titrated" with O_3 at −78°C in the presence of Sudan III as indicator (5). The result was the selective oxidation of the isolated double bond to yield, after work-up, the sensitive keto-aldehyde **16**. While the presence of methanol was necessary for clean oxidation, there was a strong tendency for addition of methanol to the aldehyde to give varying mixtures of hemiacetals, acetal, and free aldehyde. This side reaction could be circumvented by the addition of a small amount of pyridine along with dimethyl sulfide (excess) at −78°C. Warming to room temperature and concentration provided **16** free from any hemiacetal or acetal. The benzoate group in **16** proved to be labile and all attempts at aldol cyclization led to hydrolysis and internal acetal formation to yield **17***a*. Structure **17***a* was assigned on the basis of its ^{1}H nmr spectrum. The most significant changes with respect to the spectrum of **16** are as

Can. J. Chem. Downloaded from www.nrcresearchpress.com by 213.166.140.6 on 09/07/12
For personal use only.

Can. J. Chem. Downloaded from www.nrcresearchpress.com by 213.166.140.6 on 09/07/12
For personal use only.

follows: the aldehyde hydrogen is lost and a new one-hydrogen singlet appears at δ 5.32; the benzoate group is lost and the carbinol hydrogen is shifted upfield to δ 4.37; the acyl methyl group is shifted upfield to δ 1.45. The *exo* stereochemistry of the hemiacetal -OH group is assigned on the basis of the lack of coupling between the C-11 and C-12 (cyathin numbering) hydrogens (dihedral angle ≈ 90°).

Benzoate hydrolysis could be suppressed in favor of cyclization by treatment of **16** with dry *p*-toluenesulfonic acid in dry benzene (or toluene) at room temperature. In this way we could obtain a 3:1 mixture of **18** and **17***a* in 80% yield. Cyclization was always accompanied by transacylation; we were unable to detect the presence of any 11-benzoyloxy-12-hydroxy (cyathin numbering) compound in the reaction mixture. The driving force for this transacylation is, presumably, the formation of the stable internal hemiacetal. The ^{1}H nmr spectrum of **18** is fully assigned (with the exception of the C-7 and C-8 hydrogens) and is in complete accord with the indicated structure. The benzoyloxy group is assigned as *exo* due to the lack of coupling between the C-11 and C-12 hydrogens. Although the ^{1}H nmr spectrum of **18** exhibits sharp signals at room temperature, most of the resonances in the ^{13}C nmr spectrum could not be observed. This effect is due to hemiacetal–ketol interconversion. At −50°C all carbon resonances are observable and, significantly, C-14 appears at δ 108.6, indicating a predominance of the hemiacetal isomer. Interestingly, cyathin A_3 (**1***a*) shows broad signals in the ^{1}H nmr spectrum at room temperature while the ^{13}C nmr spectrum exhibits a set of signals for both the hemiacetal and ketol isomers (6).

In an effort to further characterize **18**, as well as to protect the hemiacetal, we attempted to prepare the corresponding methyl acetal **2**. In contrast to **1***a*, which readily forms **1***b* (**1***a*), we were unable to obtain **2** by treatment of **18** with methanol and acid under a variety of conditions. This result reflects the stability of the hemiacetal.[1] The preparation of **2** was finally accomplished by reaction of **18** with sodium hydride in the presence of iodomethane. With the exception of small changes in chemical shifts, the ^{1}H and ^{13}C nmr spectra of **2** are very similar to those of **18** and are fully consistent with the assigned structure.

Compound **2** possesses both the ring system and stereochemistry of the cyathins. While methods are available for introduction of a hydroxymethyl group at C-12 (7), the introduction of an isopropyl group at C-3 is not straightforward. Studies aimed at solving this problem are underway.

Experimental

All solvents except diethyl ether were distilled prior to use. ACS quality anhydrous diethyl ether was used without purification. Pyridine was distilled from CaH_2 and stored over molecular sieves, and THF was distilled under argon from potassium benzophenone ketyl. Unless otherwise noted, commercially available reagents were used as received.

Analytical thin-layer chromatography (tlc) was carried out on glass plates (70 × 20 or 70 × 50 mm) precoated (0.25 mm) with silica gel $60F_{254}$ (E. Merck, Darmstadt). Preparative thin-layer chromatography (ptlc) was carried out on glass plates (20 × 20 cm) precoated (0.25 mm) with the same adsorbent. Materials were detected by visualization under an ultraviolet (uv) lamp (254 or 350 nm), and (or) by spraying with a solution of phosphomolybdic acid (5%) containing a trace of ceric sulfate in aqueous sulfuric acid (5%, v/v), followed by charring on a hot plate. Flash column chromatography (8) was performed with Merck Silica Gel 60 (40–63 μm).

High resolution mass spectra (hrms) were recorded on an A.E.I. MS-50 mass spectrometer coupled to a DS 50 computer. Infrared (ir) spectra were recorded on a Nicolet 7199 FT interferometer on a Perkin–Elmer 781 infrared spectrophotometer. ^{1}H nuclear magnetic resonance (^{1}H nmr) spectra and ^{13}C nuclear magnetic resonance (^{13}C nmr) spectra were measured on a Bruker AM-300 spectrometer or a Bruker WH-400 spectrometer. For ^{1}H nmr, residual $CHCl_3$ in $CDCl_3$ was employed as the internal standard (assigned as 7.26 ppm downfield from tetramethylsilane (TMS)) and measurements are reported in ppm downfield from TMS (δ). For ^{13}C nmr, $CDCl_3$ was employed as the internal standard (assigned as 77.0 ppm downfield from TMS) and measurements are reported in ppm downfield from TMS (δ). The ^{1}H nmr assignments are made on the basis of chemical shift and multiplicity and, where necessary, confirmed by decoupling experiments. Coupling constants are reported to the nearest 0.5 Hz. The ^{13}C nmr assignments are made on the basis of chemical shift, multiplicity,[2] analogy with similar compounds (6), and consistency within the series of intermediates (9). Melting points were recorded on a Fisher–Johns melting point apparatus and are uncorrected.

cis-*12β-hydroxy-6β,9α,10-trimethyl-3-(phenylthio)tricyclo[7.4.0.0^{2,6}]-trideca-2,10-diene-4,8-dione* (**4**)

The 4:1 mixture of photoadducts **3***a* and **3***b* (1.009 g) was dissolved in CH_2Cl_2 (100 mL) and mCPBA (1.0 g) was added. The reaction was complete after 36 h (tlc: 5% CH_3OH in CH_2Cl_2), and $(CH_3)_2S$ (1 mL) was added. After 1 h the reaction mixture was washed with saturated $NaHCO_3$, dried with Na_2SO_4, and concentrated to give the mixture of epoxides (1.074 g, 100%). The epoxides were dissolved in dry THF (75 mL) and the solution was cooled in an ice bath. After addition of 9-BBN (0.5 *M* in THF, 9 mL) the solution was allowed to slowly warm to room temperature and the reaction was monitored by tlc (5% CH_3OH in CH_2Cl_2). After approximately 2 h starting material was consumed and CH_3OH (75 mL) was added. The solution was cooled in an ice bath and thiophenol (0.480 mL) and 2 *M* aqueous KOH (0.180 mL) were added. The solution was allowed to warm to room temperature and, after 14 h, 2 *M* aqueous KOH (5 mL) was added and the resulting solution was heated under reflux for 2 h. The reaction mixture was concentrated, diluted with water, and extracted (×3) with CH_2Cl_2. The combined CH_2Cl_2 layers were washed with dilute NaOH, water, dried (Na_2SO_4), and concentrated to give an oil, which upon trituration with ether provided crystalline **4** (mp 209–210°C, 845 mg, 78%).

cis-*12α-Benzoyloxy-6β,9α,10-trimethyl-3-(phenylthio)tricyclo-[7.4.0.0^{2,6}]trideca-2,10-diene-4,8-dione* (**6**)

The allylic alcohol **4** (845 mg) was dissolved in dry THF (100 mL), and triphenylphosphine (843 mg) and benzoic acid (424 mg) were added. Diethyl azodicarboxylate (0.61 mL) was added dropwise over 5 min, maintaining the reaction temperature at 15–20°C. After 1 h, CH_3OH (5 mL) was added and, after concentration, the reaction mixture was fractionated by flash column chromatography (gradient elution; 0–3% CH_3OH in CH_2Cl_2) to give the crude benzoate **6** (1.2 g). A sample further purified by ptlc (50% ethyl acetate – hexane) shows the following spectral characteristics: ir: 1710, 1263 cm^{-1}; ^{1}H nmr δ: 1.36 (s) and 1.39 (s) (C-6, 9 CH_3's), 1.84 (s, C-10 CH_3), 1.87 (dm, J = 14 Hz, C-13 αH), 2.05 (dt, J = 3.5, 14 Hz, C-13 βH), 2.56 (d, J = 13 Hz) and 3.00 (d, J = 13 Hz) (C-7 H's), 2.61 (AB quartet, C-5 H's), 4.24 (dd, J = 14, 3 Hz, C-1 H), 5.42 (m, C-12 H), 5.97 (d, J = 5.5 Hz, C-11 H), 7.2 (m, C_6H_5S-), 7.32, 7.52, 8.07 (m, C_6H_5CO-); ^{13}C nmr δ: 20.0 (q, C-16), 23.8 (q, C-15), 28.9 (q, C-14), 31.0 (t, C-13), 44.2 (d, C-1), 46.8 (t, C-7), 49.4 (s, C-6), 52.8 (s, C-9), 53.0 (t, C-5), 65.7 (d, C-12), 122.1 (d, C-11), 133.5 (s, C-3), 142.6 (s, C-10), 187.8 (s, C-2), 201.4 (s, C-4), 209.1 (s, C-8), 165.5, 135.2, 132.7, 130.1, 129.5, 128.9, 128.8, 128.1, 126.6 (C_6H_5CO-

[1]For acetal formation to occur, methanol must add to the (presumably protonated) carbonyl group. In **18**, methanol cannot compete with the addition of the C-11 -OH group to form the hemiacetal. By contrast, in **1***a*, the conformations of the hemiacetal and ketol isomers are different (6). Methanol can successfully add to the protonated ketol isomer to ultimately form **1***b*.

[2]Multiplicity was determined by *J*-moduation (10).

Can. J. Chem. Downloaded from www.nrcresearchpress.com by 213.166.140.6 on 09/07/12
For personal use only.

and C_6H_5S-); hrms, *m/z* calcd. for $C_{29}H_{28}O_4S$: 472.1708; found: 472.1714.

cis-*12α-Benzoyloxy-8β-hydroxy-6β,9α,10-trimethyl-3-(phenylthio)-tricyclo[7.4.0.0^{2,6}]trideca-2,10-diene-4-one (8)*

The crude benzoate **6** (1.2 g) was dissolved in CH_2Cl_2 (50 mL), and CH_3OH (50 mL) was added. The resulting solution was cooled to −78°C and $NaBH_4$ (200 mg) was added. After standing at −78°C for 14 h, acetic acid (2 mL) was added with stirring and the reaction mixture was allowed to warm to room temperature. Concentration and reconcentration from toluene provided the alcohol **8** (1.5 g), which was used without further purification. A sample purified by ptlc (2.5% CH_3OH in CH_2Cl_2) shows the following spectral characteristics: ir: 3500 (br), 1710, 1585, 1270 cm^{-1}; ^{1}H nmr δ: 0.98 (s) and 1.61 (s) (C-6, 9 CH_3's), 1.83 (s, C-10 CH_3), 1.93 (dd, *J* = 15, 3 Hz, C-7 H), 2.33 (dd, *J* = 15, 2.5 Hz, C-7 H), 2.41 (d, *J* = 18 Hz, C-5 H), 2.53 (d, *J* = 18 Hz, C-5 H), 2.83 (dt, *J* = 4, 14 Hz, C-13 βH), 3.88 (dd, *J* = 14, 2.5 Hz, C-1 H), 4.06 (brs, C-8 H), 5.46 (m, C-12 H), 6.12 (d, *J* = 5.5 Hz, C-11 H), 7.1 (m, C_6H_5S-), 7.42, 7.55, 8.09 (m, C_6H_5CO-); ^{13}C nmr δ: 18.1 (q, C-16), 24.4 (q, C-15), 31.0 (q, C-14), 31.2 (t, C-13), 39.7 (t, C-7), 40.1 (d, C-1), 42.3 (s, C-9), 44.2 (s, C-6), 54.7 (t, C-5), 66.5 (d, C-12), 72.3 (d, C-8), 124.8 (d, C-11), 133.4 (s, C-3), 143.9 (s, C-10), 190.4 (s, C-2), 203.2 (s, C-4), 126.3, 128.3, 128.5, 128.9, 129.7, 130.5, 132.8, 134.7, 165.0 (C_6H_5CO- and C_6H_5S-); hrms, *m/z* calcd. for $C_{29}H_{30}O_4S$: 474.1864; found: 474.1869.

cis-*8β,12α-Dihydroxy-6β,9α,10-trimethyl-3-(phenylthio)tricyclo-[7.4.0.0^{2,6}]trideca-2,10-diene-4-one (10)*

The crude alcohol (1.5 g) was dissolved in CH_3OH (100 mL) and 1 *M* aqueous NaOH (10 mL) was added. The reaction mixture was stirred at 50°C overnight, concentrated, diluted with water, and extracted (×3) with CH_2Cl_2 and the combined CH_2Cl_2 layers were dried (Na_2SO_4) and concentrated to give the crude diol (950 mg). A sample purified by ptlc (5% CH_3OH in CH_2Cl_2) shows the following spectral characteristics: ir: 3400 (br), 1707, 1583 cm^{-1}; ^{1}H nmr δ: 0.96 (s) and 1.58 (s) (C-6, 9 CH_3's), 1.48 (ddt, *J* = 14, 3.5, 2 Hz, C-13 αH), 1.80 (t, *J* = 1 Hz, C-10 CH_3), 1.89 (dd, *J* = 14.5, 3 Hz, C-7 H), 2.30 (dd, *J* = 14.5, 2.5 Hz, C-7 H), 2.39 (dt, *J* = 4, 14 Hz, C-13 βH), 3.68 (dd, *J* = 14, 3.5 Hz, C-1 H), 4.00 (brs, C-8 H), 4.22 (m, C-12 H), 6.00 (dq, *J* = 6, 1 Hz, C-11 H), 7.25 (m, C_6H_5S-); ^{13}C nmr δ: 17.9 (q, C-16), 24.2 (q, C-15), 30.9 (q, C-14), 33.9 (t, C-13), 39.1 (d, C-1), 39.4 (t, C-7), 42.2 (s, C-9), 43.9 (s, C-6), 54.6 (t, C-5), 62.6 (d, C-12), 71.8 (d, C-8), 127.9 (d, C-11), 132.9 (s, C-3), 140.8 (s, C-10), 190.7 (s, C-2), 203.3 (s, C-4), 126.2, 128.6, 128.8, 134.3 (C_6H_5S-); hrms, *m/z* calcd. for $C_{22}H_{26}O_3S$: 370.1602; found: 370.1586.

cis-*8β,12α-Dihydroxy-6β,9α,10-trimethyltricyclo[7.4.0.0^{2,6}]tri-deca-2,10-diene-4-one (11)*

The crude diol **10** (945 mg) was dissolved in CH_3OH (100 mL) and W2 Raney Ni (5 mL) was added with stirring. After 1.5–2 h the mixture was filtered and concentrated to give crude diol **11** (601 mg). A sample further purified by ptlc (5% CH_3OH in CH_2Cl_2) shows the following spectral characteristics: ir: 3400 (br), 1692 (sh), 1675, 1606 cm^{-1}; ^{1}H nmr δ: 0.99 (s) and 1.56 (s) (C-6, 9 CH_3's), 1.75 (dm, *J* = 14 Hz, C-13 αH), 1.81 (s, C-10 CH_3), 1.82 (dd, *J* = 14.5, 3 Hz, C-7 H), 2.24 (dd, *J* = 14.5, 2.5 Hz, C-7 H), 2.34 (s, C-5 H's), 2.74 (dt, *J* = 14, 4 Hz, C-13 βH), 3.11 (dd, *J* = 14, 3 Hz, C-1 H), 3.96 (brs, C-8 H), 4.28 (m, C-12 H), 6.00 (m, C-11 H), 6.00 (s, C-3 H); ^{13}C nmr δ: 18.0 (q, C-16), 24.0 (q, C-15), 30.2 (q, C-14), 34.5 (t, C-13), 39.8 (t, C-7), 40.5 (d, C-1), 42.2 (s, C-9), 44.1 (s, C-6), 55.6 (t, C-5), 66.2 (d, C-12), 72.0 (d, C-8), 128.0 (d, C-11), 130.0 (d, C-3), 141.2 (s, C-10), 189.1 (s, C-2), 207.8 (s, C-4); hrms, *m/z* calcd. for $C_{16}H_{22}O_3$: 262.1569; found: 262.1560.

trans-*8β,12α-Dihydroxy-6β,9α,10-trimethyltricyclo[7.4.0.0^{2,6}]tri-deca-2,10-diene-4-one (12)*

The crude *cis* diol **11** (601 mg) was dissolved in CH_3OH (100 mL) and NaOH (1.5 g) was added. The resulting solution was heated under reflux for 5 days. Normal aqueous work-up leads to a poor recovery of product, therefore a nonaqueous work-up was utilized. The reaction mixture was made slightly acidic (pH ≈ 6) by addition of 6 *M* $HCl_{(aq)}$ and $NaHCO_3$ (1 g) was added. The mixture was concentrated to dryness and the resulting solid extracted with ether (impurities and *cis* diol **11** are removed), then with 20% CH_3OH in CH_2Cl_2 (×2). Concentration of the combined methanolic dichloromethane extracts provided essentially pure **12** (391 mg, 65% overall yield from **4**); ir: 3400 (br), 1692, 1672, 1611 cm^{-1}; ^{1}H nmr δ: 0.90 (s) and 1.47 (s) (C-6, 9 CH_3's), 1.71 (dt, *J* = 10, 13 Hz, C-13 αH), 1.80 (t, *J* = 1.5 Hz, C-10 CH_3), 1.85 (dd, *J* = 15, 3 Hz, C-7 H), 2.07 (dd, *J* = 15, 2.5 Hz, C-7 H), 2.18 (dddd, *J* = 12.5, 7, 1, 1 Hz, C-13 βH), 2.24 (d, *J* = 18 Hz) and 2.34 (d, *J* = 18 Hz) (C-5 H's), 3.23 (ddd, *J* = 13, 1.5, 1 Hz, C-1 H), 4.05 (brs, C-8 H), 4.45 (m, C-12 H), 5.53 (m, C-11 H), 5.83 (d, *J* = 1.5 Hz, C-3 H); ^{13}C nmr δ: 18.0 (q, C-16), 19.3 (q, C-15), 29.7 (q, C-14), 30.4 (t, C-13), 35.3 (d, C-1), 41.9 (t, C-7), 42.9 (s, C-6), 46.7 (s, C-9), 54.1 (t, C-5), 67.3 (d, C-12), 71.6 (d, C-8), 125.9 (d, C-3), 129.2 (d, C-11), 141.4 (s, C-10), 188.6 (s, C-2), 208.6 (s, C-4); hrms, *m/z* calcd. for $C_{16}H_{23}O_3$: 262.1569; found: 262.1555.

trans-*12α-Benzoyloxy-8β-hydroxy-6β,9α,10-trimethyltricyclo-[7.4.0.0^{2,6}]trideca-2,10-diene-4-one (13)*

The *trans* diol **12** (391 mg) was dissolved in CH_2Cl_2 (70 mL) and benzoyl chloride (0.5 mL), and triethylamine (1 mL) and *N,N*-dimethylaminopyridine (20 mg) were added. The reaction mixture was kept at 3°C for 16 h and CH_3OH (2 mL) was added. After 30 min the solution was concentrated and the resulting oil was fractionated by flash column chromatography (eluting first with CH_2Cl_2, then with ethyl acetate) to give the monobenzoate **13** (514 mg, 94%); ir: 3450 (br), 1710, 1700 (sh), 1674, 1614, 1269 cm^{-1}; ^{1}H nmr δ: 0.96 (s) and 1.50 (s) (C-6, 9 CH_3's), 1.84 (t, *J* = 1.5 Hz, C-10 CH_3), 1.87 (dd, *J* = 15, 3.5 Hz, C-7 H), 1.94 (ddd, *J* = 13, 12, 10 Hz, C-13 αH), 2.10 (dd, *J* = 15, 2.5 Hz, C-7 H), 2.25 (d, *J* = 18.5 Hz) and 2.35 (d, *J* = 18.5 Hz) (C-5 H's), 2.36 (dddd, *J* = 12, 7, 1, 1 Hz, C-13 βH), 3.38 (ddd, *J* = 13, 1.5, 1 Hz, C-1 H), 4.09 (dd, *J* = 3.5, 2.5 Hz, C-8 H), 5.59 (ddq, *J* = 2, 1, 1.5 Hz, C-11 H), 5.75 (dddq, *J* = 10, 7, 2, 1.5 Hz, C-12 H), 5.81 (d, *J* = 1.5 Hz, C-3 H), 7.35 (m), 7.58 (m), 8.07 (m) (C_6H_5CO-); ^{13}C nmr δ: 18.1 (q, C-16), 19.0 (q, C-15), 26.3 (t, C-13), 29.6 (q, C-14), 35.1 (d, C-1), 41.8 (t, C-7), 42.9 (s, C-6), 46.5 (s, C-9), 53.9 (t, C-5), 70.5 (d, C-12), 71.2 (d, C-10), 124.2 (d, C-11), 125.7 (d, C-3), 188.9 (s, C-2), 207.9 (s, C-4), 128.2 (d), 129.5 (d), 130.2 (s), 132.9 (d), 166.2 (s) (C_6H_5CO-); hrms, *m/z* calcd. for $C_{23}H_{26}O_4$: 366.1831; found: 366.1831.

trans-*12α-Benzoyloxy-6β,9α,10-trimethyltricyclo[7.4.0.0^{2,6}]tri-deca-2,7,10-triene-4-one (14)*

The benzoate **13** (514 mg) was dissolved in pyridine (50 mL) and the solution was heated to 50°C. Methanesulfonyl chloride (1.0 mL) was slowly added with a syringe pump over 10–15 h while monitoring the reaction by tlc (5% CH_3OH in CH_2Cl_2). When the reaction was completed the solution was concentrated from toluene, dissolved in ethyl acetate, washed with dilute HCl, saturated $NaHCO_3$, brine, dried over Na_2SO_4, and concentrated to give the crude mesylate (663 mg); ^{1}H nmr δ: 3.08 (s, -SO_2CH_3), 5.07 (dd, *J* = 3.5, 2.5 Hz, C-8 H). The mesylate was dissolved in toluene (50 mL), DBU (1.1 g) was added, and the solution was heated under reflux for 72 h. After dilution with ethyl acetate the solution was washed with dilute HCl, saturated $NaHCO_3$, brine, dried over Na_2SO_4, and concentrated to give an oil. Purification by flash column chromatography (30% ethyl acetate in hexane) gave the triene **14** (372 mg, 76%); ir: 1712, 1635, 1620, 1270 cm^{-1}; ^{1}H nmr δ: 1.04 (s) and 1.34 (s) (C-6, 9 CH_3's), 1.88 (t, *J* = 1.5 Hz, C-10 CH_3), 2.05 (dt, *J* = 9.5, 13 Hz, C-13 αH), 2.34 (d, *J* = 17.5 Hz) and 2.40 (d, *J* = 17.5 Hz) (C-5 H's), 2.41 (ddd, *J* = 13, 7, 2 Hz, C-13 βH), 3.11 (ddd, *J* = 13, 2, 1 Hz, C-1 H), 5.43 (dq, *J* = 2, 1.5 Hz, C-11 H), 5.64 (d, *J* = 10 Hz) and 5.94 (d, *J* = 10 Hz) (C-7, 8 H's), 5.75 (dddq, *J* = 9.5, 7, 2, 1.5 Hz, C-12 H), 5.83 (d, *J* = 1 Hz, C-3 H), 7.46 (m), 7.58 (m) and 8.09 (m) (C_6H_5CO-); ^{13}C nmr δ: 19.3 (q, C-16), 24.2 (q, C-15), 26.2 (t, C-13), 29.6 (q, C-14), 41.0 (d, C-1), 44.4 (s) and 45.7 (s) (C-6,9), 50.2 (t, C-5), 70.5 (d, C-12), 121.2 (d, C-11), 124.5 (d, C-3), 131.4 (d) and 131.7 (d) (C-7,8), 145.5 (s, C-10), 185.7 (s, C-2), 207.4 (s, C-4), 128.3 (d),

Can. J. Chem. Downloaded from www.nrcresearchpress.com by 213.166.140.6 on 09/07/12
For personal use only.

129.6 (d), 130.3 (s), 132.9 (d) (C_6H_5CO-); hrms, m/z calcd. for $C_{23}H_{24}O_3$: 348.1726; found: 348.1726.

trans-*12α-Benzoyloxy-6β,9α,10-trimethyltricyclo[7.4.0.0^{2,6}]trideca-2,10-diene-4-one (**15**)*

The triene **14** (372 mg) was dissolved in benzene (50 mL) and argon was bubbled through the solution for 10 min. Wilkinson's catalyst (90 mg) was added and the solution was shaken under H_2 (50 psi) for 2 days. Concentration and fractionation by flash column chromatography (30% ethyl acetate in hexane) provided the diene **15** (345 mg, 92%); ir: 1710, 1620, 1268 cm^{-1}; ^{1}H nmr δ: 0.98 (s) and 1.29 (s) (C-6, 9 CH_3's), 1.76 (t, J = 1.5 Hz, C-10 CH_3), 1.90 (dt, J = 10, 13 Hz, C-13 αH), 2.28 (dddd, J = 13, 8, 2, 2 Hz, C-13 βH), 2.28 (d, J = 18.5 Hz) and 2.37 (d, J = 18.5 Hz) (C-5 H's), 2.77 (ddd, J = 13, 2, 1.5 Hz, C-1 H), 5.40 (ddq, J = 2, 1, 1.5 Hz, C-11 H), 5.71 (dddq, J = 10, 8, 1, 1.5 Hz, C-12 H), 5.77 (d, J = 1.5 Hz, C-3 H), 7.47 (m), 7.59 (m) and 8.09 (m) (C_6H_5CO-); ^{13}C nmr δ: 18.2 (q, C-16), 18.6 (q, C-15), 25.3 (q, C-14), 26.7 (t, C-13), 31.8 (t, C-8), 35.9 (t, C-7), 41.5 (s, C-9), 41.9 (d, C-1), 43.0 (s, C-6), 52.5 (t, C-5), 70.7 (d, C-12), 120.8 (d, C-11), 125.9 (d, C-3), 147.2 (s, C-10), 187.4 (s, C-2), 207.4 (s, C-4), 128.2 (d), 129.6 (d), 130.4 (s), 132.9 (d) (C_6H_5CO-); hrms, m/z calcd. for $C_{23}H_{26}O_3$: 350.1882; found: 350.1885.

*Preparation of keto-aldehyde **16***[3]

The diene **15** (218 mg) was dissolved in 10% methanolic dichloromethane (40 mL) containing a small amount (1–2 mg) of Sudan III and the resulting solution cooled to −78°C. A stream of ozone in air was bubbled through the solution until the red color was discharged. Argon was bubbled through the solution for 5 min. Pyridine (0.1 mL) and dimethyl sulfide (0.5 mL) were added and the solution kept at 3°C overnight. Concentration from xylenes (to remove pyridine and dimethyl sulfoxide) provided essentially homogeneous **16** (246 mg, quantitative); ir: 1705, 1620 cm^{-1}; ^{1}H nmr δ: 1.08 (s) and 1.22 (s) (C-6, 9 CH_3's), 1.82 (ddd, J = 14.5, 7.5, 1.5 Hz, C-10 H), 2.03 (ddd, J = 14.5, 10, 7.4 Hz, C-10 H), 2.23 (s, C-13 H's), 2.28 (s, C-1 H's), 3.41 (ddd, J = 10, 1.5 Hz, C-5 H), 5.23 (td, J = 7.5, 1 Hz, C-11 H), 6.10 (d, J = 1.5 Hz, C-3 H), 9.65 (d, J = 1 Hz, C-12 H); ^{13}C nmr δ: 14.6 (q, C-16), 23.6 (q, C-13), 25.4 (q, C-17), 28.1 (t, C-10), 32.2 (t, C-7), 35.7 (t, C-8), 38.1 (d, C-5), 43.3 (s, C-9), 52.0 (t, C-1), 55.5 (s, C-6), 77.5 (d, C-11), 128.3 (d, C-3), 186.6 (s, C-4), 197.4 (d, C-12), 206.2 (s, C-2), 211.0 (s, C-14), 165.8 (s), 133.6 (d), 133.1 (s), 129.8 (d) and 128.5 (d) (C_6H_5CO-); hrms, m/z calcd. for $C_{23}H_{26}O_5$: 382.1779; found: 382.1763.

*Preparation of acetal **2***[3]

The ketoaldehyde **16** (246 mg) was dissolved in benzene (40 mL) and water removed by azeotropic distillation under argon to give a dry solution (~20 mL). *p*-Toluenesulfonic acid (dihydrate, 250 mg) was suspended in toluene (40 mL) and water removed by azeotropic distillation under argon to give a dry solution (~20 mL). The two solutions were mixed under argon and allowed to stand for 48 h. The solution was washed with $NaHCO_{3(aq)}$, dried over Na_2SO_4, and concentrated to give an oil (249 mg), which consisted mainly of **18** and **17*a*** (3:1, ^{1}H nmr). Further purification by ptlc (5% CH_3OH in CH_2Cl_2) provided pure samples of **18**; ir: 3400 (br), 1705, 1620 cm^{-1}; ^{1}H nmr δ: 0.98 (s, C-16 H's), 1.32 (s, C-17 H's), 1.63 (ddd, J = 13, 4, 1.5 Hz, C-10 βH), 1.90 (ddd, J = 15, 3, 1.5 Hz, C-13 αH), 1.92 (td, J = 13, 3.5 Hz, C-10 αH), 2.29 (d, J = 18.5 Hz, C-1 H), 2.37 (d, J = 18.5 Hz, C-1 H), 2.56 (ddd, J = 13, 4, 1.3 Hz, C-5 H), 2.81 (brs, OH), 3.07 (dd, J = 15, 7.5 Hz, C-13 βH), 4.53 (dt, J = 3.5, 1.5 Hz, C-11 H), 5.27 (dd, J = 7.5, 3 Hz, C-12 H), 5.74 (d, J = 1.3 Hz, C-3 H), 7.45 (m, 2H), 7.59 (m, 1H) and 8.07 (m, 2H) (C_6H_5CO-); ^{13}C nmr (−50°C) δ: 11.6 (q, C-16), 25.9 (q, C-17), 26.1 (t, C-10), 28.1 (t, C-7), 35.2 (t, C-8), 38.1 (d, C-5), 40.1 (t, C-13), 43.1 (s, C-9), 45.2 (s, C-6), 52.1 (t, C-1), 77.4 (d) and 79.0 (d) (C-11,12), 108.4 (s, C-14), 125.7 (d, C-3), 187.8 (s, C-4), 208.9 (s, C-2), 128.3 (d), 128.7 (s), 129.6 (d), 133.5 (d), 166.4 (s) (C_6H_5CO-); hrms, m/z calcd. for $C_{23}H_{26}O_5$: 382.1779; found: 382.1768; and **17*a***; ^{1}H nmr δ: 0.87 (s, C-16 H's), 1.27 (s, C-17 H's), 1.46 (s, C-13 H's), 2.75 (brs, OH), 2.83 (ddd, J = 13.5, 4, 1.5 Hz, C-1 H), 4.33 (dd, J = 2.5, 2.5 Hz, C-11 H), 5.32 (brs, C-12 H), 5.71 (d, J = 1.5 Hz, C-3 H). In practice, the crude reaction mixture (249 mg) was dissolved in THF (25 mL), and iodomethane (0.5 mL) and NaH (50% in oil, ca. 100 mg) were added. After stirring for 1.5 h at room temperature, the reaction mixture was quenched with acetic acid, concentrated, diluted with ethyl acetate, washed with saturated $NaHCO_3$, dried over Na_2SO_4, and concentrated to give an oil. Purification by flash column chromatography (35% ethyl acetate in hexane) provided **2** (125 mg, 49% from **16**); ir: 1705, 1620 cm^{-1}; ^{1}H nmr δ: 0.92 (s, C-16 H's), 1.31 (s, C-17 H's), 1.61 (ddd, J = 13.5, 4, 1.5 Hz, C-10 βH), 1.92 (td, J = 13.5, 4 Hz, C-10 αH), 2.15 (ddd, J = 15, 2.5, 1.5 Hz, C-13 αH), 2.28 (d, J = 18.5 Hz, C-1 H), 2.35 (d, J = 18.5 Hz, C-1 H), 2.56 (ddd, J = 13.5, 4, 1.5 Hz, C-5 H), 2.60 (dd, J = 15, 7.5 Hz, C-13 βH), 3.40 (s, 3H, OCH_3), 4.48 (dt, J = 4, 1.5 Hz, C-11 H), 5.29 (dd, J = 7.5, 2 Hz, C-12 H), 5.73 (d, J = 1.5 Hz, C-3 H), 7.47 (m, 2H), 7.60 (m, 1H) and 8.07 (m, 2H) (C_6H_5CO-); ^{13}C nmr δ: 11.9 (q, C-16), 26.2 (q, C-17), 26.7 (t, C-10), 28.2 (t, C-7), 32.1 (t, C-13), 36.0 (t, C-8), 38.3 (d, C-5), 43.2 (s, C-9), 46.2 (s, C-6), 49.4 (q, OCH_3), 52.6 (t, C-1), 77.5 (d) and 78.8 (d) (C-11, 12), 111.2 (s, C-14), 125.9 (d, C-3), 186.7 (s, C-4), 207.4 (s, C-2), 128.5 (d), 129.6 (d), 129.9 (s), 133.3 (d), 166.4 (s) (C_6H_5CO-); hrms, m/z calcd. for $C_{24}H_{28}O_5$: 396.1936; found: 396.1932; and **17*b*** (32 mg, 17%); ir: 1700, 1620 cm^{-1}; ^{1}H nmr δ: 0.87 (s, C-16, H's), 1.29 (s, C-17 H's), 1.45 (s, C-13 H's), 1.54 (ddd, J = 13.5, 4, 2 Hz, C-10 βH), 1.89 (td, J = 13.5, 2.5 Hz, C-10 αH), 2.25 (d, J = 18 Hz) and 2.33 (d, J = 18 Hz) (C-1 H's), 2.83 (ddd, J = 13.5, 4, 1.5 Hz, C-5 H), 3.43 (s, OCH_3), 4.37 (dd, J = 2.5, 2 Hz, C-11 H), 5.02 (s, C-12 H), 5.70 (d, J = 1.5 Hz, C-3 H); ^{13}C nmr δ: 14.4 (q, C-16), 19.0 (q, C-17), 24.9 (q, C-13), 26.2 (t, C-10), 29.2 (t, C-7), 36.1 (t, C-8), 37.7 (d, C-5), 43.2 (s, C-9), 46.2 (s, C-6), 52.6 (t, C-1), 54.3 (q, OCH_3), 79.3 (d, C-11), 103.6 (d, C-12), 113.7 (s, C-14), 125.5 (d, C-3), 188.1 (s, C-4), 207.4 (s, C-2); hrms, m/z calcd. for $C_{17}H_{24}O_4$: 292.1674; found: 292.1662.

[3]Cyathin numbering is used in spectral assignments.

Acknowledgements

We gratefully acknowledge the financial support provided by the Natural Sciences and Engineering Research Council of Canada. We wish to thank Professor W. A. Ayer, in whose laboratories a part of this work was done, for his continuing interest in this project.

1. (*a*) W. A. Ayer and H. Taube. Can. J. Chem. **51**, 3842 (1973); (*b*) W. A. Ayer and L. L. Carstens. Can. J. Chem. **51**, 3157 (1973); (*c*) W. A. Ayer, L. M. Browne, J. R. Mercer, D. R. Taylor, and D. E. Ward. Can. J. Chem. **56**, 717 (1978); (*d*) W. A. Ayer, T. Yoshida, and D. M. J. van Schie. Can. J. Chem. **56**, 2113 (1978); (*e*) W. A. Ayer and S. P. Lee. Can. J. Chem. **57**, 3332 (1979).
2. W. A. Ayer, D. E. Ward, L. M. Browne, L. T. J. Delbaere, and Y. Hoyano. Can. J. Chem. **59**, 2665 (1981).
3. S. Krishnamurthy and H. C. Brown. J. Org. Chem. **40**, 1864 (1975).
4. O. Mitsunobu. Synthesis, 1 (1981).
5. T. Veysoglu, L. Mitscher, and J. K. Swayze. Synthesis, 807 (1980).
6. W. A. Ayer, T. T. Nakashima, and D. E. Ward. Can. J. Chem. **56**, 2197 (1978).
7. W. A. Ayer, L. M. Browne, S. Fernandez, D. E. Ward, and T. Yoshida. Rev. Latinoamer. Quim. **9**, 177 (1978).
8. W. C. Still, M. Kahn, and A. Mitra. J. Org. Chem. **43**, 2923 (1978).
9. (*a*) J. B. Stothers. Carbon-13 NMR spectroscopy. Academic Press, New York, NY. 1972; (*b*) H. Beierbeck, J. K. Saunders, and J. W. ApSimon. Can. J. Chem. **55**, 2813 (1977).
10. D. W. Brown, T. T. Nakashima, and D. L. Rabenstein. J. Magn. Reson. **45**, 302 (1981).

Chemoselective reaction of a sulfonate ester with methoxide ions in preference to benzyl mercaptide anions

RICHARD FRANCIS LANGLER[1] AND NANCY ANN MORRISON

Department of Chemistry and Chemical Engineering, Florida Institute of Technology, Melbourne, FL 32901-6988, U.S.A.

Received October 10, 1986[2]

This paper is dedicated to Professor Douglas E. Ryan on the occasion of his 65th birthday

RICHARD FRANCIS LANGLER and NANCY ANN MORRISON. Can. J. Chem. **65**, 2385 (1987).

Trifluoroethyl benzyl sulfide was prepared (in 2-propanol) and subsequently chlorinated as a further test of substituent electronegativity based regiochemical predictions. The initial attempt to prepare that sulfide by reaction of 2,2,2-trifluoroethyl methanesulfonate and benzyl mercaptide anions (in methanol) furnished benzyl methyl sulfide. Mechanistic possibilities are discussed in detail and some synthetic consequences of this novel reaction are presented.

RICHARD FRANCIS LANGLER et NANCY ANN MORRISON. Can. J. Chem. **65**, 2385 (1987).

On a préparé le sulfure de trifluoroéthyle et de benzyle (dans le propanol-2) et, dans le but de confirmer la corrélation qui existe entre l'électronégativité des substituants et les prédictions régiochimiques, on l'a ultérieurement soumis à une chloration. L'essai initial de préparer le sulfure par réaction du méthanesulfonate de trifluoro-2,2,2 éthyle avec les anions sulfures de benzyle (dans le méthanol) a conduit à la formation de sulfure de méthyle et de benzyle. On discute des diverses possibilités concernant le mécanisme et on présente quelques conséquences au niveau de la synthèse de cette nouvelle reaction.

[Traduit par la revue]

Introduction

Our longstanding interest in the chlorination of organosulfur compounds encompasses the regiochemical problem associated with sulfide chlorinations (*vide* eq. [1].) We have developed an

[1] $R^1CH_2SCH_2R^2 + Cl_2 \rightarrow R^1CH_2SCHClR^2 + R^1CHClSCH_2R^2$

1

approach (1, 2) that utilizes substituent electronegativities to successfully predict regiochemical results.[3] Our initial rationale (1) for employing substituent electronegativities to make such predictions was discredited by our own theoretical study (5). Upon completion of that work, we were left with the following positions: (*i*) according to our MNDO study of intermediate thionium ions **2**, phenyl was the best stabilizer and CF_3 was a

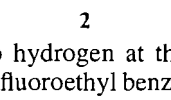

2

destabilizer (relative to hydrogen at the sp^2 carbon), so that chlorination of 2,2,2-trifluoroethyl benzyl sulfide **3**, ($R^1 = CF_3$, R^2 = Ph in **1**, eq. [1]) should occur at the benzylic carbon,[4] and (*ii*) according to substituent electronegativity predictions,[5] reaction should go exclusively into the trifluoroethyl group.

We resolved, at that time, to undertake the chlorinolysis of trifluoroethyl benzyl sulfide **3**, which we intended to prepare from trifluoroethyl methanesulfonate **4**.

Results and discussion

*Electrophilicity of **4** and the preparation of **3***

Our previous experience (8, 9) led us to treat 2,2,2-trifluoroethyl methanesulfonate **4** with the benzyl mercaptide anion in methanol as our first attempt to obtain **3**.

[2] $CF_3CH_2OSO_2CH_3 + PhCH_2SH \xrightarrow[CH_3OH]{CH_3ONa}$

4

$PhCH_2SCH_3$ + $PhCH_2SCH_2CF_3$

27% **3** (12.4%)

Several points arise from the results shown in eq. [2]. Firstly, this is clearly an unacceptable method for the preparation of **3**. However, the surprising formation of benzyl methyl sulfide does raise an interesting mechanism problem. Morever, in conjunction with the mechanism problem, the mass balance is very poor, suggesting the possibility of quantitative loss of a major product. We deal first with the origin of the benzyl methyl sulfide.

The simplest explanation for the formation of benzyl methyl sulfide, which involves what might be called an "ipso" attack, is shown as pathway *a* in Scheme 1. While we are unaware of any published precedent for nucleophilic attack at the carbon bearing sulfur in a sulfonate ester, we have observed analogous reactivity for some sulfonyl chlorides (8). Extension of this behavior to sulfonate esters would not appear to be a major step.

An alternative explanation for the formation of benzyl methyl sulfide involves attack by methoxide ions at sulfonyl sulfur (shown as pathway *b* in the scheme). Facile nucleophilic attack by an oxy-nucleophile at the sulfonyl sulfur of a sulfonate ester is readily illustrated by the following result.

[3] 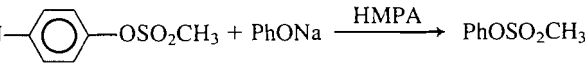

Under the same conditions, mercaptide anions attack the nitromesylate at carbon.

[4] 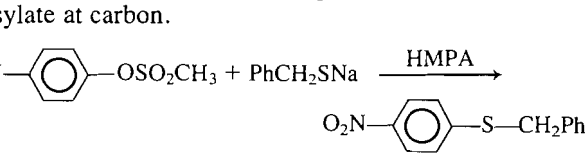

Thus, the high chemoselectivity[6] postulated for the reactions

[1] Author to whom correspondence may be addressed.

[2] Revision received May 24, 1987.

[3] For recent reviews of this area see refs. 3 and 4.

[4] This expectation assumes that the favored pathway goes through the most stable thionium ion.

[5] Pauling electronegativity of phenyl is 2.41 (6) and Pauling electronegativity of trifluoromethyl is 3.46 (7).

[6] Of course, nucleophilic attack at the methylene carbon in **4** proceeds by an S_N2 process (see pathway *c* in the scheme). In eq. [4], the corresponding nucleophilic attack at the sp^2 carbon results in substitution by an addition–elimination sequence.

Printed in Canada / Imprimé au Canada

Can. J. Chem. Downloaded from www.nrcresearchpress.com by 213.166.140.6 on 09/07/12
For personal use only.

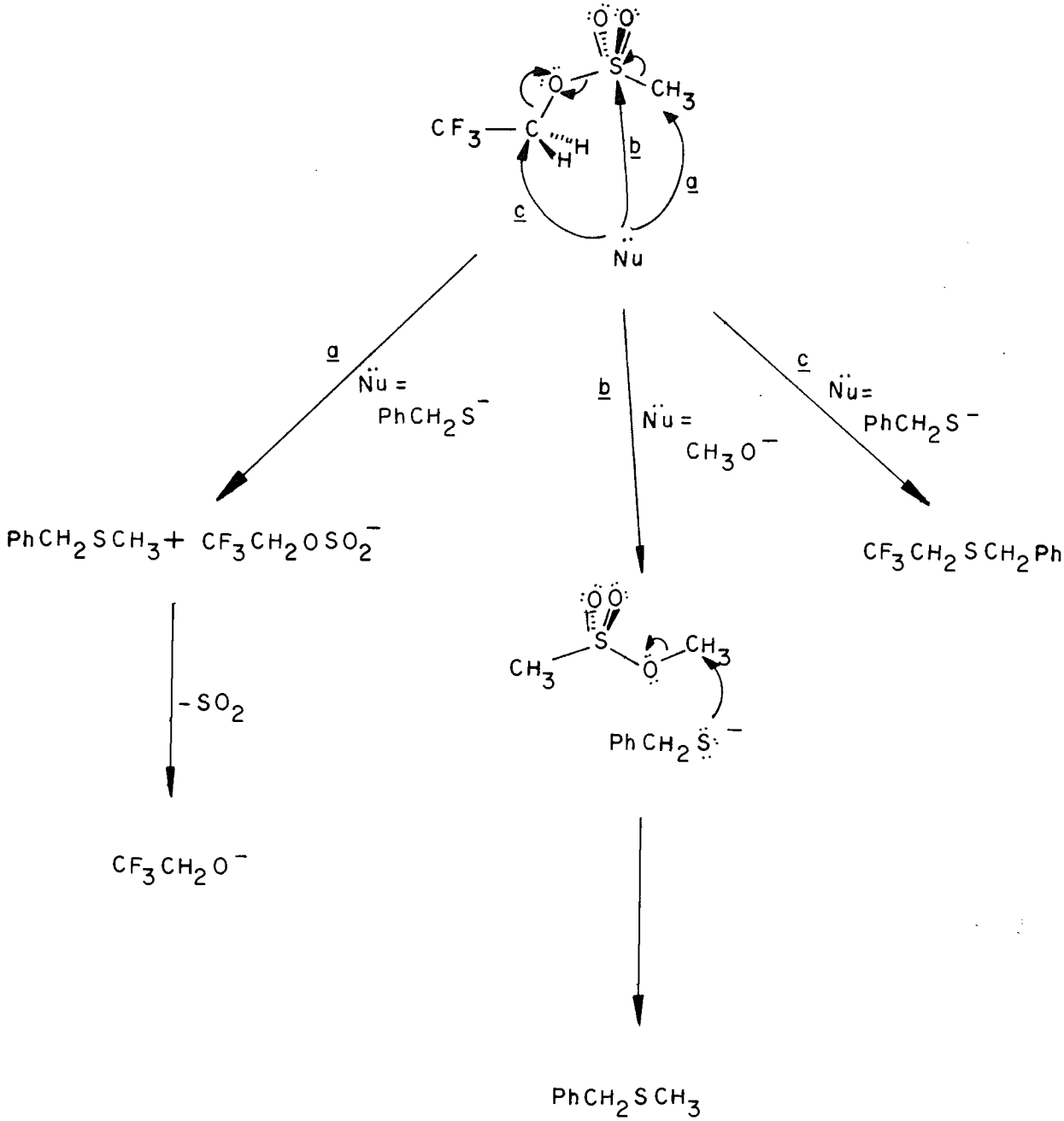

SCHEME 1

conducted in methanol (eq. [2]) can be observed in separate processes when the reactions are carried out in HMPA. HMPA, as expected, did not directly intervene in these reactions.

A simple test of the pathway by which benzyl methyl sulfide forms would involve replacing the methanol/methoxide of eq. [2] with isopropanol/isopropoxide. If the mechanism shown as pathway *a* in Scheme 1 is correct, there should be little change in the outcome of the reaction; in particular, the ratio of benzyl methyl sulfide to **3** should be essentially unchanged. However, if the pathway *b* mechanism is correct, isopropoxide ions would provide substantially greater steric hindrance, which should suppress attack at sulfonyl sulfur. This would enhance the yield of **3**. Of course, if the methyl group of benzyl methyl sulfide is derived from the methanol/methoxide, a change to isopropanol/isopropoxide would preclude formation of that sulfide. Equation [5] presents the results of this experiment.

$$[5]\quad CF_3CH_2OSO_2CH_3 + PhCH_2SH \xrightarrow[(CH_3)_2CHOH]{(CH_3)_2CHONa} \underset{\textbf{3}\ (57\%)}{PhCH_2SCH_2CF_3} + \underset{0\%}{PhCH_2SCH_3}$$

Thus the pathway *a* mechanism is ruled out and another reasonable preparation of **3**[7] has been developed. The somewhat surprising success of methoxide ions (in the pathway *b* mechanism) in a medium that must contain a substantial excess of mercaptide anions[8] leads to speculation about other processes

[7]Previous reports of the preparation of **3** may be found in ref. 10 and references therein.

[8]The pK_a of benzyl mercaptan is 12.0 (11*a*) and the pK_a of methanol is 15.5 (11*b*).

Can. J. Chem. Downloaded from www.nrcresearchpress.com by 213.166.140.6 on 09/07/12
For personal use only.

Can. J. Chem. Downloaded from www.nrcresearchpress.com by 213.166.140.6 on 09/07/12
For personal use only.

in which they might be involved. Methoxide ions could attack the methyl methanesulfonate formed *in situ* (see pathway *b*) to give dimethyl ether. The low-boiling ether would either be lost during the reaction or during work-up. The formation of dimethyl ether was confirmed as shown below.

[6] $\underset{\mathbf{4}}{CF_3CH_2OSO_2CH_3} \xrightarrow[CH_3OH]{CH_3ONa} CH_3OCH_3$

Corresponding conversions of alkoxide ions into symmetrical ethers have been reported by other workers (12*a*, *b*). Now it is clear what processes actually occurred when we carried out the eq. [2] reaction, although it was expected to proceed in a fashion similar to that shown in eq. [7] (taken from ref. 8).

[7] $PhSO_2(CH_2)_3OTs + PhCH_2SH \xrightarrow[CH_3OH]{CH_3ONa} PhSO_2(CH_2)_3SCH_2Ph$

One can begin to deal with an explanation for the unusual result shown in eq. [2] using Hard and Soft Acid and Base theory.[9] The hard base (alkoxide ion) should attack preferentially at the hard acid site (sulfonyl sulfur) and the soft base (mercaptide anion) should attack preferentially at the soft acid sites (sp^3 carbon), as observed. The unusual outcome of the reaction shown in eq. [2] would make sense if the rate of attack by mercaptide anion on the trifluoroethyl mesylate **4** was unusually slow (cf. eq. [7]). A rate retardation would necessarily be attributed to the trifluoromethyl group attached to the electrophilic carbon. Two possible origins for such an effect came to mind readily, viz: (*i*) a steric effect, or (*ii*) a field effect in which the negatively charged fluorine atoms repel approaching anionic nucleophiles. However, trifluoromethyl groups are believed to be only a little larger than methyl groups (14), which appears to rule out a steric argument. Field effects have been argued for the sulfonyl group. We have published results (15) that are inconsistent with this view for the sulfonyl group. Consequently, it is even less appealing to us as an explanation for a trifluoromethyl substituent effect. In connection with this point, we note that our MNDO gas phase results,[10] on the CF_3 containing systems **5** and **6**, show that the partial charge on fluorine is rather small (-0.17 in **5** and -0.23 in **6**) and is, to a first approximation, insensitive to demand for electron density.

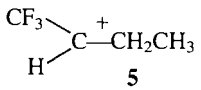

5

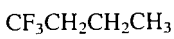

6

Another view of this problem would suppose a rate acceleration for nucleophilic attack at the sulfonyl sulfur of **4** by methoxide ions. This view is supported by the pK_a of CF_3CH_2OH, which is 12.4 (17). The pK_a suggests that the trifluoroethoxy group is a significantly better leaving group than is an alkoxy group, thereby enhancing electrophilicity at the hard acid site.

We felt that the synthetic potential for pathway *b* chemistry was worth further exploration. Among many potential methodologies, this chemistry could offer "one-pot" methodologies for symmetric ethers and for sulfides. Equations [8] and [9] give preliminary results for each of these methodologies.

[8] $PhCH_2OH + CF_3CH_2OSO_2CH_3 \xrightarrow[(CH_3)_2CHOH]{(CH_3)_2CHONa} (PhCH_2)_2O$ 23%

[9] $PhCH_2OH + PhSH + PhOSO_2CH_3 \xrightarrow[(CH_3)_3COH]{(CH_3)_3COK} PhCH_2SPh$ 50%

Further results will be communicated in due course. We note, in connection with one-pot methodologies, the highly effective method for the conversion of alcohols to sulfides developed by Nakagawa, Aki, and Hata (18).

Chlorinolysis of 3

We have attempted to chlorinate **3** with sulfuryl chloride only to find no reaction. However, facile chlorination was accomplished with molecular chlorine.

[10] $\underset{\mathbf{3}}{PhCH_2SCH_2CF_3} + Cl_2 \xrightarrow{CCl_4} \underset{\mathbf{7}\ (100\%)}{PhCH_2SCCl_2CF_3}$

The result depicted in eq. [10] is consistent with the outcome expected on the basis of substituent electronegativity difference.[5] In accord with the conclusions reached from our earlier theoretical study (5), this result suggests that the major regioisomeric thionium ion **2** is not always the most stable one and that "sulfides which have substituents with high electronegativities follow an E_{1cb}-like mechanism". Equation [10] brings the total to 51 asymmetric sulfide chlorinations for which substituent electronegativities have been successful in anticipating the regiochemistry.

Conclusions

1. CF_3 is a better directing group than Ph in asymmetric acyclic sulfide chlorination reactions, as expected on the basis of ΔXp (substituent electronegativity difference) arguments.
2. Some sulfonate esters can induce alcohols to alkylate mercaptide anions (see eq. [2]). The reaction appears to involve two highly chemoselective steps: (*i*) nucleophilic attack by alkoxide ions (particularly primary ones) at sulfonyl sulfur, then (*ii*) mercaptide anion attack at carbon of the intermediate sulfonate ester.
3. High chemoselectivity in the nucleophilic substitutions on sulfonate esters suggests a variety of possible one-pot synthetic methods. Preliminary results show potential for such syntheses of sulfides and symmetric ethers.

Experimental

General

The ir spectra were recorded on a Perkin Elmer 237B grating spectrophotometer. The nmr spectra were obtained on a Varian EM360A instrument using TMS as the internal standard. Melting points were determined on a Mel-Temp capillary melting-point apparatus and are uncorrected.

Conversion of benzyl mercaptan to benzyl methyl sulfide

Sodium metal (1.204 g, 52.3 mmol) was dissolved in methanol (100 mL) and benzyl mercaptan (6.2 mL, 50 mmol) added. 2,2,2-Trifluoroethyl methanesulfonate **4** (8.900 g, 50 mmol) (19) was added and the reaction mixture refluxed for 20 h. Water (100 mL) was added and the resultant mixture washed with methylene chloride (three 100-mL aliquots). The combined organic layers were dried ($MgSO_4$) and concentrated. The residue was rectified at reduced pressure affording a mixture (4.5579 g, bp 106–112°C/50 Torr) (1 Torr = 133.3 Pa).

[9]For a discussion of sulfur nucleophiles and electrophiles in terms of HSAB theory see ref. 13.

[10]These calculations were carried out as part of a previously published study. Details may be found in that paper (16).

Can. J. Chem. Downloaded from www.nrcresearchpress.com by 213.166.140.6 on 09/07/12
For personal use only.

A portion of the distillate (1.983 g) was chromatographed on silica gel (200 g) employing hexanes elution (100-mL fractions). Fraction 10 was concentrated, affording clean trifluoroethyl benzyl sulfide **3** (0.068 g, 0.33 mmol). Fractions 11–13 were combined and concentrated, affording more **3** (0.496 g) contaminated with benzyl mercaptan. Fractions 16–24 were combined and concentrated, affording benzyl methyl sulfide (0.8209 g, 6.09 mmol).

Chromatographed benzyl methyl sulfide (0.8209 g, 6.09 mmol) was oxidized by chromium trioxide (1.525 g, 15.2 mmol) in glacial acetic acid (50 mL) in the usual way (8). Benzyl methyl sulfone (0.362 g, 2.12 mmol) was obtained and recrystallized from methanol. It was identical to authentic material by ir, nmr, tlc, mp (123.5–124°C, lit. (20) mp 127°C), and mixture mp.

Preparation of p-*nitrophenyl methanesulfonate*

A solution of dry triethylamine (14.538 g, 143.9 mmol) and *p*-nitrophenol (19.999 g, 143.8 mmol) in dry pyridine (200 mL) was reacted with methanesulfonyl chloride (16.388 g, 143.7 mmol) in the usual way. The residue from routine work-up was recrystallized from methanol, affording clean *p*-nitrophenyl methanesulfonate (20.60 g, 94.9 mmol, 66%, mp 88–89°C). The sulfonate ester had R_f 0.81 on analytical tlc plates (0.5 mm silica gel thickness) when developed with chloroform; ir ($CHCl_3$): 1540, 1390, 1360, and 1170 cm^{-1}; uv (CH_3OH): 261 nm (ε 8 955); nmr ($CDCl_3$) δ: 8.30 (2H, d, J = 9 Hz), 7.36 (2H, d, J = 9 Hz), and 3.25 (3H, s). *Anal.* calcd. for $C_7H_7NO_5S$: C 38.70, H 3.24; found: C 38.66, H 3.19.

Reaction of p-*nitrophenyl methanesulfonate with phenoxide ions*

Phenol (2.1573 g, 22.9 mmol) in HMPA[11] (10 mL) was added dropwise to a slurry of sodium hydride (0.6111 g, 25.4 mmol) in HMPA (30 mL). Upon completion of the 5-min addition, the reaction mixture was stirred at ambient temperature for 1 h to permit complete evolution of hydrogen. *p*-Nitrophenyl methanesulfonate (5.0229 g, 23.1 mmol) was added and the reaction mixture stirred at ambient temperature for 18 h.

The reaction mixture was poured into water (400 mL) and 10% HCl (5 mL). The resultant mixture was washed with diethyl ether (three 100-mL portions). The ether was concentrated and the residue poured into water (100 mL). The aqueous layer was washed with diethyl ether (three 100-mL portions). The combined ether layers were washed with 2.5% sodium hydroxide (two 100-mL aliquots). The organic layer was dried ($MgSO_4$) and the solvent evaporated, affording crude phenyl methanesulfonate (3.3708 g, 19.5 mmol, 84%).

The crude mesylate was chromatographed on silica gel (400 g) employing chloroform elution (100-mL fractions). Fractions 12 and 13 were combined and concentrated, affording clean phenyl methanesulfonate (2.5932 g, 15.0 mmol). After recrystallization the methanesulfonate was shown to be identical to authentic material by ir, nmr, double-spotted tlc, mp (61–62°C), and mixture mp (60–61.3°C). Fractions 14 and 15 were combined, concentrated, and rechromatographed on silica gel (80 g) employing 1:1 chloroform – carbon tetrachloride elution (50-mL fractions). Fractions 8–12 were combined and concentrated, yielding more clean phenyl methanesulfonate (0.3802 g, 2.2 mmol).

Reaction of p-*nitrophenyl methanesulfonate with benzyl mercaptide anions*

Sodium hydride (0.3326 g, 13.8 mmol) was added to HMPA (30 mL). A solution of benzyl mercaptan (1.7 mL, 13.7 mmol) in HMPA (10 mL) was added dropwise over 10 min. The reaction mixture was stirred for an additional 10 min to permit complete evolution of H_2. The nitromesylate (2.9813 g, 13.7 mmol) was added and almost immediately the reaction mixture turned very deep red—almost black. The reaction mixture was stirred at ambient temperature for 2 h. Crude work-up followed the procedure used for reaction with phenoxide ions.

The residue was recrystallized from methanol, affording clean *p*-nitrophenyl benzyl sulfide (1.7561 g, 7.1 mmol, 52%, mp 119–119.5°C). The sulfide had R_f 0.46 on analytical tlc plates when developed with 3:1 carbon tetrachloride – chloroform; ir ($CHCl_3$): 1520 and 1350 cm^{-1}; nmr ($CDCl_3$) δ: 8.06 (2H, d), 7.30 (5H, s), 7.25 (2H, d), and 4.23 (2H, s). *Anal.* calcd. for $C_{13}H_{11}O_2NS$: C 63.65, H 4.51; found: C 63.46, H 4.48.

Preparation of 2,2,2-trifluoroethyl benzyl sulfide **3**

Small scale

Sodium metal (0.1233 g, 5.3 mmol) was reacted with 2-propanol (20 mL). Phenylmethanethiol (0.7 mL, 5.6 mmol) and the mesylate **4** (1.000 g, 5.6 mmol) (19) were added and the reaction mixture refluxed for 4 days. A standard extraction procedure furnished *crude product*. The crude was chromatographed on silica gel (100 g) employing hexanes for elution (100-mL fractions). Fractions 5–7 were combined and concentrated, furnishing benzylic sulfide **3** (0.660 g, 3.2 mmol, 57%) with known properties (10).

Large scale without chromatographic work-up

Reaction was carried out as outlined above using sodium metal (1.285 g, 55.8 mmol), phenylmethanethiol (7 mL, 56.4 mmol), and the trifluorosulfonate **4** (10.0145 g, 56.2 mmol) in 2-propanol (200 mL). The reaction mixture was refluxed for only 2 h. Upon completion of reflux, 3% sodium hydroxide (100 mL) was added and the reaction mixture refluxed for an additional hour. An extraction procedure furnished crude, which was added to pyridine (25 mL) and iodine (1 g) and stirred at ambient temperature for 5 min. Standard extraction furnished an organic layer, which was washed with 10% w/v sodium thiosulfate (two 50-mL aliquots). The solvent was evaporated and the residue rectified at reduced pressure, yielding **3** (6.131 g, 29.7 mmol, 52%, bp 112–120°C/35 Torr). The sulfide obtained this way is free of benzyl mercaptan and trifluoromesylate **4** but has a yellowish color.

Preparation of trifluoroethyl benzyl sulfone

The trifluorosulfide **3** (0.728 g, 3.5 mmol) in glacial acetic acid (5 mL) was added dropwise to a mixture of chromium trioxide (0.3556 g, 3.55 mmol) in glacial acetic acid (5 mL) and the oxidation carried out in the usual way (8). The crude sulfone (0.371 g, 1.5 mmol, 44%) was recrystallized from methanol, yielding clean trifluoroethyl benzyl sulfone (0.2601 g, mp 139–141°C). The sulfone had ir ($CHCl_3$): 1360 and 1145 cm^{-1}; nmr ($CDCl_3$) δ: 7.30 (5H, s), 4.26 (2H, s), and 3.50 (2H, q, J = 9 Hz). *Anal.* calcd. for $C_9H_9F_3O_2S$: C 45.37, H 3.80; found: C 45.59, H 3.76.

Reaction of trifluoroethyl mesylate **4** *with methoxide ions*

Sodium metal (1.0998 g) was dissolved in methanol (100 mL) and the trifluoroethyl mesylate (4.458 g) added. The reaction was refluxed for 0.5 h. Effluent gases were passed into a trap cooled with isopropanol/Dry Ice. Upon completion of the reflux, the trap contained dimethyl ether (0.7 mL), which was identical with authentic material by nmr.

Preparation of dibenzyl ether

Sodium metal (1.2953 g, 56.3 mmol) was dissolved in 2-propanol (100 mL) and benzyl alcohol (3.0337 g, 28.0 mmol) was added. 2,2,2-Trifluoroethyl methanesulfonate (4.9968 g, 28.0 mmol) (19) was added and the resultant mixture refluxed for 0.5 h. Acidification and extraction afforded a residue that was chromatographed on silica gel (400 g) employing chloroform elution (100-mL fractions). Fraction 12 was concentrated, affording a mixture of dibenzyl ether (0.056 g, 0.2 mmol) and benzyl trifluoroethyl ether (0.087 g, 0.4 mmol). Fractions 13–17 were concentrated and combined, affording clean dibenzyl ether (0.5775 g, 2.9 mmol). Dibenzyl ether had no OH stretch in the ir, and nmr ($CDCl_3$) δ: 7.33 (5H, s) and 4.53 (2H, s). Fractions 18–20 were concentrated and combined, yielding 2-propyl methanesulfonate (0.0754 g, 0.5 mmol). Further elution provided unchanged benzyl alcohol (1.0792 g, 9.9 mmol).

Preparation of benzyl phenyl sulfide

Potassium metal (1.0807 g, 27.7 mmol) was dissolved in *tert*-butanol (100 mL). Benzenethiol (1.5098 g, 13.7 mmol), benzyl alcohol (1.4935 g, 13.8 mmol), and phenyl methanesulfonate (2.3659 g, 13.7 mmol) were added. The reaction mixture was refluxed for 2 h.

[11] HMPA is hexamethylphosphoramide $[(CH_3)_2N]_3PO$. HMPA is toxic and carcinogenic (21).

Standard extraction gave crude, which was a mixture of ca. 2:1 benzyl phenyl sulfide – benzyl alcohol.

Half of the crude product was added to a mixture of chromium trioxide (1.9989 g, 19.9 mmol) in glacial acetic acid (50 mL). The reaction mixture was maintained at 90–100°C for 0.5 h. Standard extraction yielded clean benzyl phenyl sulfone (0.7770 g, 3.3 mmol). Upon recrystallization from methanol, the product was shown to be identical to authentic material by mp (147–149°C, lit. (ref. 20, p. 425) mp 148°C), ir, and nmr.

Chlorinolysis of **3**

Trifluoroethyl benzyl sulfide **3** (0.502 g, 2.4 mmol) was dissolved in carbon tetrachloride (5 mL), and Cl_2 (ca. 200 mL/min) was bubbled into the solution for 1 min. An nmr of the crude indicated that the reaction mixture was now ca. 28% monochlorosulfide and 72% dichlorosulfide **7**. Cl_2 was bubbled into the reaction mixture for another minute at the same rate. An nmr[12] of the crude indicated complete conversion of the starting material into the dichlorosulfide **7**.

The solvent was evaporated and the residue oxidized with chromium trioxide (0.6121 g, 6.1 mmol) in glacial acetic acid (30 mL) in the usual way (8). After recrystallization of crude dichlorotrifluorosulfone from methanol, clean sulfone (0.3497 g, 1.4 mmol, 58% after two steps, mp 78–79.5°C) was obtained. The product sulfone had R_f 0.26 on analytical tlc plates when developed with carbon tetrachloride; ir ($CHCl_3$): 1370 and 1170 cm^{-1}; nmr ($CDCl_3$) δ: 7.43 (5H, s) and 4.70 (2H, s). *Anal.* calcd. for $C_9H_7Cl_2F_3O_2S$: C 35.19, H 2.29, Cl 23.08, S 10.44; found: C 35.27, H 2.28, Cl 23.11, S 10.28.

Acknowledgements

The authors are grateful to the Florida Institute of Technology for financial support.

1. T. P. Ahern, D. G. Kay, and R. F. Langler. Can. J. Chem. **56**, 2422 (1978).
2. J. R. Hancock, W. R. Hardstaff, P. A. Johns, R. F. Langler, and W. S. Mantle. Can. J. Chem. **61**, 1472 (1983).
3. W. R. Hardstaff and R. F. Langler. *In* Sulfur in organic and inorganic Chemistry. Vol. 4. *Edited by* A. Senning. M. Dekker, Inc., New York. 1982. pp. 193–281.
4. G. E. Wilson, Jr. Tetrahedron, **38**, 2597 (1982).
5. J. L. Ginsburg and R. F. Langler. Can. J. Chem. **61**, 589 (1983).
6. W. K. Jardine, R. F. Langler, and J. A. MacGregor. Can. J. Chem. **60**, 2069 (1982).
7. J. E. Huheey. J. Phys. Chem. **69**, 3284 (1965).
8. H. O. Fong, W. R. Hardstaff, D. G. Kay, R. F. Langler, R. H. Morse, and D. N. Sandoval. Can. J. Chem. **57**, 1206 (1979).
9. T. P. Ahern, H. O. Fong, R. F. Langler, and P. M. Mason. Can. J. Chem. **58**, 878 (1980).
10. C. Bunyagidj, H. Piotrowska, and M. H. Aldridge. J. Org. Chem. **46**, 3335 (1981).
11. (*a*) R. F. Langler and J. A. Pincock. Can. J. Chem. **55**, 2316 (1977); (*b*) A. Streitwieser, Jr. and C. H. Heathcock. Introduction to organic chemistry. 3rd ed. MacMillan, New York. 1985. p. 1156.
12. (*a*) F. G. Bordwell, B. M. Pitt, and M. Knell. J. Am. Chem. Soc. **73**, 5004 (1951); (*b*) J. Ferns and A. Lapworth. J. Chem. Soc. **101**, 273 (1912).
13. T. L. Ho. Hard and soft acids and bases principle in organic chemistry. Academic Press, New York. 1977. pp. 126–146.
14. Y. Kobayashi and I. Kumadaki. Acc. Chem. Res. **14**, 76 (1981).
15. D. G. Kay, R. F. Langler, and J. E. Trenholm. Can. J. Chem. **57**, 2185 (1979).
16. A. M. Aissani, J. C. Baum, R. F. Langler, and J. L. Ginsburg. Can. J. Chem. **64**, 532 (1986).
17. L. Mukherjee and E. Grunwald. J. Phys. Chem. **62**, 1311 (1958).
18. I. Nakagawa, K. Aki, and T. Hata. J. Chem. Soc. Perkin Trans. 1, 1315 (1983).
19. R. K. Crossland and K. L. Servis. J. Org. Chem. **35**, 3195 (1970).
20. Z. Rappoport. Handbook of tables for organic compound identification. 3rd ed. Chemical Rubber Co., Cleveland, OH. 1967. p. 421.
21. N. I. Sax. Dangerous properties of industrial materials. Van Nostrand Rheinhold Co., New York. 1979. p. 721.

[12]It is important to minimize the chlorination time, since cleavage of benzylic sulfides similar to **7** is an amply precedented process (ref. 3, p. 199).

Can. J. Chem. Downloaded from www.nrcresearchpress.com by 213.166.140.6 on 09/07/12
For personal use only.

Isolation, structure, and synthesis of combretastatin A-2, A-3, and B-2[1]

GEORGE R. PETTIT[2] AND SHEO BUX SINGH
Cancer Research Institute and Department of Chemistry, Arizona State University, Tempe, AZ 85287-1604, U.S.A.

Received May 8, 1987

GEORGE R. PETTIT and SHEO BUX SINGH. Can. J. Chem. **65**, 2390 (1987).

Further investigation of the South African tree *Combretum caffrum* (Combretaceae) for murine P388 lymphocytic leukemia (PS) cell-growth inhibitory substances has led to discovery of three new active constituents designated combretastatins A-2 (**5***a*, PS ED_{50} 0.027 μg/mL), A-3 (**5***b*, PS ED_{50} 0.026 μg/mL), and B-2 (**3***b*, PS ED_{50} 0.32 μg/mL). Both combretastatins A-2 and A-3 were found to markedly inhibit tubulin polymerization. The structure of each combretastatin was firmly established by a combination of high resolution (400 MHz) ^1H and ^{13}C nuclear magnetic resonance and mass spectral analyses followed by total syntheses. The conversion of methyl gallate (**7***b*) to combretastatin A-2 via intermediates **7***c* → **7***d* → **7***e* → **7***a* and **6***a* → **5***a* illustrates the practical synthetic route utilized for obtaining these substances. The Wittig reaction employed as the penultimate step in obtaining combretastatins A-3, afforded predominantly the natural *Z* isomer.

GEORGE R. PETTIT et SHEO BUX SINGH. Can. J. Chem. **65**, 2390 (1987).

Dans le but d'isoler de nouvelles substances inhibant la croissance des cellules (PS) de la leucémie lymphocytaire de la murine P388, on a procédé à une nouvelle investigation de l'arbre sud-africain *Combretum caffrum* (Combretaceae); cette étude a conduit à la découverte de trois nouveaux constituants actifs que l'on a appelés combrétastatines A-2 (**5***a*, PS ED_{50} 0,027 μg/mL), A-3 (**5***b*, PS ED_{50} 0,026 μg/mL) et B-2 (**3***b*, PS ED_{50} 0,32 μg/mL). On a trouvé que les combrétastatines A-2 ainsi que A-3 inhibent toutes les deux la polymérisation de la tubuline. On a fermement établi la structure de chacune des combrétastatines en faisant appel à une combinaison de résonance magnétique nucléaire ^1H et ^{13}C à haute résolution (400 MHz) et de spectrométrie de masse suivis de synthèses totales. La transformation du gallate de méthyle (**7***b*) en combrétastatine A-2 (via les intermédiaires **7***c* → **7***d* → **7***e* → **7***a* et **6***a* → **5***a*) illustre bien les voies pratiques de synthèse qui peuvent être utilisées pour obtenir ces substances. La réaction de Wittig, utilisée dans l'avant-dernière étape de la synthèse des combrétastatines A-3, fournit principalement l'isomère *Z* naturel.

[Traduit par la revue]

The plant family Combretaceae is comprised of 20 genera (600 species) growing in tropical and subtropical regions as shrubs and trees (2). The genus *Combretum* with 250 climbing or erect species is known for its medicinal properties in Africa and India (3).[3] In 1979 we began an investigation directed at discovering murine P-388 lymphocytic leukemia (PS system) inhibitory components of the South African tree *Combretum caffrum* (Eckl. and Zeyh) Kuntze (or as *Salicifolium* E. Mey), a valuable lead uncovered in the U.S. National Cancer Institute's (NCI) world-wide explorations (5). Eventually we succeeded in isolating combretastatin (**1**), which was found to significantly cause astrocyte reversal in the NCI astrocytoma bioassay (6) and inhibition of tubulin polymerization (7). Isolation of diphenylethanol **1** was followed by discovery of the principal PS in vivo active constituent of *Combretum caffrum* fractions, the powerful tubulin polymerization inhibitor combretastatin A-1 (**2**, ref. 8). Subsequently, we isolated from the same tree the PS cell-growth inhibitory combretastatin B-1 (**3***a*, ref. 8) and a series of phenanthrenes (cf. **4**, ref. 1) with analogous activity. We now report discovery of two new compounds closely related to combretastatin A-1 (**2**), designated combretastatins A-2 (**5***a*) and A-3 (**5***b*), which display significant PS cell-growth and tubulin inhibitory properties. Another constituent active against the PS cell line, named combretastatin B-2 (**3***b*), was also found in this productive plant.

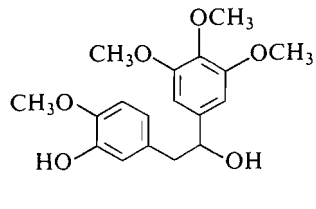

1, Combretastatin
PS ED_{50} 0.011 μg/mL

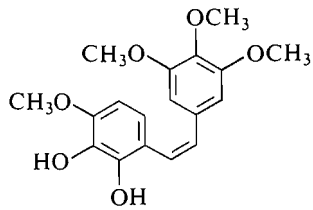

2, Combretastatin A-1
PS ED_{50} 0.99 μg/mL

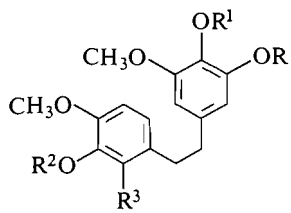

3*a*, R = R^1 = CH_3, R^2 = H, R^3 = OH
Combretastatin B-1
b, R = R^2 = R^3 = H, R^1 = CH_3
Combretastatin B-2
c, R, R^1 = —CH_2—, R^2 = R^3 = H

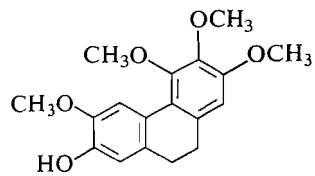

4
PS ED_{50} 2.8 μg/mL

The methylene chloride fraction (8) prepared from the original methylene chloride – methanol extract of *Combretum caffrum* stem wood (77 kg dry wt.) was employed as starting material for the present bioassay (PS) guided research. The active methylene chloride fraction was subjected to steric exclusion chromatography in methanol on Sephadex LH-20 to provide two active fractions (A and B of ref. 8). Several partition chromatography sequences of Sephadex LH-20, employing hexane–toluene–methanol (3:1:1) as solvent, afforded a set of active fractions that were further separated by ambient column and high performance silica gel chromatography, to yield combretastatin A-2 (**5***a*, NSC 383473, ED_{50} 0.027 μg/mL), combretastatin A-3 (**5***b*, NSC 382393, ED_{50} 0.026 μg/mL), and combretastatin B-2 (**3***b*, NSC 601287, ED_{50} 0.32 μg/mL). The structures of these interesting cell-growth inhibitory com-

[1]Antineoplastic agents 130; for part 129 see ref. 1.
[2]Author to whom correspondence may be addressed.
[3]Also J. A. Duke and J. K. Wain, private communications.

Printed in Canada / Imprimé au Canada

Can. J. Chem. Downloaded from www.nrcresearchpress.com by 213.166.140.6 on 09/07/12
For personal use only.

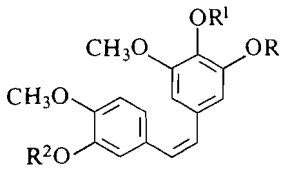

5*a*, R, R^1 = —CH_2—, R^2 = H
Combretastatin A-2
b, R = R^2 = H, R^1 = CH_3
Combretastatin A-3
c, R, R^1 = —CH_2—, R^2 = $COCH_3$
d, R, R^1 = —CH_2—, R^2 = CONH— 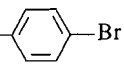 —Br
e, R = R^2 = $COCH_3$, R^1 = CH_3
f, R = R^2 = $Si(CH_3)_2C(CH_3)_3$, R^1 = CH_3

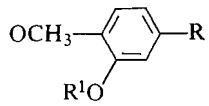

6*a*, R = CH_2P^+(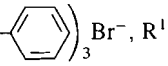)$_3$ Br^-, R^1 = H
b, R = CH_2OH, R^1 = H
c, R = CH_2Br, R^1 = H
d, R = CHO, R^1 = $Si(CH_3)_2C(CH_3)_3$

pounds were unequivocally assigned as summarized in the sequel.

Both the ultraviolet and infrared spectra of combretastatins A-2, A-3, and B-2 suggested aromatic systems and this was further supported by high resolution electron impact mass spectra (hreims) that revealed the molecular formulae $C_{17}H_{16}O_5$, $C_{17}H_{18}O_5$, and $C_{17}H_{20}O_5$ respectively. The 400-MHz ^{1}H nmr spectrum of the A-2 (**5***a*) exhibited two methoxyl group protons (δ 3.750 and 3.870), methylenedioxy protons at δ 5.935 (supported by a ^{13}C nmr signal at δ 101.35 and ir band at 930 cm^{-1}), and signals integrating for 7 protons in the aromatic region. Two sets of relatively shielded AB spin systems appeared in the ^{1}H nmr spectrum totalling four protons. One of these sets appeared as a doublet at δ 6.458 (J = 1.32 Hz) with its counterpart at δ 6.483 (J = 1.32 Hz), typical of two *meta*-coupled aromatic protons. The other AB spin system showed doublets at δ 6.383 and 6.420 (J = 12.16 Hz each). Signals for the other three aromatic protons were split into an ABC system with J_{AC} = 0.0 Hz, typical of *ortho–ortho–meta* disposed aromatic protons. A relatively upfield one-proton doublet appeared at δ 6.732 (J_{AB} = 8.4 Hz), a downfield doublet of doublets and a doublet (one proton each) at δ 6.773 (dd, J_{BA} = 8.4 and J_{BC} = 2.0 Hz) and 6.875 (J_{BC} = 2.0 Hz). Another one-proton broad singlet resonated at δ 5.520 and disappeared upon D_2O exchange, suggesting the presence of a phenolic group. Confirmation of this observation was achieved by acetylation (**5***a* → **5***c*) and conversion to *p*-bromophenylcarbamate **5***d*.

When combretastatin A-2 was catalytically hydrogenated, the mass spectrum of the dihydro product (**3***c*) gave a relatively small molecular ion at m/z 302 and two major fragment ions at m/z 165 ($C_9H_9O_3$) and 137 ($C_8H_9O_2$), resulting from cleavage of the benzyl bond. The mass spectral analysis suggested presence of a methoxyl and methylenedioxy group in one aromatic ring and a methoxyl and hydroxyl group in the other. Examination of the ^{1}H nmr spectrum of the dihydro derivative **3***c* revealed the absence of doublets at δ 6.383 and 6.420. Instead a four-proton broad singlet was displayed at δ 2.78, typical of the benzyl protons of a bibenzyl unit. On this basis, combretastatin A-2 (**5***a*) was assumed to be a stilbene.

Interpretation of the ^{13}C nmr spectra (Table 1) of combretastatin A-2 (**5***a*), its acetate (**5***c*), and dihydro derivative (**3***c*) suggested that all contained (on the basis of chemical shift additive rules, ref. 9) a 3,4-methylenedioxy-5-methoxy substitution pattern in one phenyl ring and 3′-hydroxy-4′-methoxy substitution in the other. The 3′-hydroxy-4′-methoxy substitution pattern in the latter ring was further supported by an *ortho–para* shift of +8.3 ppm at C-2′, +5.0 at C-4′, and +6.5 at C-6′ in the ^{13}C nmr, as a result of acetylation. Once the substitution pattern in the aromatic rings was securely established, the geometry at the ethylene bridge was assigned as *Z* based on the olefin ^{1}H nmr coupling constant (J = 12.16 Hz). A coupling constant of 12.2 Hz was observed in the ^{1}H nmr spectrum of combretastatin A-1 and the *cis*-olefin geometry was independently proved by an X-ray crystal structure determination (8). Therefore, combretastatin A-2 was assigned structure **5***a* and this was unequivocally confirmed by total synthesis (*vide infra*).

The 400-MHz ^{1}H nmr spectra of combretastatin A-3 showed signals corresponding to 3-methoxy groups, and in general indicated that combretastatin B-2 was its dihydro derivative. Catalytic hydrogenation of A-3 to B-2 confirmed this relationship. The ^{1}H nmr spectrum of A-3 displayed two *meta*-coupled aromatic protons at δ 6.427 and 6.535 (J = 1.72 Hz each), and a set of ABC spin system protons with J_{AC} = 0 Hz. The most shielded doublet of this set appeared at δ 6.727 (J_{AB} = 8.4 Hz) and the relatively deshielded protons at δ 6.792 (dd, J_{BA} = 8.4 Hz) and 6.897 (d, J_{CB} = 2.0 Hz). The close proximity of their signals to those in combretastatin A-2 suggested a similar substitution pattern. The ^{1}H nmr spectrum also displayed a set of AB spin system protons at δ 6.380 and 6.439 (J = 12.2 Hz each) and two phenolic group protons at δ 5.514 and 5.679, which disappeared upon D_2O exchange. The assumption of two phenol groups in A-3 was confirmed by acetylation (**5***b*–**5***e*).

The mass spectrum of combretastatin B-2 showed a molecular ion at m/z 304 and two major fragments at m/z 167 ($C_9H_{11}O_3$) and 137 ($C_8H_9O_2$) arising from cleavage of the benzyl bond. In turn this suggested that one ring contained two methoxyl and one hydroxyl groups and the other one methoxyl and one hydroxyl group. The lack of an AB spin system with J = 12.2 Hz in the ^{1}H nmr spectrum of the combretastatin A-2 hydrogenation product (*vide supra*) and appearance of a four-proton broad singlet at δ 2.785 ppm was consistent with structure **3***b* for combretastatin B-2.

Finally, the substitution pattern in the aromatic rings of both A-3 (**5***b*) and B-2 (**3***b*) was established as 3-hydroxy-4,5-dimethoxy and 3′-hydroxy-4′-methoxy by application of chemical shift additive rules (9) in interpreting the ^{13}C nmr spectra (Table 1) of these substances and diacetate **5***c*. The assignments were further supported by the acetylation shifts seen in both the ^{13}C and ^{1}H nmr spectra. These shifts were similar to those appearing in the spectra of combretastatin A-2 acetate. Thus the structure of combretastatin A-3 was established as *Z*-stilbene **5***b* and combretastatin B-2 as bibenzyl **3***b*. The structures were confirmed (as summarized below) by unambiguous syntheses. Thus combretastatins A-2 and A-3 represent valuable new additions to the rare (heretofore, seven members) *cis*-stilbene family of plant biosynthetic products (10–12).

A very practical synthesis of combretastatin A-2 was achieved,

Can. J. Chem. Downloaded from www.nrcresearchpress.com by 213.166.140.6 on 09/07/12
For personal use only.

Can. J. Chem. Downloaded from www.nrcresearchpress.com by 213.166.140.6 on 09/07/12
For personal use only.

TABLE 1. Combretastatin A-2, A-3, B-2, and acetate derivatives, ^{13}C nmr (100.6 MHz) chemical shift (δ) assignments relative to tetramethylsilane in deuteriochloroform

Carbon	3*b*	3*c*	5*a*	5*b*	5*c*	5*e*
1	138.80	136.47	131.83	133.33	131.52	132.42
2	108.05	107.76	108.57	108.92	108.36	155.74
3	145.61[a]	143.40	143.40	145.87[a]	143.51	143.91[a]
4	133.92	134.99	134.40	138.79	134.51	140.39
5	152.20	148.75	148.63	151.98	148.75	153.25
6	104.67	102.52	103.04	105.06	103.08	110.79
1a	37.14	37.48	129.23	129.59	129.38	129.00
1a′	38.07	38.09	128.88	128.96	128.29	128.52
1′	135.23	134.99	130.66	130.66	130.16	129.85
2′	114.81	114.68	115.03	115.16	123.32	123.32
3′	144.98[a]	145.51[a]	145.80[a]	145.25[a]	139.61	139.61[a]
4′	149.16	144.87[a]	145.32[a]	149.05	150.28	150.49
5′	110.82	110.63	110.45	110.45	112.19	112.24
6′	119.82	119.78	121.04	121.14	127.50	127.75

3*b*: 60.97 (OCH_3 at C-4), 56.90, 55.90 (OCH_3).
3*c*: 101.17 (OCH_2O), 56.58, 56.05 (OCH_3).
5*a*: 101.35 (OCH_2O), 56.38, 55.92 (OCH_3).
5*b*: 60.99 (OCH_3 at C-4), 55.92, 55.70 (OCH_3).
5*c*: 168.79, 101.38, 56.36, 55.96, 20.62.
5*e*: 169.05, 168.86, 60.73, 55.99, 55.95, 20.70, 20.61.
Similar superscript in vertical column may be interchanged.

based on condensing the ylide from phosphonium bromide **6***a* with aldehyde **7***a*. Methyl gallate (**7***b*) proved to be a very effective starting point for a more convenient (cf. ref. 13) preparation of aldehyde **7***a*. Reaction of phenol **7***b* with aqueous sodium borate formed the *ortho*-borate ester and allowed specific methylation of the remaining hydroxy group using dimethylsulfate. Acid hydrolysis of the borate ester afforded 3,4-dihydroxy-5-methoxybenzoate (**7***a*, 84.5% yield). Conversion to the methylenedioxy derivative (**7***d*, 98% yield) was accomplished by fluoride-assisted methylenation with dibromomethane and cesium fluoride. Benzoate **7***d* was reduced with lithium aluminum hydride to benzyl alcohol **7***e* in 98% recovery. Oxidation of benzyl alcohol (**7***e*) with pyridinium chlorochromate (PCC) led to the required aldehyde (**7***a*) in 90% yield (73% overall).

Reaction of isovanillyl alcohol **6***b* with phosphorus tribromide in benzene–tetrahydrofuran yielded benzyl bromide **6***c*. The benzyl bromide (**6***c*) was unstable (more so in dichloromethane) and immediately converted to phosphonium bromide **6***a*. The ylide prepared (two equivalents of butyllithium in tetrahydrofuran) from phosphonium bromide **6***a* was treated with aldehyde **7***a* to yield a mixture of olefins **5***a* and **8***a* in 57% yield with a *Z*/*E* ratio of 1:16 (by ^1H nmr analysis). The isomers were separated by chromatography and the yield of *Z* isomer was increased by irradiating the *E* isomer in dioxane solution with long-wave (365 nm) uv light, to provide a *Z*/*E* ratio of 2.5:1.5. The *Z* isomer was identical with natural combretastatin A-2 (**5***a*), by both spectral and chromatographic comparisons. A route analogous to that used for A-2 (**5***a*) was adopted for synthesis of combretastatin A-3 (**5***b*). Therefore, benzoic acid **7***f* was converted to silyl ether **7***g* (14) and reduced to benzyl alcohol **7***h*. Reaction of benzyl alcohol **7***h* with phosphorus tribromide was followed by conversion of benzyl bromide **7***i* to phosphonium bromide **7***j*. The ylide prepared from bromide **7***j* upon reaction with aldehyde **6***d* yielded a mixture of olefins **5***f* and **8***b* in 82% yield with a *Z*/*E* ratio of 5:1 (by ^1H nmr). The geometrical isomers were separated using multiple development preparative layer chromatography. The major product, *Z* isomer **5***f*, was deprotected using tetrabutylammonium fluoride to afford combretastatin A-3 in 84% yield, identical (by tlc, ir, nmr) with the natural product.

The quite different olefin *Z*/*E* isomeric ratios obtained in the

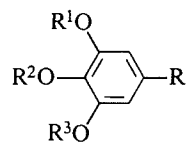

7*a*, R = CHO, R^1, R^2 = —CH_2—, R^3 = CH_3
b, R = CO_2CH_3, R^1 = R^2 = R^3 = H
c, R = CO_2CH_3, R^1 = R^2 = H, R^3 = CH_3
d, R = CO_2CH_3, R^1, R^2 = —CH_2—, R^3 = CH_3
e, R = CH_2OH, R^1, R^2 = —CH_2—, R^3 = CH_3
f, R = CO_2H, R^1 = R^2 = CH_3, R^3 = H
g, R = $CO_2Si(CH_3)_2\,C(CH_3)_3$, R^1 = R^2 = CH_3, R^3 = $Si(CH_3)_2\,C(CH_3)_3$
h, R = CH_2OH, R^1 = R^2 = CH_3, R^3 = $Si(CH_3)_2\,C(CH_3)_3$
i, R = CH_2Br, R^1 = R^2 = CH_3, R^3 = $Si(CH_3)_2\,C(CH_3)_3$
j, R = $CH_2P^+(C_6H_5)_3\,Br^-$, R^1 = R^2 = CH_3, R^3 = $Si(CH_3)_2\,C(CH_3)_3$

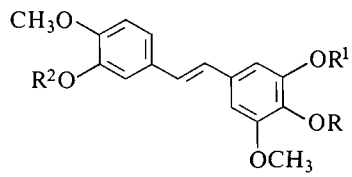

8*a*, R, R^1 = —CH_2—, R^2 = H
b, R^1 = R^2 = $Si(CH_3)_2\,C(CH_3)_3$, R = CH_3

Can. J. Chem. Downloaded from www.nrcresearchpress.com by 213.166.140.6 on 09/07/12
For personal use only.

Wittig reactions leading to A-2 and A-3 are noteworthy. In both the A-2 and A-3 syntheses, the *E* isomer(s) would normally be predicted as major product with a reaction performed in the presence of a lithium salt (15). However, in the synthesis of combretastatin A-3, the predominant product was the *Z* isomer. Apparently, the reaction is kinetically controlled due to the steric bulk (16) of the *tert*-butyldimethylsilyl group, thereby stabilizing the intermediate oxaphosphetane in the *erythro* (17) form to yield the *Z* isomer. Analogous results were realized in our parallel synthesis of combretastatin A-1 (8). Alternatively, the rate of dissociation to *cis*-stilbenes may be faster than reversal to the *threo*-oxaphosphetanes or starting ylides (18).

In experiments conducted by Dr. E. Hamel, both combretastatins A-2 and A-3 strongly inhibited tubulin polymerization (7, 8). Other biological studies with these new *cis*-stilbenes are in progress.

Experimental

Each of the synthetic intermediates was used as received from Sigma–Aldrich or from Lancaster Synthesis. All chromatographic solvents were redistilled. Sephadex LH-20 (particle size 25–100 μm) was obtained from Pharmacia Fine Chemicals AB (Uppsala, Sweden) and silica gel 60 (70–230 mesh) was supplied by E. Merck (Darmstadt, Germany). Analtech, Inc. (Newark, Delaware) silica gel GHLF U (0.25 mm layer thickness) was employed for thin-layer chromatograms and developed with an anisaldehyde – acetic acid or ceric sulfate – sulfuric acid spray reagent (heated at approximately 150°C for 5–10 min) and (or) by use of ultraviolet light.

In each of the synthetic procedures, solvent extracts of aqueous solutions were dried over anhydrous sodium sulfate. Ether refers to diethyl ether. Each pure specimen was colorless. The mutual identity of natural and synthetic specimens was established by comparison of infrared (NaCl plates) and ^{1}H nmr spectra combined with results from thin-layer chromatographic (tlc) comparisons in several solvents.

All melting points are uncorrected and were observed with a Kofler-type hot-stage apparatus. Ultraviolet spectra were obtained using a Hewlett–Packard model 8540A uv/vis spectrophotometer. Infrared spectra were measured with a Nicolet FT-IR model MX-1 unit and nuclear magnetic resonance spectra were obtained with a Bruker AM-400 instrument (deuteriochloroform as solvent and tetramethylsilane as the internal standard with chemical shifts recorded using the δ scale). The SFORD technique was used for determining multiplicities in ^{13}C nmr spectra. The mass spectral measurements were performed with a MS-50 instrument at the NSF Regional Facility, University of Nebraska, Lincoln, Nebraska. Elemental microanalyses were determined at MicAnal, Tucson, Arizona.

Plant taxonomy

Combretum caffrum (Eckl. and Zeyh.) Kuntze stem wood was collected (1979) and identified as part of the National Cancer Institute–U.S. Department of Agriculture research program directed by Drs. John Douros, Matthew I. Suffness, and James A. Duke.

Extract and solvent partition procedures

The stem wood (77 kg dry wt.) of *Combretum caffrum* was extracted with 1:1 methylene chloride – methanol and converted to a methylene chloride fraction that was partitioned between hexane and methanol–water (9:1) followed by adjustment to 3:2 methanol–water and extraction with methylene chloride as previously described (8). The methylene chloride fraction (827.9 g) from the solvent partitioning sequence was separated by steric exclusion chromatography on Sephadex LH-20 to obtain fractions A and B reported earlier (8).

*Isolation of combretastatin A-2 (**5**a), A-3 (**5**b), and B-2 (**3**b)*

Fraction A (28.6 g) was further separated on a column of Sephadex LH-20 (2.5 kg) by partition chromatography employing hexane–toluene–methanol (3:1:1) to furnish an active fraction (1.97 g, PS ED_{50} 1.8×10^{-2} μg/mL) that was redissolved in 3:1:1 hexane–toluene–methanol (20 mL), and the solution was filtered. The filtrate was chromatographed on a Sephadex LH-20 (200 g) column with the same solvent system. The resulting active fraction (1.35 g, PS ED_{50} 2.4×10^{-2} μg/mL) was dissolved in hexane – ethyl acetate (1:1, 5 mL) and chromatographed on a column (60 × 2.5 cm) of silica gel (60 g). Gradient elution, from 4:1 to 1:1 hexane – ethyl acetate, afforded in a 3:1 fraction the next PS (0.7 g, ED_{50} 1.0×10^{-2} μg/mL) active material. Rechromatography in acetone (2 mL) over a long column (100 × 1.2 cm) of silica gel (45 g) using the gradient hexane – ethyl acetate 9:1–4:1 yielded in a 4:1 fraction a pure specimen of combretastatin A-2 (**5***a*, 0.442 g, 5.74×10^{-4}% yield based on the dried plant, PS ED_{50} 2.7×10^{-2} μg/mL) as a viscous oil; R_f 0.46 (1:1 hexane – ethyl acetate); uv (CH_3OH) λ_{max} (ε): 223 (17 175), 303 (7190); ir ν_{max} (NaCl): 3490, 1508, 1452, 1440, 1427, 1272, 1196, 1129, 1114, 1085, 1042, 930 cm^{-1}; ^{1}H nmr (400 MHz): 3.750 (3H, s, OCH_3), 3.870 (3H, s, OCH_3), 5.520 (1H, s, OH, disappeared upon adding D_2O), 5.935 (2H, s, -OCH_2O-), 6.383 (1H, d, J = 12.16 Hz, -CH=CH-), 6.420 (1H, d, J = 12.16 Hz, -CH=CH-), 6.458 (1H, d, J = 1.32 Hz, H-2 or H-6), 6.483 (1H, d, J = 1.32 Hz, H-6 or H-2), 6.731 (1H, d, J = 8.4 Hz, H-5′), 6.773 (1H, dd, J = 8.4, 2.0 Hz, H-6′), 6.875 (1H, d, J = 2.0 Hz, H-2′); ^{13}C nmr (see Table 1); hreims (*m*/*z*): 300.1001 (100, M^+, calcd. for $C_{17}H_{16}O_5$: 300.0998), 285.0767 (4, $C_{16}H_{13}O_5$), 267.0666 (10, $C_{16}H_{11}O_4$), 239.0714 (17, $C_{15}H_{11}O_3$).

Active fraction B (30.6 g) was also separated in hexane–toluene–methanol (3:1:1) by partition chromatography on Sephadex LH-20 (2.5 kg). The PS active components were concentrated in two fractions: 8.11 g (PS, ED_{50} 2.7 μg/mL) and 1.57 g (ED_{50} 0.36 μg/mL). The latter fraction was chromatographed on a column (70 × 2.5 cm) of silica gel (70 g) and eluted with hexane – ethyl acetate (4:1–1:1). A fraction eluted with 4:1 hexane – ethyl acetate gave a pure specimen of combretastatin A-3 (**5***b*, 480.7 mg, 6.24×10^{-4}% yield, PS ED_{50} 2.6×10^{-2} μg/mL) as a viscous oil; R_f 0.40 (1:1 hexane – ethyl acetate); uv (CH_3OH) λ_{max} (ε): 251 (8090), 295 (8895); uv (CH_3OH + $NaOCH_3$) λ_{max}: 259 (9078), 279 (7383), 296 (7402); ir ν_{max} (NaCl): 3430, 1583, 1509, 1458, 1441, 1430, 1274, 1234, 1201, 1114, 1104 cm^{-1}; ^{1}H nmr (400 MHz): 3.668 (3H, s, OCH_3), 3.867 (3H, s, OCH_3), 3.886 (3H, s, OCH_3), 5.514, 5.680 (1H, each, brs, OH, D_2O exchanged), 6.381 (1H, d, J = 12.2 Hz, -CH=CH-), 6.427 (1H, d, J = 1.72 Hz, H-6), 6.439 (1H, d, J = 12.2 Hz, -CH=CH-), 6.535 (1H, d, J = 1.72 Hz, H-2), 6.72 (1H, d, J = 8.4 Hz, H-5′), 6.792 (1H, dd, J = 8.4 Hz, 2.0 Hz, H-6′), 6.897 (1H, d, J = 2.0 Hz, H-2′); ^{13}C nmr (refer to Table 1); hreims (*m*/*z*): 302.1156 (100, M^+, calcd. for $C_{17}H_{18}O_5$: 302.1154), 287.0919 (14, $C_{16}H_{15}O_5$), 269.0813 (14, $C_{16}H_{13}O_4$).

The active fraction weighing 8.11 g was chromatographed in ethyl acetate (20 mL) on a column of silica gel (200 g). Elution with hexane – ethyl acetate (3:1) and combination of earlier fractions furnished a 0.181-g fraction (PS, ED_{50} 0.19 μg/mL) that was further purified on a Whatman hplc column (500 × 10 mm) packed with Partisil (M-9). Elution with hexane-2-propanol (9:1) at a flow rate of 0.56 mL/min afforded pure combretastatin B-2 (**3***b*, 51.7 mg, 6.71×10^{-5}% yield, PS, ED_{50} 0.32 μg/mL) as another viscous oil; R_f 0.42 (1:1 hexane – ethyl acetate); uv (CH_3OH) λ_{max} (ε): 220 (22 902), 280 (6120); ir ν_{max} (NaCl): 3437, 1595, 1512, 1461, 1442, 1430, 1351, 1278, 1237, 1150 cm^{-1}; ^{1}H nmr (400 MHz): 2.785 (1H, brs, -CH_2—CH_2-), 3.819 (3H, s, OCH_3), 3.856 (3H, s, OCH_3), 3.866 (3H, s, OCH_3), 5.605, 5.748 (1H each, brs, OH, D_2O exchanged), 6.264 (1H, d, J = 1.88 Hz, H-6), 6.465 (1H, d, J = 1.88 Hz, H-2), 6.648 (1H, dd, J = 8.12, 2.0 Hz, H-6′), 6.760 (1H, d, J = 8.12 Hz, H-5′), 6.794 (1H, d, J = 2.0 Hz, H-2′); ^{13}C nmr (see Table 1); hreims (*m*/*z*): 304.1326 (30, M^+, calcd. for $C_{17}H_{20}O_5$: 304.1311), 167.0708 (100, $C_9H_{11}O_3$), 137.0604 (65, $C_8H_9O_2$).

*Acetylation of combretastatin A-2 (**5**a) and A-3 (**5**b)*

Both combretastatin A-2 (**5***a*, 12.0 mg) and combretastatin A-3 (**5***b*, 18.0 mg) were acetylated (separately) with acetic anhydride (1.0 mL) – pyridine (0.5 mL) at room temperature (72 h). Solvent was evaporated under a stream of nitrogen to afford acetate **5***c* and diacetate **5***e* as viscous oils; *combretastatin A-2 acetate* **5***c* displayed R_f 0.60 (1:1

hexane – ethyl acetate); ir ν_{max} (NaCl): 1767, 1510, 1430, 1264, 1199, 1127, 1112, 1086, 1042, 930, 773 cm^{-1}; ^1H nmr (400 MHz): 2.273 (3H, s, $COCH_3$), 3.731 (3H, s, OCH_3), 3.809 (3H, s, OCH_3), 5.940 (2H, s, $-OCH_2O-$), 6.410 (2H, s, -CH=CH-), 6.453 (1H, d, J = 1.1 Hz, H-2, or H-6), 6.473 (1H, d, J = 1.1 Hz, H-6 or H-2), 6.840 (1H, d, J = 8.56 Hz, H-5′), 6.977 (1H, d, J = 2.0 Hz, H-2′), 7.107 (1H, dd, J = 8.56, 2.0 Hz, H-6′); ^{13}C nmr (see Table 1); hreims (m/z): 342.1101 (59, M^+, calcd. for $C_{19}H_{18}O_6$: 342.1103), 300.0987 (100, $C_{17}H_{16}O_5$); *combretastatin A-3 diacetate* (**5***e*) showed R_f 0.54 (1:1 hexane – ethyl acetate); ir ν_{max} (NaCl): 1769, 1510, 1370, 1284, 1265, 1242, 1203, 1132, 1113, 1092 cm^{-1}; ^1H nmr (400 MHz): 2.270 (3H, s, $COCH_3$), 2.287 (3H, s, $COCH_3$), 3.675 (3H, s, OCH_3), 3.807 (3H, s, OCH_3), 3.813 (3H, s, OCH_3), 6.390 (1H, d, J = 12.2 Hz, -CH=CH-), 6.445 (1H, d, J = 12.2 Hz, -CH=CH-), 6.634 (1H, d, J = 1.76 Hz, H-6), 6.708 (1H, d, J = 1.76 Hz, H-2), 6.849 (1H, d, J = 8.46 Hz, H-5′), 7.037 (1H, d, J = 2.0 Hz, H-2′), 7.115 (1H, dd, J = 8.46, 2.0 Hz, H-6′); ^{13}C nmr (in Table 1); hreims (m/z): 386.1365 (71, M^+, calcd. for $C_{21}H_{22}O_7$: 386.1366), 344.1252 (56, $C_{19}H_{20}O_6$), 302.1146 (100, $C_{17}H_{18}O_5$).

*Hydrogenation of combretastatin A-2 (***5**a*) and combretastatin A-3 (***5**b*)

In separate experiments combretastatin A-2 (**5***a*, 12.0 mg) and combretastatin A-3 (**5***b*, 10 mg) in methanol (10 mL) and 5% Pd/C (10 mg) were each treated with a positive pressure of hydrogen at ambient temperature overnight. Catalyst was removed by filtering the solution and the product purified by preparative layer chromatography on regular (250 μm) Analtech plates with hexane – ethyl acetate (1:1) as mobile phase. The oily product from combretastatin A-3 was identical with natural *combretastatin B-2* while the dihydro product (*bibenzyl* **3***c*) from combretastatin A-2 (**5***a*) was a viscous oil exhibiting R_f 0.58 (1:1, hexane – ethyl acetate); ir ν_{max} (NaCl): 3478, 1633, 1590, 1510, 1451, 1441, 1429, 1274, 1194, 1129, 1089, 925 cm^{-1}; ^1H nmr (90 MHz): 2.78 (4H, s, $-CH_2CH_2-$), 3.86 (3H, s, OCH_3), 5.93 (2H, s, $-OCH_2O-$), 6.30 (H, d, J = 1.5 Hz, H-2 or H-6), 6.38 (1H, d, J = 1.5 Hz, H-6 or H-2), 6.63 (1H, dd, J = 8.2, 1.9 Hz, H-6′), 6.76 (1H, d, J = 8.2 Hz, H-5′), 6.77 (1H, d, J = 1.9 Hz, H-2′); ^{13}C nmr (entered in Table 1); hreims (m/z): 302.1149 (29, M^+, calcd. for $C_{17}H_{18}O_5$: 302.1154), 165.0547 (100, calcd. for $C_9H_9O_3$: 165.0552), 137.0597 (67, calcd. for $C_8H_9O_2$: 137.0603).

*Combretastatin A-2/3′-*O*-p-bromophenylcarbamate (***5**b*)

To a solution of combretastatin A-2 (**5***a*, 10 mg) in dry methylene chloride (1 mL) was added a solution of *p*-bromophenyl isocyanate (80 mg) in methylene chloride (1 mL). The mixture was stirred for 5 days at room temperature and heated at reflux for 24 h. The reaction mixture was cooled to room temperature and the solution filtered. The filtrate was concentrated and chromatographed (preparative layer) with hexane – ethyl acetate (1:1) as mobile phase. The band was eluted with acetone and crystallized from methylene chloride to afford an amorphous powder, mp 138–140°C; ir ν_{max} (NaCl): 3310, 1734, 1722, 1533, 1509, 1491, 1431, 1398, 1202, 1128, 1114, 924, 750 cm^{-1}; ^1H nmr (90 MHz): 3.75 (3H, s, OCH_3), 3.94 (3H, s, OCH_3), 5.93 (2H, s, OCH_2O), 6.43 (2H, brs, -CH=CH-), 6.48 (2H, AB_q, J = 1.1 Hz, H-2, H-6), 6.65–7.0 (3H, M, H-2′, -5′, -6′), 7.09 (1H, s, NH), 7.35 (2H, d, J = 8.5 Hz, ArH), 7.41 (2H, d, J = 8.5 Hz, ArH).

*Methyl 3,4-dihydroxy-5-methoxybenzoate (***7**c*)

Methyl gallate (**7***b*, 10 g, 54.3 mmol) was added to a solution of borax (80 g) in 800 mL of water with stirring (30 min). Dimethyl sulfate (30 mL) and a solution of sodium hydroxide (13 g in 50 mL of water) were added from two separate dropping funnels over 2.5 h and stirring was continued overnight. Concentrated sulfuric acid (50 mL) was added and stirring continued an additional hour. The product was extracted with chloroform (5 × 1 L and each time stirring the solution for 20 min). The combined chloroform extracts were washed with brine (500 mL), dried, and concentrated, and the residue crystallized from methanol–benzene to yield methyl ether **7***c* (9.1 g, 84.5%); mp 110–111°C (lit. (19) mp 112°C); ir ν_{max} (NaCl): 3380, 1700, 1696, 1611, 1436, 1341, 1314, 1229, 1204, 1089 cm^{-1}; ^1H nmr (90 MHz): 3.88 (3H, s, OCH_3), 3.94 (3H, s, OCH_3), 5.50–6.0 (2H, OH), 7.22 (1H, d, J = 1.8 Hz, ArH), 7.34 (1H, d, J = 1.8 Hz, ArH).

Under analogous experimental conditions but using continuous extraction with ethyl acetate in place of chloroform yielded a mixture of methyl gallate **7***c* (7.0 g) and 3-*O*-methyl gallic acid (1.4 g).

*Methyl 3,4-methylenedioxy-5-methoxybenzoate (***7**d*)

Cesium fluoride (24.5 g, 161.5 mmol) was added to a stirring solution of phenol **7***c* (7.3 g, 36.8 mmol) in dimethylformamide (90 mL) under argon. After stirring 20 min, dibromomethane (2.8 mL, 40.5 mmol) was added and the mixture heated for 2 h. The reaction was allowed to cool to room temperature. Ether (300 mL) was added and the ethereal solution was washed with cold water (3 × 50 mL), dried, and concentrated to afford methylenedioxy derivative **7***d* as a powder (7.62 g, 98% yield), which was recrystallized from acetone–hexane, mp 89–91°C; ir ν_{max} (NaCl): 1714, 1636, 1507, 1436, 1369, 1327, 1245, 1177, 1107, 1041 cm^{-1}; ^1H nmr (90 MHz): 3.89 (3H, s, OCH_3), 3.94 (3H, s, OCH_3), 6.06 (2H, s, $-CH_2-$), 7.21 (1H, d, J = 1.4 Hz, ArH), 7.33 (1H, d, J = 1.4 Hz, ArH); eims, m/z (rel. int.%): 210 (100, M^+), 179 (75, $M^+ - OCH_3$). *Anal.* calcd. for $C_{10}H_{10}O_5$: C 57.15, H 4.80; found: C 57.10, H 4.74.

*3,4-Methylenedioxy-5-methoxybenzyl alcohol (***7**e*)

Lithium aluminum hydride (0.50 g) was added to a stirred solution of methyl ester **7***d* (1.7 g) in ether–tetrahydrofuran (2:1, 50 mL). After stirring for 30 min, the reaction mixture was cooled to 5°C and saturated aqueous sodium sulfate was carefully added until a white solid appeared. The precipitate was collected by filtration, the solution was dried, and the solvent evaporated to give crystalline alcohol **7***e* (1.45 g, 98% yield). Recrystallization from ethyl acetate – hexane afforded an analytical sample melting at 66–67°C (lit. (4) mp 66°C); ir ν_{max} (NaCl): 3220, 1632, 1467, 1453, 1435, 1323, 1203, 1133, 1093, 1008, 918 cm^{-1}; ^1H nmr (90 MHz): 1.75 (1H, brs, OH), 3.90 (3H, s, OCH_3), 4.58 (2H, brs, $-CH_2OH$), 5.96 (2H, s, $-CH_2-$), 6.55 (2H, s, ArH).

*3,4-Methylenedioxy-5-methoxybenzaldehyde (***7**a*)

To a stirred yellow mixture of pyridinium chlorochromate (20) (1.72 g, 7.99 mmol) and anhydrous sodium acetate (0.655 g, 7.99 mmol) in methylene chloride CH_2Cl_2 (30 mL) was added at once a solution of benzyl alcohol **7***e* (1.32 g, 7.26 mmol) in methylene chloride (10 mol). The greyish solution, which formed immediately, was stirred for 2 h, and the reaction was monitored by tlc (1:1 hexane – ethyl acetate). After filtering the solution through a small silica column, colorless aldehyde **7***a* (1.18 g, 91% yield) was eluted with hexane – ethyl acetate (7:3). Recrystallization from acetone afforded needles, mp 132–133°C (lit. (13) mp 130–131°C, 129–130°C); ir ν_{max} (NaCl): 1694, 1676, 1622, 1508, 1474, 1451, 1362, 1325, 1134, 1190 cm^{-1}; ^1H nmr (90 MHz): 3.95 (3H, s, OCH_3), 6.09 (2H, s, $-CH_2-$), 7.04 (1H, d, J = 1.4 Hz, ArH), 7.12 (1H, d, J = 1.4 Hz, ArH), 9.78 (1H, s, -CHO).

*3-Hydroxy-4-methoxybenzyltriphenylphosphonium bromide (***6**a*)

A solution of phosphorus tribromide (8.51 mL) in a mixture of tetrahydrofuran–benzene (1:2, 330 mL) was added to a cool (0°C) solution of 3-hydroxy-4-methoxybenzyl alcohol (**6***b*, 6.13 g, 40 mmol) in the same solvent (75 mL) under argon. The colorless solution was stirred at room temperature for 2 h, poured onto ice water (100 mL), and extracted with ether (2 × 100 mL). The ethereal layer was washed once with water (50 mL) followed by brine (2 × 50 mL), dried, and evaporated to dryness to afford bromide **6***a* as an amorphous powder. A solution prepared from the crude bromide, anhydrous benzene (150 mL), and triphenylphosphine (15.72 g, 60 mmol) was stirred for 10 min at room temperature and heated at reflux for 2 h. On cooling to room temperature, a viscous oil separated. The upper solvent phase was decanted and the oil was crystallized from ethanol–ether to give bromide **6***a* as a powder (10.0 g, 52.4% from alcohol **6***b*); mp 262–264°C; ir ν_{max} (NaCl): 3158, 1604, 1589, 1527, 1512, 1437, 1279, 1255, 1128, 1111, 743 cm^{-1}; ^1H nmr (90 MHz, $CDCl_3$ + D_2O): 3.77 (3H, s, OCH_3), 4.95 (2H, d, J_{PCCH} = 13.7 Hz, $-CH_2-$), 6.57 (2H, brs, ArH), 6.83 (1H, brs, ArH), 7.56–7.77 (15H, ArH). *Anal.* calcd. for $C_{26}H_{24}O_2PBr$: C 65.6, H 5.05, Br 16.67; found: C 64.50, H 5.07, Br 16.78.

Can. J. Chem. Downloaded from www.nrcresearchpress.com by 213.166.140.6 on 09/07/12
For personal use only.

Can. J. Chem. Downloaded from www.nrcresearchpress.com by 213.166.140.6 on 09/07/12
For personal use only.

*3'-Hydroxy-3,4-methylenedioxy-4',5-dimethoxy-(E)- and -(Z)-stilbene (**5**a and **8**a, combretastatin A-2 (**5**a), and E isomer (**8**a)*

Phosphonium bromide **6***a* (3.35 g, 7.0 mmol) was suspended in tetrahydrofuran (100 mL), stirred, and cooled to −50°C (under argon), and *n*-butyllithium (10 mL, 15 mmol) was added using a syringe and septum technique. The solution became deep red immediately and upon reaching room temperature was stirred 20 min prior to adding a solution of aldehyde **7***a* (1.15 g, 6.39 mmol) in tetrahydrofuran (30 mL). All the aldehyde was consumed in 30 min. Cold hydrochloric acid (1 *M*, 50 mL) was added followed by water (100 mL), and the product was extracted with ethyl acetate (3 × 100 mL) from the colorless solution. The ethyl acetate extract was washed with water (50 mL), brine (50 mL), dried, and the solvent evaporated. The crude product was chromatographed on a silica gel (50 g) column. Elution with hexane – ethyl acetate (17:3) afforded a mixture of *Z*- and *E*-stilbenes (1.09 g, 57% yield, ratio *Z*/*E* 1:16). Half of the product was rechromatographed on a longer silica gel column, and elution with hexane – ethyl acetate (9:1) provided first combretastatin A-2 (40 mg) as a viscous oil identical with natural combretastatin A-2 (**5***a*) and later the *E* isomer **8***a* (0.20 g) as needles from ethyl acetate – hexane, mp 145–150°C; ir ν_{max} (NaCl): 3490, 1622, 1509, 1463, 1440, 1429, 1319, 1279, 1263, 1254, 1133 cm^{-1}; ^1H nmr (400 MHz): 3.908 (3H, s, OCH_3), 3.941 (3H, s, OCH_3), 5.598 (1H, brs, OH), 5.978 (2H, s, $-OCH_2O-$), 6.629 (1H, d, J = 1.30 Hz, H-2 or H-6), 6.729 (1H, d, J = 1.30 Hz, H-6 or H-2), 6.825 (1H, d, J = 8.32 Hz, H-5'), 6.848 (2H, s, -CH=CH-), 6.945 (1H, d, J = 8.32, 2.0 Hz, H-6'), 7.113 (1H, d, J = 2.0 Hz, H-2'). *Anal.* calcd. for $C_{17}H_{16}O_5$: C 68.00, H 5.37; found: C 67.63, H 5.37.

Photochemical isomerization of E*-stilbene **8**a to combretastatin A-2 (**5**a)*

A solution of *E* isomer **8***a* (40 mg) in dioxane (30 mL) – water (1 mL) was stirred and irradiated (directly into the solution from above) with long-wavelength (365 nm) uv for 5 h. The ultraviolet source was an uv lamp used for visualizing tlc plates equipped with both short-wave (254 nm) and long-wave (365 nm) lamps. The solvent was removed and ^1H nmr examination of the residue revealed an isomeric mixture in the ratio *Z*/*E* of 2.5:1.5. Separation by chromatography on a silica gel column and elution with hexane – ethyl acetate (9:1) yielded combretastatin A-2 (15 mg).

*3-*tert*-Butyldimethylsilyloxy-4,5-dimethoxybenzyl alcohol (**7**h)*

Diisopropylethylamine (11.3 mL, 77 mmol) was added to a stirred solution of 3-hydroxy-4,5-dimethoxybenzoic acid (**7***f*, 5.0 g, 25 mmol) in dimethylformamide (50 mL, under argon) followed by addition of *tert*-butyldimethylsilyl chloride (8.32 g, 55 mmol), and the reaction mixture was stirred for 1 h. Ice (50 g) was added and the reaction mixture was extracted with ethyl ether (200 mL). The ethereal solution was washed with cold water (3 × 50 mL), sodium bicarbonate solution (10%, 50 mL), water (50 mL), dried, and solvent evaporated to yield *tert*-butyldimethylsilyl 3-*tert*-butyldimethylsilyloxy-4,5-dimethoxybenzoate (**7***g*) as a chromatographically homogeneous oil (10.4 g, 97% yield). Attempts at high vacuum distillation (100°C at 1.0 Torr; 1 Torr = 133.3 Pa) failed and resulted in desilylation. However, the oil showed the correct ir and ^1H nmr spectral data for silane **7***g*; ir ν_{max} (NaCl): 2932, 1700, 1590, 1420, 1350, 1254, 1230, 1221, 1118, 839, 775 cm^{-1}; ^1H nmr (90 MHz): 0.107 (6H, s, 2 × $SiCH_3$), 0.276 (6H, s, 2 × $SiCH_3$), 0.922 (18H, s, 6 × CH_3), 3.751 (3H, s, OCH_3), 3.790 (3H, s, OCH_3), 7.170 (2H, AB_q, J_{AB} = 1.5 Hz, ArH).

Silyl ester **7***g* (10.0 g, 23 mmol) was dissolved in ether (300 mL) and stirred (under argon) with lithium aluminum hydride (2.0 g) at room temperature for 1 h. Saturated ammonium chloride solution (ice-cold) was added and the ether layer separated. The aqueous phase was extracted with ether (3 × 200 mL) and the combined ether extract was washed with sodium bicarbonate solution, cold water, and dried. After solvent removal, the residual oil was found to be chromatographically homogeneous alcohol **7***h* (6.0 g, 86% yield); the oil distilled at 210°C (0.04 Torr) and displayed ir ν_{max} (NaCl): 3450, 2931, 1587, 1501, 1427, 1233, 1118, 1004, 837, 782 cm^{-1}; ^1H nmr (90 MHz): 0.201 (6H, s, 2 × CH_3), 1.026 (9H, s, 3 × CH_3), 1.716 (1H, t, J = 5.9 Hz, OH, D_2O exchanged), 3.794 (3H, s, OCH_3), 4.596 (2H, d, J = 5.9 Hz, $-CH_2OH$, collapsed to a broad singlet upon D_2O exchange), 6.510 (1H, d, J = 1.9 Hz, ArH), 6.610 (1H, d, J = 1.9 Hz, ArH). *Anal.* calcd. for $C_{16}H_{26}O_4Si$: C 60.39, H 8.78; found: C 60.06, H 8.78.

*3-*tert*-Butyldimethylsilyloxy-4,5-dimethoxybenzyltriphenylphosphonium bromide (**7**j)*

Before adding phosphorus tribromide (0.95 mL) in methylene chloride (5 mL) a solution of silyloxybenzyl alcohol **7***h* (6.0, 20 mmol) in methylene chloride (anhydrous, 100 mL) was stirred and cooled (−10°C, ice–salt bath) for 15 min. The mixture was stirred 10 min and 10% aqueous sodium bicarbonate solution (50 mL) was added (slowly). The methylene chloride layer was washed with cold water (2 × 50 mL), dried, and solvent evaporated to give 3-*tert*-butyldimethysilyloxy-4,5-dimethoxybenzyl bromide (**7***i*) as a colorless oil (6.4 g, 88% yield), homogeneous by tlc. While the product (**7***i*) was heat sensitive, and distillation was unsuccessful, it did give the correct spectral data for silane **7***i*; ir ν_{max} (NaCl): 2932, 1586, 1500, 1427, 1348, 1250, 1234, 1127, 1111, 838 cm^{-1}; ^1H nmr (90 MHz): 0.183 (6H, s, 2 × CH_3), 1.006 (9H, s, 3 × CH_3), 3.777 (3H, s, OCH_3), 3.855 (3H, s, OCH_3), 4.409 (2H, s, $-CH_2-$), 6.561 (2H, AB_q, J = 2.0 Hz, ArH); ms (*m*/*z*, rel. amt.) 362, 360 (40%, M^+), 305, 303 (80, $M^+ - C_4H_9$), 281 (60, $M^+ - Br$), 253 (75, $M^+ - Br - 28$), 209 (100, $M^+ - Br - C_5H_{12}$), 166 (45, $M^+ - Br - Si(CH_3)_2C(CH_3)_3$).

To a solution of bromide **7***i* (6.0 g, 16.6 mmol) in toluene (50 mL) was added (stirring) a solution of triphenylphosphine (4.36 g, 16.6 mmol) in toluene (10 mL). The mixture was heated to reflux for 15 min. When the clear solution started to become turbid, heating was discontinued and the mixture was stirred overnight at room temperature. The solid phosphonium bromide **7***j* (7.17 g, 69% yield) was recovered by filtration as a powder melting at 248°C; ir ν_{max}(NaCl): 2957, 1586, 1502, 1453, 1436, 1344, 1253, 1113, 836, 742, 721 cm^{-1}; ^1H nmr (90 MHz): 0.58 (6H, s, 2 × CH_3), 1.48 (9H, s, 3 × CH_3), 4.15 (3H, s, OCH_3), 4.32 (3H, s, OCH_3), 5.89 (2H, d, J_{PCH} = 14 Hz, CH_2), 6.71 (1H, t, J = 2.2 Hz, ArH), 7.36 (1H, t, J = 2.2 Hz, ArH), 8.23–8.45 (15H, ArH). *Anal.* calcd. for $C_{33}H_{40}BrO_3PSi$: C 63.56, H 6.46, Br 12.81; found: C 64.04, H 6.57, Br 12.47.

*Combretastatin A-3 (**5**b)*

Butyllithium (2.47 mL, 2.2 mmol) was added to a stirred and cooled (−10°C) suspension of phosphonium bromide **7***j* (1.31 g, 2.1 mmol) in tetrahydrofuran (100 mL). The orange-red solution was stirred at room temperature 10 min. Aldehyde **6***d* (0.532 g, 2.0 mmol) was added and stirring continued another 10 min while the red solution changed to yellow. A tlc examination (4:1, hexane – ethyl acetate) showed completion of reaction. Ice water (100 mL) was added and the product extracted with ether (3 × 100 mL). The ethereal solution was washed with water (100 mL), and concentrated to a gum, which upon silica gel column (40 g) chromatography and elution with hexane – ethyl acetate (97:3) afforded a mixture of 3,3'-bis-(*tert*-butyldimethylsilyloxy)-4',4,5-trimethoxy-(*Z*)- and (*E*)-stilbene (**5***f* and **8***b*) in a ratio of 5:1 (0.870 g, 82% yield). The isomers were separated by preparative layer chromatography on silica gel (20 × 20 cm, 500 μm, E-Merck plates) employing 19:1 hexane – ethyl acetate. The short uv positive upper band was the major product and elution with hexane – ethyl acetate yielded *Z* isomer **5***f* as an oil (423 mg); ir ν_{max} (NaCl): 2930, 1575, 1509, 1250, 1231, 1118, 838, 782 cm^{-1}; ^1H nmr (400 MHz): 0.070 (6H, s, 2 × CH_3), 0.105 (6H, s, 2 × CH_3), 0.932 (9H, s, 3 × CH_3), 0.958 (9H, s, 3 × CH_3), 3.666 (3H, s, OCH_3), 3.761 (3H, s, OCH_3), 3.774 (3H, s, OCH_3), 6.366 (1H, d, J = 12 Hz, -CH=CH-), 6.413 (1H, d, J = 1.84 Hz, H-6), 6.429 (1H, d, J = 12 Hz, -CH=CH-), 6.471 (1H, d, J = 1.84 Hz, H-2), 6.718 (1H, d, J = 8.3 Hz, H-5'), 6.778 (1H, d, J = 2.0 Hz, H-2'), 6.840 (1H, dd, J = 8.3, 2.0 Hz, H-6'). The lower long uv positive band was also eluted with hexane – ethyl acetate to give *E* isomer **8***b* as an oil (80 mg); ir ν_{max} (NaCl): 2930, 1578, 1509, 1427, 1272, 1251, 1117, 838, 782 cm^{-1}; ^1H nmr (400 MHz): 0.183 (6H, s, 2 × CH_3), 0.207 (6H, s, 2 × CH_3), 1.024 (9H, s, 3 × CH_3), 1.028 (9H, s, 3 × CH_3), 3.794 (3H, s, OCH_3), 3.823 (3H, s, OCH_3), 3.901 (3H, s, OCH_3), 6.626

(1H, d, J = 1.88 Hz, H-6), 6.693 (1H, d, J = 1.88 Hz, H-2), 6.800 (1H, d, J = 16.2 Hz, -CH=CH-), 6.825 (1H, d, J = 8.3 Hz, H-5′), 6.845 (1H, d, J = 16.2 Hz, -CH=CH-), 7.020 (1H, d, J = 2.1 Hz, H-2′), 7.047 (1H, dd, J = 8.3 Hz, 2.1 Hz, H-6′). *Anal.* calcd. for $C_{29}H_{46}O_5Si_2$: C 65.62, H 8.73; found: C 66.09, H 8.97.

To a stirred solution of silyl-*Z*-stilbene **5***f* (0.25 g, 0.47 mmol) in tetrahydrofuran (10 mL under argon) was added a 1 *M* tetrahydrofuran solution of tetrabutylammonium fluoride (1 mL, 1.0 mmol). Instantaneously the solution became yellow and reaction was complete as evidenced by tlc (hexane – ethyl acetate 3:2). Ice (5 g) – water (5 mL) was added to the mixture and the product extracted with ether (2 × 25 mL). The ethanol extract was washed with cold water (20 mL) and dried. After evaporation of solvent, the residue in 1:1 hexane – ethyl acetate was filtered through a pipette filled with silica gel (2 g) to afford combretastatin A-3 as an oil (0.13 g, 91% yield), homogeneous by tlc and identical with the natural product.

Acknowledgements

For very necessary financial assistance we are pleased to thank the Arizona Disease Control Research Commission, Eleanor W. Libby, the Waddell Foundation (Donald Ware), Mrs. Lotte Flugel, the Fannie E. Rippel Foundation, Polly Trautman, Mary Dell Pritzlaff, the Olin Foundation (Spencer T. and Ann W.), Grant CA-30311-01A3 awarded by the National Cancer Institute, and Contract N01-CM-97262 with the Division of Cancer Treatment, NCI, National Institutes of Health. Other necessary assistance was contributed by Drs. M. L. Niven, D. L. Doubek, D. L. Herald, A. Goswami, P. Lohavanijaya, M. I. Suffness, and J. M. Schmidt. M.L.N. is pleased to thank the Research Grants Committee, UTC, and the CSIR, Pretoria, South Africa, for financial assistance and we also acknowledge assistance from the NSF Regional Instrumentation Facility in Nebraska (Grant CHE-8211164).

1. G. R. PETTIT, S. B. SINGH, M. L. NIVEN, and J. M. SCHMIDT. Can. J. Chem. Submitted.
2. J. C. WILLIS. A dictionary of the flowering plants and ferns. 8th ed. *Revised by* H. K. Airy Shaw. Cambridge University Press, England. 1973.
3. J. M. WATT and M. G. BRYER-BRANDWISK. The medicinal and poisonous plants of Southern and Eastern Africa. E. and S. Livingston, Ltd., London. 1962. p. 194.
4. F. DALLACKER and R. SLUYSMANS. Monatsh. Chem. **100**(2), 560 (1969).
5. M. SUFFNESS and J. DOUROS. *In* Methods in cancer research. Vol. XVI. Cancer Drug Development, Part A. *Edited by* V. De Vita and H. Busch. Academic Press, New York. 1979. p. 73.
6. G. R. PETTIT, G. M. CRAGG, D. L. HERALD, J. M. SCHMIDT, and P. LOHAVANIJAYA. Can. J. Chem. **60**, 1374 (1982).
7. E. HAMEL and C. M. LIN. Biochem. Pharmacol. **32**, 3864 (1983).
8. G. R. PETTIT, S. B. SINGH, M. L. NIVEN, E. HAMEL, and J. M. SCHMIDT. J. Nat. Prod. **50**, 119 (1987).
9. (*a*) J. B. STOTHERS. Carbon-13 NMR spectroscopy. Academic Press, New York. 1972. pp. 196–197; (*b*) E. M. SILVERSTEIN, G. C. BASSLER, and T. C. MORRILL. Spectrometric identification of organic compounds. John Wiley and Sons, New York. 1981. pp. 264–265.
10. D. E. HATHWAY. Biochem. J. **8**, 80 (1962).
11. S. E. DREWES and I. P. FLETCHER. J. Chem. Soc. Perkin Trans. 1, 961 (1974).
12. Y. KASHIWADA, G. NONAKA, and I. NISHIOKA. Chem. Pharm. Bull. **32**, 3501 (1984).
13. (*a*) Y. ASAKAWA, K. TANIKAWA, and T. ARATANI. Phytochemistry, **15**, 1057 (1976); (*b*) M. TOMITA and R. AOYAGI. Chem. Pharm. Bull. **16**, 523 (1968).
14. G. R. PETTIT, S. B. SINGH, and G. M. CRAGG. J. Org. Chem. **50**, 3404 (1985).
15. M. SCHLOSSER. Top. Stereochem. **5**, 1 (1970).
16. (*a*) M. SCHLOSSER and B. SCHAUB. J. Am. Chem. Soc. **104**, 5821 (1982); (*b*) W. E. MCEWEN and J. V. COONEY. J. Org. Chem. **48**, 983 (1983).
17. (*a*) A. B. REITZ, M. S. MUTTER, and B. E. MARYANOFF. J. Am. Chem. Soc. **106**, 1873 (1984); (*b*) B. E. MARYANOFF, A. B. REITZ, M. S. MUTTER, R. R. INNENS, and H. R. ALMOND. J. Am. Chem. Soc. **107**, 1068 (1985).
18. S. M. CAIRNS and W. E. MCEWEN. Tetrahedron Lett. **27**, 1541 (1986).
19. L. JURD. J. Am. Chem. Soc. **81**, 4606 (1959).
20. (*a*) E. J. COREY and J. W. SUGGS. Tetrahedron Lett. 2644 (1975); (*b*) J. Org. Chem. **40**, 2554 (1975).

Can. J. Chem. Downloaded from www.nrcresearchpress.com by 213.166.140.6 on 09/07/12
For personal use only.

Enzymes in organic synthesis. 37.[1] Preparation and characterization of potential decalindione substrates of horse liver alcohol dehydrogenase

J. Bryan Jones and David R. Dodds

Department of Chemistry, University of Toronto, Toronto, Ont., Canada M5S 1A1

Received March 3, 1987

J. Bryan Jones and David R. Dodds. Can. J. Chem. **65**, 2397 (1987).

The preparations of ten decalindiones for investigation as substrates of horse liver alcohol dehydrogenase are reported. The structure characterizations include clarifications of some ambiguities in the decalin literature.

J. Bryan Jones et David R. Dodds. Can. J. Chem. **65**, 2397 (1987).

On a préparé dix décalinediones dans le but d'examiner leur comportement comme substrats de la déshydrogénase d'alcool provenant du foie de cheval. Les caractérisations de leurs structures a permis de clarifier quelques ambiguités que l'on retrouve dans la littérature relativement aux décalines.

[Traduit par la revue]

Can. J. Chem. Downloaded from www.nrcresearchpress.com by 213.166.140.6 on 09/07/12
For personal use only.

The ability of enzymes to catalyze stereospecific transformations of symmetrical substrates into chiral synthons of value in asymmetric synthesis is now well established (2). Stereospecific oxidations of a broad structural range of meso diols catalyzed by horse liver alcohol dehydrogenase (HLADH) represent one of the most dramatic illustrations of this approach to chiral synthon preparation (3). The complementary process of chiron production via stereospecific reductions of symmetrical diketones is of equal asymmetric synthetic interest. As the first step in evaluating this aspect of HLADH stereospecificity we initiated an investigation of the enzyme's catalysis of the reductions of a series of the potential decalindione substrates **1**–**10** and oxidation of the meso diol **11**.

Each of the diones **1**–**11** possesses elements of rotational and (or) reflective symmetry, the respective symmetry elements being c_{2v} (**1**, **3**, **4**), i (**1**, **2**), σ_h (**1**, **4**), and σ_v (**1**, **4**–**11**). Decalins **1**, **4**–**10** are achiral, **2** and **11** are meso compounds, and **3** is a racemate.

This paper reports the preparation and characterization of **1**–**9** and **11**.

Results and discussion

Preparations and 2,6-decalindiones 1–3

This series was derived from 2,6-dihydroxynaphthalene as shown in Scheme 1.

Because hydrolysis of **12** gave both **13** and **1** in a ratio of 9:1, it was necessary to ketalize the mixture to achieve the isomer separation needed in the **13** → **2** steps. The mixture (equilibrium ratio β,γ:α,β of 1:2) of ethylenedioxymonoketals derived from **13** was readily purified into its components **14** and **15** by chromatography. Lithium in liquid ammonia reduction of **15**, followed by deketalization, yielded the desired dione **2**. Mild hydrolysis of **12** gave **1** containing 10% of **13**, and hydrogenation of **13** a 1:2 mixture of **3**:**2** even in the presence of acetic acid (4). These mixtures were readily purified by chromatography and recrystallization respectively.

Preparations of 2,7-decalindiones 4–9 and diol 11

The 2,7-decalindione **4** was obtained as shown in Scheme 2.

Unfortunately, all attempts to reduce **17** to the *trans*-2,7-dione **5** were unsuccessful. The ^{1}H nmr spectrum of **17** shows

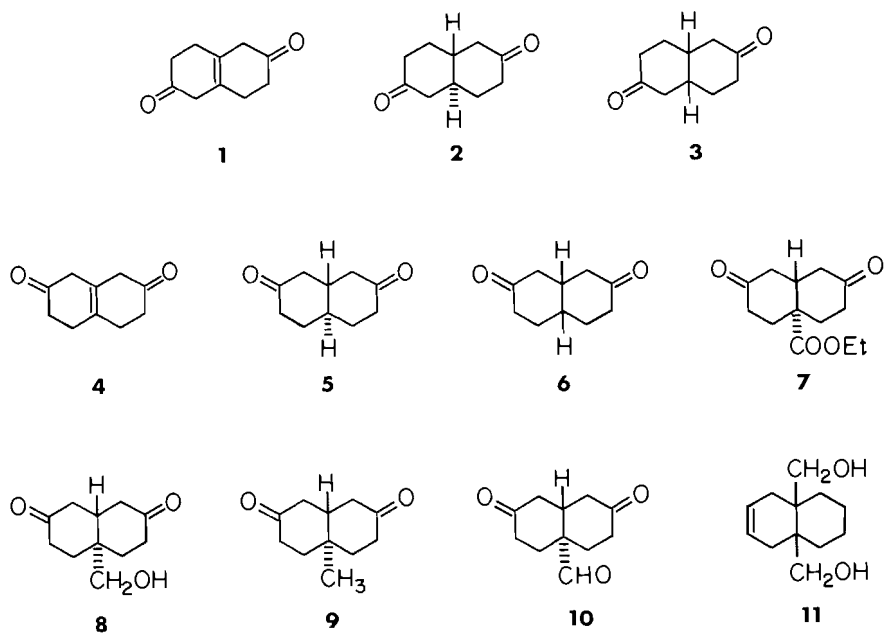

[1]For Part 36, see ref. 1.

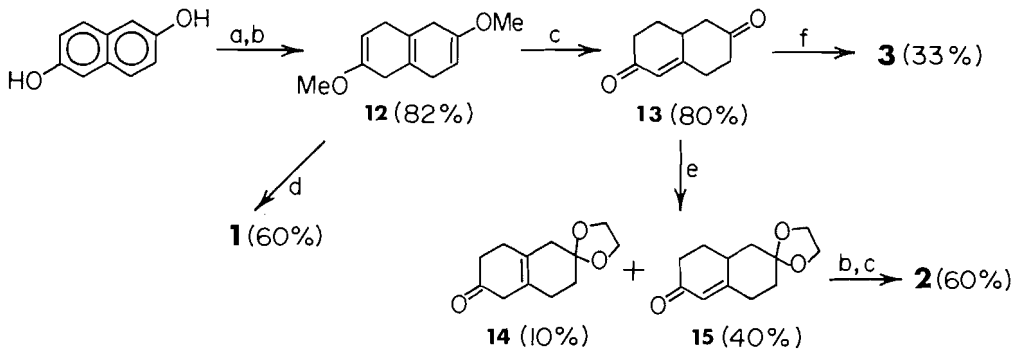

Reagents: (a) NaH/MeI (b) $Li/NH_3/EtOH$ (c) H_3O (d) $(COOH)_2/H_2O$ (e) $HO(CH_2)_2OH/H^+$ (f) H_2/Pd

SCHEME 1

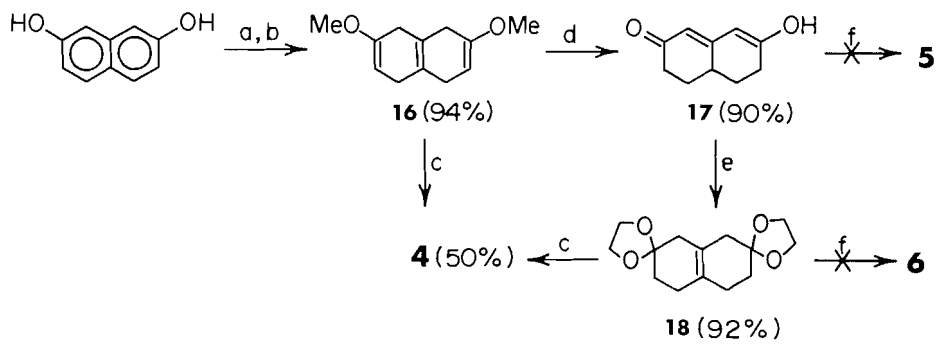

Reagents: (a) $(MeO)_2SO_2/^-OH$ (b) Li/NH_3, EtOH (c) $(COOH)_2/H_2O$ (d) H_3O^+ (e) $HOCH_2CH_2OH/H^+$ (f) reduction

SCHEME 2

only one singlet for the two olefinic protons, indicating that the enol hydroxyl proton is located between the two oxygen atoms of a fully conjugated system containing a delocalized negative charge. This situation would make reductions by the hydrogenation and dissolving metal reagents applied very difficult. Attempted reduction of **18** also failed (5). It was eventually necessary to adopt the lengthy route summarized in Scheme 3 to this compound.[2] The target dione **5** and its isomer **2** were produced in equal amounts by this method, but were readily separated. The *trans* ring junction of this series was further confirmed by hydrogenation of **20** to *trans*-2-decalone.

The *cis*-2,7-dione **6** was obtained in 65% yield by chromic acid oxidation of the diol product of high pressure hydrogenation of 2,7-dihydroxynaphthalene.

All of the C-4a substituted 2,7-diones **7–9** were derived from the same precursor **22** (Scheme 4). The bicyclic ester **21** was first observed (7) as a minor by-product, but by adding 1.5 equivalents of base, we were able to raise the yield to 36% (and occasionally 40%). Hydrogenation[3] of **21** gave mainly **22**, together with some of the hydrogenolysis product **23**. The relative ease of reduction of **21** is in sharp contrast to the resistance of **17** to the same transformations. Jones oxidation of **22** afforded the desired diketoester **7**. This was readily converted into the 4a-hydroxymethyl and 4a-methyl substrates **8** and **9** as shown.

On keeping samples of **8** under acidic conditions, up to 10% (by nmr) of the cyclic hemiketal **26** was detectable.

[2]This alternative 1,2-carbonyl shift method of Trost and Salzmann (6) was not satisfactory in this case.

[3]Attempted reduction of **21** with $LiAlH_4$, $NaBH_4$, or $Li/NH_3/EtOH$ gave only poor yields of multiproduct mixtures.

The ring junctions of all the saturated decalin derivatives of Scheme 4 are depicted in the *trans* configuration even though hydrogenation of α,β-unsaturated decalones usually results in *cis* ring junction formation (8). In this case the *trans* geometry is presumably sterically induced (9), with addition of hydrogen occurring from the direction opposite to that of the carboxyethyl group orientation. However, because of conflicting literature data (10), the *trans* nature of the ring junction was verified by the correlation outlined in the Scheme 5 conversions of **22** and **23** to the known (11) 4a-methyldecalone **28**. In addition, in view of the ambiguity in the ^{13}C nmr correlation of the ring junction literature data (12*a*) on *cis*- and *trans*-decalin systems, a further, unequivocal, synthesis of **28** was performed (Scheme 6) in which the *trans* ring junction is guaranteed by the lithium and liquid ammonia reduction of **29**. The samples of **28** from Schemes 5 and 6 were identical in every way. The α configuration of the hydroxyl group of **22** was then assigned from ^1H and ^{13}C nmr spectroscopy, which showed it to be equatorially oriented (12*b*).

Attempts to oxidize the hydroxydiketone **8** to the aldehyde **10** gave poor yields of complex mixtures. In contrast, oxidation of the triol **30** was successful but further oxidation of the initially formed aldehyde, via its hemiacetal form, during the reaction could not be prevented, resulting in the isolation of only the ketolactone **31** (Scheme 7). The dihydroxydecalin **11** was prepared by the method of Paquette *et al.* (13).

Evaluation of 1–9 and 11 as HLADH substrates

A reliable guide to the feasibility of preparative-scale HLADH-catalyzed reductions of new substrates is provided by comparison of their initial reduction rates with that of a standard reference ketone such as cyclohexanone (14). The rates of

Can. J. Chem. Downloaded from www.nrcresearchpress.com by 213.166.140.6 on 09/07/12
For personal use only.

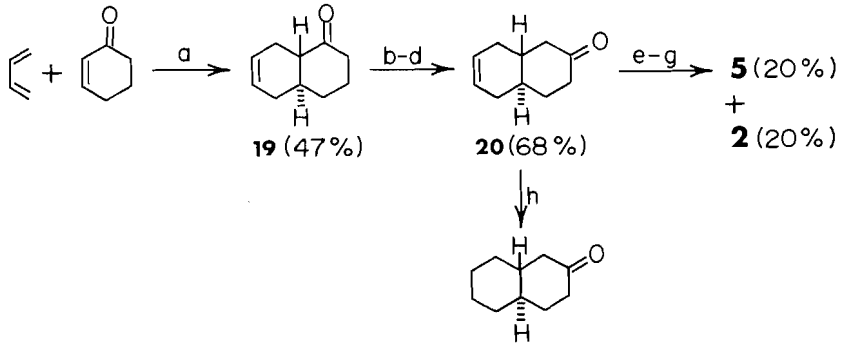

Reagents: (a) $SnCl_4$ (b) $TosNHNH_2$ (c) 1. *n*-BuLi 2. Me_2S_2 3. *n*-BuLi (d) $HgCl_2$ (e) mcpba (f) $LiAlH_4$ (g) CrO_3 (h) H_2/PdC

SCHEME 3

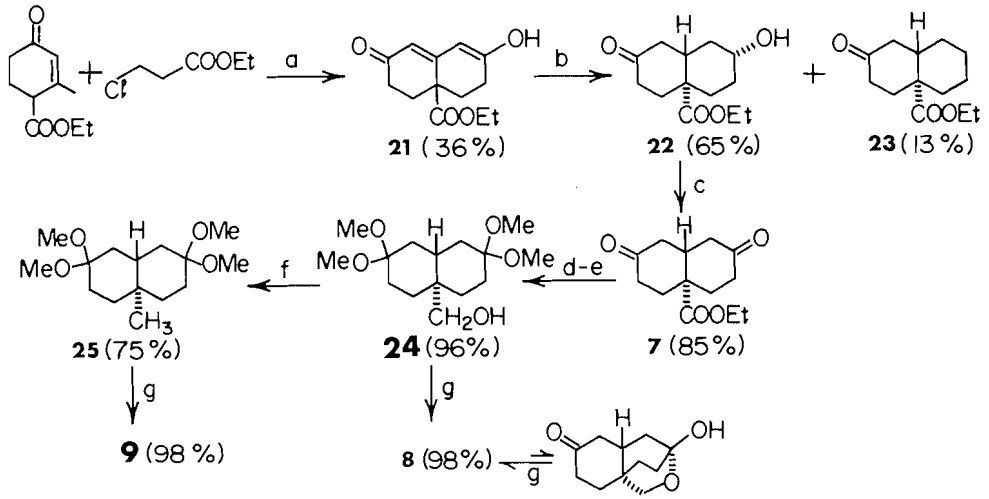

Reagents: (a) NaOEt (b) H_2/PdC (c) CrO_3 (d) MeOH/H^+/$HC(OMe)_3$ (e) $LiAlH_4$ (f) 1. *n*-BuLi 2. $ClPO(NMe_2)_2$ 3. Li/$EtNH_2$ (g) H_3O^+

SCHEME 4

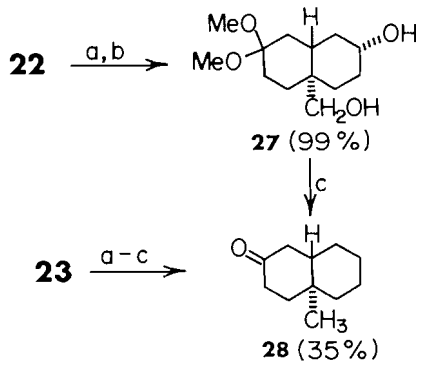

Reagents: (a) MeOH/H^+/$HC(OMe)_3$ (b) $LiAlH_4$ (c) 1. *n*-BuLi 2. $ClPO(NMe_2)_2$ 3. Li/$EtNH_2$ 4. H_3O^+

SCHEME 5

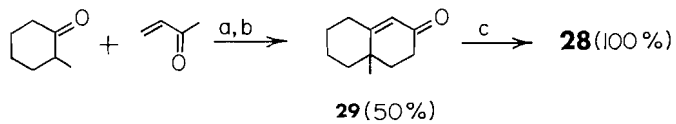

Reagents: (a) H^+/Δ (b) NaOEt (c) Li/NH_3, NH_4Cl

SCHEME 6

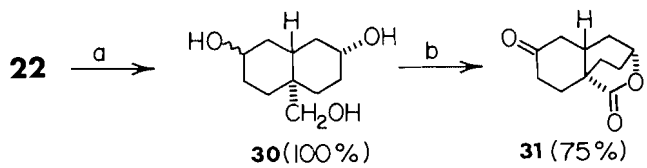

Reagents: (a) $LiAlH_4$ (b) CrO_3

SCHEME 7

reduction of **1**–**9** relative to that of cyclohexone, and of oxidation of **11**, are summarized in Table 1. Since HLADH-catalyzed reductions of ketones with relative rates of reduction >1% of that of cyclohexanone are preparatively viable (14), it is clear that the diones **1**–**6**, **8**, **9** are excellent candidates for such transformations. The full account[4] of their HLADH-catalyzed reductions will be reported shortly.

[4]A preliminary communication on some of these data has been published (15).

Experimental

All mp's were determined using an Electrothermal capillary melting point apparatus and are uncorrected. The ir spectra were recorded on films (for liquids) and KBr disks (for solids) with a Nicolet FT-IR spectrometer. The ^1H nmr spectra were recorded on a Varian T-60 instrument on $CDCl_3$ solutions with $(CH_3)_4Si$ as internal standard, and ^{13}C nmr data on a Varian CFT-20 machine with $CDCl_3$ solutions. Low and high resolution mass spectra were determined with Bell and Howell 21-490 and AEI MS3074 instruments respectively. Analytic glc was done with a Varian 2700 chromatograph with flame ionization

Can. J. Chem. Downloaded from www.nrcresearchpress.com by 213.166.140.6 on 09/07/12
For personal use only.

TABLE 1. Relative rates[a] of HLADH-catalyzed reductions of decalindiones **1**–**9**, **11**

Substrate	Relative rate	Substrate	Relative rate
Cyclohexanone	100	**6**	24
1	14[b]	**7**	Non-substrate
2	16	**8**	12
3	35	**9**	10
4	8[b]	**11**	Non-substrate
5	20		

[a]Determined spectrophotometrically by measuring optical density changes at 340 nm at 25°C in 0.1 *M* phosphate buffer of pH 6.5 with [S] = 5×10^{-3} *M* and [NADH] = 1.75×10^{-3} *M*.
[b]At pH 7.

detection, and preparative glc with a Varian 920 instrument using thermal conductivity detection. Large-scale preparative lc was carried out using the Waters Prep LC 500 system.

*Bicyclo[4.4.0]dec-1-(6)-ene-3,8-dione (**1**)*

2,6-Dihydroxynaphthalene was converted (16) to 2,6-dimethoxynaphthalene, mp 148°C (lit. (16) mp 149°C), in 92% yield, and this material then reduced with Li/liq. NH_3 (17) to give an 89% yield of 2,6-dimethoxy-2,4,6,8-tetrahydronaphthalene (**12** (18)), mp 95–96°C; ir: 1220, 1390, and 1460 cm^{-1}; ^1H nmr δ: 2.70 (s, 8H), 3.60 (s, 6H), and 4.60 (s, 2H) ppm. The bis-enolether **12** (3.0 g, 15.6 mmol) was dissolved in MeOH (100 mL) containing 1 *M* aqueous oxalic acid (40 mL) (19). The mixture was stirred at 20°C for 1 h, then neutralized slowly with saturated aqueous $NaHCO_3$ and extracted with $CHCl_3$ (4 × 25 mL). The $CHCl_3$ solution was decolourized with charcoal, dried ($MgSO_4$), and rotoevaporated. The solid obtained was recrystallized from hexanes to give bicyclo[4.4.0]dec-1(6)-ene-3,8-dione (**1**, 1.6 g, 60% yield), mp 96°C; ir: 1230 and 1710 cm^{-1}; ^1H nmr δ: 2.60 (br, 8H) and 3.00 (s, 4H) ppm; ^{13}C nmr δ: 29.38, 37.75, 43.16, 126.15, and 208.65 ppm; ms *m/e*: 164. *Anal.* calcd. for $C_{10}H_{12}O_2$: C 73.15, H 7.37; found: C 73.22, H 7.41%.

trans-*Bicyclo[4.4.0]decane-3,8-dione (**2**)*

The bis-enolether **12** (5.0 g, 26 mmol) in THF (50 mL) and 1 *M* aqueous HCl (100 mL) was heated under reflux for 1 h (16) and then cooled and extracted with $CHCl_3$ (4 × 50 mL). The dried ($MgSO_4$) $CHCl_3$ extract was rotoevaporated to give **13** (containing 10% of **1** by ^1H nmr), which was purified by chromatography on silica gel ($CHCl_3$:hexanes:MeOH, 80:19:1 elution) to give bicyclo[4.4.0]dec-1(2)-ene-3,8-dione (**13**, 3.6 g, 85% yield), mp 91°C (lit. (16) mp 93.5°C); ir: 1680 and 1720 cm^{-1}; ^1H nmr δ: 1.60–3.10 (envelope, 11H) and 6.00 (s, 1H) ppm; ^{13}C nmr δ: 29.69, 30.95, 35.86, 36.44, 38.23, 45.11, 126.04, 161.67, 198.30, and 208.34 ppm.

The diketone **13** (1.6 g, 9.75 mmol) in dry benzene (50 mL) containing 1,2-ethanediol (550 μL, 9.75 mmol) and *p*-TsOH (50 mg) was refluxed in a Dean–Stark apparatus for 30 min (20). After all water had been removed, the reaction mixture was poured into saturated aqueous $NaHCO_3$ (200 mL) and extracted with diethyl ether (4 × 50 mL). The organic layer was dried ($MgSO_4$) and rotoevaporated and the residual oil obtained chromatographed on silica gel ($CHCl_3$:hexanes:MeOH, 80:19:1 elution) to give, first, 8-ethylenedioxybicyclo-[4.4.0]dec-1(6)-en-3-one (**14**, 400 mg, 20% yield); ir: 1080, 1610, and 1720 cm^{-1}; ^1H nmr δ: 1.10–2.70 (envelope, 12H), and 3.95 (s, 4H) ppm, and, second, 8,8-(ethylenedioxy)bicyclo[4.4.0]dec-1(2)-en-3-one (**15**, 800 mg, 40% yield), mp 73–74°C; ir: 1070 and 1680 cm^{-1}; ^1H nmr δ: 1.10–2.70 (envelope, 11H), 3.95 (s, 4H), and 5.90 (s, 1H) ppm; ^{13}C nmr δ: 29.06, 32.12, 34.09, 35.05, 36.33, 41.40, 64.40, 107.73, 124.76, 164.04, and 199.29 ppm. The monoketal **15** (600 mg, 2.9 mmol) in THF (20 mL) was added rapidly with stirring at −78°C to lithium (800 mg, 43 mmol) dissolved in liquid NH_3 (150 mL). After stirring the mixture for a further 20 min, solid NH_4Cl (15 g) was added, the ammonia allowed to evaporate, and the residue taken up in water (250 mL). Extraction with $CHCl_3$ (4 × 50 mL) and rotoevaporation of the dried ($MgSO_4$) extract gave 8,8-(ethylenedioxy)-*trans*-bicyclo[4.4.0]decan-3-one (540 mg, 90% yield); ir: 1080 and 1720 cm^{-1}; ^1H nmr δ: 0.90–2.70 (envelope, 14H) and 3.95 (s, 4H) ppm; ^{13}C nmr δ: 30.92, 32.88, 33.94, 38.59, 40.95, 41.91, 47.62, 64.26, 108.75, and 210.84 ppm. This ketal (535 mg, 2.55 mmol) in THF (50 mL) and 2 *M* aqueous HCl (50 mL) was heated at 50°C for 1 h. The cooled mixture was then extracted with $CHCl_3$ (4 × 50 mL) and the $CHCl_3$ solution washed with saturated aqueous $NaHCO_3$, dried (K_2CO_3), and rotoevaporated. The white solid obtained was recrystallized from hexanes to give *trans*-bicyclo[4.4.0]decane-3,8-dione (**2**, 280 mg, 65% yield), mp 138°C (lit. (21) 139°C); ir: 1320 and 1710 cm^{-1}; ^1H nmr δ: 1.10–2.90 (envelope, peaks at 1.90, 2.20, and 2.40) ppm; ^{13}C nmr δ: 32.73, 39.91, 41.08, 46.72, and 209.25 ppm; ms *m/e*: 166.

cis-*Bicyclo[4.4.0]decane-3,8-dione ((±)**13**)*

Bicyclo[4.4.0]dec-1(2)-ene-3,8-dione (**13**, prepared as above, 2.0 g, 12.2 mmol) in 95% aqueous EtOH (200 mL) containing 10% Pd/C (100 mg) was hydrogenated under H_2 (1 Torr; 1 Torr = 133.3 Pa) until 1 equiv. of H_2 was taken up. The solid product (1.85 g, 93% yield), mp 65°C, was recrystallized from hexanes to give, first, *cis*-bicyclo[4.4.0]decane-3,8-dione ((±)**3**, 600 mg, 33% yield), mp 73°C (lit. (21) mp 73°C); ir: 1710 cm^{-1}; ^1H nmr δ: 1.60–2.90 (envelope, peaks at 1.90, 2.30, and 2.55) ppm; ^{13}C nmr δ: 27.47, 36.15, 38.51, 44.21, and 209.40 ppm; ms *m/e*: 166. The mother liquors gave *trans*-bicyclo[4.4.0]decane-3,8-dione (**2**, 1.1 g, 60% yield), mp 139°C, identical with the sample prepared above.

*Bicyclo[4.4.0]dec-1(6)-ene-3,9-dione (**4**)*

(*a*) 2,7-Dihydroxynaphthalene was converted to 2,7-dimethoxynaphthalene, mp 138°C (lit. (22) mp 138°C), in 95% yield (23). This dimethyl ether was then reduced (17) in 98% yield to 2,7-dimethoxy-1,4,5,8-tetrahydronaphthalene (**16**), mp 66°C (lit. (17) mp 68.5–69.5°C). Hydrolysis of the bisenolether **16** with aqueous oxalic acid (19) gave a 50% yield of bicyclo[4.4.0]decane-3,9-dione (**4**), mp 59°C (lit. (19) mp 59.5–60.5°C); ir: 1630 and 1710 cm^{-1}; ^1H nmr δ: 2.55 (br s, 8H) and 2.80 (s, 4H) ppm; ^{13}C nmr δ: 29.76, 38.41, 43.23, 123.96, 129.37, and 208.63 ppm; ms *m/e*: 164.

(*b*) The bis-enolether **16** was hydrolyzed with 1 *M* aqueous HCl to give a 90% yield of bicyclo[4.4.0]deca-1(2),9(10)-diene-3,9-dione (**17**),[5] mp 178–179°C (lit. (19) mp 179°C); ir: 1530, 1595, and 2600–3400 cm^{-1}; ^1H nmr (DMSO-d_6) δ: 1.00–2.70 (9H, peak at 2.25), 5.55 (s, 2H), and 8.0 (br, 1H) ppm. This dienolone **17** (5.0 g, 30.5 mmol) in dry benzene (75 mL) containing 1,2-ethanediol (15 mL, 270 mmol) and *p*-TsOH (50 mg) was refluxed in a Dean–Stark apparatus for 3 h. Work-up in the usual way (see above) gave a yellow oil that was purified by chromatography on silica gel (EtOAc:hexanes, 3:2 elution) to give 3,9-bis-ethylenedioxybicyclo[4.4.0]dec-1(6)-ene[6] (**18**, 6.8 g, 92% yield), mp 47°C (lit. (14*b*) mp 45°C).

Treatment of the diketal **18** with aqueous oxalic acid (19) as described above gave **4** identical in all respects with the previous sample.

trans-*Bicyclo[4.4.0]decane-3,9-dione (**5**)*

Cyclohexanone and butadiene was condensed (24) to give, in 47% yield, *trans*-bicyclo[4.4.0]dec-8-en-2-one (**19**), bp 80°C (0.15 Torr), bp 112°C (14 Torr), mp 44°C (lit. (25) bp 112°C (14 Torr), mp 32–34°C); ir: 1430, 1600, 1650, and 1710 cm^{-1}; ^1H nmr δ: 1.50–3.00 (envelope with peak at 2.25, 12H) and 5.70 (s, 2H) ppm; ^{13}C nmr δ: 24.32, 25.92, 32.49, 40.01, 41.79, 50.15, 125.09, 125.76, and 211.67 ppm.

The basic method of Nakai and Mimara (26) was then followed. To a solution of *trans*-ketone **19** (5.05 g, 33.6 mmol) in dry EtOH (75 mL) was added tosylhydrazine (6.25 g, 33.6 mmol) and the reaction mixture refluxed for 1 h. The EtOH was rotary evaporated to give the product

[5]All attempts to reduce this compound failed.
[6]Attempted reductions of **18**, including the method of Whitesides and Ehman (5), were unsuccessful.

Can. J. Chem. Downloaded from www.nrcresearchpress.com by 213.166.140.6 on 09/07/12
For personal use only.

Can. J. Chem. Downloaded from www.nrcresearchpress.com by 213.166.140.6 on 09/07/12
For personal use only.

tosylhydrazone as a solid foam (11.25 g, 100% yield), mp 137–139°C (dec.); ir: 1600, 1640, and 3240 cm^{-1}; ^1H nmr δ: 0.90–2.90 (envelope, 12H), 2.40 (s, 3H), 5.60 (s, 2H), and 7.00–8.00 (*para*-substituted phenyl, 4H) ppm; ^{13}C nmr δ: 21.47, 24.74, 26.19, 27.08, 32.73, 33.44, 39.11, 44.26, 124.95, 126.32, 128.10, 129.17, 135.27, 143.64, and 162.44 ppm (indicating only 1 product isomer); ms *m/e*: 318.

The above tosylhydrazone (10.57 g, 33.2 mmol) was taken up in a solution of THF (250 mL) and TMEDA (150 mL) at −35°C. To this was added *n*-BuLi (68 mmol), dropwise with stirring under argon. The resulting dark red solution was stirred at −35°C for 1 h and was then quenched with dimethyl disulphide (3.0 mL, 33.2 mmol). The reaction mixture was allowed to warm to 20°C and was then stirred for an additional 18 h. The resulting opaque, bright yellow, mixture was again cooled to −35°C and an additional aliquot of *n*-BuLi (33.2 mmol) added. *The reaction mixture was then allowed to stir at 20°C for another 24 h.* The dark mixture was then poured into saturated aqueous NH_4Cl (800 mL) and extracted with diethyl ether (6 × 100 mL). The organic layer was washed with 2 *M* aqueous HCl until the washings were acidic, then dried ($MgSO_4$) and rotoevaporated to a yellow oil. This was taken up in pentane (50 mL), filtered through a plug of alumina, and rotoevaporated to give *trans*-3-thiomethylbicyclo[4.4.0]deca-2,7-diene as a near-colourless oil (5.0 g, 85% yield); ir: 1440, 1630, and 1655 cm^{-1}; ^1H nmr δ: 1.00–2.40 (envelope, 10H), 2.30 (s, 3H), 5.20 (s, 1H), and 5.70 (s, 1H) ppm; ^{13}C nmr δ: 13.87, 29.73, 32.53, 35.96, 38.51, 122.48, 126.62, 126.91, and 133.62 ppm (indicating only 1 product isomer).

The above thiomethyl compound (4.95 g, 27.5 mmol) was dissolved in 75% aqueous CH_3CN (200 mL) and finely ground $HgCl_2$ (16.0 g, 59 mmol) added (27). The mixture was refluxed for 1 day, then cooled to 20°C, diethyl ether (800 mL) added, and the aqueous layer removed. The organic layer was washed with saturated aqueous $NaHCO_3$ until the aqueous washings were no longer turbid. The dried ($MgSO_4$) ether solution was then rotoevaporated to give a yellow crystalline solid that was chromatographed on silica gel (hexanes:diethylether:MeOH, 89:19:1 elution) to give *trans*-bicyclo[4.4.0]dec-8-en-3-one (**20**, 3.0 g, 77% yield), bp 55°C (0.05 Torr), mp 49–50°C; ir: 1440, 1645, and 1715 cm^{-1}; ^1H nmr δ: 1.10–2.60 (envelope, peaks at 1.90 and 2.40, 12H) ppm; ^{13}C nmr δ: 15.42, 31.57, 33.26, 36.29, 38.75, 41.09, 47.73, 125.11, 125.90, and 210.27 ppm; ms *m/e*: 150. *Anal.* calcd. for $C_{10}H_{14}O$: C 79.96, H 9.39; found: C 79.50, H 9.10%.

Catalytic hydrogenation of **20** gave *trans*-bicyclo[4.4.0]decan-3-one (*trans*-2-decalone), bp 70°C (1.5 Torr) (lit. (11, 29) bp 74–76°C (2 Torr)); ir: 1220, 1447, and 1715 cm^{-1}; ^1H nmr δ: 1.00–2.60 (envelope) ppm; ^{13}C nmr δ: 24.86, 25.36, 31.97, 32.87, 33.45, 40.69, 42.52, 47.65, and 209.15 ppm; ms *m/e*: 152.

A solution of 82% *m*-chloroperbenzoic acid (8.75 g, 41.6 mmol) in CH_2Cl_2 (60 mL) was added dropwise with stirring during 20 min to the ketone **20** (6.43 g, 41.6 mmol) in CH_2Cl_2 (100 mL) at 0°C. The mixture was then allowed to warm to 20°C and, after 10 min, was poured into 5% aqueous Na_2SO_3, and extracted with $CHCl_3$ (5 × 50 mL). The organic layer was washed successively with 5% aqueous $NaHCO_3$ (2 × 25 mL) and saturated aqueous NaCl (2 × 25 mL), then dried (Na_2SO_4) and rotoevaporated to yield a yellow oil (4.6 g); ir: 1720 and 1740 cm^{-1}; ^1H nmr δ: 1.10–2.60 (envelope), 3.10 (s), 3.90 (m), and 4.10 (m) ppm. These spectral data indicated the existence of the desired epoxide together with 15% lactone(s) due to Bayer–Villiger oxidation of the ketone.

The entire epoxide/lactone product mixture (4.6 g) was dissolved in dry THF (50 mL) and added dropwise with stirring to a solution of $LiAlH_4$ (2.0 g, 0.2 mmol) in dry THF (100 mL). The reaction mixture was refluxed for 4 h, then cooled to 20°C, and worked up using the standard aqueous base method (28) to give a poly-alcohol product as a viscous oil (4.5 g). This (4.4 g) was dissolved in acetone (200 mL), cooled to 0°C in an ice bath, and stirred vigorously while Jones reagent (20 mL, 80 mmol) was added dropwise during 20 min. After the addition was complete, the ice bath was removed, and the mixture stirred at 20°C for a further 2 h and then diluted with water (100 mL) and extracted with $CHCl_3$ (6 × 50 mL). The organic layer was washed with saturated aqueous $NaHCO_3$ and then dried ($MgSO_4$) and rotoevaporated to a yellow solid (3.1 g, 83% yield[7]); ^1H nmr δ: 0.90–2.50 (envelope) ppm (confirming the absence of lactone, aldehyde, or epoxide products).

This material was fractionally recrystallized from diethyl ether to yield *trans*-bicyclo[4.4.0]decane-3,8-dione (**2**, 900 mg, 20% yield from **20**), mp 140°C, identical with the previous sample. The mother liquors were chromatographically purified on silica gel (EtO_2:hexanes:MeOH, 80:19:1 elution) to give a white solid that was further purified by preparative gc (Carbowax 20M, 200°C) to give *trans*-bicyclo[4.4.0]-decane-3,9-dione (**6**) (**5**, 900 mg, 20% yield from **20**), mp 68°C; ir: 1710 and 1430 cm^{-1}; ^1H nmr δ: 1.20–2.60 (envelope) ppm; ^{13}C nmr δ: 31.73, 39.80, 40.67, 43.12, 47.68, and 208.90 ppm; ms *m/e*: 166. *Anal.* calcd. for $C_{10}H_{14}O_2$: C 72.26, H 8.49; found: C 72.04, H 8.35%.

cis-*Bicyclo[4.4.0]decane-3,9-dione (6)*

The method of Anderson and Barlow (29) was used to hydrogenate 2,7-dihydroxynaphthalene to the corresponding *cis*-decalin-2,7-diol, which was then oxidized (30) with Jones reagent to give a 65% yield of *cis*-bicyclo[4.4.0]decane (**6**), mp 64–65°C (lit. (29) mp 62–64°C); ir: 1710 cm^{-1}; ^1H nmr δ: 1.80–2.90 (envelope) ppm; ^{13}C nmr δ: 27.12, 32.83, 38.05, 39.13, 44.04, and 209.43 ppm; ms *m/e*: 166.

trans-*6-Carboethoxybicyclo[4.4.0]decane-3,9-dione (7)*

Using the basic method of Nasipur *et al.* (7), ethyl 2-methyl-4-oxo-2-cyclohexene-1-carboxylate (97.3 g, 0.53 mol) was added to a solution of sodium (18.5 g, 0.8 mol) in dry EtOH (350 mL) at 20°C during 30 min. The resulting orange anion solution was stirred for an additional 30 min, then neat ethyl-3-chloropropanoate (73.0 g, 0.53 mmol) was added with stirring during 30 min, and the resulting opaque mixture was stirred for a further 30 min. Sodium (6.5 g, 0.28 mol) in dry EtOH (150 mL) was added and the reaction mixture refluxed for 4.5 h. The orange mixture was cooled to 20°C and most of the EtOH was removed by rotoevaporation. The remaining dark orange residue was diluted with water (600 mL) and washed with diethyl ether (4 × 100 mL). The basic aqueous layer was then vigorously stirred and carefully acidified with 6 *M* aqueous HCl until a bright yellow precipitate appeared. This was collected by filtration and the aqueous filtrate extracted with $CHCl_3$ (4 × 100 mL). The $CHCl_3$ layer was washed with saturated aqueous NaCl (100 mL), dried ($MgSO_4$), and rotoevaporated to a yellow solid. This was combined with the previously collected yellow precipitate, washed with water (2 × 50 mL), and recrystallized from CH_3CN to afford 6-carboethoxybicyclo[4.4.0]deca-1,9-diene-9-ol-3-one (**21**, 42 g, 36% yield) as bright yellow crystals, mp 171°C (lit. (7) mp 171–172°C); ir: 1595, 1735, and 2600–3400 cm^{-1}; ^1H nmr (DMSO-d_6) δ: 1.10 (t, J = 6 Hz, 2H), 5.50 (s, 2H), and 10.50 (br s, 1H) ppm; ms *m/e*: 236. *Anal.* calcd. for $C_{13}H_{10}O_4$: C 66.09, H 6.83; found: C 66.17, H 6.85%.

The dienolone **21** (10.0 g, 42 mmol) and 11% Pd–C (500 mg) were suspended in diethyl ether (400 mL) and shaken under H_2 (2 atm) for 24 h, when H_2 uptake (2 equiv.) ceased. The catalyst was removed by filtration, the ether rotoevaporated, and the oily product purified by chromatography on silica gel ($CHCl_3$:MeOH, 99:1 elution) to give, first, *trans*-6-carboethoxybicyclo[4.4.0]decan-3-one (**23**, 1.3 g, 13% yield), mp 160°C; ir: 1190, 1440, and 1720 cm^{-1}; ^1H nmr δ: 1.00–2.60 (envelope, t at 1.30, J = 6 Hz, 17H), 2.60–3.30 (1H), and 4.30 (q, 2H, J = 6 Hz) ppm; ^{13}C nmr δ: 13.70, 22.75, 25.22, 28.66, 36.68, 38.51, 44.02, 44.71, 46.69, 59.68, 173.76, and 209.50 ppm; ms *m/e*: 224. *Anal.* calcd. for $C_{13}H_{20}O_3$: C 69.61, H 8.99; found: C 69.60, H 9.10%. Eluted second was *trans*-6α-carboethoxybicyclo[4.4.0]decan-3α-ol-9-one (**22**, 6.5 g, 65% yield), bp 85°C (0.15 Torr); ir: 1190, 1450, 1725, and 3400 cm^{-1}; ^1H nmr δ: 1.00–2.60 (envelope, t at 1.3, J = 7 Hz, 15H), 3.10 (br, 2H), 3.6 (br, 1H), and 4.2 (q, J = 7 Hz, 2H) ppm; ^{13}C nmr δ: 13.86, 32.06, 34.63, 35.81, 37.79, 38.39, 42.08, 44.38, 45.95, 60.22, 69.28, 173.73, and

[7]The material loss is due to removal of the lactone products as their carboxylate salts.

Can. J. Chem. Downloaded from www.nrcresearchpress.com by 213.166.140.6 on 09/07/12
For personal use only.

210.25 ppm; ms *m/e*: 240. *Anal.* calcd. for $C_{13}H_{20}O_4$: C 65.53, H 7.61; found: C 65.57, H 7.60%.

The above hydroxyketone **22** (7.6 g, 31.7 mmol) was dissolved in acetone (200 mL) at 0°C. To this was added, dropwise with vigorous stirring, Jones reagent (8.0 mL, 1.01 equiv.) and the reaction mixture stirred at 0°C for 2 h. The mixture was then diluted with water (300 mL) and extracted with $CHCl_3$ (5 × 100 mL). The organic layer was washed with saturated aqueous NaCl (100 mL), dried ($MgSO_4$), rotoevaporated, and Kugelrohr-distilled to give *trans*-6-carboethoxybicyclo[4.4.0]decane-3,9-dione (**7**, 6.3 g, 85% yield), bp 125°C (0.15 Torr), mp (recrystallized from pentanes) 83–84°C; ir: 1195 and 1720 cm^{-1}; ^1H nmr δ: 1.20–3.20 (envelope, t at 1.3, J = 7 Hz, 16H) and 4.30 (q, J = 7 Hz, 2H) ppm; ^{13}C nmr δ: 13.70, 34.87, 37.91, 42.71, 43.74, 45.50, 60.47, 172.91, and 207.54 ppm; ms *m/e*: 238. *Anal.* calcd. for $C_{13}H_{18}O_4$: C 65.53, H 7.61; found: C 65.57, H 7.60%.

trans-*6-Hydroxyethylbicyclo[4.4.0]decane-3,9-dione (8)*

trans-6-Carboethoxybicyclo[4.4.0]decane-3,9-dione (**7**, 8.8 g, 36.9 mmol) in dry MeOH (200 mL) containing trimethyl orthoformate (10 mL, 90 mmol) and *p*-TsOH (100 mg) was stirred at 25°C for 90 min. The mixture was then poured into saturated aqueous K_2CO_3 (500 mL), extracted with diethyl ether (5 × 100 mL), and the organic layers dried ($MgSO_4$) and rotoevaporated to give *trans*-6-carboethoxy-3,3,9,9-tetramethoxybicyclo[4.4.0]decane (12.3 g, quantitative yield); ir: 1050, 1100, 1455, and 1730 cm^{-1}; ^1H nmr δ: 1.00–2.10 (envelope, t at 1.20, J = 7 Hz, 13H), 3.15 (s, 6H), 3.20 (s, 6H), and 4.15 (q, J = 7 Hz, 2H) ppm; ^{13}C nmr δ: 14.17, 29.71, 33.36, 35.53, 36.63, 47.40, 59.86, 100.00, and 174.60 ppm.

The above diketal (7.5 g, 22.7 mmol) in dry THF (40 mL) was added dropwise with stirring at 20°C to $LiAlH_4$ (2.0 g, 53 mmol) in dry THF (200 mL) and the mixture refluxed for 3 h. The reaction mixture was then cooled to 20°C and worked up in the usual manner (28). After an additional 1 h of stirring, the quenched reaction mixture was allowed to settle and the inorganic salts removed by filtration and washed with THF (3 × 50 mL). Evaporation of the combined filtrate and washings left a white solid. This was recrystallized from diethyl ether to give *trans*-6-hydroxymethyl-3,3,9,9-tetramethoxybicyclo[4.4.0]decane (**24**, 6.3 g, 96% yield), mp 129–130°C; ir: 1100–1050, 1290, 1455, and 3500 cm^{-1}; ^1H nmr δ: 0.90–2.10 (envelope, 14H), 3.20 (s, 6H), 3.25 (s, 6H), and 3.70 (s, 2H) ppm; ^{13}C nmr δ: 28.16, 30.10, 34.48, 36.17, 36.71, 47.37, 57.00, and 100.20 ppm; ms *m/e*: 288. *Anal.* calcd. for $C_{15}H_{28}O_5$: C 62.47, H 9.79; found: C 62.37, H 9.70%.

The hydroxymethyldiketal **24** (5.6 g, 28.6 mmol) in THF (250 mL) and 6 *M* aqueous HCl (60 mL) was stirred at 25°C for 1 h. The mixture was then neutralized by the careful addition of solid $NaHCO_3$, and water added until the sediment dissolved. The aqueous mixture was extracted with CH_2Cl_2 (5 × 100 mL) and the organic extracts dried ($MgSO_4$) and rotoevaporated to give a solidifying oil (3.8 g, quantitative yield), which on recrystallization from diethyl ether yielded *trans*-6-hydroxymethylbicyclo[4.4.0]decane-3,9-dione (**8**, 3.6 g, 95% yield), mp 97.5°C; ir: 1045, 1720, and 3500 cm^{-1}; ^1H nmr δ: 1.00–3.20 (envelope, 14H) and 3.80–4.30 (br, 2H) ppm; ^{13}C nmr δ: 33.37, 36.43, 37.40, 43.12, 43.71, 58.21, and 209.8 ppm; ms *m/e*: 196. *Anal.* calcd. for $C_{11}H_{16}O_3$: C 67.32, H 8.22; found: C 67.12, H 8.24%.

On keeping, nmr solutions of **8** gradually developed signals due to formation of the internal hemiketal **26**; ^{13}C nmr δ: 30.57, 31.79, 32.18, 37.12, 38.29, 40.16, 43.44, 45.28, 69.50, 95.17, and 210.5 ppm.

trans-*6-Methylbicyclo[4.4.0]decane-3,9-dione (9)*

The general method of Ireland *et al.* (30) was applied. *trans*-6-Hydroxymethyl-3,3,9,9-tetramethoxybicyclo[4.4.0]decane (**24**, prepared above, 1.77 g, 6.14 mmol) was dissolved in dry THF (40 mL) and TMEDA (10 mL) at −78°C, and *n*-BuLi (1.1 equiv.) added dropwise with stirring. The mixture was stirred for 20 min and then bis(dimethylamino)phosphochloridate (4.5 mL, 30.73 mmol) was added. The mixture was allowed to warm to 25°C, at which temperature it was stirred an additional 2 h before being poured into saturated aqueous $NaHCO_3$ (300 mL), and shaken vigorously to hydrolyse the excess phosphochloridate. The aqueous solution was extracted with CH_2Cl_2 (5 × 75 mL), and the organic layers washed with saturated aqueous NaCl (2 × 100 mL), dried ($MgSO_4$), and rotoevaporated to give the phosphorylated product as a pale yellow oil (2.3 g, 88% yield); ir: 1090–1050, 1220, 1300, and 1450 cm^{-1}; ^1H nmr δ: 0.90–2.00 (envelope, 13H), 2.55 (s, 6H), 2.70 (s, 6H), 3.15 (s, 6H), 3.20 (s, 6H), and 4.00 (s, 2H) ppm.

This phosphorylation product (2.2 g, 5.2 mmol) in dry THF (25 mL) was added dropwise to lithium (350 mg, 50 mmol) in dry $EtNH_2$ (30 mL) cooled to 0°C. The blue reaction mixture was stirred for 1 h at 0°C and then quenched with water (100 mL). The $EtNH_2$ was allowed to evaporate and the remaining aqueous solution extracted with diethyl ether (5 × 50 mL). The organic layers were washed with saturated aqueous NaCl (50 mL), dried ($MgSO_4$), filtered through alumina, and rotoevaporated. The oily product was distilled to give *trans*-6-methyl-3,3,9,9-tetramethoxybicyclo[4.4.0]decane (**25**, 1.2 g, 85% yield), bp 100°C (0.15 Torr), mp 71–75°C; ir: 1050, 1110, and 1450 cm^{-1}; ^1H nmr δ: 0.90 (s, 3H), 1.00–2.00 (envelope, 13H), 3.15 (s, 6H), and 3.20 (s, 6H) ppm; ^{13}C nmr δ: 14.17, 28.22, 32.57, 34.56, 35.86, 36.70, 46.85, 46.90, and 99.97 ppm.

The diketal **25** (1.1 g, 4.1 mmol) in THF (125 mL) and 6 *M* aqueous HCl (25 mL) was stirred at 25°C for 2 h. The reaction mixture was carefully neutralized by the addition of solid $NaHCO_3$, then diluted with water until all the sediment dissolved, and extracted with diethyl ether (5 × 50 mL). The combined organic extracts were dried ($MgSO_4$), rotoevaporated, and the resulting white solid recrystallized from pentanes to give *trans*-6-methylbicyclo[4.4.0]decane-3,9-dione (**9**, 730 mg, quantitative yield), mp 114–115°C; ir: 1715 cm^{-1}; ^1H nmr δ: 1.30 (s, 3H), 1.60–2.10 (m, 5H), and 2.19–2.64 (envelope, 8H) ppm; ^{13}C nmr δ: 14.31, 32.46, 37.49, 39.14, 44.07, and 209.1 ppm; ms *m/e*: 188. *Anal.* calcd. for $C_{11}H_{16}O_2$: C 73.30, H 8.95; found: C 73.19, H 9.18%.

trans-*6-Methylbicyclo[4.4.0]decan-3-one (28)*

(a) From 22

trans-6α-Carboethoxybicyclo[4.4.0]decan-3α-ol-9-one (**22**, 2.5 g, 10.4 mmol) was dissolved in dry MeOH (125 mL) containing concentrated H_2SO_4 (100 μL). The reaction mixture was stirred at 20°C for 2 h and then poured into saturated aqueous K_2CO_3 (300 mL) and extracted with $CHCl_3$ (4 × 100 mL). The organic layer was dried (K_2CO_3) and rotoevaporated to give *trans*-6α-carboethoxy-9,9-dimethoxybicyclo[4.4.0]decan-3α-ol (2.9 g, 98% yield); ir: 1100–1050, 1725, and 3400 cm^{-1}; ^1H nmr δ: 1.00–2.20 (envelope, t at 1.1, J = 6 Hz, 17H), 3.15 (s, 3H), 3.20 (s, 3H), 3.60 (br, 1H), and 4.20 (q, J = 6 Hz, 2H) ppm.

The above dimethoxyketal (2.8 g, 9.8 mmol) in dry THF (50 mL) was added dropwise with stirring at 20°C to $LiAlH_4$ (2.0 g, 53 mmol) in THF (150 mL). The mixture was refluxed for 1 h, and then worked up in the standard way (28) to yield *trans*-6α-hydroxymethyl-9,9-dimethoxybicyclo[4.4.0]decan-3α-ol (**27**, 2.4 g, quantitative yield), mp 112–115°C; ir: 3400 cm^{-1}; ^1H nmr δ: 0.90–2.30 (envelope, 15H), 3.15 (s, 3H), 3.20 (s, 3H), and 3.80 (br, 3H) ppm; ^{13}C nmr δ: 28.01, 30.31, 30.86, 32.22, 35.00, 36.55, 37.08, 37.41, 38.62, 47.44, 57.65, 70.91, and 100.25 ppm.

Again using the basic method of Ireland *et al.* (30), the diol **27** (1.5 g, 6.15 mmol) was dissolved in a mixture of THF (40 mL) plus TMEDA (10 mL) and stirred at −78°C. To this was added *n*-BuLi (14.15 mmol) and the solution allowed to warm to 0°C. Bis(dimethylamino)phosphochloridate (9.0 mL, 30.75 mmol) was then added dropwise with stirring and the mixture stirred at 20°C for 2 h, then poured into 5% aqueous $NaHCO_3$ (300 mL), shaken vigorously to hydrolyse the remaining phosphochloridate, and extracted with CH_2Cl_2 (4 × 100 mL). The organic layer was washed with saturated aqueous NaCl (100 mL), dried ($MgSO_4$), and rotoevaporated to yield the phosphorylated product as a yellow oil (2.6 g, 83% yield); ir: 980, 1050, 1220, 1330, and 1450 cm^{-1}. This phosphorylated product (2.45 g, 4.94 mmol) in THF (30 mL) and *t*-BuOH (2.82 mL, 29.9 mmol) was then added dropwise with stirring to lithium (850 mg, 120 mol) in $EtNH_2$ at 0°C. The blue mixture was stirred at 0°C for 90 min, then

quenched with water (25 mL) and extracted with diethyl ether (4 × 50 mL). The ether solution was washed with saturated aqueous NaCl (100 mL), decolourized with charcoal, filtered through a plug of alumina, and rotoevaporated. The crude product was Kugelrohr-distilled to give *trans*-3,3-dimethoxy-6-methylbicyclo[4.4.0]decane (800 mg, 77% yield), bp 80–85°C (0.2 Torr); ir: 1050, 1105, and 1450 cm^{-1}; ^1H nmr δ: 1.05–2.00 (envelope, s at 1.05, 18H), 3.15 (s, 3H), and 3.20 (s, 3H) ppm; ^{13}C nmr δ: 14.78, 21.66, 26.49, 28.23, 33.09, 35.35, 37.82, 40.64, 46.99, and 100.42 ppm; ms *m/e*: 212.

The above dimethoxyketal (800 mg, 3.77 mmol) was dissolved in 90% formic acid (40 mL) containing water (5 mL), and THF was added until the hydrolysis mixture became clear. The solution was then stirred for 2 h at 20°C, water (250 mL) was added, and the solution was extracted with diethyl ether (5 × 100 mL). The organic layer was washed with saturated aqueous NaCl (2 × 100 mL), dried (K_2CO_3), and rotoevaporated to leave a pale yellow oil that was Kugelrohr-distilled to give *trans*-6-methylbicyclo[4.4.0]decan-3-one (**28**, 400 mg, 55% yield) (lit. (11) bp 130°C (15 Torr)); ir: 1450 and 1715 cm^{-1}; ^1H nmr δ: 1.05–2.60 (envelope, maxima at 1.05) ppm; ^{13}C nmr δ: 14.85, 21.54, 25.97, 28.94, 33.06, 38.19, 40.35, 44.67, 44.92, and 211.45 ppm. *Exact Mass* calcd. for $C_{11}H_{18}O$: 166.1358; found: 166.1351.

(b) From ***23***

trans-2-Carboethoxybicyclo[4.4.0]decan-3-one (**23**, 2.7 g, 12.1 mmol) in dry MeOH (150 mL) containing trimethyl orthoformate (2.0 mL, 18.0 mmol) and *p*-TsOH (100 mg) was stirred at 20°C for 2 h and then poured into saturated Na_2CO_3 (400 mL) and extracted with CH_2Cl_2 (4 × 100 mL). The organic layer was dried ($MgSO_4$) and rotoevaporated to yield *trans*-6-carboethoxy-3,3-dimethoxybicyclo[4.4.0]decane as a pale yellow oil (2.6 g, 80% yield); ir: 1050, 1195, 1445, and 1725 cm^{-1}; ^1H nmr δ: 0.90–2.10 (envelope, t at 1.30, J = 7 Hz, 18H), 3.15 (s, 3H), 3.20 (s, 3H), and 4.10 (q, 2H, J = 7 Hz) ppm; ms *m/e*: 270.

This ester ketal (2.5 g, 9.25 mmol) in dry THF (30 mL) was added dropwise with stirring to $LiAlH_4$ (1.5 g) in THF (100 mL). The mixture was then refluxed for 5 h and worked up as usual (28) to a clear, solidifying, oil, which was recrystallized from pentanes to give *trans*-6-hydroxymethyl-3,3-dimethoxybicyclo[4.4.0]decane (2.0 g, 95% yield), mp 83°C; ir: 1050, 1195, 1450, and 3400 cm^{-1}; ^1H nmr δ: 1.00–2.00 (envelope, 14H), 3.15 (s, 3H), 3.20 (s, 3H), and 3.80 (s, 2H) ppm; ^{13}C nmr δ: 21.28, 26.31, 27.87, 30.87, 34.05, 35.11, 37.04, 40.65, 47.21, 57.51, and 100.37 ppm; ms *m/e*: 228. *Anal.* calcd. for $C_{13}H_{24}O_3$: C 68.38, H 10.60; found: C 68.25, H 10.52%.

The Ireland (30) methodology was again applied to remove the hydroxyl function. The above hydroxymethyl ketal (1.5 g, 6.25 mmol) was dissolved in a mixture of THF (40 mL) and TMEDA (10 mL) and stirred at −78°C. To this solution was added *n*-BuLi (14.4 mmol). The resulting mixture was stirred at −78°C for a further 20 min and allowed to warm to 0°C. Bis(dimethylamino)phosphochloridate (9.1 mL, 5.0 equiv.) was added dropwise with stirring, and the mixture stirred at 25°C for a further 2 h and then poured into 5% aqueous $NaHCO_3$ solution (300 mL), shaken vigorously, and extracted with CH_2Cl_2 (4 × 75 mL). The organic layers were combined and washed with saturated aqueous NaCl (2 × 100 mL), dried ($MgSO_4$), and rotoevaporated to afford the phosphorylated product as a pale yellow oil (2.0 g, 64% yield); ir: 1050, 1220, 1300, and 1450 cm^{-1}; ^1H nmr δ: 0.90–2.00 (envelope, 15H), 2.55 (s, 6H), 2.70 (s, 6H), 3.15 (s, 3H), 3.20 (s, 3H), and 4.0 (s, 2H) ppm.

This phosphorylated product (1.5 g, 2.89 mmol) was taken up in dry THF (30 mL) and *t*-BuOH (2.1 mL, 23.1 mmol), and added with stirring to lithium metal (700 mg, 100 mmol) in dry $EtNH_2$ (30 mL) cooled at 0°C. The blue reaction mixture was stirred for an additional 90 min at 0°C and was then quenched with water (100 mL) and extracted with diethyl ether (5 × 50 mL). The organic layers were combined, washed with saturated aqueous NaCl (2 × 100 mL), decolourized with charcoal, filtered through an alumina plug, and rotoevaporated. Kugelrohr-distillation of the oily product gave *trans*-3,3-dimethoxy-6-methylbicyclo[4.4.0]decane (500 mg, 61% yield), bp 80–85°C (0.2 Torr), identical to the sample obtained in method (*a*) above. It was converted to **28** in 55% yield as described in (*a*) above.

(c) Via ***29***

Condensation of 2-methylcyclohexanone and methyl vinyl ketone by the method of Moss and Smudin (31) gave 6-methylbicyclo[4.4.0]-dec-1-en-3-one (**29**, 50% yield), bp 80–85° (0.25 Torr) (lit. (32) bp 82–83°C (0.7 Torr)); ir: 1620 and 1680 cm^{-1}; ^1H nmr δ: 1.30 (s, 3H), 1.40–1.60 (envelope, 12H), and 5.75 (s, 1H) ppm; ^{13}C nmr δ: 21.05, 21.32, 26.51, 31.99, 33.23, 35.18, 37.38, 40.87, 123.4, 169.1, and 197.9 ppm; ms, *m/e*: 164.

The α,β-unsaturated ketone **29** was reduced with lithium in liquid ammonia (11) to give a quantitative yield of **28**, identical with the samples obtained in routes (*a*) and (*b*) above.

trans-*6-Carboxybicyclo[4.4.0]decan-9-ol-3-one lactone* ***31***

trans-6α-Carboethoxybicyclo[4.4.0]decan-9α-ol-3-one (**22**, 2.0 g, 8.33 mmol) in dry THF (30 mL) was reduced with $LiAlH_4$ (1.0 g, 27 mmol) in dry THF (100 mL) in the usual (28) way to give *trans*-6α-hydroxymethylbicyclo[4.4.0]decane-3α,9-diol (**30**, quantitative yield), mp 165–169°C; ir: 1040 and 3350 cm^{-1}; ^1H nmr (DMSO-d_6) δ: 0.90–2.00 (envelope, 13H), 3.10–3.60 (envelope, 6H), and 3.80–4.50 (3H, all D_2O exchangeable) ppm.

The triol **30** (1.66 g, 8.3 mmol) was dissolved in DMF (100 mL) at 30°C (33) and Jones reagent (10 mL, 40 mmol) added dropwise with stirring during 30 min. The mixture was stirred for a further 3 h at 30°C, then cooled to 20°C, poured into water (300 mL), and extracted with diethyl ether (5 × 100 mL). The combined organic layers were decolourized with charcoal, dried ($MgSO_4$), and rotoevaporated to give *trans*-6α-carboxybicyclo[4.4.0]decan-9α-ol-3-one lactone (**31**, 1.3 g, 75% yield) as a colourless oil; ir: 1720–1740 cm^{-1}; ^1H nmr δ: 1.10–3.20 (envelope, 13H) and 4.80 (br, 1H) ppm; ^{13}C nmr δ: 25.64, 30.02, 31.29, 33.86, 37.97, 38.87, 41.23, 47.63, 75.10, 175.5, and 208.8 ppm; ms *m/e*: 194. *Anal.* calcd. for $C_{10}H_{14}O_3$: C 68.02, H 7.27; found: C 68.28, H 7.49%.

cis-*1,6-Bishydroxymethylbicyclo[4.4.0]dec-3-ene (**11**)*

This compound was prepared by the method of Paquette *et al.* (13) in 95% yield, mp 145–148°C (lit. (14) mp 147–149°C); ir: 660, 1020, 1470, 1660, and 3280 cm^{-1}; ^1H nmr (DMSO-d_6) δ: 1.40 (m, 8H), 2.00 (m, 4H), 3.40 (d, J = 4 Hz, 4H), 4.40 (t, J = 4 Hz, 2H), and 5.55 (br, 2H) ppm; ^{13}C nmr δ: 20.89, 30.33, 31.48, 38.64, 67.71, and 123.9 ppm.

Relative rates of HLADH-catalyzed reductions of ***1–9, 11***

The relative rates of reduction of **1–9**, **11**, and of the reference substrate cyclohexanone, were determined in the standard manner (34). The results are recorded in Table 1.

Acknowledgements

We gratefully acknowledge the support of the Natural Sciences and Engineering Research Council of Canada, and the award (to D.R.D.) of an NSERC fellowship, an Ontario Graduate Scholarship, and a University of Toronto Open Fellowship. We also thank Dr. P. A. Wehrli (Hoffmann-La Roche, Nutley) for a generous gift of the *cis*-decalindiol precursor of **6**, and Professor L. A. Paquette for a reference sample of the anhydride precursor of **11**.

1. J. B. Jones and R. S. Hinks. Can. J. Chem. **65**, 704 (1987).
2. C.-H. Wong and G. M. Whitesides. Angew. Chem. Int. Ed. Eng. **24**, 617 (1985); J. B. Jones. Tetrahedron, **42**, 3351 (1986).
3. I. J. Jakovac, H. B. Goodbrand, K. P. Lok, and J. B. Jones. J. Am. Chem. Soc. **104**, 4650 (1982); G. S. Y. Ng, L.-C. Yuan, I. J. Jakovac, and J. B. Jones. Tetrahedron, **40**, 1235 (1984); A. J. Bridges, P. Sundararaman, G. S. Y. Ng, and J. B. Jones. J. Am. Chem. Soc. **106**, 1461 (1984); J. B. Jones and C. J. Francis. Can. J. Chem. **62**, 2578 (1984); J. B. Jones and I. J. Jakovac. Org. Synth. **62**, 10 (1985).
4. R. L. Augustine. J. Org. Chem. **23**, 1853 (1958).

Can. J. Chem. Downloaded from www.nrcresearchpress.com by 213.166.140.6 on 09/07/12
For personal use only.

5. G. M. WHITESIDES and W. H. EHMAN. J. Org. Chem. **35**, 3565 (1970).
6. B. M. TROST and T. N. SALZMANN. J. Am. Chem. Soc. **95**, 6840 (1973).
7. D. NASIPUR, R. ROY, G. SARKAR, and M. GUHA. J. Ind. Soc. Chem. **43**, 383 (1986).
8. H. O. HOUSE. Modern synthetic reactions. Benjamin, New York. 1965. Chap. 1.
9. M. MAES, R. OTTINGER, J. REISSE, and A. CHINDOGLU. Tetrahedron, **25**, 5163 (1969); R. L. AUGUSTINE. J. Org. Chem. **28**, 152 (1963); G. STORK and D. E. KAHN. J. Am. Chem. Soc. **105**, 1072 (1983).
10. A. S. HUSSEY, H. P. LINO, and R. H. BAKER. J. Am. Chem. Soc. **75**, 4727 (1953); W. G. DAUBEN, R. C. TWEIT, and R. L. MACLEAN. J. Am. Chem. Soc. **77**, 48 (1955); E. C. DUFEU, F. J. MCQUIN, and R. ROBINSON. J. Chem. Soc. 53 (1937).
11. R. B. WOODWARD, F. SONDHEIMER, D. TAUB, K. HEUSLER, and W. M. MCLAMORE. J. Am. Chem. Soc. **74**, 4223 (1952).
12. (*a*) M. J. POUET. Org. Magn. Reson. **19**, 228 (1982); (*b*) L. M. JACKMAN. Applications of NMR spectroscopy in organic chemistry. Pergamon, New York. 1959. p. 116; J. B. STOTHERS. Carbon-13 NMR spectroscopy. Academic, New York. 1972. p. 164.
13. L. A. PAQUETTE, R. E. WING, J. C. PHILIPS, G. L. THOMPSON, L. K. READ, and J. CLARDY. J. Am. Chem. Soc. **93**, 4508 (1971).
14. (*a*) A. J. IRWIN and J. B. JONES. J. Am. Chem. Soc. **98**, 8476 (1976); (*b*) H. SCHWARTZ. Ph.D. thesis, University of Toronto. 1979.
15. D. R. DODDS and J. B. JONES. J. Chem. Soc. Chem. Commun. 1080 (1982).
16. W. KOTLAREK. J. Org. Chem. **40**, 2841 (1975).
17. N. H. ANDERSON and J. A. MARSHALL. J. Org. Chem. **30**, 1292 (1965).
18. W. KOTLAREK and M. KOCOR. Bull. Acad. Polon. Sci. Ser. Sci. Chim. **9**, 507 (1961).
19. P. RADLICK. J. Org. Chem. **30**, 3208 (1965).
20. E. J. COREY, M. OHNO, B. MITRA, and P. A. VATAKENCHERRY. J. Am. Chem. Soc. **84**, 478 (1964).
21. R. A. WILEY, B. A. FARAJ, and A. JANTZ. J. Med. Chem. **15**, 374 (1972).
22. B. WEINSTEIN and A. H. FENSELAU. J. Org. Chem. **29**, 2102 (1964).
23. G. N. VYAS and N. N. SHAH. Org. Synth. Coll. Vol. **4**, 837 (1963).
24. W. OPPOLZER and M. PETRUZILKA. J. Am. Chem. Soc. **98**, 6722 (1976).
25. J. A. MARSHALL and R. E. IRELAND. J. Org. Chem. **27**, 1620 (1962).
26. T. NAKAI and T. MIMARA. Tetrahedron Lett. 531 (1979).
27. E. J. COREY and J. I. SHULMAN. J. Org. Chem. **35**, 777 (1970).
28. M. FIESER and L. FIESER. Reagents for organic synthesis. Vol. 1. Wiley, New York. 1967. p. 435.
29. A. G. ANDERSON and D. O. BARLOW. J. Am. Chem. Soc. **77**, 5165 (1955).
30. R. E. IRELAND, D. C. MUCHMORE, and U. HENGARTNER. J. Am. Chem. Soc. **94**, 5098 (1972).
31. R. A. MOSS and D. J. SMUDIN. J. Org. Chem. **41**, 611 (1976); C. H. HEATHCOCK and J. E. ELLIS. Tetrahedron Lett. 4995 (1971).
32. J. A. MARSHALL and W. I. FANTA. J. Org. Chem. **29**, 2501 (1964).
33. E. PFENNINGER, P. E. POEL, C. BERSE, K. WEHRLI, K. SCHAFFNER, and O. JEGER. Helv. Chim. Acta, **51**, 772 (1968).
34. J. DAVIES and J. B. JONES. J. Am. Chem. Soc. **101**, 5405 (1979).

Can. J. Chem. Downloaded from www.nrcresearchpress.com by 213.166.140.6 on 09/07/12
For personal use only.

A conformational analysis of adriamycin based upon its ^{1}H nuclear magnetic resonance spectrum in various solvents

TIM ALLMAN AND R. E. LENKINSKI[1]

Department of Chemistry, University of Guelph, Guelph, Ont., Canada N1G 2W1

Received March 2, 1987

TIM ALLMAN and R. E. LENKINSKI. Can. J. Chem. **65**, 2405 (1987).

The solution conformation of adriamycin was studied by ^{1}H nuclear magnetic resonance spectroscopy. The hydrochloride was found to be rigid on the nmr time scale in each of $CDCl_3$, DMF-d_7, and DMSO-d_6. The sugar and D rings were found to have the same conformations as were found previously by X-ray crystallography. Similar results were found for the free base in DMF-d_7 and $CDCl_3$ solutions although the free base was found to be conformationally mobile in acetone-d_6 and CD_3OD solutions.

TIM ALLMAN et R. E. LENKINSKI. Can. J. Chem. **65**, 2405 (1987).

Utilisant la résonance magnétique nucléaire du ^{1}H, on a étudié la conformation de l'adriamycine en solution. On a trouvé que, en solution tant dans le $CDCl_3$ que dans le DMF-d_7 ou le DMSO-d_6, le chlorhydrate est rigide par rapport à l'échelle de temps de la rmn. On a trouvé que le cycle D ainsi que les cycles des sucres adoptent les mêmes conformations que celles qui ont été observées antérieurement par diffraction des rayons-X. On a obtenu des résultats semblables avec la base libre en solution dans le DMF-d_6 ou dans le $CDCl_3$; toutefois, on a trouvé que, en solution dans l'acétone-d_6 ou dans le CD_3OD, la base libre est conformationnellement mobile.

[Traduit par la revue]

Introduction

The mode of action of adriamycin (Adm) in the inhibition of tumours is still unknown in detail although it is known that Adm binds strongly to DNA, probably by intercalation (1–4). Adm is also known to cleave DNA and a proposed mechanism involves the interaction of the charged amino group with the phosphate backbone of DNA. Since this interaction involves the nonrigid part of Adm, the conformation of Adm in solution is of interest. A number of investigators have used a variety of approaches in determining which of the many possible conformers is the most stable and which may be the "biologically active" conformer.

Although the X-ray crystal structure of neither Adm nor Adm·HCl has been reported, those of several similar compounds have been. Of most interest are the structures of daunomycin with butanol (5) and pyridine (1) of crystallization as well as the *N*-bromoacetyl derivative of daunomycin (6). In these studies the sugar ring was found to be turned back so that there are hydrogen bonds between the 9-OH and the glycosidic oxygen atoms. The internal conformations of the daunosamine ring and the D ring are as shown in Figs. 1 and 2 respectively.

Theoretical studies (7, 8) give a slightly different result. Although the rings themselves have the same conformations, a lower energy is calculated if the glycosidic linkage is twisted back so that there is a bifurcated hydrogen bond involving the 5-O atom, the 6-OH group, and the sugar ring O atom. In fact this describes the global minimum that was found on the potential energy surface but there is a local minimum at the crystal structure conformation as well.

The conformation found in solution is obviously of greater interest than that found in the solid state because it is when it is in solution that Adm is active. The only information about the solution conformation that is so far available comes from a study of the binding of Yb(III) to Adm in methanol. This study suggests that the conformation found in solution is nearly the same as the one calculated to have minimum energy (9).

The original report of the nmr spectra of daunomycin, of its agylcone, and of daunosamine (10) stands virtually alone in the literature. This may be because Adm has been studied almost exclusively in aqueous solution. Its ^{1}H nmr spectrum in water is poorly resolved and the appearance of the spectrum is highly dependent upon concentration, pH, and temperature. This is caused by the self-association of Adm in aqueous solution, and a study of this effect has appeared in the literature (11).

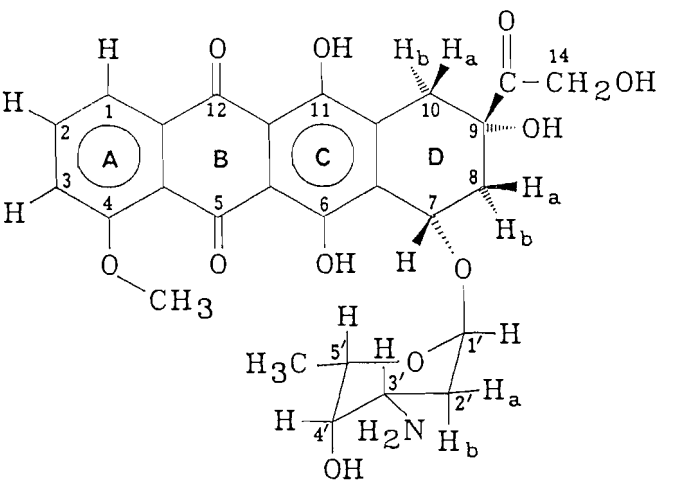

FIG. 1. Adriamycin. The portion of the molecule containing the A–D rings is referred to as the aglycone. The sugar ring is daunosamine. In daunomycin the 14-CH_2OH group is replaced by CH_3.

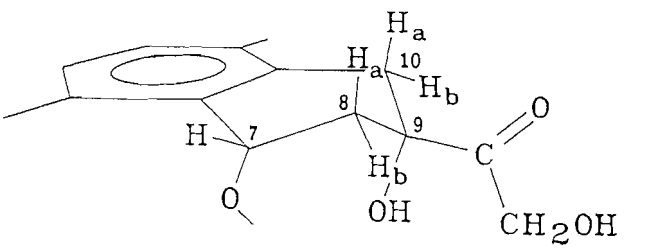

FIG. 2. The internal onformation of the D ring found in the crystal structures of related compounds. Note the planar "W" path connecting the 8b and the 10b protons.

Results

The ^{1}H nmr spectrum of daunomycin as well as several of its fragments and derivatives was first reported by Arcamone *et al.*

[1]Present address of both authors: Department of Radiology, University of Pennsylvania, Philadelphia, PA 19104, U.S.A.

Can. J. Chem. Downloaded from www.nrcresearchpress.com by 213.166.140.6 on 09/07/12
For personal use only.

Can. J. Chem. Downloaded from www.nrcresearchpress.com by 213.166.140.6 on 09/07/12
For personal use only.

in 1970 (10). This was an excellent piece of work that proved the structure of daunomycin although these workers were severely limited by the instrumentation available at the time, two cw (continuous wave) instruments operating at 60 and 100 MHz. At these low fields there was much overlap of peaks and the spin systems were too strongly coupled for complete analysis. The present study carried out at 400 MHz was much easier in the analysis of the spectra because of the better chemical shift dispersion, better sensitivity, and the availability of two-dimensional (2D) experiments, which helped to determine the spin system connectivities and the nmr parameters. For each solvent, and for each of Adm and Adm·HCl where possible, a high resolution one-dimensional spectrum was run, followed by the COSY spectrum (to confirm the assignments) and the homonuclear *J*-resolved spectrum (to see the fine structure of the multiplets). The COSY spectrum of Adm in $CDCl_3$ is shown in Fig. 3 with a high resolution spectrum plotted above it.

Assignment of the spectra

Adm in $CDCl_3$

The spectrum of Adm in $CDCl_3$ is very well resolved and is typical of the spectra seen in most other solvents. This spectrum will be treated in detail with the assignment of the other spectra following from it. The complete set of ^1H nmr data is given in Table 1.

In the 1D spectrum the aromatic region appears as two doublets flanking a triplet and the doublets appear to have some fine structure. Examination of the appropriate slices in the *J*-resolved spectrum shows that the doublets are in fact doublets of doublets and the "triplet" is a doublet of doublets, with the two coupling constants being of similar size. The centre resonance is therefore assigned to the proton at position 2. It is split by couplings of 7.7 and 8.6 Hz to the 1 and 3 protons. The H1–H3 coupling constant is 1.1 Hz. The assignment of the resonance at 7.78 to the 3 proton follows from the COSY spectrum in which there is a cross peak connecting this resonance to the one at 4.04 δ (4-OCH_3). In fact, although this coupling is not resolved here, it is well resolved in the spectrum of Adm in acetone-d_6 and is about 0.5 Hz in magnitude.

The COSY spectrum shows correlations between the strongly coupled pair of resonances at 2.08 and 2.29 δ and the resonance at 5.03 δ. These can be assigned, followed Arcamone *et al.*, to the 8 protons and the 7 proton respectively. The strongly coupled resonances at 2.89 and 3.25 δ are assigned to the protons at position 10. Each of these resonances shows a large geminal coupling of 18.5 Hz and some fine structure. The COSY spectrum indicates that there is a scalar coupling between the resonances at 2.29 δ and 3.15 δ and which is found to be 2.5 Hz from the *J*-resolved spectrum. Such a large value could only arise from coupling along a W path and is strong evidence that the D ring has the puckered conformation shown in Fig. 2. There is also a small coupling of 0.8 Hz in the resonance arising from the 10a proton. No such correlation appears on the contour plot in Fig. 3 but examination of the appropriate f_1 slices on the computer display of the COSY spectrum showed a weak cross peak at 5.03 δ, the position of the resonance of the 7 proton.

The COSY spectrum is especially useful in the assignment of the resonances of the sugar protons. The 5′ methyl group and its geminal proton provide a starting point. The 5′ proton would be expected to be a 1:3:3:1 quartet while the methyl group should appear as a doublet. These are found at 3.97 and 1.29 δ respectively. Correlations in the COSY contour plot can then be traced out to give the following assignments: 4′(3.42), 3′(3.02), 2′(1.60 and 1.70), and 1′(5.45). The only large vicinal coupling seen in the sugar system is that between the 3′ proton and the 2′ proton at 1.70 δ. Models show that this must be a *trans* coupling to the 2′b proton (12–16). Assignment of the resonance at 1.60 δ to the 2′a proton follows from this.

The presence of this single $J_{axial-axial}$ in the sugar ring is strong evidence for the chair conformation shown in Fig. 1. There is also a W coupling seen between protons 2′a and 4′. Because this coupling is very sensitive to the planarity of its coupling path, it confirms the assignment of the chair conformation.

Adm·HCl in DMF

The ^1H nmr spectrum was analysed using the same techniques as was the spectrum of Adm in $CDCl_3$. The multiplets appear much the same as they do in the previous spectrum and analysis shows that, with the exception of the aromatic protons, the coupling constants are very similar. There are, however, some fairly large changes in the chemical shifts, especially those of the sugar protons. Examination of the data in Table 1 shows that the chemical shift differences are due largely to the different atomic charge distributions in the protonated and nonprotonated molecules. Comparison of the data for Adm and Adm·HCl in both methanol and DMF shows this effect clearly. It is greatest for the 3′ proton and diminishes with increasing distance from it. A similar trend is seen when the calculated atomic charges of the protonated and nonprotonated molecule are compared (8).

Adm·HCl in CD_3OD

The assignment of this spectrum follows directly from the previous discussion. The coupling constants show little change from their values in chloroform solution, indicating that there are no significant conformational changes and that the sugar ring is locked in its chair conformation.

Adm·HCl in DMSO-d_6

DMSO is the most viscous of all of the solvents employed in this study. The higher viscosity leads to broadening of the resonances and therefore there is somewhat greater uncertainty in the coupling constants. However, the large 2′a–3′ coupling as well as the 2′a–4′ W couplings show that the conformation of the sugar ring remains the same. The D ring also appears to have the same conformation as before because of the similarity of the spectra.

Often the rate of chemical exchange of exchangeable protons is decreased in DMSO to the extent that they can be seen in the ^1H spectrum. This was found to be the case and they were assigned from the COSY spectrum. However, attempts to obtain information about the orientation of the sugar ring with respect to the rest of the molecule by nOe (nuclear Overhauser enhancement) measurements on these exchangeable protons were unsuccessful.

Adm in $(CD_3)_2CO$

The spectrum of Adm in acetone appears markedly different. The large 2′b–3′ coupling constant has been reduced to 3.2 Hz while many of the small coupling constants have increased. No amount of twisting a model of the sugar ring could account for this because every chair or boat form has one pair of diaxial protons, which should give a large coupling constant. The ring must therefore be nonrigid although it is not clear why this is the case. The D ring, in contrast, has a spectrum very similar to that found in $CDCl_3$ and the presence of ^4J(8b–10b) shows that it is rigid. The resolution of the spectrum was very good and some very small couplings (<0.5 Hz) were seen in the 1′, 3′, and 5′

Can. J. Chem. Downloaded from www.nrcresearchpress.com by 213.166.140.6 on 09/07/12
For personal use only.

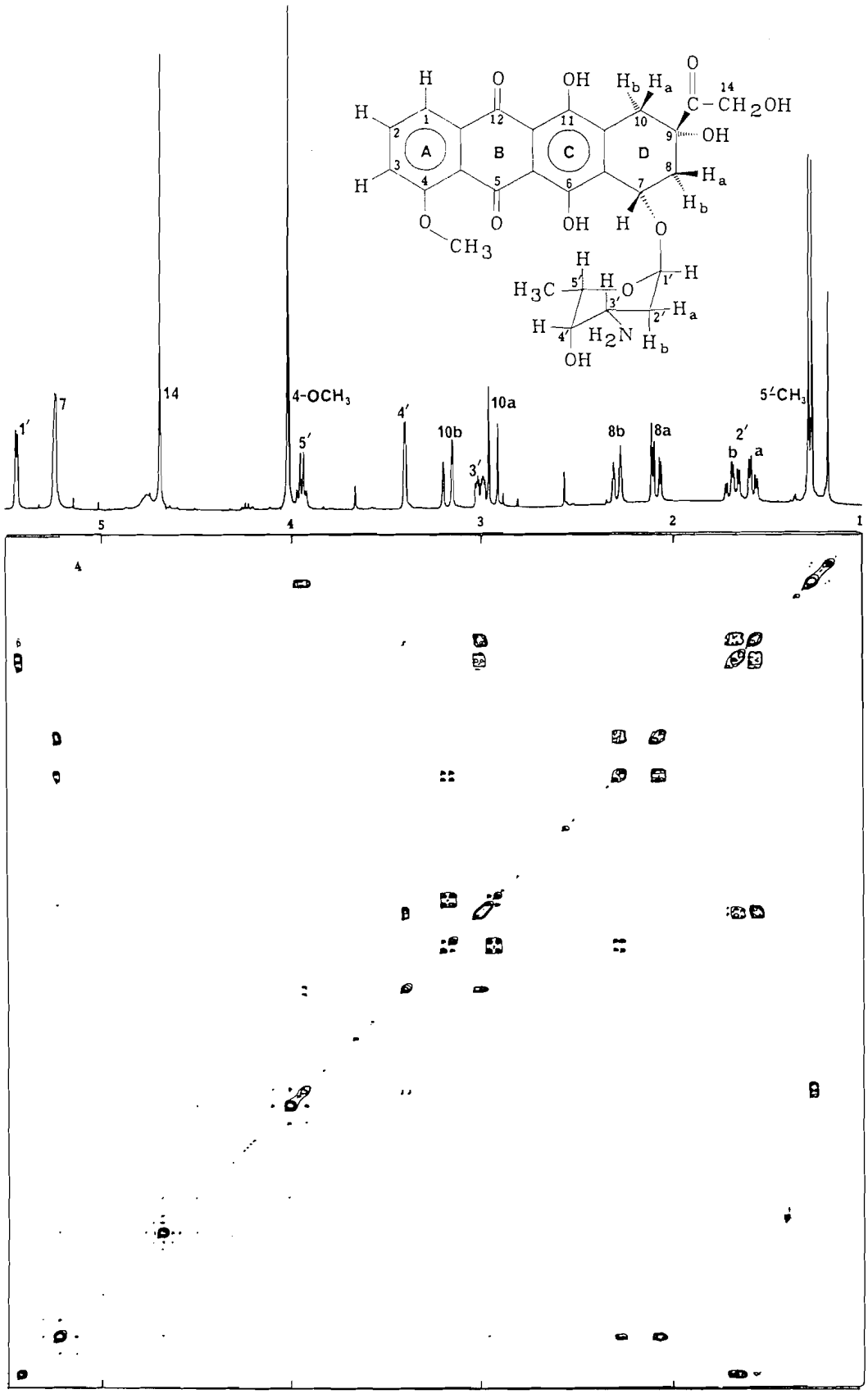

FIG. 3. The 400-MHz ^{1}H COSY spectrum of Adm in $CDCl_3$ in the region 5.5 δ to 0.0 δ with the 1D spectrum plotted above on the same scale. To improve legibility the aromatic portion is not shown. There is a cross peak (not shown) correlating the peaks at 7.32 δ and 4.02 δ. The presence of a cross peak indicates that the two resonances are scalar coupled.

Can. J. Chem. Downloaded from www.nrcresearchpress.com by 213.166.140.6 on 09/07/12
For personal use only.

TABLE 1. ^{1}H nuclear magnetic resonance parameters of Adm and Adm·HCl in various solvents

Chemical shifts of the aglycone moiety (ppm)

	Proton										
Solvent	1	2	3	7	8a	8b	10a	10b	14a	14b	4OCH$_3$
$CDCl_3$[a]	8.00	7.77	7.36	5.19	2.09	2.29	2.88	3.21	2.41		4.04
$CDCl_3$	7.95	7.73	7.32	5.03	2.08	2.29	2.89	3.15	4.71	4.71	4.02
$(CD_3)_2CO$	8.26	8.21	7.94	5.43	2.19	2.55	2.97	3.17	4.69	4.75	4.16
CD_3OD	7.87	7.77	7.48	5.08	2.10	2.34	2.87	3.04	4.70	4.71	4.00
DMF-d_7	7.93	7.70	7.93	5.04	2.23	2.37	2.95	3.14	4.79	4.79	4.05
CD_3OD*	7.92	7.82	7.57	5.27	2.14	2.34	2.91	3.06	4.68	4.74	4.04
DMF-d_7*	7.94	7.69	7.94	5.06	2.21	2.37	2.96	3.13	4.77	4.77	4.07
DMSO-d_6*[b]	7.87	7.63	7.87	5.00	2.02	2.12	2.77	2.95	4.70	4.70	3.98

Chemical shifts of the daunosamine moiety (ppm)

	Proton						
Solvent	1′	2′a	2′b	3′	4′	5′	5′-CH$_3$
$CDCl_3$[a]	5.45	1.85	1.93	4.20	3.62	4.23	1.28
$CDCl_3$	5.45	1.60	1.70	3.02	3.42	3.97	1.29
$(CD_3)_2CO$	5.76	1.72	2.24	3.17	3.95	4.09	1.16
CD_3OD	5.37	~1.7	~1.7	2.95	3.45	4.13	1.27
DMF-d_7	5.30	1.55	1.72	2.93	3.38	4.16	1.18
CD_3OD*	5.45	1.87	1.96	3.56	3.65	4.27	1.28
DMF-d_7*	5.43	1.97	2.11	3.65	3.89	4.36	1.22
DMSO-d_6*[b]	5.40	1.65	1.85	3.33	3.64	4.23	1.13

Coupling constants of the aglycone moiety (Hz)

Solvent	1–2	1–3	2–3	7–8a	7–8b	7–10a	8a–8b	8b–10b	10a–10b	14ab
$CDCl_3$[a]	7.8	1.8	7.8	2.5	3.5		15.0	<1	18.5	
$CDCl_3$	7.7	1.1	8.6	3.8	2.9	0.8	14.5	2.5	18.8	17.5
$(CD_3)_2CO$	7.8	1.4	8.4	4.4	2.3	1.0	14.7	2.0	19.0	19.8
CD_3OD	7.8	1.8	8.5	2.3	5.0		14.5	2.5	18.5	19.0
DMF-d_7	4.8	1.3	4.8	5.4	3.5		14.5	2.1	18.4	14
CD_3OD*	7.7	1.4	8.6	2.6	5.1	0.5	14.5	2.3	18.7	19.8
DMF-d_7*	4.8	1.3	4.8	5.5	3.5		14.5	2.0	18.5	14
DMSO-d_6*	8.0	1.5	8.0	5.5	6.0		14.5	1.5	18.5	

Coupling constants of the daunosamine moiety (Hz)

	Protons								
Solvent	1′–2′a	1′–2′b	2′a–2′b	2′a–3′	2′a–4′	2′b–3′	3′–4′	4′–5′	5′–5′CH$_3$
$CDCl_3$[a]							2.5	1.0	6.5
$CDCl_3$	1.6	4.1	13.8	4.8	1.6	12.0	3.2	2.1	6.6
$(CD_3)_2CO$	7.8	6.4	15.2	4.4	0.0	3.2	7.8	2.2	6.7
CD_3OD[c]	~7	~7		8.5	0.0	8.5	4.5	4.5	6.5
DMF-d_7	2.3	3.3	12.4	5.3	1	12.5	2.2	2.1	6.5
CD_3OD*	1.5	3.7	12.9	4.6	1.5	12.5	2.9	2.1	6.5
DMF-d_7*	2.3	3.3	12.5	5.5	1	13.0	2.3	2.1	6.5
DMSO-d_6*	1.8	3.5	12.5	4	1	13.5	2	1.8	6.0

*Asterisk indicates values for Adm·HCl, otherwise the values are for Adm.

[a]Results from Arcamone *et al.* (8) on *N*-acetyldaunomycin at 60 and 100 MHz. Not all values could be obtained because of limited resolution and the lower chemical shift dispersion.

[b]9-OH, 4.68; 14-OH, 4.97; 6- and 11-OH, 14.0 and 13.3; NH_3^+, 7.9; 4′-OH, 5.63.

[c]The 2′ resonances are too strongly coupled for easy extraction of their parameters.

multiplets but they could not be assigned. There was, however, a clearly resolved coupling of 0.5 Hz, connecting the 3 proton and the 4-OCH$_3$ protons.

Adm in CD_3OD

The spectrum of Adm·HCl in CD_3OD has much the same appearance as that of Adm in $CDCl_3$, indicating that in both cases the conformations are similar. However, the spectrum of Adm (the free base) in CD_3OD is quite different. The 2′ resonances are very close together, so close in fact that their separate nmr parameters could not be easily extracted although this could have been done with computer analysis. The 3′ resonance is different as well, containing two medium size couplings of 8.5 Hz rather than a large one and a small one. The

Can. J. Chem. Downloaded from www.nrcresearchpress.com by 213.166.140.6 on 09/07/12
For personal use only.

3′–4′ and 4′–5′ coupling constants are also significantly larger, each being 4.5 Hz.

Adm in DMF-d_7

The spectra of the protonated and nonprotonated molecules are virtually identical except for the deshielding of the protons caused by protonation. The sugar ring is therefore rigid and has the same conformation in both cases.

Discussion

Both crystal structures of daunomycin (5, 6) and the theoretical studies (7, 8) show that hydrogen bonding, both intramolecular and to the solvent molecules, is of great importance in determining the conformation of the molecule. It is probable that the internal conformation of the sugar ring is also stabilized by hydrogen bonding. Models show that interactions with the 5 and 6 oxygen atoms or the 9-OH group are not possible in any other chair or boat conformation.

It appears as well that the interactions that stabilize the conformation of the sugar ring are, at least partially, steric in origin. The methyl and amino groups are equatorial and therefore do not interfere. The hydroxyl group and the rest of the Adm molecule are axial but are on opposite sides of the ring. Hydrogen bonding must also play a role in stabilizing the puckered conformation of the D ring found both in the crystal and in solution. In fact the nmr results show that in each solvent this conformation is maintained even though there are marked solvent dependences in the sugar resonances.

The spectrum of Adm in methanol is quite different from that of Adm in acetone but it has the common feature that no single conformation can account for all of the magnitudes of all of the coupling constants simultaneously. It must be concluded, therefore, that the sugar ring is not rigid for the free base in these solvents. As well, because the measured nmr parameters of Adm in methanol are significantly different from those in acetone, it appears that the relative populations of the various conformers and perhaps the dynamic processes in the two solvents are quite different.

The results for the protonated and nonprotonated species in CD_3OD and DMF-d_7 clearly show the effects of protonation upon the chemical shifts of the sugar ring protons. As expected, the effect of the positive charge on the 3′ amino group is greatest for the 3′ proton and falls off with increasing distance. It would be interesting to compare the spectra of both Adm and Adm·HCl in all of the solvents but unfortunately the protonated species is insoluble in chloroform and acetone while Adm decomposes in DMSO.

Although it has been reported (11) that Adm shows no evidence for self-association in CD_3OD solution, a closer examination shows that this is not the case. Some preliminary data[2] indicate that the appearance of the ^1H nmr spectrum of Adm·HCl in methanol is both temperature and concentration dependent. The differences in the spectra of the protonated and nonprotonated forms as well as the presence of self-association of Adm in CD_3OD have important consequences with respect to the structure of adriamycin in aqueous solution. A high resolution spectrum of Adm can be obtained in D_2O only in acidic solutions (9) because the neutral species self-associates to form dimers. The reduced mobility of the dimer, its high formation constant, and the fact that it is in the fast exchange regime on the nmr time scale, all conspire to broaden the nmr resonances of Adm to the point that not much useful information can be obtained at physiologically important pH levels. The differences in conformation between Adm and Adm·HCl in CD_3OD could be looked upon as a "pH" dependence that is unobservable in D_2O but that may nonetheless exist. The conformational differences also cast doubt upon the notion that there is an "active" conformer. Adm in aqueous solution at physiological pH is partially deprotonated and therefore may be conformationally nonrigid here as well. The behaviour of Adm in methanolic solution as a function of its degree of protonation is under further investigation.

[2]T. Allman and R. E. Lenkinski, unpublished results. The spectrum of Adm·HCl in methanol at ambient temperature is sharp and shows no obvious effects that could be attributed to self-association. However, when the spectra were observed as a function of temperature below 0°C it was found that the spectra broadened as the temperature was decreased and as the concentration was increased. This mimics closely the behaviour of Adm in aqueous solution at higher temperatures.

Conclusion

We have shown that the appearance of the proton nmr spectrum of the sugar portion of adriamycin is dependent upon both the nature of the solvent and the state of protonation of the amino group. In most solvents the sugar ring is in the chair conformation in which the methyl group is equatorial. In these solvents there is no evidence for any interchange among other possible conformers although the free base in acetone and in methanol is conformationally mobile. It is interesting that there is evidence for only one conformation of the D ring. Overall, these results suggest that Adm has no strongly preferred conformation, making it likely that its interaction with DNA is controlled by intermolecular forces rather than intramolecular ones.

Experimental

Adm and Adm·HCl were prepared and purified as described elsewhere (17). All ^1H nmr spectra were recorded at the Southwestern Ontario NMR Centre on a Bruker WH-400 FT nmr spectrometer. Saturated solutions were prepared for the measurements in $CDCl_3$, $(CD_3)_2CO$, and CD_3OD. The solutions in the other solvents were approximately 10 mg L^{-1}.

2D nuclear magnetic resonance spectra

For the COSY spectra, 256 1K FIDs were acquired using the standard Bruker microprogram COSY.AU. A sine squared bell window function was applied in both dimensions before Fourier transformation. The magnitude spectrum was then symmetrized about the diagonal. The number of transients collected per FID varied depending upon the concentration of the sample but generally 16 to 64 were sufficient.

For the *J*-resolved spectra, 128 2K FIDs were acquired using the standard Bruker microprogram JRES.AU. The f_1 sweep width was ±28 Hz. The sine bell window function was applied in each dimension before transformation. A magnitude calculation was performed after which the spectra were tilted and then symmetrized about $f_1 = 0$ Hz.

1D nuclear magnetic resonance spectra

The 1D spectra were routinely acquired into 16 or 32K blocks and were Fourier transformed after the application of any of the standard window functions that was deemed to be necessary. Usually the window from 9.0 to 0.0 ppm was observed.

1. S. Neidle and G. Taylor. Biochim. Biophys. Acta, **479**, 450 (1977).
2. D. W. Henry. *In* Cancer chemotherapy. Am. Chem. Soc., Washington, DC. 1976. pp. 15–57.
3. W. J. Pigram, W. Fullier, and L. D. Hamilton. Nature (London), New Biol. **235**, 17 (1972).
4. S. Neidle. Cancer Treat. Rep. **61**, 928 (1977).
5. C. Courseille, B. Busetta, and M. Hospital. Acta Crystallogr. Sect. B: Struct. Crystallogr. Cryst. Chem. **35**, 764 (1979).

6. R. ANGUILLI, E. FORESTI, L. RIVA DI SANSERVERINO, K. W. ISAACS, O. KENNARD, W. D. S. MOTHERWELL, D. L. WAMPLER, and F. ARCAMONE. Nature (London), New Biol. **234**, 78 (1971).
7. S. NEIDLE and G. L. TAYLOR. FEBS Lett. **107**, 348 (1979).
8. Y. NAKATA and A. J. HOPFINGER. FEBS Lett. **117**, 259 (1980).
9. I. J. MCLENNAN and R. E. LENKINSKI. J. Am. Chem. Soc. **106**, 6905 (1984).
10. F. ARCAMONE, G. CASSINELLI, G. FRANCESCHI, R. MONDELLI, P. OREZZI, and S. PENCO. Gazz. Chim. Ital. **100**, 949 (1970).
11. I. J. MCLENNAN, R. E. LENKINSKI, and Y. YANUKA. Can. J. Chem. **63**, 1233 (1985).
12. M. KARPLUS. J. Chem. Phys. **30**, 11 (1959).
13. P. DURETTE and D. HORTON. Adv. Carbohyd. Chem. Biochem. **26**, 49 (1971).
14. K. BOCK and M. THOGERSON. Ann. Rep. NMR Spectrosc. **13**, 2 (1982).
15. S. STERNHELL. Q. Rev. **23**, 236 (1969).
16. L. D. HALL. *In* The Carbohydrates. *Edited by* W. Pigman and D. Horton. Wiley, New York. 1980. pp. 1300–1320.
17. T. ALLMAN and R. E. LENKINSKI. J. Inorg. Biochem. **30**, 35 (1987).

Can. J. Chem. Downloaded from www.nrcresearchpress.com by 213.166.140.6 on 09/07/12
For personal use only.

Acceleration of the mercury-induced aquation of bromopentammine Co(III) by naturally occurring glycosaminoglycans

DOUGLAS M. TEMPLETON

Department of Clinical Biochemistry, University of Toronto, 100 College St., Toronto, Ont., Canada M5G 1L5 [1]

and

Department of Biochemistry, The Hospital for Sick Children, 555 University Ave., Toronto, Ont., Canada M5G 1X8

Received March 24, 1987

FOR ERRATA SEE
V. 66 #7 1988 P. 1786

DOUGLAS M. TEMPLETON. Can. J. Chem. **65**, 2411 (1987).

The glycosaminoglycans are naturally occurring anionic polysaccharides whose polyelectrolyte properties and counterion interactions may underlie a number of biological activities. We have investigated the ability of the sulfated glycosaminoglycans to accelerate the reaction of $Br(NH_3)_5Co^{2+}$ with Hg^{2+}. Chondroitin sulfates A, B, and C, heparin, and heparan sulfates all accelerate this reaction to nearly the same extent, but do so at different optimal concentrations, above which inhibition is observed. This phenomenon of rate acceleration, sometimes called "polyelectrolyte catalysis", has previously been explained by a two-phase model, in which the reactant counterions are thought to equilibrate rapidly between the polymer domain and the bulk phase. Rate effects would then be due to higher local concentrations in the neighbourhood of the polymer. Our results show that this is an oversimplified view for the glycosaminoglycans. Rather, they demonstrate similar rate accelerations independent of net structural charge density. It is argued that counterion condensation, as described by Manning, reduces the surface potential of all glycosaminoglycans to nearly constant values. Different optimal concentrations of the glycosaminoglycans may arise in part from the unreactivity of a subpopulation of bound ions.

DOUGLAS M. TEMPLETON. Can. J. Chem. **65**, 2411 (1987).

Les glycosaminoglycanes sont des polysaccharides anioniques que l'on retrouve dans la nature dont les propriétés comme polyélectrolytes et les interactions contre-ioniques peuvent être à la base d'un grand nombre d'activités biologiques. On a étudié la facilité qu'ont des sulfates de glycosaminoglycanes d'accélérer la réaction du $Br(NH_3)_5Co^{2+}$ avec le Hg^{2+}. Les sulfates de chondritine A, B et C, l'héparine et les sulfates d'héparane accélèrent tous cette réaction de la même manière; toutefois, cette propriété n'est observée qu'à des concentrations optimales qui varient et au-dessus desquelles on observe une inhibition. Ce phénomène d'accélération des vitesses de réaction, qu'on appelle quelquefois «catalyse des polyélectrolytes», a été expliquée antérieurement par un modèle comportant deux phases; dans ce modèle, on suggère qu'il s'établit rapidement un équilibre entre les contre-ions réactifs du domaine du polymère et ceux de l'ensemble de la phase. Les effets sur les vitesses proviendraient alors de concentrations locales élevées autour du polymère. Nos résultats démontrent que cette théorie est trop simplifiée pour le glycosaminoglycanes. Nos résultats démontrent plutôt que les vitesses de réactions peuvent être accélérées de la même manière sans qu'il existe de densité nette de charge autour de la structure. On suggère donc que la condensation des contre-ions, telle que décrite par Manning, réduit le potentiel superficiel de tous les glycosaminoglycanes à des valeurs qui sont presque constantes. Il se peut donc que des concentrations optimales différentes de glycosaminoglycanes puissent provenir en partie du fait qu'une sous-population d'ions liés ne sont pas réactive.

[Traduit par la revue]

Introduction

Polyelectrolytes affect the solution properties of small ions having charges both similar (coions) and opposite (counterions) to those of the polyion. This is in large part due to electrostatic effects, which are manifest as forces concentrating counterions in the vicinity of the polymer while at the same time excluding coions from this region. Quantitative description of the concentration of counterions in the polymer domain has been approached with both Poisson–Boltzmann (1, 2) and Manning counterion condensation (3, 4) theories. Reactions in solution between small ions of like charge are in general slow, since the reactants exhibit mutual electrostatic repulsion. However, the rates of such reactions are frequently increased in the presence of polyelectrolytes of opposite charge to the reactants. This phenomenon has been called polyelectrolyte catalysis (5–8). It may be understood as arising from local concentration effects. Concentrations of both reactants are increased in the polymer domain, where the reaction then proceeds at increased rate. While this model may be of heuristic value, use of the term "catalysis" to describe the phenomenon is open to question, and has been rightly criticized (9, 10). Here we will recognize the fact that polyelectrolytes may well alter the equilibrium distribution of small ionic species, and will use the more neutral term of rate acceleration to describe the observed phenomenon.

[1]Correspondence should be sent to this address.

Acceleration of the rate of the reaction of bromopentammine Co(III) with mercuric ion,

$$Br(NH_3)_5Co(III)^{2+} + Hg^{2+} \rightarrow H_2O(NH_3)_5Co(III)^{3+} + HgBr^+$$

was studied in the presence of various ions and interpreted (11) in terms of the primary salt effect (12). Acceleration of this reaction by a biological polyelectrolyte was measured first in the presence of various polynucleotides (7) and later with chondroitin-4- and 6-sulfates (10). Booij (10) interpreted his results in terms of the two-phase model of Morawetz and Shafer (13). This model assumes that the reactants are distributed between two phases, the polymer domain with a potential ψ and the bulk solution. Rapid exchange is assumed between the phases, so that the equilibrium distribution is not affected by reaction, and the intrinsic rate constant is taken to be the same in both phases. This amounts to true catalysis and the faster rate of reaction is viewed as being due solely to the increased concentration of reactants in the polymer domain.

The glycosaminoglycans (GAGs) are a class of naturally occurring polysaccharides consisting of sulfated uronic acid – hexosamine disaccharide subunits. The exceptions are hyaluronic acid, which contains no sulfate, and keratan sulfate, in which the uronic acid is reduced to the corresponding polyol. In all cases some structural heterogeneity occurs along the length of the polymer chain, but individual GAGs are characterized by typical uronic acid – hexosamine disaccharides. Variation

Can. J. Chem. Downloaded from www.nrcresearchpress.com by 213.166.140.6 on 09/07/12
For personal use only.

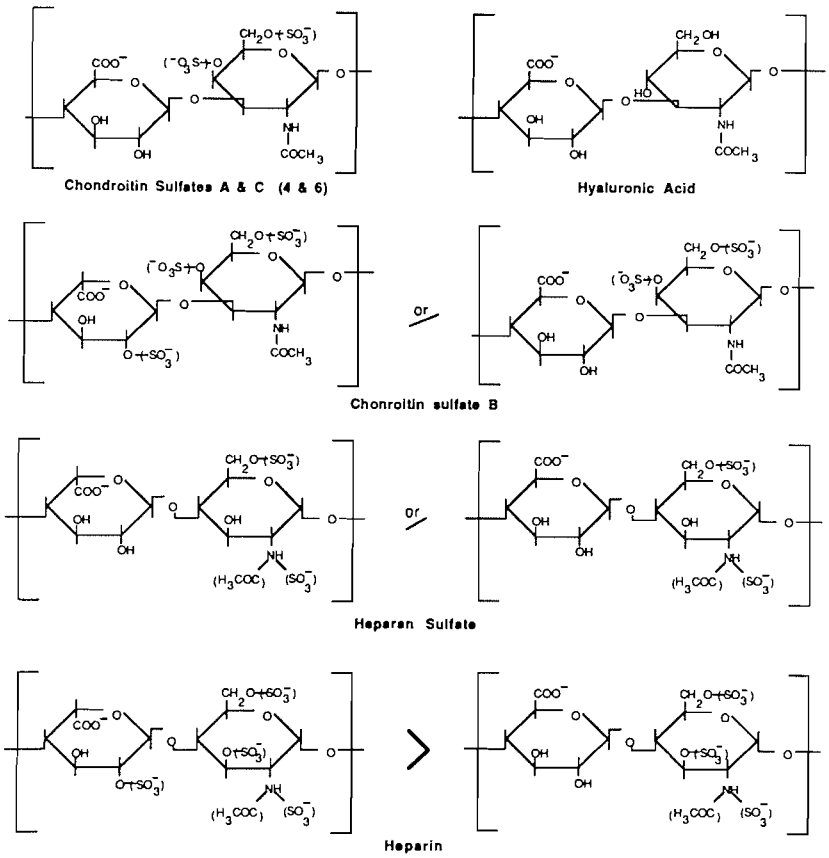

FIG. 1. Typical repeating disaccharide structures of the glycosaminoglycans used in the present study. Substituents in parentheses may alternatively be H. Iduronic acid predominates in heparin, which is also the most highly sulfated polymer of the group.

occurs in the stereochemistry of the C-5 carboxyl of the uronic acid (producing the C-5 epimers glucuronic and iduronic acid), in the extent of deacetylation of the amino group of the hexosamine, and in the degree and position of sulfation. The disaccharide structures of the GAGs used in the present study are given in Fig. 1. Clearly the GAGs are anionic polyelectrolytes with significant axial charge densities (*vide infra*). These vary from $\xi \simeq 0.7$ for hyaluronic acid to $2 < \xi < 3.5$ for various heparins (14, 15, and present work).

The electrostatic fields arising from these significant charge densities may underlie the wide range of biological functions of the GAGs. Thus electrostatic interactions have been implicated in such diverse processes as Ca^{2+} ion sequestration by chondroitins during bone mineralization (16), the anticoagulant activity of heparin (17), and the charge dependence of plasma solute filtration by the kidney (18). Our attempts to understand the latter phenomenon (19, 20) have led us to investigate the charge-dependent chemistry of these species. A number of investigators have studied metal ion binding to GAGs in isolation (21–25) and in tissue components (19). Another approach has been to study dye binding by GAGs (26), and it has been suggested that the well-known phenomenon of metachromasia may relate to the biological activity of some GAGs (17). Here we extend the work of Booij (10) to show that a wide range of GAGs from various sources exhibit polyelectrolyte rate acceleration of ionic reactions. Our results demonstrate that the two-phase model is unsuitable for describing the effects of GAGs. Significant ion binding modifies polymer charge densities, and can inhibit reaction by sequestering reactants in a manner dependent upon polymer concentration. The partitioning of ions between bulk and polymer domains is understood in terms of Manning's theory of counterion condensation (3, 4).

Theory

Two-phase model

In this model, a counterion partitions between the bulk phase and polyion domain according to the dimensionless parameter x where

$$[1] \quad x = \exp(-q\psi/kT)$$

where q is the charge on the electron, k Boltzmann's constant, and T the absolute temperature. ψ is the average potential experienced by a univalent counterion in the polymer domain. The volume of the polyion phase is approximated as that of a cylinder of radius r. If the structural radius R of the polymer is known, then the thickness ρ of the annulus in which reaction takes place can be calculated as

$$[2] \quad \rho = r - R$$

If [ua] is the concentration of uronic acid (equal to the concentration of disaccharide repeating units of the GAG polymer) in mol dm^{-3} and L is the length of the disaccharide, then with all lengths in m (metres) the volume of the polyion phase ϕ is given by

$$[3] \quad \phi = \pi r^2 LN[\text{ua}] \times 10^3$$

where N is Avogadro's number. Morawetz and Shafer (13) derived expressions for ϕ in terms of x, and for k/k_0 in terms of ϕ, where k and k_0 are the rates of the reaction in the presence and absence of polyelectrolyte, respectively. When the charges on both reactants are +2, these expressions reduce to (see

Can. J. Chem. Downloaded from www.nrcresearchpress.com by 213.166.140.6 on 09/07/12
For personal use only.

Can. J. Chem. Downloaded from www.nrcresearchpress.com by 213.166.140.6 on 09/07/12
For personal use only.

Appendix A of ref. 10)

[4] $\phi_{max} = x^{-2}$

and

[5] $(k/k_0)_{max} = x^2/4$

Equations [1] and [5] allow calculation of the effective potential from the observed rate acceleration, while eqs. [2], [3], and [4] determine the proximity of the reacting ions to the polymer.

Manning model

Partitioning of the divalent ions into the polymer domain can alternatively be described according to the empirical formulation of Manning (4), which gives the binding fraction f, defined as the fraction of polymer charge that remains uncompensated by counterion binding, by the discontinuous equation

[6] $f = (\xi Z)^{-1}, \xi > Z^{-1}$
$f = 1 \quad , \xi < Z^{-1}$

Z is the valence (charge) of the counterion and ξ is a dimensionless axial charge density given by

[7] $\xi = (q^2/4\pi\epsilon_r\epsilon_0 kT)(1/b)$
$= (\pounds/\epsilon_r T)(1/b)$

The term $(\pounds/\epsilon_r T)$ is the Landau length, where ϵ_r is the relative dielectric constant of the bulk medium and the constant $\pounds = q^2/4\pi\epsilon_0 k$. The permittivity of free space is ϵ_0 and b is the linear spacing between univalent charges on the polymer. Calculations throughout have been performed assuming T = 298 K and ϵ_r = 78.33 for water at 25°C. Note that this definition of f means that fractional charge reduction is $f - 1$, a value of $f = 1$ implies no counterion binding, and, for example, monovalent ions will not be effective in reducing polymer charge if $\xi < 1$.

In Manning's theoretical treatment of counterion condensation, the driving force for net binding may be considered to be the relief of electrostatic strain inherent in the polyion (e.g. see ref. 27). The nature of binding is not specified, all binding modes being equally effective in reducing polymer charge. Following Manning (4), we will consider binding to be either site specific or territorial. Site-specific binding refers to the complexation of counterions at fixed sites on the polymer. Territorial binding refers to all other binding modes, including, for example, metal ions concentrated in the neighbourhood of the polymer as described in double layer theory. It is only the total of both types of binding that must remain constant for counterions of a given valence, as indicated by eq. [6].

Poisson–Boltzmann model

The two-dimensional charge density per unit surface area, σ, of a cylinder of radius R and charge density ξ is given by (2)

[8] $\sigma = \xi/[2\pi R(\pounds/\epsilon_r T)]$

We will use this relation to calculate the surface potential ψ_0 of a GAG of known ξ, from the Gouy–Chapman equation, according to (28)

[9] $q\sigma/(8 \times 10^3 \cdot \epsilon_r\epsilon_0 NkTC_\infty)^{1/2} = \sinh [Zq\psi_0/2kT]$

where $\sinh(x) = \frac{1}{2}(e^x - e^{-x})$ and C_∞ is the molar concentration of counterion in the bulk solution (i.e., at an infinite distance from the polymer).

Relation of k/k_0 *to* ξ

From the above discussion it is apparent that, if the two-phase model applies, rate acceleration is related to ξ through the potential ψ that the structural charge density entails. In general,

[10] $\psi \propto -\xi/\epsilon_r$

where the proportionality term will be a function of distance from the polymer. This term has been given as $2K_0(\kappa d)$ where d is the distance from the polymer, K_0 is a zero'th order modified Bessel function of the second kind (10), and $1/\kappa$ is the Debye length defined as

[11] $1/\kappa = (8\pi \cdot 10^3 \cdot NC_\infty \pounds/\epsilon_r T)^{-1/2}$

Then for two polyions of the same signed charge and effective radius r (i.e., d constant), denoted by subscripts 1 and 2,

[12] $\psi_1/\psi_2 = \xi_1/\xi_2$

From eqs. [1], [4], and [11]

[13] $(k/k_0)_{max,1}/(k/k_0)_{max,2} = \exp[(-2q/kT)(\psi_1 - \psi_2)]$

and

[14] $\log (k/k_0)_{max,2} - \log (k/k_0)_{max,1} = 179(\psi_1 - \psi_2)$

at 25°C with ψ in volts.

Salt dependence of ion partitioning

We will consider the effects of a monovalent supporting electrolyte on the concentration of divalent counterions in the polymer domain. Because the surface potentials of the GAGs are sufficiently large ($\psi_0 < -60$ mV), linearization of the Poisson–Boltzmann equation is not justified, and the Debye–Hückel model is not valid (28). Equation [9] predicts a greater than second power dependence of ψ on ion charge. In symmetrical salts eq. [9] can be used to calculate the surface potential as a function of C_∞, from which $\psi(d)$ can be calculated according to ref. 28:

[15] $\psi(d) = (2kT/zq) \ln [(1 + \alpha e^{-\beta d})/(1 - \alpha e^{-\beta d})]$

where

$$\alpha = [\exp(zq\psi_0/2kT) - 1]/[\exp(zq\psi_0/2kT) + 1]$$

and

$$\beta = [(2q^2 C_\infty z^2)/(\epsilon_r\epsilon_0 kT)]^{1/2}$$

Here z is the valence of the electrolyte and ψ_0 is the surface potential at $d = 0$. Variation in C with distance is given by the Boltzmann relation

[16] $C(d) = C_\infty \exp[zq\psi(d)/kT]$

In mixed salts, a more general form of eq. [9] must be used, as derived by Grahame (29):

[17] $q\sigma = \{(2\epsilon_r\epsilon_0 kT)\Sigma_i C_{\infty,i} \exp(-z_i q\psi_0/kT) - 1\}^{1/2}$

where the summation is over all small ions i. In the Poisson–Boltzmann and Gouy treatments, then, the screening effects of a supporting electrolyte are understood through their concentration effects on surface potential, as revealed for example in eqs. [9] and [17] for a given structural charge density.

Salt effects on binding can also be accounted for in the Manning model. Equation [6] does not predict a concentration dependence for a single species of counterion, and this has been borne out over a wide range of conditions in polyelectrolyte solution (8). However, since the binding energy is related to the electrostatic potential in the polymer domain, a second ion will affect binding of the first if it is capable of modifying the

surface potential. In the presence of charge reduction by both monovalent and divalent ions, the contribution of each can be calculated from solution of the simultaneous equations

$$\ln [A(\theta_1/C_{\infty,1})] = -2\xi(1 - \theta_1 - 2\theta_2) \ln [1 - \exp(-b\kappa)]$$
$$\theta_2/C_{\infty,2} = A(\theta_1/C_{\infty,1})^2 \quad [18]$$

where θ_i is the extent of binding of counterions of valence i, defined as bound mole ratio per equivalent polyelectrolyte charge ($Z_i\theta_i = 1 - f_i$), and $A = e/10^3 \cdot V_p$ where V_p is the volume of the binding shell about the polymer in m^3 per mole of equivalent polyion charge and e is the base of the natural logarithms (2). Here the salt dependence of binding enters through the Debye length. Following Booij (10), we have performed most kinetic measurements at a calculated ionic strength of 0.020 *M* as a compromise between higher values, which would minimize polyelectrolyte effects by screening the polymer potential, and lower values, which would constitute a poorly controlled system. Under these conditions, the ratio of monovalent ions to divalent ions in the reaction mixture is greater than two orders of magnitude (see Methods), screening effects should be primarily due to the 1:1 salts, and the Gouy–Chapman potential should be a good approximation to the Grahame potential. The relationship between θ_2 and the observed rate of aquation depends both on the nature of binding and the reactivity of bound ions. To use eq. [18] to predict the observed ionic strength dependence of the acceleration, it will be necessary to consider the rate increase to be proportional to the increase in total concentration of divalent ions in the polymer domain, and to assume that the cobalt complex and mercuric ions are indistinguishable with respect to condensation, as implied by eq. [6].

Materials and methods

Chemicals

Chondroitin sulfates (ChS) Type A (whale cartilage), Type B (porcine skin), and Type C (shark cartilage), heparin (pig intestinal mucosa, grade I), hyaluronic acid (human umbilical cord, grade I), deoxyribonuclease I (crude, 460 Kunitz units/mg), ribonuclease (5× crystallized, 58 Kunitz units/mg), and calf thymus DNA (Type I, highly polymerized) were all obtained from Sigma Chemical Co., St. Louis, MO. The enzymes and hyaluronic acid were used without further purification. ChS(B) and heparin were purified by poly-L-lysine Sepharose chromatography. Some heparin was further fractionated by metal chelate affinity chromatography (MCAC). Chondroitin sulfates A and C were further purified by precipitation from 50 m*M* NaCl in 50 m*M* Tris-HCl, pH 7.4, with 1% cetylpyridinium chloride, redissolved in 2.5 *M* NaCl:methanol (2:1), precipitated with 5 volumes of 95% ethanol in the presence of 1% potassium acetate, dialysed extensively against deionized water, and lyophilized. $Hg(NO_3)_2$ (crystalline) was from Matheson, Coleman and Bell (Norwood, OH). $Br(NH_3)_5Co(III)\cdot Br_2$ was synthesized by the method of Diehl *et al.* (30), beginning with $CoCl_2\cdot 6H_2O$ (Anal R; BDH, Poole, UK). The product was recrystallized by dissolving 20 g in 400 mL H_2O with 20 mL NH_4OH, at 90°C. To the hot filtrate was added 36 mL of 48% HBr, and the solution was held over a steam bath for 2 h. On cooling, purple crystals were obtained ($\epsilon_{254} = 1.72 \times 10^4$ dm^3 mol^{-1} cm^{-1}). Heparan sulfates (HS) were isolated from beef lung as previously described (31), and eluted from poly-L-lysine Sepharose to yield two major fractions.

Chromatography

Cyanogen bromide activated Sepharose CL-4B was prepared and coupled with poly-L-lysine·HBr (D.P. 200; Sigma) as described (32) and poured into a 0.9 × 30 cm column. GAG samples were applied in Tris·HCl (50 m*M*, pH 7.5) and eluted with a linear gradient of NaCl (0–2 *M*, 200 mL) in the same buffer (33). Two major HS fractions eluted between the chondroitins and heparin, at 0.95 and 1.20 *M* NaCl. These are designated HS-I and HS-II respectively. MCAC was performed in disposable 10-mL plastic syringes containing iminodiacetic acid – Sepharose 6B (Pharmacia). The top two-thirds of the columns were charged with either Cu^{2+} or Ni^{2+}, and equilibrated with 50 m*M* phosphate buffer, pH 8.0. Heparin samples were loaded in this buffer, and eluted with a linear gradient of 50 m*M* phosphate (pH 8.0–pH 5.0, 200 mL). Most of the uronic-acid-positive material eluted as a single peak above pH 7. This fraction is designated non-metal-binding heparin (heparin-NMB). Less than 5% of the total uronic acid (also in polymer form) eluted as a second minor peak below pH 6. Heparin-NMB was further purified by dialysis against water, and lyophilized.

Biochemical procedures

Sulfated GAGs were estimated by the dimethylmethylene blue assay (31), using commercial heparin or chondroitin sulfates as standards, as appropriate. Uronic acid was measured by a scaled-down version of the carbazole assay (34), and sulfate by the rhodizonic acid procedure (35). For the sulfate determinations, triplicate samples were each divided in half, and one half was hydrolyzed with 1 *M* HCl (2 h, 100°C) before assay. The content of GAG sulfate ester was taken as the amount of sulfate released by hydrolysis, measured against standards of Na_2SO_4. Desulfation of ChS(A) was achieved by the method of Kantor and Schubert (36). Acetyl chloride was dissolved in methanol (0.5% by volume) and the solution let stand stoppered for 2 days. ChS(A) (100 mg) was suspended in 15 mL of this reagent, and stirred gently at room temperature for 48 h. The reagent was changed at 24 h. The product was collected by centrifugation, dialysed against water, and lyophilized. For nucleic acid digestions, 5–25 mg of GAG was dissolved in 10 mL sodium acetate buffer (0.125 *M*, pH 5.0, with 0.050 *M* $MgCl_2$) and incubated at 37°C for 48 h. Solutions of 1 mg deoxyribonuclease and 0.2 mg ribonuclease in 1 mL of the same buffer were added at 0 and 24 h. At 48 h the GAG solutions were placed in a boiling water bath for 10 min, the supernatant was cleared by centrifugation, and the GAGs were recovered by ethanol precipitation (5 vol 95% ethanol) in the presence of 1% potassium acetate.

Kinetic measurements

Water of 18 MΩ cm (Milli Q system; Millipore) was used for all solutions. Stock solutions of 1 m*M* $Br(NH_3)_5Co\cdot Br_2$ were prepared fresh each week and stored in the dark. For use each day, a 10-fold dilution was prepared, and the concentration determined from the absorbance at 254 nm. Water, $HClO_4$, $NaClO_4$, $Hg(NO_3)_2$, and the Co complex, all held at 25°C, were added in order to a quartz cuvette. The reaction was initiated by the addition of variable amounts of a GAG stock solution, which in each case was sufficient to make the final volume to 1.000 mL. Final concentrations were $[HClO_4] = 0.010$ *M*, $[Hg^{2+}] = 1.0 \times 10^{-4}$ *M*, and $[Co] = 1.0 \times 10^{-5}$ *M*. Sufficient $NaClO_4$ was added from an approximately 0.10 *M* stock solution to give a final ionic strength of 0.020 *M*, except in the ionic strength variation experiments, where variable amounts of perchlorate were used. The solution was mixed by inverting and the cuvette immediately placed in the spectrophotometer at 25 ± 0.1°C. Disappearance of the brominated Co complex was followed at 254 nm, and the initial rates were calculated assuming $\epsilon_{254} = 1.72 \times 10^4$ dm^3 mol^{-1} cm^{-1}. The pseudo-second-order rate constant k_2 was calculated according to $-d[Co]/dt = k_2[Hg][Co]$, where [Co] denotes the concentration of the brominated complex. The rate constant for aquation in the absence of GAG, $k_{2,0}$, was measured in duplicate at the beginning and end of each experiment, and the mean value used to calculate the $k_2/k_{2,0}$ ratios for that experiment. Over all experiments, a mean value of $k_{2,0} = (5.67 \pm 0.44) \times 10^4$ M^{-1} s^{-1} was found. Absorbance changes were recorded on a Perkin–Elmer Lambda 4C spectrophotometer, and analyzed in digitized form with Perkin–Elmer 7300 or 7700 computers. Each experiment consisted of concentration variation of a single GAG to encompass a maximum in the profile of $\log(k_2/k_{2,0})$ vs. [uronic acid]. Maximum rate acceleration and optimum GAG concentration were then found for the experiment from the derivative of a quadratic fit to

Can. J. Chem. Downloaded from www.nrcresearchpress.com by 213.166.140.6 on 09/07/12
For personal use only.

Can. J. Chem. Downloaded from www.nrcresearchpress.com by 213.166.140.6 on 09/07/12
For personal use only.

the profile ($R \geq 0.98$ in each case), and the values for these quantities are reported as the mean ± S.D. for several independent experiments.

Results

Chondroitin sulfate A enhances the rate of Hg^{2+}-induced aquation of bromopentammine $Co(III)^{2+}$ in 0.01 *M* perchloric acid at an ionic strength of $I = 0.020$ (Fig. 2). As the concentration of the polyelectrolyte is increased, the rate increases to a maximum, and declines thereafter. Similar behaviour is seen with ChS(B) and ChS(C) (not shown). A commercial preparation of heparin (Fig. 3), and heparan sulfates of two different compositions isolated from bovine lung (HS-I and HS-II), produce rate acceleration under similar conditions, and both show a concentration maximum for the effect. All GAGs show a concentration-dependent decrease above the maximum. At even higher concentrations, the reaction is inhibited relative to the rate of spontaneous hydrolysis in the presence of mercuric ion.

Because of microheterogeneity of these polymers, and the possibility that inhibition of the "uncatalyzed" reaction is due to site-specific binding of one or both ions by the GAG, the heparin sample was fractionated by metal chelate chromatography. On both Cu^{2+} and Ni^{2+} columns, a small fraction (<5%) of the total heparin was retained with higher affinity on the column (see Methods). The remaining heparin-NMB was also effective at enhancing the rate of the aquation reaction (Fig. 3), and was also capable of inhibiting the reaction at higher concentrations.

To demonstrate that the observed rate accelerations were due to the electrostatic fields generated by the charged functionality of the polyelectrolytes, two experiments were performed. First, the effect of hyaluronic acid on the reaction was investigated. This material is also a polymer of alternating hexosamine and uronic acid residues, but unlike the other GAGs contains no sulfate. Thus under the reaction conditions (well below the carboxyl pK_a), it is uncharged. No rate acceleration was seen with hyaluronic acid, and at increasing concentrations inhibition was noted (Fig. 4). Second, a sample of ChS(A) was desulfated by reaction with methanolic HCl. This produced a polymer with no detectable sulfate, and is also known to carboxymethylate uronic acid residues to a variable extent (36). When this desulfated chondroitin A was added to the reaction mixture, behaviour similar to hyaluronic acid was observed, i.e., no rate acceleration, and inhibition at higher concentrations (Fig. 4).

Quantitative comparison of the effects of the various polymers is achieved by determining the maximum rate acceleration produced by each, and the polymer concentration at which this maximum is reached. All sulfated GAGs give approximately the same degree of rate acceleration under a fixed set of conditions; however, they do so at quite different optimum concentrations (Table 1). From the two-phase model (eqs. [4] and [5]), the rate accelerations allow estimation of effective polymer radii and surface potentials (Table 1). For all sulfated GAGs, a mean value of $\log (k_2/\log k_{2,0}) = 1.55 \pm 0.07$ is found, corresponding to $\psi = -64 \pm 2$ mV. However, the effective polymer radius varies widely. Using published structural radii, the reaction annulus is seen to vary from 1.8 to 11.8 nm (Table 1). Under the assay conditions of 0.0197 *M* 1:1 salt, and ignoring the divalent reactants, the Debye length is 2.2 nm.

While relatively small changes in $\log (k_2/\log k_{2,0})$, and hence in the average potential ψ of the two-phase model, are observed, a much broader range of optimum GAG concentrations is seen. These range from 4.0×10^{-5} *M* for the heparin fractions to 1.6×10^{-3} *M* for the chondroitin sulfates, with intermediate values for the heparan sulfates. These concentrations are reflected in the reaction annuli. They follow the same order as the polymers' sulfate-to-uronic acid ratios, from which corresponding axial charge densities can be calculated using published structural information (Table 2). The mean repeat lengths for the fractionated lung heparan sulfates (HS-I and HS-II) have not been reported. However, if we assume both to have a disaccharide length of 0.93 nm, intermediate between heparin and the chondroitins, as reported for unfractionated heparan sulfate (14), then charge densities intermediate between heparin and the chondroitins are also calculated. The order of ξ values for all polymers follows their order of elution from the poly-L-lysine column, as expected (Fig. 5). The empirical relationship between ξ and $\log [ua]_{max}$ is shown (Fig. 6).

The surface potentials calculated from these structural charge densities by eqs. [8] and [9] (Table 3) are considerably larger

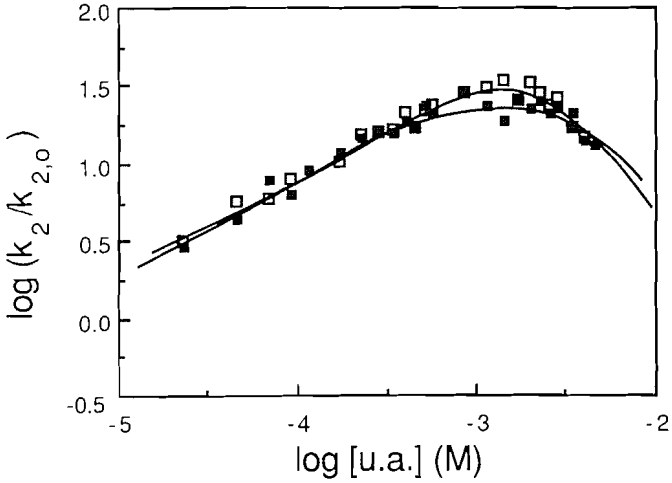

FIG. 2. Rate acceleration of the Hg^{2+}-induced aquation of $Br(NH_3)_5Co^{2+}$ in the presence of ChS(A). Polymer concentration is expressed as the molar concentration of uronic acid, [u.a.]. The reaction is carried out at 25°C in the presence of 1.0×10^{-4} *M* Hg^{2+}, 1.0×10^{-5} *M* Co(III) complex, and 0.010 *M* $HClO_4$, at an ionic strength of 0.020 adjusted with $NaClO_4$. The curves represent second-order polynomial fits to the data from two representative experiments (see Methods).

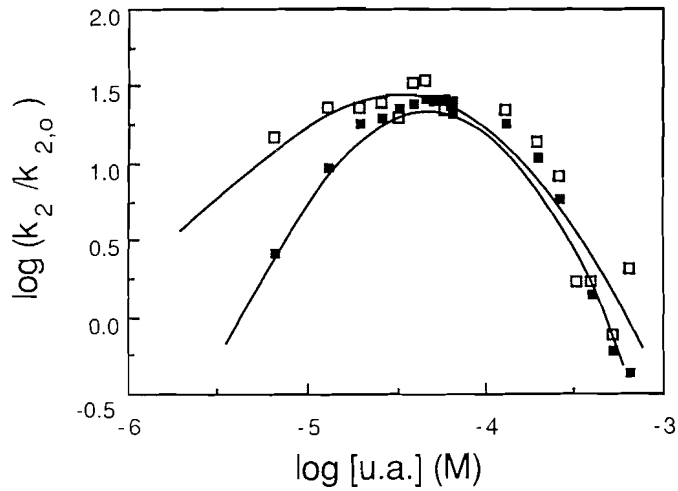

FIG. 3. Rate acceleration of the aquation reaction in the presence of native heparin (□) and the low affinity metal binding fraction heparin-NMB (■). Details are as in the legend to Fig. 2.

Can. J. Chem. Downloaded from www.nrcresearchpress.com by 213.166.140.6 on 09/07/12
For personal use only.

TABLE 1. Rate acceleration and two-phase parameters for the effect of the sulfated GAGs on the cobalt aquation reaction. The effective radii (r), reaction annulus (ρ), and average potential (ψ) are calculated from eqs. [1]–[5]. The partition factor x is as defined in eq. [1]. The mean $(k_2/k_{2,0})_{max}$ and $[ua]_{max}$ values are found from n independent experiments, such as those of Figs. 2 and 3. Values for ChS(B) are from a single experiment, since amounts of this material are limited

GAG	$\log (k_2/k_{2,0})_{max}$	$\log [ua]_{max}$ (M)	n	x	r (nm)	ρ (nm)	ψ (mV)
Heparin	1.7 ±0.3	−4.28±0.06	3	14.2	7.85	7.15	−68
Heparin-NMB	1.55±0.05	−4.49±0.02	2	11.9	11.8	11.1	−64
HS-II	1.54±0.02	−3.40±0.01	2	11.8	3.20	2.50	−63
HS-I	1.5 ±0.1	−3.49±0.03	2	11.2	3.78	3.08	−62
ChS(A)	1.48±0.07	−2.83±0.02	4	11.0	1.76	1.06	−62
ChS(C)	1.55±0.05	−2.93±0.02	4	11.9	1.83	1.13	−64
ChS(B)	1.54	−3.2	1	11.8	2.50	1.80	−63

TABLE 2. Sulfate content and charge densities of the GAGs. Because each disaccharide contains one uronic acid residue, the SO_3^-/uronic acid ratio is the number of SO_3^- groups per disaccharide. Repeat lengths are mean published lengths of the disaccharide residues (14, 15, 23), and the value for our HS-I and HS-II is taken as the value reported for "heparan sulfate" (14). Charge spacings, b, and charge densities, ξ, differ between pH 2 and 5 due to deprotonation of the carboxyl group at the higher pH, which adds one negative charge per disaccharide

GAG	SO_3^-/uronic acid	Repeat length (nm)	pH ≃ 2		pH ≥ 5	
			b (nm)	ξ	b (nm)	ξ
Heparin	1.73±0.36	0.83	0.48	1.49	0.30	2.35
Heparin-NMB	1.73±0.36	0.83	0.48	1.49	0.30	2.35
HS-II	1.69	0.93	0.55	1.3	0.35	2.07
HS-I	1.43	0.93	0.65	1.1	0.38	1.87
ChS(A)	1.28±0.09	0.97	0.76	0.94	0.43	1.68
ChS(C)	1.12±0.34	0.93	0.83	0.86	0.44	1.63
ChS(B)	1.12±0.12	0.96	0.86	0.84	0.45	1.58
Hyaluronic acid	—	1.09	—	—	1.09	0.66

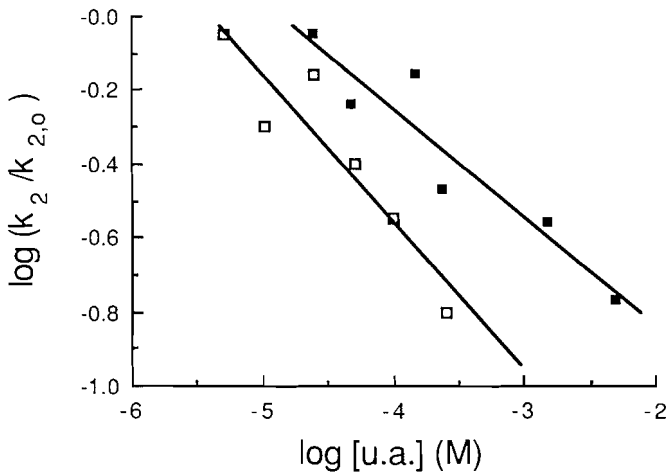

FIG. 4. Inhibition of the aquation reaction in the presence of hyaluronic acid (□) and chondroitin (desulfated ChS(A)) (■). Details are as in the legend to Fig. 2.

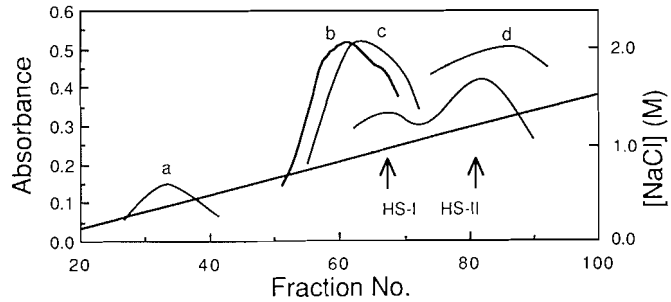

FIG. 5. Elution of glycosaminoglycans from a poly-L-lysine Sepharose CL-4B column with a linear gradient of NaCl in Tris·HCl (see Methods for details). Elution positions of standards of commercial hyaluronic acid (a), ChS(A) (b), ChS(C) (c), and heparin (d) are shown, along with those of the two components of bovine lung heparan sulfate, purified as described under Methods. The latter (HS I and II) are indicated by arrows on the figure; 1–5 mg of each glycosaminoglycan was loaded. Sulfated material was determined at 535 nm using the dimethylmethylene blue assay, as described in ref. 31, while hyaluronic acid was located by measuring its uronic acid content with the carbazole reaction, at 530 nm.

than the average potentials predicted by the two-phase model (Table 1). The potentials in Table 2 are calculated for both protonated and deprotonated carboxyl groups. In chondroitin sulfates, the carboxyl group pK_a at half ionization is about 3.8 (10), so under our experimental conditions (0.01 M $HClO_4$), ξ and ψ_0 values are due to sulfate groups alone.

Kinetic measurements at higher pH are not reported here since the Hg^{2+} ion hydrolyses to the unreactive $HgOH^+$ with a pK of 3.52 (37). We confirmed that at pH 5.5, $k_2 = k_{2,0} \simeq 0$. In the hope of investigating the reaction at higher pH, Cd^{2+} was substituted for Hg^{2+}. This choice was based on the significant stability constant of the $Cd(II)Br^+$ complex (log β_0 = 2 for

TABLE 3. GAG surface potentials. The surface charge density σ is calculated from eq. [8], assuming an average polymer radius of 0.7 nm for all GAGs. The Gouy–Chapman potentials, ψ_0^{G-C}, are calculated from eq. [9], taking into consideration only the 0.0197 *M* monovalent salts in the assay solution. The Grahame potentials, $\psi_0^{Grahame}$, from eq. [17], also include the 1.1×10^{-4} *M* divalent cations. The number of moles of divalent metal necessary to reduce ξ to $\xi_{net} = 0.5$ is calculated as $\frac{1}{2}$(uncompensated charge − net charge), where the charges are per disaccharide and net charge is given by eq. [7] with $\xi = 0.5$ and the repeat lengths of Table 3. All values are for pH ≃ 2, except for those in parentheses, which give data for hyaluronic acid at pH ≥ 5 for comparison

GAG	σ (m^{-2}, $\times 10^{-17}$)	ψ_0^{G-C} (mV)	$\psi_0^{Grahame}$ (mV)	Moles M^{2+}/mole u.a., at $\xi_{net} = 0.5$
Heparin	4.73	−115	−57	1.08
Heparin-NMB	4.73	−115	−57	1.08
HS-II	4.13	−108	−54	1.02
HS-I	3.49	−100	−50	0.89
ChS(A)	2.98	−92	−46	0.80
ChS(C)	2.73	−88	−44	0.74
ChS(B)	2.67	−87	−43	0.73
Hyaluronic acid	(2.10)	(−75)	(−37)	(0.12)

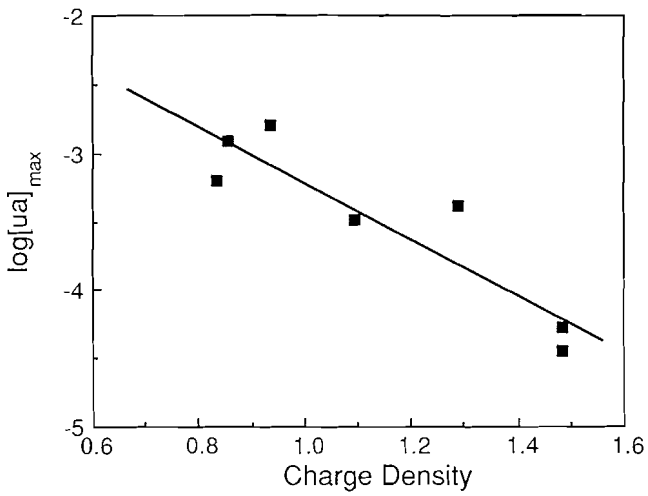

FIG. 6. Observed optimal concentrations of sulfated glycosaminoglycans as a function of linear charge density ξ. Polymer concentrations are expressed as molar concentrations of uronic acid monomers. Data are shown for heparin, heparin-NMB, HS-I, HS-II, ChS(A), ChS(B), and ChS(C). The glycosaminoglycans may be identified by their charge densities at pH ≃ 2, as given in Table 2.

$CdBr^+$ compared to $\log \beta_0 = 9$ for $HgBr^+$ (38)). No significant aquation was observed at either pH 2 or 5.5 with Cd.

No significant quantities of protein or nucleic acid were detected in any of the GAG samples, by absorbance at 280 and 260 nm. However, nucleic acids copurify with GAGs through many isolation steps based on charge properties, and because DNA has a high charge density of $\xi = 4.7$ (39), we were concerned that trace contamination with DNA could still interfere with the kinetic measurements. Indeed when DNA was substituted for GAG in a standard kinetic series (0.01 *M* $HClO_4$, $I = 0.020$), $\log (k_2/k_{2,0})_{max}$ was found to be 1.03 ± 0.02 at an optimum concentration of 1.3×10^{-4} *M* in nucleotide. Because contamination with DNA was therefore a valid concern, portions of solutions of heparin, HS-I, HS-II, and ChS(A) were used for kinetic measurements, then the remainder of the solutions were subjected to treatment with DNase and RNase and used for further kinetic measurements. No changes in the $\log (k_2/k_{2,0})_{max}$ values were found. Log $[ua]_{max}$ was increased by about 0.2 for both heparin and the more highly sulfated of the heparan sulfates, HS-II. It can be concluded that the kinetic parameters reported here are not in error due to the presence of any nucleic acid in the samples, and the increases in log $[ua]_{max}$ following enzyme treatment are probably due to some loss of labile sulfate esters in the more highly sulfated materials.

The ionic strength dependence of the reaction was investigated in the presence of a just suboptimal concentration (5.8×10^{-4} *M*) of ChS(A) (Fig. 7). We have calculated the effect of increasing monovalent salt concentration on the binding of divalent ions to the polymer, using both Poisson–Boltzmann and Manning models. For the former, the surface potential of ChS(A) is calculated from eq. [17] under the appropriate experimental conditions, using the structural parameters of Table 2. Then the concentration of bound divalent metal is found by integrating $C(d)$ (eq. [16]) over the binding shell of thickness d, with $\psi(d)$ given by eq. [15]. For the second approach, θ_2 is found within the binding shell by solving eqs. [18] with the appropriate structural parameters for ChS(A) at pH 2. In both cases, calculations have been performed for a binding shell of 1.06 nm (the reaction annulus calculated for ChS(A) from the two-phase model), or for a variable shell equal to the Debye length at each different concentration. All models show nearly similar dependence of divalent counterion binding on ionic strength (Fig. 7). The rate is assumed to be proportional to the square of the concentration of divalent ions in the polymer binding shell, with no distinction made between divalent species. For comparison with experiment, the proportionality constant is calculated at $I = 0.010$. The observed rate is much less sensitive to ionic strength than is predicted by either model (Fig. 7).

Discussion

A number of authors (15, 40) have considered that the polyelectrolyte properties of the GAGs might somehow account for their biological functions, but clear demonstration of this putative principal has remained elusive. In large part this is due to a lack of understanding of the very functions for which explanations are sought, and the teleological approach of deducing functions from polyelectrolyte properties has been favoured by some (14, 17). This potentially productive approach requires a detailed understanding of polyion–counterion interactions, and some important steps in this direction have been taken.

Can. J. Chem. Downloaded from www.nrcresearchpress.com by 213.166.140.6 on 09/07/12
For personal use only.

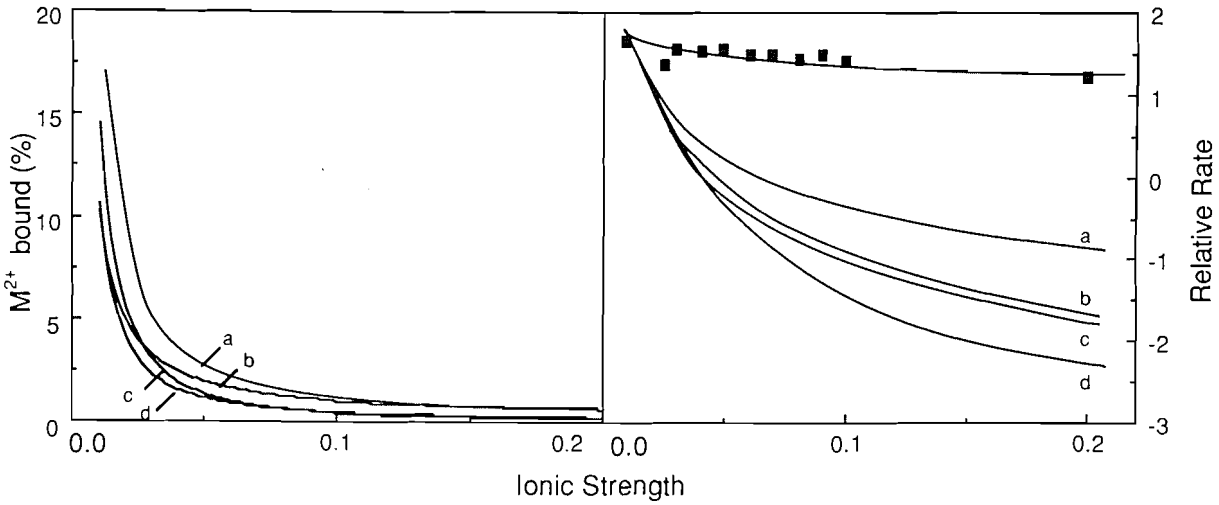

FIG. 7. Salt effects on the binding of divalent metals to ChS(A) (left panel) and on the relative rates of the aquation reaction in the presence of ChS(A) (right panel). Concentrations of Hg^{2+}, $Br(NH_3)_5Co^{2+}$, and $HClO_4$ are as in Fig. 2, and ionic strength is varied by the addition of $NaClO_4$. The concentration of uronic acid is 5.8×10^{-4} *M*. The left panel shows calculated curves for the binding of a divalent counterion, expressed as a percentage of total divalent cations present. Results are shown for the Poisson–Boltzmann model incorporating Grahame's equation, with a binding shell of 1.06 nm (b) or equal to the Debye length (a). Also shown are the predicted salt dependences of eq. [18] with a binding shell of 1.06 nm (d) or equal to the Debye length (c). The right panel shows the corresponding predictions of rate enhancement, based on k_2 proportional to $([M^{2+}]_{bound})^2$, for the same cases: Poisson–Boltzmann model with a binding shell of 1.06 nm (a) or equal to the Debye length (b), or eq. [18] with a binding shell of 1.06 nm (c), or equal to the Debye length (d). Rates are expressed as log $(k_2/k_{2,0})$, with the constant of proportionality calculated from the experimental value at $I = 0.010$. See text for details of all calculations. Experimentally determined values of log $(k_2/k_{2,0})$ are included for comparison (■).

The Manning counterion condensation model has been considered useful in describing self-diffusion of mono- and divalent ions in GAG solutions (15). While this provides a description of net binding, it does not allow distinction to be made between site-specific and territorial binding. The relative importance of these binding modes will depend on the nature of the counterion. Self-diffusion of ^{57}Co and Co^{2+} ion mobilities in ChS solutions allowed estimates of total condensed Co (41). These were compared with the site-bound fraction, deduced from the chemical shift changes in the ^1H nmr spectrum of H_2O, accompanying ion desolvation upon site binding. The net charge reduction was consistent with Manning theory. Site binding accounted for 40% of the total. Ca^{2+} and Sr^{2+} showed total binding similar to Co^{2+} in the ChS system. With the more highly sulfated heparin, Mg^{2+} bound to the extent predicted, while Ca^{2+} bound in excess of the theoretical prediction (24). If, as concluded by the authors, this is due to additional strong binding interactions in the Ca^{2+}-heparin system, then this would represent a departure from Manning behaviour. It would be interesting to distinguish site binding from territorial binding to substantiate this conclusion. Site-specific binding of Cu^{2+} to heparin, involving the carboxyl groups, has been observed in the circular dichroism spectrum (25). We have recently demonstrated that in an intact renal basement membrane, heparan sulfates account for the majority of divalent metal binding (19). Binding to these structures follows the Manning prediction (see ref. 20 for a preliminary report: full details will be published elsewhere). We can conclude at present that the Manning model is a useful starting point for the description of GAG–counterion interactions, that specific binding sites probably occur on all GAGs, and that the latter may be more important in the more highly sulfated materials.

Polyelectrolyte rate acceleration has previously been demonstrated with chondroitin sulfates A and C by Booij (10), who has discussed the phenomenon in terms of the two-phase model of Morawetz and Shafer (13). As explained above, this model assumes that the polyelectrolyte has no effect on the intrinsic rate constant and does not shift the position of equilibrium. At relatively low polymer concentrations, rate acceleration is due solely to an increased local concentration of reactants. At relatively high concentration, inhibition is due to effective separation of reactants (8). Short of detailed information on phase–phase exchange rates and intrinsic rate constants, applicability of the model can best be evaluated by testing its predictions for the relationship between ψ and rate acceleration.

The close similarity of the maximum accelerations for all polymers gives rise to closely similar effective potentials as calculated from the model. These are much closer than expected from structural information, and are more negative than even the surface charge densities predicted by the Grahame equation. Furthermore, even the small differences in the two-phase potentials predict larger differences in the maximum rates, if the assumptions inherent in eq. [12] are granted. For example, with a 6-mV difference between ψ[heparin] and ψ[ChS(A)], eq. [14] predicts a difference in maximum rates of nearly 12 times.

Clearly the assumptions of the two-phase model present an oversimplified explanation of the rate acceleration observed here for the series of GAGs. The similarity of all maximum rates supports a similar effective potential in all polymer solutions. This can only be reconciled with the known structures by assuming a reduction in ψ_0 by ion binding. Since all rates are measured in the same ionic environment, differences in screening by a double layer model cannot account for the different degrees of reduction. Rather, Manning's theory predicts that counterion condensation will reduce all polymer charge densities to $\xi_{net} = \min(\xi, N^{-1})$ (4). With divalent ions present, and all ξ's > 0.5, reduction to $\xi_{net} = 0.5$ is expected. This value predicts a Grahame potential (eq. [17]) of -31 mV

Can. J. Chem. Downloaded from www.nrcresearchpress.com by 213.166.140.6 on 09/07/12
For personal use only.

Can. J. Chem. Downloaded from www.nrcresearchpress.com by 213.166.140.6 on 09/07/12
For personal use only.

in a mixed salt solution of the composition used for the kinetic measurements at $I = 0.020$. The Gouy–Chapman potential (eq. [9]), considering monovalent salts only, is found to be −63 mV for a polyion radius of 0.7 nm. This latter value is only meaningful if we assume the charge-compensated polymer to behave as a discrete entity, which then is further screened, predominantly by the large excess of monovalent salt. Our data show the rate acceleration with ChS(A) to be much less sensitive to increases in monovalent salt than is to be expected from screening effects. This can be explained by eq. [6], since the structural charge density of the polymer is less than unity at the pH of the reaction. Only the divalent reactant counterions are effective in compensating polymer charge under these conditions. The net binding of divalent counterions required to reduce ξ from the structural value to ξ_{net} remains constant across the concentration range of monovalent ions, and this accounts for the relative insensitivity of such polyelectrolyte binding phenomena to salt effects (8).

The Gouy–Chapman potential calculated for $\xi = 0.5$ is in good agreement with the effective potentials predicted by the two-phase model. If the assumptions of the model are invalid, then this is coincidental. However, it may be consistently assumed that the charge-compensatory binding renders the ions unreactive, and the observed rate acceleration is due to the effects of the compensated polymer on the reaction of the residual reactants. Our failure to successfully predict the rate differences from eq. [14] could then be due to failure of eq. [12], which assumes that all reactions take place at the same distances from the polymers. Indeed quite dissimilar effective radii are calculated from the model. This may represent an over-interpretation of the data, since the small differences in effective potentials may not be significant.

More telling against the two-phase model are the predicted effective radii. While those calculated for the chondroitins seem reasonable, those for the more highly sulfated GAGs do not. It is unlikely that effective annuli several times thicker than the Debye length can have any meaning, since the potentials at such distances are very low. (At low surface potentials, ψ drops to $1/e$ of ψ_0 at the Debye length. At the ψ_0 values encountered here, the decrease of ψ with d is only slightly faster.) We are left with the conclusion that the model is inadequate for description of the results. In retrospect, this is not surprising, since some of the reactant ions are known to be bound to the GAGs, and to reduce their surface potentials. While the extent of site-specific binding of Hg^{2+} and the Co complex are not known, it is likely to be significant (*vide supra*). Such binding should invalidate the two main assumptions of the model, namely unaltered intrinsic rate constants and rapid exchange with the bulk phase.

At present, therefore, no theoretical description of the observed rate acceleration exists. A more complete description would consider the effects of potential on reaction rate. Detailed information on the speciation of all ions, as well as consideration of the discrete molecular nature of the solvent, would be required. The situation is further complicated by the fact that the observed rates are a composite of competing processes. Acceleration may take place due to local concentration effects and (or) changes in the free energies of the reactants in the polymer domain. Inhibition may result from binding of the reactants in unreactive form, and by separation of reactants by distinct polymers. The former cause of inhibition is likely more important for heparin, since binding of only about 30% of Hg^{2+} is necessary to reduce ξ to 0.5 at the optimum heparin concentration. However, all Hg^{2+} present would be necessary to so compensate ChS(C) at a uronic acid concentration of 4.3×10^{-4} *M*. This is only about a third of the optimum concentration of ChS(C), and with the chondroitin sulfates ion separation must be the more important cause of inhibition. The numbers of divalent ions which must bind, per disaccharide, to reduce the charge density of each GAG to 0.5, are included in Table 3.

We conclude that counterion condensation reduces all polymer charge densities to similar values and, under conditions where the volume of the polymer domain is not limiting, all GAGs achieve comparable rate accelerations as a consequence. However, at even higher polymer concentrations, two factors compete to inhibit the reaction. Those GAGs with higher charge densities may more effectively bind the reactant ions due to a greater density of potential binding sites. Those with lower charge densities eventually separate the reactive species. When these interpretations are borne in mind, the observed optimum concentrations may be useful in determining the relative sulfate-derived charge densities of unknown GAGs. Finally, under biological conditions, GAG concentrations are sufficiently low that bulk phase counterions may experience similar potentials from different classes of GAGs, if certain divalent ions are present to reduce charge densities by tight binding processes. This latter suggestion may have interesting consequences in vivo.

Conclusions

1. The GAGs are naturally occurring polyelectrolytes capable of effecting rate acceleration of ionic reactions in solution.
2. The two-phase model of polyelectrolyte catalysis is inadequate to describe the rate acceleration, probably due to significant site-specific binding to the GAGs.
3. All sulfated GAGs give similar rate accelerations, consistent with the description that counterion condensation reduces the charge density ξ of each to the same critical value, thereby producing similar surface potentials ψ_0.
4. Further investigation of these systems could yield insight into both the phenomenon of polyelectrolyte "catalysis" and the biological functions of GAGs.

Acknowledgement

This work was supported by the Medical Research Council of Canada.

1. M. Fixman. J. Chem. Phys. **70**, 4995 (1979).
2. J. Granot and D. R. Kearns. Biopolymers, **21**, 219 (1982).
3. G. S. Manning. Q. Rev. Biophys. **11**, 179 (1978).
4. G. S. Manning. Acc. Chem. Res. **12**, 443 (1979).
5. H. Morawetz and G. Gordimer. J. Am. Chem. Soc. **92**, 7532 (1970).
6. S. Brückner, V. Crescenzi, and F. Quadrifoglio. J. Chem. Soc. (A), 1168 (1970).
7. N. Ise. Nature, **225**, 66 (1970).
8. E. Baumgartner and R. Fernandez-Prini. *In* Polyelectrolytes. *Edited by* K. C. Frisch, D. Klempner, and A. V. Patsis. Technomic, Westport, CT. 1976. pp. 1–33.
9. N. Ise. *In* Polyelectrolytes and their applications. *Edited by* A. Rembaum and E. Sélégny. D. Reidel, Dordrecht, Holland. 1975. pp. 71–96.
10. M. Booij. Inorg. Chim. Acta, **55**, 109 (1981).
11. A. R. Olson and T. R. Simonson. J. Chem. Phys. **17**, 1167 (1949).
12. N. Ise and F. Matsui. J. Am. Chem. Soc. **90**, 4242 (1968).
13. H. Morawetz and J. A. Shafer. J. Phys. Chem. **67**, 1293 (1963).
14. P. Band and A. Lukton. Biopolymers, **23**, 2223 (1984).

15. B. N. PRESTON, T. C. LAURENT, and W. D. COMPER. *In* Molecular biophysics of the extracellular matrix. *Edited by* S. Arnott, D. A. Rees, and E. R. Morris. Humana Press, Clifton, NJ. 1984. pp. 119–162.
16. J. A. BUCKWALTER. Clin. Orthop. Relat. Res. **172**, 207 (1983).
17. L. B. JAQUES. *In* Polyelectrolytes and their applications. *Edited by* A. Rembaum and E. Sélégny. D. Reidel, Dodrecht, Holland. 1975. pp. 145–161.
18. Y. S. KANWAR and M. G. FARQUHAR. Proc. Natl. Acad. Sci. U.S.A. **76**, 4493 (1979).
19. D. M. TEMPLETON. Toxicology, **43**, 1 (1987).
20. D. M. TEMPLETON. *In* Bio- and toxicokinetics of metals. *Edited by* J. S. Savory and Y. Kodama. Ellis Horwood, Chichester, U.K. In press.
21. S. BALT, M. W. G. DEBOLSTER, and G. VISSER-LUIRINK. Inorg. Chim. Acta, **78**, 121 (1983).
22. S. BALT, M. W. G. DEBOLSTER, and G. VISSER-LUIRINK. Carbohydr. Res. **121**, 1 (1983).
23. K. TANAKA. J. Biochem. **83**, 647 (1978).
24. J. MATTAI and J. C. T. KWAK. Biochim. Biophys. Acta, **677**, 303 (1981).
25. D. C. MUKHERJEE, J. W. PARK, and B. CHAKRABARTI. Arch. Biochem. Biophys. **191**, 393 (1978).
26. M. D. YOUNG, G. O. PHILLIPS, and E. A. BALAZS. Biochim. Biophys. Acta, **141**, 374 (1967).
27. R. A. G. FRIEDMAN and G. S. MANNING. Biopolymers, **23**, 2671 (1984).
28. S. MCLAUGHLIN. Curr. Top. Membr. Transp. **9**, 71 (1977).
29. D. C. GRAHAME. Chem. Rev. **41**, 441 (1947).
30. H. DIEHL, H. CLARK, and H. H. WILLARD. Inorg. Synth. **1**, 186 (1939).
31. D. M. TEMPLETON. Connect. Tissue Res. In press.
32. P. CUATRECASAS, M. WILCHEK, and C. B. ANFINSEN. Proc. Natl. Acad. Sci. U.S.A. **61**, 636 (1968).
33. S. SUZUKI and A. KOIDE. Anal. Biochem. **137**, 101 (1984).
34. T. BITTER and H. M. MUIR. Anal. Biochem. **4**, 330 (1962).
35. T. T. TERHO and K. HARTIALA. Anal. Biochem. **41**, 471 (1971).
36. T. G. KANTOR and M. SCHUBERT. J. Am. Chem. Soc. **79**, 152 (1957).
37. C. F. BAES and R. E. MESMER. The hydrolysis of cations. Robert E. Krieger, Malabar, FL. 1986.
38. J. KRAGTEN. Atlas of metal–ligand equilibria in aqueous solution. Ellis Horwood, Chichester, U.K. 1978.
39. D. VASILESCU, H. GRASSI, and M. A. RIX-MONTEL. *In* Polyelectrolytes and their applications. *Edited by* A. Rembaum and E. Sélégny. D. Reidel, Dordrecht, Holland. 1975. pp. 197–216.
40. W. D. COMPER and T. C. LAURENT. Physiol. Rev. **58**, 255 (1978).
41. P. TIVANT, P. TURQ, M. CHEMLA, H. MAGDELENAT, P. SPEGT and G. WEILL. Biopolymers, **18**, 1849 (1979).

Appendix

Abbreviations

ChS(A): chondroitin sulfate A (chondroitin-4-sulfate)
ChS(B): chondroitin sulfate B (dermatan sulfate)
ChS(C): chondroitin sulfate C (chondroitin-6-sulfate)
GAG: glycosaminoglycan
HS: heparan sulfate
MCAC: metal chelate affinity chromatography
Heparin-NMB: non-metal-binding heparin (from MCAC column)

Symbols

b	linear charge spacing
C_∞	bulk counterion concentration, at infinite distance from polymer
d	radial distance from polymer surface
f	ratio of uncompensated polymer charge to net structural charge
(k/k_0)	ratio of rate constant in the presence of a polyelectrolyte to that in its absence
k_2, $k_{2,0}$	pseudo-second-order rate constants, in presence and absence of a polyelectrolyte, respectively
k	Boltzmann's constant
L	length of repeating unit of a polymer; disaccharide length for a GAG
N	Avogadro's number
q	charge on the proton, in coulombs
r	effective radius of a polymer in the two-phase model
R	radius of a polymer treated as a cylinder
T	absolute temperature
x	phase partition in the two-phase model, given by $x = e^{-q\psi/kT}$
z	electrolyte valence
Z	formal charge on a counterion in the Manning model
ϵ_r	relative dielectric constant of a solvent
ϵ_0	permittivity of free space
ξ	dimensionless linear charge density
θ_i	bound mole ratio of counterions of valence i per equivalent polyelectrolyte charge
$1/\kappa$	Debye length
ρ	thickness of reaction annulus about a polyelectrolyte
σ	surface charge density in equivalents per unit area
ψ	electrostatic potential
ψ_0	surface potential of a polyelectrolyte
$\pounds/\epsilon_r T$	Landau length

Can. J. Chem. Downloaded from www.nrcresearchpress.com by 213.166.140.6 on 09/07/12
For personal use only.

Substituent effects in cooxidation: Cr(VI) – oxalic acid – sulfoxides systems

C. Srinivasan, P. Pandarakutty Jegatheesan, S. Rajagopal, and N. Arumugam
School of Chemistry, Madurai Kamaraj University, Madurai – 625 021, India

Received January 1, 1987

C. Srinivasan, P. Pandarakutty Jegatheesan, S. Rajagopal, and N. Arumugam. Can. J. Chem. **65**, 2421 (1987).

The kinetics of cooxidation of several substituted phenyl methyl sulfoxides and oxalic acid with Cr(VI) have been carried out in the presence of perchloric acid. The reaction is first order each in sulfoxide, oxalic acid, Cr(VI), and H^+. The products of oxidation are sulfones and carbon dioxide. Electron-releasing groups in the phenyl ring accelerate the rate while electron-withdrawing groups retard it. The Hammett correlation yields a reaction constant of -0.927 ± 0.08 ($r = 0.994$) at 313 K. Addition of aluminium nitrate prevents the occurrence of cooxidation. Based on the kinetic information a suitable mechanism has been proposed. Diaryl sulfoxides behave in an analogous manner in the cooxidation.

C. Srinivasan, P. Pandarakutty Jegatheesan, S. Rajagopal et N. Arumugam. Can. J. Chem. **65**, 2421 (1987).

Opérant en présence d'acide perchlorique, on a mesuré les cinétiques de cooxydation de l'acide oxalique et de plusieurs phényl méthyl sulfoxydes substitués par le Cr(VI). La réaction est du premier ordre en sulfoxyde, en acide oxalique, en Cr(VI) et en H^+. Les produits d'oxydation sont les sulfones et le dioxyde de carbone. La présence sur le noyau phényle de groupements électrodonneurs provoque une augmentation de la vitesse de la réaction alors que les groupements électroaffinitaires la diminue. À 313 K, la corrélation de Hammett conduit à une constante de réaction de $-0{,}927 \pm 0{,}08$ ($r = 0{,}994$). L'addition de nitrate d'aluminium empêche la réaction de se produire. Sur la base des informations cinétiques, on propose un mécanisme approprié. Les sulfoxydes de diaryles se comportent d'une façon similaire lors de cooxydations.

[Traduit par la revue]

Can. J. Chem. Downloaded from www.nrcresearchpress.com by 213.166.140.6 on 09/07/12
For personal use only.

Introduction

A dramatic rate acceleration was observed by Hasan and Roček (1) in the Cr(VI) oxidation of a mixture of isopropanol and oxalic acid compared to the Cr(VI) oxidations of either of the above substrates. They attributed this rate acceleration to the phenomenon called cooxidation wherein both substrates undergo oxidation simultaneously. On the other hand, oxalic acid acts as a catalyst in the Cr(VI) oxidations of iodide (2) and ferroin (3). Recently the mechanisms of oxidation of alkyl aryl sulfoxides (4) and diaryl sulfoxides (5) by Cr(VI) have been reported and therefore the study of the influence of oxalic acid on the rates of Cr(VI) oxidation of sulfoxides will be of particular interest. In this paper we wish to report the salient features of the Cr(VI) oxidation of sulfoxides in the presence of oxalic acid.

Experimental

Materials

Alkyl aryl sulfoxides were prepared by standard procedures (6) by the oxidation of the corresponding sulfides. The diaryl sulfoxides were obtained by the Friedel–Crafts reaction of substituted benzenes with thionyl chloride (7). 4,4′-Dinitrodiphenyl sulfoxide was prepared by the oxidation of the corresponding sulfide with hydrogen peroxide (8). These sulfoxides were purified by vacuum distillation/recrystallization from suitable solvents. The physical constants of the sulfoxides were found to agree with literature values. The tlc analysis of each sulfoxide proved the presence of a single entity, and no impurity peak appears in the ^1H nmr spectra.

Potassium dichromate (BDH, AR), oxalic acid (BDH, AR), 60% perchloric acid (E. Merck, GR), and sodium perchlorate (E. Merck, GR) were employed as such. Acetic acid was purified by refluxing with chromium trioxide (9).

Kinetics

Kinetic studies were carried out in 50% acetic acid – 50% water (v/v) and in 80% acetic acid – 20% water (v/v) mixtures in the case of alkyl aryl sulfoxides and diaryl sulfoxides respectively. The rate studies were performed under pseudo first-order conditions at constant ionic strength maintained by the addition of sodium perchlorate. Freshly prepared solutions of potassium dichromate and oxalic acid were used. The unreacted Cr(VI) was estimated iodometrically (10). Pseudo first-order rate constants were evaluated from the slopes of the plots of log $(a - x)$ vs. time by the method of least squares. Reactions were generally followed to >70% completion; reproducible results giving good first-order plots (correlation coefficient, $r > 0.995$) were obtained for duplicate runs in each sulfoxide. The second-order rate constants were obtained from $k_2 = k_1/[\text{sulfoxide}]$. The precision of the k values is given in terms of 95% confidence limits of the Student t test.

Product studies

A reaction mixture (under kinetic conditions) with methyl phenyl sulfoxide (MPSO) and oxalic acid (OxH_2) was allowed to stand overnight, neutralized with sodium carbonate, and extracted with ether. The solvent was removed after drying (anhydrous Na_2SO_4) and a solid was obtained. Its mp (88°C) corresponds to the mp of methyl phenyl sulfone (6). The ir spectrum of the product was superimposable on that of an authentic sample of methyl phenyl sulfone. The product, therefore, was methyl phenyl sulfone.

The liberation of carbon dioxide during the Cr(VI) oxidation of MPSO and OxH_2 was detected as described by Vogel (11). The generation of carbon dioxide is possible only if OxH_2 is oxidized and therefore the reaction is only a cooxidation process and not a catalytic one.

Results and discussion

Detailed kinetic studies on individual Cr(VI) oxidations of alkyl aryl sulfoxides (4), diaryl sulfoxides (5), and OxH_2 (12) have already been reported. For comparison, the individual oxidations of sulfoxides and oxalic acid were carried out under conditions similar to those employed in the cooxidation. It was found that with many of the substituted sulfoxides the reaction was too slow to measure. However, at 50°C the pseudo first-order rate constants for the individual oxidations of MPSO and OxH_2 by Cr(VI) were found to be 2.17×10^{-6} s^{-1} and 1.61×10^{-5} s^{-1} respectively. When a mixture of the two substrates was taken, the reaction proceeded at an impressively faster rate, the rate constant being 2.51×10^{-4} s^{-1}. These data indicate that, for the ternary system, the cooxidation is favoured over the individual oxidation as observed by Hasan and Roček (1) with other systems.

Table 1 records the dependence of the reaction rate on the concentrations of MPSO, Cr(VI), and OxH_2. That the cooxidation is first order each in Cr(VI), MPSO, and OxH_2 has been

Can. J. Chem. Downloaded from www.nrcresearchpress.com by 213.166.140.6 on 09/07/12
For personal use only.

TABLE 1. Effect of varying the concentrations of MPSO, DPSO, Cr(VI), and OxH_2 on the rate of reaction at 30°C

10^2 [Sulfoxide] (M)	10^3 [Cr(VI)] (M)	10^3 [OxH_2] (M)	$10^4 k_1$ (s^{-1})	$10^2 k_2$ ($M^{-1} s^{-1}$)	k_3 ($M^{-2} s^{-1}$)
		MPSO[a]			
1.0	1.0	5.0	1.14±0.08	1.14±0.08	
1.5	1.0	5.0	1.68±0.06	1.12±0.04	
2.0	1.0	5.0	2.27±0.16	1.13±0.08	
5.0	1.0	5.0	5.56±0.17	1.11±0.03	
6.0	1.0	5.0	6.77±0.32	1.13±0.05	
10	1.0	5.0	10.5 ±0.19	1.05±0.02	
2.0	0.50	5.0	2.34±0.03	1.17±0.02	
2.0	1.5	5.0	2.32±0.06	1.16±0.03	
2.0	2.0	5.0	2.34±0.03	1.17±0.02	
1.0	1.0	7.5	1.93±0.11		2.57±0.15
1.0	1.0	10	2.43±0.19		2.43±0.19
1.0	1.0	15	3.79±0.15		2.53±0.10
1.0	1.0	20	5.35±0.19		2.67±0.10
		DPSO[b]			
1.0	1.0	5.0	3.82±0.21	3.82±0.21	
1.5	1.0	5.0	6.13±0.45	4.09±0.30	
2.0	1.0	5.0	7.79±0.59	3.89±0.30	
3.5	1.0	5.0	13.6 ±0.39	3.88±0.11	
5.0	1.0	5.0	19.9 ±0.64	3.98±0.13	
2.0	0.50	5.0	7.82±0.55	3.91±0.28	
2.0	1.5	5.0	7.86±0.30	3.93±0.15	
2.0	2.0	5.0	7.87±0.52	3.93±0.26	
1.0	1.0	8.0	6.35±0.21		7.94±0.26
1.0	1.0	9.0	7.04±0.32		7.82±0.36
1.0	1.0	10	7.97±0.52		7.97±0.52
1.0	1.0	20	15.5 ±0.26		7.75±0.13

[a] $[HClO_4]$ = 0.10 M; I (ionic strength) = 0.125 M; solvent 50% acetic acid – 50% water (v/v).
[b] $[HClO_4]$ = 0.10 M; I = 0.125 M; solvent 80% acetic acid – 20% water (v/v).

TABLE 2. Effect of variations of $[HClO_4]$, ionic strength (I), and solvent composition on the rate of reaction at 40°C

$[HClO_4]$ (M)	$10^4 k_1$ (s^{-1})[a]	I (M)	$10^4 k_1$ (s^{-1})[b]	AcOH–H_2O (%)	$10^4 k_1$ (s^{-1})[c]
			MPSO		
0.100	1.76±0.10	0.125	1.76±0.10	50–50	1.76±0.10
0.150	2.27±0.12	0.250	1.70±0.13	60–40	3.39±0.29
0.200	2.95±0.13	0.375	1.70±0.13	65–35	4.93±0.27
0.250	3.85±0.14	0.500	1.77±0.15	70–30	8.47±0.63
0.300	4.94±0.07	0.625	1.79±0.14		
			DPSO		
0.075	4.19±0.14	0.125	6.18±0.24	50–50	0.721±0.24
0.100	6.18±0.24	0.303	5.94±0.23	65–35	1.64±0.09
0.125	6.80±0.39	0.353	5.83±0.21	75–25	4.92±0.11
0.150	8.83±0.28	0.403	6.01±0.27	80–20	6.18±0.24

[sulfoxide] = 0.01 M; $[Cr(VI)]$ = 0.001 M; $[OxH_2]$ = 0.005 M.
[a] I = 0.35 M; solvent 50% acetic acid – 50% water (v/v) (MPSO) and 80% acetic acid – 20% water (v/v) (DPSO).
[b] $[HClO_4]$ = 0.10 M; solvent 50% acetic acid – 50% water (v/v) (MPSO) and 80% acetic acid – 20% water (v/v) (DPSO).
[c] $[HClO_4]$ = 0.10 M; I = 0.125 M.

TABLE 3. Effect of aluminium nitrate on the rate of oxidation at 50°C

$[Al(NO_3)_3]$ (M)	0.00	0.000	0.100
$[OxH_2]$ (M)	0.00	0.005	0.005
$10^6 k_1$ (s^{-1})	2.17 ± 0.01	251 ± 15	2.45 ± 0.02

[MPSO] = 0.01 M; [Cr(VI)] = 0.001 M; $[HClO_4]$ = 0.10 M; solvent 50% acetic acid – 50% water (v/v).

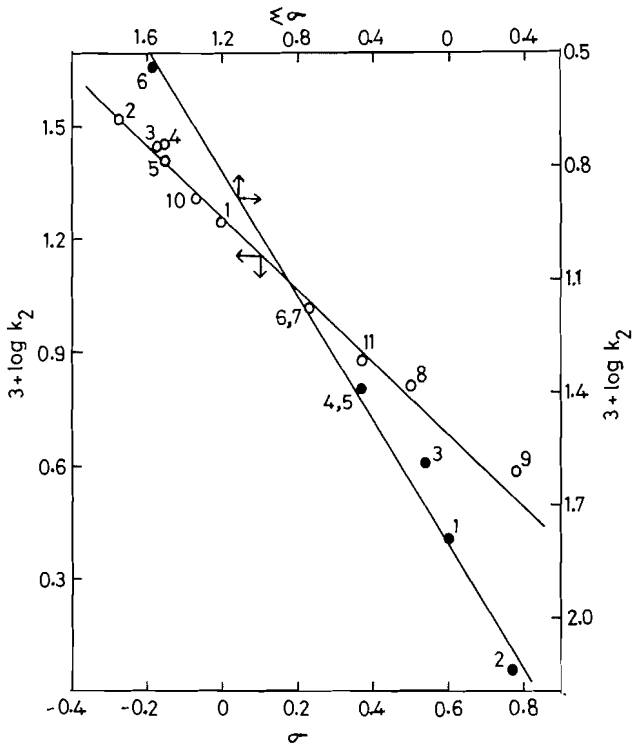

FIG. 1. Hammett plots at 40°C. ○: Substituted phenyl methyl sulfoxides (1. *p*-H, 2. *p*-OMe, 3. *p*-Me, 4. *p*-Et, 5. *p*-Pr^i, 6. *p*-Cl, 7. *p*-Br, 8. *p*-Ac, 9. *p*-NO_2, 10. *m*-Me, 11. *m*-Cl). ●: Substituted diphenyl sulfoxides (4-X-$C_6H_4)_2$ SO; X = H(1), Me(2), F(3), Cl(4), Br(5), NO_2(6).

established from the following observations: (*i*) constant k_1 values at different [Cr(VI)], constant k_2 values at various [MPSO], and constant k_3 values at different $[OxH_2]$; (*ii*) the linear plot of log k_1 against log [MPSO] with a slope of 0.976 ± 0.29 (r = 0.999, s = 0.009); and (*iii*) a slope of 1.09 ± 0.12 (r = 0.998, s = 0.018) in the double logarithmic plot of k_1 versus $[OxH_2]$. The oxidation rate increases markedly with acidity (cf. Table 2). A plot of log k_2 versus log $[H^+]$ passes through the origin with a slope of 1.02 ± 0.07 (r = 0.999, s = 0.007) showing a neat first-order dependence on $[H^+]$. The data in Table 2 show that a change in ionic strength (I) of the medium has no effect on rate and also the rate increases with decrease in polarity of the solvent.

The pseudo first-order rate constants for the cooxidation of MPSO in the absence of acrylamide and in the presence of 0.01 M and 0.05 M acrylamide are 1.76, 1.77, and 1.78 × 10^{-4} s^{-1} respectively. Thus acrylamide has no perceptible effect on the rate. This observation cannot be taken as evidence for the absence of free radicals. At high acidities it is rather not possible to detect free radicals as their own oxidation is catalyzed by acid (12). Similar results are obtained in the presence of free radical scavengers in the cooxidation of benzhydrol and oxalic acid with Cr(VI) (13).

It has been established that aluminium ions inhibit the Cr(VI) oxidation of OxH_2 by forming a complex with the latter (14). In the present system, also, when the reaction is performed in presence of aluminium nitrate the rate falls almost to the range obtained in the absence of OxH_2 (Table 3). This observation leads to the inference that complex formation between the oxidant and OxH_2 is indispensable for cooxidation to occur.

The effect of substituents on the rate of cooxidation was studied using several *meta*- and *para*-substituted phenyl methyl sulfoxides. Electron-releasing substituents accelerate the rate while electron-withdrawing groups retard it. A good Hammett correlation was obtained with a negative ρ value of −0.927 ± 0.08 (r = 0.994, s = 0.03 at 40°C) (see Fig. 1).

Mechanism

Chromic acid forms a cyclic 1:1 neutral complex, C_1, with OxH_2 (1). We propose that the complex C_1 reacts with a molecule of the sulfoxide producing another complex (C_2) in the rate-determining step. The complex C_2 on solvolysis yields the products sulfone, carbon dioxide, a $\cdot CO_2^-$ radical, and a Cr(III) species. The free radical can then undergo further oxidation with either free or complexed Cr(VI) producing carbon dioxide and Cr(V) (1) (shown in Scheme 1). This mechanism involves a two-electron oxidation of the sulfoxide part and a simultaneous one-electron oxidation of the OxH_2 part in the complex C_2. Because of the partial positive charge developed in the sulfur atom in C_2, the formation of C_2 will be favoured by electron-releasing substituents, leading to a negative ρ value.

The rate law could be written as

$$-\frac{d[Cr(VI)]}{dt} = kK[ArSOR][OxH_2][H^+][Cr(VI)]$$

$$k_{obs} = kK[ArSOR][OxH_2][H^+]$$

Kinetic studies with diaryl sulfoxides

The kinetic behavior of diaryl sulfoxides is similar to that of

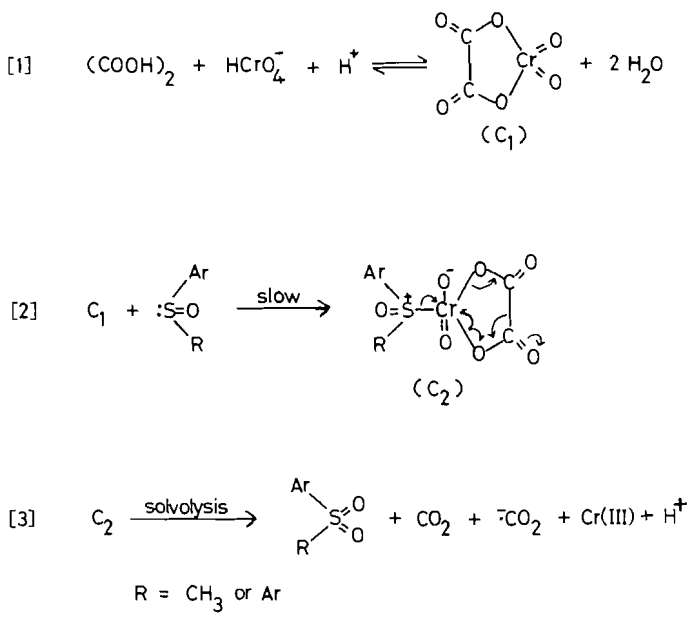

SCHEME 1

Can. J. Chem. Downloaded from www.nrcresearchpress.com by 213.166.140.6 on 09/07/12
For personal use only.

aryl methyl sulfoxides. The data in Table 1 clearly point out that the order with respect to diphenyl sulfoxide (DPSO), Cr(VI), and OxH_2 is unity in each case in the cooxidation of DPSO. The data in Table 2 also reveal that the effects of variations of $[H^+]$ and solvent composition on the rate of cooxidation of DPSO are analogous to those noticed for MPSO. These facts lead to the conclusion that the two series of sulfoxides follow the same reaction path.

In 4,4′-disubstituted diphenyl sulfoxides, electron-releasing substituents increase the rate while electron-withdrawing groups exert a retarding effect. An excellent Hammett correlation (Fig. 1) is obtained with a negative ρ value ($\rho = -0.820 \pm 0.11$, $r = 0.994$, $s = 0.06$ at 40°C).

Acknowledgement

P.P.J. thanks the UGC, New Delhi for the award of Junior Research Fellowship.

1. F. Hasan and J. Roček. J. Am. Chem. Soc. **94**, 3181 (1972).
2. G. F. Vandegrift and J. Roček. J. Am. Chem. Soc. **98**, 1371 (1976).
3. R. E. Hintze and J. Roček. J. Am. Chem. Soc. **99**, 132 (1977).
4. V. Baliah and P. V. V. Satyanarayana. Indian J. Chem. **16A**, 966 (1978).
5. C. Srinivasan, R. Venkatasamy, and S. Rajagopal. Indian J. Chem. **20A**, 505 (1981).
6. C. C. Price and J. J. Hydock. J. Am. Chem. Soc. **74**, 1943 (1952).
7. R. L. Shriner, H. C. Struck, and H. J. Jorison. J. Am. Chem. Soc. **52**, 2060 (1930).
8. H. J. Shine, M. Rahman, H. Seeger, and G. S. Wu. J. Org. Chem. **32**, 1901 (1967).
9. K. J. P. Orton and A. E. Bradfield. J. Chem. Soc. 986 (1927).
10. K. B. Wiberg and J. Mill. J. Am. Chem. Soc. **80**, 3022 (1958).
11. A. I. Vogel. A text book of micro and semi micro inorganic analysis. First Indian Edition. Orient Longmans, London. 1967. p. 326.
12. F. Hasan and J. Roček. J. Am. Chem. Soc. **94**, 9073 (1972).
13. K. Nagarajan, S. Sundaram, and N. Venkatasubramanian. Indian J. Chem. **18A**, 335 (1979).
14. S. Chandra, S. N. Shukla, and A. C. Chatterjee. Z. Phys. Chem. (Leipzig), **237**, 137 (1968).

Can. J. Chem. Downloaded from www.nrcresearchpress.com by 213.166.140.6 on 09/07/12
For personal use only.

Charge transfer complexes of diquat and paraquat with halide anions

S. G. BERTOLOTTI, J. J. COSA, H. E. GSPONER, AND C. M. PREVITALI

Departamento de Química y Física, Facultad de Ciencias Exactas Fisicoquímicas y Naturales, Universidad Nacional de Río Cuarto, 5800 Río Cuarto, Argentina

Received January 26, 1987

S. G. BERTOLOTTI, J. J. COSA, H. E. GSPONER, and C. M. PREVITALI. Can. J. Chem. **65**, 2425 (1987).

The association of methylviologen, 1,1′-dimethyl-4,4′-bipyridynium (PQ^{2+}), with halide and pseudo-halide ions was studied in water at 25°C by ultraviolet spectrophotometry. A charge transfer band could be observed in the region around 300 nm. From difference absorption measurements the first association constant (K_1) was obtained as 1.7 (Cl^-), 3.3 (Br^-), 3.9 (I^-), 0.7 (CN^-), and 2.0 (SCN^-) M^{-1}. Similar results were obtained for the dication, 6,7-dihydrodipyrido[1,2-*a*:2′,1′-*c*]pyrazinium (DQ^{2+}), with first association constants 3.3 (Cl^-), 4.1 (Br^-) and 4.6 (I^-) M^{-1}. First and second (K_2) association constants were also determined by a potentiometric technique using ion selective electrodes: $K_1 = 2.0\ M^{-1}$; $K_2 = 0.4\ M^{-1}$ for the system PQ^{2+}–Cl^- and $K_1 = 5.3\ M^{-1}$; $K_2 = 0.3\ M^{-1}$ for DQ^{2+}–Br^-.

S. G. BERTOLOTTI, J. J. COSA, H. E. GSPONER et C. M. PREVITALI. Can. J. Chem. **65**, 2425 (1987).

Faisant appel à la spectroscopie ultraviolette et opérant à 25°C, dans des solutions aqueuses, on a étudié les réactions d'association du méthylviologène, diméthyl-1,1′ bipyridinium-4,4′ (PQ^{2+}), avec divers ions halogénures et pseudo halogénures. On a observé une bande de transfert de charge dans la région de 300 nm. En se basant sur des mesures de différence d'absorption, on a obtenu les premières constantes d'association suivante (K_1) : 1,7 (Cl^-), 3,3 (Br^-), 3,9 (I^-), 0,7 (CN^-) et 2,0 (SCN^-) M^{-1}. On a obtenu des résultats similaires avec le dication, dihydro-6,7 dipyrido[1,2-*a*:2′,1′-*c*]pyrazinium (DQ^{2+}), alors que les premières constantes de vitesses sont : 3,3 (Cl^-), 4,1 (Br^-) et 4,6 (I^-) M^{-1}. Faisant appel à une technique potentiométrique utilisant des électrodes sélectives pour les ions, on a aussi déterminé les première et deuxième (K_2) constantes d'association : $K_1 = 2{,}0\ M^{-1}$ et $K_2 = 0{,}4\ M^{-1}$ pour le système PQ^{2+}–Cl^- et $K_1 = 5{,}3\ M^{-1}$ et $K_2 = 0{,}3\ M^{-1}$ pour DQ^{2+}–Br^-.

[Traduit par la revue]

Introduction

Paraquat, 1,1′-dimethyl-4,4′-bipyridinium dichloride ($PQCl_2$), and diquat, 6,7-dihydrodipyrido[1,2-*a*:2′,1′-*c*]pyrazinium dibromide ($DQBr_2$), are widely used as herbicides. They are inhibitors of electron transfer in both the cytochrome chain of mitochondria and the electron transfer chain of chloroplasts. Their use as electron relays in photochemical systems is of wide interest for solar energy conversion. It is known that they are able to form charge transfer complexes in the ground state with amines, phenols, hydroquinones, and sulfides (1), carboxylates (2), and transition metal complexes (3). However, besides this wide interest and usage, little is known about the interaction of the dications with halide anions in aqueous solutions.

Evidence of charge transfer complex formation of PQ^{2+} and DQ^{2+} with halide ions in the solid phase was given using ir spectroscopy (4). Also, the thermodynamic properties of aqueous solutions of paraquat were studied and the results suggested that, at high concentrations, this electrolyte behaves more like a 1:1 electrolyte than a 2:1 electrolyte (5).

The activity coefficients of paraquat and its mixtures with aqueous sodium chloride in the concentration range 0.1–4 molal were derived from isopiestic vapor pressure measurements (6). These results suggested that aqueous paraquat is similar in its electrochemical behavior to aqueous sulfuric acid solutions.

Conductivity measurements have been reported that indicate that the structurally similar compound, heptylviologen bromide, is completely dissociated in aqueous solution (7). However, reports based on absorption measurements and laser flash photolysis evidence (8), as well as conductance experiments (9), proposed that methylviologen is strongly associated with a chloride ion in aqueous solutions.

In view of the contradictory results given in the literature we decided to undertake a study of PQ^{2+} and DQ^{2+}–halide interaction, using ion selective electrodes and spectrophotometric techniques. In this report we present results for the association of PQ^{2+} and DQ^{2+} with chloride and bromide ions respectively. Our uv absorption results are coincident with those of Ebbesen and Ferraudi (8), but the potentiometric determinations afford a new interpretation, in terms of a weak two-step association.

Experimental

Paraquat was obtained by purification of the commercial herbicide Gramoxone through repeated recrystallization from water, ethanol, and ethanol–acetone mixtures. Diquat was prepared by refluxing a mixture of 2,2′-bipyridine and 1,2-dibromoethane (10). The yellow precipitate was filtered, washed with acetone, and recrystallized from acetone–water mixtures.

Sodium perchlorate, potassium nitrate, potassium cyanide, potassium thiocyanide, and potassium halides were Merck or Hopkins and Williams, analytical grade, and used without further purification.

The uv difference absorption measurements were obtained with a Cary 17 spectrophotometer in jacketed absorption cells at 25 ± 0.1°C. To an aqueous paraquat solution ($1.25 \times 10^{-4}\ M$ or $5 \times 10^{-4}\ M$) different potassium salts were added in varying concentrations, from 0.05 to 0.5 *M*. The reference cell was filled with $1.25 \times 10^{-4}\ M$ or $5 \times 10^{-4}\ M$ paraquat solution. At least eight runs were obtained for each anion. Some spectrophotometric measurements were also carried out in water–ethanol mixtures.

A potentiometric method was used for determination of free halide ion concentration. A bromide specific electrode (Orion model 94-35 A) or a chloride specific electrode (Orion model 94-17 A) with a double junction reference electrode (Orion model 92-02) was employed. The measurements were performed in a double-walled beaker maintained at 25 ± 0.1°C by water circulation. The electrodes were calibrated with standard solutions of 0.4 *M* total ionic strength, using sodium perchlorate or potassium nitrate as the inert electrolyte. Chloride ion measurements were done starting from a 0.2 *M* solution of $PQCl_2$ and then diluting it with a potassium nitrate or sodium perchlorate solution, with the condition that the total ionic strength was always 0.4 *M*. A similar procedure was used with $DQBr_2$.

Results and discussion

During the study of fluorescence quenching of 1-naphthylamine by paraquat in aqueous solutions (11) it was necessary to make corrections due to incident light absorption by the

Can. J. Chem. Downloaded from www.nrcresearchpress.com by 213.166.140.6 on 09/07/12
For personal use only.

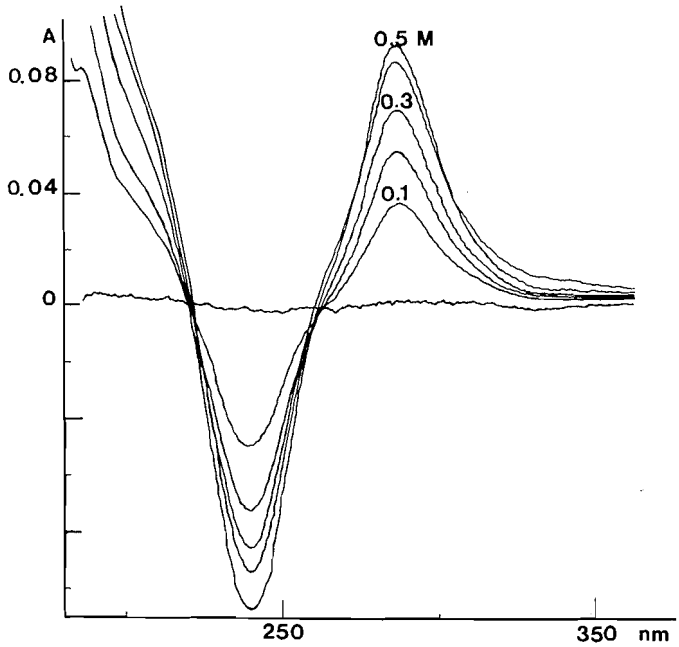

FIG. 1. The difference spectra of 1.25×10^{-4} *M* paraquat with an excess of potassium chloride.

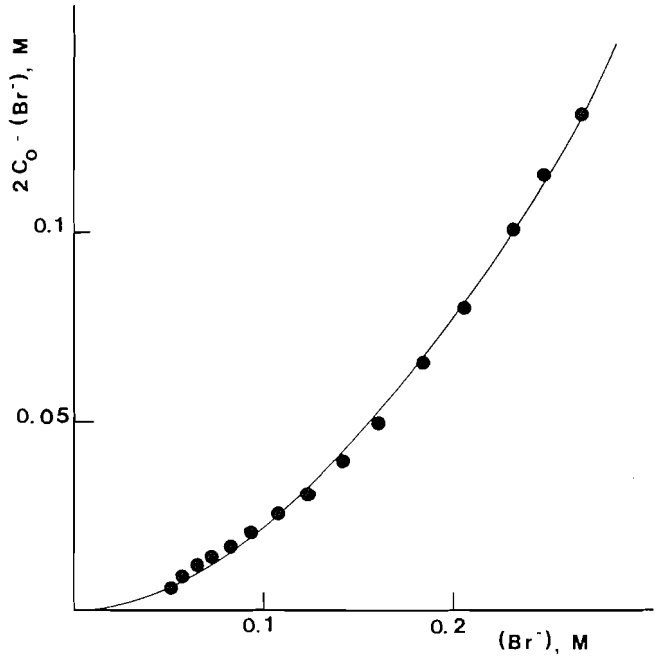

FIG. 2. Dependence of $2C_0 - [Br^-]$ vs. $[Br^-]$, experimental points by bromide selective electrode technique at 25°C, (—) line calculated according to eq. [6].

quencher at 320 nm. We found that paraquat did not obey Beer's Law at this wavelength in the concentration range 0.005–0.1 *M*. The positive deviation from Beer's Law suggested some kind of interaction between PQ^{2+} and chloride ions.

The absorption spectra of paraquat solutions containing any of the anions used in the present work confirmed that the absorption begins at longer wavelengths than those from either the potassium salt of the different anions studied or methylviologen perchlorate solutions. Therefore, difference spectra of dilute paraquat solutions, to which an excess of potassium halide was added, were obtained. As can be seen in Fig. 1 for the case of KCl, we found that the absorbance of the difference bands depends on chloride ion concentration.

Difference spectra with the addition pf potassium bromide, potassium iodide, potassium cyanide, and potassium thiocyanide were also obtained. With the exception of cyanide and thiocyanide, there is an approximately linear relationship between the wavenumber of the maxima in the difference spectra and the electronic affinity of the anions. This suggests that the difference band is of charge transfer type. Similar results were obtained with diquat solutions.

In the paraquat and diquat solutions the following association equilibria can be expected:

[1*a*] $B^{2+} + A^- \leftrightarrows BA^+ \qquad K_1$

[1*b*] $BA^+ + A^- \leftrightarrows BA_2 \qquad K_2$

where B^{2+} represents PQ^{2+} or DQ^{2+} and A^- stands for the different anions.

The equilibrium chloride and bromide concentrations were obtained by potentiometric measurements in aqueous solutions of paraquat and diquat, respectively, at different analytical concentrations, C_0. If it is assumed that the only equilibrium operating in the system is the first one, eq. [1*a*], the data for free ion and analytical concentration cannot be fitted with the resulting equation. Therefore the complete set, eqs. [1*a*] and [1*b*], was employed. The apparent equilibrium constants, K_1 and K_2, i.e., the equilibrium constants in terms of concentrations, were obtained using the following relationships:

[2] $[A^-] = [BA^+] + 2[B^{2+}]$

[3] $2C_0 = 2[BA_2] + [BA^+] + [A^-]$

Taking into account the A^- mass balance [3] and the equilibrium constants, we obtain:

$$[4] \quad [BA^+] = \frac{2C_0 - [A^-]}{1 + 2K_2[A^-]}$$

$$[5] \quad [B^{2+}] = \frac{2C_0 - [A^-]}{K_1[A^-]\{1 + 2K_2[A^-]\}}$$

then, replacing $[BA^+]$ and $[B^{2+}]$ in eq. [2]:

$$[6] \quad 2C_0 - [A^-] = \frac{K_1[A^-]^2 + 2K_1K_2[A^-]^3}{2 + K_1[A^-]}$$

Plots of $2C_0 - [A^-]$ versus $[A^-]$ are shown in Fig. 2 for aqueous solutions of diquat. Similar ones were obtained for paraquat. These plots can be fitted with K_1 and K_2 as adjustable parameters by a computer program. The values of the equilibrium constants obtained by this procedure are shown in Table 1 for diquat and paraquat.

The small differences between K_1 and K_2 can be taken as an indication that both charged groups in the molecule act almost independently of each other. This behaviour is similar to that observed in the dissociation of aliphatic organic diacids when both carboxylic groups are separated by a few carbon atoms.

These results were checked by a quantitative analysis of the difference spectra. The observed absorbance changes on addition of potassium salts to aqueous solutions of paraquat or diquat were treated by the Benesi–Hildebrand method, assuming that a 1:1 complex was formed, eq. [1*a*].

According to eqs. [1*a*] and [1*b*], a curvature could be expected in the Benesi–Hildebrand plots. However, under our

Can. J. Chem. Downloaded from www.nrcresearchpress.com by 213.166.140.6 on 09/07/12
For personal use only.

TABLE 1. Equilibrium constants between PQ^{2+} and DQ^{2+} with different anions at 25°C

Ion	λ_{max} (nm)[a]	K_1 (M^{-1})[b]		K_2 (M^{-1})	$\Delta\varepsilon$ (M^{-1} cm^{-1})
PQ^{2+}					
Cl^-	290	1.7	2.0[c]	0.39[c]	6840
Br^-	297	3.3			4600
I^-	310	3.9			1760
CN^-	295	0.71			870[d]
SCN^-	310	2.0			1680
DQ^{2+}					
Cl^-	327	3.3			6060
Br^-	329	4.1	5.3[c]	0.33[c]	8420
I^-	353	4.6			5650

[a]Wavelength in the maximum of the difference band.
[b]The uncertainties were 5%, obtained using the criteria of Pearson and Deranleau (14).
[c]Experimental values obtained by halide selective electrode technique.
[d]At λ = 325 nm.

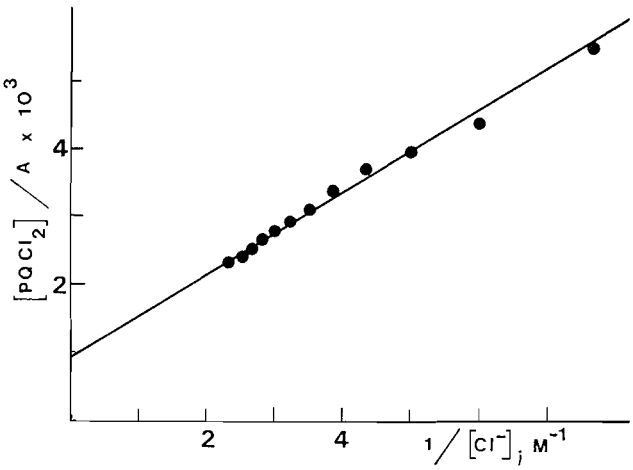

FIG. 3. Benesi–Hildebrand plot for PQ^{2+} – chloride ion. Paraquat, 1.25×10^{-4} M.

experimental conditions, deviation from a linear relationship was not observed (Fig. 3). If there was a compensating effect due to a change in the activity coefficient, we would expect a curvature in the Benesi–Hildebrand plot when the results are plotted against the chloride ion activity. However, this plot is also linear and it affords similar values of slope and intercept. The complex formation constants (K_1) and the difference of extinction coefficients ($\Delta\varepsilon$) at the maximum of the difference band were evaluated from the plots and they are given in Table 1. Although a departure from linearity could be expected according to the potentiometric results, we think that the failure to observe it is most probably due to the lack of sensitivity of the method. We assign the equilibrium constant obtained by this procedure to reaction [1*a*].

The K_1 values obtained are of the same order of magnitude as the equilibrium constant for the association between methylpyridinium and iodide (12). This is in agreement with the above conclusion that the two ammonium quaternary groups in these molecules behave almost independently.

The solvent effect on the charge transfer band observed in water–ethanol mixtures was a bathochromic shift when going to less polar solvents. Thus, for the complex of PQ^{2+} with bromide ion, the λ_{max} of the difference band are 297, 300, and 302 nm in pure water, 50%, and 75% of ethanol respectively. These results suggest the stabilization of the charge transfer state in going to less polar solvents, as was observed for other alkylpyridinium compounds (13).

The agreement between the values obtained by the two methods is satisfactory if it is realized that the experimental conditions are not exactly the same. The range of ionic strength used in the spectrophotometric method was 0.05–0.5 M. Nevertheless, the change in the activity coefficient of paraquat (6) is not high enough to invalidate the comparison of results obtained by both techniques.

In summary, we have shown that PQ^{2+} and DQ^{2+} associate with halide and pseudo-halide ions by a two-step equilibrium. This interaction is of an electron donor–acceptor type and a new charge transfer band, which manifests itself as a band in the difference spectra, is present in the electronic spectrum.

Acknowledgments

We wish to thank CONICOR and CONICET (Argentina) for financial support. The authors are also indebted to Dr. M. Marano for assistance with the computations.

1. B. G. WHITE. Trans. Faraday Soc. **65**, 2000 (1969).
2. J. R. BARNETT, A. S. HOPKINS, and A. LEDWITH. J. Chem. Soc. Perkin Trans. 2, 80 (1973).
3. R. HAQUE and S. LILLEY. J. Agric. Food Chem. **20**, 57 (1972).
4. A. NAKAHARA and J. H. WANG. J. Phys. Chem. **67**, 496 (1963).
5. G. PERRON and J. E. DESNOYERS. J. Solution Chem. **1**, 537 (1972).
6. R. F. PLATFORD. Environ. Sci. Technol. **4**, 410 (1970).
7. H. T. VAN DAM. J. Electrochem. Soc. **123**, 1181 (1976).
8. T. W. EBBESEN and G. FERRAUDI. J. Phys. Chem. **87**, 3717 (1983).
9. A. S. HOPKINS. Ph.D. thesis, University of Liverpool. 1972.
10. E. STECKHAM and T. KUWANA. Ber. Bunsenges. Phys. Chem. **78**, 253 (1974).
11. J. J. COSA, H. E. GSPONER, and C. M. PREVITALI. J. Photochem. **19**, 271 (1982).
12. E. M. KOSOWER. J. Am. Chem. Soc. **78**, 5838 (1956).
13. E. M. KOSOWER. J. Am. Chem. Soc. **80**, 3253 (1958).
14. E. G. POLLE. Russ. Chem. Rev. **43**, 631 (1974).

Can. J. Chem. Downloaded from www.nrcresearchpress.com by 213.166.140.6 on 09/07/12
For personal use only.

Contribution à l'étude des réactions d'alkylation et de polyalkylation de l'adamantane et de ses homologues

G. Molle, J. E. Dubois et P. Bauer[1]

Institut de topologie et de dynamique des systèmes de l'université Paris VII, Unité n° 34 associé au centre national de la recherche scientifique, 1 rue Guy de la Brosse, 75005 Paris, France

Reçu le 16 janvier 1987

G. Molle, J. E. Dubois et P. Bauer. Can. J. Chem. **65**, 2428 (1987).

Une méthode de préparation de dérivés alkylés de composés à structure cage est proposée. Elle repose sur la réaction de Grignard et le choix d'un solvant à haut point d'ébullition. La réaction a lieu à pression atmosphérique. Les méthylations de l'adamantane, du diamantane et de l'homoadamantane sont quantitatives. Avec d'autres groupes alkylants primaires les rendements sont supérieurs à 60%. La compétition entre la réaction d'alkylation et les réactions secondaires est discutée sur la base d'un mécanisme radicalaire.

G. Molle, J. E. Dubois, and P. Bauer. Can. J. Chem. **65**, 2428 (1987).

A method for preparing alkyl derivatives of cage-structure compounds is proposed. It relies on the use of Grignard reactions with a high boiling point solvent. The reactions take place at atmospheric pressure. Methylation of adamantane, diamantane, and homoadamantane occurs with quantitative yield. With other primary alkyl groups, yields are better than 60%. Competition between alkylation and secondary reactions is discussed on the basis of a free radical mechanism.

Can. J. Chem. Downloaded from www.nrcresearchpress.com by 213.166.140.6 on 09/07/12
For personal use only.

Introduction

Les dérivés de l'adamantane présentent un spectre très large d'applications pharmacologiques (1). L'introduction d'un groupe adamantyle sur certaines drogues peut accroître considérablement leur activité thérapeutique (2). Cette propriété est généralement attribuée au caractère lipophile très marqué de ce groupe.

Nos propres travaux sur les composés organométalliques à structure cage homologues de l'adamantane (3) ont montré que l'introduction de groupes méthyles sur les carbones apicaux de ces polycycliques exhaltait encore, dans de très larges proportions, ce caractère.

Malheureusement l'alkylation régiospécifique de l'adamantane et de ses homologues pose un certain nombre de problèmes (4–11) et ne conduit qu'à des mélanges de composés mono et polyalkylés généralement obtenus avec de faibles rendements.

Il est cependant possible de méthyler sélectivement l'adamantane (Ad—H) et ses homologues avec d'excellents rendements en utilisant les voies organométalliques (réactions [1] et [2] (12–14).

[1] $Ad—X + (CH_3)_3Al \rightarrow Ad—CH_3$

[2] $Ad—X + CH_3MgBr \rightarrow Ad—CH_3$

La voie organomagnésienne, développée pour la première fois par Schleyer et coll. (14), permet d'utiliser la plupart des réactifs de Grignard primaires mais s'effectue sous pression dans l'éther éthylique à 100°C ce qui n'est pas sans risque, la présence de peroxydes dans le milieu réactionnel pouvant dans ces conditions conduire à de violentes explosions. En outre, le rendement en produit alkylé chute d'une façon importante lorsque l'on dépasse le stade du bromure de méthylmagnésium (90% pour le méthyl-1 adamantane contre 39% pour l'éthyl-1 adamantane).

Le but de ce travail a donc été de rechercher des conditions opératoires qui permettent d'obtenir à pression atmosphérique, avec des rendements satisfaisants, des alkylations sélectives de l'adamantane et de ses homologues.

Résultats et discussion

Le fait qu'à 35°C dans l'éther éthylique la réaction d'alkylation entre les réactifs de Grignard et le bromo-1 adamantane n'ait pas lieu, alors qu'à 100°C sous pression les produits alkylés sont obtenus, tend à montrer que l'énergie d'activation de cette réaction est élevée et donc qu'à 35°C la formation de ces produits est pratiquement bloquée. Par contre il doit être possible de réaliser cette réaction, à pression atmosphérique, dans un solvant de polarité comparable mais ayant un point d'ébullition plus élevé. Des essais antérieurs (14) effectués avec le tétrahydrofuranne ou le dioxanne ont conduit à des échecs imputables, selon nous, à la trop grande basicité de ces solvants qui favorise la réaction de réduction des halogénures. L'utilisation d'un éther aliphatique tel que l'éther *n*-butylique (T_{eb} = 142°C), nous a paru plus appropriée.

1. Méthylation de l'adamantane

Les premiers essais réalisés, dans ce solvant avec l'iodo-1 adamantane **1**, le bromo-1 adamantane **2** et le chloro-1 adamantane **3** d'une part, et l'iodure ou le bromure de

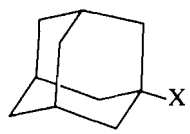

1 X = I
2 X = Br
3 X = Cl

méthylmagnésium d'autre part conduisent à des rendements en méthyl-1 adamantane supérieurs à 85% (tableau 1).

Ces rendements deviennent même quantitatifs lorsque les dérivés chloré ou bromé de l'adamantane sont condensés sur le bromure de méthylmagnésium.

Avec l'iodure de méthylmagnésium, la formation de 10% environ de carbure de réduction (adamantane) est observée. Si un prélèvement est effectué dès l'addition de ce magnésien sur le bromure **2**, on constate après hydrolyse et analyse en chromatographie en phase vapeur (cpv), la présence de 100% de l'iodure **1** indiquant que l'alcoylation est précédée dans ce cas d'une réaction très rapide d'échange.

$$CH_3MgI + 2 \rightarrow 1 + CH_3MgBr$$

L'existence de cette réaction nous a donc conduit à rejeter les dérivés iodés dans la suite de ces travaux.

Une étude cinétique réalisée, à différentes températures, lors de la condensation du bromure **2** sur le bromure de méthylmagnésium dans l'éther *n*-butylique, montre que la réaction de méthylation de l'adamantane est d'ordre 2 et que l'énergie

1. Auteur à qui adresser toute correspondance.

Printed in Canada / Imprimé au Canada

Can. J. Chem. Downloaded from www.nrcresearchpress.com by 213.166.140.6 on 09/07/12
For personal use only.

TABLEAU 1. Rendements de la méthylation de l'adamantane

R—X	CH_3MgX	T (°C)	Rendement R—CH_3	Rendement R—H
1	CH_3MgI	105	86,5	13,5
2	CH_3MgI	105	90 (70)[a]	10
2	CH_3MgI	85	91	9
2	CH_3MgBr	85	>99 (83)[a]	—
3	CH_3MgBr	85	>99	—

CH_3MgBr = 2,3 *M*; CH_3MgI = 1,8 *M*; CH_3MgX/R—X = 2.
[a]Rendements obtenus par Schleyer et coll. (14).

TABLEAU 2. Constantes cinétiques de formation du méthyl-1 adamantane

R—X	T (°C)	$k \times 10^5$ (mol L^{-1} s^{-1})
2	70	5,8
2	80	16,2
2	85	26,4
2	90	46,8

CH_3MgBr = 2,2 *M*; CH_3MgBr/R—X = 2.

d'activation est de 26,5 kcal (tableau 2). L'extrapolation, à partir de cette valeur, de la constante cinétique à 35°C donne une valeur de $k = 7{,}1 \times 10^{-7}$ mol L^{-1} s^{-1} ce qui correspond à un temps de demi-réaction de l'ordre de 7 jours.

Ces résultats confirment notre hypothèse selon laquelle la température joue un rôle déterminant dans ce type d'alkylation et justifie donc pleinement notre choix d'un solvant ayant un point d'ébullition élevé tel que l'éther *n*-butylique.

2. Méthylation des homologues de l'adamantane

L'extension de cette réaction à d'autres structures cage telles que le bromo-1 diamantane **4**, le bromo-3 homoadamantane **5** ou à des bromo-1 polyméthyladamantanes **6**, **7** et **8**, conduit à des résultats meilleurs que ceux obtenus dans l'éther éthylique sous pression à 100°C (tableau 3).

Tous les rendements sont supérieurs à 98%, avec un rapport RMgX/RX égal à 2, alors que ce même rapport est égal à 3,5 dans le protocole expérimental proposé par Schleyer et coll. (14).

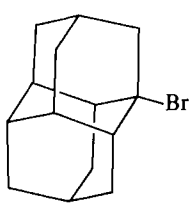

4

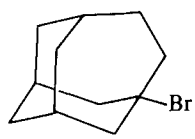

5

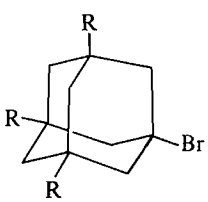

6 R = CH_3, H, H
7 R = CH_3, CH_3, H
8 R = CH_3, CH_3, CH_3

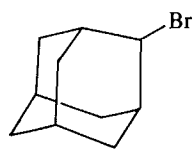

9

TABLEAU 3. Rendements des produits obtenus lors de la méthylation des homologues de l'adamantane dans l'éther *n*-butylique

R—X	T (°C)	R—CH_3	R—H
2	85	>99 (83)[a]	—
4	85	>99 (90)[a]	—
5	85	>99 (87)[a]	—
6	85	99	1
7	95	98 (92)[a]	2
8	105	>99	—
9	140	86	14

CH_3MgBr = 2,2 *M*; CH_3MgBr/RX = 2.
[a]Rendements obtenus par Schleyer et coll. (14) avec CH_3MgBr/RX = 3,5.

L'alkylation en position 2 de l'adamantane, à partir du dérivé bromé **9**, est beaucoup plus difficile et nécessite une température de 140°C, mais le rendement en méthyl-2 adamantane atteint alors 86%.

Les constantes cinétiques diminuent lorsque le nombre de groupes méthyle augmente sur le noyau (**2**, 26×10^{-5} mol L^{-1} s^{-1}; **6**, 10×10^{-5} mol L^{-1} s^{-1}; **8**, $4{,}8 \times 10^{-5}$ mol L^{-1} s^{-1}). Il est donc nécessaire pour les bromures **6**, **7** et **8** d'augmenter la température du milieu réactionnel de 85 à 105°C afin de limiter le temps de la réaction et la formation de produits secondaires.

3. Alkylation de l'adamantane

Tous les halogénures d'alkylmagnésium ont été synthétisés dans l'éther *n*-butylique puis condensés sur les halogénures **2** ou **3**. Les résultats sont réunis dans le tableau 4.

Si la condensation du bromure de méthylmagnésium sur le bromure **2** est quantitative, il n'en est pas de même pour le bromure d'éthylmagnésium. En effet le rendement en produit alkylé decroit dans ce cas à 66% (essai 1) pendant que le rendement en adamantane atteint 34%. Par contre l'augmentation de la chaine alkylée de l'organomagnésien n'influence pratiquement pas les rendements maximums obtenus puisqu'ils sont respectivement de 66, 61 et 62% pour l'éthyl, le *n*-butyl et le néopentyl-1 adamantane (essais 1, 5 et 7).

De plus les rendements en *n*-butyl-1 adamantane sont les mêmes que l'on fasse réagir le bromure **2**, sur le bromure de *n*-butylmagnésium (essai 3) ou le chlorure **3**, sur le chlorure de *n*-butylmagnésium (essai 5) avec des rapports R'MgX/RX égal à 2. Si ce rapport diminue, le rendement en *n*-butyl-1 adamantane chute à 38% (essai 4) avec les réactifs bromés mais reste sensiblement égal avec les chlorés (essai 6).

Il semblerait que la présence d'un hydrogène en β sur la chaîne aliphatique de l'organomagnésien soit responsable de la baisse de rendement constatée entre le bromure de méthylmagnésium et les autres réactifs de Grignard étudiés.

Pour vérifier cette hypothèse, nous avons synthétisé le bromure d'éthylmagnésium deutéré (C_2D_5MgBr) et condensé cet organomagnésien sur le bromure **2** (essai 2). Après hydrolyse du milieu réactionnel, une analyse effectuée par chromatographie en phase vapeur et par spectrométrie de masse donne 70% de rendement en éthyl-1 adamantane et montre que l'adamantane est deutéré à 90%.

La présence de *n*-octane semble indiquer que le magnésien qui ne conduit pas au produit alkylé attendu donne un produit de dimérisation.

Ainsi l'adamantane est vraisemblablement formé, au cours

TABLEAU 4. Rendements des réactions d'alcoylation de l'adamantane par voie magnésienne dans l'éther *n*-butylique

Essais	R—X	R'MgX	R'MgX/R—X	R—R'	R—H
1	**2**	C_2H_5MgBr	1,5/1	66[a]	34
2	**2**	C_2D_5MgBr	1,5/1	70	30
3	**2**	*n*BuMgBr	2/1	60[b]	40
4	**2**	*n*BuMgBr	1,2/1	38	62
5	**3**	*n*BuMgCl	2/1	61	39
6	**3**	*n*BuMgCl	1,2/1	62	38
7	**2**	tBuCH$_2$MgCl	3/1	62	38
8	**2**	Cyclohexyl-MgCl	2/1	20[c]	80
9	**2**	*t*BuMgCl	1,5/1	9[c]	91

T = 105°C; 1,5 < R'MgX < 1,7. Les dosages effectués après chaque essai montrent que R'MgX consommé = R—R' + R—H.

[a]85°C, $k = 1{,}33 \times 10^{-4}$ mol L^{-1} s^{-1}.

[b]Quand le rapport R'MgX/RX = 5, le rendement en R—R' = 59%.

[c]Ces produits non isolés ont été caractérisés par cpv et spectrométrie de masse.

de la réaction de réduction, par un transfert d'ion hydrure pouvant se concevoir selon un mécanisme à 6 centres du type :

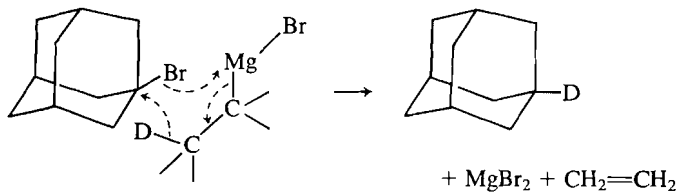

SCHÉMA 1

Cependant cette réaction secondaire de réduction est également observée lors de la condensation du bromure **2** sur le chlorure de néopentylmagnésium, bien que cet organomagnésien ne possède pas d'hydrogène en β (essai 7). Dans ce cas, outre 38% d'adamantane, une quantité importante de tétraméthyl-2,2,5,5 hexane est obtenue.

Si la présence de cet hydrocarbure n'est plus compatible avec un mécanisme à 6 centres, elle peut s'expliquer par contre par un mécanisme radicalaire faisant intervenir un transfert monoélectronique (SET) entre l'organomagnésien et le dérivé halogéné (schéma 2) (15).

Les rendements en produits d'alkylation sont toujours supérieurs à 60% pour les réactifs de Grignard primaires; ils chutent avec les organomagnésiens secondaires et tertiaires (essais 8 et 9) puisque les rendements en adamantane atteignent 80–90%.

Les échecs rencontrés surtout avec les organomagnésiens tertiaires pourraient alors s'expliquer par une diffusion hors de la cage de solvant des radicaux-anions tertiaires plus stables qui attaquent le solvant avant que la réaction d'alkylation n'ait lieu (16, 17).

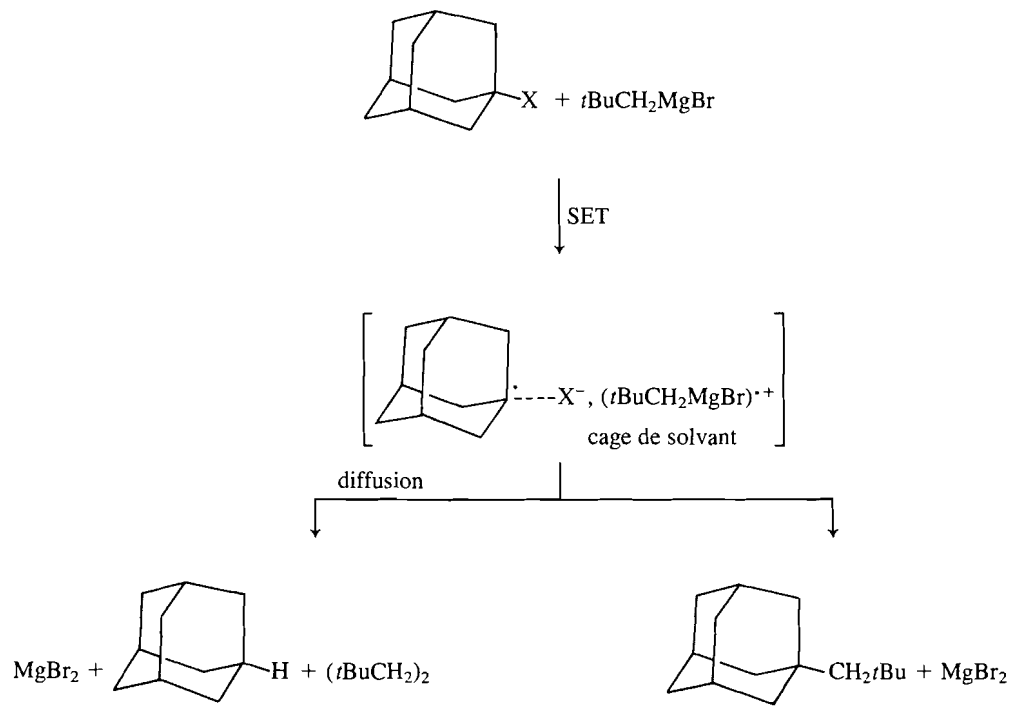

SCHÉMA 2

Can. J. Chem. Downloaded from www.nrcresearchpress.com by 213.166.140.6 on 09/07/12
For personal use only.

4. Polyalkylation de l'adamantane

La synthèse des dérivés polyalkylés s'effectue le plus souvent en plusieurs étapes :

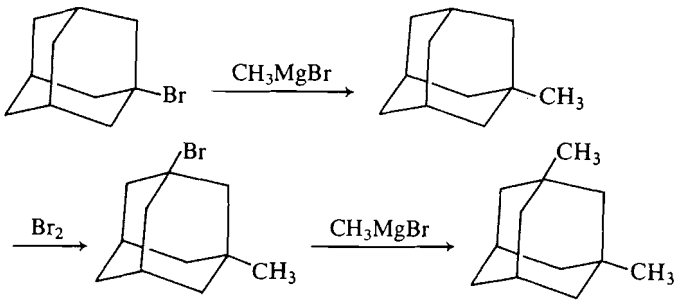

Nous avons tenté la synthèse directe du diméthyladamantane à partir du dibromo-1,3 adamantane (schéma 3).

Les premiers essais effectués montrent (tableau 5) que le rendement en diméthyladamantane est limité à 52%, le reste étant constitué de 44% de méthyladamantane et 4% d'adamantane. Or nous avons montré précédement que la réaction de réduction n'avait pas lieu lors de la méthylation des bromures **2** et **4** puisque les rendements de la réaction d'alkylation sont quantitatifs (tableaux 1 et 3).

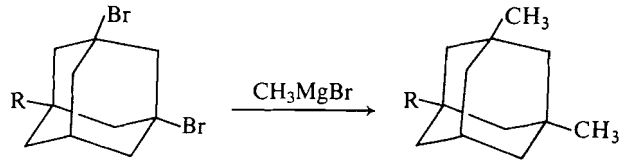

10 R = H
11 R = CH_3

SCHÉMA 3

Une deutérolyse effectuée au cours de la réaction montre que le méthyl-1 adamantane n'est pas deutéré. Il est donc très vraisemblablement formé, par diffusion du radical hors de la cage de solvant, lors de l'attaque du premier atome de brome (voie 1, schéma 4).[2]

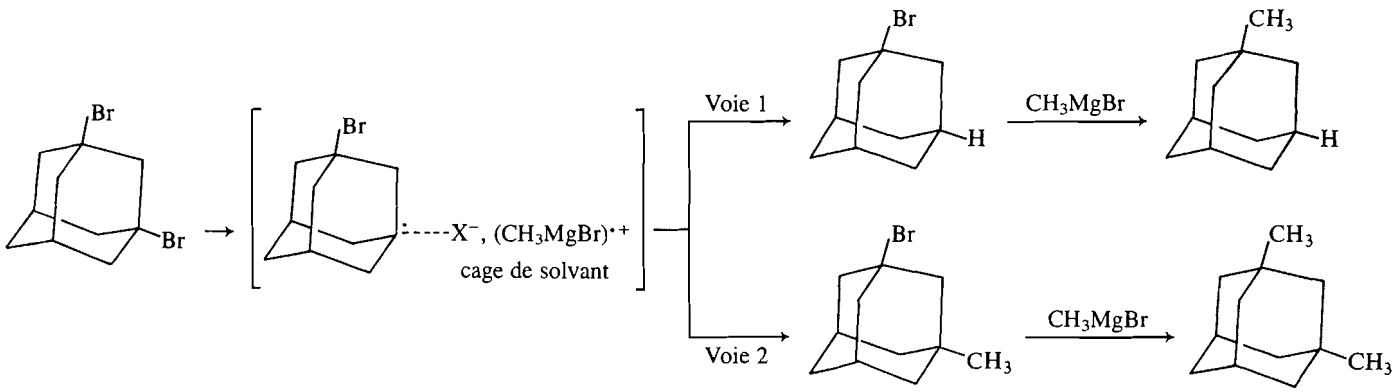

SCHÉMA 4

L'apport d'un groupe méthyle sur le noyau adamantyle conduit au même résultat (tableau 5). Dès lors on peut penser que c'est la présence de deux atomes de brome en position 1, 3 sur l'adamantane qui est responsable de la compétition entre les voies 1 et 2 du schéma 4. Cette situation est à l'origine d'une réaction secondaire qui conduit à la formation quantitative du dihydroadamantane lors de la réaction de ce dérivé dibromé avec le lithium (schéma 5) (19).

Pour vérifier ce point nous avons tenté la synthèse du 4,9-diméthyldiamantane à partir du 4,9-dichlorodiamantane

TABLEAU 5. Rendements de la méthylation des dérivés dihalogénés «cage» dans l'éther *n*-butylique à 140°C

RX_2	R—$(CH_3)_2$[a]	R—(CH_3)	RH
10	52[b]	44	4
11	51	46	3
12	97	3	—

CH_3MgBr = 2 *M*; CH_3MgBr/RX_2 = 2.

[a]Les rendements sont calculés par cpv et les produits caractérisés par spectroscopie de masse.

[b]Avec CH_3MgBr/RX_2 = 4 on obtient le même rendement.

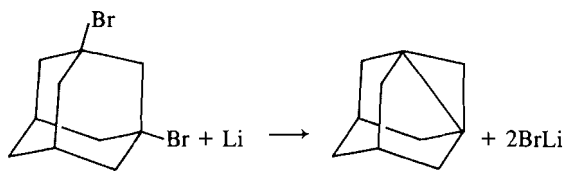

SCHÉMA 5

12, molécule dans laquelle les deux atomes de chlore sont beaucoup plus éloignés l'un de l'autre (schéma 6).

Dans ce cas on observe la formation de 97% de produit diméthylé, montrant ainsi que l'éloignement des deux atomes d'halogène élimine pratiquement la formation du produit monoalkylé.

Conclusion

Comme nous l'avions pressenti, l'utilisation d'un solvant à haut point d'ébullition nous a permis d'obtenir, à pression atmosphérique et avec des rendements parfois quantitatifs, les

2. À la température utilisée il ne nous a malheureusement pas été possible de mettre en évidence les produits intermédiaires : le bromo-1 adamantane et le méthyl-3 bromo-1 adamantane, puisque à cette température le temps de demi-réaction des voies 1 et 2 est de l'ordre de 7 s.

Can. J. Chem. Downloaded from www.nrcresearchpress.com by 213.166.140.6 on 09/07/12
For personal use only.

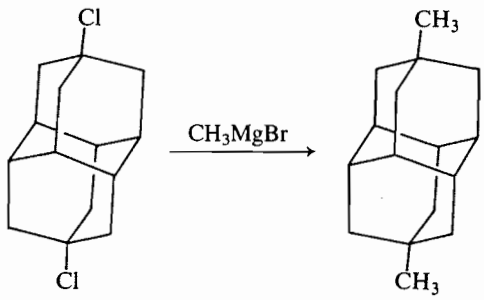

12

SCHÉMA 6

produits d'alkyation de l'adamantane et de certains de ses homologues.

L'emploi d'organomagnésiens constitue indiscutablement un progrès par rapport aux autres méthodes existantes.

Ces résultats ouvrent la voie à des études que nous comptons développer, sur le rôle de l'alkylation régiospécifique comme facteur activant le transfert de ces structures cage à travers les membranes biologiques.

Partie expérimentale

Généralités

Les points de fusion ont été déterminés sur un appareil automatique Mettler FP5. Les spectres infra-rouge ont été effectués sur un spectromètre Perkin Elmer 225 alors que les spectres de rmn ont été enrégistrés sur un appareil JEOL C 60 HL (le TMS étant pris comme référence). Les spectres de masse ont été obtenus avec un spectromètre JEOL JMS 200 connecté à un chromatographe JEOL GAS 20 K GLO et à un ordinateur JEOL Mass Data System.

Les analyses cpv ont été effectuées sur des colonnes Carbowax 20 M ou SE 30 placées sur un chromatographe Intersmat IGC 12 DFL relié à un intégrateur calculateur LTT ICAP 10. La chromatographie en phase liquide a été réalisée sur des colonnes en verre remplies d'alumine neutre (grade II) Merck en utilisant de l'éther de pétrole (30–60°C), du tétrachlorure de carbone et de l'éther éthylique comme éluants.

Réactifs

Le magnésium utilisé (Aldrich) contient 2000 ppm d'impuretés, principalement ferriques. L'éther *n*-butylique (Baker) est conservé sur sulfate de calcium anhydre et sa teneur en eau est inférieure à 40 ppm.

Les halogénures d'alkyles (Prolabo) sont préalablement distillés et stockés sur du carbonate de sodium à l'exception du bromure de méthyle gazeux (Matheson) qui est séché sur une colonne de chlorure de calcium avant introduction dans le milieu réactionnel. Le bromure d'éthyle deutéré est fourni par la Société Spin et Techniques. Les différents magnésiens sont filtrés sur cartouche d'alundum puis titrés par dosage acido-basique.

Les bromo-1 adamantane, bromo-2 adamantane, iodo-1 adamantane, bromo-1 diamantane, bromo-3 homoadamantane sont préparés selon les méthodes déjà décrites (20).

Les bromo-1 méthyl-3 adamantane et bromo-1 diméthyl-3,5 adamantane sont obtenus selon la méthode de Stetter et Wulff par bromation directe des méthyl-1 et diméthyl-3,5 adamantanes (21). Le bromo-1 triméthyl-3,5,7 adamantane est préparé par action du bromure de thionyle sur l'hydroxy-1 triméthyl-3,5,7 adamantane (22).

Synthèse des dihalogénures

Dans un tricol de 1 litre, muni d'un agitateur magnétique, d'un réfrigérant et d'une arrivée d'argon, sont introduits 40,8 g d'adamantane et 3 g de fer. À 0°C, sous agitation, sont ajoutés lentement 150 mL de brome. Un dégagement intense d'acide bromhydrique se produit. Dès que ce dégagement cesse, on monte la température à 25°C et l'agitation est maintenue 2 h, puis 200 mL de dibromoéthane sont ajoutés et la solution est versée doucement dans un bécher contenant un mélange de glace et de bisulfite de sodium. La phase organique est ensuite lavée à l'eau, puis neutralisée au bicarbonate et enfin rincée à nouveau à l'eau. La solution est séchée sur sulfate de sodium, filtrée puis évaporée à sec. La totalité du produit est reprise par 800 mL de méthanol. Après recristallisation, on obtient 75 g de dibromo-1,3 adamantane dont la pureté est de 99%. Le rendement est de 85%; F = 109,5°C (lit. (21) F 108°C).

Le dibromo-1,3 méthyl-5 adamantane est préparé selon le même mode opératoire. Le rendement est de 88%; F = 62°C.

Le dichloro-4,9 diamantane est préparé par action de l'acide chlorosulfonique sur le binor-S à basse température selon la méthode décrite par Blaney *et al.* (23).

Synthèse des halogénures d'alkylmagnésium

Dans un tricol de 1 L muni d'un agitateur et d'une garde de chlorure de calcium, on introduit 35 g de magnésium et 400 mL d'éther *n*-butylique anhydre. Après initiation du magnésium par quelques gouttes de dibromo-1,2 éthane, la température est abaissée à 5°C et on introduit l'halogénure. Au terme de la réaction le titre de la solution est déterminé par dosage acido-basique.

Alkylation des dérivés à structure cage

Synthèse du méthyl-1 adamantane

Dans un tricol de 100 mL muni d'un agitateur, d'un réfrigérant, et d'une ampoule d'addition, sont introduits, sous argon, 5 g de bromo-1 adamantane et 5 mL d'éther *n*-butylique préalablement séché sur fils de sodium. La température est portée à 105°C et 26 mL de bromure de méthylmagnésium (1,8 M) sont ajoutés goutte à goutte à raison de 2 gouttes par seconde. L'agitation à 105°C est maintenue 1 h. Après neutralisation du milieu réactionnel par HCl 1 M, la phase organique est lavée plusieurs fois à l'eau puis neutralisée au bicarbonate de sodium, avant d'être évaporée sous vide, en prenant les précautions nécessaires pour éviter une perte du produit par sublimation. Le méthyl-1 adamantane est ensuite purifié par cpl sur colonne d'alumine en utilisant le pentane comme éluant.

Les autres dérivés alkylés sont préparés selon la même méthode, seule la température du milieu réactionnel peut varier en fonction de la nature de l'organomagnésien ou du dérivé halogéné (voir les différents tableaux).

Les constantes cinétiques sont déterminées à partir des analyses chromatographiques et des dosages réalisés sur des prélèvements effectués au cours du temps.

Caractérisation des produits formés

Méthyl-1 adamantane : F = 104°C (lit. (14) F 102–103°C); rmn (CCl_4) : 0,8 (s, 3H), 1,47 (s, 6H), 1,70 (s, 6H), 1,92 (s, 3H) ppm; masse (75 eV) m/e (intensité relative) : 150 (15,7, M^+), 135 (100, $M^+ - CH_3$).

Diméthyl-1,3 adamantane : Eb = 204°C (lit. (24) Eb 204°C); rmn (CCl_4) : 0,79 (s, 6H), 1,17 (s, 2H), 1,38 (s, 8H), 1,56 (s, 2H), 1,99 (s, 2H) ppm; masse (75 eV) m/e : 164 (8,1, M^+), 149 (100, $M^+ - CH_3$).

Triméthyl-1,3,5 adamantane : Eb (760 Torr; 1 Torr = 133.3 Pa) = 210°C, Eb (0,7 Torr) = 40°C (lit. (22) Eb (19 Torr) 88°C); rmn (CCl_4) : 0,79 (s, 9H), 1,08 (s, 6H), 1,29 (s, 6H), 2,05 (s, 1H) ppm; masse (75 eV) m/e : 178 (3,3, M^+), 163 (100, $M^+ - CH_3$).

Tétraméthyl-1,3,5,7 adamantane : F = 67°C (lit. (25) F 66–67°C); rmn (CCl_4) : 0,80 (s, 12H), 1,0 (s, 12H) ppm; masse (75 eV) m/e : 192 (6,7, M^+), 177 (100, $M^+ - CH_3$).

Ethyl-1 adamantane : Eb = 229°C (lit. (24) Eb 219°C); rmn (CCl_4) : 0,77 (t, 3H), 1,05 (t, 2H), 1,42 (s, 6H), 1,67 (s, 6H), 1,95 (s, 3H) ppm; masse (75 eV) m/e : 164 (75, M^+), 135 (100, $M^+ - CH_2CH_3$).

n-Butyl-1 adamantane : Eb = 271°C (lit. (26) Eb 262°C); rmn (CCl_4) : 0,90 (t, 3H), 1,13 (s, 6H), 1,50 (s, 6H), 1,70 (s, 6H), 1,93 (s, 3H) ppm; masse (75 eV) m/e : 192 (4, M^+), 135 (100, $M^+ - n$Bu).

Néopentyl-1 adamantane : F = 69°C; rmn (CCl_4) : 0,99 (s, 9H), 1,10 (s, 2H), 1,67 (m, 12H), 1,89 (s, 3H) ppm; masse (75 eV) m/e : 206 (4, M^+), 149 (8, $M^+ - t$Bu), 135 (100, M^+ – néopentyl), 57 (50, tBu$^+$). *Anal.* calc. pour $C_{15}H_{26}$: C 87,38, H 12,62; trouvé : C 87,41, H 12,57.

Méthyl-2 adamantane : F = 144–146°C (lit. (18) F 144–146°C);

Can. J. Chem. Downloaded from www.nrcresearchpress.com by 213.166.140.6 on 09/07/12
For personal use only.

rmn (CCl_4) : 1,1 (d, 3H), 1,68 (s, 6H), 1,84 (s, 9H) ppm; masse (75 eV) *m/e* : 150 (71, M^+), 135 (100, $M^+ - CH_3$).

Méthyl-1 diamantane : F = 210–212°C (lit. (14) F 215–218°C); rmn (CCl_4) : 0,9 (s, 3H), 1,41–2,20 (m, 19H) ppm; masse (75 eV) *m/e* : 202 (12, M^+), 187 (100, $M^+ - CH_3$).

Méthyl-3 homoadamantane : F = 109–110°C (lit. (14) F 109–111°C); rmn (CCl_4) : 0,89 (s, 3H), 1,50 (m, 17H) ppm; masse (75 eV) *m/e* : 164 (3,9, M^+), 149 (100, $M^+ - CH_3$).

Diméthyl-4,9 diamantane : F = 116–117°C; rmn (CCl_4) : 0,8 (s, 6H), 1,47 (s, 12H), 1,8 (s, 6H) ppm; masse (75 eV) *m/e* : 216 (11,5, M^+), 201 (100, $M^+ - CH_3$). *Anal.* calc. pour $C_{16}H_{24}$: C 88,89, H 11,11; trouvé : C 88,82, H 11,05.

Remerciements

Nous adressons nos plus vifs remerciements à Mesdames Briand et Duchâtellier pour leur assistance technique.

1. R. C. Fort. The chemistry of adamantane. M. Dekker, New York. 1976. p. 327.
2. (*a*) K. Gerzon, E. V. Krumkalns, R. J. Brindle, F. J. Marschall et M. A. Root. J. Med. Chem. **6**, 760 (1963); (*b*) R. T. Rapalo, R. J. Kroay et K. Gerson. J. Med. Chem. **8**, 850 (1965); (*c*) Y. K. Ho, M. T. Hakala et S. F. Zarzewski. Cancer Res. **32**, 1023 (1972); (*d*) C. A. Nicol. Adv. Enzyme Regul. **6**, 305 (1968).
3. G. Molle, S. Briand, P. Bauer et J. E. Dubois. Tetrahedron, **40**, 5113 (1984).
4. (*a*) V. N. Solov'ev, E. I. Bagrii et P. I. Sanin. Neftekhimiya, **14**(6), 817 (1974); Chem. Abstr. **82**, 139476 (1975); (*b*) V. N. Solov'ev, T. F. Frid, E. I. Bagrii, D. I. Sanin et V. G. Zaikin. USSR Brevet 654, 598 (Cl. CO7C 13/54) (1979); Chem. Abstr. **91**, 019997 (1979); (*c*) V. N. Solov'ev. Mater. Resp. Nauchno. Tekh. Konf. Molodykh Uch. Pererab. Nefti Neftekhim. 3rd, **2**, 52 (1976); Chem. Abstr. **89**, 163132 (1978); (*d*) G. A. Olah, O. Farocq, G. K. Surya Prakash et K. Laali. J. Am. Chem. Soc. **107**, 7541 (1985).
5. (*a*) I. Tabushi et K. Fukunishi. U.S. Brevet 3,923,480, (Cl. 260.266 M : CO7C) (1974); Chem. Abstr. **84**, 164288 (1976); (*b*) Japan Kokai 75, 89,355, (Cl. CO7C) (1973); Chem. Abstr. **83**, 178445 (1975); (*c*) Brevet Suisse 620, 183, (Cl. CO7C) (1980); Chem. Abstr. **95**, 006641 (1981).
6. A. T. Podkhalyuzin et V. V. Vikulin. USSR Brevet 426,998, (Cl. CO7C) (1971); Otkrytiya, Izobret. Prom. Obraztsy, Tovarnye Znaki, **52**(17), 164 (1975); Chem. Abstr. **83**, 163720 (1975).
7. H. Ichikawa, H. Iida et K. Honna. Japan Kokai, 77, 12, 152, (Cl. CO7C K/10) (1977); Chem. Abstr. **87**, 039021 (1977).
8. B. G. Gavrilov et A. Apinov. Zh. Prikl. Khim. **57**(7), 1657 (1984); Chem. Abstr. **102**, 024163 (1985).
9. (*a*) Ya. M. Slobodin, V. E. Kovyazin, R. I. Frolova, V. F. Vasil'eva et V. V. Takhismov. Zh. Org. Khim. **11**, 2218 (1975); Chem. Abstr. **84**, 016845 (1976); (*b*) A. T. Saginaev et E. I. Bagrii. Neftekhimiya, **22**(6), 729 (1982); Chem. Abstr. **98**, 160281 (1983).
10. (*a*) G. I. Bolestova, Z. N. Parnes, F. M. Latypova et D. N. Kursanov. Zh. Org. Khim. **17**(7), 1357 (1981); Chem. Abstr. **95**, 168419 (1981); (*b*) E. I. Bagrii, T. N. Dolgopolova et P. N. Sapin. USSR SU 915,407 (Cl. CO7C 13/615) (1985); Chem. Abstr. **103**, 005940 (1985).
11. Y. Twiska, L. Vodicka et S. Landa. Sb. Vys. Sk. Chem.-Technol. Praze, Technol. Paliv. **D44**, 125 (1981); Chem. Abstr. **97**, 215611 (1982).
12. E. W. Della et T. K. Bradshaw. J. Org. Chem. **40**, 1638 (1975).
13. T. Mole et A. Meisters. U.S. Brevet 3,916,000 (Cl. 260–389 : CO9B) (1975); Chem. Abstr. **84**, 016914 (1976).
14. E. Osawa, Z. Majerski et P. von R. Schleyer. J. Org. Chem. **36**, 205 (1971).
15. W. F. Bailey, R. P. Gagnier et J. J. Patricia. J. Org. Chem. **49**, 2098 (1984).
16. G. Molle, P. Bauer et J. E. Dubois. J. Org. Chem. **47**, 4120 (1982).
17. G. Molle, P. Bauer et J. E. Dubois. J. Org. Chem. **48**, 2975 (1983).
18. P. von R. Schleyer et R. D. Nicholas. J. Am. Chem. Soc. **83**, 182 (1960).
19. R. E. Pincock et E. J. Torupka. J. Am. Chem. Soc. **91**, 4593 (1969).
20. G. Molle et P. Bauer. J. Am. Chem. Soc. **104**, 3481 (1982).
21. H. Stetter et C. Wulff. Ber. **93**, 1366 (1960).
22. H. Koch et J. Franken. Ber. **96**, 213 (1963).
23. F. Blaney, D. E. Johnston, M. A. McKervey et J. J. Roney. Tetrahedron Lett. 99 (1975).
24. A. Schneider, R. W. Warren et E. J. Janoski. J. Am. Chem. Soc. **86**, 5365 (1964).
25. V. S. Landa et Z. Kamycek. Collect. Czech. Chem. Commun. **24**, 4004 (1959).
26. W. Hoek, J. Strating et H. Wynsberg. Recl. Trav. Chim. Pays-Bas, **85**, 1045 (1966).

Can. J. Chem. Downloaded from www.nrcresearchpress.com by 213.166.140.6 on 09/07/12
For personal use only.

Complexes of vanadium(V) with α-hydroxycarboxylic acids studied by ^{1}H, ^{13}C, and ^{51}V nuclear magnetic resonance spectroscopy

M. Madalena Caldeira, M. Luísa Ramos, Nuno C. Oliveira, and Victor M. S. Gil
Department of Chemistry, University of Coimbra, Portugal

Received December 22, 1986

M. Madalena Caldeira, M. Luísa Ramos, Nuno C. Oliveira, and Victor M. S. Gil. Can. J. Chem. **65**, 2434 (1987).

A proton, carbon-13, and vanadium-51 nuclear magnetic resonance study is reported on the number, stoichiometry, geometry, and relative stability of the complexes that form when vanadate(V) solutions are mixed with each one of the following organic α-hydroxyacids in the pH range ~2.5–~7: glycolic, lactic, chloro-3- and phenyl-3-lactic, mandelic, glyceric, and malic acids. The predominant complexes have 1:1 composition (almost certainly in a polymeric structure) in contrast with the 1:2 (metal:ligand) stoichiometry of the corresponding Mo(VI) and W(VI) complexes.

M. Madalena Caldeira, M. Luísa Ramos, Nuno C. Oliveira et Victor M. S. Gil. Can. J. Chem. **65**, 2434 (1987).

On rapporte une étude par résonance magnétique nucléaire du ^{1}H, du ^{13}C et du ^{51}V sur le nombre, la stoechiométrie, la géométrie et la stabilité relative des complexes qui se forment lorsqu'on mélange, à des pH allant de 2,5 à 7, des solutions de vanadate(V) avec l'un des acides α-hydroxylés suivants : acides glycolique, lactique, chloro-3 et phényl-3 lactiques, mandélique, glycérique et malique. Les complexes qui se forment d'une façon prépondérante ont une composition 1 : 1 (presque certainement dans une structure polymérique); ces résultats sont en opposition avec ceux obtenus avec le Mo(VI) et le W(VI) dont les complexes sont de composition 1 : 2 (métal : ligand).

[Traduit par la revue]

Introduction

The biological role of vanadium in living plant and animal tissues recognized in recent years (1) has lent additional importance to the coordination chemistry of this essential element in aqueous solution, a current field of research of great interest.

This paper deals with the complexes that form when vanadate(V) salts are mixed with α-hydroxycarboxylic acids, in aqueous solution, for various pH and concentration conditions. ^{1}H, ^{13}C, and ^{51}V nuclear magnetic resonance spectroscopy is used, since this technique proved to be quite successful in the study of complexation of metal oxoions (MoO_4^{2-}, WO_4^{2-}, UO_2^{2+}) with such ligands (2–6). Advantage is taken of the fact that, at room temperature, ligand exchange is usually sufficiently slow to enable distinct spectra to be obtained for free and bound ligand in the various complexes. Besides ^{1}H and ^{13}C spectra of the ligand, nmr spectra of the coordinated metal (^{51}V) are readily accessible, providing an additional contribution to the full characterization of those systems.

The following acids are used as ligands in this study:

A.	Glycolic acid	CH_2—OH—CO_2H
B.	(L)-Lactic acid	CH_3—CHOH—CO_2H
C.	(L)-Phenyllactic acid	C_6H_5—CH_2—CHOH—CO_2H
D.	(D,L)-Chlorolactic acid	CH_2Cl—CHOH—CO_2H
E.	(L)-Mandelic acid	C_6H_5—CHOH—CO_2H
F.	(D,L)-Glyceric acid	CH_2OH—CHOH—CO_2H
G.	(L)-Malic acid	CO_2H—CH_2—CHOH—CO_2H

Whereas the first five acids of the general formula R—CHOH—CO_2H can behave as bidentate ligands, the last two are potentially terdentate ligands.

The systems vanadate(V) + ligands A, B, E, G have previously been the objects of study by other techniques (potentiometry, conductimetry, spectrophotometry, cryoscopy) and we shall refer to each one in the discussion.

Experimental

Analytical grade ammonium vanadate(V) and commercially available hydroxycarboxylic acids were used (unavailability of the optically active forms in two cases and failure in attempts to resolve the racemic mixture precluded us from also using one of the optical isomers in such cases). To reduce the intensity of the OH nmr signal, the reactants were lyophilized from solution in deuterium oxide, and D_2O solutions were used throughout. Previous to use, lactic, chlorolactic, and glyceric acid solutions in D_2O were heated in boiling water for 2 h to accomplish depolymerization. The concentrations of the vanadate solutions were established by weight and the acid solutions were standardized by potentiometry. The pH was adjusted (cautiously, to reduce the possibility of drastic local disturbances of equilibria that may be slow to disappear) by addition of solutions of DCl and NaOD; the pH* values quoted are the direct pH-meter readings (room temperature) after standardization with aqueous (H_2O) buffers. Whenever necessary, the ionic strength was kept approximately constant by making the solution 1 *M* in KNO_3.

The ^{1}H, ^{13}C, and ^{51}V spectra were obtained on a Varian XL-200 nmr spectrometer. Except for some ^{1}H spectra (recorded at 2°C), all spectra were obtained at probe temperature (21 ± 1°C). The ^{13}C spectra were recorded using proton-decoupling techniques with suppression of the nuclear Overhauser effect; in this manner, temperature fluctuations of the sample were reduced to ca. ± 1°C. Dioxane and DSS were used as internal references for ^{13}C and ^{1}H shifts, respectively, whereas $VOCl_3$ was the external reference for ^{51}V shifts. Typically, spectral widths of 10 000 Hz, acquisition times of 1.5 s, pulse delays of 8–12 s, and 2000 pulses were used when recording ^{13}C spectra. For ^{51}V the corresponding values were 15 000 Hz, 0.5 s, 1 s, and 10–300 pulses.

Results and discussion

Proton, carbon-13, and vanadium-51 nmr spectra were obtained for D_2O solutions of various concentrations (in the range 0.01–1.0 *M* for ^{1}H spectra, 0.2–1.0 *M* for ^{13}C spectra, and 0.01–0.2 *M* for ^{51}V spectra), of different molar ratios (3:1 to 1:3 or 1:4) of the complexing species, and of different pH* values (2.5–7.5). Spectra were recorded after equilibration had been attained; in the case of vanadate(V) + lactic acid, the slowest system to reach equilibrium, this required up to ca. 2 days after addition of the reactants. The number and intensity of ligand (free and bound) signals and their changes with molar ratio and pH, together with the number and intensity of ^{51}V signals due to complexed vanadium, enabled the number of complexes to be established. In favourable cases, Job's plots based on ^{1}H spectral intensities gave direct stoichiometric information.

Printed in Canada / Imprimé au Canada

Can. J. Chem. Downloaded from www.nrcresearchpress.com by 213.166.140.6 on 09/07/12
For personal use only.

TABLE 1. ^{1}H, ^{13}C, and ^{51}V chemical shifts[a] for the system vanadate(V) + glycolic acid

		δ_H	δ_C	δ_V[b]
pH* = 3.1	Free species	4.28 (CH_2)	61.04 (CH_2)	−502.0
			179.37 (CO_2H)	−521.0
	Complex *a*	4.82 (CH_2)[c]	77.58 (CH_2)	−525.6
			182.55 (CO_2H)	
pH* = 5.0	Free species	4.02 (CH_2)	61.99 (CH_2)	−496.5
			181.21 (CO_2H)	−512.3
	Complex *a*	4.82 (CH_2)[c]	77.54 (CH_2)	−525.6
			182.80 (CO_2H)	
	Complex *b*	4.67 (CH_2)[c]	76.30 (CH_2)	−540.8
			183.12 (CO_2H)	

[a]δ values relative to DSS (^{1}H), TMS (^{13}C, using δ_C (dioxane) = 67.4), and external $VOCl_3$ (^{51}V).

[b]For free metal, main signals of $V_{10}O_{28}^{6-}$ only (dominant species in the pH range covered).

[c]At T = 275 K, to avoid interference of the OH peak.

The ^{13}C and ^{1}H chemical shifts observed for the ligand on complexation indicate the groups bound to the metal. Vicinal proton–proton coupling constants are measured in the case of acids C, D, F, G to give information on the conformation of the bound ligand. The ^{51}V line widths for the complexed species range from 240 to 480 Hz in comparison with 200–300 Hz for vanadate solutions.

We shall now present the results obtained with each acid as ligand, and compare with results in the literature, whenever available, provided by other techniques.

(a) Glycolic acid

Irrespective of the vanadate/glycolic acid molar ratio, at pH ≅ 3 only one complex is detected by ^{13}C and ^{51}V nmr, but additional weak signals in the proton spectrum are recorded, revealing the formation of minor species as well. At pH ≅ 5 two dominant complexes are detected and at pH around 7 complexation is almost nonexistent. Table 1 shows the chemical shifts for this system.

It is noted that the ligand ^{1}H and ^{13}C signals shift to high frequency on complexation and the large shifts observed for the CH_2 group (0.7–0.8 ppm for ^{1}H and 14–15 ppm for ^{13}C, at pH* = 5.0) are a clear indication of the involvement of the hydroxyl group in complexation, together with the carboxyl group. The vanadium signal shifts to low frequency by −13 and −28 ppm for the two complexes at pH* = 5.0 with respect to the low-frequency resonance of $V_{10}O_{28}^{6-}$, which is the dominant species in vanadate(V) solutions in similar conditions (7, 13).[1]

The promixity of the proton CH_2 signal of bound ligands to the residual OH resonance did not allow a sufficiently precise determination of the stoichiometry of the complexes by measuring intensity variations with metal:ligand molar ratio, but a rough indication can be obtained that *a* is an *n*:*n* species and *b* an *n*:*m* complex with $n \geqq m$. This is supported by a comparison of ^{13}C intensities for variable molar ratios.

Previous studies of this system were based on potentiometry, leading to the proposal of 4:2 and 2:2 complexes (8, 9) as well as 1:2 species, but only in an excess of glycolic acid (8), and on spectrophotometry, pointing to 1:2 complexation (10). On the other hand, solids of composition 1:2 and 1:1 have been synthesized from vanadyl acetate and glycolic acid (11).

[1]For a review on ^{51}V nmr parameters see ref. 16.

(b) Lactic acid

The results are very similar to those obtained with glycolic acid. Figure 1 shows the ^{51}V spectrum of a 0.20 *M*:0.20 *M* vanadate(V) + lactic acid solution at pH* = 5.2, the formation of a strong complex *a* and a weaker complex *b* being suggested. Figure 2 gives the corresponding proton spectrum, which shows the presence of two additional sets of signals (A_3X spectra) of bound ligand (complexes *c* and *d*). The chemical shifts oberved at pH* = 5.0 are given in Table 2 for complexes *a* and *b*. The Job's plots shown in Fig. 3 suggest that complex *a* is an *n*:*n* species. Complex *b* seems to have an identical composition, but due to the predominance of *a* no unambiguous stoichiometry can be directly inferred from the curve, in spite of the maximum at 1:1 (see discussion of V(V) + malic acid below).

The effect of pH on the formation of *a* and *b* is illustrated in Fig. 4 for two molar ratios.

The conclusion of predominant 1:1 complexation is at variance with a previous spectrophotometric study (10), which pointed to 1:2 complexation, and with a 2:1 complexation proposed on the basis of conductimetric measurements (12). It is also contrary to what happens with Mo(VI) and W(VI), which give 1:2 complexes (4).

(c) Chloro- and phenyl-lactic acids

At low pH, the formation of two complexes (*a* and *b*, *a* being more abundant) is detected with (D,L)-chlorolactic acid, possibly due to the use of the racemic mixture. With (L)-phenyllactic acid only one complex forms, irrespective of pH and concentration conditions. Tables 3 and 4 give the corresponding nmr parameters, including the proton coupling constants arising from ABX analysis of the spectra. At pH ≅ 5, the proton spectrum in the case of vanadate(V) + chlorolactic acid becomes too broad for a complete analysis; this is probably due to a faster exchange of bound ligand, simultaneous with the presence of a third species revealed by the ^{13}C spectra (chemical shifts, identical to those of complex *a* except for -*C*HOH- with a lower δ_C value, seem to suggest that the third complex forms an acid–base pair with complex *a* via deprotonation of the hydroxyl group in -CHOH-).

At pH* = 2.7, the concentrations of bound ligand for various metal:chlorolactic acid ratios are as follows:

	Concentration (*M*)	
V:acid	Complex *a*	Complex *b*
0.2 *M*:0.1 *M*	0.060	0.026
0.1 *M*:0.1 *M*	0.061	0.029
0.05 *M*:0.1 *M*	0.037	0.012

which suggests 1:1 complexation. In line with this, the Job's plot of Fig. 5 clearly shows that the complex with phenyllactic acid has *n*:*n* composition. Again, this is contrary to what happens with W(VI) or Mo(VI), which give 1:2 complexes (4).

Another important difference with respect to W(VI) and Mo(VI) is that phenyllactic acid undergoes a drastic conformational change upon binding to vanadium(V), as the vicinal proton coupling constants clearly show (Table 4). From a mean conformation for the free ligand having a *trans* and a *gauche* HH arrangement, the ligand shows a conformation close to **I** in the *n*:*n* complex with vanadium; the small vicinal couplings are only compatible with approximately *gauche* H atoms. (A similar conformation is assumed by the ligand in the

Can. J. Chem. Downloaded from www.nrcresearchpress.com by 213.166.140.6 on 09/07/12
For personal use only.

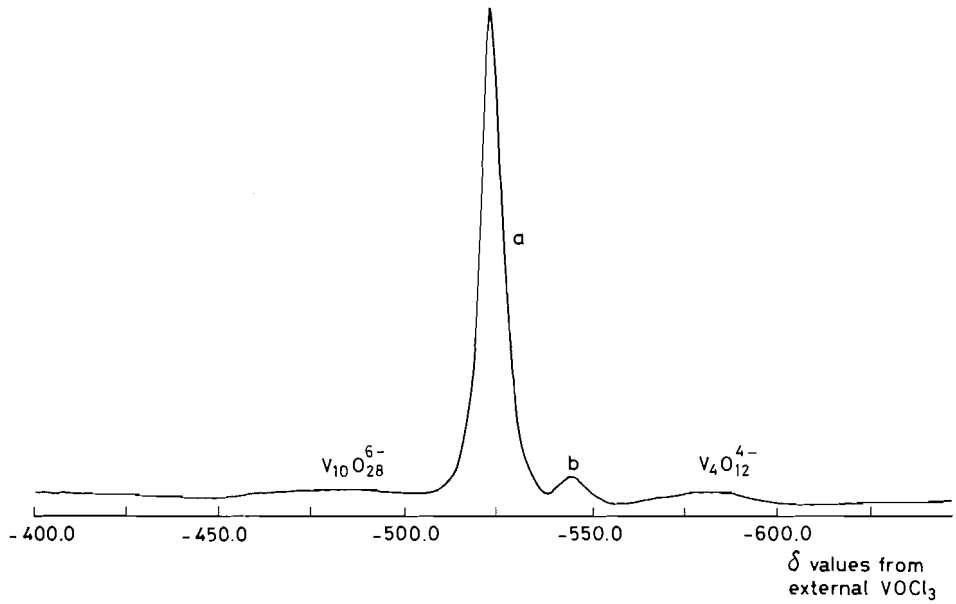

FIG. 1. The 52.6-MHz ^{51}V nmr spectrum of a 0.20 *M*:0.20 *M* D_2O solution of ammonium vanadate(V) and (L)-lactic acid (pH* = 5.2).

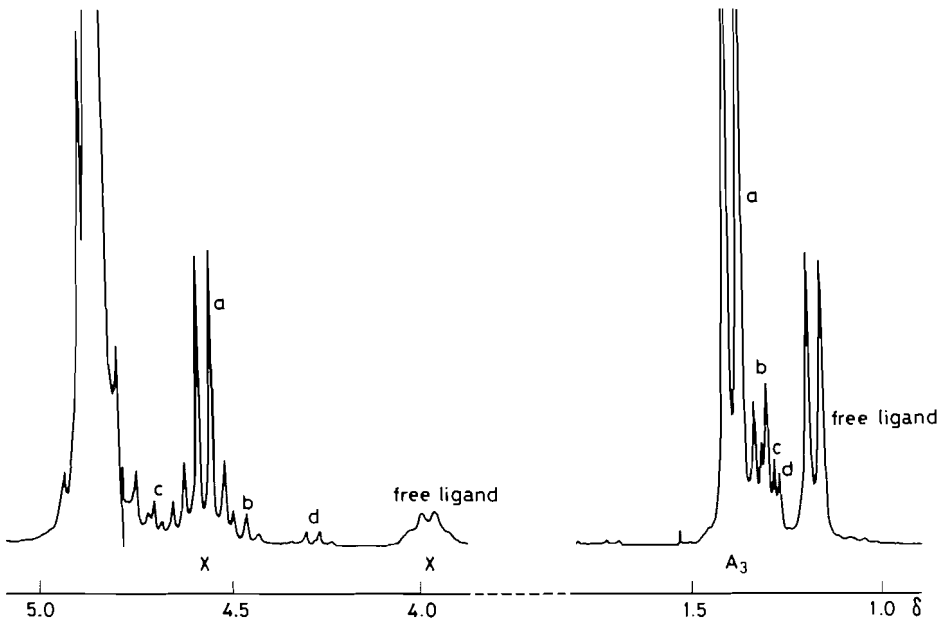

FIG. 2. The 200-MHz ^1H nmr spectrum of a 0.10 *M*:0.10 *M* D_2O solution of ammonium vanadate(V) and (L)-lactic acid (pH* = 5.2, 275 K).

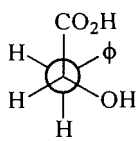

I

complexes of V(V) with chlorolactic acid.) The occurrence of conformation **I**, which is not favoured on grounds of group overcrowding in the ligand molecule, would be difficult to understand in the case of mononuclear 1:1 complex. We take this as an indication of a polymeric species being formed. Other data are, however, necessary before any nonspeculative proposal can be made about its structure.

(d) Mandelic acid

At pH ≅ 3 only one complex forms (complex *a*); at higher pH

TABLE 2. ^1H, ^{13}C, and ^{51}V chemical shifts[a] for the system vanadate(V) + (L)-lactic acid (pH* = 5.0)

	δ_H	δ_C	δ_V[b]
Free species	1.34 (CH_3)	20.48 (CH_3)	−496.5
	4.12 (CH)	69.23 (CH)	−512.3
		183.80 (CO_2H)	
Complex *a*	1.55 (CH_3)	18.87 (CH_3)	
	4.72 (CH)	84.15 (CH)	−525.0
		184.72 (CO_2H)	
Complex *b*	1.48 (CH_3)	18.87 (CH_3)	
	4.63 (CH)	83.13 (CH)	−544.1
		185.30 (CO_2H)	

[a,b]As for Table 1.

Can. J. Chem. Downloaded from www.nrcresearchpress.com by 213.166.140.6 on 09/07/12
For personal use only.

Can. J. Chem. Downloaded from www.nrcresearchpress.com by 213.166.140.6 on 09/07/12
For personal use only.

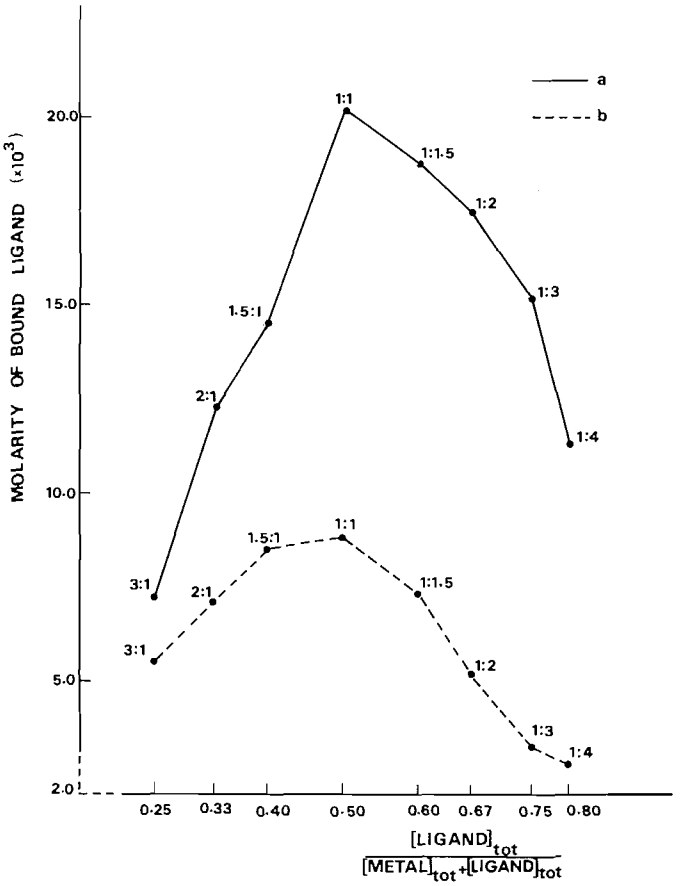

FIG. 3. Job's plots based on proton nmr spectral intensities for the system V(V) + (L)-lactic acid; total concentration of complexing species 0.080 *M* (D_2O solutions, 1 *M* in KNO_3, pH* = 5.0).

another complex (*b*) appears. Complex *a* is always dominant. This is an *n*:*n* species (as shown by a Job's plot at pH* = 2.9); *b* has a maximal concentration at 1.5:1 in a Job's plot at pH* = 5.1 but no direct conclusion on its composition can be obtained from this, because complex *a* dominates. The corresponding chemical shifts are as follows. Complex *a*: $\Delta\delta_{CHOH} = 0.53$, $\Delta\delta_{CHOH} = 14.00$, $\Delta\delta_{CO_2H} = 2.20$ relative to free ligand in the same conditions (pH* = 5.1, $\delta_{CHOH} = 5.02$, $\delta_{CHOH} = 75.99$, $\delta_{CO_2H} = 180.30$), and $\Delta\delta_V = -20.0$ relative to the low-frequency main peak of $V_{10}O_{28}^{6-}$. The equivalent values for complex *b* are, in the same order, 0.28, 12.60, 2.70, and −36.0.

The literature refers to 2:1 (12) and to 4:2, 2:2 (14, 15), and 1:2 (14) complexes on the basis of conductimetric (12, 14), spectrophotometric (14), cryoscopic (14), and potentiometric (15) studies.

(e) Glyceric acid

Two complexes form even at low pH, one (*a*) being always largely dominant. A Job's plot shows that this is an *n*:*n* complex. The corresponding spectral parameters are given in Table 5 for pH* = 3.2 (ABX proton spectrum). At this pH a full analysis of the proton spectrum of complex *a* is possible (not at pH* ≅ 5 due to overlap of the AB signals of the complex and the X signal of free ligand) but the free ligand spectrum is deceptively simple. Most of the signals of complex *b* are superimposed on those of *a*. It is clear that it is the α-hydroxyl group, rather than the β one, that is involved in complexation, together with the carboxyl group.

As for phenyllactic acid, there is a remarkable change in the vicinal HH coupling constants on complexation of glyceric acid

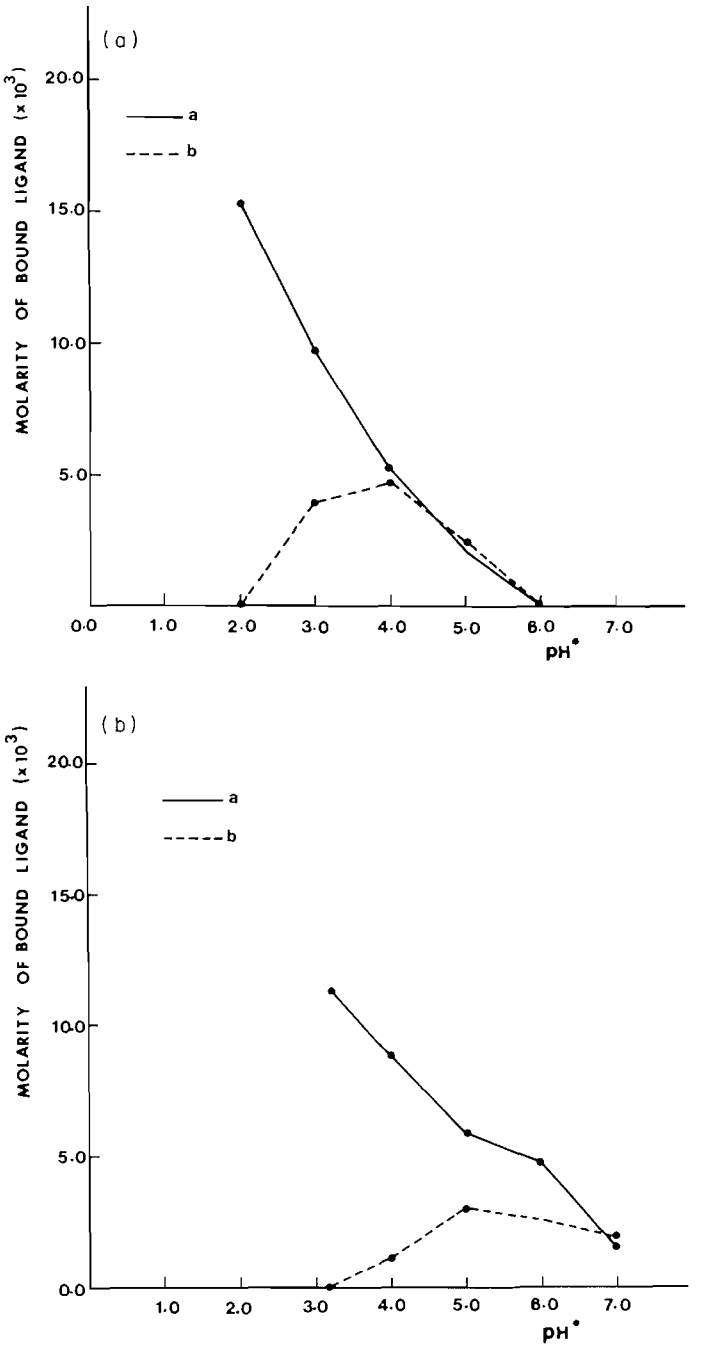

FIG. 4. Effect of pH on the concentration of the complexes V(V) + (L)-lactic acid; (*a*) 0.020 *M*:0.020 *M* (D_2O solution 1 *M* in KNO_3); (*b*) 0.020 *M*:0.040 *M* (D_2O solution 1 *M* in KNO_3).

to vanadium(V): from a sum $J_{AX} + J_{BX} = 8.9$ Hz, which presupposes a *trans* and a *gauche* arrangement of the H nuclei, to a sum of 3.0 Hz, which requires a conformation close to **II** with two *gauche* arrangements. Again, this can only be understood in terms of a special polymeric *n*:*n* structure.

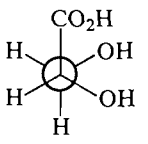

II

(f) Malic acid

Two complexes form in the pH range covered (2.0–6.5): a

Can. J. Chem. Downloaded from www.nrcresearchpress.com by 213.166.140.6 on 09/07/12
For personal use only.

TABLE 3. ^{1}H, ^{13}C, and ^{15}V nmr parameters[a] for the system vanadate(V) + (D,L)-chlorolactic acid (pH* = 2.7)

	δ_H	J_{HH}/Hz	δ_C	δ_V[b]
Free species	3.89 (CH_2, A)	11.9 ($\|J_{AB}\|$)	47.52 (CH_2)	−502.0
	3.98 (CH_2, B)	2.9 (J_{AX})	71.38 (CH)	−521.0
	4.66 (CH, X)	4.3 (J_{BX})	176.19 (CO_2H)	
Complex *a*	4.00 (A)	13.0 ($\|J_{AB}\|$)	46.25 (CH_2)	
	4.11 (B)	2.2 (J_{AX})	85.69 (CH)	−548.5
	4.97 (X)	2.0 (J_{BX})	180.32 (CO_2H)	
Complex *b*	4.20 (A)	9.4 ($\|J_{AB}\|$)	46.25 (CH_2)	
	4.23 (B)	3.0 (J_{AX})	84.58 (CH)	−532.5
	5.00 (X)	2.3 (J_{BX})	180.00 (CO_2H)	

[a,b]As for Table 1.

TABLE 4. ^{1}H, ^{13}C, and ^{51}V nmr parameters[a] for the system vanadate(V) + (L)-Phenyllactic acid (pH* = 4.5)

	δ_H	J_{HH}/Hz	δ_C	δ_V[b]
Free species	2.86 (CH_2, A)	14.0 ($\|J_{AB}\|$)	40.84 (CH_2)	−498.0
	3.09 (CH_2, B)	8.1 (J_{AX})	73.76 (CH)	−514.2
	4.26 (CH, X)	3.9 (J_{BX})	180.80 (CO_2H)	
			138.97 (ϕ; 1)	
			130.30 (ϕ; 2, 6)	
			129.43 (ϕ; 3, 5)	
			127.64 (ϕ; 4)	
Complex	3.09 (A)	14.4 ($\|J_{AB}\|$)	37.66 (CH_2)	
	3.29 (B)	2.1 (J_{AX})	88.67 (CH)	−534.0
	4.91 (X)	4.4 (J_{BX})	182.59 (CO_2H)	
			136.39 (ϕ; 1)	
			131.10 (ϕ; 2, 6)	
			129.43 (ϕ; 3, 5)	
			128.24 (ϕ; 4)	

[a,b]As for Table 1.

TABLE 5. ^{1}H, ^{13}C, and ^{15}V nmr parameters[a] for the system vanadate(V) + (D,L)-glyceric acid (pH* = 3.2)

	δ_H	J_{HH}/Hz	δ_C	δ_V[b]
Free species	~3.63 (CH_2, AB)	$J_{AX} + J_{BX}$ = 8.9	64.20 (CH_2)	−502.0
	4.34 (CH, X)		72.49 (CH)	−521.0
			177.30 (CO_2H)	
Complex *a*	3.83 (A)	10.6 ($\|J_{AB}\|$)	62.56 (CH_2)	
	4.00 (B)	1.0 (J_{AX})	87.70 (CH)	−524.5
	4.62 (X)	2.0 (J_{BX})	181.18 (CO_2H)	
Complex *b*			62.56 (CH_2)	
	4.66 (X)		86.80 (CH)	
			180.58 (CO_2H)	

[a,b]As for Table 1.

complex *a*, which dominates up to pH* ≅ 4.2, and a complex *b*, which becomes the only one detected above pH* ≅ 5. The nmr parameters for pH* ≅ 4.8 are listed in Table 6. According to a Job's plot for pH* = 4.7 (for dilute solutions and in the presence of 1 *M* KNO_3 only complex *b* is detected), *b* is an *n*:*n* complex (Fig. 6). The same conclusion is reached for complex *a* from Job's curves obtained for pH* = 2.9 (Fig. 6): a clear maximum at 1:1 is observed for complex *a*, complex *b* having then only a small concentration. It is interesting to note that at this pH the maximal concentration of *b* occurs for a 2:1 ratio and not for the stoichiometric ratio 1:1 established when *b* is practically the only complex present (pH* ≅ 5). This is an illustration of one of the limitations of Job's continuous variations method: a maximum at the right stoichiometric ratio occurs only if the species is significantly dominant in those conditions. Thus we found no evidence for the 2:1 complexation previously

TABLE 6. ^{1}H, ^{13}C, and ^{51}V nmr parameters[a] for the system vanadate(V) + (L)-malic acid (pH* = 4.8)

	δ_H	J_{HH}/Hz	δ_C	δ_V[b]
Free species	2.49 (CH_2, A)	15.7 ($\|J_{AB}\|$)	42.31 (CH_2)	−496.5
	2.74 (CH_2, B)	8.2 (J_{AX})	70.52 (CH)	−512.3
	4.34 (CH, X)	2.7 (J_{BX})	179.24 (CO_2H, α)	
			176.92 (CO_2H, β)	
Complex *a*	2.99 (A or B)	17.5 ($\|J_{AB}\|$)	39.30 (CH_2)	
	3.06 (B or A)	1.7 (J_{AX} or J_{BX})	84.46 (CH)	−534.4
	4.79 (X)	5.0 (J_{BX} or J_{AX})	183.63 (CO_2H, α)	
			181.39 (CO_2H, β)	
Complex *b*	2.87 (A or B)	15.6 ($\|J_{AB}\|$)	40.56 (CH_2)	
	2.91 (B or A)	4.2 (J_{AX} or J_{BX})	79.50 (CH)	−546.2
	5.26 (X)	9.8 (J_{BX} or J_{AX})	183.71 (CO_2H, α)	
			177.44 (CO_2H, β)	

[a,b]As for Table 1.

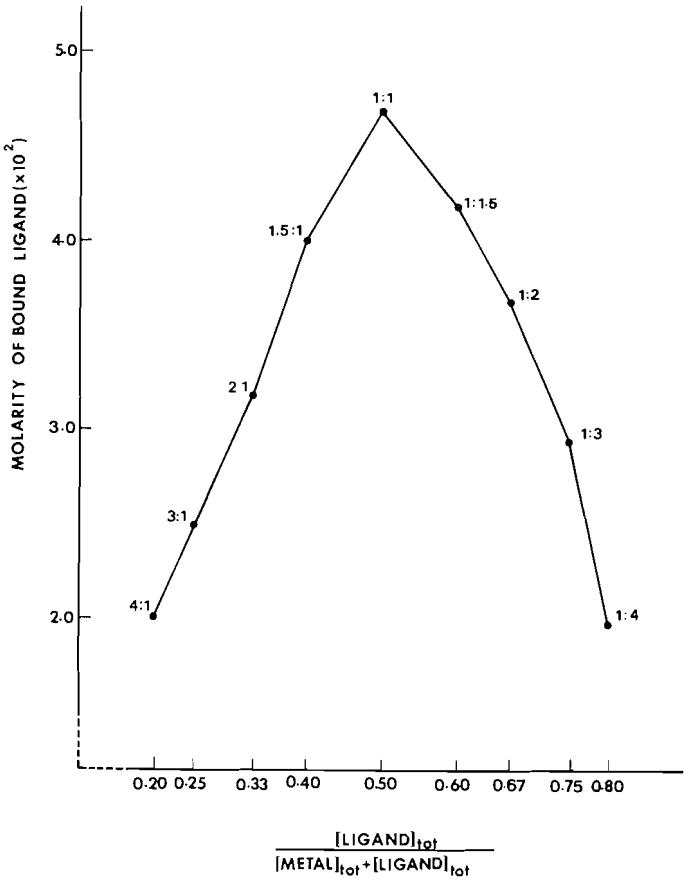

FIG. 5. Job's plots based on proton nmr spectral intensities for the system V(V) + (L)-phenyllactic acid; total concentration of complexing species 0.10 *M* (D_2O solutions, 1 *M* in KNO_3, pH* = 5.5, 275 K).

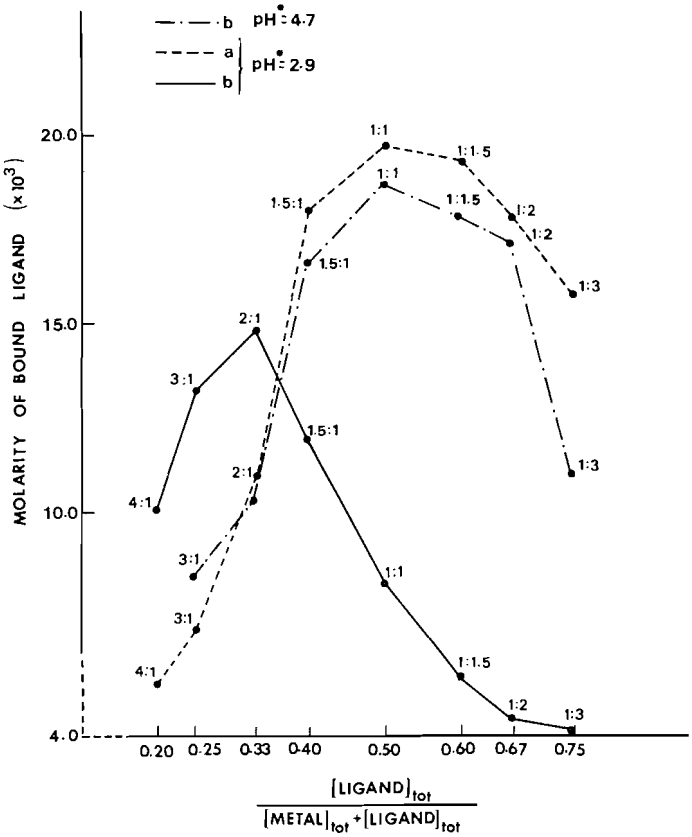

FIG. 6. Job's plots based on proton nmr spectral intensities for the system V(V) + (L)-malic acid; total concentration of complexing species 0.080 *M* (D_2O solutions 1 *M* in KNO_3).

proposed, together with 1:1 complexation, on the basis of a spectrophotometric, conductimetric, and cryoscopic study (14).

The carbon shifts for the carboxyl groups in complex *a* relative to free ligand in the same conditions (Table 6) clearly show that both groups are involved in chelation (together with the hydroxyl group). The situation is different for complex *b* where the ligand is bidentate (the β-carboxyl ^{13}C chemical shift is not significantly affected by complexation), as are the other ligands in this study.

In line with a terdentate function of malic acid in complex *a*, the vicinal coupling constants point to a conformation close to **III**, whereas in complex *b* the couplings presuppose a *trans* and a *gauche* arrangement of H atoms.

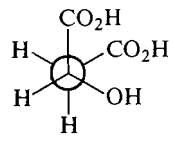

III

Can. J. Chem. Downloaded from www.nrcresearchpress.com by 213.166.140.6 on 09/07/12
For personal use only.

Conclusion

With the exception of (L)-phenyllactic acid, which forms only one strong complex with vanadium(V), all the other α-hydroxycarboxylic acids studied form two strong complexes and, in some cases, one or more minor species, in the pH range covered (~2.5–~7). The concentration of the dominant complex (complex *a*), in some cases the only one detected at pH ≅ 3, steadily decreases on increasing pH, while the concentration of the other (complex *b*) increases up to a point and then both become nearly zero for pH ≅ 6.5. In the case of malic acid as ligand, complex *b*, the least abundant in acidic medium, becomes the only complex detected at higher pH.

The acids act as bidentate ligands, but malic acid also has a terdentate function in complex *a*. The dominant complexes in all cases have *n*:*n* stoichiometry; the other strong complex is either *n*:*n* or *n*:*m* with $n > m$. With the possible exception of malic acid, mainly because of its terdentate function in complex *a*, the dominant *n*:*n* complexes are almost certainly polymeric, having the ligand in a conformation close to **IV** for R = ϕ, OH;

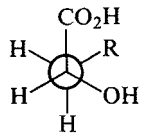

IV

this implies a drastic conformational change of the acid on complexation, which cannot easily be explained if the acid acted as a bidentate terminal ligand in a mononuclear complex. These results can be contrasted with those obtained for the corresponding W(VI) and Mo(VI) systems (4), in which the dominant complexation is 1:2 and no significant ligand conformational changes occur.

The tendency already noted with the proton and carbon chemical shifts in the tungsten and molybdenum complexes (4) is followed by vanadium, namely, the shifts on complexation decrease in the order W(VI) > Mo(VI) > V(V) for -C*H*OH-; they also decrease in that order for -*C*O_2H, but increase for -*C*HOH-.

Acknowledgements

This work is a contribution of the Centro de Investigação em Química, Coimbra, supported by the Instituto Nacional de Investigação Científica of the Portuguese Ministry of Education. The authors are indebted to Prof. C. F. Geraldes for his valuable suggestions in the early stages of this work and for the helpful discussions that followed.

1. N. D. Chasteen. Struct. Bonding (Berlin), **53**, 105 (1983).
2. M. M. Caldeira and V. M. S. Gil. Polyhedron, **5**, 381 (1986), and references therein.
3. M. M. Caldeira, N. C. Oliveira, V. M. S. Gil, and C. F. C. Geraldes. Rev. Port. Quim. **27**, 344 (1985).
4. M. M. Caldeira, M. L. Ramos, and V. M. S. Gil. Can. J. Chem. **65**, 827 (1987).
5. A. M. Cavaleiro, V. M. S. Gil, J. Pedrosa Jesus, R. D. Gillard, and P. A. Williams. Transition Met. Chem. **9**, 62 (1984).
6. M. T. Nunes and V. M. S. Gil. Inorg. Chim. Acta, **115**, 107 (1986), and reference therein.
7. E. Heath and O. W. Howarth. J. Chem. Soc. Dalton Trans. 1105 (1981).
8. B. Viossat. Bull. Soc. Chim. Fr. 113 (1975).
9. M. Bartušek and U. Šustáček. Collect. Czech. Chem. Commun. **48**, 2785 (1983).
10. A. D. Kelkar, G. V. Gholap, P. U. Khadikar, and S. G. Karmalkar. Univ. Indore Res. J.: Sci. **4**, 68 (1977); Chem. Abstr. **90**, 110799h (1979).
11. K. Dey, R. K. Maiti, and A. K. Sinha Roy. Indian J. Chem. Sect. A, **22**, 580 (1983).
12. D. K. Mullick, S. P. Moulik, and B. N. Ghosh. J. Indian Chem. Soc. **40**, 137 (1963).
13. L. Petterson, B. Hedman, A. M. Nenner, and I. Andersson. Acta Chem. Scand. Ser. A: **39**, 499 (1985).
14. F. Preuss and L. Rosenhahn. J. Inorg. Nucl. Chem. **34**, 1691 (1972).
15. J. Simon. Z. Naturforsch. B: Anorg. Chem. Org. Chem. Biochem. Biophys. Biol. **25**, 802 (1970).
16. D. Rehder. Bull Magn. Reson. **4**, 33 (1982).

Can. J. Chem. Downloaded from www.nrcresearchpress.com by 213.166.140.6 on 09/07/12
For personal use only.

Viscosity and density of isomeric butanol/water mixtures as functions of composition and temperature

P. CHANDANI SENANAYAKE, NORMAN GEE, AND GORDON R. FREEMAN
Chemistry Department, University of Alberta, Edmonton, Alta., Canada T6G 2G2

Received February 11, 1987

P. CHANDANI SENANAYAKE, NORMAN GEE, and GORDON R. FREEMAN. Can. J. Chem. **65**, 2441 (1987).

Viscosity and density of 27 binary mixtures of *sec*-, *iso*-, and *tert*-butanol with water were measured at $273 \leq T/K \leq 353$ and the results summarized using polynomials. At fixed T the density depended strongly but monotonically on mole fraction. The excess volume V^E was large and negative. In H_2O/*tert*-butanol as T increased V^E increased, while in H_2O/*sec*- or *iso*-butanol V^E decreased with increasing T. The excess viscosity was large and positive in all cases.

P. CHANDANI SENANAYAKE, NORMAN GEE et GORDON R. FREEMAN. Can. J. Chem. **65**, 2441 (1987).

Opérant à des températures allant de 273 à 353 K, on a mesuré les viscosités et les densités de 27 mélanges binaires d'eau avec les *sec*-, *iso*- et *tert*-butanols et on a résumé les résultats en utilisant des polynômes. A température constante, la densité dépend beaucoup de la fraction molaire, mais d'une façon monotone. La valeur du volume en excès V^E est importante et négative. Dans le mélange H_2O/*tert*-butanol, la valeur de V^E augmente avec une augmentation de la température; par ailleurs, dans les mélanges H_2O/*sec*- ou *iso*-butanol, les valeurs de V^E diminuent avec une augmentation de la température. Dans tous les cas, la valeur de la viscosité en excès est importante et positive.

[Traduit par la revue]

Can. J. Chem. Downloaded from www.nrcresearchpress.com by 213.166.140.6 on 09/07/12
For personal use only.

Introduction

Studies of the reactivity of solvated electrons in hydroxylic solvents utilize values of the dynamic viscosity η in examining diffusion behavior (1–3). Values of η are sometimes not available and must be measured (3). During studies in mixtures of butanols and water (4) viscosity and density values were measured for 27 binary mixtures of water with *sec*-, *iso*-, or *tert*-butanol. The results are reported here.

Experimental

A. Materials

The butanols were obtained from BDH Chemicals: *sec*- (AnalaR, >99 mol%), *iso*- (OmniSolv, >99.0 mol%), and *tert*- (BDH Assured). They were further purified by (*a*) drying for 3 weeks on Davison 3A Molecular Sieves; (*b*) treated for one day at 323 K under argon (Liquid Carbonic Canada Ultra High Purity, >99.999 mol%) with sodium borohydride (~1 g/L); (*c*) fractionally distilled from the borohydride under argon through an 80 cm long by 2.3 cm diameter glass column packed with 3 mm glass helices, discarding the first 15% and last 35%; and (*d*) holding the collected 50% in an argon-pressured syphon system until use. The residual water content was determined by Karl Fischer titration to be 0.05 mol% in *sec*- and *iso*-butanol and 0.03 mol% in *tert*-butanol.

n-Butanol (Aldrich Gold Label, >99 mol%) was bubbled with Linde UHP argon and had 0.05 mol% water by Karl Fischer titration.

Ordinary distilled water was further purified in a SYBRON/Barnstead NANOpure II system.

Aldrich HPLC *n*-heptane (99.9 mol%) and Phillips Petroleum Research Grade *n*-pentane (99.93 mol%), *n*-hexane (99.99 mol%), methylcyclohexane (99.86 mol%) and *n*-octane (99.88 mol%) were (*a*) stirred with concentrated sulphuric acid for 1 day to remove olefins; (*b*) decanted and swirled for 10 min with Davison 5A Molecular Sieves; and (*c*) bubbled with Linde UHP argon.

B. Viscosity measurements

1. Calibration with water

The kinematic viscosity ν (m^2/s) was calculated from the efflux time t measured in Ubbelohde suspended level viscometers 0_c (Schott Geräte #24501-03) and I (Schott Geräte #24501-01). An optical meniscus detection system determined t in units of 0.01 s with a precision of ±0.009% (5).

Viscometer 0_c was calibrated by measuring t for water at $283.00 \leq T/K \leq 342.42$ and comparison with literature ν values using

$$[1] \qquad \nu = At - B/t$$

where A and B are the viscometer constants. Each t was the average of ~6 determinations. Values of ν were obtained from

$$[2] \qquad \nu = \eta/\rho$$

where the dynamic viscosities η (kg/m s = Pa s) were taken from a critical review (6), and ρ were from ref. 7*a*. Values of ν (m^2/s) calculated using $A = 2.8550 \times 10^{-9}\ m^2/s^2$ and $B = 2.2823 \times 10^{-6}\ m^2$ agreed with those in ref. 6 within an average deviation of 0.08%. Equation [1] is the usual calibration relation in the literature. However, the manufacturer's table of Hagenbach corrections to t (8) showed that it used

$$[3] \qquad \nu = Kt - K_E/t^2$$

where K and K_E are the constants instead of A and B. Equation [3] was also used in another work (9). Fitting our t values for water to literature values of ν (m^2/s) yielded $K = 2.8458 \times 10^{-9}\ m^2/s^2$ and $K_E = 3.4223 \times 10^{-4}\ m^2\ s$; however, the average deviation between ν calculated from eq. [3] and the literature values increased to 0.10%. Hence we calculated ν from measured t using eq. [1].

2. Calibration with organic liquids

To calibrate viscometer I water could not be used, because its ν values have too small a range. Organic liquids were used. Although suspended level viscometers were designed to minimize the surface tension effect (10), ref. 11 suggested that calibrating with water, which at 293 K has a surface tension $\sigma = 73 \times 10^{-3}$ N/m (7*b*), would give calibrating constants 1.2% lower than if hydrocarbons or alcohols were used ($\sigma \sim 20$ to 30×10^{-3} N/m (7*b*)). Such an effect was absent in ref. 9 where constants obtained by water calibration gave viscosities of toluene ($\sigma = 29 \times 10^{-3}$ N/m at 293 K (7*b*)) at $298 \leq T/K \leq 368$ agreeing within an average deviation of 0.15% of other values in the literature.

A surface tension effect would affect studies in alcohol–water mixtures as σ changes with composition (7*b*). The possibility of a surface tension effect in the viscometers was investigated by determining flow times t (each being the average of at least three measurements) of *n*-heptane, *n*-octane, and *n*-butanol in the water-calibrated viscometer 0_c. Densities ρ used to calculate the present η are the average of values cited in the viscosity literature sources (12–14). The η values (Table 1) are in general agreement with the rather scattered earlier works and do not support consideration of a surface tension effect in the present work.

At the same time that the organic solvent measurements were done in viscometer 0_c, viscometer I was filled with that solvent and stabilized in the same bath. To calibrate viscometer I, values were correlated by eq. [1]; the resulting $A = 1.0303 \times 10^{-8}\ m^2/s^2$ and $B = 2.3128 \times$

TABLE 1. Comparison of viscosity values

Liquid	T / K	ν^a / 10^{-6} m^2/s	ρ / kg/m^3	η^b This work	Ref. 7c	Ref. 12	Other
n-C_7H_{16}	298.17	0.569	683.8[c]	0.389	0.386	0.392	0.396[d]
n-C_8H_{18}	298.24	0.726	698.4[c]	0.507	0.511	0.514	0.514[d]
n-BuOH	307.84	2.538	798.5[e]	2.027	2.034	2.026	1.993[f]
	318.23	2.005	790.7[e]	1.585	1.579	1.580	1.549[f]

[a]Measured in viscometer 0_c calibrated with water at $283.15 \leq T/K \leq 342.42$, 10^{-4} m^2/s = Stoke.
[b]Dynamic viscosity in 10^{-3} Pa s = 10^{-2} P, see eq. [2].
[c]Average of refs. 12 and 13.
[d]Reference 13.
[e]Average of refs. 12 and 14.
[f]Reference 14.

TABLE 2. Comparison of densities at 298.15 K

Liquid	ρ (kg/m^3) This work	Ref. 12	Other	Δ (%)[a]
n-C_5H_{12}	626.8	626.2	626.3[b]	0.09
n-C_6H_{14}	658.7	659.4	—	−0.11
c-C_6H_{11}—CH_3	769.2	—	769.4[c]	−0.03
n-BuOH	809.5	809.6	809.4[d]	0.00

[a]Average of percent differences from eq. [4].
[b]Reference 13.
[c]Reference 7d.
[d]Reference 14.

10^{-6} m^2 gave calculated ν values that agree with measured values, with an average deviation of 0.06%.

C. Density measurements

The liquid densities were determined from volume changes of a known mass of sample (15). Six Pyrex dilatometers, each consisting of two 1.000 mL pipettes sealed to a 10, 20, or 25 cm^3 bulb, were used. The two pipettes connected in parallel made the cell easier to clean and fill. The samples were sealed in the dilatometer using ground-glass-jointed caps and springs. The mass of sample was the difference between the filled and unfilled dilatometer, weighed at 294 ± 1 K on a Stanton Instruments Ltd. (model C.L.I.) analytical balance. Sample masses of ~9 to ~20 g were measured to 0.1 mg with a precision of ±0.1 mg as determined by repeated weighings of a given mass. The pipette scales were readable to 0.001 mL with a precision of ±0.001 mL. Each dilatometer was calibrated with water with the meniscus at positions covering the entire length of the pipette portion, and at $274.16 \leq T/K \leq 347.93$.

To estimate the reliability of the measurements, densities were measured in four liquids at 293.15 K and compared with values in the literature (Table 2). The percent deviation Δ

$$[4] \qquad \Delta = 100\left(1 - \frac{\text{lit.}}{\text{present}}\right)$$

varied from 0.09% to −0.11%. The reliability of the present densities is indicated by the average percent deviation,

$$[5] \qquad \Delta_{av} = \frac{100}{n}\sum_i |\Delta_i|$$

(n is the number of samples and subscript i denotes the ith sample) which for the liquids in Table 2 was 0.06%.

D. Temperature control

The viscometer or dilatometer was mounted in 4 L bath of light paraffin oil (Fisher Scientific) or of water. The bath was stirred using a propellor that was belt-driven by a Bodine Electric Company induction motor (model NSI-12) at about 1000 rpm. The temperature of the bath was regulated using a platinum resistance detector (Omega Engineering Inc. model TFD) in conjunction with a General Resistance Instruments temperature detector simulator (model RTD-100) in a Wheatstone bridge configuration with a Princeton Applied Research precision lock-in amplifier (model HR-8) as null detector. The lock-in amplifier in turn drove a power amplifier that controlled the heating rate of a Cenco 250 W knife heater. To get more rapid change in temperature, a 1000 W heater plugged into a standard Electrical Products voltage adjuster was used to raise the bath temperature towards the desired value, and then the lock-in amplifier controlled knife heater continued the approach toward constant temperature. At $273 \leq T/K \leq 300$ a Tecumseh (model AE 1343 AA) refrigeration unit pumped Freon-12 through a 5 cm × 10 cm expansion chamber outfitted with aluminum heat dissipation fins which was immersed in the bath, and supplied an ~45 W heat loss to the bath; the knife heater was used to balance this cooling and determined the final temperature.

The stability of the bath temperature was measured, using a second Omega FTD platinum resistance detector, to be ±0.002 K for >2 h. The bath temperature during viscosity or density measurements was recorded to 0.01 K with a Fluke 2189A platinum resistance thermometry system. The system consisted of a factory-matched Fluke 2180A digital thermometer and a Fluke Y2039 resistance temperature probe. Prior to use the system was adjusted at the ice point to 273.15 K; the accuracy at the ice point was ±0.01 K (16*b*). After all measurements were finished, the ice point check was repeated; the drift over the measurement period was less than 0.01 K. The uncertainty in temperature at ~353 K was about twice that at 273.15 K (16*a*). Hence, while the bath stability was ±0.002 K, the accuracy of temperature measurement was ±0.01 K near 273 K and ±0.02 K near 353 K.

E. Mixture composition

As in earlier work (1–3) the alcohol–water mixtures were prepared by volume measurement using pipettes cleaned by (*a*) washing with hot nitric acid; (*b*) many flushes with purified water; (*c*) *n*-hexane; (*d*) drying in an oven reserved for clean glassware. The pipette volumes were calibrated by weighing the delivered mass of water. Mole fractions were determined to ±0.0005.

Results

The density and viscosity of a mixture were measured at fixed mole fraction x as functions of temperature. More generally useful in thermodynamics are ρ and η at fixed T as functions of x. To convert the results the densities and viscosities were fitted with polynomials in temperature, and the fitting parameters were used to interpolate, typically less than 1 degree, to the desired temperatures used in Section D.

A. Temperature dependence of density

The experimental values of the densities ρ (kg/m^3) at the

Can. J. Chem. Downloaded from www.nrcresearchpress.com by 213.166.140.6 on 09/07/12
For personal use only.

TABLE 3. Temperature dependence of density[a]

x_w[b]	T/K[c] range	n[d]	a_0	a_1	$10^3\ a_2$	Δ_{av} (%)[e]	Δ_{max} (%)[f]
			H_2O in *sec*-BuOH				
0.000	283–343	5	1069.1	−0.894		0.08	0.12
0.100	275–353	7	1076.3	−0.902		0.10	0.18
0.200	283–343	5	1084.2	−0.906		0.06	0.08
0.300	275–353	7	1085.3	−0.887		0.08	0.10
0.400	275–353	7	1097.4	−0.896		0.09	0.15
0.500	275–353	7	1105.1	−0.880		0.07	0.12
0.600	284–353	6	1117.7	−0.875		0.08	0.14
0.680	275–353	7	1122.4	−0.842		0.07	0.13
0.970	275–353	7	779.3	1.716	−3.489	0.03	0.05
0.980	275–353	7	717.4	2.086	−3.982	0.02	0.03
0.990	275–353	7	708.3	2.147	−4.027	0.03	0.03
1.000[g]	278–363[g]	20	753.6	1.887	−3.594	0.02	0.05
			H_2O in *iso*-BuOH				
0.000	275–353	7	1037.0	−0.805		0.07	0.11
0.100	275–354	7	1051.1	−0.831		0.06	0.11
0.200	275–349	8	1056.0	−0.828		0.04	0.05
0.300	275–353	7	1067.9	−0.843		0.07	0.12
0.400	275–346	7	1075.9	−0.839		0.05	0.07
0.450	283–346	7	1089.2	−0.863		0.05	0.12
0.990	275–353	7	713.2	2.117	−3.985	0.04	0.06
			H_2O in *tert*-BuOH				
0.000	302–353	4	1121.5	−1.144		0.05	0.07
0.100	293–353	6	1101.0	−1.053		0.10	0.15
0.300	283–348	6	1094.3	−0.980		0.04	0.07
0.500	275–343	6	1105.6	−0.933		0.08	0.13
0.600	284–354	6	1115.8	−0.911		0.04	0.06
0.650	283–348	6	1127.2	−0.913		0.06	0.10
0.750	283–334	6	1136.2	−0.857		0.03	0.04
0.910	283–353	6	1170.3	−0.745		0.03	0.05
0.950	283–353	6	915.8	0.892	−2.374	0.02	0.03

[a]Equation [6], a_i in kg/m^3 K^i.
[b]Mole fraction of water in alcohol.
[c]Measured in 0.01 K.
[d]Number of experimental values.
[e]Average percent deviation of the calculated from the experimental densities.
[f]Largest magnitude of Δ_i.
[g]Reference 7*a*.

conditions listed in Table 3 were fitted to

$$[6] \quad \rho = a_0 + a_1 T + a_2 T^2$$

yielding the parameters values a_i (kg/m^3 K_i) in Table 3. Substituting the calculated ρ for lit. in eq. [4], the average percent deviation (eq. [5]) and largest value of Δ for each mixture fitting were obtained. Except for $x_w \geq 0.95$, a fit with $\Delta_{av} < 0.1\%$ was obtained using $a_2 = 0$. The quadratic term at $x_w \geq 0.95$ reflects the curvature of water density towards a maximum at 277.13 K (7*a*, 17).

Earlier composition studies often concentrate on the water-rich region (18*a*, 18*b*). To compare our results with literature values, densities were generated from eq. [6] and Table 3 at the temperature of the earlier study, for H_2O/*tert*-BuOH at 293.15 and 298.15 K, and for *sec*-BuOH/H_2O at 293.15 and 328.15 K, and then fitted to:

$$[7] \quad \rho\ (\text{kg/m}^3) = \sum_{j=0}^{7} c_j x^j$$

Tables of c_j are available from the Depository of Unpublished Data.[1] Our values were fitted by eq. [7] to $\Delta_{av} \approx 0.02\%$. The same calculated lines fitted literature values to typically <0.1% (11, 17, 19, 20), although one study at $x_w > 0.861$ (18*b*) differed from our and other (11, 19) data by ~0.4%.

B. Temperature dependence of viscosity

Viscosities of liquids (21) and gases (22) are often fitted to polynomials in ln T and powers of T. The present results are represented by:

$$[8] \quad \ln \eta = b_0 + b_1/T + b_2/T^2 + b_3/T^3$$

to ~0.1%. The fitting parameters b_i in K^{-i} were those in Table 4, giving η in 10^{-3} Pa s (= 10^{-2} Poise).

Discussion

The composition dependence of thermophysical properties of binary mixtures are often described in terms of properties that

[1]Complete set of data may be purchased from the Depository of Unpublished Data, CISTI, National Research Council of Canada, Ottawa, Ont., Canada K1A 0S2.

Can. J. Chem. Downloaded from www.nrcresearchpress.com by 213.166.140.6 on 09/07/12
For personal use only.

Can. J. Chem. Downloaded from www.nrcresearchpress.com by 213.166.140.6 on 09/07/12
For personal use only.

TABLE 4. Parameters[a] of temperature dependence of viscosity

x_w[b]	T/K[c] range	n[d]	b_0	$10^{-2}\,b_1$	$10^{-5}\,b_2$	$10^{-8}\,b_3$	Δ_{av} (%)[e]	Δ_{max} (%)[f]
			H_2O in *sec*-BuOH					
0.000	295–343	7	14.1616	−175.968	60.1405	−5.74516	0.01	0.03
0.100	296–363	7	8.50318	−121.966	43.5450	−4.12279	0.03	0.08
0.200	305–353	6	−2.98089	−7.35163	5.74238		0.03	0.07
0.300	297–353	7	−2.39655	−10.6417	6.22064		0.04	0.06
0.400	297–343	6	−2.13835	−12.3782	6.55305		0.02	0.04
0.500	297–343	6	−1.97165	−13.4180	6.76191		0.02	0.04
0.600	297–354	7	−1.50166	−16.3220	7.25580		0.06	0.09
0.680	296–353	8	−1.14159	−18.4122	7.58934		0.03	0.06
0.970	304–353	6	−16.7055	142.879	−47.9283	6.11713	0.03	0.07
0.980	303–354	6	−11.8145	91.3406	−29.8474	3.97164	0.00	0.01
0.990	303–354	6	−14.2332	113.215	−36.26011	4.53677	0.01	0.02
1.000	283–363[g]	9[g]	−9.24096	62.65074	−19.0815	2.53846	0.04	0.09
			H_2O in *iso*-BuOH					
0.000	297–363	8	4.73580	−91.9084	36.8499	−3.74467	0.03	0.07
0.100	299–363	8	−13.7037	89.3958	−22.3706	2.66483	0.07	0.16
0.200	298–354	7	−4.24979	2.84959	3.94311		0.05	0.11
0.300	300–363	8	−2.88761	−5.87670	5.33538		0.07	0.13
0.400	298–363	7	−3.13074	−4.57166	5.17796		0.03	0.05
0.450	299–354	7	−2.68923	−7.55512	5.69054		0.06	0.13
0.990	303–353	6	−1.41213	−13.1455	5.21390		0.08	0.14
			H_2O in *tert*-BuOH					
0.000	305–353	7	−23.0081	218.356	−80.4042	11.0575	0.02	0.04
0.100	305–353	6	3.71664	−58.1758	15.3161		0.05	0.09
0.300	303–343	5	2.32528	−47.1763	13.3169		0.02	0.04
0.500	303–343	5	1.02506	−37.7354	11.7378		0.10	0.19
0.650	303–343	5	1.88409	−41.9617	12.2517		0.04	0.08
0.750	304–353	6	2.31467	−43.6517	12.3264		0.04	0.07
0.910	303–344	5	−34.5271	323.929	−109.382	13.2601	0.00	0.01
0.950	303–344	5	−27.3695	254.761	−87.2164	10.8101	0.01	0.02

[a] b_i in K^{-i}; η in 10^{-3} Pa s.
[b] Mole fraction of water in alcohol.
[c] Measured to 0.01 K.
[d] Number of experimental values.
[e] Average absolute percent deviation; eq. [5] using calculated values as literature.
[f] Largest absolute Δ, eq. [4].
[g] Reference 6.

for ideal mixtures have values Y_{ID} that are additive in mole fraction (18, 21, 23–26):

$$[9] \quad Y_{ID} = x_1 Y_1 + x_2 Y_2$$

where $x_1 + x_2 = 1$ and Y_i is the value for pure component i. The measured Y_{EXPTL} is then related to an excess Y^E where

$$[10] \quad Y^E = Y_{EXPTL} - Y_{ID}$$

A. Excess volume

For density the additive property is molar volume $V = M/\rho$, where M the molar mass for the mixture is $M_M = \sum_i x_i M_i$. The ideal mixture volume V_{ID} is $[(x_w M_w/\rho_w) + (x_A M_A/\rho_A)]$ in our work (subscript w refers to water and A to alcohol).

Example excess volumes V^E calculated by

$$[11] \quad V^E = \frac{M_M}{\rho_{EXPTL}} - V_{ID}$$

from densities obtained from [6] and parameters in Table 3 are compared to literature values (18*c*, 20) in Fig. 1. At 298.15 K the present and ref. 18*c* results in H_2O/*tert*-BuOH were in good agreement (Fig. 1*a*). Reference 18*c* results were expressed as

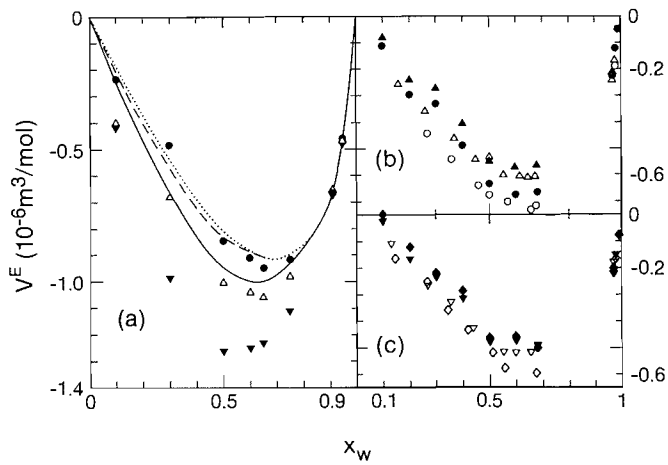

FIG. 1. Excess volume against mole fraction of water in (*a*) *tert*-BuOH at 298.15 K (●, ····), 313.15 K (△, - - -) and 353.15 K (▼, —); (●, △, ▼) are present results and lines are from ref. 18*c*. (*b*) and (*c*) *sec*-BuOH at 278.15 K (○, ●), 298.15 K (△, ▲), 328.15 K (▽, ▼), and 353.15 K (◇, ◆); solid symbols are present values and open symbols are from ref. 20.

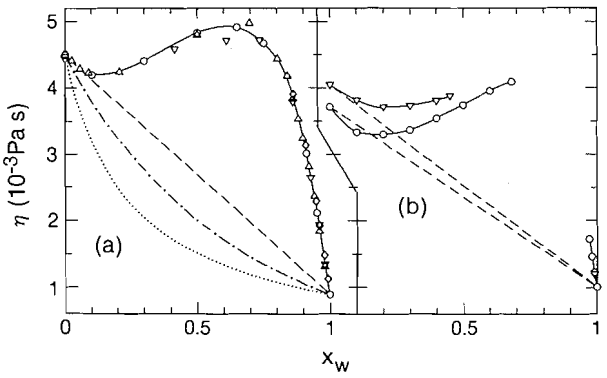

FIG. 2. Dynamic viscosity against mole fraction of water in (*a*) *tert*-BuOH at 298.15 K. η_{EXPTL} are ○ (present work), △ (ref. 11), ▽ (ref. 33), and ◇ (ref. 34). — is empirical; other lines are eq. [12] (· · · ·) and eq. [9] with $Y_i = \eta_i$ (----) or ϕ_i (· · · ·). (*b*) *sec*-BuOH (○) or *iso*-BuOH (▽) at 293.15 K. — is empirical and ---- are eq. [9] with $Y_i = \eta_i$.

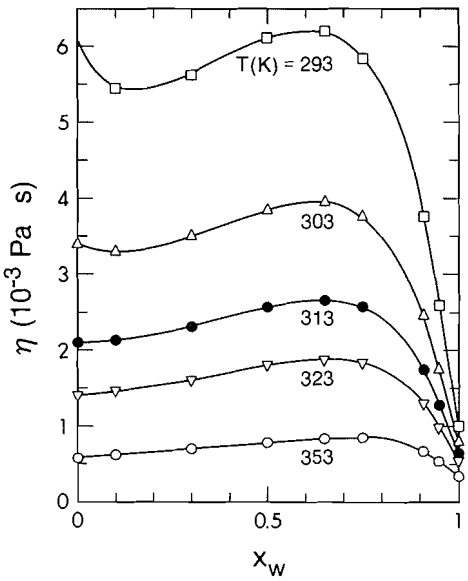

FIG. 3. .Effect of temperature on composition dependence of viscosity of *tert*-butanol/water mixtures. The value of η of pure supercooled *tert*-butanol at 293 K was obtained by extrapolation from higher temperatures.

line graphs and that same notation is used in Fig. 1*a*. The minimum in our V^E plot deepened with increasing temperature to a greater extent than indicated by ref. 18*c*, and the position of the minimum moved toward $x_w = 0.5$.

Figure 1*b* and 1*c* contain the comparison of H_2O/*sec*-BuOH results at 0.1 MPa (20). The V^E values decreased in magnitude as T increased from 278 to 328 K, but on further heating to 353 K remained approximately constant. In H_2O/*iso*-BuOH and H_2O/*sec*-BuOH V^E decreased with increasing T, which indicated that increasing thermal agitation of the molecules made these solutions less nonideal. Tables of V^E illustrating this point along with H_2O/*tert*-BuOH V^E are available from the Depository of Unpublished Data.[1]

B. Viscosity

The main problem in calculating an excess viscosity η^E is the lack of agreement about the form of the ideal mixture viscosity η_{ID}. The problem was examined in detail early in this century

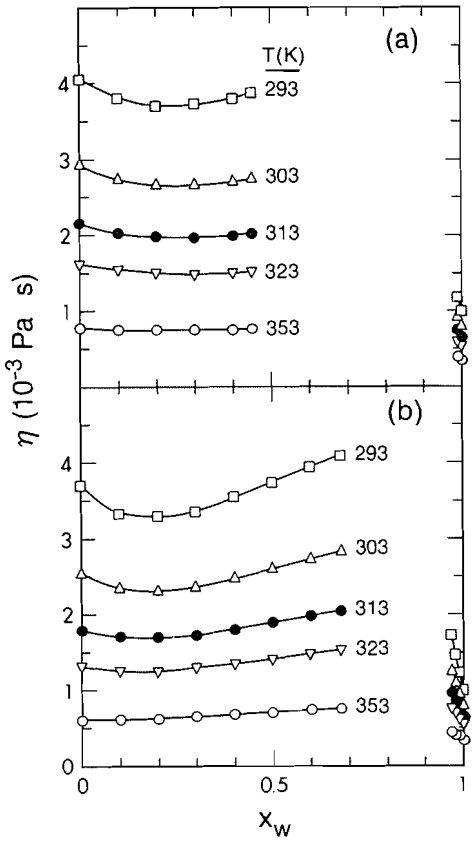

FIG. 4. Effect of temperature on composition dependence of viscosity of (*a*) *iso*-butanol/water; (*b*) *sec*-butanol/water.

(28) but is still apparent in the current literature (21, 23, 24, 27). While eqs. [9] and [10] could be used to define η^E (23, 29) the only mixture in which η could be described by eq. [9] appears to be $H_2O/HDO/D_2O$ (30), in which the components are quite similar. The most widely used relation appears to be that of Arrhenius (31) as modified by Kendall and Monroe from volume fraction to mole fraction (28), η_{AR}, that is eq. [9] with $Y_i = \ln \eta_i$,

$$[12] \quad \ln \eta_{AR} = x_1 \ln \eta_1 + x_2 \ln \eta_2$$

There is also disagreement about whether $[\ln \eta_{EXPL} - \ln \eta_{AR}]$ (21, 24, 30, 32) or $[\eta_{EXPTL} - \eta_{AR}]$ (27) is the more meaningful. Other models are power-root (28, 29) and fluidity $\phi \equiv 1/\eta$ equations (28, 33).

Example curves of η_{EXPTL} obtained from the measurements summarized by the parameters of Table 4 are shown in Fig. 2. For H_2O/*tert*-BuOH and H_2O/*sec*-BuOH the values of η_{EXPTL} in the mixtures near $x_w = 0.6$ were larger than in the pure components. The present values of η_{EXPTL} in H_2O/*tert*-BuOH are in good agreement with earlier values (11, 33, 34), except near $x_w = 0.65$ where refs. 11 and 33 differed by ~3% (Fig. 2). The relative viscosities in ref. 34 were multiplied by $\eta_w = 8.906 \times 10^{-4}$ Pa s for plotting in Fig. 2.

We tested eqs. [12] and eq. [9] with $Y_i = \eta_i$, and ϕ_i. In each case the calculated values were far from η_{EXPTL} (Fig. 2).

We also tested

$$[13] \quad \eta^P = x_1 \eta_1^P + x_2 \eta_2^P$$

with $P = 1/3$ (28), 1/2 (35), or 1/2.5 (36). The curves were intermediate to eq. [12] or [9] with $Y_i = \eta_i$ but all decrease monotonically with increasing x_w. The only clear conclusion

Can. J. Chem. Downloaded from www.nrcresearchpress.com by 213.166.140.6 on 09/07/12
For personal use only.

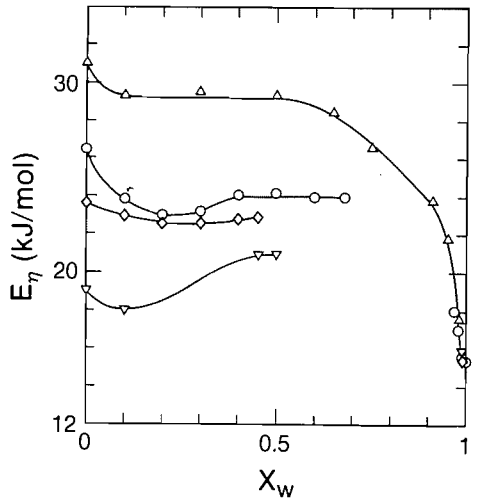

FIG. 5. Variation of energy of activation for viscous flow E_η with composition, over the range $298 < T/K < 353$. △, *tert*-butanol; ○, *sec*-butanol; ◇, *iso*-butanol; ▽, *n*-butanol (ref. 37).

from Fig. 2 is that regardless of the form for η_{ID} the present work indicates a large positive excess viscosity, consistent with stronger hydrogen bonding in the mixture than in the pure components, and consistent with the observed negative excess volume (Fig. 1).

Upon increasing the temperature the viscosities of the pure alcohols and the aqueous mixtures decreased more rapidly than did that of water. The *S*-shapes of the η against x_w curves decreased with increasing temperature (Figs. 3 and 4).

An average Arrhenius temperature coefficient of viscous flow, E_η, was obtained by fitting the measured viscosities over the temperature range $293 < T/K < 353$ to eq. [8] with $b_2 = b_3 = 0$. In this case $E_\eta = b_1 R$, where R is the gas constant. Values of E_η for binary mixtures of the four isomeric butanols with water are plotted in Fig. 5. The viscosity data for 1-butanol (37) have a lower precision (~1%) than those for the other isomers (~0.1%).

Addition of a small amount of water to a butanol disrupts the alcohol liquid structure and decreases the resistance to flow (Fig. 5). Addition of a small amount of a butanol to water stiffens the liquid structure and increases the resistance to flow. In the central composition region the viscosity and its temperature coefficient change relatively little, which probably indicates a relatively random fluid structure.

Acknowledgements

This work was financially assisted by the Natural Sciences and Engineering Research Council of Canada. The help of the staff of the Radiation Research Center in building the viscometry system is gratefully acknowledged.

1. J. CYGLER and G. R. FREEMAN. Can. J. Chem. **62**, 1265 (1984).
2. Y. MAHAM and G. R. FREEMAN. J. Phys. Chem. **89**, 4347 (1985).
3. K. M. IDRISS-ALI and G. R. FREEMAN. (*a*) Rad. Phys. Chem. **23**, 89 (1984); (*b*) Can. J. Chem. **62**, 2217 (1984).
4. P. C. SENANAYAKE and G. R. FREEMAN. J. Phys. Chem. **91**, 2123 (1987).
5. R. J. GARDNER and P. C. SENANAYAKE. Rev. Sci. Instr. **57**, 3129 (1986).
6. J. T. R. WATSON, R. S. BASU, and J. V. SENGERS. J. Phys. Chem. Ref. Data, **9**, 1255 (1980).
7. R. C. WEAST (*Editor*). Handbook of chemistry and physics. 64th ed. CRC Press, Boca Raton, FL. 1983. (*a*) p. F-11; (*b*) pp. F-33 to 36; (*c*) pp. F-39 to F-42; (*d*) p. C-249.
8. Operating Instructions KPG Ubbelohde Viscometers. Schott Geräte, Hofheim a. Ts., F.R. Germany. 1982.
9. D. F. WILLIAMS, C. H. BYERS, and C. R. YOUNG. ORNL/TM-9410. Oak Ridge National Laboratory, Oak Ridge, TN. 1985.
10. L. UBBELOHDE. Ind. Eng. Chem. (Anal. Ed.) **37**, 85 (1937).
11. T. L. BROADWATER and R. L. KAY. J. Phys. Chem. **74**, 3802 (1970).
12. N. B. VARGAFTIK. Tables on the thermophysical properties of liquids and gases. 2nd ed. J. Wiley and Sons, Halsted Press, New York. 1975.
13. A. K. DOOLITTLE and R. H. PETERSON. J. Am. Chem. Soc. **73**, 2145 (1951).
14. M. A. RAUF, G. H. STEWART, and FARHATAZIZ. J. Chem. Eng. Data, **28**, 324 (1983).
15. K. SHINSAKA, N. GEE, and G. R. FREEMAN. J. Chem. Thermodyn. **17**, 1111 (1985).
16. 2189A Thermometry System Instruction Manual. John Fluke Manufacturing Company, Inc. Everett, WA. 1981. (*a*) p. 1; (*b*) p. 8.
17. C. M. SORENSEN. J. Chem. Phys. **79**, 1455 (1983).
18. (*a*) F. FRANK and H. T. SMITH. J. Chem. Eng. Data, **13**, 538 (1968); (*b*) L. AVÉDIKIAN, G. PERRON, and J. E. DESNOYERS. J. Soln. Chem. **4**, 331 (1975); (*c*) C. DE VISSER, G. PERRON, and J. E. DESNOYERS. Can. J. Chem. **55**, 856 (1977).
19. A. HVIDT, R. MOSS, and G. NEILSEN. Acta Chem. Scand. B**32**, 274 (1978).
20. M. S. CHAUDRY and J. A. LAMB. J. Chem. Thermodyn. **18**, 665 (1986).
21. H. VOGEL and A. WEISS. Ber. Bunsenges. Phys. Chem. **86**, 193 (1982).
22. J. H. B. HOOGLAND, H. R. VAN DEN BERG, and N. J. TRAPPENIERS. Physica, **134A**, 169 (1985).
23. H. N. SÓLIMO, R. RIGGIO, J. A. ESPÍNDOLA, S. D. V. ALONSO, and M. KATZ. Can. J. Chem. **54**, 3125 (1976).
24. H. PHUONG-NGUYEN and G. DELMAS. Can. J. Chem. **64**, 681 (1986).
25. O. REDLICH and A. T. KISTER. Ind. Eng. Chem. **40**, 345 (1948).
26. J. C. G. CALADO, H. J. R. GUEDES, M. NUNES DA PONTE, L. P. N. REBELO, and W. B. STREETT. J. Phys. Chem. **90**, 1892 (1986).
27. M. A. POSTIGO, J. L. ZURITA, M. L. G. DE SORIA, and M. KATZ. Can. J. Chem. **64**, 1966 (1986).
28. J. KENDALL and K. P. MONROE. J. Am. Chem. Soc. **39**, 1777 (1917).
29. R. K. HIND, E. MCLAUGHLIN, and A. R. UBBELOHDE. Trans. Faraday Soc. **56**, 328 (1960).
30. J. KESTIN, N. IMAISHI, S. H. NOTT, J. C. NIEUWOUDT, and J. V. SENGERS. Physica, **134A**, 38 (1985).
31. S. ARRHENIUS. Z. Phys. Chem. **1**, 285 (1887).
32. (*a*) L. GRUNBERG and A. H. NISSAN. Nature, **164**, 799 (1949); (*b*) L. GRUNBERG. Trans. Faraday Soc. **50**, 1293 (1954).
33. E. P. IVANY. J. Am. Chem. Soc. **65**, 1392 (1943).
34. M. PALMA and J. P. MOREL. Can. J. Chem. **59**, 3248 (1981).
35. S. WESTMEIER. Z. Phys. Chem. **257**, 950 (1976).
36. B. REISSMANN and H. SCHUBERTH. Z. Phys. Chem. **258**, 983 (1977).
37. (*a*) W. WEBER. Rheol. Acta, **14**, 1012 (1975); (*b*) V. G. KOMARENKO, V. G. MANZHELII, and A. V. RADTSIG. Ukr. Fiz. Zh. **12**, 681 (1967); (*c*) Y. MAHAM and G. R. FREEMAN. J. Phys. Chem. **91**, 1561 (1987), and unpublished data.

Can. J. Chem. Downloaded from www.nrcresearchpress.com by 213.166.140.6 on 09/07/12
For personal use only.

Allomerization of cholic acid and conversion to petromyzonol

XINGPEI ZHU,[1] ETCHRI AMOUZOU, AND STEWART MCLEAN
Department of Chemistry, University of Toronto, Toronto, Ont., Canada M5S 1A1

Received May 13, 1987

XINGPEI ZHU, ETCHRI AMOUZOU, and STEWART MCLEAN. Can. J. Chem. **65**, 2447 (1987).

Petromyzonol, a rare bile substance, has been prepared from an abundant starting material, cholic acid. The critical conversion, the inversion of the configuration at C-5, was accomplished by oxidizing a suitably protected derivative of cholic acid to a 1,4-dien-3-one, which was then stereoselectively reduced to methyl allocholate. In a single oxidation step, the 3-hydroxy steroid was converted to the dienone by Barton's procedure using a catalytic amount of benzeneseleninic anhydride and *m*-iodoxybenzoic acid as the stoichiometric oxidant. The stereoselective reduction employed two steps: hydrogenation of the dienone to the saturated ketone (5α) in the presence of the Wilkinson catalyst, followed by reduction of the ketone with K-Selectride. Finally, methyl allocholate was reduced to petromyzonol with lithium aluminum hydride.

XINGPEI ZHU, ETCHRI AMOUZOU et STEWART MCLEAN. Can. J. Chem. **65**, 2447 (1987).

On a préparé le pétromyzonol, une substance biliaire rare, à partir d'un produit de départ abondant, soit l'acide cholique. La conversion critique, l'inversion de la configuration en C-5, a été réalisée en oxydant un dérivé de l'acide cholique protégé d'une façon appropriée en diène-1,4 one-3 qui est ensuite réduite stéréosélectivement en allocholate de méthyle. En une seule étape d'oxydation et utilisant la technique de Barton qui fait appel à une quantité catalytique d'anhydride benzèneséléninique et à une quantité stoechiométrique d'acide *m*-iodoxybenzoïque comme oxydant, on transforme l'hydroxy-3 stéroïde en dièнone. La réduction stéréosélective implique deux étapes, soit l'hydrogénation, en présence de catalyseur de Wilkinson, de la diénone en cétone saturée (5α), puis la réduction de la cétone par du K-Selectride. Finalement, l'allocholate de méthyle est réduit en pétromyzonol par l'hydrure double de lithium et d'aluminium.

[Traduit par la revue]

Can. J. Chem. Downloaded from www.nrcresearchpress.com by 213.166.140.6 on 09/07/12
For personal use only.

Petromyzonol (**1**) is a rare bile substance produced by the lamprey *Petromyzon marinus* L., but only in its larval form before it becomes parasitic (1). Petromyzonol is required for medical research on hepatic function, but supplies from natural sources are extremely limited.[2] A simple synthesis of petromyzonol from 3α,7α,12α-trihydroxy-5α-cholanic acid (allocholic acid, **2**) has been reported (1), but allocholic acid is, itself, not readily available, and was obtained in small amounts from certain lizards (family Iguanidae). However, its 5β epimer, cholic acid (**3**), is readily available and inexpensive,

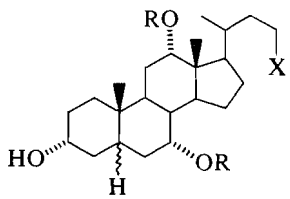

1 5α; R = H; X = CH_2OH
2 5α; R = H; X = COOH
3 5β; R = H; X = COOH
4 5β; R = CHO; X = COOMe
8 5α; R = H; X = COOMe

and is, consequently, an attractive starting material for the synthesis of petromyzonol on a large scale. The key step in the synthesis is the inversion of configuration at C-5 (allomerization). Most allomerization procedures for bile acids depend on the oxidation of ring A to a 4-en-3-one and then stereoselective reduction to a 5α compound, generally by some variant of the Birch reduction (2). Most routes to the enone involve an elimination reaction of a 4-substituted ketone (e.g., dehydrobromination of the 4-bromo ketone). The presence of a 7α hydroxyl group (usually protected as an ester) introduces complications resulting from a facile further elimination to form the 4,6-dien-3-one (2, 3). In such cases, the use of selenium dioxide to oxidize the saturated ketone directly to the 4-en-3-one has been described (4), but later workers (2) report that the method is impractical for synthetic purposes.

The introduction by Barton *et al.* (5) of benzeneseleninic anhydride (BSA) as an oxidizing agent for steroidal ketones provided a number of operational advantages, and the method was improved further when it was shown that BSA could be used in catalytic amounts with *m*-iodoxybenzoic acid as the stoichiometric oxidant (6). (Since the reagent is reduced to *m*-iodobenzoic acid, which can be isolated and oxidized back to the iodoxy level with sodium hypochlorite, the only nonrecoverable oxidizing agent is common bleach.) With this reagent a 3-hydroxycholestane can be oxidized directly to the 1,4-dien-3-one in excellent yield without the necessity of isolating any intermediates.

Consequently, we prepared the 7,12 diformate of cholic acid (7) and converted it to its methyl ester (**4**). The catalytic BSA oxidation (6) of **4** was allowed to proceed as far as the 1,4-dien-3-one **5**, which was isolated in good yield (76%); stopping the oxidation at an earlier stage led to mixtures in which both isomeric enones were present. Removal of the formate groups provided the diol **6**, which was hydrogenated in the presence of chlorotris(triphenylphosphine)rhodium (Wilkinson's catalyst). The course of the reaction was followed by observing the amount of hydrogen consumed and the tlc characteristics of aliquots of the solution. It is subject to a number of experimental variables, including the batch of catalyst used, but it is clear that a rapid reduction is followed by a slower process that forms the saturated ketone; the concentration of this ketone in the mixture increases, but it begins to undergo further reduction before all of the partially reduced material has been converted to saturated ketone. For preparative purposes the hydrogenation was allowed to proceed until the first signs of overreduction appeared, and the products were then separated by chromatography. In this way the saturated 5α ketone **7** was isolated in yields of about 50%; the 5β isomer

[1]On leave of absence from the Department of Chemistry, Beijing Normal University, People's Republic of China.

[2]Personal communication from Dr. M. M. Fisher, Department of Medicine, University of Toronto.

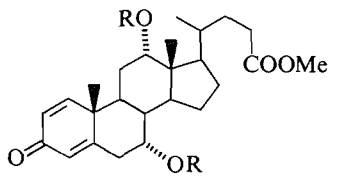

5 R = CHO
6 R = H

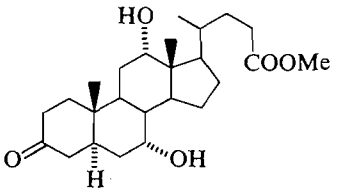

7

could not be detected by tlc. It is apparent that the 7α hydroxyl group now provides a synthetic advantage; steroidal 4-en-3-ones are normally hydrogenated extremely slowly by the Wilkinson catalyst (8), but the catalyst can complex with the 7α hydroxyl group, and then delivery of hydrogen to the 4,5 double bond is accelerated and made highly stereoselective for the α face (9).

Reduction of the ketone **7** with potassium tri-*sec*-butylborohydride (K-Selectride) (10) at low temperature proceeded with very high stereoselectivity to provide the 3α hydroxyl group, and methyl allocholate (**8**) was isolated in 95% yield. Lithium aluminum hydride was used to reduce **8** to petromyzonol (**1**) in excellent yield.

The sequence described constitutes an experimentally useful procedure for the allomerization of common (5β) bile acids incorporating a 7α hydroxyl group (and an oxygen function at C-3). The oxidation sequence is carried out in a single operation and converts the 3-hydroxy compound directly to the dienone in very good yield. The 5α stereochemistry is established with high stereoselectivity in the hydrogenation step; the yield is good, and could effectively be improved by reprocessing partially reduced by-products. Both the yield and the stereoselectivity of the reduction with K-Selectride are excellent. The overall yield from cholic acid to petromyzonol was 32%.

Experimental

Melting points were determined on a Thomas–Kofler micro hot stage. A Perkin–Elmer 243B polarimeter was used. Infrared spectra were recorded on a Nicolet 5DX FTIR spectrometer (samples in KBr discs); the frequency of selected absorptions is reported. Ultraviolet spectra were recorded on a Cary 14 spectrometer; λ_{max} values (samples in 95% EtOH) are reported. Varian XL 400 and XL 200 nmr spectrometers were used. Unless otherwise indicated, samples were dissolved in $CDCl_3$ and reported data are for ^1H spectra at 400 MHz and ^{13}C spectra at 100 MHz; for ^1H spectra, only significant resolved signals are reported as δ_H values, followed in parentheses with an indication of the multiplicity (abbreviated), coupling constants (Hz) if determined, and the number of protons associated with the signal; for ^{13}C spectra, δ_C values are reported, followed in parentheses by a figure indicating the number of protons attached to the carbon as determined by spectral editing.

Methyl 3-oxo-7α,12α-dihydroxy-1,4-choladienate (6)

The 7,12 diformate of cholic acid (7) (1.00 g; 2.16 mmol) was dissolved in a minimum of methanol and treated with diazomethane in ether to provide the methyl ester **4**, which was isolated as a white foam; ^1H nmr (200 MHz): 8.04 (s, 1H), 7.98 (s, 1H), 5.13 (narrow m, 1H), 4.90 (narrow m, 1H), 3.64 (s, 3H), 3.45 (m, 1H), 0.76 (s, 3H), 0.68 (d, *J* 6.0, 3H), 0.57 (s, 3H). Hydroxy ester **4**, *m*-iodoxybenzoic acid (2.42 g, 8.69 mmol), and diphenyl diselenide (0.17 g, 0.54 mmol) were heated in refluxing toluene (50 mL) for 18 h (6). Solvent was removed, leaving a residue that was dissolved in ethyl acetate and extracted with aqueous sodium hydrogen carbonate. The ethyl acetate solution afforded a residue that was flash chromatographed (silica gel, 1:1 ethyl acetate – hexane) to afford the dienone **5** (0.75 g, 1.64 mmol), which, on recrystallization from hexane – ethyl acetate, formed white plates, mp 183–184°C; uv: 244 nm (ε 15 200); ir: 3037, 1730, 1708, 1658, 1622, 1602 cm^{-1}; ^1H nmr: 8.08 (s, 1H), 8.04 (s, 1H), 6.93 (d, *J* 8.4, 1H), 6.25 (dd, *J* 8.4, 1.6; 1H), 6.04 (narrow m, 1H), 5.30 (narrow m, 1H), 5.24 (narrow m, 1H), 3.65 (s, 3H), 1.23 (s, 3H), 0.90 (s, 3H), 0.89 (d, *J* 6.0, 3H). Deformylation was effected by stirring a solution at **5** in methanol with sodium carbonate (ca. 2 equiv.) at room temperature for 1 h. The diol **6** was isolated in quantitative yield and, after recrystallization from acetone, obtained as fine needles, mp 212–213°C; $[\alpha]_D^{22}$ +42.6° (*c* 0.75, $CHCl_3$); uv: 244 nm (ε 18 500); ir: 3500 (br), 1714, 1656, 1617, 1599; ^1H nmr: 7.01 (d, *J* 10.4, 1H), 6.21 (dd, *J* 10.4, 2.4; 1H), 6.06 (t, *J* 2.4, 1H), 4.05 (s, 2H), 3.65 (s, 3H), 1.20 (s, 3H), 1.00 (d, *J* 6.2, 3H), 0.76 (s, 3H); ^{13}C nmr: 186.0 (0), 174.8 (0), 165.8 (0), 156.0 (1), 127.4 (1), 126.7 (1), 72.2 (1), 69.4 (1), 51.5 (3), 46.7 (1), 46.5 (0), 43.1 (0), 41.6 (1), 40.7 (2), 39.9 (1), 37.8 (1), 35.1 (1), 31.0 (2), 30.8 (2), 29.8 (2), 27.3 (2), 23.3 (2), 18.0 (3), 17.1 (3), 12.5 (3). *Anal.* calcd. for $C_{25}H_{36}O_5$: C 72.11, H 8.65; found: C 72.11, H 8.43.

Methyl 3-oxo-7α,12α-dihydroxy-5α-cholanate (7)

A solution of chlorotris(triphenylphosphine)rhodium (640 mg; 0.69 mmol) in 25 mL of a 1:1 benzene–ethanol mixture was pretreated with hydrogen in a hydrogenation flask (8). A solution of the dienone **6** (600 mg; 1.44 mmol) in 25 mL of the same solvent was introduced into the flask and the reaction mixture was stirred vigorously. Aliquots were removed periodically and examined by tlc; optimal conversion was observed after about 25 h. Removal of the solvent then afforded a dark residue, which was dissolved in chloroform and passed through a short column of silica gel with elution by 19:1 chloroform–ethanol. The colorless product was rechromatographed on a silica gel column with elution by 4:1 ether–acetone. The saturated ketone 7 (300 mg; 0.72 mmol) was obtained as the major product; a small amount (30 mg) of overreduced material was isolated, and a fraction (150 mg) consisting of underreduced material was obtained. Recrystallization of 7 from aqueous acetone afforded white crystals, mp 150–152°C (lit. (4) mp 152–154°C); $[\alpha]_D^{23}$ +43° (*c* 2.0, MeOH) (lit. (4) $[\alpha]_D$ +45°); ir: 3405, 1732, 1712 cm^{-1}; ^1H nmr: 3.94 (narrow m, 1H), 3.82 (narrow m, 1H), 3.63 (s, 3H), 0.95 (s, 3H), 0.94 (d, *J* 6.0, 3H), 0.67 (s, 3H); ^{13}C nmr: 213.2 (0), 176.0 (0), 72.6 (1), 67.3 (1), 51.5 (3), 47.2 (1), 46.5 (0), 44.1 (2), 41.2 (1), 39.6 (1), 39.1 (1), 38.7 (1), 38.03 (2), 37.96 (2), 36.5 (2), 35.3 (0), 35.1 (1), 31.0 (2); 30.8 (2), 28.7 (2), 27.3 (2), 23.1 (2), 17.3 (3), 12.6 (3), 10.3 (3).

Methyl 3α,7α,12α-trihydroxy-5α-cholenate (8)

A solution of the ketone **7** (130 mg; 0.31 mmol) in 4 mL of dry tetrahydrofuran at −78°C under nitrogen was treated with 910 μL of 1.0 *M* K-Selectride (Aldrich Chemical Co.), and the reaction mixture was stirred for 5 h at −78°C and then allowed to warm to room temperature. The mixture was treated with 0.5 mL of 10% aqueous sodium hydroxide and 0.5 mL of 30% hydrogen peroxide followed by 5 mL of water. Extraction with ether provided triol **8** (126 mg; 0.30 mmol), which, on recrystallization from dichloromethane–methanol, formed white crystals, mp 226–228°C (lit. (4) mp 225–226°C); $[\alpha]_D^{23}$ +30° (*c* 1.5, MeOH) (lit. (4) $[\alpha]_D$ +28°); ^1H nmr: 4.03 (m, 1H), 3.94 (narrow m, 1H), 3.81 (m, 1H), 3.64 (s, 3H), 0.96 (d, *J* 6.1, 3H), 0.75 (s, 3H), 0.67 (s, 3H); ^{13}C nmr: 174.8 (0), 72.9 (1), 67.9 (1), 66.4 (1), 51.5 (3), 47.1 (1), 46.4 (0), 42.1 (1), 39.7 (1), 39.2 (1), 36.2 (2), 35.8 (0), 35.5 (1), 35.1 (2), 31.9 (1), 31.5 (2), 31.0 (2), 30.9 (2), 28.8 (2), 28.0 (2), 27.3 (2), 23.0 (2), 17.3 (3), 12.6 (3), 10.0 (3).

Petromyzonol (1)

A solution of **8** (24 mg; 0.057 mmol) in 1.5 mL of tetrahydrofuran was added dropwise with stirring to lithium aluminum hydride (8 mg; 0.21 mmol) in 1.5 mL of tetrahydrofuran. The mixture was heated to reflux for 1 h and then stirred for a further 12 h. Hydrolysis by aqueous Rochelle salt (11) with heating to reflux for 1 h and to 60°C for 3 h provided petromyzonol, which was purified by flash chromatography (silica gel, 17:3 chloroform–ethanol) and obtained as white crystals (20 mg; 0.050 mmol), mp 224–226°C (lit. (1) mp 229–231°C) undepressed on admixture with an authentic sample (mp 222–224°C); $[\alpha]_D^{23}$ +29.5° (*c* 1.5, EtOH) (lit. (1) $[\alpha]_D$ 27.5°); ^1H nmr (pyridine-d_5): 5.28 (br, 4), 4.28 (t, *J* 2.5, 1H), 4.24 (t, *J* 2.5, 1H), 4.10 (m, 1H), 3.86 (t, *J* 6.6, 2H), 2.98 (m, 1H), 2.73 (td, *J* 11.5, 7.4; 1H), 2.44

Can. J. Chem. Downloaded from www.nrcresearchpress.com by 213.166.140.6 on 09/07/12
For personal use only.

(td, J 11.5, 7.4; 1H), 2.35 (m, 1H), 1.24 (d, J 6.6, 3H), 0.90 (s, 3H), 0.81 (s, 3H); ^{13}C nmr (pyridine-d_5): 72.4 (1), 67.4 (1), 65.7 (1), 62.8 (2), 47.5 (1), 46.9 (0), 42.8 (1), 40.9 (1), 40.0 (1), 37.9 (2), 36.9 (2), 36.5 (1), 36.3 (0), 32.8 (2), 32.7 (2), 32.0 (1), 30.5 (2), 29.9 (2), 29.5 (2), 28.2 (2), 23.8 (2), 18.0 (3), 13.1 (3), 10.6 (3).

Acknowledgements

Financial support from the Natural Sciences and Engineering Research Council of Canada and the Government of the People's Republic of China (to X.Z.) is gratefully acknowledged. We thank Dr. M. M. Fisher, Department of Medicine, University of Toronto, for bringing petromyzonol to our attention and for providing an authentic sample.

1. G. A. D. Haslewood and L. Tokes. Biochem. J. **114**, 179 (1969).
2. T. Iida, T. Momose, T. Nambara, and F. C. Chang. Chem. Pharm. Bull. **34**, 1929 (1986); T. Iida, T. Momose, F. C. Chang, and T. Nambara. Chem. Pharm. Bull. **34**, 1934 (1986), and references therein.
3. R. A. Leppik. Steroids, **41**, 475 (1983).
4. A. Kallner. Acta Chem. Scand. **21**, 322 (1967).
5. D. H. R. Barton, D. J. Lester, and S. V. Ley. J. Chem. Soc. Chem. Commun. 130 (1978).
6. D. H. R. Barton, C. R. A. Godfrey, J. W. Morzycki, W. B. Motherwell, and S. V. Ley. J. Chem. Soc. Perkin Trans. 1, 1947 (1982).
7. K.-Y. Tserng and P. D. Klein. Steroids, **29**, 635 (1977).
8. C. Djerassi and J. Gutzwiller. J. Am. Chem. Soc. **88**, 4537 (1966).
9. D. A. Evans, M. M. Morrissey, and R. L. Chow. Tetrahedron Lett. **26**, 6005 (1985).
10. D. M. Tal, G. D. Frish, and W. H. Elliott. Tetrahedron, **40**, 851 (1984).
11. B. P. Mundy and J. J. Theodore. J. Am. Chem. Soc. **102**, 2005 (1980).

Can. J. Chem. Downloaded from www.nrcresearchpress.com by 213.166.140.6 on 09/07/12
For personal use only.

An asymmetrical disulfide-containing photoreactive heterobifunctional reagent designed to introduce radioactive labeling into biological receptors

GILLES DUPUIS

Department of Biochemistry, Faculty of Medicine, Université de Sherbrooke, Sherbrooke, Que., Canada J1H 5N4

Received October 22, 1986[1]

GILLES DUPUIS. Can. J. Chem. **65**, 2450 (1987).

The synthesis of succinimido 1-amino-(4-azidosalicyloyl)-3,4-dithio-5-carboxylate, a heterobifunctional photoaffinity labeling reagent, is described. The cross-linker possesses an asymmetrical disulfide bond, and a general method for generating a spacer arm bearing an asymmetrical or symmetrical disulfide bond is detailed. The heterobifunctional reagent has been obtained in a minimum of steps and intermediates have been characterized. It is further shown that the reagent can be trace-labeled with [^{125}I]-iodine and it has been used to modify phytohemagglutinin, a model protein. Upon irradiation, polymeric phytohemagglutinin derivatives are produced, as evidenced by electrophoretic analysis.

GILLES DUPUIS. Can. J. Chem. **65**, 2450 (1987).

On décrit la synthèse du succinimido amino-4 (azido-4 salicyloyl) dithio-3,4 carboxylate-5, un réactif de marquage photoaffinitaire hétérobifonctionnel. L'agent réticulant possède une liaison disulfure asymétrique et on décrit une méthode générale permettant de générer un bras d'espacement portant une liaison disulfure asymétrique ou symétrique. On a obtenu le réactif hétérobifonctionnel en faisant appel à un nombre minimal d'étapes et on a caractérisé les intermédiaires. On a de plus démontré que le réactif peut être marqué à l'état de traces avec de l'iode ^{125}I et on l'a utilisé pour modifier la phytohémaglutinine, une protéine modèle. Par irradiation, il y a formation de polymères dérivés de la phytohémaglutinine qui ont été mis en évidence par analyse par électrophorèse.

[Traduit par la revue]

Can. J. Chem. Downloaded from www.nrcresearchpress.com by 213.166.140.6 on 09/07/12
For personal use only.

Introduction

Affinity labeling is a method that is increasingly used to study the molecular properties of biological receptors (1–4). In general, the strategy involves formation, under physiological conditions, of stable covalent bonds between the ligand and its receptor with the use of a cross-linking reagent. Initially, such cross-linkers were of the symmetrical type (5), but they are being largely replaced by the more versatile heterobifunctional reagents. These reagents are designed in such a manner that one of the functional groups serves to establish selectively a covalent bond with the ligand, while leaving the other function intact. This second reactive group is usually an aryl azide that can be light irradiated to generate a highly reactive nitrene (6, 7). Photoactivation of the ligand–receptor complex results in the formation of stable macromolecular species that can be analyzed by various methods. In this respect, electrophoretic analyses usually performed in the presence of sodium dodecylsulfate (SDS-PAGE)[2] have been mostly employed and have yielded valuable information concerning a variety of biological receptors (references cited in refs. 8 and 9). Such analyses can be greatly simplified if the cross-linked ligand–receptor complexes can be dissociated, as is the case of cross-linkers bearing a disulfide (4, 10–14), an azo or a *cis* glycol bond (15–17), or an ester linkage (18).

Most published reports have used radiolabeling of ligands to facilitate detection of the photolabeled complex. This approach presents disadvantages because some ligands are susceptible to denaturation during oxidative labeling (19) or may lack suitable chemical groups for introduction of label (20). Further, when cross-linked ligand–receptor complexes are dissociated by chemical treatments, radioactive label is no longer associated with the receptor, which then has to be detected by other means. A way of circumventing these problems is to use heterobifunctional reagents that bear a radioactive label. This approach has been used by Ji and Ji (21) who prepared several noncleavable aryl azido heterobifunctional reagents bearing [^{125}I]-substitution on the phenyl ring. Schwartz *et al.* (10) have also reported the synthesis and applications of a disulfide-containing heterobifunctional cross-linker that was asymmetrically [^{35}S]-labeled. Denny and Blobel (9) have described the synthesis and use of [^{125}I]-labeled *N*-4-(*p*-azido-*m*-phenylazo)benzoyl-3-aminopropyl-*N'*-oxysulfosuccinimide ester, a photoactivable heterobifunctional cross-linker that was initially synthesized by Jaffe *et al.* (15) and that can be cleaved by reduction of the azo bond. Recently, Schwartz (18) described a [^{125}I]-radiolabeled cross-linking reagent bearing an ester linkage in the spacer portion of the molecule.

In the present study, I report a facile synthesis of a reagent that possesses properties that make it highly suitable as a tool for study of biological receptors. The reagent embodies a reactive succinimidyl ester, a photolabile aryl azido group, and an easily reducible asymmetrical disulfide bond. Furthermore, the compound can be trace-labeled with 125-iodine, using the method of Bolton and Hunter (22). Photolysis of a model protein derivatized with the [^{125}I]-labeled reagent described here yields the expected products, as evidenced by electrophoretic analysis.

Results and discussion

Heterobifunctional reagent **4** was prepared according to the scheme outlined in Fig. 1. The synthetic route was designed to introduce radiolabel at the last step to minimize handling of radioactive intermediates. Discrete synthetic steps were as follows. 4-Azidosalicylic acid was obtained by a modification of the method of Husain *et al.* (23), by converting 4-aminosalicylic acid into the corresponding diazonium salt and reaction with sodium azide. The corresponding *N*-hydroxysuccinimido ester **1** was prepared in an 85% yield, by reaction of the azido

[1]Revision received June 2, 1987.

[2]The abbreviations used are: DCC, *N,N'*-dicyclohexylcarbodiimide; DCU, *N,N'*-dicyclohexylurea; DMF, *N,N*-dimethylformamide; DMSO, dimethylsulfoxide; TEA, triethylamine; THF, tetrahydrofuran; Su, succinimidyl; m, multiplet; d, doublet; s, singlet; SDS-PAGE, sodium dodecylsulfate-polyacrylamide gel electrophoresis; PHA, phytohemagglutinin from *Phaseolus vulgaris*.

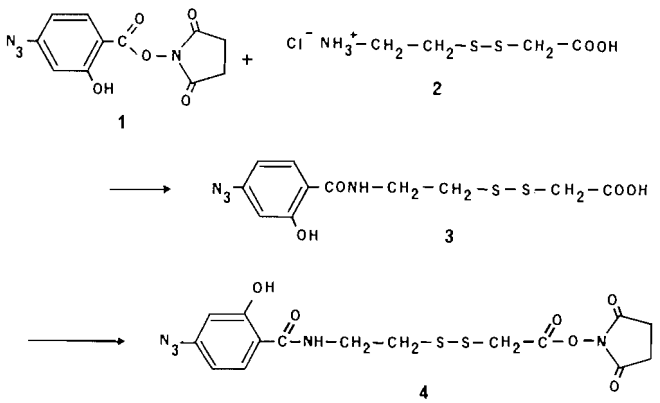

FIG. 1. Outline of the various synthetic steps used to prepare the heterobifunctional reagent **4** described in this study. Active ester **1** was allowed to react with amino acid **2** in the presence of 2 equivalents of triethylamine. Compound **3** was then converted into **4** by reaction with *N*-hydroxysuccinimide in the presence of DCC.

acid with *N*-hydroxysuccinimide in the presence of DCC according to Anderson *et al.* (24). Numerous published procedures were investigated to prepare asymmetrical disulfide **2**. For instance, controlled oxidation of a mixture (various molar ratios) of cysteamine hydrochloride and 2-mercaptoacetic acid, using H_2O_2 (25) or CNBr (26), gave **2** with poor yields. Similarly, attempts at disulfide exchange between cystamine dihydrochloride and 2-mercaptoacetic acid, in refluxing ethanol, met with little success. However, the procedure described by Schöberl and Gräfje (27), who used controlled oxidation of cystamine dihydrochloride with perbenzoic acid to the corresponding thiosulfinate, and reaction with 2-mercaptoacetic acid, proved to be satisfactory. Compound **2** was obtained after chromatographic purification, in a 45% yield, using *m*-chloroperbenzoic acid as oxidant.

Compound **3** was obtained as crystals and with a yield of 63%, by reaction of active ester **1** with asymmetrical disulfide **2**, in the presence of two equivalents of triethylamine. It was found necessary to use an aqueous DMF milieu to keep the amino component in solution. Compound **3** was easily converted into active ester **4** using the conditions described by Anderson *et al.* (24). Heterobifunctional reagent **4** was crystalline and obtained in a 71% yield. The desired product had the characteristics expected for a homogeneous product.

The ultraviolet spectrum of compound **4** is shown in Fig. 2. When aryl azido compound **4** was irradiated, a time-dependent change in its spectrum was observed. The decrease in optical density was interpreted as evidence for light-induced decomposition of **4**. Aryl azido compounds are known to decompose under light irradiation, initially giving nitrene species, followed by further reactions (2). Spectral recordings shown in Fig. 2 demonstrated that compound **4** behaves in a similar manner as other aryl azido compounds, namely, the reagents described by Ji and co-workers (28, 29), Chong and Hodges (30), Jaffé *et al.* (15), and by Dupuis and Radwan (31).

Ji and Ji (21) previously reported that salicylazido compounds can be iodinated by the procedure of Bolton and Hunter (22) if the conditions of reaction are carefully controlled. Using an organic solvent and a short time of reaction, these authors demonstrated that iodine-125 could be introduced on the aromatic ring without appreciable hydrolysis of the oxysuccinimidyl ester. This procedure was used to introduce [^{125}I]-labeling into compound **4**. Aryl azido compound **4**

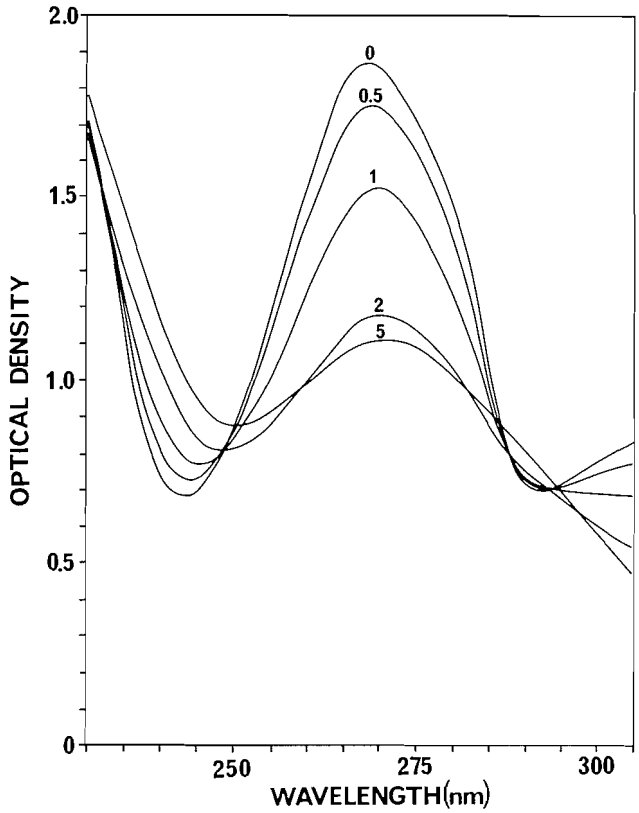

FIG. 2. Light-induced photodecomposition of cross-linking reagent **4**. The reagent was in an ethanolic solution and was irradiated for various periods of time (in minutes, as indicated) with an ultraviolet lamp as previously described (31).

was treated with one equivalent of chloramine T and Na[^{125}I] in acetone for 5–6 min at room temperature. Chloramine T/compound **4** molar ratios higher than unity led to labelled compounds that migrated in system III as multiple spots (autoradiography) with a main component of R_f^{III} 0.8, along with another spot of R_f^{III} 0.6. The fast moving compounds were thought to result from self-iodination of chloramine T. This interpretation was confirmed by allowing Na[^{125}I] to react with chloramine T under conditions described for labeling compound **4**. Chromatographic analyses (tlc) revealed (autoradiography) a profile of labeled products identical to the fast moving compounds (data not shown). Iodogen (32) behaved in a manner similar to chloramine T. The desired labeled compound **4** was freed of impurities resulting from self-iodination of chloramine T by purification on a silicic acid column. This procedure, however, did not resolve labeled and unlabeled reagents. Both compounds migrated on tlc plates at the same position as evidenced by a phenol-positive and light-sensitive spot that was superimposed on an intense radioactive spot (autoradiogram).

The use of compound **4** was investigated with a model protein. Phytohemagglutinin (PHA) from *Phaseolus vulgaris*, a tetrameric protein composed of noncovalently associated subunits (33), was allowed to react with the mixture of labeled and unlabeled heterobifunctional reagents under conditions similar to those described by Bolton and Hunter. It was found that the degree of PHA labeling was dependent on the concentration of lectin used. For instance, when the reaction was carried out at a 8 μM concentration (1 mg/mL) of PHA, the modified lectin had an activity of 3×10^5 cpm/mg.

Can. J. Chem. Downloaded from www.nrcresearchpress.com by 213.166.140.6 on 09/07/12
For personal use only.

Can. J. Chem. Downloaded from www.nrcresearchpress.com by 213.166.140.6 on 09/07/12
For personal use only.

However, when the concentration of lectin was increased by a factor of five and two treatments with the mixture of reagents were done, the protein had an activity of 7×10^5 cpm/mg. SDS-PAGE analysis of the labeled protein showed the presence of a unique protein band of M_r 29 800 ± 1 500 daltons (data not shown). This value is in agreement with results reported for the PHA subunits (33). When the modified lectin was irradiated and the products were analyzed by SDS-PAGE, the autoradiograms (data not shown) revealed the presence of bands corresponding to PHA monomer (28 000 ± 2 000), dimer (64 000 ± 4 300), trimer (80 000 ± 5 400), and faint bands that remained on top of the gel and that probably were multimeric subunits (31).

Because the reagent described in this report possesses the essential feature of being cleavable by reduction, a number of reducing compounds were evaluated for their ability to break its disulfide bond. Whereas the heterobifunctional reagent, in methanolic solution, could be easily reduced (20 min treatment) by treatment with sodium borohydride, it was only partially reduced by Cleland's reagent (DL-dithiothreitol, DTT) or by 2-mercaptoacetic acid but was not cleaved by reaction with 2-mercaptoethanol. Efficiency of reduction was evaluated by tlc in system II. However, when the reagent was covalently bound to PHA, only DTT and 2-mercaptoethanol proved to be effective to reduce the cross-linker disulfide bond, as evidenced by electrophoresis.

Conclusion

The heterobifunctional cross-linker described in this study is easy to synthesize and can be readily [^{125}I]-labeled and freed of unwanted side products by a simple chromatographic procedure. The method of disulfide bond formation described here should be of general applicability for synthesis of either symmetrical or asymmetrical heterobifunctional reagents, varying in the length of the spacer. It can be argued that although disulfide-containing compounds are prone to sulfur exchange, they can be used with sulfhydryl or disulfide-containing proteins, under controlled conditions of pH (13, 34–36). Preliminary experiments suggest that reagent **4** is of general applicability for the study of peptide hormone-receptor (Dupuis and Lehoux, unpublished).

Experimental

Chemicals were obtained from Sigma Chemical Co. (St Louis, MO), Aldrich Chemical Co. (Milwaukee, WI), from Fisher Scientific Co., or from Canlab (Montreal). [^{125}I]-iodine was from Amersham (Oakville, Ontario). Petroleum ether was the fraction boiling at 55–110°C. All evaporations were performed under reduced pressure at 40–45°C, with a rotary evaporator. Melting points were determined in capillary tubes on a Tottoli apparatus and are not corrected. Elemental analyses were determined by Galbraith Laboratories (Knoxville, TN). The ^{1}Hmr spectra were recorded on a Varian T-60 spectrometer. Chemical shifts are presented in parts per million (δ) with reference to tetramethylsilane as an internal standard. Infrared (ir) spectra were determined with a Perkin–Elmer spectrometer, model 457. Ultraviolet spectra were recorded with a Perkin–Elmer Lambda 5 instrument.

Analytical thin-layer chromatographic (tlc) analyses were performed on 0.5 mm thick silica gel G (Sigma) plates and compounds were revealed by spraying with the Ellman reagent (37), ninhydrin (38), diazotized *p*-nitroaniline followed by sodium hydroxide (39), or by exposure to ultraviolet radiation. The following chromatographic systems were used: system I, 1-butanol – acetic acid – water (3:1:1); system II, benzene–chloroform – ethyl acetate – acetic acid (1:1:1:0.1), and system III, toluene–chloroform – ethyl acetate – acetic acid (1:1:1:0.1). Currix RP1 X-ray films (Agfa–Gevaert, Belgium) were used for autoradiographies.

Synthesis of compounds

Reactions involving aryl azido compounds were carried out under dim incandescent light.

4-Azidosalicylic acid

This compound was prepared by modification of a described procedure (23). 4-Aminosalicylic acid (20.6 g; 0.15 mol) was dissolved in concentrated H_2SO_4 (50 mL) and the solution added slowly to ice-cold water (300 mL). To the ice-cold suspension was added an aqueous solution (125 mL) of sodium nitrite (13.0 g; 0.18 mol), portionwise, over a period of 20 min. Crystalline urea was added to decompose excess nitrous acid, the solution was transferred to a 4-L beaker, and an aqueous solution (100 mL) of sodium azide (20.0 g; 0.18 mol) was slowly added at 0°C. After evolution of nitrogen ceased, the suspension was further stirred for 20 min at 0°C, in the dark. The azido compound was collected by filtration, washed with ice-cold water, and crystallized from aqueous ethanol. Yield, 16.0 g (67%); mp 197°C (dec.) (lit. (23) mp 193–195°C).

*Succinimido 4-azidosalicylate (**1**)*

4-Azidosalicylic acid (3.6 g; 0.020 mol) was dissolved in CH_2Cl_2 (50 mL) and DMF (50 mL) and *N*-hydrosuccinimide (2.5 g; 0.022 mol), recrystallized from ethyl acetate, was added. The solution was cooled in an ice bath and DCC (4.2 g; 0.020 mol) in DMF (10 mL) was added. The reaction was stirred overnight at 4°C and DCU was removed by filtration. Evaporation afforded a solid that crystallized from ethyl acetate – petroleum ether. Yield, 4.7 g (85%); mp 160–161°C; R_f^{II}, 0.7; ^{1}Hmr ($CDCl_3$/DMSO-d_6): 2.87s (4H, succinimidyl protons), 6.67m and 7.83d (3H, aromatic protons). *Anal.* calcd. for $C_{11}H_8N_4O_5$ (276.2): C 47.83, H 2.92, N 20.29; found: C 47.74, H 3.12, N 20.28.

*1-Amino-3,4-dithio-5-carboxylic acid (**2**)*

This compound was prepared by modification of a described procedure (27). Cystamine dihydrochloride (11.3 g; 0.050 mol) was dissolved in absolute methanol (500 mL), the solution cooled at 4°C, and a chloroform solution (150 mL) of 3-chloroperbenzoic acid (10 g; 0.058 mol) was added dropwise, at 4°C. The reaction was further stirred in the cold room overnight and for 2 additional hours at room temperature. The mixture was evaporated, treated with ether, and the solid was suspended in absolute methanol (300 mL). Freshly distilled 2-mercaptoacetic acid (9.2 g; 0.05 mol) in methanol (50 mL) was added, and the reaction was allowed to proceed, under stirring, for 2 h at room temperature. Evaporation gave an oil that was triturated with ether and crystals were obtained from ethanol–ether. These crystals were unreacted cystamine dihydrochloride (^{1}Hmr, tlc). The oily filtrate was evaporated on silica gel G 60 (Merck) and dried in a desiccator overnight. The solid was poured into a Mitchel–Miller column (Ace Glass, Vineland, NJ) (3 × 30 cm) containing silica gel G 60 and eluted with chloroform (400 mL), ethyl acetate (400 mL), and with 5% (500 mL), 10% (500 mL), and 25% methanol (1000 mL) in ethyl acetate. Compound **2** was located (tlc) in the 25% methanol eluates. Crystals were obtained from methanol – ethyl acetate. Yield, 4.6 g (45%); R_f^I, 0.5. Compound **2** was slightly contaminated with cystamine dihydrochloride (R_f^1, 0.1) and no satisfactory elemental analysis could be obtained; ^{1}Hmr ($CDCl_3$/DMSO-d_6): 3.10m (4H, —CH_2—CH_2—S) and 3.30s (2H, S—CH_2—COOH).

*N-(4-Azidosalicyloyl)-1-amino-3,4-dithio-5-carboxylic acid (**3**)*

Disulfide **2** (3.0 g; 14.6 mmol) was dissolved in 50% aqueous DMF (50 mL) and the solution cooled in an ice bath. The pH was adjusted to 7–8 (wet pHydrion paper) by addition of TEA. Active ester **1** in DMF (40 mL) was then added and the solution was stirred at room temperature while pH was maintained at 7–8 by addition of TEA. After 16 h, the mixture was evaporated and distributed between ethyl acetate and 1 *M* citric acid. The organic phase was washed with 1 *M* citric acid, water, dried, and evaporated. The solid crystallized from ether – petroleum ether or from aqueous methanol. Yield, 3.0 g (63%); mp 99–101°C; R_f^{II}, 0.6; ^{1}Hmr ($CDCl_3$/DMSO-d_6): 3.00m (2H, CH_2—COOH), 3.3m (4H, NH—CH_2—CH_2), 6.50m and 7.80d (3H, aromatic protons). *Anal.* calcd. for $C_{11}H_{12}N_4O_4S_2$ (328.4):

C 40.23, H 3.68, N 17.06, S 19.53; found: C 40.72, H 3.95, N 17.15, S 19.15.

Succinimido 1-amino-(4-azidosalicyloyl)-3,4-dithio-5-carboxylate (4)

Compound **3** (984 mg; 3.0 mmol) was dissolved in THF (10 mL), *N*-hydroxysuccinimide (380 mg; 3.3 mmol) was added, and the solution cooled in an ice bath. DCC (618 mg; 3.0 mmol) in THF (3 mL) was added and the mixture stirred for 30 min at 4°C and overnight at room temperature. DCU was filtered and the filtrate evaporated. Evaporation from petroleum ether afforded a solid that crystallized from ethyl acetate – petroleum ether. The molar extinction coefficient was 16 000, when measured in absolute ethanol at 271 nm. Yield, 0.9 g (74%); mp 137–138°C; R_f^{II}, 0.6; R_f^{III}, 0.6; ir (Nujol): 2100 (-N_3), 1730 (-*CO*—N-oxysuccinimidyl) and 1635 (-*CO*—NH) cm^{-1}; ^{1}Hmr ($CDCl_3$/DMSO-d_6): 2.87s (4H, succinimido protons), 3.10m (4H, NH—CH_2—CH_2), 3.83s (2H, CH_2—COOH), 6.50m and 7.77d (3H, aromatic protons). *Anal.* calcd. for $C_{15}H_{15}N_5O_6S_2$ (425.4): C 42.34, H 3.55, N 16.46, S 15.07; found: C 42.78, H 3.78, N 16.12, S 14.95.

[^{125}I]-labeling of compound 4

Compound **4** (11 mg; 25 μmol) was dissolved in acetone (1 mL) and 5 μL (500 μCi) of carrier-free Na[^{125}I] neutralized with 0.01 *M* HCl (5 μL) was added. A 50% aqueous solution of chloramine T (7 mg; 25 μmol) in acetone (1 mL) was added in one portion and the reaction was allowed to proceed for 6 min. The reaction mixture was added onto a dry column (1 × 25 cm) of silica gel G 60 and elution was done by percolating solvent mixture III. Fractions were collected automatically. Under these conditions, the desired compound was freed of Na[^{125}I] that was retarded and from iodinated side products that move ahead of labelled compound **4**. Radioactive **4** was obtained by pooling and evaporating (nitrogen stream) the appropriate fractions (tlc, system III). It had an R_f value of 0.6 in system III. The labeled reagent was kept in acetone at −20°C. Under these conditions, the reagent was stable for several weeks.

Derivation of phytohemagglutinin and photolysis

Purified (33) PHA (1 mg; 7.7 μmol) in 0.1 *M* sodium borate buffer, pH 8.3 (200 μL), was added to a tube (0.5 mL) containing the mixture of [^{125}I]-labeled and unlabeled compounds **4** (30×10^6 cpm) deposited on the walls of the flask by evaporation (stream of nitrogen) of an acetone solution. The mixture was stirred for 15 min at room temperature and then allowed to react for 15 min with a second portion of labeled reagent. The reaction mixture was diluted with 0.1 *M* phosphate buffer, pH 6.6 (700 μL), dialyzed against water (200 mL) containing 10 g of mixed-bed resin RG501-X8 (Bio-Rad) for 60 min at room temperature. The suspension was cleared by centrifugation. The modified lectin was irradiated for 15 min with an ultraviolet lamp (Black-Ray lamp, Ultra-Violet Products Inc., San Gabriel, CA) placed at 10 cm from the samples that were cooled with a stream of air. SDS-PAGE analysis was done as before (31).

Acknowledgements

The author expresses his thanks to the Medical Research Council of Canada for financial support (grant MT 6343), Mrs. Bânû Bastin for assistance, and Mrs. Madeleine Paquin for typing the manuscript.

1. V. Chowdhry and F. H. Westheimer. Annu. Rev. Biochem. **48**, 293 (1979).
2. J. V. Staros. Trends Biochem. Sci. **5**, 320 (1980).
3. J. R. Knowles. Acc. Chem. Res. **5**, 155 (1972).
4. H. Bayley. *In* Laboratory techniques in biochemistry and molecular biology. *Edited by* T. S. Work and R. H. Burdon. Elsevier, Amsterdam. 1983.
5. T. H. Ji. Biochim. Biophys. Acta, **559**, 39 (1979).
6. H. Bayley and J. R. Knowles. Methods Enzymol. **46**, 69 (1972).
7. G. W. J. Fleet, R. R. Porter, and J. R. Knowles. Nature (London), **224**, 511 (1969).
8. T. H. Ji. J. Biol. Chem. **252**, 1566 (1977).
9. J. B. Denny and G. Blobel. Proc. Natl. Acad. Sci. U.S.A. **81**, 5286 (1984).
10. M. A. Schwartz, O. P. Das, and R. O. Hynes. J. Biol. Chem. **257**, 2343 (1982).
11. K. Peeters and F. M. Richards. Annu. Rev. Biochem. **46**, 523 (1977).
12. A. J. Lomant and G. Fairbanks. J. Mol. Biol. **104**, 243 (1976).
13. K. Wang and F. M. Richards. J. Biol. Chem. **249**, 8005 (1974).
14. D. J. Kiehm and T. H. Ji. J. Biol. Chem. **252**, 8524 (1977).
15. C. L. Jaffe, H. Lis, and N. Sharon. Biochemistry, **19**, 4423 (1980).
16. L. C. Lutter, F. Ortanderl, and H. Fasold. FEBS Lett. **48**, 288 (1974).
17. D. T. Browne and B. H. Kent. Biochem. Biophys. Res. Commun. **67**, 126 (1975).
18. M. A. Schwartz. Anal. Biochem. **149**, 142 (1985).
19. I. Ji, B. Y. Yoo, C. Kaltenbach, and T. H. Ji. J. Biol. Chem. **256**, 10853 (1981).
20. I. Ji and T. H. Ji. Proc. Natl. Acad. Sci. U.S.A. **78**, 5465 (1981).
21. T. H. Ji and I. Ji. Anal. Biochem. **121**, 286 (1982).
22. A. E. Bolton and N. M. Hunter. Biochem. J. **133**, 529 (1973).
23. S. N. Husain, B. Gentile, R. R. Sauers, and A. Eichholz. Carbohydr. Res. **18**, 57 (1983).
24. G. W. Anderson, J. E. Zimmerman, and F. M. Callahan. J. Am. Chem. Soc. **86**, 1839 (1964).
25. D. T. McAllan, T. V. Cullum, R. A. Dean, and F. A. Fidler. J. Am. Chem. Soc. **73**, 3627 (1951).
26. O. Abe, M. F. Lukacovic, and C. Ressler. J. Org. Chem. **39**, 253 (1974).
27. A. Schöberl and H. Gräfje. Annalen, **617**, 71 (1958).
28. E. F. Vanin and T. H. Ji. Biochemistry, **20**, 6754 (1981).
29. T. H. Ji. J. Biol. Chem. **252**, 1566 (1977).
30. P. C. S. Chong and R. S. Hodges. J. Biol. Chem. **256**, 5064 (1981).
31. G. Dupuis and F. Radwan. Can. J. Biochem. Cell Biol. **61**, 99 (1983).
32. P. J. Fraker and J. C. Speck. Biochem. Biophys. Res. Commun. **80**, 849 (1978).
33. R. L. Felsted, R. D. Leavitt, and N. R. Bachur. Biochim. Biophys. Acta, **405**, 72 (1975).
34. L. Eldjarn and A. Pihl. J. Am. Chem. Soc. **79**, 4589 (1957).
35. E. Haber and C. B. Anfinsen. J. Biol. Chem. **237**, 1839 (1962).
36. J. M. Swan. Nature (London), **180**, 643 (1957).
37. C. B. Glaser, H. Maeda, and J. Meienhofer. J. Chromatogr. **50**, 151 (1970).
38. R. L. Hill and R. Delaney. Methods Enzymol. **11**, 339 (1967).
39. E. Stahl. Thin layer chromatography, a laboratory handbook. Springer-Verlag, New York. 1969.

Can. J. Chem. Downloaded from www.nrcresearchpress.com by 213.166.140.6 on 09/07/12
For personal use only.

The gas phase ion chemistry and proton affinity of hexamethyldisiloxane studied by high pressure mass spectrometry

XIAOPING LI AND JOHN ALFRED STONE
Chemistry Department, Queen's University, Kingston, Ont., Canada K7L 3N6

Received January 27, 1987

XIAOPING LI and JOHN ALFRED STONE. Can. J. Chem. **65**, 2454 (1987).

The ion chemistry of hexamethyldisiloxane ($(CH_3)_3SiOSi(CH_3)_3$, HMDS) has been studied under chemical ionization conditions at ion source temperatures of 300–600 K and pressures of 2–4 Torr. Highly exothermic proton transfer to HMDS from CH_5^+ and $C_2H_5^+$ leads mainly to loss of CH_3 but with decreasing exothermicity the yield of $HMDSH^+$ increases such that transfer from t-$C_4H_9^+$ ($\Delta H^0 = -7.5$ kcal mol^{-1}) yields almost exclusively $HMDSH^+$. Although $HMDSH^+$ transfers $(CH_3)_3Si^+$ rather than a proton to most reference bases, the proton affinity of HMDS has been determined from van't Hoff plots using the equilibrium method with methylaromatics as reference bases. PA(HMDS) = 203.4 kcal mol^{-1} is in excellent accord with an earlier estimate of 203 kcal mol^{-1} obtained by the bracketing method. The rate constants for these proton transfer reactions show very large negative temperature coefficients in the exothermic directions which are consistent with the reactions of charge delocalized ions and/or reactions in which considerable loss of rotational freedom occurs along the reaction coordinate. The rate constants in the reverse directions have a positive temperature coefficient only when the endothermicity is significant (>2.5 kcal mol^{-1}).

XIAOPING LI et JOHN ALFRED STONE. Can. J. Chem. **65**, 2454 (1987).

Opérant dans des conditions d'ionisation chimique, à des températures de la source ionique allant de 300 à 600 K et à des pressions de 2 à 4 Torr, on a étudié la chimie ionique de l'hexaméthyldisiloxane ($(CH_3)_3SiOSi(CH_3)_3$, HMDS). Les transferts de proton des cations CH_5^+ et $C_2H_5^+$ au HMDS sont très exothermiques et ils conduisent principalement à une perte de CH_3; toutefois, lorsque l'exothermicité diminue, le rendement en $HMDSH^+$ augmente d'une façon telle que le transfert du t-$C_4H_9^+$ ($\Delta H^0 = -7{,}5$ kcal mol^{-1}) conduit presqu'exclusivement au $HMDSH^+$. Pour la plupart des bases de référence, le $HMDSH^+$ transfère du $(CH_3)_3Si^+$ plutôt qu'un proton; malgré ce fait, on a déterminé l'affinité protonique du HMDS à partir des courbes de van't Hoff et en utilisant la méthode des équilibres des produits méthylaromatiques avec les bases de référence. La valeur de PA(HMDS) = 203,4 kcal mol^{-1} est en excellent accord avec une évaluation antérieure de 203 kcal mol^{-1} obtenue à l'aide de la méthode du "bracketing". Les constantes de vitesse pour ces réactions de transfert de proton présentent d'importants coefficients négatifs de température dans les directions exothermiques et ceux-ci sont en accord avec les réactions d'ions possédant des charges délocalisées et/ou des réactions dans lesquelles il se produit une importante perte de liberté rotationnelle le long des coordonnées de la réaction. Dans la direction inverse, les constantes de vitesse ne possèdent un coefficient de température positif que lorsque l'endothermicité est importante (>2,5 kcal mol^{-1}).

[Traduit par la revue]

Can. J. Chem. Downloaded from www.nrcresearchpress.com by 213.166.140.6 on 09/07/12
For personal use only.

Introduction

There is a considerable body of qualitative information on the mass spectrometry and ion chemistry of silicon-containing compounds since derivatization of functional groups using silicon-containing reagents is a common method of increasing the volatility of compounds for gas chromatography/mass spectrometric analysis. In spite of this, quantitative thermochemical information on silicon-containing ions and indeed on organosilicon molecules is rudimentary to say the least. Even gas phase proton affinity values which are well established for organic molecules and an increasing number of organometallics, are almost non-existent for organosilicons.

Proton affinity measurements usually are most reliable when obtained by gas phase equilibrium methods, but such methods are often impossible with silicon compounds which, when protonated, show a propensity to engage in reactions competitive with proton transfer, usually the donation of a silicon-containing group. For this reason an early ion cyclotron resonance (ICR) study of proton transfer between trimethylsilyl-containing ethers and organic ethers used the double resonance technique to establish the preferred direction of proton transfer (1). Hexamethyldisiloxane (HMDS, $(CH_3)_3SiOSi(CH_3)_3$) was one of the compounds studied and, based on the results obtained, HMDS has subsequently been assigned a proton affinity (PA) of ~203 kcal mol^{-1} in a compendium of evaluated proton affinities (2).

The tendency for transfer of a silicon-containing group rather than the proton has been used to obtain both relative $(CH_3)_3Si^+$ affinities using ICR (3) and also absolute binding energies by the equilibrium method in a pulsed electron beam, high pressure ion source mass spectrometer (HPMS) (4). An interesting observation in the latter study was that the binding energies of $(CH_3)_3Si^+$ to aromatic hydrocarbons is considerably lower than that to bases such as aliphatic alcohols, esters, and ethers. Indeed, the $(CH_3)_3Si^+$ adducts of alcohols were found to transfer a proton rather than $(CH_3)_3Si^+$ to an aromatic. For example it was found that reaction [1a] rather than [1b] occurs between the $(CH_3)_3Si^+$ adduct of methanol and mesitylene.

$$[1a] \quad (CH_3)_3SiO(H)CH_3^+ + C_9H_{12} \longrightarrow (CH_3)_3SiOCH_3 + C_9H_{13}^+$$

$$[1b] \quad \not\longrightarrow (CH_3)_3SiC_9H_{12}^+ + CH_3OH$$

This suggested that it might be possible to set up proton transfer equilibria between aromatic hydrocarbons and silicon compounds of suitable proton affinities. This paper reports on such an experiment in which PA(HMDS) is determined. HMDS was chosen for this initial study for several reasons. It was one of the compounds in the original study (1) which has an estimated proton affinity in the range of readily available and suitably volatile methylaromatics. HMDS is also a very stable material which may be readily handled in our heated inlet system.

It was important initially to examine the ion chemistry of HMDS under high pressure ion source conditions to ascertain the optimal experimental parameters that will maximize proton transfer and minimize any competing reactions that might

TABLE 1. Fractional abundances of the major ions in the CI spectra of HMDS with different reagent gases

Reagent gas	Reagent ions	P (Torr)	T (K)	m/z 147	149	163	191	221	309
CH_4	CH_5^+, $C_2H_5^+$	4.1	591	0.386	0.213	0.176	0.010	0.224	0
CH_4	CH_5^+, $C_2H_5^+$	2.0	592	0.596	0.180	0.154	0.003	0.070	0
CH_4	CH_5^+, $C_2H_5^+$	4.1	412	0.003	0.003	0.095	0.020	0.003	0.895
CH_4	CH_5^+, $C_2H_5^+$	1.9	412	0.026	0.008	0.114	0.020	0.005	0.847
CH_4/C_2H_6 (9/1)	$C_2H_5^+$, $C_3H_5^+$, $C_3H_7^+$	3.7	598	0.127	0.328	0.490	0.007	0.054	0
CH_4/C_2H_6 (9/1)	$C_2H_5^+$, $C_3H_5^+$, $C_3H_7^+$	3.6	413	0.038	0.008	0.758	0.016	0.002	0.190
$CH_4/(CH_3)_3CH$ (9/1)	t-$C_4H_9^+$	4.0	592	0.003	0.038	0.946	0	0.013	0
$CH_4/(CH_3)_3CH$ (9/1)	t-$C_4H_9^+$	4.1	412	0	0	1.000	0	0	0
$CH_4/(CH_3)_3CH$ (9/1)	t-$C_4H_9^+$	2.1	593	0.014	0.041	0.938	0	0.007	0

detract from and perhaps negate proton affinity determinations by the equilibrium method.

Experimental

The pulsed electron beam, high pressure ion source mass spectrometer (HPMS) has been described previously (5).

Methane (Matheson 99.99%), ethane (Phillips Research Grade), and isobutane (Matheson 99.5%) were used as received. HMDS (Aldrich Chemical Co., Inc.) which had a stated purity of 98% + was also used as received; no peaks ascribable to impurities in this material were ever observed. The aromatic hydrocarbons 1,3-dimethylbenzene (DMB), 1,3,5-trimethylbenzene (MES), and 1,2,3,5-tetramethylbenzene (TMB) (Aldrich Chemical Co., Inc.) were of the highest purity available.

Gaseous samples, which were made up in a heated glass reservoir of 5 L volume, contained a reagent gas at ~700 Torr (1 Torr = 133.3 Pa) together with 0.05 mol% sulfurhexafluoride as an electron capture reagent, and a maximum of 0.1 mol% HMDS and/or any other reactants. In most experiments the reagent gas was a 9/1 methane/isobutane mixture. The choice of reagent gas did not affect the thermodynamic data obtained but the mixed reagent gas gave cleaner spectra and greater sensitivity. The gaseous sample was flowed into the ion source via a heated metering valve to give pressures in the range 2–4 Torr. Ion source temperatures were from 300 to 600 K.

Results and discussion

The chemical ionization (CI) mass spectra of HMDS

The CI spectra were very dependent on the reagent gas used and the ion source temperature. Typical spectra with methane and methane/10% isobutane as reagent gases are shown in Fig. 1 while Table 1 summarizes the major ions and their relative intensities obtained with several reagent gases and gas mixtures under a variety of ion source conditions.

Under methane CI conditions the reagent ions CH_5^+ and $C_2H_5^+$ appear to react with HMDS mainly by proton transfer to initially yield $HMDSH^+$ (m/z 163). A very small peak at m/z 191 containing two silicon atoms is probably the $C_2H_5^+$ adduct, $((CH_3)_2Si)_2OC_2H_5^+$). $HMDSH^+$ is never the major observable product, at high temperature m/z 147 dominates while at low temperature m/z 309 is the major product. The latter ion is completely absent at 582 K suggesting that it is possibly an ion–neutral association complex.

The normalized ion intensities plotted as functions of ion source residence times in Figs. 2 and 3 show that the major ion

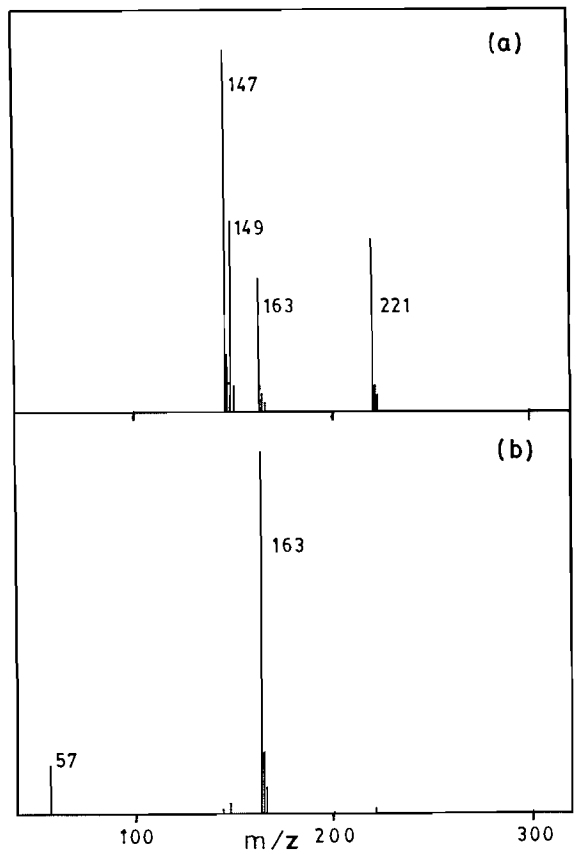

FIG. 1. Mass spectra: (*a*) CH_4/SF_6/HMDS (99.9/0.04/0.03) 4.1 Torr, 591 K; (*b*) CH_4/i-C_4H_{10}/SF_6/HMDS (85.4/14.6/0.04/0.03), 4.2 Torr, 593 K.

at short times, m/z 147, is very reactive. At 543 K (Fig. 2) it decays rapidly ($k \sim 3 \times 10^{-10}$ cm^3 molecule^{-1} s^{-1}) by reaction with HMDS to give m/z 221 and 149. m/z 309 also appears at short reaction time at this temperature and decays in parallel with m/z 147 after a very short time. This latter behaviour is independent of sample pressure in the temperature range 450–550 K. At lower temperatures when m/z 309 is the dominant ion at long reaction times the constant ratio of yields

Can. J. Chem. Downloaded from www.nrcresearchpress.com by 213.166.140.6 on 09/07/12
For personal use only.

of m/z 147 and 309 still exists, suggesting that they are in equilibrium (Fig. 3). Taking into account the number of silicon atoms in each ion as determined from the isotopic patterns then a plausible reaction scheme with CH_5^+ as protonating agent is:

[2] $(CH_3)_3SiOSi(CH_3)_3 + CH_5^+ \rightarrow [(CH_3)_3SiO(H)Si(CH_3)_3]^{+*} + CH_4$

[3a] $[(CH_3)_3SiO(H)Si(CH_3)_3]^{+*} \xrightarrow{M} (CH_3)_3SiO(H)Si(CH_3)_3^+$ (m/z 163)

[3b] $\rightarrow (CH_3)_3SiOSi(CH_3)_2^+ + CH_4$ (m/z 147)

[4] m/z 147 + $(CH_3)_3SiOSi(CH_3)_3 \rightarrow (CH_3)_3SiOSi(CH_3)_3 \cdot (CH_3)_3SiOSi(CH_3)_2^+$ (m/z 309)

[5] m/z 309 $\rightarrow$ 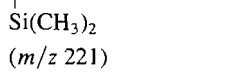 + $(CH_3)_4Si$ (m/z 221)

Ion m/z 149 appears to be formed by the reaction of m/z 147 with adventitious water since the addition of extra water results in a significant increase in its yield. Ion m/z 149 is found as a prominent ion in the electron impact mass spectra of bistrimethylsilyl ethers ($(CH_3)_3SiO(CH_2)_nOSi(CH_3)_3$) (6). It was suggested that it arises by loss of methane from m/z 165, a common rearrangement ion in the spectra of these silyl ethers

[6] 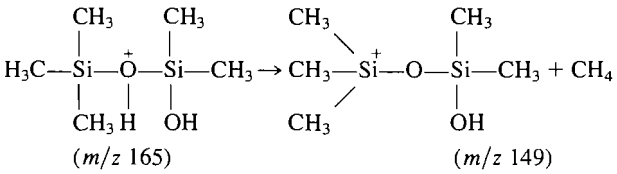
(m/z 165) (m/z 149)

Ion m/z 165 was not observed in any HMDS CI spectra which implies that the hydration of m/z 147 is sufficiently exothermic that the resulting m/z 165 has only a transitory existence.

The yields of $HMDSH^+$ (m/z 163) and $HMDS \cdot C_2H_5^+$ (m/z 191) are seen in Figs. 2 and 3 to change little with time, i.e. these ions are very unreactive towards HMDS.

Methane is obviously an unsatisfactory reagent gas for the preparation of $HMDSH^+$ in reasonable yield and in CI spectra not complicated by other silicon-containing ions. Since this behavior is presumably due to the high exothermicity of proton transfer (reaction [2]) the effect of reaction exothermicity on the decomposition of $HMDSH^+$ was studied by using mixed reagent gases. In methane/ethane mixtures the reagent ions are mainly $C_2H_5^+$, $C_3H_5^+$, and $C_3H_7^+$ while in methane/isobutane mixtures t-$C_4H_9^+$ is the only reagent ion. The results are summarized in Table 1.

The exothermicity of proton transfer may be calculated using PA(HMDS) = 203.4 kcal mol^{-1} obtained as described later. The values obtained for the different reagent ions are given in Table 2. Decomposition of the initially formed $HMDSH^+$ decreases with decreasing reaction exothermicity to such an extent that protonation by t-$C_4H_9^+$ at 4 Torr and 400 K leads exclusively to stabilized $HMDSH^+$. Even at 593 K only ~6% of the $HMDSH^+$ reacts further. A 9/1 methane/isobutane mixture was used in most of the subsequently described experiments.

Attempts to determine PA(HMDS) by studying proton transfer under equilibrium conditions with methane/isobutane mixtures and bases such as ethers, alcohols, and ketones were frustrated, as expected, by the preferred transfer of $(CH_3)_3Si^+$ rather than a proton. For example, diethyl ether formed $(C_2H_5)_2OSi(CH_3)_3^+$ rather than $(C_2H_5)_2OH^+$. However, proton transfer equilibrium measurements using HMDS and aromatic hydrocarbons were successfully accomplished.

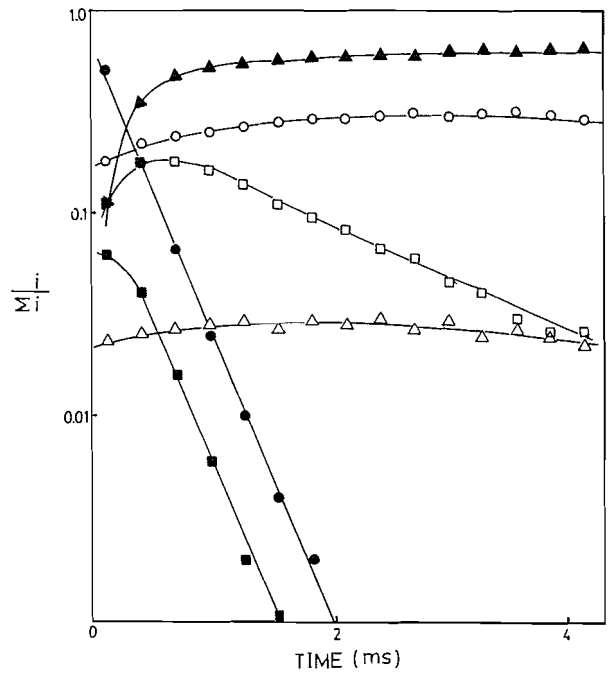

FIG. 2. Normalized ion intensities as functions of time after a 50 μs pulse of ionizing electrons for a mixture of CH_4/SF_6/HMDS 99.9/0.07/0.07 at 4.1 Torr and 543 K. ● $(CH_3)_5Si_2^+$ (m/z 147), ■ $(CH_3)_{11}Si_4O_2^+$ (m/z 309), ▲ $(CH_3)_7Si_3O_2^+$ (m/z 221), ○ $(CH_3)_6Si_2OH^+$ ($HMDSH^+$, m/z 163), □ $(CH_3)_4Si_2O_2H^+$ (m/z 149), △ $(CH_3)_6Si_2OC_2H_5^+$ (m/z 191).

Figure 4a shows the normalized yields of $HMDSH^+$ and $MESH^+$ in a HMDS/MES/CH_4/i-C_4H_{10} mixture after a 50 μs pulse of ionizing electrons. The constant ion currents after long reaction time, i_{HMDSH^+} and i_{MESH^+}, suggest that the following equilibrium has been attained.

[7] $MESH^+ + HMDS \rightleftharpoons MES + HMDSH^+$

That this was so was confirmed in the usual manner by showing that the variation of the concentration ratio of the neutrals [MES]/[HMDS] and ion source pressure had no effect on the computed equilibrium constant K.

[8] $$K = \frac{i_{HMDSH^+}}{i_{MESH^+}} \cdot \frac{[MES]}{[HMDS]}$$

K was measured over the temperature range 330–600 K; the results are shown in the van't Hoff plot of Fig. 5. Plots for reactions [9], [10], and [11] are also shown.

[9] $DMBH^+ + HMDS \rightleftharpoons DMB + HMDSH^+$

[10] $TMBH^+ + HMDS \rightleftharpoons TMB + HMDSH^+$

[11] $DMBH^+ + MES \rightleftharpoons DMB + MESH^+$

The thermodynamic data obtained from these plots which are shown in Table 3 are internally self consistent within the experimental error limits shown. The uncertainty in the ΔH^0 values is better than ±10% in all cases. This translates into a

Can. J. Chem. Downloaded from www.nrcresearchpress.com by 213.166.140.6 on 09/07/12
For personal use only.

Can. J. Chem. Downloaded from www.nrcresearchpress.com by 213.166.140.6 on 09/07/12
For personal use only.

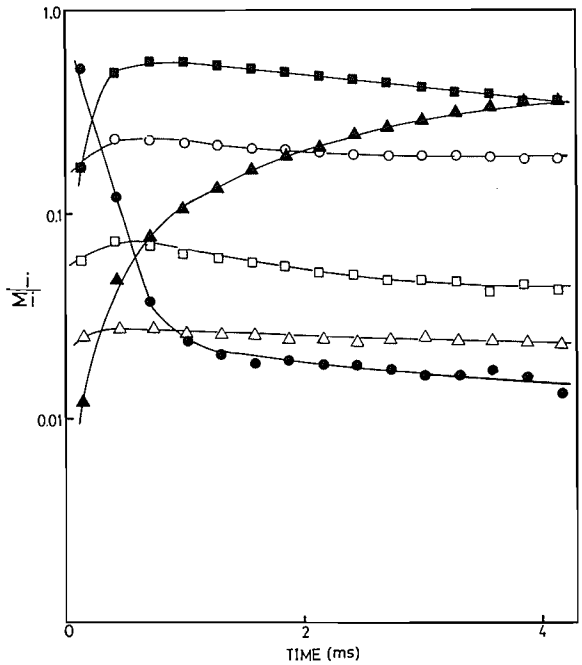

FIG. 3. Normalized ion intensities as functions of time after a 50 μs pulse of ionizing electrons for a mixture of CH_4/SF_6/HMDS (99.9/0.07/0.04) at 3.5 Torr and 478 K. ● $(CH_3)_5Si_2O^+$ (m/z 147), ○ $(CH_3)_6Si_2OH^+$ (HMDSH$^+$, m/z 163), ■ $(CH_3)_{11}Si_4O_2^+$ (m/z 309), ▲ $(CH_3)_7Si_3O_2^+$ (m/z 221), □ $(CH_3)_4Si_2O_2H^+$ (m/z 149), △ $(CH_3)_6Si_2OC_2H_5^+$ (m/z 191).

TABLE 2. Computed standard enthalpy changes (ΔH^0) for proton transfer to HMDS from CI reagent ions MH^+

MH^+	PA (M)[a] (kcal mol^{-1})	$-\Delta H^{0}$[b] (kcal mol^{-1})
CH_5^+	132	71
$C_2H_5^+$	162.6	40.8
$C_3H_7^+$	179.5	23.9
$C_3H_5^+$	186.3	17.1
t-$C_4H_9^+$	195.9	7.5

[a]All proton affinity values are from ref. 2.
[b]PA(HMDS) = 203.4 kcal mol^{-1}, this work.

small uncertainty ($< \pm 0.2$ kcal mol^{-1}) when ΔH^0 is small but ± 0.3 kcal mol^{-1} for the two largest ΔH^0 values. In determining PA(HMDS), more weight is therefore placed on the small ΔH^0 values.

We have recently determined PA(MES) to be 201.0 ± 0.2 kcal mol^{-1} using ethylacetate (PA 200.7 kcal mol^{-1}) as reference (7). This value of PA(MES) compares well with the 200.7 kcal mol^{-1} in a table of evaluated proton affinities (2). This latter value, however, is obtained from the mean of two gas phase basicity values which differ by 2 kcal mol^{-1}. An ICR proton affinity value obtained at ~320 K is 199.7 kcal mol^{-1} (8) while an HPMS value obtained at ~520 K is 201.7 kcal mol^{-1} (9), in both cases a calculated entropy change based only on symmetry numbers was employed to obtain the proton affinity from the experimental basicity. There is a growing volume of evidence that such calculations are not valid for equilibria involving charge delocalized ions (2, 7, 10). The entropy changes in Table 2 are self consistent and are presumed

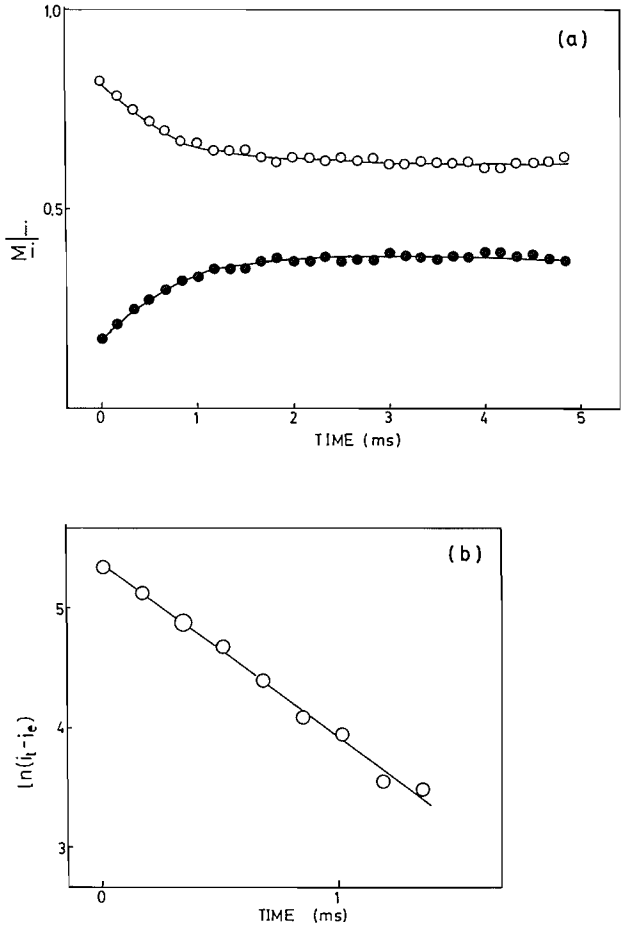

FIG. 4. (a) Normalized yields of MESH$^+$ ○ and HMDSH$^+$ ● as functions of time after a 50 μs pulse of ionizing electrons for a mixture of CH_4/i-C_4H_{10}/SF_6/MES/HMDS (91/9/0.04/0.34/0.053). (b) The kinetic plot for the approach to equilibrium in (a). The slope of the plot yields $k_{+7} + k_{-7}$. i_t and i_e are respectively the ion currents for MESH$^+$ at a time t and at equilibrium.

therefore to be reliable within the error limits given. It is noteworthy that the experimental entropy change for reaction [11] which involves two aromatic hydrocarbons differs by more than 2 cal K^{-1} mol^{-1} from the value calculated using symmetry number changes and is also of opposite sign. The calculated values for the other reactions are actually almost all in reasonable agreement with experiment, $DMBH^+$ + HMDS being the exception.

The data from Table 3 together with PA(MES) = 201.0 and PA(TMB) = 203.2 kcal mol^{-1} (7) yields PA(HMDS) = PA(MES) + 2.4 kcal mol^{-1} = 203.4 ± 0.4 kcal mol^{-1}. This value is in excellent agreement with the evaluated 203 kcal mol^{-1} (2) based on the original ICR result obtained from bracketing data viz. gas phase basicity, GB($(i$-$C_3H_7)_2O$) > GB(HMDS) > GB($(C_2H_5)_2O$). We could not confirm this ranking using HPMS because of the aforementioned problems with $(CH_3)_3Si^+$ transfer. Relative to MES, PA(DMB) is 194.9 ± 0.5 kcal mol^{-1}, a little lower than the evaluated value of 195.9 kcal mol^{-1} (2). The latter result is from an ICR determination at ~320 K and using calculated entropies (8).

An observation of significance in the ICR work (1) was that PA($((CH_3)_3C)_2O$) > PA(HMDS). Failure to observe proton transfer in the reverse direction i.e. from $HMDSH^+$ to $((CH_3)_3C)_2O$ was ascribed to a very slow reaction rate. Since no $((CH_3)_3C)_2O$ was available we attempted to prepare $((CH_3)_3C)_2OH^+$ by

TABLE 3. Standard enthalpy and standard entropy changes for proton transfer

	$-\Delta H^0$ (kcal mol^{-1})			$-\Delta S^0$ (cal K^{-1} mol^{-1})		
Hexamethyldisiloxane (HMDS)						
	2.5±0.2	0.0±0.1		2.5±0.4 (2.17)[b]	0.5±0.2 (1.37)	
1,2,3,5-Tetramethylbenzene (TMB)						
		2.2±0.2[a]	8.0±0.3		1.1±0.1[a] (0.80)	3.3±0.7 (1.37)
1,3,5-Trimethylbenzene (MES)						
	6.1±0.3			1.5±0.4 (−0.80)		
1,3-Dimethylbenzene (DMB)						

[a]Reference 7.
[b]Values in parentheses calculated from changes in rotational symmetry numbers. Si—O—Si in both HMDS and HMDS is assumed non-linear.

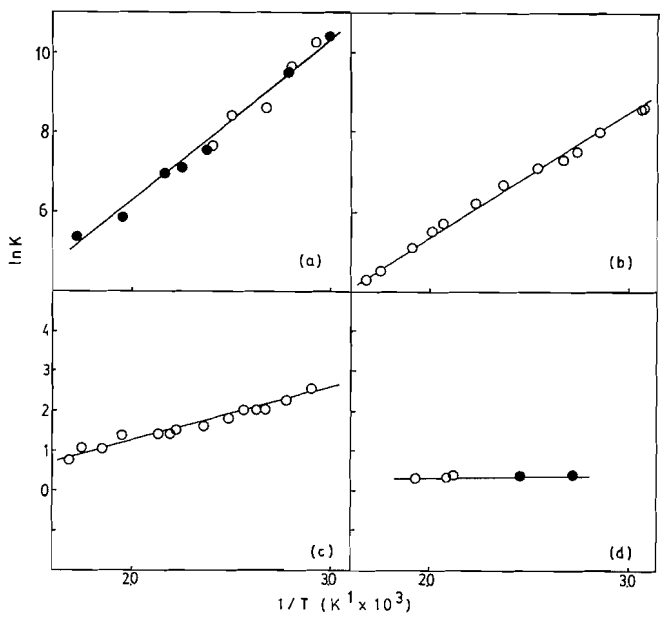

FIG. 5. van't Hoff plots (*a*) $DMBH^+ + HMDS \rightleftharpoons DMB + HMDSH^+$, (*b*) $DMBH^+ + MES \rightleftharpoons DMB + MESH^+$, (*c*) $MESH^+ + HMDS \rightleftharpoons HMDSH^+ + MES$, (*d*) $TMBH^+ + HMDS \rightleftharpoons TMB + HMDSH^+$. The closed circles show data obtained with methane only as reagent gas, open circles are for methane/isobutane mixtures.

reaction [12] with *i*-C_4H_{10} as the source of $(CH_3)_3C^+$.

[12] $(CH_3)_3C^+ + (CH_3)_3COH \rightleftharpoons (CH_3)_3CO(H)C(CH_3)_3^+$ (m/z 123)

No m/z 123 was observed even at 300 K, indicating a very weak (<15 kcal mol^{-1}) binding of cation and alcohol. It is therefore somewhat surprising that m/z 123 could be formed at low pressure under ICR conditions for the bracketing studies. The above ordering of the basicity values as determined by ICR is consistent with our observation that substitution of Si for C in $(CH_3)_3COH$ leads to a lowering of proton affinity in $(CH_3)_3SiOH$ (11).

The kinetics of proton transfer

The rate constants for both forward and reverse directions of reactions [7], [9], and [11] are readily determined by the methods which have been described previously in detail (7). Two methods may be used. The first involves treating the approach to equilibrium in the proton transfer reaction as a pseudo first order reversible reaction (12). Normalized data for reaction [7] are shown in Fig. 4(*a*) while in 4(*b*) is the appropriate kinetic plot which yields $(k_{+7} + k_{-7})$. Since the measured equilibrium constant $K = k_{+7}/k_{-7}$ the individual rate constants may be obtained. The rate constant in the forward direction may also be measured in the more usual manner by plotting log $(i/\Sigma i)$ vs. time, where the normalized ion current is that for the protonated species which decreases in intensity with time to attain equilibrium. Only the first few experimental points at low reaction time are used in such an analysis since it is only then that the reverse reaction is not significant. The results presented in Figs. 6, 7, and 8 show excellent agreement in rate constants obtained by the two methods. No kinetic data are obtainable for reaction [10] since $\Delta H^0 \sim 0$ and proton transfer equilibrium is attained during the ionizing electron pulse.

The collision rate constants k_c calculated for 300 K by the ADO theory of Su and Bowers (13) are (units 10^{-9} molecule^{-1} cm^3 s^{-1}) $MESH^+ + HMDS$, 1.4; $DMBH^+ + HMDS$, 1.4; and $DMBH^+ + MES$, 1.3. These values vary little with temperature since the molecular dipole moments are zero or very small. The experimental rate constants in the forward directions for reactions [9] and [11] are close to k_c at 300 K but decrease drastically with increase in temperature. The rate constant for reaction [7] is significantly less than k_c at 300 K and its value declines even more rapidly with increasing temperature than do those for the other two systems. These forward rate constants may be described by the equation $k = CT^n$ with $n = -6.7$, -5.9, and -3.3 for k_7, k_{11}, and k_9, respectively. These are very large negative temperature coefficients, comparable in magnitude with some found for exothermic hydride transfer in alkanes (14). The latter work showed that in general, for the reactions involving similar ions and neutrals, the value of n becomes more negative as the reaction exothermicity decreases.

Can. J. Chem. Downloaded from www.nrcresearchpress.com by 213.166.140.6 on 09/07/12
For personal use only.

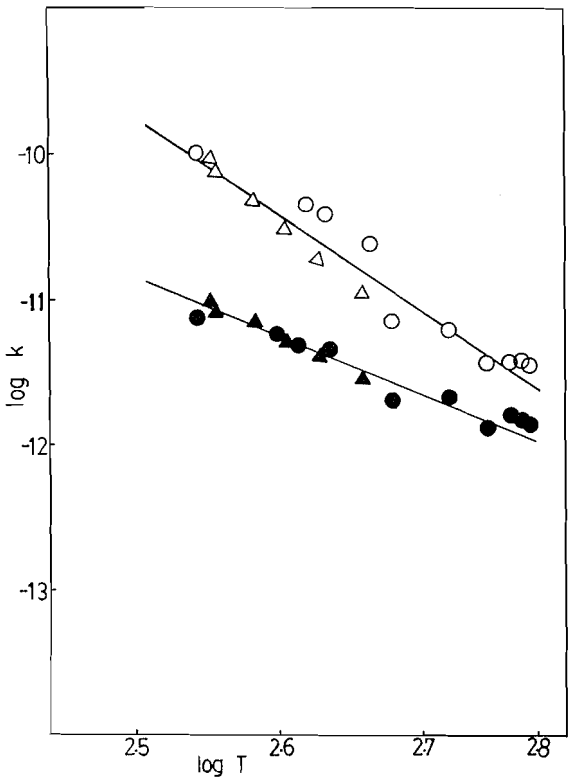

FIG. 6. The variations of the rate constants with temperature for reaction [7], $MESH^+ + HMDS \rightleftharpoons MES + HMDSH^+$. Open symbols $k_{forward}$, closed symbols $k_{reverse}$; circles, values obtained using the method illustrated in Fig. 5, triangles, values obtained from the initial slope of the decay of $MESH^+$.

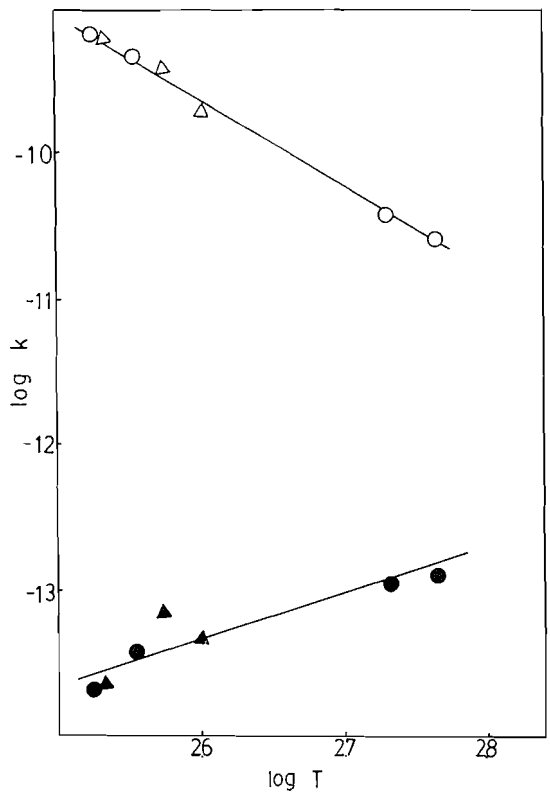

FIG. 7. The variations of the rate constants with temperature for reaction [9], $DMBH^+ + HMDS \rightleftharpoons DMB + HMDSH^+$. Upper curve $k_{forward}$, lower curve $k_{reverse}$; circles, values obtained using the method illustrated in Fig. 4, triangles, values obtained from the initial slopes of the decays of $DMBH^+$.

In like manner n for reaction [7] is more negative than n for the more exothermic reaction [9]. The value of n for reaction [11] does not fit this scheme, presumably because the neutral is MES rather than HMDS. In fact, the value is much more consistent with the lower values observed for proton transfer among aromatics where the value of n actually increases with increasing exothermicity (at least up to $\Delta H^0 \sim 5$ kcal mol^{-1}) (7). It is of significance that although each of the reactions [9] and [11] is exothermic by more than 6 kcal mol^{-1}, proton transfer is very inefficient at ~600 K.

The effect of temperature on the reverse, endothermic, proton transfer rate constants k_{-7}, k_{-9}, and k_{-11} are interesting for two reasons. In the first place two, k_{-9} and k_{-11}, have positive temperature coefficients, whereas k_{-7}, the rate constant for the least endothermic reaction has a negative temperature coefficient. Secondly the Arrhenius activation energies obtained from the temperature coefficients of k_{-9} and k_{-11}, 2.9 and 3.8 kcal mol^{-1}, respectively, are far less than the reaction endothermicities (6.1 and 8.0 kcal mol^{-1}). A similar observation was made in a study of slightly (<5 kcal mol^{-1}) endothermic proton transfer between methylbenzenes (7). For reactions such as these it is therefore not possible to obtain a measure of the reaction endothermicity from the experimental activation energy. It can be surmized from Figs. 6 and 7 that as the exothermicity of reaction involving proton transfer to HMDS from an aromatic decreases to around zero the temperature coefficients of the forward and reverse reactions will approach the same, high negative value.

Large temperature coefficients of rate constants for exothermic reactions are associated with internal barriers along the reaction coordinate, i.e., there is a maximum in the effective potential energy surface between reactants and products. The double-well theory of Farneth and Brauman (15) explains why an exothermic proton transfer reaction may be slow if the ion–molecule complex in the chemical transition state at the central barrier has a lesser density of states than it does at the centrifugal barrier for the collision. Once the collision complex (the stabilized form of which is a proton bound complex at the minimum of the first well) is formed, then return to reactants is entropically favoured. Kebarle (16) has shown that RRKM calculations do yield an appropriate negative temperature coefficient for such a model. In addition he also confirmed the validity of the suggestion of Meot-Ner (17) that an exothermic reaction may be inefficient in the forward direction if there is a considerable inhibition or even locking of external rotations on an otherwise relatively flat region of the potential energy curve along the reaction coordinate. Such would be the case when the proton is to be transferred to or from a fairly inaccessible site.

Protonated aromatics are ions in which the charge is considerably delocalized and some charge localization is probably required in the transition state at the central barrier for proton transfer (7). In addition a specific orientation of the aromatic rings will also be required implying a "tight" transition state. $HMDSH^+$ must also be a charge delocalized ion with electron transfer from Si to O as shown by its propensity to transfer $(CH_3)_3Si^+$.

HMDS has a Si—O—Si bond angle of 148 ± 3° as determined by electron diffraction in the gas phase (18) and 142.2° as determined by solid state X-ray crystallography (19). The gas phase results could be interpreted in terms of either a C_{2v} geometry or a structure with lower symmetry due to a staggering of the methyl groups. However, there are large

Can. J. Chem. Downloaded from www.nrcresearchpress.com by 213.166.140.6 on 09/07/12
For personal use only.

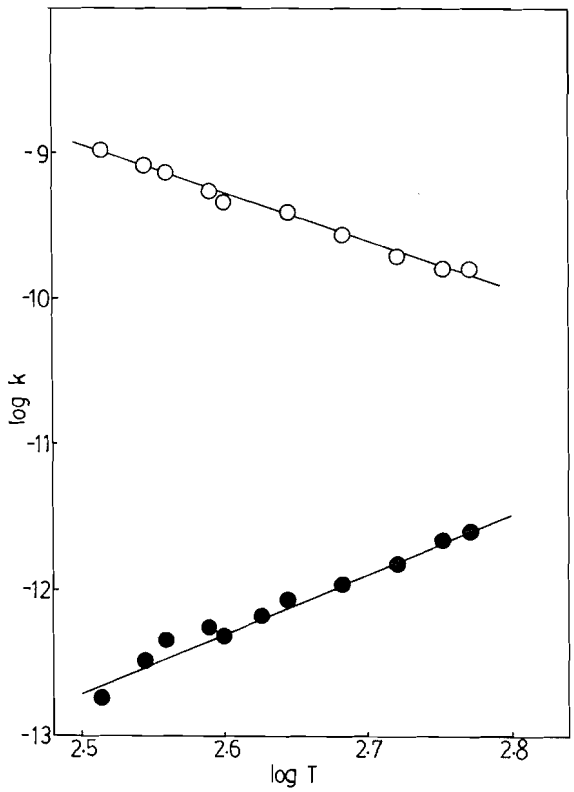

FIG. 8. The variations of the rate constants with temperature for reaction [11], $DMBH^+ + MES \rightleftharpoons DMB + MESH^+$. Upper curve $k_{forward}$, lower curve $k_{reverse}$.

amplitude motions, including twisting around the Si—O bonds (20). The very large Si—O—Si angle, which is much greater than the tetrahedral angle, will hinder access to oxygen in proton transfer. The molecular motions of HMDS along the reaction coordinate will be severely restricted as the chemical transition state is approached since not only will the external rotation of the molecule be limited but also the internal rotations of the $(CH_3)_3Si$ groups about the Si—O bonds and the CH_3 groups about the C—Si bonds will also be affected. The severe hindrance of all these rotational motions will result in large temperature coefficients for reactions involving proton transfer to or from HMDS.

The potential energy profile along the reaction coordinate in the double well potential model is defined by the depths of the two wells and the height of the central barrier. Data on the depths of the well can be obtained if the proton-bound complexes can be stabilized. Benzene forms a very weakly bonded (11 kcal mol^{-1}) proton bound dimer (21) but no aromatic proton bound dimer was observed in the present experiments. $(HMDS)_2H^+$ was not observed either in the presence or absence of aromatic and there was no evidence of a mixed dimer. Figures 2 and 3 show that $HMDSH^+$ is very unreactive towards HMDS and the non-observation of $(HMDS)_2H^+$ must therefore be due to its having only a transient existence before returning to reactants and not to its decomposition to products. Proton transfer between two HMDS molecules is probably very slow due to extreme steric constraints. In support of this contention is our inability to observe proton transfer from $HMDSH^+$ to the geometrically similar hexamethyldisilazane ($(CH_3)_3SiN(H)Si(CH_3)_3$) which has a proton affinity about 20 kcal mol^{-1} higher than HMDS.[1] When DMB is also present proton transfer is observed to occur, presumably via $DMBH^+$, although this ion was not observed. The protonated aromatic presumably can approach $HMDSH^+$ at right angles to the Si—O—Si axis without being sterically blocked whereas the large $(CH_3)_3Si$ groups in hexamethyldisilazane and $HMDSH^+$ prevent a sufficiently close encounter for measurable proton transfer in either a parallel or cruciform transition state.

[1]X. Li and J. A. Stone. Unpublished work.

Conclusions

The proton affinities of silicon compounds can be measured by the equilibrium method provided that the basicity of the competing base towards a silylium ion is low. The aromatic hydrocarbons possess the quality but their range of proton affinities does not extend very far above 200 kcal mol^{-1}. This means that aromatics may not be used to determine the proton affinities of the more basic organosilicon compounds, e.g., the silazanes. Preliminary results suggest that alkylamines may be satisfactory bases for HPMS equilibrium studies of such bases.

Acknowledgement

The authors thank the Natural Sciences and Engineering Research Council of Canada for financial support.

1. C. G. PITT, M. M. BURSEY, and D. A. CHATFIELD. J. Chem. Soc. Perkin 2, 434 (1976).
2. S. G. LIAS, J. F. LIEBMAN, and R. D. LEVIN. J. Phys. Chem. Ref. Data, **13**, 695 (1984).
3. V. C. TRENERRY, G. KLASS, J. H. BOWIE, and I. A. BLAIR. J. Chem. Res. 386 (1980).
4. A. C. M. WOJTYNIAK and J. A. STONE. Int. J. Mass Spec. Ion Proc. **74**, 59 (1986).
5. J. A. STONE and D. E. SPLINTER. Can. J. Chem. **59**, 1779 (1981).
6. J. A. MCCLOSKEY, R. N. STILLWELL, and A. M. LAWSON. Anal. Chem. **40**, 233 (1968).
7. J. A. STONE, X. LI, and P. A. TURNER. Can. J. Chem. **64**, 2021 (1986).
8. J. L. DEVLIN, J. F. WOLF, R. W. TAFT, and W. J. HEHRE. J. Am. Chem. Soc. **98**, 1990 (1976).
9. M. MEOT-NER. J. Phys. Chem. **84**, 2716 (1980).
10. K. T. FERNANDEZ, K. R. JENNINGS, and R. S. MASON. Presented at 33rd Annual Conference on Mass Spectrometry and Allied Topics; San Diego. 1985.
11. J. A. STONE, A. C. M. WOJTYNIAK, and W. WYTENBURG. Can. J. Chem. **64**, 575 (1986).
12. J. W. MOORE and R. G. PEARSON. Kinetics and mechanism. 3rd ed. John Wiley and Sons, New York. 1981.
13. T. SU and M. T. BOWERS. Int. J. Mass Spectrom. Ion Phys. **17**, 211 (1975).
14. M. MEOT-NER and F. H. FIELD. J. Am. Chem. Soc. **100**, 1356 (1978).
15. W. E. FARNETH and J. I. BRAUMAN. J. Am. Chem. Soc. **98**, 7891 (1976).
16. P. KEBARLE. *In* Ionic processes in the gas phase. *Edited by* M. A. Almoster-Ferreira. NATO ASI Series V 118 1984.
17. M. MEOT-NER. *In* Gas phase ion chemistry. Vol. 1. *Edited by* M. T. Bowers. Academic Press, New York. 1979. p. 153.
18. B. CSAKVASI, ZS. WAGNER, and P. GOMORY. J. Organomet. Chem. **107**, 287 (1976).
19. M. J. BARROW, E. A. V. EBSWORTH, and M. M. HARDING. Acta Crystallogr. B, **35**, 2093 (1979).
20. R. S. HOLLAND and C. P. SMYTH. J. Am. Chem. Soc. **77**, 268 (1955).
21. M. MEOT-NER, P. HAMLET, E. P. HUNTER, and F. H. FIELD. J. Am. Chem. Soc. **100**, 5466 (1978).

Can. J. Chem. Downloaded from www.nrcresearchpress.com by 213.166.140.6 on 09/07/12
For personal use only.

The preparation of esters of formic acid using boron oxide

CHARLES G. CARLSON, JUDITH E. HALL, YAN. Y. HUANG, SIRPA KOTILA,[1] ARVI RAUK, AND DONALD F. TAVARES[2]
Department of Chemistry, The University of Calgary, Calgary, Alta., Canada T2N 1N4

Received April 21, 1987

CHARLES G. CARLSON, JUDITH E. HALL, YAN. Y. HUANG, SIRPA KOTILA, ARVI RAUK, and DONALD F. TAVARES. Can. J. Chem. **65**, 2461 (1987).

Boron oxide has been found to act as an efficient reagent in the preparation of a number of formate esters by the direct esterification of formic acid with the alcohol. The reaction is most appropriate for primary and secondary alcohols, including unsaturated alcohols. The formate ester so produced is free of contamination by unreacted alcohol.

CHARLES G. CARLSON, JUDITH E. HALL, YAN. Y. HUANG, SIRPA KOTILA, ARVI RAUK et DONALD F. TAVARES. Can. J. Chem. **65**, 2461 (1987).

On a trouvé que l'oxyde de bore agit comme un réactif efficace pour la préparation d'un certain nombre d'esters formiques par l'estérification directe de l'acide formique avec l'alcool. La réaction est principalement appropriée pour les alcools primaires et secondaires, y compris les alcools qui ne sont pas saturés. Les esters formiques ainsi formés ne sont pas contaminés par l'alcool qui n'a pas réagi.

[Traduit par la revue]

Can. J. Chem. Downloaded from www.nrcresearchpress.com by 213.166.140.6 on 09/07/12
For personal use only.

Introduction

The course of our research required the preparation of propargyl formate in high purity, free of contamination by unreacted alcohol or acid, conditions not readily achieved in most esterification procedures involving formic acid. Acid halides or anhydrides of formic acid are unstable or not readily available (1), although formyl fluoride has been used (2). Mixed formic/acetic anhydride prepared as a mixture of formic acid and acetic anhydride serves as a general reagent for the synthesis of a variety of formates (3) but suffers from the disadvantage that the product is usually contaminated with acetates except in the case of tertiary alcohols (3). The preparation of formate esters of high purity is also besieged by difficulties in isolation, which largely ensue from similarities in the boiling points of the components of the reaction and from the susceptibility of the formyl carbonyl group to undergo nucleophilic attack and decarbonylation. The preparation of esters such as allyl or propargyl formates may be further complicated by the sensitivity of the unsaturated moiety to strong acids and (or) bases.

Direct esterification of alcohols with carboxylic acids is a readily reversible process. The position of the equilibrium is particularly unfavourable in the case of formate esters (4). By way of example, propargyl formate has been prepared in 50% yield by reacting propargyl alcohol with a twofold excess of formic acid in refluxing dichloromethane for 14 h, followed by neutralization, a water wash, and distillation (5). Among the techniques to maximize the yield of the ester is the removal of the water by-product during the course of the reaction. Where the boiling points and solubilities of the reagents are suitable, this is most readily accomplished by carrying out the esterification in refluxing benzene in a Dean–Stark apparatus (5). For formates, this technique is foiled by the low solubility of formic acid in benzene and its consequent codistillation. Dichloromethane (6) and diisopropyl ether (1) are more suitable for formates but the azeotropic mixtures have a relatively low proportion of water, 1.5 and 3.6%, respectively. Alternatively, reagents may be introduced to complex the water of reaction (7, 8). Concentrated sulfuric acid is not appropriate since formic acid is unstable under these conditions. In an adaptation of the procedure of Heaton and Noller (9) for the preparation of propargyl formate, powdered calcium chloride was used to remove the water of reaction from a boiling equimolar mixture of alcohol and acid. The ester was isolated by a double distillation. The yield was not reported (10). We have adopted the same approach for the preparation of propargyl formate, using boron oxide B_2O_3 to trap the water of reaction. As the use of this reagent had not hitherto been reported in this capacity, we investigated the general synthetic utility of the reaction and report the results below.

Experimental

Materials and equipment

All materials were reagent grade and used without further purification except as noted. Specific sources were Fischer (formic acid, *p*-toluenesulfonic acid, 1-pentanol, 2-butanol, allyl alcohol, ethylene glycol, and methylene chloride); Aldrich (boron oxide, 1-hexanol, 1-adamantanol), Columbia Organic Chemicals (3-buten-2-ol, 3-butyn-1-ol); Lancaster (phthalic anhydride); BDH (Sicapent, benzyl alcohol); MCB (cyclohexanol). The ^1H and ^{13}C nmr spectra were obtained on a Varian XL-200 FT spectrometer, mass spectra on a Kratos MS80RFA mass spectrometer. Product purity was estimated by gas chromatography using an OV-17 column.

General procedure

A mixture of the alcohol (0.25 mol), anhydrous formic acid (11) (0.29 mol), boron oxide (0.09 mol), and *p*-toluenesulfonic acid (0.025 mol) in methylene chloride (50 mL) was refluxed with vigorous stirring. After 1 h, the reaction mixture was chilled in ice water and filtered. The filtrate was treated with anhydrous potassium carbonate, refiltered, and stirred for 1 h with phosphorus pentoxide[3] to remove any residual alcohol. Decantation through a short column of silica gel over diatomaceous earth and distillation of the resulting clear solution through a Vigreux column afforded clear colorless ester. The results for specific alcohols are further delineated below and collected in Table 1. Boiling points cited are uncorrected at 660 Torr (1 Torr = 133.3 Pa).

n-*Pentyl formate*

Ester of purity >99% isolated in 66% yield; ^1H nmr ($CDCl_3$) δ: 0.86 (t, 3H, J = 7.0 Hz), 1.29 (m, 4H), 1.62 (m, 2H), 4.12 (t, 2H, J = 6.7 Hz), 8.02 (s, 1H).

n-*Hexyl formate*

Ester of 99.6% purity could be isolated in 74% yield; ^1H nmr ($CDCl_3$) δ: 0.86 (t, 3H, J = 6.6 Hz), 1.29 (m, 6H), 1.63 (m, 2H), 4.13 (t, 2H, J = 6.7 Hz), 8.04 (s, 1H).

[1]Present address: Taitoniekantie 9 D 214, 40740 Jyvaskyla, Finland.
[2]Author to whom correspondence may be addressed.

[3]For ease of manipulation, the dehydrating agent, Sicapent (BDH chemicals) may be used with similar results.

TABLE 1. Preparation of formates by B_2O_3 mediated esterification

Alcohol	Yield[a] (purity)	Yield[b] (purity)[c]	Boiling point (°C)[d] uncorr.	Ref.
1-Pentanol	66.3 (99.3)	66.3 (99.3)	127	22
1-Hexanol	73.6 (99.6)	73.6 (99.6)	150	22
Prop-2-en-1-ol	30.9 (98.0)	95.8 (41.3)	79	12
(allyl)	38.7 (96.4)[e]	50.6 (80.5)[f]		
	35.7 (99.3)[g]	35.7 (99.3)[g]		
Prop-2-yn-1-ol	81.0 (>99)	81.0 (>99)	98	9
But-3-yn-1-ol	75.0 (99.7)	76.3 (80.5)	124	
Benzyl alcohol	81.9 (100)	81.9 (100)	193	14
1,2-Ethanediol	47.9 (100)	47.9 (100)	172	15
2-Butanol	35.2 (98.6)	50.7 (74.8)	90	14
Cyclohexanol	52.4 (97)	66.9 (71)	157	14
But-3-en-2-ol	58.1 (96.5)[h]	77.3 (69.7)[h]	90	
tert-Butyl alcohol	10 (93)	25 (20)	78	16
1-Adamantanol	14 (100)		105[i]	17

[a]Based in distillation fraction collected within 2°C of boiling point.
[b]Based on total mass collected above 42°C.
[c]The principal contaminant is CH_2Cl_2.
[d]660 Torr.
[e]Diethyl ether was used instead of methylene chloride.
[f]Weight percent in ether.
[g]No solvent was used.
[h]Principal impurity is the alcohol, ~3%.
[i]4 Torr.

2-Propenyl formate (allyl formate)

Collection of all material boiling in the range 42–80°C afforded the ester in 96% yield as 41% w/w solution in CH_2Cl_2. The 78–80°C fraction is 98% chemically pure and corresponds to a yield of 31%. Because of the severe entrainment of the solvent in this case, the experiment was repeated using diethyl ether as solvent, and in the absence of solvent. In ether, ester of 96% chemical purity could be isolated in 39% yield. In the absence of solvent, >99% pure ester was obtained in 36% yield; ^{1}H nmr ($CDCl_3$) δ: 4.68 (d, 2H, J = 5.7 Hz), 5.42–5.26 (m, 2H), 6.01–5.85 (m, 2H), 8.11 (s, 1H). These results are in agreement with the data reported in the literature (12).

2-Propynyl formate (progargyl formate)

Ester of >99% purity could be isolated in 81% yield; ^{1}H nmr ($CDCl_3$) δ: 2.55 (t, 1H, J = 2.5 Hz), 4.78 (d of d, 2H, J = 2.5 Hz and J = 0.9 Hz), 8.09 (t, 1H, J = 0.9 Hz). These results agree with data previously reported (13).

3-Butynyl formate

Ester of 99.7% purity could be isolated in 75% yield; ^{1}H nmr ($CDCl_3$) δ: 2.02 (t, 1H, J = 2.6 Hz), 2.53 (t of d, 2H, J = 6.7 Hz and J = 2.6 Hz), 4.25 (t, 2H, J = 6.7 Hz), 8.05 (s, 1H); ^{13}C nmr ($CDCl_3$): 18.7 (CH_2), 61.4 (CH_2O), 70.1 (≡CH), 79.6 (≡C—), 160.5 (OC(O)H) ppm; ms m/e: 98 (missing), 55 (10), 53 (17), 52 (100), 51 (21), 50 (19), 43 (13), 40 (48), 39 (60), 38 (17), 37 (10), 31 (73). *Anal.* calcd. for $C_5H_6O_2$: C 61.22, H 6.16; found: C 61.28, H 6.37.

Benzyl formate

Ester of 100% purity could be isolated in 82% yield; ^{1}H nmr ($CDCl_3$) δ: 5.22 (s, 2H), 7.40 (s, 5H), 8.16 (s, 1H). These results agree with data previously reported (14).

Ethylene glycol diformate

The reaction was carried out as described above with the exception that the quantities of formic acid, boron oxide, *p*-toluenesulfonic acid, and methylene chloride were doubled. Diester of 100% purity was obtained in 48% yield; ^{1}H nmr ($CDCl_3$) δ: 4.36 (s, 4H), 8.04 (s, 2H). These results are in agreement with data previously reported (15).

1-Methylpropyl formate (*sec*-butyl formate)

Ester of 99% purity could be isolated in 35% yield or in 51% yield as 75% w/w solution in CH_2Cl_2; ^{1}H nmr ($CDCl_3$) δ: 0.89 (t, 3H, J = 7.5 Hz), 1.23 (d, 3H, J = 6.3 Hz), 1.57 (m, 2H), 4.95 (hextet, 1H, J = 6.4 Hz), 8.04 (s, 1H).

Cyclohexyl formate

Ester of 97% purity could be obtained in 52% yield; ^{1}H nmr ($CDCl_3$) δ: 1.20–1.90 (br m, 10H), 4.86 (br m, 1H), 8.02 (s, 1H). These data are in agreement with previously reported values (14).

1-Methyl-2-propenyl formate

Ester of 97% purity could be isolated in 58% yield, or obtained in 77% yield as a 70% w/w solution in methylene chloride; ^{1}H nmr ($CDCl_3$) δ: 1.33 (d, 3H, J = 6.6 Hz), 5.20 (m, 2H), 5.44 (quintet, 1H, J = 6.6 Hz), 5.83 (m, 1H), 8.04 (s, 1H); ^{13}C nmr ($CDCl_3$): 19.9 (CH_3), 70.9 (CH), 116.4 (=CH_2), 137.0 (=CH), 160.4 (OC(O)H) ppm; ms m/e: 100 (missing), 72 (14), 73 (52), 57 (99), 55 (85), 54 (55), 53 (34), 51 (13), 50 (13), 45 (34), 44 (33), 43 (100), 41 (14), 39 (85), 32 (14), 31 (17). *Anal.* calcd. for $C_5H_8O_2$: C 59.98, H 8.05; found: C 59.18, H 8.29.

2-Methyl-2-propyl formate (*tert*-butyl formate)

The reaction was slower than with the other alcohols. The reaction mixture was refluxed for 1.75 h and left to stand at room temperature overnight. Ester of 93% purity could be isolated in 10% yield, or obtained in 20% yield as a 53% solution in methylene chloride (analysis by gc using OV-1 column); ^{1}H nmr ($CDCl_3$) δ: 1.46 (s, 9H), 7.98 (s, 1H). These data agree with those previously reported (16).

1-Adamantyl formate

The quantities of the general procedure were scaled to 0.17 mol of 1-adamantanol. An equilibrium mixture (36% conversion to ester) was achieved after 3 h refluxing. After treatment with potassium carbonate, the filtrate was concentrated, yielding a crop of needle-like crystals of 1-adamantanol. The mother liquor, consisting of ester/alcohol in 4:1 ratio in CH_2Cl_2, was chromatographed on a silica column with hexane as eluent. Distillation afforded ester of 100% purity in 14% yield (bp 105°C at 4 Torr); ^{1}H nmr ($CDCl_3$) δ: 1.67 (m, 6H), 2.12 (m, 6H), 2.19 (br s, 3H), 8.08 (s, 1H). These data agree with those previously reported (17).

Results and discussion

Boron oxide, B_2O_3, seems not to have been used in direct esterification reactions, which formally could proceed as follows:

$$3ROH + 3R'COOH + B_2O_3 \rightarrow 3R'COOR + 2B(OH)_3$$

Several observations support the notion that boron oxide, in the

Can. J. Chem. Downloaded from www.nrcresearchpress.com by 213.166.140.6 on 09/07/12
For personal use only.

Can. J. Chem. Downloaded from www.nrcresearchpress.com by 213.166.140.6 on 09/07/12
For personal use only.

presence of free alcohol, may serve the triple role of providing the alkoxy group, trapping the water of reaction, and acting as a Lewis acid catalyst in esterification reactions. Firstly, boron oxide reacts readily with alcohols to yield alkyl borates (alkoxy boranes), whose composition depends on the relative amounts of B_2O_3 and alcohol. When the stoichiometry is 1:3, the following reaction, which yields soluble trialkyl borates (trialkoxy boranes) and insoluble boric acid, dominates (18):

$$B_2O_3 + 3ROH \rightarrow B(OR)_3 + B(OH)_3$$

Indeed, a slurry of boron oxide in methylene chloride removes approximately three quarters of an equivalent amount of propargyl alcohol from solution by chemisorption on the solid and in the form of soluble borate esters within 10 min. Secondly, trialkyl borates, $(RO)_3B$, have been used in a variety of esterifications, although not in the preparation of formates and not of esters of propargyl alcohol (ref. 18, pp. 137–138, and refs. 19–21).

$$(RO)_3B + 3R'COOH \rightarrow 3R'COOR + B(OH)_3$$

In our hands, tripropargyl borate (23) reacted with three molar equivalents of formic acid in methylene chloride to give propargyl formate in 52% yield after distillation. A moderate enhancement of the rate of reaction is observed, compared to the direct esterification without boron species present. Thirdly, boron oxide has been used as a drying agent for formic acid (11, 19). As a bonus, boron oxide is relatively inexpensive, and may also be conveniently prepared by dehydration of inexpensive boric acid (24).

While the exact nature of the participation of the boron species has not yet been elucidated, the intermediacy of the free alcohol is implicated (19–21), and the observed enhancement of the rate of the reaction suggests a role as catalyst.

The results of the reaction with a range of primary, secondary, and tertiary alcohols, some unsaturated, are shown in Table 1. Esters of high chemical purity are obtained from the primary and secondary alcohols. Both tertiary alcohols required a substantially longer reaction time and could be isolated only in low yields. *tert*-Butyl alcohol is decomposed to a large extent under the conditions of the reaction. Phenol did not react. The distillation of many of the esters is hampered by entrainment of the solvent, methylene chloride. In the worst case, allyl formate of purity >98% could only be isolated in 31% yield by careful fractionation, while almost 96% of the theoretical amount of the ester could be recovered as a solution in methylene chloride if separation was not attempted. Yields and product purities (determined by gc analysis) are reported in two ways in the table. In the first column, the maximum yield of ester of highest purity is reported. The minor impurity is a trace of methylene chloride in most cases. In the second column, the total amount of ester recovered, and the composition of the total amount of material distilling above 42°C, is reported. The only components of the distillate are ester and solvent. Two of the compounds, the formate esters of but-3-en-2-ol and but-3-yn-1-ol, have apparently not been previously reported.

In summary, the reaction time is less than an hour if a catalytic amount of *p*-toluenesulfonic acid is added. Isolation is by distillation, after treatment of the filtered reaction mixture with potassium carbonate and phosphorus pentoxide. The product is uncontaminated by formic acid, unreacted alcohol, or water. The short reaction time, availability and cost of materials, and the purity of the product, offer distinct advantages of this method over other preparations of these formates. The method is not suitable for the preparation of tertiary alcohols, for which the mixed formic/acetic anhydride method is preferred (3).

Acknowledgements

The financial support of the Natural Sciences and Engineering Research Council of Canada is gratefully acknowledged.

1. W. WERNER. J. Chem. Res. Synop. 196 (1980).
2. G. A. OLAH and S. J. KUHN. J. Am. Chem. Soc. **82**, 2380 (1960).
3. W. STEVENS and A. VAN ES. Recl. Trav. Chim. Pays-Bas, **83**, 1287 (1964).
4. E. K. EURANTO. *In* The chemistry of carboxylic acids and derivatives. *Edited by* S. Patai. Interscience Publishers, New York, NY. 1969. p. 519.
5. R. GRZESKOWIAK, G. H. GEOFFREY, and A. I. VOGEL. J. Chem. Soc. 4719 (1960).
6. H. SAATO. Suom. Kemistil. B, **38**, 76 (1965).
7. A. ARIETA, T. GARCIA, J. M. LAGO, and C. PALOMO. Synth. Commun. **13**, 471 (1983).
8. J. MARCH. Advanced organic chemistry. 3rd ed. John Wiley and Sons, New York, NY. 1985. p. 348.
9. C. D. HEATEN and C. R. NOLLER. J. Am. Chem. Soc. **71**, 2948 (1949).
10. M. J. SKEETER. U.S. Patent No. 2,958,711 (1960); Chem. Abstr. **5**, 5345a (1961).
11. D. D. PERRIN, W. L. F. ARMAREGO, and D. R. PERRIN. Purification of laboratory chemicals. Pergamon Press, New York, NY. 1966. p. 291.
12. K. HAYAMIZU and O. YAMAMOTO. J. Mol. Spectrosc. **23**, 121 (1967).
13. G. M. BLACKBURN and H. L. H. DODDS. J. Chem. Soc. B, 826 (1971).
14. J. BARLUENGA, P. J. CAMPOS, E. GONZALEZ-NUNEZ, and G. ASENSIO. Synthesis, 426 (1985).
15. N. V. RIGGS and S. M. VERMA. Tetrahedron Lett. 3767 (1968).
16. T. DRAKENBERG and S. FORSEN. J. Phys. Chem. **76**, 3582 (1972).
17. D. GRILLER and B. P. ROBERTS. J. Chem. Soc. Perkin Trans. 2, 747 (1972).
18. H. STEINBERG. Organoboron chemistry. Vol. 1. Interscience Publishers, New York, NY. 1964. p. 48.
19. V. V. GERTSEV and YA. MAKAROV-ZEMLYORSKII. Zh. Prikl. Khim. (Leningrad), **43**, 1633 (1970).
20. E. CHERBULIEZ, J.-P. LEBER, and A.-M. ULRICH. Helv. Chem. Acta, **36**, 910 (1953).
21. M. M. KREEVOY and S. S. KANTNER. Croatica Chem. Acta, **49**, 41 (1977).
22. A. I. VOGEL. J. Chem. Soc. 624 (1948).
23. M. G. VELIEV, M. M. GUEINOV, A. M. GARAMANOV, and I. A. KHUDOYAROV. Synthesis, 205 (1983).
24. W. LANGE. Inorg. Synth. **2**, 22 (1946).

Ion-pair interactions between the methyl tris(1-pyrazolyl)gallato molybdenum, tricarbonyl anion, $[MeGapz_3]Mo(CO)_3^-$, and the Na^+ cation, and the reactivity of the anion toward RX molecules (where RX = HCl, DBr, MeI, or EtBr)

EMMANUEL C. ONYIRIUKA AND ALAN STORR[1]

Chemistry Department, University of British Columbia, Vancouver, B.C., Canada V6T 1Y6

Received March 19, 1987

EMMANUEL C. ONYIRIUKA and ALAN STORR. Can. J. Chem. **65**, 2464 (1987).

Ion-pair interactions between the carbonylate anion, $[MeGapz_3]Mo(CO)_3^-$, and the Na^+ cation in THF solution have been demonstrated using ir spectroscopy. The carbonylate ion has been protonated and the resulting hydride, $[MeGapz_3]Mo(CO)_3H$, characterized. The reaction of MeI with $[MeGapz_3]Mo(CO)_3^-$ proceeds via a detectable σ-methyl derivative to the η^2-acyl complex $[MeGapz_3]Mo(CO)_2(\eta^2\text{-COMe})$, whereas an analogous reaction using EtBr leads to the formation of an unstable σ-ethyl derivative, $[MeGapz_3]Mo(CO)_3Et$, with no evidence for the (η^2-COEt) insertion product.

EMMANUEL C. ONYIRIUKA et ALAN STORR. Can. J. Chem. **65**, 2464 (1987).

Faisant appel à la spectroscopie infrarouge, on a démontre que, en solution dans le THF, il existe des interactions entre paires d'ions de l'anion carbonylate $[MeGapz_3]Mo(CO)_3^-$ et du cation Na^+. On a protoné l'ion carbonylate et on a caractérisé l'hydrure $[MeGapz_3]Mo(CO)_3H$ qui en résulte. La réaction du MeI avec l'anion $[MeGapz_3]Mo(CO)_3^-$ se produit par l'intermédiaire d'un dérivé σ-méthyle que l'on peut détecter et elle conduit au complexe η^2-acyle $[MeGapz_3]Mo(CO)_2(\eta^2\text{-COMe})$; par ailleurs, une réaction analogue impliquant le EtBr conduit à la formation d'un dérivé σ-éthyle instable, le $[MeGapz_3]Mo(CO)_3Et$, et on n'a pas pu détecter la formation du produit d'insertion (η^2-COEt).

[Traduit par la revue]

Can. J. Chem. Downloaded from www.nrcresearchpress.com by 213.166.140.6 on 09/07/12
For personal use only.

Introduction

The uninegative, tridentate, six-electron donor ligand, $MeGapz_3^-$, shows many similarities to the cyclopentadienyl, Cp^-, ligand (1). It is also closely related in properties to the $RBpz_3^-$ ligands (R = H, alkyl, aryl, or pyrazolyl), introduced some time ago by Trofimenko (2). For example, all three ligand systems yield $LMo(CO)_3^-$ (L = $RBpz_3$, $MeGapz_3$, or Cp), anions on reaction with $Mo(CO)_6$ or $(MeCN)_3Mo(CO)_3$. Differences in behaviour between the ligand systems, however, are sometimes observed. Thus, the reaction of the above $LMo(CO)_3^-$ anions with allyl halides gives directly the η^3-allyl complexes $LMo(CO)_2(\eta^3\text{-allyl})$ when L = $RBpz_3$ or $MeGapz_3$, whereas the reaction first gives a σ-allyl derivative, $CpMo(CO)_3(\sigma\text{-allyl})$ when L = Cp, and only upon uv irradiation does the decarbonylation reaction occur to yield the η^3-allyl derivative $CpMo(CO)_2(\eta^3\text{-allyl})$ (3–5). The present paper details further the properties of the $[MeGapz_3]Mo(CO)_3^-$ and $[MeGa(3,5\text{-diMepz})_3]Mo(CO)_3^-$ anions and compares and contrasts, where appropriate, their behaviour with similar complexes containing $RBpz_3^-$ or Cp^- ligands.

Experimental

Starting materials

Ph_3AsHCl (Strem Chemicals), Et_4NCl (Eastman Organic Chemicals), EtBr (Allied Chemicals), HCl (Matheson), DBr (Merck Sharpe and Dohme), and MeOH (Fisher Scientific) were used as supplied. The ligand salts, $Na^+MeGapz_3^-$ (1) and $Na^+MeGa(3,5\text{-diMepz})_3^-$ (6) were prepared as previously described. MeI (Fisher Scientific) was dried by distillation from P_2O_5 and $(MeCN)_3Mo(CO)_3$ was prepared according to a literature method (7). Air-sensitive materials were handled in a glove box under an atmosphere of oxygen-free dry nitrogen or in a nitrogen-blanketed apparatus. Tetrahydrofuran (THF) was dried by refluxing over Na/benzophenone, benzene by refluxing over potassium, CH_2Cl_2 by refluxing over CaH_2, and hexanes by refluxing over $CaSO_4$.

[1]Author to whom correspondence should be addressed.

Preparation of $Na^+[MeGapz_3]Mo(CO)_3^-$ and $Na^+[MeGa(3,5\text{-diMepz})_3]Mo(CO)_3^-$

$$Na^+MeGapz_3^- + (MeCN)_3Mo(CO)_3 \xrightarrow{THF} Na^+[MeGapz_3]Mo(CO)_3^- + 3MeCN$$

A 30 mL aliquot of the gallate ligand solution in THF containing ~0.51 mmol $Na^+MeGapz_3^-$ was added to a stirred solution of $(MeCN)_3Mo(CO)_3$ (0.154 g, 0.510 mmol) in the same solvent. The reaction mixture was stirred until the ν_{CO} bands characteristic of the $(MeCN)_3Mo(CO)_3$ starting material had disappeared. The volatiles were then allowed to evaporate to leave the $Na^+[MeGapz_3]Mo(CO)_3^-$ salt as an amber-colored solid. The $Na^+[MeGa(3,5\text{-diMepz})_3]Mo(CO)_3^-$ salt was prepared by a similar method. Both salts were very air-sensitive and satisfactory elemental analyses could not be obtained. However, solution ir and ^1H nmr spectra for the two salts were recorded.

For $Na^+[MeGapz_3]Mo(CO)_3^-$: ir (THF) ν_{CO} 1895s, 1775s, 1720s; (CH_2Cl_2) ν_{CO} 1888s, 1760br cm^{-1}. ^1H nmr (d_6-acetone, 80 MHz) 9.58s (Ga—Me), 3.83t (pz—H^4), 2.35d (pz—H^5), 2.00d (pz—H^3). ($J_{HCCH} \approx 2$ Hz for pz protons; $\tau_{(CH_3)_2CO} = 7.89$ ppm).

For $Na^+[MeGa(3,5\text{-diMepz})_3]Mo(CO)_3^-$: ir (THF) ν_{CO} 1890s, 1765s, 1710s; (CH_2Cl_2) ν_{CO} 1885s, 1745 br cm^{-1}. ^1H nmr (d_6-acetone, 80 MHz) 9.54s (Ga—Me), 7.78 (pz—Me^5), 7.19s (pz—Me^3), 4.38s (pz—H^4).

Preparation of $Et_4N^+[MeGapz_3]Mo(CO)_3^-$

$$Na^+[MeGapz_3]Mo(CO)_3^- + Et_4NCl \xrightarrow[MeOH]{THF} Et_4N^+[MeGapz_3]Mo(CO)_3^- + NaCl$$

Et_4NCl (0.169 g, 1.02 mmol), dissolved in ~5 mL MeOH, was added to an equimolar amount of the carbonylate salt $Na^+[MeGapz_3]Mo(CO)_3^-$ prepared as a THF solution as described above. The resulting cloudy yellow solution was stirred for ~1 h. The yellow precipitate formed was then collected and dried *in vacuo* to give the desired product, $Et_4N^+[MeGapz_3]Mo(CO)_3^-$ in 40% yield. This salt, like the corresponding Na^+ salt, is unstable in air: ir (THF) 1890s, 1765 br; (CH_2Cl_2) 1890s, 1760 br; (Nujol) 1885s, 1752s, 1730s cm^{-1}.

^{1}H nmr (d_6-acetone, 270 MHz): 9.57s (Ga—Me), 3.81t (pz—H^4), 2.27d (pz—H^5),1.92d (pz—H^3), 8.57br (N—CH_2—CH_3), 6.41br (N—CH_2—CH_3).

Preparation of $HAsPh_3^+[MeGapz_3]Mo(CO)_3^-$ and $HAsPh_3^+[MeGa(3,5\text{-}diMepz)_3]Mo(CO)_3^-$

$$Na^+[MeGapz_3]Mo(CO)_3^- + HAsPh_3Cl \xrightarrow[\Delta]{THF} HAsPh_3^+[MeGapz_3]Mo(CO)_3^- + NaCl$$

To a stirred THF solution of $Na^+[MeGapz_3]Mo(CO)_3^-$ (0.85 mmol) was added solid $HAsPh_3Cl$ (0.29 g, 0.85 mmol). The resulting mixture was refluxed overnight, after which the solution was cooled and the solvent removed *in vacuo*. The resulting yellow residue was extracted with benzene and filtered. Golden-yellow needles of the desired salt $HAsPh_3^+[MeGapz_3]Mo(CO)_3^-$ were obtained as a benzene solvate on slow evaporation of the solvent. The salt $HAsPh_3^+[MeGa(3,5\text{-}diMepz)_3]Mo(CO)_3^-$ was prepared in a similar manner, with the exception that the extraction and recrystallization procedure was carried out with CH_2Cl_2/hexane solvents. Both the salts obtained are considerably more air-stable than the corresponding Na^+ or Et_4N^+ salts.

Anal calcd. for $HAsPh_3^+[MeGapz_3]Mo(CO)_3^- \cdot \frac{3}{4}C_6H_6$; C 51.26, H 3.91, N 10.11; found: C 51.44, H 3.54, N 9.94. Infrared (CH_2Cl_2) ν_{CO} 1890s, 1750br; (THF) ν_{CO} 1890s, 1755br; (Nujol) ν_{CO} 1885s, 1760s, 1735s cm^{-1}. ^{1}H nmr (d_6-acetone, 80 MHz) 9.56s (Ga—Me), 3.83t (pz—H^4), 2.35d (pz—H^5), 1.98d (pz—H^3), 2.05br (As—*Ph*), 2.58s (As—H).

Anal calcd. for $HAsPh_3^+[MeGa(3,5\text{-}diMepz)_3]Mo(CO)_3^-$: C 51.83, H 4.67, N 9.81; found: C 52.23, H 4.80, N 9.72. Infrared (CH_2Cl_2) ν_{CO} 1885s, 1740br; (THF) ν_{CO} 1885s, 1750br cm^{-1}. ^{1}H nmr (d_6-acetone, 80 MHz) 9.55s (Ga—Me), 7.80s (pz—Me^5), 7.21s (pz—Me^3), 4.38s (pz—H^4), 2.09br (As—*Ph*), 2.61s (As—H).

Preparation of $[MeGapz_3]Mo(CO)_3H$

$$Na^+[MeGapz_3]Mo(CO)_3^- + HCl \xrightarrow{THF} [MeGapz_3]Mo(CO)_3H + NaCl$$

An equimolar amount of HCl gas (0.50 mmol) was condensed onto a THF solution containing the $Na^+[MeGapz_3]Mo(CO)_3^-$ salt (0.50 mmol). The reaction mixture was warmed to room temperature and the resulting orange solution was stirred for ~2 h. The solvent was then removed *in vacuo*, and the resulting residue extracted with hexane. The product hydride was obtained from the hexane filtrate as an air-sensitive orange solid in ~60% yield.

Anal calcd. for $[MeGapz_3]Mo(CO)_3H \cdot \frac{1}{2}C_6H_{14}$: C 37.67, H 3.92, N 16.48; found: C 37.21, H 3.62, N 16.41. Infrared (C_6H_{14}) 1952w, 1928s, 1908s, 1808s cm^{-1}. ^{1}H nmr (d_6-acetone, 300 MHz), 9.90s (Ga—Me), 3.60t (pz—H^4), 2.50d (pz—H^5), 2.16d (pz—H^3), 18.50s (Mo—*H*).

Attempts to prepare the corresponding deuteride, $[MeGapz_3]Mo(CO)_3D$, using DBr gas were only partially successful. A sticky orange solid was isolated that displayed three strong ν_{CO} bands at 1935, 1910, and 1840 cm^{-1} together with a weak band at 1380 cm^{-1} (assigned to $\nu_{Mo—D}$) in its ir spectrum in benzene solution.

Preparation of $[MeGapz_3]Mo(CO)_2(\eta^2\text{-}COMe)$

$$Na^+[MeGapz_3]Mo(CO)_3^- + MeI \xrightarrow{THF} [MeGapt_3]Mo(CO)_2(\eta^2\text{-}COMe) + NaI$$

To a THF solution of the carbonylate salt was added an excess of MeI in the same solvent. The resulting dark orange–red reaction mixture was stirred for ~4 days, after which the solvent and unreacted MeI were removed under vacuum. The resulting dark-red residue was extracted with CH_2Cl_2 and the solution filtered. An equal volume of hexane was added to the filtrate and the mixed solvents then allowed to evaporate. Air-sensitive, brick-red crystals of the product were obtained in ~30% yield.

Anal calcd. for $[MeGapz_3]Mo(CO)_2(\eta^2\text{-}COMe)$: C 34.95, H 3.12, N 17.48; found: C 35.10, H 3.16, N 17.15. Infrared (CH_2Cl_2) 1980s, 1855s, 1570w cm^{-1}. ^{1}H nmr (d_6-acetone, 80 MHz) 9.30s (Ga—Me), 3.63t 3.53t (pz—H^4), 2.46d 2.24d (pz—H^5), 2.06d 1.95d (pz—H^3), 6.60s (—CO*Me*). The mass spectrum of the compound displayed prominent signals due to the P^+, $P - Me^+$, $P - CO^+$, $P - CO - Me^+$, and $P - 2CO^+$, $P - 2CO - Me^+$, $P - 3CO^+$, $P - 3CO - Me^+$ ions (P^+ = parent ion).

Preparation of $[MeGapz_3]Mo(CO)_3Et$

$$Na^+[MeGapz_3]Mo(CO)_3^- + EtBr \xrightarrow{THF} [MeGapz_3]Mo(CO)_3Et + NaBr$$

An excess of EtBr in THF was added to a THF solution of the carbonylate salt (~0.68 mmol). The mixture was stirred at room temperature for ~1 day and then at reflux temperatures for a further short period. Solvent removal, followed by extraction with benzene and recrystallization from CH_2Cl_2/hexane yielded the product as a reddish-brown solid in low yield.

Anal calcd. for $[MeGapz_3]Mo(CO)_3Et$: C 36.39, H 3.44, N 16.98; found: C 36.55, H 3.28, N 16.63. Infrared (CH_2Cl_2) 1970s, 1930s, 1820s: 1890s, 1755br cm^{-1}. ^{1}H nmr (d_6-acetone, 270 MHz) 9.53s (Ga—Me), 3.81 (pz—H^4), 2.36 (pz—H^5), 1.97 (pz—H^3), 8.15br (Mo—CH_2—CH_3), 6.32br (Mo—CH_2—CH_3).

Results and discussion

The $[MeGapz_3]Mo(CO)_3^-$ and $[MeGa(3,5\text{-}diMepz)_3]Mo(CO)_3^-$ carbonylate anions have been isolated as their sodium (Na^+), tetraethylammonium (Et_4N^+), and triphenylarsonium ($HAsPh_3^+$) salts. The ir spectra of the salts in the carbonyl stretching region of the spectrum were found to be solvent and cation dependent, suggestive of ion-pair interactions in some cases. The phenomenon of ion-pair interactions between cations of Groups 1 or 2 and transition metal carbonylate anions has been well documented (8, 9). For example, the crystal structures of $[CpMo(CO)_3^-]_2Mg^{2+} \cdot 4(C_5H_5N)$ (10) and $[\{Co(salen)\}_2Na^+Co(CO)_4^- \cdot THF]$ (11) have indicated ion-pair interactions to exist between the carbonylate anions and the cations in these complexes. Generally transition metal carbonylate anion – alkali or alkaline earth cation interactions are found to occur quite extensively in basic, low polarity, donor solvents such as THF. The first ir spectroscopic evidence for this type of ion pairing in solvents of moderate polarity was reported some time ago by Edgell *et al.* (12). Since that report and subsequent work on the $Na^+Co(CO)_4^-$ salt (13), analyses of ν_{CO} ir stretching frequencies in THF solutions have successfully revealed alkali metal cation interactions with the carbonylate anions $CpFe(CO)_2^-$ (14, 15) and $CpM(CO)_3^-$ (M = Cr, Mo, or W) (16).

In the present study the ir spectra of the $M^+LMo(CO)_3^-$ salts (where M = Na, Et_4N, or $HAsPh_3$ and L = $MeGapz_3$ or $MeGa(3,5\text{-}diMepz)_3$) in CH_2Cl_2 solution displayed two strong ν_{CO} bands consistent with the symmetrical C_{3v} structure (A_1 + E modes) expected for the free carbonylate anions. However, in THF solution three strong ν_{CO} bands were observed for the Na^+ salts. Representative solution ir spectra in the ν_{CO} region of the spectrum for the $M^+[MeGapz_3]Mo(CO)_3^-$ salts are shown in Fig. 1. The presence of three strong ν_{CO} bands for the $Na^+[MeGapz_3]Mo(CO)_3^-$ salt in THF suggests that the C_{3v} symmetry of the unperturbed anion has been reduced to C_s symmetry ($2A' + A''$ modes) by an ion-pair interaction with the Na^+ cation (see Fig. 2). A listing of the ν_{CO} values for the $M^+LMo(CO)_3^-$ salts (Table 1) reveals the presence of a low-frequency band for the $Na^+LMo(CO)_3^-$ salts in THF which

Can. J. Chem. Downloaded from www.nrcresearchpress.com by 213.166.140.6 on 09/07/12
For personal use only.

TABLE 1. ν_{CO} (cm^{-1}) infrared data for $M^+LMo(CO)_3^-$ (L = $MeGapz_3$, $MeGa(3,5\text{-}Me_2pz)_3$, M^+ = Na^+, Et_4N^+, $HAsPh_3^+$) salts

Compound	Solvent	A'	A_1	A''	E	$A'(CO\cdots M^+)$
$Na^+MeGapz_3Mo(CO)_3^-$	THF	1895		1775		1720
	CH_2Cl_2		1888		1760	
$Na^+MeGa(3,5\text{-}Me_2pz)_3Mo(CO)_3^-$	THF	1890		1765		1710
	CH_2Cl_2		1885		1745	
$Et_4N^+MeGapz_3Mo(CO)_3^-$	THF		1890		1765	
	CH_2Cl_2		1890		1760	
$HAsPh_3^+MeGapz_3Mo(CO)_3^-$	THF		1890		1755	
	CH_2Cl_2		1890		1750	
$HAsPh_3^+MeGa(3,5\text{-}Me_2pz)_3Mo(CO)_3^-$	THF		1885		1750	
	CH_2Cl_2		1885		1740	

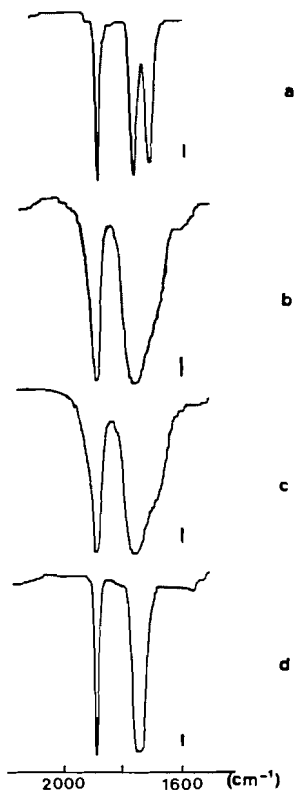

FIG. 1. Infrared spectra of $M^+[MeGapz_3]Mo(CO)_3^-$ salts in the ν_{CO} region: (*a*) $M^+ = Na^+$ in THF, (*b*) $M^+ = Na^+$ in CH_2Cl_2, (*c*) $M^+ = Et_4N^+$ in CH_2Cl_2, (*d*) $M^+ = HAsPh_3^+$ in CH_2Cl_2.

we assign to the A' (contact) vibration. Thus in the type of ion pairing proposed, substantial π-electron drift towards the CO group involved in the interaction is expected to occur (17). This is shown schematically in Fig. 3. In Fig. 3*a*, *c* the Na^+ cation is positioned for maximum interaction with both the σ and π electron density on the CO ligand. Whether this arrangement or the alternate linear arrangement (Fig. 3*b*) holds, the interaction would reduce the bond order for the CO involved, and hence lower its ν_{CO} stretching frequency.

The solution ir spectrum of the $Et_4N^+[MeGapz_3]Mo(CO)_3^-$ salt in THF displays one strong, sharp band at $\sim 1890\ cm^{-1}$ and a second continuous broad band with two or more maxima centred at $\sim 1765\ cm^{-1}$. Again, perturbation of the carbonylate anion by the Et_4N^+ cation might be occurring in the THF

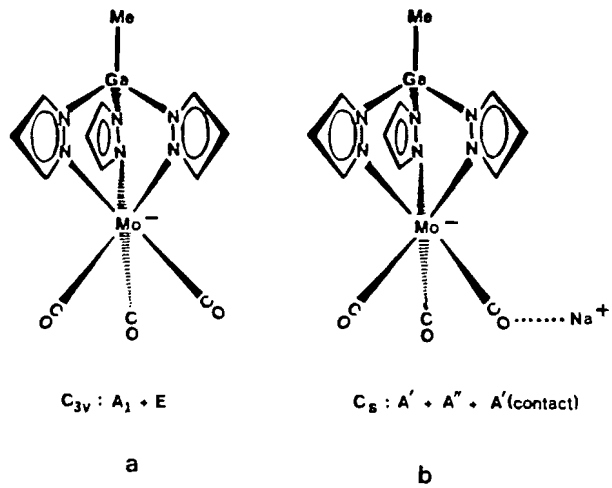

FIG. 2. Molecular arrangements for the $[MeGapz_3]Mo(CO)_3^-$ anion: (*a*) unperturbed anion, (*b*) perturbed anion.

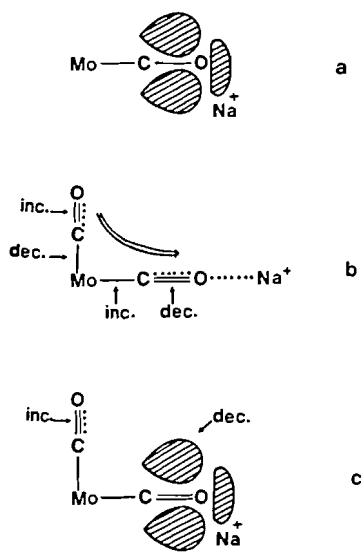

FIG. 3. Possible Na^+ interactions with the $[MeGapz_3]Mo(CO)_3^-$ anion: (*a*) Pictorial representation of electron density on CO ligand, (*b*) effects of linear interaction of coordinated CO ligand with Na^+, (*c*) non-linear interaction.

Can. J. Chem. Downloaded from www.nrcresearchpress.com by 213.166.140.6 on 09/07/12
For personal use only.

Can. J. Chem. Downloaded from www.nrcresearchpress.com by 213.166.140.6 on 09/07/12
For personal use only.

solvent. Interestingly an X-ray crystal structure of the related $Me_4N^+CpCr(CO)_3^-$ complex (18) has revealed some electrostatic interaction between the Me_4N^+ cation and the $CpCr(CO)_3^-$ anion. The ν_{CO} values for the $Na^+[MeGapz_3]Mo(CO)_3^-$ salt in THF (1895, 1775, 1720 cm^{-1}) compare favorably with the ν_{CO} values reported independently for the $Na^+CpMo(CO)_3^-$ salt (1893, 1775, 1749 cm^{-1} in pyridine (10), and 1899, 1796, 1743 cm^{-1} in THF (16)).

The ^1H nmr spectra of the salts studied in this work all showed the three pyrazolyl groups of the gallate ligands to be equivalent, with no evidence of any asymmetry of the type indicated by the ν_{CO} ir measurements. This is to be expected since oxygen-17 and carbon-13 nmr spectral studies have indicated that the lifetime of the similar $CpMo(CO)_3^-\ldots Na^+$ interactions in the related $Na^+CpMo(CO)_3^-$ salt solution is considerably shorter than the time scale of the nmr experiment (9, 16).

The reactivity of the carbonylate anion, $[MeGapz_3]Mo(CO)_3^-$, towards a variety of RX species has been probed. It had been reported earlier that acidification of the $[RBpz_3]Mo(CO)_3^-$ anions (R = H or pz) with acetic acid yields the corresponding $[RBpz_3]Mo(CO)_3H$ acids (19). Similarly, the weak acid, $CpMo(CO)_3H$, is readily obtained by protonation of the $CpMo(CO)_3^-$ anion with acetic acid (3). Consequently, the preparation of $[MeGapz_3]Mo(CO)_3H$ was attempted initially by the acidification of the $Na^+[MeGapz_3]Mo(CO)_3^-$ salt with glacial acetic acid. However, incomplete protonation of the carbonylate anion was indicated by solution ir and ^1H nmr measurements. The subsequent use of hydrogen chloride as the protonating agent was more successful and an orange-yellow, air-sensitive, solid of the correct formulation, $[MeGapz_3]Mo(CO)_3H$, was obtained in good yield. This compound displayed three strong ν_{CO} bands at 1928, 1908, and 1808 cm^{-1} and a weak ν_{Mo-H} vibration at 1952 cm^{-1} in its hexane solution ir spectrum. The assignment of the Mo—H vibration was confirmed by preparing the corresponding deuteride, $[MeGapz_3]Mo(CO)_3D$, which also gave three strong ν_{CO} bands (1935, 1910, 1845 cm^{-1}) in addition to a weak band at ~1380 cm^{-1}, assigned to the ν_{Mo-D} vibration.

The ^1H nmr spectrum of $[MeGapz_3]Mo(CO)_3H$ in d_6-acetone solution displayed one set of signals for the pyrazolyl ring protons (indicating equivalent pyrazolyl-ring environments) and a Mo—*H* signal at 18.5 τ. This result is contrary to the ir data, which showed three ν_{CO} bands, consistent with a C_s symmetry and inequivalent pyrazolyl rings for the complex. It is probable that stereochemical non-rigidity is being displayed by the hydride complex in solution. Thus, assuming the solid to possess a 3:4 piano-stool structure similar to that demonstrated recently in the crystal structure determination of the analogous compound $(\eta^5\text{-}C_5Me_5)Mo(CO)_3H$ (20), a rapid equilibration (on the nmr time scale) of the position of the three CO ligands and the hydrido ligand in the basal plane of the molecule would account for the ^1H nmr result. A similar equilibration process has been suggested for the closely similar complexes, $[HBpz_3](Mo(CO)_3X$ (X = H, Br, I) (21) and is thought to involve an intermediate C_{3v} arrangement with the X atom along the B···Mo axis. An alternative explanation of the ^1H nmr spectrum could involve a rapid rotation of the $MeGapz_3$ moiety about the Ga···Mo axis, which would also result in equalizing the environments of the pyrazolyl groups. The Mo—H signal for the $[MeGapz_3]Mo(CO)_3H$ complex (18.5 τ) appeared at a considerably higher field position than those reported for $CpMo(CO)_3H$ (12.8 τ (3)) and $[HBpz_3]Mo(CO)_3H$ (13.3 τ (19), 13.02 τ (21)). This large upfield shift is difficult to rationalize but the $MeGapz_3^-$ ligand is known to be a better electron donor than either the $HBpz_3^-$ or Cp^- ligands (1) and thus is likely to produce a more electron-rich Mo centre with concomitant increased shielding at the Mo—H proton.

An earlier report suggested that the reaction of MeI with the anion $[HBpz_3]Mo(CO)_3^-$ gave the σ-methyl derivative, $[HBpz_3]Mo(CO)_3Me$ (19). Recently, however, Curtis *et al.* communicated that the product of the above reaction was in fact an η^2-acyl complex, $[HBpz_3]Mo(CO)_2(\eta^2\text{-}COMe)$, no detectable quantities of the σ-methyl derivative being observed in solution. ^1H nmr and ir evidence for the η^2-acyl complex in solution was further substantiated by a solid state X-ray crystal structure determination (22, 23). Generally, metal η^2-acyl complexes are of interest since it is thought possible that such species may play an important role in the metal catalyzed hydrogenation of CO (24–26). The reaction of MeI with the anion $[MeGapz_3]Mo(CO)_3^-$ was carried out firstly to determine if a σ-methyl derivative could be detected and secondly to probe further this novel class of η^2-acyl molybdenum compounds. The reaction itself, in THF, was very slow and incomplete. Even after four days, the solution ir spectrum showed the three ν_{CO} bands due to the presence of unreacted carbonylate anion. However, in addition to these bands, three new ν_{CO} bands at 1970, 1920, and 1855 cm^{-1} were observed. These we assign to the presence of the σ-methyl complex $[MeGapz_3]Mo(CO)_3Me$ in THF solution.

Upon work-up of the reaction mixture brick-red crystals were isolated that displayed two strong ν_{CO} bands at 1980 and 1855 cm^{-1} and a weak band at 1570 cm^{-1} (CH_2Cl_2 solution). This pattern is consistent with the η^2-acyl formulation, $[MeGapz_3]Mo(CO)_2(\eta^2\text{-}COMe)$, for the complex (27, 28), the positions of the bands being closely similar to those reported for the $[HBpz_3]Mo(CO)_2(\eta^2\text{-}COMe)$ compound (1983, 1856, 1570 cm^{-1}) (22). It is interesting to speculate why a σ-methyl derivative is observed in our reaction, whereas Curtis *et al.* reported no detectable σ-methyl complex in the reaction involving the analogous boron-containing compound. Wax and Bergman have shown similar CO insertion reactions to be "solvent catalyzed" (29). Thus the use of the poorly coordinating solvent, THF, in our reaction sequence may have allowed the detection in solution of the σ-methyl derivative $[MeGazp_3]Mo(CO)_3Me$ whereas the use of the highly coordinating acetonitrile reaction medium by Curtis *et al.* (22, 23) may have promoted the rapid formation of the $[HBpz_3]Mo(CO)_2(\eta^2\text{-}COMe)$, thus preventing detection of the σ-methyl intermediate.

The ^1H nmr spectrum of the $[MeGapz_3]Mo(CO)_2(\eta^2\text{-}COMe)$ complex in d_6-acetone is as expected for the η^2-acyl formulation. Thus the pyrazolyl ring protons appear in the predicted 2:1 intensity ratio and the η^2-CO*Me* signal is displayed as a sharp singlet at 6.60 τ. The transformation of the σ-methyl complex, $[MeGapz_3]Mo(CO)_3Me$, to the η^2-acyl complex $[MeGapz_3]Mo(CO)_2(\eta^2\text{-}COMe)$ observed in the present study and the even more facile sequence reported for the analogous pyrazolylborate compound (22, 23) has no counterpart in cyclopentadienyl molybdenum chemistry.

The reaction of the $[MeGapz_3]Mo(CO)_3^-$ anion with EtBr afforded the metal–alkyl bonded $[MeGapz_3]Mo(CO)_3Et$ derivative in low yield. The red–brown compound decomposes slowly on storage and solutions of the complex are even less stable than the solid. Thus, the solution ir spectrum of the complex in CH_2Cl_2 shows three ν_{CO} bands at 1970, 1930, and 1820 cm^{-1} due to the ethyl complex, in addition to two ν_{CO} bands at 1890 and 1755 cm^{-1}, which increase in intensity

with time, assigned to the anion $[MeGapz_3]Mo(CO)_3^-$. It is interesting that the ir spectrum of the closely related $[HBpz_3]Mo(CO)_3Et$ complex, reported earlier by Trofimenlo (19), displayed five ν_{CO} bands (1980, 1960, 1850, 1835, and 1816 cm^{-1}, Nujol), a pattern that again may be indicative of some decomposition of this ethyl compound. The ir spectra of related cyclopentadienyl analogues are interesting in that they display only two ν_{CO} bands, $CpMo(CO)_3Et$ (2016, 1932 cm^{-1}, CCl_4 (3)) and $CpCr(CO)_3Et$ (2012, 1933 cm^{-1}, pentane (30)). The crystal structure of the $CpMo(CO)_3Et$ complex (31) has revealed a 3:4 piano-stool arrangement in the solid state and if this structure persists in solution an accidental coincidence of two ν_{CO} bands must occur in the ir spectra. The three ν_{CO} bands assigned to the $[MeGapz_3]Mo(CO)_3Et$ complex are consistent with a C_s symmetry ($2A' + A''$ modes) or a 3:4 piano-stool arrangement in solution. To explain the room-temperature ^1H nmr spectrum of the complex, which indicates equivalent environments for the three pyrazolyl rings, a fluxional process similar to that suggested earlier for the $[MeGapz_3]Mo(CO)_3H$ complex and that interchanges the Et and 3CO ligands via an average C_{3v} arrangement, could be operative.

No evidence for CO insertion into the Mo—Et bond to form an η^2-COEt complex was observed for the $[MeGapz_3]$-$Mo(CO)_3Et$ compound. It is not clear at this stage why an acyl derivative was obtained with MeI but not with EtBr. In general the rate of an alkyl to acyl conversion reaction is known to be dependent on the strengths of the M—C (alkyl) and M—CO bonds in the starting alkyl complex (32) and a recent thermodynamic study (33) might lead one to predict a more facile acyl formation should occur with the Mo—Et derivative. Perhaps the ready decomposition of the $[MeGapz_3]Mo(CO)_3Et$ complex precludes the formation of an η^2-COEt derivative.

Acknowledgements

We thank the Natural Sciences and Engineering Research Council of Canada for financial support, and Mr. P. Borda for the C, H, N analyses.

1. K. R. Breakell, S. J. Rettig, A. Storr, and J. Trotter. Can. J. Chem. **56**, 2099 (1978).
2. S. Trofimenko. J. Am. Chem. Soc. **88**, 1842 (1966).
3. T. S. Piper and G. Wilkinson. J. Inorg. Nucl. Chem. **3**, 104 (1956).
4. M. Cousins and M. L. H. Green. J. Chem. Soc. 889 (1963).
5. R. B. King. Inorg. Chem. **5**, 2242 (1966).
6. K. R. Breakell, S. J. Rettig, A. Storr, and J. Trotter. Can. J. Chem. **57**, 139 (1979).
7. D. P. Tate, W. R. Knipple, and J. M. Augl. Inorg. Chem. **1**, 433 (1962).
8. C. P. Horwitz and D. F. Shriver. Adv. Organomet. Chem. **23**, 219 (1984).
9. M. Y. Darensbourg. Prog. Inorg. Chem. **33**, 221 (1985).
10. S. W. Ullmer, P. M. Skarstad, J. M. Burlitch, and R. E. Hughes. J. Am. Chem. Soc. **95**, 4469 (1973).
11. G. Fachinetti, C. Floriani, P. F. Zanazzi, and A. R. Zanzari. Inorg. Chem. **17**, 3002 (1978).
12. W. F. Edgell, M. T. Yang, and N. Koizumi. J. Am. Chem. Soc. **87**, 2563 (1965).
13. W. F. Edgell and J. Lyford. J. Am. Chem. Soc. **93**, 6407 (1971).
14. K. H. Pannel and D. Jackson. J. Am. Chem. Soc. **98**, 4443 (1976).
15. M. Nitay and M. Rosenblum. J. Organomet. Chem. **136**, C23 (1977).
16. M. Y. Darensbourg, P. Jimenez, J. R. Sackett, J. M. Hanckell, and R. L. Kump. J. Am. Chem. Soc. **104**, 1521 (1982).
17. P. Politzer and P. H. Reggio. J. Am. Chem. Soc. **94**, 8308 (1972).
18. V. R. Feld, E. Hellner, A. Klopch, and K. Dehnicke. Z. Anorg. Allg. Chem. **442**, 173 (1978).
19. S. Trofimenko. J. Am. Chem. Soc. **91**, 588 (1969).
20. P. Leoni, E. Grilli, M. Pasquali, and M. Tomassini. J. Chem. Soc. Dalton Trans. 1041 (1986).
21. M. D. Curtis and K. Shiu. Inorg. Chem. **24**, 1213 (1985).
22. M. D. Curtis, K. Shiu, and W. M. Butler. Organometallics, **2**, 1475 (1983).
23. M. D. Curtis, K. Shiu, and W. M. Butler. J. Am. Chem. Soc. **108**, 1550 (1986).
24. C. Masters. Adv. Organomet. Chem. **17**, 61 (1979).
25. C. K. Rofer-DePoorter. Chem. Rev. **81**, 447 (1981).
26. W. A. Herrman. Angew. Chem. Int. Ed. Engl. **21**, 117 (1982).
27. F. Calderazzo. Angew. Chem. **89**, 305 (1977).
28. F. Calderazzo. Angew. Chem. Int. Ed. Engl. **16**, 299 (1977).
29. M. J. Wax and R. G. Bergman. J. Am. Chem. Soc. **103**, 7028 (1981).
30. R. M. Medina and J. R. Masaguer. J. Organomet. Chem. **299**, 341 (1986).
31. M. J. Bennett and R. Mason. Proc. Chem. Soc. 273 (1963).
32. J. P. Collman and L. S. Hegedus. Principles and applications of organo-transition metal chemistry. University Science Books, Mill Valley, CA. 1980.
33. S. P. Nolan, R. Lopez de la Vega, S. L. Mukerjee, and C. D. Hoff. Inorg. Chem. **25**, 1160 (1986).

Can. J. Chem. Downloaded from www.nrcresearchpress.com by 213.166.140.6 on 09/07/12
For personal use only.

Complexes of the dimethylgallium-1-pyrazolyl-*o*-aminophenolato ligand, $[Me_2Ga(pz)(o\text{-}NH_2C_6H_4O)]^-$. Formation and crystal structure of the molybdenum amidine complex, $Mo(CO)_2Br(\eta^3\text{-}C_3H_5)[\eta^2\text{-}HN{=}CMe(pz)]$ (where pz = pyrazolyl, $N_2C_3H_3$)

G. D. Gracey, Steven J. Rettig, Alan Storr,[1] and James Trotter[1]

Department of Chemistry, University of British Columbia, 2036 Main Mall, Vancouver, B.C., Canada V6T 1Y6

Received March 11, 1987

G. D. Gracey, Steven J. Rettig, Alan Storr, and James Trotter. Can. J. Chem. **65**, 2469 (1987).

The synthesis, characterization, and structures of complexes containing the *o*-aminophenolato ligand are detailed. A novel molybdenum amidine complex is also described. Crystals of (*o*-aminophenolato)dimethylgallium are monoclinic, a = 10.1970(9), b = 9.7597(7), c = 18.778(2) Å, β = 100.810(7)°, Z = 8, space group $C2/c$, those of bis(dimethylgallium-1-pyrazolyl-*o*-aminophenolato)nickel(II) benzene solvate are monoclinic, a = 20.491(1), b = 11.789(1), c = 15.789(1) Å, β = 103.413(7)°, Z = 4, space group $C2/c$, and those of η^3-allyl(bromo)[2-(1-pyrazolyl)ethylidenamino]dicarbonylmolybdenum(II) are monoclinic, a = 11.0278(4), b = 8.4461(2), c = 15.3747(5) Å, β = 109.208(3)°, Z = 4, space group $P2_1/c$. The structures were solved by conventional heavy atom methods and refined by full-matrix least-squares procedures to R = 0.030, 0.053, and 0.038 for 1980, 1684, and 1901 reflections, respectively. Reaction of the $[Me_2Ga(pz)(OC_6H_4NH_2)]^-$ ligand, L^-, with $[Re(CO)_4Cl]_2$ results in the formation of $LRe(CO)_3$ whose physical properties indicate a *fac* arrangement of the organogallate ligand.

G. D. Gracey, Steven J. Rettig, Alan Storr et James Trotter. Can. J. Chem. **65**, 2469 (1987).

On décrit la synthèse, la caractérisation et les structres des complexes contenant le ligand *o*-aminophénolato. On décrit aussi un nouveau complexe amidine du molybdène. Les cristaux du (*o*-aminophénolato) diméthyl gallium sont monocliniques avec a = 10,1970(9), b = 9,7597(7) et c = 18,778(2) Å, β = 100,810(7)°, Z = 8 et groupe d'espace $C2/c$; par ailleurs, ceux du bis(diméthyl gallium parazolyl-1 *o*-aminophénolato) nickel(II) solvaté par le benzène sont monocliniques avec a = 20,491(1), b = 11,789(1) et c = 15,789(1) Å, β = 103,413(7)°, Z = 4, et groupe d'espace $C2/c$ et ceux du η^3-allyl (bromo) [(pyrazolyl-1)-2 éthylidènamino] dicarbonyl molybdène(II) sont monocliniques avec a = 11,0278(4), b = 8,4461(2) et c = 15,3747(5) Å, β = 109,208(3)°, Z = 4 et groupe d'espace $P2_1/c$. On a résolu les structures par les méthodes conventionnelles aux atomes lourds et on les a affinées par les méthodes des moindres carrés (matrice entière) jusqu'à des valeurs respectives de R de 0,030, 0,053 et 0,038 pour 1980, 1684 et 1901 réflexions indépendantes. La réaction du ligand $[Me_2Ga(pz)(OC_6H_4NH_2)]^-$, L^-, avec le $[Re(CO)_4Cl]_2$ conduit à la formation du $LRe(CO)_3$ dont les propriétés physiques suggèrent une arrangement *fac* du ligand organogallate.

[Traduit par la revue]

Can. J. Chem. Downloaded from www.nrcresearchpress.com by 213.166.140.6 on 09/07/12
For personal use only.

Introduction

In our continuing investigations of the reactivity of organogallium species with "active" hydrogen compounds, and of the synthesis of anionic pyrazolylgallate ligands (1 and references therein), our attention has recently focussed on *o*-aminophenol and *o*-aminothiophenol as molecules of potential interest. Both of these compounds react readily with Me_3Ga with elimination of methane and the formation of metallocyclic gallium compounds, one of which has now been structurally characterized, $Me_2Ga(OC_6H_4NH_2)$. Further, the *o*-aminophenol molecule has been successfully incorporated into the tridentate ligand system **1**. This ligand has been used to prepare a bis-ligand nickel

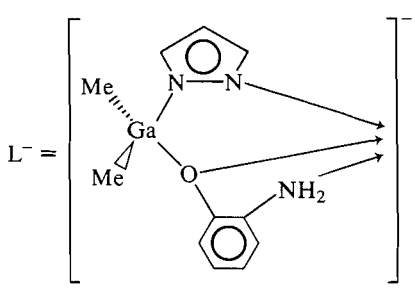

1

complex, L_2Ni, and also the rhenium tricarbonyl compound $LRe(CO)_3$. The X-ray crystal structures of the L_2Ni complex and of the molybdenum amidine complex $Mo(CO)_2Br(\eta^3\text{-}C_3H_5)[\eta^2\text{-}HN{=}CMe(pz)]$ are reported.

[1]Authors to whom correspondence should be addressed.

Experimental

Starting materials

Air-sensitive materials were handled in a nitrogen atmosphere. Tetrahydrofuran (THF), benzene, and CH_2Cl_2 were dried by refluxing over Na/benzophenone, potassium, and CaH_2, respectively, followed by distillation. $[Re(CO)_4Cl]_2$ (2), $(MeCN)_3Mo(CO)_3$ (3), $Mo(MeCN)_2(\eta^3\text{-}C_3H_5)(CO)_2Br$ (4), and Me_3Ga (5) were prepared by literature methods.

Preparation of $[Me_2Ga(XC_6H_4NH_2)]$ (where X = O or S)

$$o\text{-}HOC_6H_4NH_2 + Me_3Ga \xrightarrow[\Delta]{THF} Me_2Ga(OC_6H_4NH_2) + CH_4$$

To a solution of Me_3Ga (0.574 g, 5.00 mmol) in THF was added 2-aminophenol (0.546 g, 5.00 mmol) in the same solvent. The reaction mixture was refluxed overnight and the solvent then removed under vacuum. The crude material isolated was recrystallized from benzene to yield colorless crystals of the desired product in high yield. *Anal.* calcd. for $Me_2Ga(OC_6H_4NH_2)$: C 46.20, H 5.82, N 6.74; found: C 46.27, H 5.87, N 6.79. ^1H nmr (C_6D_6, 400 MHz, δ(C_6H_6) = 7.16 ppm) δ −0.12 s ($GaMe_2$), 2.44 s br (NH_2), 6.45 dd (J = 7.0, 1.5 Hz), 6.53 td (J = 7.0, 1.5 Hz), 7.06 td (J = 8.0, 1.5 Hz), 7.14 d (J = 8.0 Hz) (ring protons). The X-ray crystal structure of this compound is described below.

The analogous $Me_2Ga(SC_6H_4NH_2)$ complex was obtained in a similar manner using 2-aminothiophenol (0.37 g, 2.96 mmol) in the reac-

TABLE 1. Crystallographic data[a]

Compound	$Me_2Ga(OC_6H_4NH_2)$	$[Me_2Ga(pz)(OC_6H_4NH_2)]_2Ni\cdot 2C_6H_6$	$Mo(CO)_2Br(\eta^3\text{-}C_3H_5)\{\eta^2\text{-}HN{=}CMe(pz)\}$
Formula	$C_8H_{12}GaNO$	$C_{34}H_{42}Ga_2N_6NiO_2$	$C_{10}H_{12}BrMoN_3O_2$
fw	207.91	764.90	382.07
Crystal system	Monoclinic	Monoclinic	Monoclinic
Space group	$C2/c$	$C2/c$	$P2_1/c$
a (Å)	10.1970(9)	20.491(1)	11.0278(4)
b (Å)	9.7597(7)	11.789(1)	8.4461(2)
c (Å)	18.778(2)	15.749(1)	15.3747(5)
β (deg)	100.810(7)	103.413(7)	109.208(3)
V (Å^3)	1835.6(3)	3700.6(5)	1352.3(1)
Z	8	4	4
ρ_c (g/cm^3)	1.505	1.373	1.876
$F(000)$	848	1576	744
Radiation	Mo	Mo	Cu
μ (cm^{-1})	29.3	19.8	115.7
Crystal dimensions (mm)	0.38 × 0.46 × 0.58	0.15 × 0.20 × 0.38	0.28 × 0.35 × 0.43
Transmission factors	0.251–0.397	0.641–0.784	0.056–0.210
Scan type	ω–2θ	ω–2θ	ω–2θ
Scan range (deg in ω)	0.65 + 0.35 tan θ	0.65 + 0.35 tan θ	0.70 + 0.14 tan θ
Scan speed (deg/min)	1.01–10.06	0.84–6.71	1.34–10.06
Data collected	$+h, -k, \pm l$	$\pm h, +k, +l$	$+h, +k, \pm l$
$2\theta_{max}$ (deg)	65	55	150
Unique reflections	3326	4245	2770
Reflections with $I \geqq n\sigma(I)$	1980 (n = 3)	1684 (n = 1)	1901 (n = 3)
Number of variables	141	204	203
R	0.030	0.053	0.038
R_w	0.034	0.042	0.044
S	1.372	1.349	0.825
Mean Δ/σ (final cycle)	0.02	0.02	0.02
Max Δ/σ (final cycle)	0.16	0.23	0.18
Residual density (e/Å^3)	−0.67 to +0.33	−0.94 to +0.50	−1.09 to +0.58

[a]Temperature 22°C, Enraf-Nonius CAD4-F diffractometer, graphite-monochromated Mo-K_α radiation ($\lambda_{\alpha 1}$ = 0.70930, $\lambda_{\alpha 2}$ = 0.71359 Å) or nickel-filtered Cu-K_α radiation ($\lambda_{\alpha 1}$ = 1.540562, $\lambda_{\alpha 2}$ = 1.544390 Å), takeoff angle 2.7°, aperture (2.0 + tan θ) × 4.0 mm at a distance of 173 mm from the crystal, scan range extended by 25% on both sides for background measurement, $\sigma^2(I) = S + 2B + [0.04(S - B)]^2$ (S = scan count, B = normalized background count), function minimized $\Sigma w(|F_o| - |F_c|)^2$ where $w = 1/\sigma^2(F)$, $R = \Sigma||F_o| - |F_c||/\Sigma|F_o|$, $R_w = (\Sigma w(|F_o| - |F_c|)^2/\Sigma w|F_o|^2)^{1/2}$, $S = (\Sigma w(|F_o| - |F_c|)^2/(m - n))^{1/2}$. Values given for R, R_w, and S are based on those reflections with $I \geqq n\sigma(I)$.

tion with trimethylgallium (0.34 g, 2.96 mmol). Colorless, needle-like crystals were obtained from benzene in good yield. *Anal.* calcd. for $Me_2Ga(SC_6H_4NH_2)$: C 42.90, H 5.40, N 6.25; found: C 42.72, H 5.40, N 6.16. ^{1}H nmr (C_6D_6, 400 MHz) δ −0.11 s ($GaMe_2$), 2.60 s br (NH_2), 6.20 dd (J = 7.0, 2.0 Hz), 6.64 td (J = 8.0, 2.0 Hz), 6.78 td (J = 7.0, 2.0 Hz), 7.60 dd (J = 7.0, 2.0 Hz) (ring protons).

Preparation of $Na^+[Me_2Ga(pz)(OC_6H_4NH_2)]^-$ (Na^+L^-)

An equimolar amount of 2-aminophenol (1.466 g, 13.40 mmol) in THF was added to a THF solution of $Na^+Me_3Gapz^-$ (6) and the mixture refluxed for ~2 days. The resultant clear solution was cooled and made up to a standard volume with THF and this solution stored under a nitrogen atmosphere for use in subsequent reactions.

Preparation of $[Me_2Ga(pz)(OC_6H_4NH_2)]_2Ni$ (L_2Ni)

$$NiBr_2 + 2Na^+L^- \xrightarrow[rt]{THF} L_2Ni + 2NaBr$$

To a stirred slurry of $NiBr_2$ (0.118 g, 0.54 mmol) in THF was added a two molar equivalent of a THF solution of the ligand Na^+L^-. The reaction mixture was stirred for ~3 days and the solvent was then removed *in vacuo*. The residue was extracted with benzene and the solvent allowed to evaporate from the filtered solution. Purple, needle-like crystals of the product L_2Ni were obtained in approximately 60% yield as a benzene solvate. *Anal.* calcd. for $[Me_2Ga(pz)(OC_6H_4NH_2)]_2Ni\cdot 2C_6H_6$: C 53.03, H 5.50, N 11.00; found: C 52.68, H 5.51, N 11.08. The X-ray crystal structure of this complex is described below.

Preparation of $[Me_2Ga(pz)(OC_6H_4NH_2)]Re(CO)_3$ ($LRe(CO)_3$)

$$[Re(CO)_4Cl]_2 + 2Na^+L^- \xrightarrow[\Delta]{THF} 2LRe(CO)_3 + 2CO + 2NaCl$$

A two molar equivalent of the Na^+L^- ligand in THF solution was added to $[Re(CO)_4Cl]_2$ (0.450 g, 0.67 mmol) in the same solvent. The mixture was refluxed overnight and the solvent removed *in vacuo*. The residue was recrystallized from benzene to yield small colorless crystals of the product in good yield. *Anal.* calcd. for $[Me_2Ga(pz)(OC_6H_4NH_2)]Re(CO)_3$: C 30.84, H 2.77, N 7.71; found: C 31.00 H 2.80, N 7.74. ^{1}H nmr (C_6D_6, 80 MHz) δ −0.24 s, 0.45 s ($GaMe_2$), A = 2.79, B = 2.45 (J = 12.0 Hz) (NH_2). Ir (CH_2Cl_2 solution) ν_{CO} 2032, 1908, 1891 cm^{-1}.

Attempted preparation of $[Me_2Ga(pz)(OC_6H_4NH_2)]Mo(CO)_2(\eta^3\text{-}C_3H_5)$ ($LMo(CO)_2(\eta^3\text{-}C_3H_5)$)

[i] $$(MeCN)_3Mo(CO)_3 + Na^+L^- \xrightarrow{THF} Na^+LMo(CO)_3^- + 3MeCN$$

[ii] $$Na^+LMo(CO)_3^- + xsC_3H_5Br \xrightarrow{THF} LMo(CO)_2(C_3H_5) + NaBr + CO$$

$(MeCN)_3Mo(CO)_3$ (1.01 g, 3.48 mmol) in THF was reacted with a

Can. J. Chem. Downloaded from www.nrcresearchpress.com by 213.166.140.6 on 09/07/12
For personal use only.

Can. J. Chem. Downloaded from www.nrcresearchpress.com by 213.166.140.6 on 09/07/12
For personal use only.

TABLE 2. Final positional (fractional × 10^4, M and Br × 10^5, H × 10^3) and isotropic thermal parameters ($U \times 10^3$ Å^2) with estimated standard deviations in parentheses

Atom	x	y	z	U_{eq}/U_{iso}
		$Me_2Ga(OC_6H_4NH_2)$		
Ga	24667(3)	45860(3)	32521(1)	39
X(1)*	1485(2)	3250(2)	2543(1)	39
X(2)*	3350(2)	5172(2)	2432(1)	42
C(1)	1656(2)	3627(2)	1846(1)	35
C(2)	2612(2)	4618(2)	1788(1)	37
C(3)	2816(4)	5021(4)	1113(2)	53
C(4)	2054(5)	4447(4)	494(2)	68
C(5)	1099(4)	3472(4)	553(2)	64
C(6)	904(3)	3062(3)	1224(2)	48
C(7)	3723(4)	3631(5)	4000(2)	67
C(8)	1202(3)	5997(3)	3411(2)	50
H(3)	344(4)	562(4)	108(2)	66(11)
H(4)	213(4)	474(3)	10(2)	57(10)
H(5)	63(3)	302(3)	13(2)	54(8)
H(6)	26(3)	244(3)	129(2)	44(7)
H(7a)	425(7)	314(7)	376(4)	161(25)
H(7b)	421(6)	431(6)	431(4)	142(24)
H(7c)	312(5)	307(6)	428(2)	112(16)
H(8a)	159(4)	667(4)	373(2)	72(10)
H(8b)	51(5)	568(5)	355(3)	112(18)
H(8c)	101(4)	653(4)	302(2)	82(13)
H(X1a)	182	238	265	52
H(X1b)	59	326	257	52
H(X2a)	336	611	240	55
H(X2b)	421	485	251	55
		$[Me_2Ga(pz)(OC_6H_4NH_2)]_2Ni \cdot 2C_6H_6$		
Ni	0	34536(10)	25000	55
Ga	16147(3)	24240(6)	29209(4)	64
O	948(2)	3472(4)	2283(2)	62
N(1)	996(3)	1946(4)	3652(3)	60
N(2)	345(2)	2293(4)	3475(3)	60
N(3)	−133(2)	4760(4)	1529(3)	66
C(1)	2333(3)	3282(6)	3683(4)	85
C(2)	1720(3)	1203(6)	2137(4)	90
C(3)	1107(3)	1297(6)	4370(5)	76
C(4)	539(4)	1205(6)	4670(5)	82
C(5)	77(3)	1840(6)	4095(5)	73
C(6)	1045(3)	4257(6)	1702(4)	57
C(7)	510(3)	4955(6)	1312(4)	59
C(8)	594(4)	5805(6)	747(5)	77
C(9)	1205(5)	5948(7)	540(4)	91
C(10)	1739(3)	5245(8)	900(5)	87
C(11)	1657(3)	4402(6)	1476(4)	69
C(12)	3576(10)	2009(21)	2078(17)	186
C(13)	3407(9)	1688(15)	1226(22)	216
C(14)	3596(11)	2317(19)	629(11)	221
C(15)	3945(12)	3180(17)	836(14)	203
C(16)	4094(9)	3525(13)	1660(19)	236
C(17)	3956(11)	2859(20)	2222(12)	242
		$Mo(CO)_2Br(\eta^3\text{-}C_3H_5)[\eta^2\text{-}HN{=}CMe(pz)]$		
Mo	21996(6)	44531(7)	39216(4)	48
Br	42234(9)	27313(11)	38285(6)	64
O(1)	342(7)	6904(8)	4299(5)	88
O(2)	2718(7)	4106(9)	6032(4)	91
N(1)	2967(6)	6511(7)	2542(4)	53
N(2)	2176(6)	5269(6)	2530(4)	50
N(3)	3575(7)	6374(7)	4080(5)	55
C(1)	1023(9)	5993(11)	4131(6)	65
C(2)	2545(9)	4167(10)	5249(6)	64
C(3)	1487(11)	1972(12)	4193(8)	75
C(4)	955(10)	2439(11)	3269(7)	66
C(5)	91(9)	3743(12)	3120(8)	73
C(6)	2938(9)	6898(10)	1676(6)	62
C(7)	2107(11)	5901(11)	1107(7)	70
C(8)	1652(9)	4895(11)	1648(6)	61
C(9)	3753(8)	7068(9)	3409(6)	54
C(10)	4654(13)	8375(12)	3412(10)	79
H(N3)	410(10)	665(12)	453(7)	83(35)
H(3a)	217(10)	99(13)	409(7)	103(36)
H(3b)	94(13)	182(15)	458(9)	150(51)
H(4)	130(9)	208(11)	291(6)	58(32)
H(5a)	−15(10)	421(11)	246(7)	97(33)
H(5b)	−48(8)	359(10)	354(5)	63(24)
H(6)	357(8)	776(10)	153(5)	66(24)
H(7)	172(10)	590(13)	51(7)	101(39)
H(8)	98(7)	416(9)	143(5)	48(21)
H(10a)	521(10)	809(11)	308(7)	88(34)
H(10b)	396(11)	917(14)	330(8)	119(42)
H(10c)	527(9)	865(11)	394(6)	71(29)

*Refined as 50% O, 50% N.

one molar equivalent of the Na^+L^- ligand solution in the same solvent. The mixture was stirred overnight and then an excess of allyl bromide was added. The reaction mixture was stirred for an additional 2 days after which the solvent was removed under vacuum and the residue extracted with benzene solvent. Slow evaporation of the solvent from the filtrate yielded a yellowish brown oily solid. Evidence from ir, mass spectral, and ^{1}H nmr data clearly indicated the desired complex to be present in the oily solid, but satisfactory elemental analytical data could not be obtained. Attempts to obtain ^{1}H nmr spectra of the oily solid in d_6-acetone resulted in complete dissolution of the material, followed almost immediately by the deposition of a reddish-orange crystalline material. This air-stable solid was shown subsequently to be a molybdenum amidine complex. *Anal.* calcd. for $Mo(CO)_2Br(\eta^3\text{-}C_3H_5)[\eta^2\text{-}HN{=}CMe(pz)]$: C 31.43, H 3.14, N 11.00; found: C 31.53, H 3.22, N 10.68. Ir (KBr disc) ν_{CO} 1938, 1845 cm^{-1}, $\nu_{C=N}$ 1657 cm^{-1}, ν_{NH} 3340 cm^{-1}. The X-ray crystal structure of this complex is described below.

Spectra

Infrared spectra were recorded on a Perkin-Elmer 598 spectrometer, ^{1}H nmr spectra were recorded on Bruker WP-80 and Bruker WH-400 MHz instruments using FT techniques. Mass spectra were recorded on a Kratos AES MS 50 mass spectrometer. Elemental analyses were preformed by Mr. P. Borda of the UBC microanalytical laboratory.

Crystal structure analyses

Crystallographic data for $Me_2Ga(OC_6H_4NH_2)$, $[Me_2Ga(pz)(OC_6H_4NH_2)]_2Ni \cdot 2C_6H_6$, and $Mo(CO)_2Br(\eta^3\text{-}C_3H_5)[\eta^2\text{-}HN{=}CMe(pz)]$ appear in Table 1. Unit-cell parameters were refined by least-squares on 2 sin θ/λ values for 25 reflections with 2θ = 28–43, 25–32, and 81–97°, respectively, for the three compounds. The intensities of three standard reflections were measured each hour of X-ray exposure time during the data collections. For $[Me_2Ga(pz)(OC_6H_4NH_2)]_2Ni$ and $Mo(CO)_2Br(\eta^3\text{-}C_3H_5)[\eta^2\text{-}HN{=}CMe(pz)]$ only small random fluctuations were noted and for $Me_2Ga(OC_6H_4NH_2)$ the intensities of the check reflections decreased uniformly to final values 0.95 times the initial values. The data for $Me_2Ga(OC_6H_4NH_2)$ were scaled accord-

Can. J. Chem. Downloaded from www.nrcresearchpress.com by 213.166.140.6 on 09/07/12
For personal use only.

ingly. Data for the three compounds were reduced[2] and corrected for absorption.

The structures were solved by conventional heavy-atom methods, the metal and halogen atoms being positioned from the Patterson functions and the remaining atoms from subsequent difference maps. The centrosymmetric space group $C2/c$ was indicated by E-statistics and Patterson functions for $Me_2Ga(OC_6H_4NH_2)$ and L_2Ni, imposing crystallographic C_2 symmetry on molecules of the latter. The O and N atoms of the *o*-aminophenolato ligand in $Me_2Ga(OC_6H_4NH_2)$ were found to be disordered over the two positions X(1) and X(2), both positions being refined as 50% O and 50% N. Unbalanced thermal parameters resulted from both possible ordered structures in $C2/c$ and the disorder persisted when the structure was refined in the noncentrosymmetric space group Cc. Non-hydrogen atoms were refined with anisotropic thermal parameters. Hydrogen atoms were included as fixed contributors to the structure in calculated positions (N—H = 0.92, C(sp^2)—H = 0.97, C(sp^3)—H = 0.98 Å, $U_H \propto U_{\text{bonded atom}}$) for $[Me_2Ga(pz)(OC_6H_4NH_2)]_2Ni$. Hydrogen atoms associated with the disordered NH_2 group in $Me_2Ga(OC_6H_4NH_2)$ were also fixed in idealized positions while all remaining hydrogen atoms in $Me_2Ga(OC_6H_4NH_2)$ and $Mo(CO)_2Br(\eta^3\text{-}C_3H_5)[\eta^2\text{-}HN{=}CMe(pz)]$ were refined with isotropic thermal parameters. Neutral atom scattering factors and anomalous scattering corrections (Mo, Ga, Ni, and Br) were taken from ref. 7. Isotropic type I extinction corrections (Thornley–Nelmes definition of mosaic anisotropy, Lorentzian distribution) were applied for $Me_2Ga(OC_6H_4NH_2)$ and $Mo(CO)_2Br(\eta^3\text{-}C_3H_5)[\eta^2\text{-}HN{=}CMe(pz)]$ (8–10), the final values of g being $4.1(2) \times 10^4$ and $0.43(2) \times 10^4$, respectively.

Final positional and isotropic thermal parameters (U_{eq} = 1/3 trace diagonalized U) appear in Table 2. Bond lengths, bond angles, and intra-annular torsion angles are given in Tables 3–5, respectively. Calculated hydrogen atom parameters for $[Me_2Ga(pz)(OC_6H_4NH_2)]_2Ni$, anisotropic thermal parameters, bond lengths, and angles involving hydrogen, a complete listing of torsion angles (Tables 6–10), and measured and calculated structure factors have been placed in the Depository of Unpublished Data.[3]

TABLE 3. Bond lengths (Å) with estimated standard deviations in parentheses

Bond	Length (Å)	Bond	Length (Å)
	$Me_2Ga(OC_6H_4NH_2)$		
Ga —X(1)	1.994(2)	C(1)—C(2)	1.392(3)
Ga —X(2)	2.008(2)	C(1)—C(6)	1.386(4)
Ga —C(7)	1.951(3)	C(2)—C(3)	1.381(4)
Ga —C(8)	1.948(3)	C(3)—C(4)	1.389(5)
X(1)—C(1)	1.401(3)	C(4)—C(5)	1.380(6)
X(2)—C(2)	1.407(3)		
	$[Me_2Ga(pz)(OC_6H_4NH_2)]_2Ni\cdot 2C_6H_6$		
Ni —O	2.049(3)	C(4)—C(5)	1.371(8)
Ni —N(2)	2.057(5)	C(6)—C(7)	1.393(7)
Ni —N(3)	2.143(5)	C(6)—C(11)	1.392(8)
Ga —O	1.941(4)	C(7)—C(8)	1.377(8)
Ga —N(1)	1.981(5)	C(8)—C(9)	1.376(9)
Ga —C(1)	1.952(6)	C(9)—C(10)	1.384(9)
Ga —C(2)	1.941(7)	C(10)—C(11)	1.381(9)
O —C(6)	1.348(7)	C(12)—C(13)	1.36(2)
N(1)—N(2)	1.361(6)	C(12)—C(17)	1.26(2)
N(1)—C(3)	1.341(7)	C(13)—C(14)	1.32(2)
N(2)—C(5)	1.336(7)	C(14)—C(15)	1.24(2)
N(3)—C(7)	1.454(7)	C(15)—C(16)	1.33(2)
C(3)—C(4)	1.358(8)	C(16)—C(17)	1.26(2)
	$Mo(CO)_2Br(\eta^3\text{-}C_3H_5)[\eta^2\text{-}HN{=}CMe(pz)]$		
Mo —Br	2.7067(11)	N(1)—N(2)	1.360(8)
Mo —N(2)	2.239(6)	N(1)—C(6)	1.362(9)
Mo —N(3)	2.179(7)	N(1)—C(9)	1.410(10)
Mo —C(1)	1.938(10)	N(2)—C(8)	1.326(10)
Mo —C(2)	1.964(9)	N(3)—C(9)	1.257(10)
Mo —C(3)	2.324(9)	C(3)—C(4)	1.404(14)
Mo —C(4)	2.209(8)	C(4)—C(5)	1.425(14)
Mo —C(5)	2.324(9)	C(6)—C(7)	1.337(13)
Mo —A*	2.038(6)	C(7)—C(8)	1.393(12)
O(1)—C(1)	1.162(11)	C(9)—C(10)	1.484(12)
O(2)—C(2)	1.156(9)		

*Here and in Table 4 A refers to the centroid of the allyl ligand.

Results and discussion

Alkane elimination from trimethylgallium compounds and compounds containing active hydrogen has been well documented (1). The reaction of *o*-aminophenol and *o*-aminothiophenol with trimethylgallium followed the expected pattern to produce metallocyclic compounds incorporating the "Me_2Ga" moiety. The $Me_2Ga(XC_6H_4NH_2)$ (where X = O or S) complexes produced both displayed ^1H nmr spectra which indicated two equivalent Ga–Me groups and two equivalent N—H protons in the molecules. A planar structure of aromatic ring carbons and the Ga, N, and X atoms is consistent with this data. The mass spectra of the two complexes displayed prominent signals due to the parent monomer ions (P^+) with the most intense peaks being due, in each case, to the $P - Me^+$ ions. The solid state structure of $Me_2Ga(OC_6H_4NH_2)$ is shown in Fig. 1 and consists of individual monomer units linked to neighboring units by a network of N—H···O hydrogen bonds shown in Fig. 2 (X(1)—H(X1a)···X(2) ($1/2 - x$, $y - 1/2$, $1/2 - z$); X(1)—H(X1b)···X(1) ($-x$, y, $1/2 - z$); and X(2)—H(X2a)··· X(1) ($1/2 - x$, $1/2 + y$, $1/2 - z$); H···X = 2.17, 2.09, 2.09 Å; X···X = 3.009(3), 3.002(4), 3.009(3) Å; X—H···X = 152, 172, 173°; respectively). With but few exceptions (11), similar "Me_2Ga" systems have been shown by X-ray crystallographic analyses to dimerize in the solid state via the formation of four-membered $(Ga—O)_2$ rings, giving distorted trigonal bipyramidal arrangements about each five-coordinate gallium atom (12–18). As a result of the disordering of the *o*-aminophenolato ligand, the two Ga—X distances most likely represent averages of the actual Ga—N and Ga—O distances. Assuming that the Ga—O distance in $Me_2Ga(OC_6H_4NH_2)$ is the same as that in $[Me_2Ga(pz)(OC_6H_4NH_2)]_2Ni$ (1.941(4) Å), a Ga—N distance of 2.06 Å can be approximated for $Me_2Ga(OC_6H_4NH_2)$. These values are similar to the Ga—O and Ga—N distances of 1.917(4) and 2.064(8) Å in the tetrahedral complex $Me_2GaOCH_2CH_2NH_2$ (19). The aromatic ring in $Me_2Ga(OC_6H_4NH_2)$ is planar to within experimental error and the five-membered chelate ring has a flattened Ga-envelope conformation.

The reaction of the ligand **1** with $[Re(CO)_4Cl]_2$ resulted in a good yield of the rhenium tricarbonyl product $[Me_2Ga(pz)(OC_6H_4NH_2)]Re(CO)_3$. The arrangement of the tridentate ligand in this complex has been shown by ir and ^1H nmr data to

[2]The computer programs used include locally written programs for data processing and locally modified versions of the following: AGNOST, absorption corrections, by J. A. Ibers; ORFLS, full-matrix least-squares, and ORFFE, function and errors, by W. R. Busing, K. O. Martin, and H. A. Levy; FORDAP, Patterson and Fourier syntheses, by A. Zalkin; ORTEP II, illustrations, by C. K. Johnson.

[3]The structure factor table, Table 7 (anisotropic thermal parameters) and other material mentioned in the text may be purchased from the Depository of Unpublished Data, CISTI, National Research Council of Canada, Ottawa, Ont., Canada K1A 0S2.

TABLE 4. Bond angles (deg) with estimated standard deviations in parentheses*

Bonds	Angle (deg)	Bonds	Angle (deg)
	$Me_2Ga(OC_6H_4NH_2)$		
X(1)—Ga —X(2)	85.14(8)	X(1)—C(1)—C(2)	117.9(2)
X(1)—Ga —C(7)	110.37(15)	X(1)—C(1)—C(6)	122.5(2)
X(1)—Ga —C(8)	107.50(11)	C(2)—C(1)—C(6)	119.7(2)
X(2)—Ga —C(7)	111.09(14)	X(2)—C(2)—C(1)	118.0(2)
X(2)—Ga —C(8)	108.75(12)	X(2)—C(2)—C(3)	122.1(2)
C(7)—Ga —C(8)	126.3(2)	C(1)—C(2)—C(3)	119.9(2)
Ga —X(1)—C(1)	108.50(14)	C(2)—C(3)—C(4)	119.7(3)
Ga —X(2)—C(2)	107.74(15)	C(3)—C(4)—C(5)	120.3(3)
	$[Me_2Ga(pz)(OC_6H_4NH_2)]_2Ni \cdot 2C_6H_6$		
O —Ni —N(2)	87.5(2)	Ni —N(2)—C(5)	133.1(5)
O —Ni —N(3)	80.9(2)	N(1)—N(2)—C(5)	106.3(5)
O —Ni —O′	178.8(2)	Ni —N(3)—C(7)	108.1(4)
O —Ni —N(2)′	93.3(2)	N(1)—C(3)—C(4)	110.4(6)
O —Ni —N(3)′	98.2(2)	C(3)—C(4)—C(5)	104.0(6)
N(2)—Ni —N(3)	167.5(2)	N(2)—C(5)—C(4)	111.3(6)
N(2)—Ni —N(2)′	96.6(3)	O —C(6)—C(7)	118.7(6)
N(2)—Ni —N(3)′	88.9(2)	O —C(6)—C(11)	122.8(6)
N(3)—Ni —N(3)′	88.1(3)	C(7)—C(6)—C(11)	118.6(6)
O —Ga —N(1)	90.8(2)	N(3)—C(7)—C(6)	117.7(6)
O —Ga —C(1)	109.2(2)	N(3)—C(7)—C(8)	121.5(6)
O —Ga —C(2)	108.2(2)	C(6)—C(7)—C(8)	120.8(6)
N(1)—Ga —C(1)	106.4(2)	C(7)—C(8)—C(9)	119.8(7)
N(1)—Ga —C(2)	109.8(2)	C(8)—C(9)—C(10)	120.4(7)
C(1)—Ga —C(2)	126.6(3)	C(9)—C(10)—C(11)	119.7(6)
Ni —O —Ga	119.2(2)	C(6)—C(11)—C(10)	120.6(6)
Ni —O —C(6)	114.5(4)	C(13)—C(12)—C(17)	114(2)
Ga —O —C(6)	126.3(4)	C(12)—C(13)—C(14)	120(2)
Ga —N(1)—N(2)	121.7(4)	C(13)—C(14)—C(15)	121(2)
Ga —N(1)—C(3)	130.3(5)	C(14)—C(15)—C(16)	120(2)
N(2)—N(1)—C(3)	108.1(5)	C(15)—C(16)—C(17)	117(2)
Ni —N(2)—N(1)	120.2(4)	C(12)—C(17)—C(16)	127(2)
	$Mo(CO)_2Br(\eta^3\text{-}C_3H_5)[\eta^2\text{-}HN{=}CMe(pz)]$		
Br —Mo —N(2)	82.3(2)	Mo —N(2)—N(1)	114.7(4)
Br —Mo —N(3)	81.4(2)	Mo —N(2)—C(8)	140.2(6)
Br —Mo —C(1)	168.1(3)	N(1)—N(2)—C(8)	105.0(6)
Br —Mo —C(2)	96.2(3)	Mo —N(3)—C(9)	123.1(6)
Br —Mo —A	97.7(2)	Mo —C(1)—O(1)	176.9(8)
N(2)—Mo —N(3)	70.5(2)	Mo —C(2)—O(2)	175.2(8)
N(2)—Mo —C(1)	98.9(3)	C(4)—C(3)—Mo	67.5(5)
N(2)—Mo —C(2)	165.4(3)	C(3)—C(4)—C(5)	114.4(10)
N(2)—Mo —A	99.2(2)	C(3)—C(4)—Mo	76.5(5)
N(3)—Mo —C(1)	87.8(3)	C(5)—C(4)—Mo	76.1(5)
N(3)—Mo —C(2)	94.9(3)	C(4)—C(5)—Mo	67.3(5)
N(3)—Mo —A	169.8(3)	N(1)—C(6)—C(7)	106.2(8)
C(1)—Mo —C(2)	79.7(3)	C(6)—C(7)—C(8)	107.3(8)
C(1)—Mo —A	93.8(3)	N(2)—C(8)—C(7)	110.2(8)
C(2)—Mo —A	95.3(3)	N(1)—C(9)—N(3)	114.0(7)
N(2)—N(1)—C(6)	111.3(6)	N(1)—C(9)—C(10)	117.0(8)
N(2)—N(1)—C(9)	117.5(6)	N(3)—C(9)—C(10)	129.0(9)
C(6)—N(1)—C(9)	130.8(7)		

*Here and elsewhere in this report primed atoms have coordinates related to those in Table 2 by the symmetry operation: $-x$, y, $1/2 - z$.

be exclusively *facial*. Thus three strong ν_{CO} bands occur in the ir spectrum whereas for a *mer* arrangement of the unsymmetrical ligand two weak ν_{CO} bands and one strong ν_{CO} band would be predicted (20). The ^1H nmr spectrum of the complex in C_6D_6 solvent is also consistent with a *fac* arrangement of the organogallate ligand. Thus the $GaMe_2$ grouping gives rise to two sharp singlets at ~0 δ whereas for a *mer* arrangement of the ligand a plane of symmetry in the molecule would render the two GaMe groups equivalent and hence lead to one signal in this region of the spectrum. The AB quartet pattern observed for the —NH_2 grouping is also consistent with a *fac* but not a *mer* arrangement of the tridentate ligand. The mass spectrum of the $LRe(CO)_3$ complex confirms the monomeric nature of the compound in the gas phase. The parent monomer ion (P^+)

Can. J. Chem. Downloaded from www.nrcresearchpress.com by 213.166.140.6 on 09/07/12
For personal use only.

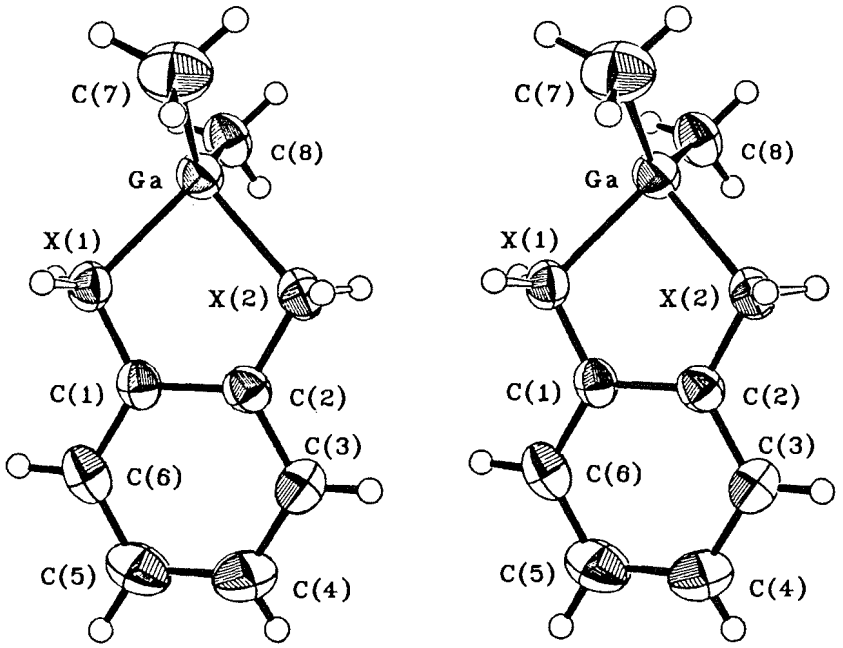

FIG. 1. Stereoscopic view of the $Me_2Ga(OC_6H_4NH_2)$ molecule; 50% probability thermal ellipsoids are shown for the non-hydrogen atoms. Hydrogen atoms have been assigned arbitrary thermal parameters for the sake of clarity.

TABLE 5. Intra-annular torsion angles (deg) standard deviations in parentheses

Atoms	Value (deg)
$Me_2Ga(OC_6H_4NH_2)$	
X(2)—Ga —X(1)—C(1)	−14.06(15)
Ga —X(1)—C(1)—C(2)	11.5(2)
X(1)—C(1)—C(2)—X(2)	0.3(3)
Ga —X(2)—C(2)—C(1)	−11.9(2)
X(1)—Ga —X(2)—C(2)	14.10(15)
$[Me_2Ga(pz)(OC_6H_4NH_2)]_2Ni\cdot 2C_6H_6$	
N(2)—Ni —O —Ga	5.5(2)
N(1)—Ga —O —Ni	−7.5(2)
O —Ga —N(1)—N(2)	7.9(4)
Ga —N(1)—N(2)—Ni	−5.6(6)
O —Ni —N(2)—N(1)	0.0(4)
N(3)—Ni —O —C(6)	2.0(4)
Ni —O —C(6)—C(7)	−0.3(6)
O —C(6)—C(7)—N(3)	−2.7(8)
Ni —N(3)—C(7)—C(6)	4.0(6)
O —Ni —N(3)—C(7)	−3.1(3)
$Mo(CO)_2Br(\eta^3\text{-}C_3H_5)[\eta^2\text{-}HN{=}CMe(pz)]$	
N(3)—Mo —N(2)—N(1)	−2.3(5)
C(9)—N(1)—N(2)—Mo	3.8(8)
N(2)—N(1)—C(9)—N(3)	−3.2(10)
Mo —N(3)—C(9)—N(1)	1.1(10)
N(2)—Mo —N(3)—C(9)	0.7(6)

pattern was observed together with prominent signals due to the $P - Me^+$ and $P - 3CO^+$ ions.

The reaction of the Na^+L^- ligand with anhydrous $NiBr_2$ has demonstrated the ability of the Ni(II) ion to accommodate two of the gallate ligands in a monomeric pseudo-octahedral complex, viz. L_2Ni. The nature of the purple crystalline product has been confirmed by elemental analysis, mass spectrometry, and X-ray crystallographic analysis. The elemental analysis indicated the presence of two benzene solvate molecules per L_2Ni molecule in the crystals and these were subsequently located in the X-ray analysis. The mass spectrum confirmed the monomeric nature of the complex in the vapor phase with weak signals due to the P^+ ion and strong signals due to the $P - Me^+$ and $P - 2Me^+$ ions being observed. The X-ray analysis of the L_2Ni complex, $[Me_2Ga(pz)(OC_6H_4NH_2)]_2Ni\cdot 2C_6H_6$, showed the ligands to be coordinated in a meridional fashion. A previous publication has documented the structures of both the *mer* and *fac* isomers of the related complex $[Me_2Ga(pz)(OCH_2CH_2NH_2)]_2Ni$ (21) and has also described how the two isomers can be interconverted by an adroit choice of recrystallization solvents. The present L_2Ni complex crystallized solely as the *mer* isomer and all attempts to convert this to the *fac* isomer proved unsuccessful. The structure of the molecule is shown in Fig. 3 and clearly establishes the tridentate chelating nature of the organogallate ligand **1**.

The crystal structure of $[Me_2Ga(pz)(OC_6H_4NH_2)]_2Ni\cdot 2C_6H_6$ consists of well-separated complex and solvent molecules. The L_2Ni molecule has crystallographic C_2 symmetry, each meridionally coordinated ligand forming a system of four fused rings which is planar to within ±0.26 Å. The pyrazolyl and phenyl rings are planar to within experimental error while the five-membered NiOGaNN and NiOCCN chelate rings have flattened Ga- and N-envelope conformations, respectively (see Table 5). The Ni—O, Ni—N(pz), and Ni—N(am) bond lengths of 2.049(3), 2.057(5), and 2.143(5) Å in $[Me_2Ga(pz)(OC_6H_4NH_2)]_2Ni$ are similar to the corresponding mean values of 2.040(3), 2.092(6), and 2.147(5) Å observed for *mer*-$[Me_2Ga(pz)(OCH_2CH_2NH_2)]_2Ni$ (21). Corresponding bond angles about Ni in the two compounds differ by a maximum of 1.7(3)°. Distances and angles involving gallium are normal.

Attempts to prepare the $LMo(CO)_2(\eta^3\text{-}C_3H_5)$ complex did not lead to a pure product. A crude material was obtained

Can. J. Chem. Downloaded from www.nrcresearchpress.com by 213.166.140.6 on 09/07/12
For personal use only.

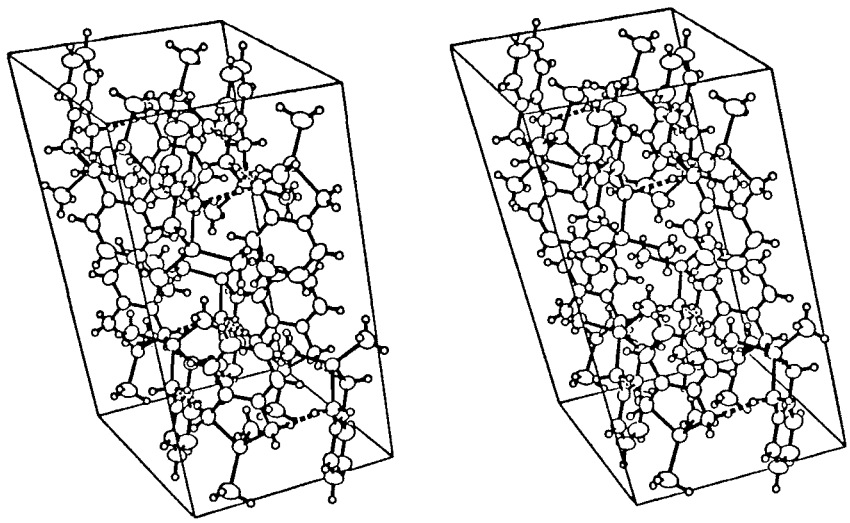

FIG. 2. Stereoview of the unit-cell of $Me_2Ga(OC_6H_4NH_2)$. Broken lines represent hydrogen bonds.

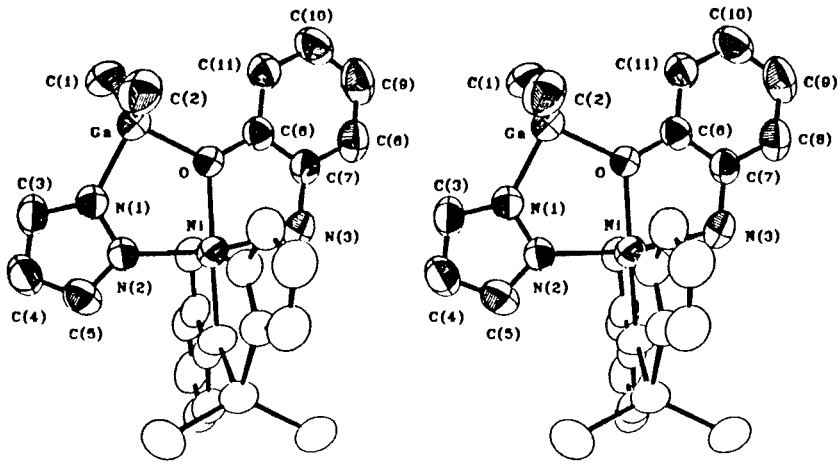

FIG. 3. Stereoscopic view of the $[Me_2Ga(pz)(OC_6H_4NH_2)]_2Ni$ molecule; 50% probability thermal ellipsoids are shown. Shaded atoms comprise the asymmetric unit.

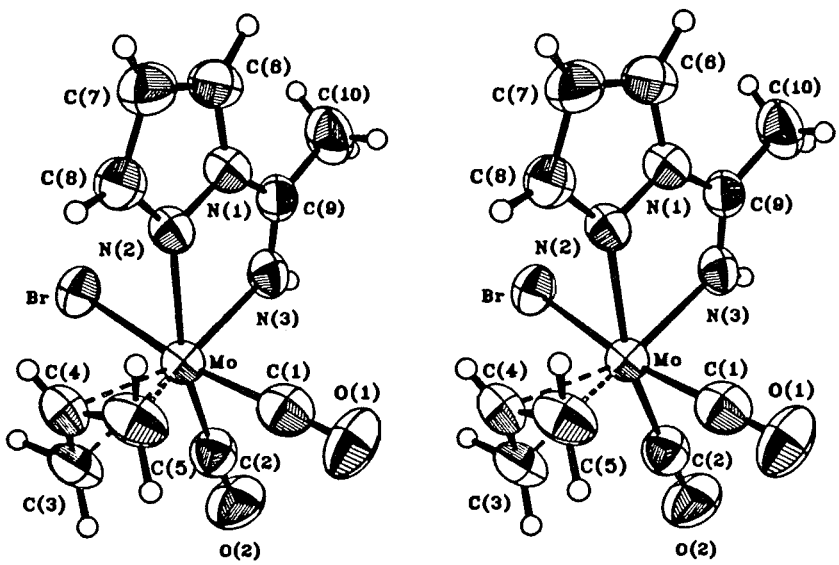

FIG. 4. Stereoscopic view of the $Mo(CO)_2Br(\eta^3\text{-}C_3H_5)[\eta^2\text{-}HN{=}CMe(pz)]$ molecule; 50% probability thermal ellipsoids are shown for the non-hydrogen atoms. Hydrogen atoms have been assigned arbitrary thermal parameters for the sake of clarity.

Can. J. Chem. Downloaded from www.nrcresearchpress.com by 213.166.140.6 on 09/07/12
For personal use only.

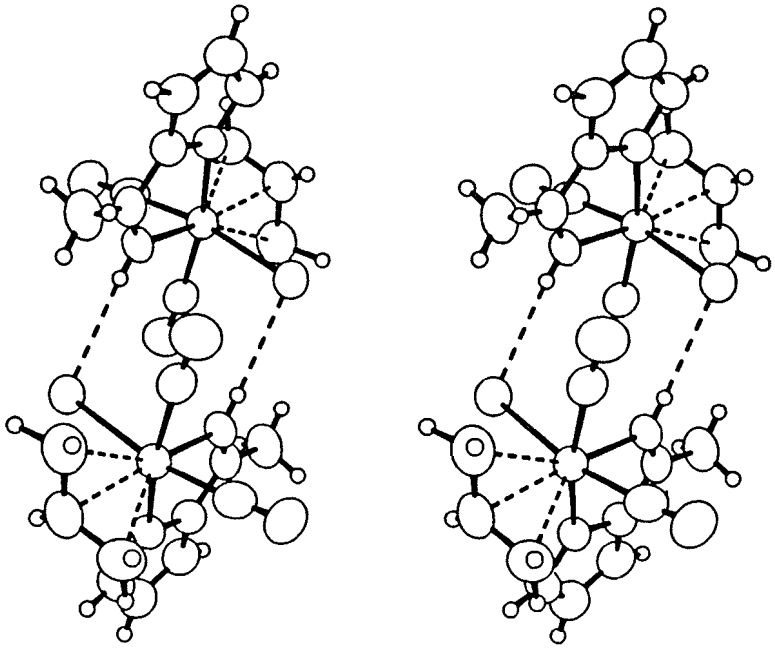

FIG. 5. Stereoscopic view of the hydrogen-bonded dimer units in the structure of $Mo(CO)_2Br(\eta^3\text{-}C_3H_5)[\eta^2\text{-}HN{=}CMe(pz)]$.

which displayed two strong ν_{CO} bands in its ir spectrum and a ^1H nmr pattern which indicated the presence of the complex with the L ligand facially coordinated. The mass spectrum of the product material also gave evidence for the presence of the $LMo(CO)_2(\eta^3\text{-}C_3H_5)$ complex with prominent signals due to P^+ and derivative ions being observed. Perhaps of more interest was the formation of the molybdenum amidine complex $Mo(CO)_2Br(\eta^3\text{-}C_3H_5)[\eta^2\text{-}HN{=}CMe(pz)]$ on treating the crude material with d_6-acetone. The X-ray structure of this complex is described below and the molecular arrangement is shown in Fig. 4. The structure represents the second of its type, a previous publication (22) having detailed the structure of the ruthenium cation $[Ru(CO)H[HN{=}CMe(Me_2pz)](PPh_3)_2]^+$. An earlier paper by Jones *et al.* (23) had suggested the existence of a similar Ru amidine cation $[Ru(\eta^6\text{-}C_6H_6)[HN{=}CMe(Me_2pz)](Me_2pzH)]^{2+}$ based primarily on ir and nmr data. It was suggested in both of these publications that the coordinated amidine ligand resulted from the addition of a dimethylpyrazole, Me_2pzH, unit across the C≡N bond of a coordinated MeCN molecule. A similar mechanism in the present case would suggest the presence of coordinated MeCN in the brown oily solid produced in the attempted preparation of the $LMo(CO)_2(\eta^3\text{-}C_3H_5)$ complex. A pyrazole molecule could conceivably originate from the ligand, L. It is not clear at this time what role the d_6-acetone plays in promoting the formation of the molybdenum amidine complex but we are planning further investigations in this area. The $\nu_{C=N}$ frequency of 1657 cm^{-1} observed for the Mo complex compares closely with the two $\nu_{C=N}$ values (1645, 1650 cm^{-1}, respectively) quoted for the Ru cations.

The molecular structure of $Mo(CO)_2Br(\eta^3\text{-}C_3H_5)[\eta^2\text{-}HN{=}CMe(pz)]$ consists of discrete monomeric units associating into centrosymmetric dimeric species (Fig. 5) via N—H···Br hydrogen bonding interactions (N(3)—H(N3)···Br($1-x$, $1-y$, $1-z$), H···Br = 2.65(10), N···Br = 3.416(7) Å, N—H···Br = 172(10)°). These dimer units are linked to one another by a pair of possible weak hydrogen bonds [C(6)—H(6)···Br($1-x$, $1/2+y$, $1/2-z$) and C(8)—H(8)···O(1) ($1-x$, $y-1/2$, $1/2-z$), H···A = 2.67(8) and 2.43(8), C···A = 3.535(9) and 3.35(1) Å, C—H···A = 137(6) and 164(6)°, respectively). The coordination geometry about Mo is irregular pseudo-octahedral if the η^3-allyl ligand is considered to occupy one coordination site. The geometry of the HN=CMe(pz) ligand is similar to, but more accurately determined than that of the related HN=CMe(Me_2pz) ligand in the Ru cation (22). The N(3)—C(9) distance of 1.257(10) Å is consistent with a C=N double bond and is not significantly different from the corresponding distance of 1.30(4) Å in the Ru cation. The pyrazolyl ring is planar to within experimental error while the five-membered chelate ring is slightly, but significantly, non-planar (maximum deviation from the mean plane = 0.023(7) Å). The Mo—N(amidine) bond, *trans* to the allyl ligand (2.179(7) Å), is significantly shorter than the Mo—N(pz) bond (2.239(6) Å). The Mo—Br distance of 2.707(1) Å is longer than other Mo(II)—Br distances reported for 6- and 7-coordinate complexes which range from 2.629 to 2.680 Å (24–27), possibly as a result of the hydrogen bonding. Other bond lengths in the complex are as expected.

Acknowledgments

We thank the Natural Sciences and Engineering Research Council of Canada for financial support and the University of British Columbia Computing Centre for assistance.

1. D. A. COOPER, S. J. RETTIG, A. STORR, and J. TROTTER. Can. J. Chem. **64**, 1643 (1986).
2. G. DOLCETTI and J. R. NORTON. Inorg. Synth. **16**, 35 (1976).
3. D. P. TATE, W. R. KNIPPLE, and J. M. AUGL. Inorg. Chem. **1**, 433 (1962).
4. R. G. HAYTER. J. Organomet. Chem. **13**, P1 (1968).
5. A. STORR and B. S. THOMAS. Can. J. Chem. **48**, 3667 (1970).
6. K. S. CHONG, S. J. RETTIG, A. STORR, and J. TROTTER. Can. J. Chem. **55**, 4166 (1977).
7. International tables for X-ray crystallography. Vol. IV. Kynoch Press, Birmingham. 1974. pp. 99–102 and 149.
8. P. J. BECKER AND P. COPPENS. Acta Crystallogr. Sect. A, **30**, 129 (1974); **30**, 148 (1974); **31**, 417 (1975).

Can. J. Chem. Downloaded from www.nrcresearchpress.com by 213.166.140.6 on 09/07/12
For personal use only.

9. P. COPPENS and W. C. HAMILTON. Acta Crystallogr. Sect. A. **26**, 71 (1970).
10. F. R. THORNLEY and R. J. NELMES. Acta Crystallogr. Sect. A, **30**, 748 (1974).
11. E. C. ONYIRIUKA, S. J. RETTIG, A. STORR, and J. TROTTER. Can. J. Chem. **65**, 782 (1987).
12. S. J. RETTIG, A. STORR, and J. TROTTER. Can. J. Chem. **52**, 2206 (1974).
13. S. J. RETTIG, A. STORR, and J. TROTTER. Can. J. Chem. **53**, 58 (1975).
14. S. J. RETTIG, A. STORR, J. TROTTER, and K. URICH. Can. J. Chem. **62**, 2788 (1984).
15. S. J. RETTIG, A. STORR, and J. TROTTER. Can. J. Chem. **54**, 1278 (1976).
16. I. WALLER, T. HALDER, W. SCHWARZ, and J. WEIDLEIN. J. Organomet. Chem. **232**, 99 (1982).
17. S. J. RETTIG, A. STORR, and J. TROTTER. Can. J. Chem. **62**, 1705 (1984).
18. G. A. BANTA, S. J. RETTIG, A. STORR, and J. TROTTER. Can. J. Chem. **63**, 2545 (1985).
19. K. S. CHONG, S. J. RETTIG, A. STORR, and J. TROTTER. Can. J. Chem. **57**, 586 (1979).
20. D. M. ADAMS. Metal–ligand and related vibrations. Edward Arnold, London. 1967.
21. K. S. CHONG, S. J. RETTIG, A. STORR, and J. TROTTER. Can. J. Chem. **56**, 1212 (1978).
22. A. ROMERO, A. VEGAS, and A. SANTOS. J. Organomet. Chem. **310**, C8 (1986).
23. C. J. JONES, J. A. MCCLEVERTY, and A. S. ROTHIN. J. Chem. Soc. Dalton Trans. 109 (1986).
24. M. G. B. DREW. J. Chem. Soc. Dalton Trans. 626 (1972).
25. M. G. B. DREW. J. Chem. Soc. Dalton Trans. 1329 (1972).
26. M. L. ZIEGLER, H.-E. SASSE, and G. NUBER. Z. Naturforsch. **30B**, 26 (1975).
27. M. G. B. DREW and J. D. WILKINS. J. Chem. Soc. Dalton Trans. 557 (1977).

Can. J. Chem. Downloaded from www.nrcresearchpress.com by 213.166.140.6 on 09/07/12
For personal use only.

FOR ERRATA SEE
66(1)1988 P. 207

The microwave spectrum and structure of bromine thiocyanate, BrSCN

H. M. JEMSON, W. LEWIS-BEVAN, AND M. C. L. GERRY[1]

Department of Chemistry, The University of British Columbia, 2036 Main Mall, Vancouver, B.C., Canada V6T 1Y6

Received February 2, 1987

H. N. JEMSON, W. LEWIS-BEVAN, and M. C. L. GERRY. Can. J. Chem. **65**, 2478 (1987).

The microwave spectra of ^{79}BrSCN and ^{81}BrSCN have been measured and analysed to give rotational, centrifugal distortion, and Br quadrupole coupling constants. The molecule has been shown unambiguously to be BrSCN rather than BrNCS. A harmonic force field has been determined from combined vibrational and distortion data. With structural parameters for the SCN chain transferred from $S(CN)_2$, both effective and ground state average values for the BrS length and BrSC angle have been estimated. The Br quadrupole tensor has been diagonalized, and the BrS bond is shown not to be bent.

H. N. JEMSON, W. LEWIS-BEVAN et M. C. L. GERRY. Can. J. Chem. **65**, 2478 (1987).

On a mesuré les spectres de micro-ondes du ^{79}BrSCN et du ^{81}BrSCN et on les a analysés pour obtenir les constantes de couplage de rotation, centrifuge et quadrupolaire du Br. On a démontré sans ambiguités que la molécule est bien BrSCN et non pas BrNCS. On a déterminé un champ de force harmonique à partir des données combinées de la vibration et de la distortion. En se basant sur les paramètres structuraux du transfert en chaîne du SCN à partir du $S(CN)_2$, on a évalué les valeurs moyennes tant efficace qu'à l'état fondamental de la longueur de la liaison BrS et de l'angle BrSC. On a diagonalisé le tenseur quadrupolaire du Br et on démontre que la liaison BrS n'est pas recourbée.

[Traduit par la revue]

Introduction

Thiocyanates, which possess the SCN moiety, have rather interesting structural properties. The group is ambidentate, and can bond to the remainder of the molecule at either the S or N atom to form, respectively, thiocyanates or isothiocyanates. There seems to be no *a priori* indication whether a molecule has a thiocyanate or isothiocyanate configuration. The H- and SiH_3-derivatives, for example, are isothiocyanates, HNCS (1) and SiH_3NCS (2). The methyl derivatives can exist in both forms, CH_3NCS and CH_3SCN (3), as can the cyano derivatives, $S(CN)_2$ (4) and NCNCS (5). Of the possible chlorine derivatives, only the thiocyanate, ClSCN, is known (6).

There have been several studies of bromine thiocyanate, BrSCN, in solution (7–10). In common with other halogen thiocyanates, it is prepared by the following scheme (7):

[1] $Pb(SCN)_2 + Br_2 \rightarrow (SCN)_2 + PbBr_2$

[2] $(SCN)_2 + X_2 \rightarrow 2XSCN$

where X is a halogen, including Br. Bromine thiocyanate undergoes addition reactions with alkenes. However, the reaction products are not unique, with both bromothiocyanato and dibromo derivatives being formed (8). It has also been used as a reagent in thiocyanation reactions (11, 12). Both infrared solution studies (10) and chemical studies (7–9) suggest that the bromine is linked via the S atom.

The only previous study of gas phase bromine thiocyanate was of its photoelectron spectrum by Frost *et al.* (13). This sprectrum was found to parallel that of chlorine thiocyanate, ClSCN. Since the configuration of the latter was found from its microwave spectrum to be indeed ClSCN (6), it seemed likely that the configuration of the bromine derivative would be the same. The aim of the present study was to confirm that this is indeed the case, and to measure the spectroscopic constants and structural parameters of the molecule.

Experimental methods

Bromine thiocyanate was prepared according to the method of Frost *et al.* (13). Freshly prepared AgSCN was loosely packed with glass wool in a U-tube, and dried under vacuum for several hours at 100°C. The solid sample was then cooled to room temperature and Br_2 vapour was added to it.

The reaction products depended on the pressure of Br_2 used and the way it came in contact with the solid. If Br_2 was simply passed through the solid sample the spectrum of $S(CN)_2$ was observed, along with some lines of SO_2 and HNCS. However, when Br_2 was passed over AgSCN at low pressure (with one end of the U-tube closed), so that the gaseous reaction products reacted with more Br_2, the spectrum of bromine thiocyanate appeared almost immediately. Its formation was entirely analogous to its formation in solution.

[3] $2AgSCN + Br_2 \rightarrow (SCN)_2 + 2AgBr$

[4] $(SCN)_2 + Br_2 \rightarrow 2BrSCN$

The microwave spectrum was observed in a conventional 100 kHz Stark modulated spectrometer, in the frequency range 8–54 GHz. The microwave source was a Watkins-Johnson 1291A Synthesizer in the range 8–18 GHz, extended to 54 GHz with Honeywell SpaceKom 14-27 and T-K_a3 multipliers. Throughout the study a flow system was used, in which the products of the reaction described above were passed immediately into the spectrometer's six foot X-band Stark cell, held at room temperature. Measurement accuracies are believed to be better than ±0.03 MHz.

Results

Assignment and analysis of the spectrum

Initial predictions of the rotational constants of both BrSCN and BrNCS were made by transferring parameters from related molecules. For BrSCN the BrS bond length was taken from S_2Br_2 (14) and the SCN parameters from $S(CN)_2$ (4); the BrSC angle was taken to be the same as the CSC angle in $S(CN)_2$ (4). For BrNCS the BrN length was transferred from BrNCO (15), as was the BrNC angle, increased by 7° following other isocyanates and isothiocyanates (3, 16); the parameters of the NCS chain were those of HNCS (16). In the two cases the molecule was predicted to be a planar near-symmetric prolate rotor, but with considerably different rotational constants.

The observed spectrum contained a series of strong *a*-type R branch clusters, along with reasonably intense *b*-type transitions. The spacing of the *a*-type R branches was found to be ~3500 MHz, in reasonable agreement with the predicted (B_0 + C_0) of BrSCN. The observed *b*-type transitions also fol-

[1]Author to whom all correspondence is to be addressed.

Can. J. Chem. Downloaded from www.nrcresearchpress.com by 213.166.140.6 on 09/07/12
For personal use only.

TABLE 1. Spectroscopic constants of bromine thiocyanate

Parameter	^{79}BrSCN	^{81}BrSCN
Rotational constants (MHz)		
A_0	10092.2012(68)[a]	10074.4731(78)
B_0	1944.40541(64)	1927.45095(82)
C_0	1627.94999(56)	1615.58914(71)
Centrifugal distortion constants (kHz)		
Δ_J	0.8477(18)	0.8272(22)
Δ_{JK}	−13.690(43)	−13.517(54)
Δ_K	104.2(12)	102.7(15)
δ_J	0.23956(43)	0.23530(56)
δ_K	2.010(39)	1.989(52)
Bromine quadrupole coupling constants (MHz)		
χ_{aa}	402.62(77)	336.4(12)
$\chi_{bb} - \chi_{cc}$	366.20(16)	304.42(20)
χ_{ab}	478.41(23)	397.74(38)
Inertial defect (amu Å^2)		
Δ	0.448	0.449
Number of rotational transitions	56	55
Standard deviation of fit (MHz)	0.044	0.055

[a]Numbers in parentheses are one standard deviation in units of the last significant figures.

Can. J. Chem. Downloaded from www.nrcresearchpress.com by 213.166.140.6 on 09/07/12
For personal use only.

lowed quite closely the pattern predicted for BrSCN. It followed that this configuration was probably the correct one.

All transitions showed quadrupole hyperfine splitting due to the Br nucleus ($I = 3/2$). Rough predictions of the coupling constants were made using those of ClSCN (6), scaled by the ratios of the quadrupole moments, and were used in first order predictions of the hyperfine patterns; these were an invaluable aid in the assignments. No ^{14}N hyperfine structure was observed for any transitions.

Significant perturbations of the hyperfine structure from the first order patterns were observed. This is not surprising, since the off-diagonal coupling constant χ_{ab} was expected to be large: with the BrS bond expected to be on or near the principal quadrupole axis, the angle between it and the a-inertial axis was anticipated to be ~33°. Also, several near-degeneracies of the type $\Delta F = 0$; $\Delta J = 0, \pm 1, \pm 2$; K_aK_c = eo ↔ oo, oe ↔ ee, were found, and transitions involving these levels were significantly shifted from their first order positions.

The analysis of the BrSCN spectrum required use of our global least-squares fitting procedure, which simultaneously produced rotational, centrifugal distortion and Br quadrupole coupling constants, including χ_{ab}. This procedure was used earlier for BrNCO (15) and INCO (19), which also have large perturbations in their hyperfine structure.

A bootstrap procedure was used to analyse the spectrum. Initial assignments were made to a-type R branch $K_a = 0$ and asymmetry split $K_a = 1$ transitions. Transitions from one asymmetry branch of the $K_a = 2 \leftarrow 1$ b-type Q branch ($J_{2,J-2}$–$J_{1,J-1}$) were also assigned; Fig. 1 shows the $13_{2,11}$–$13_{1,12}$ transition for both isotopes. These were used to obtain preliminary rotational and quadrupole constants, which were in turn used for further predictions. As further transitions were assigned they were included in successive fits, with the distortion constants now also released. Ultimately the assigned transitions included $K_a = 0$, 1, 2, and 3 a-type R branches for $J = 6$ to 12. The b-type transitions included, besides the branch mentioned above,

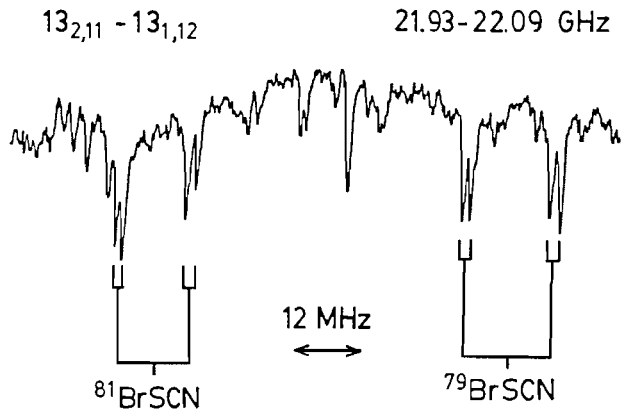

FIG. 1. The transition $13_{2,11}$–$13_{1,12}$ of ^{79}BrSCN and ^{81}BrSCN.

lines from the sub-branches $J_{3,J-3}$–$J_{2,J-2}$ and $J_{4,J-4}$–$J_{3,J-3}$; these sub-branches, which initially extend to low frequency, were easily assigned at the point where they change direction to higher frequency. An example for $J_{3,J-3}$–$J_{2,J-2}$, is in Fig. 2. Some Q branches of the series $J_{3,J-2}$–$J_{2,J-1}$, as well as some $K_a = 1 \leftarrow 0$ and $0 \leftarrow 1$ R branches, were measured to complete the analysis.

The final constants are given in Table 1. Along with rotational and Br quadrupole constants all five quartic centrifugal distortion constants (obtained in terms of Watson's A-reduction (18)) have been measured. The frequencies of all measured transitions are in Tables 2 and 3; they were weighted in the fits according to their resolvability and to whether they are partially overlapped by other transitions. These tables also contain residuals obtained when χ_{ab} is included in their calculation and when it is omitted; the latter approximates a first-order prediction. Comparison of the two sets of residuals indicates several important near degeneracies affecting primarily the a-type transitions. The closest near degeneracies separate the (unsplit)

Can. J. Chem. Downloaded from www.nrcresearchpress.com by 213.166.140.6 on 09/07/12
For personal use only.

TABLE 2. Measured rotational transitions (in MHz) of ^{79}BrSCN

Transition $F'-F''$	Normalised weight[a]	Observed frequency	Residuals[b] Without χ_{ab}	Residuals[b] With χ_{ab}
$7_{1,7}-6_{1,6}$				
17/2–15/2	1.000	23786.693	0.053	0.016
15/2–13/2	1.000	23789.286	−0.376	−0.003
11/2– 9/2	1.000	23790.086	−0.559	−0.068
13/2–11/2	1.000	23793.610	−0.092	0.018
$7_{0,7}-6_{0,6}$				
17/2–15/2	1.000	24518.481	0.052	0.008
11/2– 9/2	1.000	24520.856	−0.290	0.007
15/2–13/2	1.000	24523.468	−0.129	0.026
13/2–11/2	1.000	24526.252	−0.070	−0.028
$7_{1,6}-6_{1,5}$				
17/2–15/2	1.000	25981.968	0.172	0.053
13/2–11/2	1.000	25987.525	1.319	0.080
11/2– 9/2	0.100	25997.999	15.313	0.123
15/2–13/2	0.100	25997.999	12.732	−0.057
$8_{1,8}-7_{1,7}$				
19/2–17/2	1.000	27148.453	0.035	0.005
17/2–15/2	0.500	27149.908	−1.042	0.049
13/2–11/2	0.500	27150.324	−1.199	−0.002
15/2–13/2	1.000	27153.938	−0.139	−0.043
$8_{0,8}-7_{0,7}$				
19/2–17/2	1.000	27869.916	0.047	0.011
13/2–11/2	1.000	27871.645	−0.209	−0.018
17/2–15/2	1.000	27875.241	−0.044	0.059
15/2–13/2	1.000	27877.345	0.043	0.061
$8_{1,7}-7_{1,6}$				
13/2–11/2	0.500	29638.808	−1.297	−0.018
19/2–17/2	0.500	29639.418	0.028	−0.057
17/2–15/2	1.000	29641.682	−0.930	−0.055
15/2–13/2	1.000	29643.412	0.054	0.036
$9_{1,9}-8_{1,8}$				
19/2–17/2	1.000	30474.460	−25.762	−0.050
15/2–13/2	1.000	30488.289	−12.151	0.007
21/2–19/2	1.000	30498.014	0.045	0.019
17/2–15/2	1.000	30502.019	−0.688	−0.003
$9_{0,9}-8_{0,8}$				
21/2–19/2	1.000	31179.518	0.056	0.026
15/2–13/2	1.000	31180.779	−0.195	−0.062
19/2–17/2	1.000	31184.831	−0.036	0.038
17/2–15/2	1.000	31186.466	0.004	0.005
$9_{1,8}-8_{1,7}$				
21/2–19/2	0.100	33271.870	0.100	0.036
15/2–13/2	0.100	33271.870	−0.527	−0.128
19/2–17/2	1.000	33274.708	−0.302	−0.030
17/2–15/2	1.000	33275.656	−0.005	−0.055
$10_{1,10}-9_{1,9}$				
23/2–21/2	1.000	33835.401	0.009	−0.012
19/2–17/2	1.000	33840.263	0.775	−0.042
17/2–15/2	0.500	33855.848	18.445	−0.107
21/2–19/2	1.000	33868.105	30.638	−0.038
$10_{0,10}-9_{0,9}$				
23/2–21/2	1.000	34454.411	0.040	0.014
17/2–15/2	0.768	34455.325	−0.096	0.001
21/2–19/2	1.000	34459.303	−0.054	0.004
19/2–17/2	1.000	34460.878	−0.011	−0.004

TABLE 2 (*continued*)

Transition $F'-F''$	Normalised weight[a]	Observed frequency	Residuals[b] Without χ_{ab}	Residuals[b] With χ_{ab}
$10_{2,9}-9_{2,8}$				
17/2–15/2	0.100	35493.140	−0.192	0.154
23/2–21/2	0.100	35493.140	1.322	−0.054
21/2–19/2	1.000	35496.066	−0.189	0.033
19/2–17/2	1.000	35498.483	2.137	0.020
$10_{3,8}-9_{3,7}$				
17/2–15/2	1.000	35863.912	−0.278	0.049
23/2–21/2	1.000	35864.916	0.997	0.013
21/2–19/2	1.000	35869.046	0.118	0.014
19/2–17/2	0.500	35869.799	0.514	0.044
$10_{3,7}-9_{3,6}$				
23/2–21/2	1.000	35982.892	−5.508	0.036
19/2–17/2	1.000	35985.299	−7.246	−0.008
17/2–15/2	1.000	35988.357	−0.443	−0.131
21/2–19/2	1.000	35991.800	−0.264	−0.075
$10_{2,8}-9_{2,7}$				
21/2–19/2	1.000	36751.031	−1.152	0.085
17/2–15/2	0.500	36753.317	−1.348	0.067
19/2–17/2	0.500	36753.317	0.004	−0.031
23/2–21/2	0.500	36753.653	0.077	−0.013
$10_{1,9}-9_{1,8}$				
23/2–21/2	0.500	36874.089	0.093	0.044
17/2–15/2	0.500	36874.089	−0.266	−0.064
21/2–19/2	1.000	36877.300	−0.112	0.026
19/2–17/2	1.000	36877.877	0.089	0.043
$11_{1,11}-10_{1,10}$				
19/2–17/2	1.000	37160.568	−2.205	−0.043
25/2–23/2	1.000	37161.104	−0.002	−0.020
23/2–21/2	1.000	37161.668	−1.385	−0.019
21/2–19/2	1.000	37164.620	−0.106	−0.027
$11_{0,11}-10_{0,10}$				
25/2–23/2	1.000	37703.711	−0.035	−0.057
19/2–17/2	1.000	37705.567	−0.098	−0.007
23/2–21/2	1.000	37709.293	0.014	0.042
21/2–19/2	1.000	37709.698	−0.033	−0.016
$11_{2,10}-10_{2,9}$				
19/2–17/2	1.000	38985.034	−0.805	0.039
25/2–23/2	1.000	38985.679	0.405	−0.044
23/2–21/2	1.000	38987.672	−0.725	0.015
21/2–19/2	1.000	38990.044	0.557	−0.013
$11_{3,9}-10_{3,8}$				
19/2–17/2	0.100	39464.936	−0.039	0.074
23/2–21/2	1.000	39468.320	−0.036	0.035
25/2–23/2	1.000	39472.350	7.727	0.037
21/2–19/2	1.000	39475.583	6.809	0.002
$11_{3,8}-10_{3,7}$				
19/2–17/2	1.000	39664.034	−0.145	−0.029
23/2–21/2	1.000	39665.671	0.057	0.029
25/2–23/2	1.000	39665.155	2.528	−0.038
21/2–19/2	1.000	39669.494	3.270	−0.025
$11_{2,9}-10_{2,8}$				
21/2–19/2	1.000	40563.801	0.233	0.027
25/2–23/2	1.000	40564.123	0.042	−0.020
23/2–21/2	1.000	40568.213	5.578	0.002
19/2–17/2	1.000	40571.828	6.844	−0.014

Can. J. Chem. Downloaded from www.nrcresearchpress.com by 213.166.140.6 on 09/07/12
For personal use only.

TABLE 2 (*continued*)

Transition $F'-F''$	Normalised weight[a]	Observed frequency	Residuals[b] Without χ_{ab}	Residuals[b] With χ_{ab}
$11_{1,10}-10_{1,9}$				
25/2–23/2	0.100	40440.946	0.179	0.140
19/2–17/2	0.100	40440.946	−0.129	−0.004
23/2–21/2	0.500	40444.394	−0.067	0.019
21/2–19/2	0.500	40444.779	−0.004	−0.043
$12_{1,12}-11_{1,11}$				
27/2–25/2	1.000	40475.840	0.029	0.013
21/2–19/2	1.000	40476.624	−0.623	0.0
25/2–23/2	1.000	40477.225	−0.428	−0.001
23/2–21/2	1.000	40479.106	0.010	0.045
$12_{0,12}-11_{0,11}$				
27/2–25/2	1.000	40936.990	0.089	0.071
21/2–19/2	1.000	40937.318	−0.255	−0.083
25/2–23/2	1.000	40941.081	−0.001	0.031
23/2–21/2	1.000	40942.039	−0.209	0.001
$12_{2,11}-11_{2,10}$				
21/2–19/2	1.000	42455.891	−6.872	0.017
25/2–23/2	0.500	42457.166	−7.934	−0.001
27/2–25/2	1.000	42462.373	0.238	0.015
23/2–21/2	1.000	42465.999	0.152	0.025
$12_{3,10}-11_{3,9}$				
27/2–25/2	1.000	43051.182	−12.124	0.015
23/2–21/2	1.000	43054.541	−12.124	−0.072
21/2–19/2	1.000	43063.601	−0.110	0.006
25/2–23/2	1.000	43065.805	−0.395	−0.099
$12_{3,9}-11_{3,8}$				
27/2–25/2	0.100	43366.981	0.528	0.122
21/2–19/2	0.100	43366.981	−0.092	0.036
25/2–23/2	0.100	43366.981	−0.186	−0.114
23/2–21/2	1.000	43368.254	0.425	−0.027
$12_{2,10}-11_{2,9}$				
25/2–23/2	1.000	44368.265	−2.548	−0.004
21/2–19/2	1.000	44369.292	−3.444	−0.068
23/2–21/2	1.000	44371.522	−0.039	0.004
27/2–25/2	1.000	44372.018	0.009	−0.037
$12_{1,11}-11_{1,10}$				
27/2–25/2	1.000	43966.862	0.112	0.081
21/2–19/2	1.000	43966.862	−0.102	−0.016
25/2–23/2	0.500	43970.747	−0.034	0.028
23/2–21/2	0.500	43970.993	−0.018	−0.050
$12_{1,12}-11_{0,11}$				
27/2–25/2	0.100	42646.644	0.085	0.060
21/2–19/2	0.100	42646.644	0.592	−0.176
25/2–23/2	0.100	42659.909	0.498	−0.072
23/2–21/2	0.100	42659.909	0.285	0.209
$13_{1,13}-12_{0,12}$				
29/2–27/2	1.000	45490.044	−0.035	−0.055
23/2–21/2	1.000	45490.787	0.695	0.057
27/2–25/2	0.500	45500.964	0.466	0.070
25/2–23/2	0.500	45500.964	0.225	−0.041
$14_{1,14}-13_{0,13}$				
31/2–29/2	1.000	48404.308	0.053	0.036
25/2–23/2	1.000	48404.795	0.316	−0.018
29/2–27/2	0.500	48412.841	0.316	0.019
27/2–25/2	0.500	48412.841	−0.042	−0.031

TABLE 2 (*continued*)

Transition $F'-F''$	Normalised weight[a]	Observed frequency	Residuals[b] Without χ_{ab}	Residuals[b] With χ_{ab}
$15_{1,15}-14_{0,14}$				
33/2–31/2	1.000	51383.554	0.022	0.009
27/2–25/2	1.000	51384.158	0.280	0.016
31/2–29/2	0.100	51390.373	0.324	0.091
29/2–27/2	0.100	51390.373	−0.116	−0.114
$12_{0,12}-11_{1,11}$				
25/2–23/2	1.000	38758.334	−0.990	0.039
23/2–21/2	1.000	38761.409	−0.311	0.010
27/2–25/2	1.000	38766.203	0.050	0.041
21/2–19/2	0.500	38767.253	−1.514	0.048
$13_{0,13}-12_{1,12}$				
27/2–25/2	1.000	42446.687	−0.603	0.019
25/2–23/2	1.000	42449.203	0.026	0.052
29/2–27/2	1.000	42452.130	−0.027	−0.036
23/2–21/2	1.000	42453.392	−0.779	0.032
$15_{0,15}-14_{1,14}$				
31/2–29/2	1.000	49585.948	−0.351	−0.033
29/2–27/2	1.000	49587.495	−0.055	−0.035
33/2–31/2	1.000	49588.438	0.047	0.038
27/2–25/2	1.000	49589.282	−0.428	−0.020
$16_{0,16}-15_{1,15}$				
33/2–31/2	1.000	53058.843	−0.240	0.004
31/2–29/2	0.100	53060.202	0.080	0.095
35/2–33/2	0.100	53060.202	−0.077	−0.085
29/2–27/2	1.000	53061.064	−0.308	0.003
$13_{2,11}-13_{1,12}$				
27/2–27/2	1.000	22043.064	0.294	−0.025
25/2–25/2	1.000	22045.171	−0.036	−0.013
29/2–29/2	1.000	22064.703	0.016	0.012
23/2–23/2	0.500	22067.530	0.358	0.014
$14_{2,12}-14_{1,13}$				
29/2–29/2	1.000	23100.077	0.192	−0.010
27/2–27/2	1.000	23102.644	−0.031	−0.004
31/2–31/2	1.000	23126.847	0.045	0.032
25/2–25/2	1.000	23129.906	0.235	0.043
$15_{2,13}-15_{1,14}$				
31/2–31/2	1.000	24522.033	0.139	−0.012
29/2–29/2	1.000	24524.821	−0.040	−0.016
33/2–33/2	1.000	24553.501	0.019	−0.002
27/2–27/2	1.000	24556.832	0.090	−0.035
$16_{2,14}-16_{1,15}$				
33/2–33/2	1.000	26323.997	0.137	0.015
31/2–31/2	1.000	26327.378	0.022	0.009
35/2–35/2	1.000	26360.322	0.114	0.087
29/2–29/2	1.000	26363.405	0.074	−0.044
$17_{2,15}-17_{1,16}$				
35/2–35/2	1.000	28513.068	0.103	−0.006
33/2–33/2	1.000	28516.505	−0.021	0.035
37/2–37/2	1.000	28553.209	−0.010	−0.044
31/2–31/2	1.000	28556.745	0.128	0.091
$18_{2,16}-18_{1,17}$				
37/2–37/2	1.000	31083.442	0.117	0.016
35/2–35/2	0.500	31086.835	−0.128	−0.087
39/2–39/2	1.000	31127.053	0.060	0.020
33/2–33/2	1.000	31130.490	−0.013	−0.046

TABLE 2 (*continued*)

Transition $F'-F''$	Normalised weight[a]	Observed frequency	Residuals[b] Without χ_{ab}	Residuals[b] With χ_{ab}
$17_{3,15}-17_{2,16}$				
35/2–35/2	0.500	48953.793	0.748	0.0
33/2–33/2	0.500	48954.258	−0.202	−0.120
37/2–37/2	0.500	48979.983	−0.193	−0.135
31/2–31/2	1.000	48984.696	2.073	0.004
$18_{3,15}-18_{2,16}$				
39/2–39/2	0.500	31796.927	0.033	0.030
33/2–33/2	0.500	31796.927	0.387	0.067
37/2–37/2	0.100	31798.831	0.458	0.185
35/2–35/2	0.100	31798.831	−0.107	−0.138
$18_{3,16}-18_{2,17}$				
37/2–37/2	1.000	50483.824	0.644	0.004
35/2–35/2	1.000	50485.479	−0.062	0.007
39/2–39/2	1.000	50512.093	−0.075	−0.042
33/2–33/2	1.000	50515.192	0.649	−0.053
$19_{3,16}-19_{2,17}$				
39/2–39/2	0.500	31633.001	0.223	0.057
37/2–37/2	0.500	31633.001	0.013	−0.002
41/2–41/2	1.000	31635.683	0.024	0.017
35/2–35/2	1.000	31636.091	0.191	0.0
$19_{3,17}-19_{2,18}$				
37/2–37/2	1.000	52186.309	−0.011	0.043
41/2–41/2	1.000	52213.579	0.039	0.056
35/2–35/2	0.500	52215.793	0.464	0.125
$20_{3,17}-20_{2,18}$				
41/2–41/2	1.000	31810.444	0.130	0.016
39/2–39/2	1.000	31810.820	−0.017	−0.029
43/2–43/2	1.000	31817.705	−0.004	−0.014
37/2–37/2	1.000	31818.401	0.119	−0.007
$22_{3,19}-22_{2,20}$				
45/2–45/2	1.000	33333.022	0.070	−0.002
43/2–43/2	1.000	33334.111	−0.060	−0.039
47/2–47/2	1.000	33349.587	0.055	0.040
41/2–41/2	1.000	33350.487	−0.026	−0.069
$23_{3,20}-23_{2,21}$				
47/2–47/2	1.000	34727.587	0.141	0.077
45/2–45/2	1.000	34728.833	−0.001	0.012
49/2–49/2	1.000	34748.251	−0.043	−0.062
43/2–43/2	1.000	34749.638	0.053	0.014
$24_{3,21}-24_{2,22}$				
49/2–49/2	1.000	36562.329	0.048	−0.012
47/2–47/2	1.000	36563.859	0.003	0.016
51/2–51/2	1.000	36587.216	0.014	−0.007
45/2–45/2	1.000	36588.710	0.008	−0.023
$26_{4,22}-26_{3,23}$				
49/2–49/2	0.500	42280.139	0.155	0.056
55/2–55/2	0.500	42280.139	−0.064	−0.073
51/2–51/2	0.100	42284.232	0.200	0.176
53/2–53/2	0.100	42284.232	−0.047	−0.127
$27_{4,23}-27_{3,24}$				
57/2–57/2	0.500	41864.304	0.056	0.046
51/2–51/2	0.500	41864.304	0.048	−0.046
53/2–53/2	0.500	41864.616	0.026	−0.018
55/2–55/2	0.500	41864.616	−0.023	−0.084

TABLE 2 (*concluded*)

Transition $F'-F''$	Normalised weight[a]	Observed frequency	Residuals[b] Without χ_{ab}	Residuals[b] With χ_{ab}
$28_{4,24}-28_{3,25}$				
59/2–59/2	1.000	41842.025	0.078	0.067
53/2–53/2	1.000	41842.715	−0.002	−0.043
55/2–55/2	0.500	41838.727	0.121	0.118
57/2–57/2	0.500	41839.301	0.014	−0.041

[a]Measurements were weighted according to $1/\sigma^2$, where σ is the uncertainty in the measurements. Unit weight corresponded to an uncertainty of 0.03 MHz.

[b]Observed frequency minus the frequency calculated using the constants in Table 1.

9_{19} and 8_{27} levels by ~265 MHz for ^{79}BrSCN and ~407 MHz for ^{81}BrSCN, which in turn produce shifts in transitions involving 9_{19} of up to ~30 MHz in ^{79}BrSCN and up to ~13 MHz for ^{81}BrSCN. Table 4 indicates some of the closest near degeneracies.

Harmonic force field and structure

Despite having rotational constants for only ^{79}BrSCN and ^{81}BrSCN, we can make some deductions about the structure. In the first place, comparison of the observed rotational constants with those predicted for BrSCN and BrNCS (Table 5) indicates clearly that the molecule is the former, the thiocyanate, with Br bonded to S. Secondly, the inertial defects (Table 1) are small and positive, and essentially the same for both isotopes, consistent with a planar structure. This is confirmed by the ratio of the out-of-plane quadrupole constants $\chi_{cc}(^{81}\text{Br})/\chi_{cc}(^{79}\text{Br}) = 0.8335$, which is very close to the ratio of the quadrupole moments of the two nuclei (0.8353).

Because of the limited isotopic data only a partial set of bond lengths and angles could be obtained. These we have chosen to be the Br—S length and BrSC angle. The SCN parameters were held fixed at their values in $S(CN)_2$, in which the SCN chain is bent by 5° (4). Ground state effective (r_0) values of the two unknowns were estimated by a least-squares fit to the observed rotational constants. The results are in Table 6, along with a comparison with corresponding parameters of similar molecules. Uncertainties were estimated by varying each of the assumed parameters in turn within reasonable limits: r(SC) by 0.012 Å (to include the value assumed for CH_3SCN (3)), r(CN) by 0.003 Å (since little variation is reported in the literature (4)), and <(SCN) by 5°, to include a linear structure. Remarkably little variation in the derived parameters was found. The positions of the atoms in the inertial axis system of ^{79}BrSCN are shown in Fig. 3.

In order to evaluate ground state average (r_z) parameters it was first necessary to obtain a harmonic force field, using infrared data from the literature and the centrifugal distortion constants measured in the present work. Infrared data are, however, rather sparse, with wavenumbers of only four of the six normal modes being reported (10); these were obtained for BrSCN in solution (10), and the measurements were not made below 350 cm^{-1}. However, in the present work we were able to observe rotational transitions of molecules in the first excited state of the lowest frequency mode; from relative intensity measurements we estimate it to be at 154 ± 30 cm^{-1}.

The internal coordinates and structure used in the force field

Can. J. Chem. Downloaded from www.nrcresearchpress.com by 213.166.140.6 on 09/07/12
For personal use only.

TABLE 3. Measured rotational transitions (in MHz) of ^{81}BrSCN

Transition $F'-F''$	Normalised weight[a]	Observed frequency	Residuals[b] Without χ_{ab}	Residuals[b] With χ_{ab}
$7_{1,7}-6_{1,6}$				
17/2–15/2	1.000	23600.994	0.017	−0.011
15/2–13/2	1.000	23603.280	−0.207	0.035
11/2– 9/2	1.000	23603.993	−0.332	−0.005
13/2–11/2	1.000	23606.793	−0.067	0.008
$7_{0,7}-6_{0,6}$				
17/2–15/2	1.000	24327.058	0.026	−0.002
11/2– 9/2	1.000	24329.117	−0.199	0.011
15/2–13/2	1.000	24331.202	−0.084	0.027
13/2–11/2	1.000	24333.615	0.041	0.073
$7_{1,6}-6_{1,5}$				
17/2–15/2	1.000	25764.780	0.084	0.0
13/2–11/2	1.000	25769.026	0.654	−0.042
11/2– 9/2	0.100	25774.304	8.842	0.245
15/2–13/2	0.100	25774.304	6.733	−0.100
$8_{1,8}-7_{1,7}$				
19/2–17/2	1.000	26937.043	0.008	−0.016
17/2–15/2	0.500	26938.539	−0.596	0.081
13/2–11/2	0.500	26938.944	−0.686	0.080
15/2–13/2	1.000	26941.625	−0.121	−0.059
$8_{0,8}-7_{0,7}$				
19/2–17/2	1.000	27654.686	0.021	−0.002
13/2–11/2	1.000	27656.179	−0.156	−0.020
17/2–15/2	1.000	27659.074	−0.059	0.015
15/2–13/2	1.000	27660.763	−0.061	−0.045
$8_{1,7}-7_{1,6}$				
13/2–11/2	0.500	29392.619	−0.871	0.095
19/2–17/2	0.500	29392.907	0.032	−0.027
17/2–15/2	1.000	29394.885	−0.649	0.017
15/2–13/2	1.000	29363.091	−0.080	−0.088
$9_{1,9}-8_{1,8}$				
19/2–17/2	1.000	30253.948	−9.082	−0.045
15/2–13/2	1.000	30256.989	−6.240	−0.009
21/2–19/2	1.000	30261.182	0.018	−0.002
17/2–15/2	1.000	30264.830	−0.275	0.015
$9_{0,9}-8_{0,8}$				
21/2–19/2	1.000	30941.085	0.050	0.032
15/2–13/2	1.000	30942.180	−0.132	−0.035
19/2–17/2	1.000	30945.499	−0.013	0.041
17/2–15/2	1.000	30946.853	0.006	0.016
$9_{1,8}-8_{1,7}$				
21/2–19/2	1.000	32996.687	0.025	−0.020
15/2–13/2	1.000	32996.687	−0.360	−0.070
19/2–17/2	0.500	32999.105	−0.222	−0.024
17/2–15/2	0.500	32999.573	0.024	−0.014
$10_{1,10}-9_{1,9}$				
23/2–21/2	1.000	33573.369	−0.058	−0.076
19/2–17/2	1.000	33577.213	0.381	−0.009
17/2–15/2	1.000	33585.911	10.803	−0.011
21/2–19/2	1.000	33587.745	12.601	0.016
$10_{0,10}-9_{0,9}$				
23/2–21/2	1.000	34192.997	0.063	0.049
17/2–15/2	1.000	34193.776	−0.095	−0.018
21/2–19/2	1.000	34197.107	−0.033	0.005
19/2–17/2	1.000	34198.349	0.0	0.008
$10_{2,9}-9_{2,8}$				
17/2–15/2	0.100	35206.758	−0.131	0.095
23/2–21/2	0.100	35206.758	1.048	−0.080
21/2–19/2	1.000	35209.164	−0.145	−0.011
19/2–17/2	1.000	35211.150	1.690	0.056
$10_{3,8}-9_{3,7}$				
17/2–15/2	1.000	35567.891	−0.234	0.045
23/2–21/2	1.000	35568.498	0.612	0.060
21/2–19/2	0.500	35572.237	0.162	0.125
19/2–17/2	0.500	35572.610	0.233	0.032
$10_{3,7}-9_{3,6}$				
23/2–21/2	1.000	35682.658	−4.473	−0.044
19/2–17/2	1.000	35684.728	−5.900	0.0
17/2–15/2	1.000	35687.130	−0.338	−0.075
21/2–19/2	1.000	35690.004	−0.229	−0.082
$10_{2,8}-9_{2,7}$				
21/2–19/2	1.000	36434.114	−0.698	0.019
19/2–17/2	0.100	36435.943	0.183	0.153
17/2–15/2	0.100	36435.943	−0.937	−0.083
23/2–21/2	0.100	36435.943	−0.019	−0.083
$10_{1,9}-9_{1,8}$				
23/2–21/2	0.100	36571.444	0.169	0.134
17/2–15/2	0.100	36571.444	−0.297	−0.155
21/2–19/2	1.000	36574.014	−0.066	0.033
19/2–17/2	1.000	36574.717	−0.020	−0.049
$11_{1,11}-10_{1,10}$				
19/2–17/2	0.100	36874.010	−1.589	0.098
25/2–23/2	0.100	36874.010	−0.195	−0.211
23/2–21/2	0.100	36874.703	−1.114	−0.017
21/2–19/2	1.000	36877.209	−0.006	0.051
$11_{0,11}-10_{0,10}$				
25/2–23/2	1.000	37419.232	0.052	0.041
19/2–17/2	1.000	37420.629	−0.077	−0.034
23/2–21/2	0.500	37423.684	−0.006	0.038
21/2–19/2	0.500	37424.049	−0.108	−0.093
$11_{2,10}-10_{2,9}$				
19/2–17/2	0.500	38671.818	−0.463	0.064
25/2–23/2	0.500	38672.088	0.273	−0.059
23/2–21/2	1.000	38673.928	−0.465	−0.012
21/2–19/2	1.000	38675.751	0.429	−0.004
$11_{3,9}-10_{3,8}$				
19/2–17/2	1.000	39139.000	−0.097	−0.017
23/2–21/2	0.100	39142.099	0.173	0.222
25/2–23/2	0.100	39142.099	3.297	−0.036
21/2–19/2	1.000	39145.656	3.391	0.112
$11_{3,8}-10_{3,7}$				
19/2–17/2	1.000	39329.998	−0.005	0.077
23/2–21/2	1.000	39331.230	−0.015	−0.057
25/2–23/2	1.000	39332.084	2.545	0.065
21/2–19/2	0.500	39334.902	3.152	−0.068
$11_{2,9}-10_{2,8}$				
21/2–19/2	0.100	40213.278	0.314	0.154
25/2–23/2	0.100	40213.278	−0.112	−0.157
23/2–21/2	1.000	40216.691	4.513	0.061
19/2–17/2	1.000	40219.743	5.588	−0.009

Can. J. Chem. Downloaded from www.nrcresearchpress.com by 213.166.140.6 on 09/07/12
For personal use only.

TABLE 3 (*continued*)

Transition $F'-F''$	Normalised weight[a]	Observed frequency	Residuals[b] Without χ_{ab}	Residuals[b] With χ_{ab}
$11_{1,10}-10_{1,9}$				
25/2–23/2	0.100	40111.653	0.074	0.047
19/2–17/2	0.100	40111.653	−0.195	−0.106
23/2–21/2	0.500	40114.537	−0.070	−0.008
21/2–19/2	0.500	40114.863	−0.023	−0.049
$12_{1,12}-11_{1,11}$				
27/2–25/2	1.000	40164.185	0.028	0.013
21/2–19/2	1.000	40164.895	−0.469	−0.016
25/2–23/2	1.000	40165.308	−0.375	−0.057
23/2–21/2	1.000	40166.910	0.018	0.040
$12_{0,12}-11_{0,11}$				
27/2–25/2	0.500	40628.925	0.051	0.043
21/2–19/2	0.500	40629.218	−0.198	−0.096
25/2–23/2	1.000	40632.326	−0.021	0.0
23/2–21/2	1.000	40633.231	−0.100	−0.021
$12_{2,11}-11_{2,10}$				
21/2–19/2	1.000	42119.239	−3.274	0.066
25/2–23/2	1.000	42120.968	−3.470	−0.037
27/2–25/2	1.000	42122.147	0.167	0.004
23/2–21/2	1.000	42125.199	0.139	0.006
$12_{3,10}-11_{3,9}$				
27/2–25/2	1.000	42701.442	−16.461	0.078
23/2–21/2	1.000	42703.598	−17.110	0.072
21/2–19/2	1.000	42708.194	−0.055	0.023
25/2–23/2	1.000	42710.197	−0.124	0.045
$12_{3,9}-11_{3,8}$				
27/2–25/2	0.100	42999.136	0.464	0.151
21/2–19/2	0.100	42999.136	−0.054	0.032
25/2–23/2	0.100	42999.136	−0.183	−0.137
23/2–21/2	1.000	43000.226	0.359	0.010
$12_{2,10}-11_{2,9}$				
25/2–23/2	1.000	43985.660	−2.489	−0.025
21/2–19/2	1.000	43986.501	−3.285	−0.005
23/2–21/2	1.000	43988.768	−0.013	0.037
27/2–25/2	1.000	43989.128	−0.041	−0.074
$12_{1,11}-11_{1,10}$				
27/2–25/2	0.500	43612.402	0.030	0.008
21/2–19/2	0.500	43612.402	−0.161	−0.100
25/2–23/2	0.100	43615.752	0.077	0.121
23/2–21/2	0.100	43615.752	−0.124	−0.146
$12_{1,12}-11_{0,11}$				
27/2–25/2	0.500	42376.320	0.110	0.028
21/2–19/2	0.500	42376.320	0.548	−0.090
23/2–21/2	0.100	42387.484	0.235	0.122
25/2–23/2	0.100	42387.484	0.404	−0.123
$13_{1,13}-12_{0,12}$				
29/2–27/2	0.500	45191.522	0.031	−0.057
23/2–21/2	0.500	45191.891	0.394	−0.134
27/2–25/2	1.000	45200.618	0.283	−0.119
25/2–23/2	1.000	45200.618	0.106	−0.077
$14_{1,14}-13_{0,13}$				
31/2–29/2	0.500	48076.846	0.060	−0.036
25/2–23/2	0.500	48077.207	0.241	−0.120
29/2–27/2	0.500	48084.042	0.222	−0.119
27/2–25/2	0.500	48084.042	−0.056	−0.128

TABLE 3 (*continued*)

Transition $F'-F''$	Normalised weight[a]	Observed frequency	Residuals[b] Without χ_{ab}	Residuals[b] With χ_{ab}
$15_{1,15}-14_{0,14}$				
33/2–31/2	0.500	51027.030	0.046	−0.062
27/2–25/2	0.500	51027.401	0.133	−0.196
31/2–29/2	0.100	51032.750	0.213	−0.098
29/2–27/2	0.100	51032.750	−0.138	−0.231
$12_{0,12}-11_{1,11}$				
25/2–23/2	0.500	38410.064	−0.886	−0.020
23/2–21/2	1.000	38412.821	−0.153	0.061
27/2–25/2	1.000	38416.798	−0.023	0.035
21/2–19/2	1.000	38417.818	−1.190	0.003
$13_{0,13}-12_{1,12}$				
27/2–25/2	1.000	42077.895	−0.472	0.096
25/2–23/2	1.000	42079.944	−0.013	0.073
29/2–27/2	1.000	42082.530	−0.051	0.017
23/2–21/2	1.000	42083.585	−0.676	0.016
$15_{0,15}-14_{1,14}$				
31/2–29/2	1.000	49176.783	−0.370	0.003
29/2–27/2	1.000	49178.124	−0.086	0.023
33/2–31/2	1.000	49178.942	−0.065	0.027
27/2–25/2	1.000	49179.644	−0.469	−0.036
$16_{0,16}-15_{1,15}$				
33/2–31/2	1.000	52629.383	−0.197	0.142
31/2–29/2	0.100	52630.518	0.061	0.182
35/2–33/2	0.100	52630.518	−0.148	−0.039
29/2–27/2	1.000	52631.243	−0.338	0.045
$13_{2,11}-13_{1,12}$				
27/2–27/2	1.000	21955.197	0.296	0.063
25/2–25/2	1.000	21956.873	−0.010	0.007
29/2–29/2	1.000	21972.735	0.038	0.036
23/2–23/2	1.000	21975.046	0.336	0.082
$14_{2,12}-14_{1,13}$				
29/2–29/2	1.000	22970.004	0.183	0.038
27/2–27/2	1.000	22972.062	−0.037	−0.018
31/2–31/2	1.000	22991.750	−0.019	−0.027
25/2–25/2	1.000	22994.208	0.111	−0.029
$15_{2,13}-15_{1,14}$				
31/2–31/2	1.000	24342.389	0.122	0.015
29/2–29/2	1.000	24344.708	−0.021	−0.004
33/2–33/2	1.000	24368.156	0.022	0.008
27/2–27/2	1.000	24370.858	0.102	0.012
$16_{2,14}-16_{1,15}$				
33/2–33/2	1.000	26088.090	0.139	0.052
31/2–31/2	1.000	26090.776	−0.049	−0.048
35/2–35/2	1.000	26117.835	0.080	0.061
29/2–29/2	1.000	26120.347	0.053	−0.025
$17_{2,15}-17_{1,16}$				
35/2–35/2	1.000	28214.886	0.048	−0.029
33/2–33/2	1.000	28217.702	−0.051	−0.009
37/2–37/2	1.000	28247.880	−0.021	−0.045
31/2–31/2	1.000	28250.666	−0.030	−0.054
$18_{2,16}-18_{1,17}$				
37/2–37/2	1.000	30718.746	0.023	−0.047
35/2–35/2	1.000	30721.620	−0.087	−0.058
39/2–39/2	1.000	30754.684	0.013	−0.014
33/2–33/2	1.000	30757.595	0.031	0.007

Can. J. Chem. Downloaded from www.nrcresearchpress.com by 213.166.140.6 on 09/07/12
For personal use only.

Can. J. Chem. Downloaded from www.nrcresearchpress.com by 213.166.140.6 on 09/07/12
For personal use only.

TABLE 3 (*concluded*)

Transition $F'-F''$	Normalised weight[a]	Observed frequency	Residuals[b] Without χ_{ab}	Residuals[b] With χ_{ab}
$17_{3,15}-17_{2,16}$				
35/2–35/2	0.500	48760.444	1.370	−0.131
33/2–33/2	1.000	48761.000	−0.071	−0.013
37/2–37/2	1.000	48782.276	−0.062	−0.018
$18_{3,15}-18_{2,16}$				
35/2–35/2	1.000	31832.303	0.045	0.030
37/2–37/2	1.000	31832.654	0.229	0.024
39/2–39/2	0.500	31830.840	0.126	0.125
33/2–33/2	0.500	31830.840	0.271	0.029
$18_{3,16}-18_{2,17}$				
37/2–37/2	1.000	50257.717	0.468	−0.026
35/2–35/2	1.000	50259.092	−0.108	−0.059
39/2–39/2	1.000	50281.177	−0.051	−0.025
33/2–33/2	0.500	50283.626	0.435	−0.109
$19_{3,16}-19_{2,17}$				
39/2–39/2	1.000	31626.135	0.159	0.036
37/2–37/2	1.000	31626.135	0.023	0.012
41/2–41/2	0.500	31627.936	0.093	0.089
35/2–35/2	0.500	31628.167	0.168	0.027
$19_{3,17}-19_{2,18}$				
37/2–37/2	0.500	51924.463	0.099	0.138
41/2–41/2	0.500	51947.175	0.059	0.072
35/2–35/2	0.500	51949.413	0.401	0.133
$20_{3,17}-20_{2,18}$				
41/2–41/2	0.500	31752.252	0.169	0.086
39/2–39/2	0.500	31752.527	0.046	0.038
43/2–43/2	1.000	31757.655	−0.015	−0.022
37/2–37/2	1.000	31758.181	0.082	−0.010
$22_{3,19}-22_{2,20}$				
45/2–45/2	1.000	33141.743	0.129	0.078
43/2–43/2	1.000	33142.585	−0.024	−0.003
47/2–47/2	1.000	33154.851	0.027	0.017
41/2–41/2	1.000	33155.562	−0.006	−0.032
$24_{3,21}-24_{2,22}$				
49/2–49/2	1.000	36202.721	0.122	0.080
47/2–47/2	1.000	36203.810	−0.058	−0.048
51/2–51/2	1.000	36222.795	0.056	0.043
45/2–45/2	1.000	36223.924	−0.029	−0.051
$26_{4,22}-26_{3,23}$				
49/2–49/2	0.500	42384.580	0.149	0.077
55/2–55/2	0.500	42384.580	−0.068	−0.074
51/2–51/2	0.100	42388.465	0.098	0.081
53/2–53/2	0.100	42388.465	−0.138	−0.196
$27_{4,23}-27_{3,24}$				
57/2–57/2	1.000	41902.265	0.010	0.003
51/2–51/2	1.000	41902.265	0.046	−0.014
53/2–53/2	0.500	41903.148	0.014	−0.007
55/2–55/2	0.500	41903.148	−0.054	−0.098
$28_{4,24}-28_{3,25}$				
55/2–55/2	1.000	41796.875	−0.007	−0.007
57/2–57/2	1.000	41796.875	0.025	−0.011
59/2–59/2	0.100	41799.153	0.129	0.121
53/2–53/2	0.100	41799.153	−0.077	−0.107

[a]Measurements were weighted according to $1/\sigma^2$, where σ is the uncertainty in the measurements. Unit weight corresponded to an uncertainty of 0.03 MHz.

[b]Observed frequency minus the frequency calculated using the constants in Table 1.

TABLE 4. Closest near degeneracies having the correct symmetry to cause perturbations in hyperfine structure in the spectrum of bromine thiocyanate

Energy levels	Difference in energy (MHz) ^{79}BrSCN	Difference in energy (MHz) ^{81}BrSCN
$6_{1,5}-5_{2,3}$	−590.84	−793.51
$9_{1,9}-8_{2,7}$	−265.13	−406.54
$10_{1,9}-9_{2,8}$	1584.16	1439.67
$11_{2,9}-10_{3,7}$	1645.41	1247.23
$12_{2,11}-11_{3,9}$	−694.41	−976.20
$13_{2,12}-12_{3,10}$	2165.01	1872.17

TABLE 5. Comparison of observed rotational constants (in MHz) of BrSCN with those predicted for BrSCN and BrNCS

Parameter	Observed value[a] B_0	Observed value[a] B_z	Calculated value BrSCN	Calculated value BrNCS
^{79}BrSCN				
A	10092.201	10054.985	9888.7	41482.9
B	1944.4054	1941.715	1882.8	1187.1
C	1627.9500	1627.374	1581.7	1154.1
^{81}BrSCN				
A	10074.473	10037.426	9872.2	41412.4
B	1927.4510	1924.795	1866.3	1176.7
C	1615.5891	1615.016	1569.6	1144.2

[a]The B_0 and B_z values are the ground state effective and average values, respectively.

TABLE 6. Structural parameters of BrSCN

(*A*) Derived parameters

	Effective (r_0) values	Average (r_z) values
r(Br—S)/Å	2.180(10)[a]	2.183(10)
r(S—C)/Å	1.701[b]	1.701[b]
r(C≡N)/Å	1.156[b]	1.157[b]
<(BrSC)/deg	99.8(1.7)	99.7(1.7)
<(SCN)/deg	185[b,c]	185[b,c]

(*B*) Comparison of derived parameters with those of other molecules

r(Br—S)/Å Molecule	r(Br—S)/Å Length	<(XSC)/deg Molecule	<(XSC)/deg Angle
BrSCN	2.18	BrSCN	99.8
S_2Br_2 (14)	2.237	ClSCN(6)	99.8
$SOBr_2$ (19)	2.27	$S(CN)_2$ (4)	98.4
SO_2BrF (20)	2.155	CH_3SCN (3)	99.9
SF_5Br (21)	2.190		
Sum of single bond radii (22)	2.162		

[a]Numbers in parentheses are estimated outside uncertainty limits in units of the last significant figures (see text).

[b]Fixed at the values obtained for $S(CN)_2$ (4).

[c]The SCN chain is bent *away* from the BrS bond.

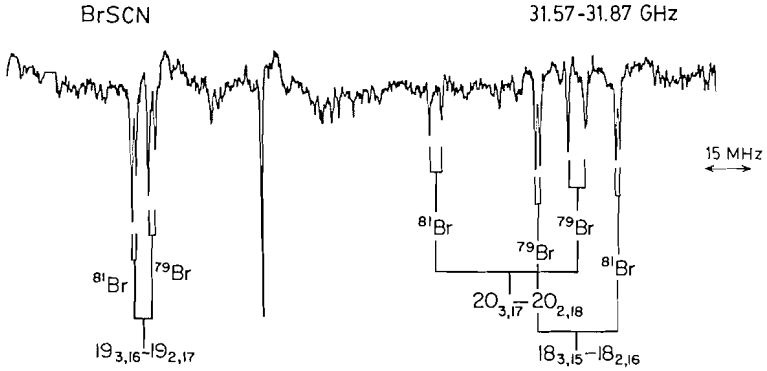

FIG. 2. Broad band scan of the spectrum of BrSCN from 31.57–31.87 GHz. Three transitions are indicated for each isotopic series.

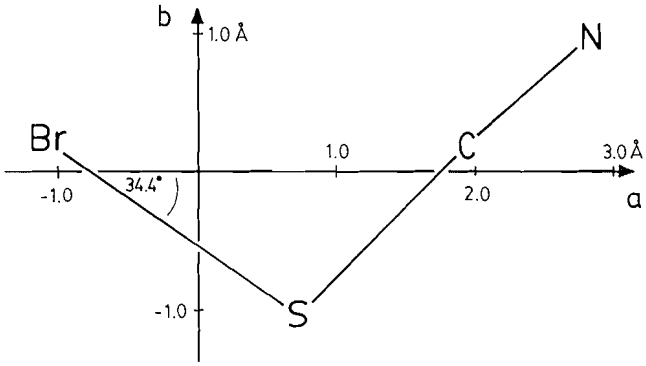

FIG. 3. The positions of the atoms of ^{79}BrSCN in the principal inertial axis system.

TABLE 7. The harmonic force field of BrSCN

Structural parameters		
r(BrS) = 2.18 Å	$<$(BrSC) = α = 99.75°	
r(SC) = 1.701 Å	$<$(SCN) = β = 185.02°[a]	
r(CN) = 1.156 Å		
Symmetry coordinates		
A': $S_1 = \Delta r$(BrS)	$S_2 = \Delta r$(SC)	$S_3 = \Delta r$(CN)
$S_4 = \Delta\alpha$	$S_5 = \Delta\beta$	
A'': $S_6 = \Delta\tau$[b]		
Harmonic force constants[c]		
f_{11} = 2.57(15) mdyn Å^{-1}	f_{44} = 0.828(24) mdyn Å rad^{-2}	
f_{14} = 0.210(49) mdyn rad^{-1}	f_{55} = 0.296(28) mdyn Å rad^{-2}	
f_{22} = 4.060(95) mdyn Å^{-1}	f_{66} = 0.00260(20) mdyn Å rad^{-2}	
f_{33} = 16.41(24) mdyn Å^{-1}		

[a]The SCN chain is bent *away* from the BrS bond.
[b]Defined as a torsion, for which **B** matrix elements are (rad Å^{-1}): Br, −0.465; S, −6.136; C, 16.503; N, −9.902.
[c]Numbers in parentheses are one standard deviation in units of the last significant figures. All other force constants were constrained to zero.

analysis are given in Table 7. All the in-plane coordinates are conventional valence coordinates. The out-of-plane coordinate we have defined as a torsion; from its **B**-matrix elements given in Table 7 it is clear that it is nevertheless essentially an SCN out-of-plane bend. We were thus able to assume that the in-plane and out-of-plane bending wavenumbers have the same value. The structure was the r_0 structure derived above.

As a starting point to the determination we estmated the SBr stretching constant to be the same as the SCl stretching constant in SCl_2 (23), and the in-plane S—C≡N constants to be the same as those of $S(CN)_2$ (4). Least-squares fits were then made to the wavenumbers and distortion constants, using first of all a diagonal force field (which gave a reasonable fit) and then including off-diagonal constants. An excellent fit was obtained including the single off-diagonal constant f_{14}, the interaction constant between the BrS stretch and the BrSC bend. The wavenumbers were assigned uncertainties of 20 cm^{-1} for ν_1 and ν_6, 30 cm^{-1} for ν_5 and 10 cm^{-1} for the remainder; the distortion constants were given uncertainties of 5%; the data were weighted as (uncertainty)$^{-2}$. The resulting force constants are in Table 7, and the goodness of the fit is indicated in Table 8. It is clear that the approximate force field obtained is very reasonable.

To evaluate the r_z parameters the harmonic parts of the α-constants were subtracted off the ground state rotational constants for the two isotopes. The resulting ground state average values are in Table 5. A least-squares fit was then made to the BrS length and BrSC angle of ^{79}BrSCN, with the remaining parameters fixed at their r_z values in $S(CN)_2$ (4). The small variation of r_z (BrS) with isotope was estimated with a Morse potential, using a = 1.542 Å^{-1} (24). The results are also in Table 6; the derived values are very similar to the corresponding r_0 values.

Discussion and conclusions[2]

This work has confirmed unambiguously that bromine thiocyanate, like chlorine thiocyanate before it, is a thiocyanate, of formula BrSCN, rather than an isothiocyanate, of formula BrNCS. Very reasonable values for the BrS bond length and BrSC angle have been obtained (Table 6): the BrS length is similar to that found in other molecules, and to the sum of the single bond radii (22), and the BrSC angle is ~99°, in common with other molecules containing the —SCN group. The similarity between the r_0 and r_z parameters is reasonable for a molecule containing entirely heavy atoms. The need to assume some structural parameters, as well as the uncertainties in the derived values, would be reduced with further isotopic substitutions, such as of ^{34}S for ^{32}S. This substitution is usually done using natural abundances; unfortunately the observed signal-to-noise ratios (Figs. 1 and 2) were too low for transitions of the ^{34}S species (~4% abundant) to be identified.

The harmonic force field obtained is remarkably good, especially considering the paucity and relatively poor quality of the infrared data. It is particularly interesting to note that it gives a

[2]NOTE ADDED IN PROOF: This paper is being published without benefit of author's correction.

Can. J. Chem. Downloaded from www.nrcresearchpress.com by 213.166.140.6 on 09/07/12
For personal use only.

TABLE 8. Goodness of fit of the harmonic force field of BrSCN

Parameter		^{79}BrSCN Value	^{79}BrSCN Obsd − calcd	^{81}BrSCN Value	^{81}BrSCN Obsd − calcd
Wavenumbers (cm^{-1})					
A'	ν_1	2157[a]	0	2157[a,b]	0
	ν_2	676[a]	−1	676[a,b]	−1
	ν_3	451[a]	−6	451[a,b]	−6
	ν_4	369[a]	3	369[a,b]	4
	ν_5	154	24	154[b]	24
A''	ν_6	369[a]	0	369[a,b]	0
Centrifugal distortion constants (kHz)					
	Δ_J	0.848	0.012	0.827	0.006
	Δ_{JK}	−13.69	−0.17	−13.52	−0.16
	Δ_K	104.2	−0.5	102.7	−1.4
	δ_J	0.2396	0.0066	0.2353	0.0075
	δ_K	2.01	−0.11	1.99	−0.11

[a]Reference 10.
[b]Not included in the least squares fit.

TABLE 9. Bromine quadrupole coupling constants in BrSCN

Parameter	^{79}BrSCN	^{81}BrSCN
Inertial axis value (MHz)		
χ_{aa}	402.62 (77)[a]	336.4 (12)
χ_{bb}	−18.21 (39)	−16.00 (20)
χ_{cc}	−384.41 (39)	−320.42 (62)
χ_{ab}	478.41 (23)	397.74 (38)
Principal values (MHz)		
χ_{zz}	714.85 (63)	595.2 (10)
χ_{xx}	−330.44 (26)	−274.82 (71)
χ_{yy}	−384.41 (39)	−320.42 (62)
θ_{za} (deg)[b]	33.12 (2)	33.05 (4)

[a]Numbers in parentheses are one standard deviation in units of the last significant figures.
[b]θ_{za} is the angle between the z-principal axis and the a-inertial axis.

calculated inertial defect of 0.436 amu Å^2 for both isotopic species, in very good agreement with the observed values near 0.448 amu Å^2. The major contributor to this is, however, the lowest frequency mode, for the approximate formula $\Delta = 4K/\omega$, with $K = h/8\pi^2$ (25). and assuming $\omega = 154 \pm 30\,cm^{-1}$, gives $\Delta = 0.438 \pm 0.08$ amu Å^2, in comparable agreement with experiment.

The Br quadrupole coupling tensors were diagonalized to give the principal values. These results are in Table 9. The angle between the z-principal axis and the a-inertial axis is also given there. It is 33.1°, slightly smaller than the angle between the Br—S bond and the a-axis (34.4°). In terms of simple bonding theories the difference is probably not significant, and the maximum electron density can be taken to lie along the BrS internuclear axis. However, it is interesting that the difference is very similar to those found for BrNCO (15), INCO (17) and ClHCCO (26). It is not immediately clear what the cause of the difference is, or even if it is significant.

The difference ($\chi_{xx} - \chi_{yy}$) is an indication of the π character of the BrS bond. Using well known equations (27) this is estimated to be ~5%, with more electron density in the Br $4p_y$ (out-of-plane) orbital than in the $4p_x$ orbital. The cause of this is unclear. One possibility is an in-plane π bond, with electron density donated from the Br atom to the S atom (presumably d-orbitals) (form **I** below).

The degree of ionic character, i.e., the contribution of form **III**, was also calculated from the quadrupole constants. Its

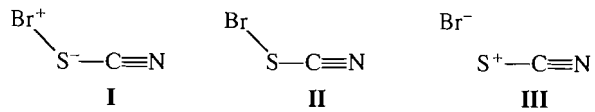

I II III

value came to 9%. Evidently the BrS bond is predominantly (~85%) covalent, in keeping with the comparable electronegativities of Br and S.

Acknowledgements

We acknowledge gratefully the support of the Natural Sciences and Engineering Research Council of Canada through research grants (to M.C.L.G.). We thank also the Atmospheric Environment Service of Canada for access to their Cray-1S computer. H.M.J. acknowledges gratefully the award of a Commonwealth Scholarship.

1. K. YAMADA, M. WINNEWISSER, G. WINNEWISSER, L. B. SZALANSKI, and M. C. L. GERRY. J. Mol. Spectrosc. **79**, 295 (1980).
2. D. R. JENKINS, R. KEWLEY, and T. M. SUGDEN. Trans. Faraday Soc. **58**, 1284 (1962).
3. R. G. LETT and W. H. FLYGARE. J. Chem. Phys. **47**, 4730 (1967).
4. L. PIERCE, R. NELSON, and C. H. THOMAS. J. Chem. Phys. **43**, 3423 (1965).
5. M. A. KING, H. W. KROTO, and B. M. LANDSBERG. J. Mol. Spectrosc. **113**, 1 (1985).
6. R. J. RICHARDS, R. W. DAVIS, and M. C. L. GERRY. J. Chem. Soc. Chem. Commun. 915 (1980).
7. C. RABY, J. CLAUDE, and J. BUXERAUD. Bull. Soc. Pharm. Bordeaux, **114**, 147 (1975).
8. C. RABY, J. CLAUDE, and J. BUXERAUD. Bull. Soc. Pharm. Bordeaux, **115**, 153 (1976).
9. C. RABY, J. BUXERAUD, C. MOESCH, and J. CLAUDE. Bull. Soc. Pharm. Bordeaux, **120**, 33 (1981).
10. M. J. NELSON and A. D. E. PULLIN. J. Chem. Soc. 604 (1960).
11. K. YAMANE, K. FUJIMORI, S. MIYOSHI, and K. HASHIZUME. Heterocycles, **20**, 1263 (1983).

Can. J. Chem. Downloaded from www.nrcresearchpress.com by 213.166.140.6 on 09/07/12
For personal use only.

12. K. FUJIMORI, N. HIRAKO, and K. YAMANE. Bull. Chem. Soc. Jpn. **56**, 1247 (1983).
13. D. C. FROST, C. B. MACDONALD, C. A. MCDOWELL, and N. P. C. WESTWOOD. J. Am. Chem. Soc. **103**, 4423 (1981).
14. R. KNIEP, L. KORTE, and D. MOOTZ. Z. Naturforsch. b**38**, 1 (1983).
15. H. M. JEMSON, W. LEWIS-BEVAN, N. P. C. WESTWOOD, and M. C. L. GERRY. J. Mol. Spectrosc. **118**, 481 (1986).
16. K. YAMADA, M. WINNEWISSER, G. WINNEWISSER, L. B. SZALANSKI, and M. C. L. GERRY. J. Mol. Spectrosc. **79**, 295 (1980).
17. H. M. JEMSON, W. LEWIS-BEVAN, N. P. C. WESTWOOD, and M. C. L. GERRY. J. Mol. Spectrosc. **119**, 22 (1986).
18. J. K. G. WATSON. *In* Vibrational spectra and structure, a series of advances. Vol. 6. *Edited by* J. R. Durig, Elsevier, Amsterdam. 1977. p. 1.
19. J. BRUNVOLL, I. HARGITTAI, and B. ROZSONDAI. J. Mol. Spectrosc. **84**, 153 (1982).
20. J. RALEY, J. E. WOLLRAB, and R. W. LOVEJOY. J. Mol. Spectrosc. **48**, 100 (1973).
21. R. JUREK, P. GOULET, C. VERRY, and A. POINSOT. Can. J. Chem. **61**, 1405 (1983).
22. L. PAULING. The chemical bond. 3rd ed. Cornell University Press, Ithaca, NY. 1960.
23. R. W. DAVIS and M. C. L. GERRY. J. Mol. Spectrosc. **65**, 455 (1977).
24. K. KUCHITSU and Y. MORINO. Bull. Chem. Soc. Jpn. **38**, 805 (1965).
25. D. R. HERSCHBACH and V. W. LAURIE. J. Chem. Phys. **40**, 3142 (1964).
26. M. C. L. GERRY, W. LEWIS-BEVAN, and N. P. C. WESTWOOD. J. Chem. Phys. **79**, 4655 (1983).
27. W. GORDY and R. L. COOK. Microwave molecular spectra. Vol. 18. 3rd ed. *In* Techniques of chemistry. *Edited by* A. Weissberger. Wiley, New York. 1984. pp. 725–802.

Can. J. Chem. Downloaded from www.nrcresearchpress.com by 213.166.140.6 on 09/07/12
For personal use only.

Coupled transport of iodide ions during interdiffusion of aqueous HCl and NaOH

DEREK G. LEAIST
Department of Chemistry, University of Western Ontario, London, Ont., Canada N6A 5B7

Received April 29, 1987

DEREK G. LEAIST. Can. J. Chem. **65**, 2489 (1987).

Stokes diaphragm cells have been used to study multicomponent diffusion in aqueous HCl–NaOH–NaI mixtures at 25°C. The nine quaternary diffusion coefficients for the mixture containing 0.025 mol L^{-1} of each electrolyte are reported. The measured coefficients are used to analyze coupled transport of iodide ions generated by interdiffusion of aqueous HCl and NaOH. The analysis shows that the gradient in concentration of NaOH is twice as effective at producing flow of iodide ions relative to the HCl gradient, and that the NaI gradient substantially alters the rates of diffusion of HCl and NaOH components. Equations are developed for predicting multicomponent transport coefficients that describe coupled transport of ions driven by interdiffusion of strong acids and bases.

DEREK G. LEAIST. Can. J. Chem. **65**, 2489 (1987).

On a utilisé des cellules à diaphragme de Stokes pour étudier la diffusion à plusieurs composantes dans des mélanges aqueux de HCl/NaOH/NaI, à 25°C. On rapporte les neuf coefficients de diffusion quaternaire pour le mélange contenant 0,025 mol L^{-1} de chacun des électrolytes. On a utilisé les coefficients ainsi déterminés pour analyser les transports couplés d'ions iodures qui sont provoqués par l'interdiffusion du HCl et du NaOH aqueux. L'analyse démontre qu'un gradient en concentration de NaOH est deux fois plus efficace qu'un gradient en concentration de HCl pour produire un écoulement des ions iodures; par ailleurs, le gradient de NaI affecte d'une façon importante les vitesses de diffusion des composantes HCl et NaOH. On a développé les équations nécessaires pour prédire les coefficients de transport dans des systèmes à plusieurs composantes qui décrivent le transport couplé des ions qui est provoqué par de l'interdiffusion d'acides forts et de bases fortes.

[Traduit par la revue]

1. Introduction

When a pH gradient is formed in a mixed electrolyte solution, the resulting flow of hydrogen or hydroxyl ions can produce large and potentially useful coupled flows of other ions (1). Recently, for example, interdiffusion of aqueous hydrochloric acid and sodium hydroxide was used to concentrate sodium(1), copper(2), and chromium(3) ions by transporting them against their concentration gradients, from regions of low concentration into regions of higher concentration. Separation of specific ions can be achieved by maintaining pH differences across liquid membranes that contain mobile carrier compounds which bind and transport selected ions (1–3).

Coupled transport of ions is often described by numerically solving the Nernst–Planck equations (4, 5)

$$[1] \qquad j_i = -D_i\nabla c_i + (z_i c_i D_i F/RT)E$$

where j_i, c_i, z_i, and D_i are the molar flux densities, concentrations, valences, and diffusion coefficients of the various ions, F is the Faraday, and E is the diffusion-induced electric field. Because ideal solutions are assumed, Nernst–Planck equations are accurate only for very dilute electrolyte solutions. If association or dissociation reactions occur, the diffusion coefficients and concentrations of certain species may be difficult to determine.

These limitations can be overcome by using multicomponent Fick equations (6, 7).

$$[2] \qquad J_i = -\sum_{k=1}^{n} D_{ik}\nabla C_k$$

Here, J_i and C_i denote the molar flux densities and concentrations of neutral solute components, such as HCl and NaOH, coefficient D_{ik} measures the flux of component i produced by the gradient in component k. Because concentrations of solute components can be measured by conventional analytical techniques, reliable values of D_{ik} can be determined by standard experimental procedures (2, 9), regardless of the number of components or reaction equilibria. The D_{ik} coefficients include the effects of the electric field implicitly. Consequently, separate calculation of E is not required. Moreover, the D_{ik} coefficients incorporate non-ideal transport behavior.

In the work reported here, multicomponent diffusion coefficients are measured for aqueous HCl–NaOH–NaI mixtures, and Fick equations are used to analyze coupled transport of iodide ion during interdiffusion of aqueous hydrochloric acid and sodium hydroxide.

2. Experimental

Diffusion in aqueous HCl(C_1)–NaOH(C_2)–NaI(C_3) mixtures was measured at 25°C by using Stokes magnetically stirred diaphragm cells. Rates of diffusion of each electrolyte were followed by determining concentration changes after diffusion for a timed interval between upper and lower solution compartments through liquid held in the pores of a sintered Pyrex disc. Details of cell construction have been reported (7, 10).

The cells were filled with the appropriate initial solutions, stirred for about 2 h to establish steady-state diffusion, then reloaded with fresh solutions and stirred for 0.5 to 4 days. At the end of a run, 10 mL samples of the upper and lower solutions were titrated against 0.1 mol L^{-1} silver nitrate. A silver indicator electrode with calomel reference and sodium sulfate bridging electrolyte was used. The volumes of titrant required to reach the first and second endpoints (11) gave the concentrations of iodide (C_3) and total halide ($C_1 + C_3$), respectively, and hence the concentrations of the HCl (C_1) and NaI components (C_3). Separate 10 mL samples of solution were titrated against standardized NaOH or HCl to determine the concentration of excess acid or base ($|C_1 - C_2|$), and hence the concentration of the NaOH component (C_2). The endpoint was detected with a glass electrode. Measured values of C_1, C_2, and C_3 were reproducible within ±0.5, 0.6, and 0.2 mmol L^{-1}, respectively.

The diaphragm cells were calibrated at frequent intervals by diffusing 0.5 mol L^{-1} KCl into pure water. Cell constants, β (2000 – 2500 m^{-2}), were computed from the relation

$$[3] \qquad \Delta C(t) = \Delta C(0)\exp(-\beta\bar{D}t)$$

where $\Delta C(t)$ is the concentration of KCl in the lower solution less the concentration in the upper solution at time t. Values of $\bar{D}$, the integral

Can. J. Chem. Downloaded from www.nrcresearchpress.com by 213.166.140.6 on 09/07/12
For personal use only.

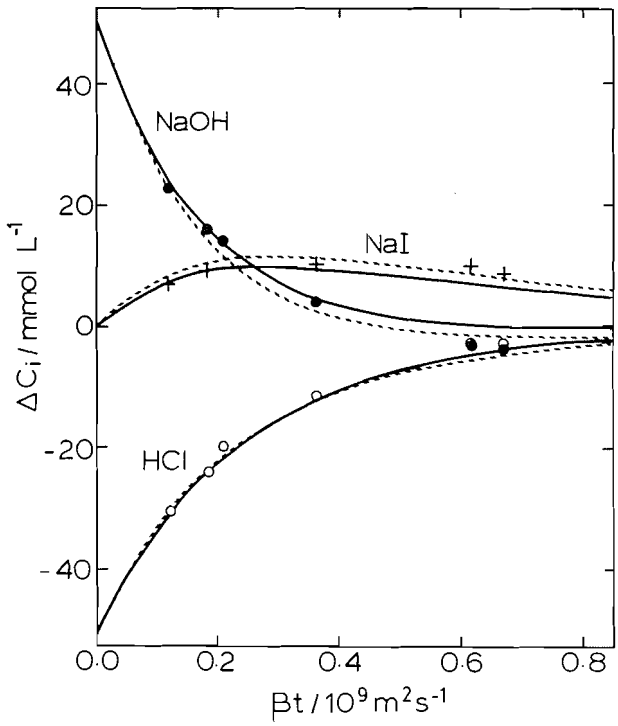

FIG. 1. Comparison of measured and predicted concentration differences during interdiffusion of 50 mmol L^{-1} NaOH + 25 mmol L^{-1} NaI solution (lower compartment) and 50 mmol L^{-1} HCl + 25 mmol L^{-1} NaI solution (upper compartment) at 25°C. Solid curve: eqs. [6] and measured $\bar{D}_{ik}$ values (Table 1). Dashed curve: eqs. [6] and predicted $\bar{D}_{ik}$ values (eqs. [11]).

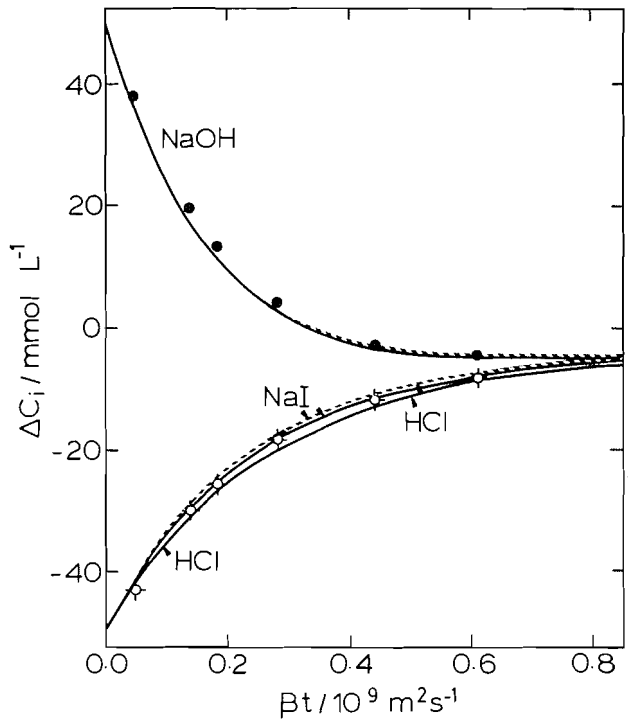

FIG. 2. Comparison of measured and predicted concentration differences during interdiffusion of 50 mmol L^{-1} NaOH and 50 mmol L^{-1} HCl + 50 mmol L^{-1} NaI.

diffusion coefficient for aqueous KCl, were interpolated from the data reported by Woolf and Tilley (12).

Reagent grade $AgNO_3$, KCl, and NaI were dried in a vacuum oven at 110°C. Solutions of the salts were prepared with de-ionized, distilled water in calibrated volumetric flasks. Stock solutions of NaOH were prepared by dilution of filtered saturated solutions, then standardized against dried potassium hydrogen phthalate. The NaOH solutions were used to standardize HCl solutions which were prepared by dilution of concentrated reagent grade acid.

3. Results and discussion

Three sets of experiments were performed at the mean cell composition: 25 mmol L^{-1} HCl + 25 mmol L^{-1} NaOH + 25 mmol NaI.

In the first set of experiments, 50 mmol L^{-1} NaOH + 25 mmol L^{-1} NaI, initially in the lower compartment, diffused into 50 mmol L^{-1} HCl + 25 mmol L^{-1} NaI, in the upper compartment. The results of these experiments are shown in Fig. 1 where the measured differences in component concentrations across the cell diaphragms are plotted against βt. Notice that interdiffusion of HCl and NaOH components causes the NaI component to diffuse into the NaOH solution, co-current to the flow of HCl. For values of βt less than about 0.3×10^9 s m^{-2}, iodide ions are driven "up" the iodide gradient. For larger values of βt, however, the gradients in HCl and NaOH decay sufficiently to allow backflow of iodide ions into the upper compartment.

When aqueous HCl and NaOH interdiffuse, an electric field is generated to maintain electroneutrality in the solutions by slowing down the highly mobile H^+ and OH^- ions (7). The electric field should drive I^- ions into the NaOH solution, which is consistent with the observed behaviour.

The binary diffusivity of aqueous HCl (13, 14) is significantly larger than the binary diffusivity of NaOH (15). In the solutions under discussion, however, the HCl and NaOH components have similar apparent diffusivities since ΔC_1(HCl) and ΔC_2(NaOH) decay at similar rates.

In this second set of experiments, 50 mmol L^{-1} NaOH solution diffused into 50 mmol L^{-1} HCl + 50 mmol L^{-1} NaI solution. The results are shown in Fig. 2. In these experiments the NaI component diffuses more rapidly than the HCl component. This result is unexpected since the binary diffusivity of aqueous HCl (13, 14) is nearly twice that of NaI (16).

Figure 3 shows the results of the final set of experiments in which 50 mmol L^{-1} NaOH + 50 mmol L^{-1} NaI solution diffused into 50 mmol L^{-1} HCl solution. Because the HCl and NaOH gradients tend to drive the NaI component back into the NaOH solution, the NaI component diffuses relatively slowly in these experiments. Study of Figs. 2 and 3 shows that diffusion of the NaOH component counter-current to NaI is almost twice as rapid as diffusion of NaOH co-current to NaI. Counter-current flow of NaI also speeds up diffusion of the HCl component, but to a lesser extent.

Measured $\bar{D}_{ik}$ coefficients

Although five different solute species (H^+, Cl^-, Na^+, OH^-, and I^-) diffuse in the HCl–NaOH–NaI solutions, electroneutrality and local equilibrium of the rapid $H^+ + OH^- = H_2O$ reaction reduce to three the number of independent solute flows. Consequently, isothermal diffusion in the solutions can be described by quaternary Fick equations (eqs. [2] with $n = 3$).

In order to provide a comprehensive description of the diffusion behavior, including the rate of diffusion of each electrolyte and its ability to produce coupled flows of the other electrolytes, all nine quaternary diffusion coefficients were measured. The coefficients were determined at the average

Can. J. Chem. Downloaded from www.nrcresearchpress.com by 213.166.140.6 on 09/07/12
For personal use only.

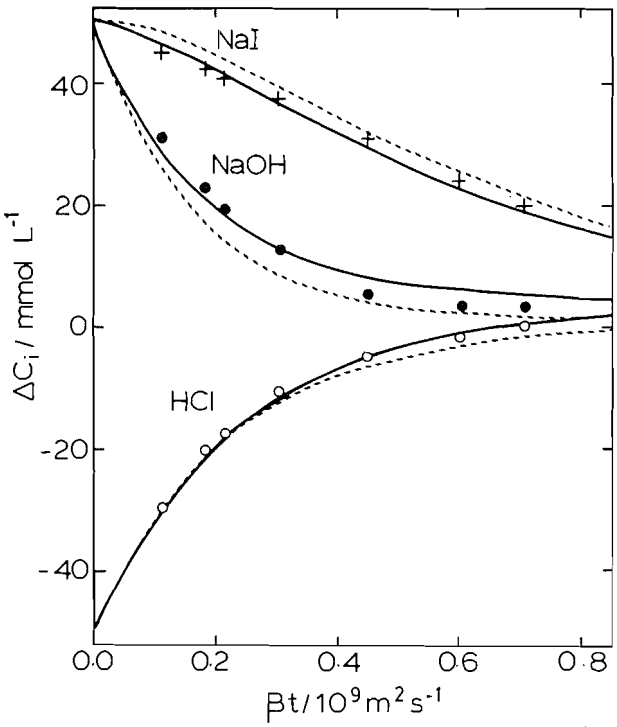

FIG. 3. Comparison of measured and predicted concentration differences during interdiffusion of 50 mmol L^{-1} NaOH + 50 mmol L^{-1} NaI and 50 mmol L^{-1} HCl.

cell composition 25 mmol L^{-1} HCl + 25 mmol L^{-1} NaOH + 25 mmol L^{-1} NaI by using Kosanovich and Cullinan's matrix procedure (9). First, data from three runs, each with different initial solutions but identical values of βt, were used to evaluate the 3 × 3 matrix **Q**

$$[4] \qquad \mathbf{Q} = [\Delta_1 C(0)\ \Delta_2 C(0)\ \Delta_3 C(0)] \times [\Delta_1 C(\beta t)\ \Delta_2 C(\beta t)\ \Delta_3 C(\beta t)]^{-1}$$

where $\Delta_i C(\beta t)$ designates the 3 × 1 column vector of component concentration differences at time t from the ith run. Integral values of D_{ik} were then calculated from the relation (9)

$$[5] \qquad \bar{\mathbf{D}} = \mathbf{P} \begin{pmatrix} \ln Q^{(1)} & 0 & 0 \\ 0 & \ln Q^{(2)} & 0 \\ 0 & 0 & \ln Q^{(3)} \end{pmatrix} \mathbf{P}^{-1}/\beta t$$

where $Q^{(i)}$ are the eigenvalues (17) of Q and the columns of **P** are the corresponding eigenvectors.

At a given mean cell composition, three runs are sufficient to determine the values of $\bar{D}_{ik}$. For improved precision, however, two additional runs were performed. The duration of each run was adjusted to give $\beta t = 0.1850 \times 10^9$ s m^2. This value was chosen so that concentration differences decayed by factors of about e^{-1} from initial values. The measured values of $\bar{D}_{ik}$ are listed in Table 1. These values were obtained by substitution of ΔC_i data from runs 1, 2, 3 or 1, 4, 5 (Table 2) into eqs. [4] and [5], then averaging the two sets of $\bar{D}_{ik}$ values.

Cross-coefficients $\bar{D}_{31}$ and $\bar{D}_{32}$, which measure the coupled flows of NaI produced by the gradients in HCl(1) and NaOH(2) components, are positive and negative, respectively. This indicates iodide ions are transported "down" HCl gradients and "up" NaOH gradients, in accordance with the behavior shown in Fig. 1. Because the magnitude of $\bar{D}_{32}$ is twice that of $\bar{D}_{31}$, NaOH gradients are twice as effective at transporting iodide compared to HCl gradients. This result is surprising since ternary diffusion experiments have shown that HCl gradients (18) produce larger coupled flows of ions than do NaOH gradients (19).

TABLE 1. Comparison of measured and predicted quaternary diffusion coefficients for 25 mmol L^{-1} HCl(1) + 25 mmol L^{-1} NaOH (2) + 25 mmol L^{-1} NaI(3) in aqueous solution at 25°C[a]

	Value	
$\bar{D}_{ik}$	Measured	Predicted
$\bar{D}_{11}$	3.01±0.16	3.24
$\bar{D}_{12}$	−1.08±0.11	−1.37
$\bar{D}_{13}$	−0.36±0.12	−0.16
$\bar{D}_{21}$	−1.83±0.16	−2.63
$\bar{D}_{22}$	4.19±0.12	4.32
$\bar{D}_{23}$	−0.85±0.12	−0.34
$\bar{D}_{31}$	0.66±0.14	1.15
$\bar{D}_{32}$	−1.31±0.10	−1.32
$\bar{D}_{33}$	2.16±0.10	1.88

[a] D_{ik} in units of 10^{-9} m^2 s^{-1}.

TABLE 2. Initial and final cell concentration differences used to calculate quaternary diffusion coefficients[a,b]

	Value				
Parameter	Run 1	Run 2	Run 3	Run 4	Run 5
$\Delta C_1(0)$	−50.0	−50.0	0.0	−50.0	50.0
$\Delta C_2(0)$	50.0	50.0	−50.0	50.0	0.0
$\Delta C_3(0)$	0.0	50.0	−50.0	−50.0	50.0
$\Delta C_1(\beta t)$	−24.0	−20.5	−9.0	−25.6	31.0
$\Delta C_2(\beta t)$	15.8	22.7	−29.4	13.4	13.1
$\Delta C_3(\beta t)$	9.2	42.4	−40.5	−25.7	31.4

[a] $\beta t = 0.1850 \times 10^9$ s m^{-2}.
[b] ΔC_i in units of mmol L^{-1}.

As mentioned earlier, the NaOH and HCl components have larger apparent diffusivities when they diffuse "up" the NaI gradient. This behavior is supported by the negative values which were determined for coefficients $\bar{D}_{13}$ and $\bar{D}_{23}$. Because $\bar{D}_{23}$ is larger than $\bar{D}_{13}$, the effect is more pronounced for the NaOH component.

A more quantitative test of the multicomponent description of the behavior shown in Figs. 1–3 can be obtained by comparing the measured concentration differences with values calculated from integrated Fick equations (20, 21). Integration of eqs. [2] for diaphragm cell diffusion gives (21)

$$[6] \qquad \Delta C_i(t) = \sum_{p=1}^{3} \sum_{q=1}^{3} A_{ip} B_{pq} \Delta C_q(0) \exp(-\beta \bar{\mathbf{D}}^{(\mathbf{P})} t)$$

where the columns of **A** are eigenvectors of $\bar{\mathbf{D}}$, $\mathbf{B} = \mathbf{A}^{-1}$, and $\bar{\mathbf{D}}^{(\mathbf{P})}$ are the eigenvalues of $\bar{\mathbf{D}}$.

The solid curves shown in Figs. 1–3 give component concentration differences that were calculated from eqs. [6] together with the experimental diffusion coefficients listed in Table 1. The measured and calculated values of $\Delta C_i(\beta t)$ are in very close agreement. The small discrepancies which are observed may be due to the concentration dependence of the integral diffusion coefficients, $\bar{D}_{ik}$. Values of $\bar{D}_{ik}$ represent averages of differential coefficients, $\bar{D}_{ik}$, taken over the range

Can. J. Chem. Downloaded from www.nrcresearchpress.com by 213.166.140.6 on 09/07/12
For personal use only.

composition between upper and lower solutions (7, 20). As a result, values of $\bar{D}_{ik}$ vary with time during each run, and a single set of $\bar{D}_{ik}$ values cannot give exact predictions of $\Delta C_i(\beta t)$ for all values of βt.

By using run combinations 1, 2, 3 and 1, 4, 5 to determine values of $\bar{D}_{ik}$, the average of the initial ($\beta t = 0$) final ($\beta t = 0.1850 \times 10^9\ m^2\ s^{-1}$) concentration differences are -18, 17, and 2 mmol L^{-1} for components HCl, NaOH, and NaI. These average differences correspond roughly to typical differences shown in Figs. 1–3. This helps to reduce the deviations between measured and calculated values of $\Delta C_i(\beta t)$. We will return to this point later in the discussion.

Predicted D_{ik} *coefficients*

A detailed interpretation of multicomponent diffusion in dilute electrolyte solutions can be made by tracing values of the D_{ik} coefficients back to the concentrations and mobilities of the various diffusing ions. The flux densities of the ions, j_i, can be expressed as (6)

$$[7] \qquad j_i = -\sum_{k=1}^{s} l_{ik} \nabla \tilde{\mu}_k$$

where $\nabla \tilde{\mu}_k$ are gradients in electrochemical potential of the ions and l_{ik} are ionic transport coefficients. At low ionic strengths it is a good approximation to neglect off-diagonal l_{ik} coefficients and write (22)

$$[8] \qquad l_{ii} = c_i u_i = c_i D_i / RT$$

where c_i, u_i, and D_i are the concentrations, absolute mobilities, and diffusivities of the ions, R is the gas constant, and T is the temperature.

This approximation can be used to estimate the Onsager coefficients of the components, L_{ik}, which are defined by flow equations (6)

$$[9] \qquad J_i = -\sum_{k=1}^{n} L_{ik} \nabla \mu_k$$

in which $\nabla \mu_k$ are the gradients in chemical potential of the neutral solute components. The multicomponent diffusion coefficients can then be estimated by using the identity (6)

$$[10] \qquad D_{ik} = \sum_{m=1}^{n} L_{im} \mu_{mk}$$

where $\mu_{mk} = \partial \mu_m / \partial C_k$. Details of the procedure for estimating values of D_{ik} are given in the Appendix.

Figure 4 shows values of D_{ik} that were predicted for compositions 50 mmol L^{-1} HCl + $(1 - x)$50 mmol L^{-1} NaOH + 25 mmol L^{-1} NaI, with $0 \leq x \leq 1$. Similar compositions are encountered along the diffusion path when 50 mmol L^{-1} NaOH + 50 mmol L^{-1} NaI solution diffuses into 50 mmol L^{-1} HCl + 25 mmol L^{-1} NaI solution, for example. The sharp changes in the diffusion coefficients at the equimolar HCl–NaOH composition closely resembles the behavior discussed previously for aqueous HCl–NaOH mixtures (7).

In order to compare measured and predicted values of the multicomponent diffusion coefficients, it is necessary to convert the predicted differential D_{ik} values to integral $\bar{D}_{ik}$ values. This is accomplished by using the expressions (7, 20)

$$[11] \qquad \bar{D}_{ik} = \int_0^1 D_{ik} \mathrm{d}\xi$$

$$[12] \qquad \xi = (C_i - \bar{C}_{iU})/(\bar{C}_{iL} - \bar{C}_{iU})$$

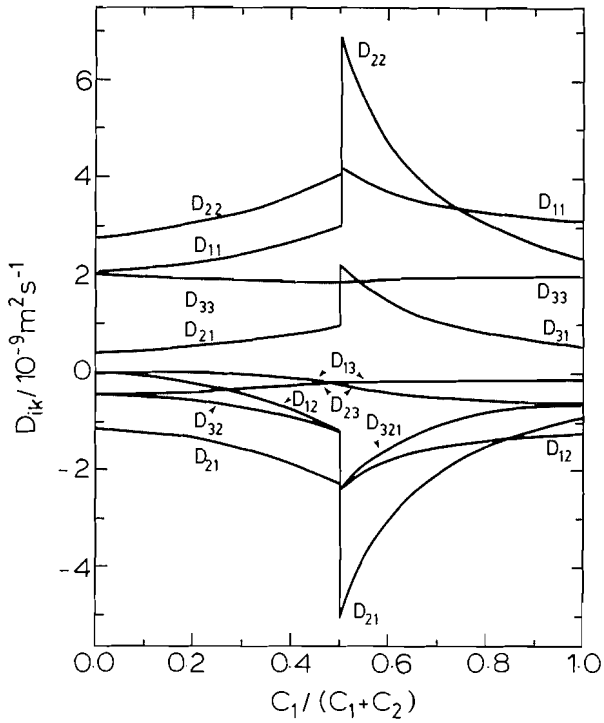

FIG. 4. Predicted values of the quaternary diffusion coefficients for aqueous HCl (50 mmol L^{-1}) – NaOH ($(1 - x)$50 mmol L^{-1}) – NaI(25 mmol L^{-1}) mixtures at 25°C with $0 \leq x \leq 1$ ($x = C_1/(C_1 + C_2)$).

where $\bar{C}_{iU}$ and $\bar{C}_{iL}$ denote mean component concentrations in the upper and lower solutions, the average of the concentrations at the beginning and end of a run for each compartment.

By averaging over run combinations 1, 2, 3 and 1, 5, 6 (Table 1), the values 34.2, 16.6, 23.9 and 15.8, 33.4, 26.1 mmol L^{-1} were obtained for $\bar{C}_{1U}$, $\bar{C}_{2U}$, $\bar{C}_{3U}$ and $\bar{C}_{1L}$, $\bar{C}_{2L}$, $\bar{C}_{3L}$, respectively. Numerical integration between these limits according to eqs. [11] and [12] gave the predicted integral values shown in Table 2. Except for the value of $\bar{D}_{21}$, which is too large, the predicted integral coefficients are in reasonable agreement with the experimental results.

To test the ability of predicted diffusion coefficients to account for the behavior shown in Fig. 1, values of $\bar{D}_{ik}$ were calculated by numerical integration of $\bar{D}_{ik}$ values from 37.5 mmol L^{-1} HCl + 12.5 mmol L^{-1} NaOH + 25 mmol L^{-1} NaI to 12.5 mmol L^{-1} HCl + 37.5 mmol L^{-1} NaOH + 25 mmol L^{-1} NaOH. These limits were obtained by averaging initial ($t = 0$) and final ($t \rightarrow \infty$) concentrations in the upper and lower cell compartments, respectively. The dashed curves shown in Fig. 1 were calculated by substitution of these $\bar{D}_{ik}$ into eqs. [6]. The dashed curves shown in Figs. 2 and 3 were obtained by similar procedures. The agreement between measured and predicted values of $\Delta C_i(\beta t)$ is almost as good as the agreement which was obtained by using experimental $\bar{D}_{ik}$ values.

The predicted values of each $\bar{D}_{ik}$ coefficient used in Figs. 1–3 differed by only $0.10 \times 10^{-9}\ m^2\ s^{-1}$ or less, which is within the present experimental error. Therefore it is a good approximation to treat integral coefficients as constants, even though the differential D_{ik} values show large variations along the diffusion path (7). This is an important result because it means that solutions to the multicomponent diffusion equations can be approximated reliably by convenient analytical expressions

Can. J. Chem. Downloaded from www.nrcresearchpress.com by 213.166.140.6 on 09/07/12
For personal use only.

without resorting to numerical methods, such as finite difference approximations.

In conclusion, this study has shown that multicomponent diffusion equations provide an accurate and detailed description of coupled diffusion during interdiffusion of a strong acid and base. The present work can be extended to weak electrolyte mixtures in which the diffusing species form ion associates.

4. Acknowledgements

The author thanks Seung Ko for technical assistance. This work was supported by The Natural Sciences and Engineering Research Council.

1. E. M. Choy, D. F. Evans, and E. L. Cussler. J. Am. Chem. Sci. **96**, 7085 (1974).
2. W. C. Babcock, R. W. Baker, E. D. Lachapelle, and K. L. Smith. J. Membr. Sci. **7**, 71 (1980); **7**, 89 (1980).
3. A. M. Hochauser and E. L. Cussler. Chem. Eng. Prog. Symp. Ser. **71**, 136 (1976).
4. A. Ekman, S. Liukkonen, and K. Kontturi. Electrochim. Acta, **23**, 243 (1978).
5. J. Garrido, S. Mafe, and J. Pellicer. J. Membr. Sci. **24**, 7 (1985).
6. D. D. Fitts. Nonequilibrium thermodynamics. McGraw-Hill, New York. 1962. Chapts. 7 and 8.
7. D. G. Leaist and B. Wiens. Can. J. Chem. **64**, 1007 (1985).
8. G. P. Rai and H. T. Cullinan, Jr. J. Chem. Eng. Data, **18**, 213 (1973).
9. G. Kosanovich and H. T. Cullinan, Jr. Can. J. Chem. Eng. **49**, 753 (1971).
10. M. V. Kulkarni, G. F. Allen, and D. A. Lyons. J. Phys. Chem. **69**, 2491 (1965).
11. A. Vogel. Textbook of quantitative inorganic analysis. 4th ed. Longman, London. 1978. p. 605.
12. L. A. Woolf and J. F. Tilley. J. Phys. Chem. **71**, 1962 (1967).
13. M. Kulkarni and P. A. Lyons. J. Phys. Chem. **69**, 2336 (1965).
14. R. H. Stokes. J. Am. Chem. Soc. **72**, 2243 (1950).
15. R. A. Noulty and D. G. Leaist. J. Solution Chem. **13**, 767 (1984).
16. R. H. Stokes and P. J. Dunlop. J. Am. Chem. Soc. **73**, 5456 (1951).
17. S. Selby (*Editor*). Standard mathematical tables. 19th ed. Chemical Rubber Co., Cleveland, OH. 1971. p. 103.
18. H. Kim, G. Reinfelds, and L. J. Gosting. J. Phys. Chem. **77**, 934 (1973).
19. D. G. Leaist and R. A. Noulty. Can. J. Chem. **63**, 476 (1985).
20. D. G. Leaist. Aust. J. Chem. **38**, 249 (1985).
21. D. G. Leaist. J. Chem. Soc. Faraday Trans. 1, **83**, 829 (1987).
22. D. G. Leaist. J. Chem. Soc. Faraday Trans. 1, **78**, 3069 (1982).
23. E. A. Guggenheim and J. C. Turgeon. Trans. Faraday Soc. **51**, 747 (1955).
24. R. A. Robinson and R. H. Stokes. Electrolyte solutions. 2nd ed. Academic Press, New York. 1959. App. 6.2.

Appendix

Expressions for the quaternary diffusion coefficients of aqueous HCl(C_1)–NaOH(C_2)–NaI(C_3) mixtures can be obtained by an extension of the procedure used for ternary HCl–NaOH mixtures (7).

The ions will be designated by subscripts: 1 = Cl^-, 2 = Na^+, 3 = H^+, 4 = OH^-, and 5 = I^-. The flux of the HCl component (total HCl) equals the flux of the Cl^- ions, and the flux of the NaI component equals the flux of I^- ions. Also, the total flux of Na^+ ions less the flux of Na^+ ions due to the NaI component gives the flux of the NaOH component (total NaOH).

[A13] $J_1(\mathrm{HCl}) = j_1(\mathrm{Cl}^-)$

[A14] $J_2(\mathrm{NaOH}) = j_1(\mathrm{Na}^+) - j_5(\mathrm{I}^-)$

[A15] $J_3(\mathrm{NaI}) = j_5(\mathrm{I}^-)$

The gradients in the chemical potentials of the components equal the sums of the gradients in the electrochemical potentials of the constituent ions, and hence

[A16] $\nabla\mu_1(\mathrm{HCl}) = \tilde{\mu}_1(\mathrm{Cl}^-) + \tilde{\mu}_3(\mathrm{H}^+)$

[A17] $\nabla\mu_2(\mathrm{NaOH}) = \tilde{\mu}_2(\mathrm{Na}^+) + \tilde{\mu}_4(\mathrm{OH}^-)$

[A18] $\nabla\mu_3(\mathrm{NaI}) = \tilde{\mu}_2(\mathrm{Na}^+) + \tilde{\mu}_5(\mathrm{I}^-)$

Electroneutrality and local equilibrium of the $H^+ + OH^- = H_2O$ reaction provide the following constraints.

[A19] $j_1(\mathrm{Cl}^-) + j_4(\mathrm{OH}^-) + j_5(\mathrm{I}^-) = j_2(\mathrm{Na}^+) + j_3(\mathrm{H}^+)$

[A20] $\nabla\tilde{\mu}_3(\mathrm{H}^+) + \nabla\tilde{\mu}_4(\mathrm{OH}^-) = 0$

Excess HCl ($C_1 > C_2$)

In mixtures containing excess HCl over NaOH, negligible amounts of OH^- ions are present

[A21] $c_4(\mathrm{OH}^-) = 0$

[A22] $j_4(\mathrm{OH}^-) = 0$

and $c_1(\mathrm{Cl}^-) = C_1$, $c_2(\mathrm{Na}^+) = C_2 + C_3$, $c_3(\mathrm{H}^+) = C_1 - C_2$, $c_4(\mathrm{OH}^-) = K_w/(C_1 - C_2) \cong 0$, and $c_5(\mathrm{I}^-) = C_3$. Upon substitution of eqs. [A13]–[A22] into eqs. [9] and elimination of any two of the five $\nabla\tilde{\mu}_i$, the following expressions are obtained

[A23] $L_{11} = l_{11}(l_{22} + l_{33} + l_{55})/H$

[A24] $L_{12} = L_{21} = l_{11}(l_{22} + l_{55})/H$

[A25] $L_{13} = L_{31} = -l_{11}l_{55}/H$

[A26] $L_{22} = (l_{11} + l_{33})(l_{22} + l_{55})/H$

[A27] $L_{23} = L_{32} = -l_{55}(l_{11} + l_{33})/H$

[A28] $L_{33} = l_{55}(l_{11} + l_{22} + l_{33})/H$

where H is an abbreviation for

[A29] $H = l_{11} + l_{22} + l_{33} + l_{55}$

Differentiation of the expressions for the chemical potentials of the components

[A30] $\mu_1(\mathrm{HCl}) = \mu_1^0 + RT \ln [(C_1 - C_2)C_1y_1y_3]$

[A31] $\mu_2(\mathrm{NaOH}) = \mu_2^0 + RT \ln [(C_2 + C_3)K_w(C_1 - C_2)^{-1}y_2y_4]$

[A32] $\mu(\mathrm{NaI}) = \mu_3^0 + RT \ln [(C_2 + C_3)C_3y_2y_5]$

gives

[A33] $\mu_{11}/RT = C_1^{-1} + (C_1 - C_2)^{-1} + G$

[A34] $\mu_{12} = \mu_{21} = (C_2 - C_1)^{-1}$

[A35] $\mu_{13} = \mu_{31} = G$

[A36] $\mu_{22} = C_2 + C_3$

[A37] $\mu_{23}/RT = \mu_{32}/RT = (C_2 + C_3)^{-1}$

[A38] $\mu_{33}/RT = C_3^{-1} + (C_2 + C_3)^{-1} + G$

where G stands for

[A39] $G = -S_f I^{1/2}/(1 + I^{1/2})^2$

Can. J. Chem. Downloaded from www.nrcresearchpress.com by 213.166.140.6 on 09/07/12
For personal use only.

These expressions were obtained by assuming that the ionic activity coefficients, y_i, are given by the semi-empirical relation (23)

[A40] $\ln y_i = -S_f z_i^2 I^{1/2}/(1 + I^{1/2})$

where I is the ionic strength in units of mol L^{-1} ($I = C_1 + C_3$ in this case) and $S_f = 1.17$ for aqueous solutions at 25°C.

The predicted values of the D_{ik} shown in Fig. 4 were obtained by substitution of eqs. [A23]–[A29] for the L_{im} coefficients and eqs. [A33]–[A39] for the μ_{mk} derivatives into eqs. [10]. The calculations employed ionic diffusivities $D_1(Cl^-) = 2.03 \times 10^{-9}$, $D_2(Na^+) = 1.33 \times 10^{-9}$, $D_3(H^+) = 9.31 \times 10^{-9}$, and $D_5(I^-) = 2.05 \times 10^{-9}$ m^2 s^{-1} which were obtained from published limiting molar ionic conductivities (24), λ_i^0, by using the relation $D_i = \lambda_i^0 RT/(z_i F)^2$.

If activity coefficient terms are dropped, the expressions for the D_{ik} coefficients simplify remarkably to give the following limiting expressions

[A41] $D_{11} = (1 - t_1)D_1 + t_1 D_3$

[A42] $D_{12} = t_1(D_2 - D_3)$

[A42] $D_{13} = t_1(D_2 - D_5)$

[A44] $D_{21} = (t_2 + t_5)(D_1 - D_3)$

[A45] $D_{22} = (1 - t_2 - t_5)D_2 + (t_2 + t_5)D_3$

[A46] $D_{23} = (1 - t_2 - t_5)(D_2 - D_5)$

[A47] $D_{31} = t_5(D_3 - D_1)$

[A48] $D_{32} = t_5(D_2 - D_3)$

[A49] $D_{33} = (1 - t_5)D_5 + t_5 D_2$

where t_i denotes the limiting transference number of ion i

[A50] $t_i = c_i z_i^2 D_i/\Sigma c_k z_k^2 D_k$

Excess NaOH ($C_2 > C_1$)

Expressions for the transport coefficients of the alkaline mixtures can be obtained by replacing l_{33} (for H^+ ions) with l_{44} (for OH^- ions), and permuting subscripts 1 and 2 on L_{ik} and μ_{ik} in eqs. [A23]–[A29] and eqs. [A33]–[A39]. The corresponding limiting expressions for the D_{ik} coefficients can be obtained by replacing D_3 with D_4 and permuting subscripts 1 and 2 on the D_{ik} in eqs. [A41]–[A50]. At 25°C the limiting value of $D_4(OH^-)$ is 5.28×10^{-9} m^2 s^{-1} (24).

Can. J. Chem. Downloaded from www.nrcresearchpress.com by 213.166.140.6 on 09/07/12
For personal use only.

Charge distributions and chemical effects. XLIII. Bond dissociation energies and radical formation

SÁNDOR FLISZÁR AND CAMILLA MINICHINO[1]

Département de Chimie, Université de Montréal, C.P. 6128, Succ. A, Montréal (Qué.), Canada H3C 3J7

Received April 2, 1987

SÁNDOR FLISZÁR and CAMILLA MINICHINO. Can. J. Chem. **65**, 2495 (1987).

The problem of bond dissociation, $R_1R_2 \rightarrow R_1\cdot + R_2\cdot$, is addressed from the viewpoint that the fragments, R_1 and R_2, may not be individually electroneutral in the host molecule, whereas the corresponding radicals certainly are. The mutual charge neutralization of R_1 by R_2 during the cleavage of the bond linking R_1 to R_2 is described by an expression featuring only molecular ground-state properties. This expression translates directly into a new energy formula for the dissociation energy, $D^*(R_1R_2) = \epsilon(R_1R_2) + CNE - E^*_{nb} + RE(R_1) + RE(R_2)$, where both the molecule and the radicals are taken at their potential minimum. The charge neutralization energy, CNE, profoundly affects the relationship between the dissociation (D^*) and contributing bond energy (ϵ), i.e., the energy in the unperturbed molecule. Nonbonded interactions between R_1 and R_2, E^*_{nb}, are almost negligible. The reorganizational energy, RE, measures the energy difference between $R\cdot$ and the corresponding electroneutral group found in the symmetric molecule RR. Numerical applications to alkanes reveal an important cancellation of individual CNE terms accompanying the mutual charge neutralization of alkyl groups during the cleavage of CC bonds, i.e., $CNE - E^*_{nb} \simeq 0$. Theoretical ϵ_{CC}'s lead to valid CC bond dissociation energies. In CH bond dissociations, on the other hand, the sum $\epsilon_{CH} + CNE$ remains nearly constant although individual ϵ_{CH}'s may differ from one another by as much as 6 kcal mol^{-1}. The appropriate approximation, $D^*_{CH} \simeq$ constant + RE, shows in what manner charge neutralization energies disguise genuine contributing CH bond energies to create a perception of seemingly constant CH bond contributions.

SÁNDOR FLISZÁR et CAMILLA MINICHINO. Can. J. Chem. **65**, 2495 (1987).

La dissociation d'un lien, $R_1R_2 \rightarrow R_1\cdot + R_2\cdot$, est décrite en tenant compte que dans la molécule les fragments R_1 et R_2 ne sont pas habituellement électriquement neutres à titre individuel, tandis que les radicaux correspondants le sont certainement. On déduit une équation pour l'énergie de neutralisation de charge, ENC, décrivant la neutralisation de R_1 par R_2. Il en découle une formule pour l'énergie de dissociation, $D^*(R_1R_2) = \epsilon(R_1R_2) + ENC - E^*_{nl} + RE(R_1) + RE(R_2)$, la molécule et les radicaux étant pris à leur minimum de potentiel, où $\epsilon(R_1R_2)$ est l'énergie de lien (qui dépend des charges) dans la molécule non perturbée. La contribution des interactions entre atomes non liés, E^*_{nl}, est pratiquement négligeable. L'énergie de réorganisation, RE, mesure la différence d'énergie entre $R\cdot$ et le groupement électriquement neutre qui lui correspond, tel qu'il est trouvé dans la molécule symmétrique RR. L'étude des alcanes révèle que $ENC - E^*_{nl} \simeq 0$ lors du clivage des liens CC. L'utilisation des énergies ϵ_{CC} théoriques permet une bonne évaluation des énergies de dissociation D^*_{CC}. D'autre part, la somme $\epsilon_{CH} + ENC$ est pratiquement constante pour les liens CH en dépit d'importantes variations individuelles des énergies de lien ϵ_{CH}. L'approximation $D^*_{CH} \simeq$ constante + RE indique bien comment l'énergie de neutralisation de charge, ENC, déguise les liens CH en les faisant paraître comme s'ils étaient tous de même énergie dans les molécules non perturbées.

[Traduit par la revue]

The concept of chemical bond is fundamental to chemistry. Its energetic aspects are at the center of this study, both for non-reacting molecules and for molecules undergoing bond cleavage.

Under laboratory conditions, molecules contain vibrational, translational, and rotational energies which are not fairly partitionable among chemical bonds. For convenience, our analysis considers the molecules at their potential minimum, i.e., with reference to their hypothetical vibrationless state at 0 K; the role of vibrational energies is treated as a separate problem. The measure for what holds the atoms together in a molecule is thus offered by the difference

ΔE^*_a = energy of all the isolated ground-state atoms minus the ground-state energy of the molecule

which is the energy required for breaking up that molecule into its constituent atoms. The atomization energy, ΔE^*_a, includes the annihilation of all interactions between atom pairs which are not chemically bonded to one another in the conventional sense, ΔE^*_{nb}, and the destruction of all chemical bonds ij, represented by their energies ϵ_{ij}, i.e.,

$$[1] \quad \Delta E^*_a = \sum_{i<j} \epsilon_{ij} + \Delta E^*_{nb}$$

It turns out that nonbonded interactions are minor (1, 2), ~0.02–0.05% of ΔE^*_a, so that the study of ΔE^*_a essentially reduces to a consideration of bond energies, $\Delta E^*_a \simeq \sum_{i<j} \epsilon_{ij}$.

We must now become familiar with the precise meaning of ϵ_{ij}. It represents the part of the total atomization energy which is contributed by a particular ij bond. This contribution is dictated by actual properties in the molecule (internuclear distance and local charge density) and should not be mistaken for the energy required to break that bond. Indeed, bond dissociation energies depend also on electronic rearrangements, such as making sure that electroneutral fragments are formed during the cleavage of a bond, and on important structural changes in polyatomic fragments. For example (1, 2), ϵ_{CH} is 104.86 kcal mol^{-1} for the CH bond in methane, in which H carries a partial charge. The actual cleavage of this bond, however, requires $D^*_{CH} = \sim 111.4$ kcal mol^{-1} and results in a neutral H atoms and a methyl radical which differs considerably from the original CH_3 group in CH_4. D^*_{ij}, expressed for a molecule and its fragments at their potential minimum, is

$$[2] \quad D^*_{ij} = \Delta E^*_a(R_iR_j) - \Delta E^*_a(R_i\cdot) - \Delta E^*_a(R_j\cdot)$$

where R_iR_j is the molecule and $R_i\cdot$, $R_j\cdot$ are the free radicals produced upon cleavage of the ij bond. The link between D^*_{ij} and ϵ_{ij} is one of the topics covered in this study.

The bond dissociation energy, D^*_{ij}, can be obtained from

[1] Visiting Scientist on leave from: Dipartimento di Chimica, Facoltà di Scienze, Via Mezzocannone 4, Napoli, I-80134, Italia.

Can. J. Chem. Downloaded from www.nrcresearchpress.com by 213.166.140.6 on 09/07/12
For personal use only.

Can. J. Chem. Downloaded from www.nrcresearchpress.com by 213.166.140.6 on 09/07/12
For personal use only.

experiment; it bears an important part in problems of chemical reactions. The contributing bond energy, ϵ_{ij}, on the contrary, can only be calculated. Of course, it has to satisfy eq. [1]. Moreover, if it is to offer a realistic understanding of the nature of chemical bonding, ϵ_{ij} should be rooted in, and derivable from, quantum theory, as opposed to purely empirical sets of bond energies constructed solely with eq. [1] in mind and involving as many parameters as required to do the job.

Let us now examine a point of utmost importance regarding theoretical bond energies. Reference energies, ϵ^0_{ij}, can be deduced (1, 2) from appropriately selected reference molecules, e.g., $\epsilon^0_{CC} = 69.633$ and $\epsilon^0_{CH} = 106.806$ kcal mol^{-1} for the ethane CC and CH bonds, respectively. A transfer of bond energies (like the ϵ^0_{CC} and ϵ^0_{CH} energies deduced for ethane) from one molecule to another implies the transfer of the bond-forming atoms as they are in the molecule for which they were derived. Such a transfer, involving invariant "local" electron populations, cannot (as a rule) describe an electroneutral molecule (1, 2). For example, if the ethane C and H net charges are 0.0351 and −0.0117 e, respectively, a methane "molecule" constructed from these "atoms" would carry a negative charge of −0.0117 e. Clearly the simple transfer of selected reference bond energies ϵ^0_{ij} would not satisfy the requirement for molecular electroneutrality. The appropriate charge renormalization accompanying the use of reference bond energies ϵ^0_{ij} leads to a description of ϵ_{ij} featuring net atomic charges, namely (1, 2),

$$[3] \quad \epsilon_{ij} = \epsilon^0_{ij} + a_{ij}\Delta q_i + a_{ji}\Delta q_j$$

Here we have ϵ^0_{ij} for a reference bond with net charges q^0_i and q^0_j at atoms i and j, respectively, whereas ϵ_{ij} corresponds to modified charges, $q_i = q^0_i + \Delta q_i$ and $q_j = q^0_j + \Delta q_j$. The a_{ij} and a_{ji} parameters, "measuring" the changes in bond energy accompanying unit charge variations at atoms i and j, respectively, are derived from theory. Typical values are, for alkanes, $a_{CC} = -0.488$, $a_{CH} = -0.247$, and $a_{HC} = -0.632$ kcal mol^{-1} me^{-1} (1 me = 10^{-3} e). The remarkable feature is that eq. [3] describes equally well the CH bonds of methane (1, 2), ethylene (3*a*), and benzene (3*b*) or the CC single bonds of ethane, propene (3*b*), biphenyl (3*b*), butadiene (3*b*), etc. The sum of these bond contributions, i.e., from eq. [1],

$$[4] \quad \Delta E^*_a = \sum_{i<j} \epsilon^0_{ij} + \sum_i \sum_j a_{ij}\Delta q_i + \Delta E^*_{nb}$$

is in all cases to its experimental counterpart, within ~0.23 kcal mol^{-1} (average deviation). Briefly, theoretical bond energies offer a consistent and quite general description of molecular energies on a conceptually simple basis, eq. [3].

Our approach differs considerably in conceptual content from earlier descriptions of alkanes (4*a*) and alkyl radicals (4*b*), in a strategy postulating electrostatic interactions between net charges, $E^{el} = \Sigma_{i<j} q_i q_j / r_{ij}$. For the alkanes, all H charges were empirically fixed at 58.1 me, with C carrying the neutralizing negative charge. This is clearly at odds with theoretical charge analyses. Still, with the aid of two additional empirical parameters, this scheme permitted evaluation of standard enthalpies of formation for the alkanes, essentially because it discriminates primary, secondary, etc., C atoms. Similarly, experimental results of seven alkyl radicals were also well reproduced (4*b*), with the introduction of four new empirical parameters in addition to those used for the alkanes. This sort of empirical duplication of experimental results is, unfortunately, not informative as regards the formal relationship between a bond dissociation energy and the energy of that bond in the unperturbed ground-state molecule. Our energy calculations, eq. [4], involve only theoretical charges, ϵ^0_{ij} and a_{ij} results.

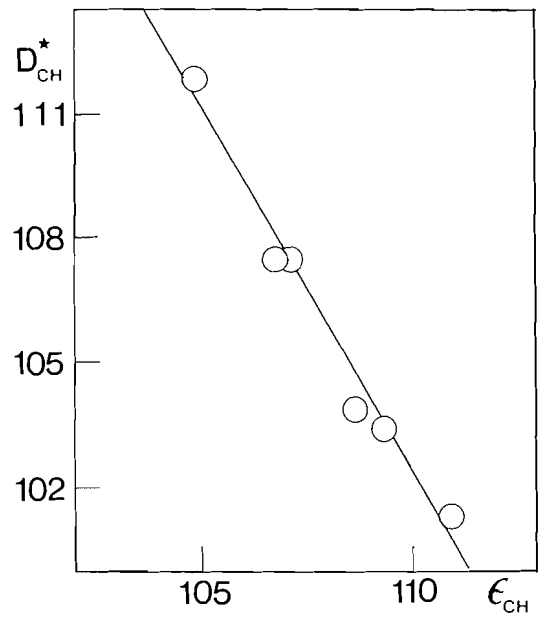

FIG. 1. Alkanes: a comparison between CH dissociation and theoretical contributing bond energies, eq. [3], in kcal mol^{-1}. The D^*_{CH} values were derived from experimental results by Castelhano and Griller (5).

Now we come to the problems. The comparison between dissociation (D^*_{CH}) and contributing (ϵ_{CH}) bond energies in alkanes is intriguing (Fig. 1). It suggests that those CH which contribute larger ϵ_{CH}'s to thermochemical stability are easier to break, certainly a point requiring clarification. In addition, Sanderson's claim (6) that all contributing CH bond energies are equal should be examined. On one hand, this claim is diametrically opposed in conceptual content to the basic tenet embodied in our description of bond energies, namely, the preservation of molecular electroneutrality. Still, on the other hand, it deserves more than passing attention because of the undisputed success of Sanderson's approach — a success largely responsible for an interesting clash of opinions.

We feel that a patient processing of general theory, rather than an accumulation of empirically generated data, should offer better insight into the energetics governing free radical formation and explain the apparent discrepancies in the interpretation of bond energies. We have opted for a fresh start, in a perspective developed from a theoretical description of chemical bonds, aimed at a general description relating dissociation energies, D^*_{ij}, and contributing bond energies, ϵ_{ij}. Numerical examples are presented for alkanes.

Theory

At the center of our description of bond energies, electroneutrality constraints are important in two ways. (*i*) For ground-state molecules, the description of contributing bond energies featuring their dependence on the charges at the bond-forming atoms, eq. [3], is rooted in the conservation of molecular electroneutrality. (*ii*) In dissociation processes, $R_1R_2 \rightarrow R_1\cdot + R_2\cdot$, the individual fragments (R_1 and R_2) may not be electroneutral while they are part of the host molecule whereas the corresponding radicals certainly satisfy electro-

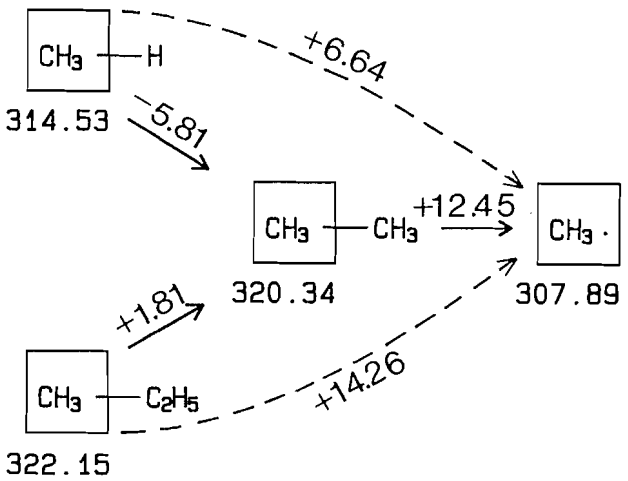

SCHEME 1. Calculated ΔE^*_a energies, eq. [4], for the methyl fragments found in methane, ethane, and propane and for the methyl radical (experimental value), in kcal mol^{-1}. The ΔE^*_a's (indicated under the corresponding boxes) illustrate how non-electroneutral CH_3 fragments (those of CH_4 and C_3H_8) compare with the electroneutral CH_3 of ethane and with the radical $CH_3\cdot$.

neutrality. This charge reneutralization represents the clue toward a realistic description of dissociation energies — a clue which can be exploited in two ways.

Our first strategy is illustrated by a numerical example, worked out for methyl groups (Scheme 1), but its conceptual content applies to any group R. Here we calculate the energies of all the bonds occurring in CH_3 and include the corresponding nonbonded contributions following eq. [1]. This gives $\Delta E^*_a(CH_3)$. Clearly, $\Delta E^*_a(CH_3)$ is deduced in the usual way (1, 2) from the appropriate atomic charges. The latter depend on what is attached to CH_3 and so does $\Delta E^*_a(CH_3)$. Thus all the CH_3 groups differ in energy from one another, and we know by how much. Therefore, it suffices to know how anyone differs from the radical $CH_3\cdot$ in order to gain the same information for the other CH_3 groups. A convenient reference is the electroneutral CH_3 of ethane, a choice which permits one to associate energy changes with charge neutralization — hence the term CNE = charge neutralization energy. The methyl of CH_4, for example, is electron deficient by 9.05 me (1, 2). When recovering that charge, its energy decreases by CNE = -5.81 kcal mol^{-1} (meaning that ΔE^*_a increases by that amount). Similarly, when the CH_3 of propane restores its electroneutrality by losing its excess electronic charge, 2.65 me (1, 2), its energy increases by CNE = $+1.81$ kcal mol^{-1}.

At this point we have acknowledged CNE as a useful concept permitting one to go from any R, described by $\Delta E^*_a(R)$, to the corresponding electroneutral R^0, described by $\Delta E^*_a(R^0)$. It suffices to know once and for all how R^0 differs from the radical $R\cdot$, i.e., the reorganization energy

$$[5] \quad RE = \Delta E^*_a(R^0) - \Delta E^*_a(R\cdot)$$

In order to learn how any R differs in energy from $R\cdot$. Having now secured this idea, there is a better way of exploiting it.

Two radicals are formed in any dissociation $R_1R_2 \rightarrow R_1\cdot + R_2\cdot$. For the problem at hand, it is more convenient to consider them jointly rather than proceeding *via* calculations of the individual CNE's, i.e., $\Delta E^*_a(R_1) - \Delta E^*_a(R_1{}^0)$ and $\Delta E^*_a(R_2) - \Delta E^*_a(R_2{}^0)$. If the portions of $\Delta E^*_a(R_1R_2)$ associated with R_1 and R_2 *as they exist in the molecule* are $\Delta E^*_a(R_1)$ and $\Delta E^*_a(R_2)$, respectively, their sum $\Delta E^*_a(R_1) + \Delta E^*_a(R_2)$ differs (in principle) from that of the corresponding electroneutral fragments, $\Delta E^*_a(R_1{}^0) + \Delta E^*_a(R_2{}^0)$. The difference between these sums is CNE, i.e.,

$$[6] \quad \Delta E^*_a(R_1) + \Delta E^*_a(R_2) = \Delta E^*_a(R_1{}^0) + \Delta E^*_a(R_2{}^0) + CNE$$

The individual ΔE^*_a's can be deduced from eq. [4]. However, this involves calculations for all the bonds found in R_1 and R_2, leaving out the only one of interest, namely, the bond linking R_1 with R_2 which is undergoing dissociation. Reverting now to a more practical strategy, we start with the energy of the molecule $\Delta E^*_a(R_1R_2)$, suppress the bond linking R_1 and R_2 and overcome the nonbonded interaction between R_1 and R_2 by supplying $\epsilon(R_1R_2) + \Delta E^*_{nb}(R_1\cdots R_2) = \epsilon(R_1R_2) - E^*_{nb}(R_1\cdots R_2)$. The energy balance gives

$$[7] \quad \Delta E^*_a(R_1R_2) - [\epsilon(R_1R_2) - E^*_{nb}(R_1\cdots R_2)] = \Delta E^*_a(R_1) + \Delta E^*_a(R_2)$$

and, using eq. [6],

$$[8] \quad CNE = \Delta E^*_a(R_1R_2) - \epsilon(R_1R_2) + E^*_{nb}(R_1\cdots R_2) - \Delta E^*_a(R_1{}^0) - \Delta E^*_a(R_2{}^0)$$

The $\Delta E^*_a(R^0)$'s are simply deduced from an application of eq. [7] to symmetric molecules RR, i.e.,

$$[9] \quad \Delta E^*_a(R^0) = \tfrac{1}{2}[\Delta E^*_a(RR) - \epsilon(RR) + E^*_{nb}(R\cdots R)]$$

Equation [8] enables the calculation of CNE energies from molecular ground-state properties. More importantly, it is the key equation for the description of bond dissociation energies. Indeed, using the definition of $D^*(R_1R_2)$, eq. [2], and that of reorganizational energy, eq. [5], it follows from eq. [8] that

$$[10] \quad D^*(R_1R_2) = \epsilon(R_1R_2) + CNE - E^*_{nb}(R_1\cdots R_2) + RE(R_1) + RE(R_2)$$

This energy formula is general and suffers from no approximations in that all the appropriate bonded and nonbonded contributions are taken care of. It is seen that CNE, eq. [8], is not just a correction term. Quite on the contrary, this particular form of electroneutrality constraint is all that is required for deducing the relationship between bond dissociation and contributing bond energies.

Numerical applications: the alkanes

Thermochemical data

Extensive studies, which are well reviewed (7), have dealt with the heats of formation of alkyl radicals. Two sets of experimental results are indicated in Table 1. Although some measurements were carried out in solution, they can be regarded as being equivalent to gas-phase data to a good approximation, for reasons given in detail elsewhere (5, 8). The sum of zero-point (ZPE) and heat content ($H_T - H_0$) energies, at 298.15 K, are also reported.

The atomization energies are conveniently deduced from the formula, valid for non-linear molecules,

$$[11] \quad \Delta E^*_a = \sum_i n_i[\Delta H_f(A_i) - \tfrac{5}{2}RT] + ZPE + (H_T - H_0) - \Delta H_f$$

where the $\Delta H_f(A_i)$'s are the standard enthalpies of formation of gaseous atoms (170.89 for C and 52.09 kcal atg^{-1} for H) (15). For all practical purposes, theoretical ΔE^*_a values for the

Can. J. Chem. Downloaded from www.nrcresearchpress.com by 213.166.140.6 on 09/07/12
For personal use only.

Can. J. Chem. Downloaded from www.nrcresearchpress.com by 213.166.140.6 on 09/07/12
For personal use only.

TABLE 1. Heats of formation, ZPE + $H_T - H_0$ and $\Delta E^*_a(R\cdot)$ energies of alkyl radicals, kcal mol^{-1} [a]

R·	$\Delta H_f(R\cdot)$ Set 1	Set 2	Selected	ZPE + $(H_T - H_0)$	$\Delta E^*_a(R\cdot)$
$CH_3\cdot$	34.4	35.1	34.0	20.65	307.89
$C_2H_5\cdot$	28.0	28.3	28.3	39.17	602.73
n-$C_3H_7\cdot$	22.8	22.6	22.7	57.09	896.88
i-$C_3H_7\cdot$	19.2	20.0	19.9	57.09	899.68
n-$C_4H_9\cdot$		17.0	17.6	75.53	1191.05
i-$C_4H_9\cdot$		15.0	14.9	75.04	1193.26
s-$C_4H_9\cdot$	13.9	13.8	13.8	75.53	1194.85
t-$C_4H_9\cdot$	9.4	10.3	9.0	75.04	1199.16

[a]Set 1 is taken from ref. 5. Set 2 is a critical selection given in ref. 9. The ZPE + $(H_T - H_0)$ energies, at 298.15 K, are based on experimental and calculated fundamental frequencies (10–12) giving, in the harmonic oscillator approximation, 20.74 ($CH_3\cdot$), 39.15 ($C_2H_5\cdot$), and 74.97 kcal mol^{-1} (t-$C_4H_9\cdot$). It is fortunate that ZPE + $(H_T - H_0)$ energies can be constructed to a good approximation by means of additivity rules (2). Theoretical foundation for this additivity, which has a long history (13), has been established (14). Present data suggest that ZPE + $(H_T - H_0)$ energies of alkyl radicals R· are systematically lower by 8.85 kcal mol^{-1} than those of their parent hydrocarbon RH. The values of the latter (2) are reported in Table 2. The $\Delta E^*_a(R\cdot)$ results were deduced from eq. [11].

hydrocarbons (1, 2), eq. [4], are the same as those deduced from eq. [11]. (Selected examples are given in Table 2.) In contrast, the study of radicals by means of eq. [4] is presently not feasible because of our lack of knowledge regarding their charges. SCF results would not provide adequate information: only charges obtained after configuration interaction would be suitable (16). Hence we resort to eq. [11] for the radicals — a task requiring a balanced selection of $\Delta H_f(R\cdot)$ values.

With the experimental data of Table 1, we obtain two sets of $\Delta E^*_a(R\cdot)$ values. From the ΔE^*_a's of the parent hydrocarbons (Table 2), we now deduce the corresponding D^*_{CH} energies, eq. [2]. (Those of Fig. 1 are for set 1.) The correlations with ϵ_{CH} bond energies (Appendix 1) are $D^*_{CH} = 296.98 - 1.77\epsilon_{CH}$ and $D^*_{CH} = 294.70 - 1.75\epsilon_{CH}$ kcal mol^{-1} from sets 1 and 2, respectively. While the correlation derived from set 1, including $CH_3\cdot$ and t-$C_4H_9\cdot$, exhibits a small and uniform scatter about the correlation line (ave. dev. $\simeq 0.38$), with set 2 the correlation is generally excellent (ave. dev. $\simeq 0.26$ kcal mol^{-1}) except for $CH_3\cdot$ and t-$C_4H_9\cdot$ which deviate by ~ 1.3 kcal mol^{-1} from the correlation line. Tentatively assuming the approximate validity of this type of empirical correlation, back calculation of $\Delta H_f(R\cdot)$ yields virtually the same results using either of these correlation lines. This strategy suggests a balanced set of $\Delta H_f(R\cdot)$ values. Of course, not too much weight should be attached to this particular selection, but it seems reasonable to expect that it would confine any scatter about the true $\Delta H_f(R\cdot)$ values within acceptable limits — a view supported by recent experimental data (5, 17) and critical review of earlier work (18). The corresponding $\Delta E^*_a(R\cdot)$ values are indicated with a precision which is not warranted by our actual knowledge. They are used here primarily in order to facilitate recalculations without being continually bothered by rounding-off errors. None of the conclusions reached in this paper critically depends on the assumed precision of the data given in Table 1.

As regards the correlation $D^*_{CH} = 295.91 - 1.76\epsilon_{CH}$ kcal mol^{-1} between dissociation and intrinsic bond energies (Table 3), a point must be made concerning radicals like $CH_3CH_2CH_2\cdot$, $C_3H_7CH_2\cdot$, and $(CH_3)_2CHCH_2\cdot$. Here we ask which of the non-equivalent CHa or CHs bonds of the parent hydrocarbon is involved (Table 4). It turns out that it is systematically the weaker of the two possible CH bonds that obeys the correlation with D^*_{CH}. Cyclohexane follows the same pattern. For the equatorial CH bond, $\epsilon_{CH} = 109.28$, we obtain D^*_{CH}(equat.) = 103.58 kcal mol^{-1}. Equation [2] and $\Delta E^*_a(C_6H_{12})$, Table 2, gives $\Delta E^*_a(C_6H_{11}\cdot) = 1657.22$ and, finally, $\Delta H_f(C_6H_{11}\cdot) = 14.6$ kcal mol^{-1}. For the axial CH bond, 111.28 kcal mol^{-1}, we find $\Delta H_f(C_6H_{11}\cdot) = 11.1$ kcal mol^{-1}. The experimental result (19)[2] is $\Delta H_f(C_6H_{11}\cdot) = 14.4 \pm 0.4$ and Allinger's calculation (21) indicates 14.01 kcal mol^{-1}. Again, it is the weaker CH bond, the equatorial one, which obeys the correlation. Hence, pending the physical explanation, when the choice between non-equivalent bonds is immaterial as regards the final products, Fig. 1 should not mislead us into concluding that the stronger bond is fated to break.

Nonbonded interactions and reorganizational energies

For nonbonded interactions we use Del Re's approximation (22)[3]

$$[12] \quad E^*_{nb} = \frac{1}{2}\sum_{k,l}\frac{q_k q_l}{r_{kl}}$$

which has recently received (3) indirect, but welcome, support as to its validity in σ systems. Equation [12] expresses Coulomb interactions between net charges of nonbonded atoms k and l at a distance r_{kl}. For the problem at hand, we are primarily interested in $E^*_{nb}(R_1\cdots R_2)$ interactions between the atoms of R_1 and those of R_2 in molecules R_1R_2 (Table 5). Negative terms are attractive. This portion of the total nonbonded interactions measures what holds R_1 and R_2 together in addition to the chemical bond joining these groups.

These results are used in calculations of $\Delta E^*_a(R^0)$, eq. [9], and reorganizational energies, eq. [5], which are reported in Table 6.

The stage is set. Now we can examine the relative importance of the various terms contributing to the dissociation of chemical bonds in saturated hydrocarbons.

Leading terms governing CC and CH bond dissociations

Let us begin with the CC bonds. Equation [1] and Tables 5 and 6 yield the CNE results which are indicated in Table 7 along with additional $\Delta E^*_a(R_1R_2)$ and ϵ_{CC} input data for a representative selection of molecules.

The CNE terms are generally small, particularly for relatively similar R_1 and R_2 partners, because charge neutralization between alkyl groups benefit from important compensations. (Citing propane as an example, experiment (23), arguments invoking inductive effects (1, 2, 24) and theoretical charge analyses (1, 2) all say the same thing, namely, that each methyl group carries an excess negative charge, −2.65 me in our calculation (1, 2). This excess charge is necessarily transferred back to the ethyl moiety when the CC bond dissociates, reducing the ΔE^*_a energy of the CH_3 part from 322.15 to 320.34 and increasing that of C_2H_5 from 610.81 to 612.78 kcal mol^{-1}, for

[2]This result is deduced from the activation energy for the gas-phase photobromination of cyclohexane, $E_{Br} = 11.53 \pm 0.32$ kcal mol^{-1}, and the Evans–Polanyi type equation (18a, 20), $E_{Br} = 0.87[DH^{298}(CH) - 82.7]$ kcal mol^{-1}, relating E_{Br} and dissociation enthalpies of CH bonds.

[3]Note that $\Delta E^*_{nb} = (0 - E^*_{nb}) = -E^*_{nb}$ because all ΔE^*'s are defined for "atoms minus molecule".

Can. J. Chem. Downloaded from www.nrcresearchpress.com by 213.166.140.6 on 09/07/12
For personal use only.

TABLE 2. Thermochemical data of selected alkanes (1, 2) kcal mol^{-1}

Molecule	ΔH^0_f (gas, 298.15)	ZPE + $H_T - H_0$	ΔE^*_a Calcd., eq. [4]	ΔE^*_a Exptl., eq. [11]
Methane	−17.89	29.50	419.35	419.24
Ethane	−20.04	48.02	710.54	710.54
Propane	−25.02	65.94	1004.29	1004.07
Butane	−30.03	84.38	1298.10	1298.15
Isobutane	−32.07	83.89	1300.02	1299.70
Cyclohexane	−29.50	107.54	1760.80	1760.80

TABLE 3. Dissociation and contributing energies of selected CH bonds, kcal mol^{-1} [a]

Bond	D^*_{CH}	ϵ_{CH}
CH_3-H	111.42	104.86
C_2H_5-H	107.81	106.81
n-C_3H_7-H	107.41	107.13
i-C_3H_7-H	104.61	108.72
n-C_4H_9-H	107.05	107.23
i-C_4H_9-H	106.76	107.59
s-C_4H_9-H	103.25	109.35
t-C_4H_9-H	100.86	110.89

[a]For internal consistency, the D^*_{CH}'s, eq. [2], were deduced from the *calculated* ΔE^*_a results indicated in Table 2 and the $\Delta E^*_a(R\cdot)$'s of Table 1. Details regarding the calculation of the ϵ_{CH} energies, eq. [3], are given in Appendix 1.

TABLE 4. Properties of selected CH bonds

Molecule	Bond	Net charge, me q_C	Net charge, me q_H	ϵ_{CH}, kcal mol^{-1}
Propane	CHa	33.64	−12.32	107.56
	CHs	33.64	−11.65	107.13
Butane	CHa	33.96	−12.54	107.62
	CHs	33.96	−11.93	107.23
Isobutane	CHa	32.37	−11.88	107.59
	CHs	32.37	−13.63	108.70
Cyclohexane	CH axial	31.86	−17.52	111.28
	CH equatorial	31.86	−14.34	109.28

a small total change − CNE = −0.16 kcal mol^{-1}).[4] As a consequence, we can approximate eq. [10] as follows

$$[13]\quad D^*_{CC} \simeq \epsilon_{CC}(R_1R_2) + RE(R_1) + RE(R_2) + 0.33 \text{ kcal mol}^{-1}$$

where the constant (0.33) is the average of the CNE and nonbonded contributions evaluated for all the 36 molecules constructed from the 8 alkyl groups considered here. The associated error (standard deviation = 0.26 kcal mol^{-1}) is acceptable. Briefly, CNE and nonbonded terms are minor contributors to the dissociation of CC bonds. This is no longer true for CH bonds (Table 8).

The CNE part accompanying CH dissociations is not only quantitatively important, but also produces an interesting effect. Indeed, CNE compensates to a large extent differences existing between ϵ_{CH} energies: ϵ_{CH} + CNE is nearly constant for all C(sp^3)—H bonds on one hand, and also for C(sp^2)—H bonds, on the other. Hence, incorporating also the small nonbonded interactions into this approximation, we rewrite eq. [10] as follows

$$[14]\quad D^*_{CH} \simeq \text{constant} + RE$$

where the constant, 98.40 or 102.65 kcal mol^{-1} for C(sp^3)

[4]Note that CNE includes the changes in nonbonded interaction energies accompanying the redistribution of electronic charge.

TABLE 5. Nonbonded interactions, kcal mol^{-1} [a]

R_1	R_2	$E^*_{nb}(R_1\cdots R_2)$	$E^*_{nb}(R_1\cdots H)$
CH_3	CH_3	−0.225	0.046
CH_3	C_2H_5	−0.196	
CH_3	n-C_3H_7	−0.189	
CH_3	i-C_3H_7	−0.175	
CH_3	n-C_4H_9	−0.196	
CH_3	i-C_4H_9	−0.181	
CH_3	s-C_4H_9	−0.171	
CH_3	t-C_4H_9	−0.164	
C_2H_5	C_2H_5	−0.167	0.039
C_2H_5	n-C_3H_7	−0.159	
C_2H_5	i-C_3H_7	−0.133	
n-C_3H_7	n-C_3H_7	−0.152	0.036
i-C_3H_7	i-C_3H_7	−0.107	0.018
n-C_4H_9	n-C_4H_9	−0.167	0.038
i-C_4H_9	i-C_4H_9	−0.138	0.028
s-C_4H_9	s-C_4H_9	−0.116	0.008
t-C_4H_9	t-C_4H_9	−0.06	−0.019

[a]The atoms are positioned as in the parent hydrocarbons, using experimental or calculated (STO-3G) geometries. The charges are those of ref. 2 (see Appendix 1).

TABLE 6. The calculation of reorganizational energies, kcal mol^{-1} [a]

R^0		$\Delta E^*_a(RR)$	$\epsilon_{CC}(RR)$	$\Delta E^*_a(R^0)$	RE
1	CH_3	710.54	69.63	320.34	12.45
2	C_2H_5	1298.10	72.38	612.78	10.05
3	n-C_3H_7	1885.69	73.39	906.07	9.19
4	i-C_3H_7	1887.16	73.71	906.67	6.99
5	n-C_4H_9	2473.21	73.06	1199.99	8.94
6	i-C_4H_9	2476.03	74.14	1200.88	7.62
7	s-C_4H_9	2473.55	74.44	1199.50	4.65
8	t-C_4H_9	2477.09	73.87	1201.61	2.45
9	c-C_6H_{11}	3401.42	75.27	1663.03	5.81

[a]The $\Delta E^*_a(RR)$ results are from ref. 2. For bicyclohexyl, see Appendix 2. The calculation of CC bond energies is outlined in Appendix 1.

Can. J. Chem. Downloaded from www.nrcresearchpress.com by 213.166.140.6 on 09/07/12
For personal use only.

TABLE 7. Charge neutralization and dissociation energies of CC bonds, kcal mol^{-1}

Bond	$\Delta E^*_a(R_1R_2)$[a]	ϵ_{CC}[b]	CNE	D^*_{CC} Exptl.	D^*_{CC} Eq. [13]
CH_3—CH_3	710.54	69.63	0	94.76	94.9
CH_3—C_2H_5	1004.29	71.14	−0.16	93.67	94.0
CH_3—n-C_3H_7	1298.10	71.56	−0.06	93.33	93.5
CH_3—i-C_3H_7	1300.02	72.42	0.43	92.45	92.2
CH_3—n-C_4H_9	1591.90	71.41	−0.04	92.96	93.1
CH_3—i-C_4H_9	1593.17	71.91	−0.13	92.02	92.3
CH_3—s-C_4H_9	1593.17	72.53	0.63	90.43	90.0
CH_3—t-C_4H_9	1596.06	73.14	0.86	89.01	88.4
C_2H_5—C_2H_5	1298.10	72.38	0	92.64	92.8
C_2H_5—n-C_3H_7	1591.90	72.89	0.00	92.29	92.5
C_2H_5—i-C_3H_7	1593.17	73.23	0.36	90.76	90.6
C_2H_5—n-C_4H_9	1885.69	72.74	0.01	91.91	92.1
C_2H_5—i-C_4H_9	1887.00	73.23	−0.03	91.01	91.2
C_2H_5—s-C_4H_9	1886.33	73.55	0.36	88.75	88.6
C_2H_5—t-C_4H_9	1888.41	73.63	0.31	86.52	86.5
n-C_3H_7—i-C_3H_7	1887.00	73.81	0.32	90.44	90.3
n-C_3H_7—s-C_4H_9	2180.15	74.10	0.34	88.42	88.3
i-C_3H_7—i-C_3H_7	1887.16	73.71	0	87.80	88.0
i-C_3H_7—s-C_4H_9	2180.32	74.05	−0.01	85.79	86.0
i-C_3H_7—t-C_4H_9	2182.36	73.88	0.15	83.52	83.7
i-C_4H_9—s-C_4H_9	2475.21	74.49	0.22	87.10	87.1
s-C_4H_9—s-C_4H_9	2473.55	74.44	0	83.85	84.1
s-C_4H_9—t-C_4H_9	2476.04	74.47	0.40	82.03	81.9
t-C_4H_9—t-C_4H_9	2477.09	73.87	0	78.77	79.1

[a] From ref. 2.
[b] See Appendix 1.

TABLE 8. Charge neutralization energies in C(sp^3)—H and C(sp^2)—H bond dissociations, kcal mol^{-1} [a]

Bond	ϵ_{CH}	CNE	ϵ_{CH} + CNE
1 CH_3—H	104.86	−5.81	99.05
2 C_2H_5—H	106.81	−9.01	97.80
3 n-C_3H_7—H	107.13	−8.87	98.26
4 i-C_3H_7—H	108.72	−11.08	97.64
5 n-C_4H_9—H	107.23	−9.08	98.15
6 i-C_4H_9—H	107.59	−8.42	99.17
7 s-C_4H_9—H	109.35	−10.74	98.61
8 t-C_4H_9—H	110.89	−12.50	98.39
9 c-C_6H_{11}—H	109.28	−11.50	97.78
10 CH_2:$CHCH_2$—H	(107.3)	(−8.6)	98.69
11 CH_2:$CHCH_2CH_2$—H	(107.4)	(−8.9)	98.52
12 $C_6H_5CH_2$—H	108.0	−9.0	99.0
13 CH_2:CH—H	105.72	−3.11	102.61
14 CH_3CH:CH—H	(106.0)	(−3.9)	102.1
15 $(CH_3)_2C$:CH—H	(104.6)	(−1.3)	103.3
16 CH_2:$C(CH_3)$—H	(109.9)	(−7.1)	102.8
17 C_6H_5—H	113.54	−10.97	102.57

[a] For **10**–**17**, the results under the heading ϵ_{CH} + CNE include $E^*_{nb}(R\cdots H)$, eq. [10]. The corresponding $\Delta E^*_a(R^0)$ values, eq. [8], are not corrected for $E^*_{nb}(R\cdots R)$, a circumstance introducing a small imprecision, <0.1 kcal mol^{-1}. The ϵ_{CH} results in parentheses (and, thus, the companion CNE results) are somewhat uncertain (≤0.3 kcal mol^{-1}) because of uncertainties affecting calculated H net charges. The $\Delta E^*_a(RH)$ values are from ref. 2 (**10**, **11**, **13**–**16**) and ref. 3*b* (**12**, **17**). The $\Delta E^*_a(RR)$ and ϵ_{CC} results for use in eq. [9] are (25), in kcal mol^{-1}, ΔE^*_a = 1593.9, ϵ_{CC} = 74.00 (1,5-hexadiene, for **10**); ΔE^*_a = 2180.99, ϵ_{CC} = 72.93 (1,7-octadiene, for **11**); ΔE^*_a = 1009.9, ϵ_{CC} = 90.81 (1,3-butadiene, for **13**); ΔE^*_a = 1603.57, ϵ_{CC} = 90.44 (*E*,*E*-2,4-hexadiene, for **14**); ΔE^*_a = 2195.98, ϵ_{CC} = 89.63 (2,5-dimethyl-2,4-hexadiene, for **15**); ΔE^*_a = 1603.0, ϵ_{CC} = 91.33 (2,3-dimethyl-1,3-butadiene, for **16**) and (3*b*) ΔE^*_a = 3203.0, ϵ_{CC} = 74.26 (1,2-diphenylethane, for **12**); ΔE^*_a = 2612.8, ϵ_{CC} = 84.94 (biphenyl, for **17**).

and C(sp^2)—H bonds, respectively, represents the average value of ϵ_{CH} + CNE − $E^*_{nb}(R\cdots H)$. The ϵ_{CH}'s examined here range from 104.86 (CH_3—H) to 110.89 kcal mol^{-1} (t-C_4H_9—H) for C(sp^3)—H bonds and from 105.72 (ethylene) to 113.54 kcal mol^{-1} (benzene) for C(sp^2)—H bonds. These are the theoretical bond energies satisfying $\Delta E^*_a \simeq \Sigma\epsilon_{ij}$. CNE disguises them in such a way that, when viewed from the perspective of dissociation energies, all CH bonds involving the same type of C are perceived as if they were equal in energy, to a good approximation. This result explains the nature of "constant CH bond energies" and vindicates Sanderson's ideas (6) concerning their use in problems of bond dissociation along the lines expressed by eq. [14]. As regards the CC bonds, however, eq. [13] commands the use of genuine ϵ_{CC}'s, whose values range from 69.63 to ~74.5 kcal mol^{-1} for the alkanes studied in this paper.[5] Their validity is illustrated by the quality of calculated D^*_{CC}'s (Table 7).

A clarification concerning reorganization energies can now be given — a problem conveniently approached by an examination of CH bonds which are not equivalent in the hydrocarbon, but whose dissociation yields the same final products.

[5] These conclusions also hold for dissociation enthalpies, $DH(R_1—R_2) = \Delta H_f(R_1\cdot) + \Delta H_f(R_2\cdot) - \Delta H_f(R_1R_2)$. Indeed, eqs. [2] and [11] lead to

$$DH(R_1 - R_2) = D^*(R_1 - R_2) + Z(R_1\cdot) + Z(R_2\cdot) - Z(R_1R_2)$$

where Z stands for ZPE + H_T − H_0. For the alkanes, taking advantage of the approximation $Z(R\cdot) \simeq Z(RH) - 8.85$ (Table 1) and (2) $Z(R_2R_2) \simeq Z(R_1H) + Z(R_2H) - 11.48$ kcal mol^{-1}, it follows from eqs. [13] and [14] that

$$DH(C—C) \simeq \epsilon_{CC} + RE(R_1\cdot) + RE(R_2\cdot) - 5.9$$

$$DH(C—H) \simeq 91.0 + RE \text{ kcal mol}^{-1}$$

Can. J. Chem. Downloaded from www.nrcresearchpress.com by 213.166.140.6 on 09/07/12
For personal use only.

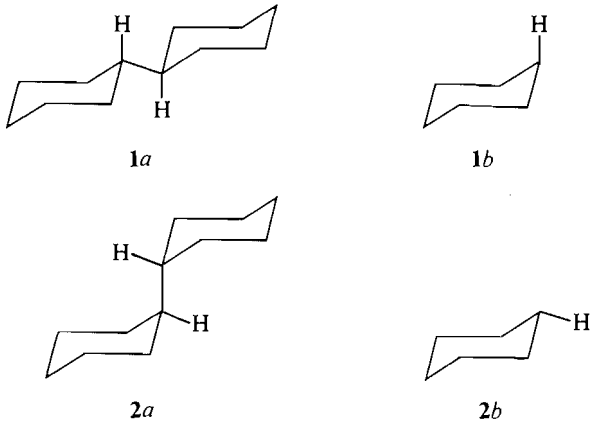

SCHEME 2. The equatorial–equatorial and axial–axial conformations of bicyclohexyl and the corresponding cyclohexyl fragments.

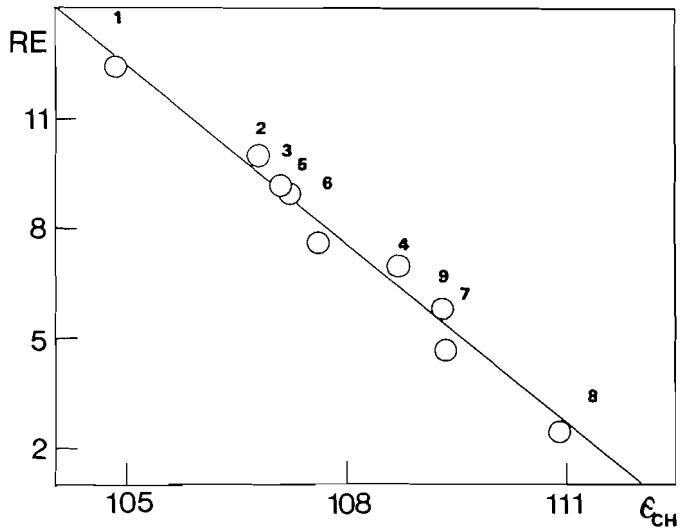

FIG. 2. A comparison between reorganizational energies, eq. [5], and theoretical CH bond energies, eq. [3], in kcal mol^{-1}. The numbering refers to that given in Table 6.

Analysis of the reorganizational energy

Let us first describe the cyclohexane system which is used as an example. Following eq. [9], the appropriate reference state R^0 is defined with respect to bicyclohexyl. The equatorial–equatorial conformation, **1***a*, is preferred over the axial–axial form **2***a* because of the four additional butane–*gauche* interactions occurring in the latter. As a consequence, **1***a* and **2***a* define reference states **1***b* and **2***b*, respectively, where $\Delta E^*_a(\mathbf{2}b) < \Delta E^*_a(\mathbf{1}b)$ (Scheme 2).

Using now eq. [14] and the definition of RE, eq. [5], we write

$$[15] \quad D^*_{CH} \simeq [98.40 - \Delta E^*_a(R\cdot)] + \Delta E^*_a(R^0)$$

A cyclohexyl radical formed from cyclohexane would not remember whether it has been formed via removal of an equatorial CH bond (corresponding to $R^0 = \mathbf{1}b$) or through abstraction of an axial CH bond (with $R^0 = \mathbf{2}b$). The term in brackets is the same in either event and we are treacherously led to think that a smaller D^*_{CH} would result if an axial rather than an equatorial CH bond was broken, because $\Delta E^*_a(\mathbf{2}b) < \Delta E^*_a(\mathbf{1}b)$. The error is that this reasoning overlooks the energy required in the process $\mathbf{1}a \rightarrow \mathbf{2}a \rightarrow \mathbf{2}b$, i.e., more precisely, the energy difference $\Delta E^*_a(\mathbf{1}b) - \Delta E^*_a(\mathbf{2}b)$ which has to be added in the computation of D^*_{CH}. Finally, D^*_{CH} is the same (or nearly so) for the dissociation of an axial or an equatorial CH bond of cyclohexane, depending on whether the ϵ_{CH} + CNE − $E^*_{nb}(R\cdots H)$ part of eq. [14] remains exactly the same in both cases.

This example illustrates the following points, equally valid for other molecules. (*i*) *The appropriate R^0 for use in the definition of RE is that deduced from eq. [9] with reference to the RR molecule at its energy minimum.* This defines the "most stable R^0". Any arbitrary selection of a "less stable R^0" reduces $\Delta E^*_a(R^0)$ in eq. [5] but, on the other hand, introduces an additional term in the calculation of D^*, namely the energy supplied in going from R^0 to the "less stable R^0". (*ii*) When non-equivalent CH bonds of a hydrocarbon can dissociate to give the same final products, *the RR molecule at its energy minimum is that constructed by replacing the weaker CH bond of RH by the appropriate CC bond linking R with R.* (For example, the CC bond between R and R replaces the equatorial CH bond of cyclohexane, the CH_s bond of propane or *n*-butane, or the CH_a bond of isobutane.) *The "most stable R^0" thus mimics the topology resulting from the abstraction of the weaker CH bond of RH* which, in quite an indirect way, is promoted to play the pivotal role in comparisons between D^*_{CH} and ϵ_{CH} energies. (*iii*) In this vein, *our earlier observation that the empirical D^*_{CH} vs. ϵ_{CH} correlation holds for the weaker bond suggests that its approximate validity is somehow linked to the implicit use of the correct R^0. A preferential cleavage of the weaker bond should not be inferred because either bond is capable of dissociating with the same D^*_{CH}, or nearly so,* although the corresponding ϵ_{CH}'s may differ significantly from one another. (*iv*) It follows that any attempt at interpreting D^*_{CH} in terms of ϵ_{CH} alone is doomed to failure. *The reason for the existence of a correlation between D^*_{CH} and ϵ_{CH} energies is given by eq. [14] and the approximate linear decrease of reorganizational energies for increasingly larger ϵ_{CH}* bond energies (Fig. 2).

In closing, let us examine a physical aspect concerning the energy involved in going from R^0 to the radical at its energy minimum. R^0 has certainly proved its merits as a convenient computational reference but, as such, does not exist as an isolated chemical species. The counterpart of R^0, considered now as an isolated species, is written R. Its geometry is that of R^0, i.e., that found in the molecule RR, and differs from that of the genuine radical R·. The change in geometry from R to R· is accompanied by an energy lowering — the relaxation energy $E(R\cdot) - E(R)$. On the other hand, bond formation to give RR also lowers the energy of this group of atoms, by $E(R) - E(R^0)$. The reorganizational energy is thus $RE = [E(R) - E(R^0)] + [E(R\cdot) - E(R)] = E(R\cdot) - E(R^0)$. The energies of R^0 and R· are readily derived from the basic equation $E = \Sigma_i E_i^{atom} - \Delta E^*_a$. The energies of R were deduced from LCAO-X_α calculations using in each case the α value which reproduces exactly $E(R\cdot)$ — an approach yielding energies of comparable quality, at the level of experimental accuracy (26) (Appendix 3). The results indicated in Table 9 are self-explanatory as regards $E(R) - E(R^0)$ and the relaxation energy $E(R\cdot) - E(R)$. It is $\Delta E^*_a(R)$ which offers the most interesting features.

Indeed, the $\Delta E^*_a(R)$ of CH_3 corresponds to CH bond energies virtually equal to ϵ_{CH} + CNE − $E_{nb}(R\cdots H)$. The results obtained for ethyl propyl, isopropyl and *tert*-butyl are equally intriguing in that their average bond energies, $\Delta E^*_a(R)/n$ with n = total number of bonds, also reflect the same regularity, as if all CH and CC bonds of R were equal in energy. These novelties seem to convey a message worth further studies.

TABLE 9. Analysis of the reorganizational energies, kcal mol^{-1}, except E(R)[a]

R	E(R), au	E(R) − E(R^0)	E(R·) − E(R)	ΔE^*_a(R)	ΔE^*_a(R)/n	ϵ_{CH} + CNE − E^*_{nb}
CH_3	−39.8279	24.10	−11.67	296.25	98.75	99.01
C_2H_5	−79.1485	24.85	−14.81	587.91	97.99	97.76
n-C_3H_7	−118.4777	21.08	−11.91	884.97	98.33	98.22
i-C_3H_7	−118.4805	19.95	−12.93	886.74	98.53	97.62
t-C_4H_9	−157.8073	19.31	−16.85	1182.29	98.52	98.41

[a]The geometries assumed for the RR molecules, defining those of R, are experimental results obtained for ethane (27), butane (28), hexane (29), 2,3-dimethylbutane and 2,2,3,3-tetramethylbutane (30). The total number of bonds in each R is n.

Conclusions

Our description of bond dissociation energies bears clear similarities with Sanderson's ideas, namely, that a dissociation energy is given by the contributing bond energy ϵ plus the appropriate reorganizational energies. The new aspects introduced by the present treatment lie (*i*) in the use of theoretical, charge-dependent, bond energies, eq. [3], which are a requirement in order to ensure molecular electroneutrality, (*ii*) in the convenient use of electroneutral reference states for defining reorganizational energies, and (*iii*) with the unavoidable introduction of a new term, the charge neutralization energy, which accounts for the fact that individual molecular fragments may not be electroneutral while they are part of the host molecule whereas the corresponding radicals certainly satisfy electroneutrality. Explicit consideration of this constraint leads directly to a general energy formula describing bond dissociation.

Numerical applications to alkanes reveal the minor role played by Coulomb interactions between nonbonded atoms. In the dissociation of carbon–carbon bonds, the mutual neutralization of charge by alkyl groups results in an important mutual cancellation of the individual energy terms associated with this neutralization. The net effect is usually small. As a consequence, the cleavage of CC bonds is primarily governed by the contributing bond energy plus the reorganizational energies of the radicals, in general accord with current views supported by Sanderson's work. The quality of our theoretical bond energies is well reflected in the quality of calculated dissociation energies. In the dissociation of carbon–hydrogen bonds, on the other hand, charge neutralization energies are entirely responsible for a peculiar perception of "seemingly constant contributing CH bond energies", leaving the reorganizational energy as the sole term regulating the dissociation of a CH bond. That this is true, at least to a good approximation, is known from Sanderson's work. Our calculations now reveal that, in fact, it is the sum of the genuine contributing bond energy plus the charge neutralization energy which remains nearly constant for CH bonds. Ultimately, this is what matters for the final result. The contributing CH bond energies, however, still obey the basic tenet, namely the preservation of molecular electroneutrality, responsible for charge-dependent bond energies. It is comforting to witness that, at times, conflicting ideas can be reconciled. In the present case, explicit consideration of charge neutralization constraints did the job.

Acknowledgements

The present work is part of a continuing effort conducted with the Chemistry Department, Università di Napoli, Italy. We thank the Italian Authorities and particularly Professor Giuseppe Del Re for promoting this cooperation and for the extraordinary hospitality extended to one of us (S.F.). We also thank Professors G. Del Re, V. Barone and D. Salahub for helpful discussions, Drs. J. Andzelm and M. Comeau for assistance, and the Natural Sciences and Engineering Research Council of Canada for financial support.

1. S. FLISZÁR. J. Am. Chem. Soc. **102**, 6946 (1980).
2. S. FLISZÁR. Charge distributions and chemical effects. Springer-Verlag, Heidelberg, New York. 1983.
3. (*a*) S. FLISZÁR, G. DEL RE, and M. COMEAU. Can. J. Chem. **63**, 3551 (1985); (*b*) S. FLISZÁR, G. CARDINAL, and N. A. BAYKARA. Can. J. Chem. **64**, 404 (1986).
4. (*a*) S. W. BENSON and M. LURIA. J. Am. Chem. Soc. **97**, 704 (1975); (*b*) M. LURIA and S. W. BENSON. J. Am. Chem. Soc. **97**, 3342 (1975).
5. A. L. CASTELHANO and D. GRILLER. J. Am. Chem. Soc. **104**, 3655 (1982).
6. R. T. SANDERSON. J. Org. Chem. **47**, 3835 (1982); R. T. SANDERSON. Chemical bonds and bond energy. 2nd ed. Academic Press, New York. 1976.
7. D. F. MCMILLEN and D. M. GOLDEN. Ann. Rev. Phys. Chem. **33**, 493 (1982); K. W. EGGER and A. T. COCKS. Helv. Chim. Acta, **56**, 1516 (1973); H. E. O'NEAL and S. W. BENSON. *In* Free radicals. Vol. 2. *Edited by* J. K. Kochi. J. Wiley and Sons, Inc., New York. 1973. pp. 275–359; D. M. GOLDEN and S. W. BENSON. Chem. Rev. **69**, 125 (1969); G. LEROY. *In* Computational theoretical organic chemistry. *Edited by* I. G. Csizmadia and R. Daudel. D. Reidel Publishing Co., Dordrecht. 1981. pp. 253–334.
8. S. W. BENSON. Thermochemical kinetics. 2nd ed. Wiley, New York. 1976.
9. J. C. SCHULTZ, F. A. HOULE, and J. L. BEAUCHAMP. J. Am. Chem. Soc. **106**, 3917 (1984).
10. A. SNELSON. J. Phys. Chem. **74**, 537 (1970).
11. J. PACANSKY and B. SCHRADER. J. Chem. Phys. **78**, 1033 (1983).
12. B. SCHRADER, J. PACANSKY, and U. PFEIFFER. J. Phys. Chem. **88**, 4069 (1984).
13. K. S. PITZER and E. CATALANO. J. Am. Chem. Soc. **78**, 4844 (1956); T. L. COTTRELL. J. Chem. Soc. 1448 (1948); K. G. PITZER. Chem. Rev. **27**, 39 (1940); K. S. PITZER. J. Chem. Phys. **8**, 711 (1940); K. S. PITZER. J. Chem. Phys. **5**, 473 (1937).
14. T. OI, A. POPOWICZ, and T. ISHIDA. J. Phys. Chem. **90**, 3080 (1986).
15. D. R. STULL and G. C. SINKE. Adv. Chem. Ser. **18** (1956).
16. S. FLISZÁR. Int. J. Quantum Chem. **29**, 305 (1986); C. MIJOULE, J.-M. LECLERCQ, S. ODIOT, and S. FLISZÁR. Can. J. Chem. **63**, 1741 (1985).
17. J. C. TRAEGER and R. G. MCLOUGHLIN. J. Am. Chem. Soc. **103**, 3647 (1981).
18. (*a*) J. A. KERR. Chem. Rev. **66**, 465 (1966); (*b*) D. R. STULL and H. PROPHET. Natl. Stand. Ref. Data Ser. (US Natl. Bur. Stand.), NSRDS-NBS **37** (1971); M. H. BAGHAL-VAYJOOSEE, A. J. COLUSSI, and S. W. BENSON. J. Am. Chem. Soc. **100**, 3214 (1978); Int. J. Chem. Kinet. **11**, 147 (1979); R. J. SHAW. J. Phys. Chem. Ref. Data, **7**, 1179 (1978).
19. K. C. FERGUSON and E. WHITTLE. Trans. Faraday Soc. **67**, 2618 (1978).

Can. J. Chem. Downloaded from www.nrcresearchpress.com by 213.166.140.6 on 09/07/12
For personal use only.

20. G. C. FETTIS and A. F. TROTMAN-DICKENSON. J. Am. Chem. Soc. **81**, 5260 (1959); J. Chem. Soc. 3037 (1961).
21. M. R. IMAM and N. L. ALLINGER. J. Mol. Struct. **126**, 345 (1985).
22. G. DEL RE. Gazz. Chim. Ital. **102**, 929 (1972).
23. V. W. LAURIE and J. S. MUENTER. J. Am. Chem. Soc. **88**, 2883 (1966).
24. S. FLISZÁR, G. KEAN, and R. MACAULAY. J. Am. Chem. Soc. **96**, 4353 (1974).
25. S. FLISZÁR and G. CARDINAL. Can. J. Chem. **62**, 2748 (1984).
26. C. MINICHINO, G. DEL RE, and S. FLISZÁR. To be published.
27. D. E. SHAW, D. W. LEPARD, and H. L. WELSH. J. Chem. Phys. **42**, 3736 (1965).
28. W. F. BRADFORD, S. FITZWATER, and L. S. BARTELL. J. Mol. Struct. **38**, 185 (1977).
29. R. A. BONHAM, L. S. BARTELL, and D. A. KOHL. J. Am. Chem. Soc. **81**, 4765 (1959).
30. L. S. BARTELL and T. L. BOATES. J. Mol. Struct. **32**, 379 (1976).
31. (*a*) S. FLISZÁR, A. GOURSOT, and H. DUGAS. J. Am. Chem. Soc. **96**, 4358 (1974); (*b*) S. FLISZÁR. *In* Applied quantum chemistry. *Edited by* V. H. Smith Jr., H. F. Schaefer III, and K. Morokuma. D. Reidel Publishing Co., Dordrecht, Holland. 1986.
32. R. S. MULLIKEN. J. Chem. Phys. **23**, 1833 (1955); **23**, 1841 (1955); **23**, 2338 (1955); **23**, 2343 (1955).
33. L. P. LINDEMAN and J. Q. ADAMS. Anal. Chem. **43**, 1245 (1971).
34. J. B. STOTHERS. Carbon-13 NMR spectroscopy. Academic Press, New York, NY. 1972.
35. H. HENRY, G. KEAN, and S. FLISZÁR. J. Am. Chem. Soc. **99**, 5889 (1977).
36. B. I. DUNLAP, J. W. D. CONNOLLY, and J. R. SABIN. J. Chem. Phys. **71**, 4993 (1979); H. SAMBE and R. H. FELTON. J. Chem. Phys. **62**, 1122 (1975).
37. S. HUZINAGA. J. Chem. Phys. **42**, 1293 (1965).
38. T. H. DUNNING. J. Chem. Phys. **55**, 716 (1970).

Appendix 1

Atomic charges were deduced from a Mulliken-type analysis allowing for an uneven partitioning of overlap populations between dissimilar atoms (1, 2, 16, 31). For the alkanes, using STO-3G Mulliken charges (32) derived will full geometry and scale factor optimizations (31), this analysis gives (1, 2) (in me) $q_C = (35.1/69.4)\ (q_C^{\text{Mulliken}} + 30.12N_{CH})$ and $q_H = (35.1/69.4)(q_H^{\text{Mulliken}} - 30.12)$, where N_{CH} = number of H atoms attached to C. The ethane net charges, $q^0_C = 35.1$ and $q^0_H = -11.70$ me, serve as references in calculations of $\Delta q_C = q_C - q^0_C$ and $\Delta q_H = q_H - q^0_H$, for use in eq. [3]. With these charges and the appropriate parameters (1, 2), eq. [3] becomes (in kcal mol^{-1})

$$\epsilon_{CH} = 106.806 - 0.247\Delta q_C - 0.632\Delta q_H$$

$$\epsilon_{CC} = 69.633 - 0.488\Delta q_{Ci} - 0.488\Delta q_{Cj}$$

For Δq_C, we can use the accurate relationship (2, 31*a*)

$$\Delta q_C = -0.148\delta_C \text{ me}$$

where δ_C is the ^{13}C nmr shift relative to ethane. The ϵ_{CC} results (Tables 6 and 7) were deduced from nmr data reported by Lindeman and Adams (33) and by Stothers (34) for bicyclohexyl.

Appendix 2

The ΔE^*_a results for alkanes with 6 or more C atoms (Tables 6 and 7) were deduced from an accurate approximation (2, 35) incorporating nonbonded contributions,

$$\Delta E^*_a \simeq 710.54(1 - m) + 290.812(n - 2 + 2m) + 0.03244\Sigma N_{CC}\delta_C + 0.05728\Sigma\delta_C \text{ kcal mol}^{-1}$$

where n = number of C atoms, m = number of cycles, and N_{CC} = number of CC bonds formed by the atom whose nmr shift is δ_C relative to ethane. This form of eq. [4], where the H charges are taken care of by charge normalization, is known to agree with experimental results, eq. [11], within 0.23 kcal mol^{-1} (average deviation). Smaller molecules were calculated with explicit consideration of nonbonded terms (1, 2). The appropriate nmr data were taken from literature (33, 34).

Appendix 3

The LCAO-Xα calculations (Table 9) were performed by means of the programs developed by Dunlap *et al.* (36). Huzinaga's (9*s*5*p*) basis (37) was used for the ground-state carbon and hydrogen was described by a (5*s*) basis obtained from Dunning's (3*s*) basis set (38). Auxiliary (9*s*5*p*3*d*) exchange and density functions were selected for carbon and (5*s*5*p*) for hydrogen. Bond-centered *s* functions were also used, as suggested by Dunlap *et al.* (26). For each radical R· we have determined the α value reproducing the total energy corresponding to the ΔE^*_a(R·) of Table 1. The same α was used for the calculation of R in the geometry of the molecule RR. This strategy allows valid energy comparisons between R·, R, and R^0 which are on the same footing as regards their quality (26).

Can. J. Chem. Downloaded from www.nrcresearchpress.com by 213.166.140.6 on 09/07/12
For personal use only.

Infrared spectra of unannealed and of annealed $Cu_4(OH)_6(NO_3)_2$

ETALO A. SECCO[1] AND GLEN G. WORTH[2]
Chemistry Department, St. Francis Xavier University, Antigonish, N.S., Canada B2G 1C0

Received March 24, 1987

ETALO A. SECCO and GLEN G. WORTH. Can. J. Chem. **65**, 2504 (1987).

The infrared spectra over the range 4000–150 cm^{-1} of $Cu_4(OH)_6(NO_3)_2$ along with site group and factor group analysis are reported for the first time. The observed absorption frequencies associated with OH and NO_3 modes show distinct individual spectral features in the unannealed and annealed $Cu_4(OH)_6(NO_3)_2$. Three distinct types of OH groups involving different degrees of H-bonding are evident. The multiple frequencies involving Cu—O—H bending modes further reflect the varying degrees of H-bonding and OH coupling in $Cu(OH)_4O_2$ and $Cu(OH)_5O$ entities paralleling their behavior in $Cu_4(OH)_6SO_4$. The NO_3 internal optic modes' activities, fundamentals along with overtones and combination bands, illustrate distinct interaction effects (OH and Cu) with respect to specific modes relative to halo-nitrates with same site symmetry. The presence of CuO in the sample after the anneal effected a striking change in ν_3. The Cu—O, O—Cu—O, and OH torsional mode frequencies show consistent behavior with $Cu_4(OH)_6SO_4$.

ETALO A. SECCO et GLEN G. WORTH. Can. J. Chem. **65**, 2504 (1987).

On a déterminé pour la première fois le spectre infrarouge du $Cu_4(OH)_6(NO_3)_2$ de 4000 à 150 cm^{-1} et on présente une analyse par groupe de position d'atomes et par groupe de facteurs. Les fréquences d'absorption observées pour les modes associés avec OH et NO_3, présentent des caractéristiques spectrales individuelles et distinctes pour les $Cu_4(OH)_6(NO_3)_2$ qu'ils soient sous forme d'anneau ou pas. On a mis en évidence trois groupes distincts de groupements OH impliquant divers degrés de liaisons-H. Les fréquences multiples impliquant les modes de déformation de l'angle Cu—O—H sont d'autres reflets des divers degrés de liaison-H et de couplage OH dans les entités $Cu(OH)_4O_2$ et $Cu(OH)_5O$ et ceux-ci sont parallèles à leur comportement dans le $Cu_4(OH)_6SO_4$. Les modes d'activité optique interne du NO_3, tant au niveau fondamental qu'au niveau des bandes harmonique ou de combinaison, illustrent les effets d'interactions distinctes (OH et Cu) par rapport aux modes spécifiques relatifs au halo-nitrates avec le même site de symétrie. La présence de CuO dans l'échantillon après l'annelation provoque un changement important dans ν_3. Les fréquences du mode de torsion Cu—O, O—Cu—O et OH présentent un comportement systématique dans le $Cu_4(OH)_6SO_4$.

[Traduit par la revue]

Introduction

The polyatomic species NO_3 can undergo various steps of reduction from its isolated point group symmetry of D_{3h} to the low site symmetry C_s in a crystalline lattice (1–3). This reduction in symmetry permits an insight into the intra-molecular effects as reflected on the internal and external optic modes of NO_3 by the surrounding molecular units or environment. Recent spectroscopic studies on crystalline Ag_2BrNO_3 and Ag_2ClNO_3 (3) provided additional information relating the magnitude of site and correlation field effects on the normal modes of NO_3 relative to $AgNO_3$ and KNO_3(II). The infrared spectra of NO_3 in Ag_2BrNO_3 and Ag_2ClNO_3 showed features more in common, to a first approximation, with $AgNO_3$ than with KNO_3(II) of same site symmetry. The interplay of other factors, e.g. dipolar coupling, etc. (4, 5) along with site symmetry contribute to specific spectroscopic properties.

The availability of the compound $Cu_4(OH)_6(NO_3)_2$ of known crystal structure presents another opportunity to observe the spectroscopic properties of NO_3 with same site symmetry C_s (1, 3) in another crystalline environment. These results can provide meaningful data for theoretical lattice or vibrational dynamics analysis using the dipolar coupling model. The prospect of obtaining useful correlations relating H-bonding effects in $OH...ONO_2$ relative to $OH...OSO_3$ as observed for $Cu_4(OH)_6SO_4$-type compounds (6) along with comparing the spectroscopic properties of OH in entities of identical coordination, viz. $Cu(OH)_4O_2$ and $Cu(OH)_5O$ in $Cu_4(OH)_6SO_4$, is another incentive for the infrared study of $Cu_4(OH)_6(NO_3)_2$. Furthermore, the infrared spectra of $Cu_4(OH)_6(NO_3)_2$ annealed just prior to the onset of decomposition might provide an insight into the elementary step leading to decomposition, viz. $Cu_4(OH)_6(NO_3)_2 \rightarrow 4CuO + 3H_2O + 2NO_2 + (1/2)O_2$.

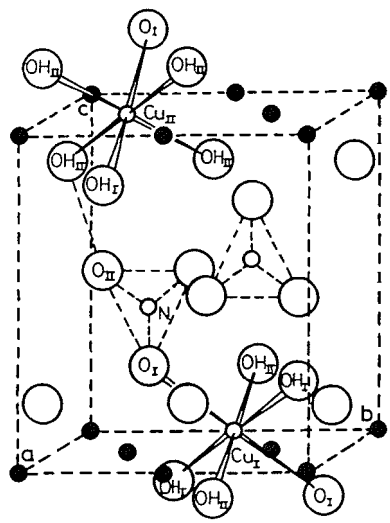

FIG. 1. Unit cell structure of $Cu_4(OH)_6(NO_3)_2$ taken from ref. 7. The filled circles ● represent the remaining Cu atoms along with Cu_I and Cu_{II} associated with the unit cell. Interatomic distances (Å): $Cu_I—Cu_I = Cu_{II}—Cu_{II} = 3.03$, $Cu_I—Cu_{II} = 3.17$, $Cu_I—OH_{II} = 2.08$, $Cu_I—OH_I = 2.00$, $Cu_{II}—OH_{II} = 2.05$, $Cu_{II}—OH_I = 2.27$, $Cu_I—O_I = 2.35$, $Cu_{II}—O_I = 2.18$, $OH_{II}—OH_{II} = 3.03$, $OH_{II}—OH_I = 4.97$, $OH_{II}—O_I = 2.60–2.46$, $OH_I—O_{II} = 2.94–2.78$, N—N = 4.01, N—O = 1.21–1.30, O—O = 2.10–2.25.

Structure of $Cu_4(OH)_6(NO_3)_2$

The structural assignment of basic copper nitrate, $Cu_4(OH)_6(NO_3)_2$, is monoclinic with space group $P2_1/m$-C_{2h}^2 (7). Using the notation given for the first setting of the C_{2h}^2 space group

[1]To whom correspondence should be addressed.

[2]Holder of Natural Sciences and Engineering Research Council of Canada Undergraduate Summer Research award.

Can. J. Chem. Downloaded from www.nrcresearchpress.com by 213.166.140.6 on 09/07/12
For personal use only.

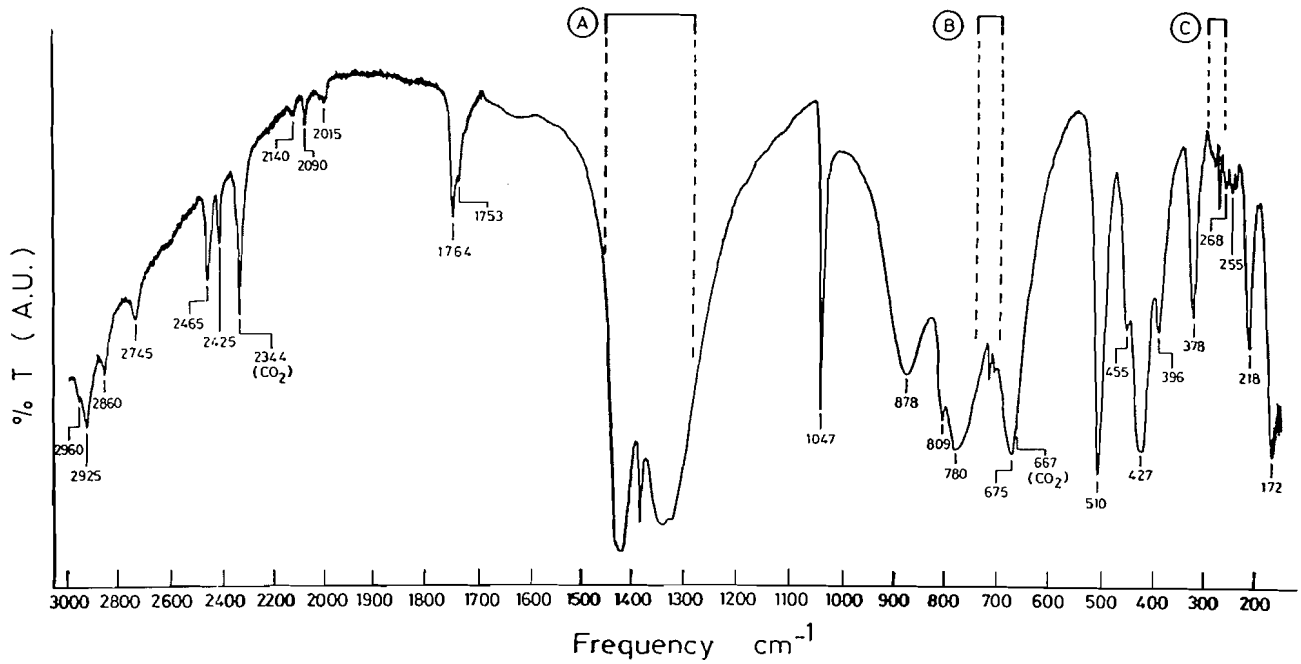

FIG. 2. Infrared spectrum of unannealed $Cu_4(OH)_4(NO_3)_2$ in KBr matrix for region 3000–150 cm^{-1}.

in the International tables for X-ray crystallography (8), we find that only the 2e sites (Wyckoff notation) with C_s symmetry are occupied. The unit cell containing one molecular or formula unit with dimensions, $a_0 = 5.57_6$ Å, $b_0 = 6.05_0$ Å, $c_0 = 6.89_6$ Å, $\beta = 94° 30'$ shown in Fig. 1 is taken from Nowacki and Scheidegger (7). The appropriate interatomic distances are noted in the caption of Fig. 1. The H atom of OH, not shown, forms Cu—O—H bond angle of 118°.

The disposition of the OH groups, their orientations and their intermolecular distances as presented in Fig. 1, suggests three classes of OH entities. The first class is essentially "free" OH with very weak H-bonding represented by OH_I and OH_{II} from Cu_{II} in $Cu_{II}(OH)_5O$ entity projecting out of the O_I—Cu_{II}—OH_{II} plane. The second and third classes are classified as varying degrees of H-bonded OH based on interatomic distances represented by $OH_{II}\ldots O_{II}$ = 2.46–2.60 Å, and $OH_I\ldots O_{II}$ = 2.78 Å.

Figure 1 shows the Cu to have a slightly distorted octahedral coordination with four equal coplanar Cu—OH bonds and two Cu—O bonds. Both oxygens in one pair of Cu_I—O are from the NO_3, i.e. $2O_I$ to form the entity $Cu_I(OH)_4O_2$. The second pair involves one oxygen from NO_3, i.e. O_I and the other oxygen from OH_{II} to form the entity $Cu_{II}(OH)_5O$. The coordination and spatial arrangements with respect to Cu and OH are identical to those in $Cu_4(OH)_6SO_4$ (6, 9). The octahedra are linked to form "layers" parallel to the [001] plane which are held together by H-bonds via NO_3 which are effectively normal to the layer planes.

Factor group analysis of $Cu_4(OH)_6(NO_3)_2$

A unit cell of $Cu_4(OH)_6(NO_3)_2$ containing 24 atoms gives rise to 72 degrees of freedom involving Cu ion motion, OH group external and intramolecular motions, and nitrate external and intermolecular motions. A free nitrate ion belongs to the molecular point group D_{3h} with irreducible representations for internal modes $\Gamma_{int} = A_1' + A_2'' + 2E'$ which correspond to the internal normal modes $\nu_1, \nu_2, \nu_3, \nu_4$, respectively. The low site symmetry C_s of the NO_3 in the cell removes all the degeneracies of the D_{3h} representations to yield nondegenerate A' and A'' representations. From correlation procedure (10) each site group A' representations is found to transfer to $A_g + B_u$ and each A'' to $B_g + A_u$ in the factor group C_{2h}. The number of irreducible representations of the modes for NO_3 is determined to be $4A_g + 4B_u + 2A_u + 2B_g$ for internal vibrational modes and 12 similar representations for translational and rotational modes or external modes. The remaining representations are identified with 6 internal modes for OH, 12 Cu—O—H bending modes, 6 Cu—O stretching modes, 12 O—Cu—O angle deformation modes, and 12 modes for Cu ion motion.

Experimental

$Cu_4(OH)_6(NO_3)_2$ was prepared according to the accepted procedure by the action of moderately concentrated solution of $Cu(NO_3)_2$ on CuO in a stoppered flask with constant stirring at ~100°C for 10 days, and analyzed as described (11, 12).

The infrared transmission spectra were recorded with a Perkin-Elmer 180 spectrophotometer using both the standard compressed KBr disc sample and the Nujol mull sample between polyethylene windows. The observed absorption frequencies were reproducible within 2 cm^{-1} for all of the overlapping spectral regions using both sample techniques. The stock sample was maintained in oven at 150°C before using. Spectra recorded for the undried sample maintained at room temperature showed no discernible difference with the dried sample spectra.

$Cu_4(OH)_6(NO_3)_2$ was annealed in two ways: (*i*) The sample contained in a pyrex tube was heated in a drying oven at 160°C up to 66 h. The sample color transformed from its initial light blue through grey–blue to eventually dark brown. The residue at different stages was used in both the Nujol mull and the KBr disc. The recorded spectra at each stage were indistinguishable from the unannealed sample spectra. (*ii*) The sample was compressed in a KBr matrix to form the disc. The KBr disc sample was annealed in a high temperature cell attachment at 190°C for 3 h. The disc color was dark brown similar to the 66 h at 160°C residue and its spectrum was recorded at room temperature.

Results and discussion

The recorded spectra for the unannealed $Cu_4(OH)_6(NO_3)_2$ are presented in Figs. 2, 3, and 4*a* and interpreted with respect to OH and NO_3 optic modes. Portions of the spectrum of the KBr disc sample annealed at 190°C for 3 h exhibiting different spectral features relative to Figs. 2 and 3 are presented in Fig. 4.

Can. J. Chem. Downloaded from www.nrcresearchpress.com by 213.166.140.6 on 09/07/12
For personal use only.

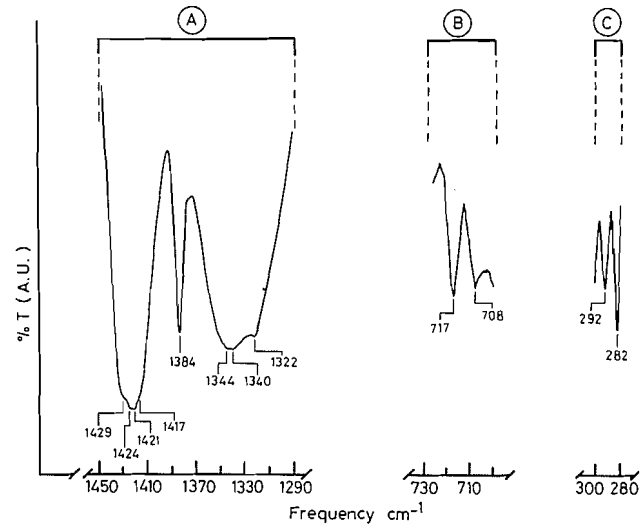

FIG. 3. Expanded portions of spectrum of Fig. 2, A, B, C.

The spectra intensities are given in arbitrary units (A.U.). No HOH bending absorption was observed.

OH absorption

The fundamental vibration frequency for OH occurs over the range 3600–3200 cm^{-1} depending on the degree of H-bonding. Tarte (12) reported the frequencies 3543, 3522, and 3428 cm^{-1} for $Cu_4(OH)_6(NO_3)_2$ whereas we record the frequencies 3550, 3475, and 3415 cm^{-1} as given in Fig. 4*a*, broken line.

The three frequencies indicate three distinct classes of hydroxy groups in the solid structure. The sharp peak at 3550 cm^{-1} is assigned to very weak H-bonded OH identified as OH_I and OH_{II} in $Cu_{II}(OH)_5O$ with interatomic distances of 2.94 and 3.03 Å. The 3550 cm^{-1} frequency is in excellent agreement with values reported for OH groups with no substantial H-bonding in lanthanide (Gd, Nd) basic nitrates (13). The shoulder at 3475 cm^{-1} and the broad band centred at 3415 cm^{-1} are consistent with different degrees of hydrogen bonding expected with OH...O separations ranging from 2.46 to 2.78 Å. These OH...O distances and their OH frequencies are in contrast with those observed for $Cu_4(OH)_6SO_4$ (6), viz. 3572–3596 cm^{-1} at 2.96 and 3.14 Å, 3396 cm^{-1} at 2.87 Å, and 3272 cm^{-1} at 2.65 Å. The distinct differences may be interpreted in terms of (*i*) weaker H-bonding in $OH...ONO_2$ relative $OH...OSO_3$ or (*ii*) non-linear or out-of-plane OH...O configuration in $OH...ONO_2$.

The absorption frequencies 878, 780, 675 cm^{-1} are assigned to Cu—O—H deformation modes paralleling the assignment of 990, 878, 780 cm^{-1} in $Cu_4(OH)_6SO_4$ (6). These assignments are based on the deuterium shift and these frequencies are within ± 2 cm^{-1} of the values reported by Tarte (12). Again the Cu—O—H bending mode frequencies reflect the varying degrees of H-bonding in the OH groups with the highest frequency associated with the strongest H-bridge, viz. 878 cm^{-1}. The fact that the relative magnitude of the shift of the bending mode frequencies, $\Delta\nu_b/\nu_b$, is larger than that of the O—H stretching mode frequencies, $\Delta\nu_s/\nu_s$, by a factor ~4, usually $\Delta\nu_b/\nu_b < \Delta\nu_s/\nu_s$ implies that the bending modes involve coupling in the coordinated units, i.e. $Cu(OH)_4O_2$ and $Cu(OH)_5O$, described above. The Cu—O—H bending mode frequencies show the same separation of ~100 cm^{-1} in both hydroxycompounds with an apparent correlation between the strength of the H-bonded OH and frequency shift. That is, ν_b = 780 cm^{-1} with ν_s = 3550–3596 cm^{-1} for very weak H-bridging and ν_b = 880 vm^{-1} with ν_s = 3400–3470 cm^{-1} for medium strength H-bridging. The extreme frequencies, however, 990 cm^{-1} in $Cu_4(OH)_6SO_4$ and 675 cm^{-1} in $Cu_4(OH)_6(NO_3)_2$ may reflect on the nature of the $Cu(OH)_5O$ entity. $Cu(OH)_5O$ shows five equal Cu—OH distances, ± 0.05 Å, in both compounds but the Cu—O distance is 2.52 Å in the sulphate and 2.18 Å in the nitrate. The assignment of the bands 255–292 cm^{-1} to OH torsional modes parallels the assignment in $Cu_4(OH)_6SO_4$-type compounds (6).

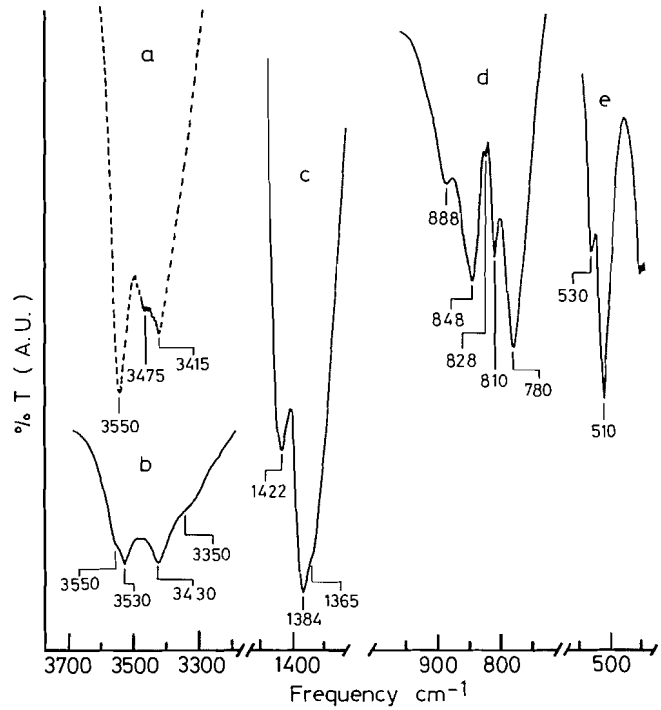

FIG. 4. Portions of infrared spectra of (*a*) unannealed $Cu_4(OH)_6(NO_3)_2$ for region 3700–3200 cm^{-1} and (*b*), (*c*), (*d*), (*e*) annealed $Cu_4(OH)_6(NO_3)_2$ in compressed KBr matrix at 190°C for 3 h.

NO_3 absorption

The reported fundamental vibration frequencies for NO_3 of D_{3h} symmetry (14) are ~1050 (A_1'), ~830 (A_2''), ~1400 (E'), and ~700 (E') where E' and A_2'' are infrared active modes. In the crystal all the fundamental vibration modes for NO_3 of reduced symmetry have been observed in the infrared (1–3) over a range of values, viz. $\nu_1(A_1')$ 1040–1067, $\nu_2(A_2'')$ 801–839, $\nu_3(E')$ 1313–1432, and $\nu_4(E')$ 702–741 cm^{-1}.

The recorded spectra for $Cu_4(OH)_6(NO_3)_2$ over the 3000–150 cm^{-1} region are given in Figs. 2 and 3 with the frequencies noted on the spectra. These frequencies with their assignments along with those of Ag_2BrNO_3, Ag_2ClNO_3, and $AgNO_3$ for comparison purposes are tabulated in Table 1. All the internal optic modes predicted by factor group analysis for NO_3 are observed and identified. It is not possible to interpret all the spectral features with a high degree of confidence but a number of definitive assignments along with comparisons, correlations, and tentative assignments can be made.

The relatively strong sharp $\nu_1(A_1')$ and $\nu_2(A_2'')$ singlet peaks at 1047 cm^{-1} and 809 cm^{-1}, respectively, are in strong contrast to the weak doublets and weak multiplets of their analogous modes in Ag_2BrNO_3 and Ag_2ClNO_3 (3).

The clearly resolved doublet of equal intensities for $\nu_4(E')$ at 708 and 717 cm^{-1} is in obvious contrast to the multiplets of

Can. J. Chem. Downloaded from www.nrcresearchpress.com by 213.166.140.6 on 09/07/12
For personal use only.

TABLE 1. Infrared frequencies of NO_3 in $Cu_4(OH)_6(NO_3)_2$ (cm^{-1})

(*a*) Internal modes

$Cu_4(OH)_6(NO_3)_2$	Ag_2BrNO_3[a]	Ag_2ClNO_3[a]	Assignment
2960, 2925, 2860			Nujol contamination
2745			$2\nu_3$
2465, 2425			$\nu_1 + \nu_3$
2140			$(\nu_3 + \nu_4)$ or $(\nu_2 + \nu_3)$
2090			$2\nu_1$ or $(\nu_3 + \nu_4)$
2015			$(2\nu_3 - \nu_4)$ or $(2\nu_3 - \nu_2)$ or $(\nu_3 + \nu_4)$
1764, 1753	1774, 1763, 1736	1762, 1745, 1740	$\nu_1 + \nu_4$
1429, 1424, 1421, 1417	1430, 1395	1432	ν_3
1384, 1344, 1340, 1322	1382, 1355	1380, 1360	
1047	1049, 1042	1050, 1040	ν_1
890	839, 824, 811, 801	838, 324, 818	ν_2
717, 708	740, 731, 715, 710	741, 732, 712, 709, 702	ν_4

(*b*) External modes

$Cu_4(OH)_6(NO_3)_2$	Ag_2BrNO_3[a]	Ag_2ClNO_3[a]	Assignment
510	520	520	
455	460, 488	462, 448	
427	—	433	
396	406, 382	408, 380	

[a]Reference 3.

varying intensities observed for Ag_2BrNO_3, Ag_2ClNO_3, and $AgNO_3$.

The multiplet structure of $\nu_3(E')$ with 8 identifiable frequencies far exceeds the maximum of 4 possible frequencies permitted by factor group analysis and reported for Ag_2BrNO_3. The 8 frequencies can be interpreted in terms of splitting in E' for each of 2 NO_3, i.e. 4 possible modes with each giving rise to splitting. Such an interpretation raises some questions. Does this splitting involve LO-TO modes and/or varying degrees of dipolar coupling? Can such splitting be specific to $\nu_3(E')$ and not $\nu_4(E')$ or is the multiplet in $\nu_4(E')$ too weak to be detected? Or are these extra features artifacts originating in a superimposed reflectivity component in the matrix?

The appearance of numerous overtone and combination bands assigned to NO_3 is in striking contrast to their absence in spectra of related nitrate compounds. The Nujol bands, viz. 2960, 2925, 2860 cm^{-1}, are included as a point of caution and to illustrate the sensitivity of the instrument in detecting Nujol presence in KBr ground in a mortar previously used to make a Nujol mull after being scrupulously cleaned. The sharp peak at 2344 cm^{-1} and spike at 667 cm^{-1} due to ν_3 and ν_2 of CO_2, respectively, serve as internal references.

The frequencies for the external and lattice modes of NO_3 are also presented in Table 1 along with those observed for Ag_2BrNO_3 and Ag_2ClNO_3. The frequencies and spectra profiles are comparable in both the hydroxy- and halonitrates but the relatively stronger peak intensities ($\times 10$) are evident in $Cu_4(OH)_6(NO_3)_2$ spectra.

Can. J. Chem. Downloaded from www.nrcresearchpress.com by 213.166.140.6 on 09/07/12
For personal use only.

TABLE 2. Remaining observed frequencies in $Cu_4(OH)_6(NO_3)_2$

$Cu_4(OH)_6(NO_3)_2$	$Cu_4(OH)_6SO_4$[a]	Assignment
328, 305	338, 318	ν_s(Cu—O)
292, 282, 268, 255	289, 260, 254	OH torsion
218, 172	228, 172	ν_b(O—Cu—O)

[a]Reference 6.

Table 2 contains the Cu—O stretching, O—Cu—O bending and OH torsional mode frequencies for $Cu_4(OH)_6(NO_3)_2$ and $Cu_4(OH)_6SO_4$. The consistency and agreement between these values and the Cu—O—H bending frequencies of both compounds support the structure and bonding character in the common coordinated units of $Cu(OH)_4O_2$ and $Cu(OH)_5O_2$.

Annealed $Cu_4(OH)_6(NO_3)_2$ in compressed KBr matrix

Most of the absorption frequencies and band profiles recorded in this spectrum are consistent with the spectrum of the unannealed sample spectrum. The portions of this spectrum exhibiting distinctly different or additional features are presented in Fig. 4.

The OH stretch frequency region, Fig. 4*b*, shows a definite change in the band profile along with lower frequency displacements of 20–80 cm^{-1}. The strong Cu—O—H bending mode at 878 cm^{-1} has shifted to 848 cm^{-1} leaving a weaker remnant at 888 cm^{-1} while the 778 cm^{-1} Cu—O—H bending frequency remains unaltered, Fig. 4*d*, suggesting a structural or coordination change in either $Cu(OH)_4O_2$ or $Cu(OH)_5O$.

Figure 4*d* shows $\nu_2(NO_3)$ at 810 cm^{-1} along with a weak satellite at 828 cm^{-1}. In Fig. 4*e* the NO_3 external mode at 510 cm^{-1} is accompanied by a weak satellite at 530 cm^{-1}. Both satellites appear ~20 cm^{-1} above its respective parent peak.

The most striking spectral change is identified with $\nu_3(NO_3)$, Fig. 4*c*. Its two main peaks at 1422 and 1384 cm^{-1} with shoulder at 1365 cm^{-1} are in strong contrast with the comple multiplet observed in the unannealed spectrum.

Due to the lack of information on the exact composition of th sample it is not possible to interpret these spectral feature with confidence. However, the dark brown color betray the presence of CuO from partial decomposition rather tha interaction with KBr. These modified spectral features sugges that CuO molecularly dispersed throughout the undecompose $Cu_4(OH)_6(NO_3)_2$ can affect specific fundamental modes o neighboring species.

Acknowledgements

The authors thank the National Research Council of Canad for an equipment grant to purchase the infrared spectromete and one of us (G.G.W.) is grateful to Natural Sciences an Engineering Research Council of Canada for the Undergraduat Summer Research Award.

1. C. H. HUANG and M. H. BROOKER. Spectrochim. Acta, Part A **32**, 1715 (1976).
2. K. AKIYAMA, Y. MORIOKA, and I. NAKAGAWA. J. Phys. Soc Jpn. (3) **48**, 898 (1979).
3. M. NATARAJAN and E. A. SECCO. J. Solid State Chem. **54** 213 (1984).
4. R. FRECH. J. Chem. Phys. **58**, 5067 (1973).
5. G. J. WU and R. FRECH. J. Chem. Phys. **66**, 1352 (1977).
6. E. A. SECCO. To be published.
7. W. NOWACKI and R. SCHEIDEGGER. Helv. Chim. Acta, **35**, 375 (1952).
8. International tables for X-ray crystallography. Vol. I. Kynoch Press, Birmingham, England. 1952. p. 92.
9. G. COCCO and F. MAZZI. Periodico Mineral. Rome, **28**, 121 (1959).
10. J. R. FERRARO and J. S. ZIOMEK. Introductory group theory and its applications to molecular structure. Plenum Press, New York. 1975.
11. P. RAMAMURTHY and E. A. SECCO. Can. J. Chem. **48**, 3510 (1970).
12. P. TARTE. Spectrochim. Acta, **13**, 107 (1958).
13. D. F. MULLICA, E. L. SAPPENFIELD, and D. A. GROSSIC. J. Solid State Chem. **63**, 231 (1986).
14. K. NAKAMOTO. Infrared spectra of inorganic and coordination compounds. Wiley, New York. pp. 92–94 and references therein. 1963.

Can. J. Chem. Downloaded from www.nrcresearchpress.com by 213.166.140.6 on 09/07/12
For personal use only.

Étude vibrationnelle du méthyl-4 triazole-1,2,4 et de son chlorhydrate

S. ZAYDOUN ET M. SAIDI IDRISSI
Laboratoire de spectroscopie infrarouge, Faculté des sciences, Rabat, Maroc

ET

C. GARRIGOU-LAGRANGE
CRPP, Domaine Universitaire, 33405, Talence, France

Reçu le 9 janvier 1987

S. ZAYDOUN, M. SAIDI IDRISSI et C. GARRIGOU-LAGRANGE. Can. J. Chem. **65**, 2509 (1987).

Les spectres de vibration du méthyl-4 triazole-1,2,4, de son chlorhydrate et de quelques uns de leurs homologues deutériés ont été examinés entre 4000 et 200 cm^{-1}. Une attribution de la plupart des modes fondamentaux a été proposée et l'effet de la protonation sur les fréquences des vibrations normales a été expliqué.

S. ZAYDOUN, M. SAIDI IDRISSI, and C. GARRIGOU-LAGRANGE. Can. J. Chem. **65**, 2509 (1987).

Vibrational spectra of 4-methyl-1,2,4-triazole, its hydrochloride salt, and some of their deuterated homologs have been studied from 4000 to 200 cm^{-1}. An attribution of most of the fundamental modes is proposed, and the effect of protonation on fundamental frequency values is explained.

Can. J. Chem. Downloaded from www.nrcresearchpress.com by 213.222.148.141 on 09/07/12
For personal use only.

Introduction

Le triazole-1,2,4 et ses dérivés jouent un rôle biologique important aussi bien dans le domaine de l'agronomie qu'en pharmacologie (1–4). Leurs sels sont des fongicides actifs (5). Depuis plusieurs années, nous nous intéressons à l'étude de ces composés. Ainsi, dans un précédent travail (6), nous avons examiné les spectres vibrationnels des triazoles-1,2,4 méthylés en position 1 qui représentent des formes «bloquées» correspondant au {1*H*} triazole-1,2,4. En vue de compléter cette étude, nous présentons ici une analyse des spectres vibrationnels du méthyl-4 triazole-1,2,4 (Me4 TA) découlant de la forme {4*H*}. Ce composé a un caractère basique et joue un rôle de donneur d'e^- dans une interaction donneur–accepteur. Nous nous sommes donc également intéressés à son chlorhydrate, afin de noter l'influence de la protonation sur les vibrations fondamentales de la base.

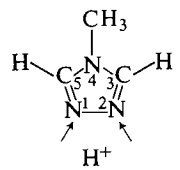

Deux sites de protonation équivalents correspondant aux deux azotes «pyridiniques» sont probables pour ce composé.

Nos résultats précédents (7) et le présent travail montrent que seule la monoprotonation est possible dans le cas des systèmes triazoliques-1,2,4.

I. Partie expérimentale

Le Me4 TA a été préparé en utilisant la méthode de Freund (8). Il a été purifié par chromatographie sur colonne de silice en utilisant un mélange benzène–chloroforme comme éluant.

L'homologue C-deutérié $Me4D_2$-3,5 TA a été obtenu en dissolvant la base dans D_2O et en portant la solution placée dans un tube scellé à 120°C pendant 2 h.

La pureté du Me4 TA ainsi que l'échange hydrogène–deutérium ont été contrôlés par rmn.

Les chlorhydrates de méthyl-4 et de méthyl-4 dideutério-3,5 triazoliums-1,2,4 (Me4 TAH^+ et $Me4D_2$-3,5 TAH^+) ont été obtenus par passage d'un courant de gaz chlorhydrique HCl sec dans une solution de la base dans le chloroforme anhydre. Le sel formé précipite, il est séparé par filtration et séché sous vide. Le Me4 TAH^+ et son dérivé N-deutérié (Me4 TAD^+) ont également été préparés par addition d'une solution aqueuse de HCl ou DCl à la base et par évaporation de l'eau sous vide.

Les dosages du carbone, de l'hydrogène, de l'azote et du chlore pour le Me4 TAH^+ ont donné les résultats suivants :

	% C	% H	% N	% Cl
Exp.	30,39	5,07	33,58	29,10
Calc.	30,13	5,02	35,15	29,71

Les spectres ir ont été enregistrés à l'aide d'un spectromètre Perkin–Elmer 577. Les solides ont été étudiés en suspension dans le Nujol ou dans le Fluorolube, entre des fenêtres de NaCl (4000–600 cm^{-1}) et de silicium ou de polyéthylène (600–200 cm^{-1}).

Les spectres Raman des composés en solution aqueuse ont été obtenus avec un appareil Coderg PH 1, la raie excitatrice étant la raie à 514,5 nm d'un laser spectra physics à gas argon ionisé.

II. Résultats et discussion

II.1. Dénombrement des modes normaux de vibration

En l'absence de données cristallographiques, nous supposons que le cycle triazole garde sa planéite dans le Me4 TA et le Me4 TAH^+ comme pour le triazole-1,2,4 (9) et que ces composés possèdent au plus la symétrie ponctuelle C_s. Dans cette hypothèse, les 27 vibrations fondamentales du Me4 TA peuvent se classer en $18A'$ $(2\nu_{CH} + 2\delta_{CH} + 7R + \nu_{N-CH_3} + \delta_{N-CH_3} + \nu_s + \nu'_s + \delta_s + \delta'_s + r_\parallel)^1$ et $9A''$ $(2\gamma_{CH} + 2R + \gamma_{N-CH_3} + \nu_a + \delta_a + r_\perp + t_{CH_3})^1$ toutes actives en ir et en Raman.

Pour le Me4 TAH^+, trois nouveaux mouvements de vibration sont introduits par addition d'un proton à la molécule (ν_{NH}, δ_{NH}, γ_{NH}).

II.2. Analyse des spectres vibrationnels

Les spectres ir des Me4 TA et Me4 TAH^+ et de leurs homologues deutériés sont représentés sur la figure 1. Les spectres Raman des dérivés hydrogénés sont donnés sur la figure 2. Les attributions des vibrations fondamentales du squelette et du groupement CH_3 sont rassemblées dans les tableaux 1 et 2.

Nous discuterons séparément les vibrations du noyau et celles des groupements exocycliques.

Vibrations des groupements C—H

On relève sur le spectre ir des Me4 TA et Me4 TAH^+ entre

1. La notation utilisée pour désigner les vibrations du noyau est celle précédemment décrite pour le triazole-1,2,4 (10). Pour le groupement CH_3, on a adopté la notation de Forel (11).

Printed in Canada / Imprimé au Canada

Can. J. Chem. Downloaded from www.nrcresearchpress.com by 213.222.148.141 on 09/07/12
For personal use only.

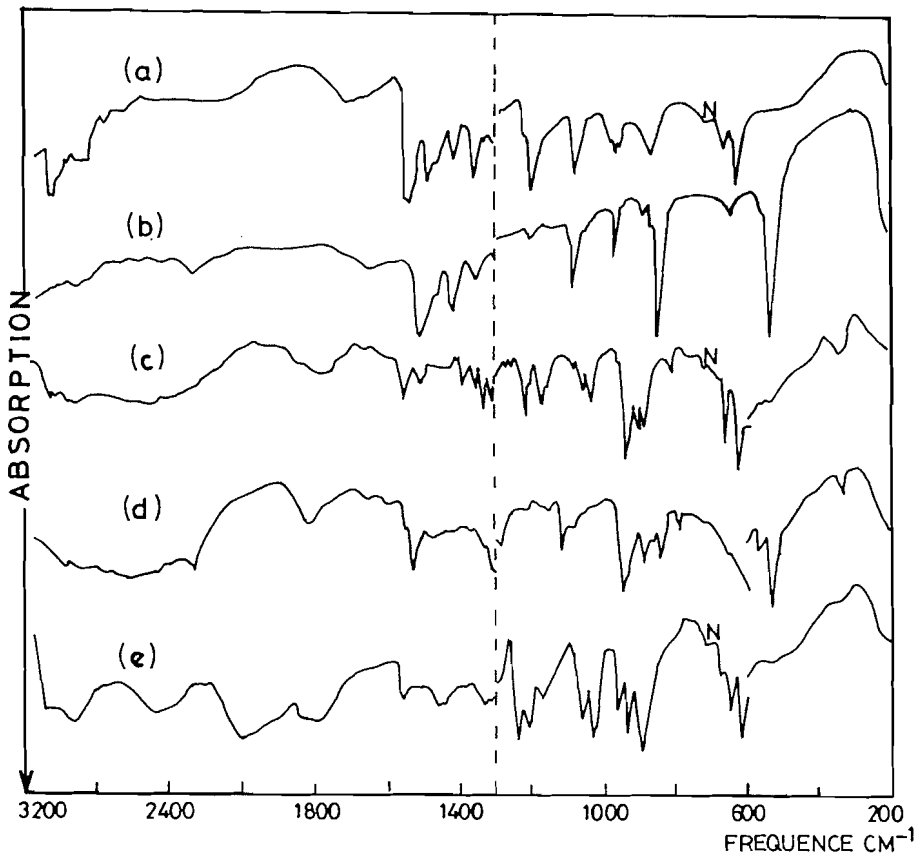

FIG. 1. Spectres infrarouges des (a) Me4 TA, (b) Me4D_2-3,5 TA, (c) Me4 TAH$^+$, (d) Me4D_2-3,5 TAH$^+$ et (e) Me4 TAD$^+$ à l'état solide entre 3200 et 200 cm^{-1}.

3150 et 3020 cm^{-1} trois absorptions situées vers 3110, 3095 et 3055 cm^{-1}. Aux deux premières correspondent en Raman des raies d'intensités moyenne et faible (figure 2). Nous les attribuons aux vibrations de valence ν_{CH} faisant intervenir leurs mouvements en phase et en opposition de phase (tableau 1). Sur le spectre ir de leurs homologues C-deutériés, elles sont remplacées par les deux bandes situées vers 2290 et 2240 cm^{-1} (figure 1). La bande faible vers 3060 cm^{-1} qui disparait par C-deutériation peut correspondre à une harmonique ou combinaison faisant intervenir le vibrateur C—H.

Les bandes observées vers 1210 et 1190 cm^{-1} sur le spectre ir du Me4 TA à l'état solide sont attribuées aux deux vibrations de déformation dans le plan δ_{CH}. En effet, la deutériation spécifique sur le carbone fait disparaître la première et diminuer considérablement l'intensité de la seconde (figure 1). Cette dernière, qui persiste sur le spectre ir du Me4D_2-3,5 TA, ne correspond pas à un reste de produit hydrogéné mais plutôt au mode R_4 superposé au mode δ_{CH} dans la molécule hydrogénée.

La comparaison des spectres ir du Me4 TAH$^+$ et du Me4D_2-3,5 TAH$^+$ (figure 1) nous permet d'attribuer la bande à 1178 cm^{-1} du premier à l'une des deux vibrations δ_{CH}. Le comportement semblable des deux bandes du Me4 TAH$^+$, obtenues à 1218 cm^{-1} et 1089 cm^{-1} par deutériation sur le carbone, et le fait que le spectre Raman du cation non deutérié présente deux raies d'intensité moyenne et forte, respectivement, et polarisées, nous incitent à attribuer celles-ci aux modes couplés $R_4 + \delta_{CH}$. Les vibrations δ_{CD} sont observées dans les composés C-deutériés vers 880 et 840 cm^{-1} (tableau 1, figure 1).

Par analogie avec le méthyl-1 triazole (6), la bande large et

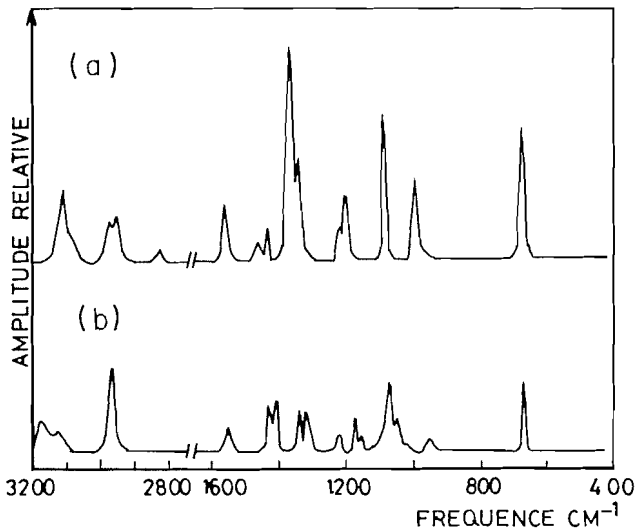

FIG. 2. Spectres Raman des (a) Me4 TA et (b) Me4 TAH$^+$ en solution aqueuse entre 3200 et 400 cm^{-1}.

dissymétrique située vers 870 cm^{-1} sur le spectre ir du Me4 TA (figure 1) est attribuée aux deux modes γ_{CH} superposés. Par contre, dans le cas du Me4 TAH$^+$, deux bandes sont vues à 902 et 889 cm^{-1}, correspondant aux deux vibrations γ_{CH}. L'apparition de ces deux bandes est vraisemblablement due au fait que les deux vibrateurs C—H sont dans un environnement différent.

Deux bandes γ_{CD} apparaissent sur les spectres ir des deux

TABLEAU 1. Attribution des vibrations fondamentales du squelette des Me4 TA, Me4 TAH^+ et de leurs dérivés C-deutériés

Me4 TA	$Me4D_2$-3,5 TA	Me4 TAH^+	$Me4D_2$-3,5 TAH^+	Attribution
3110	2290	3112	2270	$\nu_{CH(CD)}$
3095	2240	3100	—	$\nu_{CH(CD)}$
		2600	2600	ν_{NH}
1535	1494	1572	1540	R_1
1411	1403	1394	1370	R_2
1360*	1348	1315	1318	R_3
1189	1194	1218	1120	R_4; $R_4 + \delta_{CH}$
1211	876	1089	889	$\delta_{CH(CD)}$; $\delta_{CH} + R_4$
1189	842	1178	841	$\delta_{CH(CD)}$
		1163	1160	δ_{NH}
1077	1080	1062	1090	R_5
982	—	1041	1038	R_6
966	967	940	947	R_7
870	560	902	569	$\gamma_{CH(CD)}$
870	523	889	532	$\gamma_{CH(CD)}$
		940	940	γ_{NH}
669	665	660	660	R_8
627	648	623	625	R_9
676†	—	671†	—	ν_{NCH_3}
—	—	—	—	δ_{NCH_3}

*Attribution faite d'après le spectre infrarouge du composé en solution dans $CDCl_3$.
†Attribution faite d'après le spectre Raman.

TABLEAU 2. Attribution des vibrations fondamentales du groupement méthyle

Composé	Vibration							
	ν_a	ν_s	ν'_s	δ_a	δ_s	δ'_s	$r_\perp$	$r_\parallel$
Me4 TA	3010	2930	2962	1450	1350*	1480	1060	952
$Me4D_2$-3,5 TA	3005	—	2950	1450	1348	1470	1065	949
Me4 TAH^+	3000	2949	—	1432	1340	1480	1089	—
$Me4D_2$-3,5 TAH^+	3000	—	—	1430	1340	1490	1070	958

*Attribution faite d'après le spectre infrarouge du composé en solution dans $CDCl_3$.

molécules $Me4D_2$-3,5 TA et $Me4D_2$-3,5 TAH^+ vers 560 et 520 cm^{-1}.

Vibrations du noyau

Les mouvements de vibration dans le plan du noyau triazolique, R_1–R_7, donnent lieu à des absorptions auxquelles correspondent des raies de diffusion d'intensité moyenne à forte. À la bande ir à 1354 cm^{-1} observée sur le spectre du Me4 TA à l'état solide correspondent deux raies à 1361 et 1338 cm^{-1}, polarisées sur le spectre Raman de la solution aqueuse (figure 2), et deux bandes à 1360 et 1350 cm^{-1} sur le spectre ir du Me4 TA en solution dans le chloroforme deutérié. La forte intensité de la première raie nous incite à l'attribuer au mode R_3 (tableau 1).

Le tableau 1 montre que les modes R_4 et δ_{CH} sont superposés. En effet, une modification du spectre ir dans la région 1300–1100 cm^{-1} par deutériation sur le carbone est observée (figure 1).

Deux bandes intenses entre 1600 et 1500 cm^{-1} existent sur le spectre ir du cation Me4 TAH^+. L'absorption intense relevée vers 1570 cm^{-1} à laquelle correspond une raie Raman polarisée est attribuée au mode R_1 (figures 1 et 2, tableau 1). La bande située à 1525 cm^{-1} est très perturbée par la deutériation sur l'atome d'azote. Elle pourrait correspondre à une combinaison faisant intervenir le vibrateur N—H. Remarquons que le mode R_1 subit une augmentation en fréquence par protonation. Cela peut s'expliquer par l'effet électronique dû à la présence de la charge positive sans exclure un léger couplage avec le mode δ_{NH}. En effet, R_1 baisse légèrement en fréquence par N-deutériation.

Les vibrations R_2 et R_3 sont situées vers 1390 et 1315 cm^{-1} et sont abaissées par rapport au Me4 TA. L'examen des spectres du cation N-deutérié permet de conclure que ces abaissements de fréquence sont dus à une intéraction de ces modes avec la vibration δ_{NH}.

Le mode R_4 est situé vers 1218 cm^{-1}; un fort couplage a été noté pour ce mouvement avec l'une des vibrations δ_{CH} (cf. vibrations des groupements C—H).

À la vibration R_5 correspond l'absorption à 1062 cm^{-1}. La fréquence de ce mode n'est pas modifiée par N-deutériation, ce qui permet de penser que l'abaissement de sa fréquence par protonation est vraisemblablement dû à la modification de la densité de charge dans le noyau.

Les modes R_6 et R_7 sont situés à 1041 et 940 cm^{-1}; leur comportement vis à vis de la protonation est différent. La N-deutériation met en évidence une interaction de R_7 avec δ_{NH}.

Les vibrations de type A″ sont souvent faibles en Raman. Dans le cas du Me4 TA, elles n'ont pas été observées. Nous les avons donc situées à partir du spectre ir en nous basant sur la méthode des suites et la deutériation sur le carbone. Ainsi, les bandes observées vers 670 et 630 cm^{-1} sont attribuées, comme

Can. J. Chem. Downloaded from www.nrcresearchpress.com by 213.222.148.141 on 09/07/12
For personal use only.

Can. J. Chem. Downloaded from www.nrcresearchpress.com by 213.222.148.141 on 09/07/12
For personal use only.

dans les systèmes triazoliques déjà examinés (6), aux deux vibrations du cycle R_8 et R_9. Elles sont peu déplacées par protonation (tableau 1).

Vibrations du groupement N—CH_3

Le spectre Raman des Me4 TA et Me4 TAH^+ présente une raie forte et polarisée vers 660 cm^{-1} attribuable à la vibration de valence $\nu_{N—CH_3}$ (figure 2, tableau 1). L'absorption correspondant à ce mode est, comme dans le cas du méthyl-1 triazole (6), superposée à celle assigné à R_8 et située vers 670 cm^{-1} (figure 1, tableau 1). La vibration $\delta_{N—CH_3}$ n'a pas été localisée. Le mode $\gamma_{N—CH_3}$ n'est pas observé car il est situé en dessous de 200 cm^{-1}.

Vibrations du groupement méthyle

On observe sur le spectre ir du Me4 TA un massif situé entre 3010 et 2800 cm^{-1} dont l'aspect ressemble à ceux observés pour le méthyl-4 dibromo-3,5 triazole[2] et le méthyl-4 bromo-3 triazole (6). Nous avons attribué la bande de plus haute fréquence à la vibration ν'_s car il lui correspond une raie moins intense que celle correspondant à la vibration ν_s. La bande ir vers 2820 cm^{-1} est attribuable, par analogie avec d'autres composés hétérocycliques méthylés (13), à une combinaison $\delta_a + \delta_s$ ou $\delta'_s + \delta_s$. Les bandes vers 2900 et 2705 cm^{-1} peuvent correspondre, comme dans le toluène (14, 15), aux harmoniques $2\delta_a$ et $2\delta_s$, respectivement.

Dans le cas du dérivé protoné, le massif ν_{NH} masque en ir les vibrations de valence ν_{CH_3}. Les attributions que nous proposons sur le tableau 2 sont donc bassées sur les spectres Raman et sur les spectres ir des systèmes N-deutériés.

Par analogie avec les attributions déjà proposées pour les vibrations du méthyle dans plusieurs dérivés triazoliques N-méthylés (6), nous situons les modes δ'_s et δ_a vers 1480 et 1450 cm^{-1}, respectivement (tableau 2). La vibration δ_s est localisée vers 1350 cm^{-1}. On attribue l'épaulement relevé vers 1060 cm^{-1} au mouvement $r_\perp$ et la bande observée vers 950 cm^{-1} au mode $r_\parallel$. Les fréquences de ces vibrations sont peu perturbées par la protonation sur l'azote.

La vibration de torsion t_{CH_3} est attendue en dehors de notre domaine d'étude (13, 15).

Vibrations du groupement N—H

Les spectres ir des chlorhydrates sont caractérisés par l'existence d'un massif large, intense et riche en sous-maximums qui s'étend de 3200 à 1950 cm^{-1} (figure 1). Son centre de gravité est situé vers 2600 cm^{-1}. La deutériation sur l'azote provoque son déplacement vers 2010 cm^{-1}. Ce massif est attribuable comme dans les chlorhydrates d'halogéno triazoliums-1,2,4 (7) à la vibration ν_{NH} du vibrateur N—H introduit par la protonation; il est engagé dans une liaison hydrogène forte de type $NH^+ \ldots Cl^-$ avec l'anion, comme en témoigne sa fréquence de vibration. Cependant, une association de type $NH^+ \ldots IN$ ne peut pas être exclue. Les sous-maximums observés peuvent s'expliquer, comme dans le cas des ions pyridinium (16) et imidazolium (12) par l'existence d'une résonance de Fermi entre la vibration fondamentale ν_{NH} et des harmoniques ou des combinaisons binaires. La structure du massif ν_{ND} est moins complexe que celle du massif ν_{NH} du fait que ces deux massifs apparaissent dans deux régions différentes du spectre qui ne font pas appel aux mêmes combinaisons et harmoniques.

2. M. Saidi Idrissi. Travaux non publiés.

Aucune raie correspondant à la vibration ν_{NH} n'est observée en diffusion.

Les spectres ir présentent également dans cette région un massif moins large et moins intense que le premier, sous la forme d'un triplet et centré vers 1800 cm^{-1} (figure 1). La deutériation sur l'azote ne modifie ni son aspect ni la fréquence du centre de gravité.

L'absorption relevée à 1163 cm^{-1} sur le spectre ir du Me4 TAH^+ est attribuée au mode δ_{NH}, car elle disparait lors de la N-deutériation.

La bande située vers 940 cm^{-1} est assignée au mode γ_{NH} superposé à la vibration R_7 dans ce système. En effet, l'aspect de cette bande est modifié considérablement sur le spectre ir du cation Me4 TAD^+, qui présente en plus une bande à 650 cm^{-1} attribuable au mode γ_{ND} (figure 1).

Conclusion

L'analyse des spectres vibrationnels du méthyl-4 triazole et de son homologue deutérié nous a permis de proposer une attribution de la plupart des modes fondamentaux de cette molécule. La protonation du méthyl-4 triazole-1,2,4 aboutit à la fixation d'un seul proton sur l'un des azotes pyridiniques. L'étude des spectres vibrationnels du chlorhydrate obtenu montre que l'addition d'un proton provoque des variations de fréquence de la plupart des vibrations fondamentales. Les spectres des cations deutériés nous ont permis d'expliquer ces variations par deux causes :

(*i*) Couplage des mouvements de vibration avec le nouveau vibrateur N—H.

(*ii*) Modification de la répartition de la densité de charge électronique due à la présence d'une charge positive sur le cycle.

1. M. K. Mody, A. R. Prassad, T. Ramalingam et P. B. Sattur. J. Ind. Chem. Soc. **59**, 769 (1982).
2. W. Rudnicka et Z. Asmialowska. Acta Pol. Pharm. **36**, 411 (1979).
3. P. H. Freeman, P. A. Worthington et W. G. Rathmell. Eur. Pat. Appl. EP 0046, 337 (1980).
4. C. Rentzea, K. H. Fenerherd, B. Zeeh et J. Jung. Eur. Pat. Appl. EP 0044, 407 (1982).
5. K. P. Parry, P. A. Worthington et W. G. Rathmell. Eur. Pat. Appl. **15**, 756 (1980).
6. M. Saidi Idrissi, M. Sénéchal, H. Sauvaitre et C. Garrigou-Lagrange. Can. J. Chem. **61**, 2133 (1983).
7. M. Saidi Idrissi, H. Sauvaitre et C. Garrigou-Lagrange. J. Chim. Phys. **80**, 739 (1983).
8. M. Freund. Ber. **29**, 2483 (1896).
9. P. Goldstein, J. Ladell et G. Abowitz. Acta Crystallogr. Sect. B: Struct. Crystallogr. Cryst. Chem. B**25**, 135 (1969).
10. B. Saint Roch. Thèse, Bordeaux. 1972.
11. M. T. Forel et M. Fouassier. Spectrochim. Acta, Part A: **24**, 311 (1968).
12. A. M. Bellocq et C. Garrigou-Lagrange. Spectrochim. Acta, Part A: **27**, 1091 (1971).
13. M. T. Forel. Thèse, Bordeaux. 1962.
14. N. Fuson, M. L. Josien, J. Deschamps, C. Garrigou-Lagrange et M. T. Forel. Bull. Soc. Chim. Fr. 93 (1959).
15. N. Fuson, C. Garrigou-Lagrange et M. L. Josien. Spectrochim. Acta, **16**, 106 (1960).
16. R. Foglizzo et A. Novak. J. Chim. Phys. **66**, 1539 (1969).

Orientation behaviour of chlorobenzene in nematic solvents

C. T. YIM

Department of Chemistry, Dawson College, 350 Selby St., Westmount, P.Q., Canada H3Z 1W7

AND

D. F. R. GILSON

Department of Chemistry, McGill University, 801 Sherbrooke St., W., Montreal, P.Q., Canada H3A 2K6

Received April 7, 1987

C. T. YIM and D. F. R. GILSON. Can. J. Chem. **65**, 2513 (1987).

The orientational order parameters of monochlorobenzene have been determined, as functions of temperature and concentration, in two nematic solvents, EBBA and ZLI-1132. There are significant differences in the orientation of the solute molecule in the two solvents as reflected in the values of corresponding potential energy parameters as well as in the concentration dependence of the order parameters. These differences are caused mainly by a stronger interaction between the aromatic ring and the solvent ZLI-1132, since the change in the potential function terms for chlorobenzene parallel those for unsubstituted benzene. Attempts to correlate the orientation potential with molecular polarizability and molecular shape lead to the conclusion that neither of these properties plays a dominant role in determining the potential.

C. T. YIM et D. F. R. GILSON. Can. J. Chem. **65**, 2513 (1987).

On a déterminé les paramètres d'ordre orientationnel du monochlorobenzène, en fonction de la température et de la concentration, dans deux phases nématiques, soit le EBBA et le ZLI-1132. Il y a des différences importantes dans l'orientation de la molécule de soluté dans les deux solvants; ces différences sont mises en évidence par les paramètres d'énergie potentielle correspondants à chacun des solvants ainsi que par le fait que les paramètres d'ordre varient avec la concentration. Ces différences proviennent principalement d'une interaction plus forte entre le cycle aromatique et le solvant ZLI-1132; en effet, le changement dans les termes de la fonction de potentiel du chlorobenzène est parallèle à celui observé dans le benzène qui n'est pas substitué. On a effectué des essais dans le but d'établir une corrélation entre le potentiel d'orientation et la polarisabilité moléculaire et la forme moléculaire; on en déduit que ni l'une ni l'autre de ces propriétés ne joue un rôle dominant dans la détermination du potentiel.

[Traduit par la revue]

Can. J. Chem. Downloaded from www.nrcresearchpress.com by 213.166.140.6 on 09/07/12
For personal use only.

Introduction

Liquid crystals are now commonly used in display devices (1, 2). Recent developments in this area utilize the ability of the anisotropic solvent to orient dichroic dye molecules to improve contrast or add colour properties. In these applications, the degree of orientation of the solute molecule in the liquid crystal solvent is of considerable importance. The measurement of both solute and solvent orientation parameters also provides experimental data essential for the understanding of anisotropic intermolecular interactions and for testing the theories of ordered phases.

The elements of the ordering matrix for fairly simple molecules can be easily obtained from the analysis of the high resolution nmr spectrum of the solute molecule dissolved in a nematic liquid crystal solvent (3). The spectrum of the solute is dominated by the direct intramolecular dipolar couplings and may contain many lines. This direct intramolecular dipolar coupling is a function of both the internuclear distance and the average orientation of the internuclear vector with respect to the external magnetic field. Analysis of the spectrum therefore leads to information about both the geometry of the solute molecule and its orientation in the solvent. A large number of molecules have been studied by this method. However, in most of these studies the attention has been focused solely on the molecular structure, while the orientational order parameters have been treated as a "by-product" of lesser significance. Saupe has shown that calculation of the orientation parameters by a simple bond additive model gave approximate agreement with the experimental values for several fluoro- and chlorobenzenes (4, 5), and later studies have attempted to correlate the available orientation data with molecular shape (6), polarizability (7, 8, 10, 11), moments of inertia (9), repulsive forces (10, 11), and by empirical relationships (12). Recently, a few studies have been reported that specifically investigate the orientation of the solute molecule as a function of temperature and concentration in different types of nematic solvents (10, 11, 13–20). Attempts have also been made to relate the temperature and concentration dependence of the order parameters to reduced variables (13, 14).

The solute order parameters are entirely determined by the orientation dependent part of the intermolecular interaction potential. In its simplest form, the effective pseudopotential experienced by a solute molecule can be written as

$$[1] \quad V = -kT(a[1]\cos^2\theta_1 + a[2]\cos^2\theta_2 + a[3]\cos^2\theta_3)$$

where θ_i are the Euler angles specifying the orientation of the molecule-fixed 1,2,3-axial system to the director of the liquid crystal solvent, and the constants $a[i]$ characterize the interaction energy along the corresponding axis. These constants reflect both solute and solvent contributions. If the solute molecule is rigid, as in the case discussed in the present work of a planar aromatic molecule, then eq. [1] can be further simplified to a two-parameter equation. For example, if the 3-direction is taken as the long molecular axis and the 2-axis to be perpendicular to the aromatic ring,[1] Fig. 1, then the equation can be rewritten (15, 6) as

$$[2] \quad V(\theta,\phi) = -kTQ(\sin^2\theta\cos^2\phi + R\cos^2\theta)$$

where

$$Q = (a[1] - a[2])$$

[1] In refs. 6 and 15 the axes are labelled differently, with the 3-axis perpendicular to the ring and the 2-axis the long molecular axis.

and

$$R = (a[3] - a[2])/(a[1] - a[2])$$

and θ and φ are the polar and azimuthal angles, respectively. If dispersion forces play an exclusive role in determining the orientation, then the parameter R should be constant for a given solute molecule, leaving Q as the only term involving the solvent contribution. Attention is usually focused on the parameter R, which measures the relative strength of interaction along the two principal axes within the plane of the aromatic ring, and the experimental values for several different solutes have been compared with those calculated for various different molecular properties (6, 10, 11, 15, 17).

An alternative approach is possible, whereby the relative orientations can be compared by substituting the following parameters:

$$A = a[3] - (1/2)(a[1] + a[2])$$

$$B = (a[1] - a[2])/(2a[3] - a[1] - a[2])$$

and eq. [1] is rewritten as

$$[3] \quad V(\theta,\phi) = -kTA(\cos^2\theta + B\sin^2\theta\cos 2\phi)$$

Equation [3] is essentially the same as that derived by Emsley *et al.* (18). Provided that the potential function is determined by dispersion forces only, then the parameter B should be independent of temperature and solvent and dependent only on the anisotropy of polarizability of the solute molecule. Of course, eqs. [2] and [3] are equivalent and the parameters therein are related:

$$Q = 2AB$$

$$R = (1/2B) + 0.5$$

In this study we will adopt the second form, i.e., eq. [3], as the orientation potential.

In the present paper we report the results of an investigation of the temperature and concentration dependence of the orientational order of monochlorobenzene in two different nematic solvents: EBBA and ZLI-1132. This molecule has been studied previously (21–24), but not specifically in terms of its orientation in thermotropic liquid crystal solvents.

Experimental

Two liquid crystal solvents were used: (*a*) ZLI-1132, a mixture of cyanophenylcyclohexanes and cyanobiphenylcyclohexanes, which was supplied by BDH Chemicals Ltd., and (*b*) EBBA (*N*-(*p*-ethoxybenzylidine)-*p'*-*n*-butylaniline), which was synthesized and purified by literature methods (25).

Chlorobenzene (Fisher Scientific, bp 131.5–131.7°C) was used without further purification. Samples of various concentrations were prepared by weighing appropriate amounts of solute and solvent into nmr tubes and then sealing under vacuum. The concentrations of the samples studied are listed in Table 1.

The proton nmr spectra were recorded on Varian XL-200 and XL-300 spectrometers, without deuterium lock. The sample temperatures were calibrated against the proton chemical shift difference in an ethylene glycol sample. The spectra were recorded using a 5-μs pulse, an acquisition time of 1.5 s, and a spectral width of 5–12 kHz, and between 64 and 192 free induction decays were accumulated to obtain an acceptable signal-to-noise ratio, depending on the concentration. The spectral analyses were performed with a modified LAOCN 3 program using either an IBM PC or Olivetti M-24 microcomputer.

Results and discussion

The optimized geometry was obtained by fitting to the dipolar coupling constants obtained from room temperature spectra,

TABLE 1. Concentration dependence of the nematic to isotropic transition temperature and the average A' and B parameters for chlorobenzene dissolved in ZLI-1132 and EBBA

Solvent	Concentration (mol%)	$T_{N\rightarrow I}$ (K)	A' ($\times 10^{-21}$ J/mol)	B
ZLI-1132	15.5	326.2	10.8	0.591
	7.1	336.9	11.5	0.605
	2.9	341.4	11.8	0.602
	1.1	344.0	12.1	0.607
EBBA	12.7	325.3	6.87	0.249
	7.2	338.0	7.66	0.255
	3.8	346.0	8.17	0.262
	2.2	349.0	8.28	0.263

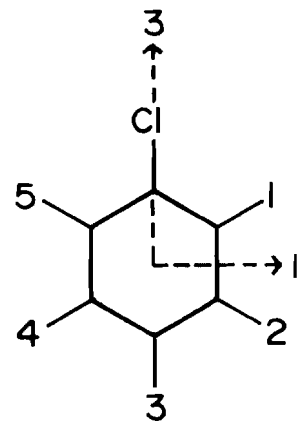

FIG. 1. Coordinate system and atomic labelling for chlorobenzene.

and the same geometry was used for analyzing the spectra recorded at other temperatures. For chlorobenzene in EBBA the geometry found is in agreement with that of Jacobsen and Schaumburg (22). The optimized geometry in ZLI-1132 is slightly different: specifically, the relative internuclear distances between H2 and H3 and between H2 and H4 are longer, and between H1 and H5 shorter, when compared with the corresponding values in EBBA (see Fig. 1 and Table 2). Vibrational effects were ignored in calculating the order parameters. Emsley *et al.* (18) have examined the effect of vibrational averaging on the derived values of order parameters and concluded that the effect is small and can be neglected in studying the orientation behavior and its variation with temperature.

Since chlorobenzene possesses two perpendicular planes of symmetry, only two of the five independent elements of the Saupe order matrix are required, and these are conveniently expressed as S_{33}, and $(S_{11} - S_{22})$. They can be obtained from the orientation potential via the expressions:

$$S_{33} = (3/2Z)\int\int(\cos^2\theta\exp\{-V(\theta,\phi)/kT\}\sin\theta\,d\theta d\phi) - (1/2)$$

$$S_{11} - S_{22} = (3/2Z)\int\int(\sin^2\theta\cos 2\phi\exp\{-V(\theta,\phi)/kT\} \times \sin\theta\,d\theta\,d\phi)$$

where

$$Z = \int\int\exp\{-V(\theta,\phi)/kT\}\sin\theta\,d\theta\,d\phi$$

Here the 3-axis is taken as the long molecular axis and the 2-axis to be perpendicular to the ring plane, Fig. 1. At any one temperature, the values of S_{33} and $S_{11} - S_{22}$ are sufficient

Can. J. Chem. Downloaded from www.nrcresearchpress.com by 213.166.140.6 on 09/07/12
For personal use only.

TABLE 2. Inter-proton distances (Å) in chlorobenzene

	ZLI-1132	EBBA	Ref. 22
r_{12}	2.486*	2.486*	2.486*
r_{13}	4.299	4.301	4.304
r_{14}	4.965	4.964	4.965
r_{15}	4.274	4.294	4.289
r_{23}	2.494	2.482	2.484
r_{24}	4.322	4.299	4.302

*Assumed.

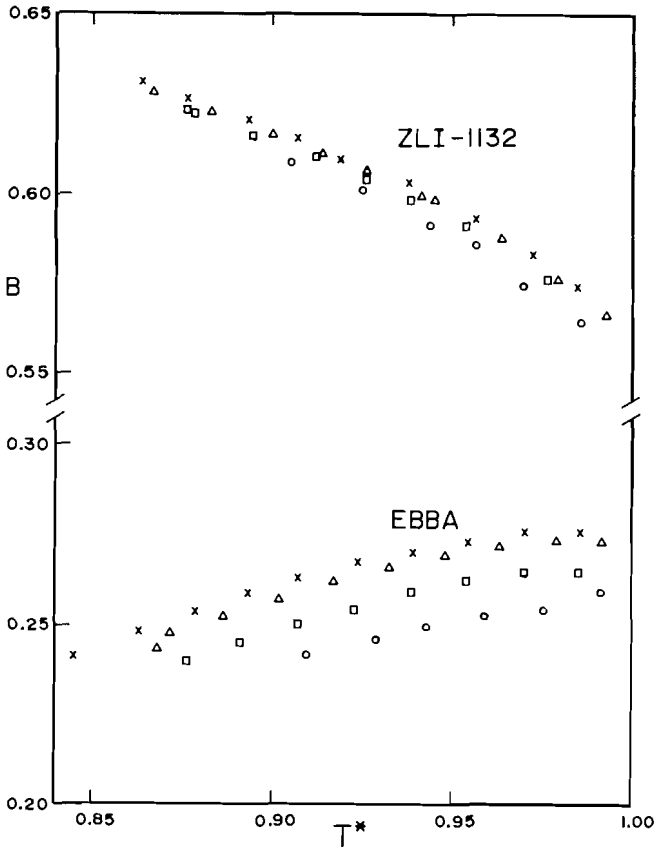

FIG. 2. Dependence of the parameter B on reduced temperature. Concentrations (in mol%) in ZLI-1132: ○, 15.5; □, 7.1; △, 2.9; ×, 1.1; and in EBBA: ○, 12.7; □, 7.2; △, 3.8; ×, 2.2.

to determine the parameters A and B in eq. [3]. The values of B so obtained are plotted against reduced temperature, T^* ($= T/T_{N\rightarrow I}$), in Fig. 2. The most obvious feature of these plots is the strong solvent dependence of B (or R in eq. [2]). Figure 2 also shows that there is a significant variation of B with both temperature and concentration. For chlorobenzene in EBBA, the value of B tends to increase with increasing temperature, while in ZLI-1132 it tends to decrease. This is in conflict with the theory, which predicts that B should be a molecular property and independent of temperature and solvent.

The average B values for each concentration are listed in Table 1. To eliminate the concentration dependence, the average B value was plotted against concentration and extrapolated to give B_0, i.e., the B value at infinite dilution, and these values are given in Table 3. For comparison, the B(pol) and B(vdW), which are calculated using polarizability (26) and van der Waals dimensions respectively, are also listed. Even if allowance is made for the uncertainties in these calculated

TABLE 3. Potential energy parameters B_0, A_0, and A_0B_0

Solvent	B_0	B_{pol}	B_{vdW}	A_0 ($\times 10^{-21}$ J/mol)	A_0B_0
ZLI-1132					
Chlorobenzene	0.610	0.486	0.437	12.1	7.39
Benzene	1.0	—	—	7.23	7.23
EBBA					
Chlorobenzene	0.267	0.486	0.437	8.66	2.31
Benzene	1.0	—	—	2.88	2.88

quantities, it is obvious there is little or no agreement with the experimental values. Therefore we conclude that neither of these properties plays a dominant role in determining the orientation behavior of chlorobenzene in the two solvents, in agreement with the results of Emsley *et al.* on the orientation of perdeuterated anthracene (20). Jokisaari and co-workers observed that, for the three solutes *ortho*- and *meta*-difluorobenzene (11, 17) and monoiodobenzene (10), similar R values are observed in solvents ZLI-1132 and ZLI-1167, and they suggested that dispersion forces are decisive in determining the solute order in these two solvents. However, variations in the solvent and temperature dependence of B and (or) R have been reported for numerous other cases (10, 11, 15–20) and specific solute–solvent interactions have been invoked to explain the observed behaviour. In their study of the orientation of perdeuterated anthracene, Emsley *et al.* (20) used six different solvents. This is the most extensive study reported so far on the effect of solvent on orientation, and yet there was no obvious correlation between the orientation and the nature of the solvent. Neither dispersion nor repulsion forces appeared to dominate. A qualitative improvement, leading to the correct temperature variation, was obtained by extending the potential function to include a fourth-rank term.

As expected, the values of A, derived by fitting the experimental order parameters, are temperature and concentration dependent. The measurements of the orientation are, of course, made at constant pressure and not at constant density, and, within the framework of the mean field theory of Maier and Saupe, the term kTA in eq. [3] is expected to be dependent on both the solvent order and on the average intermolecular separation (27, 28). Both are temperature dependent, and to include this eq. [3] is rewritten:

$$[5]\quad V(\theta,\phi) = -(A'SV_m^{-\gamma})(\cos^2\theta + B\sin^2\theta\cos 2\phi)$$

with the substitution $kTA = A'(SV_m^{-\gamma})$, where S is the solvent order, V_m is the molar volume, and the exponent γ specifies the volume dependence. A' is expected to be a constant for a given solvent–solute pair.

Experimental data on both solvent order parameters and densities are available and we will take advantage of the fact that the order parameter of the solvent is a function of reduced temperature and is, therefore, independent of the solute and its concentration (29, 30). For EBBA, the order parameters were obtained from wide-line nmr spectra[2] and the specific volumes have been measured by Bahadur and Chandra (32). For ZLI-1132, both the specific volume and order parameter data have been reported by Bahadur *et al.* (33). The dipolar splitting of the nmr absorption can be related directly to the order parameter, since it depends upon the *ortho* proton distance and

[2]D. F. R. Gilson, unpublished results.

Can. J. Chem. Downloaded from www.nrcresearchpress.com by 213.166.140.6 on 09/07/12
For personal use only.

TABLE 4. Relative values of energy parameter A_0 (the A_0 value for benzene in EBBA is taken as 1.00)

Solvent	Volume dependence	Relative A_0			
		Benzene		Chlorobenzene	
EBBA	V^0	1.00		3.01	
	V^2	1.00		3.00	
	V^4	1.00		2.98	
ZLI-1132	V^0(N)*	2.51		4.21	
	(V)*		2.53		4.26
	V^2(N)	2.39		4.00	
	(V)		2.41		4.05
	V^4(N)	2.27		3.82	
	(V)		2.29		3.84

*(N) and (V) stand for Neugebauer's and Vuks approach respectively.

orientation, but in the case of ZLI-1132, the order parameters were determined from refractive index measurements and this approach is subject to some controversy (34–38). It is claimed (34–37) that the method due to Neugebauer (39) is superior to that proposed by Vuks (40), but, in the present work, we have evaluated the A' values for ZLI-1132 based on order parameter data derived by both methods (33). The dependence of parameter A' on the volume is introduced into eq. [5] by assuming different fixed values of the exponent γ: $\gamma = 0$ (no volume dependence), $\gamma = 2$ (attractive forces), and $\gamma = 4$ (repulsive forces). The molar volume is assumed to behave in the same fashion as the order parameter, i.e., dilute solution and pure solvent will have the same volume at the same reduced temperature. The A_0 values (the A' at infinite dilution) are then obtained by extrapolation.

The results for both solvent systems are presented in Table 4. Since the values cannot be compared directly for different γ values, the A_0 values are given relative to that of benzene in EBBA. The results for chlorobenzene/ZLI-1132 clearly show that values derived for the two sets of order parameters differ only slightly, but the different volume dependence does affect the results; an increase in γ from 2 to 4 decreases the A_0 values in ZLI-1132 by 5% relative to those in EBBA. An attempt to find the "best" values of γ, by varying the exponent to yield A' values of least variance, gave exponents of 1 and 5 for ZLI-1132, using data from Neugebauer's and Vuks' approaches, respectively, and zero for EBBA. Clearly, the available data on the order parameters and molar volumes of nematic solvents are not precise enough to draw definite conclusions regarding the volume dependence, but, in spite of these uncertainties, a constant relative A_0 value is obtained.

Since neither the use of different sets of order parameters nor the different volume dependence has a significant effect, any set of A' and A_0 values can be used for further discussion of the orientation behaviour. For simplicity, we have chosen the values that are obtained assuming $\gamma = 0$, and, for ZLI-1132, using the order parameters from Neugebauer's approach. In Table 1 the resulting average A' is listed for each of the systems studied. The corresponding values of A_0, A_0B_0, and those of unsubstituted benzene[3] are given in Table 3.

The term A_0 corresponds to a potential energy difference between orientations of the solute molecules with axis-3 parallel and perpendicular to the liquid crystal director, while A_0B_0 corresponds to the difference between axis-1 and axis-2 oriented parallel to the director (see eqs. [2] and [3]). The larger A_0 and A_0B_0 values observed in ZLI-1132 imply a stronger interaction, which causes the chlorobenzene molecules to correlate their orientations with those of host molecules more effectively in ZLI-1132 than in EBBA. For solutions of different concentrations of the same solute, a plot of the order parameter of the liquid crystal solvent vs. reduced temperature, T^*, results in a universal curve (29), but attempts to show that the solute order behaves in much the same way led to contradictory conclusions (13, 14). The present results for chlorobenzene are plotted as a function of reduced temperature T^* in Fig. 3. In both solvents the results do show a small but definite concentration dependence, which is larger in EBBA than in ZLI-1132.

The variation of the nematic to isotropic transition temperature with concentration has been considered as an indication of solute–solvent compatibility (42, 43). The slopes of the $T_{N\rightarrow I}$ vs. concentration (mole fraction) plots are 133 and 216 K mol^{-1} for chlorobenzene in ZLI-1132 and in EBBA, respectively, and clearly demonstrate that chlorobenzene molecules are more capable of correlating their molecular orientations with those of ZLI-1132 than with EBBA, and hence are less effective in disordering this solvent.

A comparison of these energy parameters for chlorobenzene and benzene indicates that the replacement of a C—H by C—Cl on the benzene ring increases A_0 by approximately the same amount in both solvents. The changes in A_0B_0 are much smaller; in ZLI-1132 this quantity remains almost unchanged. The difference in A_0B_0 values of chlorobenzene in the two solvents is reasonably close to the corresponding difference for unsubstituted benzene (5.08 vs. 4.35×10^{-21} J/mol), therefore chlorine substitution is not the major contributor to the differences in orientation in these two solvents. The data in Table 3 further show that the larger B for chlorobenzene in ZLI-1132 is mainly due to the potential energy parameter A_0B_0. The contribution of A_0 is relatively small and tends to reduce the difference in B values in the two solvent systems. The strong solvent dependence of B is largely due to the difference in the contribution of the benzene ring to the total interaction energy. This may be interpreted as an indication that specific solute–solvent interactions are important in determining orientation order, in particular, the preferred location of the solute molecule at a given region of the solute.

The physical properties of a number of cyano-containing nematic liquid crystals, such as cyanobiphenyls, cyanophenylcyclohexanes, and cyanocyclohexylcyclohexanes, have been interpreted in terms of an antiparallel molecular association or correlation (44, 45). The association leads to the formation of dimers and involves both polar and apolar interactions. On the other hand, dielectric measurements have indicated that there is little dipole–dipole correlation in MBBA (31). It seems reasonable to assume that the same type of interaction exists between the aromatic moiety of the chlorobenzene molecules and the cyanophenyl group of ZLI-1132. The interaction restricts the orientation freedom of the ring plane with respect to the director, and is, therefore, responsible for the observed difference in A_0B_0 values in the two solvents.

In their recent studies of a series of molecules with C_3 or higher symmetry, dissolved in these same two solvents, Burnell and co-workers (41) concluded that the ordering of the solutes involves both the size and shape of the solute and the interaction of the molecular quadrupole moment with the solvent electric

[3]C. T. Yim and D. F. R. Gilson, unpublished results.

Can. J. Chem. Downloaded from www.nrcresearchpress.com by 213.166.140.6 on 09/07/12
For personal use only.

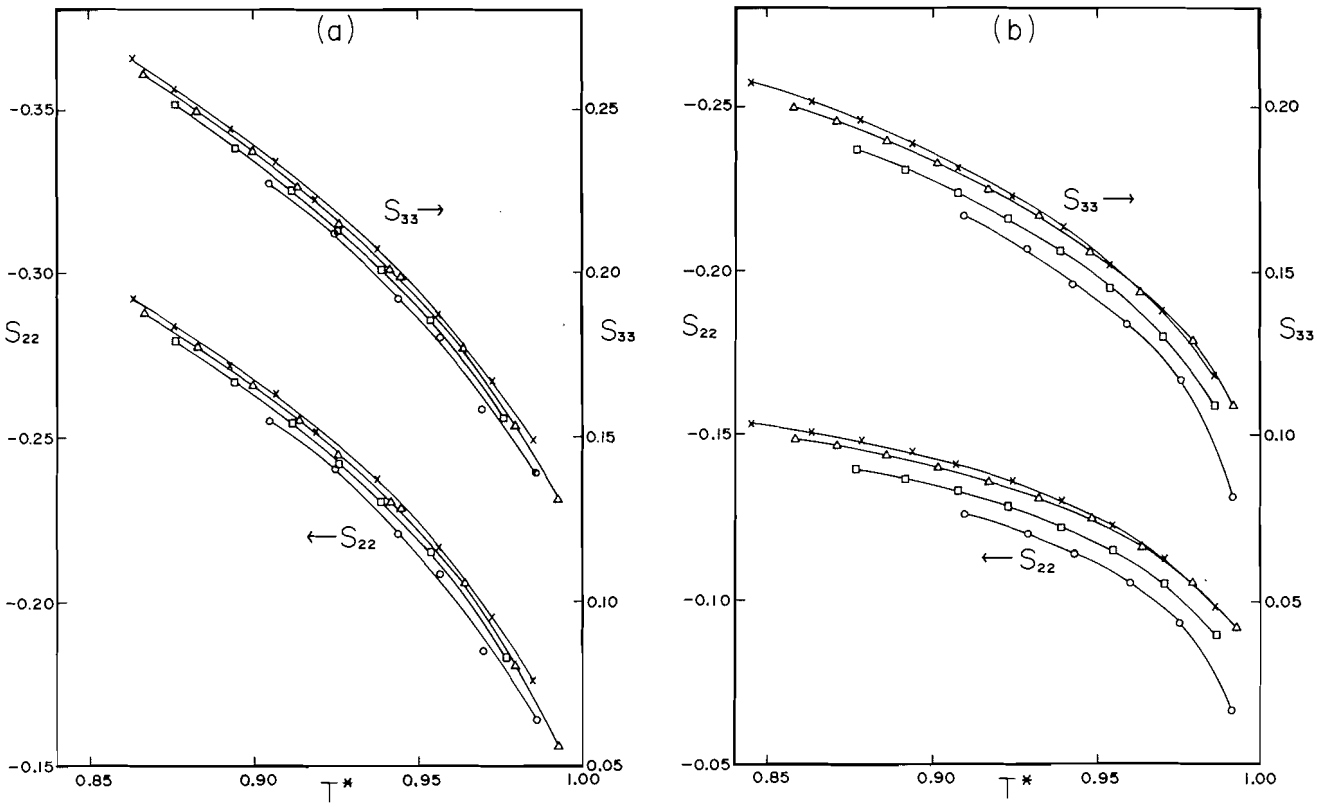

FIG. 3. Variation of order parameters, S_{33} and S_{22}, of chlorobenzene with reduced temperature; (*a*) in solvent ZLI-1132; (*b*) in solvent EBBA. Symbols as in Fig. 2.

field gradient. This model predicts that an aromatic ring system should interact more strongly with the solvent ZLI-1132, which is in agreement with the present results.

Acknowledgements

This work was supported by grants from FCAR (Quebec) (to C.T.Y.) and NSERC (to D.F.R.G.).

1. G. W. GRAY. Proc. R. Soc. London Ser. A, **402**, 1 (1985).
2. G. MEIER, E. SACKMANN, and J. G. GRABMAIER. Applications of liquid crystals. Springer Verlag, Berlin. 1975.
3. J. W. EMSLEY and J. C. LINDON. NMR spectroscopy using liquid crystal solvents. Pergamon Press, New York. 1975.
4. A. SAUPE. Mol. Cryst. **1**, 527 (1966).
5. J. NEHRING and A. SAUPE. Mol. Cryst. Liq. Cryst. **8**, 403 (1969).
6. J. C. ROBERTSON, C. T. YIM, and D. F. R. GILSON. Can. J. Chem. **49**, 2345 (1971).
7. E. SACKMANN and H. MOHWALD. Chem. Phys. Lett. **12**, 467 (1972).
8. E. SACKMANN, P. KREBS, H. U. REGA, J. VOSS, and H. MOHWALD. Mol. Cryst. Liq. Cryst. **24**, 283 (1973).
9. J. M. ANDERSON. J. Magn. Reson. **4**, 231 (1971).
10. J. JOKISAARI, T. VAANANEN, and J. LOUNILA. Mol. Phys. **45**, 141 (1982).
11. T. VAANANEN, J. JOKISAARI, and J. LOUNILA. J. Mag. Reson. **49**, 73 (1982).
12. K. G. ORRELL and V. SIK. J. Chem. Soc. Faraday Trans. 2, **71**, 1360 (1975).
13. D. F. HILLENBRAND and H. YU. J. Chem. Phys. **67**, 957 (1977).
14. Y. P. LEE and D. F. R. GILSON. J. Chem. Phys. **70**, 2042 (1979).
15. D. F. R. GILSON. Mol. Cryst. Liq. Cryst. **104**, 173 (1984).
16. D. CATALANO, C. FORTE, C. A. VERACINI, and C. ZANNONI. Israel J. Chem. **23**, 283 (1983).
17. T. VAANANEN, J. JOKISAARI, and J. LOUNILA. J. Magn. Reson. **54**, 436 (1983).
18. J. W. EMSLEY, R. HASHIM, G. R. LUCKHURST, G. N. RUMBLES, and F. R. VILORIA. Mol. Phys. **49**, 1321 (1983).
19. R. HASHIM, G. R. LUCKHURST, and S. ROMANO. Mol. Phys. **56**, 1217 (1985).
20. J. W. EMSLEY, R. HASHIM, G. R. LUCKHURST, and G. N. SHILSTONE. Liq. Cryst. **1**, 437 (1986).
21. D. CANET, E. HALOUI, and H. NERY. J. Magn. Reson. **10**, 121 (1973).
22. J. P. JACOBSEN and K. SCHAUMBURG. J. Magn. Reson. **28**, 1 (1977).
23. A. S. TRACEY. Mol. Phys. **33**, 339 (1977).
24. P. DIEHL and J. JOKISAARI. J. Mol. Struct. **53**, 55 (1979).
25. H. KELKER and B. SCHEURLE. Angew. Chem. Int. Ed. Engl. **8**, 884 (1969).
26. O. EXNER. Dipole moments in organic chemistry. George Thieme, Stuttgart. 1975.
27. G. R. LUCKHURST. *In* The molecular physics of liquid crystals. *Edited by* G. R. Luckhurst and G. W. Gray. Academic Press, London. 1979. Chap. 4.
28. D. H. CHEN, P. G. JAMES, and G. R. LUCKHURST. Mol. Cryst. Liq. Cryst. **8**, 71 (1969).
29. J. R. MCCOLL. J. Chem. Phys. **62**, 1593 (1975).
30. B. KRONBERG, D. F. R. GILSON, and D. PATTERSON. J. Chem. Soc. Faraday 2, **72**, 1673 (1976).
31. D. A. DUNMUR and W. H. MILLER. Mol. Cryst. Liq. Cryst. **60**, 281 (1980).
32. B. BAHADUR and S. CHANDRA. J. Phys. C: Solid State Phys. **9**, 5 (1976).
33. B. BAHADUR, R. K. SARNA, and V. G. BHIDE. Mol. Cryst. Liq. Cryst. **72**, 139 (1982); Mol. Cryst. Liq. Cryst. **82**, 183 (1982).
34. I. H. IBRAHIM and HAASE. Z. Naturforsch. A: Phys. Phys. Chem. Kosmophys. **31**, 1644 (1976).

Can. J. Chem. Downloaded from www.nrcresearchpress.com by 213.166.140.6 on 09/07/12
For personal use only.

35. H. S. SUBRAMHANYAM and J. S. PRASAD. Mol. Cryst. Liq. Cryst. **37**, 23 (1976).
36. H. S. SUBRAMHANYAM, C. S. PRABHA, and D. KRISHNAMURTI. Mol. Cryst. Liq. Cryst. **28**, 201 (1974).
37. D. BARBERO, R. MALVANO, and M. OMINI. Mol. Cryst. Liq. Cryst. **39**, 69 (1977).
38. W. H. DE JEU and P. BORDEWIJK. J. Chem. Phys. **68**, 109 (1978).
39. H. E. J. NEUGEBAUER. Can. J. Phys. **32**, 1 (1954).
40. M. F. VUKS. Opt. Spectrosc. (Engl. Transl.) **20**, 361 (1966).
41. A. J. VAN DER EST, M. Y. KOK, and E. E. BURNELL. Mol. Phys. **60**, 397 (1987).
42. D. E. MARTIRE. *In* The molecular physics of liquid crystals. *Edited by* G. R. Luckhurst and G. W. Gray. Academic Press, London. 1979. Chap. 10.
43. G. A. OWEIMREEN, G. C. LIN, and D. E. MARTIRE. J. Phys. Chem. **83**, 2111 (1979).
44. K. TORIYAMA and D. A. DUNMUR. Mol. Cryst. Liq. Cryst. **139**, 123 (1986).
45. N. V. MADHUSUDANA and S. CHANDRASEKHAR. Proceedings of International Liquid Crystals Conference, Bangalore, Dec. 1973. Pramana Supplement, I, p. 57.

Can. J. Chem. Downloaded from www.nrcresearchpress.com by 213.166.140.6 on 09/07/12
For personal use only.

Unambiguous structural and nuclear magnetic resonance spectral characterization of two triterpenoids of *Maprounea guianensis* by two-dimensional nuclear magnetic resonance spectroscopy

STEWART MCLEAN,[1] MARION PERPICK-DUMONT, AND WILLIAM F. REYNOLDS[1]
Department of Chemistry, University of Toronto, Toronto, Ont., Canada M5S 1A1

AND

HELEN JACOBS AND SAGAR SINGH LACHMANSING
Centre for Natural Products Chemistry, University of Guyana, Georgetown, Guyana

Received March 24, 1987

STEWART MCLEAN, MARION PERPICK-DUMONT, WILLIAM F. REYNOLDS, HELEN JACOBS, and SAGAR SINGH LACHMANSING. Can. J. Chem. **65**, 2519 (1987).

It is shown that $^{1}H-^{13}C$ shift-correlated two-dimensional spectra obtained for polarization transfer via two-bond and three-bond $^{13}C-^{1}H$ coupling can, in conjunction with related experiments, be used to assign unambiguously the molecular skeletons of two of the less common triterpenes, moretenone and 3-acetylaleuritolic acid. It is concluded that this is a technique of considerable generality for assigning structures of triterpenes and is more reliable than alternative approaches such as mass spectral fragmentation patterns. It has the additional benefit of simultaneously providing reliable ^{13}C and ^{1}H spectral assignments for these compounds.

STEWART MCLEAN, MARION PERPICK-DUMONT, WILLIAM F. REYNOLDS, HELEN JACOBS et SAGAR SINGH LACHMANSING. Can. J. Chem. **65**, 2519 (1987).

On a démontré que si on utilise les spectres de correlation homonucléaire bidimensionnels $^{1}H-^{13}C$, optimisés pour le transfert de polarisation par le biais de couplages $^{13}C-^{1}H$ à travers deux ou trois liaisons, de concert avec des expériences qui leurs sont reliées, on peut attribuer d'une façon qui n'est pas ambigue le squelette moléculaire de deux des triterpènes les moins communs, soit la moréténone et l'acide acétoxy-3 aleuritolique. On conclut que cette technique est très générale pour l'attribution de structures de triterpènes et qu'elle est plus sure que d'autres approches comme les patrons de fragmentation en spectrométrie de masse. De plus, cette technique fournit de même coup des attributions sures pour les spectres en résonance magnétique nucléaire du ^{13}C et du ^{1}H de ces composés.

[Traduit par la revue]

Can. J. Chem. Downloaded from www.nrcresearchpress.com by 213.166.140.6 on 09/07/12
For personal use only.

Triterpenoid derivatives are among the most common natural products isolated from plants (1). However, they are particularly difficult to characterize because of their extremely complex spectra, the large number of possible isomers, and the relative similarities of physical and spectral properties for different isomers. Mass spectral fragmentation patterns have been used for assigning molecular skeletons of triterpenes (2). However, as will be shown below, this is not a completely reliable technique. Consequently, there is an obvious need for an unambiguous technique for assigning structures of the less common triterpenes.

We have recently shown that two-dimensional $^{1}H-^{13}C$ shift-correlated nmr spectra optimized for polarization transfer between protons and carbons separated by two or three bonds (3–5) provide a reliable and relatively sensitive technique for total assignment of ^{13}C and ^{1}H spectra of known triterpenes (6). In this report, we demonstrate how the same approach can be used to assign the molecular structures and spectra of two uncommon triterpenoid derivatives, moretenone and 3-acetylaleuritolic acid. It is concluded that this is a technique of considerable generality for assigning structures of triterpenes.

Results and discussion

The two compounds mentioned above were isolated during the course of a detailed phytochemical investigation of *Maprounea guianensis* Aubl. (Euphorbiaceae). This plant has a reputation in Guyana as a medicinal agent (7) while the related *M. africana* has been shown to produce triterpenes with cytotoxic activity (8). Both crystalline components were isolated from the $CHCl_3$ extract of stem bark of *M. guianensis* (see Experimental). Their structural and spectral characterization is discussed below.

Characterization of moretenone

Low resolution mass spectrometry indicated a molecular weight of 424 for the first compound. The ^{1}H nmr spectrum showed six methyl singlets in the range of δ 0.69–1.08. A further slightly broadened methyl peak was observed at δ 1.68 along with a pair of weakly coupled olefinic protons at δ 4.68 and δ 4.70, indicating the presence of an isopropenyl group. No other ^{1}H signals were observed below δ 2.55. The infrared spectrum showed a strong band at 1700 cm^{-1} while the ^{13}C spectrum showed a peak at δ 218, both indicative of a carbonyl group. Normal and DEPT-edited (9) ^{13}C spectra indicated the presence of seven CH_3 groups, eleven CH_2 groups (one olefinic), five CH groups, and seven nonprotonated carbons. Allowing for one oxygen from a carbonyl group, this corresponds to an empirical formula of $C_{30}H_{48}O$, i.e., a molecular weight of 424.

A preliminary search of the literature revealed that one common triterpene, which had the correct empirical formula and which contained the anticipated functional groups, was lupenone, **1** (1). However, comparison of our ^{13}C spectral data with those reported by Wenkert *et al.* for lupenone (10) showed a number of significantly different chemical shifts, particularly for carbons assigned by Wenkert to rings D and E and the isopropenyl group. This suggested that our compound was an isomer of **1**, most likely involving structural differences in ring E. A further literature search revealed no compound with ^{13}C spectral data that were in agreement with our data.

[1]Authors to whom correspondence may be addressed.

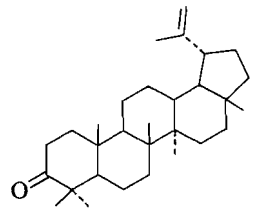

1

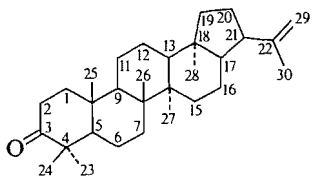

2

To elucidate the structure of this triterpene, three $^1H-^{13}C$ shift-correlated 2D nmr spectra were obtained. The first was a standard experiment with delay times optimized for $^1J_{CH}$ (11), which established connectivities between directly bonded carbons and hydrogens (Table 1). The next two experiments used delay times optimized for two-bond and three-bond $^1H-^{13}C$ couplings. They were obtained using the pulse sequence XCORFE (5). The first of the two experiments was optimized for couplings involving methyl protons ($^2J_{CH} \simeq {}^3J_{CH} \simeq 4.5$ Hz) (12). Cross-peaks involving methyl protons are particularly useful in triterpenes since the methyl groups are strategically located around the periphery of these molecules (e.g., see **1**), providing a network of two-bond and three-bond connectivities, which effectively tie the molecule together.

Results of this experiment are summarized in Table 1 with typical cross-sectional plots through specific ^{13}C frequencies shown in Fig. 1. The methodology used for making spectral assignments was similar to that described in detail by Reynolds *et al.* (6). The starting point was two methyl groups (δ_H 1.03, δ_C 26.5 and δ_H 1.08, δ_C 21.1), which showed cross-peaks with each other. This is only consistent with the presence of a *gem*-dimethyl group (6), assigned as C-23 and C-24, by analogy with **1**. In support of this assignment, both methyl protons gave additional cross-peaks with the carbonyl carbon (C-3), a quaternary carbon at δ 47.4 (C-4), and a methine carbon at δ 54.9 (C-5). The latter carbon showed an additional cross-peak with the methyl ^1H signal at δ 0.93_5, assigned as H-25 (see Fig. 1*a*).

The patterns of cross-peaks due to H-25, H-26, and H-27, as well as the chemical shifts and numbers of attached protons for carbons showing cross-peaks with these methyl protons, indicated that the structures of rings A, B, and C were identical to that shown in **1**. For example, the methine carbon at δ 49.7 (C-9) shows cross-peaks with methyl ^1H signals assigned as H-25 and H-26 (see Fig. 1*b*), as expected for **1**. However, the methine carbon assigned as C-13 showed both the expected cross-peak with H-27 and an additional cross-peak at δ 0.69 assigned to H-28 (Fig. 1*c*). This indicates that this methyl group must be bonded to C-18 (see **2**), rather than to C-17 as in **1**. The remaining cross-peaks for H-28 (see Table 1) were consistent with this assignment.

The key remaining uncertainty is the location of the isopropenyl group. The remaining methine group (δ_H 2.25, δ_C 47.9) was assigned as the point of attachment of the isopropenyl group, based on the characteristic allylic shift of the ^1H signal and an observed cross-peak of this carbon to the methyl ^1H signal at δ 1.68. This methine group was assigned as C-21, based on a second XCORFE spectrum with delay times optimized for $^nJ_{CH}$ couplings involving CH and CH_2 protons. A value of 0.062 s was chosen for the fixed delay, T_1, prior to polarization transfer. This corresponds to an optimum of $^nJ_{CH} = 8$ Hz, approximately the maximum expected value for this type of coupling (12). Results of this experiment are summarized in Table 1 with key cross-sectional spectra shown in Fig. 2. The XCORFE sequence allows distinction between $^1H-C-^{13}C(H)$ and $^1H-C-C-^{13}C(H)$ cross-peaks since the former show vicinal coupling along the f_1 (^1H) frequency axis while the latter are fully ^1H-decoupled (5). The only limitation is the f_1 data point resolution (8 Hz in this case). Peaks with vicinal couplings larger than 8 Hz appear as doublets or multiplets, peaks with couplings of ca. 8 Hz appear as broad singlets, while peaks with smaller couplings are not significantly broadened beyond the data point resolution. Bearing this in mind, a cross section through the unassigned methylene carbon at δ 27.3 shows broad ^1H peaks at δ 2.25 and δ 1.05 and a sharper peak at δ 1.51 (Fig. 1*d*). The former corresponds to the allylic methine proton while the latter two are due to the previously assigned C-19 methylene protons. Therefore, the δ 27.3 carbon must be flanked by C-19 and the allylic methine carbon, i.e., it is C-20, while the isopropenyl group must be bonded to C-21 (see **2**). The stereochemistry at C-21 was deduced from the observation of a 12-Hz coupling between H-21 and H-17, indicating an *anti* orientation for these hydro-

TABLE 1. Assigned ^{13}C and ^1H chemical shifts for **2**, along with observed $^{13}C-^1H$ cross-peaks used in making the assignments

Carbon	n_H[a]	δ_C[b]	δ_H[c]	C—H connectivities[d]
1	2	39.57	1.42, 1.94	H-25, H-2(b)[e]
2	2	34.19[f]	2.42, 2.51	—
3	0	218.14	—	H-23, H-24
4	0	47.37	—	H-23, H-24
5	1	54.85	1.32	H-23, H-24, H-25
6	2	19.74	1.46, 1.53	H-5(d),[e] H-7(d)[e]
7	2	32.58	1.31, 1.51	H-26
8	0	41.64	—	H-26, H-27
9	1	49.70	1.35	H-25, H-26, H-9,[e] H-11[e]
10	0	36.82	—	H-25
11	2	21.54	1.40, 1.52	H-9(d)[e]
12	2	23.92	1.42, 1.52	H-13(d),[e] H-11
13	1	48.71	1.45	H-27, H-28
14	0	42.31	—	H-26, H-27, H-15[e]
15	2	32.61	1.23, 1.42	H-27
16	2	20.83	1.19, 1.41	H-15(b),[e] H-17(b)[e]
17	1	53.82	1.01	H-28
18	0	44.20	—	H-28
19	2	40.17	1.05, 1.51	H-28
20	2	27.32	1.46, 1.86	H-19(b),[e] H-21(b)[e]
21	1	47.86	2.25	H-30, H-29[e]
22	0	148.09	—	H-30
23	3	26.58	1.08	H-24
24	3	21.13	1.03	H-23
25	3	15.78	0.93_5	—[g]
26	3	16.48	1.02_5	—[g]
27	3	16.51	0.95	—[g]
28	3	15.17	0.69	—[g]
29	2	109.56	4.68, 4.70	H-30
30	3	19.66	1.68	H-29[e]

[a]Number of attached hydrogens from DEPT spectra.
[b]^{13}C chemical shifts (δ scale).
[c]^1H chemical shifts (δ scale).
[d]Cross-peaks observed in $^1H-^{13}C$ shift correlated spectra optimized for polarization transfer from CH_3 protons unless otherwise indicated.
[e]Cross-peak observed in spectrum optimized for CH or CH_2 protons; (b) indicates broadened peak, while (d) indicates doublet.
[f]Assigned from cross-peaks between H-2 protons and C-1.
[g]Assigned from direct $^1H-^{13}C$ spectrum plus methyl ^1H assignments from XCORFE spectrum.

Can. J. Chem. Downloaded from www.nrcresearchpress.com by 213.166.140.6 on 09/07/12
For personal use only.

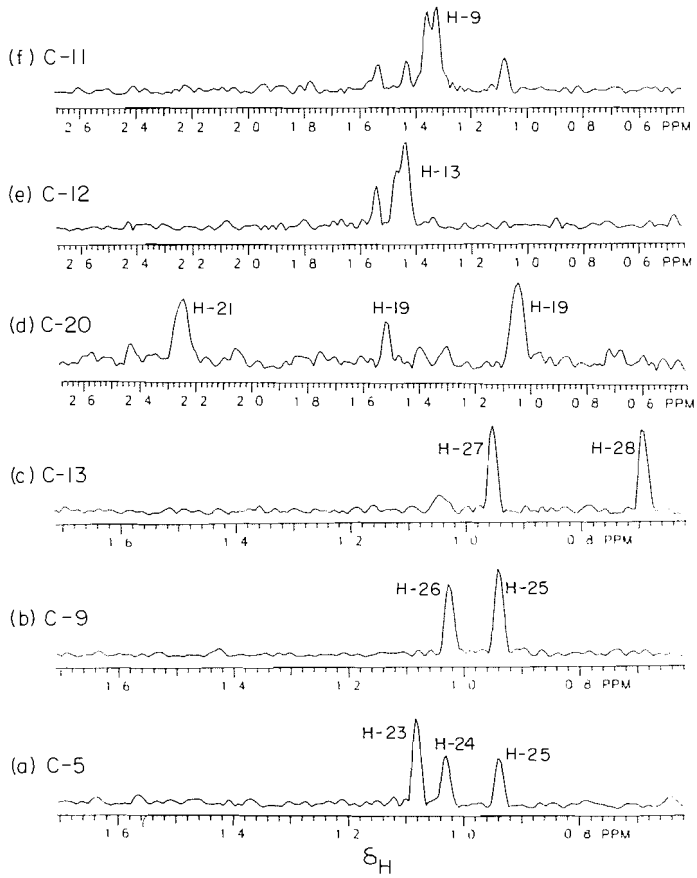

FIG. 1. Typical cross-sectional plots through specific ^{13}C (f_2) frequencies from XCORFE spectrum for **2**, illustrating two- or three-bond connectivities to the labelled ^1H (f_1) signals. Spectra 1(a)–(c) are from the XOCORFE spectrum optimized for polarization transfer from CH_3 groups, while 1(d)–(f) are from the spectrum optimized for polarization transfer from CH and CH_2 groups.

gens. Remaining carbon assignments were straightforward from the second XCORFE spectrum. For example, C-12 and C-11 were assigned on the basis that their cross sections (Figs. 1*e* and 1*f*) showed, respectively, doublets for H-13 and H-9.

A further search of the literature revealed that **2** (with the illustrated stereochemistry) has been assigned by Lavie *et al.* to moretenone, a constituent of *Euphorbia lateriflora* (13). There have been no subsequent reports of the isolation of moretenone from other plant sources. The physical constants and ^1H spectral data for our compound are in good agreement with those reported for moretenone (13) while differing significantly from those reported for hopenone, the C-21 epimer of **2** (14).

Characterization of 3-acetylaleuritolic acid

The second compound had physical and spectral properties, including mass spectral fragmentation patterns, which were very similar to those reported for 3-acetylmaprounic acid, **3**, which had been isolated from *M. africana* (8). In view of the similar plant source, we initially assumed that our compound was **3**. However, DEPT-edited ^{13}C spectra indicated two fewer methine carbons than **3** plus an additional quaternary carbon and an additional methylene carbon, i.e., our compound must be an isomer of **3**.

Consequently, we undertook a set of experiments similar to

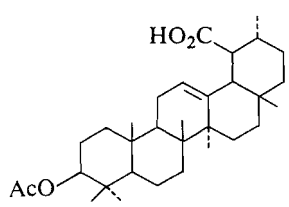

3

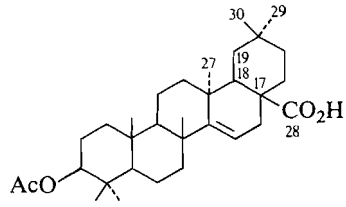

4

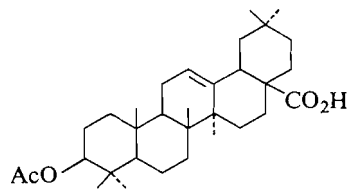

5

those used for **2**, to elucidate the structure of the second compound. The ^1H–^{13}C shift-correlated spectrum in $CDCl_3$ showed that two methyl ^1H signals (corresponding to carbons at δ 15.6 and δ 26.1) overlapped at $\delta\ 0.95_5$. A second spectrum in C_6D_6 showed overlap of a different pair of methyl ^1H signals (corresponding to carbons at δ 16.5 and δ 28.6) at $\delta\ 0.93_5$. However, comparison of the two spectra indicated that all methyl ^1H signals should be resolved in ca. 75% C_6D_6:25% $CDCl_3$ solvent mixture. This was in fact observed (see Fig. 2). Consequently this solvent mixture was used to obtain an XCORFE spectrum with delay times optimized for polarization transfer from methyl protons (Fig. 2). Results are summarized in Table 2.

Analysis of the cross-sectional spectra indicated the presence of two *gem*-dimethyl groups. One of these groups showed additional cross-peaks with a quaternary carbon and two methylene carbons while the second showed additional cross-peaks with a quaternary carbon and two methine carbons. One of the methine carbons (δ 80.5) has a chemical shift characteristic of a carbon bearing an oxygen substituent, while the second (δ 55.7) shows an additional cross-peak with a third methyl ^1H signal. This indicates a structure for ring A similar to **3** with the second *gem*-dimethyl group being C-23 and C-24 and the third methyl ^1H signal corresponding to H-25. Analysis of other cross-peaks involving H-25 and H-26 suggests that ring B is also identical to **3**. However, cross-peaks involving H-26 and H-27 revealed key differences in rings C and D. In structure **3**, both H-26 and H-27 should show cross-peaks with two quaternary carbons, C-8 and C-14. In fact, the only carbon that shows cross-peaks with both of these ^1H signals is the nonprotonated olefinic carbon (δ 160.8). The only location of C-27 and the double bond that is consistent with this observation is that shown in **4**. H-27 also shows cross-peaks with a quaternary carbon (δ 37.5), a methine carbon (δ 41.7), and a methylene carbon (δ 33.5), respectively assigned as C-13, C-18, and C-12. The carboxyl group must be bonded to a quaternary carbon to give the correct numbers of different types of carbons. Since C-18 is a methine carbon, the CO_2H group must be bonded to C-17. Finally, a direct ^1H–^{13}C shift-correlated experiment plus a ^1H COSY-45 spectrum (15) in combination with the XCORFE spectrum allowed location of the remaining *gem*-dimethyl group at C-20 rather than C-21. The first spectrum established the direct bond between C-18 and the methine proton at δ 2.28. The ^1H COSY spectrum showed that this proton was coupled to protons at δ 1.09 and δ 1.24

Can. J. Chem. Downloaded from www.nrcresearchpress.com by 213.166.140.6 on 09/07/12
For personal use only.

Can. J. Chem. Downloaded from www.nrcresearchpress.com by 213.166.140.6 on 09/07/12
For personal use only.

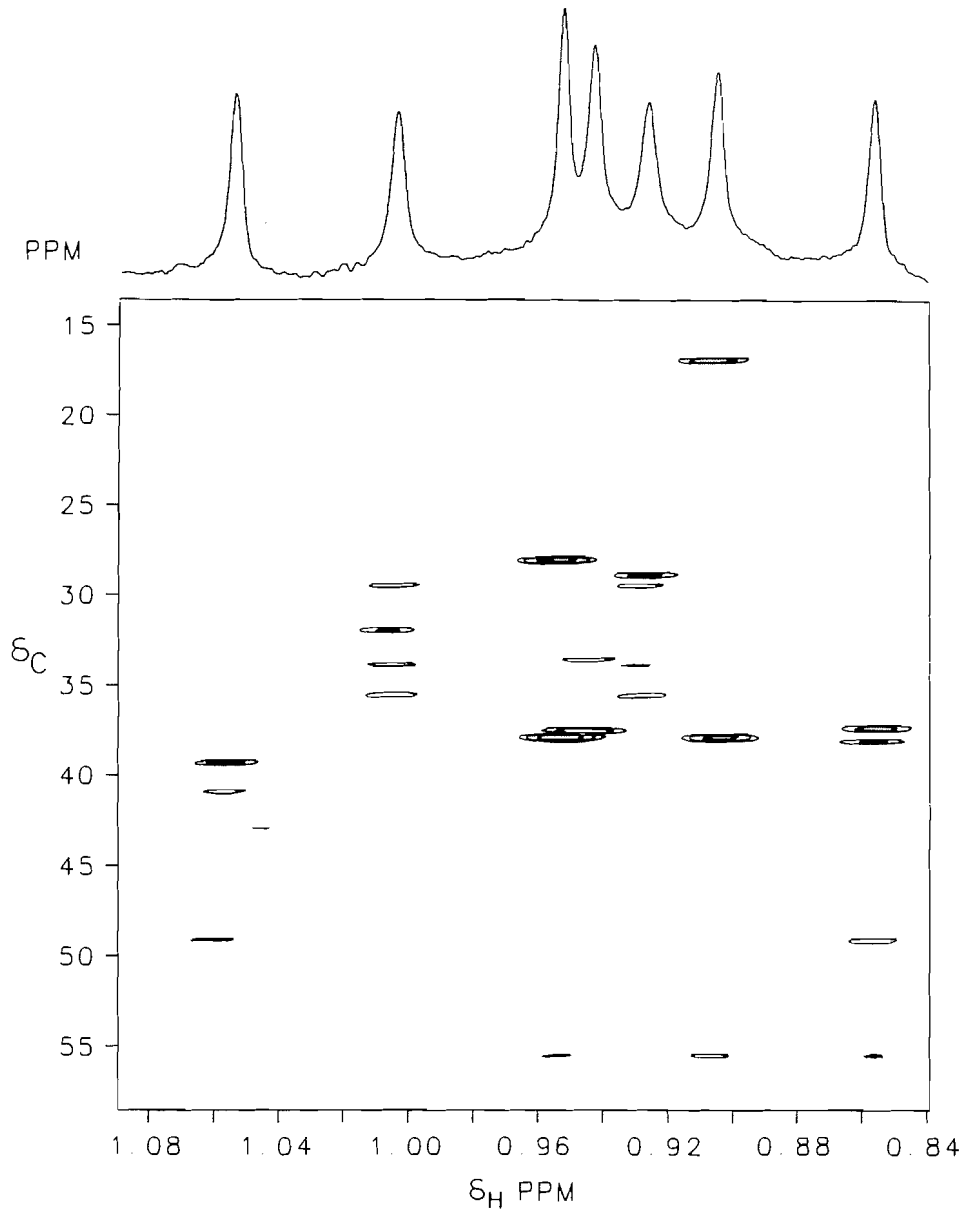

FIG. 2. Contour plot of XCORFE spectrum of **4** in 75% C_6D_6:25% $CDCl_3$. ^1H spectrum along the top shows the resolution of ^1H signals in this solvent pair.

while the direct shift-correlated experiment showed that the latter two protons were directly bonded to the carbon at δ 35.5. Thus this must be C-19. Since this carbon showed cross-peaks in the XCORFE spectrum with the two remaining *gem*-dimethyl ^1H signals, these methyl groups must be bonded to C-20. The remaining methylene carbon showing cross-peaks to these methyl protons (δ 33.8) is thus assignable as C-21.

Because of the limited amount of sample available (16 mg), it was not feasible to obtain a second XCORFE spectrum optimized for CH and CH_2 proton polarization transfer.[2] Fortunately, however, the remaining carbons (C-2, C-6, C-11, C-16, and C-22) could all be assigned from the above-mentioned combination of ^1H COSY and direct ^1H–^{13}C shift-correlated spectra. Assignments are given in Table 2. The ^1H-COSY spectra were much more informative for **4** than for **2**. This was due to the larger number of resolved ^1H signals for **4**, reflecting the larger number of functional groups in this compound.

There has been considerable confusion in the literature regarding the structure and ^{13}C spectral assignments for 3-acetyl-aleuritolic acid, **4**. This compound appears to have been first isolated by Misra and Khastigar (16), albeit with significantly different physical properties (e.g., mp 278–281°C). Subsequently, a compound (mp 301–302°C), isolated from *Phytolacca americana*, was assigned structure **4** by Woo and Wagner, mainly on the basis of mass spectral fragmentation patterns (17). They claimed that their compound was identical to that of Misra and Khastigar (based on mixture melting points) and also to a compound previously isolated by Burke and Le Quesne from *P. americana* and assigned structure **5**, also on the basis of mass spectral fragmentation patterns (18). To eliminate any possible doubts, we obtained a sample of the compound believed to be methyl aleuritolate from Professor Le Quesne and also

[2]This experiment is considerably lower in sensitivity than that involving polarization transfer from methyl protons (see ref. 6).

TABLE 2. Assigned ^{13}C and ^{1}H chemical shifts for **4** and observed $^{13}C-^{1}H$ cross-peaks used in making the assignments[a]

Carbon	n_H	δ_C ($CDCl_3$)[b]	δ_H ($CDCl_3$)	C—H connectivities
1	2	37.36 (37.35)	1.04, 1.61	H-25
2	2	23.39 (23.76)	1.61, 1.66	(3)[c]
3	1	80.79 (80.52)	4.47 (6, 10)[d]	H-23, H-24
4	0	37.59 (37.87)	—	H-23, H-24
5	1	55.50 (55.71)	0.88	H-23, H-24, H-25
6	2	18.67 (19.04)	1.49, 1.62	(5, 7)[c]
7	2	40.65 (40.85)	1.30, 1.97	H-26
8	0	38.96 (39.30)	—	H-26
9	1	48.97 (49.12)	1.42	H-26
10	0	37.85 (38.03)	—	H-25
11	2	17.23 (17.55)	1.48, 1.69	(12)[c]
12	2	33.24 (33.53)	1.60, 1.78	H-27
13	0	37.22 (37.50)	—	H-27
14	0	160.46 (160.77)	—	H-26, H-27
15	1	116.76 (117.25)	5.52 (4, 8)[d]	(16)[c]
16	2	31.25 (31.60)	1.93, 2.37	(15)[c]
17	0	51.43 (51.86)	—	—
18	1	41.29 (41.69)	2.28 (2, 14)[d]	H-27
19	2	35.23 (35.52)	1.09, 1.24	H-29, H-30
20	0	29.23 (29.44)	—	H-29, H-30
21	2	33.57 (33.84)	1.05, 1.16	H-29, H-30
22	2	30.60 (30.92)	1.44, 1.69	(21)[c]
23	3	27.88 (28.01)	0.85 (0.91)[b]	H-24
24	3	16.52 (16.92)	0.89 (0.96)[b]	H-23
25	3	15.57 (15.77)	0.95_5 (0.86)[b]	—
26	3	26.14 (26.60)	0.95_5 (1.06)[b]	—
27	3	22.39 (22.60)	0.92 (0.95)[b]	—
28	0	184.22 (185.04)	—	—
29[e]	3	31.76 (31.91)	0.94 (0.93_5)[b]	H-30
30[e]	3	28.57 (28.84)	0.91 (1.01)[b]	H-29
—O—$COCH_3$	0	170.92 (170.26)	—	OCH_3
—O—$COCH_3$	3	21.23 (20.93)	2.03	—

[a] See Table 1 for an explanation of column headings.

[b] Values in parentheses are for 75% C_6D_6:25% $CDCl_3$ mixture used for XCORFE experiment. Assignments in $CDCl_3$ were confirmed from a separate set of direct and indirect shift-correlated spectra.

[c] Proton cross-peaks in ^{1}H COSY-45 spectrum.

[d] Values in parentheses are $^{1}H-^{1}H$ coupling constants (Hz) in cases where these are clearly resolved. The $^{1}H-^{1}H$ coupling for H-3 in **4** and in methyl aleuritolate (see footnote *b*, Table 3) confirms the β orientation of the OR function in these compounds.

[e] The spectra provide no direct method for distinguishing C-29 from C-30 since they are present as a *gem*-dimethyl pair. Thus these assignments may be reversed.

converted part of our sample of **4** to this derivative. The two samples gave exactly identical ^{1}H and ^{13}C spectra (see Table 3), confirming their identity. ^{13}C and ^{1}H spectra were assigned using a combination of 2D experiments similar to that used for **4**. Thus we are confident that all compounds discussed above in this paragraph are identical. It may also be significant that the ^{1}H spectral data for **4** and for methyl aleuritolate are indistinguishable from those reported, respectively, for 3-acetylmaprounic acid **3** and methyl maprounate (8), while the mass spectral fragmentation patterns for **3** and **4** are also indistinguishable. A reinvestigation of the structure of **3** would appear to be justified.

Finally, Carpenter *et al.* have assigned the ^{13}C spectrum of **4** (19) by comparison with previously assigned spectra for oleanic acid derivatives (20). Comparison with our spectral data confirms that the compound isolated by Carpenter is identical to our sample. However, there are 11 misassignments in the earlier spectral assignments (19). This reinforces our earlier remarks concerning the unreliability of assigning spectra from model compounds (21) and the desirability of having more reliable techniques for ^{13}C spectral assignment (6, 21).

Consideration of the generality of indirect $^{13}C-^{1}H$ shift-correlated spectra for assigning structures of triterpenes

In this investigation $^{13}C-^{1}H$ shift-correlated spectra optimized for $^{n}J_{CH}$ couplings ($n = 2$ or 3) involving methyl protons have been used in conjunction with other two-dimensional (2D) nmr spectra to assign skeletal structures for two of the less common triterpenes. The first, moretenone, has been reported from only one other plant source, while the structure of the second, 3-acetylaleuritolic acid, has been in dispute. In a previous investigation, we have used a similar approach to assign ^{13}C and ^{1}H spectra of our other triterpenes (6). While these were all known compounds, the spectral data would have been sufficient to assign structures had these been unknown. Since all triterpene derivatives have a number of strategically located methyl groups (1), this approach should be generally applicable for assigning structures of this type of molecule.

Can. J. Chem. Downloaded from www.nrcresearchpress.com by 213.166.140.6 on 09/07/12
For personal use only.

TABLE 3. Assigned ^{13}C and ^{1}H chemical shifts for methyl aleuritolate in $CDCl_3$

Carbon	δ_C[a]	δ_H[b]	Carbon	δ_C[a]	δ_H[b]
1	37.78	0.95, 1.61	17	51.37	—
2	27.14	1.55, 1.63	18	41.83	2.36
3	79.05	3.18 (11, 5)	19	35.52	—
4	38.75	—	20	29.29	—
5	55.53	0.77	21	33.77	1.02, 1.16
6	18.71	1.43, 1.59	22	31.06	1.41, 1.65
7	41.07	1.28, 1.95	23	27.97	0.97
8	38.96	—	24	15.42	0.79
9	49.10	1.42	25	15.48	0.90_5
10	37.99	—	26	26.26	0.92_5
11	17.32	1.48, 1.59	27	22.41	0.93
12	33.44	1.62, 1.77	28	178.47	—
13	37.40	—	29	32.06	0.93_5
14	160.63	—	30	28.71	0.92
15	116.51	5.50 (8, 4)	CO_2CH_3	51.69	3.56
16	31.69	1.92, 2.37			

[a] ^{13}C chemical shifts (δ scale).

[b] ^{1}H chemical shifts (δ scale). Values in parentheses are $^{1}H-^{1}H$ coupling constants (in Hz) for protons where couplings are clearly resolved.

There are only three apparent limitations, all of which can be overcome. First, while the shift-correlated spectra provide no direct stereochemical information, this can be deduced either (as in this case) from vicinal $^{1}H-^{1}H$ couplings or from nuclear Overhauser enhancement measurements. Second, it is essential to have resolved methyl ^{1}H signals. As shown above, this can be achieved by judicious choice of solvent or solvent mixture. The final problem is one of sensitivity. After determining the correct solvent mixture, the three 2D spectra used to determine the structure of **4** were obtained in 26 h, using 16 mg of sample. While this represents a great sensitivity improvement over the alternative approach of 2D $^{13}C-^{13}C$ connectivity experiments (22), even greater sensitivity would be desirable. Subsequent work in our laboratory has shown that independent optimization of all three delay times can further increase sensitivity by, on average, a factor of two (23). For example, this allowed us to determine the XCORFE spectrum of methyl aleuritolate (optimized for polarization transfer from methyl protons) in 15 h, using only 5 mg of sample. However, an even more promising approach would be to use $^{1}H-^{13}C$ shift-correlated spectra obtained with ^{1}H detection since this provides one order of magnitude further increase in sensitivity (24).

Mass spectral fragmentation patterns have, in the past, been widely used for assigning structures of triterpenes (2). However, as discussed above, structures **3**, **4**, and **5** have been assigned to three different triterpene samples with very similar physical properties, including mass spectral fragmentation patterns. It has been subsequently shown that at least two of the three compounds are identical. It is this sort of ambiguity which leads us to search for a more reliable technique for structure assignment of triterpenes. We believe combinations of 2D nmr experiments of the kind used above provide this technique. Furthermore, they have the additional advantage of providing reliable ^{13}C and ^{1}H spectral assignments (6).

Experimental

General experimental procedures

Melting points were determined on a Thomas–Kofler micro hot stage. Infrared spectra were measured on a Nicolet 5DX FTIR spectrometer with samples in $CHCl_3$. Nuclear magnetic resonance spectra were obtained on a Varian XL-400 spectrometer. Mass spectra were obtained at 70 eV on a Bell and Howell CEC 21-490 mass spectrometer. Optical rotations were measured on a Perkin–Elmer 243B polarimeter.

Plant material

Maprounea guianensis was collected near the Soesdyke–Linden highway, Demerara, in May 1984. Voucher specimens are deposited in the Herbarium of the University of Guyana and at the Institute of Systematic Botany, University of Utrecht, Netherlands.

Extraction and isolation

Dried and ground bark (1.36 kg) was exhaustively extracted with cold $CHCl_3$ to afford a gum (10 g). The gum was shaken with a mixture of 9:1 MeOH–H_2O and hexane; a residue (4.4 g) remained undissolved. The material (1.9 g) obtained from the hexane solution was chromatographed on a column of silica gel; elution was first with hexane and then hexane–EtOAc of increasing polarity, and progress was monitored by tlc. Moretenone (115 mg) was the only identifiable constituent isolated. The residue (4.4 g) from the partitioning experiment was dissolved in $CHCl_3$ and chromatographed on a silica gel column with elution by hexane–EtOAc, EtOAc, then EtOAc–MeOH. This chromatography provided moretenone and 3-acetylaleuritolic acid. The MeOH aqueous fraction from the partitioning experiment also contained moretenone and 3-acetylaleuritolic acid.

Moretenone

Moretenone, **2**, recrystallized from Me_2CO, was obtained as needles, mp 194–197°C; $[\alpha]_D$ 52.5° (*c* 0.2, $CHCl_3$); ir: 1700, 1635, 881 cm^{-1}; ms M^+ 424 (lit. (13) mp 202–203°C; $[\alpha]_D$ 53° ($CHCl_3$); ir: 1710, 1640, 885 cm^{-1}; ms M^+, 424).

3-Acetylaleuritolic acid

3-Acetylaleuritolic acid, **4**, recrystallized from hexane–EtOAc, mp 297–300°C; $[\alpha]_D$ 24.3° (*c* 0.14, $CHCl_3$); ir: 3500, 1733, 1688 cm^{-1}; ms M^+, 498 (2%), 248 (31%), 234 (100%), 189 (77%) (lit. (17) mp 301–302°C; $[\alpha]_D$ 23.1° ($CHCl_3$); ir: 1735, 1689 cm^{-1}).

A sample of **4** was refluxed with K_2CO_3 in MeOH. Solvent was removed under reduced pressure and the residue was partitioned between EtOAc and 1 *M* aqueous HCl. The EtOAc solution afforded a solid, which was dissolved in Et_2O and treated with CH_2N_2. The product was chromatographed on silica gel and the fraction obtained, mp 200–203°C, was identical to the methyl aleuritolate supplied by Professor Le Quesne.

Two-dimensional nuclear magnetic resonance spectra

Experimental parameters are similar to those detailed by Reynolds *et al.* (6). However, due to the smaller amounts of sample available (36 mg for **2**, 16 mg for **4**), shorter ^{1}H relaxation delays (0.5 s) were used along with more transients per time increment (256 transients for **2**, 800 transients for **4**), to increase the signal-to-noise as much as possible for XCORFE experiments.

Acknowledgements

Research at Toronto is supported by grants from the Natural Sciences and Engineering Research Council of Canada. The Centre for Natural Products Chemistry at the University of Guyana receives generous financial support from the Canadian International Development Agency. M.P.-D. acknowledges the receipt of a University of Toronto Open Fellowship. We thank Professor P. Le Quesne for a sample of methyl aleuritolate.

1. J. D. CONNOLLY and K. H. OVERTON. *In* Chemistry of terpenes and terpenoids. *Edited by* A. A. Newman. Academic Press, New York. 1972.
2. H. BUDZIKIEWICZ, J. M. WILSON, and C. DJERASSI. J. Am. Chem. Soc. **85**, 3688 (1963).
3. K. HALLENGA and G. VAN BINST. Bull. Magn. Reson. **2**, 343 (1980).
4. H. KESSLER, C. GRIESENGER, J. ZARBOCK, and H. R. LOOSLI. J. Magn. Reson. **57**, 331 (1984).

Can. J. Chem. Downloaded from www.nrcresearchpress.com by 213.166.140.6 on 09/07/12
For personal use only.

5. W. F. REYNOLDS, D. W. HUGHES, M. PERPICK-DUMONT, and R. G. ENRIQUEZ. J. Magn. Reson. **63**, 413 (1985).
6. W. F. REYNOLDS, S. McLEAN, J. POPLAWSKI, R. G. ENRIQUEZ, L. I. ESCOBAR, and I. LEON. Tetrahedron, **42**, 3419 (1986).
7. D. B. FANSHAWE. Forest products of British Guiana. Part 2. Forest Department, British Guiana. 1950. p. 48.
8. M. C. WANI, J. P. SCHAUMBERG, H. L. TAYLOR, J. B. THOMPSON, and M. E. WALL. J. Nat. Prod. **46**, 537 (1983).
9. D. M. DODDRELL, D. T. PEGG, and M. R. BENDALL. J. Magn. Reson. **48**, 323 (1982).
10. E. WENKERT, G. V. BADDELEY, I. R. BURFITT, and L. N. MORENO. Org. Magn. Reson. **11**, 337 (1978).
11. (*a*) A. BAX and G. A. MORRIS. J. Magn. Reson. **42**, 501 (1981); (*b*) A. BAX. J. Magn. Reson. **53**, 517 (1983).
12. P. E. HANSEN. Prog. Nucl. Magn. Reson. Spectrosc. **14**, 175 (1981).
13. D. LAVIE, M. K. JAIN, and T. O. OREMBAJO. Phytochemistry, **7**, 657 (1968).
14. A. N. STARRATT. Phytochemistry, **8**, 1831 (1969); Y. TSUDA and M. HATORI. Chem. Pharm. Bull. **15**, 1073 (1967).
15. A. BAX and R. FREEMAN. J. Magn. Reson. **44**, 542 (1981).
16. D. R. MISRA and H. N. KHASTIGAR. Tetrahedron, **26**, 3017 (1970).
17. W. S. WOO and H. WAGNER. Phytochemistry, **16**, 1845 (1977).
18. D. E. BURKE and P. W. LE QUESNE. Phytochemistry, **10**, 3319 (1971).
19. R. S. CARPENTER, S. SOTHEESWARAN, M. V. S. SULTANBAWA, and B. TERNAI. Org. Magn. Reson. **14**, 462 (1980).
20. K. TORAI, S. SEO, A. SHIMAOKA, and Y. TOMITA. Tetrahedron Lett. 4227 (1974).
21. W. F. REYNOLDS, J. F. SAWYER, R. G. ENRIQUEZ, L. I. ESCOBAR, M. A. CHAVEZ, and J. N. SHOOLERY. Can. J. Chem. **63**, 1048 (1985).
22. T. H. MARECI and R. FREEMAN. J. Magn. Reson. **48**, 158 (1982).
23. M. PERPICK-DUMONT, R. G. ENRIQUEZ, S. McLEAN, F. V. PUZZUOLI, and W. F. REYNOLDS. J. Magn. Reson. In press.
24. A. BAX and M. F. SUMMER. J. Am. Chem. Soc. **108**, 2093 (1986).

Can. J. Chem. Downloaded from www.nrcresearchpress.com by 213.166.140.6 on 09/07/12
For personal use only.

Preparation, reactions, and spectroscopic investigation of the 1,1,3,3-tetramethylimidazolidinium and 1,1,4,4-tetramethylpiperazonium dications

J. ALAN CREIGHTON
Chemical Laboratories, University of Kent, Canterbury, U.K.

AND

MICHAEL J. TAYLOR
Department of Chemistry, University of Auckland, Auckland, New Zealand

Received March 9, 1987

J. ALAN CREIGHTON and MICHAEL J. TAYLOR. Can. J. Chem. **65**, 2526 (1987).

The title dications are prepared in a single step by the reaction of *N,N,N',N'*-tetramethyl-1,2-diaminoethane (tmen) with the halogenoalkanes CH_2X_2 (X = Cl, Br, or I) or CH_2XCH_2X (X = Cl or Br), respectively. These bulky dications are useful for the precipitation of complex ions from solution, and show selectivity for doubly-charged anions. Tmen also reacts with CBr_4 to yield a dibromo-imidazolidinium heterocyclic dication, whereas reaction with $CHBr_2CHBr_2$ produces the dihydrobromide of tmen. Vibrational and nmr spectra are reported, and the protons of the CH_2 group between the two quaternary nitrogen atoms of the tetramethylimidazolidinium dication are shown from the nmr data to possess acidic character.

J. ALAN CREIGHTON et MICHAEL J. TAYLOR. Can. J. Chem. **65**, 2526 (1987).

On a préparé les dications mentionnés dans le titre en une seule étape, en faisant réagir le *N,N,N',N'*-tétraméthyl diamino-1,2 éthane (tmen) respectivement avec les halogénoalcanes CH_2X_2 (X = Cl, Br ou I) ou CH_2XCH_2X (X = Cl ou Br). Ces dications très encombrants sont utiles pour provoquer la précipitation d'ions complexes à partir de solutions et ils présentent une sélectivité pour les anions doublement chargés. Le tmen réagit aussi avec le CBr_4 pour donner le dication hétérocyclique dibromo-imidazolidinium; par ailleurs, la réaction avec le $CHBr_2CHBr_2$ fournit le dibromhydrate du tmen. On rapporte les spectres de vibration et rmn; la rmn démontre que les protons du groupement CH_2 entre les deux atomes d'azote quaternaires du dication tétraméthylimidazolidinium possèdent un caractère acide.

[Traduit par la revue]

Introduction

The reaction of *N,N,N',N'*-tetramethyl-1,2-diaminoethane (tmen) with dichloromethane to form the cyclic 1,1,3,3-tetramethylimidazolidinium dication **1** has recently been reported (1). We have independently encountered the same reaction while attempting to use tmen and CH_2Cl_2 as a mixed solvent, which deposited crystals of the dichloride of **1** in a surprisingly rapid reaction. We have therefore investigated more fully the reaction of tmen with various halogenomethanes, and have also studied the similar reaction of tmen with the 1,2-dihalogenoethanes to give dihalide salts of the 1,1,4,4-tetramethylpiperazonium dication **2**. A separate report gives the structure of **2** in

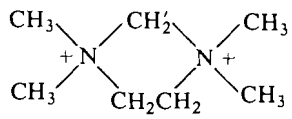

1

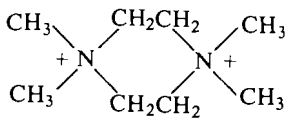

2

the salt $[C_8H_{20}N_2][InBr_5(H_2O)].H_2O$ (2), while the structure of **1** in the diiodide salt has already been determined crystallographically by Khan, Peppe, and Tuck (1). Our interest in such bulky dications is because of their potential use as counterions for the crystallization of large anions, especially those with a double negative charge (3, 4).

Quaternisation reactions of *N,N,N',N'*-tetramethyl-α,ω-diaminoalkanes with α,ω-dibromoalkanes have been previously investigated as a route to linear and cyclic polymeric quaternary ammonium cations (5, 6). However, the use of this type of reaction for the synthesis of cyclic quaternary ammonium cations does not seem to have been noted and the conventional route to such cyclic cations has been by *N*-methylation of the parent heterocycles with bromomethane or iodomethane (Menschutkin reaction) (4, 7). A low-yield synthesis of the dibromide of **2** by reaction of vinylidenebis(dimethylamine) with 1,2-dibromoethane has also been published (8).

Our investigations of the tetramethylimidazolidinium cation have also revealed that the protons of carbon atom 2 (H' in the structural formula of **1**) are appreciably acidic, and the reactivity at this carbon atom is thus a further interesting aspect of this cation.

Experimental

Preparative and spectral data

1,1,3,3-Tetramethylimidazolidinium salts

For the preparation of the dichloride salt of **1** excess dichloromethane was used as the reaction medium, and a 1:3 molar ratio of tmen to CH_2Cl_2 was found to be optimal. With this molar ratio roughly a 50% yield of the dichloride precipitated after 1 week at room temperature, whereas with methanol as the solvent it was shown by nmr spectroscopy that there was no reaction between tmen and CH_2Cl_2 (1:1) at room temperature after 1 week. It was normally possible to use reagent-grade tmen and CH_2Cl_2 without further purification, but with one batch of tmen there was no reaction with CH_2Cl_2 until after the tmen had been purified by distillation. The reaction of CH_2Br_2 or CH_2I_2 with tmen is more rapid than that of CH_2Cl_2, and precipitation of the dibromide or diiodide salt was roughly 70% complete after stirring these liquids in 3:1 mole ratio for 1 week at room temperature. The crystalline products were washed with dry ether and dried *in vacuo*. The dichloride salt was noticeably deliquescent. *Anal.* calcd. for $[C_7H_{18}N_2]Cl_2$: C 41.8, H 9.02, N 13.9; found: C 41.3, H 9.64, N 13.7. *Anal.* calcd. for $[C_7H_{18}N_2]Br_2$: C 29.0, H 6.26, N 9.66; found: C 28.6, H 6.76, N 9.42. *Anal.* calcd. for $[C_7H_{18}N_2]I_2.0.75CH_2I_2$: C 15.9, H 3.36, N 4.79; found: C 15.9, H 3.59, N 4.72. These products

Can. J. Chem. Downloaded from www.nrcresearchpress.com by 213.222.148.141 on 09/07/12
For personal use only.

TABLE 1. Vibrational data (cm^{-1}) for CBr_4 and CBr_4 – bromide ion adducts

Compound	Raman				Infrared	
	ν_1	ν_2	ν_3	ν_4	ν_3	ν_4
CBr_4*	269vs	127m	670m	183ms	670vs	183s
$[C_7H_{16}N_2Br_2]Br_2 . nCBr_4$	255vs	138vw	†	182s	660vs	183vs
$[(CH_3)_4N]Br . 2CBr_4$*	262vs	151vw	663s	186s	667vs	187s
$[(C_2H_5)_4N]Br . CBr_4$*	250vs	142w	669s	184s	667vs	185vs
$[(C_3H_7)_4N]Br . CBr_4$*	250vs	133w	647w	176mw	641vs	176m
			664m	183mw	662vs	183m
				187sh	666sh	187sh

*Reference 9.
†Out of range of measurements.

Can. J. Chem. Downloaded from www.nrcresearchpress.com by 213.222.148.141 on 09/07/12
For personal use only.

are very soluble in water and their solutions immediately precipitate silver halides on treatment with silver nitrate solution. Their identification as dihalide salts of **1** was confirmed by ^1H and ^{13}C nmr data (^1H: see ref. 1. ^{13}C: δ = 55.5, CH_3; 63.0, CH_2CH_2; 89.4, NCH_2N) recorded from their solutions in D_2O. The quantity of CH_2I_2 contained in the iodide salt is probably not stoichiometrically significant, being that remaining after partial loss of CH_2I_2 during drying *in vacuo* from a weakly-bound halide ion – iodoalkane crystalline adduct (9).

Vibrational spectroscopic data for **1**; Raman (cm^{-1}): 330w, 435w, 485m, 562m, 595w, 770vs (ring mode), 865m, 900w, 930m, 940w, 975m, 995w, 1020m, 1045vw, 1115w, 1155w, 1203m, 1250w, 1280m, 1340w, 1380w, 1405w, 1445m, 1480w, 2850w, 2900m, 2950s, 2980w, 3015vs. The infrared spectrum consisted of bands coincident with the Raman data.

1,1,4,4-tetramethylpiperazonium salts

Dihalide salts of **2** were prepared by reaction of tmen with 1,2-dichloroethane or 1,2-dibromoethane. Equimolar quantities (0.05 mol) of tmen and CH_2XCH_2X (X = Cl or Br) in 5 mL methane + 5 mL dimethylformamide as solvent were allowed to react for several days at room temperature. The solid product was washed with dry ether; yield 70%. No recrystallisation was necessary. *Anal.* calcd. for $[C_8H_{20}N_2]Cl_2$: C 44.7, H 9.37, N 13.0; found: C 44.5, H 9.83, N 12.8. *Anal.* calcd. for $[C_8H_{20}N_2]Br_2$: C 31.6, H 6.63, N 9.21; found: C 31.7, H 7.09, N 9.20. The identification of these products as dihalide salts of **2** was confirmed by nmr data (1, 5): ^1H: δ = 3.4, NCH_3; 4.0 ppm, NCH_2CH_2N; ^{13}C: δ = 54.1, CH_3; 57.5 ppm, CH_2. Vibrational spectroscopic data for **2** comprise Raman: 280m, 340m, 455m, 485m, 520w, 707vs (ring mode), 815m, 894m, 954s, 998w, 1034m, 1075vw, 1120w, 1210m, 1230m, 1285m, 1313m, 1343w, 1390w, 1410w, 1455m, 1490w, 2860w, 2935m, 2960s, 2995m, 3005vs; infrared: 265w, 360w, 455m, 632m, 735w, 870s, 920vs, 970s, 1022s, 1050w, 1060s, 1135m, 1200m, 1214s, 1308s, 1330w, 1400m, 1475m, 3010m (regions 1400–1450 and 2850–3000 cm^{-1} masked by Nujol absorption).

Complex anion salts of 1

To illustrate the use of these cations for the precipitation of doubly-charged complex anions, solutions of the dichloride of **1** in hot ethanol were mixed in 1:1 mole ratio with hot ethanolic solutions of $CoCl_2 . 6H_2O$ or $CuCl_2 . 2H_2O$ to precipitate $[C_7H_{18}N_2][CoCl_4]$ or $[C_7H_{18}N_2][CuCl_4]$ in high yield. The colours of these solids, respectively blue and yellow, were characteristic of the $[CoCl_4]^{2-}$ and $[CuCl_4]^{2-}$ ions, and it was also possible to characterise further the copper compound by obtaining its Raman spectrum using 647.1 nm excitation. This showed bands at 276s, 238w cm^{-1}, close to published wavenumbers 276, 232 cm^{-1} of the two bands of the $[CuCl_4]^{2-}$ ion observed in the Raman spectrum of the salt $[(CH_3)_4N][CuCl_4]$ (10). *Anal.* calcd. for $[C_7H_{18}N_2][CoCl_4]$: C 25.4, H 5.48, N 8.46; found: C 25.0, H 5.47, N 8.65. *Anal.* calcd. for $[C_7H_{18}N_2][CuCl_4]$: C 25.1, H 5.41, N 8.35; found: C 24.1, H 5.50, N 8.40. A similar reaction using $NiCl_2 . 6H_2O$ precipitated the $[NiCl_4]^{2-}$ salt of **1**, with the characteristic lilac colour of this anion, if the ethanol solvant was dry. *Anal.* calcd. for $[C_7H_{18}N_2][NiCl_4]$: C 25.4, H 5.49, N 8.47; found: C 25.7, H 5.27, N 8.67. If the ethanol was not dry, however, a green solid precipitated. The same green product resulted from standing $[C_7H_{18}N_2][NiCl_4]$ in moist air, and from the resulting 15.6% weight gain (constant weight), and on the basis of CHN analyses, this product is formulated as $[C_7H_{18}N_2][NiCl_4(H_2O)_2] . H_2O$. *Anal.* calcd.: C 21.8, H 6.29, N 7.28; found: C 22.1, H 6.37, N 7.45; calcd. weight increase on gaining $3H_2O$, 16.3%.

The dication **1** is also effective for the precipitation of doubly charged complex anions from aqueous solutions, and thus the tetrabromozincate salt was obtained as small, well-shaped crystals on adding an aqueous solution of the dibromide of **1** to an aqueous solution of $ZnBr_2$. *Anal.* calcd. for $[C_7H_{18}N_2][ZnBr_4]$: C 16.3, H 3.52, N 5.44; found: C 16.2, H 3.56, N 5.49. Strong bands in the ir spectrum at 220 cm^{-1}, and in the Raman spectrum at 175 cm^{-1} confirmed the presence of the $[ZnBr_4]^{2-}$ ion (11). Crystalline hexahalogenostannate salts were obtained similarly by adding the aqueous solution of the appropriate dihalide of **1** to either $SnCl_4$ in 6 ml L^{-1} HCl or $SnBr_4$ in 4 mol L^{-1} HBr. *Anal.* calcd. for $[C_7H_{18}N_2][SnCl_6]$: C 18.2, H 3.93, N 6.07; found: C 17.9, H 3.99, N 6.05. *Anal.* calcd. for $[C_7H_{18}N_2][SnBr_6]$: C 11.5, H 2.48, N 3.85; found: C 12.2, H 2.95, N 2.78. The ir and Raman spectra of these salts showed the known vibrational bands of the $[SnCl_6]^{2-}$ and $[SnBr_6]^{2-}$ ions (11) together with the bands of the dication **1**.

1,1,3,3-Tetramethyl-2,2-dibromo-imidazolidinium dibromide

The reaction of tmen with CBr_4, which in principle could result in a *spiro*-tetracation, has also been investigated. On mixing tmen with CBr_4 (1:1) in acetonitrile solution at room temperature a white solid precipitated over the course of several hours. This solid was observed to lose CBr_4 on standing in air, and it thus has a rather variable composition, depending on the washing and drying procedure. The microanalyses for two separate preparations were as follows. *Anal.* calcd. for $[C_7H_{16}N_2Br_2]Br_2 . 0.75CBr_4$: C 13.4, H 2.32, N 4.02; found: C 12.9, H 2.35, N 4.07. *Anal.* calcd. for $[C_7H_{16}N_2Br_2]Br_2 . 0.2CBr_4$: C 16.8, H 3.14, N 5.45; found: C 16.4, H 3.17, N 5.46. The Raman and far-infrared spectra of this product contained bands close to but not coincident with the vibrational bands of free CBr_4, as shown in Table 1. Similar small shifts from the free CBr_4 frequencies have previously been found in crystalline adducts of CBr_4 with tetra-alkylammonium halides (9) (see Table 1), and these adducts were shown to involve a halide ion – CBr_4 interaction (9), which persists in solution in dichloromethane or acetonitrile (12). Thus it is clear that the product precipitated from the reaction of tmen with CBr_4 is also a bromide ion – CBr_4 adduct. The formulation of the cation as 1,1,3,3-tetramethyl-2,2-dibromo-imidazolidinium was confirmed from the microanalyses and the ^1H nmr spectrum (D_2O solution), which showed two resonances at δ = 3.22, 3H; 3.70 ppm, 1H. The initially white solid decomposed slowly, becoming dark brown after several hours.

Reaction of N,N,N′,N′*-tetramethyl-1,2-diaminoethane with 1,1,2,2-tetrabromoethane*

Either five- or six-membered cyclic dications may be envisaged to result from the reaction of tmen with $CHBr_2CHBr_2$, and therefore

equimolar amounts of these reactants in carbon tetrachloride solution were allowed to react. Some crystalline solid had formed after 1 h, and this change was accompanied by the growth of a sharp peak in the nmr spectrum of the solution at $\delta = 7.1$ ppm, attributable to $CHBr{=}CBr_2$. The solid was identified from its nmr spectrum in D_2O solution as the dihydrobromide of tmen, $[(CH_3)_2HNCH_2CH_2NH(CH_3)_2]Br_2$ (^1H nmr data: $\delta = 2.93$, 3H: 3.60 ppm, 1H), which was identical with that of a sample prepared by reacting tmen with hydrobromic acid. Hence in this case the quaternization of the diamine to form a cyclic cation is supplanted by a reaction in which the diamine abstracts hydrogen halide from the halogenoalkane.

Discussion

Preparative and nmr data

Quaternary ammonium cations have been used extensively as counterions for the crystallisation of bulky anions, but little use appears to have been made of quaternary ammonium dications for this purpose. Where such dications have been synthesized, such as that derived by methylation of both nitrogen atoms in 1,4-diazabicyclooctane, the usual procedure has been to prepare the diiodide salt using iodomethane as methylating agent, and where the salt of a different anion is required, to obtain this by anion-exchange in aqueous solution (13). It is therefore of considerable advantage for the preparation of water-sensitive chloro-complexes that the dichloride of **1** can be prepared directly in an anhydrous state by such a simple and convenient reaction. As expected, the preparations of the halogeno-metallate salts reported here show the particular effectiveness of **1** and **2** as counterions for the precipitation of bulky anions which bear a 2− charge. In this respect the precipitation of the $[InBr_5(OH_2)]^{2-}$ salt is of particular note, since it is obtained from an aqueous solution containing a mixture of anionic species (14), this 2− ion containing one ligand water molecule so as to maintain the characteristic six-coordination of indium shown also in $[InBr_6]^{3-}$ and $[InBr_4(OH_2)_2]^-$ (2).

The high δ values of the ^1H and ^{13}C resonances of the NCH_2N group of **1** indicate that these atoms are considerably deshielded and suggest that the protons concerned might be appreciably acidic. This has been confirmed by showing that these hydrogen atoms undergo exchange by deuterium on the addition of OD^- or tmen as base to a solution of **1** in D_2O, the NCH_2N proton resonance at 5.4 ppm diminishing rapidly, while the signals from the other proton-containing groups were unchanged. The resulting spectrum (^1H, $\delta = 4.5$ (NCH_2CH_2N), 3.6 ppm (NCH_3)) was identical with that of the deuterated form of **1** obtained by the reaction of tmen with CD_2Cl_2. No similar exchange was observed on treating **2** with base in D_2O solution, showing that the acidic character of the methylene protons is a characteristic of the $^+NCH_2N^+$ group. This finding raises the possibility that with deprotonation **1** may act as a nucleophile or potential ligand, leading perhaps to the formation of metal–carbene complexes, or that **1** may yield a stable nitrogen ylide under strongly basic conditions.

Acknowledgements

Experimental assistance from M. J. Gallagher and N. C. Blacker (University of Kent) is acknowledged. M.J.T. is grateful for equipment grants from the New Zealand Universities Grants Committee.

1. M. A. KHAN, C. PEPPE, and D. G. TUCK. Can. J. Chem. **62**, 1662 (1984).
2. G. R. CLARK, C. E. F. RICKARD, and M. J. TAYLOR. Can. J. Chem. **64**, 1697 (1986).
3. F. BASOLO. Coord. Chem. Rev. **3**, 213 (1968).
4. A. S. N. MURTHY, J. V. QUAGLIANO, and L. M. VALLARINO. Inorg. Chim. Acta, **6**, 49 (1972).
5. H. NOGUCHI and A. REMBAUM. J. Polymer Sci. Part B, **7**, 383 (1969); Macromolecules, **5**, 253 (1972); **5**, 261 (1972).
6. R. M. OTTENBRITE and G. R. MYERS. Can. J. Chem. **51**, 3631 (1973).
7. M. H. ABRAHAM. *In* Progress in physical organic chemistry. Vol. 11. *Edited by* A. Streitwieser and R. W. Taft. Wiley, New York. 1974. p. 1.
8. C. F. HOBBS and H. WEINGARTEN. J. Org. Chem. **39**, 921 (1974).
9. J. A. CREIGHTON and K. M. THOMAS. J. Chem. Soc. Dalton Trans. 403 (1972); H. J. LINDNER and B. K. GROSS. Chem. Ber. **109**, 314 (1976).
10. J. A. CREIGHTON. *In* Essays in structural chemistry. *Edited by* D. A. Long, A. J. Downs, and L. A. K. Staverley. Macmillan, London. 1971. p. 355.
11. K. NAKAMOTO. Infrared and Raman spectra of inorganic and coordination compounds. 3rd ed. Wiley, New York. 1978.
12. J. A. CREIGHTON and K. M. THOMAS. J. Chem. Soc. Dalton, 2254 (1972).
13. S. OAE, B. HOVARTH, C. ZALUT, and R. HARRIS. J. Org. Chem. **24**, 1348 (1959); C. S. CREASER and J. A. CREIGHTON. J. Inorg. Nucl. Chem. **41**, 469 (1979).
14. M. P. HANSON and R. A. PLANE. Inorg. Chem. **8**, 746 (1969).

Can. J. Chem. Downloaded from www.nrcresearchpress.com by 213.222.148.141 on 09/07/12
For personal use only.

Benzophenone-photosensitized autoxidation of linoleate in solution and sodium dodecyl sulfate micelles

LAWRENCE ROSS COATES BARCLAY,[1] KIMBERLY ANN BASKIN, STEVEN JEFFREY LOCKE, AND TANYA DIANE SCHAEFER
Department of Chemistry, Mount Allison University, Sackville, N.B., Canada E0A 3C0

Received April 7, 1987

LAWRENCE ROSS COATES BARCLAY, KIMBERLY ANN BASKIN, STEVEN JEFFREY LOCKE, and TANYA DIANE SCHAEFER. Can. J. Chem. **65**, 2529 (1987).

Diffusion studies show that benzophenone (BP), linoleic acid, and methyl linoleate partition completely into the micelles of phosphate buffer/0.10 *M* SDS. Water-soluble compounds 4-sulphomethylbenzophenone, sodium salt (BP^-), azobis(2-amidinopropane·HCl) (ABAP) and 2,5,7,8-tetramethyl-6-hydroxychroman-2-carboxylate (Trolox) show partial partitioning into the micelles. BP- and BP^--photosensitized oxidation of linoleic acid in 0.50 *M* SDS exhibited characteristics of free radical chain reactions including: (*1*) inhibition by phenolic antioxidants, (*2*) no retardation by singlet oxygen quenchers, and (*3*) the formation of conjugated hydroperoxides with *cis,trans* to *trans,trans* ratios of geometrical isomers typical of autoxidation. Quantitative kinetic studies of the order in substrate, RH, and the rate of chain initiation, R_i, show that the classical rate law, $-d[O_2]/dt = k_p/2k_t^{1/2}[RH]R_i^{1/2}$ applies to BP-photoinitiated autoxidation of linoleic acid in SDS and the oxidizability ($k_p/2k_t^{1/2} = 4.42 \times 10^{-2}\ M^{-1/2}\ s^{-1}1/2$) is the same as that found with a thermal initiator. The rotating sector method gave absolute rate constants for linoleic acid autoxidation in 0.50 *M* SDS for propagation ($k_p = 36.2\ M^{-1}\ s^{-1}$) and termination ($2k_t = 3.52 \times 10^5\ M^{-1}\ s^{-1}$), significantly lower than values in polar organic solvents; attributed to solvation of polar peroxyls in aqueous SDS. Depressed inhibition rate constants (k_{inh}) for α-tocopherol, Trolox, and pentamethylhydroxychroman (PMHC) in 0.50 *M* SDS compared to k_{inh} in *tert*-butyl alcohol are attributed to hydrogen bonding effects on the peroxyl radicals and on the inhibitors.

LAWRENCE ROSS COATES BARCLAY, KIMBERLY ANN BASKIN, STEVEN JEFFREY LOCKE et TANYA DIANE SCHAEFER. Can. J. Chem. **65**, 2529 (1987).

Des études de diffusion démontrent que la benzophénone (BP), l'acide linoléique et le linoléate de méthyle se repartissement complètement dans les micelles du tampon de phosphate/0,10 *M* SDS. Les composés qui sont solubles dans l'eau, comme le sel de sodium de la sulfo-4 méthylbenzophénone (BP^-), l'azobis (amidino-2 propane·HCl) (ABAP) et le tétramethyl-2,5,7,8 hydroxy-6 chromanecarboxylate-2 (Trolox), ne se répartissent que partiellement dans les micelles. L'oxydation photosensibilisée par le BP ou le BP^- de l'acide linoléique dans du SDS à 0,50 *M* présente les caractéristiques des réactions radicalaires en chaînes, y compris : (*1*) l'inhibition par les antioxydants phénoliques, (*2*) le fait que les pièges à oxygène singulet ne retardent pas la réaction et (*3*) la formation d'hydroperoxydes conjugués contenant des rapports des isomères géométriques *cis,trans* à *trans,trans* qui sont typiques d'auto-oxydations. Des études cinétiques quantitatives de l'ordre en substrat, RH, et en vitesse d'initiation de chaîne, R_i, démontrent que l'équation de vitesse classique, $-d[O_2]/dt = k_p/2k_t^{1/2}[RH]R_i^{1/2}$ s'applique à l'auto-oxydation photo-initiée par le BP de l'acide linoléique dans le SDS et que la facilité d'oxyder ($k_p/2k_t^{1/2} = 4{,}42 \times 10^{-2}\ M^{-1/2}\ s^{-1/2}$) est la même que celle qui a été observée avec un initiateur thermique. Utilisant la méthode du secteur tournant, on a déterminé les vitesses absolues pour la propagation ($k_p = 36{,}2\ M^{-1}\ s^{-1}$) et pour la terminaison ($2k_t = 3{,}52 \times 10^5\ M^{-1}\ s^{-1}$) de la réaction d'oxydation de l'acide linoléique dans du SDS à 0,50 *M*; ces valeurs sont beaucoup plus basses que celles observées dans des solvants organiques polaires et on attribue ces différences à la solvatation des radicaux peroxyles polaires par le SDS aqueux. Les constantes d'inhibition de vitesse (k_{inh}) que l'on observe pour l'α-tocophérol, le Trolox et le pentaméthylhydroxychromane (PMHC), dans le SDS à 0,50 *M*, sont faibles par rapport à la valeur de k_{inh} que l'on observe dans l'alcool *tert*-butylique; on attribue ces différences à des effets de liaisons hydrogènes sur les radicaux peroxyles et sur les inhibiteurs.

[Traduit par la revue]

Introduction

The photosensitized action of oxygen on biological systems (the photodynamic effect) results in a number of known detrimental effects including membrane damage, protein damage, mutagenesis, and skin cancer (1–3). The possible involvement of singlet oxygen in the photoxidation of biological systems has attracted great interest (1–3) and even some application; as in photodynamic therapy (1).

The variety of examples in the literature where singlet oxygen is reported to be involved in photosensitization processes in model membrane environments such as phospholipid bilayers (4–9) and various types of micelles (10–22) usually involve a dye or porphyrin as sensitizer. These reports were most concerned with the detection of singlet oxygen but little attention was focused on the fate of an oxidizable substrate in these studies in microenvironments.

This investigation examines in detail the photo-oxidation of the linoleate chain in an aqueous sodium dodecyl sulfate (SDS) micellar system containing a simple aromatic ketone (benzophenone) as sensitizer. The results reported herein will show that (*1*) the benzophenone-sensitized oxidation of linoleate in 0.50 *M* SDS proceeds by a free-radical chain autoxidation reaction (Type I) rather than a reaction involving singlet oxygen (Type II); (*2*) the classical rate law

$$[1] \qquad \frac{-d[O_2]}{dt} \quad \frac{k_p[RH]R_i^{1/2}}{(2k_t)^{1/2}}$$

well known for autoxidation in homogeneous solution (23–25), is applicable to this system where RH is the linoleate concentration in the micellar phase, k_p and $2k_t$ are the chain propagation and bimolecular termination rate constants, respectively, and R_i is the rate of free radical chain initiation measured by the inhibitor method (26) using phenolic antioxidants; (*3*) the products of autoxidation of linoleate show the same trend with linoleate micellar concentration for photoinitiation with

[1]Author to whom correspondence may be addressed.

Can. J. Chem. Downloaded from www.nrcresearchpress.com by 213.166.140.6 on 09/07/12
For personal use only.

Can. J. Chem. Downloaded from www.nrcresearchpress.com by 213.166.140.6 on 09/07/12
For personal use only.

benzophenone as that found with lipid-soluble and water-soluble thermal azo initiators, and (*4*) this ketone-sensitized micellar system provides a very useful model microenvironment for *quantitative* kinetic studies of the substrate oxidizability ($k_p/2k_t^{1/2}$) and this system has important advantages for the precise determination of the absolute rate constants for chain propagation, termination, and inhibition for autoxidation of the linoleate chain.

Results

1. Partition coefficients between buffer and 0.10 M *SDS*

Whereas a previous study on thermally initiated autoxidation of linoleic acid in SDS micelles *assumed* that the substrate partitioned completely into the micellar phase (27), it was important for this quantitative study to actually determine the partition coefficients of this and other pertinent compounds between SDS micellar and phosphate buffer phases. For this purpose, we used a variation of the simple method to measure diffusion coefficients (28). The procedure and results of this study are outlined in Table 1.

TABLE 1. Distribution coefficients of organic compounds between phosphate buffer (0.01 *M*, pH 7.0) and SDS (0.10 *M*) at 25°C[a]

Compound[b]	$D \times 10^5$ cm^2 s^{-1}		
	Buffer	SDS	f[c]
Linoleic acid	0.556 ± 0.032	0.158 ± 0.013	0.952
Methyl linoleate	[d]	0.192 ± 0.012	1.0
Benzophenone	0.833 ± 0.014	0.166 ± 0.004	0.960
BP^-	0.666 ± 0.013	0.473 ± 0.044	0.366
ABAP	0.592 ± 0.013	0.180 ± 0.010	0.907
DBHN	1.013 ± 0.020	0.224 ± 0.016	0.902
Trolox	0.621 ± 0.063	0.531 ± 0.031	0.186
PMHC	0.685 ± 0.019	0.185 ± 0.001	0.914
α-Tocopherol	[d]	[e]	1.0[d]
Anthracene	[d]	0.140 ± 0.025	1.0[d]
Phenanthrene	[d]	0.138 ± 0.005	1.0[d]

[a]Diffusion coefficients were calculated from the equation (58): $D = 0.2310r^2t_r/(W_{1/2})^2$ where r is the radius of the tube, t_r is the retention time of the solute, and $W_{1/2}$ is the width of the dispersion curve at half height. The distribution coefficient, f, is then calculated from the equation $D = fD_m + (1 - f)D_w$ (28) where D and D_w are the diffusion coefficients of a solute in 0.10 *M* SDS and buffer, respectively, and D_m is the diffusion coefficient of the micelles (see footnote *d*).

[b]Concentrations of the injected samples were less than 10^{-3} *M* and the detector wavelength was such that the absorbance of the stock solution was at least 0.5.

[c]The deviation is estimated to be 5–10%.

[d]Solubility was too low for measurement. These were taken as "tracer" compounds and their average $D = D_m$ (28).

[e]Eluted peaks were not Gaussian.

2. Inhibition studies with phenolic antioxidants

Experiments were conducted on the effects of the known efficient phenolic antioxidants (29), α-tocopherol (E), 2,2,5,7,8-pentamethyl-6-hydroxychroman (PMHC), and 2,5,7,8-tetramethyl-6-hydroxychroman-2-carboxylate (Trolox) on the ketone-sensitized oxidation of linoleic acid in SDS micelles. Typical oxygen uptake traces showing the inhibition periods for these antioxidants in reactions initiated by benzophenone and by the sodium salt of 4-sulphomethylbenzophenone (BP^-) are illustrated in Fig. 1 A and B, respectively.

The relative effectiveness of the three antioxidants, E, PMHC, and Trolox, was also measured in a qualitative manner for the photoinitiated oxidation of methyl linoleate in SDS micelles. Typical traces illustrated in Fig. 2 show the relatively poor antioxidant activity of vitamin E *in this system*. Similar results (not shown) were obtained when the water-soluble thermal initiator azobis(2-amidinopropane) hydrochloride (ABAP) was used to initiate autoxidation of methyl linoleate in SDS micelles. This latter system appears to be inhomogeneous (see Discussion); therefore, subsequent quantitative studies were conducted with linoleic acid in SDS.

3. Singlet oxygen quenchers

The inhibition studies with phenolic antioxidants indicate that linoleate undergoes reaction by a free-radical chain autoxidation under our conditions. Nevertheless, a few experiments were carried out with known singlet oxygen quenchers in the aqueous and micellar phases to determine whether they had any effect on the autoxidation. Sodium azide (5×10^{-3} *M*) had no effect on the rate of oxygen uptake and this concentration of azide added with α-tocopherol did not affect the typical induction period observed for this inhibitor (Fig. 1*A*). Similarly, diphenylisobenzofuran (DPBF) did not affect the rate of oxygen uptake in concentrations of 8.2×10^{-4} *M* in the micellar phase and did not affect the length of the induction period of α-tocopherol (1.17×10^{-4} *M*).

Irradiation of aqueous SDS micellar solutions containing methylene blue is a known method to generate singlet O_2 in the aqueous phase (14, 20, 22). The effect of the free-radical trap, Trolox, on an irradiated micellar solution containing methylene blue showed a very interesting contrast with its inhibiting action in the BP-sensitized experiments. In the presence of aqueous $^1O_2$, Trolox caused a rapid upsurge in the rate of oxygen consumption which is more pronounced with increased Trolox. Similarly, injection of α-tocopherol (8.5×10^{-4} *M*) did not cause an induction period. HPLC analysis indicated consumption of E with time, presumably due to attack by singlet oxygen in the micellar phase. These results are attributed to a rapid chemical reaction between singlet oxygen and the inhibitors (30, 31). On the other hand, ground state O_2 shows a low reactivity toward the tocopheroxyl radical (32).

4. Product studies

The products of autoxidation of linoleate are known to be conjugated diene 9- and 13-hydroperoxide positional isomers, having the *trans,trans* and *cis,trans* configuration (33). Reaction of linoleate with singlet oxygen yields a different mixture with approximately equal amounts of two conjugated (9- and 13-) and two non-conjugated (10- and 12-) hydroperoxides (34). In other words, the products from the $^1O_2$ reaction are not controlled by abstraction of the reactive allylic hydrogens as is the case for the autoxidation procedure. Porter and co-workers (35–39) have conducted a detailed study of the products formed in autoxidation of linoleic acid in solution and from phospholipid emulsions using a lipid-soluble initiator (e.g. di-*tert*-butylhyponitrite, DBHN). As a result, they developed a mechanism for lipid peroxidation which involves a competition between H-atom abstraction and β-scission of peroxyl radicals to account for the dependence of the relative amounts of the kinetic (*cis,trans*) and thermodynamic (*trans,trans*) products on the hydrogen atom donating ability, i.e. linoleate concentration, of the medium.

In order to determine if the Porter mechanism for linoleate autoxidation is applicable to oxidations conducted in aqueous SDS micelles, we investigated the dependence of the ratio of the various oxidation products as a function of micellar linoleate

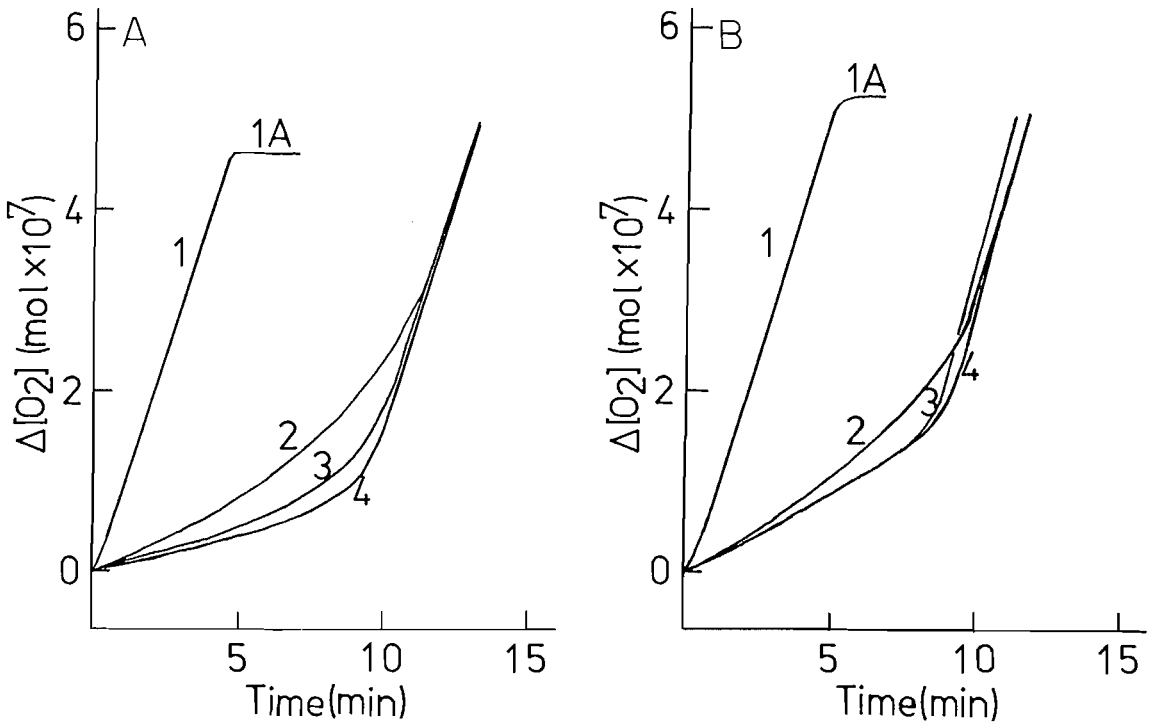

FIG. 1. (*A*) Autoxidation of linoleic acid (6.43×10^{-5} mol) in 2.00 mL of 0.50 *M* SDS (pH 7.0) at 30°C, photoinitiated by benzophenone (2.82×10^{-6} mol): *1*, uninhibited reaction (1A: lamp off); *2*, inhibited with α-tocopherol (1.67×10^{-8} mol); *3*, inhibited with Trolox (1.66×10^{-8} mol); *4*, inhibited with PMHC (1.62×10^{-8} mol). (*B*) Autoxidation of linoleic acid (4.83×10^{-5} mol) in 1.50 mL of 0.50 *M* SDS (pH 7.0) at 30°C, photoinitiated by BP^- (2.07×10^{-6} mol): *1*, uninhibited reaction (1A: lamp off); *2*, inhibited with α-tocopherol (3.75×10^{-8} mol); *3*, inhibited with Trolox (3.83×10^{-8} mol); *4*, inhibited with PMHC (3.88×10^{-8} mol).

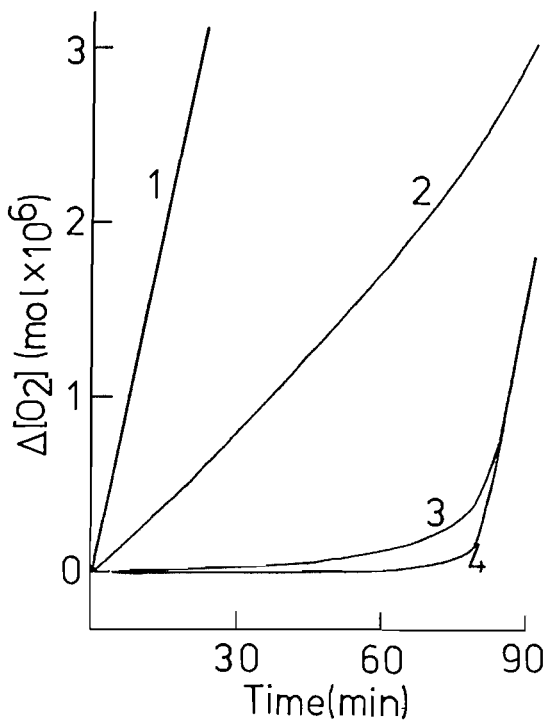

FIG. 2. Autoxidation of methyl linoleate (1.21×10^{-4} mol) in 2.00 mL of 0.50 *M* SDS (pH 7.0) at 30°C, photoinitiated by benzophenone (1.10×10^{-6} mol): *1*, uninhibited reaction; *2*, inhibited with α-tocopherol (3.70×10^{-8} mol); *3*, inhibited with Trolox (3.65×10^{-8} mol); *4*, inhibited with PMHC (3.60×10^{-8} mol).

concentration. Oxidations initiated by both water-soluble and lipid-soluble azo compounds (ABAP and DBHN, respectively) and water- and lipid-soluble benzophenones were studied. In all four cases, the products separated by HPLC (following reduction and methylation) were the alcohols known to form by free-radical autoxidation; namely **1**–**4** (Scheme 1).

The analytical data for the products of micellar linoleate autoxidations when thermally initiated by the azo compounds, ABAP and DBHN, are outlined in Table 2 while those for reactions photoinitiated by the benzophenones (BP and BP^-) are given in Table 3.

HPLC analyses were also undertaken to determine the fate of benzophenone during prolonged irradiation. A typical sample containing 1.54×10^{-4} *M* BP in 0.50 *M* SDS, saturated with O_2 *but without linoleic acid*, gave >95% recovery of benzophenone with only traces of benzhydrol and benzopinacol after $2\frac{1}{4}$ h of irradiation at full lamp intensity. Also, there was no observed uptake of oxygen during the experiment. Similar results were obtained when the experiment was carried out in the presence of linoleic acid (0.46 *M*). After $2\frac{1}{4}$ h of irradiation, greater than 90% of the BP remained while approximately 2.5% of the initial amount was accounted for by benzhydrol and a trace of benzopinacol. During the course of a typical kinetic autoxidation experiment (the equivalent of 2–3 h of continuous irradiation at full lamp intensity) essentially all of the benzophenone is recovered.

5. Kinetic results

In order to determine if the classical rate law (eq. [1]) is applicable to these photo-oxidations in SDS micelles, the

Can. J. Chem. Downloaded from www.nrcresearchpress.com by 213.166.140.6 on 09/07/12
For personal use only.

Can. J. Chem. Downloaded from www.nrcresearchpress.com by 213.166.140.6 on 09/07/12
For personal use only.

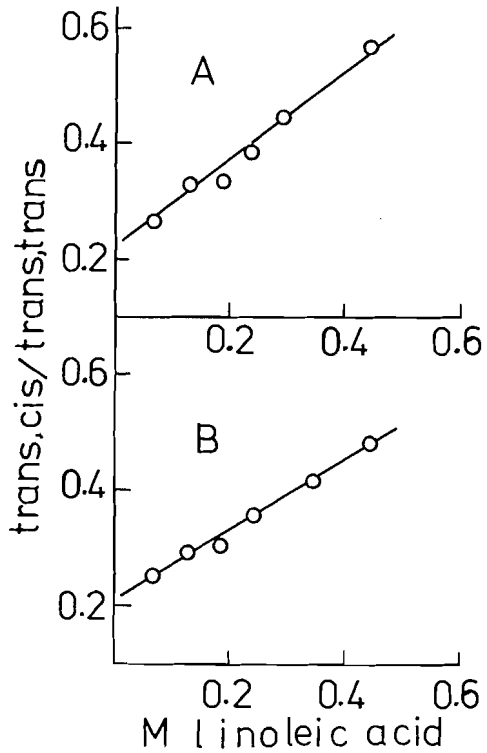

FIG. 3. Concentration dependence of product ratios (*trans,cis/trans,trans*) of hydroxy fatty esters derived from autoxidation of linoleic acid in 0.50 *M* SDS (pH 7.0) at 30°C. Values taken from Table 2. *A*, Initiation by DBHN (1.03×10^{-5} mol); *B*, initiation by ABAP (2.67×10^{-5} mol).

dependence of the rate of oxygen uptake on micellar linoleic acid concentration was measured at five concentrations over the range 0.0630 *M* to 0.459 *M* and the dependence of the rate of O_2 consumption with variation in R_i was measured by the application of five different lamp intensities at each linoleic acid concentration. The results of these experiments are summarized in Table 4.

The absolute rate constants for chain propagation, k_p, and termination, $2k_t$, were measured by the rotating sector method (40, 41).

The separation of the absolute rate constants for chain propagation and termination involves measurement of the lifetime, τ, of the reaction chain. The chain lifetime is defined by the equation

$$[2] \quad \tau = (2k_tR_i)^{1/2}$$

where R_i is the rate of photoinitiation. A sectored disc is placed in the light path between the lamp and the reaction vessel and the rate of oxygen consumption is measured at various rotation speeds of the disc. If the ratio of dark to light periods is r, the rate at fast speeds is

$$[3] \quad R_f = K[I/(r + 1)]^{1/2}$$

where $KI^{1/2}$ is the oxidation rate at a steady light intensity, I. At slow rotation speeds, the rate is

$$[4] \quad R_s = KI^{1/2}/(r + 1)$$

At intermediate sector rotation speeds, the reaction rate has a complicated dependence on the duration of the light flash, λ, and the lifetime of the reaction chain. The value of λ is

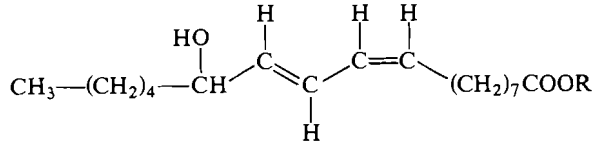

1

Methyl 13-hydroxy-*cis*-9, *trans*-11-octadecadienoate

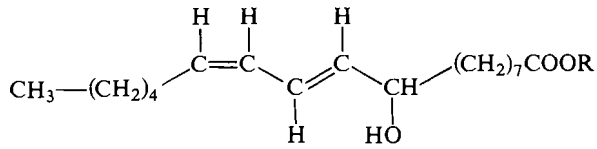

2

Methyl 9-hydroxy-*trans*-10, *cis*-12-octadecadienoate

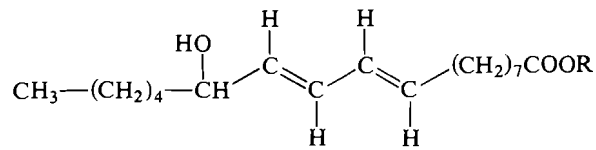

3

Methyl 13-hydroxy-*trans*-9, *trans*-11-octadecadienoate

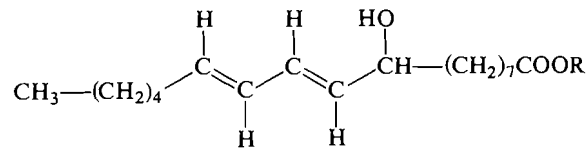

4

Methyl 9-hydroxy-*trans*-10, *trans*-12-octadecadienoate

SCHEME 1

determined by the rotation speed of the sector

$$[5] \quad \lambda = \frac{r + 1}{\text{slow speed (rpm)}}$$

Under steady illumination, the rate of oxygen consumption, R_0, can be represented by the classical rate law:

$$[1a] \quad R_0 = k_p[\text{RH}]\left(\frac{R_i}{2k_t}\right)^{1/2}$$

Burnett and Melville (40) have given values of the ratio R_λ/R_0 in terms of λ/τ for various values of r. As a result, $2k_t$ can be readily obtained from eq. [2] once the R_i has been measured. Substitution of R_i and $2k_t$ into eq. [1*a*] yields k_p. To improve the accuracy of the measurements, we used the modification (41) of finding a particular λ by varying the sector speed to obtain a rate midway between R_f and R_s and then repeatedly measured R_0 and R_λ.

In the above discussion it has been assumed that chain termination is a bimolecular process. First order chain termination, which can be represented as

$$[6] \quad \text{ROO}\cdot \rightarrow \text{inactive products}$$

causes a reduction in the value of R_f/R_0. The measured ratio enables determination of a quantity, γ, by means of the following expression:

$$[7] \quad \frac{R_f}{R_0} = \frac{\{(\gamma^2 r + 1)/(r + 1)\}^{1/2}\gamma}{1 - \gamma}$$

TABLE 2. Product ratio distribution for autoxidation of linoleic acid in 0.50 *M* SDS (pH 7.0) at 30°C; initiated by azo intiators

Initiator	Concentration (mol × 10^5)	[Linoleic acid][a] (mol L^{-1})	*t,c* products[b] / *t,t* products
DBHN	1.03	0.0631	0.264
		0.124	0.333
		0.182	0.332
		0.238	0.386
		0.292	0.450
		0.444	0.571
ABAP	2.67	0.0631	0.252
		0.124	0.296
		0.182	0.305
		0.238	0.357
		0.345	0.417
		0.444	0.483

[a]A micellar reaction volume of 2.5×10^{-4} liters for 2.00 mL of 0.50 *M* SDS was used in concentration calculations (27) in micelles throughout (Tables 2, 3, 4, 6).
[b]**(1 + 2)/(3 + 4)**. Products were analyzed as the methyl hydroxylinoleates (see text) by three HPLC analyses on each experiment. The reproducibility was approximately 5%.

TABLE 3. Product ratio distribution for autoxidation of linoleic acid in 0.50 *M* SDS (pH 7.0) at 30°C; photoinitiated by benzophenones

Initiator	Concentration (mol × 10^7)	[Linoleic acid][a] (*M*)	*t,c* products[b] / *t,t* products
BP	5.48	0.124	0.255 ± 0.007
		0.238	0.284 ± 0.019
		0.445	0.429 ± 0.032
		0.536	0.443[c]
		0.742	0.602 ± 0.034
BP^-	5.49	0.0631	0.182 ± 0.011
		0.124	0.264 ± 0.014
		0.238	0.283 ± 0.039
		0.445	0.454 ± 0.045
		0.742	0.630 ± 0.025

[a]See footnote *a*, Table 2.
[b]Results from two different experiments, also see footnote *b*, Table 2.
[c]One experiment.

where γ is defined as $k_x/(k_x^2 + 8k_tR_i)^{1/2}$. For a particular γ, the value of R_λ/R_0 yields a second quantity m, defined as

$$[8] \quad m = \frac{\lambda(k_x^2 + 8k_tR_i)^{1/2}}{2}$$

The rate constant for first order termination, k_x is readily calculated from γ and m:

$$[9] \quad k_x = \frac{2\gamma m}{\lambda}$$

The rate constants for bimolecular termination and chain propagation are then obtained from the following expressions:

$$[10] \quad 2k_t = \frac{m^2}{\lambda^2 R_i} - \frac{k_x^2}{4R_i}$$

and

TABLE 4. Kinetics of autoxidation of linoleic acid in 0.50 *M* SDS (pH 7.0) at 30°C; photoinitiated by benzophenone (1.13×10^{-2} *M*)[a]

[Linoleic acid][a]	$-d[O_2]/dt$ ($M\ s^{-1} \times 10^6$)	Transmittance[b]
0.0631	1.57	1.00
	1.43	0.794
	1.00	0.501
	0.708	0.251
	0.341	0.100
0.124	3.26	1.00
	2.82	0.794
	2.10	0.501
	1.50	0.251
	0.869	0.100
0.238	6.69	1.00
	5.99	0.794
	4.38	0.501
	3.18	0.251
	1.89	0.100
0.344	9.55	1.00
	8.39	0.794
	6.30	0.501
	4.62	0.251
	2.67	0.100
0.459	12.5	1.00
	10.8	0.794
	8.86	0.631
	8.23	0.501
	5.81	0.251
	4.42	0.159
	3.52	0.100

[a]See footnote *a*, Table 2.
[b]The transmittance was controlled by inserting neutral density filters into the light path.

$$[11] \quad k_p = \frac{R_0 2(2k_t)\gamma}{[RH]k_x(1 - \gamma)}$$

The absolute rate constants were determined in two organic solvents, acetonitrile and *tert*-butyl alcohol, by photoinitiation with benzophenone as well as the more conventional azobiscyclohexylnitrile (ACHN) (41). For each solvent, reasonably good agreement was obtained by the two methods, as illustrated in Table 5.

The rotating sector method was applied to a series of autoxidations of linoleic acid in aqueous SDS micelles with benzophenone as sensitizer. The absolute rate constants so determined are reported in Table 6.

Equation [12] is the rate equation for inhibited autoxidations,

$$[12] \quad \frac{-d[O_2]}{dt} = \frac{k_p[RH]R_i}{nk_{inh}[ArOH]}$$

where the stoichiometric factor $n = 2$ for the phenolic antioxidant (ArOH) used. Since the k_p is now known for our conditions we were able to determine inhibitor rate constants, k_{inh}, for the termination of peroxyls via the process,

$$ROO\cdot + ArOH \rightarrow ROOH + ArO\cdot$$

in homogeneous solution and in SDS micelles. Some typical value are shown in Table 7.

Can. J. Chem. Downloaded from www.nrcresearchpress.com by 213.166.140.6 on 09/07/12
For personal use only.

TABLE 5. Absolute rate constants for the autoxidation of linoleate (0.420 M) in homogeneous solution at 30°C[a]

No.[b]	Initiator ($M \times 10^3$)	Solvent	R_i[c] ($M\,s^{-1} \times 10^7$)	$\frac{-d[O_2]/dt}{[RH]R_i^{1/2}}$ ($M^{-1/2}\,s^{-1/2} \times 10^2$)	ν[e]	γ	m	k_x[d]	$2k_t$[d] ($M^{-1}\,s^{-1} \times 10^{-6}$)	k_p[d] ($M^{-1}\,s^{-1}$)
1	ACHN (6.76)	CH_3CN[f]	2.26	3.59	38	0.070	3.49	0.133	4.42	94.9
2(*a*)	BP (1.63)	CH_3CN	1.85	4.03	39	0.072	4.07	0.132	4.33	96.5
(*b*)			1.91	3.98	37	0.070	3.08	0.118	3.74	90.5
3	ACHN (6.85)	TBA[f]	6.95	1.72	30	0.075	3.75	0.153	15.1	75.6
4(*a*)	BP (1.66)	TBA	1.80	1.95	19	0.092	4.36	0.308	15.5	78.5
(*b*)	(1.68)		1.17	1.45	17	0.203		0.650	21.0	90.4
5	BP (1.63)	CH_3CN	1.71	4.37	44	0.040	4.53	0.051	2.43	70.3

[a]Under such conditions, the order with respect to the R_i (i.e. light intensity) was 0.457–0.522.
[b]Nos. 1–4 used linoleic acid, no. 5 methyl linoleate.
[c]The R_i was measured by the induction period method. The value reported is the average of at least two such measurements with Trolox.
[d]The variation in measurements of the rate constants within an experiment (by repeated measurements of R_0 and R_λ) was between 5 and 18% and generally less than 10%.
[e]The kinetic chain length; $\nu = -d[O_2]/dt//R_i$.
[f]The dielectric constants for CH_3CN = 38, for *tert*-butyl alcohol (TBA) = 11.

TABLE 6. Absolute rate constants for the benzophenone-sensitized autoxidation of linoleic acid (0.238 M)[a] in 0.50 M SDS (pH 7.0) at 30°C

No.	BP ($M \times 10^2$)	R_i[b] ($M\,s^{-1} \times 10^7$)	$\frac{-d[O_2]/dt}{[RH]R_i^{1/2}}$ ($M^{-1/2}\,s^{-1/2} \times 10^2$)	ν[d]	γ	m	k_x[c] (s^{-1})	$2k_t$[c] ($M^{-1}\,s^{-1} \times 10^{-5}$)	k_p[c] ($M^{-1}\,s^{-1}$)
1	1.01	5.20	4.94	16	0.140	2.62	0.143	4.98	44.5
2	1.01	5.05	4.78	16	0.136	3.95	0.107	3.05	35.8
3	1.01	4.22	4.46	16	0.164	4.50	0.106	2.44	30.9
4	0.203	0.914	3.95	31	0.250	2.43	0.088	3.08	32.4
5	0.203	0.803	3.95	33	0.250	2.58	0.093	4.06	37.4

[a]See footnote *a*, Table 2.
[b]See footnote *c*, Table 5.
[c]The variation in rate constants within an experiment (by repeated measurement of R_0 and R_λ) was between 8 and 30%.
[d]See footnote *e*, Table 5.

Can. J. Chem. Downloaded from www.nrcresearchpress.com by 213.166.140.6 on 09/07/12
For personal use only.

Discussion

1. Partitioning of substrates, initiators and antioxidants between the aqueous and micellar phases

The partition coefficient determinations (Table 1) reveal that the diffusion coefficients for anthracene and phenanthrene approach a limiting value, indicative of localization within micelles. As such, these highly hydrophobic compounds are said to act as "tracers" of the micellar diffusion and the average value of their diffusion coefficients is assigned to D_m (28). From the table it can also be seen that linoleic acid is completely (within experimental error) in the micellar phase. The diffusion coefficient for methyl linoleate in 0.10 M SDS is similar to that for the "tracer compounds". This and the fact that the ester has such poor solubility in the buffer used (precluding measurement of D) lead to the conclusion that both linoleates partition entirely into the micellar phase. Subsequent calculations assume this to be the case.

The partitioning of the initiators employed in this study provides some very interesting results. Benzophenone resides in the micellar phase ($f = 0.96$) while its water-soluble derivative BP^- partitions considerably ($f = 0.37$) into the micelles of 0.10 M SDS. It has been suggested earlier that BP^- was "essentially" in an aqueous environment in the presence of 0.2 M SDS from spectroscopic properties (42). It is our conclusion that the determination of diffusion coefficients provides a more sensitive quantitative measurement of partitioning than do spectroscopic methods.

The behaviour of the azo initiator, ABAP, appears to be very surprising. It is readily soluble in water (aqueous solutions of 1 M or more are easily prepared), but it partitions to the extent of 91% into 0.1 M SDS. We speculate that this may be due to electrostatic interactions between the positive amidino groups of ABAP and the anionic surface of the micelle, such as shown below

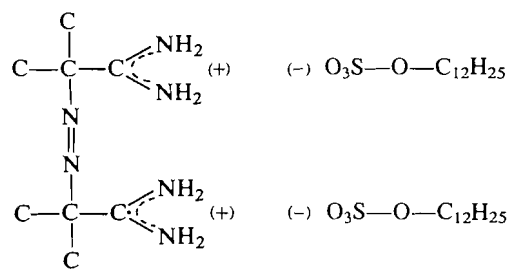

This model implies that ABAP *may* be associated with the surface of the micelles. Such electrostatic interactions could account for the unusual observation that ABAP decomposes three times *less rapidly* in 0.50 M SDS than in water or in liposome dispersions (43). We suggest that these dipolar

TABLE 7. Inhibition rate constants for phenolic antioxidants in the photo-initiated autoxidation of linoleic acid[a] in solution and in 0.50 *M* SDS (pH 7.0) at 30°C

Medium	Initiator ($M \times 10^3$)	R_i ($M\,s^{-1} \times 10^7$)	Inhibitor ($M \times 10^5$)	k_p ($M^{-1}s^{-1}$)	k_{inh}[b] ($M^{-1}\,s^{-1} \times 10^{-4}$)
TBA	BP (1.69)	1.30	α-T (7.37)	85.1	21.8 ±4.3
		1.22	(7.12)		24.2 ±4.2
		1.25	PMHC (7.67)		15.3 ±2.0
		1.12	(7.43)		26.8 ±1.8
		1.04	Trolox (7.72)		13.4 ±2.5
		1.02	(7.46)		15.9 ±2.2
CH_3CN	BP (1.63)	1.85	Trolox (10.3)	93.8	8.55±0.99
		1.74	(10.1)		11.2 ±0.9
	BP (1.63)	1.91	(10.4)		10.6 ±0.8
		1.84	(10.3)		9.27±0.99
	ACHN (6.76)	2.12	(11.1)	94.9	11.7 ±1.0
		1.93	(11.0)		12.4 ±0.8
SDS	BP (10.4)	2.04	α-T (6.19)	36.2	1.79±0.19[c]
	(11.5)	1.08	(11.7)		1.59±0.20
	(10.4)	2.12	PMHC (6.00)		4.43±0.58[c]
	(11.5)	1.74	(12.2)		2.99±0.64
	(10.4)	2.19	Trolox (6.15)		3.51±0.29[c]
	(11.5)	1.44	(16.4)		2.10±0.37

[a]Initial linoleic acid concentration was 0.420 *M* in both TBA and CH_3CN and 0.238 *M* (in the micellar phase) for 0.50 *M* SDS.

[b]Inhibition rate constants were determined for at least four points along each induction period where the chain length was in the range 2–9. The variation is shown for each induction period. The method of calculation of ref. 29 was used.

[c]The calculation for k_{inh} assumes that α-T, PMHC, and Trolox partition completely into the micellar phase in 0.50 *M* SDS (see text).

Can. J. Chem. Downloaded from www.nrcresearchpress.com by 213.166.140.6 on 09/07/12
For personal use only.

interactions act to inhibit cleavage of the molecule and reduce the rate of nitrogen liberation.

Trolox is an effective antioxidant in either organic solvents (29) or aqueous systems (43, 44). As shown in Table 1, it partitions significantly (19%)[2] into the micellar phase and its versatility as an antioxidant is undoubtedly due to this partitioning action between the two phases.

2. Product studies with azo and benzophenone initiators. The mechanism for benzophenone-initiated oxidations

The photosensitized reaction of oxygen with an organic substrate may be initiated by hydrogen abstraction from the substrate by the sensitizer triplet followed by free radical autoxidation (Type I mechanism). Alternately, the Type II process involves initial energy transfer from the sensitizer to form singlet oxygen which can react with the hydrogen donor in a variety of ways (such as the ene reaction with olefins), usually distinct from the free radical route. These two reaction types have been studied extensively and reviewed (2, 3). Product studies provide one method of distinguishing Type I from Type II (*vide supra*).

In Fig. 3 *A* and *B* are shown plots of the dependence of the ratio of *cis,trans*-substituted hydroperoxides (**1** + **2**) to *trans,trans* products (**3** + **4**) as a function of micellar linoleic acid concentration for thermal initiation by DBHN and ABAP, respectively. Good linear correlations were obtained with both lipid-soluble DBHN and water-soluble ABAP. Since ABAP is associated with the micellar phase, it most likely forms initiating peroxyls in (or near) the same region as DBHN.

Plots of *cis,trans/trans,trans* product ratios for oxidations photoinitiated by benzophenone and BP^- are shown in Fig. 4 *A* and *B*, respectively. These plots show that the ratio of kinetic (*c,t*) to thermodynamic (*t,t*) products shows a linear dependence on linoleate concentration remarkably similar to that found for the thermal azo initiators. These results are entirely consistent with the free radical autoxidation (Type I) mechanism for linoleate oxidations in micellar SDS whether thermally initiated (by DBHN or ABAP) or photoinitiated (by BP or BP^-).

At least two important factors operate to account for the occurrence of Type I mechanism in our system. (*1*) One important competition which controls whether initiation occurs by Type I (radical chain) or Type II (singlet O_2) is between substrate and oxygen for the triplet sensitizer (2). Allylic hydrogens are known to be effective quenchers of benzophenone triplets by hydrogen abstraction (45) and the doubly allylic hydrogens in linoleate are readily abstracted. (2) While singlet oxygen is known to form in micelles by various photosensitization methods (10–22) and its lifetime is "longer" (53 μs, ref. 17) in SDS, peroxyl radicals have lifetimes orders of magnitude longer. Furthermore, termination of linoleate peroxyls is very much retarded in the presence of SDS micelles (*vide infra*). As a result of these factors, $^1O_2$ quenchers such as azide and DPBF had no effect on our reactions and the peroxyl radicals carried a chain reaction as proposed in Scheme 2.

The recycling of benzophenone as initiator is an interesting characteristic of our system. This could occur via some chain

[2]This higher partition fraction over that reported (2%) is probably related to the higher SDS concentration used here compared to only 0.0150 *M* used earlier (44).

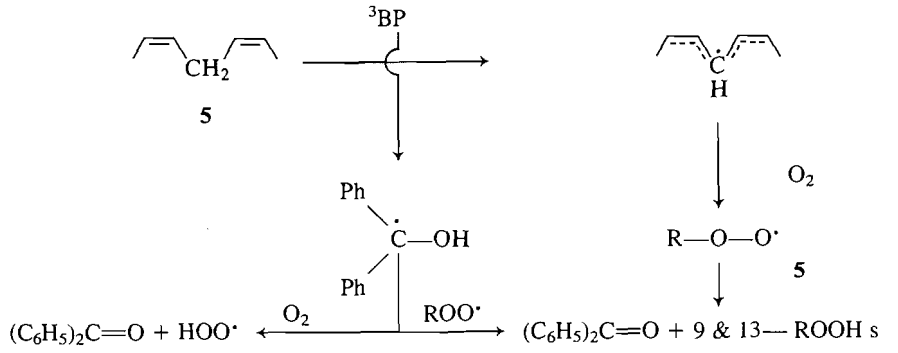

SCHEME 2

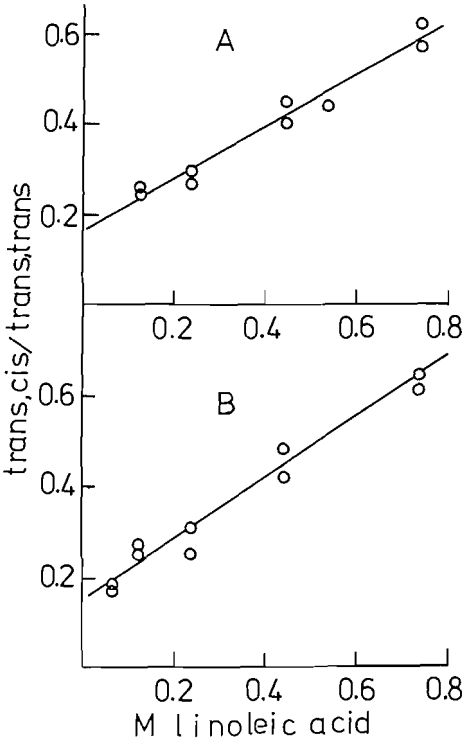

FIG. 4. Concentration dependence of product ratios (*trans,cis/trans,trans*) of hydroxy fatty esters derived from autoxidation of linoleic acid in 0.50 *M* SDS (pH 7.0) at 30°C. Values taken from Table 3. *A*, Photoinitiated by benzophenone (5.48×10^{-7} mol); *B*, photoinitiated by BP$^-$ (5.49×10^{-7} mol).

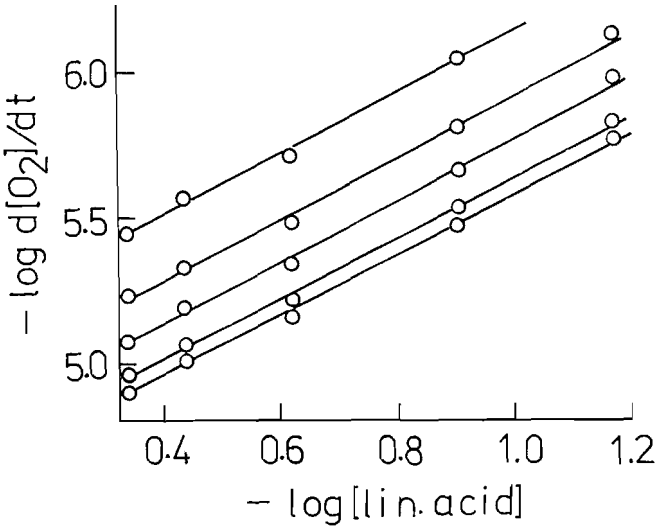

FIG. 5. Kinetic order plots for autoxidation of linoleic acid in 0.50 *M* SDS (pH 7.0) at 30°C; photoinitiated by benzophenone (1.13×10^{-2} *M*). Rate of oxygen consumption as a function of substrate concentration at five different light intensities. Values taken from Table 4.

termination by H-atom transfer from the ketyl radical to peroxyl or possibly to oxygen, a known reaction in homogeneous solution (46).

3. Kinetics for benzophenone-initiated autoxidation. Medium effects on rate constants of autoxidation and inhibition

The benzophenone-sensitized autoxidation has very significant advantages over the usual azo initiators for these quantitative measurements. Evolution of nitrogen and consumption of oxygen from the latter require large corrections to the measured rates in microenvironments (47), and such corrections are difficult to make for photo-decomposition of azo initiators since the necessary rate constants are unknown. In addition, azo initiators give thermal (dark) rates of autoxidation which can cause large errors in determinations of rate constants. These limitations do not occur in benzophenone-sensitized autoxidations; there is no dark rate and no gas is absorbed/produced when BP is irradiated in oxygenated 0.50 *M* SDS.

Log plots of the oxygen uptake for benzophenone-initiated reactions in SDS micelles are shown in Fig. 5 over a 7.3-fold change in linoleate concentration and for the five different light intensities used. Excellent linear correlations were obtained in all cases and the order in linoleate is essentially unity (1.02–1.06). Plots of the kinetic order in light transmittance shown in Fig. 6 for these conditions also exhibit linear correlations. The reaction order with respect to the rate of free radical chain initiation (R_i) obtained from the slopes vary somewhat, 0.627 to 0.540 with linoleate concentration. This is attributed to some first order chain termination[3] of peroxyls accompanying the usual bimolecular termination at low concentration. Subsequent kinetic measurements of rate constants were made at intermediate concentration (0.238 *M*) where the classical rate law for autoxidation (eq. [1]) is followed.[4]

The absolute rate constants for chain propagation, k_p, and termination, $2k_t$, for autoxidation of linoleate in two polar solvents, *tert*-butyl alcohol and acetonitrile (Table 5), provide

[3]Others (41) have postulated first order termination of peroxyls but the detailed mechanism is not known.

[4]The probability of simultaneously generating two radicals in the micelle is nil. In these and other related free radical reactions in SDS micelles (27, 44, 51), the fact that bimolecular termination occurs also implies that the radicals in question (e.g. linoleoylperoxyl) diffuse rapidly between micelles to allow radical recombination.

Can. J. Chem. Downloaded from www.nrcresearchpress.com by 213.166.140.6 on 09/07/12
For personal use only.

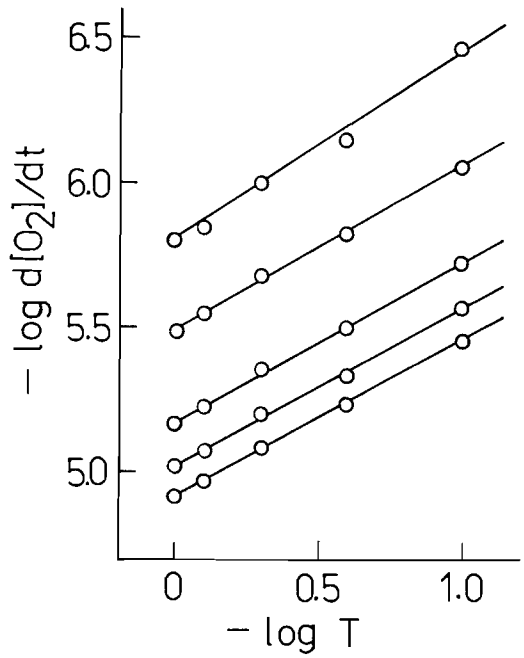

FIG. 6. Kinetic order plots for autoxidation of linoleic acid in 0.50 *M* SDS (pH 7.0) at 30°C; photoinitiated by benzophenone (1.13×10^{-2} *M*). Rate of oxygen consumption as a function of light intensity at five substrate concentrations. Values taken from Table 4.

basic data for comparison with the values obtained in micelles. As observed earlier by Howard and Ingold (48), the effect of an increase in solvent polarity is mainly on the rate of chain *termination*, which is decreased because the solvent stabilized polar peroxyl radicals (48) are destroyed in this step. Our finding that the $2k_t$ is lower in CH_3CN ($4.16 \pm 0.30 \times 10^6$ M^{-1} s^{-1}) than in *tert*-butyl alcohol ($17.2 \pm 2.7 \times 10^6$ M^{-1} s^{-1}) is consistent with the effect of the more polar solvent to decrease the termination rate.

Kinetic data for benzophenone-initiated autoxidation of linoleate (Table 6) indicate that the substrate oxidizability obtained by this method ($4.42 \pm 0.46 \times 10^{-2}$ $M^{-1/2}$ $s^{-1/2}$) is the same as that obtained earlier (4.48×10^{-2} $M^{-1/2}$ $s^{-1/2}$) using a thermal azo initiator in 0.50 *M* SDS (27).

Significant differences are shown in the absolute rate constants in micelles compared to those in organic solvents. The chain propagating rate constant in SDS (36.2 ± 4.8 M^{-1} s^{-1}) is one-half that found in acetonitrile. The effect on the $2k_t$ is more dramatic; the value in 0.50 *M* SDS ($2k_t = 3.52 \pm 0.90 \times 10^5$ M^{-1} s^{-1}) being reduced by at least an order of magnitude. We suggest that these effects on the rate constants are due, at least in part, to the polarity of peroxyl radicals.[5] Once formed, the radical centre would rapidly move to the micelle-aqueous interface where the polar environment of the aqueous buffer would substantially lower the $2k_t$ by strongly solvating the radicals by polar and hydrogen bonding interactions (50),[6] in this case of the resonance-stabilized peroxyls:

$$R{-}\ddot{O}{-}\ddot{O}\cdot \Longleftrightarrow R{-}\overset{(+)}{\dot{O}}{-}\overset{(-)}{\ddot{O}}\!: \quad \cdots \quad H{-}OH$$

Such solvation effects would also account for the lower k_p observed since the reactivity of the peroxyls would thereby be suppressed.

[5]The dipole moment of a peroxyl radical was found to be 2.4 D (49).

[6]In addition, the fact that a radical must exit a micelle in order to terminate with one in another micelle can be a controlling factor (51).

Values for inhibitor rate constants (k_{inh}) are of interest because they are an indication of the antioxidant activity. Accurate determinations are reported for various phenolic antioxidants in chlorobenzene solution (29). However, other reported values for k_{inh} in different solvents (52) and in micelles (44) can be quite unreliable because they are based on values of k_p measured in solution under different conditions. Evaluation of k_{inh} in microenvironments such as micelles and bilayers are of particular interest because they have implications for the effectiveness of antioxidants as biomembrane protectors. It is reported that the antioxidant properties of α-tocopherol and PMHC are similar within micelles and liposomes but that the phytyl side chain of α-tocopherol suppresses its transfer between liposomes (53).

Our values of k_{inh} reported in Table 7 are corrected for the k_p applicable for the medium in which the determination was made. Rather large errors are associated with these numbers (see Table 7), but they are sufficiently reliable to determine the effect of a micellar environment compared to a polar organic solvent, which is our main objective. To a certain extent, it is also possible to compare the activities of the three antioxidants in the same medium. The k_{inh} for α-tocopherol is retarded by a factor of 14 on changing from solution ($k_{inh} = 23 \pm 1.2 \times 10^4$ M^{-1} s^{-1} in *tert*-butyl alcohol) to micelles ($k_{inh} = 1.69 \pm 1.0 \times 10^4$ M^{-1} s^{-1}). This supports the proposal that diffusion of this lipophilic phenol between micelles is a limiting factor in antioxidant activity (44). The overall result of the micelles is a change in the relative activities of the three antioxidants. In 0.50 *M* SDS, PMHC and Trolox are now approximately twice as active as E; whereas in homogeneous alcohol solution, E and PMHC have the same activity, within experimental error, followed by Trolox. The absence of a definite induction period when α-tocopherol is used with methyl linoleate dispersed in SDS micelles (Fig. 2) can now be understood in terms of the reduced mobility of this inhibitor between micelles combined with a lack of homogeneity in such a system. It was suggested that methyl linoleate may "pool" (54) or form a heterogeneous microemulsion (55) in detergents (56) so that exchange of E between droplets is limiting. This demonstrates the importance of selecting the model system for quantitative study with considerable care.

Our actual values of k_{inh} are significantly different from values known in less polar solvents (e.g. α-tocopherol, $k_{inh} = 320 \times 10^4$ M^{-1} s^{-1} in chlorobenzene (29)). We suggest that a polar protic solvent (TBA) reduces the k_{inh} substantially by solvation of the polar peroxyl radicals. Trolox shows a further reduction in k_{inh} on changing from TBA ($k_{inh} = 14.7 \pm 1.3 \times 10^4$ M^{-1} s^{-1}) to more polar acetonitrile ($k_{inh} = 10.6 \pm 1.3 \times 10^4$ M^{-1} s^{-1}) most probably due to solvent effects on the peroxyl radical reactivity. The overall drop in activity of the three antioxidants observed in aqueous SDS micelles is attributed to a combination of strong hydrogen bonding aqueous solvent effects on the polar peroxyl radicals, and the effect water may have of tying up the electron lone pairs on the oxygen *para* to the phenolic hydroxyl group of the antioxidants. This latter hydrogen bonding would reduce the reactivity of the phenolic hydrogen by damping the stereoelectronic effect (29) exerted by the lone pairs on the para oxygen.

Experimental

1. Distribution coefficients

(1) Materials and preparation

The buffer used for diffusion coefficient measurements was 0.005 *M*

Can. J. Chem. Downloaded from www.nrcresearchpress.com by 213.166.140.6 on 09/07/12
For personal use only.

Can. J. Chem. Downloaded from www.nrcresearchpress.com by 213.166.140.6 on 09/07/12
For personal use only.

each of NaH_2PO_4 and Na_2HPO_4 (pH 7.0) in glass-distilled water containing 1×10^{-5} *M* EDTA. Stock 0.10 *M* SDS was prepared in this buffer. Anthracene (Eastman-Kodak) and phenanthrene (Fisher) were each recrystallized from ethanol.

Dilute solutions (generally less than 10^{-3} *M*) of the various compounds were prepared in both buffer and 0.10 *M* SDS by vortex-stirring and sonication (except DBHN and ABAP solutions). The solution concentration was such that it gave an absorbance between 0.5 and 1.5 at λ_{max} as measured in a 1.0 cm cell with a Varian Cary 219 spectrophotometer. Because of poor solubility, methyl linoleate was dissolved in 0.30 *M* SDS prior to determination of its diffusion coefficient in 0.10 *M* SDS. Also, the poor water solubility of linoleic acid necessitated the addition of sufficient aqueous NaOH to increase the pH of the injected buffer sample to 8.5.

(2) Apparatus

The Taylor diffusion apparatus used in this study is based on the design of Burkey *et al.* (28). Using a Spectra Physics SP8000 HPLC pump, the solvent was pumped at constant flow (0.2 mL/min) through 10 m of stainless steel tubing (0.03 in. i.d., Chromatographic Specialities) which was enclosed in the HPLC oven and thermostatted at 25 ± 0.1°C. A Nupro CA relief valve was placed in-line between the pressure transducer and injector of the HPLC to provide adequate back pressure (800–1200 psi) for effective flow referencing while not interfering with solute diffusion. The sample was loaded into a 10 μL loop and injected into the diffusion apparatus. Solute dispersion was detected at (or near) λ_{max} with a Schoeffel SF 770 variable wavelength detector and recorded on a Varian CDS 401 data system.

2. Autoxidations

(1) Materials and preparations

(a) Phosphate buffer

Solutions were prepared in 0.05 *M* of each of NaH_2PO_4 and Na_2HPO_4 (pH 7.0) in glass distilled water containing 1×10^{-4} *M* EDTA. Prior to use, the buffer was passed through a column of Chelex 100 (50–100 mesh) (BioRad) to remove traces of heavy metal ions (57).

(b) Solvents

Hexane, methanol, and acetonitrile were of HPLC grade and purchased from Caledon or Anachemia. *tert*-Butyl alcohol was purified by distillation.

(c) Sodium dodecyl sulfate

Electrophoresis purity SDS was purchased from BioRad. Stock solutions of 0.50 *M* SDS were prepared in the 0.10 *M* phosphate buffer (pH 7.0) described above.

(d) Linoleic acid, methyl linoleate

Linoleic acid and methyl linoleate were purchased from Nu-Chek Prep, Inc. (>99%). The lipids were found to be free of hydroperoxide by periodic TLC analysis on silica gel with *N,N*-dimethyl-*p*-phenylenediamine spray.

(e) Initiators

Di-*tert*-butylhyponitrite was synthesized and stock solutions were prepared in 0.50 *M* SDS as reported earlier (54). Azobis(2-amidinopropane·HCl) and azobiscyclohexylnitrile were obtained from Polysciences, Inc. and stored at −30°C. Benzophenone (Fisher) was recrystallized from pentane, while 4-sulphomethylbenzophenone, sodium salt (a gift from Dr. J. C. Scaiano) was used as received. Stock solutions of ABAP were prepared in phosphate buffer. BP and BP^- were dissolved in 0.50 *M* SDS by vortex-stirring and sonication. For autoxidations carried out in homogeneous solution, benzophenone and ACHN were readily dissolved in either *t*-butanol or CH_3CN. All initiator solutions were stored at 4°C.

(f) Inhibitors

For micellar autoxidations, the following procedure was used: Stock solutions of α-tocopherol (Eastman-Kodak) were prepared in 0.50 *M* SDS as previously described (27) while solid PMHC (a gift from Dr. G. W. Burton) was readily dissolved in SDS. Standard solutions of Trolox, a gift from Hoffman-LaRoche, were prepared in argon-degassed phosphate buffer. Stock solutions of PMHC, α-T and Trolox were also prepared in *t*-butanol or acetonitrile, as required. All inhibitor solutions were stored under argon and at 4°C.

(g) Quenchers

Solutions of 1,3-diphenylisobenzofuran (Aldrich) were prepared in 0.5 *M* SDS by vortex-stirring and sonication. Sodium azide and 1,4-diazabicyclo[2.2.2]octane (DABCO, Aldrich, 97%) were dissolved in argon-degassed buffer. All quencher solutions were stored refrigerated and under argon.

(2) Autoxidation procedure

Autoxidations were carried out at 30°C and 760 mm Hg of O_2 using a sensitive automatic recording gas absorption apparatus similar to that described (47). For DBHN-initiated autoxidations, a 2.00 mL aliquot of DBHN in 0.50 *M* SDS was added to a calibrated reaction cell, followed by the appropriate amount of linoleic acid and isomolar NaOH. The cell and contents were then attached to the gas absorption apparatus and the rate of O_2 consumption measured. For the ABAP-initiated autoxidations, typically 100 μL of 0.4 *M* ABAP solution in buffer was added to 2.00 mL of 0.50 *M* SDS in a calibrated cell. The cell and contents were attached to the apparatus and allowed to shake for up to 1 h (before the addition of linoleic acid and NaOH) to permit solubilization of the ABAP.

In a typical photoinitiated run, a 2.00 mL aliquot of benzophenone in the appropriate solvent (or BP^- in 0.50 *M* SDS) was added to a calibrated reaction cell followed by the desired amount of linoleic acid (and NaOH for micellar autoxidations). The cell and contents were then attached to the apparatus and shaken to thermally equilibrate. The reaction was initiated by irradiation through Pyrex with a 200 W super pressure mercury lamp, the intensity of which was monitored using fiber optics sampling of the light beam and a phototube detector. Various additives were added to the reaction mixtures from precision syringes. The extent of oxidation was generally less than 10%.

(3) Absolute rate constants

Two 45° sectors were cut from each of two discs of blackened metal with dimensions such that $r = 3$. The discs were placed back-to-back between the light source and the gas absorption apparatus equipped with a shutter. The disc nearest the lamp was driven by an electric motor through a series of gears which could be changed to provide nine different rotation speeds from 0.286 to 4.20 rpm. The disc nearer the oxidation apparatus was driven through gears which enabled rotation speeds of 700 to 2400 rpm.

The reaction order with respect to the rate of photoinitiation was determined by measuring the rate of oxygen consumption when the reaction mixture was exposed to irradiation of different intensities. A series of neutral density filters of known transmittance (Ealing Scientific) was placed in the light path, the shutter opened and the rate of oxidation measured on a strip chart recorder.

The parameter γ was determined by measuring R_f/R_0. This ratio is measured three times using the rates obtained at 2400 rpm (R_f) and steady illumination (R_0).

The next step involved a preliminary measurement of R_λ/R_0 for several of the possible slow sector speeds, λ. From ref. 40, it can be shown that for a sector with $r = 3$, the rotating sector method is most accurate when $m = 3.70$. Using the sector rotation speed which produces m nearest to 3.70, the ratio R_λ/R_0 was determined twice by alternately measuring R_λ and R_0. The R_i was then measured by the addition of an aliquot of Trolox solution (in the appropriate solvent). This process was repeated until at least four values of R_λ/R_0 (i.e. m) and two values of R_i have been determined. From this the absolute rate constants are then calculated according to eqs. [9]–[11].

HPLC analyses

(1) Linoleate autoxidation products

After 5% oxidation (as measured by the consumption of O_2), 5 mL of 10 m*M* PPh_3 was added to a 500 μL aliquot of the reaction mixture followed by the addition of 50 mL of methanol/water (50/50). The aqueous solution was extracted twice with diethyl ether; 35 and 15 mL. The combined extracts were dried over Na_2SO_4 and then treated with excess CH_2N_2 in ether at 0°C. The solution was gently warmed to room

temperature to remove excess diazomethane. Samples were then stored at −30°C until required for analysis.

Immediately prior to analysis by HPLC, the solvent was removed at reduced pressure, followed by pumping at <0.25 mm Hg for at least 30 min. The residue was brought up in 2 mL of HPLC solvent: hexane/2-propanol/acetone (992/4/4). Brief centrifugation was usually necessary to remove excess solid PPh_3. Separation of the four methyl hydroxylinoleates was achieved using a Waters 5100 HPLC pump fitted with a 30 cm × 10 μm Apex silica column (Jones Chromatography). With a flow rate of 1.6 mL/min, the products were detected by monitoring eluent absorption at 234 nm with a Schoeffel SF 770 variable wavelength detector. Identification of the four compounds was achieved by cross-comparison of an autoxidation product mixture from our lab with a reference mixture obtained and analyzed (39) under similar conditions in the laboratories of Dr. N. A. Porter of Duke University.

Relative amounts of the four hydroxylinoleates were determined by correcting the peak areas, as reported by a Varian CDS 401 data system, for the appropriate molar absorptivity (33): 13-*c*,*t* (λ_{max} 236, ϵ = 27 200); 13-*t*,*t* (λ_{max} 233 nm, ϵ = 30 500); 9-*c*,*t* (λ_{max} 236 nm, ϵ = 28 300); 9-*t*,*t* (λ_{max} 233 nm, ϵ = 31 600).

(2) Benzophenone product analysis

A 100 μL aliquot was removed from the reaction mixture and added to 1 mL of methanol/water (50/50). After vortex-stirring for 15 s, the aqueous solution was extracted twice with 1 mL of HPLC solvent: hexane/2-propanol/acetone (992/4/4). Following brief centrifugation, the organic layers were removed. To 500 μL of the combined extracts was added 25 μL of 2.82×10^{-3} *M* *p*-methoxyacetophenone (the internal standard) in hexane. The sample was eluted using the Waters 5100 pump and the Apex silica column. To aid in separation, the solvent was pumped at 0.8 mL/min for 10 min, then increased to 1.6 mL/min for the remainder of the analysis. The eluent was monitored at 225 nm with the Schoeffel SF 770 detector.

(3) α-Tocopherol analysis

A 250 μL aliquot of the reaction mixture (initially 3.94×10^{-5} *M* α-T) was removed from the reaction vessel and added to 500 μL of absolute ethanol in a small test tube. After vortex-stirring for 15 s, the solution was extracted twice with 250 μL of hexane. Brief centrifugation was necessary to aid separation of the two layers. To 250 μL of the combined hexane extracts was added 10 μL of the internal standard solution, 9.28×10^{-4} *M* PMHC in hexane. Analysis was performed by injecting 50 μL of the resulting solution onto the Apex silica column with the solvent; hexane/2-propanol (99/1) flowing at 0.9 mL/min. The column effluents were monitored at 220 nm with the Schoeffel SF 770.

Acknowledgements

Research grants from the Natural Sciences and Engineering Research Council of Canada and the Terry Fox Fund for Cancer Research are gratefully acknowledged. T.D.S. was a recipient of a NSERC Undergraduate Summer Research Scholarship. L.R.C.B. and S.J.L. acknowledge the assistance of Dr. N. A. Porter during visits to his laboratory to develop the analysis of linoleate oxidation products.

1. B. Halliwell and J. M. C. Gutteridge (*Editors*). Free radicals in biology and medicine. Oxford Science Publication. 1985.
2. C. S. Foote. *In* Free radicals in biology. Vol. II. *Edited by* W. A. Pryor. Academic Press, New York. 1980. Chap. 3. pp. 85–133.
3. R. C. Straight and J. D. Spikes. *In* Singlet O_2. Vol. IV. Polymers and biomolecules. *Edited by* A. A. Frimer. CRC Press, Boca Raton, FL. 1985. Chap. 2, pp. 91–143.
4. S. M. Anderson, N. I. Krinsky, M. J. Stone, and D. C. Clagett. Photochem. Photobiol. **20**, 65 (1974).
5. K. Suwa, T. Kimura, and A. P. Schapp. Photochem. Photobiol. **28**, 469 (1978).
6. R. Muller-Runkel, J. Blais, and L. I. Grossweiner. Photochem. Photobiol. **33**, 683 (1981).
7. S. J. Dearden, T. F. Hunter, and J. Philp. Chem. Phys. Lett. **81**, 606 (1981).
8. M. K. Logani. J. Photochem. **25**, 275 (1984).
9. R. B. Cundall, R. K. Chowdhary, A. K. Davies, and V. P. Russell. J. Photochem. **25**, 267 (1984).
10. A. A. Gorman and M. A. J. Rodgers. Chem. Phys. Lett. **55**, 52 (1978).
11. N. Barboy and J. Kraljic. J. Photochem. **9**, 336 (1978).
12. N. Miyoshi and G. Tomita. Z. Naturforsch. **33B**, 622 (1978).
13. N. Miyoshi and G. Tomita. Z. Naturforsch. **34**, 339 (1979).
14. B. A. Lindig and M. A. J. Rodgers. J. Phys. Chem. **83**, 1683 (1979).
15. B. A. Lindig and M. A. J. Rodgers. Photochem. Photobiol. **33**, 627 (1981).
16. E. Rossi, A. Van de Vorst, and G. Jori. Photochem. Photobiol. **34**, 447 (1981).
17. M. A. J. Rodgers. Photochem. Photobiol. **37**, 99 (1983).
18. J. P. Reyftmann, R. Santus, P. Morliere, and E. Kohen. Photobiochem. Photobiophys. **9**, 183 (1985).
19. I. B. C. Matheson and M. A. J. Rodgers. J. Phys. Chem. **86**, 884 (1982).
20. I. B. C. Matheson and R. Massoudi. J. Am. Chem. Soc. **102**, 1942 (1980).
21. P. C. Lee and M. A. J. Rodgers. J. Phys. Chem. **87**, 4894 (1983).
22. M. C. Hovey. J. Am. Chem. Soc. **104**, 4196 (1982).
23. F. R. Mayo. Acc. Chem. Res. **1**, 193 (1965).
24. K. U. Ingold. Acc. Chem. Res. **2**, 1 (1969).
25. J. A. Howard. *In* Free radicals. *Edited by* J. K. Kochi. Wiley, New York. 1973. Chap. 12, pp. 3–62.
26. C. E. Boozer, G. S. Hammond, C. E. Hamilton, and J. N. Sen. J. Am. Chem. Soc. **77**, 3233 (1953).
27. L. R. C. Barclay, S. J. Locke, and J. M. MacNeil. Can. J. Chem. **63**, 366 (1985).
28. T. J. Burkey, D. Griller, D. A. Lindsay, and J. C. Scaiano. J. Am. Chem. Soc. **106**, 1983 (1984).
29. G. W. Burton, T. Doba, E. J. Gabe, L. Hughes, F. L. Lee, L. Prasad, and K. U. Ingold. J. Am. Chem. Soc. **107**, 7053 (1985).
30. A. A. Gorman, I. R. Gould, I. Hamblett, and M. C. Standen. J. Am. Chem. Soc. **106**, 6956 (1984).
31. R. L. Clough, B. G. Yee, and C. S. Foote. J. Am. Chem. Soc. **101**, 683 (1979).
32. T. Doba, G. W. Burton, K. U. Ingold, and M. Matsuo. J. Chem. Soc. Chem. Commun. 461 (1984).
33. H. W.-S. Chan and G. Levett. Lipids, **12**, 99 (1977).
34. M. J. Thomas and W. A. Pryor. Lipids, **15**, 544 (1980).
35. N. A. Porter. Acc. Chem. Res. **19**, 262 (1986).
36. N. A. Porter and D. G. Wujek. J. Am. Chem. Soc. **106**, 2626 (1984).
37. H. Weenen and N. A. Porter. J. Am. Chem. Soc. **104**, 5216 (1982).
38. N. A. Porter, L. S. Lehman, B. A. Weber, and K. J. Smith. J. Am. Chem. Soc. **103**, 6447 (1981).
39. N. A. Porter, B. A. Weber, H. Weenen, and J. A. Khan. J. Am. Chem. Soc. **102**, 5597 (1980).
40. G. M. Burnett and H. W. Melville. *In* Techniques of organic chemistry. Vol. VIII. Part II. *Edited by* S. L. Friess, E. S. Lewis, and A. Weissberger. Interscience, New York. 1963. Chap. 20.
41. J. A. Howard and K. U. Ingold. Can. J. Chem. **43**, 2729 (1965); **43**, 2737 (1965).
42. J. C. Scaiano and D. J. Lougnot. J. Phys. Chem. **88**, 3379 (1984).
43. L. R. C. Barclay, S. J. Locke, J. M. MacNeil, J. VanKessel, G. W. Burton, and K. U. Ingold. J. Am. Chem. Soc. **106**, 2479 (1984).

Can. J. Chem. Downloaded from www.nrcresearchpress.com by 213.166.140.6 on 09/07/12
For personal use only.

44. L. CASTLE and M. J. PERKINS. J. Am. Chem. Soc. **108**, 6381 (1986).
45. M. V. ENCINAS and J. C. SCAIANO. J. Am. Chem. Soc. **103**, 6393 (1981).
46. J. N. PITTS, R. L. LETSINGER, R. P. TAYLOR, J. M. PATTERSON, G. RECKTENWALD, and R. B. MARTIN. J. Am. Chem. Soc. **81**, 1068 (1959).
47. L. R. C. BARCLAY and K. U. INGOLD. J. Am. Chem. Soc. **103**, 6478 (1981).
48. J. A. HOWARD and K. U. INGOLD. Can. J. Chem. **44**, 1119 (1966).
49. R. W. FESSENDEN, A. HITACHI, and V. NAGARAJAN. J. Phys. Chem. **88**, 107 (1984).
50. F. F. RUST and E. A. YOUNGMAN. J. Org. Chem. **27**, 3778 (1962).
51. T. J. BURKEY and D. GRILLER. J. Am. Chem. Soc. **107**, 246 (1985).
52. E. NIKI, T. SAITO, A. KAWAKAMI, and Y. KAMIYA. J. Biol. Chem. **259**, 4177 (1984).
53. E. NIKI, A. KAWAKAMI, M. SAITO, Y. YAMAMOTO, J. TSUCHIYA, and Y. KAMIYA. J. Biol. Chem. **260**, 2191 (1985).
54. L. R. C. BARCLAY, S. J. LOCKE, and J. M. MACNEIL. Can. J. Chem. **61**, 1288 (1983).
55. T. DOBA, G. W. BURTON, and K. U. INGOLD. Biochim. Biophys. Acta, **835**, 298 (1985).
56. Y. YAMAMOTO, S. HAGA, E. NIKI, and Y. KAMIYA. Bull. Chem. Soc. Jpn. **57**, 1260 (1984).
57. M. SCARPA, R. STEVANATO, P. VIGLINO, and A. RIGO. J. Biol. Chem. **258**, 6695 (1983).
58. D. F. EVANS, C. CHAN, and B. C. LAMARTINE. J. Am. Chem. Soc. **99**, 6492 (1977).

Can. J. Chem. Downloaded from www.nrcresearchpress.com by 213.166.140.6 on 09/07/12
For personal use only.

Autoxidation of model membranes. The kinetics and mechanism of autoxidation of mixed phospholipid bilayers

LAWRENCE ROSS COATES BARCLAY,[1] KIMBERLY ANN BASKIN, DAVID KONG, AND STEVEN JEFFREY LOCKE
Department of Chemistry, Mount Allison University, Sackville, N.B., Canada E0A 3C0

Received May 12, 1987

LAWRENCE ROSS COATES BARCLAY, KIMBERLY ANN BASKIN, DAVID KONG, and STEVEN JEFFREY LOCKE. Can. J. Chem. **65**, 2541 (1987).

Kinetics of autoxidation of bilayer mixtures of oxidizable dilinoleoylphosphatidylcholine (DLPC) with saturated phospholipids as solvents (dimyristoyl-, DMPC, and dipalmitoyl-phosphatidylcholine, DPPC) follow the classical rate law of autoxidation: $-d[O_2]/dt = k_p/2k_t^{1/2}[RH]R_i^{1/2}$. The kinetic order in substrate [RH] was found to be unity for peroxidation initiated by a lipid-soluble initiator, azobis-2,4-dimethylvaleronitrile (ADVN), and by the water-soluble azobis(2-amidinopropane·HCl) (ABAP). The kinetic order in rate of chain initiation, R_i, was found to be one-half for both initiation by ADVN, photochemically decomposed, and by ABAP. The oxidizability of unilamellar DLPC liposomes ($k_p/2k_t^{1/2} = 0.232\ M^{-1/2}\ s^{-1/2}$) is twice that of multilamellar DLPC ($k_p/2k_t^{1/2} = 0.116\ M^{-1/2}\ s^{-1/2}$). Analysis of the hydroperoxides formed during ABAP-initiated autoxidations of mixed DLPC + DPPC liposomes showed a linear trend between the ratio of *cis,trans* to *trans,*trans geometrical isomeric hydroperoxides and [DLPC], consistent with the peroxidation mechanism proposed for homogeneous systems. ^{31}P nmr spectra of mixed bilayers were used to distinguish between heterogeneous and homogeneous mixtures of DLPC + DPPC. Such spectra taken at various stages of oxidation indicate that the bilayer structure of DLPC is preserved at least to the 10% extent of oxidation used in kinetic studies. At much higher oxidative conversion, the spectra indicate changes in lamellar structures.

LAWRENCE ROSS COATES BARCLAY, KIMBERLY ANN BASKIN, DAVID KONG et STEVEN JEFFREY LOCKE. Can. J. Chem. **65**, 2541 (1987).

La cinétique de l'auto-oxydation de mélanges en double couches de dilinoléoylphosphatidylcholine (DLPC) oxydables avec des phospholipides saturés comme solvants (dimyristoyl-, DMPC et dipalmitoylphosphatidylcholine, DPPC) répond à une loi de vitesse classique pour une auto-oxydation : $-d[O_2]/dt = k_p/2k_t^{1/2[RH]}R_i^{1/2}$. On a trouvé que l'ordre en substrat [RH] est égal à un pour la peroxydation initiée par un initiateur lipo-soluble, l'azo bis(diméthyl-2,4 valéronitrile) (ADVN) et par l'initiateur soluble dans l'eau, azo bis(amidino-2 propane·HCl) (ABAP). On a trouvé que l'ordre en initiation de chaînes, R_i, est égal à une demi pour les initiations tant par l'ADVN décomposé d'une façon photochimique que par l'ABAP. La facilité d'oxyder les liposomes DLPC unilamellaires ($k_p/2k_t^{1/2} = 0{,}232\ M^{-1/2}\ s^{-1/2}$) est deux fois plus grande que celle du DLPC multilamellaire ($k_p/2k_t^{1/2} = 0{,}116\ M^{-1/2}\ s^{-1/2}$). Une analyse des hydroperoxydes qui se forment au cours des auto-oxydations initiées par l'ABAP de mélanges de liposomes de DLPC + DPPC a permis de montrer qu'il existe une tendance linéaire entre le rapport des isomères géométriques *cis,trans* et *trans,trans* des hydroperoxydes et la [DLPC]; ce résultat est en accord avec le mécanisme de peroxydation proposé pour des systèmes homogènes. On a utilisé les spectres rmn du ^{31}P des doubles couches pour établir une distinction entre les mélanges homogènes et hétérogènes du DLPC + DPPC. De tels spectres, déterminés à divers stages de l'oxydation, indiquent que la structure en double couche du DLPC est maintenue au moins jusqu'au 10% d'oxydation utilisé pour les études cinétiques. A des taux d'oxydation plus élevés, les spectres indiquent qu'il s'est produit des changements dans les structures lamellaires.

[Traduit par la revue]

Introduction

Autoxidation of unsaturated biomembrane lipids disrupts important structural and functional properties of membranes and is associated with important pathological events (1, 2) including the action of foreign toxic substances (3). Several groups have recently developed an increased interest in the *quantitative* study of autoxidation of biologically significant systems such as phospholipids in bilayers and lipids in micelles (4–31).

Most of the attention of these groups has been centred on the mechanism and activity of antioxidants (9–22), the dynamics of free radical initiation (23–26), and elucidation of the autoxidation chain mechanism from studies of trends in formation of the hydroperoxide products (27–31). We have shown that quantitative kinetic studies can be carried out in bilayers and micelles using both lipid-soluble and water-soluble initiators and inhibitors (7). This has facilitated applications to quantitative studies on natural biological fluids (32, 33). It would appear from our initial studies in bilayers (4, 5) that the kinetics of autoxidation in this phase follow the same classical rate law well known for autoxidation of organic substrates in homogeneous solution (34–37); namely, that the rate of oxygen uptake is first order in concentration of substrate (RH) and one-half order in the rate of chain initiation (R_i) as indicated in eq. [1]:

$$[1] \quad \frac{-d[O_2]}{dt} = \frac{k_p[RH]R_i^{1/2}}{2k_t^{1/2}}$$

For systems which obey eq. [1], the susceptibility of substrates to undergo autoxidation, known as *oxidizability* $k_p/(2k_t)^{1/2}$, follows from eq. [2]:

$$[2] \quad \frac{k_p}{2k_t^{1/2}} = \frac{-d[O_2]/dt}{[RH]R_i^{1/2}}$$

We have recently demonstrated that the autoxidation of linoleic acid in sodium dodecyl sulfate micelles obeys eq. [1] (8).

While it seems to be assumed that the autoxidation of unsaturated lipids in membranes follows the same classical rate law, i.e. eq. [1] (38), there are very significant deficiencies in our basic knowledge of the kinetics of membrane autoxidation. For example, the kinetic orders with respect to substrate and the rate of chain initiation have not been adequately determined in

[1]Author to whom correspondence to be addressed.

Can. J. Chem. Downloaded from www.nrcresearchpress.com by 213.166.140.6 on 09/07/12
For personal use only.

Can. J. Chem. Downloaded from www.nrcresearchpress.com by 213.166.140.6 on 09/07/12
For personal use only.

bilayers. Our earlier studies (4, 5) did show that the calculated oxidizability of egg lecithin bilayers, thermally initiated by di-*tert*-butylhyponitrite (DBHN) was "constant" for different amounts of initiator in the bilayer. On the other hand, it is also important to determine the kinetic order in substrate, RH, by employing bilayers with varying amounts of oxidizable and inert phosphatidylcholine. Obviously, *the concentration of oxidizable lipid in a single pure PPC is a fixed value*, independent of the amount used. Therefore, it is not sufficient to simply determine the effect on the rate of oxidation by varying the total amount of the sample PPC in the "aqueous emulsion" as reported (39) since this does not really vary the substrate concentration in the bilayer. Furthermore, mixtures of lipids provide a better model for a biological membrane than does a single lecithin (40).

Although the water-soluble initiator azobis(2-amidinopropane·hydrochloride) (ABAP) has been very useful in micelle and bilayer autoxidations (7, 41), both kinetic and PPC product studies are lacking for ABAP-initiated autoxidations. In order to evaluate important kinetic properties of bilayers, such as the oxidizability, a complete verification of eq. [1] is required for both water-soluble and lipid-soluble initiators. With such an objective in mind, we now report on a comprehensive quantitative investigation of bilayer autoxidation; including the following studies. (*1*) The kinetic order in oxidizable substrate, [RH], is determined by using a mixed bilayer system composed of variable amounts of non-oxidizable (saturated) dipalmitoylphosphatidylcholine, DPPC, or dimyristoylphosphatidylcholine, DMPC, mixed with the oxidizable (unsaturated) dilinoleoylphosphatidylcholine, DLPC. The effect of variation of [RH] on the rate of oxygen uptake is determined by changing the relative amounts of the two lipids in the mixture. This study is completed for a lipid-soluble initiator azobis-2,4-dimethylvaleronitrile (ADVN) and the water-soluble ABAP. (*2*) The kinetic order in the rate of chain initiation is determined for initiation in the aqueous phase by varying [ABAP] for neat DLPC and for mixtures of DLPC and DPPC. The kinetic order with respect to the R_i for DLPC autoxidations initiated by photochemically decomposed ADVN (in the bilayer) is determined by measuring the rate of O_2 consumption as a function of light intensity. (*3*) Quantitative studies of the hydroperoxides formed from ABAP-initiated autoxidation of mixtures of DLPC and DPPC are completed in order to determine whether the products and the variation in product distribution with [DLPC] are similar to those observed for autoxidations initiated in the bilayer lipid phase. The object of this study is to determine whether the mechanism for peroxidation as outlined in references 27–31 is also applicable to autoxidations initiated in the aqueous phase. (*4*) Some results are reported on ^{31}P nmr spectra of bilayers. The objectives of these studies are to determine whether (*a*) evidence of the homogeneity of the DLPC and DPPC mixed bilayers can be obtained from the spectra and (*b*) the process of oxidation alters the bilayer structure of the PPCs (multilamellar and unilamellar) as characterized by their ^{31}P nmr spectra. In this study, it was important to determine whether the integrity of the bilayer structure is retained during the usual extent of oxidation (5–10%) in our kinetic and product studies. There is widespread interest in the effects of lipid peroxidation on the structures and properties of phospholipid membranes (42–47) and pathological effects, such as "leak formation" in animal erythrocytes (48–54). To our knowledge, however, there is no evidence that relates the extent of peroxidation (as measured in a *quantitative* kinetic manner) to effects on membrane structure.

Results

1. The kinetic order in oxidizable substrate for mixed bilayers

(a) With a lipid-soluble initiator (ADVN)

Known amounts of DLPC mixed with DMPC as "solvent", containing the initiator ADVN, were prepared above the phase transition temperature, T_t.[2] Data for the rates of oxygen consumption, the measured rates of chain initiation and the oxidizabilities are given in Table 1. The data were obtained over a six-fold range of DLPC concentration. A chain length, ν, in excess of 20 was maintained even at low DLPC and a constant value (within experimental error) of the oxidizability ($k_p/2k_t^{1/2} = 0.116 \pm 0.013\ M^{-1/2}\ s^{-1/2}$) was maintained throughout. The kinetic order in DLPC concentration was found to be 1.05 ± 0.03.

(b) With a water-soluble initiator (ABAP)

It was desirable to carry out experiments using DLPC mixed with DPPC since the latter commonly occurs in natural biomembranes (56). Since DPPC has a T_t of 41°C (55) and mixing in the gel phase is "constrained" (40, 56), preparations were kept above this T_t throughout to maximize random mixing of the two phospholipids. In addition, the mixtures were extruded through a French pressure cell to produce unilamellar liposomes (20, 57). The use of unilamellar liposomes avoids the problem of inhomogeneous distribution of the initiator, reported in other studies (58) when ABAP was added to multilamellar liposomes *after sample preparation*.[3] Kinetic data obtained with these unilamellar DLPC liposomes are outlined in Table 2. A chain length in excess of 20 was achieved over the six-fold range in [DLPC] with $k_p/2k_t^{1/2} = 0.232 \pm 0.034\ M^{-1/2}\ s^{-1/2}$. The kinetic order in bilayer DLPC concentration was found to be 1.07 ± 0.06.

Some experiments were also carried out by adding the initiator, ABAP, with the aqueous buffer *before* preparing the DLPC unilamellar liposomes. The oxidizability ($k/2k_t^{1/2} = 0.239 \pm 0.031\ M^{-1/2}\ s^{-1/2}$) obtained under such conditions is similar to that reported above for experiments with ABAP added after liposome formation.

2. The kinetic order in rate of chain initiation (R_i)

(a) With a lipid-soluble initiator (ADVN)

Under ideal conditions, the rate of oxygen consumption by the organic substrate is expected to be proportional to the $R_i^{1/2}$ and therefore to the square root of the light intensity for reactions where a photochemically decomposed initiator is employed. At 30°C, the thermal decomposition of ADVN in DLPC is slow. Consequently, the kinetic order with respect to the R_i was determined by measuring rates of O_2 uptake at six different light intensities for the ADVN photoinitiated autoxidation of DLPC. From the results given in Table 3, the kinetic order in light intensity was 0.503 ± 0.032.

(b) With a water-soluble initiator (ABAP)

The reaction order with respect to the concentration of

[2]DMPC did not absorb oxygen in the presence of ADVN in blank runs. The T_t of DMPC is 23°C (55); the T_t of DLPC is not known, but it is assumed to be below our conditions used.

[3]We also found that α-tocopherol sequestered in our unilamellar liposomes gave distinct inhibition periods using our procedure. This contrasts sharply with the behaviour in multilamellar samples (58).

TABLE 1. The kinetics of autoxidation of DLPC in mixed bilayers with DMPC; thermally-initiated with lipid-soluble ADVN[a]

No.[b]	[DLPC][c] (mol L^{-1})	$-d[O_2]/dt$[d] ($M\ s^{-1} \times 10^5$)	R_i[e] ($M\ s^{-1} \times 10^7$)	ν[f]	$k_p/2k_t^{1/2}$ ($M^{-1/2} s^{-1/2}$)
1(a)	1.023	9.79	5.95	164	0.124
(b)	1.023	8.74	6.28	139	0.108
2(a)	0.512	4.14	5.12	81	0.113
(b)	0.512	3.80	5.23	73	0.102
3(a)	0.172	1.51	6.25	24	0.141
(b)	0.172	1.42	6.20	23	0.133
4(a)	0.767	7.37	6.29	117	0.121
(b)	0.767	6.65	6.00	111	0.112
5(a)	0.341	2.41	4.56	53	0.105
(b)	0.341	2.40	4.70	51	0.103

[a]In all cases, the aqueous phase was 0.10 *M* phosphate, 0.1 m*M* EDTA (pH 7.0). 8.58 μm ADVN was introduced in each run.
[b](a) and (b) refer to duplicate runs from the same liposome preparation.
[c]The concentration of oxidizable lipid, DLPC, in the mixture of DLPC and DMPC.
[d]Rates have been corrected for evolution of nitrogen and absorption of oxygen by the initiator and O_2 evolved in chain termination by adding $(1 - e)k_i[In]$ to the measured rates. The k_i for ADVN was taken as $5.25 \times 10^{-6}\ s^{-1}$ at 45°C (60) and the initiator efficiency was found to be 0.20 in the bilayers according to the equation $e = R_i/2k_i[In]$.
[e]Measured by inhibition periods with Trolox (7).
[f]The kinetic chain length where $\nu = -d[O_2]/dt//R_i$.

TABLE 2. The kinetics of autoxidation of DLPC mixed bilayers with DPPC; thermally-initiated in the aqueous phase with ABAP[a]

No.[b]	[DLPC][c] (mol L^{-1})	$-d[O_2]/dt$[d] ($M\ s^{-1} \times 10^4$)	R_i[e] ($M\ s^{-1} \times 10^6$)	ν[f]	$k_p/2k_t^{1/2}$ ($M^{-1/2} s^{-1/2}$)
1(a)	1.023	2.83	1.54	183	0.224
(b)	1.023	2.73	1.48	184	0.220
2(a)	0.180	0.431	1.60	27	0.189
(b)	0.180	0.410	1.63	26	0.179
3(a)	0.513	1.42	1.38	103	0.236
(b)	0.513	1.38	1.38	100	0.229
4(a)	0.766	2.84	1.80	158	0.276
(b)	0.766	2.56	1.84	139	0.247
5(a)	0.256	0.858	1.47	58	0.277
(b)	0.256	0.800	1.55	52	0.251
6	0.256	0.729	1.58	46	0.227

[a]ABAP used was $1.43–1.48 \times 10^{-5}$ mol.
[b]See footnote *b*, Table 1.
[c]The concentration of oxidizable lipid, DLPC, in the mixture of DLPC and DPPC. The bilayers were prepared above the phase transition temperature (see text).
[d]See footnote *c*, Table 1. The k_i for ABAP was calculated to be $4.47 \times 10^{-6}\ s^{-1}$ at 45°C (61) and the initiator efficiency was found to be 0.43.
[e]See footnote *d*, Table 1.
[f]See footnote *e*, Table 1.

water-soluble ABAP was measured conveniently by simply adding measured amounts of aqueous ABAP to DLPC and measuring the effect on the rate of oxygen consumption. Typical data for such experiments are given in Table 4. The kinetic order in [ABAP] was 0.524 ± 0.056 and 0.431 ± 0.054 for two runs, 1 and 2, with liposomes of neat DLPC. A more extensive study was carried out on a mixture of DLPC and DPPC (duplicated) giving a kinetic order of 0.538 ± 0.016.

3. *Quantitative studies of oxidation product formation from mixed DLPC + DPPC bilayers with a water-soluble initiator (ABAP)*

The products of autoxidation of linoleate are known to be the 9- and 13-hydroperoxy substituted 9-*cis*,11-*trans*; 9-*trans*,11-*trans* and 10-*trans*,12-*cis*; 10-*trans*,12-*trans* octadecadienoates which are usually analyzed by reduction and conversion to the corresponding hydroxymethyl esters as shown in Scheme 1.

Can. J. Chem. Downloaded from www.nrcresearchpress.com by 213.166.140.6 on 09/07/12
For personal use only.

Can. J. Chem. Downloaded from www.nrcresearchpress.com by 213.166.140.6 on 09/07/12
For personal use only.

TABLE 3. The dependence of the rate of oxidation of multilamellar DLPC liposomes on the light intensity, initiated by ADVN at 30°C

Relative light intensity (%)	$-d[O_2]/dt$ ($M\,s^{-1} \times 10^5$)
10.0	1.20[b]
15.9	1.60
25.1	2.05
50.1	2.87
79.4	3.82
100	3.63[c]

[a]The concentration of ADVN was 0.050 *M* in the bilayer phase.
[b]The average of two measurements: 1.19 and 1.20×10^{-5} $M\,s^{-1}$.
[c]The average of two measurements: 3.50 and 3.76×10^{-5} $M\,s^{-1}$.

TABLE 4. The dependence of the rate of oxidation of multilamellar liposomes on the concentration of initiator, ABAP, at 45°C

Run No.	ABAP (mol $\times 10^6$)	$-d[O_2]/dt$ ($M\,s^{-1} \times 10^5$)
1[a]	3.69	1.81
	7.30	2.26
	14.7	3.82
	28.7	5.03
2[a]	3.69	2.33
	7.30	3.66
	14.6	4.45
	29.2	5.85
3a (3b)[b]	1.84 (1.84)	0.605 (0.624)
	3.65 (3.65)	0.954 (1.01)
	7.38 (7.38)	1.48 (1.48)
	14.7 (14.7)	2.00 (2.32)
	29.6 (29.5)	2.96 (2.96)
	59.3 (59.3)	4.05 (4.04)

[a]Results with liposomes of neat DLPC.
[b]Separate runs on mixed bilayers of DLPC and DPPC, where [DLPC] in the bilayer is 0.523 *M*. See footnote *c*, Table 2.

Very significant information has been provided on the mechanism of autoxidation of unsaturated lipids by Porter and co-workers (27–31) through a detailed study of the dependence of the *cis,trans* to *trans,trans* ratio of geometrical isomers on the hydrogen atom donating ability of the medium. The study was also applied to the autoxidation of methyl linoleate in micelles (59) and to aqueous dispersions of lecithins (27, 29). It was most important to determine whether the same trend in product formation is observed when autoxidation is initiated in the aqueous phase. For this purpose, we undertook some studies of the dependence of the *cis,trans* to *trans,trans* product ratios on the concentration of DLPC bilayers formed from mixtures of DLPC and DPPC. The results are summarized in Table 5. The results for the product analysis from the autoxidation of 1-palmitoyl-2-linoleoylphosphatidylcholine (PLPC) are included since this is regarded as the ideal 1:1 mixture of palmitoyl and linoleoyl chains.

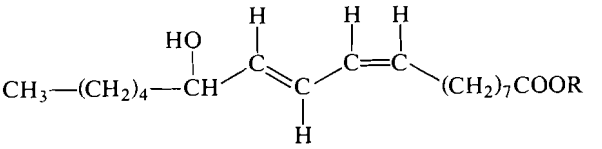

1

Methyl 13-hydroxy-*cis*-9, *trans*-11-octadecadienoate

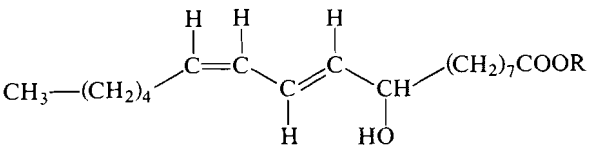

2

Methyl 9-hydroxy-*trans*-10, *cis*-12-octadecadienoate

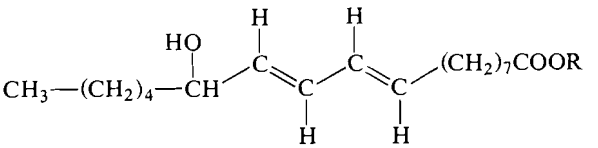

3

Methyl 13-hydroxy-*trans*-9, *trans*-11-octadecadienoate

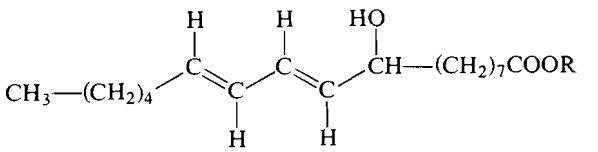

4

Methyl 9-hydroxy-*trans*-10, *trans*-12-octadecadienoate

SCHEME 1

TABLE 5. The ABAP[a]-initiated autoxidation of mixed DLPC + DPPC bilayers at 45°C; the dependence of the oxidation product distribution on the concentration of oxidizable substrate

No.[c]	[DLPC][b] (mol L^{-1})	*cis,trans*/*trans,trans*[d] (**1** + **2**)/(**3** + **4**)
1(a)	0.176	0.462
(b)	0.176	0.539
2(a)	0.259	0.547
(b)	0.259	0.625
3(a)	0.486	0.705
(b)	0.486	0.811
4	0.504	0.734
5(a)	0.765	0.955
(b)	0.765	0.940
6	1.02	1.17
7 PLPC	0.50[e]	0.656

[a]The initiator was added with the phosphate buffer (pH 7.0) before the liposomes were prepared.
[b]See footnote *c*, Table 2.
[c]Experiments (a) and (b) are duplicates with the same concentration of DLPC and initiator.
[d]The 9- and 13-hydroxy geometrically isomeric methyl esters derived from the oxidizable linoleate chains (see text).
[e]The relative concentration of linoleate in PLPC is assumed to be 0.50.

Can. J. Chem. Downloaded from www.nrcresearchpress.com by 213.166.140.6 on 09/07/12
For personal use only.

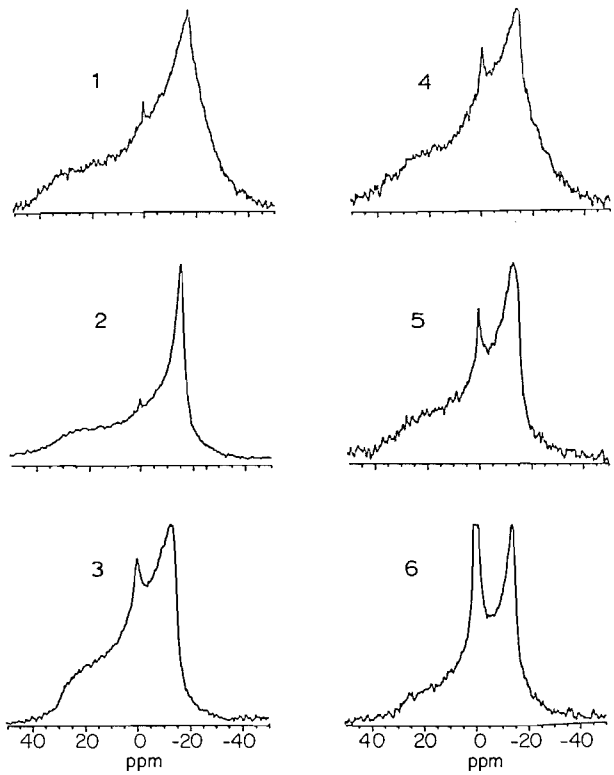

FIG. 1. ^{31}P nmr spectra of multilamellar phosphatidylcholine liposomes (0.1 mmol) in 2.00 mL of THAM buffer (pH 7.0). *1*, dipalmitoylphosphatidylcholine (DPPC) at 30°C; *2*, DPPC from *1*, at 45°C; *3*, dilinoleoylphosphatidylcholine; *4*, equimolar mixture of DLPC + DPPC, prepared (vortexed) and run at 30°C; *5*, mixture from *4*, spectrum repeated at 45°C; *6*, mixture of DLPC + DPPC prepared above 45°C (see text) and run at 45°C. The same spectrum results when run again at 30°C.

4. ^{31}P nmr spectra and autoxidation of bilayers

(a) ^{31}P nmr of DLPC and DPPC mixtures

Our kinetic and product studies and results of others (27, 29) tend to indicate that mixtures of DLPC and DPPC will form homogeneous bilayers under appropriate conditions; e.g. above their phase transition temperatures. Nevertheless, it was desirable to obtain some independent evidence on the nature of our mixtures. For this purpose we explored the application of ^{31}P nmr to mixtures of DLPC and DPPC prepared under various conditions. Some typical spectra are shown in Fig. 1 for DPPC (below and above T_t), DLPC and mixtures prepared below (30°C) and above (45°C) the T_t of DPPC.

(b) ^{31}P nmr spectra and oxidation of bilayers

Under controlled conditions, multilamellar and unilamellar liposomes (prepared from several unsaturated PPCs) were oxidized to known extents of peroxidation and their ^{31}P nmr spectra monitored during the process. Autoxidation was stopped by adding Trolox, known to be an effective antioxidant under these conditions (7) and then the ^{31}P spectra were run. Typical spectra illustrating the effects of peroxidation on multilamellar (DLPC) and unilamellar liposomes (egg lecithin, ELPC) are shown in Fig. 2.

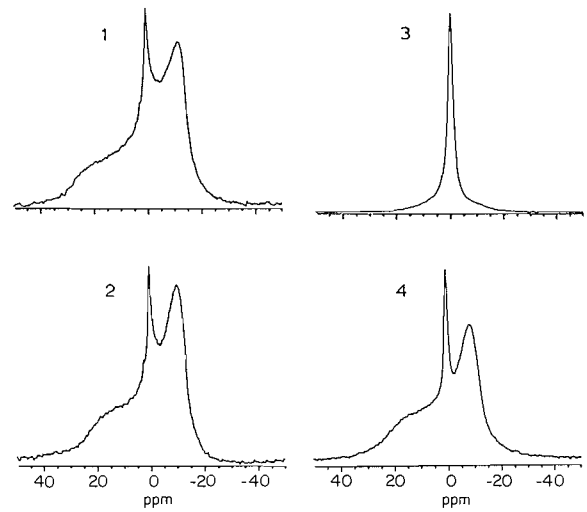

FIG. 2. ^{31}P nmr spectra of phosphatidylcholine liposomes (0.1 mmol) in 2.0 mL of THAM buffer (pH 7.0) at 40°C. *1*, multilamellar DLPC, purified by HPLC; *2*, oxidized DLPC, 60% conversion of active methylene groups; *3*, unilamellar egg lecithin; *4*, egg lecithin from *3*, after >30% oxidation.

Discussion

1. The kinetics and mechanism of autoxidation in bilayers

Rate measurements on *mixed bilayers* with various known concentrations of oxidizable DLPC with an inert PPC provide a very satisfactory method for establishing the kinetic order of oxygen uptake with substrate concentration. The results obtained with initiation by lipid-soluble ADVN in mixtures of DLPC and DMPC (Table 1) gave a good linear correlation for the order plot as shown in Fig. 3, when corrected for slight variations in the R_i. The kinetic order was unity (1.05), within experimental error, over a six-fold range of DLPC concentration and the oxidizability remained essentially constant at $k_p/2k_t^{1/2} = 0.116\,M^{-1/2}\,s^{-1/2}$.

Homogeneous mixtures of DLPC + DPPC (*vide infra*) were prepared above the phase transition temperature of DPPC. The kinetic order in DLPC was again found to be unity (1.07), within experimental error, for this system using the water-soluble initiator, ABAP. The data of Table 2 give a reasonably good correlation for the kinetic order plot shown in Fig. 4. The oxidizability of *unilamellar* DLPC was found to be $0.232\,M^{-1/2}\,s^{-1/2}$.[4]

In order to study the kinetic order with respect to the rate of chain initiation one could prepare bilayers with different (but known) concentrations of the initiator. However, due to the instability of thermal initiators such as ADVN, a study of this type with mixed bilayers is experimentally difficult (5) because significant amounts of the initiator decompose during bilayer formation. Fortunately, other studies have shown that the photocatalytic decomposition of an azo initiator could be carried out in bilayer dispersions (62). The dependence of the rate of O_2 consumption on the R_i for 0.05 *M* ADVN in multilamellar DLPC liposomes was followed by varying the light intensity. This gave a linear plot (Fig. 5) with a resulting kinetic order with respect to the R_i of one-half.

The kinetic order for the R_i for autoxidations initiated by ABAP was determined for bilayers of neat DLPC and mixtures of DLPC + DPPC. The latter study is considered to be the more significant. A plot of the order in [ABAP] gave an excellent

[4]We have recently determined the oxidizability of unilamellar 1-palmitoyl-2-linoleoylphosphatidylcholine (PLPC) to be $0.118\,M^{-1/2}\,s^{-1/2}$, which is consistent with these results since PLPC has one oxidizable chain.

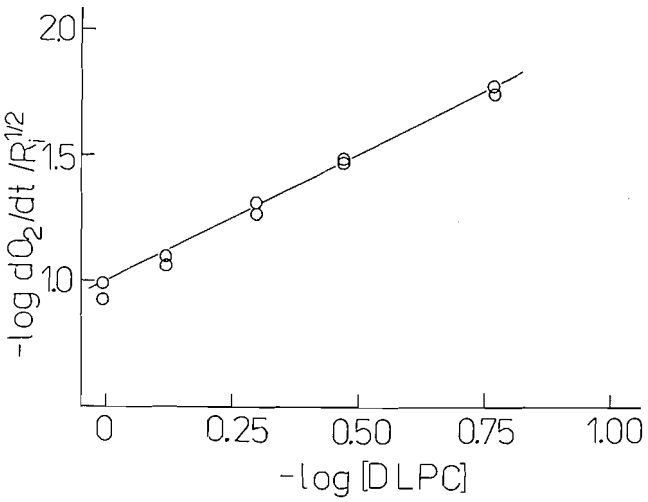

FIG. 3. Kinetic order plot for the autoxidation of mixed bilayers of DLPC + DMPC, initiated by lipid-soluble ADVN. Data taken from Table 1.

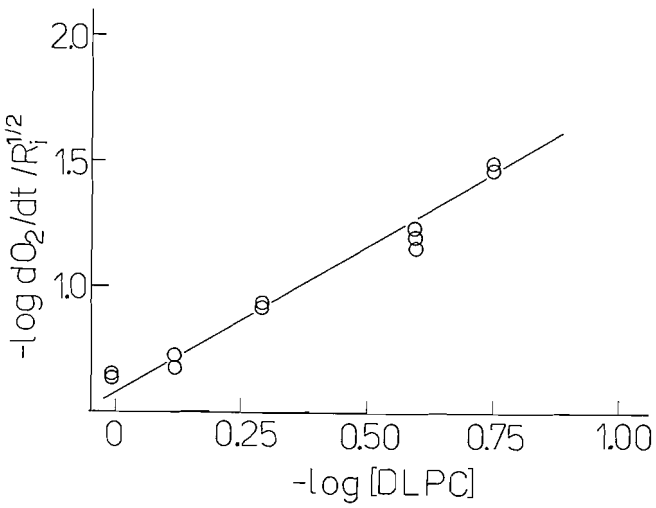

FIG. 4. Kinetic order plot for the autoxidation of mixed bilayers of DLPC + DPPC, initiated by water-soluble ABAP. Data taken from Table 2.

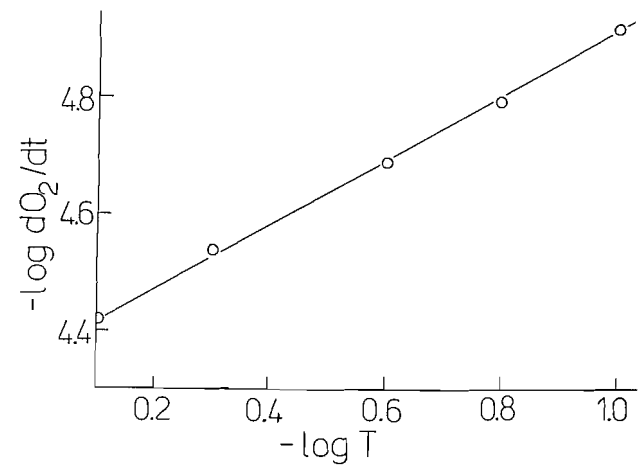

FIG. 5. Kinetic order plot of oxygen consumption as a function of light intensity for autoxidation of DLPC liposomes initiated by ADVN. Data taken from Table 3.

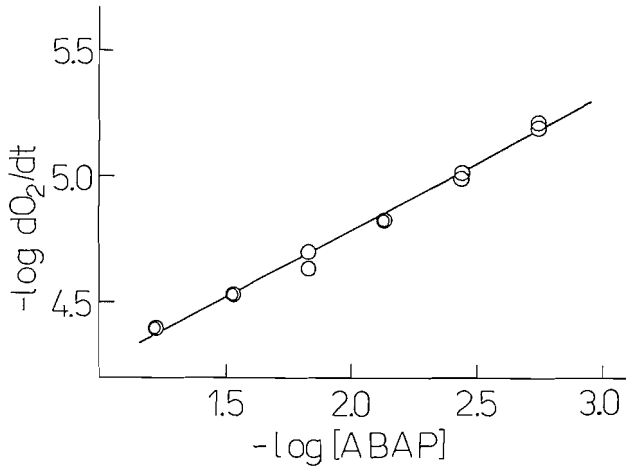

FIG. 6. Kinetic order plot of oxygen consumption with concentration of the water-soluble initiator, ABAP, for autoxidation of mixed bilayers of DLPC + DPPC. Data taken from Table 4, runs 3(a) and 3(b).

linear correlation (Fig. 6) for two runs with a kinetic order of 0.538 in the R_i.

Overall our results show that bilayer autoxidations initiated by either a lipid-soluble initiator (ADVN) or by water-soluble ABAP give rates of oxygen consumption which are first order in concentration of oxidizable substrate and half order in the R_i. This represents the first complete study showing that the classical autoxidation kinetics (eq. [1]) are applicable to PPCs as model biomembranes. Furthermore, these classical kinetics are applicable to water-soluble as well as lipid-soluble initiators. Certain interesting questions, however, remain to be answered: *(1) Why is a unilamellar system more susceptible to autoxidation than a multilamellar system?* and *(2) How does initiation with a water-soluble initiator result in the observed classical kinetics in the bilayers?*

We have not yet a satisfactory answer to question (1). However, we suspect that the higher oxidizability of unilamellar vesicles (ULV) ($k_p/2k_t^{1/2} = 0.232\,M^{-1/2}s^{-1/2}$) as compared to multilamellar vesicles (MLV) ($k_p/2k_t^{1/2} = 0.116\,M^{-1/2}s^{-1/2}$) is related to different "packing" of the lipid chains in ULV compared to those in the larger MLV systems (56). At constant R_i, identical samples of DLPC gave a higher rate of oxidation when prepared as ULV as compared to MLV. We therefore speculate that the higher oxidizability for unilamellar systems could arise from an increase in the rate of chain propagation,[5] perhaps due to a higher local concentration of oxidizable methylene groups.

In order to fully address question (2), we first examine the results of the analysis of linoleate oxidation products from mixed DLPC + DPPC bilayers when oxidation was initiated by water-soluble ABAP. A plot of the ratio of geometrical isomers (*c,t*/*t,t*) shows a linear relationship with the bilayer concentration of DLPC (Fig. 7) and the result from PLPC correlates within experimental error. In other words, the product distribution depends directly on the hydrogen atom donating ability of the medium; in this case the DLPC concentration in the bilayer. Furthermore, we found that the yield of products from addition at the C-9 position (isomers **1** + **3** = 48.9 ± 1.5%) is the same,

[5]Preliminary measurements on sonicated (unilamellar) DLPC liposomes indicate that the k_p term is higher than that for multilamellar DLPC (62).

Can. J. Chem. Downloaded from www.nrcresearchpress.com by 213.166.140.6 on 09/07/12
For personal use only.

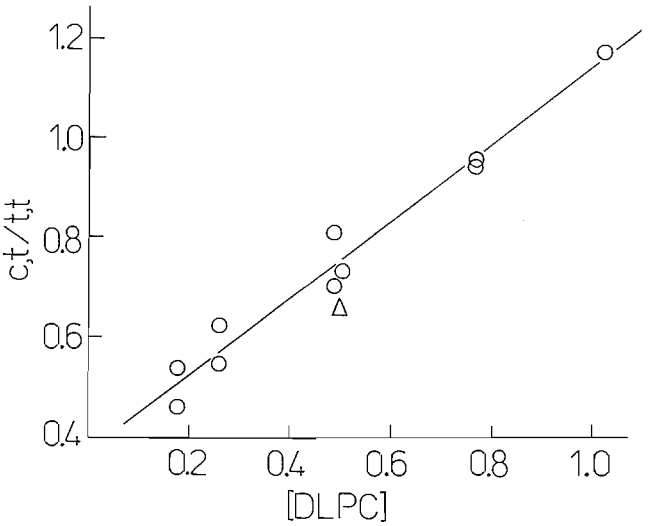

FIG. 7. Concentration dependence of the product ratios (*cis,trans/trans,trans*) of hydroxy linoleate esters derived from the autoxidation of mixtures of DLPC + DPPC. [DLPC] is the substrate concentration in the total (reaction) volume of DLPC + DPPC. The result from PLPC is shown as Δ.

within experimental error, as that for the products resulting from addition at the C-13 position (isomers **2** + **4** = 51.2 ± 1.5%). These results mean that the "Porter Mechanism" for lipid peroxidation is entirely applicable to autoxidations initiated by a water-soluble initiator. This mechanism (27, 28) involves H-atom abstraction to give a resonance-stabilized pentadienyl radical, addition of oxygen at either position 9 or 13 to give initial *c,t* and *t,c* peroxyl radicals (kinetically controlled), respectively. These radicals may abstract a hydrogen atom to produce the 9 or 13 hydroperoxide or undergo isomerization to a thermodynamically favored conformation followed by β-scission of O_2. Subsequent addition of O_2 produces *trans,trans* peroxyl radicals which may abstract a H-atom to give *trans,trans* hydroperoxides, the thermodynamic products.

These results of kinetic and product studies imply that the water-soluble initiator, ABAP, or peroxyl radicals derived thereof, "penetrate" the hydrophobic region of the bilayers sufficiently[6] to provide effective H-atom abstraction from the reactive methylene group at C-12. Mechanisms have been proposed for *trans*-bilayer transport of polar solutes. For example, inverted micelles (lipidic particles) (64–66) could form around ABAP near the membrane surface and transport it into the lipid phase.

2. ^{31}P nmr evidence of bilayer mixing and effect of oxidation

It is well known that the ^{31}P nmr spectra of multilamellar and large unilamellar PPC bilayers exhibit broad, asymmetrical line shapes due to restricted anisotropic motion of the phospholipid molecules. In these systems, the typical high field peak and low field shoulder result in a "chemical shift anisotropy" (CSA) of about −40 ppm (66). It also has been shown that line widths and line shapes can give information on the overall particle size of PPC vesicles (67).

Our ^{31}P nmr spectra provide some independent evidence on the nature of the mixtures of DLPC + DPPC. Below its T_t, DPPC exhibits a rather broad, structureless signal (Fig. 1, No. 1, CSA = 63 ppm) which appears to characterize its gel state. Above its T_t, the spectrum changes to give a sharper peak and a shoulder (No. 2, CSA = 48 ppm). Similarly, DLPC (No. 3) which is above its T_t shows the typical peak and shoulder (CSA = 45 ppm).[7] The spectrum of an equimolar mixture of DLPC + DPPC prepared by vortex-stirring of the two at 30°C (No. 4) appears identical to that of DPPC alone at 30°C. At 45°C the latter spectrum changes into a spectrum typical of the liquid crystal state (No. 5, CSA = 53 ppm) but the spectrum reverts back to that like No. 4 on cooling the sample to 30°C again. These results indicate that a heterogeneous mixture of DPPC and DLPC is present and that there is some segregation of the DLPC and DPPC from mixtures prepared under these conditions.[8]

A significant change is observed in the spectra when a film of DLPC and DPPC is converted into a bilayer above the T_t (e.g. above 45°C). Now the spectrum (No. 6, CSA = 46 ppm) is the same at 45°C and 30°C (not shown). This is taken as evidence that the DLPC and DPPC have been homogeneously mixed under these conditions. This ^{31}P nmr method has only been applied to 1:1 mixtures of the two phospholipids. We believe it is reasonable to assume that homogeneous mixtures also result at lower DLPC concentrations provided the temperature during liposome preparation and use remains above their T_t. ^{31}P nmr spectra show that phosphatidylethanolamines are miscible above their gel-liquid T_t (68).

A number of physical transformations are reported to accompany peroxidation of liposomes and thereby alter their ^{31}P nmr spectra. These changes include a decrease in PPC vesicle size (46), promotion of phase changes from bilayer to hexagonal phase in phosphatidylethanolamines (42), and enhancement of rapid transbilayer (flip-flop) movement of phospholipids which may cause non-bilayer structures (48). In addition, small unilamellar DPPC vesicles can fuse spontaneously below the T_t (69) and Ca^{2+} may cause "fast" fusion of egg lecithin – phosphatidic acid mixed vesicles (70). Despite these complications, some important conclusions can be made from our ^{31}P nmr spectra at various oxidation stages, as measured by the moles of oxygen consumed per reactive methylene group (DLPC) or per mole of lipid (ELPC). ^{31}P nmr spectra of liposomes of purified DLPC (Fig. 2, No. 1, CSA = 45 ppm) were not changed significantly after 10% oxidative conversion of the reactive methylene groups. By 60% conversion, there was a noticeable reduction in the chemical shift anisotropy (No. 2, CSA = 37 ppm). If the oxidative process causes an increase in bilayer fluidity or a decrease in the size of the liposomes (67), there could be increased motional averaging of the phosphorous-containing head group causing the observed decrease in the CSA.

Some spectral studies beginning with unilamellar vesicles which are subjected to peroxidation indicate that very significant changes can occur. A typical example is shown for egg lecithin in Fig. 2, Nos. 3 and 4. The initial unoxidized sample shows a ^{31}P spectrum with a single band attributed to smaller

[6]We have not measured the partition coefficient of ABAP between water and bilayers; however, we find that it partitions readily into 0.10 *M* SDS since $f = 0.91$ using the diffusion coefficient procedure (63).

[7]The narrower peaks which appear in most of the spectra near 0 ppm are probably due to smaller, possibly unilamellar, particles. Their proportion increases in samples prepared above the T_t (e.g. Fig. 1, No. 6).

[8]However, a referee points out that the spectrum of this mixture is expected to be dominated by the more fluid phase DLPC because of the short T_2 value of gel-state lipids.

Can. J. Chem. Downloaded from www.nrcresearchpress.com by 213.166.140.6 on 09/07/12
For personal use only.

Can. J. Chem. Downloaded from www.nrcresearchpress.com by 213.166.140.6 on 09/07/12
For personal use only.

particles, presumably unilamellar vesicles. The signal broadened as the oxidation proceeded, such that by 30% oxidative conversion the spectrum showed a signal with CSA = 34 ppm. Prolonged oxidation results in a spectrum typical of multilamellar systems (No. 4, CSA = 37 ppm). Control samples shaken under argon did not show these significant changes in their ^{31}P nmr spectra.

From these preliminary ^{31}P nmr results we conclude that: (*1*) during oxidation the bilayers retain their structural integrity to at least 10% conversion of the active methylene groups (the maximum in our kinetic studies) and (*2*) at high oxidative conversion (e.g. above about 30%), very significant changes occur. Large multilamellar liposomes appear to change to smaller average sizes while unilamellar systems are converted to multilamellar or much larger unilamellar liposomes.

Experimental

1. Materials and preparations

(a) Buffers: Phosphate buffer for autoxidation kinetic studies was prepared from 0.05 *M* each of NaH_2PO_4 and Na_2HPO_4 (pH 7.0) in glass-distilled water containing 1×10^{-4} *M* Na_2EDTA. The buffer was passed through Chelex 100 (50–100 mesh, BioRad) to remove traces of heavy metal ions. Dispersions for nmr studies were prepared in 0.054 *M* THAM (Fisher) buffer adjusted to pH 7.0 with HCl and containing 1×10^{-4} *M* Na_2EDTA.

(b) Reagents: The initiators were purchased from Polysciences and stored as the solid at −30°C. Solutions of known concentration were prepared in buffer (ABAP) and in methylene chloride or chloroform (ADVN) and stored at 4°C. Stock solutions of the inhibitor, 2,5,7,8-tetramethyl-6-hydroxychroman-2-carboxylate (Trolox) were prepared in known concentrations in the appropriate buffer shortly before use. Organic solvents used were of HPLC grade.

(c) PPCs and HPLC purification: DLPC and DMPC were purchased from Avanti Polar Lipids and DPPC was obtained from Sigma. PLPC was synthesized in the laboratory of N. A. Porter by known procedures (71). Stock solutions of DLPC in methanol (40 mg/mL) and PLPC in methanol/cyclohexane (80/20, 40 mg/mL) were prepared. Phospholipid purification was achieved by recycle HPLC using a 10 × 250 mm Vydac reverse phase column (C_{18}, 10 μm). The sample was eluted with mixed solvent: methanol/water/cyclohexane (90/10/5) pumped at 9.0 mL/min by a Waters Model 510 EF pump. Approximately 1% of the column effluent was passed through a Schoeffel SF 770 variable wavelength detector where its absorbance at 210 nm was measured. Hydroperoxide impurities eluted as a series of three peaks 2–10 min after injection of solution containing 80 mg of crude phospholipid. After the hydroperoxides were removed, the PC which had a broad elution pattern (12–30 min after injection) was recycled through the column. The purified phospholipid was then collected in an argon-filled flask at 0°C in the dark. The solvent (>200 mL) was removed by rotary evaporation at reduced pressure at 20–30°C in the dark, followed by pumping at <0.5 mm Hg to constant weight. Stock solutions of the purified lipids were then prepared in either degassed methanol (DLPC) or methylene chloride (PLPC) and stored at −30°C in the dark. The phospholipid purity was determined by spotting on silica TLC plates and development with hexane/2-propanol/acetone (992/4/4). Small traces of hydroperoxides were detected as pale pink spots with *N,N*-dimethyl-*p*-phenylenediamine dihydrochloride spray (1.5 g in methanol/water/acetic acid (128/25/1)). The phospholipid was detected with either 3.5% molybdatophosphoric acid spray (BDH) or molybdenum blue spray reagent (Sigma).

(d) Mixtures of PPCs: Homogeneous mixtures of DLPC + DPPC were prepared by slow evaporation of mixtures of known amounts from chloroform solution at 55–60°C on a water bath under a stream of argon. Final traces of solvent were removed under reduced pressure at 60°C; always keeping the sample above the phase transition temperature of DPPC. A similar procedure for DLPC + DMPC mixtures was used at 45°C. In this case, the required amount of initiator (ADVN) was added to the organic solvent containing the phospholipids. Multilamellar vesicles were prepared by vortex-stirring the film of PPCs with buffer, followed by ten freeze–thaw cycles of the aqueous dispersion by cooling in liquid nitrogen. Unilamellar vesicles were prepared by passing the multilamellar liposomes three times through a warmed French pressure cell under argon at 20 000 psi (20, 57).

2. Kinetic studies

Autoxidations were carried out at 45°C under 760 mm Hg of oxygen using a sensitive pressure transducer and an automatic recording apparatus modified from that described earlier (5, 62). The present experiments required precise measurements of rates of oxygen uptake on mixtures containing relatively small amounts of unsaturated phospholipids. In order to obviate baseline drift encountered earlier (5) due to vapour pressure of the solvent, we used a specially constructed stainless steel dual channel apparatus which has been described elsewhere (72). One channel was connected to a reaction vessel containing only the solvent used (in this case aqueous buffer); the other to a calibrated vessel containing the prepared sample in buffer. This new procedure automatically compensates for the vapour pressure due to solvent, essentially eliminating error or lag time due to baseline drift.

3. Autoxidation product analysis

Phospholipid samples were prepared as described above for kinetic experiments. After 5% oxidation, a 100 μL aliquot of the reaction mixture was added to 1 mL of 10 m*M* Ph_3P in methanol and the solution mixed. Transesterification of the phospholipid was accomplished by the addition of 1.5 mL of 0.45 *M* KOH in methanol. The mixture was stirred and then allowed to stand for 15 min at room temperature. The solution was treated with 1 mL of 1.0 *M* NH_4Cl and then extracted with 1.0 mL of HPLC solvent (*vide infra*) with brief centrifugation to aid the separation.

Separation of the four methyl hydroxylinoleates was achieved using a Waters 510 EF pump fitted with 4 × 300 mm Apex silica (10 μm) column (Jones Chromatography). With a flow rate of 1.6 mL/min, the products were detected at 234 nm with a Schoeffel SF770 variable wavelength detector. Relative amounts of the four hydroxylinoleates were determined by correcting the peak areas, as reported by a Varian CDS 401 data system, for the appropriate molar absorptivity (73): 13-*c,t* (λ_{max} 236 nm, ϵ = 27 200); 13-*t,t* (λ_{max} 233 nm, ϵ = 30 500); 9-*c,t* (λ_{max} 236 nm, ϵ = 28 300); 9-*t,t* (λ_{max} 233 nm, ϵ = 31 600).

4. ^{31}P nmr spectra

^{31}P nmr spectra were determined on bilayer dispersions containing approximately 0.1 mmol of total phospholipid in 2 mL of 0.054 *M* THAM buffer (pH 7.0). A Nicolet 360 NB FT NMR spectrometer was used at 146.15 MHz employing two-level broadband decoupling with a 90° pulse of 25 μs and decoupling power of 10 W for data acquisition and 2 W during magnetization recovery times. A delay time of 4 s was used between pulses.

An oxidation apparatus was installed adjacent to the nmr facility so that samples could be examined immediately after various stages of oxidation. Trolox[9] was added to the sample to terminate the oxidation and the samples purged with argon before ^{31}P nmr spectra were determined. Generally, 2500–4000 acquisitions were necessary to obtain satisfactory spectra. Samples of mixed bilayers (DLPC + DPPC) and those passed through the French pressure cell were similarly prepared immediately before ^{31}P nmr analysis.

Acknowledgements

This research was supported by grants from the Natural Sciences and Engineering Research Council of Canada and the Terry Fox Fund for Cancer Research which are gratefully

[9]Trolox was found to have no effect on the ^{31}P nmr spectra.

acknowledged. Important technical assistance was provided by R. D. Smith and A. H. MacDonald at Mount Allison during the design and construction of the autoxidation apparatus. We appreciated the assistance of the Chemistry Department and B. Macdonald and D. L. Hooper of the Atlantic Regional Magnetic Resonance Center at Dalhousie University during the nmr studies. We thank N. A. Porter of Duke University for his hospitality and assistance with the synthesis of phospholipids.

1. B. HALLIWELL and J. M. C. GUTTERIDGE. Free radicals in biology and medicine. Clarendon Press. 1985.
2. W. DE GRUYTER. Oxygen radicals in chemistry and biology. *Edited by* W. Bors, M. Saran, and D. Tait. Proceedings 3rd International Conference. 1984.
3. W. A. PRYOR (*Editor*). Free radicals in biology. Vols. II–IV. Academic Press, New York. 1976–1980.
4. L. R. C. BARCLAY and K. U. INGOLD. J. Am. Chem. Soc. **102**, 7792 (1980).
5. L. R. C. BARCLAY and K. U. INGOLD. J. Am. Chem. Soc. **103**, 6478 (1981).
6. L. R. C. BARCLAY, S. J. LOCKE, and J. M. MACNEIL. Can. J. Chem. **61**, 1288 (1983).
7. L. R. C. BARCLAY, S. J. LOCKE, J. M. MACNEIL, J. S. VAN KESSEL, G. W. BURTON, and K. U. INGOLD. J. Am. Chem. Soc. **106**, 2479 (1984).
8. L. R. C. BARCLAY, S. J. LOCKE, and J. M. MACNEIL. Can. J. Chem. **63**, 366 (1985).
9. Y. YAMAMATO, E. NIKI, and Y. KAMIYA. Bull. Chem. Soc. Jpn. **55**, 1548 (1982).
10. E. NIKI, R. TANIMURA, and Y. KAMIYA. Bull. Chem. Soc. Jpn. **55**, 1551 (1982).
11. J. TSUCHIYA, E. NIKI, and Y. KAMIYA. Bull. Chem. Soc. Jpn. **56**, 229 (1983).
12. E. NIKI, J. TSUCHIYA, R. TANIMURA, and Y. KAMIYA. Chem. Lett. 631 (1983).
13. E. NIKI, T. SAITO, A. KAWAKAMI, and Y. KAMIYA. J. Biol. Chem. **259**, 4177 (1984).
14. G. W. BURTON and K. U. INGOLD. J. Am. Chem. Soc. **103**, 6472 (1981).
15. G. W. BURTON, L. HUGHES, and K. U. INGOLD. J. Am. Chem. Soc. **105**, 5950 (1983).
16. T. DOBA, G. W. BURTON, and K. U. INGOLD. J. Am. Chem. Soc. **105**, 6505 (1983).
17. G. W. BURTON and K. U. INGOLD. Protective agents in cancer. Academic Press, London. 1983.
18. G. W. BURTON and K. U. INGOLD. Science, **224**, 569 (1984).
19. G. W. BURTON, T. DOBA, E. J. GABE, L. HUGHES, F. L. LEE, L. PRASAD, and K. U. INGOLD. J. Am. Chem. Soc. **107**, 7053 (1985).
20. L. R. C. BARCLAY, A. M. H. BAILEY, and D. KONG. J. Biol. Chem. **260**, 15809 (1985).
21. W. A. PRYOR, M. J. KAUFMAN, and D. F. CHURCH. J. Org. Chem. **50**, 283 (1985).
22. J. S. WINTERLE, D. DULIN, and T. MILL. J. Org. Chem. **49**, 491 (1986).
23. R. C. PETTER, J. C. MITCHELL, W. J. BRITTAIN, T. J. MCINTOSH, and N. A. PORTER. J. Am. Chem. Soc. **105**, 5700 (1983).
24. N. A. PORTER, R. C. PETTER, and W. J. BRITTAIN. J. Am. Chem. Soc. **106**, 813 (1984).
25. W. J. BRITTAIN, N. A. PORTER, and P. J. KREBS. J. Am. Chem. Soc. **106**, 7652 (1984).
26. J. S. WINTERLE and T. MILL. J. Am. Chem. Soc. **102**, 6336 (1980).
27. N. A. PORTER. Acc. Chem. Res. **19**, 262 (1986).
28. N. A. PORTER and D. G. WUJEK. J. Am. Soc. **106**, 2626 (1984).
29. H. WEENEN and N. A. PORTER. J. Am. Chem. Soc. **104**, 5216 (1982).
30. N. A. PORTER, L. S. LEHMAN, B. A. WEBER, and K. J. SMITH. J. Am. Chem. Soc. **103**, 6447 (1981).
31. N. A. PORTER, B. A. WEBER, H. WEENEN, and J. A. KHAN. J. Am. Chem. Soc. **102**, 5597 (1980).
32. D. D. M. WAYNER, G. W. BURTON, K. U. INGOLD, and S. J. LOCKE. FEBS Lett. **187**, 33 (1985).
33. Y. YAMAMATO, E. NIKI, J. EGUCHI, Y. KAMIYA, and H. SHIMASAKI. Biochim. Biophys. Acta, **819**, 29 (1985).
34. K. U. INGOLD. Acc. Chem. Res. **2**, 1 (1969).
35. F. R. MAYO. Acc. Chem. Res. **1**, 193 (1968).
36. J. A. HOWARD. *In* Free radicals. Vol. II. *Edited by* J. K. Kochi. Wiley, New York. 1973. Chap. 12, pp. 3–62.
37. J. A. HOWARD. Adv. Free Radical Chem. **4**, 49 (1972).
38. I. I. IVANOV. J. Free Radicals Biol. Med. **1**, 247 (1985).
39. Y. YAMAMATO, E. NIKI, Y. KAMIYA, and H. SHIMASAKI. Biochim. Biophys. Acta, **795**, 332 (1984).
40. P. J. DAVIS, K. P. COOLBEAR, and K. M. W. KEOUGH. Can. J. Biochem. **58**, 851 (1980).
41. T. DOBA, G. W. BURTON, and K. U. INGOLD. Biochim. Biophys. Acta, **835**, 298 (1985).
42. G. VAN DUIJN, A. J. VERKLEIJ, and B. DE KRUIJFF. Biochemistry, **23**, 4969 (1984).
43. R. C. BRUCH and W. S. THAYER. Biochim. Biophys. Acta, **733**, 216 (1983).
44. K. GAST, D. ZIRWER, A.-M. LADHOFF, J. SCHREIBER, P. KOELSCH, K. KRETSCHMER, and J. LASCH. Biochim. Biophys. Acta, **686**, 99 (1982).
45. S. NAGATSUKA and T. NAKAZAWA. Biochim. Biophys. Acta, **691**, 171 (1982).
46. M. KUNIMOTO, K. INOUE, and S. NOJIMA. Biochim. Biophys. Acta, **646**, 169 (1981).
47. D. A. BARROW and B. R. LENTZ. Biochim. Biophys. Acta, **645**, 17 (1981).
48. L. I. BARSUKOV, A. V. VICTOROV, I. A. VASILENKO, R. P. EVSTIGNEEVA, and L. D. BERGELSON. Biochim. Biophys. Acta, **598**, 153 (1980).
49. D. DEUTICKE, K. B. HELLER, and C. W. H. HAEST. Biochim. Biophys. Acta, **854**, 169 (1986).
50. S. KRISHNAMURTHY, N. J. BAI, and T. GEORGE. Ind. J. Biochem. Biophys. **21**, 361 (1984).
51. P. J. THORNALLEY, R. J. TROTTA, and A. STERN. Biochim. Biophys. Acta, **759**, 16 (1983).
52. J. F. FOSTER and R. G. SLEE. Biochim. Biophys. Acta, **752**, 233 (1983).
53. A. BENATTI, A. MORELLI, G. DAMIANI, and A. DEFLOVA. Biochim. Biophys. Res. Commun. **106**, 1183 (1982).
54. C. RICE-EVANS and P. HOCHSTEIN. Biochem. Biophys. Res. Commun. **100**, 1537 (1981).
55. B. L. SILVER. The physical chemistry of membranes. The Solomon Press, New York. 1985.
56. M. K. JAIN and R. C. WAGNER. Introduction to biological membranes. Wiley-Interscience, New York. 1980.
57. R. L. HAMILTON, J. GOERKE, L. S. S. GUO, M. C. WILLIAMS, and R. J. HAVEL. J. Lipid Res. **21**, 981 (1980).
58. T. DOBA, G. W. BURTON, and K. U. INGOLD. Biochim. Biophys. Acta, **835**, 298 (1985).
59. Y. YAMAMATO, S. HAGA, E. NIKI, and Y. KAMIYA. Bull. Chem. Soc. Jpn. **57**, 1260 (1984).
60. C. G. OVERBERGER and M. B. BERENBAUM. J. Am. Chem. Soc. **73**, 2618 (1951).
61. H. G. G. DEKKING. J. App. Polymer Sci. **9**, 1641 (1965).
62. L. R. C. BARCLAY, S. J. LOCKE, J. M. MACNEIL, and J. S. VANKESSEL. Can. J. Chem. **63**, 2633 (1985).
63. T. J. BURKEY, D. GRILLER, D. A. LINDSAY, and J. C. SCAIANO. J. Am. Chem. Soc. **106**, 1983 (1984).
64. A. J. VERKLEIJ. Biochim. Biophys. Acta, **779** 43 (1984).

Can. J. Chem. Downloaded from www.nrcresearchpress.com by 213.166.140.6 on 09/07/12
For personal use only.

65. A. J. VERKLEIJ, C. J. A. VAN ECHTELD, W. J. GERRITSEN, P. R. CULLIS, and B. DEKRUIJFF. Biochim. Biophys. Acta, **600**, 620 (1980).
66. P. R. CULLIS and B. DEKRUIJFF. Biochim. Biophys. Acta, **559**, 399 (1979).
67. E. E. BURNELL, P. R. CULLIS, and B. DEKRUIJFF. Biochim. Biophys. Acta, **603**, 63 (1980).
68. C. P. S. TILCOCK and P. R. CULLIS. Biochim. Biophys. Acta, **684**, 212 (1982).
69. S. E. SCHULLERY, C. F. SCHMIDT, P. FELGNER, T. W. TILLACK, and T. E. THOMPSON. Biochemistry, **19**, 3919 (1980).
70. M.-J. LIAO and J. H. PRESTEGARD. Biochim. Biophys. Acta, **599**, 81 (1980).
71. N. A. PORTER, R. A. WOLF, and H. WEENEN. Lipids, **15**, 163 (1980).
72. G. W. BURTON and D. D. M. WAYNER. C.R.C. Press. In press.
73. H. W.-S. CHAN and G. LEVETT. Lipids, **12**, 99 (1977).

Can. J. Chem. Downloaded from www.nrcresearchpress.com by 213.166.140.6 on 09/07/12
For personal use only.

Complexes of 18-crown-6 macrocyclic ethers containing both an alkali metal phenoxide salt and phenol. Crown:salt:phenol ratios of 1:1:1 and 1:1:2

ANDRÉ RODRIGUE, JOHN W. BOVENKAMP,[1] AND MICHAEL P. MURCHIE
Defence Research Establishment Ottawa, Ottawa, Ont., Canada K1A 0Z4

GERALD W. BUCHANAN
Ottawa–Carleton Institute for Research and Graduate Studies in Chemistry, Carleton University, Ottawa, Ont., Canada K1S 5B6

AND

SUZANNE FORTIER
Department of Chemistry, Queen's University, Kingston, Ont., Canada K7L 3N6

Received January 29, 1987

ANDRÉ RODRIGUE, JOHN W. BOVENKAMP, MICHAEL P. MURCHIE, GERALD W. BUCHANAN, and SUZANNE FORTIER. Can. J. Chem. **65**, 2551 (1987).

Sodium and potassium phenoxide, in the presence of one equivalent of dicyclohexano-18-crown-6 (*cis–anti–cis* isomer) and dibenzo-18-crown-6, form complexes that have a ratio of 1:1:1 (crown:salt:phenol) in ethereal solvents containing excess phenol. On the other hand, complexes having 1:1:2 ratios (crown:salt:phenol) are obtained under the same conditions when the macrocycle is 18-crown-6 or dicyclohexano-18-crown-6 (*cis–syn–cis* isomer). When only one equivalent of phenol is present, then 1:1:1 complexes are obtained with 18-crown-6 and dicyclohexano-18-crown-6 (*cis–syn–cis* isomer). No complexes containing only the metal salts were isolated from these solutions. The infrared spectral data obtained from the complexes show that the phenol hydroxyl hydrogens in the complexes form either strong or very strong hydrogen bonds. The nuclear magnetic resonance chemical shifts of the phenol protons in the complexes have been obtained from deuterated dimethoxyethane solutions. Comparisons are made with the chemical shifts of the phenol hydroxyl protons obtained from the corresponding solutions containing only the equivalent salt/phenol solutions.

ANDRÉ RODRIGUE, JOHN W. BOVENKAMP, MICHAEL P. MURCHIE, GERALD W. BUCHANAN et SUZANNE FORTIER. Can. J. Chem. **65**, 2551 (1987).

Dans des solvants éthérés contenant un excès de phénol, les phénolates de sodium ou de potassium, en présence d'un équivalent de dicyclohexano-18-couronne-6 (isomère *cis–anti–cis*) et de dibenzo-18-couronne-6, forment des complexes dans lesquels le rapport couronne:sel:phénol est 1:1:1. Par ailleurs, lorsqu'on travaille dans le mêmes conditions mais que le macrocycle est la 18-couronne-6 ou la dicyclohexano-18-couronne-6 (isomère *cis–syn–cis*), il se forme des complexes dans lesquels le rapport couronne:sel:phénol est 1:1:2. Lorsqu'on n'utilise qu'un seul équivalent de phénol, il se forme des complexes dans lesquels le rapport est 1:1:1, même avec la 18-couronne-6 et le dicyclohexano-18-couronne-6 (isomère *cis–syn–cis*). À partir de ces solutions, on n'a pas pu isoler de complexes ne contenant que des sels métalliques. Les données infrarouges obtenues à partir de ces complexes démontrent que les hydrogènes hydroxyliques du phénol des complexes forment des ponts hydrogènes qui sont soit forts ou très forts. Utilisant des solutions dans du diméthoxyéthane deutéré, on a pu déterminer les déplacements chimiques en résonance magnétique nucléaire des protons des phénols des complexes. On a fait une comparaison avec les déplacements chimiques des protons hydroxyliques des phénols dans des solutions correspondantes ne contenant que du phénol et le sel équivalent.

[Traduit par la revue]

Introduction

Since the isolation of the first alkali metal complexes of macrocyclic ethers (1), there has been a great deal of interest in complexes containing neutral molecules that can engage in hydrogen bonding. Pedersen (2) showed that macrocyclic ethers complexed thiourea in ratios of macrocycle to thiourea of 1:1–1:6, depending on the macrocycle used. When salts such as potassium or sodium thiocyanate were present in the reaction mixture, the complexes were found to contain one molecule of the salt and one or more molecules of thiourea. Hilgenfeld and Saenger (3) have published the crystal structure of the 1:1:1 complex of dibenzo-18-crown-6·potassium iodide·thiourea. Interestingly, it was found that the thiourea neither participates in the complexation of the metal ion, nor does it have any contact with the polyether ligand. Instead, it forms polymeric chains coupled by hydrogen bonding. The iodide is coordinated to the cation and is also hydrogen bonded to the thiourea chain. Polymeric chains involving coupling by hydrogen bonding will be discussed further (*vide infra*). Many other examples of the incorporation of neutral hydrogen bonding molecules into complexes with macrocyclic ethers have been reported in the literature (see ref. 4 for a review).

In our earlier work (5–9) we reported studies on the complexes of 18-crown-6 macrocyclic ethers with sodium and potassium salts. These complexes were obtained by precipitation from ethereal solvents. Depending on the macrocycle, the cation, and the anion of the salt used in the complexation reaction (5), the resulting complexes were found to have host:guest ratios of 1:1, 1:2, or 1:3. The complexes were studied using X-ray diffraction techniques (6), variable temperature ^{13}C nmr spectroscopy (7, 8), and CPMAS ^{13}C nmr (9). In our first attempt to prepare a suitable crystal of the 1:2 complex of DC-18-crown-6(B)·2KOPh for X-ray diffraction study,[2] rigorous anhydrous conditions were not used. Under these

[1]Author to whom correspondence may be addressed.

[2]Throughout this paper, DC-18-crown-6(A) and DC-18-crown-6(B) are used to designate the *cis–syn–cis* and the *cis–anti–cis* isomers of dicyclohexano-18-crown-6 (commonly called isomers A and B, respectively). DB-18-crown-6 refers to dibenzo-18-crown-6.

Can. J. Chem. Downloaded from www.nrcresearchpress.com by 213.166.140.6 on 09/07/12
For personal use only.

Can. J. Chem. Downloaded from www.nrcresearchpress.com by 213.166.140.6 on 09/07/12
For personal use only.

conditions, the actual crystal that was analyzed by X-ray diffraction was shown to have the unexpected 1:1:1 composition: DC-18-crown-6(B)·KOPh·HOPh (*vide infra*).[3] This result led to the work reported in the present paper.

There have been some reports of neutral substituted phenols being incorporated into complexes. For example, Poonia and Truter (10) report the synthesis of 2(benzo-15-crown-5)·K(2-nitrophenolate)·(2-nitrophenol). Poonia (11) has also synthesized complexes of benzo-15-crown-5 and dibenzo-30-crown-10 containing sodium and potassium salts and one or more molecules of 2-nitrophenol, 2,4-dinitrophenol, or 2,4,6-trinitrophenol. More recently (12), it has been shown that 3-nitrophenol can be incorporated into a complex without a salt being present. The complex was 18-crown-6·$2H_2O$·2(3-nitrophenol). To the best of our knowledge, no macrocyclic ether/salt complexes have previously been reported in which phenol itself has been incorporated.

In this paper we report a systematic study of the complexes formed when four different 18-crown-6 macrocyclic ethers were reacted with phenol in the presence of either sodium or potassium phenoxide. The use of phenol in conjunction with the sodium and potassium phenoxide salts was a deliberate choice. It was felt that this could lead to complexes with a high degree of symmetry.

The synthetic aspects, as well as the results of infrared and solution proton nmr studies are reported here. In an accompanying paper (13), the crystal structures of two of the complexes (**5** and **12**) are presented. The second accompanying paper (14) reports a high resolution ^{13}C CPMAS (cross-polarization magic angle spinning) study on the solids of three configurationally isomeric dicyclohexano-18-crown-6 ethers, as well as on three complexes derived therefrom. One of the solid complexes studied by this technique was **5**.

Results and discussion

As has been discussed previously (5), salts like sodium and potassium phenoxide form aggregates in ethereal solvents like DME, diethyl ether, and THF. The degree of association of ion pairs depends on the solvent and on the size, charge density, and hardness of both the cation and the anion (15, 16). In the absence of phenol, it has been shown that 18-crown-6 forms a 1:1 complex with KOPh when precipitated from a DME solution (5). Although we have not yet been successful in growing a suitable crystal of this complex for an X-ray diffraction structure determination, it is very likely that the 18-crown-6 macrocycle has broken up the aggregates to complex a contact ion pair. It has been shown that a dimer of KOPh is complexed in the 1:2 complex of DC-18-crown-6(B)·2KOPh and a tetramer of NaOPh is complexed in the 1:2 complex of DC-18-crown-6(A)·2NaOPh (5, 6).

In ethereal solutions of sodium and potassium phenoxide that also contain phenol (like those used in the present paper), very different aggregates are expected. The aggregates will now contain phenol, which will be coordinated to the anions with strong or very strong hydrogen bonds (*vide infra*) (see ref. 17 for a review on strong and very strong hydrogen bonding). Berny and Perrin (18, 19) have added KOPh to a benzene solution of phenol to obtain KOPh·3HOPh (mp 135°C) and, by adding potassium to a benzene solution of phenol, have isolated KOPh·2HOPh (mp 142°C). Hanson, McCulloch, and McInnes (20) have isolated a complex with the structure $[(C_6H_5OH)_4][C_6H_5O^-][Me_4N^+]$. The phenoxide oxygen was shown to be hydrogen bonded to three phenol molecules while the fourth phenol was hydrogen bonded to the oxygen of one of the three phenolic hydroxyls.

Interestingly, when larger cations such as Et_4N^+ and n-Bu_4N^+ were used, fewer phenols were found in the isolated complexes (3 and 2 molecules, respectively (20)). It can thus be expected that, in our ethereal solutions of NaOPh and KOPh, aggregates of the salts with phenol will be formed and that these will be broken up by the macrocycles as the cations are complexed.

The compositions of the complexes obtained by precipitation from ethereal solvents are shown in Table 1. The anhydrous solvent or solvent mixtures used in the complexation reactions are shown in Table 2. It was necessary to use mixtures of ethereal solvents for some of the complexation reactions to obtain the yields of the precipitated complexes shown in Table 2. A satisfactory elemental analysis has been obtained for each of the complexes (see Experimental). Also, integrated proton nmr spectra were in agreement with the ratios for the complexes shown in Table 1.

Section A of Table 1 gives the crown:salt:phenol ratios of the complexes obtained when one equivalent of macrocycle is added to a solution of the appropriate ethereal solvent containing one equivalent of phenoxide salt and three equivalents of phenol. Under these conditions, both 18-crown-6 and DC-18-crown-6(A) give complexes with 1:1:2 crown:salt:phenol ratios (**1**–**4**). By contrast, the other two macrocycles (DC-18-crown-6(B) and DB-18-crown-6) give complexes that contain only one molecule of phenol (**5**–**8**).

Section B of Table 1 shows the ratios obtained when one equivalent of 18-crown-6 and DC-18-crown-6(A) are reacted with one equivalent of salt in the presence of only 1.05 equivalents of phenol. Instead of the 1:1:2 crown:salt:phenol ratios obtained when 3 equivalents of phenol were used, the precipitated complexes have 1:1:1 ratios (**9**–**12**).

None of the macrocycles formed complexes with the salts only. Without exception, the complexes isolated contained either one or two molecules of phenol. It is interesting to note from Table 1 that, when phenol is present, the crown:salt:phenol ratio for a particular macrocycle is independent of whether the cation is K^+ or Na^+. Thus, the same ratio of 1:1:2 is obtained with 18-crown-6 when either KOPh (see **1**) or NaOPh (see **2**) is present in the reaction mixture. The same is true throughout Table 1 (e.g., compare **3** and **4**, **5** and **6**, etc). This is frequently not the case in the absence of phenol. 18-Crown-6, for example, gives a 1:1 host:guest complex with KOPh but a 1:3 host:guest complex with NaOPh (for this and other examples, see ref. 5).

One of the accompanying papers (13) reports the crystal structure determinations of two of the 1:1:1 complexes (**5** and **12**). For complex **5**, it has been found that the K^+ cation sits on a center of symmetry, in the center of the cavity formed by the six crown ether oxygens. The potassium is also coordinated to two phenol/phenoxides, one on each side of the crown cavity. Groups of phenol/phenoxide–potassium–phenol/phenoxide are linked by the hydrogen atoms to form a chain: $K^+\cdots O\cdots H\cdots O\cdots K^+$. The crystal structure of **12** is very different. In this case, the macrocyclic ring is distorted to accommodate the sodium ion. The phenol/phenoxide units are coordinated to the cation on only one side of the cavity, with one of the oxygens being coordinated to the cation and, at the

[3]Under rigorously anhydrous conditions, suitable crystals of the expected 1:2 complex were obtained for X-ray diffraction study (6).

TABLE 1. The complexes and their crown:salt:phenol ratios

Number	Macrocycle	Salt	Melting point (°C)	Crown:salt:phenol ratio
	Section A. Complexes from solutions with a 1:1:3 ratio[a]			
1	18-Crown-6	K^+OPh^-	80–82	1:1:2
2	18-Crown-6	Na^+OPh^-	82–83.5	1:1:2
3	DC-18-crown-6(A)	K^+OPh^-	84.5–86.5	1:1:2
4	DC-18-crown-6(A)	Na^+OPh^-	74–75	1:1:2
5	DC-18-crown-6(B)	K^+OPh^-	149–151	1:1:1
6[b]	DC-18-crown-6(B)	Na^+OPh^-	110–113 145–150	1:1:1
7	DB-18-crown-6	K^+OPh^-	176.5–178	1:1:1
8[b]	DB-18-crown-6	Na^+OPh^-	172–175 220–225	1:1:1
	Section B. Complexes from solutions with a 1:1:1.05 ratio[c]			
9	18-Crown-6	K^+OPh^-	113–113.5	1:1:1
10	18-Crown-6	Na^+OPh^-	96.8–97	1:1:1
11	DC-18-crown-6(A)	K^+OPh^-	102–103	1:1:1
12	DC-18-crown-6(A)	Na^+OPh^-	112.5–114.5	1:1:1

[a]The initial reaction solution had the macrocycle, metal phenoxide, and phenol in a 1:1:3 molar equivalent ratio, respectively.

[b]Two distinct mp ranges were observed. With complex **6**, the solid melts between 110 and 113°C until at 113°C the material in the tube is 80% liquid. The amount of solid then increases until melting again begins at 145°C and is complete at 150°C. Complex **8** also has two melting point ranges. It is apparent that at the first mp the original complex is broken up and a higher mp material is formed in each case.

[c]The initial reaction solution contained one equivalent each of macrocycle and metal phenoxide and 1.05 equivalents of phenol.

TABLE 2. Ethereal solvents[a] used in the complexation reactions and the yields obtained

Complex no.	Solvent used	Yield (%)	Complex no.	Solvent used	Yield (%)
1	Ether (50 mL)	86	**7**	DME (10 mL) + ether (20 mL)	92
2	Ether (40 mL)	93	**8**	THF (20 mL) + ether (20 mL)	81
3	Ether (30 mL)	88	**9**	DME (5 mL) + ether (50 mL)	81
4	Ether (30 mL)	70	**10**	THF (5 mL) + ether (30 mL)	84
5	DME (10 mL) + ether (15 mL)	75	**11**	Ether (30 mL)	70
6	Ether (20 mL)	68	**12**	DME (5 mL) + ether (20 mL)	78

[a]DME = 1,2-dimethoxyethane; THF = tetrahydrofuran; ether = diethyl ether.

same time, hydrogen bonded to the phenol hydrogen. We are currently attempting to grow crystals of the 1:1:2 complexes (**1–4**) for X-ray diffraction structure determinations.

Infrared spectra of the complexes

Infrared spectra were obtained using Nujol mulls of the complexes. We will discuss here only the peaks attributable to the phenol hydroxyl hydrogens in the spectra in the 1650–2800 cm^{-1} region (see Table 3). Additional information is difficult to extract because of the complexity of the spectra between 600 and 1650 cm^{-1} and the very large peaks due to CH stretching vibrations between 2800 and 3100 cm^{-1}.

Hadzi and Bratos (21, 22; see ref. 17 for a summary) recognized three types of spectra for hydrogen bonding systems: (*i*) the weak interaction in which the peaks are not far removed from the nonassociated AH spectrum; (*ii*) the stronger hydrogen bond that gives a very broad band absorbing at 1600–3000 cm^{-1} with three discernible maxima, which he called an ABC band; and (*iii*) very strong hydrogen bonds, which give a very broad band below 1600 cm^{-1}. None of the infrared spectra for **1–12** showed any peaks at wave numbers above 3100. Thus, all of the hydrogen bonds in the complexes are either strong (type (*ii*)) or very strong (type (*iii*)). By contrast, the Nujol mull of phenol itself shows a broad hydrogen bonding band with a maximum at about 3180 cm^{-1} (ref. 23 reports a value of 3200 cm^{-1}). In Hadzi's classification this represents type (*i*) hydrogen bonding.

The discussion of the infrared spectral information in Table 3 can be divided into three parts: that of **1–4**, **5–8**, and **9–12**. The 1:1:2 complexes **1–4** all show a broad band with two maxima in the 1650–2800 cm^{-1} region (see Fig. 1 and Table 3). Thus, this represents type (*ii*) hydrogen bonding (strong). The infrared spectrum of 18-crown-6·NaOPh·2HOPh (**2**) shown in Fig. 1 is typical for these complexes. Hadzi's spectra (21) showed a characteristic trio of bands near 2800, 2500, and 1900 cm^{-1}. Because of the very large peak due to CH stretching vibrations in our spectra between 2800 and 3100, nothing can be said about a potential third maximum expected in this region.

In contrast to **1–4**, the infrared spectra of the 1:1:1 complexes

Can. J. Chem. Downloaded from www.nrcresearchpress.com by 213.166.140.6 on 09/07/12
For personal use only.

TABLE 3. Hydrogen bonding information from infrared spectra of **1–12**

Complex no.	ν_{OH} bands in the 1650–2800 cm^{-1} region[a] (cm^{-1})	Complex no.	ν_{OH} bands in the 1650–2800 cm^{-1} region[a] (cm^{-1})
1	Maxima at 1820 and 2480	**7**	No Peaks
2	Maxima at 1880 and 2480	**8**	No Peaks
3	Maxima at 1820 and 2540	**9**	No Peaks
4	Maxima at 1880 and 2600	**10**[b]	Maxima at 1850 and 2510
5	No peaks	**11**	No Peaks
6	No peaks	**12**	No Peaks

[a]At wave numbers between 2800 and 3100, hydrogen bonding information is lost due to the very large CH stretching vibrations. Thus, nothing can be reported on the potential third maxima expected in this region (21).

[b]The magnitude of the ν_{OH} peak found for **10** is weak compared to those for **1–4**.

5–8 do not show any peaks in the 1650–2800 cm^{-1} region attributable to hydrogen bonding, indicating that very strong hydrogen bonding must occur in these complexes. The spectrum of **5** (DC-18-crown-6(B)·KOPh·HOPh) shown in Fig. 2 is representative. The very broad bands expected below 1600 cm^{-1} for very strong hydrogen bonding are difficult to identify due to the complexity of the spectrum in this region (see Fig. 2). The presence of very strong hydrogen bonding in **5** is in agreement with the crystal structure where the distance between the oxygens in the O···H···O unit is 2.48 Å (13).

Of the complexes **9–12**, only **10** exhibits strong hydrogen bonding (type (*ii*)) while **9**, **11**, and **12** have no peaks attributable to strong hydrogen bonding in the 1650–2800 cm^{-1} region and thus very strong hydrogen bonding must be involved. The crystal structure of **12** shows a PhO···H···OPh anion that is coordinated to the cation via one of the oxygens on the unhindered side of the DC-18-crown-6(A) macrocycle (13). The O···H···O distance of 2.47 Å is indicative of a very strong hydrogen bond. It is expected that the same type of hydrogen bonding and association to the cation will be present in **11**, especially since the phenolic proton chemical shift is significantly further downfield in **11** as expected (*vide infra*). Complexes **9** and **10** are the only K^+/Na^+ pair of complexes in the table that show different types of hydrogen bonding, with **9** exhibiting very strong and **10** strong hydrogen bonding. Unfortunately, X-ray diffraction data on **9** and **10** are not available to explain this difference.

Nuclear magnetic resonance chemical shifts of the phenol hydroxyl protons

The chemical shift of protons involved in hydrogen bonding has frequently been used as an indication of the strength of the hydrogen bond. Whereas weak hydrogen bonding results in only a slight downfield shift, stronger hydrogen bonding results in large downfield shifts, sometimes below 20 ppm (17). Jones and Dyer (24) found the proton chemical shift for the lithium, sodium, and potassium salts of $H(CF_3CO_2)_2^-$ in trifluoroacetic acid solutions to be 15.73, 16.94, and 19.17 ppm, respectively. One of the main conclusions of ref. 24 is that the presence of a cation near the $H(CF_3CO_2)_2^-$ anion causes the downfield shift of the proton to be smaller and dependent on the distance separating the two ions. As noted for trifluoroacetic acid solutions (24), the most upfield shift is found for the smaller, more electronegative cations, which would be expected to associate more strongly with the anion. The findings of Jones and Dyer (24) apply directly to the interpretation of the phenolic hydroxyl proton chemical shifts found in this work.

Table 4 gives the chemical shifts of the phenolic protons of **1–4**, **6**, and **8–12** as obtained from deuterated DME solutions (**5** and **7** were insoluble in this solvent). Table 4 also includes the chemical shift values found for deuterated DME solutions containing only the sodium or potassium phenoxide salts with phenol being present in the ratios of 1:1–1:4 (salt:phenol). The concentration of all solutions in Table 4 was 0.07 molar for the complexes in Section A, as well as for NaOPh and KOPh in the mixtures in Section B.

Fujio and Tsuno (25) have determined the hydroxyl chemical shifts of *m*- and *p*-substituted phenols in acetonitrile and carbon tetrachloride in the presence of benzyltri-*n*-butylphosphonium chloride. It was found that hydrogen bonding to the chloride anion shifted the hydroxyl proton signals significantly downfield with the largest shift difference being about 5.5 ppm. In our case, in DME-d_{10} the largest downfield shift difference in the absence of a macrocycle is 8.4 ppm (Table 4, Section B) for the solution containing phenol and one equivalent of KOPh.

Phenol itself has a chemical shift for the OH proton of 7.57 ppm in DME-d_{10}. A 1:1 solution of NaOPh:HOPh has an OH chemical shift of 11.02 ppm. With two and three equivalents of phenol in the solution only slight changes in chemical shifts to 11.19 and 11.10 ppm, respectively, occur. The presence of a fourth equivalent of phenol causes an upfield shift to 10.73 ppm. The relatively constant chemical shift for NaOPh solutions containing one, two, and three phenols is consistent with the cation making less contact with the anion, as the number of phenol equivalents increases, and with the effective charge on the anion consequently increasing. As a result, the chemical shift does not move upfield as would be expected. In the crystal structure of $[(C_6H_5OH)_4][C_6H_5O^-][Me_4N^+]$, three phenols are hydrogen bonded to the anion oxygen whereas the fourth phenol is hydrogen bonded to one of the other phenol oxygens (20). If this type of structure occurs in our solutions, then the upfield shift in the solution with four equivalents of phenol is readily explained.

The potassium phenoxide/phenol solutions exhibit different behaviour. The solution with one equivalent of each has an OH chemical shift of 16.00 ppm, a downfield shift more than twice as large as that found for the corresponding NaOPh solution (relative to phenol itself). Thus, as expected from the work of Jones and Dyer (24) discussed above, the potassium cation is less associated with the anion than is the smaller sodium cation. Only upfield shifts were found in solutions of potassium phenoxide containing 2, 3, and 4 equivalents of phenol.

The chemical shifts in Table 4 for the complexes are interesting from several points of view. Without exception, the

Can. J. Chem. Downloaded from www.nrcresearchpress.com by 213.166.140.6 on 09/07/12
For personal use only.

Can. J. Chem. Downloaded from www.nrcresearchpress.com by 213.166.140.6 on 09/07/12
For personal use only.

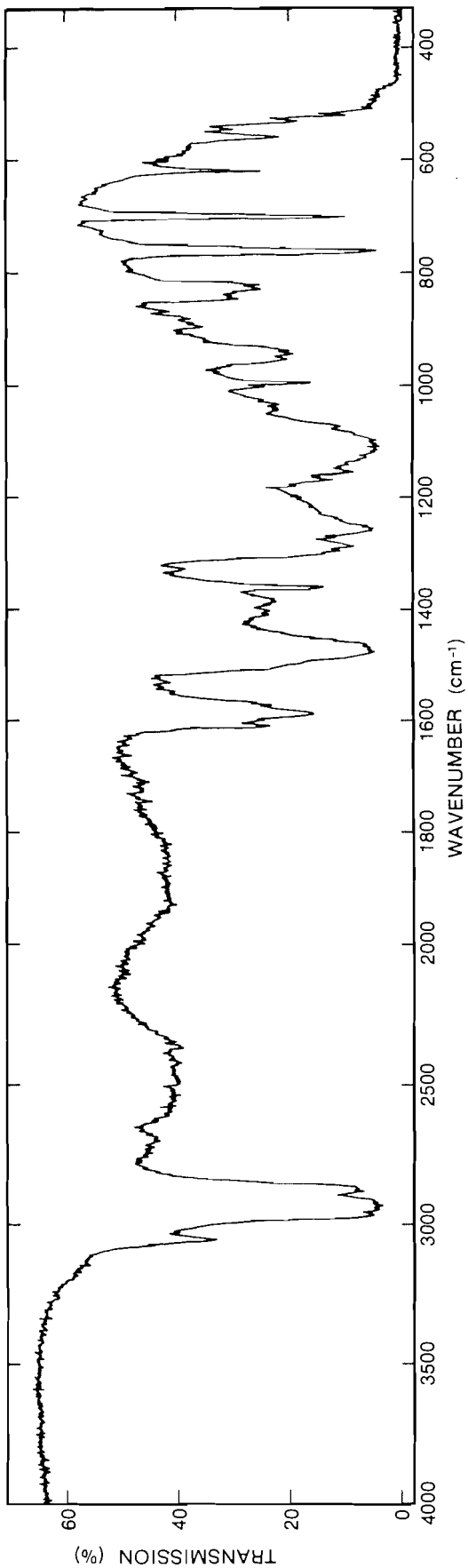

FIG. 1. Infrared spectrum of 18-crown-6·NaOPh·2HOPh (**2**), Nujol mull.

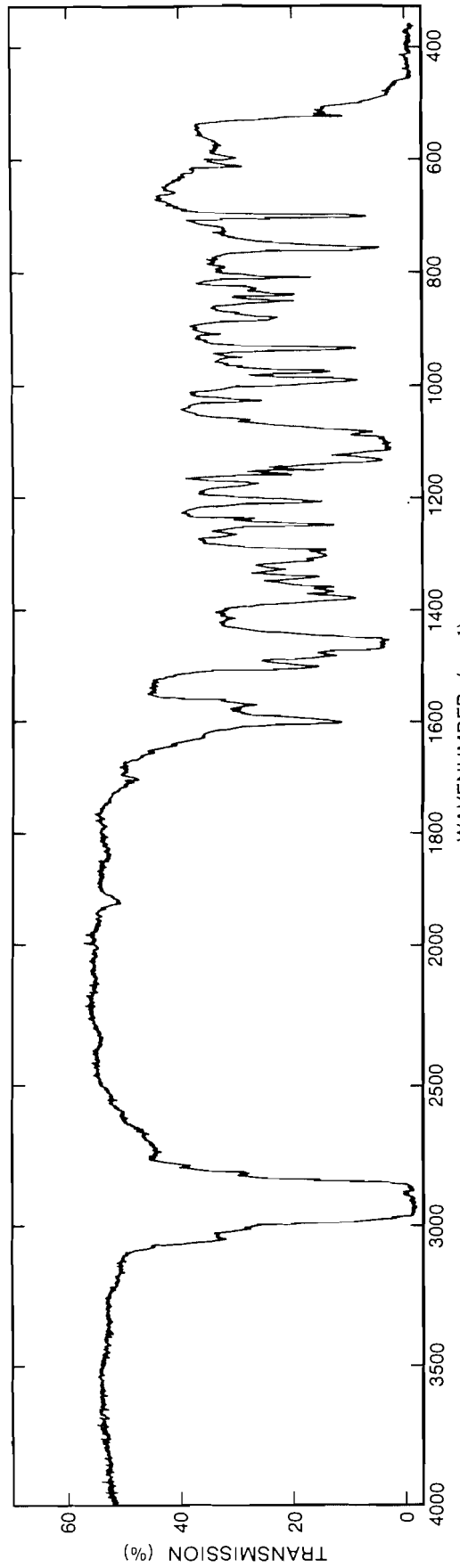

FIG. 2. Infrared spectrum of DC-18-crown-6(B)·KOPh·HOPh (**5**), Nujol mull.

TABLE 4. Chemical shifts[a,b] of the phenol hydroxyl protons in DME-d_{10}

Complex	δ_{OH} (ppm)	Complex	δ_{OH} (ppm)
	Section A. Complexes		
1 18-C-6·KOPh·2HOPh	14.15 ± 0.07	**7**[c] DB-18-C-6·KOPh·HOPh	—
2 18-C-6·NaOPh·2HOPh	13.53 ± 0.06	**8** DB-18-C-6·NaOPh·HOPh	14.20 ± 0.01
3 DC-18-C-6(A)·KOPh·2HOPh	14.00 ± 0.03	**9** 18-C-6·KOPh·HOPh	16.84 ± 0.01
4 DC-18-C-6(A)·NaOPh·2HOPh	13.65 ± 0.06	**10** 18-C-6·NaOPh·HOPh	14.94 ± 0.03
5[c] DC-18-C-6(B)·KOPh·HOPh	—	**11** DC-18-C-6(A)·KOPh·HOPh	16.75 ± 0.01
6 DC-18-C-6(B)·NaOPh·HOPh	14.40 ± 0.07	**12** DC-18-C-6(A)·NaOPh·HOPh	15.00 ± 0.03
	Section B. Phenol/phenoxide solutions		
HOPh	7.57 ± 0.01		
NaOPh + 1HOPh	11.02 ± 0.11	KOPh + HOPh	16.00 ± 0.06
NaOPh + 2HOPh	11.19 ± 0.04	KOPh + 2HOPh	13.49 ± 0.05
NaOPh + 3HOPh	11.10 ± 0.16	KOPh + 3HOPh	12.19 ± 0.23
NaOPh + 4HOPh	10.73 ± 0.09	KOPh + 4HOPh	11.15 ± 0.09

[a]Relative to internal TMS. The values shown are the average chemical shifts obtained from three different solutions except for **9** and **10** where four solutions were used. Standard deviations are shown.

[b]The concentration of the complexes (Section A) was 0.07 molar and the concentration of NaOPh and KOPh in the solutions of Section B was also 0.07 molar.

[c]Complexes **5** and **7** were not sufficiently soluble in DME-d_{10}.

chemical shifts for the phenol protons in the complexes (Section A) are downfield relative to those found for the corresponding phenol/phenoxide solutions (Section B). This is as expected since the contact of the anion and the cation should be reduced by the complexation of the cation by the macrocycle. These differences in chemical shift are much greater for the sodium complexes (differences range from 2.34 to 3.98 ppm) than for the potassium complexes (differences range from 0.51 to 0.84 ppm). This simply reflects the fact that, for the solutions in Section B, the sodium cations were much more closely associated with the anions than were the potassium cations in the corresponding solutions. It is to be noted from Table 4 that, for pairs of complexes where the same macrocycle is used but different phenoxide salts (e.g. **1** and **2**, **3** and **4**, etc.), the potassium salts have chemical shifts that are downfield to those of the corresponding sodium salts. This is in agreement with the findings of ref. 24 (*vide supra*).

The largest chemical shifts in Section A of Table 4 are exhibited by **9–12**. It is known that, in **12**, only one of the oxygens of the $PhO^- \cdots H^+ \cdots OPh^-$ unit is coordinated to the cation (13). Thus, a larger effective charge (and consequently a larger chemical shift) would likely result when compared to that for structures similar to **5** (13) where all of the oxygens are coordinated to the cation. The fact that the chemical shift for **11**, which involves the larger K^+ (which should be complexed more strongly by the cavity of the DC-18-crown-6(A) macrocycle), is further downfield by 1.75 ppm is an indication that the phenol/phenoxide orientation found in **12** could also be present in **11**. The chemical shifts for the **9** and **10** pair are very close to those for **11** and **12**, respectively.

When the chemical shifts for complexes **9–12** are compared to those of the corresponding complexes containing two molecules of phenol (**1–4**), it is seen that the chemical shifts for the potassium complexes are downfield by about 2.7 ppm and those for the sodium complexes are downfield by about 1.4 ppm. It is to be noted that the chemical shifts of the 1:1:1 complexes of **6** and **8** (14.40 and 14.20 ppm, respectively) are upfield by about 0.6–0.8 ppm to the 1:1:1 complexes **10** and **12**, which also involve the sodium cation. Interestingly, the crystal structure of complex **5** (a member of the series **5–8**) shows all of the oxygens of the phenol/phenoxide units to be coordinated to the encapsulated cations. If this type of structure is present in **6** and **8** then this would explain the upfield shift compared to **10** and **12**. It is not expected that the complexes have dissociated to any significant extent in the dry DME-d_{10} solutions used, since these complexes were obtained from ethereal solutions in the first place. From the available data, however, we cannot be certain that, even in these relatively nonpolar solutions, a proportion of the complexes has not dissociated.

It is interesting to note that relatively large downfield shifts have also been found for the OH chemical shifts of adducts of phenol with neutral bases. Thus, Eyman and Drago (26) report a value for the adduct of phenol and pyridine of 10.88 ppm in methylene chloride at 30°C.

Experimental

Commercial anhydrous diethyl ether was dried over sodium wire. Reagent grade 1,2-dimethoxyethane and tetrahydrofuran were distilled from lithium aluminum hydride using a Stedman column and a variable take-off still head. Phenol was sublimed under vacuum prior to use. Potassium and sodium phenoxide were prepared as before (5). Isomers A and B of DC-18-crown-6 were separated from the commercial mixture by the method of Izatt *et al.* (27); mp 60.2–61.2°C (lit. (27) mp 61–62°C) and mp 81.5–82.5°C (lit. (27) mp 83–84°C), respectively. DB-18-crown-6 was recrystallized from toluene; mp 161.5–163°C (lit. (28) mp 164°C and (29) mp 162.5–163.5°C). Commercial 18-crown-6 was precipitated as the acetonitrile complex (30) and the acetonitrile was removed under vacuum; mp 40.5–41.0°C (lit. (1) mp 39–40°C).

Great care was taken throughout this work to protect the samples from atmospheric moisture. All complexation reactions, the preparation of Nujol mulls, and the preparation of samples for nmr were carried out in a Dri-Lab (Vacuum Atmospheres) under an argon atmosphere.

Synthesis of complexes 1–8

Phenol (0.0051 mol) and the appropriate phenoxide salt (0.0017 mol) were stirred in dry ethereal solvent for 15 min. The macrocyclic ether was added (0.0017 mol) and, after a stirring period of 1 h, the

Can. J. Chem. Downloaded from www.nrcresearchpress.com by 213.166.140.6 on 09/07/12
For personal use only.

TABLE 5. Elemental analyses of the complexes

Complex no.	Calculated				Found			
	C	H	K	Na	C	H	K	Na
1	61.62	7.07	6.68		61.37	7.27	6.61	
2	63.36	7.26		4.04	63.15	7.35		3.94
3	65.86	7.71	5.64		65.59	7.76	5.77	
4	67.43	7.89		3.40	67.21	7.90		3.75
5	64.13	7.91	6.53		63.86	7.84	6.76	
6	65.95	8.13		3.94	65.75	8.02		3.97
7	65.60	5.92	6.66		65.22	6.05	6.61	
8	67.35	6.18		4.03	67.44	6.21		4.22
9	58.75	7.19	7.97		58.44	7.15	7.80	
10	60.74	7.43		4.84	60.77	7.30		4.71
11	64.18	7.91	6.53		63.93	7.86	6.27	
12	65.95	8.13		3.95	65.68	8.21		3.92

precipitated complex was collected by filtration and washed with dry diethyl ether. The complex was then subjected to high vacuum (<0.001 Torr; 1 Torr = 133.3 Pa) at 56°C overnight.

Table 2 gives the volume of the ethereal solvent or solvent mixture used and the yield of each complex obtained. Table 5 gives the elemental analyses for complexes **1–12**. All complexes were colourless salts.

*Synthesis of complexes **9–12***

The same procedure was used as described above except that only 1.05 equivalents of phenol were used instead of three equivalents.

The complexes with 1:1:1 ratios could be recrystallized from the same solvent or mixture of solvents used to form the complex. The only exception was the complex DC-18-crown-6(B)·NaOPh·HOPh (**6**). In this case, recrystallization gave DC-18-crown-6(B)·2NaOPh (see ref. 5 for the synthesis of this complex) as the precipitated product.

Complexes with 1:1:2 ratios could not be recrystallized from the solvents in which they were formed. The precipitated products from the recrystallizations had crown:salt:phenol ratios between 1:1:1 and 1:1:2. However, the products obtained directly from the complexation reactions gave satisfactory elemental analyses, good mp's, and integrated proton nmr spectra in agreement with the ratios shown in Table 1.

Infrared spectra of the complexes

A Perkin–Elmer infrared spectrophotometer (model 283) was used. Spectra were obtained on Nujol mulls of the complexes using ZnSe optically flat windows (25 mm diameter × 2 mm thick).

Nuclear magnetic resonance spectra of the complexes and phenol/phenoxide solutions

Proton magnetic resonance spectra were obtained at 200.058 MHz on a Varian XL-200 spectrometer using a 5-mm computer-switchable probe. Chemical shifts are relative to internal TMS. The 1,2-dimethoxyethane-d_{10} was dried over activated molecular sieves. A spectrum of the dried solvent was run at high amplitude and compared with that of the undried solvent to ensure that the trace of water present initially had been removed. We have found that even a trace of water can cause a 1-ppm or more upfield shift of the phenol hydroxyl proton peak.

Can. J. Chem. Downloaded from www.nrcresearchpress.com by 213.166.140.6 on 09/07/12
For personal use only.

Acknowledgements

The Natural Sciences and Engineering Research Council of Canada (NSERCC) is thanked for Visiting Scientist Fellowships for A.R. and M.P.M. and for financial assistance for G.W.B. and S.F. The elemental analyses were carried out by Guelph Chemical Laboratories.

1. C. J. PEDERSEN. J. Am. Chem. Soc. **89**, 7017 (1967).
2. C. J. PEDERSEN. J. Org. Chem. **36**, 1690 (1971).
3. R. HILGENFELD and W. SAENGER. Angew. Chem. Int. Ed. Engl. **20**, 1045 (1981).
4. F. VOGTLE, J. SIEGER, and W. M. MULLER. Top. Curr. Chem. **98**, 107 (1981).
5. A. RODRIGUE, J. W. BOVENKAMP, B. V. LACROIX, R. A. B. BANNARD, and G. W. BUCHANAN. Can. J. Chem. **64**, 808 (1986).
6. M. E. FRASER, S. FORTIER, A. RODRIGUE, and J. W. BOVENKAMP. Can. J. Chem. **64**, 816 (1986).
7. G. W. BUCHANAN, K. BOURQUE, J. W. BOVENKAMP, A. RODRIGUE, and R. A. B. BANNARD. Tetrahedron Lett. **25**, 3963 (1984).
8. G. W. BUCHANAN, K. BOURQUE, J. W. BOVENKAMP, and A. RODRIGUE. Can. J. Chem. **63**, 2747 (1985).
9. G. W. BUCHANAN, J. A. RIPMEESTER, J. W. BOVENKAMP, and A. RODRIGUE. Tetrahedron Lett. **27**, 2239 (1986).
10. N. S. POONIA and M. R. TRUTER. J. Chem. Soc. Dalton Trans. 2062 (1973).
11. N. S. POONIA. J. Inorg. Nucl. Chem. **37**, 1855 (1975).
12. W. H. WATSON, J. GALLOY, and D. A. GROSSIE. J. Org. Chem. **49**, 347 (1984).
13. M. E. FRASER, S. FORTIER, M. K. MARKIEWICZ, A. RODRIGUE, and J. W. BOVENKAMP. Can. J. Chem. **65**, 2558 (1987).
14. G. W. BUCHANAN, M. Z. KHAN, J. A. RIPMEESTER, J. W. BOVENKAMP, and A. RODRIGUE. Can. J. Chem. **65**, 2564 (1987).
15. L. M. JACKMAN and B. C. LANGE. Tetrahedron, **33**, 2737 (1977).
16. O. A. REUTOV and A. L. KURTS. Russ. Chem. Rev. **46**, 1040 (1977).
17. J. EMSLEY. Chem. Soc. Rev. **9**, 91 (1980).
18. M. F. BERNY and R. PERRIN. C.R. Hebd. Seances Acad. Sci. **260**, 1395 (1965).
19. M. F. BERNY and R. PERRIN. Bull. Soc. Chim. Fr. 1013 (1967).
20. A. W. HANSON, A. W. MCCULLOCH, and A. G. MCINNES. Tetrahedron Lett. **23**, 607 (1982).
21. D. HADZI. Pure Appl. Chem. **11**, 435 (1965).
22. D. HADZI and S. BRATOS. The hydrogen bond. II. Structure and spectroscopy. *Edited by* P. Schuster, G. Zundel, and C. Sandorfy. North-Holland Publishing Co., Amsterdam. 1976. Chap. 12.
23. P. V. HUONG, M. COUZI, and J. LASCOMBE. J. Chim. Phys. **64**, 1056 (1967).
24. R. G. JONES and J. R. DYER. J. Am. Chem. Soc. **95**, 2465 (1973).
25. M. FUJIO and Y. TSUNO. Mem. Fac. Sci. Kyushu Univ. Ser. C: **11**, 57 (1978).
26. D. P. EYMAN and R. S. DRAGO. J. Am. Chem. Soc. **88**, 1617 (1966).
27. R. M. IZATT, B. L. HAYMORE, J. S. BRADSHAW, and J. J. CHRISTENSEN. Inorg. Chem. **14**, 3132 (1975).
28. C. J. PEDERSEN. J. Am. Chem. Soc. **92**, 386 (1970).
29. C. J. PEDERSEN. Org. Synth. **52**, 66 (1972).
30. C. L. LIOTTA. U.S. Patent No. 3,997,562 (1976).

The crystal structures of the 1:1:1 complexes of dicyclohexano-18-crown-6 (isomer B) with potassium phenoxide and phenol and dicyclohexano-18-crown-6 (isomer A) with sodium phenoxide and phenol

MARIE E. FRASER, SUZANNE FORTIER,[1] AND MARY K. MARKIEWICZ
Department of Chemistry, Queen's University, Kingston, Ont., Canada K7L 3N6

AND

ANDRÉ RODRIGUE AND JOHN W. BOVENKAMP
Defence Research Establishment Ottawa, Ottawa, Ont., Canada K1A 0Z4

Received February 9, 1987

MARIE E. FRASER, SUZANNE FORTIER, MARY K. MARKIEWICZ, ANDRÉ RODRIGUE, and JOHN W. BOVENKAMP. Can. J. Chem. **65**, 2558 (1987).

The crystal structures of the 1:1:1 complexes of dicyclohexano-18-crown-6 (isomer B) with potassium phenoxide and phenol, and of dicyclohexano-18-crown-6 (isomer A) with sodium phenoxide and phenol have been determined. The potassium phenoxide complex crystallizes in space group *Pnca* with $a = 14.150(3)$, $b = 23.794(6)$, $c = 9.491(1)$ Å, and $Z = 4$. The sodium phenoxide complex crystallizes in space group *Pbca* with $a = 21.201(4)$, $b = 24.406(6)$, $c = 12.492(3)$ Å, and $Z = 8$. Both structures were solved by direct methods and refined by full matrix least-squares calculations to residuals, R, of 0.059 for the potassium phenoxide complex, and 0.069 for the sodium phenoxide complex. In the potassium phenoxide complex, the cation sits on a centre of symmetry, in the centre of the cavity formed by the crown ether in its regular conformation. The potassium is coordinated to all six crown oxygens as well as to two phenol/phenoxides, one on each side of the crown. Groups of phenol/phenoxide–potassium–phenol/phenoxide are linked by the hydrogen atoms to form a chain: $K^+ \ldots O \ldots H \ldots O \ldots K^+$. The distance between the oxygens of the phenol/phenoxides is short, 2.48(1) Å. The hydrogen was initially located halfway between the two oxygens, on a 2-fold axis special position. Inspection of the difference Fourier map and refinement on the hydrogen position revealed, however, the presence of statistical or dynamical disordering. In the sodium phenoxide complex, the hexaether adopts an irregular conformation. The distances between the sodium and the crown oxygens range from 2.45 to 2.89 Å, while a distance of 2.363 Å is found with the phenoxide oxygen. Strong hydrogen bonding is found between the oxygens of the phenol and phenoxide. The O....O distance is 2.471(4) Å.

MARIE E. FRASER, SUZANNE FORTIER, MARY K. MARKIEWICZ, ANDRÉ RODRIGUE et JOHN W. BOVENKAMP. Can. J. Chem. **65**, 2558 (1987).

On a déterminé les structures cristallines des complexes 1:1:1 du dicyclohexano-18-couronne-6 (isomère B) avec le phénolate de potassium et le phénol et du dicyclohexano-18-couronne-6 (isomère A) avec le phénolate de sodium et le phénol. Le complexe du phénolate de potassium cristallise dans le groupe d'espace *Pnca*, avec $a = 14,150(3)$, $b = 23,794(6)$ et $c = 9,491(1)$ Å et $Z = 4$. Le complexe du phénolate de sodium cristallise dans le groupe d'espace *Pbca*, avec $a = 21,201(4)$, $b = 24,406(6)$ et $c = 12,492(3)$ Å et $Z = 8$. On a résolu les deux structures par des méthodes directes et on les a affinées par les méthodes des moindres carrés jusqu'à des valeurs résiduelles, R, de 0,059 pour le complexe du phénolate de potassium et de 0,069 pour le phénolate de sodium. Dans le complexe du phénolate de potassium, le cation se trouve sur un centre de symétrie, au centre de la cavité qui est formée par l'éther couronne dans sa conformation régulière. Le potassium est coordonné aux six oxygènes de la couronne ainsi qu'à deux phénol/phénolate, un de chaque côté de la couronne. Les groupements phénol/phénolate–potassium–phénol/phénolate sont liés par des atomes d'hydrogènes qui forment une chaîne : $K^+ \ldots O \ldots H \ldots O \ldots K^+$. La distance entre les oxygènes du phénol/phénolates est courte, 2,48(1) Å. Au début de l'affinement, l'hydrogène se trouve à mi-chemin entre les deux oxygènes, dans une position spéciale sur un axe binaire. Une inspection de la carte différentielle de Fourier et un affinement sur la position de l'hydrogène révèle toutefois la présence d'un désordre statistique ou dynamique. Dans le complexe du phénolate de sodium, l'éther couronne adopte une conformation irrégulière. Les distances entre le sodium et les oxygènes de l'éther varient de 2,45 à 2,89 Å et on trouve une distance de 2,363 Å avec l'oxygène du phénolate. On trouve qu'il existe une forte liaison hydrogène entre les oxygènes du phénol et le phénolate. La distance O....O est égale à 2,471(4) Å.

[Traduit par la revue]

Introduction

The first ternary crown ether complexes were reported in 1971 by Pedersen (1) who obtained these 1:1:1 complexes by reaction of alkali metal thiocyanate and iodide complexes of benzo-15-crown-5 and dibenzo-18-crown-6 with thiourea in methanol. Although the exact nature of the complexes could not be established, ultraviolet spectroscopy indicated that the complexation of the metal ion in the 1:1:1 complex of dibenzo-18-crown-6, potassium thiocyanate, and thiourea was essentially the same as in the 1:1 complex of dibenzo-18-crown-6 and potassium thiocyanate. It was thus concluded that, at least in this 1:1:1 complex, the thiourea had no significant effect. This was later confirmed in the 1:1:1 complex of dibenzo-18-crown-6, potassium iodide, and thiourea, for which a crystal structure determination was reported (2). In this structure, thiourea does not participate in the coordination of the metal ion nor does it have any contact with the crown ligand. Instead, it contributes to the stabilization of the anion by forming polymeric hydrogen-bonded sheets.

In the present paper, the crystal structures of two new ternary crown ether complexes, the 1:1:1 complexes of DC-18-crown-6 (isomer B), potassium phenoxide, and phenol and DC-18-

[1]Author to whom correspondence may be addressed.

Can. J. Chem. Downloaded from www.nrcresearchpress.com by 213.222.148.141 on 09/07/12
For personal use only.

TABLE 1. Crystal data[a]

Parameter	Crystal data	
Molecular formula	$KO_8C_{32}H_{47}$	$NaO_8C_{32}H_{47}$
Molecular weight	598.83	582.72
Space group; Z	*Pnca*; 4	*Pbca*; 8
a, Å	14.150(3)	21.201(4)
b, Å	23.794(6)	24.406(6)
c, Å	9.491(1)	12.492(3)
V, Å^3	3195.4	6463.7
T, K	292	292
Number of reflections used for the determination of unit cell parameters; 2θ range, deg	25; 12–25	25; 31–76
Density (calcd.), g cm^{-3}	1.245	1.198
Number of measured reflections	3659	2981
Number of observed reflections, $I \geqslant 3\sigma(I)$	1087	1991
2θ range scanned, deg	1–55	1–90
μ, cm^{-1}	2.086 (MoKα)	7.704 (CuKα)
Crystal dimensions, mm	0.30 × 0.25 × 0.13	0.10 × 0.40 × 1.2
Isotropic secondary extinction, g	0.837 × 10^{-7}	0.366 × 10^{-7}
Final R; R_w	0.059; 0.073	0.069; 0.095
Largest shift/error in final least-squares cycle	0.01	0.02
Maximum and minimum residual electron density in final difference Fourier map, e Å^{-3}	0.22; −0.22	0.24; −0.34
Standard deviation of an observation of unit weight, σ	1.373	2.743

[a]Estimated standard deviations are shown in parentheses.

crown-6 (isomer A), sodium phenoxide, and phenol are presented. These structural results are compared to those reported in a previous publication (3) on the 1:2 host:guest complexes of DC-18-crown-6 (isomers A and B) with sodium and potassium phenoxide.

Experimental

The synthetic method used for the preparation of the two complexes has been described in a previous publication (4).

The crystal of DC-18-crown-6 (isomer B)·KOPh·HOPh was grown during an attempt to obtain suitable crystals of DC-18-crown-6 (isomer B)·2KOPh from a large amount of 1,3-dioxolane by slow evaporation of the solvent in an argon atmosphere. The solvent used was not totally anhydrous. Subsequently DC-18-crown-6 (isomer B)·KOPh·HOPh was obtained by reacting DC-18-crown-6 (isomer B) with a solution containing one equivalent of KOPh and an excess of phenol (4). Both samples had the same melting point of 149–151°C.

The crystal of DC-18-crown-6 (isomer A)·NaOPh·HOPh was obtained from a solution of DC-18-crown-6 (isomer A)·NaOPh·2HOPh in a mixture of tetrahydrofuran – diethyl ether (volume ratio of 2 to 15). The solution was slowly evaporated to dryness in an argon atmosphere. Under these conditions the complex containing two molecules of phenol gave crystals of the complex containing only one molecule of phenol. The crystallized complex had a melting point of 112.5–114.5°C.

Pertinent data about the crystals used and the measurement of diffraction intensities are summarized in Table 1. For the Na^+ complex, the crystal used in the diffraction experiment was mounted inside a glass capillary in an oxygen-free atmosphere. For the K^+ complex, the crystal was mounted in the usual manner, at the tip of a glass fibre. The intensity data were collected on an Enraf– Nonius CAD-4 diffractometer using graphite monochromated radiation, MoKα (λ = 0.71073 Å), for the K^+ complex, and CuKα (λ = 1.5418 Å), for the Na^+ complex. In each case, intensities were collected by the θ/2θ scanning procedure and three reflections were measured after every 7200 s of exposure time to check on the stability of the crystals. No evidence of crystal decay was detected for the K^+ complex. For the Na^+ complex, a 5.5% loss in intensity was observed and a linear decay correction was applied. A numerical absorption correction was also applied to the Na^+ complex intensity data. The minimum, maximum, and average transmissions were found to be 0.7014, 0.9249, and 0.8770 respectively. For both complexes, the data were corrected for Lorentz and polarization effects. The structures were solved by direct methods using the program MULTAN80 (5). For the K^+ complex, 14 of the 24 hydrogen atoms in the asymmetric unit, including the phenol hydrogen, were found in the difference Fourier map; the remaining 10 were calculated. For the Na^+ complex, the positions of all the hydrogen atoms were found in the maps. The structures were refined by full matrix least squares using all reflections with $I \geqslant 3\sigma(I)$. Anisotropic temperature factors were used for the non-hydrogen atoms. Isotropic temperature factors were used for the phenol hydrogens whose positions were also refined. The remaining hydrogen atoms were assigned temperature factors equal in magnitude to the equivalent isotropic values of their parent atoms and were included in the calculations, but neither their positions nor their temperature factors were refined. The function minimized was $\Sigma w||F_o| - |F_c||^2$, where $w = 1/\sigma^2(|F_o|)$. A correction for isotropic secondary extinction effect was included in each refinement. The scattering factors were taken from Cromer and Waber (6). All calculations were done on a PDP 11/23 computer using the Enraf–Nonius SDP program package (7).[2]

Results and discussion

The 1:1:1 complex of DC-18-crown-6 (isomer B) with potassium phenoxide and phenol

An ORTEP (8) drawing of the complex showing the atom numbering scheme is given in Fig. 1. The fractional coordinates and equivalent isotropic temperature factors of the non-hydrogen atoms are presented in Table 2. Oxygen–potassium bond lengths and angles appear in Table 4, average and range in the

[2]Tables of positional parameters, temperature factors, F values, and bond distances may be purchased from the Depository of Unpublished Data, CISTI, National Research Council of Canada, Ottawa, Ont., Canada K1A 0S2.

Can. J. Chem. Downloaded from www.nrcresearchpress.com by 213.222.148.141 on 09/07/12
For personal use only.

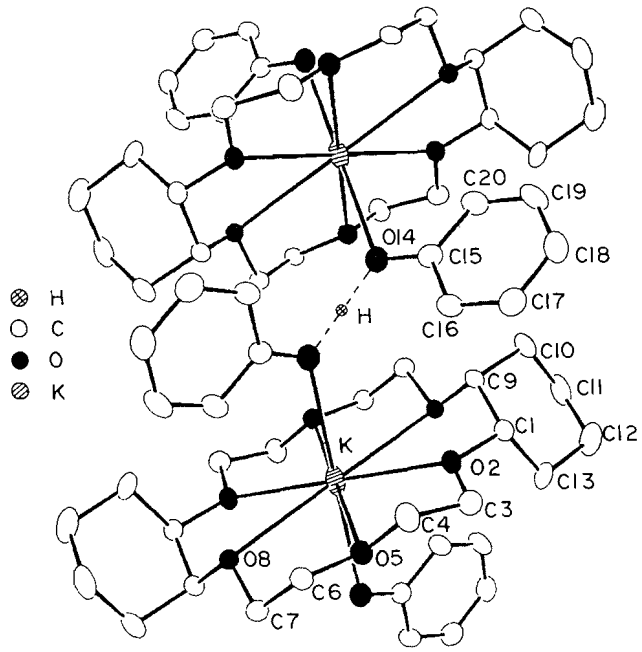

FIG. 1. ORTEP diagram and numbering scheme for the 1:1:1 complex of DC-18-crown-6 (isomer B), potassium phenoxide, and phenol.

TABLE 2. Final fractional coordinates and equivalent isotropic temperature factors for $KO_8C_{32}H_{47}$ with estimated standard deviations in parentheses

Atom	x	y	z	B_{eq} (Å^2)[a]
K	0.000	0.000	0.000	5.31(5)
O(2)	−0.0296(3)	0.0961(2)	0.1515(4)	3.7(1)
O(5)	0.0984(3)	0.0156(2)	0.2447(4)	3.8(1)
O(8)	−0.1137(3)	0.0946(2)	−0.1076(5)	3.49(9)
O(14)	0.8222(3)	−0.0289(2)	1.1771(5)	4.9(1)
C(1)	−0.0776(5)	0.1455(3)	0.1033(7)	3.5(1)
C(3)	0.0271(5)	0.1051(3)	0.2730(8)	4.6(2)
C(4)	0.0471(5)	0.0496(3)	0.3411(7)	4.6(2)
C(6)	0.1318(5)	−0.0346(3)	0.3099(7)	4.1(2)
C(7)	−0.1816(5)	0.0697(3)	−0.2001(7)	4.1(2)
C(9)	−0.1571(4)	0.1249(2)	0.0048(8)	3.6(1)
C(10)	−0.2124(5)	0.1763(3)	−0.0479(8)	5.4(2)
C(11)	−0.1471(6)	0.2161(3)	−0.1252(9)	6.2(2)
C(12)	−0.0685(6)	0.2360(3)	−0.0310(8)	6.4(2)
C(13)	−0.0116(6)	0.1871(3)	0.0329(7)	4.9(2)
C(15)	0.8205(5)	−0.0710(3)	1.2660(7)	4.0(2)
C(16)	0.7440(5)	−0.0833(3)	1.3521(7)	4.5(2)
C(17)	0.7444(6)	−0.1295(3)	1.4405(8)	5.4(2)
C(18)	0.8199(6)	−0.1650(3)	1.4479(8)	6.0(2)
C(19)	0.8978(5)	−0.1535(3)	1.3624(9)	6.4(2)
C(20)	0.8971(5)	−0.1085(3)	1.2747(9)	5.4(2)

[a] $B_{eq} = \frac{4}{3}\Sigma_i\Sigma_j\beta_{ij}(a_i \cdot a_j)$.

bond lengths and angles of the host and of the phenol/phenoxide are given in Table 5, macrocyclic ring torsion angles appear in Table 6.

Host geometry and conformation

In the present crystal structure, the *cis–anti–cis* isomer of DC-18-crown-6 has a crystallographic centre of symmetry. The crown oxygens form a nearly regular hexagon and thus outline a circular cavity. The hexaether is found in the regular conformation with all torsion angles about C—C bonds synclinal and

TABLE 3. Final fractional coordinates and equivalent isotropic temperature factors for $NaO_8C_{32}H_{47}$ with estimated standard deviations in parentheses

Atom	x	y	z	B_{eq} (Å^2)[a]
Na	0.5911(1)	0.38708(9)	0.2007(2)	4.83(5)
O(3)	0.4909(2)	0.4018(1)	0.3378(3)	4.56(9)
O(6)	0.5171(2)	0.4624(2)	0.1541(3)	5.7(1)
O(9)	0.6426(2)	0.4808(2)	0.2042(3)	4.85(9)
O(12)	0.7147(2)	0.4022(1)	0.2928(3)	4.30(9)
O(15)	0.6696(2)	0.3087(1)	0.1966(3)	4.75(9)
O(18)	0.5597(2)	0.3100(1)	0.3147(3)	4.79(9)
O(27)	0.5552(2)	0.3574(2)	0.0312(3)	6.4(1)
O(34)	0.6075(2)	0.3984(2)	−0.1255(4)	7.5(1)
C(1)	0.5243(3)	0.3167(2)	0.4115(4)	4.3(1)
C(2)	0.4674(3)	0.3517(2)	0.3837(5)	4.6(1)
C(4)	0.4436(3)	0.4324(3)	0.2814(5)	5.9(2)
C(5)	0.4746(3)	0.4814(3)	0.2332(5)	6.1(2)
C(7)	0.5536(3)	0.5036(2)	0.1004(5)	6.0(2)
C(8)	0.6048(3)	0.5257(3)	0.1673(5)	5.7(2)
C(10)	0.6830(3)	0.4951(2)	0.2923(4)	4.2(1)
C(11)	0.7383(3)	0.4567(2)	0.2888(4)	4.4(1)
C(13)	0.7566(3)	0.3634(3)	0.2493(6)	6.4(2)
C(14)	0.7259(3)	0.3087(3)	0.2565(7)	7.3(2)
C(16)	0.6323(3)	0.2609(2)	0.2055(5)	5.5(2)
C(17)	0.5959(3)	0.2603(2)	0.3114(5)	6.3(2)
C(19)	0.5658(3)	0.3407(2)	0.4985(5)	5.3(2)
C(20)	0.5252(4)	0.3487(3)	0.5987(5)	7.1(2)
C(21)	0.4693(4)	0.3862(3)	0.5752(5)	7.4(2)
C(22)	0.4298(3)	0.3619(3)	0.4880(6)	7.0(2)
C(23)	0.6483(3)	0.4909(2)	0.3973(5)	5.5(2)
C(24)	0.6919(4)	0.5029(3)	0.4917(5)	7.5(2)
C(25)	0.7478(3)	0.4650(3)	0.4891(5)	7.4(2)
C(26)	0.7834(3)	0.4682(3)	0.3838(5)	6.3(2)
C(28)	0.4973(3)	0.3381(2)	0.0098(5)	5.5(2)
C(29)	0.4620(3)	0.3125(3)	0.0879(5)	5.7(2)
C(30)	0.4037(3)	0.2927(3)	0.0719(7)	8.1(2)
C(31)	0.3763(4)	0.2972(3)	−0.0332(8)	10.6(3)
C(32)	0.4125(4)	0.3223(3)	−0.1116(7)	10.2(2)
C(33)	0.4723(3)	0.3428(3)	−0.0913(5)	6.8(2)
C(35)	0.6645(3)	0.3777(2)	−0.1445(6)	5.4(2)
C(36)	0.6975(3)	0.3478(3)	−0.0639(5)	5.7(2)
C(37)	0.7555(3)	0.3277(3)	−0.0816(5)	7.0(2)
C(38)	0.7846(3)	0.3351(3)	−0.1801(6)	7.8(2)
C(39)	0.7532(3)	0.3633(3)	−0.2581(5)	6.3(2)
C(40)	0.6944(3)	0.3851(2)	−0.2441(5)	6.0(2)

[a] $B_{eq} = \frac{4}{3}\Sigma_i\Sigma_j\beta_{ij}(a_i \cdot a_j)$.

those about C—O bonds antiplanar. As shown in Table 5, bond lengths and angles are in the expected range. The cyclohexyl ring is found in the chair conformation with an average absolute torsion angle value of 56.2°.

Host–guest interactions

The potassium ion sits on the crystallographic centre of symmetry of the hexaether, in the ideal nesting position. The average distance of 2.81 Å between the potassium and the crown oxygens is identical to the value observed in the KNCS complex of 18-crown-6 (9) in which the metal ion is also found in the ideal nesting position. The longer distance of 3.103 Å, observed between the potassium and the phenol/phenoxide oxygens, compares also with the value of 3.19 Å found between the potassium and each terminal atom, N or S, in the KNCS complex of 18-crown-6 (9). It is interesting to compare the complexation of the potassium ion in the present structure to that found in the 1:2 host:guest complex of DC-18-crown-6 (isomer

Can. J. Chem. Downloaded from www.nrcresearchpress.com by 213.222.148.141 on 09/07/12
For personal use only.

TABLE 4. Oxygen – alkali metal bond lengths and angles for (*a*) $KO_8C_{32}H_{47}$ and (*b*) $NaO_8C_{32}H_{47}$ with estimated standard deviations in parentheses[a]

Bond	Length (Å)	Bonds	Angle (deg)
(*a*) $KO_8C_{32}H_{47}$			
K—O(2)	2.734(4)	O(2)—K—O(2)′	180.0(0)
K—O(8)	2.950(4)	O(2)—K—O(5)	61.1(1)
K—O(5)	2.733(4)	O(2)—K—O(5)′	118.9(1)
K—O(14)	3.103(4)	O(2)—K—O(8)	122.7(1)
		O(2)—K—O(8)′	57.3(1)
		O(2)—K—O(14)	103.0(1)
		O(2)—K—O(14)′	77.0(1)
		O(5)—K—O(5)′	180.0(0)
		O(5)—K—O(8)′	117.9(1)
		O(5)—K—O(8)	62.1(1)
		O(5)—K—O(14)′	89.0(1)
		O(5)—K—O(14)	91.0(1)
		O(8)—K—O(8)′	180.0(0)
		O(8)—K—O(14)′	85.1(1)
		O(8)—K—O(14)	94.9(1)
		O(14)—K—O(14)′	180.0(0)
(*b*) $NaO_8C_{32}H_{47}$			
Na—O(3)	2.752(4)	O(3)—Na—O(6)	64.0(1)
Na—O(6)	2.486(4)	O(3)—Na—O(9)	101.8(1)
Na—O(9)	2.536(4)	O(3)—Na—O(12)	115.8(1)
Na—O(12)	2.886(4)	O(3)—Na—O(15)	128.1(1)
Na—O(15)	2.537(4)	O(3)—Na—O(18)	61.9(1)
Na—O(18)	2.452(4)	O(3)—Na—O(27)	110.4(2)
Na—O(27)	2.363(4)	O(6)—Na—O(9)	67.0(1)
		O(6)—Na—O(12)	124.9(1)
		O(6)—Na—O(15)	165.3(2)
		O(6)—Na—O(18)	122.1(2)
		O(6)—Na—O(27)	79.3(2)
		O(9)—Na—O(12)	59.1(1)
		O(9)—Na—O(15)	113.4(2)
		O(9)—Na—O(18)	143.0(1)
		O(9)—Na—O(27)	115.5(2)
		O(12)—Na—O(15)	60.6(1)
		O(12)—Na—O(18)	96.5(1)
		O(12)—Na—O(27)	133.5(2)
		O(15)—Na—O(18)	67.1(1)
		O(15)—Na—O(27)	87.8(2)
		O(18)—Na—O(27)	101.4(2)

[a]The primed atoms are related to the unprimed atoms by the following symmetry operation: $-x, -y, -z$.

B) with potassium phenoxide (3). In the latter complex, the potassium ions are pulled out of the approximate plane defined by the crown oxygens by a distance of 1.678 Å. Each of the potassium ions is coordinated to four crown oxygens with an average K....O distance of 2.87 Å, and to the oxygens of the two phenoxide groups with an average distance of 2.60 Å. These differences clearly show the important role played by hydrogen bonding in the structural characteristics of these host–guest complexes. In the 1:1:1 complex, groups of phenol/phenoxide–potassium–phenol/phenoxide are linked by the hydrogen atoms to form a chain: $K^+...O...H...O...K^+$. The anion is stabilized by hydrogen bonding, which facilitates complexation of the metal ion by the hexaether ligand. As a result, the ligand is left in the regular conformation with its guest in the ideal nesting position. In the 1:2 complex, on the other hand, the hard anions are strongly associated with the potassium ions and are able to pull them out of the crown cavity. The net result is an unusual 1:2 host:guest structure with a distorted hexaether ligand.

The role played by the phenol in the present structure is similar to that played by thiourea in the 1:1:1 complex of dibenzo-18-crown-6, potassium thiocyanate, and thiourea (2). The phenol stabilizes the anion through hydrogen bonding. As a result the complexation of the potassium ion by the hexaether ligand is essentially the same as was found when the counterion was the soft SCN^- anion (9).

Hydrogen bonding

The phenol hydrogen was initially located on the twofold axis special position of space group *Pnca*, thus exactly halfway between the two oxygens of the phenol/phenoxide groups. Close inspection of the difference Fourier map section defined by the O···H···O plane shows clearly, however, elongation of the hydrogen peak towards the oxygens, which suggests the presence of statistical or dynamical disordering. This is also supported by the refinement on the hydrogen position, which converges with the hydrogen being distributed on either side of the twofold axis. The hydrogen bond is strong, as can be seen from the short O···O distance of 2.48(1) Å (10, 11). With the hydrogen distributed on either side of the twofold axis, O—H distances of 0.77(6) and 1.76(7) Å are found and the O—H—O angle is 156(8)°.

The 1:1:1 complex of DC-18-crown-6 (isomer A) with sodium phenoxide and phenol

An ORTEP (8) drawing of the complex showing the atom numbering scheme is given in Fig. 2. The fractional coordinates and equivalent isotropic temperature factors of the non-hydrogen atoms are presented in Table 3. Oxygen–sodium bond lengths and angles appear in Table 4, average and range in the bond lengths and angles of the host and of the phenol and phenoxide are given in Table 5, macrocyclic torsion angles appear in Table 6.

Host geometry and conformation

As can be seen from Fig. 2 and from Table 6, the conformation of the host, the *cis–syn–cis* isomer of DC-18-crown-6, is irregular with several of the torsion angles about the C—O bonds deviating severely from the expected range. Four of the crown oxygens, O(3), O(9), O(12), and O(18) define an approximate plane that is at a distance of 1.139(3) Å from the sodium ion. The remaining two oxygens, O(6) and O(15), are folded out of the plane, towards the Na^+ ion. Distortion of the 18-crown-6 macrocycle to accommodate the sodium ion was also found in the hydrated sodium thiocyanate complex of 18-crown-6(9) and in the 1:2 host:guest complex of DC-18-crown-6 (isomer A) and sodium phenoxide (3). In each case, the distortion is due to crown oxygens folding out of the macrocycle approximate plane towards the cation guest. In the hydrated thiocyanate sodium complex of 18-crown-6, one oxygen is out of the plane, while in the 1:2 host:guest complex of DC-18-crown-6 (isomer A) and sodium phenoxide, two adjacent oxygens are involved in the distortion. In the present complex, the distortion is caused by two opposite oxygen atoms folding out of the macrocycle approximate plane.

As shown in Table 5, bond lengths and angles are in the expected range. The cyclohexyl rings are found in the chair conformation with average absolute torsion angle values of 57.3° and 56.6°.

Host–guest interactions

The sodium ion is coordinated to all six oxygens of the crown ligand. The sodium crown oxygen distances range from

Can. J. Chem. Downloaded from www.nrcresearchpress.com by 213.222.148.141 on 09/07/12
For personal use only.

TABLE 5. Average and range in the bond lengths (Å) and angles (deg) for the macrocycle rings, cyclohexyl rings, and phenoxides of (*a*) $KO_8C_{32}H_{47}$ and (*b*) $NaO_8C_{32}H_{47}$ with estimated standard deviations in parentheses

(*a*) $KO_8C_{32}H_{47}$			
Macrocycle ring			
Average C—C	1.505	Average C—O	1.426
Range of C—C	1.498–1.511(8)	Range of C—O	1.420–1.431(6)
Average C—O—C	112.5	Average C—C—O	109.4
Range of C—O—C	111.5–113.8(5)	Range of C—C—O	106.2–112.6(5)
Cyclohexyl rings			
Average C—C	1.525	Average C—C—C	110.9
Range of C—C	1.503–1.543(8)	Range of C—C—C	108.4–112.9(6)
Phenol–phenoxide			
O(14)—C(15)	1.310(7)	O(14)—C(15)—C(16)	123.7(6)
		O(14)—C(15)—C(20)	121.4(7)
Average C—C	1.382	Average C—C—C	120.0
Range of C—C	1.355–1.408(9)	Range of C—C—C	115.6–122.9(8)
(*b*) $NaO_8C_{32}H_{47}$			
Macrocycle ring			
Average C—C	1.496	Average C—O	1.426
Range of C—C	1.473–1.532(9)	Range of C—O	1.408–1.440(8)
Average C—O—C	114.2	Average C—C—O	108.3
Range of C—O—C	113.2–116.2(4)	Range of C—C—O	106.6–112.9(5)
Cyclohexyl rings			
Average C—C	1.520	Average C—C—C	110.8
Range of C—C	1.498–1.551(8)	Range of C—C—C	108.0–114.0(6)
Phenol–phenoxide			
Average C—C	1.384	C(35)—O(34)	1.332(7)
Range of C—C	1.341–1.440(13)	C(28)—O(27)	1.342(7)
Average C—C—C	120.0	C(29)—C(28)—O(27)	121.0(5)
Range of C—C—C	117.0–123.9(6)	C(33)—C(28)—O(27)	120.4(6)
		C(36)—C(35)—O(34)	120.9(6)
		C(40)—C(35)—O(34)	121.2(6)

TABLE 6. Macrocycle ring torsion angles

Bonds	Angle (deg)	Bonds	Angle (deg)
$KO_8C_{32}H_{47}$		$NaO_8C_{32}H_{47}$	
C(1)—O(2)—C(3)—C(4)	161.4(5)	C(1)—C(2)—O(3)—C(4)	164.0(4)
O(2)—C(3)—C(4)—O(5)	61.8(7)	C(2)—O(3)—C(4)—C(5)	−177.0(4)
C(3)—C(4)—O(5)—C(6)	171.4(5)	O(3)—C(4)—C(5)—O(6)	66.4(6)
C(4)—O(5)—C(6)—C(7)	177.4(6)	C(4)—C(5)—O(6)—C(7)	−177.8(5)
O(5)—C(6)—C(7)—O(8)	−73.7(6)	C(5)—O(6)—C(7)—C(8)	74.6(6)
C(6)—C(7)—O(8)—C(9)′	175.5(5)	O(6)—C(7)—C(8)—O(9)	54.7(6)
C(7)—O(8)—C(9)′—C(1)′	−175.4(5)	C(7)—C(8)—O(9)—C(10)	−164.0(5)
O(8)—C(9)′—C(1)′—O(2)′	59.6(6)	C(8)—O(9)—C(10)—C(11)	−153.9(4)
C(9)—C(1)—O(2)—C(3)	162.7(5)	O(9)—C(10)—C(11)—O(12)	−56.8(5)
		C(10)—C(11)—O(12)—C(13)	156.6(5)
		C(11)—O(12)—C(13)—C(14)	−178.9(5)
		O(12)—C(13)—C(14)—O(15)	61.1(6)
		C(13)—C(14)—O(15)—C(16)	−173.5(5)
		C(14)—O(15)—C(16)—C(17)	77.2(6)
		O(15)—C(16)—C(17)—O(18)	56.2(6)
		C(16)—C(17)—O(18)—C(1)	−177.8(4)
		C(17)—O(18)—C(1)—C(2)	−152.5(4)
		O(18)—C(1)—C(2)—O(3)	−56.6(5)

Can. J. Chem. Downloaded from www.nrcresearchpress.com by 213.222.148.141 on 09/07/12
For personal use only.

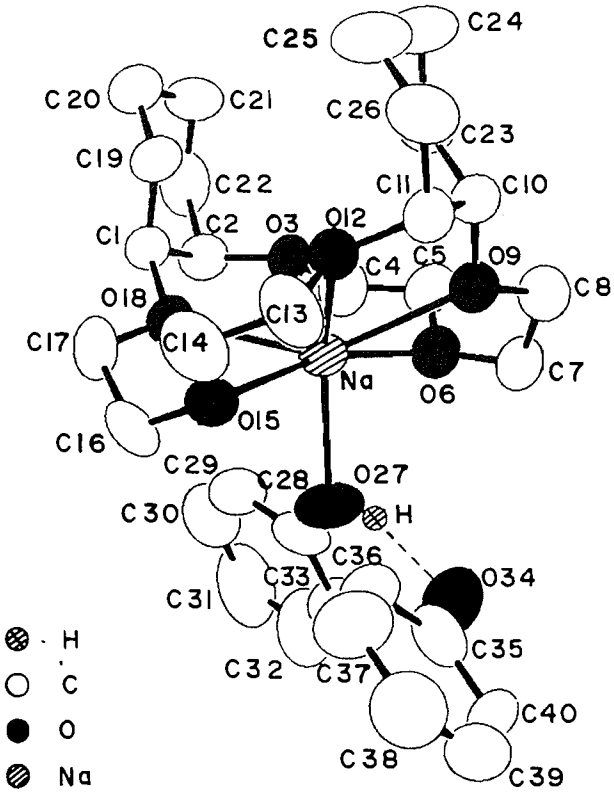

FIG. 2. ORTEP diagram and numbering scheme for the 1:1:1 complex of DC-18-crown-6 (isomer A), sodium phenoxide, and phenol.

2.452(4) to 2.886(4) Å with an average value of 2.608 Å. These distances are relatively long but are in the range of values observed in other 18-crown-6 complexes with sodium ion guests (12, 13). A distance of 2.363(3) Å is found between the sodium and the phenoxide[3] oxygen, while the phenol oxygen is found at a distance of 4.106(3) Å from the sodium. As in the potassium complex, the anion is stabilized by the phenol through hydrogen bonding.

In the 1:2 host:guest complex of DC-18-crown-6 and sodium phenoxide, on the other hand, the two sodium ions are strongly associated with the phenolate anion. One sodium is coordinated to only one crown oxygen at a distance of 2.425 Å and to three phenoxide oxygens at an average distance of 2.23 Å. The second sodium is coordinated to all six crown oxygens at distances ranging from 2.358 to 2.842 Å, with an average value of 2.55 Å, and to one phenoxide oxygen located at a distance of 2.323 Å.

Hydrogen bonding

A strong hydrogen bond is found between the phenol and phenoxide oxygens. The O...O distance is 2.471(3) Å and the O—H, O...H distances are found to be 1.35(4) and 1.38(4) Å. The O—H—O angle, at a value of 130(3)°, shows a strong deviation from linearity that is unusual for a hydrogen bond of this strength (10, 11). This result, however, must be taken with caution in view of the imprecision associated with the hydrogen position, as apparent in the large values of the standard deviation.

[3]From the O—H distances, it is not possible to distinguish the phenol from the phenoxide oxygen. We are using the term phenoxide oxygen to refer to the oxygen that is coordinated to the sodium ion.

Conclusions

Several factors contribute to the structural characteristics of host–guest complexes. It is well known that ligand and salt (both cation and anion), as well as solvent parameters, play a role in the structural features of these complexes (14). In the present paper, two examples are given of complexes in which hydrogen bonding is seen to have a marked effect. In particular, comparison of the present 1:1:1 complexes of DC-18-crown-6 (isomers A and B) with sodium and potassium phenoxide and phenol with the 1:2 complexes of DC-18-crown-6 (isomers A and B) with sodium and potassium phenoxide shows that stabilization of the anion by hydrogen bonding affects the cation–anion interaction as well as the ligand – metal ion complexation and, in turn, the ligand conformation.

Acknowledgements

Financial assistance in equipment grants and scholarships from the Natural Sciences and Engineering Research Council of Canada is gratefully acknowledged.

1. C. J. PEDERSEN. J. Org. Chem. **36**, 1690 (1971).
2. R. HILGENFELD and W. SAENGER. Angew. Chem. Int. Ed. Engl. **20**, 1045 (1981).
3. M. E. FRASER, S. FORTIER, A. RODRIGUE, and J. W. BOVENKAMP. Can. J. Chem. **64**, 816 (1986).
4. A. RODRIGUE, J. W. BOVENKAMP, M. P. MURCHIE, G. W. BUCHANAN, and S. FORTIER. Can. J. Chem. **65**, 2551 (1987).
5. P. MAIN, S. J. FISKE, S. E. HULL, L. LESSINGER, G. GERMAIN, J.-P. DECLERCQ, and M. M. WOOLFSON. MULTAN80. A system of computer programs for the automatic solution of crystal structures from X-ray diffraction data. Univs. of York, England, and Louvain, Belgium. 1980.
6. D. T. CROMER and J. T. WABER. International tables for X-ray crystallography. Vol. IV. Kynoch Press, Birmingham. 1974.
7. Enraf–Nonius. Structure determination package. Revised by B. A. Frenz. Enraf–Nonius, Delft. 1979.
8. C. K. JOHNSON. ORTEP. Report ORNL-3794, Oak Ridge National Laboratory, Tennessee. 1965.
9. M. DOBLER, J. D. DUNITZ, and P. SEILER. Acta. Crystallogr. Sect. B: Struct. Crystallogr. Cryst. Chem. **30**, 2741 (1974).
10. I. OLOVSSON and P. G. JONSOSON. The hydrogen bond. Recent developments in theory and experiments. *Edited by* P. Schuster, G. Zundel, and C. Sandorfy. North-Holland, Amsterdam. 1976. pp. 393–456.
11. C. CECCARELLI, G. A. JEFFREY, and R. TAYLOR. J. Mol. Struct. **70**, 255 (1981).
12. M. A. BUSH and M. R. TRUTER. J. Chem. Soc. (B), 1440 (1971).
13. D. BRIGHT and M. R. TRUTER. J. Chem. Soc. (B), 1545 (1970).
14. R. HILGENFELD and W. SAENGER. *In* Host guest complex chemistry. II. *Edited by* F. Vogtle. Springer Verlag, Berlin, Heidelberg, New York. 1982. pp. 1–82.

Can. J. Chem. Downloaded from www.nrcresearchpress.com by 213.222.148.141 on 09/07/12
For personal use only.

^{13}C nuclear magnetic resonance spectra in the solid state of 18-crown-6·NaNCS·H_2O, some dicyclohexyl-18-crown-6 ethers, and their complexes with phenoxides and phenol[1]

G. W. BUCHANAN[2] AND M. Z. KHAN
Ottawa–Carleton Chemistry Institute, Department of Chemistry, Carleton University, Ottawa, Ont., Canada K1S 5B6
J. A. RIPMEESTER
Division of Chemistry, National Research Council of Canada, Ottawa, Ont., Canada K1A 0R9
AND
J. W. BOVENKAMP AND A. RODRIGUE
Defence Research Establishment Ottawa, Ottawa, Ont., Canada K1A 0Z4

Received January 29, 1987

G. W. BUCHANAN, M. Z. KHAN, J. A. RIPMEESTER, J. W. BOVENKAMP, and A. RODRIGUE. Can. J. Chem. **65**, 2564 (1987).

High resolution ^{13}C CPMAS spectra for three configurationally isomeric dicyclohexyl-18-crown-6 ethers and three complexes derived therefrom are presented. Spectra are consistent with conformationally locked crown ether structures at 298 K. Data are discussed in terms of the symmetry properties of the macrocycles and stereochemical effects on ^{13}C chemical shifts in the solid phase. For the complex of 18-crown-6 with NaSCN and H_2O, a single line is observed at 298 K. Temperature reduction removes the chemical shift averaging as the different torsional angles of the solid crown ether undergo distortions that become slow on the nuclear magnetic resonance timescale.

G. W. BUCHANAN, M. Z. KHAN, J. A. RIPMEESTER, J. W. BOVENKAMP et A. RODRIGUE. Can. J. Chem. **65**, 2564 (1987).

On rapporte les CPMAS du ^{13}C à haute résolution de trois éthers dicyclohexyl-18-couronnes-6 qui sont configurationnellement isomères. Les spectres sont en accord avec des structures d'éthers couronnes qui seraient conformationnellement figées à 298 K. On discute des données en fonction des propriétés de symétrie des macrocycles et des effets stéréochimiques, dans la phase solide, sur les déplacements chimiques en résonance magnétique nucléaire du ^{13}C. À 298 K et dans le H_2O, on n'observe qu'une seule bande pour le complexe de l'éther 18-couronne-6 avec le NaSCN. Une diminution de la température élimine les déplacements chimiques moyens alors que les différents angles de torsion de l'éther couronne solide subissent des distorsions qui deviennent lentes sur l'échelle de temps de la résonance magnétique nucléaire.

[Traduit par la revue]

Introduction

In the past two years, several attempts have been made to apply solid phase ^{13}C nmr spectroscopy via the CPMAS (cross-polarization magic angle spinning) technique, to the stereochemical analysis of crown ethers and their complexes (1–3). The success of such efforts, however, depends greatly on the quality of spectra obtained. In the first report by Belton *et al.* involving dibenzo-30-crown-10, dibenzo-24-crown-10, and benzo-15-crown-5 systems, resolution of 0.1 ppm was obtained (1) at 75.5 MHz with high signal-to-noise ratios.

Unfortunately, this was followed by publication of 75.5-MHz spectra of inferior quality by Tabeta and Saito (2), which led to some erroneous conclusions regarding the stereochemical features of two dicyclohexyl-18-crown-6 isomers. Our early communication in the field (3) illustrated some high resolution ^{13}C spectra at 45.3 MHz for one isomer of dicyclohexyl-18-crown-6 and two complexes thereof.

Presently we report results of our studies on three configurationally isomeric dicyclohexyl-18-crown-6 ethers and some unique complexes with alkali metal phenoxides and phenol. Specifically the free *cis-syn-cis* (**1**), *cis-anti-cis* (**2**), and *trans-syn-trans* (**3**) isomers depicted below have been examined.

In addition, the 1:2 complex of **1** with sodium phenoxide, the 1:2 complex of **2** with potassium phenoxide, and the 1:1:1 complex of **2** with phenol and phenoxide have been studied. One complex of 18-crown-6 has also been included. Conclusions regarding symmetry are compared with those from X-ray data and stereochemical features of ^{13}C shieldings in solids are discussed.

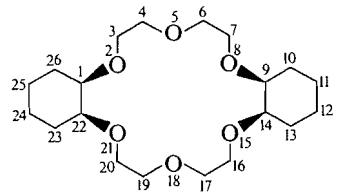

Results and discussion

Free crown ethers

The 45.3-MHz ^{13}C CPMAS spectra of **1**, **2**, and **3** are presented in Fig. 1. For **1**, which is also known as isomer A, there are seven resolved carbon resonances in the 19–32 ppm region, corresponding to non-oxygenated carbons, with one instance of peak overlap. This indicates the absence of any symmetry in the crystal structure of **1**, since eight non-oxygenated carbons would be expected in such a case. By contrast, Tabeta and Saito (2) report just two resolved resonances in this region. An examination of their published spectra indicates that the ^1H decoupling power employed appears to be only about 50% of that required for adequate removal of all ^{13}C–^1H coupling effects. Hence the published spectra (2)

[1]NRCC No. 27804.
[2]Author to whom correspondence may be addressed.

Can. J. Chem. Downloaded from www.nrcresearchpress.com by 213.166.140.6 on 09/07/12
For personal use only.

Can. J. Chem. Downloaded from www.nrcresearchpress.com by 213.166.140.6 on 09/07/12
For personal use only.

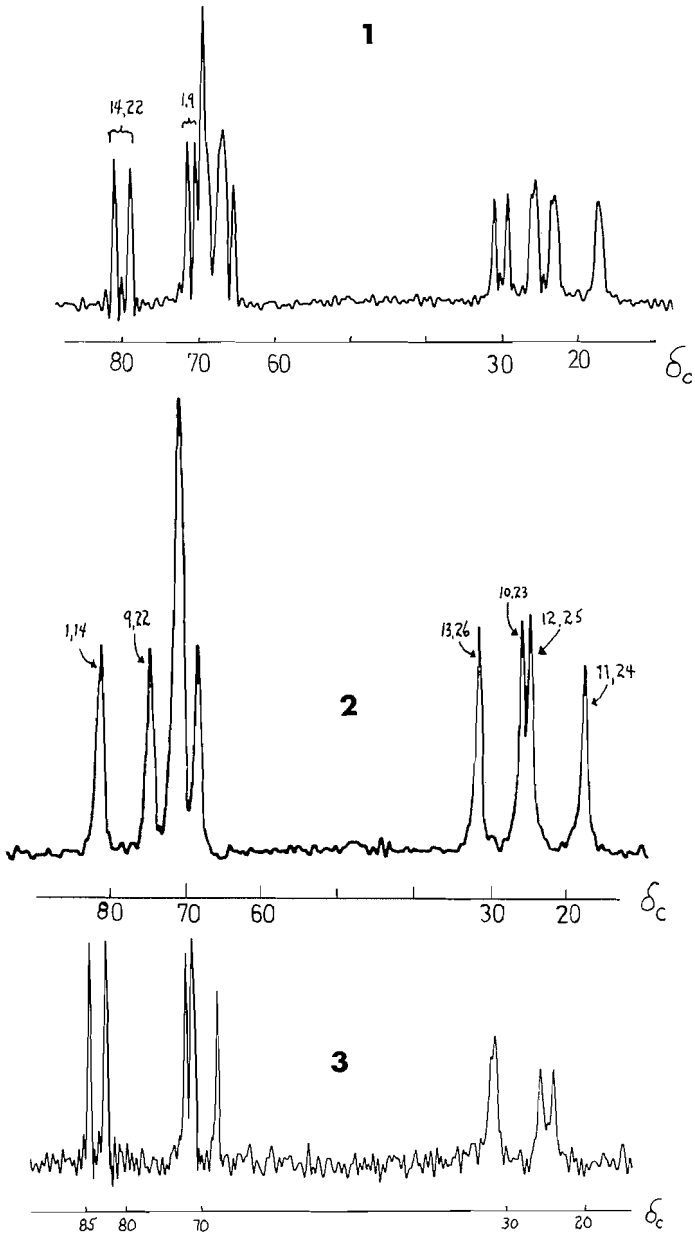

FIG. 1. The 45.3-MHz ^{13}C CPMAS spectra of *cis-syn-cis* (**1**), *cis-anti-cis* (**2**), and *trans-syn-trans* (**3**) dicyclohexano-18-crown-6 ethers.

appear as broad multiplets that are barely visible above the baseline noise in many cases.

Further evidence for the complete lack of symmetry in **1** comes from the observation of two resonances at 81.2 and 79.0 ppm arising from the cyclohexyl methine carbons bearing equatorial oxygen. Similarly the lines at 70.5 and 71.5 ppm are due to their axially oxygenated counterparts. A preliminary report of the X-ray structure of **1** has been communicated by Dalley *et al.* (4). There is distortion in the central cavity of the molecule as reflected in the oxygen–oxygen contact distances, leading to complete loss of symmetry. Somewhat surprisingly, this point was not emphasized by the authors at the time.

By contrast, it was found (4) that the *cis-anti-cis* isomer (**2**), also known as isomer B (B′ polymorph), shows no distortions in the macrocyclic cavity and there is a crystallographic centre of symmetry.

The ^{13}C CPMAS spectrum is consistent with a conformationally locked crown ether in which there is a centre of symmetry

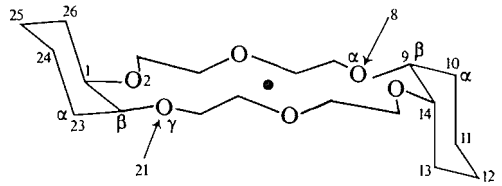

and the asymmetric unit is half the molecule. In such a structure, one would expect to observe 10 ^{13}C resonances in the absence of any accidental peak overlap. The spectrum (Fig. 1) shows four non-oxygenated carbons, with the symmetry equivalent C-11,24 resonance at highest field (19.6 ppm) due to the γ-*gauche* relationship with the axial O-8 and O-21 sites respectively (5). Appearing at 26.6 ppm is the resonance due to the C-12,25 pair, which are *trans*-γ to the equatorial O-15 and O-2 sites respectively. This assignment is made by analogy with the spectrum observed in solution at 183 K (6) where ring inversion is effectively stopped on the nmr timescale. Ring carbons which are β to equatorial oxygen, i.e., C-13 and C-26, give rise to the line at 33.0 ppm, so that the remaining resonance at 27.2 must be due to C-10,23.

In the oxygenated carbon region, the intensities are in the ratio of 1:3:1:1 with two instances of peak overlap. The resonance at 81.1 ppm arises from C-1,14, which bear equatorial oxygens. The corresponding carbons C-9,22, bonded to axial oxygens, appear at 75.0 ppm. Interestingly, in the solid there is no evidence for minor conformations of **1** or **2**, in contrast to their behaviour in solution (5, 6). The chemical shifts in the solid are, however, within 1–2 ppm of those found for the major conformation in solution at 183 K where ring inversion is slow on the nmr timescale (6).

For the *trans-syn-trans* isomer **3** below (7), no X-ray data are available. The CPMAS spectrum shows four non-oxygenated carbons in the range of 23.5–31.6 ppm and six resonances (allowing for one peak overlap) in the 67.8–84.6 ppm range. These results indicate that the asymmetric unit in the crystal of **3** is one-half the molecule, which could arise due to a centre of symmetry or a C_2 axis most likely passing through the O-5 and the O-18 atoms of the macrocycle.

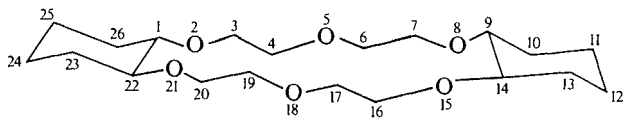

3

Interestingly, the highest field resonance of **3** is at 23.5 ppm, whereas **1** and **2**, which both possess a *cis* linkage, have resonances near 19.5 ppm. In **3** there are only *trans*-γ interactions involving the C-11, -12, -24, and -25 sites whereas in **1** and **2** there are an equal number of *trans*-γ and *gauche*-γ interactions experienced by these sites. It is well known (5) that *gauche*-γ interactions involving carbon and oxygen induce upfield shifts of 4–6 ppm at the carbon relative to the corresponding *trans*-γ interactions, so that the result is consistent with the all-*trans* stereochemistry of **3**. Similarly the C-1, -9, -14, -22 resonances appearing at 82.4 and 84.6 ppm are downfield of those for corresponding carbons of **1** and **2** since there are only β-equatorial effects of oxygen present in **3**.

Complexes

The ^{13}C CPMAS spectra of the three dicyclohexyl-18-crown-6 complexes examined are illustrated in Fig. 2.

*(i) The 1:2 complex of **1** with sodium phenoxide*

Preparation and characterization of this complex were reported

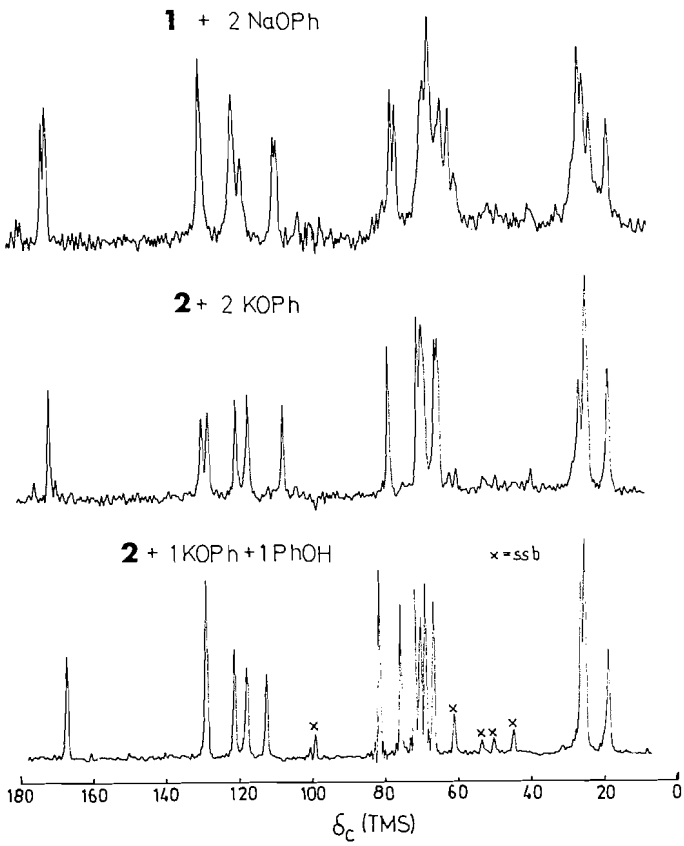

FIG. 2. The 45.3-MHz ^{13}C CPMAS spectra of complexes of **1** and **2**.

recently (8) and its X-ray structure has been published (9). The X-ray results indicate an irregular macrocyclic ring conformation in which no elements of symmetry exist. The solid phase ^{13}C spectrum reflects this despite several instances of peak overlap. For example there are two resonances near 82 ppm indicating that the cyclohexyl carbons bearing equatorial oxygens are different, as they were in free **1**, which lacks any elements of symmetry.

From inspection of the aromatic region one can draw some conclusions regarding the phenoxide environment. There are seven clearly visible lines in the range of 110–180 ppm with several instances of accidental peak overlap. This includes two resonances for oxygenated aromatic carbon near 178 ppm. Hence the two phenoxide rings must be in different environments in the crystal structure. Such a conclusion is in accord with the X-ray data (9).

*(ii) The 1:2 complex of **2** with potassium phenoxide*

The ^{13}C CPMAS spectrum of this complex (8) has just one resonance near 81 ppm, indicative of a single type of equatorially oxygenated cyclohexyl carbon. Allowing for two instances of peak overlap there are a total of 10 resonances in the aliphatic region, which suggests an element of symmetry must be present in the crown ether (either a centre or a plane).

In addition, there are six aromatic carbon resonances with no apparent peak overlap in the 110–180 ppm range. This suggests that the two phenoxide moieties are present in the crystal such that they are equivalent, but that the magnetic environment of each of the aromatic carbons is unique. These conclusions are in agreement with the recently completed X-ray study (9) on this novel structure. In the absence of X-ray data, an alternative rationale for the observed carbon nonequivalence could have been that the chemically equivalent (in solution) C-2,6 and C-3,5 sites are rendered magnetically nonequivalent in the solid by crystal packing forces. Such effects have been observed earlier for benzo-15-crown-5 ether (1).

*(iii) The 1:1:1 complex of **2** with phenol and potassium phenoxide*

The spectrum for this material (10) in Fig. 2 shows six clear resonances in the saturated oxygen-bearing carbon range of 60–82 ppm and three in the 20–35 ppm region. Assuming one instance of peak overlap in the latter group of lines, it therefore appears that there is an asymmetric unit of one-half a molecule for the crown ether itself in this complex. X-ray data (11) indicate that there is a centre of symmetry in the crown ether portion of this complex, in agreement with the nmr results.

In addition, there are five distinct resonances resolved in the aromatic region of 110–170 ppm. Given one instance of peak overlap near 130 ppm, one is forced to conclude that the aromatic rings of the phenoxide and phenol are equivalent in the crystal, but each aromatic unit lacks any symmetry elements, so that six ^{13}C resonances result. As shown by Figs. 1 and 2 of an accompanying paper (11), the hydroxyl proton and the potassium ion are situated so that they are equally "shared" between the oxygenated aromatic rings, rendering the latter equivalent.

In this complex, the aromatic carbon bearing oxygen resonates about 5 ppm upfield of those for the complexes involving only phenoxide. This is consistent with the approximately 50% phenolic character at this site. In solution, C-1 of phenol resonates ca. 12 ppm upfield of that for phenoxide (12, 13) and similar differences appear to exist in the solid.

(iv) The 1:1 complex of 18-crown-6 with H_2O and NaSCN

Finally, we have recorded the ^{13}C CPMAS spectrum of the complex of 18-crown-6 with NaSCN and one equivalent of water. In this spectrum at 298 K there is a single broad line at 68.6 ppm for the crown ether carbons. The linewidth at half-height is about 360 Hz, however, which is at least an order of magnitude greater than that normally seen in the spectra of these materials.

Results of the X-ray crystallographic analysis (14) indicate that there is a highly distorted crown structure in this complex, so that there is a complete lack of symmetry. The macrocyclic cavity adopts a conformation in which five approximately coplanar oxygen atoms surround the sodium ion. The remaining oxygen of the crown ether and a water molecule complete the distorted pentagonal bipyramidal coordination of the cation. It was found that the vibrational ellipsoids of the carbons in the irregular part of the macrocycle are large and anisotropic, suggesting that internal motions of the molecule are occurring to a substantial extent.

Accordingly we have recorded the ^{13}C CPMAS spectrum of this complex at lower temperatures in an attempt to slow down these internal motions sufficiently to produce resolvable signals for the macrocyclic carbons. As the spectra in Fig. 3 illustrate, partial success has been achieved with resolution of 7 out of the possible 12 resonances expected for the completely nonaveraged situation.

The chemical shifts for the 18-crown-6 carbons at 233 K range from 63.9 to 73.0 ppm. It is likely that these shift differences arise primarily from differences in the torsional angles present at each carbon, since it is well known (15) that ^{13}C shieldings are profoundly affected by *gauche* vs. *trans* torsional arrangements (or γ effects) depicted below. Carbons at

Can. J. Chem. Downloaded from www.nrcresearchpress.com by 213.166.140.6 on 09/07/12
For personal use only.

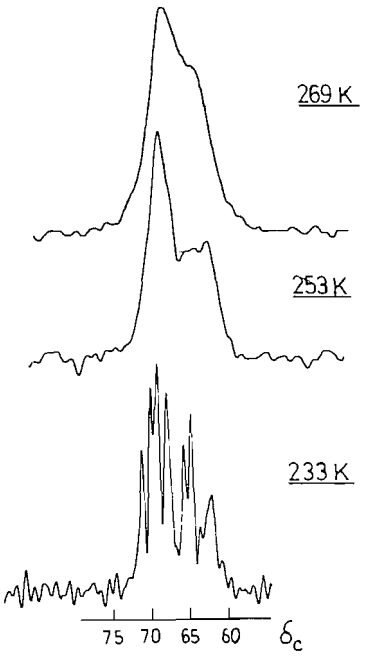

FIG. 3. The 45.3-MHz ^{13}C CPMAS spectra of the $NaNCS \cdot H_2O$ complex of 18-crown-6 as a function of temperature.

the termini, as well as at the central positions of the *gauche* arrangements are generally shifted upfield by 4–6 ppm relative to their counterparts in *trans* orientations.

From the X-ray data for this complex (14), one can group the carbons of 18-crown-6 into four general classes based on the number of *gauche*- and *trans*-type networks in which each is involved. There are 4 carbons (Class 1), which partake in 1 *gauche* and 3 *trans* interactions. Class 2 contains 5 carbons, which are involved in 2 *trans* and 2 *gauche* effects, while Class

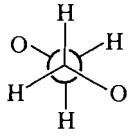

trans

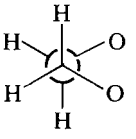

gauche

3 contains 2 carbons, which experience 1 *trans*, 2 *gauche*, and one 115° torsional geometries. Finally, Class 4 has just one carbon, which experiences no *trans* effects, 3 *gauche* effects, and one dihedral angle of 115°.

For the reasons outlined above, Class 1 carbons will resonate at lowest field while there will be a steady progression to higher field for Classes 2, 3, and 4 respectively. Since there is a difference of 2 *gauche* effects between Class 1 and Class 4, the total range of chemical shifts expected is 8–10 ppm. This agrees with experimental observations. Also the asymmetry in the spectrum at 233 K reflects, at least to a first approximation, the relative populations of Classes 1–4.

In conclusion, it is apparent that solid phase ^{13}C nmr represents a valuable addition to the available methods for examining crown ether stereochemistry, especially for the determination of asymmetric units in the crystal. The low temperature results reflect the potential of this technique for the observation of individual carbon environments that are not detectable in solution.

Experimental

Spectra

A Bruker CXP-180 spectrometer was employed to obtain the spectra at 45.3 MHz. Cross-polarization times of 2–5 ms were used with rf field amplitudes being 60 kHz. Normally 400–800 scans were accumulated. Sweep width was 20 kHz with a 4-s recycle time. Typically 2K data points were collected and FID's were zero filled to 8K before Fourier transformation. Magic angle spinning rates of ca. 3 kHz were achieved by using Kel-F spinners of the Andrew-Beams type. For the low temperature spectra, recycle times of 30–40 s were used due to the long ^1H T_1's. A probe supplied by Doty Scientific with spinners of a double air-bearing design was employed.

Materials

Compounds **1** and **2** were available from earlier work (5). The literature procedure (7) was followed for the preparation of **3**. Methods for preparation of phenoxide complexes have been reported (8). Synthesis of the 1:1:1 complex of **2** is reported in an accompanying paper (10) and the $NaSCN \cdot H_2O$ complex of 18-crown-6 has been described earlier (14).

Acknowledgements

G.W.B. thanks the Natural Sciences and Engineering Research Council of Canada for continuing financial support via operating grants.

1. P. S. BELTON, S. F. TANNER, K. M. WRIGHT, M. P. PAYNE, M. R. TRUTER, and J. N. WINGFIELD. J. Chem. Soc. Perkin Trans. 2, 1307 (1985).
2. R. TABETA and H. SAITO. Bull. Soc. Chem. Jpn. **58**, 3215 (1985).
3. G. W. BUCHANAN, J. A. RIPMEESTER, J. W. BOVENKAMP, and A. RODRIGUE. Tetrahedron Lett. **27**, 2239 (1986).
4. N. K. DALLEY, J. S. SMITH, S. B. LARSON, J. J. CHRISTENSEN, and R. M. IZATT. J. Chem. Soc. Chem. Commun. 43 (1975).
5. G. W. BUCHANAN, K. BOURQUE, J. W. BOVENKAMP, A. RODRIGUE, and R. A. B. BANNARD. Tetrahedron Lett. **25**, 3964 (1984).
6. G. W. BUCHANAN, K. BOURQUE, J. W. BOVENKAMP, and A. RODRIGUE. Can. J. Chem. **63**, 2747 (1985).
7. R. C. HAYWARD, C. H. OVERTON, and G. H. WHITHAM. J. Chem. Soc. Perkin Trans. 1, 2413 (1976).
8. A. RODRIGUE, J. W. BOVENKAMP, B. V. LACROIX, R. A. B. BANNARD, and G. W. BUCHANAN. Can. J. Chem. **64**, 808 (1986).
9. M. E. FRASER, S. FORTIER, A. RODRIGUE, and J. W. BOVENKAMP. Can. J. Chem. **64**, 816 (1986).
10. A. RODRIGUE, J. W. BOVENKAMP, M. P. MURCHIE, G. W. BUCHANAN, and S. FORTIER. Can. J. Chem. **65**, 2551 (1987).
11. M. E. FRASER, S. FORTIER, M. K. MARKIEWICZ, J. W. BOVENKAMP, and A. RODRIGUE. Can. J. Chem. **65**, 2558 (1987).
12. P. C. LAUTERBUR. J. Am. Chem. Soc. **83**, 1846 (1961).
13. G. E. MACIEL and J. J. NATTERSTAD. J. Chem. Phys. **42**, 2427 (1965).
14. M. DOBLER, J. D. DUNITZ, and P. SEILER. Acta Crystallogr. Sect. B: Struct. Crystallogr. Cryst. Chem. **30**, 2741 (1974).
15. N. K. WILSON and J. B. STOTHERS. Top. Stereochem. **8**, 1 (1973).

Can. J. Chem. Downloaded from www.nrcresearchpress.com by 213.166.140.6 on 09/07/12
For personal use only.

Reactions of some *N*-acyl-1-alkylamines with polyphosphoric ester PPE: nuclear magnetic resonance and stereochemistry of reaction products

ELBA N. ALESSO, DORA G. TOMBARI, AND GRACIELA Y. MOLTRASIO IGLESIAS[1]

Departmento de Química Orgánica, Facultad de Farmacia y Bioquímica, Universidad de Buenos Aires, Buenos Aires, Argentina

AND

JOSÉ M. AGUIRRE

Departmento de Ciencias Básicas, Universidad Nacional de Luján, Luján, Argentina

Received February 17, 1987

ELBA N. ALESSO, DORA G. TOMBARI, GRACIELA Y. MOLTRASIO IGLESIAS, and JOSÉ M. AGUIRRE. Can. J. Chem. **65**, 2568 (1987).

Phenylindanes were obtained from the reaction of *N*-acyl-1-arylalkylamines with polyphosphoric ester (PPE). *cis*-1-Methyl-3-(3,4-dimethoxyphenyl)-5,6-dimethoxyindane was synthesized to determine which stereoisomer was produced by *N*-formyl and *N*-acetyl-1-(3,4-dimethoxyphenyl)ethylamine with PPE. Nuclear magnetic resonance specra (^{1}H and ^{13}C) of several mono-, 1,3-di-, and 1,2,3-tri-substituted indanes were fully analyzed to provide information on steric interactions and conformation of the cyclopentene ring. Possible cyclodimerization pathways are proposed.

ELBA N. ALESSO, DORA G. TOMBARI, GRACIELA Y. MOLTRASIO IGLESIAS et JOSÉ M. AGUIRRE. Can. J. Chem. **65**, 2568 (1987).

On a obtenu des phénylindanes par la réaction de *N*-acyl arylalkyl-1 amines avec l'ester polyphosphorique (EPP). On a réalisé la synthèse du méthyl-1 (diméthoxy-3,4 phényl)-3 diméthoxy-5,6 indane afin de déterminer quel stéréoisomère est formé par la réaction du EPP avec les *N*-formyl et *N*-acétyl (diméthoxy-3,4 phényl)-1 éthylamines. Dans le but d'obtenir des informations sur les interactions stériques et la conformation du noyau cyclopentène, on a complètement analysé les spectres en résonance magnétique nucléaire du ^{1}H et du ^{13}C de plusieurs indanes mono-, di-1,3 et tri-1,2,3 substitués. On propose divers mécanismes possibles pour la cyclodimérisation.

[Traduit par la revue]

In previous work (1) polyphosphoric ester (PPE) has been found to act as a highly effective desamidation agent on *N*-acyl-1,2-diarylethylamines to produce *trans*-stilbenes. However, in some special cases, indane-type derivatives were obtained along with the *trans*-stilbenes.

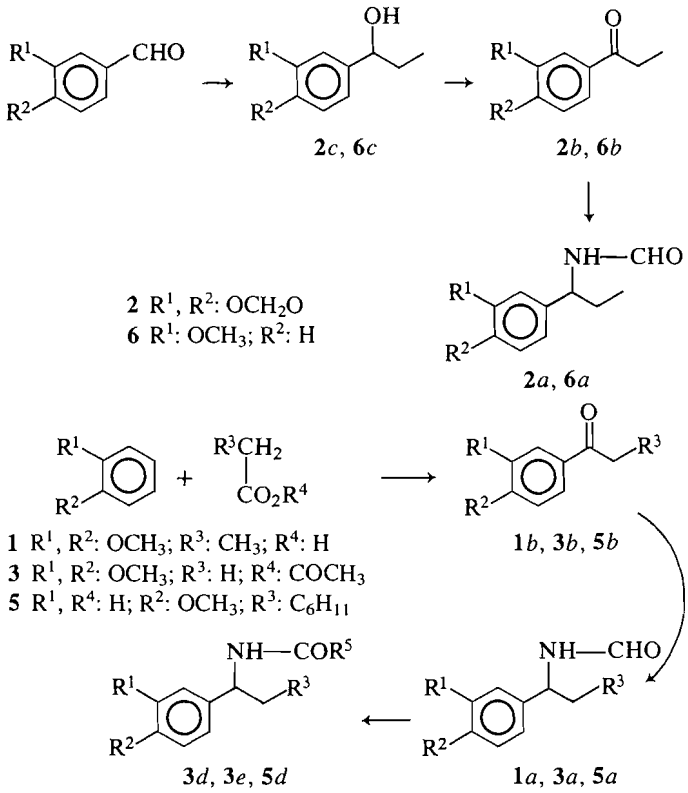

SCHEME 1

Reactions of *N*-acyl-1-arylalkylamines, prepared as illustrated in Scheme 1, with PPE in chloroform–ether solution, were attempted in order to learn more about the reaction scope and the nature of the products, including their stereochemistry. As shown in eq. [1] and outlined in Table 1, amides **1***a*, **2***a*, **3***a*, **3***d*, and **3***e* rendered indanes **7**, **8**, and **10** as major products, whereas amides **5***a*, **5***d*, and **6***a* gave only the styrenes, which were detected as their bromo derivatives. Cyclodimerization thus depends essentially on the degree of aryl ring substitution.

[1]

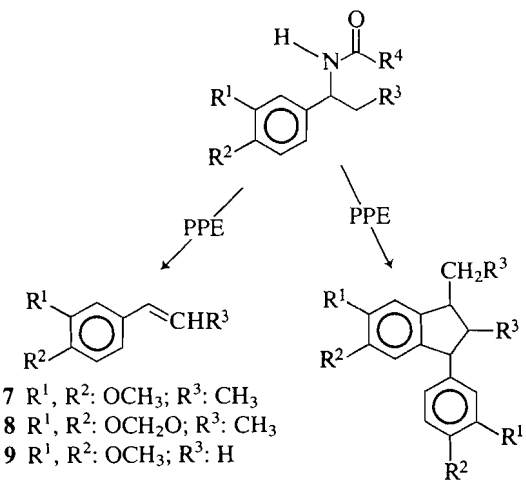

Catalyzed dimerization of isohomogenol and isosafrol has been reported (2) to give the 1,2-*cis*-2,3-*trans*-(α-racemate) diisohomogenol **7** and diisosafrol **8** as major products, with the all *trans*-(γ-racemate) isomers as minor products. Amides **1***a* and **2***a* rendered only the α-racemate. Likewise, **3***a*, **3***d*, and **3***e* gave a stereoisomer of **10** as the major product, with traces of the other one.

Having isolated and purified the two possible stereoisomers of **10**, a synthetic sample of the *cis*-indane **10** was then prepared

[1]Author to whom correspondence may be addressed.

Can. J. Chem. Downloaded from www.nrcresearchpress.com by 213.222.148.141 on 09/07/12
For personal use only.

TABLE 1. Reaction of *N*-acyl-1-arylalkylamines with PPE

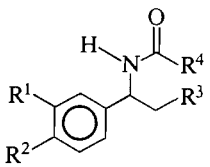

Amide	R^1	R^2	R^3	R^4	Yield (%; compound) Styrene	Indane
1*a*	CH_3O	CH_3O	CH_3	H	—	56; **7**
2*a*	O—CH_2—O		CH_3	H	—	78; **8**
3*a*	CH_3O	CH_3O	H	H	—	56; **10**
3*b*	CH_3O	CH_3O	H	CH_3	—	50; **10**
3*c*	CH_3O	CH_3O	H	C_6H_5	—	57; **10**
4	H	H	H	H	—	—
5*a*	H	CH_3O	C_6H_{11}	H	48; **19**	—
5*d*	H	CH_3O	C_6H_{11}	CH_3	43; **19**	—
6*a*	CH_3O	H	CH_3	H	51; **20***	—

*Detected as bromo derivative.

following Scheme 2 reactions (3, 4). An alternative synthesis of compound **10** (Scheme 3) was attempted using indanone **15**, as reported by Feeman and Amstutz (6), but cyclization of **14** was unsuccessful after boiling in phosphorus oxychloride solution for 3 min. Instead, **15** was obtained by using PPA (polyphosphoric acid). The cyclized product was a colourless solid, mp 75°C, characterized by its spectral data.

Spectral data for the synthetic sample allowed direct identification of the minor **10** isomer as the *cis* isomer. Comparison of 80-MHz spectra enabled the following conclusions to be drawn:

1. Stereochemical assignments of indane **10** are further supported by the H-2a and H-2b chemical shifts, whose variation over a 1.1-ppm range in the *cis* isomer is attributable to the diverse degrees of H-2a shielding by the C-1 methyl and C-3 aryl groups. In the *trans* isomer these two protons are collapsed in a complex multiplet and appear at intermediate field. The observed difference in chemical shift between the geminal protons in the *cis* isomer is not unexpected when the cyclopentene ring conformation is locked (7).

2. Strikingly, H-4 in either stereoisomer is clearly shielded in comparison to the same proton in 5,6-dimethoxyindane **16**. The minimal H-4 chemical shift difference observed (Δ = 0.1 ppm) between the two stereoisomers **10** and 3-(3,4-dimethoxyphenyl)-5,6-dimethoxyindane **17** seems attributable to the similar *pseudo*-equatorial C-3 aryl group position, with the aryl group at right angles to the plane of the indane nucleus, the only conformation in which the C-3 aryl group is close enough to H-4 to exert a shielding effect (8).

3. The observed shielding effect of H-3 (Δ = 0.20 ppm) between the *cis* and *trans* isomers of **10** is not unexpected, given the strong H-3 *pseudo*-axial – CH_3 *pseudo*-axial repulsion leading to considerable van der Waals deshielding (7) of H-3 in the *trans* isomer.

4. The different displacement of the C-1 methyl group signal in either stereoisomer is indicative (9) of the different angle subtended by the aromatic ring plane and defined by the bonds joining C-1 and the methyl group (10). Preliminary data on H-4 in *cis*- and *trans*-**10** support the *pseudo*-equatorial position of the C-3 aryl group, so it is reasonable to assume that equilibria must be shifted in the direction of the conformers shown in Fig. 1. Besides, on comparing the methyl group shift in 5,6-dimethoxy-1-methylindane **18** and the chemical shifts of the same group in *cis*- and *trans*-**10**, it proves quite similar to that of the *trans* isomer. It could thus be expected that the

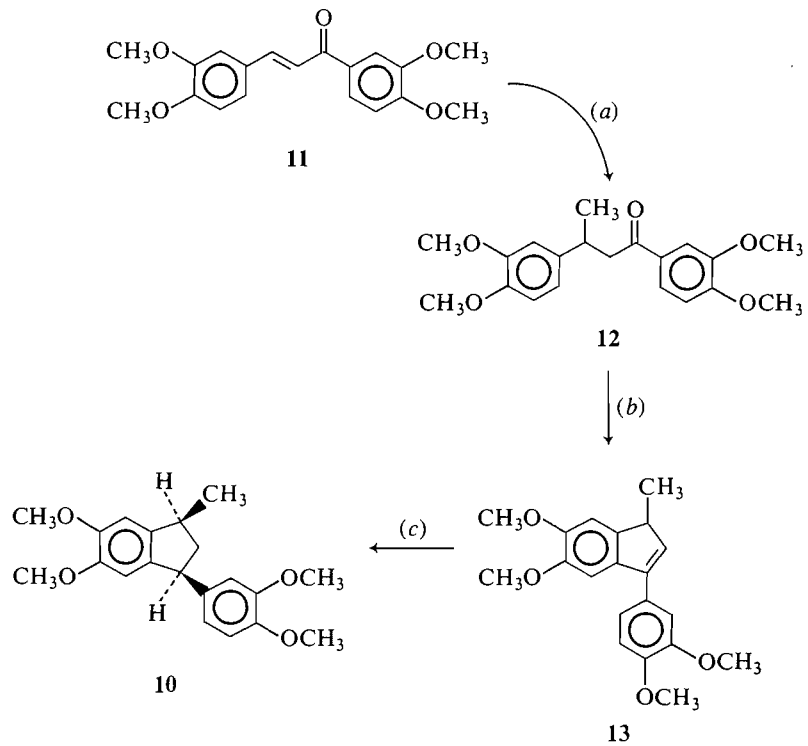

(*a*) CH_3MgI, $ClCu/Et_2O$; (*b*) H_2SO_4/H_3PO_4; (*c*) PtO_2/AcOEt

SCHEME 2

Can. J. Chem. Downloaded from www.nrcresearchpress.com by 213.222.148.141 on 09/07/12
For personal use only.

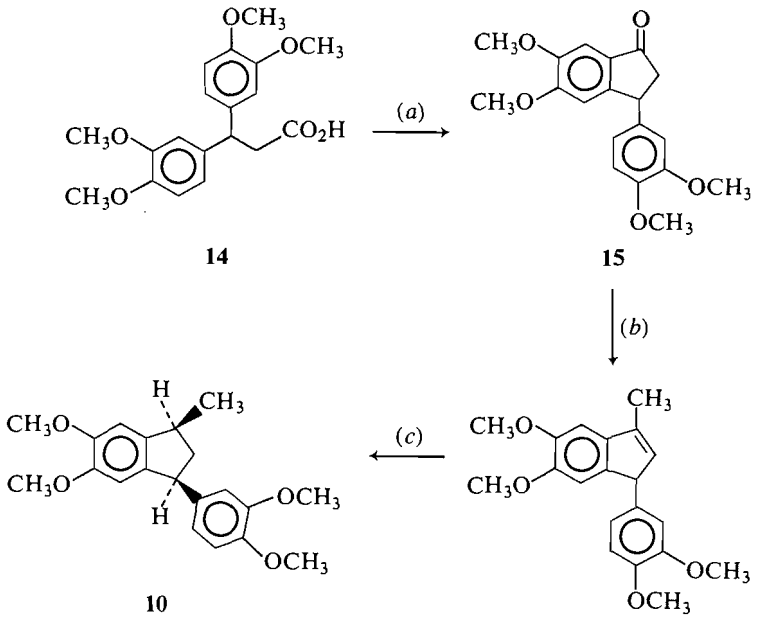

(*a*) PPA; (*b*) CH_3MgI/Et_2O; (*c*) $PtO_2/AcOEt$

SCHEME 3

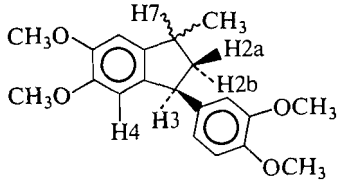

10

The ^1H nmr spectra of **10** (80 MHz)

	cis	*trans*
H1	3.20	3.31
H2a	1.60	2.22
H2b	2.70	2.22
H3	4.14	4.34
H4	6.45	6.54
CH_3	1.36	1.26

methyl group in **18** would preferably be in the *pseudo*-axial position. Dreiding models indicate that the H-3 *pseudo*-axial to CH_3 *pseudo*-axial distance is greater than the CH_3 *pseudo*-equatorial to H-7 distance.

The ^{13}C chemical shifts for seven indanes are given in Table 2. Cyclopentene ring carbon shifts were determined by means of model values and APT (Attached Protons Test) experiments. Besides evaluating substitution effects on ^{13}C nmr shielding data, steric factors and epimeric shift differences were compared with results obtained from substituted cyclopentanes (11). To start with, the ^{13}C signal was compared for C-3 in **18** versus C-1 in **16**. The former compound shows a larger shielding than the latter (Δ = 1.72 ppm). Although the steric origin of γ effects in indane seems unquestionable, this effect is minor when compared to the same effect exerted by the introduction of an

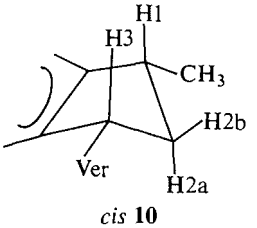

cis **10**

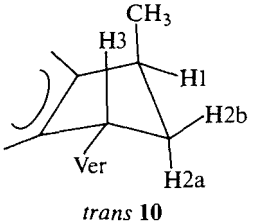

trans **10**

Ver = 3,4-dimethoxyphenyl

FIG. 1

axial methyl group in cyclohexane, and may be ascribed to reduced steric interaction in the indane system due to less ring puckering. Moreover, C-3 in the *trans* isomer is shielded by 1 ppm in comparison to the *cis* isomer. In the epimeric indanes, C-3 shielding variations arise from the γ effect of equatorial versus axial methyl groups (12, 13). The ^{13}C signals from C-2 show greater shielding for the *trans*-**10** than for the *cis*-**10** epimer (Δ = 1.61 ppm). In methylindane **18**, the β effect is

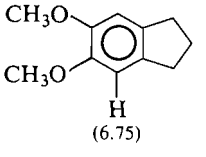

16

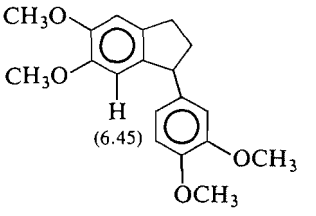

17

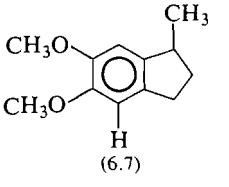

18

9.18 ppm, greater than for an axial methyl group in cyclopentane or cyclohexane. This feature may also be associated with less ring puckering. The C-1 shielding variation in stereoisomers **10** is rather small (Δ = 0.12 ppm), in agreement with Roberts and co-workers (11), who considered that the α effect in substituted cyclopentanes is hardly influenced by steric hindrance (Table 2).

Lastly, ^{13}C nmr data for diisosafrol closely agree with those for diisohomogenol (10), lending further support to the conclusion that diisosafrol and diisohomogenol obtained by PPE desamidation share the same stereochemistry.

To clarify feasible cyclodimerization pathways, it was therefore of interest to determine whether *trans*-styrenes and

Can. J. Chem. Downloaded from www.nrcresearchpress.com by 213.222.148.141 on 09/07/12
For personal use only.

TABLE 2. ^{13}C nuclear magnetic resonance chemical shifts of indanes

Carbon	**16**	**18**	**17**	**10*t***	**10*c***	**7**	**8**
1	32.80	39.24	51.04	37.7	37.82	48.3	48.22
2	25.69	34.87	36.91	45.2	46.81	49.3	49.31
3	32.80	31.08	31.27	48.9	49.91	56.7	56.62
4	107.84	107.75*	107.75	107.7	107.58	107.9	105.45
5	147.82	147.78*	145.85*	147.1*	147.87	147.4	145.96
6	147.82	147.87*	145.21*	148.2*	148.07	147.2	146.23
7	107.84	106.71	107.19	106.2	105.85	107.9	105.28
8	135.60	135.12	135.57	138.3	138.10	137.7	139.14
9	135.60	140.32	138.03	137.1	137.51	136.3	138.00
1′			138.08	140.6	140.25	139.0	140.31
2′			110.81	110.7	110.92	110.7	107.75
3′			148.70*	148.6*	148.69	148.6	145.96
4′			147.94*	147.9*	147.09	147.8	147.51
5′			110.92	110.8	110.97	111.0	108.27
6′			119.67	119.3	120.10	120.4	121.57
CH_3		20.1		20.4	19.37	13.6	13.57
CH_2						22.2	22.16
CH_2CH_3						12.0	11.95
OCH_2O							100.63
CH_3O	55.98	55.87	55.64	55.58	55.5	55.5	
		55.94	55.52	55.75	55.7	55.8	
			55.48				

*May be interchanged.

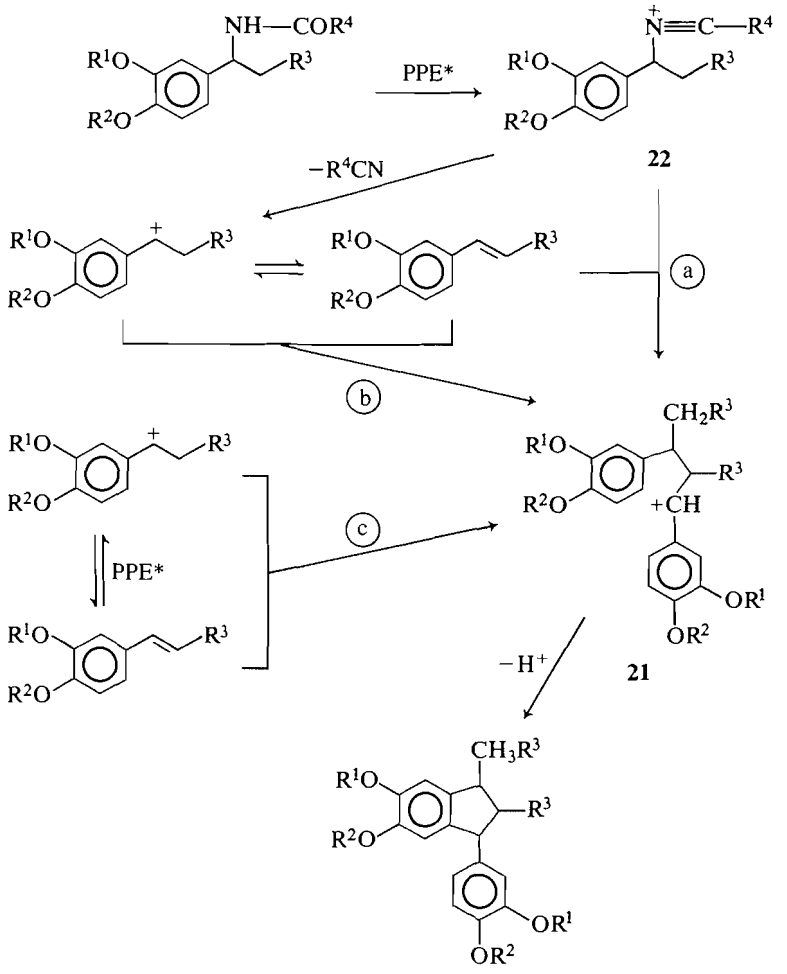

* 0.8 H^+/4 atoms of P (ref. 22)

SCHEME 4

Can. J. Chem. Downloaded from www.nrcresearchpress.com by 213.222.148.141 on 09/07/12
For personal use only.

Can. J. Chem. Downloaded from www.nrcresearchpress.com by 213.222.148.141 on 09/07/12
For personal use only.

N-acyl-1-arylalkylamines having the same aryl ring substitution produce the same indanes, given the fact that *trans*-styrenes were isolated when unfavourably substituted aryl groups were present in the starting amides. When 1,2-(methylenedioxy)-*trans*-4-propenylbenzene, synthesized by a Wittig reaction, and amide **2***a* were likewise treated with PPE, only the α stereoisomer of indane **8** was obtained, clearly indicating that cyclodimerization involves the common intermediary **21** (Scheme 4). However, the yield from amide **2***a* was significantly higher than from the styrene (78 versus 20%), which may be accounted for by assuming that **21** might have been formed by routes a and (or) b from the amide, as well as by route c from the styrene. It is thus evident that the monomeric cations formed by pathways a and c are identical but differ in formation capability.

The existence of nitrilium ions **22** was supported by the isolation of benzonitrile as one of the reaction products from amide **3***e*. These ions are the most commonly invoked intermediaries in the mechanism of the Bischler–Napieralski synthesis and von Braun amide degradation reaction (14, 23).

Experimental

Infrared spectra were obtained on a Shimadzu IR 440 spectrometer. The ^1H and ^{13}C spectra were recorded on a Bruker WO 80 SYFT or a Varian FT 80 A spectrometer with $CDCl_3$ as solvent. Both spectra were referenced to internal Me_4Si and are reported on the δ scale. Mass spectra were recorded on a Varian Mat Mod CH7 A instrument. Elemental analyses were carried out in our laboratories using a Colemann Analyzer. Melting points (uncorrected) were obtained on a Thomas Hoover apparatus. Polyphosphoric ester (PPE) was prepared by the method of Pollmann and Schramm (15). Polyphosphoric acid was prepared by heating P_2O_5 (100 g) with H_3PO_4 (85%, 120 g) during 4 h at 120°C. Formamide was prepared by heating $(NH_4)_2CO_3$ (80 g) with HCOOH (80 g) during 1 h at 160°C.

1-(3,4-Methylenedioxyphenyl)-1-propanol **2**c

Ethyl bromide (0.5 mL) was added to a mixture of 10.7 g (0.44 g-atom) of Mg and 80 mL of dry ether. After starting the stirring, a solution of 48 g of ethyl bromide in 100 mL of ether was slowly added to the mixture (over 2 h). To the freshly prepared ethyl Grignard reagent was added dropwise 19.5 g (0.13 mol) of 3,4-dimethylenedioxybenzaldehyde in 20 mL of ether. When the addition was complete, the mixture was heated gently under reflux for 1 h and allowed to cool to room temperature. The mixture was hydrolyzed with saturated aqueous NH_4Cl and the aqueous layers were extracted with ether. The ethereal solution was dried ($MgSO_4$) and concentrated *in vacuo* to yield an oil, which was purified by dry column chromatography (silica gel). Elution with cyclohexane yielded the desired product. Yield 82%; ir (neat): 3450 (O—H) cm^{-1}; ^1H nmr: 0.85 (t, 3H, CH_3), 1.65 (m, 2H, CH_2), 2.15 (s, 1H, O*H*), 4.40 (t, 1H, C*H*), 5.9 (s, 2H, OCH_2O), 6.75 (m, 3H, Ar). *Anal.* calcd. for $C_{10}H_{12}O_3$: C 66.72, H 6.72; found: C 66.65, H 6.70.

1-(3-Methoxyphenyl)-1-propanol **6**c

This alcohol was prepared by the same procedure as described for **2***c* and isolated as an oil using a dry column (silica gel) with benzene as eluent. Yield 69.2%; ir (neat): 3480 (O—H) cm^{-1}; ^1H nmr: 0.86 (t, 3H, CH_3), 1.65 (m, 2H, CH_2), 2.75 (s, 1H, O*H*), 3.70 (s, 3H, OCH_3), 4.40 (t, 1H, C*H*), 6.7–7.2 (m, 4H, Ar). *Anal.* calcd. for $C_{10}H_{14}O_2$: C 72.35, H 8.50; found: C 72.40, H 8.52.

1-(3,4-Methylenedioxyphenyl)-1-propanone **2**b

A mixture of 7 g (0.070 mol) of chromium trioxide in 10 mL of water was immersed in an ice bath and 11.2 g of concentrated (18 *M*) H_2SO_4 followed by 20 mL of water was added cautiously with manual stirring. The solution was cooled to 0–5°C. The cooled oxidation reagent was added with vigorous stirring to a solution of 18 g (0.1 mol) of alcohol in 60 mL of acetone, cooled to 0–5°C at such a rate as to maintain the temperature of the reaction mixture at about 20°C. The stirring was continued for 3 h after the addition was completed. Sodium bisulfite was added and the mixture was extracted with chloroform and acetone. The extracts were combined, washed sucessively with saturated sodium bicarbonate solution and water, and dried ($MgSO_4$). The solvent was removed and the residue was chromatographed on a dry column (silica gel) with benzene as eluent. Yield 64.06% of a white solid, mp 36–37°C; ir (mull): 1670 (C=O) cm^{-1}; ^1H nmr: 1.21 (t, 3H, CH_3), 2.90 (c, 2H, CH_2), 6.00 (s, 2H, OCH_2O), 6.8 (d, 1H, Ar-5), 7.40 (d, 1H, Ar-2), 7.55 (dd, 1H, Ar-6). *Anal.* calcd. for $C_{10}H_{10}O_3$: C 67.47, H 5.66; found: C 67.37, H 5.63.

1-(3-Methoxyphenyl)-1-propanone **6**b

This ketone was prepared by the same procedure as described for **2***b* and isolated as an oil using a dry column (silica gel) with benzene as eluent (16). Yield 77.7%; ir (neat): 1660 (C=O) cm^{-1}; ^1H nmr: 1.23 (t, 3H, CH_3), 2.95 (c, 2H, CH_2), 3.85 (s, 3H, OCH_3), 6.95–7.90 (m, 4H, Ar).

1-(3,4-Dimethoxyphenyl)-1-propanone **1**b

A mixture of recently prepared polyphosphoric acid (220 g), veratrole (0.20 mol), and propionic acid (0.20 mol) was stirred during 4 h at 70–80°C. Water was added and the mixture was extracted with $CHCl_3$, and the organic phase was washed with NaOH solution (10%) and water. The chloroform solution was dried over Na_2SO_4 and evaporated to dryness. The residue was crystallized from methanol. Yield 55%, mp 58–59°C (EtOH) (lit. (17*a*) mp 58–59°C).

1-(3,4-Dimethoxyphenyl)ethanone **3**b

This ketone was prepared by using a modification of the procedure described before, using acetic anhydride as the electrophilic reagent. It was isolated as an oil and was purified by distillation at 160°C and 10 Torr (1 Torr = 133.3 Pa). Yield 69%, mp 48–49°C (lit. (17*b*) mp 49–51°C).

1-(4-Methoxyphenyl)-2-cyclohexylethanone **5**b

This ketone was prepared in an analogous manner to **1***b*. The residue was crystallized from EtOH–H_2O. Yield 85%, mp 44–45°C (lit. (18) mp 43°C).

N-*1-(3,4-Dimethoxyphenyl)propylformamide* **2**a

A mixture of 1.78 g (0.01 mol) of the ketone **2***b* and 15 mL of freshly prepared formamide was heated at 180–190°C for 8 h. The water formed was removed during the reaction. The reaction mixture was diluted with water and extracted twice with $CHCl_3$. The combined organic layers were dried (Na_2SO_4) and finally the solvent was removed *in vacuo*. The amide was isolated as an oil using dry column (silica gel) with benzene–ethanol (95:5) as eluent. Yield 52.2%; ir (neat): 3352 (N—H), 1660 (C=O) cm^{-1}; ^1H nmr: 0.85 (t, 3H, CH_3), 1.75 (m, 2H, CH_2), 4.75 (m, 1H, C*H*), 5.85 (s, 2H, OCH_2O), 6.40 (m, 1H, N*H*), 6.75 (s, 3H, Ar), 8.10 (s, 1H, C*H*O). *Anal.* calcd. for $C_{11}H_{13}NO_3$: C 63.82, H 6.33, N 6.77; found: C 63.70, H 6.30, N 6.79.

The following compounds were prepared in a manner similar to that described for **2***a*.

N-*1-(3-Methoxyphenyl)propylformamide* **6**a

Isolated as an oil using dry column (silica gel) and benzene–ethanol (95:5) as eluent. Yield 85%; ir: 3345 (N—H), 1665 (C=O) cm^{-1}; ^1H nmr: 0.90 (t, 3H, CH_3), 1.76 (m, 2H, CH_2), 3.75 (s, 3H, OCH_3), 4.85 (m, 1H, C*H*), 6.5 (s, br, 1H, N*H*), 6.6–7.25 (m, 4H, Ar), 8.1 (s, br, 1H, C*H*O). *Anal.* calcd. for $C_{11}H_{15}NO_2$: C 68.45, H 7.83, N 7.26; found: C 68.50, H 7.78, N 7.30.

N-*1-(3,4-Dimethoxyphenyl)propylformamide* **1**a

Isolated as an oil using a dry column (silica gel) and benzene as eluent. Yield 58%; ir: 3350 (N–H), 1680 (C=O) cm^{-1}; ^1H nmr: 0.90 (m, 3H, CH_3), 1.80 (m, 2H, CH_2), 3.85 (s, 6H, OCH_3), 4.83 (m, 1H, C*H*), 6.1 (s, br, 1H, N*H*), 6.77 (s, 3H, Ar), 8.10 (s, br, 1H, C*H*O). *Anal.* calcd. for $C_{12}H_{17}NO_3$: C 64.63, H 7.68, N 6.28; found: C 64.66, H 7.71, N 6.30.

Can. J. Chem. Downloaded from www.nrcresearchpress.com by 213.222.148.141 on 09/07/12
For personal use only.

N-*1-(3,4-Dimethoxyphenyl)ethylformamide* ***3***a

Yield 52%, mp 115–116°C (benzene); ir: 3250 (N—H); 1685 (C=O) cm^{-1}; ^1H nmr: 1.47 (d, 3H, CH_3), 3.82 (s, 6H, OCH_3), 5.05 (m, 1H, C*H*), 6.1 (s, br, 1H, N*H*), 6.84 (s, 3H, Ar), 8.1 (s, br, 1H, C*H*O). *Anal.* calcd. for $C_{11}H_{15}NO_3$: C 63.21, H 7.23, N 6.70; found: C 63.35, H 7.30, N 6.75.

N-*1-(4-Methoxyphenyl)-2-cyclohexylethylformamide* ***5***a

Yield 55%; mp 66–68°C (benzene); ir: 3350 (N—H), 1660 (C=O) cm^{-1}; ^1H nmr: 0.75–1.9 (m, 13H, CH_2—C_6H_{11}), 3.70 (s, 3H, OCH_3), 5.10 (dd, 1H, C*H*), 5.90 (s, br, 1H, N*H*), 6.85 (d, 2H, Ar-3,5), 7.15 (d, 2H, Ar-2,6), 8.05 (s, br, 1H, C*H*O). *Anal.* calcd. for $C_{16}H_{23}NO_2$: C 73.62, H 8.88, N 5.37; found: C 73.70, H 8.91, N 5.50.

N-*1-(3,4-Dimethoxyphenyl)ethylacetamide* ***3***d

A mixture of 1.5 g of ***3a***, 25 mL of HCl (δ 1.19), and 75 mL of water was heated under reflux for 1 h. After cooling, the clear solution was extracted with ether and the aqueous solution was made strongly alkaline with 20% NaOH solution. The resulting solution was extracted with ether. The ether layers were washed (H_2O) and dried ($MgSO_4$). Evaporation left the crude amine, which was converted to its acetyl derivative in the usual way. Yield 67%; ir: 3250 (N—H), 1640 (C=O) cm^{-1}; ^1H nmr: 1.35 (d, J = 6 Hz, 3H, CH_3), 1.86 (s, 3H, CH_3), 3.73 (s, 6H, OCH_3), 4.95 (m, 1H, C*H*), 6.10 (s, br, 1H, N*H*), 6.72 (s, 3H, Ar). *Anal.* calcd. for $C_{12}H_{17}NO_3$: C 64.63, H 7.68, N 6.28; found: C 64.69, H 7.71, N 6.32.

N-*1-(4-Methoxyphenyl)-2-cyclohexylethylacetamide* ***5***d

This acetamide was prepared from ***5a*** in an analogous manner to ***3d***. Yield 73%, mp 131–133°C (EtOH); ir: 3230 (NH), 1650 (C=O) cm^{-1}; ^1H nmr: 1–2.05 (m, 13H, CH_2—C_6H_{11}), 2.15 (s, 3H, CH_3), 4.0 (s, 3H, OCH_3), 5.25 (dd, 1H, C*H*), 6.0 (s, br, 1H, N*H*), 6.90 (d, 2H, Ar-3,5), 7.35 (d, 2H, Ar-2,6). *Anal.* calcd. for $C_{17}H_{25}NO_2$: C 74.24, H 9.16, N 5.09; found: C 74.36, H 9.13, N 5.16.

N-*1-(3,4-Dimethoxyphenyl)ethylbenzamide* ***3***e

This compound was prepared by hydrolysis of ***3a*** and then the amine was treated with benzoyl chloride in dry pyridine to give white crystals, mp 123–124°C (EtOH–H_2O). Yield 84%; ir: 3310 (NH), 1640 (C=O) cm^{-1}; ^1H nmr: 1.6 (d, 3H, CH_3), 3.85 (s, 6H, OCH_3), 5.30 (m, 1H, C*H*), 6.45 (s, br, 1H, N*H*), 6.85 (d, 2H, Ar), 6.90 (s, 1H, Ar), 7.45 (m, 3H, Ar), 7.80 (m, 2H, Ar). *Anal.* calcd. for $C_{17}H_{19}NO_3$: C 71.64, H 6.72, N 4.92; found: C 71.70, H 6.70, N 4.96.

1,3-Bis-(3,4-dimethoxyphenyl)-1-butanone ***12***

A solution of chalcone **11**, 3.28 g (0.01 mol), in anhydrous benzene was added slowly to a 100% excess of methyl magnesium iodide containing 0.1 mol of cuprous chloride (19). During the addition, the temperature of the reaction mixture was maintained at 0–5°C. After addition was complete, the reaction mixture was stirred for an additional 30 min, then the temperature was allowed to rise. Finally, the mixture was refluxed for 1 h. The reaction mixture was decomposed by pouring it into cracked ice mixed with acetic acid. The solution was filtered, the benzene layer was separated, and the aqueous layer was extracted with methylene chloride. The combined organic layers were dried ($MgSO_4$) after being washed with aqueous bicarbonate and water. The solvent was finally evaporated and the extract was purified by column chromatography (silica gel) with benzene as eluent. The ketone was obtained as colourless crystals from acetone. Yield 52%, mp 94–95°C; ^1H nmr: 1.3 (d, J = 6.7 Hz, 3H, CH—CH_3), 3.0–3.5 (m, 3H, C*H*—CH_2), 3.84, 3.86, 3.92 (s, 12H, OCH_3), 6.82–7.6 (m, 6H, Ar). *Anal.* calcd. for $C_{20}H_{24}O_5$: C 69.83, H 7.03; found: C 69.82, H 7.09.

cis-*3-(3,4-Dimethoxyphenyl)-1-methyl-5,6-dimethoxyindane* ***10***

A solution of the ketone **12** (1.97 mol) in 0.9 mL of 85% phosphoric acid was added slowly with vigorous stirring to 0.9 mL of concentrated H_2SO_4 at 0°C. The reaction mixture was heated at 60–70°C for 30 min at which time the colour changed from yellow to red. The crude product was obtained by pouring the reaction mixture into ice water. The solid was dissolved in methylene chloride and the solution shaken exhaustively with a solution of NaOH (2%), then with water. Drying and evaporation of the solvent yielded the indene **13**, which was used without any other purification. Hydrogenation of 0.0026 mol of **13** in 6 mL of ethyl acetate with 5.3 mg of platinum dioxide at room temperature and 40 psi (1 psi = 6.9 kPa) for 2 h afforded a pale yellow oil. Yield 82%; ^1H nmr: 1.36 (d, 3H, CH_3), 1.60 (m, 1H, H-2a), 2.70 (m, 1H, H-2b), 3.2 (m, 1H, H-1), 3.70, 3.80, 3.86, 3.90 (s, 12H, OCH_3), 4.14 (m, 1H, H-3), 6.45 (s, 1H, Ar-4), 6.6–6.75 (m, 4H, Ar); ms: M^+ 328 (100%); *m/e*: 313 (62%), 297 (89%), 191 (15%), 190 (36.7%), 175 (28%), 165 (18%), 164 (19%), 159 (21%), 149 (16.1%).

trans-*3-(3,4-Dimethoxyphenyl)-1-methyl-5,6-dimethoxyindane* ***10*** (ref. 1): ms: M^+ 328 (100%); *m/e*: 313 (37%), 297 (6.25%), 191 (9.8%), 190 (36.7%), 175 (21.4%), 165 (3.9%), 164 (8.1%), 149 (25.4%).

3-(3,4-Dimethoxyphenyl)-5,6-dimethoxyindanone ***15***

A mixture of 2.3 g (6.6 mmol) of **14** and 23 g of freshly prepared PPA was heated with stirring for 8 h at 100–110°C. The mixture was cooled and the excess of PPA was destroyed by addition of water. The crude product was extracted with methylene chloride and the organic layer was washed with water and NaOH (5%). The organic extract was dried ($MgSO_4$) and after removal of the solvent it was purified by column chromatography (silica gel) using methylene chloride as eluent. Recrystallization from acetone gave 1.3 g of nearly colourless solid. Yield 51.2%, mp 74–75°C (lit. (6) mp 124–125°C); ^1H nmr: 2.55 (dd, J_{gem} = 20 Hz, J_{vic} *cis* = 4 Hz, 1H, H-2b), 3.20 (dd, J_{gem} = 20 Hz, J_{vic} *trans* = 8 Hz, 1H, H-2a), 3.75, 3.80, 3.90 (s, 12H, OCH_3), 4.4 (dd, J_{vic} *trans* = 8 Hz, J_{vic} *cis* = 4 Hz, 1H, H-3), 6.5–6.75 (m, 4H, Ar), 7.20 (s, 1H, Ar-7). *Anal.* calcd. for $C_{19}H_{20}O_6$: C 69.57, H 6.15; found: C 69.35, H 6.18.

cis-*3-(3,4-Dimethoxyphenyl)-1-methyl-5,6-dimethoxyindane* ***10***

A solution of the indanone **15** (300 mg, 0.97 mol) in anhydrous benzene was added to a 100% excess of methyl magnesium iodide in anhydrous ether. During the addition the temperature of the reaction was maintained at 5–10°C. After addition was complete the mixture was refluxed on a water bath for 2 h; the organic solution was poured into a mixture of acetic acid, water, and crushed ice. The organic layer was separated and the aqueous solution was extracted with two portions of ether. The combined organic extracts were washed with a dilute solution of sodium bicarbonate, followed by water, and finally were dried ($MgSO_4$). The solvent was evaporated and the residue was purified by preparative tlc, using plates of silica gel with fluorescent indicator and benzene–ethanol (9:1) as eluent. Without further purification the indene was hydrogenated in a manner similar to indene **13**. Yield 53%. This material was identical (ir, nmr) with that prepared by the alternative method.

5,6-Dimethoxyindane ***16***

This compound was obtained from the 5,6-dimethoxyindanone (5) and zinc amalgam (20). Yield 71%, mp 50°C (lit. (21) mp 50°C); ^1H nmr: 2.05 (q, 2H, CH_2), 2.80 (t, 4H, CH_2), 3.80 (s, 6H, OCH_3), 6.75 (s, 2H, Ar).

3-(3,4-Dimethoxyphenyl)-5,6-dimethoxyindane ***17***

This compound was prepared from **15** according to the literature experimental procedure (6). Yield 83%, mp 84–85°C (EtOH) (lit. (5) mp 85.0–86.8°C); ^1H nmr: 2.50 (m, 2H, CH_2), 2.85 (m, 2H, CH_2), 3.75, 3.83, 3.90 (s, 12H, OCH_3), 4.20 (m, 1H, C*H*), 6.45 (s, 1H, Ar-7), 7.25 (m, 4H, Ar).

1-Methyl-5,6-dimethoxyindane ***18***

The 5,6-dimethoxyindanone (280 mg, 1.35 mmol) dissolved in anhydrous benzene was added drop by drop to an excess of methyl Grignard reagent (6.75 mol) at 0–5°C. After addition was complete the mixture was refluxed for 2 h. The reaction mixture was decomposed by pouring it into cracked ice mixed with acetic acid and methylene chloride. The combined organic layers were dried ($MgSO_4$) after

Can. J. Chem. Downloaded from www.nrcresearchpress.com by 213.222.148.141 on 09/07/12
For personal use only.

being washed with aqueous bicarbonate and water. The solvent was finally evaporated and the residue, without further purification, was hydrogenated in a similar manner to indene **13** and crystallized from benzene–hexane to afford colourless crystals. Yield 78%, mp 88–89°C; ^{1}H nmr: 1.25 (d, 3H, CH_3), 1.65 (m, 1H, CH_2-2), 2.25 (m, 1H, CH_2-2), 2.75 (m, 2H, CH_2-3), 3.10 (m, 1H, C*H*), 3.73, 3.80 (s, 6H, OCH_3), 6.65, 6.70 (s, 2H, Ar). *Anal.* calcd. for $C_{12}H_{16}O_2$: C 75.06, H 8.40; found: C 74.93, H 8.30. For the indene, ^{1}H nmr: 2.12 (d, 3H, CH_3), 3.22 (s, br, 2H, CH_2), 3.80, 3.85 (s, 6H, OCH_3), 6.05 (m, 1H, C*H*), 6.8 (s, 1H, Ar-4), 6.93 (s, 1H, Ar-7).

General procedure for the cyclodimerization reaction with PPE (ref. 1)

A solution of amide or styrene (1 mmol) and PPE (2.56 g) in chloroform–ether was warmed at 80°C for 8 h. After removing the solvent *in vacuo*, water and methylene chloride were added to the crude product. The organic layer was separated, then washed with NaOH (5%) and water. The organic extract was dried ($MgSO_4$) and the solvent was removed. Chromatography of the crude product on alumina column (eluent benzene–hexane) afforded the indanes.

1-Ethyl-2-methyl-3-(3,4-dimethoxyphenyl)-5,6-dimethoxyindane 7

Only the α isomer was obtained from the amide **1***a*. Yield 56%, mp 104–105°C (lit. (2) mp 104–106°C). The ^{1}H nmr of this material was identical with that prepared by an alternate method (2).

1-Ethyl-2-methyl-3-(3,4-methylenedioxyphenyl)-5,6-methylenedioxyindane 8

Only the α isomer was obtained from the amide **2***a*. Yield 78%, mp 92–93°C (lit. (2) mp 92–93°C). The ^{1}H nmr of this material was identical with that prepared by an alternate method (2). From the isosafrol the α isomer was obtained in 20% yield.

trans-*1-Methyl-3-(3,4-dimethoxyphenyl)-5,6-dimethoxyindane 10*

This isomer was obtained from the amides **3***a*, **3***d*, and **3***e* in 56, 50, and 57% yield respectively, mp 118–119°C.

trans-*1-Methoxy-4-(2-cyclohexylethenyl)benzene 19*

This compound was obtained from the amides **5***a* and **5***d*, mp 39–40°C (EtOH); ^{1}H nmr: 1.1–1.9 (m, 11H, C_6H_{11}), 3.79 (s, 3H, OCH_3), 5.99 (dd, J = 15.2 Hz, J = 6.4 Hz, 1H, C*H*—C_6H_{11}), 6.31 (d, J = 15.2 Hz, 1H, C*H*-Ar), 6.81 (d, J = 8.8 Hz, 2H, Ar-3,5), 7.25 (d, J = 8.8 Hz, 2H, Ar-2,6). *Anal.* calcd. for $C_{15}H_{20}O$: C 83.40, H 9.33; found: C 83.25, H 9.38.

1,2-Dibromo-1-(3-bromo-4-methoxyphenyl)-cyclohexylethene

Bromine (0.5 mL) was added, dropwise, to a solution of *trans*-styrene (0.2 mL) in CCl_4 (1 mL). The solid obtained was filtered and washed with cold MeOH. Recrystallization from methanol gave white crystals, mp 87–88°C; ^{1}H nmr: 1.2–1.9 (m, 11H, C_6H_{11}), 3.85 (s, 3H, OCH_3), 3.90–4.25 (m, 2H, C*H*-Br), 6.95 (d, J = 6 Hz, 1H, Ar-5), 7.20 (dd, J = 6 Hz, J = 1.2 Hz, 1H, Ar-6), 7.45 (d, J = 1.2 Hz, 1H, Ar-2). *Anal.* calcd. for $C_{15}H_{19}Br_3O$: C 39.59, H 4.21; found: 39.61, H 4.25.

1,2-Dibromo-1-(2-bromo-5-methoxyphenyl)propane 20

The crude product of the reaction of **6***a* with PPE was treated with bromine and carbon tetrachloride. The bromine derivative was isolated as an oil by preparative tlc on silica gel with fluorescent indicator and benzene as solvent; ^{1}H nmr: 2.00 (d, J = 6.4 Hz, 3H, CH_3), 3.80 (s, 3H, OCH_3), 4.55 (m, 1H, C*H*Br), 5.50 (d, J = 12 Hz, 1H, C*H*Br), 6.7 (dd, J_{H3-H4} = 8 Hz, J_{H4-H6} = 3 Hz, 1H, Ar-4), 7.03 (d, J = 3 Hz, 1H, Ar-6), 7.40 (d, J = 8 Hz, 1H, Ar-3). *Anal.* calcd. for $C_{10}H_{11}Br_3O$: C 31.03, H 2.87, Br 61.96; found: C 31.10, H 2.89, Br 61.78.

Acknowledgements

This research work was supported by Grant No. 3031400/85 from CONICET and Grant No. 1679/85 from SECYT, Argentina. The authors are indebted to Dr. M. González Sierra for recording some of the nmr spectra and to Dr. E. Rúveda for valuable criticism.

1. J. M. Aguirre, E. N. Alesso, C. Somoza, D. G. Tombari, G. Y. Moltrasio, and J. D. Bonafede. An. Asoc. Quim. Argent. **73**, 391 (1985).
2. J. MacMillan, I. L. Martin, and D. J. Morris. Tetrahedron, **25**, 905 (1969).
3. E. Rohrmann, R. G. Jones, and H. A. Shonle. J. Am. Chem. Soc. **66**, 1855 (1944).
4. M. S. Kharasch and D. C. Sayles. J. Am. Chem. Soc. **64**, 2972 (1942).
5. J. Koo. J. Am. Chem. Soc. **75**, 2000 (1953).
6. J. F. Feeman and E. D. Amstutz. J. Am. Chem. Soc. **72**, 1526 (1950).
7. W. D. Cotterill and, in part, R. Livingstone, K. D. Bartle, and D. W. Jones. Tetrahedron, **24**, 1981 (1965).
8. T. Gilchrist, R. Hodges, and A. L. Porte. J. Chem. Soc. 1780 (1962).
9. A. L. Campbell, H. H. Leader, M. Gonzalez Sierra, C. L. Spencer, and J. D. McChesney. J. Org. Chem. **44**, 2755 (1979).
10. E. Wenkert, A. Afonso, P. Beak, R. Carney, P. Jeffs, and J. D. McChesney. J. Org. Chem. **30**, 713 (1965).
11. M. Christi, H. Y. Reich, and J. D. Roberts. J. Am. Chem. Soc. **93**, 3454 (1971).
12. D. K. Dalling and D. M. Grant. J. Am. Chem. Soc. **89**, 6612 (1967).
13. P. K. Agrawal, H. J. Schneider, M. S. Malik, and S. N. Rastogi. Org. Magn. Reson. **21**, 146 (1983).
14. J. Gal, R. J. Wienkam, and N. Castanogli, Jr. J. Org. Chem. **39**, 418 (1974).
15. W. Pollman and G. Schramm. Biochem. Biophys. Acta, **80**, 1 (1964).
16. R. W. Hartmann, A. Heindl, and H. Schoenenberger. J. Med. Chem. **27**, 577 (1984).
17. (*a*) C. Hell and B. Portmann. Chem. Ber. **28**, 2092 (1895); (*b*) L. Bouveault. Bull. Soc. Chim. Fr. 1021 (1987).
18. J. R. Barrio, M. C. G. de Barrio, and M. J. Vernengo. J. Med. Chem. **14**, 898 (1971).
19. R. N. Killer and H. D. Wycoff. Inorg. Synth. 1 (1946).
20. C. Manning, M. R. McClong, and J. J. McCullough. J. Org. Chem. **46**, 919 (1981).
21. W. H. Mills and I. G. Nixon. J. Chem. Soc. 2510 (1930).
22. W. Wieker, H. P. Walter, and E. Thilo. Chem. Ber. **97**, 2385 (1964).
23. S. Nagubandi and G. Fodor. J. Heterocycl. Chem. **17**, 1457 (1980).

Conformational analysis of 3-substituted-2,3,4,5-tetrahydro-1-benzoxepin by ^1H and ^{13}C nuclear magnetic resonance

A. LACHAPELLE AND M. ST-JACQUES[1]

Département de chimie, Université de Montréal, C.P. 6128, Succ. A, Montréal (Qué.), Canada H3C 3J7

Received May 5, 1987

A. LACHAPELLE and M. ST-JACQUES. Can. J. Chem. **65**, 2575 (1987).

2,3,4,5-Tetrahedro-1-benzoxepin (**8**) and its 3-substituted derivatives (**9–13**) have been studied by ^1H and ^{13}C dynamic nuclear magnetic resonance in a few solvent systems. The results show that, while **8** and its methyl derivative **9** exist solely in chair forms (*C* for **8** and C_e:C_a (96:4) for **9**), the twist-boat (*TB*) conformation contributes significantly to the conformational equilibria of the derivatives 3-methoxy **10** (C_a:C_e:*TB*, 70:20:10), 3,3-dimethyl **11** (*C*:*TB*, 90:10), 3,3-methylmethoxy **12** (C_a:C_e:*TB*, 89:4:7), and 3,3-dimethoxy **13** (*C*:*TB*, 92:8). The analysis of several factors (steric, electrostatic, and electronic) on the conformational behaviour of these molecules shows why the *TB* form is a viable conformational alternative to destabilized chair forms in this benzoxepin system.

A. LACHAPELLE et M. ST-JACQUES. Can. J. Chem. **65**, 2575 (1987).

Faisant appel à la résonance magnétique nucléaire dynamique du ^1H et du ^{13}C, on a étudié la tétrahydro-2,3,4,5 benzoxépine-1 (**8**) ainsi que ses dérivés portant des substituants en position 3 (**9–13**), dans divers solvants. Les résultats démontrent que, alors que **8** et son dérivé méthylé **9** existent uniquement dans des formes chaises (*C* pour **8** et C_e:C_a (96:4) pour **9**), la conformation bateau croisé (*BC*) apporte une contribution importante à l'équilibre conformationnel des dérivés méthoxy-3 (**10**) (C_a:C_e:*BC*, 70:20:10), diméthyl-3,3 (**11**) (*C*:*BC*, 90:10), méthyl-3 méthoxy-3 (**12**) (C_a:C_e:*BC*, 89:4:7) et diméthoxy-3,3 (**13**) (*C*:*TB*, 92:8). Une analyse de l'influence de plusieurs facteurs (stérique, électrostatique et électronique) sur le comportement conformationnel de ces molécules démontre pourquoi la forme *BC* est une alternative conformationnelle viable pour les formes chaises déstabilisées de ce système benzoxépine.

[Traduit par la revue]

Over the last two decades, various studies of substituted six-membered ring heterocycles (tetrahydropyran (1), 1,3-dioxane (2), etc...) have revealed the importance of steric and electrostatic effects on conformational stability. While most molecules investigated were shown to exist as chair forms, only extremely crowded derivatives were found (3) to adopt predominantly the twist-boat (*TB*) form, in order to minimize the strong nonbonding interactions. Recent work by St-Jacques and co-workers (4, 5) showed that replacement of the 5- or 2-methylene groups in the 1,3-dioxane **1** ring by an *ortho*-benzo group, leading to 2,3-dihydro-2,4-benzodioxepin **2** and to 2,3-dihydro-1,5-benzodioxepin **5**, stabilizes the *TB* conformation significantly (about 20% is detected for both compounds in CHF_2Cl between −100 and −150°C). Furthermore, *TB* stabilization is increased substantially by substitution at the 3-position with a *gem*-dimethyl group (as in **3** or **6**) or with a polar methoxy group (as in **4** or **7**).

Because both series of molecules contain interactions involving two ring oxygen atoms, we wished to characterize the effect of only one oxygen atom in the seven-membered ring. We therefore report a high-field ^1H and ^{13}C nmr (1D and 2D) investigation of molecules **8–13**, containing a single oxygen adjacent to the aromatic ring, whose results contribute to understanding the various factors (steric, stereoelectronic, electrostatic, etc...) favouring the twist form.

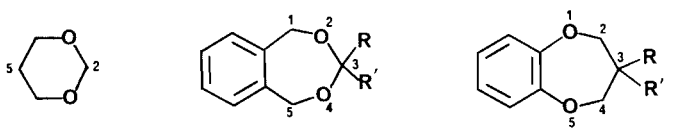

1

2: R = R' = H

3: R = R' = CH_3

4: R = H, R' = OCH_3

5: R = R' = H

6: R = R' = CH_3

7: R = H, R' = OCH_3

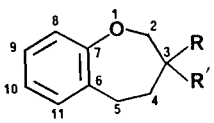

8: R = R' = H

9: R = H, R' = CH_3

10: R = H, R' = OCH_3

11: R = CH_3, R' = CH_3

12: R = CH_3, R' = OCH_3

13: R = R' = OCH_3

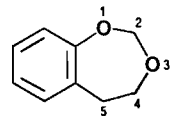

14

Results

The ^1H and ^{13}C nmr spectra of all six compounds (**8–13**) studied were obtained at different temperatures between −5 and −125°C. Three different solvent systems were used: a polar CHF_2Cl–CD_2Cl_2 (80:20) mixture for both ^1H and ^{13}C spectra and less polar combinations such as CF_2Cl_2–acetone-d_6 (94:6) for ^1H and CH_3OCH_3–CD_2Cl_2 (80:20) for ^{13}C spectra. All pertinent nmr parameters are summarized in Tables 1 and 2.

The ^{13}C spectra of **8** in both the polar and the less polar solvent systems revealed no spectral modifications upon lowering the temperature. Aliphatic carbon atoms were identified through selective proton irradiations at −120°C while the aromatic carbon signals were assigned using aromatic carbon chemical shifts of a similar molecule (6) (4,5-dihydro-1,3-benzodioxepin **14**). The observed signals were attributed to the chair (*C*) form, as will be further discussed in the next section.

The 400.13-MHz ^1H spectra of **8** in both solvent systems, however, showed one spectral modification on going from −10 to −125°C, as illustrated in Fig. 1. At −10°C, the aliphatic region consists of four multiplets corresponding to the four methylene groups of the molecule. The most deshielded one (3.90 ppm) can easily be assigned to H-2, because of the

[1]Author to whom correspondence should be addressed.

Can. J. Chem. Downloaded from www.nrcresearchpress.com by 213.222.148.141 on 09/07/12
For personal use only.

Can. J. Chem. Downloaded from www.nrcresearchpress.com by 213.222.148.141 on 09/07/12
For personal use only.

TABLE 1. Carbon-13 chemical shifts[a,b] of compounds **8–13** at high and low temperatures

Compound	Solvent	Temperature (°C)	Conformation (populations (%))	C-2	C-3	C-4	C-5	C-6	C-7	C-8	C-9	C-10	C-11	Substituent on C-3
8	CHF_2Cl	−25	—	74.88	33.75	27.41	35.54	137.64	161.86	122.37	128.37	124.62	131.54	—
(H,H)		−120	*C*[c] (>98)	75.04	33.42	26.93	35.31	138.12	161.38	122.61	128.40	124.82	131.66	—
	CH_3OCH_3	−24	—	74.15	33.74	27.46	35.36	136.74	161.78	122.08	128.05	124.12	131.08	—
		−120	*C* (>98)	74.03	33.50	27.10	35.07	136.88	161.37	122.13	128.09	124.30	131.08	—
9	CHF_2Cl	−25	—	80.14	38.46	35.62	33.69	137.74	161.55	122.31	128.50	124.79	131.49	17.82
(H,CH_3)		−120	C_e (97)	80.14	38.60	35.23	33.84	138.23	161.23	122.53	128.52	125.00	131.53	18.06
			C_a (3)	79.03	34.29	32.47	29.36	—[d]	—[d]	—[d]	128.23	—[d]	131.24	15.86
	CH_3OCH_3	−15	—	79.32	38.19	35.54	33.39	136.68	161.69	121.95	128.11	124.20	130.98	17.78
		−120	C_e (96)	79.11	38.53	35.28	33.56	136.94	161.21	122.00	128.16	124.43	130.89	17.96
			C_a (4)	77.86	34.36	32.61	29.04	—[d]	—[d]	—[d]	—[d]	—[d]	—[d]	15.87
10	CHF_2Cl	−20	—	80.81	75.00	28.89	31.41	136.48	161.36	122.20	128.70	124.92	131.62	56.99
(H,OCH_3)		−125	C_a (70)	78.71	74.59	27.69	29.31	137.93	161.07	122.54	128.71	125.89	131.51	56.43
			C_e (20)	81.29	75.22	29.12	32.46	137.04	160.53	122.5[e]	128.99	125.42	131.76	57.80
			TB (10)	81.29	71.81	29.02	29.95	130.54	160.43	120.68	128.10	123.11	133.02	56.73
	CH_3OCH_3	−20	—	80.53	74.35	28.80	31.76	135.73	161.11	121.76	128.21	124.25	131.07	56.55
		−120	C_a (44)	78.30	72.94	27.66	30.16	137.29	161.09	122.06	128.13	124.55	130.74	55.74
			C_e (50)	80.95	74.94	28.91	32.38	136.15	160.58	121.98	128.55	124.80	131.10	56.91
			TB (6)	80.45	71.76	28.17	29.07	129.86	—[d]	120.25	127.48	122.34	132.25	56.16
11	CHF_2Cl	−15	—	83.12	36.52	40.26	30.55	136.86	161.86	121.99	128.37	124.47	131.57	25.59
(CH_3,CH_3)		−120	*C* (90)	83.06	36.45	39.55	30.30	138.01	161.42	122.37	128.42	124.87	131.44	27.62, 23.01
			TB (10)	80.90	36.23	38.00	28.99	131.10	—[d]	—[d]	127.84	122.53	132.94	—[d]
	CH_3OCH_3	−15	—	82.35	36.32	40.24	30.35	135.93	161.82	121.76	128.06	123.99	131.17	25.52
		−115	*C* (89)	82.06	36.30	39.67	30.06	136.99	161.58	122.02	128.18	124.43	130.93	27.42, 23.01
			TB (11)	79.78	36.13	38.28	28.62	130.00	—[d]	120.00	127.43	—[d]	132.29	—[d]

Can. J. Chem. Downloaded from www.nrcresearchpress.com by 213.222.148.141 on 09/07/12
For personal use only.

TABLE 1 (*concluded*)

Compound	Solvent	Temperature (°C)	Conformation (populations (%))	C-2	C-3	C-4	C-5	C-6	C-7	C-8	C-9	C-10	C-11	Substituent on C-3
12	CHF_2Cl	−20	—	78.93	77.21	28.76	35.94	136.34	161.25	121.95	128.50	124.72	131.45	20.98(Me), 49.33(OMe)
(CH_3,OCH_3)		−95	C_a (89)	79.52	76.80	34.10	27.98	137.74	160.81	122.32	128.65	125.27	131.25	21.23(Me), 49.23(OMe)
			TB (7)	76.51	79.77	35.66	29.23	130.29	160.11	—[d]	128.04	122.98	132.73	19.10(Me), 49.65(OMe)
			C_e (4)	—[d]	77.31	36.34	29.39	—[d]	—[d]	—[d]	128.8	—[d]	131.66	19.52(Me), 49.50(OMe)
	CH_3OCH_3	−25	—	77.60	76.46	28.63	36.71	135.61	161.21	121.54	128.02	124.06	131.08	20.91(Me), 49.10(OMe)
		−120	C_a (85)	76.35	75.80	27.81	36.46	137.31	160.96	121.90	128.13	124.60	130.71	20.75(Me), 49.03(OMe)
			TB (8)	79.54	—[d]	28.17	36.03	—[d]	160.04	120.13	127.53	122.41	132.21	19.19(Me), 48.87(OMe)
			C_e (7)	—[d]	—[d]	29.04	—[d]	136.43	—[d]	—[d]	128.55	124.85	131.17	19.19(Me), —[d]
13	CHF_2Cl	−25	—	74.55	101.84	34.21	28.46	135.70	161.06	121.92	128.76	124.98	131.71	48.60
(OCH_3,OCH_3)		−110	*C* (89)	74.37	100.98	33.84	27.95	136.85	160.67	122.67	128.94	125.52	131.62	48.67, 48.48
			TB (11)	73.36	—[d]	32.39	28.34	—[d]	—[d]	120.71	128.23	123.37	132.80	48.95
	CH_3OCH_3	−20	—	73.63	101.06	34.26	28.38	135.39	161.06	121.54	128.27	124.42	131.24	48.05
		−120	*C* (94)	73.04	100.29	34.09	28.01	136.19	160.80	121.74	128.45	124.85	131.20	48.26, 47.46
			TB (6)	72.45	—[d]	32.76	—[d]	—[d]	—[d]	120.25	127.68	122.63	132.19	48.11

[a]All spectra were taken on a Bruker WH-400 spectrometer operating at 100.62 MHz.
[b]Solutions containing 20% CD_2Cl_2 for locking purposes and tetramethylsilane as internal standard.
[c]The symbols *C*, C_e, C_a, and *TB* refer to conformations defined in the text.
[d]These signals were not observed, either because of peak overlapping or too small signal-to-noise ratio.
[e]C-8 resonances for C_a and C_e conformations are overlapping.

Can. J. Chem. Downloaded from www.nrcresearchpress.com by 213.222.148.141 on 09/07/12
For personal use only.

TABLE 2. Proton (^{1}H) chemical shifts[a,b] for compounds **8–13**, at high and low temperatures

Compound (R,R')	Solvent	Temperature (°C)	Conformation (population (%))	H-2e	H-2a	H-3e	H-3a	H-4e	H-4a	H-5e	H-5a	Substituent on C-3
8 (H,H)	CHF_2Cl	−10	—	3.97 m	3.97 m	1.96 m	1.96 m	1.71 m	1.71 m	2.81 m	2.81 m	—
		−125	*C*[c] (>95)	4.46 d	3.51 t	1.96[d]	1.92[d]	2.02[d]	1.38 q	2.74 d × d	2.90 t	—
	CF_2Cl_2	−10	—	3.90 t	3.90 t	1.92 m	1.92 m	1.69 m	1.69 m	2.77 m	2.77 m	—
		−120	*C* (>95)	4.36 d	3.41 t	1.95[d]	1.92[d]	2.01[d]	1.36 q	2.65 d × d	1.85 t	—
9 (H,CH_3)	CHF_2Cl	−10	—	4.21 d	3.28 t	—	2.11 m	1.98 m	1.21 q	2.73 d × d	2.89 t	0.89 d
		−120	C_e (97)	4.29 d	3.18 t	—	2.13 br	2.00 d	1.11 q	2.72 d × d	2.92 t	0.85 d
			C_a (3)	—[e]	3.70 br	—	—[e]	1.82 br	1.68 br	2.50 br	—[e]	1.28 d
	CF_2Cl_2	−20	—	4.13 d × d	3.21 t	—	2.05 m	1.92 m	1.19 q	2.66 d × d	2.85 t	0.89 d
		−120	C_e (96)	4.17 d	3.07 t	—	2.07 d	1.94 d	1.09 q	2.62 d × d	2.97 t	0.85 d
			C_a (4)	4.09 d	3.61 d	—[e]	—	1.79 br d	1.66 br t	2.40 br	—[e]	1.27 d
10 (H,OCH_3)	CHF_2Cl	−10	—	4.03 d	3.95 s	3.52 br s	—	2.00 m	1.85 br	2.64 t	2.99 t	3.43 s
		−125	C_a (70)	4.52 d	3.59 t	3.56 s	—	2.37 d	1.55 t	2.48 d × d	3.22 t	3.45 s
			C_e (20)	4.45 d	3.2 —	—	—[e]	2.4 —	1.29 q	2.6–2.8	2.6–2.8[d]	—[e]
			TB (10)	—[e]	4.19 d	—[e]	—	—[e]	1.95 q	—[e]	2.98 t	—[e]
	CF_2Cl_2	−20	—	4.08 d	3.65 br s	3.45 m	—	2.05 m	1.63 m	2.61 t	2.89 d × d	3.38 s
		−120	C_a (44)	4.48 d	3.42 t	3.43 t	—	2.18 d	1.49 t	2.32 d × d	3.27 t	3.38 s
			C_e (50)	4.34 d	3.11 t	—	3.40 s	2.31 d	1.19 q	2.63 d × d	2.71 t	3.37 s
			TB (6)	4.10 br	3.63 br	—[e]	—	2.08 br	2.02 br	—[e]	2.88 d × d	—[e]
11 (CH_3,CH_3)	CHF_2Cl	−10	—	3.61 s	3.61 s	—	—	1.56 m	1.56 m	2.80 m	2.80 m	1.01 s
		−120	*C* (90)	3.87 d	3.31 d	—	—	1.65 d	1.37 t	2.52 d	3.06 t	1.20, 0.82 s
			TB (10)	3.7 br	3.7 br	—	—	1.79 br	1.79 br	2.9 br	2.9 br	1.02 s
	CF_2Cl_2	−20	—	3.56 s	3.56 s	—	—	1.54 m	1.54 m	2.75 m	2.75 m	1.01 s
		−120	*C* (89)	3.76 d	3.20 d	—	—	1.61 d	1.36 t	2.44 d	3.00 t	1.20, 0.81 s
			TB (11)	3.5 br	3.5 br	—	—	1.75 br	1.75 br	2.8 br	2.8 b	1.04 s

Can. J. Chem. Downloaded from www.nrcresearchpress.com by 213.222.148.141 on 09/07/12
For personal use only.

TABLE 2 (*concluded*)

Compound (R,R′)	Solvent	Temperature (°C)	Conformation (population (%))	H-2e	H-2a	H-3e	H-3a	H-4e	H-4a	H-5e	H-5a	Substituent on C-3
12	CHF_2Cl	−10	—	4.09 d	3.55 d	—	—	2.09 d × d	1.58 t	2.54 d × d	3.10 t	1.12 s, 3.31 s
(CH_3,OCH_3)		−115	C_a (—)[f]	4.18 d	3.45 d	—	—	2.25 d	1.39 t	2.48 d × d	3.09 t	1.05 s, 3.33 s
			TB (—)	3.96 d	4.2[d]	—	—	2.15 br	2.05 br	2.95 br	2.8 br	1.22 s, 3.29 s
			C_e (—)	—[e]	—[e]	—	—	—[e]	—[e]	—[e]	—[e]	1.48 s, 3.27 s
	CF_2Cl_2	−20	—	3.99 d	3.52 d	—	—	1.93 d × d	1.61 t	2.46 d × d	3.10 t	1.13 s, 3.23 s
		−120	C_a (—)[f]	4.21 d	3.20[d]	—	—	1.98 d	1.37 t	2.30 d × d	3.2[d]	0.99 s, 3.27 s
			TB (—)	3.8[d]	4.3[d]	—	—	—[e]	—[e]	—[e]	—[e]	1.27 s, 3.22 s
			C_e (—)	3.96 d	3.78 d	—	—	—[e]	1.71 br t	—[e]	—[e]	1.40 s, 3.18 s
13	CHF_2Cl	−10	—	3.91 s	3.91 s	—	—	1.94 m	1.94 m	2.82 m	2.82 m	3.30 s
(OCH_3,OCH_3)		−120	*C* (92)	4.42 d	3.33 t	—	—	2.34 d	1.48 t	2.65 d × d	2.95 t	3.36, 3.20 s
			TB (8)	4.22 br	4.22 br	—	—	2.19 br	2.19 b	2.89 br	2.89 b	3.31 s
	CF_2Cl_2	−10	—	3.78 br s	3.78 br s	—	—	1.85 m	1.85 m	2.78 m	2.78 m	3.25 s
		−120	*C* (93)	4.21 d × d	—[d]	—	—	2.21 d	1.32 t	2.50 d × d	1.99 t	3.30, 3.14 s
			TB (7)	4.03 br	4.03 br	—	—	2.05 br	2.05 br	2.82 br	2.82 br	3.17 s

[a]All spectra were taken on a Bruker WH-400 spectrometer operating at 400.13 MHz for solutions containing tetramethylsilane as internal standard and 20% CD_2Cl_2 (for CHF_2Cl) or 6% acetone-d_6 (for CF_2Cl_2) for locking purposes.

[b]The aromatic signals are not reported here because of solvent (CHF_2Cl) overlapping peaks. All aromatic signals for compounds **8–13** appear between 6.85 and 7.10 ppm in the CF_2Cl_2/acetone-d_6 solvent system.

[c]The symbols *C*, C_e, C_a, and *TB* refer to conformations defined in the text.

[d]Multiplicity of the signal could not be resolved due to peak overlapping.

[e]These signals were not identified, either because of peak overlapping or too small signal-to-noise ratio.

[f]Precise integration of the signals was not possible due to peak overlapping.

Can. J. Chem. Downloaded from www.nrcresearchpress.com by 213.222.148.141 on 09/07/12
For personal use only.

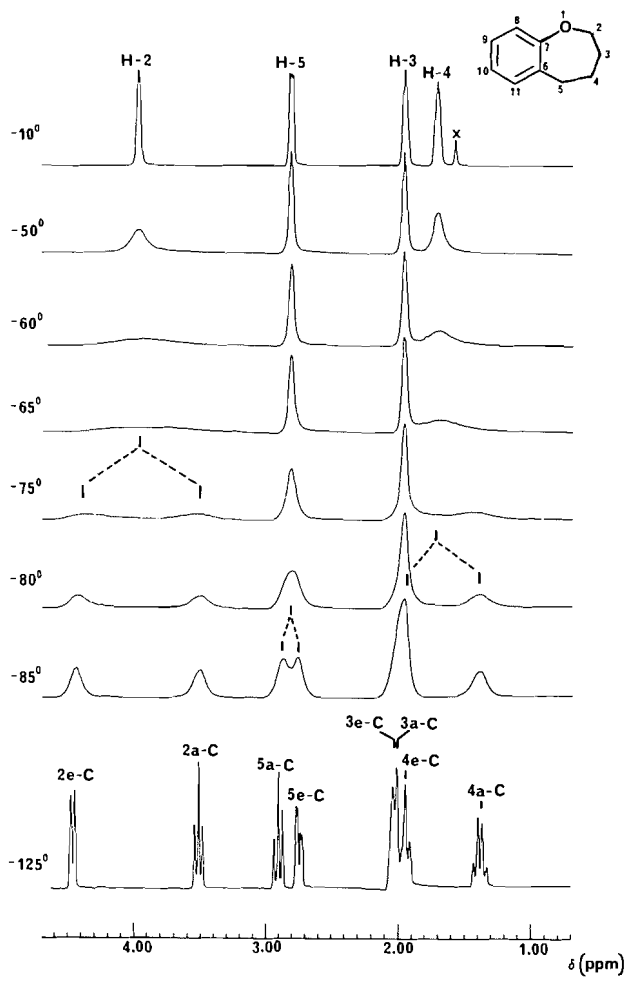

FIG. 1. Aliphatic portion of the 400.13-MHz ^{1}H nmr spectra of **8** in CHF_2Cl–CD_2Cl_2 (80:20) at several temperatures. The numbers and letters over the signals at −120°C refer to the position and the orientation of the protons, as well as to the nature of the ring conformation, as described in the text. "X" denotes an impurity, while broken lines link together exchanging protons.

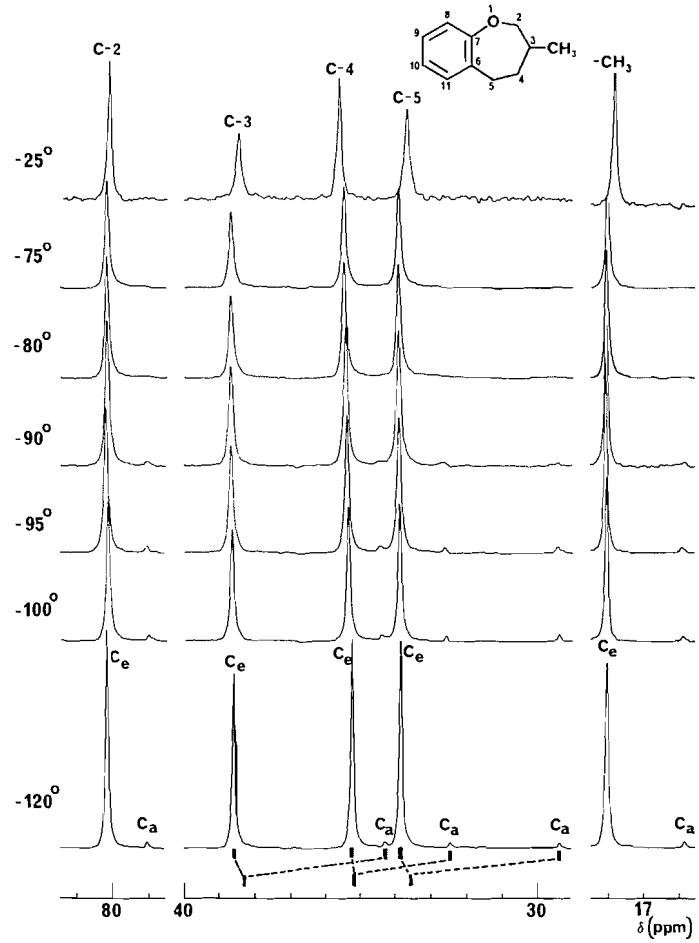

FIG. 2. Aliphatic portion of the 100.62-MHz ^{13}C nmr spectra of **9** in CHF_2Cl–CD_2Cl_2 (80:20) at several temperatures. C_e and C_a refer to conformations described in the text.

deshielding effect of the oxygen atom. Irradiation of that multiplet permits the identification of the H-3 multiplet, and subsequent irradiations readily identify the H-4 and H-5 multiplets. Each signal broadens at lower temperatures to give, at −120°C, five distinct signals, each integrating for one proton, and a multiplet at 2 ppm integrating for three other protons. The deshielded doublet at 4.46 ppm can readily be identified as 2e-*C*,[2] showing only one strong geminal coupling ($^2J_{HH}$ = −12.2 Hz) with 2a-*C*, as confirmed by selective irradiation of the doublet at 4.46 ppm, which transformed the triplet at 3.51 ppm (2a-*C*) into a doublet. The shielded quartet at 1.38 ppm could be assigned to either 3a-*C* or 4a-*C*, but since irradiation of the 2a-*C* resonance left that signal unperturbed, it is unequivocally identified as 4a-*C*. Subsequent irradiations established the identity of all the other aliphatic resonances (Table 2).

The 100.62-MHz ^{13}C spectra of **9** (R = H, R′ = CH_3) in both solvent systems showed one spectral change upon lowering the temperature. As shown in Fig. 2, the aliphatic portion of the ^{13}C spectrum of **9** in CHF_2Cl at −25°C consists of five peaks, of which the C-3 signal could easily be identified by an off-resonance experiment. While the deshielded C-2 carbon can be readily assigned, the C-4 and C-5 signals were identified by selective proton irradiation of 4a-*C*, at −25°C. Finally, the aromatic carbon chemical shifts were assumed to exhibit the same order as in the parent compound **8**, as reported in Table 1.

All aliphatic carbon signals broaden at low temperatures to give, at −120°C, two sets of signals of unequal intensities (97:3 in CHF_2Cl–CD_2Cl_2 shown in Fig. 2 and 96:4 in CH_3OCH_3–CD_2Cl_2), which can be assigned to the C_e (major set) and C_a forms (minor set), as will be discussed in the next section. The aromatic signals of the minor set cannot be detected either because of low signal-to-noise ratio (quaternary carbons) or overlap with the major set (protonated aromatic carbons).

The 400.13-MHz ^{1}H spectrum of **9**, at −10°C, in CHF_2Cl–CD_2Cl_2, consists of eight distinct signals that could be assigned by comparison with proton chemical shifts of the parent compound **8** (at −120°C), and by selective irradiation of the methyl doublet at 1.11 ppm, leading to the identification of H-3. All signals broaden slightly as the temperature is lowered to give, at −125°C, in addition to eight intense signals corresponding to the C_e form, a very weak doublet at 1.28 ppm, which can be associated with the C_a form (see next section). The other resonances of the minor form either overlap with the

[2]Protons are identified by a symbol composed of two parts: the first one gives the position and orientation of the proton while the second part specifies the nature of the ring conformation. Thus 2e-*C* refers to the 2-equatorial proton of the chair form.

Can. J. Chem. Downloaded from www.nrcresearchpress.com by 213.222.148.141 on 09/07/12
For personal use only.

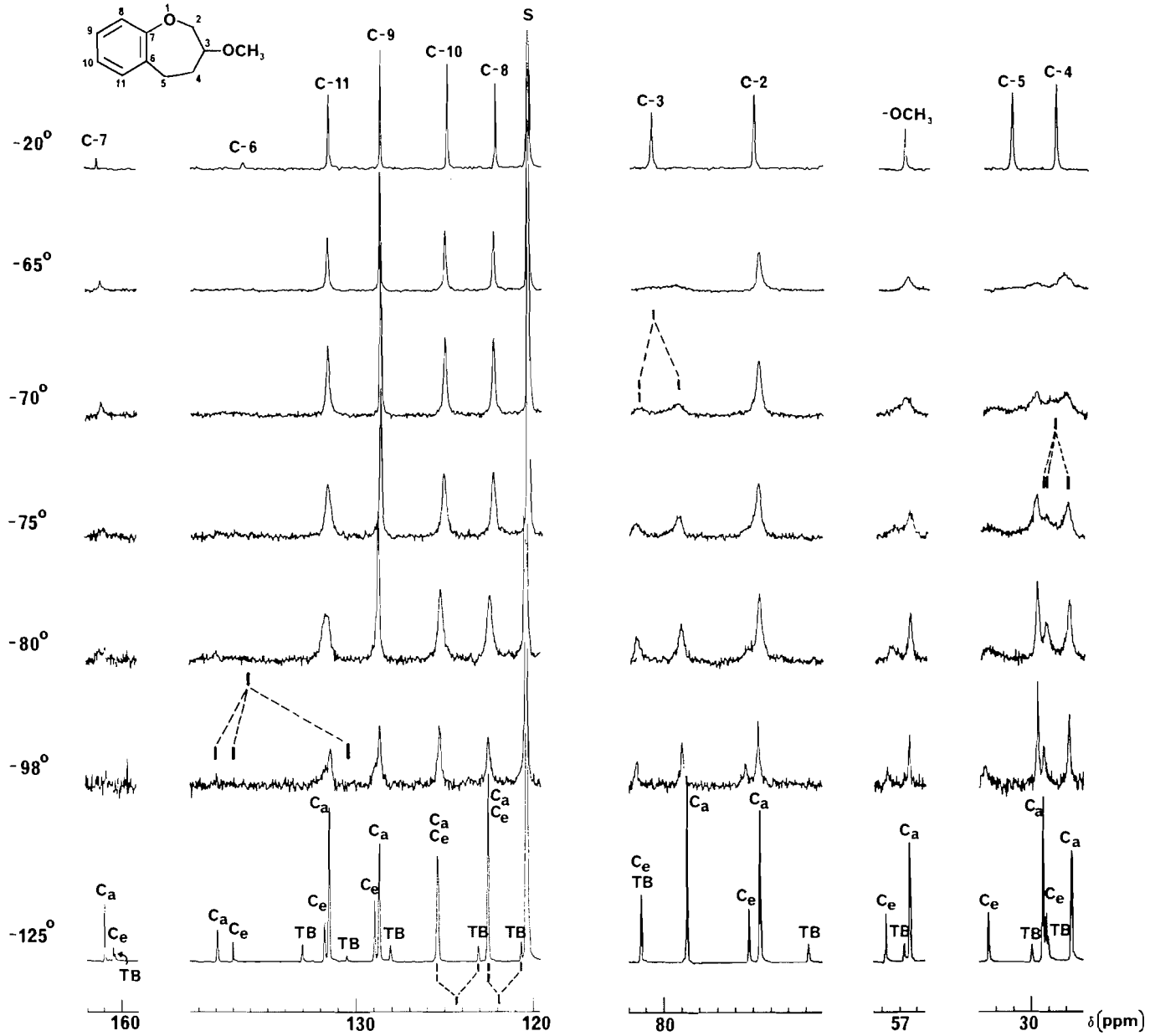

FIG. 3. The 100.62-MHz ^{13}C nmr spectra of **10** in CHF_2Cl–CD_2Cl_2 (80:20) at several temperatures. C_a, C_e, and *TB* refer to conformations described in the text. "S" defines a solvent (CHF_2Cl) line, while broken lines link together signals corresponding to the same carbon atom position.

intense signals or cannot be clearly distinguished from the background noise in that solvent system. However, a better signal-to-noise ratio is observed in the ^1H spectrum of **9** in CF_2Cl_2–acetone-d_6 at $-120°C$, and allows the identification of 2e-C_a and 2a-C_a as doublets. Other weak resonances appear in the spectrum, but they could not be correlated precisely with the remaining protons of the C_a form.

In contrast, both ^{13}C and ^1H spectra of compound **10** (R = H, R′ = OCH_3) exhibit spectacular changes (Figs. 3 and 4) as the temperature is lowered. At $-20°C$, the ^{13}C spectrum of **10** in the polar CHF_2Cl–CD_2Cl_2 solvent system shows five resonances for the aliphatic carbons and six resonances for the aromatic carbons. All aromatic signals can be easily assigned through direct comparison with those of the parent molecule **8** (see Table 1). The oxygen-bound carbon atoms, namely C-2, C-3, and the methoxy carbons, can be differentiated by an off-resonance proton decoupling experiment, while C-4 and C-5 were identified through selective proton irradiations.

All signals of **10** broaden at lower temperatures to give, at $-125°C$ (Fig. 3), three different sets of carbon resonances, integrating for 70:20:10. The intensity ratio is associated to the C_a, C_e, and *TB* forms respectively, as will be discussed in the next section. Integration shows that the tall signal at 122.54 ppm contains two superimposed signals, one for the C_a form (70%) and one for the C_e form (20%). A change for the less polar solvent system (CH_3OCH_3–CD_2Cl_2) modifies the relative intensities of the sets at $-125°C$ (44:50:6 for C_a, C_e, and *TB* respectively). The nmr parameters characteristic of each form are summarized in Table 1.

The ^1H spectrum of **10** in CHF_2Cl–CD_2Cl_2, at $-10°C$, shows seven aliphatic signals integrating each for one proton and a taller methoxy signal (Fig. 4). The two most deshielded

Can. J. Chem. Downloaded from www.nrcresearchpress.com by 213.222.148.141 on 09/07/12
For personal use only.

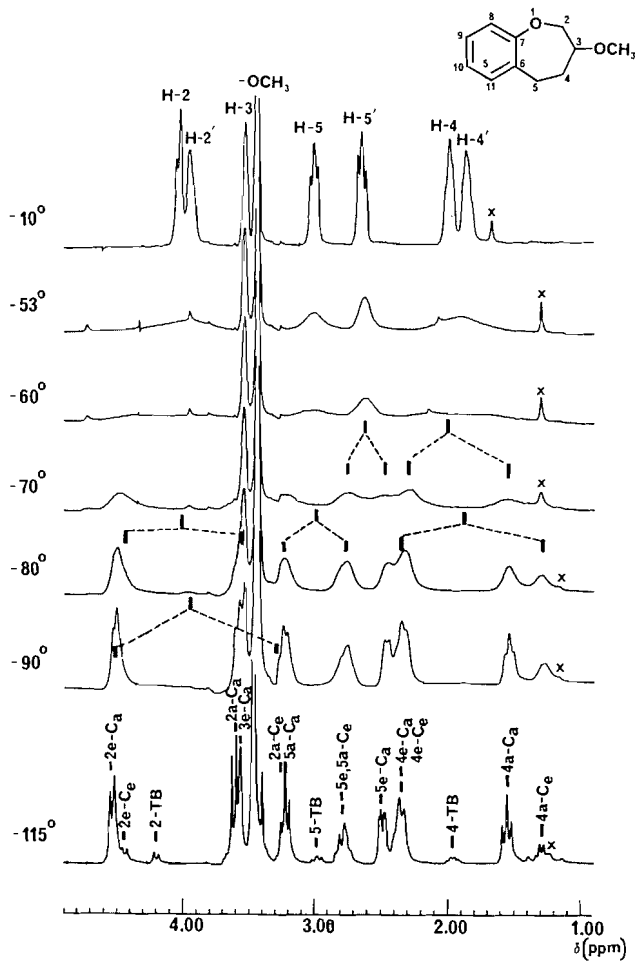

FIG. 4. Aliphatic portion of the 400.13-MHz ^{1}H nmr spectra of **10** in CHF_2Cl–CD_2Cl_2 (80:20) at several temperatures. The numbers and letters refer to the position and the orientation of the protons, while C_e, C_a, and *TB* refer to conformations described in the text. "X" identifies an impurity.

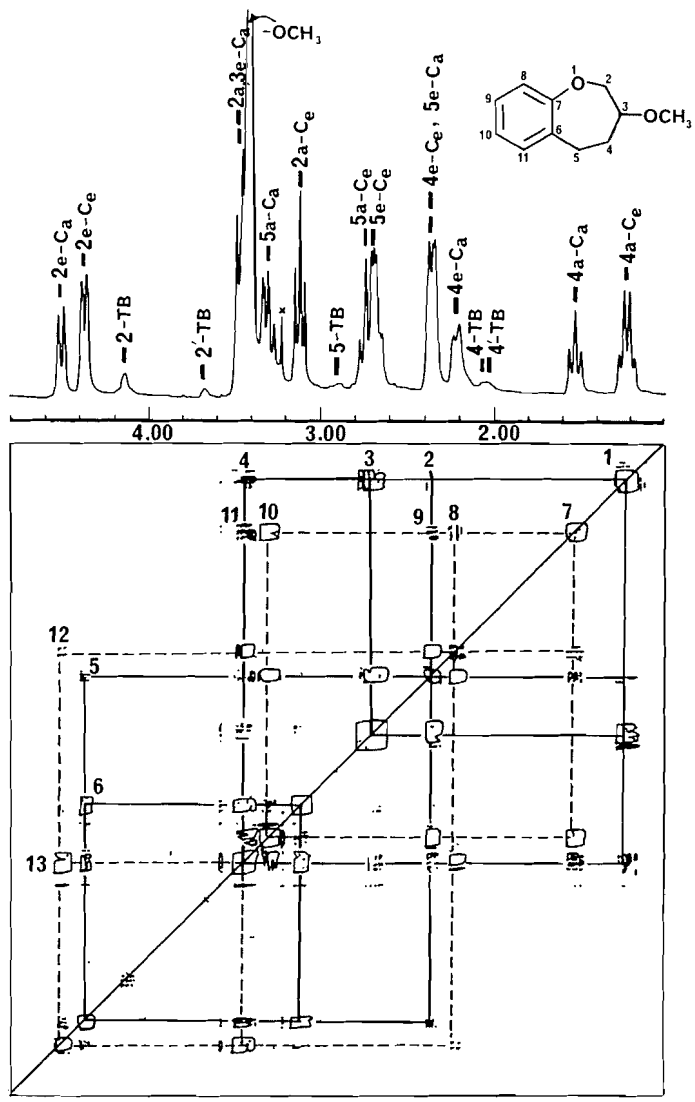

FIG. 5. Proton (^{1}H) 2D-homonuclear COSY spectrum, with double quantum filtering of the aliphatic signals of **10**, in CF_2Cl_2–acetone-d_6 (94:6), at −120°C. The numbers and letters refer to the position and the orientation of the protons, while C_a, C_e, and *TB* refer to conformations described in the text.

signals can be attributed to the 2-protons next to the oxygen atom. The other resonances given in Table 2 were assigned by double irradiations. All those signals broaden at lower temperatures to give, at −115°C, three sets of signals in a ratio 70:20:10, as also found in the ^{13}C spectrum. The signals of the major C_a form (70% of the total spectrum) were assigned without much difficulty through double irradiations and by comparison with previous proton patterns of chair forms (as for compounds **8** and **9**). Thus, it was found that 3e-C_a overlaps with the most shielded line of the triplet (3.59 ppm) corresponding to 2a-C_a. Identification of the C_e (20%) and *TB* (10%) proton resonances is difficult in that solvent system because of their low abundance and possible overlap with the major peaks. However, a change to the less polar CF_2Cl_2–acetone-d_6 solvent system increases the amount of C_e form appreciably (44:50:6 for C_a:C_e:*TB*) and facilitates the assignation of its resonances.

Unequivocal assignations of C_a and C_e resonances of **10** in the CF_2Cl_2–acetone-d_6 mixture at −120°C are possible using the 2D-COSY technique, with double quantum filtering (7) to remove as much as possible the interference caused by the intense methoxy signal, as shown in Fig. 5.

The 2D contour plot consists of correlation peaks appearing either *on* or *off* the diagonal line (lower left to upper right); the diagonal peaks arise from individual protons whose chemical shifts and multiplicities are obtained directly from the 1D spectrum above, while the off-diagonal peaks relate two diagonal peaks through coherence transfer via *J* coupling. Unequivocal identification of a "base" diagonal peak for each conformation is the starting point that enables us to sort out the chemical shifts of all coupled protons to this base peak and, hence, to secure the position of all resonances for each conformation.

For example, the quartet at 1.19 ppm is unambiguously assigned to 4a-C_e, since 4a-protons in chair forms of this system always appear as the most shielded protons in the ^{1}H nmr spectrum (Table 2). Now, correlations 2, 3, and 4, on the same horizontal line as the diagonal peak 1, correspond to protons in the C_e conformation coupling with 4a-C_e. Thus, correlation peak 4 can confidently be attributed to 3a-C_e (methine proton at 3.40 ppm), while correlation 2 identifies 4e-C_e (2.31 ppm), since protons at position 4 in both **8** and **9** were shown (Table 2) to be more shielded than the benzylic protons (position 5). Additional evidence for this last assignment is given by the presence of correlation 5 between the 2e-C_e proton (character-

Can. J. Chem. Downloaded from www.nrcresearchpress.com by 213.222.148.141 on 09/07/12
For personal use only.

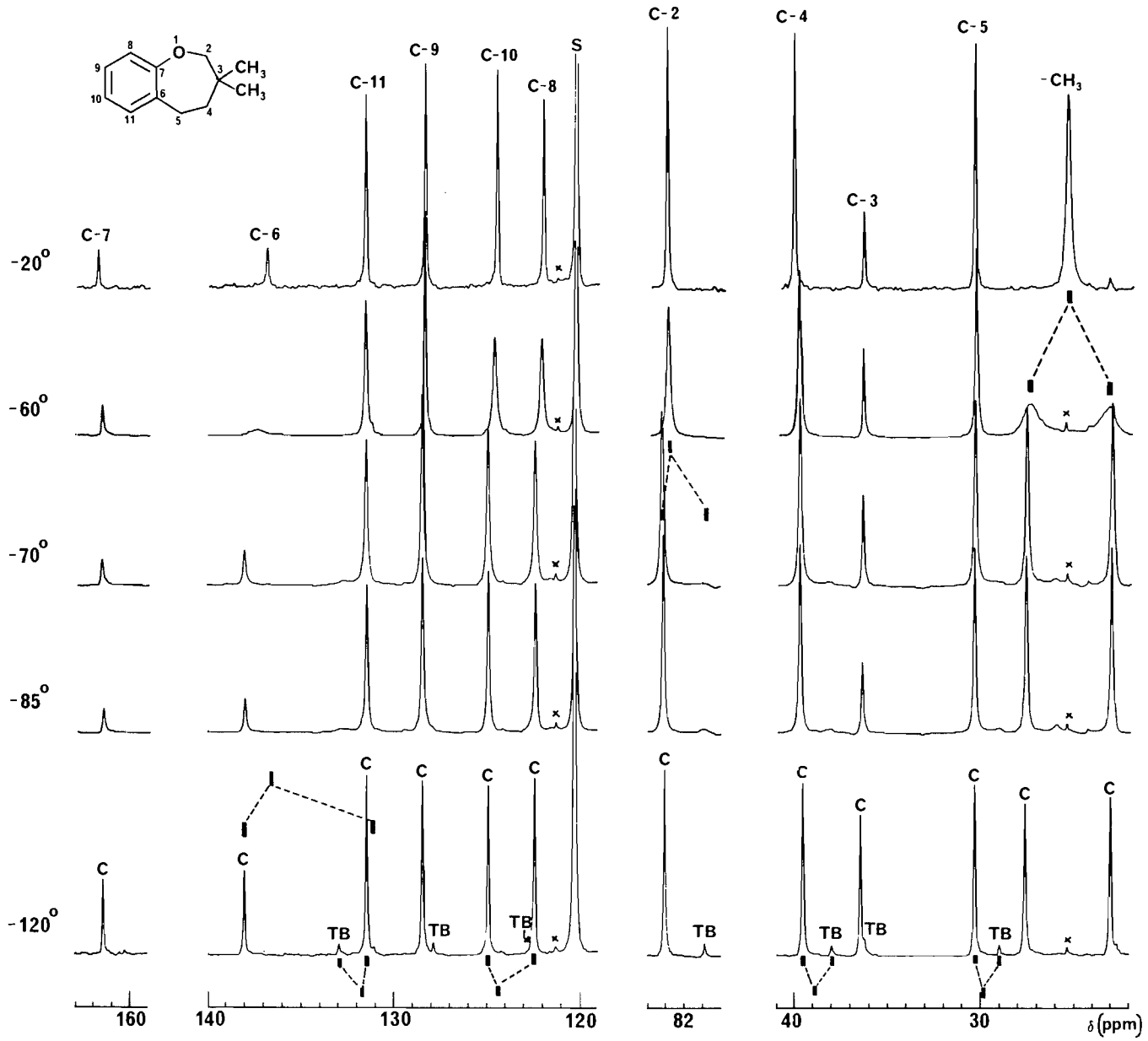

FIG. 6. The 100.62-MHz ^{13}C nmr spectra of **11** in CHF_2Cl–CD_2Cl_2 (80:20) at several temperatures. *C* and *TB* refer to conformations described in the text. Broken lines link together signals corresponding to the same carbon atom position. "S" defines a solvent (CHF_2Cl) line, while "X" denotes an impurity.

istically the most deshielded seven-membered ring proton in this system) and the 4e-C_e proton (diagonal peak 14). Correlation peak 5 arises from "W"-coupling between 2e-C_e and 4e-C_e, which cannot exist between 2e-C_e and either 5e-C_e or 5a-C_e. Correlation peak 3, together with careful integration of the 1D spectrum, can then be attributed to the two benzylic protons (5a-C_e and 5e-C_e). Finally, the diagonal peak 15 belongs to 2a-C_e, a triplet at 3.11 ppm, since correlation peak 6 relates it to the 2e-C_e proton via geminal coupling.

Signals of the less abundant C_a form can be identified through a similar procedure in which the 4a proton (4a-C_a) is taken as a reference point (base peak 7 on the diagonal). Figure 5 shows four off-diagonal correlation peaks (numbered 8, 9, 10, and 11) related horizontally by dotted lines to base peak 7. Correlation peak 8 is attributed to 4e-C_a (broad doublet at 2.18 ppm), since it can explain correlation peak 12 relating it to 2e-C_a (diagonal peak 16) via W-coupling. All other signals assigned in Fig. 5 were identified by straightforward analysis of the 2D spectrum and by direct comparison with the low temperature ^1H nmr spectrum of the same compound at −115°C, in CHF_2Cl–CD_2Cl_2 (80:20), shown in Fig. 4. For example, the presence of the 2a-C_a proton at 3.42 ppm (diagonal peak 17) is confirmed by the presence of correlation 13, which relates it to 2e-C_a via geminal coupling.

Correlation peaks for the minor *TB* resonances were not observed in the 2D-COSY spectrum of Fig. 5; these signals were assigned by direct comparison with *TB* resonances in the ^1H spectrum of **10** at −115°C, in CHF_2Cl–CD_2Cl_2 (80:20), shown in Fig. 4.

Changes were also observed in the ^{13}C and ^1H spectra of compound **11** (R = R′ = CH_3), on going from −10 to −120°C. As seen in Fig. 6, the ^{13}C spectrum of **11**, in CHF_2Cl–CD_2Cl_2

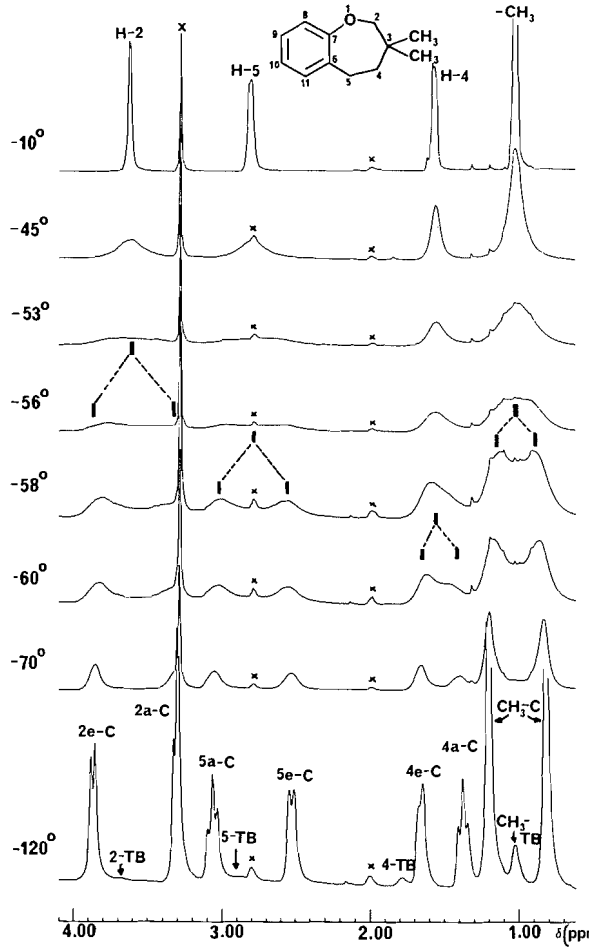

FIG. 7. Aliphatic portion of the 400.13-MHz ^{1}H nmr spectra of **11** in CHF_2Cl–CD_2Cl_2 (80:20) at several temperatures. The numbers and letters refer to the position and the orientation of the protons, while *C* and *TB* refer to conformations described in the text. Broken lines link together exchanging protons, while "X" denotes an impurity.

(80:20) at −15°C, consists of 11 signals, which were readily assigned by off-resonance experiments and by using the known substituent chemical shift (SCS) effect of a *gem*-dimethyl group on a chair form (8). The methyl carbon signal at 25.59 ppm shows appreciable broadening at that temperature, and coalesces at lower temperature to give, at −60°C, two distinct broad signals corresponding to axial and equatorial methyl groups on the chair conformation. A broad signal corresponding to the methyl groups of the twist-boat conformation is also apparent at −80°C near 26.5 ppm. All other carbon resonances also broaden at lower temperature to give, at −120°C, two sets of signals (integration = 90:10) assigned to the chair (*C*) and the twist-boat (*TB*) conformations, as will be discussed in the next section. Minor *TB* signals for quaternary carbons C-6 and C-7 could not be distinguished from the base line, while that of C-8 was hidden under the large solvent (CHF_2Cl) line. A decrease in the polarity of the solvent mixture (CH_3OCH_3–CD_2Cl_2, 80:20) only led to small variations in the relative populations of the two conformations (*C*:*TB*, 89:11).

The partial ^{1}H spectrum of **11** at −10°C in CHF_2Cl–CD_2Cl_2 (Fig. 7) shows four distinct broad signals corresponding to the three methylene groups and to the *gem*-dimethyl moiety. All these signals broaden as the temperature is lowered to give, at −120°C, two sets of signals with unequal intensities (90:10), as was also noted in the ^{13}C spectrum and assigned to the chair (*C*) and twist-boat (*TB*) conformations. Precise assignment of the individual ^{1}H resonances is done by direct comparison with the analogous signals observed for the parent compound **8** at the same temperature. The doublet corresponding to 2a-*C* (3.31 ppm) partially overlaps with an impurity line, but its presence is unambiguously ascertained by selective decoupling of the 2e-*C* doublet (3.87 ppm). The minor set consists of only two detectable aliphatic signals at 1.02 and 1.79 ppm, which are assigned respectively to the methyl groups and to H-4. Better signal-to-noise ratio in the less polar CF_2Cl_2–acetone-d_6 (94:6) mixture allowed the detection at −120°C of the two other missing *TB* signals, namely those for H-5 (2.8 ppm) and for H-2 (3.5 ppm).

Appreciable variations (shown in Figs. 8 and 9) also occur in the ^{13}C and ^{1}H spectra of **12** (R = CH_3, R′ = OCH_3) in CHF_2Cl–CD_2Cl_2 (80:20) as the temperature is lowered. The ^{13}C spectrum of **12** at −20°C, for example (Fig. 8), shows 12 resonances, most of which are assigned by techniques mentioned earlier. The most deshielded signal in the 25–35 ppm region is assigned to C-4 because of the known downfield β-effect created by the introduction of the methyl group at the 3-position (*5a,b*). Lowering the temperature broadens all the signals, although the C-9 and methoxy resonances remain sharper at −70°C. Further cooling produces, at −95°C, three sets of signals of unequal intensities (89:4:7) for the C-4, C-5, methyl, and methoxy resonances: these sets are assigned respectively to the C_a, C_e, and *TB* conformations, as will be discussed in the next section. Signals for the least stable of the three conformations (C_e) could, however, not be detected for all the other carbon atoms, which show only two signals.

The assignment of individual aromatic carbon atoms for the *TB* set is possible through direct comparison with aromatic *TB* resonances of **10** and **11**; this procedure allows the detection of the C-8 (*TB*) signal under the solvent (CHF_2Cl) line near 120 ppm. Finally, the identification of the C-2 and C-3 *TB* signals is done using the known intimate relation between the coalescence temperature for a given dynamic process and the chemical shift difference between the two exchanging sites (9). Extensive broadening at −70°C for the C-2 and C-3 resonances, for example, compared to that observed for the methoxy signal, corresponds to a larger chemical shift difference between C_a and *TB* signals than for the methoxy case. This deduction leads to the assignment of the small 79.77-ppm signal to C-3 of *TB* and the signal at 76.52 ppm to C-2 of *TB*, in line with trends observed in C_a and *TB* signals of the monomethoxy derivative **10**.

The partial ^{1}H spectrum of **12** (Fig. 9) in CHF_2Cl–CD_2Cl_2 (80:20) at −15°C shows six multiplets, corresponding to the six aliphatic protons of the aliphatic portion of the molecule, and two singlets corresponding to the methoxy and methyl groups. All those resonances broaden as the temperature is lowered to give, at −115°C, a major set of signals that could be easily analyzed through selective irradiations; this set is attributed to the C_a conformation, in agreement with the ^{13}C spectrum of the same molecule at −95°C. A minor set of resonances is also detected and attributed to the *TB* form, but clear identification of individual resonances is possible only by considering the signals in the fast exchange limit (−10°C) as somewhat weighted averages of signals appearing in the slow exchange limit

Can. J. Chem. Downloaded from www.nrcresearchpress.com by 213.222.148.141 on 09/07/12
For personal use only.

Can. J. Chem. Downloaded from www.nrcresearchpress.com by 213.222.148.141 on 09/07/12
For personal use only.

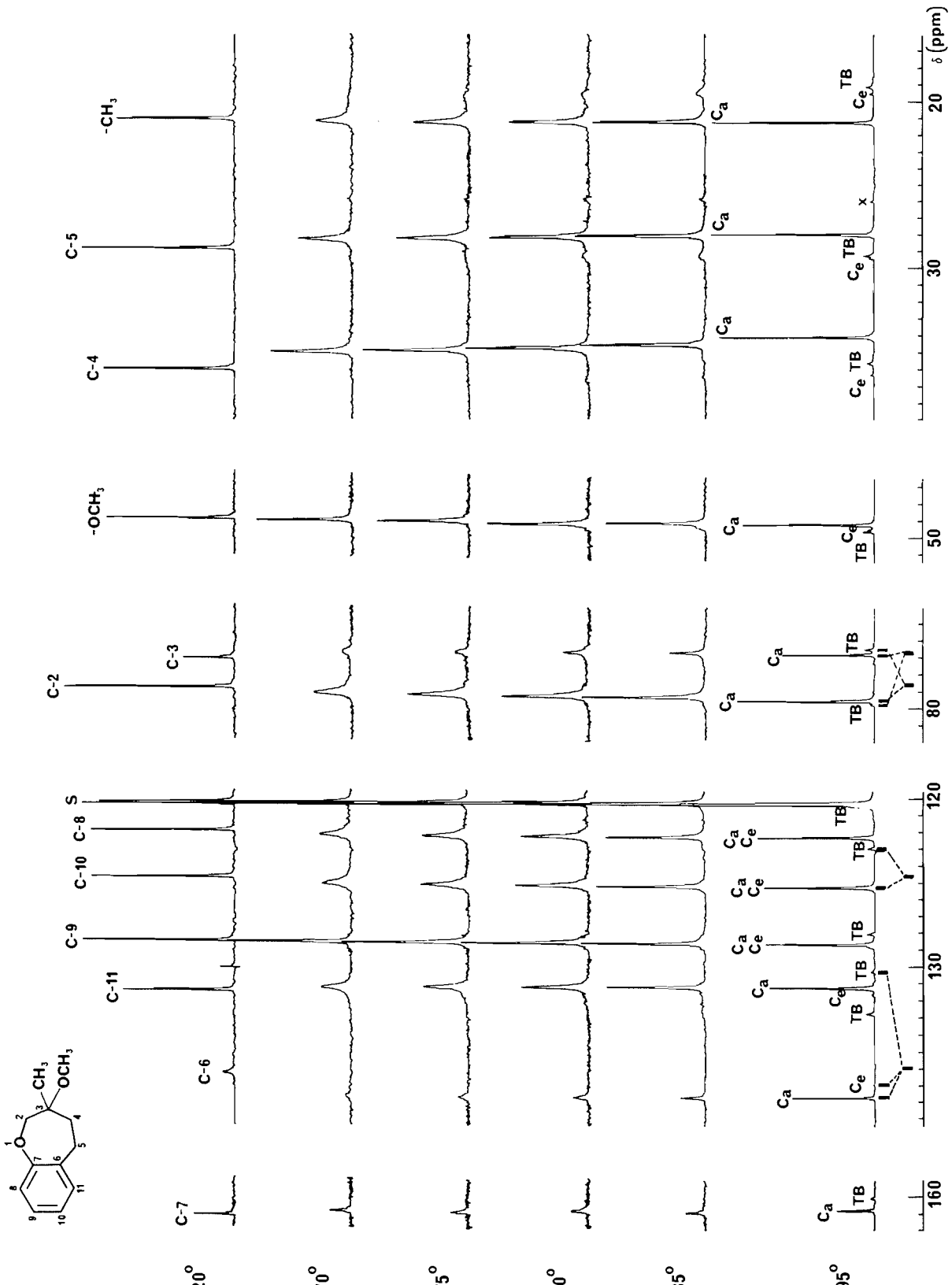

FIG. 8. The 100.62-MHz ^{13}C nmr spectra of **12** in CHF_2Cl–CD_2Cl_2 (80:20) at several temperatures. C_a, C_e, and *TB* refer to conformations described in the text. Broken lines link together signals corresponding to the same carbon atom position.

Can. J. Chem. Downloaded from www.nrcresearchpress.com by 213.222.148.141 on 09/07/12
For personal use only.

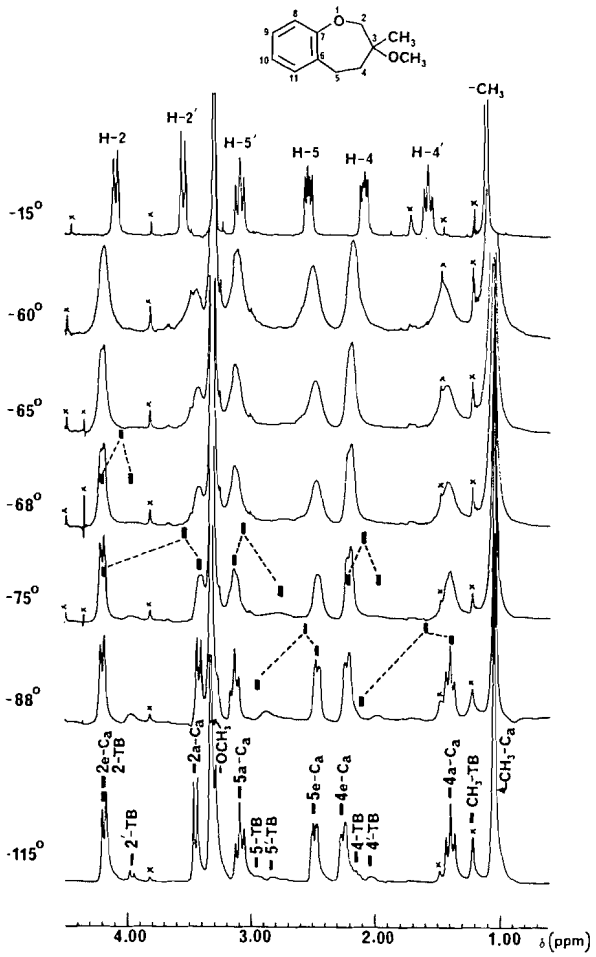

FIG. 9. Aliphatic portion of the 400.13-MHz ^{1}H nmr spectra of **12** in CHF_2Cl–CD_2Cl_2 (80:20) at several temperatures. Numbers and letters over the signals refer to the position and to the orientation of the protons, while C_a and *TB* correspond to conformations described in the text. "X" denotes an impurity.

(−110°C). Observation, for example, of the 2a-C_a signal, at −115°C, at higher field than the H-2′ signal at −15°C, points to a corresponding signal at lower field, which was detected as a broad peak around 4.1 ppm. Other minor resonances were assigned in the same fashion. Changing the solvent medium to a less polar combination only resulted in a small change of population for the three conformers present, namely C_a (85); *TB* (7) and C_e (8).

Finally, significant changes were also observed in the ^{13}C and ^{1}H nmr spectra of **13** (R = R′ = OCH_3) upon temperature lowering. For example, the ^{13}C spectrum of **13** in CHF_2Cl–CD_2Cl_2 (80:20) (Fig. 10) at −25°C shows 10 of the 11 signals of the molecule, which were assigned through direct comparison with the ^{13}C spectrum of **12** at −20°C. All those signals broaden as the temperature is lowered, although the phenomenon is much more pronounced for signals corresponding to C-6, C-8, C-9, C-11, C-2, and C-4. At −110°C, two sets of signals of different intensities (89:11) are detected; they are attributed respectively to the chair (*C*) and twist-boat (*TB*) conformations, as will be discussed in the next section. Again, lowering the polarity of the solvent mixture only resulted in a small population variation of *C* and *TB* forms (94:6).

The partial ^{1}H nmr spectrum of **13** in CHF_2Cl–CD_2Cl_2 (80:20), at −10°C (Fig. 11) shows three broad multiplets for the three methylene groups of the molecule and one singlet for the methoxy groups. All signals coalesce as the temperature is lowered, and split at −120°C into two sets of unequal intensities (92:8) assigned to the chair (*C*) and twist-boat (*TB*) forms, as previously deduced by ^{13}C. Careful integration of all aliphatic signals shows the presence of only three broad *TB* resonances, corresponding each to two protons, which could mean that the pseudorotation ($TB \rightleftharpoons TB^*$) process is still relatively rapid at that temperature (−120°C).

Discussion

Conformations of the seven-membered ring in compounds 8–13

Previous investigations (4–6, 10, 11) of various heterocyclic compounds of the benzocycloheptene family have demonstrated the frequent existence of two seven-membered ring geometries for such molecules, namely the chair (*C*) and the twist-boat (*TB*) conformations. However, as was the case for benzocycloheptene itself (12*a*), only the chair form has been detected (10*a*, 12*b*) by dynamic nmr for the unsubstituted benzoxepins **15** and **16**. The absence of a ^{13}C spectral change for **8** (in both polar and nonpolar solvent systems) confirms the existence of a single chair (*C*) conformation for that molecule. The $C \rightleftharpoons C^*$ conformational inversion possible for **8** is revealed by the ^{1}H spectral modification from which an activation barrier of 9.2 ± 0.3 kcal mol^{-1} is estimated (13). This value is comparable to those observed for the same process in **15** (9.5 ± 0.2 kcal mol^{-1}) (12*b*) and in **16** (9.4 ± 0.3 kcal mol^{-1}) (10*a*).

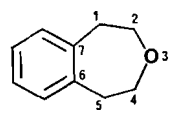

15

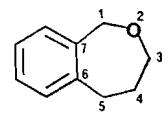

16

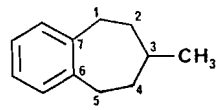

17

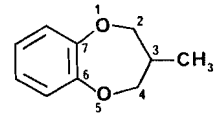

18

The presence of two sets of carbon resonances in the ^{13}C nmr spectrum of **9** (R = H, R′ = CH_3), at −120°C, reveals the presence of two distinct conformations at that temperature. The identification of these conformations makes use of experimental methyl substituent effects (α, β, and γ) (14) for **9** compared with those obtained for the chair forms of two model compounds 3-methylbenzocycloheptene **17** (15) and 3-methyl-1,5-benzodioxepin **18** (5*b*). The major set of signals of **9** gives ^{13}C methyl chemical shift effects (β (on C-2) = +5.10 ppm, β (on C-4) = +8.30 ppm, and γ (on C-5) = −1.47 ppm) similar to those found for an equatorial methyl group on the chair conformation of **18** (β (on C-2) = +5.11 ppm) (5*b*) and of **17** (β (on C-4) = +7.80 ppm and γ (on C-5) = −1.24 ppm) (15), in agreement with a C_e (chair with an equatorial methyl) form for **9**. A similar treatment for the minor set of signals relates it to the C_a (axial methyl) conformation, because the β-effect observed on C-2 (+3.99 ppm) agrees fairly well with that of an axial methyl group on the chair form of **18** (β (on C-2) = +4.07 ppm) (5*b*). The presence of a strongly shielding γ-effect (−5.95 ppm) noted for the weaker C-5 resonance of **9** corroborates this C_a assignment.

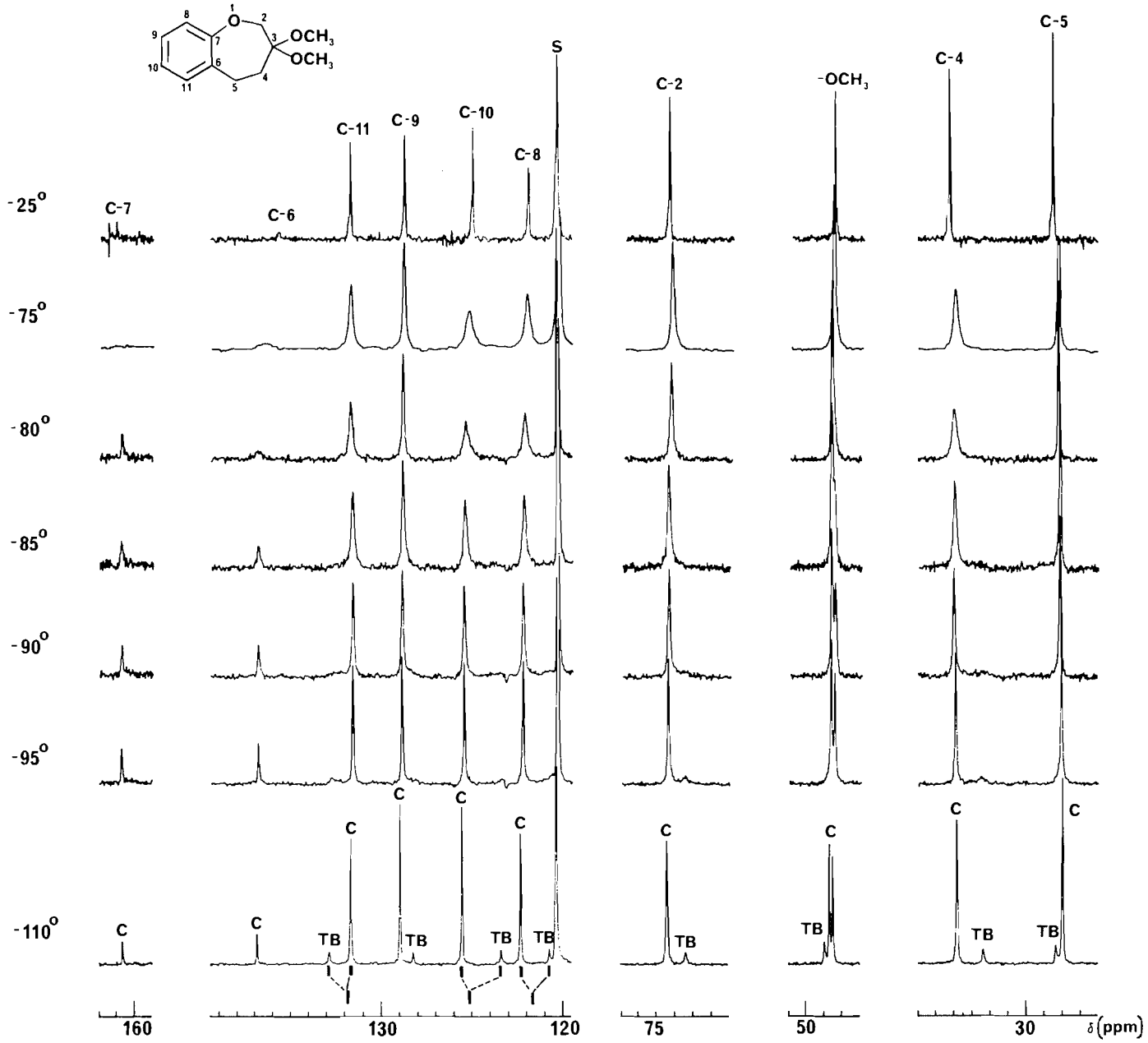

FIG. 10. The partial 100.62-MHz ^{13}C nmr spectra of **13** in CHF_2Cl–CD_2Cl_2 (80:20) at several temperatures. *C* and *TB* refer to conformations described in the text. Broken lines link together signals corresponding to similar carbon atom positions.

Similarly, at −120°C, the chemical shift difference between the geminal protons at the 2-position in **18** was found (5*b*) to be quite sensitive to the methyl orientation on the chair conformation (equatorial $\Delta\delta$ = 0.97 ppm and axial $\Delta\delta$ = 0.46 ppm). The observation of similar chemical shift differences for the two sets of signals of **9** (major $\Delta\delta$ = 0.90 ppm and the minor $\Delta\delta$ = 0.40 ppm) therefore supports the above conformational assignments.

The above method must be used with great caution for derivatives **10–13** because additional factors, such as solvation owing to the presence of a polar substituent and ring deformation resulting from increased substitution, could lead to misleading results, especially for the identification of twist-boat conformations, because no reference *TB* signal is detected in the low-temperature nmr spectra of the parent compound **8**. More reliable conformational assignments can be obtained using the chemical shifts of the protonated aromatic carbons C-8 to C-11 as "conformational probes".

^{13}C chemical shifts are known to be quite sensitive to small changes in local environments (14). Analysis of Dreiding models for the chair and the twist-boat conformations for compounds **8–13** shows that interactions of the phenolic-type oxygen atom with the aromatic ring are significantly different in the *C* and *TB* conformations. Because changes in orientation of the substituents at the distant 3-position should not affect aromatic chemical shifts significantly for a particular ring geometry, those signal positions should reflect mainly on the geometry of the seven-membered ring.

The usefulness of the aromatic carbons as a probe is illustrated by analysis of the low-temperature ^{13}C spectrum

Can. J. Chem. Downloaded from www.nrcresearchpress.com by 213.222.148.141 on 09/07/12
For personal use only.

Can. J. Chem. Downloaded from www.nrcresearchpress.com by 213.222.148.141 on 09/07/12
For personal use only.

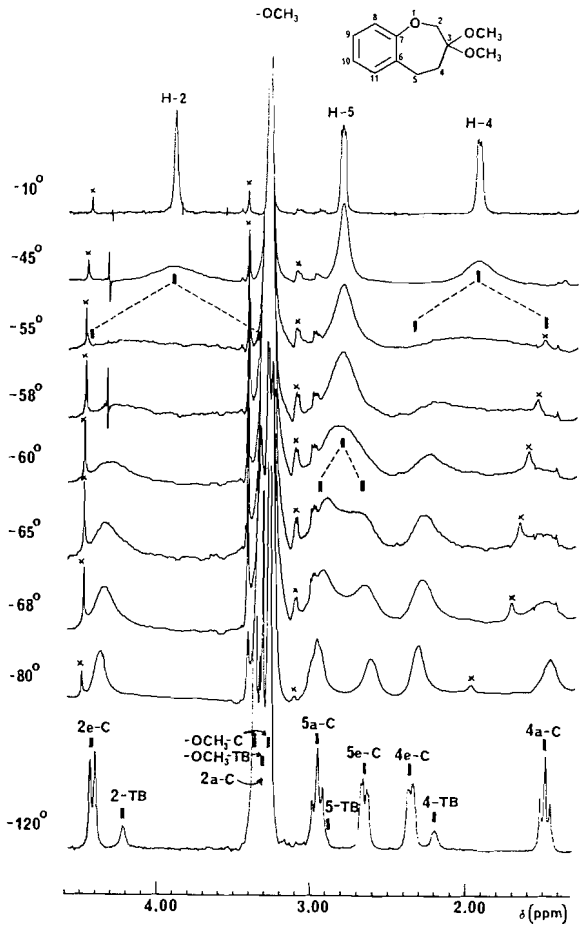

FIG. 11. Aliphatic portion of the 400.13-MHz ^{1}H nmr spectra of **13** in CHF_2Cl–CD_2Cl_2 (80:20) at several temperatures. Letters and numbers over individual signals describe the position and the orientation of the corresponding protons. *C* and *TB* refer to conformations described in the text. "X" denotes an impurity.

of the monomethoxy derivative **10**. The examination of the 120–135 ppm aromatic region in Table 1 shows that of the three resonances for each carbon, the two more intense (70% and 20% of the total signal intensity) have chemical shifts similar to those observed for the chair conformation of the parent compound **8** as well as the monomethyl derivative **9**. These signals, then, most probably belong to the two possible chair conformations C_a and C_e. Now, the association of each of the chair forms to the appropriate set of resonances can be done through the analysis of the C-6 and C-7 signals. For example, the fact that the less shielded C-6 and C-7 signals belong to the most intense set (70%) relates them to the C_a form, since axial methoxy groups are known (5*b*, 15) to have a less pronounced shielding δ-effect than equatorial ones. This assignment is corroborated by the observations of the 4a proton resonance as a triplet for this set in the ^{1}H spectrum of **10** at −120°C, owing to strong couplings with both H-4e and H-5a.

Finally, population variations induced by changing the polarity of the solvent are in line with the above identification of the C_e and C_a signals. Existing knowledge (16) holds that increasing the solvent dielectric constant should stabilize the more polar conformation, because of better solvation and attenuation of unfavorable dipole–dipole interactions. Precise dipole moment determination for the C_a and C_e conformations of **10** is not feasible because many geometrical variables (exact lone-pair locations, bond lengths, etc...) are unknown for this system. Only a qualitative assessment of the relative dipole moments of the two conformations can be utilized throughout this work. Such an analysis, applied previously to the 1,5-benzodioxepin family (5*b*), considered only the C—O bonds and the lone pairs of the oxygen atom as major contributors to the resultant dipole moment of the molecule. The resulting dipoles about each oxygen atom are represented as arrows bisecting the lone pairs and the C—O—C angle in structures **19** and **20**, and pointing towards the negative end of the dipole.

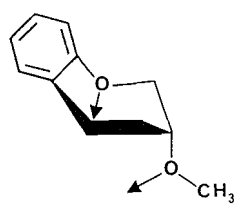

19 (C_a)

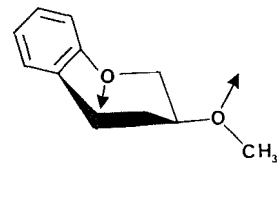

20 (C_e)

The dipole orientations of the methoxy group on both the C_a and C_e conformations do not have a fixed spatial direction and are represented as the mean of the most probable rotamers.

The relative orientations of the two resulting dipoles clearly indicate that C_a (**19**, with dipoles pointing in the same direction) should be more polar than C_e (**20**, with dipoles oriented in opposite directions). Such a conclusion is then consistent with the association of the major set of resonances in CHF_2Cl with C_a, since lowering the solvent polarity actually reduces the population of this form from 70% (in CHF_2Cl) to 44% (in CF_2Cl_2).

Association of the minor (10%) set of ^{13}C resonances of **10** in CHF_2Cl to the twist-boat (*TB*) family is straightforward from the chemical shift analysis of the aromatic carbons, which are quite distinct from those observed for the chair form of **8** as well as **9**. All *TB* resonances for those carbon atoms (except C-11) are more shielded than their chair counterpart. Indeed, the shielding is quite spectacular for the quaternary C-6 resonance, for which a chemical shift difference of more than 7 ppm is observed between the C_a and the *TB* signals (Table 1). Such a difference can be rationalized by the fact that C-6 is *ortho* to the phenolic oxygen and lone-pair delocalization contributes appreciably to its electron density. Because a change from the *C* to the *TB* geometry alters the angular relationship about the phenolic oxygen bonds, the extent of electron delocalization is modified. This change then gives rise to the dramatic upfield displacement of the C-6 chemical shift.

Now, two *TB* conformations are possible for **10** depending on the orientation of the methoxy group, namely TB_g (**21**) and TB_a (**22**). In **21**, the external C—O bond is *gauche* (g) to the internal C—O bond while in **22**, it is *anti* (a). Observation of only one set of *TB* carbon resonances in the ^{13}C spectrum of **10**, at −120°C, suggests either the predominance of one of these conformations or a rapid equilibrium of the two forms. The absence of suitable ^{13}C reference chemical shifts for those *TB* conformations unfortunately restricts the use of ^{13}C parameters in this pursuit.

The multiplicity of the ^{1}H *TB* signals for **10** at −120°C (in CHF_2Cl) is useful to sort out the various conformational possibilities, since H-2a′ and H-4a′ should show characteristic coupling patterns for each form (the prime indicates pseudo-axial orientation in *TB*). For example, Dreiding models of the two *TB* forms (see also projections **23** and **24**) reveal that the 2a′

Can. J. Chem. Downloaded from www.nrcresearchpress.com by 213.222.148.141 on 09/07/12
For personal use only.

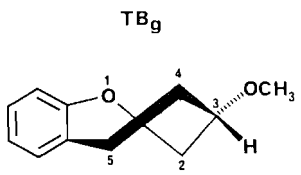

21

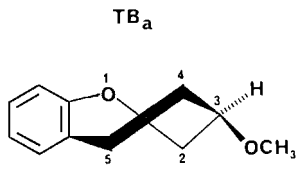

22

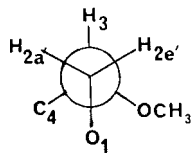

23

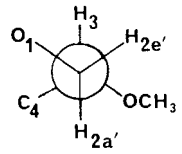

24

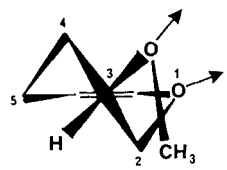

25

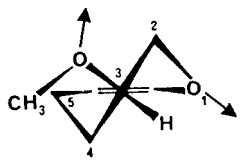

26

proton should give rise to a triplet due to strong coupling with H-2e′ and H-3 for TB_a, while in TB_g it should give a doublet (strong coupling with H-2e′ only).

The observation that the *TB*-2a′ signal is a doublet (4.19 ppm) in the ^{1}H nmr spectrum of **10** therefore suggests a predominant TB_g conformation. This conclusion is corroborated by the appearance of the H-4a′ as a quartet (1.95 ppm) (strong couplings with the 4e′, 3, and 5a′ protons). Exact determination of the TB_g:TB_a ratio cannot, however, be deduced from such an approach (since the *TB* geometries described are flexible enough to be distorted significantly in solution).

The TB_g predominance over TB_a can also be appreciated from the effect produced by a change in the solvent polarity. Table 2 shows that substitution of the polar CHF_2Cl–CD_2Cl_2 mixture by the less polar CH_3OCH_3–CD_2Cl_2 system reduces the relative populations of the *TB* and C_a forms relative to C_e, inferring roughly similar dipole moments for the *TB* and C_a conformations. Structures **25** and **26** confirm that a similar resultant orientation of internal dipole moments exists in both C_a and TB_g conformations (**19** and **25**), in agreement with the observed solvent effect.

The evaluation of the conformational preferences of compounds **11** (R = R′ = CH_3), **12** (R = CH_3; R′ = OCH_3), and **13** (R = R′ = OCH_3) is rather straightforward through the use of the aromatic ^{13}C signals as probes. Thus, the similar aromatic resonances observed for the chair form of the unsubstituted compound **8** and of **11**, **12**, and **13** clearly indicate a predominance of the chair (*C*) conformation in all three cases. The presence of two sets of chair resonances in the low temperature ^{13}C nmr spectrum of the methylmethoxy derivative **12** refers to different spatial arrangements of the substituents at the 3-carbon, namely to C_a and C_e conformations, as defined earlier in the text. Previous studies (2*a*) on the analogous 5,5-methylmethoxy-1,3-dioxane compound showed that the methyl group appears at higher field in the ^{1}H nmr spectrum when in an equatorial position than in an axial one. Assuming the same order in the seven-membered ring, the methyl group on the major chair conformation of **12** should be equatorial, since no methyl signals at higher field can be detected in the low temperature ^{1}H nmr spectra of that compound. The exact position of this major methyl signal (1.05 ppm) can also be used as an indication of its equatorial orientation since it correlates fairly with the ^{1}H nmr chemical shift (1.04 ppm) of the equatorial methyl group in the similar C_a conformation of 5-methyl-5-methoxy-1,5-benzodioxepin (5*b*).

Aromatic signals for the *TB* conformations of all three disubstituted compounds (e.g., **11**, **12**, and **13**) were identified by comparison with those of the monomethoxy derivative **10**. Finally, two *TB* forms (TB_g and TB_a, as defined in the text for **10**) are possible in solution for **12**, but careful analysis of the experimental results could not establish their individual relative contribution to the conformational equilibrium of the molecule.

Origin of the conformational preferences

Benzocycloheptene, the basic carbon framework of this study, was shown, by ^{1}H nmr spectroscopy (12*a*), to exist solely in the chair form (*C*), as predicted from theoretical calculations by Favini and Nava (17). Further studies (4, 5) demonstrated that the introduction of two oxygen atoms at either the 1,5 or the 2,4 position stabilizes the twist-boat conformation (*TB*) relative to the chair (*C*) conformation, due to more favorable dipolar as well as electronic or stereoelectronic interactions between both oxygen atoms.

Such a stabilization is, however, not apparent a priori for compound **8**, in which only one benzylic CH_2 group is replaced by an oxygen atom. Qualitative assessment of the various parameters involved can be achieved through the use of a phenomenological approach described by Kaloustian (16) and Zefirov (18). This method defines the total energy (*E*) of a conformer as the sum of energies relating to structural (E_{ST}), dipolar (E_D), and solvent (E_S) interactions. Therefore, the energy difference (ΔE) between two conformers corresponds to the sum of the differences in each sub-term, as described in eq. [1]:

$$[1]\quad \Delta E_{(C/TB)} = \Delta E_{ST}(C/TB) + \Delta E_D(C/TB) + \Delta E_S(C/TB)$$

In benzocycloheptene, the large energy difference (ΔE) between the *C* and *TB* conformations is attributed mainly to the ΔE_{ST} sub-term (notably to the van der Waals interactions and to the torsional strain, which both favor the *C* form). The introduction of an oxygen atom next to the benzene ring to give compound **8** should raise the contribution of the other ΔE sub-terms, since significant dipolar interactions are created. However, the overall effect of these changes on $\Delta E(C/TB)$ cannot be determined experimentally since no *TB* signal is detected in the low temperature ^{1}H and ^{13}C nmr spectra of **8**.

The presence of a methyl group at the 3-position as in **9** does not significantly perturb the conformational behavior of the seven-membered ring, since only chair conformations (C_e (major) and C_a (minor)) are detected in the low temperature nmr spectra of **9**. The presence of minor C_a signals is not unexpected for **9**, since replacement of a benzylic methylene group of benzocycloheptene by an oxygen atom is expected to reduce the 1,3-diaxial interactions that would characterize an axial methyl group. By comparison, no C_a form is detected for 5-methylbenzocycloheptene **17** (15). A similar increase in the amount of the C_a form upon substituting methylene groups by oxygen atoms was noted for methyl derivatives of the analogous saturated six-membered ring system (19).

In contrast, the change from a methyl group at the 3-position

Can. J. Chem. Downloaded from www.nrcresearchpress.com by 213.222.148.141 on 09/07/12
For personal use only.

to a polar methoxy group (compound **10**) brings radical changes to the conformational equilibrium of the system. The earlier analysis of the dipole orientations in the possible chair conformations of **10** (structures **19** and **20**) showed that the C_a conformer should have a greater dipole moment than C_e. The predominance of the C_e conformation for **10** in a relatively nonpolar medium (CH_3OCH_3–CD_2Cl_2, 80:20) can thus be explained by the less destabilizing dipolar interactions (E_D term less positive) in that conformation. Increasing the polarity of the medium (CHF_2Cl–CD_2Cl_2, 80:20) reverses the relative conformational stabilities, as C_a becomes the predominant conformation in solution. Increased solvation (E_S term more negative) and decreased dipolar interactions (E_D term less positive) should stabilize the C_a form relative to the C_e form. Finally, effective overlap between bonding σ and antibonding σ^* orbitals (the so-called "attractive *gauche* effect" (20)) should also stabilize the C_a form, although the quantitative assessment of the effect of this factor on the conformational equilibrium is beyond the scope of this study.

Quite interestingly, *TB* signals are detected in the low temperature nmr spectra of compound **10**, indicating that the introduction of a methoxy group at the 3-position is much more stabilizing for the *TB* form than for the *C* form. This observation is compatible with the great flexibility of the twist-boat conformation, which allows structural distortions in order to minimize the total energy of the conformer through reduced dipolar interactions or better orbital overlap. A similar observation (10*a*) was made upon introduction of a methoxy group at the 3-position of 2,3,4,5-tetrahydro-2-benzoxepin (**16**).

Two twist-boat conformations (TB_g and TB_a, as defined earlier by structures **21** and **22**) are possible in solution for **10**; the predominance of the TB_g conformer, at least in the polar solvent system (CHF_2Cl–CD_2Cl_2), can be rationalized through consideration of dipolar and orbital interactions in both *C* and *TB* conformations. The examination of Dreiding models described in the preceding section indicates similar spatial *gauche* arrangements for the —O—C—C—O— fragment in both TB_g and C_a, whereas an *anti* arrangement exists in both TB_a and C_e. Therefore, on a qualitative basis, the stabilizing factors shown previously to favor C_a over C_e in a polar medium should also favor TB_g over TB_a.

The presence of two geminal substituents at the 3-position as in compounds **11**, **12**, and **13** also stabilizes the *TB* form relative to the *C* form. In the case of the dimethyl derivatives **11**, it results in large part from destabilizing 1,3-diaxial CH_3–H interactions on the chair form, which can be alleviated by placing these substituents in the sterically less demanding isoclinal positions of the *TB* form.

A combination of factors governing conformational preferences in both the monomethyl (**9**) and the monomethoxy (**10**) derivatives can then be used to analyse the methylmethoxy (**12**) case. As expected, C_a (axial methoxy and equatorial methyl groups) is the predominant conformation of **12** in solution, for it combines the favorable arrangements of the C_a form of **10** and the C_e form of **9**. Furthermore, *TB* signals are detected in solution for **12**. Because the addition of a 3-methyl group does not change significantly the *C*:*TB* ratio from that observed for **10**, the origin of the relative stabilization of the *TB* form for **12** should be related to that for compound **10**.

Finally, the presence of only 8% of *TB* form in solution for the dimethoxy derivative **13** indicates that the addition of a second methoxy group at the 3-position of **10** does not change significantly the *C*:*TB* ratio of this system. The observation of similar *TB* populations for both the dimethyl (**11**) and the dimethoxy (**13**) derivatives also suggests that increased dipolar interactions in the latter must be compensated for by reduced 1,3-diaxial steric interactions, in the chair as well as in the twist-boat conformations. This result also apparently implies that the effect of geminal disubstitution at the 3-position on the $C \rightleftharpoons TB$ conformational equilibrium is relatively independent of the nature (polar or nonpolar) of the substituting groups.

Experimental

All syntheses requiring anhydrous conditions were performed under argon with techniques described elsewhere (21). Anhydrous solvents were obtained by distilling over various drying agents: $LiAlH_4$ for ether, sodium–benzophenone for tetrahydrofuran, $CaCl_2$ for benzene and xylene, and Mg for methanol. Flash chromatography was performed on 230–400 mesh silica gel (Merck) under standard conditions described by Still *et al.* (22). Preparative vapor phase chromatography was performed on a Varian model 920 apparatus using a 5 ft. × 3/8 in. stainless steel column containing 30% SE-30(P-HMDS) on Chromosorb-P. The sample to be purified is vaporized at 200°C in the injection port, passed through the separating column on a stream of helium gas (carrier gas), detected at 200°C by thermal conductivity, and condensed in an acetone – Dry Ice bath. Column temperatures and retention times are specified when necessary.

Melting points were determined on a Thomas–Hoover (Unimelt) apparatus and were not corrected. Boiling points were determined by either simple or bulb-to-bulb (Kugelrohr) distillation for which the temperature reported represents the lowest one at which the vapors condensed on the receiving bulbs. Infrared spectra were taken on a Perkin–Elmer (Model 783) spectrometer. Low resolution mass spectra were recorded at 70 eV, in the chemical ionization mode, on a V.G. Micromass (Model 12-12) spectrometer, while those at high resolution were recorded at 70 eV, in the electron impact mode, on a modified MS-9 spectrometer. Routine ^1H nmr spectra were taken on a Bruker WH-90 spectrometer; solutions were typically 5% (w/v) $CDCl_3$ containing Me_4Si as internal reference. The following abbreviations are used to describe the signal multiplicity: s: singlet; d: doublet; t: triplet; q: quartet; m: multiplet; br: broad.

The variable temperature ^1H nmr spectra at 400.13 MHz and the ^{13}C nmr spectra at 100.62 MHz were obtained using a Bruker WH-400 spectrometer equipped with a B-VT-1000 variable temperature unit. Calibration using a copper–constantan thermocouple inside a solvent-containing nmr tube indicates that the temperatures reported are precise within ±3°C.

Proton samples in standard 5-mm tubes (degassed and sealed) were studied as 0.20 *M* solutions in either CHF_2Cl–CD_2Cl_2 (80:20) or CF_2Cl_2–acetone-d_6 (94:6) solvent systems containing a small amount of TMS. The following instrumental parameters are typical: flip angle, 15°; SW (scan width), 4500 Hz; number of scans, 100–1000. Gaussian multiplication was applied on all FID's. Data size was 8K (AQ (acquisition time), 0.91 s) for low temperature spectra (−100 to −125°C), and 16 and 32K (AQ, 1.81 and 3.64 s) for all others (+10 to −100°C). All 8 and 16K FID's were zero filled to 32K prior to the Fourier transformation.

Carbon-13 samples in standard 10-mm tubes (degassed and sealed) were studied as 0.40 *M* solutions in either CHF_2Cl–CD_2Cl_2 (80:20) or CH_3OCH_3–CD_2Cl_2 (80:20) solvent systems, containing a small amount of TMS. The following instrumental parameters are typical: flip angle, 60–70°; SW, 18 000 Hz; relaxation delay, 0.20 s; number of scans, 100–3000. Gaussian multiplication was applied on all FID's; data size, 16K (AQ, 0.46 s), zero filled to 32K prior to Fourier transformation.

Conformation populations derived from integration of proton signals represent averages of five integrations for a defined set of signals, while reliable integrations from carbon-13 spectra were obtained using a 0.1–0.2 s delay between pulses and by comparing results with at least two other sets of carbon resonances of the same compound. All integration figures are therefore precise within 2%.

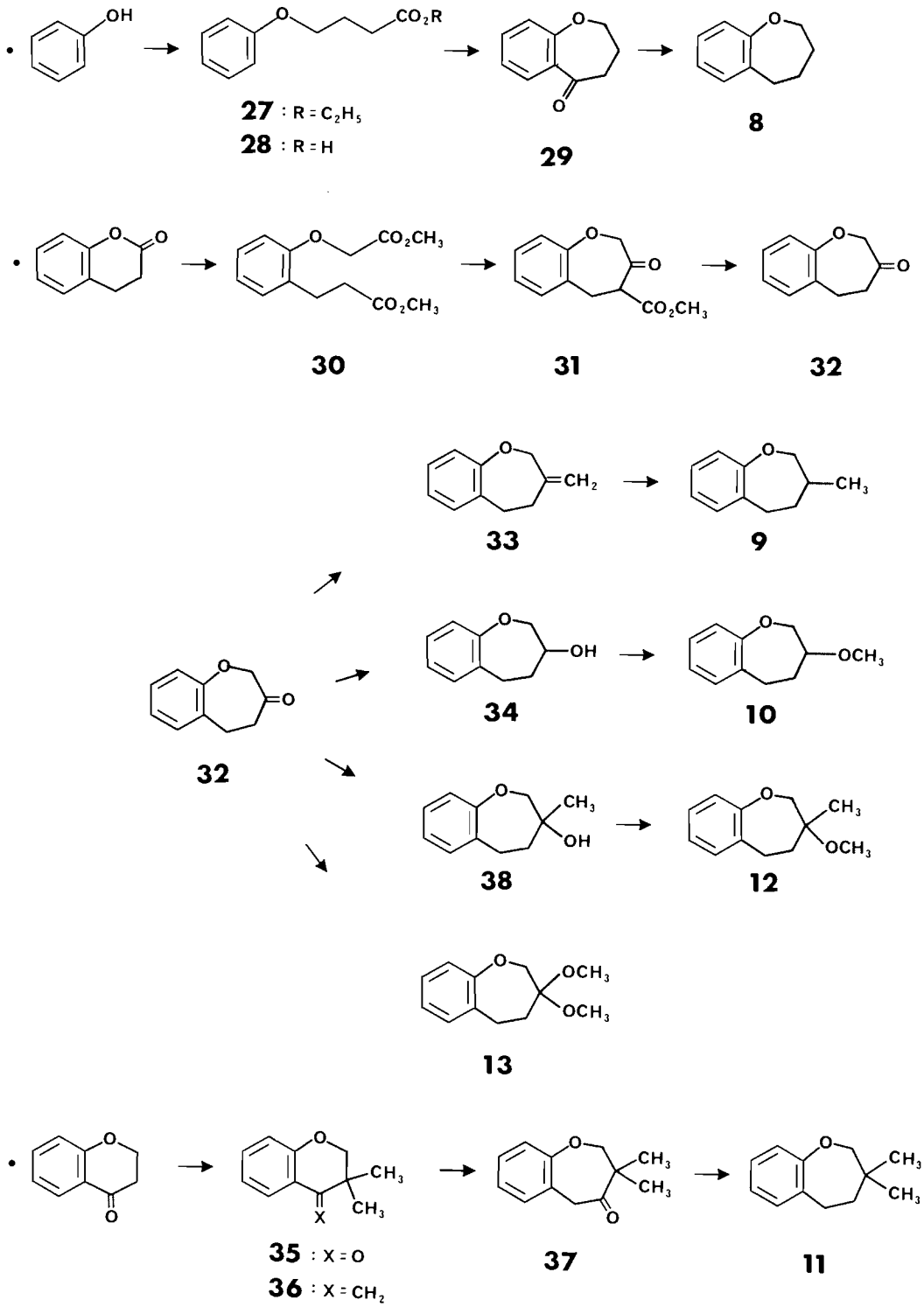

SCHEME 1

The rate constant for **8** was determined by nmr at the coalescence temperature using the equation $\pi((\Delta\nu)^2 + 6J^2)^{1/2}/\sqrt{2}$ for singlet to AB spectral change. The free-energy barrier for this compound was calculated from standard equations (13) using a transmission coefficient of one (*vide infra*).

The two-dimensional (2D) ^{1}H nmr COSY experiment with double quantum filtering (7) was performed using the standard Bruker hardward and software (COSYDQF.AU). The pulse sequence utilized was D1–90°–D0–D2–90°–D3–90°–D2–FID, with the following delays: D1, 0.6 s; D2, 5 μs; D3, 5 μs. A spectral width of 2200 Hz and quadrature detection were used to collect a 97 FID × 2K data matrix (zero filled to 1K × 2K) using 96 scans; digital resolution was then 2.14 Hz/point. A sine bell square function was applied in both dimensions and absolute display was used.

Compounds **8–13** were obtained by multistep synthesis from commercially available products, as described in Scheme 1.

γ-Phenoxybutyric acid ethyl ester 27

To 150 cm^3 of a 1.05 *M* sodium ethoxide solution in ethanol (10.75 g of sodium in 150 cm^3 of ethanol) was added with stirring, at 40°C, 40.00 g (0.425 mol) of phenol in four portions, over a period of 2 h. γ-Chlorobutyric acid ethyl ester (Aldrich, 64.01 g, 0.425 mol) was

Can. J. Chem. Downloaded from www.nrcresearchpress.com by 213.222.148.141 on 09/07/12
For personal use only.

Can. J. Chem. Downloaded from www.nrcresearchpress.com by 213.222.148.141 on 09/07/12
For personal use only.

then added dropwise during 2 h, and the resultant cloudy solution was refluxed for 16 h. The solution was then cooled to room temperature, filtered on sintered glass, and evaporated under reduced pressure; the residue was dissolved in 300 cm^3 of ether, and this organic phase was washed successively by 3 × 75 cm^3 10% NaOH and by 3 × 75 cm^3 brine. The organic phase was then separated, dried over anhydrous magnesium sulfate, and filtered on sintered glass. Evaporation under reduced pressure yielded an oil, which was distilled under reduced pressure (120–125°C/0.5 Torr; 1 Torr = 133.3 Pa) (lit. (23) bp 170–173°C/25 Torr) to give 53.29 g (60% yield) of a clear and pleasant smelling oil whose ^1H nmr spectrum agreed with the proposed structure; ^1H nmr (90 MHz, $CDCl_3$) δ: 1.24 (t, 3H, CH_3), 2.09 (m, 2H, —CH_2—), 2.50 (t, 2H, —CH_2—CO—), 3.98 (t, 2H, —O—CH_2—), 4.13 (q, 2H, —CO—O—CH_2—), 6.83–7.36 (m, 4H, arom. protons).

γ-Phenoxybutyric acid ***28***

A quantity of 50.00 g (0.240 mol) of **27** was mixed, at room temperature, with 75.00 g (1.34 mol) of KOH and 350 cm^3 of absolute ethanol in a one-necked round-bottomed flask, and the resulting solution was stirred during 1.5 h. A white precipitate gradually appeared as the reaction proceeded; the mixture was then filtered on sintered glass, and the recovered white solid was dissolved in 600 cm^3 H_2O. The resulting solution was made acidic (pH 3) by slow addition of concentrated HCl, which precipitated the desired acid. Filtration on a Büchner funnel and drying over $CaCl_2$ for 24 h afforded 36.3 g (84% yield) of a white fluffy solid, whose melting point (63.0–64.0°C) agrees fairly well with that reported in the literature (62–63°C (ref. 24)); ^1H nmr (90 MHz, $CDCl_3$) δ: 2.12 (m, 2H, —CH_2—), 2.59 (t, 2H, —CH_2—CO—), 4.01 (t, 2H, —O—CH_2—), 6.84–7.38 (m, 4H, arom. protons), 10.01 (br, 1H, —COOH, exchangeable with D_2O).

*2,3-Dihydro-1-benzoxepin-5(4*H*)-one* ***29***

This compound was prepared by cyclization of γ-phenoxybutyric acid **28** with polyphosphoric acid, as described by Fontaine (25). A 65% yield of the desired ketone was thus obtained as a clear and dense oil, whose boiling point (120.8–125.0°C/1 Torr) is similar to that reported (106°C/2 Torr) (ref. 26), while its ^1H nmr spectrum (in $CDCl_3$) is identical with the one already published (25).

2,3,4,5-Tetrahydro-1-benzoxepin ***8***

To 12.21 g of zinc powder (Aldrich) in a 250-cm^3 three-necked flask, were added 1.12 g (0.004 mol) of mercuric chloride (Aldrich), 12.0 cm^3 of distilled water, and 1.1 cm^3 of concentrated HCl; the mixture was stirred at room temperature for 1 h, and then allowed to settle for 10 min. The Zn–Hg amalgam was ready for use after decanting the milky liquid phase. To that amalgam were added 9.6 cm^3 of distilled water, 21.6 cm^3 of concentrated HCl, and 6.0 g of ketone **29**. The mixture was then allowed to cool and filtered through a Büchner funnel; the solid particles were crushed on the filter and thoroughly washed with water (150 cm^3) and ether (200 cm^3). The organic layer from the filtrate was then separated and the aqueous layer extracted with 2 × 100 cm^3 ether. The combined organic phases were washed with 5 × 75 cm^3 of a saturated $NaHCO_3$ solution, dried on $MgSO_4$, filtered on a Büchner funnel, and evaporated under reduced pressure to give 3.90 g of a yellow oil. Distillation on a Kugelrohr apparatus (145°C/0.7 Torr) yielded a clear oil, which was flash-chromatographed on silica gel using dichloromethane–hexane (10:90) as eluant. The first compound eluted was identified as 2,3-dihydro-1-benzoxepin (oil), R_f 0.19 (CH_2Cl_2–hexane, 10:90); ^1H nmr ($CDCl_3$) δ: 2.66 (2H, m, H-3), 4.23 (2H, t, H-2), 5.99 (1H, td, H-4), 6.34 (1H, td, H-5), 6.88–7.25 (4H, m, arom. protons), while the more polar compound was the desired benzoxepin **8** (oil, 1.42 g, 26% yield). An analytically pure sample could be obtained from a preparative gc experiment (column temperature, 140°C; gas flow rate, 30 cm^3 min^{-1}; retention time, 3.0 min). The ^{13}C and ^1H nmr spectra described in Tables 1 and 2 confirm the identity of **8**. *Exact Mass* calcd. for **8** (EI ms), $C_{10}H_{12}O$, *m/e*: 148.0888; found: 148.0882.

2-(Carbomethoxyethyl)-phenoxyacetic acid methyl ester ***30***

In a 300-cm^3 three-necked flask containing 120 cm^3 of a sodium methylate solution (prepared from 6.6 g of sodium and 120 cm^3 of anhydrous methanol) was added dropwise, under argon, 35.9 cm^3 (42.0 g) of dihydrocoumarin (Aldrich). The resulting solution was refluxed for 45 min, followed by the dropwise addition to this refluxing solution of 29.5 cm^3 (47.67 g; 1.1 equiv.) of bromomethylacetate (Aldrich) and the cloudy solution was kept at reflux for another 16 h; it was then cooled, filtered on sintered glass, and evaporated under reduced pressure. The residue was dissolved in ether (200 cm^3) and washed successively with 3 × 50 cm^3 10% NaOH and 3 × 50 cm^3 brine. The organic phase was then dried on $MgSO_4$, filtered on a Büchner funnel, and evaporated under reduced pressure. The oily yellowish liquid obtained was distilled under vacuum (162–168°C/1.3 Torr) to give 56.00 g (78% yield) of **30** as a pleasant smelling oil; ir (neat): 1720 (C=O; ester) cm^{-1}; ^1H nmr ($CDCl_3$) δ: 2.56–3.08 (4H, m, Ph—*CH_2*—*CH_2*—$COOCH_3$), 3.63 and 3.75 (6H, s, 2 × -OCH_3), 4.64 (2H, s, —O—CH_2—), 6.65–7.23 (4H, m, arom. protons); ms (EI): 252 ($M^{+\cdot}$) (25), 192 (100).

*4-Carbomethoxy-3,4-dihydro(2*H*)-1-benzoxepin-3-one* ***31***

The procedure described here is a slightly modified version of the one presented in a U.S. patent (26). To 16.44 g of a 50% (w/w) dispersion of NaH in mineral oil, in 300 cm^3 of anhydrous THF, was added dropwise, under argon, a solution of 40.00 g of **30** in 200 cm^3 of anhydrous THF. The rate of addition was chosen to maintain gentle boiling without external heating. The greenish solution thus obtained was then refluxed for 16 h. After cooling, it was poured in 1.0 dm^3 of ice water, stirred for 0.5 h, and acidified to pH 2 with concentrated HCl. The organic layer was removed and the aqueous phase was extracted with 4 × 100 cm^3 ether; the combined organic phases were washed with brine (4 × 100 cm^3), dried on anhydrous $MgSO_4$, filtered on a Büchner funnel, and evaporated under reduced pressure to give a red oily liquid. Distillation at 140–144°C under 1 Torr yielded 20.05 g (57% yield) of a thick yellow oil. The ^1H nmr spectrum of this substance indicates the presence of the 4-carbomethoxy derivative **31** as the major product; ir (neat): 1720 and 1740 (C=O; ketone and ester) cm^{-1}; ^1H nmr ($CDCl_3$) (400.13 MHz) δ: 3.32 (1H, dd, H-5), 3.47 (1H, dd, H-5), 3.69 (1H, t, H-4), 4.55 (2H, AB pattern, —O—CH_2—), 7.00–7.25 (4H, m, arom. protons); ^{13}C nmr (100.62 MHz, $CDCl_3$) δ: 29.93 (C-5), 52.48 (C-4), 54.59 (—OCH_3), 78.30 (—O—CH_2—), 121.53, 124.71, 128.16, 131.00 (arom. protonated carbons), 157.31 (quaternary arom. carbon), 169.50 (C=O; ester), 205.74 (C=O; ketone); *Exact Mass* calcd. for **31** (EI ms), $C_{12}H_{12}O_4$, *m/e*: 220.0736; found: 220.0742.

*3,4-Dihydro-2*H*-1-benzoxepin-3-one* ***32***

A quantity of 18.00 g of **31**, together with 60 cm^3 of absolute ethanol and 60 cm^3 of 5% HCl, was mixed in a 300-cm^3 round-bottomed flask and refluxed with stirring for 16 h. The solution was then cooled, poured into 200 cm^3 of brine water, and extracted with ether (4 × 150 cm^3); the organic phases were then dried on $MgSO_4$, filtered on a Büchner funnel, and evaporated under reduced pressure to yield 12.68 g (95% yield) of a slightly yellow liquid. The product was used as such for further experiments. Analytically pure **32** could be obtained by vacuum distillation (160–163°C/1 Torr; lit. (27) bp 100–105°C/0.5 Torr); ir (neat): 1720 (C=O; ketone) cm^{-1}; ^1H nmr ($CDCl_3$) δ: 2.80–3.20 (4H, m, Ar—*CH_2*—*CH_2*—), 4.50 (2H, s, —O—CH_2—), 6.97–7.28 (4H, m, Ar); ms (CI): 163 ($M^{+\cdot}$ + 1) (100).

*3,4-Dihydro-2*H*-1-benzoxepin-3-methylene* ***33***

To 5.26 g (15 mmol) of methyltriphenylphosphonium bromide in 60 cm^3 of anhydrous THF, at 0°C, was added dropwise, under argon, 8.7 cm^3 (15 mmol) of *n*-BuLi (1.6 *M* in hexane). The solution turned orange as the addition proceeded. After stirring at 0°C for 30 min, a solution of 1.43 g (9 mmol) of **32** in 20 cm^3 of anhydrous THF was added dropwise. The solution was stirred for 2 h at 0°C, then allowed to warm to room temperature, and stirred for another 16 h. The solution was then poured in 300 cm^3 of pentane, and filtered through a 3 cm thick silica bed, using pentane as a washing solvent (200 cm^3). The filtrate was evaporated under reduced pressure to yield 1.11 g (78% yield) of **33** as a yellow oil. The product was used as such

Can. J. Chem. Downloaded from www.nrcresearchpress.com by 213.222.148.141 on 09/07/12
For personal use only.

without further purification; ^{1}H nmr ($CDCl_3$) δ: 2.40–2.92 (4H, m, —CH_2—CH_2—), 4.40 (2H, s, —O—CH_2—), 4.97 (2H, s, C=CH_2), 6.98–7.25 (4H, m, arom. protons).

2,3,4,5-Tetrahydro-3-methyl-1-benzoxepin ***9***

Hydrogen (1 atm (101.3 kPa)) was bubbled through a stirred solution of **33** (0.95 g) in 50 cm^3 of absolute ethanol containing 200 mg of 10% Pd/C, during 48 h. The solution was then filtered through Celite and the solids washed with 100 cm^3 EtOH; the filtrate was evaporated under reduced pressure, yielding a yellow oil that was purified by flash chromatography on silica gel, using dichloromethane–hexane (25:75) as eluant. The first compound eluted (major component) proved to be the desired **9** (420 mg; 43% yield), as a colorless liquid (bp (Kugelrohr) 59°C/1.1 Torr). The ^{13}C and ^{1}H nmr spectra are described in Tables 1 and 2; ms (CI): 163 ($M^{+\bullet}$ + 1) (36), 147 (10), 71 (100). *Exact Mass* calcd. for $C_{11}H_{14}O$, *m/e*: 162.1045; found: 162.1055.

The minor compound (more polar) was identified as (3-methylbutyl)-phenol: ^{1}H nmr ($CDCl_3$) δ: 0.95 (6H, d, 2 × CH_3), 1.26–1.60 (3H, m, —*CH_2*—*CH*—), 2.62 (2H, t, Ar—*CH_2*—), 4.78 (1H, s, phenolic OH), 6.70–7.23 (4H, m, arom. protons).

2,3,4,5-Tetrahedro-1-benzoxepin-3-ol ***34***

To 3.00 g of $LiAlH_4$ in 20 cm^3 of anhydrous ether was added dropwise, under argon, a solution of 4.00 g of **32** in 10 cm^3 of ether. The exothermic reaction brought the solution to reflux, maintained by external heating for an additional hour, after which the solution was cooled and treated carefully with 10% NaOH. The organic layer was separated and the aqueous phase extracted with ether (3 × 50 cm^3). The combined organic layers were dried on sodium carbonate, filtered, and evaporated under reduced pressure to give 2.50 g (62% yield) of **34** as a white, fluffy solid (mp 87–91°C; lit. (27) mp 86–88°C); ^{1}H nmr ($CDCl_3$) δ: 1.87–2.00 (2H, m, H-4), 2.38 (1H, br, —OH, exchangeable with D_2O), 2.65–3.03 (2H, m, H-5), 3.99 (2H, s, H-2), 4.01 (1H, br s, H-3), 6.92–7.17 (4H, m, arom. protons).

2,3,4,5-Tetrahedro-3-methoxy-1-benzoxepin ***10***

To 351 mg of NaH (50% dispersion in mineral oil, washed with hexane) in 20 cm^3 of anhydrous THF, was added dropwise, under argon, a solution of 1.00 g of **34** in 10 cm^3 of anhydrous THF. The solution was stirred at room temperature for 15 min and then 5 cm^3 (13 equiv.) of CH_3I was added dropwise. The resulting red solution was stirred at room temperature for 48 h, during which period a white precipitate appeared. This pinkish solution was filtered on sintered glass and the filtrate evaporated under reduced pressure; the residue was dissolved in 10 cm^3 of CCl_4 and filtered. The filtrate was again evaporated under reduced pressure to give 1.04 g (96% yield) of a yellow oil, identified as **10** by its ^{1}H and ^{13}C nmr spectra (Tables 1 and 2). Analytically pure **10** could be obtained by preparative gc (column temperature, 100°C; He flow rate, 60 cm^3/min; retention time, 6.0 min). *Exact Mass* calcd. for $C_{11}H_{14}O_2$, *m/e*: 178.0994; found: 178.0993.

2,3-Dihydro-3,3-dimethyl-1-benzopyran-4-one ***35***

This compound was prepared from dihydro-2,3-chromanone-4 (Aldrich) by following the general procedure described by Klemm *et al.* (28), with modifications proposed later by Zimmermann and Factor (29). A 39% yield of the desired product was obtained upon distillation (98.0°C/2.5 Torr (lit. (28) bp 88–89°C/1 Torr). The ^{1}H nmr spectra of **35** was found to be similar to the one described in ref. 29.

2,3-Dihydro-3,3-dimethyl-4-methylene-1-benzopyran ***36***

To 20.33 g (57 mmol) of methyltriphenylphosphonium bromide (Aldrich) in 300 cm^3 of anhydrous THF was added dropwise, under argon, at 0°C, 35.4 cm^3 (57 mmol) of a 1.55 *M* *n*-BuLi solution in hexane, and the resulting solution was stirred at 0°C for an additional half hour. A solution of 6.00 g (34 mmol) of the ketone **35** in 60 cm^3 of anhydrous THF was then added dropwise; the resulting mixture was warmed to room temperature and stirred for 36 h; it was then poured in 500 cm^3 of pentane followed by filtration on a silica gel pad (3 cm thick), which was washed several times with pentane (total volume of washing solvent: 500 cm^3). The filtrate was evaporated under reduced pressure to give a residual yellow oil, which was vacuum distilled to give 4.57 g (77% yield) of the desired olefin **36** (bp 76.0–80.0°C/1.0 Torr); ir (neat), ν: 1600, 1640 (C=C) (cm^{-1}); ^{1}H nmr ($CDCl_3$) δ: 1.16 (s, 6H, 2 × CH_3), 3.81 (s, 2H, -CH_2-), 5.02, 5.48 (2s, 2H, =CH_2), 6.79–7.62 (m, 4H, arom. protons); ms (CI), *m/e*: 175 ($M^{+\bullet}$ + 1) (100), 174 ($M^{+\bullet}$) (75), 159 (15). *Exact Mass* calcd. for $C_{12}H_{14}O$, *m/e*: 174.1045; found: 174.1022.

2,3,4,5-Tetrahedro-3,3-dimethyl-1-benzoxepin-4-one ***37***

This compound was prepared by a ring expansion of **36** mediated by thallium(III) nitrate, as described by Taylor *et al.* (30). To a stirred solution of 10.63 g (24 mmol) of thallium(III) nitrate in 90 cm^3 methanol was added as rapidly as possible a solution containing 4.17 g (24 mmol) of ketone **36** in 90 cm^3 methanol. The resulting mixture rapidly turns red as a voluminous white precipitate (probably thallium(I) nitrate) appears; it is stirred for an additional 3 min, then poured into 200 cm^3 chloroform. The solution is then filtered on sintered glass and the filtrate washed successively with 3 × 100 cm^3 of a saturated $NaHCO_3$ solution and with 3 × 10 cm^3 brine. The organic phase is then dried on $MgSO_4$, filtered on a Büchner funnel, and evaporated under reduced pressure to give a yellow oil, which, by vacuum distillation, yields the desired seven-membered ring ketone **37** as a clear yellow oil (3.88 g; 85% yield); bp (Kugelrohr) 100°C/1.5 Torr; ir (neat), ν: 1740 (C=O) (cm^{-1}); ^{1}H nmr ($CDCl_3$) δ: 1.24 (s, 6H, 2 × CH_3), 3.95, 4.08 (2s, 4H, 2 × -CH_2-), 6.86–7.26 (m, 4H, arom. protons). *Exact Mass* calcd. for $C_{12}H_{14}O_2$ (EI ms), *m/e*: 190.0994; found: 190.0953.

2,3,4,5-Tetrahedro-3,3-dimethyl-1-benzoxepin ***11***

This compound was prepared by a Zn–Hg/HCl Clemmensen reduction similar to that described for compound **8**. The crude product was purified by flash chromatography on silica gel using CH_2Cl_2–hexane (5:95) as eluent. The first fractions gave dihydro-2,3-dimethyl-3,3-benzoxepin-1, identified by its ^{1}H nmr spectra ($CDCl_3$) δ: 1.12 (s, 6H, 2 × -CH_3), 3.88 (s, 2H, -CH_2-), 5.70, 6.13 (AB, 2H, —CH=CH—), 6.93–7.11 (m, 4H, arom. protons). Subsequent fractions yielded pure **11** (692 mg, 25%) as a clear oil; R_f 0.17 (CH_2Cl_2–hexane, 5:95); bp (Kugelrohr) 80°C/1.6 Torr. The ^{13}C and ^{1}H nmr spectra are described in Tables 1 and 2. *Exact Mass* calcd. for **11** (ms), $C_{12}H_{16}O$, *m/e*: 176.1201; found: 176.1209.

2,3,4,5-Tetrahedro-3-methyl-1-benzoxepin-3-ol ***38***

To 270 mg (11 mmol) of magnesium turnings and an iodine crystal in 5 cm^3 of anhydrous ether was slowly added dropwise, under argon and with stirring, a solution of 1.2 cm^3 of CH_3I (19 mmol) in 10 cm^3 of anhydrous ether; the rate of addition was adjusted to maintain the solution to reflux (addition period, 0.5 h) and the solution was then stirred for an additional 30 min. To this mixture was added a solution of 1.50 g (9 mmol) of ketone **32** in 10 cm^3 of anhydrous ether and the resulting solution was stirred at room temperature for 16 h, during which period a white precipitate gradually appeared. The milky solution was then neutralized with 50 cm^3 of a 10% NH_4Cl solution followed by the addition of 50 cm^3 of ether. The organic phase was washed with 3 × 50 cm^3 brine, and the combined aqueous phases were backwashed with 3 × 50 cm^3 ether. The combined ethereal phases were dired over Na_2CO_3, filtered, and the solvent was evaporated under reduced pressure to yield 1.60 g (97% yield) of a yellow oil whose ^{1}H nmr spectrum is similar to the one described in the literature (31). The product was used as such, without further purification, for the next step.

2,3,4,5-Tetrahedro-3-methyl-3-methoxy-1-benzoxepin ***12***

This compound was obtained by methylation of the tertiary alcohol **38** using the procedure described earlier for the formation of the monomethoxy derivative **10**. Distillation of the crude product under reduced pressure gave 1.03 g (73% yield) of **12**, as a slightly yellow oil (bp 98–100°C/0.5 Torr). The ^{13}C and ^{1}H nmr spectra are described in Tables 1 and 2. *Exact Mass* calcd. for **12** (EI ms), $C_{12}H_{16}O_2$, *m/e*: 192.1150; found: 192.1151.

2,3,4,5-Tetrahedro-3,3-dimethoxy-1-benzoxepin ***13***

A mixture of 1.00 g (6 mmol) of ketone **32**, 6.8 cm^3 (62 mmol) of trimethylorthoformate (Aldrich), 25 mg (0.2 mmol) of *p*-toluene-

sulfonic acid, and 175 cm^3 of anhydrous methanol was refluxed and stirred, under argon, for 16 h. The resulting solution was afterwards brought back to room temperature, and evaporated under reduced pressure to distill off the methanol. The residue was dissolved in 125 cm^3 of benzene and washed successively with 2×50 cm^3 of a 20% NaOH solution and with 2×50 cm^3 brine after which the organic phase was separated, dried on K_2CO_3, filtered, and evaporated under reduced pressure to yield a yellow oil, which gave pure **13** (1.10 g; 86% yield) when distilled on a Kugelrohr apparatus. Crystallization occurred on standing for 24 h at 0°C (white crystals, mp 60.0–62.0°C). The ^{13}C and ^1H nmr spectra are described in Tables 1 and 2. *Exact Mass* calcd. for **13** (EI ms), $C_{12}H_{16}O_3$, *m/e*: 208.1099; found: 208.1099.

Acknowledgments

We acknowledge the assistance of Dr. M. T. Phan Viet, manager of the "Laboratoire Régional de RMN à Haut Champ", in Montreal. We are grateful for financial assistance from the Natural Sciences and Engineering Research Council of Canada.

1. (*a*) E. L. Eliel, K. D. Hargrave, K. M. Pietrusiewicz, and M. Manoharan. J. Am. Chem. Soc. **104**, 3635 (1982), and references cited therein; (*b*) E. L. Eliel and M. Pietrusiewicz. Pol. J. Chem. **55**, 1265 (1981); (*c*) C. B. Anderson and M. P. Geis. Tetrahedron, **31**, 1149 (1975); (*d*) E. L. Eliel, M. Manoharan, K. M. Pietrusiewicz, and K. D. Hargrave. Org. Magn. Reson. **21**, 94 (1983).
2. (*a*) R. M. Enamoza and E. L. Eliel. J. Am. Chem. Soc. **94**, 8072 (1972); (*b*) F. G. Riddell. The conformational analysis of heterocyclic compounds. Academic Press, London. 1980. Chap. 4. pp. 70–78.
3. (*a*) M. J. O. Anteunis and G. Swaelens. Org. Magn. Reson. **2**, 389 (1970); (*b*) K. Pihlaja, G. M. Kellie, and F. G. Riddell. J. Chem. Soc. Perkin Trans. 2, 252 (1972).
4. A. Blanchette, F. Sauriol-Lord, and M. St-Jacques. J. Am. Chem. Soc. **100**, 4055 (1978).
5. (*a*) D. Ménard and M. St-Jacques. Can. J. Chem. **59**, 1160 (1981); (*b*) J. Am. Chem. Soc. **106**, 2055 (1984).
6. R. St-Amour, M. T. Phan Viet, and M. St-Jacques. Can. J. Chem. **62**, 2830 (1984).
7. (*a*) A. Wokaun and R. R. Ernst. Chem. Phys. Lett. **52**, 407 (1977); (*b*) U. Piantini, O. W. Sorensen, and R. R. Ernst. J. Am. Chem. Soc. **104**, 6800 (1982); (*c*) A. J. Shaka and R. Freeman. J. Mag. Reson. **51**, 169 (1983).
8. F. W. Wehrli and T. Wirthlin. Interpretation of carbon-13 NMR spectra. Heyden & Son, London. 1978. Chap. 2. p. 45.
9. J. Sandström. Dynamic NMR spectroscopy. Academic Press, London. 1982. Chap. 7. p. 96.
10. (*a*) S. Désilets and M. St-Jacques. J. Am. Chem. Soc. **109**, 1641 (1987); (*b*) P. Dionne and M. St-Jacques. J. Am. Chem. Soc. **109**, 2616 (1987).
11. (*a*) B. A. Arbusov, E. N. Klimovitskii, G. N. Sergeeva, D. Yu. Strel'nik, and N. I. Monakhova. Izv. Akad. Nauk SSSR Ser. Khim. **5**, 1077 (1986), and references cited therein; (*b*) B. A. Arbusov, E. N. Klimovitskii, G. N. Sergeeva, D. Yu. Strel'nik, K. M. Enikeev, and A. V. Il'yasov. Izv. Akad. Nauk SSSR Ser. Khim. **5**, 1072 (1986), and references cited therein; (*c*) I. A. Litvinov, Yu. T. Struchkov, E. N. Klimovitskii, M. B. Timirbaev, and B. A. Arbusov. Zh. Obshch. Khim. **56**, 155 (1986), and references cited therein.
12. (*a*) C. Vaziri and M. St-Jacques. Org. Magn. Reson. **4**, 77 (1972); (*b*) L. Canuel and M. St-Jacques. Can. J. Chem. **52**, 3581 (1971).
13. (*a*) D. Kost, E. H. Carlson, and M. Raban. J. Chem. Soc. D, 656 (1971); (*b*) F. A. L. Anet, P. J. Deger, and J. Krane. J. Am. Chem. Soc. **98**, 2059 (1976).
14. N. K. Wilson and J. B. Stothers. Top. Stereochem. **8**, 1 (1974).
15. D. Ménard and M. St-Jacques. Tetrahedron, **39**, 1041 (1983).
16. M. K. Kaloustian. J. Chem. Educ. **51**, 777 (1974).
17. G. Favini and A. Nava. Gazz. Chim. Ital. **104**, 621 (1974).
18. N. S. Zefirov. Tetrahedron, **33**, 3193 (1977).
19. E. L. Eliel and M. C. Knoeber. J. Am. Chem. Soc. **90**, 3444 (1968).
20. (*a*) S. Wolfe. Acc. Chem. Res. **5**, 102 (1972); (*b*) E. Juaristi. J. Chem. Educ. **56**, 438 (1979).
21. (*a*) C. F. Lane and G. W. Kramer. Aldrichimica Acta, **10**, 11 (1977); (*b*) G. B. Gill and D. A. Whiting. Aldrichimica Acta, **19**, 31 (1986).
22. W. C. Still, M. Kahn, and A. Mitra. J. Org. Chem. **43**, 2923 (1978).
23. S. G. Powell and R. Adams. J. Am. Chem. Soc. **42**, 646 (1920).
24. O. Dann and W. D. Arnott. Ann. **587**, 38 (1954).
25. G. Fontaine. Ann. Chim. **3**, 179 (1968).
26. U.S. Patent No. 3,799,892 (1974).
27. D. Huckle, I. M. Lockhart, and M. Wright. J. Chem. Soc. Perkin Trans. 1, 2425 (1972).
28. L. H. Klemm, J. Shabtai, and D. R. Taylor. J. Org. Chem. **33**, 1480 (1968).
29. H. E. Zimmermann and R. E. Factor. J. Am. Chem. Soc. **102**, 3538 (1980).
30. E. C. Taylor, C.-S. Chiang, and A. McKillop. Tetrahedron Lett. 1827 (1977).
31. K. J. Baird and M. F. Grundon. J. Chem. Soc. Perkin Trans. 1, 1820 (1980).

Can. J. Chem. Downloaded from www.nrcresearchpress.com by 213.222.148.141 on 09/07/12
For personal use only.

Ion–ion–solvent interactions in aqueous ionic cosolvent systems. II. Single-ion transfer free energies and entropies using tetraphenylarsonium tetraphenylborate reference electrolyte assumption in aqueous sodium nitrate solvent system

SIBAPRASAD RUDRA, HIMANSU TALUKDAR, AND KIRON K. KUNDU[1]
Physical Chemistry Laboratories, Jadavpur University, Calcutta – 700 032, India

Received February 19, 1987

SIBAPRASAD RUDRA, HIMANSU TALUKDAR, and KIRON K. KUNDU. Can. J. Chem. **65**, 2595 (1987).

Single-ion tranfer free energies $\Delta G_t^0(i)$ and entropies $\Delta S_t^0(i)$ of some electrolytes from water to 1, 2, and 4 *m* aqueous $NaNO_3$ solvents have been determined at 25°C using the widely used tetraphenylarsonium tetraphenylborate (Ph_4AsBPh_4) reference electrolyte assumption, after due modification for this solvent system. The required ΔG_t^0 and $T\Delta S_t^0$ values of Ph_4AsPi, $KBPh_4$, KPi, AgPi, $PbPi_2$, Ag_2CrO_4, and AgCl where Pi = picrate, were determined by measuring solubilities at 15–35°C of the solutes except AgCl, the values of which were determined from emf measurements. Analysis of $\Delta G_t^0(i)$ and $T\Delta S_t^0(i)$ values of the ions as well as their respective true interaction effects, $\Delta G_{t,tr.int}^0(i)$ and $T\Delta S_{t,tr.int}^0(i)$ as obtained after correcting for their cavity effects $\Delta G_{t,cav}^0(i)$ and $T\Delta S_{t,cav}^0(i)$ estimated by the scaled particle theory (SPT) and Born-type electrostatic effects, $\Delta G_{t,Born}^0(i)$ and $T\Delta S_{t,Born}^0(i)$ computed by simple Born equation, reveals that the behaviour of the ions in this ionic cosolvent system is chiefly guided by one or several effects of ion–ion–solvent, Born and cavity forming interactions. Moreover, a rational explanation has been offered to explain the observed mirror-image entropic behaviour of simple cations and anions in light of Kundu *et al.*'s four-steps transfer process.

SIBAPRASAD RUDRA, HIMANSU TALUKDAR et KIRON K. KUNDU. Can. J. Chem. **65**, 2595 (1987).

Opérant à 25°C et utilisant l'hypothèse du tétraphénylborate de tétraphénylarsonium (Ph_4AsBPh_4), un électrolyte de référence fréquemment utilisé, et après avoir fait les modifications appropriées pour le système de solvant, on a mesuré les énergies $G_t^0(i)$ et les entropies $\Delta S_t^0(i)$ libres de transferts mono-ioniques de quelques électrolytes de l'eau vers des solutions aqueuses 1, 2 et 4 *m* en $NaNO_3$. On a déterminé les valeurs requises de ΔG_t^0 et ΔS_t^0 du Ph_4AsPi, du $KBPh_4$, du KPi, du AgPi, du $PbPi_2$, du Ag_2CrO_4 et du AgCl (dans lesquels Pi = picrate) en mesurant leurs solubilités à des températures allant de 15 à 35°C; dans le cas du AgCl, on a déterminé ces valeurs à partir de mesures de fem. Une analyse des valeurs de $\Delta G_t^0(i)$ et $T\Delta S_t^0(i)$ des ions ainsi que de leurs effets respectifs d'interaction réelle, $\Delta G_{t,ver.int}^0(i)$ et $T\Delta S_{t,ver.int}^0(i)$, obtenues après avoir corrigé les effets de cavités $\Delta G_{t,cav}^0(i)$ et $T\Delta S_{t,cav}^0(i)$ qui ont été évalués par la théorie de la particule scalaire (TPS) et par les effets électrostatiques du type de Born, $\Delta G_{t,Born}^0(i)$ et $T\Delta S_{t,Born}^0(i)$, calculés par l'équation simple de Born, révèle que le comportement des ions dans ce système de cosolvant ionique résulte principalement d'un ou de plusieurs effets ion/solvant ionique ainsi que d'interactions de Born qui se produisent dans la cavité. De plus, utilisant le processus de transfert en quatre étapes proposé par Kundu et ses collaborateurs, on offre une explication rationnelle du comportement entropique d'image miroir qui a été observé avec des cations et des anions simples.

[Traduit par la revue]

Introduction

In the previous paper (1) we have reported for the first time the transfer thermodynamics of HCl and the related "ion–ion–solvent" interactions and solvent structuredness in 1, 2, and 4 *m* $NaNO_3$ solutions taking each composition as an individual solvent and taking the infinitely dilute solution of solutes in each solvent as the standard state, exactly similar to what is being done in aquo-organic solvent systems. As a part of our comprehensive studies and especially for better understanding of the individual ion behaviour in this solvent system, we are now reporting free energies of transfer, ΔG_t^0, and also entropies of transfer, $T\Delta S_t^0$, of some electrolytes and their constituent ions from water to the aqueous mixtures of 1, 2, and 4 *m* $NaNO_3$ at 25°C taking each composition as the individual solvent referred to above. These are determined by the widely used tetraphenylarsonium tetraphenylborate (Ph_4AsBPh_4) reference electrolyte (RE) assumption (2) which has been duly modified in the aquo-ionic solvent system as discussed later on.

Since the solubility of this RE itself is too low to be determined accurately in this ionic cosolvent system $\Delta X_t^0(Ph_4AsBPh_4)$ (X = G and S) values were obtained indirectly by relation [1]

$$[1] \quad \Delta X_t^0(Ph_4AsBPh_4) = \Delta X_t^0(Ph_4AsPi) + \Delta X_t^0(KBPh_4) - \Delta X_t^0(KPi)$$

where Pi = picrate. ΔX_t^0 values of the salts Ph_4AsPi, $KBPh_4$, and KPi were determined by solubility measurements (3, 4) at different temperatures. Moreover, to help determine $\Delta X_t^0(i)$ values for Cl^- and hence H^+ from $\Delta X_t^0(HCl)$ values reported in the previous paper, ΔX_t^0 values of AgPi have been determined by measuring the solubility of the compound spectrophotometrically and that of AgCl by emf measurements of cell [A] (5) at different temperatures

$$[A] \quad Ag/AgNO_3(m), NaNO_3 + water//AgCl, KCl(m), NaNO_3 + water/Ag$$

using 0.1 *m* NH_4NO_3 as the salt bridge in the respective solvent system.

Moreover, in order to facilitate understanding of the behaviour of divalent cations and anions in this solvent we have also determined ΔX_t^0 values of Ag_2CrO_4 and $PbPi_2$ from solubility measurements at different temperatures. Also, to verify the validity of the emf method adopted for AgCl, the solubilities of Ag_2CrO_4 were determined from emf measurements at 25°C using cell [B]

$$[B] \quad Ag/AgNO_3(m), NaNO_3 + water//Ag_2CrO_4, K_2CrO_4(m), NaNO_3 + water/Ag$$

Experimental

Sodium nitrate and other salts used were of AR quality. The method of preparation of $NaNO_3$ solutions has been described (1). Methods of

[1]Author to whom all correspondence should be addressed.

Can. J. Chem. Downloaded from www.nrcresearchpress.com by 213.222.148.141 on 09/07/12
For personal use only.

Can. J. Chem. Downloaded from www.nrcresearchpress.com by 213.222.148.141 on 09/07/12
For personal use only.

TABLE 1. Solubility products (K_{sp}) of Ph_4BK, Ph_4AsPi, KPi, AgPi, AgCl, Ag_2CrO_4, and $PbPi_2$ in H_2O and in aqueous $NaNO_3$ solvents at different temperatures

	pK^c_{sp} for H_2O					pK^c_{sp} for 1 *m* $NaNO_3$				
Solute	15°C	20°C	25°C	30°C	35°C	15°C	20°C	25°C	30°C	35°C
Ph_4BK	7.68	7.60	7.52 (7.53)[a]	7.47	7.41	5.71	5.64	5.57	5.49	5.41
Ph_4AsPi	9.16	9.02	8.93 (8.92)[a]	8.76	8.64	8.57	8.48	8.36	8.28	8.18
KPi	3.74	3.56	3.41 (3.41)[a]	3.25	3.09	3.52	3.28	3.05	2.84	2.62
AgPi	3.03	2.92	2.80	2.69	2.59	3.79	3.50	3.26	3.05	2.87
Ag_2CrO_4	11.90	11.40	11.07 (11.06)[b]	10.85	10.72	10.12	9.96	9.80 (9.79)[b]	9.59	9.35
$PbPi_2$	5.25	4.97	4.66	4.44	4.11	5.52	5.16	4.83	4.48	4.14
AgCl(pK^m_{sp})	10.24	10.04	9.81	9.66	9.48	9.58	9.38	9.21	9.02	8.84
	pK^c_{sp} for 2 *m* $NaNO_3$					pK^c_{sp} for 4 *m* $NaNO_3$				
Solute	15°C	20°C	25°C	30°C	35°C	15°C	20°C	25°C	30°C	35°C
Ph_4BK	5.16	5.10	5.03	5.00	4.95	4.34	4.29	4.25	4.21	4.17
Ph_4AsPi	8.65	8.34	8.44	8.33	8.21	8.98	8.78	8.64	8.54	8.45
KPi	3.80	3.66	3.50	3.33	3.13	4.25	4.09	3.92	3.78	3.61
AgPi	4.00	3.80	3.59	3.44	3.29	4.29	4.13	3.95	3.83	3.68
Ag_2CrO_4	9.58	9.44	9.33 (9.31)[b]	9.20	9.10	9.45	9.27	9.09 (9.06)[b]	8.88	8.67
$PbPi_2$	6.09	5.81	5.54	5.29	5.05	6.69	6.42	6.18	5.96	5.74
AgCl(pK^m_{sp})	9.44	9.24	9.05	8.86	8.68	9.30	9.08	8.86	8.66	8.46

[a]References 5 and 35.
[b]Electromotive force method.

preparation and purification of the salts Ph_4AsPi, $KBPh_4$, and KPi as well as the procedure for the determination of saturated solubilities of Ph_4AsPi and $KBPh_4$ in these solvents by spectrophotometric measurements were essentially similar to those described earlier (3–5). AgPi and $PbPi_2$ were prepared from $AgNO_3$ and $Pb(NO_3)_2$, respectively, by a process similar to that adopted for KPi. As the solubilities of these salts are rather large, we determined them spectrophotometrically at different "ionic strengths" using up to 0.15 *m* $KClO_4$ as the inert electrolyte and each composition of the solvent system as the standard reference state. The solubilities thus obtained at different "ionic strengths" arising from the added inert electrolyte and the saturated solutions of the respective salts were then extrapolated to "zero ionic strength" of the same at each solvent composition, which gives the solubilities of salts in the respective solvent composition. Notably, in view of the fact that in our treatment the salt solutions are assumed to be in their respective standard reference states, the "ionic strength" at any composition of the salt solution does not vary significantly due to small addition of $KClO_4$ and the effect of involved activity coefficient term is always small and disappears upon extrapolation to zero "ionic strength".

Ag_2CrO_4 was prepared by mixing equivalent amounts of $AgNO_3$ and K_2CrO_4 and washed several times with triple distilled water. Its solubilities were measured spectrophotometrically at the wavelength 364 nm where the molar extinction coefficient is 3490. The dilution of the aliquot of the saturated solution of each salt was made with triple distilled water. The appropriately diluted solutions were analyzed spectrophotometrically using a Perkin-Elmer (model 200) spectrophotometer. Constancy of two or three successively measured concentrations of each of the solutions to within ±1% was taken as the criterion for the attainment of the saturated solubility of the salts. At least two sets of measurements were made for all the solutes and the results were found to agree to within ±1%. Emf measurements of cell [A] and cell [B] were made by a Leeds and Northrup K_3-potentiometer and a Cambridge moving coil galvanometer. Ag/Ag^+ electrodes were prepared by electrochemical deposition of Ag on Pt-wire base from $K[Ag(CN)_2]$ solution using 5 mA current for 10–15 min. Electrodes having less than ±0.1 mV asymmetry potential were used. The emf's of cell [A] and cell [B] were measured for different molalities of KCl and K_2CrO_4 equilibrated with solid AgCl and Ag_2CrO_4, respectively, so as to determine pK_{sp} at "zero ionic strength."

Results

The observed saturated solubilities (S) in mol dm^{-3} at different temperatures for the salts Ph_4AsPi, $KBPh_4$, KPi, AgPi, Ag_2CrO_4, and $PbPi_2$ in different compositions of aqueous $NaNO_3$ solvent and also in water are given elsewhere.[2] Assuming that the salts are completely ionized the thermodynamic solubility products K_{sp} of the salts Ph_4AsPi, $KBPh_4$, KPi, AgPi, Ag_2CrO_4, and $PbPi_2$ were computed on the molar scale by relation [2]

$$[2] \quad pK^c_{sp} = -\log (\nu_+^{\nu_+} . \nu_-^{\nu_-}) S^{\nu_+ + \nu_-}$$

where ν_+ and ν_- represent the number of cation and anion, respectively, of the electrolyte. The corresponding mean molar activity coefficients $\gamma_\pm$ of the salts have been neglected for low soluble salts like $KBPh_4$, Ph_4AsPi, Ag_2CrO_4 and that of KPi, $PbPi_2$, and AgPi have been accounted for by determining the solubilities at zero "ionic strength" referred to above, by the usual extrapolation procedure. pK^c_{sp} values thus obtained at different temperatures are listed in Table 1. Estimated uncertainties in pK_{sp} values are within ±0.01.

[2]A complete set of the data referred to above may be purchased from the Depository of Unpublished Data, CISTI, National Research Council of Canada, Ottawa, Ont., Canada K1A 0S2.

Can. J. Chem. Downloaded from www.nrcresearchpress.com by 213.222.148.141 on 09/07/12
For personal use only.

TABLE 2. Coefficients a, b, and c in eq. [4] for Ph_4AsPi, KPi, Ph_4BK, AgPi, AgCl, Ag_2CrO, and $PbPi_2$ in H_2O and also in aqueous $NaNO_3$ solvents and transfer energetics (ΔG_t^0 and $T\Delta S_t^0$) of the salts from water to aqueous $NaNO_3$ solvents at 25°C (mole fraction scale)

	H_2O		
Solute	a/kJ mol^{-1}	b/kJ mol^{-1} K^{-1}	c/kJ mol^{-1} K^{-1}
Ph_4BK	121.5810	−2.1222	0.3315
Ph_4AsPi	−102.2828	3.3148	−0.4916
KPi	30.4168	0.4290	−0.0818
AgPi	50.3670	−0.3561	0.0423
Ag_2CrO_4	2361.0672	−50.9552	7.5906
$PbPi_2$	−129.3614	4.8249	−0.7549
AgCl	283.2739	−4.9417	0.7336

	1 m $NaNO_3$				
Solute	a/kJ mol^{-1}	b/kJ mol^{-1} K^{-1}	c/kJ mol^{-1} K^{-1}	ΔG_t^0/kJ mol^{-1}	$T\Delta S_t^0$/kJ mol^{-1}
Ph_4BK	−112.5379	3.1236	−0.4633	−11.36	14.21
Ph_4AsPi	25.2058	0.2314	−0.0273	−3.16	−7.78
KPi	96.5269	−0.6536	0.0682	−1.92	23.30
AgPi	645.7986	−12.9609	1.9056	2.51	37.38
Ag_2CrO_4	−675.7629	16.6165	−2.4857	−7.42	−25.17
$PbPi_2$	−60.3365	3.6861	−0.5952	0.69	20.72
AgCl	−5.8451	1.5046	−0.2297	−3.87	1.94

	2 m $NaNO_3$				
Solute	a/kJ mol^{-1}	b/kJ mol^{-1} K^{-1}	c/kJ mol^{-1} K^{-1}	ΔG_t^0/kJ mol^{-1}	$T\Delta S_t^0$/kJ mol^{-1}
Ph_4BK	155.6961	−3.0642	0.4631	−14.37	9.24
Ph_4AsPi	−125.2793	3.6861	−0.5448	−2.80	−4.35
KPi	−434.4353	10.9165	−1.6485	0.45	1.80
AgPi	403.9377	−7.8508	1.1522	4.33	18.32
Ag_2CrO_4	133.1282	−2.0326	0.3098	−10.04	−47.13
$PbPi_2$	201.4298	−2.7292	0.3791	4.91	−12.02
AgCl	51.2842	0.2568	−0.0448	−4.95	5.04

	4 m $NaNO_3$				
Solute	a/kJ mol^{-1}	b/kJ mol^{-1} K^{-1}	c/kJ mol^{-1} K^{-1}	ΔG_t^0/kJ mol^{-1}	$T\Delta S_t^0$/kJ mol^{-1}
Ph_4BK	43.1136	−0.6143	0.0967	−19.08	10.61
Ph_4AsPi	706.7576	−14.8718	2.2232	−1.83	1.45
KPi	−26.3107	1.7009	−0.2698	2.86	−3.53
AgPi	179.6275	−2.9720	0.4292	6.30	7.60
Ag_2CrO_4	−327.4032	8.8003	−1.3213	−11.77	−19.62
$PbPi_2$	265.8547	−4.3209	0.6227	8.17	−23.68
AgCl	102.4791	−0.7671	0.1041	−6.60	13.58

The free energies of solution of the salts (ΔG_s^0) on the molar scale were calculated for each solvent using relation [3]

$$[3] \quad \Delta G_s^0 = 2.303RT\mathrm{p}K_{sp}^c$$

and were fitted by the method of least squares to an equation of form [4]

$$[4] \quad \Delta G_s^0 = a + bT + cT \ln T$$

where T is the absolute temperature. The values of the coefficient, a, b, and c thus obtained are listed in Table 2. These values when applied to eq. [4] reproduce ΔG_s^0 values to within ±0.02 kJ mol^{-1}. The standard free energies of transfer ΔG_t^0 from water to the solvents were computed at 25°C on the mole fraction scale using relation [5]

$$[5] \quad \Delta G_t^0 = (a_s - a_w) + (b_s - b_w)T + (c_s - c_w)T \ln T + \text{scale effect}$$

where the scale effect is $\nu RT \ln M_w d_s / M_s d_w$. The subscripts s and w represent the quantities for solvent and water, respectively. M represents the appropriate molar mass of the solvent, and d is the density of the solvent (1), T = 298.15 K and $\nu = (\nu_+ + \nu_-) = 2$ for 1:1 electrolyte and 3 for 2:1 or 1:2 electrolyte.

The corresponding standard entropies of transfer were computed from eq. [6]

$$[6] \quad \Delta S_t^0 = (b_w - b_s) + (c_w - c_s) + (c_w - c_s) \ln T - \text{scale effect}$$

Can. J. Chem. Downloaded from www.nrcresearchpress.com by 213.222.148.141 on 09/07/12
For personal use only.

where the scale effect is $[\nu R \ln M_w d_s/M_s d_w + \nu RT(\mathrm{d} \ln d_s/\mathrm{d}T - \mathrm{d} \ln d_w/\mathrm{d}T)]$, temperature coefficient of the density being obtained from ref. 1. ΔG_t^0 and ΔS_t^0 values thus obtained are given in Table 2.

Assuming negligible junction potential across the salt bridge the emf (E_A) of cell [A] is given by [7]

$$[7] \quad E_A = \frac{RT}{F} \ln (a_{Ag^+})_l/(a_{Ag^+})_r$$

where the subscripts l and r refer to the left and right hand half cells, respectively. This E_A is related to K_{sp} of AgCl by [8]

$$[8] \quad pK'_{sp} = \frac{E_A \cdot F}{2.303RT} - \log (m_{Ag^+})_l - \log (m_{Cl^-})_r = pK_{sp} + 2 \log (\gamma_\pm) = pK_{sp} + f(\mu)$$

which has been obtained as a result of the experimental condition for that $(m_{Ag^+})_l = (m_{Cl^-})_r$ and hence assuming that $(\gamma_{Ag^+})_l = (\gamma_{Cl^-})_r = (\gamma_\pm)$.

The pK_{sp} values at infinite dilution were then determined by extrapolating the function of the observed linear plots pK'_{sp} defined by eq. [8], against the ionic strength μ to $\mu = 0$. The pK_{sp} values thus obtained on molal scale, pK^m_{sp} are reported in Table 1. Moreover, to verify the pK^m_{sp} values of AgCl obtained by this method, the pK^m_{sp} values of Ag_2CrO_4 were also determined at 25°C by the method using cell [B]. The pK^m_{sp} values of Ag_2CrO_4 thus obtained on the molal scale were then transformed to the molar scale. Notably, the pK^c_{sp} values of Ag_2CrO_4 obtained both by emf and spectroscopic methods are in fair agreement to within the limit ±0.02 as presented in Table 1. Evidently uncertainties to liquid junction potential are within experimental error.

The free energies of solution (ΔG^0_s) on the molal scale of AgCl were calculated using eq. [3] and fitted by the method of least squares to eq. [4]. ΔG^0_t(AgCl) and ΔS^0_t(AgCl) values on mole fraction scale were then calculated using [5] and [6], respectively, with the scale effect as $\nu RT \ln M_w/M_s$ for eq. [5] and $\nu R \ln M_w/M_s$ for eq. [6]. Those values are listed in Table 2. The estimated uncertainties in ΔG^0_t and ΔS^0_t for the different salts are ±0.03 kJ mol^{-1} and ±2 J K^{-1} mol^{-1}, respectively.

The transfer free energies of the relevant individual ions $\Delta G^0_t(i)$ were then computed by use of TATB assumption which has been widely used not only in pure solvents but also in various aquo-organic solvents because of its intrinsic merits (6). True, there might be some doubts on the validity of this assumption for the mixed solvents as there might be preferential solvation of cations or anions by the components of the mixed solvents. But whether that "preferential" solvation will really affect the relative solvation of these big Ph_4As^+ and Ph_4B^- ions is indeed highly questionable. However, in our aquo-ionic cosolvent system, because of the possible difference in Ph_4B^-–Na^+ and Ph_4As^+–NO_3^- interactions we have calculated our data in the following way. Since

$$[9] \quad {}_s\bar{X}^0(Ph_4AsBPh_4)^N = \Delta X^0_t(Ph_4AsBPh_4)^N + {}_w\bar{X}^0(Ph_4AsBPh_4)^N$$

$$[10] \quad {}_w\bar{G}^0(Ph_4AsBPh_4)^N = {}_w\bar{G}^0(Ph_4AsBPh_4)^c + 2RT \ln 1000\, d_w/M_w$$

and

$$[11] \quad {}_w\bar{S}^0(Ph_4AsBPh_4)^N = {}_w\bar{S}^0(Ph_4AsBPh_4)^c - 2R \ln 1000\, d_w/M_w - 2RT(\mathrm{d} \ln d_w/\mathrm{d}T)$$

where the superscripts N and c refer to mole fraction and molar scales, respectively, we have obtained the values of ${}_s\bar{G}^0(Ph_4AsBPh_4)^N$ by use of eqs. [9] and [10] as ${}_w\bar{G}^0(Ph_4AsBPh_4)^c$ is obtained by use of [4] in pure water. Similarly ${}_s\bar{S}^0(Ph_4AsBPh_4)^N$ is obtained using eqs. [9] and [11] and the temperature derivative of eq. [4] for pure water.

Now assuming that Ph_4B^-–Na^+ and Ph_4As^+–NO_3^- interactions are governed chiefly by coulombic interaction we have,

$$[12] \quad \frac{{}_s\bar{G}^0(Ph_4B^-)}{{}_s\bar{G}^0(Ph_4As^+)} = \frac{Ne^2[\epsilon_s(r_{Ph_4B^-} + r_{Na^+})]^{-1}}{Ne^2[\epsilon_s(r_{Ph_4As^+} + r_{NO_3^-})]^{-1}} = \frac{r_{Ph_4As^+} + r_{NO_3^-}}{r_{Ph_4B^-} + r_{Na^+}} = 1.05$$

taking $r_{Ph_4B^-} = r_{Ph_4As^+} = 0.420$ nm (7), $r_{Na^+} = 0.097$ nm (8), and $r_{NO_3^-} = 0.124$ nm (9). As TATB reference electrolyte assumption is also likely to be true regardless of temperatures, then as per above-noted assumption we have

$$[13] \quad \frac{{}_s\bar{S}^0(Ph_4B^-)}{{}_s\bar{S}^0(Ph_4As^+)} = \frac{-Ne^2[\epsilon_s\theta_s(r_{Ph_4B^-} + r_{Na^+})]^{-1}}{-Ne^2[\epsilon_s\theta_s(r_{Ph_4As^+} + r_{NO_3^-})]^{-1}} = \frac{r_{Ph_4As^+} + r_{NO_3^-}}{r_{Ph_4B^-} + r_{Na^+}} = 1.05$$

where θ_s^{-1} is given by $-\mathrm{d} \ln \epsilon_s/\mathrm{d}T$. Thus from eqs. [12] and [13] we get

$$[14] \quad \frac{{}_s\bar{X}^0(Ph_4B^-) + {}_s\bar{X}^0(Ph_4As^+)}{{}_s\bar{X}^0(Ph_4As^+)} = 2.05$$

or

$${}_s\bar{X}^0(Ph_4As^+) = \frac{1}{2.05}\,{}_s\bar{X}^0(Ph_4BAsPh_4)$$

and

$$[15] \quad {}_s\bar{X}^0(Ph_4B^-) = 1.05\,{}_s\bar{X}^0(Ph_4As^+)$$

The required values were therefore obtained by

$$[16] \quad \Delta\bar{X}^0_t(Ph_4B^-) = {}_s\bar{X}^0(Ph_4B^-) - {}_w\bar{X}^0(Ph_4B^-)$$

and

$$[17] \quad \Delta\bar{X}^0_t(Ph_4As^+) = {}_s\bar{X}^0(Ph_4As^+) - {}_w\bar{X}^0(Ph_4As^+)$$

The transfer free energies and entropies of the relevant individual ions, $\Delta X^0_t(i)$ were then computed by use of additivity relations. The results thus obtained for the solvents are presented in Table 3. The estimated uncertainties of the values are within ±0.1 kJ. Notably, as would be discussed later, the observed $\Delta S^0_t(i)$ values especially for small sized cations and anions, are very much similar to those observed in various aquo-organic solvents. And this seemingly suggests that TATB method is not only valid in aquo-organic solvents but also in aquo-ionic cosolvent systems like this, provided reasonable modification is made for the latter, as has been done in the present case.

Discussion

Free energies of transfer

ΔG^0_t–composition profiles for the salts and HCl are illustrated in Fig. 1. From this figure it appears that whilst the salts AgPi and $PbPi_2$ are increasingly destabilized and KPi, Ph_4AsPi, and HCl are increasingly destabilized after an initial stabilization up to 1–2 *m* $NaNO_3$, the salts AgCl, Ag_2CrO_4, and $KBPh_4$ are, however, increasingly stabilized with the increased

Can. J. Chem. Downloaded from www.nrcresearchpress.com by 213.222.148.141 on 09/07/12
For personal use only.

TABLE 3. Values of free energies and enthalpies of cavity formation ($\bar{G}_c$) and ($\bar{H}_c$) and standard free energies of transfer $\Delta G_t^0(i)$, $\Delta G_{t,cav}^0(i)$, $\Delta G_{t,Born}^0(i)$, and $\Delta G_{t,tr.int}^0(i)$ and entropies of transfer $T\Delta S_t^0(i)$, $T\Delta S_{t,cav}^0(i)$, $T\Delta S_{t,Born}^0(i)$, and $T\Delta S_{t,tr.int}^0(i)$ (mole fraction scale) in kJ mol^{-1} of the individual ions from water to aqueous $NaNO_3$ solvents at 25°C

	1 *m* $NaNO_3$											
Ions	$\bar{G}_c{}^a$ (water)	$\bar{G}_c{}^a$ (solvent)	$\bar{H}_c{}^a$ (water)	$\bar{H}_c{}^a$ (solvent)	$\Delta G_t^0(i)$	$\Delta G_{t,cav}^0(i)^a$	$\Delta G_{t,Born}^0(i)^b$	$\Delta G_{t,tr.int}^0(i)$	$T\Delta S_t^0(i)$	$T\Delta S_{t,cav}^0(i)^a$	$T\Delta S_{t,Born}^0(i)^b$	$T\Delta S_{t,tr.int}^0(i)$
Ph_4B^-	88.9	84.0	12.9	21.9	−5.3	−4.9	0.3	−0.7	−9.6	13.9	−0.4	−23.1
Ph_4As^+	88.9	84.0	12.9	21.9	−7.3	−4.9	0.3	−2.7	−7.2	13.9	−0.4	−20.7
K^+	13.1	12.4	1.7	2.9	−6.1	−0.7	1.0	−6.4	23.9	1.9	−1.2	23.2
Ag^+	11.8	11.2	1.5	2.6	−1.6	−0.6	1.0	−2.0	37.9	1.7	−1.3	37.5
H^+	13.5	12.8	1.8	3.1	0.6	−0.7	0.5	0.8	42.3	2.0	−0.6	40.9
Pb^{2+}	11.0	10.4	1.4	2.4	−7.6	−0.6	4.3	−11.3	21.8	1.6	−1.3	21.5
Pi^-	67.2	63.5	9.7	16.4	4.1	−3.7	0.4	7.4	−0.6	10.4	−0.4	−10.6
Cl^-	20.7	19.6	2.8	4.8	−2.2	−1.1	0.7	−1.8	−36.0	3.1	−0.9	−38.2
CrO_4^{2-}	17.0	16.1	2.3	3.9	−4.2	−0.9	3.2	−6.5	−101.1	2.5	−1.0	−102.6

	2 *m* $NaNO_3$									
Ions	$\bar{G}_c{}^a$	$\bar{H}_c{}^a$	$\Delta G_t^0(i)$	$\Delta G_{t,cav}^0(i)^a$	$\Delta G_{t,Born}^0(i)^b$	$\Delta G_{t,tr.int}^0(i)$	$T\Delta S_t^0(i)$	$T\Delta S_{t,cav}^0(i)^a$	$T\Delta S_{t,Born}^0(i)^b$	$T\Delta S_{t,tr.int}^0(i)$
Ph_4B^-	78.7	26.1	−7.9	−10.3	0.6	1.8	0.6	23.5	−1.0	−21.9
Ph_4As^+	78.7	26.1	−9.8	−10.3	0.6	−0.1	2.5	23.5	−1.0	−20.0
K^+	11.7	3.5	−6.5	−1.5	2.0	−7.0	8.7	3.3	−3.1	8.5
Ag^+	10.5	3.1	−2.6	−1.4	2.1	−3.3	25.2	3.0	−3.3	25.5
H^+	12.1	3.6	1.7	−1.5	1.0	2.2	20.5	3.3	−1.5	18.7
Pb^{2+}	9.8	2.9	−9.0	−1.3	8.9	−16.6	1.7	2.8	−3.4	2.3
Pi^-	59.5	20.0	7.0	−7.8	0.7	14.1	−6.9	18.1	−1.2	−23.8
Cl^-	18.4	5.7	−2.3	−2.4	1.5	−1.4	−20.1	5.3	−2.3	−23.1
CrO_4^{2-}	15.1	4.6	−4.8	−2.0	6.7	−9.5	−97.5	4.3	−2.6	−99.2

	4 *m* $NaNO_3$									
Ions	$\bar{G}_c{}^a$	$\bar{H}_c{}^a$	$\Delta G_t^0(i)$	$\Delta G_{t,cav}^0(i)^a$	$\Delta G_{t,Born}^0(i)^b$	$\Delta G_{t,tr.int}^0(i)$	$T\Delta S_t^0(i)$	$T\Delta S_{t,cav}^0(i)^a$	$T\Delta S_{t,Born}^0(i)^b$	$T\Delta S_{t,tr.int}^0(i)$
Ph_4B^-	69.4	22.6	−11.0	−19.6	1.3	7.3	7.0	29.3	−5.1	−17.2
Ph_4As^+	69.4	22.6	−12.8	−19.6	1.3	5.5	8.6	29.3	−5.1	−15.6
K^+	10.4	3.1	−8.1	−2.8	4.1	−9.4	3.6	4.2	−16.0	15.4
Ag^+	9.4	2.8	−4.6	−2.5	4.4	−6.5	14.8	3.8	−16.9	27.9
H^+	10.7	3.2	2.6	−2.9	2.0	3.5	−0.1	4.3	−7.7	3.3
Pb^{2+}	8.8	2.6	−13.7	−2.3	18.3	−29.7	−9.4	3.5	−17.7	4.8
Pi^-	52.5	17.0	10.9	−14.8	1.5	24.2	−7.2	22.1	−5.9	−23.4
Cl^-	16.3	5.0	−2.0	−4.5	3.0	−0.5	−1.2	6.7	−11.8	3.9
CrO_4^{2-}	13.4	4.1	−2.5	−3.7	13.7	−12.5	−49.1	5.5	−13.3	−41.3

[a]The required diameters of the solvent constituents and the values of the scale effect $RT \ln V_w/V_s$ are taken as given in ref. 1, $\alpha = -d \ln d_s/dT$, also taken from the same paper, and those for the solute species $b_{Ph_4B^-} = 0.84$ nm (7), $b_{Pi} = 0.72$ nm as tentatively taken to be equal to that of pNA given in ref. 13(*b*), $b_{Cl^-} = 0.362$ nm (32), $b_{K^+} = 0.270$ nm (32), $b_{H_3O^+} = 0.276$(1), $b_{Ag^+} = 0.252$ nm (32), $b_{Pb^{2+}} = 0.240$ nm (8), $b_{CrO_4^{2-}} = 0.320$ nm (9).

[b]The required radii of the ionic species are obtained from the corresponding diameters of the species as indicated in *a* and that of H^+ as equal to 0.276 nm (1).

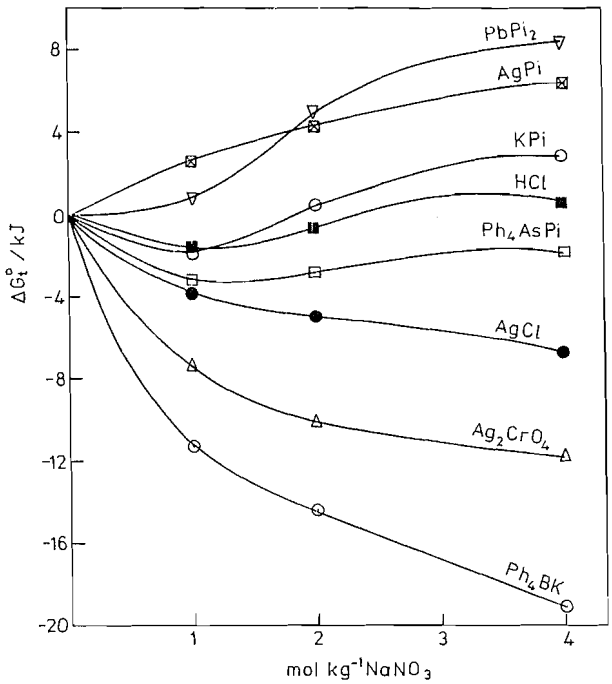

FIG. 1. Variation of ΔG_t^0 of different electrolytes with molality of $NaNO_3$ in aqueous $NaNO_3$ solutions.

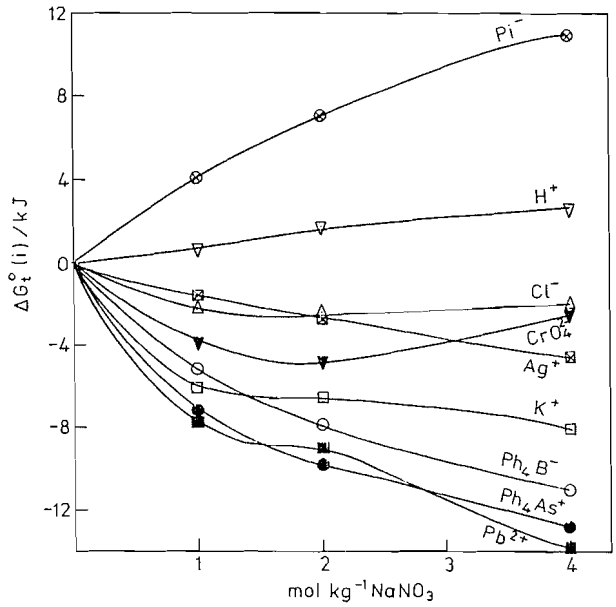

FIG. 2. Variation of $\Delta G_t^0(i)$ of different ions with molality of $NaNO_3$ in aqueous $NaNO_3$ solutions.

molality of $NaNO_3$. But as indicated in our previous paper for HCl (1), the behaviour of these salts like the acid HCl is also likely to be chiefly guided by the combined effects of "ion–ion–solvent" interactions of the cations and anions of the solutes with the oppositely charged ionic constituents of the ionic cosolvent $NaNO_3$ and the possible repulsive interactions between the similarly charged ions (1) besides the destabilizing Born-type electrostatic interactions arising from the difference of the dielectric constant of solvent (10, 11). Thus a discussion of $\Delta G_t^0(i)$ values of single ions rather than those of the electrolytes should be more informative regarding the involved ion–ion–solvent interactions and the $\Delta G_t^0(i)$–composition profiles for single ions are illustrated in Fig. 2. Significantly enough, $\Delta G_t^0(i)$–composition profiles for anions like Cl^- and CrO_4^{2-} show an upward trend after passing through a shallow minimum around 1–2 *m* $NaNO_3$ while those for Pi^- and Ph_4B^- move increasingly upward and downward, respectively, right from the beginning. But while $\Delta G_t^0(i)$ values for cations like Ag^+, K^+, and Pb^{2+} are more or less increasingly negative those for H^+ are increasingly positive. Evidently the behaviour of Ph_4B^- or H^+ seems to be "odd man out" in the respective cases.

As per discussion in our previous paper (1), transfer energetics ΔX_t^0 (X = G, H, and S) can be taken to compose of cavity forming effect $\Delta X_{t,cav}^0$, Born-type electrostatic effect $\Delta X_{t,Born}^0$ and the true interaction effect $\Delta X_{t,tr.int}^0$ i.e.

$$[18]\quad \Delta X_t^0(i) = \Delta X_{t,cav}^0 + \Delta X_{t,Born}^0(i) + \Delta X_{t,tr.int}^0(i)$$

Thus the discussion of true transfer free energies of ions $\Delta G_{t,tr.int}^0(i)$ rather than $\Delta G_t^0(i)$ should be more informative. Consequently we have tentatively computed $\Delta G_{t,Born}^0(i)$ and $\Delta G_{t,cav}^0(i)$ terms for the different ions by the simple Born equation (10) and scaled particle theory (SPT) (12), respectively, as per formulations described and referred to in the previous papers (1, 13). These and the required solvent and solute parameters are given in Table 3. The values of $\Delta G_{t,Born}^0(i)$ and $\Delta G_{t,cav}^0(i)$ and also $\Delta G_{t,tr.int}^0(i)$ so obtained are given in Table 3 and depicted in Fig. 3.

Significantly enough, in the case of small sized ions like Cl^-, H^+, Ag^+, and K^+ the cavity effect is smaller and in fact gets nullified to a larger extent by the opposing Born effect. In the case of bivalent ions like Pb^{2+} and CrO_4^{2-} $\Delta G_{t,tr.int}^0(i)$–composition profiles become more negative than the $\Delta G_t^0(i)$–composition profiles, indicating larger stabilization of these ions due to true interaction effects.

As indicated in the previous paper (1), consequent to the assumed standard state in this ionic cosolvent system $\Delta G_{t,tr.int}^0(i)$ values of the transferred small-sized ions are likely to be chiefly guided by the ion–ion–solvent interactions with the constituent ions of the ionic cosolvent $NaNO_3$ relative to that in water. Various spectroscopic (14–16) and other evidences (17) indicate that in the solvent composition up to 1.5 *m* $NaNO_3$ the prevalent ionic species are $(Na^+)_{aq}$ and NO_3^-.

The observed stabilization of Cl^- or CrO_4^{2-} in this region therefore suggests that the resulting attractive interaction of these ions and $(Na^+)_{aq}$ over the repulsive interaction of Cl^- or CrO_4^{2-} and NO_3^- exceeds the Cl^-–H_2O or CrO_4^{2-}–H_2O interaction in pure water. This is probably due to the fact that H_2O molecules in the hydration cosphere round Na^+ have more protonic character (δ^+) than that in pure water and hence are likely to induce more "acid–base" type (18) short range interaction with Cl^- or CrO_4^{2-} ion than that in pure water. The observed more downward trend of CrO_4^{2-} than that of Cl^- indicates that CrO_4^{2-} interacts more strongly with $(Na^+)_{aq}$ due to its doubly charged character.

On the other hand, the observed increased stabilization of cations such as Ag^+, K^+, and Pb^{2+} suggests that the attractive interactions between these ions and the unhydrated NO_3^- are so strong that these seemingly overcome the combined opposite effects of Born-type electrostatic and weak cation–$(Na^+)_{aq}$ repulsive interactions. The observed larger stabilization of the divalent Pb^{2+} than the univalent Ag^+ and K^+ is evidently the result of its more attractive interaction with NO_3^- ion. The observed increased destabilization of H^+ is, however, indicative of the resultant effect of smaller attractive interactions between H_3O^+ (rather than bare proton) with delocalised (δ^+) charge on 3-H atom, and NO_3^- and the destabilizing repulsive interactions of H_3O^+ with $(Na^+)_{aq}$ bearing more protonic

Can. J. Chem. Downloaded from www.nrcresearchpress.com by 213.222.148.141 on 09/07/12
For personal use only.

Can. J. Chem. Downloaded from www.nrcresearchpress.com by 213.222.148.141 on 09/07/12
For personal use only.

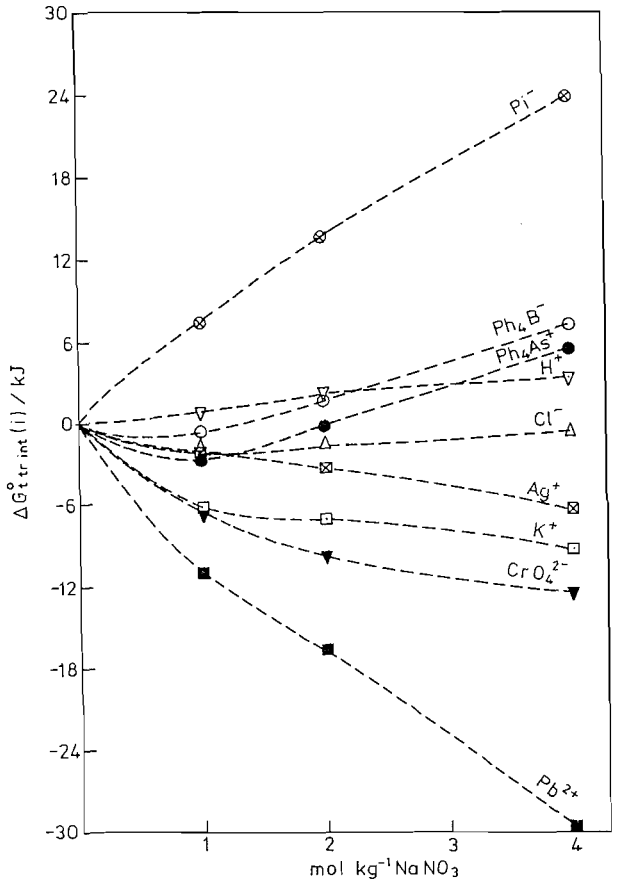

FIG. 3. Variation of $\Delta G^0_{t,tr.int}(i)$ of different ions with molality of $NaNO_3$ in aqueous $NaNO_3$ solutions.

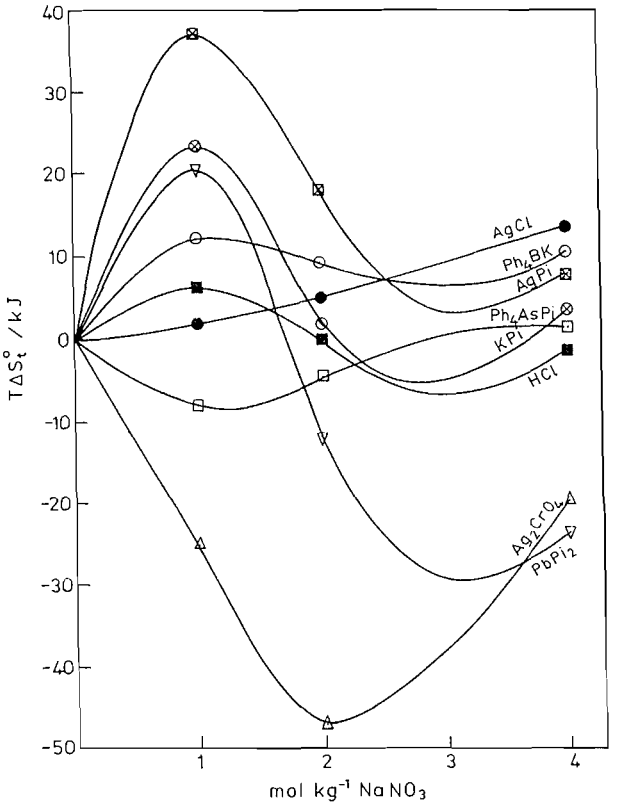

FIG. 4. Variation of $T\Delta S^0_t$ of different electrolytes with molality of $NaNO_3$ in aqueous $NaNO_3$ solutions.

character of H_2O molecules in the hydration cosphere around Na^+. More importantly, the effect of structural propensity of H_3O^+ in 3-D structures in pure water also augments largely the observed destabilization of H_3O^+ in these aqueous $NaNO_3$ solutions. All this explains the odd-man-out behaviour of H^+ compared to other cations.

From Figs. 2 and 3 it appears that while $\Delta G^0_t(i)$–compositions for Ph_4B^- and Ph_4As^+ become increasingly negative, $\Delta G^0_{t,tr.int}(i)$–composition profiles become increasingly positive after passing through a shallow minimum around 1 *m* $NaNO_3$. This implies that the observed stabilization of Ph_4B^- and Ph_4As^+ as reflected in $\Delta G^0_t(i)$ values, is dictated by the pronounced cavity effect, since the solvation of large hydrophobic molecular ions is always associated with the creation of cavity inside the bulk of the solvent (7, 12, 19, 20) and that the salting-out of these hydrophobic Ph_4B^- and Ph_4As^+ ions become increasingly predominant with the increased proportion of the ionic cosolvent $NaNO_3$, as expected from the larger hydrophobic effect in salt solution than in water.

Similarly, the relative positions of $\Delta G^0_t(i)$ and $\Delta G^0_{t,tr.int}(i)$–composition profiles for Pi^- are also indicative of the fact that the pronounced cavity-effect partly opposes the "true interaction" effects of the species. The latter effects are largely guided by the "salting-out" effect on the hydrophobic parts of the species overcoming the relatively smaller stabilization effect of the anionic features of Pi^- in this ionic cosolvent system compared to that in pure water. Moreover, the pronounced H-bonding stabilization of Pi^- through three NO_2 groups in water also contribute to the observed destabilization of Pi^- in the salt solutions.

Notably, the observed near invariance of $\Delta G^0_{t,tr.int}(i)$ values of the smaller ions beyond 1.5 *m* $NaNO_3$ is indicative of the effect of constitutional features of the aqueous ionic cosolvent system beyond 1–15 *m* as obtained from various spectroscopic evidences (14–16) indicated earlier (1). Evidently, the solvent separated ion-pairs (SSIP) present beyond 1.5 *m* $NaNO_3$ diminish the intensity of cation–anion or anion–cation attractive interactions to a large extent particularly for the small sized cations and anions.

Entropies of transfer

Figure 4 depicts the $T\Delta S^0_t$–composition profiles of some salts at 25°C. Strikingly enough, $T\Delta S^0_t$–composition profiles of AgPi, KPi, $PbPi_2$, and $KBPh_4$, unlike that of AgCl, pass through a maximum whilst those of Ph_4AsPi and Ag_2CrO_4 pass through a minimum around 1–1.5 *m* $NaNO_3$. Since the discussion of $T\Delta S^0_t(i)$ values of single ions rather than those of the electrolytes should provide more information on solvent structuredness, $T\Delta S^0_t(i)$–composition profiles for the ions are illustrated in Fig. 5. Significantly enough, $T\Delta S^0_t(i)$–composition profiles for all cations pass through a maximum whilst those for all anions pass through a minimum. Pi^- is seemingly the odd-man-out as its profile passes through a slight maximum.

Notably, the observed mirror-image behaviour of $T\Delta S^0_t(i)$ for these small hydrophilic cations and anions may lead one to wonder if it is due to the possible uncertainties of the involved modification of the RE assumption. But the fact that similar type of behaviour has also been observed in the aqueous mixtures of Bu^{t}OH (21), DMSO (4*b*, 22), ACN (4*d*, 23), DMF (24), MeOH (25), urea (26), and glycerol (26) lead us to believe that as in aquo-organic solvents, the basic RE assumption and its modification for the present solvent system are free from uncertainties. Notably, Marcus (6), Juillard *et al.* (21), and

Can. J. Chem. Downloaded from www.nrcresearchpress.com by 213.222.148.141 on 09/07/12
For personal use only.

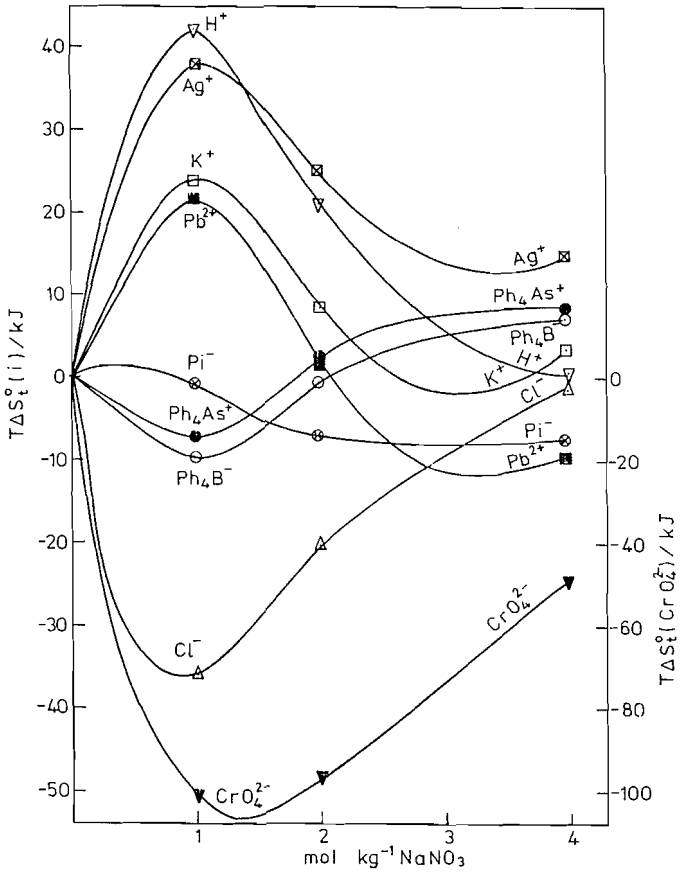

FIG. 5. Variation of $T\Delta S_t^0(i)$ of different ions with molality of $NaNO_3$ in aqueous $NaNO_3$ solutions.

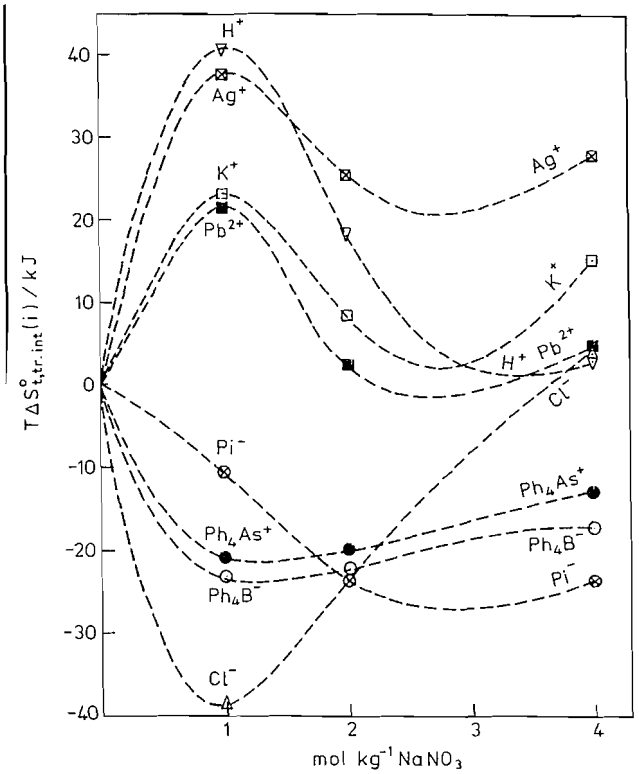

FIG. 6. Variation of $T\Delta S^0_{t,tr.int}(i)$ of different ions with molality of $NaNO_3$ in aqueous $NaNO_3$ solutions.

Abraham *et al.* (25) also indicated that the widely used RE assumption for $\Delta G_t^0(i)$ at 25°C should be equally true irrespective of temperatures and hence $T\Delta S_t^0(i)$ data for the individual ions should be no less meaningful.

But the question why cations and anions show opposite behaviour in $T\Delta S_t^0(i)$–composition profile is not yet accounted for satisfactorily. Indeed the cationic behaviour in some cosolvent systems (21, 23, 25) has been adduced in light of the effects of structural changes of the solvents, relative hydration/solvation and preferential solvation of the cations, solvent sorting in the coordination sphere of the cations (23*b*), no tangible explanation has yet been offered for the anions.

Thus before we analyse the implications of the observed maxima and minima in this solvent system let us make at least a tentative estimate of (*a*) the Born-type electrostatic contribution, $\Delta S^0_{t,Born}(i)$ with the help of the simple Born equation as described in our previous paper (27) and (*b*) the cavity effect term $\Delta S^0_{t,cav}(i)$ through SPT using the formulations described in our previous papers (13). Since the required temperature coefficients of dielectric constants ($\theta^{-1} = -d \ln \epsilon / dT$) are not known at different compositions for the solvent system, we have tentatively obtained them by assuming $(\theta_s)_{NaNO_3} = (\theta_s)_{NaCl}$ in the corresponding compositions for NaCl. θ_s values for different molalities of NaCl system are obtained from the slope of the observed linear plots of ln ϵ_s vs. T, ϵ_s values being obtained from Akhadov's monograph (28). The values of $\Delta S^0_{t,Born}(i)$, $\Delta S^0_{t,cav}(i)$, and $\Delta S^0_{t,tr.int}(i)$ so obtained are given in Table 3. The latter values are also illustrated in Fig. 6. Significantly enough there are little differences between $T\Delta S_t^0(i)$ and $T\Delta S^0_{t,tr.int}(i)$–composition profiles for most of the ions save Pi^- and Ph_4B^-/Ph_4As^+ which become fairly more negative.

Following Kundu *et al.*'s four-step transfer process (27*b*, 29) and the discussion in our previous paper (1), we may try to explain the observed results for different cations and anions as follows. It is well known that due to low ionic force field hydrophilic anions like Cl^- are generally less hydrated and often designated as structure breakers (17). As a result ΔS_1^0 the entropy change accompanying step 1, i.e., breaking down of hydration sphere round the anions is more or less fairly small. However, the secondary solvation zone (SSZ) is fairly large in these cases, $|-\Delta S_2^0|$, the entropy change, accompanying step 2, i.e., the formation of three dimensional (3D) ice-like water structure out of the released disordered water molecules from the SSZ, is largely negative. The net contributions ($\Delta S_1^0 - \Delta S_2^0$) are therefore likely to be largely negative for different anions.

Now at initial compositions, i.e., below 1.5 *m* $NaNO_3$ the prevalent ionic species are free $(Na^+)_{aq}$ and NO_3^- (14–17). Since the anions are likely to be stabilized by $(Na^+)_{aq}$, as indicated earlier, the entropy change ΔS_3^0 associated with the step 3, i.e. the breakdown of the relevant structure of the solvents or of the solvating species in the solvent, would be zero. Also, as the anions are likely to induce more order by restricting the translation degree of freedom of $(Na^+)_{aq}$ round the added anions, $|-\Delta S_4^0|$ the entropy change in the step 4, i.e., for the formation of ion–ion solvated species with the incoming ions in $NaNO_3$ solution, will be increasingly negative. This is also true for overall contributions ($\Delta S_1^0 - \Delta S_2^0$) + ($\Delta S_3^0 - \Delta S_4^0$) or $\Delta S^0_{t,tr.int}(i)$, as have been observed for the anions like Cl^-.

But after about 1.5 *m* $NaNO_3$ where the ionic species are being increasingly replaced by solvent-separated ion-pairs

Can. J. Chem. Downloaded from www.nrcresearchpress.com by 213.222.148.141 on 09/07/12
For personal use only.

(SSIP), ΔS_3^y would be more and more positive for breaking down the SSIP first to free NO_3^- and $(Na^+)_{aq}$ and then to free NO_3^- and Na^+ especially when water content diminishes at still higher concentration of $NaNO_3$. Evidently at higher $NaNO_3$ compositions while ΔS_3^0 will be increasingly positive, ΔS_4^0 will be increasingly less negative and thus $(\Delta S_3^0 - \Delta S_4^0)$ increasingly positive. Consequently the opposing effects of $(\Delta S_1^0 - \Delta S_2^0)$ and $(\Delta S_3^0 - \Delta S_4^0)$ will result in a minimum in $\Delta S_{t,tr.int}^0(i)$–composition profiles for the anions as have been observed. The observed relative position of the said profile for CrO_4^{2-} also conforms to the effect of divalent character of CrO_4^{2-} as compared to the monovalent Cl^-.

On the other hand, the relative positions of the composition profiles of $T\Delta S_t^0(i)$ and $T\Delta S_{t,tr.int}^0(i)$ for Pi^- suggest that the cavity effect plays an important role (also see Table 3). Moreover, the essentially similar nature of the latter profile with that of Cl^- or CrO_4^{2-} is indicative of the fact that entropic contributions of the characteristic features of the hydrophilic anions as discussed above are somewhat subdued by the opposing hydrophobic effects of the aromatic ring of Pi^-. In the cases of Ph_4B^- and Ph_4As^+, cavity effect of course plays an important role (see Table 3 and Fig. 6). As their solvation is chiefly guided by water molecules rather than $(Na^+)_{aq}$ or NO_3^-, respectively, their initial downward trends followed by the upward bent are also indicative of the fact that $NaNO_3$ is a 3D structure breaker up to about 1.5 *m*, thus causing the observed downward trend (13, 29). Since the water molecules are increasingly engaged for the SSIP, they impart the observed upward trends in $T\Delta S_t^0$ at higher compositions.

On analyzing the cations we find that, unlike the anions, $T\Delta S_t^0(i)$ and $T\Delta S_{t,tr.int}^0(i)$–composition profiles pass through maxima around 1–1.5 *m* $NaNO_3$ and their relative order is $H^+ > Ag^+ > K^+ > Pb^{2+}$. In view of the fact that small hydrophilic cations like these are usually largely hydrated, ΔS_1^0 values are expected to be large positive quantities. Since $|-\Delta S_2^0|$ is the entropy change accompanying the formation of 3D water structure by the water molecules set free in step 1, it would be smaller than the corresponding ΔS_1^0. This is because in step 1 we have to dismantle larger order induced by ionic force field around these cations, while in step 2 ordering is induced by the weaker H-bonding interactions around the central water molecules. As a result the difference $(\Delta S_1^0 - \Delta S_2^0)$ is a large positive quantity characteristic to the cations concerned.

Now in the initial compositions of the aqueous $NaNO_3$ solvent system, where prevalent NO_3^- ions are free to "solvate" the added cations, $\Delta S_3^0 = 0$. However, electrostatic interactions between cations and NO_3^- ions cause ΔS_4^0 to be increasingly negative. Consequently, the negative $(\Delta S_3^0 - \Delta S_4^0)$ would increasingly nullify the positive $(\Delta S_1^0 - \Delta S_2^0)$. Beyond about 1.5 *m* $NaNO_3$ where the free ions are gradually replaced by SSIP, $(Na^+)_{aq}NO_3^-$, and NO_3^- side being relatively free as compared to $(Na^+)_{aq}$ of the SSIP, added cations are likely to interact directly with the SSIP through the NO_3^- ions causing ΔS_3^0 to be zero and ΔS_4^0 to be increasingly negative. Consequently the difference $(\Delta S_3^0 - \Delta S_4^0)$ will ultimately overcome the positive contribution of $(\Delta S_1^0 - \Delta S_2^0)$ and thus result in a maximum in $T\Delta S_{t,tr.int}^0$–composition profile, as observed.

The observed relative positions of the $\Delta S_{t,tr.int}^0(i)$–composition profiles of cations around the maximum, viz. $H^+ > Ag^+ > K^+ > Pb^{2+}$ are also fairly in conformity with the relative hydration of these cations. In fact, of all these cations H^+ is highly hydrated because it easily fits in the water lattice and also facilitates to form not only H_3O^+ but also $H_9O_4^+$ (30), as detected in the gas phase from mass spectra by Kebarle (31). The crystallographic radius of Ag^+ (0.126 nm) (32) is not much smaller than that of K^+ (0.135 nm) (32) and the remarkably enhanced maximum for Ag^+ compared to K^+ is the reflection of larger hydration of Ag^+ than K^+. This is evident from the viscosity *B*-coefficients (17); $B_{Ag^+} = 0.089$ vs. $B_{K^+} = 0.007$ and also from the hydration numbers (*n*) obtained by the mobility method (33): $n_{Ag^+} = 2.4$ compared to that for $n_{K^+} = 1.00$. Similarly, although Pb^{2+} is doubly charged and is likely to be highly hydrated, due to the screening effect on nuclear charge by the surrounding multi-electron atmosphere in the outer orbits, the effective force field and hence the hydration is likely to be fairly small compared to other bivalent cations like Mg^{2+}, Ca^{2+} etc. In fact, while the hydration number as obtained by acidity function method (34) for $n_{Mg^{2+}} = 7.4$, $n_{Ba^{2+}} = 6.6$, $n_{Sr^{2+}} = 5.8$, and $n_{Pb^{2+}} = 1.9$. All these values thus reflect smaller hydration of Pb^{2+} compared to that of other bivalent cations. This result seemingly substantiates the observed relative position of $T\Delta S_{t,tr.int}^0$–composition profile of Pb^{2+} compared to the monovalent cations studied here.

Conclusions

The results of the present study reveal that the entropic contributions of the ionic constituents of electrolytes like MX (X = Cl and the like, and M = H, K, and the like) in this ionic cosolvent system behave, on the one hand, almost opposite to each other, while on the other hand, exactly similar to that observed in some aqueous nonionic cosolvent systems referred to earlier. Moreover, since $\Delta S_t^0(i)$ is guided by the ion–ion–solvent interactions of the oppositely charged constituents of the ionic cosolvent, rather by water molecules, neither the transfer entropies of the electrolytes nor those of their ionic constituents would directly or unambiguously reflect the structuredness of the solvents. Consequently, $\Delta S_t^0(HX)$ or rather $\Delta S_{t,tr.int}^0(HX)$ in aqueous ionic cosolvent systems which are usually considered 3D water structure breakers (17), can be hardly used to provide the desired extra confidence to its use as a structural probe for aquo-organic solvents, as envisaged by us earlier (1).

Acknowledgement

We wish to thank the University Grants Commission, New Delhi, for financial assistance.

1. S. Rudra, H. Talukdar, B. P. Chakravarty, and K. K. Kundu. Can. J. Chem. **64**, 1960 (1986).
2. B. G. Cox, G. R. Hedwig, A. J. Parker, and D. W. Watts. Aust. J. Chem. **27**, 477 (1974) and relevant references therein.
3. O. Popovych. Crit. Rev. Anal. Chem. **1**, 73 (1970) and relevant references therein.
4. A. K. Das and K. K. Kundu. (*a*) Ind. J. Chem. **16**A, 467 (1978); (*b*) J. Soln. Chem. **8**, 259 (1979); (*c*) I. N. Basu-Mullick and K. K. Kundu. Can. J. Chem. **58**, 79 (1980); (*d*) K. Das, A. K. Das, and K. K. Kundu. Electrochim. Acta, **26**, 471 (1981); (*e*) A. Bhattacharya, J. Datta, K. Das, and K. K. Kundu. Ind. J. Chem. **21**A, 9 (1982) and relevant references therein.
5. K. K. Kundu and A. J. Parker. J. Soln. Chem. **10**, 8471 (1981).
6. Y. Marcus. (*a*) Pure Appl. Chem. **55**, 977 (1983); **57**, 1103 (1985); (*b*) J. Chem. Soc. Faraday Trans. I, **83**, 339 (1987).
7. C. Treiner. Can. J. Chem. **55**, 682 (1977).
8. R. C. Weast. Handbook of Chemistry and physics. 52nd ed. The Chemical Rubber Co., Cleveland, OH. 1971–1972, p. F-171.
9. J. V. Leyendekkers. J. Chem. Soc. Faraday Trans. I, **78**, 357 (1982).

10. M. BORN. Z. Physik, **1**, 45 (1920).
11. R. G. BATES. *In* Hydrogen-bonded solvent systems. *Edited by* A. K. Covington and P. Jones. Taylor and Francis, London. 1968. p. 49.
12. R. A. PIEROTTI. J. Phys. Chem. **67**, 1840 (1963); **69**, 281 (1965); Chem. Rev. **76**, 717 (1976).
13. J. DATTA and K. K. KUNDU. (*a*) Can. J. Chem. **61**, 625 (1983); (*b*) J. Phys. Chem. **86**, 4055 (1982).
14. D. E. IRISH and A. R. DAVIS. Can. J. Chem. **46**, 943 (1968).
15. M. M. VOILMAR. J. Chem. Phys. **39**, 2236 (1963).
16. R. L. FROST and D. W. JAMES. J. Chem. Soc. Faraday Trans. I, **78**, 3223 (1982).
17. M. KAMINSKY. Discuss. Faraday Soc. **24**, 171 (1957).
18. D. FEAKINS. *In* Physico-chemical processes in mixed aqueous solvents. *Edited by* F. Franks. Heinemann, London. 1967. p. 71.
19. N. DESROSIERS and J. E. DESNOYERS. Can. J. Chem. **54**, 3800 (1976).
20. C. TREINER, P. TZIAS, and M. CHEMLA. J. Chem. Soc. Faraday Trans. I, **72**, 2007 (1977).
21. (*a*) J. JUILLARD. J. Chem. Soc. Faraday Trans. I, **78**, 43 (1982); (*b*) J. JUILLARD, C. TISSIER, J. BARCZYNSKA, J. MOKRZAN, and S. TANIEWSKA-OSINSKA. J. Chem. Soc. Faraday Trans. I, **81**, 3081 (1985).
22. (*a*) P. K. BISWAS and M. N. DAS. J. Chem. Soc. Faraday Trans. I, **82**, 1973 (1986); (*b*) R. FUCHS, C. P. HAGEN, and R. F. RODEWALD. J. Phys. Chem. **78**, 1509 (1974).
23. (*a*) K. MIYAJI and K. MORINAGA. Bull. Chem. Soc. Jpn. **59**, 1695 (1986); (*b*) B. G. COX, R. NATARAJAN, and W. S. WAGHORNE. J. Chem. Soc. Faraday Trans. I, **75**, 86 (1979).
24. M. BOOIJ and G. SOMSEN. Electrochim. Acta, **28**, 1883 (1983).
25. M. H. ABRAHAM, T. HILL, H. C. LING, R. A. SCHULZ, and R. A. C. WATT. J. Chem. Soc. Faraday Trans. I, **80**, 489 (1984).
26. H. TALUKDAR, S. RUDRA, and K. K. KUNDU. Electrochim. Acta. To be published.
27. (*a*) U. SEN, K. K. KUNDU, and M. N. DAS. J. Phys. Chem. **71**, 3665 (1967); (*b*) K. K. KUNDU and K. MAZUMDAR. J. Chem. Soc. Faraday Trans. I, **69**, 806 (1973).
28. Y. Y. AKHADOV. Dielectric properties of binary solutions. Pergamon Press, 1980.
29. K. BOSE, K. DAS, A. K. DAS, and K. K. KUNDU. J. Chem. Soc. Faraday Trans. I, **74**, 1051 (1978).
30. J. O'M. BOCKRIS and A. K. N. REDDY. Modern electrochemistry. Vol. 1. Plenum Press, New York. 1970. p. 470.
31. P. KEBERLE. J. Am. Chem. Soc. **89**, 6393 (1967).
32. H. S. HARNED and B. B. OWEN. Physical chemistry of electrolyte solutions. Reinhold Publication, New York. 1958. p. 651.
33. H. SADEK. J. Electroanal. Chem. **11**, 144 (1983).
34. L. LEIFER and H. HAGFELDT. Proc. 1st Australian Conference on Electrochemistry. Sydney, 1963. p. 107.
35. O. POPOVYCH, A. GIBOFSKY, and D. H. BERNE. Anal. Chem. **44**, 811 (1972).

Can. J. Chem. Downloaded from www.nrcresearchpress.com by 213.222.148.141 on 09/07/12
For personal use only.

Forbeside C, a saponin from *Asterias forbesi*. Complete structure by nuclear magnetic resonance methods[1]

JOHN A. FINDLAY AND MAHESH JASEJA
Department of Chemistry, University of New Brunswick, Fredericton, N.B., Canada E3B 6E2

AND

JEAN-ROBERT BRISSON
Division of Biological Sciences, National Research Council of Canada, 100 Sussex Drive, Ottawa, Ont., Canada K1A 0R6

Received March 23, 1987

This paper is dedicated to the memory of Professor Karel Wiesner

JOHN A. FINDLAY, MAHESH JASEJA, and JEAN-ROBERT BRISSON. Can. J. Chem. **65**, 2605 (1987).

The structure of forbeside C, a saponin from the starfish *Asterias forbesi*, has been deduced totally by nuclear magnetic resonance methods applied to the undegraded molecule. Using principally 2D-COSY, HCORR, RCT, and 1D-nOe experiments, forbeside C is shown to be the hydrate of the monosodium salt of 6α-*O*-{β-D-fucopyranosyl(1→2)-*O*-β-D-fucopyranosyl(1→4)-*O*-[β-D-quinovopyranosyl(1→2)]-*O*-β-D-quinovopyranosyl(1→3)-*O*-6-deoxy-β-D-*xylo*-hexos-4-ulopyranosyl}-20S-hydroxy-3β-sulfo-oxy-5α-cholest-9(11)-en-23-one, the structure reported previously for ovarian asterosaponin **1**.

JOHN A. FINDLAY, MAHESH JASEJA et JEAN-ROBERT BRISSON. Can. J. Chem. **65**, 2605 (1987).

Appliquant des méthodes de la résonance magnétique nucléaire à la molécule qui n'a pas été dégradée, on a déterminé la structure du forbeside C, une saponine provenant de l'étoile de mer *Asterias forbesi*. Faisant principalement appel à des expériences de COSY-2D, HCORR, RCT et d'eOn-1D, on a démontré que le forbeside C est l'hydrate du monosel de sodium de la *O*-{β-D-fucopyrannosyl(1→2)-*O*-β-D-fucopyrannosyl(1→4)-*O*-[β-D-quinovopyrannosyl(1→2)]-*O*-β-D-quinovopyrannosyl(1→3)-*O*-désoxy-6 β-D-*xylo*-hexosulo-4 pyrannosyl}-6α hydroxy-20(S) sulfoxy-3β 5α-cholestène-9(11) one-23, la structure qui avait été rapportée antérieurement pour l'astérosaponine ovarienne **1**.

[Traduit par la revue]

Recently, we reported (1) the structures of the major saponins, forbeside A and forbeside B, from the starfish *Asterias forbesi* (Desor). We have now assigned the structure **1** to a third saponin, forbeside C, from the same source. As in the case of the major saponins, the structure of forbeside C has been deduced entirely by nmr methods and corroborated, in part, by FAB mass spectrometric data.

The ^{1}H nmr spectrum of forbeside C in pyridine-d_5/D_2O (5:1) at 500 MHz shows, in the downfield region, five anomeric sugar proton signals as doublets at δ 5.108 (7.9 Hz), δ 5.057 (7.9 Hz), δ 4.997 (8.0 Hz), δ 4.947 (7.7 Hz), and δ 4.838 (7.7 Hz). The high coupling constant values are consistent only with the β configuration for all anomeric linkages. The region δ 3.5–4.5 ppm shows the overlapping resonances of the oligosaccharide ring protons. Five sugar methyl doublets at δ 1.828 (6.1 Hz), δ 1.770 (6.5 Hz), δ 1.724 (6.1 Hz), δ 1.482 (6.2 Hz), and δ 1.445 (6.2 Hz) attest to the presence of five deoxy sugars. The rest of the signals in the upfield region δ 0.90–2.90 ppm are assigned to the aglycone moiety. The signals of the five aglycone methyl groups are easily recognizable, three of them are tertiary (δ 0.99 s, δ 0.95 s, δ 1.67 s) and are assigned to C18, C19, and C21 protons, respectively. Isopropyl doublets appear at δ 0.94 and δ 0.92, corresponding to the C26 and C27 methyls. In addition, doublets are observed at δ 2.95 and δ 2.80 for the C22 methylene protons and two overlapping AB quartets are observed at δ 2.53, corresponding to the C24 protons. A broad signal for the olefinic proton at C11 is clearly seen at δ 5.20 and a multiplet at δ 4.89 for the C3α

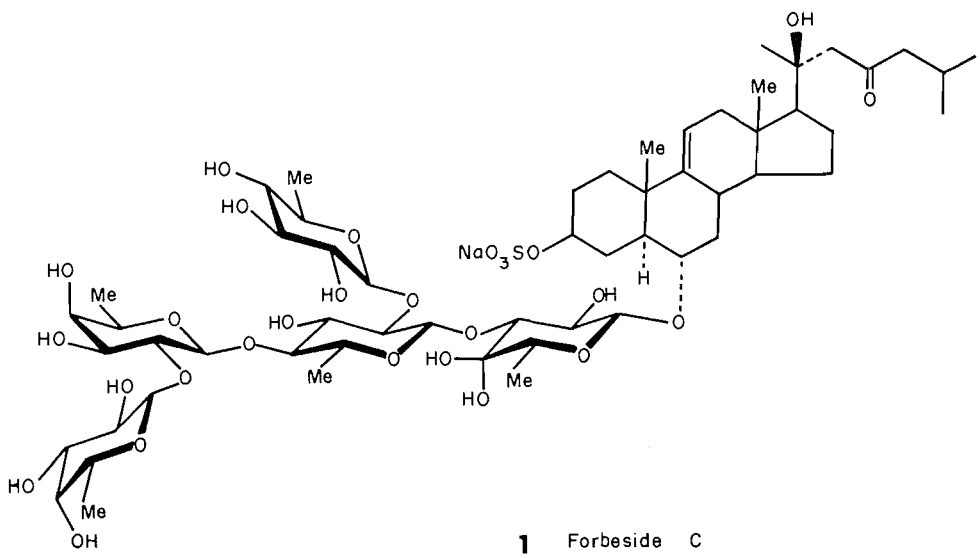

1 Forbeside C

[1]NRCC No. 28067.

Can. J. Chem. Downloaded from www.nrcresearchpress.com by 213.222.148.141 on 09/07/12
For personal use only.

Can. J. Chem. Downloaded from www.nrcresearchpress.com by 213.222.148.141 on 09/07/12
For personal use only.

TABLE 1. The nmr assignments of aglycone moiety of forbeside C in pyridine-d_5/D_2O (5:1)

Carbon no.	^{13}C shift[a]	^{1}H shift(s)[b]
1	35.9	1.63, 1.41
2	29.2	2.78, 1.92
3	78.0	4.89
4	30.6	3.32, 1.81
5	49.1	1.54
6	79.9	3.93
7	41.2	2.73, 1.31
8	35.3	2.07
9	145.4	—
10	38.3	—
11	116.7	5.20
12	42.3	2.30, 2.11
13	41.5	—
14	54.0	1.28
15	23.2	2.25, 1.87
16	25.1	1.80, 1.26
17	59.2	1.84
18	13.6	0.99
19	19.3	0.95
20	73.9	—
21	26.8	1.67
22	55.2	2.95, 2.80
23	212.3	—
24	53.9	2.53, 2.53
25	24.6	2.22
26	22.6	0.94
27	22.5	0.92

[a]From comparison with forbeside A and forbeside B data (1).
[b]From ^{1}H–^{13}C correlation using CHORTLE technique.

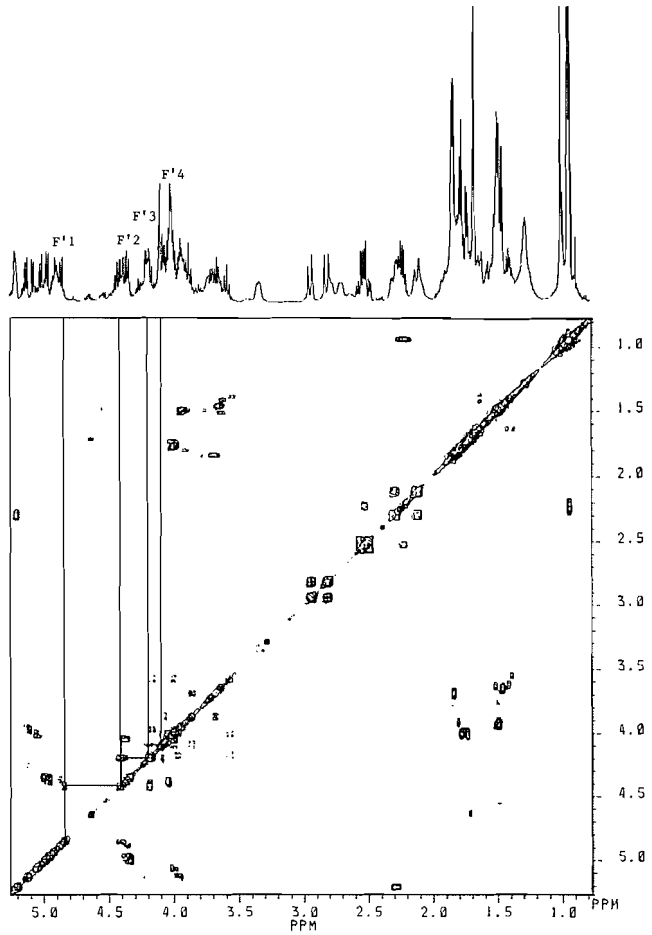

FIG. 1. 2D-nuclear proton correlation (COSY) spectrum (δ 0.95–5.15) of forbeside C.

proton. These findings indicate the presence of a thornasterol A aglycone moiety (1, 2). This was confirmed by ^{13}C nmr spectroscopy. The ^{13}C signals (Table 1) of the aglycone of forbeside C are virtually coincident with those of forbeside A (1) and consistent with those of thornasteroside A (3). The ^{13}C nmr spectrum also shows five anomeric carbon signals at 106.4, 105.8, 104.5, 103.5, and 102.3 ppm and five sugar methyls at 18.0, 18.0, 16.9, 16.6, and 13.4 ppm, consistent with the presence of five deoxy sugars in the oligosaccharide moiety. Distortionless enhancement by polarization transfer (DEPT) (4) analysis showed the absence of methylene carbons (-CH_2-) in the region 60–65 ppm. Thus, a preliminary review of nmr data indicated that forbeside C features a pentasaccharide chain attached to thornasterol A at position C6. With the aid of ^{1}H–^{13}C correlation spectra using "CHORTLE" (5) technique, all the proton resonances of the thornasterol A aglycone could be identified in the ^{1}H nmr spectrum of forbeside C. The assignments are listed in Table 1.

The complete structure of the oligosaccharide chain was determined by two-dimensional nuclear proton correlation (2D-COSY) (6), relayed coherence transfer (2D-RCT) (7), one-dimensional nuclear Overhauser enhancement (nOe) (8) difference spectroscopy, spin simulation, and heteronuclear ^{13}C–^{1}H correlation (HCORR) spectroscopy. The carbon and proton chemical shifts and coupling constant values of the oligosaccharide moiety of forbeside C are summarized in Table 2.

The anomeric doublet at δ 4.838 is designated as F′1, and the others are designated as F″1, Z1, Q″1, and Q′1 sequentially downfield.

From the 2D-COSY spectrum (Fig. 1), the anomeric proton signal for F′1 at δ 4.838 is coupled to the F′2 proton signal at δ 4.408 and, continuing this J-connectivity path, it was possible to locate F′3 at δ 4.182, and F′4 at δ 4.081. These assignments are confirmed by the 2D-RCT spectrum (Figs. 2*a*,*b*), which also shows that the signal at δ 4.081 (F′4) correlates with the signals at δ 3.927 and δ 1.482. Since the doublet at δ 1.482 belongs to the F′6 methyl, the signal at δ 3.926 is assigned to F′5. In the 2D-COSY spectrum the correlation between the F′4 and F′5 protons is not apparent since the $J_{4,5}$ coupling value is very small. Furthermore, the irradiation of the F′1 proton signal (δ 4.838) in the nOe difference spectrum (Fig. 3) induces substantial enhancements at δ 4.182 (F′3), δ 3.927 (F′5), and δ 3.565, the site of interglycosidic linkage. From the COSY spectrum (Fig. 1) and nOe spectra (Fig. 3), it is clear that the $J_{3,4}$ coupling value is small. From the J values in Table 2, which were refined by spin simulation (Fig. 4), it is evident that F′ must be a β-fucose unit.

Similarly, from the second anomeric doublet F″1 (δ 4.947), the J-connectivity pathway can be traced out from the 2D-COSY spectrum (Fig. 1) identifying all the couplings belonging to the sugar network F″, i.e., F″2 at δ 4.365, F″3 at δ 4.036, F″4 at δ 3.997, F″5 at δ 3.639, and F″6 at δ 1.455. The small couplings as observed from F″3/F″4, F″4/F″5 cross peaks and

TABLE 2. The nmr assignments and coupling constant data for oligosaccharide portion of saponin forbeside C in pyridine-d_5/D_2O (5:1)

Sugar/carbon	No.	^1H shift[a,b] (ppm)	Coupling constant $J_{(H,H)}$[b] (Hz)	^{13}C shift[c] (ppm)	(Δ)[e]
Z	1	4.997	$J_{(1,2)}$ = 8.0	104.5	
	2	4.328		73.1	
	3	4.073[d]	$J_{(2,3)}$ = 9.0[d]	92.7[d]	
	4	—		90.4	
	5	3.993	$J_{(5,6)}$ = 6.5	73.1	
	6	1.770		13.4	
Q′	1	5.108	$J_{(1,2)}$ = 7.9	103.5	
	2	3.961	$J_{(2,3)}$ = 9.0	83.4	(+7.4)
	3	4.165	$J_{(3,4)}$ = 9.0	74.7	
	4	3.565	$J_{(4,5)}$ = 9.0	84.8	(+9.3)
	5	3.997	$J_{(5,6)}$ = 6.1	73.1	
	6	1.724		18.0	
Q″	1	5.057	$J_{(1,2)}$ = 7.9	105.8	
	2	3.993	$J_{(2,3)}$ = 9.0	76.0	
	3	4.075	$J_{(3,4)}$ = 9.0	76.5	
	4	3.857	$J_{(4,5)}$ = 9.0	75.5	
	5	3.675	$J_{(5,6)}$ = 6.1	73.9	
	6	1.828		18.0	
F′	1	4.838	$J_{(1,2)}$ = 7.7	102.3	
	2	4.408	$J_{(2,3)}$ = 9.5	81.6	(+8.3)
	3	4.182	$J_{(3,4)}$ = 3.6	74.5	
	4	4.081	$J_{(4,5)}$ = 0.6	71.6	
	5	3.927	$J_{(5,6)}$ = 6.2	71.6	
	6	1.482		16.6	
F″	1	4.947	$J_{(1,2)}$ = 7.7	106.4	
	2	4.365	$J_{(2,3)}$ = 9.5	73.3	
	3	4.036	$J_{(3,4)}$ = 3.6	74.5	
	4	3.997	$J_{(4,5)}$ = 0.6	72.2	
	5	3.639	$J_{(5,6)}$ = 6.2	71.7	
	6	1.445		16.9	

[a]Assignments from 2D-COSY and 2D-RCT experiments.
[b]Parameters refined by spin simulations.
[c]Obtained from ^1H–^{13}C correlation using CHORTLE technique.
[d]Appears after equilibration with pyridine-d_5/H_2O (5:1).
[e]Δ ppm in comparison with same position without interglycosidic linkage in this molecule.

the $J_{(AB)}$ values of each of the proton couplings derived by spin simulation show sugar F″ to be a β-fucose unit.

The irradiation of the F″1 proton signal (δ 4.947) in the nOe difference spectrum (Fig. 3) causes marked enhancements of signals at δ 4.036 (F″3) and δ 3.639 (F″5), and also a substantial enhancement at δ 4.407, showing the site of interglycosidic linkage at the neighbouring sugar unit to be F′2.

From the 2D-COSY spectrum (Fig. 1) one can trace out the *J*-connectivity pathway starting from Q″1 at δ 5.057 to Q″6 at δ 1.828, thus assigning all the ring protons in sugar Q″. Irradiation at δ 5.057 (Q″1) (Fig. 3) induces enhancements at δ 4.075 (Q″3) and δ 3.675 (Q″5) and a marked enhancement at δ 3.961 (Q′2), the site of interglycosidic linkage to the neighbouring sugar Q′.

The last anomeric doublet at δ 5.108 (Q′1) is seen coupled to a signal at δ 3.961 (Q′2) in the 2D-COSY spectrum (Fig. 1) and, continuing this pathway, the protons Q′3, Q′4, Q′5, and Q′6 are identified at δ 3.961, δ 4.165, δ 3.565, δ 3.997, and δ 1.724, respectively. The nOe difference spectrum (Fig. 3) shows enhancement at δ 4.165 (Q′3) and δ 3.997 (Q′5) in agreement with the assigned quinovose structure.

In the 2D-COSY spectrum (Fig. 1) the anomeric doublet for sugar Z at δ 4.997 (Z1) is seen to be coupled to the signal at δ 4.328 (Z2) but this latter proton has no further coupling partner. Also, one can see the remaining methyl doublet at δ 1.770 (Z6) coupled to the signal at δ 3.993 (Z5), which in turn shows no further coupling partner. The 2D-RCT spectrum (Fig. 2) gives no evidence of proton substitution at Z3 and Z4.

The proton chemical shifts obtained from the 2D-COSY and 2D-RCT experiments and coupling constant information for various sugar protons were refined by spin simulation (Fig. 4) until excellent agreement between experimental and calculated spectra was obtained (Table 2). This confirmed the absence of signals due to proton substitution at Z3 and Z4.

The sequencing of the sugars was completed with the help of 1D nOe difference spectroscopy (Fig. 3) by irradiating each of the anomeric signals separately. The nOe data for the oligosaccharide chain is summarized in Table 3. Thus, the positions of three interglycosidic linkages, their preferred conformations, and the position of attachment of sugar Z to the aglycone were readily revealed from inter-residue nOe. However, irradiation of signal Q′1 did not reveal the location of interglycosidic

Can. J. Chem. Downloaded from www.nrcresearchpress.com by 213.222.148.141 on 09/07/12
For personal use only.

Can. J. Chem. Downloaded from www.nrcresearchpress.com by 213.222.148.141 on 09/07/12
For personal use only.

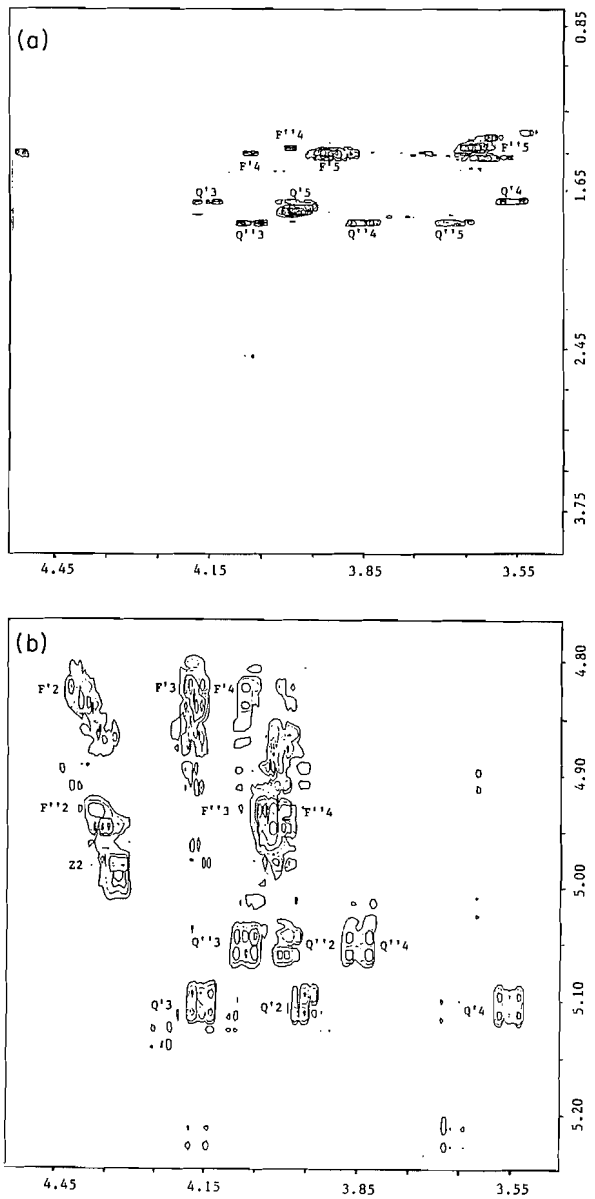

FIG. 2. (*a*) 2D-Relayed coherence transfer (RCT) spectrum (δ 3.45–4.55/δ 0.85–3.85) of forbeside C. (*b*) 2D-Relayed coherence transfer (RCT) spectrum (δ 3.45–4.55/δ 4.75–5.25) of forbeside C.

linkage to sugar Z, implying that this site on Z was substituted by either a deuterium (D_2O) exchangeable hydrogen or no hydrogen. Alternatively, the transglycosidic nOe may be negligible for reasons of conformation. The sequencing of the sugars as deduced from nOe data can be summarized as follows:

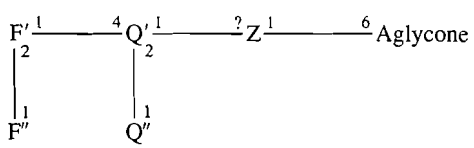

Corroboration of the location of the interglycosidic linkages comes from the ^{13}C shift data (Table 2) since the chemical shifts of carbons involved in the interglycosidic linkages invariably occur at lower field than when simply hydroxylated. Thus Q′ is seen to be linked at C2 and C4 since their signals, 83.4 and 84.8 ppm, respectively, are substantially downfield from the

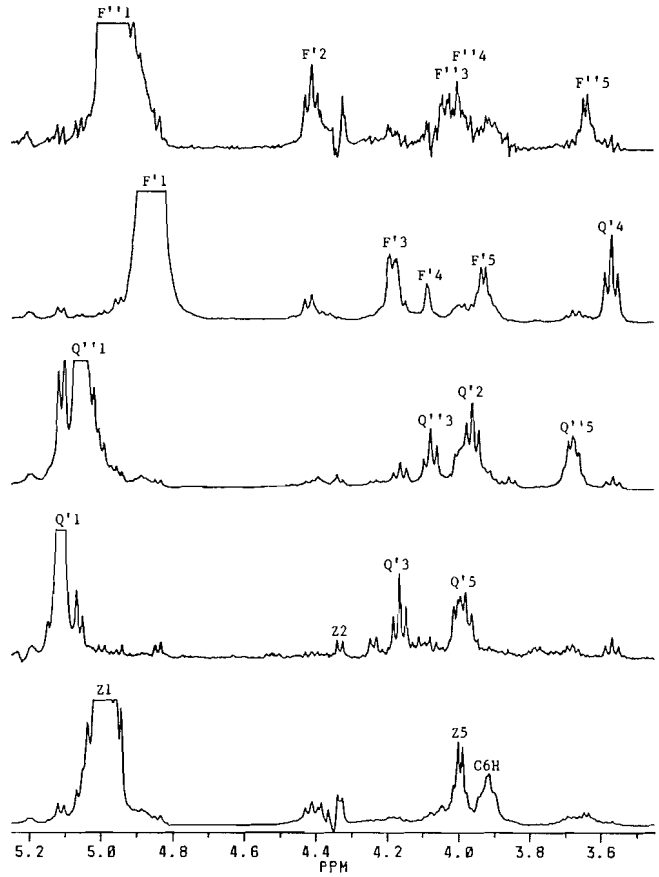

FIG. 3. The nOe difference spectra for forbeside C.

corresponding signals in Q″ (i.e., 76.0 and 75.5, respectively). Similarly F′ must be linked at C2 since its chemical shift, 81.6 ppm, is 7.3 ppm lower than its counterpart in F″. Thus the ^{13}C nmr data fully support this assigned sequence and also allow insight into the connectivity of Q′ to Z. The signal at δ 92.7 for the fully substituted carbon in the ^{13}C spectrum (pyridine-d_5/D_2O, 5:1) of forbeside C must belong to either Z3 or Z4 since all other signals are satisfactorily accommodated. Furthermore, it is evident that, in this medium, one of the sugar Z carbons (Z3 or Z4) fails to give rise to a discernible ^{13}C signal.

This dilemma was overcome by assigning the δ 92.7 signal to a *gem* diol carbon at C4. The inclusion of an extra oxygen atom is in full agreement with the molecular ion from positive ion FAB (fast-*atom bombardment*) mass spectral data (*vide infra*). The placement of the *gem* diol at C4 allows for the exchange of C3H for deuterium via the anticipated C4 *gem* diol ⇌ C4 ketone + water equilibrium in pyridine-d_5/D_2O. In confirmation of these assignments, recovery of the nmr sample followed by equilibration in pyridine-d_5/H_2O (5:1) for seven days afforded a ^{13}C nmr spectrum featuring an additional methine signal at 90.3 ppm. Therefore the interglycosidic linkage must be at C3, the carbon that gives rise to the elusive 90.3-ppm signal and whose hydrogen is D_2O exchangeable. This lower field chemical shift is in accord with expectation.

To determine the relative configuration of C3H in sugar Z, the 2D-COSY spectrum of forbeside C was recorded in pyridine/H_2O (5:1) and it showed the Z3 proton at δ 4.073 coupled with a large (9.0 Hz) coupling constant to Z2 at δ 4.328. Sugar Z is, therefore, a β-linked 6-deoxy-*xylo*-4-hexulose unit in hydrated form.

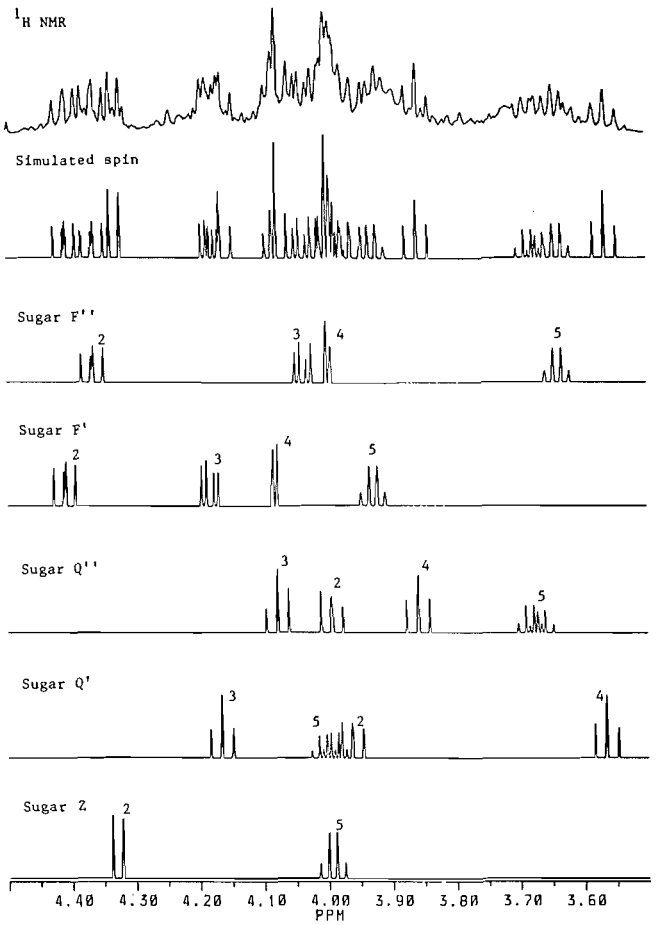

FIG. 4. Spin simulation of the ^{1}H nmr spectra for the sugar moiety of forbeside C.

TABLE 3. The nOe data for forbeside C obtained from nOe difference spectroscopy

Irradiation at ^{1}H (ppm)	nOe enhancements at ^{1}H shift: Intraresidual 1–3	Axial–axial 1–5	Interresidual through glycosidic bond to
4.997 (Z1)	—	3.993	(C_6 of aglycone) 3.93
5.108 (Q′1)	—	3.997	—
5.057 (Q″1)	4.075	3.675	3.961 (Q′2)
4.838 (F′1)	4.182	3.927	3.565 (Q′4)
4.947 (F″1)	4.036	3.639	4.408 (F′2)

The positive ion FAB mass spectrum (Fig. 5) of forbeside C exhibits prominent ions at m/z 1303.3 (M + Na), 1281.2 (M + H), 1201.5 (M + H + Na − $NaSO_3$), and 1183.5 (M + H + Na − $NaSO_3$ − H_2O), confirming the elemental composition $C_{57}H_{93}NaO_{28}S$, while other ions provide corroboration of aspects of the oligosaccharide chain as shown in Scheme 1. Thus cleavage of the oligosaccharide moiety furnishes an ion m/z 769, which is subject to further fragmentation corresponding to loss of one or two sugars by fission on each side of the glycosidic oxygens.

Thus, assuming D-family sugars, forbeside C possesses structure **1**, the hydrate of the monosodium salt of 6α-*O*-{β-D-fucopyranosyl(1→2)-*O*-β-D-fucopyranosyl(1→4)-*O*-[β-D-quinovopyranosyl(1→2)]-*O*-β-D-quinovopyranosyl(1→3)-*O*-6-deoxy-β-D-*xylo*-hexos-4-ulopyranosyl}-2OS-hydroxy-3β-sulfo-oxy-5α-cholest-9(11)-en-23-one. This same structure has been assigned to ovarian asterosaponin **1** from the starfish *Asterias amurensis* by Ikegami and co-workers (9) and was deduced principally from examination of various hydrolysis and degradation products. It has also been found by Itakura and

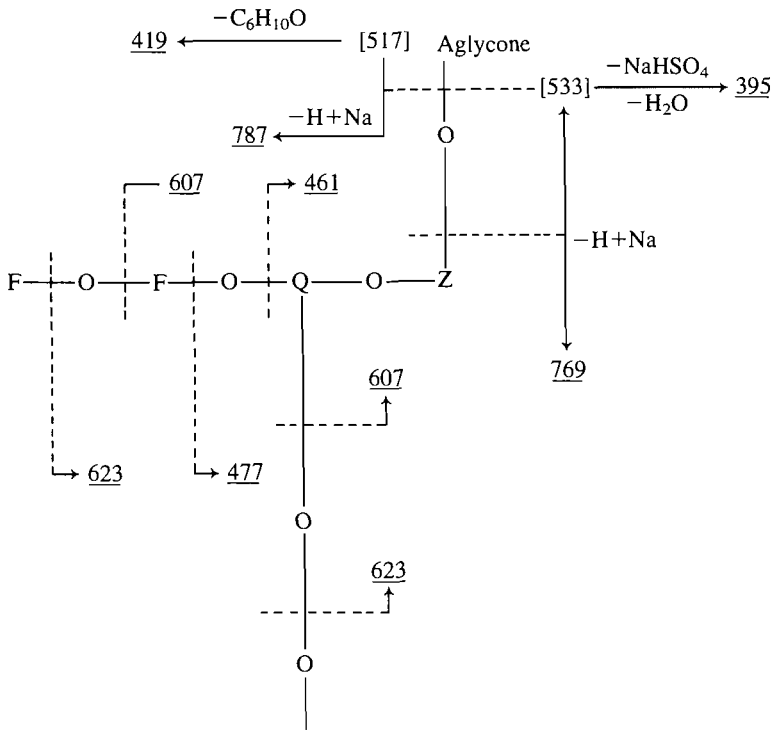

SCHEME 1. FAB$^+$ fragmentation of forbeside C.

Can. J. Chem. Downloaded from www.nrcresearchpress.com by 213.222.148.141 on 09/07/12
For personal use only.

Can. J. Chem. Downloaded from www.nrcresearchpress.com by 213.222.148.141 on 09/07/12
For personal use only.

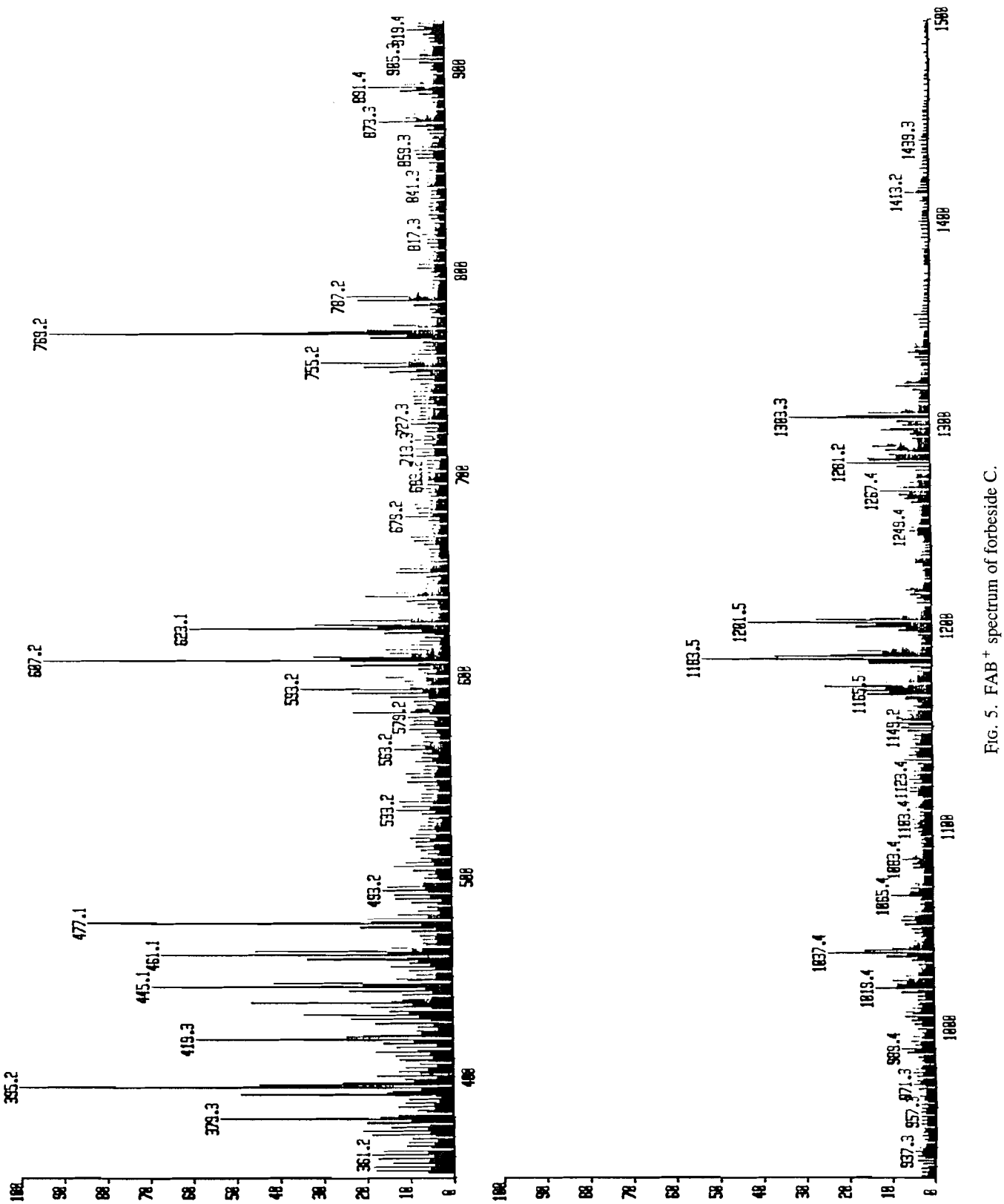

FIG. 5. FAB$^+$ spectrum of forbeside C.

Komori (10) in *Asterias amurensis* (cf.) *versicolor* Sladen. Very recently we have also isolated **1** from the starfish *Asterias vulgaris*, Verrill.[2]

Experimental

Forbeside C

Forbeside C (30 mg) was obtained via fractionation of crude saponin (3 g) obtained from specimens of *Asterias forbesi* (Desor) (collected in Passamaquoddy Bay, August 1984) as previously described (1). This saponin was obtained as a glassy solid (mp 180–182°C uncorrected).

Nuclear magnetic resonance spectra

The nmr spectra were recorded on a Bruker AM-500 spectrometer at 300 K using forbeside C (25 mg) in 0.5 mL of pyridine-d_5/D_2O (5:1) unless otherwise indicated.

All one-dimensional and two-dimensional nmr experiments were performed using the standard pulse sequences provided by Bruker (DISNMRP).

One-dimensional nuclear Overhauser enhancement difference experiments

The 1D-nOe difference experiments were performed as previously described (11). However, instead of irradiation at a single frequency of the whole multiplet, each line in the multiplet was sequentially irradiated 100 ms for a total time of 1 s per multiplet (12). A line broadening factor of 2 Hz was used prior to Fourier transformation to improve signal-to-noise ratio.

2D-COSY and 2D-RCT experiments

2D-COSY and 2D-RCT experiments were performed using the standard pulse sequences. The initial matrix of 256 × 2048 data points over a sweep width of 5.4 ppm in both dimensions was zero-filled to 1024 × 2048 points for a final resolution of 2.6 Hz/point. Sine-bell functions were used for resolution enhancement. Magnitude calculations and symmetrization about the diagonal were used to represent the data. For the two-step RCT experiment, a delay of 32 ms was used.

The heteronuclear $^{13}C-^{1}H$ correlation

The heteronuclear $^{13}C-^{1}H$ correlation was done by a least-squares analysis of the ^{13}C intensities as a function of proton evolution times according to Pearson (5). Five evolution times of 0.16, 0.4, 1.0, 2.4, and 3.2 ms were used.

Spin simulations

The spin simulations were done using the Bruker programme PANIC. A linewidth of 0.5 Hz was used in all cases.

[2]Larry Calhoun and John A. Findlay, unpublished results.

Fast-atom bombardment (FAB) mass spectra

The FAB mass spectra were obtained on VG 7070E and VG ZAB-SE mass spectrometers employing xenon as an ionizing gas, accelerating voltages of 5 and 10 kV, respectively, and "MAGIC BULLET" was used as matrix (13).

Acknowledgements

The authors are grateful to Professor K. L. Rinehart, University of Illinois at Urbana–Champaign, for providing mass spectra and to Larry Calhoun, Department of Chemistry, University of New Brunswick, for helpful discussions on aspects of 2D nmr. This study was funded with a grant from the Natural Sciences and Engineering Research Council of Canada.

1. JOHN A. FINDLAY, MAHESH JASEJA, D. JEAN BURNELL, and JEAN-ROBERT BRISSON. Can. J. Chem. **65**, 1384 (1987).
2. M. HONDA and T. KOMORI. Tetrahedron Lett. **27**, 3369 (1986).
3. Y. ITAKURA, T. KOMORI, and T. KAWASAKI. Liebig's Ann. Chem. **1983**, 2079–2091 (1983).
4. D. M. DODDRELL, D. T. PEGGY, and M. R. BANDALL. J. Magn. Reson. **48**, 323 (1982).
5. G. A. PEARSON. J. Magn. Reson. **64**, 487 (1985).
6. A. BAX. Two-dimensional NMR in liquids. Riedel, Boston. 1982; A. BAX and R. FREEMAN. J. Magn. Reson. **44**, 542 (1981); A. BAX, R. FREEMAN, and G. MORRIS. J. Magn. Reson. **42**, 164 (1981).
7. G. EICH, G. BODENHAUSEN, and R. R. ERNST. J. Am. Chem. Soc. **104**, 3731 (1982); A. BAX and G. DROBNY. J. Magn. Reson. **61**, 306 (1985).
8. J. K. M. SANDERS and J. D. MERSCH. Progress in nuclear magnetic resonance spectroscopy. Vol. 15. *Edited by* J. W. Emsley, J. Feeney, and L. H. Sutcliffe. Pergamon Press, Oxford. 1983. p. 353.
9. K. OKANO, T. NAKAMURA, Y. KAMAIYA, and S. IKEGAMI. Agric. Biol. Chem. **45**, 805 (1981).
10. Y. ITAKURA and T. KOMORI. Liebig's Ann. Chem. **1986**, 359 (1986).
11. J.-R. BRISSON and J. P. CARVER. J. Biol. Chem. **258**, 1431 (1983).
12. D. MENHAUS. J. Magn. Reson. **53**, 109 (1983); M. KINNS and J. K. M. SANDERS. J. Magn. Reson. **56**, 518 (1984).
13. J. L. WHITTEN, M. H. SCHAFFER, M. O'SHEA, J. C. COOK, M. E. HEMLING, and K. L. RINEHART, JR. Biochem. Biophys. Res. Commun. **124**, 350 (1984).

Can. J. Chem. Downloaded from www.nrcresearchpress.com by 213.222.148.141 on 09/07/12
For personal use only.

Convenient synthesis and cycloaddition reactions of 2-phenylseleno-1,3-butadiene and 2-trialkylstannyl-1,3-butadienes

GORDON S. BATES,[1] MICHAEL D. FRYZUK,[1,2] AND CHARLES STONE
Department of Chemistry, University of British Columbia, 2036 Main Mall, Vancouver, B.C., Canada V6T 1Y6

Received May 20, 1987

GORDON S. BATES, MICHAEL D. FRYZUK, and CHARLES STONE. Can. J. Chem. **65**, 2612 (1987).

The facile preparation of 2-trialkylstannyl-1,3-butadienes and 2-phenylseleno-1,3-butadiene by reaction of 2-(1,3-butadienyl)magnesium chloride with trialkylstannyl chlorides and phenylselenium chloride, respectively, is reported. The Diels–Alder reactivity of these dienes with a variety of activated dienophiles is also described. Finally, a novel transmetallation of tin, in vinyl stannanes, to selenium by use of phenylselenium chloride is outlined.

GORDON S. BATES, MICHAEL D. FRYZUK et CHARLES STONE. Can. J. Chem. **65**, 2612 (1987).

On rapporte une méthode facile de préparer les trialkylstannyl-2 et phénylséléno-2 butadiènes-1,3 qui implique la réaction du chlorure du butadiène-1,3 yle-2 magnésium avec les chlorures soit de trialkylstannyles soit de phénylsélénium. On décrit aussi la réactivité de ces dienes, dans la réaction de Diels–Alder, avec divers diénophiles activés. Enfin, on décrit une nouvelle réaction de transmétallation de l'étain, dans des stannanes de vinyles, vers le sélénium du chlorure de phénylsélénium.

[Traduit par la revue]

Can. J. Chem. Downloaded from www.nrcresearchpress.com by 213.166.140.6 on 09/07/12
For personal use only.

Introduction

As part of our interest in the Diels–Alder reactivity of 1,3-dienes with metalloid (1) or transition metal substituents, we have examined the synthesis of 2-substituted 1,3-butadienes of the formula **1** (ML_n = metalloid or transition metal complex). Our rational approach was to use the readily available, inexpensive starting material chloroprene **2**, and examine its conversion to **1** via the Grignard reagent **3**. It had been reported that attempts to prepare **3** from chloroprene gave polymers; however, the preparation of this Grignard reagent could be achieved from the less accessible 4-chloro-1,2-butadiene (2). More recently, a modification was published that allows **3** to be prepared directly from **2** by first activating the magnesium (3). We have used this procedure to prepare 2-trialkylstannyl-1,3-butadienes **4** and 2-phenylseleno-1,3-butadiene **5** in a one-step, facile synthesis. While our work was in progress, reports on alternative syntheses and Diels–Alder reactivity of **4** and **5** were communicated. A "tin-cupration" of 2-butyne-1,4-diol followed by "silyl-cupration" generated **4***a* in reasonable yield (4), while an equally elaborate Wurtz-type coupling yielded **4***b* (5). The preparation and isolation of **5** have never been reported to our knowledge, although the synthesis of the SO_2-masked derivative **6** has been recently described along with a study of its Diels–Alder reactivity (6).

In this paper we describe the following: (*i*) full details for the one-pot synthesis of **4** and **5**, (*ii*) cycloaddition reactions of these dienes with a variety of dienophiles, and (*iii*) the first example of transmetallation from tin to selenium.

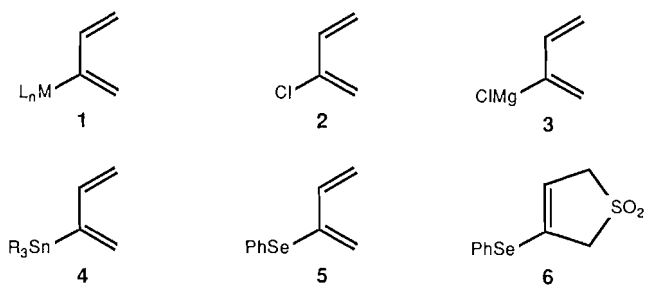

1 2 3 4 5 6

4*a* R = n-Bu

4*b* R = Me

[1]Authors to whom correspondence may be addressed.
[2]Fellow of the Alfred P. Sloan Foundation (1984–1987).

Results and discussion

Synthesis of dienes

Chloroprene **2** is readily converted to the corresponding Grignard reagent **3** by activating the magnesium with 1–3 mol% anhydrous $ZnCl_2$ and small amounts of 1,2-dibromoethane. In this fashion, 0.25–0.60 *M* solutions of **3** in tetrahydrofuran (THF) can be obtained. The subsequent reaction with the commercially available stannyl halides and phenylselenium chloride provides for the convenient, one-pot preparation of the dienes **4** and **5** on a multi-gram scale (see eq. [1]). Diene **5**, previously uncharacterized due to its ready polymerization (6), was isolated and found to be stable for long periods at low temperature (−20°C).

Diels–Alder reactions

Reaction of 2-trialkylstannyl-1,3-butadienes **4** with a variety of activated dienophiles leads to the preparation of substituted cyclohexenes containing a vinyl stannane functionality. This latter functionality has been shown to have great synthetic potential via transition metal catalysed cross-coupling with vinyl halides (7) and vinyl triflates (8). The results of the preparation of such trialkylstannyl-substituted cyclohexenes **7–11** are summarized in Table 1. In general, the reactions proceeded smoothly at elevated temperatures to give good yields of the Diels–Alder cycloadducts. However, reaction of **4***a* with maleic anhydride for extended periods of time at room temperature gave the best yields of cycloadduct **7**. In the work-up of **9**, by column chromatography on silica gel, enolization took place producing small quantities of the corresponding hydroquinone. Hydroquinone production was also observed when reaction times in excess of 12 h were used. Similar results were noted in the preparation and work-up of **14** (see Table 2), albeit to a lesser extent.

The trialkylstannane substituted diene allows for facile reaction with electron-deficient dienophiles, as is evidenced by its ready cycloaddition with dimethyl acetylenedicarboxylate. Extended periods (several days) of reflux in toluene with diphenylacetylene, an electron-rich dienophile, led only to isolation of starting materials.

In an attempt to determine the directing effect of the stannyl

TABLE 1. Reaction of 2-trialkylstannyl-1,3-butadienes **4***a*/**4***b*

Entry	Dienophile	Conditions	Products	Yields
1	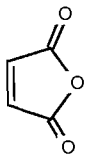	$PhCH_3$, room temp., 2 days	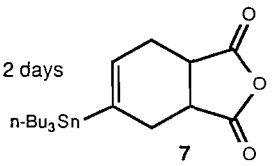 **7**	75%
2	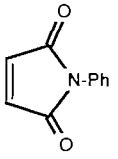	$PhCH_3$, reflux, 8 h	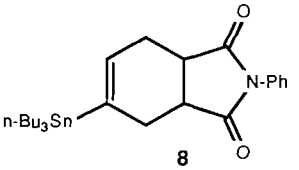 **8**	90%
3	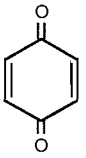	$PhCH_3$, reflux, 5 h	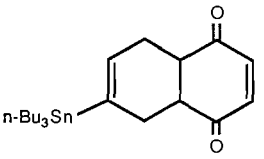 **9**	69%
4	$MeO_2CC{\equiv}CCO_2Me$	$PhCH_3$, reflux, 18 h	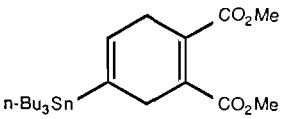 **10**	71%
5	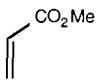	$PhCH_3$, reflux, 18 h	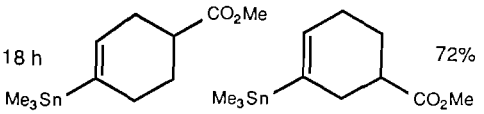 **11a** **11b** 2 : 1	72%

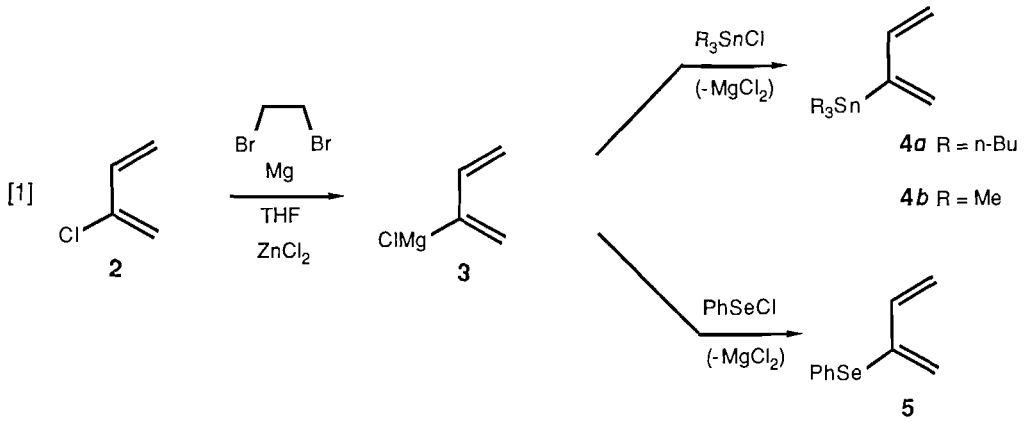

moiety, the reaction of **4***b* with methyl acrylate at reflux in toluene was examined. In analogy to results previously observed in cycloaddition reactions of silylbutadienes (9), the stannyl moiety was found to exhibit only a weak directing effect, resulting in a 2:1 mixture of *para*:*meta* regioisomers **11***a*:**11***b*.[3] Other workers have shown (4*b*) that the use of 15% $AlEt_2Cl$ in the reaction of **4***a* with ethyl acrylate gave a 10:1 ratio of *para*:*meta* regioisomers.

The assignment of **11***a* (*para*) as the major regioisomer is based on much literature precedent, both theoretical and experimental (6, 10). Attempts to separate mixtures of **11***a*/**11***b* using column chromatography proved difficult; however, an enriched 7:1 (**11***a*:**11***b*) mixture was obtained. It was hoped that by use of ^1H nmr NOEDIFF (nuclear Overhauser effect difference) spectroscopy (11), on this enriched mixture, more physical evidence for the assignment of the major regioisomer

[3]The best yields of **11***a*/**11***b* were obtained by use of several equivalents of freshly distilled methyl acrylate containing 2 mol% (based on diene) 2,6-di-*tert*-butyl-4-methylphenol (BHT).

Can. J. Chem. Downloaded from www.nrcresearchpress.com by 213.166.140.6 on 09/07/12
For personal use only.

TABLE 2. Reaction of 2-phenylseleno-1,3-butadiene **5**

Entry	Dienophile	Conditions	Products	Yields
1	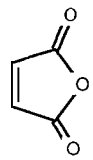	$PhCH_3$, room temp., 2 days	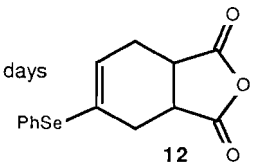 **12**	70%
2	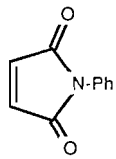	$PhCH_3$, reflux, 8 h	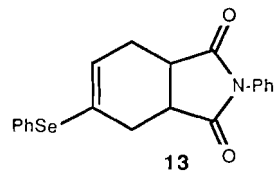 **13**	76%
3	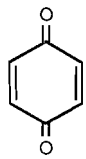	$PhCH_3$, reflux, 2 h	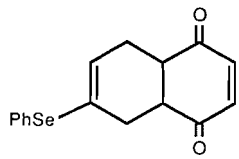 **14**	64%
4	$MeO_2CC{\equiv}CCO_2Me$	$PhCH_3$, reflux, 18 h	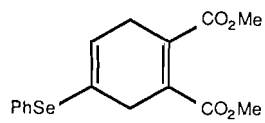 **15**	81%
5	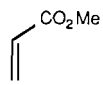	$PhCH_3$, reflux, 18 h	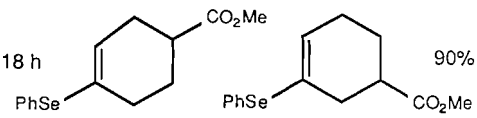 **16a** **16b** 4:1	90%

could be achieved. Unfortunately, the results of such experiments at 400 MHz were equivocal.

The results of the cycloaddition reactions of the phenylseleno diene **5** with a variety of activated dienophiles are outlined in Table 2. The reaction of **5** at room temperature with maleic anhydride and at elevated temperature with less activated dienes yielded cycloadducts **12–16**.[4]

The synthetic utility of the vinyl selenide functionality is realized most readily in its role as a masked carbonyl (12). Other uses involve cross-coupling reactions with Grignard reagents in the presence of nickel-phosphine catalysts (13) and oxidative cleavage with hydrogen peroxide (14). Evidence that the selenenyl substituted diene permits facile reaction with electron-deficient dienophiles is seen in the ready formation of **12–16** and in its total lack of reactivity with diphenylacetylene.

Regiochemical investigation of the Diels–Alder reactivity of **5** involved reaction with methyl acrylate at reflux in toluene. A 4:1 mixture[5] of *para*:*meta* regioisomers was obtained in excellent chemical yield. This result was in complete agreement with published data, based on theoretical calculations, on the products obtained by reaction of **6** with ethyl acrylate (6). The results of our study show that, in reaction with methyl acrylate, the selenenyl moiety has a greater directing effect than the stannyl substituent.

Transmetallation from tin to selenium

Other results from our laboratory (1) have shown that addition of phenylselenium chloride (PhSeCl) to solution of zirconium dienyl complexes results in smooth transmetallation from zirconium to selenium with immediate discharge of the deep red colour of PhSeCl. A similar result was obtained when the stannyl diene **4***b* was reacted with PhSeCl at room temperature (see eq. [2]). Work-up of the reaction mixture yielded a yellow oil that had identical spectral data to diene **5**, indicating that the transmetallation reaction had proceeded without rearrangement. In an attempt to gain further comparative information on the reaction of the dienes **4***a* and **5** with methyl acrylate, a solution of PhSeCl was added to a 2:1 *para*:*meta* mixture of the Diels–Alder adducts **11***a*/**11***b*. Stirring the mixture overnight at room temperature caused discharge of the deep red colour of the PhSeCl, which on work-up yielded a 2:1 *para*:*meta* mixture of **16***a*/**16***b* as determined by ^1H nmr (see eq. [3]). This result indicates that the major regioisomer formed in reaction **4***b* and **5**, with methyl acrylate, was the same in each case.

Transmetallation of tin in vinyl stannanes has precedence in

[4]Addition of 2 mol% (based on diene) BHT was used in all reactions of **5**.

[5]No attempt was made to separate this mixture.

Can. J. Chem. Downloaded from www.nrcresearchpress.com by 213.166.140.6 on 09/07/12
For personal use only.

[2] 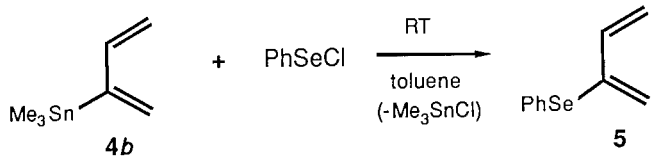

[3] 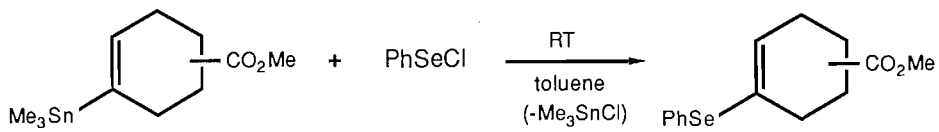

11a/11b
2:1
para:meta

16a/16b
2:1
para:meta

reactions at low temperature with alkyl lithium reagents (15), and in coupling reactions catalysed by palladium complexes (7). Stereoselective transmetallation from mercury to selenium by reaction of vinyl mercuric compounds with PhSeCl has also been observed (16).

The reaction of vinyl stannanes with PhSeCl is analogous to a previously reported reaction in which iodine is used to cleave the tin–carbon bond producing a vinyl iodide (17). Much work has already been done on the mechanism of areneselenenyl chloride addition to alkenes. Schmid and Garratt (18) have proposed three possible mechanisms, which differ only in the relative amount of carbon–selenium bond making and selenium–chlorine bond breaking leading up to the formation of the seleniranium ion. In our system, collapse of seleniranium ion **17** to give diene **5** could proceed via attack of chloride at the

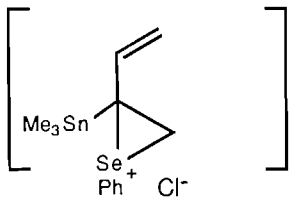

17

least-substituted carbon or at tin, followed by elimination of Me_3SnCl.[6] No spectroscopic evidence for the formation of allenic species was observed.

This transmetallation reaction appears to be general for vinyl stannanes. It exhibits interesting chemoselectivity as shown in eq. [2], with no products of addition to the isolated double bond being observed. To our knowledge, this is the first example of transmetallation from tin to selenium. Further studies in this area will involve investigation of the stereochemistry of this metal-transfer reaction.

Experimental

The ^1H nmr spectra were recorded on a Bruker WH-400 equipped with Aspect 2000 computer software. Signal positions are given in delta (δ) with reference to C_6D_5H at 7.15 ppm. Infrared spectra were run on a Nicolet 5D-X spectrophotometer. Low resolution and high resolution mass spectra (hrms) were determined on a Kratos MS-50 spectrometer. Gas–liquid chromatography was performed on a Hewlett–Packard model 5880a gas chromatograph using a 12 m × 0.2 mm column (Carbowax 10M). Column chromatography was carried out using Merck Kieselgel 60 (230–400 mesh ASTM). For thin-layer chromatography (tlc) silica gel 13181 (Eastman chromagram) sheets were used. Microanalyses were performed by Mr. P. Borda, Microanalytical Laboratory, University of British Columbia.

Dry solvents were used in all experiments. Tetrahydrofuran (THF) and toluene were dried by refluxing over and then distilling from sodium-benzophenone ketyl. All Diels–Alder reactions were carried out in the absence of light. In addition, reactions of **5** and reactions involving methyl acrylate contained 2 mol% (based on diene) 2,6-di-*tert*-butyl-4-methylphenol (BHT). No microanalysis is given for previously prepared compounds. For cycloadduct **9**, satisfactory microanalysis could not be obtained; instead, hrms is given for the hydroquinone. Grignard reagent **3** was prepared according to Method A in ref. 3.

*2-Tri-*n*-butylstannyl-1,3-butadiene,* ***4****a*

Tri-*n*-butyltin chloride (14.64 g, 45 mmol) dissolved in 25 mL THF was added dropwise, at room temperature, to a stirred solution of Grignard **3** (75 mL, 45 mmol; 0.6 *M* solution in THF) under nitrogen. The mixture was stirred at room temperature for a further 6 h, and then 10 mL of water was added to decompose any unreacted Grignard reagent. At this stage most of the THF was evaporated, leaving a white slurry that was extracted with 3 × 100 mL portions of diethyl ether. The ether layer was washed with 2 × 100 mL portions of aqueous 2 *M* potassium fluoride to remove any unreacted n-Bu_3SnCl. Finally, the organic layer was washed with 2 × 100 mL water and dried over anhydrous $MgSO_4$. Evaporation of the solvent and distillation under high vacuum yielded one fraction (40–50°C/10^{-3} Torr; 1 Torr = 133.3 Pa) of a colourless liquid **4***a* (10.9 g, 71%).

Spectroscopic data for **4***a* were consistent with those reported in ref. 4*a*.

2-Trimethylstannyl-1,3-butadiene, ***4****b*

Trimethyltin chloride (6.0 g, 30 mmol) dissolved in 25 mL THF was added dropwise, at room temperature, to a solution of Grignard **3** (50 mL, 30 mmol; 0.6 *M* in THF) under nitrogen. The mixture was stirred at room temperature for a further 6 h. The work-up was identical to that described for **4***a*. Distillation, at reduced pressure, yielded **4***b* (4.35 g, 65%) as a colourless liquid, distilling at 42°C/11 Torr.

Spectroscopic data for this compound were identical to those reported in ref. 5.

2-Phenylseleno-1,3-butadiene, ***5***

Phenylselenium chloride (4.78 g, 25 mmol) dissolved in 25 mL THF was added dropwise, at room temperature, to a stirred solution of Grignard **3** (100 mL, 25 mmol; 0.25 *M* in THF) under nitrogen. The deep red colour of the PhSeCl dissipated immediately on addition to **3**; the reaction was then stirred at room temperature for a further hour. The work-up was identical to that described for **4***a*, with the omission of the aqueous KF washings. After drying the organic layer, evaporation of the solvent yielded a yellow oil. Distillation of the latter under high

[6]A similar argument is put forward to explain the stereospecific cleavage of an E/Z mixture of $PhCH{=}CHSnMe_3$ by Br_2 (19).

Can. J. Chem. Downloaded from www.nrcresearchpress.com by 213.166.140.6 on 09/07/12
For personal use only.

Can. J. Chem. Downloaded from www.nrcresearchpress.com by 213.166.140.6 on 09/07/12
For personal use only.

vacuum (10^{-3} Torr) gave a pale yellow oil **5** (3.66 g, 70%); ν_{max} (film): 1620, 1572, 1477, 1439, 1214, 914, and 735 cm^{-1}; δ (C_6D_6, 400 MHz): 5.00 (1H, d, J = 10.5 Hz), 5.34 (1H, s), 5.53 (1H, s), 5.62 (1H, d, J = 17 Hz), 6.24 (1H, dd, J = 10.5 Hz, 17 Hz), 6.94 (3H, m), and 7.44 (2H, m). *Anal.* calcd. for $C_{10}H_{10}Se$: C 57.43, H 4.82; found: C 57.66, H 4.81.

Preparation of ***7***

A solution of **4***a* (500 mg, 1.46 mmol) and maleic anhydride (143 mg, 1.46 mmol) in 2 mL of toluene was stirred at room temperature under nitrogen for 48 h. The solvent was evaporated and the residue was purified directly by column chromatography (eluent: ether/petroleum ether 1:2) yielding **7** (482 mg, 75%) as a white solid.

Spectroscopic data for **7** were identical to those reported in ref. 4*a*.

Preparation of ***8***

A solution of **4***a* (500 mg, 1.46 mmol) and *N*-phenylmaleimide (252 mg, 1.46 mmol) in 3 mL of toluene was refluxed for 8 h. The solvent was evaporated and the residue was subjected to column chromatography (eluent: ether/petroleum ether 1:3), which yielded **8** (675 mg, 90%) as a yellow oil; ν_{max} (film): 1779, 1712, 1499, 1456, 1378, 1190, 1171, and 690 cm^{-1}; δ (C_6D_6, 400 MHz): 0.90 (15H, m), 1.29 (6H, m), 1.48 (6H, m), 1.84 (1H, m), 1.99 (1H, m), 2.53 (2H, m), 2.63 (1H, dd, J = 6 Hz, 15 Hz), 2.85 (1H, d, J = 15 Hz), 6.01 (1H, m), 7.00 (1H, m), 7.15 (2H, m), and 7.41 (2H, m). *Anal.* calcd. for $C_{26}H_{39}NO_2Sn$: C 60.49, H 7.61, N 2.71; found: C 60.60, H 7.79, N 2.60.

Preparation of ***9***

A solution of **4***a* (500 mg, 1.46 mmol) and benzoquinone (158 mg, 1.46 mmol) in 3 mL toluene was refluxed under nitrogen for 5 h. The solvent was evaporated and the residue was purified by column chromatography (eluent: dichloromethane) to give **8** as a yellow oil (453 mg, 69%); ν_{max} (film): 1684, 1602, 1260, 1090, and 850 cm^{-1}; δ (C_6D_6, 400 MHz): 0.90 (15H, m), 1.32 (6H, m), 1.32 (6H, m), 1.54 (6H, m), 1.84 (1H, m), 2.17 (1H, m), 2.39 (1H, m), 2.57 (1H, m), 2.63 (1H, m), 2.70 (1H, m), 5.72 (1H, m), and 6.05 (2H, s). From the chromatography of **9** a white solid (53 mg, 8%) was obtained, Spectroscopic data, as follows, indicated that this solid was the hydroquinone of **9**; ν_{max} (Nujol): 3286, 1625, 1595, 1311, 1242, 992, 807, and 743 cm^{-1}; δ (C_6D_6, 400 MHz): 0.93 (9H, t, J = 7 Hz), 0.99 (6H, t, J = 8 Hz), 1.37 (6H, m), 1.58 (6H, m), 3.27 (2H, m), 3.63 (2H, m), 3.83 (2H, br s, δ was concentration dependent and signal disappeared on D_2O exchange), 6.06 (1H, m), 6.10 (1H, d, J = 8.5 Hz), and 6.22 (1H, d, J = 8.5 Hz); *m/e* (relative intensity) with ^{120}Sn: 395 (14.3), 338 (6.4), 281 (13.4), 161 (98.1), 147 (70.0), and 56 (93.1). *Mol. Wt.* calcd. for $C_{18}H_{27}O_2Sn$ ($M - n$-Bu)$^+$: 395.1033; found (hrms): 395.1027.

Preparation of ***10***

A solution of **4***a* (500 mg, 1.46 mmol) and dimethyl acetylene dicarboxylate (207 mg, 1.46 mmol) in 3 mL toluene was refluxed overnight under nitrogen. The solvent was evaporated and the residue was purified by column chromatography (eluent: ether/petroleum ether 1:7) to give **10** (503 mg, 71%) as a colourless liquid; ν_{max} (film): 1736, 1726, 1668, 1618, 1434, 1261, and 1065 cm^{-1}; δ (C_6D_6, 400 MHz): 0.91 (15H, m), 1.32 (6H, m), 1.51 (6H, m), 2.93 (2H, m), 3.27 (2H, m), 3.42 (3H, s), 3.45 (3H, m), and 5.63 (1H, m). *Anal.* calcd. for $C_{22}H_{38}O_4Sn$: C 54.46, H 7.89; found: C 54.61, H 7.87.

Preparation of ***11***a/***11***b

A solution of **4***b* (1.73 g, 7.98 mmol) and methyl acrylate (3.43 g, 39.92 mmol) in 10 mL toluene was refluxed overnight under nitrogen. The solvent and excess methyl acrylate were evaporated and the residue was subjected to column chromatography (eluent: ether/petroleum ether 1:20) yielding **11***a*/**11***b* (1.74 g, 72%). Capillary glc and ^1H nmr indicated that the regioisomers **11***a*/**11***b* were present in a 2:1 ratio. The following data were obtained for this mixture: ν_{max} (film): 1737, 1618, 1437, 1166, and 767 cm^{-1}; δ (C_6D_6, 400 MHz): 0.07 (9H, s), 1.67–2.54 (7H, m), 3.36 and 3.37 (3H, 2 singlets; **11***a* and **11***b*, respectively), and 5.75 (1H, m). *Anal.* calcd. for $C_{11}H_{20}O_2Sn$: C 43.61, H 6.65; found: C 43.91, H 6.80.

Preparation of ***12***

A solution of **5** (750 mg, 3.59 mmol) and maleic anhydride (351 mg, 3.59 mmol) in 3 mL toluene was stirred at room temperature for 48 h under nitrogen. A mass of white crystals gradually deposited from solution. Low temperature recrystallization of this material (from ether/petroleum ether) yielded pure **12** (771 mg, 70%); ν_{max} (Nujol): 1845, 1780, 1245, 1010, and 942 cm^{-1}; δ (C_6D_6, 400 MHz): 1.42 (1H, m), 1.76 (1H, m), 2.04 (1H, m), 2.11 (2H, m), 2.37 (1H, m), 5.61 (1H, m), 6.97 (3H, m), and 7.33 (2H, m). *Anal.* calcd. for $C_{14}H_{12}O_3Se$: C 54.74, H 3.94; found: C 54.56, H 3.92.

Preparation of ***13***

A solution of **5** (1.00 g, 4.78 mmol) and *N*-phenylmaleimide (829 mg, 4.78 mmol) in 3 mL toluene was refluxed for 8 h under nitrogen. The solvent was evaporated and the residue was chromatographed (eluent: ether/petroleum ether 1:3) to give **13** as a yellow oil (1.39 g, 76%); ν_{max} (film): 1960, 1882, 1782, 1715, 1597, 1575, 1384, 1180, and 745 cm^{-1}; δ (C_6D_6, 400 MHz): 1.75 (1H, m), 2.08 (1H, m), 2.40 (2H, m), 2.49 (1H, m), 2.78 (1H, m), 5.92 (1H, m), and 6.98–7.50 (10H, m). *Anal.* calcd. for $C_{20}H_{17}NO_2Se$: C 62.83, H 4.48, N 3.66; found: C 62.91, H 4.63, N 3.80.

Preparation of ***14***

A solution of **5** (657 mg, 3.14 mmol) and benzoquinone (340 mg, 3.14 mmol) in 2 mL toluene was refluxed for 2 h under nitrogen. Upon cooling the reaction to room temperature a white solid deposited. After evaporation of the bulk of the solvent the residue was dissolved in CH_2Cl_2 and passed through a short column (2 cm × 2 cm) of silica to remove small traces of a highly coloured material. Removal of the solvent and recrystallization from toluene/petroleum ether yielded a white solid **14** (638 mg, 64%); ν_{max} (KBr): 1676, 1598, 1577, 1475, 1435, 1263, and 737 cm^{-1}; δ (C_6D_6, 400 MHz): 1.68 (1H, m), 2.05 (1H, m), 2.17 (1H, m), 2.41 (2H, m), 2.59 (1H, m), 5.87 (1H, m), 5.92 (1H, s), 5.93 (1H, s), 7.00 (3H, m), and 7.47 (2H, m). *Anal.* calcd. for $C_{16}H_{14}O_2Se$: C 60.58, H 4.45; found: C 60.56, H 4.52. Purification of **14** using long columns of silica (> 10 cm × 2 cm) led to significant decomposition, as well as formation of small quantities (generally <3%) of what appeared to be the corresponding hydroquinone. The ^1H nmr data of the latter are as follows: δ (C_6H_6, 400 MHz): 3.21 (2H, m), 3.58 (2H, m), 3.77 and 3.90 (2 broad singlets, δ was concentration dependent; signals disappeared on D_2O exchange), 6.08 (1H, d, J = 8.5 Hz), 6.13 (1H, d, J = 8.5 Hz), 6.20 (1H, m), 6.93 (3H, m), and 7.46 (2H, m).

Preparation of ***15***

A solution of **5** (1.00 g, 4.78 mmol) and dimethyl acetylene dicarboxylate (680 mg, 4.78 mmol) in 3 mL toluene was refluxed overnight under nitrogen. The solvent was evaporated and the residue subjected directly to column chromatography (eluent: ether/petroleum ether 1:7), yielding **15** as a yellow oil (1.36 g, 81%); ν_{max} (film): 1731, 1669, 1640, 1578, 1434, 1263, 1064, 742, and 689 cm^{-1}; δ (C_6D_6, 400 MHz): 2.78 (2H, m), 3.16 (2H, m), 3.27 (3H, s), 3.41 (3H, s), 5.80 (1H, m), 6.96 (3H, m), and 7.42 (2H, m). *Anal.* calcd. for $C_{16}H_{16}O_4Se$: C 54.71, H 4.59; found: C 55.00, H 4.67.

Preparation of ***16***a/***16***b

A solution of **5** (1.30 g, 6.22 mmol) and methyl acrylate (1.60 g, 18.66 mmol) in 3 mL toluene was refluxed overnight under nitrogen. The solvent was evaporated and the resulting yellow liquid was distilled, under high vacuum (10^{-3} Torr), to yield a pale yellow oil (1.65 g, 90%). All data reported are for the 4:1 mixture of *para*:*meta* regioisomers **16***a*/**16***b*, the ratio having been determined by ^1H nmr and capillary glc; ν_{max} (film): 1738, 1578, 1475, 1437, 1169, 1020, 738, and 692 cm^{-1}; δ (C_6D_6, 400 MHz): 1.46–2.71 (7H, m), 3.23 and 3.30 (3H, 2 singlets; **16***b* and **16***a*, respectively), 6.00 and 6.03 (1H, 2 multiplets), 6.97 (3H, m), 7.44 and 7.47 (2H, 2 multiplets). *Anal.* calcd. for $C_{14}H_{16}O_2Se$: C 56.96, H 5.46; found: C 56.71, H 5.49.

Reaction of **4**b *with phenylselenium chloride*

To a solution of **4***b* (200 mg, 0.92 mmol) in 1 mL toluene was added, dropwise, a toluene solution of phenylselenium chloride (176 mg,

0.92 mmol). On addition, the deep red colour of the PhSeCl dissipated immediately. The mixture was stirred overnight at room temperature, after which 75 mg of KF and 3 mL of THF were added to destroy the Me_3SnCl by-product. After a further 2 h at room temperature, the resulting slurry was filtered through a short column of basic alumina. Evaporation of the solvent yielded a yellow oil (164 mg, 85%), spectroscopic data for which were identical to those reported for the phenylseleno diene **5**.

Reaction of ***11****a*/***11****b with phenylselenium chloride*

To a solution of **11***a*/**11***b* 2:1 *para*:*meta* (150 mg, 0.50 mmol) in 1 mL toluene was added a solution of phenylselenium chloride (95 mg, 0.50 mmol). The mixture was stirred overnight at room temperature during which time the deep red colour of the mixture had changed to a bright yellow. The reaction work-up was identical to that described above. A yellow oil (122 mg, 84%) was isolated whose spectroscopic data were consistent with those reported for **16***a*/**16***b*, with ^{1}H nmr and capillary glc indicating a *para*:*meta* ratio of 2:1.

Acknowledgements

Financial support was provided by NSERC of Canada in the form of operating grants (M.D.F. and G.S.B.) and by the Alfred P. Sloan Foundation (M.D.F.).

1. M. D. Fryzuk, G. S. Bates, and C. Stone. J. Org. Chem. **52**, 2334 (1987).
2. C. A. Aufdermarsh. J. Am. Chem. Soc. **29**, 1994 (1964).
3. S. Nunomoto and Y. Yamashita. J. Org. Chem. **44**, 4788 (1979).
4. (*a*) I. Fleming and M. Taddei. Synthesis, 899 (1985); (*b*) M. Taddei and A. Mann. Tetrahedron Lett. **27**, 2913 (1986).
5. P. Vanderlinden and S. Bone. J. Organomet. Chem. **87**, 183 (1975).
6. C. L. Liotta and J. W. Verbicky. Tetrahedron Lett. **26**, 1395 (1985).
7. W. J. Scott and J. K. Stille. J. Am. Chem. Soc. **108**, 3033 (1986).
8. J. K. Stille and B. L. Groh. J. Am. Chem. Soc. **109**, 813 (1987).
9. (*a*) D. G. Batt and B. Ganen. Tetrahedron Lett. **19**, 3323 (1978); (*b*) I. Fleming and A. Percival. J. Chem. Soc. Chem. Commun. 278 (1978).
10. (*a*) O. Eisenstein, J. M. Lefour, and N. T. Anh. Tetrahedron, **33**, 523 (1977); (*b*) Yu. A. Titov. Russ. Chem. Rev. **31**, 267 (1962).
11. R. A. Bell and J. K. Saunders. Can. J. Chem. **48**, 1114 (1970).
12. N. Petragnani, R. Rodrigues, and J. V. Comasseto. J. Organomet. Chem. **114**, 281 (1976).
13. H. Okamura, M. Miura, K. Kosugi, and H. Takei. Tetrahedron Lett. **21**, 87 (1980).
14. M. Sevrin, W. Dumont, and A. Krief. Tetrahedron Lett. **18**, 3835 (1977).
15. D. Seyferth and M. A. Weiner. J. Am. Chem. Soc. **83**, 3583 (1961).
16. S. Raucher, M. R. Hansen, and M. A. Colter. J. Org. Chem. **43**, 4885 (1978).
17. P. Baekelmans, M. Gielman, P. Malfroid, and J. Nasielski. Bull. Soc. Chim. Belg. **77**, 85 (1968).
18. G. H. Schmid and D. G. Garratt. J. Org. Chem. **48**, 4169 (1983).
19. A. Alvanipour, C. Eaborn, and D. R. M. Walton. J. Organomet. Chem. **201**, 233 (1980).

Can. J. Chem. Downloaded from www.nrcresearchpress.com by 213.166.140.6 on 09/07/12
For personal use only.

Characterization of a γ-radiation-induced decomposition product of thymidine. Crystal and molecular structure of the (−)*cis*(5*R*,6*S*) thymidine glycol

FRANK E. HRUSKA AND RUDY SEBASTIAN
Chemistry Department, University of Manitoba, Winnipeg, Man., Canada R3T 2N2

AND

ANDRÉ GRAND, LUCIENNE VOITURIEZ, AND JEAN CADET
Laboratoire de Chimie, Département de Recherche Fondamentale, Centre d'Etudes Nucléaires de Grenoble, 85X, F.38041 Grenoble Cedex, France

Received December 23, 1986[1]

FRANK E. HRUSKA, RUDY SEBASTIAN, ANDRÉ GRAND, LUCIENNE VOITURIEZ, and JEAN CADET. Can. J. Chem. **65**, 2618 (1987).

X-ray crystallography was used to determine the structure of (−)*cis*(5*R*,6*S*)-5,6-dihydroxy-5,6-dihydrothymidine, a γ-radiation induced product of thymidine. The crystals belong to the orthorhombic space group $P2_12_12_1$ and have cell dimensions a = 8.420(1) Å, b = 10.422(1) Å, and 13.552(1) Å. The half-chair pucker of the 5,6-saturated pyrimidine ring is similar to that observed for the isolated base with the *cis* configuration, and is described by the Cremer–Pople parameters Q = 0.48 Å, θ = 62°, and φ = 272°. The conformation about the *N*-glycosyl bond is *anti*; the χ angle (−111.6(5)°) lies at one extreme of the range previously seen for nucleosides (−180 to −115°). The pucker $^2T_1$ of the sugar (P = 151.2°; τ_m = 36.5°) contrasts with the O4′-*endo* type of pucker seen in 5,6-dihydrothymidine ($^0T_4$) and (5*S*)-5-hydroxy-5,6-dihydrothymidine ($^0T_1$). The conformation about the C4′—C5′ bond is *gauche*$^+$. The solid state structure is similar to that determined in aqueous solution by ^{1}H nmr.

FRANK E. HRUSKA, RUDY SEBASTIAN, ANDRÉ GRAND, LUCIENNE VOITURIEZ et JEAN CADET. Can. J. Chem. **65**, 2618 (1987).

On a utilisé la diffraction des rayons-X pour déterminer la structure de la (−)-dihydroxy-5,6 dihydro-5,6 thymidine-(5*R*,6*S*)-*cis*, un produit de la thymidine induit par les radiations-γ. Les cristaux appartiennent au groupe d'espace orthorhombique $P2_12_12_1$, avec a = 8,420(1), b = 10,422(1) et c = 13,522(1) Å. La forme demi-chaise de la pyrimidine saturée en 5,6 est semblable à celle qui a été observée avec la base isolée ayant la configuration *cis*; on peut décrire cette demi-chaise par les paramètres de Cremer-Pople Q = 0,48 Å, θ = 62° et φ = 272°. La conformation de la liaison *N*-glycosyle est *anti*; l'angle χ (−111,6(5)°) se trouve à la limite extrême de la fourchette qui avait été observée antérieurement avec les nucléosides (−180° à −115°). La conformation $^2T_1$ du sucre (P = 151,2° et τ_m = 36,5°) est en opposition avec le type de conformation *endo*-O4′ que l'on a observé dans la dihydro-5,6 thymidine ($^0T_4$) et dans l'hydroxy-5 dihydro-5,6 thymidine-(5*S*) ($^0T_1$). La conformation autour de la liaison C4′—C5′ est *gauche*$^+$. La structure observée à l'état solide est semblable à celle qui a été déterminée en solution aqueuse, par rmn du ^{1}H.

[Traduit par la revue]

Introduction

The free radical reactions in γ-irradiated, aerated or oxygen-free, aqueous solutions of thymine (Thy) (or thymidine (dThd)) leads to, *inter alia*, the *cis*- and *trans*-5,6-dihydroxy-5,6-dihydrothymine derivatives (1, 2). These thymine diols (or glycols) are a major class of base damage in DNA exposed to ionizing radiation or near-ultraviolet light (3–5), and to certain oxidants (4). The biological significance of these damaged bases is evidenced by the presence of *N*-glycosylase activities which lead to their excision (6). The addition of the hydroxyl groups to the thymine base, with the concomitant 5,6-saturation of the ring, should have important effects on its base stacking and hydrogen bonding properties. At present only limited information is available on the effects of 5,6-saturation of pyrimidine rings on ordered nucleic acids (7). Our understanding of the effects of thymine diol formation on the physical properties and biological behavior of DNA would be furthered by the availability of the precise structural details provided by X-ray diffraction. However, such data have been reported (8) for only a single base, the *cis*-5,6-dihydroxy-5,6-dihydrothymine, and no data are available at the nucleoside level. Cadet and Teoule (9) have prepared the four isomers of 5,6-dihydroxy-5,6-dihydrothymidine; a ^{1}H nmr study of their conformational properties followed (10). The present work describes our crystallographic study of the (−)(5*R*,6*S*) thymidine glycol (*cis* configuration for the two hydroxyl groups) (Fig. 1). Our data are compared with those for other crystalline 5,6-saturated pyrimidine derivatives and with the nmr solution data.

[1]Revision received May 25, 1987.

Experimental

The (−)(5*R*,6*S*) isomer of 5,6-dihydroxy-5,6-dihydrothymidine (**I**) was prepared according to the literature (10) and was crystallized from a saturated aqueous solution. A crystal with dimensions 0.2 mm × 0.2 mm × 0.3 mm was chosen for data collection on an experimental ENRAF-NONIUS CAD4 diffractometer.

$C_{10}H_{16}N_2O_7$ F_w = 276.248

Orthorhombic, $P2_12_12_1$; a = 8.420(1), b = 10.422(1), c = 13.522(1) Å; V = 1186.6 Å^3; Z = 4; ρ_c = 1.547 g cm^{-3}; μ = 0.799 cm^{-1}; MoK$_\alpha$: 0.71069 Å (monochromatized); 20°C; scan mode: ω; scan rate: 1° min^{-1}; max shift/esd final cycle 0.42.

The intensities of the reflections were corrected for Lorentz and polarization factors but not for absorption. The structure was solved by direct methods using MULTAN (11). An *E*-map based on 190 phased reflections with $E > 1.6$ revealed the positions of all non-hydrogen atoms. The structure was refined by least-squares XFLSN methods (12) with 985 reflections (of 1250 unique data) for which $|F_o| > 2.5\sigma(F_o)$. The refinement of 169 variables yielded values of R = 0.091 and R_w = 0.081 ($R = \Sigma||F_o| - |F_c||/\Sigma|F_o|$; $R_w = [\Sigma w(|F_o| -$

Can. J. Chem. Downloaded from www.nrcresearchpress.com by 213.222.148.141 on 09/07/12
For personal use only.

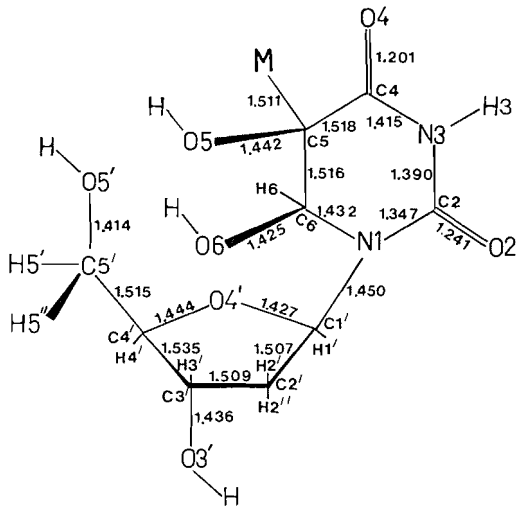

FIG. 1. Structure of (−)*cis*(5*R*,6*S*)-5,6-dihydroxy-5,6-dihydrothymidine (**I**) and bond lengths (Å) involving the heavy atoms. The estimated standard deviations are less than 0.009 Å.

$|F_c|)^2/\Sigma w|F_o|^2]^{1/2}$) for non-hydrogens only. (The weights were based on counting statistics.) The positions of all hydrogen atoms were determined from a difference Fourier map and were fixed in subsequent cycles of refinement. In the final stages of refinement non-hydrogen atoms were assigned anisotropic temperature factors whereas the hydrogens were assumed to have isotropic thermal motions ($B = 5$ Å^2). The refinement converged at $R = 0.061$ and $R_w = 0.047$. The final Fourier difference map shows no electron density larger than 0.4 e Å^{-3}. The choice of the proper enantiomorph was based on the known D configuration of the 2-deoxyribose unit.

Further data are provided in Table 1 (atomic coordinates), Fig. 1 (bond lengths), Table 2 (bond angles), Table 3 (torsion angles), Table 4 (Cremer–Pople (CP) parameters (13) for the pyrimidine ring), and Table 5 (hydrogen bond geometries). A stereoscopic view of the packing is shown in Fig. 2. The molecules represented by the symbols **I**, **II**, etc. are given in a footnote of Table 4. Lists of anisotropic temperature parameters and of final hydrogen coordinates (unrefined) are available.[2]

Results and discussion

Structure of the pyrimidine ring

The bond lengths and bond angles of **I** are given in Fig. 1 and Table 2, respectively. Figure 3 shows a comparison of the bond lengths and bond angles of the 5,6-saturated pyrimidine rings of **I** and **II**. (**II** is the free thymine diol base with the *cis* configuration of the hydroxyl groups (8).) The bond lengths and endocyclic bond angles of **I** and **II** are similar. Significant differences are noted in some of the exocyclic angles at C5 and C6.

Figure 3 also provides a comparison of **I** and an "average" thymine base which allows us to assess the effect of 5,6-saturation on the geometry of the pyrimidine ring. The data for the thymine base are the averages of six sets of literature values (14–18) used previously (19). Relative to the thymine base, **I** shows a large extension at C5—C6 (0.18 Å), and smaller extensions of C4—C5 (0.08 Å) and N1—C6 (0.05 Å), a reflection of the loss of π-electron density due to 5,6-saturation (20). The N1—C2 and C2—O2 bonds are, respectively, shortened and extended by 0.03 Å; a similar trend has been observed in other 5,6-saturated pyrimidines (21, 22) and attributed to stronger conjugation of the lone electron pair on N1 with the C2—O2 carbonyl group.

The pyrimidine ring of **I** exhibits an approximate half-chair conformation (Figs. 2, 4). The best contiguous four-atom plane is defined by the N1, C2, N3, and C4 atoms; their average displacement from this plane is 0.04 Å. The C5 and C6 atoms are displaced respectively 0.28 Å to the left and 0.42 Å to the right of the plane, with left and right displacements defined by Fig. 5. (When **I** is viewed in its *anti* conformation about the *N*-glycosyl bond, left and right represent displacements towards

[2]These tables may be purchased from the Depository of Unpublished Data, CISTI, National Research Council of Canada, Ottawa, Ont., Canada K1A 0S2.

TABLE 1. Final atomic coordinates* and their estimated standard deviations†

Atom	*x*	*y*	*z*	B_{eq}
N1	7187(6)	4486(4)	4636(4)	2.46
C2	5940(8)	4256(6)	5235(4)	3.31
O2	5897(5)	4559(4)	6122(3)	4.05
N3	4650(6)	3605(5)	4835(3)	3.09
C4	4389(8)	3421(6)	3811(4)	3.21
O4	3235(5)	2853(5)	3526(3)	4.39
C5	5635(7)	4056(6)	3164(4)	2.55
O5	5825(5)	3332(4)	2263(3)	3.31
M5	5184(8)	5430(6)	2944(4)	3.55
C6	7240(7)	3939(6)	3665(4)	2.65
O6	7688(5)	2629(4)	3781(3)	3.49
C1′	8464(7)	5304(6)	4979(4)	2.76
C2′	10137(7)	4815(6)	4859(4)	3.04
C3′	11083(7)	6044(7)	4833(4)	2.63
O3′	11471(5)	6419(4)	5826(3)	3.67
C4′	9968(7)	7021(6)	4344(4)	3.06
C5′	10362(9)	7337(7)	3279(5)	4.75
O5′	10856(6)	6244(5)	2740(3)	5.83
O4′	8407(5)	6450(4)	4404(3)	3.04

*Multiplied by 10^4.
†M5 = 5-methyl carbon.

TABLE 2. Bond angles (deg) of the (−)(5*R*,6*S*) *cis* thymidine diol*

Bonds	Angle	Bonds	Angle
(*a*) C6—N1—C2	120.3(4)	(*d*) O4′—C1′—C2′	104.8(5)
N1—C2—N3	117.5(5)	C1′—C2′—C3′	102.0(5)
C2—N3—C4	124.6(5)	C2′—C3′—C4′	104.5(5)
N3—C4—C5	113.4(5)	C3′—C4′—O4′	105.0(5)
C4—C5—C6	108.9(5)	C4′—O4′—C1′	110.2(4)
C5—C6—N1	110.5(4)	N1—C1′—C2′	117.4(5)
		N1—C1′—O4′	107.0(4)
(*b*) C1′—N1—C2	119.3(4)	O3′—C3′—C2′	109.3(5)
C1′—N1—C6	120.3(3)	O3′—C3′—C4′	111.1(5)
O2—C2—N1	124.0(6)	C5′—C4′—C3′	114.8(5)
O2—C2—N3	118.5(6)	C5′—C4′—O4′	110.0(5)
O4—C4—N3	120.4(6)	O5′—C5′—C4′	112.3(5)
O4—C4—C5	126.1(6)		
(*c*) M—C5—C4	110.7(5)		
M—C5—C6	112.8(5)		
M—C5—O5	111.0(5)		
O5—C5—C4	109.6(5)		
O5—C5—C6	103.7(5)		
O6—C6—N1	106.7(4)		
O6—C6—C5	111.2(5)		

*M = 5-methyl carbon.

Can. J. Chem. Downloaded from www.nrcresearchpress.com by 213.222.148.141 on 09/07/12
For personal use only.

TABLE 3. Torsion angles (deg) of the (−)(5*R*,6*S*) *cis* thymidine diol*†

Bonds	Torsion angle	Bonds	Torsion angle
(*a*) N1—C2—N3—C4	−14.9	(*c*) O4′—C1′—N1—C2(χ)	−111.6
C2—N3—C4—C5	−2.3	O4′—C1′—N1—C6(χ′)	67.6
N3—C4—C5—C6	37.0	C2′—C1′—N1—C2	131.0
C4—C5—C6—N1	−56.5	C2′—C1′—N1—C6	−49.8
C5—C6—N1—C2	43.3	C4′—O4′—C1′—C2′	−27.5
C6—N1—C2—N3	−7.3	O4′—C1′—C2′—C3′	36.5
		C1′—C2′—C3′—C4′	−32.0
(*b*) C1′—N1—C2—N3	172.0	C2′—C3′—C4′—O4′	16.6
C1′—N1—C2—O2	−10.2	C3′—C4′—O4′—C1′	6.7
C1′—N1—C6—C5	−135.9		
C1′—N1—C6—O6	103.0	(*d*) O3′—C3′—C2′—C1′	87.0
O2—C2—N3—C4	167.1	O3′—C3′—C4′—O4′	−101.2
O2—C2—N1—C6	170.6	O3′—C3′—C4′—C5′	137.9
O4—C4—N3—C2	−179.5	O5′—C5′—C4′—C3′(γ)	39.1
O4—C4—C5—C6	−146.0	O5′—C5′—C4′—O4′	−79.0
O4—C4—C5—M	89.4		
O4—C4—C5—O5	−33.2		
M—C5—C6—N1	66.8		
M—C5—C4—N3	−87.5		
M—C5—C6—O6	−174.8		
O5—C5—C6—N1	−173.1		
O5—C5—C4—N3	149.8		
O5—C5—C6—O6	−54.7		
O6—C6—N1—C2	−77.7		
O6—C6—C5—C4	61.9		

*M = 5-methyl carbon.
†Standard deviations 0.5–1.1°.

TABLE 4. Cremer–Pople puckering parameters for a series of 5,6-saturated pyrimidine bases

Molecule	*Q* (Å)	θ (deg)	φ (deg)	Molecule	*Q* (Å)	θ (deg)	φ (deg)
I*†	0.48	62	272	**VII**	0.45	66	283
II	0.49	59	265	**VIII**	0.41	63	271
III	0.44	66	272	**IX**	0.45	119	95
IV	0.40	67	289	**X**	0.49	114	113
V	0.44	60	283	**XI**	0.31	120	86
VI	0.43	66	260	**XII**	0.24	123	141

*I: title molecule; II: *cis* thymine diol base; III: (5*S*)-5-hydroxy-5,6-dihydrothymidine; IV: 5,6-dihydrouridine-3′-monophosphate; V: 5,6-dihydrouridine (molecule **1**); VI: 5,6-dihydroisocytidine; VII: 5,6-dihydro-2,4-dithiouridine; VIII: 5,6-dihydro-2-thiouridine; IX: 5,6-dihydrothymidine; X: molecule **2** of V; XI and XII: [p]T and T[p] units of the cyanoethylester of d(T[p]T).
†I: this work; II: calculated from coordinates in ref. 8; III–X: from ref. 24; XI–XII: from ref. 23.

the O4′ and C2′ sides of the sugar, respectively.) Following Hruska *et al.* (23), we can denote this as a $_5H^6$ pucker (H means half chair with C6 showing the greater displacement to the right of the four-atom plane, and C5 the lesser displacement to the left). In this conformation the 5-methyl and 6-hydroxyl groups occupy pseudoaxial positions whereas the 5-hydroxyl group is pseudoequatorial and *gauche* to the 6-hydroxyl (see Fig. 2 and torsion angles in Table 3*b*). Note in the tabulation of torsion angles (Table 3*a*,*b*) that the substituent atoms on the C5—C6 fragment are oriented only 5° (average) from the classically-staggered saturated system (±60°, 180°).

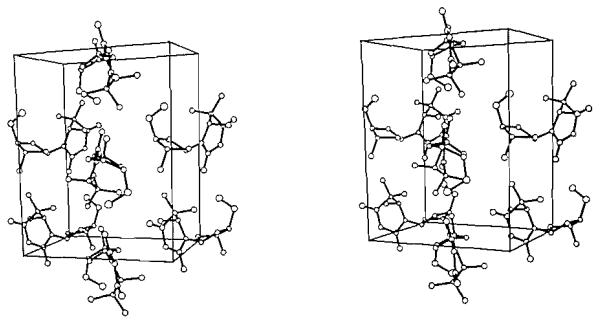

FIG. 2. Stereoscopic packing diagram. The hydrogen atoms and hydrogen bonds are not shown.

The overall conformation of the pyrimidine base is similar in **I** and **II**, that is, the attachment of the sugar has little effect on the base pucker. The endocyclic torsion angles of **I** (Table 3*a*) differ from those of **II** (8) by 3° (average) and by no more than 6° (at N3—C4). This similarity is also apparent in their CP parameters (Table 4) which indicate the extent of puckering (*Q*, the total puckering amplitude) and the mode of puckering (θ and φ, the angular descriptors) (13).

For comparison with **I** and **II**, Table 4 provides CP data for other 5,6-saturated pyrimidine nucleosides. Molecules lying in the "northern" CP hemisphere (N(CP)) ($0° < \theta < 90°$) have *Q* values in the range 0.45 ± 0.04 Å. The diols **I** and **II** show the most pronounced extent of puckering (largest *Q*), presumably a reflection of the presence of three bulky groups (methyl and hydroxyl) on the C5—C6 fragments. **III** (5*S*-5-hydroxy-5,6-dihydrothymidine), which lacks a 6-hydroxyl group, has a smaller *Q* (0.44 Å) as do the remaining N(CP) entries (**IV–VIII**)

Can. J. Chem. Downloaded from www.nrcresearchpress.com by 213.222.148.141 on 09/07/12
For personal use only.

TABLE 5. Distances and angles for hydrogen bonds

D	A	Acceptor (A) at	Distance (Å) D—H	Distance (Å) H···A	Distance (Å) D···A	Angle (deg) D—H···A
N3—H···O6		$-\frac{1}{2}+x, \frac{1}{2}-y, 1-z$	1.12	1.71	2.807(6)	164
O5—H···O3′		$-\frac{3}{2}-x, 1-y, -\frac{1}{2}+z$	0.97	1.99	2.755(5)	134
O6—H···O5′		$2-x, -\frac{1}{2}+y, \frac{1}{2}-z$	1.12	1.99	2.797(6)	126
O3′—H···O4′		$\frac{1}{2}+x, \frac{3}{2}+y, \frac{3}{2}-z$	1.12	1.65	2.771(6)	175
O5′—H···O2		$\frac{3}{2}-x, 1-y, \frac{1}{2}+z$	1.22	2.16	2.769(6)	106

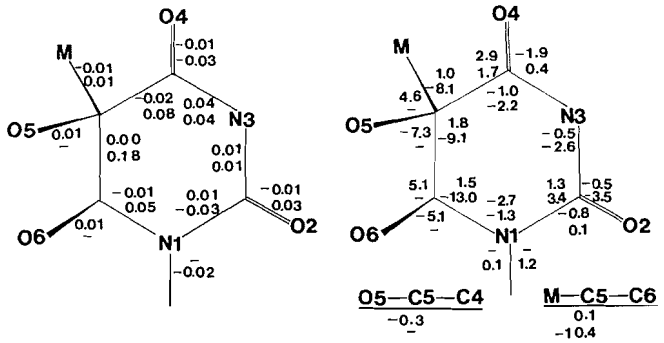

FIG. 3. Left. Differences between the bond lengths (Å) of the *cis* thymidine diol (**I**) and the *cis* thymine diol (**II**) (top number) and an "average" thymine base (bottom number). Right. Similar comparison of bond angles. Data for **I**: Fig. 1 and Table 2; for **II**, ref. 8; for the average thymine: refs. 14–18. See text for details. A positive number means that the bond length or angle is larger in **I**.

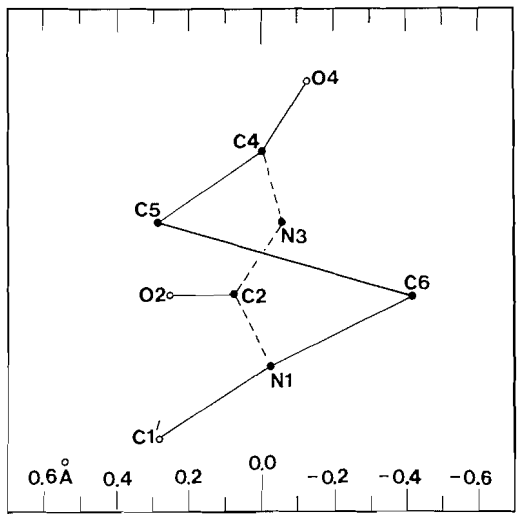

FIG. 4. Schematic view of the base from its front edge (C5—C6) to its back edge (C2—N3) which illustrates the ring puckering. Solid circles: ring atoms; open circles: atoms directly bonded to the ring. The horizontal axis gives deviations (Å) to the left (positive) and to the right (negative) of the best four-atom plane, N1—C2—N3—C4.

which are not substituted on C5—C6. The θ and φ entries for **I**–**VIII** lie in the narrow ranges 63 ± 4° and 274 ± 9°, respectively.

Table 4 lists four nucleosides with 5,6-saturated pyrimidine rings in the "southern" CP hemisphere (S(CP)) (90° < θ < 180°). **IX** (5,6-dihydrothymidine) and **X** (molecule **2** of 5,6-dihydrouridine) have Q values (0.45 Å, 0.49 Å) similar to those of the N(CP) entries, whereas those of the two rings of the thymine photodimer (**XI** and **XII**) are significantly reduced (0.31 Å, 0.24 Å). The S(CP) entries lie in a narrow range of θ values (119 ± 5°), but have a larger range of φ values (114 ± 27°).

At present no crystallographic data are available for the three isomers of **I** having the 5*R*–6*R*, 5*S*–6*R*, or 5*S*–6*S* configurations at C5 and C6. A ^{1}H nmr study of the four thymidine diols in aqueous solution has been reported (10) but it provided no information about the pyrimidine ring pucker since no vicinal pair of protons is located on the ring. However, our crystal structure of **I** (in conjunction with molecular models) suggests that the favored conformation is that which places the 6-hydroxyl in a pseudoaxial orientation, and thereby minimizes crowding between this group and the 5-hydroxyl and 5-methyl groups. On this basis we expect an N(CP) pucker to be favored by the 5*S*–6*S* isomer and an S(CP) pucker by the 5*R*–6*R* and 5*S*–6*R* isomers.

The N*-glycosyl bond (*χ,χ′*)*

The N1—C1′ bond length of **I** (Fig. 1) and the bond angles involving the N1—C1′ bond (Table 2*b*,*d*) are similar to those of the other 5,6-saturated pyrimidine-2′-deoxynucleosides, **III** (26) and **IX** (27). The χ(O4′—C1′—N1—C2) and χ′(O4′—C1′—N1—C6) torsion angles (Table 3) show that **I** has the *anti* conformation about the *N*-glycosyl bond. The χ angle (−111.6°) lies at one extreme of the range of χ angles seen for nucleosides (−180 – −115°) (28). It is noteworthy that the two 2′-deoxyribonucleosides with N(CP) puckers of the saturated pyrimidine ring (**I**, **III**) have similar χ(−111.6°, −110.6°) and χ′(67.6°, 68.7°) angles, even though the 6-OH of **I** is replaced by a hydrogen in **III**. On the other hand, molecule **IX**, a 2′-deoxyriboside with an S(CP) pucker of the pyrimidine ring, has significantly different χ(−117.3°) and χ′(52.8°) angles. (χ and χ′ for **IX** were calculated by G. I. Birnbaum from data in ref. 27; data for **III** in ref. 26). A similar (but less pronounced) trend is noted for the two independent molecules of the *riboside*, 5,6-dihydrouridine; the N(CP) molecule (**V**) and the S(CP) molecule (**X**) have χ′ angles of 65.6 and 57.3°, respectively (averages of data from Suck *et al.* (29) and Sundaralingam *et al.* (30)).

With an N(CP) pucker and χ′ = 67.6° in **I**, H6 occupies a pseudoequatorial position on the left face of the pyrimidine ring (left and right defined in Fig. 4), and is positioned over the sugar ring as shown in Fig. 5*a*. A close contact is made between this hydrogen and O5′ (2.191 Å separation). The 6-OH group occupies a pseudoaxial position on the right face, and is located off the sugar ring on the C2′ side. As noted in the previous section, the 5*S*–6*S* isomer of **I**, is expected to favor an N(CP)

Can. J. Chem. Downloaded from www.nrcresearchpress.com by 213.222.148.141 on 09/07/12
For personal use only.

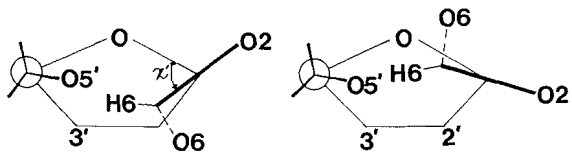

FIG. 5. Left (*a*): view of **I**, the 5*R*,6*S* thymidine diol which shows the position of the pseudoequatorial H6 and pseudoaxial 6-OH relative to the sugar ring. A similar arrangement of these atoms is postulated in the text for the 5*S*,6*S* diol. Right (*b*): approximate positions predicted for the pseudoequatorial 6H and pseudoaxial 6-OH of the 5*R*,6*R* and 5*S*,6*R* diols.

pucker, and thus the disposition of its H6 and 6-OH should be similar to that noted in **I** (Fig. 5*a*). On the other hand, the 5*R*–6*R* and 5*S*–6*R* isomers are expected to favor the S(CP) pucker (see previous section). Examination of molecular models leads us to predict that the pseudoequatorial H6 (on the right face) will lie over the sugar ring (Fig. 5*b*) whereas the pseudoaxial 6-OH (on the left face) will lie off the ring on the O4′ side.

The sugar geometry

The bond lengths (Fig. 1) and bond angles (Table 2) of the sugar moiety of **I** are not unusual. The furanose ring adopts an S-type pucker (31) with a phase angle of pseudorotation (P) of 151.2° ($^2T_1$) and a maximum amplitude of pucker (τ_m) of 36.5°. The pucker of dThd is not very different: P = 187.5° ($_3T^2$) and τ_m = 38.2° (18, 32). In contrast **III** and **IX** (the other 2′-deoxyribosides with 5,6-saturated bases) are located in the O4′-*endo* quadrant of the pseudorotational cycle: P = 95.5° ($^0T_1$) and 84.4° ($^0T_4$), respectively (26, 31). Furthermore, **IX** shows a considerable flattening of the ring (τ_m = 31.6°) whereas **III** does not (τ_m = 37.4°) (26, 31).

The conformation of **I** about the C4′—C5′ bond (γ) is *gauche*$^+$ (γ = 39.1°). This angle falls just outside of the lower extreme of γ values observed for S-type nucleosides (28). *Anti*-2′*endo* deoxynucleosides such as dThd show a slight bias for the *trans* over the *gauche*$^+$ γ torsion angle (32). Considering the other 2′-deoxyribosides, we note that **III** is also *gauche*$^+$ (γ = 49.4°) (25) whereas **IX** shows disorder at the C4′—C5′ bond (2:1 *trans*:*gauche*$^+$ distribution) (27).

Comparison with solution

A ^{1}H nmr study of **I** as well as of its 5*R*–6*R*, 5*S*–6*R*, and 5*S*–6*S* isomers has appeared (10). Each of the four isomers prefers the *anti* conformation in aqueous solution. Evaluation of the C4′—C5′ orientation according to Haasnoot *et al.* (33) gives the following narrow ranges of populations: *gauche*$^+$ (47 ± 2%); *trans* (37 ± 2%); *gauche*$^-$ (16 ± 2%). No significant effect of the configuration at C5 and C6 is apparent; the bias towards the *gauche*$^+$ rotamer and the minimal contribution from *gauche*$^-$ are standard features of normal 2′-deoxyribosides (34). Like most 2′-deoxyribosides, the four diols show a bias towards the S(2′*endo*) type of sugar pucker, the pucker of I in the crystal state. However, this bias is slightly stronger in the 6*S* pair of isomers (70% *S*) than in the 6*R* pair (60% *S*).

Hydrogen bonding and molecular packing

The molecular packing of **I** can be seen in three dimension in Fig. 2. No strong intramolecular hydrogen bonds are found though a close contact is made between H6 and O5′ (2.191 Å). The packing is stabilized by two strong and three weak hydrogen bonds in the networks N3—H3···O6—H···O5′—H···O2 and O5—H···O3′—H···O4′. Thus all potential donors are involved. The O3′, O5′, and O6 donor atoms also serve as acceptors but N3 and O5 do not. It is interesting that O2 participates in a weak bond, and O4 does not participate at all. In contrast with **I**, the 5-OH of the free base (**II**) serves as both a donor and an acceptor, whereas the 6-OH serves only as a donor; both keto groups of **II** serve as acceptors (8). No base stacking interactions occur in **I**.

Acknowledgements

NSERC operating grants to F.E.H. and T. Schaefer (for support of R.S.) are acknowledged. We thank Drs. G. I. Birnbaum and A. S. Secco for useful discussions, and Nola Li for help with the diagrams.

1. G. SCHOLES. *In* Photochemistry and photobiology of nucleic acids. Vol. 1. *Edited by* S. Y. Wang. Academic Press, New York. 1976. p. 521.
2. R. TEOULE AND J. CADET. *In* Molecular biology, biochemistry and biophysics. *Edited by* J. Hutterman, W. Kohnlein, R. Teoule, and A. J. Bertinchamps. Springer-Verlag, Berlin. 1978. pp. 171–203.
3. P. V. HARIHARAN and P. A. CERUTTI. J. Mol. Biol. **66**, 65 (1972).
4. K. FRENKEL, M. S. GOLDSTEIN, and G. W. TEEBOR. Biochemistry, **20**, 7566 (1981).
5. R. TEOULE, C. BERT, and A. BONICEL. Radiat. Res. **72**, 190 (1977).
6. L. H. BREIMER and T. LINDAHL. J. Biol. Chem. **259**, 1 (1984).
7. J. SWINEHART, A. BOBST, and P. CERUTTI. FEBS Lett. **21**, 56 (1972).
8. J. L. FLIPPEN. Acta Crystallogr. B**29**, 1756 (1973).
9. J. CADET and R. TEOULE. Bull. Soc. Chim. Fr. 891 (1975).
10. J. CADET, R. DUCOLOMB, and F. E. HRUSKA. Biochim. Biophys. Acta, **563**, 206 (1979).
11. J. P. DECLERCQ, G. GERMAIN, P. MAIN, and M. M. WOOLFSON. Acta Crystallogr. A**29**, 231 (1973).
12. W. R. BUSING, K. O. MARTIN, and H. A. LEVY. ORFELS3, Report ORNL 59-4-37. 1971. Oak Ridge National Laboratory, Oak Ridge, TN.
13. D. CREMER and J. A. POPLE. J. Am. Chem. Soc. **97**, 1354 (1975).
14. T. ISHIDA, S. MITOGUCHI, Y. MIYAMOTO, K.-I. TOMITA, and M. INOUE. Biochim. Biophys. Acta, **609**, 158 (1980).
15. C.-H. CHANG, J. PLETCHER, W. FUREY JR., and M. SAX. Acta Crystallogr. B**36**, 2655 (1980).
16. D. SUCK, W. SAENGER, and W. RHODE. Biochim. Biophys. Acta, **361**, 1 (1974).
17. D. J. HUNT and E. SUBRAMANIAN. Acta Crystallogr. B**25**, 2144 (1969).
18. D. W. YOUNG, P. TOLLIN, and H. R. WILSON. Acta Crystallogr. B**25**, 1423 (1969).
19. G. I. BIRNBAUM, K. L. SADANA, W. J. P. BLONSKI, and F. E. HRUSKA. J. Am. Chem. Soc. **108**, 1671 (1986).
20. M. GELLER, A. KALINSKI, W. KOLOS, and M. KOPCZYNSKI. Biochim. Biophys. Acta, **287**, 1 (1972).
21. D. C. ROHRER and M. SUNDARALINGAM. Acta Crystallogr. B**26**, 546 (1970).
22. B. KOJIC-PRODIC, Z. RUZIC-TOROS, and E. COFFOU. Acta Crystallogr. B**32**, 1090 (1976).
23. F. E. HRUSKA, L. VOITURIEZ, A. GRAND, and J. CADET. Biopolymers, **25**, 1399 (1986).
24. J. EMERSON and M. SUNDARALINGAM. Acta Crystallogr. B**36**, 537 (1980).

Can. J. Chem. Downloaded from www.nrcresearchpress.com by 213.222.148.141 on 09/07/12
For personal use only.

25. F. E. HRUSKA, M. BERGER, J. CADET, and M. REMIN. Can. J. Chem. **63**, 15 (1985).
26. A. GRAND and J. CADET. Acta Crystallogr. B**34**, 1524 (1978).
27. J. KONNERT, I. L. KARLE, and J. KARLE. Acta Crystallogr. B**26**, 770 (1970).
28. W. SAENGER. Principles of nucleic acid structure. Springer Verlag, New York. 1983. Chap. 4.
29. D. SUCK, W. SAENGER, and K. ZECHMEISTER. Acta Crystallogr. B**28**, 596 (1972).
30. M. SUNDARALINGAM, S. T. RAO, and J. A. ABOLA. J. Am. Chem. Soc. **93**, 7055 (1971).
31. C. ALTONA and M. SUNDARALINGAM. J. Am. Chem. Soc. **94**, 8205 (1972).
32. H. P. M. DE LEEUW, C. A. G. HAASNOOT, and C. ALTONA. Israel J. Chem. **20**, 108 (1980).
33. C. A. G. HAASNOOT, F. A. A. M. DE LEEUW, H. P. M. DE LEEUW, and C. ALTONA. Recl. Trav. Chim. Pays-Bas, **98**, 576 (1980).
34. B. D. ALLORE, A. QUEEN, W. J. BLONSKI, and F. E. HRUSKA. Can. J. Chem. **61**, 2397 (1983).

Can. J. Chem. Downloaded from www.nrcresearchpress.com by 213.222.148.141 on 09/07/12
For personal use only.

Enthalpies of interaction of nonpolar solutes with nonpolar solvents. The role of solute polarizability and molar volume in solvation

RICHARD FUCHS, ERIC J. CHAMBERS, AND W. KIRK STEPHENSON
Department of Chemistry, University of Houston, Houston, TX 77004, U.S.A.

Received January 20, 1987

RICHARD FUCHS, ERIC J. CHAMBERS, and W. KIRK STEPHENSON. Can. J. Chem. **65**, 2624 (1987).

Heats of solution of 10 nonpolar solutes (carbon tetrachloride, perfluoroheptane, diiodomethane, benzene, hexane, decane, hexadecane, cyclohexane, toluene, and mesitylene) in 11 nonpolar solvents (heptane, cyclohexane, carbon tetrachloride, benzene, carbon disulfide, diiodomethane, toluene, mesitylene, tetrachloroethylene, 1,1,2-trichlorotrifluoroethane, and hexadecane) have been combined with solute heats of vaporization to give enthalpies of transfer from vapor to solvent ($\Delta H(v \rightarrow S)$). The heat of vaporization of diiodomethane has been measured (11.70 ± 0.01 kcal/mol). Correlations of the form $\Delta H(v \rightarrow S) = a + b\text{MMR} + c\text{MV}$ describe the solvent–solute interaction enthalpies with high precision (correlation coefficients 0.991–0.999). Earlier correlations with only the molar refraction are limited to solutes of similar refractive index. In each solvent $\Delta H(v \rightarrow S)$ becomes more exothermic with an increase in the solute molar refraction term, and less exothermic with an increase in the solute molar volume term. These terms represent solvent–solute dispersion interaction enthalpies, and solvent cavity formation enthalpies, respectively.

RICHARD FUCHS, ERIC J. CHAMBERS et W. KIRK STEPHENSON. Can. J. Chem. **65**, 2624 (1987).

On a combiné les chaleurs de solution de 10 solutés non-polaires (chlorure de carbone, perfluoroheptane, diiodométhane, benzène, hexane, décane, hexadécane, cyclohexane, toluène et mésitylène) dans 11 solvants non-polaires (heptane, cyclohexane, tétrachlorure de carbone, benzène, disulfure de carbone, diiodométhane, toluène, mésitylène, tétrachloroéthylène, trichloro-1,1,2 trifluoroéthane et hexadécane) avec les chaleurs de vaporisation des solutés et on en a déduit les enthalpies de transfert de la vapeur au solvent ($\Delta H(v \rightarrow S)$). On a mesuré la chaleur de vaporisation du diiodométhane (11,70 ± 0,01 kcal/mol). Les corrélations de la forme $\Delta H(v \rightarrow S) = a + b\text{MMR} + c\text{MV}$ décrivent les enthalpies d'interaction solvant–soluté avec une grande précision (coefficients de corrélation 0,991–0,999). Des corrélations antérieures avec uniquement la réfraction molaire sont limitées à des solutés d'indices de réfraction semblables. Dans chacun des solvants, la valeur du $\Delta H(v \rightarrow S)$ devient plus exothermique avec une augmentation du terme de la réfraction molaire du soluté et moins exothermique avec une augmentation du terme du volume molaire du soluté. Ces termes représentent respectivement les enthalpies d'interaction de dispersion solvant–soluté et les enthalpies de formation de la cavité du solvant.

[Traduit par la revue]

In an interesting series of recent articles Solomonov and coworkers (1–3) suggested that solvation enthalpies ($\Delta H(v \rightarrow S)$) of a variety of organic solutes in polar and nonpolar solvents depend (in a given solvent) on the molar refractions (MR = $(((n^2 - 1)/(n^2 + 2)) \times$ molar volume) of the solutes, and in many cases are independent of solute dipolarity. Molar refraction may reasonably be taken as a measure of the capability of each solute to undergo dispersion interactions with a particular solvent. By contrast, correlations of solvation enthalpies (4–9) with the Taft–Kamlet π^* solvatochromic parameter (10, 11) imply the importance of polar (dipolarity–polarizability) interactions. Although π^* values were designed as *solvent* parameters, the role of the *solute* π^* in solvation has also been demonstrated (12). For the "select solvent set" of nonaromatic and nonhalogenated solvents π^* is approximately linear with the dipole moment μ (13), and dispersion interactions are believed to be relatively constant. We are therefore presented with two quite different viewpoints of the factors involved in solvation in organic solutions. Resolution of this question will be important in the treatment of future data, and in our understanding of the intermolecular forces operative.

In the present study we begin an examination of molar refraction correlations with the simplest possible systems, nonpolar solutes in nonpolar solvents. We will consider whether, in the absence of polar effects, MR is a general predictor of relative solvation enthalpies of solutes.

Dissolution of a gaseous species in a liquid is an exothermic process, a result of solvent–solute dispersion interactions. However, there is an endothermic contribution to $\Delta H(v \rightarrow S)$, the enthalpy of formation of cavities within the solvent structure, required to accommodate the dissolving solute molecules. If ΔH_{cav} is dependent (in a given solvent) on solute molar volume (MV), then $\Delta H(v \rightarrow S)$ might be expected to be correlated with both MR and MV

$$\Delta H(v \rightarrow S) = a + b\text{MR} + c\text{MV}$$

where coefficient b is negative and c is positive. However, this results in two MV terms

$$\Delta H(v \rightarrow S) = a + b\left[\frac{n^2 - 1}{n^2 + 2}\right]\text{MV} + c\text{MV}$$

Most of the organic liquid solutes considered by Solomonov *et al.* (1) have refractive indices of 1.4–1.5, and polarizability functions (PF) $((n^2 - 1)/(n^2 + 2))$ of 0.24–0.29. With PF nearly constant it would be unlikely that correlations with MR and (MR + MV) could be distinguished. We will therefore include in the present study solutes of extremely low (1.26) and extremely high (1.74) refractive index (PF = 0.16–0.40). Throughout this study we assume that polar interactions make a negligible contribution to the interactions of slightly polar diiodomethane ($\mu = 1.10$), and that the solvation enthalpies of perfluoroheptane are not appreciably affected by the presence of an isomeric impurity. We will also consider a modified molar refraction (MMR) based on an alternative polarizability function: $\text{MMR} = ((n^2 - 1)/(2n^2 + 1))(\text{MV})$, which might provide a better measure of dispersion interactions.

Experimental

Solutes and solvents were commercial samples in excess of 99% purity, and were dried with 4A molecular sieve. An exception was perfluoroheptane (3M Co.), which was fractionally distilled through a 200 plate Teflon spinning band column to give material consisting

Can. J. Chem. Downloaded from www.nrcresearchpress.com by 213.222.148.141 on 09/07/12
For personal use only.

TABLE 1. Heats of solution of nonpolar solutes in nonpolar solvents at 25°C[a]

Solvent	Heat of solution when solute is									
	Hexane[b]	Decane[b]	$C_{16}H_{34}$[b]	c-C_6H_{12}[b]	Benzene[b]	Toluene[b]	Mes[b]	CCl_4	C_7F_{16}	CH_2I_2
Benzene	1.17	1.80	2.70	0.87	0	0.12	0.62	0.13	6.72	0.94
Heptane	0.00	0.00	0.11	0.19	0.79	0.49	0.30	0.29	3.70	2.68
Carbon disulfide[c]	0.87	1.22	1.76	0.53	0.62	0.45	0.55	0.34		1.14
Carbon tetrachloride	0.43	0.72	1.11	0.20	0.13	−0.04	0.18	0	4.49	1.69
Mesitylene	0.30	0.34	0.52	0.47	0.38	0.13	0	0.11	4.99	0.77
Toluene	0.61	0.96	1.48	0.60	0.06	0	0.17	0.01	5.74	0.71
Cyclohexane[d]	0.27	0.56	0.97	0	0.91	0.77	0.99	0.41	5.19	2.48
Tetrachloroethylene	0.39	0.52	0.75	0.46	0.45	0.21	0.10	0.05	4.84	1.86
CCl_2FCClF_2[e]	0.45	0.75	1.38	0.51	0.60	0.40	0.44	0.31	1.44	2.72
Hexadecane	0.10	0.03	0	0.37	0.83	0.50	0.22	0.39		2.39
Diiodomethane	3.48	(4.22)[f]	7.25	2.56	1.01	1.08				0
Solute ΔH_v[g]	7.54	12.28	19.45	7.90	8.09	9.08	11.35	7.75	8.69	11.70[h]

[a]In kcal/mol, at solute concentrations of $1–5 \times 10^{-3} M$. Each value is the mean of three or more determinations, with uncertainties of 0.01–0.05 kcal/mol.
[b]Values for these solutes in benzene, heptane, carbon tetrachloride, mesitylene, toluene, and cyclohexane from ref. 5.
[c]ΔH_s of carbon disulfide is 0.
[d]ΔH_s of carbon disulfide is 0.37 (ref. 1), 0.41 (this work).
[e]ΔH_s of 1,1,2-trichlorotrifluoroethane is 0.
[f]ΔH_s of octane.
[g]References 15, 16. Values ±0.01–0.02 kcal/mol except C_7F_{16} (±0.10) and hexadecane (±0.08).
[h]This work.

TABLE 2. Solvation enthalpies ($\Delta H(v \rightarrow S)$) of nonpolar solutes in nonpolar solvents at 25°C

Solvent	$\Delta H(v \rightarrow S)$ when solute is									
	Hexane	Decane	$C_{16}H_{34}$[b]	c-C_6H_{12}	Benzene	Toluene	Mes	CCl_4	C_7F_{16}	CH_2I_2
Benzene	−6.37	−10.48	−16.75	−7.03	−8.09	−8.96	−10.73	−7.62	−1.97	−10.76
Heptane	−7.54	−12.28	−19.34	−7.71	−7.30	−8.59	−11.05	−7.46	−4.99	−9.02
Carbon disulfide[b]	−6.67	−11.06	−17.69	−7.37	−7.47	−8.63	−10.80	−7.41		−10.56
Carbon tetrachloride	−7.11	−11.56	−18.34	−7.70	−7.96	−9.12	−11.17	−7.75	−4.20	−10.01
Mesitylene	−7.24	−11.94	−18.93	−7.43	−7.71	−8.95	−11.35	−7.64	−3.70	−10.93
Toluene	−6.93	−11.32	−17.97	−7.30	−8.03	−9.08	−11.18	−7.74	−2.95	−10.99
Cyclohexane[c]	−7.27	−11.72	−18.48	−7.90	−7.18	−8.31	−10.36	−7.34	−3.53	−9.22
Tetrachloroethylene	−7.15	−11.76	−18.70	−7.44	−7.64	−8.87	−11.25	−7.70	−3.85	−9.84
CCl_2FCClF_2[d]	−7.09	−11.53	−18.07	−7.39	−7.49	−8.68	−10.91	−7.44	−7.25	
Hexadecane	−7.44	−12.25	−19.45	−7.53	−7.26	−8.58	−11.13	−7.36		−9.31
Diiodomethane	−4.06	(−5.70)[e]	−12.20	−5.34	−7.08	−8.00				−11.70

[a]In kcal/mol.
[b]$\Delta H(v \rightarrow S)$ of carbon disulfide is −6.61 kcal/mol.
[c]$\Delta H(v \rightarrow S)$ of carbon disulfide is −6.20 kcal/mol.
[d]$\Delta H(v \rightarrow S)$ of 1,1,2-trichlorotrifluoroethane is −6.84 kcal/mol.
[e]$\Delta H(v \rightarrow S)$ of octane.

of 65% perfluoro-*n*-heptane, 34% perfluoromethylhexane, and the remainder other C-7 perfluoroalkanes + homologs. The calorimetric procedure (25.0°C) was previously described (4), except the calorimeter remained sealed at all times, and sample addition (10, 20, or 50 μL syringe) was made through a Teflon-faced septum.

The heat of vaporization of diiodomethane at 25.0°C was measured by evaporation of 100 μL samples into a slow nitrogen stream, using a vaporization calorimeter and technique reported previously (14).

Results and discussion

The measured heats of solution (kcal/mol at 25.0°C) are listed in Table 1. Calculated solvation enthalpies ($\Delta H(v \rightarrow S) = \Delta H_s - \Delta H_v$) are listed in Table 2. Table 3 presents the molar refraction, modified molar refraction, and molar volume of each solute.

Based on Solomonov's correlations (1–3) we should expect similar solvation enthalpies in a particular solvent for various solutes with similar molar refractions. It is important to estab-

TABLE 3. Properties of nonpolar solutes

Solute	n_D	MV (cm^3)	MR (cm^3)	MMR (cm^3)
Hexane	1.3751	130.5	29.89	24.31
Decane	1.4113	194.9	48.43	38.79
Hexadecane	1.4345	292.9	76.36	60.57
Cyclohexane	1.4266	108.1	27.73	22.07
Benzene	1.5011	88.9	26.20	20.23
Toluene	1.4961	106.3	31.06	24.03
Mesitylene	1.4994	138.9	40.81	31.54
Carbon tetrachloride	1.4601	96.5	26.43	20.75
Perfluoroheptane	1.2618	223.9	36.90	31.68
Diiodomethane	1.7425	80.7	32.63	23.23
Carbon disulfide	1.6270	60.1	15.73	21.31
Octane	1.3974	162.6	39.19	31.58
CCl_2FCClF_2	1.3578	119.0	26.11	21.42

Can. J. Chem. Downloaded from www.nrcresearchpress.com by 213.222.148.141 on 09/07/12
For personal use only.

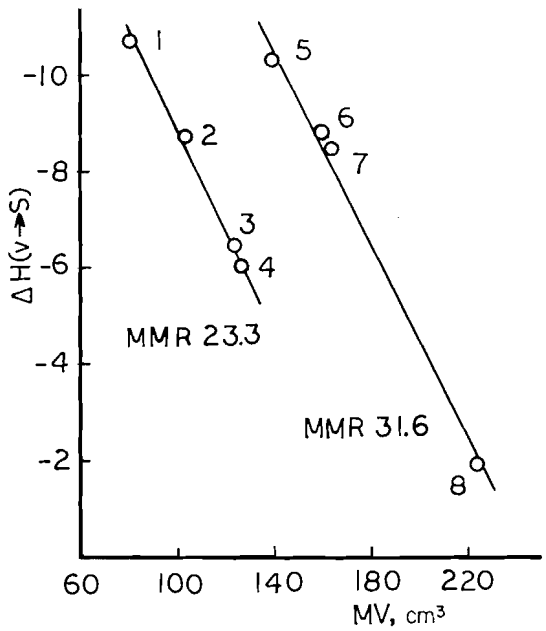

FIG. 1. The effect of molar volume on solvation enthalpies in benzene for solutes of the same modified molar refraction. Points are *1*, diiodomethane; *2*, $C_6H_5C_{0.81}H_{2.62}$; *3*, $C_{3.9}H_{8.8}CH{=}CH_2$, *4*, $C_{5.72}H_{13.44}$ alkane; *5*, mesitylene; *6*, $C_{6.13}H_{13.26}CH{=}CH_2$, *7*, *n*-octane; and *8*, perfluoroheptane.

lish whether molar volume separately influences $\Delta H(v \rightarrow S)$. Experimentally, the problem is to find a varied series of solutes with the same molar refraction. We make use of the observation that $\Delta H(v \rightarrow S)$ of alkanes (5) is linear with carbon number (and MR) (as are values for monoalkylbenzenes and for the series benzene, toluene, and mesitylene), and use Solomonov's interpolative procedures (1) to estimate $\Delta H(v \rightarrow S)$ of alkanes, alkenes, and alkylbenzenes of intermediate carbon number and chosen molar refraction. Figure 1 is a plot of $\Delta H(v \rightarrow$ benzene) vs. MV for (*1*) four solutes with modified molar refractions of 31.6 cm^3 and molar volumes of 138.9–223.9 cm^3, and (*2*) four solutes with MMR = 23.3 cm^3 and MV = 80.7–126.2 cm^3. Both groups show a strong decrease in solvation with increasing molar volume (Group 1: $\Delta H(v \rightarrow Bz) = -10.73$ to -1.97 kcal/mol; Group 2: -10.76 to -6.07 kcal/mol). The same trend is observed with other solvents. It is apparent that molar refraction alone does not properly predict solvation enthalpy when a series of solutes of greatly differing molar volume (and refractive index) is considered.

In correlations of $\Delta H(v \rightarrow S)$ of solutes with molar refraction and molar volume the results with MMR are somewhat better than those with MR, and the former are reported below. In Solomonov-type correlations with molar refraction only, MR is somewhat superior to MMR. Equations in MR are listed below for comparison with the two parameter correlations. The number of solutes, n, correlation coefficient, r, and uncertainties in the coefficient a, b, and c are furnished for each equation. All solutes for which $\Delta H(v \rightarrow S)$ is listed in Table 2 are included in the correlations.

In diiodomethane

[1] $\Delta H(v \rightarrow S) = (-2.1739 \pm 0.1525) - (1.0255 \pm 0.0226)MMR + (0.1778 \pm 0.0044)MV$
$n = 7, \quad r = 0.9992$

[2] $\Delta H(v \rightarrow S) = (3.5237 \pm 2.5615) - (0.1118 \pm 0.0625)MR$
$n = 7, \quad r = 0.6244$

In benzene

[3] $\Delta H(v \rightarrow S) = (-1.9448 \pm 0.1922) - (0.7607 \pm 0.0156)MMR + (0.1073 \pm 0.0028)MV$
$n = 10, \quad r = 0.9987, \quad$ std. error $= 0.2212$

[3a] $\Delta H(v \rightarrow S) = (-1.690 \pm 0.378) - (0.4970 \pm 0.0198)MR + (0.07884 \pm 0.00437)MV$
$n = 10, \quad r = 0.9950$

[4] $\Delta H(v \rightarrow S) = (-2.0239 \pm 2.4308) - (0.1820 \pm 0.0602)MR$
$n = 10, \quad r = 0.7300$

[5] $\Delta H(v \rightarrow S) = (-2.4077 \pm 0.8813) - (0.1850 \pm 0.0212)MR$
$n = 8, \quad r = 0.9628$

[6] $\Delta H(v \rightarrow S) = (-1.9928 \pm 0.2222) - (0.7740 \pm 0.0504)MMR + (0.1101 \pm 0.0101)MV$
$n = 8, \quad r = 0.9981$

In heptane

[7] $\Delta H(v \rightarrow S) = (-0.4519 \pm 0.4005) - (0.6406 \pm 0.0325)MMR + (0.0664 \pm 0.0058)MV$
$n = 10, \quad r = 0.9948$

[8] $\Delta H(v \rightarrow S) = (-0.45178 \pm 1.4490) - (0.2411 \pm 0.0359)MR$
$n = 10, \quad r = 0.9216$

In carbon disulfide

[9] $\Delta H(v \rightarrow S) = (-1.2639 \pm 0.1825) - (0.6960 \pm 0.0297)MMR + (0.0879 \pm 0.0057)MV$
$n = 10, \quad r = 0.9985$

[10] $\Delta H(v \rightarrow S) = (-2.1493 \pm 0.7438) - (0.2017 \pm 0.0190)MR$
$n = 10, \quad r = 0.9664$

In carbon tetrachloride

[11] $\Delta H(v \rightarrow S) = (-1.4826 \pm 0.2292) - (0.6757 \pm 0.0186)MMR + (0.0803 \pm 0.0033)MV$
$n = 10, \quad r = 0.9981$

[12] $\Delta H(v \rightarrow S) = (-1.5103 \pm 1.7903) - (0.2120 \pm 0.0444)MR$
$n = 10, \quad r = 0.8606$

In mesitylene

[13] $\Delta H(v \rightarrow S) = (-1.0398 \pm 0.1479) - (0.7460 \pm 0.0120)MMR + (0.0933 \pm 0.0021)MV$
$n = 10, \quad r = 0.9993$

[14] $\Delta H(v \rightarrow S) = (-1.0623 \pm 2.0183) - (0.2263 \pm 0.0500)MR$
$n = 10, \quad r = 0.8470$

Can. J. Chem. Downloaded from www.nrcresearchpress.com by 213.222.148.141 on 09/07/12
For personal use only.

In toluene

[15] $\Delta H(v \rightarrow S) = (-1.6014 \pm 0.1241) - (0.7551 \pm 0.0101)MMR + (0.1005 \pm 0.0018)MV$
$n = 10, \quad r = 0.9995$

[16] $\Delta H(v \rightarrow S) = (-1.6516 \pm 2.2279) - (0.2045 \pm 0.0552)MR$
$n = 10, \quad r = 0.7947$

In cyclohexane

[17] $\Delta H(v \rightarrow S) = (-0.5780 \pm 0.4792) - (0.6829 \pm 0.0423)MMR + (0.0784 \pm 0.0074)MV$
$n = 11, \quad r = 0.9901$

[18] $\Delta H(v \rightarrow S) = (-0.9527 \pm 1.5758) - (0.2189 \pm 0.0404)MR$
$n = 11, \quad r = 0.8740$

In tetrachloroethylene

[19] $\Delta H(v \rightarrow S) = (-0.9512 \pm 0.2698) - (0.7055 \pm 0.0219)MMR + (0.0855 \pm 0.0039)MV$
$n = 10, \quad r = 0.9976$

[20] $\Delta H(v \rightarrow S) = (-0.9816 \pm 1.8544) - (0.2242 \pm 0.0460)MR$
$n = 10, \quad r = 0.8651$

In 1,1,2-trichlorotrifluoroethane

[21] $\Delta H(v \rightarrow S) = (-1.5331 \pm 0.2135) - (0.4829 \pm 0.0183)MMR + (0.0435 \pm 0.0034)MV$
$n = 10, \quad r = 0.9980$

[22] $\Delta H(v \rightarrow S) = (-1.233 \pm 0.7477) - (0.2171 \pm 0.0188)MR$
$n = 10, \quad r = 0.9714$

In hexadecane

[23] $\Delta H(v \rightarrow S) = (-0.6256 \pm 0.0881) - (0.5458 \pm 0.0137)MMR + (0.0487 \pm 0.0026)MV$
$n = 9, \quad r = 0.9998$

[24] $\Delta H(v \rightarrow S) = (-0.8786 \pm 0.3431) - (0.2427 \pm 0.0084)MR$
$n = 9, \quad r = 0.9958$

One may conclude from eqs. [1]–[24] that correlations of $\Delta H(v \rightarrow S)$ with both MMR and MV are far superior to correlations with MR alone. In all solvents the latter predict values of $\Delta H(v \rightarrow S)$ which are insufficiently exothermic for solutes of high refractive index, and too exothermic for solutes of low n_D. These are the solutes which, for a given molar refraction, have particularly small and large molar volumes, respectively. If the extreme solutes are omitted, correlations with MR improve (eq. [5] vs. eq. [4]), but are still not comparable to the two parameters correlation (eq. [3]). If C_7F_{16} and CH_2I_2 are omitted the two parameter correlations are not greatly improved (eq. [6] vs. eq. [3]). The intercept and coefficients (a, b, c) are only slightly affected. These observations indicate that the two extreme solutes are not "forcing" the correlation. Solvation enthalpies can also be estimated from the Hildebrand-Scatchard equation

$$\Delta H(v \rightarrow S) = (-2\delta_H{}^B\delta_H{}^A MV^B)((\delta_H{}^A)^2 MV^B) - RT$$

where $\delta_H{}^A$ and $\delta_H{}^B$ represent the Hildebrand solubility parameters of the solvent and solute, respectively. Solomonov obtained poor results by this method (1). The correlation of calculated H.–S. solvation enthalpies with our experimental values for 10 solutes in benzene is poor ($r = 0.934$, std. error = 1.45 kcal/mol).

In equations of the form $\Delta H(v \rightarrow S) = a + b\text{MMR} + c\text{MV}$ which solvent properties determine the coefficients, b and c? Because b and c are related ($r = 0.987$) correlations of b with polarizability functions, and c with Hildebrand δ^2 (or δ)

$$b = (0.279 \pm 0.092) - (4.551 \pm 0.413)((n^2 - 1)/(2n^2 + 1)) \qquad r = 0.976$$

$$c = -(0.023 \pm 0.008) + (0.148 \pm 0.010)(\delta_H{}^2/100) \qquad r = 0.987$$

for eight of the solvents (CS_2, C_2Cl_4, hexadecane omitted) suggest, but do not prove, that solvent capability for dispersion interactions, and solvent cohesiveness and cavity formation enthalpy are principal factors determining b and c, respectively.

Acknowledgement

This study was supported by the Robert A. Welch Foundation (Grant E-136).

1. B. N. Solomonov, I. S. Antipin, V. B. Novikov, and A. I. Konovalov. J. Gen. Chem. USSR, **52**, 2364 (1982).
2. B. N. Solomonov, A. I. Konovalov, V. B. Novikov, A. N. Vedernikov, M. D. Borisover, V. V. Gorbachuk, and I. S. Antipin. J. Gen. Chem. USSR, **54**, 1444 (1984).
3. B. N. Solomonov, A. I. Konovalov, V. B. Novikov, V. V. Borbachuk, and S. A. Neklyudov. J. Gen. Chem. USSR, **55**, 1681 (1985).
4. W. K. Stephenson and R. Fuchs. Can. J. Chem. **63**, 336 (1985).
5. R. Fuchs and W. K. Stephenson. Can. J. Chem. **63**, 349 (1985).
6. W. K. Stephenson and R. Fuchs. Can. J. Chem. **63**, 342 (1985).
7. W. K. Stephenson and R. Fuchs. Can. J. Chem. **63**, 2529 (1985).
8. W. K. Stephenson and R. Fuchs. Can. J. Chem. **63**, 2535 (1985).
9. W. K. Stephenson and R. Fuchs. Can. J. Chem. **63**, 2540 (1985).
10. M. J. Kamlet, J.-L. M. Abboud, and R. W. Taft. Prog. Phys. Org. Chem. **13**, 485 (1981).
11. M. J. Kamlet, J.-L. M. Abboud, M. H. Abraham, and R. W. Taft. J. Org. Chem. **48**, 2877 (1983).
12. R. Fuchs and W. K. Stephenson. J. Am. Chem. Soc. **105**, 5159 (1983).
13. J.-L. M. Abboud, M. J. Kamlet, and R. W. Taft. J. Am. Chem. Soc. **99**, 8325 (1977).
14. R. Fuchs, J. H. Hallman, and M. O. Pearlman. Can. J. Chem. **60**, 1832 (1982).
15. V. Majer and V. Svoboda. Enthalpies of vaporization of organic compounds. Blackwell Scientific Publications, Oxford. 1985.
16. J. B. Pedley and J. Rylance. Sussex-N.P.L. computer analyzed thermochemical data: organic and organometallic compounds. University of Sussex, Brighton. 1977.

Can. J. Chem. Downloaded from www.nrcresearchpress.com by 213.222.148.141 on 09/07/12
For personal use only.

Synthesis of ^{31}P nmr spectroscopic study of $[Ag(\mu\text{-}R_2PCH_2PR_2)_3Ag]^{2+}$ (R = Me or Ph). Observation of an intramolecular "end-over-end" exchange of bridging $R_2PCH_2PR_2$ [1]

PHILIP A. W. DEAN,[2] JAGADESE J. VITTAL, AND RADHEY S. SRIVASTAVA[3]
The Department of Chemistry, University of Western Ontario, London, Ont., Canada N6A 5B7

Received April 21, 1987

PHILIP A. W. DEAN, JAGADESE J. VITTAL, and RADHEY S. SRIVASTAVA. Can. J. Chem. **65**, 2628 (1987).

Reaction of $AgAsF_6$ with $R_2PCH_2PR_2$ (R = Ph or Me) in a 2:3 ratio in $MeNO_2$ or Me_2CO produces the new compounds $[Ag_2(R_2PCH_2PR_2)_3](AsF_6)_2$, which have been isolated in good yield. The analogous ^{107}Ag-enriched compounds are produced using $^{107}AgAsF_6$. The 2:3 compounds have interesting variable temperature ^{31}P nmr spectra which have been studied in detail using the ^{107}Ag-enriched compounds. The ^{31}P nmr spectra of $[^{107}Ag_2(Ph_2PCH_2PPh_2)_3](AsF_6)_2$:$[^{107}Ag_2(Me_2PCH_2PMe_2)_3](AsF_6)_2$ mixtures at ambient probe temperature show the formation of the mixed ligand binuclear cations $[^{107}Ag_2(Ph_2PCH_2PPh_2)_{3-x}(Me_2PCH_2PMe_2)_x]^{2+}$ (x = 1 or 2). By analogy, the two parent complexes also contain binuclear cations, and the limiting low temperature ^{31}P nmr spectra of these can be interpreted in terms of the manxane structure, $[^{107}Ag(\mu\text{-}R_2PCH_2PR_2)_3{}^{107}Ag]^{2+}$. With increase in temperature, the ^{31}P nmr spectra of the parents provide evidence for an intramolecular exchange process which is faster for R = Ph than for R = Me and which is shown to involve "end-over-end" exchange of bridging $R_2PCH_2PR_2$. This type of exchange has not been observed previously for these ligands. With Me_2CO as solvent, an approximate value of the enthalpy of activation for exchange is 59 kJ mol^{-1} for $[^{107}Ag(\mu\text{-}Ph_2PCH_2PPh_2)_3{}^{107}Ag]^{2+}$ and 50 kJ mol^{-1} for $[^{107}Ag(\mu\text{-}Me_2PCH_2PMe_2)_3{}^{107}Ag]^{2+}$.

PHILIP A. W. DEAN, JAGADESE J. VITTAL et RADHEY S. SRIVASTAVA. Can. J. Chem. **65**, 2628 (1987).

La réaction du $AgAsF_6$ avec le $R_2PCH_2PR_2$ (R = Ph ou Me), dans un rapport de 2 à 3, dans le $MeNO_2$ ou le Me_2CO, conduit à la formation des nouveaux produits $[Ag_2(R_2PCH_2PR_2)_3](AsF_6)_2$ qui ont été isolés avec de bons rendements. On a préparé les produits analogues enrichis en ^{107}Ag en utilisant du $^{107}AgAsF_6$. Les spectres rmn du ^{31}P, à température variable, des composés 2:3 sont intéressants et on les a étudiés en détail en utilisant les composés enrichis en ^{107}Ag. Les spectres rmn du ^{31}P, à la température ambiante, de mélanges de $[^{107}Ag_2(Ph_2PCH_2PPh_2)_3](AsF_6)_2$:$[^{107}Ag_2(Me_2PCH_2PMe_2)_3](AsF_6)_2$ montrent qu'il y a formation de cations binucléaires à ligands mixtes du type $[^{107}Ag_2(Ph_2PCH_2PPh_2)_{3-x}(Me_2PCH_2PMe_2)_x]^{2+}$ (x = 1 ou 2). Par analogie, les deux complexes parents contiennent aussi des cations binucléaires et les spectres rmn du ^{31}P aux limites de la basse température peuvent être interprétés en fonction de la structure du manxane, $[^{107}Ag(\mu\text{-}R_2PCH_2PR_2)_3{}^{107}Ag]^{2+}$. Par augmentation de la température à laquelle on détermine les spectres rmn du ^{31}P des composés parents, on obtient des indications à l'effet qu'il se produit un processus d'échanges intramoléculaires qui est plus rapide avec les produits RPh qu'avec les produits RMe et on démontre de plus que ce processus implique un échange "tête à queue" du ligand $R_2PCH_2PR_2$ qui sert de pont. Ce type d'échange n'avait pas été observé antérieurement avec ces ligands. Avec le Me_2CO comme solvant, la valeur approximative de l'enthalpie d'activation est de 59 kJ mol^{-1} pour le $[^{107}Ag(\mu\text{-}Ph_2PCH_2PPh_2)_3{}^{107}Ag]^{2+}$ et de 50 kJ mol^{-1} pour le $[^{107}Ag(\mu\text{-}Me_2PCH_2PMe_2)_3{}^{107}Ag]^{2+}$.

[Traduit par la revue]

Can. J. Chem. Downloaded from www.nrcresearchpress.com by 213.222.148.141 on 09/07/12
For personal use only.

Introduction

A variety of stoichiometries and structures are known for complexes of silver(I) with bis(diphenylphosphino)methane (dppm) and related 1,1-ditertiaryphosphinoalkanes. For the 2:1 Ag:L complexes $(Ph_2PCHRPPh_2)(AgO_2CR')_2$ (R = H or Me; R' = Me, Et, *i*-Pr, and Ph) in solution, the bridging bidentate nature of the ligands has been demonstrated using ^{1}H and ^{31}P nmr spectroscopy (1). The $Ag(\mu\text{-dppm})Ag$ unit has been established (2) in the cluster $[Ag_2Ru_4(\mu_3\text{-}H)_2(\mu\text{-dppm})(CO)_{12}]$ and its occurrence in $(dppm)(AgNO_3)_2$ has been postulated (3). From an nmr study (1) and an X-ray structural study (4), the ligands also occupy bridging bidentate positions in the 2:2 complexes $[Ag(\mu\text{-}Ph_2PCHRPPh_2)_2Ag](BF_4)_2$ (R = H or Me) and $(Ag_2(dppm)_2(NO_3)_2)$, respectively. In addition, a wide range of related heterometallic binuclear complexes containing the skeleton $M(\mu\text{-}Ph_2PCH_2PPh_2)_2Ag$ have been described (5). X-ray analysis of the 3:3 compound of AgBr with dppm has revealed the ligand-bridged trimeric structure $[Ag_3(\mu\text{-dppm})_3(\mu_3\text{-}Br)_2]Br$ (6). The same technique was used to characterize a 4:4 cation in $[\{Ag_2(dppm)_2\}_2(NO_3)_2](PF_6)_2$ (4). In this cation two $Ag(\mu\text{-dppm})_2Ag$ subunits are evident. The complex $(dppm)(AgO_3SMe)$ is trimeric in $CHCl_3$ (7), and so might have a dppm-bridged structure. In contrast, the 1:2 complex $(dppm)_2(AgO_3SMe)$ is monomeric in $CHCl_3$ (7); its structure is unknown.

To our knowledge, there has been no report of a 2:3 Ag:L silver(I) complex with a ligand of the general type $R_2PCH_2PR_2$. We describe here the ready synthesis of two such complexes, one with dppm and one with $Me_2PCH_2PMe_2$ (dppm). These are shown by nmr spectroscopy to contain $[Ag(\mu\text{-}R_2PCH_2PR_2)_3Ag]^{2+}$, analogous to the cation $[Au(\mu\text{-dmpm})_3Au]^{2+}$ for which structural data were reported very recently (8). The new silver complex with dppm is isoelectronic with $Pd_2(dmpm)_3$. The palladium complex is of unknown structure but it is thought likely (9) to have the same structure as $[Pt(\mu\text{-dppm})_3Pt]$ which has been fully characterized both in solution and in the solid state (9).

The ^{31}P nmr spectra of both new silver complexes exhibit interesting temperature dependence. This has been studied in detail and provides evidence for a novel intramolecular exchange process.

Experimental

Materials and general procedures

Isotopically-enriched silver metal (98.22% ^{107}Ag) from Oak Ridge National Laboratory, and natural silver of 99.999% purity (Alfa) were

[1]Presented in part at the 67th Canadian Chemical Conference and Exhibition, Montreal, June, 1984. Abstract IN 12-10.

[2]To whom all correspondence should be addressed.

[3]On leave from 1983 to 1985 from Department of Chemistry, M. G. Degree College, Gorakhpur 273001, India.

converted into the corresponding silver hexafluoroarsenates by treatment with AsF_5 in SO_2 (10). 1,2-Bis(dimethylphosphino)methane was the gift of Professor R. J. Puddephatt and Mr. R. Ramachandran of this Department. All other chemicals were of reagent grade and were used as received from commercial sources. All solvents were dried over 3A Molecular Sieves and thoroughly deoxygenated in a flow of Ar before use. Silver hexafluoroarsenate was handled in a glove box under an atmosphere of dry nitrogen.

Carbon, hydrogen, silver, and phosphorus microanalyses were performed by Analytische Laboratorien, Gummersbach, West Germany.

Synthesis

The following syntheses were performed under an atmosphere of Ar gas. However, the air-sensitivity of the compounds described here, once they are formed, does not seem to be high.

$[Ag_2(dppm)_3](AsF_6)_2$ (1). A solution of $AgAsF_6$ (0.499 g, 1.68 mmol) in 5 mL of $MeNO_2$ was added with stirring to a solution of dppm (0.990 g, 2.58 mmol) in 10 mL of $MeNO_2$. The light yellow solution was filtered and the solvent was removed *in vacuo*. The crude product was recrystallized from warm acetone and dried under vacuum. Yield 1.25 g (85%). *Anal.* calcd. for $C_{75}H_{66}Ag_2As_2F_{12}P_6$: C 51.57, H 3.81, Ag 12.35, P 10.64; found: C 51.48, H 3.98, Ag 12.20, P 10.70. ^1H nmr (CD_3NO_2, 294 K): δ_H 3.77 (s, CH_2), 7.15–7.43 (phenyl H atoms).

$[Ag_2(dmpm)_3](AsF_6)_2$ (2). Starting from $AgAsF_6$ (0.509 g, 1.71 mmol) and dmpm (0.35 g, 1.7 mmol), this compound was prepared and purified in a manner identical to that used for **1**. Yield 0.67 g (78%). *Anal.* calcd. for $C_{15}H_{42}Ag_2As_2F_{12}P_6$: C 17.98, H 4.23, Ag 21.53, P 18.55; found: C 17.97, H 4.12, Ag 21.30, P 18.69. ^1H nmr (CD_3NO_2, 294 K): δ_H 1.57 (CH_3), 2.24 (CH_2, septet, J_{obs} = $(1/3)[^2J(^{31}P—^1H) + ^4J(^{31}P—^1H)]$ = 3.0 Hz).

$[^{107}Ag_2(dppm)_3](AsF_6)_2$ (1) and $[^{107}Ag_2(dmpm)_3](AsF_6)_2$ (2*).* These compounds were prepared in the same way as **1** and **2**, but starting with $^{107}AgAsF_6$.

Nuclear magnetic resonance spectra

All nmr samples were prepared on a mass of solute/volume of solvent basis. The tube size was 5 mm od for measurement of proton spectra on a Varian XL-200 spectrometer system and for measurement of ^{13}C and some of the ^{31}P spectra on a Varian XL-300 Spectrometer System. In these cases the deuterated solvent was the ^2D field/frequency lock substance. Some of the ^{31}P nmr spectra were measured on the XL-200 spectrometer using protiated solvents and no field/frequency lock. (Field drift $\ll$ 1 Hz/day.) Samples for measurements at or below ambient probe temperature were then contained in 10 mm od nmr tubes, while samples which would be measured at elevated temperatures were contained in sealed 9 mm od standard wall tubes that were a tight sliding fit inside a standard thin-walled 10 mm od nmr tube.

References used were internal TMS for ^1H and ^{13}C nmr spectra and external 85% H_3PO_4 (by sample interchange) for ^{31}P nmr. In the last case no corrections for volume susceptibility difference were made.

Probe temperatures were measured by means of a calibrated thermocouple probe in a stationary dummy sample of the appropriate solvent for ambient probe temperature or below, or of ethylene glycol for elevated temperatures.

Simulation of nuclear magnetic resonance spectra

Spectra were simulated using a version of LAOCN3 (11) adapted locally[4] to run on a Victor 9000 computer. This adaptation can handle up to an 8-spin system.

Results and discussion

When progressive amounts of $Ph_2PCH_2PPh_2$ are added to $AgAsF_6$ in $MeNO_2$ or Me_2CO, ^{31}P nmr shows that at Ag:dppm = 2:1 the known (1) complex $[Ag(\mu\text{-dppm})Ag]^{2+}$ is formed quantitatively. Additional amounts of dppm up to Ag:dppm = 1:1 lead to quantitative formation of $[Ag(\mu\text{-dppm})_2Ag]^{2+}$, which is also known (1, 4). The 2:2 complex in the presence of further dppm reacts quantitatively to give a third species that has not been noted previously. From the composition of the solution together with integration of the ^{31}P nmr spectrum, it is evident that this species has a 2:3 stoichiometry, and indeed analytically pure $Ag_2(dppm)_3(AsF_6)_2$ (**1**) is isolable in good yield from solutions that contain it (see Experimental section). This 2:3 complex seems to have escaped attention in previous work (1, 4), perhaps because a restricted range of compositions was investigated. Addition of more dppm to the 2:3 compound does not produce further silver complexes. Indeed, the ^{31}P nmr spectrum shows signals from the 2:3 complex and free dppm. A 1:2 complex might have been anticipated from the earlier isolation of $(dppm)_2(AgO_3SMe)$ (7).

By substitution of Me_2PCH_2PMe for dppm it was possible to produce the 2:3 compound $Ag_2(dmpm)_3(AsF_6)_2$ (**2**) quantitatively in $MeNO_2$ or Me_2CO solution. Again this new compound was isolated in good yield (see Experimental section).

The variable temperature ^{31}P nmr spectra of **1** and **2** show interesting changes. As an example, Fig. 1 shows the ^{31}P nmr spectra of **2** in Me_2CO at ambient probe temperature and reduced temperature. At 295 and 213 K these spectra are centered at −20.7 and −20.0 ppm, respectively. The spectra of **1** are generally similar[5] and centered at 5.9 and 5.0 ppm at 295 and 213 K, respectively. Three things are immediately evident from the spectra: (*i*) from the similarity of the spectra at reduced temperature the cations in **1** and **2** must have the same structure; (*ii*) the complexes contain symmetrical spin systems, judging from the symmetrical if complicated spectra obtained at low temperature; and (*iii*) there is the onset of an exchange process as the temperature is increased to ambient probe temperature. As exemplified by the 213 K spectrum in Fig. 1, the ^{31}P nmr spectra at reduced temperature show the expected couplings to ^{109}Ag and ^{107}Ag. These isotopes both have spin, $I = \frac{1}{2}$, and their natural abundances are 48.18 and 51.82%, respectively (12). The largest doublet separation in each low temperature spectrum is a result of coupling to ^{109}Ag and the smallest of coupling to ^{107}Ag. At 213 K the ratio of the largest to smallest doublet separations is (358 ± 1 Hz)/(310 ± 1 Hz) (= 1.15) for **1**, and (368 ± 1 Hz)/(319 ± 1 Hz) (= 1.15) for **2**, both identical with $\gamma(^{109}Ag)/\gamma(^{107}Ag)$ which is 1.150 (12). In each spectrum at 213 K there is a third doublet with an intermediate coupling, 334 ± 1 Hz for **1** and 343 ± 1 Hz for **2**, providing evidence that the cations have a polynuclear structure. From the formulae of **1** and **2** a binuclear structure is the simplest possibility. In a dimeric Ag_2 complex the statistical (13) fractional populations of the $(^{109}Ag)_2$, $(^{109}Ag)(^{107}Ag)$, and $(^{107}Ag)_2$ isotopomers are 0.232, 0.499, and 0.269, respectively. In order of increasing separation, the approximate relative intensities of the three major doublets are 1.3:2.0:1 in the spectrum of **1*** at 213 K, and 1.5:2.2:1 in the spectrum of **2*** at 213 K. These are in fair agreement with expectation for a binuclear complex. However, since these are previously unreported complexes, further proof of their structure seemed desirable. The occurrence of three isotopomers with comparable populations makes the detailed interpretation of the spectra of **1** and **2** a difficult task. To

[4]We thank Dr. R. H. Hill, previously of this Department, for making available to us his adaptation which could handle up to seven spins and which we modified to handle up to eight spins.

[5]Copies of these spectra may be purchased from the Depository of Unpublished Data, CISTI, National Research Council of Canada, Ottawa, Ont., Canada K1S 0S2.

Can. J. Chem. Downloaded from www.nrcresearchpress.com by 213.222.148.141 on 09/07/12
For personal use only.

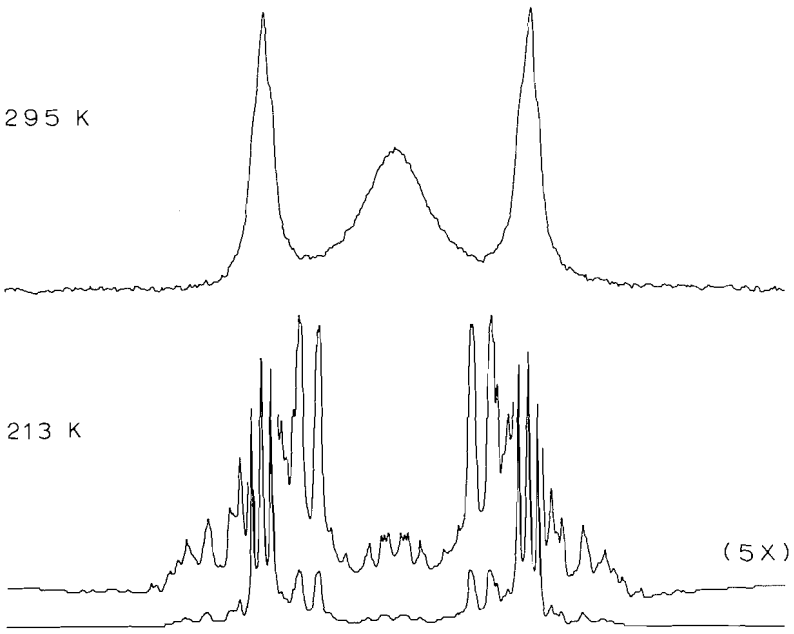

FIG. 1. The 80.98 MHz ^{31}P nmr spectra at 213 and 295 K of $[Ag(\mu\text{-dmpm})_3Ag](AsF_6)_2$ (**2**) (0.01 mol/L of acetone). The spectra are 1000 Hz wide and have been plotted using a 1 Hz exponential line broadening. The lower spectrum is shown with a 5× vertical expansion.

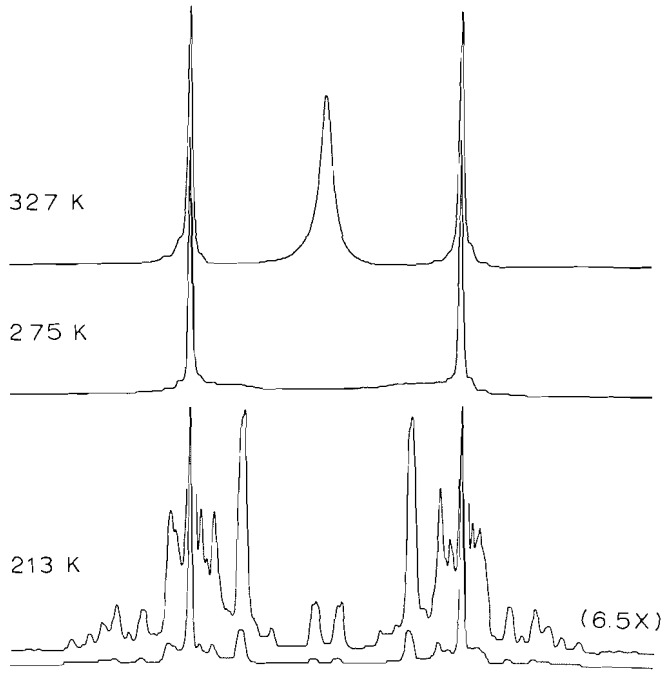

FIG. 2. Representative variable temperature ^{31}P nmr spectra of $[^{107}Ag(\mu\text{-dmpm})_3{}^{107}Ag](AsF_6)_2$ (**2***) (0.01 mol/L of acetone). The spectra are 750 Hz wide and were plotted using a 1 Hz (bottom) or 2 Hz (middle and top) exponential line broadening. The bottom spectrum is shown with a 6.5× vertical expansion.

simplify this problem the ^{107}Ag-enriched complexes **1*** and **2***, containing 98.2% ^{107}Ag were synthesized and studied.

Representative variable temperature ^{31}P nmr spectra, those of **2*** in Me_2CO, are shown in Fig. 2. The spectra of **1*** exhibit parallel behaviour.[5] In each case the most noticeable feature of the limiting low temperature spectrum is the intense doublet that was associated above with coupling to ^{107}Ag. At 213 K, the doublet is centred at $\delta_P = 4.9$ and has a separation of 310 ± 1 Hz for **1***. For **2*** under the same conditions the corresponding values are $\delta_P = -20.0$ and a separation of 318 ± 1 Hz. It is most significant that for both complexes *this doublet is retained when the effects of exchange on the spectra become evident as the temperature is raised*. This shows that the exchange process that is occurring is *intramolecular*. At a phenomenological level, it is very useful to have only the simpler part of the spectrum, the intense doublet, unaffected as the temperature is raised. As a result of this behaviour, the ^{31}P nmr spectra of **1***:**2*** mixtures at ambient or higher temperature both allow a chemical proof of the dimeric structure and give an indication of the type of exchange process that occurs in the complexes.

In **1***:**2*** mixtures, only two new species are formed. Figure 3(*a*) shows the ^{31}P nmr spectrum at 304 K of a solution in which **1***:**2*** = 1.9:1. In this spectrum, a sharp doublet of triplets of relative intensity 2 is observed at $\delta_P = 6.4$ ppm, in the dppm-on-^{107}Ag region. By comparison with the spectrum of **1*** itself, the large doublet splitting of 305 ± 1 Hz must be associated with coupling to ^{107}Ag. The smaller splitting of 56 ± 1 Hz between the components of the triplets also occurs in the dmpm-on-^{107}Ag region (see following) and so is $^{31}P—^{31}P$ coupling. In the dmpm-on-^{107}Ag region there is a doublet of quintets of relative intensity 1 centered at $\delta_P = -20.4$ ppm. Again the large doublet splitting, 327 ± 1 Hz, must be associated with coupling to ^{107}Ag, while the quintets show the 56 Hz $^{31}P—^{31}P$ coupling. In both regions the sharp signals are accompanied by broader resonances from the parts of the spectrum that are affected by the exchange process that is known to be occurring at this temperature (see above). The relative intensities of the sharp signals in the two regions together with their multiplicities show that the new species must contain two dppm ligands and one dmpm. Taken with the known overall stoichiometries of **1*** and **2*** it is evident that the new complex must be binuclear and of composition $[^{107}Ag_2(dppm)_2(dmpm)]^{2+}$.

The second binuclear complex with mixed ligands is formed in **2***-rich mixtures of **1*** and **2***. Figure 3(*b*) presents the ^{31}P nmr spectrum at 295 K of a mixture in which **1***:**2*** = 1:2.4. This shows the doublet spectrum of **2***. Also in the dmpm-on-^{107}Ag region, at $\delta_P = -20.6$ ppm, there can be seen sharp

Can. J. Chem. Downloaded from www.nrcresearchpress.com by 213.222.148.141 on 09/07/12
For personal use only.

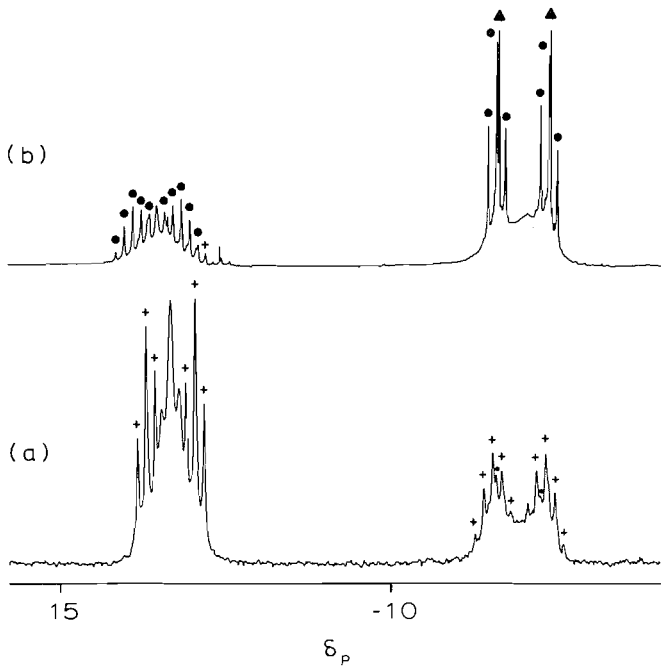

FIG. 3. The 80.98 MHz ^{31}P nmr spectra of **1***:**2*** mixtures (total concentration 0.01 mol/L of acetone), showing the sharp resonances of $[^{107}Ag(\mu\text{-dppm})_{3-x}(dmpm)_x{}^{107}Ag]^{2+}$. (*a*) **1***:**2*** = 1.9:1; (*b*) **1***:**2*** = 1:2.4. Spectrum (*a*) was recorded using a 2 Hz exponential line broadening, spectrum (*b*) using 1 Hz. Key: + = $[^{107}Ag(\mu\text{-dppm})_2(dmpm)^{107}Ag]^{2+}$; ○ = $[^{107}Ag(\mu\text{-dppm})(\mu\text{-dmpm})_2{}^{107}Ag]^{2+}$; △ = $[^{107}Ag(\mu\text{-dmpm})_3{}^{107}Ag]^{2+}$.

signals (once more there occur accompanying broad signals) due to the new complex. The observed pattern is a doublet of triplets of relative intensity 2, with a 321 ± 1 Hz doublet splitting from ^{107}Ag and a 52 ± 1 Hz ^{31}P—^{31}P coupling within the triplets. The other sharp part, occurring in the dppm-on-^{107}Ag region, is a doublet of quintets of relative intensity 1 centered at δ_P = 7.4 ppm, and having a 302 ± 1 Hz coupling to ^{107}Ag and the same 52 Hz ^{31}P—^{31}P coupling. Following our previous reasoning, this second new complex is clearly binuclear $[^{107}Ag(dppm)(dmpm)_2]^{2+}$.

With the occurrence of the two binuclear mixed ligand complexes proven, it is clear that **1*** (and **1**) and **2*** (and **2**) must also be binuclear. The two complexes with mixed ligands are then formed by simple ligand redistribution, as in eq. [1].

$$[1]\quad [^{107}Ag_2(dppm)_3]^{2+} + [^{107}Ag_2(dmpm)_3]^{2+} \rightleftharpoons [^{107}Ag_2(dppm)_{3-x}(dmpm)_x]^{2+}$$

The symmetries of the limiting low temperature ^{31}P nmr spectra of **1*** (and **1**) and **2*** (and **2**) (see above) are quite consistent with the complexes having the "manxane" structure **I**.[6] With such a structure, **1*** and **2*** will have ^{31}P nmr spectra that are the A part of an AA′A″A‴A⁗A⁗′XX′ spectrum. In such spectra, the A part is symmetrical and contains a doublet with half the total intensity and a separation of $(J(A—X) + J(A—X'))$ (14). Thus $(^1J(^{107}Ag—^{31}P) + {}^3J(^{107}Ag—^{31}P))$ = 310 Hz in **1***, and 318 Hz in **2***. The other half of the intensity in the A part of the spectrum occurs as an AA′A″BB′B″ subspectrum. By trial and error, a convincing simulation[7] of the 213 K ^{31}P nmr spectrum of **1*** was obtained using $^1J(^{107}Ag—^{31}P)$ = 309 Hz, $^2J(^{31}P—Ag—^{31}P)$ = 100 Hz, $^2J(^{31}P—C—^{31}P)$ = 148 Hz, and $^4J(^{31}P—Ag—P—C—^{31}P)$ = 3 Hz. Evidently $^3J(^{107}Ag—^{31}P)$ is small, approximately 1 Hz. Similarly, the ^{31}P nmr spectrum of **2*** at 213 K was satisfactorily reproduced with the three non-zero coupling constants $^1J(^{107}Ag—^{31}P)$ = 317 Hz, $^2J(^{31}P—Ag—^{31}P)$ = 115 Hz, and $^2J(^{31}P—C—^{31}P)$ = 141 Hz. Here both $^3J(^{107}Ag—^{31}P)$ and $^4J(^{31}P—Ag—P—C—^{31}P)$ must be very small. For **1***, the smallness of $^3J(^{107}Ag—^{31}P)$ is consistent with results for other complexes with the Ag(μ-dppm)Ag unit (1, 2), while the values found for $^2J(^{31}P—C—^{31}P)$, $^2J(^{31}P—M—^{31}P)$, and $^4J(^{31}P—^{31}P)$ are comparable to those reported for [Pt(μ-dppm)$_3$Pt] (9). Also, the values found for $^1J(^{107}Ag—^{31}P)$ in **1*** and **2*** are in the range reported (15) for monomeric tris(phosphine) complexes, $Ag(PR_3)_3X$ (X = weakly coordinating anion), adding strong support to the proposed structure **I**. For the complexes $[Ag(\mu\text{-dppm})_nAg]^{2+}$, $^1J(^{107}Ag—^{31}P)$

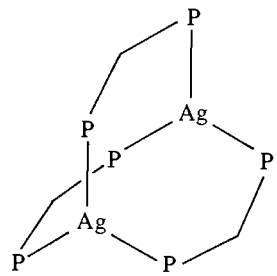

I

varies with *n* in the order 1 > 2 > 3 (ref. 1 and see above), as expected if the couplings vary with the 5*s* character of the hybrid orbitals of the silver atom, i.e. are dominated by the Fermi contact mechanism. We note that the values of $^2J(^{31}P—^{31}P)$ obtained for **1*** and **2*** are roughly twice the values found for the ^{31}P—^{31}P couplings in the ^{31}P nmr spectra of $[^{107}Ag_2(dppm)_{3-x}(dmpm)_x]^{2+}$ (x = 1 or 2) at ambient probe temperature (see above). However, the couplings found for the complexes with mixed ligands are the exchange-average of $^2J(^{31}P—^{31}P)$ and $^4J(^{31}P—^{31}P)$ (see below) and as just described the four-bond coupling is small.

It is now possible to account for the reduced temperature ^{31}P nmr spectra of **1** and **2** (see Fig. 1). These spectra are composites: they contain the two different AA′A″A‴A⁗′A⁗⁗XX′ spectra of the isotopomers $[^{107}Ag(\mu\text{-L—L})_3{}^{107}Ag]^{2+}$ and $[^{109}Ag(\mu\text{-L—L})_3{}^{109}Ag]^{2+}$, and spectrum of the isotopomer $[^{107}Ag(\mu\text{-L—L})_3{}^{109}Ag]^{2+}$ which will be of the type AA′A″A‴A⁗′A⁗⁗MX or AA′A″BB′B″B‴MX depending on whether the isotope effect is or is not negligible. The relative intensities are those of the combinations $^{107}Ag_2$, $^{109}Ag_2$, and $^{107}Ag^{109}Ag$, i.e. 0.269, 0.232, and 0.499 (see above).

There remains the nature of the intramolecular exchange process that occurs in the 2:3 complexes as the temperature is raised. It is clear from the exchange-averaged spectra of

[6]The CH_2 signals in the ^1H nmr spectra of **2** and **2*** in CD_3NO_2 at ambient probe temperature are consistent with a manxane structure also. These signals are *septets*. In the manxane structure the apparent coupling in the expected septet is $(1/3)[^2J(^{31}P—^1H) + 2^4J(^{31}P—^1H)]$.

[7]For speed and ease of computation the spectra were simulated as the appropriately weighted composite of two A_3 subspectra and an AA′A″BB′B″ subspectrum. The last of these results from complexes in which the spins of Ag are opposed. The form of the centre of the six-spin subspectrum, in particular, is very sensitive to the values chosen for the various coupling constants. It should be noted, however, that the combination of coupling constants obtained by trial and error may not be unique.

Can. J. Chem. Downloaded from www.nrcresearchpress.com by 213.222.148.141 on 09/07/12
For personal use only.

$[^{107}Ag(\mu\text{-dppm})_{3-x}(\mu\text{-dmpm})_x{}^{107}Ag]^{2+}$ ($x = 1$ or 2) (see Fig. 3 and the discussion above) that this process renders both ends of the bridging ligands equivalent on a time-average. Thus the process must involve overall "end-over-end" ligand exchange as shown in reaction [2]. This type of intramolecular exchange

[2] 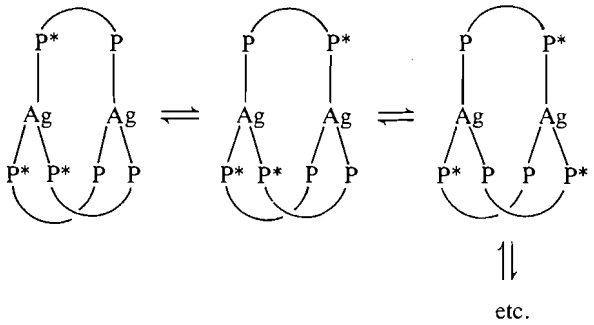

does not seem to have been observed previously for a bridging dppm. However, intramolecular "end-over-end" exchange of η^1-dppm is well-established. (See, for examples, refs. 5*a* and 16.) A plausible mechanism for the exchange is via the short-lived complex $[Ag(\mu\text{-dppm})_2Ag(\eta^2\text{-dppm})]^{2+}$, as shown in reaction [3].[8]

[3] 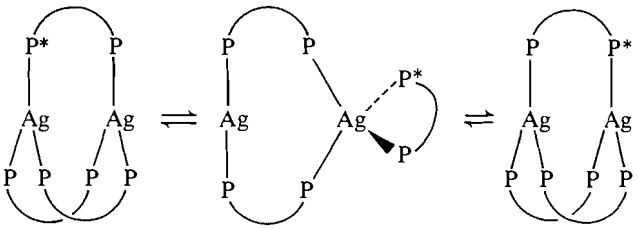

For the exchange process shown in reaction [2], the $[^{107}Ag(\mu\text{-L—L})^{107}Ag]^{2+}$ complexes with different combinations of ^{107}Ag nuclear spins count as different sites. The possible combinations of silver spins are αα, ββ, and αβ/βα with relative populations 1, 1, and 2, respectively. When the spins are αα or ββ, the exchange process does not result in a change of site for the two ^{31}P nuclei that interchange places. On the other hand when the silver spins are αβ/βα, the two ^{31}P nuclei on the ligand undergoing exchange do change sites (and hence resonance frequencies) as a result of the exchange, and thus their resonances collapse together as the exchange rate becomes appreciable on the nmr timescale. Therefore, exactly half of the total intensity in the ^{31}P nmr spectra of **1*** and **2*** should remain sharp during the end-over-end exchange process,[9] while the other half should collapse together and eventually become a singlet when the exchange rate becomes fast enough. This is just what is observed in the variable temperature spectra of **1*** and **2***, as exemplified in Fig. 2. The same explanation accounts for the spectra of the complexes $[^{107}Ag(dppm)_{3-x}(dmpm)_x{}^{107}Ag]^{2+}$ ($x = 1$ or 2) at ambient probe temperature (see Fig. 3). Here the exchange in the complexes with αα or ββ spins of silver causes averaging of ^{31}P—^{31}P couplings but not of different sites (i.e. resonance frequencies). In complexes with opposed silver spins, both averaging of coupling constants and site exchange (at an intermediate rate) occur, and this accounts for the broad signals seen in Fig. 3(*a*) and (*b*). Similarly, the couplings to $^{109/107}Ag$ persist in just half the intensity of the spectra of **1** and **2** at 295 K, while the other half of the intensity is in the form of a single broad resonance (e.g. Figs. 1 and 2). Again this observation is quite consistent with the occurrence of the intramolecular exchange process shown in reaction [2].

After the complicated subspectrum[7] of the Ag(α)Ag(β)/Ag(β)Ag(α) spin isomers of **1*** and **2*** has collapsed to a single line, it seems reasonable that the behaviour of this line should be just that expected for exchange between two different equally populated sites, i.e. the α and β spins of silver. In this region of exchange-narrowing, the exchange rate is inversely proportional to $(\Delta\nu_{1/2}(\text{excess}))^{-1}$ (17). In the present case $\Delta\nu_{1/2}(\text{excess}) = [\Delta\nu_{1/2}(\text{collapsed singlet}) - \Delta\nu_{1/2}(\text{uncollapsed doublet})]$.[10] Thus from an Eyring plot of $\ln [\Delta\nu_{1/2}(\text{excess}) \times T]^{-1}$ vs. $1/T$, for the region of exchange-narrowing, it is possible to obtain the enthalpy of activation, $\Delta H^{\ddagger}$, for the exchange process shown in reaction [2]. From a regression analysis of the Eyring plot, $\Delta H^{\ddagger}$ for intramolecular ligand exchange in **1*** in Me_2CO is found to be 58.7 ± 1.4 kJ mol^{-1} (from five points covering the temperature range −4.1 to 22.4°C; the correlation coefficient is 0.999). The same approach (with four points covering the range 36.0–54.4°C; the correlation coefficient is 0.999) yields 49.9 ± 1.5 kJ mol^{-1} for $\Delta H^{\ddagger}$ for exchange in **2*** in Me_2CO. The standard deviations from such Eyring plots can be serious underestimates (18).[11] With the small temperature range that could be used here, and the consequent small number of points collected, the values of $\Delta H^{\ddagger}$ should be taken as approximate. However, the relative values of $\Delta H^{\ddagger}$, **1*** > **2***, together with the observed rates of exchange, **1*** > **2***, suggest that there is a difference in the entropies of activation between **1*** and **2*** that favours the intramolecular ligand exchange in **1***.

Acknowledgments

We thank the Natural Sciences and Engineering Research Council of Canada for financial support of this work in the form of an Operating Grant to P.A.W.D. We are grateful to Professor R. J. Puddephatt and Mr. R. Ramachandran for their kind gift of dmpm. We acknowledge with thanks the expert technical assistance of Mrs. V. M. Richardson and Ms. S. Wilson in obtaining some of the nmr spectra reported herein.

1. A. F. M. J. Van der Ploeg and G. Van Koten. Inorg. Chim. Acta, **51**, 225 (1981).
2. S. S. D. Brown, I. J. Colquhoun, W. McFarlane, M. Murray, I. D. Salter, and V. Sik. J. Chem. Soc. Chem. Commun. 53 (1986).
3. W. Levason and C. A. McAuliffe. Inorg. Chim. Acta, **8**, 25 (1974).
4. D. M. Ho and R. Bau. Inorg. Chem. **22**, 4073 (1983).
5. (*a*) A. T. Hutton, C. R. Langrick, D. M. McEwan, P. G. Pringle, and B. L. Shaw. J. Chem. Soc. Dalton Trans. 2121 (1985), and references therein; (*b*) P. A. W. Dean and R. S.

[8] We find that the ^{31}P nmr spectrum of $[^{107}Ag(\mu\text{-dppm})_2{}^{107}Ag]^{2+}$ does not show evidence for the same type of exchange that occurs in **1***. Possibly two anchored bridging ligands are necessary before end-over-end exchange can occur. Alternatively, as suggested by one of the referees, stronger ligand binding in the 2:2 complex makes it less susceptible to the initial dissociative rupture required for a process like [3].

[9] *General* broadening can occur if there is *inter*molecular ligand exchange. This is clearly the case for the dppm complex around ambient probe temperature.

[10] Use of this difference minimizes the effect of any general broadening.

[11] We thank a referee for drawing our attention to this point.

Can. J. Chem. Downloaded from www.nrcresearchpress.com by 213.222.148.141 on 09/07/12
For personal use only.

SRIVASTAVA. Can. J. Chem. **63**, 2829 (1985); (*c*) M. LUSSER and P. PERINGER. Polyhedron, **4**, 1997 (1985).
6. A. A. M. ALY, D. NEUGEBAUER, O. ORAMA, U. SCHUBERT, and H. SCHMIDBAUR. Angew. Chem. Int. Edn. Engl. **17**, 125 (1978); U. SCHUBERT, D. NEUGEBAUER, and A. A. M. ALY. Z. Anorg. Chem. **464**, 217 (1980).
7. N. KUHN and P. SARTORI. Chem. Z. **105**, 87 (1981).
8. W. BENSCH, M. PRELATI, and W. LUDWIG. J. Chem. Soc. Chem. Commun. 1762 (1986).
9. L. MANOJLOVIC-MUIR, K. MUIR, M. C. GROSSEL, M. P. BROWN, C. D. NELSON, A. YAVARI, E. KALLAS, R. P. MOULDING, and K. R. SEDDON. J. Chem. Soc. Dalton Trans. 1955 (1986).
10. P. A. W. DEAN, D. G. IBBOTT, and J. B. STOTHERS. Can. J. Chem. **54**, 166 (1976).
11. A. A. BOTHNER-BY and S. M. CASTELLANO. LAOCN3. The Mellon Institute, Pittsburgh.
12. R. K. HARRIS. Nuclear magnetic resonance spectroscopy. Pitman, London. 1983. p. 230.
13. G. CALINGAERT and H. A. BEATTY. J. Am. Chem. Soc. **61**, 2748 (1934).
14. R. K. HARRIS. Inorg. Chem. **5**, 701 (1966).
15. P. S. PREGOSIN and R. W. KUNZ. ^{31}P and ^{13}C nmr of transition metal phosphine complexes. Springer-Verlag, Berlin. 1979. Table 15, p. 107, and references therein.
16. M. P. BROWN, J. R. FISHER, R. H. HILL, R. J. PUDDEPHATT, and K. R. SEDDON. Inorg. Chem. **20**, 3516 (1983).
17. L. H. PIETTE and W. A. ANDERSON. J. Chem. Phys. **30**, 899 (1959); A. ALLERHAND, W. A. ANDERSON, H. S. GUTOWSKY, J. JONAS, and R. A. MEINZER. J. Am. Chem. Soc. **88**, 3185 (1966).
18. J. SANDSTROM. Dynamic NMR spectroscopy. Academic Press, London. 1982. Chap. 7.

Can. J. Chem. Downloaded from www.nrcresearchpress.com by 213.222.148.141 on 09/07/12
For personal use only.

Seven coordination. 1. Synthesis, structure, and fluxionality of $(CH_3)_2AsC(CF_3)=C(CF_3)As(CH_3)_2W(CO)_2I_2P(OCH_3)_3$

LYNN M. MIHICHUK,[1] CAROLYN L. GIESINGER, BEVERLY E. ROBERTSON, AND RICHARD J. BARTON
Department of Chemistry, University of Regina, Regina, Sask., Canada S4S 0A2

Received May 7, 1987

LYNN M. MIHICHUK, CAROLYN L. GIESINGER, BEVERLY E. ROBERTSON, and RICHARD J. BARTON. Can. J. Chem. **65**, 2634 (1987).

(L—L)W(CO)$_4$ (L—L = $(CH_3)_2AsC(CF_3)=C(CF_3)As(CH_3)_2$) is oxidized by I_2 to yield the seven-coordinate complex (L—L)W(CO)$_3I_2$ which reacts with monodentate phosphines or phosphites to form (L—L)W(CO)$_2I_2$P (P = phosphine or phosphite). Crystals of (L—L)W(CO)$_2I_2P(OCH_3)_3$ are monoclinic, space group $P2_1/c$, a = 15.711(3), b = 13.134(2), c = 13.800(3) Å, β = 111.81(2)° with Z = 4. The structure was solved from a Patterson map and anisotropically refined by least squares to a conventional R value of 0.039 using 3737 independent reflections. The crystal structure showed the tungsten atom to be seven-coordinate with a geometry most closely approximated by a capped octahedral environment, the capping group being a carbonyl moiety ([W—C] = 1.95(1) Å). The capped face consists of the carbon atom ([W—C] = 1.98(1) Å) of the remaining carbonyl, an arsenic atom ([W—As] = 2.556(1) Å), and the phosphorus atom ([W—P] = 2.466(3) Å). The W—As bond *trans* to a phosphite group is longer (by 0.050(2) Å) than the W—As bond *trans* to an iodine atom. ^{1}H nmr data indicate the complex to be fluxional at 298 K and rigid at lower temperatures, the data at lower temperatures being consistent with the configuration found in the crystal. The nmr data at lower temperatures suggest two exchange processes are occurring; one which averages two sets of As—CH_3 groups and another process which averages all four As—CH_3 groups.

LYNN M. MIHICHUK, CAROLYN L. GIESINGER, BEVERLY E. ROBERTSON et RICHARD J. BARTON. Can. J. Chem. **65**, 2634 (1987).

L'oxydation du (L—L)W(CO)$_4$ (L—L = $(CH_3)_2AsC(CF_3)=C(CF_3)As(CH_3)_2$) par du I_2 conduit à un complexe hepta-coordonné (L—L)W(CO)$_3I_2$ qui réagit avec les phosphines ou les phosphites monodentates pour former (L—L)W(CO)$_2I_2$P (P = phosphine ou phosphite). Les cristaux de (L—L)W(CO)$_2I_2P(OCH_3)_3$ sont monocliniques, groupe d'espace $P2_1/c$ avec a = 15,711(3), b = 13,134(2) et c = 13,800(3) Å, β = 111,81(2)° et Z = 4. On a résolu la structure par une carte de Patterson et on l'a affinée d'une façon anisotrope par la méthode des moindres carrés jusqu'à une valeur conventionnelle de R de 0,039 pour 3737 réflexions uniques. La structure cristalline démontre que l'atome de tungstène est hepta-coordonné avec une géométrie qui se rapproche beaucoup d'un environnement octaédrique cappé, dans lequel le groupe qui agit comme cap est une portion carbonyle ([W—C] = 1,95(1) Å). La face cappée comporte l'atome de carbone ([W—C] = 1,98(1) Å) de l'autre carbonyle, un atome d'arsenic ([W—As] = 2,556(1) Å) et l'atome de phosphore ([W—P] = 2,466(3) Å). La liaison W—As est *trans* par rapport à un groupement phosphite et elle est plus longue (par 0,050(2) Å) que la liaison W—As qui est *trans* par rapport à un atome d'iode. Les données relatives à la rmn du ^{1}H indiquent que le complexe est fluxionnel à la température ambiante (298 K) et qu'il est rigide à des températures plus basses; les données obtenues à des températures plus basses sont en accord avec la configuration trouvée dans le cristal. Les données de la rmn à basse température suggèrent qu'il y a deux processus d'échanges qui sont impliqués; un fait que la position des deux ensembles de groupements As—CH_3 devient moyenne et un autre processus provoque une moyenne des quatre groupements As—CH_3.

[Traduit par la revue]

Can. J. Chem. Downloaded from www.nrcresearchpress.com by 213.222.148.141 on 09/07/12
For personal use only.

Introduction

The relevant seven-vertex polytopal polyhedra are the pentagonal bipyramid (D_{5h}), the monocapped octahedron (C_{3v}) and the quadrilaterally monocapped trigonal prism (C_{2v}). X-ray crystallographic studies of seven-coordinate complexes of transition metal carbonyls have shown that they generally adopt either of the latter two types of geometry (1–4). However, the actual structures seldom match the ideal polyhedral arrangements but various criteria have been proposed to aid in the assignment of the most appropriate description to an experimentally determined coordination polyhedron (5–7).

Another phenomenon commonly associated with seven coordination is fluxional behavior (8), which results in the room temperature nmr spectra often not being consistent with the X-ray crystal structure. Variable-temperature nmr studies may provide the appropriate data representative of the slow-exchange limit. Previous work in the area of seven coordination by one of us described the fluxional behavior of a series of related complexes utilizing ^{1}H, ^{19}F, and ^{31}P nmr studies (9). However, no crystallographic studies were available, making the assignment of the static structure and the discussion of the exchange processes uncertain! We are now compiling structural data (10) in order to better understand the behavior of these complexes and to elucidate the mechanism of the ligand motion, which is generally poorly understood in seven coordination. In view of the fluxional phenomenon we thus believe that spectroscopic assignment of seven-coordinate complexes should be substantiated with a crystallographic structural analysis.

In this paper we describe the synthesis, X-ray structure, and fluxional behavior of the seven-coordinate complex $(CH_3)_2AsC(CF_3)=C(CF_3)As(CH_3)_2W(CO)_2I_2P(OCH_3)_3$.

Experimental section

A. General comments

All preparations were carried out under an argon atmosphere using standard Schlenk techniques. The ligand *cis*-2,3-bis(dimethylarsino)-1,1,1,4,4,4-hexafluorobut-2-ene, (L—L), and the complex (L—L)W(CO)$_3I_2$ were prepared as previously described (9, 11).

^{1}H nmr data were obtained using a Perkin-Elmer R12-B nmr spectrometer. Chemical shifts are reported in parts per million from internal Me_4Si for ^{1}H. Low temperature ^{1}H nmr data were obtained using a Bruker HX-90 NMR spectrometer with $CFCl_3$ as solvent. Infrared spectra were recorded using a Beckman IR-12 spectrophotometer.

[1]Author to whom correspondence may be addressed.

Can. J. Chem. Downloaded from www.nrcresearchpress.com by 213.222.148.141 on 09/07/12
For personal use only.

TABLE 1. Crystallographic experimental data

Molecular formula	$C_{13}H_{21}As_2F_6I_2O_5PW$
mol. wt.	989.80
a, Å	15.711(3)
b, Å	13.134(2)
c, Å	13.800(3)
β, deg	111.81(2)
ρ(calc), g cm^{-3}	2.487
V, Å^3	2643.6
Z	4
μ(MoKα), cm^{-1}	93.75
Takeoff angle, deg	3.6
$F(000)$	1820
Residual electron density, e/Å^3	1.4
Temperature, K	290
Space group	$P2_1/c$
Radiation (MoKα), λ, Å	0.71069
Monochromator	Graphite
Data collection method	θ–2θ
Scan speed, deg/min	2.0
Scan width, deg	0.9 + 0.692 tan θ
Orientation reflections, number, range (2θ)	32, 30° < 2θ < 35°
2θ limits, deg	3–55
Standard intensity decay, %	11
Background time	9.96 s/side
Reflections collected	$\pm h, +k, +l$
Total	6771
Unique	6069
Used	3737
$I/\sigma(I)$	3.0
R	0.039
R_w	0.049
Maximum shift/error	3.1×10^{-3}
Average shift/error	1.1×10^{-4}
GOF	1.30
Weighting scheme	$1/\sigma^2$

B. Preparation of (L—L)W(CO)$_2$I$_2$P(OCH$_3$)$_3$

A solution of (L—L)W(CO)$_3$I$_2$ (0.196 g, 2.17 × 10^{-4} mol) and P(OCH$_3$)$_3$ (0.035 g, 2.82 × 10^{-4} mol) in 35 mL degassed benzene was refluxed for 21.5 h. The benzene was removed under reduced pressure and recrystallization from dichloromethane–hexane solution yielded yellow crystals of (L—L)W(CO)$_2$I$_2$P(OCH$_3$)$_3$; 0.146 g, 69%; mp 136–138°C; ir (CH$_2$Cl$_2$) ν(CO) 1953, 1874 cm^{-1}; ^{1}H nmr (CDCl$_3$) δ 3.87 (d, 9H, P(OCH$_3$)$_3$, J_{P-H} = 10.5 Hz), 2.16 (s, 12H, As(CH$_3$)$_2$).

C. X-ray structure analysis

A yellow plate of (L—L)W(CO)$_2$I$_2$P(OCH$_3$)$_3$ with approximate dimensions 0.09 × 0.2 × 0.35 mm was mounted on a modified Picker FACS-1 four-circle diffractometer. Intensity data were collected using the NRCC diffractometer control system (12).

The effects of absorption were corrected using the Gaussian method and the XTAL system of programs (13). Scattering factors were also assigned by XTAL. Dispersion corrections for the tungsten, iodine, arsenic, and phosphorus atoms were taken from the International tables for X-ray crystallography, Vol. IV (14).

The structure was solved by applying the Patterson method followed by use of electron density and difference Fourier maps. It was refined by full-matrix least squares applied to the structure amplitudes using anisotropic temperature factors. The hydrogen atoms were not located.

Table 1 contains crystallographic experimental data, Tables 2 and 3 contain atomic and thermal parameters and important bond lengths and bond angles, respectively.[2] The atomic labelling is given in Fig. 1 and a stereoscopic view of the molecule with thermal ellipsoids represented at 50% probability is shown in Fig. 2. Figure 3 shows the torsional angles in the five-membered ring of the chelate ligand and their estimated standard deviations for the title compound and the related complex (L—L)W(CO)Br$_2$[P(OCH$_3$)$_3$]$_2$ (10). Figure 4 shows an enantiomeric inversion pathway to partially explain the fluxional behavior of the title compound.

[2]Tables of observed and calculated structure factor amplitudes, anisotropic temperature factors and additional bond lengths and angles may be purchased from the Depository of Unpublished Data, CISTI, National Research Council of Canada, Ottawa, Ont., Canada K1A 0S2.

TABLE 2. Atomic and thermal parameters with estimated standard deviations in parentheses

Atom	x	y	z	U_{eq},[a] Å^2
W	0.21662(3)	−0.07761(3)	0.76852(3)	4.48
I(1)	0.31032(5)	−0.11663(6)	0.98807(5)	6.28
I(2)	0.05276(6)	−0.06149(7)	0.81359(8)	8.83
As(1)	0.37336(6)	−0.14014(7)	0.77721(7)	4.48
As(2)	0.19684(6)	−0.27481(7)	0.75930(8)	4.99
P	0.2288(2)	0.1014(2)	0.8263(3)	6.7
F(1)	0.5109(6)	−0.3930(7)	0.9170(8)	13.0
F(2)	0.5487(5)	−0.2604(6)	0.8590(9)	13.2
F(3)	0.4972(6)	−0.3823(8)	0.7627(8)	13.1
F(4)	0.3720(7)	−0.5078(5)	0.7746(8)	12.7
F(5)	0.3455(8)	−0.4842(6)	0.9091(7)	13.5
F(6)	0.2371(6)	−0.5001(5)	0.7653(8)	12.8
O(1)	0.2637(8)	0.0459(7)	0.6021(8)	10.8
O(2)	0.0588(8)	−0.1030(9)	0.5494(8)	13.0
O(3)	0.237(1)	0.1281(8)	0.9407(9)	13.8
O(4)	0.1561(9)	0.1797(7)	0.760(1)	15.1
O(5)	0.3228(6)	0.1460(6)	0.8296(9)	10.0
C(1)	0.2478(9)	−0.0006(9)	0.666(1)	7.7
C(2)	0.117(1)	−0.0931(9)	0.630(1)	8.7
C(3)	0.187(2)	0.163(3)	0.992(2)	25
C(4)	0.096(1)	0.178(1)	0.657(1)	10.4
C(5)	0.349(1)	0.249(1)	0.852(1)	12
C(6)	0.3895(7)	−0.2887(7)	0.8074(7)	5.0
C(7)	0.3169(7)	−0.3445(7)	0.7950(8)	5.1
C(8)	0.4874(8)	−0.3302(9)	0.837(1)	7.4
C(9)	0.3195(9)	−0.4569(8)	0.811(1)	7.5
C(10)	0.4809(8)	−0.0680(8)	0.8767(9)	6.9
C(11)	0.4027(8)	−0.1384(8)	0.6525(9)	6.7
C(12)	0.1210(9)	−0.3376(9)	0.623(1)	8.0
C(13)	0.1488(9)	−0.3352(9)	0.861(1)	8.2

[a]$U_{eq} = (1/3) \sum_{i=1}^{3} \sum_{j=1} [U_{ij} a_i^* a_j^* (\mathbf{a}_i \cdot \mathbf{a}_j)]$. Values listed are multiplied by 10^2.

Results and discussion

The tungsten atom is seven-coordinate with the coordination sphere containing the two arsenic atoms of the L—L ligand, two iodine atoms, the two carbon atoms of the carbonyl groups, and the phosphorus atom of the trimethyl phosphite group. The coordination polyhedron about the tungsten atom for the title compound is similar to that of (L—L)W(CO)Br$_2$[P(OCH$_3$)$_3$]$_2$ (10). In order to compare the two compounds we have used the δ parameters of Porai-Koshits and Aslanov (15), as calculated by Muetterties and Guggenberger. However, we have modified the experimentally determined polyhedron by moving each ligand along its radius vector to the surface of a unit sphere. The modified coordination polyhedron in both compounds is intermediate between the monocapped octahedron (C_{3v}) and the quadrilaterally monocapped trigonal prism (C_{2v}). The δ values which are most sensitive to changes in polyhedral shape and which are best used to compare experimentally determined polyhedra with the relevant polytopes are the three δ values for the edges which form the capped face in the monocapped

TABLE 3. Selected bond distances Å and angles (deg) with estimated standard deviations in parentheses

Bond	Distance
W—I(1)	2.8801(9)
W—I(2)	2.872(1)
W—As(1)	2.556(1)
W—As(2)	2.606(1)
W—P	2.466(3)
W—C(1)	1.95(1)
W—C(2)	1.98(1)
As(1)—C(6)	1.991(9)
As(1)—C(10)	1.98(1)
As(1)—C(11)	1.94(1)
As(2)—C(7)	1.99(1)
As(2)—C(12)	1.99(1)
As(2)—C(13)	1.99(2)
C(1)—O(1)	1.17(2)
C(2)—O(2)	1.16(2)
C(6)—C(7)	1.31(1)
C(6)—C(8)	1.54(2)
C(7)—C(9)	1.49(1)

Bonds	Angle
I(1)—W—I(2)	86.23(3)
I(1)—W—As(1)	77.67(3)
I(1)—W—As(2)	83.09(3)
I(1)—W—P	83.21(8)
I(1)—W—C(1)	133.7(3)
I(1)—W—C(2)	155.2(5)
I(2)—W—As(1)	159.88(3)
I(2)—W—As(2)	89.06(3)
I(2)—W—P	80.1(1)
I(2)—W—C(1)	127.4(4)
I(2)—W—C(2)	76.3(5)
As(1)—W—As(2)	77.19(3)
As(1)—W—P	109.46(9)
As(1)—W—C(1)	72.7(4)
As(1)—W—C(2)	114.6(5)
As(2)—W—P	163.0(1)
As(2)—W—C(1)	122.5(4)
As(2)—W—C(2)	79.2(3)
P—W—C(1)	74.4(4)
P—W—C(2)	110.4(4)
C(1)—W—C(2)	80.0(6)
W—As(1)—C(6)	111.7(3)
W—As(1)—C(10)	116.0(4)
W—As(1)—C(11)	119.8(3)
C(6)—As(1)—C(10)	108.3(4)
C(6)—As(1)—C(11)	98.2(5)
C(10)—As(1)—C(11)	100.8(5)
W—As(2)—C(7)	111.1(3)
W—As(2)—C(12)	118.5(3)
W—As(2)—C(13)	115.5(4)
C(7)—As(2)—C(12)	102.9(5)
C(7)—As(2)—C(13)	102.4(5)
C(12)—As(2)—C(13)	104.4(5)
W—C(1)—O(1)	178(1)
W—C(2)—O(2)	179(1)
As(1)—C(6)—C(7)	118.9(7)
As(1)—C(6)—C(8)	116.1(7)
C(7)—C(6)—C(8)	124.8(9)
As(2)—C(7)—C(6)	118.3(7)
As(2)—C(7)—C(9)	117.6(8)
C(6)—C(7)—C(9)	124(1)

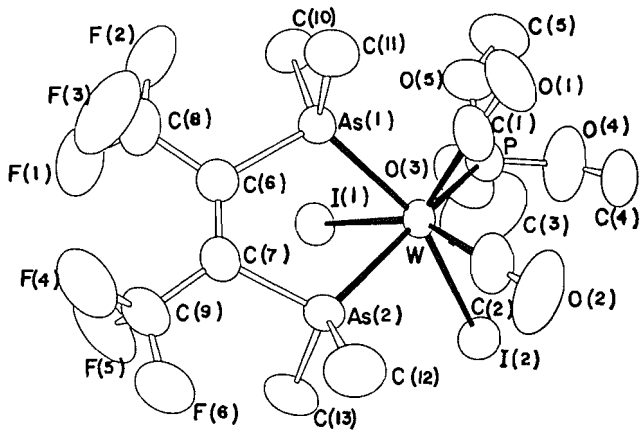

FIG. 1. Atomic labelling for $(CH_3)_2AsC(CF_3)=C(CF_3)As(CH_3)_2$-$W(CO)_2I_2P(OCH_3)_3$.

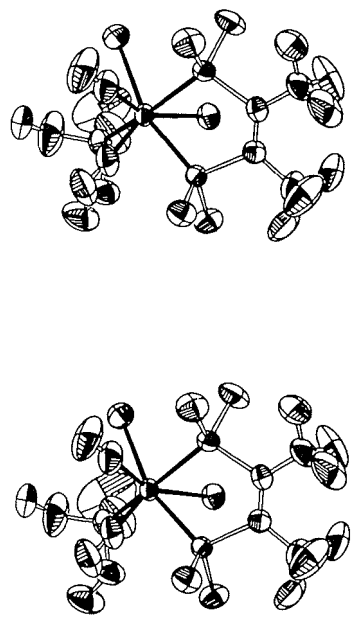

FIG. 2. Stereoscopic view of the molecule with thermal ellipsoids represented at 50% probability.

octahedral description. These three δ values are (24.2°, 24.2°, 24.2°), (7°, 16°, 23°), (4°, 8°, 30°), and (0°, 0°, 41.5°) for the idealized monocapped octahedron, (L—L)$W(CO)_2I_2P(OCH_3)_3$, (L—L)$W(CO)Br_2[P(OCH_3)_3]_2$, and the idealized monocapped trigonal prism, respectively. The compound reported here is marginally better described as a distorted capped octahedron, while (L—L)$W(CO)Br_2[P(OCH_3)_3]_2$ is marginally better described as a monocapped trigonal prism (10).

These small differences are readily attributed to the lesser bulk of the second carbonyl group, which replaces a $P(OCH_3)_3$ ligand and the greater radius of I(1) which replaces Br(1) in (L—L)$W(CO)Br_2[P(OCH_3)_3]_2$.

In the capped octahedral description, the capping atom is the C(1) carbonyl group. In the capped trigonal prism description I(1) is the capping atom. In both compounds the bidentate ligand bridges an edge joining the capped trilateral face of the octahedron to the trilateral face formed by the remaining three ligands, and an edge of the capped quadrilateral face of the trigonal prism which joins the two trilateral faces of the prism.

Can. J. Chem. Downloaded from www.nrcresearchpress.com by 213.222.148.141 on 09/07/12
For personal use only.

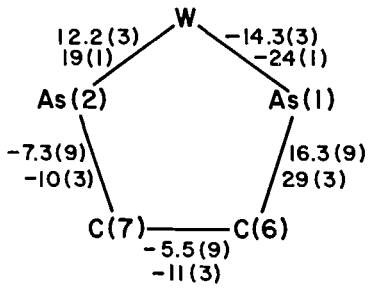

FIG. 3. Schematic diagram showing the torsional angles in the five-membered ring of the chelate ligand and their estimated standard deviations (in brackets) for the title compound (top numbers) and the related complex (L—L)W(CO)Br_2[$P(OCH_3)_3$]$_2$ (bottom numbers).

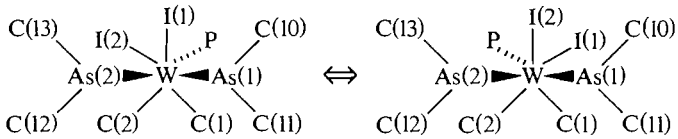

FIG. 4. Schematic diagram showing an enantiomeric inversion pathway for the molecule.

Kepert (16) reports this as the normal configuration for polyhedra with one bidentate ligand with a *bite* on the unit sphere greater than 1.20. The *bite* on the unit sphere for the iodine and bromine compounds are 1.23 and 1.25, respectively.

The stereochemistry of seven-coordinate complexes, in particular substituent site preferences, have been discussed by Hoffmann *et al.* (17). For d^4 cations containing molybdenum or tungsten, Hoffmann *et al.*, from considerations of bond energies, conclude that in the monocapped octahedron description, strong π-acceptors such as the carbonyl substituent will prefer to occupy the three vertices of the capped face over the capping vertex itself, with the three vertices of the uncapped face least preferred. However, from simple steric considerations ligands with a small radius, such as a carbon atom, should prefer vertices with a minimum number of neighboring vertices; i.e. the capping vertex would be most preferred and the vertices of the capped face least preferred.

Hoffmann *et al.* conclude that strong π-donors, such as the halides would prefer the vertices of the uncapped face of the monocapped octahedron. From simple steric considerations, these large ligands would be expected to occupy the vertices of the capped face, each of which has five neighboring vertices.

If we consider both polyhedra from the point of view of the monocapped trigonal prism, Hoffmann *et al.* conclude that the acceptors would prefer either the vertices of the quadrilaterally capped face or the vertices of the opposite edge over the vertex of the capping vertex. They conclude that the π-donors would prefer the capping vertex of the monocapped trigonal prism. From simple steric considerations, the vertices of the capped quadrilateral face would be preferred.

A detailed analysis of the stereochemistry of (L—L)W-$(CO)_2I_2P(OCH_3)_3$ and (L—L)W(CO)Br_2[$P(OCH_3)_3$]$_2$ from the point of view of the monocapped octahedron and from the point of view of the monocapped trigonal prism shows that it is generally consistent with these considerations, but when steric and bond energy preferences are in conflict it is not possible to predict which will prevail.

The puckering of the ring is qualitatively the same in both compounds, as shown in Fig. 3, but of lesser magnitude in the compound reported here. The ring puckering parameters, according to the method of Cremer and Pople (18), are $q = 0.26$ and $\phi = 10.1°$, compared to $q = 0.43$ and $\phi = 13.2°$ for (L—L)W(CO)Br_2[$P(OCH_3)_3$]$_2$. These parameters imply a moderate degree of puckering, intermediate between twist and envelope conformation. The greater degree of puckering in the bromine complex is primarily due to the greater bulk of the second phosphite group.

Significant shortening of the W—As bonds from a predicted value of 2.73 Å (4) to the experimental values of 2.556(1) and 2.606(1) Å is a result of double-bond character in the W—As bonds caused by $d\pi$–$d\pi$ back donation from the tungsten atom. The lengths of the two W—As bonds are also significantly different from each other which can be explained by a consideration of their respective *trans* ligands. The I(2) atom *trans* to As(1) is not as strong a $d\pi$ acceptor as the P atom *trans* to As(2), resulting in greater back donation to As(1). This results in a shortening of the W—As(1) bond compared to the W—As(2) bond, the difference being 0.050(2) Å.

Fluxional behavior of (L—L)W(CO)$_2$I$_2$P(OCH$_3$)$_3$

The observation of a single As—CH_3 resonance in the room temperature ^{1}H nmr spectrum of the title compound is not consistent with the structure in the solid state and this led us to variable-temperature nmr studies. The static structure consistent with the solid-state structure is frozen out at 216 K. The solid-state structure shows all four As—CH_3 groups to be chemically nonequivalent and thus four resonances are found at 2.09, 2.39, 2.97, and 3.09. As the temperature is increased, the four peaks broaden and coalesce into two peaks with coalescence temperatures of 218 K for the two lower field peaks and 224 K for the two higher field peaks; as the temperature is further increased the two peaks broaden and coalesce into a single peak with a coalescence temperature of 239 K. The single resonance line becomes very sharp at 298 K indicative of a fast-exchange limiting spectrum. Thus the ^{1}H nmr results suggest that there are two exchange processes occurring; one process which averages two pair of As—CH_3 groups (process 1) and another process which averages all four As—CH_3 groups (process 2). Using the relationships $k = \pi\Delta\nu/\sqrt{2}$ and $k = (k_BT/h)\exp(-\Delta G^{\ddagger}/RT)$ (19) values of $\Delta G^{\ddagger} = 46.6 \pm 0.3$ kJ mol^{-1} for process 1 and 48.3 ± 0.3 kJ mol^{-1} for process 2 are obtained.

There exists the possibility that the changes in the nmr spectra may be associated with only one process. We had hoped to obtain $\Delta H^{\ddagger}$ and $\Delta S^{\ddagger}$ values using the value of $\Delta G^{\ddagger}$ calculated from the variable temperature ^{19}F nmr spectra. However, the ^{19}F nmr spectra showed further complications due to the presence of an A_3B_3 spin system at lower temperatures. We intend to pursue these phenomena by investigating other related seven-coordinate complexes using ^{1}H, ^{13}C, ^{19}F, and ^{31}P nmr spectroscopy.

If we assume the model involving two exchange processes for the related complex (L—L)W(CO)Br_2[$P(OCH_3)_3$]$_2$, there is only evidence for process 2. At room temperature two As—CH_3 resonances are observed which remain sharp at 223 K. Thus it was not possible to obtain a low-temperature slow-exchange limiting spectrum consistent with the solid-state structure. With increased temperatures the two resonances broaden, collapse, and coalesce into a single line with a coalescence temperature of

Can. J. Chem. Downloaded from www.nrcresearchpress.com by 213.222.148.141 on 09/07/12
For personal use only.

Can. J. Chem. Downloaded from www.nrcresearchpress.com by 213.222.148.141 on 09/07/12
For personal use only.

343 K. At the coalescence temperature a value of 70.8 kJ mol^{-1} for $\Delta G^{\ddagger}$ is obtained.[3]

Therefore, our proposed mechanism must account for the fact that process 2 occurs at a temperature approximately 80° higher in the bromo complex than in the iodo complex, and, given that in the bromo complex the two As—CH_3 resonances remain sharp down to 223 K, and give no indication of the onset of a transition at a lower temperature, process 1 occurs at a lower temperature in the bromo complex than in the iodo complex.

A seven-vertex polyhedron with the C_{2v} symmetry required to produce a single As—CH_3 resonance, and which is consistent with the stoichiometry of (L—L)$W(CO)_2I_2P(OCH_3)_3$ is the pentagonal bipyramid with the (L—L) ligand, the phosphite ligand and either the two iodine atoms or two carbonyl groups in the equatorial plane. The adoption of a C_{2v} pentagonal bipyramidal geometry at higher temperatures would involve a rearrangement, not a coalescence phenomenon such as that observed. Furthermore, the equatorial plane of a pentagonal bipyramid would seem to be unreasonably crowded.

Other explanations of the nmr spectra must involve equilibration of the As—CH_3 resonances through fluxional behavior of the remaining ligands. The mechanism must also explain the intermediate spectra which shows a doublet resonance.

Process 1, the transition to the intermediate state with an activation energy of 46.6 kJ mol^{-1} might involve a random scrambling of the atoms I(2), C(1), C(2), and P, leaving the atom I(1) rigidly held in the "pocket" of the chelate ring. This would equilibrate the atoms C(11) and C(12) as one pair and the atoms C(10) and C(13) as the other pair. Process 2, the coalescence to a single resonance, with an activation energy of 48.3 kJ mol^{-1} would then involve the addition of the atom I(1) to the random scrambling motion.

Alternatively, process 1 may involve a scrambling of the atoms I(1), I(2), C(1), C(2), and P that is not completely random. The doublet resonance state would exist if the scrambling motion did not permit an enantiomeric inversion. This would equilibrate the atoms C(10) and C(12) as one pair and the atoms C(11) and C(13) as the other pair. An enantiomeric inversion of the $W(CO)_2I_2P(OCH_3)_3$ portion of the molecule would then result in the coalescence of the nmr spectrum to one As—CH_3 resonance. Examination of Fig. 2 suggests that the enantiomeric inversion might be accomplished by a mirror operation on the atoms I(1), I(2), and the $P(OCH_3)_3$ group as illustrated in Fig. 4.

In both proposed models for the fluxional behavior process 2 might be expected to be controlled primarily by the overall degree of crowding of the ligands. Specifically, the presence of the extra phosphite ligand in the bromo complex forces the chelate ligand to enclose the Br(1) atom more completely in its pocket than is the I(1) atom enclosed in the iodo complex. This effect is evident in Fig. 2. It is also illustrated by the observation that the puckering parameter in the bromo complex is 1.65 times that for the iodo complex and the Br(1) atom is 2.60 Å from the W, As(1), As(2) plane compared to 2.81 Å for the I(1) atom. Therefore the activation energy for process 2 may be raised by the presence of the second phosphite group in the bromo complex, which restricts the motion of the halogen atom in the pocket of the chelate ring, either in a random scrambling or in a mirror inversion with the other halogen atom.

However, the greater radius of the iodine atom over that of the bromine atom would also contribute to the overall crowding of the complex and we would expect that in a complex with one phosphite and two bromine ligands, process 2 would occur at a lower temperature than in (L—L)$W(CO)_2I_2P(OCH_3)_3$. This expectation is consistent with results obtained for a related complex, (L—L)$Mo(CO)_2Br_2P(OCH_3)_3$ (9). Assuming a similar structure as the title compound, but with molybdenum replacing tungsten and bromine replacing iodine a single As—CH_3 resonance is observed at room temperature which remains sharp down to 193 K. The reason that process 1 occurs at a lower temperature in the bromo complex than in the iodo complex is not clear, but it presumably involves the relative radius of the halogen atoms.

We have tried unsuccessfully to synthesize the complex (L—L)$W(CO)I_2[P(OCH_3)_3]_2$ to compare its anticipated dynamic behavior to (L—L)$W(CO)Br_2[P(OCH_3)_3]_2$ and further illustrate the steric effect of the halogens.

[3]This value was obtained at a field strength of 60 MHz.

Acknowledgments

We are grateful to Natural Sciences and Engineering Research Council of Canada for financial support of this work in the form of operating grants to R.B., L.M., and B.R. and a summer research award to C.G. L.M. gratefully acknowledges the University of Regina for financial support of this work. Technical assistance from Yaoguang Luo and Suzanne Manley, University of Regina, Regina, Saskatchewan, is gratefully acknowledged. The authors thank the University of Regina for provision of computational facilities.

1. A. L. Beauchamp, F. Belanger-Gariepy, and S. Arali. Inorg. Chem. **24**, 1860 (1985).
2. M. G. B. Drew and J. D. Wilkins. J. Chem. Soc. Dalton Trans. 2664 (1973).
3. A. Mercer and J. Trotter. Can. J. Chem. **52**, 3331 (1974).
4. F. A. Cotton, L. R. Falvello, and J. H. Meadows. Inorg. Chem. **24**, 514 (1985).
5. M. G. B. Drew. Prog. Inorg. Chem. **23**, 67 (1977).
6. M. G. B. Drew and C. J. Rix. J. Organomet. Chem. **102**, 467 (1975).
7. E. L. Muetterties and L. J. Guggenberger. J. Am. Chem. Soc. **96**, 1748 (1974).
8. F. A. Van-Catledge, S. D. Ittel, and J. P. Jesson. Organometallics, **4**, 18 (1985), and references therein.
9. W. R. Cullen and L. M. Mihichuk. Can. J. Chem. **54**, 2548 (1976).
10. L. Mihichuk, M. Pizzey, B. Robertson, and R. Barton. Can. J. Chem. **64**, 991 (1986).
11. J. P. Crow, W. R. Cullen, F. G. Herring, J. R. Sams, and R. L. Tapping. Inorg. Chem. **10**, 1616 (1971).
12. A. C. Larson and E. J. Gabe. Computing in crystallography. *Edited by* H. Shenk, R. Olthof-Hazekamp, H. Van Koningsveld, and G. C. Bassi. Delft University Press. 1978. pp. 81–89.
13. J. M. Stewart, S. R. Hall, R. A. Alden, R. Olthof-Hazekamp, and R. M. Doherty. The XTAL system of crystallographic programs: users manual. Computer Science Centre, University of Maryland, College Park, MD. September, 1983.
14. International tables for X-ray crystallography. Vol. 4. Kynoch Press, New York. 1974. pp. 99, 149.
15. M. A. Porai-Koshits and L. A. Aslanov. Zh. Strukt. Khim. **13**, 266 (1972).
16. D. L. Kepert. Inorganic chemistry concepts 6. Inorganic stereochemistry. Springer Verlag, New York. 1982.
17. R. Hoffmann, B. F. Beier, E. L. Muetterties, and A. R. Rossi. Inorg. Chem. **16**, 511 (1977).
18. D. Cremer and J. A. Pople. J. Am. Chem. Soc. **97**, 1354 (1975).
19. H. Kessler. Angew. Chem. Int. Ed. **9**, 219 (1970).

Some thermodynamic aspects of organic eutectic in a monotectic type system

U. S. Rai,[1] O. P. Singh, and Narsingh B. Singh[2]
Chemistry Department, Banaras Hindu University, Varanasi-221005, India

Received October 20, 1986[3]

U. S. Rai, O. P. Singh, and Narsingh B. Singh. Can. J. Chem. **65**, 2639 (1987).

Phase diagram and heat of fusion of succinonitrile–phenanthrene system have been studied. Heat of mixing, entropy of fusion, and excess thermodynamic functions such as h^E, s^E, and g^E have also been calculated. The results have been explained on the basis of cluster formation and the interactions among the components forming the eutectic melt. Solid–liquid and liquid–liquid interfacial energies calculated from the heats of fusion of the pure components suggest the validity of Cahn wetting condition and predict the monotectic solidification morphology in the present system.

U. S. Rai, O. P. Singh et Narsingh B. Singh. Can. J. Chem. **65**, 2639 (1987).

On a étudié le diagramme de phase et la chaleur de combustion du système succinonitrile/anthracène. On a aussi calculé la chaleur de mélange, l'entropie de fusion et les fonctions thermodynamiques en excès. On explique les résultats en faisant appel à la formation d'agrégats et en faisant intervenir les interactions entre les composants qui forment un mélange eutectique. Les énergies interfaciales solide/liquide et liquide/liquide, calculées à partir des chaleurs de fusion des composants à l'état pur, suggèrent d'une part que la condition de mouillage de Cahn est valide et, de plus, elles prédisent la morphologie de solidification monotectique qu'on retrouve dans le présent système.

[Traduit par la revue]

Can. J. Chem. Downloaded from www.nrcresearchpress.com by 213.166.140.6 on 09/07/12
For personal use only.

Introduction

In the recent past the chemistry of eutectic (1–3) and monotectic systems (4) has been a field of active investigation due to their unusual physical properties not normally shown by the parent components. The metallic eutectics constitute an interesting area of investigation in metallurgy and material science, but they require complicated experimental techniques. Due to low transformation temperature, ease in purification, transparency, and wider choice of material, organic eutectics have attracted the attention of a number of research groups (5–7). Apart from these, the small density difference of the two components forming the organic eutectics minimises the density-driven convection effects on solidification. Succinonitrile (SCN), a material of low entropy of fusion, simulates the metallic solidification and phenanthrene (Ph), a material of high entropy of fusion, simulates nonmetallic solidification. As such, the SCN–Ph system can be chosen as a suitable analogue of Al–Si (metal–nonmetal) system for direct observation on solidification. The results of linear velocity of crystallization, diffusion coefficient measurement, and microstructure of succinonitrile–phenanthrene system were reported by Singh and co-workers (8). In the present article the data on phase diagram, heats of fusion, and interfacial energy have been discussed in detail. Making use of the heats of fusion some excess thermodynamic functions such as g^E, s^E, and h^E and entropy of fusion and heat of mixing have been calculated. The results have been analysed in light of cluster formation and interactions among the components forming the eutectic melts. The interfacial energies which decide the mode of solidification of monotectic alloys have been calculated from the heats of fusion data.

Experimental

Phase diagram

The phase diagram of the SCN–Ph system was determined by thaw–melt method (9, 10). The mixtures of different compositions were prepared by weighing phenanthrene and succinonitrile in a long-necked test tube which was sealed before the melting of any of the components. The test tube was immersed in an oil bath to ensure complete melting. The test tube was taken out and shaken periodically to mix the liquids. At this state, we could find out that both liquids had a miscibility gap and the melting point of the mixture could not be determined by taking a small amount of solid mixtures as there was always the possibility of the heavier component settling down. The thaw temperature, melt temperature, and temperature of complete miscibility were observed by immersing the same sealed test tube in which the mixtures were prepared in a bath.

Heats of fusion

Heats of fusion for SCN, Ph, and their eutectic were determined using a Perkin-Elmer DSC-2 with computer-aided data requisition and analysis by differential scanning calorimeter. Whenever a transition such as melting, boiling, dehydration, or crystallization occurs in the sample material, an endothermic or exothermic reaction takes place. The change in power required to maintain the sample holder at the same temperature as that of the reference holder during transition is recorded from the peak obtained in the pattern. The chart abscissa indicates the transition temperature and the peak area indicates the total energy transfer to or from the sample. In the present system under investigation all runs were carried out with a range of 2 m cal s^{-1}, chart speed of 5 mm min^{-1}, and chart range of 10 mV. The heating rate was 1.25 K min^{-1} and the sample weight range was 5–10 mg for each estimation.

Interfacial energies

Solid–liquid and liquid–liquid interfacial energies are required to verify the theory of monotectic solidification in SCN–Ph system. Measurement of solid–liquid interface energy is extremely difficult and unfortunately, the reported data show wide variation. Only few workers like Glicksman *et al.* (11) and Jones and Hardy (12) have claimed suitable values which are well within 10% of total error. Fortunately, these values lie between the theoretically predicted values by Spapen (13). Glicksman has shown that solid–liquid interface energy is given by a fraction of the heat of fusion of the molecules on unit area of the surface. A similar method of calculation was adopted to obtain solid–liquid interface energies in the SCN–Ph system. Liquid–liquid interfacial energy was calculated by a method reported earlier (14).

Results

The enthalpy of fusion, the values of $\ln \gamma_i^l$ and $\partial \ln \gamma_i^l / \partial T$ at the eutectic temperature, the excess thermodynamic functions for the eutectic, the entropy of fusion of succinonitrile–phenan-

[1]To whom all correspondence should be addressed.
[2]Present address: Westinghouse Electric Corporation, Research and Development Center, 1310 Beulah Road, Pittsburgh, PA, U.S.A.
[3]Revision received July 7, 1987.

Can. J. Chem. Downloaded from www.nrcresearchpress.com by 213.166.140.6 on 09/07/12
For personal use only.

TABLE 1. Enthalpy of fusion

Material	Enthalpy of fusion (kJ/mol)
SCN	3.704
Ph	18.627
SCN–Ph eutectic (experimental)	10.071
SCN–Ph eutectic (by mixture law)	4.076

TABLE 2. Values of $\ln \gamma_i^l$ and $\partial \ln \gamma_i^l/\partial T$ at eutectic temperature

Material	$\ln \gamma_i^l$	$\frac{\partial \ln \gamma_i^l}{\partial T}$
SCN	−0.0167	−0.0061
Ph	−2.9045	−0.0242

TABLE 3. Excess thermodynamic functions for the eutectic

Function	Value (J/mol)
g^E	−57.9
s^E	−4.1
h^E	−1410.0

TABLE 4. Entropy of fusion of succinonitrile, phenanthrene and their eutectic

Material	Entropy of fusion (kJ M^{-1} K^{-1})
SCN	0.0111
Ph	0.0499
Eutectic	0.0306

TABLE 5. Interfacial energies in the SCN–Ph system

Parameter	Value (erg/cm^2)
$\gamma_{SL_2(SCN)}$	8.89
$\gamma_{SL_1(Ph)}$	23.00
$\gamma_{L_1L_2(SCN—Ph)}$	3.29

threne and their eutectic, and the interfacial energies in the SCN–Ph system are listed in Tables 1 to 5, respectively.

Discussion

Phase diagram

The phase diagram of the SCN–Ph system is shown in Fig. 1 which clearly shows that Ph forms a monotectic (0.225 mole fraction of SCN) and a eutectic (0.975 mole fraction of SCN). Monotectic (15) is another important three-phase reaction of the eutectic class in which one liquid phase decomposes with decreasing temperature into a solid phase and a new liquid phase

$$L_2 \rightleftharpoons S_2 + L_1$$

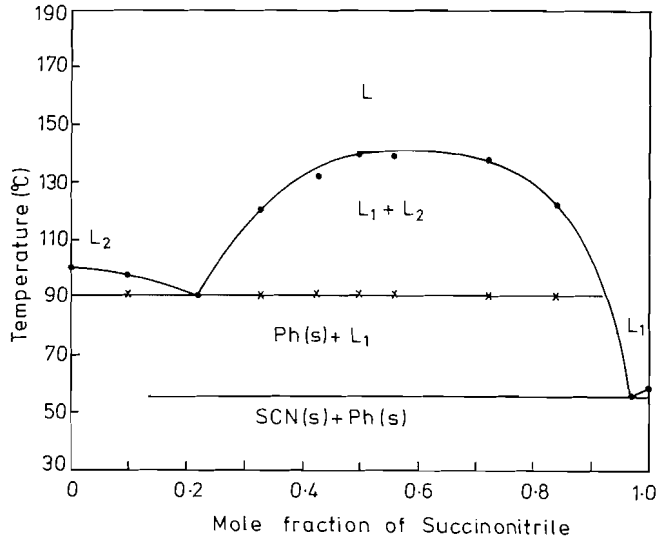

FIG. 1. Phase diagram of the SCN–Ph system.

Over a certain composition range, the two liquids are mutually immiscible and they constitute individual phases. The boundary of the $L_1 + L_2$ field is the limit of liquid immiscibility. The field of $L_1 + L_2$ may be regarded as being made up of an infinite number of tie-lines. The tie-lines connect the two liquid phases L_1 and L_2, the composition of each liquid phase varies with temperature. With increasing temperature the tie-lines become progressively shorter until the ultimate tie-line, at the top of the area, has zero length. This is known as critical point where the two liquid phases, having identical composition, become indistinguishable. The temperature corresponding to this point is known as consolute temperature and it is found to be 49°C above the monotectic horizontal in the SCN–Ph system. Above the critical temperature, there is complete miscibility in the liquid state, i.e., there is only one liquid phase called L in the entire composition range. At the invariant monotectic temperature L_2 (liquid rich in Ph), L_1 (liquid rich in SCN), and solid Ph are in equilibrium.

Thermochemical studies

The heats of fusion of pure components and eutectic are reported in Table 1. For the purpose of comparison, the heat of fusion of eutectic was calculated, using mixture law, and is given in the same table. In order to assess the nature of interaction between the components forming the eutectic melts, the activities of components and their excess thermodynamic functions were also calculated, and the results are given in the Tables 2 and 3, respectively.

(a) Heat of fusion of eutectic

If an eutectic is a simple mixture of two components, involving neither heat of mixing nor any type of association in the melt, heat of fusion may simply be given by the mixture law:

$$[1] \quad (\Delta_f h)_e = x_1 \Delta_f h_1^0 + x_2 \Delta_f h_2^0$$

where x and $\Delta_f h^0$ are mole fraction and heat of fusion, respectively, of the component indicated by the subscript. But when a solid eutectic melts, there is a considerable possibility of association and heat of mixing, both causing violation of the mixture law. Besides the heat of mixing, another factor, the interfacial tension, may also affect the magnitude of the heat of fusion. The comparison of the experimental value (vide Table 1) of heat of fusion with that calculated from eq. [1] indicates that the calculated value is lower than the experimental value. This

Can. J. Chem. Downloaded from www.nrcresearchpress.com by 213.166.140.6 on 09/07/12
For personal use only.

difference may be attributed to the formation of a quasieutectic (16) structure of the eutectic melt. During cluster formation, there may be liberation of heat which will lower the actual value of the heat content of the eutectic. The cluster formation will be favoured due to the molecular association by certain weak intermolecular forces.

(b) Entropy of fusion and excess thermodynamic functions of eutectics

The deviation from ideal behaviour can best be expressed in terms of excess thermodynamic functions which gives the quantitative nature of molecular interactions. These functions are also of much use in the development of statistical theories based on fluid models. The difference between the thermodynamic function of mixing for a real system and the corresponding value for an ideal system at the same temperature and pressure is called excess thermodynamic function. This quantity represents the excess of a given thermodynamic property of the solution over that in the ideal solution and can be expressed as follows:

$$[2] \quad Y^{E} = \Delta Y_{mix}(\text{real}) - \Delta Y_{mix}(\text{ideal})$$

where Y can be taken as any of the thermodynamic functions.

Theoretical studies (17, 18) on the entropy of fusion and calculation of some excess thermodynamic functions of eutectics predict the structure, stability, and ordering in the eutectic melts. The excess thermodynamic functions and entropy of fusion of eutectics are given in Tables 3 and 4, respectively. The entropy of fusion, ΔS, has been calculated from the following relation:

$$[3] \quad \Delta S = \Delta_f h/T$$

where $\Delta_f h$ is the heat of fusion and T is the fusion temperature. The positive entropy of fusion in the system studied indicates an increase in the randomness of the system during melting.

To understand the nature of interaction between the components forming the eutectic, some thermodynamic functions such as the excess free energy, g^E, excess enthalpy of mixing, h^E, and excess entropy of mixing, s^E, have been calculated by the procedure below.

The eutectic temperature and composition can be determined from the phase diagram of a system. Using eutectic temperature and composition, one can calculate the excess thermodynamic function with eqs. [4] to [6].

$$[4] \quad g^{E} = RT(x_1 \ln \gamma_1^1 + x_2 \ln \gamma_2^1)$$

$$[5] \quad s^{E} = -R(x_1 \ln \gamma_1^1 + x_2 \ln \gamma_2^1 + x_1 T\frac{\partial \ln \gamma_1^1}{\partial T} + x_2 T\frac{\partial \ln \gamma_2^1}{\partial T}$$

$$[6] \quad h^{E} = -RT^2\left(x_1\frac{\partial \ln \gamma_1^1}{\partial T} + x_2\frac{\partial \ln \gamma_2^1}{\partial T}\right)$$

The activity coefficient, γ_i, of component i present in the system is given by

$$[7] \quad -\ln x_i^1\gamma_i^1 = \frac{\Delta_f h_i^0}{R}(T^{-1} - T_i^{0-1})$$

where x_i^1, γ_i^1, $\Delta_f h_i^0$, and T_i^0 are the mole fraction, activity coefficient, heat of fusion, and melting temperature of component i, respectively; R is the gas constant; and T is the melting temperature of the system. The values of $\partial \ln \gamma_i/\partial T$ can be determined by the slope of the liquidus curve in the phase diagram, using eq. [8] obtained after differentiating eq. [7].

$$[8] \quad x_i\frac{\partial \ln \gamma_i^1}{\partial T} = x_i\frac{\Delta_f h_i^0}{RT^2} - \frac{\partial x_i}{\partial T}$$

The liquidus curves in the phase diagram are virtually straight lines in the region of eutectic composition. The value of $\partial x_i/\partial T$ can be calculated as

$$[9] \quad x_i = \alpha + \beta T$$

where α and β are constants and $\beta = \partial x_i/\partial T$.

It is evident from the Table 3 that the value of excess thermodynamic functions are all negative. The value of excess free energy is a measure of the departure (19) of the system from ideal behaviour. Thus, it reveals some interaction among the components of the system in the present investigation. The negative value of excess enthalpy and excess entropy correspond to excess free energy, and are measures of excess enthalpy of mixing and excess entropy of mixing, respectively, and thereby suggest an appreciable interaction among the two components of the eutectic. Similar results were reported (20) in the case of *m*-aminophenol–pyrogallol system in which excess free energy, g^E, excess entropy, s^E, and excess enthalpy, h^E, are -478.0, -11.1, and $-1044.0\ \text{J mol}^{-1}$, respectively.

The activity coefficients of components 1 and 2 for the present system were computed from eq. [7] and are given in Table 2. In each case, the activity coefficient is not equal to unity and therefore it is not possible to predict the eutectic composition and temperature.

(c) Heat of mixing

The heat of mixing, ΔH_m, of a eutectic can be very easily calculated by following equation, and thereby an insight into the structure (21) of melt in binary eutectics may be obtained:

$$[10] \quad \Delta H_m = (\Delta_f h)_{exp} - \Sigma x_i \Delta_f h_i^0$$

where $(\Delta_f h)_{exp}$ is the heat of fusion of the system determined experimentally, x_i, and $\Delta_f h_i^0$ are the mole fraction and heat of fusion, respectively, for component i. The heat of mixing of eutectic in the present system was calculated using eq. [10] and was found to be 5.995 kJ/mol. In the present system, eutectic composition is far from equimolar composition and the enthalpy of mixing is reasonably high. The eutectic point is shifted towards the component of lower melting temperature. Recently, Singh and co-workers (16) have reported that eutectic composition is connected with enthalpy of mixing in a definite manner. This type of behaviour was observed by Zalkin (22, 23) in the metallic system and he explained the eutectic structure on the basis of colloidal theory. Thermochemical studies suggested that structure of eutectic melts depends on the sign and magnitude of enthalpy of mixing, ΔH_m. Based on the above observations, three different structures have been suggested; quasieutectic for $\Delta H_m > 0$, clustering of molecules for $\Delta H_m < 0$, and molecular solution for $\Delta H_m = 0$. The magnitude of enthalpy of mixing indirectly gives (24) an idea about the composition of eutectics in a system. In the present system, the value of ΔH_m is highly positive which suggests firstly that the eutectic is on one side of the phase diagram and there is miscibility gap in the system, and secondly that the structure is of quasieutectic type.

Interfacial energies

The influence of surface energy on monotectic solidification morphology is discussed in this section. In the last few years, several articles have been published (25, 26) which explain various interesting phenomena during the solidification of a monotectic alloy. Specifically, the role of wetting in a phase

separation process has been the subject of great discussion. The wetting (26) condition is given as:

$$[11] \quad \gamma_{SL_2} < \gamma_{SL_1} + \gamma_{L_1L_2}$$

where γ is the interface energy between the faces denoted by the subscripts. Two important views have been put forward: (*a*) if the minor component wets the wall of the container in preference to the major component, the separation is possible by capillarity because the minor component easily spreads on the wall of the container, (*b*) at the monotectic temperature, if there is perfect wetting, a film of the liquid of the first component intrudes between its own solid and liquid of the second. As the temperature goes below the critical temperature $\gamma_{L_1L_2}$ increases more rapidly than γ_{SL_2}. This increases the critical wetting condition. In case the critical wetting temperature is below the monotectic temperature, the liquid of the first component will intrude between the growing solid and liquid of the second component. This will tend to push the liquid ahead of the growth front with a force determined by the disjoining pressure.

In order to check the validity of Cahn (26) wetting condition and to predict the mode of solidification morphology, in the present system, the interfacial energies were calculated at the monotectic temperature and results are included in Table 5. It is evident from the numerical values of interfacial energies that Cahn's wetting condition given by eq. [11] is obeyed in the present system. If we apply the wetting idea, the Ph–SCN liquid wets the solidified Ph perfectly and SCN-rich droplets will be surrounded by the SCN–Ph liquid. In this situation there is the possibility of capillary instabilities (27). Accordingly, if the cell depths are greater than the droplet circumference, capillary instabilities will develop SCN droplets and they will pinch off into spheres, Ph-rich liquid solidifies behind these spheres afterwards. Repetition of this process produces a very well arranged array of spheres (8). At low growth rates, droplets will not have enough time to develop capillary instabilities. These SCN droplets get surrounded by solidified Ph in such a way that cylindrical rods of SCN freeze as the solidification proceeds further.

Acknowledgements

The authors thank Professor S. M. Verma, Head, Chemistry Department, Banaras Hindu University, Varanasi, for providing necessary facilities. The authors are also thankful to Dr. Namwar Singh and Dr. N. P. Singh, T. D. College, Jaunpur, U.P. (India) for their assistance during the course of this study.

1. R. Elliot. Int. Met. Rev. **22**, 161 (1977).
2. K. A. Jackson and J. D. Hunt. Trans. Met. Soc. AIME, **236**, 1129 (1966).
3. W. Kurz and J. D. Fischer. Acta Metall. **28**, 777 (1980).
4. R. N. Grugel, T. A. Lograsso, and A. Hellawell. Metall. Trans. **15**A, 1003 (1984).
5. W. E. Kaukler and D. O. Frazer. J. Cryst. Growth, **71**, 340 (1985).
6. M. E. Glicksman, N. B. Singh, and M. Chopra. Manuf. Space, **11**, 207 (1983).
7. N. B. Singh and K. D. Dwivedi. J. Sci. Ind. Res. **41**, 96 (1982).
8. N. B. Singh, U. S. Rai, and O. P. Singh. J. Cryst. Growth, **71**, 353 (1985).
9. N. B. Singh and N. B. Singh. Krist. Tech. **13(10)**, 1175 (1978).
10. R. P. Rastogi, N. B. Singh, and N. B. Singh. J. Cryst. Growth, **37**, 329 (1977).
11. R. Schaefer, M. E. Glicksman, and J. D. Ayers. Phil. Mag. **32**, 125 (1975).
12. H. Jones and S. Hardy. Phil. Mag. **35**, 471 (1977).
13. F. Spapen. Acta Metall. **32**, 729 (1975).
14. R. Good. Ind. Eng. Chem. **62**, 54 (1970).
15. F. N. Rhines. Phase diagrams in metallurgy. McGraw Hill Book Co., Inc., New York. 1956. p. 72.
16. N. Singh, N. B. Singh, U. S. Rai, and O. P. Singh. Thermochim. Acta, **95**, 291 (1985).
17. R. P. Rastogi, N. B. Singh, P. Rastogi, and N. B. Singh. J. Cryst. Growth, **40**, 234 (1977).
18. N. Singh, D. P. Singh, and N. B. Singh. Krist. Tech. **15(1)**, K4 (1980).
19. S. Glasstone. Thermodynamics for chemists. D. Van Nostrand Company, Inc. 1960. p. 375.
20. U. S. Rai, O. P. Singh, N. P. Singh, and N. B. Singh. Thermochim. Acta, **71**, 373 (1983).
21. N. P. Singh, B. M. Shukla, N. Singh, and N. B. Singh. J. Chem. Eng. Data, **30(1)**, 49 (1985).
22. V. M. Zalkin. Z. Fiz. Khim. **40**, 2655 (1966).
23. V. M. Zalkin. Russ. J. Phys. Chem. **46**, 5 (1972).
24. N. Singh and N. B. Singh. Thermochim. Acta, **57**, 241 (1982).
25. J. W. Cahn. J. Chem. Phys. **66**, 667 (1977).
26. J. W. Cahn. Trans. Met. Soc. **10**A, 119 (1979).
27. C. Schafer, M. H. Johnston, and R. A. Parr. Acta Metall. **31**, 1221 (1983).

Can. J. Chem. Downloaded from www.nrcresearchpress.com by 213.166.140.6 on 09/07/12
For personal use only.

The X-ray crystal structure of bis(pentafluorophenyl)tellurium difluoride

J. ARAMINI, R. J. BATCHELOR, C. H. W. JONES,[1] F. W. B. EINSTEIN,[1] AND R. D. SHARMA
Department of Chemistry, Simon Fraser University, Burnaby, B.C., Canada V5A 1S6

Received February 20, 1987

J. ARAMINI, R. J. BATCHELOR, C. H. W. JONES, F. W. B. EINSTEIN, and R. D. SHARMA. Can. J. Chem. **65**, 2643 (1987).

Bis(pentafluorophenyl)tellurium difluoride crystallizes, in the space group *Cc*, as a molecular solid in which pairs of crystallographically independent molecules are linked by two weak secondary Te···F interactions. ($C_{12}F_{12}Te$; a = 11.088(6), b = 20.040(10), c = 13.208(5); β = 109.07(4); U = 2774; Z = 8; fw = 499.7). The structural model was refined by full-matrix least-squares methods to a final residual of R_1 = 0.035 for 1621 observed reflections. The stereochemistry of the primary bonding about Te is ψ-trigonal bipyramidal as for other R_2TeX_2 species and is compared with that of diphenyltellurium difluoride. Differences in the stereochemistry of the primary bonding about tellurium can be attributed to the influence of the more electron-withdrawing C_6F_5 group, and relates to the different secondary bonding and the crystal packing. ^{125}Te nmr coupling constants, $J_{^{125}Te-^{19}F}$, are reported for this and two related compounds. Previous ^{125}Te Mössbauer data is discussed in the light of the structure.

J. ARAMINI, R. J. BATCHELOR, C. H. W. JONES, F. W. B. EINSTEIN et R. D. SHARMA. Can. J. Chem. **65**, 2643 (1987).

Le difluorure du bis(pentafluorophényl)tellure qui cristallise dans le dans le groupe d'espace *Cc* est un solide moléculaire dans lequel des paires de molécules qui sont cristallographiquement indépendantes sont liées par deux interactions Te···F secondaires et faibles. ($C_{12}F_{12}Fe$; a = 11,088(6), b = 20,040(10), c = 13,208(5); β = 109,07(4); U = 2774; Z = 8; fw = 499,7). On a affiné la structure par les méthodes des moindres carrés (matrice entière) jusqu'à une valeur finale de R_1 = 0,035 pour 1621 réflexions observées. La stéréochimie de la liaison primaire autour du Te est ψ-trigonale bipyramidale comme dans le cas des autres espèces R_2TeX_2 et elle se compare à celle du difluorure du diphényltellure. On peut attribuer les différences dans la stéréochimie de la liaison primaire autour du tellure à l'influence du groupement C_6F_5 qui est plus électroaffinitaire et on peut les relier à la liaison secondaire différente et à l'entassement du cristal. On rapporte les constantes de couplage, $J_{^{125}Te-^{19}F}$, de ce composé et de deux autres composés apparentés. En se basant sur la structure qui a été déterminée, on discute de données de Mössbauer du ^{125}Te qui ont été publiées antérieurement.

[Traduit par la revue]

Introduction

The diorganyltellurium dihalides R_2TeX_2, X = Cl, Br, or I, are found to occur as molecular solids in which some weak intermolecular secondary bonding takes place (1). The molecules have an irregular trigonal bipyramidal stereochemistry with *trans*-axial halogens. The only diorganotellurium difluoride whose structure has been reported previously is that of diphenyltellurium difluoride (2), which, like the other dihalides, exhibits a ψ-tbp stereochemistry. The other tellurium fluorides for which crystal structures have been determined are TeF_4 (3) and $C_2F_5TeF_3$ (4). These compounds crystallize as *cis*-μ-bridged infinite chain polymers having ψ-octahedral stereochemistry about tellurium.

In the present work we report the X-ray crystal structure of bis(pentafluorophenyltellurium difluoride), the first perfluorinated difluoride for which the structure has been determined. A recent ^{125}Te Mössbauer spectroscopic investigation (5) of $(C_6F_5)_2Te$ and its dihalides $(C_6F_5)_2TeX_2$, X = F, Cl, or Br, showed these compounds to have very different quadrupole splittings from the corresponding phenyl compounds and this could be interpreted as evidence for the greater electronegativity of the C_6F_5 ligand compared with C_6H_5. Alternatively, the Mössbauer data could be interpreted as evidence for a somewhat different coordination geometry about the tellurium in the perfluorinated compounds than that in the phenyl compounds and the determination of the X-ray crystal structure of $(C_6F_5)_2TeF_2$ was undertaken to resolve this question.

The ^{125}Te solution nmr spectra for $(C_6F_5)_2Te$ and its dihalides have also previously been studied and compared with those of the corresponding phenyl compounds (5). In the present paper we also report the ^{125}Te—^{19}F coupling constants for $(C_6F_5)_2TeF_2$, $(C_6H_5)_2TeF_2$, and $(C_6F_5)_2Te$ and these constants are discussed.

Experimental

Crystals of $(C_6F_5)_2TeF_2$ (5) were obtained from chloroform solution by slow evaporation of the solvent. Crystal data, acquisition, and refinement details are given in Table 1. Cell parameter determination and data acquisition were performed at 20°C using an Enraf-Nonius CAD-4F diffractometer and Mo K_α radiation, graphite monochromated. Standards were measured every hour of acquisition time and showed no systematic variation in intensity.

Data reduction, including Lorentz and polarization corrections, was applied to the raw data. No absorption correction was applied, which may result in possible errors of ±4% in F_{obs}. Systematic absences in the diffractometer data coincided with those for the space groups $C2/c$ and Cc. Intensity statistics favoured the choice of the non-centrosymmetric space group Cc. This choice was subsequently confirmed by the successfully refined structure.

The structural solution was arrived at by the heavy atom method using Patterson and Difference Fourier syntheses. Full-matrix least-squares refinement of 329 variables for 1621 observed reflections, included anisotropic thermal parameters for the Te and F atoms. The x and z coordinates of Te(1) were fixed to define the origin. Seven poorly centered, high angle reflections with poor agreement were excluded from the refinement. No extinction correction was deemed necessary.

The programs used for data reduction and structure refinement were from the NRC VAX Crystal Structure System (6) and used scattering factors and anomalous dispersion corrections for neutral atoms from International tables (7). Plots were generated by the program SNOOPI (8). The final positional and isotropic thermal parameters are given in Table 2. Tables of anisotropic thermal parameters and of calculated and observed structure factors and σ values for the 1628 observed reflections are deposited as supplementary information and are available upon request.[2]

[1]To whom correspondence may be addressed.

[2]A complete set of data may be purchased from the Depository of Unpublished Data, CISTI, National Research Council of Canada, Ottawa, Ont., Canada K1A 0S2.

Can. J. Chem. Downloaded from www.nrcresearchpress.com by 213.222.148.141 on 09/07/12
For personal use only.

TABLE 1. Crystal data, acquisition, and refinement details for bis(pentafluorophenyl)-tellurium difluoride

Formula $C_{12}F_{12}Te$	a = 11.088(6) Å
Space group Cc	b = 20.040(10) Å
Z = 8	c = 13.208(5) Å
fw = 499.7	β = 109.07(4)°
ρ_{obsd} = 2.38 g cm^{-1} (floatation)	U = 2774 Å^3
ρ_{calcd} = 2.393 g cm^{-1}	μ(Mo K_α) = 22.83 cm^{-1}
Crystal dimensions (mm) 0.15 × 0.25 × 0.30	
Temperature = 20°C	
Radiation: Mo K_α, graphite monochromator, 0.71069 Å	
Scan mode: Ω-2θ	Max. 2θ: 45°
Scan width:[a] 0.85° + 0.35 tan θ	Reflections: 1806 (h, k, $\pm l$)
Scan speeds: 3.3–0.78° min^{-1}	1628 ($I \geq 2.5\sigma$)
	7 (rejected)
	Variables: 329
$R_f = \Sigma(\lvert F_o\rvert - \lvert F_c\rvert)/\Sigma\lvert F_o\rvert = 0.035$	
$R_{wf} - [\Sigma w(\lvert F_o\rvert - \lvert F_c\rvert)^2/\Sigma(wF_o^2)]^{1/2} = 0.046$	
$w = [\sigma^2(F) + 0.0002F^2]^{-1}$	
Maximum shift/error 0.01	Goodness of fit = 2.1[b]
Final difference: highest peak 0.86(10) e Å^{-3} 0.914(18) Å from Te(1)	

[a]Background intensities were measured by extending the scans by 25% of the scan width on either side.

[b]Goodness of fit = $\Sigma w(\lvert F_o\rvert - \lvert F_c\rvert)^2$/degrees of freedom.

The ^{125}Te nmr spectra were recorded on a Bruker WM400 spectrometer at 126.24 MHz and ambient temperature using the methods previously described (5). A sample spectrum showing the tellurium fluorine couplings is given in Fig. 2.

Results and discussion

The structure of bis(pentafluorophenyl)tellurium difluoride (Fig. 1) appears to be a molecular solid in which pairs of crystallographically independent molecules are mutually linked by secondary Te···F interactions. Each of the two independent molecules displays the approximate ψ-trigonal bipyramidal geometry typical of R_2TeX_2 species, having pseudo-*trans*-axial fluorine atoms while the pentafluorophenyl groups and, presumably, the formally non-bonding pair of electrons on tellurium occupy the equatorial plane. Each molecule is distorted from the ideal trigonal bipyramidal geometry because of the greater stereochemical influence of the non-bonding pair of electrons as evidenced by the F—Te—F and C—Te—C bond angles. These and other bond angles, as well as selected bond distances, are given in Table 3.

One other R_2TeF_2 crystal structure is known, that of diphenyltellurium difluoride (2). This structure and that of the title compound may be compared in terms of the bonding and geometry about tellurium. Both molecules of $(C_6F_5)_2TeF_2$ and that of $(C_6H_5)_2TeF_2$ display the usual ψ-trigonal bipyramidal geometry of R_2TeX_2 species. The primary Te—F bond lengths range from 1.932(11) to 1.990(11) Å for $(C_6F_5)_2TeF_2$, as compared to 2.006(2) Å for $(C_6H_5)_2TeF_2$. The Te—C distances are not significantly different in the two compounds; $(C_6F_5)_2TeF_2$, 2.064(16) to 2.157(19); $(C_6H_5)_2TeF_2$, 2.115(3) Å. The F—Te—F bond angles are more acute in the molecules of $(C_6F_5)_2TeF_2$, 164.0(5) and 161.5(5)°, than in $(C_6H_5)_2TeF_2$, 173.1(1)°, while the C—Te—C bond angles are more obtuse in $(C_6F_5)_2TeF_2$, 102.0(6)° and 104.1(6)°, as compared to 96.9(1)° for $(C_6H_5)_2TeF_2$. The average C—Te—F bond angle is 85.7° for $(C_6F_5)_2TeF_2$. All eight values which give rise to this average are smaller than the value for $(C_6H_5)_2TeF_2$, 87.6(1)°, seven of them significantly. The fact that the F—Te—F bond angle is smaller in $(C_6F_5)_2TeF_2$ than in $(C_6H_5)_2TeF_2$, together with the observation that the C—Te—C bond angle is larger, suggests that the non-bonding pair of electrons on tellurium has a larger stereochemical influence in $(C_6F_5)_2TeF_2$ than in $(C_6H_5)_2TeF_2$.

The above observations may be directly or indirectly attributable to the greater electron-withdrawing power of the C_6F_5 group compared to C_6H_5. The effect of crystal packing and secondary bonding forces and the interrelationship between these and the much stronger primary bonds in determining the net geometry about tellurium is, however, a moot point. In the structure of the title compound there are obvious correlations between secondary interactions and the primary bond lengths. In $(C_6F_5)_2TeF_2$ each tellurium atom has only one secondary contact to a fluorine on an adjacent molecule, whereas in $(C_6H_5)_2TeF_2$ each tellurium atom has two such interactions (symmetry equivalent). One feature of this is that in $(C_6H_5)_2TeF_2$ every fluorine atom is involved in a secondary interaction, though weak, 3.208(2) Å. In $(C_6F_5)_2TeF_2$, on the other hand, there are both Te—F···Te interactions as well as purely terminal Te—F bonds. The secondary Te···F interactions in $(C_6F_5)_2TeF_2$, 2.952(11) Å and 2.846(11) Å, are considerably shorter than that in $(C_6H_5)_2TeF_2$, although still quite weak (estimated bond valences 0.05 and 0.07).[3] This appears to be consistent with a possible correlation between secondary bond length and the number of such interactions to Te.

The primary Te—F bonds in $(C_6F_5)_2TeF_2$ range from 1.932(11) to 1.990(11) Å as compared to 2.006(2) Å in $(C_6H_5)_2TeF_2$. The variation in Te—F bonds, while crystallographically significant, does not appear to reflect chemical differences beyond the overall shortening on changing from C_6H_5 to C_6F_5 substituents.

The geometries and dimensions of the C_6F_5 groups are not significantly different from those previously reported (10).

[3]Bond valences calculated by the empirical method proposed by Brown and Altermatt (9). Using the same method a Te(IV)···F separation of 3.52 Å (the sum of the Van der Waals radii) corresponds to a bond valence of .011.

Can. J. Chem. Downloaded from www.nrcresearchpress.com by 213.222.148.141 on 09/07/12
For personal use only.

Can. J. Chem. Downloaded from www.nrcresearchpress.com by 213.222.148.141 on 09/07/12
For personal use only.

TABLE 2. Fractional atomic coordinates and B_{eq} (Å^2) for $(C_6F_5)_2TeF_2$ (esd's refer to the last digit printed)

Atom	x	y	z	B_{eq}[a]
Te(1)	1/2	0.38023(5)	1/2	3.11(5)
Te(2)	0.41197(12)	0.40957(6)	0.77478(11)	3.59(5)
F(1)	0.5818 (10)	0.3824 (5)	0.6584 (9)	4.4 (6)
F(2)	0.4516 (10)	0.3571 (6)	0.3500 (8)	5.0 (5)
F(3)	0.3231 (10)	0.3886 (5)	0.6249 (9)	4.2 (5)
F(4)	0.4627 (10)	0.4549 (6)	0.9165 (7)	5.3 (6)
F(12)	0.6520 (11)	0.2587 (5)	0.4227 (10)	5.3 (6)
F(13)	0.8890 (10)	0.2536 (6)	0.4134 (9)	6.0 (6)
F(14)	1.0538 (11)	0.3586 (10)	0.4875 (12)	7.8 (9)
F(15)	0.9732 (10)	0.4672 (6)	0.5691 (10)	6.3 (6)
F(16)	0.7335 (10)	0.4735 (5)	0.5752 (9)	5.0 (5)
F(22)	0.2445 (11)	0.3104 (8)	0.4057 (10)	6.6 (7)
F(23)	0.1568 (15)	0.1866 (9)	0.4190 (15)	10.5 (11)
F(24)	0.309 (3)	0.0974 (8)	0.5479 (24)	16.8 (23)
F(25)	0.5568 (22)	0.1262 (8)	0.6591 (17)	11.7 (14)
F(26)	0.6435 (13)	0.2485 (6)	0.6435 (10)	6.3 (6)
F(32)	0.2299 (9)	0.5201 (5)	0.6076 (8)	5.1 (5)
F(33)	0.2895 (14)	0.6366 (8)	0.5341 (11)	7.1 (7)
F(34)	0.5388 (15)	0.6778 (7)	0.6019 (12)	8.4 (9)
F(35)	0.7213 (12)	0.6047 (7)	0.7433 (11)	7.6 (7)
F(36)	0.6592 (9)	0.4900 (6)	0.8219 (8)	5.3 (6)
F(42)	0.1955 (11)	0.3057 (6)	0.7318 (11)	6.1 (6)
F(43)	−0.0374 (12)	0.3032 (7)	0.7544 (12)	8.1 (8)
F(44)	−0.1292 (13)	0.4151 (9)	0.8187 (14)	8.5 (10)
F(45)	0.0071 (13)	0.5284 (8)	0.8543 (12)	8.7 (8)
F(46)	0.2418 (12)	0.5317 (6)	0.8338 (9)	5.9 (6)
C(11)	0.6878 (16)	0.3674 (8)	0.5009 (13)	3.0 (3)
C(12)	0.7289 (19)	0.3123 (10)	0.4588 (17)	4.9 (4)
C(13)	0.8538 (18)	0.3078 (10)	0.4566 (15)	4.5 (4)
C(14)	0.9336 (19)	0.3618 (11)	0.4909 (15)	4.1 (4)
C(15)	0.8962 (18)	0.4183 (9)	0.5337 (15)	4.5 (4)
C(16)	0.7717 (16)	0.4189 (9)	0.5371 (14)	3.6 (3)
C(21)	0.4473 (16)	0.2837 (8)	0.5208 (13)	3.7 (3)
C(22)	0.3196 (20)	0.2675 (11)	0.4625 (16)	5.3 (4)
C(23)	0.2738 (24)	0.2015 (13)	0.4776 (20)	7.0 (5)
C(24)	0.3475 (24)	0.1570 (13)	0.5363 (20)	7.0 (6)
C(25)	0.4758 (24)	0.1772 (14)	0.6011 (20)	7.1 (6)
C(26)	0.5245 (19)	0.2344 (10)	0.5879 (16)	4.7 (4)
C(31)	0.4409 (14)	0.5022 (8)	0.7162 (12)	3.0 (3)
C(32)	0.3519 (17)	0.5404 (9)	0.6440 (14)	4.0 (3)
C(33)	0.3784 (20)	0.5986 (10)	0.6053 (17)	4.6 (4)
C(34)	0.5056 (21)	0.6189 (11)	0.6410 (18)	5.5 (4)
C(35)	0.5991 (21)	0.5839 (11)	0.7089 (17)	4.7 (4)
C(36)	0.5694 (16)	0.5264 (9)	0.7500 (14)	3.8 (3)
C(41)	0.2236 (19)	0.4166 (9)	0.7882 (15)	4.2 (4)
C(42)	0.1520 (18)	0.3602 (10)	0.7624 (15)	4.4 (4)
C(43)	0.0287 (20)	0.3604 (11)	0.7739 (16)	5.3 (4)
C(44)	−0.0095 (19)	0.4186 (10)	0.8105 (17)	4.6 (4)
C(45)	0.0533 (20)	0.4723 (11)	0.8290 (17)	5.6 (4)
C(46)	0.1756 (18)	0.4768 (10)	0.8159 (14)	4.5 (4)

[a] B_{eq} is the arithmetic mean of the principal axes of the thermal ellipsoid.

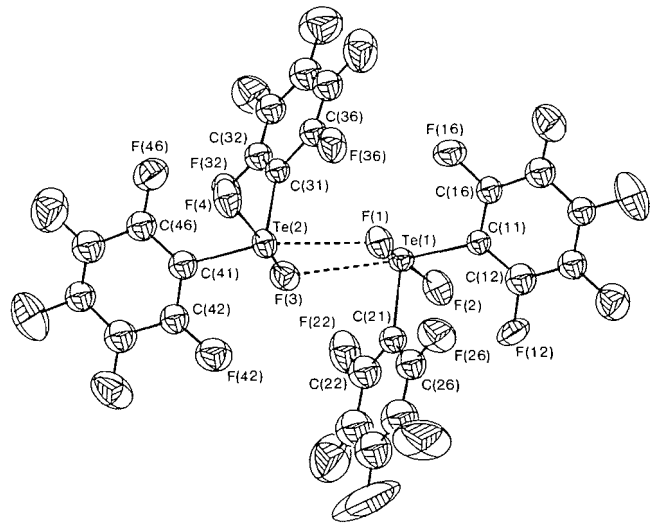

FIG. 1. Molecular structure of $(C_6F_5)_2TeF_2$.

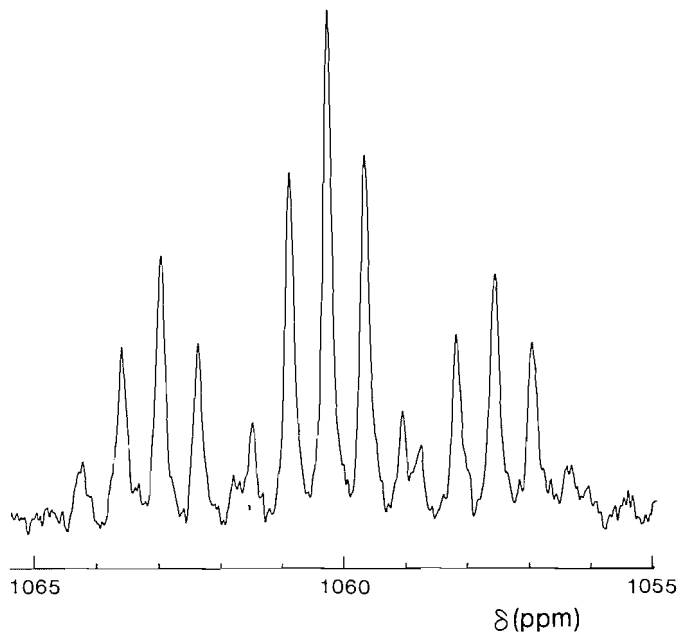

FIG. 2. ^{125}Te nmr spectrum of $(C_6F_5)_2TeF_2$ measured in $CDCl_3$ solution at ambient temperature.

Mössbauer data

With regard to the Mössbauer data, the ^{125}Te Mössbauer quadrupole splitting is smaller in $(C_6F_5)_2TeF_2$ (8.78(8) mm s^{-1}) than in $(C_6H_5)_2TeF_2$ (10.4(1) mm s^{-1}). If the non-bonding electrons were dominant in determining the magnitude of the quadrupole splitting in these compounds, i.e., if the principal component of the electric field gradient tensor was in the direction of the non-bonding pair, then we would have anticipated that the quadrupole coupling in $(C_6F_5)_2TeF_2$ would be larger than that in $(C_6H_5)_2TeF_2$, the non-bonding pair being more stereochemically active in the former than the latter. It appears then that the electric field gradient is not determined by the stereochemically active lone pair or the small changes in coordination about the tellurium but is in fact dominated by the difference in tellurium *p*-orbital populations between the axial Te—F bonds and the equatorial Te—C bonds. This difference must then be smaller in $(C_6F_5)_2TeF_2$ than in the diphenyl compound, presumably as a result of the difference in electronegativity of the C_6H_5- and C_6F_5-ligands, i.e., the more electronegative C_6F_5-ligand withdraws more electron density from tellurium in the equatorial plane than does C_6H_5- and $(C_6F_5)_2TeF_2$ yields a smaller Δ value.

The question as to the role that the tellurium non-bonding pair may play in determining the quadrupole couplings in Te(IV) compounds of the type R_2TeX_2 is one which has been difficult to answer. Because of the broad natural linewidth of the ^{125}Te Mössbauer transition and the small magnetic moments of the

Can. J. Chem. Downloaded from www.nrcresearchpress.com by 213.222.148.141 on 09/07/12
For personal use only.

TABLE 3. Interatomic distances and bond angles for $(C_6F_5)_2TeF_2$

(*i*) Tellurium coordination sphere

(*a*) Bond lengths and bond angles

Bond	Length	Bond	Angle (°)
	Molecule 1		
Te(1)—F(1)	1.990(11)	F(1)—Te(1)—F(2)	164.0(5)
Te(1)—F(2)	1.932(11)	F(1)—Te(1)—C(11)	83.5(5)
Te(1)—C(11)	2.094(17)	F(1)—Te(1)—C(21)	86.1(6)
Te(1)—C(21)	2.064(16)	F(2)—Te(1)—C(11)	85.3(5)
		F(2)—Te(1)—C(21)	85.2(6)
		C(11)—Te(1)—C(21)	102.0(6)
	Molecule 2		
Te(2)—F(3)	1.947(11)	F(3)—Te(2)—F(4)	161.5(5)
Te(2)—F(4)	1.989(10)	F(3)—Te(2)—C(31)	84.4(5)
Te(2)—C(31)	2.077(16)	F(3)—Te(2)—C(41)	85.1(6)
Te(2)—C(41)	2.157(19)	F(4)—Te(2)—C(31)	84.9(6)
		F(4)—Te(2)—C(41)	82.9(6)
		C(31)—Te(2)—C(41)	104.1(6)

(*b*) Secondary contacts

Contact	Length (Å)	Contact	Length (Å)
Te(1)···F(3)	2.952(1)	Te(2)···F(1)	2.846(11)

Contact	Angle (deg)	Contact	Angle (deg)
F(1)—Te(1)···F(3)	64.5(4)	F(1)···Te(2)—F(3)	67.3(4)
F(2)—Te(1)···F(3)	125.1(4)	F(1)···Te(2)—F(4)	124.2(4)
F(3)—Te(1)—C(11)	147.7(5)	F(1)···Te(2)—C(31)	152.4(6)
F(3)···Te(1)—C(21)	73.2(5)	F(1)···Te(2)—C(41)	161.5(5)

(*ii*) Perfluorinated phenyl rings

Bond	Length (Å)	Bonds	Angle (deg)
	Molecule 1: ring 1		
C(11)—C(12)	1.38(3)	Te(1)—C(11)—C(12)	123.8(13)
C(12)—C(13)	1.40(3)	Te(1)—C(11)—C(16)	118.1(12)
C(13)—C(14)	1.38(3)	C(12)—C(11)—C(16)	117.9(16)
C(14)—C(15)	1.39(3)	F(12)—C(12)—C(11)	121.5(17)
C(15)—C(16)	1.40(3)	F(12)—C(12)—C(13)	117.0(17)
C(16)—C(11)	1.37(2)	C(11)—C(12)—C(13)	121.4(18)
C(12)—F(12)	1.36(2)	F(13)—C(13)—C(12)	119.3(17)
C(13)—F(13)	1.34(2)	F(13)—C(13)—C(14)	122.1(17)
C(14)—F(14)	1.35(2)	C(12)—C(13)—C(14)	118.5(18)
C(15)—F(15)	1.28(2)	F(14)—C(14)—C(13)	119.1(19)
C(16)—F(16)	1.33(2)	F(14)—C(14)—C(15)	118.9(19)
		C(13)—C(14)—C(15)	122.0(18)
		F(15)—C(15)—C(14)	121.2(17)
		F(15)—C(15)—C(16)	122.0(17)
		C(14)—C(15)—C(16)	116.7(17)
		F(16)—C(16)—C(11)	119.3(15)
		F(16)—C(16)—C(15)	117.3(15)
		C(11)—C(16)—C(15)	123.4(16)
	Molecule 2: ring 2		
C(41)—C(42)	1.36(3)	Te(2)—C(41)—C(42)	115.3(14)
C(42)—C(43)	1.42(3)	Te(2)—C(41)—C(46)	122.2(14)
C(43)—C(44)	1.38(3)	C(42)—C(41)—C(46)	122.4(18)
C(44)—C(45)	1.26(3)	F(42)—C(42)—C(41)	121.8(17)
C(45)—C(46)	1.42(3)	F(42)—C(42)—C(43)	119.9(18)
C(46)—C(41)	1.41(3)	C(41)—C(42)—C(43)	118.2(18)
C(42)—F(42)	1.31(2)	F(43)—C(43)—C(42)	117.4(18)
C(43)—F(43)	1.34(3)	F(43)—C(43)—C(44)	125.4(19)

TABLE 3 (*concluded*)

Bond	Length (Å)	Bonds	Angle (deg)
C(44)—F(44)	1.37(2)	C(42)—C(43)—C(44)	117.1(19)
C(45)—F(45)	1.32(3)	F(44)—C(44)—C(43)	113.7(18)
C(46)—F(45)	1.30(2)	F(44)—C(44)—C(45)	121.0(20)
		C(43)—C(44)—C(45)	125.1(21)
		F(45)—C(45)—C(44)	122.7(20)
		F(45)—C(45)—C(46)	116.1(19)
		C(44)—C(45)—C(46)	121.1(21)
		F(46)—C(46)—C(41)	122.1(17)
		F(46)—C(46)—C(45)	122.3(17)
		C(41)—C(46)—C(45)	115.6(18)
	Molecule (1): ring 2		
C(21)—C(22)	1.41(3)	Te(1)—C(21)—C(22)	114.9(13)
C(22)—C(23)	1.45(3)	Te(1)—C(21)—C(26)	126.8(13)
C(23)—C(24)	1.29(4)	C(22)—C(21)—C(26)	118.3(17)
C(24)—C(25)	1.43(4)	F(22)—C(22)—C(21)	121.1(18)
C(25)—C(26)	1.39(3)	F(22)—C(22)—C(23)	120.7(19)
C(26)—C(21)	1.42(3)	C(21)—C(22)—C(23)	117.9(19)
C(22)—F(22)	1.26(3)	F(23)—C(23)—C(22)	116.7(22)
C(23)—F(23)	1.31(3)	F(23)—C(23)—C(24)	120.7(25)
C(24)—F(24)	1.29(3)	C(22)—C(23)—C(24)	122.2(23)
C(25)—F(25)	1.34(3)	F(24)—C(24)—C(23)	122.8(28)
C(26)—F(26)	1.31(2)	F(24)—C(24)—C(25)	115.4(27)
		C(23)—C(24)—C(25)	121.6(25)
		F(25)—C(25)—C(24)	123.0(24)
		F(25)—C(25)—C(26)	118.1(22)
		C(24)—C(25)—C(26)	117.8(23)
		F(26)—C(26)—C(21)	119.4(16)
		F(26)—C(26)—C(25)	118.9(19)
		C(21)—C(26)—C(25)	121.6(19)
	Molecule (2): ring 3		
C(31)—C(32)	1.36(2)	Te(2)—C(31)—C(32)	126.8(12)
C(32)—C(33)	1.34(3)	Te(2)—C(31)—C(36)	116.5(11)
C(33)—C(34)	1.39(3)	C(32)—C(31)—C(36)	116.7(15)
C(34)—C(35)	1.33(3)	F(32)—C(32)—C(31)	119.7(16)
C(35)—C(36)	1.36(3)	F(32)—C(32)—C(33)	116.6(16)
C(36)—C(31)	1.43(2)	C(31)—C(32)—C(33)	123.7(17)
C(32)—F(32)	1.34(2)	F(33)—C(33)—C(32)	123.6(18)
C(33)—F(22)	1.35(2)	F(33)—C(33)—C(34)	119.8(18)
C(34)—F(34)	1.38(3)	C(32)—C(33)—C(34)	116.6(19)
C(35)—F(35)	1.35(2)	F(34)—C(34)—C(33)	119.1(19)
C(36)—F(36)	1.34(2)	F(34)—C(34)—C(35)	117.2(20)
		C(33)—C(34)—C(35)	123.7(20)
		F(35)—C(35)—C(34)	122.8(20)
		F(35)—C(35)—C(36)	118.4(18)
		C(34)—C(35)—C(36)	118.7(20)
		F(36)—C(36)—C(31)	118.0(14)
		F(36)—C(36)—C(35)	121.4(16)
		C(31)—C(36)—C(35)	120.6(16)

Can. J. Chem. Downloaded from www.nrcresearchpress.com by 213.222.148.141 on 09/07/12
For personal use only.

nuclear states involved, it is not possible to determine the signs of the quadrupole coupling constants for ^{125}Te, a measurement which would clarify, for example, whether or not the principal component of the electric field gradient lies in the direction of the non-bonding pair. The X-ray structural data, together with the relative magnitudes of the quadrupole splittings, has answered this question for $(C_6H_5)_2TeF_2$ and $(C_6F_5)_2TeF_2$, following the arguments outlined above.

Nuclear magnetic resonance data

The ^{125}Te nmr chemical shifts for $(C_6F_5)_2TeF_2$ (1060 ppm) and $(C_6H_5)_2TeF_2$ (1125 ppm) are very similar. There are no alkyl- or aryltellurium(IV) fluorides with which to compare these shifts but they are similar to those of TeF_4 (1316 ppm) and TeF_3^+ (1381 ppm) (11) where the shifts are relative to neat Me_2Te. The Te(VI) phenyltellurium fluorides have shifts ranging from 659 ppm for $(C_6H_5)_2TeF_2$ to 805 ppm for $(C_6H_5)_2TeF_4$ (12), while in $Te(OTeF_5)_4$ the central Te(IV) has a shift of 1104 ppm and the ligand Te′(VI) a shift of 868 ppm (11) at 297 K. Assuming that that ^{125}Te nmr chemical shifts are dominated by the Ramsey paramagnetic shielding term, these trends correspond to less shielding at Te(IV) than at Te(VI).

The shifts for $(C_6F_5)_2TeX_2$ (X = F, Cl, Br) have been compared with those of $(C_6H_5)_2TeX_2$ in ref. 5, as have those of $(C_6F_5)_2Te$ and $(C_6H_5)_2Te$.

The $^1J_{^{125}Te—^{19}F}$ coupling constants observed for $(C_6F_5)_2TeF_2$

TABLE 4. ^{125}Te nmr data for $(C_6F_5)_2TeF_2$, $(C_6H_5)_2TeF_2$, and $(C_6F_5)_2Te$

Compound	δ^a (ppm)	$^1J_{^{125}Te-^{19}F}$ (Hz)	$^3J_{^{125}Te-^{19}F}$ (Hz)
$(C_6F_5)_2TeF_2$	1060.3	342	77
$(C_6H_5)_2TeF_2$	1125.1	548	
$(C_6F_5)_2Te$	298.0		50

[a] δ, measured in $CDCl_3$ solution with respect to neat Me_2Te at ambient temperature.

(342 Hz) and $(C_6H_5)_2TeF_2$ (548 Hz) are significantly smaller than those for TeF_3^+ (2905 Hz) or for $TeF_2(OTeF_5)_2$, where $^1J_{^{125}Te-^{19}F}$ = 2736 Hz and $^1J_{^{125}Te'-^{19}F}$ = 3724 (equatorial) or 3656 (axial) (11). In $(C_6H_5)_2TeF_4$ the corresponding coupling constant was 3000 Hz (12). These data can be understood assuming that the coupling constants are dominated by the Fermi contact term and hence the *s*-character in the Te—F bond. In $(C_6H_5)_2TeF_2$ and $(C_6F_5)_2TeF_2$ the axial F—Te—F linkage may be viewed as a $3c$—$2e$ bond in which a tellurium $5p$ orbital is dominant. This would be consistent with the relatively large Te—F bond length. The small $^1J_{^{125}Te-^{19}F}$ values would result from the small amount of *s*-character in the Te—F bonds. In comparison, for the other cases noted above a considerable amount of *s*-character would be anticipated in the Te—F bonds resulting in the much larger coupling constants.

However, the fact that $(C_6F_5)_2TeF_2$ has a smaller $^1J_{^{125}Te-^{19}F}$ coupling constant than $(C_6H_5)_2TeF_2$ is less readily rationalised. The F—Te—F bond angle is more acute in the former than the latter and the Te—F bond length is marginally smaller, suggesting a greater *s*-character in the Te—F bond.

The $^3J_{^{125}Te-^{19}F}$ coupling constants in $(C_6F_5)_2TeF_2$ (77 Hz) and $(C_6F_5)_2Te$ (50 Hz) are somewhat larger than those observed in $Te(OTeF_5)_4$ ($^3J_{^{125}Te-^{19}F}$ = 31.8 Hz) (11), reflecting a greater covalency and a greater *s*-character in the F—C—C—Te linkage. The Te—F coupling pattern observed in Fig. 2 reflects a 1:2:1 triplet, from the directly coupled axial fluorines, of 1:4:6:4:1 quintets arising from the three-bond coupling to the four equivalent fluorines of the pentafluorophenyl rings.

Acknowledgements

C. H. W. Jones and F. W. B. Einstein wish to acknowledge a grant in support of this research from the Natural Sciences and Engineering Research Council of Canada, and J. Aramini acknowledges support through a NSERC Undergraduate Research Award.

1. N. W. ALCOCK. Adv. Inorg. Chem. Radiochem. **15**, 1 (1972).
2. F. S. BERRY and A. J. EDWARDS. J. Chem. Soc. Dalton Trans. 2306 (1980).
3. A. J. EDWARDS and F. I. HEWAIDY. J. Chem. Soc. Sect. A, 2977 (1968).
4. C. LAU, J. PASSMORE, E. K. RICHARDSON, T. K. WHIDDEN, and P. S. WHITE. Can. J. Chem. **63**, 2273 (1985).
5. C. H. W. JONES and R. D. SHARMA. Can. J. Chem. **64**, 980 (1986).
6. E. J. GABE, A. C. LARSON, F. L. LEE, and Y. LEPAGE. NRC VAX Crystal Structure System. Ottawa, National Research Council. 1984.
7. International tables for X-ray crystallography. Vol. 4. Birmingham, Kynoch Press (1974).
8. E. K. DAVIS. SNOOPI Plot Program. Chemical Crystallography Laboratory, University of Oxford. 1984.
9. I. D. BROWN and D. ALTERMATT. Acta Crystallogr. Sect. B, B**41**, 244 (1985).
10. C. M. WOODWARD, D. S. BROWN, J. D. LEE, and A. G. MASSEY. J. Organomet. Chem. **121**, 333 (1976).
11. M. J. COLLINS and G. J. SCHROBILGEN. Inorg. Chem. **24**, 2608 (1985).
12. K. ALAN and A. F. JANZEN. J. Fluorine Chem. **27**, 467 (1985).

Can. J. Chem. Downloaded from www.nrcresearchpress.com by 213.222.148.141 on 09/07/12
For personal use only.

The synthesis and characterisation of hetero-bimetallic sulfonate bridged coordination polymers of the type $M^{II}Sn^{IV}(SO_3X)_6$ with X = F or CF_3

S. P. MALLELA, K. LEE, P. F. GEHRS, J. I. CHRISTENSEN, J. R. SAMS, AND F. AUBKE[1]

Department of Chemistry, The University of British Columbia, Vancouver, B.C., Canada V6T 1Y6

Received February 7, 1986[2]

S. P. MALLELA, K. LEE, P. F. GEHRS, J. I. CHRISTENSEN, J. R. SAMS, and F. AUBKE. Can. J. Chem. **65**, 2649 (1987).

The synthesis of a series of hetero-bimetallic fluorosulfate bridged coordination polymers of the type $M(II)Sn(SO_3F)_6$, with M(II) = Mn, Fe, Co, Ni, or Cu, by interaction of the metal bisfluorosulfate with the strong fluorosulfate acceptor $Sn(SO_3F)_4$ in fluorosulfuric acid is described. Subsequent solvolysis of either stoichiometric 1:1 mixtures of $M(SO_3F)_2$ and $Sn(SO_3F)_4$ or the bimetallic polymer $M(II)Sn(IV)(SO_3F)_6$ in an excess of trifluoromethyl sulfuric acid affords the corresponding SO_3CF_3-bridged polymers of the composition $M(II)Sn(SO_3CF_3)_6$ with M(II) = Mn, Fe, Co, Ni, or Cu. The new compounds are characterized by infrared and ^{119}Sn Mössbauer spectroscopy.

S. P. MALLELA, K. LEE, P. F. GEHRS, J. I. CHRISTENSEN, J. R. SAMS et F. AUBKE. Can. J. Chem. **65**, 2649 (1987).

On décrit la synthèse d'une série de polymères de coordination pontés de fluorosulfates hétérobimétalliques du type $M(II)Sn(SO_3F)_6$, dans lesquels M(II) = Mn, Fe, Co, Ni ou Cu et qui sont produits par une interaction entre le bisfluorosulfate métallique et l'accepteur fluorosulfate puissant $Sn(SO_3F)_4$, dans l'acide fluorosulfurique. La solvolyse subséquente, soit des mélanges stoechiométriques 1:1 de $M(SO_3F)_2$ et $Sn(SO_3F)_4$ ou du polymère bimétallique $M(II)Sn(IV)(SO_3F)_6$, dans un excès d'acide trifluorométhylsulfurique conduit aux polymères pontés SO_3CF_3 correspondants, de composition $M(II)Sn(SO_3CF_3)_6$, dans lesquels M(II) = Mn, Fe, Co, Ni ou Cu. On a caractérisé les nouveaux produits par spectroscopies infrarouge et de Mössbauer du ^{119}Sn.

[Traduit par la revue]

Introduction

The first two examples of sulfonate bridged polymers of the type $M^{II}M^{IV}(SO_3X)_6$ with X = F or CF_3 were discovered and identified by us some time ago, $Sn(SO_3CF_3)_3$, where ^{119}Sn Mössbauer spectra suggested formulation as a mixed valency compound $Sn^{II}Sn^{IV}(SO_3CF_3)_6$ (2), and $Pd(SO_3F)_3$, with formulation as $Pd^{II}Pt^{IV}(SO_3F)_6$ based on magnetic susceptibility measurements (3).

Both compounds may be viewed as homo-bimetallic sulfonates with the metal in the 2+ and 4+ oxidation states. Subsequently the first hetero-bimetallic fluorosulfates, $Pd^{II}Pd^{IV}(SO_3F)_6$ and $Pd^{II}Sn^{IV}(SO_3F)_6$ (4), were obtained with identification relying again on magnetic susceptibility studies, ligand field and vibrational spectra. The ir spectra for the Pd(II)–Sn(IV) complex were distinctly different from those previously reported for salts of the type $M'_2[Sn(SO_3F)_6]$, with M' = K, Cs, NO, and ClO_2 (5), and an "aniso bidentate" bridging function of the fluorosulfate group, with strong bonding to Sn(IV) and weak coordination to Pd(II), producing an octahedral environment for both metallic centers was suggested (4). The polymeric nature was deduced from the lack of solubility in strongly ionizing HSO_3F, which is in contrast to high solubility and weakly basic behavior found for the $M'_2[Sn(SO_3F)_6]$ salts (5) as well as for $Ba[Pt(SO_3F)_6]$ (6).

The magnetic and spectroscopic study on the Pd^{II}—M^{IV} fluorosulfates and a parallel investigation of the corresponding silver(II) salts, $Ag^{II}Sn(SO_3F)_6$ and $Ag^{II}Pt(SO_3F)_6$ (6), suggested a magnetically dilute environment for the paramagnetic ions Ag^{2+} and more surprisingly Pd^{2+}, where an $^3A_{2g}$ ground state is rather uncommon and only encountered in PdF_3 (7–9) or related fluoro complexes. The study of Pd(II) fluorosulfate complexes suggested a closer approach to a bare Pd^{2+} ion for M^{IV} being Sn rather than Pt or Pd (4).

The objective then became to study a wider range of divalent metal ions in such a magnetically dilute environment produced by weakly coordinated fluorosulfate and trifluoromethyl sulfates. Metal ions from the 3*d* series became interesting because a number of detailed magnetic susceptibility studies on some of the divalent metal sulfonates such as $Co(SO_3F)_2$ (10), $Co(SO_3CF_3)_2$, $Cu(SO_3F)_2$ (11*a*), $Fe(SO_3F)_2$ (11*b*), and $Fe(SO_3CF_3)_2$ (11*c*) had been reported. An infrared study on a wide range of metal bisfluorosulfates (12) and a general synthetic route to such metal fluorosulfates via the solvolysis of the corresponding benzoates in HSO_3F (12) provided a good basis as well.

More recent work from our laboratory provided additional encouragement: metal oxidation by $S_2O_6F_2$ in HSO_3F as solvent represented a simple and facile general route to both $Sn(SO_3F)_4$ (13) and $Pt(SO_3F)_4$ (14), and the conversion of the more readily accessible fluorosulfates into the corresponding trifluoromethyl sulfates by solvolysis in excess HSO_3CF_3 was systematically explored (15). The preparation of one of the desired bimetallic polymers, $Mn^{II}Sn(SO_3CF_3)_6$, was quoted as an example (15). The general preparative route, SO_3X-abstraction (X = F or CF_3) by strong acceptors according to:

$$[1]\quad M^{II}(SO_3X)_2 + M^{IV}(SO_3X)_4 \xrightarrow{HSO_3X} M^{II}M^{IV}(SO_3X)_6$$

with M^{IV} = Sn or Pt and X = F or CF_3 had been explored most recently in attempts to stabilize the divalent cations Sn^{2+} and $(CH_3)_2Sn^{2+}$ in this manner (16). The potential of this general route had been demonstrated by the successful isolation of $HgSn(SO_3F)_6$, obtained from $Hg(SO_3F)_2$ (12, 17) and $Sn(SO_3F)_4$ (13, 18).

It was decided to use only $Sn(SO_3F)_4$ and $Sn(SO_3CF_3)_4$ as acceptors for the following reasons: (*i*) previous work discussed above (4, 6) had established $Sn(SO_3F)_4$ as a stronger acceptor than $Pt(SO_3F)_4$. (*ii*) ^{119}Sn Mössbauer spectra would allow us to monitor the abstraction reaction. (*iii*) The $Sn(SO_3X)_6$ moiety, X = F or CF_3, transparent in the visible – near ir region, would permit observation of ligand field bands in this region, while ligand-to-metal charge transfer bands are observed for platinum(IV) fluorosulfate complexes (14). (*iv*) The small but

[1]To whom all correspondence should be addressed.

[2]Revision received July 8, 1987.

Can. J. Chem. Downloaded from www.nrcresearchpress.com by 213.222.148.141 on 09/07/12
For personal use only.

Can. J. Chem. Downloaded from www.nrcresearchpress.com by 213.222.148.141 on 09/07/12
For personal use only.

measurable TIP (temperature independent paramagnetism) contributions found in otherwise diamagnetic Pt(IV) compounds (14) would require correction in a magnetic study. (*v*) Finally, only $Pt(SO_3F)_4$ appears to have been reported so far, but not $Pt(SO_3CF_3)_4$.

The present study reports the synthesis, analysis, ^{119}Sn Mössbauer spectra and infrared spectra for the complete series $M^{II}Sn^{IV}(SO_3X)_6$ where M^{II} = Mn, Fe, Co, Ni, and Cu, and X = F or CF_3. Extension to the corresponding Cr^{II} compounds is explored and additional synthetic routes are discussed.

Experimental

Metalfluorosulfates $M^{II}(SO_3F)_2$ (M = Mn, Fe, Co, Ni, and Cu) were prepared by solvolysis of the corresponding benzoates in HSO_3F and identified by their infrared spectra (12). The benzoates were obtained from Dr. R. C. Thompson of this Department, whose help is gratefully acknowledged. $Sn(SO_3F)_4$ was prepared as described earlier (13). Technical grade fluorosulfuric acid was doubly distilled at atmospheric pressure in a counter stream of dry nitrogen. Trifluoromethyl sulfuric acid (3M Co.) was freshly distilled from concentrated H_2SO_4 in a stream of dry nitrogen before each reaction.

A Perkin Elmer 598 grating infrared spectrophotometer was used with samples pressed between AgCl or AgBr windows (Harshaw Chemicals).

The ^{119}Sn Mössbauer spectra were recorded in transmission mode with a constant acceleration spectrometer of conventional design. Pulses were accumulated in a Tracor-Northern TN-1706 multichannel analyser, whence the data were transmitted via an IBM PC to the mainframe computer for curve fitting. The latter was accomplished using a standard non-linear regression programme with no constraints imposed on the fitting parameters (19). In every case, the spectra were satisfactorily fitted to a single Lorentzian line whose full width at half maximum did not exceed 1.34 mm s^{-1}. The Doppler velocity scale was calibrated using an iron foil absorber and ^{57}Co source. Isomer shifts are reported relative to $BaSnO_3$ at 77 K.

All reactions were performed in Pyrex reaction vials of about 40 mL capacity, fitted with Kontes Teflon stem valves and equipped with Teflon coated spin bars. Volatile materials were handled by using vacuum-line techniques. Solids were handled in a Vacuum Atmospheres Corp. Dri Lab, Model No. HE-43-2, filled with purified dry nitrogen and equipped with a Dri-Train Circulating unit, Model No. HE-92-B.

All reactions were followed by weight. Vacuum filtration of moisture-sensitive material was performed in an apparatus described by Shriver (20). Chemical analysis was carried out by Analytische Laboratorium, Gummersbach, West Germany. The carbon content was determined by Mr. P. Borda of this Department.

General procedure for the synthesis of M(II)[Sn(SO$_3$F)$_6$]

To an equimolar mixture of $M(II)(SO_3F)_2$ and $Sn(SO_3F)_4$ approximately 10 mL HSO_3F were distilled *in vacuo*. In no instance was complete dissolution of the fluorosulfates noted during reaction. The product isolation was accomplished by vacuum filtration and subsequent repeated washing with doubly distilled HSO_3F. The product was dried *in vacuo*, usually at ~40°C, and manipulated inside the dry box.

For the syntheses of compounds of the type $M(II)[Sn(SO_3CF_3)_6]$ two alternative approaches were used: The solvolysis of $M(II)[Sn(SO_3F)_6]$ in HSO_3CF_3 and the co-solvolysis of $M(II)(SO_3F)_2$ and $Sn(SO_3F)_4$ in HSO_3CF_3.

Details of this general reaction type have been reported earlier (15).

Individual preparations, specific details

(i) MnSn(SO$_3$F)$_6$: To $Mn(SO_3F)_2$ (336 mg, 1.33 mmol) and $Sn(SO_3F)_4$ (691 mg, 1.34 mmol) ~10 mL of HSO_3F were distilled. The reaction mixture was heated at 60°C for 5 days. The white hygroscopic product did not decompose or melt below 310°C.

(ii) CuSn(SO$_3$F)$_6$: To $Cu(SO_3F)_2$ (593 mg, 2.27 mmol) and (1167 mg, 2.27 mmol) $Sn(SO_3F)_4$ ~15 mL HSO_3F were distilled. The reaction mixture was heated to ~70°C for 6 days. The product was dried *in vacuo* at ~40°C for 2 days. The white hygroscopic product did not decompose or melt below 300°C.

(iii) NiSn(SO$_3$F)$_6$: $Ni(SO_3F)_2$ (333 mg, 1.296 mmol) were mixed with (668 mg, 1.297 mmol) $Sn(SO_3F)_4$ and ~15 mL HSO_3F were added. The reaction mixture was subsequently heated to ~60°C for 4 days. The yellow color of $Ni(SO_3F)_2$ changed to light yellow during the reaction. The product was dried *in vacuo* at 40°C for 2 days. The light yellow hygroscopic solid did not decompose or melt below 310°C.

(iv) CoSn(SO$_3$F)$_6$: To $Co(SO_3F)_2$ (375 mg, 1.46 mmol) and $Sn(SO_3F)_4$ (751 mg, 1.46 mmol) ~15 mL HSO_3F were distilled and the mixture kept for 2 days at room temperature. The purple color of $Co(SO_3F)_2$ gradually turned to light purple as the reaction proceeded. The light purple hygroscopic solid did not decompose or melt below 300°C.

(v) FeSn(SO$_3$F)$_6$: $Fe(SO_3F)_2$ (194 mg, 0.76 mmol) and $Sn(SO_3F)_4$ (393 mg, 0.76 mmol) were stirred in ~5 mL HSO_3F at 60°C for 7 days. The resulting white hygroscopic product turned to very light green at 265°C on heating.

(vi) FeSn(SO$_3$CF$_3$)$_6$: To $Fe(SO_3F)_2$ (641 mg, 2.52 mmol) and $Sn(SO_3F)_4$ (1229 mg, 2.52 mmol) ~15 mL of HSO_3CF_3 were distilled. The reaction mixture was then gradually heated to 70°C for 12 days. The hygroscopic solid did not decompose or melt below 330°C.

(vii) CoSn(SO$_3$CF$_3$)$_6$: $Co(SO_3F)_2$ (360 mg, 1.40 mmol) and $Sn(SO_3F)_4$ (721 mg, 1.40 mmol) plus 10 mL HSO_3CF_3 were gradually heated to 70°C for 11 days; the pink color of $Co(SO_3F)_2$ gradually turned to light pink during the reaction. The light pink product did not decompose or melt below 300°C.

(viii) NiSn(SO$_3$CF$_3$)$_6$: $Ni(SO_3F)_2$ 360 mg, (1.40 mmol) and 721 mg (1.40 mmol) of $Sn(SO_3F)_4$ were transferred into a reaction vial in the drybox. Excess (~10 mL) HSO_3CF_3 were distilled onto it and the resultant mixture was heated at 70°C for 10 days. The yellow color of $Ni(SO_3F)_2$ gradually turned to light yellow. The product was finally dried *in vacuo* at ~40° for 2 days. The light yellow, hygroscopic solid did not melt or decompose below 300°C.

(ix) CuSn(SO$_3$CF$_3$)$_6$: For method (*a*) 944.6 mg of $CuSn(SO_3F)_6$ were solvolysed in excess (10 mL) HSO_3CF_3 at 60°C for 8 days. The synthesis of $MnSn(SO_3CF_3)_6$ in a similar manner was reported previously (15) by this method. (*b*) To an equimolar mixture of $Cu(SO_3F)_2$ (395 mg, 1.51 mmol) and $Sn(SO_3F)_4$ (778 mg, 1.51 mmol) about 10 mL HSO_3CF_3 were distilled. Stirring was continued at ~60°C for 11 days. The white hygroscopic solid (1625 mg, 1.5 mmol) did not decompose or melt below 300°C.

Results and discussion

(a) Synthesis

The general synthetic route to the bimetallic fluorosulfates is in principle adopted from the reported preparations of $AgPt(SO_3F)_6$ (6), $PdPt(SO_3F)_6$ (4), and $PdSn(SO_3F)_6$ (4). There are important differences: $Pt(SO_3F)_4$ is sufficiently soluble to allow its dissolution in HSO_3F prior to reaction and there are distinct color changes, and precipitation, during the reaction which make it rather easy to judge its completion.

This is somewhat more difficult with $Sn(SO_3F)_4$. The bulk of the materials remain solid throughout and color changes as observed e.g., for the reaction of cobalt and nickel fluorosulfate are very subtle. These color changes are sufficient to reduce the reaction times for the preparations of $NiSn(SO_3F)_6$ and $CoSn(SO_3F)_6$ to 4 and 2 days, respectively. Heating to ~60–70°C is found to be advantageous.

Reaction times and conditions chosen for the remaining three preparations in the absence of any noticeable changes during the reactions are intended to allow completion of the abstraction reaction within a sufficiently large time limit.

The abstraction reaction with $Sn(SO_3F)_4$ as acceptor and $M(SO_3F)_2$ as donor may be viewed as an acid–base reaction in HSO_3F, in spite of the apparent lack of solubility of both reactants. However, for the reaction to occur at all, some limited

TABLE 1. Analytical data for M(II)[$Sn(SO_3X)_6$] with X = F or CF_3

Compound	Metal %		Sn %		F %		C %	
	Calcd.	Found	Calcd.	Found	Calcd.	Found	Calcd.	Found
$FeSn(SO_3F)_6$	7.26	7.49	15.44	15.70	14.82	14.52		
$MnSn(SO_3F)_6$	7.15	7.28	15.45	15.35	14.84	14.71		
$CoSn(SO_3F)_6$	7.63	7.79	15.37	15.32	14.77	14.88		
$NiSn(SO_3F)_6$	7.61	7.78			14.77	14.67		
$CuSn(SO_3F)_6$	8.18	8.30	15.28	15.30	14.68	14.62		
$FeSn(SO_3CF_3)_6$	5.22	5.42	11.10	11.15	31.99	31.75	6.74	6.62
$CoSn(SO_3CF_3)_6$	5.49	5.63	11.07	11.00	31.90	31.65	6.72	6.62
$NiSn(SO_3CF_3)_6$	5.47	5.85	11.08	11.70	31.90	28.53	6.72	6.47
$CuSn(SO_3CF_3)_6$	5.90	6.05	11.02	11.20	31.76	31.53	6.69	6.29

solubility of the two reactants at the reaction temperature is required.

An alternate, more convenient and direct route to bimetallic fluorosulfates, the simultaneous or successive oxidation of both metals by $S_2O_6F_2$, exemplified by the preparation of $AgSn(SO_3F)_6$ (6):

$$[2]\quad Ag + Sn + 3S_2O_6F_2 \xrightarrow{HSO_3F} AgSn(SO_3F)_6$$

is not feasible on two accounts: (*i*) tin is oxidized within 12 h at room temperature (13), however, the transition metals are found to react either not at all or extremely slowly and often only incompletely, even at elevated temperatures, and (*ii*) some of all five *d*-block metals may possibly be partly oxidized beyond the 2+ oxidation state. Recently the synthesis of $Mn(SO_3F)_3$ by metal oxidation has been reported (21).

Some effort has been expended to include $CrSn(SO_3F)_6$ in this study. However, the solid product of the reaction between $Cr(SO_3F)_2$ and $Sn(SO_3F)_4$ has been found to contain only small amounts of tin(II) and tin(IV) according to its Mössbauer spectrum. The bulk was identified as $Cr(SO_3F)_3$ by its infrared spectrum (22). It is suggested that oxidation of $Cr(SO_3F)_2$ rather than complexation, has occurred according to:

$$[3]\quad 2Cr(SO_3F)_2 + Sn(SO_3F)_4 \xrightarrow{HSO_3F} 2Cr(SO_3F)_3 + Sn(SO_3F)_2$$

with the reduced product $Sn(SO_3F)_2$ fairly soluble in HSO_3F (16).

This result is not surprising. Of the reduction potentials ϵ^0 (23) in aqueous medium for the M^{2+}/M^{3+} couples, with M ranging from Cr to Cu in the 3*d* series, only the ϵ^0 value for Cr^{2+}/Cr^{3+}, +0.41 V is positive, and hence oxidation of Cr^{2+} by Sn(IV) is likely. Redox potentials ϵ^0 are strictly valid in aqueous medium only, but our observation points to a comparable situation in HSO_3F, favoring oxidation over complexation for Cr^{2+} only.

The Mössbauer data, summarized in Table 2 and to be discussed later, provide the most unambiguous evidence for a successful complexation. Analytical data, listed in Table 1, confirm the suggested overall composition and are valuable because they rule out unexpected side reactions, such as hydrolysis or partial product decomposition. The thermal behaviour of the fluorosulfato complexes is inconsistent with the presence of mere mixtures of the starting materials. Polymeric $Sn(SO_3F)_4$ is found to have rather sharp decomposition points at +196°C (13) or +216°C (18), depending on the method of preparation used. None of the reaction products melt or decompose below 300°C.

Conversion of the $MSn(SO_3F)_6$ compounds into the corresponding trifluoromethyl sulfates proceeds for the most part very cleanly and completely as is evident from the analytical data in Table 1. Only in the case of $NiSn(SO_3CF)_6$ do the analytical data indicate an incomplete conversion, even after prolonged reaction times and a reaction temperature of 70°C. A similar situation was found previously for polymeric $Hg(SO_3F)_2$ (15). It is not immediately obvious why $NiSn(SO_3F)_6$ should be so difficult to convert to the corresponding SO_3CF_3 compound. It appears to make very little difference whether a stoichiometric mixture of $M(SO_3F)_2$ and $Sn(SO_3F)_4$ or the bimetallic $MSn(SO_3F)_6$ are used as starting materials as exemplified by two different preparations of $CuSn(SO_3CF_3)_6$.

The reason for a complete conversion is seen in a degradation of HSO_3F, initially formed in the solvolysis reaction, by an excess of HSO_3CF_3 to form a number of fairly volatile products such as CO_2, COF_2, SO_2, CF_3SO_3F, $CF_3SO_3CF_3$, and SiF_4 which seemingly do not interfere in the product isolation. However, the formation of SiF_4, a secondary product from the reaction of HF with glass, suggests the formation of water as well. It is therefore not surprising that in products of the conversion reaction, micro analysis and ir spectra will indicate the presence of variable amounts of water in the trifluoromethyl sulfates obtained, and careful drying *in vacuo* at ~40°C is needed.

TABLE 2. ^{119}Sn Mössbauer data for M(II)[$Sn(SO_3X)_6$] with X = F or CF_3 at 80 K[a]

Compound	δ (mm s^{-1})	Γ (mm s^{-1})
$MnSn(SO_3F)_6$	−0.271	1.124
$FeSn(SO_3F)_6$	−0.277	1.132
$CoSn(SO_3F)_6$	−0.287	1.327
$NiSn(SO_3F)_6$	−0.283	1.230
$CuSn(SO_3F)_6$	−0.251	1.290
$AgSn(SO_3F)_6$[b]	−0.211	
$HgSn(SO_3F)_6$[c]	−0.267	1.148
$SnSn(SO_3F)_6$[c,d]	−0.272	1.240
$BaSn(SO_3F)_6$[c]	−0.305	1.337
$PdSn(SO_3F)_6$[e]	−0.254	1.133
$MnSn(SO_3CF_3)_6$	−0.257	1.063
$FeSn(SO_3CF_3)_6$	−0.247	1.114
$CoSn(SO_3CF_3)_6$	−0.227	1.262
$NiSn(SO_3CF_3)_6$	−0.259	0.938
$CuSn(SO_3CF_3)_6$	−0.253	1.067

[a]Relative to $BaSnO_3$.
[b]ΔE_q = 0.53 mm s^{-1} (6).
[c]Reference 16.
[d]Sn(IV) part only.
[e]Reference 4.

Can. J. Chem. Downloaded from www.nrcresearchpress.com by 213.222.148.141 on 09/07/12
For personal use only.

Can. J. Chem. Downloaded from www.nrcresearchpress.com by 213.222.148.141 on 09/07/12
For personal use only.

TABLE 3. Infared spectra of $M^{II}Sn(SO_3F)_6$ and $K_2[Sn(SO_3F)_6]$ for M^{II} = Mn, Fe, Co, Ni, Cu, Ag, and Pd[e]

$MnSn(SO_3F)_6$	$FeSn(SO_3F)_6$	$CoSn(SO_3F)_6$	$NiSn(SO_3F)_6$	$CuSn(SO_3F)_6$	$AgSn(SO_3F)_6$[a]	$PdSn(SO_3F)_6$[b]	$K_2[Sn(SO_3F)_6$[c]	Approximate description[d]
ν (cm^{-1}) Int.	ν (cm^{-1}) Int.	ν (cm^{-1}) Int.	ν (cm^{-1}) Int.	ν (cm^{-1}) Int.	ν (cm^{-1}) Int.	ν (cm^{-1}) Int.	ν (cm^{-1}) Int.	
~1430 m, sh	~1430 w, sh	~1425 w, sh	~1420 mw, sh	~1430 m, sh	1425 ms, sh	1425 m, sh		Asymmetric
1395 s, sh	1409 vs	1410 vs, b		1400 vs		1405 vs		SO_2 stretch
1380 vs	1390 s, sh	1385 s, sh	1395 s, b	1390 vs	1395 vs, b	1385 s	1380 vs, b	
				1310 vs				Combination
~1280 vw	1285 m	~1270 m, sh	1270 m, sh	1270 vw, sh		1250 ms, sh		mode
				1205 vs, sh	1227 s		1220 s, sh	Symmetric
1195 vs, b	1210 vs	1210 vs, b	1195 vs, b	1195 vs	1170 vs, b	1195 vs, b	1190 s, b	SO_2 stretch
1140 w, sh	~1155 vw, sh	1145 vw	1145 vw, sh					Combination
1105 vw	1110 w	1110 w, b	1112 vw	1105 vw, sh		1105 w		mode
				1040 vs, b	1040 s			
1015 vs, b	1032 vs	1020 vs, b	1030 s, b	1020 vs	1010 s, sh	1028 vs, b	990 s, b	S—O···Sn
					984 s, b			Stretch
825 vs	845 vs	840 vs, b	838 vs, b	845 v	865 s	865 m, sh	820 s, sh	S—F
					835 s	855 vs	810 s, b	Stretch
	640 m, sh							Sn—O skeletal
638 ms, sh	630 ms	640 s, sh	640 ms	635 m, b	640 s, b	648 ms		stretch + SO_3F
620 ms	612 ms	630 ms	625 m	605 vw	625 s	630 ms	620 s	deformation
592 m	596 ms	595 ms	592 m	595 mw	590 s	590 s	571 m	FSO_3 bend, assym.
555 ms	556 s	565 s	560 ms	560 m	555 ms	562 m	555 s	FSO_3 bend,
						551 m		sym.
		455 ms		460 m	452 m			SO_3F wagging
		438 ms		435 m, sh	448 s	445 ms, sh	430 m	mode

[a]Reference 6.
[b]Reference 4.
[c]Reference 5.
[d]Based on previous assignment in ref. 5.
[e]Abbreviations: Int. = estimated intensity, s = strong, m = medium, w = weak, v = very, sh = shoulder, b = broad.

TABLE 4. Infrared spectra of $M^{II}Sn(SO_3CF_3)_6$ with M = Mn, Fe, Co, Ni, Cu, and Sn

$MnSn(SO_3CF_3)_6$[a]	$FeSn(SO_3CF_3)_6$	$CoSn(SO_3CF_3)_6$	$NiSn(SO_3CF_3)_6$	$CuSn(SO_3CF_3)_6$	$SnSn(SO_3CF_3)_6$[b]
ν (cm^{-1}) Int.	ν (cm^{-1}) Int.	ν (cm^{-1}) Int.	ν (cm^{-1}) Int.	ν (cm^{-1}) Int.	ν (cm^{-1}) Int.
	1390 m, sh	1395 m, sh	~1400 m, sh		
1375 vs	1373 vs	1372 vs	1377 vs	1380 vs	1375 s
1360 s, sh	1360 m, sh	1360 s, sh	1360 s, sh		1350 ms, sh
				1280 w, sh	
1240 s, sh	1225 s	1225 s, sh	1230 vs, b	1220 s, sh	1240 ms
1200 s, b	1200 vs	1198 vs, b	1197 vs	1200 vs	1210 vs, b
1125 s	1120 ms	1127 s	1121 s	1116 vs	1155 s
1100 m, sh	1071 mw	1068 m	1060 ms	1062 m, sh	
980 m, sh	1012 m, sh	992 s, sh	1010 ms	985 ms, sh	985 vs, b
960 vs, b	962 vs	962 vs	962 s	968 s	940 m
870 vw, sh	~870 vw, sh	~870 vw	871 w		
775 s	775 m	774 m	774 m	776 m	780 m
674 m, sh	~655 m, sh	~670 m, sh		~670 w, sh	
639 s	636 s	640 s	659 s	640 s	640 m, sh
606 s	610 ms	610 s	620 s	610 ms	630 s
585 s	585 s	589 m	583 m, sh	585 ms	570 w, sh
535 s, sh	545 s, sh	543 ms, sh	540 m, sh	545 m, sh	
525 s	531 s	531 s	535 s	533 s	520 ms
507 m	510 vw	~510 m, sh	~510 m, sh	~510 m, sh	
452 w	472, 455 w	475–452 vw			
422 w	425 mw	420 w	432 m	426 w	
398 ms	400 ms	400 ms		403 ms	
361 s	372 m	369 ms	372 ms	380–373 m-w	380 m, sh
351 s, sh	355 m	351 m, sh	350 m, sh	350 w	345 ms
335 m	330 w				

[a]Reference 15.
[b]Reference 2.

The evolution of volatile by-products during the conversion reaction results in a rather slight pressure increase over the reaction mixture, insufficient to reliably estimate when a reaction is complete. As a precaution rather long reaction times of up to 12 days are chosen with reaction temperatures usually at ~70°C.

The resulting products, like their SO_3F counterparts, are seemingly insoluble in the parent acid and are usually stable at least up to 300°C. For polymeric $Sn(SO_3CF_3)_4$, depending on the method of preparation lower melting points, 225–227°C (2) and 235°C (15), respectively, are reported.

In summary, it appears that the general synthetic routes described here can be extended to a wider range of bimetallic polymers of the general type $M^{II}M^{IV}(SO_3X)_6$ with X = F or CF_3 than had been reported previously (2–4, 6, 16). The synthetic approach is successful as long as the $M(SO_3X)_2$ precursors are readily obtainable and will not reduce the M^{IV} species. Besides the reduction of Sn^{IV} by Cr^{II} described here, we have previously noted a similar redox-reaction between Sn^{II} and Pt^{IV} (16).

Infrared spectra

The infrared spectra obtained on solid films pressed between AgCl or occasionally AgBr windows resulted in rather broad bands. The band positions are tabulated for $M^{II}Sn(SO_3F)_6$ in Table 3 and for $M^{II}Sn(SO_3CF_3)_6$ in Table 4, together with an approximate band description for the fluorosulfates. The spectra of the fluorosulfate complexes are less complicated than those of their trifluoromethyl sulfate analogues and permit comparison with published data on $PdSn(SO_3F)_6$ (4), $AgSn(SO_3F)_6$ (6) and the ionic salts $K_2[Sn(SO_3F)_6]$ (5).

Comparison to published infrared data for either $Sn(SO_3F)_4$ (18) or $M(SO_3F)_2$ (12) with M = Fe, Co, or Ni is difficult even for the fluorosulfates, due to the complex spectra obtained. However, both the positions of the band centers and the band intensities differ markedly in the SO_3-stretching range; e.g. very strong bands at 1260 cm^{-1} and strong sharp bands at 1120 cm^{-1} noted for $M(SO_3F)_2$ (12) are absent in the spectra reported here or are slightly shifted and of very low intensity. The band center at ~1400 cm^{-1} of the rather intense SO_3 stretch of highest frequency differs also from the reported strong band at 1438 cm^{-1} in the infrared spectrum of $Sn(SO_3F)_4$. Additional but admittedly subtle differences are also noted in the SF-stretching range, while the rather narrowly spaced deformation modes provide little useful information in this regard.

For all bimetallic fluorosulfate stannates, the bands due to the three expected S—O stretching vibrations are found at ~1400, ~1200, and ~1025 cm^{-1} with little variations noted for the five new complexes. Pronounced band-splittings of 10 to 20 cm^{-1} are observed only for $CuSn(SO_3F)_6$ and appear to be caused by a distorted environment around the Cu^{2+} ion. Even more pronounced splitting of the three fundamentals are reported for $AgSn(SO_3F)_6$ (6), and even ν_{SF} shows a splitting of 30 cm^{-1} for this compound. Assuming the distortions to be due to the Jahn–Teller effect in both instances, this effect is more pronounced for Ag^{2+}.

Can. J. Chem. Downloaded from www.nrcresearchpress.com by 213.222.148.141 on 09/07/12
For personal use only.

Can. J. Chem. Downloaded from www.nrcresearchpress.com by 213.222.148.141 on 09/07/12
For personal use only.

Additional, weaker band features in the SO_3 stretching region at ~1270, ~1150, and ~1105 cm^{-1} are common to all five new complexes and found for $PdSn(SO_3F)_6$ (3) as well, but are not observed for $K_2[Sn(SO_3F)_6]$ (5) or $Ba[Sn(SO_3F)_6]$ (16).

Spectral features found for the ionic hexakis (fluorosulfato) stannates, which differ from the spectra of the bimetallic polymers are briefly summarized: (*i*) the observed spectra are considerably simpler, (*ii*) principle bands in the SO_3F stretching region are shifted to lower frequencies by ~20 to 30 cm^{-1}, and (*iii*) a skeletal ν_{SnO} at 620 cm^{-1} is unsplit and a SO_3F wagging mode at ~455 is absent.

The features found for the bimetallic polymers are consistent with monodentate —OSO_2F groups, strongly bonded to tin and coordinated more weakly to M^{2+} through a second oxygen, where M is a transition metal. This bonding type has been described previously as "aniso bidentate bridging" (4, 16).

The general impression that band positions, intensities, and shapes for the bimetallic fluorosulfate complexes are relatively independent of the divalent cation, with distortions around M^{2+} barely detectable, is reinforced by the infrared spectra for the series $M^{II}Sn(SO_3CF_3)_6$ listed in Table 4. For the mixed valency compound $Sn^{II}Sn^{IV}(SO_3CF_3)_6$ (2) a similar band pattern is reported, some small frequency shifts not withstanding. Incomplete conversion to $NiSn(SO_3CF_3)_6$ suggested by the analytical data is not evident from the infrared data, which compare well with those for the other compounds. Band splittings due to Jahn–Teller distortions of the Cu^{2+} ion as had been found for $CuSn(SO_3F)_6$, but are not observed for the SO_3CF_3 analogue. This is presumed to be due to both extensive vibrational mixing between SO_3 and CF_3 modes and the near coincidence of their bands, which results in greater complexity and makes it more difficult to detect possible distortions reflected in the SO_3 vibrations around Cu^{2+}.

A detailed band description is rather problematic on account of this vibrational mixing and only a few tentative suggestions are made. It appears reasonable in view of assignments proposed for the SO_3F-series, to attribute three band features at 1370–1360, ~1200, and 980–960 cm^{-1} to the three SO_3 stretching modes, shifted by ~10 to ~40 cm^{-1} to lower frequencies for the SO_3CF_3 compounds, which would imply a similar coordination mode for the sulfonate groups. From this follows assignment of bands at ~1230, 1120, and ~1070 cm^{-1} as primarily caused by CF_3 stretching vibrations.

A rather sharp medium intensity band at 775 cm^{-1} is found in all spectra. This band is strongly Raman active (2, 15) and found in a very narrow frequency range for SO_3CF_3 compounds. Not surprisingly, bands at 640–630 cm^{-1}, attributed predominantly to Sn—O skeletal vibrations, are found for both series of compounds in the same frequency range with rather similar band shapes and relative intensities.

All these features point to a strong structural similarity between the two series of compounds. Due to the spectral complexity of the SO_3CF_3 vibrations, it is not quite as easy as had been for the fluorosulfates to differentiate between true compounds and mere mixtures, but a careful comparison to ir spectra of previously (2) and recently (15) reported Sn^{IV}—SO_3CF_3 derivatives reveals several differences both in band position and intensity patterns.

^{119}Sn Mössbauer spectra

In previous ^{119}Mössbauer spectra studies of hexakis(fluorosulfato)stannate(IV) derivatives $R_2[Sn(SO_3F)_6]$ with monovalent cations ($R = K^+, Cs^+, NO^+, ClO_2^+, Br(SO_3F)_2^+$) (1, 5) single-line absorptions with $\delta = -0.27 \pm 0.04$ mm s^{-1} (at ~80 K, relative to $BaSnO_3$) and line widths from 1.1 to 1.4 mm s^{-1} have been observed. These results were interpreted (5, 22) as indicating a regular, or nearly regular, octahedral environment about tin(IV). The corresponding $M[Sn(SO_3F)_6]$ salts with the divalent cations $M = Hg^{2+}, Sn^{2+}, Ba^{2+}, Pd^{2+}$ were also found (4, 16) to exhibit unsplit resonances with isomer shifts again in the region of -0.27 mm s^{-1}. In all instances where $Sn(SO_3F)_4$ was used as starting material, its doublet with $\Delta E_a = 1.34$ mm s^{-1} (18) had collapsed to a single line on complexation.

On the other hand, the ^{119}Sn Mössbauer spectrum of $Ag[Sn(SO_3F)_6]$ exhibits (6) a quadrupole splitting of 0.53 mm s^{-1} and a slightly more positive isomer shift of -0.21 mm s^{-1}. Two reasonable explanations of the distorted environment of tin in this complex are (*i*) diminished ionic character due to the strongly polarizing Ag^{2+} ion, and (*ii*) a Jahn–Teller distortion of the Ag^{2+} ion transmitted to tin via bridging fluorosulfate groups. Either of these effects would be consistent with the more positive isomer shift, but comparison with $Hg[Sn(SO_3F)_6]$, where the small Hg^{2+} ion is also strongly polarizing and which shows a narrow single-line absorption, suggests that the quadrupole splitting in the silver complex is most likely a result of Jahn–Teller distortion of the Ag^{2+} ion (6).

The present results (Table 2) for the 3*d* transition metal derivatives $M[Sn(SO_3F)_6]$ and $M[Sn(SO_3CF_3)_6]$ (M = Mn, Fe, Co, Ni, Cu) are interesting in that in every case the ^{119}Sn Mössbauer spectrum consists of a single line of width 1.06–1.33 mm s^{-1}. We might well have expected to observe quadrupole splitting in the two Cu^{2+} complexes arising from Jahn–Teller distortion of the d^9 cations. However, neither the line widths nor the isomer shifts are exceptional for the copper salts, and it seems that any distortion due to the Jahn–Teller effect is not being effectively relayed to the tin site via bridging sulfonate groups. Another possibility is that of a dynamic Jahn–Teller distortion that is too rapid to be observed on the Mössbauer time scale.

In neither the $M[Sn(SO_3F)_6]$ nor the $M[Sn(SO_3CF_3)_6]$ series of compounds is there a discernible trend in either isomer shift or line width as the electronic configuration of the cations changes from d^5 to d^9. In each series the isomer shifts are identical within experimental error, although on average the values for the trifluoromethyl sulfates are approximately 0.02–0.03 mm s^{-1} more positive than those for the fluorosulfates. This difference is barely large enough to be significant, but is consistent with previously reported isomer shift differences in the following pairs of complexes where X = F, CF_3: $Sn(SO_3X)_4$ (2), $Sn[Sn(SO_3X)_6]$ (anionic species (16)), and $(CH_3)_2Sn[Sn(SO_3X)_6]$ (anionic species (16)). If these differences are indeed genuine, they indicate a very slightly more positive effective nuclear charge on tin in the fluorosulfate derivatives.

Finally, it should be noted that all the new derivatives show weak but resolvable Mössbauer spectra at room temperature. This fact presumably reflects the bridging function of the SO_3X^- (X = F, CF_3) moieties and significant covalent cation–anion interactions, without however, causing more than a minor perturbation of the near-spherical charge distribution at tin in the anions.

Conclusions

Metal bis(fluorosulfates), $M(SO_3F)_2$ with M = Mn, Fe, Co, Ni, or Cu react with $Sn(SO_3F)_4$ in fluorosulfuric acid at

reaction temperatures of 25 to 70°C to give bimetallic coordination polymers. Solvolysis of these SO_3F-containing polymers in trifluoromethylsulfuric acid leads to the corresponding $MSn(SO_3CF_3)_6$ compounds.

Characterisation is based on chemical analysis, vibrational spectra, and on single line ^{119}Sn Mössbauer spectra at 298 and 80 K. A common structural type, involving octahedral environments for both tin and the transition metal ion is suggested in all instances except for possible Jahn–Teller distortions for Cu^{2+}. The suggested anisobidentate bridging mode for the fluorosulfate group — strong oxygen bonding to tin and weak coordination to M^{2+} — should provide a magnetically dilute environment for the paramagnetic M^{2+} ions and a detailed magnetic study involving both sets of compounds is presently underway.

Acknowledgements

Financial support by the Natural Sciences and Engineering Research Council of Canada in the form of operating grants (to J.R.S. and F.A.) and summer student scholarships (to P.F.G. and K.L.) is most gratefully acknowledged. We are thankful to Mrs. L. Sallos for recording the Mössbauer spectra, Mr. P. Borda for chemical analysis (carbon) and great patience, and to Professor R. C. Thompson for many helpful discussions.

1. P. A. Yeats, B. Landa, J. R. Sams, and F. Aubke. Inorg. Chem. **15**, 1452 (1976).
2. R. T. Batchelor, J. N. R. Ruddick, J. R. Sams, and F. Aubke. Inorg. Chem. **16**, 1414 (1977).
3. K. C. Lee and F. Aubke. Can. J. Chem. **55**, 2473 (1977).
4. K. C. Lee and F. Aubke. Can. J. Chem. **57**, 2058 (1979).
5. P. A. Yeats, J. R. Sams, and F. Aubke. Inorg. Chem. **12**, 328 (1973).
6. P. C. Leung and F. Aubke. Inorg. Chem. **17**, 1765 (1978).
7. A. G. Sharpe. J. Chem. Soc. 3444 (1950).
8. N. Bartlett and P. R. Rao. Chem. Soc. Proc. 393 (1964); P. R. Rao. Ph.D. Thesis. University of British Columbia, Vancouver, B.C. 1965.
9. A. Tressaud, M. Wintenberger, N. Bartlett, and P. Hagenmüller. C.R. Acad. Sci. Ser. C, **282**, 1069 (1976).
10. J. M. Taylor and R. C. Thompson. Can. J. Chem. **49**, 511 (1971).
11. (*a*) A. L. Arduini, M. Garnett, R. C. Thompson, and T. C. T. Wong. Can. J. Chem. **53**, 3812 (1975); (*b*) J. R. Sams, R. C. Thompson, and T. B. Tsin. Can. J. Chem. **55**, 115 (1977); (*c*) J. S. Haynes, J. R. Sams, and R. C. Thompson. Can. J. Chem. **59**, 669 (1981).
12. C. S. Alleyne, K. O'Sullivan-Mailer, and R. C. Thompson. Can. J. Chem. **52**, 336 (1974).
13. S. P. Mallela, K. C. Lee, and F. Aubke. Inorg. Chem. **23**, 653 (1984).
14. K. C. Lee and F. Aubke. Inorg. Chem. **23**, 124 (1984).
15. S. P. Mallela, J. R. Sams, and F. Aubke. Can. J. Chem. **63**, 3305 (1985).
16. S. P. Mallela, S. T. Tomic, K. Lee, J. R. Sams, and F. Aubke. Inorg. Chem. **25**, 2039 (1986).
17. S. P. Mallela and F. Aubke. Can. J. Chem. **62**, 382 (1984).
18. P. A. Yeats, B. L. Poh, B. F. E. Ford, J. R. Sams, and F. Aubke. J. Chem. Soc. A, 2188 (1970).
19. P. A. Yeats, J. R. Sams, and F. Aubke. Inorg. Chem. **11**, 2634 (1972).
20. D. F. Shriver. The manipulation of air sensitive compounds. McGraw-Hill, New York. 1969.
21. S. P. Mallela and F. Aubke. Inorg. Chem. **24**, 2969 (1985).
22. S. D. Brown and G. L. Gard. Inorg. Nucl. Chem. Lett. **11**, 19 (1975).
23. W. M. Latimer. The oxidation states of the elements and their potentials in aqueous solution. 2nd ed. Prentice-Hall Inc., New York. 1952.

Can. J. Chem. Downloaded from www.nrcresearchpress.com by 213.222.148.141 on 09/07/12
For personal use only.

Interactions between cations and sugars. III. Free energies, enthalpies, and entropies of association of Ca^{2+}, Sr^{2+}, Ba^{2+}, La^{3+}, Gd^{3+} with D-ribose in water at 25°C

ALFREDO MAESTRE ALVAREZ,[1] NICOLE MOREL-DESROSIERS, AND JEAN-PIERRE MOREL[2]

Laboratoire d'Etude des Interactions Solutés–Solvants, U.A. au C.N.R.S. n° 434, Université de Clermont-Ferrand 2, 63170 Aubière, France

Received March 3, 1987

ALFREDO MAESTRE ALVAREZ, NICOLE MOREL-DESROSIERS, and JEAN-PIERRE MOREL. Can. J. Chem. **65**, 2656 (1987).

The standard enthalpies of transfer of ribose and arabinose from water to aqueous solutions of electrolytes ($CaCl_2$, $SrCl_2$, $BaCl_2$, $LaCl_3$, and $GdCl_3$) have been measured at 25°C. A method is described to calculate from these data the equilibrium constant and the enthalpy for the association between the cations and the complexing isomers of ribose. Mean values relative to these isomers are given: the constants vary from 2.0 to 4.3 and the enthalpies from −5.9 to −17.9 kJ mol^{-1} for the different cations studied. The thermodynamic properties of association are not related to the size nor to the charge of the complexed cation in a simple way. On the other hand, the enthalpies of reaction are linearly correlated to the entropies of reaction.

ALFREDO MAESTRE ALVAREZ, NICOLE MOREL-DESROSIERS et JEAN-PIERRE MOREL. Can. J. Chem. **65**, 2656 (1987).

Les enthalpies standard de transfert du ribose et de l'arabinose entre l'eau et les solutions aqueuses d'électrolytes ($CaCl_2$, $SrCl_2$, $BaCl_2$, $LaCl_3$ et $GdCl_3$) sont mesurées à 25°C. Une méthode est décrite qui permet, à partir de ces grandeurs, de calculer la constante d'équilibre et l'enthalpie de la réaction d'association entre les cations et les formes isomères complexantes du ribose. Des valeurs moyennes relatives à ces isomères sont données (les constantes varient de 2,0 à 4,3 et les enthalpies de −5,9 à −17,9 kJ mol^{-1}) pour les différents cations étudiés. Les grandeurs thermodynamiques de la réaction d'association ne sont pas reliées de façon claire à la taille ou à la charge du cation complexé. Cependant, pour la série des cations étudiés, il existe une corrélation linéaire de pente unité entre les enthalpies et les entropies de réaction.

Introduction

Recently, we have reported the thermodynamic properties characterizing the reaction of association of the cation Ca^{2+} with the suitably positioned sequences of hydroxyls of ribose in aqueous solutions (1, 2). Values of the constant of this equilibrium, mainly determined by nmr data, had already been proposed (3–5). Our value (1) was evaluated from the electrochemically measured free energies of transfer of $CaCl_2$ from water to aqueous solutions of ribose and arabinose (taken as the reference pentose which characterizes the non-specific interactions between the sugar and the electrolyte). By using a liquid membrane electrode selective to Ca^{2+} ions (ORION 93-20) it was possible to perform very sensitive emf measurements and the results obtained showed to be in satisfactory agreement with those published previously (4, 6).

To have a better understanding of the association process between the cations and the complexing sequences of hydroxyls (*axial–equatorial–axial* for the pyranose forms and *cis–cis* for the furanose forms), we felt it was necessary to study the association of ribose with other cations. It is known, for instance, that the other alkaline-earth cations (3, 7) and some trivalent cations like La^{3+} (4, 7, 8) are notably associated with ribose or other sugars and derived species in aqueous solutions. Unfortunately, our potentiometric method cannot be used with these species because of the lack of sensitive selective electrodes; in particular, some attempts with a liquid membrane electrode selective to divalent cations (ORION 93-32) have shown that the electrode is not sufficiently sensitive and that the results are not reproducible (the involved emf are of the order of a few mV and should be known to better than 0.05 mV). On the other hand, it is known that some calorimetric methods can lead simultaneously to the association constant and to the enthalpy of reaction. We have thus tried to apply such a method to the determination of the free energies and enthalpies of association of ribose and arabinose with Ca^{2+} (for which we have comparative results and can thus check the validity of the method), Sr^{2+}, Ba^{2+}, La^{3+}, and Gd^{3+} in aqueous solutions at 25°C.

Theoretical relations

The standard enthalpy of transfer of a sugar S at infinite dilution from water to a solution of electrolyte E at molality m_E corresponds to the difference between the enthalpies of dilution of a concentrated solution of the sugar in water and in the electrolytic solution (2)

$$[1] \quad \Delta_t H_S^\theta(m_E) = \Delta_{dil} H_S(m_S, m_E) - \Delta_{dil} H_S(m_S)$$

The final concentration in sugar, m_S, must be the same for both dilution processes and sufficiently low. This enthalpy of transfer can be expressed as a power series in concentration of the electrolyte (2)

$$[2] \quad \Delta_t H_S^\theta(m_E) = 2\nu h_{SE} m_E + 3\nu^2 h_{SEE} m_E^2 + \ldots$$

where h_{SE}, h_{SEE}, ... are parameters characteristic of the pair, triplet, and higher-order interactions between the sugar and the electrolyte and ν is the number of ions into which E dissociates. Similarly, the standard enthalpy of transfer of the electrolyte E from water to the solution of sugar at molality m_S can be written

$$[3] \quad \Delta_t H_E^\theta(m_S) = \Delta_{dil} H_E(m_E, m_S) - \Delta_{dil} H_E(m_E) = 2\nu h_{SE} m_S + 3\nu h_{SSE} m_S^2 + \ldots$$

with the following correspondence

$$[4] \quad \left(\frac{\partial \Delta_t H_E^\theta}{\partial m_S}\right)_{m_S=0} = \left(\frac{\partial \Delta_t H_S^\theta}{\partial m_E}\right)_{m_E=0} = 2\nu h_{SE}$$

The pair interaction parameter h_{SE} is a mean parameter characterizing the interactions between all the sugar-ion pairs. For an electrolyte like $CaCl_2$, for instance, $\nu = 3$ and it follows that

$$[5] \quad 3h_{SE} = h_{SCa^{2+}} + 2h_{SCl^-}$$

[1]On leave of absence from the Facultad de Farmacia, Universidad de Sevilla, España.

[2]To whom all correspondence should be addressed.

Can. J. Chem. Downloaded from www.nrcresearchpress.com by 213.166.140.6 on 09/07/12
For personal use only.

By comparing ribose (R), which can interact specifically with Ca^{2+} through the suitably positioned sequences of hydroxyls, with arabinose (A), which is taken as the reference pentose since it does not show specific interactions with this cation, we get (1)

$$[6] \quad 2\nu(h_{RE} - h_{AE}) = 2h_{RCa^{2+}}$$

where $h_{RCa^{2+}}$ characterizes only the specific interaction between Ca^{2+} and ribose. The point particularly interesting is that the pair interaction parameters are related to the thermodynamic properties of association (1, 2, 9). For instance, the parameters relative to the pair RCa^{2+} are related to the properties of the reaction

$$[7] \quad R_{(aq)} + Ca^{2+}{}_{(aq)} = RCa^{2+}{}_{(aq)}$$

characterized by the equilibrium constant β_1. It can be shown (1, 9) that the pair interaction parameter relative to the free energy, $g_{RCa^{2+}}$, that we have measured in a previous work (1) corresponds to

$$[8] \quad -2g_{RCa^{2+}} = RT\beta_1$$

from which it follows that

$$[9] \quad 2h_{RCa^{2+}} = \beta_1 \Delta_R H^\theta$$

where $\Delta_R H^\theta$ is the standard enthalpy of reaction [7]. If relation [2] is restricted to the first-order term in m_E and is successively applied to S ≡ R and S ≡ A we get

$$[10] \quad \delta\Delta_t H^\theta = \Delta_t H_R{}^\theta(m_E) - \Delta_t H_A{}^\theta(m_E) = 2h_{RCa^{2+}} m_E = \beta_1 \Delta_R H^\theta m_E$$

and, from the known β_1 and $h_{RCa^{2+}}$, $\Delta_R H^\theta$ may be estimated. In fact, relations [2] and [4] are not exactly linear with m_E and it is important to understand what is the origin of the second-order term. Rigorously, it can be shown from the equations relating the coefficients of the power series in m_E to the constants of the successive equilibria corresponding to the formation of pairs, triplets, etc... (see, for example, ref. 9) that the coefficient of the second-order term (g_{SEE} in the present case) is related to the two successive association constants β_1 and β_2. The deviation from linearity of relation [2] thus results from the formation of the triplet SEE ($RCa^{2+}Ca^{2+}$ in the present case) which is characterized by the constant β_2, on the one hand, and from the formation of the complex SE itself (reaction [7] characterized by the constant β_1) when m_E is large, on the other hand. Although both reasons can be put forward in the general case, it is obvious that in the present study the formation of the triplet $RCa^{2+}Ca^{2+}$ is totally unlikely. As regards the second reason, let us explain its origin. Considering only reaction [7] and taking into account the assumption relative to the non-specific interactions, we may write

$$[11] \quad \delta\Delta_t H^\theta(m_E) = \alpha(m_E)\Delta_R H^\theta$$

where α, which is a function of m_E, is the extent of association of ribose with Ca^{2+} (reaction [7]). α is generally calculated from β_1, m_R, and m_E but at infinite dilution of ribose it reduces to

$$[12] \quad \alpha(m_E) = \beta_1 m_E/(1 + \beta_1 m_E)$$

The first-order assumption would simply lead back, by introduction of $\alpha(m_E) = \beta_1 m_E$ into [11], to relation [10]. In the general case,

$$[13] \quad \delta\Delta_t H^\theta(m_E) = \frac{\beta_1 m_E}{(1 + \beta_1 m_E)}\Delta_R H^\theta$$

which can be written

$$[14] \quad \frac{\delta\Delta_t H^\theta(m_E)}{m_E} = \beta_1 \Delta_R H^\theta - \beta_1 \delta\Delta_t H^\theta(m_E)$$

It is thus possible to get simultaneously the association constant β_1 and the enthalpy of reaction $\Delta_R H^\theta$ from the sole determination of the enthalpies of transfer at different m_E.

Experimental

D-Arabinose and D-ribose (Fluka puriss.) were dried under vacuum, stored in a desiccator, and used as such. The solutions of $CaCl_2$, $SrCl_2$, $BaCl_2$ (Merck pro analysi), $LaCl_3$ (Fluka puriss.), and $GdCl_3$ (Prolabo rectapur) were titrated by EDTA. All solutions were prepared by weight from triply distilled water degassed prior to use.

The enthalpies of dilution were measured with a LKB 8700 calorimeter by using the classical ampoule breaking technique. The measurements were carried out at 25.00 ± 0.01°C.

Results

The concentrated (0.650 mol kg^{-1}) solutions of ribose and arabinose in water have been diluted to a final molality of 0.0200 mol kg^{-1}. It follows that the enthalpies of dilution of these two sugars in pure water are, respectively,

$$\Delta_{dil}H_R = -0.14 \text{ kJ mol}^{-1}$$

$$\Delta_{dil}H_A = -0.12 \text{ kJ mol}^{-1}$$

By introducing into relation [1] these data and the enthalpies of dilution in the electrolytic solutions of various molalities, we get the standard enthalpies of transfer of ribose and arabinose given in Table 1. In the particular case of $CaCl_2$, the enthalpies of transfer of the electrolyte from water to the solutions of sugar have also been studied in order to check the reciprocity postulated in relation [4]. The initial concentration of $CaCl_2$ is 0.650 mol kg^{-1} and it is diluted to a final molality of 0.0200 mol kg^{-1}. However, since the heat of dilution of $CaCl_2$ varies noticeably with concentration, it is necessary to correct for the fact that the final concentration in pure water is not exactly the same as that in the sugar solution in order to get the enthalpies of transfer of $CaCl_2$ reported in Table 1 (it was not necessary to make such a correction to get the enthalpy of transfer of ribose since the enthalpy of dilution of the sugar is not so much concentration dependent). By plotting $\delta\Delta_t H^\theta/m_E$ versus $\delta\Delta_t H^\theta$ we can evaluate β (corresponding to the β_1 of the theoretical section since the formation of the triplet is unlikely) and $\Delta_R H^\theta$ as shown in relation [14]. The plots obtained, for instance, with the data of $SrCl_2$ and $BaCl_2$ are shown in Fig. 1. The vertical bars indicate the estimated uncertainties of the $\delta\Delta_t H^\theta/m_E$ values. The sets of β and $\Delta_R H^\theta$ values (in kJ) thus obtained are (0.86, −15.1), (1.87, −5.9), (1.60, −5.9), (1.20, −9.2), and (1.78, −17.9) for the cations Ca^{2+}, Sr^{2+}, Ba^{2+}, La^{3+}, and Gd^{3+}, respectively. The uncertainties are not easy to evaluate but we can estimate that β is determined to ±0.2 and $\Delta_R H^\theta$ to ±0.5 kJ.

Discussion

The β and $\Delta_R H^\theta$ values we get here are overall values characteristic of the association of all the complexing forms of ribose. This comes from the fact that solutions of ribose present anomeric and conformational equilibria and that only the isomers which have suitably positioned sequences of hydroxyls can specifically interact with the cation. The existence of these equilibria makes it necessary to specify clearly which processes are involved in the course of the measurement.

Can. J. Chem. Downloaded from www.nrcresearchpress.com by 213.166.140.6 on 09/07/12
For personal use only.

TABLE 1. Standard enthalpies of transfer of $CaCl_2$ from water to aqueous solutions of ribose (R) and arabinose (A), and of transfer of ribose and arabinose from water to aqueous solutions of $CaCl_2$, $SrCl_2$, $BaCl_2$, $LaCl_3$, $GdCl_3$ at 25°C[a]

m_R	$-\Delta_t H^\theta(CaCl_2)$	m_A	$-\Delta_t H^\theta(CaCl_2)$
0.0194	0.38	0.0389	0.10
0.0389	0.66	0.0777	0.21
0.0583	0.94	0.117	0.45
0.0777	1.26	0.155	0.55
0.0970	1.55	0.194	0.57
0.146	2.28		
0.194	2.91		
m_E	$-\Delta_t H^\theta(R)$	m_E	$-\Delta_t H^\theta(A)$
		$E \equiv CaCl_2$	
0.0193	0.32	0.0194	0.08
0.0388	0.65	0.0388	0.16
0.0582	0.96	0.0581	0.23
0.0776	1.26	0.0777	0.30
0.0922	1.51	0.0923	0.36
0.0972	1.56	0.145	0.60
0.145	2.26	0.194	0.74
0.194	3.02		
		$E \equiv SrCl_2$	
0.0449	0.63	0.0450	0.16
0.0954	1.20	0.0955	0.34
0.142	1.75	0.142	0.54
0.194	2.23	0.194	0.65
0.242	2.70	0.242	0.84
0.282	3.03		
		$E \equiv BaCl_2$	
0.0582	0.75	0.0485	0.20
0.0967	1.19	0.0970	0.39
0.145	1.66	0.145	0.60
0.194	2.15	0.194	0.75
0.251	2.70	0.251	1.00
0.290	3.04		
		$E \equiv LaCl_3$	
0.0484	0.76	0.0484	0.30
0.0969	1.46	0.0969	0.48
0.145	2.10	0.145	0.68
0.191	2.71	0.191	0.97
0.242	3.32	0.285	1.54
0.285	3.86		
		$E \equiv GdCl_3$	
0.0289	1.02	0.0493	0.23
0.0375	1.33	0.0698	0.29
0.0481	1.69	0.0969	0.41
0.0562	1.84	0.124	0.57
0.0726	2.33	0.144	0.66
0.0936	2.92	0.241	1.22
0.115	3.55		
0.140	4.28		
0.172	4.81		
0.180	5.06		
0.187	5.21		
0.213	6.23		
0.239	6.59		

[a] m, in mol kg^{-1}; $\Delta_t H^\theta$, in kJ mol^{-1}.

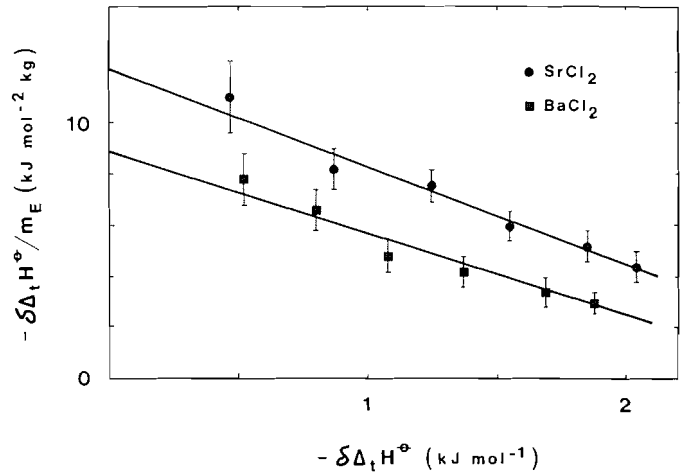

FIG. 1. Determination of β and $\Delta_R H^\theta$ for $SrCl_2$ and $BaCl_2$ ($\delta\Delta_t H^\theta/m_E$ in kJ mol^{-2} kg and $\delta\Delta_t H^\theta$ in kJ mol^{-1}).

If we let $[R_i]$ be the concentration of the isomer R_i and m_R be the total analytical concentration of pure ribose we may write

$$[15] \quad [R_i] = r_i m_R$$

r_i, the fraction of the isomer R_i in solution at equilibrium, can be considered as a thermodynamic constant if the concentrations of the studied solutions are low enough to be assimilated to activities. The two conformers of the α-pyranose ($r_a = 0.22$), the 1C4 conformer of the β-pyranose ($r_b = 0.14$), and the α-furanose ($r_c = 0.07$) bear a sequence of hydroxyls suitably positioned for association with Ca^{2+}. The r_i values given in parentheses have been determined by Angyal (10) at 31°C; they do not differ very much from those found at 40°C (11). Each of the active isomers is characterized by its complexation constant

$$[16] \quad \beta_i = \frac{[R_i M^{z+}]}{[R_i][M^{z+}]}$$

From nmr measurements, it is possible to determine the constants relevant to each isomer. At 31°C, Angyal (3) has found $\beta_a = 4.6$, $\beta_b = 1.2$, and $\beta_c = 5.0$ for the isomers indicated above, respectively. Lenkinski and Reuben (4) have found $\beta_a = 3.4$, $\beta_b = 0.8$, and $\beta_c = 5.3$ at 27°C. The constant β_b relevant to β-pyranose is not known with good accuracy (4). In fact, only the 1C4 conformer of β-pyranose is active and when $CaCl_2$ is added the equilibrium between the two conformers is displaced in favour of the 1C4 form. If we consider that the β_b value given above reflects the sum of the concentrations of both conformers, we then understand why it is much smaller than the constant of α-pyranose; but if we take into account the fact that the 1C4 conformer represents only 25% of β-pyranose (11) we calculate for the active isomer a constant which is close to the α-pyranose one (see below). We thus notice that all the active isomers of ribose form with Ca^{2+} complexes of comparable stabilities.

Our method does not allow differentiation between the isomers but gives an overall constant which has the advantage of being determined at sufficiently low concentration to be considered as a real thermodynamic constant. This overall constant may be written

$$[17] \quad \beta = \frac{\sum_i [R_i M^{z+}]}{[M^{z+}][R]}$$

Can. J. Chem. Downloaded from www.nrcresearchpress.com by 213.166.140.6 on 09/07/12
For personal use only.

where R_i is an active isomer and [R] is the total concentration of all the forms, active or not, of the free ribose. It can easily be shown that

$$[18] \quad \beta = \sum_i r_i \beta_i$$

Considering the values given above, we may assume that all the β_i constants are identical and may define a mean association constant $\overline{\beta}_i$ such that

$$[19] \quad \beta = \overline{\beta}_i \sum_i r_i$$

with $\sum_i r_i = 0.22 + 0.14 + 0.07 = 0.43$ (the r_b value given in our previous work (1) was wrong). We find $\beta = 0.86$ whereas from Lenkinski and Reuben's values, which are the most precise nmr-determined values at a temperature close to 25°C, we get $\beta = 0.22 \times 3.4 + 0.14(0.8 \times 4) + 0.07 \times 5.3 = 1.56$. The agreement is not perfect since the mean association constant deduced from nmr data is almost twice the one we get from calorimetry. Let us notice, however, that our value is in excellent agreement with the electrochemically determined one (1). In fact, the nmr method necessitates to work on concentrated solutions (0.634 *M* in ribose and up to 2.76 *M* in $CaCl_2$ (4)) and thus leads to apparent constants which can differ noticeably from thermodynamic constants.

If we examine the variations of the enthalpies of transfer of ribose with m_{CaCl_2} and of $CaCl_2$ with m_R we observe, as in a previous work (2), that both curves almost overlap over the studied concentration range. This means that the triplets $RCa^{2+}Ca^{2+}$ and $RRCa^{2+}$ do not participate to these processes. For both transfers, the deviation from linearity is solely due to the variation of the extent of association.

What do the values of $\Delta_R H^\theta$ deduced from the extrapolation of the straight lines of Fig. 1 represent? The β_1 which appears in the relation between $\delta\Delta_t H^\theta(m_E)$ and $\Delta_R H^\theta$ [13] corresponds to the overall association constant defined by [19]. Accordingly, the plots of Fig. 1 lead to a mean enthalpy of association of the metal cation with the different complexing isomers of ribose (let us notice also that $2h_{RCa^{2+}}/\beta_1$ leads directly to $\Delta_R H^\theta$, as shown by relation [9], whereas we had mistakenly said in our previous paper (2) that it was leading to $\sum_i r_i \Delta_R H^\theta$). The thermodynamic properties for the association of different cations with a complexing isomer of ribose are given in Table 2.

Some interesting observations can be made regarding these data:

(*a*) although always small, the association constants vary noticeably from one cation to the other;

(*b*) *neither the charge nor the size of the cation is determinant of the value of the association constant:* in fact, it appears, on the one hand, that the extent of association of cations of similar size but differently charged is not proportional to the valence of the ion (divalent strontium is more associated than trivalent lanthanum) and, on the other hand, that the extent of association of like-valence ions is not clearly related to the size of the ion (within the divalent cations strontium is more associated than smaller calcium whereas within the trivalent cations gadolinium is more associated than larger lanthanum);

(*c*) the enthalpy of reaction is favourable to the association process but is largely compensated by an unfavourable entropy of reaction which thus leads to small association constants.

Figure 2 shows that there is a good linear correlation of slope close to unity between $\Delta_R H^\theta$ and $T\Delta_R S^\theta$ and that it extrapolates

TABLE 2. Thermodynamic properties of association of ribose with different cations in water at 25°C

Ions	r^a	$\overline{\beta}_i{}^b$	$\Delta_R G^{\theta c}$	$\Delta_R H^{\theta c}$	$T\Delta_R S^{\theta c}$
Ca^{2+}	0.99	2.0	−1.7	−15.1	−13.4
Sr^{2+}	1.13	4.3	−3.6	−5.9	−2.3
Ba^{2+}	1.35	3.7	−3.2	−5.9	−2.7
La^{3+}	1.15	2.8	−2.5	−9.2	−6.7
Gd^{3+}	1.02	4.1	−3.5	−17.9	−14.4

[a] Pauling's radii in Å.
[b] Association constant: mean value for the whole of the complexing forms.
[c] kJ mol^{-1}.

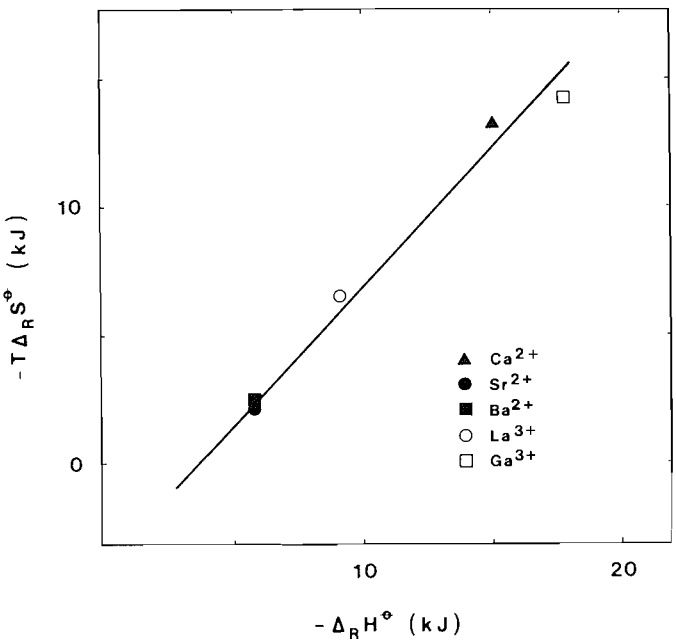

FIG. 2. Correlation between the entropies and the enthalpies (kJ mol^{-1}) of association of ribose with Ca^{2+}, Sr^{2+}, Ba^{2+}, La^{3+}, and Gd^{3+} in water at 25°C.

to $T\Delta_R S^\theta = 6$ kJ. The existence of such a correlation indicates that the association phenomenon is essentially controlled by the hydration of the different species involved in the process. This implies, in fact, the replacement of the water molecules solvating the ion by the three hydroxyls of the complexing forms of the sugar. During this process, which corresponds to a reorganization of the hydration spheres of the cation and of the sugar, the nature of the interactions involved is not fundamentally modified. The fact that the straight line of Fig. 2 does not pass through the origin is not easy to interpret but it is not a pronounced effect.

Conclusion

By using a calorimetric method, we have determined the equilibrium constants and the enthalpies of the reaction of association of Ca^{2+}, Sr^{2+}, Ba^{2+}, La^{3+}, and Gd^{3+} with ribose. We get mean values relative to the whole of the isomers of the sugar which present sequences of three hydroxyls in a position suitable for complexation (*axial–equatorial–axial* for the pyranose forms and *cis–cis* for the furanose forms).

Can. J. Chem. Downloaded from www.nrcresearchpress.com by 213.166.140.6 on 09/07/12
For personal use only.

We show that the values of the stability constant and of the enthalpy of association are not related to the size nor to the charge of the complexed cation in a simple way. The existence of a linear correlation of slope close to unity between the enthalpies and the entropies of reaction indicates that the process is essentially controlled by the hydration of the species.

1. J. P. MOREL and C. LHERMET. Can. J. Chem. **63**, 2639 (1985).
2. J. P. MOREL, C. LHERMET, and N. MOREL-DESROSIERS. Can. J. Chem. **64**, 996 (1986).
3. S. J. ANGYAL. Aust. J. Chem. **25**, 1957 (1972).
4. R. E. LENKINSKI and J. REUBEN. J. Am. Chem. Soc. **98**, 3089 (1976).
5. M. C. R. SYMONS, J. A. BENBOW, and H. PELMORE. J. Chem. Soc. Faraday Trans. 1, **78**, 3671 (1982).
6. L. G. EKSTRÖM and A. OLIN. Acta Chem. Scand. A**31**, 838 (1977).
7. A. VESALA, H. LÖNNBERG, R. KÄPPI, and J. ARPALAHTI. Carbohydr. Res. **102**, 312 (1982).
8. A. VESALA and H. LÖNNBERG. Acta Chem. Scand. A**35**, 123 (1981).
9. R. H. WOOD, T. H. LILLEY, and P. T. THOMPSON. J. Chem. Soc. Faraday Trans. 1, **74**, 1301 (1978).
10. S. J. ANGYAL. Advances in carbohydrate chemistry and biochemistry. Academic Press, Orlando. 1984. Vol. 42. p. 15.
11. S. J. ANGYAL. Angew. Chem. **8**, 157 (1969).

Can. J. Chem. Downloaded from www.nrcresearchpress.com by 213.166.140.6 on 09/07/12
For personal use only.

Complexation of aqueous ammonia by cyclodextrins

WARREN HIRSCH, CAROL DIMARTINI, AND VOJTECH FRIED[1]
Brooklyn College of the City University of New York, Brooklyn, NY 11210, U.S.A.

AND

WILLIAM LING
Edward R. Murrow High School, Brooklyn, NY 11230, U.S.A.

Received February 24, 1987

WARREN HIRSCH, CAROL DIMARTINI, VOJTECH FRIED, and WILLIAM LING. Can. J. Chem. **65**, 2661 (1987).

The complexation of aqueous ammonia with α, β, and γ cyclodextrins has been monitored by pH measurements at (23 ± 1)°C. A mathematical model has been developed yielding reproducible equilibrium association constants for the formation of these complexes. The constants are quite large, suggesting the possibility of hydrogen bond formation.

WARREN HIRSCH, CAROL DIMARTINI, VOJTECH FRIED et WILLIAM LING. Can. J. Chem. **65**, 2661 (1987).

Opérant à 23 ± 1°C et faisant appel à des mesures de pH, on a déterminé les taux de complexation de l'ammoniac aqueux avec les cyclodextrines α, β et γ. On a développé un modèle mathématique qui permet de reproduire les constantes d'équilibre d'association pour la formation de ces complexes. Les constantes sont assez élevées et elles suggèrent la possibilité de formation de ponts hydrogènes.

[Traduit par la revue]

Introduction

The cyclic oligosaccharides α, β, and γ cyclodextrin (cyclohexaamylose, cycloheptaamylose, and cyclooctaamylose) have been the subject of much intensive research (1, 2). The above cyclodextrins are structured in doughnut shapes which are composed of six, seven, or eight glucose units, respectively. Some reasons for the interest in the cyclodextrins are their ability to mimic enzymes, their catalytic ability, and their ability to form inclusion complexes in aqueous solution with molecules and anions. The relatively large interior of the cyclodextrins allow suitably sized molecules or anions to get trapped within the cavity, conformational changes perhaps aiding the process (3–5). The pH change of systems of acids and their anionic conjugate bases upon cyclodextrin addition has provided much information on stability constants (6, 7). Possible binding forces within these inclusion complexes may involve hydrophobic, Van der Waals, hydrogen bonding, or dipole interaction (1, 2, 6). In the present work, the complexation of an electrically neutral base, ammonia, has been studied by a novel pH method since there is a scarcity of information on the inclusion of this type of guest.

Experimental section

The α, β, and γ cyclodextrins, obtained from Aldrich Inc., were used as received. Information on the water contents was obtained from the manufacturer. Hydration did not affect the calculated results within experimental error. Solutions of cyclodextrins were prepared by dissolving weighed portions in volumetric flasks. The ammonia was reagent grade, from Baker Chemical Company. Distilled, degassed water was used to prepare the desired solution concentrations. Solutions were freshly prepared before a series of measurements were made. The solutions of known concentration, which were prepared by dilution of the reagent, showed pH values equal to the calculated values within experimental error. Therefore, no purification was deemed necessary.

A Beckman model Φ 43 pH meter accurate to ±0.01 pH unit was employed. The meter was calibrated with two primary standard buffers, tetraborate (pH 9.18) and phosphate (pH 7.41), before each series of readings were taken. The combined AgCl/glass electrode was rinsed with distilled water and blotted dry with clean tissue before use. pH measurements were made at the room temperature: (23 ± 1)°C. Some measurements were made with a combined glass–calomel electrode to insure that complexation of AgCl by the very dilute ammonia solutions was negligible. Aqueous ammonia was introduced into a modified graduated cylinder equipped with a side-arm sealed with synthetic rubber. The initial pH was recorded. Cyclodextrin solutions were added to the ammonia solution in several 1 mL portions by hypodermic syringe. The pH electrode fit tightly within the cylinder to prevent escape of ammonia. After each addition, the solution was stirred manually and the stable pH was recorded; then additional cyclodextrin was added to the solution. At least three aliquots of cyclodextrin were added in each experiment. Not less than five such experiments were performed for each cyclodextrin.

Results

Computerized linear least square plots were prepared for the pH of the aqueous ammonia–cyclodextrin solutions vs. $v/(V + v)$, where the V represents the initial volume and the v represents the volume of aqueous cyclodextrin (Cy) of known molar concentration (about 10^{-3} M) added in millilitre (see Tables 1–3). The correlation coefficients of these empirical plots were all close to one.

Calculations of K_{CyNH_3} were based on the predicted values for the pH of the last point on each plot and for the intercept (pure NH_3(aq)).

The following equations describe the equilibria occurring in the solutions being studied as well as the charge and mass balance.

[1] $NH_3 + H_2O \rightleftarrows NH_4^+ + OH^-$

with

$$K_b = \frac{(NH_4^+)(OH^-)}{(NH_3)} = 1.74 \times 10^{-5} \text{ (at 23°C)} \quad (8)$$

[2] $Cy + NH_3 \rightleftarrows CyNH_3$

with

$$K_{CyNH_3} = \frac{(CyNH_3)}{(Cy)(NH_3)}$$

where $(CyNH_3)$ is the molar concentration of the cyclodextrin–ammonia complex.

[1]To whom correspondence should be addressed.

Printed in Canada / Imprimé au Canada

Can. J. Chem. Downloaded from www.nrcresearchpress.com by 213.166.140.6 on 09/07/12
For personal use only.

Can. J. Chem. Downloaded from www.nrcresearchpress.com by 213.166.140.6 on 09/07/12
For personal use only.

TABLE 1. Effect of α cyclodextrin on the pH of NH_3(aq)

Run	Molarity of Cy added	V (mL)	V (mL)	$v/(V+v)$	pH	Correlation coefficient	Slope	Intercept
1	8.72×10^{-4}	0	10.0	0.000	9.02			
		1		0.0909	8.91			
		2		0.167	8.80			
		3		0.231	8.67			
		4		0.286	8.55			
		5		0.333	8.47	0.994	−1.69	9.05
2	8.72×10^{-4}	0	9.5	0.000	8.99			
		1		0.0952	8.82			
		2		0.174	8.71			
		3		0.240	8.57			
		4		0.296	8.50			
		5		0.345	8.41	0.998	−1.71	8.99
3	9.07×10^{-4}	0	10.0	0.000	9.00			
		1		0.0909	8.87			
		2		0.167	8.71			
		3		0.231	8.56	0.994	−1.91	9.02
4	9.07×10^{-4}	0	10.0	0.000	9.08			
		1		0.0909	8.93			
		2		0.167	8.76			
		3		0.231	8.61	0.997	−2.04	9.09
5	9.07×10^{-4}	0	10.0	0.000	9.05			
		1		0.0909	8.90			
		2		0.167	8.73			
		3		0.231	8.53	0.990	−2.22	9.07

TABLE 2. Effect of β cyclodextrin on the pH of NH_3(aq)

Run	Molarity of Cy added	V (mL)	V (mL)	$v/(V+v)$	pH	Correlation coefficient	Slope	Intercept
1	1.17×10^{-3}	0	10.5	0.000	9.01			
		1		0.0870	8.86			
		2		0.160	8.72			
				0.222	8.63	0.999	−1.73	9.01
2	1.17×10^{-3}	0	9.5	0.000	9.05			
		1		0.0952	8.91			
		2		0.174	8.81			
		3		0.240	8.77			
		4		0.296	8.67			
		4.6		0.326	8.60	0.992	−1.30	9.05
3	1.20×10^{-3}	0	10.0	0.000	9.03			
		1		0.0909	8.95			
		2		0.167	8.86			
		3		0.231	8.77			
		4		0.286	8.68			
		5		0.333	8.61	0.994	−1.28	9.05
4	1.20×10^{-3}	0	10.0	0.000	9.00			
		1		0.0909	8.88			
		2		0.167	8.79			
		3		0.231	8.71	0.999	−1.25	9.00
5	1.20×10^{-3}	0	10.0	0.000	9.10			
		1		0.0909	9.00			
		2		0.167	8.90			
		3		0.231	8.78			
		4		0.286	8.68	0.993	−1.47	9.12
6	1.22×10^{-3}	0	10.0	0.000	9.03			
		1		0.0909	8.95			
		2		0.167	8.85			
		3		0.231	8.75	0.992	−1.21	9.04

TABLE 3. Effect of γ cyclodextrin on the pH of NH_3(aq)

Run	Molarity of Cy added	V (mL)	V (mL)	$v/(V+v)$	pH	Correlation coefficient	Slope	Intercept
1	1.05×10^{-3}	0	10.0	0.000	9.03			
		1		0.0909	8.93			
		2		0.167	8.82			
		3		0.231	8.72			
		4		0.286	8.63	0.997	−1.41	9.04
2	1.05×10^{-3}	0	10.0	0.000	9.04			
		1		0.0909	8.93			
		2		0.167	8.85			
		3		0.231	8.75			
		4		0.286	8.65	0.994	−1.34	9.05
3	1.05×10^{-3}	0	10.0	0.000	9.02			
		1		0.0909	8.93			
		2		0.167	8.84			
		3		0.231	8.76	0.999	−1.13	9.03
4	1.03×10^{-3}	0	10.0	0.000	9.08			
		1		0.0909	8.99			
		2		0.167	8.90			
		3		0.231	8.83	0.999	−1.09	9.08
5	1.03×10^{-3}	0	10.0	0.000	9.07			
		1		0.0909	8.94			
		2		0.167	8.80			
		3		0.231	8.67	0.997	−1.73	9.08
6	1.01×10^{-3}	0	15.0	0.000	8.98			
		1		0.0625	8.86			
		2		0.118	8.75			
		3		0.167	8.66	0.999	−1.93	8.98
7	1.03×10^{-3}	0	10.0	0.000	9.06			
		1		0.0909	8.96			
		2		0.167	8.83			
		3		0.231	8.70	0.991	−1.56	9.08
8	1.04×10^{-3}	0	10.0	0.000	8.99			
		1		0.0909	8.88			
		2		0.167	8.77			
		3		0.231	8.68			
		4		0.286	8.62	0.999	−1.32	8.99

[3] $F_{NH_3} = (NH_3) + (NH_4^+) + (CyNH_3)$

where F_{NH_3} represents the total molar concentration of ammonia.

[4] $F_{Cy} = (Cy) + (CyNH_3)$

where F_{Cy} is the total molar cyclodextrin concentration.

[5] $K_w = (H^+)(OH^-)$

[6] $(NH_4^+) + (H^+) = (OH^-)$

from electroneutrality.

Gelb and co-workers report the existence of complexes formed between OH^- and α and β Cy, each with formation constants ≈ 50 (6). The concentrations of these complexes were found to be too small to affect eqs. [4] and [6], and hence the K_{CyNH_3} values within experimental error.

F_{NH_3} was obtained from the predicted initial value of (OH^-), employing eqs. [1], [5], and [6] and the dilution factor $V/(V + v)$. Next, (NH_3) and (NH_4^+) were obtained from the same equations using the value for (OH^-) for the predicted last point in each plot. Then, $(CyNH_3)$ was obtained from eq. [3] and after determining F_{Cy} from the concentration of Cy titrant and the dilution factor $v/(V + v)$, (Cy) was obtained from eq. [4]. Finally, K_{CyNH_3} was obtained for each run from eq. [2]. The average results of the runs and their standard deviations are listed in Table 4.

TABLE 4. Formation constants for cyclodextrin–ammonia complexes in aqueous solutions

Cyclodextrin	K_{CyNH_3} at (23 ± 1)°C
α	$(6.1 \pm 0.9) \times 10^4$
β	$(1.5 \pm 0.3) \times 10^4$
γ	$(2.2 \pm 0.8) \times 10^4$

The preceding model equations assume a 1:1 molecular ratio of NH_3 to Cy in each complex. This assumption seems warranted under the experimental conditions, i.e. $F_{Cy} > F_{NH_3}$. Moreover, the constancy of the calculated equilibrium constants between the runs, which employed different values for F_{Cy} and F_{NH_3}, seems to justify the assumption. Since the ionic strength of these dilute solutions was very low, activity coefficients are assumed to be unity.

The model equations assume that the ammonium cation is not included at all by the cyclodextrins. As a test of this assumption, the other assumptions above, and the validity of the method in general, aniline solutions were reacted with aqueous β cyclo-

Can. J. Chem. Downloaded from www.nrcresearchpress.com by 213.166.140.6 on 09/07/12
For personal use only.

dextrin, monitoring the pH as with ammonia above. The results of six trials using three separate cyclodextrin concentrations yield a formation constant for the inclusion complex (at 23°C) of 46 ± 8. This value is in good agreement with a literature value of 50 ± 3, which was obtained by uv–visible absorption spectrophotometry (9).

Discussion of results

The interactions of α, β, and γ cyclodextrins with aqueous ammonia produced significant pH decreases. The decrease in pH can be attributed to the formation of the inclusion complex $CyNH_3$. The decrease suggests that an ammonia molecule is being trapped inside the cavity of the cyclodextrins, and is not free to react with water. Hence, the solution becomes less alkaline. As the Cy concentration increases in the solution, the molar concentration of free ammonia decreases resulting the noted pH decreases. The binding constants of α, β, and γ cyclodextrins were $(6.1 \pm 0.9) \times 10^4$, $(1.5 \pm 0.3) \times 10^4$, and $(2.3 \pm 0.8) \times 10^4$, respectively. All three of the binding constants are quite large compared to those of acids and their anions, which were explained by dipole forces (6, 7). However, previous experiments (10, 11) have obtained binding constants in the order of magnitude of 10^4.

While there is about a four-fold decrease in the binding constant in going from the α to the β form, the constants for the β and γ are indistinguishable within experimental error. Apparently, the "tightness of fit" effect is not very important and after a certain ring size becomes negligible.

Gelb and associates (7) determined ΔS^0 and ΔH^0 for the complexation of 28 different guests by Cy, utilizing the temperature dependencies of the formation constants. For these guests, which were quite diverse in nature (anions, aliphatic and aromatic carboxylic acids, and other small organic molecules such as alcohols), the following empirical relationship was determined from a linear least-squares plot of ΔH^0 vs. ΔS^0

$$[7] \quad \Delta H^0 = (410 \pm 15)\Delta S^0 - (1.2 \pm 0.2) \times 10^3$$

where the units for ΔH^0 are cal mol^{-1} and those for ΔS^0 are cal mol^{-1} K^{-1}. However, there is apparently a scarcity of data on electrically neutral bases such as ammonia. Assuming that eq. [7] holds true for NH_3, since

$$[8] \quad \Delta G^0 = -RT \ln K = \Delta H^0 - T\Delta S^0$$

one calculates from Table 4 that for the α Cy–NH_3 complex,

$$\Delta G^0 = -6.49 \text{ kcal mol}^{-1}$$

$$\Delta S^0 = -46 \text{ cal mol}^{-1} \text{ K}^{-1}$$

$$\Delta H^0 = -20 \text{ kcal mol}^{-1}$$

The very large negative ΔH^0 in conjunction with only a small "tightness of fit" effect suggest that the intermolecular forces are strong and short range. Therefore, we suspect that hydrogen bonds augment the dipole forces postulated by Gelb *et al.* (7). In particular, the lone pair of NH_3 may hydrogen bond with —OH groups in the ring while its hydrogens may interact with —O— in the ring. Gelb *et al.* explain the fact that their standard entropy changes are consistently quite negative by conformational changes in the ring. This idea has also been advanced by others (5), and probably occurs with NH_3. The previous experiments (10, 11) which yielded binding constants of the order 10^4 involved the inclusion of the phenolphtalein and oxalate anions, respectively. Both of these contain —O's which may hydrogen bond to —OH groups in the Cy ring.

1. M. L. Bender and M. Komiyama. Cyclodextrin chemistry. Springer-Verlag, New York. 1978.
2. W. Saenger. Angew. Chem. Int. Ed. Engl. **19**, 344 (1980).
3. M. L. Bender. Cyclodextrins as enzyme models. *In* Proceedings of the First International Symposium on Solution Behavior, Theoretical and Practical Aspects. Vol. 2. *Edited by* K. J. L. Mittal and E. J. Fendler. Plenum Press, New York. 1982.
4. J. Szejtli. Cyclodextrins and their inclusion compounds. Akademiai Kiado, Budapest. 1982.
5. R. P. Rohrbach, L. J. Rodriguez, and E. M. Eyring. J. Phys. Chem. **81**, 944 (1976).
6. R. I. Gelb, L. M. Schwartz, B. Carelino, H. S. Fuhrman, R. R. Johnson, and D. A. Laufer. J. Am. Chem. Soc. **103**, 1750 (1981).
7. R. I. Gelb, L. M. Schwartz, M. Radeos, and D. A. Laufer. J. Phys. Chem. **87**, 3349 (1983).
8. R. G. Bates and G. D. Pinching. J. Am. Chem. Soc. **72**, 1393 (1950).
9. M. Hoshino, I. Masashi, I. Kiyoshi, and H. Yoshimasa. J. Phys. Chem. **85**, 1820 (1981).
10. A. Buvari and L. Barzca. Inorg. Chim. Acta, **33**, 179 (1980).
11. W. Hirsch, V. Fried, and L. Altman. J. Pharm. Sci. **74**, 1123 (1985).

Can. J. Chem. Downloaded from www.nrcresearchpress.com by 213.166.140.6 on 09/07/12
For personal use only.

The reactions of the chromate, dichromate, and permanganate ions with 100% sulfuric acid and dilute oleum

R. J. GILLESPIE AND R. KAPOOR
Department of Chemistry, McMaster University, Hamilton, Ont., Canada L8S 4M1

Received November 18, 1986[1]

R. J. GILLESPIE and R. KAPOOR. Can. J. Chem. **65**, 2665 (1987).

Solutions of potassium chromate and potassium dichromate in 100% sulfuric acid and dilute oleum have been investigated by cryoscopic and conductimetric methods. It is shown that they both react to give the compound $CrO_2(HSO_4)_2$. The absorption spectra of solutions of potassium chromate and dichromate in 100% sulfuric acid are very similar to the spectra of species of the type CrO_2X_2. Potassium permanganate dissolves in 100% sulfuric acid to give green solutions which are shown to contain $MnO_3 \cdot SO_4H$. The formation of this compound has been further confirmed by conductimetric measurements in dilute oleum. The absorption spectra of these green solutions are also consistent with the formation of a species of the type MnO_3X.

R. J. GILLESPIE et R. KAPOOR. Can. J. Chem. **65**, 2665 (1987).

Faisant appel à des méthodes cryoscopiques et conductimétriques, on a étudié des solutions de chromate et de bichromate de potassium dans l'acide sulfurique à 100% et dans de l'oléum dilué. On a démontré que chacun de ces composés réagit pour donner le composé $CrO_2(HSO_4)_2$. Les spectres d'absorption des solutions de chromate et de bichromate de potassium dans l'acide sulfurique à 100% sont très semblables à ceux des espèces du type CrO_2X_2. Le permanganate de potassium dissout dans l'acide sulfurique à 100% pour donner des solutions vertes et on a démontré qu'elles contiennent du $MnO_3 \cdot SO_4H$. On a de plus confirmé la formation de ce composé à l'aide de mesures conductimétriques dans l'oléum dilué. Les spectres d'absorption de ces solutions vertes sont aussi en accord avec la formation d'une espèce du type MnO_3X.

[Traduit par la revue]

Can. J. Chem. Downloaded from www.nrcresearchpress.com by 213.222.148.141 on 09/07/12
For personal use only.

Ever since the discovery of the NO^+ and NO_2^+ cations (1) there has been considerable speculation about the existence of other similar oxocations and there have been a number of studies which had the objective of establishing the existence of such ions. The existence of the dioxochlorine cation ClO_2^+ has been certainly established by X-ray crystallography and other studies on its salts with the anions AsF_6^- (2), SbF_6^-, and $Sb_3F_{16}^-$ (3). Although evidence has also been presented for ions that may be written as IO^+, IO_2^+ (4, 5), and AsO^+ (6), it is very probable that in fact they exist only in solvated forms even in highly acidic media, or as polymeric chains in the solid state. There is even less evidence for other oxocations. For example, phosphoric acid is converted to $H_4PO_4^+$ in solution in 100% sulfuric acid and PO_2^+ ion is not formed (7). Ammonium metavanadate and vanadium pentoxide have been shown to be solvolyzed to $OV(HSO_4)_3$ in 100% sulfuric acid and there is no evidence for the oxocation VO_2^+ as a discrete species (7) although it is known in strongly solvated forms such as $[VO_2(H_2O)_4]^+$ (8). The existence of other oxometal cations such as TiO^{2+}, ZrO^{2+}, and MoO_2^{2+} as discrete species has also not been established although they are known when they are coordinated with ligands to give anionic species.

In this paper we report a study of the possible formation of the oxocations of Cr(VI) and Mn(VII) in which we investigated the species formed by some of their compounds when they are dissolved in 100% sulfuric acid and dilute oleum.

Chromium(VI) compounds

Hayek and Engelbrecht (9) reported the formation of $CrO_2(SO_4)_2$ by the reaction of chromyl chloride, CrO_2Cl_2, with SO_3. Woolf (10) suggested that this compound is an ionic CrO_2^{2+} salt, i.e., $(CrO_2)^{2+}S_2O_7^{2-}$. Yatsimirskii and Vasil'eva (11) postulated the formation of $H_2Cr_2O_7$, and $H_2Cr_4O_{13}$ and other related compounds in solutions of chromates in 50–80% sulfuric acid. Symons and co-workers (12), from their study of the absorption spectrum of potassium chromate in 100% sulfuric acid, tentatively suggested that chromyl ion, CrO_2^{2+}, is formed in these solutions. But later Mishra and Symons (13) reported the conductivities of solutions of potassium chromate in 100% sulfuric acid. Their results are consistent with the formation of $CrO_2(OH)(HSO_4)$,

$$K_2CrO_4 + 4H_2SO_4 \rightarrow 2K^+ + CrO_2(OH)(HSO_4) + H_3O^+ + 3HSO_4^-$$

and are not in such good agreement with the formation of CrO_2^{2+}. However, the conductivity results alone are not sufficient to establish the mode of ionization unambiguously. We now report the results of cryoscopic and conductimetric measurements on solutions of potassium chromate and potassium dichromate in 100% sulfuric acid and dilute oleum.

Solutions in 100% H_2SO_4

Some difficulty was experienced in the preparation of solutions of potassium chromate and dichromate in 100% sulfuric acid. If the mixture was not vigorously stirred immediately after addition of the solute to 100% sulfuric acid a yellow solid compound separated out, which was insoluble even on heating. The identity of this solid could not be established with certainty, since it was very difficult to filter a significant amount from the sulfuric acid solution. It seems likely that this solid is CrO_3 which is insoluble in 100% sulfuric acid even at high temperatures. However, if the sulfuric acid was vigorously stirred on addition of the solute a clear solution was obtained. The results of the cryoscopic and conductimetric studies on these solutions are given in Table 1. We obtained a value of $\gamma = 4$ from the conductivity data rather than $\gamma = 3$ as reported by Mishra and Symons (13) and a value of $\nu = 9.0$.[2] Possible modes of ionization are

$$[1a] \quad K_2CrO_4 + 2H_2SO_4 \rightarrow 2K^+ + H_2CrO_4 + 2HSO_4 \qquad \nu = 5; \gamma = 2$$

[1]Revision received July 2, 1987.

[2]γ is the number of moles of HSO_4^- formed by one mole of the solute and ν is the total number of moles of ions and molecules produced in solution by one mole of the solute (1).

Can. J. Chem. Downloaded from www.nrcresearchpress.com by 213.222.148.141 on 09/07/12
For personal use only.

TABLE 1. Freezing points and conductivities of solutions of K_2CrO_4 and $K_2Cr_2O_7$ in 100% sulfuric acid

Solute	$10^2\ m$	Freezing point (°C)	ν	$10^2\ \kappa$ (ohm^{-1} cm^{-1})	γ
K_2CrO_4					
	0.4	10.245	9.2	1.2960	
	1.2	9.872	9.2	1.5000	
	1.6	9.668	9.1	1.7000	4.0
	2.0	9.461	9.1	1.9040	
	2.4	9.255	9.0	2.1090	
	2.8	9.048	8.9	—	
	3.2	8.828	8.9	—	
$K_2Cr_2O_7$	0.2			1.0675	
	0.4			1.1400	
	0.6			1.2350	
	0.8			1.3525	
	1.0			1.4725	5.0
	1.2			1.5950	
	1.4			1.7125	
	1.6			1.8350	
	1.8			1.9500	
	2.0			2.0675	

[2a] $K_2CrO_4 + 3H_2SO_4 = 2K^+ + H_3CrO_4^+ + 3HSO_4^-$ $\quad \nu = 6; \gamma = 3$

[3a] $K_2CrO_4 + 6H_2SO_4 = 2K^+ + CrO_2^{2+} + 2H_3O^+ + 6HSO_4^-$ $\quad \nu = 11; \gamma = 6$

[4a] $K_2CrO_4 + 9H_2SO_4 = 2K^+ + CrO^{4+} + 3H_3O^+ + 9HSO_4^-$ $\quad \nu = 15; \gamma = 9$

[5a] $K_2CrO_4 + 4H_2SO_4 = 2K^+ + CrO_2(OH)(HSO_4) + H_3O^+ + 3HSO_4^-$ $\quad \nu = 7; \gamma = 3$

[6a] $K_2CrO_4 + 7H_2SO_4 = 2K^+ + CrO(SO)_4)_2 + 3H_3O^+ + 5HSO_4^-$ $\quad \nu = 11; \gamma = 5$

[7a] $K_2CrO_4 + 5H_2SO_4 \rightarrow 2K^+ + CrO_2(SO_4) + 2H_3O^+ + 4HSO_4^-$ $\quad \nu = 9; \gamma = 4$

[8a] $K_2CrO_4 + 6H_2SO_4 \rightarrow 2K^+ + CrO_2(HSO_4)_2 + 2H_3O^+ + 4HSO_4^-$ $\quad \nu = 9; \gamma = 4$

These results support the formation of $CrO_2(HSO_4)_2$ or $CrO_2(SO_4)$ in sulfuric acid (eqs. [7a] and [8a]). It is not possible to distinguish between these two possibilities on the basis of the cryoscopic and conductimetric results because they differ only by a solvent molecule, but it is very probable that the compound formed in a large excess of sulfuric acid is $CrO_2(SO_4H)_2$.

The conductivity results on solutions of potassium dichromate in 100% sulfuric acid (Table 1) can be accounted for by a reaction similar to that proposed for potassium chromate, namely

$$K_2Cr_2O_7 + 9H_2SO_4 \rightarrow 2K^+ + 2CrO_2(HSO_4)_2 + 3H_3O^+ + 5HSO_4^- \qquad \gamma = 5$$

For the formation of $CrO_2(OH)(HSO_4)$ as suggested by Mishra and Symons (13),

$$K_2Cr_2O_7 + 5H_2SO_4 = 2K^+ + 2CrO_2(OH)(HSO_4) + H_3O^+ + 3HSO_4^-$$

a γ value of 3 would be expected.

TABLE 2. Conductivities of solutions of K_2CrO_4 and $K_2Cr_2O_7$ in dilute oleum

$r = \frac{n_b}{n_a}$	$10^2\ \kappa$ (ohm^{-1} cm^{-1})	$r = \frac{n_b}{n_a}$	$10^2\ \kappa$ (ohm^{-1} cm^{-1})
K_2CrO_4		$K_2Cr_2O_7$	
#1 Initial molality of $H_2S_2O_7 = 0.083$		#1 Initial molality of $H_2S_2O_7 = 0.077$	
0.000	1.427	0.000	1.398
0.086	1.226	0.062	1.244
0.141	1.155	0.090	1.189
0.175	1.128	0.115	1.149
0.237	1.129	0.148	1.115
0.284	1.185	0.170	1.110
0.346	1.310	0.223	1.143
#2 Initial molality of $H_2S_2O_7 = 0.099$		#2 Initial molality of $H_2S_2O_7 = 0.059$	
0.000	1.499	0.000	1.301
0.086	1.264	0.019	1.260
0.135	1.175	0.050	1.204
0.169	1.146	0.084	1.155
0.191	1.136	0.107	1.128
0.219	1.146	0.138	1.104
0.266	1.201	0.160	1.095
0.313	1.311	0.195	1.101
		0.236	1.134

Solutions in dilute oleum

Further evidence for the ionization of potassium chromate and dichromate in sulfuric acid has been obtained by conductimetric titrations in dilute oleum at 25°C, the results of which are shown in Table 2 and Fig. 1.

The reaction of potassium chromate with dilute oleum can be conveniently considered to take place in two stages: first the reaction of potassium chromate with 100% H_2SO_4

$$K_2CrO_4 + 4H_2SO_4 = 2K^+ + 2HSO_4^- + CrO_2(HSO_4)_2 + 2H_2O$$

followed by the reaction of $H_2S_2O_7$ with H_2O and HSO_4^-. Two moles of $H_2S_2O_7$ are needed to react with two moles of H_2O and $2(1/0.56)$ moles of $H_2S_2O_7$ are needed to react with two moles of HSO_4^- to give a conductivity minimum (14). Thus a conductivity minimum in the titration of n_a moles of $H_2S_2O_7$ with n_b moles of K_2CrO_4 will be obtained at the ratio

$$n_b/n_a = 1/[2 + 2(1/0.56)] = 0.18$$

which is very close to the experimental value of 0.19.

Addition of potassium dichromate to dilute oleum gives a minimum at $r_{min} = n_b/n_a = 0.16$ (Table 2 and Fig. 1). The reaction of potassium dichromate in 100% sulfuric acid can be written as

$$K_2Cr_2O_7 + 6H_2SO_4 = 2K^+ + 2HSO_4^- + 2CrO_2(HSO_4)_2 + 3H_2O$$

Thus the minimum in the conductivity curve for this reaction would be expected at

$$n_b/n_a = 1/[3 + 2(1/0.56)] = 0.15$$

where n_b and n_a are the molalities of potassium dichromate and initial acid, respectively.

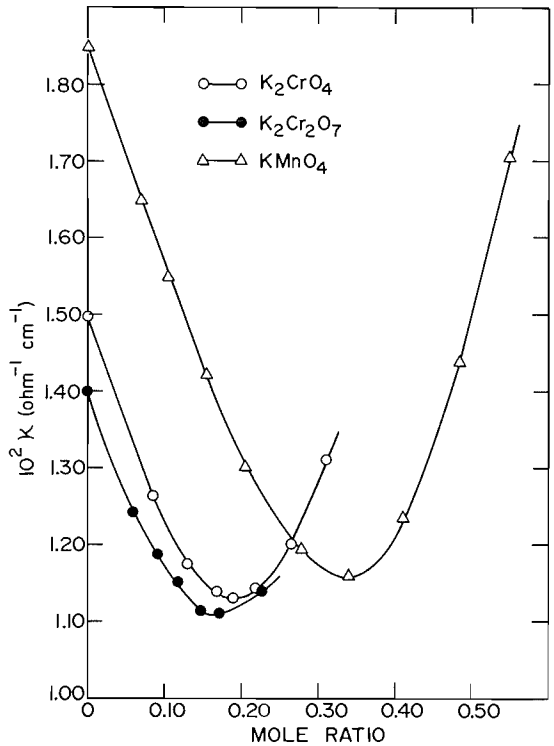

FIG. 1. Conductivities of solutions of potassium chromate, potassium dichromate, and potassium permanganate in dilute oleum.

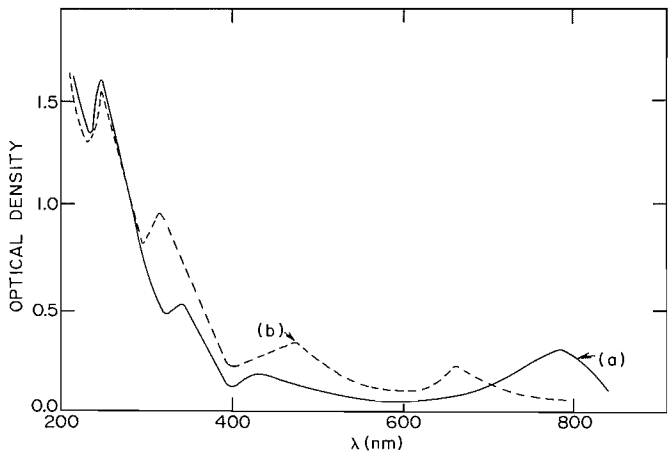

FIG. 2. Absorption spectra of a solution of (*a*) potassium chromate/potassium dichromate, and (*b*) potassium permanganate in 100% sulfuric acid.

Absorption spectra

The visible and ultraviolet absorption spectra of solutions of potassium chromate and potassium dichromate in 100% sulfuric acid have been studied and a typical spectrum is given in Fig. 2. Absorption maxima occur at 250, 340, 420, and 780 nm. The solutions obey Beer's law and the values for the molar extinction coefficients are given in Table 3.

It is seen that both potassium chromate and potassium dichromate give the same absorption spectrum and the values for the molar extinction coefficient for $K_2Cr_2O_7$ are twice those observed for K_2CrO_4. This strongly suggests that both these compounds give the same species in 100% sulfuric acid.

TABLE 3. Absorption maxima for solutions of potassium chromate and potassium dichromate in 100% sulfuric acid

K_2CrO_4		$K_2Cr_2O_7$	
λ (nm)	ϵ	λ (nm)	ϵ
250	5 500	250	11 000
340	1 400	340	2 750
420	300	420	600
780	400	780	780

It has been pointed out that the ultraviolet and visible spectrum of Cr^{VI} in 72% perchloric acid is close to that expected for H_2CrO_4 (12) and resembles the spectrum of CrO_2Cl_2 (15). The spectrum obtained for potassium chromate and dichromate in 100% sulfuric acid (Fig. 2) is similar to that reported by Mishra and Symons (13) and is very similar to that of CrO_2Cl_2. The similarity between these spectra strongly suggests that they all arise from species of the type CrO_2X_2. It is concluded that in 72% $HClO_4$ chromate is converted to $CrO_2(OH)_2$ while in 100% H_2SO_4 both chromate and dichromate are converted to $CrO_2(HSO_4)_2$.

Potassium permanganate

It has been known for a long time that the dissolution of a small amount of potassium permanganate in concentrated sulfuric acid produces a green solution (16). Franke (17) suggested that the green colour was due to $(MnO_3)_2SO_4$, but he gave no direct evidence for this species.

Symons and co-workers (12), from their study of the absorption spectrum of potassium permanganate in 100% sulfuric acid, postulated that the green species is permanganic acid. Royer (18) has studied the conductivity and freezing point of $KMnO_4$ in slightly aqueous sulfuric acid. He explained his results in terms of the formation of the permanganyl ion, MnO_3^+, according to the following equation

$$KMnO_4 + 3H_2SO_4 \rightarrow K^+ + MnO_3^+ + H_3O^+ + 3HSO_4^- \quad \nu = 6; \gamma = 3$$

He also suggested that the absorption spectrum of the green species was consistent with the formation of the planar MnO_3^+ ion.

Subsequently Mishra and Symons (13) studied the behaviour of $KMnO_4$ in 100% sulfuric acid. They obtained a γ value of 2.0–2.2 and taking into account the average of Royer's ν values, which is in fact closer to 5 than 6, they proposed the reaction

$$KMnO_4 + 3H_2SO_4 \rightarrow K^+ + MnO_3{\cdot}SO_4H + H_3O^+ + 2HSO_4^- \quad \nu = 5; \gamma = 2$$

These authors also carried out a conductimetric titration of $KMnO_4$ in dilute oleum and found $r_{min} = n_{KMnO_4}/n_a = 0.28$, although as we shall show the above equation would predict a conductivity minimum at $r_{min} = 0.36$.

Because the previous cryoscopic and conductimetric work did not lead to unambiguous conclusions, we made some further studies on solutions of $KMnO_4$ in 100% sulfuric acid and dilute oleum.

Can. J. Chem. Downloaded from www.nrcresearchpress.com by 213.222.148.141 on 09/07/12
For personal use only.

Can. J. Chem. Downloaded from www.nrcresearchpress.com by 213.222.148.141 on 09/07/12
For personal use only.

TABLE 4. Freezing points and conductivities of solutions of potassium permanganate in 100% sulfuric acid

$10^2\ m$	Freezing point (°C)	ν	$10^2\ \kappa$ ($ohm^{-1}\ cm^{-1}$)	γ
0.02	9.970	4.9	1.345	
0.03	9.690	4.9	1.620	
0.04	9.385	4.9	1.900	
0.05	9.075	4.9	2.170	2.0
0.06	8.780	4.9	2.430	
0.07	8.475	4.9	2.710	

TABLE 5. Conductivities of solutions of potassium permanganate in dilute oleum

$r = \frac{n_b}{n_a}$	$10^2\ \kappa$ ($ohm^{-1}\ cm^{-1}$)
Initial molality of $H_2S_2O_7$ = 0.185	
0.000	1.848
0.069	1.648
0.105	1.550
0.154	1.421
0.206	1.303
0.274	1.196
0.341	1.162
0.411	1.236
0.484	1.437
0.550	1.706

Potassium permanganate dissolves both in 95% and 100% sulfuric acid to give green solutions which if they are less concentrated than 0.05 molal are reasonably stable for about 24 h. More concentrated solutions were less stable, becoming turbid after 3–4 h, and eventually depositing MnO_2 with the evolution of oxygen gas.

The results of the cryoscopic and conductimetric studies are given in Table 4. Possible reactions are

[1b] $KMnO_4 + H_2SO_4 = K^+ + HMnO_4 + HSO_4^-$ $\quad \nu = 3; \gamma = 1$

[2b] $KMnO_4 + 2H_2SO_4 = K^+ + H_2MnO_4^+ + 2HSO_4^-$ $\quad \nu = 4; \gamma = 2$

[3b] $KMnO_4 + 3H_2SO_4 = K^+ + MnO_3^+ + H_3O^+ + 3HSO_4^-$ $\quad \nu = 6; \gamma = 3$

[4b] $KMnO_4 + 3H_2SO_4 = K^+ + MnO_3SO_4H + H_3O^+ + 2HSO_4^-$ $\quad \nu = 5; \gamma = 2$

It is clear from Table 4 that the results are consistent with the formation of MnO_3SO_4H (eq. [4b]).

The results of a conductimetric titration of $KMnO_4$ in dilute oleum at 25°C are given in Table 5 and Fig. 1. If there are initially n_a moles of $H_2S_2O_7$, and n_b moles of $KMnO_4$ are added to give a conductivity minimum and assuming ionization according to eq. [4b]

$$n_b/n_a = 1/(1 + 1/0.56) = 0.36$$

at the conductivity minimum. The experimental value of $n_b/n_a = 0.36$ is in good agreement with the value calculated on the basis of eq. [4b] above although the value of Mishra and Symons of $n_b/n_a = 0.28$ is not in such good agreement with our experimental value or the calculated value. If the product of the ionization had been the MnO_3^+ ion a conductivity minimum would have been expected at

$$n_b/n_a = 1/[1 + (2/0.56)] = 0.22$$

The previous evidence did not clearly establish the mode of ionization of $KMnO_4$ but our new results confirm the suggestion of Mishra and Symons that it ionizes according to eq. [4b] above.

TABLE 6. Absorption maxima for solutions of potassium permanganate in 100% sulfuric acid

λ (nm)	ε
250	4 400
310	2 500
460	480
650	140

Absorption spectra

The visible and ultraviolet absorption spectrum of green solutions of potassium permanganate in 100% sulfuric acid is shown in Fig. 2. Four absorption maxima were found at 250, 310, 460, and 650 nm. The solutions obey Beer's law and the values for the molar extinction coefficient are given in Table 6. The spectrum is very similar to that observed for CrO_3Cl^- and CrO_3F^- (12, 15), and is also in accord with the changes expected in going from MnO_4^- (symmetry T_d) to the MnO_3X species (symmetry C_{3v}). This is consistent with the other evidence that the green species is $MnO_3 \cdot SO_4H$.

Experimental section

The freezing-point depression and electrical conductivities of solutions were measured by methods described previously (19–21). Potassium chromate, potassium dichromate, and potassium permanganate were (BDH, AnalaR) samples and were kept over P_4O_{10} in a desiccator before use.

The preparation of the 100% sulfuric acid solvent has been described previously (19, 20). Oleums of known composition were obtained by distilling sulfur trioxide into a weighed amount of 100% sulfuric acid.

1. R. J. GILLESPIE and E. A. ROBINSON. *In* Non-aqueous solvents. *Edited by* T. C. Waddington. Academic Press. 1965.
2. C. J. SHACK and D. PILIPOVITCH. Inorg. Chem. **9**, 387 (1970).
3. J. J. RENARD and H. I. BOLKER. Chem. Rev. **76**, 487 (1976).
4. R. J. GILLESPIE and J. B. SENIOR. Inorg. Chem. **3**, 972 (1964).
5. J. R. DALZIEL, H. A. CARTER, and F. AUBKE. Inorg. Chem. **15**, 1247 (1976).
6. R. J. GILLESPIE and E. A. ROBISON. Can. J. Chem. **41**, 450 (1963).
7. R. J. GILLESPIE, R. KAPOOR, and E. A. ROBINSON. Can. J. Chem. **44**, 1203 (1966).
8. F. A. COTTON and G. WILKINSON. Advanced inorganic chemistry. John Wiley and Sons, New York. 1980. p. 712.
9. E. HAYEK and A. ENGELBRECHT. Monatsh. Chem. **80**, 640 (1949).
10. A. A. WOOLF. Chem. Ind. London, 1320 (1954).
11. K. B. YATSIMIRSKII and V. N. VASIL'EVA. Zhur. Neorg. Khim. **1**, 1983 (1956).

12. N. BAILEY, A. CARRINGTON, K. A. K. LOTT, and M. C. R. SYMONS. J. Chem. Soc. 290 (1960).
13. H. C. MISHRA and M. C. R. SYMONS. J. Chem. Soc. 4411 (1962).
14. R. H. FLOWERS, R. J. GILLESPIE, and E. A. ROBINSON. Can. J. Chem. **38**, 1363 (1960).
15. L. HELMHOLZ, H. BRENNAN, and M. WOLFSBERG. J. Chem. Phys. **23**, 853 (1955).
16. H. ASCHOFF. J. Prakt. Chem. (1) **81**, 29 (1860); Chem. News, **6**, 57 (1861).
17. B. FRANKE. J. Prakt. Chem. (2) **36**, 31 (1887).
18. D. J. ROYER. J. Inorg. Nucl. Chem. **17**, 159 (1961).
19. R. J. GILLESPIE, J. O. V. OUBRIDGE, and C. SOLOMONS. J. Chem. Soc. 1804 (1957).
20. R. J. GILLESPIE, E. D. HUGHES, and C. K. INGOLD. J. Chem. Soc. 2504 (1950).
21. R. H. FLOWERS, R. J. GILLESPIE, and E. A. ROBINSON. Can. J. Chem. **41**, 264 (1963).

Can. J. Chem. Downloaded from www.nrcresearchpress.com by 213.222.148.141 on 09/07/12
For personal use only.

The oxidation of stannous halides by tetrahalogeno-*ortho*-quinones, and the crystal structure of bis[2-(dimethylamino)ethyldimethylammonium] tris(tetrachlorocatecholato)tin(IV), $(Me_2NC_2H_4NMe_2H)_2[Sn(O_2C_6Cl_4)_3]$

THEODORE A. ANNAN
Department of Chemistry and Biochemistry, University of Windsor, Windsor, Ont., Canada N9B 3P4

RAJ K. CHADHA
Department of Chemistry, University of Manitoba, Winnipeg, Man., Canada R3T 2N2

AND

DENNIS G. TUCK AND KATHERINE D. WATSON
Department of Chemistry and Biochemistry, University of Windsor, Windsor, Ont., Canada N9B 3P4

Received April 2, 1987

THEODORE A. ANNAN, RAJ K. CHADHA, DENNIS G. TUCK, and KATHERINE D. WATSON. Can. J. Chem. **65**, 2670 (1987).

The reaction between SnX_2 (X = Cl, Br, I), 1,10-phenanthroline (phen) and $Y_4C_6O_2$ (Y = Cl, Br) yields $Y_4C_6O_2SnX_2$.phen with the *o*-quinone being converted to the corresponding catecholate anion. Reactions in which phen is replaced by $Me_2NC_2H_4NMe_2$ (tmen) are more complex, and the products depend in part on the solvent. These products include $Cl_4C_6O_2SnCl_2$.tmen, and products arising from solvation by ROH (R = CH_3, C_2H_5). An X-ray crystallographic study of $(tmenH)_2[Sn(O_2C_6Cl_4)_3]$ shows that the anion contains a six-coordinate tin atom bonded to substituted catecholate anions. Hydrogen-bonding between cation and anion appears to be an important factor in the stability of the lattice.

THEODORE A. ANNAN, RAJ K. CHADHA, DENNIS G. TUCK et KATHERINE D. WATSON. Can. J. Chem. **65**, 2670 (1987).

La réaction du SnX_2 (X = Cl, Br, I) phénanthroline (phen) avec le $Y_4C_6O_2$ (Y = Cl, Br) conduit au $Y_4C_6O_2SnX_2$.phen alors que la *o*-quinone est transformée en anion catécholate correspondant. Les réactions dans lesquelles le phen est remplacé par le $Me_2NC_2H_4NMe_2$ (tmen) sont plus complexes et la nature des produits dépend du solvant. Parmi ces produits, on retrouve le $Cl_4C_6O_2SnCl_2$.tmen et des produits qui proviennent de la solvatation par ROH (R = CH_3, C_2H_5). Une étude par diffraction des rayons-X du $(tmenH)_2[Sn(O_2C_6Cl_4)_3]$ démontre que l'anion contient un atome de Sn(IV) qui est hexacoordonné et qui est lié aux anions catécholates substitués. Les liaisons hydrogènes entre le cation et l'anion semblent être des facteurs importants dans la stabilité du réseau.

[Traduit par la revue]

Introduction

Although there is considerable literature on the reactions between *ortho*-quinones and transition metal ions, the corresponding oxidations of lower state Main Group metals have not been widely studied. In recent work, we have investigated the reaction of indium(I) halides (InX) in non-aqueous media with a variety of substituted *o*-quinones to give the corresponding XIn^{III}(catecholate) species. Electron spin resonance spectroscopy shows that these redox reactions proceed via one-electron, rather than two-electron, processes (1). We now report the results of a parallel preparative study of the reaction between stannous halides (SnX_2) and the tetrahalogeno-substituted *o*-quinones $Y_4C_6O_2$ (X = Cl, Br) to give the corresponding catecholate $Y_4C_6O_2SnX_2$, which were isolated as the adducts with bidentate neutral donors. During an investigation of the possible insertion of indium(I) chloride into the Sn—X bond of one of these products, we recovered the rearranged product $(tmenH)_2[Sn(O_2C_6Cl_4)_3]$ (tmen = *N,N,N',N'*-tetramethylethanediamine), whose structure was determined by X-ray crystallography.

Experimental

General

Tin(II) halides (Alfa), tetrahalogeno-*o*-quinones, 1,10-phenanthroline (phen), and tmen (Aldrich) were used as supplied. Solvents were dried by conventional methods, and stored over drying agents. All reactions were carried out in an atmosphere of dry nitrogen.

Tin analysis was by atomic absorption spectrophotometry, and microanalysis was carried out by Guelph Chemical Laboratory. Total halogen analysis of reaction products by the Oakdale–Thompson method proved unreliable, and the presence of the *o*-quinone in acidified aqueous solution prevented the use of the Volhard method. Proton nmr spectra were recorded on a Varian EM 360 instrument, and ^{13}C spectra on a General Electric GN 300 instrument at Wayne State University, Detroit, MI. Mass spectrometry was carried out on a Varian MAT CH-5DF instrument operating in the electron impact or field desorption modes. Infrared spectroscopy involved the use of samples in KBr discs with a Nicolet 5DX instrument.

Preparative

(*a*) A solution of $SnCl_2$ (0.39 g, 2 mmol) and tetrachloro-*o*-quinone (0.50 g, 2 mmol) in acetone (50 mL) was stirred mechanically for 1 h at room temperature to give a yellow–orange solution. Addition of phen (0.31 g, 2 mmol) precipitated $Cl_4C_6O_2SnCl_2$.phen in quantitative yield. Later work showed that the synthesis is more conveniently carried out by refluxing equimolar quantities of $SnCl_2$, $Cl_4C_6O_2$ (or $Br_4C_6O_2$), and phen in acetone for 1 h, and this technique was used in the preparation of analogous compounds listed in Table 1, since direct reaction at room temperature is unsatisfactory with $SnBr_2$ or SnI_2. The yellow–orange solids were collected, washed successively with acetone (2 × 20 mL) and *n*-pentane (20 mL), and dried *in vacuo*.

(*b*) $Cl_4C_6O_2SnI_2$.phen can also be prepared by refluxing tin metal (0.4 g, 2.4 mmol), iodine (0.86 g, 3.4 mmol calculated as I_2), and $Cl_4C_6O_2$ (0.83 g, 3.4 mmol) in toluene (50 mL) for 3 h, by which time the tin had dissolved to give a light green solution. An equimolar quantity of phen was then added, and refluxing stopped. The mixture was stirred for 1 h as it cooled; the orange solid which formed was then collected and washed as described above.

(*c*) $SnCl_2$ (0.39 g, 2 mmol) was suspended in toluene (50 mL) containing an equimolar quantity of $Cl_4C_6O_2$ (0.5 g), and tmen (0.35 g, 3 mmol) added to the red solution. The mixture was stirred at room temperature for 16 h, and then filtered, to give an off-white solid which

Can. J. Chem. Downloaded from www.nrcresearchpress.com by 213.166.140.6 on 09/07/12
For personal use only.

TABLE 1. Analytical results

Compound	Found/calcd. (%) Sn	C	H	N	Molar mass
$Cl_4C_6O_2SnCl_2$.phen	19.0(19.3)	36.0(35.1)	1.59(1.31)	4.6(4.6)	616
$Cl_4C_6O_2SnBr_2$.phen	14.4(15.0)	27.7(27.2)	1.21(1.02)	3.3(3.5)	704
$Cl_4C_6O_2SnI_2$.phen	16.9(16.8)	—	—	—	—
$Br_4C_6O_2SnCl_2$.phen	13.7(13.5)	—	—	—	794
$Br_4C_6O_2SnBr_2$.phen	15.0(14.9)	—	—	—	—
$Br_4C_6O_2SnI_2$.phen	11.8(12.2)	—	—	—	—
$Cl_4C_6O_2SnCl_2$.tmen	21.3(21.5)	—	—	—	552
$Cl_4C_6O_2SnCl_2$.tmen.$2CH_3OH$	18.8(19.3)	—	—	—	—
$Cl_4C_6O_2Sn(OCH_3)_2$	27.6(27.8)	—	—	—	—
$Cl_4C_6O_2SnCl_2$.tmen.C_2H_5OH	19.8(19.9)	—	—	—	—
$Cl_4C_6O_2Sn(OC_2H_5)_2$	25.9(26.1)	—	—	—	—
$(tmenH)_2[Sn(O_2C_6Cl_4)_3]$	10.6(10.9)	32.3(33.0)	3.26(3.14)	5.1(5.1)	—

was washed with toluene and then *n*-pentane, and dried *in vacuo*. This solid was identified as $Cl_4C_6O_2SnCl_2$.tmen on the basis of metal analysis, infrared and ^1H nmr spectroscopy. Repetition of this procedure with $Br_4C_6O_2$ in place of the tetrachloro-*o*-quinone gave as the final insoluble product a beige-coloured solid which contained tmen and the $Br_4C_6O_2^{2-}$ ligand, but did not correspond analytically to $Br_4C_6O_2SnCl_2$.tmen (calcd Sn 16.3%; found Sn 24.7%). ^1H nmr, singlets at 2.72 and 3.33 ppm from Me_4Si, in d_6-dmso.

(*d*) A mixture of $SnCl_2$ and $Cl_4C_6O_2$ (quantities as in (*c*)) was dissolved in acetone, and tmen (0.35 g, 3 mmol) added; the solution darkened in colour, and a slight cloudiness developed. After 1 h, the now pale yellow solution was filtered to remove a white solid, and the solution evaporated *in vacuo* to yield crystals of $Cl_4C_6O_2SnCl_2$.tmen. The white solid collected by filtration contained Sn (32%) and $Cl_4C_6O_2$, but no tmen. This material was not investigated further.

(*e*) Stannous chloride (0.56 g, 3.0 mmol) was dissolved in dry methanol (50 mL), and tmen (0.35 g, 3.0 mmol) added dropwise to the stirred solution. The slight cloudiness disappeared on warming the solution. A methanol solution of $Cl_4C_6O_2$ (0.73 g, 3.0 mmol in 50 mL) was added dropwise over 1 h. Some slight precipitation was obvious at this point, and on refluxing over 4 h considerable quantities of solid were thrown down. This solid was collected, washed with hot methanol (2 × 20 mL), and dried *in vacuo*. This material was identified as $Cl_4C_6O_2SnCl_2$.tmen.$2CH_3OH$ (A) on the basis of metal analysis (Table 1), infrared and ^1H nmr spectroscopy (Table 5). Yield 0.87 g. No spectroscopic or weight changes were detected after heating the substance *in vacuo* (60°C, 6 h).

The filtrate from this reaction was taken to dryness *in vacuo*, giving a mixture of colourless and yellow powders. The former was found to be insoluble in most common organic solvents, and the compounds were separated by treatment with hot acetonitrile. The insoluble colourless solid (weight 0.24 g) was identified as the salt $(tmenH_2)Cl_2$ (B) (analysis: found Cl 37.4, calcd 37.5%). ^1H nmr in D_2O showed singlets at 3.7 (4H) and 3.0 (12H) ppm from internal sodium 3-(trimethylsilyl)propionate. The molar conductivity of a m*M* solution in H_2O was 209 $ohm^{-1}\ mol^{-1}\ cm^2$, slightly less than the classical value of 240 $ohm^{-1}\ mol^{-1}\ cm^2$ for 2:1 electrolytes.

The acetonitrile extract of the above solid mixture was subsequently taken to dryness *in vacuo*. Analysis and spectroscopy showed that this compound is $Cl_4C_6O_2Sn(OCH_3)_2$ (C).

The total mass of products A, B, and C was 1.72 g, to be compared with 1.64 g of reactants used. After making appropriate allowance for the MeOH and MeO incorporated into A and C, the mass balance accounts for 94% of the starting materials.

(*f*) Stannous chloride (0.50 g, 2.6 mmol) and $Cl_4C_6O_2$ (0.65 g, 2.6 mmol) were dissolved in dry ethanol (50 mL), and 0.4 mL (2.6 mmol) of tmen added to the pale yellow solution. An instant opalescence was followed by the formation of a white precipitate. The mixture was refluxed for 12 h under nitrogen, after which the precipitate was collected by filtration, washed with hot ethanol (2 × 20 mL) and dried overnight *in vacuo*. This solid is $Cl_4C_6O_2SnCl_2$.tmen.C_2H_5OH. The filtrate was treated by the method described above for the methanol solution, and the products identified were $(tmenH_2)Cl_2$ and $Cl_4C_6O_2Sn(OC_2H_5)_2$.

(*g*) The compound $(tmenH)_2[Sn(O_2C_6Cl_4)_3]$ was produced in the course of an unsuccessful attempt to insert indium(I) chloride into a Sn—Cl bond of $Cl_4C_6O_2SnCl_2$. Tin(II) chloride (0.39 g, 2 mmol) and $Cl_4C_6O_2$ (0.5 g, 2 mmol) were stirred together in methanol (25 mL), and the resultant solution added dropwise to a solution of InCl (0.31 g, 2 mmol) in 50 mL tmen/toluene (1:50) at −40°C (cf. ref. 3). The mixture was stirred for 1 h to give a clear solution, after which the cooling bath was removed, and stirring continued for 1 h as the solution reached room temperature (~25°C). After filtration to remove impurities, the solution was evaporated *in vacuo*; the resultant solid was recrystallized from methanol, and the crystals washed with *n*-pentane and dried *in vacuo*. Analysis, spectroscopy, and a subsequent X-ray crystallographic study showed that this product is $(tmenH)_2[Sn(O_2C_6Cl_4)_3]$.

X-ray crystallographic analysis

A single crystal of $(tmenH)_2[Sn(O_2C_6Cl_4)_3]$ (**1**) was mounted along the largest dimension, and the cell parameters obtained from 15 strong reflections with $15° < 2\theta < 30°$. Data were collected on a Syntex $P2_1$ diffractometer following the procedure described previously (4). The intensities of three monitored reflections did not change significantly during data collection. The data were corrected for Lorentz and polarization effects; no absorption correction was deemed necessary because of the low absorption coefficient. Details of the X-ray data collection are given in Table 2.

The systematic absences (hkl, $h + k = 2n + 1$; $h0l$, $l = 2n + 1$) indicated the space groups $C2/c$ or Cc. The former was used and later assumed to be correct because of the successful refinement of the structure. Computation was carried out on the University of Manitoba Computer Services Department's Amadahl 580/5850 mainframe computer. The position of the tin atom was obtained from a sharpened Patterson synthesis using SHELX, 1976, and was found to be on a twofold axis. The positions of remaining non-hydrogen atoms were determined from a difference Fourier map. The structure was refined anisotropically using full-matrix least-squares methods, and the refinement converged at $R = (\Sigma||F_o| - |F_c||/\Sigma|F_o|) = 0.0369$. Hydrogen atoms were included in subsequent refinement in ideal positions (C—H 0.95 Å and CCH 109.5°), leading to the final values $R = 0.0324$ and $R_w = [E_w\Delta^2/\Sigma_w F_o^2]^{1/2} = 0.0378$. The function $(|F_o| - |F_c|)^2$ was minimized during least-squares refinement; in the final cycles, a weighting scheme of the form $w = 1/[\sigma^2(F) + pF]^2$ was employed, with a final p value of 0.0011. No evidence of secondary extinction was found.

Can. J. Chem. Downloaded from www.nrcresearchpress.com by 213.166.140.6 on 09/07/12
For personal use only.

Can. J. Chem. Downloaded from www.nrcresearchpress.com by 213.166.140.6 on 09/07/12
For personal use only.

TABLE 2. Summary of crystal intensity data, collection, and structural refinement for $(tmenH)_2[Sn(O_2C_6Cl_4)_3]$

Cell constants	$a = 20.501(8)$ Å, $b = 12.607(3)$ Å $c = 17.357(7)$ Å; $\beta = 113.53(5)°$
Cell volume (Å^3)	4113(4)
Crystal system	Monoclinic
Space group	$C2/c$
Mol. wt.	1090.6
Z, $F(000)$	4, 2168
ρ_c, ρ_0 (g cm^{-3})	1.76, 1.80
Crystal dimensions (mm)	0.21 × 0.27 × 0.28
Absorption coefficient, μ (cm^{-1})	13.33
Radiation	MoKα, $\lambda = 0.71069$ Å
Monochromator	Highly oriented graphite
Temperature (°C)	24
2θ angle (deg)	45
Scan type	coupled θ (crystal)/2θ (counter)
Scan width	$K_{\alpha_1} - 1°$ to $K_{\alpha_2} + 1°$
Scan speed (deg min^{-1})	variable, 2.02–4.88
Background time/scan time	0.5
Total reflections measured	4133 $[+h, +k, \pm l)$
Unique data used	2901 $[I > 3\sigma(I)]$
No. of parameters (NP)	240
$R = (\Sigma\|\|F_o\| - \|F_c\|\|/\Sigma\|F_o\|)$	0.0324
$R = [\Sigma w(\|\|F_o\| - \|F_c\|\|)^2/\Sigma w\|F_o\|^2]^{1/2}$	0.0378

TABLE 3. Final fractional coordinates and isotropic thermal parameters for non-hydrogen atoms of $(tmenH)_2[Sn(O_2C_6Cl_4)_3]$ with standard deviations in parentheses[a]

Atom	x	y	z	U_{eq}^* (Å^2 × 10^3)
Sn	0.0	0.10175(3)	0.25000	33.1(2)
Cl(1)	0.0225(1)	0.1369(1)	0.5487(1)	57(1)
Cl(2)	0.1415(1)	0.2992(1)	0.6501(1)	66(1)
Cl(3)	0.2310(1)	0.4124(1)	0.5629(1)	56(1)
Cl(4)	0.1990(1)	0.3598(1)	0.3741(1)	50(1)
Cl(5)	−0.1628(1)	−0.2073(1)	0.1420(1)	73(1)
Cl(6)	−0.0827(1)	−0.4257(1)	0.1960(1)	104(1)
O(1)	0.0820(1)	0.2084(2)	0.2976(2)	42(2)
O(2)	−0.0011(1)	0.1209(2)	0.3685(2)	39(1)
O(3)	−0.0707(1)	−0.0221(2)	0.2089(2)	28(1)
N(1)	0.1453(2)	0.1180(3)	0.1330(2)	48(2)
N(2)	0.0850(2)	0.3319(3)	0.0781(2)	51(2)
C(1)	0.0958(2)	0.2315(3)	0.3777(2)	35(2)
C(2)	0.0537(2)	0.1831(3)	0.4161(2)	34(2)
C(3)	0.0699(2)	0.2032(3)	0.4999(2)	41(2)
C(4)	0.1239(2)	0.2736(4)	0.5459(2)	42(2)
C(5)	0.1641(2)	0.3242(3)	0.5078(3)	42(2)
C(6)	0.1497(2)	0.3014(3)	0.4234(2)	38(2)
C(7)	−0.0378(2)	−0.1149(3)	0.2269(2)	43(2)
C(8)	−0.0729(3)	−0.2112(4)	0.2023(3)	56(3)
C(9)	−0.0368(3)	−0.3073(4)	0.2262(3)	66(3)
C(11)	0.1594(3)	0.0893(5)	0.0574(3)	76(3)
C(12)	0.1709(3)	0.0319(4)	0.1966(3)	64(3)
C(13)	0.1800(2)	0.2196(4)	0.1745(3)	59(3)
C(14)	0.1602(2)	0.3130(4)	0.1158(3)	63(3)
C(15)	0.0604(3)	0.3895(4)	0.1343(3)	65(3)
C(16)	0.0634(3)	0.3870(4)	−0.0011(3)	71(3)

[a] U_{eq}^* is calculated from the refined anisotropic thermal parameter $U_{eq} = \frac{1}{3}\Sigma_i\Sigma_j U_{ij} a^*_i a^*_j a_i \cdot a_j$.

Sources of scattering factors and computer programs have been given elsewhere (4). The final atomic coordinates for non-hydrogen atoms are given in Table 3 and important distances and angles in Table 4. List of structure factors, anisotropic thermal parameters, and fractional coordinates for hydrogen atoms are available as deposited material.[1] The structure of the $[Sn(O_2C_6Cl_4)_3]^{2-}$ anion is shown in Fig. 1, and the crystal packing of $(tmenH)_2[Sn(O_2C_6Cl_4)_3]$ in the unit cell in Fig. 2.

Results and discussion

Preparative

The six compounds $Y_4C_6O_2SnX_2$.phen (X = Cl, Br, I; Y = Cl, Br) are the result of adduct formation by the dihalogenotin(IV)catecholate species, which are themselves generated by the redox reaction

[1] 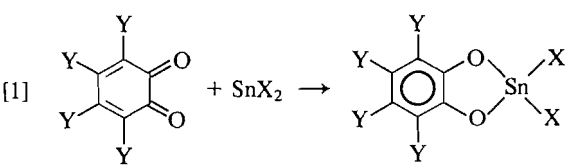

The products were characterized by elemental analysis, and by infrared and ^{1}H nmr spectroscopy, all of which confirmed the presence of the neutral donor and the catecholate ligands, and also demonstrated the absence of the original *o*-quinone (no ν(C=O) at 1700 cm^{-1}). In three cases, the molar mass of the product was confirmed by field desorption mass spectrometry, with the manifold of peaks from the molecular ion appearing as the most abundant species. The values given in Table 1 correspond to the most intense line in the manifold, and in each case computer simulation of the isotopic distribution within the manifold agreed with the experimental results. Similar determinations could not be carried out for the other products because of the limitations imposed by the m/e range of the mass spectrometer.

Reaction [1] is formally equivalent to oxidative addition. Given our results on indium(I) systems, and the work on transition metals such as the copper complexes of semiquinones (5), it seems very probable that reaction [1] actually proceeds

[1] Complete set of material may be purchased from the Depository of Unpublished Data, CISTI, National Research Council of Canada, Ottawa, Ont., Canada K1A 0S2.

TABLE 4. Interatomic distances (Å) and angles (deg) for $(tmenH)_2[Sn(O_2C_6Cl_4)_3]$[a,b]

Atoms	Distance	Bonds	Angle
Sn—O(1)	2.051(3)	O(1)—Sn—O(1)′	98.1(2)
Sn—O(2)	2.079(3)	O(1)—Sn—O(2)	81.7(1)
Sn—O(3)	2.055(3)	O(1)—Sn—O(3)	171.5(1)
Cl(1)—C(3)	1.737(4)	O(2)—Sn—O(3)	98.5(1)
Cl(2)—C(4)	1.729(4)	O(3)—Sn—O(3)′	81.1(2)
Cl(3)—C(5)	1.728(4)	Sn—O(1)—C(1)	111.2(2)
Cl(4)—C(6)	1.729(4)	Sn—O(2)—C(2)	109.8(2)
Cl(5)—C(8)	1.719(5)	Sn—O(3)—C(7)	111.5(2)
Cl(6)—C(9)	1.731(5)	C(11)—N(1)—C(12)	109.9(4)
O(1)—C(1)	1.335(4)	C(11)—N(1)—C(13)	114.1(4)
O(2)—C(2)	1.349(5)	C(12)—N(1)—C(13)	107.8(4)
O(3)—C(7)	1.324(5)	C(14)—N(2)—C(15)	111.9(4)
N(1)—C(11)	1.494(6)	C(14)—N(2)—C(16)	112.2(4)
N(1)—C(12)	1.487(6)	C(15)—N(2)—C(16)	110.0(4)
N(1)—C(13)	1.502(6)	O(1)—C(1)—C(2)	118.5(3)
N(2)—C(14)	1.434(6)	O(1)—C(1)—C(6)	121.6(3)
N(2)—C(15)	1.457(6)	O(2)—C(2)—C(1)	118.4(3)
N(2)—C(16)	1.443(6)	O(2)—C(2)—C(3)	118.6(4)
		Cl(1)—C(3)—C(2)	118.6(3)
Ring C(1)—C(6)*		Cl(1)—C(3)—C(4)	119.9(3)
Mean C—C	1.398(8)	Cl(2)—C(4)—C(3)	120.3(3)
Mean C—C—C	120.0(6)	Cl(2)—C(4)—C(5)	119.5(3)
		Cl(3)—C(5)—C(4)	121.3(3)
Ring C(7)—C(9),C(7)′—C(9)′		Cl(3)—C(5)—C(6)	120.0(3)
Mean C—C	1.400(9)	Cl(4)—C(6)—C(1)	118.4(3)
Mean C—C—C	120.0(7)	Cl(4)—C(6)—C(5)	120.5(3)
N(2)—H...Cl(1)	2.626	O(3)—C(7)—C(8)	123.1(4)
		O(3)—C(7)—C(7)′	117.9(4)
		Cl(5)—C(8)—C(7)	117.4(4)
		Cl(5)—C(8)—C(9)	121.2(4)
		Cl(6)—C(9)—C(8)	120.0(4)
		Cl(6)—C(9)—C(9)′	120.4(4)
		N(1)—C(13)—C(14)	113.2(4)
		N(2)—C(14)—C(13)	113.0(4)
		N(2)—H...Cl(1)	144.8

[a]Symmetry equivalent position for primed atoms is $-x, y, 0.5 - z$.
[b]Estimated standard deviations on mean values have been calculated with the use of the scatter formula $\sigma = [\Sigma(d_i - \bar{d})^2/(N-1)]^{1/2}$; where d_i is the ith and $\bar{d}$ is the mean of N equal measurements.

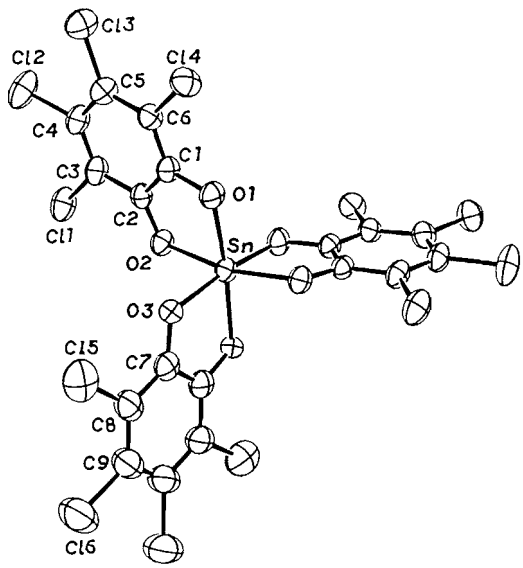

FIG. 1. ORTEP diagram of $[Sn(O_2C_6Cl_4)_3]^{2-}$: thermal ellipsoids are drawn at 50% probability levels.

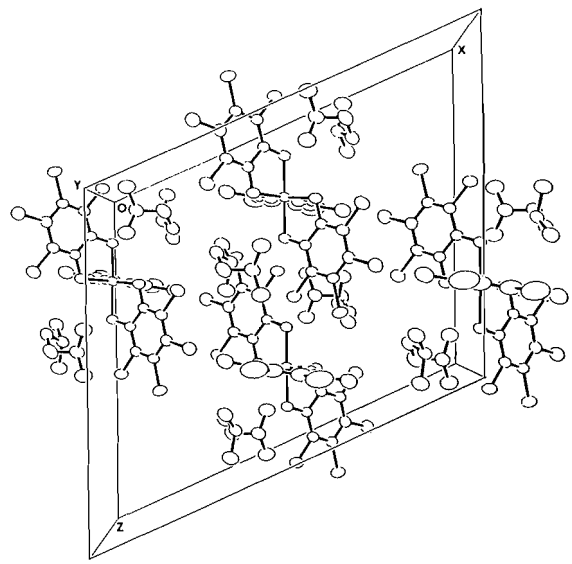

FIG. 2. Crystal packing diagram of $(tmenH)_2[Sn(O_2C_6Cl_4)_3]$.

Can. J. Chem. Downloaded from www.nrcresearchpress.com by 213.166.140.6 on 09/07/12
For personal use only.

Can. J. Chem. Downloaded from www.nrcresearchpress.com by 213.166.140.6 on 09/07/12
For personal use only.

via successive one-electron transfers, but the experimental conditions of these systems did not permit detailed studies by esr spectroscopy. It is clear that the mechanism proposed to account for the insertion of InX into M—M and M—X bonds (6, 7) cannot apply in the case of eq. [1], since neither the ground state nor any readily accessible excited state of the quinone can act as an electron pair acceptor, but a detailed discussion of this point must await further investigations of related systems.

The $Y_4C_6O_2SnX_2$ molecules identified as the primary product in eq. [1] are clearly Lewis acids, in keeping with the presumption that the coordination number at tin is four. The adducts formed with 1,10-phenanthroline are thermally stable, and only slightly soluble in most common organic solvents. The tmen derivatives of $Cl_4C_6O_2SnCl_2$ are more labile, and the reactions leading to these compounds merit some discussion. The preparations in either toluene or acetone give the expected 1:1 adduct, but in methanol or ethanol the product is solvated by strongly bound ROH which is probably hydrogen-bonded either to a chloride ligand or to an oxygen atom of the catecholate ligand. The other products obtained from this reaction mixture are the salt $(tmenH_2)Cl_2$ and the tin alkoxide derivatives $Cl_4C_6O_2Sn(OR)_2$. On the basis of the experimental evidence, we suggest that the reaction sequence is

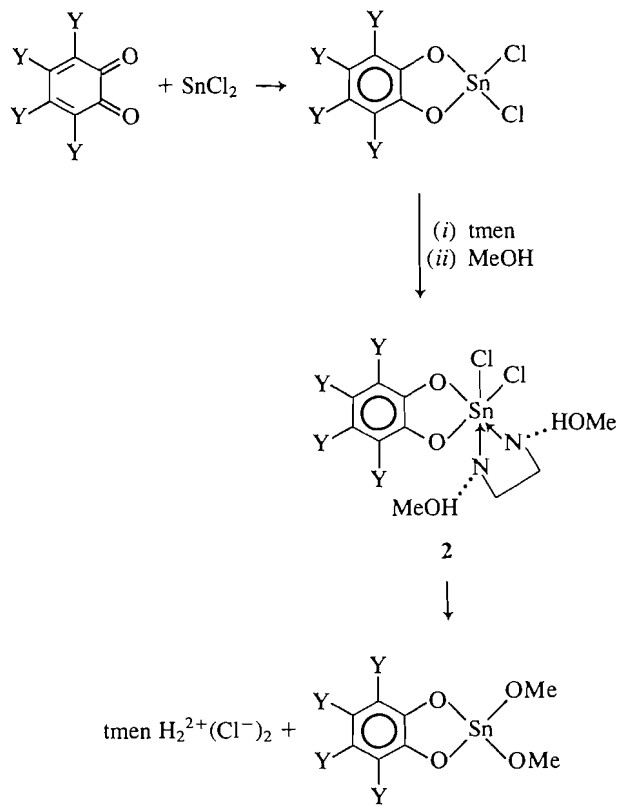

This sequence implies that the difference between CH_3OH and C_2H_5OH resides in the composition of the solvate **2** formed in the second step. The formation of such solvates, and the subsequent intramolecular reaction, are common features of tin(IV) chemistry. The products $Cl_4C_6O_2Sn(OR)_2$ may be stabilized by intermolecular Sn...O bonding.

The unexpected formation of the $[Sn(O_2C_6Cl_4)_3]^{2-}$ anion took place during experiments designed to investigate the insertion of InCl into the Sn—Cl bond of $Cl_4C_6O_2SnCl_2$, following earlier work on such insertion reactions between InX and Ph_3SnX (7). The following sequence is in keeping with the known reactions of SnX_2 and $Cl_4C_6O_2$ (= Q), as demontrated in this work, and of InX and InX_3.

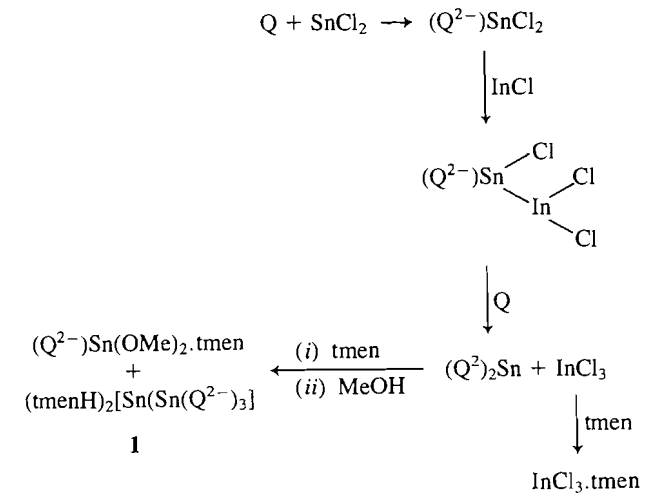

TABLE 5. ^1H nmr spectra of tin(IV) derivatives of *o*-$Cl_4C_6O_2$ (ppm, relative to Me_4Si)

Compound[a]	Chemical shift	Assignment
1,10-Phenanthroline[b]	9.2 (m, 2H)	C2,C9 (phen)
	7.7 (m, 2H)	C3,C8
	8.4 (m, 2H)	C4,C7
	7.9 (m, 2H)	C5,C6
$Cl_4C_6O_2SnCl_2$.phen	9.25 (m, 2H)	C2,C9 (phen)
	8.00 (m, 2H)	C3,C8
	8.70 (m, 2H)	C4,C7
	8.25 (m, 2H)	C5,C6
$Br_4C_6O_2SnCl_2$.phen	9.25 (m, 2H)	C2,C9 (phen)
	8.20 (m, 2H)	C3,C8
	8.75 (m, 2H)	C4,C7
	8.55 (m, 2H)	C5,C6
$Cl_4C_6O_2SnCl_2$.tmen	2.93 (s, 1H)	CH_2 } tmen
	2.50 (s, 3H)	CH_3 }
$Cl_4C_6O_2SnCl_2$.tmen.$2CH_3OH$	6.35 (br, 2H)	CH_3OH
	3.20 (s, 6H)	CH_3OH
	2.95 (s, 4H)	CH_2 } tmen
	2.60 (s, 12H)	CH_3 }
$Cl_4C_6O_2SnCl_2(OCH_3)_2$	3.25 s	CH_3
$Cl_4C_6O_2SnCl_2$.tmen.C_2H_5OH	6.15 (br, 1H)	C_2H_5OH
	3.45 (q, 2H)	CH_3CH_2OH
	2.90 (s, 4H)	CH_2 } tmen
	2.55 (s, 12H)	CH_3 }
	1.05 (t, 3H)	CH_3CH_2OH
$(tmenH)_2[Sn(O_2C_6Cl_4)_3]$	2.90 (s, 2H)	CH_2N
	3.60 (t, 2H)	CH_2N^+
	2.45 (s, 6H)	CH_3N
	3.20 (s, 6H)	CH_3N^+
	5.50 (br, 1H)	N—H

[a]All compounds run in d_6-dmso solution.
[b]In d_6-acetone; results from ref. 13.

The structure of $(tmenH)_2[Sn(O_2C_6Cl_4)_3]$ (1)

The crystal structure of **1** confirms the presence of the anionic triscatecholato complex of tin(IV). The $tmenH^+$ cations show no unusual stereochemical features except that there is clear evidence of hydrogen-bonding at Cl(1) of two $Cl_4C_6O_2^{2-}$ ligands, with Cl(1)---H—N = 2.626 Å, and N(2)—H---Cl(1) = 144.8° (Fig. 2). There are no significant non-bonded distances involving the hydrogen atoms of the cation (Cl(1)—

TABLE 6. ^{13}C nmr spectra of tin(IV) derivatives of *o*-$Cl_4C_6O_2$ (ppm, relative to Me_4Si)

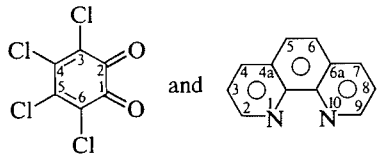

Compound	Solvent	$Cl_4C_6O_2$	tmen	phen	other
o-$Cl_4C_6O_2$	$CDCl_3$	131.9 C4,C5 143.7 C3,C6 168.8 C1,C2			
o-$Cl_4C_6(OH)_2$[a]	Acetone-d_6	119.5 C4,C5 122.5 C3,C6 143.0 C1,C2			
tmen	Neat		45.2 CH_2 57.6 CH_3		
phen	dmso-d_6			123.0 C5,C6 126.4 C4a,C6a 128.1 C4,C7 135.3 C3,C8 145.4 C4b,C6b 149.7 C2,C9	
$Cl_4C_6O_2SnCl_2$.phen	dmso-d_6	113.9 C4,C5 115.0 C3,C6 146.7 C1,C2		124.1 C5,C6 126.1 C4a,C6a 128.1 C4,C7 137.5 C3,C8 139.7 C4b,C6b 145.0 C2,C9	
$Cl_4C_6O_2SnCl_2$.tmen.EtOH	dmso-d_6	115.6 C4,C5 117.0 C3,C6 148.5 C1,C2	42.9 CH_2 50.9 CH_3		18.0 CH_3CH_2OH 56.1 CH_3CH_2OH
$(tmenH)_2[Sn(O_2C_6Cl_4)_3]$	dmso-d_6	115.9 C4,C5 117.2 C3,C6 149.0 C1,C2	44.0 $CH_2{}^+N$ 47.4 CH_2N 53.7 CH_3N^+ 54.9 CH_3N		

[a]Results from ref. 14.

H(12A) = 2.936 Å; Cl(2)—H(13A) = 2.908 Å; Cl(4)—H(13B) = 2.953 Å; Cl(5)—H(11) = 3.052 Å; Cl(5)—H(13A) = 2.901 Å; Cl(6)—H(16A) = 2.943 Å). It seems reasonable to conclude that the hydrogen-bonding is responsible in part for the stability of the crystals isolated.

The bond distances observed in the $[Sn(O_2C_6Cl_4)_3]^{2-}$ anion (Fig. 1) are typical of those reported for other tin(IV) complexes. The average Sn—O bond length is 2.062(3) Å, in good agreement with the values reported for $CF_3CO_2^-$ ligands coordinated to octahedral tin(IV) in the complex $[Sn^{II}Sn^{IV}O(O_2CCF_3)_4]_2$ (range 2.040(6)–2.070(7) Å) (8). Some older results include $Sn(OCCH_3)_4$ (mean *r*(Sn—O) = 2.22, range 2.13–2.29 Å) (9) and $[Sn^{II}Sn^{IV}(O_2CC_6H_4NO_2\text{-}o).THF]_2$ (mean *r*(Sn—O) at octahedral tin(IV) = 2.059, range 2.047(6)–2.067(7)) (10); the latter paper reviews earlier results for Sn^{IV}—O bonds in a variety of stereochemistries. In the present structure, the Sn—O_6 kernel is distorted octahedral, with the average O—Sn—O bite angle = 81.5(2)°.

The coordinated $Cl_4C_6O_2$ ligands are aromatic, with planar hexagonal C_6 rings, with *r*(C—C)(av) = 1.400(9) Å, and C—C—C(av) = 120.0(7)°. The C—Cl distances are typical of those in aromatic compounds, as are the C—O values, but these bonds (av. 1.336(5) Å) are significantly longer than the average of 1.29 Å found in a variety of transition metal complexes of the 3,5-di-*tert*-butyl-*o*-semiquinato ligand (11, 12), thus confirming that the reduction of the $Cl_4C_6O_2$ ligand has indeed proceeded beyond the semiquinone state to the dianion. In summary, there is ample confirmation from the crystallographic results that the reaction product in this case is a tin(IV)—catecholate derivative. The remaining features of the structure do not call for any comment.

Spectroscopic results

The most informative region of the infrared spectra is the ν(C=O) mode, which occurs at ~1700 cm^{-1}, vs, in both tetrahalogeno-*o*-quinones. This band is absent in all the tin compounds prepared in this work, being replaced by ν(C—O) vibrations at 1430m + 1240s cm^{-1}, indicating the presence of the *o*-$Cl_4C_6O_2^{2-}$ ligand.

The ^1H nmr spectra have been noted in the Experimental

Can. J. Chem. Downloaded from www.nrcresearchpress.com by 213.166.140.6 on 09/07/12
For personal use only.

Section and are tabulated in Table 5. The ^{13}C spectra of those products which are sufficiently soluble for such measurements are summarized in Table 6. Significant changes occur in the ^{13}C resonance spectrum of $Cl_4C_6O_2$ following reduction from the quinone to the catechol form, and these same changes are apparent in the spectra of the neutral adducts with tmen or phen, and in the $[Sn(O_2C_6Cl_4)_3]^{2-}$ anion, again confirming the presence of the reduced form in each of these species. Smaller changes are observed in the spectrum of tmen or phen upon coordination, or on formation of the protonated species. It is rather surprising that $tmenH^+$ cation shows two sets of resonances, and we conclude that the hydrogen-bonding evident in the solid state (Fig. 2) persists in solution, thus removing the degeneracy observed in the spectrum of the free ligand.

In general, we conclude that the spectroscopic evidence is exactly congruent with that from X-ray crystallography, and shows clearly that the reaction of SnX_2 with the tetrahalogeno-*o*-quinones is an oxidative addition process to give the appropriate tin(IV) species.

Acknowledgements

This work was supported in part by Operating Grants (to D.G.T.) from the Natural Sciences and Engineering Research Council of Canada.

1. T. A. Annan, P. E. Doan, D. McConville, B. R. McGarvey, A. Ozarowski, and D. G. Tuck. Unpublished results.
2. W. J. Geary. Coord. Chem. Rev. **7**, 81 (1971).
3. C. Peppe, D. G. Tuck, and L. Victoriano. J. Chem. Soc. Dalton Trans. 2165 (1982).
4. M. A. Khan, R. C. Steevensz, D. G. Tuck, J. G. Noltes, and P. W. R. Corfield. Inorg. Chem. **19**, 3407 (1980).
5. G. A. Abakumov, A. V. Lobanov, V. K. Cherkasov, and G. A. Razuvaev. Inorg. Chim. Acta, **49**, 135 (1981).
6. C. Peppe and D. G. Tuck. Can. J. Chem. **62**, 2793 (1984); **62**, 2798 (1984).
7. T. A. Annan and D. G. Tuck. J. Organomet. Chem. **325**, 83 (1987).
8. T. Birchall and J. P. Johnson. J. Chem. Soc. Dalton Trans. 69 (1981).
9. N. W. Alcock and V. L. Tracy. Acta Crystallogr. B**35**, 80 (1979).
10. P. F. R. Ewings, P. G. Harrison, A. Morris, and T. J. King. J. Chem. Soc. Dalton Trans. 1602 (1976).
11. J. S. Thompson and J. C. Calabrese. J. Am. Chem. Soc. **108**, 1903 (1986).
12. C. G. Pierpoint and R. M. Buchanan. Coord. Chem. Rev. **38**, 45 (1981).
13. M. F. A. Dove and J. G. Hallett. J. Chem. Soc. (A), 1204 (1969).
14. J. Knuutinen, R. Laatikainen, and J. Passivirta. Org. Mag. Reson. **14**, 5 (1980).

Can. J. Chem. Downloaded from www.nrcresearchpress.com by 213.166.140.6 on 09/07/12
For personal use only.

Electrocatalytic reduction of molecular oxygen by mononuclear and binuclear cobalt phthalocyanines

MICHAEL R. HEMPSTEAD,[1] A. B. P. LEVER,[1] AND CLIFFORD C. LEZNOFF
Department of Chemistry, York University, North York, Ont., Canada M3J 1P3

Received March 25, 1987

MICHAEL R. HEMPSTEAD, A. B. P. LEVER, and CLIFFORD C. LEZNOFF. Can. J. Chem. **65**, 2677 (1987).

Investigations of the electrocatalytic activity of mononuclear and binuclear cobalt phthalocyanines for the reduction of molecular oxygen established that the latter compounds are more effective catalysts than the corresponding mononuclear species. A correlation between the half-bandwidths for the Q band of these species and their catalytic efficiency, expressed as a kinetically-limited current, suggests that the increase in activity may be attributed to electronic coupling between the phthalocyanine rings.

MICHAEL R. HEMPSTEAD, A. B. P. LEVER et CLIFFORD C. LEZNOFF. Can. J. Chem. **65**, 2677 (1987).

Des études sur l'activité électrocatalytique des phtalocyanines de cobalt mononucléaires et binucléaires pour la réduction de l'oxygène moléculaire ont permis d'établir que les derniers composés sont des catalyseurs plus efficaces que les espèces mononucléaires correspondantes. Une corrélation entre les demi-largeurs des bandes Q de ces espèces et leur efficacité catalytique, exprimée sous la forme de courant limite cinétique, suggère que l'augmentation de l'activité peut être attribuée au couplage électronique entre les cycles phtalocyanines.

[Traduit par la revue]

Introduction

If a fuel cell is to operate efficiently, a catalyst must be embedded in the cathode to accelerate the reduction of oxygen gas. This catalyst must be capable of withstanding the operating conditions of the fuel cell (strong acid or base, fairly high temperatures), for long periods of time, without loss of activity. Platinum is commonly used as a fuel cell catalyst, but is expensive, representing some 10% of the total fuel cell cost. Catalysts which are more effective and less expensive are needed, if fuel cell applications are to become viable.

Many mononuclear metal porphyrins act as electrocatalysts (1–21) but the work of Collman and Anson (22–28) and Chang and co-workers (29–35) has revealed that certain binuclear porphyrins are much more effective. Similarly, mononuclear phthalocyanines of iron and cobalt are effective (36–50), but some ill-characterised "dimeric" and polymeric phthalocyanines appear more effective (51–62). Savy and co-workers (54–56) performed ESCA, esr, Mössbauer and optical spectroscopic studies to establish correlations between the spectroscopic properties of polymeric and monomeric iron phthalocyanines and the electrocatalytic activity of these species towards oxygen reduction. We consider here a correlation between the optical spectra of a series of well-characterized mono- and binuclear cobalt phthalocyanines and their electrocatalytic activity.

The binuclear porphyrins studied by Collman and Anson are too fragile for long-term use under fuel cell conditions and therefore our studies have been directed towards thermally more stable binuclear phthalocyanine compounds. We have recently reported (63–65) a series of binuclear phthalocyanine complexes of the general formula [M—tri(neopentoxy)phthalocyanine]$_2$(bridge) where the bridge may contain 1, 2, 4, or 5 atoms, and where M may be H_2, Cu, or Co. The three neopentoxy groups are randomly distributed in the 4 or 5 positions of the three unbridged benzene rings, providing solubility in many organic solvents, e.g., toluene, *o*-dichlorobenzene, and dichloroethane, but generally not acetone and ethanol.

Of relevance to this presentation are the following species, with their abbreviations (the number in parentheses is the number of bridging atoms connecting the two phthalocyanine rings): CoTNPc, 2,9,16,23-tetraneopentoxyphthalocyanatocobalt(II). This is the mononuclear control molecule. O(1)[CoTrNPc]$_2$, bis-2-(9,16,23-trineopentoxyphthalocyaninylcobalt(II))ether; two phthalocyanine rings linked by a single oxygen (ether) bridge. C(2)[CoTrNPc]$_2$, 1,2-bis-2′-(9′,16′,23′-trineopentoxyphthalocyaninylcobalt(II))ethane; two phthalocyanine rings linked by an ethane —CH_2CH_2— bridge. Cat(4)[CoTrNPc]$_2$, 1,2-bis-2′-(9′,16′,23′-trineopentoxyphthalocyaninoxycobalt(II))benzene; two phthalocyanine rings linked by a catechol —O—C_6H_4—O— bridge. EtMeO(5)[CoTrNPc]$_2$, 1,3-bis-2′-(9′,16′,23′-trineopentoxyphthalocyaninoxycobalt(II))-2-ethyl-2-methylpropane; two phthalocyanine rings linked by a —$OCH_2C(Et)(Me)CH_2O$— bridge.

Earlier investigations of the metal-free analogues of these species (66) established properties of these compounds which are relevant to the observations reported here. These properties are as follows. (*i*) In condensed phases (frozen solution glass, Nujol mull, etc.), these complexes may exhibit *inter*molecular aggregation. In dilute solution, $<5 \times 10^{-5}$ *M*, *inter*molecular aggregation is generally absent (67). (*ii*) Some binuclear phthalocyanines may close upon themselves ("clamshell" behaviour) to aggregate via cofacial *intra*molecular aggregation. Specifically, of the metal-free species, only Cat(4)[TrNPcH$_2$]$_2$ and EtMeO(5)[TrNPcH$_2$]$_2$ are capable of such *intra*molecular aggregation. Such species exist in a dynamic equilibrium with "open" conformations. (*iii*) The electronic spectra of the metal-free species show evidence of the coupling of the transition moments on each phthalocyanine ring (66). Thus direct through space coupling is observed in the cofacial conformations, giving rise to a blue shift in the Q and Soret absorptions. However, a blue shift is also observed in the other metal-free species, as a consequence of coupling through space (or through the bridge) in "open", non-aggregated conformations.

Note that electronic coupling is more readily detected in the electronic spectra of binuclear phthalocyanine species, relative to comparable porphyrin species, because the visible region transition moments are much larger in the former case (68).

Experimental

The species Co(II)TNPc (64), EtMeO(5)[Co(II)TrNPc]$_2$ (64), C(2)[Co(II)TrNPc]$_2$ (65), Cat(4)[Co(II)TrNPc]$_2$ (65), and O(1)-[Co(II)TrNPc]$_2$ (69) were prepared by literature routes. Aldrich Gold

[1]Author to whom correspondence may be addressed.

Can. J. Chem. Downloaded from www.nrcresearchpress.com by 213.222.148.141 on 09/07/12
For personal use only.

Can. J. Chem. Downloaded from www.nrcresearchpress.com by 213.222.148.141 on 09/07/12
For personal use only.

Label *o*-dichlorobenzene (DCB) was used without further purification and Fisher certified 1 *N* sodium hydroxide was diluted as required for the aqueous studies. Water was purified by double-distillation over $KMnO_4$ followed by passage through a Barnstead organic removal cartridge and two Barnstead mixed resin ultrapure cartridges. Stress-annealed pyrolytic graphite (SAPG) and ordinary pyrolytic graphite (OPG), obtained from Union Carbide, were used as electrode materials. The graphite was mounted in Teflon to expose a circular area of 0.490 cm^2 for the SAPG electrode and 0.493 cm^2 for the OPG electrode. Before each experiment, the OPG electrode surface was cleaned by successive polishings with 1.0 μm, 0.3 μm, and 0.05 μm alumina (Linde) suspended in water on Metron polishing cloth. Argon gas (Linde) was purified by passage through heated copper filings, anhydrous $CaSO_4$ (Drierite), molecular sieves (BDH Type 3A), and glass wool. Oxygen gas (Linde) was purified by passage through anhydrous $CaSO_4$, NaOH pellets (AnalaR analytical grade), anhydrous $CaSO_4$, molecular sieves, and glass wool. Tetrabutylammonium perchlorate (TBAP) (Eastman Kodak) was recrystallized from absolute ethanol and dried in a vacuum oven at 50°C for 2 days. Potential scans were performed with a Pine Instruments RD3 potentiostat and the rotation studies with a Pine Instruments PIR rotator. The cell for the adsorption experiments employed a medium frit to separate a silver wire quasi-reference electrode from the main chamber containing the OPG working electrode and a platinum wire counter electrode. The cell for the aqueous studies comprised a separate chamber for each electrode with a Luggin capillary extending from the reference chamber to the proximity of the OPG surface. For all aqueous experiments, the potential was measured versus a saturated calomel electrode (sce).

Phthalocyanine solutions were prepared in DCB with 0.1 *M* TBAP as supporting electrolyte, such that the concentration was ca. 10 μ*M* with respect to the TNPc unit. These solutions were purged with argon for about an hour before scanning the working electrode at a rate of 100 mV/s over the range 0.00 to +1.00 V versus the silver wire. Adsorbed layers on OPG or SAPG electrodes were obtained by cycling until the anodic and cathodic peak currents associated with the adsorbed species remained constant over 5 min of continuous scanning. When this condition was satisfied, the adsorbed layer was assumed to have reached a steady coverage. Scans at various rates were then recorded to determine the surface coverage (*vide infra*).

The catalytic efficiency of the various phthalocyanine compounds was investigated with the adsorbed species on the OPG electrode. This modified electrode was removed from the phthalocyanine solution, washed with ethanol, then with water, and finally placed in the cell for the aqueous studies. The 0.10 *M* NaOH solution in this cell had been purged with oxygen for several hours to ensure saturation. The electrode was then scanned over the range 0.00 to −1.00 V versus sce at a rate of 10 mV/s for rotation rates ranging from 400 to 10 000 rpm. After each scan, the electrode was held at 0.00 V for 1 min to permit the rotation rate to be changed for the next scan.

Results

(I) Adsorption studies

Some preliminary adsorption experiments were performed on a SAPG electrode to determine the electronic nature and orientation of the adsorbed species. The cyclic voltammograms for a solution of 2.5×10^{-5} *M* CoTNPc in DCB and 0.1 *M* TBAP studied at a SAPG working electrode, as shown in Fig. 1, display two couples in close proximity. Following deconvolution of these waves,[2] a plot (Fig. 2*A*) of cathodic peak current, $i_{p,c}$, versus scan rate, ν, for couple I ($R = 0.999$) and a

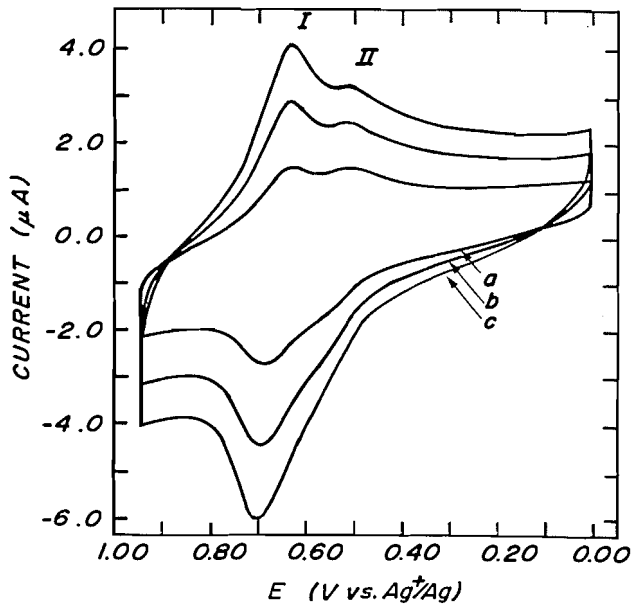

FIG. 1. Cyclic voltammograms at scan rates of (*a*) 50 mV/s, (*b*) 100 mV/s, and (*c*) 150 mV/s for 2.5×10^{-5} *M* CoTNPc in DCB and 0.1 *M* TBAP under argon at a SAPG working electrode. Couples I and II are both associated with the $[Co(II)TNPc(-1)]^+/Co(II)TNPc(-2)$ process. The nature of these couples is investigated more fully in Fig. 2.

plot (Fig. 2*B*) of $i_{p,c}$ versus $\sqrt{\nu}$ for couple II ($R = 0.998$) indicated that these couples were adsorption and diffusion processes (71), respectively. From the relative positions of couples I and II, it follows that the adsorbed species binds most strongly in the reduced form associated with couple II (72), although the presence of a reductive adsorption wave indicates that the oxidized form associated with this couple also binds to the electrode. Couple II is associated with the ligand process $[Co(II)TNPc(-1)]^+/Co(II)TNPc(-2)$ (73) and therefore CoTNPc binds to the graphite surface most strongly as $Co(II)TNPc(-2)$. The binding between the CoTNPc and the SAPG electrode can be explained by π−π interactions between the phthalocyanine ring and the graphite lattice, if the CoTNPc is adsorbed flat to the SAPG surface. This mode of adsorption has also been suggested in a similar investigation (41) by Yeager and co-workers who studied cobalt tetrasulphonate phthalocyanine (CoTSPc).

In addition to the electronic nature and orientation of the adsorbed molecule, the extent of coverage of the catalyst on the electrode surface must be known. Quantitative analysis requires the selection of an appropriate adsorption isotherm to describe the cyclic voltammetric response of the adsorbate. An adsorption isotherm describes the relationship between the concentrations of the adsorbate in the adsorption layer and in the bulk phase from which the adsorption takes place. Appropriate isotherms may also yield information about interactions between molecules in the adsorption layer.

The Langmuir isotherm was used to analyse the adsorption of CoTNPc on a SAPG electrode. This isotherm applies to systems in which there are no interactions between the adsorbed molecules (72). For systems which satisfy these conditions, the value of n may be calculated from the peak-width-at-half-height, $W_{1/2}$, from the expression

$$[1] \quad n = \frac{2RT}{W_{1/2}F} \ln (3 + 2\sqrt{2})$$

[2]The cathodic waves for these couples were deconvoluted by subtracting the background from a neat DCB solution to obtain a baseline followed by construction of a symmetric wave about the peak of couple I. The contribution of the symmetric wave in the region of mixed currents was subtracted from the observed response to obtain the current associated with couple II. Complete details of this deconvolution are described in ref. 1.

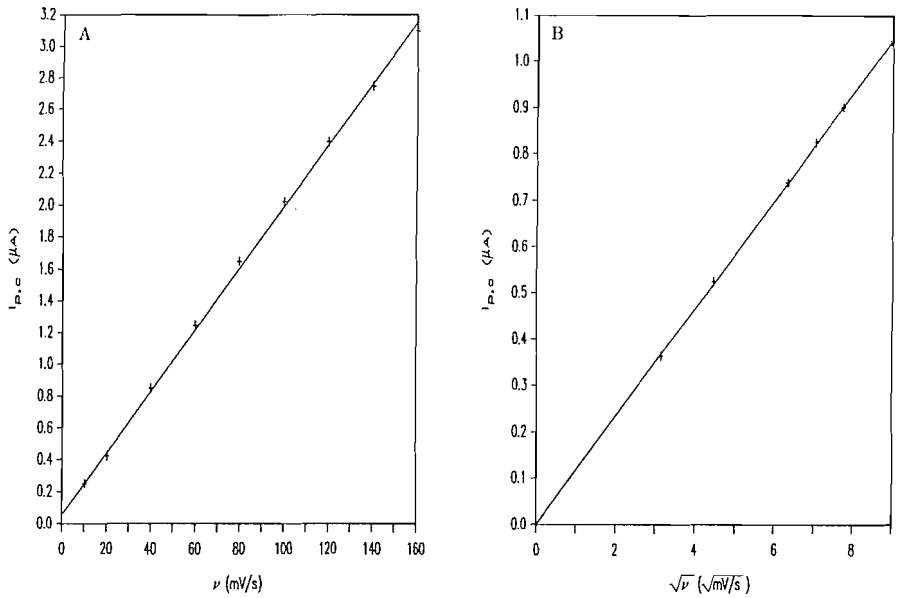

FIG. 2. Plots of the dependence of cathodic peak current with scan rate for (*A*) couple I and (*B*) couple II, as designated in Fig. 1 (2.5×10^{-5} *M* CoTNPc in DCB and 0.1 *M* TBAP at a SAPG working electrode).

The average value of n calculated in this fashion was 1.00 ± 0.02 in excellent agreement with our expectation of a one-electron process. By calculating the charge under the adsorption peak and assuming the area of a phthalocyanine molecule, A_{pc}, is 200 Å^2 (41), the coverage of CoTNPc on a SAPG electrode was determined to be about 0.30 ± 0.1 monolayers. This low level of coverage is consistent with another study (41) in which CoTSPc adsorbed on SAPG to the extent of 0.4 monolayers.

Since a coverage of between one and two monolayers was desired for these oxygen reduction studies, SAPG was not used for these investigations. (Recent studies have established a method for obtaining a coverage of one monolayer on SAPG which will be employed in later investigations.) Yeager and co-workers (42) found that CoTSPc could be adsorbed on OPG to about four times the coverage on SAPG; the greater adsorption on the OPG electrode was attributed to a higher density of surface defects assumed to be critical to adsorption (74). Adsorption experiments with CoTNPc and an OPG electrode did show enhanced adsorption, as shown in Fig. 3. This increased adsorption affects the cyclic voltammograms in many ways. The most readily apparent effect is the loss of the diffusion wave which had been observed in conjunction with an adsorption wave when using SAPG. Since the adsorption wave overwhelms the diffusion wave under the conditions employed for this experiment (71), later calculations of surface coverage disregard contributions from diffusion and treat this as a pure adsorption process. The other noticeable effect in Fig. 3 is the large peak separation observed at higher scan rates. This probably arises from the larger currents observed in this scan and the high *iR* drop in these DCB solutions.

The adsorption studies with the OPG electrode were analysed with the Langmuir isotherm which gave an average n value of 0.72 ± 0.04, suggesting that the use of the Langmuir isotherm was not appropriate for this system. An alternate choice, the Frumkin isotherm (75–78) is useful for systems in which there are interactions between adsorbed molecules. A recent investigation (78) of several isotherms suggests that the Frumkin isotherm is most appropriate for electrochemical processes involving the adsorption of organic compounds. According to the Frumkin isotherm, the peak current and the value of n are

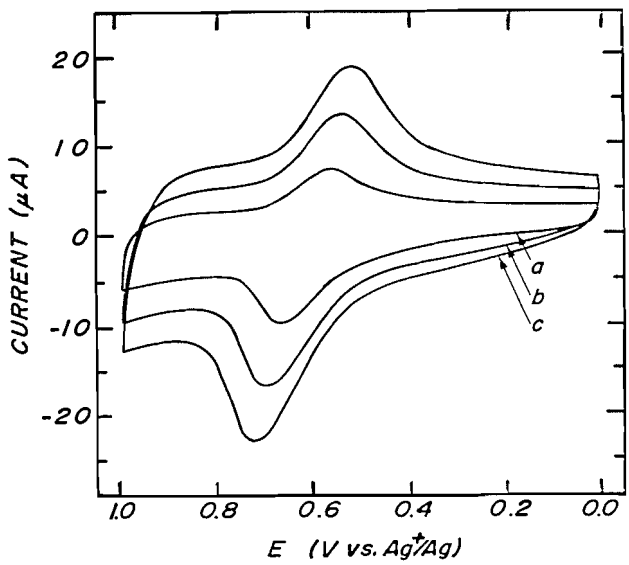

FIG. 3. Cyclic voltammograms at scan rates of (*a*) 50 mV/s, (*b*) 100 mV/s, and (*c*) 150 mV/s for 1.0×10^{-5} *M* TNPcCo in DCB and 0.1 *M* TBAP at an OPG working electrode. The waves shown here are associated with the $[Co(II)TNPc(-1)]^+/Co(II)TNPc(-2)$ couple.

given by the expressions (77)

$$[2] \quad i_p = \frac{n^2F^2A\Gamma\nu}{RT(4 - 2r\Gamma)}$$

$$[3] \quad n = \frac{2RT}{W_{1/2}F}\left[\ln P - r\Gamma\frac{P-1}{P+1}\right]$$

where r is an interaction parameter (cm^2/mol), Γ is the surface concentration of the adsorbed species (mol/cm^2), and P is given by

$$[4] \quad P = 3 - r\Gamma + (r^2\Gamma^2 - 6r\Gamma + 8)^{1/2}$$

Repulsive interactions are denoted by negative values of r while stabilizing interactions are denoted by positive values of r. If the interactions between adsorbed molecules are repulsive, the wave broadens and the peak decreases, but if the interactions

Can. J. Chem. Downloaded from www.nrcresearchpress.com by 213.222.148.141 on 09/07/12
For personal use only.

TABLE 1. Average values of θ and $r\Gamma$ for an OPG electrode modified with CoTNPc or one of its binuclear derivatives

Compound	θ	$r\Gamma$
CoTNPc	1.4 ± 0.4	−0.77 ± 0.14
O(1)[CoTrNPc]$_2$	1.3 ± 0.4	−1.36 ± 0.11
C(2)[CoTrNPc]$_2$	1.8 ± 0.1	−0.87 ± 0.13
Cat(4)[CoTrNPc]$_2$	2.2 ± 0.2	−0.88 ± 0.06
EtMeO(5)[CoTrNPc]$_2$	2.2 ± 0.4	−0.85 ± 0.01

are attractive, the wave narrows and the peak increases. If the interaction parameter is zero, then the Frumkin isotherm expressions simplify to those given by the Langmuir isotherm.

The cyclic voltammograms from the adsorption studies on OPG displayed waves which were broader and more rounded than those observed for the SAPG experiments. This change in waveshape indicates that at these higher coverages, repulsive interactions exist between molecules adsorbed on the electrode surface. The voltammograms which had been analysed by the Langmuir isotherm to give an average n value of 0.72 ± 0.04 when analysed by the Frumkin isotherm yielded 0.93 ± 0.03 in much better agreement with the expected value of unity.

Average values of the dimensionless parameters $r\Gamma$ and the average surface coverage, θ (where $\theta = \Gamma A_{pc}$), are presented in Table 1 for an OPG electrode modified with CoTNPc or one of its binuclear derivatives. The surface coverage calculations for the binuclear compounds used the same area approximation per phthalocyanine unit as had been used for CoTNPc since these calculations were designed to estimate the number of cobalt atoms on the electrode surface, not the number of phthalocyanine molecules. As a means of clarifying this point, consider the following example. If a value of 2.0 is calculated for θ, this could indicate that the electrode is covered by two monolayers of the mononuclear species, two layers of a binuclear species in an "open" configuration, or one layer of a binuclear species in a cofacial configuration. Consideration of steric restraints in these molecules and the behaviour of these species in solution is required to infer the manner in which these molecules adsorb on the electrode surface.

The θ value of 1.4 ± 0.4 for CoTNPc-modified OPG electrodes is most likely indicative of a coverage of one monolayer. The reported θ may be somewhat high as it is based on the geometric area of the electrode and does not account for the inherent roughness of the surface. It is improbable that a second layer forms on the surface since none of the adsorbate is lost after washing and transferring to an aqueous solution. A weakly bound second layer of CoTSPc on OPG has been reported (74), but it was readily removed by washing.

The average coverage for the molecule O(1)[CoTrNPc]$_2$ was 1.3 ± 0.4, which is quite similar to that found for CoTNPc. The adsorption of O(1)[CoTrNPc]$_2$ was anticipated to be similar to that of CoTNPc because this binuclear species can only exist in an "open" conformation. The O(1)[CoTrNPc]$_2$ molecule would adsorb with one ring flat on the OPG surface while the other ring lies at some oblique orientation. The ring in the oblique orientation would give this surface a highly disordered structure and, from the $r\Gamma$ value in Table 1, it would appear that it also leads to abnormally high repulsive interactions.

The remaining binuclear phthalocyanines have average θ values near two. If these molecules adsorbed on to the electrode surface in an "open" conformation then a θ value near two would not be expected since, as noted earlier, the π–π

TABLE 2. Half-bandwidths of the Q band for CoTNPc and its binuclear derivatives as Co(III) and also as Co(I)[a]

Compound	Half-bandwidths (cm^{-1}) Co(III)	Co(I)
CoTNPc	680	660
C(2)[CoTrNPc]$_2$	765	735
Cat(4)[CoTrNPc]$_2$	800	775
EtMeO(5)[CoTrNPc]$_2$	785	775
O(1)[CoTrNPc]$_2$	1000	920

[a]These half-bandwidths were calculated from the spectra obtained by bulk electrolysis of DCB solutions containing these species along with an excess of tetrabutylammonium-hydroxide and 0.1 *M* TBAP (80).

interactions which arise between the first and second layer of phthalocyanine molecules adsorbed on the electrode surface are too weak to stabilize a second layer. It would therefore appear that most of these binuclear species adsorb on to the electrode surface in some sort of cofacial arrangement. This configuration is easily obtained by Cat(4)[CoTrNPc]$_2$ and EtMeO(5)[CoTrNPc]$_2$, but the stacking of C(2)[CoTrNPc]$_2$ would necessitate that the phthalocyanine rings in the second layer lie above a surface bound ring of an adjacent C(2)[CoTrNPc]$_2$ molecule. The values of $r\Gamma$ reported for these binuclear compounds are fairly consistent and are quite similar to the value of −0.7 reported by Collman and Anson (28) for one of their cofacial cobalt porphyrins. It has been suggested that the source of repulsions observed for flatly adsorbed aromatic molecules such as these, is the parallel orientation of their dipoles (79).

Another interesting feature of these adsorption studies is illustrated in Fig. 4. The cyclic voltammograms for O(1)[CoTrNPc]$_2$ and Cat(4)[CoTrNPc]$_2$ display one adsorption wave for the [Co(II)TrNPc(−1)]$^+$/Co(II)TrNPc(−2) couple, just like that observed for the adsorption of CoTNPc on OPG (see Fig. 3). However, the cyclic voltammograms for C(2)[CoTrNPc]$_2$ and EtMeO(5)[CoTrNPc]$_2$ display two couples in the same potential region. Plots of i_p versus ν for the two couples are linear, thus both couples arise from adsorption processes. Frumkin isotherm analysis yielded values of n close to unity which, when combined with the potential of these couples, suggests that these couples are both associated with the [Co(II)TrNPc(−1)]$^+$/Co(II)TrNPc(−2) process. The origin of these two adsorption processes may be explained in terms of the electronic coupling inherent in these binuclear compounds.

The theory of intramolecular coupling in these binuclear phthalocyanines has been presented elsewhere (66). In solution, these binuclear species are expected to exist in a dynamic equilibrium between various conformations, dependent upon the nature of the bridge since, in some cases, steric effects may provide barriers to free rotation. Therefore, the electronic absorption spectrum of a solution of one of these binuclear species would represent the summation of the spectra of a mixture of these conformers. The coupling in these species resulted in a blue-shifted Q band which was also broadened, the degree of this broadening being a qualitative measure of the degree of electronic coupling in these binuclear species.

The half-bandwidths of the five phthalocyanine species investigated in this study are presented in Table 2 (80). The relative extent of coupling in these compounds, as established

Can. J. Chem. Downloaded from www.nrcresearchpress.com by 213.222.148.141 on 09/07/12
For personal use only.

Can. J. Chem. Downloaded from www.nrcresearchpress.com by 213.222.148.141 on 09/07/12
For personal use only.

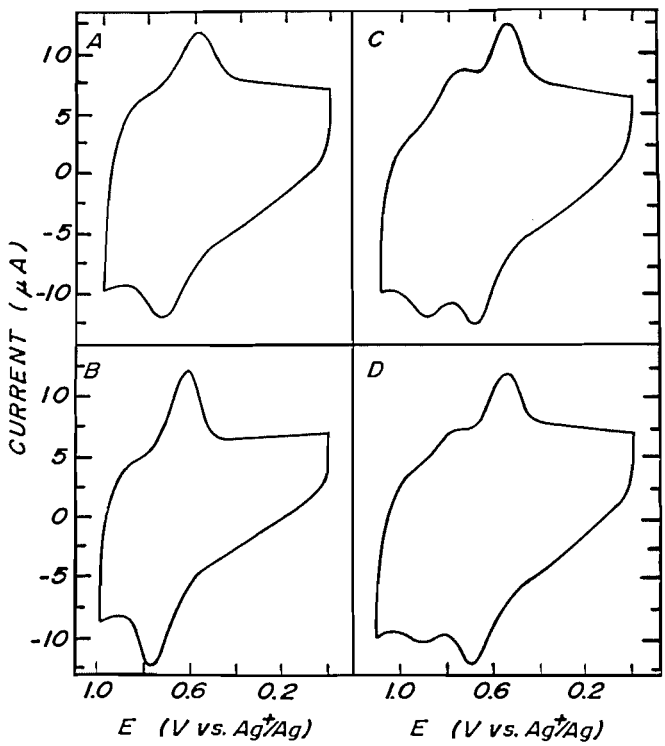

FIG. 4. Cyclic voltammograms displaying adsorption features of (*a*) O(1)[TNPcCo]$_2$, (*b*) Cat(4)[TNPcCo]$_2$, (*c*) C(2)[TNPcCo]$_2$, and (*d*) EtMeO(5)[TNPcCo]$_2$. All voltammograms were recorded at a scan rate of 100 mV/s for a binuclear concentration of ca. 5 μM in DCB and 0.1 *M* TBAP. The waves shown here are associated with the [Co(II)TNPc(−1)]$^+$/Co(II)TNPc(−2) couple.

by these half-bandwidths, is as follows:

[5] O(1)[CoTrNPc]$_2$ > EtMeO(5)[CoTrNPc]$_2$ ≃ Cat(4)[CoTrNPc]$_2$ > C(2)[CoTrNPc]$_2$ > CoTNPc

Cyclic voltammograms of each of the binuclear species are presented in Fig. 4. In the voltammograms of C(2)[CoTrNPc]$_2$ and EtMeO(5)[CoTrNPc]$_2$, two adsorption waves are observed which arise from two distinct redox couples in close proximity. Similar voltammograms have been reported previously (28, 81) but, in these earlier reports, both of the redox processes could be observed when the species was in solution, not bound to the electrode surface. For each of the adsorbed binuclear species, one phthalocyanine ring lies on the electrode surface while the other ring is not in contact with it. The two redox couples, therefore, are regarded to arise from the bound Pc ring, and the bridged Pc ring which is not bound directly to the electrode. In solution, only one redox process is observed, common to both rings. In the more highly coupled species, namely O(1)[CoTrNPc]$_2$ and Cat(4)[CoTrNPc]$_2$, electron transfer across the bridge to the outer phthalocyanine ring is facile and therefore only one redox couple is observed. However, electron transfer across the saturated C(2)[CoTrNPc]$_2$ and EtMeO(5)[CoTrNPc]$_2$ bridges is inhibited and therefore the redox potential for the outer phthalocyanine ring could differ from that of the inner phthalocyanine ring. Although the O(1)[CoTrNPc]$_2$ bridge is, technically, also a saturated bridge, it is apparent from the half-bandwidth studies mentioned above, that electron transfer across this bridge is permissible. This proposal could explain the differences between the cyclic voltammograms given in Fig. 4, although further study would be necessary to establish the source of this behaviour conclusively.

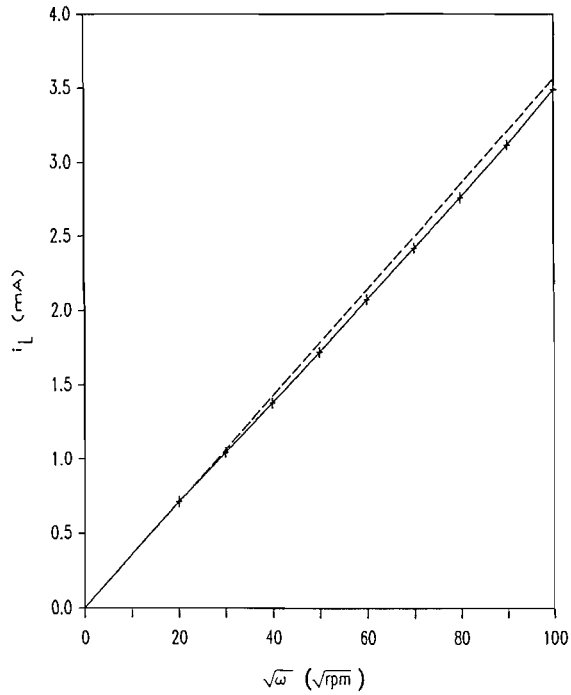

FIG. 5. Levich plot of the diffusion-limited O_2 reduction current at a CoTNPc-modified OPG electrode. The dashed line is the response predicted by eq. [6] and the solid line is the fit through the experimental data denoted by + signs.

(II) Oxygen studies

The catalytic properties of these phthalocyanine species were investigated by means of rotating disc electrode (RDE) studies. The diffusion-limited current for such an experiment, expressed in mA, is described by the expression (82)

$$[6] \quad i_L = 1000nAFC\left(\frac{2\pi\upsilon\omega}{60}\right)^{1/2} \times \left[\frac{0.62048S^{-2/3}}{1 + 0.2980S^{-1/3} + 0.14514S^{-2/3}}\right]$$

where υ is the kinematic viscosity (cm^2/s), ω is the rotation rate (rpm), S is the Schmidt number ($S = \upsilon/D$), A is the electrode area (cm^2), F is Faraday's constant, and C is the concentration of O_2 (mol/cm^3). A Levich plot (i_L versus $\omega^{1/2}$) of the diffusion-limited O_2 reduction current at a CoTNPc-modified OPG electrode is shown in Fig. 5. In the calculation of i_L for this Levich plot, the diffusion coefficient and concentration of O_2 were taken as 1.67×10^{-5} cm^2/s (42) and 1.38×10^{-6} mol/cm^3 (83), respectively, the kinematic viscosity was estimated at 9.97×10^{-3} cm^2/s (84), the Schmidt number was calculated to be 597, and the value used for n was two. The good agreement between the calculated diffusion-limited current and the experimentally observed limiting current suggests that O_2 is undergoing a two-electron reduction to peroxide rather than a four-electron reduction to water. Further evidence for this two-electron reductive pathway will be presented later.

If an electrode process is hindered by a kinetic step, a plot of i_L, or i, versus $\omega^{1/2}$ deviates from the linear relationship given in eq. [6] (71). The effect of this kinetic step on the current that flows in the potential region of mixed diffusion-kinetic control for a first-order process under steady-state conditions is given by the expression (85–88):

$$[7] \quad 1/i = 1/i_k + 1/i_L$$

TABLE 3. Average values of n for the electrocatalytic reduction of oxygen in 0.10 M NaOH at an OPG electrode modified with CoTNPc or one of its binuclear derivatives

	n			
	Potential (V versus sce)			
Compound	−0.450	−0.500	−0.550	−0.600
CoTNPc	1.94±0.17	1.93±0.11	1.91±0.10	1.93±0.06
O(1)[CoTrNPc]$_2$	2.07±0.02	2.04±0.02	2.02±0.02	2.01±0.01
C(2)[CoTrNPc]$_2$	2.09±0.01	2.05±0.01	2.01±0.01	1.99±0.02
Cat(4)[CoTrNPc]$_2$	2.10±0.09	2.03±0.01	1.99±0.01	1.98±0.02
EtMeO(5)[CoTrNPc]$_2$	1.94±0.01	1.94±0.02	1.94±0.01	1.96±0.01

TABLE 4. Kinetic currents, in mA, and normalized kinetic currents (in parentheses) for oxygen reduction in 0.10 M NaOH at OPG electrodes modified with CoTNPc or one of its binuclear derivatives (electrode area = 0.493 cm^2)

	Potential (V versus sce)				Average normalized i_k
Compound	−0.450	−0.500	−0.550	−0.600	
CoTNPc	1.51	3.00	5.58	9.95	
	(1)	(1)	(1)	(1)	—
C(2)[CoTrNPc]$_2$	1.64	3.20	5.90	11.01	
	(1.09)	(1.07)	(1.06)	(1.11)	1.08±0.02
Cat(4)[CoTrNPc]$_2$	1.84	3.91	7.95	16.01	
	(1.22)	(1.30)	(1.42)	(1.61)	1.39±0.17
EtMeO(5)[CoTrNPc]$_2$	2.35	4.38	7.68	13.08	
	(1.56)	(1.46)	(1.38)	(1.31)	1.43±0.10
O(1)[CoTrNPc]$_2$	2.45	4.61	8.15	13.89	
	(1.62)	(1.54)	(1.46)	(1.40)	1.50±0.10

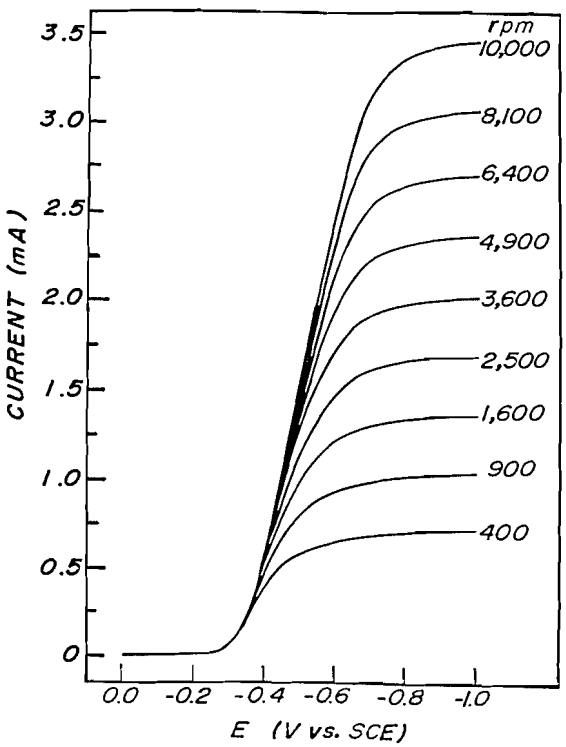

FIG. 6. Reduction of molecular oxygen at a rotating OPG electrode modified CoTNPc in an O_2-saturated 0.10 M NaOH solution.

in which i_k is the kinetically-limited current. A plot of $1/i$ versus $1/\omega^{1/2}$, known as the Koutecky–Levich plot, establishes this kinetically-limited current which is equivalent to the current that would flow if the concentration of O_2 at the electrode surface could be maintained at its bulk concentration during the reduction process. Therefore, i_k at a given potential is directly proportional to the maximum rate at which O_2 can be reduced to peroxide at the catalyst-modified electrode at that potential (89).

The reduction of O_2 at an OPG electrode modified with CoTNPc is shown in Fig. 6. These scans were recorded at 10 mV/s, but may be considered to be steady-state curves since no hysteresis was observed between the forward and reverse scans. Following the procedures presented by Frumkin and Tedoradse (90), Koutecky–Levich plots at −0.450 V, −0.500 V, −0.550 V, and −0.600 V were constructed. Koutecky–Levich plots of O_2 reduction at −0.450 V for OPG electrodes modified with CoTNPc and each of its binuclear derivatives are given in Fig. 7. The scatter for Koutecky–Levich plots was small ($R > 0.999$) and the n values calculated from the slopes of these plots (Table 3) were consistent with a two-electron process yielding peroxide as the reduction product. The different intercepts for the Koutecky–Levich plots illustrate that the catalytic activity of these species differ. The kinetically-limited currents for oxygen reduction are presented in Table 4. These kinetically-limited currents have been normalized to the CoTNPc data to rank the catalytic efficiency of the binuclear species and these normalized kinetically-limited currents are presented in parentheses in Table 4.

Can. J. Chem. Downloaded from www.nrcresearchpress.com by 213.222.148.141 on 09/07/12
For personal use only.

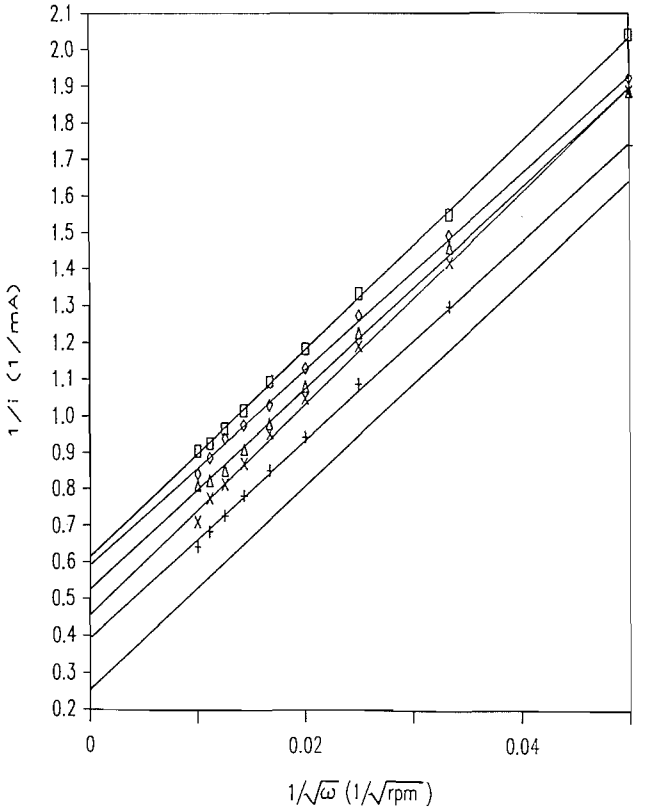

FIG. 7. Koutecky–Levich plots for the reduction of molecular oxygen in 0.10 *M* NaOH at −0.450 V versus sce on OPG electrodes modified with □, CoTNPc; +, O(1)[CoTrNPc]$_2$; ◇, C(2)[CoTrNPc]$_2$; △, Cat(4)[CoTrNPc]$_2$; or ×, EtMeO(5)[CoTrNPc]$_2$. A theoretical two-electron line is shown at the bottom of the graph for comparison.

The standard deviation for the average normalized kinetically-limited currents is less than 15% which though somewhat large, is similar to the deviation reported in another study (91). These normalized currents indicate the reactivities of these species towards oxygen reduction are as follows:

[8] O(1)[CoTrNPc]$_2$ > EtMeO(5)[CoTrNPc]$_2$ ≃ Cat(4)[CoTrNPc]$_2$ > C(2)[CoTrNPc]$_2$ > CoTNPc

It is surely significant that this ranking is the same as given for the electronic coupling of these species.

Although the binuclear CoTNPc compounds have shown increased activity towards the electrocatalytic reduction of molecular oxygen, the potential at which this process occurs in pH 13 NaOH solution is approximately the same as that for CoTSPc under the same conditions (41), and rather too negative to be practical for a fuel cell catalyst. Present studies are being directed towards the shifting of the molecular oxygen reduction potential to more positive values by performing these experiments under acidic conditions, and also to devise conditions under which the direct four-electron reduction process will be favoured.

Summary

In basic media, binuclear cobalt phthalocyanines were shown to be more active towards the electrocatalytic reduction of molecular oxygen than the corresponding mononuclear species. The increased activity of these binuclear compounds has been attributed to the increased electronic coupling between the phthalocyanine rings of these species. Current studies include CoPc species showing a much greater degree of intramolecular coupling than observed here (92). A mechanistic study of CoTNPc over the pH range 1 to 13 will also be reported shortly.

Acknowledgements

Gratitude is extended to the Natural Sciences and Engineering Research Council of Canada for financial support in the forms of an operating grant and a postgraduate scholarship (M.R.H.). Support from the Office of Naval Research (Washington) is also appreciated. The authors also wish to express their gratitude to Dr. Pavel Janda for beneficial discussions.

1. T. KUWANA, M. FUJIHIRA, K. SUNAKAWA, and T. OSA. J. Electroanal. Chem. **88**, 299 (1978).
2. A. BETTELHEIM and T. KUWANA. Anal. Chem. **51**, 2257 (1979).
3. A. BETTELHEIM, R. J. H. CHAN, and T. KUWANA. J. Electroanal. Chem. **99**, 391 (1979).
4. N. KOBAYASHI, T. MATSUE, M. FUJIHIRA, and T. OSA. J. Electroanal. Chem. **103**, 427 (1979).
5. M. R. TARASEVICH and K. A. RADYUSHKINA. Russ. Chem. Rev. Engl. Transl. **49**, 1498 (1980).
6. J. A. R. VAN VEEN, J. F. VAN BAAR, C. J. KROESE, J. G. F. COOLEGEM, N. DE WIT, and H. A. COLIJN. Ber. Bunsenges. Phys. Chem. **85**, 693 (1981).
7. J. A. R. VAN VEEN and H. A. COLIJN. Ber. Bunsenges. Phys. Chem. **85**, 700 (1981).
8. P. A. FORSHEY, T. KUWANA, N. KOBAYASHI, and T. OSA. Adv. Chem. Ser. **201**, 601 (1982).
9. N. KOBAYASHI, M. FUJIHIRA, T. OSA, and S. DONG. Chem. Lett. 575 (1982).
10. A. BETTELHEIM, R. PARASH, and D. OZER. J. Electrochem. Soc. **129**, 2247 (1982).
11. N. KOBAYASHI and T. OSA. J. Electroanal. Chem. **157**, 269 (1983).
12. A. BETTELHEIM, D. OZER, and R. PARASH. J. Chem. Soc. Faraday Trans. 1, **79**, 1555 (1983).
13. P. A. FORSHEY and T. KUWANA. Inorg. Chem. **22**, 699 (1983).
14. K. OKABAYASHI, O. IKEDA, and H. TAMURA. J. Chem. Soc. Chem. Commun. 684 (1983).
15. O. IKEDA, K. OKABAYASHI, and H. TAMURA. Chem. Lett. 1821 (1983).
16. O. IKEDA, H. FUKUDA, and H. TAMURA. J. Chem. Soc. Chem. Commun. 567 (1984).
17. D. OZER, R. PARASH, F. BROITMAN, U. MOR, and A. BETTELHEIM. J. Chem. Soc. Faraday Trans. 1, **80**, 1139 (1984).
18. O. IKEDA, H. FUKEDA, T. KOJIMA, and H. TAMURA. J. Electrochem. Soc. **132**, 3069 (1985).
19. C.-L. NI and F. C. ANSON. Inorg. Chem. **24**, 4754 (1985).
20. F. BEDIOUI, C. BONGARS, C. HINNEN, C. BIED-CHARRETON, and J. DEVYNCK. Bull. Chim. Soc. Fr. 679 (1985).
21. O. IKEDA, K. OKABAYASHI, N. YOSHIDA, and H. TAMURA. J. Electroanal. Chem. **191**, 157 (1985).
22. J. P. COLLMAN, M. MAROCCO, P. DENISEVICH, C. KOVAL, and F. C. ANSON. J. Electroanal. Chem. **101**, 117 (1979).
23. J. P. COLLMAN, P. DENISEVICH, Y. KONAI, M. MAROCCO, C. KOVAL, and F. C. ANSON. J. Am. Chem. Soc. **102**, 6027 (1980).
24. R. R. DURAND, JR., J. P. COLLMAN, and F. C. ANSON. J. Electroanal. Chem. **151**, 289 (1983).
25. J. P. COLLMAN, F. C. ANSON, C. E. BARNES, C. S. BENCOSME, T. GEIGER, E. R. EVITT, R. P. KREH, K. MEIER, and R. B. PETTMAN. J. Am. Chem. Soc. **105**, 2694 (1983).
26. J. P. COLLMAN, C. S. BENCOSME, R. R. DURAND, JR., R. P. KREH, and F. C. ANSON. J. Am. Chem. Soc. **105**, 2699 (1983).
27. J. P. COLLMAN, F. C. ANSON, C. E. BARNES, and B. D. MILLER. J. Am. Chem. Soc. **105**, 2704 (1983).
28. R. R. DURAND, JR., C. S. BENCOSME, J. P. COLLMAN, and F. C. ANSON. J. Am. Chem. Soc. **105**, 2710 (1983).
29. C. K. CHANG. J. Chem. Soc. Chem. Commun. 800 (1979).

Can. J. Chem. Downloaded from www.nrcresearchpress.com by 213.222.148.141 on 09/07/12
For personal use only.

30. C. K. CHANG. Biochem. Clin. Aspects Oxygen, 437 (1978).
31. C. K. CHANG. Adv. Chem. Ser. **173**, 162 (1979).
32. H. Y. LIU, M. J. WEAVER, C.-B. WANG, and C. K. CHANG. J. Electroanal. Chem. **145**, 439 (1983).
33. C. K. CHANG and I. ABDALMUHDI. Angew. Chem. Int. Ed. Engl. **23**, 164 (1984).
34. C. K. CHANG, H. Y. LIU, and I. ABDALMUHDI. J. Am. Chem. Soc. **106**, 2725 (1984).
35. H.-Y. LIU, I. ABDALMUHDI, C. K. CHANG, and F. C. ANSON. J. Phys. Chem. **89**, 665 (1985).
36. R. JASINSKI. J. Electrochem. Soc. **112**, 526 (1965).
37. A. KOZAWA, V. E. ZILIONIS, and R. J. BRODD. J. Electrochem. Soc. **117**, 1470 (1970).
38. A. KOZAWA, V. E. ZILIONIS, and R. J. BRODD. J. Electrochem. Soc. **117**, 1474 (1970).
39. A. KOZAWA, V. E. ZILIONIS, and R. J. BRODD. J. Electrochem. Soc. **118**, 1705 (1971).
40. J.-P. RANDIN. Electrochim. Acta, **19**, 83 (1974).
41. J. ZAGAL, R. K. SEN, and E. YEAGER. J. Electroanal. Chem. **83**, 207 (1977).
42. J. ZAGAL, P. BINDRA, and E. YEAGER. J. Electrochem. Soc. **127**, 1506 (1980).
43. F. VAN DEN BRINK, W. VISSCHER, and E. BARENDRECHT. J. Electroanal. Chem. **157**, 283 (1983).
44. F. VAN DEN BRINK, W. VISSCHER, and E. BARENDRECHT. J. Electroanal. Chem. **157**, 305 (1983).
45. F. VAN DEN BRINK, W. VISSCHER, and E. BARENDRECHT. J. Electroanal. Chem. **172**, 301 (1984).
46. F. VAN DEN BRINK, W. VISSCHER, and E. BARENDRECHT. J. Electroanal. Chem. **175**, 279 (1984).
47. J. H. ZAGAL, M. PAEZ, J. STURM, and S. URETA-ZANARTU. J. Electroanal. Chem. **181**, 295 (1984).
48. T. OSAKA, K. NAOI, T. HIRABAYASHI, and S. NAKAMURA. Bull. Chem. Soc. Jpn. **59**, 2717 (1986).
49. A. ELZING, A. VAN DER PUTTEN, W. VISSCHER, and E. BARENDRECHT. J. Electroanal. Chem. **200**, 313 (1986).
50. A. VAN DER PUTTEN, A. ELZING, W. VISSCHER, and E. BARENDRECHT. J. Electroanal. Chem. **214**, 523 (1986).
51. D. WOHRLE. Fortschr. Hochpolym. Forsch. **10**, 35 (1972).
52. M. SAVY, P. ANDRO, C. BERNARD, and G. MAGNER. Electrochim. Acta, **18**, 191 (1973).
53. M. SAVY, P. ANDRO, and C. BERNARD. Electrochim. Acta, **19**, 403 (1974).
54. A. J. APPLEBY and M. SAVY. Natl. Bur. Stand. (U.S.), Spec. Publ. **455**, 241 (1976).
55. A. J. APPLEBY, J. FLEISCH, and M. SAVY. J. Catal. **44**, 281 (1976).
56. S. MAROIE, M. SAVY, and J. J. VERBIST. Inorg. Chem. **18**, 2560 (1979).
57. L. KREJA and A. PLEWKA. Electrochim. Acta, **25**, 1283 (1980).
58. H. BEHRET, H. BINDER, G. SANDSTEDE, and G. G. SCHERER. J. Electroanal. Chem. **117**, 29 (1981).
59. J. BLOMQUIST, U. HELGESON, and L. C. MOBERG. Electrochim. Acta, **27**, 1445 (1982).
60. J. BLOMQUIST, U. HELGESON, and L. C. MOBERG. Electrochim. Acta, **27**, 1453 (1982).
61. L. KREJA. Electrochim. Acta, **28**, 1807 (1983).
62. T. HIRAI and J.-I. YAMAKI. J. Electrochem. Soc. **132**, 2125 (1986).
63. C. C. LEZNOFF, S. GREENBERG, S. M. MARCUCCIO, P. C. MINOR, P. SEYMOUR, and A. B. P. LEVER. Inorg. Chim. Acta, **89**, L35 (1984).
64. C. C. LEZNOFF, S. M. MARCUCCIO, S. GREENBERG, A. B. P. LEVER, and K. B. TOMER. Can. J. Chem. **63**, 623 (1985).
65. S. M. MARCUCCIO, P. I. SVIRSKAYA, S. GREENBERG, A. B. P. LEVER, and C. C. LEZNOFF. Can. J. Chem. **63**, 3057 (1985).
66. E. S. DODSWORTH, A. B. P. LEVER, P. SEYMOUR, and C. C. LEZNOFF. J. Phys. Chem. **89**, 5698 (1985).
67. W. A. NEVIN, W. LIU, and A. B. P. LEVER. Can. J. Chem. **65**, 855 (1987).
68. M. GOUTERMAN. The porphyrins. Vol. III. *Edited by* D. Dolphin. Pt. A, Academic Press, New York. 1978. p. 1.
69. S. GREENBERG, S. M. MARCUCCIO, C. C. LEZNOFF, and K. B. TOMER. Synthesis, 406 (1986).
70. M. R. HEMPSTEAD. Ph.D. Thesis, York University. 1987.
71. A. J. BARD and L. R. FAULKNER. Electrochemical methods. John Wiley and Sons, New York. 1980.
72. R. H. WOPSCHALL and I. SHAIN. Anal. Chem. **39**, 1514 (1967).
73. W. A. NEVIN, M. R. HEMPSTEAD, W. LIU, C. C. LEZNOFF, and A. B. P. LEVER. Inorg. Chem. **26**, 570 (1987).
74. J. H. ZAGAL. Ph.D. Thesis, Case Western Reserve University. 1978.
75. A. N. FRUMKIN. Z. Phys. **35**, 792 (1926).
76. E. LAVIRON. J. Electroanal. Chem. **52**, 395 (1974).
77. J. SCHREURS and E. BARENDRECHT. Recl. Trav. Chim. Pays-Bas, **103**, 205 (1984).
78. P. NIKITAS. J. Chem. Soc., Faraday Trans. 1, **81**, 1767 (1985).
79. A. N. FRUMKIN and B. B. DAMASKIN. Pure Appl. Chem. **15**, 263 (1967).
80. A. B. P. LEVER, M. R. HEMPSTEAD, C. C. LEZNOFF, W. LIU, M. MELNIK, W. A. NEVIN, and P. SEYMOUR. Pure Appl. Chem. **58**, 1467 (1986).
81. A. P. BROWN, C. KOVAL, and F. C. ANSON. J. Electroanal. Chem. **72**, 379 (1976).
82. J. NEWMAN. J. Phys. Chem. **70**, 1327 (1966).
83. W. F. LINKE. Solubilities of inorganic and metal organic compounds. Vol. II. 4th ed. Am. Chem. Soc. Washington, D.C., 1965. p. 1219.
84. R. C. WEAST (*Editor*). Handbook of chemistry and physics. 57th ed., CRC Press, Cleveland, OH. 1977.
85. J. KOUTECKY and V. G. LEVICH. Zh. Fiz. Khim. **32**, 1565 (1957).
86. YU. V. PLESKOV and V. YU. FILINOVSKI (*Editors*). Studies in Soviet science: the rotating disc electrode. Consultants Bureau, New York. 1976. p. 90.
87. P. N. ROSS and P. C. ANDRICACOS. J. Electroanal. Chem. **154**, 205 (1983).
88. F. OPEKAR and P. BERAN. J. Electroanal. Chem. **69**, 1 (1976).
89. K. SHIGEHARA and F. C. ANSON. J. Phys. Chem. **86**, 2776 (1982).
90. A. FRUMKIN and G. TEDORADSE. Z. Elektrochem. **62**, 251 (1958).
91. T. E. MALLOUK, V. CAMMARATA, J. A. CRAYSON, and M. S. WRIGHTON. J. Phys. Chem. **90**, 2150 (1986).
92. C. C. LEZNOFF, H. LAM, S. M. MARCUCCIO, W. A. NEVIN, P. JANDA, N. KOBAYASHI, and A. B. P. LEVER. J. Chem. Soc. Chem. Commun. 699 (1987).

Can. J. Chem. Downloaded from www.nrcresearchpress.com by 213.222.148.141 on 09/07/12
For personal use only.

ADDITIONS AND CORRECTIONS / AJOUTS ET CORRECTIONS

C. L. Chakrabarti, D. Ferrarotto, S. J. Cathum, and C. J. Rademeyer. Atomization efficiency of a graphite furnace in atomic absorption spectrometry at high heating rates. Can. J. Chem. **65**, 1079 (1987).

In the label of curves B, D, and E in Fig. 3, "slope" should read "2.303 × slope"; the remaining parts of the labels, which are $-k_1$, $-k_2$, and $-(k_1 + k_3)$, and their values remain unchanged.

Can. J. Chem. Downloaded from www.nrcresearchpress.com by 213.222.148.141 on 09/07/12
For personal use only.

Structure of kerlinic acid from *Salvia keerlii*. Chemical correlation with melisodoric acid[1]

LYDIA RODRÍGUEZ-HAHN,[2] ADRIANA GARCÍA, BALDOMERO ESQUIVEL, AND JORGE CÁRDENAS
Instituto de Química, Universidad Nacional Autónoma de México, Circuito Exterior, Ciudad Universitaria, Coyoacán 04510, México, D.F.

Received March 11, 1987

LYDIA RODRÍGUEZ-HAHN, ADRIANA GARCÍA, BALDOMERO ESQUIVEL, and JORGE CÁRDENAS. Can. J. Chem. **65**, 2687 (1987).

The structure of kerlinic acid, a *neo*-clerodane diterpenoid isolated from *Salvia keerlii* (Labiatae), was deduced from spectral data and chemical correlation with melisodoric acid.

LYDIA RODRÍGUEZ-HAHN, ADRIANA GARCÍA, BALDOMERO ESQUIVEL et JORGE CÁRDENAS. Can. J. Chem. **65**, 2687 (1987).

En se basant sur des données spectrales et sur une corrélation chimique avec l'acide mélisodorique, on a déduit la structure de l'acide kerlinique, un diterpénoïde de la famille du *néo*-clérodane qui a été isolé du *Salvia keerlii* (Labiatae).

[Traduit par la revue]

Introduction

Plants of the Labiatae family have attracted much attention due to a variety of biological activities and medicinal properties attributed to them (1). The bi- and tricyclic diterpenoids isolated from plants of this family have shown antifeedant (2), antitumor, antibacterial, or antifungal properties (3, 4).

Salvia L. is the largest genus of the Labiatae family with over 900 species widespread all over the world. This genus has been divided into four Subgenera (*Sclarea*, *Salvia*, *Leonia*, and *Calosphace*), according to morphological characteristics. In México *Salvia* L. is represented by almost 300 species all of which belong to *Salvia* subgenus *Calosphace* (5, 6). In recent years we have undertaken a systematic study of the Mexican *Salvia* spp. We have found that the diterpenoid content of the *Salvia* species studied depends on the section to which it belongs (7–11). Over 80% of the diterpenoids isolated up to now from Mexican *Salvia* spp. are *neo*-clerodane diterpenoids (10–12, 14).

Some years ago (12) we described the structural elucidation of melisodoric acid **1***a*, a clerodane diterpenoid isolated from *Salvia melissodora* Lag. *Salvia melissodora* has been classified in the section *Scorodonia* (S. subgenus *Calosphace*) (5). Melisodoric acid and some of its derivatives showed antifeedant activity (M. Taboada, personal communication). We have been trying to find an adequate natural source of melisodoric acid and have studied different populations of *S. melissodora* and of *S. keerlii* Bentham (*S.* section *Scorodonia*), a species botanically related to *S. melissodora* (5, 6).

A phytochemical study of *S. keerlii* collected in Oaxaca (México) yielded (13) two *neo*-clerodane diterpenoids, kerlin and kerlinolide. Herein we describe the isolation and structural elucidation of kerlinic acid **2***a*, the main diterpenoid constituent of a population of *S. keerlii* collected in a semiarid region near Querétaro (México).

Results and discussion

Kerlinic acid **2***a*, $C_{20}H_{28}O_4$, showed in the ir spectrum the presence of a hydroxyl group (3500 cm^{-1}), a carboxyl function (3200–2700, 1670 cm^{-1}), and a furan ring (1560, 1510, and 870 cm^{-1}). The ^1H nmr spectrum of **2***a* (Table 1) confirmed the presence of a β-substituted furan ring. A multiplet at δ 5.6 was ascribed to the H-3 vinylic proton, which was shown to be coupled to the vinylic methyl group bound to C-4 by double resonance experiments. A double doublet at δ 3.45 (1H, J = 4 and 10 Hz) was assigned to the geminal proton of a secondary hydroxyl group. It also showed signals due to a tertiary, a secondary, and a vinylic methyl group. Treatment of **2***a* with ethereal diazomethane gave the methyl ester **2***b*. Acetylation (Ac_2O, py) of **2***b* gave the acetate derivative **2***c* whose ^1H nmr spectrum (Table 1) showed the acetate geminal proton at δ 4.75 (dd, J = 4 and 10 Hz).

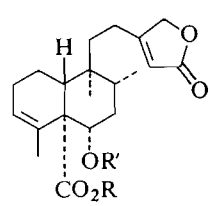

1*a* R = R′ = H
b R = Me, R′ = H
c R = Me, R′ = Ac

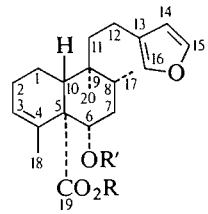

2*a* R = R′ = H
b R = Me, R′ = H
c R = Me, R′ = Ac
d R = H, R′ = Ac

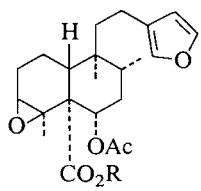

3 R = Me

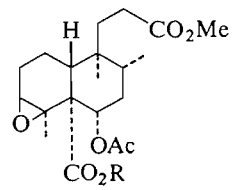

4 R = Me

The resemblance of the spectral data of kerlinic acid to those of melisodoric acid, **1***a*, suggested structure **2***a* for the former. To prove the structural relationship between kerlinic acid **2***a* and melisodoric acid **1***a*, we decided to transform it into the dimethyl ester derivative **4**, which had been previously (12) obtained from melisodoric acid.

Treatment of **2***c* with one equivalent of *m*-chloroperbenzoic acid gave mainly polar products and recovered starting material after 24 h of reaction. The polar products were isolated and characterized as a mixture of the 3,4-epoxy-hydroxy lactones **5** and **6**. Treatment of **2***c* with three equivalents of *m*-chloroperbenzoic acid gave the 3,4-epoxy-hydroxy lactones **5** and **6** in 90% yield as a crystalline mixture that could not be resolved. Their structures were deduced from the spectral data. The mixture showed hydroxyl absorptions in the ir spectrum at 3583 and 3480 cm^{-1} and a band at 1766 cm^{-1} that was attributed to

[1]This work was presented in part at the XIII International Symposium of Natural Products Chemistry, Monterrey, México, 1986.

[2]Author to whom correspondence may be addressed.

Printed in Canada / Imprimé au Canada

Can. J. Chem. Downloaded from www.nrcresearchpress.com by 213.222.148.141 on 09/07/12
For personal use only.

TABLE 1. ^{1}H nuclear magnetic resonance spectral data*

H	Compound								
	2*a*	**2***b*	**2***c*	**3**	**5**	**6**	**7**	**8**	**9**
3	5.6 m	5.55 m	5.5 m	2.92 d (4)	2.95 d (4)	2.95 d (4)	2.95 d (4)	2.92 d (5)	2.92 d (5)
6	3.45 dd (4, 10)	3.37 dd (4, 10)	4.75 dd (4, 10)	4.9 dd (4, 12)	4.83 dd (5, 10)	4.9 dd (5, 10)	4.9 dd (5, 10)	4.85 dd (4, 10)	4.85 dd (4, 10)
14	6.2 dd (2, 1)	6.2 m	6.2 m	6.2 m	6.8 m	6.2 m	6.55 t (2)	5.80 m	7.05 m
15	7.3 t (2)	7.3 t (2)	7.3 t (2)	7.3 t (2)	5.8 br s	—	—	—	4.7 br s
16	7.15 br s	7.15 br s	7.15 m	7.15 m	—	5.97 s	—	4.67 d (2)	—
17(Me)	0.85 d (7)	0.85 d (7)	0.85 d (7)	0.80 d (7)	0.82 d (7)	0.82 d (7)	0.85 d (7)	0.8 d (7)	0.8 d (7)
18(Me)	1.9 br s	1.87 br d (2)	1.62 br d (2)	1.25 s	1.25 s	1.25 s	1.25 s	1.25 s	1.25 s
20(Me)	0.75 s	0.62 s	0.75 s	0.58 s	0.65 s	0.60 s	0.65 s	0.65 s	0.60 s
O*Me*	—	3.67 s	3.70 s	3.75 s	3.80 s	3.80 s	3.78 s	3.75 s	3.73 s
OCO*Me*	—	—	2.05 s	2.05 s	2.07 s	2.07 s	2.05 s	2.05 s	2.05 s

*Run at 80 MHz in $CDCl_3$ using TMS as internal standard. Coupling constants in Hz are in parentheses.

the α,β-unsaturated γ-lactone function. In the ^{1}H nmr spectrum (Table 1), H-3 was observed as a broad doublet (J = 4 Hz) at δ 2.95. Two multiplets at δ 6.8 and 6.2 were ascribed to the H-14 of **5** and **6** respectively. A broad singlet at δ 5.8 was assigned to H-15 of **5** and a singlet at δ 5.97 to H-16 of **6**.

Manganese dioxide oxidation of the mixture of hydroxy lactones gave the epoxy anhydride **7**. The anhydride moiety was evidenced by the ir bands at 1843 and 1775 cm^{-1} and a triplet (1H, J = 2 Hz) at δ 6.55 in the ^{1}H nmr spectrum (Table 1) ascribed to H-14.

Ozonolysis of the mixture of 3,4-epoxy-hydroxy lactones **5** and **6**, followed by oxidative treatment of the ozonide and esterification with ethereal diazomethane, gave the dimethyl ester **4** identical (see Experimental) to the product previously obtained from melisodoric acid (12). Reduction of the hydroxy lactones **5** and **6** with sodium borohydride (14) gave a mixture of 3,4-epoxy lactones **8** and **9** in a 4:3 ratio. The presence of product **8** in the mixture was proved by comparison of its ^{1}H nmr spectrum with that of the product obtained by epoxidation of melisodoric acid acetate methyl ester **1***c* (12). In this way, the structural correlation between kerlinic acid **2***a* and melisodoric acid **1***a* was established.

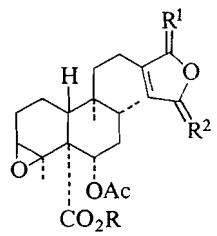

R	R^1	R^2
5 Me	O	H,OH
6 Me	H,OH	O
7 Me	O	O
8 Me	H_2	O
9 Me	O	H_2

The stereochemistry proposed for kerlinic acid **2***a* rests on a careful analysis of the ^{13}C nmr data of **2***a* and some of its derivatives (Table 2). Recently (15) the ^{13}C chemical shifts of the pendant methyl groups in a clerodane skeleton have been proposed as a useful tool to distinguish between *cis* and *trans* A/B ring junctions. In *cis*-clerodanes the equatorial C-20 resonates at δ 21–29; a chemical shift of δ 17–19 is expected for the axial C-20, and about δ 15 for the equatorial C-17 in *trans-neo*-clerodanes. In the ^{13}C nmr spectra of **2***a* and its

TABLE 2. ^{13}C data for kerlinic acid and derivatives*

C	Compound				
	2*a*†	**2***d*	**2***c*	**5**	**6**
1	38.9 (t)	38.7 (t)	38.7 (t)	38.4 (t)	38.4 (t)
2	17.5 (t)	17.7 (t)	17.7 (t)	16.2 (t)	16.2 (t)
3	127.6 (d)	127.8 (d)	127.2 (d)	63.7 (d)	63.7 (d)
4	136.2 (s)	135.6 (s)	135.8 (s)	62.8 (s)	62.8 (s)
5	53.7 (s)	53.1 (s)	53.4 (s)	53.2 (s)	53.4 (s)
6	76.0 (d)	76.8 (d)	77.1 (d)	75.12 (d)	75.12 (d)
7	38.8 (t)	33.8 (t)	33.9 (t)	33.2 (t)	35.0 (t)
8	35.5 (d)	34.8 (d)	34.8 (d)	34.54 (d)	34.5 (d)
9	38.9 (s)	38.7 (s)	38.5 (s)	38.2 (s)	38.2 (s)
10	48.4 (d)	48.3 (d)	48.25 (d)	41.9 (d)	41.9 (d)
11	26.3 (t)	26.4 (t)	26.5 (t)	23.0 (t)	23.0 (t)
12	17.5 (t)	17.7 (t)	18.2 (t)	22.7 (t)	22.7 (t)
13	125.2 (s)	125.1 (s)	125.22 (s)	137.9 (s)	170.5 (s)
14	110.9 (d)	110.8 (d)	110.9 (d)	143.9 (d)	117.2 (d)
15	142.8 (d)	142.8 (d)	142.8 (d)	99.26 (d)	170.48 (s)
16	138.5 (d)	138.5 (d)	138.5 (d)	170.41 (s)	97.0 (d)
17	16.1 (q)	15.8 (q)	15.9 (q)	15.4 (q)	15.4 (q)
18	23.3 (q)	22.2 (q)	22.15 (q)	22.2 (q)	22.2 (q)
19	181.0 (s)	180.0 (s)	173.3 (s)	172.8 (s)	172.7 (s)
20	15.15 (q)	15.3 (q)	15.4 (q)	15.7 (q)	15.7 (q)
21	—	170.5 (s)	170.5 (s)	171.8 (s)	171.5 (s)
22	—	21.7 (q)	21.8 (q)	21.7 (q)	21.7 (q)
23	—	—	51.5 (q)	51.6 (q)	51.6 (q)

*Recorded at 20 MHz. Chemical shifts in δ values from TMS. SFORD multiplicities in parentheses.

†The methyl signals were assigned by selective decoupling experiments.

derivatives (Table 2), C-20 and C-17 resonate at δ 15–16. These chemical shifts indicate an axial orientation for C-20, an equatorial orientation for C-17, and a steroidal A/B *trans* ring junction for kerlinic acid **2***a*.

The coupling constants observed for H-6 in the ^{1}H nmr spectrum of kerlinic acid **2***a* and its derivatives (Table 1) indicate an axial–axial and axial–equatorial interaction of this proton with H-7α and H-7β, hence the C-6 hydroxyl group is α-equatorially oriented.

Can. J. Chem. Downloaded from www.nrcresearchpress.com by 213.222.148.141 on 09/07/12
For personal use only.

Can. J. Chem. Downloaded from www.nrcresearchpress.com by 213.222.148.141 on 09/07/12
For personal use only.

The β-orientation proposed for the 3,4-epoxide in **5** and **6** was deduced from the upfield shift observed for C-10 in these products with respect to the chemical shift of C-10 in compounds **2***a*–**2***d* (Table 2). The application of the Tori (16) equation was not useful in our case.

In the structural elucidation of melisodoric acid (12), its relative stereochemistry was not ascertained. The chemical correlation established between **2***a* and **1***a*, mainly the formation of product **4** with the same optical rotation (see Experimental) from both acids, allowed us to assign the stereochemistry shown in **1***a* for melisodoric acid.

In a series of papers on the chemistry of the diterpenoid constituents of *Solidago* species, McCrindle *et al.* (17) described the *m*-chloroperbenzoic acid epoxidation reaction of a number of furyl olefins, in which the furyl 3,4-epoxides were obtained in 10–50% yields. In some examples they describe the formation of polar compounds whose structures were not analysed. We think that those polar compounds were the corresponding hydroxy lactone derivatives formed by attack of the *m*-chloroperbenzoic acid on the β-substituted furan ring present in all the products described.

Experimental

Melting points are uncorrected. The uv spectra were run in methanol solutions, and the ir spectra were recorded in chloroform solutions. Mass spectra were obtained by direct inlet at 70 eV. The ^{1}H nmr spectra were obtained at 80 MHz in $CDCl_3$ solutions with TMS as internal standard, the ^{13}C nmr spectra at 20 MHz, also in $CDCl_3$ solutions with TMS as internal standard. Assignments of ^{13}C nmr chemical shifts were made with the aid of off-resonance, noise-decoupled, APT and gated decoupling ^{13}C nmr spectra.

Plant material was collected in August 1985, 15 km SW of Querétaro, México, and the voucher specimen (MEXU 211417) was deposited at the Herbarium of the Instituto de Biología, UNAM.

Isolation of kerlinic acid **2**a

Dried aerial parts of *S. keerlii* (1.7 kg) were extracted with acetone (10 L) for 1 week. The solvent was removed under reduced pressure and the gummy residue obtained (140 g) was chromatographed over silica gel (1 kg, deactivated with 5% H_2O). Elution with light petroleum – EtOAc (9:1) gave kerlinic acid **2***a* (11 g, 0.68% dry weight), mp 183–185°C from acetone – light petroleum; $[\alpha]_D^{25}$ −236.8 (*c* 0.19, $CHCl_3$); λ_{max}: 205 nm (14 500); ν_{max}: 3500, 3200–2500, 1670, 1560, 1510, 870 cm^{-1}; ^{1}H nmr, see Table 1; *m/z*: 332 (M^+, 8), 314 (2), 270 (7), 189 (2), 175 (30), 105 (43), 95 (30), 81 (100%). *Anal.* calcd. for $C_{20}H_{28}O_4$: C 72.26, H 8.49; found: C 71.65, H 8.43.

Kerlinic acid methyl ester **2**b

Kerlinic acid **2***a* (1 g) in ethyl ether was treated with ethereal diazomethane solution in the usual manner. The crude product obtained was passed through SiO_2 to yield kerlinic acid methyl ester **2***b* (850 mg) as an oily product; ν_{max}: 3510, 1690, 1560, 1090, 1060, 870 cm^{-1}; ^{1}H nmr, see Table 1; *m/z*: 346 (M^+, 30), 328 (2), 296 (10), 269 (20), 173 (30), 105 (25), 95 (25), 91 (35), 81 (100%) ($C_{21}H_{30}O_4$ requires M^+, 346).

Kerlinic acid methyl ester acetate **2**c

Treatment of kerlinic acid methyl ester **2***b* (450 mg) with Ac_2O (1 mL) in pyridine (1 mL) at 90°C gave the acetate derivative **2***c* after chromatography over SiO_2. The acetate **2***c* showed mp 107–108°C from light petroleum; ν_{max}: 1720, 1650, 1495, 870 cm^{-1}; ^{1}H nmr, see Table 1; *m/z*: 388 (M^+, 8), 328 (9), 314 (5), 296 (20), 269 (25), 233 (40), 173 (58), 105 (45), 95 (30), 81 (100%), 43 (90) ($C_{23}H_{32}O_5$ requires M^+, 388).

Epoxidation of **2**c

The acetate **2***c* (100 mg) in dry carbon tetrachloride (5 mL) was treated with *m*-chloroperbenzoic acid (75 mg) at room temperature with stirring for 4 h. Water was added and the reaction mixture extracted twice with dichloromethane. The organic solution was washed with saturated aqueous $NaHCO_3$ solution and brine, dried, and the solvent removed under reduced pressure. The crude product obtained was chromatographed over SiO_2. Elution with light petroleum gave the epoxide **3** (5 mg), mp 107–111°C, from light petroleum; ν_{max}: 1732, 1560, 873 cm^{-1}; ^{1}H nmr, see Table 1; *m/z*: 404 (M^+, 8), 309 (35), 249 (50), 217 (25), 289 (31), 175 (8), 105 (10), 95 (25), 81 (80), 43 (100%) ($C_{23}H_{32}O_6$ requires M^+, 404). Elution with light petroleum – EtOAc (1:1) gave the hydroxy lactones **5** and **6** (65 mg).

Preparation of hydroxy lactones **5** *and* **6**

To a cooled (ice bath) solution of the acetate **2***c* (250 mg) in dichloromethane (10 mL), *m*-chloroperbenzoic acid (388 mg) was added. The reaction mixture was warmed to room temperature and stirred for 8 h. Water was added and extracted with EtOAc. The organic solution was washed with saturated aqueous $NaHCO_3$ solution and brine, dried, and the solvents removed under reduced pressure. The solid product obtained was recrystallized from acetone – light petroleum to yield a 2:3 mixture of the hydroxy lactones **5** and **6** (225 mg); mp 198–200°C; λ_{max}: 206 nm (10 400); ν_{max}: 3583, 3540, 1766, 1730, 1650, 1248, 864 cm^{-1}; ^{1}H nmr, see Table 1; ^{13}C nmr, see Table 2; *m/z*: 436 (M^+, 2), 377 (10), 344 (15), 277 (15), 259 (10), 249 (15), 217 (35), 189 (15), 161 (19.5), 91 (25.8), 43 (100%) ($C_{23}H_{32}O_8$ requires M^+, 436).

Treatment of the acetate **2***c* with *m*-chloroperbenzoic acid following Wiesner conditions (14) gave the hydroxy lactones **5** and **6** in a 1:1 ratio (mp 176–178°C).

Manganese dioxide oxidation of the hydroxy lactones **5** *and* **6**

The hydroxy lactones mixture (25 mg) in dichloromethane was treated with manganese dioxide (250 mg) stirring at room temperature for 5 h. The reaction mixture was filtered through Celite, the solvent removed, and the residue chromatographed over SiO_2. The crystalline anhydride **7** showed mp 146–150°C from light petroleum; λ_{max}: 204 nm (9000); ν_{max}: 1843, 1775, 1731, 1641, 897 cm^{-1}; ^{1}H nmr, see Table 1; *m/z*: 403 ($M^+ - 31$, 2), 375 ($M^+ - 59$, 35), 359 (50), 342 (22), 315 (15), 275 (12), 217 (18), 189 (8), 161 (15), 119 (19), 105 (22), 97 (8), 91 (26), 43 (100%) ($C_{23}H_{30}O_8$ requires M^+, 434); by chemical ionization *m/z*: 435 ($M^+ + 1$, 12), 463 ($M^+ + 29$, 5).

Preparation of the dimethyl ester derivative **4**

The hydroxy lactones (100 mg) in dichloromethane (20 mL) were treated with ozone at −70°C. The reaction mixture was warmed to room temperature and treated with a saturated aqueous solution of $NaHCO_3$ (0.5 mL), and hydrogen peroxide (30%, 0.2 mL) in MeOH, for 2 h, then acidified and extracted with EtOAc. The organic solution was washed with brine, dried, and the solvent removed. The oily product obtained was treated with ethereal diazomethane solution and passed through SiO_2 gel to yield the dimethyl ester **4**, mp 92–94°C, $[\alpha]_D^{25}$ −29.4° (*c* 0.17, $CHCl_3$), identical (mp, mmp, ir) to the product obtained from melisodoric acid (12), $[\alpha]_D^{25}$ −29°.

Sodium borohydride reduction of the hydroxy lactones (ref. 14)

The hydroxy lactones (**5** and **6**, 60 mg) in dichloromethane at 0°C were treated with sodium borohydride (60 mg) and methanol (0.1 mL). The reaction mixture was stirred for 1 h at room temperature, acidified, and extracted with EtOAc, washed with brine, dried, and the solvent removed. The crude reaction product was chromatographed over SiO_2 to yield the mixture of lactones **8** and **9** in 4:3 ratio, mp 145–148°C (**8** showed (12) mp 168–170°C). Attempts to obtain pure **8** and **9** were unsuccessful, as use of silver nitrate impregnated SiO_2 preparative plates produced decomposition; ν_{max}: 1784, 1749, 1615, 1602, 1246 cm^{-1}; ^{1}H nmr, see Table 1; *m/z*: 420 (M^+, 1), 389 (2), 360 (12), 328 (20), 301 (30), 261 (40), 189 (50), 119 (80), 91 (87), 79 (78), 55 (100%) ($C_{23}H_{32}O_7$ requires M^+, 420).

Acknowledgements

We thank Dr. T. P. Ramamoorthy (Instituto de Biología, UNAM) for the classification of the plant and for fruitful discussions, and Miss E. Argüelles for her help in the collection of the plant material. We also thank Messrs. R. Villena, M.

Torres, H. Bojórquez, L. Velasco, and R. Gaviño for technical assistance. We are very grateful to Dr. L. A. Maldonado for drawing our attention to Professor Wiesner's work. This work was supported in part by CONACyt, México (Project PCCBBNA 021142).

1. J. R. HANSON. *In* Terpenoids and steroids. Vol. 11. The Chemical Society, London. 1982. See also preceding volumes.
2. F. CAMPS, J. COLL, and A. CORTELL. Rev. Latinoam. Quím. **12**, 81 (1981).
3. J. FAYOS, F. FERNÁNDEZ-GADEA, C. PASCUAL, A. PERALES, F. PIOZZI, M. RICO, B. RODRÍGUEZ, and G. SAVONA. J. Org. Chem. **49**, 1789 (1984), and references cited therein.
4. E. FUJITA and M. NODE. Prog. Chem. Org. Nat. Prod. **46**, 77 (1984).
5. C. EPLING. Rep. Spec. Nov. Regni Veg. **110**, 1 (1939).
6. T. P. RAMAMOORTHY. Plant Syst. Evol. **146**, 141 (1984).
7. X. DOMÍNGUEZ, F. GONZÁLEZ, R. ARAGÓN, M. GUTIÉRREZ, J. S. MARROQUÍN, and W. WATSON. Planta Med. **30**, 237 (1976).
8. L. RODRÍGUEZ-HAHN, B. ESQUIVEL, C. SÁNCHEZ, J. CÁRDENAS, L. ESTEBANES, M. SORIANO-GARCÍA, A. TOSCANO, and T. P. RAMAMOORTHY. Tetrahedron Lett. 5459 (1986).
9. M. HERNÁNDEZ, B. ESQUIVEL, J. CÁRDENAS, T. P. RAMAMOORTHY, and L. RODRÍGUEZ-HAHN. Phytochemistry. In press.
10. B. ESQUIVEL, J. CÁRDENAS, A. TOSCANO, M. SORIANO-GARCÍA, and L. RODRÍGUEZ-HAHN. Tetrahedron, **41**, 3213 (1985).
11. B. ESQUIVEL, J. CÁRDENAS, T. P. RAMAMOORTHY, and L. RODRÍGUEZ-HAHN. Phytochemistry, **25**, 2381 (1986).
12. L. RODRÍGUEZ-HAHN, G. MARTÍNEZ, and J. ROMO. Rev. Latinoam. Quím. **4**, 93 (1973).
13. B. ESQUIVEL, A. MENDEZ, A. ORTEGA, M. SORIANO-GARCÍA, A. TOSCANO, and RODRÍGUEZ-HAHN. Phytochemistry, **24**, 1769 (1985).
14. T. Y. TSAI, A. MINTA, and K. WIESNER. Heterocycles, **12**, 1397 (1979).
15. S. MANABE and C. NISHINO. Tetrahedron, **42**, 3461 (1986).
16. K. TORI, T. KOMEIRO, and T. NAKAGAWA. J. Org. Chem. **29**, 1136 (1964).
17. R. MCCRINDLE, E. NAKAMURA, and A. B. ANDERSON. J. Chem. Soc. Perkin Trans. 1, 1590 (1976), and references therein.

Can. J. Chem. Downloaded from www.nrcresearchpress.com by 213.222.148.141 on 09/07/12
For personal use only.

^{15}N nuclear magnetic resonance spectra of nucleoside compounds. Reflection of modifications at N1 and N^6 of adenosine derivatives

JUN UZAWA AND KENTARO ANZAI[1]

The Institute of Physical and Chemical Research, Wako-shi, Saitama 351, Japan

Received May 1, 1987

JUN UZAWA and KENTARO ANZAI. Can. J. Chem. **65**, 2691 (1987).

^{15}N nuclear magnetic resonance spectra of adenosine derivatives were taken at the natural abundance level, and the reflection of structural modifications on the spectra was considered on the basis of the electronic behaviour of the molecules.

JUN UZAWA et KENTARO ANZAI. Can. J. Chem. **65**, 2691 (1987).

Opérant au niveau de l'abondance naturelle, on a déterminé les spectres en résonance magnétique nucléaire du ^{15}N de dérivés de l'adénosine; on a observé des variations dans les spectres qui résultaient de modifications de structure et on les a considérées en fonction du comportement électronique des molécules.

[Traduit par la revue]

Can. J. Chem. Downloaded from www.nrcresearchpress.com by 213.222.148.141 on 09/07/12
For personal use only.

Introduction

Several papers have been published regarding the ^{15}N nmr spectra of nucleosides (1). We would like to present here the ^{15}N nmr spectra of some adenosine derivatives to cast light on the spectral changes caused by structural modifications at N1 and N^6 of adenosine.

Results and discussion

Morris (2) has presented a method of taking ^{15}N nmr spectra at the natural abundance level, using INEPT (insensitive nuclei enhanced by polarization transfer). To assign the signals of nitrogen unambiguously, Bax, Niu, and Live (3) have adopted the selective INEPT, including the use of refocussed pulse sequence and broad band proton decoupling. If a compound has several nitrogen atoms whose $^nJ_{N,H}$ values are similar, as in the case of polypeptides (3), the selective INEPT would be effective because a τ value can be chosen unequivocally based on a J value. A preliminary study has suggested that the nitrogen atoms in adenosine have $^2J_{N,H}$ values ranging widely (8–15 Hz), and setting a τ value based on a $^2J_{N,H}$ value seems to be difficult. Deviation from the optimum τ values ($\tau = 1/4J$) causes, if the refocussing period is included in the sequence, the decrease of the S/N ratio (4). Thus, we adopted the basic INEPT pulse sequence,[2] and τ values were chosen experimentally to reach analyzable spectra (Table 1). The assignment of nitrogen resonance signals in adenine compounds at the natural abundance level was accomplished as follows: selective irradiation[3] at the H-2 resonance resulted in the appearance of two antiphase doublets assignable to N1 and N3 (8). In the same manner the signals of N7 and N9 were observed by irradiating the H-8 signal. Distinction between N1 and N3 signals was accomplished by the method of Städeli, Bigler, and Philipsborn (5), which included the combination of INEPT with selective ^{1}H decoupling. Because of the coupling (<2 Hz) between N1 and one (two) hydrogen(s) at N^6, the N1 signal was broader than the N3 signal, being sharpened by weak irradiation[4] at the N^6-H resonance during the time of acquisition.

The position of protonation on adenosine was determined to be N1, based on the fact that addition of an acid causes upfield shifts of the N1 signal without affecting the other nitrogen signals (6). From a different viewpoint this experiment seems to illustrate the localization of positive charge without perturbing the π-electron sextet, which would have caused upfield shifts of other N atoms.

To extend the above reasoning, the ^{15}N nmr spectra of compounds having various functional groups at N1 of adenosine ($\gtrless$N→O, $\gtrless$N$^+$—OR, $\gtrless$N$^+$—R, $\succ$N—R) were inspected. Unexpectedly, adenosine **1** and adenosine *N*-oxide **15** were found to have almost the same ^{15}N chemical shifts, giving no information about the position of oxygen. Wasylishen and Schaefer (7) reported that protonation of azines was accompanied by the decrease of $^2J_{N,H}$ and, in fact, a small value of $^2J_{N1,H\text{-}2}$ (4.9 Hz) in **15** compared to **1** (16 Hz) was observed. Other N1-modified derivatives of adenosine showed a $^2J_{N1,H\text{-}2}$ value of 8.8 Hz, compared to a value of 16 Hz in N^6-substituted adenosine derivatives.

The introduction of positive charge at N1 seemed not to affect the π-electron sextet, as was shown by the ^{15}N chemical shifts of **11**, **12**, and **13**.

We previously reported that zinc bromide coordinates at N1 and N7 to the same extent, as is known by upfield shifts of the ^{15}N signals (9). The present study revealed that both $^2J_{N1,H\text{-}2}$ and $^2J_{N7,H\text{-}8}$ were not altered by coordination of the zinc cation until a salt concentration of 0.5 equivalents,[5] in spite of large upfield shifts of the N1 and N7 signals (N1, $\Delta\delta$ 24; N7, $\Delta\delta$ 18).

The fact that the resonance signal of N7 in **6** was at high field compared to **7** ($\Delta\delta$ 5) led us to the assumption that the bulkiness of the di-*p*-methoxytrityl group at N6 in **6** forced hydrogen bonding between N^6*H* and N7. In the case of 7-deazaadenosine compounds **19** and **20**, the ^{13}C chemical shifts of C7 were similar (**19**, δ_{C7} 100.0; **20**, δ_{C7} 100.5).

Effects of the substituents at N^6 seemed to be explicable by Hammett's rule: electron-releasing alkyl and electron-withdrawing acyl or trityl groups exerted opposite effects on the electron densities at N^6, N1, and N3. The ^{15}N chemical shifts of N7 and N9 were not altered, showing that the nature of 10π-electron aromatics could hardly be attributed to adenine compounds. Modifications of the imidazole ring as were seen in 8-bromoadenosine and 7-deazaadenosine did not alter the ^{15}N chemical shifts of N^6, N1, and N3.

[1]Author to whom correspondence may be addressed.

[2]$90°_x(^1H)$–τ–$180°_x(^1H)$, (^{13}C)–τ–$90°_y(^1H)$, $90°_\phi(^{13}C)$-acquisition.

[3]$\gamma B_2/2\pi$ = 21 Hz; pulse width 11 ms.

[4]$\gamma B_2/2\pi$ = 16 Hz.

[5]At the concentration of 1.5 equivalents $ZnBr_2$, all of the $^2J_{N,H}$ values were found to decrease to the same extent (10–20%), the reason being unknown.

TABLE 1. ^{15}N chemical shifts and spin coupling constants of adenosine derivatives[a]

Compound	N1	N3	N7	N9	N^6
1	215.3 (15.6)[b]	202.6 (14.6)	219.5 (11.7)	150.3 (8.8)	62.5 (90.3)
2	218.6 (16.6)	201.9 (15.6)	[c]	[c]	65.4 (90.4)
3	217.6 (18.6)	204.1 (15.6)	222.6 (12.7)	151.7 (8.8)	63.3 (90.3)
4	218.4 (15.6)	203.3 (15.6)	[c]	[c]	64.6 (90.3)
5	214.1 (18.6)	201.5 (15.6)	[c]	[c]	59.5 (95.7)
6	216.4 (16.6)	205.1 (15.6)	223.0 (11.7)	151.9 (8.8)	63.1 (90.3)
7	223.8 (18.5)	207.1 (15.6)	217.9 (11.7)	152.5 (8.8)	87.9 (89.8)
8	217.4 (18.6)	204.8 (15.6)	222.6 (11.7)	150.6 (8.8)	62.9 (90.3)
9	240.9 (17.6)	225.3 (16.6)	226.3 (11.7)	150.6 (8.8)	[d]
10	250.0 (15.6)	231.3 (14.6)	221.8 (11.7)	152.0 (8.8)	[c]
11	134.1 (8.8)	206.4 (13.7)	223.6 (11.7)	159.1 (8.8)	—
12	135.7 (8.8)	205.9 (12.7)	[c]	[c]	—
13	193.2 (8.8)	207.6 (12.7)	225.8 (12.7)	160.6 (8.8)	—
14	131.0 (8.8)	186.1 (12.7)	224.5 (11.7)	155.7 (8.8)	—
15	215.9 (4.9)	200.2 (13.7)	219.7 (12.6)	153.0 (8.8)	57.6 (91.3)
16	217.5 (4.9)	200.8 (13.7)	219.5 (12.6)	153.8 (8.8)	—
17			241.9 (12.7)	168.0 (7.8)	84.3 (93.8)
18	211.5 (16.6)	204.2 (15.6)		135.2 (7.8)	—
19	211.4 (15.6)	205.5 (14.6)		135.5 (7.8)	63.5 (89.4)
20	220.8 (18.6)	207.1 (15.6)		134.7 (7.8)	88.0 (89.9)

[a]*Solvent: DMSO-d_6.*

[b]The minus sign for all of the $^2J_{N,H}$ values listed here is quite likely according to literature values, although the sign assignment experiments were not carried out.

[c]No detection of signal based on the principle of INEPT.

[d]The signals were not obtained.

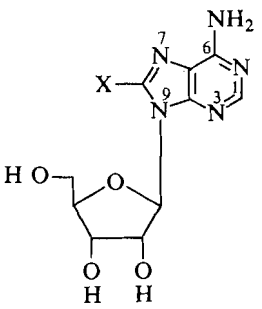

1 X = H
2 X = Br

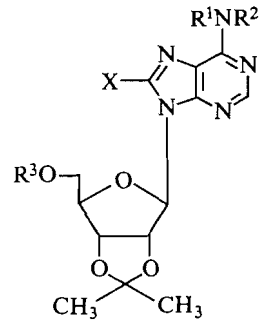

3 X, R^1, R^2, R^3 = H
4 X = Br, R^1, R^2, R^3 = H
5 X = Br, R^1 = CH_3, R^2, R^3 = H
6 X, R^1, R^2 = H, R^3 = (p-$OCH_3C_6H_4)_2C_6H_5$—
7 X, R^1 = H, R^2, R^3 = (p-$OCH_3C_6H_4)_2C_6H_5$—
8 X, R^1, R^2 = H, R^3 = p-$CH_3C_6H_4CO$—
9 X, R^1 = H, R^2, R^3 = p-$CH_3C_6H_4CO$—
10 X = H, R^1, R^2, R^3 = p-$CH_3C_6H_4CO$—

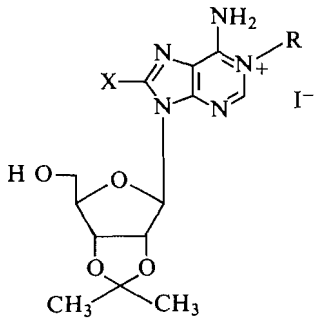

11 X = H, R = CH_3
12 X = Br, R = CH_3
13 X = H, R = OCH_3

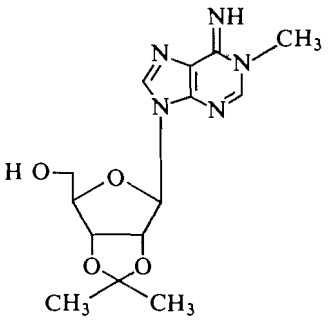

14

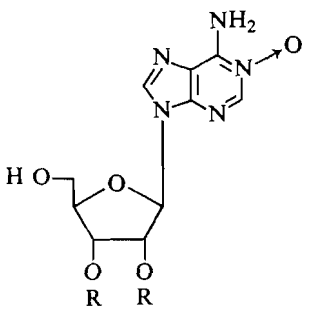

15 R = H
16 R, R = $(CH_3)_2C$

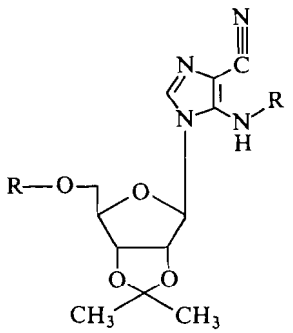

17 R = p-$CH_3C_6H_4CO$—

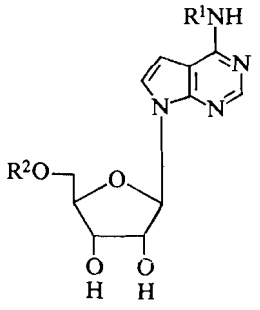

18 R^1, R^2 = H
19 R^1 = H, R^2 = $(C_6H_5)_3C$—
20 R^1, R^2 = $(C_6H_5)_3C$—

Can. J. Chem. Downloaded from www.nrcresearchpress.com by 213.222.148.141 on 09/07/12
For personal use only.

Can. J. Chem. Downloaded from www.nrcresearchpress.com by 213.222.148.141 on 09/07/12
For personal use only.

In conclusion, although recent advances in nmr techniques enable us to take ^{15}N nmr spectra at the natural abundance level, the procedure for taking the spectra is still less accessible than for ^{1}H and ^{13}C nmr measurements. However, the laboriousness of taking the spectra may be balanced by the information obtained about the electronic states of nitrogen (lone-pair existence, metal coordination, protonation, and salt formation). Thus, detailed information about the structure of nitrogen compounds is made available, as exemplified in this paper.

Experimental[6]

^{15}N nuclear magnetic resonance measurements

The ^{15}N nmr spectra were recorded on a JEOL FX-100 spectrometer at 10.10 MHz; τ value, 25 ms or 2.8 ms; proton pulse width, 240 μs or 11 ms (for selective INEPT); repetition time, 1.8 s; 15 000–125 000 transients; sample concentration, 0.6–0.1 mol in DMSO-d_6; ^{15}N chemical shifts were measured relative to external standard of aqueous $^{15}NH_4NO_3$.

N^6,5′-O-Bis(4,4′-dimethoxytrityl)-2′,3′-O-isopropylideneadenosine (7)

The isolation of 5′-*O*-(4,4′-dimethoxytrityl)-2′,3′-*O*-isopropylideneadenosine from the reaction mixture of **3** (1.04 g, 5 mmol) and 4,4′-dimethoxytrityl chloride (1.8 g, 5.3 mmol) in pyridine (50 mL) as the main product (yield 1.6 g, 53%) has been reported (9). The presence of two minor products was observed on tlc and the less polar one was isolated by silica gel chromatography (4:1 C_6H_6–EtOAc), yield 370 mg (8%), mp 104–108°C (ligroin); ^{1}H nmr data (100 MHz, $CDCl_3$) δ: 3.72 and 3.76 (2s, 6H, $2CH_3O$). *Anal.* calcd. for $C_{55}H_{53}N_5O_8$: C 72.43, H 5.86, N 7.68; found: C 72.78, H 5.94, N 7.38.

8-Bromo-9-(2′,3′-O-isopropylidene-β-D-ribofuranosyl)-1-methyladeninium iodide (12)

A solution of **4** (386 mg, 1 mmol) and CH_3I (1 mL) in DMF (20 mL) was left standing at room temperature for 5 days. The solvent was removed by evaporation to obtain a solid, which was dissolved in hot PrOH. A powder decomposing in the range 290–300°C separated when this solution was left in a refrigerator, yield 405 mg (77%); ^{1}H nmr data (100 MHz, DMSO-d_6) δ: 1.40 and 1.62 (2s, 6H, two isopropylidene methyls), 3.84 (s, 3H, N1-methyl), 6.14 (d, 1H, H-1′, J = 3 Hz), 8.16 and 8.68 (2s, 2H, H-8 and H-2). *Anal.* calcd. for $C_{14}H_{19}N_5O_4BrI$: C 31.83, H 3.63, N 13.26, I 24.03; found: C 32.08, H 3.68, N 13.44, I 23.64.

8-Bromo-2′,3′-O-isopropylidene-N^6-methyladenosine (5)

A solution of **7** (528 mg, 1 mmol) in 0.1 *M* NaOH (20 mL) was left standing at room temperature overnight to give a precipitate, which was crystallized from toluene, yield 300 mg (75%), mp 175–177°C; ^{1}H nmr data (100 MHz, $CDCl_3$) δ: 1.43 and 1.72 (2s, 6H, two isopropylidene methyls), 3.40 (d, 3H, $HNCH_3$, J = 5 Hz), 6.10 (d, 1H, H-1′, J = 4 Hz), 8.35 (s, 1H, H-2). *Anal.* calcd. for $C_{14}H_{18}N_5O_4Br$: C 42.15, H 4.52, N 17.46; found: C 42.10, H 4.45, N 17.46.

2′,3′-O-Isopropylidene-1-methyladenosine (14)

This compound has already been synthesized (10) and the following is our method of preparation. The adeninium iodide **11** (449 mg, 1 mmol) was dissolved in 0.3 *M* NaOH (40 mL) and the product was immediately extracted with $CHCl_3$. The solvent was removed by evaporation and the residue was crystallized from toluene, yield 370 mg (87%), mp 180–181°C; ^{1}H nmr data (100 MHz, $CDCl_3$) δ: 1.42 and 1.68 (2s, 6H, two isopropylidene methyls), 3.60 (s, 3H, $=N—CH_3$), 5.81 (d, 1H, H-1′, J = 3 Hz), 7.72 and 7.80 (2s, 2H, H-8 and H-2). *Anal.* calcd. for $C_{14}H_{19}N_5O_4$: C 52.33, H 5.92, N 21.80; found: C 52.27, H 5.94, N 21.73.

5′-O-Trityltubercidin (19) and N^6,5′-O-ditrityltubercidin (20)

To a solution of **18** (2.66 g, 10 mmol) in pyridine (50 mL) was added trityl chloride (5.57 g, 20 mmol) portionwise. After leaving it at room temperature for 2 days, the solution was poured into an ice-cooled solution of $NaHCO_3$. The products were extracted with $CHCl_3$ and separated on a silica gel column. Compound **20** was eluted with EtOAc and obtained as a glass from EtOAc–ligroin, yield 1.63 g (22%); uv λ_{max} (MeOH): 283 nm (ε 17 600); ^{1}H nmr data (100 MHz, DMSO-d_6) δ: 3.2 (m, 2H, H-5′), 6.10 (d, 1H, H-1′, J = 4 Hz), 7.76 (s, 1H, H-2), 8.1 (s, 1H, NH, quenched with D_2O); ^{13}C nmr data (25 MHz, DMSO-d_6) δ: 87.3 (C1′), 73.7 (C2′), 70.3 (C3′), 82.4 (C4′), 64.1 (C5′), 149.9 (C2 and C4), 104.9 (C5), 155.4 (C6), 100.5 (C7), 121.6 (C8), 86.1 (Ph_3C—O), 70.3 (Ph_3C—N), 143.6 (phenyl C1 of Ph_3C—O), 145.4 (phenyl C1 of Ph_3C—N). *Anal.* calcd. for $C_{49}H_{42}N_4O_4$: C 78.37, H 5.64, N 7.46; found: C 78.15, H 5.42, N 7.22.

Compound **19** was eluted with 9:1 EtOAc–MeOH. The crystals precipitated during concentration of the eluate were washed with benzene, yield 2.9 g (57%), mp 210–212°C ($CHCl_3$–benzene); uv λ_{max} (MeOH): 270 nm (ε 13 500); ^{1}H nmr data (100 MHz, DMSO-d_6) δ: 3.2 (m, 2H, H-5′), 6.14 (d, 1H, H-1′, J = 4 Hz), 8.10 (s, 1H, H-2), 7.05 (s, 2H, NH_2, quenched with D_2O); ^{13}C nmr data (25 MHz, DMSO-d_6) δ: 87.3 (C1′), 73.7 (C2′), 70.4 (C3′), 82.2 (C4′), 64.0 (C5′), 151.8 (C2), 150.3 (C4), 102.8 (C5), 157.5 (C6), 100.0 (C7), 121.3 (C8), 86.1 (Ph_3C—O), 143.6 (phenyl C1 of Ph_3C—O). *Anal.* calcd. for $C_{30}H_{27}N_4O_4$: C 70.99, H 5.36, N 11.04; found: C 70.69, H 5.22, N 10.89.

[6]For the preparation of **13**, **15**, and **16** see refs. 11, 13, and 14, respectively. The present authors have reported the synthesis of **6**, **8**, **9**, **10**, and **17** (9, 12).

1. V. Markowski, G. R. Sullivan, and J. D. Roberts. J. Am. Chem. Soc. **99**, 714 (1977); P. Büchner, W. Maurer, and H. Rüterjans. J. Magn. Reson. **29**, 45 (1978); G. Remaud, X-x. Zhou, C. J. Welch, and J. Chattopadhyaya. Tetrahedron, **42**, 4057 (1986); H. Sierzputowska-Gracz, H. D. Gopal, and P. F. Agris. Nucleic Acids Res. **14**, 7783 (1986).
2. G. A. Morris. J. Am. Chem. Soc. **102**, 428 (1980).
3. A. Bax, C. Niu, and D. Live. J. Am. Chem. Soc. **106**, 1150 (1984).
4. H. Nöth and B. Wrackmeyer. J. Magn. Reson. **69**, 492 (1986).
5. W. Städeli, P. Bigler, and W. Philipsborn. Org. Magn. Reson. **16**, 170 (1981).
6. N. C. Gonnella, H. Nakanishi, J. B. Holtwick, D. S. Horowitz, K. Kanamori, N. J. Leonard, and J. D. Roberts. J. Am. Chem. Soc. **105**, 2050 (1983).
7. R. Wasylishen and T. Schaefer. Can. J. Chem. **50**, 2989 (1972).
8. K. Anzai and J. Uzawa. Nucleic Acids Symp. Ser. **15**, 49 (1984).
9. K. Anzai and J. Uzawa. Can. J. Chem. **64**, 2109 (1986).
10. B. Zagalak and J. Pawelkiewicz. Acta Biochim. Polon. **12**, 103 (1965).
11. T. Fujii, C. C. Wu, T. Itaya, S. Moro, and T. Saito. Chem. Pharm. Bull. **21**, 1676 (1973).
12. K. Anzai and J. Uzawa. J. Org. Chem. **49**, 5076 (1984).
13. M. A. Stevens, D. I. Magrath, H. W. Smith, and G. B. Brown. J. Am. Chem. Soc. **80**, 2755 (1958).
14. T. Fujii, T. Saito, T. Itaya, and K. Yokoyama. Chem. Pharm. Bull. **21**, 209 (1973).

Déplacements homolytiques intramoléculaires. 14. Additions radicalaires à des peroxydes de δ-alcényle et de *tert*-butyle : accès à des tétrahydrofurannes et des tétrahydropyrannes substitués

M. AGORRODY ET E. MONTAUDON[1]

Laboratoire de chimie appliquée, Université de Bordeaux 1, 351, cours de la Libération, F-33405, Talence-CEDEX, France

ET

B. MAILLARD[1]

Laboratoire de chimie organique et organométallique, Unité associée n° 35 au centre national de la recherche scientifique, Université de Bordeaux 1, 351, cours de la Libération, F-33405, Talence-CEDEX, France

Reçu le 4 février 1987

M. AGORRODY, E. MONTAUDON et B. MAILLARD. Can. J. Chem. **65**, 2694 (1987).

Les additions radicalaires de composés donneurs d'hydrogène ZH aux peroxydes δ-insaturés conduisent à des éthers cycliques à 5 ou 6 chaînons, avec des rendements compris entre 40 et 70%, selon la substitution de la double liaison.

M. AGORRODY, E. MONTAUDON, and B. MAILLARD. Can. J. Chem. **65**, 2694 (1987).

Free radical additions of hydrogen donors of type ZH to δ-unsaturated organic peroxides give 5- or 6-membered cyclic ethers in yields varying from 40 to 70%, depending on the substitution of the double bond.

[Journal translation]

Can. J. Chem. Downloaded from www.nrcresearchpress.com by 213.222.148.141 on 09/07/12
For personal use only.

Dans un travail précédent (1), il a été montré que le peroxyde de *tert*-butyle et de pentène-4 yle, **P1**, se comporte comme ses homologues inférieurs, le peroxyde d'allyle et de *tert*-butyle et le peroxyde de *tert*-butyle et de butène-3 yle, et subit une décomposition induite au cours de sa thermolyse dans des solvants bons donneurs d'hydrogène.

La phase de propagation de cette décomposition induite en chaîne est la suivante :

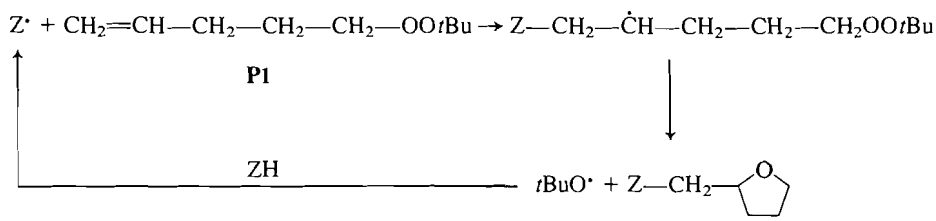

Le rendement obtenu en (tétrahydrofuryl-2 méthyl)-2 tétrahydrofuranne lors de cette étude préliminaire (1), où le solvant est le THF, est de 50%. Ceci laisse présager que ces réactions peuvent constituer une voie d'accès facile à des tétrahydrofurannes fonctionnels substitués en 2. Notre travail, dont le but est d'explorer les possibilités synthétiques de la décomposition induite de peroxydes δ-insaturés, se limitera uniquement à la recherche et à la séparation des éthers cycliques. Une définition préalable des modalités permettant d'atteindre les meilleurs rendements est indispensable.

1. Détermination des conditions optimales

L'expérience acquise conduit à opérer dans des conditions d'additions radicalaires afin d'éviter la disparition du peroxyde par thermolyse. L'amorceur et les paramètres qui ont donné les meilleurs résultats lors de la décomposition de peroxydes allyliques (2) et homoallyliques (3) sont les suivants : chauffage en présence de peracétate de *tert*-butyle (PA) à 110°C durant 12 h.

Les premiers essais ont mis en évidence l'influence primordiale des proportions relatives **P1**/PA sur les rendements de la réaction. En effet, au-dessous d'une certaine valeur de ce rapport, la décomposition de **P1** est incomplète. Ce facteur doit être déterminé en premier lieu.

*1.1. Rapport molaire **P1**/PA*

Le solvant utilisé pour cette étude est le cyclohexane. Le rapport molaire cyclohexane/**P1** est arbitrairement fixé à 100/1. Les rendements en (cyclohexylméthyl)-2 tétrahydrofuranne sont rassemblés dans le tableau 1.

L'examen de ce tableau impose d'utiliser un rapport molaire **P1**/PA égal à 2 si l'on veut que la décomposition de **P1** soit complète. Cette proportion d'amorceur est beaucoup plus importante que celle déterminée dans le cas d'autres dérivés peroxydiques : en effet, avec le peroxyde d'allyle et de *tert*-butyle (2), le peroxyde de butène-3 yle et de *tert*-butyle (3), un rapport molaire peroxyde/PA de 10 est suffisant. La nécessité d'utiliser ici davantage d'amorceur traduit l'intervention d'une réaction en chaîne très courte. Ce résultat est surprenant si l'on considère que les décompositions induites des trois modèles cités s'effectuent avec le même mécanisme en trois étapes.

Précisons que si, dans l'étude des peroxydes de butényle (3), le rapport peroxyde/PA utilisé était de 1/0,5 et non de 1/0,1, ce choix avait été établi non pas à partir du peroxyde de butène-3 yle et de *tert*-butyle mais à partir du peroxyde de méthyl-4

1. Auteurs à qui adresser toute correspondance.

TABLEAU 1. Addition radicalaire du cyclohexane à **P1** (110°C; 12 h). Influence du rapport molaire **P1**/PA

Rapport molaire **P1**/PA	1/0,1	1/0,2	1/0,3	1/0,5	1/0,75	1/1
Rendement (%)[a]	43[b]	49[b]	63[b]	70	65	60

[a]Déterminé relativement au peroxyde mis en jeu par dosage du produit brut en cpg.
[b]Présence de peroxyde **P1** qui n'a pas réagi.

TABLEAU 2. Additions radicalaires à **P1** (110°C; 12 h). Influence du rapport molaire ZH/**P1** sur les rendements en tétrahydrofurannes substitués en 2

	Rendement (%)[b]		
	ZH		
ZH/**P1**[a]	Cyclohexane	Propionate de méthyle	Chlorure de méthylène
100/1	62	75	46
50/1	70	58	42
20/1	51	35	32

[a]Rapport molaire **P1**/PA = 1/0,5.
[b]Déterminé relativement au peroxyde **P1** mis en jeu par analyse du produit réactionnel brut en cpg.

pentène-3 yle et de *tert*-butyle, afin de pouvoir effectuer des comparaisons dans toute cette série : en effet, le peroxyde disubstitué sur le carbone sp^2 terminal nécessitait, lui et lui seul, un tel taux d'amorceur.

1.2. Rapport molaire optimal ZH/P1

La détermination du «meilleur» rapport molaire ZH/**P1** a été réalisée à partir des essais décrits dans le tableau 2.

On observe que, si l'on excepte le cas du cyclohexane, le rendement maximum en tétrahydrofuranne substitué correspond à un rapport ZH/**P1** = 100. Ces proportions seront retenues et utilisées pour tous les solvants et tous les peroxydes étudiés dans cette série.

Les additions radicalaires de solvants ZH aux peroxydes δ-éthyléniques seront donc réalisées en présence de peracétate de *tert*-butyle dans les conditions suivantes : rapport molaire ZH/peroxyde/PA = 100/1/0,5; 110°C; 12 h.

2. Additions radicalaires au peroxyde de *tert*-butyle et de pentène-4 yle, P1

La réaction a été effectuée dans divers solvants, fonctionnels ou non : dichlorométhane, cyclohexane, propionate de méthyle, acétonitrile, dioxanne-1,4, acide propionique, anhydride propionique, acétone, dans les conditions déterminées dans le paragraphe précédent.

Les rendements en produits isolés relativement au peroxyde mis en jeu dans la réaction sont rassemblés dans le tableau 3.

Dans la majorité des cas, un seul tétrahydrofuranne substitué est identifié; seul le propionate de méthyle fait exception.

Les rendements en hétérocycles oxygénés, **1***x*, compris entre 40 et 70% sont relativement bons, bien que légèrement inférieurs à ceux obtenus à partir du peroxyde d'allyle et de *tert*-butyle (2); ils confèrent donc à la méthode un intérêt synthétique.

3. Additions radicalaires aux peroxydes δ-éthyléniques

Compte-tenu de la potentialité synthétique de l'addition radicalaire de dérivés à hydrogène mobile ZH au peroxyde **P1**, nous avons préparé les peroxydes **P2**, **P3**, **P4**, dans le but de déterminer l'influence des substituants présents sur ou au voisinage des deux fonctions réactives sur le cours de la réaction.

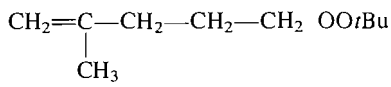

P2

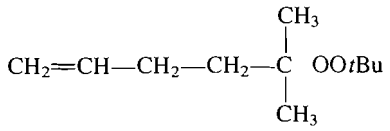

P3

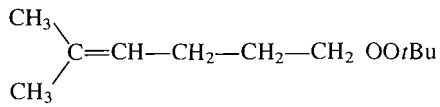

P4

Nous allons essayer d'interpréter les résultats enregistrés avec chacun des peroxydes sur la base du mécanisme en deux étapes établi dans le cas du peroxyde **P1** (1).

3.1. Additions radicalaires au peroxyde P2

Le tableau 4 regroupe les résultats obtenus à partir du peroxyde **P2**.

La comparaison des résultats des peroxydes **P1** et **P2** montre que l'on peut classer les solvants ZH en deux catégories, une augmentation du rendement étant observée avec la première (dichlorométhane, acétonitrile, propionate de méthyle, acide propionique, acétone), alors que pour la seconde, il n'y a que peu de variation (cyclohexane) ou diminution (dioxanne).

Si l'on se réfère au caractère polaire des radicaux issus de ces deux catégories de solvants — électrophile pour la première, nucléophile pour la seconde — on est tenté d'attribuer cette différence de résultats à l'étape d'addition; en effet, la nature du radical additionné ne devrait avoir aucune influence sur l'étape de substitution homolytique intramoléculaire.

3.2. Additions radicalaires au peroxyde P3

Le tableau 5 regroupe les résultats obtenus à partir du peroxyde **P3**.

De la comparaison des résultats obtenus avec les peroxydes **P1** et **P3**, il ressort que la substitution des deux hydrogènes en α de la liaison peroxydique par deux groupements méthyle est sans effet majeur sur la formation de tétrahydrofuranne et n'entraîne une diminution du rendement nette que dans le seul cas du dioxanne.

3.3. Additions radicalaires au peroxyde P4

Le tableau 6 regroupe les résultats obtenus à partir de ce peroxyde.

Le peroxyde **P4** conduit à des tétrahydropyrannes alors que les peroxydes **P1**, **P2**, **P3** sont des précurseurs de tétrahydrofurannes. Ce résultat est conforme aux règles gouvernant la réactivité et la régiosélectivité de l'étape d'addition, à savoir : l'orientation de l'addition d'un radical à une double liaison est contrôlée par la substitution de cette dernière.

Lorsque le substrat ZH est le cyclohexane, l'hétérocycle attendu ne semble pas se former; une partie du peroxyde **P4** est

Can. J. Chem. Downloaded from www.nrcresearchpress.com by 213.222.148.141 on 09/07/12
For personal use only.

Can. J. Chem. Downloaded from www.nrcresearchpress.com by 213.222.148.141 on 09/07/12
For personal use only.

TABLEAU 3. Additions radicalaires à **P1**. Produits formés et rendements : rapport molaire ZH/**P1**/PA = 100/1/0,5; 110°C; 12 h

Solvant	Produit		Rendement (%)[a]
CH_2Cl_2	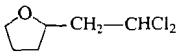	**1***a*	42
	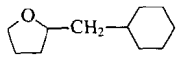	**1***b*	54
$CH_3—CH_2—COOCH_3$	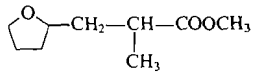	**1***c*	71[b]
CH_3CN	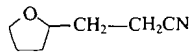	**1***d*	50
	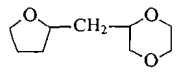	**1***e*	67
$CH_3—CH_2—COOH$ $C_2H_5—C(=O)—O—C(=O)—C_2H_5$[c]	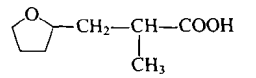	**1***f*	44 48
$CH_3—C(=O)—CH_3$	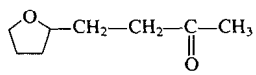	**1***g*	49

[a]Déterminé sur le produit isolé relativement au peroxyde mis en jeu dans la réaction.
[b]Présence, à côté de **1***c*, d'une impureté, probablement le propionate de (tétrahydrofuryl-2)-2 éthyle issu de la substitution d'un hydrogène du méthoxyle du propionate de méthyle (proportions relatives : 97/3).
[c]Le composé hétérocyclique initialement formé est transformé en acide **1***f* par hydrolyse.

TABLEAU 4. Additions radicalaires de ZH à **P2**. Rapport molaire ZH/**P2**/PA = 100/1/0,5; 110°C; 12 h

Solvant	Produits		Rendement (%)[a]
CH_2Cl_2	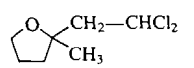	**2***a*	47 (42)
	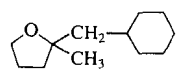	**2***b*	55 (54)
$CH_3—CH_2—COOCH_3$	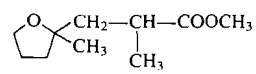	**2***c*	79 (71)
CH_3CN	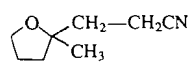	**2***d*	55 (50)
	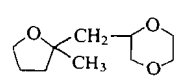	**2***e*	47 (67)
$CH_3—CH_2—COOH$	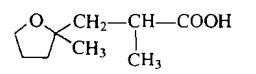	**2***f*	58 (44)
$CH_3—C(=O)—CH_3$	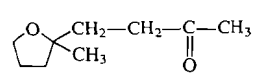	**2***g*	54 (49)

[a]Déterminé sur le produit isolé relativement au peroxyde mis en jeu dans la réaction. Entre parenthèses : rappel des rendements en tétrahydrofurannes obtenus à partir de **P1**.

Can. J. Chem. Downloaded from www.nrcresearchpress.com by 213.222.148.141 on 09/07/12
For personal use only.

TABLEAU 5. Additions radicalaires de ZH à **P3**. Rapport molaire ZH/**P3**/PA = 100/1/0,5; 110°C; 12 h

Solvant	Produits		Rendement isolé (%)[a]
CH_2Cl_2	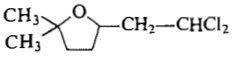	**3***a*	41 (42)
	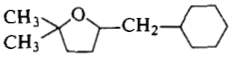	**3***b*	49 (54)
$CH_3—CH_2—COOCH_3$	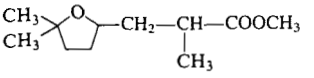	**3***c*	70 (71)
CH_3CN	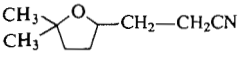	**3***d*	43 (50)
	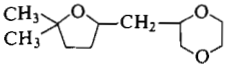	**3***e*	38 (67)
$CH_3—CH_2—COOH$	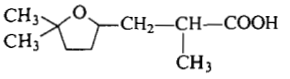	**3***f*	46 (44)
$CH_3—C(=O)—CH_3$	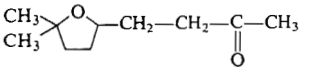	**3***g*	41 (49)

[a]Déterminé sur le produit isolé relativement au peroxyde mis en jeu dans la réaction. Entre parenthèses : rappel des rendements en tétrahydrofurannes obtenus à partir de **P1**.

TABLEAU 6. Additions radicalaires de ZH/**P4**. Rapport molaire ZH/**P4**/PA = 100/1/0,5; 110°C; 12 h

Solvant	Produits		Rendement (%)[a]
CH_2Cl_2	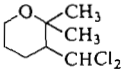	**4***a*	39
$CH_3—CH_2—COOCH_3$	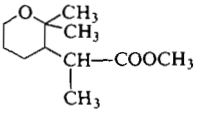	**4***c*	37
CH_3CN	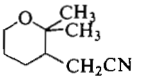	**4***d*	40
	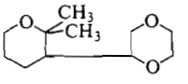	**4***e*	23[b]
$CH_3—CH_2—COOH$	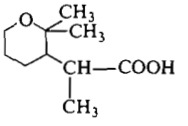	**4***f*	46
$CH_3—C(=O)—CH_3$	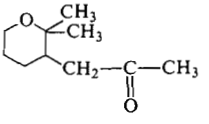	**4***g*	41

[a]Déterminé sur le produit isolé, relativement au peroxyde mis en jeu dans la réaction.
[b]Présence à côté de **4***e* de composés dont nous n'avons pas recherché la structure.

Can. J. Chem. Downloaded from www.nrcresearchpress.com by 213.222.148.141 on 09/07/12
For personal use only.

récupérée après réaction, indiquant que l'addition du radical cyclohexyle à la double liaison ne se fait pas, vraisemblablement pour des raisons stériques.

Les rendements en hétérocycles formés à partir du peroxyde **P4** sont plus faibles que dans le cas du peroxyde **P1**. Aucune comparaison directe ne peut être effectuée, puisque les chaînes séparant le centre radicalaire de la liaison peroxydique n'ont pas la même longueur.

Conclusion

L'addition radicalaire de composés donneurs d'hydrogène au peroxyde de *tert*-butyle et de pentène-4 yle conduit avec des rendements intéressants à des tétrahydrofurannes substitués en 2 par un groupement fonctionnel ou non. La ramification de la chaîne du peroxyde ne semble pas être un obstacle au succès de la réaction.

Notre méthode permet de synthétiser aisément et avec de bons rendements : (*i*) certains tétrahydrofurannes substitués en 2 à partir du peroxyde de *tert*-butyle et de pentène-4 yle; (*ii*) certains tétrahydrofurannes-2,2 disubstitués à partir de peroxydes d'alkyl-4 pentène-4 yle et de *tert*-butyle; (*iii*) certains tétrahydrofurannes-2,2,5 trisubstitués à partir de peroxydes d'alkyl-2 hexène-5 yle-2 et de *tert*-butyle; (*iv*) certains tétrahydropyrannes-2,2,3 trisubstitués à partir de peroxydes d'alkyl-5 alcène-4 yle et de *tert*-butyle.

Partie expérimentale

Techniques utilisées

Les analyses en cpg ont été effectuées sur un chromatographe Intersmat ICG 112 F (ionisation de flamme; gaz vecteur : azote), équipé de colonnes d'acier inox (longueur = 1,50 m ou 2 m; diamètre intérieur = 2 mm). Deux phases ont été utilisées : FFAP (10%) et OV 17 (10%).

Les identifications ont été réalisées par comparaison des temps de rétention avec ceux des échantillons préparés en référence. Les dosages ont été effectués par la méthode de l'étalon interne. En l'absence de produits de référence, après vérification de la pureté des produits par cpg, les techniques spectroscopiques ont permis de confirmer la structure des composés.

Les spectres de rmn ^{1}H ont été enregistrés sur des appareils Perkin Elmer R 12 B opérant à 60 MHz et Bruker WP 60 CW fonctionnant à 60 MHz; le solvant utilisé est CCl_4 contenant 10% de TMS (étalon interne).

Les spectres de rmn ^{13}C ont été effectués sur un appareil Bruker AC 200 fonctionnant à 50,3 MHz; le solvant utilisé est $CDCl_3$ contenant 5% de TMS (étalon interne).

Les séparations en chromatographie liquide à haute performance (hplc) ont été réalisées sur un appareil Prep LC/System 500 Waters, équipé d'une cartouche Prep Pak-500/Silica.

Les spectres de masse ont été enregistrés sur des appareils Micromass 16 F et 70-70, en ionisation électronique (70 eV) ou ionisation chimique, couplés avec un chromatographe en phase gazeuse de type Pye–Unicam, série 204.

Matières premières

Tous les solvants utilisés sont des produits commerciaux, distillés avant emploi.

Le peracétate de *tert*-butyle est préparé par action de l'hydroperoxyde de *tert*-butyle sur le chlorure d'acétyle en présence de pyridine (4).

Peroxyde de pentène-4 yle et de tert*-butyle,* ***P1*** : il a été préparé selon la réf. 1, par action de *t*BuOOH sur le bromo-1 pentène-4 (Rdt 39%), et possède des constantes physiques en accord avec la littérature.

Peroxyde de tert*-butyle et de méthyl-4 pentène-4 yle,* ***P2*** : il a été préparé selon la réf. 5, par action de *t*BuOOH sur le mésylate du méthyl-4 pentène-4 ol-1 (6), Eb_{25} 75°C (litt. (6) Eb_{19} 67,5–69°C); rmn ^{1}H δ(ppm) : 4,7 (s, 2H, CH_2=), 4–3,4 (m, 3H, CH_2OH), 2,3–1,5 (m, 7H, autres protons). **P2** est purifié par chromatographie sur gel de silice; Rdt = 39%; n_D^{20} = 1,4225; rmn ^{1}H δ(ppm) : 4,8 (s, 2H, CH_2=), 3,9 (t, J = 8 Hz, 2H, CH_2O), 2,2–1,3 (m, 7H, autres H), 1,2 (s, 9H, $(CH_3)_3C$).

Peroxyde de tert*-butyle et de méthyl-2 hexène-5 yle-2,* ***P3*** : il a été préparé selon la réf. 7, par action de *t*BuOOH sur le bromo-2 méthyl-2 hexène-5 (8), Eb_{90} 82°C (litt. (8) Eb_{95} 87–89°C); rmn ^{1}H δ(ppm) : 6–4,8 (m, 3H, CH_2=CH), 2,8–1,8 (m, 4H, autres CH_2), 1,2 (s, 6H, $(CH_3)_2C$). **P3** est isolé par distillation; Rdt = 28%; Eb_1 43°C; n_D^{20} = 1,4198; rmn ^{1}H δ(ppm) : 6–4,9 (m, 3H, CH_2=CH), 2,3–1,3 (m, 4H, autres CH_2), 1,2 et 1,15 (2s, 15H, $(CH_3)_3C$ et $(CH_3)_2C$).

Peroxyde de tert*-butyle et de méthyl-5 hexène-4 yle,* ***P4*** : il a été obtenu selon la réf. 5, par action de *t*BuOOH sur le mésylate du méthyl-5 hexène-4 ol-1 (9), Eb_{30} 86°C (litt. (9) Eb_{15} 79°C); rmn ^{1}H δ(ppm) : 5,1 (t, J = 8 Hz, 1H, =CH), 3,6–3,2 (m, 3H, CH_2OH), 2,2–1,8 (m, 4H, autres CH_2), 1,65 et 1,6 (2s, 6H, $CH_3)_2C$). **P4** est purifié par chromatographie sur gel de silice; Rdt = 40%; n_D^{20} = 1,4329; rmn ^{1}H δ(ppm) : 5,3–5 (m, 1H, =H), 3,9 (t, J = 8 Hz, 2H, CH_2O), 2,5–1,3 (m, 10H, $(CH_3)_2C$ et autres CH_2), 1,2 (s, 9H, $(CH_3)_3C$).

Additions radicalaires

Les études analytiques ont été réalisées en introduisant 2 cm^3 de solution dans des ampoules en Pyrex scellées, placées 12 h dans un bain thermostaté à 110°C (rapport molaire 100/1).

Les études préparatives ont été effectuées sur des volumes de 90 ou 180 cm^3 dans des autoclaves de 125 ou 250 cm^3 placés pendant 12 h dans une étuve préalablement portée à 110°C. Les rapports molaires substrat/composé insaturé/amorceur sont de 100/1/0,5.

Après élimination du solvant en excès, les produits de réaction sont isolés par les méthodes habituelles (distillation, chromatographie sur gel de silice ou hplc).

Produits de reactions[2]

1. Additions radicalaires à ***P1***

(Dichloro-2,2 éthyl)-2 tétrahydrofuranne, ***1***a : $Eb_{0,5}$ 45°C; n_D^{20} = 1,4842; rmn ^{1}H δ(ppm) : 6 (t, J = 8 Hz, 1H, $CHCl_2$), 4,25–3,5 (m, 3H, CH_2—O—CH), 2,5–1,5 (m, 6H, autres protons); principaux pics du spectre de masse, m/z (abondance) : 27 (32), 39 (24), 41 (41), 42 (21), 43 (35), 71 (100), 85 (19).

Cyclohexylméthyl-2 tétrahydrofuranne, ***1***b : $Eb_{0,35}$ 77°C; n_D^{20} = 1,4721 (litt. (10) $Eb_{0,1}$ 45°C; n_D^{20} = 1,471); rmn ^{1}H δ(ppm) : 4,25–3,5 (m, 3H, CH_2—O—CH), 2,25–1 (m, 17H, autres protons); principaux pics du spectre de masse, m/z (abondance) : 41 (35), 43 (30), 55 (21), 71 (100).

Méthyl-2 (tétrahydrofuryl-2)-3 propionate de méthyle, ***1***c : $Eb_{0,45}$ 55°C; n_D^{20} = 1,4422; rmn ^{1}H δ(ppm) : 4,1–3,6 (m, 3H, CH_2—O—CH), 3,5 (s, 3H, OCH_3), 2,75–1,3 (m, 7H, autres CH_2 et CH), 1,1 (d, J = 8 Hz, 3H, CH_3—CH); principaux pics du spectre de masse, m/z (abondance) : 45 (36), 71 (100), 85 (32).

(Tétrahydrofuryl-2)-3 propanenitrile, ***1***d : Eb_4 74°C; n_D^{20} = 1,4499 (litt. (11) Eb_8 92–94°C; n_D^{20} = 1,4468); rmn ^{1}H δ(ppm) : 4–3,5 (m, 3H, CH_2—O—CH), 2,5–1,3 (m, 8H, autres protons); principaux pics du spectre de masse, m/z (abondance) : 39 (28), 41 (53), 42 (24), 43 (74), 55 (22), 71 (100).

(Tétrahydrofuryl-2) méthyl dioxanne-1,4, ***1***e : $Eb_{0,5}$ 74°C; n_D^{20} = 1,4661; rmn ^{1}H δ(ppm) : 4,3–4 (m, 10H, CH_2—O et CH—O), 2–1,2 (m, 6H, autres protons); principaux pics du spectre de masse, m/z (abondance) : 31 (17), 41 (29), 43 (75), 71 (100), 87 (16).

Acide méthyl-2 (tétrahydrofuryl-2)-3 propionique, ***1***f : $Eb_{0,35}$ 92°C; n_D^{20} = 1,4590 (litt. (12) Eb_{13} 154°C; n_D^{20} = 1,4561); rmn ^{1}H δ(ppm) : 11,2 (s, 1H, $COOH$), 4–3,5 (m, 3H, CH_2—O—CH), 2,8–2,2 (m, 1H, CH—COO), 2,1–1,3 (m, 6H, autres CH_2), 1,2 (d, J = 8 Hz, 3H, CH_3); principaux pics du spectre de masse, m/z (abondance) : 41 (36), 42 (19), 43 (55), 71 (100), 85 (21).

2. La pureté des produits nouveaux isolés ayant été vérifiée par cpg sur deux colonnes de polarités différentes et l'étude spectroscopique (rmn, masse) accréditant leurs structures, il ne nous a pas paru nécessaire d'effectuer leur analyse centésimale.

Can. J. Chem. Downloaded from www.nrcresearchpress.com by 213.222.148.141 on 09/07/12
For personal use only.

(Tétrahydrofuryl-2)-4 butanone, ***1***g : $Eb_{0,8}$ 61°C; n_D^{20} = 1,4464 (litt. (13) Eb_2 81°C; n_D^{19} = 1,4459); rmn ^1H δ(ppm) : 4–3,5 (m, 3H, CH_2—O—CH), 2,6 (t, J = 8 Hz, 2H, CH_2—CO), 2 (s, 3H, CH_3), 2–1,3 (m, 6H, autres protons); principaux pics du spectre de masse, m/z (abondance) : 41 (28), 43 (100), 71 (69), 84 (40).

2. Additions radicalaires à ***P2***

(Dichloro-2,2 éthyl)-2 méthyl-2 tétrahydrofuranne, ***2***a : $Eb_{0,3}$ 76°C; n_D^{20} = 1,4767; rmn ^1H δ(ppm) : 5,9 (t, J = 8 Hz, 1H, $CHCl_2$), 3,9–3,6 (m, 2H, CH_2—O), 2,5–1,3 (m, 6H, autres CH_2), 1,2 (s, 3H, CH_3); principaux pics du spectre de masse, m/z (abondance) : 42 (29), 43 (100), 85 (70).

Cyclohexylméthyl-2 méthyl-2 tétrahydrofuranne, ***2***b : $Eb_{0,8}$ 86°C; n_D^{20} = 1,4696; rmn ^1H δ(ppm) : 3,8–3,5 (m, 2H, CH_2—O), 2–1,2 (m, 17H, autres CH_2 et CH), 1,1 (s, 3H, CH_3); principaux pics du spectre de masse, m/z (abondance) : 43 (34), 85 (100).

Méthyl-2 (méthyl-2 tétrahydrofuryl-2)-3 propionate de méthyle, ***2***c : $Eb_{0,5}$ 74°C; n_D^{20} = 1,4402; rmn ^1H δ(ppm) : 3,9–3,6 (m, 2H, CH_2—O), 3,5 (s, 3H, OCH_3), 2,6–1,25 (m, 7H, autres CH_2 et CH), 1,2 (d, J = 8 Hz, 3H, CH_3—CH), 1,1 (s, 3H, CH_3—C—O); principaux pics du spectre de masse, m/z (abondance) : 43 (48), 85 (100).

(Méthyl-2 tétrahydrofuryl-2)-3 propanenitrile, ***2***d : Eb_3 80°C; n_D^{20} = 1,4507; rmn ^1H δ(ppm) : 3,9–3,6 (m, 2H, CH_2—O), 2,5–1,5 (m, 8H, autres CH_2), 1,2 (s, 3H, CH_3); principaux pics du spectre de masse, m/z (abondance) : 41 (29), 42 (22) 43 (100), 82 (46), 85 (55), 124 (17).

(Méthyl-2 tétrahydrofuryl-2) méthyl dioxanne-1,4, ***2***e : $Eb_{0,6}$ 56°C; n_D^{20} = 1,4603; rmn ^1H δ(ppm) : 4–3,4 (m, 9H, CH_2—O et CH—O), 2,1–1,2 (m, 6H, autres CH_2), 1,1 (s, 3H, CH_3); principaux pics du spectre de masse, m/z (abondance) : 32 (24), 43 (83), 85 (100), 87 (17).

Acide méthyl-2 (méthyl-2 tétrahydrofuryl-2)-3 propionique, ***2***f : $Eb_{0,25}$ 95°C; n_D^{20} = 1,4801; rmn ^1H δ(ppm) : 11,2 (s, 1H, $COOH$), 4–3,5 (m, 2H, CH_2—O), 2,6–1,3 (m, 7H, autres CH_2 et CH), 1,25 (d, J = 8 Hz, 3H, CH_3—CH), 1,1 (s, 3H, CH_3—C—O); principaux pics du spectre de masse, m/z (abondance) : 28 (20), 43 (41), 85 (100).

(Méthyl-2 tétrahydrofuryl-2)-4 butanone, ***2***g : $Eb_{0,4}$ 76°C; n_D^{20} = 1,4547 (litt. (14) $Eb_{0,5}$ 80–81°C); rmn ^1H δ(ppm) : 3,8–3,5 (m, 2H, CH_2—O), 2,5–1,25 (m, 8H, autres CH_2), 2 (s, 3H, CH_3—C), 1,1 (s, 3H, CH_3—C—O); principaux pics du spectre de masse, m/z (abondance) : 43 (100), 85 (64).

3. Additions radicalaires à ***P3***

(Dichloro-2,2 éthyl)-2 diméthyl-5,5 tétrahydrofuranne, ***3***a : Eb_{10} 98°C; n_D^{20} = 1,4592; rmn ^1H δ(ppm) : 5,9 (t, J = 8 Hz, 1H, $CHCl_2$), 4,25–4 (m, 1H, CH—O), 2,5–1,5 (m, 6H, CH_2), 1,2 (s, 6H, CH_3); principaux pics du spectre de masse, m/z (abondance) : 43 (100), 55 (28), 59 (39), 70 (33), 81 (39), 99 (51), 181 (68), 183 (42).

Cyclohexylméthyl-2 diméthyl-5,5 tétrahydrofuranne, ***3***b : $Eb_{0,3}$ 63°C; n_D^{20} = 1,4597; rmn ^1H δ(ppm) : 3,8–3,5 (m, 1H, CH—O), 1,8–1,3 (m, 17H, autres CH et CH_2), 1,1 (s, 6H, CH_3); principaux pics du spectre de masse, m/z (abondance) : 43 (21), 55 (20), 81 (56), 99 (100).

(Diméthyl-5,5 tétrahydrofuryl-2)-3 méthyl-2 propionate de méthyle, ***3***c : Eb_8 110°C; n_D^{20} = 1,4364; rmn ^1H δ(ppm) : 4–3,5 (m, 1H, CH—O), 3,5 (s, 3H, OCH_3), 2,8–1,8 (m, 7H, autres CH et CH_2), 1,6 (d, J = 8 Hz, 3H, CH_3—CH), 1,1 (s, 6H, autres CH_3); principaux pics du spectre de masse, m/z (abondance) : 41 (30), 43 (100), 55 (39), 70 (25), 81 (79), 88 (43), 99 (83) 112 (36), 144 (43).

(Diméthyl-5,5 tétrahydrofuryl-2)-3 propanenitrile, ***3***d : $Eb_{0,5}$ 49°C; n_D^{20} = 1,4330; rmn ^1H δ(ppm) : 4–3,7 (m, 1H, CH—O), 2,5–1,3 (m, 8H, CH_2), 1,1 (s, 6H, CH_3); principaux pics du spectre de masse, m/z (abondance) : 41 (22), 43 (100), 55 (33), 59 (23), 138 (29).

(Diméthyl-5,5 tétrahydrofuryl-2) méthyl dioxanne-1,4, ***3***e : $Eb_{0,1}$ 55°C; n_D^{20} = 1,4557; rmn ^1H δ(ppm) : 3,8–3,4 (m, 8H, CH_2—O et CH—O), 1,8–1,3 (m, 6H, autres CH_2), 1,1 (s, 6H, CH_3); principaux pics du spectre de masse, m/z (abondance) : 29 (15), 31 (17), 32 (42), 41 (26), 43 (79), 55 (26), 81 (100), 86 (30), 87 (65), 89 (99), 144 (21).

Acide (diméthyl-5,5 tétrahydrofuryl-2)-3 méthyl-2 propionique, ***3***f : Eb_2 113°C; n_D^{20} = 1,4506; rmn ^1H δ(ppm) : 9,8 (s, 1H, $COOH$), 4–3,7 (m, 1H, CH—O), 2,8–1,7 (m, 7H, autres CH et CH_2), 1,6 (d, J = 8 Hz, 3H, CH_3—CH), 1,1 (s, 6H, autres CH_3); principaux pics du spectre de masse, m/z (abondance) : 39 (24), 41 (43), 43 (100), 55 (34), 81 (33), 99 (26).

(Diméthyl-5,5 tétrahydrofuryl-2)-4 butanone, ***3***g : $Eb_{0,5}$ 78°C; n_D^{20} = 1,4396; rmn ^1H δ(ppm) : 4–3,7 (m, 1H, CH—O), 2,5–1,3 (m, 8H, CH_2), 2 (s, 3H, CH_3—C=O), 1,2 (s, 6H, autres CH_3); principaux pics du spectre de masse, m/z (abondance) : 43 (100), 55 (17), 81 (23), 99 (16), 112 (15).

4. Additions radicalaires à ***P4***

Dichlorométhyl-3 diméthyl-2,2 tétrahydropyranne, ***4***a : $Eb_{0,5}$ 46°C; n_D^{20} = 1,4870; rmn ^1H δ(ppm) : 6 (d, J = 8 Hz, 1H, $CHCl_2$), 3,7–3,4 (m, 2H, CH_2—O), 2,4–1,5 (m, 5H, autres CH et CH_2), 1,25 et 1,2 (2s, 6H, CH_3); rmn ^{13}C δ(ppm) : 74,9 ($CHCl_2$), 73,7 ($C(CH_3)_2$), 61,2 (CH_2O), 56,1 (CH—$CHCl_2$), 29,5 et 19,5 (CH_3), 25,8 et 19,1 (autres CH_2); principaux pics du spectre de masse, m/z (abondance) : 41 (33), 43 (100), 55 (16), 68 (18), 85 (67).

(Diméthyl-2,2 tétrahydropyrannyl-3)-2 propionate de méthyle, ***4***c : $Eb_{0,8}$ 66°C; n_D^{20} = 1,4566; rmn ^1H δ(ppm) : 4–3,3 (m, 2H, CH_2—O), 3,6 (s, 3H, OCH_3), 2,8–1,3 (m, 6H, autres CH_2 et CH), 1,5 (d, J = 8 Hz, 3H, CH_3—CH), 1,2 et 1,1 (2s, 6H, autres CH_3); principaux pics du spectre de masse, m/z (abondance) : 39 (24), 41 (59), 43 (93), 55 (100), 59 (33), 85 (22), 88 (52), 99 (57), 113 (31), 114 (20), 125 (23), 127 (28), 142 (59).

(Diméthyl-2,2 tétrahydropyrannyl-3) éthanenitrile, ***4***d : $Eb_{0,2}$ 59°C; n_D^{20} = 1,4670; rmn ^1H δ(ppm) : 3,7–3,4 (m, 2H, CH_2—O), 2,4–1,3 (m, 7H, autres CH_2 et CH), 1,1 et 1,2 (2s, 6H, CH_3); rmn ^{13}C δ(ppm) : 118,8 (CN), 73,2 ($C(CH_3)_2$), 61,1 (CH_2O), 41,3 (CH—CH_2CN), 28,1 et 18,9 (CH_3), 24,9 et 19,8 (autres CH_2); principaux pics du spectre de masse, m/z (abondance) : 41 (33), 43 (100), 55 (16), 66 (18), 85 (67).

(Diméthyl-2,2 tétrahydropyrannyl-3) dioxanne-1,4, ***4***e : ***4e*** n'a pu être obtenu parfaitement pur après distillation (cpg); $Eb_{0,4}$ 52°C; n_D^{20} = 1,4339; rmn ^1H δ(ppm) : 3,8–3,3 (9H, CH_2—O et CH—O), 2,8–1,3 (m, 5H, autres CH et CH_2), 1,2 et 1,1 (2s, 6H, CH_3); principaux pics du spectre de masse, m/z (abondance) : 27 (15), 29 (17), 31 (25), 41 (52), 43 (31), 45 (15), 55 (100), 69 (71), 73 (18), 81 (37), 86 (48), 87 (84), 96 (40), 97 (20), 125 (24).

Acide (diméthyl-2,2 tétrahydropyrannyl-3)-2 propionique, ***4***f : $Eb_{0,2}$ 92°C; n_D^{20} = 1,4691; rmn ^1H δ(ppm) : 10,5 (s, 1H, $COOH$), 3,75–3,25 (m, 2H, CH_2—O), 2,75–1,3 (m, 6H, autres CH_2 et CH), 1,5 (d, J = 8 Hz, 3H, CH_3—CH), 1,2 et 1,1 (2s, 6H autres CH_3); principaux pics du spectre de masse, m/z (abondance) : 32 (15), 39 (23), 41 (49), 43 (91), 55 (97), 56 (19), 58 (29), 59 (100), 74 (46), 83 (28), 85 (31), 87 (26), 113 (24), 128 (74).

(Diméthyl-2,2 tétrahydropyrannyl-3) acétone, ***4***g : $Eb_{0,5}$ 55°C; n_D^{20} = 1,4639; rmn ^1H δ(ppm) : 3,75–3,25 (m, 2H, CH_2—O), 2,5–1,4 (m, 7H, autres CH_2 et CH), 2,1 (s, 3H, CH_3—C=O), 1,2 et 1,1 (2s, 6H, autres CH_3); principaux pics du spectre de masse, m/z (abondance) : 41 (19), 43 (100), 59 (21), 112 (25).

Remerciements

Les auteurs remercient Monsieur le Professeur Lalande pour l'intérêt qu'il a porté à ce travail.

1. M. J. Bourgeois, E. Montaudon et B. Maillard. Tetrahedron, **42**, 5309 (1986).
2. E. Montaudon, F. Rakotomanana et B. Maillard. Bull. Soc. Chim. Fr. 198 (1985).
3. M. Agorrody, M. Campagnole, E. Montaudon et B. Maillard. Tetrahedron, **43**, 3429 (1987).
4. P. D. Bartlett et R. R. Hiatt. J. Am. Chem. Soc. **80**, 1398 (1958).
5. F. W. Homer, R. Williams et H. S. Mosher. J. Am. Chem. Soc. **77**, 551 (1955); W. A. Pryor et E. P. Pultinas. J. Am. Chem. Soc. **85**, 133 (1963); W. A. Pryor, D. M. Huston, T. R. Fisher et T. L. Pichering. J. Am. Chem. Soc. **86**, 4237 (1964);

R. K. CROSSLAND et K. L. SERVIS. J. Org. Chem. **35**, 3195 (1970).
6. M. F. ANSELL et D. A. THOMAS. J. Chem. Soc. 1163 (1958).
7. P. G. COOKSON, A. G. DAVIES et B. P. ROBERTS. J. Chem. Soc. Chem. Commun. 1022 (1976).
8. M. A. CHEL'TSOVA, E. A. CHERNYSHEV et A. D. PETROV. Bull. Acad. Sci. USSR, Div. Chem. Sci. (Engl. Transl.) 459 (1955).
9. C. CRISAN. Ann. Chim. **13**, 436 (1956).
10. E. E. SCHWEIZER, W. S. CREASY, K. K. LIGHT et E. T. SHAFFER. J. Org. Chem. **34**, 212 (1969).
11. C. G. GALUST'YAN et C. S. KADYROV. Khim. Geterotsikl. Soedin. 376 (1967).
12. J. COLONGE et A. LAGIER. Bull. Soc. Chim. Fr. 17 (1949).
13. W. E. KAUFMANN et R. ADAMS. J. Am. Chem. Soc. **45**, 3043 (1923).
14. A. CITTERIO, A. ARNOLDI et A. GRIFFINI. Tetrahedron, **38**, 393 (1982).

Can. J. Chem. Downloaded from www.nrcresearchpress.com by 213.222.148.141 on 09/07/12
For personal use only.

Préparation et détermination des configurations des dihydroxy-10,11 dihydro-10,11 quinidines 10(*R*) et 10(*S*), des métabolites de la quinidine

FRANÇOIS-XAVIER JARREAU ET J. J. KOENIG
Centre de recherche du Laboratoire Nativelle, 34, rue de la Fédération, 75015 Paris, France

MICHEL PAYS ET ROBERT LEROYER
Unité d'enseignement et de recherche des sciences pharmaceutiques, 1, rue de Vaubénard, 1403, Caen CEDEX France

ET

FRANÇOIS BRISSE ET JEAN-CLAUDE RICHER
Département de chimie, Université de Montréal, C.P. 6128, Succ. A, Montréal (Qué.), Canada H3C 3J7

Reçu le 13 mars 1987

FRANÇOIS-XAVIER JARREAU, J. J. KOENIG, MICHEL PAYS, ROBERT LEROYER, FRANÇOIS BRISSE et JEAN-CLAUDE RICHER. Can. J. Chem. **65**, 2701 (1987).

Dans ce travail, on décrit la préparation chimique des dihydroxy-10,11 dihydroquinidines, des métabolites de la quinidine. La séparation des isomères 10(*R*) et 10(*S*) a été réalisée à l'aide des dérivés isopropylidènes. On a déterminé les caractéristiques physiques de chacun des isomères et on a déterminé leur structure respective par résonance magnétique nucléaire du ^{1}H à 400 MHz. Grâce à la diffraction des rayons X, il a été établi que le composé majoritaire, de point de fusion 239°C, possède la configuration 10(*R*). Ce composé cristallise avec une molécule d'eau, dans une maille orthorhombique de dimensions a = 8,756(2), b = 11,499(7) et c = 19,123(5) Å et le groupe spatial est $P2_12_12_1$. La structure a été affinée jusqu'à une valeur finale de R = 0,040 pour 2039 réflexions observées.

FRANÇOIS-XAVIER JARREAU, J. J. KOENIG, MICHEL PAYS, ROBERT LEROYER, FRANÇOIS BRISSE, and JEAN-CLAUDE RICHER. Can. J. Chem. **65**, 2701 (1987).

This paper describes the chemical preparation of the 10,11-dihydroxyquinidines, some of the metabolites of quinidine. The 10(*R*) and 10(*S*) isomers have been separated using the isopropylidene derivatives. The physical characteristics of each of these isomers have been determined and their respective structures have also been determined using ^{1}H nuclear magnetic resonance at 400 MHz. On the basis of an X-ray diffraction structure determination, it has been shown that the main product, melting point 239°C, is the 10(*R*) isomer. This product crystallizes with one molecule of water in the orthorhombic system with a = 8.756(2), b = 11.499(7), and c = 19.123(5) Å and space group $P2_12_12_1$. The structure has been refined to a final value of R = 0.040 for 2039 observed reflections.

[Journal translation]

Can. J. Chem. Downloaded from www.nrcresearchpress.com by 213.222.148.141 on 09/07/12
For personal use only.

Introduction

La dégradation oxydative de la quinidine, aussi bien chez l'animal que chez l'homme, conduit aux principaux produits suivants (pour revues, voir la réf. 1) : l'hydroxy-3(*S*) quinidine (2, 3); la desméthylquinidine (cupréidine) (4); la *N*-oxyde de quinidine (5); l'hydroxy-2′ quinidine (2, 3) et la dihydroxy-10,11 dihydroquinidine (6) qui n'a été observée jusqu'à maintenant que chez l'animal.

La préparation par synthèse des trois premiers de ces composés a déjà été réalisée (5, 7, 8). Celle du quatrième présente des difficultés liées au caractère polyfonctionnel de la molécule (9). Enfin, les tentatives de préparation du «dihydrodiol» (5, 10) n'ont pas permis jusqu'à récemment de l'isoler à l'état pur (5, 11). Par ailleurs, une combinaison des deux techniques décrites antérieurement nous a récemment permis d'isoler une faible quantité de l'isomère le plus polaire.[1]

Résultats et discussion

Dans le but d'élucider définitivement la structure du métabolite naturel de la quinidine dihydroxylée en 10 et 11 et de déterminer sa configuration absolue, une synthèse efficace en a été réalisée selon le schéma 1.

Par oxydation au moyen de OsO_4 (12), l'acétyl quinidine (**1**) est transformée en deux produits qui ont été séparés par chromatographie après transformation en dérivés isopropylidènes **2** et **3**. La déprotection de chacun de ces dérivés livre un composé pur cristallisé.

Les structures de ces deux molécules ont été établies sur la base de leurs caractéristiques spectrales. Alors que les spectres de masse à haute résolution confirment les compositions attendues, les spectres ir et uv des produits **4** et **5**, marqués par le noyau méthoxyquinoléine, sont identiques entre eux et avec ceux de la quinidine et de la dihydroquinidine. De plus, les deux $[\alpha]_D$ ont des valeurs peu différentes et très positives comme celles des dérivés quinidiniques, quoique sensiblement plus faibles.

Ce n'est que par rmn du ^{1}H à 400 MHz que l'on a pu mettre en évidence des différences entre **4** et **5**; dans ces conditions, tous les protons sont distincts (tableaux 1 et 2). Il apparaît clairement que la transformation chimique a affecté la chaîne vinyle, devenue éthyle disubstituée, sans altérer le reste de la molécule. Les différences entre les deux spectres sont le reflet d'une stéréoisomérie au niveau de l'hydroxyle en 10. L'attribution des massifs a été établie par analogie avec les spectres de la quinidine **1** et confirmée par découplage dans la partie modifiée de la molécule, c'est-à-dire sur les protons en 3 et en 10 (sur l'isopropylidène du majoritaire, **2**) et par rapprochement avec les spectres à haute résolution des dérivés hydroxy-3 de la quinidine et de la dihydroquinidine.[2]

Donc, compte tenu du réactif employé pour l'oxydation de la quinidine, des transformations chimiques appliquées ensuite et

1. T. Ogerau et A. Bossard. Laboratoire Nativelle. Communication personnelle.

2. J. J. Koenig, S. Fenard et F.-X. Jarreau. Hydroxy-3*S* dihydro-10,11 quinidine, nouvel antiarythmique; à paraître.

Can. J. Chem. Downloaded from www.nrcresearchpress.com by 213.222.148.141 on 09/07/12
For personal use only.

TABLEAU 1. Résonance magnétique nucléaire du ^1H 400 MHz dans CD_3OD. Déplacements chimiques par rapport à TMS/$CDCl_3$ en ppm

	H-Quinoléine									H-Quinuclidine										
Composé n°	H-2′	H-8′	H-3′	H-7′	H-5′	H-9	H-10	H-11	H-11	H-2q*	H-8	H-2	H-6a*	H-6s*	H-7s*	H-4	H-3	H-5s*–H-5a*	H-7a*	MeO
	d	d	d	dd	d	d	ddd	dd	dd	ddd	ddd	dd	tm	dt	dddd	mfin	ddd	d	ddd	s
5	8,65	7,94	7,70	7,41	7,37	5,68	3,91	3,62	3,44	3,44	3,04	2,85	2,93	2,82	2,25	2,03	1,64	1,54	1,04	3,97
4	8,66	7,95	7,69	7,41		5,67	4,01	3,69	3,49	3,74	3,07	2,94	2,93	2,80	2,18	1,80	1,72	1,54	1,12	3,98
2	8,66	7,94	7,70	7,41	7,40	5,67	4,55	4,10	3,55	3,72	3,08	2,95	2,91	2,81	2,18	1,59	1,73	1,53	1,11	3,98
1	8,64	7,92	7,69	7,40	7,38	5,63	6,16	5,11 ddd	5,07 ddd	3,56	3,08	2,92	2,92	2,84	2,25	1,74	2,32	1,58	1,11	3,96

TABLEAU 2. Résonance magnétique nucléaire du ^1H 400 MHz dans CD_3OD. Constantes de couplage en Hz

Composé n° 4

$J_{2q,2} = 13{,}5$, $J_{2q,3} = 8$, $J_{2q,6*} = 2$, $J_{2,3} = 10$, $J_{3,10} = 9$, $J_{4,5} \leqslant 3$, $J_{4,7a} = 4$, $J_{5,6} = 9$, $J_{5s,7s} \leqslant 2$, $J_{6,6} = 13$, $J_{7,7} = 13$, $J_{7,8} = 9$, $J_{8,9} = 3$, $J_{10,11} = 3$ et 6, $J_{11,11} = 11{,}5$

Composé n° 5

$J_{2q,2} = 12{,}5$, $J_{2q,3} = 7{,}5$, $J_{2q,6a} = 2$, $J_{2,3} = 10{,}5$, $J_{3,10} = 9$, $J_{4,5} \leqslant 3$, $J_{4,7a} = 4$, $J_{5,6} = 10$, $J_{5s,7s} \leqslant 2$, $J_{6,6} = 13$, $J_{7,7} = 13$, $J_{7,8} = 9$, $J_{8,9} = 3$, $J_{10,11} = 2{,}5$ et 6,5, $J_{11,11} = 11{,}5$

Légende : H_{2q} = H-2 voisin de quinoléine; a = anti, s = syn, par rapport à C-3.

Can. J. Chem. Downloaded from www.nrcresearchpress.com by 213.222.148.141 on 09/07/12
For personal use only.

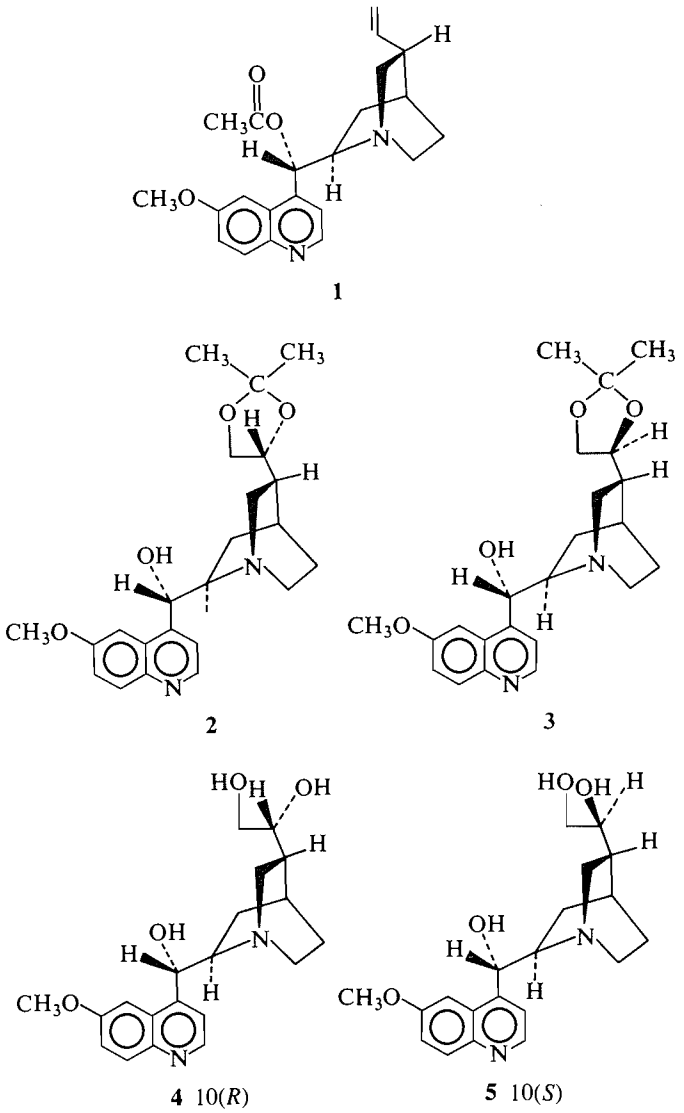

SCHÉMA 1

des caractéristiques spectrales des deux produits formés, il est possible d'affirmer qu'il s'agit bien des deux dihydroxy-10,11 dihydroquinidines stéréoisomères par rapport au carbone secondaire 10. Toutefois, l'attribution de la stéréochimie à chacun de ces deux isomères n'est pas possible avec ces seuls éléments. Aussi la détermination de la structure et de la configuration absolue de l'isomère majoritaire a été réalisée par diffraction des rayons X.

Les coordonnées atomiques finales, leurs écarts-types et les facteurs thermiques équivalents U_{eq} sont présentés dans le tableau 3.[3] Ces coordonnées correspondent à la configuration absolue, telle que déterminée en tenant compte de la dispersion anormale des atomes d'oxygène et d'azote (17). La configuration absolue ainsi trouvée est en accord avec celle du parent quinidine, elle aussi établie par diffraction des rayons X par Carter, McPhail et Sim (18). La numérotation des atomes est indiquée sur la figure 1 alors que la conformation moléculaire adoptée par l'isomère 10(*R*) est représentée par la paire stéréo

3. Les tables des coordonnées des atomes d'hydrogène, des facteurs thermiques anisotropes, des plans moyens et la liste des facteurs de structure observés et calculés sont disponibles. On peut les acheter en s'adressant au Dépôt de données non publiées, ICIST, Conseil National de Recherches du Canada, Ottawa (Ontario), Canada K1A 0S2.

TABLEAU 3. Coordonnées atomiques finales de $C_{20}H_{26}N_2O_4 \cdot H_2O$ ($\times 10^5$) et U_{eq} (Å^2, $\times 10^3$). $U_{eq} = \frac{1}{3}\sum_i \sum_j U_{ij} a_i^* a_j^* a_i \cdot a_j$

Atom	x	y	z	U_{eq}
O(9)	46293(19)	5373(15)	97595(8)	290
O(10)	37204(19)	40706(14)	94984(8)	288
O(11)	5780(19)	37681(15)	89334(9)	330
O(6′)	106028(21)	−22173(16)	83923(12)	423
N(1)	68805(21)	16128(17)	86372(9)	237
N(1′)	48884(26)	−37197(18)	92083(10)	330
C(2)	60645(25)	26100(20)	89526(12)	253
C(3)	47080(25)	30181(19)	84916(11)	242
C(4)	44515(25)	20664(20)	79348(11)	261
C(5)	58528(28)	20423(23)	74533(12)	309
C(6)	72927(27)	19210(22)	79106(12)	302
C(7)	43185(25)	8671(19)	82874(11)	254
C(8)	58814(25)	5673(19)	86184(10)	226
C(9)	57799(25)	−34(19)	93484(10)	228
C(10)	33098(26)	32826(19)	89485(11)	253
C(11)	19595(29)	37603(23)	85396(13)	337
C(2′)	38398(31)	−29728(22)	94195(12)	324
C(3′)	40896(28)	−17595(21)	94728(11)	299
C(4′)	54753(25)	−13033(19)	92848(10)	239
C(5′)	81060(26)	−17030(20)	88326(12)	266
C(6′)	91696(29)	−24873(22)	86070(13)	314
C(7′)	88271(31)	−36946(22)	85849(14)	368
C(8′)	74217(32)	−40681(21)	87896(14)	355
C(9′)	66262(26)	−20754(19)	90401(11)	241
C(10′)	62803(29)	−32891(20)	90194(12)	283
C(Me)	109594(33)	−10094(27)	83410(21)	543
O(W)	47884(19)	34583(16)	8217(9)	324

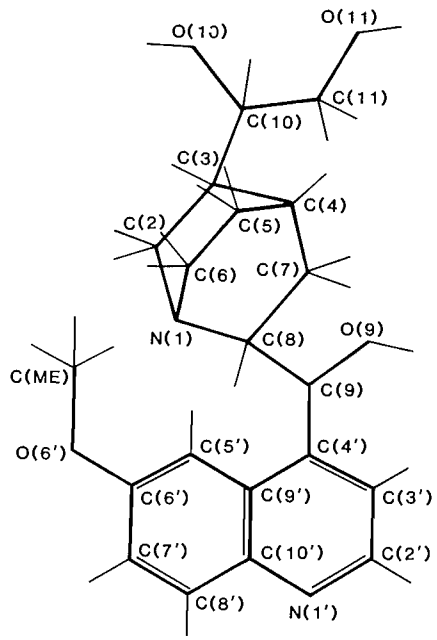

FIG. 1. Numérotation des atomes de l'isomère 10(*R*).

de la figure 2. Les longueurs des liaisons, les angles de valence et leurs écarts-types sont donnés dans le tableau 4, alors que les principaux angles de torsion sont rassemblés au tableau 5.

Les résultats obtenus au cours de ce travail démontrent que l'oxydation de la double liaison de la quinidine se produit principalement par la face supérieure de la double liaison du composé dans lequel la chaîne latérale éthylénique adopte une

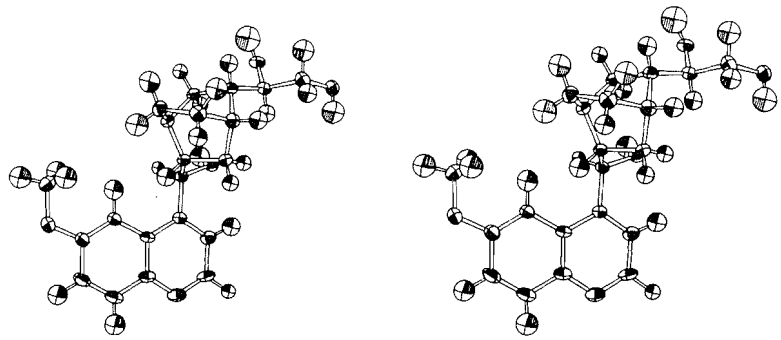

FIG. 2. Paire stéréoscopique montrant la conformation de l'isomère 10(*R*).

TABLEAU 4. Distances (Å), angles de valence (°) et leurs écarts-types

Liaison	Distance	Liaison	Distance	Liaison	Distance
C(9)—O(9)	1,421(3)	C(4)—C(7)	1,539(3)	C(4′)—C(9′)	1,422(2)
C(10)—O(10)	1,434(3)	C(5)—C(6)	1,541(3)	C(5′)—C(6′)	1,366(3)
C(11)—O(11)	1,425(3)	C(7)—C(8)	1,547(3)	C(5′)—C(9′)	1,421(3)
N(1)—C(2)	1,480(3)	C(8)—C(9)	1,545(3)	C(6′)—O(6′)	1,356(3)
N(1)—C(6)	1,479(3)	C(10)—C(11)	1,520(3)	C(6′)—C(7′)	1,421(4)
N(1)—C(8)	1,487(3)	C(9)—C(4′)	1,523(3)	C(7′)—C(8′)	1,361(4)
C(2)—C(3)	1,552(3)	N(1′)—C(2′)	1,321(3)	C(8′)—C(10′)	1,412(4)
C(3)—C(4)	1,543(3)	N(1′)—C(10′)	1,364(3)	C(9′)—C(10′)	1,429(3)
C(3)—C(10)	1,535(3)	C(2′)—C(3′)	1,416(4)	O(6′)—C(Me)	1,427(4)
C(4)—C(5)	1,534(3)	C(3′)—C(4′)	1,370(3)		

Angle	Valeur	Angle	Valeur	Angle	Valeur
C(2)—N(1)—C(6)	108,4(2)	C(7)—C(8)—C(9)	114,4(2)	N(1′)—C(10′)—C(9′)	122,5(2)
C(2)—N(1)—C(8)	110,6(2)	N(1)—C(8)—C(9)	110,8(2)	C(4′)—C(9′)—C(5′)	123,4(2)
C(6)—N(1)—C(8)	108,3(2)	O(9)—C(9)—C(8)	110,8(2)	C(4′)—C(9′)—C(10′)	118,0(2)
N(1)—C(2)—C(3)	116,9(2)	O(9)—C(9)—C(4′)	110,5(2)	C(5′)—C(9′)—C(10′)	118,7(2)
C(2)—C(3)—C(4)	106,8(2)	O(10)—C(10)—C(3)	110,1(2)	C(8′)—C(10′)—C(9′)	118,6(2)
C(2)—C(3)—C(10)	110,3(2)	C(3)—C(10)—C(11)	113,5(2)	C(7′)—C(8′)—C(10′)	122,0(2)
C(4)—C(3)—C(10)	114,7(2)	O(10)—C(10)—C(11)	110,1(2)	C(6′)—C(7′)—C(8′)	119,4(2)
C(3)—C(4)—C(5)	108,1(2)	O(11)—C(11)—C(10)	113,0(2)	O(6′)—C(6′)—C(5′)	120,7(2)
C(3)—C(4)—C(7)	110,1(2)	C(9)—C(4′)—C(3′)	120,7(2)	O(6′)—C(6′)—C(7′)	114,2(2)
C(5)—C(4)—C(7)	107,9(2)	C(9)—C(4′)—C(9′)	121,0(2)	C(5′)—C(6′)—C(7′)	120,7(2)
C(4)—C(5)—C(6)	108,4(2)	C(2′)—C(3′)—C(4′)	119,7(2)	C(6′)—C(5′)—C(9′)	120,7(2)
N(1)—C(6)—C(5)	110,8(2)	N(1′)—C(2′)—C(3′)	123,7(2)	C(6′)—O(6′)—C(Me)	116,5(2)
C(4)—C(7)—C(8)	108,2(2)	C(2′)—N(1′)—C(10′)	117,8(2)	C(9′)—C(4′)—C(3′)	118,3(2)
N(1)—C(8)—C(7)	110,5(2)	N(1′)—C(10′)—C(8′)	119,0(2)	C(8)—C(9)—C(4′)	110,8(2)

TABLEAU 5. Les principaux angles de torsion (°) et leurs écarts-types

Angle	Valeur	Angle	Valeur
N(1)—C(2)—C(3)—C(4)	12,3(3)	C(2)—C(3)—C(10)—O(10)	52,5(4)
N(1)—C(6)—C(5)—C(4)	12,2(3)	C(4)—C(3)—C(10)—O(10)	173,1(4)
N(1)—C(8)—C(7)—C(4)	13,0(3)	C(2)—C(3)—C(10)—C(11)	176,4(4)
C(2)—C(3)—C(4)—C(5)	−66,3(3)	C(4)—C(3)—C(10)—C(11)	−63,0(4)
C(3)—C(4)—C(5)—C(6)	52,9(3)	C(3)—C(10)—C(11)—O(11)	167,3(4)
C(2)—C(3)—C(4)—C(7)	51,4(3)	O(10)—C(10)—C(11)—O(11)	−68,8(4)
C(3)—C(4)—C(7)—C(8)	−66,2(3)	C(7)—C(4)—C(3)—C(10)	−71,1(3)
C(5)—C(6)—N(1)—C(8)	53,0(3)	C(5)—C(4)—C(3)—C(10)	171,2(3)
C(5)—C(6)—N(1)—C(8)	−68,1(3)	N(1)—C(8)—C(9)—O(9)	85,0(3)
		C(7)—C(8)—C(9)—O(9)	−40,7(3)
		N(1)—C(8)—C(9)—C(4′)	−152,1(3)
O(9)—C(9)—C(4′)—C(3′)	13,5(3)	C(7)—C(8)—C(9)—C(4′)	82,2(3)
O(9)—C(9)—C(4′)—C(9′)	−165,5(3)		
C(8)—C(9)—C(4′)—C(3′)	−109,6(3)	C(5′)—C(6′)—O(6′)—C(Me)	−6,0(4)
C(8)—C(9)—C(4′)—C(9′)	71,4(3)	C(7)—C(6′)—O(6′)—C(Me)	174,3(4)

Can. J. Chem. Downloaded from www.nrcresearchpress.com by 213.222.148.141 on 09/07/12
For personal use only.

TABLEAU 6. Caractéristiques géométriques des ponts-hydrogène

D[a]	A	O_D—H (Å)	O_D.....O_A (Å)	H.....O_A (Å)	O_D—H.....O_A (°)
O(9)—H(09)...O(11)	[002, 3][b]	0,93(3)	2,752(12)	1,85(3)	166(3)
O(10)—H(010)...N(1′)	[010, 1]	0,91(4)	2,795(3)	1,96(4)	152(4)
O(11)—H(011)...O(W)	[$\bar{1}$01, 3]	0,87(5)	2,693(3)	1,83(5)	173(4)
O(W)—H(W2)...O(10)	[00$\bar{1}$, 1]	0,81(3)	2,788(2)	2,00(3)	164(4)
O(W)—H(W1)...N(1)	[$\bar{1}$01, 3]	0,93(3)	2,750(2)	1,83(3)	174(3)

[a]D : donneur; A : accepteur.
[b][Translation, symétrie]; symétrie 1 = x, y, z; symétrie 3 = $\frac{1}{2} + x, \frac{1}{2} - y, -z$.

conformation parallèle à l'axe N—C(4) du noyau quinuclidine et orientée en direction opposée de l'azote. Cette conformation, qui semble la préférée pour les fins de l'oxydation, est vraisemblablement aussi favorisée dans l'état fondamental. Ces connaissances sont d'une importance capitale dans la compréhension des réactions qui se produisent en milieux biologiques, qui ont été examinées et dont les résultats feront l'objet d'une communication ultérieure.

Distances et angles

Les distances interatomiques C(sp^3)—C(sp^3) observées dans l'intervalle 1,520(3)–1,552(3) Å ont une moyenne de 1,539 Å. Les trois distances C(sp^3)—N sont très voisines et ont une moyenne de 1,482 Å. Les trois distances C(sp^3)—OH sont aussi très voisines et leur moyenne est de 1,426 Å. Les angles de valence du cycle quinuclidique impliquant les atomes de C ont une moyenne de 109,2° qui ne diffère pas significativement des angles de valence à l'azote dont la moyenne est 109,1°. Il faut toutefois noter que ce sont les trois atomes de carbone liés à l'azote qui ont les angles de valence les plus ouverts. Dans le noyau méthoxyquinoléique on retrouve une alternance de liaisons courtes et longues telle que rapportée pour le naphtalène, et ses dérivés (16). Les longueurs observées ici, qui varient de 1,321(3) à 1,429(3) Å, sont quelque peu perturbées au voisinage de N(1′). En ce qui concerne les angles de valence, ils ont une moyenne de 120,0° et ce sont les angles à N(1′), C(2′) et C(10′) qui s'écartent le plus de la moyenne. Le noyau méthoxyquinoléique est pratiquement plan, les déviations des atomes du plan moyen n'excédant pas 5σ. L'atome O(6′) fait aussi partie du plan moyen tandis que C(Me) s'en écarte de 0,153(4) Å.

Le système de ponts-hydrogène

La présence d'une molécule d'eau de cristallisation a été révélée au cours de la détermination structurale. Elle est associée par ponts-hydrogène à O(11), O(10) et N(1). Les caractéristiques géométriques de ces liaisons sont données dans le tableau 6. On y remarque des liaisons hydrogène de forces moyennes puisque les distances O...O* varient de 2,693(3) à 2,788(3) Å. Les deux atomes d'azote N(1) et N(1′) sont impliqués dans ces interactions avec la molécule d'eau et l'oxygène alcoolique O(10) respectivement. Les distances O...N* ont les valeurs de 2,750(2) et 2,795(3) Å.

Partie expérimentale

Les points de fusion ont été mesurées sur un banc Kofler et ne sont pas corrigés. Les spectres infrarouges ont été déterminés sur un appareil Perkin Elmer, modèle 157-G. Les spectres ultraviolets ont été déterminés sur un appareil Perkin Elmer modèle 402. Les indices de rotation ont été mesurés à l'aide d'un polarimètre Perkin Elmer modèle 141MC. Les spectres rmn du ^{1}H ont été déterminés à l'aide d'appareils Varian, modèle EM-360, et Bruker, modèle WM 400; ces mesures ont été faites dans le méthanol-d_4 et les déplacements chimiques, exprimés en ppm, sont déterminés par rapport au TMS. Les spectres de masse ont été déterminés à l'aide d'un appareil AEI, modèle MS-901. Les chromatographies analytiques ont été réalisées sur des plaques de 0,25 mm, type 60F-254, de silice (Merck 5719) ou d'alumine (Merck 5731) alors que les chromatographies préparatives ont été réalisées sur une colonne de gel de silice 60H (Merck 7736), sous une pression de 300 mbar (1 bar = 100 kPa) («chromatographie flash»).

Diméthyl méthylène dioxy)-10,11 dihydro-10,11 quinidine 5 (2 et 3)

À une solution, refroidie à 10°C et agitée, de 5,00 g (13,6 mmol) d'acétylquinidine (**1**) dans 52 mL de pyridine, on ajoute 3,50 g (13,8 mmol) de OsO_4 et on laisse reposer 1 nuit à 20°C; après traitement (12), 4,58 g de bases sont obtenus. À 4,30 g de ces bases, on ajoute 65 mL de DMF, 75 mL de diméthoxypropane et 2,90 g d'acide tosylique; après 1 nuit à 20°C, on procède à l'extraction pour obtenir 4,99 g de bases. Enfin, si on traite 4,88 g de celles-ci par 0,2 mL de NaOH 10 M dans 100 mL de MeOH à 20°C pendant 2,5 h, on obtient 4,07 g d'un mélange d'alcaloïdes qui présente en ccm trois taches distinctes et qu'on a séparé par chromatographie sur colonne (support, 140 g de silice 60H Merck 7736; éluant CH_2Cl_2 : EtOH : NH_4OH, 91 : 8,0 : 0,8; pression de 300 mbar). On obtient ainsi par ordre de polarité croissant : 1,91 g (4,8 mmol) de l'isomère majoritaire 10(*R*), la dihydroxy-10,11 dihydro-10,11 quinidine sous la forme de dérivé di-*O*-isopropylidène-10,11 (**2**); 1,00 g (2,5 mmol) de l'isomère minoritaire 10(*S*) (**3**); 463 mg (1,4 mmol) de dihydroquinidine et 360 mg de mélange de fractions intermédiaires.

Le rendement est d'environ 60% en dihydrodiols purs et séparés en ses deux stéréoisomères (en proportion 1,9/1); le rendement est calculé à partir de la *O*-acétylquinidine et tient compte du fait que le produit initial contient environ 10–15% de dérivé dihydro.

L'isomère majoritaire 10(*R*) (**2**) présente les caractéristiques suivantes : *F* 196°C (AcOEt); rmn ^{1}H ($CDCl_3$) δ : 1,34 et 1,37 (2s, 2Me), 3,50 et 4,0 (t, 2H-11), 3,26 (s, OMe), 4,45 (q, H-10), 5,69 (s, H-9), 7,23, 7,47, 7,87 et 8,40 (5H, aromatiques) ppm. L'isomère minoritaire 10(*S*) (**3**) présente les caractéristiques suivantes : *F* 188°C (AcOEt); rmn ^{1}H ($CDCl_3$) δ : 1,37 (2Me), 3,47 et 3,97 (2t, 2H-11), 3,73 (s, OMe), 4,37 (m, H-10), 7,10, 7,53, 7,78 et 8,40 (5H, aromatiques) ppm.

Dihydroxy-10,11 dihydro-10,11 quinidines (4 et 5)

*Isomère majoritaire 10(*R*) (4)*

On dissout 500 mg de diméthyl méthylènedioxy-10,11 dihydroquinidine-10(*R*) dans 2,3 mL de MeOH et on ajoute 2,5 mL (4,8 milliéquivalents) de résine IR 120-H^+ en suspension dans l'eau et on agite la suspension à température ambiante pendant 1 nuit.

Can. J. Chem. Downloaded from www.nrcresearchpress.com by 213.222.148.141 on 09/07/12
For personal use only.

Can. J. Chem. Downloaded from www.nrcresearchpress.com by 213.222.148.141 on 09/07/12
For personal use only.

TABLEAU 7. Données cristallographiques

$C_{20}H_{26}N_2O_4 \cdot H_2O$	P.M. = 376,46	$F(000)$ = 808 e	orthorhombique
a = 8,756(2) Å	b = 11,499(7) Å	c = 19,123(5) Å	V = 1925,4 Å^3
$P2_12_12_1$	Z = 4	d_0 = 1,28	d_c = 1,298 g cm^{-3}
μ(CuKα) = 7,27 cm^{-1}		λ(CuK$\bar{\alpha}$) = 1,54178 Å	T = 190 K

Par la suite, on filtre, rince et élue les bases par un mélange de $MeOH/NH_4OH$ et on concentre à sec avant de cristalliser le résidu (405 mg) dans du EtOH aqueux pour obtenir 343 mg de cristaux de dihydroxy-10,11 dihydro-10,11-quinidine 10(*R*) (**4**) qui présente les caractéristiques suivantes : *F* 239°C (*i*-PrOH); $[\alpha]_D$ +188° (*c* 1,09, EtOH 95); uv (EtOH) λ_{max} : 233 (30 200), 280 (3600), 290 (3100), 322 (4100), 333 (4600) nm; masse calculée pour $C_{20}H_{26}N_2O_4$: 358.4; trouvée (par sm) : 358 (ions principaux à *m/e* 340 (10), 283 (10) et 227 (100)).

*Isomère minoritaire 10(*S*) (**5**)*

De la même manière, à partir de 250 mg du produit **3**, on obtient 174 mg de cristaux (acétonitrile) de dihydroxy-10,11 dihydro-10,11-quinidine 10(*S*) (**5**) qui présentent les caractéristiques suivantes : *F* 228°C (*i*-PrOH–AcOEt); $[\alpha]_D$ +182° (*c* 1,03, EtOH 95); masse calculée pour $C_{20}H_{26}N_2O_4$: 358,4; trouvée (par SM) : 358 (ions principaux à *m/e* 340 (100), 221 (60) et 181 (100)).

*Étude structurale de l'isomère majoritaire 10(*R*) (**4**)*

Le composé 10(*R*), recristallisé à partir de sa solution dans l'isopropanol, se présente sous forme de cristaux prismatiques, incolores et de dimensions 0,16 × 0,25 × 0,35 mm. La détermination précise de la maille cristalline a été faite à partir de 25 réflexions bien centrées mesurées dans l'intervalle $25 \leqslant 2\theta \leqslant 70°$. Les seules absences systématiques rencontrées, du type $h00$, $h \neq 2n$; $0k0$, $k \neq 2n$ et $00l$, $l \neq 2n$, sont caractéristiques du groupe spatial $P2_12_12_1$. Les données cristallographiques d'intérêt sont rapportées dans le tableau 7. La collection des intensités diffractées sur un diffractomètre automatique Nonius CAD4 a été effectuée par la méthode de balayage ω–2θ avec une largeur de balayage $\Delta\omega = (1{,}00 + 0{,}14 \text{ tg } \theta)°$ en utilisant la radiation du cuivre et un monochromateur de graphite à 190 K. L'orientation et la stabilité du cristal ont été suivies grâce à 7 réflexions de référence dont les intensités étaient mesurées toutes les heures et l'orientation vérifiée à toutes les 100 mesures. Les intensités de 2188 réflexions ont été enregistrées dans la sphère de réflexion limitée par $2\theta_{max} = 150°$, $0 \leqslant h \leqslant 10$, $0 \leqslant k \leqslant 14$ et $0 \leqslant l \leqslant 23$. La fluctuation maximum des intensités de référence n'a pas dépassé 3,2%. Au total, les 2039 réflexions pour lesquelles $I \geqslant 3{,}0\sigma(I)$ sont considérées observées et servent à la détermination et à l'affinement de la structure. Les coordonnées de la majorité des atomes de la molécule ont été établies grâce au programme MULTAN.[4] Tous les atomes, y compris une molécule d'eau de cristallisation, ont été trouvés à la suite d'une série d'affinement et de synthèses de différence Fourier. Les atomes semi-lourds ont été affinés anisotropiquement alors que les atomes d'hydrogène, trouvés sur les cartes de différence Fourier, étaient isotropes. La quantité minimisée est $\Sigma w(|F_o| - |F_c|)^2$ où les poids w sont dérivés des statistiques de comptage. L'affinement a convergé quand $\Delta/\sigma_{max} = 0{,}37$ et $\Delta/\sigma_{moyen} = 0{,}06$, alors $R = \Sigma||F_o| - |F_c||/\Sigma|F_o| = 0{,}0399$, $R_w = [\Sigma w(|F_o| - |F_c|)^2/\Sigma w|F_o|^2]^{1/2} = 0{,}0496$ et $S = [\Sigma w(|F_o| - |F_c|)^2/(m - n)]^{1/2} = 2{,}026$. La configuration absolue correspond à celle établie pour la quinidine (18). Les valeurs extrêmes de la densité électronique résiduelle de la dernière synthèse de différence Fourier sont −0,22 et +0,20 e Å^{-3}. Les courbes de diffusion de C, N, O sont tirées de Cromer et Mann (14) et celles de l'hydrogène viennent de Stewart, Davidson et Simpson (15). Pour l'autre configuration, S prend la valeur de 2,043 alors que R et R_w prennent les valeurs de 0,0402 et 0,050 respectivement.

4. Les programmes utilisés pour ce travail sont mentionnés dans la référence 13.

Remerciements

Les auteurs remercient le Conseil de recherches en sciences naturelles et en génie du Canada et l'Institut de recherches en santé et sécurité au travail pour l'aide financière apportée sous la forme de bourses et d'octrois de recherches. Nous remercions aussi M. J. Olivier pour la mesure des intensités diffractées.

1. G. GRETHE et M. R. USKOVIC. Heterocycl. Compd. **25**, 1983; L. S. GOODMAN et A. GILMAN. The pharmacological basis of therapeutics. 7e ed., MacMillan Publishing Company. 1985. p. 759.
2. B. B. BRODIE, J. E. BAER et L. C. CRAIG. J. Biol. Chem. **188**, 567 (1951).
3. K. H. PALMER, B. MARTIN, B. BAGGETT et M. E. WALL. Biochem. Pharmacol. **18**, 1845 (1969).
4. D. E. DRAYER, C. E. COOK et M. M. REIDENBERG. Clin. Res. **24**, 623A (1976).
5. T. W. GUENTERT, J. J. DALY et S. RIEGELMAN. Eur. J. Drug Metab. Pharmacokinet. **7**, 31 (1982).
6. S. E. BARROW, R. A. TAYLOR et M. G. HORNING. J. Chromatogr. **181**, 219 (1980).
7. F. I. CARROLL, A. PHILIP et M. C. COLEMAN. Tetrahedron Lett. 1757 (1976).
8. L. D. SMALL, H. ROSENBERG, P. U. NWANGWU, T. L. HOLCSLAW et S. J. STOHS. J. Med. Chem. **22**, 1014 (1979).
9. E. OCHIAI. J. Org. Chem. 534 (1953).
10. Y. YANUKA, J. YOSSELSON-SUPERSTINE, A. GERYES et E. SUPERSTINE. J. Pharm. Sci. **70**, 675 (1980).
11. A. RAKHIT, N. H. G. HOLFORD, T. W. GUENTERT, K. MALONEY et S. RIEGELMAN. J. Pharmacokin. Biopharm. **12**, 1 (1984).
12. J. S. BARAN. J. Org. Chem. **25**, 257 (1960).
13. A. PALMER, S. POULIN-DANDURAND et F. BRISSE. Can. J. Chem. **63**, 3079 (1985).
14. D. T. CROMER et J. B. MANN. Acta Crystallogr. Sect. A: Cryst. Phys. Diffr. Theor. Gen. Crystallogr. **24**, 321 (1968).
15. R. F. STEWART, E. R. DAVIDSON et W. T. SIMPSON. J. Chem. Phys. **42**, 3175 (1965).
16. M. J. BERTRAND, L. MALTAIS, F. BRISSE et M. J. OLIVIER. Can. J. Chem. **63**, 3386 (1985).
17. D. T. CROMER et D. LIBERMAN. J. Chem. Phys. **53**, 1891 (1970).
18. D. L. CARTER, A. T. MCPHAIL et G. A. SIM. J. Chem. Soc. A, 365 (1967).

The influence of charge on nuclear magnetic resonance isotope effects

RODERICK E. WASYLISHEN[1] AND NEIL BURFORD
Department of Chemistry, Dalhousie University, Halifax, N.S., Canada B3H 4J3

Received May 22, 1987

RODERICK E. WASYLISHEN and NEIL BURFORD. Can. J. Chem. **65**, 2707 (1987).

Deuterium isotope effects on the ^{31}P shielding constants and spin–spin coupling constants in the isoelectronic series, PH_2^-, PH_3, PH_4^+, are examined. Also, deuterium isotope effects on the nuclear magnetic resonance parameters of SnH_3^- are examined and compared with our earlier results on SnH_4 and SnH_3^+. The experimental results are analyzed using the models of Jameson and Osten. In each isoelectronic series it is found that the isotope effects on the heavy atom chemical shifts are largest for the negatively charged ions and essentially zero for the positively charged ions, as predicted by recent molecular orbital calculations. The primary isotope effects on J(A,H) are positive for all species containing lone-pair electrons, otherwise $\Delta_p\,{}^1J$(A,H) is negative. The primary and secondary isotope effects on J(Sn,H) in the SnH_3^- ion are the largest reported to date.

RODERICK E. WASYLISHEN et NEIL BURFORD. Can. J. Chem. **65**, 2707 (1987).

On a étudié les effets isotopiques du deutérium sur les constantes d'écran du ^{31}P et sur les constantes de couplage spin–spin de la série isoélectronique PH_2^-, PH_3 et Ph_4^+ : On a aussi étudié les effets isotopiques du deutérium sur les paramètres en résonance magnétique nucléaire du SnH_3^- et on les a comparés avec nos résultats antérieurs sur le SnH_4 et le SnH_3^+. On a analysé les résultats expérimentaux en utilisant les modèles de Jameson et Osten. Dans chacune des séries isoélectroniques, on a trouvé que les effets isotopiques sur les déplacements chimiques de l'atome lourd sont les plus importants pour les ions chargés négativement et essentiellement zéro pour les ions chargés positivement; ces résultats sont en accord avec les prédictions dérivées de calculs récents d'orbitales moléculaires. Les effets isotopiques primaires sur J(A,H) sont positifs pour toutes les espèces contenant des paires libres d'électrons; autrement, la valeur de $\Delta_p\,{}^1J$(A,H) est négative. Les valeurs des effets électroniques primaire et secondaire sur J(Sn,H) dans l'ion SnH_3^- sont les valeurs les plus élevées à être rapportées à date.

[Traduit par la revue]

Can. J. Chem. Downloaded from www.nrcresearchpress.com by 213.222.148.141 on 09/07/12
For personal use only.

Introduction

It has been known for several years that in simple hydrides, AH_x, replacement of a hydrogen atom by deuterium leads to increased shielding of nucleus A (1–3). Recently, Jameson and Osten (4) have developed a simple model that allows qualitative estimate of $^{2/1}H$-induced one-bond isotope effects on the shielding constant of A in any simple hydride. The model predicts isotope effects on the shielding constant to increase as one moves across any row or down any group of the periodic table due to the periodicity of $\langle r^{-3}\rangle_A$ for the valence p or d orbitals of atom A. This general periodic variation of $^{2/1}H$ isotope effects in simple hydrides is supported by recent theoretical calculations of Chesnut and Foley (5, 6), which show that the shielding derivative with respect to bond extension, $(\partial\sigma^A/\partial\Delta r)_e$, also exhibits a systematic variation as one moves across either the first or second row of the periodic table. The shielding derivative is intimately related to the isotope effect on σ^A because the main influence of deuterium substitution is to decrease the average mean bond displacement, $\Delta r_{A-^{2/1}H}$ (3, 7–9).

For any particular isotope, A, it has also been recognized that the extent of the $^{2/1}H$ isotope effect on σ^A will show some variation depending upon the detailed electronic structure of the molecule (2, 3). For example, the $^{2/1}H$ isotope effect on the ^{15}N chemical shift of ammonia is -0.62 ppm/^2H, about twice the shift observed in the isoelectronic ammonium ion, -0.29 ppm/^2H (10–12). The detailed explanation for this observation is not entirely clear; however, it does appear that the gross atomic charge on the central atom is important (5). To examine further the influence of charge we have measured very accurate $^{2/1}H$ induced isotope effects on ^{31}P and ^{119}Sn chemical shifts in PH_2^-, PH_4^+, and SnH_3^-, respectively. This allows us to compare our results with earlier experimental data on PH_3 (13) and on SnH_4 and SnH_3^+ (14). Investigation of these two series of isoelectronic molecules also permits us to make a systematic experimental study of isotope effects on spin–spin coupling constants (15).

[1]Author to whom correspondence may be addressed.

Theory

The one-bond isotope shift is defined by eq. [1],

$$[1]\quad {}^1\Delta A(^{2/1}H) = \sigma^A(A—{}^1H) - \sigma^A(A—{}^2H)$$

and for end atom isotopic substitution in a simple hydride, eq. [2] is a good approximation (3, 4, 8),

$$[2]\quad {}^1\Delta A(^{2/1}H) \cong (\partial\sigma^A/\partial\Delta r_{AH})_e[\langle\Delta r_{A—H}\rangle - \langle\Delta r_{A—D}\rangle] \cong (\partial\sigma^A/\partial\Delta r_{AH})_e(1/4)\langle\Delta r_{AH}\rangle$$

where $\langle\Delta r_{AH}\rangle$ is the mean bond displacement, 15–20 $\times$ 10^{-3} Å (9). As mentioned in the introduction, $\sigma^A(A—{}^2H) > \sigma^A(A—{}^1H)$; hence ${}^1\Delta A(^{2/1}H)$ and $(\partial\sigma^A/\partial\Delta r_{AH})$ are invariably negative. A more complete analysis of isotope effects on σ^A involves contributions from mean square bond displacements and mean bond angle displacements. Thus terms such as $(\partial^2\sigma^A/\partial\Delta r_{AH}{}^2)_e\langle(\Delta r_{AH})^2\rangle$ and $(\partial\sigma^A/\partial\Delta\alpha)_e[\langle\Delta\alpha\rangle_{light} - \langle\Delta\alpha\rangle_{heavy}]$ must be considered; however, it is generally thought that these contributions to ${}^1\Delta A(^{2/1}H)$ are relatively small (3, 4, 8, 9, 16).

Recently, Jameson and Osten (15) have summarized isotope effects on spin–spin coupling constants. They define the primary and secondary isotope effect on spin–spin coupling constants using eqs. [3] and [4], respectively.

$$[3]\quad \Delta_p{}^1J(A,^{2/1}H) = |{}^1J(A,D)|(\gamma_H/\gamma_D) - |{}^1J(A,H)|$$

$$[4]\quad \Delta_s{}^1J(A,B)[^{2/1}H] = |{}^1J(A,B)_D| - |{}^1J(A,B)_H|$$

where B is either ^1H or ^2H. The interpretation of isotope effects on spin–spin coupling constants is similar to that of isotope effects on shielding constants (13, 15, 17, 18). Primary isotope effects on J can be estimated by eq. [5] (15),

$$[5]\quad \Delta_p{}^1J(A,^{2/1}H) = (\partial J/\partial\Delta r_{AH})_e[\langle\Delta r_{A—D}\rangle - \langle\Delta r_{A—H}\rangle]$$

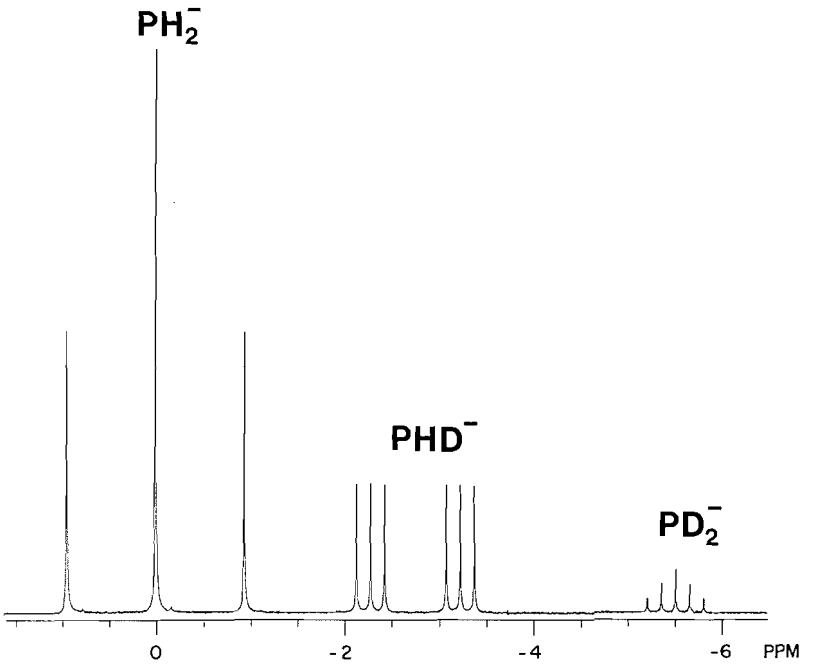

FIG. 1. Phosphorus-31 nmr spectrum of $PH_{2-n}D_n^-$ ($n \leq 2$) at 20°C in liquid ammonia.

Experimentally, primary isotope effects on $^1J(A,^{2/1}H)$ are generally negative unless atom A has one or more electron lone pairs (e.g., PH_3, H_2Se), in which case they are positive (15). Secondary isotope effects on spin–spin coupling constants are usually much smaller than primary isotope effects, and they are more difficult to interpret. The interested reader should consult ref. 15.

Experimental

A sample of $PH_{4-n}D_n^+$ ($n \leq 4$) (~0.7 *M*) was prepared by condensing phosphine (2.7 mmol) into a mixture of boron trifluoride (2.5 mL), CH_3OH (0.5 mL), and CH_3OD (1.5 mL) (19*a*). Potassium phosphide was prepared from potassium metal (0.12 g, 3 mmol) and phosphine (excess) in ammonia (5 mL) (19*b*). The ammonia and excess phosphine were removed under vacuum and the remaining white solid was dissolved in a 1:2 mixture of ammonia and ammonia-d_3. A sample of $NaSnH_{3-n}D_n$ ($n \leq 3$) was prepared by condensing stannane into a solution of sodium (0.07 g, 3 mmol) in a 1:2 mixture of NH_3 and ND_3 (20). Ammonia was dried over sodium before use in all cases. The solutions were all sealed in thick-walled 10 mm o.d. nmr tubes. We would like to point out that $NaSnH_3$ in liquid ammonia undergoes slow decomposition with the evolution of hydrogen gas at 20°C. We stored our sample at liquid nitrogen temperatures; however, after remaining at 20°C for 3 to 5 h the sealed nmr tube exploded violently.

The nmr spectra were obtained using a high-frequency broadband multinuclear nmr probe in a Nicolet-360 spectrometer operating at B_0 = 8.48 T. Phosphorus-31 and ^{119}Sn chemical shifts were referenced with respect to external 85% H_3PO_4 and neat $SnCl_4$, respectively, at 20°C.

Results and discussion

1. $^{2/1}H$ induced isotope effects on shielding constants

(a) PH_2^-, PH_3, and PH_4^+

Phosphorus-31 nmr spectra of $PH_{2-n}D_n^-$ and $PH_{4-n}D_n^+$ at 20°C are shown in Figs. 1 and 2 and the measured isotope shifts are summarized in Tables 1 and 2. The corresponding $^{2/1}H$ isotope effects on the ^{31}P chemical shifts in phosphine are summarized in Table 3; the data are from Jameson and Jameson (13). The first point to note is the decrease in $|^1\Delta^{31}P(^{2/1}H)|$: −2.76, −0.85, and 0.00 ppm/D on going from PH_2^- to PH_3 to PH_4^+. Assuming eq. [2] applies we calculate $(\partial\sigma^P/\partial\Delta r)_e$ values of −585 ± 65, −180 ± 20, and 0 ± 10 ppm/Å, respectively, for PH_2^-, PH_3, and PH_4^+. The observed trend is in agreement with the proposal of Chesnut (5) that the gross charge is related to $(\partial\sigma^P/\partial\Delta r)_e$ and hence the isotope shift. The derivative calculated for phosphine is in excellent agreement with the theoretical value of −150.8 ppm/Å (6). The good agreement suggests that bond angle deformation must make minor contributions to the isotope shift in phosphine. This conclusion is supported by the theoretical calculations of Chesnut and Foley (6) and the arguments of Jameson and Osten (16).

In the case of PH_2^- we also believe that the isotope shift is dominated by $(\partial\sigma^P/\partial\Delta r)_e$; the large derivative is due to both the increased electron density at the phosphorus and to the larger paramagnetic shielding that results from the two groups of lone pairs of electrons on the phosphorus atom. Unfortunately, high-level molecular orbital calculations of the various shielding derivatives are not available for PH_2^-.

To our knowledge the phosphonium ion is the first example where a one-bond $^{2/1}H$ isotope shift is observed to be positive, i.e., $\sigma(PH_4^+) - \sigma(PD_4^+)$ is positive. The calculations of Chesnut (5) predict $(\partial\sigma^P/\partial\Delta r)_e = -52.9$ ppm/Å; this would correspond to a $^1\Delta^{31}P(^{2/1}H)$ of approximately −0.25 ppm. Considering the range of observed $\partial\sigma^P/\partial\Delta r_{PH}$ values, the possible influence of solvent effects, and anion–cation interactions (2, 3, 21), the agreement between theory and experiment is good. It is of interest to point out that the molecular orbital calculations (5) predict a small positive value for $(\partial\sigma^{Al}/\partial\Delta r)_e$ in AlH_4^-, +11.6 ppm/Å; however, experiments imply a small negative value. The isotope shifts, $^1\Delta Al(^{2/1}H)$, reported in three independent studies are very small, 0 ppm/^2H (22), −0.04 ± 0.02 ppm/^2H (23), and −0.1 ppm/^2H (24); again considering the possible influence of intermolecular interactions, the agreement between theory and experiment is good.

Can. J. Chem. Downloaded from www.nrcresearchpress.com by 213.222.148.141 on 09/07/12
For personal use only.

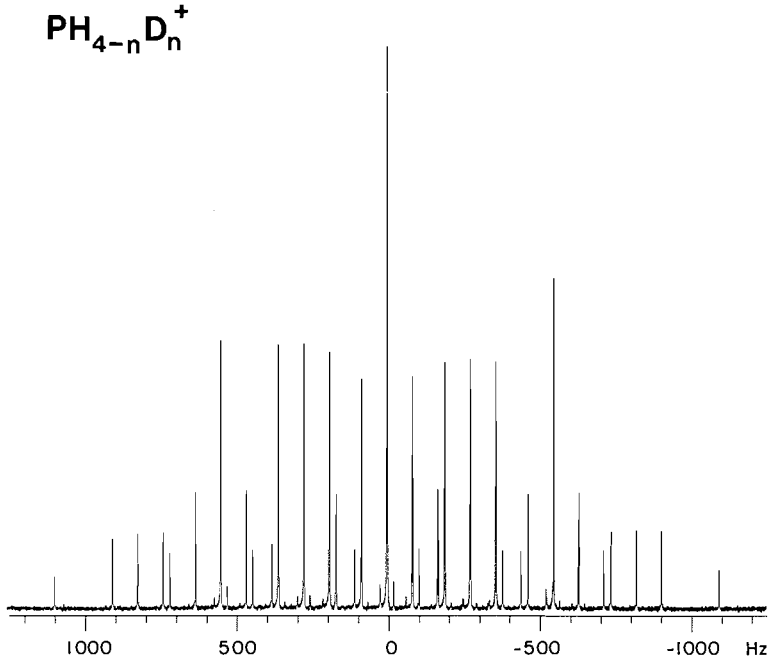

FIG. 2. Phosphorus-31 nmr spectrum of $PH_{4-n}D_n^+$ ($n \leq 4$) in BF_3 and methanol at 20°C.

TABLE 1. Phosphorus-31 chemical shifts for $PH_{2-n}D_n^-$ ($n \leq 2$) in liquid ammonia at 20°C

Molecule	$^1\Delta^{31}P(^{2/1}H)_{obs}$[a]	$^1\Delta^{31}P(^{2/1}H)_{add}$	Δ
PH_2^-	0.0000 ppm	0.0000 ppm	0
PHD^-	−2.7613	−2.7599	0.0014
PD_2^-	−5.5197	−5.5197	0

[a]Error ±0.0002 ppm; the chemical shift of PH_2^- w.r.t. 85% H_3PO_4 is −279.4 ppm.

TABLE 2. Phosphorus-31 chemical shifts and spin–spin coupling constants for the $PH_{4-n}D_n^+$ ($n \leq 4$) ion in methanol and boron trifluoride at 20°C

Molecule	$^1\Delta^{31}P(^{2/1}H)_{obs}$[a]	$^1J(^{31}P,H)$[b]	$^1J(^{31}P,D)$[c]
PH_4^+	0.000 ppm	547.98 Hz	—
PH_3D^+	−0.004	547.78	83.32 Hz
$PH_2D_2^+$	−0.002	547.56	83.81
PHD_3^+	+0.006	547.37	83.76
PD_4^+	+0.018	—	83.66[d]

[a]Error ±0.001 ppm; the chemical shift is −105.3 ppm w.r.t. 85% H_3PO_4.
[b]Error ±0.05 Hz; $\Delta_s\ ^1J(^{31}P,H)\ [^{2/1}H] = -0.20 \pm 0.05$ Hz.
[c]Error ±0.10 Hz; $\Delta_p\ ^1J(^{31}P,H) = -1.68 \pm 0.35$ Hz.
[d]Error ±0.10 Hz.

(b) SnH_3^-, SnH_4, and SnH_3^+

The ^{119}Sn nmr spectrum of $NaSnH_{3-n}D_n$ at −50°C is shown in Fig. 3 and the results are summarized in Table 4. The isotope shifts, $^1\Delta Sn(^{2/1}H)$, in the series SnH_3^-, SnH_4, and SnH_3^+ are −3.09, −0.40, and −0.05 ppm/D, respectively. The trend observed in this isoelectronic series of hydrides is the same as that observed for the phosphorus hydrides, and similar qualitative arguments can be used to rationalize the variation in isotope shifts. One point to note is that on going from PH_3 to PH_2^- there is not a significant change in the HPH bond angle (93.5 ± 2° in both compounds (25, 26)); however, on going from SnH_4 to SnH_3^- there will be a substantial change in the HSnH bond angle from 109.47° to 92.5 ± 4° (27, 28). This change in geometry, concomitant with the lone-pair contribution, in part accounts for the large change in $^1\Delta^{119}Sn(^{2/1}H)$ between SnH_3^- and SnH_4. Assuming that only differences in the mean bond displacement are responsible for the isotope shift, we calculate $(\partial\sigma^{Sn}/\partial\Delta r_{SnH})_e = -700 \pm 100$ ppm/Å. If other terms contribute to the isotope shift the value of −700 ppm/Å is probably an upper limit to the bond displacement derivative (3).

TABLE 3. Phosphorus-31 chemical shifts for $PH_{3-n}D_n$ ($n \leq 3$)[a]

Molecule	$^1\Delta^{31}P(^{2/1}H)_{obs}$	$^1\Delta^{31}P(^{2/1}H)_{add}$	Δ
PH_3	0.0000 ppm	0.0000 ppm	0
PH_2D	−0.8045	−0.8458	−0.0413
PHD_2	−1.6491	−1.6916	−0.0425
PD_3	−2.5373	−2.5373	0

[a]Results from ref. 13.

TABLE 4. $^{2/1}H$ isotope effects on ^{119}Sn chemical shifts in $SnH_{3-n}D_n^-$ ($n \leq 3$) at −50°C

Molecule	$^1\Delta Sn(^{2/1}H)_{obs}$[a]	$^1\Delta Sn(^{2/1}H)_{additivity}$	Δ
SnH_3^-	0.000 ppm	0.000 ppm	0
SnH_2D^-	−3.093	−3.108	−0.015
$SnHD_2^-$	−6.202	−6.217	−0.015
SnD_3^-	−9.325	−9.325	0

[a]Estimated error is less than ±0.002 ppm except for SnD_3^- where the error is ±0.003 ppm; at 20°C the chemical shift of SnH_3^- is −634.7 ppm with respect to external $SnCl_4$ (1), thus with respect to $Sn(CH_3)_4$ the chemical shift of SnH_3^- is approximately −782.5 ppm (ref. 30).

Can. J. Chem. Downloaded from www.nrcresearchpress.com by 213.222.148.141 on 09/07/12
For personal use only.

Can. J. Chem. Downloaded from www.nrcresearchpress.com by 213.222.148.141 on 09/07/12
For personal use only.

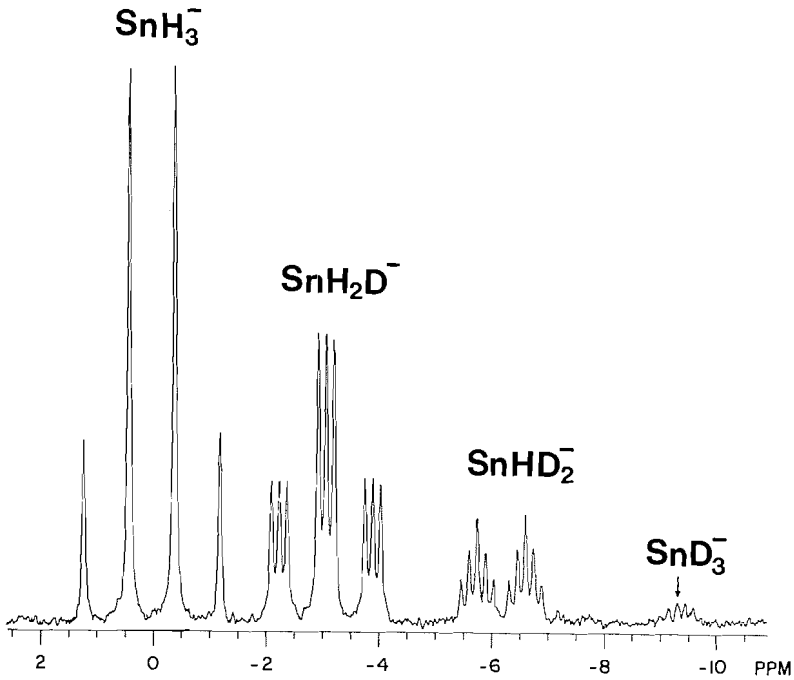

FIG. 3. Tin-119 nmr spectrum of $SnH_{3-n}D_n^-$ ($n \leq 3$) at −50°C in liquid ammonia.

TABLE 5. Isotope effects on spin–spin coupling constants in $PH_{2-n}D_n^-$ ($n \leq 2$), all values in Hz

Molecule	$^1J(^{31}P,H)^a$	$^1J(^{31}P,D)^a$	$\gamma_H/\gamma_D\,^1J(^{31}P,H)^b$	$\Delta_p\,^1J(^{31}P,H)$
PH_2^-	138.235	—	—	—
PHD^-	138.930	21.74	141.62	2.69 ± 0.1
PD_2^-	—	21.85	142.34	—

[a]Error ±0.01 Hz; $\Delta_s\,^1J(^{31}P,H)\,[^{2/1}H] = 0.70 \pm 0.02$ Hz.
[b]$\gamma_H/\gamma_D = 6.51440$ (ref. 15); error ±0.06 Hz.

TABLE 6. Isotope effects on spin–spin coupling constants in $PH_{3-n}D_n$ ($n \leq 3$)[a]

Molecule	$^1J(^{31}P,H)^b$	$J(^{31}P,D)$	$\gamma_H/\gamma_D\,^1J(^{31}P,D)^c$	$\Delta_p\,^1J(^{31}P,H)$
PH_3	185.6	—	—	—
PH_2D	184.4	30.36	197.8	13.4
PHD_2	183.1	30.05	195.8	12.7
PD_3	—	29.79	194.1	—

[a]All values in Hz; results from ref. 13.
[b]$\Delta_s\,^1J(^{31}P,H)\,[^{2/1}H] = -1.2$ Hz.
[c]$\gamma_H/\gamma_D = 6.51440$ (ref. 15).

The $^{2/1}H$ isotope effects on the ^{119}Sn chemical shifts of SnH_2D^+ and $SnHD_2^+$ deviate from additivity by the same amount, −0.015 ppm. Interestingly, the deviations from additivity are negative, i.e., each replacement of a hydrogen in SnH_3^- by deuterium results in a larger change in $^1\Delta^{119}Sn$ (−3.093, −3.109, and −3.123 ppm, respectively). Negative deviations are also observed for phosphine (13); however, for all other molecules that we have studied (NH_4^+, NH_3, PH_2^-, and SnH_4) deviations are positive.

2. Isotope effects on spin–spin coupling constants

Spin–spin coupling constants involving ^{31}P in the series $PH_{2-n}D_n^-$, $PH_{3-n}D_n$, and $PH_{4-n}D_n^+$ are given in Tables 5, 6, and 2, respectively. The coupling constants involving ^{119}Sn in $SnH_{3-n}D_n^-$ are given in Table 7. A single table summarizes all spin–spin coupling constants in the phosphorus and tin hydrides (Table 8).

Primary isotope effects on J are positive for all species with one or more lone pairs (PH_2^-, PH_3, and SnH_3^-); otherwise they are negative (PH_4^+, SnH_4, and SnH_3^+). This observation is attributed to a negative derivative, $(\partial K/\partial \Delta r)_e$, for those molecules with one or more lone pairs; otherwise $(\partial K/\partial \Delta r)_e$ is positive. For example, in the case of PH_2^-, theoretical molecular orbital calculations by Lazzeretti *et al.* (26) predict $\delta\partial J/\partial \Delta r \cong -700$ Hz/Å; also these same calculations predict bond angle deformations to have a relatively small influence on

TABLE 7. $^{2/1}$H isotope effects on spin–spin coupling constants (Hz) in $SnH_{3-n}D_n^-$ ($n \leq 3$) at −50°C

Molecule	$\lvert {}^1J(^{119}Sn,H)^a \rvert$	$\lvert {}^1J(^{119}Sn,D) \rvert$	$(\gamma_H/\gamma_D)\lvert {}^1J(^{119}Sn,D)^b \rvert$	$\Delta_p {}^1J(^{119}Sn,H)$
SnH_3^-	108.54 ± 0.05	—	—	—
SnH_2D^-	111.55 ± 0.10	18.73 ± 0.10	122.0 ± 0.7	10.4[5]
$SnHD_2^-$	114.43 ± 0.15	19.17 ± 0.15	124.9 ± 1.0	10.4[5]
SnD_3^-	—	19.73 ± 0.30	128.5 ± 2.0	—

[a] $\Delta_s {}^1J(^{119}Sn,H)$ [$^{2/1}$H] = 3.0 ± 0.2 Hz.
[b] (γ_H/γ_D) = 6.51440 (ref. 15).

TABLE 8. Spin–spin coupling constants and $^{2/1}$H isotope effects on $^1J(^{31}P,H)$ and $^1J(^{119}Sn,H)$ in some phosphorus and tin hydrides (all values in Hz)

Molecule	$^1J(A,H)$	$\Delta_p {}^1J(A,H)$	$\Delta_s {}^1J(A,H)[^{2/1}H]$	Reference
PH_2^-	138.24	2.69 ± 0.1	0.70 ± 0.02	Present study
PH_3	185.6	13.4	−1.2	13
PH_4^+	547.98	−1.68 ± 0.35	−0.20 ± 0.05	Present study
SnH_3^-	108.54	10.45 ± 1.0	3.0 ± 0.2	Present study
SnH_4	1933.3	−2.7 ± 0.6	−1.7 ± 0.1	14
SnH_3^+	2906.8	−11.6 ± 7	—	14

J compared to bond length deformations. Assuming eq. [5] is valid (i.e., ignoring terms involving $(\partial J/\partial\Delta\alpha)_e$), we calculate $(\partial J/\partial\Delta r)_e = -570$ Hz/Å, in good agreement with the molecular orbital calculations. Jameson and Osten (15) have proposed that in the case of H_2Se and PH_3 the negative derivative, $(\partial J(A,H)/\partial\Delta r_{AH})_e$, arises from the molecular orbital which has nonbonding character (i.e., the heavy atom lone pair).

In discussing the isotope effects where one of the nuclei has a negative magnetogyric ratio (e.g., ^{119}Sn) it is important to work with reduced coupling constants, $K(A,B) = 4\pi^2 J(A,B)/h\gamma_A\gamma_B$. Using the definitions outlined in ref. 15, $\Delta_p {}^1K(A,^{2/1}H)$ will always have the same sign as $\Delta_p {}^1J(A,^{2/1}H)$; however, the sign of any given derivative involving J will be opposite to the corresponding derivative involving K if A has a negative magnetogyric ratio. Thus, for SnH_3^-, $\partial J(Sn,H)/\partial\Delta r$ is positive (+2400 Hz/Å); however, $\partial K(Sn,H)/\partial\Delta r$ is negative as found in all other hydrides where "A" has one or more lone pairs. We have also carried out measurements on the same sample of $SnH_{3-n}D_n^-$ ($n \leq 3$) at 20°C; as expected, $^1J(^{119}Sn,H)$ decreased with increasing temperature; however, within experimental error $\Delta_p {}^1J(^{119}Sn,H)$ was independent of temperature. At 20°C, $^1J(^{119}Sn,H) = 101.00 \pm 0.05$ Hz in SnH_3^-. The primary isotope effect on J observed for SnH_2D^- at 20°C is the largest isotope effect on J, 10.7 ± 1%, of which we are aware (29).

The secondary isotope effects on $J(A,H)$ [$^{2/1}$H] observed for the tin and phosphorus hydrides show no obvious trends. The value of $\Delta_s J(^{119}Sn,H)$ [$^{2/1}$H] in SnH_3^- is 3% of $J(^{119}Sn,H)$ and is the largest secondary isotope effect on J reported to date.

Acknowledgements

We wish to thank Professor C. J. Jameson for her interest in this study, Mr. Brian Millier for rebuilding one of our nmr probes, and Mr. Jürgen Mueller for the construction of thick-walled nmr tubes and some specialized glassware. We are grateful to NSERC for financial support. All nmr spectra were recorded at the Atlantic Magnetic Resonance Centre.

1. H. BATIZ-HERNANDEZ and R. A. BERNHEIM. Prog. Nucl. Magn. Reson. Spectrosc. **3**, 63 (1967).
2. P. E. HANSEN. Annu. Rep. NMR Spectrosc. **15**, 105 (1983).
3. C. J. JAMESON and H. J. OSTEN. Annu. Rep. NMR Spectrosc. **17**, 1 (1986).
4. C. J. JAMESON and H. J. OSTEN. J. Am. Chem. Soc. **107**, 4158 (1985).
5. D. B. CHESNUT. Chem. Phys. **110**, 415 (1986).
6. D. B. CHESNUT and C. K. FOLEY. J. Chem. Phys. **85**, 2814 (1986).
7. C. J. JAMESON. J. Chem. Phys. **66**, 4983 (1977).
8. C. J. JAMESON and H. J. OSTEN. J. Chem. Phys. **81**, 4293 (1984).
9. C. J. JAMESON and H. J. OSTEN. J. Chem. Phys. **81**, 4300 (1984).
10. W. H. LITCHMAN, M. ALEI, and A. E. FLORIN. J. Chem. Phys. **50**, 1897 (1969).
11. R. E. WASYLISHEN and J. O. FRIEDRICH. J. Chem. Phys. **80**, 585 (1984).
12. R. E. WASYLISHEN and J. O. FRIEDRICH. Can. J. Chem. **65**, 2238 (1987).
13. A. K. JAMESON and C. J. JAMESON. J. Magn. Reson. **32**, 455 (1978).
14. K. L. LEIGHTON and R. E. WASYLISHEN. Can. J. Chem. **65**, 1469 (1987).
15. C. J. JAMESON and H. J. OSTEN. J. Am. Chem. Soc. **108**, 2497 (1986).
16. H. J. OSTEN and C. J. JAMESON. J. Chem. Phys. **82**, 4595 (1985).
17. W. T. RAYNES and N. PANTELI. Chem. Phys. Lett. **94**, 558 (1983).
18. P. LAZZERETTI, R. ZANASI, and W. T. RAYNES. J. Chem. Soc. Chem. Commun. 57 (1986).
19. (*a*) G. M. SHELDRICK. J. Chem. Soc. Faraday Soc. Trans. **63**, 1077 (1967); (*b*) J. Chem. Soc. Faraday Soc. Trans. **63**, 1065 (1967).
20. A. LYČKA and P. E. HANSEN. Mag. Reson. Chem. **23**, 973 (1985).
21. T. BIRCHALL and A. R. PEREIRA. J. Chem. Soc. Dalton Trans. 1087 (1975).
22. S. HEŘMÁNEK, O. KŘIŽ, J. PLEŠEK, and T. HANSLIK. Chem. Ind. (London), 42 (1975).
23. H. NÖTH, R. RURLÄNDER, and P. WOLFGARDT. Z. Naturforsch. **356**, 31 (1980).

Can. J. Chem. Downloaded from www.nrcresearchpress.com by 213.222.148.141 on 09/07/12
For personal use only.

24. V. P. TARASOV, V. I. PRIVALOV, Y. A. BUSLAEV, and U. ERCHHOFF. Z. Naturforsch. B: Anorg. Chem. Org. Chem. **39**, 1230 (1984).
25. G. MCRAE, M. C. L. GERRY, and E. A. COHEN. J. Mol. Spectrosc. **116**, 58 (1986).
26. P. LAZZERETTI, E. ROSSI, F. TADDEI, and R. ZANASI. J. Chem. Phys. **77**, 408 (1982).
27. K. OHNO, H. MATSUURA, Y. ENDO, and E. HIROTA. J. Mol. Spectrosc. **118**, 1 (1986).
28. G. THIRASE, E. WEISS, H. J. HENNIG, and H. LECHERT. Z. Anorg. Allg. Chem. **417**, 221 (1975).
29. R. E. WASYLISHEN and N. BURFORD. J. Chem. Soc. Chem. Commun. In press.
30. C. R. LASSIGNE and E. J. WELLS. Can. J. Chem. **55**, 927 (1977).

Can. J. Chem. Downloaded from www.nrcresearchpress.com by 213.222.148.141 on 09/07/12
For personal use only.

A 2-methylthio-3,5-diaryl-1,3,4-thiadiazolium cation; its reactions, and further exploration of the chemistry of 2-alkyl-3,5-diaryl-1,3,4-thiadiazolium cations

HAROLD MASTALERZ, TAJ MOHAMMAD, AND MARTIN S. GIBSON[1]

Department of Chemistry, Brock University, St. Catharines, Ont., Canada L2S 3A1

Received March 13, 1987

HAROLD MASTALERZ, TAJ MOHAMMAD, and MARTIN S. GIBSON. Can. J. Chem. **65**, 2713 (1987).

Activation of a representative 3,5-diaryl-1,3,4-thiadiazole-2-thione by thione S-methylation gives a cation that is readily susceptible to nucleophilic substitution. Reactions with diethyl malonate, ethyl acetoacetate, acetylacetone, cyclopentan-1,3-dione, or 3-ethylrhodanine under basic conditions lead to β,β-disubstituted methine bases and (or) β-substituted methine bases in cases where deacetylation occurs under the reaction conditions. This cation and the 2-alkyl-3,5-diaryl-1,3,4-thiadiazolium cation are convenient sources of a series of neutral and cationic dyes containing the 1,3,4-thiadiazole ring system.

HAROLD MASTALERZ, TAJ MOHAMMAD et MARTIN S. GIBSON. Can. J. Chem. **65**, 2713 (1987).

L'activation d'une diaryl-3,5 thiadiazole-1,3,4 thione-2 caractéristique par une S-méthylation de la thione conduit à un cation qui peut facilement subir une réaction de substitution nucléophile. Les réactions avec le malonate de diéthyle, l'acétoacétate d'éthyle, l'acétylacétone, la cyclopentanedione-1,3 ou l'éthyl-3 rhodanine, dans des conditions basiques, conduisent à des bases méthines β,β-disubstituées et (ou) à des bases méthines β-substituées, dans les cas où une déacétylation se produit dans les conditions de la réaction. Ce cation ainsi que le cation alkyl-2 diaryl-3,5 thiadiazole-1,3,4 ium sont des sources intéressantes d'une série de colorants neutres ou cationiques contenant le système cyclique thiadiazole-1,3,4.

[Traduit par la revue]

Can. J. Chem. Downloaded from www.nrcresearchpress.com by 213.222.148.141 on 09/07/12
For personal use only.

We have previously described syntheses of a number of 1,3,4-thiadiazolium perchlorates **1**, together with a study of their reactions (1). The 2-alkyl substituted salts **1** are synthetically useful for elaboration at the 2-position since they react with electrophiles in the presence of a base, reactions which are considered to proceed by electrophilic substitution of an intermediate methine base. The related 2-alkyl-2-alkoxy-2,3-dihydrothiadiazoles react similarly with electrophiles when thermolysed; again, an intermediate methine base is assumed to be involved. We now report a complementary approach to 2-functionalization in which a representative 2-methylthio-1,3,4-thiadiazolium salt **2** (Ar = $C_6H_3Br_2$-2,4) is used, together with additional reactions of **1** (Ar = $C_6H_3Br_2$-2,4).

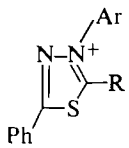

1 ClO_4^-

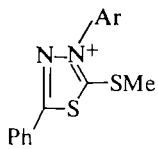

2*a* $MeSO_4^-$ **2***b* ClO_4^-

The methosulfate **2***a* was prepared by methylating the corresponding 3-aryl-5-phenyl-1,3,4-thiadiazole-2-thione (2) with dimethyl sulfate; subsequent treatment with sodium perchlorate gave **2***b*. The site of methylation (thione sulfur) and the susceptibility of the 2-substituent in **2** to nucleophilic displacement were confirmed by hydrolysis of **2***a* to the corresponding 3-aryl-5-phenyl-1,3-4-thiadiazol-2-one (2, 3) and methanethiol. Further, treatment of **2***a* with aqueous sodium hydrosulfide regenerated the original thione.

Compound **2***a* was found to condense readily with diethyl malonate in acetonitrile solution in the presence of triethylamine as added base to give **3***a* (eq. [1]). Deprotonation of diethyl malonate generates the carbanion that displaces methylthiolate ion, and a further deprotonation then gives **3***a*. A similar reaction of **2***a* with ethyl acetoacetate gave **3***b* as the major product. The two compounds **3***a*, **3***b* are of interest in that the methylene proton signals in their ^1H nmr spectra appear as multiplets rather than quartets at ambient temperature, perhaps indicative of restricted rotation. Their mass spectra show molecular ions and expected fragmentation patterns. The reaction of **2***a* with ethyl acetoacetate also gave a second product, **3***c*, resulting from deacetylation of the primary product **3***b*. Methylthiolate ion is assumed to be the deacetylating agent, although methyl thiolacetate was not detected among the products. In a similar way, condensation of **2***a* with acetylacetone gave the known 2-acetonylidene-2,3-dihydro-1,3,4-thiadiazole **3***d* (4); none of the diacetyl derivative (**3**; X,Y = COMe) was isolated. We have since noted a related deacetylation phenomenon in some reactions of 1,1-dimorpholinoethene and 1,1-dipiperidinoethene (5), an example being provided by the formation of ethyl (*E*)-3-(1-piperidino)crotonate from 1,1-dipiperidinoethene and ethyl acetoacetate. However, deacylation in the present series of reactions seems unusual and is probably not general. For instance, substitution of cyclopentan-1,3-dione for acetylacetone in the foregoing reaction with **2***a* led to **3***e*, with little or no sign of acyl cleavage. In a final example, 3-ethylrhodanine condensed readily with **2***a* to give **3***f*. The formulation **3***f* is consistent with the ^1H nmr and mass spectra of the compound, the mass spectrum exhibiting features resulting from fragmentation of the rhodanine-derived ring; the base peak (*m/z* 359) arises from the molecular ion through loss of EtNCS, CO, and Br.

[1] 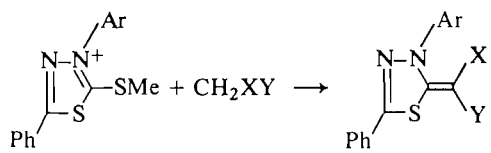

2 **3** (*a–f*)

a X, Y = COOEt
b X, Y = COMe, COOEt
c X, Y = H, COOEt
d X, Y = H, COMe
e X, Y = —$COCH_2CH_2CO$—
f X, Y = —SCSNEtCO—

(Ar = $C_6H_3Br_2$-2,4)

Compounds **3***b*, *c*, *d*, and *f* may formally exist as two geometrical isomers. The reactions leading to their formation appear stereospecific, only one compound being obtained in each case. We now have the results of an X-ray crystallographic

[1]Author to whom correspondence may be addressed.

Can. J. Chem. Downloaded from www.nrcresearchpress.com by 213.222.148.141 on 09/07/12
For personal use only.

study[2] of compound **3** (Ar = $C_6H_3Br_2$-2,4; X,Y = H, COPh) (4), which is closely related to **3***d*. These establish (*Z*) geometry for this compound, with a close oxygen–sulfur contact (the oxygen–sulfur interatomic distance is 2.629(5) Å), indicating an oxygen–sulfur interaction as foreshadowed in our earlier work (6). Of additional interest is the revelation that the 3-aryl substituent is skewed out of the plane of the thiadiazolene ring. Since this substituent is unsymmetrically substituted (2,4-dibromophenyl), the molecule is chiral, and an energy barrier to rotation may be assumed for this and related compounds. From these and spectroscopic correlations, we therefore assign (*Z*) geometry to **3***d* (i.e., X = H, Y = COMe), with similar geometry probably also applying to **3***c*. The geometries of **3***b* and *f* are not known at this point.

This method can evidently be extended to allow for interpolation of a double bond. For example, the thione sulfur in the known 2-thioacetonylidene-2,3-dihydro-1,3,4-thiadiazole **4** (6) was activated to nucleophilic displacement by methylation (methyl iodide); treatment of the resulting salt with 3-ethylrhodanine, as in the preparation of **3***f*, resulted in the formation of **5** (eq. [2]; Ar = $C_6H_3Br_2$-2,4).

[2] 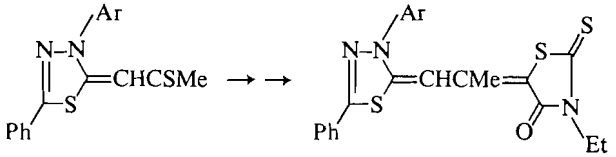

4 **5**

Dyes (for pertinent review and references, see ref. 7) of type **5** should also be accessible from salts of type **1** (R = Me, Et). We first attempted to extend the chain from the 2-position of **1** (R = Me) by condensation with *N*,*N*′-diphenylformamidine and acetylation, to be followed by condensation with 3-ethylrhodanine (8). This was unsuccessful, only tars being obtained. Success was achieved by reversing the order of assembly. 3-Ethylrhodanine was condensed with ethyl *N*-phenylisoformamidate, this being preferable to the earlier procedure (8) using *N*,*N*′-diphenylformamidine, and the product was then acetylated. Condensation of this acetyl derivative with **1** (R = Me) gave **6***a* (R′ = H), while similar treatment of **1** (R = Et) gave **6***b* (R′ = Me) (eq. [3]).

[3] 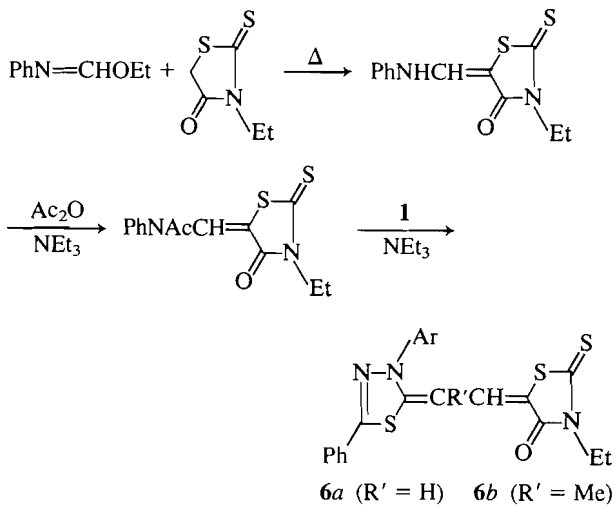

6*a* (R′ = H) **6***b* (R′ = Me)

Visible spectral data (λ_{max}) are reported in the experimental section for **3***f*, **5**, **6***a*, and **6***b*, from which we note that interpolation of a double bond in the system of **3***f* produces a bathochromic shift of some 90–100 nm, similar to that noted in other systems of this type.

We have also explored the preparation of some simple cationic dyes (7) based on these thiadiazolium salts. In the first of these, the perchlorate **1** (R = Me) was deprotonated to the methine base in the presence of the perchlorate **2***b*. In this reaction, the nucleophilic methine base displaces methylthiolate ion from **2***b*, and subsequent deprotonation then gives the dye **7** (eq. [4]). Compound **7** was also prepared by extension of our earlier nuclear synthesis (1), providing independent evidence of structure. The benzothiohydrazide **8** (2 mol) was condensed with malononitrile (1 mol) in acetic acid containing perchloric acid to give **7**; the overall reaction course is shown in eq. [5]. The related dye **9** containing an interpolated double bond was prepared directly from **1** (R = Me) and triethyl orthoformate (8) (eq. [6]). Finally, **10** was prepared by condensing **1** with *p*-dimethylaminobenzaldehyde in acetic anhydride as solvent (9) (eq. [7]).

[4] 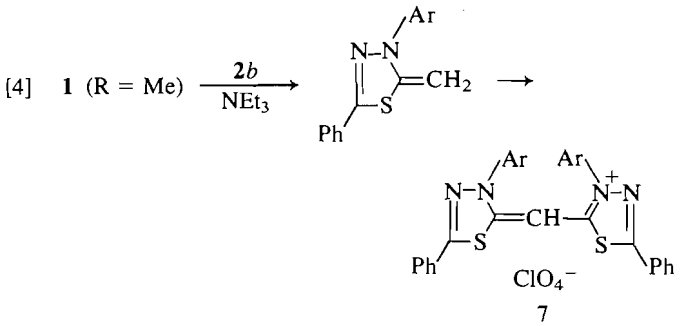

7

[5]

[6] 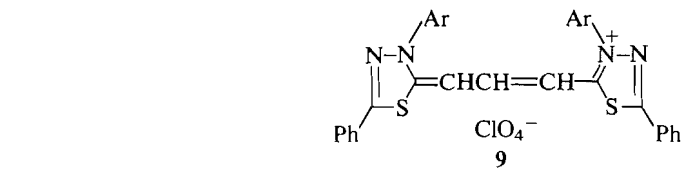

9

[7] 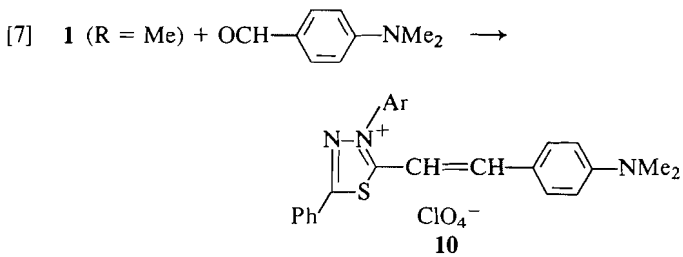

10

A wide variety of 1,3,4-thiadiazole derivatives is thus readily available from cations such as **1** and **2** and similar approaches are likely to find continued use with related systems.

Experimental

Visible spectra were recorded on a Hitachi Perkin Elmer (Coleman 124 model) double beam grating spectrophotometer; absorption maxima are quoted in nm (log ε in parentheses). The ir spectra were recorded for KBr discs on a Perkin Elmer model 237B instrument. The ^{1}H nmr spectra were recorded on a Bruker WP 60 spectrometer (tetramethylsilane as internal reference). Mass spectra were determined with an AEI MS-30 double beam spectrometer; *m*/*z* values are

[2]M. F. Richardson, personal communication.

Can. J. Chem. Downloaded from www.nrcresearchpress.com by 213.222.148.141 on 09/07/12
For personal use only.

reported for the lowest isotopic species unless noted otherwise (relative intensities in parentheses). Melting point data are uncorrected.

3-(2,4-Dibromophenyl)-2-methylthio-5-phenyl-1,3,4-thiadiazolium methosulfate **2**a *and perchlorate* **2**b*; hydrolysis and thiohydrolysis thereof*

A solution of 3-(2,4-dibromophenyl)-5-phenyl-1,3,4-thiadiazole-2-thione (2) (20.0 g, 0.047 mol) and dimethyl sulfate (13.6 g, 0.108 mol) in dry benzene (50 mL) was boiled under reflux for 12 h, cooled, and refrigerated for 24 h. The methosulfate **2***a* (24.8 g, 96%) separated as colourless prisms, mp 200–205°C, raised to mp 208–210°C by crystallization from acetic acid – benzene. Though not analytically pure, this was sufficiently pure for further preparative work. *Anal.* calcd. for $C_{16}H_{14}Br_2N_2O_4S_3$: C 34.67, H 2.55, N 5.05; found: C 33.88, H 2.35, N 4.86.

A solution of sodium perchlorate (75.0 g) in water (150 mL) was added to a stirred solution of **2***a* (24.0 g) in acetic acid (500 mL). After 10 min, water (500 mL) was added and the precipitated solid (20.3 g, 86%) was collected and dried. Crystallization from acetic acid gave the perchlorate **2***b* as colourless prisms, mp 210–212°C. *Anal.* calcd. for $C_{15}H_{11}Br_2ClN_2O_4S_2$: C 33.20, H 2.04, N 5.16; found: C 33.24, H 2.09, N 5.26.

(*i*) A suspension of **2***a* (500 mg) in water (25 mL) was stirred overnight. The strong stench of methyl mercaptan was noticed. The solid was collected, washed with water, and crystallized from ethanol. This gave 3-(2,4-dibromophenyl)-5-phenyl-1,3,4-thiadiazol-2-one (200 mg, 53%), mp 150–152°C (lit. (2) mp 148–150°C), identical (mixture mp; tlc) with an authentic sample (3).

(*ii*) A suspension of **2***a* (470 mg) in a solution of sodium hydrosulfide (3.0 g) in water (25 mL) was stirred for 6 h. The solid was collected, washed with water, and crystallized from ethanol. This gave 3-(2,4-dibromophenyl)-5-phenyl-1,3,4-thiadiazole-2-thione (290 mg, 80%), mp and mixture mp 128–129°C (lit. (2) mp 129°C).

Reaction of 3-(2,4-dibromophenyl)-2-methylthio-5-phenyl-1,3,4-thiadiazolium methosulfate **2**a *with carbon acids: General procedure*

A mixture of **2***a* (5 mmol), the carbon acid (5.5 mmol), and triethylamine (8 mmol) in dry acetonitrile (18 mL) was refluxed under nitrogen for 30 min. In cases (*a*)–(*c*), the reaction mixture was concentrated to ca. half volume and then chilled. In the remaining two cases, the reaction mixture was simply cooled. In all cases, the solid products were collected, washed with acetonitrile, and purified as noted below.

(a) From diethyl malonate

Compound **3***a* (48%) crystallized from ethanol as cream prisms, mp 175–177°C; ir: 1725 and 1650 (C=O) cm^{-1}; ^1H nmr ($CDCl_3$) δ: 1.20 (t, 6H, $-CH_2CH_3$), 3.93 (m, sharpening to q at 50°C, 4H, $-CH_2CH_3$), and 7.2–8.0 (m, 8H, arom.) ppm; mass spectrum *m/z*: 552 (M^+, 18), 507 ($M^+ - OC_2H_5$, 7), 480 ($M^+ - CO_2C_2H_4$, 8), 473 ($M^+ - Br$, 22), 435 ($480 - OC_2H_5$, 5), 408 ($480 - CO_2C_2H_4$, 9), and 103 (C_6H_5CN, 100). *Anal.* calcd. for $C_{21}H_{18}Br_2N_2O_4S$: C 45.51, H 3.27, N 5.05; found: C 45.58, H 3.24, N 5.08.

(b) From ethyl acetoacetate

The crude product consisted of two components (tlc), which were separated chromatographically (silica; benzene as eluant).

First eluted, compound **3***c* (22%) crystallized from ethanol as fluffy cream needles, mp 147–148°C; ir: 1655 (C=O) cm^{-1}; ^1H nmr ($CDCl_3$) δ: 1.25 (t, 3H, $-CH_2CH_3$), 4.20 (q, 2H, $-CH_2CH_3$), 4.83 (s, 1H, HC=C), and 7.2–8.0 (m, 8H, arom.) ppm; mass spectrum *m/z*: 480 (M^+, 57; base peak at *m/z* 482), 435 ($M^+ - OC_2H_5$, 9), 408 ($M^+ - CO_2C_2H_4$, 23), 401 ($M^+ - Br$, 71), 373 ($401 - C_2H_4$, 11), 356 ($401 - OC_2H_5$, 39), and 322 ($401 - Br$, 24). *Anal.* calcd. for $C_{18}H_{14}Br_2N_2O_2S$: C 44.84, H 2.93, N 5.81; found: C 44.77, H 2.96, N 5.70.

Second eluted, compound **3***b* (30%) crystallized as cream prisms, mp 180–183°C; ir: 1710 and 1605 (C=O) cm^{-1}; ^1H nmr ($CDCl_3$) δ: 1.26 (t, 3H, $-CH_2CH_3$), 2.46 (s, 3H, CH_3CO), 3.67 (m, 2H, $-CH_2CH_3$), and 7.26–8.03 (m, 8H, arom.) ppm; mass spectrum *m/z*: 522 (M^+, 18), 507 ($M^+ - CH_3$, 5), 477 ($M^+ - OC_2H_5$, 7), 443 ($M^+ - Br$, 46), 435 ($477 - CH_2CO$, 16), 415 ($443 - C_2H_4$, 10), 401 ($443 - CH_2CO$, 96; base peak at *m/z* 403), and 356 ($401 - OC_2H_5$, 68). *Anal.* calcd. for $C_{20}H_{16}Br_2N_2O_3S$: C 45.82, H 3.08, N 5.34; found: C 46.09, H 3.13, N 5.22.

(c) From acetylacetone

Compound **3***d* (47%) crystallized from acetonitrile as tan prisms, mp 153–156°C, raised by recrystallization to mp 155–157°C; mixture mp 155–157°C (lit. (4) mp 154–155°C).

(d) From cyclopentan-1,3-dione

Compound **3***e* was obtained as a cream solid (82%), mp 209–211°C (mp 207–208°C after crystallization from ethanol); ir: 1690 and 1620 (C=O) cm^{-1}; ^1H nmr ($CDCl_3$) δ: 2.53 (s, 4H, $-CH_2-$), and 7.23–7.98 (m, 8H, arom.) ppm; mass spectrum *m/z*: 411 ($M^+ - Br$, 98; base peak at *m/z* 413) (no molecular ion observed). *Anal.* calcd. for $C_{19}H_{12}Br_2N_2O_2S$: C 46.37, H 2.46, N 5.69; found: C 45.89, H 2.22, N 5.99.

(e) From 3-ethylrhodanine

Compound **3***f* (76%) crystallized from acetone–benzene as bright yellow prisms, mp 240–242°C; vis (EtOH): 424 nm (4.70); ir: 1650 (C=O) cm^{-1}; ^1H nmr ($CDCl_3$) δ: 1.26 (t, 3H, $-CH_2CH_3$), 4.14 (q, 2H, $-CH_2CH_3$), and 7.2–8.0 (m, 8H, arom.) ppm; mass spectrum *m/z*: 553 (M^+, 40), and 359 ($C_{15}H_8BrN_2S_2$, 91; base peak at *m/z* 361). *Anal.* calcd. for $C_{19}H_{13}Br_2N_3OS_3$: C 41.10, H 2.36, N 7.57; found: C 41.11, H 2.19, N 7.58.

Conversion of **4** *into* **5**

Compound **4** (ref. 6) (1.28 g, 2.34 mmol) was heated under reflux with methyl iodide (3.65 g, 25.7 mmol) in dry benzene (40 mL) for 1 h. The salt (1.6 g, 99%) separated as an orange solid, mp 185–190°C (dec.). This was used without further purification as partial decomposition occurred on attempted crystallization.

A mixture of the foregoing salt (1.0 g, 1.45 mmol), 3-ethylrhodanine (320 mg, 1.99 mmol), triethylamine (330 mg, 3.27 mmol), and dry ethanol (20 mL) was heated under reflux for 1 h. When cool, the precipitate was collected and washed with ethanol. Crystallization from methanol–pyridine gave **5** (810 mg, 93%) as red prisms, mp 247–249°C; vis (EtOH): 510 nm (4.65); ir: 1650 (C=O) cm^{-1}; mass spectrum *m/z*: 593 (M^+, 20) and 103 (C_6H_5CN, 100). *Anal.* calcd. for $C_{22}H_{17}Br_2N_3OS_3$: C 44.38, H 2.88, N 7.06; found: C 44.82, H 2.89, N 6.82.

5-Anilinomethylene-3-ethylrhodanine and its acetyl derivative

A mixture of 3-ethylrhodanine (4.0 g, 24.8 mmol), ethyl *N*-phenylisoformamidate (4.5 g, 32.4 mmol), and ethanol (5 mL) was heated under reflux for 25 min. When cool, the red solid (6.0 g, 95%), mp 181–184°C (lit. (8) mp 184–186°C), was collected, washed with methanol, and dried.

The red solid (6.0 g) was heated under reflux with a mixture of acetic anhydride (25 mL) and triethylamine (3.2 mL) for 10 min. When cool, the solid was collected and washed with methanol. Crystallization from methanol gave the acetyl derivative as yellow needles (4.9 g, 70%), mp 90–94°C, resolidifying, and then mp 123–125°C (lit. (8) mp 85–87°C and 128–130°C, respectively).

Condensation of the foregoing acetyl derivative with 2-alkylthiadiazolium perchlorates **1** *(Ar =* $C_6H_3Br_2$*-2,4)*

(*a*) A mixture of **1** (R = Me) (1) (1.0 g, 1.96 mmol), the foregoing acetyl derivative (780 mg, 2.64 mmol), triethylamine (400 mg, 3.95 mmol), and ethanol (20 mL) was heated under reflux for 30 min. When cool, the precipitate (940 mg, 82%; mp 240–244°C) was collected, washed with ethanol, and dried. Crystallization from methanol–pyridine gave **6***a* as red prisms, mp 242–244°C; vis (EtOH): 517 nm (4.79); ir: 1695 (C=O) cm^{-1}; mass spectrum *m/z*: 579 (M^+, 26) and 103 (C_6H_5CN, 100). *Anal.* calcd. for $C_{21}H_{15}Br_2N_3OS_3$: C 43.39, H 2.60, N 7.23; found: C 43.39, H 2.47, N 7.14.

(*b*) The perchlorate **1** (R = Et) (1) (1.0 g, 1.91 mmol), similarly treated (2 h reflux), gave **6***b* as red prisms (630 mg, 55%), mp 213–215°C; vis (EtOH): 519 nm (4.74); ir: 1690 (C=O) cm^{-1}; mass spectrum *m/z*: 593 (M^+, 22) and 103 (C_6H_5CN, 100). *Anal.* calcd. for

$C_{22}H_{17}Br_2N_3OS_3$: C 44.38, H 2.88, N 7.06; found: C 44.89, H 2.93, N 6.91.

Alternative syntheses of **7**

(a) From **1** *(R = Me; Ar = $C_6H_3Br_2$-2,4) and* **2**b *(Ar = $C_6H_3Br_2$-2,4)*

A suspension of perchlorate **1** (1.9 g, 3.72 mmol) and perchlorate **2***b* (2.0 g, 3.69 mmol) in ethanol (40 mL) and triethylamine (0.41 g, 4.03 mmol) was heated under reflux for 30 min. When cool, the precipitated solid was collected and washed with ethanol. Crystallization from methanol–pyridine gave the carbocyanine perchlorate **7** (2.63 g, 79%) as yellow prisms, mp >325°C; vis (EtOH): 427 nm (4.70); ir: 1515, 1490, 1470, 1450, 1280, 1100, and 770 cm^{-1}. *Anal.* calcd. for $C_{29}H_{17}Br_4ClN_4O_4S_2$: C 38.50, H 1.89, N 6.19; found: C 38.44, H 1.93, N 6.10.

(b) From N′*-(2,4-dibromophenyl)benzothiohydrazide and malononitrile*

A mixture of *N′*-(2,4-dibromophenyl)benzothiohydrazide **8** (10) (2.0 g, 5.18 mmol), malononitrile (170 mg, 2.58 mmol), acetic acid (4 mL), and 70% perchloric acid (2 mL) was heated under reflux for 5 min, and then allowed to cool. Water (40 mL) was added slowly, whereupon the colorless precipitate dissolved and a yellow gum (which solidified on trituration with water) separated. Crystallization from methanol–pyridine gave **7** (1.8 g, 77%) as yellow prisms, mp >325°C, with an ir spectrum identical to that of the foregoing sample.

Condensation of **1** *(R = Me; Ar = $C_6H_3Br_2$-2,4) with triethyl orthoformate*

A mixture of the perchlorate **1** (1.0 g, 1.96 mmol), triethyl orthoformate (0.89 g, 6.02 mmol), and pyridine (10 mL) was heated under reflux for 45 min. Crystallization of the precipitated solid from methanol–pyridine gave the tricarbocyanine perchlorate **9** (740 mg, 81%) as lustrous golden-green prisms, mp 290–295°C. These crystals retained pyridine, and an analytical sample, mp 298–303°C, was obtained by recrystallization from aqueous dimethyl sulfoxide; vis (EtOH): 560 nm (5.01); ir: 1560, 1475, 1360, 1300, 1200, 1180, 1090, and 880 cm^{-1}. *Anal.* calcd. for $C_{31}H_{19}Br_4ClN_4O_4S_2$: C 40.01, H 2.06, N 6.02, S 6.89; found: C 40.00, H 2.32, N 5.89, S 6.60.

Condensation of **1** *(R = Me; Ar = $C_6H_3Br_2$-2,4) with* p*-dimethylaminobenzaldehyde*

A mixture of the perchlorate **1** (500 mg, 0.98 mmol), *p*-dimethylaminobenzaldehyde (180 mg, 1.21 mmol), and acetic anhydride (5 mL) was heated under reflux for 20 min. The precipitated solid was collected and crystallized from methanol–pyridine to give the styryl dye **10** (510 mg, 81%) as green prisms, mp 263–265°C; vis (EtOH): 555 nm (4.91); ir: 1580, 1530, 1470, 1440, 1380, 1275, 1175, and 1100 cm^{-1}. *Anal.* calcd. for $C_{24}H_{20}Br_2ClN_3O_4S$: C 44.92, H 3.14, N 6.55; found: C 45.09, H 3.03, N 6.38.

Acknowledgement

We thank the Natural Sciences and Engineering Research Council of Canada for partial financial support.

1. H. Mastalerz and M. S. Gibson. J. Chem. Soc. Perkin Trans. 1, 245 (1983).
2. R. Fusco and C. Musante. Gazz. Chim. Ital. **68**, 147 (1938); Gazz. Chim. Ital. **68**, 665 (1938).
3. I. T. Barnish, S. C. Fung, M. S. Gibson, S. R. Khan, G. A. Pawelchak, and K. M. Tse. J. Heterocycl. Chem. **23**, 417 (1986).
4. P. D. Callaghan, A. J. Elliott, S. S. Gandhi, M. S. Gibson, H. Mastalerz, and D. J. Vukov. J. Chem. Soc. Perkin Trans. 1, 2948 (1981).
5. S. S. Gandhi and M. S. Gibson. Can. J. Chem. **65**, 2717 (1987).
6. H. Mastalerz and M. S. Gibson. J. Chem. Soc. Perkin Trans. 1, 2952 (1981).
7. D. J. Fry. *In* Supplement to the 2nd Edition of Rodd's Chemistry of Carbon Compounds. *Edited by* M. F. Ansell. Vol. IV, Part B. Elsevier, Amsterdam. 1985. Chap. 15.
8. L. G. S. Brooker, G. H. Keyes, R. H. Sprague, R. H. VanDyke, E. VanLare, G. VanZandt, F. L. White, H. W. J. Cressman, and S. G. Dent. J. Am. Chem. Soc. **73**, 5332 (1951); L. G. S. Brooker, G. H. Keyes, and D. W. Heseltine. J. Am. Chem. Soc. **73**, 5350 (1951), and references cited.
9. G. V. Boyd. Chem. Commun. 954 (1967).
10. P. Wolkoff and S. Hammerum. Acta Chem. Scand. Ser. B, **30**, 831 (1976), and references cited.

Can. J. Chem. Downloaded from www.nrcresearchpress.com by 213.222.148.141 on 09/07/12
For personal use only.

Condensation reactions of 1,1-dimorpholinoethene and of 1,1-dipiperidinoethene with carbon acids

SHAM S. GANDHI AND MARTIN S. GIBSON[1]

Department of Chemistry, Brock University, St. Catharines, Ont., Canada L2S 3A1

Received March 13, 1987

SHAM S. GANDHI and MARTIN S. GIBSON. Can. J. Chem. **65**, 2717 (1987).

1,1-Dimorpholinoethene and 1,1-dipiperidinoethene condense with such compounds as malononitrile, ethyl cyanoacetate, cyanoacetamide, and diethyl malonate to give the corresponding β,β-disubstituted enamine, a molecule of morpholine or piperidine being eliminated in the process. Similar reactions with acetylacetone and ethyl acetoacetate proceed with loss of the acetyl group to give the β-substituted enamine. 1,1-Dipiperidinoethene and nitromethane give the β-nitroenamine. Secondary processes of either hydrolysis or further Michael addition and elimination are noted in condensations of 1,1-dimorpholinoethene or 1,1-dipiperidinoethene with cyanoacetamide under more basic conditions. 1,1-Dipiperidinoethene is arylated at the 2-position by 2,4-dinitrochlorobenzene.

SHAM S. GANDHI et MARTIN S. GIBSON. Can. J. Chem. **65**, 2717 (1987).

Le dimorpholino-1,1 éthène et le dipipéridino-1,1 éthène se condensent avec des composés comme le malononitrile, le cyanoacétate d'éthyle, le cyanoacétamide et le malonate de diéthyle pour conduire à la formation des ènamines β,β-disubstituées correspondantes alors qu'une molécule de morpholine ou de pipéridine est éliminée au cours de la réaction. Des réactions semblables avec l'acétylacétone ou l'acétoacétate d'éthyle se produisent avec la perte d'un groupement acétyle et elles conduisent à la formation d'ènamines β-substituées. Lorsqu'on effectue des condensations entre le dimorpholino-1,1 éthène ou le dipipéridino-1,1 éthène, en utilisant des conditions expérimentales beaucoup plus basiques, on note aussi des réactions secondaires impliquant soit des hydrolyses ou des additions de Michael accompagnées d'éliminations. Par réaction avec le dinitro-2,4 chlorobenzène, le dipipéridino-1,1 éthène subit une réaction d'arylation en position 2.

[Traduit par la revue]

Methine bases ("anhydro-bases") (**1**) have been implicated as intermediates in various reactions of 1,3,4-thiadiazolium salts (**2**) (1) and of analogous salts in many other aromatic heterocyclic systems (2). Often, however, evidence for the involvement of such methine bases has been indirect, stemming from trapping experiments using electrophilic reagents or, in the absence of such reagents, from isolation of methine base dimers or other artifacts (1). We have latterly been interested in the 1,1-enediamines **3** and **4** (3) as usable models for methine base studies, and we now report details of their reactions with a variety of carbon acids.

1,1-Dimorpholinoethene (**3**) and 1,1-dipiperidinoethene (**4**) are basic, electron-rich alkenes, giving amidinium salts when treated with acids, and are prone to hydrolysis, giving the corresponding amide and amine (**5** and morpholine, **6** and

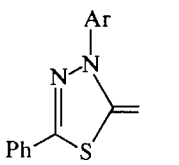

1

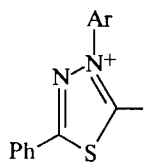

2

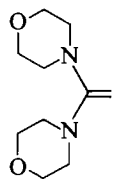

3

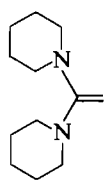

4

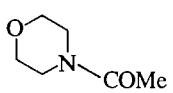

5

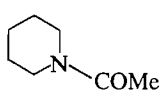

6

piperidine, respectively) (3); **4** has been shown to form 1:1 adducts with boron halides via the 2-carbon atom (4). As nucleophiles, **3** and **4** undergo a variety of substitution reactions at the 2-carbon atom when treated with electrophiles. Generally these reactions yield mono- or di-substitution products, but cases involving subsequent cyclization or hydrolysis have been noted. Examples include their reactions (*a*) with alkyl halides (*N*-alkylation is a possible side reaction in related cases) (5), (*b*) with ketene and with acyl chlorides (6), (*c*) with sulfonyl halides (7), (*d*) with phenyl isocyanate and with phenyl isothiocyanate (5), (*e*) with aromatic aldehydes (8), and (*f*) with α,β-unsaturated carbonyl compounds and with Mannich bases (9). Monosubstitution occurs in the reaction of **4** with 1-(2,2-dicyanovinyl)-4-methyl-1,2,3-triazole (10). The electron-rich double bonds of **3** and **4** can participate in cycloaddition reactions of the 1,3-dipolar and Diels–Alder types (11, 12) and of the 2 + 2 type (7, 13), some of which are succeeded by fragmentation reactions. A case of electron transfer from **3** to an electron-deficient substrate, ethyl benzoylazocarboxylate, has also been recorded (14). Not surprisingly, the reactivity of these 1,1-enediamines has at times led to complex reaction mixtures, with attendant difficulties in complete characterization of the reaction products and delineation of reaction pathways.

With basicity and nucleophilicity of these 1,1-enediamines manifested at the 2-carbon atom, it seemed likely that a general synthesis of enamines substituted with electron-attracting group(s) at the β-position could be developed by reacting **3** and **4** respectively with various carbon acids. Proton transfer between the two reactants would provide the corresponding amidinium ion and carbanion; combination of the ions, followed by elimination of morpholine or piperidine as appropriate, should then lead to the substituted enamine. These transformations are summarized in Scheme 1 for **3** → **7** and **4** → **8**.

We prepared **3** and **4** by known methods (3) and fractionated the compounds before use to limit the extent of contamination by their hydrolysis products, as the presence of these might complicate the isolation of the desired reaction products, **7** and **8**, respectively. We found that **3** and **4** each reacted readily with a variety of well-known carbon acids when refluxed in dry ether

[1]Author to whom correspondence may be addressed.

Can. J. Chem. Downloaded from www.nrcresearchpress.com by 213.222.148.141 on 09/07/12
For personal use only.

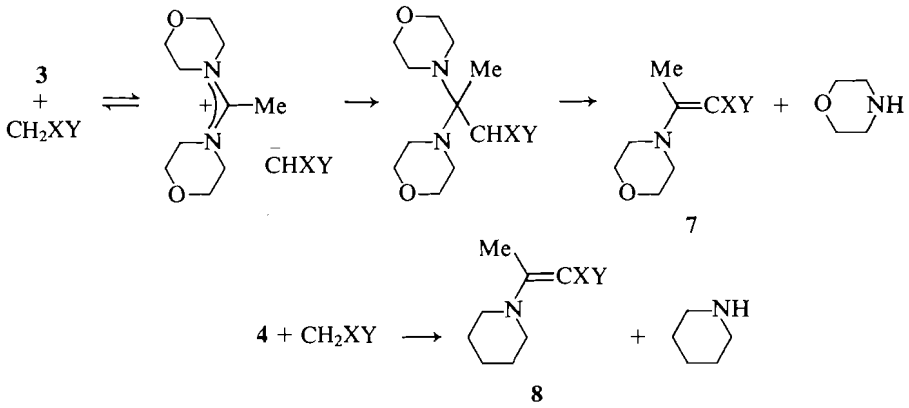

a X, Y = CN; *b* X = CN, Y = COOEt; *c* X = CN, Y = $CONH_2$; *d* X, Y = COOEt;
e X = H, Y = COMe; *f* X = H, Y = COOEt; *g* X = H, Y = NO_2

SCHEME 1

or tetrahydrofuran. Thus **3** reacted with malononitrile, with ethyl cyanoacetate, and with cyanoacetamide to give **7***a*, *b*, and *c*, respectively, as crystalline solids. In each case these products were accompanied by morpholine, as expected, and also by **5**, indicating that some hydrolysis of **3** had occurred as a side reaction. This hydrolysis proved to be an ubiquitous feature of these reactions. From **3** and diethyl malonate, **7***d* was isolated in poor yield as an oil, contaminated with **5**. The reactions of **3** with acetylacetone and with ethyl acetoacetate gave **7***e* and *f*, respectively, loss of an acetyl group accompanying the reaction (the crude materials from these reactions apparently contained traces of the expected products (^{1}H nmr) in each case). Our assumption here is that morpholine generated during the reaction (as well as by hydrolysis of **3**) was the deacetylating agent, being transformed in the process to **5**. A similar deacetylation process has been noted in condensations of a 2-methylthio-1,3,4-thiadiazolium salt with acetylacetone and with ethyl acetoacetate in the presence of triethylamine, the displaced methylthiolate ion being the presumed nucleophile in these cases (1).

Reaction also clearly occurred between **3** and ethyl nitroacetate, but the only characterizable products were the morpholinium salt of ethyl nitroacetate, recovered in low yield, and **5**. Our interpretation is that hydrolysis of the amidinium ion salt supervenes, and little or no condensation occurs. Interestingly, the less basic 1,1-diethoxyethene has been found to condense with ethyl nitroacetate to yield the corresponding β,β-disubstituted vinyl ether (15). The last carbon acids examined were the weakly acidic fluorene and xanthene. These were recovered from attempted reactions (at the bp of diethyl ether) with **3** and with **4**.

We also attempted the condensation of **3** with cyanoacetamide in isopropanol containing sodium isopropoxide, primarily to determine whether further reaction of the condensation product **7***c* would occur under these conditions. The normal isolation procedure was modified to include an acid treatment. From this experiment, we isolated a small yield of (*Z*)-2-cyano-3-hydroxycrotonamide (**9**), with properties corresponding to those reported for the compound produced by hydrolysis of 5-amino-4-cyano-3-methylisothiazole (16). This amide is formally a product of hydrolysis of **7***c*, i.e., of enamine to ketone (enol) function (cf. ref. 15). The relative solubility of **9** or hydrolysis to simpler products may account for low recovery in this experiment.

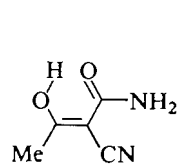

9

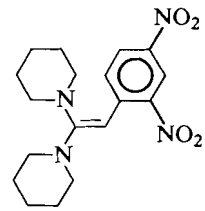

10

Turning to the chemistry of **4**, we noted that, although its reactions with simple alkyl halides were known (5), apparently no case of nucleophilic aromatic substitution had been examined. We found that **4** reacted with 2,4-dinitrochlorobenzene to give **10**, together with piperidinium chloride and **6**, the latter compounds presumably arising from proton transfer to **4** and subsequent hydrolysis. Compound **4** could be utilized somewhat more efficiently by incorporating triethylamine as base in this reaction, but purification of **10** was still rather tedious.

Mutatis mutandis, reactions of **4** with carbon acids were conducted as for **3** with carbon acids. Pure crystalline products, **8***b* and *e*, were obtained using ethyl cyanoacetate and acetylacetone (again one acetyl group was displaced). Further, condensation of **4** with nitromethane provided a simple alternative route to **8***g* (17). Reaction of **4** was also effected with malononitrile and with ethyl acetoacetate (acetyl loss observed) to give **8***a* and *f*, respectively, as oils.

With the exception of **7***a*, **7***d*, and **8***a*, all compounds **7** and **8** prepared in this series may exist as geometrical isomers. The indications are that we obtained only one isomer from each reaction, with the possible exception of **8***f*, which may contain a small amount of the second isomer. Thus, the ^{1}H nmr spectrum of **8***f* exhibits, for the major component, signals at δ 2.42 (CH_3 C=C) and 4.75 (HC=C) ppm, confirming (*E*) geometry (18), and similarly for **7***f* (19). The downfield shift for this methyl proton signal arises from deshielding of the methyl protons by the *cis*-carbonyl function and, applied to the cases of **7***e* and **8***e*, allows the assignment of (*E*) geometry to these compounds also (19); by extension, (*E*) geometry can similarly be assigned to **8***g* (17). The ^{1}H nmr spectra of **7***a* and **8***a* reveal signals (for CH_3 C=C) at δ 2.32 and 2.29 ppm respectively. For compounds **7***b*, **7***c*, and **8***b*, the corresponding signals appear at δ 2.47, 2.43, and 2.47 ppm, respectively, suggesting that this methyl group lies *cis* to a carbonyl rather than a

Can. J. Chem. Downloaded from www.nrcresearchpress.com by 213.222.148.141 on 09/07/12
For personal use only.

nitrile group and again implying (*E*) geometry. The foregoing assignments would conform to the view that the thermodynamically more stable isomer (17, 18) is obtained from these reactions. We make a further comment about **8***f*; like the other compounds which we obtained as oils, this was not 100% pure and its ^{1}H nmr spectrum contained a low intensity peak at δ 2.07 ppm that may suggest the presence (<10%) of the (*Z*) isomer (18).

A variety of "push–pull" olefins, **7** and **8**, is thus available from these reactions of **3** and of **4** with carbon acids. The resulting β-substituted enamines are of interest to us as polyfunctional synthetic intermediates and in this context we have briefly examined the reaction of **4** with cyanoacetamide in ethanol containing sodium ethoxide. This reaction gave 2-amino-5-cyano-6-hydroxy-4-methylnicotinamide (**11**). We envisage this process as involving Michael addition of cyanoacetamide (anion) to the intermediate **8***c*, followed by loss of piperidine and ring closure by dehydration. The factors that favour production of a polyfunctional pyridine over hydrolysis, as in **7***c* → **9**, remain to be examined and we hope to develop a more general pyridine synthesis using this approach.

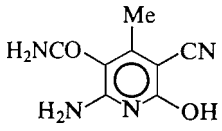

11

Our syntheses of **7** and **8** have a bearing on the production of pyrazole derivatives from a variety of 2-substituted 1,3,4-oxadiazolium salts (the correspondence is with our amidinium ion intermediates) and carbon acids in the presence of triethylamine (20). The latter reactions were interpreted as proceeding with ring opening of the heterocyclic ring to yield a labile β,β-disubstituted enehydrazide (corresponding to our **7**, **8**), which then underwent cyclization to the pyrazole; one such intermediate was isolated and shown to cyclize in this way. This interpretation is reinforced by our current study, although no such secondary cyclization is possible with our series of compounds.

Experimental

Instrumental techniques were as noted in the preceding publication (1*a*).

1,1-Dimorpholinoethene (3)

This was prepared by the literature method (3) and was characterized by reaction with *p*-methoxybenzaldehyde to give (*E*)-*p*-methoxycinnamomorpholide, mp 100–101°C (from ether – light petroleum (bp 60–80°C)) (lit. (8) mp 100–101°C). Compound **3** was freshly prepared and fractionated prior to use in the following reactions.

Reaction of 3 with carbon acids: General procedure

A mixture of **3** (0.01 mol) and the carbon acid (0.01 mol) in dry ether or tetrahydrofuran (15–40 mL) was refluxed under nitrogen. Reactions were monitored chromatographically for consumption of **3** and in most cases were complete within 8 h. The solvent was then removed by evaporation *in vacuo* and the residue was submitted to analysis by glc or glc/ms. The desired product was normally accompanied by morpholine and **5**.

The crude reaction product was triturated with light petroleum (bp 40–60°C). In cases where this procedure induced crystallization, the solid material was collected and purified by recrystallization from aqueous ethanol or occasionally from water. In the remaining cases, the light petroleum layer was decanted and the residual oil was chromatographed and (or) distilled *in vacuo*; working on this scale, we were not able to obtain pure compounds in this way and identification is based on spectroscopic correlations, where possible with published data (18, 19).

The following compounds were obtained as solids (from the carbon acids noted in parentheses):

(*a*) 2-Cyano-3-(1-morpholino)crotononitrile (**7***a*) (74%), mp 105–106°C (prepared from malononitrile); ir: 2200 and 2180 (C≡N) cm^{-1}; ^{1}H nmr ($CDCl_3$) δ: 2.32 (s, 3H, CH_3) and 3.79 (s, 8H, CH_2 of morpholino ring); mass spectrum, *m/z*: 117 (M^+). *Anal.* calcd. for $C_9H_{11}N_3O$: C 61.00, H 6.26, N 23.71; found: C 60.99, H 6.26, N 23.54.

(*b*) Ethyl (*E*)-2-cyano-3-(1-morpholino)crotonate (**7***b*) (50%), mp 95–96°C (prepared from ethyl cyanoacetate); ir: 2200 (C≡N) and 1675 (C=O) cm^{-1}; ^{1}H nmr ($CDCl_3$) δ: 1.23 (t, 3H, CH_2CH_3), 2.47 (br s, 3H, CH_3), 3.76 (br s, 8H), and 4.18 (q, 2H, CH_2CH_3); mass spectrum, *m/z*: 224 (M^+, 21), 152 (80), and 151 (100). *Anal.* calcd. for $C_{11}H_{16}N_2O_3$: C 58.91, H 7.19, N 12.49; found: C 58.80, H 7.14, N 12.50.

(*c*) (*E*)-2-Cyano-3-(1-morpholino)crotonamide (**7***c*) (36%), mp 160–162°C (prepared from cyanoacetamide); ir: 3365 and 3175 (N—H), 2180 (C≡N) and 1640 (C=O) cm^{-1}; ^{1}H nmr ($CDCl_3$) δ: 2.43 (br s, 3H, CH_3), 3.45–4.0 (m, 8H), and 5.75 (br s, 2H, NH_2); mass spectrum, *m/z*: 195 (M^+, 29), 178 (100), and 151 (43). *Anal.* calcd. for $C_9H_{13}N_3O_2$: C 55.37, H 6.71, N 21.52; found: C 55.54, H 6.67, N 21.15.

The following compounds were obtained as oils; yields (in parentheses) are for distilled compounds containing small amounts of retained acetomorpholide (**5**) and other minor products:

(*d*) Ethyl 2-ethoxycarbonyl-3-(1-morpholino)crotonate (**7***d*) (10%), bp 180–185°C/20 Torr (1 Torr = 133.3 Pa) (prepared from diethyl malonate); ir: 1755 sh, 1740, and 1655 (C=O) cm^{-1}; ^{1}H nmr ($CDCl_3$) δ: 1.28 (t, 6H, CH_2CH_3), 2.27 (s, 3H, CH_3), 3.36–3.75 (m, 8H), and 4.20 (q, 4H, CH_2CH_3); mass spectrum, *m/z*: 271 (M^+, 11), 198 (43), 152 (64), 150 (57), and 127 (100).

(*e*) (*E*)-4-(1-Morpholino)-3-pentenone (**7***e*) (33%), bp 135–136°C/20 Torr (lit. (19) mp 46–47°C) (prepared from acetylacetone); ir: 1640 (C=O) cm^{-1}; ^{1}H nmr ($CDCl_3$) δ: 2.09 (s, 3H, CH_3CO), 2.47 (s, 3H, CH_3), 3.30–3.81 (m, 8H), and 5.25 (s, 1H, HC=C); mass spectrum, *m/z*: 169 (M^+, 47), 154 (50), 152 (100), and 126 (75).

(*f*) Ethyl (*E*)-3-(1-morpholino)crotonate (**7***f*) (31%), bp 154–156°C/20 Torr (lit. (19) bp 124–128°C/1 Torr (prepared from ethyl acetoacetate); ir: 1690 (C=O) cm^{-1}; ^{1}H nmr ($CDCl_3$) δ: 1.22 (t, 3H, CH_2CH_3), 2.44 (s, 3H, CH_3), 3.57—3.75 (m, 8H), 4.06 (q, 2H, CH_2CH_3), and 4.75 (s, 1H, HC=C); mass spectrum, *m/z*: 199 (M^+, 33) and 126 (100).

Reaction of 3 with ethyl nitroacetate

Compound **3** and ethyl nitroacetate reacted exothermically in dry ether under the conditions of the foregoing general procedure (5 h reflux). Crystallization from light petroleum (bp 80–100°C) of the yellowish gummy solid resulting from trituration gave yellowish needles (420 mg, 20%) of the morpholine salt of ethyl nitroacetate, mp 125–127°C, identical with a sample prepared by mixing equivalent quantities of morpholine and ethyl nitroacetate in dry ether (colourless needles, mp 123–125°C); ir: 1675 (C=O), 1460 and 1280 (NO_2) cm^{-1}.

Reaction of 3 with cyanoacetamide in 2-propanol containing sodium 2-propoxide

Cyanoacetamide (769 mg, 9.15 mmol), dissolved in dry 2-propanol (15 mL), was added to a warm stirred solution of sodium 2-propoxide (from 421 mg sodium, 18.3 mmol) in 2-propanol (70 mL). After 15 min, a solution of **3** (1.814 g, 9.24 mmol) in 2-propanol (25 mL) was added and the stirred mixture was refluxed for 4 h. The solvent was then removed by evaporation *in vacuo* and the residue was triturated with dry light petroleum (bp 60–80°C). The resulting hygroscopic yellow solid (350 mg) was dissolved in water (7 mL) and the solution was acidified to pH 3 using concentrated hydrochloric acid. On standing overnight, the solution deposited colourless plates of (*Z*)-2-cyano-3-hydroxycrotonamide (**9**) (30 mg, 2.6%), mp 174–176°C (lit. (16) mp 171–173°C). Identity was established by correlation of ir and mass

Can. J. Chem. Downloaded from www.nrcresearchpress.com by 213.222.148.141 on 09/07/12
For personal use only.

Can. J. Chem. Downloaded from www.nrcresearchpress.com by 213.222.148.141 on 09/07/12
For personal use only.

spectra with published data and from the ^{1}H nmr spectrum; δ (DMSO-d_6): 2.20 (s, 3H, CH_3) and 3.43–3.56 (br, ca. 3H, exchangeable with D_2O) (lit. (16) δ (perdeuterioacetic acid): 1.85 (s, CH_3)).

*1,1-Dipiperidinoethene (**4**)*

This was prepared by the literature method (3) and was characterized both by reaction with methyl iodide to give *N,N'*-bispentamethylenepropionamidinium iodide, mp 158–160°C (from acetone – ethyl acetate) (lit. (5) mp 158–159°C), and by reaction with ethyl iodide to give *N,N'*-bispentamethylenebutyramidinium iodide, mp 213–215°C (from acetone – ethyl acetate) (lit. (5) mp 212–212.5°C). (**Note**: exclusion of moisture is necessary to prevent contamination of these derivatives by products from hydrolysis reactions.) Compound **4** was freshly prepared and fractionated prior to use in the following reactions.

*2,4-Dinitrophenylation of **4***

A freshly prepared solution of **4** (2.26 g, 11.8 mmol) in dry dichloromethane (30 mL) was added under nitrogen to a stirred, freshly prepared solution of 1-chloro-2,4-dinitrobenzene (2.35 g, 11.6 mmol) and triethylamine (1.35 g, 13.3 mmol) in dichloromethane (40 mL). The solution immediately became dark red-brown in colour. After 24 h, the solvent was evaporated *in vacuo* and the residue was then stirred with 5% hydrochloric acid for 3 h. Extraction with dichloromethane, followed by washing, drying, and evaporation of the organic extract gave a dark brown gum. Several crystallizations from benzene gave an analytically pure sample (190 mg, 4.6%) of 1-(2,4-dinitrophenyl)-2,2-di(1-piperidino)ethene (**10**) as dark brown crystals, mp 192–194°C; ir: 1515 and 1320 (NO_2) cm^{-1}; ^{1}H nmr ($CDCl_3$) δ: 1.66 (br s, 12H), 3.21 (br s, 8H), 5.52 (s, 1H, HC=C), 6.65 (d, 1H, arom H-6; J = 9.5 Hz), 7.99 (dd, 1H, arom H-5; J = 9.5 and 2.0 Hz), and 8.84 (d, 1H, arom H-3; J = 2.0 Hz); mass spectrum, *m/z*: 360 (M^+). *Anal.* calcd. for $C_{18}H_{24}N_4O_4$: C 59.99, H 6.71, N 15.55; found: C 60.20, H 6.76, N 15.56.

*Reaction of **4** with carbon acids: General procedure*

The procedure followed was the same as that described for corresponding reactions of **3**; the desired product was normally accompanied by piperidine and **6**.

The following compounds were obtained as solids (from the carbon acids noted in parentheses):

(*a*) Ethyl (*E*)-2-cyano-3-(1-piperidino)crotonate (**8***b*) (22%), mp 75–76°C (prepared from ethyl cyanoacetate); ir: 2195 (C≡N) and 1680 (C=O) cm^{-1}; ^{1}H nmr ($CDCl_3$) δ: 1.30 (t, 3H, CH_2CH_3), 1.72 (br s, 6H, 3 × CH_2 of piperidino ring), 2.47 (s, 3H, CH_3), 3.55 (br s, 4H, 2 × CH_2 of piperidino ring), and 4.17 (q, 2H, CH_2CH_3); mass spectrum, *m/z*: 222 (M^+, 10) and 149 (100). *Anal.* calcd. for $C_{12}H_{18}N_2O_2$: C 64.84, H 8.16, N 12.60; found: C 64.62, H 8.10, N 12.66.

(*b*) (*E*)-4-(1-Piperidino)-3-pentenone (**8***e*) (28%), mp 45–47°C (lit. (19) mp 47–48°C) (prepared from acetylacetone); ir: 1650 (C=O) cm^{-1}; ^{1}H nmr ($CDCl_3$) δ: 1.62 (m, 6H), 2.07 (s, 3H, CH_3CO), 2.51 (s, 3H, CH_3), 3.36 (m, 4H), and 5.22 (s, 1H, HC=C); mass spectrum, *m/z*: 167 (M^+, 36), 152 (60), 150 (100), and 124 (89). *Anal.* calcd. for $C_{10}H_{17}NO$: C 71.81, H 10.24, N 8.37; found: C 71.45, H 10.17, N 8.21.

(*c*) (*E*)-1-Nitro-2-(1-piperidino)propene (**8***g*) (43%), mp 86–87°C (lit. (17) mp 84°C) (prepared from nitromethane); ^{1}H nmr ($CDCl_3$) δ: 1.69 (m, 6H), 2.60 (s, 3H, CH_3), 3.43 (m, 4H), and 6.91 (s, 1H, HC=C); mass spectrum, *m/z*: 170 (M^+, 37) and 124 (100). *Anal.* calcd. for $C_8H_{14}N_2O_2$: C 56.45, H 8.29, N 16.46; found: C 56.09, H 8.40, N 16.03.

The following compounds were obtained as oils; yields (in parentheses) are for chromatographed or distilled compounds containing small amounts of acetopiperidide (**6**) and other minor products:

(*d*) 2-Cyano-3-(1-piperidino)crotononitrile (**8***a*) (36%) (prepared from malononitrile); ir: 2210 and 2190 (C≡N) cm^{-1}; ^{1}H nmr ($CDCl_3$) δ: 1.75 (m, 6H), 2.29 (s, 3H, CH_3), and 3.72 (m, 4H); mass spectrum, *m/z*: 175 (M^+).

(*e*) Ethyl (*E*)-3-(1-piperidino)crotonate (**8***f*) (25%), bp 112–114°C/1 Torr (lit. (19) bp 122°C/0.6 Torr) (prepared from ethyl acetoacetate); ir: 1690 (C=O) cm^{-1}; ^{1}H nmr ($CDCl_3$) δ: 1.23 (t, 3H, CH_2CH_3), 1.59 (m, 6H), 2.42 (s, 3H, CH_3), 3.27 (m, 4H), 4.06 (q, 2H, CH_2CH_3), and 4.75 (s, 1H, HC=C); mass spectrum, *m/z*: 197 (M^+, 17) and 124 (100).

*Reaction of **4** with cyanoacetamide in ethanol containing sodium ethoxide*

Cyanoacetamide (635 mg, 7.55 mmol) was dissolved in a warm stirred solution of sodium ethoxide (from 450 mg sodium, 19.6 mmol) in absolute ethanol (75 mL). A solution of **4** (1.468 g, 7.63 mol) in ethanol (15 mL) was then added and the mixture was refluxed for 3 h. When cool, the mixture was filtered to remove a small amount of yellow solid and the filtrate was then evaporated *in vacuo*. The residue was dissolved in water (10 mL) and the solution was acidified to pH 3 using concentrated hydrochloric acid. On standing overnight the solution deposited a light brown solid (350 mg, 48% based on **4**). Crystallization from aqueous ethanol gave 2-amino-5-cyano-6-hydroxy-4-methylnicotinamide (**11**), mp 309–310°C (dec.); ir: 2220 (C≡N), 1660 and 1640 (C=O) cm^{-1}; ^{1}H nmr (D_2O/DMSO-d_6) δ: 2.32 (s, CH_3); mass spectrum, *m/z*: 192 (M^+, 20), 175 (55), 174 (50), 149 (45), 147 (20), 131 (15), 119 (20), 106 (40), 105 (50), 93 (23), and 69 (100). *Anal.* calcd. for $C_8H_8N_4O_2$: C 50.00, H 4.20, N 29.15; found: C 49.64, H 4.17, N 28.53. *Mol. Wt.* calcd. for $C_8H_8N_4O_2$: 192.0647; found (ms): 192.0586.

Acknowledgements

We thank Mrs. Laurie Raimondo for technical help and the Natural Sciences and Engineering Research Council of Canada for partial financial support.

1. (*a*) H. Mastalerz, T. Mohammad, and M. S. Gibson. Can. J. Chem. **65**, 2713 (1987); (*b*) H. Mastalerz and M. S. Gibson. J. Chem. Soc. Perkin Trans. I, 245 (1983), and references cited.
2. (*a*) T. L. Gilchrist. Heterocyclic chemistry. Pitman, London. 1985. pp. 267, 282; (*b*) J. W. Bunting. *In* Advances in heterocyclic chemistry. Vol. 25. *Edited by* A. Katritzky and A. J. Boulton. Academic Press, Toronto. 1979. p. 47; (*c*) M. Coenen. Angew. Chem. **61**, 11 (1949).
3. H. Bohme and F. Soldan. Chem. Ber. **94**, 3109 (1961); H. Baganz and L. Domaschke. Chem. Ber. **95**, 2095 (1962).
4. J. S. Hartman and E. C. Kelusky. Can. J. Chem. **59**, 1284 (1981).
5. D. H. Clemens, A. J. Bell, and J. L. O'Brien. J. Org. Chem. **29**, 2932 (1964); C. F. Hobbs and H. Weingarten. J. Org. Chem. **39**, 918 (1974).
6. G. Opitz and F. Zimmerman. Chem. Ber. **97**, 1266 (1964); R. H. Hasek, P. G. Gott, and J. C. Martin. J. Org. Chem. **29**, 2514 (1964); A. Armati, P. De Ruggieri, E. Rossi, and R. Stradi. Synthesis, 573 (1986).
7. R. H. Hasek, P. G. Gott, R. H. Meen, and J. C. Martin. J. Org. Chem. **28**, 2496 (1963); W. E. Truce and P. N. Son. J. Org. Chem. **30**, 71 (1965); G. Opitz and H. Schempp. Liebigs Ann. Chem. **684**, 103 (1965); W. E. Truce, D. J. Abraham, and P. Son. J. Org. Chem. **32**, 990 (1967).
8. D. H. R. Barton, G. Hewitt, and P. G. Sammes. J. Chem. Soc. C, 16 (1969).
9. (*a*) J. Ficini, J. Besseyre, J. D'Angelo, and C. Barbara. C. R. Seances Acad. Sci. Ser. C: **271**, 468 (1970); J. H. Hall and M. Wojciechowska. J. Org. Chem. **43**, 3348 (1978); G. Tacconi, M. Leoni, P. Righetti, G. Desimoni, R. Oberti, and F. Conim. J. Chem. Soc. Perkin Trans. 1, 2687 (1979); R. A. Jeffreys and S. M. Mellows. U.S. Patent No. 3, 672, 905 (1972); Chem. Abstr. **77**, 116067 (1972); (*b*) M. von Strandtmann, M. P. Cohen, and J. Shavel. U.S. Patent No. 3, 752, 830 (1973); Chem. Abstr. **79**, 92193 (1973).
10. H. Schubert, I. Bart, and M. Regitz. Synthesis, 661 (1983).

11. S. MINAMI and J. MATSUMOTO. Jap. Patent No. 73, 34, 158 (1973); Chem. Abstr. **79**, 32028 (1973); D. POCAR, L. H. ROSSI, and R. STRADI. Synthesis, 684 (1976).
12. V. N. CHARUSHIN and H. C. VAN DER PLAS. Tetrahedron Lett. 3965 (1982); J. Org. Chem. **48**, 2667 (1983), and references cited.
13. K. C. BRANNOCK, R. D. BURPITT, and J. G. THWEATT. J. Org. Chem. **28**, 1697 (1963).
14. H. J. HALL and M. WOJCIECHOWSKA. J. Org. Chem. **43**, 4869 (1978).
15. K. K. BABIEVSKY and V. M. BELIKOV. Synth. Commun. **7**, 269 (1977).
16. R. C. ANDERSON and Y. Y. HSIAO. J. Heterocycl. Chem. **12**, 883 (1976).
17. C. D. HURD and L. T. SHERWOOD. J. Org. Chem. **13**, 471 (1948); S. RAJAPPA. Tetrahedron, **37**, 1453 (1981); M. FAULQUES, L. RENE, and R. ROYER. Synthesis, 260 (1982).
18. J.-C. CHALCHAT, F. THÉRON, and R. VESSIÈRE. Bull. Soc. Chim. Fr. 711 (1970).
19. P. W. HICKMOTT and G. SHEPPARD. J. Chem. Soc. Perkin Trans. 1, 1038 (1972).
20. G. V. BOYD and S. R. DANDO. J. Chem. Soc. C, 225 (1971).

Can. J. Chem. Downloaded from www.nrcresearchpress.com by 213.222.148.141 on 09/07/12
For personal use only.

Enzymes in organic synthesis. 40.[1] Evaluation of the enantioselectivity of the pig liver esterase catalyzed hydrolyses of racemic piperidine carboxylic acid esters

ERIC J. TOONE AND J. BRYAN JONES
Department of Chemistry, University of Toronto, Toronto, Ont., Canada M5S 1A1

Received April 29, 1987

ERIC J. TOONE and J. BRYAN JONES. Can. J. Chem. **65**, 2722 (1987).

Pig liver esterase (PLE) catalyzed hydrolysis of racemic piperidine esters proceeds enantioselectively to give product acids and recovered esters in 0–47% enantiomeric excess.

ERIC J. TOONE et J. BRYAN JONES. Can. J. Chem. **65**, 2722 (1987).

L'hydrolyse, catalysée par l'EFC (estérase du foie de cochon), d'esters racémiques de la pipéridine se produit d'une façon énantiosélective pour conduire à des produits acides et à des esters récupérés dont l'excès énantiomérique varie de 0 à 47%.

[Traduit par la revue]

Can. J. Chem. Downloaded from www.nrcresearchpress.com by 213.222.148.141 on 09/07/12
For personal use only.

Introduction

Enzymes are now established as important tools in the field of asymmetric synthesis (2), with the resolution of racemates being one area in particular where the utility of enzymes has been traditionally recognized (3). While the resolution approach to the preparation of pure stereoisomers suffers from the disadvantage that only half of the starting material is transformed into the desired product, it is often possible to recycle the unwanted enantiomer by epimerization to the racemic form. Furthermore, in many cases a racemic starting material can be very cheap. Resolution can then offer the most cost efficient route to enantiomerically pure chiral synthons (4).

Esterases are a very attractive class of enzymes for use in resolution and other aspects of organic synthesis since they do not require expensive cofactors. One of the most promising of the esterases is pig liver esterase (PLE, E.C. 3.1.1.1). PLE is a commercially available enzyme that catalyses the hydrolysis of a broad range of ester substrates. While several reports of the use of PLE in the asymmetric hydrolysis of symmetrical diesters have appeared (5), there have been relatively few examples of resolution of racemates using PLE (6).

The enzymatic production of enantiomerically pure amino acids for use as chirons in organic synthesis is of considerable interest (7). Enzyme-catalyzed methods for the production of pure enantiomers of natural amino acids are well documented (8), but so far the use of enzymes for the resolution of racemates of unnatural amino acids of chiron value has not been widely explored. We have now begun to investigate the utility of enzymes in the resolution of unnatural amino acids. In this paper, we report on the potential of PLE for the resolution of some unnatural amino acid derivatives of the N-protected monosubstituted piperidine types represented by structures (+/−) **1–6**.

Results

The N-acylated piperidine substrates **1–6** were prepared as outlined in Scheme 1.

Each of compounds **1–6** was a substrate for PLE. Despite the fact that (+/−)-**1** and (+/−)-**2** were hydrolyzed much more slowly than the reference substrate ethyl butyrate (Table 1), all were sufficiently active to be considered good candidates for preparative scale resolution.

The resolutions were evaluated for each of compounds **1–6** on a 1–1.5 g scale at pH 7. The results are summarized in Scheme 2.

[1]For Part 39 see ref. 1.

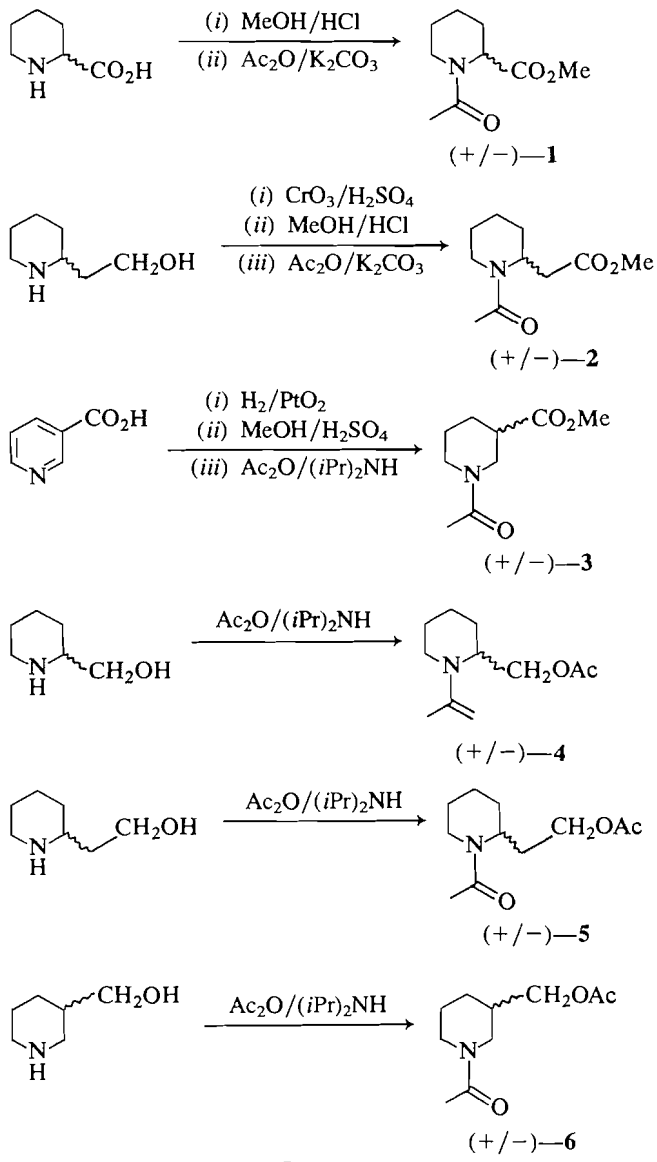

SCHEME 1

For the product acids (−)-**7**, (−)-**8**, and (+/−)-**9**, the enantiomeric excess (ee) values were determined by 200-MHz ^{1}H nmr examination of the diastereomeric salts formed between product acids and (−)-*S*-phenethylamine (9). For substrates (+/−) **4–6** the product alcohols **10–12** were converted by Jones oxidation to the corresponding carboxylic acids, **7–9**,

Can. J. Chem. Downloaded from www.nrcresearchpress.com by 213.222.148.141 on 09/07/12
For personal use only.

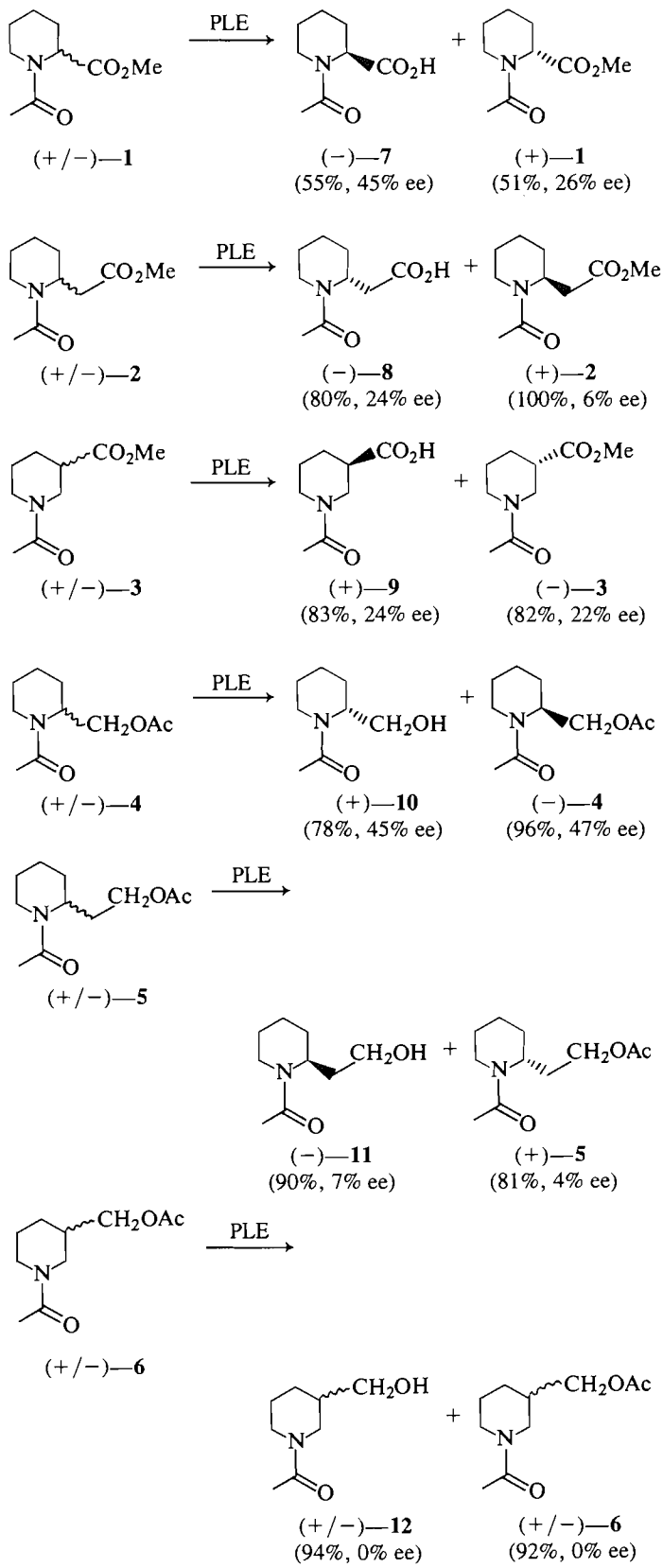

SCHEME 2

and their (−)-*S*-phenethyl amine salts again examined. The enantiomeric excesses of the unhydrolyzed acetates (−)-**4** and (+)-**5** were determined similarly, following their conversion to their alcohols (−)-**10** and (+)-**11** by base hydrolysis, and then oxidation to the corresponding acids **7** and **8**. The enantiomeric excesses of unhydrolyzed esters **1**–**3** were determined by esterification of the optically active acids **7**–**9** of known absolute configuration with diazomethane, and comparison of optical rotations.

TABLE 1. Relative rates of PLE hydrolysis[a]

Substrate	Relative rate
Ethyl butyrate	100
(+/−)-**1**	<0.01
(+/−)-**2**	<0.01
(+/−)-**3**	14
(+/−)-**4**	1
(+/−)-**5**	3
(+/−)-**6**	1

[a]Determined at pH 7.0, 25°C, in distilled water.

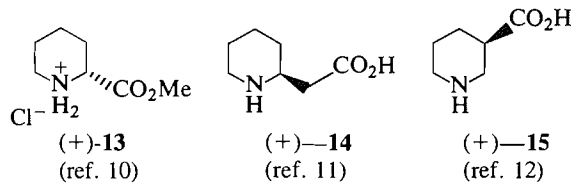

FIG. 1

The absolute configurations were all assigned by optical rotation correlations with known compounds as follows: (−)-**7**, (+)-**1**, (+)-**10**, and (−)-**4** with (+)-**13** (10); (−)-**8**, (+)-**2**, (−)-**11**, and (+)-**5** with (+)-**14** (11); and (+)-**9** and (−)-**3** with (+)-**15** (12).

Discussion

The preparations of substrates were routine, as were their preparative-scale PLE-catalyzed hydrolyses. Hydrolyses were stopped after 50% conversion. The hydrolyses were carried out at pH 7.0 to avoid the possibility of competing chemical hydrolysis or epimerization under the higher pH conditions that have been used in other applications (13). This would have been a significant problem for substrates (+/−)-**1** and (+/−)-**2**, due to the long reaction time. In fact, even at pH 7.0, it appears that some epimerization of optically active ester took place during the relatively long reaction times, as indicated by the fact that for (+/−)-**1** and (+/−)-**2** the enantiomeric excesses of the recovered esters are substantially lower than those of the product acids. In these cases, epimerization of the product acids would be virtually nonexistent since they are present in solution as their carboxylate salts.

The piperidine esters **1**–**6** represent a new class of PLE substrates whose structures are of clear synthetic value, for example as chirons for alkaloids such as coniine and sedrine. While the enantiomeric excess levels observed in the initial study are below the levels required for asymmetric synthesis, they demonstrate that PLE does possess significant enantiomeric stereoselectivity towards each of **1**–**6**. It is possible to increase the enantiomeric excess values of PLE-catalyzed reactions to acceptable asymmetric synthetic levels by manipulation of reaction conditions, particularly by varying organic solvent composition and temperature (14), and we are now exploring this aspect. In addition, in resolutions of this nature, it is always possible to reesterify the product acids and subject optically enriched material to a second enzymic hydrolysis (15). This approach will also be followed if the reaction conditions' improvement of ee is not satisfactory.

Can. J. Chem. Downloaded from www.nrcresearchpress.com by 213.222.148.141 on 09/07/12
For personal use only.

Experimental

All melting points were taken on a Electrothermal capillary melting point apparatus, and are uncorrected. The ir spectra were recorded as films for liquids and KBr discs for solids on a Nicolet 5DX FTIR spectrophotometer. All routine ^{1}H nmr spectra were recorded in $CDCl_3$ on a Varian T60 instrument. High field ^{1}H nmr spectra were recorded on a Varian XL200 instrument. Optical rotations were measured in a Perkin–Elmer 141 polarimeter in a thermostated cell. Elemental analyses were carried out by Galbraith Laboratories. Analytical glc work was carried out on a Varian Series 2700 gas chromatograph. The pH stat used was a Radiometer REA 270 pH stat, equipped with a TTT80 titrator and an ABU 80 autoburette. Pig liver esterase (EC 3.1.1.1) was obtained from Sigma Chemical Company.

Synthesis of substrates

N-*Acetyl-2-carbomethoxypiperidine (**1**)*

2-Piperidinecarboxylic acid (Aldrich, 1.5 g, 11.5 mmol) in HCl-saturated methanol (100 mL) was stirred at 21°C for 24 h. The methanol was removed by rotary evaporation and the yellow solid recrystallized once from methanol – ethyl acetate (1:1) to yield (+/−)-2-carbomethoxypiperidine hydrochloride (1.62 g, 78% yield), mp 212°C (lit. (16) mp 213–214°C); ir ν: 1748 cm^{-1}; ^{1}H nmr δ: 1.9–2.1 (m, 6H), 3.1–3.3 (m, 3H), 3.95 (s, 3H), 5.1 (br s, 1H) ppm. To this ester (0.75 g, 4.2 mmol) in ethyl acetate (15 mL) was added K_2CO_3 (2.1 g, 21 mmol) in water (5 mL), and acetic anhydride (1.1 g, 10 mmol), and the mixture was stirred for 24 h at 21°C. The layers were separated and the aqueous phase extracted with ethyl acetate (2 × 25 mL). The combined organic phases were washed with 1 M hydrochloric acid (15 mL), 5% aqueous Na_2CO_3 (15 mL), and saturated aqueous NaCl (15 mL), dried ($MgSO_4$), and concentrated *in vacuo* on a rotary evaporator. The residual oil was Kugelrohr distilled (bp 80°C/0.1 Torr; 1 Torr = 133.3 Pa) to yield *N*-acetyl-2-carbomethoxypiperidine **1** (0.44 g, 56% yield); ir ν: 1748, 1649 cm^{-1}; ^{1}H nmr δ: 1.5–1.9 (m, 6H), 2.2 (s, 3H), 3.2–3.5 (m, 2H), 3.8 (s, 3H), 5.4 (br, 1H) ppm. *Anal.* calcd. for $C_9H_{15}NO_3$: C 58.37, H 8.11, N 7.46; found: C 58.16, H 8.18, N 7.46%.

N-*Acetyl-2-carbomethoxymethylpiperidine (**2**)*

2-Carboxymethylpiperidine was prepared by the method of Marshall *et al.* (17), and esterified as above to give 2-carbomethoxymethylpiperidine hydrochloride, in 83% yield, mp 218–221°C (lit. (17) mp 218–220°C); ir ν: 1741 cm^{-1}; ^{1}H nmr δ: 1.7–2.1 (m, 6H), 2.9–3.1 (m, 5H), 3.7 (s, 3H) ppm. This ester (0.42 g, 2.2 mmol) was acetylated with acetic anhydride (0.45 g, 4.4 mmol) and K_2CO_3 (1.2 g, 8.8 mmol) as above to yield *N*-acetyl-2-carbomethoxymethylpiperidine **2** (0.3 g, 72% yield), bp 85°C/0.1 Torr; ir ν: 1737, 1644 cm^{-1}; ^{1}H nmr δ: 1.6–2.0 (m, 6H), 2.1 (s, 3H), 2.7–2.9 (m, 3H), 4.8–5.1 (m, 2H) ppm. *Anal.* calcd. for $C_{10}H_{17}NO_3$: C 60.28, H 8.60, N 7.03; found: C 60.31, H 8.66, N 6.99%.

N-*Acetyl-3-carboxymethylpiperidine (**3**)*

To nicotinic acid (10 g, 80 mmol) in water (100 mL) was added 6 M hydrochloric acid (13.5 mL, 6 M, 1 equiv.). PtO_2 (200 mg) was added and the mixture was stirred under hydrogen (50 psi; 1 psi = 6.9 kPa). After 24 h (3 equiv. H_2 uptake), the water was removed by rotary evaporation, and the residual solid recrystallized from absolute EtOH to give 3-carboxypiperidine hydrochloride (12.7 g, 95% yield), mp 239–240°C (dec.) (lit. (18) mp 240–242°C); ir ν: 1625 cm^{-1}; ^{1}H nmr δ: 1.8–2.1 (m, 6H), 3.2–3.4 (m, 5H), 9.2 (s, 1H) ppm. This ester (1.0 g, 6 mmol) was dissolved in dry MeOH (50 mL) containing 2 drops concentrated sulfuric acid and the mixture was stirred for 24 h at 20°C. The methanol was removed by rotary evaporation and the residual oil taken up in THF (50 mL) and cooled to 0°C. Acetic anhydride (6.2 g, 60 mmol), diisopropyl amine (4.0 g, 40 mmol), and catalytic dimethylaminopyridine (DMAP) were then added and the solution warmed to 20°C. After stirring for 24 h the solvent was removed and the desired product was obtained in pure form by Kugelrohr distillation (bp 85°C/0.25 Torr) (0.67 g, 58% yield); ir ν: 1733, 1648 cm^{-1}; ^{1}H nmr δ: 1.8–2.1 (m, 4H), 2.2 (s, 3H), 2.8–3.6 (m, 4H), 3.8 (s, 3H) ppm. *Anal.* calcd. for $C_9H_{15}NO_3$: C 58.37, H 8.11, N 7.46; found: C 58.37, H 8.08, N 7.50%.

N-*Acetyl-2-acetoxymethylpiperidine (**4**)*

2-Hydroxymethylpiperidine (1.5 g, 13 mmol) was dissolved in dry diethyl ether (50 mL). To this was added dropwise at 0°C acetic anhydride (16.2 g, 130 mmol), diisopropyl amine (3.95 g, 39 mmol), and catalytic DMAP, and the resulting solution was stirred at 20°C for 2 days. The solvent was removed by rotary evaporation, and the excess acetic anhydride and diisopropyl amine by Kugelrohr distillation (40°C/0.25 Torr). The residual oil was taken up in ethyl acetate (50 mL) and washed with 1 M hydrochloric acid (2 × 20 mL), followed by saturated aqueous $NaHCO_3$ (2 × 20 mL) and saturated aqueous NaCl (2 × 20 mL). The organic phase was dried ($MgSO_4$) and concentrated *in vacuo* on a rotary evaporator. The residual oil was purified by flash chromatography on silica (ether–methanol (5:1) elution) to give *N*-acetyl-2-acetoxymethylpiperidine (**4**, 1.05 g, 38% yield); ir ν: 1742, 1644 cm^{-1}; ^{1}H nmr δ: 1.7 (m, 6H), 2.15 (s, 3H), 2.2 (s, 3H), 2.45 (m, 2H), 4.1–4.4 (m, 3H) ppm. *Anal.* calcd. for $C_{10}H_{17}NO_3$: C 60.35, H 8.54, N 7.01; found: C 60.29, H 8.60, N 7.11%.

N-*Acetyl-2-acetoxyethylpiperidine (**5**)*

This was prepared, as was **4** above, from 2-hydroxyethylpiperidine (2 g, 17 mmol), acetic anhydride (15.8 g, 155 mmol), and diisopropyl amine (4.56 g, 45 mmol) with ether–methanol (4:1) elution from silica, giving pure *N*-acetyl-2-acetoxyethylpiperidine (**5**, 1.4 g, 40% yield); ir ν: 1736, 1618 cm^{-1}; ^{1}H nmr δ: 1.7 (br s, 6H), 2.15 (s, 3H), 2.20 (s, 3H) 2.3–2.6 (m, 2H), 3.6 (br s, 2H), 3.8–4.2 (m, 3H) ppm. *Anal.* calcd. for $C_{11}H_{19}NO_3$: C 61.95, H 8.98, N 6.57; found: C 62.01, H 8.88, N 6.49%.

N-*Acetyl-3-acetoxymethylpiperidine (**6**)*

This was prepared, as was **4** above, from 3-hydroxymethylpiperidine (2 g, 17 mmol), acetic anhydride (21.6 g, 170 mmol), and diisopropyl amine (5.3 g, 52 mmol), to give *N*-acetyl-3-acetoxymethylpiperidine (**6**, 1.5 g, 38% yield); ir ν: 1742, 1618 cm^{-1}; ^{1}H nmr δ: 1.2–1.8 (m, 5H), 2.05 (s, 6H), 2.2–2.5 (m, 2H), 3.6 (m 1H), 3.9 (m, 2H), 4.2–4.4 (m, 1H) ppm. *Anal.* calcd. for $C_{10}H_{17}NO_3$: C 60.35, H 8.54, N 7.01; found: C 59.96, H 8.44, N 6.92.

*Preparative-scale PLE-catalysed hydrolyses of racemic esters **1**–**6***

(a) Of N-*acetyl-2-carbomethoxypiperidine ((+/−)-**1**)*

The ester (+/−)-**1** (1 g, 5.4 mmol) was dissolved in distilled water (75 mL), pH was adjusted to 7.0 with 0.25 M NaOH, and PLE (3600 units) was added. The pH was held constant at 7.0 by addition of 0.25 M aqueous NaOH from a pH stat. When one-half equivalent of base had been added (10 days) there was no further uptake of base, and the reaction was stopped by saturating the solution with NaCl. The pH was readjusted to 7.0 and the solution extracted with ethyl acetate (3 × 50 mL). The combined organic phase was dried ($MgSO_4$) and concentrated *in vacuo* on a rotary evaporator to give (2*R*)-*N*-acetyl-2-carbomethoxypiperidine ((+)-**1**, 260 mg, 51% yield, 26% ee), $[\alpha]_D^{25}$ +19.4° (*c* 5.44, $CHCl_3$); spectral characteristics were identical to those of racemic **1** above. The aqueous solution was then acidified to pH 2.0 with 6 M hydrochloric acid and reextracted with ethyl acetate (3 × 50 mL). The combined organic phase was dried ($MgSO_4$) and concentrated *in vacuo* on a rotary evaporator to give (2*S*)-*N*-acetyl-2-piperidinecarboxylic acid ((−)-**7**, 259 mg, 55% yield, 45% ee) as a slowly crystallizing oil, mp 140–141°C; $[\alpha]_D^{25}$ −7.4° (*c* 10, $CHCl_3$); ir ν: 1728, 1608 cm^{-1}; ^{1}H nmr δ: 1.6–2.0 (m, 6H), 2.25 (s, 3H), 3.4–3.8 (m, 2H), 5.5 (m, 1H), 8.8 (s, 1H) ppm.

(b) Of N-*acetyl-2-carbomethoxymethylpiperidine ((+/−)-**2**)*

The above procedure was followed using (+/−)-**2** (1 g, 5 mmol) in water (25 mL) and PLE (1774 units) for 2.5 days, yielding (2*S*)-*N*-acetyl-2-carbomethoxymethylpiperidine ((+)-**2**, 502 mg, 100% yield, 6% ee); $[\alpha]_D^{25}$ +1.0 (*c* 11.6, $CHCl_3$) (spectra identical to racemic **2** above) and (2*R*)-*N*-acetyl-2-carboxymethylpiperidine ((−)-**8**, 372 mg, 80% yield, 24% ee), mp 91–93°C; $[\alpha]_D^{25}$ −1.7° (*c* 7.2, $CHCl_3$); ir ν: 1722, 1588 cm^{-1}; ^{1}H nmr δ: 1.5–1.7 (m, 6H), 2.1 (br s, 2H), 2.2 (s, 3H), 2.4–2.8 (m, 2H), 4.6 (br, 1H), 10.5 (s, 1H) ppm.

(c) Of N-acetyl-3-carboxymethylpiperidine ((+/−)-**3**)

The above procedure was followed using (+/−)-**3** (1.0 g, 5.3 mmol) in water (25 mL) and PLE (260 units) for 2.6 h, yielding (3*R*)-*N*-acetyl-

Can. J. Chem. Downloaded from www.nrcresearchpress.com by 213.222.148.141 on 09/07/12
For personal use only.

3-carbomethyoxypiperidine ((−)-**3**, 411 mg, 82% yield, 22% ee); $[\alpha]_D^{25}$ −14.6° (*c* 8.2, $CHCl_3$) (spectra identical to racemic ester **3** above), and (3*S*)-*N*-acetyl-3-piperidinecarboxylic acid ((+)-**9**, 385 mg, 83% yield, 24% ee), mp 114–116; $[\alpha]_D^{25}$ +11.6° (*c* 4.1, $CHCl_3$); ir *ν*: 1604, 1703 cm^{-1}; ^1H nmr δ: 1.6–1.8 (m, 4H), 2.1 (s, 3H), 2.4–2.8 (m, 2H), 3.6–3.8 (m, 2H), 10.7 (s, 1H) ppm.

(d) Of N-acetyl-2-acetoxymethylpiperidine ((+/−)-*4*)

(+/−)-**4** (1.0 g, 5 mmol) was dissolved in distilled water (20 mL). The pH was adjusted to 7.0 with 0.25 M NaOH, and PLE (523 units) was added. The pH was kept constant at 7.0 with 0.25 M NaOH, using a pH stat. After addition of one-half equivalent of base (10.5 h), the reaction was stopped by freezing, followed by lyophilization. The residual product was taken up in ethyl acetate (2 × 50 mL), filtered through Celite, dried ($MgSO_4$), and concentrated *in vacuo* on a rotary evaporator. The remaining oil was separated using a Chromatatron (silica, ether–acetone (3:2) development). The high R_f fraction was identified as (2*R*)-*N*-acetyl-2-acetoxymethylpiperidine ((−)-**4**, 494 mg, 96% yield, 47% ee); $[\alpha]_D^{25}$ −18.3 (*c* 9.6, $CHCl_3$) (spectra identical to racemic acetate **4** above), The low R_f fraction was identified as (2*S*)-*N*-acetyl-2-hydroxymethylpiperidine ((+)-**10**, 326 mg, 78% yield, 45% ee); $[\alpha]_D^{25}$ +20.5 (*c* 4.0, $CHCl_3$); ir *ν*: 3400 (br), 1618 cm^{-1}; ^1H nmr δ: 1.4–1.8 (m, 6H), 2.2 (s, 3H), 3.6–3.8 (m, 3H), 4.0–4.3 (m, 2H), 4.8 (br, 1H) ppm.

(e) Of N-acetyl-2-acetoxyethylpiperidine ((+/−)-*5*)

The above procedure was followed using (+/−)-**5** (1.0 g, 4.7 mmol) in water (20 mL) with PLE (300 units) for 4 h, followed by chromatography on silica (ether–THF (4:1)), yielding (2*R*)-*N*-acetyl-2-acetoxyethylpiperidine ((+)-**5**, 507 mg, 100% yield, 4% ee); $[\alpha]_D^{25}$ +2.6° (*c* 14, $CHCl_3$) (spectra identical to racemic acetate **5** above), and (2*S*)-*N*-acetyl-2-hydroxyethylpiperidine ((−)-**11**, 383 mg, 90% yield, 7% ee); $[\alpha]_D^{25}$ −1.7° (*c* 16, $CHCl_3$); ir *ν*: 3400 (br), 1625 cm^{-1}; ^1H nmr δ: 1.4–1.6 (m, 6H), 2.1 (s, 3H), 2.8–3.0 (m, 2H), 3.4–3.6 (m, 2H), 3.8–4.2 (m, 2H), 4.5–5.0 (m, 2H) ppm.

(f) Of N-acetyl-3-acetoxymethylpiperidine ((+/−)-*6*)

The above procedure was followed using (+/−)-**6** (1.0 g, 5 mmol) in water (30 mL) with PLE (110 units) for 12 h, followed by chromatography on silica (ethyl acetate – methanol (98:2) elution) yielding racemic *N*-acetyl-3-acetoxymethylpiperidine ((+/−)-**6**, 496 mg, 94% yield); $[\alpha]_D^{25}$ 0.0 (*c* 9.4, $CHCl_3$) (spectra identical to racemic acetate **6** above), and racemic *N*-acetyl-3-hydroxymethylpiperidine ((+/−)-**12**, 384 mg, 92% yield); $[\alpha]_D^{25}$ 0.0° (*c* 12.0, $CHCl_3$); ir *ν*: 3370 (br), 1622 cm^{-1}; ^1H nmr δ: 1.2–1.8 (m, 5H), 2.1 (s, 3H), 2.6–3.0 (m, 1H), 3.3–3.6 (m, 3H), 3.8–4.5 (m, 3H) ppm.

Enantiomeric excess determinations

(A) By nuclear magnetic resonance

The method of Schneider *et al.* (9) was employed. The general method was as follows: to approximately 20 mg optically active acid was added 1.5 equivalents of (−)-(*S*)-phenethylamine. The resulting oil was dissolved in $CDCl_3$ and the proton spectrum examined at 200 MHz. In all cases, the separation of the diastereotopic *N*-acetate methyl peaks was sufficient to permit the ee values to be determined. The racemic acids (+/−) **1**–**3**, were used as standards.

This technique was applied to the product acids (−)-**7**, (−)-**8**, and (+)-**9** directly, and to alcohol products (+)-**10** and (−)-**11** following oxidation.

*Oxidation of optically active alcohols **10** and **11***

1. Of N-*acetyl-2-hydroxymethylpiperidine ((+)-**10**)*

N-Acetyl-2-hydroxymethylpiperidine ((+)-**10**, 100 mg, 0.6 mmol) from PLE hydrolysis was dissolved in 1 M aqueous phosphate buffer (20 mL, pH 6.5). To this was added $KMnO_4$ (0.7 g, 3 mmol), and the mixture stirred at 70°C for 8 h. The mixture was cooled to 20°C and $Na_2S_2O_5$ added until the purple colour was destroyed. The resulting mixture was filtered through Celite, and the filtrate saturated with NaCl. The pH was readjusted to 6.5 and the solution extracted with dichloromethane (2 × 25 mL). The aqueous phase was acidified to pH 2.0 with 6 M hydrochloric acid and reextracted with dichloromethane (3 × 25 mL). The pH 2.0 extract was dried ($MgSO_4$) and concentrated *in vacuo* on a rotary evaporator to give (2*S*)-*N*-acetyl-2-piperidinecarboxylic acid ((−)-**7**, 22 mg, 21% yield); $[\alpha]_D^{25}$ −7.5° (*c* 2.0, $CHCl_3$). Spectra were identical to **7** above.

2. Of N-*acetyl-2-hydroxyethylpiperidine ((+)-**11**)*

The above procedure was followed with *N*-acetyl-2-hydroxyethylpiperidine ((+)-**11**, 100 mg, 0.5 mmol) and $KMnO_4$ (0.7 g, 3 mmol) for 7 h to yield (2*S*)-*N*-acetyl-2-carboxymethylpiperidine ((+)-**8**, 15 mg, 16% yield); $[\alpha]_D^{25}$ +0.65° (*c* 1.4, $CHCl_3$). Spectra were identical to **8** above.

(B) By optical rotation

The enantiomeric excesses of the remaining products were determined by comparison of optical rotations with compounds of known enantiomeric excess. Thus, optically active acids **7**–**9** were esterified, giving the enantiomeric excesses of product esters **1**–**3** by rotation. Optically active acetates **4** and **5** were deacylated and enantiomeric excesses obtained by comparison of rotations with product alcohols **10** and **11**.

1. Esterification of optically active acids 7–9

(a) Of (2S)-N-*acetyl-2-piperidinecarboxylic acid ((−)-7).* Optically active *N*-acetyl-2-piperidinecarboxylic acid ((−)-**7**, 290 mg, 1.7 mmol) from PLE catalysed hydrolysis was dissolved in methanol (5 mL). Ethereal diazomethane was added until persistence of colour. Colour was removed by dropwise addition of acetic acid. The resulting solution was dried ($MgSO_4$) and concentrated *in vacuo* on a rotary evaporator to give (2*S*)-*N*-acetyl-2-carbomethoxypiperidine ((−)-**1**, 305 mg, 95% yield); $[\alpha]_D^{25}$ −33.1° (*c* 6.0, $CHCl_3$). Spectra were identical to racemic **1** above.

(b) Of (2R)-N-*acetyl-2-carboxymethylpiperidine ((−)-8).* The above procedure was followed with *N*-acetyl-2-carboxymethylpiperidine ((−)-**8**, 210 mg, 1.7 mmol) to give (2*R*)-*N*-acetyl-2-carbomethoxypiperidine ((−)-**2**, 241 mg, 93% yield); $[\alpha]_D^{25}$ −4.3° (*c* 2.1, $CHCl_3$). Spectra were identical to racemic **2** above.

(c) Of (3S)-N-*acetyl-3-piperidinecarboxylic acid ((+)-9).* The above procedure was followed with *N*-acetyl-3-piperidinecarboxylic acid ((+)-**9**, 50 mg, 0.2 mmol), to give (3*S*)-*N*-acetyl-3-carbomethoxypiperidine ((+)-**3**, 36 mg, 96% yield); $[\alpha]_D^{25}$ +13.3 (*c* 4.0, $CHCl_3$). Spectra were identical to racemic **3** above.

2. Deacetylation of optically active acetates 4 and 5

(a) Of (2S)-N-*acetyl-2-acetoxymethylpiperidine ((−)-4).* (2*S*)-*N*-Acetyl-2-acetoxymethylpiperidine ((−)-**4**, 352 mg, 1.8 mmol) from PLE hydrolysis, was dissolved in distilled water (25 mL). To this was added NaOH (72 mg, 1.8 mmol) and the solution stirred for 10 h. The mixture was saturated with NaCl, and extracted with dichloromethane (3 × 50 mL). The combined organic phase was dried ($MgSO_4$), and concentrated *in vacuo* on a rotary evaporator to give (2*S*)-*N*-acetyl-2-hydroxymethylpiperidine ((−)-**10**, 265 mg, 79% yield); $[\alpha]_D^{25}$ −22.9° (*c* 3.95, $CHCl_3$). Spectra were identical to **10** above.

(b) Of (2R)-N-*acetyl-2-acetoxymethylpiperidine ((+)-5).* The above procedure with (2*R*)-*N*-acetyl-2-acetoxymethylpiperidine ((+)-**5**, 200 mg, 1 mmol) in water (25 mL) and NaOH (40 mg, 1 mmol) for 10 h gave (2*R*)-*N*-acetyl-2-hydroxymethylpiperidine ((+)-**11**, 143 mg, 79% yield); $[\alpha]_D^{25}$ +0.48° (*c* 12 in $CHCl_3$). Spectra were identical to **11** above.

Absolute configuration determinations

(a) N-*Acetyl-2-carbomethoxypiperidine (1)*

2-Piperidinecarboxylic acid was resolved as its (+)-tartrate salt according to the method of Portoghese *et al.* (10), to yield (2*R*)-(+)-2-carbomethoxypiperidine hydrochloride, mp 175–176°C (lit. (10) mp 177–180°C); $[\alpha]_D^{25}$ +9.3° (*c* 9, H_2O) (lit. (9) $[\alpha]_D^{25}$ +9.8 (*c* 1, 6 M HCl)). Optically active ester (200 mg, 1.4 mmol) was dissolved in dry THF (25 mL). To this was added acetic anhydride (1.43 g, 14 mmol) and diisopropyl amine (0.7 g, 7 mmol). This was stirred at 20°C for 48 h. THF was removed by rotary evaporation and excess acetic anhydride and diisopropyl amine removed by Kugelrohr distillation (40°C/0.25 Torr). The residual oil was purified by flash chromatography (silica, diethyl ether elution) to yield (2*R*)-(+)-*N*-acetyl-2-carbomethoxypiperidine (2*R*-(+)-**1**, 140 mg, 53% yield); $[\alpha]_D^{25}$ +65.2° (*c* 9.53, $CHCl_3$). Spectra were identical to racemic **1** above.

(b) N-*Acetyl-2-carboxymethylpiperidine (8)*

(2*R*)-*N*-Acetyl-2-carboxymethylpiperidine (−)-**8**, 180 mg, 1 mmol) from the PLE catalysed hydrolysis was dissolved in water (25 mL). To this was added NaOH (100 mg, 2.5 mmol) and the solution stirred at 70°C for 12 h. The solution was cooled to 20°C and extracted with methylene chloride (4 × 50 mL). The combined organic phase was dried ($MgSO_4$) and concentrated *in vacuo* on a rotary evaporator to yield (2*R*)-(−)-2-carboxymethylpiperidine, the enantiomer of which is of known absolute configuration (11) (128 mg, 78% yield), mp 216–220°C (lit. (11) mp 218–221°C); $[\alpha]_D^{25}$ −8.2° (*c* 9, H_2O) (lit. (11) $[\alpha]_D^{25}$ +22.1° (*c* 0.6, H_2O), 64% ee reported); ir *ν*: 3400, 1591 cm^{-1}; ^1H nmr (D_2O/ppts) δ: 1.5–1.7 (m, 6H), 2.1 (br s, 2H), 2.4–2.8 (m, 2H), 4.6–5.5 (m, 3H), 11.2 (s, 1H) ppm.

(c) N-*Acetyl-3-piperidinecarboxylic acid (9)*

The above procedure was followed using (3*S*)-*N*-acetyl-3-piperidinecarboxylic acid ((+)-**9**, 210 mg, 1.2 mmol) in water (25 mL) with NaOH (121 mg, 3 mmol) for 10 h, yielding (3*S*)-(+)-3-piperidinecarboxylic acid of known absolute configuration (12) (125 mg, 69% yield), mp 255–258°C (dec.) (lit. (12) mp 259–260°C); $[\alpha]_D^{25}$ +0.9° (*c* 11.5, H_2O) (lit. (12) $[\alpha]_D^{25}$ +3.6° (*c* 5, H_2O)). Spectra were identical to racemic acid above.

1. G. Sabbioni and J. B. Jones. J. Org. Chem. In press.
2. (*a*) G. M. Whitesides and C. H. Wong. Angew. Chem. Int. Ed. Engl. **8**, 617 (1985); (*b*) J. B. Jones. Tetrahedron, **42**, 3351 (1986).
3. J. B. Jones and J. F. Beck. Tech. Chem. **10**, 107 (1976).
4. (*a*) W. E. Ladner and G. M. Whitesides. J. Am. Chem. Soc. **106**, 7250 (1984); (*b*) H. A. Kita, H. Matsukaura, and T. Oishi. Tetrahedron Lett. **27**, 5241 (1986); (*c*) Q-M. Gu, D. R. Reddy, and C. J. Sih. Tetrahedron Lett. **27**, 5203 (1986).
5. (*a*) G. Sabbioni, M. L. Shea, and J. B. Jones. J. Chem. Soc. Chem. Commun. 236 (1984); (*b*) F-C. Huang, L. F. H. Lee, R. S. D. Mittal, P. R. Ravikumar, J. A. Chan, C. J. Sih, E. Casou, and C. R. Eck. J. Am. Chem. Soc. **97**, 4144 (1975); (*c*) S. Kobayashi, M. Kurihara, K. Kaniyama, and M. Ohno. Tetrahedron Lett. **26**, 5831 (1985); (*d*) J. B. Jones, R. S. Hinks, and P. G. Hultin. Can. J. Chem. **63**, 452 (1985).
6. (*a*) A. J. H. Klunder, W. B. Huizinga, A. J. M. Hulshof, and B. Zwaneburg. Tetrahedron Lett. **27**, 2543 (1986); (*b*) C. Papageorgiou and C. Benezra. J. Org. Chem. **50**, 1144 (1985); (*c*) C. J. Morrow. J. Org. Chem. **48**, 3960 (1983).
7. (*a*) A. I. Meyers, D. A. Dickman, and T. R. Bailey. J. Am. Chem. Soc. **107**, 7974 (1985); (*b*) L. A. Trimble and J. C. Vederas. J. Am. Chem. Soc. **108**, 6397 (1986); (*c*) D. A. Evans, T. C. Britton, R. L. Dorow, and J. F. Dellaria. J. Am. Chem. Soc. **108**, 6395 (1986).
8. (*a*) J. P. Greenstein. Adv. Protein Chem. **9**, 122 (1954); (*b*) I. Chibata, T. Tosa, T. Sato, and K. Yammamoto. Methods Enzymol. **44**, 746 (1986).
9. M. Schneider, N. Engel, D. Honicke, G. Heinemann, and H. Gorisch. Angew. Chem. Int. Ed. Engl. **23**, 67 (1981).
10. P. S. Portoghese, T. L. Pazdernid, W. L. Kuhn, G. Hite, and A. Shafi'ee. J. Med. Chem. **11**, 12 (1968).
11. T. Wakabayashi, K. Watanabe, and Y. Kato. Synth. Commun. **7**, 239 (1977).
12. A. M. Akkerman, D. K. DeJong, and H. Veldstra. Recl. Trav. Chem. Pays-Bas, **70**, 899 (1951).
13. (*a*) C-S. Chen, Y. Fujimoto, and C. J. Sih. J. Am. Chem. Soc. **103**, 3580 (1981); (*b*) M. Ohno, S. Kobayashi, T. Imori, Y. F. Wanh, and T. Izawa. J. Am. Chem. Soc. **105**, 2405 (1981).
14. L. K. P. Lam, R. A. H. F. Hui, and J. B. Jones. J. Org. Chem. **51**, 2047 (1986).
15. C-S. Chen, Y. Fujimoto, G. Girdankas, and C. J. Sih. J. Am. Chem. Soc. **104**, 7294 (1982).
16. H. T. Nagasawa, J. A. Elberling, P. S. Fraser, and N. S. Mizuno. J. Med. Chem. **14**, 501 (1971).
17. W. D. Marshall, T. T. Nguyen, D. B. MacLean, and I. D. Spenser. Can. J. Chem. **53**, 41 (1975).
18. S. M. McElvain and R. Adams. J. Am. Chem. Soc. **45**, 2738 (1924).

Can. J. Chem. Downloaded from www.nrcresearchpress.com by 213.222.148.141 on 09/07/12
For personal use only.

Reactions of dimethylsilylene with pinenes

DONG WANG AND T. H. CHAN[1]
Department of Chemistry, McGill University, Montreal, P.Q., Canada H3A 2K6

Received May 26, 1987

DONG WANG and T. H. CHAN. Can. J. Chem. **65**, 2727 (1987).

Photolysis of β-pinene and dodecamethylhexasilane (**2**) followed by methanol quenching gave the allylsilane **5** and the methoxysilane **6**. The intermediacy of the silirane **7** was proposed. Photolysis of α-pinene and **2** gave **6** only. The formation of another silirane **15** as intermediate was verified by deuterium labelling experiment. The potential of silylene chemistry in organic synthesis was examined.

DONG WANG et T. H. CHAN. Can. J. Chem. **65**, 2727 (1987).

La photolyse du β-pinène en présence de dodécaméthylhexasilane **2**, suivie d'un piégeage au méthanol, conduit à l'allylsilane **5** et au méthoxysilane **6**. On suggère que le silirane **7** est un intermédiaire dans la réaction. La photolyse de l'α-pinène en présence du composé **2** ne fournit que le composé **6**. Faisant appel à une expérience de marquage au deutérium, on a démontré que le silirane **15** est un intermédiaire dans cette réaction. On a examiné le potentiel de la chimie du silylène en synthèse organique.
[Traduit par la revue]

Can. J. Chem. Downloaded from www.nrcresearchpress.com by 213.222.148.141 on 09/07/12
For personal use only.

Introduction

Silylene, the silicon analog of carbene, has been a subject of intensive investigation in the last decade (1–4). In the presence of alkenes or alkynes, dimethylsilylene is known to add to the double bond to form the corresponding siliranes (5) or silirenes (6). Thus, photolysis of decamethyltetrasilane (**3**) with cyclohexene gave the bicyclic compound **4** (Scheme 1) (7). Siliranes such as **4** are quite unstable. They can rearrange to an allylsilane. In addition, the endocyclic silicon–carbon bond can be cleaved under very mild conditions with polar reagents (e.g., CH_3OH) to give ring-opened adducts (for a review of silylene chemistry, see ref. 1).

In this paper we report the reactions of dimethylsilylene with pinenes in the hope of exploring the factors that may be significant in defining the use of silylene chemistry in organic synthesis (for examples of the use of dimethylsilylene in organic synthesis, see refs. 8 and 9).

Results and discussion

1. Reaction of dimethylsilylene with β-pinene

Dimethylsilylene (**1**) was generated by the photolysis of dodecamethylcyclohexasilane (**2**) (10). Thus, a mixture of β-pinene and **2** in cyclohexane was photolysed in a Rayonet photochemical reactor. At the end of reaction, the mixture was quenched with methanol and the products purified by distillation and then flash chromatography. Two main products, **5** and **6**, in a combined yield of about 60–69% (based on **2**) were identified (Scheme 2).

The structure of **5** was quite evident from its spectroscopic data. Its identity was further confirmed by synthesis from an independent route according to Scheme 3, using conventional chemistry.

By analogy with the known rearrangement of **4** to allylsilane, it was likely that the silirane **7** was formed in the photolysis of **2** with β-pinene. Compound **5** was then derived from **7** by a similar process. Efforts to isolate **7** were not successful. Its presence was inferred as well from the other product of the reaction, compound **6**, formed by the methanolysis of the silirane **7**. Heterolysis of siliranes has been reported previously (6). The present methanolysis of **7** to give **6** is noteworthy in two respects. The first is that the reaction is regiospecific. In the opening of the unsymmetrical silirane **7**, we observed cleavage of the silicon–carbon bond where the carbon is less substituted. The other expected regioisomer, compound **8** (9), was not detected in the reaction mixture. Regiospecificity in the heterolysis of unsymmetrical siliranes has been noted in the literature before (6). The present example indicates that a silicon – primary carbon bond is cleaved preferentially over a silicon – tertiary carbon bond (*vide infra*). The second interesting feature is the stereochemistry of **6**. Because the two faces of the

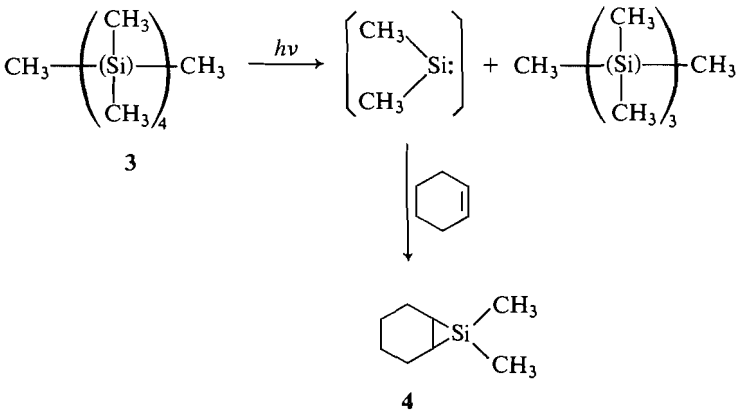

SCHEME 1

[1]Author to whom correspondence may be addressed.

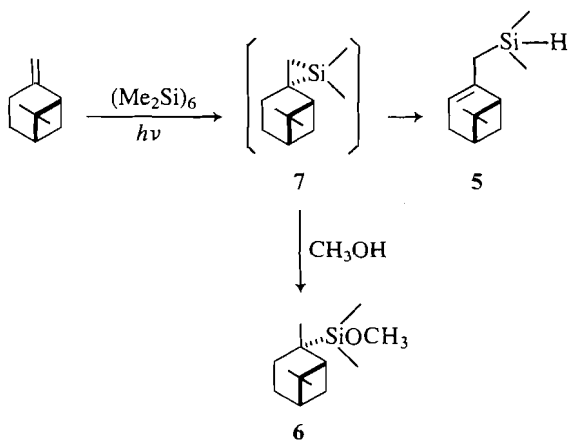

SCHEME 2

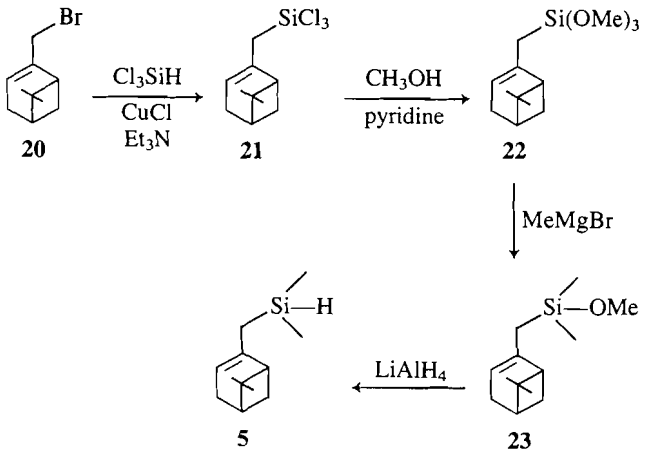

SCHEME 3

β-pinene double bond are not equivalent, dimethylsilylene can add *syn* or *anti* to the *gem*-dimethyl carbon bridge to give **7** or **9**. On methanolysis, two stereoisomers, **6** or **10**, can result. In the

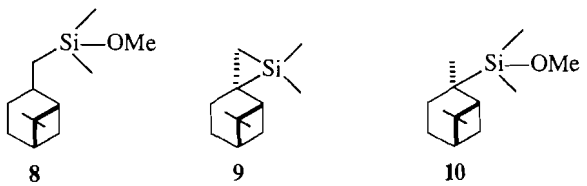

reaction mixture, only one stereoisomer was found. On steric grounds, one assumes that the dimethylsilylene would add to the double bond from the less hindered side to give **7**. We thus assigned structure **6** rather than **10** to the product isolated. This structural assignment was supported by ^{1}H nmr data. The

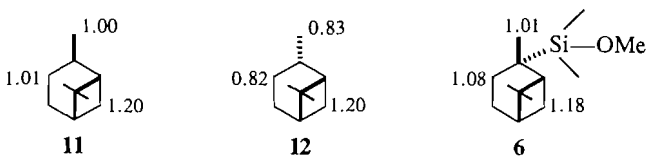

C10-methyl and the *syn*-methyl of *cis*-pinane (**11**) both resonate at about 1.01 ppm. By contrast, the C10-methyl and the *syn*-methyl of *trans*-pinane (**12**) both resonate at about 0.82 ppm. In the case of **6**, the C10-methyl resonates at 1.01 ppm, more in line with **11**.

Normally, in the trapping of silylene with simple alkenes, the alkene was used in large excess. We found that the combined yield of **5** and **6** diminished only slightly from 69% to 60% even if the ratio of β-pinene to **2** was reduced from 40:1 to 4:1. Furthermore, the relative amount of **5** to **6** could be modified by a change in the length of photolysis time.

2. Reaction of dimethylsilylene with α-pinene

When a mixture of α-pinene and **2** in cyclohexane was photolysed under similar conditions, compound **6** was obtained on quenching the reaction mixture with methanol. The yield of **6** was about 27%. Various attempts to change the reaction conditions by using different ratios of α-pinene to **2** or different lengths of photolysis time, etc., did not lead to significant improvement in the yield of **6**. Nor was it possible to detect or isolate the allylsilanes **13** or **14** from the reaction mixture (Scheme 4).

The formation of **6** can be explained on the basis of methanolysis of the silirane **15**. Again, efforts to isolate **15** were not successful. The formation of the same product **6** from the reactions of the two pinenes raised the question whether two different siliranes, **7** and **15**, were involved as the intermediates. We were able to resolve this question by quenching the photolysis mixture with CH_3OD. When the reaction from the photolysis of β-pinene and **2** was treated with CH_3OD at the end, compound **6***a* was obtained, with deuterium incorporation at the C10-methyl. On the other hand, compound **6***b* obtained from α-pinene contained deuterium at the ring methylene (Scheme 5). This experiment established clearly that two distinct siliranes were involved. Furthermore, it also suggests that in the methanolysis of unsymmetrical siliranes, cleavage of a silicon – secondary carbon bond is preferred over a silicon – tertiary carbon bond.

3. Potential of silylene chemistry in organic synthesis

Activation of the allylic position of an alkene is an important operation in synthetic organic chemistry. The use of palladium or other metals to activate an allylic compound for nucleophilic substitution reactions has proved useful in synthesis. The ability of silylene to react with alkenes to yield the corresponding allylsilanes provides activation in a complementary fashion since allylsilanes are known to react with electrophiles to give substitution products (Scheme 6). The formation of the allylsilane **5** in the reaction of β-pinene with dimethylsilylene is therefore an activation of β-pinene, permitting the synthesis of substituted β-pinenes. We demonstrated this by the reaction of the allylsilane **5** with a number of electrophiles (Scheme 7). Reaction of **5** with 10% HCl in $CHCl_3$ gave β-pinene in 90% yield. With bromine as the electrophile in the presence of pyridine, the bromo compound **16** was obtained presumably by addition and elimination, followed by rearrangement. The isomeric bromo compound was known to rearrange to **16** on column chromatography. Epoxidation of **5** with *m*-chloroperbenzoic acid (MCPBA) followed by acid opening of the epoxide gave the hydroxy compound **17**, again with the hydroxy group *trans* to the *gem*-dimethyl bridge. Finally, the reaction of **5** with acetyl chloride/aluminum chloride gave the acetyl compound **18**, which upon column chromatography rearranged to the more stable α,β-unsaturated ketone **19**. The last reaction is particularly instructive in demonstrating the use of silylene chemistry for the formation of new carbon–carbon bonds.

Can. J. Chem. Downloaded from www.nrcresearchpress.com by 213.222.148.141 on 09/07/12
For personal use only.

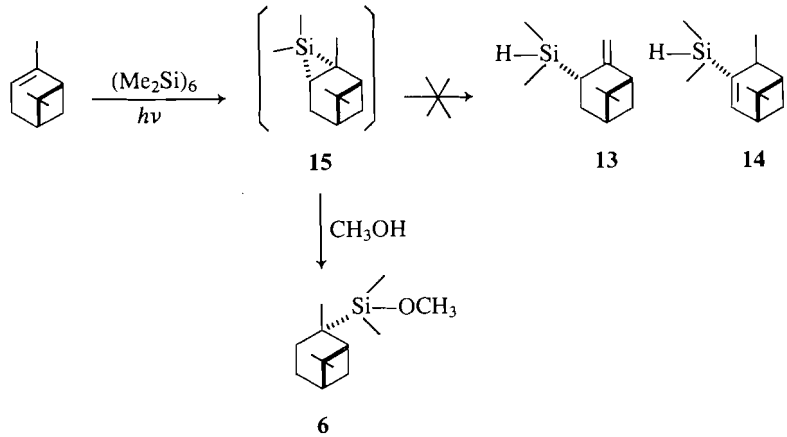

15 13 14 6

SCHEME 4

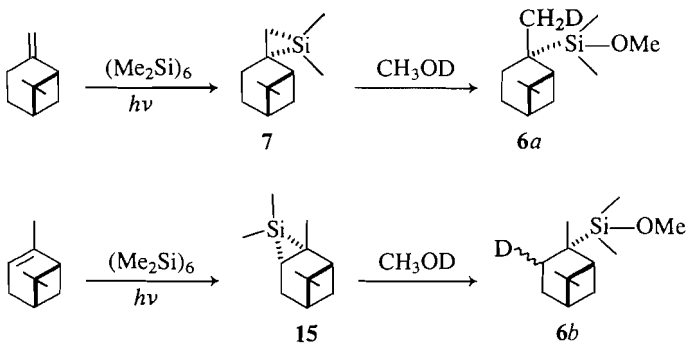

7 6a 15 6b

SCHEME 5

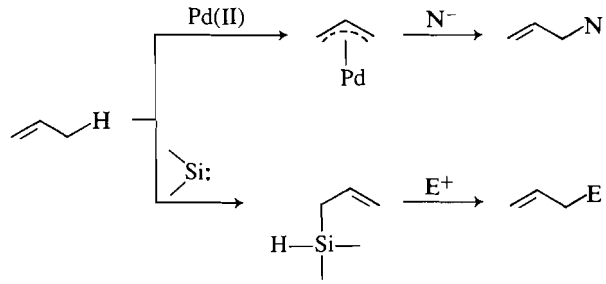

SCHEME 6

Conclusion

The present study demonstrates that the addition of dimethylsilylene to the double bond of pinenes occurs on the less hindered face. The methanolysis of unsymmetrical siliranes is regiospecific, with cleavage of a silicon – primary carbon bond or a silicon – secondary carbon bond preferred over a silicon – tertiary carbon bond. Dimethylsilylene reaction with β-pinene can be used as a way to introduce electrophiles into the allylic position. In spite of many obvious problems, silylene chemistry appears to be potentially useful in organic synthesis (8).

Experimental

Boiling points and melting points are reported uncorrected. Nuclear magnetic resonance spectra were recorded on Varian XL-200 and T-60A spectrometers. Low and high resolution EI mass spectra were determined on a Dupont 21-492B instrument and gc/ms were done on a Hewlett–Packard 5980A instrument. Infrared spectra were recorded on Perkin–Elmer-297 or Nicolet 7002 MC spectrophotometers. Analytical gas chromatography was performed on a Hewlett–Packard 5730A

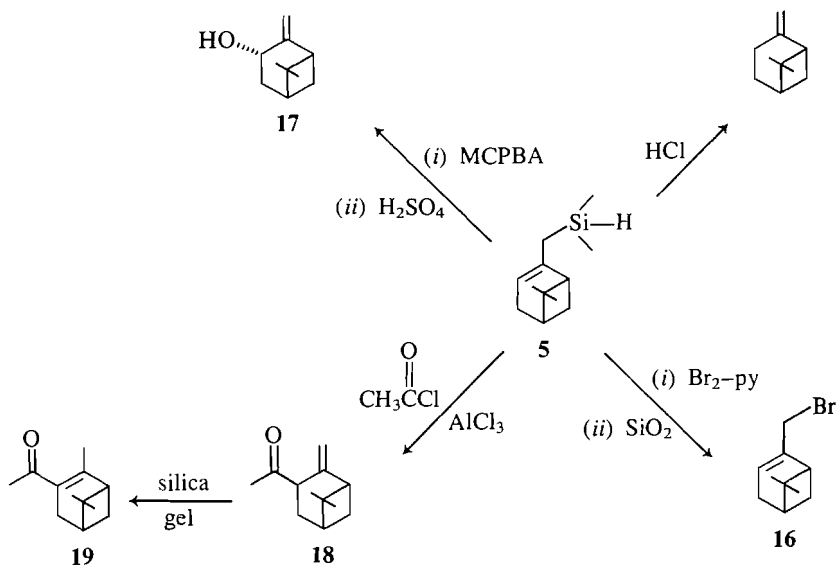

17 5 16 19 18

SCHEME 7

Can. J. Chem. Downloaded from www.nrcresearchpress.com by 213.222.148.141 on 09/07/12
For personal use only.

Can. J. Chem. Downloaded from www.nrcresearchpress.com by 213.222.148.141 on 09/07/12
For personal use only.

instrument equipped with a flame ionization detector using helium carrier gas flow. The column used was a 10 ft × 0.125 in. 6% OV-101 on Chromosorb W. HP. 80/100. Elemental analyses were performed using a Carlo Erba Elemental Analyses MOD-1102.

Photolysis of β-pinene with 2

A mixture of 1.95 g (14 mmol) of β-pinene and 1.25 g (3.6 mmol) of **2** in 85 mL of cyclohexane in a quartz flask was photolysed under nitrogen with low pressure mercury lamps (254 nm) in a Rayonet photochemical reactor. At the end of the reaction (20–40 h), 3 mL of dry methanol was added to the mixture. The reaction mixture was concentrated and distilled under reduced pressure. The first fraction (bp 45°C/10 Torr; 1 Torr = 133.3 Pa) was mainly unreacted β-pinene. The second fraction (bp 95–105°C/10 Torr) was a mixture of 10-dimethylsilyl-α-pinene (**5**) and 2-dimethylmethoxysilyl-pinane (**6**) in a combined yield of 60%. The mixture was purified by silica gel flash chromatography eluting with pentane – ethyl acetate (100:1) to give compounds **5** and **6**.

Compound 5: ir: 2080 cm^{-1}; ^1H nmr ($CDCl_3$) δ: 0.00 (d, 6H), 0.82 (s, 3H), 1.22 (s, 3H), 1.47 (m, 2H), 1.62–2.47 (m, 6H), 3.83 (m, 1H), 5.04 (m, 1H); gc/ms, *m/z*: 194 (M^+, 8%), 179 (2), 149 (24), 59 (100). The spectroscopic data were identical to those for the same compound synthesized by an independent route (see below).

Compound 6: ir: 1090 cm^{-1}; ^1H nmr ($CDCl_3$) δ: 0.04 (s, 6H), 1.01 (s, 3H), 1.08 (s, 3H), 1.18 (s, 3H), 1.50–2.30 (m, 8H), 3.42 (s, 3H); gc/ms: 226 (0.1%), 136 (2), 121 (3), 89 (100).

The total yield of **5** and **6** was slightly greater (69%) if a larger excess of β-pinene was used (ratio of β-pinene to **2**, 40-fold excess). The work-up was somewhat more difficult in removing the excess β-pinene. The use of β-pinene to **2** in a ratio of about 4:1 was to be preferred.

The proportion of **5** to **6** in the reaction mixture was dependent on the length of photolysis time. For a photolysis of 20 h before methanol quenching, the ratio of **5** to **6** was 1:4. If photolysis was extended to 40 h, the ratio of **5** to **6** was 2.

2-Dimethylmethoxysilyl-10-deutero-pinane-(6a)

Photolysis of β-pinene with **2** was carried out as described above for 20 h. The mixture was quenched with methanol-O-*d*. Compound ***6a*** was obtained after column chromatography. Its ^1H nmr spectrum was the same as that of compound **6** with the exception of the peak at 1.01, which was changed into a 1:1:1 triplet with J_{HD} = 2 Hz and a relative intensity of ~2H. It had gs/ms: 227 (0.1%), 137 (2), 122 (3), 89 (100).

Photolysis of α-pinene with 2

A mixture of α-pinene and **2** in cyclohexane was photolysed under nitrogen in the same manner as described for β-pinene. After quenching the reaction mixture with methanol, and work-up, compound **6** was obtained in 27% yield after column chromatography. It had identical properties to those of the compound obtained from the photolysis of β-pinene. Varying the amount of α-pinene or photolysis time did not lead to significant change in the outcome of the reaction.

2-Dimethylmethoxysilyl-3-deutero-pinane (6b)

Photolysis of α-pinene (2.0 mL) with **2** (1.02 g) in 85 mL cyclohexane was carried out as described above for 30 h. The mixture was quenched with methanol-O-*d* and worked up as above. Compound ***6b*** was obtained after column chromatography. Its ^1H nmr spectrum was identical to that of compound **6** with the exception that the multiplet at ~1.9–2.2 ppm was reduced in intensity. It has gc/ms: 227 (0.1%), 137 (2), 122 (3), 89 (100).

10-Trimethoxysilyl-α-pinene (22)

10-Bromo-α-pinene (**20**) was prepared from myrtenol according to literature procedure (11). To a mixture of trichlorosilane (1.7 g, 11 mmol) and compound **20** (2.5 g, 11 mmol) was added dropwise under nitrogen a mixture of triethylamine (1.2 g, 12 mmol), cuprous chloride (0.06 g, 6 mmol), and 25 mL of ether. After the mixture was stirred for 4 h at room temperature, the solid was removed by filtration. To the ether solution, a solution of 2.6 mL pyridine and 1.3 mL methanol was added. The mixture was stirred overnight at room temperature. The mixture was filtered and the filtrate was evaporated *in vacuo* to yield crude 10-trimethoxysilyl-α-pinene (**22**); ^1H nmr ($CDCl_3$) δ: 0.85 (s, 3H), 1.25 (s, 3H), 1.52 (m, 2H), 1.80–2.50 (m, 6H), 3.52 (s, 9H), 5.15 (m, 1H); ms, *m/e*: 256 (M^+, 14%), 241 (20), 181 (55), 121 (100). *Anal.* calcd. for $C_{13}H_{24}O_3Si$: C 60.89, H 9.43; found: C 60.44, H 9.36.

10-Dimethylmethoxysilyl-α-pinene (23)

To the solution of crude **22** in 30 mL of ether, methylmagnesium bromide solution (~2.0 M, 20 mL) was added. The mixture was stirred for 15 h at room temperature. The excess Grignard reagent was destroyed by aqueous ammonium chloride solution. The organic solvent was dried and distilled under reduced pressure to give 1.5 g of 10-dimethylmethoxysilyl-α-pinene (**23**) (63% yield), bp 80–83°C/0.5 Torr. *Anal.* calcd. for $C_{13}H_{24}OSi$: C 69.58, H 10.78; found: C 69.76, H 10.76.

10-Dimethylsilyl-α-pinene (5)

To a suspension of lithium aluminum hydride (1.2 g) in ether (25 mL), compound **23** (2.0 g, 8.8 mmol) was added. The mixture was stirred overnight at room temperature. The excess hydride was destroyed by aqueous ammonium chloride. The organic layer was washed with water, dried ($MgSO_4$), and filtered. The filtrate was distilled under reduced pressure to give 1.4 g of compound **5** (82% yield), bp 62–64°C/1 Torr. The spectroscopic data of this compound were identical to those of the compound prepared via the photolysis of β-pinene with **2**. *Anal.* calcd. for $C_{12}H_{22}Si$: C 74.15, H 11.41; found: C 74.50, H 11.75.

Protodesilylation of 5

A mixture of **5** (0.1 g) and 0.5 mL of 10% HCl in 3 mL of chloroform was stirred at room temperature for 24 h. The main product (90%) was identified to be β-pinene by ^1H nmr and gc.

Bromodesilylation of 5

To a solution of **5** (0.15 g) and pyridine (0.06 mL) in hexane (5 mL) at −78°C, bromine (0.22 g) was added dropwise. After stirring for 0.5 h, the mixture was warmed to room temperature and stirred for another 0.5 h. The mixture was concentrated *in vacuo* and the product passed through a silica gel column, eluting with pentane – ethyl acetate (75:1). 10-Bromo-α-pinene was isolated in 65% yield, and identified by ^1H nmr and gc comparison with an authentic sample.

3-Hydroxy-β-Pinene (17)

1. From β-pinene

An authentic sample of compound **17** was prepared by lead tetraacetate oxidation of β-pinene followed by base hydrolysis according to literature procedure (12). It had bp 83–85°C/10 Torr.

2. From oxidation of 5

A mixture of compound **5** (0.2 g, 1 mmol), MCPBA (0.4 g), and sodium bicarbonate (4 g) in dichloromethane (15 mL) was stirred at room temperature for 3 days. The solid was filtered and the filtrate was evaporated to dryness. The residue was stirred with dilute sulfuric acid at room temperature for 1 h. The mixture was extracted with ethyl acetate. The organic solution was washed with water, dried ($MgSO_4$), and filtered. The filtrate was evaporated and the residue purified by flash chromatography (pentane – ethyl acetate 15:1) to give compound **17** in 72% yield.

3-Acetyl-α-pinene (18)

To a solution of compound **5** (0.40 g, 2 mmol) and acetyl chloride (0.19 g, 2.4 mmol) in 10 mL of dichloromethane at −78°C, a solution of $TiCl_4$ (0.41 g, 2.2 mmol) in 2 mL of CH_2Cl_2 was added. The mixture was stirred for 1 h, poured into an aqueous solution of sodium bicarbonate, and then extracted with ethyl acetate. The organic layer was washed with water, dried ($MgSO_4$), and filtered. The filtrate was evaporated to dryness. The residue was purified by column chromatography (pentane – ethyl acetate 75:3) to give compound **18** in 57% yield. It had spectral data in agreement with the structure and similar to those reported in the literature (13).

Acknowledgements

We thank NSERC and FCAC for financial support of our research. D.W. thanks NSERC for an International Scientific Exchange Award.

1. (*a*) M. ISHIKAWA and M. KUMADA. Advances in organometallic chemistry. Vol. 19. *Edited by* F. G. A. Stone and R. West. Academic Press, New York. 1981; (*b*) P. P. GASPAR. *In* Reactive intermediates. Vols. 1–3. *Edited by* M. Jones and R. A. Moss. Wiley, New York. 1978, 1981, 1985.
2. T. D. DRAHNAK, J. MICHL, and R. WEST. J. Am. Chem. Soc. **101**, 5427 (1979).
3. V. J. TORTORELLI and M. JONES, JR. J. Am. Chem. Soc. **102**, 1425 (1980); V. J. TORTORELLI, M. JONES, JR., S. HU, and Z. LI. Organometallics, **2**, 759 (1983).
4. J. L. MARGRAVE and P. W. WILSON. Acc. Chem. Res. **4**, 145 (1971).
5. D. SEYFERTH and D. C. ANNARELLI. J. Am. Chem. Soc. **97**, 2273 (1975).
6. D. SEYFERTH and D. C. ANNARELLI. J. Organometal. Chem. **117**, C51 (1976); M. ISHIKAWA, K. NAKAGAWA, M. ISHIGMO, F. OHI, and M. KUMADE. J. Organometal. Chem. **152**, 155 (1978).
7. M. ISHIKAWA and M. KUMADA. J. Organometal. Chem. **81**, C3 (1974).
8. T. H. CHAN and D. WANG. J. Chem. Soc. Chem. Commun. 1273 (1984).
9. D. WANG and T. H. CHAN. Tetrahedron Lett. 1573 (1983).
10. M. LAGUERRE, J. DUNOGUES, and R. CALAS. J. Chem. Soc. Chem. Commun. 272 (1978).
11. B. HENC, H. PAULING, and G. WILKE. Liebigs Ann. Chem. 1820 (1974).
12. M. P. HARTSHORN, D. N. KIRKLAND, and A. F. A. WALLIS. J. Chem. Soc. 5294 (1964).
13. J. P. PILLOT, G. DÉLÉRIS, J. DUNOQUÉS, and R. CALAS. J. Org. Chem. **44**, 3397 (1979).

Can. J. Chem. Downloaded from www.nrcresearchpress.com by 213.222.148.141 on 09/07/12
For personal use only.

Synthesis of optically active forms of the δ-lactone of 3,5-dihydroxydecanoic acid

TSUGUO SATŌ
Tōhoku College of Pharmacy, Komatsushima, Sendai, Miyagi, Japan

Received April 14, 1987

TSUGUO SATŌ. Can. J. Chem. **65**, 2732 (1987).

The δ-lactone of 3,5-dihydroxydecanoic acid was synthesized from methyl-3-oxooctanoate by utilizing its baker's yeast reduction.

TSUGUO SATŌ. Can. J. Chem. **65**, 2732 (1987).

Utilisant l'oxo-3 octanoate de méthyle comme produit de départ qui est réduit par de la levure de pain, on a réalisé la synthèse de la δ-lactone de l'acide dihydroxy-3,5 décanoïque.

[Traduit par la revue]

Can. J. Chem. Downloaded from www.nrcresearchpress.com by 213.222.148.141 on 09/07/12
For personal use only.

Introduction

In 1972 R. F. Vesonder *et al.* isolated the δ-lactone of 3,5-dihydroxydecanoic acid from culture liquor of the fungus (1). However, the absolute configuration of this compound has yet to be defined. Recently, utilization of the biochemical system has been reported as an effective method in asymmetric synthesis (2). This has prompted me to present the enantiomerically pure forms of the δ-lactone.

Results and discussion

I describe a simple synthesis of the optically active forms of the δ-lactone of 3,5-dihydroxydecanoic acid starting from methyl (*R*)-3-hydroxydecanoate **2**, which was readily obtainable in 99% optical purity by reduction of ethyl-3-oxooctanoate **1** with baker's yeast (3). The optical purity was estimated by hplc analysis. The synthetic route is shown in Scheme 1.

Protection of the OH group of (*R*)-**2** as a tetrahydropyranyl (THP) ether gave (*R*)-**3**. This was reduced with DIBAL-H and condensed with ethyl acetate, treating with LDA to give **5**. Removal of the THP protective group of **5** with pyridinium-*p*-toluenesulfonate (PPTS) yielded **6**. Then **6** was treated with *p*-toluenesulfonic acid (PTS) to give the desired lactone **7**. This diastereomeric mixture **7** could be separated by tlc to give **8** as a colourless oil. The nmr spectrum of **8** coincided with the spectrum of the lactone that was reported by R. F. Vesonder (1). On the other hand, A. Numata *et al.* (5) isolated (3*S*,5*S*)-3-hydroxyhexan-5-olide (4) from *Osmunda japonica* Thunb. In the nmr data of this compound, the signal due to CHOH was reported at δ 4.36 (q, J = 4 Hz). According to the above nmr spectral properties, the absolute configuration of the CHOH of lactone **8** was assigned to be (3*R*). In conclusion, I propose (3*R*,5*R*)-(+)-3-hydroxydecan-5-olide.

Experimental

The ir spectra were determined as film on a Shimadzu IR-430 spectrometer. The nmr spectra were recorded at 60 or 90 MHz with TMS as an internal standard and $CDCl_3$ as a solvent on a JEOL PMX-60 and FX90Q spectrometer. Optical rotations were measured on a Jasco DIP-360 polarimeter. High resolution mass spectra (hrms) were obtained with a Hitachi M-80A spectrometer and Data Processing System M-003. Microelemental analyses were performed at Kobe Women's College of Pharmacy.

Ethyl 3-oxooctanoate ***1***

This was prepared from *n*-butylbromide and ethyl acetoacetate in 70% yield (6); ir ν: 1740, 1715, 1630, 1235, 1150 cm^{-1}; ^1H nmr δ: 1.13 (3H, t, J = 4 Hz), 1.50 (3H, t, J = 7 Hz), 2.76 (2H, t, J = 7 Hz), 3.63 (2H, s), 4.43 (2H, q, J = 7 Hz); ms, m/z: 186 (M^+, 3.8), 99 (100). *Mol. Wt.* calcd. for $C_{10}H_{18}O_3$: 186.1277; found (hrms) m/z: 186.1266. *Anal.* calcd. for $C_{10}H_{18}O_3$: C 64.49, H 9.74; found: C 64.71, H 10.14.

*Methyl (*R*)-(−)-3-hydroxydecanoate* ***2***

A solution of **1** (3.945 g) was reduced according to the reported procedure (3). The acidified filtrate was concentrated and treated with CH_2N_2 in ether to give crude **2**, which was chromatographed on an SiO_3 column to afford oily **2** (1.20 g, 32%); $[\alpha]_D^{18}$ −11.65 (*c* 2.3, $CHCl_3$); ir ν: 3400, 1720, 1188, 1160, 1120 cm^{-1}; ^1H nmr δ: 2.4 (2H, d, J = 2 Hz), 4.06 (1H, m), 3.7 (3H, s); ms m/z: 175 (M^+ + 1,

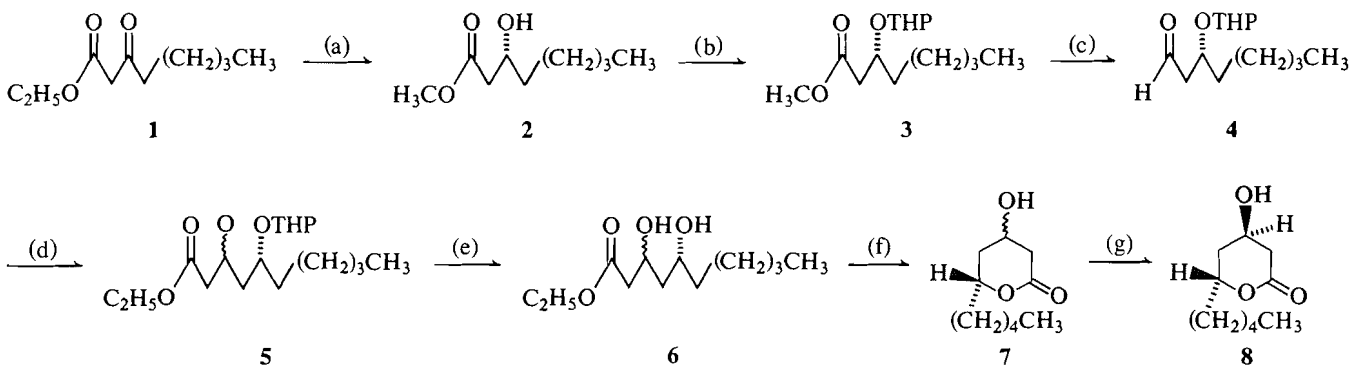

(a) baker's yeast, CH_2N_2; (b) 2,3-DHP, PTS, CH_2Cl_2; (c) DIBAL-H/−78°C, THF;
(d) LDA, $CH_3COOC_2H_5$/−78°C, THF; (e) PPTS/60°C, EtOH, 1 h; (f) PTS/90°C, benzene, 1 h;
(g) preparative tlc

SCHEME 1

1.5), 103 (100). *Mol. Wt.* calcd. for $C_9H_{19}O_3$: 175.1322; found (hrms) *m/z*: 175.1366. *Anal.* calcd. for $C_9H_{18}O_3$: C 62.04, H 10.41; found: C 61.98, H 10.25.

Determination of the optical purity of **2**

To a solution of **2** (4 mg, toluene 0.3 mL) was added 3,5-dinitrophenylisocyanate (10 mg) and pyridine (0.5 mL) at room temperature. After being kept 1 h, the reaction mixture was evaporated, followed by hplc analysis (column: Sumipax OA-4000 25 × 4 mm; solvent:hexane–1,2-dichloroethane–ethanol (100:20:1), 1 mL/min; pressure: 35 kg/cm^2; detector: 254 nm). The two diastereomers showed retention times of 12 min 3 s and 14 min, respectively. (*R*)-**2** was shown to be 99.9% pure.

*Methyl (*R*)-(−)-3-tetrahydropyranyloxyoctanoate* **3**

To a stirred solution of **2** (1.20 g, 6.9 mmol) and *p*-toluenesulfonate (7.2 mg, 0.042 mmol) in dry CH_2Cl_2 was added dropwise 2,3-dihydropyran (0.50 g, 6.0 mmol). The mixture was stirred for 1 h at room temperature. It was then washed with saturated $NaHCO_3$ solution and brine, dried ($MgSO_4$), and concentrated *in vacuo* to give **3**, which was chromatographed on an SiO_2 column to afford oily **3** (1 g, 56%); $[\alpha]_D^{28}$ −5.90 (*c* 1.033, $CHCl_3$); ir *ν*: 1725, 1190, 1160, 1120, 1070, 1020 cm^{-1}; ^{1}H nmr δ: 0.79–1.0 (3H, m), 2.46–2.63 (2H, br s), 3.66 (3H, s); ms *m/z*: 258 (M^+, 6.1), 85 (100). *Mol. Wt.* calcd. for $C_{14}H_{25}O_4$: 257.1687; found (hrms) *m/z*: 257.1719. *Anal.* calcd. for $C_{14}H_{26}O_4$: C 65.08, H 10.14; found: C 64.74, H 9.50.

*(*R*)-3-Tetrahydropyranyloxyoctanal* **4**

A solution of **3** (1.0 g, 3.9 mmol) in dry toluene (12 mL) was added dropwise at −78°C to a stirred and cooled solution of *i*-Bu_2AlH in toluene (16%, 4 mL) under Ar. After the addition, the mixture was kept at −78°C for 10 min. The saturated NH_4Cl solution was added dropwise to the stirred mixture, then the reaction temperature was gradually raised to room temperature. The reaction mixture was continuously extracted with ether for 1 h. The organic extract was washed with $NaHCO_3$ solution, dried ($MgSO_4$), and concentrated *in vacuo*. The residue was chromatographed on an SiO_2 column to afford oily **4** (0.82 g, 92%); $[\alpha]_D^{28}$ −4.20 (*c* 2.0, $CHCl_3$); ir *ν*: 2540, 1740, 1195, 1140, 1080, 1030, 1020 cm^{-1}; ^{1}H nmr δ: 2.5–2.81 (2H, m), 4.81 (1H, br s), 9.83 (1H, br s); ms, *m/z*: 228 (M^+, 1.5), 85 (100). *Mol. Wt.* calcd. for $C_{13}H_{24}O_3$: 228.1740; found (hrms) *m/z*: 228.1737. *Anal.* calcd. for $C_{13}H_{24}O_3$: C 68.38, H 10.59; found: C 67.91, H 10.12.

*Ethyl (3*RS,5R*)-3-hydroxy-5-tetrahydropyranyloxydecanoate* **5**

A solution of LDA was prepared by the addition of *n*-BuLi in *n*-hexane (1.5 M, 3.6 mL) to a stirred and cooled solution of $(i\text{-Pr})_2NH$ (0.6 mL, 4.6 mmol) in dry THF (15 mL) at −78°C under Ar. After stirring for 10 min at −78°C, the mixture was warmed to room temperature and stirred for 10 min. It was then cooled to −78°C. Ethyl acetate (0.45 mL, 4.6 mmol) was added dropwise to the resulting slurry, which was then stirred for 15 min; next a solution of **4** (0.820 g, 3.6 mmol) in dry THF (4 mL) was added slowly to the stirred solution during 10 min. Saturated NH_4Cl solution was then added to the mixture. After the addition the reaction temperature was gradually raised to room temperature. The mixture was diluted with ether. The ether solution was washed with saturated $NaHCO_3$ solution, dried ($MgSO_4$), and concentrated *in vacuo*. The residue was chromatographed on an SiO_2 column; 0.45 g of **5** (oil, 40%); $[\alpha]_D^{28}$ −13.22 (*c* 0.930, $CHCl_3$); ir *ν*: 3450, 1730, 1130, 1075, 1022 cm^{-1}; ^{1}H nmr δ: 2.50 (2H, dd, *J* = 6 Hz, *J* = 2 Hz), 4.25 (2H, q, *J* = 7 Hz); ms, *m/z*: 299 (20). *Anal.* calcd. for $C_{17}H_{32}O_5$: C 64.52, H 10.19; found: C 64.20, H 9.87.

*Ethyl (3*RS,5R*)-3,5-dihydroxydecanoate* **6**

PPTS (13.15 mg, 0.052 mmol) was added to a solution of **5** in EtOH (0.100 g, 0.349 mmol). The mixture was stirred for 2 h. It was then washed with saturated $NaHCO_3$ solution, saturated NH_4Cl solution, dried ($MgSO_4$), and concentrated *in vacuo*. The residue was chromatographed on an SiO_2 column to afford oily **6** (0.086 g, 97%); ir *ν*: 3350, 1720, 1150, 1020 cm^{-1}; ^{1}H nmr δ: 2.58 (2H, br s, *J* = 4 Hz), 4.26 (2H, q, *J* = 6 Hz). *Anal.* calcd. for $C_{12}H_{24}O_4$: C 62.04, H 10.41; found: C 61.66, H 10.39.

*(3*R,5R*)-(+)-3-Hydroxydecan-5-olide* **8**

PTS (48.91 mg, 0.25 mmol) in benzene (12 mL) was added dropwise to a solution of **6** (86 mg, 0.427 mmol) in benzene (2 mL). The mixture was stirred and heated for 30 min. It was then washed with saturated $NaHCO_3$ solution, saturated NH_4Cl solution, dried ($MgSO_4$), and concentrated *in vacuo* to give 67 mg (84%) of **7**. This residue was purified by preparative tlc on a silica gel plate (Merck, Kieselgel 60 F_{254}, 0.5 mm) using a mixture of ether and *n*-hexane (1:1 v/v) to give 33 mg (42%) of **8**; $[\alpha]_D^{24}$ +24.9 (*c* 0.825, $CHCl_3$); ir *ν*: 3425, 1715, 1255, 1165, 1065, 1040 cm^{-1}; ^{1}H nmr δ: 0.88 (3H, t, *J* = 4 Hz), 2.68 (2H, d, *J* = 4 Hz), 4.36 (1H, q, *J* = 4 Hz), 4.50–4.80 (1H, m); ms, *m/z*: 187 (M^+ + 1, 58), 169 (100). *Mol. Wt.* calcd. for $C_{10}H_{19}O_3$: 187.1335; found (hrms) *m/z*: 187.1334. *Anal.* calcd. for $C_{10}H_{18}O_3$: C 64.49, H 9.74; found: C 64.14, H 9.72.

Acknowledgement

I am grateful to Associate Professor Dr. Masahiro Hirama, Tōhoku University, for useful discussion and generous support.

1. R. F. Vesonder, F. H. Stodola, and W. K. Rohwedder. Can. J. Biochem. **50**, 363 (1972).
2. (*a*) M. Hirama, T. Noda, and S. Itō. J. Org. Chem. **50**, 127 (1985); (*b*) K. Mori, H. Mori, and T. Sugai. Tetrahedron, **41**, 919 (1985).
3. M. Hirama, M. Shimizu, and M. Iwashita. J. Chem. Soc. Chem. Commun. 599 (1983).
4. R. Tscheshe, H.-J. Hoppe, G. Snatzke, G. Wulff, and H.-W. Fehlhaber. Chem. Ber. **104**, 1420 (1971).
5. A. Numata, K. Hokimoto, T. Takemura, T. Katsuno, and K. Yamamoto. Chem. Pharm. Bull. **32**, 2815 (1984).
6. E. M. Kaiser, J. D. Petty, and L. A. Knutson. Synthesis, 509 (1977).

Can. J. Chem. Downloaded from www.nrcresearchpress.com by 213.222.148.141 on 09/07/12
For personal use only.

1,*n*-Radical ions. The photosensitized (electron transfer) formation of 1,5-radical cations[1]

DONALD R. ARNOLD,[2] BRIAN J. FAHIE, LAURIE J. LAMONT, JACEK WIERZCHOWSKI, AND KENT M. YOUNG
Department of Chemistry, Dalhousie University, Halifax, N.S., Canada B3H 4J3

Received May 6, 1987

DONALD R. ARNOLD, BRIAN J. FAHIE, LAURIE J. LAMONT, JACEK WIERZCHOWSKI, and KENT M. YOUNG. Can. J. Chem. **65**, 2734 (1987).

The photosensitized (electron transfer) reactions of 3-phenyl-2,3-dihydrobenzofuran (**8***a*), 5-methyl-3-phenyl-2,3-dihydrobenzofuran (**8***b*), *cis* and *trans*-2-methoxy-1-phenylindane (**9**, *cis* and *trans*), 3,3-diphenyltetrahydrofuran (**10**), and 2,2-diphenyl-1-methoxycyclopentane (**11**) have been studied using 1,4-dicyanobenzene as an electron-accepting photosensitizer and acetonitrile–methanol (3:1) as solvent. These reaction conditions cause carbon–carbon bond cleavage of analogous acyclic β,β-diphenylethyl ethers to give products derived from the diphenylmethyl radical and the α-oxycarbocation intermediates. The purpose of this study was to determine if this reaction could be applied to five-membered cyclic derivatives to give 1,5-radical cations.

The primary products from **8***a* and **8***b* were the dehydrogenated, aromatized 3-phenylbenzofurans **14***a* and **14***b*. These products react further; continued irradiation gave the methanol adducts, *cis* and *trans*-2-methoxy-3-phenyl-2,3-dihydrobenzofuran (**15***a* and **15***b*, *cis* and *trans*). The only observed reaction of the indanes (**9**, *cis* and *trans*) was *cis–trans* isomerization. Deuterium was incorporated at the bis-benzylic position of **8** and **9** when the irradiation was carried out in acetonitrile–methanol-O-*d*. These results are consistent with reversible deprotonation from the radical cations. There was no evidence for carbon–carbon bond cleavage with either **8** or **9**. The relative rate, deprotonation faster than carbon–carbon bond cleavage, is explained in terms of the conformation of the bond that cleaves in relation to the singly occupied molecular orbital (SOMO) of the radical cation. Oxidation potential measurements support the conclusion that the SOMO of **8** and **9** is largely associated with the fused phenyl ring and is therefore orthogonal to the benzylic carbon–carbon bond. Irradiation of *cis* or *trans*-2-methoxy-3-phenyl-2,3-dihydrobenzofuran (**15***a*, *cis* or *trans*), under these conditions, leads to *cis–trans* isomerization. The mechanism in this case involves the reversible loss of methanol. There is evidence that the addition of methanol to **14** involves the sensitizer radical anion – **14** radical cation pair.

In contrast with the fused bicyclic systems, the monocyclic tetrahydrofuran **10** and the methoxycyclopentane **11** both cleave under these conditions; the products are the expected acetals **22** and **29** formed from the intermediate 1,5-radical cations. In **10** and **11** the SOMO, which is largely associated with the diphenylmethyl moiety, can overlap with the adjacent carbon–carbon bond and cleavage occurs as in analogous acyclic systems. Both **10** and **11** are relatively stable to irradiation under conditions that are identical except with acetonitrile as solvent (without methanol). We found no evidence for cyclization of the intermediates (1,5-radical cation or 1,5-diradical) into the terminal phenyl ring.

DONALD R. ARNOLD, BRIAN J. FAHIE, LAURIE J. LAMONT, JACEK WIERZCHOWSKI et KENT M. YOUNG. Can. J. Chem. **65**, 2734 (1987).

Utilisant le dicyano-1,4 benzène comme photosensibilisateur accepteur d'électrons et un mélange d'acétonitrile–méthanol (3:1) comme solvant, on a étudié les réactions photosensibilisées (transferts d'électrons) du phényl-3 dihydro-2,3 furanne (**8***a*), du méthyl-5 phényl-3 dihydro-2,3 benzofuranne (**8***b*), des méthoxy-2 phényl-1 indanes *cis* et *trans* (**9**-*cis* et -*trans*), du diphényl-3,3 tétrahydrofuranne (**10**) et du diphényl-2,2 méthoxy-1 cyclopentane (**11**). Lorsqu'on soumet les éthers acycliques β,β-diphényléthyliques analogues aux mêmes conditions, il se produit une rupture de la liaison carbone–carbone qui conduit à des produits provenant du radical diphénylméthyle et des intermédiaires α-oxycarbocationiques. Le but du présent travail était de déterminer si cette réaction pouvait être appliquée à des dérivés cycliques à cinq chaînons pouvant conduire à des cations radicaux-1,5.

Les produits primaires des réactions des produits **8***a* et **8***b* sont les phényl-3 benzofurannes déshydrogénés et aromatisés **14***a* et **14***b*. Ces produits donnent lieu à des réactions subséquentes; si l'on continue l'irradiation, il y a formation des adduits avec le méthanol, les méthoxy-2 phényl-3 dihydro-2,3 benzofuranne *cis* et *trans* (**15***a* et **15***b*, *cis* et *trans*). Dans le cas des indanes (**9**, *cis* et *trans*), la seule réaction observée est l'isomérisation *cis–trans*. Lorsqu'on effectue l'irradiation dans un mélange d'acétonitrile–méthanol-O-*d*, il y a incorporation de deutérium à la position bis-benzylique des produits **8** et **9**. Ces résultats sont en accord avec une déprotonation réversible des cations radicaux. Aucun résultat ne nous permettrait de croire que les produits **8** ou **9** donnent lieu à une rupture de la liaison carbone–carbone. Le fait que la réaction de déprotonation est plus rapide que la réaction de rupture de la liaison carbone–carbone est expliqué en fonction de la conformation de la liaison qui se brise par rapport à l'orbitale moléculaire occupée seule (OMOS) du cation radical. Des mesures de potentiels d'oxydation sont en accord avec la conclusion que les OMOS des composés **8** et **9** sont largement associées avec le cycle phényle condensé et qu'elles sont donc orthogonales à la liaison carbone–carbone benzylique. Dans ces conditions, l'irradiation des composés méthoxy-2 phényl-3 dihydro-2,3 benzofurannes *cis* et *trans* (**15***a*, *cis* et *trans*) conduit à une isomérisation *cis–trans*. Dans ce cas, le mécanisme implique la perte réversible de méthanol. On a des indications à l'effet que l'addition de méthanol au composé **14** implique la paire anion radical sensibilisateur – cation radical **14**.

Par opposition avec les résultats obtenus avec les systèmes bicycliques condensés, les composés monocyliques comme le tétrahydrofuranne **10** et le méthoxycyclopentane **11** se clivent tous les deux dans ces conditions; les produits obtenus sont les acétals attendus **22** et **29** qui se forment à partir des cations radicaux-1,5 intermédiaires. Dans les cas des produits **10** et **11**, les OMSO, qui sont largement associées avec la portion diphénylméthyle, et la liaison carbone–carbone voisine peuvent se recouvrir et un clivage se produit alors comme dans les systèmes acycliques. Si les conditions des réactions ne sont modifiées que par l'élimination du méthanol dans le solvant, les composés **10** ainsi que **11** sont relativement stables. Les résultats obtenus ne suggèrent pas que les intermédiaires cation radical-1,5 ou diradical-1,5 se cyclisent dans le noyau phényle terminal.

[Traduit par la revue]

[1]This is also part 19 of the series Radical Ions in Photochemistry. Preceding publications in these series are refs. 1 and 2.

[2]Author to whom correspondence may be addressed.

Can. J. Chem. Downloaded from www.nrcresearchpress.com by 213.222.148.141 on 09/07/12
For personal use only.

Can. J. Chem. Downloaded from www.nrcresearchpress.com by 213.222.148.141 on 09/07/12
For personal use only.

Introduction

Radical ions have received the least attention of all the common intermediates in organic chemistry. Most research in this area has focused on those special examples which are stable and are consequently the least interesting from the point of view of reactivity (3). Of the reactive species, 1,2-radical ions are the most studied. This class includes the alkene radical cations (4) and the ketyls generated by the one-electron reduction of carbonyl compounds (5). Reactions involving 1,3-radical ions are much less common although both theoretical and experimental interest in these species has increased markedly in recent years (2, 6). These intermediates have been formed by the cleavage of three-membered ring compounds. Addition of a 1,2-radical ion to a double bond or cleavage of a four-membered ring compound can lead to a 1,4-radical ion. A few examples of this class have been studied (4, 7). 1,*n*-Radical ions with $n > 4$ are virtually unknown (8),[3] this is in spite of the fact that these intermediates should also be readily available by cleavage of the molecular ions or larger membered ring compounds. In fact, the relationship between the ring-closed (the one-electron two-center bond) and ring-opened species is one of the interesting aspects of this area.

We have earlier shown (1*a*, 1*b*, and 10) that the radical cations of methyl 2,2-diphenylethyl ether (**1**) and 2-methoxy-2-diphenylmethylnorbornane (**2**, *endo* and *exo*) are readily formed by photosensitization (electron transfer) and that they cleave, giving the radical and the carbocation intermediates (reactions [1] and [2]). The mechanism of these reactions is

[1] $Ph_2CHCH_2OCH_3$ (**1**) $\xrightarrow[CH_3CN,\ CH_3OH]{h\nu,\ \text{Sens.}}$ Ph_2CH_2 (**5**) + $CH_3OCH_2OCH_3$ (**6**)

[2] **2**, *exo, endo* $\xrightarrow[CH_3CN,\ CH_3OH]{h\nu,\ \text{Sens.}}$ + 5 (**7**, $(OCH_3)_2$)

Sens.: 1,4-dicyanobenzene (**3**) or
1,4-dicyanonaphthalene (**4**)

summarized in abbreviated form in Scheme 1. 1,4-Dicyanobenzene (**3**) and 1,4-dicyanonaphthalene (**4**) have been used as electron-accepting photosensitizers for these reactions in the solvent acetonitrile–methanol (3:1).

The stability of the diphenylmethyl radical and α-oxycarbocation help to lower the bond dissociation energy of the central bond of the radical cations of **1** and **2**. Thus, the radical cation cleavage (Scheme 1, step 4) occurs rapidly enough to compete

[3]The nomenclature in this area has not been fully defined. We recognize a difference between 1,*n*-radical ions and distonic radical ions (9). Distonic radical ions are coordinatively saturated at the ionic site and are not available by one-electron transfer involving a stable precursor without extensive rearrangement. They are common products of gas phase ionization reactions, and are occasionally encountered as intermediates in solution. The 1,5-ammonium salt – alkyl radical intermediate in the Hofmann–Loffler–Freytag reaction is a distonic radical cation.

1. Sensitizer (A) $\xrightarrow{h\nu}$ A*
2. $Ph_2CH—R + A^* \longrightarrow Ph_2CH—R^{\ddagger} + A^{-}$
3. $Ph_2CH—R^{\ddagger} + A^{-} \longrightarrow Ph_2CH—R + A$
4. $Ph_2CH—R^{\ddagger} \longrightarrow Ph_2CH\cdot + R^{+}$
5. $R^{+} + CH_3OH \longrightarrow R—OCH_3 + H^{+}$
6. $Ph_2CH\cdot + A^{-} \longrightarrow Ph_2CH^{-} + A$
7. $Ph_2CH^{-} + CH_3OH \longrightarrow Ph_2CH_2 + CH_3O^{-}$
8. $Ph_2CH—R^{\ddagger} \longrightarrow Ph_2C(\cdot)—R + H^{+}$
9. $Ph_2C(\cdot)—R + A^{-} \longrightarrow Ph_2C(^{-})—R + A$
10. $Ph_2C(^{-})—R + H^{+} \longrightarrow Ph_2CH—R$

SCHEME 1. The mechanism for the photosensitized (electron transfer) carbon–carbon bond cleavage.

effectively with other fast reactions, particularly deactivation by back electron transfer (Scheme 1, step 3) and deprotonation from the bis-benzylic position (Scheme 1, step 8).

We have studied the photosensitized (electron transfer) reactions of **8**–**11** (Chart 1) (and **15**) under conditions identical

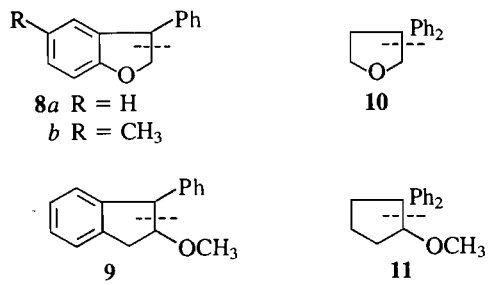

8*a* R = H
b R = CH_3

10

9 **11**

CHART 1

with those used previously in reactions [1] and [2]. Compounds **8**–**11** are cyclic analogs of **1** and **2**. They incorporate the β,β-diphenylethyl ether moiety so the radical cation might be expected to undergo the cleavage process, at the bond indicated (Chart 1), to give 1,5-radical cations. However, the carbon–carbon bond that would be expected to cleave in **8** and **9** is conformationally constrained by virtue of the fused bicyclic structure. Also, **8** is a dihydroaromatic compound. These features may be important in influencing the ultimate reactivity of **8** and **9**.

Results and discussion

The fused phenyl bicyclic systems 8, 9, and 15

3-Phenyl-2,3-dihydrobenzofuran (**8***a*) is a known compound (11*d*). It and 5-methyl-3-phenyl-2,3-dihydrobenzofuran (**8***b*) were prepared by the reported procedure (Scheme 2) (11). The 5-methyl derivative was used in our preliminary study because it can be prepared in higher yield than the unsubstituted compound and because the distinctive proton nuclear magnetic resonance (^{1}H nmr) signal due to the 5-methyl protons provides a useful probe for following the progress of reactions of **8***b*.

Irradiation of **8***a* in acetonitrile–methanol (3:1), with 1,4-dicyanobenzene (**3**) as the electron-accepting photosensitizer (conditions identical to those used for reactions [1] and [2]) led to a relatively inefficient consumption of **8***a*. Analysis of the photolysate by capillary column vapour phase chromatography with a mass selective detector (gc/ms) indicated two major volatile products were formed. These products constituted more than half of the reacted starting material; no other product of similar retention time was detected. The crude photolysis mixture was separated by column chromatography and the products were identified by spectroscopic techniques (infrared

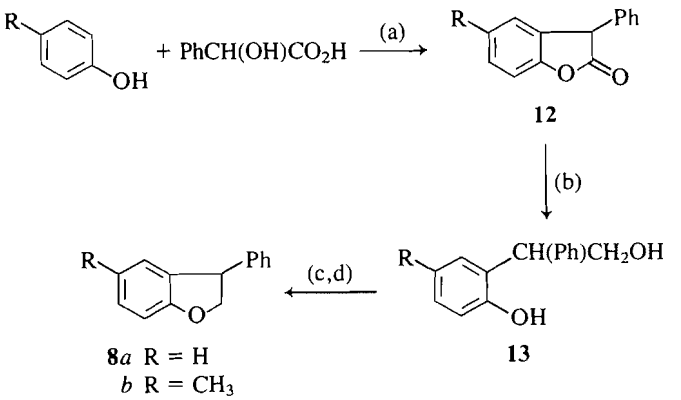

SCHEME 2. The synthesis of 3-phenyl-2,3-dihydrobenzofurans (**8***a* and **8***b*) (11). (a) 75% H_2SO_4, 130°C, 45 min; (b) $LiAlH_4$; (c) phthalic anhydride, pyridine, 48 h; (d) 2% NaOH, reflux 1 h.

(ir), ^{1}H nmr, and mass spectrometry (ms)). They are the isomeric *cis* and *trans*-2-methoxy-3-phenyl-2,3-dihydrobenzofurans (**15***a*, *cis* and *trans*) (reaction [3]).

It seemed probable that these products resulted from a photosensitized (electron transfer) addition of methanol to the 3-phenylbenzofuran formed as a primary product. Control experiments supported this conclusion. Irradiation of 3-phenylbenzofuran (**14***a*) (12) under these conditions led to the same methanol adducts in good yield, and **14***a* was formed by irradiation of **8***a* under identical conditions but in acetonitrile without added methanol.

Similar results were obtained starting with **8***b* (reaction [3]).

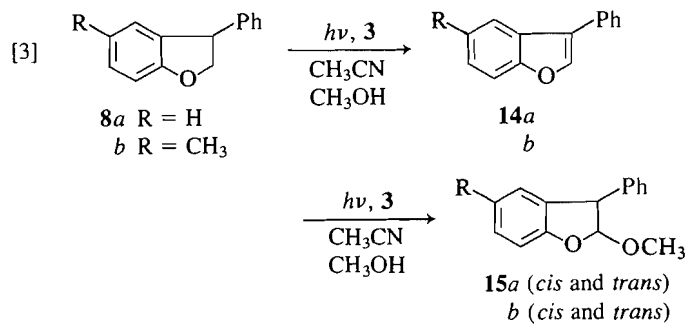

A possible first step in the formation of **14** from the radical cation of **8** is deprotonation from the bis-benzylic (i.e., 3) position. Subsequent loss of the hydrogen from the 2-position, either by disproportionation or by hydrogen transfer to the sensitizer radical anion, has aromatization as a driving force and therefore should be favoured. Reversible deprotonation of radical cations similar to those of **8***a* and **8***b* has been observed under these conditions (Scheme 1, step 8) (1*a*); this possibility was tested.

The photosensitization (electron transfer) of **8***b* was carried out in acetonitrile–methanol-O-*d* until reaction [3] was 20% complete. The unreacted starting material was isolated from the reaction mixture and the deuterium content was determined by ^{1}H and ^{2}H nmr. The proton at the bis-benzylic position was more than 90% exchanged for deuterium. There was no evidence for deuterium incorporation at either the methylene position (i.e., 2) or the 5-methyl group (reaction [4]).

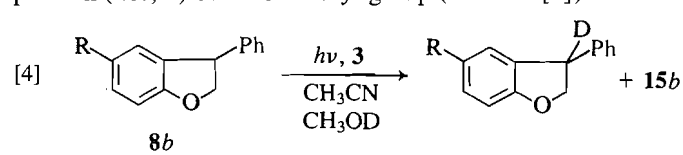

Our study was next extended to the isomeric methanol adducts **15**, *cis* and *trans*. The radical cation of **15** should be even more prone to carbon–carbon bond cleavage than **8** since cleavage would result in a carbocation stabilized by two electron-donating oxygen atoms.[4] Furthermore, with **15**, *cis–trans* isomerization that would accompany reversible cleavage could be observed.

The photosensitized (electron transfer) reactions of **15** *cis* and *trans* were carried out in the usual way. The *cis–trans* isomerization was observed but none of the products expected from carbon–carbon bond cleavage were formed, even after prolonged irradiation.

An alternative mechanism for configurational isomerization would involve the reversible deprotonation at the bis-benzylic position analogous to that observed with **8**. To test this possibility **15***b* *cis* and **15***b* *trans* were irradiated as before except that the solvent was acetonitrile-d_3–methanol-d_4 (3:1). Analysis (^{1}H nmr) of the isomerized product and the recovered starting material, as a function of irradiation time, indicated that *exchange of both the bis-benzylic proton and the methoxy group had occurred in both isomers, and that the rate of exchange was essentially the same at both positions* (reaction [5]).

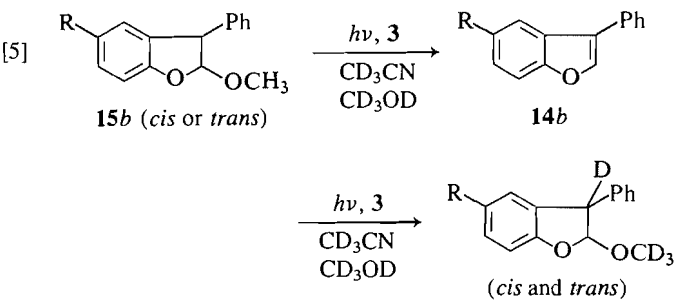

In the case of **15***b* *cis* yielding **15***b* *trans*, there was some evidence that the exchange of the bis-benzylic proton may have been somewhat more rapid than the exchange of the methoxy group; but, the difference in rate was small so that a mechanism that exchanges protons at both positions must dominate.

To explain these results we propose that following deprotonation from the bis-benzylic position (i.e., 3), the resulting radical aromatizes to **14** by loss of the methoxy radical. Then perdeutero methanol adds to the radical cation of **14** (reaction [3]).

This mechanism requires loss of the methoxy radical from the same radical that was invoked as an intermediate during the addition of methanol to the radical cation of **14**. The difference may be that the addition of methanol occurs while the radical cation of **14** is still in the solvent cage with the sensitizer radical anion. Under these conditions the radical would be reduced rapidly by back electron transfer from the sensitizer radical anion and the anion would be protonated. This would effectively prevent reversal by loss of methoxy radical in this case. The deprotonation of the radical cation of **15** and subsequent loss of methoxy radical would then occur outside the radical ion cage. A similar proposal of addition of methanol to the radical cation of an alkene held within a solvent cage of a radical ion pair has recently been reported (13).

The 2-methoxy-1-phenylindanes (**9**, *cis* and *trans*) were

[4]Cleavage of the radical cation of acyclic β,β-diphenylethyl acetals is a facile reaction. For example, 2-(2,2-diphenylethyl)-1,3-dioxalane gives a good yield of diphenylmethane and 2-methoxy-1,3-dioxalane under these conditions (D. R. Arnold, L. J. Lamont, and J. Trottier, unpublished results).

Can. J. Chem. Downloaded from www.nrcresearchpress.com by 213.222.148.141 on 09/07/12
For personal use only.

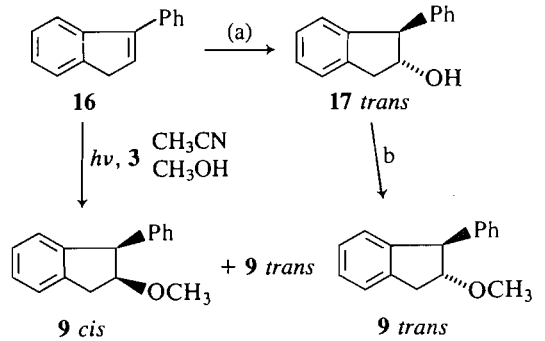

SCHEME 3. The synthesis of 2-methoxy-1-phenylindane (**9**). (a) 9-BBN, THF, reflux; NaOH, H_2O_2, aq.; (b) NaH, dimethyl sulfate, reflux, 24 h (14).

prepared by two methods starting with 1-phenylindene (**16**) (Scheme 3). The hydroboration sequence (14) gave exclusively **17** *trans*, while the photosensitized (electron transfer) addition of methanol to the indene (4, 15) gave predominantly **17** *cis* (*cis*:*trans*, 6:1). These are new compounds; the structural assignments were firmly established by spectral methods (^{1}H nmr).

The photosensitization (electron transfer) of either **9** *cis* or **9** *trans* led to inefficient configurational isomerization (reaction [6]). Isomerization was accompanied by incorporation of

[6] 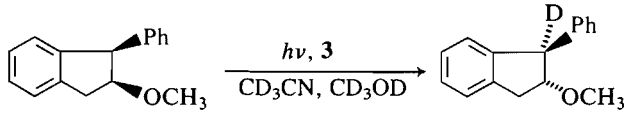

9 *cis* 9 *trans*

deuterium in the bis-benzylic position when acetonitrile-d_3–methanol-d_4 (3:1) was used as the solvent. Analysis of the isomers recovered after prolonged irradiation in this perdeutero solvent mixture indicated that exchange also occurred, albeit much less efficiently, at the mono-benzylic position (i.e., 3) and at the methoxy.

Apparently reversible deprotonation of the radical cation is again the dominant process. Deprotonation from the bis-benzylic position is favoured. Deprotonation from the mono-benzylic position and loss of methoxy radical followed by readdition of methanol to **16** both occur but are relatively inefficient processes. The loss of the methoxy radical does not have the driving force of aromatization in this case.

This efficiency of exchange at the bis-benzylic position relative to that at the mono-benzylic position was also observed upon irradiation of 1-phenylindane (**18**). Irradiation of **18** under the usual conditions, with acetonitrile–methanol-O-*d* (3:1) as the solvent, led to incorporation of deuterium at the bis-benzylic position (reaction [7]). Prolonged irradiation in this medium

[7] 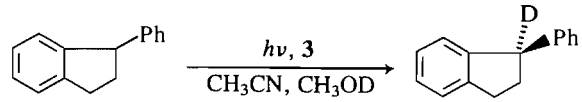

18

led to further incorporation of deuterium in the mono-benzylic position; however, the relative rate of exchange at these two positions is in the order of 100:1. The kinetic acidity of the radical cation of **18** therefore follows the thermodynamic acidity. The pK_a of the proton at the bis-benzylic position must be considerably more negative by virtue of the additional resonance stabilization of the radical, which weakens the carbon–hydrogen bond (1*a*, 16).

TABLE 1. The oxidation potential of some diphenylmethyl compounds[a]

Diphenylmethyl compound	E_p (V)[b]	$E_p - E_p/2$ (mV)
Diphenylmethane	2.17[c]	120
1,1-Diphenylethane	2.16[d]	—
1	2.16[d]	—
2, *exo* and *endo*	1.95[c]	120
8*b*	1.47	105
9, *trans*	2.04	112
10	2.22	113
11	2.16	150
1-Phenylindane, **18**	2.14	156

[a]Measured by cyclic voltammetry at a sweep rate of 100 mV s^{-1}, in acetonitrile (0.1 M tetraethylammonium perchlorate).
[b]Peak potential versus SCE. The estimated error is ±0.02 V. The oxidation potential ($E^{ox}_{1/2}$) can be taken as 0.03 V less than the anodic peak potential.
[c]Reference 1*a*.
[d]Reference 10.

All of these reactions (reactions [3]–[7]) can be accounted for by a first step involving the deprotonation of the radical cation (Scheme 1, step 8). We found no evidence for carbon–carbon bond cleavage of the radical cations of these fused phenyl bicyclic systems. In contrast, in reactions [1] and [2] carbon–carbon bond cleavage is much more favourable than deprotonation. This dichotomy may appear surprising at first, but it can be explained in terms of the conformation of the singly occupied molecular orbital (SOMO) of the radical cation relative to the bond (carbon–carbon versus carbon–hydrogen) that cleaves.

Table 1 lists the oxidation potentials of **1**, **2**, **8***b*, **9**, **17**, and some other compounds of interest. The SOMO of **1** and **2** is largely associated with the diphenylmethyl moiety (1*a*, 10). The oxidation potential of **8** is considerably lower than that of **1**, **2**, and other diphenylmethyl derivatives listed in Table 1. This is consistent with the SOMO of **8** being largely associated with the fused phenyl ring. This is expected since this ring is substituted with an electron-donating group (that is, the oxygen atom) that lowers the oxidation potential.

In the case of **1** and **2** there are favourable conformations of the radical cation that allow the SOMO to be parallel to the σ-orbital involved in the carbon–carbon bond that cleaves. This conformation is not possible for the bicyclic structure of **8** and **15**. Instead, the carbon–hydrogen bond is held more closely parallel with the SOMO.

The loss of methanol from the radical cations of **15***b*, *cis* and *trans*, is also a dominant process in the gas phase. The question that arises is whether the mechanism of this reaction involves a concerted loss of the methanol molecule, which might be favoured in the case of the *trans* isomer (where the methoxy group and the proton are *cis*), or whether a stepwise loss of a proton and a methoxy radical is involved. The base peak in the mass spectrum of both isomers is the molecular ion (m/z = 240). The relative abundance of the 208 m/z peak (that is, the molecular ion minus methanol) versus the ionizing voltage is shown for the two isomers in Fig. 1. Loss of methanol from the radical cation of the *trans* isomer is only about twice as efficient as from the *cis* isomer. Furthermore, a significant metastable peak at 180.3 m/z in the spectrum of both isomers provides additional evidence that methanol is lost from the molecular ion of both. We found no evidence that loss of methanol occurs by different mechanisms in these two isomers.

Can. J. Chem. Downloaded from www.nrcresearchpress.com by 213.222.148.141 on 09/07/12
For personal use only.

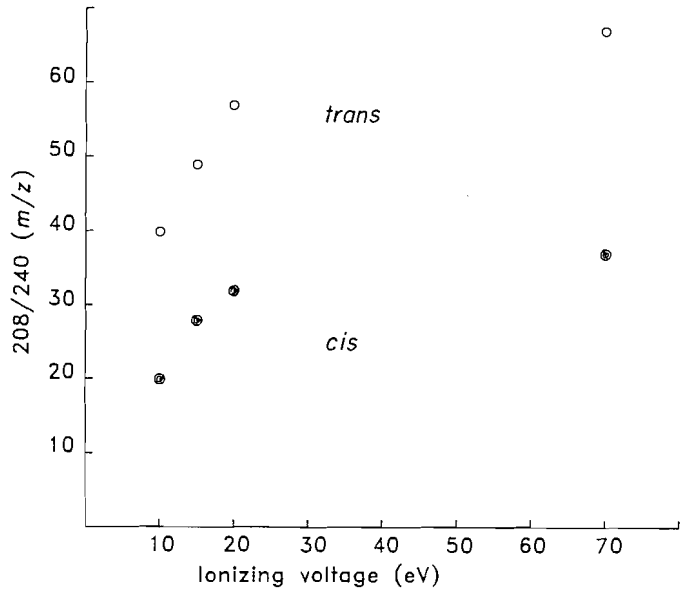

FIG. 1. The relative abundance of the 208 m/z fragment (molecular ion minus methanol) as a function of ionizing voltage for **15***b* *cis* and *trans*.

It would seem likely that for **9** *cis* and *trans* the SOMO would at least partially reside on the unfused phenyl ring and that carbon–carbon bond cleavage could then occur. However, the oxidation potential of **9** *trans* is also somewhat lower than that of **1**, **2**, and other diphenylmethyl compounds listed in Table 1. We suggest that in these radical cations also the SOMO is associated largely with the fused phenyl ring and is therefore orthogonal to the benzylic carbon–carbon bond.[5]

*The monocyclic systems **10** and **11***

The radical cations of 3,3-diphenyltetrahydrofuran (**10**) and 2,2-diphenyl-1-methoxycyclopentane (**11**) should be able to attain a conformation that would allow sufficient overlap of the SOMO associated with the diphenylmethyl moiety with the σ-orbital of the benzylic carbon–carbon bond so that cleavage will occur. The preferred conformation of **10**, in the crystal, has been determined by X-ray analysis.[6] The bis-benzylic carbon–carbon bond of **10** forms an angle of 62° with the plane of one of the phenyl rings.

The preparation of the tetrahydrofuran (**10**) has been reported (17*a*). The synthetic procedure used is shown in Scheme 4.

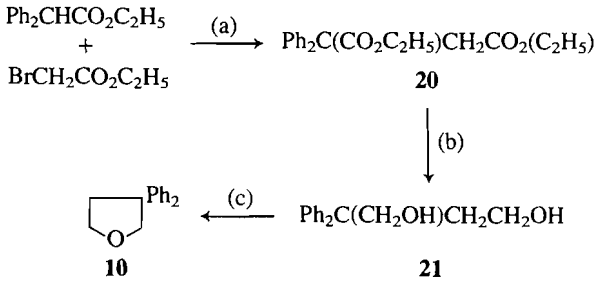

SCHEME 4. The synthesis of 3,3-diphenyltetrahydrofuran (**10**) (17). (a) NaH, ether; (b) $LiAlH_4$, ether; (c) HBr 49% aq., reflux.

[5]The site of the SOMO can be changed to the unfused phenyl ring of **9** by appropriate substitution. For example, carbon–carbon bond cleavage occurs when 2-methoxy-1-(4-methoxyphenyl)indane is subjected to these conditions (D. R. Arnold and K. Henseleit, unpublished results).

[6]T. S. Cameron and B. Vincent, unpublished results.

Irradiation of an acetonitrile–methanol (3:1) solution of 1,4-dicyanobenzene **3** and **10** under the usual conditions gave a good yield of methyl (3,3-diphenylpropyl) formaldehyde acetal **22** (reaction [8]).

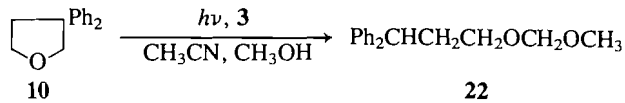

The proof of structure for **22** rests upon an analysis of the ^1H and ^{13}C nmr spectra and upon the isolation and characterization of 3,3-diphenyl-1-propanol (**23**), a known compound (18), following hydrolysis of the crude photolysate.

Carbon–carbon bond cleavage of the radical cation (step 4, Scheme 1) gives the 1,5-radical cation, which is trapped by the nucleophile methanol. Similar irradiation of **10** in acetonitrile without added methanol causes relatively little reaction. There was no evidence (gc/ms) for formation of any rearranged or isomerized product. This indicates that in the absence of an effective nucleophilic trapping reagent, the intermediate 1,5-radical cation returns to the starting tetrahydrofuran.[7] It is not clear whether back electron transfer precedes (in which case the intermediate 1,5-diradical would be involved) or is subsequent to ring closure.

The cyclopentane **11** was prepared from the known alcohol **28** (20*a*) by treatment with sodium hydride followed by dimethylsulphate (Scheme 5).

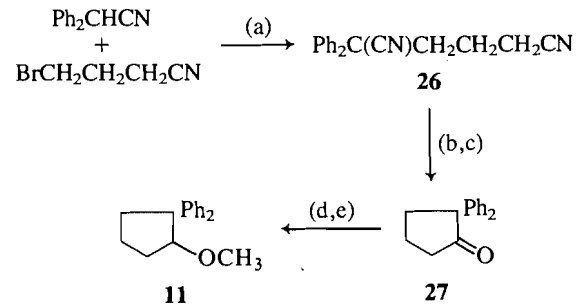

SCHEME 5. The synthesis of 2,2-diphenyl-1-methoxycyclopentane (**11**) (20). (a) $NaNH_2$, NH_3, benzene; (b) KOH aq., ethylene glycol; (c) acetic anhydride; (d) $LiAlH_4$; (e) NaH, dimethyl sulfate.

Irradiation of an acetonitrile–methanol (3:1) solution of 1,4-dicyanobenzene (**3**) and **11** under the usual conditions led to the efficient formation of 5,5-diphenylpentanal dimethylacetal **29** (reaction [9]). The structure assigned to **29** is consistent with

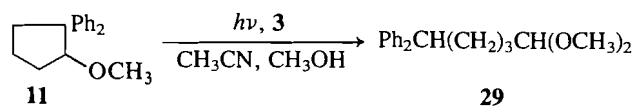

the spectral (^1H nmr and ms) data. The aldehyde **30**, obtained upon hydrolysis of the crude photolysate, was also fully characterized.

Again in this case **11** was relatively stable to irradiation under conditions identical to earlier experiments except that no methanol was used. The 1,5-radical cation is efficiently trapped with added nucleophile, but no evidence was found for rearrangement or isomerization of **11** in the absence of the trapping agent.

[7]A pattern of reactivity of 1-phenyl-1,*n*-radical cations seems to be emerging. The 1,3- and 1,5-radical cations apparently do not cyclize into the terminal phenyl while the 1,4-homologues do (2*a*, 4, 19). The transition state is 6-*endo*–*trig* in the reactive case.

Can. J. Chem. Downloaded from www.nrcresearchpress.com by 213.222.148.141 on 09/07/12
For personal use only.

Can. J. Chem. Downloaded from www.nrcresearchpress.com by 213.222.148.141 on 09/07/12
For personal use only.

The oxidation potentials of **10** and **11** are listed in Table 1. Incorporation of the diphenylmethyl moiety in a five-membered ring has little effect on the oxidation potential. The SOMO of both **10** and **11** can overlap sufficiently with the σ-orbital of the benzylic carbon–carbon bond so that cleavage can occur.

The marked difference in reactivity of the bicyclic fused radical cations and the monocyclic analogues illustrates the importance of overlap of the SOMO with the bond that cleaves. This concept has been recognized as an important factor directing the deprotonation from the carbon α to the nitrogen of the radical cation of tertiary amines (21), and from the benzylic position of alkyl aromatic radical cations (22). There are exceptions, however. We know of two examples where cleavage of a carbon–carbon bond that is orthogonal to the SOMO does occur. The photosensitized (electron transfer) irradiation of *meso*-1,2-dimethyl-1,2-dimethoxyacenaphthene (**31**) and *rac*-9,10-dimethoxy-9,10-dimethyl-9,10-dihydro-

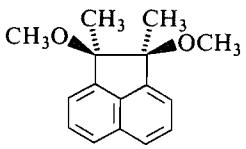

31

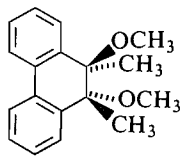

32

phenanthrene (**32**) in acetonitrile with **4** as the electron acceptor leads to formation of the diastereomers (**8***a*, **8***b*). As both the radical and the cationic centers are conjugatively coupled through the π-system in both of these cases, factors other than conformation (e.g., orbital symmetry) may be involved.

In summary, 1,5-radical cations are formed as intermediates upon cleavage of the radical cation of five-membered cyclic compounds. In the presence of nucleophiles, reaction proceeds as with acyclic analogues. For example, the acetals **22** and **29** are formed in high yield in reactions [8] and [9]. The bond cleavage process requires orbital overlap with the SOMO. When the SOMO is held orthogonal to the adjacent bond, as in the bicyclic systems **8**, **9**, and **15**, deprotonation of the radical cation occurs instead. Product formation is then dependent upon the subsequent reactivity of the radical.

Experimental

General information

The ^{1}H nmr spectra were recorded on a Varian Associates EM360L, CFT-20, T-60 or a Nicolet Industries narrow bore 360-MHz spectrometer and are reported in parts per million downfield from TMS. The ^{2}H nmr spectra were obtained on the Nicolet instrument operating at 55.4 MHz. The ^{13}C nmr spectra were recorded on the CFT-20 or on the Nicolet spectrometer operating at 90 MHz. Infrared spectra were recorded on an air-purged Perkin Elmer 180 grating spectrometer, a Perkin Elmer 233B, or a Perkin Elmer 1320 spectrometer and are reported in wavenumbers (relative to the 1601.8 cm^{-1} absorption of polystyrene). Mass spectra were recorded on a modified Du Pont CEC Model 21-104 mass spectrometer, except where noted.

The gc/ms analyses were done on an Hewlett Packard 5890A GC/5970 mass selective detector interfaced with an H.P. 9816 microcomputer. The columns used for analyses were 25 m × 0.2 mm methyl silicone or 5% phenyl methyl silicone on fused silica, with a film thickness of 0.25 μm, or a 25 m × 0.2 mm Carbowax 20M, with a film thickness of 0.25 μm where noted. Product analyses were determined by vapor phase chromatography (gc) using a Varian Aerograph 1200 chromatograph with flame ionization detection. The column used was 1/8 in. × 6 ft copper packed with 8% SE-30 on Chromosorb G 60/80. An Aerograph Autoprep A-700 (3.8 in. × 6 ft aluminum columns packed with 5 or 10% SE-30 on Chromosorb 60/80 NAW) was used for prep-gc. Preparative medium pressure liquid chromatography (mplc) was carried out using a 25 × 1000 mm column packed with tlc grade silica gel (without binder) (Merck) at 15 psi (helium) (1 psi = 6.9 kPa) with hexanes. The columns were eluted with a hexanes/methylene chloride gradient and the eluate was monitored/collected by a uv spectrometer/fraction collector. Ultraviolet–visible absorption spectra were recorded on a Cary–Varian 219 absorption spectrophotometer and are reported in nanometers. Melting points were taken on a Thermolyne melting point apparatus, and are uncorrected. Combustion analyses were performed by Canadian Microanal. Service Ltd., Vancouver, B.C.

Proton nmr spectra for **9** and **17** were simulated using the Lame (Laocoon with magnetic equivalence) simulation program on a CDC Cyber 170-730 mainframe computer. Irradiations were done in Pyrex tubes using a General Electric Co. 1-kW medium pressure mercury vapor lamp (CGE HR 1000 DX 36-15) with a quartz cooling jacket immersed in a constant temperature bath at 10°C.

Oxidation potentials were obtained by cyclic voltammetry using a three-electrode cell that has been previously described (2*a*). The working electrode was a platinum sphere (1 mm diameter) and the counter electrode was a Pt wire. The reference electrode was a saturated calomel electrode (SCE). The electrolyte used was 0.1 M tetraethylammonium perchlorate in acetonitrile. Substrate concentrations were typically 1 mM.

Materials

All solvents used were distilled prior to use. Acetonitrile, 1,4-dicyanobenzene (**3**), and 1,4-dicyanonaphthalene (**4**) for photochemical use were purified as previously described (1*a*). Deuterated acetonitrile and methanol-d_4 were obtained from Stohler Isotopes. Methanol-O-*d* was obtained from Aldrich Chemical Co.

*3-Phenyl-2,3-dihydrobenzofuran (8*a*)*

This compound was prepared starting with mandelic acid and phenol using reported procedures (11). The colourless needles of **8***a* obtained upon recrystallization from 95% ethanol had mp 37.5°C (lit. (11*e*) mp 38–39°C); ^{1}H nmr (360 MHz) in $CDCl_3$: 6.83–7.30 (m, 9H), 4.87 (dd, 1H, J = −8.85 Hz, J = 9.7 Hz), 4.64 (dd, 1H, J = 9.7 Hz, J = 7.3 Hz), 4.39 (dd, 1H, J = −8.85 Hz, J = 7.3 Hz).

*5-Methyl-3-phenyl-2,3-dihydrobenzofuran (8*b*)*

The methyl derivative was prepared by a procedure similar to that used for **8***a* except *para*-cresol was used instead of phenol. The intermediate 5-methyl-3-phenyl-2-coumaranone (**12***b*) is a known compound (11*c*). Recrystallization (95% ethanol) gave **12***b* as colourless crystals. From **12***b* (4 g, 0.02 mol), **8***b* (1.7 g, 8.1 × 10^{-3} mol, 45% yield) was obtained as colourless crystals, mp 60.5°C; ^{1}H nmr (360 MHz) in $CDCl_3$: 6.74–7.30 (m, 8H), 4.83 (dd, 1H, J = −8.85 Hz, J = 9.5 Hz), 4.57 (dd, 1H, J = 9.5 Hz, J = 7.3 Hz), 4.36 (dd, 1H, J = −8.85 Hz, J = 7.3 Hz), 2.2 (s, 3H); ^{13}C nmr (90 MHz) in $CDCl_3$: 158.0, 142.9, 130.5, 130.1, 128.9, 128.7, 127.9, 126.9, 125.7, 109.1, 79.2, 48.6, 20.8. *Anal.* calcd. for $C_{15}H_{14}O$: C 85.68, H 6.71; found: C 85.66, H 6.77.

*3-Phenylbenzofuran and 5-methyl-3-phenylbenzofuran (**14**a and b)*

These known compounds were prepared by the reported procedure (23). The intermediate aryloxyacetophenones were cyclodehydrated using polyphosphoric acid, keeping the temperature below 45°C to avoid rearrangement of the initial products. 3-Phenylbenzofuran (**14***a*) was purified by recrystallization from methanol (Dry Ice – acetone) to colourless crystals, mp 41–43°C (lit. (23*a*) mp 41–42°C); ^{1}H nmr (T-60) in $CDCl_3$: 7.0–7.7 (m). The methyl derivative (**14***b*) was also purified by recrystallization from methanol at low temperature; the crystals melt upon warming to room temperature; ^{1}H nmr (T-60) in $CDCl_3$: 7.65–6.9 (m, 9H), 2.4 (s, 3H) (in agreement with the reported spectrum (23*b*)).

*Irradiation of 5-methyl-3-phenyl-2,3-dihydrobenzofuran (8*b*)*

A solution of 5-methyl-3-phenyl-2,3-dihydrobenzofuran (**8***b*) (0.50 g, 2.38 × 10^{-3} mol) and 1,4-dicyanobenzene (**3**) (0.30 g, 2.34 ×

Can. J. Chem. Downloaded from www.nrcresearchpress.com by 213.222.148.141 on 09/07/12
For personal use only.

10^{-3} mol) in acetonitrile–methanol (3:1) (30 mL) was placed in a Pyrex tube, purged with nitrogen, and irradiated for 20 h with a 1-kW medium pressure mercury vapor lamp. Analysis of the reaction mixture by gc/ms indicated that two products were formed with the composition of methanol adducts. There was no evidence for formation of the dehydrogenation product **14***b*. After prolonged irradiation the solvent was evaporated and the crude photolysate was chromatographed on silica gel using hexanes – diethyl ether (3:1). Unreacted starting material (0.17 g) was recovered, followed by a mixture (0.18 g) of the isomeric methanol adducts **15***b*, *cis* and *trans* (45% yield). Analysis of the mixture by ^{1}H nmr indicated that the *cis*:*trans* ratio was 1:0.85. This mixture was rechromatographed on silica gel using mplc, eluting with ethyl ether (4%) in hexanes. The *trans* isomer eluted first.

The *trans* isomer (**15***b trans*) was recrystallized from ethanol giving colourless prisms (mp 48°C); ^{1}H nmr (EM360L) in $CDCl_3$: 6.9–7.3 (m, 8H), 5.4 (d, 1H, J = 1.9 Hz), 4.4 (d, 1H, J = 1.9 Hz), 3.6 (s, 3H), 2.2 (s, 3H). *Anal.* calcd. for $C_{16}H_{16}O_2$: C 79.97, H 6.71; found: C 79.79, H 6.66.

The *cis* isomer (**15***b cis*) was an oil; ir (PE 180), neat: 3020 (w), 2920 (m), 2835 (w), 1600 (w), 1480 (s), 1650 (w), 1225 (w), 1180 (w), 1110 (m), 1090 (s), 930 (m), 910 (s), 800 (m), 720 (w), 685 (s); ^{1}H nmr (EM360L) in $CDCl_3$: 6.8–7.3 (m, 8H), 5.6 (d, 1H, J = 6.5 Hz), 4.6 (d, 1H, J = 6.5 Hz), 3.4 (s, 3H), 2.2 (s, 3H). *Anal.* calcd. for $C_{16}H_{16}O_2$: C 79.97, H 6.71; found: C 79.99, H 6.71.

*Irradiation of 3-phenyl-2,3-dihydrobenzofuran (**8**a)*

The irradiation procedure used for this unsubstituted compound was essentially the same as that used for the methyl derivative. The isomers were separated by chromatography (mplc). The *trans* isomer (**15***a trans*) was eluted first. Recrystallization from ethanol gave colourless needles, mp 95°C; ir (PE 180), KBr: 3060 (m), 3020 (m), 2985 (m), 2960 (m), 2940 (s), 2840 (m), 1600 (s), 1500 (s), 1470 (s), 1450 (m), 1370 (s), 1220 (s), 1100 (s), 920 (s), 860 (s), 740 (s), 690 (s); ^{1}H nmr (EM360L) in $CDCl_3$: 6.8–7.4 (m, 9H), 5.4 (d, 1H, J = 2.4 Hz), 4.4 (d, 1H, J = 2.4 Hz), 3.5 (s, 3H). *Anal.* calcd. for $C_{15}H_{14}O_2$: C 79.62, H 6.24; found: C 79.39, H 6.20.

The *cis* isomer (**15***a cis*) is an oil; ir (PE 180), neat: 3060 (sh), 3020 (m), 2935 (b), 2840 (m), 1600 (m), 1500 (m), 1470 (s), 1450 (s), 1210 (m), 1180 (s), 1100 (s), 920 (s), 870 (s), 740 (s), 690 (s); ^{1}H nmr (EM360L) in $CDCl_3$: 6.8–7.3 (m, 9H), 5.6 (d, 1H, J = 6.5 Hz), 4.7 (d, 1H, J = 6.5 Hz), 3.4 (s, 3H). *Anal.* calcd. for $C_{15}H_{14}O_2$: C 79.62, H 6.24; found: C 79.69, H 6.28.

*Irradiation of 3-phenyl-2,3-benzofuran (**14**a) and 5-methyl-3-phenyl-2,3-benzofuran (**14**b)*

The methanol adducts **15***a* and **15***b cis* and *trans* were formed in good yield (90%) when **14***a* and **14***b* were irradiated under the conditions described above.

*Deuterium exchange experiment with 5-methyl-3-phenyl-2,3-dihydrobenzofuran (**8**b)*

A solution of 5-methyl-3-phenyl-2,3-dihydrobenzofuran (**8***b*) (0.15 g) and 1,4-dicyanobenzene (**3**) (0.10 g, 4.8×10^{-4} mol) in acetonitrile–methanol-O-*d* (1:1) (10 mL) was purged with nitrogen and irradiated for 6 days. Analysis of the photolysate by gc (8% SE-30) indicated the reaction was 20% complete, giving the methanol adducts (**15***b cis* and *trans*). The solvent was evaporated and a sample of unreacted starting material was recovered by prep-gc (5% SE-30). Integration of the ^{1}H nmr spectrum showed that 90% of the proton resonance at 4.57 ppm had exchanged; the other two protons at 4.36 and 4.83 ppm appeared as doublets with a coupling constant J = −8.8 Hz; ^{2}H nmr showed a single peak at 4.5 ppm. There was no evidence for deuterium at any other position; as much as 5% incorporation would have been detected.

*Deuterium exchange experiment with 2-methoxy-5-methyl-3-phenyl-2,3-dihydrobenzofuran (**15**b, cis and trans)*

1. The photolysis mixture consisted of 2-methoxy-5-methyl-3-phenyl-2,3-dihydrobenzofuran **15***b cis* and *trans* (1:1) (0.05 g, 2.1×10^{-4} mol) and 1,4-dicyanobenzene (**3**) (0.01 g, 7.8×10^{-5} mol) in acetonitrile (0.5 mL) – methanol-d_4 (0.2 mL) placed in a Pyrex nmr tube. The solution was purged with nitrogen and irradiated. Progress of the reaction was followed by ^{1}H nmr, integrating the region for the 2-H and 3-H protons of the two isomers. After 4 days of irradiation the ratio of isomers was *cis*:*trans* 20:80. The solvent was evaporated and the isomers were separated by preparative gas chromatography. Analysis of the ^{1}H nmr of the *cis* isomer showed that the 3-H proton (4.65 ppm) was 40% exchanged while the methoxy protons (3.38 ppm) were 23% exchanged for deuterium. The results for the *trans* isomer were 14% exchange of the 3-H proton (4.27 ppm) and 12% exchange of the methoxy protons (3.52 ppm). Integration of the ^{2}H nmr spectra gave similar results; there was no evidence for deuterium incorporation at the 2-H or 5-methyl positions (<5%).

2. The experiment described above was repeated starting with the pure isomers in acetonitrile-d_3 and methanol-d_4 solution. The progress of the reaction was followed by ^{1}H nmr. The degree of isomerization was calculated from the integration of the signals due to the 2-H protons. The extent of deuterium incorporation was assessed by integration of the signals due to the 3-H and methoxy protons in comparison to the signal due to the proton at 2-H, which does not exchange. Integration of the methoxy proton signal was complicated by the overlapping signal due to the residual protons in the methanol. Experimental accuracy was ±5%.

The isomerization of the *cis* isomer was significantly more efficient than that of the *trans* isomer. After irradiating the *cis* isomer for 36 h the ratio of *cis*:*trans* was 80:20, the *trans* product had incorporated 60% deuterium at the 3-H position and 43% deuterium at the methoxy position, while the *cis* isomer had incorporated 20% deuterium at the 3-H position and 11% at the methoxy position. Starting with the *trans* isomer, after 36 h *trans*:*cis* = 95:5; after 80 h *trans*:*cis* = 90:10. The *cis* product incorporated >90% deuterium at the 3-H position and 65% deuterium at the methoxy position, while the *trans* isomer incorporated 16% deuterium at the 3-H and 16% at the methoxy position.

*2-Methoxy-1-phenylindane (**9**, cis and trans)*

Two methods were used for the preparation of these compounds starting with 1-phenylindene (**16**) (23).

Method 1 (4*a*, 15)

A solution of 1-phenylindene (0.50 g, 2.78×10^{-3} mol) and 1,4-dicyanobenzene (0.237 g, 1.85×10^{-3} mol) in acetonitrile (30 mL) – methanol (10 mL) was irradiated in a Pyrex tube at 10°C. After 20 h irradiation, gc analysis showed that reaction was complete. The solvent was evaporated and the product purified by mplc. Both the *cis* and *trans* isomers of **9** were obtained.

cis **9**: ir (PE 180), neat: 3060 (w), 3020 (m), 2920 (m), 2900 (m), 2820 (m), 1600 (w), 1500 (m), 1450 (s), 1105 (s), 1090 (s), 720 (s), 700 (s), 680 (s); ^{1}H nmr (360 MHz) in C_6D_6: 7.15 (m, 9H), 4.18 (d, 1H, J = 6.2 Hz), 3.89 (dd, 1H, J = 6.2 Hz, J = 4.0 Hz, J = 6.0 Hz), 2.87 (dd, 1H, J = 15.7 Hz, J = 4.0 Hz), 3.00 (dd, 1H, J = 15.4 Hz, J = 6.0 Hz), 2.82 (s, 3H).

trans **9**: ir (PE 180), neat: 3060 (w), 3020 (m), 2920 (m), 2900, 2820 (w), 1600 (w), 1500 (m), 1450 (m), 1105 (s), 1090 (s), 730 (s), 680 (s); ^{1}H nmr (360 MHz) in C_6D_6: 6.8 (m, 9H), 4.05 (d, 1H, J = 6.3 Hz), 3.72 (ddd, 1H, J = 6.3 Hz, J = 6.57 Hz, J = 6.60 Hz), 2.77 (dd, 1H, J = 15.7 Hz, J = 6.57 Hz), 2.74 (s, 3H), 2.56 (dd, 1H, J = 15.7 Hz, J = 6.60 Hz).

Method 2 (14)

To a stirred solution of 0.50 M 9-borabicyclo[3.3.1]nonane (9-BBN) (60 mL, 0.03 mol) in tetrahydrofuran under nitrogen purge was added dropwise 1-phenylindene (5.4 g, 0.03 mol). The reaction was then refluxed for 7 h, cooled, and then 20 mL of water was added. To this mixture was added dropwise a solution of sodium hydroxide (4.0 g, 0.10 mol) in water (35 mL), and hydrogen peroxide (15 mL, 30% aq.). This mixture was stirred for 2 h at room temperature and was extracted with diethyl ether. The combined organic layers were washed with water, saturated aqueous sodium chloride, saturated aqueous ammonium chloride, dried over magnesium sulfate, and the solvent evaporated to give a pale yellow liquid (6.7 g). This product was then purified by liquid column chromatography over silica gel, eluting with

Can. J. Chem. Downloaded from www.nrcresearchpress.com by 213.222.148.141 on 09/07/12
For personal use only.

a hexane – diethyl ether gradient to give 3.20 g (0.016 mol, 80%) of *trans*-1-phenyl-2-indanol (**17**); ir (PE 1320), neat: 3340 (b), 3060 (m), 3040 (m), 2940 (s), 2900 (s), 2840 (m), 1600 (w), 1500 (s), 1450 (s), 1055 (s), 725 (s), 680 (s); ^{1}H nmr (EM360L) in $CDCl_3$: 7.2 (m, 9H), 4.4 (m, 2H), 3.1 (m, 3H).

An ethereal solution of the indanol (**17** *trans*) (3.0 g, 0.014 mol) was added dropwise to a stirred suspension of sodium hydride (3.48 g, 0.14 mol) and diethyl ether. Then dimethyl sulfate (3.60 g, 0.03 mol) was added, and the reaction mixture was refluxed for 24 h. The reaction was then poured into iced aqueous hydrochloric acid, and the layers separated. The organic layer was washed with aqueous ammonia (to remove excess dimethyl sulfate), water, and saturated aqueous sodium chloride, dried over magnesium sulfate (anhydrous), and the solvent evaporated. The product was purified by liquid column chromatography using silica gel, eluting with 10% diethyl ether in hexane to give 2.80 g (0.013 mol, 87%) of the methyl ether. The ir (PE 180), neat, was superimposable upon that of *trans* **9** as prepared above. The ^{1}H nmr (60 MHz) in $CDCl_3$ was also identical. *Anal.* calcd. for $C_{16}H_{16}O$: C 85.68, H 7.19; found: C 85.83, H 7.20.

*1-Phenylindane (**18**)*

A solution of 1-phenylindene (2.0 g, 0.01 mol) was stirred under an atmosphere of nitrogen with 0.5 M 9-BBN (25 mL, 0.013 mol) in tetrahydrofuran for 16 h and then refluxed for 6 h. The solvent was removed by rotary evaporation and the residue was dissolved in diglyme (50 mL) and propionic acid (1.2 g, 0.016 mol). This mixture was stirred at room temperature for 4 h and then refluxed for 2 h. The reaction was then quenched by the addition of 1 M sodium hydroxide (100 mL) and pentane (75 mL). The layers were separated and the aqueous layer extracted twice with pentane; the combined organic layers were washed with 50 mL water (5×), dried over anhydrous magnesium sulfate, and the solvent evaporated to give a pale yellow oil. The gc/ms analysis showed a trace amount of starting material present. The olefin in the mixture was oxidized using *meta*-chloroperbenzoic acid in methylene chloride. Subsequent purification by column chromatography over silica gel yielded 1.0 g (0.005 mol, 49.5%) of 1-phenylindane (**18**) as a colourless oil (23); ^{1}H nmr (360 MHz) in $CDCl_3$: 7.2 (m, 9H), 4.31 (dd, 1H, J = 8.215 Hz, J = 8.218 Hz), 3.03 (ddd, 1H, J = −15.73 Hz, J = 3.50 Hz, J = 8.89 Hz), 2.93 (ddd, 1H, J = −15.73 Hz, J = 8.40 Hz, J = 8.14 Hz), 2.56 (dddd, 1H, J = 8.218 Hz, J = 3.50 Hz, J = 8.40 Hz, J = −12.85 Hz), 2.04 (dddd, 1H, J = 8.215 Hz, J = 8.89 Hz, J = 8.14 Hz, J = −12.85 Hz); ms (155°C, 70 eV) m/z: 194 (M^+, 100), 115 (29.6), 91 (9.2).

Irradiation of trans *1-phenyl-2-methoxyindane (**9**)*

1. A solution of *trans* **9** (0.064 g, 2.86×10^{-4} mol) and 1,4-dicyanobenzene (0.018 g, 1.43×10^{-4} mol) in acetonitrile (30 mL) was irradiated through Pyrex at 10°C for 170 h. The reaction progress was monitored by gc/ms. After 170 h no significant reaction was observed, the starting material remaining unconsumed.

2. A solution of *trans* **9** (0.040 g, 1.79×10^{-4} mol) and 1,4-dicyanobenzene (0.015 g, 1.17×10^{-4} mol) in acetonitrile–methanol (1.0 mL, 3:1 ratio) was irradiated at 10°C through Pyrex, and the reaction progress monitored by gc/ms using a Carbowax 20M capillary column. The solution became an amber colour after approximately 20 h irradiation. After 92 h approximately 1.3% conversion to the *cis* isomer of **9** was detected. Irradiation for an additional 100 h did not change the *cis* to *trans* ratio. No other efficient processes were detected.

3. A solution of *trans* **9** (0.040 g, 1.79×10^{-4} mol) and 1,4-dicyanobenzene (0.015 g, 1.17×10^{-4} mol) in acetonitrile-d_3–methanol-O-*d* (1.0 mL, 3:1 ratio) was irradiated at 10°C through Pyrex. After 55 h irradiation deuterium was detected at the methoxy position. Also observed at this time, by ^{2}H nmr, was a deuterium resonance for the methoxy group of the *cis* isomer of **9**. The ratio of the *cis* to *trans* isomers at this time was approximately 1:3; ^{2}H nmr (55.4 MHz) in $CHCl_3$: 3.25 (s), 3.10 (s). After an additional 70 h irradiation the ^{2}H nmr showed a new resonance due to deuterium at the bis-benzylic (C-1) position. The ratio of the *cis* to *trans* isomer at this time was approximately 1:1.85; ^{2}H nmr (55.4 MHz) in $CHCl_3$: 4.12 (s), 3.27 (s), 3.11 (s).

*Irradiation of 1-phenylindane (**18**)*

1-Phenylindane (45 mg, 2.32×10^{-4} mol) and 1,4-dicyanobenzene (15 mg, 1.17×10^{-4} mol) in acetonitrile–methanol-O-*d* (1 mL, 3:1) was placed in a Pyrex tube and was irradiated in a constant temperature bath (10°C). Reaction progress was monitored by ^{1}H nmr, ^{2}H nmr, and gc/ms. After 12 h irradiation the ^{1}H nmr spectrum showed a significant (>90%) reduction in the intensity of the bis-benzylic proton at 4.33 ppm. The ^{2}H nmr spectra, at this time, also showed significant incorporation of deuterium at this position, but little or no (<5%) incorporation of deuterium at the mono-benzylic position (3 ppm).

*3,3-Diphenyltetrahydrofuran (**10**)*

The diester, diethyl-2,2-diphenylsuccinate, was prepared according to the reported synthesis (17*b*) with the exception that anhydrous ether was used instead of DMF. The reduction to form the diol (**21**) was done according to the reported procedure (17*a*). The diol (1.0 g) was then cyclized by refluxing for 1 h with an excess (2–3 mL) of hydrobromic acid (49%). The cooled reaction mixture was diluted with water and the organic layer was extracted with ether, washed with saturated sodium bicarbonate solution, dried over magnesium sulfate, and the solvent was evaporated to yield 80% of the ether (**10**). The product (**10**) was purified by chromatography on silica gel using hexanes and methylene chloride as eluants. The product was recrystallized from 95% ethanol, mp 57–59°C; ir (PE 180), KBr: 3050 (m), 3020 (m), 2980 (m), 2940 (m), 2880 (s), 2840 (s), 1600 (w), 1485 (s), 1440 (s), 1100 (s), 755 (s), 690 (s); ^{1}H nmr (360 MHz) in $CDCl_3$: 7.13–7.27 (m, 10H), 4.28 (s, 2H), 3.91–3.95 (t, 2H, J = 7.0 Hz), 2.51–2.55 (t, 2H, J = 7.0 Hz); ^{13}C nmr (90 MHz) in $CDCl_3$: 145.8, 128.3, 127.4, 126.3, 77.2, 67.1, 55.4, 38.6.

*1-Methoxy-2,2-diphenylcylopentane (**11**)*

The preparation of 2,2-diphenylcyclopentanone (**27**) was previously described (20*b*). The reduction of ketone **27** to the corresponding alcohol was carried out by the reported procedure (20*a*). 2,2-Diphenylcyclopentanol (**28**) (2 g, 0.0084 mol) dissolved in anhydrous ether was added dropwise to a stirred suspension of NaH (2 g, 0.084 mol) in anhydrous ether. After the addition was complete, dimethyl sulfate (3.18 g, 0.025 mol) was added slowly. The mixture was stirred for 1 h and then refluxed overnight. The reaction mixture was poured into water and extracted with ether. The combined organic layers were washed three times with aqueous ammonia, twice with brine, dried (magnesium sulfate), and the solvent was evaporated. The product was purified by vacuum distillation (bp 125°C/0.25 Torr; 1 Torr = 133.3 Pa) and by chromatography using silica gel (Kieselgel 60) with hexanes and methylene chloride as eluants; ir (PE 180), neat: 3080 (m), 3060 (m), 3020 (m), 2980 (b), 2880 (m), 2820 (m), 1600 (s), 1500 (s), 1450 (s), 1100 (s), 750 (s), 685 (s); ^{1}H nmr (360 MHz) in $CDCl_3$: 7.2 (m, 10H), 4.30 (t, 1H, J = 4.5 Hz), 3.29 (s, 3H), 2.5 (m, 2H), 1.8 (m, 4H); ^{13}C nmr (90 MHz) in $CDCl_3$: 147, 146, 128.5, 128, 127.6, 126.8, 125.7, 125.5, 87.1, 57, 56, 35, 28, 20. $E^{ox}_{1/2}$ = 2.13 ± 0.02 V (taken as 0.03 V before anodic peak potential).

*Irradiation of 3,3-diphenyltetrahydrofuran (**10**)*

A solution of **10** (40 mg, 1.8×10^{-4} mol) and 1,4-dicyanobenzene (**3**) (15 mg, 1.1×10^{-4} mol) in acetonitrile was irradiated for 170 h through Pyrex. The reaction was monitored by gc/ms using a methyl silicone column. No major volatile product was observed but the mixture became dark yellow.

A solution of **10** (0.443 g, 1.98×10^{-3} mol) and 1,4-dicyanobenzene (**3**) (0.150 g, 1.17×10^{-3} mol) in acetonitrile–methanol (30 mL; 3:1 ratio) was irradiated for 170 h through Pyrex. The reaction progress was monitored by gc/ms using the 5% phenyl capillary column. In this reaction, **3** was partially consumed. Three minor products were detected but were not isolated. Comparison of their mass spectra with those in the N.B.S. library indicated that they may be benzonitrile, *para*-cyanotoluene, and *para*-cyanobenzyl alcohol.

Can. J. Chem. Downloaded from www.nrcresearchpress.com by 213.222.148.141 on 09/07/12
For personal use only.

The major product of this irradiation was methyl 3,3-diphenylpropyl formaldehyde acetal (**22**). The starting material and product were not separated. The ^{1}H nmr (360 MHz) and ^{13}C nmr (90 MHz) spectra were recorded using the mixture of **10** and the photochemical product. Peaks attributed to **29** were determined by subtraction; ^{1}H nmr (360 MHz) in $CDCl_3$: 7.1–7.2 (m, 10H), 4.54 (s, 2H), 4.13 (t, 1H, J = 7.9 Hz), 3.45 (t, 2H, J = 6.8 Hz), 3.38 (s, 3H), 2.34 (m, 2H); ^{13}C nmr (90 MHz) in $CDCl_3$: 144.4, 128.4, 127.8, 126.1, 96.4, 65.8, 55.1, 47.4, 35.5. The acetal was acid hydrolyzed by heating the mixture dissolved in ethylene glycol with a catalytic amount of *para*-toluenesulfonic acid for 1.5 h. The reaction mixture was poured into saturated sodium bicarbonate solution, extracted with methylene chloride, washed with water, dried (magnesium sulfate), and the solvent was evaporated. The gc/ms (5% phenyl) determined that a small amount of the acetal had been converted to the alcohol, 3,3-diphenylpropanol (**23**). The identity of this product was confirmed by direct comparison with an authentic sample of **23** prepared by the reported procedure (18).

A solution of **10** (0.225 g, 1.0×10^{-3} mol) and **3** (0.124 g, 9.7×10^{-4} mol) in acetonitrile–water (30 mL, 3:1 ratio) was irradiated for 170 h through Pyrex. The reaction progress was monitored by gc/ms (5% phenyl) capillary column. The alcohol, 3,3-diphenylpropanol (**23**), was formed in essentially quantitative yield at 10% conversion. The reaction mixture was separated by column chromatography using silica gel. Comparison of the product with an authentic sample of 3,3-diphenylpropanol (18) established the structure (**23**); ^{1}H nmr (360 MHz) in $CDCl_3$: 7.1–7.3 (m, 10H), 4.11 (t, 1H, J = 7.9 Hz), 3.57 (t, 2H, J = 6.5 Hz), 2.29 (dt, 2H, J = 7.9 Hz, J = 6.5 Hz), 1.63 (br s, 1H); ^{13}C nmr (90 MHz) in $CDCl_3$: 144.5, 128.5, 127.8, 126.2, 61.1, 47.4, 38.3.

*Irradiation of 1-methoxy-2,2-diphenylcyclopentane (**11**)*

A solution of **11** (0.502 g, 1.99×10^{-3} mol) and **3** (0.20 g, 1.6×10^{-3} mol) in acetonitrile–methanol (30 mL, 3:1 ratio) was irradiated at 10°C through Pyrex. The reaction was monitored by gc/ms (5% phenyl) capillary column. After 170 h of irradiation the starting material had been converted to 1,1-dimethoxy-5,5-diphenylpentane (**29**); ^{1}H nmr (360 MHz) in $CDCl_3$: 7.1–7.3 (m, 10H), 4.35 (t, 1H, J = 5.8 Hz), 3.94 (t, 1H, J = 7.7 Hz), 3.31 (s, 6H), 2.12 (dt, 2H, J = 7.7 Hz, J = 10.1 Hz), 1.6 (m, 2H), 1.3 (m, 2H); ^{13}C nmr (90 MHz) in $CDCl_3$: 144.7, 128.1, 127.5, 125.8, 104.2, 52.4, 51.1, 35.3, 32.2, 22.8.

The reaction mixture was dissolved in 75 mL of 3–5% aqueous HCl. Dioxane was added to increase the solubility of the acetal. The mixture was refluxed for 45 min. The aqueous layer was extracted with ether, washed with saturated sodium bicarbonate solution, dried (magnesium sulfate), and the solvent was evaporated to yield 60% (overall from **11**) of the aldehyde, 5,5-diphenylpentanal (**30**). The aldehyde was purified by column chromatography (silica gel); ir (PE233B) in CCl_4: 3080 (m), 3040 (m), 3100 (s), 2960 (b), 2720 (s), 1720 (s), 1600 (m), 1500 (s), 1450 (s), 1030 (m); ^{1}H nmr (360 MHz) in $CDCl_3$: 9.68 (t, 1H, J = 1.4 Hz), 7.1–7.3 (m, 10H), 3.88 (t, 1H, J = 7.0 Hz), 2.4 (dt, 2H, J = 7.4 Hz, J = 7.2 Hz), 2.0 (m, 2H), 1.6 (m, 2H); ^{13}C nmr (90 MHz) in $CDCl_3$: 202.2, 144.5, 128.5, 127.7, 126.2, 51.2, 43.8, 35.1, 20.7.

Acknowledgments

Acknowledgment is made to the Donors of the Petroleum Research Fund, administered by the American Chemical Society, and to the Natural Sciences and Engineering Research Council of Canada for support of this research. We also thank D. L. Hooper and the Atlantic Regional Magnetic Resonance Centre at Dalhousie University for the 360-MHz nmr spectra, and T. S. Cameron and B. Vincent (also at Dalhousie) for the X-ray analysis of **10**.

1. (*a*) A. Okamoto, M. S. Snow, and D. R. Arnold. Tetrahedron, **42**, 6175 (1986); (*b*) A. Okamoto and D. R. Arnold. Can. J. Chem. **63**, 2340 (1985); (*c*) D. R. Arnold and S. A. Mines. Can. J. Chem. **65**, 2312 (1987).
2. (*a*) D. D. M. Wayner and D. R. Arnold. Can. J. Chem. **63**, 871 (1985); (*b*) D. D. M. Wayner, R. J. Boyd, and D. R. Arnold. Can. J. Chem. **63**, 3283 (1985).
3. (*a*) E. T. Kaiser and L. Kevan (*Editors*). Radical ions. Interscience Pub., New York. 1968; (*b*) O. Hammerich and V. D. Parker. Adv. Phys. Org. Chem. **20**, 55 (1984).
4. (*a*) R. A. Neunteufel and D. R. Arnold. J. Am. Chem. Soc. **95**, 4080 (1973); (*b*) D. R. Arnold, R. M. Borg, and A. Albini. J. Chem. Soc. Chem. Commun. 138 (1981).
5. N. Hirota. *In* Radical ions. *Edited by* E. T. Kaiser and L. Kevan. Interscience Pub., New York. 1968. Chap. 2.
6. (*a*) A. Albini and D. R. Arnold. Can. J. Chem. **56**, 2985 (1978); (*b*) X.-Z. Qin and F. Williams. Tetrahedron, **42**, 6301 (1986); (*c*) V. R. Rao and S. S. Hixson. J. Am. Chem. Soc. **101**, 6458 (1979); (*d*) K. Mizuno, J. Ogawa, and Y. Otsuji. Chem. Lett. 741 (1981).
7. (*a*) T. R. Evans, R. W. Wake, and O. Jaemicke. *In* The exciplex. *Edited by* M. Gordon and W. R. Ware. Academic Press Inc., New York. 1975; (*b*) T. Majima, C. Pac, and H. Sakurai. J. Am. Chem. Soc. **102**, 5265 (1980); (*c*) Y. Yamamoto, M. Irie, Y. Yamamoto, and K. Hayashi. J. Chem. Soc. Perkin Trans. 2, 1517 (1979); (*d*) T. Gotoh, M. Kato, M. Yamamoto, and Y. Nishijima. J. Chem. Soc. Chem. Commun. 90 (1981).
8. (*a*) H. F. Davis, P. K. Das, L. W. Reichel, and G. W. Griffin. J. Am. Chem. Soc. **106**, 6968 (1984); (*b*) L. W. Reichel, G. W. Griffin, A. J. Muller, P. K. Das, and S. N. Ege. Can. J. Chem. **62**, 424 (1984); (*c*) H. D. Roth, M. L. M. Schilling, and C. J. Abelt. Tetrahedron, **42**, 6157 (1986).
9. (*a*) B. F. Yates, W. J. Bouma, and L. Radom. Tetrahedron, **42**, 6225 (1986); (*b*) B. F. Yates, W. J. Bouma, and L. Radom. J. Am. Chem. Soc. **106**, 5805 (1984); (*c*) J. L. Homes, F. P. Lossing, J. K. Terlouw, and P. C. Burgers. Can. J. Chem. **61**, 2305 (1983).
10. D. R. Arnold and A. J. Maroulis. J. Am. Chem. Soc. **98**, 5931 (1976).
11. (*a*) R. C. Elderfield and T. P. King. J. Am. Chem. Soc. **76**, 5439 (1954); (*b*) A. Padwa, D. Dehm, T. Oine, and G. A. Lee. J. Am. Chem. Soc. **97**, 1837 (1975); (*c*) P. Karafiloglou, J.-P. Catteau, A. Lablache-Combier, and H. Ofenberg. J. Chem. Soc. Perkin Trans. 2, 1545 (1977); (*d*) C. O. Guss, H. R. Williams, and L. H. Jules. J. Am. Chem. Soc. **73**, 1257 (1951); (*e*) C. O. Guss. J. Am. Chem. Soc. **73**, 608 (1951).
12. (*a*) W. Davies and S. Middleton. J. Chem. Soc. 822 (1958); (*b*) J. R. Collier, M. K. Dirania, and J. Hill. J. Chem. Soc. Part C. 155 (1970); (*c*) G. Y. Kuo and S. T. Ross. J. Heterocycl. Chem. **15**, 1489 (1978).
13. (*a*) S. L. Mattes and S. Farid. J. Am. Chem. Soc. **108**, 7356 (1986); (*b*) *In* Organic photochemistry. Vol. 6. *Edited by* A. Padwa. Marcel Dekker, New York. 1983. p. 233.
14. (*a*) H. C. Brown, E. F. Knights, and C. G. Scouten. J. Am. Chem. Soc. **96**, 7765 (1974); (*b*) H. C. Brown and C. P. Garg. J. Am. Chem. Soc. **83**, 2951 (1961).
15. (*a*) C. Pac, A. Nakasone, and H. Sakurai. J. Am. Chem. Soc. **99**, 5806 (1977); (*b*) T. Ansanuma, T. Gotoh, A. Tsuchida, M. Yamamoto, and Y. Nishijima. J. Chem. Soc. Chem. Commun. 485 (1977).
16. A. M. de P. Nicholas and D. R. Arnold. Can. J. Chem. **60**, 2165 (1982).
17. (*a*) M. M. Kayser and P. Morand. J. Org. Chem. **44**, 1338 (1979); (*b*) A. Brault. Bull. Soc. Sci. Bretagne, 42 (1967); Chem. Abstr. **70**, 67825m (1969); (*c*) G. Poulain. Bull. Soc. Chem. Fr. 913 (1964).
18. N. M. Vinokurova and I. Kh. Fel'dman. Khim.-Farm. Zh. **2**, 25 (1968); Chem. Abstr. **69**, 86494y (1968).
19. (*a*) C. Pac, T. Ohtsuki, T. Fukunaga, S. Yanagida, and H. Sakurai. Chem. Lett. 1855 (1985); (*b*) K. Yamaguchi, S.-C. Oh, and Y. Shirota. Chem. Lett. 1445 (1986); (*c*) T. Asanuma, M. Yamamoto, and Y. Nishijima. J. Chem. Soc. Chem. Commun. 608 (1975).

20. (*a*) H. E. ZIMMERMAN and D. J. KREIL. J. Org. Chem. **47**, 2060 (1982); (*b*) F. S.-LEGAGNEUR and J. RABADEUX. Bull. Soc. Chem. Fr. 1310 (1967).
21. F. D. LEWIS. Acc. Chem. Res. **19**, 401 (1986).
22. (*a*) L. M. TOLBERT and R. K. KHANNA. J. Am. Chem. Soc. **109**, 3477 (1987); (*b*) T. SHONO and Y. MATSUMURA. J. Org. Chem. **35**, 4157 (1970); (*c*) P. J. WAGNER, R. J. TRUMAN, A. E. PUCHALSKI, and R. WAKE. J. Am. Chem. Soc. **108**, 7727 (1986); (*d*) D. N. R. RAO, H. CHANDRA, and M. C. R. SYMONS. J. Chem. Soc. Perkin Trans. 2, 1201 (1984).
23. (*a*) W. E. PARHAM and C. D. WRIGHT. J. Org. Chem. **22**, 1473 (1957); (*b*) E. W. VALYOCSIK and P. SIGAL. J. Org. Chem. **36**, 66 (1971).

Can. J. Chem. Downloaded from www.nrcresearchpress.com by 213.222.148.141 on 09/07/12
For personal use only.

FOR ERRATA SEE
V.66(10)1988 P.2671

The preparation of SeI_3SbF_6 and TeI_3SbF_6; the X-ray crystal structures of SBr_3AsF_6, SeI_3AsF_6, SeI_3SbF_6, and TeI_3SbF_6; some considerations of the energetics of the formation of SBr_3AsF_6 and SeI_3AsF_6

JAMES P. JOHNSON, MICHAEL MURCHIE, JACK PASSMORE, MAHMOUD TAJIK, PETER S. WHITE, AND CHI-MING WONG
Department of Chemistry, University of New Brunswick, Fredericton, N.B., Canada E3B 6E2

Received March 24, 1987

JAMES P. JOHNSON, MICHAEL MURCHIE, JACK PASSMORE, MAHMOUD TAJIK, PETER S. WHITE, and CHI-MING WONG. Can. J. Chem. **65**, 2744 (1987).

The crystal structures of the compounds SBr_3AsF_6 (**1**), SeI_3AsF_6 (**2**), SeI_3SbF_6 (**3**), and TeI_3SbF_6 (**4**) are reported and the quantitative preparation of the hitherto unknown **3** and **4** from SbF_5 and the respective elements in SO_2 are given. Crystal data are as follows: **1**, monoclinic, space group $P2_1/c$, with $a = 8.015(1)$ Å, $b = 9.342(1)$ Å, $c = 12.126(2)$, $\beta = 97.81(1)°$, and $Z = 4$; **2**, monoclinic, space group $P2_1/c$, with $a = 8.380(2)$ Å, $b = 10.237(1)$ Å, $c = 12.524(1)$ Å, $\beta = 99.36(1)°$, and $Z = 4$; **3**, monoclinic, space group $P2_1/c$, with $a = 8.548(2)$ Å, $b = 10.297(6)$ Å, $c = 12.877(8)$ Å, $\beta = 98.70(3)°$, and $Z = 4$; **4**, monoclinic, space group $P2_1/c$, with $a = 8.463(1)$ Å, $b = 10.676(2)$ Å, $c = 13.121(4)$ Å, $\beta = 100.05(1)$, and $Z = 4$. Compounds **1**, **2**, **3**, and **4** are isostructural and were refined to a final R values of 0.040, 0.051, 0.047, and 0.037, respectively. The structures of these salts consist of essentially discrete MX_3^+ cations and $M'F_6^-$ anions (M = S, Se, Te; X = Br, I; M′ = As, Sb) with some cation–anion interactions. The SeI_3^+ bond distances and angles were essentially identical in both AsF_6^- and SbF_6^- salts (average Se—I distance and I—Se—I angle for AsF_6^- salt; 2.508(2) Å, 102.4(1)° and for SbF_6^- salt; 2.512(1) Å, 102.3(1)°). Similarly the average Te—I bond distance and I—Te—I angle for TeI_3SbF_6 were 2.666(1) Å and 99.8(1)° which are essentially identical to those in the previously reported TeI_3AsF_6. The average S—Br distance and Br—S—Br angle were 2.142(6) Å and 103.4(2)° in SBr_3AsF_6. Estimates of the S—I bond distance and I—S—I bond angle in the as yet unknown $SI_3M'F_6$ are made from the extrapolation of MX_3^+ data. The bond distances observed in the simple MX_3^+ cations (M = S, Se, Te; X = Cl, Br, I) with anions of very low basicity are within 0.02 Å of the corresponding distances calculated by the Schomaker–Stevenson equation. The observed and estimated bond distances in SBr_3^+, SI_3^+, and SeI_3^+ are significantly longer than the corresponding S—Br, S—I, and Se—I distances in S_7I^+, S_7Br^+, and $Se_6I_2^{2+}$. This observation is used to support the thesis that the long intra-cationic halogen–chalcogen contacts in polychalcogen–halogen cations are weakly bonding, and responsible for the cluster-like nature of these cations. The heats of formation of **1** and **2** from their respective elements and AsF_5 were estimated.

JAMES P. JOHNSON, MICHAEL MURCHIE, JACK PASSMORE, MAHMOUD TAJIK, PETER S. WHITE et CHI-MING WONG. Can. J. Chem. **65**, 2744 (1987).

On a déterminé les structures cristallines des composés SBr_3AsF_6 (**1**), SeI_3AsF_6 (**2**), SeI_3SbF_6 (**3**) et TeI_3SbF_6 (**4**) et on a aussi réalisé la préparation quantitative des composés **3** et **4** (inconnus jusqu'à maintenant) à partir du SbF_5 et de leurs éléments respectifs mis en solution dans du SO_2. Les données cristallographiques sont les suivantes : **1**, monoclinique, groupe d'espace $P2_1/c$ avec $a = 8{,}015(1)$, $b = 9{,}342(1)$ et $c = 12{,}126(2)$ Å, $\beta = 97{,}81(1)°$ et $Z = 4$; **2**, monoclinique, groupe d'espace $P2_1/c$ avec $a = 8{,}380(2)$, $b = 10{,}237(1)$ et $c = 12{,}524(1)$ Å, $\beta = 99{,}36(1)$ Å et $Z = 4$; **3**, monoclinique, groupe d'espace $P2_1/c$ avec $a = 8{,}548(2)$, $b = 10{,}297(6)$ et $c = 12{,}877(8)$ Å, $\beta = 98{,}70(3)°$ et $Z = 4$; **4**, groupe d'espace $P2_1/c$ avec $a = 8{,}463(1)$, $b = 10{,}676(2)$ et $c = 13{,}121(4)$ Å, $\beta = 100{,}05(1)$ et $Z = 4$. Les composés **1**, **2**, **3** et **4** sont isostructuraux et on les a affinés jusqu'à des valeurs finales respectives de R de 0,040, 0,051, 0,047 et 0,037. Les structures de ces sels sont formées essentiellement de cations MX_3^+ et d'anions $M'F_6^-$ discrets (M = S, Se, Te; X = Br, I; M′ = As, Sb) et d'un peu d'interactions cations–anions. Les longueurs des distances et des angles du SeI_3^+ sont essentiellement identiques aux valeurs observées dans les sels de AsF_6^- et de SbF_6^- (distances Se—I et angles I—Se—I moyens : pour le sel de AsF_6^-, 2,508(2) Å et 102,4(1)°, et pour le sel de SbF_6^-, 2,512(1) Å et 102,3(1)°). De la même manière, les moyennes des longueurs des liaisons Te—I et des angles I—Te—I du TeI_3SbF_6 sont respectivement 2,666(1) Å et 99,8(1)°, pratiquement identiques à celles rapportées antérieurement pour le TeI_3AsF_6. Dans le SBr_3AsF_6, les moyennes des distances S—Br et des angles Br—S—Br sont respectivement 2,142(6) Å et 103,4(2)°. En faisant une extrapolation à partir des données relatives aux MX_3^+, on propose des évaluations pour les distances S—I et les angles I—S—I des $SI_3M'F_6$ qui sont inconnus jusqu'à maintenant. Les longueurs des liaisons que l'on a observé dans les cations MX_3^+ simples (M = S, Se, Te; X = Cl, Br, I) associés à des anions de basicité faible sont identiques, à 0,02 Å près, aux distances correspondantes calculées en utilisant l'équation de Schomaker–Stevenson. Les longueurs des liaisons, tant évaluées qu'observées, dans les ions SBr_3^+, SI_3^+ et SeI_3^+ sont beaucoup plus longues que les distances S—Br, S—I et Se—I correspondantes des ions S_7I^+, S_7Br^+ et $Se_6I_2^{2+}$. On utilise cette observation pour supporter la thèse selon laquelle les contacts intra-ioniques halogènes–chalcogènes, qui sont longs dans les cations polychalcogènes–halogènes, provoquent une liaisons faible qui est responsable du fait que ces cations sont pratiquement des agrégats. On a évalué les chaleurs de formation des composés **1** et **2** à partir du AsF_5 et de leurs éléments respectifs.

[Traduit par la revue]

Introduction

The structures of the Group V trihalides both in the gas phase and in the solid state are well established (1). The structures are of interest in terms of the bonding and stereochemistry in these simple molecules, and also of interest in terms of the secondary interactions which are observed in the solid state (1–7). Before the present work was carried out the crystal structures of salts containing most of the isoelectronic Group VI trihalide cations, MX_3^+ (M = S, Se, Te; and X = F, Cl, Br, I) were known, with the exceptions of the SBr_3^+, SI_3^+, and SeI_3^+ salts. The preparation (8, 9), Raman spectra (10), and cell parameters (11) of $SBr_3M'F_6$ (M′ = As, Sb) obtained from X-ray powder data

Can. J. Chem. Downloaded from www.nrcresearchpress.com by 213.222.148.141 on 09/07/12
For personal use only.

Can. J. Chem. Downloaded from www.nrcresearchpress.com by 213.222.148.141 on 09/07/12
For personal use only.

have been reported. Cell parameters for SeI_3AsF_6 obtained from single crystal data have been obtained, and the volume per formula unit of 257.1 Å^3 was shown to be consistent with the presence of SeI_3^+ and AsF_6^- ions, which were estimated to be 161 Å^3 and 100 Å^3, respectively (12). However, vibrational spectroscopic data for $SeI_3M'F_6$ (M' = As, Sb) are not available. Our attempts to prepare SI_3^+ salts have so far been unsuccessful, although bond distances and angles in the hypothetical SI_3^+, and in SeI_3^+ and SBr_3^+, have been predicted by extrapolation from the structural data for related Group V trihalides and Group VI trihalide cations (11).

Well-determined X-ray crystal structures of SBr_3AsF_6, SeI_3AsF_6, SeI_3SbF_6, and TeI_3SbF_6 are reported below. These are the first structural determinations of salts of the SBr_3^+ and SeI_3^+ cations by X-ray diffraction, and the first structural determination of the SeI_3^+ cation by any method. The X-ray structure of the TeI_3^+ cation, as the AsF_6^- salt, has previously been reported (13). This structural information can be used to obtain a better estimate of the S—I bond distance in the hypothetical SI_3^+ and therefore an estimate of the corresponding sulphur–iodine bond strength. The structures of the SX_3^+ and SeX_3^+ cations (X = Br, I) are of interest, as these are the simplest binary cations which contain the M(IV)$^+$—X (M = S, Se) bond. Therefore they can be used as benchmarks for comparison with corresponding bond distances in more complicated sulphur—bromine, sulphur—iodine, and selenium—iodine cations. These include S_7Br^+ (14), S_7I^+ (15, 16), $(S_7I)_2I^{3+}$ (16), $Se_2I_4^{2+}$ (17), and $Se_6I_2^{2+}$ (18) containing S(IV)$^+$—Br, S(IV)$^+$—I, and Se(IV)$^+$—I covalent bonds. A preliminary report of the selenium—iodine bond distance in SeI_3AsF_6 has been published (17).

Experimental

The apparatus and techniques used in this work are as previously described (9), except where stated. Elemental sulphur (Fisher Scientific), selenium (B.D.H.), tellurium (B.D.H.), iodine (B.D.H.) and AsF_5 (Ozark-Mahoning) were used without further purification. Bromine (Fisher Scientific) was stored over PO_{10} and SbF_5 (Ozark-Mahoning) was triply distilled in a glass vessel prior to use. $Se_4(AsF_6)_2$ and $I_2Sb_2F_{11}$ were prepared by their published procedures described in refs. 19 and 20. SO_2 (Matheson) and AsF_3 (Ozark-Mahoning) were distilled onto, and stored over, CaH_2 and NaF, respectively.

A glass extracting vessel (21), designed to allow continuous extraction of sparingly soluble material from insoluble products by liquid SO_2, was used to separate SeI_3SbF_6 and TeI_3SbF_6 from their reduced products. Single crystals of SeI_3SbF_6, SeI_3AsF_6, TeI_3SbF_6, and SBr_3AsF_6 were mounted and flame sealed in rigorously dried Pyrex capillaries as described in ref. 22.

Infrared spectra were obtained with a Perkin-Elmer 687 spectrometer using AgCl and KBr plates. Nuclear magnetic resonance spectra were recorded unlocked at −80°C with a Varian XL-200 spectrometer using a 10 mm probe (broad-band over the frequency range 20–125 MHz) tuned to 38.164 MHz, to obtain ^{77}Se nmr spectra. ^{19}F nmr spectra were obtained with the same probe using the ^{1}H decoupler coil, retuned to 188.220 MHz, as the observe coil. Typically, ^{77}Se and ^{19}F nmr spectra were accumulated in 32 kwords of memory over a spectral width of 100 kHz (6.1 Hz/data point, line broadening of 5 Hz, acquisition time of 0.16 s) with pulse widths of 20 and 6 μs, in 2000–7000 and 1000–3000 scans, respectively. Samples were prepared in a 10 mm o.d. thick walled nmr tubes fitted with J. Young (O-ringette PTFE stopcock; model BST/2) valves and were referenced externally to $(CH_3)_2Se$ and CCl_3F. Powder X-ray diffraction photographs were obtained from a Philips Debye-Scherrer camera with Straumanis mounting using nickel filtered Cu-Kα radiation. Samples were mounted and flame sealed in 0.5 mm o.d. glass capillary tubes.

Preparation of SeI_3SbF_6

A preweighed quantity of SbF_5 (0.97 g, 4.48 mmol) was condensed onto a mixture of Se (0.20 g, 2.57 mmol), I_2 (1.01 g, 3.98 mmol), and SO_2 (14.34 g) in a glass extracting vessel (21), forming a dark brown solution over a gray–black solid, on warming to room temperature. The mixture was stirred for 1 day, producing a brown–black solution over a dark brown precipitate. The solution and precipitate were poured through the pressure equalizing bridge and placed above the sintered glass frit in the extractor. A brown–black soluble product was separated from a white insoluble solid after 10 min of continuous extraction with SO_2. The volatile material was removed by pumping under dynamic vacuum leaving 1.85 g and 0.34 g of crystalline brown–black soluble and white insoluble solids (calculated weights of SeI_3SbF_6 and $(SbF_3)_3SbF_5$, based on Se, are 1.79 and 0.32 g, according to eq. [1]). The Raman spectrum and X-ray powder diffraction photograph of the insoluble white solid confirmed the presence of $(SbF_3)_3SbF_5$ (23). The infrared spectrum of the brown–black soluble solid gave peaks at 677 w, 640 sh, 620 vs, 608 sh, 526 sh, and 362 m, cm^{-1} consistent with the presence of the SbF_6^- anion (24). A sample of the soluble solid (0.36 g), redissolved in SO_2 (4.35 g), was identified as SeI_3SbF_6 by ^{77}Se and ^{19}F nmr spectroscopy. The chemical shifts were $\delta_{(CH_3)_2Se}$ = 832 ppm (cf. $\delta_{(CH_3)_2Se}(SeI_3^+)$ in SeI_3AsF_6 dissolved in SO_2 = 842 ppm (25)) and δ_{CCl_3F} = −114.6 ppm (cf. $\delta_{CCl_3F}(SbF_6^-)$ in $(CH_3)_3CSbF_6$ dissolved in SO_2ClF = −117.9 ppm (26)).

Brown–black single crystals of SeI_3SbF_6 were obtained in the following reaction. A mixture of SbF_5 (3.47 g, 16.05 mmol) and SO_2 (7.4 g) were poured onto a mixture of Se (0.63 g, 8.03 mmol) and I_2 (3.03 g, 11.95 mmol), in a two-bulbed vessel equipped with a coarse sintered glass frit. A red–brown solution over a dark precipitate was formed after less than 5 min. After 4 days, the red supernatant was filtered into the second bulb of the vessel, leaving behind a brown crystalline material. The solvent was slowly condensed back onto this solid material by cooling the bulb containing the solid material with running tap water (ca. 10°C). After 10 h, a highly crystalline brown product was obtained in the second bulb. The volatile materials were removed by pumping under dynamic vacuum overnight. Several crystals from the second bulb were mounted in capillaries and subsequently identified as SeI_3SbF_6 by X-ray diffraction analysis.

Preparation of TeI_3SbF_6

Tellurium (0.21 g, 1.64 mmol), I_2 (0.66 g, 2.61 mmol), and SbF_5 (0.58 g, 2.66 mmol) in SO_2 (11.50 g) were reacted in an extracting vessel (21) in a manner identical to that described for the quantitative preparation of SeI_3SbF_6. The mixture was stirred for 1 day, producing a dark brown solution over a brown–beige precipitate. A highly brown–yellow soluble solid was separated from a light gray–white insoluble solid, after less than 1 day of continuous extraction with SO_2. The volatile material was removed, leaving a total of 1.42 g of soluble and insoluble solids (total calculated for a 6:1 mixture of TeI_3SbF_6 and $(SbF_3)_3SbF_5$ is 1.39 g according to eq. [1]). Attempts to obtain a Raman spectrum of the gray–white insoluble solid were unsuccessful. However, X-ray powder diffraction photography confirmed the presence of the $(SbF_3)_3SbF_5$ in the reduced product (23). The infrared spectrum of the brown–yellow soluble solid showed peaks at 642 s, sh, 630 vs, and 560 sh, cm^{-1} confirming the presence of the SbF_6^- anion (24).

Single crystals of TeI_3SbF_6 were obtained by the following reaction. A solution of $I_2Sb_2F_{11}$ (0.54 g, 0.77 mmol) in liquid SO_2, (5.20 g) was poured onto elemental Te (0.20 g, 1.57 mmol) in a two-bulbed vessel equipped with a coarse sintered glass frit. A brown solution over a dark solid was observed after less than 5 min. After 3 days, a brown transparent solution was filtered into the second bulb, leaving behind a dark brown solid. Red–black crystalline plates were formed under the transparent brown solution after standing at room temperature for 1 week. The solvent was decanted into the first bulb, and the volatile materials were removed by pumping under dynamic vacuum. Several of the red–black crystals were mounted in capillaries, and were subsequently identified as TeI_3SbF_6 by X-ray diffraction analysis.

TABLE 1. Crystal data

Parameter	Value			
	SBr_3AsF_6	SeI_3AsF_6	SeI_3SbF_6	TeI_3SbF_6
System	Monoclinic	Monoclinic	Monoclinic	Monoclinic
Space group	$P2_1/c$	$P2_1/c$	$P2_1/c$	$P2_1/c$
a (Å)	8.015(1)	8.380(2)	8.548(2)	8.463(1)
b (Å)	9.342(1)	10.237(1)	10.297(6)	10.676(2)
c (Å)	12.126(1)	12.524(1)	12.877(8)	13.121(4)
β (deg)	97.81(1)	99.36(1)	98.70(3)	100.05(1)
V (Å)	899.6	1060.0	1120.4	1167.3
Z	4	4	4	4
Crystal size (mm)	0.40 × 0.35 × 0.30	0.35 × 0.30 × 0.28	0.40 × 0.60 × 0.28	0.29 × 0.29 × 0.14
μ (mm^{-1})	17.2	15.3	13.9	12.7
D_{calcd} (Mg m^{-3})	3.40	4.06	4.12	4.23
$F(000)$	832	1120	1192	1264
Diffractometer	CAD4	CAD4	FACS-I	FACS-I
Scan type	ω–2θ	ω–2θ	ω–2θ	ω–2θ
Scan width (deg 2θ corrected for dispersion)	2	2	2	2
Scan speed (deg 2θ min^{-1})	2	2	2	2
$2\theta_{max}$	50	50	50	50
Number of standards/interval	3/200	3/200	3/150	3/100
No. of measured reflections	1694	2522	2093	2810
No. of observed reflections ($I \geqq 3\sigma(I)$)	1575	1860	1582	1592
λ-MoKα (Å)	0.71073	0.71073	0.71073	0.71073
Temperature (K)	293	293	293	293
$R (= \Sigma\|\Delta F\|/\Sigma\|F\|)$				
Observed data	0.040	0.051	0.047	0.037
All data	0.061	0.083	0.053	0.091
$R = (\Sigma w\|\Delta F\|^2/\Sigma wF_o^2)^{1/2}$				
Observed data	0.052	0.054	0.063	0.043
All data	0.073	0.063	0.065	0.066
No. of refined parameters	100	100	100	100
Final difference synthesis maximum (e/Å^3)	1.1	1.7	1.0	0.9

Preparation of SeI_3AsF_6

A detailed account of the quantitative preparation of SeI_3AsF_6 has been reported in ref. 12.

Single crystals of SeI_3AsF_6, used in the X-ray crystal structure determination, were obtained in the following reaction. $Se_4(AsF_6)_2$ (0.68 g, 0.97 mmol) and I_2 (0.50 g, 1.96 mmol) were reacted in AsF_3 (6.36 g) in a two-bulbed vessel equipped with a coarse sintered glass frit. A red–brown solution over unreacted I_2 was noted after 10 min. After 1 day, the I_2 appeared to have completely reacted. The solution was very slowly concentrated (approximately 2 weeks) by condensing the solvent into the second bulb which was held at ~10°C, producing a black crystalline solid under a viscous red–brown solution. On removal of the volatile material, the red–brown solution became a tarry froth. Examination of the product in the dry box revealed that it was a mixture of small black crystals and a red–brown paste. Several of the black crystals were mounted in glass capillaries and shown to be SeI_3AsF_6 by X-ray diffraction analysis. The paste was not identified.

Preparation of SBr_3AsF_6

The quantitative preparation of SBr_3AsF_6 has been previously described (8, 9). Single crystals of SBr_3AsF_6 were obtained in the following reaction. AsF_5 (2.35 g, 13.8 mmol) was condensed onto a mixture of S_8 (0.296 g, 1.15 mmol), Br_2 (2.21 g, 13.8 mmol), and SO_2 (7.52 g) in a two-bulb vessel equipped with a course sintered glass frit. A reddish-orange solution was formed with no precipitate, on warming to room temperature. The solution was cooled to 10°C for 5 min, which resulted in the formation of a yellow microcrystalline precipitate. The reddish-orange solution above the precipitate was filtered into the second bulb. The solvent was slowly (2 days) condensed back into the first bulb, producing a large quantity of yellow–orange crystals in the other bulb which was at room temperature. The crystals were then held at 0°C while the volatile materials were removed. The total yield of the solid material in both bulbs was 4.20 g (calculated for SBr_3AsF_6 based on sulphur is 4.25 g). Several crystals from the second bulb were quickly mounted in the dry box. The crystals were stored at −20°C prior to X-ray analysis. One of the crystals was identified as SBr_3AsF_6 by single crystal X-ray diffraction analysis. The X-ray powder photograph of the crystals corresponded to that reported previously (11).

In contrast to solid SeI_3AsF_6, SeI_3SbF_6, and TeI_3SbF_6, which appear to be stable at room temperature when stored under dry nitrogen, solid SBr_3AsF_6 slowly gives off bromine (8) under these conditions. It does appear to be stable at −20°C and in sulphur dioxide solution. Previous attempts to obtain single crystals of SBr_3AsF_6 were unsuccessful. The difference between this and earlier work appear to be that in this work a more dilute solution was used, the crystals were held at 0°C while the volatiles were removed, and the crystals were mounted quickly and stored at −20°C.

Single crystal X-ray diffraction studies

Crystals were examined in a dry box filled with dry nitrogen using a Wild M3 microscope of long focal length mounted outside the box. A number of crystals were flame sealed in rigorously dried capillary tubes and specimens for further study were selected on the basis

Can. J. Chem. Downloaded from www.nrcresearchpress.com by 213.222.148.141 on 09/07/12
For personal use only.

Can. J. Chem. Downloaded from www.nrcresearchpress.com by 213.222.148.141 on 09/07/12
For personal use only.

of X-ray diffraction photographs. Initial cell dimensions and crystal symmetry were established by precession photography after which the crystals were mounted on either a Picker FACS-I or an Enraf-Nonius CAD-4 diffractometer, both of which were equipped with graphite monochromated MoKα radiation. After alignment, intensity data were collected using ω–2θ scans, full details of the data collection parameters and other crystallographic information for each crystal are given in Table 1. The intensity data were averaged and reduced to structure factors using the routine DATRD2 (27).

Although the compounds are isostructural with TeI_3AsF_6 and $TeBr_3AsF_6$ it was found necessary to redetermine each structure using the MULTAN-80 suite of programs (28). The program SHELX-76 (29) was used for least-squares refinement. None of the four crystals had a well-defined shape, making an analytical absorption correction difficult, so after refinement of the structures with isotropic thermal parameters, the empirical absorption correction, DIFABS, of Walker and Stuart (30) was applied to the unaveraged data. Final cycles of least squares were performed with all atoms assigned anisotropic thermal parameters. Final atomic coordinates are given in Table 2.[1] All computations were performed on a Wicat Systems microcomputer using local implementations of the software.

Discussion

Preparation of SBr_3AsF_6, SeI_3AsF_6, SeI_3SbF_6, TeI_3SbF_6

This is the first report of the preparations of SeI_3SbF_6 and TeI_3SbF_6. The preparations of SBr_3^+, SeI_3^+, and TeI_3^+ cations as salts of the AsF_6^- anion have been reported earlier (8, 9, 12, 13). SeI_3SbF_6 and TeI_3SbF_6 were prepared essentially quantitatively from the respective chalcogen, iodine, and antimony pentafluoride in liquid sulphur dioxide solution according to reaction [1].

$$[1]\quad 6M + 9X_2 + 10SbF_5 \xrightarrow{SO_2} 6MX_3SbF_6 + (SbF_3)_3SbF_5$$
(M = Se, Te, X = I; and M = S, X = Br)

SBr_3SbF_6 has also been prepared quantitatively in a similar manner, although the reduced product was not known to be $(SbF_3)_3SbF_5$ at that time (8). Reaction [1] likely represents a general route to the preparations of the hexafluoroantimonate salts of the Group VI trihalide cations with the exception of SI_3^+.

SBr_3AsF_6 and SeI_3AsF_6 may be readily prepared quantitatively from the respective chalcogen, halogen, and arsenic pentafluoride in liquid sulphur dioxide according to reaction [2], or with an excess of arsenic pentafluoride.

$$[2]\quad 2M + 3X_2 + 3AsF_5 \xrightarrow{SO_2} 2MX_3AsF_6 + AsF_3$$
(M = S, Se, Te; X = Br, I (except for SI_3^+), and likely Cl)

$SBr_3M'F_6$ (M′ = As, Sb) have been identified in solution and in the solid state by Raman spectroscopy (8, 10). The cell parameters of SBr_3AsF_6 obtained from X-ray powder photographs (11) are similar to those obtained from single crystals and the composition of the bulk material is therefore SBr_3AsF_6. Vibrational spectroscopic data for the SeI_3^+ and TeI_3^+ cations in $SeI_3M'F_6$ and $TeI_3M'F_6$ have not been reported. However, SeI_3AsF_6 and SeI_3SbF_6 have been identified in solution by ^{77}Se nmr spectroscopy (ref. 25 and this work). $TeI_3M'F_6$ are sparingly soluble in sulphur dioxide and therefore is not readily identified in solution by ^{125}Te nmr. The Group VI trihalide cations are of interest in their own right, and in addition are potentially useful reagents (31) in the synthesis of novel chalcogen–halide cations, e.g. in the synthesis of $Se_6I_2^{2+}$ and $Se_4I_4^{2+}$ according to reactions [3] and [4].

$$[3]\quad 2SeI_3^+ + 2Se_8^{2+} \xrightarrow{SO_2} 3Se_6I_2^{2+}$$

$$[4]\quad 4SeI_3^+ + Se_8^{2+} \xrightarrow{SO_2} 3Se_4I_4^{2+}$$

The crystal structures of SBr_3AsF_6, SeI_3AsF_6, SeI_3SbF_6, and TeI_3SbF_6

The crystal structures of SBr_3AsF_6, SeI_3AsF_6, SeI_3SbF_6,

TABLE 2. Fractional atomic coordinates with esd's in parentheses

Atom	x	y	z
		SBr_3AsF_6	
S	0.6940 (6)	0.2977 (6)	0.2095 (4)
Br(1)	0.7606 (3)	0.4403 (2)	0.3458 (2)
Br(2)	0.7061 (3)	0.0904 (2)	0.2875 (3)
Br(3)	0.9103 (3)	0.2963 (3)	0.1235 (2)
As	0.2896 (3)	0.2307 (2)	0.4417 (2)
F(1)	0.3386 (18)	0.2840 (15)	0.3155 (10)
F(2)	0.2087 (19)	0.3945 (15)	0.4626 (13)
F(3)	0.2458 (17)	0.1760 (18)	0.5678 (10)
F(4)	0.0947 (20)	0.1741 (17)	0.3825 (15)
F(5)	0.3649 (18)	0.0638 (14)	0.4185 (12)
F(6)	0.4828 (20)	0.2850 (16)	0.4986 (12)
		SeI_3AsF_6	
Se	0.18914(22)	0.18275(17)	0.19815(14)
I(1)	0.26749(15)	0.04264(11)	0.36201(9)
I(2)	0.21215(17)	0.41213(13)	0.26842(15)
I(3)	0.43631(18)	0.17620(13)	0.10763(11)
As	0.80442(21)	0.22566(17)	0.93270(13)
F(1)	0.8445 (15)	0.2819 (11)	0.8112 (8)
F(2)	0.7194 (16)	0.3751 (12)	0.9517 (10)
F(3)	0.7692 (18)	0.1701 (14)	1.0576 (9)
F(4)	0.6187 (16)	0.1726 (13)	0.8748 (13)
F(5)	0.8826 (16)	0.0745 (10)	0.9107 (10)
F(6)	0.9866 (16)	0.2783 (14)	0.9951 (10)
		SeI_3SbF_6	
Se	0.18842(14)	0.30735(12)	0.70538(9)
I(1)	0.26300(10)	0.45030(10)	0.86310(10)
I(2)	0.21120(10)	0.08220(10)	0.78170(10)
I(3)	0.43070(10)	0.31560(10)	0.61690(10)
Sb	0.80090(10)	0.27910(10)	0.43220(10)
F(1)	0.8583 (11)	0.2189 (9)	0.3050 (6)
F(2)	0.7196 (12)	0.1155 (11)	0.4604 (7)
F(3)	0.7504 (12)	0.3381 (11)	0.5605 (7)
F(4)	0.6006 (12)	0.3221 (11)	0.3656 (9)
F(5)	0.8748 (11)	0.4454 (7)	0.4041 (7)
F(6)	0.4974 (12)	0.2312 (10)	0.5012 (7)
		TeI_3SbF_6	
Te	0.32159(9)	0.17724(7)	0.30291(6)
I(1)	0.21459(14)	0.04684(9)	0.13233(7)
I(2)	0.27813(13)	0.41254(9)	0.23519(10)
I(3)	0.06645(13)	0.16558(10)	0.39719(9)
Sb	0.31725(10)	0.72453(8)	0.92236(6)
F(1)	0.3810 (12)	0.7844 (8)	0.8022 (6)
F(2)	0.2411 (13)	0.8841 (10)	0.9482 (9)
F(3)	0.2652 (13)	0.6607 (11)	1.0467 (8)
F(4)	0.1134 (12)	0.6811 (12)	0.8517 (8)
F(5)	0.3854 (13)	0.5657 (8)	0.8923 (9)
F(6)	0.5182 (11)	0.7639 (11)	0.9932 (8)

[1]Tables of anisotropic thermal parameters, and observed and calculated structure factors have been deposited and may be obtained, at a nominal charge, from the Depository of Unpublished Data, CISTI, National Research Council of Canada, Ottawa, Ont., Canada K1A 0S2.

Can. J. Chem. Downloaded from www.nrcresearchpress.com by 213.222.148.141 on 09/07/12
For personal use only.

TABLE 3. Bond lengths (Å)[a] with estimated standard deviations in parentheses for SBr_3AsF_6, SeI_3AsF_6, SeI_3SbF_6, TeI_3AsF_6,[b] and TeI_3SbF_6

Bond	Length				
	SBr_3AsF_6	SeI_3AsF_6	SeI_3SbF_6	TeI_3AsF_6[b]	TeI_3SbF_6
M[c]—X(1)	2.133(6)	2.502(2)	2.511(1)	2.633(1)	2.657(1)
—X(2)	2.151(6)	2.504(2)	2.514(1)	2.665(2)	2.669(1)
—X(3)	2.141(6)	2.519(2)	2.512(1)	2.674(2)	2.672(1)
M′[c]—F(1)	1.704(13)	1.710(10)	1.884(7)	1.720(9)	1.866(8)
F(2)	1.695(15)	1.721(11)	1.879(8)	1.675(11)	1.873(10)
F(3)	1.694(14)	1.734(12)	1.871(8)	1.716(9)	1.889(9)
F(4)	1.712(16)	1.696(12)	1.849(9)	1.687(15)	1.869(9)
F(5)	1.709(14)	1.720(10)	1.879(8)	1.704(12)	1.855(8)
F(6)	1.686(15)	1.686(11)	1.849(9)	1.695(11)	1.838(8)
M[c]—F(1)	[e]	[e]	3.28(1)	3.16(1)	3.10(1)
—F(5)	2.94(2)	2.98(1)	2.92(1)	2.90(1)	2.86(1)
—F(6)	2.97(2)	2.98(1)	2.97(1)	2.88(1)	2.93(1)
	[0.17][d]	[0.22][d]	[0.30][d]	[0.50][d]	[0.51][d]
X(1)—F(2)	2.77(2)	2.88(1)	2.82(1)	3.11(1)	3.02(1)
X(2)—F(1)	3.12(1)	3.30(1)	3.32(1)	[e]	3.43(1)
—F(3)	3.04(2)	3.41(1)	3.22(1)	[e]	[e]
—F(4)	3.27(2)	[e]	[e]	[e]	3.46
X(3)—F(3)	2.87(1)	2.96(1)	2.94(1)	3.04(1)	3.02(1)

[a]All interactions less than the sum of van der Waals' radii are included (r_S = 1.85, r_{Se} = 2.00, r_{Te} = 2.20, r_{Br} = 1.95, r_I = 2.15, and r_F = 1.35 Å, ref. 48).
[b]Reference 13.
[c]M = S, Se, and Te; M′ = As and Sb; and X = Br and I.
[d]Sum of bond valences of the M---F contacts (valence unit, v.u.). Bond valence in valence unit (v.u.), $S = (R/R_0)^{-N}$, ref. 6, where R is the observed bond distance (Å), R_0 = 1.550, N = 3.8 for S(IV)—F, R_0 = 1.71, N = 4.0 for Se(IV)—F, and R_0 = 1.779, N = 3.5 for Te(IV)—F.
[e]In these cases the bond distances are longer than the sum of the corresponding van der Waals' radii.

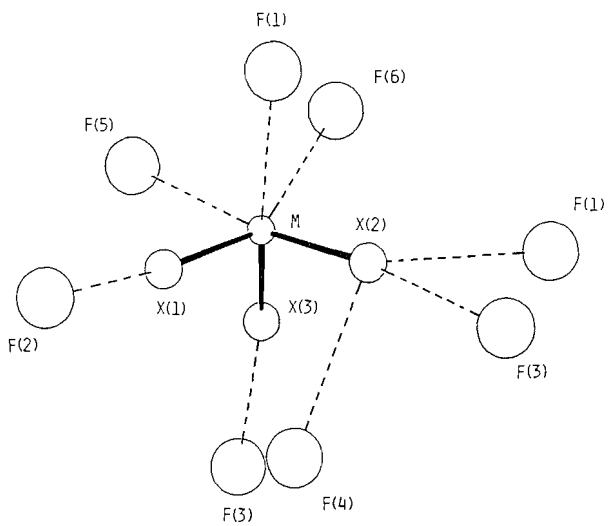

FIG. 1. MX_3^+ cation (M = S, Se, Te; and X = Br, I) with anion contacts. Corresponding bond distances and angles are listed in Tables 3 and 4. S—F(1) in SBr_3AsF_6, Se—F(1) and I(2)—F(4) in SeI_3AsF_6, I(2)—F(4) in SeI_3SbF_6, and I(2)—F(3) in TeI_3SbF_6 are longer than their corresponding sum of Van der Waals' radii.

TeI_3SbF_6 salts consist of discrete MX_3^+ cations (M = S, Se, Te; and X = Br, I), and $M'F_6^-$ anions (M′ = As, Sb) with definite cation–anion interactions. Figure 1 shows the MX_3^+ cation with anion contacts; corresponding bond distances and angles are presented in Tables 3 and 4. The SBr_3AsF_6, SeI_3AsF_6, SeI_3SbF_6, and TeI_3SbF_6 salts are isostructural with $TeBr_3AsF_6$ and TeI_3AsF_6. The packing in all these compounds are similar to that in $TeBr_3AsF_6$ which has been illustrated in ref. 11.

The geometry of the SBr_3^+, SeI_3^+, and TeI_3^+ cations

The SBr_3^+, SeI_3^+, and TeI_3^+ cations are of approximately C_{3v} symmetry. The average bond distances and angles in the SBr_3^+ cation are 2.142(6) Å and 103.4(2)°, those of the SeI_3^+ cation in both AsF_6^- and SbF_6^- salts (2.508(2) Å, 102.4(1)° and 2.512(1) Å, 102.3(1)°, respectively) are essentially identical. The average bond distance and angle of TeI_3^+ cation in SbF_6^- salt (2.666(1) Å, 99.8(1)°) are also identical to those in the AsF_6^- salt (2.667(1) Å, 99.9(3)°) (13). For Group VI trihalide cations with counterions of very different basicity, the more basic the counterion, the longer the chalcogen halide bond, e.g. the average $SeCl_3^+$ distance in $SeCl_3MoOCl_4$ is 2.148(2) Å (32), longer than those in the less basic $AlCl_4^-$ and $SbCl_6^-$ salts, $SeCl_3AlCl_4$ (2.11(1) Å) (33) and $SeCl_3SbCl_6$ (2.10(1) Å) (34). Presumably the more basic anion donates electron density into the antibonding σ* orbitals of the cation more effectively, leading to chalcogen–halide bond lengthening (2, 34). Clearly, the difference in basicity of the AsF_6^- and SbF_6^- anions is not sufficiently large to affect the geometry of the SeI_3^+, TeI_3^+, or $TeCl_3^+$ cations (Table 5), or alternatively the differences in geometry are too small to be detected by our experiments. Consistently, the vibrational data of the SBr_3^+ cation for both the AsF_6^- and the SbF_6^- salts are also very similar (8, 10).

All the chalcogen–halogen bond distances in the MX_3^+ salts of very weakly basic anions, including those in SBr_3^+, SeI_3^+, and TeI_3^+, are within 0.02 Å of the corresponding distances calculated by the Schomaker–Stevenson equation (35). The exceptions are the M—F bonds in MF_3^+ (M = S, Se, Te) which are ~0.10 Å shorter than the values calculated by the Schomaker–Stevenson equation (Table 6). However, it is well-known that bond distances of related perfluoro compounds

TABLE 4. Bond angles (deg)[a] with estimated standard deviations in parentheses for SeI_3AsF_6, SeI_3SbF_6, TeI_3AsF_6,[b] and TeI_3SbF_6

Bonds	Angle				
	SBr_3AsF_6	SeI_3AsF_6	SeI_3SbF_6	TeI_3AsF_6[b]	TeI_3SbF_6
X(1)—M—X(2)[c]	103.3(2)	104.7(1)	103.3(1)	103.40(5)	101.9(1)
—X(3)	104.3(2)	103.2(1)	102.8(1)	100.86(5)	100.5(1)
X(2)—M—X(3)	102.6(2)	99.3(1)	100.8(1)	95.42(5)	97.0(1)
F(1)—M′—F(2)	90.6(7)	88.3(6)	91.5(4)	88.4(6)	90.0(5)
—F(3)	178.6(7)	178.4(6)	178.2(4)	178.6(6)	176.6(4)
—F(4)	91.3(8)	91.5(7)	91.2(5)	93.0(7)	92.5(5)
—F(5)	89.4(7)	91.4(6)	89.6(4)	90.6(6)	89.3(4)
—F(6)	88.2(7)	90.6(6)	89.9(4)	90.2(6)	88.3(4)
F(2)—M′—F(3)	90.4(8)	91.8(7)	88.8(5)	91.6(7)	91.9(5)
F(4)	89.7(7)	88.4(7)	87.8(5)	86.9(10)	89.9(5)
F(5)	178.1(7)	177.8(6)	177.9(4)	176.8(9)	177.6(5)
F(6)	90.9(7)	90.9(7)	90.1(4)	93.8(9)	91.0(5)
F(3)—M′—F(4)	89.8(8)	90.1(7)	90.6(5)	88.4(7)	90.3(5)
F(5)	89.7(8)	88.5(6)	90.2(4)	89.5(7)	88.9(5)
F(6)	90.7(7)	87.7(7)	88.3(4)	88.4(6)	88.9(5)
F(4)—M′—F(5)	88.4(7)	89.4(6)	90.4(5)	90.1(9)	87.8(5)
F(6)	179.2(8)	177.7(8)	177.6(5)	176.7(7)	178.8(4)
F(5)—M′—F(6)	91.0(7)	91.3(7)	91.7(4)	89.3(8)	91.2(5)
X(1)—M—F(6)	151.9(4)	157.5(3)	154.8(2)	170.2(3)	165.9(2)
X(2)—M—F(5)	171.6(3)	170.9(2)	172.0(2)	172.5(3)	174.8(2)
X(3)—M—F(1)	173.5(3)	[d]	175.2(2)	173.5(2)	175.0(2)
M—X(1)—F(2)	168.9(4)	167.2(2)	168.5(2)	151.3(3)	156.1(2)
M—X(2)—F(1)	130.8(3)	141.8(2)	137.0(2)	[d]	142.2(2)
—F(3)	170.2(3)	160.6(2)	164.1(2)	[d]	[d]
—F(4)	85.6(3)	[d]	[d]	[d]	84.6(2)
M—X(3)—F(3)	163.7(3)	165.7(2)	167.2(2)	165.3(2)	166.6(2)
F(1)—M—F(5)	98.9(4)	[d]	98.7(2)	99.8(3)	101.1(2)
—F(6)	84.5(4)	[d]	86.2(2)	94.0(3)	94.7(2)
F(5)—M—F(6)	74.5(4)	81.7(2)	76.5(2)	87.8(4)	83.6(2)

[a]All interactions less than sum of van der Waals radii are included.
[b]Reference 13.
[c]M = S, Se, and Te; M′ = As and Sb; and X = Br and I.
[d]In these cases the bond distances are longer than the sum of the corresponding van der Waals' radii.

Can. J. Chem. Downloaded from www.nrcresearchpress.com by 213.222.148.141 on 09/07/12
For personal use only.

are also shorter than the corresponding distances calculated by the Schomaker–Stevenson equation, e.g. PF_3 (36), CF_4 (37), and SiF_4 (38) (observed bond distances 1.570(1), 1.32, and 1.56(1) Å; calculated bond distances, 1.66, 1.36, and 1.70 Å, respectively; see Table 6). The agreement of the observed bond distances in the known MCl_3^+, MBr_3^+, and MI_3^+ (M = S, Se, Te) cations with the corresponding values calculated by the Schomaker–Stevenson equation is within 0.02 Å. This is remarkable in view of the fact that the Schomaker–Stevenson equation utilizes covalent radii and electronegativity values for neutral dico-ordinate chalcogens (i.e. (M(II)), whereas the central atoms in the MX_3^+ salts are all positively charged with a formal valence of IV. However, the M—X bond distance in the MX_3^+ cation are slightly shorter than those in the related M[II] compounds (e.g. SCl_3^+, 1.970; SCl_2 (39), 2.014(5); CF_3SCl (40), 2.015(3); SBr_3^+, 2.142(8); CF_3SBr (41), 2.162(6); $SeCl_3^+$, 2.10(1); $SeCl_2$ (42), 2.157(3) Å).

The small variations of the bond angles (X—M—X) within the SBr_3^+, SeI_3^+, and TeI_3^+ are consistent with VSEPR theory (5), i.e. the longer the adjacent bonds, the smaller the corresponding angles (Tables 3 and 4).

The SBr_3^+, SeI_3^+, and TeI_3^+ cations all can be regarded as having AX_3E tetrahedral geometry in VSEPR terms (5) with the lone pair of electrons, E, occupying one of the vertices. The structures of SBr_3^+, SeI_3^+, and TeI_3^+ cations are very similar to those of their isoelectronic counterparts, PBr_3 (43), AsI_3 (44), and SbI_3 (45) in the solid state. The shorter bond distances and slightly larger angles in Group VI trihalide cations (SBr_3^+, 2.142(8) Å, 103.4(2)°; SeI_3^+, 2.510(2) Å, 102.4(1)°; and TeI_3^+, 2.667(1) Å, 99.9(3)°) than those in Group V trihalides (PBr_3(s), 2.213(4) Å, 100.5(2)° (43); AsI_3(s), 2.591(1) Å, 99.67(5)° (44); and SbI_3(s), 2.87(1) Å, 95.8(3)° (45)) are consistent with the greater charge and smaller size of the formerly positively charged sulphur, selenium, and tellurium atoms.

The variation of bond angles in group VI trihalide cations

The average bond angles (X—M—X) in the Group VI trihalide cations, MX_3^+, decreases as the electronegativity of M decreases (S → Te) and as the electronegativity of the ligand X increases (I → F) as shown in Table 5 and consistent with VSEPR theory (5). Alternatively, the bond angle variations can be understood in terms of relative size, e.g. the larger the halogen, X, the larger the X—M—X angle (46, 47). The observed angles are consistent with both models except for the angle in $SeCl_3^+$ in $SeCl_3SbCl_6$ (see Table 5), which appears to be too large.

Cation–anion interactions

Table 4 includes all cation–anion contacts that are less than the sum of the appropriate van der Waals radii (48). There are two to three fluorine cation–anion contacts, M---F (M = S, Se, Te), to the central atoms of the MX_3^+ cations. In terms of

TABLE 5. Average bond distances (Å), bond angles (deg), and sum of M---F bond valences (valence unit) in the Group VI trihalide cations[a]

Cation Anion	SF_3^+ BF_4^- [b]	SeF_3^+ $Nb_2F_{11}^-$ [c]	TeF_3^+ $Sb_2F_{11}^-$ [d]
Average d(M—X)	1.496(2)	1.66(2)	1.84(4)
Average X—M—X	97.5(1)	94.2(4)	90(2)
Sum of M---F bond valences	0.41	0.72	1.16
Cation Anion	SCl_3^+ AsF_6^- [e]	$SeCl_3^+$ $SbCl_6^-$ [f]	$TeCl_3^+$ AsF_6^- [f] SbF_6^- [f]
Average d(M—X)	1.970	2.10(1)	2.264(2), 2.258(3)
Average X—M—X	102.3	103.1(4)	96.0(1), 95.8(1)
Sum of M---F bond valences	0.28	—	0.88, 0.84
Cation Anion	SBr_3^+ AsF_6^- [g]	$SeBr_3^+$ SbF_6^- [h]	$TeBr_3^+$ AsF_6^- [h]
Average d(M—X)	2.142(8)	2.269(8)	2.432(3)
Average X—M—X	103.4(2)	100.9(3)	97.9(1)
Sum of bond valences	0.17	0.44	0.69
Cation Anion	SI_3^+ —	SeI_3^+ AsF_6^- [g] SbF_6^- [g]	TeI_3^+ AsF_6^- [j] SbF_6^- [g]
Average d(M—X)	[2.38(1)] [i]	2.508(2), 2.512(1)	2.667(2), 2.666(1)
Average X—M—X	[104(2)] [i]	102.4(1), 102.3(1)	99.9(1), 99.8(1)
Sum of M---F bond valences	—	0.22, 0.30	0.50, 0.51

[a]Data from the available salts with the anions of lowest basicity are included.
[b]Reference 61.
[c]Reference 62.
[d]Reference 63.
[e]Reference 64.
[f]Reference 34.
[g]This work.
[h]Reference 11.
[i]Estimated, see text.
[j]Reference 13.

VSEPR model, these contacts are grouped around the lone pair electrons of the MX_3^+ cation. With inclusion of the M---F contacts, the overall geometry around the sulphur and selenium atoms can be described as AX_3Y_2E in SBr_3AsF_6 and SeI_3AsF_6 and AX_3Y_3E around the selenium and tellurium atoms in SeI_3SbF_6 and TeI_3SbF_6. Various overall geometries including the more complicated $AX_3Y_3Y'E$, $AX_3Y_3Y'_2E$, $AX_3Y_3Y'_3E$, and AX_5Y_4E of the central atoms in other Group VI trihalide cations have been observed and discussed (34). The strength of the M---F contacts can be assessed by the relative magnitude of the bond valences, as defined by Brown (6). The sum of the bond valences of the M---F contacts, listed in Tables 3 and 5, increases as the electronegativity of the ligand, X, increases or the electronegativity of the central atom, M, decreases. This is consistent with the charge being more localized on the trico-cordinate atom, as the differences in electronegativity between M and X increase.

Contacts between X and the anionic fluoride (or chloride) are not common in Group VI trifluoride and trichloride cations. However, significant X---F contacts have been observed in $SeBr_3SbF_6$, $TeBr_3AsF_6$, and TeI_3SbF_6. These contacts are also observed in SBr_3AsF_6, SeI_3AsF_6, SeI_3SbF_6, and TeI_3AsF_6, and are consistent with the higher polarizability and more electropositive nature of Br and I. Consistently, the weaker M---F contacts in the tribromide and triiodide cations lead to more and/or stronger X---F contacts (see Table 3). The weak M---F contacts and the relatively strong X---F contacts in SBr_3^+ and SeI_3^+ can be attributed to the similarity in electronegativity of M and X ($\chi_S = 2.58$, $\chi_{Se} = 2.55$, $\chi_{Br} = 2.96$, $\chi_I = 2.66$ (49)). Thus the positive charge is more delocalized in SBr_3^+ and SeI_3^+ than in the other MX_3^+ cations.

A prediction of the geometry of SI_3^+ in the non-existent $SI_3M'F_6$ ($M' = As, Sb$)[2]

An estimate of bond distances and angles in MX_3^+ cations, for which structures were unknown, were determined by extrapolation of known data from Group V trihalides and Group VI trihalide cations (11). The estimated bond distances and angles for SBr_3^+, SeI_3^+, and TeI_3^+ deviated (~0.02 Å and 1°) from the values obtained in the present work and for TeI_3^+ in TeI_3AsF_6 (13).[3] A more accurate fit is desirable, and in addition the method cannot give an accurate estimate of the S—I distance in $SI_3M'F_6$, as the method relies on the structural determination of the isoelectronic Group V trihalide (PI_3) in the gas phase, for which an accurate structure is not available

[2]Various attempts to prepare solid $SI_3M'F_6$ in our laboratory led in all cases to $S_2I_4(MF_6)_2 + I_2$ solids (19, 51).

[3]SBr_3^+, estimated 2.164(5) Å, 101.1(9)°, observed 2.142(6) Å, 103.4(2)°; SeI_3^+, estimated 2.492(5) Å, 101.0°, observed 2.510(2) Å, 102.4(1)°; TeI_3^+, estimated 2.650 Å, 99.2°, observed 2.667(2) Å, 99.9(2)°.

Can. J. Chem. Downloaded from www.nrcresearchpress.com by 213.222.148.141 on 09/07/12
For personal use only.

TABLE 6. Variations of M—X bond distances (Å) and X—X distances (Å) of the Group VI trihalide cations, MX_3^+ [a]

Cation Anion	SF_3^+ BF_4^-	SeF_3^+ $Nb_2F_{11}^-$	TeF_3^+ $Sb_2F_{11}^-$	Average values
Average d(M—F)	1.496(2)	1.66(2)	1.84(4)	
d(M—F) calculated by Schomaker–Stevenson equation[b]	1.63	1.76	1.92	
d(M—F) − d(M—Cl)	−0.474	−0.45	−0.42	−0.448 ± 0.027
Average d(F---F)	2.250	2.428	2.602	
Ratio of d(F---F) to d(Cl---Cl)	0.733	0.735	0.755	0.741 ± 0.012
Cation Anion	**SCl_3^+ AsF_6^-**	**$SeCl_3^+$ $SbCl_6^-$**	**$TeCl_3^+$ AsF_6^-, SbF_6^- [c]**	**Average value**
Average d(M—Cl)	1.970	2.10(1)	2.261(3)	
d(M—Cl) calculated by Schomaker–Stevenson equation[b]	1.98	2.11	2.26	
d(M—Cl) − d(M—Br)	−0.172	−0.169	−0.171	−0.170 ± 0.002
Average d(Cl---Cl)	3.069	3.289	3.358	
Ratio of d(Cl---Cl) to d(Br---Br)	0.913	0.940	0.915	0.923 ± 0.015
Cation Anion	**SBr_3^+ AsF_6^-**	**$SeBr_3^+$ SbF_6^-**	**$TeBr_3^+$ AsF_6^-**	**Average value**
Average d(M—Br)	2.142(8)	2.269(8)	2.432(3)	
d(M—Br) calculated by Schomaker–Stevenson equation[b]	2.15	2.27	2.44	
d(M—Br) − d(M—I)	—	−0.242	−0.235	−0.238 ± 0.003
Average d(Br---Br)	3.362	3.499	3.668	
Ratio of d(Br---Br) to d(I---I)	—	0.894	0.898	0.896 ± 0.002
Cation Anion	**SI_3^+ —**	**SeI_3^+ AsF_6^-, SbF_6^- [c]**	**TeI_3^+ AsF_6^+, SbF_6^- [c]**	
Average d(M—I)	—	2.510(2)	2.667(2)	
d(M—I) calculated by Schomaker–Stevenson equation[b]	2.36	2.49	2.65	
Average d(I---I)	—	3.912	4.083	

[a]Data from the available salts containing the anions of lowest basicity are used.
[b]From Schomaker–Stevenson equation (35): Schomaker–Stevenson distance for M—X = $r_m + r_x - 0.09|\chi_m - \chi_x|$(Å) where r_m and r_x are the covalent radii (35) and χ_m and χ_x are Pauling's electronegativities (49).
[c]Average values of the two salts are used.

(P—I distance in PI_3(g) = 2.43(3) Å (50)). We have therefore developed another approach using only the data for the known Group VI trihalide cations of low basicity. The differences in bond distance, i.e. d(M—I) − d(M—Br), d(M—Br) − d(M—Cl), d(M—Cl) − d(M—F), in the appropriate cations are essentially constant as shown in Table 6. The S—I bond distance in $SI_3M'F_6$ can therefore be estimated as equal to the S—Br distance in SBr_3^+ plus the average of (d(M—I) − d(M—Br)) and equals to 2.38(1) Å. The accuracy of all the structures is high, which lends confidence to the estimation. The chalcogen–iodine distances calculated by the Schomaker–Stevenson equation are 0.02 Å shorter than the observed or estimated distances in SI_3^+, SeI_3^+, and TeI_3^+. This consistency supports the estimation of the S—I distance in SI_3^+ as 2.38(1) Å.

The ratio of d(Br—Br)/d(I—I), d(Cl—Cl)/d(Br—Br), and d(F—F)/d(Cl—Cl) in corresponding pairs of MX_3^+ cations are essentially constant (Table 6). Therefore the I—I separation in the hypothetical SI_3^+ cation is estimated as (Br—Br separation in SBr_3^+)/0.896 = 3.752 Å, leading to a predicted angle of 104(2)°.

A comparison of the chalcogen–halide bond distances in SBr_3^+ and that estimated for SI_3^+ with the chalcogen–halide distances in the binary polychalcogen–halogen cations

Recently, a number of novel binary sulphur and selenium–iodine cations, including S_7I^+ (15, 16), $(S_7I)_2I^{3+}$ (16), $S_2I_4^{2+}$ (51), $Se_2I_4^{2+}$ (17), $[Se_6I]_n^{n+}$ (52), and $Se_6I_2^{2+}$ (18), and the sulphur—bromine cation, S_7Br^+ (14), have been prepared and structurally characterized. The iodine and bromine atoms form formally single covalent bonds with the positively charged trico-ordinate sulphur and selenium atoms in these cations except in $S_2I_4^{2+}$ and the polymeric $[Se_6I]_n^{n+}$ cations. A major motivation for this work was to accurately determine the structures of SBr_3^+, SeI_3^+, and estimate that of SI_3^+, in order to compare the "bench mark" chalcogen—halogen bond distances in these simple cations, with those in the more complex cations. In this way it was hoped to aid in a better understanding of the geometry and bonding in these novel polychalcogen–halogen cations. Such a comparison is given in Table 7.

The M—X (M = S, Se; X = Br, I) bond distances in S_7Br^+, S_7I^+, $(S_7I)_2I^{3+}$, $Se_2I_4^{2+}$, and $Se_6I_2^{2+}$ cations are all significantly shorter (Table 7) than the corresponding bond distances

Can. J. Chem. Downloaded from www.nrcresearchpress.com by 213.222.148.141 on 09/07/12
For personal use only.

TABLE 7. Comparison of the chalcogen–halide bond distances (Å) in the chalcogen trihalide cations, MX_3^+, and polychalcogen–halogen cations

Compound	Average M—X distances	Differences[a]	References
SBr_3AsF_6	2.142(8)	—	—
$(S_7Br)_4S_4(AsF_6)_6$	2.11(2)	−0.03	14
$SI_3M'F_6$ (M' = As, Sb)	2.38(1)[b]	—	—
S_7IAsF_6	2.33(3)	−0.05	15
S_7ISbF_6	2.342(3)	−0.038	15
$(S_7I)_4S_4(AsF_6)_6$	2.314(9)	−0.066	16
$[(S_7I)_2I](AsF_6)_3 \cdot 2AsF_3$	2.335(6)	−0.045	16
	2.674(7)[c]	+0.29	—
$S_2I_4(AsF_6)_2$	3.027(7)[d]	+0.65	51
$SeI_3M'F_6$ (M' = As, Sb)	2.510(2)	—	—
$Se_2I_4(Sb_2F_{11})_2$	2.447(2)	−0.063	17
$[Se_6I]_n \cdot n AsF_6$	2.736(3)[c]	+0.23	52
$Se_6I_2(AsF_6)_2 \cdot 2SO_2$	2.454(2)	−0.056	18

[a]Differences = M—X bond distance − M—X bond distance in MX_3^+.
[b]Estimated, see text.
[c]Bridging M---I bond, with bond order of approximately 0.5.
[d]The S—I interaction is via a π^*—π^* bond. An average value is quoted.

in the Group VI trihalide cations. The shorter Se—I bond in $Se_2I_4^{2+}$ relative to that in SeI_3^+ has been attributed to the presence of π-bonding which results in a formal bond order of 1.25 per Se—I bond (17). The exocyclic chalcogen—halogen bonds in the other binary polychalcogen—halogen cation are also shorter than those in the corresponding simple chalcogen trihalide cations, MX_3^+ (Table 7). This suggests that they may also have some π-bonding character. It is conceivable that there is some π-bonding in MX_3^+ themselves, but this will be spread over three bonds, and will be less than that in the one chalcogen—halogen bond in the polychalcogen—halogen cations. Thus the shorter exocyclic M—X bonds in the binary polychalcogen—halogen cations may arise from some localisation of the positive charge onto the exocyclic halogen atoms and therefore some contribution to the overall structure by valence bond structures **I** and **II** for $S_7I(Br)^+$ and $Se_6I_2^{2+}$ respectively.

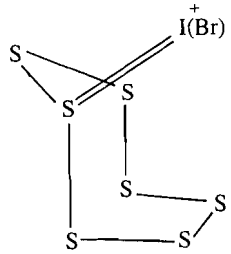

I

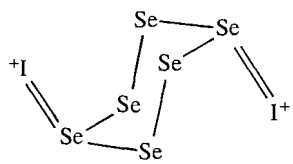

II

Although the contribution from valence bond structures **I** and **II** may be small, the I(Br)---F interionic contacts in these cations are significant (d(I---F) for S_7ISbF_6, 2.926(9) Å (15); for $Se_6I_2(AsF_6)_2.2SO_2$, 3.16(1) and 3.17(1) Å (18); the sum of van der Waal's radii is 3.50 Å) and consistent with some positive charge localisation on the exocyclic halogen atoms. The trico-ordinate chalcogen atom presumably carries the greatest positive charge, and in addition there will be charge delocalisation into the ring giving rise, in part, to the observed chalcogen–chalcogen bond distance alternation in the ring.

The exocyclic halogen atoms in the $S_7I(Br)^+$ and $Se_6I_2^{2+}$ cations adopt the *endo*-configuration (**III***a* and **VI***a*) and form the weak, but definite, intra-cationic contacts (e.g. d(I---S(6)) for S_7ISbF_6(15), 3.394(3) Å; d(I—Se(1′)) and d(I—Se(3′)) for $Se_6I_2(AsF_6)_2.2SO_2$(18), 3.719(2) and 3.709(2) Å; where the sum of van der Waals' radius is 4.00 Å for S—I and 4.15 Å for Se—I). Presumably the intra-ionic contacts reflect attraction (weakly bonding or electrostatic), or the sterically less hindered isomer **III***b* and **IV***b* would be preferred. In $S_7I(Br)^+$ (**III***a*), the I(Br)S(1)S(7)S(6) atoms lie in a plane, which is at 90.2° to the S(4)S(5)S(6)S(7) plane and is reminiscent of the planar I_4^{2+} cation (53) and the S_2I_2 units in $S_2I_4^{2+}$ cations (51), both of which contain dimers joined by π^*—π^* bonds. The electron density in the π^* antibonding orbital of the exocyclic chalcogen—halogen bond may be delocalised into the ring through I(Br)---S(6) interactions. This then would lead to a reduction of π^* electron density in the I(Br)—S(6) bond, and therefore an increase in π bonding and corresponding decrease in bond length. A similar situation can hold in $Se_6I_2^{2+}$. Thus the relatively short exocyclic chalcogen—halogen bonds in the

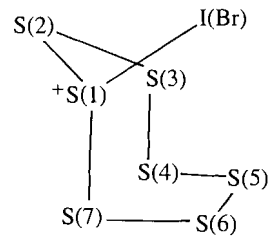

III*a*

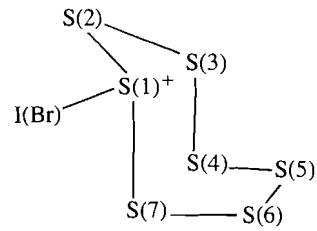

III*b*

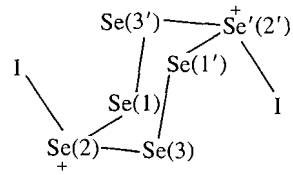

IV*a*

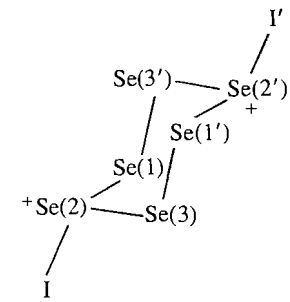

IV*b*

Can. J. Chem. Downloaded from www.nrcresearchpress.com by 213.222.148.141 on 09/07/12
For personal use only.

TABLE 8. Thermodynamic data

Reaction	ΔH (kcal mol^{-1})	Reference
Se(hexagonal) → Se(g)	54	65
(1/8)S_8(s) → S(g)	66.6	65
I_2(s) → I_2(g)	14.9	65
$\frac{1}{2}I_2$(s) → I(g)	25.5	65
$\frac{1}{2}Br_2$(l) → Br(g)	26.5	65
S(g) + 2I(g) → SI_2(g)	−95	*a*
Se(g) + 2I(g) → SeI_2(g)	−82	*a*
SI_2(g) → SI_2(s)	−15	*b*
SeI_2(g) → SeI_2(s)	−20	*b*
Se(g) → Se^+(g) + e	226	65
S(g) → S^+(g) + e	240	65
$3AsF_5$(g) + $2e^-$ → $2AsF_6^-$(g) + AsF_3(g)	−233	*c*
AsF_3(l) → AsF_3(g)	9	65
SeI_3^+(g) → Se^+(g) + 3I(g)	124	*d*
SBr_3^+(g) → S^+(g) + 3Br(g)	168	*d*
SeI_3^+(g) + AsF_6^-(g) → SeI_3AsF_6(s)	−123 ± 5	*e*
SBr_3^+(g) + AsF_6^-(g) → SBr_3AsF_6(s)	−128 ± 5	*e*

[a]The S—I bond energy in SI_2 was calculated to be 47.5 kcal mol^{-1} by Sanderson (66), assuming d(S—I) = 2.37 Å (sum of nonpolar covalent radii). This is similar to the experimental S—I bond energy of 49.4 ± 2 kcal mol^{-1} in H(S—I) (67). The Se—I bond energy in SeI_2 was calculated to be 41.2 kcal mol^{-1} by using Sanderson's approach (assuming d(Se—I) = 2.50 Å, sum of nonpolar covalent radii). Johnson (68) estimated the Se—I bond energy in SeI_2 to be 42 kcal mol^{-1}. No experimentally determined Se—I bond energy is available. In order to keep the estimations of the heat of formations consistent, the calculated bond energies in SI_2 and SeI_2 by Sanderson are used (i.e. D(S—I) = 47.5 and D(Se—I) = 41.2 kcal mol^{-1}).

[b]The sublimation energies are expected to be similar to those of SiI_4 (69), PI_3 (65, 69), and CII (70) (18, 15, and 13 kcal mol^{-1}, respectively) for SI_2, and to those of GeI_4 (65), AsI_3 (70), and BrI (65) (20, 23, and 12 kcal mol^{-1}) for SeI_2. Thus, the sublimation energies of SI_2 and SeI_2 are estimated to be 15 and 20 kcal mol^{-1}, respectively.

[c]The heat of reaction for the formation of $2AsF_6^-$(g) and AsF_3(g) may be estimated as follows:

Reaction	ΔH
As(s) + (3/2)F(g) → AsF_3(g)	−187.8 (ref. 65)
AsF_5(g) → As(s) + (5/2)F_2(g)	295.6 (ref. 71)
F_2(g) + $2e^-$ → $2F^-$(g)	−119 (ref. 71)
$2AsF_5$(g) + $2F^-$(g) → $2AsF_6^-$(g)	−222 (refs. 72, 73)
$3AsF_5$(g) + $2e^-$ → $2AsF_6^-$(g) + AsF_3(g)	−233 kcal mol^{-1}

[d]The atomization energies of SeI_3^+(g) and SBr_3^+(g) were estimated from the sums of the respective bond dissociation energies. It is reasonable to assume that the Se(IV)$^+$—I and S(IV)$^+$—Br bond energies are similar to the energies of iodine bonded to neutral Se(II) and bromine bonded to neutral S(II), respectively, because the M(IV)$^+$—X bond lengths are similar to those in M(II)—X (Schomaker–Stevenson distances, Table 6). The Se(IV)$^+$—I and S(IV)$^+$—Br bond strengths can therefore be considered to be similar to the Se(II)—I bond in SeI_2 (41.2 kcal mol^{-1}, footnote *a*) and S(II)—Br bond in S_2Br_2 (56 kcal mol^{-1}, calculated by Sanderson (66)). Thus, the atomization energies for SeI_3^+(g) and SBr_3^+(g) are as follows:

$$SeI_3^+(g) \rightarrow Se^+(g) + 3I(g) \qquad \Delta H = 3(41.2) = 124 \text{ kcal mol}^{-1}$$

$$SBr_3^+(g) \rightarrow S^+(g) + 3Br(g) \qquad \Delta H = 3(56) = 168 \text{ kcal mol}^{-1}$$

On the other hand, it can be argued that the bond dissociation energies are higher than this because bond cleavage is accompanied by charge delocalisation on the chalcogen. Thus the estimated bond dissociation energies are in fact lower limits of the actual values.

[e]Bartlett and co-workers (72, 73) have shown that there is an essentially linear relationship, for simple A^+B^- salts (e.g. NaCl, KBr, KI) between the lattice energies and (molecular volume)$^{1/3}$, where the equation of the line may be represented by ΔU = (556.3(molecular volume)$^{-1/3}$ + 26.3) kcal mol^{-1}. Therefore the crystal lattice energies of SeI_3AsF_6 and SBr_3AsF_6 (molecular volumes are 265 and 225 Å^3, respectively) are estimated as 113 ± 5 kcal mol^{-1} and 118 ± 5 kcal mol^{-1}. However, Bartlett and co-workers noted that for species such as ClO_2BF_4 and SF_3BF_4, there was a positive deviation (~6–8 kcal mol^{-1}) from the line, which was attributed to the dispersion energies of these salts being greater than those of the simple salts (e.g. NaCl, KBr). A conservative estimate of 10 kcal mol^{-1} has been used for the positive deviation of SeI_3AsF_6 and SBr_3AsF_6, and, therefore, ΔU (corrected) for SeI_3AsF_6 and SBr_3AsF_6 are estimated as 123 ± 5 kcal mol^{-1} and 128 ± 5 kcal mol^{-1}, respectively. A more sophisticated treatment would give improved estimates of the dispersion energies of SBr_3^+ and SeI_3^+, which are undoubtedly greater than those of ClO_2^+ or SF_3^+.

Can. J. Chem. Downloaded from www.nrcresearchpress.com by 213.222.148.141 on 09/07/12
For personal use only.

Can. J. Chem. Downloaded from www.nrcresearchpress.com by 213.222.148.141 on 09/07/12
For personal use only.

polychalcogen—halogen cations support the thesis that the long intracationic contacts are bonding in nature and responsible for the cluster-like geometries of this and related cations and molecules. It is likely that both the localisation of the positive charge onto the halogen atom (resonance structures **I** and **II**) and the delocalisation of the π^* electron density in the M—X bond onto the chalcogen ring both contribute to the shortening of the exocyclic M—X bond.

The AsF_6^- and SbF_6^- anions

The average M′—F distances and F—M′—F angles (M′ = As, Sb) in $SBrAsF_6$ (1.70(1) Å, 90.0(8)°), SeI_3AsF_6 (1.71(1) Å, 90.0(8)°), SeI_3SbF_6 (1.87(1) Å, 89.9(5)°), and TeI_3SbF_6 (1.87(1) Å, 90.0(5)°) are similar to those in $TeBr_3AsF_6$ (1.86(4) Å and 90(2)°) and $SeBr_3SbF_6$ (1.71(1) Å, 90.0(7)°). The AsF_6^- and SbF_6^- anions have distorted octahedral geometry as a result of the cation—anion contacts. A correlation between the M′—F bond distances and cation—anion contact distances is not observed.

The thermodynamic stability of SBr_3AsF_6 and SeI_3AsF_6

The neutral binary sulphur and selenium iodides are unstable and were once considered to be non-existent (54). Since then S_2I_2 has been prepared and characterized at −90°C (55, 56), and SI_2 has been detected at −246°C (57). Neutral binary selenium iodides remain uncharacterized (58). The heat of formation of $SI_2(s)$ and $SeI_2(s)$ according to reactions [5] and [6] are estimated to be positive, i.e. $SI_2(s)$ and $SeI_2(s)$ are unstable with respect to the elements. Entropy considerations further favour the elements rather than the binary iodides.

[5] $(1/8)S_8(s) + I_2(s) \rightarrow SI_2(s)$

$$\Delta H(\text{eq. [5]}) = \Delta H(\text{Atom.E., S(g)}) + 2\Delta H(\text{Atom.E., I(g)}) - 2D(\text{S—I}) - \Delta H(\text{Subl.E., } SI_2(g))^4$$
$$= 66.6 + 51 - 95 - 15$$
$$= 8 \text{ kcal mol}^{-1}$$

[6] $Se(\text{hexagonal}) + I_2(s) \rightarrow SeI_2(s)$

$$\Delta H(\text{eq. [6]}) = \Delta H(\text{Atom.E., Se(g)}) + 2\Delta H(\text{Atom.E., } I_2(g)) - 2D(\text{Se—I}) - \Delta H(\text{Subl.E., } SeI_2(g))$$
$$= 54 + 51 - 82 - 20$$
$$= 3 \text{ kcal mol}^{-1}$$

The heat of reaction [7] accompanying the formation of $SeI_3AsF_6(s)$ is estimated to be about -24 kcal mol^{-1}.

[7] $2Se(\text{hexagonal}) + 3I_2(s) + 3AsF_5(g) \rightarrow 2SeI_3AsF_6(s) + AsF_3(l)$

$$\Delta H(\text{eq. [7]}) = 2\Delta H(\text{Atom.E., Se(g)}) + 2\text{IP}(Se^+(g)) + 6\Delta H(\text{Atom.E., I(g)}) - 6D(Se^+—I) - \Delta H(3AsF_5(g) + 2e \rightarrow 2AsF_6^-(g) + AsF_3(g)) - 2U(SeI_3AsF_6) - \Delta H(\text{Vap.E., } AsF_3(g))$$
$$= 108 + 452 + 153 - 248 - 233 - 246 - 9$$
$$= -24 \text{ kcal mol}^{-1}$$

The major energy terms favouring the formation of SeI_3AsF_6 are its crystal lattice energy (2×123 kcal mol^{-1}), and the energy associated with the reduction of AsF_5 ($3AsF_5(g) + 2e \rightarrow 2AsF_6^-(g) + AsF_3(l)$, $\Delta H = -242$ kcal mol^{-1}) which more than offset (by -36 kcal mol^{-1}) the energy needed to ionise $2Se(g)$ to $2Se^+(g)$ (2×226 kcal mol^{-1}). The atomisation energy of selenium and iodine is almost compensated ($+13$ kcal mol^{-1}) by the formation of $2SeI_3^+$ from $2Se^+(g) + 6I(g)$. Thus the overall reaction is exothermic. The actual value of the heat of reaction [7] (and [8]) is likely more negative than shown, as the value of the bond dissociation energy of SeI_3^+ (and SBr_3^+) used in the estimation is a lower limit (see Table 8, footnote *c*). Entropy strongly favours the reactants, and therefore this must be offset by a significant negative reaction enthalpy as the reaction is observed to readily proceed at room temperature. Thus SeI_3AsF_6 is stable, formally a salt of the non-existent SeI_4. This is reminiscent of the existence, in the solid state, of various salts of $S_2I_4^{2+}$ (51), NF_4^+ (59), and ClF_6^+ (60) cations, which are formally salts of the non-existent I_3SSI_3, NF_5, and ClF_7.

The heat of reaction [8] leading to SBr_3AsF_6 is estimated in a similar manner to be exothermic (data given in Table 8).

[8] $(1/4)S_8(s) + 3Br_2(l) + 3AsF_5(g) \rightarrow 2SBr_3AsF_6(s) + AsF_3(l)$

$\Delta H(\text{eq. [8]}) = -62$ kcal mol^{-1}

The higher enthalpy of reaction [8] leading to SBr_3AsF_6 relative to reaction [7] giving SeI_3AsF_6 is largely due to the greater strength of the S^+—Br bond (56 kcal mol^{-1}) relative to the Se^+—I bond (41 kcal mol^{-1}). Nevertheless, SBr_3AsF_6 slowly dissociates, or disproportionates at room temperature, although it is stable at −20°C. Thus the decomposition is likely entropy controlled.

Acknowledgement

We wish to thank the Natural Science and Engineering Research Council of Canada for financial support.

1. J. Galy and R. Enjalbert. J. Solid State Chem. **44**, 1 (1982).
2. N. W. Alcock. Adv. Inorg. Radiochem. **15**, 1 (1973).
3. N. W. Alcock. J. Chem. Soc. Dalton Trans. 1709 (1984) and references therein.
4. R. J. Gillespie and J. F. Sawyer. *In* Progress in inorganic chemistry. *Edited by* S. Lippard. Wiley Interscience. 1985. Vol. 34 and references therein.
5. R. J. Gillespie. Molecular geometry. Van Nostrand Reinhold, London. 1972.
6. I. D. Brown. *In* Structure and bonding in crystals. Vol. II. *Edited by* M. O'Keefe and A. Navrotsky. Academic Press, London. 1981. p. 1.
7. I. D. Brown and D. Altermatt. Acta Crystallogr. B**41**, 244 (1985).
8. J. Passmore, E. K. Richardson, and P. Taylor. Inorg. Chem. **17**, 1681 (1978).
9. M. Murchie and J. Passmore. Inorg. Synth. **24**, 76 (1986).
10. W. V. F. Brooks, J. Passmore, and E. K. Richardson. Can. J. Chem. **57**, 3230 (1979).
11. J. Passmore, E. K. Richardson, T. K. Whidden, and P. S. White. Can. J. Chem. **58**, 851 (1980).
12. J. Passmore and P. Taylor. J. Chem. Soc. Dalton Trans. 804 (1976).
13. J. Passmore, G. Sutherland, and P. S. White. Can. J. Chem. **59**, 2876 (1981).
14. J. Passmore, G. Sutherland, T. K. Whidden, P. S. White, and C.-M. Wong. Can. J. Chem. **63**, 1209 (1985).
15. J. Passmore, G. Sutherland, P. Taylor, T. K. Whidden, and P. S. White. Inorg. Chem. **20**, 3839 (1981).
16. J. Passmore, G. Sutherland, and P. S. White. Inorg. Chem. **21**, 2717 (1982).

[4]The thermodynamic quantities used in all estimates of ΔH values are given in Table 8 in the deposited material. ΔH(Atom.E., X(g)) is the atomization energy per mole of X(g) from standard state. D(M—X) is the bond energy. ΔH(Subl.E., X(g)) is the sublimation energy of X. IP(X^+(g)) is the ionization energy of X in gas phase. U(X) is the crystal lattice energy. ΔH(Vap.E., X(g)) is the vaporization energy of X.

17. W. A. S. NANDANA, J. PASSMORE, P. S. WHITE, and C.-M. WONG. J. Chem. Soc. Chem. Commun. 1098 (1982).
18. J. PASSMORE, P. S. WHITE, and C.-M. WONG. J. Chem. Soc. Chem. Commun. 1178 (1985).
19. J. PASSMORE, G. SUTHERLAND, and P. S. WHITE. J. Chem. Soc. Chem. Commun. 330 (1980); M. MURCHIE. Ph.D. Thesis, University of New Brunswick. 1986.
20. J. PASSMORE, E. K. RICHARDSON, and P. TAYLOR. J. Chem. Soc. Dalton Trans. 1006 (1976).
21. R. W. H. SMALL, A. J. BANISTER, and Z. V. HAUPTMAN. J. Chem. Soc. Dalton Trans. 1377 (1984).
22. A. APBLETT, F. GREIN, J. P. JOHNSON, J. PASSMORE, and P. S. WHITE. Inorg. Chem. **25**, 422 (1986).
23. W. A. S. NANDANA, J. PASSMORE, D. C. N. SWINDELLS, P. TAYLOR, P. S. WHITE, and J. E. VEKRIS. J. Chem. Soc. Dalton Trans. 619 (1983).
24. G. M. BEGUN and A. C. RUTENBERG. Inorg. Chem. **6**, 2212 (1967).
25. M. M. CARNELL, F. GREIN, M. MURCHIE, J. PASSMORE, and C.-M. WONG. J. Chem. Soc. Chem. Commun. 225 (1986); J. PASSMORE and C.-M. WONG. Unpublished results.
26. J. BACON, P. A. W. DEAN, and R. J. GILLESPIE. Can. J. Chem. **48**, 3413 (1970).
27. E. J. GABE, F. L. LEE, and Y. LEPAGE. The N.R.C. VAX crystal structure system. *In* Crystallographic computing 3: data collection, structure determination, proteins and databases. *Edited by* G. M. Sheldrick, C. Kruger, and R. Goddard. Clarendon Press, Oxford. 1985. pp. 167–174.
28. P. MAIN. MULTAN-80. A system of computer programs for the automatic solution of crystal structures from X-ray diffraction data. University of York. 1980.
29. G. M. SHELDRICK. SHELX-76, Program for crystal structure determination. University of Cambridge. 1976.
30. N. WALKER and D. STUART. Acta Crystallogr. A**39**, 158 (1983).
31. J. PASSMORE and C.-M. WONG. Unpublished results.
32. A. GLEIZES and J. GALY. C. R. Hebd. Seances Acad. Sci. Ser. C. **286**, 29 (1978).
33. B. A. STORK-BLAISSE and C. ROMERS. Acta Crystallogr. B**27**, 386 (1971).
34. B. H. CHRISTIAN, M. J. COLLINS, R. J. GILLESPIE, and J. F. SAWYER. Inorg. Chem. **25**, 777 (1986).
35. V. SCHOMAKER and D. P. STEVENSON. J. Am. Chem. Soc. **63**, 37 (1941).
36. Y. MORINO, K. KUCHITSU, and T. MORTANI. Inorg. Chem. **8**, 867 (1969).
37. R. L. LIVINGSTON. Ann. Rev. Phys. Chem. **5**, 395 (1954).
38. M. ATOJI and W. N. LIPSCOMB. Acta Crystallogr. **7**, 597 (1954).
39. J. T. MURRAY, W. A. LITTLE, Q. WILLIAMS, and T. L. WEATHERLY. J. Chem. Phys. **65**, 985 (1976).
40. H. OBERHAMMER, W. GOMBLER, and H. WILLNER. J. Mol. Spectrosc. **70**, 273 (1981).
41. R. MINKWITZ, R. LEKIES, and A. RADÜNZ. Z. Anorg. Allg. Chem. **531**, 31 (1985).
42. L. FERNHOLT, A. HAALAND, R. SEIP, R. KNIEP, and L. KORTE. Z. Naturforsch. **38**b, 1072 (1983).
43. K. KICHITSU, T. SHIBATA, A. YOKOZEKI, and C. MATSUMURA. Inorg. Chem. **10**, 2584 (1971).
44. R. ENJALBERT and J. GALY. Acta Crystallogr. B**36**, 914 (1980).
45. J. TROTTER and T. ZOBEL. Z. Kristallogr. **123**, 67 (1966).
46. G. GLIDEWELL. Inorg. Chim. Acta, **12**, 219 (1975).
47. G. GLIDEWELL. Inorg. Chim. Acta, **20**, 113 (1976).
48. L. PAULING. The nature of chemical bond. 3rd ed. Cornell University Press, New York. 1960.
49. A. L. ALLRED. J. Inorg. Nucl. Chem. **17**, 215 (1961).
50. P. W. ALLEN and L. E. SUTTON. Acta Crystallogr. **3**, 46 (1950).
51. J. PASSMORE, G. SUTHERLAND, T. K. WHIDDEN, and P. S. WHITE. J. Chem. Soc. Chem. Commun. 289 (1980), and unpublished results.
52. W. A. S. NANDANA, J. PASSMORE, and P. S. WHITE. J. Chem. Soc. Chem. Commun. 526 (1983).
53. R. J. GILLESPIE, R. KAPOOR, R. FAGGIANI, C. J. L. LOCK, M. MURCHIE, and J. PASSMORE. J. Chem. Soc. Chem. Commun. 8 (1983).
54. W. E. DASENT. Non-existent compounds. Marcel Dekker, New York. 1965.
55. G. VAHL and R. MINKWITZ. Z. Anorg. Allg. Chem. **443**, 217 (1978).
56. G. KRUMMEL and R. MINKWITZ. Inorg. Nucl. Chem. Lett. **13**, 213 (1977).
57. M. FEUERHAHN and G. VAHL. Inorg. Nucl. Chem. Lett. **16**, 5 (1980).
58. Gmelin handbook of inorganic chemistry. 8th ed. Selenium (supplement volume B2). Springer–Verlag, Berlin. 1984. p. 272.
59. K. O. CHRISTE and W. W. WILSON. Inorg. Chem. **25**, 1904 (1986) and references therein.
60. K. O. CHRISTE, W. W. WILSON, and E. C. CURTIS. Inorg. Chem. **22**, 3056 (1983).
61. D. D. GIBLER, C. J. ADAMS, M. FISCHER, A. ZALKIN, and N. BARLETT. Inorg. Chem. **11**, 2325 (1972).
62. A. J. EDWARDS and G. R. JONES. J. Chem. Soc. A, 1491 (1970).
63. A. J. EDWARDS and P. TAYLOR. J. Chem. Soc. Dalton Trans. 2150 (1973) and references therein.
64. R. MINKWITZ, K. JÄNICHEN, H. PRENZEL, and V. WÖLFEL. Z. Naturforsch. **40**b, 53 (1985).
65. D. D. WAGMAN, W. H. EVANS, V. B. PARKER, R. H. SCHUMM, I. HALOW, S. M. BAILEY, K. L. CHRUNEY, R. L. NUTTALL. J. Phys. Chem. Ref. Data, **11**, Supplement 2 (1982).
66. R. T. SANDERSON. Chemical bonds and bond energy. Academic Press, New York. 1971.
67. R. J. HWANG and S. W. BENSON. J. Am. Chem. Soc. **101**, 2615 (1979).
68. D. A. JOHNSON. *In* Sulfur in organic and inorganic chemistry. Vol. 2. *Edited by* A. Senning. Marcel Dekker, New York. 1971.
69. I. BARIN, O. KNACKE, and O. KUBASCHEWSKI. *In* Thermochemical properties of inorganic substances and supplement. Springer–Verlag, New York. 1977.
70. A. J. DOWNS and C. J. ADAMS. *In* Comprehensive inorganic chemistry. Vol. 2. *Edited by* J. C. Bailar, H. J. Emeleus, R. Nyholm, and A. F. Trotman-Dickenson. Pergamon Press, New York. 1973.
71. R. BOUGON, T. BUI HUY, J. BURGESS, K. O. CHRISTE, and R. D. PEACOCK. J. Fluorine Chem. **19**, 263 (1982).
72. T. E. MALLOUK, G. L. ROSENTHAL, G. MÜLLER, R. BRUSASCO, and N. BARLETT. Inorg. Chem. **23**, 3167 (1984).
73. T. J. RICHARDSON, F. L. TANZELLA, and N. BARLETT. J. Am. Chem. Soc. **108**, 4937 (1986).

Can. J. Chem. Downloaded from www.nrcresearchpress.com by 213.222.148.141 on 09/07/12
For personal use only.

Structure and absolute configuration of [1-(*N*,*N*-dimethylammonium)ethyl]ferrocene tartrate dihydrate

YAO GUANG LUO, RICHARD J. BARTON, AND BEVERLY E. ROBERTSON
Department of Chemistry, University of Regina, Regina, Sask., Canada S4S 0A2

Received May 12, 1987

YAO GUANG LUO, RICHARD J. BARTON, and BEVERLY E. ROBERTSON. Can. J. Chem. **65**, 2756 (1987).

Crystals of [1-(*N*,*N*-dimethylammonium)ethyl]ferrocene tartrate dihydrate are triclinic, space group $P\bar{1}$, $a = 7.235(1)$, $b = 11.372(2)$, $c = 12.724(3)$ Å, $\alpha = 90.78(1)$, $\beta = 102.75(1)$, $\gamma = 91.76(2)°$, $V = 1020.3$ Å^3 at 20 ± 2°C with $Z = 2$. The structure was solved by direct methods. The correct enantiomer was chosen based on full-matrix least-square refinements of each enantiomer. For the correct enantiomer, $R = 0.031$, $R_w = 0.035$ for 11052 reflections with $I \geq 2\sigma(I)$. Although the two crystallographically independent units of the complex in the structure are chemically equivalent, they are structurally different. The absolute configuration of the amino-substituted carbon atom is (*S*), and that of the tartrate anion is (*R*,*R*). The mean ferrocenyl Fe—C bond lengths are 2.037(2) Å and 2.027(3) Å for each molecule, respectively. The NMe_2 group is located outside the planes of the cyclopentadienyl rings. The tartrate ions are connected through water molecules by hydrogen bonds.

YAO GUANG LUO, RICHARD J. BARTON et BEVERLY E. ROBERTSON. Can. J. Chem. **65**, 2756 (1987).

Les cristaux du tartrate de [(*N*,*N*-diméthylammonium)-1 éthyl]ferrocène dihydraté sont tricliniques, groupe d'espace $P\bar{1}$ avec $a = 7,235(1)$, $b = 11,372(2)$ et $c = 12,724(3)$ Å, $\alpha = 90,78(1)$, $\beta = 102,75(1)$ et $\gamma = 91,76(2)°$, $V = 1020,3$ Å^3 à 20 ± 2°C et $Z = 2$. On a résolu la structure par des méthodes directes. On a choisi l'énantiomère correct en se basant sur un affinement par la méthode des moindres carrés (matrice entière) de chacun des énantiomères. Dans le cas du bon énantiomère, on a obtenu des valeurs de $R = 0,031$ et $R_w = 0,035$ pour 11052 réflexions avec $I \geq 2\sigma(I)$. Les deux unités qui forment la structure complexe sont indépendantes d'un point de vue cristallographique alors qu'elles sont équivalentes d'un point de vue chimique; toutefois, elles sont différentes du point de vue de la structure. La configuration absolue de l'atome de carbone portant le groupement aminé est (*S*) alors que celle de l'anion tartrate est (*R*,*R*). Les longueurs moyennes des liaisons Fe—C sont respectivement 2,037(2) et 2,027(3) Å pour chacune des molécules. Le groupement NMe_2 est situé à l'extérieur des plans des noyaux cyclopentadiènyles. Les ions tartrates sont reliés par des liaisons hydrogènes de molécules d'eau.

[Traduit par la revue]

Introduction

Resolved optically active *N*,*N*-dimethyl-α-ferrocenylethylamine (DMFEA) has been widely employed as a starting material in the preparation of optically active ferrocenyl derivatives, with planar chirality or both planar and central chirality, which are useful in asymmetrically induced syntheses (1, 2). Optically active ferrocenyl derivatives are also used as a precursor for the chiral ferrocenylphosphine used in the preparation of several transition metal complexes which have been found to have catalytic activity in: (*i*) the asymmetric hydrogenation of olefins and ketones (3–6); (*ii*) the asymmetric hydrosilation of olefins and ketones (7, 8); (*iii*) the asymmetric isomerization of allylamines to enamines (9); (*iv*) Grignard cross-coupling reactions (10). Several structures and absolute configurations of these derivatives and related complexes have been well characterized (2, 4, 11, 12). The absolute configuration of the compound itself, however, was only determined by optical methods (13). This paper reports the results of an X-ray crystallographic determination of the crystal structure and absolute configuration of the title compound.

Experimental

$C_{18}H_{29}FeNO_8$ fw = 443.27

Triclinic. Space group $P\bar{1}$, from structure analysis. $a = 7.235(1)$, $b = 11.372(2)$, $c = 12.724(3)$ Å, $\alpha = 90.78(1)$, $\beta = 102.75(1)$, $\gamma = 91.76(2)°$, $V = 1020.3$ Å^3. $T = 20 \pm 2$°C. $Z = 2$, $D_x = 1.445$ g/cm^3, $D_m = 1.44$ g/cm^3. $F(000) = 468$, $\mu(\text{MoK}\alpha) = 7.78$ cm^{-1}.

The compound was synthesized and provided by W. R. Cullen of the University of British Columbia. The compound was synthesized by the reaction between α-ferrocenylethyl acetate and dimethylamine in methanol solution overnight at room temperature. After the evaporation of the solvent, the oily residue was swirled with aqueous phosphoric acid and benzene. The acid solution was then separated and treated with sodium carbonate until the pH reached about 10. The product was then extracted with dichloromethane, and the enantiomer was resolved by crystallization with (*R*)-tartaric acid from methanol (14). A recrystallization at room temperature from a methanol/water solution yielded yellow–orange crystals.

Unit-cell parameters were measured by least-squares refinement on the positions of 50 reflections. The density of the crystal was determined by the flotation method. Intensities were measured with graphite-monochromated MoKα radiation ($\lambda = 0.71069$ Å) on a modified Picker FACS-1 diffractometer, using the NRCC diffractometer control system (15) employing the θ–2θ scan technique. Data were measured in the range of $3° \leq 2\theta \leq 60°$, using a scan speed of 2°/min. The intensities of three reference reflections, measured after every 47 reflections throughout the data collection, showed less than 7% drift. A total of 11862 Freidel related reflections were collected of which 11052 were considered as observed with $I/\sigma(I) \geq 2.0$ and were used in the structure determination.

The data were corrected for the Lorentz effect and polarization. All calculations were carried out with the XTAL system of crystallographic programs (16). The Gaussian integration method was used for absorption corrections giving minimum and maximum transmission factors of 0.679 and 0.841. Scattering factors were taken from the XTAL system. A dispersion correction, taken from International tables for X-ray crystallography, Vol. 4 (17), was applied to the scattering factor of the iron atom.

The structure was solved by direct methods; the Fe positions were obtained from the *E*-map. Several subsequent electron density and difference Fourier syntheses revealed all non-hydrogen atoms. The structure was refined on *F* with anisotropic temperature factors using each enantiomer. Convergence was reached at $R = 0.044$, $R_w = 0.057$ (where $R = \Sigma||F_o| - |F_c||/\Sigma|F_o|$, $R_w = (\Sigma w(|F_o| - |F_c|)^2/\Sigma w|F_o|^2)^{1/2}$, and $w = 1/\sigma^2(F)$), for one enantiomer, compared to $R = 0.059$, $R_w = 0.075$ for the other. Hydrogen atoms were then obtained either from difference Fourier syntheses or from calculated positions. Hydrogen atoms assigned to calculated positions were constrained to have their C—H bond lengths fixed at 1.0 Å. All other hydrogen atoms were constrained to maintain their original bond lengths as found from the difference map. The temperature factors for all hydrogen atoms were refined isotropically during subsequent

Can. J. Chem. Downloaded from www.nrcresearchpress.com by 213.222.148.141 on 09/07/12
For personal use only.

Can. J. Chem. Downloaded from www.nrcresearchpress.com by 213.222.148.141 on 09/07/12
For personal use only.

TABLE 1. Fractional atomic coordinates with esd's in parentheses and thermal parameters ($Å^2 \times 10^2$)[a]

Atom	x	y	z	U_{eq}
Fe(1)	0.0000	0.0000	0.0000	3.8
C(1)	−0.0544(3)	−0.0855(2)	0.1304(1)	3.6
C(2)	−0.2136(3)	−0.0189(2)	0.0803(2)	4.8
C(3)	−0.2738(3)	−0.0614(3)	−0.0283(2)	6.0
C(4)	−0.1552(4)	−0.1528(2)	−0.0447(2)	5.6
C(5)	−0.0204(3)	−0.1680(2)	0.0519(2)	4.4
C(6)	0.1814(6)	0.1410(3)	0.0441(3)	9.8
C(7)	0.0316(6)	0.1697(3)	−0.0402(4)	10.4
C(8)	0.0338(4)	0.0980(3)	−0.1282(3)	8.1
C(9)	0.1821(4)	0.0245(2)	−0.0991(2)	6.1
C(10)	0.2748(4)	0.0500(3)	0.0064(2)	7.2
N(1)	−0.0392(3)	−0.1482(2)	0.3193(1)	5.0
C(11)	0.0519(3)	−0.0698(2)	0.2454(2)	4.2
C(12)	0.2613(3)	−0.0932(3)	0.2641(2)	6.9
C(13)	−0.2399(4)	−0.1189(3)	0.3146(2)	6.1
C(14)	−0.0230(5)	−0.2764(2)	0.3024(2)	7.6
Fe(1′)	0.43507(5)	0.52206(3)	0.93371(3)	4.4
C(1′)	0.4913(3)	0.4150(2)	0.8153(2)	4.1
C(2′)	0.6338(3)	0.5064(2)	0.8449(2)	5.0
C(3′)	0.7166(3)	0.4956(3)	0.9574(2)	6.7
C(4′)	0.6265(4)	0.4012(3)	0.9956(2)	6.7
C(5′)	0.4875(3)	0.3498(2)	0.9099(2)	5.4
C(6′)	0.1773(5)	0.5912(4)	0.8907(4)	11.2
C(7′)	0.3144(5)	0.6818(3)	0.9103(3)	7.9
C(8′)	0.4102(5)	0.6740(3)	1.0155(3)	7.6
C(9′)	0.3399(6)	0.5829(4)	1.0608(3)	9.6
C(10′)	0.1947(6)	0.5272(3)	0.9891(6)	12.0
N(1′)	0.4894(3)	0.3143(2)	0.6409(2)	5.9
C(11′)	0.3757(3)	0.3881(2)	0.7038(2)	4.4
C(12′)	0.1857(4)	0.3275(3)	0.6982(3)	7.2
C(13′)	0.6331(5)	0.3853(4)	0.6002(3)	10.2
C(14′)	0.5771(7)	0.2129(4)	0.7028(3)	11.8
C(15)	1.1195(2)	0.3975(2)	0.3155(2)	3.6
C(16)	0.9050(2)	0.3933(2)	0.3089(2)	3.5
C(17)	0.8238(2)	0.2680(2)	0.2890(2)	3.4
C(18)	0.6118(2)	0.2627(2)	0.2917(2)	3.6
O(1)	1.1667(2)	0.3437(1)	0.2360(1)	4.7
O(2)	1.2300(2)	0.4471(2)	0.3891(2)	6.9
O(3)	0.8706(2)	0.4419(1)	0.4050(1)	5.0
O(4)	0.9265(2)	0.1902(1)	0.3642(1)	4.8
O(5)	0.5107(2)	0.3375(1)	0.2356(1)	4.4
O(6)	0.5580(2)	0.1859(2)	0.3453(2)	7.1
C(15′)	0.7206(2)	0.7669(2)	0.6113(1)	3.6
C(16′)	0.5089(2)	0.7659(2)	0.6112(2)	3.6
C(17′)	0.4425(2)	0.8917(2)	0.6178(1)	3.3
C(18′)	0.2267(2)	0.8868(2)	0.6103(1)	3.3
O(1′)	0.8261(2)	0.8294(1)	0.6889(1)	4.7
O(2′)	0.7796(2)	0.7128(2)	0.5434(1)	6.1
O(3′)	0.4095(2)	0.7056(1)	0.5178(1)	5.2
O(4′)	0.4926(2)	0.9579(1)	0.5352(1)	4.6
O(5′)	0.1737(2)	0.8401(1)	0.6877(1)	4.3
O(6′)	0.1235(2)	0.9291(1)	0.5289(1)	4.4
O(7)	0.1148(2)	0.5877(1)	0.5626(1)	5.2
O(8)	0.3065(2)	0.1708(1)	0.4681(1)	5.1
O(9)	0.8437(2)	0.0866(1)	0.5463(2)	6.0
O(10)	0.5633(2)	0.5762(2)	0.3601(2)	6.5

[a]Fe(1) to C(14) belong to cation(I), Fe(1′) to C(14′) belong to cation(II). C(15) to O(6) belong to anion(I), C(15′) to O(6′) belong to anion(II). O(7) to O(10) are water oxygens.

[b]$U_{eq} = \frac{1}{3}\Sigma_i\Sigma_j U_{ij} a_i^* a_j^* \mathbf{a}_i \mathbf{a}_j$.

TABLE 2. Bond lengths (Å) with esd's in parentheses

Bond	Length	Bond	Length
Fe(1)—C(1)	2.041(2)	Fe(1′)—C(1′)	2.042(2)
Fe(1)—C(2)	2.040(3)	Fe(1′)—C(2′)	2.025(3)
Fe(1)—C(3)	2.034(2)	Fe(1′)—C(3′)	2.025(2)
Fe(1)—C(4)	2.044(2)	Fe(1′)—C(4′)	2.023(3)
Fe(1)—C(5)	2.042(2)	Fe(1′)—C(5′)	2.038(4)
Fe(1)—C(6)	2.032(4)	Fe(1′)—C(6′)	2.012(4)
Fe(1)—C(7)	2.022(3)	Fe(1′)—C(7′)	2.037(3)
Fe(1)—C(8)	2.043(4)	Fe(1′)—C(8′)	2.038(3)
Fe(1)—C(9)	2.031(3)	Fe(1′)—C(9′)	2.014(4)
Fe(1)—C(10)	2.035(3)	Fe(1′)—C(10′)	2.017(6)
C(1)—C(2)	1.431(3)	C(1′)—C(2′)	1.427(3)
C(2)—C(3)	1.428(3)	C(2′)—C(3′)	1.434(4)
C(3)—C(4)	1.409(4)	C(3′)—C(4′)	1.388(4)
C(4)—C(5)	1.408(3)	C(4′)—C(5′)	1.416(3)
C(5)—C(1)	1.426(3)	C(5′)—C(1′)	1.428(3)
C(1)—C(11)	1.502(2)	C(1′)—C(11′)	1.501(3)
C(6)—C(7)	1.397(6)	C(6′)—C(7′)	1.389(5)
C(7)—C(8)	1.380(6)	C(7′)—C(8′)	1.370(5)
C(8)—C(9)	1.369(4)	C(8′)—C(9′)	1.334(6)
C(9)—C(10)	1.386(4)	C(9′)—C(10′)	1.363(6)
C(10)—C(6)	1.389(5)	C(10′)—C(6′)	1.440(8)
N(1)—C(11)	1.540(3)	N(1′)—C(11′)	1.529(3)
N(1)—C(13)	1.488(3)	N(1′)—C(13′)	1.482(5)
N(1)—C(14)	1.483(4)	N(1′)—C(14′)	1.484(5)
C(11)—C(12)	1.513(3)	C(11′)—C(12′)	1.506(3)

refinement. The structure was refined further using the enantiomer with lower R value by minimizing $\Sigma w(|F_o| - |F_c|)^2$. The final value of R and R_w were 0.032 and 0.036 for 11052 reflections with $I \geq 2\sigma(I)$. For all 11862 reflections $R = 0.034$. A final difference map showed a maximum fluctuation of 0.56 e $Å^{-3}$ at a position located 0.87 Å from the Fe atom. The average shift/error and maximum shift/error were 2.2×10^{-4} and 5.7×10^{-3}, respectively, at the termination of refinement. The atomic coordinates and their equivalent isotropic temperature factors are given in Table 1.[1] The important bond lengths and angles are given in Tables 2 and 3, respectively. Figure 1 shows the stereo view of one of the ferrocenyl cation and Fig. 2 shows the packing diagram.

Results and discussion

The choice of correct absolute configuration of the compound is verified by using Hamilton's significance test (18), which shows that the choice of enantiomer is correct with a significance level better than 99.5%. A Bijvoet ratio test (19) of 10 reflections also supports this assignment.

The unit cell contains two ferrocene cations, two tartrate anions, and four waters of crystallization. The result shows the anticipated (*R*,*R*)-configuration for the two tartrate ions and shows that the two crystallographically independent ferrocene moieties have an (*S*)-configuration in a right handed coordinate system.

The iron atom is π-bonded to two cyclopentadienyl rings. The two cyclopentadienyl rings are planar and deviate slightly from a parallel arrangement; the angles between two cyclopentadienyl planes are 1.8° in cation(I) and 4.0° in cation(II). The structure of ferrocene in the solid state shows the two cyclopentadienyl rings nearly eclipsed (20). They are also

[1]Tables of observed and calculated structure factor amplitudes, anisotropic temperature factors, hydrogen atom parameters, and Bijvoet test are available at a minimal charge from the Depository of Unpublished Data, CISTI, National Research Council of Canada, Ottawa, Ont., Canada K1A 0S2.

TABLE 3. Bond angles (deg) with esd's in parentheses

Bonds	Angle	Bonds	Angle
C(2)—C(1)—C(5)	107.4(2)	C(2′)—C(1′)—C(5′)	107.3(2)
C(2)—C(1)—C(11)	124.9(2)	C(2′)—C(1′)—C(11′)	126.1(2)
C(5)—C(1)—C(11)	127.6(2)	C(5′)—C(1′)—C(11′)	126.4(2)
C(1)—C(2)—C(3)	107.3(2)	C(1′)—C(2′)—C(3′)	107.6(2)
C(2)—C(3)—C(4)	108.4(2)	C(2′)—C(3′)—C(4′)	108.1(2)
C(3)—C(4)—C(5)	108.3(2)	C(3′)—C(4′)—C(5′)	109.2(2)
C(4)—C(5)—C(1)	108.5(2)	C(4′)—C(5′)—C(1′)	107.7(2)
C(10)—C(6)—C(7)	106.9(3)	C(10′)—C(6′)—C(7′)	107.1(3)
C(6)—C(7)—C(8)	108.8(3)	C(6′)—C(7′)—C(8′)	107.2(3)
C(7)—C(8)—C(9)	107.4(3)	C(7′)—C(8′)—C(9′)	109.6(3)
C(8)—C(9)—C(10)	109.2(3)	C(8′)—C(9′)—C(10′)	110.7(4)
C(9)—C(10)—C(6)	107.7(3)	C(9′)—C(10′)—C(6′)	105.3(4)
C(11)—N(1)—C(13)	112.0(2)	C(11′)—N(1′)—C(13′)	112.8(2)
C(11)—N(1)—C(14)	114.7(2)	C(11′)—N(1′)—C(14′)	112.6(2)
C(13)—N(1)—C(14)	110.6(2)	C(13′)—N(1′)—C(14′)	110.9(3)
C(1)—C(11)—N(1)	110.3(2)	C(1′)—C(11′)—N(1′)	109.8(2)
C(1)—C(11)—C(12)	114.4(2)	C(1′)—C(11′)—C(12′)	115.5(2)
N(1)—C(11)—C(12)	109.5(2)	N(1′)—C(11′)—C(12′)	109.0(2)

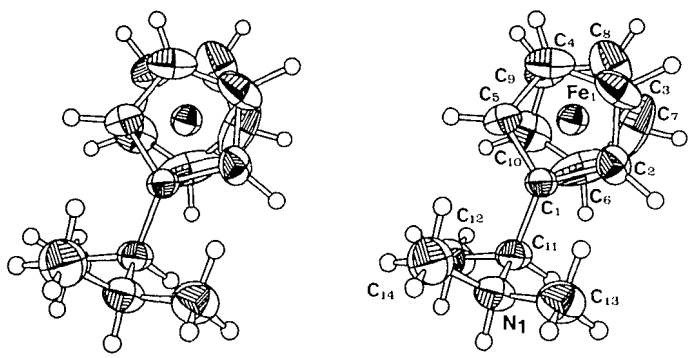

FIG. 1. Stereo view of a ferrocenyl cation.

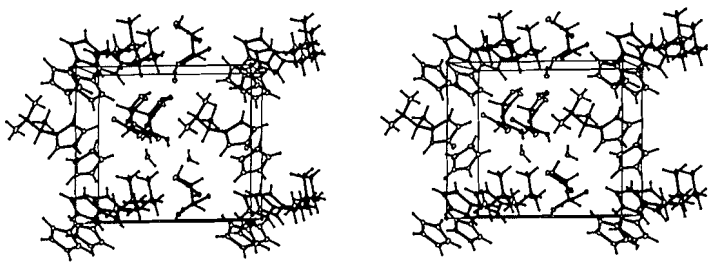

FIG. 2. Packing diagram of a ferrocenyl cation.

nearly eclipsed in a series of ferrocene derivatives which are related to DMFEA such as *N*-formylaminomethylferrocene (21), (*p*-methoxyphenyl)hydroxymethyl-3*N*,*N*-dimethyl-1-ferrocenylamine (2), [1-(2-diphenylphosphinoferrocenyl)ethyl]dimethylamine (12) and $Fe(\eta^5\text{-}C_5H_3\text{-}(PMe_3)_2\text{-}1,3)(\eta^5\text{-}C_5H_3\text{-}(CHMeNMe_2)P(CMe_3)_2\text{-}1,2)$ (4). However, in 2-(α-(dimethylamino)ethyl)-1,1′,3-tris(trimethylsilyl)ferrocene (11), which was prepared from DMFEA, the cyclopentadienyl rings are staggered. In the title compound, the situation is quite unusual. In cation(I), the two cyclopentadienyl rings are close to the eclipsed conformation with rotation angles from 4.5 to 6.6° (average 5.4°). (The rotation angle is defined in terms of vectors from each cyclopentadienyl ring atom to the mean ring center.) However, in cation(II), the two cyclopentadienyl rings are closer to the ideal staggered conformation with the rotation angles from 24.2 to 25.1° (average 24.7°). This difference is presumably caused by packing effects.

The averages of the ferrocenyl Fe—C distances are 2.037(2) and 2.027(3) Å in cation(I) and (II), respectively. These distances are similar to the equivalent distances in other derivatives (2, 4, 11, 12). The distances from the Fe atom to the cyclopentadienyl ring planes are 1.643(1) and 1.656(2) Å in cation(I); and 1.633(1) and 1.649(2) Å in cation(II).

The carbon atoms in the unsubstituted cyclopentadienyl rings show slightly greater thermal motion than those in the substituted rings. The average C—C bond lengths in cation(I) are 1.421(5) Å for the substituted ring and 1.384(5) Å for the unsubstituted ring. The equivalent values for cation(II) are 1.419(8) and 1.379(18) Å, respectively. These values and their differences are similar to those reported for other derivatives of DMFEA (2, 4, 11, 12). However, greater variations are observed for the individual bond lengths. Within the cyclopentadienyl rings, the C—C bond lengths vary from 1.334(6) to 1.440(8) Å. We have carried out an analysis of these differences in order to determine the significance of environmental (i.e. packing) effects according to the method of Taylor and Kennard (22). The result shows that the variation is greater than 9 times the semi-weighted average standard deviation of the C—C bond lengths. Consistent with the variation among the C—C bond lengths, the maximum variation from 105.3(4) to 110.7(4)° among the C—C—C angles is more than 10 times the semi-weighted average standard deviation of the ring C—C—C bond angles. Based on the assumption made by Taylor and Kennard, we must conclude that parts of these differences are real.

The difference map shows peaks at positions approximately 0.90 Å from the N atoms of the amino-substituted ethyl groups. We interpret these peaks as representing hydrogen atoms and, therefore, the amino group must be positively charged. This conclusion is supported by the fact that the C—N—C bond angles around the N atoms range from 110.6(2) to 114.7(2)°. If there is only lone pair electron density on the N atom one would expect that the C—N—C bond angles would be less than 109°.

Can. J. Chem. Downloaded from www.nrcresearchpress.com by 213.222.148.141 on 09/07/12
For personal use only.

TABLE 4. Hydrogen bond lengths (Å) and angles (deg) with esd's in parentheses

Atoms	Distance O(N)···O	Distance H···O	Angles O(N)—H···O
O(3′)—H(03′)···O(7)	2.654(2)	1.660(2)	149.3(2)
O(8)—H(082)···O(6)	2.651(3)	1.833(3)	163.1(2)
O(3)—H(03)···O(10)	2.697(2)	1.843(2)	167.1(2)
N(1)—H(01)···O(6′)	2.787(2)	1.876(2)	173.1(2)
O(8)—H(081)···O(4)	2.792(2)	1.927(2)	175.8(2)
N(1′)—H(01′)···O(8)	2.781(3)	1.931(3)	155.1(2)
O(9)—H(092)···O(6′)	2.786(2)	1.965(2)	156.2(2)
O(9)—H(091)···O(4′)	2.867(3)	2.018(3)	166.3(2)
O(4)—H(04)···O(9)	2.786(3)	2.066(3)	153.4(2)
O(4′)—H(04′)···O(8)	2.855(2)	2.078(2)	155.5(2)
O(10)—H(0102)···O(2)	2.881(3)	2.131(3)	145.9(2)
O(10)—H(0101)···O(3′)	2.905(3)	2.189(3)	139.4(4)
O(10)—H(0101)···O(2′)	2.905(2)	2.203(2)	137.6(3)

This conclusion is consistent with evidence that the tartrate ions carry negative charges. The H—N—C bond angles range from 104 to 110°.

The three N—C bond lengths are of the order of 1.482(5) to 1.540(3) Å which is longer than average N—C single bond lengths. In both cations, atom C(11) lies in the same plane as the C(1)—C(5) cyclopentadienyl ring, the C(12) methyl group lies between two cyclopentadienyl ring planes and the NMe_2 group is outside the ring planes. The distance from C(12) to the C(1)—C(5) ring plane is 0.737(6) and 0.515(6) Å in cation(I) and (II), respectively. The C(12)—C(11)—C(1)—C(5) torsional angles are 33.7(3) and 29.5(3)°, respectively. The N(1)—C(11) bond is nearly perpendicular to the cyclopentadienyl ring plane; the torsional angles C(2)—C(1)—C(11)—N(1) are 88.8(2) and 81.4(3)°, respectively. The distances from N(1), C(13), and C(14) to the ring (C(1)—C(5)) plane are 1.462(4), 2.202(5), and 2.240(5) Å in cation(I), and 1.531(5), 2.012(7), and 2.449(6) Å in cation(II). Viewed down the N(1)—C(11) bond, the $CHMeNMe_2$ group adopts a staggered conformation in both cations. The torsional angle defined by C(13)—N(1)—C(11)—C(12) is 173.0(2)° in cation(I) and 154.5(2)° in cation(II). It was thought that the initial site of lithiation of DMFEA would be the position next to the ethyl-substituted carbon atom (11). Therefore the NMe_2 group would be expected to be oriented in such a way that the lone pair on the nitrogen atom is directed toward this position. However, the result shows that the lone pair on the nitrogen atom is directed away from the ring in both cations. This result supports the suggestion that "only small barriers exist for the rotation of all or part of the $CHMeNMe_2$ group attached to a substituted ferrocene ring" (11).

Bond lengths and angles in the tartrate anion are normal. One noteworthy feature is the C—O distances for the carboxyl groups in both ions. On one end they are similar (average 1.234(2) Å for C=O bond and 1.257(2) Å for C—O bond) but on the other end they are significantly different (average 1.212(3) Å for C=O bond and 1.292(3) Å for C—O bond). This similarity of the bond lengths at one end implies delocalization of electron density among the O—C—O atoms, and suggests that the negative charge is associated with this end of the ion.

The shortest intermolecular distance between cation and anion is 1.876(2) Å (O(6′)···H(01)) and the shortest contact between adjacent cations is 2.818(4) Å (C(8′)···H(2)). The tartrate anions are connected by water molecules through hydrogen bonds with bond lengths and angles listed in Table 4.

Acknowledgements

B. E. Robertson and R. J. Barton thank the Natural Sciences and Engineering Research Council of Canada for an operating grant. Y. G. Luo thanks the Canadian International Development Agency for financial support, and thanks Dr. L. Mihichuk of the University of Regina for very helpful discussion. We also thank the University of Regina for computing time.

1. D. MARQUARDING, H. KLUSACEK, G. W. GOKEL, P. HOFFMANN, and I. UGI. J. Am. Chem. Soc. **92**, 5389 (1970).
2. L. F. BATTELLE, R. BAU, G. W. GOKEL, R. T. OYAKWA, and I. K. UGI. J. Am. Chem. Soc. **95**, 482 (1973).
3. W. R. CULLEN and J. D. WOOLLINS. Can. J. Chem. **60**, 1793 (1982).
4. T. D. APPLETON, W. R. CULLEN, S. V. EVANS, T. J. KIM, and J. TROTTER. J. Organomet. Chem. **279**, 5 (1985).
5. K. YAMAMOTO, J. WAKATSUKI, and R. SUGIMOTO. Bull. Chem. Jpn. Soc. **53**, 1132 (1980).
6. T. HAYASHI, T. MISE, and M. KUMADA. Tetrahedron Lett. 4351 (1976).
7. T. HAYASHI, K. TAMAO, and M. KUMADA. Tetrahedron Lett. 4405 (1974).
8. T. HAYASHI, K. TAMAO, Y. KATSURO, I. NAKAE, and M. KUMADA. Tetrahedron Lett. 1871 (1980).
9. H. KUMOBAYASHI, S. AKUTAGAWA, and S. OTSUKA. J. Am. Chem. Soc. **100**, 3949 (1978).
10. T. HAYASHI, M. KONISHI, M. FUKUSHIMA, T. MISE, M. KAGOTANI, M. TAJIKA, and M. KUMADA. J. Am. Chem. Soc. **104**, 180 (1982).
11. I. R. BUTLER, W. R. CULLEN, and S. J. RETTIG. Organometallics, **5**, 1320 (1986).
12. F. W. B. EINSTEIN and A. C. WILLIS. Acta Crystallogr. B**36**, 39 (1980).
13. G. W. GOKEL and I. K. UGI. Chem. Edu. **49**, 294 (1972).
14. W. R. CULLEN. Private communication.
15. A. C. LARSON and E. J. GABE. Computing in crystallography. *Edited by* H. Shenk, K. Olthof-Hazekamp, H. van Konigsveld, and G. C. Bassi. Delf University Press. 1978. pp. 81–89.
16. J. M. STEWART and S. R. HALL. Technical Report TR-873.2, Computer Science Center, University of Maryland, College Park, Maryland, MD. 1984.
17. International tables for X-ray crystallography. Vol. 4. Kynoch Press, New York. 1974. p. 149.
18. W. C. HAMILTON. Acta Crystallogr. **18**, 502 (1965).
19. J. M. BIJVOET, A. F. PEERDEMAN, and A. J. VAN BOMMEL. Nature, **168**, 271 (1951).
20. P. SEILER and J. D. DUNITZ. Acta Crystallogr. B**35**, 1068 (1979).
21. L. H. HALL and G. M. BROWN. Acta Crystallogr. B**27**, 81 (1971).
22. R. TAYLOR and O. KENNARD. Acta Crystallogr. B**39**, 517 (1983).

Can. J. Chem. Downloaded from www.nrcresearchpress.com by 213.222.148.141 on 09/07/12
For personal use only.

Dielectric polarization and molecular interaction. Part I. Acetoacetanilide and benzoylacetanilide–triethylamine–benzene systems

MAGDI M. NAOUM, GAMAL R. SAAD, MOHAMED M. ABDEL-MOTELEB, HAKIM G. SHINOUDA, AND HANNA A. RIZK[1]
Department of Chemistry, Faculty of Science, University of Cairo, Cairo, Egypt

Received May 1, 1987

MAGDI M. NAOUM, GAMAL R. SAAD, MOHAMED M. ABDEL-MOTELEB, HAKIM G. SHINOUDA, and HANNA A. RIZK. Can. J. Chem. **65**, 2760 (1987).

The apparent molecular polarization at infinite dilution of acetoacetanilide, and benzoylacetanilide in five constant-ratio mixtures of triethylamine in benzene leads to the inference that the equilibrium constants of the association process between the anilide and the amine in benzene are 357 and 600, and that the dipole moments of the complexes formed are 4.43 and 5.25 D, respectively.

MAGDI M. NAOUM, GAMAL R. SAAD, MOHAMED M. ABDEL-MOTELEB, HAKIM G. SHINOUDA et HANNA A. RIZK. Can. J. Chem. **65**, 2760 (1987).

On a mesuré les polarisations moléculaires apparentes, à dilution infinie, des acétyl- et benzoyl-acétanilides, dans cinq mélanges à rapports constants de triéthylamine dans le benzène; les résultats obtenus suggèrent que les constantes d'équilibre des processus d'association entre les anilides et l'amine, en présence de benzène, sont respectivement 357 et 600 alors que les moments dipôlaires des complexes qui se forment sont respectivement 4,43 et 5,25 D.

[Traduit par la revue]

Can. J. Chem. Downloaded from www.nrcresearchpress.com by 213.222.148.141 on 09/07/12
For personal use only.

Several papers (1–3) have described the application of dielectric polarization measurements to the problem of molecular interaction in solution but only one (3) article by Few and Smith reports extensive data for a range of compounds. Their method (3) involved the determination of apparent molecular polarization at infinite dilution of a compound A in an active solvent B, in an inert solvent S, and in mixtures of B and S in constant proportion. By so doing, they were able to deduce the equilibrium constant, K, of the association process as well as the dipole moment, μ_{AB}, of the complex formed.

We are currently studying molecular interactions between amines and amides in solution by static dielectric measurements. This paper is concerned with interactions between triethylamine and acetoacetanilide and benzoylacetanilide, respectively, in benzene solution. For this purpose, the method developed by Few and Smith (3) has been utilized.

Experimental and results

Acetoacetanilide and benzoylacetanilide were prepared as described before (4). Benzene and triethylamine were purified according to recommended procedures (5). The purity of compounds was checked by comparing their physical constants with those cited in the literature (4, 5).

Five mixtures of different concentrations of triethylamine, B, in inert solvent benzene, S, were made up having weight fractions, w_B, varying between 0.01 and 0.1. Then a group of dilute solutions of the anilide, A, in each of these constant-ratio solvent mixtures, BS, were made by weight, and all solutions were left to stand at 30°C for 24 h to equilibrate before measurements.

The static dielectric constant, ϵ, density, d, and refractive index for the sodium-D line, n_D, were measured at 30°C for these solutions as described earlier (6).

For the calculation of the equilibrium constant, K, of the association process and the dipole moment, μ_{AB}, of the complex, the following equation derived by Few and Smith (3) was used.

$$[1] \quad \frac{\Delta P}{P_A^* - P_A} = 1 + \frac{M_B}{K w_B d}$$

[1]Author to whom correspondence should be addressed.

Herein, we have P_A^* = molecular polarization at infinite dilution of the anilide, A, in a constant-ratio mixture of the active polar solvent, triethylamine, B, and the inert, non-polar solvent benzene, S; P_A = molecular polarization at infinite dilution of the anilide, A, in the inert solvent benzene, S; ΔP = increase in molecular polarization at infinite dilution attending the formation of 1 mol of the association complex AB from the anilide, A, and the amine, B, i.e., equals $P_{AB} - P_A - P_B$; w_B = weight fraction of the amine, B, in a given solvent mixture, BS, which, at the same time, was considered to be approximately equal to that of the amine in very dilute solution of the anilide, A, in the same solvent mixture; M_B = molecular weight of the amine, B; d = density of the solvent mixture, BS, which was also taken to be approximately equal to the density of very dilute solutions of the anilide, A, in the same solvent mixture; and K = equilibrium constant of the association process A + B = AB, where the active masses of the reactants and resultants were expressed in terms of their concentrations in mol per cm^3.

Obviously, this equation would first permit the values of K and P_{AB} to be deduced from a plot of $1/(P_A^* - P_A)$ against $1/w_B d$, provided, of course, that the plot is linear. In this case, the slope of the line would be equal to $M_B/K\Delta P$, and the intercept on the y-axis, $1/\Delta P$. Subsequently, for the determination of the apparent solution moment, μ_{AB}, of the complex, the molecular refraction, R_{AB}, was deduced the same way as that of the molecular polarization. That is, the equation

$$[2] \quad \frac{\Delta R}{R_A^* - R_A} = 1 + \frac{M_B}{K w_B d}$$

which is analogous to eq. [1], was used to deduce from the slope of the linear plot of $1/(R_A^* - R_A)$ against $1/w_B d$, which is equal to $1/\Delta R$, the value of R_{AB}. Consequently, from a knowledge of P_{AB} and R_{AB} the dipole moment, μ_{AB}, of the complex was calculated in the usual way by refractivity method.

The results obtained are summarized in Tables 1 and 2 for acetoacetanilide-, and benzoylacetanilide–triethylamine–benzene systems, respectively.[2]

[2]Tables 3 to 9 of original data have been deposited with the Depository of Unpublished Data, CISTI, National Research Council of Canada, Ottawa, Ont., Canada K1A 0S2.

TABLE 1. Polarization data of acetoacetanilide (A) in triethylamine (B) – benzene (S) mixtures

% amine (= w_B)	d_{BS} (g/cm^3)	P_A^* (cm^3)	R_A^*	$1/(P_A^* - P_A)$	$1/(R_A^* - R_A)$	$1/w_B d_{BS}$	μ_2 (D)
0.000	0.8685	267.8	55.9	—	—	—	—
2.776	0.8632	274.1	54.1	0.1577	−0.5376	41.73	3.26
4.458	0.8601	277.0	49.4	0.1082	−0.1534	26.08	3.37
5.626	0.8579	280.2	49.2	0.0808	−0.1481	20.72	3.39
9.241	0.8512	286.9	48.4	0.0523	−0.1335	12.71	3.45
11.474	0.8470	307.9	47.5	0.0249	−0.1195	10.29	3.61

$M_B/K\Delta P$ (slope)	$1/\Delta P$ (intercept)	ΔP (cm^3)	K (cm^3/mol)	P_{AB} (cm^3)	R_{AB} (cm^3)	μ_{AB} (D)
3.65×10^{-3}	7.36×10^{-3}	135.9	357	450.0	51.2	4.43

Since triethylamine has an appreciable dipole moment (~0.7 D), it follows that the constant-ratio solvent mixtures of the amine and benzene definitely increase in polar character with increasing amine content. This suggests the use of the following equation, which was previously (9) derived from Onsager's equation (8), rather than from the usual Debye equation (7), for the determination of the apparent solution moment, μ_2, of the anilide in these mixtures.

$$[3]\quad \mu_2^2 = F\left(\frac{d\epsilon_{12}}{dC_2}\right)_{C_2\to 0}\frac{1}{A_2} + \frac{A_1\mu_1^2C_1^0V_2 + B_1C_1^0V_2 - B_2}{A_2}$$

Here C_2 = the number of gram-molecules of solute per L of solution; C_1^0 = the molar concentration of pure solvent; V_2 = the molar volume (in L) of pure solute;

$$A_1 = \frac{4\pi N}{9000kT}\frac{(n_1^2+2)^2\epsilon_{12}(2\epsilon_{12}+1)}{(2\epsilon_{12}+n_1^2)^2}$$

$$A_2 = \frac{4\pi N}{9000kT}\frac{(n_2^2+2)^2\epsilon_{12}(2\epsilon_{12}+1)}{(2\epsilon_{12}+n_2^2)^2}$$

$$B_1 = 3V_1\frac{\epsilon_{12}(n_1^2-1)}{(2\epsilon_{12}+n_1^2)}$$

$$B_2 = 3V_2\frac{\epsilon_{12}(n_2^2-1)}{(2\epsilon_{12}+n_2^2)}$$

and

$$F = 1 - C_2\mu_2^2A_2\frac{(n_2^2+4\epsilon_{12}n_2^2-2\epsilon_{12})}{\epsilon_{12}(2\epsilon_{12}+1)(2\epsilon_{12}+n_2^2)} - C_1\mu_1^2A_1\frac{(n_1^2+4\epsilon_{12}n_1^2-2\epsilon_{12})}{\epsilon_{12}(2\epsilon_{12}+1)(2\epsilon_{12}+n_1^2)} - C_2B_2\frac{n_2^2}{\epsilon_{12}(2\epsilon_{12}+n_2^2)} - C_1B_1\frac{n_1^2}{\epsilon_{12}(2\epsilon_{12}+n_1^2)}$$

The slope $d\epsilon_{12}/dC_2$ in the limit as C_2 approaches zero was determined and the terms A_1, A_2, B_1, and B_2 were calculated using the dielectric constant of the solvent, ϵ_1, instead of that of the solution, ϵ_{12}. Similarly, in deriving the numerical value of the factor F for the condition of infinite dilution, the second and fourth terms of F involving C_2 disappear; C_1 becomes C_1^0, and ϵ_{12} becomes equal to ϵ_1. The dipole moment of the solvent mixture, μ_1, was approximated by $(N_B\mu_B^2)^{1/2}$, where N_B is the mole fraction of triethylamine in this mixture, and μ_B (= 0.74 D) its dipole moment in benzene. The results obtained are summarized in Tables 10 and 11.

Based on precisions of ±0.0005 in static dielectric constant, ±0.0001 in density and refractive index, and ±0.05% in solution concentration, the uncertainty of molecular polarization is of the order of 2%. Accordingly, the dipole moments obtained are accurate to ±0.03 D, and the equilibrium constants are in error by ±3%.

Discussion

It will be seen from Tables 2 and 11 that the apparent solution moments of the anilides in the various constant-ratio mixtures obtained by the usual Debye equation are in close agreement with those obtained using the modified Onsager equation, so that it might first be inferred that under such conditions when the polarity of the solvent is sufficiently low, both equations would practically lead to identical dipole moments.

On the other hand, if one accepts *a priori* that complex formation between the anilide and the amine takes place through one or another type of reaction, then the applicability of the Onsager equation, in which no account was taken of such interactions (10) would be as inappropriate as use of the usual Debye equation. Accordingly, the observed agreement between the dipole moments obtained by using these two equations can be considered only coincidental.

Although "incorrect" dipole moments are obtained this way, the apparent increase of the moment with increasing concentration of the amine can be taken as evidence of an increase in complex formation. This, in turn, suggests an estimate can be made of the fraction of anilide introduced in the constant-ratio mixture of triethylamine and benzene, which is complexed with the amine at infinite dilution. For this purpose, the following equation also suggested by Few and Smith (3) in their derivation of eq. [1] has been used.

$$[4]\quad P_A^* - P_A = \Delta P(\Delta w_A/w_A)$$

The values of this fraction expressed as $\Delta w_A/w_A$ are listed in Table 12. It is obvious from this table that an increase in the proportion of triethylamine in the solvent mixture favours complex formation, as is to be expected. Also, for a given solvent mixture, benzoylacetanilide has a greater tendency to form complex with triethylamine than does acetoacetanilide. This agrees with the fact that the equilibrium constant, K, is higher in the former case than in the latter. Both observations are also consistent with the fact that acetoacetanilide is less acidic than benzoylacetanilide, pK_a values being 10.7 and 9.8, respectively (11).

Can. J. Chem. Downloaded from www.nrcresearchpress.com by 213.222.148.141 on 09/07/12
For personal use only.

TABLE 2. Polarization data of benzoylacetanilide (A) in triethylamine (B) – benzene (S) mixtures

% amine ($= w_B$)	d_{BS} (g/cm^3)	P_A^* (cm^3)	R_A^* (cm^3)	$1/(P_A^* - P_A)$	$1/(R_A^* - R_A)$	$1/w_B d_{BS}$	μ_2 (D)
0.000	0.8685	335.1	78.0	—	—	—	—
2.068	0.8648	350.3	76.4	0.0659	−0.6289	55.92	3.68
3.452	0.8620	353.3	73.5	0.0548	−0.2242	33.61	3.69
5.047	0.8590	361.3	73.3	0.0381	−0.2160	23.07	3.77
6.560	0.8562	367.6	72.1	0.0308	−0.1704	17.80	3.81
7.966	0.8534	382.6	71.4	0.0210	−0.1517	14.71	3.91

$M_B/K\Delta P$ (slope)	$1/\Delta P$ (intercept)	ΔP (cm^3)	K (cm^3/mol)	P_{AB} (cm^3)	R_{AB} (cm^3)	μ_{AB} (D)
1.47×10^{-3}	3.68×10^{-3}	271.8	600	654.1	91.9	5.25

TABLE 10. Apparent solution moments of acetoacetanilide in triethylamine–benzene mixtures using modified Onsager's equation

% amine (w_B)	μ_1 (D)	V_1 (cm^3)	C_1^0	n_2^2	V_2 (cm^3)	$\left(\frac{d\epsilon_{12}}{dC_2}\right)_{C_2=0}$	F_2	μ_2 (D)
2.776	0.12	91.24	10.96	2.487	156.6	1.393	0.819	3.28
4.458	0.15	92.02	10.87	2.217	149.3	1.423	0.819	3.37
5.626	0.17	92.60	10.80	2.382	151.7	1.443	0.819	3.39
9.241	0.21	94.30	10.61	2.381	147.9	1.500	0.818	3.45
11.474	0.24	95.41	10.49	2.376	145.4	1.633	0.818	3.61

TABLE 11. Apparent solution moments of benzoylacetanilide in triethylamine–benzene mixtures using modified Onsager's equation

% amine (w_B)	μ_1 (D)	V_1 (cm^3)	C_1^0	n_2^2	V_2 (cm^3)	$\left(\frac{d\epsilon_{12}}{dC_2}\right)_{C_2=0}$	F_2	μ_2 (D)
2.068	0.10	90.90	11.00	2.536	202.8	1.773	0.819	3.68
3.452	0.13	109.24	10.92	2.553	200.7	1.793	0.819	3.69
5.047	0.16	108.35	10.84	2.524	202.0	1.860	0.819	3.77
6.560	0.18	93.00	10.73	2.521	199.2	1.891	0.818	3.81
7.966	0.20	93.70	10.67	2.513	198.6	1.992	0.818	3.91

TABLE 12. Fraction of the anilides introduced in triethylamine–benzene solvent mixtures which pass into the form of complex at infinite dilution

Acetoacetanilide		Benzoylacetanilide	
% amine ($= w_B$)	$(\Delta w_A/w_A)_{w_A=0}$	% amine ($= w_B$)	$(\Delta w_A/w_A)_{w_A=0}$
2.776	0.046	2.068	0.056
4.458	0.068	3.452	0.067
5.626	0.091	5.047	0.096
9.241	0.141	6.560	0.120
11.474	0.295	7.966	0.175

However, owing to their insolubility, an estimate could not be made of the fraction of both anilides which complexes at infinite dilution in pure triethylamine.

Finally, from the values of the apparent solution moments, μ_{AB}, μ_A, and μ_B in benzene, an estimate can be made of the dipole moment change, $\Delta\mu$ ($= \mu_{AB} - \mu_A - \mu_B$), accompanying the formation of the complex AB. Thus the fact that $\Delta\mu$ is 0.46 D for acetoacetanilide–triethylamine complex, and 1.01 D for benzoylacetanilide–triethylamine complex, might be taken as a confirmation of the above conclusion that the extent to which such complexes are formed is lower in the former case than in the latter.

Many theories (12–15) have been advanced concerning the nature of interaction involved in complex formation. One theory, known as charge-transfer interaction, was first recognized by Mülliken (16) as a result of the discovery of a new absorption band in some systems (17). The other type of interaction is hydrogen bonding in which the hydrogen bridge is regarded (15, 18) as a path for the flow of charge between the atoms it connects, so that both types are now considered (19, 20) as electron donor–acceptor interactions.

In our present study the anilide in dilute solutions of the triethylamine–benzene solvent mixtures mainly exists (21) in the enolic form and hence, complex formation expectedly takes place through hydrogen-bonding action between the enolic proton and the amine nitrogen, this proton being more acidic in benzoylacetanilide than that in acetoacetanilide.

An investigation of the influence of changes in the dielectric constants of the inert non-polar solvent on the equilibrium

Can. J. Chem. Downloaded from www.nrcresearchpress.com by 213.222.148.141 on 09/07/12
For personal use only.

constants obtained above is required before a final conclusion can be reached.

1. J. S. EARP and GLASSTONE. J. Chem. Soc. 1709 (1935).
2. D. L. HAMMICK, A. NORRIS, and L. E. SUTTON. J. Chem. Soc. 1755 (1935).
3. A. V. FEW and J. W. SMITH. J. Chem. Soc. 2781 (1949).
4. A. S. SHAWALI, M. M. NAOUM, and S. A. IBRAHIM. Bull. Chem. Soc. Jpn. **45**, 2501 (1972); H. PFEIFFER. J. Prakt. Chem. **111**, 240 (1925).
5. A. WEISSBERGER and E. PROSKAUER. Organic solvents, physical constants, and methods of purification. The Clarendon Press, Oxford. 1935.
6. A. R. TURKY, H. A. RIZK, and Y. M. GIRGIS. J. Phys. Chem. **64**, 565 (1960).
7. P. DEBYE. Phys. Z. **13**, 97 (1912).
8. L. ONSAGER. J. Am. Chem. Soc. **58**, 1487 (1936).
9. H. A. RIZK and I. M. ELANWAR. Can. J. Chem. **46**, 507 (1968); H. A. RIZK, N. Y. YOUSSEF, and H. GRACE. Can. J. Chem. **47**, 3767 (1969).
10. J. G. KIRKWOOD. J. Chem. Phys. **7**, 911 (1939); Ann N.Y. Acad. Sci. **40**, 315 (1940); Trans. Faraday Soc. A, **42**, 7 (1946).
11. E. E. FERGUSON and F. A. MATSEN. J. Chem. Phys. **29**, 105 (1958); J. Am. Chem. Soc. **82**, 3268 (1960).
12. A. S. SHAWALI and M. S. ELEZABY. J. Inorg. Nucl. Chem. **31**, 3149 (1976).
13. N. D. SOKOLOV. Ann. Chim. Paris, **10**, 497 (1965).
14. S. BRATOS. Adv. Quantum Chem. **3**, 209 (1967).
15. A. S. N. MURTY and C. N. R. RAO. J. Mol. Struct. **6**, 253 (1970).
16. R. S. MÜLLIKEN. J. Am. Chem. Soc. **74**, 811 (1952).
17. H. A. NENESI and J. H. HILDBRAND. J. Am. Chem. Soc. **70**, 3978 (1948).
18. P. SHUSTER. Intern. J. Quantum Chem. **3**, 851 (1969).
19. R. S. MÜLLIKEN and W. B. PERSON. Ann. Rev. Phys. Chem. **13**, 107 (1962).
20. H. RATAJCZAK and W. J. ORVILLE-THOMAS. J. Chem. Phys. 911 (1973).
21. L. W. REEVES. Can. J. Chem. **35**, 1351 (1957).

Can. J. Chem. Downloaded from www.nrcresearchpress.com by 213.222.148.141 on 09/07/12
For personal use only.

Synthetic oligosaccharides related to Group B streptococcal polysaccharides. The rhamnotriose moiety of the common antigen[1]

VINCE POZSGAY, JEAN-ROBERT BRISSON, AND HAROLD J. JENNINGS
Division of Biological Sciences, National Research Council of Canada, Ottawa, Ont., Canada K1A 0R6

Received May 15, 1987

VINCE POZSGAY, JEAN-ROBERT BRISSON, and HAROLD J. JENNINGS. Can. J. Chem. **65**, 2764 (1987).

The methyl glycoside (**1**) of the α-L-Rha*p*-(1→2)-α-L-Rha*p*-(1→2)-α-L-Rha*p*-(1→ portion of the group-specific, common antigen polysaccharide of Group B Streptococci has been synthesized. The key compound of the synthesis was methyl 3,4-di-*O*-benzyl-α-L-rhamnopyranoside (**4**). Controlled acetolysis of **4** gave 1,2-di-*O*-acetyl-3,4-di-*O*-benzyl-α-L-rhamnopyranose (**10**), which upon reaction with **4** under catalysis by trimethylsilyl trifluoromethanesulfonate (TMS-Tf) yielded the α-(1→2)-linked dirhamnoside. Subsequent rhamnosylation followed by deprotection gave **1**. TMS-Tf was also used in rhamnosylation reactions with tetra-*O*-acetyl-α-L-rhamnopyranose. Acetylation of acceptor alcohols was found to be a major side reaction in the TMS-Tf assisted glycosylations. One-dimensional nuclear Overhauser enhancement differential spectroscopy indicated that, in solution, **1** takes up a bent instead of an extended conformation.

VINCE POZSGAY, JEAN-ROBERT BRISSON et HAROLD J. JENNINGS. Can. J. Chem. **65**, 2764 (1987).

On a synthétisé le glycoside de méthyle (**1**) de la portion α-L-Rha*p*-(1→2)-α-L-Rha*p*-(1→2)-α-L-Rha*p*-(1→ du polysaccharide antigénique commun et spécifique du streptocoque du groupe B. Le composé clé de la synthèse est le di-*O*-benzyl-3,4 α-L-rhamnopyrannoside de méthyle (**4**). Une acétolyse contrôlée du produit **4** conduit au di-*O*-acétyl-1,2 di-*O*-benzyl-3,4 α-L-rhamnopyrannose (**10**) qui, par une réaction avec le composé **4** catalysée par le trifluorométhanesulfonate de triméthylsilyle (Tf-TMS), conduit au dirhamnoside qui comporte la liaison α-(1→2). Une rhamnosylation subséquente, suivie d'une déprotection, conduit au composé **1**. On a aussi utilisé le Tf-TMS dans des réactions de rhamnosylation impliquant le tétra-*O*-acétyl α-L-rhamnopyrannose. On a trouvé que l'acétylation des alcools accepteurs est une réaction secondaire importante dans les réactions de glycosylation assistées par le Tf-TMS. La spectroscopie différentielle, unidimensionnelle de l'effet Overhauser nucléaire indique que, en solution, la conformation du composé **1** est plutôt repliée qu'étendue.

[Traduit par la revue]

Introduction

Group B Streptococci are the major causative organisms of bacterial meningitis in newborn infants (1) and are responsible for a number of serious infections in adults (2). These organisms have been classified into four distinct serotypes (1), each type being characterized by a unique, immunodeterminant capsular polysaccharide (3–5). At the same time, each type of the group possesses a complex, group-specific common antigen polysaccharide ("C-substance"), which has been shown by studies in our laboratories to contain a backbone polymer of the pentasaccharide repeating unit (6):

α-L-Rha*p*-(1→2)-α-L-Rha*p*-(1→2)-α-L-Rha*p*-(1→1)-D-Glcol-(3←1)-α-L-Rha*p*

Also, the isolation (6) from the common antigen polysaccharide of the octasaccharide

α-L-Rha*p*-(1→3)-α-D-Gal*p*-(1→3)-β-D-GlcNAc*p*-(1→4)-[α-L-Rha*p*-(1→2)]-α-L-Rha*p*-(1→2)-α-L-Rha*p*-(1→1)-D-Glcol-(3←1)-α-L-Rha*p*

showed that some of the pentasaccharide repeating units are substituted by the trisaccharide α-L-Rha*p*-(1→3)-α-D-Gal*p*-(1→3)-β-D-GlcNAc*p*. Although the exact nature of this heterogeneity associated with the Group B streptococcal common antigen remains to be established (6), the recognition of its structural units is expected to make possible the identification of its major, immunodominant region(s). As a tool for mapping these regions, and those of other Group B streptococcal polysaccharides, we have currently been using synthetic approaches to obtain oligosaccharides related to these polymers. The tailored oligosaccharides together with those obtained in limited quantities by degradation from polysaccharides will then be used in serological experiments. In addition, conformational data obtained on the synthetic oligosaccharides are expected to help understanding the properties of the native, Group B streptococcal polysaccharides. In this paper we report the synthesis of the methyl glycoside (1) of the rhamnotriose fragment of the common antigen polysaccharide.

Results and discussion

Our synthetic strategy was based on chain elongation starting at the reducing end. This strategy avoids the formation of anomeric mixtures that might be formed due to the nonparticipating (7) nature of a glycosyl group (8).

The synthetic route described here required a methyl α-L-rhamnopyranoside (**2**) derivative as the reducing terminal moiety, selectively protected at HO-3 and -4. Dibenzyl derivative **4** was selected; it was first prepared by Lipták *et al.* (9) by $LiAlH_4$–$AlCl_3$ reduction of methyl 4-*O*-benzyl-2,3-*O*-*exo*-benzylidene-α-L-rhamnopyranoside in ca. 21% overall yield from **2**. Subsequently, **4** was obtained (10) in 9% yield as the minor product in phase-transfer catalyzed benzylation of methyl 4-*O*-benzyl-α-L-rhamnopyranoside (**3**). Also, **4** was obtained from **3** using tributyltin oxide-mediated regioselective benzylation, in 65% yield (11). David *et al.* (12) reported that alkylation of stannylene derivatives of polyhydroxy compounds is greatly accelerated in the presence of quaternary ammonium halides. Using this observation, we were now able to convert **3** to **4** in 91% yield, with an equimolar amount of Bu_2SnO, Bu_4NBr, and a slight excess of benzyl bromide. Although not part of the present synthetic work, we tested the scope of this technique and found that it is equally successful for the preparation of the 3-*O*-allyl (**8**, ref. 10) and 3-*O*-(4-methoxybenzyl) derivative (**9**) using allyl bromide and 4-methoxybenzyl chloride, respectively, as alkyl donors. The corresponding derivatives of methyl α-L-thiorhamnopyranoside are also accessible, in similar

[1]NRCC No. 28120.

Can. J. Chem. Downloaded from www.nrcresearchpress.com by 213.222.148.141 on 09/07/12
For personal use only.

Can. J. Chem. Downloaded from www.nrcresearchpress.com by 213.222.148.141 on 09/07/12
For personal use only.

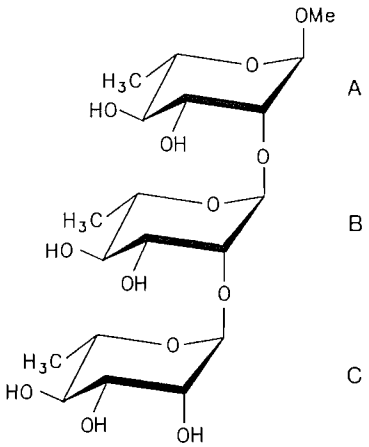

1

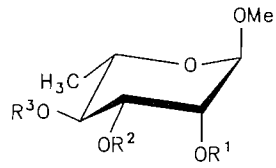

2 $R^1=R^2=R^3=H$
3 $R^1=R^2=H$, $R^3=Bn$
4 $R^1=H$, $R^2=R^3=Bn$
5 $R^1=Ac$, $R^2=R^3=Bn$
6 $R^1=R^3=Bn$, $R^2=H$
7 $R^1=R^3=Bn$, $R^2=Ac$
8 $R^1=H$, $R^2=All$, $R^3=Bn$
9 $R^1=H$, $R^2=MBn$, $R^3=Bn$

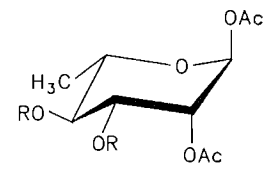

10 R=Bn
11 R=Ac

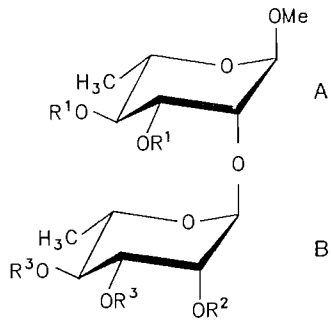

12 $R^1=R^3=Bn$, $R^2=H$
13 $R^1=Bn$, $R^2=R^3=Ac$
14 $R^1=R^2=R^3=H$

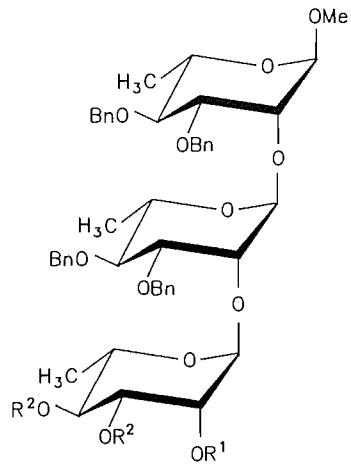

15 $R^1=H$, $R^2=Bn$
16 $R^1=R^2=H$

yields.[2] As **3** can be obtained from **2** in three steps (isopropylidenation, benzylation, acid hydrolysis) in a combined yield of >90%, the methodology suggested here is clearly the method of choice for the synthesis of 3-*O*-ether derivatives of **3**.

As the rhamnosyl donor for the "middle" unit, 1,2-di-*O*-acetyl-3,4-di-*O*-benzyl-α-L-rhamnopyranose (**10**) (13) was envisaged. In **10** the acetoxy group at C-1 would function as the leaving group in the glycosylation reaction whilst the acetyl group at HO-2 would fulfill a dual functional role; as a participating group (7) it should assist the formation of the new, 1,2-*trans* interglycosidic linkage and as a "temporary" protecting group it is selectively removable after glycosylation, making thus available the site of subsequent chain elongation. Compound **10** was prepared earlier by one of us (13) by acetylation of 2-*O*-acetyl-3,4-di-*O*-benzyl-L-rhamnopyranose. We have obtained crystalline **10** now simply by acetolysis of the key compound of this study, namely **4**, in 76.5% yield.

Reaction of **4** with **10** under catalysis by trimethylsilyl trifluoromethanesulfonate (TMS-Tf), as suggested by Paulsen and Paal (14) in the presence of powdered 4 Å molecular sieves followed by deacetylation (Zemplén), gave the partially blocked disaccharide **12** in 64.9% yield. In this reaction the formation of 1,2-*cis* linked disaccharide was not observed and the benzyl protecting groups were sufficiently stable in both the glycosyl donor and glycosyl acceptor to survive the acidic conditions (14) of the reaction. In addition to the efficiency of its preparation and its high reactivity under catalysis by TMS-Tf, the new rhamnosyl donor **10** has the advantage of stability during storage. A noteworthy side reaction in this glycosylation was the formation of trisaccharide **15** in 4.9% yield, the structure of which was proven by its nmr spectra and by the fact that its hydrogenolytic debenzylation gave **1**. Rhamnosylation of **12** with crystalline 2,3,4-tri-*O*-acetyl-α-L-rhamnopyranosyl bromide (15) under $Hg(CN)_2$ catalysis (16) followed by deacetylation (Zemplén) gave the partially protected trirhamnoside **16**, hydrogenolysis of which afforded **1**.

TMS-Tf catalysis was used also to synthesize disaccharides **14** (9) and **18** (9). Reaction of 1,2,3,4-tetra-*O*-acetyl-α-L-rhamno-

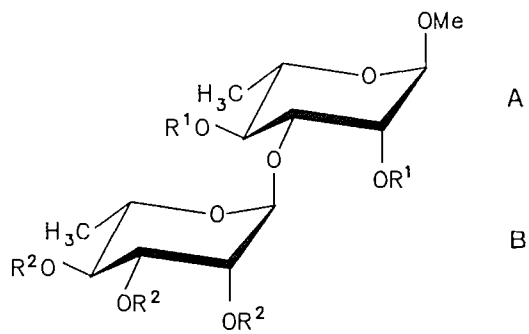

17 $R^1=Bn$, $R^2=Ac$
18 $R^1=R^2=H$

[2]V. Pozsgay and H. J. Jennings, unpublished results.

Can. J. Chem. Downloaded from www.nrcresearchpress.com by 213.222.148.141 on 09/07/12
For personal use only.

pyranose (**11**, refs. 13, 17) with glycosyl acceptors **4** and **6** (9, 10) gave the desired disaccharides **13** (9) and **17** (9) in 36.7 and 70.8% yields, respectively. These glycosylations were accompanied by extensive acetylation of the acceptors **4** and **6**, giving acetates **5** and **7** in 22.3 and 14.8% yields, respectively.

This type of side reaction has been reported recently by Kováč (18), who observed that TSM-Tf catalysed reaction between 1,2,3,4,6-penta-*O*-acetyl-β-D-galactopyranose and methyl 2,3,4-tri-*O*-benzoyl-β-D-galactopyranoside gave, in addition to the desired disaccharide, the 6-*O*-acetate of the glycosyl acceptor in 28% yield. The observations reported (18) and observed by us show that acetylation of acceptor alcohols is a major side reaction in TMS-Tf assisted glycosylation, the occurrence of which is not related to molecular sieves. Removal of the blocking groups from **13** and **17** as above gave **14** and **18**. The yields of the glycosylation reactions between **10** and **4** (64.9%) and between **11** and **4** (36.7%) reflect the increased reactivity of glycosyl donor **10** versus **11**, in agreement with the observations by Paulsen and Paal (14) for a partially benzylated galactopyranosyl donor. It is also apparent that HO-2 of L-rhamnose is less nucleophilic than HO-3 towards the cyclic 1,2-*O*-dioxocarbenium cation, which is the probable reactive intermediate generated (14) by TMS-Tf.

Structures of the compounds described in this study were verified by combined application of high-resolution, Fourier-transform ^1H and ^{13}C nmr spectroscopic measurements performed at 500 and 200 MHz for protons and at 125 and 50 MHz for carbons, respectively.

Published ^{13}C nmr assignments for key compounds **4** (9), **6** (9), and **10** (13) could now be confirmed by the use of two-dimensional C–H heteronuclear correlated spectroscopy with a composite pulse sequence (19). For **4**, the line reported (9) at 80.2 ppm is resolved at the higher field used by us into two separate resonances, which were individually assigned (Experimental).

The ^{13}C chemical shifts of the free disaccharides **14** and **18** and trisaccharide **1** (Table 1) were assigned by using the CHORTLE technique (20). Our assignments for **14** and **18** are in agreement with those published by Lipták *et al.* (9) except for the relative assignments of C-2_A and C-3_B in **18**. We want to note that the difference between these shifts is small and that their reassignment was made possible by using techniques and high field strength not available at the time of the original assignment. Carbon T_1 values of **1** were also determined, using the inversion–recovery technique to obtain insight into the relative segmental motion of the individual sugar units. Segmental motion of the individual units within an oligosaccharide was originally demonstrated by Allerhand and Doddrell (21), who found that in stachyose the carbon T_1 values of the α-(1→6)-linked terminal D-galactopyranosyl group were larger than those of the identically linked, internal D-galactopyranosyl unit. Carbon T_1 data for **1** (Table 2) are in agreement with the expected trend and further confirm the ^{13}C assignments for **1**. In the absence of any bulky terminal anchor (22, 23), the middle unit has the shortest T_1 values, indicating the slowest segmental motion among the individual units.

The ^1H nmr spectra of **1**, **14**, and **18** were unambiguously assigned (Table 3) by the use of 500 MHz one-dimensional and two-dimensional (2-D) homonuclear correlation spectroscopy (COSY) (24) and for **1** also homonuclear, relayed-correlation spectroscopy (RELAYED-COSY) (25). The assignments were aided by heteronuclear, proton–carbon chemical-shift correlation experiments (CHORTLE) (*vide supra*). For example, in **14** the heteronuclear shift-correlation experiment established that the proton (H-2_A) attached to the linkage carbon (C-2_A, 79.36 ppm) resonates at 3.922 ppm. Sequential connectivities in the 2-D COSY spectrum of **14** unambiguously identified the remaining protons. The proton spectrum of **18** was assigned in a similar way. The assignment of the proton spectrum of **1** was assisted by nOe measurements. Saturation of the anomeric proton resonating at 4.754 ppm resulted in a significant nOe for the aglycon methyl group whilst no such enhancement was observed upon saturation of the other two anomeric resonances. Assignment of the resonance at 4.754 ppm to H-1_A was then straightforward, and connectivities in the 2-D COSY spectrum of **1** established the identities of the other resonances belonging to the reducing end unit. Starting point for identification of

TABLE 1. ^{13}C nuclear magnetic resonance chemical shifts[a] for **1**, **14**, and **18** and heteronuclear coupling constants[b] for the anomeric carbon atoms of **1**

Carbon atom[c]	Compound		
	1[d]	**14**[e]	**18**[e]
1_A	100.34 (170.7, 4.4)	100.39	101.64
2_A	78.85	79.36	70.64
3_A	70.89	70.81	78.82
4_A	72.87	72.94	72.23
5_A	69.29	69.41	69.40
6_A	17.47	17.44	17.39
1_B	101.52 (171.8, 4.5)	103.06	103.17
2_B	78.95	70.85	70.96
3_B	70.58	70.85	70.93
4_B	72.87	72.82	72.84
5_B	69.95	69.96	69.89
6_B	17.47	17.44	17.43
1_C	102.89 (170.4, 4.5)		
2_C	70.78		
3_C	70.83		
4_C	72.74		
5_C	69.85		
6_C	17.41		

[a]In D_2O. Other conditions are to be found in the Experimental.
[b]The one-bond ^{13}C–^1H and three-bond ^{13}C–O–C–^1H coupling constants (in Hz) are given in parentheses.
[c]For designations A–C see formulae **1**, **14**, and **18**.
[d]At 50 MHz.
[e]At 125 MHz.

TABLE 2. Spin-lattice relaxation time (T_1) values[a,b] for the ^{13}C nuclei of **1**

Carbon atom	Unit[c]		
	A	B	C
1	0.345	0.295	0.361
2	0.332	0.296	0.351
3	0.314	0.282	0.350
4	—[d]	—[d]	0.336
5	0.317	0.286	0.330

[a]In s.
[b]Standard deviation: 0.001–0.004 s.
[c]For designations A–C see formula **1**.
[d]Individual values could not be determined because of completely overlapping resonances.

Can. J. Chem. Downloaded from www.nrcresearchpress.com by 213.222.148.141 on 09/07/12
For personal use only.

TABLE 3. ^{1}H nuclear magnetic resonance data[a] for **1**, **14**, and **18**

	Chemical shifts[b] (ppm)			Coupling constants[b] (Hz)			
H atom[c]	**1**	**14**	**18**	J_{H-H}	**1**	**14**	**18**
1_A	4.754	4.784	4.666	1_A-2_A	1.7	1.6	1.7
2_A	3.922	3.922	3.999	2_A-3_A	3.4	3.3	3.3
3_A	3.820	3.814	3.763	3_A-4_A	9.7	9.8	9.7
4_A	3.467	3.461	3.529	4_A-5_A	9.6	9.6	9.7
5_A	3.675	3.670	3.708	5_A-6_A	6.2	6.2	6.2
6_A	1.307	1.305	1.284				
1_B	5.109	4.960	5.027	1_B-2_B	1.8	1.7	1.6
2_B	4.075	4.064	4.058	2_B-3_B	3.3	3.4	3.3
3_B	3.894	3.794	3.831	3_B-4_B	9.7	9.8	9.7
4_B	3.475	3.449	3.455	4_B-5_B	9.4	9.6	9.6
5_B	3.734	3.749	3.799	5_B-6_B	6.3	6.2	6.3
6_B	1.287	1.276	1.303				
1_C	4.969			1_C-2_C	1.8		
2_C	4.064			2_C-3_C	3.4		
3_C	3.785			3_C-4_C	9.7		
4_C	3.445			4_C-5_C	9.4		
5_C	3.723			5_C-6_C	6.3		
6_C	1.266						
OCH_3	3.401	3.401	3.401				

[a]Measured at 310 K in D_2O.
[b]First-order data.
[c]For designations A–C see formulae **1**, **14**, and **18**.

TABLE 4. Observed nuclear Overhauser enhancements for **1**

Saturated proton[a]	Observed nOe[b]		
H-1_A	H-2_A 3.1%	H-5_B 3.4%	OCH_3 4.3%
H-1_B	H-2_A 6.9%	H-2_B 3.6%	H-5_C 4.6%
H-1_C	H-2_B + H-2_C 10.9%		

[a]For designations A–C see formula **1**.
[b]Intensity of the irradiated resonance is taken as 100%. Estimated error of measurement is ca. 10%.

the protons of the middle ring was the recognition that the linkage carbon (C-2_B) of this unit resonates at 78.95 ppm. The proton–carbon heteronuclear correlation experiment then identified the position of H-2_B as 4.075 ppm and the 2D-COSY spectrum led to the assignment of the remaining resonances. The nOe measurements (Table 4) confirmed the ^{1}H nmr assignments and also revealed the proximity of H-1_A and H-5_B and H-1_B and H-5_C. Analogous nOes were reported by Bock *et al.* (26) between the corresponding protons of α-(1→2)-linked L-rhamnopyranosyl units in oligosaccharides related to the *Shigella flexneri* O-antigen. This geometry is, however, not general for α-L-Rhap-(1→2)-α-L-Rhap disaccharide units, as Christian *et al.* (27) found no nOe between the corresponding protons of α-(1→2)-linked L-rhamnopyranosyl units within a glycan composed of the →2)-α-L-Rhap-(1→2)-α-L-Rhap(1→3)-β-L-Rhap-(1→ repeating unit. The nOe data for **1** show that the inter-residue geometry for rings A and B corresponds to that of B and C and is in agreement with the geometry proposed (26) for α-L-Rhap(1→2)-α-L-Rhap with φ and ψ values around both interglycosidic linkages of about 45° and 15° (26), respectively. The three-bond, heteronuclear $^{13}C-O-C-^1H$ coupling constants (Table 1) across the glycosidic linkage are also in support of this (26).

Compound **1** proved to be an excellent inhibitor in serological inhibition experiments[3] between the common antigen polysaccharide and antibodies raised against it. This observation strongly indicates that the conformational determinant represented by **1** is crucial to the serological specificity of the common antigen polysaccharide. Further work along these lines is in progress in our laboratories.

Experimental

Anhydrous dichloromethane used in glycosylation reactions was purchased from Aldrich (Gold label) and was transferred using the syringe technique. Other solvents were of hplc quality. Syrupy and solid compounds and reagents were dried in high vacuum using a liquid nitrogen trap. All glycosylation reactions were performed under nitrogen. Column chromatography was made on silica gel 60 (0.063–0.2 mm, E. Merck, Cat. No. 7734).

Melting point was determined on a Fisher–Johns apparatus and is uncorrected. Optical rotations were measured with a Perkin–Elmer 243 automatic polarimeter at 20°C. The nmr spectra were measured with a Bruker AM-500 or an AM-200 spectrometer at 500 and 200 MHz for protons and 125 or 50 MHz for carbons, using standard Bruker software DISNMR, at 300 K if not stated otherwise. Referencing was made to internal acetone (2.225 ppm for protons or 31.07 ppm for carbons) or to internal $CDCl_3$ (77.0 ppm for the central line of its triplet for carbons). Assignments given in Tables 1 and 3 and those for **4** and **9** are definitive; others are tentative. Proton-coupled ^{13}C nmr spectra were measured using the WALTZ decoupling (28).

*Methyl 3,4-di-O-benzyl-α-L-rhamnopyranoside (**4**)*

A solution of methyl 4-*O*-benzyl-α-L-rhamnopyranoside (**3**) (20.0 g, 74.6 mmol) and dibutyltin oxide (19 g, 76.3 mmol) in dry benzene (300 mL) was refluxed for 14 h under stirring under a Dean–Stark trap, followed by concentration to ca. 150 mL. After cooling to ca. 65°C, tetrabutylammonium bromide (24 g, 74.5 mmol) and benzyl bromide (10 mL, 84.1 mmol) were added and the mixture was further stirred at 65°C for 2 h. Concentration followed by chromatography (ethyl acetate–hexane, 1:1) gave syrupy **4** (24.3 g, 91.0%); $[\alpha]_D$ −45 (*c* 0.8, CH_2Cl_2) (lit. (10) $[\alpha]_D$ −44 ($CHCl_3$)); ^{13}C nmr (50 MHz, $CDCl_3$): 138.35, 137.86 (2 aromatic quat. carbons), 128.47–127.63 (aromatic carbons), 99.00 (C-1), 79.97 (C-3), 79.84 (C-4), 75.27, 71.91 ($2CH_2$ (Bn)), 68.37 (C-2), 67.07 (C-5), 54.67 (OCH_3), 17.83 (C-6).

*Methyl 3-O-allyl-4-O-benzyl-α-L-rhamnopyranoside (**8**)*

Compound **8** was prepared and isolated similarly to **4**, using allyl bromide as the alkyl donor. Yield: 92%, syrup; $[\alpha]_D$ −70 (*c* 0.9, CH_2Cl_2) (lit. (10) $[\alpha]_D$ −71 ($CHCl_3$).

*Methyl 4-O-benzyl-3-O-(4-methoxybenzyl)-α-L-*rhamnopyranoside (*9*)

Compound **9** was prepared and isolated similarly to **4**, using 4-methoxybenzyl chloride as the alkyl donor. Yield: 91%, syrup; $[\alpha]_D$ −42.1 (*c* 1.6, CH_2Cl_2); ^{13}C nmr (50 MHz, $CDCl_3$): 159.19 (C-4 (MBn)), 138.34 (aromatic quat. carbon), 129.90, 129.36, 128.18, 127.70, 127.48 (aromatic carbons), 113.72 (C-3 + C-5 (MBn)), 99.94 (C-1), 79.72 (C-4), 79.53 (C-3), 76.36 (CH_2 (Bn)), 71.46 (CH_2 (MBn)), 68.23 (C-2), 66.99 (C-5), 55.02, 54.51 ($2OCH_3$), 17.75 (C-6). *Anal.* calcd. for $C_{22}H_{28}O_6$: C 68.02, H 7.26; found: C 68.10, H 7.36.

*1,2-Di-O-acetyl-3,4-di-O-benzyl-α-L-rhamnopyranose (**10**)*

To an ice-cold stirred solution of **4** (3.5 g, 9.78 mmol) in acetic anhydride (20 mL) was added concentrated sulfuric acid (0.3 mL). After 30 min the mixture was poured into a stirred, ice-cold solution of

[3]F. Michon, A. Gamian, V. Pozsgay, and H. J. Jennings. In preparation.

Can. J. Chem. Downloaded from www.nrcresearchpress.com by 213.222.148.141 on 09/07/12
For personal use only.

sodium hydrogen carbonate (5 g) in water (200 mL). After 30 min the crystalline solid was filtered and washed with water. Yield: 3.2 g (76.5%); mp 107–109°C (MeOH) (lit. (13) mp 106–107°C); $[\alpha]_D$ −20 (*c* 1.1, CH_2Cl_2) (lit. (13) $[\alpha]_D$ −20 ($CHCl_3$)). The ^1H and ^{13}C nmr data are identical with those reported (13).

*Methyl 3,4-di-*O*-benzyl-2-*O*-(3,4-di-*O*-benzyl-α-L-rhamnopyranosyl)-α-L-rhamnopyranoside (12)*

A solution of **4** (2.52 g, 7.04 mmol) and **10** (3.66 g, 8.55 mmol) in anhydrous dichloromethane (20 mL) was stirred with powdered, 4 Å molecular sieves (~2 g) for 30 min at room temperature. Trimethylsilyl trifluoromethanesulfonate (0.4 mL, 2.07 mmol) was added and stirring was continued for 2 h. The mixture was filtered, and the filtrate extracted with ice-cold, 5% aqueous sodium hydrogen carbonate solution. The organic layer was dried ($CaSO_4$) and concentrated under reduced pressure. The residual syrup was dissolved in anhydrous methanol (100 mL) containing a catalytic amount of sodium methoxide. After 4 h the solution was neutralized with acetic acid, followed by concentration. Chromatography on silica gel with hexane – ethyl acetate (3:1) first gave syrupy **15** (350 mg, 4.9%); ^{13}C nmr (50 MHz, $CDCl_3$): 138.20, 137.95, 137.77 (quat. aromatic carbons), 128.05, 127.57, 127.33 (aromatic carbons), 100.24, 100.11, 99.63 (C-1_A, C-1_B, C-1_C), 80.09, 79.79 (2×), 79.26, 79.20, 78.82 (C-3_A, C-3_B, C-3_C, C-4_A, C-4_B, C-4_C), 74.98, 74.85 (2×) (3 CH_2 (Bn)), 73.97, 73.78 (C-2_A, C-2_B), 71.95, 71.73, 71.60 (3 CH_2 (Bn)), 68.39, 68.15, 67.73, 67.47 (C-2_C, C-5_A, C-5_B, C-5_C), 54.18 (OCH_3), 17.74, 17.66, 17.49 (C-6_A, C-6_B, C-6_C).

Further elution gave syrupy **12** (3.12 g, 64.9%); $[\alpha]_D$ −16.2 (*c* 0.37, CH_2Cl_2); ^{13}C nmr (50 MHz, $CDCl_3$): 138.4, 138.2, 138.1, 137.7 (aromatic quat. carbons), 128.2, 127.7, 127.5 (aromatic carbons), 100.6 (C-1_A), 99.8 (C-1_B), 80.1, 79.9, 79.7, 79.3 (C-3_A, C-4_A, C-3_B, C-4_B), 75.1, 75.0 (2 CH_2 (Bn)), 74.2 (C-2_A), 71.2 (2×) (2 CH_2 (Bn)), 68.5 (C-2_B), 67.8 (C-5_B), 67.5 (C-5_A), 54.4 (OCH_3), 17.9, 17.8 (C-6_A, C-6_B). *Anal.* calcd. for $C_{41}H_{48}O_9$: C 71.90, H 7.06; found: C 71.75, H 7.20.

*Methyl 2-*O*-(2,3,4-tri-*O*-acetyl-α-L-rhamnopyranosyl)-3,4-di-*O*-benzyl-α-L-rhamnopyranoside (13)*

To a stirred mixture of **4** (480 mg, 1.34 mmol), **11** (560 mg, 1.68 mmol), and powdered 4 Å molecular sieves (0.5 g) in anhydrous dichloromethane (10 mL), trimethylsilyl trifluoromethanesulfonate (60 μL, 0.31 mmol) was added at room temperature and the mixture was further stirred for 3 h. Triethylamine (1 mL) was added, the mixture was filtered, and the solution concentrated. Silica gel chromatography of the residual syrup (hexane – ethyl acetate, 3:1) gave first syrupy **5** (120 mg, 22.3%); ^{13}C nmr (50 MHz, $CDCl_3$): 170.09 (*C*=O), 138.38, 137.9 (2 aromatic quat. carbons), 128.2, 127.9, 127.7, 127.5 (aromatic carbons), 98.53 (C-1), 79.85 (C-4), 77.85 (C-3), 75.2, 71.5 (2 CH_2 (Bn)), 68.72 (C-2), 67.36 (C-5), 54.60 (OCH_3), 20.90 (CH_3CO), 17.85 (C-6). Further elution gave syrupy **13** (310 mg, 36.7%); $[\alpha]_D$ −44.5 (*c* 0.33, CH_2Cl_2) (lit. (9) mp 124–126°C; $[\alpha]_D$ −38.4 (*c* 0.53, $CHCl_3$). For ^{13}C nmr see ref. 9.

*Methyl 2-*O*-(α-L-rhamnopyranosyl)-α-L-rhamnopyranoside (14)*

Compound **14** was obtained from **13** by Zemplén deacetylation followed by hydrogenolysis (10% Pd–C), gel filtration through Sephadex G-10 (water), and freeze-drying; $[\alpha]_D$ −48 (*c* 0.9, H_2O) (lit. (9) $[\alpha]_D$ −92 (*c* 1.28, H_2O); lit (29) $[\alpha]_D$ −46 (*c* 1, H_2O)). For ^1H nmr and ^{13}C nmr see Tables 3 and 1, respectively.

*Methyl 3,4-di-*O*-benzyl-2-*O*-[3,4-di-*O*-benzyl-2-*O*-(α-L-rhamnopyranosyl)-α-L-rhamnopyranosyl]-α-L-rhamnopyranoside (16)*

A mixture of **12** (670 mg, 0.978 mmol), mercuric cyanide (1.1 g, 4.35 mmol), powdered 4 Å molecular sieves (~1.5 g), and anhydrous acetonitrile (10 mL) was stirred for 1 h, then crystalline 2,3,4-tri-*O*-acetyl-α-L-rhamnopyranosyl bromide (15) (1.1 g, 3.11 mmol) was added and stirring was continued for 12 h. The mixture was filtered and concentrated; the residue was dissolved in chloroform (20 mL) and extracted with 5% aqueous potassium iodide, then with water. Drying ($CaSO_4$) and concentration left a syrup, which was dissolved in anhydrous methanol (20 mL) to which a catalytic amount of sodium methoxide was added. The solution was kept at room temperature for 4 h, neutralized with acetic acid, and concentrated. Chromatography of the residue (ethyl acetate – hexane, 2:1) gave syrupy **16** (597 mg, 73.4%); $[\alpha]_D$ −35.8 (*c* 0.43, CH_2Cl_2); ^{13}C nmr (50 MHz, $CDCl_3$): 138.32, 138.17 (aromatic quat. carbons), 128.42–127.65 (aromatic carbons), 100.84, 100.42, 99.82 (C-1_A, C-1_B, C-1_C), 80.45, 80.22, 79.44, 79.05 (C-3_A, C-3_B, C-4_A, C-4_B), 75.19 (2 CH_2 (Bn)), 74.33, 74.19 (C-2_A, C-2_B), 73.13 (C-4_C), 72.39 (CH_2 (Bn)), 72.01 (CH_2 (Bn)), 71.54 (C-3_C), 70.88 (C-2_C), 68.55, 68.41 (C-5_A, C-5_B), 67.68 (C-5_C), 54.54 (OCH_3), 17.98 (2×), 17.45 (C-6_A, C-6_B, C-6_C). *Anal.* calcd. for $C_{47}H_{58}O_{13}$: C 67.93, H 7.03; found: C 66.67, H 6.99.

*Methyl 3-*O*-(2,3,4-tri-*O*-acetyl-α-L-rhamnopyranosyl)-2,4-di-*O*-benzyl-α-L-rhamnopyranoside (17)*

A mixture of **6** (350 mg, 0.976 mmol), **11** (1.5 g, 4.5 mmol), powdered 4 Å molecular sieves (2 h), and anhydrous dichloromethane (10 mL) was stirred at room temperature for 1 h. Trimethylsilyl trifluoromethanesulfonate (100 μL, 0.517 mmol) was added and stirring was continued for 3 h. Work-up, similar to that for **13**, gave syrupy **7** (58 mg, 14.8%); ^{13}C nmr (50 MHz, $CDCl_3$): 170.14 (*C*=O), 138.25 (aromatic quat. carbons), 129.7–126.8 (aromatic carbons), 98.67 (C-1), 79.00 (C-4), 76.08 (C-2), 74.82, 73.01 (2CH_2 (Bn)), 73.72 (C-3), 67.54 (C-5), 54.68 (OCH_3), 20.98 (CH_3CO), 17.94 (C-6); and **17** (432 mg, 70.1%); $[\alpha]_D$ −46.2 (*c* 1.64, CH_2Cl_2) (lit. (9) $[\alpha]_D$ −46.1 (*c* 0.56, $CHCl_3$). For ^{13}C nmr of **17** see ref. 9.

*Methyl 3-*O*-(α-L-rhamnopyranosyl)-α-L-rhamnopyranoside (18)*

Compound **18** was obtained from **17** as described for **14**; $[\alpha]_D$ −81 (*c* 0.4, H_2O) (lit. (9) $[\alpha]_D$ −78 (*c* 1.52, H_2O). For ^1H nmr and ^{13}C nmr see Tables 3 and 1, respectively.

*Methyl-2-*O*-[2-O-(α-L-rhamnopyranosyl)-α-L-rhamnopyranosyl]-α-L-rhamnopyranoside (1)*

1. A mixture of 10% palladium on carbon (0.5 g) in 95% ethanol (5 mL) and acetic acid (5 mL) was stirred under hydrogen under atmospheric pressure for 2 h. A solution of **16** (530 mg) in 95% ethanol (10 mL) was then added and stirring was continued for 14 h. Removal of catalyst followed by concentration left a syrup, which was purified on a column of Sephadex G-15 (water). The major fraction was freeze-dried to give **1** as a white amorphous powder (252 mg, 84.0%); $[\alpha]_D$ −57.7 (*c* 1, H_2O). For ^1H nmr and ^{13}C nmr see Tables 3 and 1, respectively. *Anal.* calcd. for $C_{19}H_{34}O_{13}$: C 48.50, H 7.28; found: C 48.29, H 7.39.

2. Hydrogenolysis of **15** as described for **16** gave **1** (86%) having identical $[\alpha]_D$ and ^1H nmr and ^{13}C nmr spectra to the compound obtained from **16** by hydrogenolysis.

Acknowledgment

We thank Mr. H. Seguin for the elemental analyses.

1. H. J. Jennings. Adv. Carbohydr. Chem. Biochem. **41**, 155 (1983).
2. A. Verghese, K. Mireault, and R. D. Arbeit. Rev. Infect. Dis., **8**, 912 (1986).
3. H. J. Jennings, E. M. Katzenellenbogen, C. Lugowski, and D. L. Kasper. Biochemistry, **22**, 1258 (1983).
4. M. R. Wessels, V. Pozsgay, D. L. Kasper, and H. J. Jennings. J. Biol. Chem. **262**, 8262 (1987).
5. H. J. Jennings, K.-G. Rosell, E. Katzenellenbogen, and D. L. Kasper. J. Biol. Chem. **258**, 1793 (1983).
6. F. Michon, E. Katzenellenbogen, D. L. Kasper, and H. J. Jennings. Biochemistry, **26**, 476 (1987).
7. H. Paulsen. Angew. Chem. Int. Ed. Engl., **21**, 155 (1982).
8. V. Pozsgay, P. Nánási, and A. Neszmélyi. Carbohydr. Res. **75**, 310 (1979).
9. A. Lipták, P. Nánási, A. Neszmélyi, and H. Wagner. Tetrahedron, **36**, 1261 (1980).
10. V. Pozsgay. Carbohydr. Res. **69**, 284 (1979).
11. V. Pozsgay and A. Neszmélyi. Carbohydr. Res. **85**, 143 (1980).

12. S. DAVID, A. THIEFFRY, and A. VEYRIÈRES. J. Chem. Soc. Perkin Trans. 1, 1796 (1981).
13. V. POZSGAY and A. NESZMÉLYI. Carbohydr. Res. **80**, 196 (1980).
14. H. PAULSEN and M. PAAL. Carbohydr. Res. **135**, 53 (1984).
15. E. FISCHER, M. BERGMANN, and H. RABE. Chem. Ber. **53**, 2362 (1920).
16. B. HELFERICH and K.-F. WEDEMEYER. Justus Liebigs Ann. Chem. **563**, 139 (1949).
17. R. S. TIPSON. J. Biol. Chem. **130**, 55 (1939).
18. P. KOVÁČ. Carbohydr. Res. **153**, 237 (1986).
19. J. A. WILDE and P. H. BOLTON. J. Magn. Reson. **59**, 343 (1984).
20. G. A. PEARSON. J. Magn. Reson. **64**, 487 (1985).
21. A. ALLERHAND and D. DODDRELL. J. Am. Chem. Soc. **93**, 2777 (1971).
22. A. NESZMÉLYI, K. TORI, and G. LUKACS. J. Chem. Soc. Chem. Commun. 613 (1977).
23. H. GUINAUDEAU, O. SELIGMANN, H. WAGNER, and A. NESZMÉLYI. Phytochemistry, **20**, 1113 (1981).
24. W. P. AUE, E. BARTHOLDI, and R. R. ERNST. J. Chem. Phys. **64**, 2229 (1976).
25. G. EICH, G. BODENHAUSEN, and R. R. ERNST. J. Am. Chem. Soc. **104**, 3731 (1982).
26. K. BOCK, S. JOSEPHSON, and D. R. BUNDLE. J. Chem. Soc. Perkin Trans. 2, 59 (1982).
27. R. CHRISTIAN, G. SCHULZ, F. M. UNGER, P. MESSNER, Z. KÜPCÜ, and U. B. SLEYTR. Carbohydr. Res. **150**, 265 (1986).
28. A. J. SHAKA, J. KEELER, T. FRENKIEL, and R. FREEMAN. J. Magn. Reson. **52**, 335 (1983).
29. T. NORBERG, S. OSCARSON, and M. SZÖNYI. Carbohydr. Res. **156**, 214 (1986).

Can. J. Chem. Downloaded from www.nrcresearchpress.com by 213.222.148.141 on 09/07/12
For personal use only.

Bicyclization of aza-compounds by positive halide ions. II. Lactams and some related cyclizations[1,2]

RICHARD M. ELOFSON, FAHMI F. GADALLAH, AND JAMES K. LAIDLER
Alberta Research Council, 250 Karl Clark Road, Edmonton, Alta., Canada T6H 5X2

Received April 22, 1986[3]

This paper is dedicated to Dr. O. E. (Ted) Edwards

RICHARD M. ELOFSON, FAHMI F. GADALLAH, and JAMES K. LAIDLER. Can. J. Chem. **65**, 2770 (1987).

Anodic oxidation of lactams in the presence of halide ions produced excellent yields of bicyclic compounds with reactants having rings in the range of eight to ten atoms (C_7 to C_9). Smaller rings did not react to form bicyclic products and larger rings gave reduced yields. Attempts were made to cyclize non-cyclic amides and to bicyclize cycloheptyl and cyclooctyl acetamide with limited success.

RICHARD M. ELOFSON, FAHMI F. GADALLAH et JAMES K. LAIDLER. Can. J. Chem. **65**, 2770 (1987).

Lorsqu'on soumet des lactames cycliques comportant de huit à dix atomes (C_7 à C_9) à une oxydation anodique en présence d'ions halogénures, on obtient des composés bicycliques avec d'excellents rendements. Lorsqu'on soumet des composés cycliques plus petits à cette réaction, ils ne donnent pas de produits bicycliques alors que les composés dont le cycle est plus grand donnent de moins bons rendements. Lorsqu'on a essayé de cycliser des amides non-cycliques ou de provoquer une bicyclisation des cycloheptyl- et cyclooctyl-acétamides, les résultats ont été mitigés.

[Traduit par la revue]

Introduction

We have previously reported (1) the bicyclization of cyclic amines in moderate yields by anodic oxidation in the presence of halide ions, particularly bromide ion. Following the example of Edwards and co-workers (2–4) it was decided to attempt the bicyclization of a number of lactams by electrochemical means. Since amides are not readily attacked at anodes (5) and are much more resistant to chemical reagents, it was anticipated that more severe conditions in the form of higher anode potentials and/or higher temperatures might be required. On the other hand, since amides are resistant to direct anodic attack, any bicyclic products produced by indirect processes as described in the previous paper (1) should be safe from further degradation at the electrode. These postulates have been confirmed in the experiments described below.

Because of the success with lactams it was decided to attempt to bicyclize cycloheptylacetamide and cyclooctylacetamide and to cyclize non-cyclic amides. These results, to date much less successful and preliminary in nature, are included only because no further work in this area is likely from this laboratory.

Results

The first attempt to bicyclize lactams was to duplicate the conditions for bicyclization of amines with the addition of $Ca(OH)_2$ to maintain alkaline conditions. Under these conditions very little bicyclization occurred. The temperature was then raised to 60°C but this resulted in attack of the acetonitrile to produce succinonitrile and bromoform. Acetonitrile was finally replaced with dioxane and the electrolyses were conducted at the elevated temperature of 85°C. The results for bicyclization of a number of lactams are shown in Table 1.

As shown in Table 1 the yields of bicyclic products from C_7 to C_9 lactams were near quantitative. No bicyclization of C_6 lactam occurred and the C_{10} and C_{12} lactams were bicyclized in reduced but significant yields. As expected the C_7 lactam produced only one isomer **a** with two five-membered rings

TABLE 1. Bicyclization of lactams at 100 mA, 85°C, C anode, $Ca(OH)_2$, LiBr (0.1 *M*), 20% H_2O in dioxane

Lactam	Time (h)	Starting material (%)	Bicyclic products (%)
$C_6H_{11}NO$	5	100	0
$C_7H_{13}NO$	3.5	12	85
$C_8H_{15}NO$	3	Trace	89[a]
$C_9H_{17}NO$	12	16	83
$C_{10}H_{19}NO$	6	49	46[b]
$C_{12}H_{23}NO$	6	61	10

[a]In CH_3OH bicyclic yield 82%.
[b]No change after 8 h.

[1] 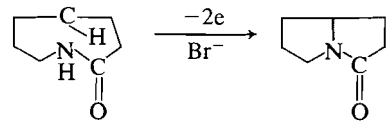

(reaction [1], Fig. 1). The C_8 amide produced two isomers, **b** and **c** each with one five-membered ring and one six-membered ring but with the carbonyl function reversed. The ratio of the respective isomers varied somewhat but was in approximate agreement with Edwards (4), viz. about 1:3 to 1:5. From the C_9 lactam three bicyclic products **d**, **e**, and **f** were obtained, viz. 1-azabicyclo[4,4,0]decan-2-one, 1-azabicyclo[5,3,0]decan-10-one, and 1-azabicyclo[5,3,0]decan-2-one. Again the ratios varied, but for the run reported in Table 1 the ratio was 11:1:3 for the respective isomers. Bicyclization of the C_{10} lactam produced three isomers **g**, **h**, and **i**, viz. 1-azabicyclo[6,3,0]-undecan-2-one, 1-azabicyclo[6,3,0]undecan-11-one, and 1-azabicyclo[5,4,0]undecan-2-one in a ratio 23:8:16, respectively. For the C_{12} lactam, yields were very much reduced and no attempt was made to sort out the isomers that were produced. In the case of the C_{10} lactam, the yield did not increase when the reaction time was increased to 8 h but the amount of starting material declined.

Table 2 depicts the results of attempts to cyclize primary amides under the conditions used in Table 1. When aqueous methanol was used as the solvent together with higher current more complex products were obtained. Methoxylation was

[1]ARC Contribution Number 1482.

[2]Parts of this paper were presented at: (*a*) The North American Chemical Congress, Mexico City, December 1975; (*b*) The Electrochemistry Society Meeting, Washington, D.C., April 1976; and (*c*) 6th North American Meeting of the Catalysis Society, Chicago, 1979.

[3]Revision received July 21, 1987.

Can. J. Chem. Downloaded from www.nrcresearchpress.com by 213.222.148.141 on 09/07/12
For personal use only.

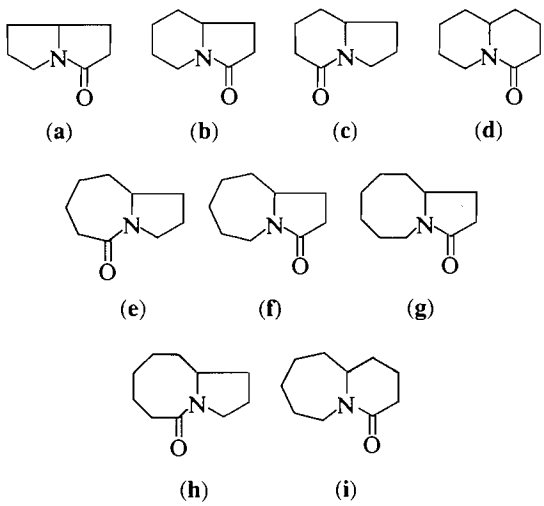

FIG. 1. Structures of bicyclic lactams.

TABLE 2. Anodic oxidation of amides at C anode, $Ca(OH)_2$, LiBr (0.1 *M*), 20% H_2O in dioxane

Compound	*I* (mA)	*I* (°C)	Time (h)	Starting material (%)	Cyclization products (%)
Pentylacetamide	100	85	4.5	78	6.5
Isohexylacetamide	100	85	3	92	Nil
Cycloheptylacetamide	200	85	3	77	13.4
Cyclooctylacetamide	200	85	3	53	17

involved but otherwise the products were not established. *N*-Pentyl acetamide produced a 6.5% yield of 2-methyl-*N*-acetylpyrolidine after 4.5 h, in dioxane, according to reaction [2]. No *N*-acetylpiperidine was detected. This would seem to agree with the well-known propensity of free radicals to extract secondary hydrogen atoms instead of primary hydrogen atoms.

[2] 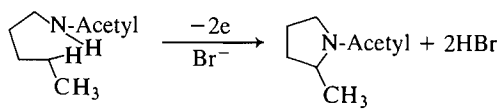

Isohexylacetamide in methanol yielded two products, not including the expected 2,2-dimethyl-*N*-acetylpyrolidine in methanol. The retention times and molecular ions corresponded to methoxylated and brominated cyclized products but were not otherwise characterized. No identifiable products were obtained in dioxane. Large amounts of starting material were recovered from each of the last two reactions.

Cycloheptylacetamide was subjected to electrolysis under the conditions listed in Table 2. After 3 h at 200 mA the reaction mixture was worked up and yielded 13.4% of a product that came 0.9 min before the starting material, by glc, with the correct molecular ion for the bicyclized material of 153 mass units, but which was not identified further. The reaction presumably is depicted in [3].

[3] 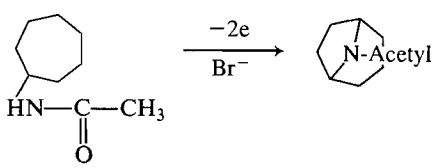

TABLE 3. $E_{1/2}$ vs. sce, of secondary amines and amides and halide ions

Species	E_1 (*V*)	E_2 (*V*)
Amines	1.2–1.3	
Amides	1.7–1.8	
Cl^-	1.1	1.7
Br^-	1.0	1.4
I^-	0.25	0.55

TABLE 4. Effect of anion on bicyclization of C_8 lactam at 100 mA, 85°C, C anode, $Ca(OH)_2$, LiBr (0.1 *M*), 20% H_2O in dioxane

Electrolyte	Time (h)	Starting material (%)	Bicyclic product (%)
$LiClO_4$	6.5	90	0
LiCl	12	29	55
LiBr	3	Trace	89
LiI	3	95	Trace

Cyclooctylacetamide produced a mixture of bicyclized products which after reduction with lithium aluminum hydride yielded 17% bicyclic material with a retention time shorter than that of the starting material according to reaction [4]. The primary products of the reaction could not be separated by glc so the bicyclic amides were reduced with $LiAlH_4$ and produced three products, with the correct molecular ions by mass spectrometry.

[4] 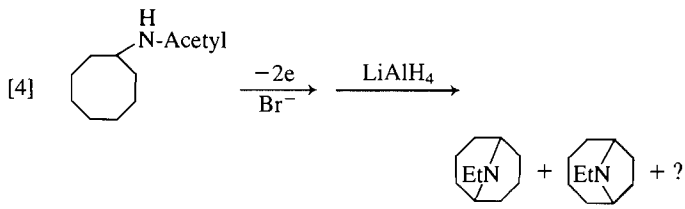

Discussion

Table 3 illustrates the point that lactams are indeed very resistant to anodic attack (5). In fact in these experiments there was little evidence in the absence of halide ion of direct attack on the lactams, Table 4, reaction [1]. In order to obtain significant yields of bicyclized material, halide ions must be present as shown in Table 4.

As in the case of the bicyclization of the amines, bromide ions gave the best results (Table 4). Possibly the advantage of bromide over chloride was not as great for bicyclization of the lactams as for the cyclic amines. Not surprisingly iodine was not effective since iodine in any form would not be expected to react with lactams. These results are consistent with the mechanistic proposals made in [1], namely oxidation of the halide ion at the electrode followed by reaction of the halide cation species produced with the amide. The work of Anson (6), as discussed previously (1), accounts nicely for this sequence of adsorption and oxidation. The high anodic potentials of amides make the hypothesis for removal of two electrons from the halide moiety before reaction with the organic species even more plausible than in the case of bicyclization of cyclic amines.

The results shown in Table 5 indicate that the mechanism for the next step probably does not simply involve formation of

Can. J. Chem. Downloaded from www.nrcresearchpress.com by 213.222.148.141 on 09/07/12
For personal use only.

TABLE 5. Bicyclization of C_7 lactam and N—Cl analogue with and without current

Electrolyte	I (mA)	Time (h)	Bicyclic (%)	N—Cl (%)	NH (%)
LiCl[a]	0	5.5	12.2	(87)	
LiCl[a]	0	21.5	20.9	28	50
LiCl[a]	100	5.5	10.1	39	3
LiCl	100	13	38.3		22
LiBr[a]	0	5.5	6.3	51	36
LiBr[a]	100	5.5	59.7	6	10
LiBr	100	3.5	87		13

[a]Starting material N—Cl lactam, remainder lactam.

N-haloamides and their subsequent thermal decomposition. Not enough additional work has been done to support the proposal that the X^+ species first produced at the anode in the triplet state (Hund's Rule) reacts directly with the amide. It could be argued that the higher temperatures required for the amide reactions support a conventional electrophilic mechanism with a significant energy of activation. Clearly, the environment of the X^+ species produced at the electrode must be important in order to account for the results shown in Table 5. Steric or entropy factors are responsible for the high yields upon bicyclization of lactams of moderate ring size and the low yields for cyclization of amides studied here.

Experimental

The reaction conditions were similar to those already described (1). For the results described in this paper a three-necked round bottom flask, 200 mL, was fitted with a condenser to minimize solvent loss and flushed with a slow stream of nitrogen. A stainless steel rod (SS-304), 0.3 cm in diameter was used as the cathode. The anode was a rod 1.5 cm by 5 cm of carbon (Union Carbide S2408-60). Two millimoles of amide were dissolved in 100 mL of solvent, usually 20% water in dioxane with the electrolyte as specified. The current was maintained at 100 mA unless specified otherwise. Under these conditions the initial anode potential was found to be about 2.3 V at a current of 100 mA. All electrochemical operations were accomplished with a Princeton Applied Research Electrochemical System, Model 170.

Quantitative analyses were done by glc (Hewlett-Packard F&M 810) with the columns and packing as specified in Table 6. The temperature was programmed as specified in Table 6. Helium flow was 60 mL/min. Retention times and molecular ions are presented in Table 6.

Qualitative analyses were done by glc and mass spectrometry using known compounds as standards or simply by glc – mass spectrometry as indicated. Mass spectra were obtained with a Perkin Elmer GLC Mass Spectrometer Model 270.

The work up procedure for electrolysis with 20% dioxane as solvent consisted of filtration to remove $Ca(OH)_2$, solid washed with dioxane, water added, extracted 5 times with benzene, benzene washed 4 times with water, benzene solution dried, and concentrated as required.

The C_6, C_7, C_8, and C_{12} lactams were obtained from Aldrich Chemical Co., Milwaukee, WI. The C_9 and C_{10} lactams were prepared from the respective cyclic ketones (Aldrich) using the Beckmann rearrangement. N—Cl—C_7 lactam was prepared according to the procedure of Edwards (2).

The C_7 bicyclic lactam was isolated from the electrolysis reaction and identified by nmr and mass spectrometry (2). The C_8 and C_9 bicyclic lactams were identified by comparison with authentic samples supplied through the courtesy of Dr. M. H. Benn, University of Calgary. The C_{10} bicyclic lactams were identified with the aid of data from the thesis of K. N. Vohra, University of Calgary, 1973.

No attempt was made to identify the individual C_{12} bicyclic lactams except to note that their unseparated retention time was shorter than that of the parent lactam and their molecular ions by mass spectra corresponded to the required formulae. In all cases reported in this paper the bicyclized material had retention times shorter than the parent compounds.

TABLE 6. Gas–liquid chromatography retention times and molecular ions of reagents and products from Table 1[a]

Compound (from Fig. 1)	Retention time (min)	Mass ions		
Column conditions: 10% Versamid 900, 1/8 in. × 6 ft, 20 to 180°C (15°C/min)				
a	5.7	125	97	69
C_7 lactam	7.1	127	99	55
b	7.5	139	83	
c	9.2	139	111	83
C_8 lactam	10.6	141	124	98
Column conditions: 10% Versamid 900, 1/8 in. × 6 ft, Iso at 180°C				
d	6.9	153	97	
e	7.15	153		
f	7.35	153	70	
C_9 lactam	8.35	155	138	98
Column conditions: 10% Versamid 900, 1/8 in. × 12 ft, 20 to 240°C (15°C/min)				
γ	17.0	167	84	
h	17.5	167	73	
i	18.0	167	70	
C_{10} lactam	18.8	169	84	73
Column conditions: 10% Versamid 900, 1/8 in. × 12 ft, Iso at 240°C				
C_{12} bicyclo	5.18	197	152	72
C_{12} lactam	7.6	199	182	100

[a]Compounds **b**, **c**, **d**, **e**, and **f** are identical to compounds provided by M. Benn; compounds **g**, **h**, and **i** are identified from Vohra's Thesis.

n-Pentylacetamide was prepared by acetylation of *n*-pentylamine; purity was checked by glc on SE30 and Versamid 900 columns.

Isohexylacetamide was prepared by acetylation of the amine; purity checked by glc on SE30, and mass spectra. The amine was prepared by reduction of the amide of 4-methyl pentanoic acid with lithium aluminum hydride in ether.

Cycloheptylacetamide was prepared by acetylation of the amine (Aldrich). Purity was checked by glc and mass spectra.

Cyclooctylacetamide was prepared by acetylation of cyclooctylamine (Aldrich) with acetic anhydride and recrystalized from *n*-pentane. The electrolysis of this amide produced a mixture of bicyclic amides and starting material which resisted separation by glc. Reduction of the mixed amides with $LiAlH_4$ in ether was followed by destruction of excess reagent with HCl. Extraction of this solution with ether, after basification with NaOH, produced a solution which after drying yielded the ethyl amines with retention times as shown in Table 7.

Mass spectra and retention times indicated that bicyclization had taken place as indicated in Table 2.

2-Methylpyrrolidine was prepared by photolysis of *N*-chloro-*n*-pentylamine (8, 9). Gas–liquid chromatography on Versamid 900 and mass spectra showed that the product of acetylation of this reaction corresponded to the product of the electrolysis of *n*-pentylacetamide.

Can. J. Chem. Downloaded from www.nrcresearchpress.com by 213.222.148.141 on 09/07/12
For personal use only.

TABLE 7. Gas–liquid chromatography retention times and mass ions of reagents and products from Table 2

Compound	Retention time (min)	Mass ions			
Column conditions: 10% Versamid 900, 1/8 in. × 12 ft, 20 to 240°C (15°C/min)					
2-Methyl-*N*-acetylpyrrolidine	11.9	127	112	70	
Pentylacetamide	12.9	129	114	84	
Acetylpiperidine	12.15	127	84		
Isohexylacetamide	14.0	143			
Methoxylated and cycl. isohexyl.	14.7	171			
Brominated compound	19.9				
Bicycl. cycloheptylacetamide	28.8	153	82	56	
Cycloheptylacetamide	29.7	155	98	60	56
Column conditions: 10% SE 30, 1/8 in. × 12 ft, 20 to 280°C (8°C/min)					
Bicycl. cyclooctylethylamine	17.4	139			
ditto	18.1	139			
ditto	18.9	139			
N-Ethylcyclooctylamine	19.5	141			
Cyclooctylacetamide[a]	24.9	169			

[a]Mass spectra of cyclooctyl derivatives lost. Record of mole ions only.

Acknowledgements

The authors are grateful to O. E. Edwards and M. H. Benn for their helpful discussions and supplying some of the bicyclic chemicals. Thanks are also due to G. Spratt and M. Rawluk of this laboratory for mass spectral analysis.

1. R. M. ELOFSON, F. F. GADALLAH, and J. K. LAIDLER. Can. J. Chem. **63**, 1170 (1985).
2. O. E. EDWARDS, D. VOCELLE, J. W. APSIMON, and F. HAGUE. J. Am. Chem. Soc. **87**, 678 (1965).
3. O. E. EDWARDS and D. VOCELLE. Can. J. Chem. **50**, 1167 (1972).
4. O. E. EDWARDS, J. M. PATON, M. H. BENN, R. E. MITCHELL, C. WATANATADA, and K. N. VOHRA. Can. J. Chem. **49**, 1648 (1971).
5. C. K. MANN and K. K. BARNES. Electrochemical reactions in nonaqueous systems. Debber, New York. 1970. Chap. 9.
6. F. C. ANSON. Acc. Chem. Res. **8**, 400 (1975).
7. K. N. VOHRA. Ph.D. Thesis, U. of Calgary. 1975.
8. G. E. COLEMAN and G. E. GOHEEN. J. Am. Chem. Soc. **60**, 730 (1938).
9. S. WAWZONEK and T. P. CULBERTSON. J. Am. Chem. Soc. **81**, 3367 (1959).

Can. J. Chem. Downloaded from www.nrcresearchpress.com by 213.222.148.141 on 09/07/12
For personal use only.

The effect of electron-pair donor solvents on methylene reactivity

MIQUEL MORENO, JOSÉ M. LLUCH, ANTONIO OLIVA, AND JUAN BERTRÁN
Departament de Química, Universitat Autònoma de Barcelona, Bellaterra, Barcelona, Spain

Received March 5, 1987

MIQUEL MORENO, JOSÉ M. LLUCH, ANTONIO OLIVA, and JUAN BERTRÁN. Can. J. Chem. **65**, 2774 (1987).

The effect of electron pair donor solvents on methylene reactivity has been theoretically studied by means of *ab initio* methods, using the split valence 3-21G basis set. The calculations have been done on the well-known methylene addition to ethylene, taking one water molecule in order to represent the donor solvent. We have shown that the process takes place via the formation of a reversible complex between water and methylene, the formation of this complex permitting to explain the experimentally observed decrease of methylene's electrophilicity. The analysis of the variation of the electronic charge density and of the solvation parameters along the reaction coordinate have also allowed to interpret the reaction in terms of the transfer of an electrophile (methylene) from a nucleophile (water) to another nucleophile (ethylene).

MIQUEL MORENO, JOSÉ M. LLUCH, ANTONIO OLIVA et JUAN BERTRÁN. Can. J. Chem. **65**, 2774 (1987).

Faisant appel à des méthodes *ab initio* et utilisant un ensemble de base 3-21G, on a réalisé une étude théorique de l'effet des solvants donneurs de paires d'électrons sur la réactivité du méthylène. On a réalisé les calculs en prenant comme exemple l'addition bien connue de méthylène sur l'éthylène et en utilisant une molécule d'eau pour représenter le solvant donneur de paires d'électrons. On a démontré que le processus se produit par le biais de la formation d'un complexe réversible entre l'eau et le méthylène; la formation de ce complexe permet d'expliquer le fait observé expérimentalement selon lequel le caractère électrophile du méthylène diminue. Une analyse de la variation de la densité de la charge électronique et des paramètres de solvatation en fonction des coordonnées de la réaction a aussi permis d'interpréter la réaction en fonction du transfert d'un électrophile (méthylène) d'un nucléophile (l'eau) vers un autre nucléophile (éthylène).

[Traduit par la revue]

Introduction

It is well known that solvent greatly influences reactions in which ionic species intervene (1). It is equally well recognized that the reactivity of neutral species such as free radicals and carbenes is generally insensitive to the nature of the solvent. However, recent experimental works (2–4) have shown that some electron-pair donor solvents modify the reactivity of carbenes. For instance, competition between pairs of alcohols in their reactions with arylcarbenes indicate that the O—H insertion selectivity is drastically increased in the presence of 1,4-dioxane with respect to that encountered in the same reactions without solvent. Similar competition between alcohol and olefin again shows that the O—H insertion/addition selectivities of arylcarbenes are also considerably enhanced by 1,4-dioxane.

This experimental behaviour has been interpreted by the reversible formation of a complex between the carbene and the solvent. Given that most singlet carbenes are known to react as electrophiles, it seems quite reasonable to assume that they can form complexes with electron-pair donor solvents through the interaction between the vacant *p* orbital of the carbene and the lone pair electrons of the solvent. This complexation is expected to reduce the electrophilicity of the carbene, its selectivity being consequently increased according to the Reactivity–Selectivity Principle. If the interaction between the carbene and the solvent is too strong the formation of the complex would not be reversible and the reaction would give rise to solvent-incorporated products. As a matter of fact, this is presumably what occurs in the case of ethers more basic than 1,4-dioxane, e.g. THF.

A related case to this change of reactivity is presented by chlorophenylcarbene. This is a typically electrophilic carbene that should exhibit preferential reactivity versus nucleophilic olefins (5–7). However, chlorophenylcarbene reacts with electrophilic olefins, such as vinyl ethers and α,β-unsaturated carbonyl compounds, to form cyclopropane products in high yields (8). Here the interpretation again involves the formation of a complex between the carbene and the corresponding olefin, in such a way that the carbene is displaced to a more nucleophilic zone of the spectrum of carbene philicity.

To our knowledge, until now no theoretical works have been devoted to the study of the modification of singlet carbene reactivities by electron-pair donor solvents. The object of this study is to reach a more thorough understanding of the experimental facts. To this aim, we have studied the well known methylene addition reaction to ethylene, taking one water molecule to represent the donor solvent. It is true that methylene and water actually react to give methanol (9–11) but it has recently been found (12) that the complex methylene–water exists as a local energy minimum. In any case water is a good theoretical model to simulate an ether which is not excessively basic.

Methodology

Ab initio SCF calculations were done with the GAUSSIAN 80 and 82 series of programs (13) using the double ζ quality 3-21G basis set (14). Some points have been recalculated with the 6-31G** basis set (15) where the electron correlation has been introduced using the Møller–Plesset perturbation theory up to third order, MP3 (16). Geometry optimization and location of stationary points were carried out with the Schlegel gradient minimization algorithm (17). Analytical second derivatives of energy with respect to the cartesian coordinates (18) were used to characterize the nature of the stationary points, since, as it is well known, the force constant matrix presents no negative eigenvalues for an equilibrium structure and only one negative eigenvalue for a transition state.

Results and discussion

First, we have studied the structure of the complex between singlet methylene and water. In fact, the interaction between these two molecules can lead to two different complexes, depending on whether water acts as an electrophile (one hydrogen atom interacts with the HOMO of methylene) or as

Printed in Canada / Imprimé au Canada

Can. J. Chem. Downloaded from www.nrcresearchpress.com by 213.222.148.141 on 09/07/12
For personal use only.

TABLE 1. Relative energies[a] for the located stationary points

	Relative energy at stationary point		
	3-21G//3-21G[b]	6-31G**//3-21G[b]	MP3/3-21G//3-21G[b]
Complex + ethylene	−20.3	−6.6	−26.6
Intermediate	−21.1	−7.5	−28.1
Transition state	−20.0	−8.5	−28.1
Cyclopropane + water	−93.1	−61.0	−105.4

[a]In kcal mol^{-1} referred to the isolated methylene + ethylene + water molecules.
[b]"//" stands for "at the geometry of".

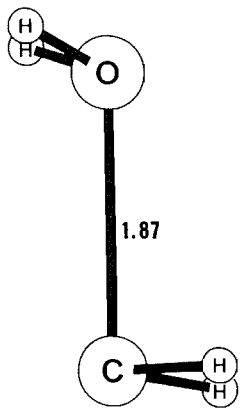

FIG. 1. Equilibrium structure of the water–methylene complex (distances in Å).

a nucleophile (the oxygen atom interacts with the LUMO of methylene). We have only considered the second case, in which the interaction is more favourable (9, 10) and might be responsible for the experimental results mentioned in the introduction.

Figure 1 presents the equilibrium structure of the complex obtained by complete geometry optimization. It belongs to the C_s point group, with its plane of symmetry bisecting ∠HOH and ∠HCH. This structure is similar to that found by Pople *et al.* (9, 10) using another basis set. It is worthy to note the existence of an important charge transfer (0.188 au) from water to methylene, in spite of the great value of the C—O distance between both molecules. This important charge transfer indicates the great electrophilicity of singlet methylene, which has a vacant *p* orbital and is therefore an electron-deficient molecule. As a direct consequence, the interaction between water and methylene is rather strong and the complex formed is well stabilized (20.3 kcal mol^{-1}) with respect to the isolated constituents.

It is interesting to discuss how this interaction energy changes when larger basis sets and correlation corrections are included. To this aim we have recalculated the stabilization energy of the methylene–water complex at several levels of calculation. The results are shown in the first row of Table 1. One can observe that the depth of the well decreases with increasing size in the basis set. This was to be expected since the basis set superposition error exaggerates the stabilization of the complex when small basis sets are used. On the other hand, the introduction of electron correlation increases the depth of the well. So, both effects tend to compensate each other as already found by Pople *et al.* (9). These authors obtained a binding energy of 14.7 kcal mol^{-1} with the MP4/6-31G**//MP2/6-31G* level of calculation, their highest.

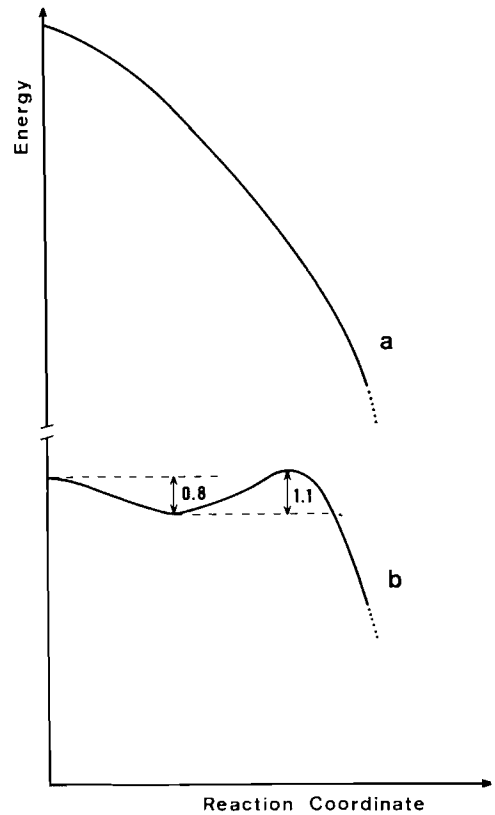

FIG. 2. Schematic representation of the energy profiles in kcal mol^{-1} for the non-solvated (*a*) and solvated (*b*) methylene addition to ethylene.

To study the solvent effect on the reactivity of singlet methylene, we have studied its addition and the addition of the CH_2–H_2O complex to ethylene. For the reaction with non-solvated methylene we have obtained the reaction path using the reaction coordinate method; as independent variable we have chosen the distance between the midpoint of the C—C bond of ethylene and the C atom of methylene, all the remaining geometrical parameters being optimized for each value of the independent variable. In the case of reaction with the complex methylene–water, the stationary points of the potential energy hypersurface have been directly located. Figure 2 schematically presents the energy profiles so obtained.

One can observe that the reaction of ethylene with isolated singlet methylene takes place with no energy barrier, in good agreement with *ab initio* calculations previously done by other authors (19, 20). Thus, the energy monotonically decreases until cyclopropane is reached, the reaction being highly exothermic (93.1 kcal mol^{-1}). On the other hand, the introduction

Can. J. Chem. Downloaded from www.nrcresearchpress.com by 213.222.148.141 on 09/07/12
For personal use only.

TABLE 2. Net charges[a] over water, methylene, and ethylene for the located stationary points

	Complex + ethylene	Intermediate	Transition state	Cyclopropane + water
Water	0.1875	0.1714	0.0934	0.0
Methylene	−0.1875	−0.1764	−0.1214	0.0
Ethylene	0.0	0.0050	0.0280	0.0

[a]In atomic units.

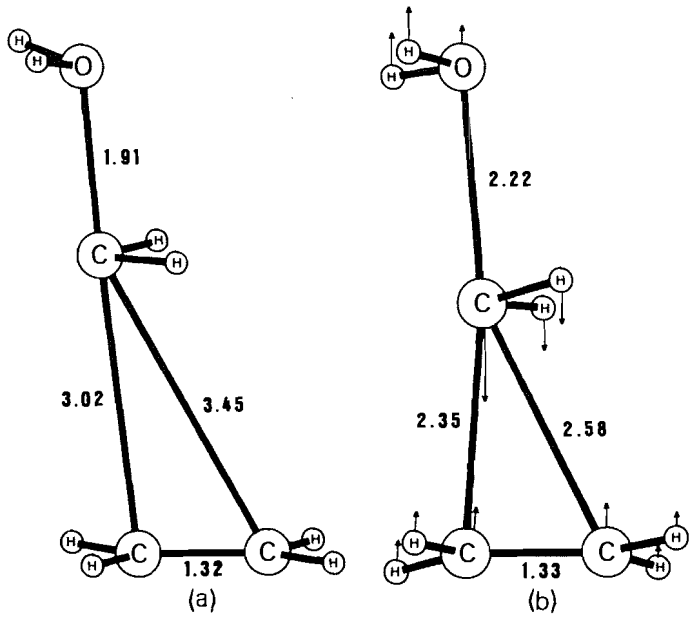

FIG. 3. Geometrical structure of the intermediate (*a*) and of the transition state (*b*) for the addition of the water–methylene complex to ethylene (distances in Å).

of one water molecule solvating methylene leads to a drastically different energy profile, since now there exists an intermediate situated in a well of very shallow depth (0.8 kcal mol^{-1}), followed by a small energy barrier of 1.1 kcal mol^{-1} with respect to the intermediate. Furthermore, the presence of one water molecule notably reduces the exothermicity of the process, the energy of the reaction now being −72.8 kcal mol^{-1}.

As we have already done with the binding energy of the methylene–water complex, let us now discuss the effect of the size of the basis set and of the correlation energy in the energy profiles in Fig. 2. The results obtained are in the three last rows in Table 1. The shape of the non-solvated energy profile (Fig. 2*a*) is independent of the level of calculation, but, as can be observed in the last row in Table 1, its exothermicity decreases with larger basis sets and increases when electron correlation is introduced. The effect on the solvated energy profile (Fig. 2*b*) is more complicated, since the second and third rows of data in Table 1 show that the intermediate and the subsequent energy barrier disappear at the 6-31G**//3-21G and MP3/3-21G//3-21G levels of calculation. However, these calculations are subjected to some important limitations. First, there is the assumption of unchanged 3-21G geometries. Secondly, this basis set does not give significant correlation corrections. These limitations prevent us from knowing if an intermediate does exist. However, in all cases the slope of the solvated energy profile is drastically reduced. Thus it is important for us to note that the solvent does noticeably change the energy profile of the addition in the sense of reducing the reactivity of singlet methylene.

To understand this change of energy profile it is interesting to analyze the variation of the most important geometrical parameters along the reaction path. Figure 3 presents the structures corresponding to the intermediate (*a*) and to the transition state (*b*) of the reaction with solvated methylene. In the transition state, the components over each atom of the transition vector are also drawn. The final product structure is not presented, since it corresponds to cyclopropane and water situated very far apart as expected, given that cyclopropane has no vacant *p* orbitals and has, therefore, a hydrophobic behaviour. One can observe that solvated methylene and ethylene approach each other in parallel planes, in such a way that the predominant frontier orbital interaction will be between the HOMO of ethylene and the LUMO of the complex methylene–water. In other words, this complex, as isolated methylene, is acting as an electrophile.

One can also observe that the approach between the two reactants is accompanied by a progressive desolvation of methylene, as indicated by the evolution of bond distance C—O. In the intermediate, the interaction between methylene and ethylene is still quite weak and the desolvation has scarcely begun. On the contrary, it is already noticeable in the transition state. Desolvation is clearly in progress at this point of the energy profile as indicated by components of the transition vector. Methylene is moving away from water as it approaches ethylene. Furthermore, the greater component of the transition vector over the carbon atom of methylene with respect to those on the hydrogen atoms shows that methylene has already begun to rotate in order to adopt the position it has in cyclopropane.

Let us now analyze the progress of charge transfer along the reaction path. Table 2 presents the net charges over the three groups (water, methylene, and ethylene). One can observe that charge transfer from water to methylene decreases monotonically from reactants to products, the decrease is intimately related to the increase in desolvation. On the other hand, the charge transfer from ethylene to methylene increases initially, and then decreases to zero in cyclopropane where the three CH_2 groups are equivalent. It is interesting to mention that the corresponding values of the charge transfer from ethylene to methylene in the absence of water are notably greater than those presented in Table 2 for the same value of the reaction coordinate. For instance, charge transfers of 0.041 and 0.095 au have been obtained in the absence of water for the values of the reaction coordinate corresponding to the intermediate and the transition state of the hydrated reaction. This decrease in charge transfer in the presence of solvent clearly shows that the electrophilicity of the complex methylene–water is much smaller than that of free methylene.

A deeper insight into the mechanism of the process can be achieved by inspecting the topology of the electronic charge density at the complex, intermediate, and transition state. Figure 4 presents the isodensity contour plots of these three

Can. J. Chem. Downloaded from www.nrcresearchpress.com by 213.222.148.141 on 09/07/12
For personal use only.

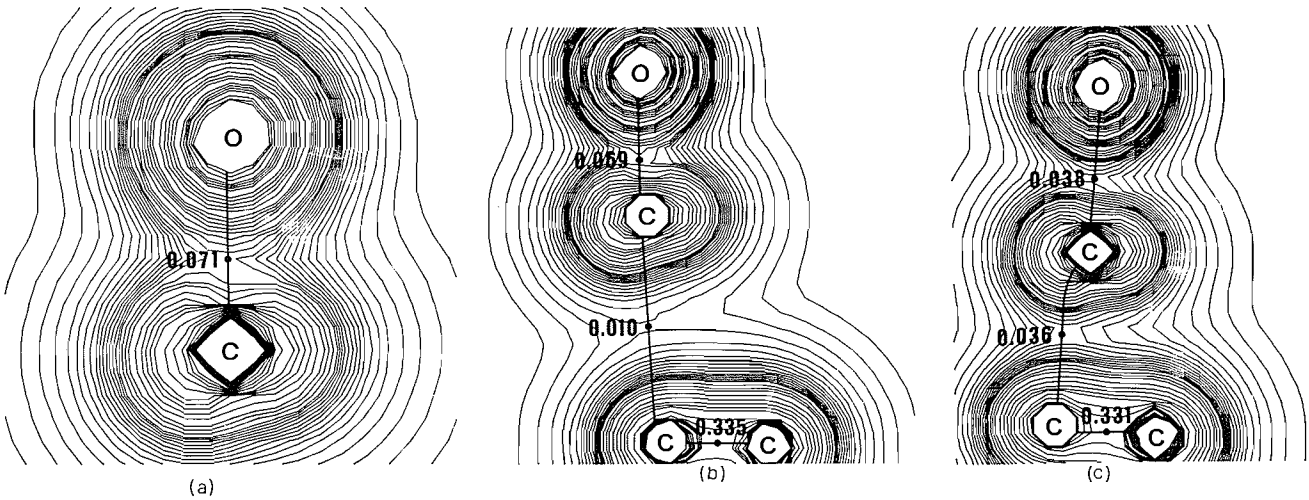

FIG. 4. Isodensity contour plots in the plane formed by the heavy atoms in the water–methylene complex (*a*), the intermediate (*b*), and the transition state (*c*). Numbers indicate electron density in the bond critical points (.).

structures in the plane which contains the heavy atoms of the system. Bond critical points and bond paths linking the atoms on the planes of the figure are also shown. According to the Bader terminology (21), bond paths are a unique pair of gradient paths which originate at each bond critical point, i.e. at the saddle point situated between two linked atoms. Two interesting facts can be observed in Fig. 4. First, the charge density at the critical point linking the carbon atom in methylene to the oxygen atom in water decreases from the complex to the transition state, again showing the desolvation of methylene. Thus, desolvation is small in the intermediate, but already rather important in the transition state. Secondly, the carbon atom in methylene is initially bonded to only one of the carbon atoms in ethylene. A similar asynchronous approach had previously been found (19, 20) for the addition to ethylene in free methylene.

The change in the energy profile when methylene is solvated by one water molecule can be now easily understood. As one can observe in Fig. 2, the addition of free methylene to ethylene is accompanied by a strong energy decrease from the beginning of the process. On the other hand, the introduction of one water molecule stabilizes all points in the energy profile, and this stabilization decreases as desolvation increases according to the sequence reactant > intermediate > transition state > product. As a direct consequence, the initial part of the energy profile is rather flat and the exothermicity of the process clearly decreases. The presence or absence of an intermediate depends on a subtle balance between the slope of the energy profile in the absence of water and the decrease in stabilization on desolvation.

The energy profile of the addition of $CH_2.H_2O$ to ethylene can be related to those found in several electron, proton, or group transfer processes. In these cases, the energy profile frequently presents a double-well shape, and the process occurs via a three-step mechanism: formation of a first intermediate without energy barrier, subsequent isomerization through a transition state to a second intermediate where the transfer has already been produced, and final dissociation to the reaction product. In our case the second intermediate does not appear, since it would correspond to the hydrophobic interaction between cyclopropane and water. The first intermediate only appears at the 3-21G//3-21G level of calculation, although we observe a drastic reduction in slope of the energy profile in this zone at all the levels of calculation. In any case, the reaction we studied can be interpreted as the transfer of an electrophile (methylene) from a nucleophile (water) to another nucleophile (ethylene).

Conclusions

Using water as a model of lone-pair donor solvent, we have shown that the addition of methylene takes place via the formation of a reversible complex between water and methylene. The electrophilicity of methylene is thus noticeably reduced, leading to an important decrease in the exothermicity of the process, resulting in an energy profile very similar to those in group transfer reactions. In conclusion, this work enables one to reach a theoretical interpretation of the experimental behavior of electrophilic carbenes in the presence of electron-pair donor solvents.

1. R. A. MOSS and M. JONES JR. Reactives intermediates. Wiley, New York. 1978.
2. W. GRIMME, J. REISDORFF, W. JÜNEMANN, and E. VOGEL. J. Am. Chem. Soc. **92**, 6335 (1970).
3. R. A. MOSS and C. B. MALLON. J. Org. Chem. **40**, 1368 (1975).
4. H. TOMIOKA, Y. OZAKI, and Y. IZAWA. Tetrahedron, **41**, 4987 (1985).
5. R. A. MOSS. Acc. Chem. Res. **13**, 58 (1980).
6. N. J. TURRO, J. A. BUTCHER JR., R. A. MOSS, W. GUO, R. C. MUNJAL, and M. FEDORYNSKI. J. Am. Chem. Soc. **102**, 7576 (1980).
7. R. A. MOSS, J. R. WHITTLE, and P. FREIDENREICH. J. Org. Chem. **34**, 2220 (1969).
8. M. P. DOYLE, J. W. TERPSTRA, and C. H. WINTER. Tetrahedron Lett. **25**, 901 (1984).
9. L. B. HARDING, H. B. SCHLEGEL, R. KRISHNAN, and J. A. POPLE. J. Phys. Chem. **84**, 3394 (1980).
10. J. A. POPLE, K. RAGHAVACHARI, M. J. FRISCH, J. S. BINKLEY, and P. VON R. SCHLEYER. J. Am. Chem. Soc. **105**, 6389 (1983).
11. W. KIRMSE. Carbene chemistry. Academic Press, New York. 1970.
12. C. WESDEMIOTIS, R. FENG, P. O. DANIS, R. WILLIAMS, and F. W. MCLAFFERTY. J. Am. Chem. Soc. **108**, 5847 (1986).
13. J. S. BINKLEY, R. A. WHITESIDE, R. KRISHNAN, R. SEEGER, D. J. DEFREES, H. B. SCHLEGEL, S. TOPIOL, L. R. KAHN, and

Can. J. Chem. Downloaded from www.nrcresearchpress.com by 213.222.148.141 on 09/07/12
For personal use only.

J. A. POPLE. QCPE, **13**, 406 (1980); J. S. BINKLEY, M. J. FRISCH, D. J. DEFREES, R. KRISHNAN, R. A. WHITESIDE, H. B. SCHLEGEL, E. M. FLUDER, and J. A. POPLE. GAUSSIAN 82, Carnegie Mellon University, Pittsburgh, PA.
14. J. S. BINKLEY, J. A. POPLE, and W. J. HEHRE. J. Am. Chem. Soc. **102**, 939 (1980).
15. W. J. HEHRE, R. DITCHFIELD, and J. A. POPLE. J. Chem. Phys. **56**, 2257 (1972).
16. J. A. POPLE, R. KRISHNAN, H. B. SCHLEGEL, and J. S. BINKLEY. Int. J. Quantum Chem. **14**, 545 (1978).
17. H. B. SCHLEGEL. J. Comput. Chem. **3**, 214 (1982).
18. J. A. POPLE, R. KRISHNAN, H. B. SCHLEGEL, and J. S. BINKLEY. Int. J. Quantum Chem. **S13**, 225 (1979).
19. B. ZURAWSKI and W. KUTZELNIGG. J. Am. Chem. Soc. **100**, 2654 (1978).
20. N. G. RONDAN, K. N. HOUK, and R. A. MOSS. J. Am. Chem. Soc. **102**, 1770 (1980).
21. R. F. W. BADER, Y. TAL, S. G. ANDERSON, and T. T. NGUYEN-DANG. Israel J. Chem. **19**, 8 (1980) and references cited therein.

Can. J. Chem. Downloaded from www.nrcresearchpress.com by 213.222.148.141 on 09/07/12
For personal use only.

Surface tension and density of the molten $LaCl_3$–NaCl binary system

G. Liu, J. M. Toguri, and N. M. Stubina

Department of Metallurgy and Materials Science, University of Toronto, 184 College Street, Toronto, Ont., Canada M5S 1A4

Received February 19, 1987[1]

G. Liu, J. M. Toguri, and N. M. Stubina. Can. J. Chem. **65**, 2779 (1987).

The surface tension and density of the $LaCl_3$–NaCl system were determined as a function of temperature by the maximum bubble pressure technique. The surface tension and density were found to vary linearly with temperature ($1123 < T < 1248$ K). At constant temperature, the surface tensions of $LaCl_3$–NaCl melts showed a small negative deviation from Guggenheim's Equation.

G. Liu, J. M. Toguri et N. M. Stubina. Can. J. Chem. **65**, 2779 (1987).

Faisant appel à la technique de la pression maximale de la bulle, on a déterminé la tension superficielle et la densité du système LaCl–NaCl en fonction de la température. On a trouvé que la tension superficielle et la densité varient d'une façon linéaire avec la température ($1123 < T < 1248$ K). A température constante, les tensions superficielles de mélanges fondus de $LaCl_3$–NaCl présentent une légère déviation par rapport à l'équation de Guggenheim.

[Traduit par la revue]

Can. J. Chem. Downloaded from www.nrcresearchpress.com by 213.222.148.141 on 09/07/12
For personal use only.

Introduction

One method of producing lanthanum metal is by fused-salt electrolysis of a chloride melt containing lanthanum. A possible electrolyte for this process would be a $LaCl_3$–NaCl mixture. Kim and Ejima (1) and Cho and Kuroda (2) have measured the density of $LaCl_3$–NaCl binary melts. Foerthmann *et al.* (3) measured the electrical conductivity of this system. However, surface tension data for $LaCl_3$–NaCl melts are not available in the literature.

In the present study, surface tensions and densities of binary $LaCl_3$–NaCl melts were measured.

Experimental

The experimental apparatus and procedure for the present study have been described in detail previously (4) and thus only a brief description is given here. The well established maximum bubble pressure technique was selected for the determination of surface tension and density of the $LaCl_3$–NaCl system. With this technique, surface tension and density of the salt can be measured simultaneously. Briefly, it involves the slow formation of a gas bubble at the tip of a capillary immersed in the molten salt. Schrödinger (5) developed the following equation which relates the surface tension to the maximum bubble pressure:

$$[1] \quad \gamma = \frac{rP_\gamma}{2}\left[1 - (2/3)\left(\frac{r\rho g}{P_\gamma}\right) - (1/6)\left(\frac{r\rho g}{P_\gamma}\right)^2\right]$$

where γ is the surface tension, r is the radius of the capillary, P_γ is the maximum pressure difference inside and outside the bubble at the level of the end of the tip, ρ is the density difference between the liquid salt and the gas, and g is the acceleration due to gravity.

Apparatus

A schematic diagram of the experimental apparatus is shown in Fig. 1. The furnace had a uniform temperature (±2.5 K) region of 5.0 cm. The salt mixture was contained in a quartz crucible under an argon atmosphere. The crucible had an inner diameter of 20 mm and a height of 60 mm. The quartz capillary was 50 mm long, with an outer diameter of ~2.2 mm, and an inner diameter of ~1.08 mm.

Procedure

The sodium chloride used in this work was obtained from Baker Chemical Co. ("Baker Analysed" reagent grade). Lanthanum chloride was obtained from Aldrich Chemical Co. Inc. These materials were predried in a vacuum oven at 400 K for 3 days and then analyzed by DTA. The argon (99.999%) used to form the bubble was passed through a copper getter furnace and through two drying columns (drierite and phosphoric anhydride) in order to remove any traces of oxygen or water.

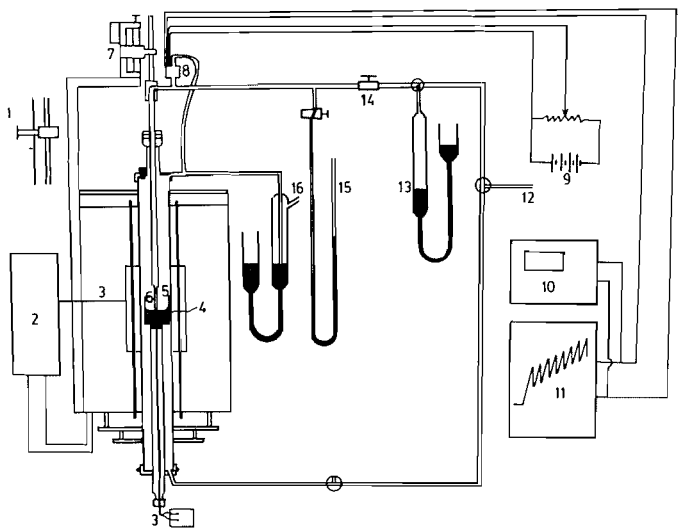

FIG. 1. Experimental apparatus: (*1*) cathetometer; (*2*) temperature controller; (*3*) thermocouple; (*4*) sample; (*5*) graphite crucible; (*6*) capillary; (*7*) capillary drive; (*8*) pressure transducer; (*9*) dry cell; (*10*) digital multimeter; (*11*) recorder; (*12*) purified argon inlet; (*13*) gas reservoir; (*14*) needle valve; (*15*) manometer; (*16*) gas outlet.

The quartz crucible containing the required salt mixture was positioned in the furnace and heated to the desired temperature under a flowing argon atmosphere. Excess pressure was applied to the capillary while it was lowered towards the melt surface. The capillary was then lowered very slowly until a sudden pressure jump was registered by the pressure transducer, indicating that the capillary had touched the melt surface and the surface position was recorded.

The bubbling rate was adjusted to about 1 bubble/min which was in the region where the transducer output was independent of the gas flowrate. The pressure was increased linearly with immersion depth until a bubble was released at the capillary tip followed by a sudden decrease in pressure. The capillary immersion depth was changed several times while the maximum pressure was recorded.

The density of the molten salt mixture was calculated from the slope of the maximum pressure versus immersion depth data, while the surface tension was evaluated from the obtained maximum pressure for zero immersion using Schrödinger's equation.

The temperature effect on surface tension and density was deter-

[1]Revision received August 11, 1987.

TABLE 1. Surface tension values for the $LaCl_3$–NaCl system[a]

Composition (mol%)		Surface tension at temperature (K) =						$\gamma = A + BT$		
NaCl	$LaCl_3$	1123	1148	1173	1198	1223	1248	A	$B \times 10^2$	Standard error of estimation
0	100		119.4	117.2	114.4	111.4	107.7	253.9	−11.68	0.50
15	85	119.6	116.3	112.6	109.0	107.0	104.0	259.8	−12.51	0.56
30	70		112.8	110.1	108.2	105.1	102.6	229.5	−10.16	0.30
45	55		111.6	109.2	106.5	104.8	102.5	215.2	−9.04	0.29
60	40		110.2	108.0	106.0	104.1	102.3	200.5	−7.88	0.11
75	25	111.2	109.1	107.4	105.3	103.2	101.4	199.5	−7.86	0.10
87.5	12.5		109.0	107.1	105.3	103.7	101.2	196.3	−7.60	0.24
100	0	110.2	108.5	106.6	104.9	102.8	101.6	189.5	−7.06	0.22

[a]Surface tension values are given in mN/m.

TABLE 2. Density values for the $LaCl_3$–NaCl system[a]

Composition (mol%)		Density value at temperature (K) =						$\rho = C + DT$		
NaCl	$LaCl_3$	1123	1148	1173	1198	1223	1248	C	$D \times 10^4$	Standard error of estimation
0	100		3.16	3.14	3.13	3.11	3.09	3.94	−6.80	3.2
15	85	3.03	3.01	2.99	2.99	2.98	2.96	3.75	−6.40	3.5
30	70		2.85	2.84	2.83	2.81	2.80	3.45	−5.20	2.9
45	55		2.63	2.62	2.61	2.59	2.58	3.23	−5.20	3.1
60	40		2.42	2.41	2.39	2.38	2.36	3.11	−6.00	3.3
75	25	2.18	2.16	2.15	2.13	2.11	2.09	2.98	−7.08	3.2
87.5	12.5		1.85	1.84	1.82	1.80	1.78	2.68	−7.20	3.6
100	0	1.54	1.52	1.50	1.49	1.48	1.46	2.22	−6.06	4.2

[a]Density values are given in g/mL.

Can. J. Chem. Downloaded from www.nrcresearchpress.com by 213.222.148.141 on 09/07/12
For personal use only.

mined during both heating and cooling cycles. Since the salts wetted the capillary tip, the inner radius of the capillary tip was used for surface tension calculation. All measurements were corrected for thermal expansion of the capillary orifice.

Results and discussion

Surface tension and density data determined in the present study for NaCl, $LaCl_3$, and $LaCl_3$–NaCl mixtures are listed in Tables 1 and 2, respectively.

The dependence of surface tension on temperature, over a range from 1120 to 1250 K, for pure $LaCl_3$ and pure NaCl is shown in Fig. 2. In both cases, a linear relationship was observed. Results obtained by Smirnov and Stepanov (6) for pure $LaCl_3$ and by Sokolova and Voskresenskaya (7) for NaCl are included in the diagram. The results from this study are in excellent agreement with those from other investigators.

Density curves for the two pure salts are shown in Fig. 3. For pure NaCl, the data obtained by Van Artsdalen and Yaffe (8) are included as a comparison. For $LaCl_3$, data recommended by Janz *et al.* (9) are systematically higher than the results obtained in this study, as shown in Fig. 3. While the reasons for the consistently lower values for $LaCl_3$ are not clear, the results are in accord if an overall accuracy limit of $\sim \pm 1\%$ is assumed.

In Fig. 4, the surface tension measurements for various $LaCl_3$–NaCl mixtures are presented. The surface tension of each melt decreases with increasing temperature in the range investigated. The curves for 12.5 and 25.0 mol% $LaCl_3$ are almost superimposed.

The corresponding density values for these melts are shown in Fig. 5. Included in Fig. 5 are density results obtained by Cho and Kuroda (2). The results from this study are in excellent agreement with their findings. A decrease in density with an increase in temperature was observed. Linear relationships of the form:

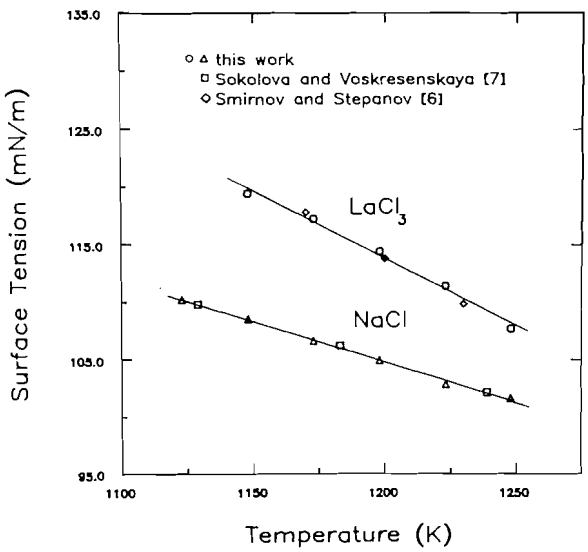

FIG. 2. Surface tensions of pure $LaCl_3$ and NaCl.

[2] $\gamma = A + BT(\mathrm{K})$ (mN/m)

and

[3] $\rho = C + DT(\mathrm{K})$ (g/mL)

Can. J. Chem. Downloaded from www.nrcresearchpress.com by 213.222.148.141 on 09/07/12
For personal use only.

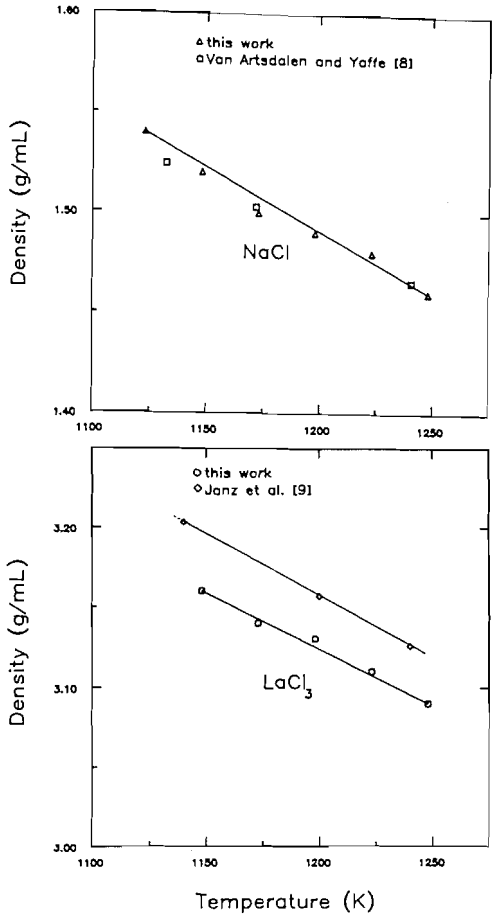

FIG. 3. Densities of pure $LaCl_3$ and NaCl.

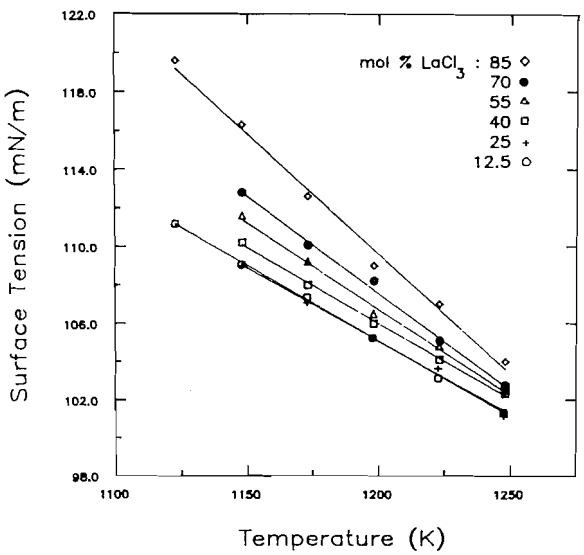

FIG. 4. Effect of temperature on the surface tension of $LaCl_3$–NaCl melts.

were obtained. The linear regression coefficients (A, B, C, and D) are summarized in Tables 1 and 2. The standard error of estimation is also included.

A surface tension isotherm for the $LaCl_3$–NaCl system at 1148 K is shown in Fig. 6. There is only a small negative departure from Guggenheim's equation for ideal solutions (10). The maximum deviation between the measured results and Guggenheim's equation was less than 2%. This indicates that

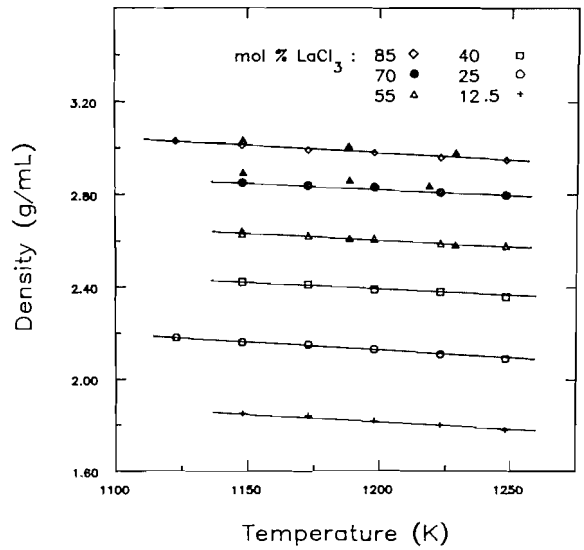

FIG. 5. Effect of temperature on the density of $LaCl_3$–NaCl melts. Data by Cho and Kuroda (2) are designated by ▲.

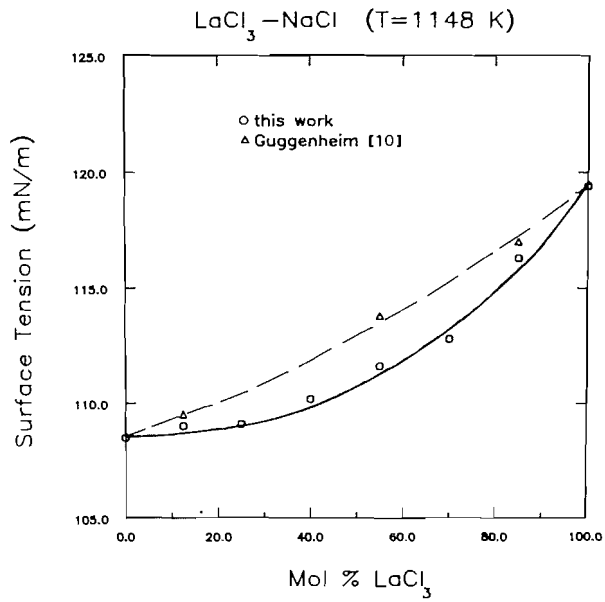

FIG. 6. Surface tension isotherm for the $LaCl_3$–NaCl system at 1148 K.

this molten binary system can be regarded as a simple mixture of components that do not form complexes. This result could also be explained by examining the nature of Na and La ions. The radii of Na and La are similar, 0.97 and 1.016 Å, respectively (11). Moreover, the difference in electronegativity between Na and La is not very large.

Molar volumes (V) for the molten $LaCl_3$–NaCl system were calculated from the density data using the following equation:

$$[4] \quad V = \frac{\sum^{i} X_i M_i}{\rho}$$

where M_i is the molecular weight of component i and X_i is the mole fraction of component i. The molar volumes obtained in this study, as well as the values obtained from a simple additive relationship, are listed in Table 3 for a temperature of 1248 K. The deviations from ideality are small. This confirms the result that the binary $LaCl_3$–NaCl system can be regarded as a simple mixture that does not form complexes.

TABLE 3. Molar volume and deviation from additivity at 1248 K

Parameter	Value when mol% $LaCl_3$ =					
	85	70	55	40	25	12.5
Molar volume (g/mL)	73.6	67.6	62.5	56.4	50.3	45.9
Values of additivity (g/mL)	73.5	67.6	61.7	55.8	49.9	44.9
Deviation (g/mL)	0.1	0.0	0.8	0.6	0.4	1.0

Acknowledgement

Financial support from the Natural Sciences and Engineering Research Council of Canada (NSERC) is gratefully acknowledged.

1. K. H. KIM and T. EJIMA. Taehan Kumsok Hakhoechi. **22**, 91 (1984).
2. K. CHO and T. KURODA. Denki Kagaku, **40**, 45 (1972).
3. R. FOERTHMANN, G. VOGEL, and A. SCHNEIDER. Z. Anorg. Allg. Chem. **367**, 19 (1969).
4. T. FUJISAWA, T. UTIGARD, and J. M. TOGURI. Can. J. Chem. **63**, 1132 (1985).
5. E. SCHRÖDINGER. Ann. Physik. **46**, 488 (1917).
6. M. V. SMIRNOV and V. P. STEPANOV. Electrochemistry of molten and solid electrolytes. Vol. 9. 1972. p. 5.
7. I. D. SOKOLOVA and N. K. VOSKRESENSKAYA. Russ. J. Phys. Chem. **36**, 502 (1962).
8. E. R. VAN ARTSDALEN and I. S. YAFFE. J. Phys. Chem. **59**, 118 (1955).
9. (*a*) Chemistry Division Semiannual Progress Report, Oak Ridge National Laboratory, ORNL-2159 (1956); (*b*) G. J. JANZ, F. W. DAMPIER, G. R. LAKSHMINARAYANAN, P. K. LORENZ, and R. P. T. TOMKINS. Molten salts. Vol. 1. Electrical conductance, density, and viscosity data. U.S. Department of Commerce National Bureau of Standards, Report NSRDS-NBS 15. 1968. p. 52.
10. E. A. GUGGENHEIM. Mixtures. Oxford University Press, London. 1952. p. 176.
11. R. C. WEAST (*Editor*). Handbook of chemistry and physics. CRC Press, Cleveland. 1976–7. p. F-213.

Can. J. Chem. Downloaded from www.nrcresearchpress.com by 213.222.148.141 on 09/07/12
For personal use only.

Réactivité du trioxyde de chlore avec des chlorures, des nitrates, des carbonates et des perchlorates hydratés. Synthèse et analyse structurale de complexes de Cd(II) et Hg(II) : $Cd(ClO_4)_2$, $Hg(ClO_4)_2$, $ClO_2Cd(ClO_4)_3$, $NO_2Cd(ClO_4)_3$, $(NO_2)_2Hg(ClO_4)_4$ et $HgClClO_4$

MOHIEDDINE FOURATI ET MONCEF CHAABOUNI

École nationale d'ingénieurs de Sfax, Laboratoire de chimie physique et inorganique, B.P. W. 3038 Sfax, Tunisie

ET

JEAN-LOUIS PASCAL ET JACQUELINE POTIER[1]

Université des sciences et techniques du Languedoc, Laboratoire des agrégats moléculaires et matériaux inorganiques (Laboratoire des acides minéraux), Unité associée 79, Centre national de la recherche scientifique, 2, place Eugène Bataillon, 34060 Montpellier CEDEX, France

Reçu le 26 mai 1987

MOHIEDDINE FOURATI, MONCEF CHAABOUNI, JEAN-LOUIS PASCAL et JACQUELINE POTIER. Can. J. Chem. **65**, 2783 (1987).

Afin d'optimiser la préparation de complexes perchlorato de Cd(II) et Hg(II), on a testé successivement les réactions de Cl_2O_6 avec $CdCl_2$, $CdCO_3$, $Cd(NO_3)_2 \cdot nH_2O$, $HgCl_2$, $Hg(ClO_4)_2 \cdot 6H_2O$ et $Hg(NO_3)_2 \cdot H_2O$. Les complexes $Cd(ClO_4)_2$, $ClO_2Cd(ClO_4)_3$, $NO_2Cd(ClO_4)_3$, $HgClClO_4$, $Hg(ClO_4)_2$ et $(NO_2)_2Hg(ClO_4)_4$ ont été caractérisés. Parmi ces complexes seul $HgClClO_4$ est ionique avec $HgCl^+$ polymère en chaîne; les autres sont des complexes perchlorato. $Cd(ClO_4)_2$ s'apparente aux complexes à structure en couches $M(ClO_4)_2$ (M = Co, Ni, Zn), dans lesquels le groupe ClO_4 est tridenté en pont. $Hg(ClO_4)_2$ se rapproche de $HgCl_2$ ou de $Hg(SR)_2$ (SR : thiocarbamate) avec des groupes ClO_4 monodentés en interaction avec les molécules voisines. Dans les sels $ClO_2Cd(ClO_4)_3$, $NO_2Cd(ClO_4)_3$ et $(NO_2)_2Hg(ClO_4)_4$, les anions sont des polymères; leurs structures sont analogues respectivement à celles de $ACuCl_3$, $NO_2Co(ClO_4)_3$ et $(NO_2)_2Cu(ClO_4)_4$.

MOHIEDDINE FOURATI, MONCEF CHAABOUNI, JEAN-LOUIS PASCAL, and JACQUELINE POTIER. Can. J. Chem. **65**, 2783 (1987).

To improve the synthesis of perchlorato complexes of Cd(II) and Hg(II), reactions of Cl_2O_6 with $CdCl_2$, $CdCO_3$, $Cd(NO_3)_2 \cdot nH_2O$, $HgCl_2$, $Hg(ClO_4)_2 \cdot 6H_2O$, and $Hg(NO_3)_2 \cdot H_2O$ were tried. The complexes $Cd(ClO_4)_2$, $ClO_2Cd(ClO_4)_3$, $NO_2Cd(ClO_4)_3$, $HgClClO_4$, $Hg(ClO_4)_2$, and $(NO_2)_2Hg(ClO_4)_4$ were characterized. Among these complexes only $HgClClO_4$ is ionic ($HgCl^+$ is a polymeric chain); the others are perchlorato complexes. $Cd(ClO_4)_2$ is related to the layered complexes $M(ClO_4)_2$ (M = Co, Ni, Zn) in which ClO_4 is a bridging tridentate. $Hg(ClO_4)_2$ is close to $HgCl_2$ or $Hg(SR)_2$ (SR: thiocarbamate); ClO_4 is a monodentate and it interacts with neighbouring molecules. In the salts $ClO_2Cd(ClO_4)_3$, $NO_2Cd(ClO_4)_3$, and $(NO_2)_2Hg(ClO_4)_4$ the anions have polymeric arrangements; their structures are analogous to those of $ACuCl_3$, $NO_2Co(ClO_4)_3$, and $(NO_2)_2Cu(ClO_4)_4$, respectively.

Introduction

La synthèse et l'analyse structurale de complexes perchlorato non solvatés par des molécules d'eau ou des bases organiques dans lesquels les groupements ClO_4 sont fortement liés à l'élément central ont connu un essor important ces dernières années (1). Ceci a été rendu possible par l'utilisation d'agents perchloratants performants : Cl_2O_6 (1*b*), $ClOClO_3$ (2), $HClO_4$–Cl_2O_7 (3), NO_2ClO_4 (4) et la mise en oeuvre de nombreuses méthodes d'analyses structurales : spectroscopie de vibration (1*b*, 5), diffraction des rayons X sur poudre et monocristaux (1*c*, 6), EXAFS (7), etc. Une mise au point récente résume ces travaux (1*a*).

En 1982, certains d'entre nous avaient présenté une préparation originale de $Zn(ClO_4)_2$ et de $ClO_2Zn(ClO_4)_3$ par action de Cl_2O_6 sur un métal (8), puis complété cette étude par la synthèse de sels de nitryle (9) et l'analyse par EXAFS de $Zn(ClO_4)_2$ (7*c*). Récemment, Rosolovskii et coll. (10) ont proposé de nouvelles synthèses : action de NO_2ClO_4 sur $ZnCl_2$, déshydratation par voie thermique de $Zn(ClO_4)_2 \cdot 6H_2O$. Leurs résultats sont analogues aux nôtres.

Il a paru logique d'étudier les complexes perchlorato des autres éléments de la colonne IIB (colonne 12 selon la nouvelle nomenclature de l'IUPAC et de l'ACS (11)) afin de pouvoir comparer les complexes de Cd et Hg à ceux de Zn et suivre leur condition de formation en fonction de l'acidité décroissante selon Pearson (12*a*) lorsqu'on passe de Zn à Hg.

Lorsqu'a débuté ce travail (15) seule l'enthalpie de formation de $Cd(ClO_4)_2$ avait été calculée (13) et sa densité mesurée (14). Récemment Nikitina et Rosolovskii (16) ont publié une étude portant notamment sur la synthèse de $Cd(ClO_4)_2$ par déshydratation thermique de $Cd(ClO_4)_2 \cdot 6H_2O$. Cette voie de synthèse est toutefois aléatoire puisqu'elle peut conduire soit à des composés légèrement hydratés soit à des oxohydroxo-perchlorates. Jusqu'à maintenant, l'étude des complexes perchlorato de Hg(II) non solvatés était plus réduite (17). Il était fait état de la formation possible de $Hg(ClO_4)_2$ par chauffage de $Hg(ClO_4)_2 nL$ (L : pyridine, dioxane, quinoline), avec les très graves dangers d'une telle voie de préparation (18).

Dans les lignes suivantes, nous présentons les synthèses et l'étude structurale par spectroscopie de vibration et diffraction des rayons X sur poudre de divers complexes perchlorato de Cd(II) et Hg(II).

Partie expérimentale

Attention : Le trioxyde de chlore et les perchlorates anhydres sont des composés très réactifs, particulièrement au contact des matières organiques et sous les chocs (19). Les réactions doivent être surveillées attentivement, les complexes sont extrêmement hygroscopiques et sont manipulés sur une ligne vide (1*b*) ou dans une boîte à gants contenant de l'azote ou de l'argon très pur et sec (<5 ppm en H_2O ou O_2). D'une façon générale, les expériences sont conduites dans une pièce faiblement éclairée et en l'absence de lumière fluorescente. Au cours de ce travail, un complexe résultant de la décomposition thermique de $(NO_2)_x Hg(ClO_4)_{2+x}$ a explosé spontanément et violemment dès qu'il a été exposé à la lumière du jour.

1. Auteur à qui adresser toute correspondance.

Printed in Canada / Imprimé au Canada

Can. J. Chem. Downloaded from www.nrcresearchpress.com by 213.222.148.141 on 09/07/12
For personal use only.

Can. J. Chem. Downloaded from www.nrcresearchpress.com by 213.222.148.141 on 09/07/12
For personal use only.

TABLEAU 1. Synthèse et analyse de complexes perchlorato de cadmium (II) et mercure (II)

Produits de base[a]		Cl_2O_6[a]	T[b]	t[c]	Produits obtenus	N,C[d]	Analyses (%)[e] M^{2+}	ClO_4^-	ClO_2^+	Cl^-	NO_2^+	m[f]
$CdCl_2$[g]	(0,776)	>20	10	25	$Cd(ClO_4)_2 + xCdCl_2$[h]	s, b	—	—	—	—	—	1,281 (1,317)
$CdCO_3$[i]	(0,3688)	4	5–7 −5[j]	3 24[j]	$ClO_2Cd(ClO_4)_3$	s, o	23,69 (23,51)	62,21 (62,39)	14,09 (14,10)	—	—	0,9754 (1,0229)
$Cd(NO_3)_2 \cdot 6{,}5H_2O$[k]	(1,9736)	12	10–15	20	$Cd(ClO_4)_2 + NO_2Cd(ClO_4)_3$[h]	s, bj	—	—	—	—	—	—
$Cd(NO_3)_2 \cdot 1{,}8H_2O$[l]	(0,8458)	20	10–15	50	$(NO_2)_2Cd(ClO_4)_4$[m,h] ε $Cd(NO_3)_2 \cdot xH_2O$	s, bj	—	—	—	—	—	1,9743 (1,8948)
$ClO_2Cd(ClO_4)_3$	—	—	40–50	1	$Cd(ClO_4)_2$	s, b	36,36 (36,11)	63,64 (63,89)	—	—	—	—
$(NO_2)_2Cd(ClO_4)_4$ + ε $Cd(NO_3)_2 \cdot xH_2O$	(1,1347)	—	95–100	12	$NO_2Cd(ClO_4)_3$ + ε $Cd(NO_3)_2 \cdot xH_2O$	s, b	25,96 (24,61)	64,36 (65,32)	—	—	—	0,9069 (0,8635)
$HgCl_2$[n]	(4,054)	15	10	6	$HgClClO_4 + \varepsilon\ HgCl_2$	s, b	60,69 (59,79)	27,71 (29,64)[o]		11,59 (10,57)		4,9337 (5,0131)
	(2,359)	18	10	20	$Hg(ClO_4)_2$	s, b	50,28 (50,18)	49,43 (49,81)				3,430 (3,457)
$HgClClO_4 + \varepsilon\ HgCl_2$	—	—	110	4	$HgClClO_4$	s, b	59,95 (59,79)	29,43 (29,64)		10,96 (10,57)		—
$Hg(ClO_4)_2 \cdot 6H_2O$[p]	(1,2882)	8	10–15	16	$Hg(ClO_4)_2$	s, b	49,8 (50,2)	50,5 (49,8)	—	—	—	—
$Hg(NO_3)_2 \cdot 1H_2O$[q]	(1,7456)	18	10–15	65	$(NO_2)_2Hg(ClO_4)_4$	s, jo	28,81 (29,04)	57,88 (57,63)	—	—	13,61 (13,33)	3,391 (3,518)

[a]Quantité en gramme (expérience type).
[b]Température de la réaction ou de la transformation (°C).
[c]Temps (heure).
[d]Nature et couleur à température ambiante; s : solide; b : blanc; o : orange; bj : blanc jaune; jo : jaune orange.
[e]Les valeurs théoriques sont données entre parenthèse; les méthodes de dosage sont spécifiées dans le texte et dans les références 22, 23, 24.
[f]Masse en grammes obtenue après réaction ou transformation; la masse attendue est donnée entre parenthèses.
[g]Prolabo Rectapur (sauf indication les produits sont utilisés sans purification préalable).
[h]Identifié par spectroscopie Raman.
[i]Merck très pur.
[j]Pompage dynamique de l'excès de Cl_2O_6.
[k]Merck pour analyse vendu comme contenant $4H_2O$ (!).
[l]Préparé à partir du produit (*k*) placé sous vide dynamique (10^{-2} Torr) durant 60 h à T ambiante.
[m]$(NO_2)_2Cd(ClO_4)_4$: $NO_2Cd(ClO_4)_3 + NO_2ClO_4$.
[n]Merck pour analyse.
[o]Sur la base de $HgClClO_4$.
[p]Ce produit est préparé par dissolution de HgO dans un minimum d'acide perchlorique commercial à 72%; la solution est ensuite concentrée à chaud puis évaporée lentement sous vide.
[q]Prolabo pur en plaque.
$\varepsilon < 0{,}05$.

Produits de base

L'agent perchloratant, le trioxyde de chlore est préparé et purifié selon les méthodes déjà décrites (20). La provenance, la pureté et l'utilisation des sels de base qui sont transformés en perchlorates sont reportées dans le tableau 1.

Méthodes d'analyses

Les appareils d'analyse infra-rouge (ir), Raman, rayons X (RX) sur poudre ainsi que les méthodes d'échantillonnage ont été présentés par ailleurs (1*b*, 21) de même que les protocoles de dosage des cations métalliques (22), de l'ion perchlorate (23) et du cation ClO_2^+ (ClO_3^- dans l'eau) (24). L'ion NO_2^+ (NO_3^- en solution) n'est pas dosé, sa quantité est déterminée par différence ou sa présence est décelée par spectroscopie de vibration.

D'une façon générale, moyennant le respect de précautions élémentaires (1*b*), ces analyses sont effectuées sans difficultés majeures. Notons cependant la nécessité de complexer au préalable Hg(II) par l'EDTA 0,1 ou 0,01 M avant d'analyser ClO_4^- par potentiométrie. Les résultats analytiques sont reportés dans le tableau 1.

Résultats et discussion

Synthèse des complexes perchlorato de cadmium (II) et de mercure (II)

Quel que soit le complexe perchlorato le principe de la synthèse est le même; nous n'y reviendrons pas (1*b*).

Notons cependant que devant les difficultés rencontrées, les synthèses sont recommencées plusieurs fois. Seuls les résultats d'expériences types sont donnés dans le tableau 1.

(a) Synthèse à partir de chlorures

La séquence habituellement rencontrée (1*b*, 5) :

[1] $$MCl_2 \xrightarrow[(3+n)Cl_2O_6]{} ClO_2M(ClO_4)_3 nCl_2O_6 \xrightarrow[T]{} M(ClO_4)_2$$

s'observe difficilement avec $CdCl_2$ et jamais avec $HgCl_2$. Dans ces deux cas le remplacement de Cl par ClO_4 est délicat et il reste toujours des traces de $CdCl_2$ ou $HgCl_2$ n'ayant pas réagi.

Le sel de chloryle de Cd est peu stable et perd facilement Cl_2O_6 à température ambiante sous vide dynamique. En outre, si n est trop grand (cf. réaction [1]), on obtient une phase unique, liquide rouge sang instable qui se décompose à température ambiante pour donner directement $Cd(ClO_4)_2$ sans permettre d'isoler le sel de chloryle.

Avec le mercure, il y a une étape intermédiaire avant d'obtenir $Hg(ClO_4)_2$:

[2] $$HgCl_2 + Cl_2O_6 \rightarrow HgClClO_4 + \tfrac{1}{2}Cl_2 + ClO_2$$

$HgClClO_4$ est un complexe ionique défini. Ce sel peut être souillé soit par $HgCl_2$ si le temps de contact des réactifs n'est pas suffisant, soit par $Hg(ClO_4)_2$ si l'excès de Cl_2O_6 et le temps de contact des réactifs sont trop importants. Dans le premier cas, on peut purifier $HgClClO_4$ par sublimation de $HgCl_2$ à 110°C sous 1,33 Pa.

Soulignons que :

(*i*) le remplacement partiel des chlorures a déjà été observé avec le gallium (25), le bore (21), le germanium (26), le titane (27) et l'étain (6*a*); avec les deux derniers éléments il y a oxydation partielle.

(*ii*) il est possible d'obtenir $Hg(ClO_4)_2$ à partir de $HgClClO_4$, mais cette opération est fastidieuse car elle demande plusieurs additions successives de Cl_2O_6 et des temps de contact importants.

Afin de pallier les difficultés précédentes, deux réactions originales ont été effectuées pour préparer les perchlorates de Cd et Hg.

(b) Synthèse des perchlorates de cadmium à partir de $CdCO_3$

Cette réaction s'inspire des synthèses classiques des perchlorates hydratés par action de l'acide perchlorique commercial sur les carbonates (28).

$CdCO_3$ réagit très facilement et très rapidement dans le milieu très acide que constitue Cl_2O_6 pour donner $ClO_2Cd(ClO_4)_3$ selon les réactions :

[3] $$CdCO_3 + 2Cl_2O_6 \rightarrow Cd(ClO_4)_2 + CO_2 + 2ClO_2 + \tfrac{1}{2}O_2$$

[4] $$Cd(ClO_4)_2 + Cl_2O_6 \rightarrow ClO_2Cd(ClO_4)_3$$

La formation de ClO_2 et CO_2 au cours de la réaction [3] a été vérifiée en ir selon un procédé déjà décrit (20*b*).

Les observations faites plus haut sur la formation et la stabilité de $ClO_2Cd(ClO_4)_3$ sont valables dans le cadre de la réaction [4].

(c) Synthèse de $Hg(ClO_4)_2$ à partir de $Hg(ClO_4)_2 \cdot 6H_2O$

Les propriétés déshydratantes de Cl_2O_6 (1*b*, 9) permettent de synthétiser $Hg(ClO_4)_2$ à partir de $Hg(ClO_4)_2 \cdot 6H_2O$. Cette méthode dérive de la préparation des perchlorates à partir des chlorures hydratés (1*b*, 5, 9). Rappelons que la préparation se fait en deux étapes : Cl_2O_6 réagit d'abord sur le chlorure hydraté pour donner un perchlorate hydraté puis il y a déshydratation.

Notons que quel que soit l'excès de Cl_2O_6, il est impossible d'isoler à température ambiante un perchlorato mercurate de chloryle stable.

(d) Synthèse de perchlorato cadmiates et mercurates à partir de nitrates hydratés

La réaction de Cl_2O_6 avec des nitrates hydratés a déjà été éprouvée (1*b*, 9, 15, 29). On a pu préparer des perchlorato métallates de Mn, Fe, Co, Ni, Cu, Zn, Th et Al, et proposer une méthode simple de préparation de NO_2ClO_4 à partir de HNO_3 (29*b*).

Cette réaction obéit généralement aux équations :

[5] $$M(NO_3)_n \cdot mH_2O + (2n+m)Cl_2O_6 \rightarrow (NO_2)_nM(ClO_4)_{2n} + 2nClO_2 + n/2O_2 + mHClO_4 + mHClO_3$$

[6] $$(NO_2)_nM(ClO_4)_{2n} \rightarrow (NO_2)_{n-1}M(ClO_4)_{2n-1} + NO_2ClO_4$$

(n, degré d'oxydation du métal)

Les étapes intermédiaires conduisant à [5] ont été explicitées par ailleurs (1*b*, 9). On a pu montrer que la réaction [5] était tributaire de l'engagement du nitrate vis à vis du métal dans le sel de base, et du degré d'hydratation (m) du sel : si $m < 2$ la réaction est difficile, si $m > 5$ il y a compétition entre la réaction [5] et la réaction parasite :

[7] $$ClO_2^+ + NO_3^- \rightarrow NO_2 + \tfrac{1}{2}O_2 + ClO_2$$

Le nitrate est détruit totalement ou partiellement et une réaction analogue à [1] a lieu. Ceci conduit à la formation du mélange : $(ClO_2)_xM(ClO_4)_{(n+x)}$, $(NO_2)_mM(ClO_4)_{(n+m)}$ (cas des complexes perchlorato de Co (1*b*, 9), d'Al (15)). Lorsque Cl_2O_6 réagit avec $Cd(NO_3)_2 \cdot 6{,}5H_2O$ (tableau 1) on obtient un mélange de $Cd(ClO_4)_2$ et $NO_2Cd(ClO_4)_3$. Le faible stabilité de $ClO_2Cd(ClO_4)_3$ ne permet pas d'observer sa formation.

Avec $Cd(NO_3)_2 \cdot 1{,}8H_2O$ et $Hg(NO_3)_2 \cdot 1H_2O$, les réactions obéissent à l'équation [5] mais sont lentes et nécessitent un large excès de Cl_2O_6 pour être complètes. Pour le complexe de cadmium, l'analyse chimique révèle des traces ($\varepsilon < 0{,}05$) de nitrate de base mais la spectroscopie de vibration et les diagrammes de poudre ne permettent pas de le détecter. La phase $NO_2Cd(ClO_4)_3$ a pu être caractérisée sans ambiguïté.

Le complexe de mercure attendu dans la première étape, $(NO_2)_2Hg(ClO_4)_4$, a été préparé, par contre son chauffage sous vide selon la méthode décrite (15) n'a pas permis d'isoler $NO_2Hg(ClO_4)_3$ mais un complexe de stoechiométrie voisine :

Can. J. Chem. Downloaded from www.nrcresearchpress.com by 213.222.148.141 on 09/07/12
For personal use only.

Can. J. Chem. Downloaded from www.nrcresearchpress.com by 213.222.148.141 on 09/07/12
For personal use only.

$(NO_2)_{0,8}Hg(ClO_4)_{2,8}$. Ce dernier composé est un mélange. Une tentative pour le purifier à 126°C durant 14 h a conduit à un produit qui a explosé à température ambiante dès qu'il a été exposé à la lumière du jour.

(e) Remarques sur la synthèse des complexes perchlorato de Cd et Hg

Au cours de ce travail, nous avons montré que la faisabilité des synthèses des complexes perchlorato était liée à l'environnement du centre métallique. Nous avons déjà exploité et expliqué ces faits (1*b*, 5, 9, 15). Cependant, la colonne IIB présente une particularité évidente : la réactivité des chlorures anhydres de ces éléments vis à vis de Cl_2O_6 décroît nettement quant le numéro atomique croît.

Par exemple, il y a substitution partielle des atomes de chlore de $HgCl_2$ avec formation de $HgClClO_4$, et l'obtention de $Hg(ClO_4)_2$ est difficile.

Par ailleurs, $ClO_2Zn(ClO_4)_3$ est stable (1*b*), $ClO_2Cd(ClO_4)_3$ est instable, alors que $ClO_2Hg(ClO_4)_3$ n'a pas pu être isolé à température ambiante.

Cette réactivité décroissante des éléments du groupe IIB liée à la stabilité des composés formés, peut s'expliquer aisément en faisant appel au concept H.S.A.B. (Hard and Soft Acid and Bases) de Pearson (12*a*) :

(*i*) quand on passe de Zn à Hg, la mollesse des centres acides M^{2+} augmente (Zn^{2+} est considéré comme un acide frontière (ou limite), Cd^{2+} comme un acide mou et Hg^{2+} comme un acide très mou), ceci défavorise la coordination de ClO_4^- : base parmi les moins dures.

(*ii*) il est difficile pour ClO_4^- de remplacer des bases plus dures que lui, tel que Cl^-, déjà liées à des acides mous. Remarquons ici que la substitution relativement facile de CO_3^{2-} par ClO_4^-, rencontrée lors de l'utilisation de $CdCO_3$, s'explique par la dureté sensiblement comparable de ces deux ligands.

Remarquons également que l'accroissement des rayons des cations M^{2+} (Zn < Cd < Hg) peut rendre compte des difficultés de perchloratation lorsqu'on passe de Zn à Hg.

Analyse structurale

Si l'on exclut $HgClClO_4$ qui est un composé ionique, tous les composés isolés au cours de ce travail sont, d'après leurs spectres de vibration (figures 1, 2, 5, 6, 7, 9), des complexes perchlorato dans lesquels le groupement ClO_4 est lié au métal.

Seule l'étude du diagramme X de poudre de $Cd(ClO_4)_2$ a pu être menée à bien (tableau 2); les autres produits présentent les diagrammes complexes (tableau 4) et les composés auxquels on pourrait éventuellement les comparer ont des symétries cristallines trop faibles pour que l'on puisse établir surement un isomorphisme.

La comparaison des spectres de vibration montre que les complexes sont différents dans leur arrangement moléculaire.

(a) Le perchlorate de chloro-mercure : $HgClClO_4$

Seul le spectre Raman de ce composé a pu être enregistré avec précision (fig. 1). Le spectre infra-rouge est largement perturbé par un effet Christiansen (30) et sa qualité n'a pu être améliorée en utilisant une suspension dans du Nujol, car le produit est très réactif.

On relève sur le spectre Raman les raies caractéristiques d'un groupement ClO_4 ionique : 460 cm^{-1} $\delta_s(E)$; 622 $\delta_{as}(F_2)$; 924–935 $\nu_s(A_1)$ (dédoublée par effet de cristal); 1025–1101 cm^{-1} $\nu_{as}(F_2)$. Le cation associé est donc $HgCl^+$. Les vibrations de valence de $HgCl_2$ interviennent à 313 et 375 cm^{-1} (31). Si $HgCl^+$ était monomère, HgCl serait détecté à une fréquence supérieure ou égale à la moyenne des fréquences ν HgCl dans $HgCl_2$ (344 cm^{-1}). Sur le spectre Raman on relève deux raies à 247 et 272 cm^{-1} et un épaulement à 286 cm^{-1}. Leur nombre et les fréquences observées sont l'indication de la formation de $(HgCl^+)_n$ et de ponts Hg–Cl–Hg. Ce fait n'est pas surprenant puisque de nombreux complexes HgXL (X = I, L = NO_3^- (32); X = OH, L = ClO_4^- (33); X = OH, L = ClO_3^- ou BrO_3^- (34); X = NH_2, L = Cl^- (34) etc.) présentent des cations HgX^+ polymères en chaîne analogues à HgO (34).

TABLEAU 2. Indexation du diagramme de poudre de $Cd(ClO_4)_2$

d^a	I^b	$d_{mes}{}^b$	$d_{calc}{}^b$	h	k	l^b
—	25	4,89	4,92	0	0	3
4,19	25	4,24	4,22	2	0	1
3,75	30	3,78	3,78	2	0	2
3,42	25	3,45	3,53	1	1	3
			3,40	1	0	4
2,96	45	2,98	2,99	1	1	4
—	7	2,82	2,83	2	0	4
			2,80	1	0	5
2,53	100	2,55	2,54	2	2	0
—	20	2,35	2,32	3	1	2
2,24	7	2,25	2,26	2	2	3
2,09	15	2,10	2,11	4	0	2
1,98	—	—				
1,92	20	1,93	1,93	2	2	5

[a]Rosolovskii et coll. (réf. 10).
[b]Ce travail : groupe d'espace $R\bar{3}$; a = 10,18; c = 14,78 Å.

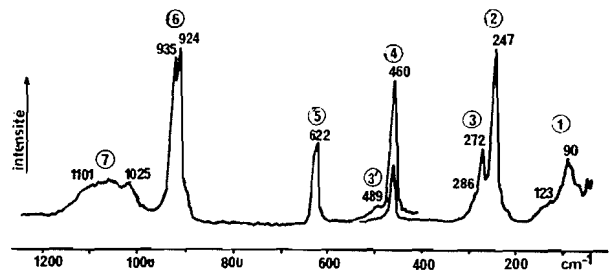

FIG. 1. Spectre Raman de $HgClClO_4$ (1) : vibrations de réseau + $\delta(HgCl)_n$; (2) ν_s HgCl; (3) (et 3' ?); ν_{as} HgCl; (4) δ_s ClO_4; (5) δ_{as} ClO_4; (6) ν_s ClO_4; (7) ν_{as} ClO_4.

Compte tenu de ces remarques, nous avons porté sur le spectre Raman (fig. 1) les principales attributions des fréquences observées.

(b) Le bis(perchlorato cadmium) : $Cd(ClO_4)_2$

Les spectres infra-rouge et Raman de ce complexe sont reproduits sur la figure 2 et sont comparés à ceux de $Ni(ClO_4)_2$. L'allure de ces spectres montre qu'il existe une grande analogie entre les structures moléculaires des deux complexes.

Il a été possible d'indexer le diagramme de poudre de $Cd(ClO_4)_2$ dans le même groupe d'espace $R\bar{3}$ (système trigonal) que $Ni(ClO_4)_2$ (tableau 2), bien que Nikitina et Rosolovskii (16) aient considéré une maille cubique. Les paramètres de la maille de $Cd(ClO_4)_2$ se rapprochent de celle de $Zn(ClO_4)_2$ (tableau 3), qui comme $Ni(ClO_4)_2$ possède une structure lamellaire (7*c*) et des groupements ClO_4 tridentés en pont.

On considère que $Cd(ClO_4)_2$ a le même arrangement (fig. 3). L'environnement du métal est octaédrique comme cela a été trouvé pour de nombreux complexes de Cd (39).

Les principales attributions des bandes ou raies sont notées

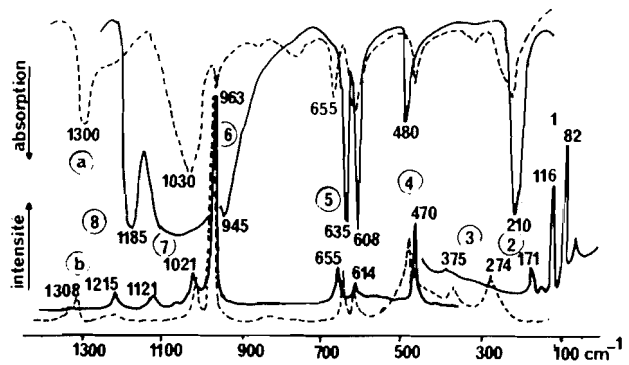

FIG. 2. Spectres (a) infra-rouge et (b) Raman de $Cd(ClO_4)_2$ (—) comparés à ceux de $Ni(ClO_4)_2$ (-----) : (1) réseau + déf. MO_6; (2) ν_{as} MO_6; (3) ν_s MO_6; (4) ρ_r ClO_4; (5) δ_s et δ_{as} ClO_{3p}; (6) ν_s ClO_p; (7) ν_{as} ClO_p; (8) ν ClO_t; O_p : oxygène lié à M; O_t : oxygène non lié.

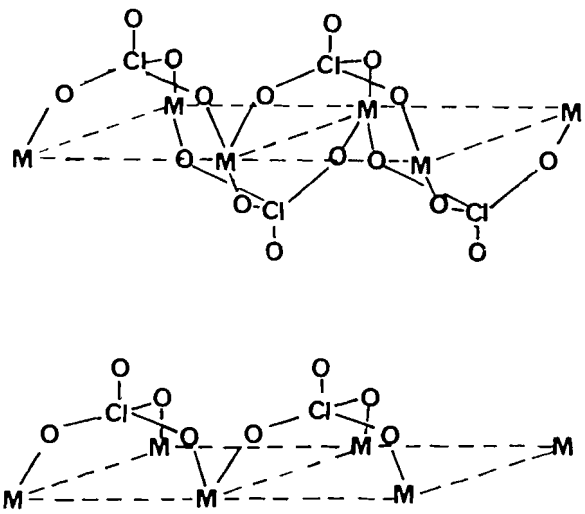

FIG. 3. Modèle possible pour $Cd(ClO_4)_2$: structure en couche analogue à celle de $Zn(ClO_4)_2$ (7*c*) et $Ni(ClO_4)_2$ (7*c*).

sur la figure 2. Les fréquences observées indiquent que l'interaction élément central (Cd) ↔ ClO_4 est plus faible que dans $M(ClO_4)_2$ (M = Ni, Co, Zn). Ceci est particulièrement vérifié avec la fréquence peu élevée (1185 cm^{-1}) relative à la vibration ν_{as} ClO_t (O_t : oxygène terminal non lié). Dans le cas d'un groupement ClO_4 fortement lié à un métal, la liaison ClO_t prend le caractère d'une double liaison et la vibration correspondante apparaît vers 1300 cm^{-1} (cf. $Ni(ClO_4)_2$). D'après la courbe ν ClO = $f(d\text{ClO})$ (1*c*) on en déduit, pour $Cd(ClO_4)_2$, que $d\text{ClO}_t$ = 1,40 Å et $d\text{ClO}_p$ = 1,43 Å (O_p : oxygène lié au métal). $[ClO_4]$ est peu perturbé; ceci est en accord avec la remarque précédente.

Les vibrations de valence symétriques du squelette CdO_6 apparaissent sous forme d'une bande intense en ir à 210 cm^{-1} et d'une raie de faible intensité vers 375 cm^{-1} en Raman.

Si l'on se réfère aux données relatives à divers complexes de cadmium dans lequels le centre Cd^{2+} est lié à des bases organiques : 2,22 < d(Cd—O) < 2,33 Å (39); la distance Cd—O dans $Cd(ClO_4)_2$ doit être supérieure à 2,22 Å. Cette hypothèse est en accord avec une valeur d(Cd—O) ≃ 2,40 Å, déduite de la relation dMO = f(R) (35) (R : rayons ionique effectif selon Brown et Shannon (36)). Cette distance M—O est nettement plus grande que celles habituellement observées dans des complexes perchlorato (Ni—O : 2,04 (7*b*); Co—O : 2,09

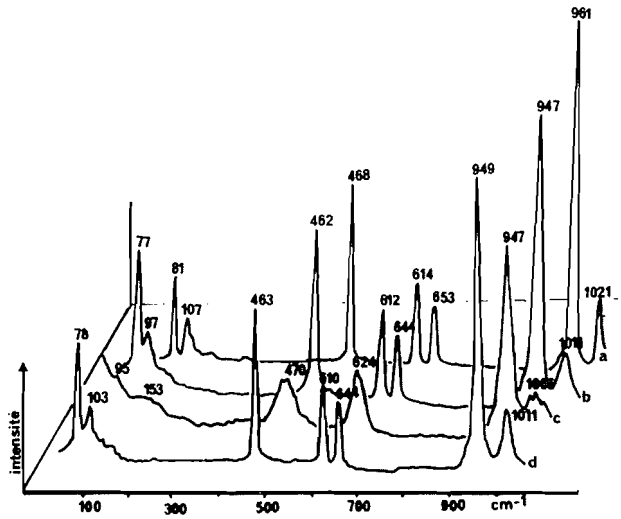

FIG. 4. Transformation de phase dans $Cd(ClO_4)_2$ suivie par spectroscopie Raman : (a) température ambiante; (b) 248°C; (c) 273°C; (d) 170°C (au refroidissement).

(7*b*); Cu—O : 1,95 (7*a*); Ti—O : 2,06 (1*c*)). Elle pourrait expliquer la variation des paramètres cristallins de $Cd(ClO_4)_2$ par rapport à ceux des complexes voisins.

Remarque : $Cd(ClO_4)_2$ présente une transformation de phase autour de 273°C et elle est réversible. Ce phénomène a pu être suivi par spectroscopie Raman (fig. 4). À cette température élevée, $Cd(ClO_4)_2$ est quasiment ionique.

(c) Le bis(perchlorato) mercure (II) : $Hg(ClO_4)_2$

Les spectres infra-rouge et Raman de ce complexe sont reproduits sur la figure 5. Ils sont différents de ceux de $Zn(ClO_4)_2$ ou $Cd(ClO_4)_2$. Alors que les spectres de ces derniers sont caractéristiques de groupements ClO_4 tridentés, ceux de $Hg(ClO_4)_2$ présentent des bandes ou raies de groupements ClO_4 monodentés. Elles sont localisées pour les vibrations de valence, autour de 800 (ν ClO_p), 1000 (ν_s ClO_t) et 1150 cm^{-1} (ν_{as} ClO_t). La raie relative à ν_s ClO_t apparaît à une fréquence anormalement basse. Rappelons qu'elle est habituellement située autour de 1050 cm^{-1} (21). On peut lier ce phénomène à une interaction secondaire similaire à celle notée pour $HgCl_2$ (37) et $Hg(SCNEt_2)_2$ (38), ou le ligand interéagit avec les atomes de mercure des molécules voisines. Le mercure est alors dans un environnement octaédrique déformé comme cela est habituellement rencontré (34).

La symétrie locale élevée autour de Hg se traduit par l'activité sélective infra-rouge–Raman et par le dédoublement des bandes et raies. Une attribution est proposée sur la figure 5. Les fréquences des vibrations de valence de ClO_4 montrent que la variation des distances ClO est importante : $d(ClO_p)$ ≈ 1,55 Å, $d(ClO_t)$ ≈ 1,40 Å. Elles classent $Hg(ClO_4)_2$ parmi les complexes où les groupements ClO_4 sont très fortement engagés.

(d) Le perchlorato cadmiate de chloryle : $ClO_2Cd(ClO_4)_3$

Les spectres ir et Raman de $ClO_2Cd(ClO_4)_3$ sont représentés sur la figure 6. Il existe une similitude du spectre Raman de ce complexe avec celui de $ClO_2Cu(ClO_4)_3$ (1*b*).

On note en tout premier lieu les raies et bandes relatives au cation ClO_2^+ : ν_{as} : 1295 et 1280 (ir) et 1307 et 1293 (R); ν_s : 1064 et 1056 (R); δ : 510 (ir) et 519 (R) cm^{-1}. Sur le spectre Raman mieux résolu que le spectre ir les autres raies sont attribuées à $Cd(ClO_4)_3^-$. Dans cet anion coexistent des groupements ClO_4

Can. J. Chem. Downloaded from www.nrcresearchpress.com by 213.222.148.141 on 09/07/12
For personal use only.

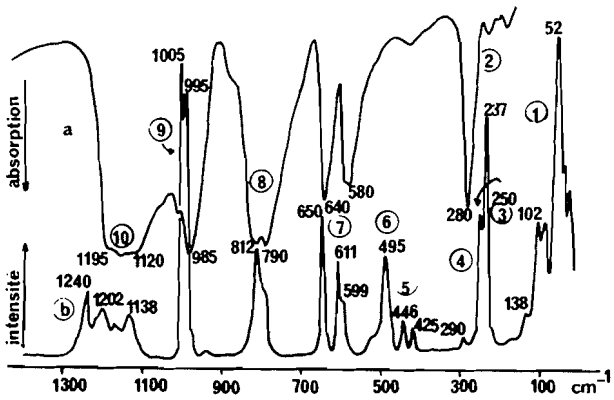

FIG. 5. Spectres (a) infra-rouge et (b) Raman de $Hg(ClO_4)_2$: (1) réseau + déf. HgO_2O_4 (cf. texte); (2) ν_s HgO; (3) ρ_r ClO_4; (4) ν_{as} HgO; (5) ν_{as} HgO + δ_s ClO_3; (6) δ_s ClO_3; (7) δ_{as} ClO_3; (8) ν ClO_p; (9) ν_s ClO_t; (10) ν_{as} ClO_t.

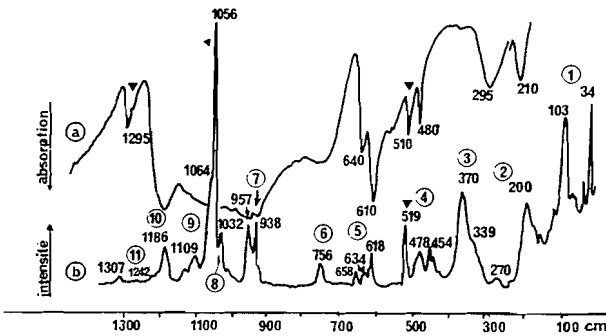

FIG. 6. Spectres (a) infra-rouge et (b) Raman de $ClO_2Cd(ClO_4)_3$: ▼ ClO_2^+; sur le spectre Raman les autres raies ou bandes sont attribuées à $Cd(ClO_4)_3^-$: (1) réseau; (2) ν MO; (3) ρ_r (m); (4) δ_s ClO_2 (m, b); (5) δ_{as} ClO_2 (m, b), ρ_w, ρ_r (b); (6) ν ClO_p (m); (7) ν_s, ν_{as} ClO_p (b); (8) ν_s ClO_t (m); (9) ν_s ClO_t (b); (10) ν_{as} ClO_t (b); (11) ν_{as} ClO_t (m) (m : monodenté, b : bidenté).

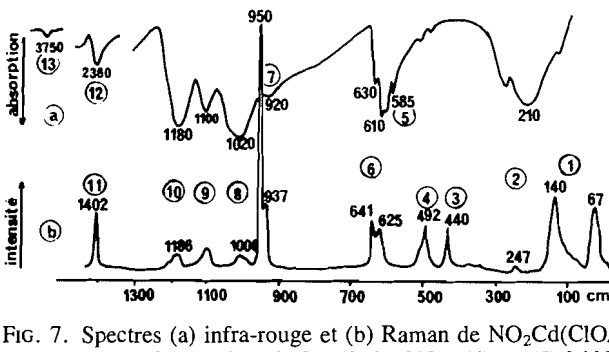

FIG. 7. Spectres (a) infra-rouge et (b) Raman de $NO_2Cd(ClO_4)_3$: (1) réseau + déf. CdO_6; (2) ν CdO_6; (3) δ_s ClO_2; (4) ρ_t; (5) δ NO_2^+; (6) δ_{as} ClO_2 + ρ_r + ρ_w; (7) ν_s ClO_p; (8) ν_{as} ClO_p; (9) ν_s ClO_t; (10) ν_{as} ClO_t; (11) ν_s NO_2^+; (12) ν_{as} NO_2^+; (13) (ν_s + ν_{as}) NO_2^+.

monodentés et bidentés; les principales attributions sont notées sur le spectre. On a déjà montré que les structures des perchlorato complexes dérivaient de celles de chlorures correspondants (7); $ClO_2Cd(ClO_4)_3$ doit se rapprocher de $ACdCl_3$ ou des composés $ACuCl_3$ (40), polymères avec des ligands pontants et terminaux.

(e) Le tris(perchlorato) cadmiate de nitryle : $NO_2Cd(ClO_4)_3$

Les spectres infra-rouge et Raman de $NO_2Cd(ClO_4)_3$ sont reproduits sur la figure 7. Ils sont semblables à ceux de $NO_2Ni(ClO_4)_3$ (1*b*) et sont comparables aux spectres infra-

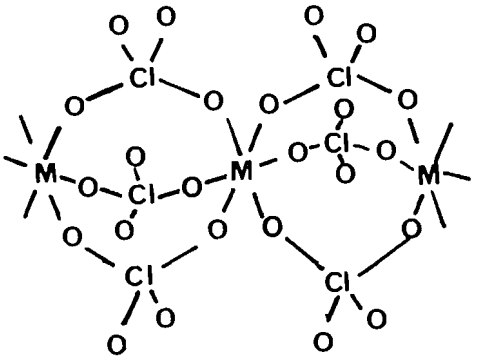

FIG. 8. Structure de l'anion $M(ClO_4)_3^-$ d'après des données EXAFS (41).

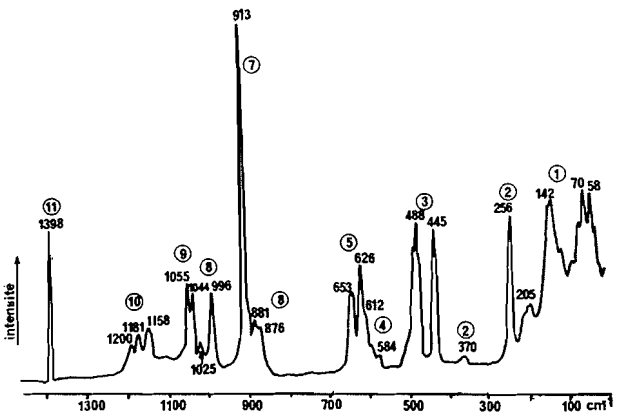

FIG. 9. Spectre Raman de $(NO_2)_2Hg(ClO_4)_4$: (1) δ HgO_6 + réseau; (2) ν HgO_6; (3) δ_s ClO_2 (m, b); (4) δ NO_2^+; (5) δ_{as} ClO_2 (m, b), ρ_r + ρ_w (b); (6) ν_{as} ClO_p (b) + ν ClO_p (m); (7) ν_s ClO_p (b); (8) ν_s ClO_t (m, en interaction); (9) ν_s ClO_t (m, libre); (10) ν_s, ν_{as} ClO_t (b), ν_{as} ClO_t (m); (11) ν_s NO_2^+.

TABLEAU 3. Données radiocristallographiques pour divers complexes perchlorato à structure en couche et pour CdI_2

Complexe	Groupes d'espaces	Paramètres		Référence
$Ni(ClO_4)_2$	$R\bar{3}$	4,77	21,85	7*b*
$Co(ClO_4)_2$	$R\bar{3}$	4,77	22,05	7*b*
$Zn(ClO_4)_2$	$P\bar{4}m2$	10,91	11,94	7*c*
$Ga(ClO_4)_3$	$R\bar{3}$	8,16	23,57	7*c*
$In(ClO_4)_3$	$P\bar{3}m1$	8,29	23,01	7*c*
$Tl(ClO_4)_3$	$P\bar{3}$	8,35	23,32	5
$NO_2Co(ClO_4)_3$	$R\bar{3}$	9,02	18,83	41
$Cd(ClO_4)_2$	$R\bar{3}$	10,18	14,75	[a]
CdI_2	$R\bar{3}m$	4,24	6,84	45

[a]Ce travail.

rouge de divers complexes $ACd(ClO_4)_3$ (A = Li, Na, K, Rb, Cs, Bu_4N) isolés récemment par Rosolovskii et coll. (10).

Le diagramme de poudre de $NO_2Cd(ClO_4)_3$ est très proche de celui du sel de césium préparé par Rosolovskii et coll., mais diffère de ceux de la série isomorphe $NO_2M(ClO_4)_3$ (M = Mn, Co, Ni, Zn) et $ClO_2M'(ClO_4)_3$ (M' = Co, Ni) (1*b*, 9).

Les résultats de la spectroscopie de vibration indiquent que l'arrangement moléculaire de $NO_2Cd(ClO_4)_3$ est identique à celui de $NO_2Ni(ClO_4)_3$. Une étude EXAFS récente (41) a montré que le sel de nickel (ou de cobalt) était analogue aux chlorures $ANiCl_3$ (A = R_4N) à structure polymère en chaîne

Can. J. Chem. Downloaded from www.nrcresearchpress.com by 213.222.148.141 on 09/07/12
For personal use only.

TABLEAU 4. Données radiocristallographiques pour des complexes perchlorato synthétisés dans le cadre de ce travail

$NO_2Cd(ClO_4)_3$		$HgClClO_4$		$Hg(ClO_4)_2$		$(NO_2)_2Hg(ClO_4)_4$	
d_{obs}	I	d_{obs}	I	d_{obs}	I	d_{obs}	I
13,93	15	9,40	15	14,01	10	7,25	20
9,17	55	8,34	15	11,93	7	5,53	25
8,60	10	8,18	15	10,03	10	4,79	15
7,96	10	7,96	15	9,30	30	4,72	20
6,99	20	7,19	8	8,41	20	4,45	25
6,63	35	7,00	8	8,04	20	4,37	20
5,40	25	6,36	5	7,13	15	3,98	60
4,67	50	5,50	95	6,60	10	3,42	100
3,51	50	5,03	8	5,43	45	3,22	45
3,29	100	4,46	55	4,67	40	3,25	30
3,10	30	4,23	5	4,52	50	3,17	90
2,94	85	3,71	35	4,43	20	2,94	40
2,83	5	3,45	100	4,15	15	2,78	40
2,80	15	3,42	95	4,11	15	2,62	30
2,68	65	3,36	15	3,81	15	2,57	30
2,57	20	3,22	15	3,73	100	2,38	25
2,39	10	2,95	15	3,51	45	2,34	15
2,35	10	2,84	100	3,46	20	2,27	15
2,24	5	2,79	90	3,26	35	2,25	25
2,19	25	2,71	75	3,22	25	2,22	25
2,12	10	2,45	25	2,94	25	2,20	25
2,07	50	2,34	8	2,91	14	2,17	25
2,02	15	2,30	40	2,89	55	2,01	20
1,89	10	2,23	35	2,81	15	1,95	25
1,85	15	2,22	35	2,66	35	1,88	20
		2,16	10	2,49	15		
		2,08	35	2,44	15		
		2,03	10	2,39	10		
				2,32	10		
				2,42	30		
				2,174	40		
				2,169	45		
				2,087	15		
				2,069	15		
				2,043	15		
				2,025	15		
				1,960	10		
				1,930	10		

(42) (fig. 8). Les groupements ClO_4 sont bidentés en pont et l'environnement du métal est octaédrique. Les principales attributions sont notées dans la légende de la figure 7. Les fréquences observées indiquent que le groupement ClO_4 dans $NO_2Cd(ClO_4)_3$ est peu perturbé; il a un caractère ionique important.

(f) Le tétrakis(perchlorato) mercurate de nitryle : $(NO_2)_2$-$Hg(ClO_4)_2$

Le spectre Raman de ce complexe est reproduit sur la figure 9. Il ne présente aucune raie caractéristique de NO_2ClO_4 (29*b*). C'est un complexe défini. La comparaison du diagramme de poudre et du spectre Raman de ce produit avec ceux de $(NO_2)_2Cu(ClO_4)_4$ (1*b*, 9) montre que ces complexes sont isomorphes et ont le même arrangement moléculaire. Sur le spectre (fig. 9) pour $Hg(ClO_4)_4^{2-}$, dans le domaine des vibrations de valence symétrique, on relève des raies caractéristiques de groupements ClO_4 monodentés libres ou perturbés par des interactions (respectivement à 1055, 1044 et 996 cm^{-1}). La raie intense à 913 cm^{-1} dénote la présence de groupements ClO_4 bidentés.

L'anion pourraît adopter un arrangement analogue à celui trouvé pour des motifs polymères HgX_4^{2-} (43), différent des anions monomères HgI_4^{2-} (43) et $Hg(NO_2)_4^{2-}$ (44). Les principales attributions sont notées dans la légende de la figure 9.

Conclusion

Avec ce travail, la connaissance des complexes perchlorato de la colonne IIB (ou 12) a progressé. Si les complexes de cadmium se rapprochent de ceux du zinc, du cobalt ou du nickel (avec modifications des paramètres cristallins dues, certainement, aux rayons ioniques effectifs différents des cations métalliques), les complexes du mercure en diffèrent totalement contrairement aux complexes fluorosulfato de la même série (46). Le comportement des complexes perchlorato semble être dû à l'acidité différente, selon Pearson, des cations M^{2+} (M = Zn, Cd, Hg). Ces différences d'acidité influent aussi bien sur les préparations que sur l'arrangement structural. Cependant, d'une façon générale, les complexes perchlorato isolés ont des structures qui dérivent de celles des halogénures correspondants.

Can. J. Chem. Downloaded from www.nrcresearchpress.com by 213.222.148.141 on 09/07/12
For personal use only.

Remerciements

Les auteurs remercient le C.N.R.S. (France) et la D.R.S.T. (Tunisie) pour l'aide financière qu'ils leur ont apportée.

NOTE : Alors que la rédaction de cet article était achevée, nous avons eu connaissance du travail de Rosolovskii et coll. (47) sur $Hg_2(ClO_4)_2$ et $Hg(ClO_4)_2$. Leurs méthodes de synthèses diffèrent des nôtres (déshydratation par voie thermique des complexes hydratés) pour $Hg(ClO_4)_2$. Leurs résultats spectroscopiques sont analogues aux nôtres. On note cependant de légères différences dans les données des diagrammes de poudre X.

1. (*a*) J. L. PASCAL et J. POTIER. Le courrier du C.N.R.S. Image de la chimie Supp. **60**, 14 (1985); (*b*) J. L. PASCAL, J. POTIER et C. S. ZHANG. J. Chem. Soc. Dalton Trans. 297 (1985), et références citées; (*c*) M. FOURATI, M. CHAABOUNI, C. BELIN, M. CHARBONNEL, J. L. PASCAL et J. POTIER. Inorg. Chem. **25**, 1386 (1986).
2. C. J. SHACK, D. PILIPOVICH et K. O. CHRISTE. J. Inorg. Nucl. Chem. Supp. **76**, 207 (1976).
3. Z. K. NIKITINA, A. I. KARELIN et V. YA. ROSOLOVSKII. Russ. J. Inorg. Chem. (Trad. Anglaise), **25**, 71 (1980).
4. Z. K. NIKITINA et V. YA. ROSOLOVSKII. Russ. J. Inorg. Chem. (Trad. Anglaise), **25**, 715 (1980).
5. M. FOURATI, M. CHAABOUNI, H. F. AYEDI, J. L. PASCAL et J. POTIER. Can. J. Chem. **63**, 3499 (1985), et références citées.
6. (*a*) C. BELIN, M. CHAABOUNI, J. L. PASCAL, J. POTIER et J. ROZIERE. J. Chem. Soc. Chem. Commun. 105 (1980); (*b*) Inorg. Chem. **21**, 3557 (1982); (*c*) E. A. GENKINA, V. P. BABAEVA et V. YA. ROSOLOVSKII. Koord. Khim. **10**, 1415 (1984).
7. (*a*) J. L. PASCAL, J. POTIER, D. J. JONES, J. ROZIERE et A. MICHALOWICZ. Inorg. Chem. **23**, 2068 (1984); (*b*) Inorg. Chem. **24**, 238 (1985); (*c*) J. POTIER, J. ROZIERE, A. SEIGNEURIN, D. J. JONES, J. L. PASCAL et A. MICHALOWICZ. Nouv. J. Chim. **11**, 641 (1987).
8. J. L. PASCAL, J. POTIER et C. S. ZHANG. C.R. Acad. Sci. Ser. 2, **295**, 1097 (1982).
9. C. S. ZHANG. Thèse, Université des Sciences et Techniques du Languedoc. Montpellier, France (1984).
10. Z. K. NIKITINA, YU. V. CHUPRAKOV et V. YA. ROSOLOVSKII. Russ. J. Inorg. Chem. (Trad. Anglaise), **31**, 691 (1986).
11. R. L. RAWIS. Chem. Eng. News, **64** (4), 22 (1986).
12. (*a*) R. G. PEARSON. J. Am. Chem. Soc. **85**, 3533 (1963); (*b*) S. YAMADA et M. TANAKA. J. Inorg. Nucl. Chem. **37**, 587 (1974); (*c*) W. B. JENSEN. Chem. Rev. **78**, 1 (1978); (*d*) S. AHRLAND. XXIV International Conference on coordination chemistry. Athènes, Grèce. Août 1986.
13. V. YA. ROSOLOVSKII et N. V. KRIVTSOV. Russ. J. Inorg. Chem. (Trad. Anglaise), **13**, 18 (1968).
14. G. LUYBIMOVA, A. P. RAZUMOVA et V. YA. ROSOLOVSKII. Russ. J. Inorg. Chem. (Trad. Anglaise), **28**, 1687 (1983).
15. A. HASSAN. Thèse, Université des Sciences et Techniques du Languedoc. Montpellier, France (juillet 1986).
16. Z. K. NIKITINA et V. YA. ROSOLOVSKII. Russ. J. Inorg. Chem. (Trad. Anglaise), **31**, 827 (1986).
17. P. PASCAL. Complément au Nouv. Traité de chimie minérale. Vol. 9. *Édité par* Masson, H. Brusset. Paris. 1977. p 168.
18. A. PICOT et P. GRENOUILLET. Actual. Chim. 41 (avril 1986).
19. (*a*) R. E. COOK et P. J. ROBINSON. Nature (Londres), **299**, 674 (1982); (*b*) R. L. ELSENBAUMER et G. G. MILLER. Chem. Eng. News, **63** (25), 4 (1985).
20. (*a*) A. C. PAVIA, J. L. PASCAL et A. POTIER. C.R. Seances. Acad. Sci. Paris, Ser. C, **272**, 1495 (1971); (*b*) J. L. PASCAL. Thèse. Université des Sciences et Techniques du Languedoc. Montpellier, France (1978).
21. T. CHAUSSE, J. L. PASCAL, A. POTIER et J. POTIER. Nouv. J. Chem. **5**, 261 (1981).
22. Méthodes d'analyses complexométriques par les titriplex. 3^e éd. E. Merck, Darmstadt, R.F.A.
23. (*a*) R. J. BACZUK et W. G. BOTTELER. Anal. Chem. **40**, 687 (1968); (*b*) Guide des méthodes analytiques. 9^e éd. Orion Research, Küsnacht, Suisse. 1979.
24. H. MATHIEU. Analyse quantitative. Masson, Paris. 1946.
25. M. CHAABOUNI, J. L. PASCAL, A. C. PAVIA, A. POTIER et J. POTIER. J. Chim. Phys. **74**, 1083 (1977).
26. M. FOURATI, J. L. PASCAL, M. CHAABOUNI et J. POTIER. Polyhedron. Sous presse.
27. M. FOURATI, M. CHAABOUNI, J. L. PASCAL et J. POTIER. J. Mol. Struct. **143**, 147 (1986).
28. A. A. SCHILT. Perchloric acid and perchlorates. G. Frederick Smith Chemical Company, Columbus, OH. 1979.
29. (*a*) J. L. PASCAL, J. POTIER et C. S. ZHANG. C.R. Acad. Sci. Paris, Ser. 2, **298**, 579 (1984); (*b*) J. L. PASCAL, A. HASSAN et J. POTIER. C.R. Acad. Sci. Paris, Ser. 2, **302**, 817 (1986).
30. D. REDFIELD et R. L. BAUM. J. Opt. Soc. Am. **51**, 184 (1961).
31. H. SIEBERT. Anwendungen der Schwingungsspektroskopie in der Anorganischen Chemie. Springer Verlag, Berlin. 1966.
32. K. PEARSON et B. HOLMBERG. Acta Crystallogr. Sect. B: Struct. Crystallogr. Cryst. Chem. **38**, 900 (1982).
33. G. JOHANSSON et E. HANSEN. Acta Chem. Scand. **26**, 796 (1972).
34. D. GRDENIC. Q. Rev. Chem. Soc. **19**, 303 (1965).
35. H. F. AYEDI, M. CHAABOUNI, M. FOURATI, J. POTIER, J. L. PASCAL et A. HASSAN. Rapport interne CNRS–DRST (1986).
36. J. E. HUHEEY. Inorganic chemistry. Principles of structures and reactivity. 2^e éd. Harper and Row, New York. 1978. p. 71.
37. A. F. WELLS. Structural inorganic chemistry. 4^e éd. Oxford University Press, Londres. 1975.
38. (*a*) H. IWASAHI. Acta Crystallogr. Sect. B: Struct. Crystallogr. Cryst. Chem. **29**, 2115 (1973); (*b*) P. C. HEALY et A. H. WHITE. J. Chem. Soc. Dalton Trans. 284 (1973).
39. (*a*) D. G. TUCK. Rev. Inorg. Chem. **1**, 209 (1979); (*b*) L. BUSTOS, J. N. GREEN, J. L. HENCHER, M. A. KHAN et D. G. TUCK. Can. J. Chem. **61**, 2141 (1983).
40. U. GEISER, R. M. GAURA, R. D. WILLET et D. X. WEST. Inorg. Chem. **25**, 4203 (1986), et références citées.
41. M. FOURATI, M. CHAABOUNI, J. L. PASCAL et J. POTIER. XXIVth International Conference on Coordination Chemistry. Athènes, Grèce. Août 1986.
42. G. STUCKY. Acta Crystallogr. Sect. B: Struct. Crystallogr. Cryst. Chem. **24**, 330 (1968).
43. R. H. FENN. Acta Crystallogr. **20**, 24 (1966).
44. L. F. POWER, J. A. KING et F. H. MOORE. J. Chem. Soc. Dalton Trans. 93 (1976).
45. W. G. WYCKOFF. Crystal structures. Interscience Publishers, New York. 1960. pp. 1, 266, 1069.
46. S. P. MALLELA et F. AUBKE. Can. J. Chem. **62**, 382 (1984).
47. Z. K. NIKITINA et V. YA. ROSOLOVSKII. Zh. Neorg. Khim. **31**, 2925 (1986).

Can. J. Chem. Downloaded from www.nrcresearchpress.com by 213.222.148.141 on 09/07/12
For personal use only.

Use of Pd/sepiolite systems as hydrogenation catalysts. II. Hydrogenolysis of *N*-blocked amino acids and dipeptides by hydrogen transfer

A. ARAMENDIA, V. BORAU, C. JIMENEZ, J. M. MARINAS, AND M. E. SEMPERE
Department of Organic Chemistry, Faculty of Sciences, Córdoba University, 14004 Córdoba, Spain

Received January 16, 1986[1]

A. ARAMENDIA, V. BORAU, C. JIMENEZ, J. M. MARINAS, and M. E. SEMPERE. Can. J. Chem. **65**, 2791 (1987).

We have carried out the deprotecting of various *N*-protected amino acids and dipeptides by subjecting them to hydrogen transfer with several palladium catalysts supported on different solids. The hydrogen donor itself has been used "*in situ*" to reduce the corresponding Pd salt on the support. We have also analyzed the effect of various factors on the deprotecting rate for Z-glycine. Such factors include the procedure used in synthesizing the catalysts ("*in situ*" or by conventional reduction), the type of support, hydrogen donor, promoting effect of alkaline hydroxides, type of reactor (closed or open), and magnetic or ultrasonic agitation. We have found that the ease of adsorption of the protected amino groups (*Z*—NH—) is fundamental in accounting for the order of deprotecting rates found. We have compared the activity of new catalysts in the deprotecting process with that of a commercial one containing 10% Pd over carbon, supplied by Fluka (ref. 75990).

A. ARAMENDIA, V. BORAU, C. JIMENEZ, J. M. MARINAS et M. E. SEMPERE. Can. J. Chem. **65**, 2791 (1987).

On a effectué la déprotection de divers acides aminés et de divers dipeptides portant un groupement protecteur sur le N; pour ce faire, on les a soumis à un transfert d'hydrogène avec plusieurs catalyseurs de palladium supportés sur divers solides. Le donneur d'hydrogène lui-même a été utilisé *in situ* afin de réduire le sel de palladium correspondant sur le support. En plus de ce travail, on a analysé l'influence de divers facteurs sur le taux de déprotection de la Z-glycine. Parmi ces facteurs, on note la procédure utilisée pour synthétiser les catalyseurs (*in situ* ou réduction conventionnelle), le type de support, le donneur d'hydrogène, l'effet activant des hydroxydes alcalins, le type de réacteur (ouvert ou fermé) et la méthode d'agitation (magnétique ou ultrasonique). On a trouvé que la facilité d'adsorption des groupements aminés protégés (*Z*—NH—) est fondamentale pour expliquer l'ordre que l'on a trouvé pour les taux de déprotection. On a comparé l'activité des nouveaux catalyseurs dans le processus de déprotection avec celle d'un catalyseur commercial contenant 10% de Pd sur du charbon et qui avait été fourni par Fluka (ref. 75990).

[Traduit par la revue]

Introduction

The reduction of different organic functions by hydrogen transfer (1) plays a major role in the field of organic synthesis nowadays. In the last few years, transfer reduction processes have been applied as a convenient method for removal of some protecting groups commonly used in peptide synthesis (2–8) such as *N*-benzyloxycarbonyl groups, C-terminal benzyl ester, the nitro function of nitroarginine or the *N*-benzyl grouping of N^2-benzylhistidine. In some instances, the reduction has been carried out in solid phase (Bradykinin synthesis) (4). The following are used as hydrogen donors: cyclohexene (2, 4, 7), cyclohexadiene (3), formic acid (5, 6), and ammonium formate (9). On the other hand, the process of deprotecting, by hydrogen transfer, showed negligible racemization (8).

In this paper we report the deprotecting of various *N*-blocked amino acids and dipeptides blocked in their amino function by the action of the benzyloxycarbonyl group (Z), using various hydrogen donors such as cyclohexene, formic acid, α-Phellandrene (5,6-dihydro-*p*-methylisopropylbenzene) and the formic acid – triethylamine at room temperature.

The following have been used as catalysts: Pd deposited at low concentration (3% by weight) on aluminium ortophosphate, aluminium ortophosphate – silica, aluminium ortophosphate – alumina, and a sepiolite from Vallecas (Madrid, Spain) supplied by TOLSA S.A.

Catalytic systems of $Pd/AlPO_4$, $Pd/AlPO_4–SiO_2$, and $Pd/AlPO_4–Al_2O_3$ had been employed earlier in transfer reductions of nitro groups (10) and α,β-unsaturated carbonyl compounds (11–14), as well as in the decarbonilation of aromatic aldehydes (15). Likewise, Pd–sepiolite catalysts are now being used as reduction catalysts for aromatic nitro-compounds and imines (16, 17).

[1]Revision received July 10, 1987.

Experimental

Supports

We have used eight different supports, as shown in Table 1. Support S is made of commercial silica from Merck (Kieselgel, 200–250 mesh). The sepiolite (Sep) was supplied by TOLSA S.A. (Madrid, Spain) and was extracted from their deposite in Vallecas (Madrid). The thus-labelled Sep_{300} was calcined at 300°C for 4 h. Whereas sepiolite Sep_{400} was calcined over the same period at 400°C. Support B consists of aluminium ortophosphate synthesized in our laboratory (18), whereas supports E, P2, and F72 contain $SiO_2–AlPO_4$ (80:20 by weight) and were obtained by different procedures reported elsewhere (19, 20). Support CB consists of $Al_2O_3–AlPO_4$ (25:75 by weight), the synthesis of which was described in an earlier paper (21). Table 1 gives a summary of the texture properties of the different supports used.

Table 2 lists the titration results of the acidic, basic, oxidizing, and reducing sites of the supports with cyclohexylamine (CHA), *m*-nitrobenzoic acid (MNBA), phenothiazine (PT), and tetracyanoethylene (TCNE), respectively, using a procedure developed by our team (22, 23) described below.

All supports were sifted through 200–250 mesh.

Surface chemical properties

Surface acidity and basicity of the catalysts were determined by the titration method with cyclohexylamine (CHA pK_a = 10.6), and *m*-nitrobenzoic acid (*m*-NB pK_a = 3.47), respectively. One-electron donor and one-electron acceptor properties were determined on the basis of adsorption on the catalyst surface of tetracyanoethylene (TCNE, electron affinity 2.88 eV) or phenothiazine (Ft, ionization energy 7.13 eV) using the same spectrophotometric method already cited.

In each experiment a freshly prepared titrant agent solution (10 mL) is pippeted into a cylindrical glass tube previously was loaded with the solid (about 0.1 g). The tube is fitted with a ground glass stopper, shaken for 1 h at constant temperature (298 K), and the concentration of substrate in solution, in equilibrium with the adsorbed substrate, is determined spectrophotometrically.

Sorption experiments are developed at the maximum absorption

Can. J. Chem. Downloaded from www.nrcresearchpress.com by 213.222.148.141 on 09/07/12
For personal use only.

Can. J. Chem. Downloaded from www.nrcresearchpress.com by 213.222.148.141 on 09/07/12
For personal use only.

TABLE 1. Textural properties of supports

System	Composition	(wt %)	Gelifying agent	$S_{BET\,N_2}$[c] ($m^2\,g^{-1}$)	V_p[a] ($mL\,g^{-1}$)	$\bar{r}$[b] (Å)
B	Pure $AlPO_4$		Ethylene oxide	256	0.60	40
CB	$AlPO_4$–Al_2O_3	(75/25)	Ethylene oxide	263	0.53	30
E	SiO_2–$AlPO_4$	(80/20)	Ethylene oxide	327	0.46	30
EL	SiO_2–$AlPO_4$	(80/20)	Ethylene oxide	420	0.57	32
P2	SiO_2–$AlPO_4$	(80/20)	Propylene oxide	410	0.54	35
F72	SiO_2–$AlPO_4$	(80/20)	Ammonia	280	0.46	35
S	SiO_2			395	0.55	32
$Sep_{(400)}$				280	0.48	35

[a]Accumulated pore volume.
[b]Average pore radius.
[c]Specific surface area.

TABLE 2. Determination of active sites with CHA, *m*-NB, Ft, and TCNE[a]

	Sites			
Support catalyst	Acidic ($X_m \pm 0.4$) $\times 10^4$	Basic ($X_m \pm 0.1$) $\times 10^6$	Oxidizing ($X_m \pm 0.1$) $\times 10^6$	Reducing ($X_m \pm 0.1$) $\times 10^6$
F-72	18.9	0.2	—	—
P2	15.8	1.9	—	—
S	15.5	—	—	1.0
Sep_{400}	3.4	2800.0	1.5	2.0
B	7.1	120.0	1.2	0.2
CB	6.2	53.0	0.5	0.8
E	6.9	4.6	$<1\times10^{-7}$	$<1\times10^{-7}$

[a]X_m = moles of titrant/g support, CHA = cyclohexylamine, *m*-NB = *m*-nitrobenzoic acid, Ft = phenothiazine, TCNE = tetracyanoethylene.

wavelength (λ_{max}, nm) and between the titrant concentrations where the Lambert–Beer law is fitted. The time required for the system to reach equilibrium at constant temperature was checked for each solid and titrant, and it was never more than 45 min.

The chemical interaction between the adsorbate and the surface is consistent with the Langmuir adsorption isotherm equation:

$$c/X = (1/bX_m) + c/X_m$$

where c is the concentration of substrate in solution, in equilibrium with the adsorbed substrate; b is a constant; X is the amount of adsorbed substrate per g of solid, and X_m is the monolayer coverage, which corresponds to the theoretical amount of solute by 1.0 g of solid system if all sites are covered.

The method is capable of providing useful data not only on the total concentration of sites but also on their strength as well as the relative number of sites accessible to adsorbed molecules, by the use of compounds with different pK_a (or ionization energy, or election affinity) and steric hindrance.

The determination of surface chemical properties by the spectrophotometric method was carried out in cyclohexane solutions (spectroscopic grade, Merck) at 298 K.

Catalysts

The catalysts obtained "*in situ*" were prepared by adding over the corresponding support the amount of salt required for each reaction and, over both and in this order, the donor and the protected amino acid or dipeptide, previously dissolved in methanol or a methanol – acetic acid mixture.

The catalyst not obtained "*in situ*" was prepared by incipient impregnation with Na_2PdCl_4, drying in an oven at 110°C for 24 h, calcination (by increasing the temperature at a rate of 1°C min^{-1} up to 250°C) and subsequent reduction in a hydrogen stream at a flow-rate of 60 mL min^{-1}, following the same thermal treatment as for its calcination. It is labelled Pd_3F-72, the postscript indicating the Pd content (%).

Catalysts promoted by alkaline hydroxides

In this case, the amount of alkaline hydroxide needed was added over the support – metal salt mixture, and the remainder of reagents were then added as for the catalysts not promoted by alkaline hydroxides. The metal precursor used in this case was always $PdCl_2$ from Riedel (ref. 14757).

The commercial catalyst used as reference consists of 10% Pd over carbon (Fluka, ref. 75990).

Chemicals

Both Pd salts, hydrogen donors, and protected amino acids and dipeptides used were commercial reagents supplied by Merck, Fluka and Sigma. All were distilled or recrystallized prior to use.

Product analysis

The reaction products, once homogenized with excess methanol, were analyzed by hplc, using a Perkin-Elmer series 2 liquid chromatograph furnished with a variable-wave LC-75 ultraviolet detector. The working wavelength was 254 nm. An LKB column (LiChrosorb RP-18, 5 μm 4 × 250 mm) was used. A methanol–water mixture (75:25 by volume) with a flow of 0.8 mL min^{-1} were used as carrier. The internal standard employed was naphthalene.

In addition to the deprotecting product, the deprotecting of the benzyloxycarbonyl group (Z) yields CO_2 and toluene. Cyclohexene used as a donor is transformed into benzene. The occurrence of both toluene and benzene has been checked by gc–ms, using the Hewlett-Packard 5990B system and a column (2 m long, 1/8 in. wide) containing 5% polyphenyl ether over chromosorb GAW-DMCS. Free amino acids and peptides were recovered by distillation of the solvent and subsequent recrystallization. Their melting points were checked

TABLE 3. Influence of the temperature on the hydrogenation reaction (transfer) of Z-glycine

(*a*) Donor concentration, 3.94×10^{-2} mol; acceptor concentration, 1.44×10^{-3} mol; solvent, 5 mL MeOH; catalyst, Pd_3 F-72, 0.5 g; *t*, 6 h

Donor	X_{30} (%)	X_{80} (%)
Cyclohexene	100.0	100[a]
Formic acid	12.8	49.7

[a]Reaction time, 2 h.

(*b*) Donor (cyclohexene) concentration, 3.94×10^{-2} mol; acceptor concentration; 1.44×10^{-3} mol; solvent, 5 mL MeOH; catalyst, Pd_3Sep_{400}, 0.5 g, reactions in a closed reactor; *t*, 3 min

Temperature	*X* (%)
30	7
40	23
50	56
60	100

on an oil-bath apparatus and were consistent with those given in the literature for the pure products.

Thermogravimetric analysis

The catalyst was placed in the thermogravimetric analyser (Cahn 2000) and allowed to dry under flowing N_2 overnight. The TGA was conducted in an air atmosphere at a heating rate of 10 K/min.

X-Ray diffraction analysis

X-Ray diffractograms were recorded on a Siemens D 500-1 apparatus, by using the Cu K_α radiation, with $\lambda = 1.5418$ Å.

Determination on the Pd content

The chemical analysis of the metal content was made by atomic absorption spectrometry using a Perkin-Elmer 370 instrument with a hollow cathode lamp, at $\lambda = 247.8$ nm.

Experimental setup and conditions

The reactions were carried out in a two-necked flask fitted with a reflux condenser and septum for all the samples, using 1.44×10^{-3} mol of protected amino acid or dipeptide, 0.5 g of 3% palladium supported catalyst and 3.97×10^{-2} mol of hydrogen donor and 5 mL of methanol as solvent. Some acetic acid had to be added in order to facilitate the dissolution of the starting product in the case of the dipeptides. The reaction mixture was placed on a silicone bath at 30°C and stirred magnetically at 700 rpm. Under these conditions we have verified that the process is not diffusion-controlled. Moreover, blank runs indicated a lack of activity in the absence of metallic phase, even in the presence of pure supports.

Results and discussion

Table 3 lists the results obtained on the effect of temperature on the deprotecting rate of Z-glycine. As can be seen, the effect is significant. When using cyclohexene as a donor, the time needed to achieve 100% conversion is three times shorter at 80°C than at 30°C. Nevertheless, for subsequent experiments, we chose a temperature of 30°C because the thermal lability of some groups occurring in natural products.

As can be seen in Table 4, the catalyst reduced "*in situ*" is much more active than that prepared by a conventional incipient impregnation procedure when using the commonest hydrogen donors cyclohexene and formic acid. For this reason, we only employed catalysts reduced "*in situ*" in all subsequent experiments.

TABLE 4. Effect of preparation procedure on catalyst[a]

Donor	Catalyst "*in situ*" *X* (%)	$t_{reaction}$ (h)	Pd_3 F-72[b] *X* (%)	$t_{reaction}$ (h)
Cyclohexene	100	2	40.0	2[c]
Formic acid	19	6	12.8	6

[a]Support, F-72; salt, Cl_4PdNa_2; donor, 3.94×10^{-2} mol cyclohexene; acceptor, 1.44×10^{-3} mol Z-Gly. Solvent, 5 mL methanol; reaction temperature, 30°C. We have used only formic acid both as the solvent and the donor, the resulting yield is the same.

[b]Catalyst prepared by incipient impregnation as described under "Experimental".

[c]*X* (%) = 100 at $t_{reaction} = 6$ h.

Table 5 lists the results obtained in analyzing the influence of the precursor salt. The reaction rate decreases in the order $(CH_3COO)_2Pd > Na_2PdCl_4 > Pd(NO_3)_2$ for salts dissolved in dimethylformamide. For a given salt (e.g. Na_2PdCl_4 dissolved in H_2O or DMF), the activity of the catalyst obtained is higher for aqueous solutions than for organic solvent.

The results of the XPS experiments, carried out with an Mg excitation source and an MgK_α anode at a potential of 12 kV, an intensity of 20 mA, a multiplier potential of 2.8 kV, and a vacuum of 10^{-8} mbar by recording at a constant *E*, are shown in Figs. 1–4 for the systems obtained using Na_2PdCl_4, $Pd(NO_3)_2$, $Pd(CH_3COO)_2$, and $(NH_3)_4PdCl_2$, respectively, as precursors. As can be seen, the results show that the systems formed from the precursors Na_2PdCl_4, $Pd(NO_3)_2$, and $(CH_3COO)_2Pd$ contain no unreduced Pd. On the other hand, some Pd^{2+} was found in the $Cl_2(NH_3)_4Pd$ sample. The high stability of the Pd—NH_2 bond obviously hinders the precursor reduction.

By using molecular hydrogen we have checked that Na_2PdCl_4, $Pd(CH_3COO)_2$, and $Pd(NO_3)_2$ also reduced much more readily than $(NH_3)_4PdCl_2$. Since the dispersion of Pd in these systems generated "*in situ*" is similar, their differences in activity must be related (at least in part) to the ease of reduction of the different precursors. This points to Pd^0 rather than to any Pd^{2+} salt or complex as the actual catalytic species.

To demonstrate that the catalytic activity is related to the Pd^0 content, we carried out the following experiments: (*a*) determination of Pd^{2+} in the liquid phase and on the support after 5 min reaction for all Pd precursors used. (*b*) Determination of Pd^{2+} from precursor Na_2PdCl_4 after reacting for 5 min in the absence of support. No Pd^{2+} from the Na_2PdCl_4 remains in solution after reacting for 5 min while both Pd^0 and Pd^{2+} from $Pd(NO_3)_2$ and $(CH_3COO)_2Pd$ are found. On the other hand, only Pd^{2+} (2.5% in solution and the remainder adsorbed on the support) is found from $Cl_2(NH_3)_4Pd$. (*c*) TGA studies of the catalyst samples from Na_2PdCl_4 as precursor, both in the absence and presence of the support. A weight increase equivalent to 95% of that theoretically corresponding to the full conversion of Pd^0 present to PdO was found. (*d*) X-Ray diffraction studies of the catalyst samples prior to and following the TGA: The results obtained allow us to state that the samples are Pd^0 ($2\theta = 40.4$; $2\theta = 47.2$), see Fig. 5*a*, and PdO ($2\theta = 34$; $2\theta = 55$), see Fig. 5*b*, before and after the TGA, respectively.

We therefore believe the Pd^0 content is the determining factor of the rates found.

As for hydrogen donors (Table 6), cyclohexene yields much

Can. J. Chem. Downloaded from www.nrcresearchpress.com by 213.222.148.141 on 09/07/12
For personal use only.

TABLE 5. Influence of precursor salt on hydrogenolysis (transfer) of Z—glycine[a]

Precursor salt	d (A)	Solvent	X_1 (%)	t_1 (h)	t_2 (h)	X_2 (%)
Cl_4PdNa_2	40	H_2O	100.0	2	$1\frac{1}{2}$	89.0
$(NO_3)_2Pd$	52	DMF	60.1	8		
$Cl_2(NH_3)_4Pd$	42	H_2O	100.0	8	$1\frac{1}{2}$	23.0
$(CH_3COO)_2Pd$	45	DMF	87.1	8		
Cl_4PdNa_2	58	DMF	65.4	8		

[a]Support, F-72; donor, 3.94×10^{-2} mol cyclohexene; acceptor, 1.44×10^{-3} mol Z-Gly; solvent, 5 mL MeOH; reaction temperature, 30°C; catalyst: 0.5 g; d (A): average particle diameter by XRD.

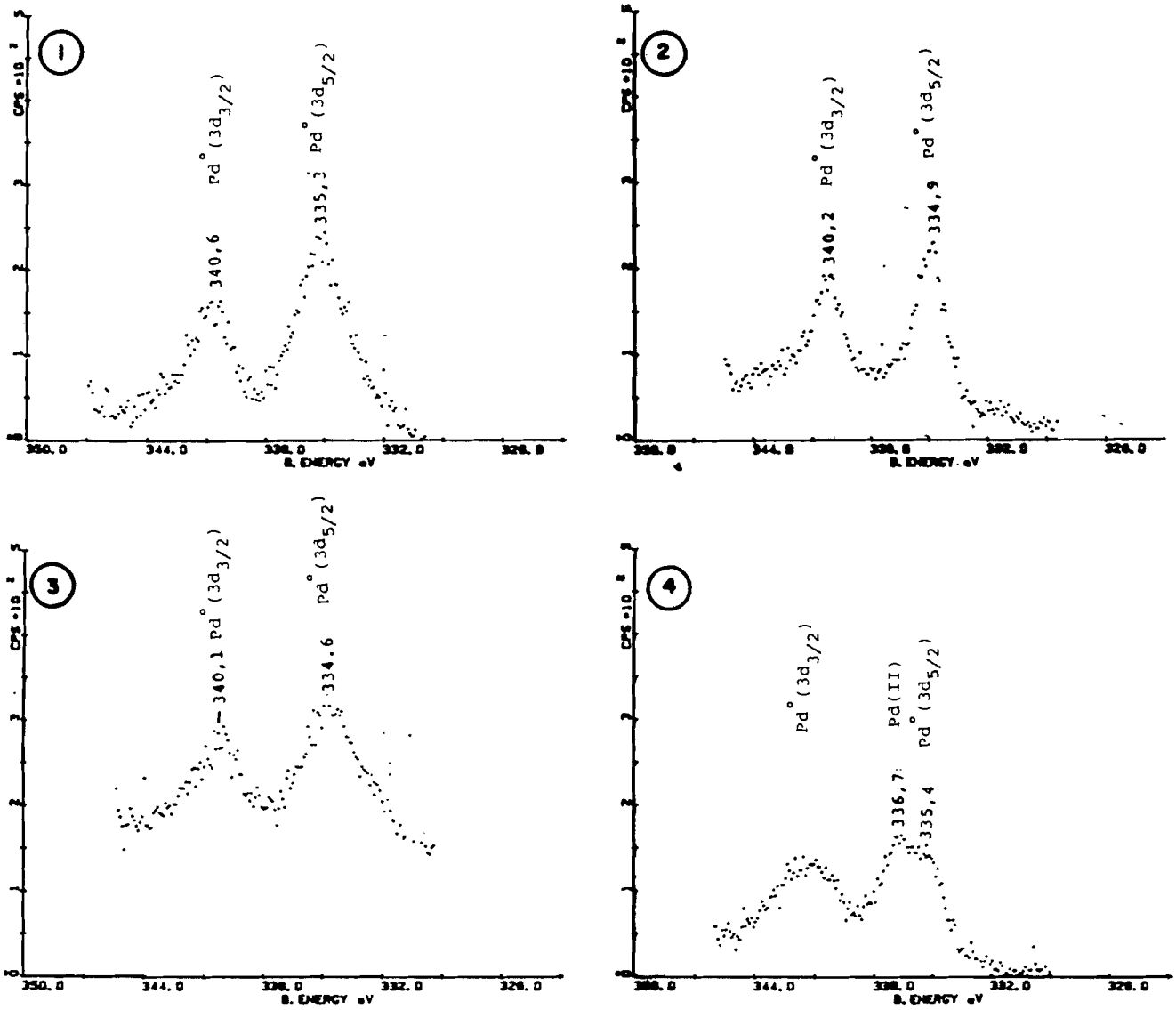

FIGS. 1–4. Results of the XPS experiments carried out on the systems obtained from the precursors Na_2PdCl_4, $Pd(NO_3)_2$, $(CH_3COO)_2Pd$, and $(NH_3)_4PdCl_2$, respectively.

better results than the others. Moreover, neither limonene nor tetralin used at 30°C for 2 h allows the desired deprotecting. In both cases Na_2PdCl_4 remains unchanged.

Silica has proved to be the most efficient support (Table 7), followed by the SiO_2–$AlPO_4$ systems. Thus, the order of activity found according to the support used was F-72 > P2 > E > CB > Sep. This order can be accounted for by the acidic sites of these supports (see Table 2). The higher the density of acidic sites, the more favourable the hydrogenolysis of the protecting group. The order varies inversely with the number of basic sites: the higher their density, the lower the hydrogenolysis rate. In fact, it is the silica support which contains a large number of acidic sites and a high density of reducing sites, but virtually no basic centres, which yields the best results.

Can. J. Chem. Downloaded from www.nrcresearchpress.com by 213.222.148.141 on 09/07/12
For personal use only.

Can. J. Chem. Downloaded from www.nrcresearchpress.com by 213.222.148.141 on 09/07/12
For personal use only.

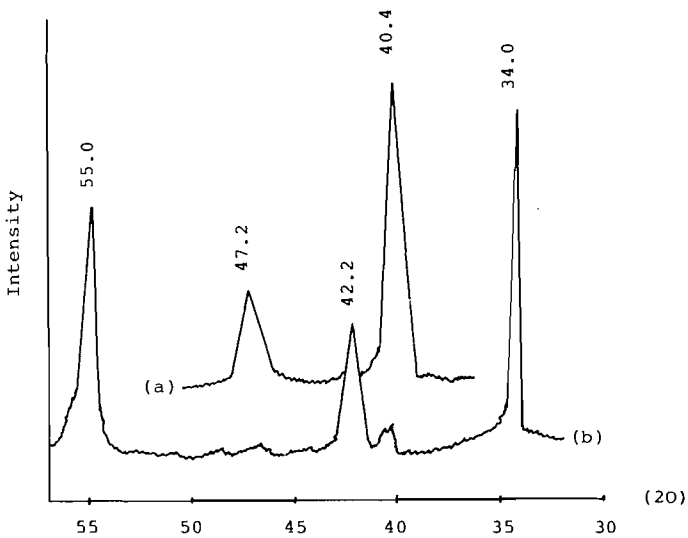

FIG. 5. X-ray diffractograms of the catalyst samples prior to (*a*) and following (*b*) the TGA.

TABLE 6. Influence of the type of donor on the hydrogenolytic reaction (transfer)[a]

Donor	Toluene (%)
Cyclohexene	100.0
Formic acid	4.5
Formic acid – triethylamine	10.5
Limonene	0.0
Tetralin	0.0

[a]Support, F-72; salt, Cl_4PdNa_2; solvent, 5 mL MeOH; donor, 3.97×10^{-2} mol; acceptor, 1.44×10^{-3} mol; reaction temperature, 30°C. Neither limonene nor tetralin tarnish the catalyst at this temperature. The use of tetralin at 80°C results in reduction of the catalyst, although the reaction does not develop. Limonene does not even bring about catalyst reduction. *t*, 2 h.

TABLE 7. Influence of support on hydrogenolysis (transfer) of Z—glycine[a]

Support	X_1 (%)	t_1 (h)	t_2 (h)	X_2 (%)
F-72	100.0	2	1½	89.0
P-2	100.0	2.5	1½	66.0
E	100.0	4	1½	41.1
CB	100.0	8	1½	16.0
B	100.0	8	1½	12.0
SiO_2	100.0	1.5		
Sepiolite 300	79.3	8		
Sepiolite 400	80.7	8		
Unsupported	25.0	8		

[a]Salt, Cl_4PdNa_2; donor, 3.94×10^{-2} mol cyclohexene; acceptor, 1.44×10^{-3} mol; solvent, 5 mL MeOH; reaction temperature, 30°C.

On the other hand, the yields obtained in the absence of support (Table 7) are substantially lower than those achieved with any of the supports assayed.

Table 8 shows the results found in the possible promoting effect of NaOH. We found an optimum molar ratio of NaOH-to-Pd of 4. The influence of alkaline hydroxides on the promotion of Pd catalysts has been widely discussed by several authors (24), and our team encountered this effect in earlier works (e.g. in the reduction of benzylidene derivatives (25) and other organic functions (26)). Table 9 also shows the effect of the type of alkaline hydroxide on the optimum ratio found. The order found was $Na^+ > K^+ > Li^+$. The greater similarity between the ionic radii of Na and Pd ($r_{Pd^{2+}} = 0.86$, $r_{Na^+} = 0.95$, $r_{Li^+} = 0.60$, $r_{K^+} = 1.33$ Å) could account for this order. Other authors (27) have found that LiOH exerts a more marked effect on the promotion of Ni catalysts, which is logical taking into account the greater similarity between the ionic radii of Ni^{2+} and Li^+ ($r_{Ni^{2+}} = 0.63$ Å).

The strong promoting effect of alkaline hydroxides is attributed in this particular case to the formation of a Pd^{2+} hydroxide reported as an active catalyst (7), or its precursor (28) in hydrogenolytic processes. On the other hand, we have verified that the NaOH-to-Pd ratio influences the Pd dispersion (25, 26) as stated by other authors who have used Pd/C (28) and $Co/\gamma\text{-}Al_2O_3$ catalysts (29).

Table 10 compares the conversions obtained with different amino acids protected in their amino group by a benzyloxycarbonyl function (Z). The presence of sulphur (e.g. in methionine) inhibits the deprotecting as the Pd salt remains dissolved and does not allow the formation of the catalytic species. The rate order found for the different amino acids glycine > alaline > valine coincides with an increasing order of steric hindrance of the adsorption of the protected amino group on the catalyst. In comparing serine and alanine, the higher rate of the former could be attributed to the negative interaction of the OH group, since its binding to the catalyst via this position would hinder the hydrogenolysis of the Z—N— group. The adsorption mechanism also seems to be a decisive factor for the dipeptides analyzed (see Table 11). These compounds bear two —NH— groups which can bind to the catalyst. The introduction of CH_3— groups next to the peptide —NH— groups will indirectly favour the adsorption via blocked —NH— and hence the hydrogenolysis Z—Gly—Gly > Z—Gly—Ala. As can be seen, the introduction of an aromatic ring in the vicinity of a peptide —NH— group which is strongly absorbed on the catalyst (Z—Gly—Gly—nitrophenylester) hinders the deblocking. Again, in Z—Valyl—Ala methyl ester, the presence of the isopropyl group of valine slows down the reaction through the steric hindrance of the adsorption via Z—NH— group.

In summary, the ease of adsorption on the catalyst is a decisive factor in accounting for the order of deblocking rates found. The deblocking rates obtained with our catalysts are much higher than that of the Pd(10%)/C catalyst supplied by Fluka (ref. 75990): in fact, this commercial catalyst achieves a deblocking less than 1% for Z—glycine after 2 h, whereas support F-72 and the use of the optimum NaOH-to-Pd ratio for 1 h allows 100% conversion. Further experiments made by our team have shown that our catalysts are highly active in the hydrogenolysis of benzyl ethers and esters. On the other hand, we have started to perform the deblocking in a closed reactor (Berghol Heiz) by hydrogen transfer at 40°C, achieving 100% conversion in 5 min by using the optimum catalyst reported in this paper and the amounts of hydrogen donor and substrate described under "Experimental". Ultrasonic agitation (see Table 10) yielded better results than magnetic stirring (48% and 10% respectively, at 20°C for 5 min).

TABLE 8. Optimization of the NaOH-to-Pd ratio for hydrogenolysis (transfer) of Z—glycine[a]

Mol Na^+/g cat	Molar Pd/Na ratio	X_1 (%)	t_1 (h)	X_2 (%)	t_2 (h)
0	1:0	100	5	9	1/2
5.5×10^{-4}	1:2	100	2	30	1/2
8.3×10^{-4}	1:3	100	1½	37	1/2
1.1×10^{-3}	1:4	100	1	56	1/2
1.4×10^{-3}	1:5	100	5	17	1/2

[a]Support, F-72; salt, Cl_4PdNa_2; donor, 3.94×10^{-2} mol cyclohexene; acceptor, 1.44×10^{-4} mol; solvent, 5 mL MeOH; reaction temperature, 30°C; amount of catalyst, 0.5 g.

TABLE 9. Effectiveness of Li^+, Na^+, and K^+ as promoters[a]

Promoter-to-catalyst (mol/g cat)	Molar Pd/M^+ ratio	Promoter	X_1 (%) (1 h)	X_2 (%) (½ h)
1.1×10^{-3}	1:4	Li^+	100	38
1.1×10^{-3}	1:4	K^+	100	40
1.1×10^{-3}	1:4	Na^+	100	56

[a]Support, F-72; salt, Cl_2Pd; donor, 3.94×10^{-2} mol cyclohexene; acceptor, 1.44×10^{-3} mol; solvent, 5 mL MeOH; reaction temperature, 30°C. All promoters were added as hydroxides dissolved in water.

TABLE 10. Deprotecting of various Z — amino acids[a]

Product	X (%)	Reaction time (h)
Z—Met	0.0	1
Z—Val	80.5	1 (100% 1½ h)
Z—Ser	55.0	1 (80.2% 1½ h)
Z—Ala	83.8	1 (100% 1½ h)
Z—Gly	100.0	1
Z—Gly	100.0	5 min (1)
Z—Gly	48.0	5 min (2)

[a]Donor, 3.94×10^{-2} mol cyclohexene; support, F-72; salt, Cl_4PdNa_2; acceptor, 1.44×10^{-3} mol; solvent, 5 mL MeOH. These reactions were carried out under optimum conditions Pd^{2+}/Na^+ = 1:4. Reaction temperature, 30°C; (*1*) reaction in a closed reactor by hydrogen transfer at 40°C; (*2*) reaction in a closed reactor by hydrogen transfer at 20°C and stirred ultrasonically.

TABLE 11. Deprotecting reactions (transfer) of Z—dipeptide carboxy-derivatives[a]

Product	X_1 (%) at 1 h	X_2 (%) at 8 h
Z—Gly—Gly	22	100
Z—Gly—Ala	34	100
Z—Gly—Gly—*p*-nitrophenyl ester	<2	24.6
Z—Val—Ala—methyl ester	<5	33.8

[a]Donor, 3.94×10^{-2} mol cyclohexene; support, F-72; salt, Cl_4PdNa_2; acceptor, 1.44×10^{-3} mol; solvent, 1:1 MeOH/AcH; reaction temperature, 30°C.

We also performed tests to determine the possible racemization caused by the support or the reaction medium. As far as Z—L-alanine is concerned, the specific optical activity of the reaction product allows one to state that racemization is negligible. We have applied Izumiya's test to Z—L-alanyl—L-phenylalanine, finding no diastereoisomers when using the optimum catalyst.

Acknowledgements

This work was financially supported by a grant from the "Consejería de Educación y Ciencia de la Junta de Andalucía".

The authors are grateful to Professors G. Munuera and A. R. González-Elipe, of the XPS service of the Department of Inorganic Chemistry, University of Seville, for realization of the XPS experiments.

1. (*a*) G. BRIEGER and T. NESTRICK. Chem. Rev. **74**, 567 (1974); (*b*) R. A. W. JOHNSTONE, H. WILBY, and I. A. ENTWISTLE. Chem. Rev. **85**, 129 (1985).
2. G. M. ANANTHARAMAIAH and K. M. SIVANANDAIAH. J. Chem. Soc. Perkin Trans. I, 490 (1977).
3. A. M. FELIX, E. P. HEIMER, T. J. LAMPROS, CH. TZOUGRAKI, and J. MEIENHEFER. J. Org. Chem. **43**, 4194 (1978).
4. S. A. KHAN and K. M. SIVANANDAIAH. Synthesis, 750 (1978).
5. B. ELAIM, G. M. ANANTHARAMAIAH, G. P. ROYER, and G. E. MEANS. J. Org. Chem. **44**, 3442 (1979).
6. K. M. SIVANANDAIAH and S. GURUSIDDAPPA. J. Chem. Res. **5**, 108 (1979).
7. S. HANESSIAN, T. J. LIAK, and B. VENESSE. Synthesis, 396 (1981).
8. A. E. JACKSON and R. A. W. JOHNSTONE. Synthesis, 685 (1976).
9. (*a*) M. K. ANNER and A. F. SPATOLA. Synthesis, 929 (1980); (*b*) K. MOHMED, A. SPATOLV, and A. SPATOLA. J. Org. Chem. **48**, 3503 (1983).
10. A. ARAMENDIA, V. BORAU, C. JIMENEZ, J. M. MARINAS, and A. PAJARES. J. Catal. **78**, 188 (1982).
11. A. ARAMENDIA, V. BORAU, M. C. GOMEZ, C. JIMENEZ, and J. M. MARINAS. Appl. Catal. **8**, 177 (1983).
12. A. ALBA, A. ARAMENDIA, V. BORAU, A. GARCIA RASO, C. JIMENEZ, and J. M. MARINAS. Can. J. Chem. **62**, 917 (1984).
13. A. ALBA, A. ARAMENDIA, V. BORAU, C. JIMENEZ, and J. M. MARINAS. React. Kinet. Catal. Lett. **25**, 45 (1984).
14. A. ARAMENDIA, V. BORAU, C. JIMENEZ, and J. M. MARINAS. Gazz. Chim. Ital. **114**, 451 (1984).
15. M. A. ARAMENDIA, V. BORAU, C. JIMENEZ, and J. M. MARINAS. React. Kinet. Catal. Lett. **19**, No 1-2, 233 (1982).
16. M. A. ARAMENDIA, V. BORAU, J. F. GOMEZ, and J. M. MARINAS. Appl. Catal. **10**, 347 (1984).
17. M. A. ARAMENDIA, V. BORAU, J. F. GOMEZ, C. JIMENEZ, and J. M. MARINAS. React. Kinet. Catal. Lett. In press.
18. A. ALBEROLA and J. M. MARINAS. An. Quim. **65**, 1001 (1969).
19. C. JIMENEZ, J. M. MARINAS, R. PEREZ-OSSORIO, and J. V. SINISTERRA. An. Quim. **73**, 1164 (1977).
20. C. JIMENEZ, J. M. MARINAS, J. V. SINISTERRA, and V. BORAU. An. Quim. **73**, 561 (1977).
21. J. M. CAMPELO, J. M. MARINAS, and R. PEREZ-OSSORIO. An. Quim. **72**, 698 (1976).
22. J. M. MARINAS, C. JIMENEZ, J. M. CAMPELO, M. ARAMENDIA,

Can. J. Chem. Downloaded from www.nrcresearchpress.com by 213.222.148.141 on 09/07/12
For personal use only.

V. Borau, and D. LUNA. 7th Simp. Ibero-Amer. de Catal. La Plata (Argentina) 79 (1980).
23. M. A. ARAMENDIA, C. JIMENEZ, V. BORAU, and J. M. MARINAS. Acta Cient. Venezolana, **32**, 369 (1983).
24. (*a*) W. D. MROSS. Catal. Rev. Sci. Eng. **25**(4), 951 (1983); (*b*) A. LYCOURGHIOTIS, C. DEFOSSE, and B. DELMON. Rev. Chim. Minerale, **16**, 473 (1979).
25. A. ALBA, A. ARAMENDIA, V. BORAU, C. JIMENEZ, and J. M. MARINAS. Can. J. Chem. **63**, 3471 (1985).
26. M. A. ARAMENDIA, V. BORAU, C. JIMENEZ, J. M. MARINAS, and M. E. SEMPERE. React. Kinet. Catal. Lett. **27**, No 1, 133 (1985).
27. R. B. BLANCE and D. T. GIDSON. J. Chem. Soc. 2487 (1954).
28. R. J. CARD, J. L. SCHMITT, and J. M. SIMPSON. J. Catal. **79**, 13 (1983).
29. A. LYCOURGHIOTIS, C. DEFOSSE, F. DELAUNAY, J. LEMAITRE, and B. DELMON. J. Chem. Soc. Faraday I, **76**, 1677 (1980).

Can. J. Chem. Downloaded from www.nrcresearchpress.com by 213.222.148.141 on 09/07/12
For personal use only.

Analytical potentiometric data analyses of metal–ligand equilibria by microcomputer. A general procedure for minimizing potential sources of errors and a fast linear-scaled least-squares algorithm[1]

PATRICK DECOCK[2] AND BIBUDHENDRA SARKAR[3]

Research Institute, The Hospital for Sick Children, Toronto, Ont., Canada M5G 1X8
and Department of Biochemistry, University of Toronto, Toronto, Ont., Canada M5S 1A8

Received January 19, 1987[4]

PATRICK DECOCK and BIBUDHENDRA SARKAR. Can. J. Chem. **65**, 2798 (1987).

Analytical potentiometry is a powerful technique to investigate multiple species in solution and their formation constants. However, there have been some difficulties in this method resulting primarily from the theoretical approach. In this paper we critically examined them and improvements have been implemented successfully. Suitable experimental designs are adapted and preliminary computation of potentiometric data are performed to minimize potential sources of errors. Criteria are proposed to choose the best set of titration curves. A correction is introduced to partially minimize the errors originating from the volume variation. A linear-scaled minimization algorithm has been implemented to extract the value of the complex stability constants from the experimental free ion concentrations. This has two advantages over the earlier non-linear minimization process. The execution time is faster and it facilitates the selection of the best fit of species. A series of 14 programs are introduced to run on a low memory microcomputer.

PATRICK DECOCK et BIBUDHENDRA SARKAR. Can. J. Chem. **65**, 2798 (1987).

Il est reconnu que la méthode de potentiométrie analytique présente un grand intérêt dans l'étude de la répartition des espèces en solution. Elle permet d'accéder à la valeur de leur constante de formation. L'approche théorique de cette technique repose sur des approximations conceptuelles qui n'ont pas pu être totalement contournées dans les versions antérieures. Nous avons examiné les points les plus critiques afin d'y pallier. (Aucun programme, aussi sophistiqué soit il, ne peut aboutir à des résultats valables qu'avec des données qui le sont également.) Aussi une méthodologie expérimentale, liée à des calculs préliminaires sur les données potentiométriques, est proposée. Elle contribue à minimiser les sources d'erreurs expérimentales potentielles. Des critères ayant pour but de sélectionner les meilleurs jeux de courbe de titration sont décrits. Des corrections, réduisant les effects des variations des volumes, sont exposées. Un processus de minimisation linéaire, permettant d'extraire les valeurs des constantes de formation des complexes de celles des concentrations en ions libres expérimentales a été introduite avec succès. Ce type de minimisation présente deux avantages essentiels sur les techniques non linéaires utilisées antérieurement. Elle est rapide en temps d'exécution machine et elle est en soit un critère de selection du choix des espèces présentes en solution. Une série de 14 programmes, concus spécialement dans le contexte de la microinformatique est introduite.

Can. J. Chem. Downloaded from www.nrcresearchpress.com by 213.222.148.141 on 09/07/12
For personal use only.

Introduction

Based on a procedure by Lefebvre (1), Österberg (2) and Sarkar and co-workers (3–5) had developed a method for determining the concentration of free ligand(s) and metal as a function of pH in a multicomponent system at equilibrium. Subsequently, this laboratory has used this technique extensively to study a variety of metal–ligand equilibria of biological interest (6–14). There are variations of this procedure which are alternatively called as FICS (free ion concentrations in solution) or analytical potentiometry (15–17). There are also other techniques (18–25) available to study species distribution and formation constants which employ different approaches to calculate free concentrations of ions. They all need high speed and large memory computers.

Successful application of analytical potentiometry requires a large quantity of data and high degree of experimental accuracy. The last difficulty can be partially solved by using high concentration of ligands and metal if there is no problem of solubility. Attempts have been made to minimize potential sources of errors by adapting newer experimental designs (15). In this paper we propose a general method which reduces the number of experimental data and at the same time increases the overall accuracy. A correction is included which takes into account the volume variation during the titration. A linear-scaled least-squares algorithm is proposed to expedite the microcomputer solution of metal complex stability constants from potentiometric data. Contrary to the non-linear procedures, this method of minimization allows one to choose the correct set of species easily.

Theory

In analytical potentiometry, the basic relationship for determining the average free concentrations $\bar{C}_i^{\nu}$ at pH = ν in complex equilibria is

$$[1] \quad p\bar{C}_i^{\nu} = p\bar{C}_i^{0} - \int_{pH^0}^{pH} \left(\frac{\partial T_{i,j}^{*\nu}}{\partial T_{i,j}^{\nu}} \right)_{T_{s,j}^{\nu}(s \neq i),\, pH,\, \theta,\, v} dpH$$

where C_i^0 is the average free concentration of ion i (for metal $i = 1$, for ligand 1 and 2, $i = 2$ and 3) at initial pH (pH^0). $T_{i,j}^{\nu}$ and $T_{i,j}^{*\nu}$ are the analytical concentration of ion i and the concentration of protons liberated, respectively, at pH = ν.

To evaluate the derivative part of eq. [1], we assume that the hypersurface which is determined by the ratio of pH and the concentrations $T_{i,j}^{\nu}$ ($i = 1$ to 3) is flat (1). This condition must be examined carefully for all titration sets. With the above assumption as well as taking into consideration of all the constants of eq. [1], a linear correlation between $T_{i,j}^{*\nu}$ and $T_{i,j}^{\nu}$ can be expected. Consequently the derivative term of eq. [1] is the slope (S_i^{ν}) of this straight line. However, establishing such ideal conditions is not feasible, hence we decided to make an

[1]Details concerning the availability of programs, list data and results, and a comprehensive user's manual can be obtained by writing to the authors.

[2]Permanent address: Laboratoire de Chimie Minerale et Methodologie Analytique, Universite des Sciences et Techniques de Lille, U.E.R. de Chimie, Villeneuve, d'Ascq Cedex, France.

[3]To whom all correspondence should be addressed.

[4]Revision received July 31, 1987.

Can. J. Chem. Downloaded from www.nrcresearchpress.com by 213.222.148.141 on 09/07/12
For personal use only.

approximation relating $T_{i,j}{}^{*\nu}$ and $T_{i,j}{}^{\nu}$ by a linear least-squares line passing through three different values of j. Our objective is to increase the probability of keeping the line in a flat region of the hypersurface. This is closely approximated by limiting the titration set to three curves and using the differences between $T_{i,j}{}^{\nu=\mathrm{pH}_0}$. Satisfactory results have been obtained with several systems following such an approach (26).

All our titrations are carried out in the presence of an excess of strong acid. This serves three important functions: it enables one to verify the electrode response; low pH causes complete protonation of ligand(s); and it facilitates the measurement of the accurate amount of ligand(s) in the complex solution. We take into account the excess of strong acid (NH_j) in the following eq. [2]

$$[2]\quad T_{i,j}{}^{*\nu} = \frac{V_j{}^{\nu} \times \mathrm{CB}_j + \mathrm{NH}_j}{V_j{}^{0} + V_j{}^{\nu}}$$

where $V_j{}^0$ is the initial volume of the solution, CB_j is the base concentration of the titration j, $V_j{}^{\nu}$ is the added volume of base at pH = ν for the titration j.

The analytical concentration of metal and ligand(s) are given in eq. [3]

$$[3]\quad T_{i,j}{}^{\nu} = \frac{N_{i,j}}{V_j{}^{0} + V_j{}^{\nu}}$$

where $N_{i,j}$ is the analytical mole number of ion i.

Calculations of the slopes $S_j{}^{\nu}$ are performed for all the combinations of ligand(s) or metal variations by sets of three titrations. The best set of curves is chosen using the following criteria:

1. Lowest sum of standard deviations of the least squares lines calculated at each pH.
2. Minimum value at each pH of the quantities appearing in

$$\frac{T_{i,2}{}^{*\nu} - T_{i,1}{}^{\nu}}{T_{i,2}{}^{\nu} - T_{i,1}{}^{\nu}} - S_i{}^{\nu} \quad \text{and} \quad S_i{}^{\nu} - \frac{T_{i,3}{}^{*\nu} - T_{i,2}{}^{\nu}}{T_{i,3}{}^{\nu} - T_{i,2}{}^{\nu}}$$

3. Lowest degree of curvature (DC_i) of the function $T_{i,j}{}^{*\nu}$ against $T_{i,j}{}^{\nu}$ at each pH as it is defined in eq. [4]

$$[4]\quad \mathrm{DC}_i = \sum_{\nu=\mathrm{pH}^0}^{\mathrm{pH}} T_{i,2}{}^{*\nu} - (T_{i,3}{}^{*\nu} - T_{i,1}{}^{*\nu}) \times (T_{i,2}{}^{\nu} - T_{i,1}{}^{\nu})/(T_{i,3}{}^{\nu} - T_{i,1}{}^{\nu}) - T_{i,1}{}^{*\nu}$$

The coefficients j (1 to 3) are such that

$$[5]\quad T_{i,j=1}^{\nu} < T_{i,j=2}^{\nu} < T_{i,j=3}^{\nu}$$

4. In the case of metal variation (i = 1), an additional criterion is adopted: Minimum deviation between the volume of added base extracted from the set of three titrations at the extrapolated (β^{ν}) zero metal concentration and the same volume calculated from $\mathrm{p}K_a$ values. It is performed utilizing the following equations:

$$[6]\quad H^* = [\mathrm{H_3O^+}] - K_w/[\mathrm{H_3O^+}]$$

$$[7]\quad \mathrm{NU}_t{}^{\nu} = \mathrm{NP}_t + \sum_{r=1}^{\mathrm{NP}_t} (\mathrm{NP}_t - r) \frac{[\mathrm{H_3O^+}]}{\prod_{k=1}^{r} K_{\mathrm{a}_{t,k}}}$$

where NP_t is the number of titratable protons of ligand(s) ($t = i - 1$) and $K_{\mathrm{a}_{t,k}}$ the kth acidity constant of ligand t.

$$[8]\quad \mathrm{DE}_t{}^{\nu} = 1 + \sum_{r=1}^{\mathrm{NP}_t} \frac{[\mathrm{H_3O^+}]}{\prod_{k=1}^{r} K_{\mathrm{a}_{t,k}}}$$

$$[9]\quad \mathrm{DB}^{\nu} = \frac{B^{\nu}}{C_m} + \mathrm{NH_m} - \left(\sum_{t=1}^{\substack{nb\ of \\ ligands}} \left(N_{t+1,\mathrm{m}} \frac{\mathrm{NU}_t{}^{\nu}}{\mathrm{DE}_t{}^{\nu}} \right) + \mathrm{NH_m} - H^* V_m{}^{0} \right) \div \left(\mathrm{CB_m} + H^* \right)$$

In the above eq. [9] the subscript m indicates values corresponding to the middle point titration curve. The results are computations of all combinations of sets of three titration curves. The above-mentioned criteria allow one to choose the best set of titration curves.

The integral of eq. [1] is evaluated by Simpson's numerical integration taking into account the volume variation as follows:

$$[10]\quad I_i{}^{\nu} = I_i{}^{\nu-1} - \log (V_m{}^{0} + V_m{}^{\nu-1}) + \log (V_m{}^{0} + V_m{}^{\nu}) + f(\mathrm{pH}, S_i{}^{\nu})$$

where $f(\mathrm{pH}, S_i{}^{\nu})$ is the classical Simpson's function. The initial value of $I_i{}^{\nu}$ corresponding to pH^0 ($I_i{}^{\mathrm{pH}^0}$) is given for metal ion by eq. [11] and for the fully protonated ligand(s) by eq. [12]

$$[11]\quad I_1{}^{\mathrm{pH}^0} = -\log N_{1,m} + \log (V_m{}^{0} + V_m{}^{\mathrm{pH}^0})$$

$$[12]\quad I_i{}^{\mathrm{pH}^0}(i = 2 \text{ or } 3) = -\log N_{1,\mathrm{m}} + \log (V_m{}^{0} + V_m{}^{\mathrm{pH}^0}) + \log \left(1 + \sum_{r=\mathrm{NP}_t}^{1} \frac{\prod_{k=\mathrm{NP}_t}^{r} K_{\mathrm{a}_{t,k}}}{[\mathrm{H}^0]^r} \right)$$

For metal ion

$$[13]\quad \mathrm{p}\bar{C}_1{}^{\nu} = I_1{}^{\nu}$$

For ligand(s), the concentration of completely deprotonated form is determined at each pH as follows

$$[14]\quad \mathrm{p}\bar{C}_i{}^{\nu}(i = 2 \text{ or } 3) = I_i{}^{\nu} + \sum_{k=1}^{\mathrm{NP}_t} \mathrm{p}K_{\mathrm{a}_{t,k}} - \mathrm{NP}_t \times \mathrm{pH}$$

At each pH, there are N species $\mathrm{M}_x\mathrm{H}_y\mathrm{L}_z(\mathrm{Kt})$ in equilibria. The concentration of each species l ($\mathrm{CS}_l{}^{\nu}$) is given by eq. [15]

$$[15]\quad \mathrm{CS}_l{}^{\nu} = \beta_l \prod_i (C_{i,l}{}^{\nu\, q_{l,i}})$$

where β_l is the formation constant and $q_{l,i}$ are the stoichiometric coefficients of species l.

In analytical potentiometry an excess of ligand is used so that only the metal mass balance equation is considered in solving β_l values.

$$[16]\quad T_{1,\mathrm{m}}{}^{\nu} = \bar{C}_1{}^{\nu} + \sum_{l=1}^{N} \beta_l q_{l,1} \prod_i (\bar{C}_i{}^{\nu})^{q_{l,i}}$$

In this equation the values of $\bar{C}_1{}^{\nu}$ can closely approach to $\bar{C}_{i,m}{}^{\nu}$. Each element of Jacobian matrix in relation to metal ion is

$$[17]\quad J_{l,1}{}^{\nu} = \frac{\partial T_{1,\mathrm{m}}}{\partial \beta_l}$$

From eq. [16] and eq. [17] we obtain:

$$[18]\quad J_{l,1}{}^{\nu} = q_{l,1} \prod_i (\bar{C}_i{}^{\nu})^{q_{l,i}}$$

Equation [16] can be written as a matrix equation as following

[19] $\mathbf{JB} = \mathbf{\Delta}$

where $\mathbf{J}$ is the Jacobian matrix and each β_l forms the $\mathbf{B}$ matrix. The elements of matrix $\mathbf{\Delta}$ are given by the following equation for each pH.

[20] $\delta^\nu = T_{l,m}{}^\nu - \bar{C}_l{}^\nu$

Equation [19] is in fact a set of overdetermined equations of N unknowns. Theoretically, it can be solved by a fast and direct minimization process.

[21] $\mathbf{J}^T\mathbf{JB} = \mathbf{J}^T\mathbf{\Delta}$

[22] $\mathbf{B} = (\mathbf{J}^T\mathbf{J})^{-1}\mathbf{J}^T\mathbf{\Delta}$

For the purpose of inverting the wide range of values in matrix $\mathbf{J}^T\mathbf{J}$, an effective scaling is necessary for the overall goal of refinement and reducing the rounding errors (27). It should be pointed out that the use of β_l values greater than 10^{37} also poses a problem.

To circumvent these difficulties we propose the following way to decompose matrix $\mathbf{B}$ to two matrices.

[23] $\mathbf{B} = \xi\mathbf{M}$

$\mathbf{M}$ has the mantissa elements of β_l and the diagonal ξ matrix has the exponents of β_l.

A scale factor is calculated by eq. [24]

[24] $$S = 1 \Big/ \sum_{\nu=1}^{NN} \delta^\nu$$

where NN is the number of pH values considered in the minimization step. Combining eqs. [21], [23], and [24] we obtain

[25] $(\mathbf{SJ}\xi)^T(\mathbf{SJ}\xi)\mathbf{M} = \mathbf{S}(\mathbf{SJ}\xi)^T$

It is now easy to obtain a triangular inferior matrix $\mathbf{L}$ with units on the principal diagonal and a triangular superior matrix $\mathbf{R}$ solving eq. [26]

[26] $(\mathbf{SJ}\xi)^T(\mathbf{SJ}\xi) = \mathbf{LR}$

Matrix $\mathbf{M}$ is obtained by solving the following matrix equations

[27] $\mathbf{LRM} = \mathbf{S}(\mathbf{SJ}\xi)^T\mathbf{\Delta}$

[28] $\mathbf{RM} = \mathbf{L}^{-1}\mathbf{S}(\mathbf{SJ}\xi)^T\mathbf{\Delta}$

[29] $\mathbf{M} = \mathbf{R}^{-1}\mathbf{L}^{-1}\mathbf{S}(\mathbf{SJ})^T\mathbf{\Delta}$

And finally β_l values are given in log form by eq. [30].

[30] $\log \beta_l = \log m_l + e_l$

The strategy adopted in the calculations consist of determining the scaler followed by the matrix $\mathbf{J}\xi$. Each element of $\mathbf{J}$ or ξ can be larger than $10^{\pm 37}$, but the product of each element performed in log units is in the scale of δ^{-1}. Matrix $\mathbf{SJ}\xi$ is obtained and multiplied by $(\mathbf{SJ}\xi)^T$. Matrix $\mathbf{S}(\mathbf{SJ}\xi)^T\mathbf{\Delta}$ is also calculated. Subsequently $\mathbf{R}$ and $\mathbf{L}$ are determined, inverted, and multiplied by $\mathbf{S}(\mathbf{SJ}\xi)^T\mathbf{\Delta}$ in sequential order.

It could happen that some elements m_l of $\mathbf{M}$ are negative. In this case the species with the more negative value is rejected and a new minimization is performed with $N - 1$ species.

Data analysis

Calculations are performed by a series of programs written in BASIC APPLESOFT or in compiled language for a 48 Kb computer. These are designed to be used quite easily. The few questions asked to the users are clearly explained and any unscaled or wrong inputs are critically monitored. The following programs are utilized by data analysis (Fig. 1).

Program 1: DATA ENTRY

Two programs are involved at this stage. With one, the data (pH, volume of base) are entered in the keyboard, titration curves are displayed or printed, and data files are created. The second one is an on-line data acquisition system monitoring titration experiments.

Program 2: CONVERSION

The main objective of this program is to move the P-1 data files in random access files. In this way 20 titrations of 300 experimental values each can be computed in the subsequent programs.

Program 3: VARIATIONS

With this program the best set of titration curves is determined and eqs. [1] and [11] solved.

Program 4: PROPOSITIONS

An estimation of β values, a probability of the existence of the proposed species, and the pH where their concentrations are maximum, are obtained with this program.

Program 5: MINIMIZATION COMBINATION

Equations [16] to [30] are computed in this program whereby the final concentration of species as a function of pH are obtained.

Program 6: GRAPHICS

It is an utility program to display a graph of the data saved in files created by P-3 and P-5. The same program saves the screen display in binary files which are adapted to a commercial software PHOTO (Program 7) (28). With this program it is possible to display quickly on the screen a "photo" saved on the disc and transmit it on to any type of printer.

Other programs listed in Fig. 1 do not directly concern the theoretical part of the method of analytical potentiometry as has been described. However, these programs are used in conjunction with the above programs in order to obtain the necessary essential parameters for the purpose of data analysis. Following is a brief description of the other programs.

Program 8: DERIVATION

It performs the calculation of dV/dpH as a function of volume of base added through a least-squares polynomial filter of 3, 5, 7, 9, or 11 points moving along the titration curve. Equivalent volumes are calculated from the intercept of two least-squares lines. We included the possibility of obtaining the second derivative.

Program 9: IONIZATION

This program uses the data of base titration against phthalate or strong acid. Its output is pK_w.

Program 10: ACTIVITY

This program is used to calculate the relation between activity of H_3O^+ and its concentration. It is performed by calculating the deviation between the theoretical slope and the least squares line of pH read against $-$ log [HCl] in the acidic and basic range where electrode response is more linear.

Program 11: ELECTRODE

This program calculates the theoretical initial pH's from the real concentrations of ions i and strong acid in a titration mixture (P-8). A comparison of the experimental pH values with those of the theoretical enables one to decide whether to reject the

Can. J. Chem. Downloaded from www.nrcresearchpress.com by 213.222.148.141 on 09/07/12
For personal use only.

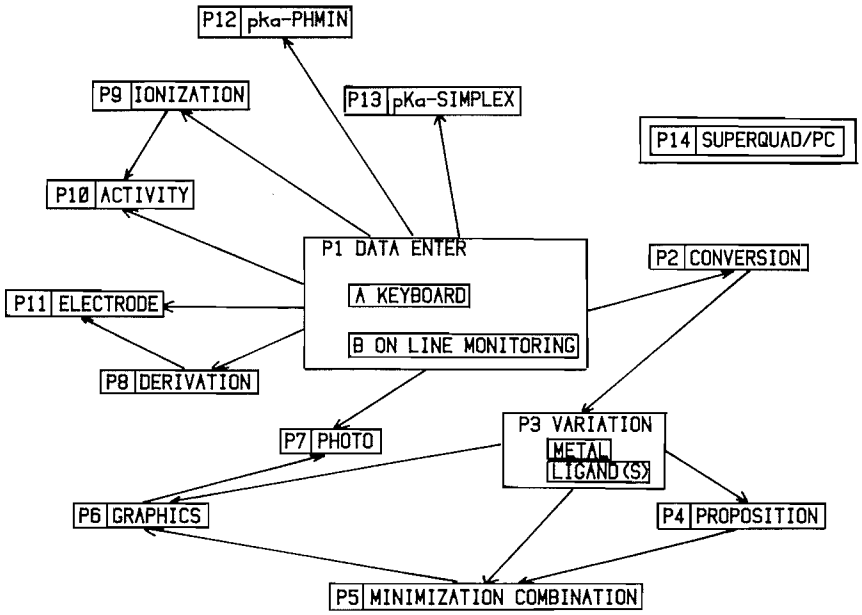

FIG. 1. Programs utilized for data analysis.

titration data or to make suitable pH adjustments necessitated by improving electrode response.

Program 12: PKA-PHMIN

This program calculates the values of pK_a's of ligand(s) through the process of minimization at each pH values.

Program 13: PKA-SIMPLEX

It is a program which refines all the wanted titration parameters simultaneously using a simplex algorithm. The minimization is done with respect to the volumes of base added (29).

Program 14: SUPERQUAD/PC

This program (25) has been used to determine the species and their stability constants in an equilibrium mixture containing metal and ligand(s) in solution. The program has recently been modified by one of us (P.D.) to run in Fortran 77 on an IBM-PC microcomputer with 8087 coprocessor. The compiled program occupies about 140 Kbytes of space.

Methods and discussion

In potentiometry, equations and algorithms used to obtain free ion concentrations are essential. Equally important is the process of minimization to obtain the best ion mass balance. However, the corrections of experimental data introduced in the programs of analytical potentiometry is most crucial. In this connection, two major difficulties are encountered: (1) the exact nature and the analytical amounts of chemicals introduced in the titration solutions and (2) the quality of electrode response during the titration. From our experience, we have noticed that these difficulties are the major sources of erroneous results. In order to circumvent these problems, we propose the following steps.

Solutions

A probable source of error may be caused by the limited amount of materials available for titration. This can be partially overcome by preparing the solutions in certain ways. One can prepare four solutions in all. First a stock solution S in 0.15 *M* background electrolyte in strong acid. Second, a solution SL_1 is obtained by dilution of weighted amount of ligand in solution S. This solution must have an excess of strong acid in order to fully protonate the ligand. The third and fourth SL_2 and SL_3 are also prepared by dilution of SL_1, with S. Solution SL_2, for instance, could be adjusted to the ligand concentration at the middle point.

Titrations

Electrodes are calibrated with buffers in terms of activity. At least three titrations of solution S are performed. The exact amount of strong acid in the titration solution is obtained with P-8. Thereafter, the relation between pH and $-\log [H_3O^+] (\gamma L)$ is obtained with P-10 using the pK_w value calculated by P-9.

Purity and pK_a's of ligand

Titrations of solutions SL_1, SL_2, and SL_3 are carried out and the purity and the amount of ligand are determined using the program P-8. More often, the results of P-8 on the three different titrations show a difference with the expected value. This may be due to the method of manipulation rather than the presence of an impurity. This can be discerned from the output of P-8. If the presence of protonated impurity is not detected, the concentration of ligand is corrected and the study is allowed to continue. If the impurity has ionizable protons, the studies are undertaken as though it is a two ligand system.

Titration data corrected from γL by following equation:

$$-\log [H_3O^+] = pH + \gamma L$$

are introduced sequentially in P-12, P-13, and P-14. In this manner, pK_a's are calculated and the values of ligand concentrations are adjusted.

Metal variation

At least three titrations of solution SL_2 added with different amounts of metal are performed. Ligand(s) and strong acid concentrations are estimated by P-8 and eventually corrected. Alongside, electrode response is tested by P-11. If necessary, a correction of pH is applied. Actually, the amount of metal introduced in the titration is most critical. It would be important to have an independent verification of this amount. Attempts are under way using cyclic voltamperometry for such a verification.

Program 3 is run with at least three data files created by P-2.

Can. J. Chem. Downloaded from www.nrcresearchpress.com by 213.222.148.141 on 09/07/12
For personal use only.

Can. J. Chem. Downloaded from www.nrcresearchpress.com by 213.222.148.141 on 09/07/12
For personal use only.

At this stage the correction of volume variation is initiated. It should be pointed out that this correction can influence the species distribution particularly at high pH.

Ligand variation

Solutions SL_1 and SL_3 with added amounts of metal corresponding to the middle point concentration are titrated and corrected by P-8 and P-11. These two titrations are analyzed along with the one containing solution SL_2 having the same amount of metal (obtained from the metal variation experiment) by P-3. This step does not present any difficulty as there is very little correction to be made for the ligand and strong acid. Experimentally it can be shown that the standard deviations in metal variation are on the average of 10 to 20 times higher than in ligand variation. At this step $p\bar{C}_i^{\nu}$ values have been determined in the best case, with only five titrations.

Propositions

The proposition program P-4 is run with the data file created by P-3. One can propose an extensive set of stoichiometric coefficients of species (<31). An approximate β value and the pH of its maximum concentration are calculated for each species. In general, when the criterion of curvature DC_i is too high, it is often preferable to introduce multimetal and multiligand species. The program P-4 calculates the Jacobian elements $\mathbf{J}_{l,1}^{\nu}$ of each species as a function of pH. If the variation of $\mathbf{J}_{l,1}^{\nu}$ on the pH range does not pass by a maximum, the probability of the existence of the species l is negligible. Finally, the knowledge of the pH region, where these species are likely to be present, is very helpful in the subsequent minimization steps.

Minimization

The minimization based on a linear least squares method is performed by P-5 with data files created by P-3 and P-4. When a right set of proposed species is introduced in the minimization process, the β_l values are obtained quickly without giving rise to false minima. It is possible that some calculated elements m_l of matrix **M** are negative which indicates that the proposed set of species has no chemical meaning. In this instance P-5 rejects the species with the more negative value and performs a new minimization with the remaining $N - 1$ species. One should be cautioned here, that this procedure may result in the rejection of a real species if a false species is introduced at the initial stage. In order to overcome this problem we have introduced a procedure to propose a higher than real number of species, chosen on the basis of "chemical intuition". The minimization process is carried out for each possible set of proposed species and standard deviations are calculated. The knowledge of the frequency of rejection of each species facilitates the choice of best set of species. However, the above method of analysis does not detract from the fact that some mathematical set of species without any chemical meaning may provide a better standard deviation than that given by the real set of species.

Two other difficulties should be pointed out regarding the minimization procedure. Firstly, the postulation that the values of $\bar{C}_i^{\nu}$ can closely approach $C_{i,m}^{\nu}$ is an approximation. Secondly, β_l values are calculated on the basis of the lowest sum of δ_1^{ν} terms as it has been shown in eq. [20]. This equation shows that δ_1^{ν} is the difference between $T_{1,m}^{\nu}$ and $\bar{C}_1^{\nu}$. The volume correction is certainly helpful in the reduction of errors. However, it has been shown that for the purpose of volume correction, $T_{1,m}^{\nu}$ is calculated from $N_{1,m}$ which could have large errors. The resultant effect of such errors can be amplified at the level of δ_1^{ν} values. In analytical potentiometry one uses excess ligand(s) which justifies the use of metal mass balance in the calculation. Unfortunately, the minimization provides the lowest least-squares sum of δ_1^{ν} which is related to metal mass balance equation. Thus one should be aware of the possible errors in δ_1^{ν} values arising from the methodology. We have incorporated the possibility of minimization at a restricted part of pH range. In the end of minimization the species distribution is calculated and displayed on screen by P-6 along with standard deviations at each pH.

Conclusion

1. A general procedure is proposed for analytical potentiometry which includes minimization of potential sources of errors and a fast linear-scaled least-squares algorithm to expedite the microcomputer solution of metal complex stability from potentiometric data.

2. Programs have been written in BASIC APPLESOFT on a microcomputer Apple II. They allow the computation of at least 40 titration curves of 300 data each and in theory 20 species.

3. Besides dealing with the theoretical part of analytical potentiometry, programs are also written to obtain the necessary essential parameters for the purpose of data analysis.

4. An additional amount of acid in titration solutions and variation of volumes, previously neglected, have now been incorporated in this procedure. Attempts have been made to control the exact amount of metal introduced in the titration vessel.

5. The method reduces the number of experimental data and at the same time increases the overall accuracy.

Acknowledgements

The research was supported by a grant from the Medical Research Council of Canada. P.D. was a recipient of a NATO grant. The authors thank Dr. S. Lau for many helpful discussions.

1. J. Lefebre. J. Chem. Phys. **57**, 553 (1957).
2. R. Österberg. Acta Chem. Scand. **14**, 471 (1960).
3. B. Sarkar and T. P. A. Kruck. Can. J. Chem. **51**, 3541 (1973).
4. S. H. Laurie, D. H. Prime, and B. Sarkar. Can. J. Chem. **57**, 1411 (1979).
5. D. M. Templeton and B. Sarkar. Can. J. Chem. **63**, 3122 (1985).
6. K. S. N. Iyer, S. Lau, S. H. Laurie, and B. Sarkar. Biochem. J. **169**, 61 (1978).
7. H. Lakusta and B. Sarkar. J. Inorg. Biochem. **11**, 303 (1979).
8. S. Lau and B. Sarkar. J. Chem. Soc. Dalton Trans. 491 (1981).
9. S. Lau and B. Sarkar. Biochem. J. **199**, 649 (1981).
10. J. D. Glennon and B. Sarkar. Biochem. J. **203**, 15 (1982).
11. J. D. Glennon and B. Sarkar. Biochem. J. **203**, 25 (1982).
12. D. Muller, B. Decock-Le Reverend, and B. Sarkar. J. Inorg. Biochem. **21**, 215 (1984).
13. M. Tabata and B. Sarkar. Can. J. Chem. **63**, 3111 (1985).
14. M. Tabata and B. Sarkar. Can. J. Chem. **63**, 3117 (1985).
15. R. Guevremont and D. L. Rabenstein. Can. J. Chem. **55**, 4211 (1977).
16. A. Avdeef and K. N. Raymond. Inorg. Chem. **18**, 1605 (1979).
17. A. Avdeef. Inorg. Chem. **19**, 3081 (1980).
18. N. Ingri and L. G. Sillen. Acta Chem. Scand. **18**, 1085 (1964).
19. I. G. Sayce. Talanta, **18**, 653 (1971).
20. P. Gans, A. Sabatini, and A. Vacca. Inorg. Chim. Acta, **18**, 237 (1978).
21. M. Wozniak and G. Nowogrocki. Talanta, **25**, 643 (1978).
22. F. Gaiser and A. Puskas. Talanta, **28**, 565 (1981).

23. R. J. MOTEKAITIS and A. E. MARTELL. Can. J. Chem. **60**, 2403 (1982).
24. K. MURRAY and P. M. MAY. ESTA equilibrium simulation for titration analysis, UWIST, Cardiff (1984).
25. P. GANS, A. SABATINI, and A. VACCA. J. Chem. Soc. Dalton Trans. 1195 (1985).
26. P. DECOCK and B. SARKAR. Can. J. Chem. **65**, 2804 (1987).
27. G. E. FORSYTHE and C. B. MOLER. Computer solution of linear algebraic systems. Prentice Hall, Inglewood Cliffs. 1967.
28. D. K. HUDSON. Combined enhanced graphics, Software (c) 1979-82. Computer Stations, Inc. Release 2.0.
29. Actas sur les methods informatiques dans l'enseignement de la chimie. Vol. 2. Universite de Lille. 1985. p. 17.

Can. J. Chem. Downloaded from www.nrcresearchpress.com by 213.222.148.141 on 09/07/12
For personal use only.

Application of an advanced technique of data analysis by analytical potentiometry and comparison of results by SUPERQUAD. Studies of nickel(II) – glycine, copper(II) – glycylglycyl-L-tyrosine-*N*-methyl amide, and zinc(II) – 3,6-diazaoctane-1,8-diamine systems

PATRICK DECOCK[1] AND BIBUDHENDRA SARKAR[2]

Research Institute, The Hospital for Sick Children, Toronto, Ont., Canada M5G 1X8; and Department of Biochemistry, University of Toronto, Toronto, Ont., Canada M5S 1A8

Received January 19, 1987[3]

PATRICK DECOCK and BIBUDHENDRA SARKAR. Can. J. Chem. **65**, 2804 (1987).

An advanced methodology for the data analysis by analytical potentiometry (Decock and Sarkar. Can. J. Chem. **65**, 0000 (1987)) has been utilized to analyze three different metal–ligand systems. The results are compared with those obtained by SUPERQUAD adapted for microcomputer. An excellent agreement has been attained with the stability constant data of Ni(II)–glycine complexes of an earlier multi-laboratory study. The technique has been utilized to investigate the effect of ligand concentration in the equilibria of Cu(II) complexes of glycylglycyl-L-tyrosine-*N*-methyl amide. The third system studied by this technique was Zn(II) complexes of 3,6-diazaoctane-1,8-diamine, a ligand of potential therapeutic efficacy against metal toxicity.

PATRICK DECOCK et BIBUDHENDRA SARKAR. Can. J. Chem. **65**, 2804 (1987).

Des modifications apportées à la méthode de potentiométrie analytique, décrites dans la première partie de cette publication, sont utilisées pour analyser les équilibres de complexes dans trois systèmes métal–ligand différents. Les résultats obtenus sont comparées à ceux issus du programme SUPERQUAD, que nous avons adapté pour être utiliser sur un microordinateur. Les résultats acquis, pour les complexes du Ni(II) et de la glycine sont très proches de ceux publiés dans un travail antérieur par une série de laboratoires différents. La technique préconisée est également appliquée à l'analyse de système Cu(II) – glycylglycyl-L-tyrosine-*N*-méthyl amide et les effets de l'influence de la concentration du ligand sont considérés. Le troisième système étudié est relatif au Zn(II) associé au diaza-3,6 octanediamine-1,8 qui est un ligand présentant une efficacité térapeutique potentielle à l'encontre de la toxicité des métaux.

Introduction

We have proposed an advanced methodology for the data analysis of metal–ligand equilibria by analytical potentiometry (AP) (1). In this article we report the application of this method in the studies of equilibria involving three different metals Ni(II), Cu(II), and Zn(II) with different ligands. We have examined the procedure by studying the Ni(II)–glycine system since it was chosen as a test system for a previous inter-laboratory procedure evaluation (2). We also report an analysis of Cu(II) complexation of a peptide, glycylglycyl-L-tyrosine-*N*-methyl amide (GGTNMA). The third system we examined is Zn(II) complexation of 3,6-diazaoctane-1,8-diamine (Trien), a ligand of potential therapeutic efficacy against metal toxicity. The results obtained by AP were further compared with those from SUPERQUAD (3) adapted for microcomputer (SPC).

Experimental

Potentiometric studies were performed using both AP and SPC procedures. The solutions were prepared in deionized and twice redistilled water under argon atmosphere ($R > 1$ MΩ). Carbonate-free sodium hydroxide solutions were prepared and stored under argon and standardized against N.B.S. grade potassium hydrogen phthalate. HCl solutions were standardized with 0.1013 *M* NaOH and checked by the program DERIVATION (1). Puratronic metal chloride was used to prepare a 0.2 *M* (in HCl) solution which was checked by titration with EDTA.

Glycine (Fluka) was recrystallized from water–ethanol mixtures prior to use. For the Ni(II)–glycine system, ligand concentrations varied between 0.6×10^{-2} and 1.5×10^{-2} *M* and metal between 10^{-3} and 3×10^{-3} *M*. The peptide, glycylglycyl-L-tyrosine-*N*-methyl amide, was synthesized as reported earlier (4). For Cu(II)–GGTNMA, five different order of concentrations were studied with respect to the same average ligand-to-metal ratio of 5:1 as indicated in Table 1. 3,6-Diazaoctane-1,8-diamine tetrahydrochloride has been purified as previously reported (5). Purity was checked by high voltage paper electrophoresis at pH 6.9 (phosphate buffer). A total of 41 different titrations were performed to study the Zn(II)–Trien system (Table 2). All solutions were prepared in 0.15 *M* NaCl.

The potentiometric titrations were carried out on a Tacussel ISIS 20000 pH meter at 25 ± 0.03°C with a TB 10/HA glass electrode and a KCl-saturated reference electrode. All calculations were performed on APPLE II or IBM PC computers for AP and SPC programs, respectively.

Results and discussion

Nickel(II)–glycine

Studies were carried out in the pH range 3 to 9 using a high ligand and metal concentration to minimize the errors. Best mathematical fit of the data resulted in the identification of three species: NiL, NiL_2, and NiL_3. We were not able to detect any species such as $NiH_{-1}L$. Stability constants calculated by AP are compared with those obtained by SPC as well as with those of earlier studies (Table 3). All results are quite consistent. When volume corrections are incorporated in AP there is a better agreement between AP and SPC. Results also indicate the SPC programs designed for a microcomputer is operating successfully.[4]

*Copper(II) – glycylglycyl-L-tyrosine-*N*-methylamide*

This system was chosen to investigate the capability of the method (1) to analyze the chelation of Cu(II) by a peptide. The

[1]Permanent address: Laboratoire de Chimie Minerale et Methodologie Analytique, Universite des Sciences et Techniques de Lille, U.E.R. de Chimie, Villeneuve d'Ascq Cedex, France.

[2]To whom correspondence should be addressed.

[3]Revision received July 31, 1987.

[4]These programs are modified by one of us (P.D.) to operate on IBM-PC. Please direct any enquiries to P.D.

Can. J. Chem. Downloaded from www.nrcresearchpress.com by 213.222.148.141 on 09/07/12
For personal use only.

TABLE 1. Concentrations of Cu(II) and glycylglycyl-L-tyrosine-*N*-methyl amide used in titrations[a]

No.	Total ligand (mg)	[HCl]	[Ligand]	[Cu(II)]	Ratio
I	86.5	2×10^{-3}	3×10^{-4} 5×10^{-4}, 4×10^{-5}(2) 1×10^{-3}	1×10^{-4} 1×10^{-4}(4), 2×10^{-4}(2) 1×10^{-4}	3 12.5, 5, 2.5 10
II	31.5	2×10^{-4}	1.38×10^{-4} 2.3×10^{-4}, 2×10^{-5} 4.6×10^{-4}	5.2×10^{-5} 5.2×10^{-5}, 1×10^{-4} 5.2×10^{-5}	2.6 1.1, 4.4, 2.3 8.8
III	21.5	2×10^{-4}	7.5×10^{-4}, 1×10^{-5} 1.25×10^{-4}, 1×10^{-5} 2.49×10^{-4}	2.8×10^{-5} 2.8×10^{-5}, 5.2×10^{-5} 2.8×10^{-5}	2.7 12.5, 4.4, 2.4 8.9
IV	12.1	2×10^{-4}	4.2×10^{-5} 7×10^{-5}, 4×10^{-6} 7.4×10^{-4}	1.6×10^{-5} 1.6×10^{-5}, 3.2×10^{-5} 1.6×10^{-5}	2.7 17.5, 4.4, 2.2 8.7
V	10	2×10^{-3}	3.8×10^{-5} 5.8×10^{-4}, 4×10^{-6} 1.16×10^{-4}	1.2×10^{-5} 1.2×10^{-5}(2), 2.4×10^{-5}(2) 1.2×10^{-5}	2.9 14, 4.8, 2.4 9.7

[a]Column 2 represents total quantity of ligand used; column 3 indicates the concentration of HCl (mol L^{-1}) in solution S (ref. 1); in columns 4 and 5 are given concentrations in mol L^{-1} of ligand and metal for each titration; column 6 indicates the different metal/ligand ratio used. Numbers in parentheses represent the number of titrations.

TABLE 2. Concentrations (mol L^{-1}) of Zn(II) and 3,6-diazaoctane-1,8-diamine used in titrations[a]

[Ligand]	[Zn(II)]
8.1×10^{-4}(3)	6×10^{-5}(2)
7.2×10^{-4}(3)	6×10^{-5}(2)
6.5×10^{-4}(4)	6×10^{-5}(2)
4.9×10^{-4}(4), 1.6×10^{-5}(3), 3×10^{-5}(3)	6×10^{-5}(4), 9×10^{-5}(3), 1.2×10^{-4}(3)
3.3×10^{-4}	6×10^{-5}(3)
1.6×10^{-4}	6×10^{-5}(3)

[a]Numbers in parentheses represent the number of titrations.

TABLE 3. Stability constants of the Ni(II)—glycine species; entries are log β_{pqr} values for species $Ni_pH_qGly_r$[a]

							(*e*)						
p	*q*	*r*	(*a*)	(*b*)	(*c*)	(*d*)	1	2	3	4	5	6	7
1	1	1	5.23	5.51	5.59	5.55	5.80	5.52	5.62	5.62	5.60	5.62	5.66
1	0	2	10.14	10.25	10.44	10.31	10.59	10.26	10.36	10.40	10.32	10.38	10.43
1	0	3	13.75	13.92	13.46	13.85	14.31	13.59	13.75	13.91	13.65	13.80	14.08

[a](*a*) AP without volume correction (APPLE II), present work; (*b*) AP with volume correction (APPLE II), present work; (*c*) AP: Fletcher-Powell minimization (MAC INTOSH), ref. 7; (*d*) SUPERQUAD (IBM-PC); (*e*) ref. 2.

TABLE 4. p*K*'s of glycylglycyl-L-tyrosine-*N*-methyl amide (H_qL_r)

q	*r*	P13 PKA:SIMPLEX[b]	P17 PKA:PH-MIN	P14 SUPERQUAD	AP[a]
1	1	9.55	9.61 (0.05)	9.71 (0.01)	9.85
2	1	7.85	7.85 (0.04)	7.89 (0.01)	7.94

[a]Reference 6.
[b]pK_a values are estimated to be reliable to ±0.02 log units.

Can. J. Chem. Downloaded from www.nrcresearchpress.com by 213.222.148.141 on 09/07/12
For personal use only.

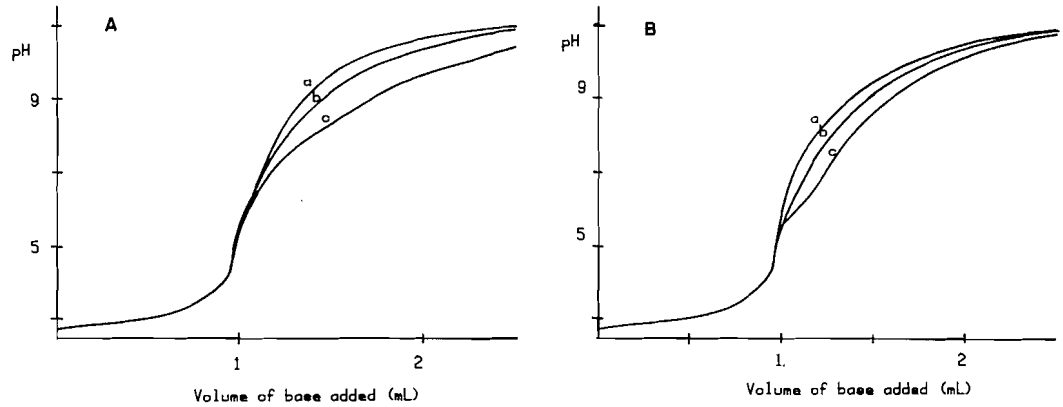

FIG. 1. Original titration data of Cu(II) – glycylglycyl-L-tyrosine-*N*-methyl amide with 0.1013 *M* NaOH. Conditions are given in the Experimental Section. (*A*) Ligand variation at [Cu] = 1×10^{-4} *M* and [GGTNMA] = 3×10^{-4} *M* (*a*), 5×10^{-4} (*b*), and 1×10^{-3} *M* (*c*). (*B*) Metal variation at [GGTNMA] 5×10^{-4} *M* and [Cu] = 4×10^{-5} *M* (*a*), 1×10^{-4} *M* (*b*), and 2×10^{-4} *M* (*c*).

TABLE 5. Stability constants of the Cu(II) – glycylglycyl-L-tyrosine-*N*-methyl amide species and the pH of maximum species concentration; entries are log β_{pqr} values for species $Cu_pH_qGGTNMA_r$[a]

			AP						SPC	
			(*a*)		(*b*)		(*c*)			
p	*q*	*r*	log β	pH	log β	pH	log β	pH	log β	pH
1	1	1	14.25	6	14.27	6	14.61	6	14.64	6
1	0	1	8.79	6.6	8.80	6.7	9.24	6.7	9.21	6.8
1	−1	1	1.37	8.1	1.51	8	1.90	8.2	1.79	7.7
1	−2	1	−7.31	9.2	−7.15	9	−6.71	9.3	−6.29	8.8
1	−3	1	−17.21	9.9	−16.34	9.1	−16.96	>10	−15.69	9
1	−2	2	−4.23	9.8			−3.22	>10		

[a](*a*) AP without volume correction (APPLE II); (*b*) AP with volume correction (APPLE II); (*c*) AP early version (ref. 6) (G.E. 400).

two pK_a values of the peptide calculated by programs PKA-PHMIN, PKA-SIMPLEX, and SPC (1) are presented in Table 4 where they are compared with the previous results. The metal peptide titrations were carried out using the condition I as described in Table 1. Titration data are shown in Fig. 1. Complexation begins with the species CuHL and following deprotonation the last species $CuH_{-3}L$ is formed at high pH. The result of log β values (Table 5) and the pH of the maximum concentration of species (Fig. 2) are consistent with both AP and SPC, although some minor differences are observed in the concentration of species as a function of pH. The new version of AP eliminates the species $CuH_{-2}L_2$ which was previously described at high pH (6). It is also rejected by SPC. An increasing shift in the species distribution is observed at high pH using the two AP methods.

We have examined the influence of concentration in this study. Five different concentrations of Cu(II)–peptide have been investigated. The average ratio of metal-to-ligand was kept constant. The total amount of peptide used to perform a complete set of data analysis, as described previously (1), is in the scale of 10 to 86.5 mg (Table 1). The results are summarized in Table 6 where these are compared to SPC. In systems II and V species $CuH_{-2}L_2$ is rejected by both programs. $CuH_{-3}L$ is also eliminated in the refinement of system V. In all cases, the formation constants of the highest concentration species are

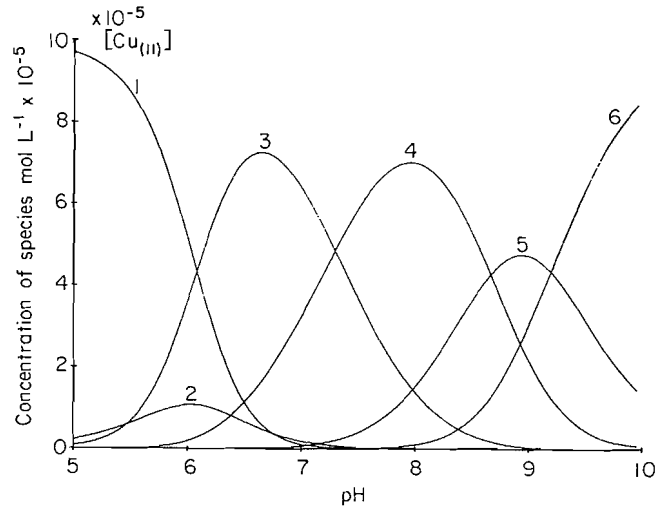

FIG. 2. Species distribution as a function of pH for Cu(II) – glycylglycyl-L-tyrosine-*N*-methyl amide. *1*, Cu; *2*, CuHL; *3*, CuL; *4*, $CuH_{-1}L$; *5*, $CuH_{-2}L$; *6*, $CuH_{-3}L$.

consistent with SPC results. No particular effect of ligand concentration was observed.

From a theoretical standpoint it could be assumed that the β values obtained from low ligand concentration systems are

Can. J. Chem. Downloaded from www.nrcresearchpress.com by 213.222.148.141 on 09/07/12
For personal use only.

Can. J. Chem. Downloaded from www.nrcresearchpress.com by 213.222.148.141 on 09/07/12
For personal use only.

better. In this case the approximations of the method supporting AP programs are minimized. This point has been verified by the results of the partial volume correction. On the other hand, the errors expected on the initial concentrations of ligands and protons, recalculated by program DERIVATION, are higher.

Both AP and SPC, although based on two different mathematical approaches, lead to the same type of complexes. The difference in the β-values are small but somewhat larger than those in the Ni(II)–glycine system. This difference could result from the approximation $C_l^{\nu} \simeq \bar{C}_{l,m}^{\nu}$ (1). The other possibility would be an error in the metal concentration which is not treated in the same manner by the two programs. The satisfactory convergence of results obtained by both methods could be attributed to the system which has only a series of mononuclear species in different protonation states. However, the deviation may be more pronounced in complicated systems such as the one described below.

Zinc(II) – 3,6-diazooctane-1,8-diamine (Trien)

The results of the four pK_a's of Trien and the stability constants of the complexed species are given in Table 7, and they are compared with the literature values. The titration data are presented in Fig. 3. It is shown in Fig. 4 that the complexation begins above pH 5 with the formation of the species ZnH_2L. Subsequently, the species ZnH_2L_2 is formed which predominates over the pH range 6.5 to 8. This is the major species around pH 7.8 containing approximately 90% of Zn(II). At pH 8 the species $ZnHL_2$ starts to form, reaching a maximum at pH 8.4. Finally the completely deprotonated species ZnL_2 is formed which starts to predominate at pH 9 and above.

No precise structural assignments of the Zn(II)–Trien species are possible from the presently available data. However, some of the possibilities can be discussed. The low pH species ZnH_2L is most likely from two of the closest proton bearing sites enabling the formation of a stable five-membered chelate ring. The next species ZnH_2L_2 is most likely an octahedral species where both the ligands in this species could form two five-membered rings each. The high pH species $ZnHL_2$ and ZnL_2 are formed from ZnH_2L_2 by the subsequent ionization of protons. This contention is substantiated by the similar log K values calculated for the formation of $ZnHL_2$ and ZnL_2 species (Table 8).

AP and SPC programs lead to the same kind of species. However, the differences on calculated values of formation constants are higher than those observed for Ni(II)—glycine and Cu(II)—peptide. This difference increases with the higher pH species. This may be due to the uncertainties of the exact concentration of Zn(II) introduced in each titration solutions. It could also be assumed that if some error occurs in the values of S_i^{ν} (1) at a pH range, the same error will greatly increase past the pH of complexation of all Zn(II). Subsequently an error propagation could result at higher pH on $\bar{C}_i^{\nu}$. The real problem of the approximation of $C_{i,m}^{\nu}$ by $\bar{C}_i^{\nu}$ (1) will be crucial in such a system. Th minimization procedure on $\bar{C}_i^{\nu}$ values could also contribute to propagation of errors. In SPC errors are also expected, but the different mathematical approach does not lead to the same kind of error values and so of formation constants.

Conclusions

1. An advanced method of data analysis by analytical potentiometry utilizing a series of programs running on microcomputer (1) has been used successfully to obtain accurate data

TABLE 6. Stability constants of the species in the Cu(II) – glycylglycyl-L-tyrosine-*N*-methyl amide system and the pH maxima of species concentrations; entries are log β_{pqr} values for species Cu_pH_q GGTNMA$_r$[a]

System	log β_{111}	pH	log β_{101}	pH	log β_{1-11}	pH	log β_{1-21}	pH	log β_{1-31}	pH	log β_{1-22}	pH	ST	%ERR	
I	14.25	6	8.79	6.6	1.37	8.1	−7.37	9.2	−17.21	9.9	−4.23	9.8	2.11×10^{-7}	0.23	POTENTIOMETRY
II	14.52	6.1	8.84	6.7	1.46	7.9	−6.95	9	−16.43	10			6.7×10^{-8}	0.2	ANALYTICAL APPLICATIONS
III	14.71	6.3	8.85	6.8	1.43	7.9	−7.01	9	−16.72	9.9	−2.82	9.7	4×10^{-8}	0.2	
IV	15.44	6.3	8.94	6.9	1.70	7.9	−6.7	9	−17.6	9.9	−2.64	9.9	9×10^{-8}	0.8	
V	15.08	6.5	8.48	7.2	0.98	8.4	−8.66	9.9					1.4×10^{-8}	1.7	
	14.61	6	9.24	6.7	1.90	8.2	−6.71	9.3	−16.76	>10	−3.23	>10			[b]
VI	14.64	6	9.21	6.8	1.79	7.7	−6.29	8.8	−15.69				0.7	$X = 7.2$ (SPC)	IBM PC

[a]Refer to Table 1 for ligand concentrations.
[b]Reference 6.

TABLE 7. pK's of 3,6-diazaoctane-1,8-diamine (H_pL_r)

q	r	P13/PKA:SIMPLEX	P12/PH-MIN	P14/SUPERQUAD	Value Ref. 5	Ref. 8	Ref. 9
1	1	9.91	10.065 (0.033)	9.929 (0.055)	9.81 (0.020)	9.74	9.92
2	1	9.22	9.253 (0.020)	9.214 (0.043)	9.22 (0.020)	9.08	9.20
3	1	6.64	6.713 (0.086)	6.632 (0.048)	6.77 (0.015)	6.55	6.67
4	1	3.45	3.84 (0.058)	3.412 (0.055)	3.59 (0.015)	3.25	3.32

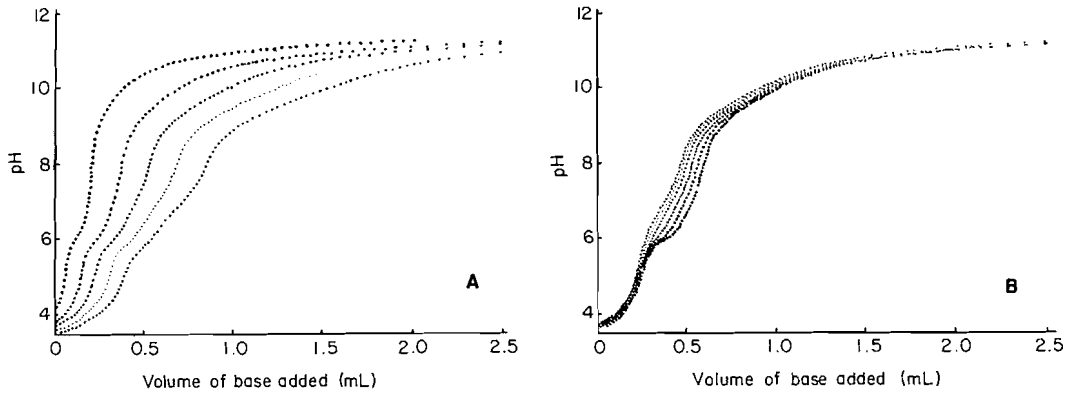

FIG. 3. Original titration data of Zn(II) – 3,6-diazaoctane-1,8-diamine with 0.1013 M NaOH. Conditions are given in the Experimental Section. (A) Ligand variation at [Zn] = 6×10^{-5} M and [Trien] = 1.6×10^{-4} M, 3.3×10^{-4} M, 4.9×10^{-4} M, 6.5×10^{-4} M, 7.2×10^{-4} M, and 8.1×10^{-4} M. (B) Metal variation at [Trien] = 4.9×10^{-4} M and [Zn] = 0 M, 1.6×10^{-5} M, 3×10^{-5} M, 6×10^{-5} M, 9×10^{-5} M, and 1.2×10^{-4} M.

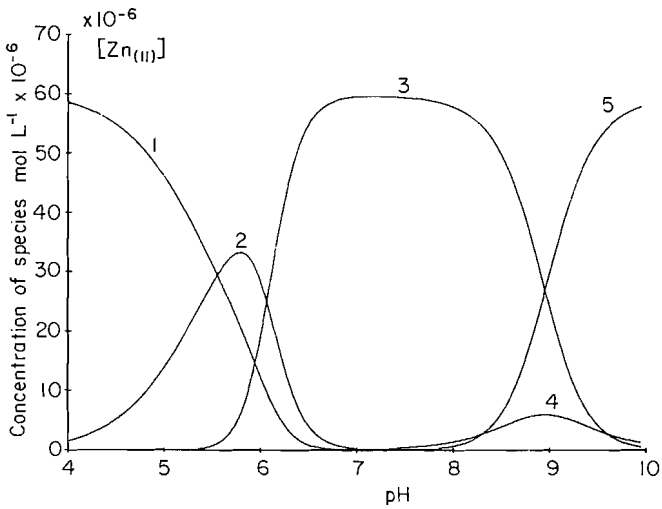

FIG. 4. Species distribution as a function of pH for Zn(II) – 3,6-diazaoctane-1,8-diamine. *1*, Zn; *2*, ZnH_2L; *3*, ZnH_2L_2; *4*, $ZnHL_2$; *5*, ZnL_2.

TABLE 8. Stability constants of the species in Zn(II) – diazaoctane-1,8-diamine system and the pH of maxima of species concentrations; entries are log β_{pqr} values for species $Zn_pH_qTrien_r$ as determined by analytical potentiometry (AP) and SUPERQUAD (SPC)

p	q	r	AP log β	AP pH	SPC log β	SPC pH
1	2	1	23.58	5.7	23.75 (0.19)	5.7
1	2	2	34.63	7.5	35.94 (0.04)	6.8
1	1	2	25.03	9.1	27.89 (0.09)	8.4
1	0	2	16.73	9.5	19.18 (0.08)	>9.2

for the determination of stability constants and the distribution of simultaneously existing multiple species of three different metal–ligand systems.

2. Potential sources of errors have been minimized by introducing preliminary computations of titration curves.

3. Consideration of the volume variations, selection criteria of the best set of titration curves, and the implementation of a different algorithm of a linear minimization technique — all contributed to the power of the technique.

4. The data analysis technique has been utilized to study the Ni(II)–glycine system the results of which are in good agreement with those obtained earlier by an inter-laboratory study.

5. The stability constants of Cu(II) – glycylglycyl-L-tyrosine-*N*-methyl amide and Zn(II) – 3,6-diazaoctane-1,8-diamine complex species have been derived by the above method.

Acknowledgements

The research was supported by a grant from the Medical Research Council of Canada. P.D. was a recipient of a NATO grant. The authors thank Dr. S. Lau for many helpful discussions and Mrs. Virginia Del Castillo for technical assistance.

1. P. DECOCK and B. SARKAR. Can. J. Chem. **65**, 2798 (1987).
2. E. BOTTARI, A. BRAIBANTI, L. CIAVATTA, A. M. CORRIE, P. G. DANIELE, F. DALLAVALLE, M. GRIMALDI, A. MASTROIANNI,

Can. J. Chem. Downloaded from www.nrcresearchpress.com by 213.222.148.141 on 09/07/12
For personal use only.

G. MORI, G. OSTACOLI, P. PAOLETTI, E. RIZZARELLI, S. SAMMARTANO, C. SEVERINI, A. VACCA, and D. R. WILLIAMS. Ann. Chim. **68**, 813 (1978).
3. P. GANS, A. SABATINI, and A. VACCA. J. Chem. Soc. Dalton Trans. 1195 (1985).
4. J. D. GLENNON and B. SARKAR. Biochem. J. **203**, 25 (1982).
5. S. H. LAURIE and B. SARKAR. J. Chem. Soc. Dalton Trans. 1822 (1977).
6. D. MULLER, B. DECOCK-LE REVEREND, and B. SARKAR. J. Inorg. Biochem. **21**, 215 (1984).
7. D. M. TEMPLETON and B. SARKAR. Can. J. Chem. **63**, 3122 (1985).
8. D. W. MARGERUM, D. B. RORABACHER, and J. F. G. CLARKE. Inorg. Chem. **2**, 669 (1953).
9. G. SCHWARZENBACH. Helv. Chim. Acta, **33**, 974 (1950).

Can. J. Chem. Downloaded from www.nrcresearchpress.com by 213.222.148.141 on 09/07/12
For personal use only.

Heat capacities and volumes of some non-electrolytes in *N*,*N*-dimethylformamide at 298.15 K

HENRYK PIEKARSKI[1]

Department of Physical Chemistry, Free University, De Boelelaan 1083, 1081 HV Amsterdam, The Netherlands

Received March 5, 1987

HENRYK PIEKARSKI. Can. J. Chem. **65**, 2810 (1987).

Heat capacities and densities of dilute solutions of formamide, acetone, tetrahydrofuran, ethylene glycol, 2-methoxyethanol, and 2-ethoxyethanol in *N*,*N*-dimethylformamide were determined at 298.15 K. Apparent molal heat capacities and volumes for these solutes in DMF were calculated and compared with the analogous data for other substances in DMF solution as well as with the data concerning solutions in methanol and water. Heat capacities of cavity formation (ΔC_{cav}) in DMF were calculated on the basis of the Scaled Particle Theory. ΔC_{cav} appeared to be linearly correlated with the standard partial molal volume of corresponding solutes in DMF. Similar dependences were also found for aqueous and methanolic solutions of the non-electrolytes.

HENRYK PIEKARSKI. Can. J. Chem. **65**, 2810 (1987).

Opérant à 298,15 K, on a déterminé les capacités calorifiques et les densités de solutions diluées de formamide, d'acétone, de tétrahydrofuranne, d'éthylèneglycol, de méthoxy-2 éthanol et d'éthoxy-2 éthanol dans le *N*,*N*-diméthylformamide. On a calculé les volumes et les capacités calorifiques molals apparents de ces solutés dans le DMF et on a comparé ces valeurs avec des données semblables d'autres substances en solution dans le DMF ainsi qu'avec des données concernant des solutions dans le méthanol ainsi que dans l'eau. En se basant sur la théorie de la particule scalaire, on a calculé les capacités calorifiques de la formation de la cavité (ΔC_{cav}) dans le DMF. Il semble exister une corrélation linéaire entre les valeurs de ΔC_{cav} et le volume molal partiel standard des solutés correspondants dans le DMF. On a trouvé des corrélations semblables pour les solutions aqueuses et méthanoliques de non-électrolytes.

[Traduit par la revue]

Introduction

Physicochemical properties of the mixtures of *N*,*N*-dimethylformamide with different compounds are a subject of numerous investigations today. The present of "peptide-like" and methyl groups in molecules makes DMF an "attractive solvent" in view of the model function for the interior of a protein. Moreover, its molecules are highly polar, but practically non-associated, which makes DMF a good solvent for different groups of compounds.

Molar heat capacities and volumes are among the most frequently examined properties of binary mixtures. Many of the above mentioned investigations have been devoted to systems containing DMF (1–7). The present study is aimed at determining molar heat capacities and molar volumes of the solutions of several substances not investigated till now (namely: formamide, acetone, tetrahydrofuran, ethylene glycol, 2-methoxyethanol, and 2-ethoxyethanol) in DMF solvent. The results were to be compared with the analogous data concerning the other DMF–non-electrolyte mixtures investigated earlier. Moreover, it is of interest to see whether some close correlations exist between the volumetric functions and C_p for the different solutes in a solvent as relatively unstructured as DMF.

Experimental

Materials

The origin, and purification of the chemicals are as follows: *N*,*N*-dimethylformamide, formamide, 2-methoxyethanol, and 2-ethoxyethanol (all Baker Analyzed Reagents) were stored over molecular sieves 4 Å for at least one week and used without further purification. Acetone and tetrahydrofuran (Baker Analyzed Reagents) were purified by distillation and dried with molecular sieves. Ethylene glycol (also Baker A.R.) was distilled under reduced pressure. Their water content determined by the modified Karl Fischer procedure (8) was less than 1×10^{-4} volume fraction. Gas–liquid chromatography showed a mole-fraction purity higher than 0.995 for each compound.

Procedure

Liquid mixtures of DMF with the solutes were prepared by mass, avoiding contact with air. Further uptake of water was reduced as much as possible by storing the polyethylene vials with pure solvent and the mixtures in dessicators under nitrogen and above granulated P_2O_5. After these manipulations the water content did not increase by a detectable amount.

Densities of mixtures, ρ, relative to the density of reference liquid were measured using a digital flow densimeter (Sodev, Model 03, Sherbrooke, Quebec). Heat capacities per unit volume (C_p/V) were measured with a Picker flow microcalorimeter (Setaram, Model "chaleur specifique", Lyon, France). The procedure was as reported previously (5, 7).

Results

Densities, ρ, of the investigated solutions in *N*,*N*-dimethylformamide at 298.15 K relative to that of pure DMF ρ_1^* are presented in Table 1 as a function of the molality m of the solute.[2] The density of pure DMF as measured with respect to pure water was $\rho_1^* = 0.943286\ \mathrm{g\ cm^{-3}}$ (7), corresponding to to a molar volume $V_1^* = 77.49\ \mathrm{cm^3\ mol^{-1}}$.

Changes in the heat capacities per unit volume with respect to that of DMF

$$\Delta(C_p/V) = [(C_p/V) - (C_{p,1}^*/V_1^*)]$$

are also reported in Table 1. The results refer to a mean temperature 298.15 K. For heat capacity calculations $(C_{p,1}^*/V_1^*) = 1.9146\ \mathrm{J\ K^{-1}\ cm^{-3}}$ was adopted (3).

The apparent molal volume $V_{\Phi,2}$ and heat capacity $C_{\Phi,2}$ of the solute in the mixtures were calculated from the data using the following equations:

$$[1] \quad V_{\Phi,2} = M_2/\rho - 1000(\rho - \rho_1^*)/m\rho\rho_1^*$$

[1]On leave from the University of Łódź, Department of Physical Chemistry, ul. Nowotki 18, 91-416 Łódź, Poland.

[2]Throughout this paper, subscript 1 refers to the pure solvent (DMF) and 2 to the solute while asterisks refer to the pure liquid.

Printed in Canada / Imprimé au Canada

Can. J. Chem. Downloaded from www.nrcresearchpress.com by 213.222.148.141 on 09/07/12
For personal use only.

Can. J. Chem. Downloaded from www.nrcresearchpress.com by 213.222.148.141 on 09/07/12
For personal use only.

TABLE 1. Experimental differences in density ($\rho - \rho^*_1$) and in heat capacity divided by volume $\Delta(C_p/V)$, and apparent molal quantities in DMF solution at 298.15 K

m	$10^3(\rho - \rho^*_1)$	$V_{\Phi,2}$	$10^3\Delta(C_p/V)$	$C_{\Phi,2}$
mol kg^{-1}	g cm^{-3}	cm^3 mol^{-1}	J K^{-1} cm^{-3}	J K^{-1} mol^{-1}
		Acetone		
0.20161	−1.950	72.59	−2.725	124.48
0.28192	−2.702	72.55	−3.756	124.50
0.59057	−5.597	72.65	−7.919	124.32
0.96141	−8.890	72.65	−12.668	124.16
1.29638	−11.707	72.62	−16.720	124.20
1.64011	−14.528	72.65	−20.680	124.23
2.05749	−17.791	72.66	−25.210	124.29
		Tetrahydrofuran		
0.25403	−1.079	81.31	−5.750	130.36
0.38721	−1.619	81.28	−8.939	130.42
0.52554	−2.177	81.27	−11.970	130.51
0.85302	−3.447	81.28	−19.311	130.05
1.11176	−4.395	81.26	−24.641	130.15
1.55237	−6.025	81.32	−33.910	129.79
1.90996	−7.275	81.35	−41.229	129.51
		Formamide		
0.29533	+2.337	38.76	+10.190	111.21
0.67920	+5.318	38.73	+23.289	111.39
1.00040	+7.746	38.73	+33.689	111.16
1.26177	+9.648	38.76	+42.091	111.19
1.69174	+12.662	38.82	+55.089	111.03
2.08025	+15.295	38.86	+66.692	111.00
		Ethylene glycol		
0.28235	+2.695	54.92	+11.769	149.98
0.57970	+5.431	54.95	+23.856	150.16
0.88415	+8.147	54.97	+35.771	150.10
1.19076	+10.787	54.99	+46.860	149.58
1.45894	+13.026	55.00	+56.739	149.67
1.83799	+16.082	55.02	+69.990	149.58
		2-Methoxyethanol		
0.21416	+0.377	78.69	+4.611	173.87
0.36796	+0.624	78.68	+7.785	173.82
0.54873	+0.886	78.74	+11.388	173.83
0.83176	+1.292	78.79	+16.494	173.24
1.11136	+1.726	78.75	+21.587	173.13
1.42471	+2.115	78.79	+26.988	173.11
1.83080	+2.634	78.80	+33.391	172.79
		2-Ethoxyethanol		
0.23711	−0.212	96.57	+5.489	209.96
0.55948	−0.519	96.64	+12.500	209.92
0.86885	−0.802	96.66	+18.979	210.05
1.17879	−1.082	96.68	+25.020	210.02
1.52907	−1.391	96.71	+31.440	210.00
1.97609	−1.765	96.73	+39.010	209.90

and

[2] $$C_{\Phi,2} = M_2 c_p + 1000(c_p - c_{p,1})/m$$

where M_2 is the solute molecular weight, m is the molality, and $c_p = C_p/V\rho$ the gravimetric (specific) heat capacity. Calculated values of $V_{\Phi,2}$ and $C_{\Phi,2}$ are also given in Table 1.

The apparent molal volumes and heat capacities were next fitted by least-squares methods to equations of the form:

[3] $$V_{\Phi,2} = V^\infty_{\Phi,2} + b_v m$$

or

[4] $$C_{\Phi,2} = C^\infty_{\Phi,2} + b_c m$$

The limiting partial molal quantities ($V^\infty_{\Phi,2} = V^\infty$ and $C^\infty_{\Phi,2} = C^\infty_{p,2}$) and the empirical constants b_v and b_c, as well as the molar values V^*_1 and $C^*_{p,2}$ for pure solutes are summarized in Table 2.

It is known that $C^\infty_{p,2}$, the partial molal heat capacity of the solute at infinite dilution, contains the heat capacity of the solute along with the solute–solvent interaction term. $C^*_{p,2}$ is usually chosen to represent the heat capacity of the liquid solute when solute–solvent interactions are absent (20). As can be seen from the data in Table 2, as well as from the literature (1–7), the limiting partial molal heat capacities for most of the solutes in DMF solution are not too different from the molar quantities ($C^\infty_{p,2} - C^*_{p,2} = \Delta C_{p,2} \approx 0$). Relatively small $\Delta C_{p,2}$ values in DMF are probably connected with the fact that DMF is unstructured and for this reason it is not too sensitive to the presence of the solute. Moreover, this suggests that any specific interactions with DMF in these systems if present at all are very small. Figure 1 presents the heat capacity of solvation of non-electrolytes in DMF, $\delta C^\infty_{p,2} = C^\infty_{p,2} - C^g_{p,m}$ (where $C^g_{p,m}$ is the molal heat capacity of the non-electrolyte in gas phase) as a function of the molecular polarizability (α) of the non-electrolyte. Observed linear correlation of $\delta C^\infty_{p,2}$ and α suggests that electrostatic interactions are dominating forces in most of the analyzed systems.

Partial molal volumes for most of the investigated thus for non-electrolytes are a bit lower in DMF solution than are the corresponding molar volumes ($V^\infty_2 - V^*_2 = \Delta V_2 < 0$). Alkanols higher than C_4, for which $\Delta V_2 > 0$, are the exception in this case.

Much attention has been devoted to finding whether any direct relations exist between the heat capacities and volumetric properties of the solutions in a given solvent. Among others Arnett and co-workers analyzed different dependences between molar volumes of alcohols in aqueous solution and some functions derived from the heat capacities of these solutions (20). It appeared that some simple dependences existed only for solutions of closely related compounds like normal alkanols.

No simple correlations between V^∞_2 and $C^\infty_{p,2}$ could be found for solutions in DMF. Since the partial molal volume of a solute in a given solvent is related to the dimension of a cavity created in the solvent structure, it can be supposed that a correlation exists between V^∞_2 and heat capacity of the cavity creation (ΔC_{cav}). The cavity term can be calculated from the Scaled Particle Theory (21):

[5] $$\Delta C_{cav} = A\sigma_2^2 + B\sigma_2 + C$$

where

[6] $$A = [3J/((1-y)^2\sigma_1^2)] \times [Z(1+2y)(1-y) - y\alpha_p(4y+5)]$$

[7] $$B = [3J/((1-y)\sigma_1)][Z(1-y) - 2y\alpha_p]$$

[8] $$C = J[Z(1-y) - y\alpha_p]$$

and

[9] $$J = RT^2 y\alpha_p/(1-y)^2$$

[10] $$Z = 2/T - \alpha_p + (1/\alpha_p)(\partial\alpha_p/\partial T_p)$$

where

σ_1 = hard sphere diameter of solvent molecule

TABLE 2. Partial molal volumes and heat capacities of several solutes in *N*,*N*-dimethylformamide[a]

Solute	V_2^∞ / cm^3 mol^{-1}	b_v / cm^3 mol^{-2} kg	V_2^* / cm^3 mol^{-1}	$C_{p,2}^\infty$ / J K^{-1} mol^{-1}	b_c / J K^{-1} mol^{-2} kg	$C_{p,2}^*$ / J K^{-1} mol^{-1}
Acetone	72.58 (0.02)	0.04 (0.02)	74.02 74.02 (9) 74.01 (10)	124.44 (0.08)	−0.13 (0.06)	126.36 (11)
Tetrahydrofuran	81.27 (0.02)	0.03 (0.02)	81.82 81.76 (12)	130.63 (0.09)	−0.55 (0.08)	123.56 (12)
Formamide	38.70 (0.03)	0.07 (0.02)	39.88 39.89 (13)	111.38 (0.09)	−0.18 (0.07)	107.6 (14) 107.9 (15)
Ethylene glycol	54.91 (0.01)	0.06 (0.01)	55.93 55.92 (16)	150.22 (0.24)	−0.28 (0.21)	149.9 (17)
2-Methoxyethanol	78.68 (0.02)	0.07 (0.02)	79.22 79.25 (18)	174.04 (0.10)	−0.71 (0.10)	176.4 (18) 174.9 (19)
2-Ethoxyethanol	96.57 (0.02)	0.08 (0.01)	97.17 97.15 (18)	210.00 (0.05)	−0.01 (0.04)	210.3 (18) 210.8 (19)

[a]Standard deviations in parentheses below each result. References in parentheses next to the literature result.

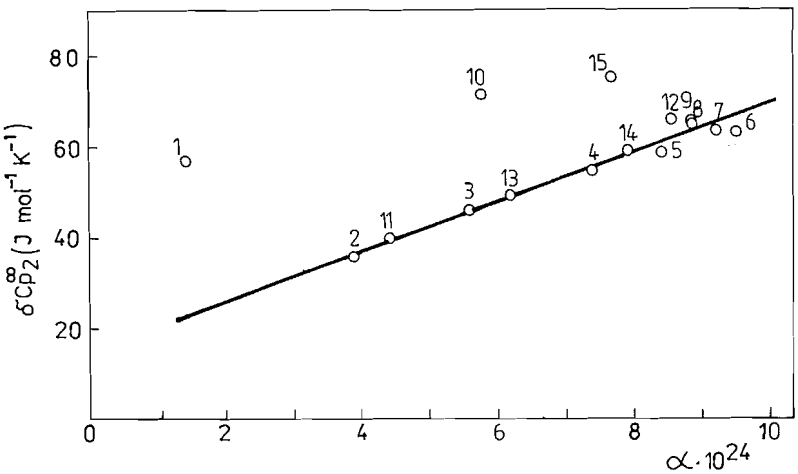

FIG. 1. The dependence of standard molal heat capacity of solvation of non-electrolytes in DMF ($\delta C_{p,2}^\infty = C_{p,2}^\infty - C_{p,m}^g$) on molecular polarizability of the non-electrolyte (α). *1*, Water; *2*, methanol; *3*, ethanol; *4*, propanol; *5*, *i*-propanol; *6*, *n*-butanol; *7*, *i*-butanol; *8*, *s*-butanol; *9*, *t*-butanol; *10*, ethylene glycol; *11*, acetonitrile; *12*, dimethylsulfoxide; *13*, acetone; *14*, *N*,*N*-dimethylformamide; *15*, 2-methoxyethanol.

and

σ_2 = hard sphere diameter of solute molecule

[11] $y = \pi N_A \sigma_1^3 / 6 V_1^*$

The parameters, necessary for these calculations, are given in Table 3. The hard sphere diameters of the solute, σ_2, were taken from Kim's compilation (10), or were calculated using the method proposed in his paper. Table 4 presents the cavity term ΔC_{cav} for several solutes in *N*,*N*-dimethylformamide. The same data are plotted as a function of the standard partial molal volumes of the corresponding solutes in DMF solution in Fig. 2. For the sake of comparison the analogous dependences for aqueous and methanolic solutions are also presented in the figure. The ΔC_{cav} and V_2^∞ values in the latter solvents are taken from the papers of French and Criss (21, 24) and of Cabani and co-workers (25), or calculated (some for ΔC_{cav} in water) using the hard sphere diameters σ_2 given in Kim's paper (10). To make possible a comparison of these data the same values of σ_2 were used for ΔC_{cav} calculations in each solvent.

As can be seen in Fig. 2 there are good linear correlations in all systems studied. The equations correlating ΔC_{cav} and V_2^∞ have a form:

$$\Delta C_{cav} = (1.676 \pm 0.065) V_2^\infty + (49.680 \pm 4.475) \quad \text{in DMF solution}$$

$$\Delta C_{cav} = (2.632 \pm 0.068) V_2^\infty + (51.963 \pm 4.619) \quad \text{in water}$$

TABLE 3. *N*,*N*-Dimethylformamide parameters for Scaled Particle Theory calculations of ΔC_{int}

Parameter	Value
$10^8\sigma$	4.98 cm[a]
V	77.49 cm^3 mol^{-1}
$10^3\alpha_p$	1.015 K^{-1} [b]
$10^6(\partial\alpha_p/\partial T)_p$	5.22 K^{-2} [c]
y	0.503

[a]Reference 10.
[b]Reference 22.
[c]Calculated from data in ref. 23.

Can. J. Chem. Downloaded from www.nrcresearchpress.com by 213.222.148.141 on 09/07/12
For personal use only.

TABLE 4. Scaled Particle Theory cavity and interaction contributions to $\delta C_{p,2}^{\infty}$ in DMF and heat capacity of the solute transfer from DMF to water at 298.15 K[a]

Solute	ΔC_{cav}	$\delta C_{p,2}^{\infty}$	ΔC_{int}	ΔC_p^{∞} (DMF → W)
Water	70.5	56.9	−14.2	−15.1
Methanol	110.8	35.9	−75.5	+78.4
Ethanol	144.3	46.4	−98.4	+148.5
Propanol	164.8	54.4	−111.0	+211.4
i-Butanol	201.4	62.6	−139.4	+260.1
2-Methoxyethanol	183.6	76.5	−107.6	+112.7
2-Ethoxyethanol	209.3	89.1	−120.8	+173.5
Ethylene glycol	146.0	72.2	−74.3	+41.7
Acetonitrile	136.7	39.7	−97.6	+118
Dimethylsulfoxide	178.0	66.0	−112.6	+30.7
Formamide	123.2	64.9	−58.9	−29.3
N-Methylformamide	153.2	46.5	−107.3	+46.0
N,*N*-Dimethylformamide	181.7	59.5	−122.8	+76.7
Acetone	168.3	49.6	−119.3	+117.1

[a]All C_p values in J K^{-1} mol^{-1}.

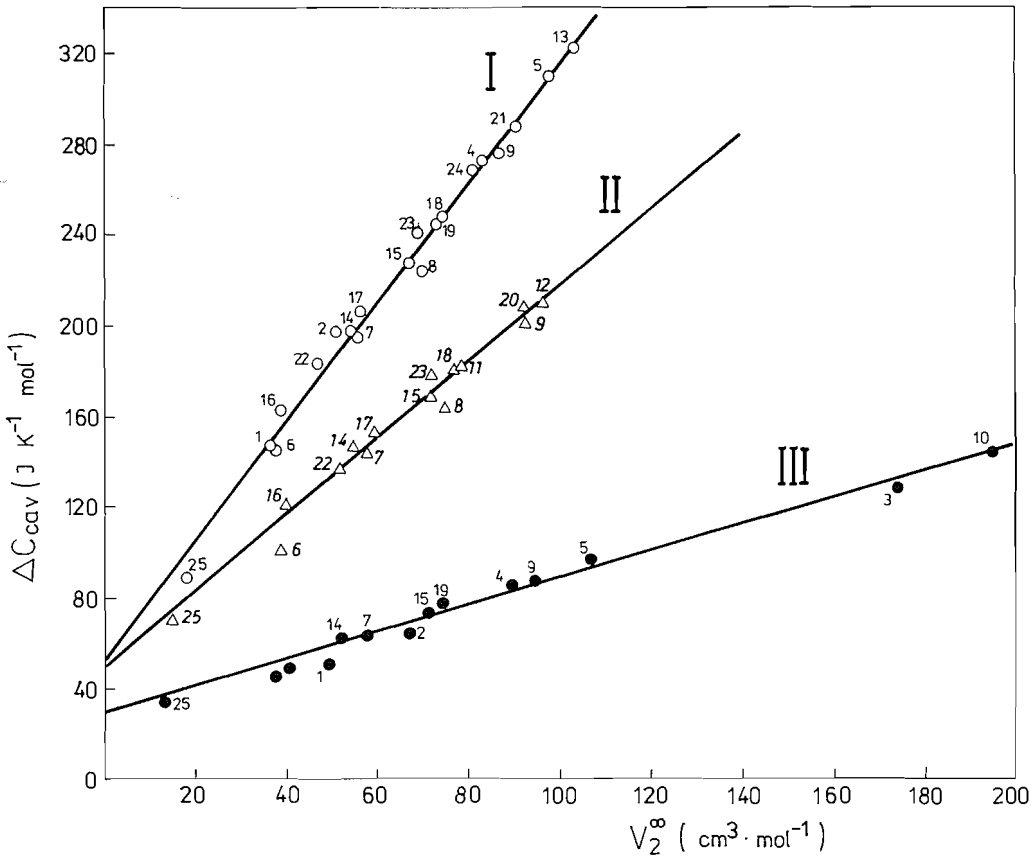

FIG. 2. Correlation between heat capacity of formation of cavity, ΔC_{cav}, and standard partial molal volume of the solutes in water (I), DMF (II), and methanol (III) at 298.15 K. *1*, Methane; *2*, ethane; *3*, octane; *4*, benzene; *5*, toluene; *6*, methanol; *7*, ethanol; *8*, propanol; *9*, *i*-butanol; *10*, *n*-decanol; *11*, 2-methoxyethanol; *12*, 2-ethoxyethanol; *13*, cyclohexanol; *14*, ethylene glycol; *15*, acetone; *16*, formamide; *17*, *N*-methylformamide; *18*, *N*,*N*-dimethylformamide; *19*, *N*-methylacetamide; *20*, *N*,*N*-dimethylacetamide; *21*, *N*-butylacetamide; *22*, acetonitrile; *23*, dimethylsulfoxide; *24*, dioxane; *25*, water.

and

$$\Delta C_{cav} = (0.608 \pm 0.028)V_2^{\infty} + (27.190 \pm 2.894) \quad \text{in methanol}$$

The observed dependence appears to be especially surprising in aqueous solutions since it encompasses both solutes which are able to interact with water through H-bond formation and the compounds that are hydrophobically hydrated such as hydrocarbons and higher alkanols. This observation seems to confirm Stillinger's opinion that in aqueous solution, the formation of a cage around the hydrophobic solute contributes to $C_{p,2}^{\infty}$ through an interaction term ΔC_{int} but not through the cavity term ΔC_{cav} (26). Comparison of the slopes of these functions indicates that the expansion of the cavity dimension in DMF is less related to the solvent structure disturbance than it is in water. The opposite appears to be true when comparing

Can. J. Chem. Downloaded from www.nrcresearchpress.com by 213.222.148.141 on 09/07/12
For personal use only.

DMF with methanol. The values of isothermal compressibility coefficient β_T of these solvents (DMF, 6.3×10^{-5} atm^{-1} (27); water, 4.63×10^{-5} atm^{-1} (21); methanol, 12.64×10^{-5} atm^{-1} (21)) confirm this opinion.

The correlations makes it possible to find the cavity term for a solute for which V_2^∞ is given.

The knowledge of the cavity term and limiting partial molal heat capacity allows us to calculate the solute–solvent "interaction term", ΔC_{int}, according to a formula given by SPT (21):

$$[12] \quad \Delta C_{int} = \delta C_{p,2}^\infty - \Delta C_{cav} - R[2\alpha_p T + (\partial\alpha_p/\partial T)_p T^2 - 1]$$

where, as defined earlier, $\delta C_{p,2}^\infty = C_{p,2}^\infty - C_{p,m}^g$. The values of ΔC_{int} and $\delta C_{p,2}^\infty$ for several solutes in DMF are also presented in Table 4. These values show that ΔC_{int} in DMF solution is negative for all non-electrolytes investigated, just as it was found for methanolic solutions (water was an exception), and for aqueous solutions of substances that were capable of interacting strongly with water (methanol, NMA, acetone, DMSO, water) (24). The positive ΔC_{int} values, characteristic of aqueous solutions of hydrophobic substances were not found in DMF solution. This observation seems to confirm the conclusion reached earlier (21) that positive ΔC_{int} in water were related to the formation of cages around the hydrophobic solutes.

The change in heat capacities of the solute transfer from DMF to water ΔC_p^∞(DMF→ W) Table 4 for most of the examined systems are large and positive. This is caused by large, negative ΔC_{int} for these solutes in DMF and ΔC_{cav} values generally lower than that in aqueous solutions. Negative values of ΔC_p^∞(DMF→ W) observed in the case of water and formamide as solutes are probably joined with relatively high negative interaction term of these solutes in water owing to their molecular structure, possibility of strong H-bond formation, and lack of hydrocarbon groups that bring in positive interaction contributions.

Acknowledgement

The author is grateful to the authorities of the Free University of Amsterdam for the generous grant of a post-doctoral fellowship at their Thermochemical Laboratory.

1. C. DE VISSER and G. SOMSEN. J. Solution Chem. **8**, 593 (1979).
2. O. D. BONNER, J. M. BEDNAREK, and R. K. ARISMAN. J. Am. Chem. Soc. **99**, 2898 (1977).
3. H. C. ZEGERS and G. SOMSEN. J. Chem. Thermodyn. **16**, 225 (1984).
4. H. C. ZEGERS and G. SOMSEN. Fluid Phase Equilibria, **18**, 299 (1984).
5. H. C. ZEGERS, R. BOEGSCHOTEN, W. MELS, and G. SOMSEN. Can. J. Chem. **64**, 40 (1986).
6. V. P. KOROLEV, V. A. KUKHARENKO, and G. A. KRESTOV. Zhur. Fiz. Khim. **60**, 1854 (1986).
7. H. PIEKARSKI and G. SOMSEN. J. Chem. Soc. Faraday Trans. I. In press.
8. J. C. VERHOEF and E. BARENDRECHT. Anal. Chim. Acta, **94**, 395 (1977).
9. J. TIMMERMANS. Physico-chemical constants of pure organic compounds. Vol. II. Elsevier Publishing Co., New York. 1965.
10. J. I. KIM. Z. Physik. Chem. Neue Folge, **113**, 129 (1978).
11. Handbook of chemistry and physics. 65th ed. CRC Press Inc. Boca Raton, FL. 1985.
12. O. KIYOHARA, P. J. D'ARCY, and G. C. BENSON. Can. J. Chem. **57**, 1006 (1978).
13. E. N. VASENKO and S. M. DUBROVSKII. Zhur. Fiz. Khim. **27**, 281 (1953).
14. G. SOMSEN. Thesis, Free University, Amsterdam. 1964.
15. C. DE VISSER, W. J. M. HEUVELSLAND, L. A. DUNN, and G. SOMSEN. J. Chem. Soc. Faraday Trans. I, **74**, 1159 (1978).
16. Y. MATSUMOTO, H. TOUHARA, K. NAKANISHI, and N. WATANABE. J. Chem. Thermodyn. **9**, 801 (1977).
17. M. A. STEPHENS and W. S. TAMPLIN. J. Chem. Eng. Data, **24**, 81 (1979).
18. G. ROUX, G. PERRON, and J. E. DESNOYERS. J. Solution Chem. **7**, 639 (1978).
19. K. KUSANO, J. SUURKUUSK, and I. WADSÖ. J. Chem. Thermodyn. **5**, 757 (1973).
20. E. M. ARNETT, W. B. KOVER, and J. V. CARTER. J. Am. Chem. Soc. **91**, 4028 (1969).
21. R. N. FRENCH and C. M. CRISS. J. Solution Chem. **10**, 713 (1981).
22. A. ROUW. Thesis, Free University, Amsterdam. 1982.
23. B. S. KRUMGALZ and J. G. M. BARTHEL. Z. Physik Chem. Neue Folge, **142**, 167 (1984).
24. R. N. FRENCH and C. M. CRISS. J. Solution Chem. **10**, 699 (1981).
25. S. CABANI, P. GIANNI, V. MOLLICA, and L. LEPORI. J. Solution Chem. **10**, 563 (1981).
26. F. H. STILLINGER. J. Solution Chem. **2**, 141 (1973).
27. J. JUILLARD. Pure Appl. Chem. **49**, 885 (1977).

Can. J. Chem. Downloaded from www.nrcresearchpress.com by 213.222.148.141 on 09/07/12
For personal use only.

Copper(II) complexes of a macrocyclic binucleating ligand which exhibit two-electron oxidation and two-electron reduction. Structure of $[Cu_2(C_{24}H_{34}N_4O_2)(CH_3OH)_2](ClO_4)_2$, a macrocyclic dicopper(II) complex involving coordinated methanol[1]

SANAT K. MANDAL AND LAURENCE K. THOMPSON[2]
Department of Chemistry, Memorial University of Newfoundland, St. John's, Nfld., Canada A1B 3X7

KAMALAKSHA NAG
Department of Inorganic Chemistry, Indian Association for the Cultivation of Science, Calcutta, 100032, India

AND

JEAN-PIERRE CHARLAND AND ERIC J. GABE
Division of Chemistry, National Research Council of Canada, Ottawa, Ont., Canada K1A 0R6

Received May 11, 1987

SANAT K. MANDAL, LAURENCE K. THOMPSON, KAMALAKSHA NAG, JEAN-PIERRE CHARLAND, and ERIC J. GABE. Can. J. Chem. **65**, 2815 (1987).

The saturated ligand H_2L1, derived by template condensation of 4-methyl-2,6-diformylphenol and 1,3-diaminopropane, followed by borohydride reduction, generates binuclear, antiferromagnetically coupled, copper(II) complexes which exhibit cyclic voltammetry involving two one-electron oxidation steps ($E_{1/2}$ = 1.1 to 1.2 V, 1.3 to 1.4 V; $Pt/CH_3CN/SCE$) and two one-electron reduction steps ($E_{1/2}$ = −0.75 to −0.76 V, −0.89 to −0.90 V (GC/DMSO/SCE) with the formation of Cu(III)–Cu(III) and Cu(I)–Cu(I) and mixed oxidation state species. A trinuclear derivative, $[Cu_2(L1)(CuCl_4)]$, appears to contain a spin-coupled binuclear species bound to a magnetically isolated tetrachlorocuprate(II) entity. The complex $[Cu_2(L1)(CH_3OH)_2](ClO_4)_2$ forms brown crystals with a = 8.6516(7), b = 11.6832(9), c = 16.7205(6) Å, β = 92.596(5)°, $P2_1/n$, Z = 2, R_f = 0.037 and has a copper–copper separation of 3.088(1) Å and two weakly bound *trans*-axial methanol molecules (Cu—O, 2.413(4) Å). Variable temperature magnetic studies on $[Cu_2(L1)(ClO_4)_2]$ and $[Cu_2(L1)](ClO_4)_2$ indicate strong antiferromagnetic exchange ($-2J$ = 824 ± 5 cm^{-1}, 827 ± 7 cm^{-1}, respectively) in both cases.

SANAT K. MANDAL, LAURENCE K. THOMPSON, KAMALAKSHA NAG, JEAN-PIERRE CHARLAND et ERIC J. GABE. Can. J. Chem. **65**, 2815 (1987).

On peut obtenir le ligand saturé H_2L1 par une condensation du méthyl-4 diformyl-2,6 phénol avec du diamino-1,3 propane, suivie d'une réduction par le borohydrure; il génère des complexes binucléaires du cuivre(II) qui sont couplés d'une façon antiferromagnétique et qui présentent un voltamétrie cyclique impliquant deux étapes d'oxydation par un électron ($E_{1/2}$ = 1,1 à 1,2 V et 1,3 à 1,4 V; $Pt/CH_3CN/SCE$) et deux étapes de réduction par un électron ($E_{1/2}$ = −0,75 à −0,76 V et −0,89 à −0,90 V; GC/DMSO/SCE) avec la formation d'espèces Cu(III)–Cu(III), Cu(I)–Cu(I) et d'espèces de niveaux d'oxydation mixtes. Un dérivé trinucléaire, $[Cu_2(L1)(CuCl_4)]$, semble contenir une espèce binucléaire couplés par les spin à une entité tétrachlorocuprate(II) isolée d'un point de vue magnétique. Le complexe $[Cu_2(L1)(CH_3OH)_2](ClO_4)_2$ forme des cristaux bruns avec a = 8,6516(7), b = 11,6832(9) et c = 16,7205(6) Å, β = 92,596(5)°, $P2_1/n$, Z = 2, R_f = 0,037; ils comportent une séparation cuivre–cuivre de 3,088(1) Å et deux molécules de méthanol faiblement liées en positions trans et axiales (Cu—O, 2,413(4) Å). Des études magnétiques à température variable sur le $[Cu_2(L1)(ClO_4)_2]$ et sur le $[Cu_2(L1)](ClO_4)_2$ indiquent que, dans chaque cas, il se produit un fort échange antiferromagnétique ($-2J$ = respectivement 824 ± 5 cm^{-1} et 827 ± 7 cm^{-1}).
[Traduit par la revue]

Introduction

Binuclear copper(II) complexes of the unsaturated macrocyclic ligand H_2L3 and its derivatives have been the focus of extensive studies (1–13) but the half saturated macrocycle, H_2L2 (14, 15), and the fully saturated macrocycle, H_2L1 (16), have received much less attention (Fig. 1). Structural studies on $[Cu_2(L3)Cl_2].6H_2O$ (4, 5) and the mixed valence state species $[Cu(II)Cu(I)(L3)]ClO_4.0.5CH_3OH$ (13), involving the unsaturated macrocycle, have been reported and indicate square-pyramidal copper(II) centres and essentially square planar copper centres, respectively. In both cases the two copper centres are bound by four in-plane donors: two azomethine nitrogen centres and two oxygen atoms from the phenoxide bridges. In a recent report (16) the structure of the complex $[Cu_2(L1)(ClO_4)_2]$, involving the fully saturated macrocycle, has been shown to consist of two copper(II) centres bridged by the two phenoxide oxygen atoms with two secondary amine nitrogen donors completing the in-plane donor sets, and two axially bound, bidentate perchlorates forming distorted, axially elongated, octahedra. This complex exhibits remarkable electrochemistry involving two one-electron oxidation steps (cyclic voltammetry, $E_{1/2}$ = 1.21 V, 1.41 V; $Pt/CH_3CN/SCE$) and two one-electron reduction steps ($E_{1/2}$ = −0.76 V, −0.90 V; GC/DMSO/SCE) with the formation of Cu(III)–Cu(III), Cu(I)–Cu(I), and mixed oxidation state species. Electron spin resonance data indicate that the odd electron is localised on one copper centre only in both the half-oxidized and half-reduced species (16).

In the present study we report the crystal structure of the complex $[Cu_2(L1)(CH_3OH)_2](ClO_4)_2$, an unusual binuclear, five-coordinate, copper(II) species involving in-plane N_2O_2 coordination and *trans*-coordination of two methanol molecules with relatively long Cu—O (MeOH) separations (2.413 Å). Variable temperature magnetic studies indicate very strong antiferromagnetic exchange between the copper(II) centres in $[Cu_2(L1)](ClO_4)_2$ and $[Cu_2(L1)(ClO_4)_2]$ ($-2J$ = 827 ± 7 cm^{-1}, 824 ± 5 cm^{-1}, respectively). Other copper(II) derivatives of this ligand are also described, including the trinuclear species $[Cu_2(L1)(CuCl_4)]$, which appears to consist of a

[1]NRC No. 28162.
[2]Author to whom correspondence should be addressed.

Can. J. Chem. Downloaded from www.nrcresearchpress.com by 213.222.148.141 on 09/07/12
For personal use only.

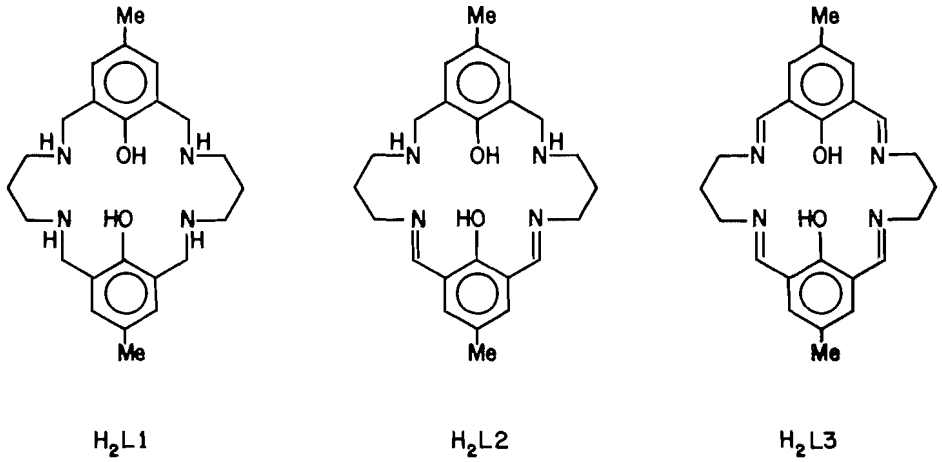

FIG. 1. Structure of H_2L1, H_2L2, and H_2L3.

TABLE 1. Analytical and other data

	Compound	Color	Found (%)			Calcd (%)		
			C	H	N	C	H	N
II	$[Cu_2(L1)(H_2O)_2](ClO_4)_2$	Green	37.65	4.67	7.36	37.30	4.92	7.25
III	$[Cu_2(L1)](ClO_4)_2$	Brown	38.95	4.59	7.54	39.10	4.62	7.60
IV	$[Cu_2(L1)(CuCl_4)]$	Green–brown	38.75	4.62	7.55	38.79	4.62	7.54
V	$[Cu_2(L1)(SCN)_2].H_2O$	Green	46.40	5.23	12.29	46.49	5.40	12.52

strongly coupled binuclear entity bound to an essentially magnetically isolated tetrachlorocuprate(II) anion.

Experimental

Synthesis of the ligand and complexes

The ligand, H_2L1, was synthesized according to the published procedure (16).

*$[Cu_2(L1)(CH_3OH)_2](ClO_4)_2$ (**I**), $[Cu_2(L1)(H_2O)_2](ClO_4)_2$ (**II**), $[Cu_2(L1)](ClO_4)_2$ (**III**)*

H_2L1 (0.41 g, 0.001 mol) was dissolved in a mixture of dry methanol (5 mL) and 2,2-dimethoxypropane (10 mL) and $Cu(ClO_4)_2.6H_2O$ (0.75 g, 0.002 mol) was dissolved separately in a similar solvent mixture. The solutions were refluxed separately for 30 min, cooled to room temperature, and mixed. After 30 min green needles formed (**II**), which were removed by decanting. On further standing a mixture of brown and green crystals was obtained (yield 0.23 g) and was decanted. Finally a third crop of brown crystals (**I**) was obtained (yield 0.06 g). This original complex was studied by X-ray crystallography (see Discussion), but in all subsequent preparations only mixtures of **II** and **III** were obtained. If the ligand and copper perchlorate are refluxed separately with excess 2,2-dimethoxypropane in methanol for 5–6 h, cooled, and then mixed, the brown product **III** is obtained as the exclusive product.

*$[Cu_2(L1)(CuCl_4)]$ (**IV**)*

H_2L1 (0.41 g, 0.001 mol) was dissolved in methanol (5 mL) and a solution of $CuCl_2.2H_2O$ (0.35 g, 0.002 mol) in methanol (10 mL) was added and the mixture left for several hours. Green–brown crystals formed and were filtered off, washed with methanol, and air dried (yield 0.25 g).

*$[Cu_2(L1)(NCS)_2].H_2O$ (**V**)*

H_2L1 (0.41 g, 0.001 mol) was dissolved in butanol (30 mL) and a solution of $Cu(ClO_4)_2.6H_2O$ (0.75 g, 0.002 mol) in butanol (20 mL) added. After 5 to 6 h green crystals formed and were filtered off, washed with butanol, and air dried. The green crystalline compound (0.2 g) was dissolved in hot acetonitrile (30 mL) and a saturated aqueous solution of NH_4SCN (10 mL) added with stirring. On reducing the volume of the solution a green compound (**V**) formed and was separated by filtration, washed with water and ethanol, and air dried (yield 0.12 g).

Analytical data for compounds **II**–**V** are given in Table 1.

Electrochemical measurements

The electrochemical experiments were performed at room temperature in dimethylsulfoxide (spectroscopic grade, dried over molecular sieves) and acetonitrile (spectroscopic grade, dried over molecular sieves) under O_2-free conditions using a BAS CV27 Voltammograph and a Houston Omnigraph 2000XY recorder. A three-electrode system was used (cyclic voltammetry) in which the working electrode was either glassy carbon (reduction in DMSO) or platinum (oxidation in acetonitrile), the counter electrode platinum, with a standard calomel (SCE) electrode as reference. For coulometry measurements a three-electrode system was employed consisting of a platinum mesh flag working electrode, a platinum mesh counter electrode, and a silver rod as reference electrode. The supporting electrolyte was tetraethylammonium perchlorate (TEAP) (0.1 *M*) and all solutions were 10^{-3}–10^{-4} in complex. The best combination of experimental conditions (working electrode, scan rates, solvent etc.) was determined by preliminary experiment.

Magnetic measurements

Room-temperature magnetic moments were measured by the Faraday method using a Cahn 7600 Faraday magnetic susceptibility system. Variable-temperature magnetic susceptibility data were obtained in the range 5–300 K (compounds **III**, **VI**) using an Oxford Instruments superconducting Faraday magnetic susceptibility system with a Sartorius 4432 microbalance. A main solenoid field of 1.5 Tesla and a gradient field of 10 T m^{-1} were employed.

Data for X-ray crystallographic analysis for $[Cu_2(L1)(CH_3OH)_2](ClO_4)_2$ (**I**) are as follows:

Can. J. Chem. Downloaded from www.nrcresearchpress.com by 213.222.148.141 on 09/07/12
For personal use only.

TABLE 2. Atomic positional parameters and equivalent isotropic temperature factors (esd's) for $[Cu_2(L1)(CH_3OH)_2](ClO_4)_2$ (**I**)

Atom	*X*	*Y*	*Z*	B_{iso}
Cu1	0.48848(7)	0.01098(5)	0.59156(3)	3.00(3)
Cl1	0.00112(17)	−0.07793(11)	0.71219(8)	4.21(7)
O1	0.5565(3)	0.09452(21)	0.49759(15)	2.95(14)
O2	−0.1572(4)	−0.09697(29)	0.69881(24)	7.78(24)
O3	0.0578(6)	−0.12693(31)	0.78407(22)	10.56(28)
O4	0.0794(4)	−0.13117(33)	0.65053(22)	8.20(24)
O5	0.0388(4)	0.04083(25)	0.71220(19)	6.01(19)
O6	0.2451(4)	0.11206(35)	0.59013(24)	5.72(22)
N1	0.5661(5)	0.1326(3)	0.66641(22)	3.3(2)
N2	0.4322(6)	−0.1078(3)	0.67050(22)	3.2(2)
C1	0.6060(5)	0.2042(3)	0.49485(24)	2.64(22)
C2	0.6800(5)	0.2541(4)	0.56253(23)	2.96(21)
C3	0.7249(6)	0.3672(4)	0.55937(29)	3.91(26)
C4	0.7051(6)	0.4340(4)	0.49186(30)	3.85(26)
C5	0.6343(6)	0.3821(4)	0.42526(27)	3.43(24)
C6	0.5848(5)	0.2703(3)	0.42574(23)	2.71(21)
C7	0.7095(7)	0.1857(5)	0.63691(29)	3.73(26)
C8	0.5844(7)	0.1056(5)	0.75307(27)	3.70(29)
C9	0.4525(8)	0.0354(5)	0.78137(31)	4.39(32)
C10	0.4620(8)	−0.0878(5)	0.75842(29)	3.97(29)
C11	0.4954(7)	−0.2211(4)	0.64779(29)	3.39(27)
C12	0.7540(11)	0.5580(5)	0.48941(50)	5.75(44)
C13	0.1581(11)	0.1309(9)	0.51789(51)	7.04(47)
H1	0.498(4)	0.1815(29)	0.6635(22)	1.8(11)
H2	0.343(4)	−0.1126(31)	0.6636(21)	1.0(11)
H3	0.768(4)	0.3977(25)	0.6032(17)	1.2(8)
H5	0.619(4)	0.4238(24)	0.3808(16)	1.0(8)
H6	0.181(6)	0.0971(50)	0.6250(30)	9.0(21)
H71	0.782(4)	0.1226(32)	0.6315(20)	3.6(12)
H72	0.751(4)	0.2370(28)	0.6820(20)	3.8(10)
H81	0.680(4)	0.0623(27)	0.7615(20)	3.2(11)
H82	0.596(5)	0.1786(30)	0.7843(21)	4.5(11)
H91	0.450(4)	0.0403(27)	0.8344(19)	2.8(10)
H92	0.358(4)	0.0697(27)	0.7689(19)	1.7(10)
H101	0.394(4)	−0.1321(31)	0.7862(20)	3.1(11)
H102	0.576(5)	−0.1140(35)	0.7720(24)	5.6(14)
H111	0.608(5)	−0.2099(32)	0.6431(22)	4.1(13)
H112	0.483(4)	−0.2692(27)	0.6914(19)	2.0(8)
H121	0.753(6)	0.5874(40)	0.5284(24)	4.7(17)
H122	0.885(8)	0.5700(47)	0.4912(35)	13.1(25)
H123	0.725(6)	0.5989(41)	0.4480(28)	7.9(19)
H131	0.083(7)	0.1875(47)	0.5311(34)	10.3(26)
H132	0.230(7)	0.1694(48)	0.4854(32)	10.1(24)
H133	0.126(8)	0.0650(44)	0.4985(39)	12.8(31)

$C_{26}H_{42}N_4O_{12}Cl_2Cu_2$ fw = 796.29
Monoclinic, $P2_1/n$, a = 8.6516(7), b = 11.6832(9), c = 16.7205(6) Å, β = 92.596(5)°, V = 1679.6 Å^3, Z = 2(MoKα, $\lambda\alpha$ = 0.70930 Å); μ = 1.49 mm^{-1}, D_{calcd} = 1.575 g cm^{-3}.

Crystals of **I** are brown in colour. The diffraction intensities of an approximately 0.30 × 0.30 × 0.20 mm crystal were collected with graphite monochromatized MoKα radiation using the ω scan mode to $2\theta_{max}$ = 44° using a Nonius diffractometer. A total of 2284 reflections were measured, of which 2172 were considered unique, and 1769 reflections were considered to be significant with $I_{net} > 2.5\sigma(I_{net})$. Lorentz and polarization factors were applied and no correction was made for absorption. The cell parameters were obtained by the least-squares refinement of the setting angles of 44 reflections with 2θ in the range 40–45° (λMoKα = 0.70930 Å). The structure was solved by direct methods using MULTAN (17) and refined by full-matrix least-squares methods to final residuals of R_f = 0.037 and R_w = 0.022 for the significant data (0.049 and 0.022 for all data) with weights based on counting statistics. All hydrogen atoms were located from a difference map and refined. All calculations were performed with the NRCVAX system of programs (18). Scattering factors were taken from ref. 19. The final atomic positional parameters and equivalent isotropic temperature factors are listed in Table 2, thermal parameters in Table 3, and observed and calculated structure factors in Table 4.[3]

Results and discussion

Description of the structure of $[Cu_2(L1)(CH_3OH)_2](ClO_4)_2$ (I)

The crystal structure of **I** is shown in Fig. 2 and consists of two square-pyramidal copper(II) centres bridged by two phenoxide oxygen atoms with two secondary amine nitrogen donors completing the distorted CuN_2O_2 plane. Interatomic distances and angles relevant to the copper coordination spheres

[3]Photocopies of Tables 3, 4 may be purchased from the Depository of Unpublished Data, CISTI, National Research Council of Canada, Ottawa, Ont., Canada K1A 0S2.

Can. J. Chem. Downloaded from www.nrcresearchpress.com by 213.222.148.141 on 09/07/12
For personal use only.

Can. J. Chem. Downloaded from www.nrcresearchpress.com by 213.222.148.141 on 09/07/12
For personal use only.

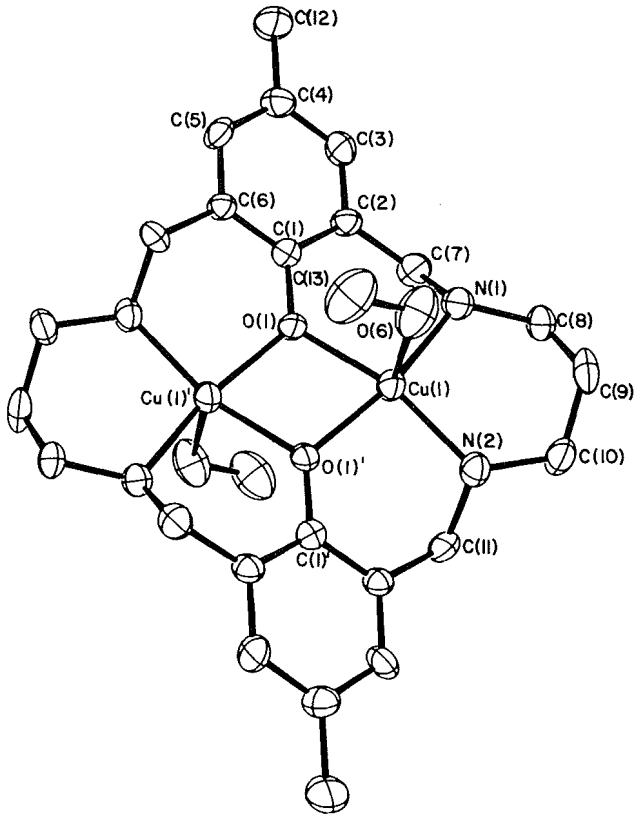

FIG. 2. Structural representation of $[Cu_2(L1)(CH_3OH)_2]^{2+}$ (**I**) with hydrogen atoms omitted (40% probability thermal ellipsoids).

are listed in Table 5. The distortion in the CuN_2O_2 plane involves an acute angle O(1)—Cu(1)—O(1)′ of 76.1° and the copper centre is displaced from the mean plane of the atoms O(1), N(1), N(2), O(1)′, toward the coordinated methanol by 0.11 Å. The oxygen bridge angles, Cu—O(1)—Cu, are 103.9° and the two copper centres are separated by 3.088 Å. The methanol molecules are bound in a *trans* fashion, above and below the binuclear centre, with Cu—O separations of 2.413 Å. Coordinated methanol molecules have been observed for a number of other mononuclear and binuclear copper(II) complexes and copper–oxygen separations are found in the range 2.16–2.48 Å in a literature sampling (20–28). The methanol–copper interaction in **I** is relatively weak and the overall *trans* arrangement of the two methanol molecules about the diphenoxide bridged binuclear centre is similar to that observed for the bistriketonate system $[Cu_2(HXFDAA)_2(CH_3OH)_2]$ (HXFDAA = 1,1,1,7,7,7-hexafluoro-2,4,6-heptanetrionate) (27), which involves two *trans* square-pyramidal CuO_5 chromophores with two ketonic oxygen bridges and relatively short copper–methanol separations (2.223 Å).

The structure of **I** is very similar to that of the complex $[Cu_2(L3)Cl_2].6H_2O$ (5), which involves a *trans* arrangement of two axially bound chlorine atoms (Cu—Cl 2.582 Å) about the binuclear centre. Similar distortions were observed in the CuN_2O_2 planes with slightly shorter Cu—N and slightly longer Cu—O distances than those observed for **I**. The copper–copper separation (3.133 Å) and the Cu—O—Cu angle (104.5°) are larger for this compound also. The binuclear centre in **I** also compares closely with that of the complex $[Cu_2(L1)(ClO_4)_2]$ (**VI**) (16), which has the same basic structure but with two weakly bound bidentate axial perchlorate groups forming what is best described as a severely distorted, elongated octahedron at each copper centre.

Synthesis, spectral, magnetic, and electrochemical properties of the complexes

The copper coordination chemistry of H_2L1 is quite complicated and even relatively subtle differences in reaction conditions can lead to different compounds using the same copper salt. In the case of the perchlorate derivatives three different compounds have been obtained from methanol/2,2-dimethoxypropane mixtures. The green diaquoderivative (**II**) clearly results from incomplete drying of the solvent while the anhydrous brown compound $[Cu_2(L1)](ClO_4)_2$ is formed when all the water in the solvent mixture has been consumed by reaction with 2,2-dimethoxypropane. The dimethanol complex (**I**), which was characterized by X-ray crystallography, was obtained from the original synthesis (Experimental), but in all subsequent preparations only the brown compound $[Cu_2(L1)](ClO_4)_2$ was obtained in addition to compound **II**. Consequently, although compound **I** has been characterized structurally, no other physical characterization has been carried out on this complex. Structurally, however, the binuclear macrocyclic entity $[Cu_2(L1)]^{2+}$ will likely be the same in all three systems.

The infrared spectra of **II** and **III** are very similar with strong ν_3 perchlorate vibrations at 1100 cm^{-1} indicative of ionic perchlorate and NH stretching absorptions at 3230 and 3250 cm^{-1}, respectively. Two strong absorptions at 3490 and 3560 cm^{-1} suggest that in **II** both water molecules are coordinated. Compound **II** has a visible absorption at 17 400 cm^{-1} while compound **III** absorbs at 16 600 cm^{-1} (Table 6). The blue complex $[Cu_2(L1)(ClO_4)_2]$(VI), which involves very long axial Cu—O (perchlorate) interactions (2.821 Å), has a visible absorption at 17 700 cm^{-1} and exhibits three ν_3 perchlorate absorptions (1120, 1085, 1025 cm^{-1}) (16) in the infrared indicative of low symmetry, coordinated perchlorate. Structurally all three complexes are clearly closely related and it seems reasonable to assume that for **II** the water molecules are bound in a *trans*-axial square-pyramidal arrangement while for compound **III** a binuclear square-planar structure exists.

Room temperature magnetic moments for compounds **II**, **III**, and **VI** are around 0.5 BM (Table 6) indicating strong spin exchange between the copper(II) centres. Variable temperature magnetic susceptibility measurements were performed on powdered samples of **III** and **VI** in the temperature range 5–300 K. The results are summarised in Figs. 3 and 4, respectively. The best-fit lines were calculated from the Van Vleck equation (29) for exchange-coupled pairs of copper(II) ions (eq. [1]):

$$[1]\quad \chi_M = \frac{N\beta^2 g^2}{3kT}\left[1 + \frac{1}{3}\exp(-2J/kT)\right]^{-1}(1-\rho) + \left[\frac{N\beta^2 g^2}{4kT}\right]\rho + N\alpha$$

In this expression $2J$ (in the spin Hamiltonian $H = 2J\hat{s}_1.\hat{s}_2$) is the singlet–triplet splitting or exchange integral and other symbols have their usual meaning. ρ represents the fraction of a possible magnetically dilute copper(II) impurity. The temperature-independent paramagnetism for a binuclear copper(II) complex, $N\alpha$, was taken as 120×10^{-6} cgs units/mol. The parameters giving the best fit were obtained by using a non-linear regression analysis with ρ as a floating parameter. The exchange integral ($-2J$) for **III** was found to be 827 ± 7 cm^{-1} ($g = 2.14 \pm 0.03$, $\rho = 0.00055$) and for **VI** was found to be 824 ± 5 cm^{-1} ($g = 2.17 \pm 0.02$, $\rho = 0.00075$) indicating very strong exchange between the copper(II) centres in both cases.

It is of interest to compare the magnetism of **III** and **VI**

TABLE 5. Selected bond distances (Å) and angles (deg) (esd's) for $[Cu_2(L1)(CH_3OH)_2](ClO_4)_2$ (**I**)

Bond	Length	Bond	Length
Cu(1)—Cu(1)′	3.088(1)	N(1)—C(8)	1.484(6)
Cu(1)—O(1)	1.963(3)	N(2)—C(10)	1.498(6)
Cu(1)—O(1)′	1.9590(25)	N(2)—C(11)	1.488(7)
Cu(1)—N(1)	1.989(4)	C(1)—C(2)	1.400(6)
Cu(1)—N(2)	1.991(4)	C(1)—C(6)	1.395(6)
Cu(1)—O(6)	2.413(4)	C(2)—C(3)	1.379(6)
Cl(1)—O(2)	1.395(4)	C(2)—C(7)	1.490(6)
Cl(1)—O(3)	1.399(4)	C(3)—C(4)	1.376(7)
Cl(1)—O(4)	1.405(4)	C(4)—C(5)	1.385(7)
Cl(1)—O(5)	1.425(3)	C(4)—C(12)	1.511(8)
O(1)—C(1)	1.353(5)	C(5)—C(6)	1.375(6)
O(6)—C(13)	1.410(8)	C(6)—C(11)′	1.497(6)
N(1)—C(7)	1.492(7)	C(8)—C(9)	1.500(9)
		C(9)—C(10)	1.493(8)

Bonds	Angle	Bonds	Angle
O(1)—Cu(1)—O(1)′	76.12(10)	Cu(1)—N(2)—C(10)	120.4(3)
O(1)—Cu(1)—N(1)	92.49(14)	Cu(1)—N(2)—C(11)	110.3(3)
O(1)—Cu(1)—N(2)	165.64(14)	C(10)—N(2)—C(11)	109.9(4)
O(1)′—Cu(1)—N(1)	167.73(15)	O(1)—C(1)—C(2)	120.0(3)
O(1)′—Cu(1)—N(2)	91.15(14)	O(1)—C(1)—C(6)	121.5(3)
N(1)—Cu(1)—N(2)	99.58(16)	C(2)—C(1)—C(6)	118.5(4)
O(1)—Cu(1)—O(6)	92.48(13)	C(1)—C(2)—C(3)	119.1(4)
O(1)′—Cu(1)—O(6)	99.13(12)	C(1)—C(2)—C(7)	120.3(4)
N(1)—Cu(1)—O(6)	85.71(16)	C(3)—C(2)—C(7)	120.6(4)
N(2)—Cu(1)—O(6)	96.13(17)	C(2)—C(3)—C(4)	123.4(4)
O(2)—Cl(1)—O(3)	112.0(3)	N(1)—C(8)—C(9)	112.1(4)
O(2)—Cl(1)—O(4)	108.39(23)	C(8)—C(9)—C(10)	113.2(5)
O(2)—Cl(1)—O(5)	112.21(22)	N(2)—C(10)—C(9)	113.1(4)
O(3)—Cl(1)—O(4)	106.7(3)	N(2)—C(11)—C(6)	112.9(4)
O(3)—Cl(1)—O(5)	109.12(21)	C(3)—C(4)—C(5)	116.4(4)
O(4)—Cl(1)—O(5)	108.22(23)	C(3)—C(4)—C(12)	122.8(5)
Cu(1)—O(1)—Cu(1)′	103.88(12)	C(5)—C(4)—C(12)	120.8(5)
Cu(1)—O(1)—C(1)	127.26(23)	C(4)—C(5)—C(6)	122.5(4)
Cu(1)′—O(1)—C(1)′	128.47(24)	C(1)—C(6)—C(5)	120.1(4)
Cu(1)—N(1)—C(7)	110.5(3)	C(1)—C(6)—C(11)′	120.4(4)
Cu(1)—N(1)—C(8)	118.7(3)	C(5)—C(6)—C(11)′	119.5(4)
C(7)—N(1)—C(8)	111.1(4)	N(1)—C(7)—C(2)	112.7(4)

TABLE 6. Electronic spectral and magnetic data

	Complex	Mull transmittance (cm^{-1})	μ_{eff}(BM) (rt)
II	$[Cu_2(L1)(H_2O)_2](ClO_4)_2$	29000, 17400	0.50
III	$[Cu_2(L1)](ClO_4)_2$	[27000], 16600	0.50
IV	$[Cu_2(L1)(CuCl_4)]$	23800, 18000	1.30
V	$[Cu_2(L1)(SCN)_2].H_2O$	16100, 14900	0.50
VI	$[Cu_2(L1)(ClO_4)_2]$	17700	0.51

with that of $[Cu_2(L3)Cl_2].6H_2O$ ($-2J$ = 588 cm^{-1}) (11). Structurally all the compounds are similar with weakly bound axial ligands in two cases. The dominant structural feature, which is likely to influence the antiferromagnetic exchange between the copper centres the most, is the planar arrangement of oxygen bridges and the phenoxide bridge angle. It is well established that magnetic exchange in a series of dihydroxo-bridged binuclear copper(II) complexes, $[Cu_2B_2(OH)_2]^{2+}$ (B = bidentate nitrogen donor) varies as a function of hydroxide bridge angle (30), and for a hydroxide bridge angle of 104.1° $-2J$ was found to be 508 cm^{-1}. This value compares with that for $[Cu_2(L3)Cl_2].6H_2O$, which has a slightly larger bridge angle (104.5°). However, the value associated with **VI** is much larger for what is a smaller oxygen bridge angle (102.8° (16)). A comparable angle is found for compound **I** (103.9°). The dominant exchange pathway, through the two oxygen bridge atoms, involves interaction of the two copper $d_{x^2-y^2}$ orbitals and s and p orbitals on the oxygen with a predominantly σ overlap. Out-of-plane distortions at the copper centres will, no doubt, lead to some reduction in σ overlap and hence exchange, but the effect on exchange is likely to be small (31). The copper centres are displaced from the mean planes of the N_2O_2 donor sets in **I** and $[Cu_2(L3)Cl_2].6H_2O$(5) by 0.11 and 0.21 Å, respectively. For **VI**, although the copper centres lie in the mean plane of the N_2O_2 donor set, the magnetic orbital is not planar (O ± 0.097(5) Å, N ± 0.209(8) Å versus mean N_2O_2 plane) (16). In addition, the spin exchange between copper(II) centres bridged by oxygen donors (e.g. alkoxide, phenoxide) has been shown to be dependent on the degree of pyramidal distortion at the oxygen bridge (32, 33) and that in severe cases the overall exchange situation can be dominated by a ferromagnetic component. The complex $[Cu_2(L3)Cl_2].6H_2O$ has a solid angle at the phenoxide bridge of 357.4° (5), whereas

Can. J. Chem. Downloaded from www.nrcresearchpress.com by 213.222.148.141 on 09/07/12
For personal use only.

Can. J. Chem. Downloaded from www.nrcresearchpress.com by 213.222.148.141 on 09/07/12
For personal use only.

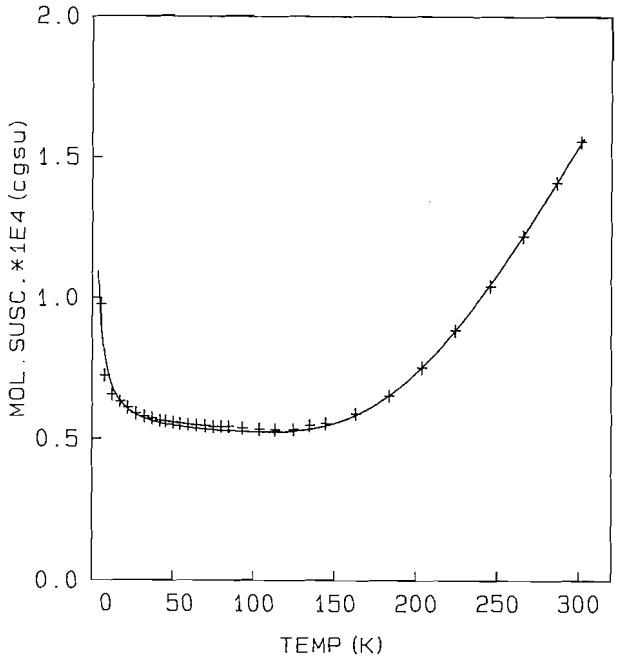

FIG. 3. Magnetic susceptibility data for $[Cu_2(L1)](ClO_4)_2$ (**III**). The solid line was calculated from eq. [1] with $g = 2.14 \pm 0.03$, $-2J = 827 \pm 7\ cm^{-1}$, and $N\alpha = 60 \times 10^{-6}$ cgs units ($cm^3\ mol^{-1}$)/Cu and assuming 0.055% paramagnetic impurity ($\rho = 0.00055$).

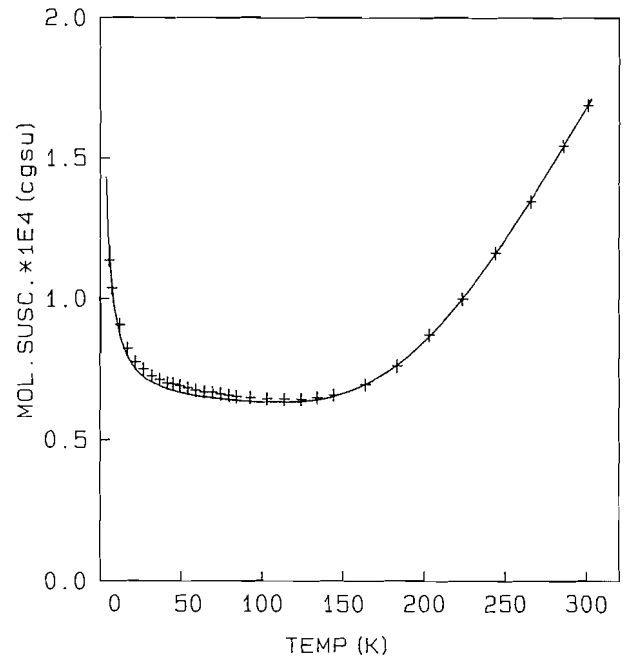

FIG. 4. Magnetic susceptibility data for $[Cu_2(L1)(ClO_4)_2]$ (**VI**). The solid line was calculated from eq. [1] with $g = 2.17 \pm 0.02$, $-2J = 824 \pm 5\ cm^{-1}$, and $N\alpha = 60 \times 10^{-6}$ cgs units ($cm^3\ mol^{-1}$)/Cu and assuming 0.075% paramagnetic impurity ($\rho = 0.00075$).

for **I** and **VI** solid oxygen angles of 359.6° and 360.0° are found, respectively. However, such a small pyramidal distortion for $[Cu(L3)Cl_2].6H_2O$ is not considered significant in terms of reducing the net antiferromagnetic exchange by in excess of $200\ cm^{-1}$.

Another factor, which appears to contribute to the exchange situation, is the degree of saturation at the nitrogen donor centres. It has been established that as the extent of saturation

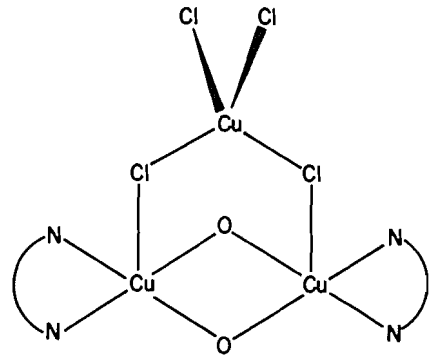

FIG. 5. Proposed structural representation for $[Cu_2(L1)(CuCl_4)]$ (**IV**).

at these centres increases ($H_2L3 \rightarrow H_2L2 \rightarrow H_2L1$) the first one-electron reduction potential exhibits a dramatic negative shift in DMSO for the complexes $[Cu_2(L3)](ClO_4)_2.2H_2O$, $[Cu_2(L2)](ClO_4)_2.2H_2O$, and $[Cu_2(L1)(ClO_4)_2]$ (**VI**) ($E_{1/2} = -0.43$ V, -0.58 V, -0.76 V, respectively) (16). This trend can be interpreted in terms of a stabilising effect of the copper(I) state with increasing unsaturation and has been observed before for macrocyclic (N_4), mononuclear copper(II) (34), and nickel(II) (35) complexes. The copper–nitrogen bonds can be considered to be more strongly polarized when the nitrogen centres are unsaturated, which would lead to a situation where the copper(II) ions would become reduced more readily. This charge delocalization effect will, no doubt, polarize the electron density in the copper magnetic orbital, with the result that exchange will diminish as unsaturation increases. This is reflected in the room temperature magnetic moments for the copper perchlorate complexes of H_2L3, H_2L2, and H_2L1 ($\mu_{eff} = 0.72$ BM (12), 0.71 BM (14), and 0.51 BM ($-2J = 824 \pm 5\ cm^{-1}$ for **VI**), respectively), which indicate that any nitrogen unsaturation causes reduced antiferromagnetic exchange. The presence of *trans*-axial chlorines in $[Cu_2(L3)Cl_2].6H_2O$ appears to exert an additional electron delocalization effect, despite the fact that they are bound orthogonally to the copper magnetic orbital (μ_{eff}(rt) = 0.80 BM) (11).

The trinuclear complex, $[Cu_2(L1)(CuCl_4)]$ (**IV**), is most unusual, and exhibits far-infrared bands which can be associated with both terminal and bridging Cu—Cl bonds (280, $260\ cm^{-1}$). A relatively low energy charge transfer absorption at $23\,800\ cm^{-1}$ can be associated with halogen-to-metal charge transfer. The room temperature magnetic moment (μ_{eff} = 1.30 BM) would be the average of the contributions of the three copper centres. On the assumption that the binuclear fragment $[Cu_2(L1)]^{2+}$ in **IV** is similar to that in **VI** an estimate of its room temperature contribution to the magnetic moment would be based on a value of μ_{eff} of about 0.5 BM. If the mononuclear fragment was considered to be $CuCl_4^{2-}$ then a contribution from this species based on a room temperature magnetic moment (μ_{eff}) of 1.9 BM would not be unreasonable. Assuming these values the average magnetic moment (μ_{eff}) for **IV** becomes 1.3 BM, in good agreement with the observed value. In the absence of structural data a reasonable suggestion for the structure of **IV** would involve a binuclear, cationic fragment similar to that in **I** and **VI** with a distorted $CuCl_4^{2-}$ moiety associated with the cation via a *cis*-axial interaction (Fig. 5). A similar situation was found to exist for the complex $[Cu_2(PPDMe)(OH)Cl_2][CuCl_3(H_2O)].H_2O$ (PPDMe = 3,6-bis(3,5-dimethyl-1-pyrazolyl)pyridazine (μ_{eff} = 1.03 BM)) (36) which has a long copper–chlorine axial interaction (2.955 Å)

TABLE 7. Electrochemical data for reduction and oxidation

	Complex	Cu^{II}/Cu^{II} $\Delta E_p{}^a$ (mV)	$\rightleftharpoons$ Cu^{II}/Cu^{I} $E_{1/2}{}^b$ (V)	Cu^{II}/Cu^{I} $\Delta E_p{}^a$ (mV)	$\rightleftharpoons$ Cu^{I}/Cu^{I} $E_{1/2}{}^b$ (V)	(GC/DMSO/SCE/TEAP) ΔE^c (V)	$K_{con}{}^e$
III	$[Cu_2(L1)](ClO_4)_2$	100[d]	−0.76	100[d]	−0.90	0.14	2.3×10^2
V	$[Cu_2(L1)(SCN)_2].H_2O$	80[d]	−0.76	100[d]	−0.90	0.14	2.3×10^2
IV	$[Cu_2(L1)(CuCl_4)]$	100[d]	−0.75	100[d]	−0.89	0.13	1.6×10^2

	Complex	Cu^{II}/Cu^{II} $\Delta E_p{}^a$ (mV)	$\rightleftharpoons$ Cu^{II}/Cu^{III} $E_{1/2}{}^b$ (V)	Cu^{II}/Cu^{III} $\Delta E_p{}^a$ (mV)	$\rightleftharpoons$ Cu^{III}/Cu^{III} $E_{1/2}{}^b$ (V)	(Pt/CH_3CN/SCE/TEAP) ΔE^c (V)	$K_{con}{}^e$
III	$[Cu_2(L1)](ClO_4)_2$	80[d]	1.18	90[d]	1.34	0.16	5.1×10^2
V	$[Cu_2(L1)(SCN)_2].H_2O$	80[d]	1.17	90[d]	1.35	0.18	1.1×10^3

[a] $\Delta E_p = E_{p,c} - E_{p,a}$ at scan rate 200 mV s^{-1}.
[b] $E_{1/2} = 0.5(E_{p,c} + E_{p,a})$ at 200 mV s^{-1}.
[c] $\Delta E = [E_{1/2}(1) - E_{1/2}(2)]$.
[d] Quasi-reversible.
[e] $K_{con} = \dfrac{[Cu^{II}Cu^{I}L]^2}{[Cu^{II}Cu^{II}L][Cu^{I}Cu^{I}L]}$

or

$$\frac{[Cu^{II}Cu^{III}L]^2}{[Cu^{II}Cu^{II}L][Cu^{III}Cu^{III}L]} = \exp(nF.\Delta E/RT).$$

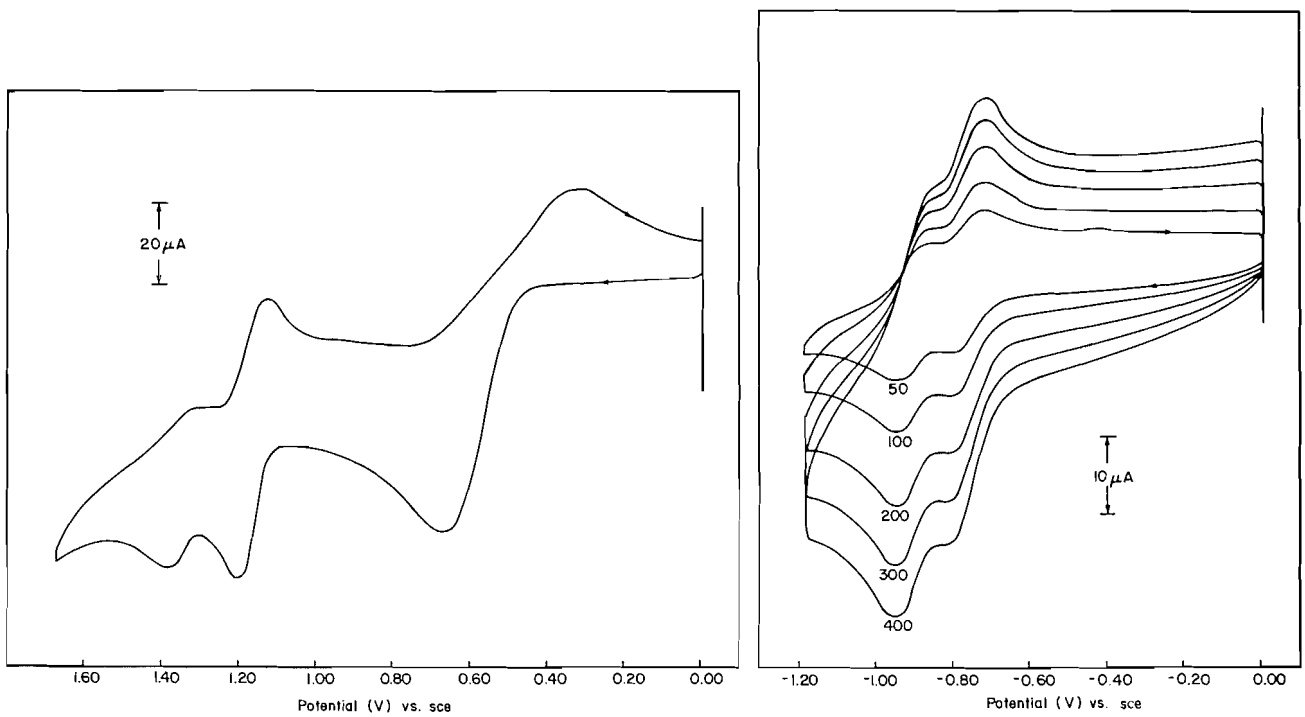

FIG. 6. Cyclic voltammograms for $[Cu_2(L1)(SCN)_2].H_2O$ (**V**) at positive (200 mV s^{-1}) (GC/CH_3CN/TEAP/SCE) and negative (50, 100, 200, 300, 400 mV s^{-1}) potentials (GC/DMSO/TEAP/SCE).

and a very strongly coupled binuclear cation. The proposed axial copper–chlorine interaction in **IV** would represent an orthogonal, magnetically isolated situation and so a chlorine bridge would not be involved in mediating spin exchange between the binuclear entity and the $CuCl_4{}^{2-}$ group.

The thiocyanate derivative **V** exhibits two infrared bands associated with thiocyanate, νCN, stretch at 2058 and 2035 cm^{-1}, which can be associated with two *cis*-isothiocyanate groups bound to the binuclear, macrocyclic entity. Two visible bands are observed for this compound (Table 5), clearly distinguishing it from the other derivatives, and indicating the involvement of thiocyanate as a ligand. The low room temperature magnetic moment indicates the presence of very strong exchange between the two copper(II) centres, with an exchange integral that is likely to be comparable with that found for **III** and **VI**.

The electrochemical properties of **II** and **III** are essentially identical and compare very closely with those of **V** on reduction. Two clearly defined cyclic voltammetry waves are observed at

Can. J. Chem. Downloaded from www.nrcresearchpress.com by 213.222.148.141 on 09/07/12
For personal use only.

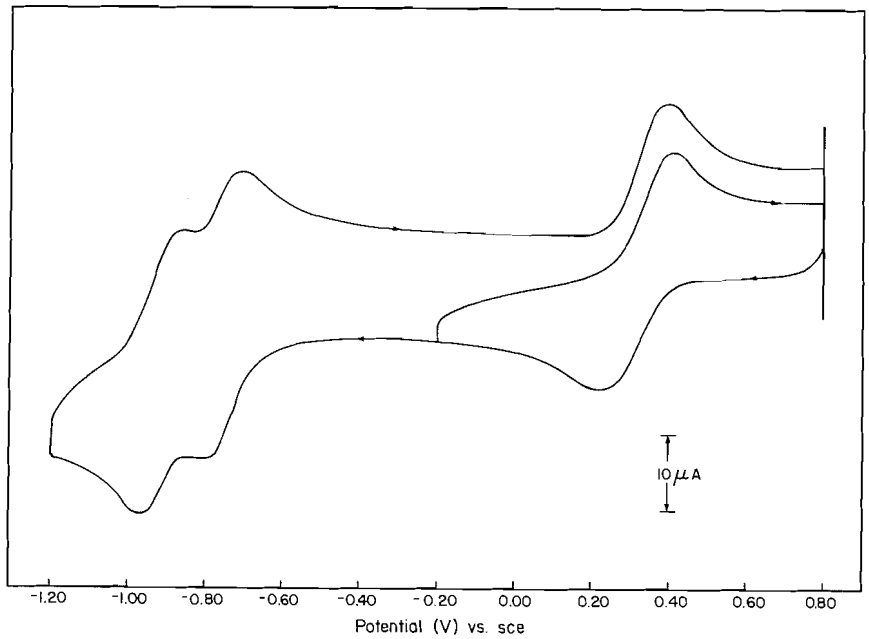

FIG. 7. Cyclic voltammograms for $[Cu_2(L1)(CuCl_4)]$ (**IV**) (200 mV s^{-1}) (GC/DMSO/TEAP/SCE).

negative potentials in DMSO in all cases, associated with two single electron reduction steps, while two waves are observed in CH_3CN at positive potentials for **II** and **V** only associated with two single electron oxidation steps (Table 7). All three complexes exhibit cyclic voltammetry which compares very closely with that of $[Cu_2(L1)(ClO_4)_2]$ (16), which exhibits two one-electron reduction steps and two one-electron oxidation steps under similar conditions. Figure 6 illustrates cyclic voltammograms for **V** at both positive and negative potentials. The peak-to-peak separations (ΔE_p) vary slightly as a function of scan rate at negative potentials indicating quasi-reversible redox processes. The broad, irreversible wave at $E_{1/2} = 0.51$ V (GC/CH_3CN/SCE/TEAP) is associated with thiocyanate and a similar wave is observed for sodium thiocyanate under similar conditions. The potentials associated with these redox processes and the conproportionation constants representing the stability of the mixed oxidation state intermediates compare closely with the complex $[Cu_2(L1)(ClO_4)_2]$ and it is assumed that in solution the active species in all cases is the solvated cation $[Cu_2(L1)]^{2+}$. This is supported by conductance data which indicate all species to be 1:2 electrolytes in these solvents.

The trinuclear complex, **III**, exhibits reduction waves similar to the other complexes, but at positive potentials the electrochemistry is dominated by a redox wave at 0.30 V (GC/DMSO/SCE/TEAP) (Fig. 7) and 0.45 V (Pt/CH_3CN/SCE/TEAP) associated with a mononuclear copper entity. Controlled potential electrolysis of **III** in DMSO at −0.09 V involved passage of 0.97 equivalents of charge indicating one electron reduction of the mononuclear copper species. Other waves, which can be attributed to chloride, prevent observation of any oxidation waves due to the binuclear copper species. The difference in potential for this species as a function of solvent indicates some solvation at this site. Conductance measurements in DMSO indicate that compound **III** is a 1:1 electrolyte. The dissociation of this complex is perhaps most likely to occur with the formation of the cation $[Cu_2(L1)]^{2+}$ and a solvated chlorocuprate anion.

Acknowledgement

We thank the Natural Sciences and Engineering Research Council of Canada for financial support for this study.

1. S. E. GROH. Isr. J. Chem. **15**, 277 (1976–7).
2. N. H. PILKINGTON and R. ROBSON. Aust. J. Chem. **23**, 2225 (1970).
3. H. OKAWA and S. KIDA. Bull. Chem. Soc. Jpn. **45**, 1759 (1972).
4. B. F. HOSKINS and G. A. WILLIAMS. Aust. J. Chem. **28**, 2607 (1975).
5. B. F. HOSKINS, N. J. MCLEOD, and H. A. SCHAAP. Aust. J. Chem. **29**, 515 (1976).
6. A. W. ADDISON. Inorg. Nucl. Chem. Lett. **12**, 899 (1976).
7. R. R. GAGNÉ, C. A. KOVAL, T. J. SMITH, and M. C. CIMOLINO. J. Am. Chem. Soc. **101**, 4571 (1979).
8. R. R. GAGNÉ, C. L. SPIRO, T. J. SMITH, C. A. HAMANN, W. R. THIES, and A. K. SHIEMKE. J. Am. Chem. Soc. **103**, 4073 (1981).
9. C. L. SPIRO, S. E. LAMBERT, T. J. SMITH, E. N. DUESLER, R. R. GAGNÉ, and D. N. HENDRICKSON. Inorg. Chem. **20**, 1229 (1981).
10. R. C. LONG and D. N. HENDRICKSON. J. Am. Chem. Soc. **105**, 1513 (1983).
11. S. L. LAMBERT and D. N. HENDRICKSON. Inorg. Chem. **18**, 2683 (1979).
12. S. K. MANDAL and K. NAG. J. Chem. Soc. Dalton Trans. 2429 (1983).
13. R. R. GAGNÉ, L. M. HENLING, and T. J. KISTENMACHER. Inorg. Chem. **19**, 1226 (1980).
14. S. K. MANDAL and K. NAG. J. Chem. Soc. Dalton Trans. 2141 (1984).
15. S. K. MANDAL, B. ADHIKARY, and K. NAG. J. Chem. Soc. Dalton Trans. 1175 (1986).
16. S. K. MANDAL, L. K. THOMPSON, K. NAG, J.-P. CHARLAND, and E. J. GABE. Inorg. Chem. **26**, 1391 (1987).
17. G. GERMAIN, P. MAIN, and M. M. WOOLFSON. Acta Crystallogr. A27, 368 (1971).
18. E. J. GABE, F. L. LEE, and Y. LEPAGE. Crystallographic computing III. *Edited by* G. Sheldrick, C. Kruger, and R. Goddard. Clarendon Press, Oxford. 1985. p. 167.

Can. J. Chem. Downloaded from www.nrcresearchpress.com by 213.222.148.141 on 09/07/12
For personal use only.

19. International tables for X-ray crystallography. Vol. IV. Kynoch Press, Birmingham, England. 1974. p. 99. Table 2.2B.
20. O. KAHN, J. GALY, Y. JOURNAUX, J. JAUD, and I. MORGENSTERN-BADARAU. J. Am. Chem. Soc. **104**, 2165 (1982).
21. M. I. BRUCE, J. K. WALTON, M. L. WILLIAMS, J. M. PATRICK, B. W. SKELTON, and A. H. WHITE. J. Chem. Soc. Dalton Trans. 815 (1983).
22. Y. JOURNAUX, O. KAHN, J. ZAREMBOWITCH, J. GALY, and J. JAUD. J. Am. Chem. Soc. **105**, 7585 (1983).
23. A. W. ADDISON, P. J. BURKE, K. HENRICK, T. N. RAO, and E. SINN. Inorg. Chem. **22**, 3645 (1983).
24. H. C. FREEMAN and N. D. HUTCHINSON. Acta Crystallogr. Sect. B, **35**, 2045 (1979).
25. V. M. RAO, D. N. SATHYANARAYANA, H. MANOHAR. J. Chem. Soc. Dalton Trans. 2167 (1983).
26. W. HAASE and S. GEHRING. J. Chem. Soc. Dalton Trans. 2609 (1985).
27. J. W. GUTHRIE, R. L. LINTVEDT, and M. D. GLICK. Inorg. Chem. **19**, 2949 (1980).
28. J. GALY, J. JAUD, O. KAHN, and P. TOLA. Inorg. Chim. Acta, **36**, 229 (1979).
29. J. H. VAN VLECK. The theory of electric and magnetic susceptibilities. Oxford University Press, London. 1932. Chap. 9.
30. V. H. CRAWFORD, H. W. RICHARDSON, J. R. WASSON, D. J. HODGSON, and W. E. HATFIELD. Inorg. Chem. **15**, 2107 (1976).
31. O. KAHN. Angew. Chem. Int. Ed. Engl. **24**, 834 (1985).
32. K. S. MURRAY. *In* Copper coordination chemistry: inorganic and biological perspectives. *Edited by* K. D. Karlin and J. Zubieta. Adenine Press, New York. 1985.
33. W. MAZUREK, B. J. KENNEDY, K. S. MURRAY, M. J. O'CONNOR, J. R. RODGERS, M. R. SNOW, A. G. WEDD, and P. R. ZWACK. Inorg. Chem. **24**, 3258 (1985).
34. D. C. OLSON and J. VASILEVSKIS. Inorg. Chem. **3**, 463 (1971).
35. F. V. LOVECCHIO, E. S. GORE, and D. H. BUSCH. J. Am. Chem. Soc. **96**, 3109 (1974).
36. L. K. THOMPSON, T. C. WOON, D. B. MURPHY, E. J. GABE, F. L. LEE, and Y. LE PAGE. Inorg. Chem. **24**, 4719 (1985).

Can. J. Chem. Downloaded from www.nrcresearchpress.com by 213.222.148.141 on 09/07/12
For personal use only.

Some phase relationships between basic bismuth chlorides in aqueous solutions at 25°C[1]

PETER TAYLOR AND VINCENT J. LOPATA

Research Chemistry Branch, Atomic Energy of Canada Limited, Whiteshell Nuclear Research Establishment, Pinawa, Man., Canada R0E 1L0

FOR ERRATA SEE 66(6)19 88 P. 1540

Received June 23, 1987

PETER TAYLOR and VINCENT J. LOPATA. Can. J. Chem. **65**, 2824 (1987).

Observations are reported on the interconversion of solid α-Bi_2O_3, $Bi_{12}O_{17}Cl_2$, BiOCl, and a daubréeite-like phase tentatively identified as $Bi_2O_2(OH)Cl$, in aqueous chloride solutions at 25°C. Equilibrium constants, K, for these interconversions are expressed as anion activity ratios, $\{Cl^-\}/\{OH^-\}$. Experimental values of K for equilibrium between Bi_2O_3 and each of the chlorides are $10^{0.56 \pm 0.20}$ for $Bi_{12}O_{17}Cl_2$, $10^{1.5 \pm 0.4}$ for $Bi_2O_2(OH)Cl$, and $10^{3.13 \pm 0.04}$ for BiOCl; the latter two represent metastable equilibria. These equilibrium constants yielded the following estimates of Gibbs energies of formation: $Bi_{12}O_{17}Cl_2$, -3141 ± 6 kJ mol^{-1}; "$Bi_2O_2(OH)Cl$", -696 ± 4 kJ mol^{-1}; BiOCl, -321.5 ± 1.3 kJ mol^{-1}. Phase relationships among these solids are discussed, with reference to natural occurrence, other bismuth oxychlorides, and the stability of other basic salts of bismuth.

PETER TAYLOR et VINCENT J. LOPATA. Can. J. Chem. **65**, 2824 (1987).

On rapporte des observations relatives à l'interconversion, dans des solutions aqueuses de chlorure, à 25°C, d'α-Bi_2O_3, de $Bi_{12}O_{17}Cl_2$, de BiOCl et d'une phase qui ressemble à de la daubréeite que l'on a identifiée provisoirement comme du $Bi_2O_2(OH)Cl$. On exprime les constantes d'équilibre, K, pour ces interconversions sous la forme de rapports d'activités d'anions, $\{Cl^-\}/\{OH^-\}$. Les valeurs expérimentales de K pour l'équilibre entre Bi_2O_3 et chacun des chlorures sont $10^{0.56 \pm 0.20}$ pour le $Bi_{12}O_{17}Cl_2$, $10^{1.5 \pm 0.4}$ pour le $Bi_2O_2(OH)Cl$ et $10^{3.13 \pm 0.04}$ pour le BiOCl; dans les deux derniers cas, il s'agit d'équilibres métastables. Ces constantes d'équilibre ont permis d'évaluer que les énergies de Gibbs de formation sont respectivement de -3141 ± 6 kJ mol^{-1} pour le $Bi_{12}O_{17}Cl_2$, de -696 ± 4 kJ mol^{-1} pour le "$Bi_2O_2(OH)Cl$" et de $-321{,}5 \pm 1{,}3$ kJ mol^{-1} pour le BiOCl. On discute des relations de phase entre ces solides en fonction de leur état naturel, d'autres oxychlorures de bismuth et de la stabilité d'autres sels basiques du bismuth.

[Traduit par la revue]

Introduction

Bismuth(III) oxychloride chemistry is complex, with four intermediate compounds between BiOCl and Bi_2O_3. One such compound, $Bi_7O_9Cl_3$, was reported as long ago as 1844 (1). This report was viewed with skepticism, but was finally vindicated almost a century later by Sillen and Edstrand (2), who showed, however, that the correct stoichiometry is $Bi_{24}O_{31}Cl_{10}$. Another oxychloride, $Bi_{12}O_{15}Cl_6$, was identified by Hopfgarten (3). Two further compounds, Bi_3O_4Cl and $Bi_{12}O_{17}Cl_2$, have been reported by Nurgaliev *et al.* (4–6) as products of both dry and hydrothermal syntheses, and Aurivillius (7) has reported some additional crystallographic information on these phases. As well as these anhydrous compounds, the hydroxychloride $BiO(OH)_xCl_{1-x}$ ($x \simeq 0.5$) has been reported both as a mineral, daubréeite (8), and as a synthetic material (9). The only other bismuth oxychloride mineral is bismoclite, BiOCl (8).

We have recently measured the stability limits of basic bismuth carbonates and iodides in aqueous solutions at or near 25°C (10, 11). Some of these compounds show promise as waste forms for immobilization and disposal of ^{14}C and ^{129}I, which are long-lived radioactive waste products from nuclear power generation. We need information on the stability of bismuth chlorides, to help predict the behavior of the carbonates and iodides in saline groundwaters. Here we report observations on the preparation and interconversion of basic bismuth chlorides in aqueous solutions.

Our experimental strategy was to examine the conditions under which various basic bismuth chlorides are formed, in aqueous solutions at or near 25°C, and hence to determine whatever equilibrium relationships we could. We have examined the sequential hydrolysis of BiOCl and the reaction of Bi_2O_3 with dissolved chloride, and analysed solutions in contact with combinations of Bi_2O_3 and three basic chlorides: $Bi_{12}O_{17}Cl_2$, BiOCl, and a daubréeite-like compound with approximate composition $Bi_2O_2(OH)Cl$.

[1]AECL No. 9448.

Background on phase relationships

The $BiCl_3$–Bi_2O_3 phase diagram, determined by Nurgaliev *et al.* (4), indicates that all five bismuth oxychlorides (BiOCl, $Bi_{12}O_{15}Cl_6$, $Bi_{24}O_{31}Cl_{10}$, Bi_3O_4Cl, and $Bi_{12}O_{17}Cl_2$) are stable with respect to disproportionation at room temperature. In the aqueous system, $BiCl_3$–Bi_2O_3–H_2O–[pH],[2] interconversion of these solids can be represented by a series of equilibria similar to those we have previously described (11) for the sequential hydrolysis of BiI_3:

$$[1] \quad (1/2)BiCl_3(s) + OH^-(aq) \rightleftharpoons (1/2)BiOCl(s) + (1/2)H_2O(l) + Cl^-(aq)$$

$$[2] \quad 2BiOCl(s) + OH^-(aq) \rightleftharpoons (1/6)Bi_{12}O_{15}Cl_6(s) + (1/2)H_2O(l) + Cl^-(aq)$$

$$[3] \quad Bi_{12}O_{15}Cl_6(s) + OH^-(aq) \rightleftharpoons (1/2)Bi_{24}O_{31}Cl_{10}(s) + (1/2)H_2O(l) + Cl^-(aq)$$

$$[4] \quad (1/2)Bi_{24}O_{31}Cl_{10}(s) + OH^-(aq) \rightleftharpoons 4Bi_3O_4Cl(s) + (1/2)H_2O(l) + Cl^-(aq)$$

$$[5] \quad 2Bi_3O_4Cl(s) + OH^-(aq) \rightleftharpoons (1/2)Bi_{12}O_{17}Cl_2(s) + (1/2)H_2O(l) + Cl^-(aq)$$

$$[6] \quad (1/2)Bi_{12}O_{17}Cl_2(s) + OH^-(aq) \rightleftharpoons 3Bi_2O_3(s) + (1/2)H_2O(l) + Cl^-(aq)$$

[2]Here, [pH] denotes a non-interacting acid or base, i.e. one that is not incorporated in any of the solids.

Can. J. Chem. Downloaded from www.nrcresearchpress.com by 213.222.148.141 on 09/07/12
For personal use only.

TABLE 1. Gibbs energies of formation, $\Delta_f G^0$ (298.15 K) of species discussed[a]

Species	$\Delta_f G^0$, kJ mol^{-1}		
	Ref. 12	Ref. 13	This work
$BiCl_3$(s)	−315.0	—	—
BiOCl(s)	−322.1	—	−321.5 ± 1.3
$Bi_2O_2(OH)Cl$(s)	—	—	−696 ±4[b]
$Bi_{12}O_{17}Cl_2$(s)	—	—	−3141 ±6[b]
α-Bi_2O_3(s)	−493.7	−493.5 ±1.5	—
H_2O(l)	−237.13	−237.14 ± 0.08	—
OH^-(aq)	−157.24	−157.33 ± 0.09	—
Cl^-(aq)	−131.23	−131.27 ± 0.11	—

[a]For Gibbs energy calculations, we used $\Delta_f G^0$ values from ref. 12, and uncertainties from ref. 13. The major sources of uncertainties in our Gibbs energy data are $\Delta_f G^0$ for α-Bi_2O_3, and our own experimental errors.
[b]From experiments on poorly crystalline material.

When the reactions are expressed in this way, all the equilibrium constants (K_1, K_2, ... K_6) take the form $\{Cl^-\}/\{OH^-\}$, and are expected to decrease in this order. The stability field of each solid can then be expressed in terms of this activity ratio, for example $Bi_{12}O_{15}Cl_6$ will be stable in contact with a solution having $\{Cl^-\}/\{OH^-\}$ between K_2 and K_3. It is possible, however, that the stability fields of hydrous chlorides, such as daubréeite, might encroach on, or eliminate, those of some of the anhydrous solids.

We make a distinction here between the activity {X} and concentration [X] of a given species. Since all of the experimental equilibrium constants discussed below are ratios of activities of singly charged anions, $\{Cl^-\}/\{OH^-\}$, activity coefficients virtually cancel out and this term is interchangeable with $[Cl^-]/[OH^-]$. The distinction is maintained, however, to indicate whether a measured quantity is a concentration or an activity, and to assure that activities and concentrations are not mixed in the same expression. Similarly, the distinction between molarity and molality virtually cancels out in the term $\{Cl^-\}/\{OH^-\}$, and is inconsequential at the level of accuracy of these experiments.

Gibbs energies of formation, $\Delta_f G^0$, are available for solid $BiCl_3$, BiOCl, and Bi_2O_3, but not for any of the other oxychlorides (12, 13). These and other relevant Gibbs energies are listed in Table 1. The value of −322.1 kJ mol^{-1} recommended for BiOCl dates back to a 1918 electrochemical study of reaction [7] by Noyes and Chow (14):

[7] $BiOCl(s) + (3/2)H_2(g) \rightleftharpoons Bi(s) + H_2O(l) + H^+(aq) + Cl^-(aq)$

Vasil'ev and Grechina (15, 16) have recommended slightly less negative values, based on reinterpretation of the data of Noyes and Chow (−321.0 ± 0.3 kJ mol^{-1}), and on their own electrochemical measurements (−319.4 ± 0.2 kJ mol^{-1}). Other work on the solubility of BiOCl has been concerned principally with the speciation of bismuth in solution, and has not explicitly addressed the thermodynamics of BiOCl (17, 18). Sammour and Moussa, however, do mention that some of their emf measurements were consistent with those of Noyes and Chow (14, 19). Thus, although there may be some cause for revising the recommended value of $\Delta_f G^0$ for BiOCl, any change is likely to be small, probably <3 kJ mol^{-1}.

Using the Gibbs energies in Table 1, and the standard relationship between Gibbs energy of reaction, $\Delta_r G^0$, and equilibrium constant, K [8]:

[8] $\Delta_r G^0 = -RT \ln K$

we obtain $\log_{10} K_1 = 16.8$. This indicates that $BiCl_3$ is unstable with respect to hydrolysis to BiOCl, even in concentrated HCl. This is consistent with various studies on BiOCl in acidic media (14–19). We can also calculate a metastable equilibrium constant for coexisting BiOCl and Bi_2O_3:

[9] $BiOCl(s) + OH^-(aq) \rightleftharpoons (1/2)Bi_2O_3(s) + (1/2)H_2O(l) + Cl^-(aq)$

$\Delta_r G^0 = -17.3$ kJ mol^{-1}

$K_9 = \{Cl^-\}/\{OH^-\} = 10^{3.03}$

Experimental

Starting materials were reagent-grade $Bi(NO_3)_3 \cdot 5H_2O$, α-Bi_2O_3, NaCl, KCl, and carbonate-free aqueous solutions of NaOH and KOH. It was sometimes necessary to remove traces of bismuth carbonates (10) from Bi_2O_3 by heating at 550°C for 2 h, or by washing overnight with concentrated NaOH, then filtering and washing with freshly deionized water immediately before use.

Bismuth oxychloride, BiOCl, was prepared in 10 to 50 g quantities by adding $Bi(NO_3)_3 \cdot 5H_2O$ to water, and mixing the resulting milky suspension of basic bismuth nitrate(s) with a slight excess of NaCl solution. The net hydrolysis of Bi^{3+} to $(BiO)_n^{n+}$ was accompanied by production of acid, in accordance with the overall reaction:

[10] $Bi(NO_3)_3 + H_2O + NaCl \rightleftharpoons BiOCl + NaNO_3 + 2HNO_3$

The pH was adjusted to neutral, and the white precipitate was filtered and washed. The product gave a well-resolved X-ray diffraction pattern, in excellent agreement with the published pattern of BiOCl (20).

Solutions of desired chloride and hydroxide concentration were prepared using deionized water. Adjustments and measurements of pH were made with automatic titration equipment (Metrohm E526 titrator and E535 dosimat, or Mettler DV/DK modular system), calibrated with standard buffer solutions at pH = 6.86 and 9.18. Chloride activities were determined using Orion chloride-ion specific and double-junction reference electrodes, calibrated with solutions of known activity (10^{-2} to 10^{-5} mol dm^{-3}).

Preparative experiments were performed in screw-top Teflon bottles or flame-sealed Pyrex vials, at ambient temperature (22 ± 2°C) unless otherwise stated. Titrations were run in a nitrogen-purged vessel, thermostatted at 25.0°C. Solids were identified by X-ray powder diffraction (XRD), using a Rigaku Rotaflex diffractometer system with a 12 kW rotating-anode CuKα X-ray source; some measurements were also made with a Philips PW-1150 diffractometer.

Results and discussion

(a) Preparative experiments

(i) Hydrolysis of BiOCl

Samples of BiOCl (0.5 g) were allowed to react for 8 days with 100 cm^3 of solutions containing NaCl + NaOH, or KCl + KOH, in different proportions, with a total concentration of 1 mol dm^{-3}. No change was detected by XRD in the BiOCl recovered from solutions with $[Cl^-]/[OH^-] = 4$ or 9. In the solution with $[Cl^-]/[OH^-] = 1$, the BiOCl was partly converted to a near-amorphous material with very broad XRD features at $d \approx 3.4$ Å and 3.0 Å. This may have been $Bi_{24}O_{31}Cl_{10}$, which has several XRD features grouped near these positions (2).

In solutions with $[Cl^-]/[OH^-] = 0.25$ and 0.11, the BiOCl was converted to a bright yellow solid. Peaks in the diffraction pattern of this material were broad, but their positions are in good agreement with the $Bi_{12}O_{17}Cl_2$ pattern reported by Nurgaliev *et al.* (5) and corroborated by Aurivillius (7), as shown in Table 2. We generally observed somewhat higher

Can. J. Chem. Downloaded from www.nrcresearchpress.com by 213.222.148.141 on 09/07/12
For personal use only.

TABLE 2. X-ray diffraction data for $Bi_{12}O_{17}Cl_2$

Nurgaliev *et al.* (5)			This work[a]	
hkl[b]	d_{obs}	I/I_0	d_{obs}	I/I_0[c]
002	17.67	1	—[d]	—
004	8.793	3	8.87	15
006	5.875	3	5.88	5
008	4.405	3	4.42	5
111	3.824	5	3.84	10
113	3.660	5	3.67	10
115	3.379	30	3.38	30
117	3.056	100	3.06	100
00$\underline{12}$	2.934	20	2.94	30
119	2.744	10	2.73	80
200	2.722	80		
00$\underline{14}$	2.515	3	2.52	10
21$\underline{2}$	2.414	3	2.42	5
21$\underline{10}$	2.001	3	1.998	20
20$\underline{12}$	1.994	5		
220	1.924	20	1.928	30
20$\underline{14}$	1.847	3	1.847	10
307	1.706	3	1.706	10
315	1.672	3	1.673	20
317	1.629	5	1.630	30
319	1.575	3	1.578	10
			Plus eight weak broad peaks to $2\theta = 85°$.	

[a]Diffractometer data, CuKα radiation, $2\theta = 5$–$85°$.
[b]Based on tetragonal unit cell, $a = 5.443$ Å, $c = 35.20$ Å (ref. 5). Aurivillius (7) reported a $4a$, a, c orthorhombic superlattice, based on Weissenberg data.
[c]Peak heights.
[d]$2\theta < 5°$.

TABLE 3. X-ray diffraction data for "$(BiO)_2(OH)Cl$" and BiOCl

	"$(BiO)_2(OH)Cl$"			BiOCl			
	d			*d*		I/I_0	
hkl	Calc.[a]	Obs.	I/I_0[b]	Lit.[c]	Obs.	Lit.	Obs.[d]
001	7.578	7.615	50	7.38	7.400	38	41
002	3.789	3.789	15	3.69	3.687	16	13
101	3.403	3.410	90	3.442	3.442	100	100
110	2.693	2.693	100	2.753	2.753	76	85
102	2.686			2.667	2.667	97	90
111	2.537	2.525	20	2.577	2.577	10	9
003	2.526			2.457	2.458	12	10
112	2.195	2.195	15	2.205	2.207	28	23
103	2.105	2.1sh	5	2.076	2.078	1	2
200	1.904	1.904	20	1.946	1.946	34	35
201	1.847	1.852	20	1.881	1.881	9	9
113	1.842			1.833	1.833	25	22
202	1.701	1.696	15	1.720	1.720	8	8
104	1.696			1.665	1.665	17	18
211	1.662	1.660	20	1.694	1.693	25	30
212	1.553	1.558	15	1.574	1.574	31	35
203	1.520	1.523	10	1.528	1.525	11	10
005	1.516			1.473	1.473	2	2
105	1.408	1.405	5	[1.378][e]	—	—	—
220	1.346	1.345	10	1.376	1.376	12	12
204	1.343			1.338	1.338	2	2
221	1.326	1.33sh	5	1.352	1.352	3	3
115	1.321			1.299	1.298	3	3
222	1.269	1.26br	15	1.289	1.289	3	3
214	1.267			1.266	1.265	14	13
301	1.252			1.278	1.278	6	6

[a]Tetragonal, $a = 3.808$ Å, $c = 7.578$ Å.
[b]Approximate integrated intensities (product of peak height and full width at half-maximum).
[c]Tetragonal, $a = 3.891$ Å, $c = 7.369$ Å, ref. 20.
[d]Peak heights.
[e]Calculated.

intensities than Nurgaliev *et al.* for the weaker peaks. Chloride analyses were also consistent with $Bi_{12}O_{17}Cl_2$ (experimental, 2.66 to 2.95%; calculated, 2.49%).

The hydrolysis of BiOCl provided a convenient method for preparing up to 10 g of $Bi_{12}O_{17}Cl_2$, although the product often contained traces of α-Bi_2O_3. Prolonged exposure of the wet solid to air also resulted in contamination with basic bismuth carbonates. The traces of oxide persisted when the $Bi_{12}O_{17}Cl_2$ was contacted for up to 12 days with solutions having $[Cl^-]/[OH^-]$ between 0.1 and 1.0. At still lower ratios, further conversion to α-Bi_2O_3 was observed. Both BiOCl and $Bi_{12}O_{17}Cl_2$ were converted quantitatively to α-Bi_2O_3 in a few hours in initially chloride-free 1.0 mol dm^{-3} NaOH solution. Traces of Bi_2O_3 were removed from 0.3 g samples of $Bi_{12}O_{17}Cl_2$ by exposure to solutions with $[Cl^-]/[OH^-]$ between 2.3 and 9 for about 10 days.

These observations of the interconversion of Bi_2O_3 and $Bi_{12}O_{17}Cl_2$ indicate that K_6 lies between 0.1 and 2.3. However, the apparent kinetic stability of BiOCl at $[Cl^-]/[OH^-]$ ratios down to 4 (cf. $\log K_9 = 3.03$, above), and the ill-defined hydrolysis product at $[Cl^-]/[OH^-] = 1$, prevented the acquisition of other equilibrium information from hydrolysis reactions.

(ii) Reaction of α-Bi_2O_3 with chloride solutions

Samples of α-Bi_2O_3 (0.5 g) were allowed to react for 8 days with solutions identical to those used in the BiOCl hydrolysis experiments, as well as 1 mol dm^{-3} NaCl and KCl solutions. The Bi_2O_3 was unchanged by solutions with $[Cl^-]/[OH^-] \leq 1$, except for traces of basic bismuth carbonates (10). In solutions with $[Cl^-]/[OH^-] \geq 9$, Bi_2O_3 was converted (>80%, estimated from XRD intensities) to a solid with a rather diffuse diffraction pattern, similar but not identical to that of BiOCl, as shown in Table 3. The unit cell of BiOCl is tetragonal (9), with $a = 3.891$ Å, $c = 7.369$ Å, $c/a = 1.894$.

The XRD peak positions varied slightly between preparations, corresponding to variations in cell dimensions within the limits $a = 3.80$–3.82, $c = 7.50$–7.58 Å, $c/a = 1.97$–1.99. Although the diffraction peaks were broad, the variation in c, at least, exceeded the experimental uncertainty. The cell dimensions were significantly different from both BiOCl and natural daubréeite, BiO(OH,Cl) ($a = 3.85$ Å, $c = 7.40$ Å, $c/a = 1.922$, ref. 20).

The pattern was too poor for the usual unit-cell refinement methods. The 002 and 200 peaks, however, were reasonably sharp, yielding the estimated cell dimensions $a = 3.80_8$ Å, $c = 7.57_8$ Å, $c/a = 1.990$, from which the calculated pattern in Table 3 was derived. The data in Table 3 are from the purest sample prepared from Bi_2O_3; it contained about 6 wt.% chlorine (calc. for $Bi_2O_2(OH)Cl$, 7.1%; BiOCl, 13.6%).

Bannister and Hey reported identical diffraction patterns for natural daubréeite and a synthetic material containing 7.5% and 10.25% chlorine, respectively. Our data indicate some variation in composition of our products, with a stoichiometry near

Can. J. Chem. Downloaded from www.nrcresearchpress.com by 213.222.148.141 on 09/07/12
For personal use only.

Can. J. Chem. Downloaded from www.nrcresearchpress.com by 213.222.148.141 on 09/07/12
For personal use only.

$Bi_2O_2(OH)Cl$. We have assumed this stoichiometry for estimation of Gibbs energies and phase relationships, below. We did not observe any other solid products in reactions between Bi_2O_3 and neutral or alkaline chloride solutions at room temperature.

(iii) Other preparative experiments

We tried two other approaches to clarify the sequence of interconversion of basic bismuth chlorides, namely, reaction of Bi_2O_3 with chloride/hydroxide solutions at 70 and 100°C, and reaction of bismuth nitrate with chloride/hydroxide solutions at 22°C. After 2 days at 70 and 100°C, partial conversion of Bi_2O_3 to Bi_3O_4Cl was observed at $[Cl^-]/[OH^-] \geq 10$. Daubréeite was formed together with Bi_3O_4Cl at $[Cl^-]/[OH^-] \geq 16$ at 70°C. No reaction was observed at $[Cl^-]/[OH^-] \leq 5$.

About 2 mmol of bismuth nitrate was contacted at 22°C with solutions (100 cm^3) containing a total of 39 mmol of sodium chloride and hydroxide, with the $[Cl^-]/[OH^-]$ ratio ranging from 0.016 to 3.3. Daubréeite was formed at $[Cl^-]/[OH^-] = 3.3$, and Bi_3O_4Cl at $[Cl^-]/[OH^-] = 1.6$. An unidentified phase, with a diffraction pattern resembling that of $Bi_{12}O_{17}Cl_2$, was obtained at $[Cl^-]/[OH^-]$ ratios between 0.065 and 0.85. Bismuth oxide was precipitated at $[Cl^-]/[OH^-] \leq 0.1$, and was the sole product at $[Cl^-]/[OH^-] \leq 0.03$.

Although both these series of experiments revealed conditions under which Bi_3O_4Cl can occur, they offered little prospect of further clarification of phase relationships.

(b) Heterogeneous titrations

We have attempted to measure equilibrium chloride activities, as a function of pH, by adding successive aliquots of NaOH to stirred, thermostatted suspensions of the following three solid mixtures, at 25°C: (*i*) Bi_2O_3 + BiOCl, (*ii*) Bi_2O_3 + "$Bi_2O_2(OH)Cl$", (*iii*) Bi_2O_3 + $Bi_{12}O_{17}Cl_2$.

No more than one of these mixtures can be a stable phase assemblage at a given temperature. However, the sluggish interconversion of many of the solids gave some hope of measuring metastable equilibria, and hence deducing the true equilibrium phase relationships. We did not attempt to measure any equilibria involving the other three oxychlorides ($Bi_{12}O_{15}Cl_6$, $Bi_{24}O_{31}Cl_{10}$, Bi_3O_4Cl), since they occurred rarely (or not at all) in preparative experiments.

In these titrations we used 5 g of solid, initially suspended in 40 cm^3 of water. The chloride activity and pH usually stabilized within about an hour of addition of aliquots of NaOH. Solids were filtered and washed between titrations.

(i) Bi_2O_3 + BiOCl

The results of two titrations of a mixture of Bi_2O_3 and BiOCl with NaOH solution are shown in Fig. 1. The data are consistent with the metastable equilibrium [9], with $\log K_9 = 3.13 \pm 0.04$. This is in good agreement with the value of 3.03 derived above from literature values for Gibbs energies (Table 1). The difference corresponds to a discrepancy in Gibbs energies of only 0.6 kJ mol^{-1}; we obtain $\Delta_f G^0$ (BiOCl, s, 298 K) = -321.5 ± 1.3 kJ mol^{-1}.

(ii) Bi_2O_3 + "$(BiO)_2(OH)Cl$"

Bismuth oxide (5 g, 10.7 mmol) was pretreated with either NaCl or HCl (1 mmol) to convert it partly to the hydroxychloride (confirmed by XRD), then filtered, washed, and titrated with NaOH in the manner described above. Data are presented in Fig. 2. There was more variation between runs than in the titrations with Bi_2O_3 + BiOCl, but the behaviour was otherwise similar, with $\{Cl^-\}/\{OH^-\} \sim 30$. Assuming the formula $Bi_2O_2(OH)Cl$, we can write the following relationship:

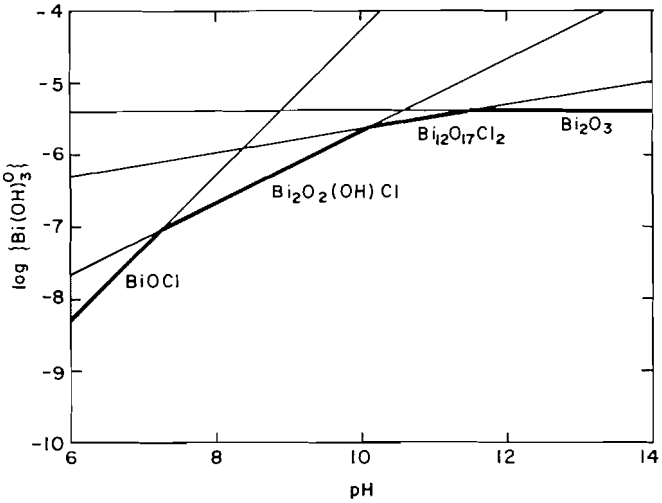

FIG. 1. Measured pH and chloride activity of solutions in contact with α-Bi_2O_3 + BiOCl. First titration, ○; second titration, ●; increasing pH and $\{Cl^-\}$ corresponds to successive additions of NaOH.

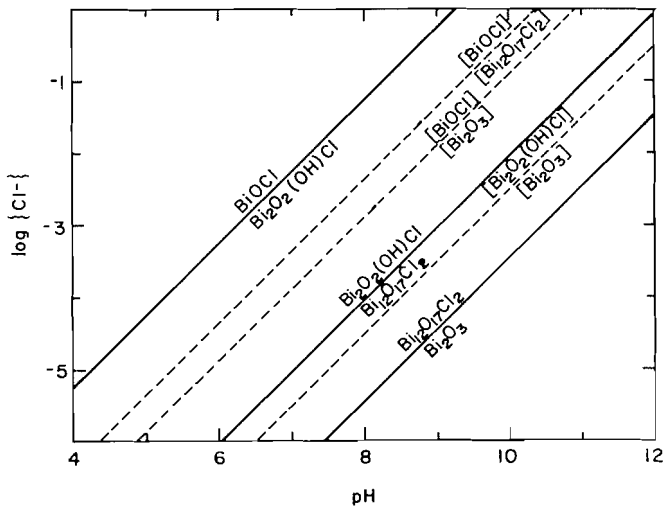

FIG. 2. Measured pH and chloride activity of solutions in contact with α-Bi_2O_3 + "$Bi_2O_2(OH)Cl$". Oxide pretreated with HCl (○) or NaCl (◒, ●).

[11] $Bi_2O_2(OH)Cl(s) + OH^-(aq) \rightleftharpoons Bi_2O_3(s) + H_2O(l) + Cl^-(aq)$

$K_{11} = \{Cl^-\}/\{OH^-\} = 10^{1.5 \pm 0.4}$

$\Delta_f G^0(Bi_2O_2(OH)Cl, s, 298\ K) = -696 \pm 4$ kJ mol^{-1}

Since the hydroxychloride was rather poorly crystalline, as indicated by XRD, there is probably a positive bias of a few kilojoules per mole, in addition to the stated uncertainty.

(iii) Bi_2O_3 + $Bi_{12}O_{17}Cl_2$

A sample of $Bi_{12}O_{17}Cl_2$ (5 g), containing traces of α-Bi_2O_3 (see "Hydrolysis of BiOCl" above), was suspended in deionized water under a nitrogen purge, and titrated with NaOH. Data for three successive titrations are presented in Fig. 3.

In the first titration, the chloride activities showed a persistent downward drift, resulting in a slope of about 0.6 in the plot of $\log\{Cl^-\}$ vs. pH. The second and third titrations, however, showed reproducible equilibrium behaviour of the type expected from eq. [6]. We conclude that there was insufficient Bi_2O_3 in the initial sample to sustain equilibrium, or there was some aging of the $Bi_{12}O_{17}Cl_2$, in the early stages of the first titration.

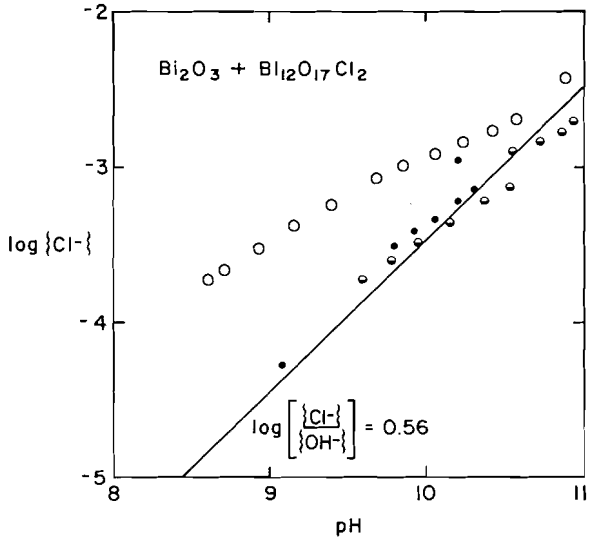

FIG. 3. Measured pH and chloride activity of solutions in contact with α-Bi_2O_3 + $Bi_{12}O_{17}Cl_2$. Three successive titrations (○, ◒, ●).

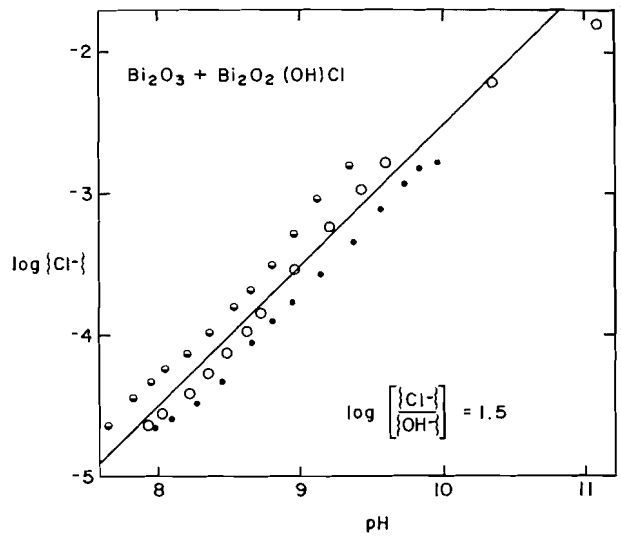

FIG. 4. Phase relationships between α-Bi_2O_3, $Bi_{12}O_{17}Cl_2$, "$Bi_2O_2(OH)Cl$", and BiOCl, calculated from equilibrium data in Figs. 1 to 3.

Based on the two subsequent titrations, we estimate that $\log K_6 = 0.56 \pm 0.20$, whence $\Delta_f G^0(Bi_{12}O_{17}Cl_2, s, 298\,K) = -3141 \pm 6\,kJ\,mol^{-1}$. Again, there is probably a small positive bias in this value, because of the poor crystallinity of the $Bi_{12}O_{17}Cl_2$.

(c) Deduction of phase relationships

The descending order of the observed equilibrium constants, $K_9 > K_{11} > K_6$, follows the descending order of Cl:Bi ratios in the solids, 1:1 (BiOCl) > 1:2 ($Bi_2O_2(OH)Cl$) > 1:6 ($Bi_{12}O_{17}Cl_2$). This indicates that all three solids have stability fields within the system $BiCl_3$–Bi_2O_3–H_2O–[pH] at 25°C; these fields are bounded by equilibria [12], [13], and [6].

[12] $2BiOCl(s) + OH^-(aq) \rightleftharpoons Bi_2O_2(OH)Cl(s) + Cl^-(aq)$

$$\log K_{12} = 2 \log K_9 - \log K_{11} = 4.76 \pm 0.48$$

(using our value of K_9)

[13] $(3/2)Bi_2O_2(OH)Cl(s) + OH^-(aq) \rightleftharpoons (1/4)Bi_{12}O_{17}Cl_2(s) + (5/4)H_2O(l) + Cl^-(aq)$

$$\log K_{13} = 1.5 \log K_{11} - 0.5 \log K_6 = 1.97 \pm 0.70$$

In addition, we can calculate the metastable equilibrium relationship, [14]:

[14] $(6/5)BiOCl(s) + OH^-(aq) \rightleftharpoons (1/10)Bi_{12}O_{17}Cl_2(s) + (1/2)H_2O(l) + Cl^-(aq)$

$$\log K_{14} = 1.2 \log K_9 - 0.2 \log K_6 = 3.65 \pm 0.09$$

These relationships are all depicted in Fig. 4. Stated uncertainties do not include the bias arising from poor crystallinity of $Bi_2O_2(OH)Cl$ and $Bi_{12}O_{17}Cl_2$.

The relatively broad stability field of $Bi_2O_2(OH)Cl$ implies that it may have supplanted some of the other anhydrous phases ($Bi_{12}O_{15}Cl_6$, $Bi_{24}O_{31}Cl_{10}$, Bi_3O_4Cl) in the low-temperature aqueous system. The relative stability of the hydrous phase is expected to decrease with increasing temperature; there is some evidence that $Bi_2O_2(OH)Cl$ is itself supplanted by Bi_3O_4Cl above about 70°C.

Figure 4 indicates that BiOCl is stable in acidic, or concentrated neutral, chloride solutions, whereas $Bi_2O_2(OH)Cl$ is stable in more dilute neutral, or concentrated and slightly alkaline solutions. This probably has some bearing on the occurrence of the minerals bismoclite and daubréeite. The narrow stability field of $Bi_{12}O_{17}Cl_2$ is consistent with its apparent absence in nature; similar observations have been made (10, 21) on the absence or scarcity of $(BiO)_4(OH)_2CO_3$ (basobismutite?) and $Pb_{10}O(OH)_6(CO_3)_6$ (plumbonacrite).

(d) Solubility relationships

The stability data also allow us to estimate the relative solubilities of the basic bismuth chlorides. The predominant hydrolysed bismuth species at pH 7–13 is neutral $Bi(OH)_3$, with a Gibbs energy of formation of about -571.6 kJ mol^{-1} (22–24). Bismuth chloride complexes appear to be stable only in acidic solutions (17). The solubilities of α-Bi_2O_3 and the bismuth oxychlorides in neutral to basic solutions can thus be approximated by equilibria [15] to [18]:

[15] $(1/2)Bi_2O_3(s) + (3/2)H_2O(l) \rightleftharpoons Bi(OH)_3(aq)$

$$K_{17} = \{Bi(OH)_3\} = 10^{-5.4}$$

[16] $(1/12)Bi_{12}O_{17}Cl_2(s) + (1/6)OH^-(aq) + (17/12)H_2O(l) \rightleftharpoons Bi(OH)_3(aq) + (1/6)Cl^-(aq)$

$$K_{18} = \{Bi(OH)_3\}\{Cl^-\}^{1/6}/\{OH^-\}^{1/6} = 10^{-5.3}$$

[17] $(1/2)Bi_2O_2(OH)Cl(s) + (1/2)OH^-(aq) + H_2O(l) \rightleftharpoons Bi(OH)_3(aq) + (1/2)Cl^-(aq)$

$$K_{19} = \{Bi(OH)_3\}\{Cl^-\}^{1/2}/\{OH^-\}^{1/2} = 10^{-4.7}$$

[18] $BiOCl(s) + OH^-(aq) + H_2O(l) \rightleftharpoons Bi(OH)_3(aq) + Cl^-(aq)$

$$K_{20} = \{Bi(OH)_3\}\{Cl^-\}/\{OH^-\} = 10^{-2.4}$$

(using BiOCl data from ref. 12)

Equilibrium $Bi(OH)_3$ activities as a function of pH, at a chloride-ion activity of 10^{-2} mol dm^{-3}, are shown in Fig. 5. This figure helps to rationalize some of our experimental observations. Within its stability range, $Bi_{12}O_{17}Cl_2$ is only marginally less soluble than Bi_2O_3, but about two orders of magnitude less soluble than BiOCl. Thus, BiOCl can provide a much higher supersaturation than Bi_2O_3, which may explain why we were able to form $Bi_{12}O_{17}Cl_2$ easily from BiOCl, but not from Bi_2O_3. Bismuth oxide, however, can provide over an order of magnitude of bismuth supersaturation with respect to $Bi_2O_2(OH)Cl$, which we did obtain from the oxide. The low solubility of BiOCl within most of the stability field of

Can. J. Chem. Downloaded from www.nrcresearchpress.com by 213.222.148.141 on 09/07/12
For personal use only.

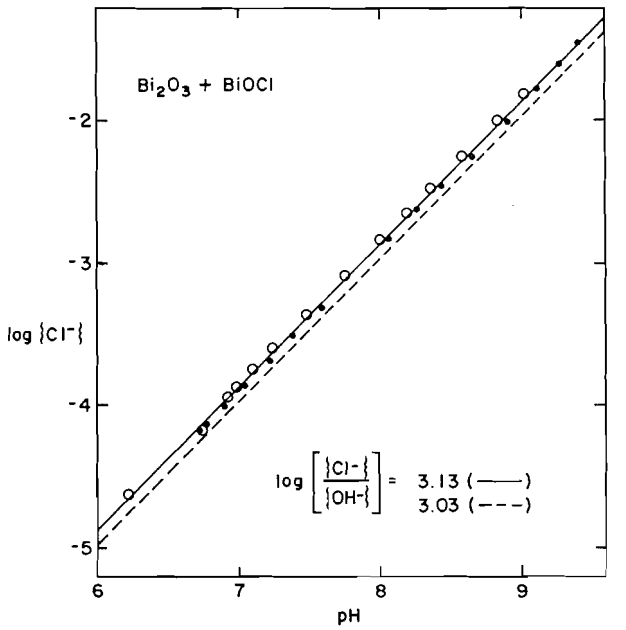

FIG. 5. Calculated $Bi(OH)_3^0$ activities in contact with bismuth oxide and oxychlorides at a Cl^- activity of 10^{-2} mol dm^{-3}, as a function of pH. For any change in log {Cl^-}, change the pH scale by an equal and opposite quantity. The $Bi(OH)_3^0$ activity approximates total bismuth within the pH limits 7–13. Bold portions of lines represent the range over which each solid is stable.

$Bi_2O_2(OH)Cl$ (and vice versa) may also explain why these solids do not easily interconvert. Interconversion of these two phases by direct anion exchange would not depend on solubilities, but on solid-state interdiffusion of OH^- and Cl^-. This is also expected to be slow, however, since the anion sites between the $(BiO)_n^{n+}$ layers are fully occupied, and efficiently packed (9, 25).

(e) Comparison with other basic bismuth salts

The two chloride-deficient phases, $Bi_2O_2(OH)Cl$ and $Bi_{12}O_{17}Cl_2$, are stable within a narrow band of solution conditions, between K_6 and K_{12}, which brackets about four pH units at a given chloride activity. This contrasts with the basic iodide, Bi_5O_7I, whose stability field spans seven pH units at a given iodide activity (11). Also, Bi_5O_7I is more resistant to hydrolysis than $Bi_{12}O_{17}Cl_2$:

[19] $Bi_5O_7I(s) + OH^-(aq) \rightleftharpoons (5/2)Bi_2O_3(s) + (1/2)H_2O(l) + I^-(aq)$
$K_{19} = \{I^-\}/\{OH^-\}$; $\log K_{19} = -3.4$ (ref. 11) cf. $\log K_6 = 0.6$.

The relative stability of Bi_5O_7I may arise from better steric accommodation of iodide in the $[Bi_5O_7]_n^{n+}$ cation network, compared with chloride and $[Bi_{12}O_{17}]_n^{2n+}$ (neither structure is known, but both are presumed to contain extensive polymeric bismuth–oxygen networks; this is the case with $Bi_{24}O_{31}Cl_{10}$ (2), $Bi_{12}O_{15}Cl_6$ (3), and β-Bi_5O_7I (26)). It is also possible that some weak Bi...I covalent interaction contributes to the iodide's stability.

Even though Bi_5O_7I is much more stable than the basic bismuth chlorides towards hydrolysis, it is susceptible to "anion exchange" reaction with concentrated chloride solutions:

[20] $2Bi_5O_7I + 5Cl^- + 4H_2O \rightleftharpoons 5Bi_2O_2(OH)Cl + 2I^- + 3OH^-$
$K_{20} = \{OH^-\}^3\{I^-\}^2/\{Cl^-\}^5 = 10^{-14.3 \pm 2.4}$
(based on K_{11} and data for Bi_5O_7I from ref. 11)

We have found that Bi_5O_7I is converted to $Bi_2O_2(OH)Cl$ by concentrated chloride solutions ($>10^{-2}$ mol dm^{-3}). A sample prepared by contacting 0.5 g Bi_5O_7I with 1.0 mol dm^{-3} NaCl at 90°C for 48 h contained 7.2 wt.% chlorine (calculated for $Bi_2O_2(OH)Cl$, 7.1%). This reaction is a major limiting factor on the performance of the suggested bismuth oxyiodide waste form for iodine-129 (11, 27). Bismutite ($(BiO)_2CO_3$), however, is sufficiently stable that exchange reactions with chloride are unlikely to limit its performance as a waste form for carbon-14 (10, 22).

Acknowledgements

We are grateful to A. M. Duclos and J. M. Snider for the X-ray diffraction measurements, D. D. Wood for the chloride analyses, and J. Paquette and D. W. Shoesmith for helpful comments.

1. A. E. ARPPE. De chloreto bismutico. Specimen academicum, Helsingforsiae 1844; Pogg. Ann. **64**, 246 (1845).
2. L. G. SILLEN and M. EDSTRAND. Z. Kristallogr. **104**, 178 (1942).
3. F. HOPFGARTEN. Acta Crystallogr. B**32**, 2570 (1976).
4. B. Z. NURGALIEV, T. F. VASEKINA, A. E. BARON, B. A. POPOVKIN, and A. V. NOVOSELOVA. Russ. J. Inorg. Chem. **28**, 415 (1983) (Zh. Neorg. Khim. **28**, 735 (1983)).
5. B. Z. NURGALIEV, B. A. POPOVKIN, and S. YU. STEFANOVICH. Russ. J. Inorg. Chem. **28**, 1252 (1983) (Zh. Neorg. Khim. **28**, 2207 (1983)).
6. B. Z. NURGALIEV, M. L. BARSUKOVA, V. A. KUZNETSOV, and B. A. POPOVKIN. Zh. Neorg. Khim. **30**, 1665 (1985).
7. B. AURIVILLIUS. Chem. Scr. **24**, 125 (1984).
8. A. H. MEANS. Am. J. Sci. **41**, 125 (1916).
9. F. A. BANNISTER and M. H. HEY. Mineral. Mag. **24**, 49 (1935).
10. P. TAYLOR, S. SUNDER, and V. J. LOPATA. Can. J. Chem. **62**, 2863 (1984).
11. P. TAYLOR and V. J. LOPATA. Can. J. Chem. **64**, 290 (1986).
12. D. D. WAGMAN, W. H. EVANS, V. B. PARKER, R. H. SCHUMM, I. HALOW, S. M. BAILEY, K. L. CHURNEY, and R. L. NUTTALL. J. Phys. Chem. Ref. Data, Vol. 11, Suppl. 2, 392 pp. (1982).
13. R. A. ROBIE, B. S. HEMINGWAY, and J. R. FISHER. U.S. Geol. Surv. Bull. 1452 (reprinted with corrections, 1979).
14. A. A. NOYES and M. CHOW. J. Am. Chem. Soc. **40**, 739 (1918).
15. V. P. VASIL'EV and N. K. GRECHINA. Russ. J. Inorg. Chem. **12**, 315 (1967) (Zh. Neorg. Khim. **12**, 605 (1967)).
16. V. P. VASIL'EV and N. K. GRECHINA. Soviet Electrochem. **5**, 386 (1969) (Elektrokhimiya, **5**, 426 (1969)).
17. L. JOHANSSON. Acta Chem. Scand. **23**, 548 (1969).
18. A. A. MOUSSA and H. M. SAMMOUR. J. Chem. U.A.R. **9**, 73 (1966).
19. H. M. SAMMOUR and A. A. MOUSSA. J. Chem. Soc. 1762 (1958).
20. H. E. SWANSON, R. K. FUYAT, and G. M. UGRINIC. Natl. Bur. Stand. (U.S.) Circ. No. 539, vol. 4, p. 54 (1955) (JCPDS File Card. No. 6-0249).
21. P. TAYLOR and V. J. LOPATA. Can. J. Chem. **62**, 395 (1984).
22. P. TAYLOR. Atomic Energy of Canada Ltd. Report No. AECL-9073 (1987).
23. C. F. BAES, JR., and R. E. MESMER. The hydrolysis of cations. Wiley-Interscience, New York. 1976. p. 382.
24. T. F. BIDLEMAN. Anal. Chim. Acta, **56**, 221 (1971).
25. A. F. WELLS. Structural inorganic chemistry. 4th ed. Clarendon Press, Oxford. 1975. p. 408.
26. J. KETTERER, E. KELLER, and V. KRAMER. Z. Kristallogr. **172**, 63 (1985).
27. P. TAYLOR, V. J. LOPATA, and D. D. WOOD. Proceedings of ASTM 4th International Hazardous Waste Symposium, Atlanta, GA. May 1987.

Can. J. Chem. Downloaded from www.nrcresearchpress.com by 213.222.148.141 on 09/07/12
For personal use only.

The reaction of 3,5-diphenyl-1,2-dithiolium-4-olate with aniline: the crystal structure of 1-phenylimino-2-phenylamino-3-phenylindene

DAVID M. MCKINNON AND PETER D. CLARK
Chemistry Department, University of Manitoba, Winnipeg, Man., Canada R3T 2N2

ROBERT O. MARTIN AND LOUIS T. J. DELBAERE
Department of Biochemistry, University of Saskatchewan, Saskatoon, Sask., Canada S7N 0W0

AND

J. WILSON QUAIL
Department of Chemistry, University of Saskatchewan, Saskatoon, Sask., Canada S7N 0W0

Received June 2, 1987

DAVID M. MCKINNON, PETER D. CLARK, ROBERT O. MARTIN, LOUIS T. J. DELBAERE, and J. WILSON QUAIL. Can. J. Chem. **65**, 2830 (1987).

3,5-Diphenyl-1,2-dithiolium-4-olate (**1**) reacts with aniline to form 1-phenylimino-2-phenylamino-3-phenylindene (**3***a*). Under suitable conditions, 6-phenylbenzo[*b*]indeno[1,2-*e*]-1,2-thiazine is also formed. These structures are confirmed by alternative syntheses. The molecular structure of **3***a* has been determined by single crystal X-ray diffraction. Compound **3***a* crystallizes in the monoclinic space group $C2/c$ with unit cell dimensions $a = 20.777(3)$ Å, $b = 6.130(3)$ Å, $c = 31.327(3)$ Å, $\beta = 99.59(1)°$, and $Z = 8$. The structure was solved by direct methods and refined by least squares to a final $R = 0.055$. The molecular structure of **3***a* shows the three phenyl containing substituents to have the planes of their ring systems tilted between 40° and 60° from the plane of the indene system due to steric repulsions.

DAVID M. MCKINNON, PETER D. CLARK, ROBERT O. MARTIN, LOUIS T. J. DELBAERE et J. WILSON QUAIL. Can. J. Chem. **65**, 2830 (1987).

Le diphényl-3,5 dithiolium-1,2 olate-4 (**1**) réagit avec l'aniline pour former le phénylimino-1 phénylamino-2 phényl-3 indène (**3***a*). Dans certaines conditions appropriées, il se forme aussi du phényl-6 benzo[*b*]indéno[1,2-*e*]thiazine-1,2. On a confirmé ces structures en se basant sur d'autres synthèses. On a déterminé la structure moléculaire du composé **3***a* à l'aide de la diffraction de rayons-X. Le composé **3***a* cristallise dans le groupe d'espace monoclinique $C2/c$, avec $a = 20,777(3)$, $b = 6,130(3)$ et $c = 31,327(3)$ Å, $\beta = 99,59(1)°$ et $Z = 8$. On a résolu la structure par des méthodes directes et on l'a affinée par la méthode des moindres carrés jusqu'à une valeur finale de $R = 0,055$. La structure moléculaire du composé **3***a* démontre que, pour des raisons stériques, les plans des systèmes cycliques des trois substituants portant des noyaux phényles sont décalés de 40° à 60° du plan du système indénique.

[Traduit par la revue]

Introduction

The reaction of 3,5-diphenyl-1,2-dithiolium-4-olate (**1**) with aniline has been reported by Chinone *et al.* (1) to give a blue material, assigned the structure of 3,4,5-triphenylisothiazole (**2**). Since such a reaction would involve some unusual chemistry it has been reinvestigated. The results are reported below.

Results and discussion

When the reaction was performed as described, using redistilled aniline, a dark red mixture was obtained from which the only material isolated in any quantity was a dark red solid, mp 184–195°C. However, when the dithiole was treated with unpurified aniline, the red material was accompanied by greater or lesser amounts of a violet crystalline material whose mp (169°C) corresponds to that of the material reported (1). Its mass spectrum indicates a molecular weight of 311.007, which corresponds to a formula of $C_{21}H_{13}NS$, confirmed by analysis; Chinone *et al.* (1) have suggested a formula of $C_{21}H_{15}NS$. The analysis and mass spectrum of the red material were consistent with a formula of $C_{21}H_{20}N_2$.

While the ^1H nmr spectrum of the violet material only showed a complex series of absorptions in the aromatic region, the decoupled ^{13}C spectrum was more informative. Nine tertiary carbons were evident, of which two were at double intensity, consistent with the presence of a monosubstituted aromatic ring. There were eight quaternary carbon atoms of which three were of lesser intensity, consistent with their not being adjacent to tertiary carbon atoms. The presence of a thiocarbonyl function could be eliminated since the spectrum lacked a signal in that range (2, 3). Also the compound was unaffected by cold potassium permanganate in acetone. It thus appears that the sulfur atom present in the material is part of a heterocyclic ring.

Since blue colours are characteristic of pseudoazulenes and if the carbon skeleton of the starting dithiole were intact, a number of possible structures consistent with the above data may be advanced. Of these, fused benzothiopyrano[4,3-*b*] indoles may be eliminated on the basis of earlier studies (4). The red material, unlike the violet material, was amenable to X-ray structural determination (*vide infra*), which identified it as 1-phenylimino-2-phenylamino-3-phenylindene (**3***a*). On this basis the fused indene structures **4***a* and **5***a* were considered for the violet material.

It is reported that the system **5***a* may be made from indanedione by condensation with 2-aminobenzenethiol (5). While the isomeric system **4***b* could possibly have been formed by an alternative condensation mode (4), another synthesis of benzo[*b*]indeno[1,2-*e*]-1,4-thiazine (6) confirmed the structure as type **5**. Accordingly, 3-phenylindane-1,2-dione was treated with 2-aminobenzenethiol. A violet material was obtained, which was identical to that obtained above, establishing its formula as **5***a*.

Treatment of 3-phenylindane-1,2-dione with aniline afforded a dark red material that was identical with the red material **3***a* isolated above.

Can. J. Chem. Downloaded from www.nrcresearchpress.com by 213.222.148.141 on 09/07/12
For personal use only.

Can. J. Chem. Downloaded from www.nrcresearchpress.com by 213.222.148.141 on 09/07/12
For personal use only.

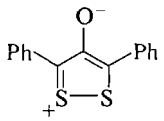

1

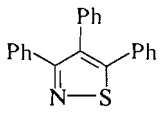

2

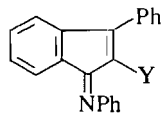

3
a Y = NHPh
b Y = OH
c Y = SH

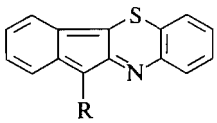

4
a R = Ph
b R = H

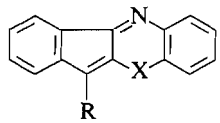

5
a R = Ph, X = S
b R = H, X = S
c R = Ph, X = NMe
d R = Ph, X = O

Compound **4***a*, compared to **5***a*, would also require bond fixation in one of the aromatic rings, and be less stable (compare data for related benzoindenothiopyrans (7)). In addition, the violet material failed to react with dimethyl acetylenedicarboxylate. A compound such as **4***a* with an *o*-quinonoid structure would be expected to react readily.

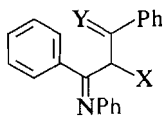

6
a X = OH, Y = S
b X = NHPh, Y = S
c X = NHPh, Y = NPh

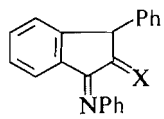

7
a X = O
b X = S

Since the compound **1** reacts with hydrazine according to observed patterns for 1,2-dithiolium salts (8, 9), its reaction with aniline, as for 1,2-dithiolium salts (10), could form the compound **6***a*. Cyclization of **6***a* by known modes forms the indan-2-one **7***a* or its tautomer **3***b*, which react further with aniline to provide the indene **3***a*. Alternatively the compound **6***a* could react with aniline to give **6***b* or **6***c*, which cyclize to form **3***a* directly. The reactions forming **5***a* are not so clear, since they involve forming a sulfur bond to the central carbon atom that did not initially bear one, but a plausible reaction process would involve an intermediate compound of type **7***b*, which could have been formed from compounds such as **3***a* or **3***b* by reaction with hydrogen sulfide. The role of the impure aniline may be to provide some material that can reversibly associate with hydrogen sulfide eliminated in the initial reactions forming compounds of type **6**. A pericyclic or possibly radical reaction of compound **7***b* followed by dehydrogenation would form compound **5***a*. In support of this, the reaction of the 1,2-dithiole with redistilled aniline gave **5***a* when the reaction mixture was treated with hydrogen sulfide.

Two related pseudoazulenes, the pyrazine (**5***c*) and the 1,4-oxazine (**5***d*), were made by related methods, the condensation of 3-phenylindane-1,2-dione with 2-methylaminoaniline and 2-aminophenol, respectively.

The molecular structure of 1-phenylimino-2-phenylamino-3-phenylindene (**3***a*) has been determined by single crystal X-ray diffraction. Selected bond distances and angles of **3***a* are given in Tables 2 and 3, respectively. A view of the molecule is given in Fig. 1. The bond distances and angles in the phenyl rings of **3***a* are similar to those found for these groups in other structure determinations. The six-membered ring in the indene group has carbon–carbon bonds similar to other aromatic groups, whereas the bonds involving C(1), C(2), and C(3) are similar to either single or double bonds. For example, C(1)—N(1) is 1.274 Å, compared to values between 1.38 and 1.42 Å for all of the other C—N bonds in the molecule. The distance between C(2) and C(3) is 1.358 Å, compared to values between 1.47 and 1.49 Å for the other C—C distances involving these atoms. Thus, in the indene group there is an aromatic benzene ring and an α,β unsaturated imine.

The indene group (plane A), C(1)–C(9), is planar within 0.032 Å. The phenylimino group (plane B), C(10)–C(15), is planar within 0.007 Å, with N(1) out of the plane by 0.10 Å. The phenylamino group (plane C), C(16)–C(21) is planar within 0.016 Å, with N(2) and H(N2) out of the plane by 0.011 and 0.55 Å, respectively. The phenyl ring (plane D), C(22)–C(27), is planar within 0.0034 Å. The angles between the above planes are:

Plane 1	Plane 2	Angle (degrees)
A	B	60.2
A	C	39.9
A	D	51.6

The steric repulsions of groups B, C, and D with each other and with group A prevent the molecule from attaining a structure with delocalization of electrons between the separate π systems.

Experimental

The ^{1}H nmr and ^{13}C spectra were obtained in deuterochloroform solution using tetramethylsilane as an internal standard on Varian model 56/60 and Bruker WH90 spectrometers respectively. Mass spectra were obtained on a Finnigan Model 1015 mass spectrometer or, for accurate mass, on a VG7070-EHF mass spectrometer. Chromatography was performed on Merck silica gel Kieselgel PF-254, or on Camag alumina type 507C-1.

*Preparation of 6-phenylbenzo[*b*]indeno[1,2-*e*]-1,4-thiazone (**5**a)*

3-Phenylindane-1,2-dione (1.11 g, 5.0 mmol) and 2-aminobenzenethiol (0.62 g, 5 mmol) in acetic acid (10 mL) containing concentrated sulfuric acid (2 drops) was heated under reflux 10 min. The bluish solution was poured into water, neutralized with dilute sodium hydroxide solution, and extracted with chloroform. The dried extract was evaporated, and chromatographed in benzene on alumina. A fast running dark blue band was collected. Evaporation gave a violet oil, which crystallized under ethanol. It was recrystallized from an ethanol–dimethylformamide 1:1 mixture as fine dark violet needles, mp 168°C (yield 63%). The ^{1}H nmr spectrum has δ: 8.4–7.2 (complex bands) ppm. The ^{13}C nmr spectrum δ: 156.80(4°)*, 142.77(4°), 138.94(4°), 133.78(4°), 133.05(4°), 132.71(3°), 132.52(4°)*, 131.07(3°), 128.91(3°, on phenyl substituent), 128.47(3°), 128.19(3°), 127.58(3°, on phenyl substituent), 126.59(3°), 125.97(3°), 124.37(3°), 122.48(3°), 120.85(4°), 118.53(3°), 116.03(4°)*. *Anal.* calcd. for $C_{21}H_{13}NS$: C 81.03, H 4.18, N 4.50, S 10.29; found: C 81.11, H 4.06, N 4.39, S 10.44. The mass spectrum M^+: 311.0775; M^+ calcd. for $C_{21}H_{13}NS$: 311.0781.

*These correspond to 4° carbon atoms *not* attached to 3° carbon atoms.

*Preparation of 1-phenylimino-2-phenylamino-3-phenylindene (**3**a)*

3-Phenylindan-1,2-dione (1.11 g, 5.0 mmol) and excess aniline (3 mL) were heated together under reflux for 5 min. The initially violet colored solution became dark red. The mixture was poured into 20%

Can. J. Chem. Downloaded from www.nrcresearchpress.com by 213.222.148.141 on 09/07/12
For personal use only.

TABLE 1. Fractional coordinates and average thermal parameters for **3***a* (estimated standard deviation of the last digit is given in parentheses; $U_{eq} = (U_{11} + U_{22} + U_{33})/3$)

Atom	x/a	y/b	z/c	$10^3\ U_{eq}$
N(1)	0.6270(1)	0.0038(4)	0.09010(7)	46(1)
N(2)	0.5214(1)	−0.2622(4)	0.07415(7)	50(1)
C(1)	0.6103(1)	−0.0899(4)	0.12289(9)	42(1)
C(2)	0.5524(1)	−0.2375(4)	0.11639(9)	43(1)
C(3)	0.5414(1)	−0.3169(4)	0.15500(8)	41(1)
C(4)	0.6054(1)	−0.2702(5)	0.2328(1)	50(1)
C(5)	0.6597(1)	−0.1736(5)	0.2580(1)	52(1)
C(6)	0.7017(1)	−0.0442(5)	0.2397(1)	55(1)
C(7)	0.6898(1)	−0.0020(5)	0.1954(1)	49(1)
C(8)	0.6362(1)	−0.0957(4)	0.17024(8)	42(1)
C(9)	0.5941(1)	−0.2336(4)	0.18865(9)	42(1)
C(10)	0.6790(1)	0.1559(5)	0.09318(9)	44(1)
C(11)	0.6798(1)	0.3494(5)	0.1163(1)	52(1)
C(12)	0.7285(1)	0.5009(5)	0.1158(1)	58(1)
C(13)	0.7774(1)	0.4621(6)	0.0918(1)	62(1)
C(14)	0.7767(1)	0.2725(6)	0.0682(1)	61(1)
C(15)	0.7278(1)	0.1199(5)	0.0686(1)	53(1)
C(16)	0.4772(1)	−0.4249(5)	0.05632(8)	41(1)
C(17)	0.4322(1)	−0.3750(5)	0.01918(9)	49(1)
C(18)	0.3884(2)	−0.5305(6)	0.0005(1)	60(1)
C(19)	0.3875(2)	−0.7368(6)	0.0184(1)	63(1)
C(20)	0.4328(2)	−0.7873(5)	0.0547(1)	57(1)
C(21)	0.4783(1)	−0.6344(5)	0.07334(9)	49(1)
C(22)	0.4873(1)	−0.4539(4)	0.16465(8)	42(1)
C(23)	0.4227(1)	−0.3975(5)	0.14894(9)	48(1)
C(24)	0.3714(1)	−0.5288(6)	0.1564(1)	60(1)
C(25)	0.3845(2)	−0.7207(7)	0.1795(1)	69(1)
C(26)	0.4481(2)	−0.7800(6)	0.1953(1)	70(1)
C(27)	0.4999(2)	−0.6479(5)	0.1882(1)	56(1)

TABLE 2. Selected bond distances for **3***a* (Å, estimated standard deviation of the last digit is given in parentheses)

Bond	Distance	Bond	Distance
N(1)—C(1)	1.274(4)	C(11)—C(12)	1.376(4)
N(1)—C(10)	1.418(3)	C(12)—C(13)	1.381(5)
N(2)—C(2)	1.380(3)	C(13)—C(14)	1.376(5)
N(2)—C(16)	1.408(4)	C(14)—C(15)	1.382(5)
C(1)—C(2)	1.492(4)	C(16)—C(17)	1.399(4)
C(1)—C(8)	1.492(4)	C(16)—C(21)	1.389(4)
C(2)—C(3)	1.358(4)	C(17)—C(18)	1.380(4)
C(3)—C(9)	1.479(3)	C(18)—C(19)	1.386(5)
C(3)—C(22)	1.473(4)	C(19)—C(20)	1.384(4)
C(4)—C(5)	1.397(4)	C(20)—C(21)	1.389(4)
C(4)—C(9)	1.381(4)	C(22)—C(23)	1.395(4)
C(5)—C(6)	1.374(5)	C(22)—C(27)	1.400(4)
C(6)—C(7)	1.392(4)	C(23)—C(24)	1.386(5)
C(7)—C(8)	1.377(4)	C(24)—C(25)	1.384(5)
C(8)—C(9)	1.406(4)	C(25)—C(26)	1.380(5)
C(10)—C(11)	1.389(4)	C(26)—C(27)	1.393(5)
C(10)—C(15)	1.388(4)		

concentrated hydrochloric acid in water, and the crude dark material collected. Chromatography on alumina in benzene indicated a dark red band, which was collected and evaporated. The dark red oil crystallized under ethanol and was recrystallized from hexane as dark red prisms, mp 184–185°C (yield 81%). The ^{1}H nmr spectrum δ: 8.5–7.2 (complex bands) ppm. *Anal.* calcd. for $C_{27}H_{20}N_2$: C 87.1, H 5.38, N 7.53; found: C 87.18, H 6.04, N 7.61. The mass spectrum M^+: 372; M^+ calcd.: 372.

Reaction of 3,5-diphenyl-1,2-dithiolium-3-olate with aniline

(a) With impure aniline

The reaction was performed as described (1), but the residue from evaporation of excess aniline was examined by tlc. Two bands were evident, a dark red and a dark blue one; these were isolated. Work-up gave the products **3***a* (yield 43%) and **5***a* (yield 24%), which were identical (ms, mixture mp) to the compounds prepared above.

(b) With redistilled aniline

Performed as above (1), the major product of the reaction was the indene **3***a*. None of the **5***a* was evident, but traces of yellow material were present.

(c) With redistilled aniline and hydrogen sulfide

This was performed as in (*b*) but a slow stream of hydrogen sulfide was passed through for the first 30 min; then the solution was refluxed a further 1 h. Work-up afforded the indene **3***a* and the thiazine **5***a* (yields 40 and 15%, respectively).

*Preparation of 6-phenylbenzo[*b*]indeno[1,2-*e*]pyrazine (***5***c)*

3-Phenylindane-1,2-dione (222 mg, 1.0 mmol) and 2-methylaminoaniline (108 mg, 1.0 mmol) in ethanol (5 mL) were refluxed 10 min. The dark blue solution was evaporated, then purified by chromatography on silica gel in benzene. Collection and evaporation of a dark blue band gave an oil, which crystallized under methanol. It recrystallized from toluene as dark blue needles, mp 172°C (yield 55%). The ^{1}H nmr spectrum, δ: 3.48 (3H, s, the methyl protons), 7.47–8.28 (13H, bands, the aromatic protons) ppm. *Anal.* calcd. for $C_{22}H_{16}N_2$: C 85.71, H 5.19, N 9.09; found: C 85.83, H 5.06; N 9.20. The mass spectrum M^+: 308; calcd. for $C_{22}H_{16}N_2$: 308.

*Preparation of 6-phenylbenzo[*b*]indeno[1,2-*e*]-1,4-oxazine (***5***d)*

3-Phenylindane-1,2-dione (222 mg, 1.0 mmol) and 2-aminophenol (109 mg, 1.0 mmol) in acetic acid (5 mL) and sulfuric acid (1 drop) were heated at 100°C for 1 h. Dilution with water afforded a crude product that was collected and purified by chromatography on silica gel, in a benzene–chloroform (5:1) mixture. Collection and evaporation of a purple band gave a dark oil that solidified under methanol. It recrystallized from toluene as dark purple needles, mp 185–186°C, subliming above 140°C (yield 40%). The ^{1}H nmr spectrum, δ: 7.25–8.09 (bands, the aromatic protons) ppm. *Anal.* calcd. for $C_{21}H_{13}NO$: C 85.42, H 4.41, N 4.75; found: C 85.27, H 4.56, N 4.51. The mass spectrum, M^+: 295; calcd. for $C_{21}H_{13}NO$: 295.

Crystallographic data collection and analysis

Crystals of **3***a* were grown from a supersaturated solution in methanol. The red crystals of **3***a* exhibited the forms {001}, {010}, and {100}. The crystal data were the following:

$C_{27}H_{20}N_2$ mw = 372.45

Monoclinic, $C2/c$, a = 20.777(3) Å, b = 6.130(3) Å, c = 31.327(3) Å, β = 99.59(1)°, Z = 8, V = 3934.1 Å^3, ρ_o = 1.243 g cm^{-3}, ρ_c = 1.258 g cm^{-3}, $F(000)$ = 1568 e, radiation Ni-filtered Cu K_α (λ = 1.5418 Å), $(\sin\theta/\lambda)_{max}$ = 0.6095, crystal dimensions (mm) 0.09 × 0.28 × 0.35, max. decay correction 1.02, T = 11°C. Quantitative data collection was carried out on a single crystal mounted about the c-axis on an Enraf–Nonius CAD4F diffractometer with an $\omega/2\theta$ scan. A total of 3739 reflections was collected, of which 2939 unique reflections had a net $I > 3\sigma(I)$. Lorentz and polarization corrections were applied. Intensities of three standard reflections were monitored throughout the data collection. No absorption correction was applied. Observed weights for the reflections were taken as $1/[\sigma(F)]^2$.

X-ray diffraction data collected on the **3***a* crystal were processed using the XTAL system (11) of crystallographic programs. The structure was solved using the structure solution part of the XTAL system. The figures of merit CFOM and AMOS were used to choose the best set of phases used in the structure determination. The values were 0.96 and 82%, respectively. The positions of 23 of the 29 non-hydrogen atoms were determined from a calculated E map. The remaining non-hydrogen atoms were found in difference Fourier maps. Least-squares isotropic refinement gave an R value of 0.126. Anisotropic refinement was then carried out and gave an R value of

TABLE 3. Selected bond angles for **3***a* (degrees, estimated standard deviation of the last digit is given in parentheses)

Bonds	Angle	Bonds	Angle
C(2)—C(1)—C(8)	105.7(2)	C(10)—C(11)—C(12)	121.0(3)
C(2)—C(1)—N(1)	119.0(2)	C(11)—C(12)—C(13)	120.0(3)
C(8)—C(1)—N(1)	135.3(2)	C(12)—C(13)—C(14)	119.6(3)
C(1)—C(2)—C(3)	110.3(2)	C(13)—C(14)—C(15)	120.6(3)
C(1)—C(2)—N(2)	115.7(2)	C(10)—C(15)—C(14)	120.2(3)
C(3)—C(2)—N(2)	133.9(2)	C(2)—N(2)—C(16)	128.9(2)
C(2)—C(3)—C(9)	107.2(2)	N(2)—C(16)—C(17)	118.4(3)
C(2)—C(3)—C(22)	129.4(2)	N(2)—C(16)—C(21)	122.3(2)
C(9)—C(3)—C(22)	123.4(2)	C(17)—C(16)—C(21)	119.2(3)
C(5)—C(4)—C(9)	118.9(3)	C(16)—C(17)—C(18)	120.3(3)
C(4)—C(5)—C(6)	121.2(3)	C(17)—C(18)—C(19)	120.7(3)
C(5)—C(6)—C(7)	120.2(3)	C(18)—C(19)—C(20)	118.9(3)
C(6)—C(7)—C(8)	119.1(3)	C(19)—C(20)—C(21)	121.1(3)
C(1)—C(8)—C(7)	133.0(3)	C(16)—C(21)—C(10)	119.7(3)
C(1)—C(8)—C(9)	106.0(2)	C(3)—C(22)—C(23)	120.6(2)
C(7)—C(8)—C(9)	120.9(2)	C(3)—C(22)—C(27)	120.7(2)
C(3)—C(9)—C(4)	129.7(3)	C(23)—C(22)—C(27)	118.7(3)
C(3)—C(9)—C(8)	110.6(2)	C(22)—C(23)—C(24)	121.3(3)
C(4)—C(9)—C(8)	119.6(2)	C(23)—C(24)—C(25)	119.5(3)
C(1)—N(1)—C(10)	123.3(2)	C(24)—C(25)—C(26)	120.3(3)
N(1)—C(10)—C(11)	122.6(3)	C(25)—C(26)—C(27)	120.5(3)
N(1)—C(10)—C(15)	118.4(3)	C(22)—C(27)—C(26)	119.8(3)
C(11)—C(10)—C(15)	118.6(3)		

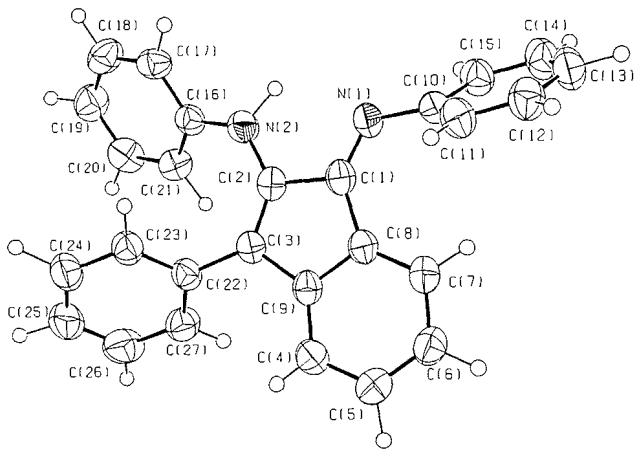

FIG. 1. ORTEP perspective drawing of **3***a*.

0.105. The positions of the hydrogen atoms were located by using difference Fourier maps. Finally, full matrix least-squares refinement of anisotropic temperature factors for the non-hydrogen atoms and isotropic refinement for the hydrogen atoms converged to an R index of 0.055, $R = \Sigma||F_o| - |F_c||/\Sigma|F_o|$. The R_w was 0.046, $R_w = (\Sigma w\Delta^2/\Sigma wF_o^2)^{1/2}$. The number of parameters refined was 342. The largest and average shift/error ratios were 0.034 and 0.0023, respectively, in the final cycle. The largest residual peaks on a ΔF map were 0.247 e Å^{-3}. The value of the Goodness of Fit was 1.574. An ORTEP (12) representation of the molecule is shown in Fig. 1 and all final atomic coordinates are given in Table 1. Crystallographic computations were carried out using the XTAL system (11) on a VAX 8600 computer at the University of Saskatchewan.[1]

[1]Tables of observed and calculated structure factors, atomic parameters of H-atoms, and anisotropic thermal parameters are included as supplementary material and may be purchased from the Depository of Unpublished Data, CISTI, National Research Council of Canada, Ottawa, Ont., Canada K1A 0S2.

Acknowledgements

We are grateful to Mr. K. Marat and Mr. W. Buchannon for the preparation of spectra, and to the Natural Sciences and Engineering Research Council of Canada and the Medical Research Council of Canada for financial support.

1. A. CHINONE, K. INOUYE, and M. OHTA. Bull. Chem. Soc. Jpn. **45**, 213 (1972).
2. H.-O. KALINOWSKI and H. KESSLER. Angew. Chem. Int. Ed. Engl. **13**, 90 (1974).
3. I. W. J. STILL, N. PLAVAC, D. M. McKINNON, and M. S. CHAUHAN. Can. J. Chem. **54**, 280 (1976).
4. D. M. McKINNON and P. D. CLARK. Can. J. Chem. **60**, 243 (1982).
5. D. LEAVER, G. SMOLICZ, and W. H. STAFFORD. J. Chem. Soc. 740 (1962).
6. F. G. BORDWELL, T. W. CUTSHALL, and T. S. RINDESPACHER. J. Org. Chem. **33**, 3308 (1968).
7. N. K. DASGUPTA and F. W. BIRSS. Tetrahedron, **36**, 2711 (1980).
8. A. SCHONBERG and E. FRESE. Chem. Ber. **103**, 3885 (1970).
9. E. KLINGSBERG. J. Am. Chem. Soc. **83**, 2934 (1961).
10. D. LEAVER, D. M. McKINNON, and W. A. H. ROBERTSON. J. Chem. Soc. 32 (1965).
11. J. M. STEWART and S. R. HALL. The XTAL system of crystallographic programs. The University of Maryland Computer Science Center, College Park, MD 20742. 1983.
12. C. K. JOHNSON. ORTEP-II: A Fortran thermal-ellipsoid plot program for crystal structure illustrations. Oak Ridge National Laboratory, Oak Ridge, TN, U.S.A. 1976.

Can. J. Chem. Downloaded from www.nrcresearchpress.com by 213.222.148.141 on 09/07/12
For personal use only.

Controlled formation of dipyranoside derivatives through C6 and O4.[1] Pyranosidic homologation. VII[2,3]

BRUCE FRANCIS MOLINO[4] AND BERT FRASER-REID[5]

Department of Chemistry, University of Maryland, College Park, MD 20742, U.S.A.
and Department of Chemistry, Paul M. Gross Chemical Laboratory, Duke University, Durham, NC 27706, U.S.A.

Received March 18, 1987

BRUCE FRANCIS MOLINO and BERT FRASER-REID. Can. J. Chem. **65**, 2834 (1987).

A procedure has been developed for pyranosidic homologation of methyl α-D-glucopyranoside via C4 and C6. Reaction of the aldehydo group of compound **2** with the Wittig–Bestmann reagent, $Ph_3P{=}CHCH(OEt)_2$, gave an *E*/*Z* mixture of acetals, **4**, which cyclizes under the specific catalysis of pyridinium *p*-toluenesulfonate and in the presence of alcohols to give anomerically pure olefinic bipyranosides, **6***a–d*. A general procedure for epoxidation of the latter involves osmium tetroxide hydroxylation, followed by reaction with phosgene iminium chloride (Viehe's salt) to give chlorocarbamates **12** and **13**, which are then subjected to the action of sodium methoxide. This allows for the formation of a single series of diastereomeric epoxides, **7**, and controlled cleavage of the latter with nucleophiles then follows well-established precedents. Selective access to the "ends" of the bipyranosides **7***c* and *d* can be obtained by oxidative removal of the activated benzyl glycosides with DDQ.

BRUCE FRANCIS MOLINO et BERT FRASER-REID. Can. J. Chem. **65**, 2834 (1987).

On a développé un méthode pour effectuer l'homologation de l'α-D-glucopyrannoside de méthyle via C4 et C6. La réaction du groupement aldéhydique du composé **2** avec le réactif de Wittig–Bestmann, $Ph_3P{=}CHCH(OEt)_2$, conduit à un mélange *E*/*Z* des acétals **4** qui, en utilisant des conditions de catalyse spécifique du *p*-toluènesulfonate de pyridinium et en présence d'alcools, se cyclise pour donner les bipyrannosides oléfiniques anomériquement purs **6***a–d*. Une méthode générale pour effectuer l'époxydation de ces derniers composés implique une hydroxylation par le tétroxyde d'osmium, suivie par une réaction avec le chlorure d'iminium phosgène (sel de Viehe), qui conduit aux chlorocarbamates **12** et **13** qui sont alors soumis à l'action du méthylate de sodium. Cette procédure permet de former une seule série d'époxydes diastéréomères (**7**); un clivage sélectif de ces derniers à l'aide de nucléophiles se produit en suivant les précédents bien établis. On peut accéder d'une façon sélective aux «bouts» des bipyrannosides **7***c* et **7***d* en procédant à un enlèvement oxydatif des glycosides de benzyle activés par du DDQ.

[Traduit par la revue]

In an effort to extend the range of simple sugar derivatives to accommodate increased numbers of contiguous chiral centers, we have developed a process termed pyranosidic homologation in which a "satellite" pyranose ring is appended to a "primary" ring (1). The assembly obtained thereby provides additional stereogenic centers, which can be manipulated according to well-precedented transformations from the carbohydrate literature. This principle is illustrated in Chart 1 for the bipyranose **I**, whose substituents, X and Y, can be introduced into **II** by taking advantage of the highly developed chemistry of unsaturated sugars (2, 3). The efficient formation of bipyranose **II** from a monopyranose precursor, **III**, is an obvious first step. In this manuscript, we give details of our studies related to the transformations **III** → **II** → **I**.[6]

Methyl 2,3-di-*O*-benzyl-α-D-glucopyranoside **1***a* (5) was a convenient starting material for model studies. By routine protecting group strategies, the primary alcohol in **1***d* was exposed in 87% overall yield from **1***a*. Oxidation to aldehyde **2** proceeded cleanly both with Collin's reagent (6) and pyridinium chlorochromate (7) in yields of approximately 60%. However, Swern oxidation using trifluoracetic anhydride, dimethylsulfoxide, and triethylamine (8) proved to be more adaptable to large-scale preparation, with the aldehyde **2** being isolated in yields of 72%.

The formation of **II** required a *Z* olefinic precursor. 2,2-Diethoxyethylidenetriphenylphosphorane, **3**, had been shown by Bestmann *et al.* (9) to react with aldehydes to give *Z*-α,β-unsaturated diethoxy acetals with typically 10:1 *Z*/*E* ratios. Indeed, reaction of phosphorane **3** with aldehyde **2** proceeded smoothly to give an unsaturated acetal, **4**, in excellent yields; however, the *Z*/*E* ratio could not be determined because the mixture was inseparable chromatographically, and the olefinic region in the ^1H nmr spectrum was too complex for assignment. However, subsequent transformations were to show that the olefinic geometry was of no importance to our future plans. Thus, when the crude unsaturated acetal **4** (undoubtedly a *Z*/*E* mixture) was treated with methanol and pyridinium *p*-toluenesulfonate (PPTS) (10) under reflux, cyclization occurred to give a single product whose structure, as the bicyclic olefin **6***a*, was suggested by the value $J_{6,7}$ = 10.1 Hz. Similarly, use of benzyl alcohol, as well as its 4-methoxy and 3,4-dimethoxy derivatives, in refluxing benzene gave the corresponding products, **6***b*, **6***c*, and **6***d*, respectively.

In the transformations of **4** into **6**, four acid-catalyzed processes were occurring *in situ*, which may be rationalized as shown in Chart 2. Probable steps are (*a*) cleavage of the α-ethoxyethyl group from O4; (*b*) cleavage of the allylic diethylacetal to give a stabilized carbocation, e.g., **IV** (*E*/*Z*); (*c*) cyclization with the C4-OH to give the ethyl enoside, **V**; (*d*) glycosidic exchange at the activated anomeric center with the alcohol ROH to give **6**. Formation of the axial glycoside was expected to be favored in view of the anomeric effect (11). However, the reactions here were more selective than with simple alkyl hex-2-enopyranosides (2), where anomeric mixtures are usually much richer. Thus, in the present case, regardless of the alcohol used, only the axial product was detected.

[1]Taken in part from Ph.D. thesis of B.F.M., University of Maryland, 1984.

[2]For Part III, see ref. 1*a*.

[3]For a preliminary account of this work, see ref. 1*b*.

[4]Present address: Rorer Central Research, 900 Business Center Drive, Bldg. 3, Horsham, PA 19044.

[5]Author to whom correspondence should be addressed at Duke University.

[6]For some recent studies from other laboratories, see ref. 4.

Can. J. Chem. Downloaded from www.nrcresearchpress.com by 213.222.148.141 on 09/07/12
For personal use only.

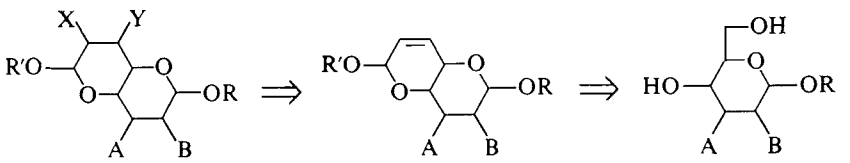

I II III

CHART 1

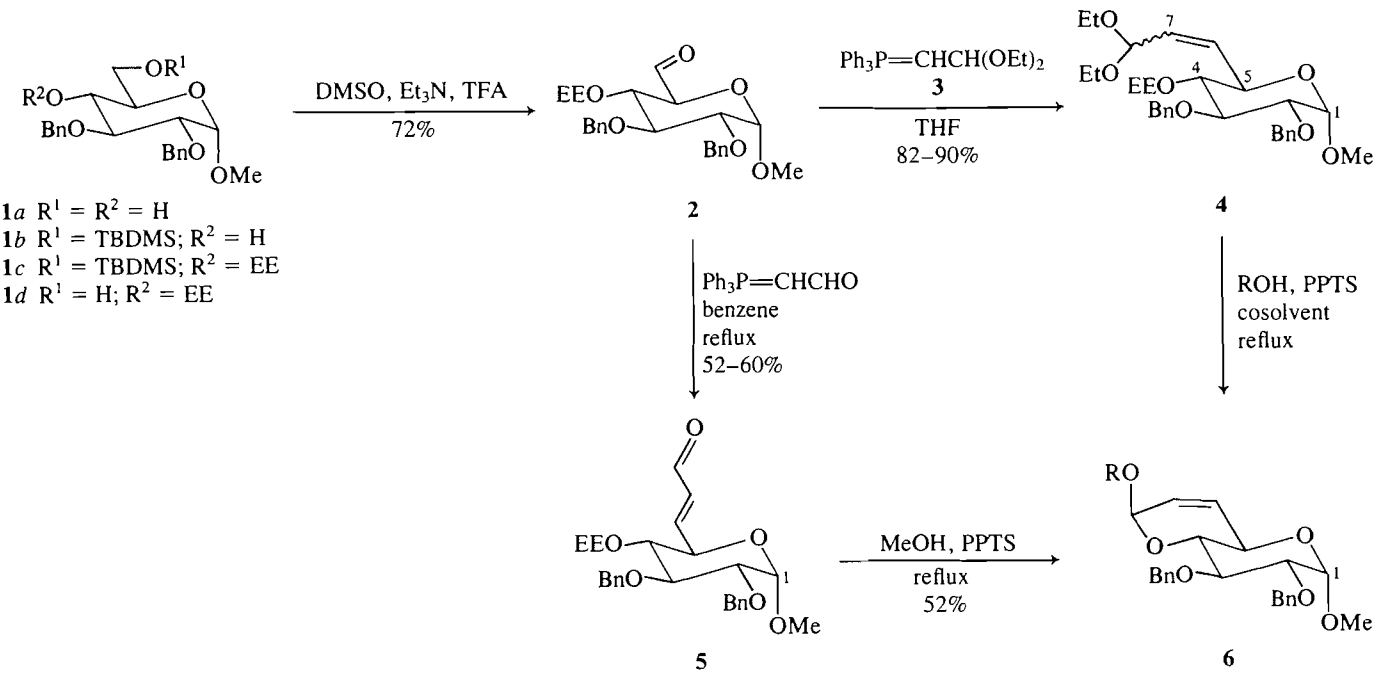

1*a* $R^1 = R^2 = H$
1*b* R^1 = TBDMS; $R^2 = H$
1*c* R^1 = TBDMS; R^2 = EE
1*d* $R^1 = H$; R^2 = EE

2 **4** **5** **6**

ROH	Cosolvent	**6** Yield (%)
MeOH	—	*a* 74
benzyl alcohol	benzene	*b* 60–70
4-methoxybenzyl alcohol	benzene	*c* 73
3,4-dimethoxybenzyl alcohol	benzene	*d* 71

SCHEME 1

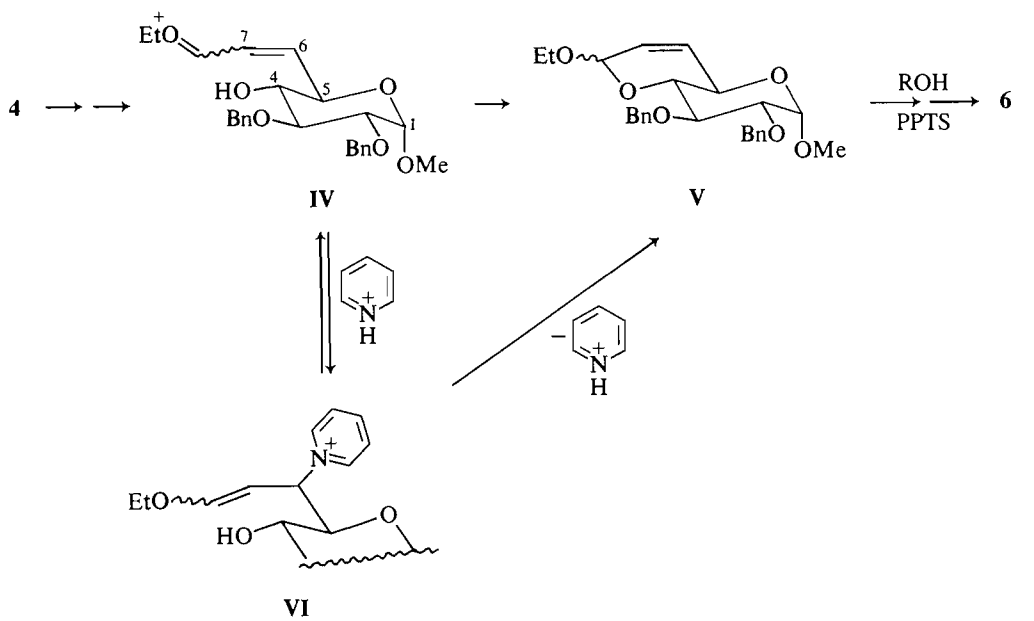

IV V VI

CHART 2

Can. J. Chem. Downloaded from www.nrcresearchpress.com by 213.222.148.141 on 09/07/12
For personal use only.

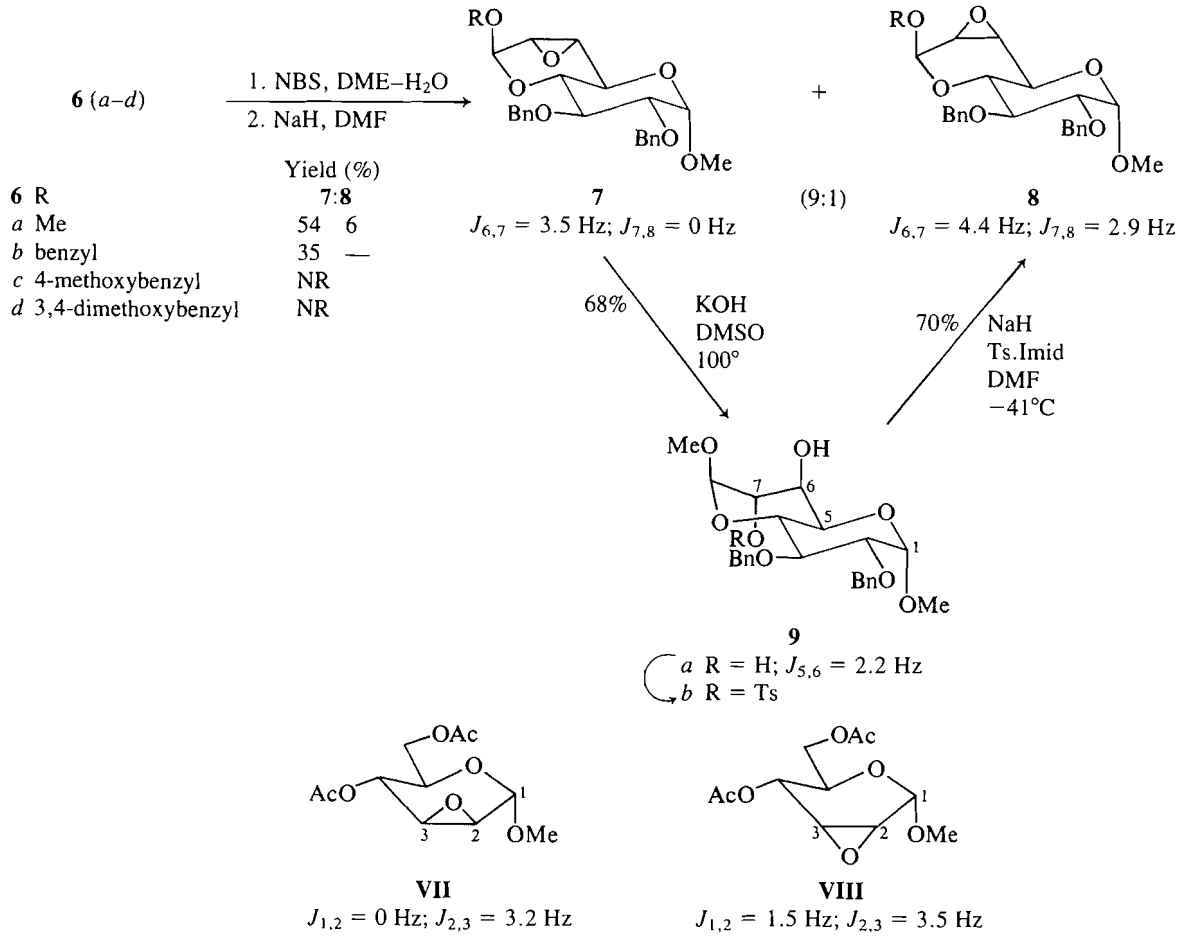

SCHEME 2

A second gratifying observation was that there was no trace of any *trans*-unsaturated acetal (i.e., **4***E*), or the aldehyde obtained therefrom (i.e., **5**) at the end of the reaction. *This implied that both* Z *and* E *forms of* **4** *had cyclized.* A control experiment was therefore carried out to determine the fate of the *E*-α,β-unsaturated aldehyde, **5**. The desired material was prepared by reaction of formylmethylene triphenylphosphorane (12) with aldehyde **2**. Acid-catalyzed methanolysis of the product, **5** ($J_{6,7}$ = 16.0 Hz), did give **6** in 52% yield.

During attempts to optimize the yields in this series of reactions, it became apparent that the cyclization of **4** or **5** would not proceed with acid catalysts other than pyridinium *p*-toluenesulfonate (10). For example, acetic acid, trifluoroacetic acid, *p*-toluenesulfonic acid, or α-pyridone led either to decomposition or simply removal of the protecting groups. *Thus, with these other acids, even the* Z *isomer did not cyclize!!* The specific action of pyridinium *p*-toluenesulfonate implies that the reagent is functioning as something other than a simple acid. This effect can be rationalized by postulating the intermediacy of the salt, **VI** (Chart 2), formed by conjugate addition of pyridine to **IV** *E*/*Z*. Cyclization of **VI** would then occur, regardless of the *Z* or *E* configuration of the precursor, with subsequent or concomitant β-elimination of pyridine to give **V**.

Epoxidation of the bicyclic olefin **6***a* was effected by treating the mixture of bromohydrins obtained from reaction with *N*-bromosuccinimide with sodium hydride. A 9:1 mixture of **7** and **8** was thereby obtained in 60% overall yield from olefin **6***a*.

The stereochemical assignments for the epoxides **7** and **8** were made on the basis of favorable comparisons of the coupling constants with those of related epoxides, **VII** and **VIII** (13), as shown in Scheme 2. Nevertheless, the stereochemistry was confirmed by interconversion of the epoxides. Thus, solvolysis of **7** with potassium hydroxide gave the expected *trans* diol **9***a* ($J_{5,6}$ = 2.2 Hz) and, following the precedent of Hicks and Fraser–Reid (14), the material was treated with sodium hydride and tosyl imidazole, whereupon selective sulfonation occurred at O7 to give **9***b*, followed by *in situ* ring closure to give epoxide **8** in 70% overall yield. The configurations of epoxides **7** and **8** were thereby confirmed.

While the bromohydrin route for epoxidation of the methyl glycoside **6***a* was satisfactory, it transpired that this would not be a general method for the benzylated analogues **6***b*–*d*. Thus, under these conditions, the yield of the epoxide **7***b* from the benzyl glycoside **6***b* was only 35%, and the methoxybenzyl analogue, **6***c*, did not form a bromohydrin at all. This meant that benzyl glycosides could not be used for the "top" ring if the bromohydrin route was to be relied upon, and would have imposed a serious limitation because differentiation of the two glycosidic centers was clearly a valuable asset of **6** (*b*, *c*, and *d*).

It therefore became necessary to develop an alternative method for epoxidation, and an indirect procedure eventually proved best (15). Hydroxylation of **6***a*–*d* proceeded cleanly under standard conditions to give, in each case, a single product, **10***a*–*d* ($J_{5,6} \cong 9.7$ Hz), in keeping with precedent (16).

In keeping with the work of Copeland and Stick (17) on methyl 4,6-*O*-benzylidene-α-D-mannopyranoside, the diol **10***a*

Can. J. Chem. Downloaded from www.nrcresearchpress.com by 213.222.148.141 on 09/07/12
For personal use only.

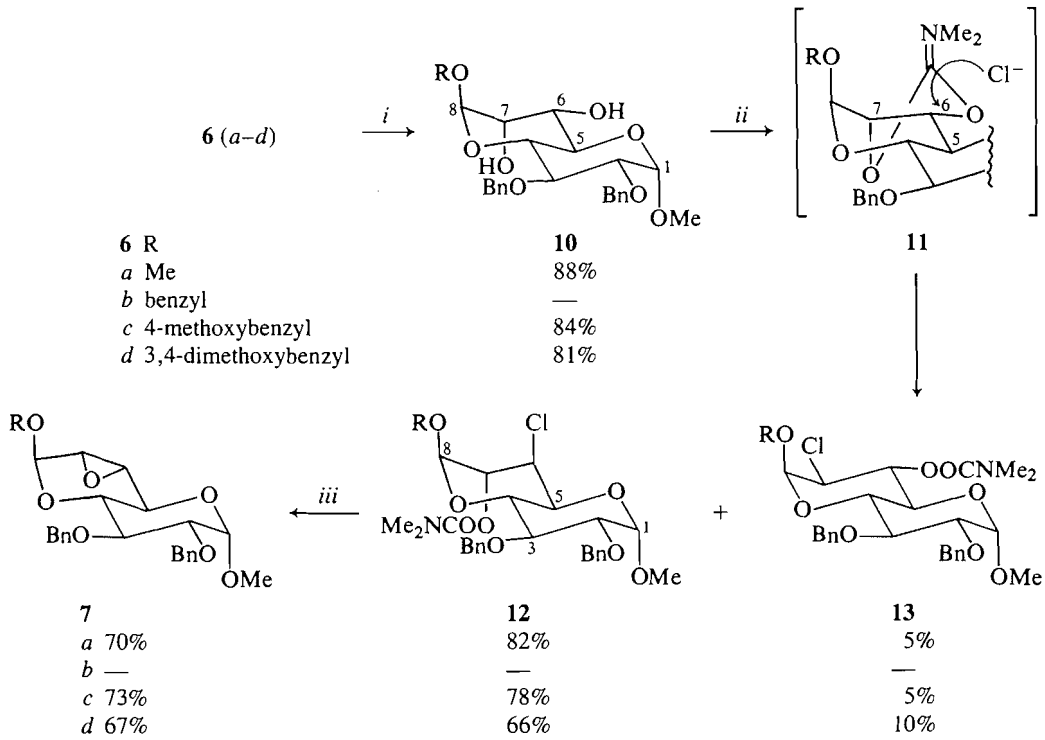

6 R	10	11	7	12	13
a Me	88%		70%	82%	5%
b benzyl	—		—	—	—
c 4-methoxybenzyl	84%		73%	78%	5%
d 3,4-dimethoxybenzyl	81%		67%	66%	10%

Reagents: *i*. OsO_4 (1–5 mol%), *N*-methylmorpholine-*N*-oxide (NMMO), acetone–H_2O; *ii*. $Cl_2C{=}NMe_2Cl$, Et_3N, $ClCH_2CH_2Cl$, reflux; *iii*. MeONa, MeOH, reflux.

SCHEME 3

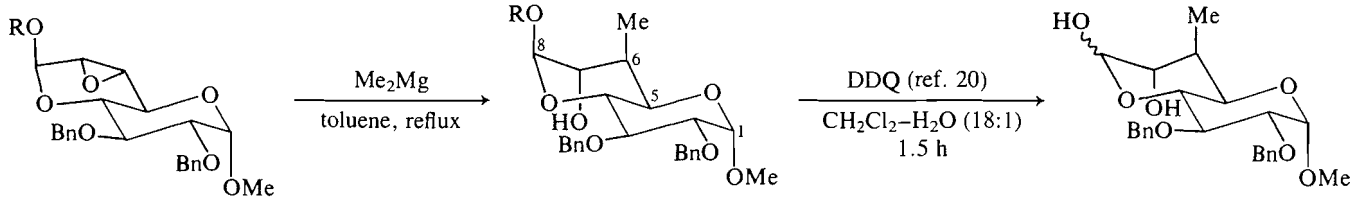

7 R	14	$J_{5,6}$	15
a Me	86%	5.3 Hz	
b benzyl	82%	5.3 Hz	
c 4-methoxybenzyl	89%	5.3 Hz	
d 3,4-dimethoxybenzyl	83%	5.3 Hz	

SCHEME 4

was treated with Viehe's salt (phosgene iminium chloride) (18) and triethylamine in refluxing 1,2-dichloroethane. Two isomers were formed in ~16:1 ratio, a result that is in keeping with the proposed cyclic iminium carbonate intermediate **11**, which would be expected to undergo nucleophilic attack at C6 and (less preferably) at C7, leading to **12** and **13**, respectively. Thus, when the mixture of chlorocarbamates **12***a* and **13***a* was treated with sodium methoxide in methanol under reflux, the epoxide **7***a* was obtained in good yield, along with small amounts of the unreacted chlorocarbamate **13***a*. Similarly, the benzyl glycosides **6***c* and *d* were converted into epoxides **7***c* and *d* via the relevant intermediates **10**, **12**, and **13**.

Although the method in Scheme 3 for making the epoxide **7** required one more step than going through the bromohydrin intermediates (Scheme 2), it had the advantage that none of the diastereomeric epoxide **8** was formed. Furthermore, the reaction worked well on all scales attempted (0.1–1.5 mmol) without any diminution of yield.

With respect to cleavage of the epoxides, Parker and Babine (19) had shown that dimethylmagnesium was a preferred reagent for opening 2,3-epoxides having the α-D-*manno* configuration. Accordingly, exposure of the bicyclic epoxide **7** to a large excess of this reagent gave **14** as the only product in excellent yields. The stereochemistry of the products was apparent from the values $J_{5,6}$ = 5.3 Hz, in all cases.

It was desirable to see whether the two "ends" of the bipyranosides **14** could be differentiated. Acid-catalyzed hydrolysis did not seem to be a promising procedure. However, the studies of Oikawa *et al.* (20) on selective oxidations of activated benzyl ethers proved to be timely. Thus, oxidation of the 4-methoxybenzyl glycosides **14***c* with 2,3-dichloro-5,6-dicyanobenzoquinone (DDQ) gave the anomeric mixture **15** in 41% yield. We found that this low yield was due to some loss of the benzyl groups at C2 and C3. Hence the more readily oxidizable 3,4-dimethoxybenzyl group was examined, since it is known to be more readily cleaved by DDQ (20). This indeed proved

Can. J. Chem. Downloaded from www.nrcresearchpress.com by 213.222.148.141 on 09/07/12
For personal use only.

Can. J. Chem. Downloaded from www.nrcresearchpress.com by 213.222.148.141 on 09/07/12
For personal use only.

to be the case, with compound **14***d* affording the product **15** in 70% yield.

In summary, an efficient synthetic route has been developed for the preparation of bipyranose derivatives via pyranosidic homologation of methyl α-D-glucopyranoside. The net result is the extension of the carbon chain at C6 with stereoselective formation of two new chiral centers on a rigid bicyclic framework. Application of Viehe's salt to the formation of an epoxide from a *cis* diol (Scheme 3) is a valuable development, and selective access to the anomeric center of the top ring (**14***d*→ **15**) enhances the value of these intermediates for further transformations.

Experimental

General procedures

Melting points were determined in capillary tubes using a Buchi Model 510 melting point apparatus, and are uncorrected. Elemental analyses were performed by Dr. F. Kasler, University of Maryland, or by M-H-W Laboratories, PO Box 15149, Phoenix, AZ. The ir spectra were recorded on a Perkin–Elmer model 298 spectrometer using sodium chloride plates for thin films of liquids, syrups, or solids in Nujol mulls. Optical rotations were determined at the sodium D line using a Perkin–Elmer 241 polarimeter. The ^{1}H nmr spectra were determined on the following spectrometers: Varian XL-100, Varian XL 200, or Brucker WM-250. Unless otherwise stated, the solvent used was $CDCl_3$ with internal tetramethylsilane or $CHCl_3$ as the standard. The coupling constants were verified by homonuclear decoupling experiments. For the purpose of ^{1}H nmr interpretation, compound structures have been numbered in the schemes. High resolution mass spectra (hrms) were performed at the Research Triangle Park, North Carolina, with a VG707OF instrument. The progress of all reactions was monitored by thin-layer chromatography (tlc), which was performed on aluminum plates precoated with silica gel HF-254 (0.2-mm layers) containing a fluorescent indicator (Merck, 5539). The following solvent systems were used: EtOAc – petroleum ether mixtures, A = 1:9; B = 1:4; C = 3:7; D = 1:1; E = 7:3; F = 2% MeOH in CH_2Cl_2. Detection was first by uv (254 nm), then charring with sulfuric acid spray, or charring with a solution of ammonium molybdate(VI) tetrahydrate (12.5 g) and cerium(IV) sulfate tetrahydrate (5.0 g) in 10% aqueous sulfuric acid (500 mL). Flash chromatography was performed using Kieselgel 60 (230–400 mesh, E. Merck).

Selective silylation of primary alcohols

tert-Butyldimethylsilyl or *tert*-butyldiphenylsilyl chloride (1.5 mmol per mmol of alcohol) was added to a solution of triethylamine (1.7 mmol per mmol of alcohol), 4-dimethylaminopyridine (0.05 mmol per mmol of alcohol), and the alcohol in dry methylene chloride (10 mL per mmol of alcohol). The reaction was usually complete after 16 h at room temperature, at which time the solution was diluted with methylene chloride and washed successively with saturated solutions of sodium bicarbonate and sodium chloride. The organic phase was dried over anhydrous sodium sulfate, filtered, and evaporated *in vacuo*. The crude residue was purified by flash chromatography.

Swern oxidation

A solution of dimethylsulfoxide (2.0 equiv.) in dry methylene chloride (4 mL/mmol) was added dropwise to a cooled (−78°C) solution of oxalyl chloride in dry methylene chloride (4 mL/mmol) under an argon atmosphere. The solution was stirred for 15 min at −78°C and then a solution of the alcohol in methylene chloride (5 mL/mmol) was added dropwise. The reaction was stirred for 20–30 min and dry triethylamine (5 equiv.) was added dropwise. The reaction mixture was warmed to room temperature and quenched with an aqueous saturated sodium bicarbonate solution (10 mL). The methylene chloride layer was separated and the aqueous layer extracted with methylene chloride (3 × 10 mL). The combined methylene chloride layers were dried over anhydrous sodium sulfate and then concentrated *in vacuo*. The residue was purified by flash silica gel chromatography.

*Methyl 2,3-di-*O*-benzyl-4-*O*-(1-ethoxyethyl)-α-D-glucopyranose (**1***d*)*

A solution of methyl 2,3-di-*O*-benzyl-α-D-glucopyranoside (4) (**1***a*, 3.00 g, 8.01 mmol) in dry methylene chloride (30 mL) was selectively silylated by the general procedure. The resulting product, **1***b* (2.50 g, 5.10 mmol, R_f = 0.52 (D)), was dissolved in dry methylene chloride (25 mL) and treated at room temperature with pyridinium *p*-toluenesulfonate (0.0935 g, 0.765 mmol) and ethyl vinyl ether (5 mL). After 16 h, two products were observed by tlc and the reaction mixture was diluted with methylene chloride (50 mL), and washed with saturated sodium bicarbonate and sodium chloride solutions. The organic layer was separated, dried (Na_2SO_4), filtered, and concentrated *in vacuo* to give methyl 6-*O*-*tert*-butyldimethylsilyl-2,3-di-*O*-benzyl-4-*O*-(α-ethoxyethyl)-α-D-glucopyranoside (**1***c*) as a diastereomeric mixture (2.87 g, 94%); R_f = 0.44 and 0.38 (B). The crude oil **1***c* (2.70 g, 4.82 mmol) was dissolved in tetrahydrofuran (40 mL) and treated with tetra-*n*-butylammonium fluoride (5.3 mL of a 1 M tetrahydrofuran solution) at room temperature. After 3 h, the brown reaction mixture was concentrated *in vacuo* and the oily residue was purified by flash chromatography (D) to give a pale yellow oil **1***d* (2.04 g, 95%); tlc R_f = 0.50 and 0.43 (D); ^{1}H nmr (60 MHz, $CDCl_3$) δ: 1.00–1.52 (m, 6), 2.12 (br s, 1, OH, D_2Oex), 3.53 (s, 3, OCH_3), 3.53–4.22 (m, 8), 4.62–5.23 (m, 6), 7.50 (s, 10, $PhCH_2$). *Anal.* calcd. for $C_{25}H_{34}O_7$: C 67.24, H 7.67; found: C 67.50, H 7.68.

*Methyl 2,3-di-*O*-benzyl-4-*O*-(1-ethoxyethyl)-α-D-*gluco*-hexodialdo-1,5-pyranoside (**2**)*

Oxidation of **1***d* (1.76 g, 3.95 mmol) under Swern conditions (see General) gave a yellow oil, which was subjected to flash chromatography (C followed by D) to give the aldehyde **2** as a pale yellow oil (1.29 g, 74%); R_f = 0.55 (20:1 methylene chloride – methanol); ir (neat): 2930, 1742, 1050 cm^{-1}; ^{1}H nmr (60 MHz, $CDCl_3$) δ: 0.90–1.50 (m, 6), 3.37 (s, 3, OCH_3), 3.40–4.30 (m, 6), 4.50–5.11 (m, 6), 7.35 (s, 10, $PhCH_2$), 9.80 (d, 1, $J_{5,6}$ = 4.0 Hz, CHO); hrms *m*/*e* (M^+) calcd.: 444.2148; found: 444.2145.

*Methyl (E,Z)-2,3-di-*O*-benzyl-6,7-dideoxy-4-*O*-(1-ethoxyethyl)-α-D-*gluco*-octodiald-6-eno-1,5-pyranoside diethyl acetal (**4**)*

Formylmethylene triphenylphosphorane (12) (1.55 g, 4.73 mmol) was refluxed with freshly distilled bromoethane (80 mL) under an argon atmosphere overnight. Dry tetrahydrofuran (80 mL) was added and, after refluxing for another 3 h, the excess bromoethane was removed by standard fractional distillation. The resulting solution was cooled to room temperature and the oily product was treated with sodium ethoxide (3 equiv.) prepared fresh from the reaction of oil-free sodium hydride and ethanol. The mixture was stirred for 0.5 h under an argon atmosphere, during which time the oily residue and sodium ethoxide dissolved, resulting in an orange-red solution of **3**. The aldehyde **2** (0.700 g, 1.58 mmol) was added in tetrahydrofuran solution (5 mL) at room temperature. After 0.5 h, the reaction mixture was quenched with saturated ammonium chloride solution and extracted with ether. The combined organic layers were dried (K_2CO_3), filtered, and concentrated *in vacuo*. Purification of the residue by flash chromatography (C) gave **4** as a yellow oil (0.799 g, 82%); R_f = 0.58 (C); ^{1}H nmr (200 MHz, $CDCl_3$) δ: 0.90–1.30 (m, 12), 3.35–3.95 (m, 10), 4.42–5.20 (m, 9), 5.25–5.80 (m, 3), 7.38 (s, 10); hrms *m*/*e* ($M^+ - CH_3CH_2OH$) calcd.: 498.2617; found: 498.2620.

*Methyl (E)-2,3-di-*O*-benzyl-6,7-dideoxy-4-*O*-(1-ethoxyethyl)-α-D-*gluco*-octodiald-6-eno-1,5-pyranoside (**5**)*

Aldehyde **2** (380 mg, 0.856 mmol) was refluxed with formylmethylene triphenylphosphorane (Ph_3P=CHCHO) (840 mg, 2.57 mmol) in dry benzene for 2 h. The reaction mixture was concentrated *in vacuo* and the residue was purified by flash column chromatography to give **5** (298 mg, 74%) as a pale yellow oil; R_f = 0.33 and 0.40 (1:2 ethyl acetate – hexane); ir (neat): 2940, 1692, 1452, 1372, 1100, 1045, 738, 690 cm^{-1}; ^{1}H nmr (250 MHz, $CDCl_3$) δ: 1.01–1.32 (m, 6), 3.37 and 3.38 (two s, 3, OCH_3), 3.32–3.82 (m, 3), 3.97 (t, 1, $J_{2,3}$ = $J_{3,4}$ = 9.0 Hz, H3), 4.28–4.41 (m, 1, H5), 4.58–5.07 (m, 6),

Can. J. Chem. Downloaded from www.nrcresearchpress.com by 213.222.148.141 on 09/07/12
For personal use only.

6.28–6.44 (m, 1, H6), 6.96 (br dd, 1, $J_{6,7}$ = 16 Hz, $J_{7,8}$ = 4.2 Hz, H7), 7.28–7.45 (m, 10, *Ph*CH_2), 9.61 (dd, 1, $J_{6,8}$ = 1 Hz, H8); hrms *m/e* (M^+) calcd.: 470.2304; found: 470.2301.

*Dimethyl (8*R*)-2,3-di-*O*-benzyl-6,7-dideoxy-α-*D*-*gluco*-octodiald-6-eno-1,5:8,4-dipyranoside (**6**a)*

(*a*) A solution of the unsaturated acetal **4** (1.02 g, 1.87 mmol), pyridinium *p*-toluenesulfonate (0.1 equiv.), and absolute methanol (80 mL/mmol) was refluxed under argon in a round bottom flask fitted with a magnetic stirring bar and a condenser. After 24 h, the reaction mixture was concentrated *in vacuo* and the residue was purified by flash chromatography (C) to give **6***a* as a pale yellow oil (0.508 g, 74%); tlc R_f = 0.55 (1:2 ethyl acetate – hexane); $[\alpha]_D^{24}$ +0.67° (*c* 1.04, $CHCl_3$); ir (neat); 3025, 2900, 1368, 1092, 1043 cm^{-1}; ^1H nmr (200 MHz, $CDCl_3$) δ: 3.38 (s, 3, OCH_3), 3.46 (s, 3, OCH_3), 3.53 (dd, 1, $J_{1,2}$ = 3.3 Hz, $J_{2,3}$ = 9.5 Hz, H2), 3.58 (t, 1, $J_{3,4}$ = $J_{4,5}$ = 9.4 Hz, H4), 3.90 (t, 1, H3), 4.13 (m, 1, H5), 4.58 (d, 1, H1), 4.76 (ABq, 2, *J* = 12 Hz, Δδ = 0.19 ppm, Ph*CH*$_2$), 4.91 (ABq, 2, *J* = 11 Hz, Δδ = 0.09 ppm, Ph*CH*$_2$), 4.91 (m, 1, H8), 5.70 (dt, 1, $J_{6,7}$ = 10.1 Hz, $J_{5,7}$ = $J_{7,8}$ = 2.4 Hz, H7), 5.95 (dt, 1, $J_{5,6}$ = $J_{6,8}$ = 1 Hz, H6), 7.30 (m, 10, *Ph*CH_2). *Anal.* calcd. for $C_{24}H_{28}O_6$: C 69.88, H 6.84; found: C 69.89, H 6.84.

(*b*) The *E*-α,β-unsaturated aldehyde **5** (145 mg, 0.308 mmol) was refluxed with pyridinium *p*-toluenesulfonate (20 mol%) in absolute methanol (10 mL) under argon. After 0.5 h, a more polar product was detected by tlc (R_f = 0.22 (C)) due to loss of the 4-(α-ethoxyethyl) protecting group. Refluxing was continued for 72–96 h, when further monitoring by tlc showed the formation of a less polar product (R_f = 0.55 (C)). The reaction mixture was concentrated *in vacuo* and the residue was purified by flash column chromatography (C) to give a pale yellow oil, **6***a* (66.1 mg, 52%). The physical properties of this material were identical with **6***a* described in part (*a*).

*Methyl-(1) benzyl-(8) (8*R*)-2,3-di-*O*-benzyl-6,7-dideoxy-α-*D*-*gluco*-octodiald-6-eno-1,5:8,4-dipyranoside (**6**b)*

The benzyl glycoside **6***b* was prepared, as described above, for the methyl analogue **6***a*, except that the benzyl alcohol (10 equiv.) in dry benzene (40 mL/mmol) was used. For **6***b* (~65% yield) R_f = 0.43 (C); $[\alpha]_D^{25}$ +4.2° (*c* 0.98, $CHCl_3$); ^1H nmr (200 MHz, $CDCl_3$) δ: 3.40 (s, 3, OCH_3), 3.57 (dd, 1, $J_{1,2}$ = 3.9 Hz, $J_{2,3}$ = 9.1 Hz, H2), 3.72 (t, 1, $J_{3,4}$ = $J_{4,5}$ = 9.4 Hz, H4), 3.96 (t, 1, H3), 4.17 (br d, 1, H5), 4.61 (d, 1, H1), 4.55–5.15 (m, 6, 3 Ph*CH*$_2$), 5.10 (br s, 1, H8), 5.74 (dt, 1, $J_{6,7}$ = 10.2 Hz, $J_{5,7}$ = $J_{7,8}$ = 2.5 Hz, H7), 5.98 (dt, $J_{5,6}$ = $J_{6,8}$ = 1 Hz), 7.35 (m, 15, 3, *Ph*CH_2). *Anal.* calcd. for $C_{30}H_{32}O_6$: C 73.75, H 6.60; found: C 73.79, H 6.72.

*Methyl-(1) 4-methoxybenzyl-(8) (8*R*)-2,3-di-*O*-benzyl-6,7-dideoxy-α-*D*-*gluco*-octodiald-6-eno-1,5:8,4-dipyranoside (**6**c)*

The title compound was prepared in 73% yield, as described in the preceding section, except that 4-methoxybenzyl alcohol was used; R_f = 0.31 (C); $[\alpha]_D^{25}$ +18.8° (*c* 1.35, $CHCl_3$); ^1H nmr (200 MHz, $CDCl_3$) δ: 3.40 (s, 3, OCH_3), 3.57 (dd, 1, $J_{1,2}$ = 3.7 Hz, $J_{2,3}$ = 9.2 Hz, H2), 3.70 (t, 1, $J_{3,4}$ = $J_{4,5}$ = 9.4 Hz, H4), 3.80 (s, 3, *p*-CH_3O*Ph*CH_2), 3.95 (t, 1, H3), 4.17 (br d, 1, H5), 4.61 (d, 1, H1), 4.64 (ABq, 2, *J* = 11.2 Hz, Δδ = 0.23 ppm, *p*-CH_3O*Ph*CH_2), 4.76 (ABq, 2, *J* = 11.0 Hz, Δδ = 0.18 ppm, Ph*CH*$_2$), 4.96 (ABq, 2, *J* = 11.3 Hz, Δδ = 0.09 ppm, Ph*CH*$_2$), 5.08 (br s, 1, H8), 5.71 (dt, 1, $J_{5,7}$ = $J_{7,8}$ = 2.5 Hz, $J_{6,7}$ = 10.3 Hz, H7), 5.97 (dt, 1, $J_{5,6}$ = $J_{6,8}$ = 1 Hz, H6), 6.8 (d of ABq, 2, *p*-CH_3O*Ph*CH_2), 7.20–7.52 (m, 12, *Ph*CH_2, *p*-CH_3O*Ph*CH_2). *Anal.* calcd. for $C_{31}H_{34}O_7$: C 71.80, H 6.61; found: C 71.75, H 6.73.

*Methyl-(1) 3,4-dimethoxybenzyl-(8) (8*R*)-2,3-di-*O*-benzyl-6,7-dideoxy-α-*D*-*gluco*-octodiald-6-eno-1,5:8,4-dipyranoside (**6**d)*

The title compound was prepared in 71% yield, as described in the preceding section, except that 3,4-dimethoxybenzyl alcohol was used; R_f = 0.20 (C); $[\alpha]_D^{19}$ +11.5° (*c* 1.08, $CHCl_3$); ^1H nmr (250 MHz, $CDCl_3$) δ: 3.39 (s, 3, CH_3), 3.53 (dd, 1, $J_{1,2}$ = 3.6 Hz, $J_{2,3}$ = 9.4 Hz, H2), 3.70 (t, 1, $J_{3,4}$ = $J_{4,5}$ = 9.5 Hz, H4), 3.76 and 3.85 (two s, 6, 3,4-di-CH_3O*Ph*CH_2), 3.94 (t, 1, H3), 4.16 (m, 1, H5), 4.60 (d, 1, H1), 4.63 (ABq, 2, *J* = 11.1 Hz, Δδ = 0.30 ppm, 3,4-di-CH_3O*Ph*CH_2), 4.74 (ABq, 2, *J* = 12.1 Hz, Δδ = 0.17 ppm, Ph*CH*$_2$), 4.94 (ABq, 2 = 11.2 Hz, Δδ = 0.08 ppm, Ph*CH*$_2$), 5.08 (br d, 1, $J_{7,8}$ = 2.9 Hz, H7), 5.71 (dt, 1, $J_{6,7}$ = 10.2 Hz, $J_{5,7}$ = 2.9 Hz, H7), 5.95 (dt, 1, $J_{5,6}$ = $J_{6,8}$ = 1 Hz, H6), 6.82 (m, 3, 3,4-di-CH_3O*Ph*CH_2), 7.24–7.47 (m, 10, 2*Ph*CH_2). *Anal.* calcd. for $C_{32}H_{36}HO_8$: C 70.05, H 6.61; found: C 69.94, H 6.72.

*Dimethyl (8*R*)-6,7-anhydro-2,3-di-*O*-benzyl-β-*L*-erythro-*D*-gluco-octodialdo-1,5:8,4-dipyranoside (**7**a)*

(*a*) A solution of the methyl enoside **6***a* (492 mg, 1.19 mmol) in dimethoxyethane–water (3:1 v/v, 10 mL) was treated with *N*-bromosuccinimide (2 equiv.). The reaction mixture was stirred in the dark at room temperature for 16 h, after which time a mixture of bromohydrins (R_f = 0.21 and 0.25 (C)) was observed. (If the reaction was allowed to continue for too long, decomposition was observed by tlc.) The reaction mixture was diluted with ether (3 volumes) and washed successively with 10% sodium thiosulfate and saturated sodium bicarbonate solutions. The organic layer was separated, dried ($MgSO_4$), filtered, and concentrated *in vacuo*. The resulting crude mixture of bromohydrins was dissolved in dry dimethylformamide (5 mL) and added to a vigorously stirred slurry of sodium hydride (2 equiv., oil-free) in dry dimethylformamide (10 mL) at 0°C under argon. The reaction mixture was warmed slowly to room temperature. After 2 h, methanol (1 mL) was carefully added to quench the excess sodium hydride. The reaction mixture was diluted with water and extracted with ether. The combined ether portions were washed with water and saturated sodium chloride solutions. The organic layer was separated, dried (Na_2SO_4), filtered, and concentrated *in vacuo*. The residue was purified by flash column chromatography (C) to afford **7***a* as a colorless syrup (275 mg, 54%); tlc R_f = 0.55 (C); $[\alpha]_D^{25}$ −1.36° (*c* 1.77, $CHCl_3$); ^1H nmr (600 MHz, $CDCl_3$) δ: 3.23 (br d, 1, $J_{6,7}$ = 3.5 Hz, H6), 3.38 (d, 1, H7), 3.42 (dd, 1, $J_{3,4}$ = 9.5 Hz, $J_{4,5}$ = 10.0 Hz, H4), 3.43 (s, 3, OCH_3), 3.45 (s, 3, OCH_3), 3.48 (dd, 1, $J_{1,2}$ = 3.7 Hz, $J_{2,3}$ = 9.3 Hz, H2), 3.67 (br d, 1, H5), 4.57 (d, 1, H1), 4.73 (ABq, 2, *J* = 11.8 Hz, Δδ = 0.18 ppm, Ph*CH*$_2$), 4.85 (ABq, 2, *J* = 10.8 Hz, Δδ = 0.06 ppm, Ph*CH*$_2$), 4.90 (s, 1, H8), 7.34 (m, 10, *Ph*CH_2). *Anal.* calcd. for $C_{24}H_{28}O_7$: C 67.27, H 6.59; found: C 66.94, H 6.59.

(*b*) A solution of the chlorocarbamate mixture **12***a* and **13***a* (40 mg, 0.075 mmol) in absolute methanol was added to a freshly prepared solution of sodium methoxide (5 equiv.) in absolute methanol (5 mL). The reaction mixture was refluxed for 6–8 h and monitored by tlc (D). Upon completion, the reaction mixture was concentrated *in vacuo*; the residue was dissolved in methylene chloride and washed with water and saturated sodium chloride solutions. The methylene chloride layer was dried (Na_2SO_4), filtered, and concentrated *in vacuo* and the residue purified by flash chromatography (D) to afford **7***a* as a colorless syrup (23 mg, 70%). The physical properties were identical with **7***a* described above in part (*a*).

Unreacted chlorocarbamate **13***a* was recovered (3.8 mg) as the only other product.

*Methyl-(1) benzyl-(8) (8*R*)-6,7-anhydro-2,3-di-*O*-benzyl-β-*L*-erythro-*D*-gluco-octodialdo-1,5:8,4-dipyranoside (**7**b)*

The epoxide **7***b* was prepared in 58% yield, as described above for **7***a*; tlc R_f = 0.53 (C); ^1H nmr (200 MHz, $CDCl_3$) δ: 3.18 (d, 1, $J_{6,7}$ = 3.6 Hz, H6), 3.38 (d, 1, H7), 3.48 (s, 3, OCH_3), 3.50–3.63 (m, 2, H2 + H4), 3.72 (d, 1, $J_{4,5}$ = 10.4 Hz, H5), 3.90 (t, 1, $J_{2,3}$ = $J_{3,4}$ = 10.0 Hz, H3), 4.48–5.00 (m, 5, H1, Ph*CH*$_2$), 5.09 (s, 1, H8), 7.30–7.45 (m, 10, *Ph*CH_2). *Anal.* calcd. for $C_{30}H_{32}O_7$: C 71.41, H 6.39; found: C 71.30, H 6.30.

*Methyl-(1) 4-methoxybenzyl-(8) (8*R*)-6,7-anhydro-2,3-di-*O*-benzyl-β-*L*-erythro-*D*-gluco-octodialdo-1,5:8,4-dipyranoside (**7**c)*

The epoxide **7***c* was prepared as described above for the conversion **12***a* → **7***a*, using the chlorocarbamate mixture **12***c* and **13***c* (545 mg, 0.849 mmol). Compound **7***c* was obtained as a white solid (329 mg, 73%), mp 60–61°C; tlc R_f = 0.50 (D); $[\alpha]_D^{19}$ −12.3° (*c* 1.67, $CHCl_3$); ^1H nmr δ (250 MHz, $CDCl_3$) δ: 3.13 (d, 1, $J_{6,7}$ = 3.6 Hz, H6), 3.33 (d, 1, H7), 3.43 (s, 3, OCH_3), 3.47–3.57 (m, 2, H2, H4), 3.68 (d, 1, $J_{4,5}$ = 10.2 Hz, H5), 3.81 (s, 3, CH_3OPhCH$_{22}$), 3.86 (t, 1, $J_{2,3}$ =

$J_{3,4}$ = 9.3 Hz, H3), 4.59 (d, 1, $J_{1,2}$ = 3.8 Hz, H1), 4.62 (ABq, 2, J = 11.1 Hz, $\Delta\delta$ = 0.28 ppm, p-CH_3OPhCH_2), 4.74 (ABq, 2, J = 12.0 Hz, $\Delta\delta$ = 0.28 ppm, PhCH_2), 4.91 (ABq, 2, J = 11.5 Hz, $\Delta\delta$ = 0.05 ppm, PhCH_2), 5.06 (s, 1, H8), 7.03 (ABq, 2, J = 8.6 Hz, $\Delta\delta$ = 0.35 ppm, p-CH_3OPhCH_2), 7.25–7.44 (m, 10, $Ph$$CH_2$). *Anal.* calcd. for $C_{32}H_{34}O_8$: C 69.65, H 6.41; found: C 69.41, H 6.70.

*Methyl-(1) 3,4-dimethoxybenzyl-(8) (8*R*)-6,7-anhydro-2,3-di-*O*-benzyl-β-*L*-*erythro*-*D*-gluco-octodialdo-1,5:8,4-dipyranoside (7*d*)*

The epoxide **7***d* was prepared as described above for the conversion **12***a* → **7***a*, using the chlorocarbamate mixture **12***d* and **13***d* (546 mg, 0.812 mmol). Compound **7***d* was obtained as a white solid (305 mg, 67%), mp 86.5–88.5°C; tlc R_f = 0.44 (D); $[\alpha]_D^{19}$ −1.9° (*c* 1.37, $CHCl_3$); ^{1}H nmr (250 MHz, $CDCl_3$) δ: 3.15 (d, 1, $J_{6,7}$ = 3.6 Hz, H6), 3.34 (d, 1, H7), 3.44 (s, 3, OCH_3), 3.46–3.59 (m, 2, H2, H4), 3.69 (d, 1, $J_{4,5}$ = 10.2 Hz, H5), 3.82–3.92 (m, 1, H3), 3.75 and 3.87 (two s, 6, 3,4-di-CH_3OPhCH_2), 4.60 (d, 1, $J_{1,2}$ = 3.8 Hz, H1), 4.63 (ABq, 2, J = 10.9 Hz, $\Delta\delta$ = 0.30 ppm, 3,4-CH_3OPhCH_2), 4.74 (ABq, 2, J = 12.1 Hz, $\Delta\delta$ = 0.17 ppm, PhCH_2), 4.91 (ABq, 2, J = 11.1 Hz, $\Delta\delta$ = 0.06 ppm, PhCH_2), 5.09 (s, 1, H8), 6.82 (m, 3, 3,4-di-CH_3OPhCH_2), 7.20–7.40 (m, 10, $Ph$$CH_2$). *Anal.* calcd. for $C_{32}H_{36}O_9$: C 68.07, H 6.43; found: C 68.21, H 6.24.

Unreacted chlorocarbamate **13***d* was recovered (70 mg) as the only other product.

*Dimethyl (8*R*)-6,7-anhydro-2,3-di-*O*-benzyl-α-*D*-gluco-octodialdo-1,5:8,4-dipyranoside (8)*

(*a*) The chromatography in the preceding experiment also provided the *D-erythro* diastereomer **8** as a colorless syrup (30.7 mg, 6%); tlc R_f = 0.31 (C); $[\alpha]_D^{25}$ −8.7° (*c* 1.59, $CHCl_3$); ^{1}H nmr (600 MHz, $CDCl_3$) δ: 3.39 (dd, 1, $J_{5,6}$ = 1.2 Hz, H6), 3.42 (s, 3, OCH_3), 3.46 (s, 3, OCH_3), 3.47 (dd, 1, $J_{7,8}$ = 2.9 Hz, H7), 3.47 (dd, 1, $J_{1,2}$ = 13.7 Hz, $J_{2,3}$ = 9.5 Hz, H2), 3.74 (t, 1, $J_{3,4}$ = $J_{4,5}$ = 9.5 Hz, H4), 3.84 (t, 1, H3), 3.92 (dd, 1, H5), 4.59 (d, 1, H1), 4.72 (ABq, 2, J = 12.1 Hz, $\Delta\delta$ = 0.18 ppm, PhCH_2), 4.83 (ABq, 2, J = 11.4 Hz, $\Delta\delta$ = 0.05 ppm, PhCH_2), 4.89 (d, 1, H8), 7.23–7.40 (m, 10, $Ph$$CH_2$). *Anal.* calcd. for $C_{24}H_{28}O_7$: C 67.27, H 6.59; found: C 66.95, H 6.68.

(*b*) A vigorously stirred solution of the diol **9***a* (68.3 mg, 0.153 mmol) in dry dimethylformamide (1 mL) was treated with oil-free sodium hydride (3.7 mg, 0.153 mmol) at −41°C under argon. After 0.5 h, tosyl imidazole (51.1 mg, 0.230 mmol) in dimethylformamide (0.5 mL) was slowly added and the resulting solution was stirred for 6 h at −41°C to give the sulfonate **9***b*. An additional equivalent of sodium hydride (3.7 mg) was then added and the reaction mixture was warmed to room temperature. After 2 h, several drops of methanol were added to the reaction mixture, followed by careful addition of water. The aqueous mixture was extracted with ether and the combined ether portions were washed with water, dried (Na_2SO_4), filtered, and concentrated *in vacuo*. The residue was purified by flash column chromatography (D) to give **8** (45.9 mg, 70%), identical to the material in part (*a*).

*Dimethyl (8*R*)-2,3-di-*O*-benzyl-β-*L*-threo-*D*-gluco-octodialdo-1,5:8,4-dipyranoside (9*a*)*

The epoxide **7***a* (120 mg, 0.281 mmol) was stirred with potassium hydroxide (236 mg, 4.2 mmol) in dimethyl sulfoxide and water (5 mL, 9:1 v/v) at 100°C for 20 h. The reaction mixture was cooled to room temperature, diluted with water, and extracted with ether. The combined ether portions were washed with saturated sodium chloride solution (3 × 25 mL), dried (Na_2SO_4), filtered, and concentrated *in vacuo*. The residue was purified by flash column chromatography to give the diol **9***a* (85 mg, 68%) as a colorless syrup; tlc R_f = 0.08 (E); $[\alpha]_D^{25}$ −26.0° (*c* 1.21, $CHCl_3$); ir (neat): 3485, 2940, 1052 cm^{-1}; ^{1}H nmr (600 MHz, $CDCl_3$) δ: 1.22 (br s, 1, OH), 2.98 (br s, 1, OH), 3.39 (s, 3, OCH_3), 3.44 (s, 3, OCH_3), 3.51 (dd, 1, $J_{1,2}$ = 3.7 Hz, $J_{2,3}$ = 9.2 Hz, H2), 3.85 (dd, 1, $J_{3,4}$ = 8.8 Hz, $J_{4,5}$ = 10.3 Hz, H4), 3.88 (dd, 1, $J_{5,6}$ = 2.2 Hz, H5), 3.98 (m, 2H, H6, H7), 4.00 (t, 1, H3), 4.64 (d, 1, H1), 4.72 (br s, 1, H8), 4.74 (ABq, 2, J = 12.5 Hz, $\Delta\delta$ = 0.18 ppm, PhCH_2), 4.89 (ABq, 2, J = 11.03 Hz, $\Delta\delta$ = 0.05 ppm, PhCH_2), 7.25–7.42 (m, 10, $Ph$$CH_2$). *Anal.* calcd. for $C_{24}H_{30}O_8$: C 64.56, H 6.77; found: C 64.18, H 6.82.

*Dimethyl (8*R*)-2,3-di-*O*-benzyl-β-*L*-erythro-*D*-gluco-octodialdo-1,5:8,4-dipyranoside (10*a*)*

N-methyl morpholine-*N*-oxide (1.1 equiv., 60 wt.% in water) and osmium tetroxide (1 mol%, 2.5 wt.% in *tert*-butanol) were added to a solution of the methyl enoside **6***a* (287 mg, 0.696 mmol) in acetone–water (5:1, 15 mL). The reaction mixture was stirred for 48 h at room temperature under argon and, upon completion (tlc, C), was quenched with sodium bisulfite (25 mg), diluted with water, and extracted with ethyl acetate. The combined ethyl acetate portions were dried (Na_2SO_4), filtered, and concentrated *in vacuo*. The residue was purified by filtration through a short silica gel column (E) to afford the diol **10***a* as a white amorphous solid (273 mg, 88%), mp 141–143.5°C; tlc R_f = 0.07 (D); $[\alpha]_D^{19}$ −5.4° (*c* 0.71, $CHCl_3$); ^{1}H nmr (250 MHz, $CDCl_3$) δ: 2.40 (d, 1, J = 1.5 Hz, OH, D_2Oex), 2.45 (d, 1, J = 1.5 Hz, OH, D_2Oex), 3.39 (s, 3, OCH_3), 3.40 (s, 3, OCH_3), 3.47 (dd, 1, $J_{1,2}$ = 3.7 Hz, $J_{2,3}$ = 9.4 Hz, H2), 3.51 (t, 1, $J_{3,4}$ = $J_{4,5}$ = 9.5 Hz, H4), 3.79 (t, 1, $J_{5,6}$ = 9.7 Hz, H5), 3.89 (dt, 1, $J_{OH,6}$ = $J_{6,7}$ = 1.5 Hz, H6), 3.95–4.03 (m, 2, H3, H7), 4.57 (d, 1, H1), 4.75 (ABq, 2, J = 12.2 Hz, $\Delta\delta$ = 0.19 ppm, PhCH_2), 4.88 (ABq, 2, J = 11.0 Hz, $\Delta\delta$ = 0.10 ppm, PhCH_2), 7.20–7.45 (m, 10, $Ph$$CH_2$). *Anal.* calcd. for $C_{24}H_{30}O_8$: C 64.56, H 6.77; found: C 64.52, H 6.80.

*Methyl-(1) 4-methoxybenzyl-(8) (8*R*)-2,3-di-*O*-benzyl-β-*L*-erythro-*D*-gluco-octodialdo-1,5:8,4-dipyranoside (10*c*)*

The diol **10***c*, prepared as described for **10***a* from the benzyl enoside **6***c* (4.33 mg, 0.834 mmol), was obtained as a white crystalline solid (388 mg, 84%), mp 136–137°C (recrystallized from ether); tlc R_f = 0.18 (E); $[\alpha]_D^{19}$ −27.7° (*c* 1.15, $CHCl_3$); ^{1}H nmr (250 MHz, $CDCl_3$) δ: 2.42 (d, 1, J = 4.0 Hz, OH, D_2Oex), 2.45 (d, 1, J = 3.0 Hz, OH, D_2Oex), 3.40 (s, 3, OCH_3), 3.81 (s, 3, CH_3OPh), 3.49 (dd, 1, $J_{1,2}$ = 3.7 Hz, $J_{2,3}$ = 9.3 Hz, H2), 3.62 (t, 1, $J_{3,4}$ = $J_{4,5}$ = 9.5 Hz, H4), 3.76–4.06 (m, 4, H3, H5, H6, H7), 4.55 (ABq, 2, J = 11.5 Hz, $\Delta\delta$ = 0.24 ppm, p-CH_3OPhCH_2), 4.58 (d, 1, H1), 4.76 (ABq, 2, J = 12.1 Hz, $\Delta\delta$ = 0.18 ppm, PhCH_2), 4.92 (br d, 1, $J_{7,8}$ = 1.2 Hz, H8), 4.94 (ABq, 2, J = 11.1 Hz, $\Delta\delta$ = 0.10 ppm, PhCH_2), 7.04 (ABq, 4, J = 8.2 Hz, $\Delta\delta$ = 0.35 ppm, p-CH_3OPhCH_2), 7.25–7.50 (m, 10, $Ph$$CH_2$). *Anal.* calcd. for $C_{31}H_{36}O_9$: C 67.38, H 6.57; found: C 67.26, H 6.49.

*Methyl-(1) 3,4-dimethoxybenzyl-(8) (8*R*)-2,3-di-*O*-benzyl-β-*L*-erythro-*D*-gluco-octodialdo-1,5:8,4-dipyranoside (10*d*)*

The diol **10***d*, prepared as described above for **10***a* from the corresponding benzyl enoside **6***d* (763 mg, 1.39 mmol), was obtained as a white crystalline solid (653 mg, 81%), mp 169–170°C (recrystallized from ether); tlc R_f = 0.02 (D); $[\alpha]_D^{19}$ −30.9° (*c* 1.44, $CHCl_3$); ^{1}H nmr (250 MHz, $CDCl_3$) δ: 2.50 (d, 1, J = 4.0 Hz, OH, D_2Oex), 2.54 (d, 1, J = 2.9 Hz, OH, D_2Oex), 3.40 (s, 3, OCH_3), 3.47 (dd, 1, $J_{1,2}$ = 3.6 Hz, $J_{2,3}$ = 9.3 Hz, H4), 3.76 and 3.87 (two s, 6, 3,4-di-CH_3OPhCH_2), 3.78–4.07 (m, 4, H3, H5, H6, H7), 4.58 (ABq, 2, J = 11.3 Hz, $\Delta\delta$ = 0.23 ppm, 3,4-di-CH_3OPhCH_2), 4.58 (d, 1, H1), 4.75 (ABq, 2, J = 12.1 Hz, $\Delta\delta$ = 0.18 ppm, PhCH_2), 4.95 (ABq, 2, J = 11.3 Hz, $\Delta\delta$ = 0.10 ppm, PhCH_2), 6.80 (m, 3, 3,4-di-CH_3OPhCH_2), 7.24–7.48 (m, 10, $Ph$$CH_2$). *Anal.* calcd. for $C_{32}H_{38}O_{10}$: C 65.97, H 6.57; found: C 65.82, H 6.65.

*Dimethyl (8*R*)-2,3-di-*O*-benzyl-6-chloro-6-deoxy-7-*O*-(N,N-dimethylcarbamoyl)-(8*R*)-β-*L*-threo-*D*-gluco-octodialdo-1,5:8,4-dipyranoside (12*a*) and dimethyl (8*R*)-2,3-di-*O*-benzyl-7-chloro-7-deoxy-6-*O*-(N,N-dimethylcarbamoyl)-α-*D*-threo-*D*-gluco-octodialdo-1,5:8,4-dipyranoside (13*a*)*

A solution of the *cis* diol **10***a* (58 mg, 0.13 mmol) in dry 1,2-dichloroethane (5 mL) and triethylamine (0.5 mL) was treated with phosgene iminium chloride (1.5 equiv.) and refluxed with vigorous stirring for 0.5–1 h under argon. The dark brown reaction mixture was cooled to room temperature, quenched with saturated sodium bicarbonate solution, and extracted with methylene chloride. The combined methylene chloride portions were washed with saturated sodium bicarbonate solution, dried (Na_2SO_4), filtered, and concentrated *in vacuo*. The residue was fractionated by flash column chromatography (D) to give **12***a* (57 mg, 82%) and **13***a* (3.8 mg, 5%). For **12***a*: tlc R_f = 0.25 (D); $[\alpha]_D^{19}$ −11.9° (*c* 0.77, $CHCl_3$); ir (neat):

Can. J. Chem. Downloaded from www.nrcresearchpress.com by 213.222.148.141 on 09/07/12
For personal use only.

Can. J. Chem. Downloaded from www.nrcresearchpress.com by 213.222.148.141 on 09/07/12
For personal use only.

2900, 1709, 1454, 1397, 1184, 1049, 747 cm^{-1}; ^1H nmr (250 MHz, $CDCl_3$) δ: 2.94 (br s, 6, Me_2NCO_2), 3.41 (s, 3, OCH_3), 3.42 (s, 3, OCH_3), 3.55 (dd, 1, $J_{7,8}$ = 3.6 Hz, $J_{2,3}$ = 8.9 Hz, H2), 3.90–4.10 (m, 3, H5, H4, H3), 4.27 (m, 1, H6), 4.69 (br s, 1H, H8), 4.75 (ABq, 2, J = 12.2 Hz, Δδ = 0.18 ppm, PhCH_2), 4.89 (ABq, 2, J = 10.2 Hz, Δδ = 0.06 ppm, PhCH_2), 5.06 (br d, 1, $J_{6,7}$ = 2.0 Hz, H7), 7.20–7.50 (m, 10, $Ph$$CH_2$); hrms m/e (M^+) calcd.: 535.1973; found: 535.1976.

For **13***a*: tlc R_f = 0.29 (D); ir ($CDCl_3$): 2925, 1712, 1455, 1392, 1052, 737 cm^{-1}; ^1H nmr (250 MHz, $CDCl_3$) δ: 2.92 (br s, 6, Me_2NCO_2), 3.34 (s, 3, OCH_3), 3.45 (s, 3, OCH_3), 3.41–3.59 (m, 2), 3.72 (t, 1, J = 10.0 Hz), 3.82–3.92 (m, 2), 4.55 (d, 1, J = 3.7 Hz, H1), 4.61 (d, J = 12.2 Hz, 1, PhCH), 4.80–4.87 (m, 4), 5.30 (t, 1, $J_{6,7}$ = $J_{5,6}$ = 9.8 Hz, H6), 7.26–7.42 (m, 10, $Ph$$CH_2$); hrms m/e (M^+) calcd.: 535.1973; found: 535.1975.

*Methyl-(1) 3,4-dimethoxybenzyl-(8) (8*R*)-2,3-di-*O*-benzyl-6-chloro-6-deoxy-7-*O*-(*N,*N-dimethylcarbamoyl)-β-*L*-threo-*D*-gluco-octodialdo-1,5:8,4-dipyranoside (**12**d) and methyl-(1) 3,4-dimethoxybenzyl-(8) (8*R*)-2,3-di-*O*-benzyl-7-chloro-7-deoxy-6-*O*-(*N,*N-dimethylcarbamoyl)-α-*D*-threo-*D*-gluco-octodialdo-1,5:8,4-dipyranoside (**13**d)*

The chlorocarbamate **12***d*, prepared as described above for **12***a* from the diol **10***d* (630 mg, 1.08 mmol), was obtained as a colorless syrup (480 mg, 66%); tlc R_f = 0.26 (D); $[\alpha]_D^{19}$ −60.2° (*c* 1.02, $CHCl_3$); ir (neat): 2940, 3040, 1711, 1516, 1090, 1042, 730 cm^{-1}; ^1H nmr (250 MHz, $CDCl_3$) δ: 2.91 (br s, 6, Me_2NCO_2), 3.42 (s, 3, OCH_3), 3.56 (dd, 1, $J_{2,3}$ = 9.4 Hz, $J_{1,2}$ = 3.6 Hz, H2), 3.80 and 3.87 (two s, 6, 3,4-di-CH_3OPhCH_2), 3.95–4.19 (m, 3, H5, H4, H3), 4.30 (m, 1, H6), 4.47 (d, 1, J = 11.8 Hz, 3,4-di-CH_3OPhCH_2), 4.63–4.86 (m, 7, H1, H8, 2PhCH_2, 3,4-di-CH_3OPhCH_2), 5.11 (d, 1, $J_{6,7}$ = 2.4 Hz, 1, H7), 6.80–6.9 (m, 3, 3,4-di-CH_3O-Ph-CH_2), 7.21–7.45 (m, 10, PhCH_2); hrms m/e (M^+) calcd.: 671.2497; found: 671.2494.

For **13***d* (75 mg, 10%); tlc R_f = 0.30 (D); $[\alpha]_D^{19}$ −75° (*c* 0.49, $CHCl_3$); ir ($CDCl_3$): 2935, 1711, 1505, 1264, 1141 cm^{-1}; ^1H nmr (250 MHz, $CDCl_3$) δ: 2.91 (br s, 6, Me_2NCO_2), 3.34 (s, 3, OCH_3), 3.47–3.61 (m, 2), 3.75–3.92 (m, 3), 3.80 and 3.88 (two s, 6, 3,4-di-O-CH_3OPhCH_2), 4.56 (d, 1, $J_{1,2}$ = 3.8 Hz, H1), 4.62 (ABq, 2, J = 12.0 Hz, Δδ = 0.25 ppm, 3,4-di-CH_3OPhCH_2), 4.73 (ABq, 2, J = 12.3 Hz, Δδ = 0.20 ppm, PhCH_2), 4.89 (br s, 1, PhCH_2), 4.95 (d, 1, $J_{7,8}$ = 3.6 Hz, H8), 5.37 (t, 1, $J_{6,7}$ = $J_{5,6}$ = 10.1 Hz, H3), 6.76–6.95 (m, 3, 3,4-di-CH_3OPhCH_2), 7.20–7.47 (m, 10, $Ph$$CH_2$); hrms m/e (M^+) calcd.: 671.2497; found: 671.2494.

*Methyl-(1) 4-methoxybenzyl-(8) (8*R*)-2,3-di-*O*-benzyl-6-chloro-6-deoxy-7-*O*-(*N,*N-dimethylcarbamoyl)-β-*L*-threo-*D*-gluco-octodialdo-1,5:8,4-dipyranoside (**12**c)*

The chlorocarbamate **12***c*, prepared as described for **12***a* from the diol **10***c* (722 mg, 1.31 mmol), was obtained as a colorless syrup (545 mg, 78%); tlc R_f = 0.38 (E); ir (neat): 2920, 1712, 1514, 1392, 1230, 1042 cm^{-1}; ^1H nmr (250 MHz, $CDCl_3$) δ: 2.91 and 2.92 (two s, 6, Me_2NCO_2), 3.41 (s, 3, OCH_3), 3.58 (dd, $J_{2,3}$ = 9.3 Hz, $J_{1,2}$ = 3.6 Hz), 3.80 (s, 3, *p*-CH_3OPhCH_2), 3.95–4.19 (m, 3, H5, H4, H3), 4.28 (br t, 1, H6), 4.61 (ABq, 2, J = 11.9 Hz, Δδ = 0.32 ppm, *p*-CH_3OPhCH_2), 4.71 (d, 1, H8), 4.75 (ABq, 2, J = 12.1 Hz, Δδ = 0.18 ppm, PhCH_2), 4.80 (br s, 1, H8), 4.93 (ABq, 2, J = 12.3 Hz, Δδ = 0.05 ppm, PhCH_2), 5.09 (d, 1, $J_{6,7}$ = 3.5 Hz, H7), 7.05 (ABq, 4, J = 9.03 Hz, Δδ = 0.37 ppm, *p*-CH_3OPhCH_2), 7.27–7.45 (m, 10, $Ph$$CH_2$); hrms m/e (M^+) calcd.: 641.2392; found: 641.2394.

*Dimethyl (8*R*)-2,3-di-*O*-benzyl-6-deoxy-6-*C*-methyl-β-*L*-threo-*D*-gluco-octodialdo-1,5:8,4-dipyranoside (**14**a)*

Dimethyl magnesium was generated *in situ* by adding methyllithium (9.9 equiv., stock ether solution, low lithium halide content) dropwise to methyl magnesium chloride (10.0 equiv., stock tetrahydrofuran solution) with stirring at 0°C under an argon atmosphere. A white precipitate (presumably lithium chloride) formed almost immediately upon complete addition of methyllithium. After 0.5 h, the epoxide **7***a* (150 mg, 0.281 mmol) dissolved in dry toluene (7 mL) was added to the dimethyl magnesium solution. The reaction mixture was refluxed for 3–5 h and monitored by tlc (D). Upon completion, it was cooled to 0°C, carefully quenched with saturated ammonium chloride solution, and extracted with ethyl acetate. The combined organic phases were dried over anhydrous sodium sulfate, filtered, and concentrated *in vacuo* and the residue was purified by filtration through a short silica gel column (D), followed by solvent evaporation to give **14***a* as the only product (133 mg, 86%); tlc R_f = 0.24 (D); $[\alpha]_D^{25}$ −27.1° (*c* 1.01, $CHCl_3$); ^1H nmr (200 MHz, $CDCl_3$) δ: 1.08 (d, 3, J_{6,CH_3} = 7.5 Hz, CH_3), 1.76 (d, 1, J = 6.5 Hz, OH, D_2Oex), 2.22 (m, 1, H6), 3.38 (s, 6, OCH_3), 3.42–3.51 (m, 1, H2), 3.65–3.78 (m, 2, H4, H7), 3.89–4.05 (overlapping dd and t, $J_{2,3}$ = $J_{3,4}$ = 9.2 Hz, $J_{5,6}$ = 4.7 Hz, H3, H5), 4.59–4.65 (m, 2, H1, H8), 4.75 (ABq, 2, J = 11.6 Hz, Δδ = 0.17 ppm, PhCH_2), 4.89 (ABq, 2, J = 11.2 Hz, Δδ = 0.08 ppm, PhCH_2), 7.30–7.44 (m, 10, $Ph$$CH_2$). *Anal.* calcd. for $C_{25}H_{32}O_7$: C 67.55, H 7.26; found: C 67.89, H 7.43.

*Methyl-(1) benzyl-(8) (8*R*)-2,3-di-*O*-benzyl-6-deoxy-6-*C*-methyl-β-*L*-threo-*D*-gluco-octodialdo-1,5:8,4-dipyranoside (**14**b)*

Compound **14***b*, prepared as described above for **14***a* from epoxide **7***b* (80.0 mg, 0.159 mmol), was obtained as a colorless syrup (67.8 mg, 82%); tlc R_f = 0.29 (D); $[\alpha]_D^{25}$ −52.1° (*c* 1.29, $CHCl_3$); ^1H nmr (200 MHz, $CDCl_3$) δ: 1.12 (d, 3, J_{6,CH_3} = 7.4 Hz, CH_3), 1.81 (br s, 1, OH, D_2Oex), 2.23 (m, 1, H6), 3.39 (s, 3, OCH_3), 3.48 (dd, 1, $J_{1,2}$ = 3.7, $J_{2,3}$ = 9.8 Hz, H2), 3.74–3.93 (m, 2, H4, H7), 3.92–4.09 (overlapping dd and t, 2, $J_{2,3}$ = $J_{3,4}$ = 9.8 Hz, $J_{5,6}$ = 5.3 Hz, H3, H5), 4.62 (d, 1, H1), 4.62 (ABq, 2, J = 12.2 Hz, Δδ = 0.33 ppm, PhCH_2), 4.75 (ABq, 2, J = 12.2 Hz, Δδ = 0.16 ppm, PhCH_2), 4.76 (br s, 1, H8), 4.93 (ABq, 2, J = 11.1 Hz Δδ = 0.08 ppm, PhCH_2), 7.30–7.47 (m, 15, $Ph$$CH_2$). *Anal.* calcd. for $C_{31}H_{36}O_7$: C 71.52, H 6.97; found: C 71.23, H 7.09.

*Methyl-(1) 4-methoxybenzyl-(8) (8*R*)-2,3-di-*O*-benzyl-6-deoxy-6-*C*-methyl-β-*L*-threo-*D*-gluco-octodialdo-1,5:8,4-dipyranoside (**14**c)*

Compound **14***c*, prepared as described above for **14***a* from epoxide **7***c* (329 mg, 0.615 mmol), was obtained as a colorless syrup (300 mg, 89%); tlc R_f = 0.20 (D); $[\alpha]_D^{19}$ −51.2° (*c* 1.25, $CHCl_3$); ^1H nmr (250 MHz, $CDCl_3$) δ: 1.10 (d, 3, J_{6,CH_3} = 7.5 Hz, CH_3), 1.85 (d, 1, $J_{7,OH}$ = 6.4 Hz, OH, D_2Oex), 2.22 (m, 1, H6), 3.39 (s, 3, OCH_3), 3.49 (dd, 1, $J_{1,2}$ = 3.7 Hz, $J_{2,3}$ = 9.1 Hz, H2), 3.70–3.87 (m, 2, H4, H7), 3.80 (s, 3, *p*-CH_3OPhCH_2), 3.98 (t, 1, $J_{3,4}$ = 9.1 Hz, H3), 4.02 (dd, 1, $J_{4,5}$ = 10.4 Hz, $J_{5,6}$ = 5.3 Hz, H5), 4.57 (ABq, 2, J = 11.7 Hz, Δδ = 0.31 ppm, *p*-CH_3OPhCH_2), 4.63 (d, 1, H1), 4.73 (br s, 1, H8), 4.76 (ABq, 2, J = 12.6 Hz, Δδ = 0.16 ppm, PhCH_2), 4.95 (ABq, 2, J = 11.2 Hz Δδ = 0.08 ppm, PhCH_2), 7.03 (ABq, 4, J = 8.6 Hz, 0.35 ppm, *p*-CH_3OPhCH_2), 7.17–7.47 (m, 10, $Ph$$CH_2$). *Anal.* calcd. for $C_{32}H_{38}O_8$: C 69.80, H 6.96; found: C 69.60, H 6.99.

*Methyl-(1) 3,4-dimethoxybenzyl-(8) (8*R*)-2,3-di-*O*-benzyl-6-deoxy-6-*C*-methyl-β-*L*-threo-*D*-gluco-octodialdo-1,5:8,4-dipyranoside (**14**d)*

Compound **14***d*, prepared as described above for **14***a* from epoxide **7***d* (284 mg, 0.503 mmol) was obtained as a colorless syrup (243 mg, 83%); tlc R_f = 0.14 (D); $[\alpha]_D^{19}$ −49.5° (*c* 3.13, $CHCl_3$); ^1H nmr (250 MHz, $CDCl_3$) δ: 1.10 (d, 3, J_{6,CH_3} = 7.4 Hz, CH_3), 1.87 (br d, 1, OH, D_2Oex), 2.24 (m, 1, H6), 3.40 (s, 3, OCH_3), 3.47 (dd, 1, $J_{1,2}$ = 3.6 Hz, $J_{2,3}$ = 9.3 Hz, H2), 3.72–3.85 (m, 2, H4, H7), 3.78 and 3.87 (two s, 6, 3,4-di-CH_3OPhCH_2), 3.95–4.06 (overlapping dd and t, 2, $J_{2,3}$ = $J_{3,4}$ = 9.3 Hz, 2, $J_{5,6}$ = 5.3 Hz, H3, H5), 4.43 (d of ABq, 1, J = 11.6 Hz, 3,4-di-CH_3OPhCH_2), 4.64 (d, 1, H1), 4.64–4.81 (m, 3, H8, PhCH, 3,4-di-CH_3OPhCH_2), 4.83 (d of ABq, J = 12.2 Hz, 1, PhCH), 4.95 (ABq, 2, J = 11.1 Hz Δδ = 0.08 ppm, PhCH_2), 6.82 (m, 3, 3,4-di-CH_3OPhCH_2), 7.22–7.47 (m, 10, $Ph$$CH_2$). *Anal.* calcd. for $C_{33}H_{40}O_9$: C 68.26, H 6.94; found: C 68.42, H 7.04.

*Methyl (8*R*,8*S*)-2,3-di-*O*-benzyl-6-deoxy-6-*C*-methyl-β-*L*-threo-*D*-gluco-octodialdo-8,4-pyranoso-1,5-pyranoside (**15**)*

(*a*) The *p*-methoxybenzyl methyl bipyranoside **14***c* (41.0 mg, 0.0745 mmol) was stirred with 2,3-dichloro-5,6-dicyano-1,4-benzoquinone (20) (DDQ, 25.4 mg, 0.112 mmol) in methylene chloride and water (18:1 v/v, 5 mL) under argon at room temperature. A dark green charge-transfer complex formed immediately and gradually faded to orange-yellow after 2 h. Thin-layer chromatography (E) showed significant starting material remained. An additional equivalent of

DDQ was added, and stirring continued for 2.5 h. The crude reaction mixture was filtered through a Celite pad and the solid residue was washed with methylene chloride (15 mL). The filtrate was concentrated *in vacuo* and the residue was dissolved in toluene (10 mL) and concentrated *in vacuo* to remove water as an azeotrope. The residue was purified by flash chromatography (D followed by E) to give the anomeric mixture **15** as a colorless syrup (13.3 mg, 41%); tlc R_f = 0.24 (E); ir (neat): 3430, 2900, 1452, 1358, 1030 cm^{-1}; ^1H nmr (250 MHz, $CDCl_3$) δ: 0.95 and 1.10 (two d, 2:1 respective ratio, CH_3), 1.18 and 0.36 (two m, 1:2 respective ratio, H6), 2.50 and 3.09 (two d, 2, OH, D_2Oex), 3.38 (s, 3, OCH_3), 3.40–3.58 (m, 2), 3.67–4.40 (m, 3), 4.58–6.04 (m, 6), 7.22–7.41 (m, 10). *Anal.* calcd. for $C_{24}H_{30}O_7$: C 66.96, H 7.02; found: C 66.81, H 7.13.

(*b*) Compound **15** was prepared in an improved yield when 3,4-dimethoxybenzyl methyl bipyranoside **14***d* (113 mg, 0.195 mmol) was stirred with DDQ (48.6 mg, 0.214 mmol) in methylene chloride – dioxane–water (10 mL, 18:2:1 v/v) under argon at room temperature. After 4 h, the dark green charge-transfer complex faded to an orange-yellow color. Thin-layer chromatography (E) showed some starting material still present so additional DDQ (10 mg) was added. After 2 h, only a trace of starting material was left. The reaction work-up was the same as previously described and **15** was obtained as a colorless syrup (58.8 mg, 70%). The physical properties were identical to the material in part (*a*).

Acknowledgements

We are grateful to the National Science Foundation (CHE 8304283), Duke University, and the University of Maryland for support of this work.

1. (*a*) B. Fraser-Reid, L. Magdzinski, and B. Molino. J. Am. Chem. Soc. **106**, 731 (1984); (*b*) B. F. Molino, L. Magdzinski, and B. Fraser-Reid. Tetrahedron Lett. **24**, 5819 (1983); (*c*) L. Magdzinski, B. Cweiber, and B. Fraser-Reid. Tetrahedron Lett. **224**, 5823 (1983).
2. R. J. Ferrier. Adv. Carbohydr. Chem. Biochem. **24**, 199 (1969); **20**, 67 (1965).
3. B. Fraser-Reid. Acc. Chem. Res. **8**, 192 (1975); **18**, 347 (1985).
4. H. C. Jarrell and W. A. Szarek. Can. J. Chem. **57**, 924 (1979); K. Tatsuta, K. Akimoto, H. Takahashi, T. Hamatsu, M. Annaka, and M. Kinoshita. Tetrahedron Lett. **24**, 4868 (1983); O. R. Martin and W. A. Szarek. Carbohydr. Res. **130**, 195 (1984); D. Nicoll-Griffith and L. Weiler. J. Chem. Soc. Chem. Commun. 659 (1984).
5. D. J. Bell and J. Lorber. J. Chem. Soc. 453 (1940).
6. J. C. Collins, W. W. Hess, and F. J. Frank. Tetrahedron Lett. 3363 (1968).
7. D. H. Hollenberg, R. S. Klein, and J. J. Fox. Carbohydr. Res. **67**, 491 (1978).
8. K. Omura, A. K. Sharma, and D. Swern. J. Org. Chem. **41**, 957 (1976).
9. H. J. Bestmann, K. Roth, and M. Ettlinger. Chem. Ber. **115**, 161 (1982); Angew. Chem. Int. Ed. Engl. **18**, 687 (1979).
10. M. Miyashita, A. Yoshikosi, and P. A. Grieco. J. Org. Chem. **42**, 3772 (1977).
11. R. U. Lemieux. *In* Molecular rearrangements. Vol. 2. *Edited by* P. De Mayo. Interscience, New York. 1964. p. 709; A. J. Kirby. The anomeric effect and related stereoelectronic effects at oxygen. Springer Verlag, New York. 1983.
12. S. Trippett and D. M. Walker. J. Chem. Soc. 1266 (1961).
13. R. J. Ferrier and N. Prasad. J. Chem. Soc. (C), 575 (1969).
14. D. R. Hicks and B. Fraser-Reid. Synthesis, 203 (1974).
15. U. Sunay, D. Mootoo, B. Molino, and B. Fraser-Reid. Tetrahedron Lett. **27**, 4697 (1986).
16. S. McNally and W. G. Overend. J. Chem. Soc. (C), 1978 (1966).
17. C. Copeland and R. V. Stick. Aust. J. Chem. **35**, 2257 (1982).
18. H. G. Viehe and A. Janousek. Angew. Chem. **85**, 837 (1973); Angew. Chem. Int. Ed. Engl. **12**, 806 (1973).
19. K. A. Parker and R. E. Babine. Tetrahedron Lett. **23**, 1763 (1982).
20. Y. Oikawa, T. Yoshioka, O. Yonemitsu. Tetrahedron Lett. **23**, 885 (1982).

Can. J. Chem. Downloaded from www.nrcresearchpress.com by 213.222.148.141 on 09/07/12
For personal use only.

Ion–ion–solvent interactions in aqueous ionic cosolvent systems. III. Thermodynamics of hydrogen bromide and hydrogen iodide from water to aqueous solutions of sodium nitrate from emf measurements at different temperatures and the structuredness of the solvents

SIBAPRASAD RUDRA, HIMANSU TALUKDAR, AND KIRON K. KUNDU[1]
Physical Chemistry Laboratory, Jadavpur University, Calcutta – 700 032, India

Received April 6, 1987

SIBAPRASAD RUDRA, HIMANSU TALUKDAR, and KIRON K. KUNDU. Can. J. Chem. **65**, 2843 (1987).

Standard free energies (ΔG_t^0) and entropies (ΔS_t^0) of transfer of hydrogen bromide and iodide from water to the aqueous 1, 2, and 4 *m* of sodium nitrate have been determined by measuring the emf's of the cell: Pt, H_2(g, 1 atm)/KOH(m_1), KX(m_2), solvent/AgX–Ag where X = Br or I at five equidistant temperatures ranging from 15–35°C. ΔG_t^0 values of HBr, HI as well as that of HCl obtained from earlier paper and particularly of the individual ions ΔG_t^0(i), obtained by use of modified TATB assumption reported earlier and also $\Delta G_{t,tr.int}^0$(i) obtained after correcting for "cavity" effect and Born-type electrostatic effect estimated tentatively by the scaled particle theory (SPT) and simple Born equation, respectively, reveal the relative order of stabilisation of Cl^-, Br^-, and I^- ions. Analysis of $T\Delta S_t^0$(HX)–composition profile (X = Cl, Br, and I) exhibits a characteristic "maxima" around 1.5 *m* $NaNO_3$ with the relative order HI > HBr > HCl in the region of maxima. Moreover, dissection of $T\Delta S_t^0$(HX) values into the individual ion contributions by use of the modified TATB assumption reported earlier, results in the characteristic "maxima" around 1.5 *m* $NaNO_3$ in $T\Delta S_t^0$(i) or $T\Delta S_{t,tr.int}^0$(i)–composition profiles for H^+ and "minima" for Cl^-, Br^-, and I^-. The results are discussed in terms of ion–ion–solvent interactions as well as the structural changes of the solvents.

SIBAPRASAD RUDRA, HIMANSU TALUKDAR et KIRON K. KUNDU. Can. J. Chem. **65**, 2843 (1987).

Opérant à des températures équidistantes entre 15 et 35°C et faisant appel à des mesures de fem de la cellule Pt, H_2(g, 1 atm)/KOH(m_1), KX(m_2), solvent/AgX–Ag, dans laquelle X = Br ou I, on a déterminé les énergies libres standard (ΔG_t^0) et les entropies (ΔS_t^0) pour le transfert du bromure et de l'iodure d'hydrogène de l'eau vers des solutions aqueuses 1, 2 et 4 *m* en nitrate de sodium. En se basant sur les valeurs des ΔG_t^0 du HBr et du HI, sur la valeur équivalente du HCl qui a été déterminée antérieurement, sur les valeurs des ΔG_t^0(i) des ions individuels qui ont été obtenues en utilisant l'hypothèse TATB proposée antérieurement ainsi que sur les valeurs de $\Delta G_{t,tr.int}^0$(i) obtenues après avoir effectué des corrections pour l'effet de «cavité» ainsi que pour l'effet électrostatique du type de Born évalués respectivement par la théorie des particules scalaires (TPS) et par une équation simple de Born, on peut en déduire l'ordre relatif de stabilisation des ions Cl^-, Br^- et I^-. Une analyse du profil $T\Delta S_t^0$(HX)/composition (X = Cl, Br, I) présente un "maximum" caractéristique autour de 1,5 *m* $NaNO_3$ et, dans cette région, l'ordre relatif est HI > HBr > HCl. De plus, une dissection des valeurs de $T\Delta S_t^0$(HX) en contributions ioniques individuelles, en utilisant l'hypothèse TATB modifiée proposée antérieurement, conduit à des "maxima" caractéristiques autour de 1,5 *m* en $NaNO_3$ dans les profils de $T\Delta S_t^0$(i) ou $T\Delta S_{t,tr.int}^0$(i)/composition pour H^+ et à des "minima" pour Cl^-, Br^- et I^-. On discute des résultats en fonction d'interactions ion–ion–solvent ainsi qu'en fonction de changements structuraux des solvants.

[Traduit par la revue]

Introduction

Systematic studies on different physico-chemical properties including thermodynamics of electrolytes and non-electrolytes, in aqueous ionic cosolvent systems parallel to that in aquo-organic cosolvent systems, constitute a new approach for understanding the thermodynamic and kinetic behaviour of electrolytes and non-electrolytes in salt solutions. In the previous papers (1, 2) we have reported for the first time the transfer energetics of HCl (1), free energies of transfer (ΔG_t^0), and entropies of transfer ($T\Delta S_t^0$) of some electrolytes and their constituent ions (2) from water to the aqueous mixtures of 1, 2, and 4 *m* $NaNO_3$ at 25°C, taking each composition as the individual solvent and the infinitely dilute solution of solute in each solvent as the standard state, exactly similar to what are usually done in aquo-organic solvent systems.

Recent studies (3–6) on the standard potentials (E^0) of the Ag–AgX (X = Cl, Br, and I) electrodes at different temperatures in different aquo-organic solvents and the related transfer energetics of HX are found to be amply useful in furnishing important reflections on the ion–solvent interactions as well as the structural features of the solvents relative to that of water. We have therefore extended the above idea to the aquo-ionic solvent system. As E^0 values of the Ag–AgCl electrode at different temperatures are already reported in the previous paper (1) we are now reporting the same for Ag–AgBr and Ag–AgI electrodes.

Since Pt/H_2 electrode is found to behave irratically in low pH solution of I^- in these solvents, a cell of the type

[A] Pt, H_2(g, 1 atm)/KOH(m_1), KX(m_2), solvent/AgX–Ag

has been used for both X = I and Br. The required autoionization constant (K_s) values of the solvents have of course been determined earlier and reported in another paper (7). In these aqueous ionic solvents the E^0 values have been determined at five equidistant temperatures ranging from 15–35°C for each composition.

Experimental

The method of preparation of solvent has been described earlier (1). Water used was triple distilled. Both KI and KBr (Merck, G.R.) were used after drying at 150°C and then in a vacuum desiccator for about 12 h. Ag–AgI and Ag–AgBr electrodes were of the thermal type and prepared by the method described earlier (8). Other experimental details including the preparation of solutions, platinized electrodes, and also the method of measurements were exactly the same as those described in the preceding papers (3*c*,*d*). The behaviour of electrodes, the time of attainment of equilibrium and criteria of equilibrium of the

[1]Author to whom all correspondence should be addressed.

Can. J. Chem. Downloaded from www.nrcresearchpress.com by 213.222.148.141 on 09/07/12
For personal use only.

TABLE 1. The values of E^0_m (in V) of the Ag–AgBr and Ag–AgI electrodes at different temperatures for aqueous solutions of $NaNO_3$

$NaNO_3$ (mol kg^{-1})	Ag–AgBr					Ag–AgI				
	15°C	20°C	25°C	30°C	35°C	15°C	20°C	25°C	30°C	35°C
0.0	0.0756	0.0734	0.0711	0.0685	0.0658	−0.1494	−0.1508	−0.1524	−0.1541	−0.1559
1.0	0.0916	0.0908	0.0896	0.0880	0.0864	−0.1327	−0.1330	−0.1333	−0.1338	−0.1343
2.0	0.0600	0.0754	0.0738	0.0700	0.0686	−0.1470	−0.1497	−0.1528	−0.1546	−0.1558
4.0	—	—	—	—	—	−0.1710	−0.1740	−0.1764	−0.1786	−0.1806

cells were also essentially similar to that described in the said papers (3*c*,*d*).

Results

The emf (E) of cell [A] at any solvent composition is given by

$$[1]\quad E = E^0 - \frac{2.303\,RT}{F}\log(a_{H^+}\cdot a_{X^-})$$

where X = Br^- and I^- and the other terms have the usual significance. Replacing a_{H^+} in terms of K_s by $K_s a_{H_2O}/a_{OH^-}$, a_i of the ionic species by the product of molality (m_i) and the molal activity coefficient γ_i and 2.303 RT/F by k, we have an extrapolation function, $E^{0'}$ defined by [2]

$$[2]\quad E^{0'} = E + k\log\frac{m_{X^-}}{m_{OH^-}} + k\log K_s$$

$$= E^0 - k\log\frac{a_{H_2O}\gamma_{X^-}}{\gamma_{OH^-}} = E^0 + f(\mu)$$

As in previous cases (1, 3*c*,*d*), the standard states are so chosen that at infinite dilution in each solvent mixture the activity coefficient of ions concerned, as well as the activity of water (a_{H_2O}) are unity. Also, as the term $\log a_{H_2O}\gamma_{X^-}/\gamma_{OH^-}$ in dilute solution in each solvent mixture is as before (1, 3*c*,*d*) likely to be proportional to the "ionic strength" μ, extrapolation of the function $E^{0'}$ to $\mu = 0$ would yield E^0 values on the molal scale, henceforth denoted as E^0_m.

Notably, the values of K_s in eq. [2] are also based on this very assumption (see ref. 7) and not on the usual assumption of taking pure water as the standard state. Had the latter case been true the activity of water a_{H_2O} in each composition of the respective ionic and non-ionic cosolvent systems should have been accounted for. Eventually K_s values in the respective composition would have been altered by a constant factor $|-\log a_{H_2O}|$ depending upon the composition and the temperature. Evidently as in the cases of aquo-organic solvents (3*c*,*d*), E^0 values, though not K_s values, in this ionic cosolvent system would be independent of the assumed standard states.

Moreover, the "ionic strength" μ referred to above stands for that due to the "added" electrolytes viz. KX and KOH, in the respective compositions of $NaNO_3$ solutions. As indicated earlier (2) in our treatment the molalities of the added electrolytes are so small compared to the molalities of $NaNO_3$ in any composition that the "ionic strength" arising from the added electrolytes does not vary significantly and the effect of involved activity coefficient term is always small and disappears upon extrapolation to zero "ionic strength".

The E values of cell [A] at different temperatures after due correction to b_{H_2} = 1 atm, and the corresponding molalities of KOH, KI/KBr for each of the solvent mixtures are given elsewhere.[2] The required partial pressures of the mixed solvents for correcting b_{H_2} = 1 atm are taken from ref. 1.

Assuming as before (3*c*,*d*) that KOH and KI/KBr are completely dissociated in all these solvents m_{OH^-} and m_{I^-} or m_{Br^-} are taken as equal to m_1 and m_2, respectively, and $\mu = (m_1 + m_2)d_s$ where d_s is the density of the solvent. The values of d_s were obtained from the previous paper (1). The values of $E^{0'}$ computed by use of equation [2] at any temperature for any composition were then plotted against μ. And the resulting linear plots on extrapolation yielded the values of E^0_m which are given in Table 1. The uncertainties in the values of E^0_m so obtained lie within ±0.3 mV. Notably due to poisoning effect E^0_m values at 4 *m* $NaNO_3$ for Ag–AgBr electrode could not be determined.

As before (1), the E^0_m values at different temperatures for each solvent composition were then fitted into the E^0_m–temperature quadratic equation [3].

$$[3]\quad E^0_m = a + b(t - 25) + c(t - 25)^2$$

by the method of least squares where t is the temperature in degree Celcius. The coefficients a, b, and c for each of the solvent mixtures as well as for water are listed in Table 2. The E^0_m values in water for the Ag–AgBr and the Ag–AgI electrodes were taken from refs. 9 and 10, respectively.

The free energy changes ΔG^0_t accompanying the transfer of 1 mole of HX from the standard state in water (w) to that in each composition of $NaNO_3$ salt solution (s), i.e. of the process HX(w) → HX(s) were computed on the mole fraction scale at t = 25°C using the relation [4].

$$[4]\quad \Delta G^0_t(HX) = -F[(E^0_m)^{25}_s - (E^0_m)^{25}_s] - 2RT\ln\frac{M_s}{M_w}$$

where T = 298.15 and M_s and M_w are the average and pure molar mass of the mixed solvent and water, respectively. The corresponding entropy changes ΔS^0_t(HX) at 25°C were obtained by the use of eq. [5].

$$[5]\quad \Delta S^0_t(HX) = F(b_s - b_w) + 2F(t - 25)(c_s - c_w) + 2R\ln\frac{M_s}{M_w}$$

The values of ΔG^0_t and ΔS^0_t so obtained for HX for all the solvent compositions are presented in Table 2. The average estimated uncertainties (11) in ΔG^0_t and ΔS^0_t at 25°C for these mixed solvents are respectively ±0.03 kJ mol^{-1} and ±2 J K^{-1} mol^{-1}.

[2]A complete set of data referred to above may be purchased from the Depository of Unpublished Data, CISTI, National Research Council of Canada, Ottawa, Ont., Canada K1A 0S2.

Can. J. Chem. Downloaded from www.nrcresearchpress.com by 213.222.148.141 on 09/07/12
For personal use only.

Can. J. Chem. Downloaded from www.nrcresearchpress.com by 213.222.148.141 on 09/07/12
For personal use only.

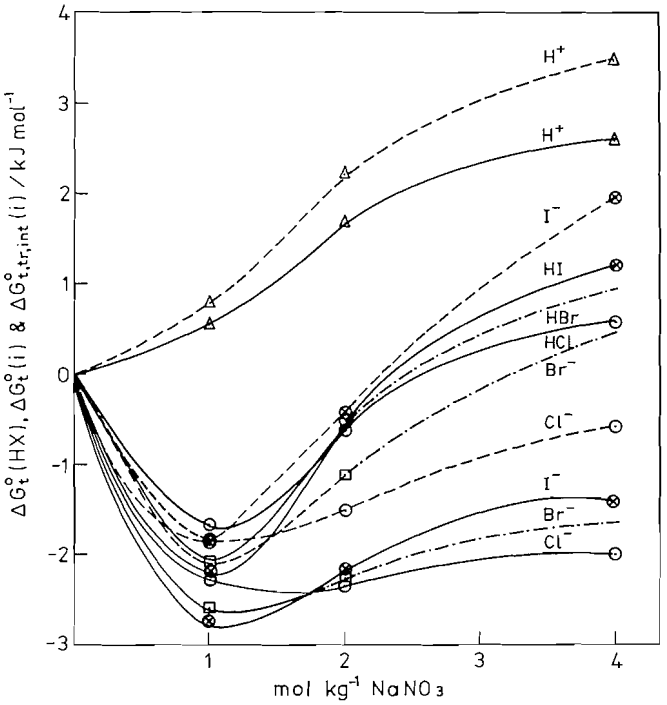

FIG. 1. Variation of ΔG_t^0(HX) of hydrogen halides, ΔG_t^0(i) (solid lines), and $\Delta G_{t,tr.int}^0$(i) (dotted lines) of different ions with molality of $NaNO_3$ in aqueous $NaNO_3$ solutions at 25°C.

Discussion

Free energy of transfer

ΔG_t^0(HX)–composition profiles are illustrated in Fig. 1. From Fig. 1 it is observed that ΔG_t^0–composition profiles of HX exhibit a slight roller-coaster type behaviour. A perusal of ΔG_t^0(HX) values (Table 2) including those for HCl (Table 3) as obtained from previous paper (*1*), reveals that up to 1.5 *m* $NaNO_3$ the downward trend of ΔG_t^0(HX) is in the order of HI > HBr > HCl but after 1.5 *m* $NaNO_3$ the upward trend of HI > HBr > HCl. So from Fig. 1 it can be said that the order of stabilisation of $I^- > Br^- > Cl^-$ in the initial compositions but the reverse is true at higher compositions. It is also evident from the ΔG_t^0(i)–composition profiles of H^+ and X^- as obtained by using the modified form of widely used tetraphenylarsonium tetraphenylborate reference electrolyte assumption (2) and are illustrated in Fig. 1.

In the previous paper (2) we have already accounted for the nature of ΔG_t^0(i)–composition profiles of H^+ and Cl^-. The behaviour of both Br^- and I^- being exactly similar to that of Cl^- we are now trying to account for the relative order of stabilization and destabilisation of the halide ions. Before doing so let us at first calculate tentatively the Born-type electrostatic effect $\Delta G_{t,Born}^0$ and cavity effect $\Delta G_{t,cav}^0$ by the simple Born equation (12) and the scaled particle theory (SPT) (13), respectively, as per formulation described and referred to in the previous papers (1, 2, 14). These and the required solvent and solute parameters are given in Table 3. Now the values of $\Delta G_{t,Born}^0$(i) and $\Delta G_{t,cav}^0$(i) when subtracted from the corresponding ΔG_t^0(i) values yielded $\Delta G_{t,tr.int}^0$(i) values, which are also illustrated in Fig. 1.

Significantly enough the composition profiles of $\Delta G_{t,tr.int}^0(X^-)$ are more or less similar to each other as well as to the respective profiles of $\Delta G_t^0(X^-)$. Their relative positions are of course

TABLE 2. Coefficients *a*, *b*, and *c* of eq. [3] for Ag–AgBr and Ag–AgI electrodes and the transfer energetics (ΔG_t^0 and $T\Delta S_t^0$) of HBr and HI from water to aqueous $NaNO_3$ solvents at 25°C (mole fraction scale)

	Ag–AgBr					Ag–AgI				
$NaNO_3$ (mol kg^{-1})	*a*/V	$b \times 10^4$/ V(°C)$^{-1}$	$c \times 10^6$/ V(°C)$^{-2}$	ΔG_t^0/kJ mol^{-1}	$T\Delta S_t^0$/ kJ mol^{-1}	*a*/V	$b \times 10^4$/ V(°C)$^{-1}$	$c \times 10^6$/ V(°C)$^{-2}$	ΔG_t^0/kJ mol^{-1}	$T\Delta S_t^0$/ kJ mol^{-1}
0.0	0.0711	−4.90	−3.70	—	—	−0.1524	−3.26	−2.57	—	—
1.0	0.0899	−2.64	−13.30	−2.10	6.8	−0.1333	−0.80	−1.71	−2.16	7.4
2.0	0.0730	−5.64	8.57	−0.58	−1.8	−0.1526	−4.50	12.30	−0.56	−3.0
4.0	—	—	—	—	—	−0.1764	−4.76	6.29	1.21	−3.2

Can. J. Chem. Downloaded from www.nrcresearchpress.com by 213.222.148.141 on 09/07/12
For personal use only.

TABLE 3. Values of free energies and enthalpies and cavity formation ($\bar{G}_c$) and ($\bar{H}_c$) and standard free energies of transfer $\Delta G_t^0(i)$, $\Delta G_{t,cav}^0(i)$, $\Delta G_{t,Born}^0(i)$ and $\Delta G_{t,tr.int}^0(i)$ and entropies of transfer $T\Delta S_t^0(i)$, $T\Delta S_{t,cav}^0(i)$, $T\Delta S_{t,Born}^0(i)$, and $T\Delta S_{t,tr.int}^0(i)$ (mole fraction scale in kJ mol^{-1} of the individual ions from water to aqueous $NaNO_3$ solvents at 25°C)

	G_c[a]		H_c[a]									
Ions	Water	Solvent	Water	Solvent	ΔG_t^0(i)	$\Delta G_{t,cav}^0$(i)[a]	$\Delta G_{t,Born}^0$(i)[b]	$\Delta G_{t,tr.int}^0$(i)	$T\Delta S_t^0$(i)	$T\Delta S_{t,cav}^0$(i)[a]	$T\Delta S_{t,Born}^0$(i)[b]	$T\Delta S_{t,tr.int}^0$(i)
						1 *m* $NaNO_3$						
H^+	13.5	12.8	1.8	3.1	0.6	−0.7	0.5	0.8	42.3	2.0	−0.6	40.9
Cl^-	20.7	19.6	2.8	4.8	−2.2	−1.1	0.7	−1.8	−36.0	3.1	−0.9	−38.2
Br^-	23.3	22.1	3.2	5.5	−2.6	−1.2	0.7	−2.1	−35.5	3.5	−0.8	−38.2
I^-	27.8	26.3	3.9	6.6	−2.7	−1.5	0.6	−1.8	−34.9	4.2	−0.7	−38.4
						2 *m* $NaNO_3$						
H^+	—	12.1	—	3.6	1.7	−1.5	1.0	2.2	20.5	3.3	−1.5	18.7
Cl^-	—	18.4	—	5.7	−2.3	−2.4	1.5	−1.4	−20.1	5.3	−2.3	−23.1
Br^-	—	20.8	—	6.5	−2.3	−2.6	1.4	−1.1	−22.3	5.9	−2.1	−26.1
I^-	—	24.7	—	7.8	−2.3	−3.2	1.2	−0.3	−23.5	7.1	−1.9	−28.7
						4 *m* $NaNO_3$						
H^+	—	10.7	—	3.2	2.6	−2.9	2.0	3.5	−0.1	4.3	−7.7	3.3
Cl^-	—	16.3	—	5.0	−2.0	−4.5	3.0	−0.5	−1.2	6.7	−11.8	3.9
Br^-	—	18.4	—	5.8	(−1.7)[c]	−4.9	2.8	0.4	(−2.5)[c]	7.5	−10.9	0.9
I^-	—	21.9	—	6.9	−1.4	−6.0	2.5	2.1	−3.1	9.0	−9.8	−2.3

[a]The required diameters of the solvent constituents and the values of the scale effect $RT \ln V_w/V_s$ are taken from previous paper (1) and $\alpha = -\mathrm{d} \ln d_s/\mathrm{d}T$ also taken from that paper (1) and for solute species, $b_{Cl^-} = 0.362$ nm (9), $b_{Br^-} = 0.390$ nm (9), $b_{I^-} = 0.434$ nm (9).

[b]The required radii of the ionic species are obtained from the corresponding diameters of the species as indicated in *a* and that of H^+ as equal to 0.276 nm (1).

[c]The values within the parentheses are obtained by smooth extrapolation of the curve.

Can. J. Chem. Downloaded from www.nrcresearchpress.com by 213.222.148.141 on 09/07/12
For personal use only.

shifted upward as the magnitudes of $\Delta G^0_{t,tr.int}(X^-)$ are becoming increasingly less negative and in the case of I^- at higher composition of $NaNO_3$ these become even positive. However, it appears from the nature of $\Delta G^0_{t,tr.int}(X^-)$–composition profiles as well as their relative positions that X^- ions are stabilized at initial compositions. But beyond 1.5 *m* $NaNO_3$ composition X^- ions tend to become increasingly less stabilized and even destabilized, and the larger the size of X^- ion the greater is the tendency of destabilization.

As indicated in the previous papers (1, 2) and evidenced from various spectroscopic (15–17) and other evidences (18) in the solvent compositions up to 1.5 *m* $NaNO_3$ the prevalent ionic species are $(Na^+)_{aq}$ and NO_3^-. Now the observed stabilization of halide ions in the region therefore suggests that the attractive interaction of halide ions and $(Na^+)_{aq}$ over the repulsive interaction of halide ions and NO_3^- exceeds halide ion – H_2O interactions in pure water. This is probably due to the fact that the H_2O molecules in the hydration sphere round Na^+ have more protonic character (δ^+) than that in pure water and hence are likely to induce more "acid–base" type (19) short range attractive interaction with X^- than that in pure water. Now among Cl^-, Br^-, and I^- the charge density of $Cl^- > Br^- > I^-$, hence the repulsive interaction with unhydrated NO_3^- will be in the order of $Cl^- > Br^- > I^-$ but the attractive interaction with hydrated Na^+ is more for Cl^- than Br^- and I^- and hence the overall result is that the observed stabilization of Cl^-, Br^-, and I^- ions are more or less the same in the region.

But after 1–1.5 *m* $NaNO_3$ the reverse order, i.e., the order of less stabilization and even destabilization $I^- > Br^- > Cl^-$ is perhaps due to the change in solvating species. As various spectroscopic evidences (15–17) referred to earlier (1, 2) indicate, around 1.5–6.0 *m* $NaNO_3$ the constituent ions $(Na^+)_{aq}$ and NO_3^- are increasingly replaced by the solvent separated ion-pair (SSIP) viz. $(Na^+)_{aq}NO_3^-$. In SSIP the positive character round Na^+ is reduced to a greater extent by accompanying NO_3^- and consequently halide ions become increasingly destabilized with increasing concentration of $NaNO_3$. Now the relative order of destabilization $I^- > Br^- > Cl^-$ is probably due to the fact that owing to its smaller size and larger ionic force field the interaction of Cl^- with SSIP is greater than that of Br^- and I^- and also that of Br^- is greater than that of I^- ion.

Entropy of transfer

Figure 2 depicts the $T\Delta S^0_t$–composition profiles of HX at 25°C. The observed $T\Delta S^0_t$–composition profiles exhibit the characteristic maxima around 1.5 *m* $NaNO_3$ and after that show a downward trend followed by a slight upward trend at higher compositions. The maxima and also the downward trend follow the order HI > HBr > HCl. The nature of these profiles is of course contrary to the observed downward trend of non-electrolyte like *p*-nitroaniline (*p*NA) and benzoic acid (HBz) from the very beginning in aqueous $NaNO_3$ solutions (7) and as expected from the observed three-dimensional (3D) structure-breaking propensity of $NaNO_3$ (18). Of course, there is also a break around 1.5 *m* $NaNO_3$ in the case of *p*NA and HBz. Evidently complex structural contributions are involved in the transfer of hydrogen halides unlike that of *p*NA and HBz where the solvating species is only water.

Since the discussion of $T\Delta S^0_t(i)$–composition profile of H^+ and halide ions would be more informative about the involved ion–ion–solvent interactions and solvent structuredness, dissection of $T\Delta S^0_t(HX)$ into its ionic constituents are made by the modified form of the widely used tetraphenylarsonium tetraphenylborate RE assumption described in the previous paper (2) and are illustrated in Fig. 2. Figure 2 also depicts the $T\Delta S^0_{t,tr.int}(i)$–composition profiles of the halide ions and H^+, as obtained after subtracting $T\Delta S^0_{t,cav}(i)$ and $T\Delta S^0_{t,Born}(i)$ values from the corresponding $T\Delta S^0_t(i)$ values, the cavity and Born effects being computed by use of the formulations described in the previous paper (2). From Fig. 2 it is observed that as in the case of Cl^-, $\Delta S^0_t(i)/\Delta S^0_{t,tr.int}(i)$–composition profiles for Br^- and I^- also pass through a minimum around 1.5 *m* $NaNO_3$. But while the relative order of the downward trend of $\Delta S^0_t(X^-)$ values at initial compositions is $Cl^- > Br^- > I^-$, the upward trend at higher compositions is $Cl^- > Br^- > I^-$. On the other hand, while the $\Delta S^0_{t,tr.int}(X^-)$–composition profiles more or less overlap at the initial compositions the relative order of the upward trend at higher composition remains unaltered, i.e., $Cl^- > Br^- > I^-$.

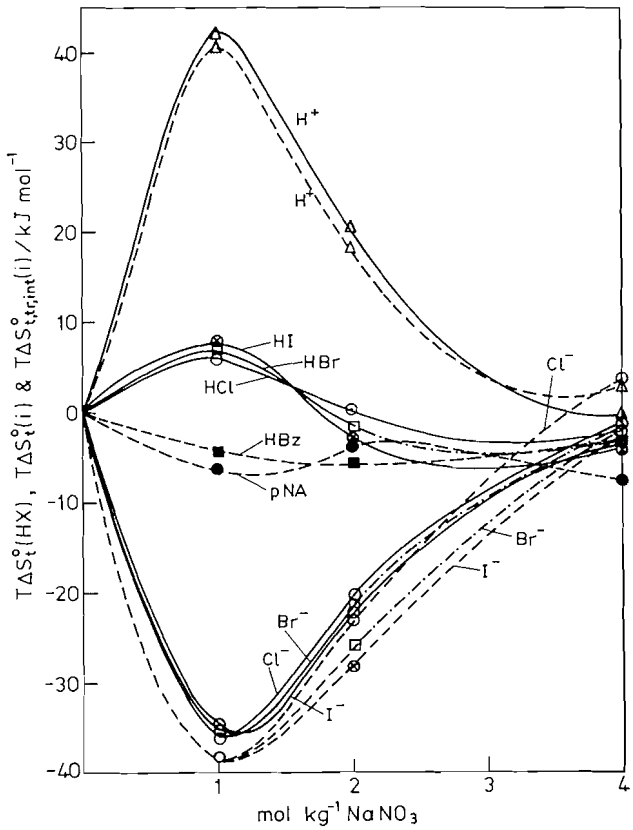

FIG. 2. Variation of $T\Delta S^0_t(HX)$ of hydrogen halides, $T\Delta S^0_t(i)$ (solid lines), and $T\Delta S^0_{t,tr.int}(i)$ (dotted lines) of different ions and also of pNA and HBz (dotted-lines) as obtained from ref. 7 with molality of $NaNO_3$ in aqueous $NaNO_3$ solutions at 25°C.

If we recall Kundu *et al.*'s four-step transfer process (1, 3*a*, 20) we have

$$\Delta S^0_{t,tr.int}(i) = (\Delta S^0_1 - \Delta S^0_2) + (\Delta S^0_3 - \Delta S^0_4)$$

where ΔS^0_1 is the positive entropy change accompanying the dehydration of the ion, if any, $|-\Delta S^0_2|$ is that accompanying the formation of 3D structure of water out of the molecules released from dehydration, ΔS^0_3 is the entropy change accompanying the break down of relevant structure of the solvents or of the solvating species in the solvent and $|-\Delta S^0_4|$ is that accompanying the interaction of the transferred ion with the solvating species in the solvent.

As indicated in course of explaining $\Delta S^0_{t,tr.int}(i)$–composition

profile for Cl^- (2) due to the large size, anions like Cl^-, Br^-, and I^- are nearly unhydrated and hence $\Delta S_1^0 \simeq 0$. But since the solvent molecules in the secondary solvation zone (SSZ) are in the disordered state, $|-\Delta S_2^0|$ and hence $|\Delta S_1^0 - \Delta S_2^0|$ will be a large negative quantity. And the SSZ around I^- being larger in size the magnitudes of $(\Delta S_1^0 - \Delta S_2^0)$ will be more negative for I^- than Br^- and Cl^-. But in the lower composition region, the halide ions are interacted upon by $(Na^+)_{aq}$ with $\Delta S_3^0 = 0$, and the order due to the interaction of Cl^- with $(Na^+)_{aq}$ will be greater than that of Br^- and I^- i.e. $(\Delta S_3^0 - \Delta S_4^0)$ will be more negative for Cl^- than Br^- and I^- and the overall magnitude $[(\Delta S_1^0 - \Delta S_2^0) + (\Delta S_3^0 - \Delta S_4^0)]$ might be more or less the same for the halide ions, as has been observed. But beyond 1.5 *m* $NaNO_3$ the "solvating" or interacting species are solvent-separated ion-pairs and hence the magnitude of ΔS_3^0 will be greater for Cl^- than that of Br^- and I^- and consequently the overall magnitude $[(\Delta S_1^0 - \Delta S_2^0) + (\Delta S_3^0 - \Delta S_4^0)]$ will be greater for Cl^- than Br^- and I^- and hence the observed order.

Notably, the mirror-image behaviour of $\Delta S_{t,tr.int}^0(i)$–composition profile of H^+ and also of other cations, which is true not only in this solvent system but also in other aquo-organic solvents (21–25), has been duly explained in our earlier paper (2).

Thus it appears that the order of $\Delta S_{t,tr.int}^0(i)$ rather than that of $\Delta S_t^0(i)$, conforms with what is expected from the four-step transfer process. And this substantiates our earlier contention (1, 2, 14) that $\Delta S_{t,tr.int}^0(i)$ should be a better indicator than $\Delta S_t^0(i)$ for inferring the relative structuredness of solvents.

Acknowledgement

We record our thanks to the University Grants Commission, New Delhi for financial assistance.

1. S. P. Rudra, H. Talukdar, B. P. Chakravarty, and K. K. Kundu. Can. J. Chem. **64**, 1960 (1986).
2. S. P. Rudra, H. Talukdar, and K. K. Kundu. Can. J. Chem. To be published.
3. (*a*) K. Bose, K. Das, A. K. Das, and K. K. Kundu. J. Chem. Soc. Faraday Trans. I, **74**, 1051 (1978) and references therein; (*b*) I. N. Basumallick and K. K. Kundu. Can. J. Chem. **57**, 961 (1979); (*c*) J. Dutta and K. K. Kundu. Can. J. Chem. **59**, 3141 (1981); (*d*) P. K. Guha and K. K. Kundu. Can. J. Chem. **63**, 798 (1985).
4. R. N. Roy, J. J. Gibons, K. Buechter, and S. Faszhoiz. J. Chem. Thermodyn. **13**, 537 (1981).
5. S. V. Venkateswara and C. Kalidas. J. Chem. Eng. Data, **28**, 5 (1983).
6. M. M. Elsemongy, I. M. Kenawy, and A. S. Fouda. J. Chem. Soc. Faraday Trans. I, **78**, 897 (1982); **78**, 1257 (1982) and references therein.
7. S. P. Rudra, H. Talukdar, and K. K. Kundu. Can. J. Chem. To be published.
8. D. J. G. Ives and J. Janz. Reference electrodes – theory and practice. Academic Press, New York. 1969. p. 208.
9. H. S. Harned and B. B. Owen. Physical chemistry of electrolytic solutions. 3rd ed. Reinhold, New York. 1958. pp. 496, 164.
10. H. B. Hetzer, R. A. Robinson, and R. G. Bates. J. Phys. Chem. **68**, 1929 (1964).
11. N. W. Please. Biochem. J. 196 (1954).
12. R. G. Bates. *In* Hydrogen-bonded solvent systems. *Edited by* A. K. Covington and P. Jones. Taylor and Francis, London. 1968. p. 49.
13. R. A. Pierotti. J. Phys. Chem. **67**, 1840 (1963); **69**, 281 (1965); Chem. Rev. **76**, 717 (1976).
14. J. Datta and K. K. Kundu. (*a*) Can. J. Chem. **61**, 625 (1983); (*b*) J. Phys. Chem. **86**, 4055 (1982).
15. D. E. Irish and A. R. Davis. Can. J. Chem. **46**, 943 (1968).
16. M. M. Vollmar. J. Chem. Phys. **39**, 2236 (1963).
17. D. L. Frost and D. H. James. J. Chem. Soc. Faraday Trans. I, **78**, 3223 (1982).
18. M. Kaminsky. Discuss. Faraday Soc. **24**, 171 (1957).
19. D. Feakins. *In* Physico-chemical processes in mixed aqueous solvents. *Edited by* F. Franks. Heinemann, London. 1967. p. 71.
20. K. K. Kundu and K. Mazumdar. J. Chem. Soc. Faraday Trans. I, **69**, 806 (1973).
21. (*a*) J. Juillard. J. Chem. Soc. Faraday Trans. I, **78**, 43 (1982); (*b*) J. Juillard, C. Tissier, J. Barczynska, J. Mokrzan, and S. Taniewska-Osinska. J. Chem. Soc. Faraday Trans. I, **81**, 3081 (1985).
22. (*a*) P. K. Biswas and M. N. Das. J. Chem. Soc. Faraday Trans. I, **82**, 1973 (1986); (*b*) R. Fuchs, C. P. Hagen, and R. F. Rodewald. J. Phys. Chem. **78**, 1509 (1974).
23. M. H. Abraham, T. Hill, H. C. Ling, R. A. Schuiz, and R. A. C. Watt. J. Chem. Soc. Faraday Trans. I, **80**, 489 (1984).
24. (*a*) K. Miyaji and K. Morinaga. Bull. Chem. Soc. Jpn. **59**, 1695 (1986); (*b*) B. G. Cox, R. Natarajan, and W. E. Waghorne. J. Chem. Soc. Faraday Trans. I, **75**, 86 (1979).
25. M. Booij and G. Somsen. Electrochim. Acta, **28**, 1883 (1983).

Can. J. Chem. Downloaded from www.nrcresearchpress.com by 213.222.148.141 on 09/07/12
For personal use only.

The formation of $(CH_3)_7Si_2^+$ in $(CH_3)_4Si/CH_4$ mixtures and CH_3^- exchange reactions between $(CH_3)_4Si$, $(CH_3)_4Ge$, and $(CH_3)_4Sn$ studied by high pressure mass spectrometry

ANASTASIA C. M. WOJTYNIAK, XIAOPING LI, AND JOHN A. STONE
Chemistry Department, Queen's University, Kingston, Ont., Canada K7L 3N6

Received May 1, 1987

ANASTASIA C. M. WOJTYNIAK, XIAOPING LI, and JOHN A. STONE. Can. J. Chem. **65**, 2849 (1987).

The association equilibrium $(CH_3)_4Si + (CH_3)_3Si^+ \rightleftharpoons (CH_3)_7Si_2^+$ has been studied in a high pressure mass spectrometer ion source using tetramethylsilane/methane mixtures. Measurement of the equilibrium constant over a range of temperatures yields $\Delta H^0 = -22.3 \pm 0.4$ kcal mol^{-1} and $\Delta S^0 = -35.2 \pm 0.9$ cal mol^{-1} K^{-1}. Collision-assisted dissociation experiments suggest that the methyl groups retain their integrity in $(CH_3)_7Si_2^+$. Mixed ions such as $(CH_3)_7SiGe^+$ and $(CH_3)_7GeSn^+$ were not observed in mixtures of $(CH_3)_4X$ and $(CH_3)_4Y$ (X ≠ Y = Si, Ge, Sn). Instead CH_3^- transfer equilibrium reactions were observed viz. $(CH_3)_3Si^+ + (CH_3)_4Ge \rightleftharpoons (CH_3)_4Si + (CH_3)_3Ge^+$ ($\Delta H^0 = -10.2 \pm 1.2$ kcal mol^{-1}, $\Delta S^0 = -3.7 \pm 2.4$ cal K^{-1} mol^{-1}) and $(CH_3)_3Ge^+ + (CH_3)_4Sn \rightleftharpoons (CH_3)_4Ge + (CH_3)_3Sn^+$ ($\Delta H^0 = -8.1 \pm 0.9$ kcal mol^{-1}, $\Delta S^0 = -0.9 \pm 1.6$ cal K^{-1} mol^{-1}). These are in excellent agreement with some published differences in appearance potentials for $(CH_3)_3X^+$ from $(CH_3)_4X$ (X = Si, Ge, Sn).

ANASTASIA C. M. WOJTYNIAK, XIAOPING LI et JOHN A. STONE. Can. J. Chem. **65**, 2849 (1987).

Utilisant des mélanges de tétraméthylsilane/méthane, on a étudié l'équilibre d'association $(CH_3)_4Si + (CH_3)_3Si^+ \rightleftharpoons (CH_3)_7Si_2^+$ dans un spectromètre de masse à haute pression. En mesurant les constantes d'équilibre à diverses températures, on peut en déduire le $\Delta H^0 = -22{,}3 \pm 0{,}4$ kcal mol^{-1} et le $\Delta S^0 = -35{,}2 \pm 0{,}9$ cal mol^{-1} K^{-1}. Des expériences de dissociations assistées par des collisions suggèrent que les groupements méthyles conservent leur identité dans l'ion $(CH_3)_7Si_2^+$. On n'a pas observé la présence d'ions mixtes comme le $(CH_3)_7SiGe^+$ ou le $(CH_3)_7GeSn^+$ dans des mélanges de $(CH_3)_4X$ et $(CH_3)_4Y$ (X ≠ Y = Si, Ge, Sn). Toutefois, on a observé des réactions d'équilibre de transfert de CH_3^-; par exemple, $(CH_3)_3Si^+ + (CH_3)_4Ge \rightleftharpoons (CH_3)_4Si + (CH_3)_3Ge^+$ ($\Delta H^0 = -10{,}2 \pm 1{,}2$ kcal mol^{-1}, $\Delta S^0 = -3{,}7 \pm 2{,}4$ cal K^{-1} mol^{-1}) et $(CH_3)_3Ge^+ + (CH_3)_4Sn \rightleftharpoons (CH_3)_4Ge + (CH_3)_3Sn^+$ ($\Delta H^0 = -8{,}1 \pm 0{,}9$ kcal mol^{-1}, $\Delta S^0 = -0{,}9 \pm 1{,}6$ cal K^{-1} mol^{-1}). Ces valeurs sont en bon accord avec des valeurs publiées pour les différences dans les potentiels d'apparition des ions $(CH_3)_3X^+$ à partir des composés $(CH_3)_4X$ (X = Si, Ge, Sn).

[Traduit par la revue]

Introduction

The ion chemistry of $(CH_3)_4X$ (X = Si, Ge, Sn) is characterized by the formation of $(CH_3)_3X^+$. In the absence of other neutral molecules, $(CH_3)_3X^+$ associates with $(CH_3)_4X$ to yield ions which are described as $(CH_3)_7X_2^+$ although their structures have never been determined. $(CH_3)_7Si_2^+$ (m/z 161) was first reported in the mass spectrum of tetramethylsilane at a pressure of 5×10^{-3} Torr (1). Its formation was ascribed to the reaction

[1] $(CH_3)_4Si^+ + (CH_3)_4Si \rightarrow (CH_3)_7Si_2^+ + CH_3$

The formation of $(CH_3)_7Si_2^+$ was later observed in pure tetramethylsilane in a chemical ionization (CI) source at pressures up to 0.6 Torr (2). The suggested structure for $(CH_3)_7Si_2^+$ contained an Si—Si bond, one of the silicons being in the pentavalent state. This structure was proposed by analogy with pentavalent carbon containing ions such as CH_5^+. It is now known that CH_5^+ is better described in terms of CH_3^+ interacting with H_2, i.e., a structure with essentially a three centre, two electron bond (3). Klevan and Munson (4) studied the formation of $(CH_3)_7Si_2^+$ under similar CI conditions and showed that its relative intensity decreased with increasing ion source temperature. They confirmed, in agreement with ref. 2, that $(CH_3)_7Si_2^+$ is formed mainly by reaction of $(CH_3)_3Si^+$ with tetramethylsilane.

[2] $(CH_3)_3Si^+ + (CH_3)_4Si \rightarrow (CH_3)_7Si_2^+ * \xrightarrow{M} (CH_3)_7Si_2^+$

A kinetic analysis of the ion currents at low pressures and small extents of conversion as functions of temperature yielded an apparent activation energy for reaction [2] of −12 kcal mol^{-1}. Since ion–molecule association reactions have no activation energies the bond energy in the association complex was taken to be 12 kcal mol^{-1}. This is such a weak bond that at the temperatures employed, 343 to 443 K, only the presence of the high concentrations of $(CH_3)_4Si$ could allow observation of the association ion. Such a small binding energy is, however, not consistent with our observation of $(CH_3)_7Si_2^+$ in dilute mixtures (<3%) of tetramethylsilane in methane at 4 Torr and temperatures up to 500 K (5). Under these ion source conditions we never observe complexes with such small dissociation energies. We here report a more detailed study of reaction [2], in particular the determination of the reaction enthalpy and entropy.

We have previously reported the observation of $(CH_3)_7Sn_2^+$ in tetramethylstannane/methane mixtures (6) and of $(CH_3)_7Ge_2^+$ in tetramethylgermane/methane mixtures (7). No information was obtained on the binding energies in the complexes but the experimental conditions under which they were observed indicate binding energies considerably greater than 12 kcal mol^{-1}. Both tin and germanium have numerous stable isotopes and the isotopic patterns of $(CH_3)_7Sn_2^+$ and $(CH_3)_7Ge_2^+$ are complex and cover large m/z ranges. Mixed in with these $(CH_3)_7X_2^+$ ions is $(CH_3)_6X_2OH^+$ a protonated ether formed via the addition of adventitious water to $(CH_3)_3X^+$.

[3] $(CH_3)_3X^+ + H_2O \rightarrow (CH_3)_3XOH_2^+ \xrightarrow{(CH_3)_4X} (CH_3)_7XOH^+ + CH_4$

The spectrum is therefore very complex and we have not attempted to study it further. We have been unsuccessful in our attempts to observe mixed association ions of the form $(CH_3)_7XY^+$ (X ≠ Y = Si, Ge, Sn) but this study has led to

Can. J. Chem. Downloaded from www.nrcresearchpress.com by 213.222.148.141 on 09/07/12
For personal use only.

observation of the CH_3^- transfer reactions described by reaction [4] for which we have been able to obtain both thermochemical and kinetic data.

[4] $(CH_3)_3X^+ + (CH_3)_4Y \rightleftharpoons (CH_3)_4X + (CH_3)_3Y^+$

Experimental

The high pressure ion source mass spectrometer equipped with pulsed electron beam has been described previously as has the method of preparing samples and collecting data (6, 7).

Collision assisted dissociation (CAD) spectra were obtained using a ZAB-2FQ reverse geometry instrument at the Ontario Regional Ion Chemistry Laboratory, Toronto, Canada. In this instrument $(CH_3)_7Si_2^+$ was prepared in 20/1 methane/tetramethylsilane mixtures at ~170°C and an ion source pressure of ~0.2 Torr. The collision gas was helium which was fed into the second field-free region after the magnetic analyzer at pressure sufficient to decrease the $(CH_3)_7Si_2^+$ beam intensity by ~5%.

Tetramethylsilane (MSD Isotopes, Montreal, Canada) and tetramethyltin (Strem Chemicals Inc., Newburyport, MA.) were dried over molecular sieve before use. Tetramethylgermanium (Alfa Inorganic) was purified by gas liquid chromatography to remove tetrahydrofuran and then dried over molecular sieve. Methane was from Matheson and was 99.99% pure.

Results

The normalized ion intensities for a $(CH_3)_4Si/CH_4$ (1/200) mixture after a short ionizing pulse of electrons at similar ion source pressures but two different temperatures are shown in Fig. 1. The reagent ions from methane (CH_5^+ and $C_2H_5^+$) react with $(CH_3)_4Si$ to give $(CH_3)_3Si^+$ and the subsequent reaction of this ion with $(CH_3)_4Si$ and adventitious water leads to the array of ions shown in the figure (5). It is immediately apparent that the reaction leading to $(CH_3)_7Si_2^+$ is much faster than any other reaction of $(CH_3)_3Si^+$ and indeed the build-up of the $(CH_3)_7Si_2^+$ ion intensity is not observed on the time scale shown. It occurs during the electron beam pulse. The parallellism between the yield curves for $(CH_3)_3Si^+$ and $(CH_3)_7Si_2^+$ strongly suggests that the following equilibrium occurs.

[5] $(CH_3)_3Si^+ + (CH_3)_4Si \rightleftharpoons (CH_3)_7Si_2^+$

Computed equilibrium constants for this reaction were found to be independent of total pressure and $(CH_3)_4Si$ concentration. Figure 2 shows the results for a temperature of 431 K when the equilibrium constant may be measured over particularly large ranges of composition and ion source pressure. The van't Hoff plot shown in Fig. 3 yields $\Delta H_5^0 = -22.3 \pm 0.4$ kcal mol^{-1} and $\Delta S_5^0 = -35.2 \pm 0.9$ cal mol^{-1} K^{-1}. This measured binding energy, $D((CH_3)_3Si^+ - (CH_3)_4Si)$ is almost double that suggested by Klevan and Munson (4) and the accompanying very large decrease in entropy shows that a covalent condensation product rather than a much looser cluster is probably being formed. Clustering is associated with standard entropy changes of ~20 cal K^{-1} mol^{-1} (8).

Information regarding the structure of $(CH_3)_7Si_2^+$ (m/z 161) was sought from its unimolecular dissociation and from ions formed by its collision assisted dissociation. The ion source conditions in the ZAB-2FQ instrument were not comparable to those in the high pressure, field-free ion source in which the thermochemical measurements were made. The much lower pressure in the more open source allowing some acceleration field penetration and the high ambient ion source temperature in the ZAB-2FQ almost certainly led to the ions under study being non-thermalized. For example, in the low pressure ZAB-2FQ source m/z 145 and 131 were equally as prominent as m/z 161

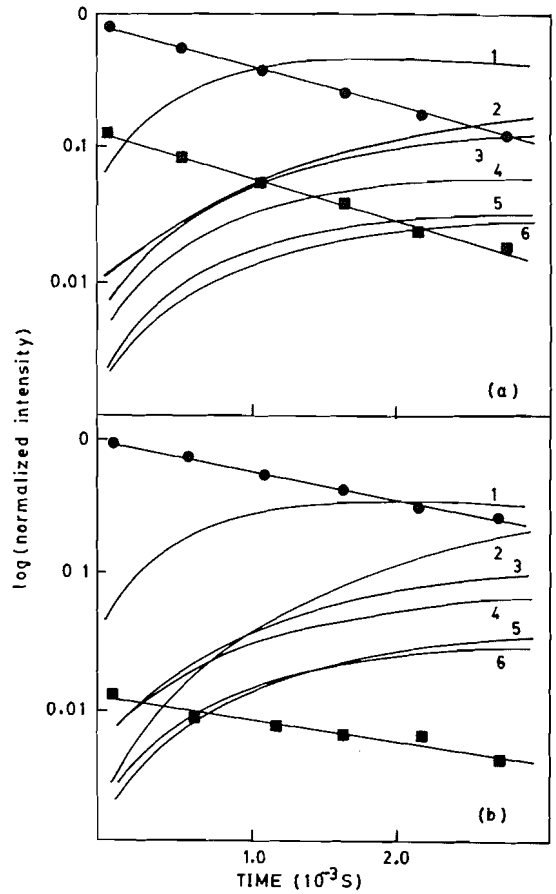

FIG. 1. Normalized ion intensities vs. time after a 30 μs ionizing pulse of electrons in a tetramethylsilane/methane (1/200) mixture at 4.5 Torr and (*a*) 429 K and (*b*) 468 K. ● $(CH_3)_3Si^+$, ■ $(CH_3)_7Si_2^+$. For clarity the experimental points are not shown for the other ions. The curves are for: *1*, $(CH_3)_3SiOH_2^+$; *2*, $(CH_3)_6Si_2OH^+$; *3*, $(CH_3)_3Si_2^+$; *4*, $(CH_3)_6Si_2H^+$; *5*, $C_4H_{13}SiO^+$; *6*, $C_4H_{11}SiO^+$.

whereas m/z 131 was small in the high pressure source and m/z 145 was never observed. m/z 145 and 131 have been reported in earlier CI studies (2, 4, 9) and in particular m/z 145 increased in yield with increasing pressure. Klevan and Munson (4) report that m/z 145 is kinetically one order higher than m/z 161 and that it arises from the reaction of m/z 161 with tetramethylsilane, although the nature of this reaction is not spelled out.

The unimolecular and the CAD spectra of $(CH_3)_7Si_2^+$ are shown in Table 1. There are only three significant ions in the unimolecular spectrum and it is to be noted that m/z 145 is not one of them and indeed it is absent from the spectrum. H_2 loss leads to m/z 159, an ion whose intensity is only ~1% of that of m/z 161 in the main beam. The major unimolecular decomposition leads to regeneration of $(CH_3)_3Si^+$. It could not be determined whether the two silicon atoms in the reactants which form $(CH_3)_7Si_2^+$ lose their identities or whether the reversal of reaction [5] preserves the initial identities. The only other significant unimolecular dissociation leads to m/z 87 which arises by loss of trimethylsilane.

[6] $(CH_3)_7Si_2^+ \rightarrow C_4H_{11}Si^+ + (CH_3)_3SiH$
(m/z 87)

The yields in the CAD spectrum relative to those in the unimolecular spectrum show slight reductions in relative abundances for all the common ions but the absolute intensites

Can. J. Chem. Downloaded from www.nrcresearchpress.com by 213.222.148.141 on 09/07/12
For personal use only.

Can. J. Chem. Downloaded from www.nrcresearchpress.com by 213.222.148.141 on 09/07/12
For personal use only.

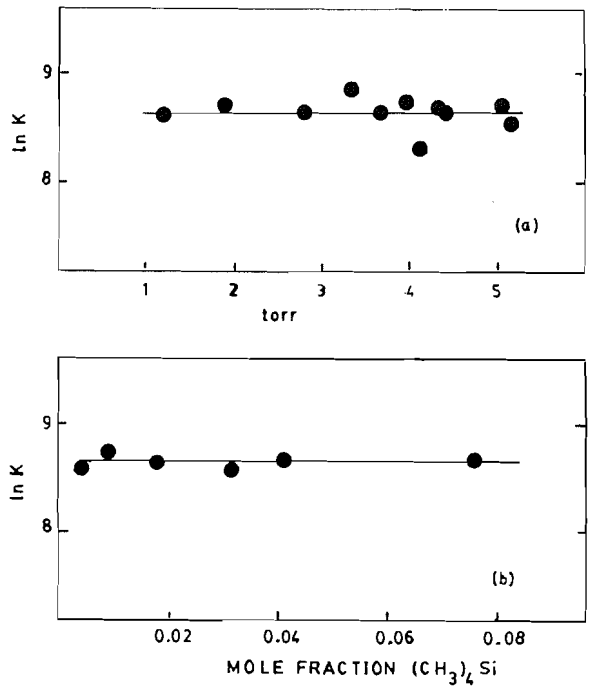

FIG. 2. The constancy with (*a*) total ion source pressure and (*b*) mole fraction of $(CH_3)_4Si$ of the equilibrium constant for the reaction $(CH_3)_4Si + (CH_3)_3Si^+ \rightleftharpoons (CH_3)_7Si_2^+$. Temperature 431 K. Mole fraction $(CH_3)_4Si$ in (*a*) is 0.018; ion source pressure in (*b*) is ~4 Torr.

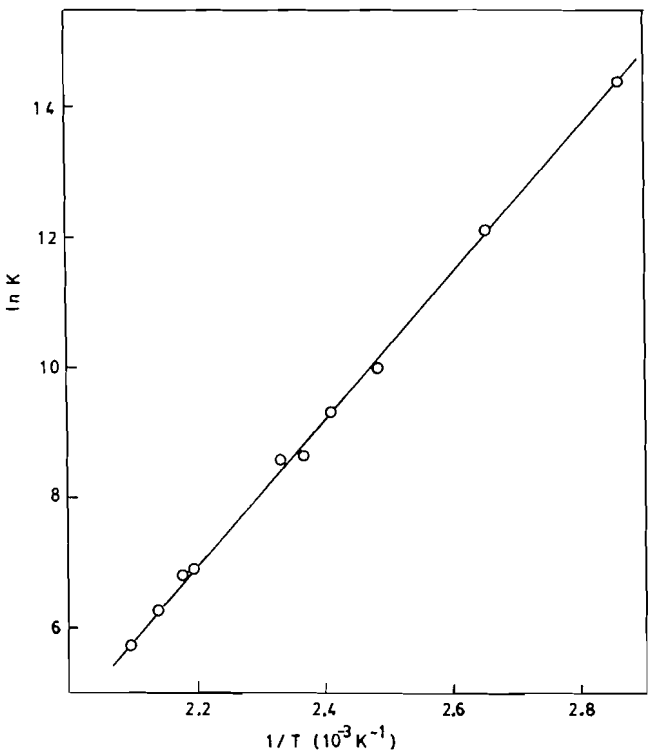

FIG. 3. van't Hoff plot for the equilibrium $(CH_3)_3Si^+ + (CH_3)_4Si \rightleftharpoons (CH_3)_7Si_2^+$.

are actually much greater, i.e., these ions are also produced as major ions by collsional excitation. The loss of $(CH_3)_4Si$ to give $(CH_3)_3Si^+$ accounts for 75% of total decomposition in both unimolecular and CAD spectra. In the CAD spectrum the groups of peaks around m/z values, 145, 131, 115 attest to the losses of 1, 2, and 3 methyl groups leaving ions still retaining both Si atoms. The most significant of these is m/z 145 resulting from the loss of CH_4.

TABLE 1. Relative abundances of fragment ions from m/z 161 in MIKE spectra

			Relative abundance	
m/z	Ion	Loss	Unimolecular	CAD[a]
160	$C_7H_{20}Si_2^+$	H	—	2
159	$C_7H_{19}Si_2^+$	H_2	10	5
146	$C_6H_{18}Si_2^+$	CH_3	—	2
145	$C_6H_{17}Si_2^+$	CH_4	—	4
133	$C_5H_{17}Si_2^+$	C_2H_4	2	1
131	$C_5H_{15}Si^{2+}$	C_2H_6	—	1
129	$C_5H_{13}Si^{2+}$		—	1
119	$C_4H_{15}Si_2^+$	C_3H_6	2	—
117	$C_4H_{13}Si_2^+$	C_3H_8	—	1
115	$C_4H_{11}Si_2^+$	$C_3H_8 + H_2$	—	1
101	$C_3H_9Si_2^+$	$C_4H_{10} + H_2$	1	2
87	$C_4H_{11}Si^+$	$(CH_3)_3SiH$	11	3
73	$(CH_3)_3Si^+$	$(CH_3)_4Si$	74	76

[a]He introduced as collision gas.

[7] $(CH_3)_7Si_2^+ \rightarrow C_6H_{17}Si_2^+ + CH_4$
(m/z 145)

The observation of this ion in earlier CI studies and in particular the kinetics of its formation observed by Klevan and Munson (4) show that it was most probably formed by the collisional dissociation of $(CH_3)_7Si_2^+$. m/z 145 was observed in the mass spectrum of tetramethylsilane/methane mixtures under CI conditions in the ZAB-2FQ but since no unimolecular dissociation corresponding to reaction [7] was observed it must be formed in a very fast reaction involving an excited $(CH_3)_7Si_2^+$.

$(CH_3)_7Si_2^+$ has been described as $(CH_3)_3Si—Si(CH_3)_4^+$ (2), $(CH_3)_3SiCH_2Si(CH_3)_3H^+$ (1), and as a product of the insertion of $(CH_3)_3Si^+$ into either an Si—C or C—H bond of $(CH_3)_4Si$ (4). The first structure involving a silicon–silicon bond can be ruled out since it involves the formation of pentavalent silicon. Neutral hypervalent silicon compounds have only been observed in structurally stabilized species with electron donor ligands such as oxygen atoms (10) or in anions (11). The electrophilic $(CH_3)_3)Si^+$ cation is not expected to induce hypervalency in the silicon of $(CH_3)_4Si$. SiH_5^+ (like CH_5^+) is best described as H_3Si^+ added across H—H (12). The second structure appears to be the equivalent of a protonated, substituted methane which would be unstable towards proton transfer. There is no evidence for m/z 161 being a Brønsted acid. The two possible structures resulting from insertion are:

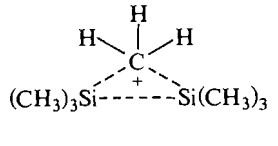

I

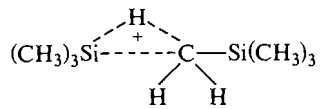

II

Klevan and Munson (4) favoured **I** over **II** for several reasons. They surmised that hydride transfer to yield m/z 87 (reaction [6]) would be sufficiently endothermic for **II** to prevent its decomposition by this path. In addition they suggested that **I** can

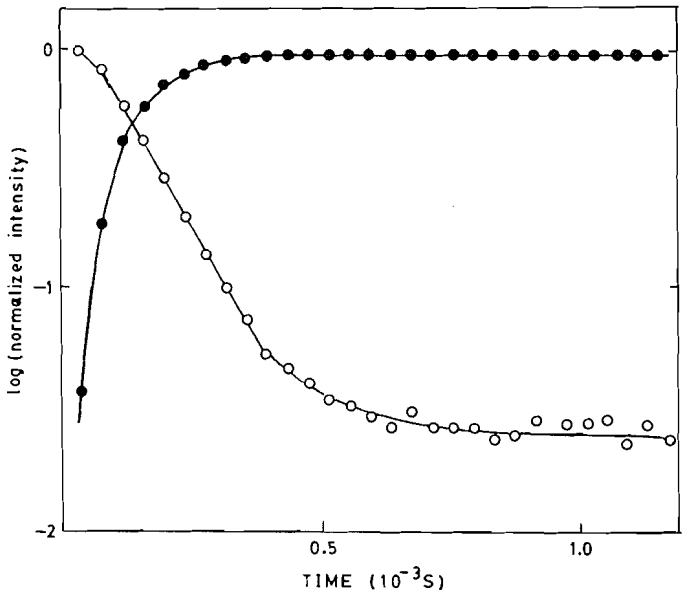

FIG. 4. The normalized intensities of $(CH_3)_3Sn^+$ ● and $(CH_3)_3Ge^+$ ○ in a $(CH_3)_4Sn/(CH_3)_4Ge/CH_4$ (0.0053/0.00026/1) mixture at 2.45 Torr and 565 K. The equilibrium constant for the CH_3^- transfer process $(CH_3)_3Ge^+ + (CH_3)_4Sn \rightleftharpoons (CH_3)_4Ge + (CH_3)_3Sn^+$ is obtained from the constant ratio of normalized ion intensities at long reaction times. The rate constant for the forward reaction is obtained from the slope of the initial linear portion of the $(CH_3)_3Ge^+$ curve.

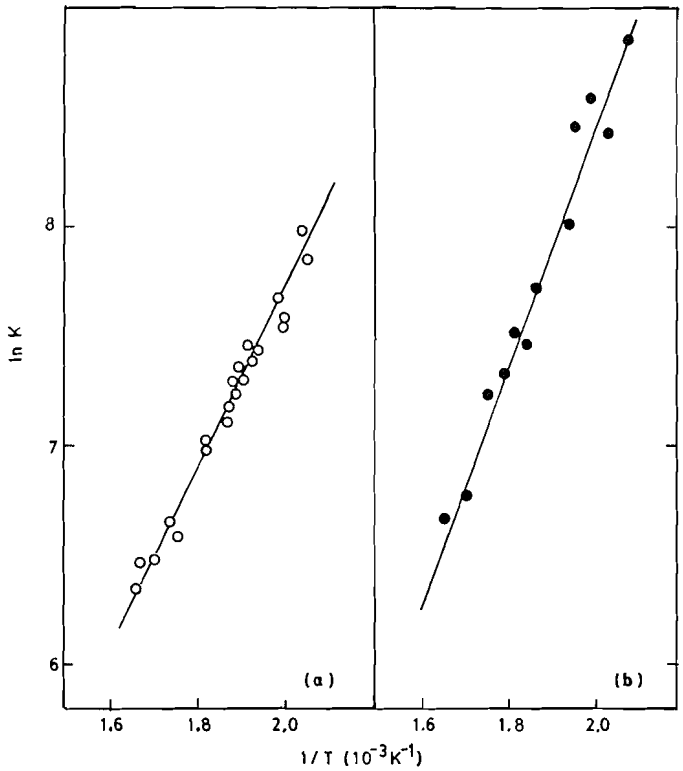

FIG. 5. van't Hoff plots for the equilibria (*a*) $(CH_3)_3Ge^+ + (CH_3)_4Sn \rightleftharpoons (CH_3)_4Ge + (CH_3)_3Sn^+$ and (*b*) $(CH_3)_3Si^+ + (CH_3)_4Ge \rightleftharpoons (CH_3)_4Si + (CH_3)_3Ge^+$.

react more readily than **II** by elimination of methane to give m/z 145 (reaction [7]). They also made analogies with carbon chemistry which are not supported by later experimental and theoretical results. For example, Hiraoka and Kebarle examined the reaction of $C_2H_5^+$ with ethane and provide thermodynamic data consistent with insertion into the alkane C—H bond followed by further rearrangement leading to loss of molecular hydrogen (13). We have shown above that reaction [7] involves an excited m/z 161 and therefore Klevan and Munson's arguments regarding ions in their ground states are not valid. Hydrogen loss is observed and m/z 145 is absent in the unimolecular decomposition spectrum m/z 161 and by analogy with Hiroaka and Kebarle's results a case may be made for structure **II**. Our experiments do not allow us to decide in favour of one structure or the other. We have found, however, that CH_3^- transfer occurs in mixtures of trimethylsilylalkyl compounds under CI conditions (14). Such reactions most probably proceed via a complex of the form $(CH_3)_6Si_2R^+$ which implies that a structure such as **I** is present on the reaction coordinate.

Methide transfer reactions

Since $(CH_3)_7X_2^+$ ions were found for X = Si, Ge, and Sn a search was made using the high pressure source for mixed ions, e.g., $(CH_3)_7SiGe^+$ in $(CH_3)_4Ge/(CH_3)_4Si/CH_4$ mixtures. None was ever observed. We also failed to observe the mixed ion $(CH_3)_7CSi^+$ in $(CH_3)_4C/(CH_3)_4Si/CH_4$ mixtures whose existence was speculated upon by Klevan and Munson (4). They could not draw any conclusion regarding its presence in their system since $(CH_3)_7CSi^+$ (m/z 145) is isobaric with $(CH_3)_5Si_2^+$. We had no such problem. In such "mixed" systems each of the different $(CH_3)_7X_2^+$ ions (X = Si, Ge, Sn) could be observed under suitable conditions, the relative yields, however, being regulated by the competing CH_3^- transfer reactions [8]–[10].

[8] $(CH_3)_3Si^+ + (CH_3)_4Ge \rightleftharpoons (CH_3)_4Si + (CH_3)_3Ge^+$

[9] $(CH_3)_3Si^+ + (CH_3)_4Sn \rightleftharpoons (CH_3)_4Si + (CH_3)_3Sn^+$

[10] $(CH_3)_3Ge^+ + (CH_3)_4Sn \rightleftharpoons (CH_3)_4Ge + (CH_3)_3Sn^+$

Equilibria [8] and [10] could be studied under suitable experimental conditions as illustrated in Fig. 4. The van't Hoff plots in Fig. 5 provide the thermodynamic data in Table 2. The error limits in Table 2 are one standard deviation from a least squares regression analysis of the data. These error limits are <6% of the absolute values of ΔH^0. The equilibrium constant for reaction [9] is very large and it was possible to attain equilibrium at long reaction times only at the highest attainable temperature (600 K). The measured equilibrium constant gave $\Delta G_9^0 = -15.9$ kcal mol^{-1} in excellent agreement with the sum $\Delta G_8^0 + \Delta G_{10}^0 = -15.7$ kcal mol^{-1} at the same temperature.

$(CH_3)_7XY^+$ ions are probably formed as unstable intermediates in reactions [8], [9], and [10] but fast exothermic, bimolecular dissociation precludes collisional stabilization. It might be possible to observe these weakly bonded complexes as stabilized ions by working at significantly higher pressure or at sub-ambient temperatures. Neither of these options is presently available in our laboratory.

Experimentally determined enthalpies of formation of silicon, germanium, and tin compounds are few and those that are available are not mutually consistent. Walsh (15, 16) has discussed the available data for some organosilicon compounds and cations and notes the high uncertainties prevalent in the literature for their enthalpies of formation. In particular and relevant to this study, $\Delta H_f^0((CH_3)_3Si^+)$ has a spread in literature values from 141 to 151 kcal mol^{-1}. There are similar uncertainties in the measured enthalpies of formation of neutral

Can. J. Chem. Downloaded from www.nrcresearchpress.com by 213.222.148.141 on 09/07/12
For personal use only.

TABLE 2. Thermodynamic data for the equilibria $(CH_3)_3X^+ + (CH_3)_4Y \rightleftharpoons (CH_3)_4X + (CH_3)_3Y^+$

X	Y	$-\Delta H^{0a}$ (kcal mol^{-1})	$-\Delta S^{0a}$ (cal K^{-1} mol^{-1})	$-\Delta H^0$(calc)^b (kcal mol^{-1})
Si	Ge	10.2 ± 0.6^c	3.7 ± 1.2	9.8
Ge	Sn	8.1 ± 0.5	0.9 ± 0.8	8.1
Si	Sn	18.4^d	4.6 ± 2.0^e	17.9

[a]Thermodynamic data from Fig. 5.
[b]Calculated from standard enthalpies of formation in ref. 21.
[c]Error limits are one standard deviation from a least-squares analysis.
[d]Calculated using the experimentally determined $\Delta G^0_{600} = -15.9$ kcal mol^{-1} and $\Delta S^0 = 4.6$ cal M^{-1} mol^{-1}.
[e]The sum of the two above values.

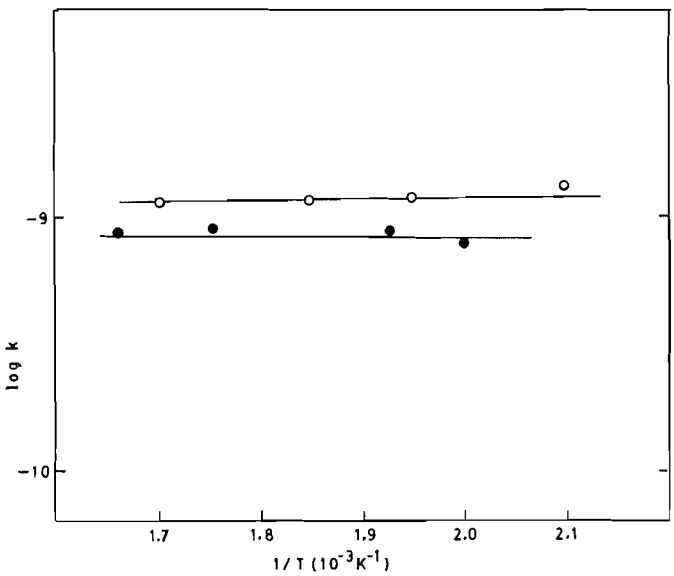

FIG. 6. Rate constants for CH_3^- transfer: ○, $(CH_3)_3Si^+ + (CH_3)_4Ge \rightarrow (CH_3)_4Si + (CH_3)_3Ge^+$; ●, $(CH_3)_3Ge^+ + (CH_3)_4Sn \rightarrow (CH_3)_4Ge + (CH_3)_3Sn^+$. The units of k are cm^3 molecule^{-1} s^{-1}.

organosilicon compounds. For example a tabulated value of -58.7 ± 2.4 kcal mol^{-1} (17) for $\Delta H_f^0((CH_3)_4Si)$ is close to a more recently determined value of -55.4 kcal mol^{-1} (18) but both are very different from the mass spectrometric value of -42.4 kcal mol^{-1} (19) favoured by Davidson (20) in his listing of self-consistent enthalpies of formation of the methylsilanes.

Relevant thermochemical data for silicon, germanium, and tin neutrals and ions are contained in a set of internally "self-consistent" values based on mass spectrometric ionization and appearance energies (21). The preferred value of $\Delta H_f^0((CH_3)_4Si) = -48.25$ kcal mol^{-1} is considerably different from the -55.4 kcal mol^{-1} preferred by Walsh (16) in his critical analysis of the thermochemistry of some silicon compounds. $\Delta H_f^0((CH_3)_4Ge) = -32.0 \pm 3.0$ kcal mol^{-1} is estimated in ref. 16 using unpublished results on $(C_2H_5)_4Ge$ and an assumed small correction for the change from ethyl to methyl. This value is lower than a recent bomb calorimetric determination of -24.5 ± 2.0 kcal mol^{-1} (22) and much lower than the value of -16.9 ± 2.3 kcal mol^{-1} given in a later compendium of thermochemical data (17). The latter collection does, however, retain essentially the same value of -3.35 kcal mol^{-1} for $\Delta H_f^0((CH_3)_4Sn)$.

Obviously there are no "accepted values" of thermochemical data with which to compare the present results. Surprisingly the results from these methide transfer experiments are in remarkably good agreement with the "self consistent" data of ref. 21 as shown in Table 2. This becomes understandable if the enthalpy change for CH_3^- transfer is written in terms of X—C bond dissociation energies, $D((CH_3)_3X—CH_3)$ and ionization energies of the trimethyl radicals, IE$((CH_3)_3X)$. For example, for reaction [8]:

$$\Delta H^0 = \mathrm{IE}((CH_3)_3Ge) + D((CH_3)_3Ge—CH_3) - \mathrm{IE}((CH_3)_3Si) - D((CH_3)_3Si—CH_3) = \mathrm{AP}((CH_3)_3Ge^+) - \mathrm{AP}((CH_3))_3Si^+)$$

$\mathrm{AP}((CH_3)_3X^+)$ is the appearance energy of $(CH_3)_3X^+$ from $(CH_3)_4X$. The concordance of our CH_3^- transfer results therefore validates the *relative* AP values for $(CH_3)_3Si^+$, $(CH_3)_3Ge^+$, and $(CH_3)_3Sn^+$ used in ref. 21 to derive ΔH_f^0 values. The absolute values are probably not too accurate, for example $\mathrm{AP}((CH_3)_3Si^+) = 242.4 \pm 4.6$ kcal mol^{-1} compared with a value of 235.95 ± 6.2 kcal mol^{-1} deducible from the data of Walsh (16) which is in agreement with the experimental 236.5 kcal mol^{-1} of Potzinger, Ritter, and Krause (19). The wide error limits for each value attest to the present state of knowledge.

Using the latest calorimetric value of $\Delta H_f^0((CH_3)_4Ge) = -24.5$ kcal mol^{-1} (22) together with $\Delta H_f^0((CH_3)_3Si^+) = 145.8$ kcal mol^{-1} (15), $\Delta H_f^0((CH_3)_4Si) = -55.7$ kcal mol^{-1} (18), and $\Delta H_8 = -10.2$ kcal mol^{-1} then $\Delta H_f^0((CH_3)_3Ge^+) = 166.8$ kcal mol^{-1}. This value, together with $\Delta H_f^0(\cdot CH_3) = 34.4$ kcal mol^{-1} (23) yields an appearance energy for $(CH_3)_3Ge^+$ from $(CH_3)_4Ge$ of 225.7 kcal mol^{-1} (9.79 eV). This is a significantly lower value than the 10.05 eV of ref. 21 but is tied to the more acceptable appearance potential for $(CH_3)_3Si^+$ from $(CH_3)_4Si$ of 10.23 eV calculable from the data of ref. 15.

Methide transfer equilibrium measurements such as the ones described in this paper provide precise information on appearance potential differences and might be used to more precisely define the thermochemistry of gas phase silicon ions and molecules if a link could be established by equilibrium methods to ions and neutrals with known thermochemical properties. We have been unsuccessful so far in establishing such a link to either hydrocarbons or halocarbons. We are pursuing such ideas.

The rate constants for methide ion transfer were measured for the forward directions of reactions [8] and [10]. Both reactions proceed with virtually unit efficiency; the calculated Langevin collision rate constants are 1.22×10^{-9} and 1.06×10^{-9} cm^3 molecule^{-1} s^{-1} for reactions [8] and [10], respectively. As seen in Fig. 6 the rate constants are independent of temperature as expected for fast exothermic reactions involving non-polar neutrals.

Acknowledgements

The authors thank the Natural Sciences and Engineering Research Council of Canada for financial assistance. The advice and assistance of Drs. A. G. Harrison and A. B. Young is gratefully acknowledged. A referee is thanked for pointing out ref. 22.

1. P. POTZINGER and F. W. LAMPE. J. Phys. Chem. **75**, 13 (1971).
2. T. J. ODIORNE, D. J. HARVEY, and P. VOUROS. J. Phys. Chem. **76**, 3217 (1972).
3. K. HIRAO and S. YAMABE. Chem. Phys. **89**, 237 (1984).
4. L. KLEVAN and B. MUNSON. Int. J. Mass Spectrom. Ion Phys. **13**, 261 (1974).

Can. J. Chem. Downloaded from www.nrcresearchpress.com by 213.222.148.141 on 09/07/12
For personal use only.

5. A. C. M. WOJTYNIAK and J. A. STONE. Int. J. Mass Spectrom. Ion Proc. **74**, 59 (1986).
6. J. A. STONE and D. E. SPLINTER. Can. J. Chem. **59**, 1779 (1981).
7. J. A. STONE and W. J. WYTENBERG. Can. J. Chem. To be published.
8. M. MEOT-NER, M. M. ROSS, and J. E. CAMPANA. J. Am. Chem. Soc. **107**, 4839 (1985).
9. J. R. KRAUSE and P. POTZINGER. Int. J. Mass Spectrom. Ion Phys. **18**, 303 (1975).
10. J. C. MARTIN, W. H. STEVENSONA, and D. Y. LEE. *In* Organosilicon and bioorganosilicon chemistry. *Edited by* H. Sakurai. Ellis Horwood, Chichester, England. 1985. p. 137.
11. R. R. SQUIRES. Proceedings 34th Annual Conference on Mass Spectrometry and Allied Topics, Cincinnati, OH. June 1986.
12. S. IKUTA, S. K. SUDOH, S. KATAGISI, and O. NOMURA. *In* Applied quantum chemistry. *Edited by* V. H. Smith, H. F. Schaefer, and K. Mosokuma. D. Reidel Publishing Co., Dordrecht, Holland. 1986. p. 313.
13. K. HIRAOKA and P. KEBARLE. Can. J. Chem. **58**, 2262 (1980).
14. X. LI and J. A. STONE. To be published.
15. R. WALSH. J. Phys. Chem. **90**, 389 (1986).
16. R. WALSH. Acc. Chem. Res. **14**, 246 (1981).
17. J. B. PEDLEY and J. RYLANCE. N.P.L. computer analysed thermochemical data. University of Sussex, Sussex, England. 1977.
18. W. V. STEELE. J. Chem. Thermodyn. **15**, 595 (1983).
19. P. POTZINGER, A. RITTER, and J. KRAUSE. Z. Naturforsch. **30**a, 347 (1975).
20. I. M. T. DAVIDSON. J. Organomet. Chem. **170**, 365 (1979).
21. M. F. LAPPERT, J. B. PEDLEY, J. SIMPSON, and T. R. SPALDING. J. Organomet. Chem. **29**, 195 (1971).
22. L. H. LONG and C. I. PULFORD. J. Chem. Soc. Faraday 2, **82**, 567 (1986).
23. J. C. TRAEGER and R. G. MCLOUGHLIN. J. Am. Chem. Soc. **103**, 3647 (1981).

Can. J. Chem. Downloaded from www.nrcresearchpress.com by 213.222.148.141 on 09/07/12
For personal use only.

Platinum complexes with sterically demanding ligands: *trans*-bis(2,7-diazatetracyclo[6.3.0.0^{4,9}.0^{5,11}]undecane-*N*,*N*′)platinum(II) dichloride tetrahydrate

B. E. Brown, R. Faggiani, D. Hughes, and C. J. L. Lock[1]

The Laboratories for Inorganic Medicine, McMaster University, SSC-426, Hamilton, Ont., Canada L8S 4M1

Received May 7, 1987

B. E. Brown, R. Faggiani, D. Hughes, and C. J. L. Lock. Can. J. Chem. **65**, 2855 (1987).

The complex $[Pt(C_9H_{14}N_2)_2]Cl_2.4H_2O$ was isolated from a reaction mixture containing $K_2[PtCl_4]$ and a norbornane-based diamine, $C_9H_{14}N_2$. This product was analyzed with use of elemental analysis, nuclear magnetic resonance spectroscopy, and X-ray crystallography. $[Pt(C_9H_{14}N_2)_2]Cl_2.4H_2O$ crystallized in the triclinic system, space group $P\bar{1}$, a = 9.437(1) Å, b = 9.975(1) Å, c = 6.888(1) Å, α = 109.54(1)°, β = 109.71(1)°, γ = 93.63(1)°, Z = 1. The X-ray data were collected with use of a Syntex $P2_1$ diffractometer and MoKα radiation and the structure solved by the heavy atom method. Based on 1983 reflections, the structure was refined to R = 0.0310 and R_w = 0.0408. The platinum resides on an inversion center and is coordinated to the nitrogen atoms of the secondary amines. The chelating N—Pt—N angle is 79° but otherwise the bond lengths and angles agree well with values for similar structures.

B. E. Brown, R. Faggiani, D. Hughes et C. J. L. Lock. Can. J. Chem. **65**, 2855 (1987).

On a isolé le complexe $[Pt(C_9H_{14}N_2)_2]Cl_2.4H_2O$ d'un mélange réactionnel contenant du $K_2[PtCl_4]$ et une diamine, $C_9H_{14}N_2$, dérivée du norbornane. On a analysé ce produit en faisant appel à l'analyse centésimale, à la résonance magnétique nucléaire et à la diffraction des rayons-X. Le $[Pt(C_9H_{14}N_2)_2]Cl_2.4H_2O$ cristallise dans le système triclinique, groupe d'espace $P\bar{1}$, avec a = 9,437(1), b = 9,975(1) et c = 6,888(1) Å, α = 109,54(1), β = 109,71(1) et γ = 93,63(1)° et Z = 1. On a accumulé les données à l'aide d'un diffractométre Syntex $P2_1$ et de la radiation MoKα et on a résolu la structure par la méthode des atomes lourds. En se basant sur 1983 réflexions, on a affiné la structure jusqu'à des valeurs de R = 0,0310 et R_w = 0,0408. Le platine se trouve sur un centre d'inversion et il est coordonné aux atomes d'azote des amines secondaires. L'angle de chélation N—Pt—N est de 79°; par ailleurs, les longueurs des liaisons et les angles sont en bon accord avec les valeurs observées dans des structures semblables.

[Traduit par la revue]

Introduction

The anti-cancer drug *cis*-dichlorodiammineplatinum(II), cisplatin, represents a group of platinum(II) complexes that show anti-tumour activities (1). The major drawback to administering cisplatin is its renal toxicity (2). It has been shown, however, that replacement of the amine ligands by either cyclic amines or bulky amines reduces the toxicity (3, 4). We have attempted to prepare platinum complexes of the bulky polycyclic amine 2,7-diazatetracyclo[6.3.0.0^{4,9}.0^{5,11}]undecane, $C_9H_{14}N_2$. Two compounds were isolated from the reaction, the first a brown, insoluble powder, probably of a polymeric nature, and the second as colourless, plate-like crystals. This second compound was identified by single crystal X-ray diffraction and was shown to be *trans*-bis(2,7-diazatetracyclo[6.3.0.0^{4,9}.0^{5,11}]undecane-*N*,*N*′)platinum(II) dichloride tetrahydrate, **A**. The compounds were also examined by infrared and ^{1}H and ^{13}C nmr spectroscopy. The expected 1:1 platinum:diamine complex, *cis*-dichloro(2,7-diazatetracyclo[6.3.0.0^{4,9}.0^{5,11}]undecane-*N*,*N*′)-platinum(II), **B**, was not isolated.

Experimental procedures

The 2,7-diazatetracyclo[6.3.0.0^{4,9}.0^{5,11}]undecane was supplied by Dr. D. N. Butler at York University, Toronto, Ontario. The $K_2[PtCl_4]$ was prepared according to Kauffman and Cowan (5).

Preparation of $[Pt(C_9H_{14}N_2)_2]Cl_2.4H_2O$, A

A was prepared by dissolving 0.344 g $K_2[PtCl_4]$ (0.83 mmol) and 0.125 g of $C_9H_{14}N_2$ (0.83 mmol) in 50 mL of N_2-purged distilled water. The reaction was carried out under a nitrogen atmosphere, with the exclusion of light. The pH was maintained at 7.0–7.5 by reaction, as necessary, with dilute aqueous $NaHCO_3$ and HCl solutions. After 5 h a light brown powder had formed and was filtered off and the colourless filtrate evaporated to yield colourless plate-like crystals (yield ≤10%).

Infrared spectra were recorded on a Perkin-Elmer 283 grating spectrometer in the range 4000–200 cm^{-1}. The samples were prepared as KBr pellets. Spectra were calibrated against polystyrene and indene. Raman spectra from powder samples were excited by a Coherent Radiation Argon Laser Model 52 and measured in the range 3000–50 cm^{-1} on a Spex spectrometer Model 14018. Satisfactory spectra were obtained from the ligand, but the platinum complex, **A**, decomposed in the beam, even when the sample was cooled to 77 K. Spectral calibrations were made with use of $HgCl_2$.

Proton nmr spectra were recorded at 500.137 MHz on a Bruker AM-500 spectrometer. The single-pulse spectra were recorded over a 5.0 kHz sweep width in 32K data points (3.277 s acquisition time). Suppression of the HDO resonance was achieved by pre-saturation during the 1.0 s delay before acquisition. Sample temperature was maintained at 30 ± 1°C by a Bruker B-VT1000 variable temperature unit. The free induction decays were processed with use of Gaussian multiplication for resolution enhancement.

The ^{13}C nmr spectra were obtained at 125.759 MHz over a sweep width of 29.4 kHz in 32K data points (0.557 s acquisition time). A 2 Hz exponential line broadening was applied to the FID before Fourier transformation. The number of directly bonded protons was determined with use of the standard J-modulated spin echo pulse sequence with a 1.0 s relaxation delay and ^{13}C 90° pulse of 6.8 μs.

The ^{1}H COSY 2-D nmr spectra of the diamine were acquired with use of the pulse sequence 90°–z–90° sequence. The 90° ^{1}H pulse on the 5 mm dual frequency probe was 18.0 μs. The HDO resonance was suppressed by pre-saturation during the 2.0 s relaxation delay and evolution time before acquisition. Spectra were acquired over a sweep width of 1449.28 Hz in 1K data points in F2 with 64 scans for each of the 256 FID's. Zero-filling in the F1 dimension during 2-D Fourier transformation produced a 512 × 512 data matrix with a digital resolution of 2.831 Hz/point in both dimensions. All spectra were transformed with the application of the squared sine-bell function in both dimensions, followed by symmetrization of the transformed matrix.

[1]To whom correspondence should be addressed.

Can. J. Chem. Downloaded from www.nrcresearchpress.com by 213.222.148.141 on 09/07/12
For personal use only.

Can. J. Chem. Downloaded from www.nrcresearchpress.com by 213.222.148.141 on 09/07/12
For personal use only.

TABLE 1. Crystal data for $[Pt(C_9H_{14}N_2)_2]Cl_2.4H_2O$

Compound	$[Pt(C_9H_{14}N_2)_2]Cl_2.4H_2O$, $C_{18}H_{36}Cl_2N_4O_4Pt$
f.w. (Daltons)	638.45
Crystal size (mm)	Cylinder, $r = 0.095$, $l = 0.45$
Systematic absences	None
Space group	$P\bar{1}$ (No. 2)
Unit cell parameters (Å and deg)	$a = 9.437(1)$, $\alpha = 109.54(1)$
	$b = 9.975(1)$, $\beta = 109.71(1)$
	$c = 6.888(1)$, $\gamma = 93.63(1)$
Volume (Å^3)	563.8(1)
Z	1
μ, linear absorption coefficient (cm^{-1})	6.81
ρ_{calc}, ρ_{obs} (g cm^{-3})	1.880, 1.883(4) in $CHCl_3/CH_2I_2$ mixture
Standard reflections (esd %)	3 1 $\bar{4}$ (1.4), 4 4 $\bar{1}$ (1.7)
Max 2θ, reflections	50°, $h \pm k \pm l$
Temperature (°C)	22
Total number of reflections measured	2113
Number of independent reflections	1983
Number with $I > 0$ (used)	1983
R_{int}	0.0216
Final R, R_w[a]	0.0310, 0.0408
Final shift/error max (ave.)	0.339, (0.004)
Final difference map	
highest peak, lowest valley (e Å^{-3})	1.081, −1.432
Weighting	$w = (\sigma_F^2 + 0.001126F_o^2)^{-1}$
Secondary extinction correction (x)[b]	0.0066(13)
$F(000)$	314.0
Number of variables	190
Error in obs. of unit wt.	1.1914

[a] $R = [\Sigma||F_o| - |F_c||]/\Sigma|F_o|$; $R_w = (\Sigma w(|F_o| - |F_c|)^2/\Sigma wF_o^2)^{1/2}$.

[b] x is the secondary extinction factor given by the equation $F_c^* = F_c(1 - 0.0001(x)F_c^2/\sin\theta)$, where F_c^* and F_c are the values of the calculated structure factor corrected and not corrected for secondary extinction.

Samples were dissolved in 99.8% D_2O (MSD Isotopes) to concentrations of 3×10^{-4} M for the diamine and 1×10^{-4} M for the Pt-complex. Proton chemical shifts are reported in ppm relative to external sodium 4,4-dimethy-4-silapentan-1-sulfonate while ^{13}C chemical shifts are in ppm relative to external tetramethylsilane.

Collection of diffraction data and structure solution

A colourless, plate-like crystal was cut and ground to an acicular crystal of suitable size and sealed in a Lindemann capillary. Space groups $P1$ or $P\bar{1}$ were consistent with precession photographs. The latter was chosen and justified by the successful solution of the structure. A Delaunay reduction revealed no hidden symmetry. The cell parameters were determined by a least-squares refinement based on 15 automatically centered independent reflections in the range $21° \leq 2\theta \leq 29°$. Intensities were measured at 22°C on a Syntex $P2_1$ diffractometer with the use of graphite monochromatized MoKα radiation ($\lambda = 0.71069$ Å). Crystal data and other numbers related to data collection are summarized in Table 1. Corrections were made for Lorentz-polarization and absorption.[2]

The platinum atom was located on the inversion center, 0,0,0. The positions of the remaining atoms were obtained from subsequent full-matrix least-squares refinement and electron density difference calculations. Further refinement with use of anisotropic temperature factors for all non-hydrogen atoms, minimized $\Sigma w(|F_o| - |F_c|)^2$ until the final maximum shift/error was $\simeq 0.3$. Corrections were made for secondary extinction by the SHELX method (6). Scattering curves were taken from Cromer and Waber (7). Anomalous dispersion corrections were applied to the scattering curves for Pt and Cl (8). The atom parameters are listed in Table 2.[3]

TABLE 2. Atomic positional parameters and temperature factors (Å^2) for $[Pt(C_9H_{14}N_2)_2]Cl_2.4H_2O$, A[a]

Atom	x ($\times 10^4$)	y ($\times 10^4$)	z ($\times 10^4$)	U_{eq}[b] ($\times 10^3$)
Pt	0(0)	0(0)	0(0)	20.4
Cl	532(6)	2983(6)	3081(9)	27.8
N2	242(6)	2178(5)	661(8)	23.9
C3	1590(7)	2814(6)	299(10)	31.7
C4	2719(7)	3741(6)	2626(11)	33.4
C5	3636(6)	2923(6)	4075(10)	30.6
C6	3294(6)	1266(7)	2998(11)	31.7
N7	1755(5)	822(6)	3071(8)	26.5
C8	1439(6)	2167(6)	4512(9)	27.0
C9	1678(8)	4378(6)	3855(11)	32.3
C10	2594(9)	4702(7)	6291(12)	37.4
C11	2992(7)	3202(7)	5921(11)	30.8
Cl	2631(2)	−916(2)	6389(3)	45.8
O1	−2513(6)	2984(6)	−1661(9)	50.1
O2	4635(7)	−1848(6)	317(9)	50.5

[a] Pt lies on an inversion center and thus x, y, and z were not refined.

[b] $U_{eq} = (1/3)(U_{11} + U_{22} + U_{33} + 2U_{23}\cos\alpha + 2U_{13}\cos\beta + 2U_{12}\cos\gamma)$.

[2]The programs DATCO5, ABSORB, and DATRDN from the XRAY76 program (9) were used for preliminary data treatment. The structure was solved with use of SHELX (6). The above calculations were carried out on a Cyber 170/815 computer. The following calculations were carried out on a VAX 8600 computer. Plane calculations were made using LSQPL (10) and torsional angles obtained from CHEMX (11). Molecule and cell packing diagrams were obtained from SNOOPI (12).

[3]Tables of anisotropic temperature factors, hydrogen atom positional parameters and temperature factors, interatomic distances and angles involving hydrogen atoms, torsional angles, and the moduli of F_o and F_c have been deposited. They may be purchased from the Depository of Unpublished Data, CISTI, National Research Council of Canada, Ottawa, Ont., Canada K1A 0S2.

TABLE 3. Interatomic distances (Å) and bond angles (deg)

(*a*) non-hydrogen atoms for $[Pt(C_9H_{14}N_2)_2]Cl_2.4H_2O$

Atoms	Distance	Atoms	Distance	Atoms	Distance
Pt—N7	2.048(4)	Pt—N2	2.046(5)	N7—C8	1.495(8)
N7—C6	1.514(9)	C8—C1	1.557(10)	C8—C11	1.528(8)
C5—C4	1.569(11)	C10—C11	1.525(11)	C1—C9	1.521(9)
C5—C6	1.529(9)	C3—N2	1.516(10)	C4—C9	1.538(11)
C3—C4	1.514(7)	C10—C9	1.514(10)	C5—C11	1.539(9)
C1—N2	1.506(8)				

Atoms	Angle	Atoms	Angle	Atoms	Angle
N2—Pt—N7	78.9(2)	Pt—N7—C6	113.4(4)	Pt—N7—C8	109.4(4)
C8—N7—C6	105.9(5)	N7—C8—C1	110.5(5)	N7—C8—C11	106.1(5)
C1—C8—C11	103.3(6)	C8—C11—C5	97.7(5)	C8—C11—C10	103.7(6)
C10—C11—C5	104.5(7)	C11—C5—C4	103.3(6)	C11—C5—C6	102.4(6)
C6—C5—C4	116.7(5)	C5—C4—C9	102.1(6)	C5—C4—C3	116.8(5)
C3—C4—C9	103.3(5)	C4—C9—C1	98.0(5)	C4—C9—C10	105.5(6)
C10—C9—C1	104.5(7)	C11—C10—C9	95.4(5)	C9—C1—C8	102.9(5)
C9—C1—N2	106.4(6)	C8—C1—N2	110.2(5)	Pt—N2—C1	109.2(4)
Pt—N2—C3	114.4(4)	C1—N2—C3	105.6(4)	N2—C3—C4	104.3(6)
N7—C6—C5	104.1(6)				

(*b*) Hydrogen bonds

Atoms	Distance	Atoms	Distance	Atom	Distance	Atoms	Angle
O1...Cl	3.179(7)	O2...Cl	3.216(6)				
O2...O1	2.78(1)	O2[a]...Cl	3.190(8)				
N2...O1	2.876(9)	N2—H2	0.8(1)	H2...O1	2.3(2)	N2—H2...O1	138(14)
N7...Cl	3.221(8)	N7—H7	0.95(8)	H7...Cl	2.42(7)	N7—H7...Cl	142(4)

[a]Atom related to O(2) by the transformation, $1 - x, -y, 1 - z$.

Discussion

The identity of the minor product, bis(2,7-diazatetracyclo-[6.3.0.0^{4,9}.0^{5,11}]undecane-*N*,*N*′)platinum(II) dichloride tetrahydrate, **A**, was established by X-ray crystallography. The structure of the cation of **A** is shown in Fig. 1 and bond lengths and angles are given in Table 2. The platinum atom lies on an inversion center and the usual square planar arrangement of ligands in a platinum(II) complex is attained by coordination of the amine nitrogen atoms. The Pt—N distances found here (2.048(4), 2.046(5) Å), are similar to those reported for other Pt–amine complexes (13, 14). The rigidity of the tetracyclic ligand has produced a N1—Pt—N3 chelating angle of 79°, which is less than the 83–90° usually observed for square-planar platinum(II) complexes (13–18). The remaining bond lengths and angles of the organic framework agree well with values reported for similar structures (19–21).

The packing of **A** in the unit cell is shown in Fig. 2. The packing arrangement can be described as comprising alternating cation layers and chloride and water layers. Within these latter layers there are chains consisting of six-membered hydrogen bonded rings O1..O2..Cl..O1′..O2′..Cl′ alternating with four-membered hydrogen bonded rings Cl..O2..Cl′..O2′. The cations are bound to the six-membered rings by N7..Cl and N2..O1 hydrogen bonds. Interatomic distances indicating hydrogen-bonding interactions have been included in Table 3.

The results of ^{1}H nmr studies of **A** and the ligand, 2,7-diazatetracyclo[6.3.0.0^{4,9}.0^{5,11}]undecane are reported in Table 4. The amine proton signals were unresolved because of rapid exchange with the solvent, D_2O. The two doublets for H_{10a} and H_{10s}, centered at 1.443 and 1.523 ppm, respectively,

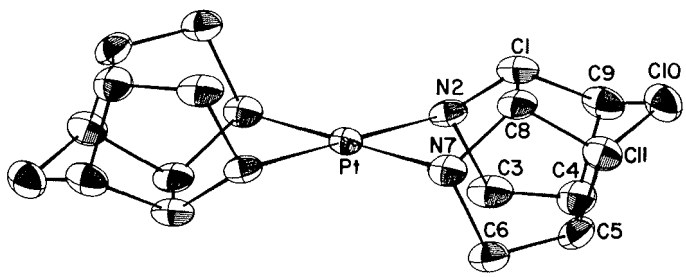

FIG. 1. The cation *trans*-bis(2,7-diazatetracyclo[6.3.0.0^{4,9}.0^{5,11}]-undecane-*N*,*N*′)platinum(II), showing the atom numbering.

represent an AB type system with a geminal coupling of −11.2 Hz. The H_{10s} proton also couples with the two bridgehead protons, H_9 and H_{11}, ($^3J_{10s,9(11)}$ = 1.7 Hz). A singlet at 2.209 ppm represents the H_4 and H_5 protons. The bridgehead protons, H_9 and H_{11}, appear as a singlet at 2.306 ppm. Another AB system caused by $H_{3e}(H_{6e})$ and $H_{3i}(H_{6i})$ is represented by the doublets centered at 2.706 and 2.894 ppm, respectively, with a geminal coupling of −11.6 Hz. The doublet arising from H_{3e} and H_{6e} is further split by coupling to H_4 and H_5, respectively, ($^3J_{3e(6e),4(5)}$ = 2.3 Hz). The H_1 and H_8 protons produced a singlet at 3.058 ppm.

Platination of the ligand results in a withdrawal of electron density from the hydrogen atoms. The extent of this withdrawal is reflected in the relative proton shifts to lower field. The reduction in the geminal coupling constants indicates that the platinum is siphoning electron density away from nitrogen atoms, making them more electronegative or/and the H—C—H bond angle is reduced upon platination of the ligand. The errors

Can. J. Chem. Downloaded from www.nrcresearchpress.com by 213.222.148.141 on 09/07/12
For personal use only.

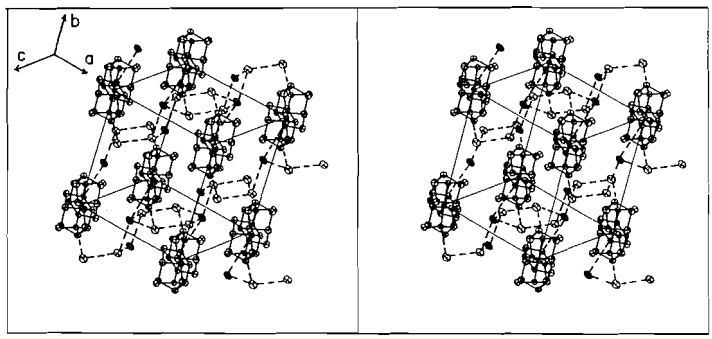

FIG. 2. The packing of **A** within the unit cell. The view is roughly down [1 1 1]. Hydrogen bonds are shown by dotted lines.

TABLE 4. ^{1}H nmr results for $C_9H_{14}N_2$ and $[Pt(C_9H_{14}N_2)_2]Cl_2.4H_2O$, **A**[a]

	$C_9H_{14}N_2$		$[Pt(C_9H_{14}N_2)_2]Cl_2.4H_2O$, **A**	
Proton	Chemical shift (ppm)	Relative intensity	Chemical shift (ppm)	Relative intensity
H-10a	1.443	1	1.623	1
H-10s	1.523	1	2.164	1
H-4,5	2.209	2	2.347	2
H-9,11	2.306	2	2.445	2
H-3e,6e	2.706	2	3.170	2
H-3i,6i	2.894	2	3.550	2
H-1,8	3.058	2	3.777	2

Coupling constants (Hz)	$C_9H_{14}N_2$	**A**
$^2J_{3i,3e;(6i,6e)}$	−11.6	−12.5
$^2J_{10s,10a}$	−11.2	−11.6
$^3J_{10s,9(11)}$	1.7	1.6
$^3J_{3e,4(6e,5)}$	2.3	2.2

[a]Chemical shifts are relative to external sodium 4,4-dimethyl-4-silapentan-1-sulfonate.

TABLE 5. ^{13}C chemical shifts for $C_9H_{14}N_2$ and $[Pt(C_9H_{14}N_2)_2]Cl_2.4H_2O$, **A**

	Chemical shift[a] (ppm)	
Carbon	$C_9H_{14}N_2$	**A**
C-10	27.6	32.9
C-4,5	42.1	41.9
C-9,11	46.6	44.4
C-3,6	47.2	55.7
C-1,8	60.7	72.5

[a]Chemical shifts are relative to external tetramethylsilane.

in the respective geminal H—C—H bond angles, however, do not allow us to confirm or refute any such reduction in these angles. Assignments of the signals were confirmed with use of COSY nmr experiments.

The ^{13}C nmr results are listed in Table 5. Assignments for $C_{4,5}$ and $C_{9,11}$ are not definitive from these experiments alone and may be interchanged. Comparison with similar compounds, however, supports our assignments (22). As expected, the relative shifts of ^{13}C nmr peaks upon platination are much smaller than those observed in the ^{1}H spectra.

The major product, the brown powder, was not satisfactorily identified. It was insoluble in common solvents and this precluded the use of many physical techniques in its identification. The material may have been a mixture containing the desired product, (L—L)$PtCl_2$, and the insolubility suggests a polymeric nature. The vibrational spectra were ambiguous. A poorly resolved band at 316 cm^{-1} might have been $\upsilon_{Pt—Cl}$, but we cannot be certain because it was part of a broad ligand vibrational manifold centered at 330 cm^{-1}. Analytical measurements showed that chlorine was present in the brown solid, but at nowhere near the level needed for (L—L)$PtCl_2$ (*Anal.* calcd. for (L—L)$PtCl_2$: C 26.0, H 3.4, N 6.7, Cl 17.0; found: C 21.4, H 3.2, N 5.8, Cl 10.2).

The question arises as to why it was difficult to obtain (L—L)$PtCl_2$ rather than the (L—L)$_2Pt^{2+}$ compound. This is the second time we have run into this problem recently (18). The problem is more general, however. Magnus' green salt, $[Pt(NH_3)_4][PtCl_4]$, is always formed in small amounts in the normal preparation of *cis*-$Pt(NH_3)_2Cl_2$ (23). It seems that the reaction

$$(L—L)PtCl_2 + L—L \rightarrow (L—L)_2Pt^{2+} + 2Cl^-$$

must be faster than, or at least competitive with, the reaction

$$PtCl_4^{2-} + L—L \rightarrow (L—L)PtCl_2 + 2Cl^-$$

and so (L—L)$PtCl_2$ is converted to (L—L)$_2Pt^{2+}$ as it is formed. To obtain the pure desired product, (L—L)$PtCl_2$, one clearly needs alternative methods of preparation.

Acknowledgements

We acknowledge, with thanks, financial support from the National Cancer Institute of Canada and the Natural Sciences and Engineering Research Council of Canada, and Dr. D. N. Butler, York University, Canada, for providing the sample of amine ligand.

1. Papers in J. Clin. Hematol. Oncol. **7**(1) and **7**(2) (1977). These papers were presented at the 3rd International Conference on Platinum Coordination Complexes in Cancer Chemotherapy, Dallas, TX. October, 1976.
2. W. J. M. HRUSHESKY. *In* Platinum coordination complexes in cancer chemotherapy. *Edited by* M. P. Hacker, E. B. Douple, and I. H. Krakoff. Martin Nijhoff Publishers, Boston. 1984. pp. 165–186.
3. M. L. TOBE and A. R. KHOKHAR. J. Clin. Hemat. Oncol. **7**, 114 (1977) and references therein.
4. P. C. HYDE. *In* Platinum coordination complexes in cancer chemotherapy. *Edited by* M. P. Hacker, E. B. Douple, and I. H. Krakoff. Martin Nijhoff Publishers, Boston. 1984. pp. 216–227.
5. G. B. KAUFFMAN and D. O. COWAN. Inorg. Synth. **7**, 240 (1963).

Can. J. Chem. Downloaded from www.nrcresearchpress.com by 213.222.148.141 on 09/07/12
For personal use only.

6. G. M. SHELDRICK. SHELX. Program for crystal structure determination. University of Cambridge, England. 1976.
7. D. T. CROMER and J. T. WABER. International tables for X-ray crystallography. Vol. IV. *Edited by* J. A. Ibers and W. C. Hamilton. Kynoch Press, Birmingham, England. 1974. Table 2.2B. pp. 99–101.
8. D. T. CROMER and J. T. WABER. International tables for X-ray crystallography. Vol. IV. *Edited by* J. A. Ibers and W. C. Hamilton. Kynoch Press, Birmingham, England. 1974. Table 2.3.1 pp. 149, 150.
9. J. M. STEWART. The XRAY 76 System Tech. Report TR-446, Computer Science Center, University of Maryland, College Park, MD. 1976.
10. LSQPL, Calculation of Least-squares Planes, George Davenport, Crystallography Center, Univ. of Western Australia, Nedlands, WA. Australia 6009. Part of the XTAL System of Crystallographic Programs, eds. J. M. Stewart and S. R. Hall, Computer Science Technical Report Series, TR-1364, December, 1983, Univ. of Maryland, College Park, MD 30742, U.S.A.
11. K. DAVIES. Chem-X, developed and distributed by Chemical Design Ltd., Oxford, England. 1986.
12. K. DAVIES. CHEMGRAF Suite: Program SNOOPI, Chemical Design Ltd., Oxford, England. January, 1983.
13. C. J. L. LOCK, R. A. SPERANZINI, and M. ZVAGULIS. Acta Crystallogr. B**36**, 1789 (1980) and references therein.
14. H. E. HOWARD-LOCK, C. J. L. LOCK, G. TURNER, and M. ZVAGULIS. Can. J. Chem. **59**, 2737 (1981) and references therein.
15. R. FAGGIANI, B. LIPPERT, and C. J. L. LOCK. Inorg. Chem. **19**, 295 (1980).
16. R. BAU, R. W. GELLERT, S. M. LEHOVEC, and S. LOUIE. J. Clin. Hemat. Oncol. **7**, 5 (1977).
17. C. J. L. LOCK and P. PILON. Acta Crystallogr. B**37**, 45 (1981).
18. B. E. BROWN and C. J. L. LOCK. Acta Crystallogr. C**43**, 12 (1987).
19. A. S. SECCO and J. TROTTER. Acta Crystallogr. C**39**, 782 (1983).
20. M. CATELLANI, G. P. CHINSOLI, and P. SGARABOTTO. J. Organomet. Chem. **240**, 311 (1982).
21. T. A. HAMOR and D. J. WATKIN. J. Chem. Soc. Perkin II, 140 (1974).
22. A. P. MARCHAND. Texas A & M NMR Newsletter, Jan. No. 340. 1987. p. 10.
23. G. B. KAUFFMAN and D. O. COWAN. Inorg. Synth. **7**, 241 (1963).

Can. J. Chem. Downloaded from www.nrcresearchpress.com by 213.222.148.141 on 09/07/12
For personal use only.